Table of Contents

General_Authors_Publications.....2
LI-263682_Permeable_pavement-Water_Environment_Research.....7
Microorganism_Removal_in_Permeable_Pavement_Parking_Lots_in_Edison_Environment16
Permeable_pavement-Water_Environment_Research.....17
Record_of_Percentage-Selvakumar.....26
RecordofPercentage-OConnor.....27
WEF_letter_-_one_of_the_top_cited.....28

United States Environmental Protection Agency
Washington, DC 20460

STAA REPORT FOR THE SCIENTIST NOMINATIONS

General Information:

Nomination ID/App ID:	20-069
Research Category Primary:	Other Environmental Research (OR)
Research Category Secondary:	Other Environmental Research (OR)
Laboratory/Office Name:	ORD
Nomination Entered By:	Ariamalar Selvakumar

Eligibility Checklist:

[Y] The nominated publication(s) has not been submitted to a previous STAA competition.

[Y] The nominated publication(s) was published on or before January 1, 2017 and on or after January 1,2012

[Y] The principal author was an EPA employee or a PHS employee assigned to EPA when the research was performed

[Y] The EPA authors (includes PHS employees assigned to EPA) contributed collectively a minimum of 50% toward the publication(s)

Nominating Official Name:	Regan Murray
Nominating Official Title:	SUPERVISORY INTERDISCIPLINARY SCIENTIST
Nominating OfficialEmail:	murray.regan@epa.gov
STAA Coordinator Name:	Kathleen Wiser
STAA Coordinator Email:	wiser.kathi@epa.gov

Justifications:

Justification 1:

Nearly half of the nation’s assessed surface waters remain incapable of maintaining water quality adequate for supporting one or more designated uses, such as recreational swimming, fishing, or drinking water supply. National biennial water quality surveys consistently indicate waters are impaired by bacterial indicators, nutrients, sediments, and assorted toxic chemical loadings. A leading cause of this impairment is non-point source stormwater runoff from agricultural and urban areas. Stormwater runoff is commonly treated by stormwater control measures (SCMs), which include wet ponds, wetlands, bioretention areas, dry detention basins, permeable pavements, rain gardens, and proprietary devices. Permeable pavement is an infiltration system where the stormwater runoff infiltrates through a permeable layer of pavement or other stabilized surface, reducing the need for runoff drainage and treatment offsite. This research was conducted to evaluate the performance of permeable pavement in removing indicator organisms such as fecal coliform, enterococci, and E. coli from infiltrating stormwater runoff. The results from this research are intended to assist U.S. EPA program and regional offices to implement Clean Water Act (CWA) and Safe Drinking Water Act (SDWA) requirements; to help states and tribes meet their programmatic requirements; and to assist utilities to more effectively implement comprehensive management of stormwater runoff.

Justification 2A:

N/A

Justification 2B:

N/A

Justification 2C:

N/A

Justification 2D:

N/A

Justification 2E:

N/A

Justification 3A:

This paper addresses the performance of permeable pavements in reducing the concentration of microorganisms in stormwater runoff. Three types of permeable pavements were monitored at the Edison Environmental Center in Edison, New Jersey, for indicator organisms such as fecal coliform, enterococci, and Escherichia coli. Results showed that porous asphalt had a much lower concentration in monitored infiltrate compared to pervious concrete and permeable interlocking concrete pavers; concentrations of monitored organisms in infiltrate from porous asphalt were consistently below the bathing water quality standard. Concentration reductions greater than 90% were observed for all three indicator organisms for porous asphalt and fecal coliform and E. coli for pervious concrete when compared to runoff values, while permeable interlocking concrete pavers only had a modest (39%) observable reduction for E. coli only. This information is very useful to municipalities and developers in selecting the type of pavement for their intended purpose. This article was read by many people with interest and was among the journal's top cited papers for 2018-2019 as tracked by publisher John Wiley. This article was cited 5 times since January 2018.

Justification 3B:

There were several levels of peer-review associated with the publication of the nominated article. The article was internally reviewed by EPA staff, branch chief and division director including an internal QA review and cleared for publication. In addition, *Journal of Water Environment Research* utilizes three peer reviewers and a Managing Editor from the Board of Editorial Review to decide whether or not a paper is accepted. The process is highly competitive.

AUTHORS

Principal Author

Author Name:	Ariamalar (Ari) Selvakumar	
Professional Title:		Salutation:
Email:	selvakumar.ariamalar@epa.gov	Organization:
Mailing Address:		
Street Line 1:		
City:		
Zip Code:		State:
At time of research was:	EPA Employee	
Separation Date:		
% of Effort:	70	

Contributing Author

Author Name:	Thomas OConnor	
Professional Title:		Salutation:
Email:	oconnor.thomas@epa.gov	Organization:
Mailing Address:		
Street Line 1:		
City:		
Zip Code:		State:
At time of research was:	EPA Employee	
Separation Date:		
% of Effort:	30	

PUBLICATIONS

Publication 1:

Publication Title:	Organism Detection in Permeable Pavement Parking Lot Infiltrates at the Edison Environmental Center,		
Publication Date:	Mon Jan 01 00:00:00 GMT 2018		
Journal/Publication Method:	Water Environment Research		
All Author(s):			
Volume:	90	Number:	1
Pages:	21-29	Immediately Index:	Immediately Index:
Citation ½ Life:	8.40	Impact Factor:	0.5

Organism Detection in Permeable Pavement Parking Lot Infiltrates at the Edison Environmental Center, New Jersey

Ariamalar Selvakumar[1*], Thomas P. O'Connor[2]

ABSTRACT: Three types of permeable pavements were monitored at the Edison Environmental Center in Edison, New Jersey, for indicator organisms such as fecal coliform, enterococci, and *Escherichia coli*. Results showed that porous asphalt had a much lower concentration in monitored infiltrate compared to pervious concrete and permeable interlocking concrete pavers; concentrations of monitored organisms in infiltrate from porous asphalt were consistently below the bathing water quality standard and actually had limited detection. Fecal coliform and enterococci exceeded bathing water quality standards more than 72 and 34% of the time for permeable interlocking concrete pavers and pervious concrete, respectively. Concentration reductions greater than 90% were observed for all three indicator organisms for porous asphalt and fecal coliform and *E. coli* for pervious concrete when compared to runoff values, while permeable interlocking concrete pavers only had a modest (39%) observable reduction for *E. coli* only. The near absence of indicator organisms observed in the porous asphalt infiltrate may be due to the high pH potentially due to asphalt processing. Neither rain intensity nor temperature was demonstrated to have an observable effect in both concentrations of organisms and performance of permeable pavement; but this may due to the limitations of the dataset consisting of 16 events over an 8-month period. *Water Environ. Res.*, **90,** 21 (2018).

KEYWORDS: permeable pavement, indicator organisms, bathing water quality standard, infiltrate, stormwater runoff.

doi:10.2175/106143017X14902968254575

[1*] National Risk Management Research Laboratory, Office of Research and Development, U.S. Environmental Protection Agency, 2890 Woodbridge Avenue, Edison, NJ 08837; e-mail: selvakumar.ariamalar@epa.gov

[2] National Risk Management Research Laboratory, Office of Research and Development, U.S. Environmental Protection Agency, Edison, New Jersey

Introduction

Since the inception of the Clean Water Act in 1972, the United States has made great efforts in restoring and preserving the physical, chemical, and biological integrity of the nation's waters. However, nearly half of the nation's assessed surface waters remain incapable of maintaining water quality adequate for supporting one or more designated uses, such as recreational swimming, fishing, or drinking water supply (U.S. EPA, 2007). National biennial water quality surveys consistently indicate waters are impaired by bacterial indicators, nutrients, sediments, and assorted toxic chemical loadings. A leading cause of this impairment is non-point source stormwater runoff from agricultural and urban areas affecting an estimated 46% of impaired rivers and streams, 22% of impaired lake areas, and 22% of impaired estuaries (U.S. EPA, 2009). More river and stream miles were affected by pathogenic indicator microorganisms than any other pollutant (U.S. EPA, 2009).

Stormwater discharges release pathogenic bacteria, protozoan, and viruses to receiving waters (Pandey et al., 2014). Tata-Maharaj and Scholz (2010) reported typical concentrations in urban runoff as *Escherichia coli* (*E. coli*) (10^2 to 10^7 colony forming unit [CFU/100 mL]), fecal streptococci (10^2 to 10^6 CFU/100 mL) and fecal coliforms (10^3 to 10^7 CFU/100 mL). Selvakumar and Borst (2006) reported concentration ranges for fecal coliforms (5.6×10^3 to 2.2×10^4 CFU/100 mL), enterococci (1.0×10^3 to 6.6×10^3 CFU/100 mL), and *E. coli* (1.5×10^3 to 8.5×10^3 CFU/100 mL) in urban stormwater runoff. Pitt (2011) reported similar nationwide median concentrations for fecal coliform and *E. coli* using data from a number of National Pollutant Discharge Elimination System (NPDES) Municipal Separate Storm Sewer System (MS4) stormwater permit holders.

Fecal indicator microorganisms are found in feces from both human sources (e.g., sewer discharges, and failing septic systems) and domestic and wild animals (Whitlock, et al., 2002). Burton and Pitt (2002) also note potential sources to paved areas from atmospheric deposition and erosion of previously contaminated soils. Indicator microorganisms tested by public health agencies include total coliform, fecal coliform, fecal

streptococci, *E. coli,* and enterococci. The concentrations of these indicators are used to determine the potential for fecal contamination and to compare to public health-based thresholds. These species may not be harmful to humans themselves; however, their presence can indicate fecal contamination. Indicator microorganisms are used to test surface waters. They serve as a proxy because it is difficult to measure the actual pathogens.

In 1976, the U.S. Environmental Protection Agency's (U.S. EPA) recommended that states adopt a bathing water quality standard (BWQS) of fecal coliforms not to exceed 200 organisms/100 mL (U.S. EPA, 1976). In 1986, based on statistical analysis, U.S. EPA recommended that states revise the recreational water quality microbial criteria to use enterococci for marine waters and *E. coli* or enterococci for freshwaters as *E. coli* and enterococci are more representative of warm-blooded animal fecal contamination in water than total or fecal coliforms. Suggested criteria are 35 enterococci per 100 mL for marine waters and 33 enterococci per 100 mL and 126 *E. coli* per 100 mL for freshwaters (U.S. EPA, 1986).

Stormwater runoff is commonly treated by stormwater control measures (SCMs), which include wet ponds, wetlands, bioretention areas, dry detention basins, permeable pavements, rain gardens, and proprietary devices. Increasingly, SCMs are being incorporated on-site as low impact development (LID) or as green infrastructure (GI) in the municipal right of way. A combination of factors (e.g., predation, sedimentation, sorption, filtration, light, pH, biological oxygen demand, and dissolved oxygen) can contribute significantly to the inactivation of indicator bacteria in SCMs (Struck et al., 2008). Permeable pavement, an alternative to conventional pavement, is a LID/GI infiltration system where the stormwater runoff infiltrates through a permeable layer of pavement or other stabilized surface, reducing the need for runoff drainage and treatment offsite (Field and Sullivan, 2003). Permeable pavement systems can enhance stormwater quality after infiltrating through the system (Clausen and Gilbert, 2003; Ellis, et al., 2004; Gilbert and Clausen, 2006; James and Thompson, 1997; Rushton, 2001). There are a variety of permeable pavements and each has unique characteristics that lend themselves to application in specific environments. Permeable pavement usually diverts stormwater runoff into an underground stone reservoir before gradually exfiltrating out of the stone reservoir into the subsoil (Field and Sullivan, 2003) though there are also systems that have a limited storage reservoir for various reasons (e.g., high groundwater, significant underground infrastructure) that discharge to the nearest conveyance system or surface water.

Although many SCMs have been studied for removal of microorganisms, there are limited studies on the effectiveness of porous pavements (Hathaway and Hunt, 2012; Hathaway et al., 2009). Tata-Maharaj and Scholz (2010) found that permeable pavement was effective in removing microorganisms such as total coliforms, *E. coli*, and fecal streptococci by 98 to 99%. Similarly, few studies have assessed the effectiveness of SCMs on the seasonal removal of microorganisms (Hathaway and Hunt, 2012). Li and Davis (2009) observed the highest *E. coli* and fecal coliform concentrations in the runoff during the summer; however, SCM removal efficiency remained same and was not correlated to the temperature. Tata-Maharaj and Scholz (2010) found that the rates of microbiological degradation remained constant and were not negatively affected by temperature variations due to seasonal changes.

The objectives of this study were to: 1) evaluate the performance of permeable pavement in removing indicator organisms such as fecal coliform, enterococci, and *E. coli* from infiltrating stormwater runoff; and 2) evaluate potential seasonal effects and rainfall intensity on infiltrate concentrations of indicator organisms.

Methods

U.S. EPA's Office of Research and Development operates the Urban Watershed Research Facility (UWRF) at the Edison Environmental Center (EEC) in Edison, New Jersey. The UWRF serves as a location to perform both laboratory-scale and field-scale studies to test monitoring methods and performance of SCMs. The UWRF allows U.S. EPA to better understand SCM performance and monitoring methods with a high level of control over external factors. The EEC is a 200-acre campus that has been shown to have representative runoff comparable to literature values (e.g., Brown and Borst, 2015, specifically relate for nutrients and total organic carbon) and is subject to many of the same potential suburban fecal inputs of wild animals to storm systems, namely deer, geese, pigeons, and seagulls.

At the EEC in 2009, U.S. EPA constructed a functional, 0.4 ha, 110-space parking lot that is surfaced with three different permeable pavement types: permeable interlocking concrete pavers (PICP), pervious concrete (PC), and porous asphalt (PA). The site, depicted in Figure 1, was opened for use in October 2009 and it is used daily by EEC staff and visitors.

The three head-to-head parking rows with permeable pavement systems are 11.58 m wide by 42.67 m long while the 7.62 m wide travel lanes are paved with traditional impervious hot mix asphalt. There is a 1.6% surface slope so that each permeable surface receives runoff from the adjacent travel lanes to the north. All surfaces were constructed over an open-graded subbase reservoir of recycled concrete aggregate (RCA) crushed on site to the size of American Association of State Highway and Transportation Officials (AASHTO) No. 2 size aggregate. Five sections of each permeable pavement system allow water to infiltrate the underlying soil while four of the sections have an impermeable liner 40 cm below each permeable surface, which allows infiltrate to be collected for measurement and sampling. The thickness of each permeable surface varies depending on structural needs for that particular application. The PA is 8 cm thick and PC is 15 cm thick. The individual pavers are 9 cm thick and were placed on a 5-cm layer of AASHTO No. 8 aggregate, which also filled spaces between pavers; an additional 10-cm layer of AASHTO No. 57 aggregate separated the AASHTO No. 8 and common RCA aggregate for PICP. The infiltration capacity of all three surfaces is very large; the infiltration rate of PC was approximately twice that of PICP. Permeable interlocking concrete pavers and PC had infiltration

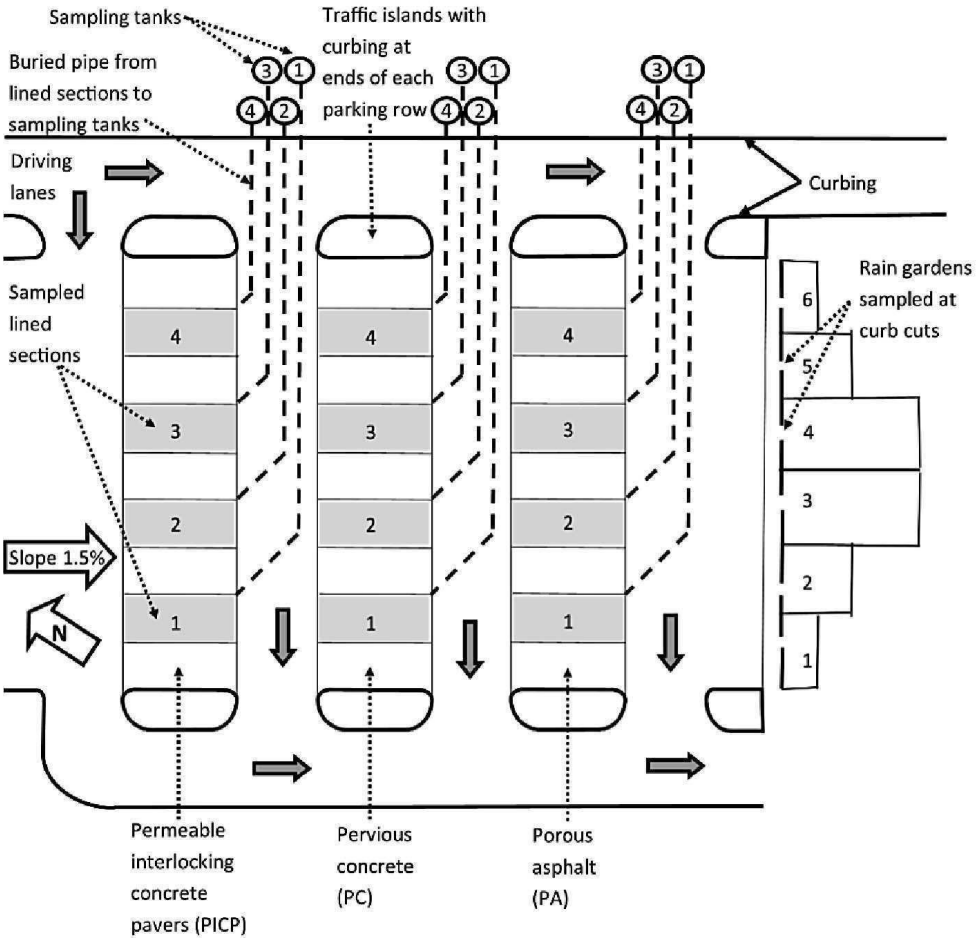

Figure 1—Plan view of parking lot.

rates that were more than one order of magnitude larger than PA. Although the surface infiltration rates vary by more than an order of magnitude, each is much larger than the reasonably expected rain event (Brown and Borst, 2014; U.S.EPA, 2010). A more detailed description of the liners, permeable surfaces and drainage piping is provided in Brown and Borst (2014).

Flow-weighted samples were collected using programmable automatic samplers. Samples were collected from the drainage pipes for collection tanks for permeable surfaces 1 and 3 (see Figure 1) for each permeable surface. Surface runoff samples were also collected at two curb cuts (CC) (4 and 5 rain gardens) at the south end of the parking lot that collects runoff from impermeable asphalt surface. The automatic sampler collected discrete samples in up to 24 1-l HDPE bottles. The sampling interval was set using the forecast duration from the National Weather Service.

Sixteen sampling events were conducted between July 2015 and February 2016. Collected samples were transported to the UWRF laboratory and analyses were initiated within the standard holding time of 6 hours. Samples were analyzed for

Table 1—Summary statistics of fecal coliform for monitored storm events.

Statistics	Driving lane surface runoff (CC)	Permeable interlocking concrete pavers (PICP)	Porous concrete (PC)	Porous asphalt (PA)
Detection frequency (%)	88	94	100	6
Geometric mean (MPN/100 mL)	**412**[a]	**601**[a]	60	NA
Arithmetic mean (MPN/100 mL)	**5054**[a]	**1911**[a]	177	NA
Median (MPN/100 mL)	2254	1065	58	NA
Maximum (MPN/100 mL)	24 196	8665	692	331
Minimum (MPN/100 mL)	0	0	3	0
Standard deviation (MPN/100 mL)	8118	2289	232	NA

[a] Mean concentration exceeds BWQS (bolded).
NA: cannot be calculated as it was detected only once.

Table 2—Summary statistics of enterococci for monitored storm events.

Statistics	Driving lane surface runoff (CC)	Permeable interlocking concrete pavers (PICP)	Porous concrete (PC)	Porous asphalt (PA)
Detection frequency (%)	100	100	100	87.5
Geometric mean (MPN/100 mL)	**66**[a]	**115**[a]	25	3
Arithmetic mean (MPN/100 mL)	**1070**[a]	**212**[a]	**72**[a]	9
Median (MPN/100 mL)	37	171	30	3
Maximum (MPN/100 mL)	12 243	578	338	39
Minimum (MPN/100 mL)	2	5	1	0
Standard deviation (MPN/100 mL)	3076	191	96	12

[a] Mean concentration exceeds BWQS (bolded).

indicator microorganisms such as fecal coliform, enterococci, and *E. coli*. Fecal coliform and *E. coli* were enumerated using Colilert incubating at 35 and 44.5 °C for 24 hours, respectively and enterococci was enumerated using Enterolert incubating at 41 °C for 24 hours (IDEXX Laboratories, Inc., Westbrook, Maine). Colilert and Enterolert are commercially available enzyme-substrate liquid-broth mediums (IDEXX Laboratories, Inc., Westbrook, Maine). All enumerations were performed using Quanti-tray 2000 trays, which use a most probable number (MPN)-based protocol with a quantitation range from less than 1 colony forming unit (CFU)/100 mL to 2419.6 CFU/100 mL without sample dilution. Each sample was analyzed with and without dilution; infiltrate was analyzed at 10 times dilution (observable range of 10 to 24 196 CFU/100 mL) and runoff samples were analyzed at 20 times dilution (observable range 20 to 48 392 CFU/100 mL). Results were reported as the average of the undiluted and diluted analysis. When there were no observed concentrations for both the undiluted and diluted analysis, the sample concentration was zero as no organisms were present.

Rainfall was measured using a 0.1-mm tipping bucket rain gauge and recorded with a Campbell Scientific CR1000 data logger (Logan, Utah) set to record at 10-minute intervals. The tipping bucket rain gauge is located in the field adjacent to the collection tanks to the east of the parking lot. All storms had at least 2.54 mm (0.1 in.) of rainfall as per NPDES guidance (U.S. EPA, 1992). Air temperature was measured at the UWRF weather station.

Statistical analysis was conducted to evaluate the performance of permeable pavement parking lots in treating stormwater infiltrate except for fecal coliform and *E. coli* in the PA infiltrate which were detected at a frequency $< 10\%$, which effectively restricts statistical analysis (U.S. EPA, 2000). For all other infiltrate and runoff concentration, detection frequency was 50% or greater. Summary statistics, that is, geometric and arithmetic means, medians, standard deviations, were performed in Excel. To calculate the geometric means, a substitution was required for non-detects (0) and unity (1) was used (UWRRC, 2014). Atchison's Method (U.S. EPA, 2000), a conservative method, was used to calculate arithmetic mean and standard deviation. Atchison's method adjusts the arithmetic mean and standard deviation by assuming that non-detects are actually zero, which is the case in this study as described above.

Normality of data sets were tested by the Shapiro-Wilk W test using Satistica 10 (StatSoft, 2011). A nonparametric Wilcoxon Matched Pair Test (StatSoft, 2011) was used to determine concentration differences between and within permeable surfaces; nonparametric methods can reduce the influence of outliers such as non-detects and values greater than maximum reporting limit. A statistical significance value of $p \leq 0.05$ was used for all statistical analysis. Box and whisker plots were created to display the data with median as the center point and 25 and 75% as quartiles.

Probability plots were developed in Excel spreadsheets (Microsoft, 2013) to evaluate the performance of different permeable surfaces. Probability was calculated using the following equation (Burton and Pitt, 2002):

$$p = \frac{i - 0.5}{n} \tag{1}$$

where, p is probability of given observation; i is rank of observation within group n; and n is total number of observations within a given data set. These probability values

Table 3—Summary statistics of *E. coli* for monitored storm events.

Statistics	Driving lane surface runoff (CC)	Permeable interlocking concrete pavers (PICP)	Porous concrete (PC)	Porous asphalt (PA)
Detection frequency (%)	75	81	50	0
Geometric mean (MPN/100 mL)	13	8	2	NA
Arithmetic mean (MPN/100 mL)	**1315**[a]	49	2	NA
Median (MPN/100 mL)	6	8	1	NA
Maximum (MPN/100 mL)	12 141	344	7	0
Minimum (MPN/100 mL)	0	0	0	0
Standard deviation (MPN/100 mL)	3604	104	3	NA

[a] Mean concentration exceeds BWQS (bolded).
NA: cannot be calculated as it was not detected.

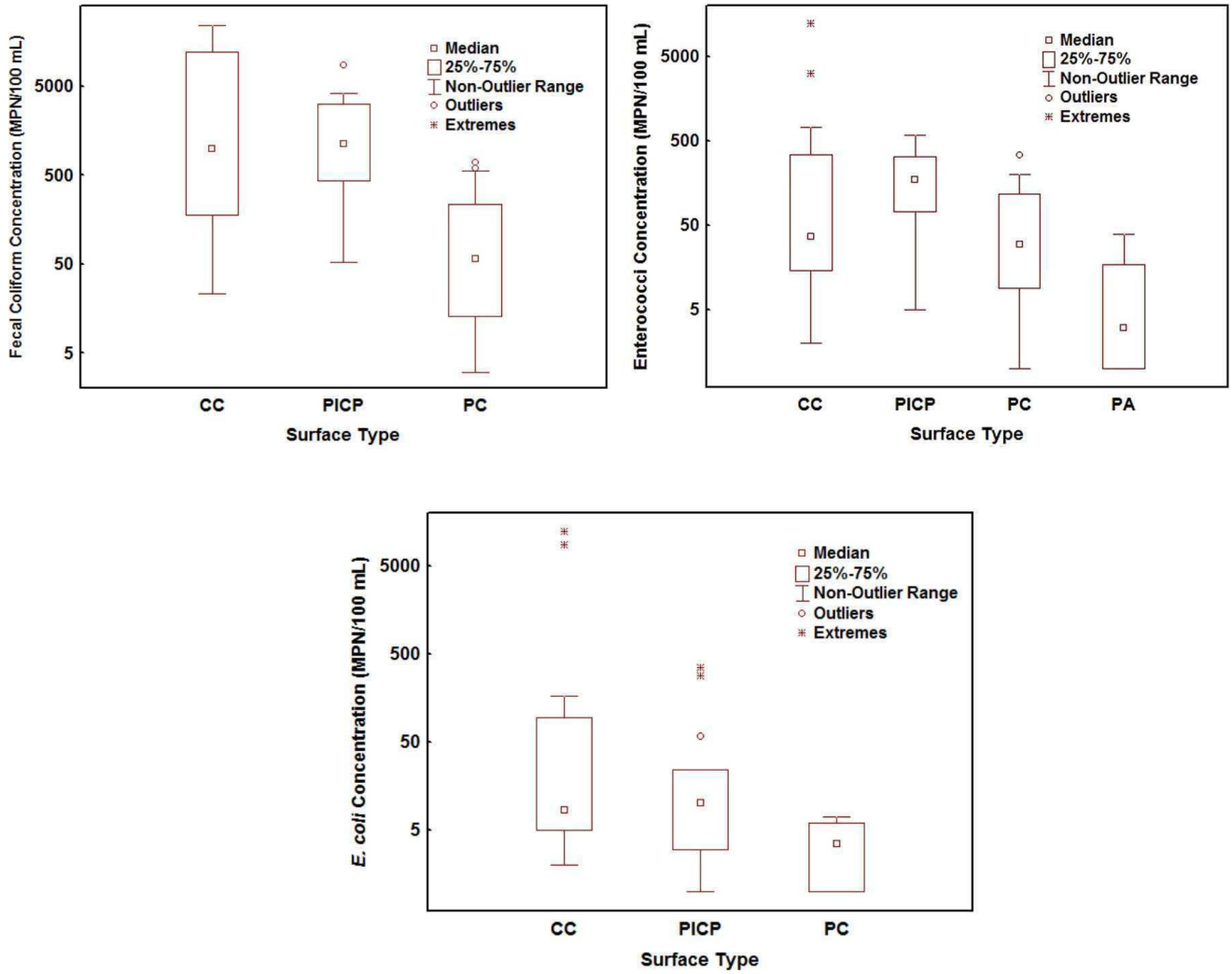

Figure 2—Box and whisker plots for permeable surface infiltrate concentrations.

(ordinate) were then plotted against organism concentrations (abscissa) and compared against a vertical straight line representing the BWQS (freshwater criteria, if applicable) for respective microorganisms to demonstrate exceedance occurrences.

Treatment by infiltration through the pavement surfaces was determined by calculating percent removal of infiltrate concentration of each surface in comparison to common driving lane surface runoff values collected at the CCs. Geometric mean concentrations were used for the calculation. A nonparametric Wilcoxon Matched Pair Test (StatSoft, 2011) was used to determine statistical significance of the differences between driving lane surface runoff and permeable surface infiltrate concentrations.

A least squares log normal regression analysis was performed on rainfall and temperature in comparison to microbial indicator organism concentrations.

Results and Discussion

Summary statistics for the sampling events are presented in Tables 1 to 3 and Box and Whisker plots are shown in Figure 2. Fecal coliform was detected in infiltrates from both PICP and PC; it was only detected once in PA. The geometric mean fecal coliform concentration in the runoff (represented by CC for curb

Table 4—Indicator organism concentration differences within surfaces.

	Fecal coliform		Enterococci		*E. coli*	
Pavement types	***p*-value**	**Statistical significance**	***p*-value**	**Statistical significance**	***p*-value**	**Statistical significance**
PICP-1 vs. PICP-3	**0.0007**	Yes	0.121	No	0.15	No
PC-1 vs. PC-3	**0.007**	Yes	0.078	No	1.0	No

Table 5—Indicator organism concentration differences between surfaces

	Fecal coliform		Enterococci		*E. coli*	
Pavement types	***p*-value**	**Statistical significance**	***p*-value**	**Statistical significance**	***p*-value**	**Statistical significance**
PICP vs. PC	0.0027	Yes	0.0007	Yes	0.0047	Yes
PICP vs. PA	0.0007	Yes	0.0004	Yes	0.0015	Yes
PC vs. PA	0.0004	Yes	0.0024	Yes	0.0117	Yes

cuts in Figure 2) was 412 MPN/100 mL. The geometric mean fecal coliform concentrations in infiltrates from PICP and PC were 601 and 60 MPN/100 mL, respectively; the geometric mean for PICP infiltrate exceeded the BWQS of 200 MPN/100 mL.

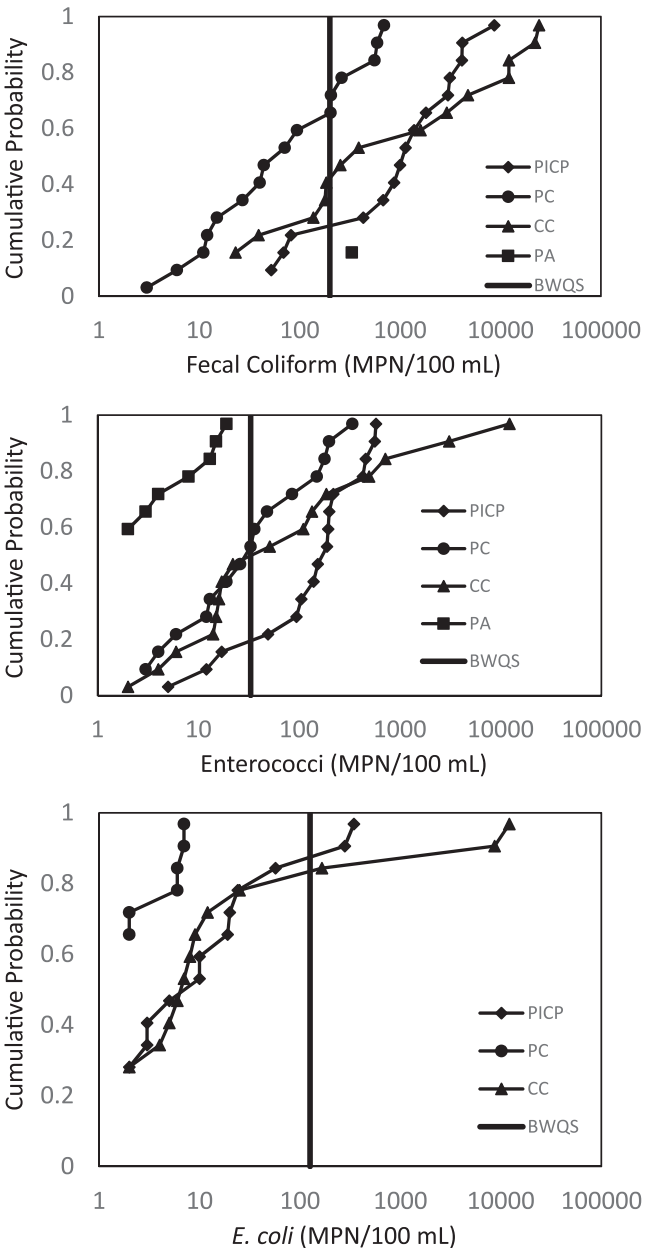

Figure 3—Cumulative probability plots of indicator organisms.

Geometric mean for PA infiltrate was not calculated as it was detected only once.

The geometric mean of fecal coliform concentration in PICP infiltrate was greater than the concentration in the runoff. However, the arithmetic mean concentrations in the infiltrates are less than the concentration in the runoff. The concentrations of PICP and PC infiltrate were log normally distributed over the 16 events. Concentrations of fecal coliform in the infiltrate of PICP were always higher than that of PC and PA.

The geometric mean enterococci concentration in the runoff was 66 MPN/100 mL. The enterococci were detected 100% of the time for PICP and PC and was the most observed microorganism in PA infiltrate at 87.5% of events, even though the PA MPN were very low in comparison to PICP and PC. The geometric mean enterococci concentration in infiltrates from PICP, PC, and PA were 115, 25, and 3 MPN/100 mL, respectively, with only PICP mean exceeding BWQS of 33 MPN/100 mL.

E. coli was detected in PICP during 81% of the events. It was detected in only 50% of the events in PC and at concentrations lower than the PICP. The geometric mean *E. coli* concentrations in infiltrates from PICP and PC were 8 and 2 MPN/100 mL, respectively, while *E. coli* was not detected in PA. The geometric mean concentration in the runoff was 13 MPN/100 mL.

Wilcoxon Matched Pair Test (StatSoft, 2011) indicated there was a statistically significant difference within surfaces for PICP and PC for fecal coliform as shown in Table 4. There was no statistically significant difference within surfaces for enterococci and *E. coli* (Table 4). There is statistically significant difference

Table 6—Percent indicator organism concentrations reductions for permeable pavement infiltrates based on difference of geometric means to runoff.

Organism	Surface type	Concentration reduction (%)
Fecal Coliform	PICP	0[a]
	PC	**93**
	PA	**94[b]**
Enterococci	PICP	0[a]
	PC	**62**
	PA	**100**
E. coli	PICP	**39**
	PC	**100**
	PA	**100**

[a] Concentration in PICP infiltrate was greater than concentration in runoff.
[b] Based on 6% detection frequency.

Table 7—Results of Wilcoxon Matched Pair Test.

	Fecal coliform		Enterococci		*E. coli*	
Surface type	*p*-value	Statistical significance	*p*-value	Statistical significance	*p*-value	Statistical significance
PICP	0.3066	No	0.4228	No	0.9770	No
PC	0.0151	**Yes**	0.5180	No	0.0063	**Yes**
PA	0.0009	**Yes**	0.0110	**Yes**	0.0022	**Yes**

between all three surfaces ($p < 0.05$) (Table 5) for all three microorganisms.

Exceedance of Bathing Water Quality Standards. Probability of exceedance of U.S. EPA BWQS are shown in Figure 3 with the vertical line representing the respective BWQS for each microorganism. The probability of exceedance is where the curve crossed the BWQS. The BWQS of 200 MPN/100 mL for fecal coliform was exceeded 72 and 34% of the time for PICP and PC, respectively. The BWQS of 33 MPN/100 mL for enterococci was exceeded 78 and 47% of times for PICP and PC, respectively. The BWQS of 126 MPN/100 mL for *E. coli* was exceeded only 9% of times for PICP.

Potential Reduction in Concentration of Indicator Organisms. Estimated concentration reductions of microorganisms based on geometric means for each permeable pavement type in comparison to the common driving lane surface runoff collected at the rain garden CCs is documented in Table 6. Permeable interlocking concrete pavers reduced concentrations for only 1 of the three organisms studied, *E. coli* at 55%. Concentration reductions of greater than 90% were observed for PC infiltrate for fecal coliform and *E. coli*, while enterococci had a 62% reduction. The highest reductions were observed in PA infiltrate for all three organisms.

Results of Wilcoxon Matched Pair Test are shown in Table 7. Porous asphalt significantly reduced the concentration of all three organisms ($p \leq 0.05$), whereas PC reduced fecal coliform and *E. coli*. Permeable interlocking concrete pavers did not significantly reduce any of the organisms. Statistical analyses agreed with the concentration reductions listed in Table 6.

The large reductions from runoff by and near complete absence of observed organisms in the PA system is most likely due to the high pH of the PA infiltrate. The high pH of the infiltrate systems was previously presented in Brown and Borst (2015), though their paper focused on the initial 13 storm events sampled from October 2010 until September 2011. These high pH observations have continued through 2015 (O'Connor and Borst, 2017), which coincides with the time period of this current study. The infiltrate from PC and PICP was observed to be around 9; however, pH of infiltrate from PA was consistently as high as 11 (O'Connor and Borst, 2017), which may explain why microorganism concentrations in the infiltrate from PA are low or non-existent compared to the other two surfaces. The cause of this high pH in the PA infiltrate is suspected to be asphalt emulsions, which are used in the asphalt processing. Specifications called for asphalt mix between 4.0 and 4.5% asphalt and liquid anti-stripping agent. Anionic emulsions have a high pH (e.g., pH 10 to 12) (Transportation Research Board, 2006), which is in the range of the pH observations for the PA infiltrate. Alternatively, asphalt emulsions can be cationic as well with correspondingly acidic pH (e.g., pH 1 to 4) (Transportation Research Board, 2006).

Effects of Weather. Between July 2015 and February 2016, 16 sampling events were conducted, which equates to two events per month. Rain depth ranged from 3.4 to 39.4 mm with the mean size of 18.6 mm and median size of 19.7 mm. Rain depth is normally distributed as shown in Figure 4. Least-square log normal regression analysis of rain depth and indicator organism concentrations for all the surfaces had low coefficient of determination ($R^2 \leq 0.33$), which agrees with findings by other researchers (Hathaway et al., 2010; McCarthy et al., 2007).

Event temperatures ranged from –1.1 °C to 26.4 °C with a mean of 15 °C and median of 13.58 °C (Figure 5). Least-squares log normal regression analysis of temperature and indicator organism concentrations for all three surfaces had low coefficient of determinations ($R^2 \leq 0.20$).

Conclusion

Porous pavements function as infiltration SCMs, with stormwater runoff passing through the permeable surface where pollutants are removed and stored in the storage gallery. This study's research suggests that, of the three pavement types tested, PA consistently had the lowest concentration of indicator microorganisms' load and the concentrations of organisms in the infiltrate water were below the bathing water quality standards. There was a statistically significant difference between all three surfaces for all three organisms with PICP having the highest observed concentrations and frequency of detection.

As expected, impervious driving lane runoff mean concentrations exceed BWQS for all microbial indicators. Results of the probability plots (Figure 3), estimated percent removals (Table 6), and Wilcoxon Matched Pair Test (Table 7) show consistently that permeable asphalt had large reductions of indicator microorganism concentrations. No reduction in concentrations of fecal coliform and enterococci were observed in PICP infiltrate as the geometric concentrations in the infiltrate were greater than the concentrations in the runoff. Concentration reductions of greater than 90% were observed with the exception of enterococci (62%) in PC infiltrate. PICP was most prone to not to reduce concentrations significantly and to have mean concentrations exceeding BWQS for fecal coliform and enterococci.

Despite PA having the shortest profile of 8 cm above the common gallery of RCA, it had the lowest observed concen-

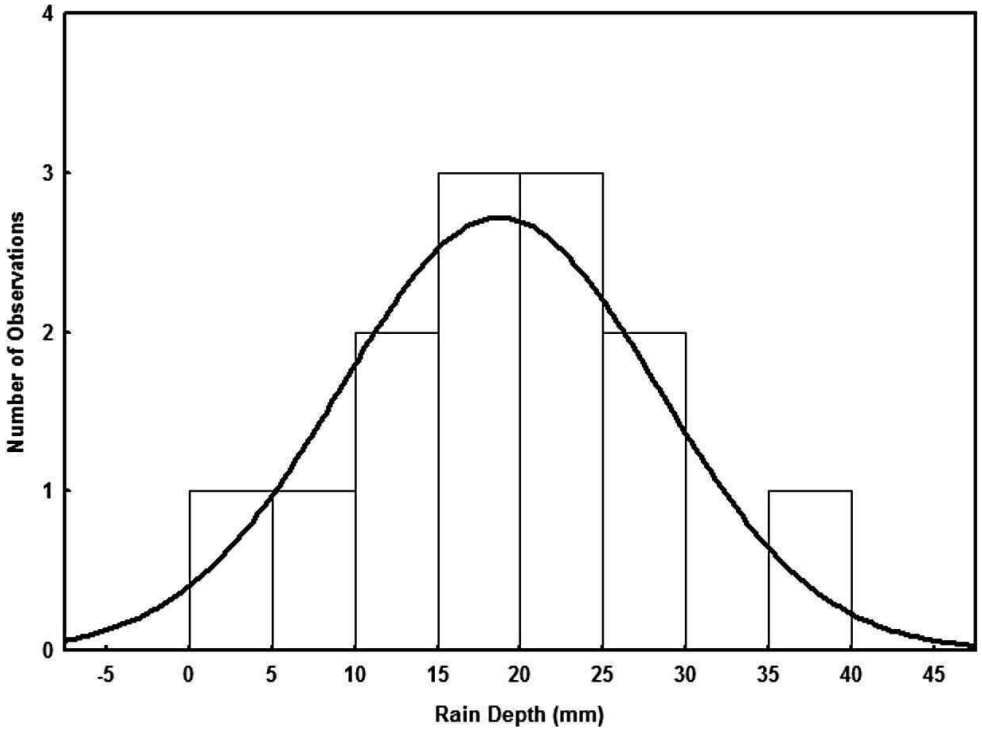

Figure 4—Rain depth distribution of events sampled.

tration of indicator bacteria, while PICP with a total profile depth of 24 cm above the RCA had the highest concentrations. The large pore space of the PICP would appear to let the bacteria through with the infiltrate water while the PA reductions of indicator bacteria may have been assisted by the high observed pH in the infiltrate. The PC with 15-cm profile depth had removal performance between these two extremes.

The observed highly basic infiltrate of the PA potentially resulted from processing of the asphalt itself, which appears to be manufactured in this case with alkaline asphalt emulsion. In general, anionic or cationic asphalt emulsion may potentially affect the pH of the infiltrate of permeable asphalt systems. The high pH observed in the permeable pavement infiltrate, particularly for PA, which even exceeded the expected high pH of the concrete permeable systems, was previously presented in Brown and Borst (2015) and continued through the period of this study (O'Connor and Borst, 2016).

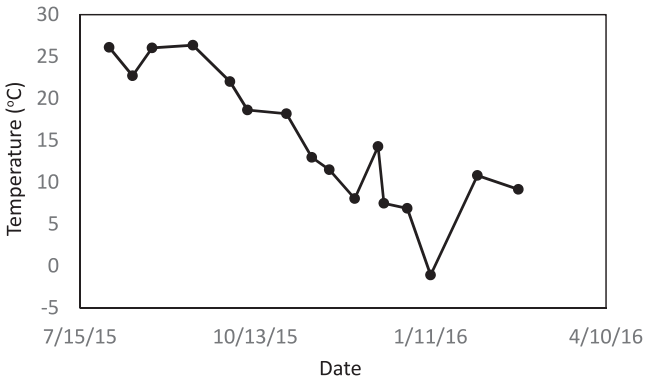

Figure 5—Mean temperature on event days.

Rain depth and temperature did not appear to have any effect on either concentration of organisms or the performance of permeable pavement in this small data set; this observation should be confirmed with a larger data set.

Acknowledgments

The authors would like to thank PARS Environmental Inc. for collection and analysis of samples. The parking lot was constructed as a joint project with U.S. EPA Office of Administration and Resources Management and U.S. EPA Region 2.

Submitted for publication February 2, 2017; accepted for publication May 22, 2017.

Disclaimer

The U.S. Environmental Protection Agency, through its Office of Research and Development, funded and managed, or partially funded and collaborated in, the research described herein. It has been subjected to the Agency's peer and administrative review and has been approved for external publication. Any opinions expressed in this paper are those of the author(s) and do not necessarily reflect the views of the Agency, therefore, no official endorsement should be inferred. Any mention of trade names or commercial products does not constitute endorsement or recommendation for use.

References

Borst, M.; Brown, R. A. (2014) Chloride Released from Three Permeable Pavement Surfaces After Winter Salt Application. *J. Am. Water Resour. Assoc.*, 50 (1), 29–41.

Brown, R. A.; Borst, M. (2014) Evaluation of Surface Infiltration Testing Procedures in Permeable Pavement Systems. *J. Environ. Eng.,* **140** (3), 04014001.

Brown, R. A.; Borst, M. (2015) Nutrient Infiltrate Concentrations from Three Permeable Pavement Types. *J. Environ. Manage.*, **164**, 74–85.

Burton, G. A.; Pitt, R. E. (2002) *Stormwater Effects Handbook: A Tool Box for Watershed Managers, Scientists, and Engineers*; CRC: Boca Raton, Florida.

Clausen, J. C.; Gilbert, J. K. (2003) *Annual Report, Jordan Cove Urban Watershed Section 319 National Monitoring Program Project*; Department of Natural Resources and Engineering, College of Agriculture and Natural Resources, University of Connecticut: Storrs, Connecticut.

Ellis, J. B., Scholes, L., Revitt, D. M.; Oldham, J. (2004) Sustainable Urban Development and Drainage. *Proc. Inst. Civ. Eng.: Munic. Eng.*, 157 (4), 245–250.

Field, R.; Sullivan, D., Eds. (2003) *Proceedings of the Institution of Civil Engineers—Municipal Engineer*; Lewis Publishers/CRC Press: Boca Raton, Florida. ISBN 1-56676-916-7.

Gilbert, J. K.; Clausen, J. C. (2006) Stormwater Runoff Quality and Quantity from Asphalt, Paver, and Crushed Stone Driveways in Connecticut. *Water Res.* **40**, 826–832.

Hathaway, J. M.; Hunt, W. F.; Jadlocki, S. J. (2009) Indicator Bacteria Removal in Stormwater Best Management Practices in Charlotte, North Carolina. *J. Environ. Eng.*, **135** (12), 1275–1285.

Hathaway, J. M.; Hunt, W. F.; Simmons, O. D. (2010) Statistical Evaluation of Factors Affecting Indicator Bacteria in Urban Stormwater Runoff. *J. Environ. Eng.,* **136** (12), 1360–1368.

Hathaway, J. M.; Hunt, W. F. (2012) Indicator Bacteria Performance of Stormwater Control Measures in Wilmington, NC. *J. Irrig. Drain. Eng.*, **138** (2), 185–197.

James, W.; Thompson, M. K. (1997) Contaminants from Four New Pervious and Impervious Pavements in a Parking-Lot. In *Advances in Modeling the Management of Stormwater Impacts*; James, W., Ed.; Computational Hydraulics, Inc.: Guelph, Ontario, Canada; Vol. 5, pp 207–222.

Li, H.; Davis, A. P. (2009) Water Quality Improvement Through Reductions of Pollutant Loads Using Bioretention. *J. Environ. Eng.*, **135** (8), 567–576.

McCarthy, D. T.; Mitchell, V. G.; Deletic, A.; Diaper, C. (2007) *Escherichia coli* in Urban Stormwater: Explaining Their Variability. *Water Sci. Technol.*, **56** (11), 27–34.

Microsoft Office Excel (2013) (15.0.4805.1001) MSO (15.0.4805.1001) 32-bit Part of Microsoft Office 365 ProPlus; Microsoft: Redmond, Washington.

O'Connor, T. P.; Borst, M. (2017) Update to Permeable Pavement Research at the Edison Environmental Center. Proceedings of the *2016 EWRI International Low Impact Development Conference*, Portland, Maine, August 2016.

Pandey, P. K.; Kass, P. H.; Soupir, M. L.; Biswas, S.; Singh, V. P. (2014) Contamination of Water Resources by Pathogenic Bacteria. *AMB Express*, **4**, 51.

Pitt, R. (2011) The National Stormwater Quality Database, Version 3.1. http://unix.eng.ua.edu/~rpitt/Research/ms4/mainms4.shtml (accessed May 2017).

Rushton, B. T. (2001) Low-Impact Parking Lot Design Reduces Runoff and Pollutant Loads. *ASCE J. Water Resour. Plan. Manage.*, **127** (3), 172–179.

Selvakumar, A.; Borst, M. (2006) Variation of Microorganism Concentrations in Urban Stormwater Runoff with Land Use and Seasons. *J. Water Health*, **4** (1), 109–124.

StatSoft, Inc. (2011) Statistica (data analysis software system), version 10. www.statsoft.com.

Struck, S.; Selvakumar, A.; Borst, M. (2008) Prediction of Effluent Quality from Retention Ponds and Constructed Wetlands for Managing Bacterial Stressors in Storm Water Runoff. *ASCE J. Irrig. Drain. Eng.*, **134** (5).

Tata-Maharaj, K.; Scholz, M. (2010) Efficiency of Permeable Pavement Systems for the Removal of Urban Runoff Pollutants Under Varying Environmental Conditions. *Environ. Prog. Sustainable Energy*, **29** (3), 358–369.

Transportation Research Board (2006) *Asphalt Emulsion Technology, Circular No. E-C102*. http://onlinepubs.trb.org/onlinepubs/circulars/ec102.pdf (accessed May 2017).

U.S. Environmental Protection Agency (1976) *Quality Criteria for Water;* EPA/440/9–76/023; U.S. Environmental Protection Agency, Office of Water: Washington, D.C.

U.S. Environmental Protection Agency (1986) *Ambient Water Quality Criteria for Bacteria—1986;* EPA/440/5–84/002; U.S. Environmental Protection Agency, Office of Water: Washington, D.C.

U.S. Environmental Protection Agency (1992) *NPDES Stormwater Sampling Guidance Document*; EPA/833/8–82/001; U.S. Environmental Protection Agency, Office of Water: Washington, D.C.

U.S. Environmental Protection Agency (2000) *Guidance for Data Quality Assessment: Practical Methods for Data Analysis*; EPA/600/R-96/084; U.S. Environmental Protection Agency, Office of Water: Washington, D.C.

U.S. Environmental Protection Agency (2007) National Water Quality Inventory: Report to Congress, 2002 Reporting Cycle; EPA/841/R-07/001; U.S. Environmental Protection Agency, Office of Water: Washington, D.C.

U.S. Environmental Protection Agency (2009) National Water Quality Inventory: Report to Congress, 2004 Reporting Cycle; EPA/841/R-08/001; U.S. Environmental Protection Agency, Office of Water: Washington, D.C.

U.S. Environmental Protection Agency (2010) Surface Infiltration Rates of Permeable Surfaces: Six Month Update (November 2009 through April 2010); EPA/600/R-10/083; U.S. Environmental Protection Agency, Office of Research and Development: Cincinnati, Ohio.

Urban Water Resources Research Council (2014) *Pathogens in Urban Stormwater Systems*; Pathogens in Wet Weather Flows Technical Committee, Environmental and Water Resources Institute, American Society of Civil Engineers: Reston, Virginia. http://collaborate.asce.org/HigherLogic/System/DownloadDocumentFile.ashx?DocumentFileKey=c468710e-971d-4284-a052–0efae9e25d3d (accessed May 2017).

Whitlock, J. E.; Jones, D. T.; Harwood, V. J. (2002) Identification of the Sources of Fecal Coliforms in an Urban Watershed Using Antibiotic Resistance Analysis, *Water Res.*, **36** (17), 4273–4282.

Microorganism Removal in Permeable Pavement Parking Lots in Edison Environmental Center, New Jersey

Ariamalar Selvakumar and Thomas P. O'Connor
Office of Research and Development, National Risk Management Research Laboratory
U.S. Environmental Protection Agency, Edison, NJ 08837

Abstract

Three types of permeable pavements (pervious concrete, permeable interlocking concrete pavers, and porous asphalt) were monitored at the Edison Environmental Center in Edison, New Jersey for indicator organisms such as fecal coliform, enterococci, and *E. coli*. Results showed that porous asphalt had much lower concentration in monitored infiltrate compared to pervious concrete and permeable interlocking concrete pavers. Concentrations of monitored organisms in infiltrate from porous asphalt were consistently below the bathing water quality standard. Fecal coliform and enterococci exceeded bathing water quality standards more than 72% and 34% of the time for permeable interlocking concrete pavers and pervious concrete, respectively.

Objectives

- Evaluate the performance of permeable pavement in removing indicator organisms from infiltrating stormwater runoff
- Evaluate effects of season and rainfall intensity on infiltrate concentrations of indicator organisms.

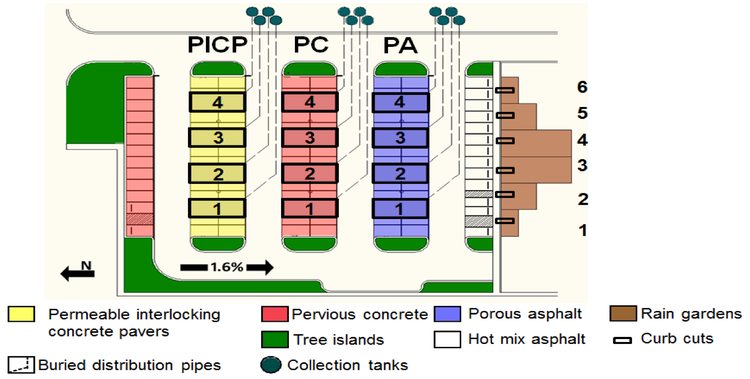

Figure 1. Plan View of Parking Lot

Methods

- Sixteen sampling events were conducted between July 2015 and February 2016.
- Flow-weighted samples were collected using programmable automatic samplers.
- Samples were analyzed for indicator microorganisms such as fecal coliform, enterococci, and *E. coli*.

Statistical Analysis

- Atchison's Method was used to calculate mean and standard deviation. Geometric mean was also calculated.
- A nonparametric Wilcoxon Matched Pair Test was used to determine concentration differences between and within permeable surfaces.
- Probability plots were developed to evaluate the performance of different permeable surfaces.

$$p = \frac{i - 0.5}{n}$$

Results

Table 1. Summary Statistics of Indicator Organisms

Sampling Location	Driving Lane Surface Runoff (CC)	Permeable Interlocking Concrete Pavers (PICP)	Porous Concrete (PC)	Porous Asphalt (PA)
Fecal Coliform				
Detection Frequency (%)	88	94	100	6
Arithmetic Mean (MPN/100 mL)	**5054[a]**	**1911[a]**	177	NA
Geometric Mean (MPN/100 mL)	**412[a]**	**601[a]**	60	NA
Enterococci				
Detection Frequency (%)	100	100	100	87.5
Arithmetic Mean (MPN/100 mL)	**1070[a]**	**212[a]**	**72[a]**	9
Geometric Mean (MPN/100 mL)	**66[a]**	**115[a]**	25	3
E. Coli				
Detection Frequency (%)	75	81	50	0
Arithmetic Mean (MPN/100 mL)	**1315[a]**	49	2	NA
Geometric Mean (MPN/100 mL)	13	8	2	NA

Figure 2. Box and Whisker Plots for Indicator Organisms

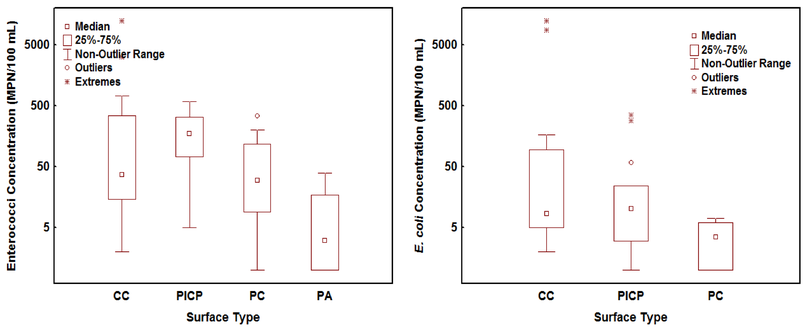

Table 2. Indicator Organism Concentration Differences between Surfaces

Pavement Types	Fecal Coliform		Enterococci		*E. coli*	
	p-value	Statistical Significance	p-value	Statistical Significance	p-value	Statistical Significance
PICP vs. PC	0.0027	Yes	0.0007	Yes	0.0047	Yes
PICP vs. PA	0.0007	Yes	0.0004	Yes	0.0015	Yes
PC vs. PA	0.0004	Yes	0.0024	Yes	0.0117	Yes

There is statistically significant difference between all three surfaces ($p < 0.05$) for all three microorganisms.

Figure 3. Cumulative Probability Plot of Indicator Organisms

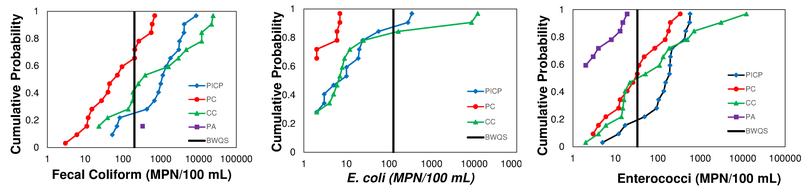

The BWQS of 200 MPN/100 mL for fecal coliform was exceeded 72% and 34% of the time for PICP and PC, respectively. BWQS of 33 MPN/100 mL for enterococci was exceeded 78% and 47% for PICP and PC, respectively. BWQS of 126 MPN/100 mL for *E. coli* was exceeded only 9% times for PICP.

Table 3. Indicator Organism Concentrations Reduction

Organism	Surface Type	Concentration Reduction (%)
Fecal Coliform	PICP	0
	PC	**93**
	PA	**94**
Enterococci	PICP	0
	PC	62
	PA	**100**
E. coli	PICP	39
	PC	**100**
	PA	**100**

The highest reduction was observed in PA.

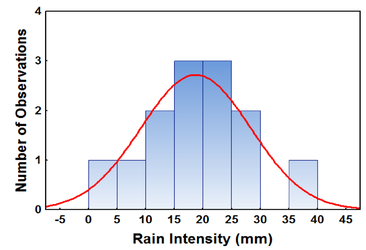

Figure 4. Rain Intensity

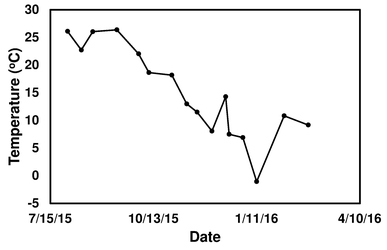

Figure 5. Mean Temperature

Conclusions

- Porous asphalt and porous concrete reduced the concentrations of all three organisms studied.
- Concentrations of organisms in the infiltrate water from porous asphalt were below the BWQS.
- Concentrations of organisms in the infiltrate water from PA had the lowest concentrations.
- PA reductions may have been assisted by the high observed pH in the infiltrate due to asphalt emulsion.
- Concentrations of organisms in the infiltrate water from PICP had the highest concentrations.
- The large pore space of the PICP appear to let the bacteria through with the infiltrate water.
- Rain intensity and temperature did not appear to have any effect on the performance of permeable pavements.

Organism Detection in Permeable Pavement Parking Lot Infiltrates at the Edison Environmental Center, New Jersey

Ariamalar Selvakumar[1*], Thomas P. O'Connor[2]

ABSTRACT: Three types of permeable pavements were monitored at the Edison Environmental Center in Edison, New Jersey, for indicator organisms such as fecal coliform, enterococci, and *Escherichia coli*. Results showed that porous asphalt had a much lower concentration in monitored infiltrate compared to pervious concrete and permeable interlocking concrete pavers; concentrations of monitored organisms in infiltrate from porous asphalt were consistently below the bathing water quality standard and actually had limited detection. Fecal coliform and enterococci exceeded bathing water quality standards more than 72 and 34% of the time for permeable interlocking concrete pavers and pervious concrete, respectively. Concentration reductions greater than 90% were observed for all three indicator organisms for porous asphalt and fecal coliform and *E. coli* for pervious concrete when compared to runoff values, while permeable interlocking concrete pavers only had a modest (39%) observable reduction for *E. coli* only. The near absence of indicator organisms observed in the porous asphalt infiltrate may be due to the high pH potentially due to asphalt processing. Neither rain intensity nor temperature was demonstrated to have an observable effect in both concentrations of organisms and performance of permeable pavement; but this may due to the limitations of the dataset consisting of 16 events over an 8-month period. *Water Environ. Res.*, **90,** 21 (2018).

KEYWORDS: permeable pavement, indicator organisms, bathing water quality standard, infiltrate, stormwater runoff.

doi:10.2175/106143017X14902968254575

[1*] National Risk Management Research Laboratory, Office of Research and Development, U.S. Environmental Protection Agency, 2890 Woodbridge Avenue, Edison, NJ 08837; e-mail: selvakumar.ariamalar@epa.gov

[2] National Risk Management Research Laboratory, Office of Research and Development, U.S. Environmental Protection Agency, Edison, New Jersey

Introduction

Since the inception of the Clean Water Act in 1972, the United States has made great efforts in restoring and preserving the physical, chemical, and biological integrity of the nation's waters. However, nearly half of the nation's assessed surface waters remain incapable of maintaining water quality adequate for supporting one or more designated uses, such as recreational swimming, fishing, or drinking water supply (U.S. EPA, 2007). National biennial water quality surveys consistently indicate waters are impaired by bacterial indicators, nutrients, sediments, and assorted toxic chemical loadings. A leading cause of this impairment is non-point source stormwater runoff from agricultural and urban areas affecting an estimated 46% of impaired rivers and streams, 22% of impaired lake areas, and 22% of impaired estuaries (U.S. EPA, 2009). More river and stream miles were affected by pathogenic indicator microorganisms than any other pollutant (U.S. EPA, 2009).

Stormwater discharges release pathogenic bacteria, protozoan, and viruses to receiving waters (Pandey et al., 2014). Tata-Maharaj and Scholz (2010) reported typical concentrations in urban runoff as *Escherichia coli* (*E. coli*) (10^2 to 10^7 colony forming unit [CFU/100 mL]), fecal streptococci (10^2 to 10^6 CFU/100 mL) and fecal coliforms (10^3 to 10^7 CFU/100 mL). Selvakumar and Borst (2006) reported concentration ranges for fecal coliforms (5.6×10^3 to 2.2×10^4 CFU/100 mL), enterococci (1.0×10^3 to 6.6×10^3 CFU/100 mL), and *E. coli* (1.5×10^3 to 8.5×10^3 CFU/100 mL) in urban stormwater runoff. Pitt (2011) reported similar nationwide median concentrations for fecal coliform and *E. coli* using data from a number of National Pollutant Discharge Elimination System (NPDES) Municipal Separate Storm Sewer System (MS4) stormwater permit holders.

Fecal indicator microorganisms are found in feces from both human sources (e.g., sewer discharges, and failing septic systems) and domestic and wild animals (Whitlock, et al., 2002). Burton and Pitt (2002) also note potential sources to paved areas from atmospheric deposition and erosion of previously contaminated soils. Indicator microorganisms tested by public health agencies include total coliform, fecal coliform, fecal

streptococci, *E. coli,* and enterococci. The concentrations of these indicators are used to determine the potential for fecal contamination and to compare to public health-based thresholds. These species may not be harmful to humans themselves; however, their presence can indicate fecal contamination. Indicator microorganisms are used to test surface waters. They serve as a proxy because it is difficult to measure the actual pathogens.

In 1976, the U.S. Environmental Protection Agency's (U.S. EPA) recommended that states adopt a bathing water quality standard (BWQS) of fecal coliforms not to exceed 200 organisms/100 mL (U.S. EPA, 1976). In 1986, based on statistical analysis, U.S. EPA recommended that states revise the recreational water quality microbial criteria to use enterococci for marine waters and *E. coli* or enterococci for freshwaters as *E. coli* and enterococci are more representative of warm-blooded animal fecal contamination in water than total or fecal coliforms. Suggested criteria are 35 enterococci per 100 mL for marine waters and 33 enterococci per 100 mL and 126 *E. coli* per 100 mL for freshwaters (U.S. EPA, 1986).

Stormwater runoff is commonly treated by stormwater control measures (SCMs), which include wet ponds, wetlands, bioretention areas, dry detention basins, permeable pavements, rain gardens, and proprietary devices. Increasingly, SCMs are being incorporated on-site as low impact development (LID) or as green infrastructure (GI) in the municipal right of way. A combination of factors (e.g., predation, sedimentation, sorption, filtration, light, pH, biological oxygen demand, and dissolved oxygen) can contribute significantly to the inactivation of indicator bacteria in SCMs (Struck et al., 2008). Permeable pavement, an alternative to conventional pavement, is a LID/GI infiltration system where the stormwater runoff infiltrates through a permeable layer of pavement or other stabilized surface, reducing the need for runoff drainage and treatment offsite (Field and Sullivan, 2003). Permeable pavement systems can enhance stormwater quality after infiltrating through the system (Clausen and Gilbert, 2003; Ellis, et al., 2004; Gilbert and Clausen, 2006; James and Thompson, 1997; Rushton, 2001). There are a variety of permeable pavements and each has unique characteristics that lend themselves to application in specific environments. Permeable pavement usually diverts stormwater runoff into an underground stone reservoir before gradually exfiltrating out of the stone reservoir into the subsoil (Field and Sullivan, 2003) though there are also systems that have a limited storage reservoir for various reasons (e.g., high groundwater, significant underground infrastructure) that discharge to the nearest conveyance system or surface water.

Although many SCMs have been studied for removal of microorganisms, there are limited studies on the effectiveness of porous pavements (Hathaway and Hunt, 2012; Hathaway et al., 2009). Tata-Maharaj and Scholz (2010) found that permeable pavement was effective in removing microorganisms such as total coliforms, *E. coli*, and fecal streptococci by 98 to 99%. Similarly, few studies have assessed the effectiveness of SCMs on the seasonal removal of microorganisms (Hathaway and Hunt, 2012). Li and Davis (2009) observed the highest *E. coli* and fecal coliform concentrations in the runoff during the summer; however, SCM removal efficiency remained same and was not correlated to the temperature. Tata-Maharaj and Scholz (2010) found that the rates of microbiological degradation remained constant and were not negatively affected by temperature variations due to seasonal changes.

The objectives of this study were to: 1) evaluate the performance of permeable pavement in removing indicator organisms such as fecal coliform, enterococci, and *E. coli* from infiltrating stormwater runoff; and 2) evaluate potential seasonal effects and rainfall intensity on infiltrate concentrations of indicator organisms.

Methods

U.S. EPA's Office of Research and Development operates the Urban Watershed Research Facility (UWRF) at the Edison Environmental Center (EEC) in Edison, New Jersey. The UWRF serves as a location to perform both laboratory-scale and field-scale studies to test monitoring methods and performance of SCMs. The UWRF allows U.S. EPA to better understand SCM performance and monitoring methods with a high level of control over external factors. The EEC is a 200-acre campus that has been shown to have representative runoff comparable to literature values (e.g., Brown and Borst, 2015, specifically relate for nutrients and total organic carbon) and is subject to many of the same potential suburban fecal inputs of wild animals to storm systems, namely deer, geese, pigeons, and seagulls.

At the EEC in 2009, U.S. EPA constructed a functional, 0.4 ha, 110-space parking lot that is surfaced with three different permeable pavement types: permeable interlocking concrete pavers (PICP), pervious concrete (PC), and porous asphalt (PA). The site, depicted in Figure 1, was opened for use in October 2009 and it is used daily by EEC staff and visitors.

The three head-to-head parking rows with permeable pavement systems are 11.58 m wide by 42.67 m long while the 7.62 m wide travel lanes are paved with traditional impervious hot mix asphalt. There is a 1.6% surface slope so that each permeable surface receives runoff from the adjacent travel lanes to the north. All surfaces were constructed over an open-graded subbase reservoir of recycled concrete aggregate (RCA) crushed on site to the size of American Association of State Highway and Transportation Officials (AASHTO) No. 2 size aggregate. Five sections of each permeable pavement system allow water to infiltrate the underlying soil while four of the sections have an impermeable liner 40 cm below each permeable surface, which allows infiltrate to be collected for measurement and sampling. The thickness of each permeable surface varies depending on structural needs for that particular application. The PA is 8 cm thick and PC is 15 cm thick. The individual pavers are 9 cm thick and were placed on a 5-cm layer of AASHTO No. 8 aggregate, which also filled spaces between pavers; an additional 10-cm layer of AASHTO No. 57 aggregate separated the AASHTO No. 8 and common RCA aggregate for PICP. The infiltration capacity of all three surfaces is very large; the infiltration rate of PC was approximately twice that of PICP. Permeable interlocking concrete pavers and PC had infiltration

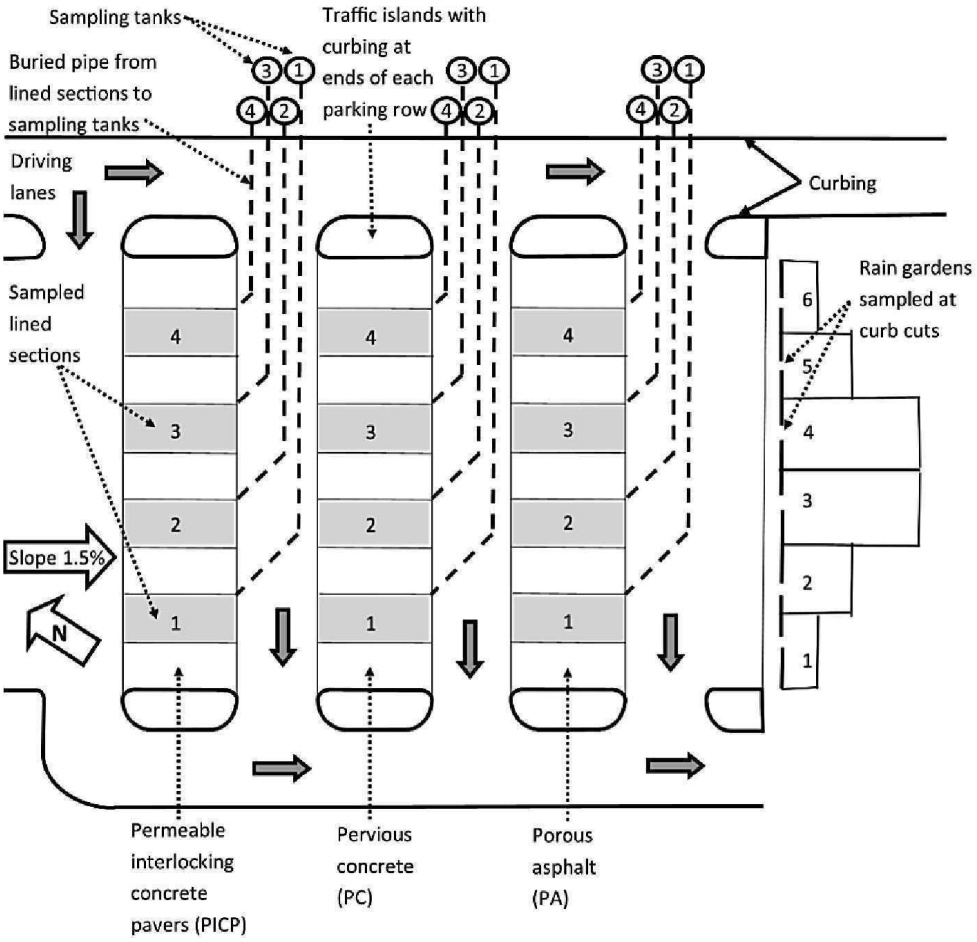

Figure 1—Plan view of parking lot.

rates that were more than one order of magnitude larger than PA. Although the surface infiltration rates vary by more than an order of magnitude, each is much larger than the reasonably expected rain event (Brown and Borst, 2014; U.S.EPA, 2010). A more detailed description of the liners, permeable surfaces and drainage piping is provided in Brown and Borst (2014).

Flow-weighted samples were collected using programmable automatic samplers. Samples were collected from the drainage pipes for collection tanks for permeable surfaces 1 and 3 (see Figure 1) for each permeable surface. Surface runoff samples were also collected at two curb cuts (CC) (4 and 5 rain gardens) at the south end of the parking lot that collects runoff from impermeable asphalt surface. The automatic sampler collected discrete samples in up to 24 1-l HDPE bottles. The sampling interval was set using the forecast duration from the National Weather Service.

Sixteen sampling events were conducted between July 2015 and February 2016. Collected samples were transported to the UWRF laboratory and analyses were initiated within the standard holding time of 6 hours. Samples were analyzed for

Table 1—Summary statistics of fecal coliform for monitored storm events.

Statistics	Driving lane surface runoff (CC)	Permeable interlocking concrete pavers (PICP)	Porous concrete (PC)	Porous asphalt (PA)
Detection frequency (%)	88	94	100	6
Geometric mean (MPN/100 mL)	**412**[a]	**601**[a]	60	NA
Arithmetic mean (MPN/100 mL)	**5054**[a]	**1911**[a]	177	NA
Median (MPN/100 mL)	2254	1065	58	NA
Maximum (MPN/100 mL)	24 196	8665	692	331
Minimum (MPN/100 mL)	0	0	3	0
Standard deviation (MPN/100 mL)	8118	2289	232	NA

[a] Mean concentration exceeds BWQS (bolded).
NA: cannot be calculated as it was detected only once.

Table 2—Summary statistics of enterococci for monitored storm events.

Statistics	Driving lane surface runoff (CC)	Permeable interlocking concrete pavers (PICP)	Porous concrete (PC)	Porous asphalt (PA)
Detection frequency (%)	100	100	100	87.5
Geometric mean (MPN/100 mL)	**66**[a]	**115**[a]	25	3
Arithmetic mean (MPN/100 mL)	**1070**[a]	**212**[a]	**72**[a]	9
Median (MPN/100 mL)	37	171	30	3
Maximum (MPN/100 mL)	12 243	578	338	39
Minimum (MPN/100 mL)	2	5	1	0
Standard deviation (MPN/100 mL)	3076	191	96	12

[a] Mean concentration exceeds BWQS (bolded).

indicator microorganisms such as fecal coliform, enterococci, and *E. coli*. Fecal coliform and *E. coli* were enumerated using Colilert incubating at 35 and 44.5 °C for 24 hours, respectively and enterococci was enumerated using Enterolert incubating at 41 °C for 24 hours (IDEXX Laboratories, Inc., Westbrook, Maine). Colilert and Enterolert are commercially available enzyme-substrate liquid-broth mediums (IDEXX Laboratories, Inc., Westbrook, Maine). All enumerations were performed using Quanti-tray 2000 trays, which use a most probable number (MPN)-based protocol with a quantitation range from less than 1 colony forming unit (CFU)/100 mL to 2419.6 CFU/100 mL without sample dilution. Each sample was analyzed with and without dilution; infiltrate was analyzed at 10 times dilution (observable range of 10 to 24 196 CFU/100 mL) and runoff samples were analyzed at 20 times dilution (observable range 20 to 48 392 CFU/100 mL). Results were reported as the average of the undiluted and diluted analysis. When there were no observed concentrations for both the undiluted and diluted analysis, the sample concentration was zero as no organisms were present.

Rainfall was measured using a 0.1-mm tipping bucket rain gauge and recorded with a Campbell Scientific CR1000 data logger (Logan, Utah) set to record at 10-minute intervals. The tipping bucket rain gauge is located in the field adjacent to the collection tanks to the east of the parking lot. All storms had at least 2.54 mm (0.1 in.) of rainfall as per NPDES guidance (U.S. EPA, 1992). Air temperature was measured at the UWRF weather station.

Statistical analysis was conducted to evaluate the performance of permeable pavement parking lots in treating stormwater infiltrate except for fecal coliform and *E. coli* in the PA infiltrate which were detected at a frequency $< 10\%$, which effectively restricts statistical analysis (U.S. EPA, 2000). For all other infiltrate and runoff concentration, detection frequency was 50% or greater. Summary statistics, that is, geometric and arithmetic means, medians, standard deviations, were performed in Excel. To calculate the geometric means, a substitution was required for non-detects (0) and unity (1) was used (UWRRC, 2014). Atchison's Method (U.S. EPA, 2000), a conservative method, was used to calculate arithmetic mean and standard deviation. Atchison's method adjusts the arithmetic mean and standard deviation by assuming that non-detects are actually zero, which is the case in this study as described above.

Normality of data sets were tested by the Shapiro-Wilk W test using Satistica 10 (StatSoft, 2011). A nonparametric Wilcoxon Matched Pair Test (StatSoft, 2011) was used to determine concentration differences between and within permeable surfaces; nonparametric methods can reduce the influence of outliers such as non-detects and values greater than maximum reporting limit. A statistical significance value of $p \leq 0.05$ was used for all statistical analysis. Box and whisker plots were created to display the data with median as the center point and 25 and 75% as quartiles.

Probability plots were developed in Excel spreadsheets (Microsoft, 2013) to evaluate the performance of different permeable surfaces. Probability was calculated using the following equation (Burton and Pitt, 2002):

$$p = \frac{i - 0.5}{n} \tag{1}$$

where, p is probability of given observation; i is rank of observation within group n; and n is total number of observations within a given data set. These probability values

Table 3—Summary statistics of *E. coli* for monitored storm events.

Statistics	Driving lane surface runoff (CC)	Permeable interlocking concrete pavers (PICP)	Porous concrete (PC)	Porous asphalt (PA)
Detection frequency (%)	75	81	50	0
Geometric mean (MPN/100 mL)	13	8	2	NA
Arithmetic mean (MPN/100 mL)	**1315**[a]	49	2	NA
Median (MPN/100 mL)	6	8	1	NA
Maximum (MPN/100 mL)	12 141	344	7	0
Minimum (MPN/100 mL)	0	0	0	0
Standard deviation (MPN/100 mL)	3604	104	3	NA

[a] Mean concentration exceeds BWQS (bolded).
NA: cannot be calculated as it was not detected.

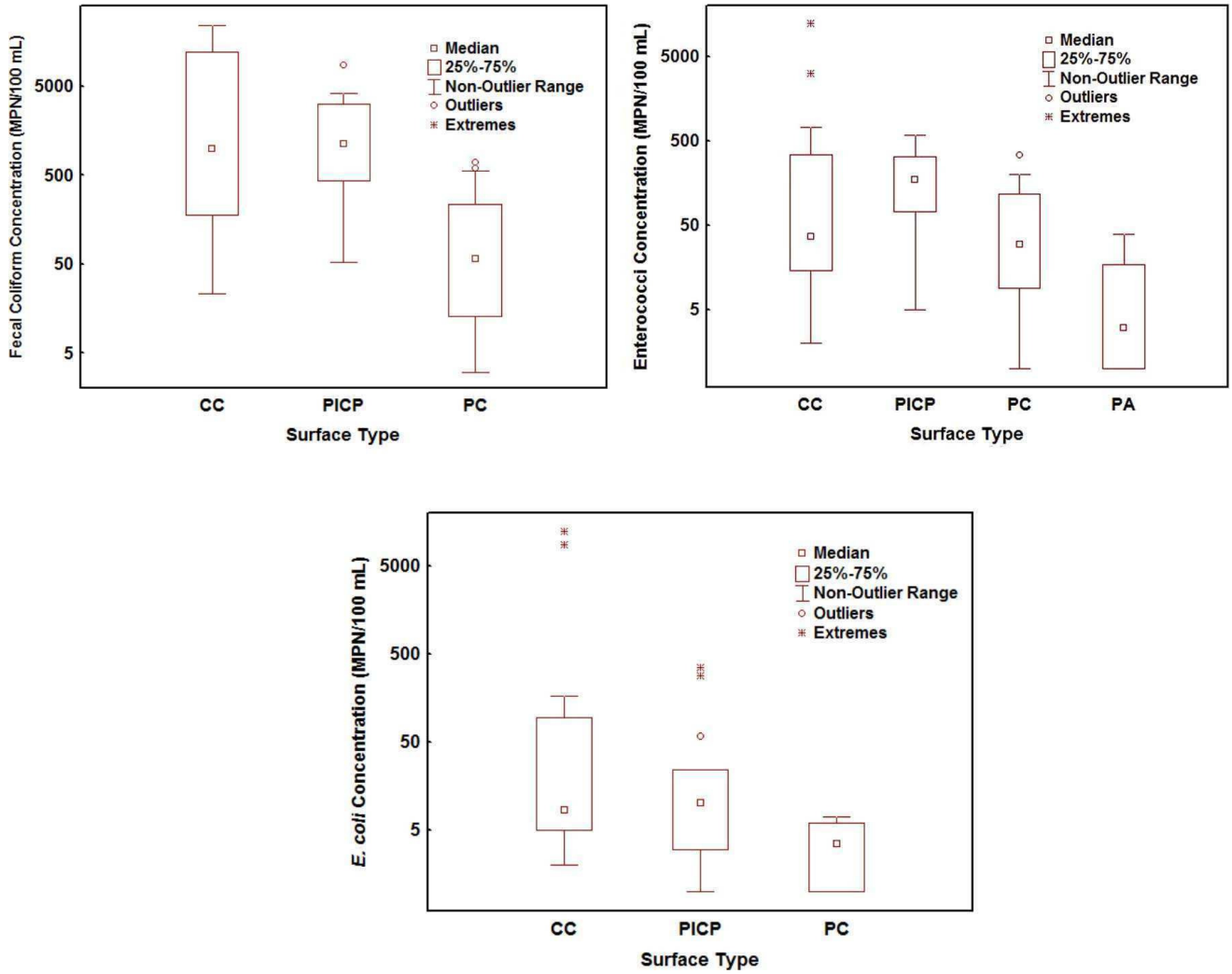

Figure 2—Box and whisker plots for permeable surface infiltrate concentrations.

(ordinate) were then plotted against organism concentrations (abscissa) and compared against a vertical straight line representing the BWQS (freshwater criteria, if applicable) for respective microorganisms to demonstrate exceedance occurrences.

Treatment by infiltration through the pavement surfaces was determined by calculating percent removal of infiltrate concentration of each surface in comparison to common driving lane surface runoff values collected at the CCs. Geometric mean concentrations were used for the calculation. A nonparametric Wilcoxon Matched Pair Test (StatSoft, 2011) was used to determine statistical significance of the differences between driving lane surface runoff and permeable surface infiltrate concentrations.

A least squares log normal regression analysis was performed on rainfall and temperature in comparison to microbial indicator organism concentrations.

Results and Discussion

Summary statistics for the sampling events are presented in Tables 1 to 3 and Box and Whisker plots are shown in Figure 2. Fecal coliform was detected in infiltrates from both PICP and PC; it was only detected once in PA. The geometric mean fecal coliform concentration in the runoff (represented by CC for curb

Table 4—Indicator organism concentration differences within surfaces.

	Fecal coliform		Enterococci		*E. coli*	
Pavement types	***p*-value**	**Statistical significance**	***p*-value**	**Statistical significance**	***p*-value**	**Statistical significance**
PICP-1 vs. PICP-3	**0.0007**	Yes	0.121	No	0.15	No
PC-1 vs. PC-3	**0.007**	Yes	0.078	No	1.0	No

Table 5—Indicator organism concentration differences between surfaces

	Fecal coliform		Enterococci		*E. coli*	
Pavement types	***p*-value**	**Statistical significance**	***p*-value**	**Statistical significance**	***p*-value**	**Statistical significance**
PICP vs. PC	0.0027	Yes	0.0007	Yes	0.0047	Yes
PICP vs. PA	0.0007	Yes	0.0004	Yes	0.0015	Yes
PC vs. PA	0.0004	Yes	0.0024	Yes	0.0117	Yes

cuts in Figure 2) was 412 MPN/100 mL. The geometric mean fecal coliform concentrations in infiltrates from PICP and PC were 601 and 60 MPN/100 mL, respectively; the geometric mean for PICP infiltrate exceeded the BWQS of 200 MPN/100 mL.

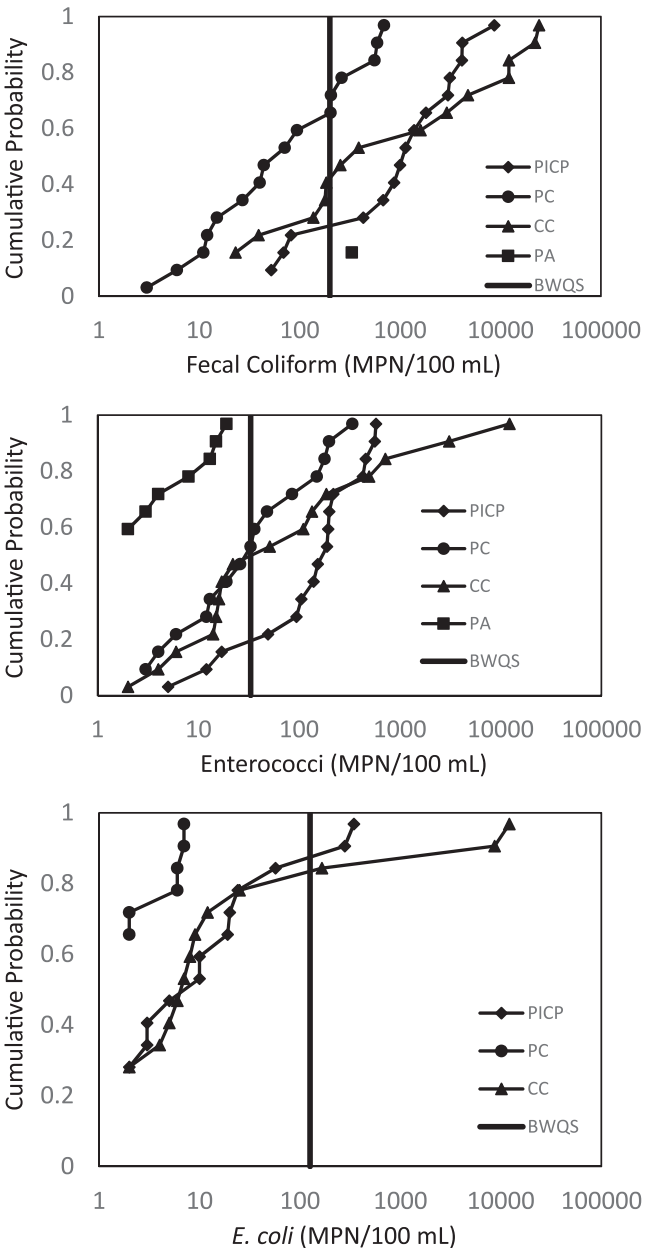

Figure 3—Cumulative probability plots of indicator organisms.

Geometric mean for PA infiltrate was not calculated as it was detected only once.

The geometric mean of fecal coliform concentration in PICP infiltrate was greater than the concentration in the runoff. However, the arithmetic mean concentrations in the infiltrates are less than the concentration in the runoff. The concentrations of PICP and PC infiltrate were log normally distributed over the 16 events. Concentrations of fecal coliform in the infiltrate of PICP were always higher than that of PC and PA.

The geometric mean enterococci concentration in the runoff was 66 MPN/100 mL. The enterococci were detected 100% of the time for PICP and PC and was the most observed microorganism in PA infiltrate at 87.5% of events, even though the PA MPN were very low in comparison to PICP and PC. The geometric mean enterococci concentration in infiltrates from PICP, PC, and PA were 115, 25, and 3 MPN/100 mL, respectively, with only PICP mean exceeding BWQS of 33 MPN/100 mL.

E. coli was detected in PICP during 81% of the events. It was detected in only 50% of the events in PC and at concentrations lower than the PICP. The geometric mean *E. coli* concentrations in infiltrates from PICP and PC were 8 and 2 MPN/100 mL, respectively, while *E. coli* was not detected in PA. The geometric mean concentration in the runoff was 13 MPN/100 mL.

Wilcoxon Matched Pair Test (StatSoft, 2011) indicated there was a statistically significant difference within surfaces for PICP and PC for fecal coliform as shown in Table 4. There was no statistically significant difference within surfaces for enterococci and *E. coli* (Table 4). There is statistically significant difference

Table 6—Percent indicator organism concentrations reductions for permeable pavement infiltrates based on difference of geometric means to runoff.

Organism	Surface type	Concentration reduction (%)
Fecal Coliform	PICP	0[a]
	PC	**93**
	PA	**94[b]**
Enterococci	PICP	0[a]
	PC	**62**
	PA	**100**
E. coli	PICP	**39**
	PC	**100**
	PA	**100**

[a] Concentration in PICP infiltrate was greater than concentration in runoff.
[b] Based on 6% detection frequency.

Table 7—Results of Wilcoxon Matched Pair Test.

	Fecal coliform		Enterococci		*E. coli*	
Surface type	*p*-value	Statistical significance	*p*-value	Statistical significance	*p*-value	Statistical significance
PICP	0.3066	No	0.4228	No	0.9770	No
PC	0.0151	**Yes**	0.5180	No	0.0063	**Yes**
PA	0.0009	**Yes**	0.0110	**Yes**	0.0022	**Yes**

between all three surfaces ($p < 0.05$) (Table 5) for all three microorganisms.

Exceedance of Bathing Water Quality Standards. Probability of exceedance of U.S. EPA BWQS are shown in Figure 3 with the vertical line representing the respective BWQS for each microorganism. The probability of exceedance is where the curve crossed the BWQS. The BWQS of 200 MPN/100 mL for fecal coliform was exceeded 72 and 34% of the time for PICP and PC, respectively. The BWQS of 33 MPN/100 mL for enterococci was exceeded 78 and 47% of times for PICP and PC, respectively. The BWQS of 126 MPN/100 mL for *E. coli* was exceeded only 9% of times for PICP.

Potential Reduction in Concentration of Indicator Organisms. Estimated concentration reductions of microorganisms based on geometric means for each permeable pavement type in comparison to the common driving lane surface runoff collected at the rain garden CCs is documented in Table 6. Permeable interlocking concrete pavers reduced concentrations for only 1 of the three organisms studied, *E. coli* at 55%. Concentration reductions of greater than 90% were observed for PC infiltrate for fecal coliform and *E. coli*, while enterococci had a 62% reduction. The highest reductions were observed in PA infiltrate for all three organisms.

Results of Wilcoxon Matched Pair Test are shown in Table 7. Porous asphalt significantly reduced the concentration of all three organisms ($p \leq 0.05$), whereas PC reduced fecal coliform and *E. coli*. Permeable interlocking concrete pavers did not significantly reduce any of the organisms. Statistical analyses agreed with the concentration reductions listed in Table 6.

The large reductions from runoff by and near complete absence of observed organisms in the PA system is most likely due to the high pH of the PA infiltrate. The high pH of the infiltrate systems was previously presented in Brown and Borst (2015), though their paper focused on the initial 13 storm events sampled from October 2010 until September 2011. These high pH observations have continued through 2015 (O'Connor and Borst, 2017), which coincides with the time period of this current study. The infiltrate from PC and PICP was observed to be around 9; however, pH of infiltrate from PA was consistently as high as 11 (O'Connor and Borst, 2017), which may explain why microorganism concentrations in the infiltrate from PA are low or non-existent compared to the other two surfaces. The cause of this high pH in the PA infiltrate is suspected to be asphalt emulsions, which are used in the asphalt processing. Specifications called for asphalt mix between 4.0 and 4.5% asphalt and liquid anti-stripping agent. Anionic emulsions have a high pH (e.g., pH 10 to 12) (Transportation Research Board, 2006), which is in the range of the pH observations for the PA infiltrate. Alternatively, asphalt emulsions can be cationic as well with correspondingly acidic pH (e.g., pH 1 to 4) (Transportation Research Board, 2006).

Effects of Weather. Between July 2015 and February 2016, 16 sampling events were conducted, which equates to two events per month. Rain depth ranged from 3.4 to 39.4 mm with the mean size of 18.6 mm and median size of 19.7 mm. Rain depth is normally distributed as shown in Figure 4. Least-square log normal regression analysis of rain depth and indicator organism concentrations for all the surfaces had low coefficient of determination ($R^2 \leq 0.33$), which agrees with findings by other researchers (Hathaway et al., 2010; McCarthy et al., 2007).

Event temperatures ranged from –1.1 °C to 26.4 °C with a mean of 15 °C and median of 13.58 °C (Figure 5). Least-squares log normal regression analysis of temperature and indicator organism concentrations for all three surfaces had low coefficient of determinations ($R^2 \leq 0.20$).

Conclusion

Porous pavements function as infiltration SCMs, with stormwater runoff passing through the permeable surface where pollutants are removed and stored in the storage gallery. This study's research suggests that, of the three pavement types tested, PA consistently had the lowest concentration of indicator microorganisms' load and the concentrations of organisms in the infiltrate water were below the bathing water quality standards. There was a statistically significant difference between all three surfaces for all three organisms with PICP having the highest observed concentrations and frequency of detection.

As expected, impervious driving lane runoff mean concentrations exceed BWQS for all microbial indicators. Results of the probability plots (Figure 3), estimated percent removals (Table 6), and Wilcoxon Matched Pair Test (Table 7) show consistently that permeable asphalt had large reductions of indicator microorganism concentrations. No reduction in concentrations of fecal coliform and enterococci were observed in PICP infiltrate as the geometric concentrations in the infiltrate were greater than the concentrations in the runoff. Concentration reductions of greater than 90% were observed with the exception of enterococci (62%) in PC infiltrate. PICP was most prone to not to reduce concentrations significantly and to have mean concentrations exceeding BWQS for fecal coliform and enterococci.

Despite PA having the shortest profile of 8 cm above the common gallery of RCA, it had the lowest observed concen-

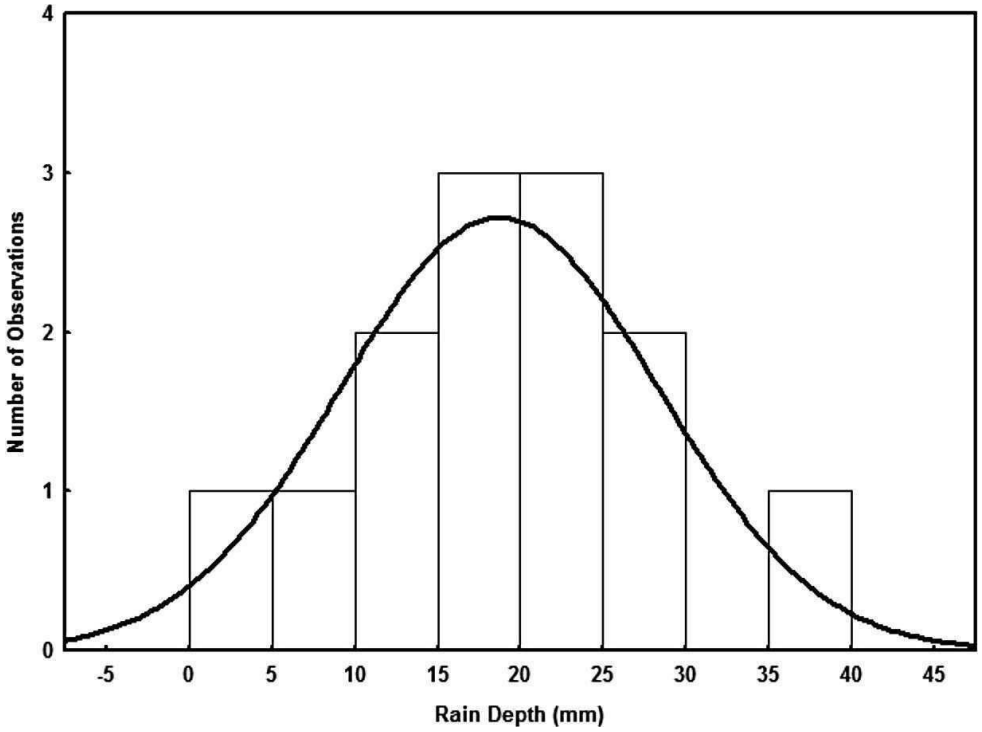

Figure 4—Rain depth distribution of events sampled.

tration of indicator bacteria, while PICP with a total profile depth of 24 cm above the RCA had the highest concentrations. The large pore space of the PICP would appear to let the bacteria through with the infiltrate water while the PA reductions of indicator bacteria may have been assisted by the high observed pH in the infiltrate. The PC with 15-cm profile depth had removal performance between these two extremes.

The observed highly basic infiltrate of the PA potentially resulted from processing of the asphalt itself, which appears to be manufactured in this case with alkaline asphalt emulsion. In general, anionic or cationic asphalt emulsion may potentially affect the pH of the infiltrate of permeable asphalt systems. The high pH observed in the permeable pavement infiltrate, particularly for PA, which even exceeded the expected high pH of the concrete permeable systems, was previously presented in Brown and Borst (2015) and continued through the period of this study (O'Connor and Borst, 2016).

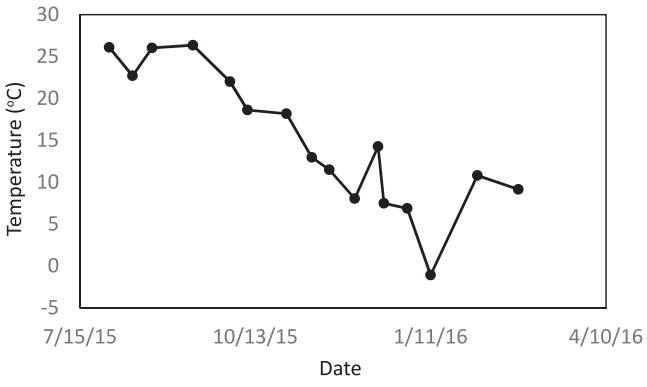

Figure 5—Mean temperature on event days.

Rain depth and temperature did not appear to have any effect on either concentration of organisms or the performance of permeable pavement in this small data set; this observation should be confirmed with a larger data set.

Acknowledgments

The authors would like to thank PARS Environmental Inc. for collection and analysis of samples. The parking lot was constructed as a joint project with U.S. EPA Office of Administration and Resources Management and U.S. EPA Region 2.

Submitted for publication February 2, 2017; accepted for publication May 22, 2017.

Disclaimer

The U.S. Environmental Protection Agency, through its Office of Research and Development, funded and managed, or partially funded and collaborated in, the research described herein. It has been subjected to the Agency's peer and administrative review and has been approved for external publication. Any opinions expressed in this paper are those of the author(s) and do not necessarily reflect the views of the Agency, therefore, no official endorsement should be inferred. Any mention of trade names or commercial products does not constitute endorsement or recommendation for use.

References

Borst, M.; Brown, R. A. (2014) Chloride Released from Three Permeable Pavement Surfaces After Winter Salt Application. *J. Am. Water Resour. Assoc.*, 50 (1), 29–41.

Brown, R. A.; Borst, M. (2014) Evaluation of Surface Infiltration Testing Procedures in Permeable Pavement Systems. *J. Environ. Eng.,* **140** (3), 04014001.

Brown, R. A.; Borst, M. (2015) Nutrient Infiltrate Concentrations from Three Permeable Pavement Types. *J. Environ. Manage.*, **164**, 74–85.

Burton, G. A.; Pitt, R. E. (2002) *Stormwater Effects Handbook: A Tool Box for Watershed Managers, Scientists, and Engineers*; CRC: Boca Raton, Florida.

Clausen, J. C.; Gilbert, J. K. (2003) *Annual Report, Jordan Cove Urban Watershed Section 319 National Monitoring Program Project*; Department of Natural Resources and Engineering, College of Agriculture and Natural Resources, University of Connecticut: Storrs, Connecticut.

Ellis, J. B., Scholes, L., Revitt, D. M.; Oldham, J. (2004) Sustainable Urban Development and Drainage. *Proc. Inst. Civ. Eng.: Munic. Eng.*, 157 (4), 245–250.

Field, R.; Sullivan, D., Eds. (2003) *Proceedings of the Institution of Civil Engineers—Municipal Engineer*; Lewis Publishers/CRC Press: Boca Raton, Florida. ISBN 1-56676-916-7.

Gilbert, J. K.; Clausen, J. C. (2006) Stormwater Runoff Quality and Quantity from Asphalt, Paver, and Crushed Stone Driveways in Connecticut. *Water Res.* **40**, 826–832.

Hathaway, J. M.; Hunt, W. F.; Jadlocki, S. J. (2009) Indicator Bacteria Removal in Stormwater Best Management Practices in Charlotte, North Carolina. *J. Environ. Eng.*, **135** (12), 1275–1285.

Hathaway, J. M.; Hunt, W. F.; Simmons, O. D. (2010) Statistical Evaluation of Factors Affecting Indicator Bacteria in Urban Stormwater Runoff. *J. Environ. Eng.,* **136** (12), 1360–1368.

Hathaway, J. M.; Hunt, W. F. (2012) Indicator Bacteria Performance of Stormwater Control Measures in Wilmington, NC. *J. Irrig. Drain. Eng.*, **138** (2), 185–197.

James, W.; Thompson, M. K. (1997) Contaminants from Four New Pervious and Impervious Pavements in a Parking-Lot. In *Advances in Modeling the Management of Stormwater Impacts*; James, W., Ed.; Computational Hydraulics, Inc.: Guelph, Ontario, Canada; Vol. 5, pp 207–222.

Li, H.; Davis, A. P. (2009) Water Quality Improvement Through Reductions of Pollutant Loads Using Bioretention. *J. Environ. Eng.*, **135** (8), 567–576.

McCarthy, D. T.; Mitchell, V. G.; Deletic, A.; Diaper, C. (2007) *Escherichia coli* in Urban Stormwater: Explaining Their Variability. *Water Sci. Technol.*, **56** (11), 27–34.

Microsoft Office Excel (2013) (15.0.4805.1001) MSO (15.0.4805.1001) 32-bit Part of Microsoft Office 365 ProPlus; Microsoft: Redmond, Washington.

O'Connor, T. P.; Borst, M. (2017) Update to Permeable Pavement Research at the Edison Environmental Center. Proceedings of the *2016 EWRI International Low Impact Development Conference*, Portland, Maine, August 2016.

Pandey, P. K.; Kass, P. H.; Soupir, M. L.; Biswas, S.; Singh, V. P. (2014) Contamination of Water Resources by Pathogenic Bacteria. *AMB Express*, **4**, 51.

Pitt, R. (2011) The National Stormwater Quality Database, Version 3.1. http://unix.eng.ua.edu/~rpitt/Research/ms4/mainms4.shtml (accessed May 2017).

Rushton, B. T. (2001) Low-Impact Parking Lot Design Reduces Runoff and Pollutant Loads. *ASCE J. Water Resour. Plan. Manage.*, **127** (3), 172–179.

Selvakumar, A.; Borst, M. (2006) Variation of Microorganism Concentrations in Urban Stormwater Runoff with Land Use and Seasons. *J. Water Health*, **4** (1), 109–124.

StatSoft, Inc. (2011) Statistica (data analysis software system), version 10. www.statsoft.com.

Struck, S.; Selvakumar, A.; Borst, M. (2008) Prediction of Effluent Quality from Retention Ponds and Constructed Wetlands for Managing Bacterial Stressors in Storm Water Runoff. *ASCE J. Irrig. Drain. Eng.*, **134** (5).

Tata-Maharaj, K.; Scholz, M. (2010) Efficiency of Permeable Pavement Systems for the Removal of Urban Runoff Pollutants Under Varying Environmental Conditions. *Environ. Prog. Sustainable Energy*, **29** (3), 358–369.

Transportation Research Board (2006) *Asphalt Emulsion Technology, Circular No. E-C102*. http://onlinepubs.trb.org/onlinepubs/circulars/ec102.pdf (accessed May 2017).

U.S. Environmental Protection Agency (1976) *Quality Criteria for Water;* EPA/440/9–76/023; U.S. Environmental Protection Agency, Office of Water: Washington, D.C.

U.S. Environmental Protection Agency (1986) *Ambient Water Quality Criteria for Bacteria—1986;* EPA/440/5–84/002; U.S. Environmental Protection Agency, Office of Water: Washington, D.C.

U.S. Environmental Protection Agency (1992) *NPDES Stormwater Sampling Guidance Document*; EPA/833/8–82/001; U.S. Environmental Protection Agency, Office of Water: Washington, D.C.

U.S. Environmental Protection Agency (2000) *Guidance for Data Quality Assessment: Practical Methods for Data Analysis*; EPA/600/R-96/084; U.S. Environmental Protection Agency, Office of Water: Washington, D.C.

U.S. Environmental Protection Agency (2007) National Water Quality Inventory: Report to Congress, 2002 Reporting Cycle; EPA/841/R-07/001; U.S. Environmental Protection Agency, Office of Water: Washington, D.C.

U.S. Environmental Protection Agency (2009) National Water Quality Inventory: Report to Congress, 2004 Reporting Cycle; EPA/841/R-08/001; U.S. Environmental Protection Agency, Office of Water: Washington, D.C.

U.S. Environmental Protection Agency (2010) Surface Infiltration Rates of Permeable Surfaces: Six Month Update (November 2009 through April 2010); EPA/600/R-10/083; U.S. Environmental Protection Agency, Office of Research and Development: Cincinnati, Ohio.

Urban Water Resources Research Council (2014) *Pathogens in Urban Stormwater Systems*; Pathogens in Wet Weather Flows Technical Committee, Environmental and Water Resources Institute, American Society of Civil Engineers: Reston, Virginia. http://collaborate.asce.org/HigherLogic/System/DownloadDocumentFile.ashx?DocumentFileKey=c468710e-971d-4284-a052–0efae9e25d3d (accessed May 2017).

Whitlock, J. E.; Jones, D. T.; Harwood, V. J. (2002) Identification of the Sources of Fecal Coliforms in an Urban Watershed Using Antibiotic Resistance Analysis, *Water Res.*, **36** (17), 4273–4282.

Record of Percentage Agreement - Ariamalar Selvakumar
Co-Author's First and Last Name

Co-Author's Name: Ariamalar Selvakumar

Organization: SMB, WID, CESER

Address: 2890 Woodbridge Avenue (MS-104), Edison, NJ 08837

Phone #: 732-906 6990

Email: selvakumar.ariamalar@epa.gov

Nominee's Name: Ariamalar Selvakumar

Proposed Percentage(s): Nominee - 70 % Co-Author - __

Title(s) of Nominated Publication(s):

1) Organism Detection in Permeable Pavement Parking Lot Infiltrates at the Edison Environmental Center, New Jersey

2) _____

_____

3) _____

_____

I am in agreement with my designated percentage of contribution as stated on the Scientific and Technological Achievement Awards 2020 Nomination Form.

A Selvakumar
_____ 04/15/2020
Signature Date

Ariamalar Selvakumar
Name (Please Print)

Record of Percentage Agreement - Thomas O'Connor
Co-Author's First and Last Name

Co-Author's Name: Thomas O'Connor

Organization: SMB, WID, CESER

Address: 2890 Woodbridge Avenue (MS-104), Edison, NJ 08837

Phone #: 732-321 6723

Email: OConnor.thomas@epa.gov

Nominee's Name: Ariamalar Selvakumar

Proposed Percentage(s): Nominee - 30 % Co-Author - __

Title(s) of Nominated Publication(s):

1) Organism Detection in Permeable Pavement Parking Lot Infiltrates at the Edison Environmental Center, New Jersey

2) _____

_____

3) _____

_____

I am in agreement with my designated percentage of contribution as stated on the Scientific and Technological Achievement Awards 2020 Nomination Form.

Thomas P. O'Connor _____ 04/6/2020
Signature Date

Thomas O'Connor
Name (Please Print)

Selvakumar, Ariamalar

From: Wiley <e-service@wiley.com>
Sent: Tuesday, January 28, 2020 2:43 PM
To: Selvakumar, Ariamalar
Subject: Your work was among the top cited articles in recent publication history!

[redacted]

ter
RESEARCH

Water Fe
the w

gratulations! Your work was one of our top cited articles in recent publication history!

olished in *Water Environment Research*, is among the journal's top cited papers!

avement Parking Lot Infiltrates at the Edison Environmental Center, New Jersey

anuary 2018 and December 2019, your article received some of the highest count of citations.*
act and helped to raise the visibility of *Water Environment Research*.

o offer you a certificate of achievement.

Download Certificate

ur journal so that work like yours is more discoverable.

---

ic news? Post this on social media using #TopCitedArticle

rticle until March 1, 2020 – unless you've published open access, in which case your research will remain free to read, download, and share

This e-mail message was sent to selvakumar.ariamalar@epa.gov. Update your subscription preferences.
You may also unsubscribe here, or by forwarding this email to e-service@wiley.com.

Please consider the environment before you print.

AMERICAS
John Wiley & Sons, Inc.
111 River Street,
Hoboken, NJ 07030-5774 USA
Phone: +1 877 762 2974

Customer Service
Web:
https://hub.wiley.com/community/support

© John Wiley & Sons. All rights reserved. Privacy Policy.

WILEY

Table of Contents

General_Authors_Publications.....2
LI-264488_jam13284-sup-0001-supinfo.....16
LI-264488_Wood_et_al-2016-Journal_of_Applied_Microbiology_(1).....22
Re__[EXTERNAL]_Record_of_Percentage_Agreement__Abderrahmane_(Dahman)_Touati_-_35
Re__[Non-DoD_Source]_Record_of_Percentage_Agreement__Vipin_Rastogi_-_for_STAA_36
Re__Record_of_Percentage_Agreement_Leroy_Mickelsen_-_for_STAA_award.....38
RE__Record_of_Percentage_Agreement_Lisa_Smith_-_for_STAA_award.....39
RE__Record_of_Percentage_Agreement_M_Worth_Calfee_-_for_STAA_award.....41
Re__Record_of_Percentage_Agreement_Matt_Clayton_-_for_STAA_award.....42
Re__Record_of_Percentage_Agreement_Nicole_Griffin-Gatchalian_-_for_STAA_award.44
Re__Record_of_Percentage_Agreement_Shawn_Ryan-_for_STAA_award.....46
Supp_Item_1_EPA_Strategic_Plan.....48
Supp_Item_2_HS_StRap.....103
Supp_Item_3_National-Biodefense-Strategy.....146
Supp_Item_4_Mickelsen_et_al-2019-Remediation.....182
Supp_Item_5_EPA_report_R18-215_anthracis_high_low_concs_HPV.....192
Supp_Item_6_acsest9b06034_EBOV.....315
Supp_Item_7_LCHPV_vehicle_EPA_Conf_2019_Final.....325
Supp_Item_8_LCHPV_chem_agents.....348
Supp_Item_9_Mickelsen_Lab_decon_LCHP.....349
Supp_Item_10_Singapore_presentation_LCHP_lab_tests.....364

United States Environmental Protection Agency
Washington, DC 20460

STAA REPORT FOR THE SCIENTIST NOMINATIONS

General Information:

Nomination ID/App ID:	20-071
Research Category Primary:	Homeland Security (HS)
Research Category Secondary:	
Laboratory/Office Name:	ORD
Nomination Entered By:	Joseph Wood

Eligibility Checklist:

[Y] The nominated publication(s) has not been submitted to a previous STAA competition.

[Y] The nominated publication(s) was published on or before January 1, 2017 and on or after January 1,2012

[Y] The principal author was an EPA employee or a PHS employee assigned to EPA when the research was performed

[Y] The EPA authors (includes PHS employees assigned to EPA) contributed collectively a minimum of 50% toward the publication(s)

Nominating Official Name:	Gregory Sayles
Nominating Official Title:	DIRECTOR, NHSRC
Nominating OfficialEmail:	sayles.gregory@epa.gov
STAA Coordinator Name:	Kathleen Wiser
STAA Coordinator Email:	wiser.kathi@epa.gov

Justifications:

Justification 1:

The nominated research furthers the science and engineering related to decontamination of materials contaminated with biological agents and thus assists the US EPA to prepare for a large-scale release of a biological agent. Preparing for events of national significance, such as a biological agent release, is an EPA responsibility as described under Goal 1 (A Cleaner, Healthier Environment) of the EPA's Strategic Plan (Supplemental Item 1). According to the Strategic Plan, "EPA homeland security research fills critical scientific and technological gaps, enhancing the Agency's ability to carry out its mandated national preparedness and emergency response and recovery obligations, and informing disaster response and guidance." The nominated research was performed under the Homeland Security Research Program (the most recent Homeland Security Strategic Research Action Plan [StRAP] is listed as Supplemental Item 2). The nominated research falls under Research Topic Two of the HS StRAP, specifically in the Wide-Area Decontamination sub-topic. The nominated research also fulfills Goal 3 of the National Biodefense Strategy (Supplemental Item 3), to "Ensure Biodefense Enterprise Preparedness to Reduce the Impacts of Bioincidents", and in particular, enhance preparedness to support decontamination.

In summary, the research and development of techniques to decontaminate and remediate areas contaminated with anthrax spores and other biological agents clearly supports and is relevant to EPA's mission. Specifically, the technique described in the nominated manuscript increases our nation's capacity and ability to recover and reduce the time to recover from a wide-area, intentional release of *Bacillus anthracis* spores.

The nominated research is innovative in that it describes a simple, practical technique that can be used to generate low concentration hydrogen peroxide vapor (LCHPV), which can then be used to inactivate biological agents such as *Bacillus anthracis* spores at conditions determined through the nominated research. The LCHPV is generated through inexpensive yet practical means such as off-the-shelf humidifiers along with using off-the-shelf 3 or 8% aqueous solutions of hydrogen peroxide as described in the nominated publication. This "low-tech" approach would be

advantageous where specialized equipment and financial resources are limited. In addition, because of this low cost, simple approach and its wide availability, it could be implemented on a large-scale and utilized in the event of a wide release of *B. anthracis* spores. The nominated work outlines

in detail the decontamination operational and environmental conditions necessary to obtain effective inactivation of *B. anthracis* spores using LCHPV.

Hydrogen peroxide vapor delivered at relatively higher concentrations is used for decontamination of healthcare, pharmaceutical, animal and food industry facilities. The generating equipment used in these facilities can cost upwards of $100,000. In contrast, the approach described in this published paper can generate LCHPV from off the shelf supplies for only a few hundred dollars. Most laboratory efficacy testing (for bioagents such as *B. anthracis* spores) of HPV has been focused on high concentrations (>200 ppm) as well. While this approach may be appropriate for routine decontamination of facilities in regular use, implementation on a large scale and in a field-setting would be problematic due to a limited number of these expensive generators. It is also difficult to attain and maintain high concentrations of hydrogen peroxide vapor in a building without large generating equipment. The isolation of the high concentration fumigant also poses a safety challenge. In contrast, the use of LCHPV generated through off the shelf equipment, as discussed in the nominated publication, could be implemented on a large scale by lay personnel in the event of a large area release of a biological agent. This would potentially reduce the time for recovery.

The nominated research is highly influential in that it has led to a large body of additional EPA research that has been conducted or is currently underway. This additional research is summarized as follows:

· A study was conducted to demonstrate the use of humidifiers to generate LCHPV at full-scale in a test house, to effectively inactivate *B. anthracis* spore surrogates (Supplemental Item 4)

· A laboratory study was conducted following the nominated work to further elucidate some of the factors affecting efficacy of LCHPV against *Bacillus anthracis* Ames and Vollum spores. (Supplemental Item 5).

· A study was recently conducted and published evaluating the use of LCHPV for the inactivation of Ebola virus surrogates Phi6 and Ms2 bacteriophages. (Supplemental Item 6).

· Although not yet published, a study was conducted evaluating the use of LCHPV disseminated using humidifiers to decontaminate a light duty vehicle. This work was presented at the recent US EPA decontamination conference; (Supplemental Item 7).

· A study was recently conducted to evaluate the material compatibility aspects of using LCHPV. The report is being drafted as of the writing of this STAA nomination form. The results showed that LCHPV had minimal impacts on equipment and electronics.

· A field test was recently conducted to demonstrate the use of LCHPV to decontaminate a Coast Guard vessel. This work was funded by the Department of Homeland Security.

· Research is currently underway to examine the use of LCHPV to neutralize chemical warfare agents. A poster for this work was presented at the recent EPA decontamination conference; (Supplemental Item 8).

· LCHPV is currently being used for decontaminating some our own EPA laboratory facilities, to prevent cross-contamination. Tests have been conducted in one of our decontamination labs as well as our aerosol wind tunnel. (Supplemental Item 9)

· Lab experiments are currently underway (during the writing of this STAA nomination form) to investigate the use of LCHPV to inactivate the SARS CoV2 virus. The LCHPV conditions found to inactivate the Phi6 and MS2 viruses (50 ppm-hr dose) would presumably be effective as well for the SARS-CoV2 virus, since this dose inactivated the MS2 phage, a non-enveloped virus. The current research is looking at what conditions this dose could be achieved using off the shelf equipment such as humidifiers, foggers, and natural evaporation, to generate and disseminate the LCHPV. The goal of this work is to apply for a crisis exemption under Section 18 of the Federal Insecticide, Fungicide, and Rodenticide Act, to allow use of this approach to inactivate the SARS CoV2 virus.

· Research plans have been made to investigate the use of LCHPV to neutralize ricin toxin.

Justification 2A:

N/A

Justification 2B:

Joseph Wood

2018 (July) US EPA STAA Honorable Mention - Demonstration of methyl bromide as an effective decontamination technique for inactivation of Bacillus anthracis spores

Leroy Mickelsen

2018 (July) US EPA STAA Honorable Mention - Demonstration of methyl bromide as an effective decontamination technique for inactivation of Bacillus anthracis spores

Worth Calfee

2018 (July) US EPA STAA Honorable Mention - Demonstration of methyl bromide as an effective decontamination technique for inactivation of Bacillus anthracis spores

2018 (July) US EPA STAA Honorable Mention - Research to Increase our Nation’s Capabilities in Responding to Biological Contamination Incidents

2015 (October) EPA STAA Level III – Development and Application of Test Methods to Evaluate Biological-Terror-Agent Surface Sampling

Shawn Ryan

2015 (October) EPA STAA Level III – Development and Application of Test Methods to Evaluate Biological-Terror-Agent Surface Sampling

Justification 2C:

The previous nomination entitled “2018 (July) US EPA STAA Honorable Mention - Demonstration of methyl bromide as an effective decontamination technique for inactivation of Bacillus anthracis spores” is different from the current nomination in that it deals with a different chemical decontaminant and is applied differently. The current nomination relates to the use of hydrogen peroxide vapor, while the previous nomination dealt with methyl bromide gas. Additionally, the current nomination’s main technical advancement is how the hydrogen peroxide vapor is generated (i.e., through the use of off the shelf humidifiers), whereas the former is already a gas.

The previous nomination entitled “2015 (October) EPA STAA Level III – Development and Application of Test Methods to Evaluate Biological-Terror-Agent Surface Sampling” dealt with surface sampling for *B. anthracis*, while the current nomination is about decontamination and inactivation of *B. anthracis*.

The previous nomination entitled “2018 (July) US EPA STAA Honorable Mention - Research to Increase our Nation’s Capabilities in Responding to Biological Contamination Incidents” dealt with evaluating liquid spray disinfectants for the inactivation of *Burkholderia pseudomallei*, whereas the present nomination is for a novel technique to generate HPV to inactivate *B. anthracis* spores.

Justification 2D:

N/A

Justification 2E:

N/A

Justification 3A:

The primary author was invited to present the nominated research at the 8th Singapore International Symposium on Protection Against Toxic Substances (SISPAT), in March 2017. Refer to Supplemental Item 10.

Funding provided by Department of Homeland Security for a research program to develop restoration plans for US Coast Guard facilities following a biological agent attack, was used to demonstrate the nominated research in the decontamination of a Coast Guard vessel.

The nominated research was featured in EPA's Science Newsletter Sept 2017.

An "On the Spot" award was received in 2017 for the nominated research (as well as other research).

Receipt of an S award in 2019 for nominated research (as well as other research).

Per Google Scholar, the nominated article has been cited 11 times.

Justification 3B:

The nominated journal article underwent extensive internal EPA review, followed by the peer review process for the journal. The Journal of Applied Microbiology typically enlists three peer reviewers with appropriate expertise to provide substantive comments, and then these reviewers make a recommendation to the editor for acceptance or not. The nominated paper received comments from two reviewers on the initial submission to the journal, and then the paper was revised based upon the comments received. The article was then resubmitted to the journal and then accepted for publication, following an editorial review to ensure comments were addressed adequately.

AUTHORS

Principal Author

Author Name:	Joseph P. (Joe) Wood		
Professional Title:		Salutation:	
Email:	wood.joe@epa.gov	Organization:	
Mailing Address:			
Street Line 1:			
City:			
Zip Code:		State:	
At time of research was:	EPA Employee		
Separation Date:			
% of Effort:	20		

Contributing Author

Author Name:	M. Worth Calfee		
Professional Title:		Salutation:	Dr.
Email:	calfee.worth@epa.gov	Organization:	
Mailing Address:			
Street Line 1:			
City:			
Zip Code:		State:	
At time of research was:	EPA Employee		

Separation Date:			
% of Effort:	15		

Contributing Author

Author Name:	Shawn Ryan		
Professional Title:		Salutation:	Dr.
Email:	ryan.shawn@epa.gov	Organization:	
Mailing Address:			
Street Line 1:			
City:			
Zip Code:		State:	
At time of research was:	EPA Employee		
Separation Date:			
% of Effort:	5		

Contributing Author

Author Name:	Leroy Mickelsen		
Professional Title:		Salutation:	
Email:	mickelsen.leroy@epa.gov	Organization:	
Mailing Address:			
Street Line 1:			
City:			
Zip Code:		State:	
At time of research was:	EPA Employee		

Separation Date:			
% of Effort:	10		

Contributing Author

Author Name:	Vipin Rastogi		
Professional Title:		Salutation:	Dr.
Email:	vipin.k.rastogi.civ@mail.mil	Organization:	
Mailing Address:			
Street Line 1:			
City:			
Zip Code:		State:	
At time of research was:	Non EPA Personnel		
Separation Date:			
% of Effort:	15		

Contributing Author

Author Name:	Matthew Clayton		
Professional Title:		Salutation:	
Email:	matt@wildscallionsfarm.com	Organization:	
Mailing Address:			
Street Line 1:			
City:			
Zip Code:		State:	
At time of research was:	Non EPA Personnel		

Separation Date:			
% of Effort:	10		

Contributing Author

Author Name:	Dahman Touati		
Professional Title:		Salutation:	Dr.
Email:	touati.dahman@epa.gov	Organization:	
Mailing Address:			
Street Line 1:			
City:			
Zip Code:		State:	
At time of research was:	Non EPA Personnel		
Separation Date:			
% of Effort:	10		

Contributing Author

Author Name:	Nicole Griffin-Gatchalian		
Professional Title:		Salutation:	
Email:	nicole.griffin@gmail.com	Organization:	
Mailing Address:			
Street Line 1:			
City:			
Zip Code:		State:	
At time of research was:	Non EPA Personnel		

Separation Date:			
% of Effort:	5		

Contributing Author

Author Name:	Lisa Smith		
Professional Title:		Salutation:	
Email:	smith.lisas@epa.gov	Organization:	
Mailing Address:			
Street Line 1:			
City:			
Zip Code:		State:	
At time of research was:	Non EPA Personnel		
Separation Date:			
% of Effort:	10		

PUBLICATIONS

Publication 1:

Publication Title:	A Simple Decontamination Approach Using Hydrogen Peroxide Vapour for Bacillus anthracis Spore Inacti		
Publication Date:	Mon Aug 29 00:00:00 GMT 2016		
Journal/Publication Method:	Journal of Applied Microbiology		
All Author(s):			
Volume:	121	Number:	6
		Immediately	Immediately

Pages:	1603-1615	Index:	Index:
Citation ½ Life:	10.2	Impact Factor:	2.68

Supporting Information

Table S1 Biological Indicator Test Results

Test ID	*G.s.* BI results (# exhibiting growth/# tested)
Test C1	0/3
Test C2	0/9
Test C3	0/9
Test C4	0/9
Test C5	0/9
Test C6	0/9
Test C7	1/6
Test C8	1/9
Test C9	0/9
Test C10	0/9

- All tests used *G. stearothermophilus* (var. 12980) BIs, nominally 10^6 CFU per stainless steel carrier. Each disc was enclosed in a Tyvek pouch.
- The BIs were produced from Mesa Labs, Bozeman MT, USA, and cultured/analyzed per manufacturer instructions, incubated 7 days at 55-60 °C.
- All COMMANDER tests utilized 3 BIs for each of the 3 test chamber locations (n=9) - co-located with coupons - except as noted in table.
- There were only 2 BIs showing growth (incomplete inactivation of carrier) out of a total of 81 tested.

Figure S1 Photos of humidifiers used in testing

Sponge/Evaporative type humidifier

Ultrasonic humidifier

Heated vaporizer

Table S2 Decontamination efficacy results, average ± SD log reduction values, by test #/material/chamber location

Test #	Above Ceiling	On Desk	Under Desk	avg	sd
C1					
Carpet	5.63	7.72	7.75	7.04	1.21
Ceiling Tile	5.84	6.77	6.77	6.46	0.54
Concrete	0.64	2.65	2.42	1.90	1.10
Glass	4.39	7.48	7.48	6.45	1.78
Drywall	5.15	6.56	5.98	5.90	0.71
Laminate	5.35	7.56	7.55	6.82	1.27
C2					
Carpet	7.61	7.61	7.61	7.61	0.00
Ceiling Tile	6.77	6.77	6.77	6.77	0.00
Galvanized Steel	7.46	7.46	7.46	7.46	0.00
Glass	7.17	7.18	7.17	7.17	0.00
Drywall	7.45	7.45	7.45	7.45	0.00
Laminate	7.54	7.54	7.55	7.54	0.01
Wood	7.90	7.89	7.86	7.88	0.02
C3					
Carpet	7.60	7.59	7.60	7.60	0.01
Ceiling Tile	6.66	6.66	6.66	6.66	0.00
Galvanized Steel	7.36	7.35	7.35	7.35	0.01
Glass	7.33	7.33	7.21	7.29	0.07
Drywall	7.67	7.55	7.68	7.63	0.07
Laminate	7.80	7.79	7.80	7.80	0.01
Wood	7.78	7.77	7.78	7.78	0.00
C4					
Carpet	7.50	7.50	7.49	7.50	0.01
Ceiling Tile	6.56	6.56	6.56	6.56	0.00
Galvanized Steel	7.43	7.43	7.44	7.43	0.00
Glass	7.39	7.52	7.52	7.48	0.07
Drywall	7.36	7.36	7.35	7.36	0.01
Laminate	7.47	7.46	7.46	7.46	0.00
Wood	7.73	7.78	7.77	7.76	0.03

Test #	Above Ceiling	On Desk	Under Desk	avg	sd
C5					
Carpet	7.39	6.98	7.39	7.25	0.24
Ceiling Tile	6.62	6.62	6.62	6.62	0.00
Galvanized Steel	7.48	7.46	7.46	7.47	0.01
Glass	7.19	7.34	7.33	7.28	0.08
Drywall	7.19	7.20	7.18	7.19	0.01
Laminate	7.54	7.54	7.54	7.54	0.00
Wood	7.00	7.53	7.54	7.36	0.31
C6					
Carpet	6.24	7.59	6.83	6.89	0.68
Ceiling Tile	4.67	5.32	4.57	4.85	0.41
Galvanized steel	7.47	7.48	4.90	6.62	1.48
Glass	7.75	7.74	7.74	7.74	0.00
Drywall	7.58	7.46	7.46	7.50	0.07
Laminate	6.92	7.56	6.92	7.13	0.37
Wood	7.89	7.88	7.89	7.89	0.01
C7					
Carpet	5.68	4.88	6.91	5.83	1.02
Ceiling Tile	5.07	5.29	6.77	5.71	0.92
Galvanized steel	2.80	6.68	2.65	4.04	2.29
Glass	5.79	7.38	6.93	6.70	0.82
Drywall	3.97	6.00	6.63	5.53	1.39
Laminate	7.30	6.16	7.60	7.02	0.76
Wood	7.78	7.77	7.30	7.62	0.27
C8					
Carpet	7.50	7.81	7.80	7.70	0.17
Ceiling Tile	5.80	6.62	6.62	6.35	0.48
Galvanized steel	7.29	7.42	5.66	6.79	0.98
Glass	7.15	7.27	7.15	7.19	0.07
Drywall	7.29	5.96	7.42	6.89	0.81
Laminate	7.55	7.55	7.55	7.55	0.00
Wood	7.69	7.55	7.71	7.65	0.09

Test #	Above Ceiling	On Desk	Under Desk	avg	sd
C9					
Carpet	3.65	7.63	6.98	6.08	2.13
Ceiling Tile	6.56	6.68	6.68	6.64	0.07
Galvanized steel	4.59	6.88	6.88	6.12	1.32
Glass	6.40	7.22	4.87	6.16	1.19
Drywall	6.99	5.44	7.34	6.59	1.01
Laminate	7.30	7.30	7.29	7.30	0.00
Wood	7.34	7.35	7.24	7.31	0.06
C10					
Carpet	7.75	7.75	7.74	7.75	0.00
Ceiling Tile	6.23	6.66	6.66	6.52	0.25
Galvanized steel	3.41	5.79	7.41	5.54	2.02
Glass	6.47	6.23	7.59	6.76	0.73
Drywall	5.75	7.41	6.28	6.48	0.85
Laminate	7.63	7.62	7.63	7.63	0.00
Wood	7.63	7.66	7.63	7.64	0.02

LR values in red signify complete inactivation of spores for the 3 replicates at a particular chamber location

Journal of Applied Microbiology

Journal of Applied Microbiology ISSN 1364-5072

ORIGINAL ARTICLE

A simple decontamination approach using hydrogen peroxide vapour for *Bacillus anthracis* spore inactivation

J.P. Wood[1], M.W. Calfee[1], M. Clayton[2], N. Griffin-Gatchalian[2], A. Touati[3], S. Ryan[1], L. Mickelsen[4], L. Smith[5] and V. Rastogi[5]

1 National Homeland Security Research Center, United States Environmental Protection Agency, Research Triangle Park, NC, USA
2 ARCADIS, Inc., Durham, NC, USA
3 Jacobs Technology Inc., Research Triangle Park, NC, USA
4 Consequence Management Advisory Division, United States Environmental Protection Agency, Research Triangle Park, NC, USA
5 US Army Edgewood Chemical and Biological Center, Gunpowder, MD, USA

Keywords
antimicrobials, *Bacillus anthracis*, bacterial spores, biocides, hydrogen peroxide vapour, sterilization.

Correspondence
Joseph P. Wood, National Homeland Security Research Center, U.S. Environmental Protection Agency, Research Triangle Park, NC Mail Code E343-06, USA.
E-mail: wood.joe@epa.gov

2016/1389: received 28 June 2016, revised 17 August 2016 and accepted 24 August 2016

doi:10.1111/jam.13284

Abstract

Aims: To evaluate the use of relatively low levels of hydrogen peroxide vapour (HPV) for the inactivation of *Bacillus anthracis* spores within an indoor environment.

Methods and Results: Laboratory-scale decontamination tests were conducted using bacterial spores of both *B. anthracis* Ames and *Bacillus atrophaeus* inoculated onto several types of materials. Pilot-scale tests were also conducted using a larger chamber furnished as an indoor office. Commercial off-the-shelf (COTS) humidifiers filled with aqueous solutions of 3 or 8% hydrogen peroxide (H_2O_2) were used to generate the HPV inside the mock office. The spores were exposed to HPV for periods ranging from 8 h up to 1 week.

Conclusions: Four- to seven-day exposures to low levels of HPV (average air concentrations of approx. 5–10 parts per million) were effective in inactivating *B. anthracis* spores on multiple materials. The HPV can be generated with COTS humidifiers and household H_2O_2 solutions. With the exception of one test/material, *B. atrophaeus* spores were equally or more resistant to HPV inactivation compared to those from *B. anthracis* Ames.

Significance and Impact of the Study: This simple and effective decontamination method is another option that could be widely applied in the event of a *B. anthracis* spore release.

Introduction

Deliberate dissemination of *Bacillus anthracis* (Ames strain) endospores (referred to as spores for the rest of this manuscript) through letters processed by the US Postal Service in the fall of 2001 led to the contamination of numerous offices, buildings and residences across Florida, New Jersey, New York and Washington DC. Hydrogen peroxide vapour (HPV) was used to decontaminate two of the affected buildings (Canter 2005). At that time, the optimal application conditions (concentration, contact time, temperature and relative humidity (RH)) for use of HPV to inactivate *B. anthracis* spores in a building were unknown. For one of the contaminated buildings (Department of State SA-32), it was decided to fumigate using a target HPV concentration of 216 parts per million (ppm) for 4 h, with temperature held above 21°C (US EPA 2005). Special efforts were required (e.g. complete removal of all interior materials and equipment to reduce demand for the HPV fumigant, subdividing the building into 10 separate decontamination zones to reduce needed capacity to generate the HPV, the use of several modified HPV generators), and difficulties were encountered, in order to reach and maintain the target HPV concentration.

HPV has been widely used for decontamination of healthcare, pharmaceutical, animal and food industry facilities (Klapes and Vesley 1990; McDonnell and Russell

Published 2016. This article is a U.S. Government work and is in the public domain in the USA.

1999; Krause *et al.* 2001; Johnston *et al.* 2005; Barbut *et al.* 2009). Effective decontamination using HPV has been demonstrated against a wide range of micro-organisms, including vegetative bacteria (French *et al.* 2004; Kahnert *et al.* 2005; Rogers *et al.* 2008), viruses (Heckert *et al.* 1997), and bacterial spores (Johnston *et al.* 2005; Rogers *et al.* 2005; Rastogi *et al.* 2009; Lawley *et al.* 2010; Malik *et al.* 2013). HPV has also been shown to inactivate prions (Fichet *et al.* 2007).

Laboratory testing of HPV as a sterilant has typically focused on exposure of relatively short durations (2–4 h) at high concentration (>200 ppm) using specialized equipment and concentrated liquid feedstock, for example, 35% concentration of H_2O_2 in aqueous solution. While this approach may be appropriate for routine decontamination of facilities in regular use, implementation on a large scale and in a field setting would be problematic. It is also difficult to attain and maintain high concentrations of HPV in a building without large generating equipment (this is actually a problem for any fumigant), and isolation of the fumigant poses a safety challenge. In addition, high concentrations were found to pose a risk of material incompatibility and resulted in off-gassing of HPV for extended periods in lined ventilation duct (Meyer *et al.* 2014). These results, and reports of other HPV outgassing research (Baron *et al.* 2007), led to the present study, which investigated the sporicidal effects of relatively long durations of low concentration HPV generated with simple, readily available commercial off-the-shelf (COTS) humidifiers.

Decontamination tests were conducted at EPA's Research Triangle Park (NC) laboratories using *Bacillus atrophaeus* spores, with the HPV disseminated using COTS humidifiers in a pilot-scale chamber. Laboratory (bench-scale) tests were also conducted at the Edgewood Chemical and Biological Center (ECBC) facility in Edgewood, MD, with spores of both *B. anthracis* Ames and *B. atrophaeus*. Tests were conducted to assess the effect of operational variables such as the type of humidifier; quantity and concentration of the aqueous H_2O_2 solution; and contact time, on decontamination efficacy. In addition, the tests in the pilot-scale chamber allowed us to assess the effect of location within the chamber on decontamination efficacy, while the bench-scale tests allowed us to compare the degree of inactivation between the two species.

Materials and methods

Test organisms and inoculation procedures

Dried spores of *B. atrophaeus* (ATCC 9372; formerly *Bacillus subtilis* var. *niger* and *Bacillus globigii*) were obtained from the US Army Dugway Proving Ground Life Science Division, and were prepared as described previously (Brown *et al.* 2007). Briefly, *B. atrophaeus* was cultivated, then allowed to sporulate, centrifuged, then spray dried. This spore product was then blended with silicon dioxide particles. Refer to Brown *et al.* (2007) for further details. The surfaces of the materials were inoculated with *B. atrophaeus* spores via a metered dose inhaler (MDI) according to the aerosol deposition-based inoculation methods described previously (Lee *et al.* 2011), yielding approx. 1×10^7 spores over a 18 mm diameter coupon surface. Each inoculation event consisted of one actuation from the MDI.

The *B. anthracis* Ames spores were prepared as detailed in Rastogi *et al.* (2009). Briefly, an overnight tryptic soy broth culture was seeded on Lab Lemko agar plates and incubated at 37 ± 2°C. The plates were daily monitored microscopically for sporulation progression for a period of 7–9 days. When the sporulation reached ≥95%, the spores were harvested from the plates using cold sterile water. The suspension was washed three times in cold sterile water by repeated centrifugations (9 300 ***g*** for 30 min) to remove cell debris and media co-contaminants. The spore suspension was heat-treated at 65°C for 30 min before use. The master stock was enumerated and diluted to a working stock of 2×10^8 CFU ml^{-1} in sterile distilled water containing 0·1% Tween-80 and stored at 4°C until use, within 1 month.

The *B. anthracis* Ames spores were inoculated onto test coupons the afternoon before each experiment as follows. Test coupons were placed flat in a biological safety cabinet (BSC) and inoculated at approx. 10^7 CFU per coupon. A 50 μl aliquot of the well-mixed stock suspension of spores was dispensed with a micropipette via five droplets across the surface of the test coupon. This approach provided more uniform distribution of spores across the coupon surface, as opposed to application of a single drop of the suspension. After inoculation, the test coupons remained undisturbed for an hour in the BSC to initially dry under ambient conditions. The coupons, in Petri plates, were covered and then moved to an incubator at room temperature to finish drying overnight.

Test material coupons

All materials used for decontamination testing were fabricated into circular coupons 18 mm in diameter (Fig. 1) as follows. Oak wood coupons were 8-mm-thick plugs (part SPO750; Woodworks Ltd, Haltom City, TX), while the borosilicate glass coupons were 3·3-mm-thick plugs (Prism Research Glass, Inc., Research Triangle Park, NC). The 18 mm discs were cut from 26-gauge galvanized steel (East Coast Metal, Durham, NC), carpet (Multiplicity

 Published 2016. This article is a U.S. Government work and is in the public domain in the USA.

Figure 1 Photograph of 18 mm diameter coupons of materials mounted on stubs and placed in holder trays.

54594; Shaw Industries Group, Dalton, GA), laminate flooring (Pergo Estate Oak Laminate Flooring from Home Depot, Atlanta, GA; SKU 257063 – no longer available) and ceiling tile (Armstrong, Lancaster, PA; P/N 949, Lowes SKU 40684). Concrete coupons were cast from sand and cement mix (Quikrete Model 110360, Atlanta, GA). The front facing of the wallboard (Gold-Bond, Mooresville, NC; P/N GB00090800, Lowes SKU 34137) was primed (Kilz, Masterchem Industries, Imperial, MO; 2-gal, P/N 20005; Home Depot SKU 317390) and painted (Behr Premium Plus Flat White Latex, Atlanta, GA, P/N 105001, Home Depot SKU 923827). The paper was then removed from the gypsum before 18-mm discs were cut from the paper. All aforementioned materials were then mounted to 18 mm aluminium stubs (P/N 16119; Ted Pella, Inc., Redding, CA) using double-sided adhesive tape (P/N 16073-2; Ted Pella, Inc.) and placed in holder trays. To prevent contamination and bias of results due to nontarget organisms, all coupons and stubs were sterilized prior to tests by exposure to ethylene oxide per procedures specified by manufacturer (Anderson EOGas AN333 Sterilization System, Haw River, NC).

Pilot-scale decontamination chamber and mock office test environment

Decontamination tests using only *B. atrophaeus* spores were conducted in a pilot-scale stainless steel-lined chamber built specifically for decontamination testing, with internal dimensions of approx. 3·4-m wide by 2·5-m deep by 2·8-m high. We have named this chamber the Consequence Management and Decontamination Evaluation Room, or COMMANDER. Refer to Wood *et al.* (2013) for additional details on the overall design and operation of COMMANDER. Briefly, at the entrance to the inner chamber is an airlock compartment, and enclosing the chamber and airlock is an exterior steel shell. All three components of COMMANDER are kept under slight cascading negative pressure (most negative within the innermost compartment) with the use of separate air streams, with valve controls on the inlet and outlet of each to minimize leakage of hazardous materials to occupational areas in proximity to the chamber. Air entering the decontamination chamber passes through a high efficiency particulate air (HEPA) filter, and exhaust air from the decontamination chamber is ducted to an activated carbon bed and HEPA filter prior to release to the facility exhaust system. Within the chamber, temperature and RH data are continuously monitored and logged using a supervisory control and data acquisition (SCADA) system. Other operational parameters of the chamber system, such as air pressures, flow rate, and air duct valves are controlled and/or their data logged via the SCADA system. Valves in the ducts at the inlet and outlet of the inner chamber were shut to prevent air flow during tests, except when air exchange was used (discussed later). The HPV levels within the chamber were measured continuously with an electrochemical sensor (Model B12; Analytical Technology Inc., Collegeville, PA), which was connected to the SCADA system. This HPV sensor had a range of 0–1000 ppm, and was calibrated prior to each test using ambient air as zero and the head space equilibrium concentration (varied between 250 and 300 ppm depending on ambient temperature) of an aqueous H_2O_2 solution. In the first test (Test C1), we used a similar sensor with a range of 0–10 ppm tied into a feedback loop set at 5 ppm, such that the humidifier would be shut off

when the HPV concentration rose above the set point. Temperature and RH within the decontamination chamber were measured with a Vaisala Model 333 sensor and transmitter. This instrument was calibrated prior to each test by comparing its RH data with known RH values generated in the sealed headspace above individual saturated solutions of various salt compounds (Vaisala HMK15, Helsinki Finland).

The stainless steel surfaces of the decontamination chamber were covered by materials typical of an indoor office setting. The mock office arrangement allows for a realistic setting to conduct the tests, and in particular, the materials in the office may absorb or react with the HPV, thus creating a demand or challenge to maintaining desired concentration. The floor was covered with plywood and then carpet, the walls were finished with painted wallboard, and a drop ceiling was installed with acoustic ceiling tiles. The 'office' itself was furnished with equipment consisting of a laminated desk, an office chair, a file cabinet, pin cushion screen, books/catalogues and a computer with monitor and keyboard. A small oscillating fan was also included in the office to assist with distribution of the HPV. Refer to US EPA (2014) for further details on the mock office. For the pilot-scale tests, a set of four coupons (three test coupons, and one negative coupon) of each material was inserted at each testing location immediately before the start of the experiment. Coupon locations within the mock office were on the desk, on the floor beneath the desk, and in the plenum above the drop ceiling (with one ceiling tile panel removed). The humidifier was placed on the floor in the centre of the chamber. Positive controls (coupons of each material inoculated with the target organism but not exposed to the HPV) were kept undisturbed in a sealed container adjacent to but outside of the decontamination chamber.

Small chamber test environment

The chamber used for the ECBC tests using *B. anthracis* Ames is described in Rastogi *et al.* (2009). Briefly, the custom made 0·23 m^3 volume chamber is constructed with 316L stainless steel with four sanitary ports and a sampling port. Temperature, RH and HPV concentration were measured and recorded using similar methods and equipment as described for the mock office tests. A small fan was installed in the chamber to facilitate air and HPV circulation. After the desired contact time, the coupons were withdrawn from the chamber and aerated in a BSL-2 hood before processing.

Test conditions

The test matrix for the pilot-scale experiments is shown in Table 1. All tests were conducted at the laboratory

Table 1 Pilot-scale test conditions

Test ID	Humidifier type	Starting H_2O_2 concentration in aqueous solution (%)	H_2O_2 solution disseminated, ml per m^3 of chamber volume	Air exchange used (fraction of chamber volume replaced each hour)	Average HPV concentration ppm	Max HPV concentration ppm	HPV dose (ppm h)	Avg RH (%)	Max RH (%)
Test C1*	Ultrasonic	8	128	None	5·5	7·3	889	74	81
Test C2	Ultrasonic	8	164	None	11	78	1900	75	93
Test C3	Sponge evaporation	8	154	None	9	43	1430	72	88
Test C4	Ultrasonic	8	173	0·3	11	59	1716	54	91
Test C5	Heated vaporizer	8	161	None	7·5	69	1224	77	94
Test C6	Sponge evaporation	3	148	None	2·2	10	362	78	93
Test C7†	Sponge evaporation	3	148	None	2·5	11	428	72	85
Test C8	Sponge evaporation	3	200	None	3·2	11	543	82	89
Test C9	Sponge evaporation	3	224	0·3	6·4	24	1067	62	85
Test C10	Sponge evaporation	3	224	0·5	3·55	21	597	50	89

HPV, hydrogen peroxide vapour; RH, relative humidity.
All air temperatures at 21 ± 2°C. All tests conducted with 1 week contact time.
*Used a set point of 5 ppm.
†Humidifier turned off and on every 30 min using the SCADA system.

Published 2016. This article is a U.S. Government work and is in the public domain in the USA.

ambient temperature of approx. 21°C. Three types of humidifiers were used to disperse the aqueous H_2O_2 feedstock into the air: an ultrasonic (Vicks P/N V5100NS; The Procter and Gamble Company, Cincinnati, OH), heated vaporizer (P/N 975CVS; CVS Corporation, Woonsocket, RI) and sponge evaporation (P/N HCM-6009; Honeywell, Morristown, NJ). These humidifiers have a capacity of approx. 4–6 l, and varying quantities of the aqueous H_2O_2 solution were disseminated into the mock office as an experimental variable. In Table 1, the amount of solution disseminated in each test is normalized by the chamber volume (24·4 m^3) to allow for extrapolation/comparison of results from other tests. The amount of solution ranged from 128 to 224 ml m^{-3} for the pilot-scale tests. Two feedstocks of aqueous H_2O_2 solution were used in the study: 3% H_2O_2 (CVS, Woonsocket, RI) and 8% H_2O_2 (Family Health News, Miami Shores, FL). Both concentrations can be shipped without hazardous labelling, but 3% is more readily available. The contact time for all of the pilot-scale tests was 1 week, that is, the test coupons were recovered from the chamber 1 week after the humidifier was turned on. With the exception of the first test (C1) and Test C7, the humidifiers ran uncontrolled until the aqueous H_2O_2 feedstock solution was disseminated. In Test C1, the HPV level was held to 5 ppm by turning on and off the humidifier automatically as needed via a feedback loop controlled by the SCADA. The 5 ppm HPV level was selected in light of previous research, for example, Meyer *et al.* (2014), as well as observations of low HPV levels following facility reset operations. In Test C7, the humidifier was turned on and off every 30 min until the aqueous solution was vaporized. Finally, in a majority of the tests, the chamber was sealed and allowed for no air flow. However, in a few of the tests, air ducts at the inlet and outlet of the chamber were left slightly open, which allowed for some air flow. This is noted in Table 1 as air exchange, which is defined as the fraction of the volume of the chamber replaced each hour.

For the bench-scale tests (using spores of both *B. atrophaeus* and *B. anthracis* Ames), the HPV was produced by sparging air through a glass tube fritted at the end (Prism Research Glass, RTP, NC) and immersed in a 1 l Pyrex beaker containing an 8% aqueous solution of H_2O_2. A small pump was used to bubble air through the sparger (Aquaculture MX-1504). Similar to Test C1 described above, all tests at bench-scale used a target HPV concentration of either 5 or 10 ppm, which was maintained by turning on and off the air pump to the sparger via a feedback loop controlled by a SCADA system. Temperature, RH and HPV concentration data were logged continuously via the SCADA system. Although all of the pilot-scale tests used a week contact time (to focus on experimental variables other than contact time), the contact time was an experimental variable for the bench-scale test programme, and ranged from 8 h to 7 days. Table 2 summarizes of the bench-scale experimental matrix.

Recovery of bacterial spores from coupons

At the end of each decontamination test (either pilot-scale or bench-scale), the 18-mm test, procedural blank, and positive control coupons were recovered from the test chambers and sealed containers (for positive controls) and transferred aseptically into empty 50-ml sterile tubes. Bacterial spores were recovered from the coupons according to the methods described by Meyer *et al.* (2014). Briefly, the coupons in the sample vials were extracted in 10 ml of sterile Phosphate Buffered Saline plus Tween® 20 (PBST; Part number 3563; Sigma Aldrich, St. Louis, MO). The samples were then sonicated for 10 min using an 8510 Branson (Danbury, CT) ultrasonic cleaner at 44 kHz and 250 Watts. The sonication step was immediately followed by two continuous minutes of vortexing to further dislodge any viable spores from the coupons. Each vial was briefly re-vortexed immediately before any solution was withdrawn for analysis. The suspension was then subjected to a five-stage, 10-fold serial dilution. Each dilution (0·1 ml) was plated in triplicate on tryptic soy agar (TSA), spread using sterile cell spreaders (Model COPTS-01; Hardy Diagnostics, Santa Maria, CA) and incubated at 35 ± 2°C for 18–24 h. Plates with 30–300 CFU were enumerated manually or using an automated colony counter (Spiral Biotech Q-Count; Advanced Instruments, Norwood, MA). Any samples below enumerable criteria (30 CFU) on the primary dilution plates were filtered. The filters (0·2 μm; Nalgene Analytical, Thermo Scientific P/N 130-4020, Waltham, MA) were plated onto TSA and incubated at 35 ± 2°C for 18–24 h prior to manual enumeration. The number of CFU ml^{-1} was then determined by multiplying the average number of colonies per plate by the reciprocal of the dilution.

Table 2 Bench-scale test conditions

Test run	HPV set point (ppm)	Average actual HPV (ppm)	Contact time (days)	HPV dose (ppm h)	Average RH (%)
1	5	5·87	7	986	41·7
2	5	5·6	4	538	47·3
3	5	6·18	1	148	44·9
4	10	8·46	1	203	56·7
5	10	11·32	0·33	91	49·4

HPV, hydrogen peroxide vapour; RH, relative humidity.
All tests conducted with air temperatures at 26 ± 1°C

Recovery and decontamination efficacy calculations

Decontamination efficacy for a particular material was determined by comparing the number of recovered spores from positive control coupons ($n = 3$ for pilot-scale tests; $n = 5$ for bench-scale tests) and test coupons ($n = 3$ for pilot-scale tests; $n = 5$ for bench-scale tests). That is, efficacy was expressed as $\log_{10}$ reduction (LR) per Eqn (1):

$$\text{Efficacy} = \overline{(\log_{10} \text{CFUc})} - \overline{(\log_{10} \text{CFUt})} \qquad (1)$$

where CFUc is the number of CFU recovered from the positive control coupons and CFUt is the number of CFU recovered from the test coupons. When filter plates had no CFU detected, a value of 1 CFU was inputted, resulting in a log value of 0. Many of the decontamination efficacy results are presented or discussed in terms of whether a 6 LR of the micro-organism population was obtained for a particular material and test condition. The 6 LR benchmark is used since a decontaminant that achieves a LR of 6 or greater (when a 6–7 log challenge is used) for a particular material is considered an effective sporicidal decontaminant (US EPA 2007). We caution, however, that effective decontamination in the laboratory setting may not always transfer to similar efficacy in a field- or full-scale, more realistic setting. Further, a 6 LR still might not be safe for a highly contaminated area. For example, a 6 LR of spores against a spore loading of 8 or 9 log CFU would leave significant remaining viable spores and could potentially present a health hazard.

Statistical analyses

Statistical analyses were performed with SAS 9.4 for Windows (SAS Institute Inc., Cary, NC). The null hypothesis testing was conducted at the 5% level of significance. Decontamination efficacies associated with study parameters were compared using one-way analysis of variance (ANOVA) and the Least-Squares Means (LS Means) multiple comparison test. Diffograms were constructed to visualize pair-wise LS means differences. Linear mixed models were considered for assessing fixed and random effects of experimental variables. Interaction effects were as well analysed. The Wilcoxon rank-sum/Exact test and Kruskal–Wallis test were applied for statistical comparisons of groups of non-normal data. The *P*-value from two-sided (nondirectional) tests were used to test hypotheses. Correlations (Pearson product-moment correlation coefficient, *r*) were analysed using MS Excel, and only include materials that were common to all tests: carpet, ceiling tile, glass, painted wallboard and laminate.

Results

Pilot-scale tests with *Bacillus atrophaeus* spores

The results for the fumigation parameter measurements for the 10 decontamination tests conducted in COMMANDER are summarized in Table 1. Five of the tests were conducted using an 8% aqueous solution of H_2O_2, and the other five tests used a 3% aqueous solution. The average concentration of HPV for each test ranged from 2 to 11 ppm, with the highest HPV levels associated with the 8% aqueous solution (C2–C5). For a given aqueous H_2O_2 concentration, HPV levels generally increased with greater quantities of solution disseminated. For example, Test C2, which used 164 ml m^{-3} of 8% solution, resulted in the highest maximum HPV level of 78 ppm. In Test C9, 224 ml m^{-3} of the 3% aqueous solution was used, resulting in the highest HPV levels for the tests using the 3% solution (e.g. 24 ppm). The use of air exchange or increase in air exchange reduced HPV levels in COMMANDER when compared to similar tests without it, for example, compare C2 to C4; compare C9 to C10. However, in comparing Tests C8 and C9, the use of air exchange is accompanied by a higher HPV level. This unexpected result may be explained in part by an increase in H_2O_2 solution that was disseminated (In Test C9, we disseminated an additional 24 ml m^{-3} of solution compared to C8.), or may be due to erroneous measurement of an experimental parameter such as air flow.

Figure 2 shows the HPV concentration profiles following dispersion of 8% H_2O_2 solution with the three humidifier types, from tests C2, C3 and C5. The general shape of these concentration profiles was typical of all the tests except C1 and C7. In C1, the HPV level was held to a constant level of 5 ppm for the entire week, and in Test C7, the HPV level fluctuated as the humidifier was turned on and off every 30 min. As illustrated in Fig. 2, the HPV concentration increased to its maximum level (data shown in Table 1) within approx. 12 h, and then gradually decayed back to nondetectable levels of HPV within the week's contact time. The HPV dose (ppm HPV h) results reported in Table 1 were calculated by integrating the area under these HPV concentration profile curves. Of the three concentration profiles shown in Fig. 2, the ultrasonic humidifier produced the highest HPV dose (Test C2; 1900 ppm h), followed by the sponge evaporator, and then the heated vaporizer.

Similar to the rise in HPV levels, with the start of the humidifiers, the RH levels in the decontamination chamber increased from ambient levels of between 40 and 50% to the maximum levels ranging between 81 and 94%. Air temperatures within the decontamination chamber were consistent throughout the study and averaged 21 ± 2°C.

Published 2016. This article is a U.S. Government work and is in the public domain in the USA.

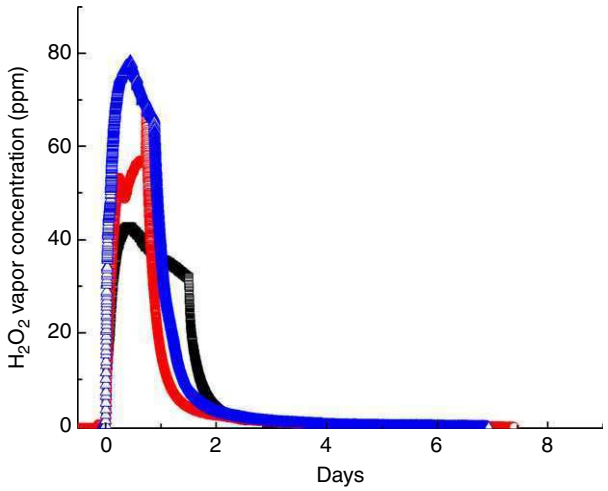

Figure 2 Hydrogen peroxide vapour concentration profiles of the different humidifier types. Data are from Tests C2, C3 and C5. Ultrasonic = blue triangles; sponge evaporation = black squares; heated = red circles.

Overall results and effect of material on efficacy

In Table 3 we present a summary of the decontamination efficacy results for the pilot-scale tests conducted in COMMANDER. The results are summarized by the average LR for each material for each test. At the bottom of Table 3 are the average LR values for each material for all of the pilot-scale tests. Because the concrete material was poorly decontaminated (1·90 average LR), we discontinued this material from further testing. In the place of concrete, we added wood and galvanized metal materials to the test matrix. With the exception of concrete (used only in the first test), all of the materials were decontaminated on average above 6 LR for the COMMANDER tests. The LR results shown in bold in Table 3 indicate that all test coupons for that particular material (3 replicates × 3 chamber locations = 9 total) were completely decontaminated, that is, there were no detectable spores following treatment. The laminate material had the greatest number of tests in which all of its coupons were completely decontaminated (7), while carpet had the fewest number of tests (only 3) in which all of its coupons were completely decontaminated. With the exception of concrete, ceiling tile had the lowest overall average LR (6·31) for the pilot test programme.

Biological indicators (BIs) comprised of *Geobacillus stearothermophilus* on steel discs were also used in the COMMANDER tests as another tool to assess the efficacy of HPV generated via the humidifiers. Only two out of the 81 BIs used in the overall study exhibited growth following HPV exposure. Further information and detailed results for this additional assay are presented in the Supporting Information.

Effect of HPV levels and quantity of solution disseminated on efficacy

The average LR values across all materials that were common for each test (carpet, ceiling tile, glass, painted wallboard and laminate) are shown in the last column in Table 3, and were all greater than 6·0 for every test (We note that some materials within a particular test may have been decontaminated at an average level <6 LR, while the overall average for all the materials in a test was >6 LR. In

Table 3 Summary of pilot-scale decontamination efficacy results for *Bacillus atrophaeus* spores

Test ID	Carpet	Ceiling tile	Unpainted concrete†	Glass	Painted wallboard	Laminate	Wood	Galvanized metal	Avg by test*
Test C1	7·04 ± 1·21	6·46 ± 0·54	1·90 ± 1·10	6·45 ± 1·78	5·90 ± 0·71	6·82 ± 1·27			6·53 ± 0·43
Test C2	**7·61 ± 0·00**	**6·77 ± 0·00**		**7·17 ± 0·00**	**7·45 ± 0·00**	**7·54 ± 0·01**	**7·88 ± 0·02**	**7·46 ± 0·00**	7·31 ± .34
Test C3	**7·61 ± 0·00**	**6·66 ± 0**		7·29 ± 0·07	7·63 ± 0·07	**7·80 ± 0·01**	**7·78 ± 0·00**	**7·35 ± 0·00**	7·40 ± .45
Test C4	7·50 ± 0·01	**6·56 ± 0**		**7·48 ± 0·07**	**7·36 ± 0**	**7·46 ± 0**	**7·76 ± 0·02**	**7·43 ± 0**	7·27 ± .4
Test C5	7·25 ± 0·23	**6·62 ± 0**		7·28 ± 0·08	**7·19 ± 0·01**	**7·54 ± 0**	7·36 ± 0·31	**7·47 ± 0**	7·18 ± .34
Test C6	6·89 ± 0·68	4·85 ± 0·41		**7·74 ± 0**	7·50 ± 0·07	7·13 ± 0·37	**7·89 ± 0·01**	6·62 ± 1·48	6·82 ± 1·15
Test C7	5·83 ± 1·02	5·71 ± 0·92		6·70 ± 0·82	5·53 ± 1·39	7·02 ± 0·76	7·62 ± 0·27	4·04 ± 2·29	6·16 ± .66
Test C8	7·70 ± 0·17	6·35 ± 0·48		7·19 ± 0·07	6·89 ± 0·81	**7·55 ± 0**	7·65 ± 0·09	6·79 ± 0·98	7·14 ± .54
Test C9	6·08 ± 2·13	6·64 ± 0·07		6·16 ± 1·19	6·59 ± 1·01	**7·30 ± 0**	7·31 ± 0·06	6·12 ± 1·32	6·55 ± .49
Test C10	**7·75 ± 0**	6·52 ± 0·25		6·76 ± 0·73	6·48 ± 0·85	**7·63 ± 0**	**7·64 ± 0·02**	5·54 ± 2·02	7·03 ± .62
Avg by material	7·13 ± 0·62	6·31 ± 0·68	1·09 ± 1·63	7·02 ± 0·50	6·85 ± 0·71	7·38 ± 0·30	7·65 ± 0·19	6·45 ± 1·12	

Results are average of log reductions ± SD on coupons for each of the three locations where coupons were placed: above ceiling tile, on desk and below desk. Log reduction results in bold indicate all test coupons (n = 9; 3 replicates at each location) for that material were completely decontaminated.

*Average LR by test calculated using materials common for all tests (carpet, ceiling tile, glass, painted wallboard and laminate).

†Unpainted concrete was only included in first test.

Published 2016. This article is a U.S. Government work and is in the public domain in the USA.

addition, replicates of a material placed at a particular location within the chamber may have been decontaminated at a level <6 LR while the overall average for that material may be >6 LR. Indeed, coupons placed at the ceiling location tended to be decontaminated to a lesser degree than the two other locations, and this is discussed in more detail below. Summary data for the average LR values for each material/test/chamber location are provided in Supporting Information.) Tests C1, C6 and C7 each had at least one material which was decontaminated at an average LR level less than 6·0. From this result, we observe that approx. 160 ml m^{-3} was the minimum amount of 8% solution needed for effective decontamination (>6 LR) for all materials used in our study; similarly, 200 ml m^{-3} was the minimum amount of the 3% solution needed to effectively decontaminate the materials included in our study. In terms of HPV dose, Test C1 had the highest dose (889 ppm h) in which not all of the materials were decontaminated with a LR >6·0, suggesting that a dose higher than this would be needed for effective decontamination across a range of materials. Test C2 was the only test in which every test coupon for every material was completely decontaminated, and this test also had the highest HPV values (in terms of average and maximum concentration, as well as dose). The average LR value for a test correlated with HPV dose ($r = 0{\cdot}63$), but was lesser correlated with maximum HPV ($r = 0{\cdot}48$) and average HPV ($r = 0{\cdot}41$). The average LR for each test was minimally but negatively correlated with average RH ($r = -0{\cdot}24$).

Effect of humidifier type on efficacy

Comparison of the LR results for Tests C2, C3 and C5 could potentially allow one to interpret the effect of humidifier type on decontamination efficacy, since a different humidifier type was used in each of these three tests, all three tests used an 8% solution with similar quantity of the H_2O_2 solution disseminated (154–164 ml m^{-3}), with no air exchange. While many of the materials from these three tests were completely decontaminated, and all of the materials were effectively decontaminated, significance testing found that the decontamination efficacy of the heated vaporizer (irrespective of material) was statistically lower than the other two types of humidifiers. (As mentioned previously, the heated vaporizer (Test C5) also resulted in the lowest HPV dose of the three tests being compared.) We do acknowledge, however, that the maximum difference in efficacy between the humidifier types was less than 0·5 LR, and that the heated vaporizer was only tested once. No other significant differences in decontamination efficiency by type of humidifier were found. For this reason, in all of the subsequent tests using the 3% solution, we used the sponge evaporator humidifier, which had a higher reservoir capacity and thus allowed us to disseminate greater amounts of the aqueous solution.

Effect of test coupon location on efficacy

In Table 4, we show decontamination efficacy results as a function of the test coupon location in the COMMANDER test chamber. The results are shown in terms of the fraction (per cent) of the number of samples in which no viable spores were detected, as well as fraction of instances when the LR <6·0. Coupons located on the desk were easiest to decontaminate, as indicated by having the highest percentage (75%) of samples with no detectable spores. Coupons located above the ceiling tiles were the most difficult to decontaminate, exemplified by having the lowest percentage of occurrences in which a material had no detectable spores (52%), as well as by having the most number of occurrences in which the decontamination efficacy was not effective (LR <6·0). Statistical analysis confirmed that the overall efficacy for the coupons located above the ceiling tiles is statistically lower ($\alpha = 0{\cdot}05$) than the other two locations.

Small chamber results using spores of *Bacillus anthracis* Ames and *Bacillus atrophaeus*

The decontamination efficacy results for the laboratory-scale tests using both *B. anthracis* Ames and *B. atrophaeus* spores are summarized in Table 5. Five tests were conducted with both species, with average actual HPV levels ranging from approx. 5 to 11 ppm; contact times ranged from 8 h to 1 week, and actual RH levels ranged from 45 to 57%; refer to Table 2 for actual fumigation conditions.

In the first three tests, we used a target HPV concentration of 5 ppm, but varied the contact time to assess the effect of this parameter. In Test 1, with a 1-week contact time, nearly every material, for both species, was completely decontaminated. After reducing the contact

Table 4 Effect of location of decontamination efficacy in COMMANDER

	Above ceiling	On desk	Under desk
Per cent of occurrences in which all three replicates for a material in a given test had no detectable spores	52	75	72
Per cent of occurrences in which the average LR for a material in a given test was <6·0	32	23	17

Published 2016. This article is a U.S. Government work and is in the public domain in the USA.

Table 5 Summary of bench-scale decontamination efficacy results

	Carpet		Ceiling tile		Wood		Glass		Painted wallboard		Laminate	
Test ID	Ames	Bg	Ames	Bg	Ames	Bg	Ames	Bg	Ames	Bg	Ames	Bg
1	**7·33 ± 0**	**7·42 ± 0**	**7·25 ± 0**	**7·48 ± 0**	**7·09 ± 0**	**7·47 ± 0**	**6·35 ± 0**	7·07 ± 0·41	**7·13 ± 0**	**7·45 ± 0**	7·05 ± 0·4	6·29 ± 1·26
2	6·53 ± 0·49	6·28 ± 1·0	**7·18 ± 0**	6·74 ± 0·57	**07·24 ± 0**	6·50 ± 1·0	**7·21 ± 0**	7·65 ± 0·17	7·13 ± 0·13	6·59 ± 0·51	NA	6·98 ± 0·69
3	2·28 ± 0·19	1·88 ± 0·44	6·75 ± 0·76	2·48 ± 0·69	5·80 ± 1·74	2·29 ± 0·55	7·02 ± 0	2·74 ± 0·75	5·18 ± 1·93	2·15 ± 0·4	**6·48 ± 0**	2·53 ± 0·48
4	4·89 ± 1·01	6·96 ± 0·77	**7·37 ± 0**	6·96 ± 0·63	**7·28 ± 0**	7·12 ± 0·68	**7·63 ± 0**	7·53 ± 0·23	6·85 ± 1·88	6·12 ± 0·91	**7·51 ± 0**	6·83 ± 1·09
5	2·90 ± 0·05	0·79 ± 0·16	4·25 ± 1·30	1·17 ± 0·19	5·83 ± 1·64	1·33 ± 0·19	5·11 ± 2·32	1·68 ± 0·33	3·15 ± 0·29	3·02 ± 0·4	6·20 ± 2·01	2·58 ± 0·31

Results are presented as average LR ± SD, with values in bold indicating complete inactivation. Ames refers to *Bacillus anthracis* Ames; Bg refers to *Bacillus globigii* aka *B. atrophaeus*.

time to 4 days (Test 2), efficacy remained high, with greater than 6 LR for both species and material. In Test 3, using a target concentration of 5 ppm HPV and 1 day contact time, *B. anthracis* spores were inactivated at a LR >6·0 for three of the six materials. But maintaining the 1-day contact time and raising the target HPV level to 10 ppm (Test 4), decontamination efficacy was significantly improved compared to Test 3, for all materials for both species. In particular, with an actual average HPV concentration of 8·5 ppm held for 24 h, we were able to achieve over 6 LR in *B. anthracis* spores on all materials except carpet (average LR for this material was 4·89). With Test 5, the actual HPV level was 11·32 ppm, and with a contact time of 8 h, this resulted in the lowest HPV dose of the bench-scale tests, at approx. 91 ppm h. Correspondingly, the LR results for Test 5 were generally the lowest for the bench-scale tests, with the majority of LR values less than 5·0.

Excluding tests in which one or both species were completely inactivated on all replicates for a particular material (e.g. this occurred for every material in Test 1 except laminate), the LR values were all higher for *B. anthracis* compared to *B. atrophaeus* with the exception of the carpet material in Test 4. Comparing the decontamination efficacy results for the two species for the two tests in which the kill was incomplete (Tests 3 and 5) allows us to more readily analyse statistical differences. In these two tests, statistical analyses showed that the LR values for the materials inoculated with *B. atrophaeus* spores were significantly less than for *B. anthracis* Ames spores. In the tests where there was sufficient HPV dosing (Tests 1, 2 and 4), that is, the HPV treatment was effective in most cases, there was no significant difference in efficacy between the two species.

Statistical comparisons of the effect of material on efficacy were also conducted for Tests 3 and 5, in which fractionated kill was observed. With respect to the Ames strain, decontamination efficacy was significantly lower for carpet compared to the rest of the materials. Wallboard was the next most difficult material to decontaminate for *B. anthracis* Ames: the painted wallboard LR values were not significantly different compared to ceiling tile, but were significantly lower than the rest of the materials. With respect to *B. atrophaeus*, carpet, ceiling tile and wood, were significantly more difficult to decontaminate compared to glass, laminate, and wallboard.

Comparing *B. atrophaeus* efficacy results for Test 1 of the bench-scale tests and Test C1 for the pilot-scale tests allows us to confirm any differences that may have arisen due to differences in test venue or scale, since both tests were conducted at constant 5 ppm HPV for 1 week. The materials in common for both these tests were carpet, ceiling tile, glass, painted wallboard and laminate. In Test 1 of the

bench-scale tests, four of the five materials (carpet, ceiling tile, glass and wallboard) were completely decontaminated of *B. atrophaeus*, while none of the materials in pilot-scale Test C1 were completely decontaminated. Nevertheless, statistical comparisons provide evidence to suggest that both test environments were equally effective for all materials, with the exception that ceiling tile and painted wallboard were significantly more difficult to decontaminate at the pilot-scale. That said, these minor differences in efficacy between test venues may be due to differences in the venues' HPV dissemination techniques, or due to differences in temperature. For example, the average temperature for testing at the bench-scale was 26°C, while the average temperature of the pilot-scale tests was 21°C.

Discussion

Several studies have demonstrated the use of HPV for inactivating virulent bacterial spores from species such as *B. anthracis* and *Clostridium difficile* (Johnston *et al.* 2005; Rogers *et al.* 2005; Rastogi *et al.* 2009; Lawley *et al.* 2010). However, these studies and the actual use of HPV in practice typically require sophisticated and expensive equipment to generate the HPV, and usually at relatively high levels (200–500 ppm). In contrast, our study demonstrated that generating relatively low levels of HPV with easy to use equipment and readily available H_2O_2 solutions is an effective and inexpensive technique for inactivating *B. anthracis* spores on a number of materials. Average HPV levels of 5–10 ppm, coupled with contact times between 4 and 7 days, were shown to be effective in inactivating *B. anthracis* and *B. atrophaeus* spores at levels greater than 6 LR for all of the materials tested except for concrete. Studies by Meyer *et al.* (2014) and Baron *et al.* (2007) provided initial evidence suggesting that desorption of HPV from materials results in the production of low levels of HPV over extended time periods, and leads to inactivation of spores. Our robust test programme and research, through the use of several materials and other experimental variables, builds on and corroborates these studies. We are not aware of any other peer reviewed scientific literature reporting the use of such low levels of HPV for bacterial spore inactivation.

We have also demonstrated in pilot-scale experiments that simply disseminating aqueous solutions of H_2O_2 via COTS humidifiers, without control of the HPV concentration, is an effective decontamination technique. This approach is effective provided that a sufficient quantity of solution is disseminated as vapour and/or a high enough dose of HPV is obtained, coupled with sufficient contact time. For example, 200 ml m^{-3} was the minimum amount of 3% H_2O_2 solution found to be effective (>6 LR) on the all materials tested, while a minimum of approx. 160 ml m^{-3} of 8% solution was effective on all materials – with both tests using a 7-day contact time. While we did not vary contact time for the pilot-scale tests using humidifiers (all tests were conducted with a 7-day contact time), most likely similar decontamination efficacy results would have been obtained had we used a shorter contact time such as 4 days, consistent with the small chamber tests. In addition, Fig. 2 shows that 99% of the HPV dose is obtained within 4 days, further indication that a full week contact time may not have been needed. Relative to the HPV dose, the results suggest that a dose of at least 1000 ppm h HPV would be effective for a range of materials, under the conditions tested in our experiments.

We also found that the three types of COTS humidifiers we tested (ultrasonic, heated vaporizer, and sponge evaporation) were generally similarly effective in decontamination at the conditions we tested them, for example, using an 8% aqueous solution. We do note, however, that when we compare the results for Tests C2, C3 and C5, in which the three different types of humidifiers were used with similar amounts of 8% solution, the heated vaporizer was slightly (but statistically significant) less efficacious. In comparing these same three tests, the HPV concentration (in terms of average, maximum and dose) for the ultrasonic type (Test C2) was the highest among the three tests, while the heated vaporizer resulted in the lowest HPV concentrations. Although we do not have enough data to definitively conclude that the ultrasonic device is more effective in producing the HPV, further research may be warranted to investigate this matter. Additional experiments at less than ideal conditions may also produce additional data to better characterize or elucidate differences in efficacy by the type of humidifier.

With the exception of unpainted concrete, low levels of HPV were predominantly effective on all the materials we tested. While there was some variation in decontamination efficacy among some of the materials, as would be expected, the variation was relatively minor. For example, ceiling tile and galvanized metal were slightly more difficult to decontaminate in pilot test experiments, a result consistent with Rogers *et al.* (2005). Inactivation of *B. atrophaeus* on ceiling tile, carpet and wood was slightly but significantly more difficult compared to the other materials in the laboratory-scale tests.

With respect to unpainted concrete being the most difficult to decontaminate, this result is consistent with Rastogi *et al.* (2009), who found that the LR on concrete via HPV was less than 1·0 under variable spore loadings. Rogers *et al.* (2005) did achieve effective inactivation of *B. anthracis* spores on concrete using HPV, but the concrete was painted. The low efficacy of HPV on unpainted concrete may be due to the high demand this material

 Published 2016. This article is a U.S. Government work and is in the public domain in the USA.

places on HPV concentration (US EPA, 2010). Although it is conceivable that HPV would be efficacious on concrete provided a sufficiently high enough concentration and contact time is allowed, finding these required conditions was beyond the scope of this study.

While most materials were effectively decontaminated, decontamination of the materials placed above the ceiling tile panels was not as effective as those placed at other locations. This is most likely due to insufficient mixing of the heavier-than-air HPV. Full removal of the ceiling panels, as well as raising the humidifier outlet, may be warranted to facilitate exposure at all elevations within a room.

One purpose of this study was to compare the small-scale decontamination results between the virulent *B. anthracis* (Ames) and *B. atrophaeus*, to confirm the latter micro-organism as an appropriate surrogate in the pilot-scale COMMANDER experiments, as well as future decontamination studies. For spore inactivation studies, the nonpathogenic substitute organism should possess resistance to the decontamination treatment equivalent to or greater than the virulent species (Wood *et al.* 2011). Our results show that *B. atrophaeus* may be a suitable surrogate for *B. anthracis* Ames in HPV decontamination studies. In this study, there was only one case (material/test combination) in which *B. atrophaeus* was inactivated to a significantly greater degree than *B. anthracis*. We acknowledge that each species was inoculated on coupons using a different technique, and that this difference in spore inoculation method may confound comparison of efficacy between the two species. The *B. anthracis* spores were deposited onto coupons using a liquid inoculation method, while *B. atrophaeus* spores were deposited onto coupons as an aerosol via the use of an MDI. Ryan *et al.* (2014) found that the spore inoculation method did affect decontamination efficacy results, but the effect varied by material and decontaminant. Nevertheless, our *B. anthracis* Ames and *B. atrophaeus* decontamination efficacy results agree well with Rogers *et al.* (2005), who showed that with the exception of just a few instances, *B. subtilis* was inactivated to a lesser degree than *B. anthracis* Ames when exposed to HPV on a number of materials. While we were unable to find any study in the literature specifically comparing the resistance of *B. anthracis* Ames to *B. atrophaeus* (aka *B. subtilis* var Niger) upon exposure to HPV, *B. atrophaeus* is phenotypically similar to *B. subtilis* except for the production of pigment (Sella *et al.* 2014).

From the bench-scale experiments in which contact time was varied, we found that 4 days was the minimum contact time needed for effective decontamination with HPV at an average level of 5 ppm. Based on this result and the fact that all but one material was effectively decontaminated at 10 ppm HPV with 1-day exposure, this would suggest that a contact time of between 2 and 3 days should be sufficient for effective decontamination at 10 ppm HPV at the bench-scale.

In summary, the use of relatively low levels of HPV coupled with extended contact times (e.g. 4–7 days) represents a new, straightforward methodology for the decontamination of many types of surfaces contaminated with *B. anthracis* spores. The approach can be implemented by holding HPV levels constant at 5–10 ppm, or by simply disseminating the vapour with COTS humidifiers using readily available (e.g. 3–8% concentration) aqueous solutions of H_2O_2. This is a practical, safe and economical decontamination technique useful for when financial resources may be limited, and when the volume being decontaminated is not overly large and can be left undisturbed for a few days. We also foresee this easy to use decontamination method applied to the inactivation of other pathogenic micro-organisms that have already been demonstrated to be susceptible to HPV, although further research is needed to confirm required contact times for the different types of materials and biological agents. In conclusion, we caution that effective decontamination in the laboratory setting may not always transfer to similar efficacy in a field- or full-scale, more realistic setting. Therefore, further testing of this low-level HPV decontamination approach, using a larger, more realistic test bed, is recommended.

Acknowledgements

The authors gratefully acknowledge the statistical analyses provided by Patrick Pancras and the dedicated microbiological laboratory support provided by Christina Slone. Expert technical assistance of LTC (retired) Laura Burton is also gratefully acknowledged for experimental preparation and processing the *B. atrophaeus* samples at the ECBC facility.

Disclaimer

The US Environmental Protection Agency (EPA) through its Office of Research and Development funded and directed the research described herein under contract EP-C-09-027 with ARCADIS, Inc. It has been subjected to the Agency's review and has been approved for publication. Note that approval does not signify that the contents necessarily reflect the views of the Agency. Mention of trade names, products or services does not convey official EPA approval, endorsement or recommendation.

Conflict of Interest

The authors declare no conflict of interest.

References

Barbut, F., Menuet, D., Verachten, M. and Girou, E. (2009) Comparison of the efficacy of a hydrogen peroxide dry-mist disinfection system and sodium hypochlorite solution for eradication of *Clostridium difficile* spores. *Infect Control Hosp Epidemiol* **30**, 507–514.

Baron, P.A., Estill, C.F., Beard, J.K., Hein, M.J. and Larsen, L. (2007) Bacterial endospore inactivation caused by outgassing of vapourous hydrogen peroxide from polymethyl methacrylate (Plexiglas). *Lett Appl Microbiol* **45**, 485–490.

Brown, G.S., Betty, R.G., Brockmann, J.E., Lucero, D.A., Souza, C.A., Walsh, K.S., Boucher, R.M., Tezak, M. *et al.* (2007) Evaluation of a wipe surface sample method for collection of *Bacillus* spores from nonporous surfaces. *Appl Environ Microbiol* **73**, 706–710.

Canter, D.A. (2005) Remediating anthrax-contaminated sites: learning from the past to protect the future. *Chem Health Saf* **12**, 13–19.

Fichet, G., Antloga, K., Comoy, E., Deslys, J.P. and McDonnell, G. (2007) Prion inactivation using a new gaseous hydrogen peroxide sterilisation process. *J Hosp Infect* **67**, 278–286.

French, G.L., Otter, J.A., Shannon, K.P., Adams, N.M.T., Watling, D. and Parks, M.J. (2004) Tackling contamination of the hospital environment by methicillin-resistant *Staphylococcus aureus* (MRSA): a comparison between conventional terminal cleaning and hydrogen peroxide vapour decontamination. *J Hosp Infect* **57**, 31–37.

Heckert, R.A., Best, M., Jordan, L.T., Dulac, G.C., Eddington, D.L. and Sterritt, W.G. (1997) Efficacy of vaporized hydrogen peroxide against exotic animal viruses. *Appl Environ Microbiol* **63**, 3916–3918.

Johnston, M.D., Lawson, S. and Otter, J.A. (2005) Evaluation of hydrogen peroxide vapour as a method for the decontamination of surfaces contaminated with *Clostridium botulinum* spores. *J Microbiol Methods* **60**, 403–411.

Kahnert, A., Seiler, P., Stein, M., Aze, B., McDonnell, G. and Kaufmann, S.H.E. (2005) Decontamination with vaporized hydrogen peroxide is effective against *Mycobacterium tuberculosis*. *Lett Appl Microbiol* **40**, 448–452.

Klapes, N.A. and Vesley, D. (1990) Vapor-phase hydrogen peroxide as a surface decontaminant and sterilant. *Appl Environ Microbiol* **56**, 503–506.

Krause, J., McDonnell, G. and Riedesel, H. (2001) Biodecontamination of animal rooms and heat-sensitive equipment with vaporized hydrogen peroxide. *Contemp Top Lab Anim Sci* **40**, 18–21.

Lawley, T.D., Clare, S., Deakin, L.J., Goulding, D., Yen, J.L., Raisen, C. and Brandt, C. (2010) Use of purified *Clostridium difficile* spores to facilitate evaluation of health care disinfection regimens. *Appl Environ Microbiol* **76**, 6895–6900.

Lee, S.D., Ryan, S.P. and Snyder, E.G. (2011) Development of an aerosol surface inoculation method for *Bacillus* spores. *Appl Environ Microbiol* **77**, 1638–1645.

Malik, D.J., Shaw, C.M., Rielly, C.D. and Shama, G. (2013) The inactivation of *Bacillus subtilis* spores at low concentrations of hydrogen peroxide vapour. *J Food Eng* **114**, 391–396.

McDonnell, G. and Russell, A.D. (1999) Antiseptics and disinfectants: activity, action, and resistance. *Clin Microbiol Rev* **12**, 147–179.

Meyer, K.M., Calfee, M.W., Wood, J.P., Mickelsen, L., Attwood, B., Clayton, M., Touati, A. and Delafield, R. (2014) Fumigation of a laboratory-scale HVAC system with hydrogen peroxide for decontamination following a biological contamination incident. *J Appl Microbiol* **116**, 533–541.

Rastogi, V.K., Wallace, L., Smith, L.S., Ryan, S.P. and Martin, B. (2009) Quantitative method to determine sporicidal decontamination of building surfaces by gaseous fumigants, and issues related to laboratory-scale studies. *Appl Environ Microbiol* **75**, 3688–3694.

Rogers, J.V., Sabourin, C.L., Choi, Y.W., Richter, W.R., Rudnicki, D.C., Riggs, K.B., Taylor, M.L. and Chang, J. (2005) Decontamination assessment of *Bacillus anthracis*, *Bacillus subtilis*, and *Geobacillus stearothermophilus* spores on indoor surfaces using a hydrogen peroxide gas generator. *J Appl Microbiol* **99**, 739–748.

Rogers, J.V., Richter, W.R., Shaw, M.Q. and Choi, Y.W. (2008) Vapour-phase hydrogen peroxide inactivates *Yersinia pestis* dried on polymers, steel, and glass surfaces. *Lett Appl Microbiol* **47**, 279–285.

Ryan, S.P., Lee, S.D., Calfee, M.W., Wood, J.P., McDonald, S., Clayton, M., Griffin-Gatchalian, N., Touati, A. *et al.* (2014) Effect of inoculation method on the determination of decontamination effiacy against *Bacillus* spores. *World J Microbiol Biotechnol* **30**, 2609–2623.

Sella, S.R.B.R., Vandenberghe, L.P.S. and Soccol, C.R. (2014) *Bacillus atrophaeus*: main characteristics and biotechnological applications-a review. *Crit Rev Biotechnol* 1–13.

U.S. Environmental Protection Agency (2005) *Compilation of available data on building decontamination alternatives*. Washington, DC: EPA Report 600/R-05/036, March 2005.

U.S. Environmental Protection Agency (2007) *Transmittal of meeting minutes of the FIFRA scientfic advisory panel meeting held July 17-18, 2007 on guidance on test methods for demonstrating the efficacy of antimicrobial products for inactivating Bacillus anthracis spores on environmental surfaces*. http://archive.epa.gov/scipoly/sap/meetings/web/pdf/july2007_sap_finalreport.pdf (Accessed from the World Wide Web on February 22, 2016).

U.S. Environmental Protection Agency (2010) *Material Demand Studies: Materials Sorption of Vaporized Hydrogen Peroxide*. Washington, DC: US EPA Report EPA/600/R-10/002, May 2010.

 Published 2016. This article is a U.S. Government work and is in the public domain in the USA.

U.S. Environmental Protection Agency (2014) *Decontamination of a mock office using chlorine dioxide gas*. Washington, DC: US EPA, report EPA/600/R-14/208, August 2014.

Wood, J.P., Choi, Y.W., Rogers, J.V., Kelly, T.J., Riggs, K.B. and Willenberg, Z.J. (2011) Efficacy of liquid spray decontaminants for inactivation of *Bacillus anthracis* spores on building and outdoor materials. *J Appl Microbiol* **110**, 1262–1273.

Wood, J.P., Calfee, M.W., Clayton, M., Griffin-Gatchalian, N., Touati, A. and Egler, K. (2013) Evaluation of peracetic acid fog for the inactivation of *Bacillus anthracis* spore surrogates in a large decontamination chamber. *J Hazard Mater* **250**, 61–67.

Supporting Information

Additional Supporting Information may be found in the online version of this article:

Figure S1 Photos of humidifiers.

Table S1 Biological indicator test results.

Table S2 Decontamination efficacy results for the large test chamber, average ± SD log reduction values, by test number/material/chamber location.

Published 2016. This article is a U.S. Government work and is in the public domain in the USA.

From: Touati, Abderrahmane
To: Wood, Joe
Cc: Winterrowd, Chris; Brixey, Laurie
Subject: Re: [EXTERNAL] Record of Percentage Agreement: Abderrahmane (Dahman) Touati - for STAA award
Date: Monday, April 13, 2020 8:10:11 PM

I concur
Dahman Touati
Sent from my iPhone

> On Apr 13, 2020, at 5:55 PM, Wood, Joe <Wood.Joe@epa.gov> wrote:
>
> Co-author Dahman Touati, US EPA, Jacobs Technology (at time of research)
>
> Nominee name: Joseph Wood
>
> Nominated publication: A simple decontamination approach using hydrogen peroxide vapour for Bacillus anthracis spore inactivation
>
> Dahman, I have designated you as contributing 10% toward the study/publication. Please reply back that you concur with this amount.
>
> Thank you.
>
> Joseph Wood, M.S., P.E.
> Senior Research Engineer
> US EPA Office of Research and Development
> Center for Environmental Solutions and Emergency Response
> Homeland Security and Materials Management Div.
> Research Triangle Park, NC 27711
> Mail Code E343-06
> mobile phone: 919 482-3996
> http://www2.epa.gov/homeland-security-research

NOTICE - This communication may contain confidential and privileged information that is for the sole use of the intended recipient. Any viewing, copying or distribution of, or reliance on this message by unintended recipients is strictly prohibited. If you have received this message in error, please notify us immediately by replying to the message and deleting it from your computer.

From: Rastogi, Vipin K CIV USARMY CCDC CBC (USA)
To: Wood, Joe
Subject: Re: [Non-DoD Source] Record of Percentage Agreement: Vipin Rastogi - for STAA award
Date: Monday, April 13, 2020 7:58:19 PM

Joe,

I concur with the level of my contribution to the said published paper l.

Thanks.

Vipin

Sent from my iPhone

> On Apr 13, 2020, at 6:46 PM, Wood, Joe <Wood.Joe@epa.gov> wrote:
>
> All active links contained in this email were disabled. Please verify the identity of the sender, and confirm the authenticity of all links contained within the message prior to copying and pasting the address to a Web browser.
>
> ---
>
> Co-author Vipin Rastogi, US Army Edgewood Chemical and Biological Center
>
> Nominee name: Joseph Wood
>
> Nominated publication: A simple decontamination approach using hydrogen peroxide vapour for Bacillus anthracis spore inactivation
>
> Vipin, I have designated you as contributing 15% toward the study/publication. Please reply back that you concur with this amount.
>
> Thank you.
>
> Joseph Wood, M.S., P.E.
> Senior Research Engineer
> US EPA Office of Research and Development
> Center for Environmental Solutions and Emergency Response
> Homeland Security and Materials Management Div.
> Research Triangle Park, NC 27711
> Mail Code E343-06
> mobile phone: 919 482-3996
> Caution-http://www2.epa.gov/homeland-security-research < Caution-http://www2.epa.gov/homeland-security-research >

From: Mickelsen, Leroy
To: Wood, Joe
Subject: Re: Record of Percentage Agreement, Leroy Mickelsen - for STAA award
Date: Monday, April 13, 2020 6:05:45 PM

Concur

Sent from my iPhone

> On Apr 13, 2020, at 5:47 PM, Wood, Joe <Wood.Joe@epa.gov> wrote:
>
> Co-author Leroy Mickelsen, US EPA, Office of Research and Development, National Homeland Security Research Center (at time of research)
>
> Nominee name: Joseph Wood
>
> Nominated publication: A simple decontamination approach using hydrogen peroxide vapour for Bacillus anthracis spore inactivation
>
> Leroy, I have designated you as contributing 10% toward the study/publication. Please reply back that you concur with this amount.
>
> Thank you.
>
> Joseph Wood, M.S., P.E.
> Senior Research Engineer
> US EPA Office of Research and Development
> Center for Environmental Solutions and Emergency Response
> Homeland Security and Materials Management Div.
> Research Triangle Park, NC 27711
> Mail Code E343-06
> mobile phone: 919 482-3996
> http://www2.epa.gov/homeland-security-research

From: Smith, LisaS
To: Wood, Joe
Subject: RE: Record of Percentage Agreement, Lisa Smith - for STAA award
Date: Tuesday, April 14, 2020 8:43:50 AM

Hi Joe! Yes that percentage is fine. Good luck!

Thanks,
Lisa

From: Wood, Joe <Wood.Joe@epa.gov>
Sent: Monday, April 13, 2020 6:14 PM
To: Smith, LisaS <smith.lisas@epa.gov>
Subject: Record of Percentage Agreement, Lisa Smith - for STAA award

Lisa, I hope you are doing well in the time of COVID19, as best as can be expected.

I am putting in our publication for an EPA Science and Technology Achievement Award. Part of the application process is to get confirmation from co-authors on their percentage contribution.

I have designated you as contributing 10% toward the study/publication. Please reply back that you concur with this amount. If not, please let me know what percentage you'd be ok with.

Take care, Lisa.

****
Co-author Lisa Smith, US Army Edgewood Chemical and Biological Center, Inc. (At time of publication)

Nominee name: Joseph Wood

Nominated publication: A simple decontamination approach using hydrogen peroxide vapour for Bacillus anthracis spore inactivation

Thank you.

Joseph Wood, M.S., P.E.
Senior Research Engineer
US EPA Office of Research and Development
Center for Environmental Solutions and Emergency Response
Homeland Security and Materials Management Div.
Research Triangle Park, NC 27711
Mail Code E343-06
mobile phone: 919 482-3996
http://www2.epa.gov/homeland-security-research

From: Calfee, Worth
To: Wood, Joe
Subject: RE: Record of Percentage Agreement, M. Worth Calfee - for STAA award
Date: Monday, April 13, 2020 9:23:20 AM

Concur

M. Worth Calfee, Ph.D.
Microbiologist
Homeland Security and Materials Management Division
US Environmental Protection Agency
Research Triangle Park, NC
O: 919.541.7600
M: 919.423.3837

From: Wood, Joe <Wood.Joe@epa.gov>
Sent: Monday, April 13, 2020 9:22 AM
To: Calfee, Worth <Calfee.Worth@epa.gov>
Subject: Record of Percentage Agreement, M. Worth Calfee - for STAA award

Co-author Worth Calfee, US EPA, Office of Research and Development, National Homeland Security Research Center (at time of research)

Nominee name: Joseph Wood

Nominated publication: A simple decontamination approach using hydrogen peroxide vapour for Bacillus anthracis spore inactivation

Worth, I have designated you as contributing 15% toward the study/publication. Please reply back that you concur with this amount.

Thank you.

Joseph Wood, M.S., P.E.
Senior Research Engineer
US EPA Office of Research and Development
Center for Environmental Solutions and Emergency Response
Homeland Security and Materials Management Div.
Research Triangle Park, NC 27711
Mail Code E343-06
mobile phone: 919 482-3996
http://www2.epa.gov/homeland-security-research

From: wildscallionsfarm@yahoo.com
To: Wood, Joe
Subject: Re: Record of Percentage Agreement, Matt Clayton - for STAA award
Date: Tuesday, April 14, 2020 8:33:53 AM

Hi Joe,

Yes, we are doing okay in COVID 19 times. Living outdoors, planting food, sequestering carbon, life goes on.

Of course, in my heart, I will never forget how much I had to fight you and everyone to investigate this.
This is 100% mine.
I agree with 5%.

Be well,
Matt

On Monday, April 13, 2020, 06:05:05 PM EDT, Wood, Joe <wood.joe@epa.gov> wrote:

Matt, I hope you are doing well in the time of COVID19, as best as can be expected.

I am putting in our publication for an EPA Science and Technology Achievement Award. Part of the application process is to get confirmation from co-authors on their percentage contribution.

I have designated you as contributing 5% toward the study/publication. Please reply back that you concur with this amount. If not, please let me know what percentage you'd be ok with.

Take care, Matt.

****

Co-author Matt Clayton, US EPA, Office of Research and Development, National Homeland Security Research Center (at time of research)

Nominee name: Joseph Wood

Nominated publication: A simple decontamination approach using hydrogen peroxide vapour for Bacillus anthracis spore inactivation

Thank you.

Joseph Wood, M.S., P.E.
Senior Research Engineer

US EPA Office of Research and Development
Center for Environmental Solutions and Emergency Response

Homeland Security and Materials Management Div.
Research Triangle Park, NC 27711
Mail Code E343-06
mobile phone: 919 482-3996

http://www2.epa.gov/homeland-security-research

From: Nicole Gatchalian
To: Wood, Joe
Subject: Re: Record of Percentage Agreement, Nicole Griffin-Gatchalian - for STAA award
Date: Monday, April 13, 2020 6:20:36 PM

Hi Joe,

I hope you are doing well, staying safe and healthy.
Wonderful news on applying for the STAA. I am fine with a 5% contribution.
Please let me know the outcome of the submission.

All the best,
Nicole

On Mon, Apr 13, 2020 at 6:09 PM Wood, Joe <Wood.Joe@epa.gov> wrote:

> Nicole, I hope you are doing well in the time of COVID19, as best as can be expected.
>
> I am putting in our publication for an EPA Science and Technology Achievement Award. Part of the application process is to get confirmation from co-authors on their percentage contribution.
>
> I have designated you as contributing 5% toward the study/publication. Please reply back that you concur with this amount. If not, please let me know what percentage you'd be ok with.
>
> Take care, Nicole.
>
> **********
>
> Co-author Nicole Griffin-Gatchalian, Arcadis, Inc. (At time of publication)
>
> Nominee name: Joseph Wood
>
> Nominated publication: A simple decontamination approach using hydrogen peroxide vapour for Bacillus anthracis spore inactivation

Thank you.

Joseph Wood, M.S., P.E.
Senior Research Engineer

US EPA Office of Research and Development
Center for Environmental Solutions and Emergency Response

Homeland Security and Materials Management Div.
Research Triangle Park, NC 27711
Mail Code E343-06
mobile phone: 919 482-3996

http://www2.epa.gov/homeland-security-research

From: Ryan, Shawn
To: Wood, Joe
Subject: Re: Record of Percentage Agreement, Shawn Ryan- for STAA award
Date: Monday, April 13, 2020 9:00:58 PM

Concur

Shawn

_____

Shawn P. Ryan, Ph.D.
Director, Homeland Security and Materials Management Division
U.S. Environmental Protection Agency (MD-E343-06)
Office of Research and Development
109 T.W. Alexander Dr., Research Triangle Park, NC 27711
Phone 919-541-0699

http://www2.epa.gov/homeland-security-research

> On Apr 13, 2020, at 5:47 PM, Wood, Joe <Wood.Joe@epa.gov> wrote:
>
> Co-author Shawn Ryan, US EPA, Office of Research and Development, National Homeland Security Research Center (at time of research)
>
> Nominee name: Joseph Wood
>
> Nominated publication: A simple decontamination approach using hydrogen peroxide vapour for Bacillus anthracis spore inactivation
>
> Shawn, I have designated you as contributing 5% toward the study/publication. Please reply back that you concur with this amount.
>
> Thank you.
>
> Joseph Wood, M.S., P.E.
> Senior Research Engineer
> US EPA Office of Research and Development
> Center for Environmental Solutions and Emergency Response
> Homeland Security and Materials Management Div.
> Research Triangle Park, NC 27711
> Mail Code E343-06
> mobile phone: 919 482-3996
> http://www2.epa.gov/homeland-security-research

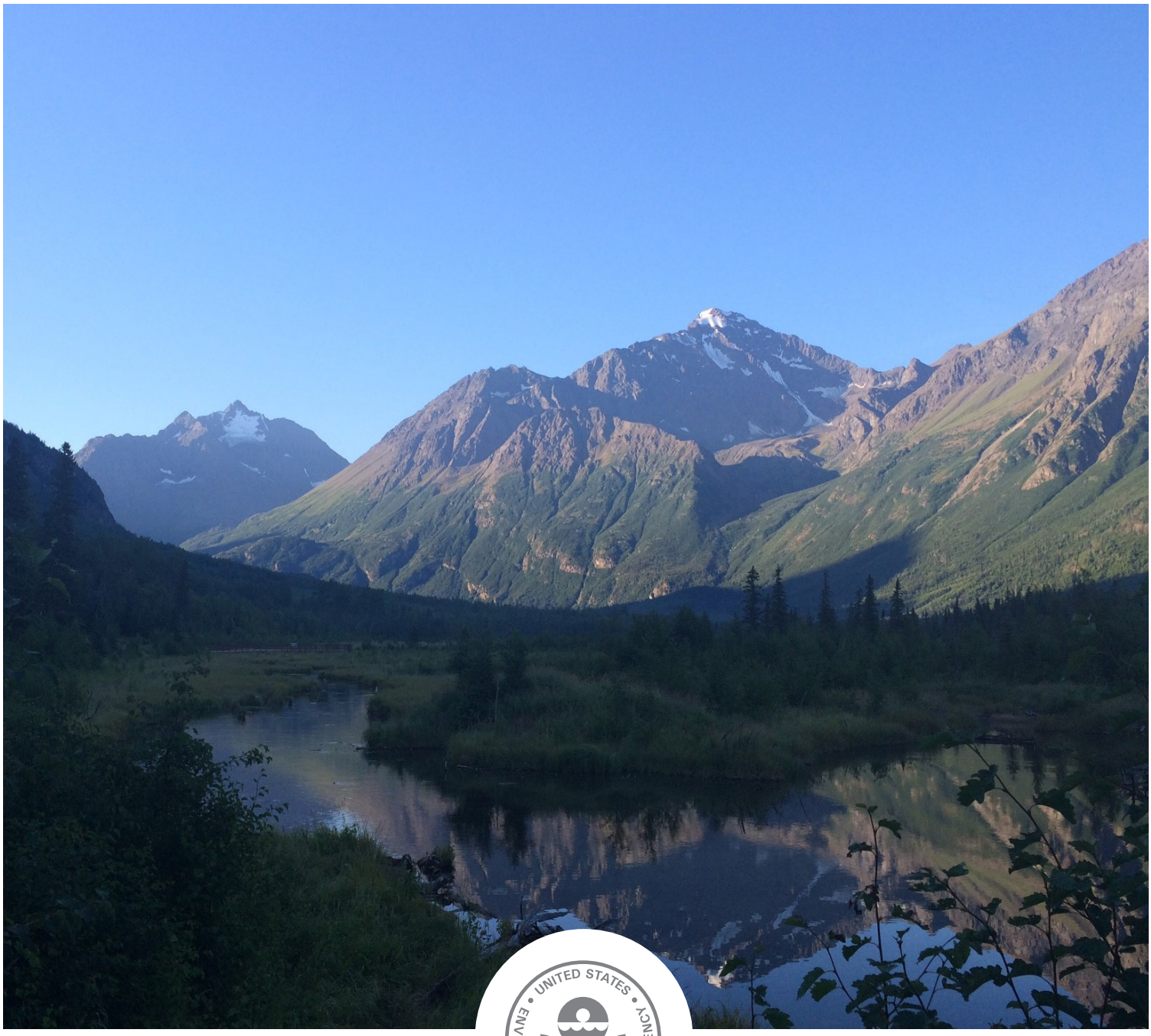

Working Together

FY 2018-2022 U.S. EPA Strategic Plan

February 2018 (Updated: September 2019)

EPA's Mission

Protect Human Health and the Environment

Goal 1

A Cleaner, Healthier Environment:

Deliver a cleaner, safer, and healthier environment for all Americans and future generations by carrying out the Agency's core mission.

Goal 2

More Effective Partnerships:

Provide certainty to states, localities, tribal nations, and the regulated community in carrying out shared responsibilities and communicating results to all Americans.

Goal 3

Greater Certainty, Compliance, and Effectiveness:

Increase certainty, compliance, and effectiveness by applying the rule of law to achieve more efficient and effective agency operations, service delivery, and regulatory relief.

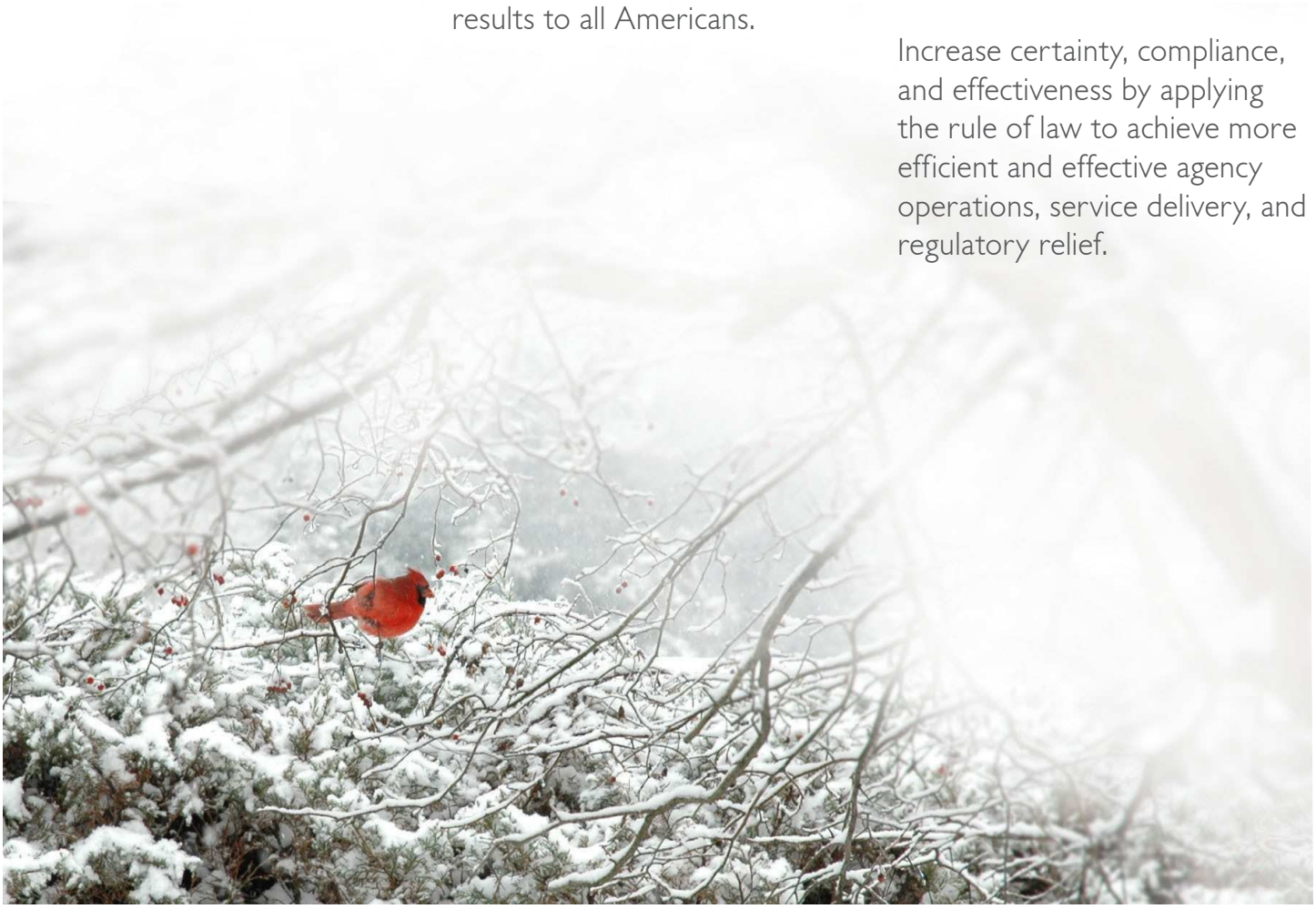

Table of Contents

Introduction 4

Goal 1: A Cleaner, Healthier Environment 6

Objective 1.1: Improve Air Quality 8

Objective 1.2: Provide for Clean and Safe Water 11

Objective 1.3: Revitalize Land and Prevent Contamination 15

Objective 1.4: Ensure Safety of Chemicals in the Marketplace 19

Goal 2: More Effective Partnerships 24

Objective 2.1: Enhance Shared Accountability 26

Objective 2.2: Increase Transparency and Public Participation 30

Goal 3: Greater Certainty, Compliance, and Effectiveness 34

Objective 3.1: Compliance with the Law 36

Objective 3.2: Create Consistency and Certainty 39

Objective 3.3: Prioritize Robust Science 42

Objective 3.4: Streamline and Modernize 46

Objective 3.5: Improve Efficiency and Effectiveness 48

The GPRA (Government Performance and Results Act) Modernization Act of 2010 directs agencies to consult with the Congress and requires that they solicit and consider the views and suggestions of those entities likely to be interested in or potentially affected by a strategic plan. Consultation with EPA's federal, state, tribal, and local government partners and its many stakeholders is integral to the Agency's strategic planning process. In developing the FY 2018-2022 EPA Strategic Plan, EPA issued a Federal Register notice and used www.regulations.gov to encourage and share feedback on the draft Plan. The Agency also sent notifications on the availability of the draft Plan to leaders of the Agency's Congressional authorizing, appropriations, and oversight committees, and notified all federally-recognized Indian tribes of the opportunity for consultation and coordination. These outreach efforts resulted in unique submissions from approximately 5,000 organizations and individuals.

Message from EPA

The U.S. Environmental Protection Agency's FY 2018–FY 2022 Strategic Plan, emphasizes the EPA's "Back-to-Basics" agenda. The agenda set out in this plan has three over-arching goals*: (1) Deliver a cleaner, safer, and healthier environment for all Americans and future generations by carrying out the Agency's core mission; (2) Provide certainty to states, localities, tribal nations, and the regulated community in carrying out shared responsibilities and communicating results to all Americans; and (3) Increase certainty, compliance, and effectiveness by applying the rule of law to achieve more efficient and effective agency operations, service delivery, and regulatory relief. The agency's mission of protecting human health and the environment resonates with all Americans; we all can agree that we want our future generations to inherit a cleaner, healthier environment that supports a thriving economy.

Our nation has made great progress in making rivers and lakes safer for swimming and boating, reducing the smog that clouded city skies, cleaning up lands that were once used as hidden chemical dumps and providing Americans greater access to information on chemical safety. However, we still have important work to do.

We must create a sense of shared accountability between states, tribes and the federal government to achieve positive environmental results. Along with faithfully applying the rule of law, improving the processes by which the EPA has operated is crucial in advancing the agency's mission.

Air

Over the next five years, the EPA will prioritize key activities to support attainment of the national ambient air quality standards (NAAQS) and implementation of stationary source regulations.

We will work with our state and tribal partners to rapidly approve their implementation plans for attaining air quality standards to reduce contaminants that cause or exacerbate health issues.

Water

We will modernize and update aging drinking water, wastewater and stormwater infrastructure which the American public depends on.

The agency will continue to leverage the State Revolving Funds (SRFs) and Water Infrastructure Finance and Innovation Act (WIFIA) to assist states, tribes, municipalities and private entities to finance high-priority infrastructure investments that protect human health and the environment.

Land

The Administration is placing particular emphasis on the top priority list of Superfund sites and will implement Superfund Task Force recommendations to accelerate the pace of cleanups and promote site reuse, while addressing risks to human health and the environment.

The agency will accelerate cleanup by re-prioritizing some resources to focus on remedial actions, construction completions, ready-for-reuse determinations and National Priorities List site deletions.

Chemicals

We will prioritize the safety of chemicals in the marketplace in the implementation of the new Frank R. Lautenberg Chemical Safety for the 21st Century Act, which modernizes the Toxic Substances and Control Act (TSCA).

To achieve this, the EPA will focus on meeting its statutory requirements and mandatory deadlines of TSCA and ensure our reviews are efficient, effective and transparent to stakeholders.

More than 45 years after the creation of the EPA most states, and to a lesser extent territories and tribes, are authorized to implement delegated federal environmental programs within their jurisdictions. Recognizing the congressionally intended responsibilities of our state, local and tribal partners, we must adapt and modernize our practices to reduce duplication of effort and tailor oversight of delegated programs.

For example, the EPA will expand its compliance assistance work by continuing to partner with third-party organizations and federal agencies to support existing web-based, sector-specific compliance assistance centers and seek to develop new centers. EPA will assess our shared governance to clarify the agency's statutory roles and responsibilities and tailor state oversight to maximize our return on investment and reduce burden on states.

Over the next five years, the EPA will increase certainty, compliance, and effectiveness by applying the rule of law to achieve more efficient and effective agency operations, service delivery, and regulatory relief.

Federal agencies exist to administer laws passed by Congress, in accordance with the will of this body. The EPA will ensure compliance with the law by providing consistency and certainty for the regulated community and clarify the impact of proposed actions on human health, the environment and the economy to provide a clear path and timeline for entities to achieve compliance.

Further, we will reform our approach to regulatory development and prioritize meeting our statutory deadlines to ensure that expectations for the regulated community and the public are clear and comprehensive. The EPA will also employ business process improvement strategies, such as Lean, to improve efficiencies in all permitting processes, working alongside states to streamline the review of state-issued permits and to improve our internal business processes.

EPA can accomplish the environmental and human health outcomes outlined in this Strategic Plan by increasing collaboration with other external partners and striving to achieve improved consistency and certainty for the regulated community.

**In September 2019, EPA updated language in this Plan to better reflect the Agency's environmental and policy goals. While the update does not change the Agency's Strategic Objectives or Long-Term Performance Goals, re-framing EPA's overarching strategic goals will help communicate the Agency's priority to deliver tangible results to further the Agency's mission to protect human health and the environment. The changes are as follows:*

STRATEGIC GOALS	PREVIOUS LANGUAGE	UPDATED LANGUAGE
GOAL 1	**Core Mission:** Deliver real results to provide Americans with clean air, land, and water, and ensure chemical safety.	**A Cleaner, Healthier Environment:** Deliver a cleaner, safer, and healthier environment for all Americans and future generations by carrying out the Agency's core mission.
GOAL 2	**Cooperative Federalism:** Rebalance the power between Washington and the states to create tangible environmental results for the American people.	**More Effective Partnerships:** Provide certainty to states, localities, tribal nations, and the regulated community in carrying out shared responsibilities and communicating results to all Americans.
GOAL 3	**Rule of Law and Process:** Administer the law as Congress intended, to refocus the Agency on its statutory obligations under the law.	**Greater Certainty, Compliance, and Effectiveness:** Increase certainty, compliance, and effectiveness by applying the rule of law to achieve more efficient and effective agency operations, service delivery, and regulatory relief.

Introduction

Goal 1

A Cleaner, Healthier Environment: Deliver a cleaner, safer, and healthier environment for all Americans and future generations by carrying out the Agency's core mission.

Goal 2

More Effective Partnerships: Provide certainty to states, localities, tribal nations, and the regulated community in carrying out shared responsibilities and communicating results to all Americans.

Goal 3

Greater Certainty, Compliance, and Effectiveness: Increase certainty, compliance, and effectiveness by applying the rule of law to achieve more efficient and effective agency operations, service delivery, and regulatory relief.

The U.S. Environmental Protection Agency (EPA) developed this *FY 2018-2022 EPA Strategic Plan* (the *Plan*) to: (1) deliver a cleaner, safer, and healthier environment for all Americans and future generations by carrying out the Agency's core mission; (2) provide certainty to states, localities, tribal nations, and the regulated community in carrying out shared responsibilities and communicating results to all Americans; and (3) increase certainty, compliance, and effectiveness by applying the rule of law to achieve more efficient and effective agency operations, service delivery, and regulatory relief. The *Plan* supports states, localities, and federally-recognized Indian tribes[1] by streamlining programs and processes, reducing duplication of effort, providing greater transparency and listening opportunities, and enabling the Agency to focus on its core mission.

EPA's senior managers will use this *Plan* routinely as a management tool to guide the Agency's path forward, tracking progress and assessing and addressing risks and challenges that could potentially interfere with EPA's ability to accomplish its goals. The three strategic goals established in the *Plan* are supported by strategic objectives and long-term performance goals[2] focused on advancing human health and environmental results over the next five years. These long-term performance goals are supported by annual performance goals included in the annual performance plans and budgets that EPA submits to Congress. The strategies and long-term performance goals in this *Plan* highlight key areas in which the Agency will make the most dramatic changes over the next five years and are not intended to address all ongoing programs. The annual performance plans and budgets, and supporting annual and operational measures, address a broader range of the Agency's work. In addition, the Agency will hold quarterly and monthly meetings to assess progress toward annual and long-term performance goals.

The EPA Administrator established two-year agency priority goals (APGs) for accelerating progress on EPA priorities. APGs reflect agency leadership's top near-term priorities for implementing performance improvement. EPA's APGs were selected from among the suite of long-term performance goals. EPA will support these priority goals by developing two-year implementation plans and reporting quarterly progress.

The *FY 2018-2022 EPA Strategic Plan* is supported by other, more detailed Agency plans in specific areas. For example, EPA's Human Capital Operating Plan details the

[1] Tribes include all federally-recognized tribes, including Alaska Native Villages (as issued by the Secretary of the Interior).

[2] Long-term performance goals are the measurable results the Agency is working to achieve over the life of the Plan and are supported by data quality records (DQRs), which provide details such as the methods of measurement and other important contextual information such as baselines. DQRs can be found at **https://www.epa.gov/planandbudget/results**.

FY 2018-2019 Agency Priority Goals

APG-1: Improve air quality by implementing pollution control measures to reduce the number of nonattainment areas. By September 30, 2019, EPA, in close collaboration with states, will reduce the number of nonattainment areas to 138 from a baseline of 166.

APG-2: Empower communities to leverage EPA water infrastructure investments. By September 30, 2019, EPA will increase by $16 billion the non-federal dollars leveraged by EPA water infrastructure finance programs (Clean Water and Drinking Water State Revolving Funds and the Water Infrastructure Finance and Innovation Act).

APG-3: Accelerate the pace of cleanups and return sites to beneficial use in their communities. By September 30, 2019, EPA will make an additional 102 Superfund sites and 1,368 brownfields sites ready for anticipated use (RAU).

APG-4: Meet new statutory requirements to improve the safety of chemicals in commerce. By September 30, 2019, EPA will complete in accordance with statutory timelines (excluding statutorily-allowable extensions): 100% of required EPA-initiated Toxic Substances Control Act (TSCA) risk evaluations for existing chemicals; 100% of required TSCA risk management actions for existing chemicals; and 80% of TSCA pre-manufacture notice final determinations.

APG-5: Increase environmental law compliance rate. Through September 30, 2019, EPA will increase compliance by reducing the percentage of Clean Water Act (CWA) National Pollutant Discharge Elimination System (NPDES) permittees in significant noncompliance with their permit limits to 21% from a baseline of 24%.

APG-6: Accelerate permitting-related decisions. By September 30, 2019, EPA will reduce by 50% the number of permitting-related decisions that exceed six months.

actions the Agency will execute to achieve its overarching human capital goals, and EPA's Information Technology/Information Management Strategic Plan will guide efforts to support and modernize the Agency's technology and data infrastructure. The EPA's workforce and reform efforts will support streamlining efforts to work more efficiently and effectively in the future. The many activities described in these plans align with and help position the Agency to achieve the strategic goals and objectives presented in this *Plan*.

EPA is also in the process of deploying a Lean management system specifically designed to deliver measurable results that align with this Plan. Lean is a set of principles and tools designed to identify and eliminate waste from processes while maximizing customer value and return on taxpayer investment. EPA will standardize and streamline processes to strengthen efficiency and quality to better meet mission goals and objectives. Under the Administrator's leadership, EPA will become a Lean organization.

Strategies to achieve EPA's goals and objectives are also informed by gathering evidence related to environmental problems and evaluating the effectiveness of the strategies that the programs use to address them. Examples of recent evidence and evaluation efforts used to develop this *FY 2018-2022 EPA Strategic Plan* and a preliminary list of future planned efforts can be found at **https://www.epa.gov/planandbudget/strategicplan.**

1

A Cleaner, Healthier Environment

Deliver a cleaner, safer, and healthier environment for all Americans and future generations by carrying out the Agency's core mission.

Pollution comes in many forms with myriad impacts on human health and the environment. With the goal of clean and safe air, water, and land for all Americans, Congress enacted a range of environmental statutes that spell out EPA's core responsibilities. Our nation has come a long way since EPA was established in 1970. We have made great progress in making rivers and lakes safe for swimming and boating, reducing the smog that clouded city skies, cleaning up lands that were once used as hidden chemical dumps, and providing Americans greater access to information on the safety of the chemicals all around us. Today we can see enormous progress—yet we still have important work to do.

EPA has established priorities for advancing progress over the next five years in each of its core mission areas—land, air, water—as well as chemicals. The Agency will focus on speeding the cleanup of Superfund and brownfields sites, and will use a list of top priority sites to advance progress on Superfund sites of particular concern. We will work with states and tribes to more rapidly approve their implementation plans for attaining air quality standards, reducing contaminants that can cause or exacerbate health issues. We will work with our state and tribal partners to provide for clean and safe water by updating aging infrastructure, both for drinking water and wastewater systems. EPA's top priority for ensuring the safety of chemicals in the marketplace is the implementation of the new Frank R. Lautenberg Chemical Safety for the 21st Century Act, which modernizes the Toxic Substances and Control Act (TSCA) by creating new standards and processes for assessing chemical safety within specific deadlines. These efforts will be supported by strong compliance assurance and enforcement in collaboration with our state and tribal partners, up-to-date training for partners, and use of the best available science and research to address current and future environmental hazards, develop new approaches, and improve the foundation for decision making.

The Agency will collaborate more efficiently and effectively with other federal agencies, states, tribes, local governments, communities, and other partners and stakeholders to address existing pollution and prevent future problems. EPA will directly implement federal environmental laws in Indian country where eligible tribes have not taken on program responsibility.

With our partners, we will pay particular attention to vulnerable populations. Children and the elderly, for example, may be at significantly greater risk from elevated exposure or increased susceptibility to the harmful effects of environmental contaminants. Some low-income and minority communities may face greater risks because of proximity to contaminated sites or because fewer resources are available to avoid exposure to pollutants. Tribal ways of life such as traditional subsistence hunting, fishing, and gathering also may increase exposure to contaminants and increase risks. Much work remains and, together with our partners, we will continue making progress in protecting human health and the environment.

Objective 1.1 Improve Air Quality

Work with states and tribes to accurately measure air quality and ensure that more Americans are living and working in areas that meet high air quality standards.

Introduction

As part of its mission to protect human health and the environment, EPA is dedicated to improving the quality of the nation's air. From 1970 to 2016, aggregate national emissions of the six criteria air pollutants[3] were reduced over 70 percent, while gross domestic product grew by over 253 percent. Despite this progress, in 2016, more than 120 million people lived in counties with monitored air quality that did not meet standards for at least one criteria pollutant. EPA's work to control emissions of air pollutants is critical to continued progress in reducing public health risks and improving the quality of the environment. Over the next five years, EPA will conduct a wide range of activities that contribute to improving air quality and protecting human health and the environment.

Long-Term Performance Goal

LTPG-1.1.1 By September 30, 2022, reduce the number of nonattainment areas to 101.[4]

Strategies for Achieving the Objective

EPA works in cooperation with states, tribes, and local governments to design and implement air quality standards and programs. EPA relies on other federal agencies, academia, researchers, industry, other organizations, and the public. These partnerships are critical to achieving improvements in air quality and reducing public health risks.

EPA will prioritize key activities to support attainment of the national ambient air quality standards (NAAQS) and implementation of stationary source regulations. The Agency will address its Clean Air Act (CAA) responsibilities by collaborating with and providing technical assistance to states and tribes to develop plans and implement decisions that administer the NAAQS and

[3] The Clean Air Act (CAA) requires EPA to set National Ambient Air Quality Standards (NAAQS) for six common air pollutants including carbon monoxide, lead, ground-level ozone, nitrogen dioxide, particulate matter, and sulfur dioxide.

[4] The baseline is 166 nonattainment areas as of 10/1/2017.

visibility programs; taking federal oversight actions such as approving state implementation plan/tribal implementation plan (SIP/TIP) submittals consistent with statutory obligations; developing regulations and guidance to implement standards; and addressing transported air pollution. EPA will focus on ways to improve the efficiency and effectiveness of the SIP/TIP process, including the Agency's own review process, with a goal of maximizing timely processing of state/tribal-requested implementation plan actions to help move more quickly to attainment.

EPA will operate effective nationwide and multi-state programs, such as the acid rain program and the cross-state air pollution rule, which address global, national, and regional air pollutants from the power sector and other large stationary sources. The Agency also will develop and provide data, analysis, and technical tools and assistance to industries, states, tribes, and communities to meet CAA obligations and other statutory requirements.

EPA also develops, implements, and ensures compliance with national emission standards to reduce mobile source-related air pollution from light-duty cars and trucks, heavy-duty trucks and buses, nonroad engines and vehicles, and their fuels—a priority for the Agency to ensure that industry has the certainty it needs while protecting human health and the environment and to support improvements in air quality and moving areas into attainment. The Agency evaluates new emission control technologies and provides information to state, tribal, and local air quality managers on a variety of transportation programs. EPA will review and approve vehicle and engine emissions certification applications and perform its compliance oversight functions on priority matters where there is evidence to suggest noncompliance. The Agency will also conduct pre-certification confirmatory testing for emissions and fuel economy for passenger cars.

EPA develops and implements national emission standards for stationary and mobile sources and works with state, tribal, and local air agencies to address air toxics problems in communities. For stationary sources, pursuant to the CAA, EPA develops initial air toxics emissions standards for categories of industrial sources and reviews these standards' risk reduction and technological currency according to timeframes set by the Act. EPA will conduct these reviews to meet CAA requirements and to ensure that the air toxics rules appropriately protect public health.

To support our partners in meeting their CAA obligations, EPA will provide grants and technical assistance to state, tribal, and local air pollution control agencies to manage and implement their individual air quality programs, including funding for air quality monitoring. State and tribal air quality monitoring, which provides critical information for developing clean air plans, for research, and for public awareness, will be a focus of the Administration.

EPA will prioritize efforts to reduce the production, import, and use of ozone depleting substances (ODS), including reviewing and listing alternatives that are safer for the stratospheric ozone layer through implementation of Title VI of the CAA and the Montreal Protocol.

EPA also is responsible for measuring and monitoring ambient radiation and radioactive materials and assessing radioactive contamination in the environment. The Agency supports federal radiological emergency response and recovery operations under the National Response Framework and the National Oil and Hazardous Substances Pollution Contingency Plan and will assist states, tribes, and other partners, as appropriate. EPA will design essential training and conduct exercises to improve our nation's radiation response preparedness.

External Factors and Emerging Issues

Emerging measurement and information technologies are shifting the paradigm for air quality data. Traditionally, state, tribal, and local air programs, along with EPA, have been the primary resource for collecting, storing, sharing, and communicating air data. Increasingly, air quality information is also available from nontraditional sources, such as satellites or sensors. Additionally, big data companies are becoming involved in storing, analyzing, and presenting publicly available air quality data alongside other data sets. These developments are expected to have profound influence on understanding air quality, as well as determining the most cost-effective ways to improve air quality. EPA partners with states and tribes through efforts such as E-Enterprise, and with other entities in a variety of ways to ensure that the Agency advances appropriate technologies and stays abreast of emerging technologies.

EPA engages in both domestic and international forums to address the depletion of the stratospheric ozone layer, a global problem that cannot be solved by domestic action alone. Success relies on joint action.

Lastly, there are several emerging issues and external factors that will affect how EPA protects the public from unnecessary exposure to radiation, including evolving policies on radioactive waste management, uranium extraction and processing technologies, a decrease in available radiation expertise, and new science on radiation health effects. The Agency will focus on education, including formal and informal training in the areas of health physics, radiation science, radiation risk communications, and emergency response to fill existing and emerging gaps.

Objective 1.2
Provide for Clean and Safe Water

Ensure waters are clean through improved water infrastructure and, in partnership with states and tribes, sustainably manage programs to support drinking water, aquatic ecosystems, and recreational, economic, and subsistence activities.

Introduction

The nation's water resources are the lifeblood of our communities, supporting our economy and way of life. Across the country we depend upon reliable sources of clean and safe water. Just a few decades ago, many of the nation's rivers, lakes, and estuaries were grossly polluted, wastewater sources received little or no treatment, and drinking water systems provided very limited treatment to water coming through the tap. Now over 90 percent of the population receives safe drinking water from community water systems regulated by EPA or delegated states and tribes, and many formerly impaired waters have been restored and support recreational and public health uses that contribute to healthy economies.

We have made significant progress since enactment of the Clean Water Act (CWA); Safe Drinking Water Act; and Marine Protection, Research, and Sanctuaries Act. However, serious water resource and water infrastructure challenges remain. Many communities need to improve and maintain both drinking water and wastewater infrastructure and develop the capacity to comply with new and existing standards. Tens of thousands of homes, primarily in tribal and disadvantaged communities and the territories, lack access to basic sanitation and drinking water.

Over the next five years, EPA will work with states, tribes, territories, and local communities to better safeguard human health; maintain, restore, and improve water quality; and make America's water systems sustainable and secure, supporting new technology and innovation wherever possible.

Long-Term Performance Goals

LTPG-1.2.1 By September 30, 2022, reduce the number of community water systems out of compliance with health-based standards to 2,700.[5]

LTPG-1.2.2 By September 30, 2022, increase by $40 billion the non-federal dollars leveraged by EPA water infrastructure finance programs (CWSRF, DWSRF, and WIFIA).[6]

LTPG-1.2.3 By September 30, 2022, reduce the number of square miles of watershed with surface water not meeting standards by 37,000 square miles.[7]

Strategies for Achieving the Objective

Invest in Infrastructure to Spur Environmental Benefits and Economic Growth

Supporting state, tribal, and local efforts to modernize the outdated drinking water, wastewater, and stormwater infrastructure on which the American public depends is a top priority for EPA. The Agency will promote construction of infrastructure in tribal and, small, rural, and disadvantaged communities. EPA's state revolving fund (SRF) and Water Infrastructure Finance and Innovation Act (WIFIA) programs will allow the Agency, states, tribes, municipalities, and private entities to finance high-priority infrastructure investments that protect human health and the environment. The revolving nature of the SRFs and the leveraging capacity of WIFIA greatly multiply the federal investment. For the clean water SRF, EPA estimates that every federal dollar contributed thus far has resulted in close to three dollars of investment in water infrastructure. For the drinking water SRF, for every one dollar the federal government has invested, the states, in total, delivered $1.80 in assistance to drinking water systems. For WIFIA, for every $1 million in credit subsidy appropriations, EPA could potentially provide approximately $100 million in direct credit assistance, resulting in an estimated $200 million in total infrastructure investment.

[5] Baseline is 3,508 community water systems out of compliance with health-based standards as of FY 2017. (Footnote updated from *FY 2018-2022 EPA Strategic Plan* published February 12, 2018.)

[6] The baseline is $32 billion in non-federal dollars leveraged from the CWSRF and DWSRF between FY 2013 and FY 2017 (i.e., loans made from recycled loan repayments, bond proceeds, state match, and interest earnings). The baseline does not include WIFIA leveraged dollars because no loans were closed prior to FY 2018. (Footnote updated from *FY 2018-2022 EPA Strategic Plan* published February 12, 2018.)

[7] Draft baseline is 464,020 square miles of impaired waters as of September 2017, to be updated in FY 2019. (Footnote updated from *FY 2018-2022 EPA Strategic Plan* published February 12, 2018.)

Protect Human Health

Sustaining the quality of our water resources is essential to safeguarding human health. More than 300 million people living in the United States rely on the safety of tap water provided by public water systems that are subject to national drinking water standards. EPA will help protect human health and make America's water systems secure by:

- Providing financial assistance to states, tribes, and territories to assist public water systems in protecting and maintaining drinking water quality;
- Strengthening compliance with drinking water standards to ensure protection of public health by enhancing the technical, managerial, and financial capability of those systems;
- Continuing to protect and restore water resources, including sources of drinking water, from contamination;
- Taking actions to address known and emerging contaminants that endanger human health;
- Supporting states, tribes, territories, and local communities in implementing water programs by providing guidance, training, and information;
- Ensuring the security and preparedness of the nation's drinking water supplies by implementing EPA's national security responsibilities for the water sector; and
- Protecting underground sources of drinking water by providing for the safe injection of fluids underground for storage, disposal, enhanced recovery of oil and gas, or minerals recovery.

Recent challenges in Flint, Michigan and elsewhere highlighted the need to strengthen EPA's implementation of the Safe Drinking Water Act to ensure we protect and build upon the enormous public health benefits achieved through the provision of safe drinking water throughout the country. The Agency's highest priorities include reducing exposure to lead in the nation's drinking water systems, ensuring continuous compliance with contaminant limits, responding quickly to emerging concerns, and improving the nation's aging and insufficient drinking water infrastructure to address significant needs. EPA is also collaborating with states and tribes to share more complete data from monitoring at public water systems through the Safe Drinking Water Information System (SDWIS). This will allow for better targeting of funding and technical assistance resources, and improve data quality while increasing public access to drinking water data.

Human health and recreational criteria are the foundation for state, tribal, and territorial tools to safeguard human health. Over the next five years we will improve our understanding of emerging potential waterborne threats to human health; provide technical assistance and resources to help the states, tribes, and territories monitor and prevent harmful exposures; and develop new or revised criteria as needed.

External Factors and Emerging Issues

Water quality programs face challenges such as increases in nutrient loadings, nonpoint source[8] and stormwater runoff, and aging infrastructure. EPA is carefully examining the potential impacts of and solutions to these issues. Many important water quality problems have complex causes that can only be addressed through strategic use of federal, state, tribal, and local authorities. EPA will work closely with its partners to ensure that these issues are addressed in a coordinated and effective manner, particularly

[8] Read more about nonpoint source pollution: https://www.epa.gov/nps

where water quality issues cross jurisdictional lines. The Agency will implement the National Aquatic Resource Surveys to support collection of nationally-consistent data to support these efforts.

EPA is working with external partners and stakeholders to address the barriers to and incentives for ways that technology and innovation can accelerate improvements in water infrastructure and protection and restoration of waters. Some key market opportunities for innovative practices and technology to help address current and emerging water resource issues are identified in EPA's Blueprint for Integrating Technology Innovation into the National Water Program.[9]

Protect and Restore Water Quality

Protecting the nation's waters relies on cooperation among EPA, states, tribes, territories, and local communities and involves a suite of programs to protect and improve water quality in the country's rivers, lakes, wetlands, and streams, as well as in estuarine, coastal, and ocean waters. EPA will foster strong partnerships with other federal agencies, states, tribes, local governments, and other organizations that facilitate achieving water quality goals while supporting robust economic growth. In partnership with states, tribes, territories, and local governments, EPA core water programs will:

- Develop recommended water quality criteria for protecting designated uses of water;
- Assist states, authorized tribes, and territories in adopting water quality standards that support designated uses;
- Establish pollution reduction targets for impaired waters;
- Improve water quality by financing traditional and nature-based wastewater treatment infrastructure;
- Develop national effluent guidelines that set a technology-based floor;
- Work with partners to protect and restore wetlands and coastal and ocean water resources;
- In cooperation with the Army Corps of Engineers, work with states and tribes interested in assuming the Clean Water Act Section 404 program;
- Prevent or reduce the discharge of pollutants;
- Update analytical methods that enable precise analysis; and
- Conduct monitoring and assessment so we know the status of the nation's waters.

EPA will partner with states and tribes to implement the National Aquatic Resource Surveys (NARS)[10] to provide nationally-consistent and scientifically-defensible assessments of America's waters. These surveys will support EPA and its partners in identifying actions to protect and restore water quality and in assessing whether these efforts are improving water quality over time.

[9] Read more about the technology blueprint: **https://www.epa.gov/innovation/water-technology-innovation-blueprints**

[10] Read more on NARS: **https://www.epa.gov/national-aquatic-resource-surveys**

Objective 1.3
Revitalize Land and Prevent Contamination

Provide better leadership and management to properly clean up contaminated sites to revitalize and return the land back to communities.

Introduction

EPA works to improve the health and livelihood of all Americans by cleaning up and returning land to productive use, preventing contamination, and responding to emergencies. Challenging and complex environmental problems persist at many contaminated properties, including contaminated soil, sediment, surface water, and groundwater that can cause human health concerns.

One of EPA's top priorities is accelerating progress on Superfund sites. EPA recently convened a Superfund Task Force that identified 42 recommendations to streamline and improve the Superfund process. Over the next five years, these recommendations and other innovative ideas will be considered and applied to Superfund sites with priority given to addressing National Priority List (NPL) sites.[11]

EPA collaborates with other federal agencies, industry, states, tribes, and local communities to enhance the livability and economic vitality of neighborhoods. The Agency works with international, state, tribal, and local governments, and other federal agencies to achieve goals and help communities understand and address risks posed by releases of hazardous substances into the environment. EPA's efforts are guided by scientific data, tools, and research that inform decisions on addressing contaminated properties and preparing for and addressing emerging contaminants.

[11] Please see the Superfund Task Force Recommendations at https://www.epa.gov/sites/production/files/2017-07/documents/superfund_task_force_report.pdf

Long-Term Performance Goals

LTPG 1.3.1 By September 30, 2022, make 255 additional Superfund sites ready for anticipated use (RAU) site-wide.[12]

LTPG 1.3.2 By September 30, 2022, make 3,420 additional brownfields sites RAU.[13]

LTPG 1.3.3 By September 30, 2022, make 536 additional Resource Conservation and Recovery Act (RCRA) corrective action facilities RAU.[14]

LTPG 1.3.4 By September 30, 2022, complete 56,000 additional leaking underground storage tank (LUST) cleanups that meet risk-based standards for human exposure and groundwater migration.[15]

Strategies for Achieving the Objective

Cleaning Up Contaminated Sites

Over the next five years, EPA will focus special attention on the Administrator's top priority Superfund sites and will implement Superfund Task Force recommendations to accelerate the pace of cleanups and promote reuse, while addressing risks to human health and the environment. Cleanup actions can take from a few months for relatively straight-forward soil excavation or capping remedies to several decades for complex, large, area-wide groundwater, sediment, or mining remedies. NPL sites in the investigation stages will be expedited by developing strategies that apply new technologies and innovative approaches. NPL sites at which remedies already have been selected will be prioritized for faster completion and deletion from the NPL, as will sites that have been on the NPL for five years or longer without significant progress. Finally, the Agency will aim to accelerate cleanup by re-prioritizing some resources to focus on remedial actions, construction completions, ready-for-reuse determinations, and NPL site deletions.

[12] By the end of FY 2017, 836 Superfund sites had been made RAU site-wide.

[13] From FY 2006 through the end of FY 2017, 5,993 brownfield properties/sites had been made RAU. (Footnote updated from *FY 2018-2022 EPA Strategic Plan* published February 12, 2018.)

[14] From FY 1987 through FY 2017, 1,232 of the universe of 3,779 high priority RCRA corrective action facilities had been made RAU site-wide. (Footnote updated from *FY 2018-2022 EPA Strategic Plan* published February 12, 2018.)

[15] By the end of FY 2017, 469,898 LUST cleanups had been completed.

In addition, EPA will work with communities to revitalize their brownfield sites and return them to productive use, advancing environmental and human health protection while stimulating economic development and job creation. EPA will award competitive grants to communities, states, and tribes to assess, clean up, and plan reuse of brownfield properties that are contaminated or perceived to be contaminated. To reduce risks from exposure to waste, consistent with RCRA, EPA or authorized states will oversee and manage cleanups by the owners or operators. There are currently 3,779 facilities subject to RCRA corrective action. EPA will support, along with its state and tribal partners, the cleanup of LUST sites and work to revitalize abandoned facilities. These cleanups protect people from exposure to contaminants, and can improve property values[16] and provide redevelopment opportunities.

Preparedness and Response

EPA prepares for the possibility of nationally-significant incidents and provides guidance and technical assistance to state, tribal, and local planning and response organizations to strengthen their preparedness. During an incident, EPA works to prevent, mitigate, or contain the release of chemical, oil, radiological, biological, or hazardous materials. The Agency will work with industry, states, tribes, and local communities to ensure national safety and security for responses. EPA homeland security research fills critical scientific and technological gaps, enhancing the Agency's ability to carry out its mandated national preparedness and emergency response and recovery obligations, and informing disaster response and guidance. EPA develops the tools, methods, and data needed to implement our environmental statutes effectively and support EPA and local emergency responders in characterizing chemical, biological, or radiological (CBR) contamination; assessing exposure and risks to human health; cleaning up impacted areas; and improving community resilience.

Preventing Contamination

With its state and tribal partners, EPA works to prevent releases of contamination, allowing the productive use of facilities and land and contributing to communities' economic vitality.[17] In partnership with tribes, the Agency directly provides training, compliance assistance, and inspection support to implement the updated underground storage tank (UST) regulations in Indian country. EPA also helps to prevent chemical releases by reviewing approximately 12,500 risk management plans (RMPs) and delivering RMP inspector training for federal and state inspectors. EPA seeks to prevent and prepare for accidental releases from chemical facilities that store hazardous chemicals by requiring chemical facilities that store a certain amount of hazardous chemicals to analyze the potential for accidental releases and possible consequences, develop an accident prevention program, and coordinate with communities to ensure that all are prepared to respond to a release.

EPA will update and improve the efficiency of the RCRA hazardous waste regulations to meet the needs of today's business and industry to ensure protective standards for managing hazardous waste. To prevent future environmental contamination and to protect the health of the estimated 20 million people living within a mile of a hazardous waste management facility,[18] EPA will support states to issue, update, or maintain RCRA permits for the approximately 20,000 hazardous waste units (such as incinerators and landfills) at these facilities. EPA also will issue polychlorinated biphenyl (PCB) cleanup, storage, and disposal approvals, since this work cannot be delegated to states or tribes.

[16] A 2016 study found that high profile UST releases decrease nearby property values by 4% - 6%. Once cleanup is completed, nearby property values rebound by a similar margin. (Guignet, Dennis, Robin Jenkins, Matthew Ranson, and Patrick Walsh (2016), "Do Housing Values Respond to Underground Storage Tank Releases? Evidence from High-Profile Cases across the United States," U.S. EPA National Center for Environmental Economics Working Paper, 2016-01, Washington, DC, March.) Available at: https://www.epa.gov/sites/production/files/2016-05/documents/2016-01.pdf

[17] This work will be done consistent with the government-wide National Response Framework and the National Disaster Recovery Framework.

[18] U.S. EPA, Office of Land and Emergency Management Estimate. 2014. Data collected includes: (1) site information as of the end of FY 2011 from RCRAInfo, and (2) census data from the 2007-2011 American Community Survey.

EPA will improve and modernize hazardous waste transportation and tracking by implementing the Hazardous Waste Electronic Manifest Establishment Act, enacted on October 5, 2012. The fee-based e-Manifest system will provide better knowledge of waste generation and final disposition, enhanced access to manifest information, and greater transparency for the public about hazardous waste shipments. It will also reduce the burden associated with paper manifests by between 300,000 and 700,000 hours.[19]

As authorized in the Water Infrastructure Improvements for the Nation Act of 2016, EPA will help states develop plans, work to approve state permit programs for coal ash disposal, coordinate closely with the states on guidance for evaluating state permit programs, and implement a coal ash permit program in Indian country.

Over the next five years, EPA will provide technical assistance, assets, and outreach to industry, states, tribes, and local communities as part of its effort to ensure national safety and security for inland oil incidents. There are approximately 580,000 spill prevention, control, and countermeasure facilities, including a high-risk subset of 4,600 facility response plan facilities required to ensure that resources will be available to respond in the event of a discharge.

External Factors and Emerging Issues

A number of factors may delay cleanup timelines. For example, new scientific information (such as new toxicity information or a new analytical method) can call previous determinations into question. In general, cleanup standards have become more stringent over the years, and discovery of new pathways and emerging contaminants (such as vapor intrusion and per- and polyfluoroalkyl substances [PFAS]) have made remediation of remaining Superfund sites more challenging. Many of the Superfund sites remaining on the National Priorities List–including sediment, mining, and large groundwater sites–are large, contain multiple areas of contamination, and require more complex remediation efforts. Discovery of new sites, newly detected contamination, or emerging contaminants can also impact cleanup schedules.

Several external factors and emerging issues may affect the overall success of EPA's waste management and chemical facility risk programs. Rapidly changing technology, emerging new waste streams, and aging infrastructure present challenges, as does the complexity of issues and consideration of specific solutions for varying waste streams and situations.

The Agency recognizes that our state, tribal, local, and regional government partners face challenges in fully characterizing environmental outcomes associated with land. Over the next five years, EPA will emphasize the importance of engaging stakeholders at all levels and from all perspectives in making cleanup and land revitalization decisions.

[19] From a 2009 programmatic estimate, cited in Hazardous Waste Management System; Modification of the Hazardous Waste Manifest System; Electronic Manifests; Final Rule. 40 CFR § 260, 262, 263, 264, 265, and 271.

Objective 1.4
Ensure Safety of Chemicals in the Marketplace

Effectively implement the Toxic Substances Control Act, and the Federal Insecticide, Fungicide, and Rodenticide Act, to ensure new and existing chemicals and pesticides are reviewed for their potential risks to human health and the environment and actions are taken when necessary.

Introduction

Chemicals and pesticides released into the environment as a result of their manufacture, processing, use, or disposal can threaten human health and the environment. EPA gathers and assesses information about the risks associated with chemicals and pesticides and implements risk management strategies when needed. EPA's research efforts will help advance the Agency's ability to assess chemicals more rapidly and accurately.

In 2016, TSCA was amended by the Frank R. Lautenberg Chemical Safety for the 21st Century Act. The amendments give EPA significant new, as well as continuing, responsibilities for reviewing chemicals in or entering commerce to prevent unreasonable risks to human health and the environment, including unreasonable risks to potentially exposed or susceptible subpopulations. Proper implementation, as Congress intended, of the TSCA amendments is one of EPA's top priorities.

The Federal Insecticide, Fungicide, and Rodenticide Act (FIFRA) is the primary federal law governing oversight of pesticide manufacture, distribution, and use in the United States. FIFRA requires EPA to register pesticides based on a finding that they will not cause unreasonable adverse effects on people and the environment, taking into account the economic, social, and environmental costs and benefits of the use of the pesticide. Each time the law was amended, Congress strengthened FIFRA's safety standards while continuing to require consideration of pesticide benefits. In addition to FIFRA, the Federal Food, Drug, and Cosmetic Act (FFDCA) governs the maximum allowable level of pesticides in and on food grown and sold in the United States. The legal level of a pesticide residue on a food or food item is referred to as a tolerance. FFDCA requires that the establishment, modification, or revocation of tolerances be based on a finding of a "reasonable certainty of no harm." When evaluating the establishment, modification, or revocation of a tolerance, EPA tries to harmonize the tolerance with the maximum residue levels (MRLs) set by other countries to enhance the trade of agricultural commodities.

Long-Term Performance Goals

LTPG 1.4.1 By September 30, 2022, complete all EPA-initiated TSCA risk evaluations for existing chemicals in accordance with statutory timelines.[20]

LTPG 1.4.2 By September 30, 2022, complete all TSCA risk management actions for existing chemicals in accordance with statutory timelines.[21]

LTPG 1.4.3 By September 30, 2022, complete all TSCA pre-manufacture notice final determinations in accordance with statutory timelines.[22]

LTPG 1.4.4 By September 30, 2022, complete all cases of Federal Insecticide, Fungicide, and Rodenticide Act (FIFRA)-mandated decisions for the pesticides registration review program.[23]

LTPG 1.4.5 By September 30, 2022, reduce the Pesticide Registration Improvement Act (PRIA) registration decision timeframe by an average of 60 days.[24]

Strategies for Achieving the Objective

Chemicals

Over the next five years, EPA will focus on meeting the statutory requirements and mandatory deadlines of the amended TSCA and ensuring that the reviews are efficient, effective, and transparent to EPA's stakeholders. EPA will ensure that decisions are based on science, are transparent, use methods and tools that are based on the weight of scientific evidence, are consistent with the best available scientific information, and are reasonable and consistent with the intended use of the information.

Under the chemical data reporting (CDR) rule, EPA collects basic exposure-related information from manufacturers (including importers) on the types, quantities, and uses of chemical substances produced domestically or imported into the United States. Since the enactment of TSCA in 1976, many new chemicals have entered commerce following review by EPA under the TSCA new chemicals program. Once in commerce, these chemicals are considered existing chemicals in commerce. The amended

[20] There is no baseline for this measure, as the program is operating under new statutory authority.
[21] There is no baseline for this measure, as the program is operating under new statutory authority.
[22] Baseline is 58.4% of determinations made within 90 days in FY 2018. (Footnote updated from *FY 2018-2022 EPA Strategic Plan* published February 12, 2018.)
[23] Baseline is 239 decisions completed by the close of FY 2017 out of the known universe of 725. (Footnote updated from *FY 2018-2022 EPA Strategic Plan* published February 12, 2018.)
[24] Baseline is an average timeframe of 655 days (range: 93-2,086 days) for PRIA decisions for 68 new active ingredients completed in FY 2015-2017.

EPA works closely with public health officials, researchers, and agricultural experts to identify emerging pests; and, with industry, to expeditiously register pesticides that address issues while ensuring pesticide safety.

TSCA provides a framework for making progress in understanding and managing the risks associated with existing chemicals to prevent unreasonable risk posed by their manufacturing, processing, distribution, use or disposal. The Act requires EPA to identify high- and low-priority existing chemicals and evaluate high-priority chemicals against a new risk-based safety standard. By December 2019, EPA must complete risk evaluations for the first ten high-priority chemicals, ramp up the risk evaluation process so that 20 high-priority chemicals are under evaluation at all times, and identify 20 low-priority chemicals which will not undergo further evaluation at this time. Chemical risk evaluations of existing chemicals must be completed within three years. Transparency and stakeholder engagement are vital parts of the process, as they help inform EPA's prioritization and risk evaluation of existing chemicals.

The Agency has two years to address unreasonable risks identified as warranted for action by the findings of the chemical risk evaluations.[25] Risk management actions may include prohibiting, restricting, or modifying the manufacture, processing, distribution in commerce or commercial use, modifying the labeling, recordkeeping, and other restrictions.

For new chemicals, EPA reviews and takes action on approximately 1,000 new chemical notices –including exemption notices– submitted by industry annually, including pre-manufacture notices (PMNs), to ensure that the chemicals are not likely to pose unreasonable risk before being allowed to commercialize. To prevent such risk, EPA may establish risk reduction/management requirements through the new chemical review process to protect workers, consumers or the environment. The 2016 TSCA amendments created additional new requirements for positive determinations of chemical safety, which have resulted in changes to EPA's assessment process for new chemicals. In particular, for each new chemical notice, EPA now has 90 days to make an affirmative determination of safety based on whether the chemical substance will present, may present, or is not likely to present an unreasonable risk to human health or the environment, or that the available information is insufficient to enable the Agency to make any of the above determinations. All four of these outcomes constitute final determinations on pre-manufacture notices and thus count toward EPA's strategic target of completing 100% of such determinations within statutory timelines. Under the TSCA amendments, if EPA makes an "insufficient information" determination, the Agency will work with the submitter to conduct testing needed to make a determination or will impose restrictions on the substance that prevent exposure from occurring.

EPA will protect legitimate claims of confidentiality of the identity of chemicals. With limited exceptions provided by statute, the Agency will review within 90 days all chemical identity confidential business information (CBI) claims requiring substantiation under TSCA Section 14(c)(3) and a representative subset, comprising at least 25 percent, of all other CBI claims. Timely review of CBI claims will help to increase transparency of chemical data. Additionally, EPA is developing guidance required by TSCA, as amended, to address how states, tribes, and medical professionals in an emergency situation may gain access to CBI information.

The Agency uses a variety of tools and approaches to assess, prevent, and reduce chemical releases and exposures, and empowers stakeholders by ensuring access to chemical data and other information and expertise. EPA annually publishes the Toxics Release Inventory (TRI), a public database that contains release and other waste management information (e.g., recycling) and pollution prevention data on over 650 toxic chemicals from approximately 20,000 industrial and federal facilities.

[25] TSCA section 6(c)(1) requires final regulatory action within 2 years of publication of the final risk evaluation but allows for an extension to this deadline "for not more than 2 years."

Pesticides

EPA is responsible for licensing (registering) and periodically reevaluating (registration review) pesticides to protect consumers, pesticide users, workers who may be exposed to pesticides, children, and other sensitive populations, while considering the benefits associated with the use of the pesticide. EPA seeks public input on all pesticide reevaluations; all new active ingredients; first food uses; and the establishment, modification, or revocation of tolerances. For example, the rules governing the registration review program[26] typically provide for three distinct comment periods at various stages of the review process. In making pesticide decisions, the Agency often seeks input from stakeholders to address specific information, such as real-world use patterns and benefits to the user community.

EPA works with other federal, state, and tribal agencies, trade organizations, industry, and non-governmental organizations to ensure the effective and safe use of pesticides. EPA also has long provided financial support and expertise to states and tribes so that they can provide training, education, and outreach to pesticide applicators about the safe, proper, and legal use of pesticides. States and tribes work with farmers, businesses, and public agencies to protect human health and the environment and serve as a critical part of job training and business growth in rural areas.

External Factors and Emerging Issues

The amended TSCA provides EPA the authority to collect user fees designed to defray 25 percent of the Agency's costs to administer TSCA Sections 4, 5, 6, and 14. While EPA is directed by the statute to design the fees to collect 25 percent of the costs of administering these sections, it has no control over exactly how much revenue the fees will generate. That will be determined in large part by how the fee-paying community responds to the new fees in terms of their number of fee-related submissions or requests.

New pests and disease vectors carried by pests create challenges for managing pesticides. EPA works closely with public health officials, researchers, and agricultural experts to identify emerging pests; and, with industry, to expeditiously register pesticides that address issues while ensuring pesticide safety. Assessing and appropriately addressing risks is complex. The Agency must determine safe, effective methods of pesticide use, weighing differing risks for humans and ecosystems. For example, one pesticide may have lower risks for humans than do other pesticides, but have increased risks for pollinators or endangered species. Similarly, a pesticide may have risks for humans, but may be appropriate to fight mosquitos that carry diseases that also pose risks to humans.

EPA continues to conduct education and outreach with tribes. One challenge is ensuring that the flow of information on the safe use of pesticides reaches all federally-recognized tribes across the country, and comes in forms that result in protective actions on the ground.

[26] 40 CFR 155 – Registration Standards and Registration Review

2 More Effective Partnerships

Provide certainty to states, localities, tribal nations, and the regulated community in carrying out shared responsibilities and communicating results to all Americans.

The idea that environmental protection is a shared responsibility between the states, tribes, and the federal government is embedded in our environmental laws, which in many cases provide states and tribes the opportunity and responsibility for implementing environmental protection programs. More than 45 years after the creation of EPA and the enactment of a broad set of federal environmental protection laws, most states, and to a lesser extent territories and tribes, are authorized to implement environmental programs within their jurisdictions in lieu of EPA-administered federal programs. Specifically, states have assumed more than 96 percent of the delegable authorities under federal law.[27] EPA retains responsibility for directly implementing federal environmental programs in much of Indian country where eligible tribes have not received delegable authorities. There are also programs that by statute may not be delegated to the states or tribes. Recognizing these evolving responsibilities, EPA headquarters and regions will facilitate constructive dialogue with states and tribes to ensure maximum utilization of resources. EPA will adapt its practices to reduce duplication of effort with authorized states and tribes, and tailor its oversight of delegated programs.

An effective partnership (or cooperative federalism) between states, tribes and EPA–is not just about who makes decisions, but about how decisions are made and a sense of shared accountability to provide positive environmental results. EPA understands that improvements to protecting human health and the environment cannot be achieved by any actor operating alone, but only when the states, tribes, and EPA, in conjunction with affected communities, work together in a spirit of trust, collaboration, and partnership. Effective environmental protection is best achieved when EPA and its state and tribal partners work from a foundation of transparency, early collaboration –including public participation–and a spirit of shared accountability for the outcomes of this joint work. This foundation involves active platforms for public participation, including building the capacity of the most vulnerable community stakeholders to provide input. With these public participation opportunities, the beneficiaries of environmental protection–the American people–will be able to more meaningfully engage through their communities, their local governments, and their state and tribal governments. Including the public's voice, particularly the voices of the most vulnerable to environmental and public health challenges among us, in EPA's policy, regulatory, and assistance work is essential to meeting their needs as the Agency implements its statutory responsibilities.

EPA also recognizes that meeting the needs of states, tribes, local governments, and communities, and achieving environmental improvements cannot be done in isolation from economic growth. Opportunities for prosperous economic growth and clean air, water, and land are lost without effective infrastructure investments that align with community needs. This is especially true for infrastructure investments that repair existing systems, support revitalization of existing communities and buildings, take advantage of existing roads, and lead to the cleanup and redevelopment of previously-used sites and buildings. Currently, there is a need for significant infrastructure investments. EPA will play a role in meeting this need by aligning its relevant programs to catalyze other resources, supporting beneficial infrastructure investments, and meeting community needs for thriving economies and improved environmental and human health outcomes.

[27] Environmental Council of the States (ECOS) Paper, "Cooperative Federalism 2.0," June 2017

Objective 2.1
Enhance Shared Accountability

Improve environmental protection through shared governance and enhanced collaboration with state, tribal, local, and federal partners using the full range of compliance assurance tools.

Introduction

In the spirit of cooperative federalism, EPA and its partners have made enormous progress in protecting air, water, and land resources. EPA recognizes that states and tribes vary in the environmental challenges that they face due to variations in geography, population density, and other factors. EPA will maximize the flexibilities provided by law to take each state's unique situation into account when making regulatory and policy decisions. EPA directly implements the majority of federal environmental programs in Indian country. The Agency actively works with tribes to develop their capacity to administer environmental programs and to enable tribes that choose to implement federal environmental laws and programs for their lands. The unique relationship among EPA and its co-regulators is the foundation of the nation's environmental protection system; each organization fulfills a critical role based on its expertise, abilities, and responsibilities in protecting and improving human health and the environment.

EPA recognizes the advances states and tribes have made in implementing environmental laws and programs. This Administration will undertake a series of initiatives to rethink and assess where we are and where we want to be with respect to shared governance. These initiatives will clarify the Agency's statutory roles and responsibilities and tailor state and tribal oversight to maximize our return on investment and reduce burden on states and tribes, while ensuring continued progress in meeting environmental laws.

In addition, EPA, with its state, tribal, and local partners, ensures consistent and fair enforcement of federal environmental laws and regulations. The Agency works jointly with its co-regulators to protect human health and the environment, using a full set of compliance assurance tools, such as compliance assistance and monitoring; electronic reporting; traditional enforcement; grants to states and tribes; and tribal capacity building. EPA is building on progress made using E-Enterprise for the Environment, a platform for transformative change that operationalizes cooperative federalism principles. EPA's E-Enterprise partnership with states and tribes modernizes the way we do the business of environmental protection.

Long-Term Performance Goals

LTPG 2.1.1 By September 30, 2022, increase the number of grant commitments achieved by states, tribes, and local communities.[28]

LTPG 2.1.2 By September 30, 2022, increase the use of alternative shared governance approaches to address state, tribal, and local community reviews.[29]

Strategies for Achieving the Objective

Shared Governance

To develop a future model of shared governance that takes into account the progress states and tribes have made in protecting human health and the environment, the Agency will undertake an analysis of EPA's statutory roles and responsibilities to determine what we have to do and assess what we want to do in light of priorities. The Agency will work with states and tribes to find alternative approaches to shared governance, seeking to provide flexibility and streamline oversight of state and tribal programs. As part of this process, the Agency will seek to understand which approaches currently are working well for state, tribal and local co-regulators. EPA will pilot new approaches to oversight (e.g., permit reviews) where we have the legal flexibility to do so and streamline those processes by which EPA reviews and approves state and tribal actions. EPA will continue to work with states and tribes through E-Enterprise, focused on how we work and plan together, agree on priorities, and allocate roles and responsibilities to update processes and programs. Through shared governance–engaging early and meaningfully with states and tribes–the Agency will use E-Enterprise to deliver streamlined processes as well as accessible, reliable information and data that benefit co-regulators and the regulated community.

The National Environmental Performance Partnership System (NEPPS) has long served as a model for advancing cooperative federalism by providing the flexibility needed to address the unique needs of individual states and tribes to achieve the best environmental results. NEPPS is a performance-based approach for organizing working relationships with states and many tribes, providing specific benefits, such as greater flexibility to assess environmental conditions, shared priorities, and strategically leveraged resources, thus improving cooperative federalism, shared governance, and shared accountability. EPA will work with states and tribes to strengthen cooperative federalism principles through NEPPS, and intends to make NEPPS training available for state and tribal stakeholders.

EPA will work closely with states and tribes on NEPPS, Performance Partnership Grants (PPGs), and related policies. PPGs are a financial tool that allows states and tribes to combine separate "streams" of categorical grant funding, from across 20 eligible categorical grants, into one multi-program grant with a single budget. The goal of the review is to understand PPG utilization and outline a course of action addressing the challenges, leveraging lessons learned and progress achieved over the last 22 years.

[28] Universe (number of commitments contained in Performance Partnership Grants) and FY 2020 target will be determined in FY 2019. (Footnote updated from *FY 2018-2022 EPA Strategic Plan* published February 12, 2018.)

[29] There is no baseline for this measure. (Footnote updated from *FY 2018-2022 EPA Strategic Plan* published February 12, 2018.)

The intent is to provide states and tribes the flexibility to maximize human health and environmental protection achieved by the funds; further enhance the federal, state, and/or tribal partnership; and promote the goals of NEPPS.

EPA will respect the important role governors play in cooperative federalism and will seek their views and perspectives on compliance assistance and other opportunities to improve EPA-state partnerships. In addition, the Agency will work to strengthen intergovernmental consultation methods to engage stakeholders and hear diverse views on the impacts of prospective regulations.

Local governments also have a unique relationship with EPA as partners and often as innovative problem solvers. EPA works with local governments to build stronger and more robust partnerships and bring local concerns forward into Agency decision making. As part of these efforts, EPA seeks advice from the Local Government Advisory Committee (LGAC), a chartered policy committee comprising elected and appointed local officials, on the impacts of the Agency's regulations and policies on local governments.

Consistent with the 1984 Indian Policy and EPA Policies on consultation and treaty rights,[30] EPA will work on a government-to-government basis to build tribal capacity to implement federal programs through delegations, authorizations, and primacy designations to enable tribes to meaningfully participate in the Agency's policy making, standard setting, and direct implementation activities under federal environmental statutes.[31] EPA will work with individual tribes to develop and implement an EPA-Tribal Environmental Plan (ETEP), a joint planning document for achieving stronger environmental and human health protection in Indian country. ETEPs identify tribal, EPA, and shared priorities, and the roles and responsibilities for addressing those priorities.

EPA will focus its direct implementation efforts on areas of high need for human health or environmental protection, including programs identified in the ETEP for which tribes are not eligible, as well as those for which tribes do not currently anticipate seeking delegation, authorization, or primacy. In carrying out its direct implementation activities, EPA will work closely with tribes to develop tribal capacity for programs for which they do not anticipate seeking delegation, authorization, or primacy. EPA will also encourage tribes to participate in policy making and to assume appropriate partial roles in the implementation of programs, including through the use of Direct Implementation Tribal Cooperative Agreements (DITCAs) or other agreements, as available.

Compliance Assurance

Over the next five years, the Agency will look for cost-effective ways to enhance the compliance assurance tool box in collaboration with its state, tribal, local, federal, and industry partners. For example, the E-Enterprise Web Portal offers a platform or gateway for making shared services available to states, tribes, and EPA to transact business (e.g., e-permitting and reporting). It also provides information for the regulated community (e.g., compliance assistance information). Tools and services are designed to enhance efficiency, reduce burden on the regulated community, and improve environmental outcomes. EPA will expand its compliance assistance work by continuing to partner with third-party organizations and federal agencies to support the 17 existing web-based, sector-specific compliance assistance centers[32] and developing new centers. In general, an expanded and modernized compliance assurance tool box will enhance EPA's ability to tailor compliance assurance approaches to the differing needs and challenges among states and regulated entities. EPA is also working closely with states and tribes to develop new compliance tools and approaches to make programs more effective and efficient in promoting compliance and remedying violations. Some of the

[30] There is no baseline for this measure. (Footnote updated from *FY 2018-2022 EPA Strategic Plan* published February 12, 2018.)

[31] The Tribal Consultation Opportunities Tracking System (TCOTS) publicizes upcoming and current EPA consultation opportunities for tribal governments and can be located here: **https://TCOTS.epa.gov**.

[32] For more information on compliance assistance centers, see **https://www.epa.gov/compliance/compliance-assistance-centers**.

Agency's ongoing collaborative efforts with the Environmental Council of the States (ECOS) include[33] producing webinars to help identify new compliance approaches that EPA could pilot and evaluate, increasing availability of training, and preparing for advances in pollution monitoring technology.[34]

A key component of EPA's overall compliance assurance program is compliance monitoring. Compliance monitoring allows the regulatory agencies to detect noncompliance and promote compliance with the nation's environmental laws. Effective targeting of compliance monitoring plays a central role in achieving the goals EPA has set for protecting human health and the environment. EPA, state, and tribal inspectors often provide regulated entities with compliance assistance during the inspection process. On a national level, EPA works closely with individual states, tribes, and state and tribal associations to develop, modernize, and implement national compliance monitoring strategies to ensure a level playing field for regulated entities across the country. EPA principally focuses compliance monitoring activities, such as field inspections, electronic reporting, and data analysis tools, for those programs that are not delegated to states and tribes. The Agency provides monitoring, program evaluations, and capacity building to support and complement authorized state, tribal, and local government programs. The Agency will work with its state and tribal partners to enhance compliance monitoring tools and increase the use of Lean practices. Through E-Enterprise for the Environment, EPA, states, tribes, and territories will collaborate to develop smart mobile tools to enhance the effectiveness and efficiency of state, tribal, and EPA inspectors, and support advanced monitoring technology.

International Partnerships

To achieve the Agency's domestic environmental and human health objectives, the EPA will work with international partners to address international sources of pollution, as well as the impacts of pollution from the United States on other countries and the global environment. Pollution impacts air, water, food crops, and food chains, and can accumulate in foods such as fish. EPA efforts will include working with international partners to strengthen environmental laws and governance to more closely align with U.S. standards and practices and to help level the playing field for U.S. industry.

External Factors and Emerging Issues

Advances in the field of information technology and social science research may offer innovative ways to promote compliance. EPA is partnering with states to help prepare for and use these technologies and research to carry out our statutory obligations. The Agency also is working with the academic community on additional research to develop innovation in promoting compliance. EPA also will work closely with ECOS; the National Tribal Caucus; state and tribal program associations; and individual states, tribes, and territories to implement the Administrator's vision for cooperative federalism. In partnership with ECOS, EPA plans to develop principles and best practices for enhancing collaboration among EPA and states on compliance assurance work. In addition, EPA will continue to work with ECOS, the Association of State and Territorial Solid Waste Management Officials (ASTSWMO), and individual states to develop an integrated hardware/software solution that supports documenting and conducting inspections.

[33] For more information on OECA's collaboration with ECOS via E-Enterprise, see Article: Advanced Monitoring Technology: Opportunities and Challenges. A Path Forward for EPA, States, and Tribes.

[34] For more information on a broader range of collaborations between OECA and ECOS, see Compendia of Next Generation Compliance Examples in Water, Air, Waste, and Cleanup Programs.

Objective 2.2
Increase Transparency and Public Participation

Listen to and collaborate with impacted stakeholders and provide effective platforms for public participation and meaningful engagement.

Introduction

EPA will strengthen its community-driven approach, which emphasizes public participation to better partner with states, tribes, and communities and to maximize the support and resources of the entire Agency to create tangible environmental results. The Agency will deploy its collective resources and expertise to collaborate with states, tribes, and communities and support locally-led, community-driven solutions to improved environmental protection and economic growth. EPA will increase transparency with industry, environmental groups, and other stakeholders, and will facilitate public participation, emphasizing cooperation and collaboration, especially at the early stages of Agency actions. This will provide a more comprehensive understanding of community needs.

The Agency also will coordinate better across its programs and with federal partners to ensure mutual efforts are aligned. EPA will include consideration of vulnerable groups and communities in decisions, and will reflect community needs in its actions and investments, recognizing that the needs of rural communities may not be the same as urban areas. Increasing transparency and public participation in EPA's work with other agencies will enhance the Agency's ability to partner with states, tribes, and local governments and increase responsiveness to the needs of their most vulnerable communities. EPA will serve as a convener and leverage resources with new and existing partners to deliver services more efficiently and effectively. The Agency also will engage with regulated entities to identify reforms to more efficiently and effectively meet the nation's environmental goals.

Long-Term Performance Goal

LTPG 2.2.1 By September 30, 2022, eliminate the backlog and meet statutory deadlines for responding to Freedom of Information Act (FOIA) requests.[35]

Strategies for Achieving the Objective

Over the next five years, EPA will meet community needs through public participation and will build community capacity through grants, technical assistance, partnering, and meaningful engagement. The Agency will leverage recommendations provided by federal advisory committees, such as the National Environmental Justice Advisory Council (NEJAC), LGAC, and Children's Health Protection Advisory Committee (CHPAC), and focus on partnerships representing vulnerable populations, such as youth, the elderly, and low-income communities. Specifically, the Agency will engage with the focus communities identified by EPA regions to understand each community's goals and identify its environmental priorities and needs, recognizing that rural communities and more urban areas may have different priorities.

EPA will continue to provide loans and grants to states and tribes to improve infrastructure. Given that investment in infrastructure is necessary for economic growth and environmental protection and that EPA investments are catalytic to both, the Agency's efforts will be used to support private and public investment in economic revitalization and improved environmental outcomes across the country. This requires that EPA strengthen its infrastructure and community assistance programs (e.g., the clean water SRF, drinking water SRF, Water Infrastructure Finance and Innovation Act, environmental justice, community revitalization, and brownfields area-wide planning grant programs) to better align EPA investments with each other and with other federal investments in pursuit of economic revitalization and improved environmental outcomes. At the same time, EPA will ensure that it is serving disadvantaged communities, leveraging private investment to improve the economy, and protecting human health and the environment.

EPA will work in a focused manner to make infrastructure and public health protection investments in communities with and through partners such as states and tribes. To further integrate and implement community environmental considerations within EPA programs, the Agency will create tools to facilitate incorporation of community understanding, needs, and concerns across program activities, and advance more systematic incorporation of existing tools and needs, such as use of the Environmental Justice Screening and Mapping Tool (EJSCREEN) and EnviroAtlas. EPA will develop a cross-Agency communities team to lead regional involvement in and resourcing of community-based environmental work through a fully-integrated resource platform.

The Agency will coordinate across the federal government–EPA regions partnering with federal agencies in focus communities –to deliver services more efficiently and effectively. EPA will utilize such partnerships to leverage resources and expertise from across EPA and a range of outside partners to advance economic revitalization through the environmental and health goals of communities. EPA will look for opportunities for early engagement with state, local, and tribal co-regulators through existing advisory committees and other forums. The Agency will also continue leadership of and involvement in the Office of Management and Budget (OMB) Community Solutions Taskforce to better access and leverage resources from across federal agencies, and will strengthen coordination with the Interagency Working Group on Environmental Justice to better integrate EPA priorities and support and engage communities. In addition, EPA will support and align its work with the activities and priorities of the President's Task Force on Environmental Health Risks and Safety Risks to Children.

[35] As of April 2018, there were 2,537 overdue FOIA requests in the backlog. (Footnote updated from *FY 2018-2022 EPA Strategic Plan* published February 12, 2018.)

The Agency will seek to increase the number and type of public participation platforms it has to ensure that the public can meaningfully participate in all of EPA's work—including policy making, regulatory development, outreach, education, and community engagement.

EPA will work on the E-Enterprise Web Portal's Assistance Gateway, which provides tools and resources for communities to facilitate two-way communication between the public and environmental agencies. The Agency will determine how EPA, states, and tribes can most effectively harness and benefit from the recent, rapid development of environmental monitoring technologies that are smaller, more portable, and less expensive than traditional methods. EPA will pursue innovative technologies without compromising the accuracy of the information collected. In consultation with state, tribal, and local partners, EPA will make monitoring data publicly available, providing context and relevancy. EPA will support the E-Enterprise Assistance Gateway that will enhance collaboration and communication with communities. The Agency will seek to increase the number and type of public participation platforms it has to ensure that the public can meaningfully participate in all of EPA's work—including policy making, regulatory development, outreach, education, and community engagement.

EPA will also focus on reducing the FOIA backlog the Agency has built up over the years, and enhancing the FOIA process. The complexity and volume of electronic documents required to be searched, collected, and reviewed has increased over time. The Agency will ensure that it can support the timely searching and collection of electronically-stored information for purposes of responding to FOIA requests and other information needs in a cost-effective, sustainable manner. This should not only help the Agency provide the public information requested, but also reduce the fees and lawsuits the Agency incurs from missing FOIA response deadlines.

External Factors and Emerging Issues

Resources are critical to the expansion of technical assistance directed at communities and state, tribal, and local government partners that support community-focused engagement and collaboration. Staff must be available for a wide variety of implementation activities such as direct community engagement and support, intra- and inter-agency coordination, and partnering effectively with states and tribes.

In addition, the challenges of coordinating across offices within EPA and with other federal agencies can inhibit the identification and delivery of creative solutions and services that can lead to tangible results for communities and a more effective leveraging of government resources. EPA recognizes the need to communicate successes and achievements related to this work, both to market its effectiveness and to teach new partners and practitioners how to replicate successful models and approaches.

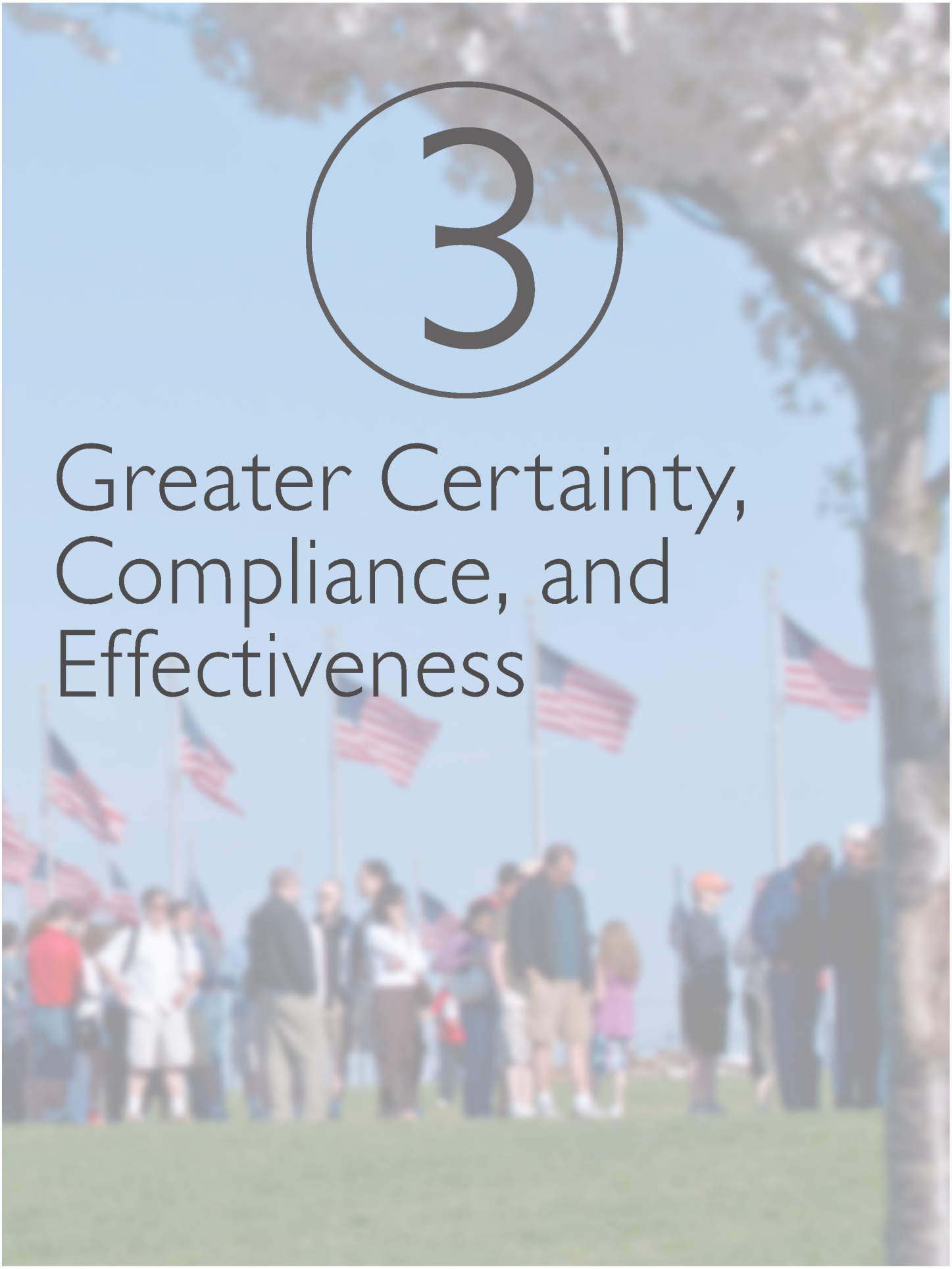

3

Greater Certainty, Compliance, and Effectiveness

Increase certainty, compliance, and effectiveness by applying the rule of law to achieve more efficient and effective agency operations, service delivery, and regulatory relief.

EPA will seek to increase certainty, compliance, and effectiveness. To accomplish this, EPA will work cooperatively with states and tribes to ensure compliance with the law, as well as to create consistency and certainty for the regulated community. Of course, EPA will take civil or criminal enforcement action against violators of environmental laws.

A robust enforcement program is critically important for addressing violations and promoting deterrence, and supports the Agency's mission of protecting human health and the environment. Ensuring compliance with the law also ensures consistency and certainty for the regulated community so it has a complete understanding of the impact of proposed actions on human health, the environment, and the economy, and a clear path and timeline to achieve that compliance. EPA's policies and rules will reflect common sense, consistent with the Agency's statutory authorities, and provide greater regulatory and economic certainty for the public. EPA will enforce the rule of law in a timely manner and take action against those that violate environmental laws to the detriment of human health or the environment.

One of EPA's highest priorities must be to create consistency and certainty for the regulated community. Consistency in how the laws and regulations are applied across the country is part of that process. EPA will undertake a variety of efforts to ensure that consistency in application of laws and regulations is evaluated and addressed, while respecting the unique circumstances of each state and tribe.

EPA recognizes the importance of applying rules and policies consistently as well as creating certainty by meeting the statutory deadlines that are required for EPA's actions. The rule of law must also be built on the application of robust science that is conducted to help the Agency meet its mission and support the states and tribes in achieving their environmental goals. Research, in conjunction with user-friendly applications needed to apply the science to real-world problems, will help move EPA and the states forward in making timely decisions based on science.

Carrying out this goal requires that EPA improve the efficiency of its internal business and administrative operations. First, EPA's business operations, specifically the vast permitting processes established by the different environmental statutes, are key to ensuring economic growth and human health and environmental protection. Over the next five years, EPA will modernize its permitting practices to increase the timeliness of reviews and decisions, while working more collaboratively, transparently, and cost effectively to achieve the Agency's mission. The second part of improving internal operations includes reducing EPA's overhead and creating more efficient and effective administrative processes (e.g., acquisition) that allow EPA to accomplish its core mission work.

Objective 3.1 Compliance with the Law

Timely enforce environmental laws to increase compliance rates and promote cleanup of contaminated sites through the use of all of EPA's compliance assurance tools, especially enforcement actions to address environmental violations.

Introduction

For decades, the protections mandated by federal environmental laws have been essential to the growth of American prosperity. Noncompliance with those laws diminishes shared prosperity and unfairly tilts the field of economic competition in favor of those that skirt the law. To carry out its mission to protect human health and the environment, EPA, in collaboration with state and tribal partners, relies on a strong national compliance assurance and cleanup enforcement program. An effective enforcement program is key to ensuring that the ambitious goals of the nation's environmental statutes are realized.

EPA's enforcement priorities remain focused on cleaning up hazardous waste sites and addressing the most significant violations consistent with EPA's statutory authorities. EPA takes the overwhelming majority of its enforcement actions in programs that are: (1) not delegable to a state or tribe; (2) in states or tribes that have not sought authorization to implement a delegable program; or (3) in states or tribes that do not have the resources or expertise, or that seek assistance from the Agency—and these actions are taken in coordination with the states and tribes. For states and tribes with authorized programs, EPA, states, and tribes share enforcement responsibility, with primary enforcement responsibility residing with the state[36] or tribe. Further, EPA is responsible for addressing violations that occur in Indian country in the absence of an approved program.

Even in states or tribes authorized to implement a program, EPA serves a critical role in addressing serious national noncompliance problems, such as those affecting multiple states or tribes, and in serving as a backstop for instances when a state or tribe does not timely or appropriately address serious noncompliance. EPA also may assist a state or tribe in remedying noncompliance problems when the state or tribe is unable to address the problem because it lacks the capability or resources, such as in actions against other federal or state agencies. For some serious violations, the Agency and states or tribes may decide that the best approach is a joint enforcement action. Further, EPA will take immediate action when there is an environmental emergency, such as an oil spill or chemical

[36] See e.g., ECOS Resolution 98-9, U.S. EPA Enforcement in Delegated States (revised September 28, 2016), describing the EPA and state roles in enforcement in authorized states: "WHEREAS, U.S. EPA and the States have bilaterally developed policy agreements which reflect those roles and which recognize the primary responsibility for enforcement action resides with the States, with U.S. EPA taking enforcement action principally where the State requests assistance, is unwilling or unable to take timely and appropriate enforcement actions, or in actions of national interest, or in actions involving multiple state jurisdictions."

accident. Through the State Review Framework (SRF), EPA periodically reviews authorized state compliance monitoring and enforcement programs, using criteria agreed upon by states, to evaluate performance against national compliance monitoring or enforcement program standards. When states do not achieve standards, the Agency works with them to make progress. However, EPA may also take a lead implementation role when authorized states have a documented history of failure to make progress toward meeting national standards. In all of its work, EPA's enforcement program strives to address noncompliance in an efficient and timely manner, applying a broad range of enforcement and compliance tools to achieve the goal of reducing noncompliance.

Long-Term Performance Goals

LTPG 3.1.1 By September 30, 2022, reduce the average time from violation identification to correction.[37]

LTPG 3.1.2 By September 30, 2022, increase the environmental law compliance rate.[38]

Strategies for Achieving the Objective

Civil Enforcement

The overall goal of EPA's civil enforcement program is to maximize compliance with the nation's environmental laws and regulations to protect human health and the environment. The Agency works closely with the U.S. Department of Justice, states, tribes, territories, and local agencies to ensure consistent and fair enforcement of all major environmental statutes. EPA will seek to strengthen environmental partnerships with its state and tribal partners, encourage regulated entities to correct violations rapidly, ensure that violators do not realize an economic benefit from noncompliance, and pursue enforcement to deter future violations.

EPA recognizes that significant environmental progress has been made over the years, much of it due to enforcement efforts by EPA, states, tribes, and local communities. To maximize compliance over the next five years, the Agency will refocus efforts toward areas with significant noncompliance issues and where enforcement can address the most substantial impacts to human health and the environment. EPA also recognizes the role of states and tribes as the primary implementers, where authorized by EPA to implement the federal statutes, and will focus compliance assurance and enforcement resources on direct implementation responsibilities, addressing the most significant violations, and assisting authorized states and tribes in meeting national standards. For example, the Agency will provide expertise and implement compliance monitoring strategies that will ensure a level playing field. EPA is responsible for direct implementation for programs that are not delegable or where a state or tribe has not sought or obtained

[37] Baseline will be determined in FY 2018.

[38] This concept will be piloted by focusing initially on decreasing the percentage of Clean Water Act (CWA) National Pollutant Discharge Elimination System (NPDES) permittees in significant noncompliance with their permit limits. The baseline and targets will be determined in FY 2019. Other program areas may be included in this long-term performance goal during the FY 2018-2022 timeframe. (Footnote updated from *FY 2018-2022 EPA Strategic Plan* published February 12, 2018.)

the authority to implement a particular program (or program component). Examples of non-delegable programs include the CAA mobile source program, pesticide labeling and registration under FIFRA, virtually all compliance assurance and enforcement in Indian country, enforcement of the federal Superfund cleanup program, and enforcement of non-delegated portions of various other laws, including RCRA, the CWA, and stratospheric ozone under the CAA. EPA also will pursue enforcement actions at federal facilities where significant violations are discovered, will ensure that federal facilities are held to the same standards as the private sector, and will provide technical and scientific support to states and tribes with authorized programs.

Criminal Enforcement

EPA's Criminal Enforcement program enforces the nation's environmental laws through targeted investigation of criminal conduct committed by individual and corporate defendants that threaten public health and the environment. Over the next five years, EPA will collaborate and coordinate with the U.S. Department of Justice and state, tribal, and local law enforcement counterparts to ensure that the Agency responds to violations as quickly and effectively as possible. EPA enforces the nation's environmental laws through targeted investigation of criminal conduct committed by individual and corporate defendants that threatens human health and the environment. The Agency plays a critical role across the country since states and tribes have limited capacity to prosecute environmental crimes. The Agency will focus resources on the most egregious environmental cases (i.e., those presenting significant human health and environmental impacts).

Cleanup Enforcement

Through the Comprehensive Environmental Response, Compensation, and Liability Act (CERCLA, or Superfund), EPA will facilitate prompt site cleanup and use an "enforcement first" approach that maximizes the participation of liable and viable parties in performing and paying for cleanups. The Agency will protect communities by ensuring that potentially responsible parties (PRPs) conduct cleanups at Superfund sites, preserving federal taxpayer dollars for sites where there are no viable contributing parties, and by recovering costs if the EPA expends Superfund-appropriated dollars to clean up sites. EPA also will address liability concerns that can be a barrier to potential reuse. Addressing the risks posed by Superfund sites and returning them to productive use strengthens the economy and spurs economic growth.

Over the next five years, EPA will focus its resources on the highest priority sites, particularly those that may present an immediate risk to human health or the environment. In accordance with the Superfund Task Force Report, the Agency will improve and revitalize the Superfund program to ensure that contaminated sites across the country are remediated to protect human health and the environment, and returned to beneficial reuse as expeditiously as possible. At federally-owned sites, EPA will also focus on resolving formal disputes under the federal facility agreements.

External Factors and Emerging Issues

Advanced monitoring technology and information technology are rapidly evolving, and advances in these fields offer great opportunities for improving the ability of EPA, states, and tribes to ensure compliance. EPA, states, and tribes do, however, face challenges in keeping up with the rapid pace of change in these technologies. In addition, social science research and knowledge may offer innovative ways to promote compliance. EPA is partnering with states and tribes to help prepare for and use these advanced monitoring technologies, consistent with statutory and regulatory obligations. The Agency will collaborate with ECOS and state associations to maximize the use of these technologies and modernize programs. EPA, in collaboration with states, is working with the academic community to identify new ways to improve compliance. For example, EPA will work with states and academics to pilot and evaluate innovative compliance methods.[39] EPA will work with states to integrate advanced pollution monitoring and information technology into Agency work.

[39] ECOS Resolution 17-2: On the Value of Diverse and Innovative Approaches to Advance Compliance (2017)

Objective 3.2
Create Consistency and Certainty

Outline exactly what is expected of the regulated community to ensure good stewardship and positive environmental outcomes.

Introduction

The regulatory framework is inherently dynamic. As part of its statutory obligations, EPA is required to publish many regulations within a set timeframe each year that implement environmental programs and assist the Agency in meeting its core mission. These regulations address newly mandated responsibilities as well as updates and revisions to existing regulations. As EPA meets its obligations to protect human health and the environment through regulatory action, it must also meet another key responsibility – minimizing "regulatory uncertainty" that unnecessarily causes businesses and communities to face delays, planning inefficiencies, and compliance complexities that impede environmental protection, economic growth, and development. EPA will employ a set of strategies to reduce regulatory uncertainty while continuing to improve human health and environmental outcomes consistent with the Agency's authorities as established by Congress and while considering unique state, tribal, and local circumstances. These strategies, which reflect EPA's commitment to cooperative federalism and commitment to the rule of law, will also help advance Agency goals for streamlining and modernizing permitting and enhancing shared accountability.

Long-Term Performance Goals

LTPG 3.2.1 By September 30, 2022, meet 100% of legal deadlines imposed on EPA.[40]

LTPG 3.2.2 By September 30, 2022, eliminate unnecessary or duplicative reporting burdens to the regulated community by 10,000,000 hours.[41]

Strategies for Achieving the Objective

As EPA issues new or revised regulations, businesses and individuals can find it challenging to know which rules apply to them and to adjust their compliance strategies. Over the next five years, EPA will reinvigorate its approach to regulatory development and

[40] Baseline will be determined in FY 2019. (No footnote in *FY 2018-2022 EPA Strategic Plan* published February 12, 2018.)
[41] Baseline is estimated at 173,849,665 information collection and reporting hours.

prioritize meeting its statutory deadlines to ensure that expectations for the regulated community and the public are clear and comprehensive and that Agency actions are defensible and consistent with its authorities. The Agency will use new approaches and flexible tools to minimize regulatory uncertainty and will communicate more comprehensively to realize more consistent and better environmental outcomes, while centering work on statutory and regulatory obligations. EPA will strengthen working relationships with industry sectors to better understand their needs and challenges in implementing Agency requirements and with communities to understand their concerns. This knowledge will enable the Agency to develop better policies and regulations to protect human health and the environment in line with the authorities given to EPA by Congress.

On average, the EPA faces approximately 20 legal challenges under the various environmental statutes each year that assert that the Agency missed a statutory or regulatory deadline for taking an action or unreasonably delayed taking an action. In addition, the Agency faces nearly the same number of legal challenges under FOIA for failure to comply with the deadlines in that law. Responding to these challenges often diverts significant EPA resources away from priority activities, and could impact the Agency's ability to fulfill its commitments. In order to facilitate achievement of this goal, EPA will undertake a systematic mapping of the processes associated with these obligations and implement improvements where needed.

In addition, EPA will develop and engage stakeholders in reviewing a draft base catalog of responsibilities that statutes require EPA to perform in programs delegated to states and tribes. The base catalog, to be complete by 2019 and subsequently updated as necessary, will provide EPA a foundation to make decisions that reduce contradictory policy determinations at headquarters and across regions. It will also support EPA cooperative federalism commitments aimed at minimizing duplication and overlap among regions, headquarters, states, and tribes. This effort also leverages the commitment that EPA is making under cooperative federalism to identify, for all environmental media, an inventory and timeline for state-led permits that EPA reviews.

The Agency will ensure consistent implementation of policies across all regions. EPA will also work towards more cooperative decision making between EPA's regions and headquarters, when necessary. EPA will review regulatory guidance documents to

identify key opportunities and will clarify and realign Agency approaches to improve consistency and clarity. EPA will strengthen working relationships with states, tribes, and local communities to transfer knowledge, leveraging its commitments under cooperative federalism, such as collaboration under E-Enterprise for the Environment. EPA will make available to states and tribes tools or services designed by other federal agencies, states, tribes, or local communities that enhance efficiency and reduce burden on the regulated community while ensuring protection of human health and the environment.

EPA will work with states and tribes to achieve this objective without overburdening those entities with costly unnecessary reporting systems and technology. Building on efforts to date, such as under E-Enterprise, EPA will collaborate with its partners on systems and services, including but not limited to:

- E-reporting: A systematic digital approach that enables states, tribes, and the regulated community to move from paper-based to electronic reporting.
- The Environmental Information Exchange Network: Managed under the collaborative leadership of EPA, states, territories, and tribes, a communication, data, and services platform for submitting and sharing environmental information among partners to foster informed decision making.
- SPeCS for SIPs (State Plan Electronic Collection System for State Implementation Plans): A web-based system for authorized state, tribal, and local governments to submit and manage SIPs under the Clean Air Act.

External Factors and Emerging Issues

A number of factors and emerging issues may impede the Agency's ability to meet this strategic objective. Sustainable resource levels and a strong workforce are critical to success. Proposing and finalizing regulations is often a multi-year process, which can be challenged by lawsuits causing further delays. For example, technical complexity also creates challenges in meeting aggressive deadlines.

Objective 3.3
Prioritize Robust Science

Refocus the EPA's robust research and scientific analysis to inform policy making.

Introduction

EPA will identify, assess, conduct, and apply the best available science to address current and future environmental hazards, develop new approaches, and improve the scientific foundation for environmental protection decisions. EPA conducts problem-driven, interdisciplinary research to address specific environmental risks, and is committed to using science and innovation to reduce risks to human health and the environment, based on needs identified by EPA's program and regional offices and as well as state and tribal partners. Specifically, over the next five years, the Agency will strengthen alignment of its research to support EPA programs, regions, states, and tribes in accomplishing their top human health and environmental protection priorities for improved air quality, clean and safe water, revitalized land, and chemical safety.[42] Working closely with ECOS and its subsidiary, the Environmental Research Institute of the States (ERIS), the Agency will strive to connect state research needs with Agency priorities, and work to improve communication of research results. Through the public-private coalition Interstate Technology and Regulatory Council,[43] EPA will encourage the adoption of innovative technologies and solutions. The Agency will also emphasize the translation of its work products for end user application and feedback.

EPA research will be reviewed by various scientific advisory boards (e.g., Board of Scientific Counselors) that are made up of recognized experts in various scientific, engineering, and social science fields and may be from industry; business; public and private research institutes or organizations; academia; federal, state, tribal, and local governments; nongovernmental organizations; and other relevant interest areas.

[42] EPA research under Homeland Security supports efforts outlined in A Cleaner, Healthier Environment (Goal 1) objectives.
[43] For more information on the Interstate Technology and Regulatory Council, go to http://www.itrcweb.org/.

Long-Term Performance Goal

LTPG 3.3.1 By September 30, 2022, increase the percentage of research products meeting customer needs.[44]

Strategies for Achieving the Objective

Air Quality

EPA's research will advance the science and provide the information critical to improve air quality and to inform stationary source regulations; vehicle and fuel standards and certification; emission inventories; air quality assessments; and domestic ozone actions. The results of Agency research to support air quality program priorities will inform EPA programs; state, tribal, and local air programs; communities; and individuals about measures and strategies to reduce air pollution. Researchers will publish peer-reviewed scientific journal articles to disseminate research findings as appropriate and consistent with resource and program needs.

Over the next five years, the Agency will:

- Deliver state-of-the-art tools for states and tribes to use in identifying effective emission reduction strategies to meet national ambient air quality standards and enhance air quality measurement methods used to ascertain compliance with NAAQS.
- Assess human and ecosystem exposures and effects associated with air pollutants on individual, community, regional, and global scales.
- Develop and evaluate approaches to prevent and reduce pollution, particularly sustainable, cost-effective, and innovative multi-pollutant and sector-based approaches.
- Provide human exposure and environmental modeling, monitoring, metrics, and information needed to inform air quality decision making at the state, tribal, and local level.

Safe and Sustainable Water Resources

EPA will develop innovative, cost-effective solutions to current, emerging, and long-term water resource challenges for complex chemical and biological contaminants. Using a systems approach to develop scientific and technological solutions for protecting human health and aquatic ecosystems, EPA researchers partner with program experts; federal and state agencies; tribes; local communities; academia; nongovernmental organizations; and private stakeholders.

[44] Measure text updated from "By September 30, 2022, increase the number of research products meeting customer needs." Based on a pilot survey, 77% of products were delivered in FY 2018 that met customer needs. (Footnote updated from *FY 2018-2022 EPA Strategic Plan* published February 12, 2018.)

Over the next five years, the Agency will:

- Support safe drinking water by focusing research on assessing the distribution, composition, remediation, and health impacts of known and emerging chemical and biological contaminants.
- Improve methods for fast and efficient waterborne pathogen monitoring in recreational waters.
- Investigate health impacts from exposure to harmful algal/cyanobacteria toxins, and develop innovative methods to monitor, characterize, and predict blooms for early action.
- Support states and tribes in meeting their priorities and setting water quality and aquatic life thresholds.
- Assist states, tribes, communities, and utilities in addressing stormwater and wastewater infrastructure needs through applied modeling, technical assistance, and capture-and-reuse risk assessments.
- Provide water reuse research support on potable and non-potable use guidance for states and tribes.

Sustainable and Healthy Communities

EPA will conduct research to support regulatory activities and protocol development for the National Oil and Hazardous Substances Pollution Contingency Plan and provide on-demand technical support at cleanup sites managed by federal, state or tribal governments, as well as assistance during emergencies. The Agency conducts health, environmental engineering, and ecological research and prepares planning and analysis tools for localities nationwide to use in facilitating regulatory compliance and improving environmental and health outcomes.

Over the next five years, EPA will:

- Provide technical support to the states and tribes through technical support centers for remediating CERCLA-designated contaminated sites and returning them to productive use.
- Assist regional, state, tribal, and local leaders in reducing costs and setting science-based cleanup levels in areas designated under CERCLA.
- Characterize sites and contaminants released from leaking underground storage tanks identified under the LUST Trust Fund.
- Work with the ECOS/ERIS to evaluate the causal relationships between ecosystem goods and services and human health, and to document these relationships using EnviroAtlas.
- Assess the impact of pollution (e.g., health impact assessments) on such vulnerable groups as children, tribes, environmental justice communities, and other susceptible populations.

Chemical Safety

EPA will evaluate and predict impacts from chemical use and disposal, and provide states and tribes with information, tools, and methods to make better informed, more timely decisions about the thousands of chemicals in the United States. The Agency will produce innovative tools that accelerate the pace of data-driven evaluations, enable knowledge-based decisions that protect human health, and advance the science required to anticipate and solve problems.

Over the next five years, EPA will:

- Provide tools to more efficiently and cost-effectively evaluate the biological activity and health risks of chemicals and reduce the use of toxicity tests to animals.
- Use ToxCast/Tox21 data to develop high-throughput risk assessments, particularly for chemicals for which adequate risk assessment information has been historically unavailable.
- Develop online software tools to provide information on thousands of chemicals and integrate health, environmental, and exposure data to support regulatory and prioritization decisions.
- Explore how high-throughput exposure and hazard information can be combined to predict the potential for exposure and risk to susceptible subpopulations.
- Conduct nanoparticle research by using life-cycle analyses, evaluating impacts on ecosystem health, and supporting the development of safer nanomaterials in private industry.

Human Health Risk Assessment

EPA also will focus on the science of assessments that inform Agency, state, and tribal decisions and policies. These risk assessments provide the research and technical support needed to ensure safety of chemicals in the marketplace, revitalize and return land to communities, provide clean and safe water, and work with states and tribes to improve air quality.

Over the next five years, EPA will:

- Develop a portfolio of chemical evaluation products that use the best available science for use by EPA, states, tribes, and other federal agencies.
- Provide research and scientific support for proper TSCA implementation, as Congress intended.
- Develop assessment products, peer-reviewed toxicity values, and advanced exposure assessment tools to help inform Superfund and hazardous waste cleanups as required by RCRA and CERCLA.
- Provide scientific support to the risk and technology reviews conducted under the CAA.
- Provide integrated science assessments (ISAs) to support decisions to retain or revise the national ambient air quality standards. ISAs also inform benefit-cost and other analyses conducted by state, tribal, and local officials to support implementation of air quality management programs.
- Provide research and technical support to deliver safe drinking water by evaluating exposures to and health impacts of known and emerging chemical and biological contaminants.
- Work with states and tribes on research and development of new assessment technologies.

External Factors and Emerging Issues

EPA faces a number of challenges in its commitment to conducting robust science. For example, aging information technology infrastructure presents a risk to information security and limits the capacity for information management. Recruiting and maintaining a strong workforce with appropriate scientific and technical skillsets are also critical to EPA's research efforts.

Objective 3.4
Streamline and Modernize

Issue permits more quickly and modernize our permitting and reporting systems.

Introduction

EPA implements a host of environmental statutes that affect the regulated community. Permitting requirements under these statutes can impose a variety of costs, including direct costs and opportunity costs related to uncertainty, delay, and cancellation. Delays in the approval of permits and modifications by federal, state, or tribal permitting authorities can postpone or prevent manufacturers from building, expanding, or beginning operations, even if the affected operations ultimately may be deemed suitable as proposed. Delays can also impact construction of major infrastructure projects. EPA is committed to speeding up the processing of permits and modifications to create certainty for the business community, leading to more jobs, increased economic prosperity, and streamlined permit renewals, which incorporate up-to-date information and requirements more quickly, thereby improving environmental protection. Further, EPA will continue to convert permit applications and reports that rely on paper submissions to electronic processing in order to reduce burden, shorten the wait for approval decisions, and increase the opportunity for public transparency.

Long-Term Performance Goal

LTPG 3.4.1 By September 30, 2022, reach all permitting-related decisions within six months.[45]

Strategies for Achieving the Objective

Over the next five years, EPA will systematically collect and report permitting data for each of its permitting programs. The Agency will employ business process improvement strategies, such as Lean, to increase efficiencies in all permitting processes and meet our commitments. The Agency will also work with states and use Lean techniques to streamline the review of state-issued permits. Solutions may include conducting earlier triage and communications, conducting Agency reviews in parallel with public reviews, and/or focusing reviews where they add the most value.

EPA will consider where policy changes can improve permitting efficiency without sacrificing environmental results. Examples include expanding the scope of minor permit modifications to reduce the number of permit reviews required, reinvigorating the use of plant-wide applicability limits (PALs) to reduce unnecessary permitting transactions, and increasing states' ability to incorporate federal regulations by reference, enabling them to adjust quickly and efficiently to new regulatory provisions.

[45] Baseline and FY 2020 target will be determined in FY 2019. (No footnote in *FY 2018-2022 EPA Strategic Plan* published February 12, 2018.)

EPA will modernize permitting and reporting processes through efforts such as E-Enterprise for the Environment, a shared governance model with EPA, states, and tribes. EPA will work with states and tribes to achieve this objective without overburdening those entities with costly unnecessary reporting systems and technology. Building on efforts to date, EPA will collaborate with its partners on the following systematic process improvements:

- E-Enterprise Web Portal: A web portal that allows the states, tribes, regulated community, and EPA to transact business, such as permitting and reporting, and provides easy access to needed information.
- E-permitting: An online system to ensure the ability to apply for, track the status of, and receive a permit electronically.

External Factors and Emerging Issues

Sustainable resource levels for states, tribes, and EPA are critical to efforts to streamline and modernize permitting processes. Support from states and tribes, including state and tribal capacity for maintaining and increasing delegation, is also critical to streamlining and modernizing permitting processes. The global shift to digital services for communication and transaction raises expectations of EPA stakeholders and provides more robust approaches and technologies for developing electronic services.

EPA will modernize permitting and reporting processes through efforts such as E-Enterprise for the Environment, a shared governance model with EPA, states, and tribes.

Objective 3.5
Improve Efficiency and Effectiveness

Provide proper leadership and internal operations management to ensure that the Agency is fulfilling its mission.

Introduction

To support its mission to protect human health and the environment, EPA will improve the efficiency and effectiveness of its business processes. Focus areas will include financial, facility, human resource, contract, grant, and information technology/information management. EPA will improve its future workforce, modernize and streamline its business practices, and take advantage of new collaborative and cost-effective tools and technologies. The Agency will build a modern and secure work environment that will protect critical information and support its efforts to address the environmental problems of the 21st century. EPA will work to alleviate challenges associated with outdated or non-existent policies, tension between centralized and decentralized approaches, myriad federal acquisition and grants requirements, complex processes, and fluctuating levels of expertise across Agency programs.

Long-Term Performance Goals

LTPG 3.5.1 By September 30, 2022, reduce unused office and warehouse space by 850,641 sq. feet.[46]

LTPG 3.5.2 By September 30, 2022, reduce procurement processing times by achieving 100% of procurement action lead times (PALT).[47]

LTPG 3.5.3 By September 30, 2022, improve 250 operational processes.

LTPG 3.5.4 By September 30, 2022, increase enterprise adoption of shared services by four.[48]

[46] Baseline is 5,264,846 square feet as of FY 2017.
[47] Baseline, as of September 30, 2018 is 77% for all contract actions awarded within PALT. (Footnote updated from *FY 2018-2022 EPA Strategic Plan* published February 12, 2018.)
[48] Baseline is 5 administrative systems/operations shared services in FY 2017.

Strategies for Achieving the Objective

EPA will modernize and improve business processes and operations to promote transparency, efficiency, and effectiveness; enhance collaborative, results-driven partnerships with internal and external business partners; recruit, develop, and maintain a highly-skilled, diverse, and engaged workforce; and improve the capabilities and cost-effectiveness of its information technology (IT) and information management (IM) systems.

EPA will apply Lean principles and will leverage input from customer-focused councils, advisory groups, surveys, workgroups, acquisition partnership initiatives, technical user groups, portfolio reviews, and federal advisory committees to identify business process streamlining opportunities. To improve the efficiency and cost effectiveness of its operations, EPA will standardize and streamline internal business processes in its acquisition and grants processes and systems, and use additional federal and/or internal shared services when supported by business case analysis.

EPA will ensure its workforce is positioned to accomplish the Agency's mission effectively by providing access to quality training and development opportunities that will improve staff's and managers' skills, knowledge, and performance, and prepare them to capitalize on opportunities that advance progress. EPA will improve its workforce planning and management, strengthen its Senior Executive Service, and focus on developing and maintaining a highly-skilled technical workforce.

EPA also will transform and modernize its information systems, tools, and processes to improve how the Agency collaborates both internally and with external stakeholders. EPA will enhance the power of information by delivering on-demand data to the right people at the right time. To enable the Agency, its partners, and the public effectively to acquire, generate, manage, use, and share information–a critical resource in protecting human health and the environment–EPA will improve its IT/IM capabilities and customer experiences. EPA will employ enterprise risk management and financial data analytics to support data management decision making, using the enterprise risk management framework mandated by OMB Circular A-123.

To ensure that critical environmental and human health information is adequately protected, EPA will strengthen its cybersecurity posture. The Agency will focus on implementing two key cybersecurity priorities–the mandated federal-government-wide Continuous Diagnostics and Mitigation (CDM) effort, and the complementary EPA-specific Cyber Risk Mitigation Projects (CRMPs). These two priorities introduce or improve upon dozens of cybersecurity capabilities, enhance the Agency's ability to respond to threats, and improve EPA's privacy posture via the Privacy Act of 1974. EPA will work closely with the Department of Homeland Security and other partners in implementing CDM capabilities.

To better understand complex interactions between pollutants and the environment and address the environmental problems of the 21st century effectively and efficiently, EPA and its partners analyze large volumes of data. EPA will develop a comprehensive data management strategy that addresses the collection, management, and use of data generated both internally and from external partners including states, tribes, grantees, the regulated community, and citizen science. The Agency will deploy new data analysis, data visualization, and geospatial tools in a Cloud-based framework to enable analysis and provide the basis for informed decision making.

Environmental decision making across media programs requires access to high-quality data and analytics. EPA will build shared IT services, maximizing the benefits of our investments and ensuring consistency and scalability in tools and services. Over the next five years, EPA programs that receive submissions from outside the Agency, whether from the reporting community, states, tribes, or local governments, will rely increasingly on centrally-developed and maintained information services, decreasing the volume of computer code each program must develop and maintain. Shared services will reduce reporting burden for submitting entities and improve data quality for EPA. EPA programs, states, and tribes must establish a common catalog of shared services and agree to a minimum set of common standards and practices.

The Agency will enhance its extensive information resources by designing an enterprise-wide information architecture that will facilitate the electronic management of data and information, as well as multimodal access, effective searching, and ease of use. The Agency's future information management architecture will support official recordkeeping requirements, as well as daily document management, business processes, information access, and legal needs of EPA employees and organizations, while also being flexible, scalable, and cost effective.

External Factors and Emerging Issues

EPA faces a number of factors that may impede its ability to promote effective and efficient internal operations. The Agency's ability to attract and retain staff skilled in human resources, IT/IM, cybersecurity, and acquisition management and staff with scientific and technical expertise is a continuing challenge in improving Agency operations. A lack of category-focused skills and business acumen can negatively affect strategic sourcing decisions. Myriad federal acquisition and grant requirements, complex processes, and varying levels of expertise across Agency programs often prevent the timely awarding of contract and grant vehicles to meet Agency demands. EPA must increase its competencies in these areas through a robust training program for staff and managers.

Without standard business processes, EPA cannot achieve its objectives. For example, tension between local needs and Agency-wide strategies may result in missed opportunities to make effective strategic sourcing decisions. This not only impedes Agency efforts to modernize business processes and streamline IT infrastructure, but also affects the ability of government shared service providers to serve additional customers and use standard software to achieve efficiencies and cost savings. Furthermore, continually changing IT/IM and security requirements and variation among states and tribes require development of a holistic "Enterprise-Level Vision and Data Strategy" that optimizes both business processes and solutions; aligns all data programs, resources, and budgets; and strengthens the Agency's enterprise risk strategies. Demands for IT/IM services will continue to grow, due to the increasing volume of environmental data and increased expectations of other agencies, regulated entities, the public, and EPA staff. As cybersecurity risks evolve, protecting EPA's information assets will continue to be a priority.

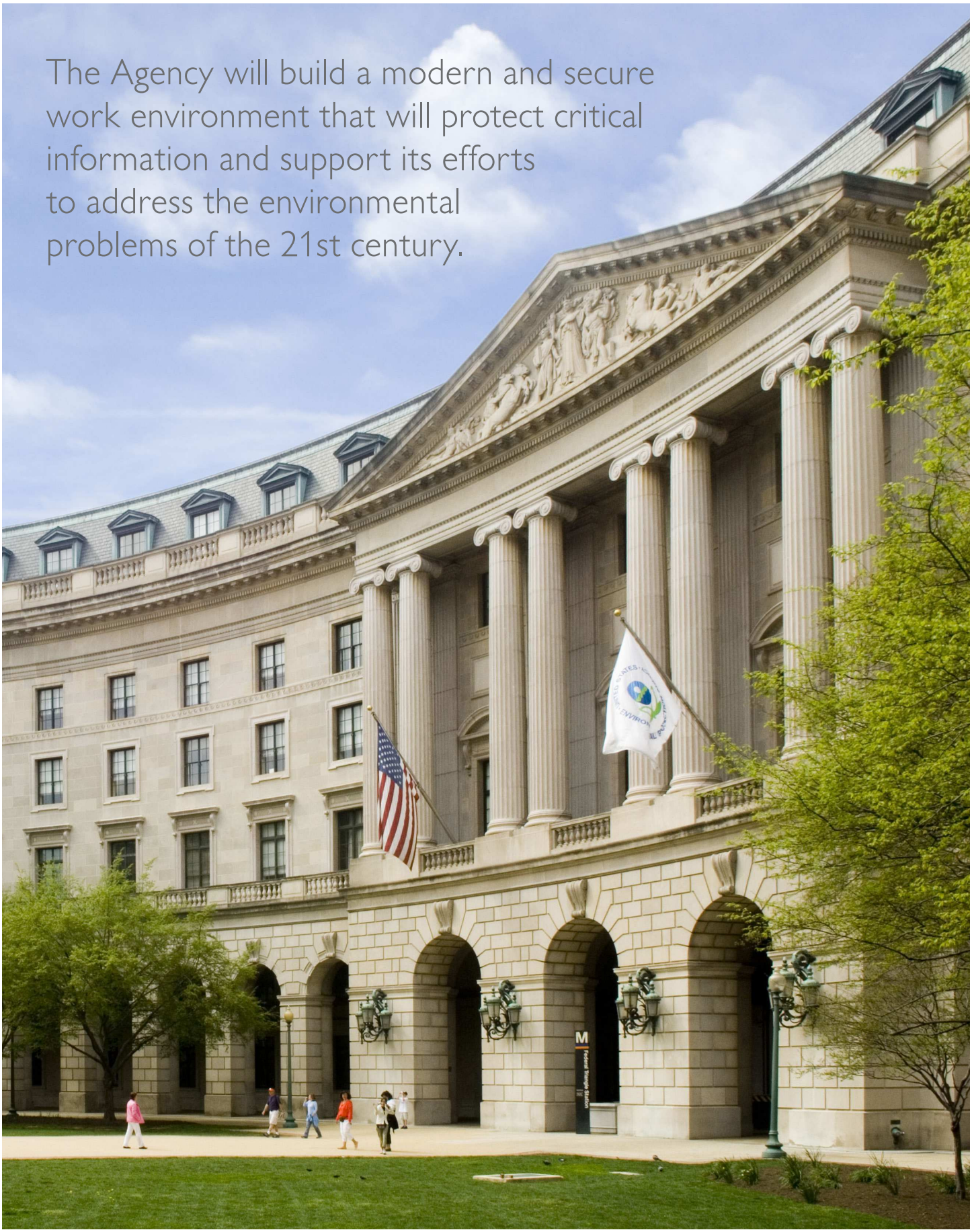
The Agency will build a modern and secure work environment that will protect critical information and support its efforts to address the environmental problems of the 21st century.

photos:	cover/back	Nate McMichael - Chugach State Park, Alaska
	inside cover	EPA Staff Submission - Washington, DC Metro Area
	page 6	David Iacono - Lewes, Delaware
	page 21	Eric Vance - Pesticide Application
	page 24	Eric Vance - Meeting
	page 32	Eric Vance - Gully Branch Tree Farm - Cochran, Georgia
	page 34	Eric Vance - Washington Monument
	page 40-41	Paymon Danesh - Glacier National Park, Montana
	page 51	Eric Vance - Ariel Rios Building, EPA HQ

Office of the Chief Financial Officer
Office of Planning, Analysis, and Accountability (2721A)

United States Environmental Protection Agency
1200 Pennsylvania Avenue, NW
Washington, DC 20460

www.epa.gov/planandbudget/strategicplan

EPA-190-R-18-003

February 2018 (Updated: September 2019)

EPA 601K20002 March 2020 www.epa.gov/research

United States
Environmental Protection
Agency

Homeland Security

STRATEGIC RESEARCH ACTION PLAN
2019-2022

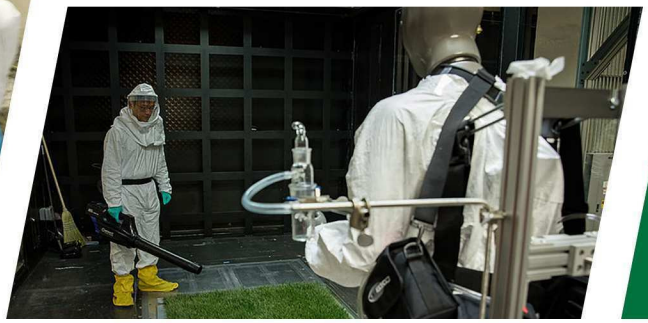

Office of Research and Development
Homeland Security

Homeland Security

National Research Program

Strategic Research Action Plan

2019 – 2022

Table of Contents

LIST OF ACRONYMS ..... **III**

EXECUTIVE SUMMARY **1**

INTRODUCTION **2**

Research to Support the EPA Strategic Plan 3

Statutory and Policy Context 3

ENVIRONMENTAL PROBLEMS AND PROGRAM PURPOSE **4**

Problem Statement 7

Program Vision 7

Program Objectives 7

RESEARCH TOPICS **7**

Topic 1: Contaminant Characterization and Consequence Assessment 8

Topic 2: Environmental Cleanup and Infrastructure Remediation 13

Topic 3: Systems Approaches to Preparedness and Response 23

PROGRAM DESIGN **24**

Program Components 25

Solutions-Driven Research 26

EPA Partner and Stakeholder Involvement 26

ANTICIPATED RESEARCH ACCOMPLISHMENTS AND PROJECTED IMPACTS **28**

CONCLUSION **29**

REFERENCES **30**

APPENDICES **31**

Appendix 1: Summary Table of Proposed Outputs for Homeland Security Research Program (FY2019 - 2022) 31

Appendix 2: Homeland Security Research Program Supports Decisions Mandated by Legislation and Executive Actions 37

List of Acronyms

ASTHO	Association of State and Territorial Health Officials
ASTWMO	Association of State and Territorial Waste Management Officials
CAA	Clean Air Act
CBRN	Chemical, biological, radiological, and nuclear
CERCLA	Comprehensive Environmental Response, Compensation, and Liability Act
CIPAC	Critical Infrastructure Protection Advisory Committee
CONOPS	Concept of operations
CSS	Chemical Safety for Sustainability
CWA	Clean Water Act
HHS	U.S. Department of Health and Human Services
DHS	U.S. Department of Homeland Security
DOD	U.S. Department of Defense
DPAS	Decontamination Preparedness and Assessment Strategy
DWH	Deepwater Horizon
EO	Executive Order
EPA	U.S. Environmental Protection Agency
EPCRA	Emergency Planning and Community Right-to-Know Act
ERLN	Environmental Response Laboratory Network
ESAM	Environmental Sampling and Analytical Methods
ESF	Emergency Support Function
FAD	Foreign animal diseases
FIFRA	Federal Insecticide, Fungicide, and Rodenticide Act
FSMA	Food Safety Modernization Act
HERA	Health and Environmental Risk Assessment
HSA	Homeland Security Act
HSPD	Homeland Security Presidential Directive
HSRP	Homeland Security Research Program
ICCOPR	Interagency Coordinating Committee for Oil Pollution Research
IMO	International Maritime Organization
NCP	National Contingency Plan
NCPPS	National Contingency Plan Product Schedule
NDRF	National Disaster Recovery Framework
NEBA	Net Environmental Benefit Analysis
NEMA	National Emergency Management Association
NOAA	National Oceanic and Atmospheric Administration
NRDA	Natural Resource Damage Assessment
NRF	National Response Framework
NRP	National Response Plan
NRT	National Response Team
NSPM	National Security Presidential Memorandum
NSTC	(White House) National Science and Technology Council
OAR	U.S. EPA Office of Air and Radiation
OCSPP	U.S. EPA Office of Chemical Safety and Pollution Prevention
OECA	U.S. EPA Office of Enforcement and Compliance

OEM	U.S. EPA Office of Emergency Management
OLEM	U.S. EPA Office of Land and Emergency Management
OPA	Oil Pollution Act
ORCR	U.S. EPA Office of Resource Conservation and Recovery
ORD	U.S. EPA Office of Research and Development
OW	U.S. EPA Office of Water
OWM	U.S. EPA Office of Waste Management
PAL	Provisional Advisory Level
PFAS	Per- and polyfluorinated alkyl substance
PFOA	Perfluorooctanoic acid
PPD	Presidential Policy Directive
RCRA	Resource Conservation and Recovery Act
R&T	Research and Technology
SBIR	Small Business Innovation Research
SDWA	Safe Drinking Water Act
SHC	Sustainable and Healthy Communities
SSWR	Safe and Sustainable Water Resources
S&T	Science and technology
StRAP	Strategic Research Action Plan
USDA	U.S. Department of Agriculture
WCIT	Water Containment Information Tool
WLA	Water Laboratory Alliance
WSD	U.S. EPA Water Security Division
WSTB	Water Security Test Bed

Executive Summary

Caused naturally or by humans, environmental emergencies continue to challenge our nation. The use of chemical threats in Syria and the United Kingdom, the opioid epidemic, and several recent water system contamination incidents that affected hundreds of thousands of people, remind us of the impact that chemical contaminants can have on public health. Further, the radiological contamination following the Fukushima Daiichi nuclear disaster in 2011 demonstrated the significant impact and challenge of cleaning up large-scale contamination incidents. Smaller-scale incidents, such as the attempted ricin poisonings in several communities around the country, also highlight the ever-present threat of terrorism post 2001.

The U.S. Environmental Protection Agency (EPA) is responsible for helping communities prepare for and recover from disasters that result in threats to public health and the environment. The Office of Research and Development's (ORD) Homeland Security Research Program (HSRP) aims to increase the United States' capabilities to prepare for and respond to releases of oil and hazardous substances into the environment, as mandated by Congress. The hazardous substances involved can include chemical, radiological, nuclear, and biological materials. There are considerable gaps in our capabilities to address these risks, including understanding the behavior of contaminants when released into the environment, potential public exposures, determining where contamination is present that may pose an exposure risk, and cleaning up contaminated areas and infrastructure. Enhancing capabilities for response and remediation of contaminated areas and protecting water systems will improve our nation's resilience to environmental catastrophes.

The *Homeland Security Strategic Research Action Plan (StRAP)*, 2019-2022, is a four-year research strategy designed to achieve the following objectives: advance EPA's capabilities and those of our state, tribal, and local partners to respond to and recover from wide-area contamination incidents; and, improve the ability of water utilities to prevent, prepare for, respond to, and recover from water contamination incidents that threaten public health.

EPA's HSRP is organized into three topics supporting these objectives: (1) contaminant characterization and consequence assessment; (2) environmental cleanup and infrastructure remediation; and (3) systems approaches to preparedness and response. Short- and long-term goals accomplished through research areas within these topics outline a strategy for addressing the objectives.

HSRP performs applied research that delivers relevant and timely methods, tools, data, technologies, and technical expertise in support of federal, regional, state, tribal, water system, and local community resilience. HSRP engages partners throughout the research life-cycle to ensure their needs are being met – from identifying scientific capability gaps, to performing research to address those gaps, to formulating and delivering timely and reliable products that fill those gaps, to transitioning and implementing the products via collaborative field studies and exercises. HSRP products provide systems-based approaches to site characterization, risk assessment, and remediation (which includes waste management) to address large-scale contaminated areas and water systems. Federal, state, tribal, and local decision makers will have access to the information and tools they need to prepare for and recover from catastrophes involving environmental contamination incidents that threaten public health.

Introduction

The Homeland Security Strategic Research Action Plan (StRAP) for 2019-2022 is a four-year strategy to deliver research necessary to support the Environmental Protection Agency's (EPA) overall mission to protect human health and the environment, fulfill the EPA's legislative mandates, and advance cross-agency priorities identified in the FY2018-FY2022 EPA Strategic Plan (U.S. EPA, 2018a). This StRAP outlines how EPA's Office of Research and Development's (ORD) Homeland Security Research Program (HSRP) aims to meet the homeland security science needs of the EPA partners and stakeholders. EPA partners include EPA program and regional offices, federal agencies, and state and tribal governments supporting the protection of human health and the environment; stakeholders include local governments, non-governmental organizations, private industries, academic institutions, and others with an interest or investment in public and environmental health.

The Homeland Security StRAP is one of six research plans, one for each of EPA's national research programs in ORD. The six research programs are:

- Air and Energy (A-E)
- Chemical Safety for Sustainability (CSS)
- Homeland Security Research Program (HSRP)
- Health and Environmental Risk Assessment (HERA)
- Safe and Sustainable Water Resources (SSWR)
- Sustainable and Healthy Communities (SHC)

EPA's six strategic research action plans lay the foundation for EPA's research programs to provide focused research that meets the Agency's legislative mandates and the goals outlined in the EPA and ORD Strategic Plans (U.S. EPA, 2018a, 2018c). The StRAPs are designed to guide an ambitious research portfolio that delivers the science and engineering solutions EPA needs to meet its goals now and into the future, while also cultivating an efficient, innovative, and responsive research enterprise.

HSRP addresses science gaps related to remediation of environmental contamination that threatens public health and welfare, as well as science gaps related to environmental quality before, during, and after a disaster. HSRP helps EPA carry out its homeland security and emergency response mission by working closely with its partners to understand the potential threats and consequences of hazardous substance release. HSRP works in coordination with its partners and stakeholders to conduct research that gives decision makers the information they need for their communities and environments to rapidly recover after a disaster.

HSRP's general research approach is to adapt suitable methodologies that have proven effectiveness in a laboratory setting for success in real-world settings. Real-world settings can be challenging because affected environments are not pristine; grime and biofilms complicate the behaviors of sampling and cleanup technologies, thereby affecting responders' ability to sample and remediate sites. Furthermore, some response activities and decisions may occur in sequence where such activities are coupled to, or are dependent on, other response activities and decisions. Human behavior is not always predictable, stakeholder relationships must be negotiated, and risks can be difficult to communicate. HSRP develops information and tools for cleanup, waste management, characterization and assessment of hazards, and application of the latest information in decision-making.

Research to Support the EPA Strategic Plan

The FY2018-FY2022 EPA Strategic Plan is designed to implement the Administrator's priorities for the next five years. This Strategic Plan identifies three overarching strategic goals: 1) A Cleaner, Healthier Environment, 2) More Effective Partnerships, and 3) Greater Certainty, Compliance, and Effectiveness. EPA's research programs are aligned to the Strategic Plan and designed to ensure that the Agency successfully meets the goals and objectives articulated in the Strategic Plan.

The first goal emphasizes EPA's mission of providing a Cleaner, Healthier Environment by improving air quality, providing clean and safe water, revitalizing land and preventing contamination, and ensuring chemical safety. HSRP directly supports this mission through its applied research in response and remediation, a critical component of building resilience.

The second goal of EPA's Strategic Plan is More Effective Partnerships, which enhances shared accountability and increases transparency and public participation for states and tribes.
HSRP works with EPA regional offices to support state and tribal needs and continues to strengthen its direct relationship with states and tribes through partnerships with national associations such as the Environmental Council of the States (ECOS) and the Environmental Research Institute of the States (ERIS), National Environmental Health Association (NEHA) and the Association of State and Territorial Health Officials (ASTHO), the Association of State and Territorial Waste Management Officials (ASTWMO) and the National Emergency Management Association (NEMA).

Greater Certainty, Compliance, and Effectiveness is the final goal of EPA's Strategic Plan. This goal includes the specific objective to prioritize robust science. HSRP helps achieve this by conducting research and providing EPA programs and regions with the scientific support they need to develop innovative solutions to environmental challenges.

Statutory and Policy Context

Since the attacks of September 11, 2001 on the United States, the nation's homeland security enterprise was reconstructed, ultimately leading to better national protection from both natural and anthropogenic disasters. Several statutes give EPA the authority and obligation to respond to emergencies, such as oil spills, and to develop research that would improve hazardous material removal actions primarily through the Comprehensive Environmental Response, Compensation, and Liability Act (CERCLA), Clean Water Act (CWA), and Safe Drinking Water Act (SDWA). The Public Health Security and Bioterrorism Preparedness and Response Act required EPA and its partners to help water utilities conduct vulnerability assessments and develop emergency response plans (U.S. EPA, 2018d).

In addition to statutory authorities, the federal government has established many policies through Presidential Directives and National Frameworks that outline EPA's responsibilities with respect to emergencies including acts of terrorism. For example, Homeland Presidential Directive (HSPD) 7[1] helped define federal government roles and responsibilities within the homeland security enterprise for U.S. critical infrastructure, designating EPA as the lead for drinking water and water treatment systems. The National Response Framework (NRF) assigns EPA as the lead agency to take "appropriate actions to prepare for and respond to a threat to public health, welfare, or the environment caused by actual or

[1] HSPD 7 was revoked by Presidential Policy Directive (PPD) 21, which states all plans developed pursuant to HSPD 7 remain in effect until specifically revoked or superseded.

potential oil and hazardous materials incidents… [including those involving] … chemical, biological, radiological, and nuclear substances, whether accidentally or intentionally released."

An extensive listing of statutes and policies that influence EPA's homeland security research is provided in Appendix 2.

Environmental Problems and Program Purpose

In 2001, a few grams of *Bacillus anthracis* (*B. anthracis)* spores (the causative agent for the bacterial disease anthrax) mailed through the U.S. Postal Service resulted in the contamination of several postal facilities and public and private buildings. EPA was tasked to support the cleanup of numerous facilities, facing many challenges. At the time, there were no methods to determine which facilities were contaminated, no capabilities for cleaning up contaminated areas, no means to manage waste generated from cleanup activities, and the government did not fully understand the risk to workers and the public. The ultimate development and adaptation of methods for sampling, analysis, cleanup, waste management, and risk assessment were created on a site-by-site basis and resulted in cleanup efforts taking years and costing taxpayers hundreds of millions of dollars.

The resulting exposure of workers and the public, including five deaths attributed to inhalation of *B. anthracis* spores, made bioterrorism a reality in the United States. The reality of bioterrorism also highlighted the possibility of an ever-growing list of other potential threats (including biological, chemical, and radiological contaminants) being released in urban/suburban environments and the intentional contamination of water systems.

EPA and other federal agencies have invested considerable effort since the incidents in 2001 to build the nation's capabilities. Incremental advances have been made and standardized in: (1) early warning for biological threat release; (2) sampling and analysis methods for indoor areas; (3) cleanup methods for facilities; (4) waste management approaches; and (5) biological risk assessment methodologies. However, the United States continues to lack the full capability and capacity to effectively address large, wide-spread contamination incidents the size of, for example, lower Manhattan, or Washington D.C.'s drinking water distribution system.

The scenarios that challenge our current capabilities are real threats. The 2011 Fukushima nuclear power plant disaster resulted in immense impacts to the public, environment, and the economy of Japan, further exacerbated by the lack of tools and technologies to address the challenge of large and complex environmental cleanup in an area the size of Maryland. The international Ebola outbreak in 2014 demonstrated the challenges of environmental decontamination to stop the spread of disease and manage voluminous biological wastes resulting from cleanup actions and health care delivery. The few Ebola cases in the United States were enough to spotlight the challenges that would be faced in a wide-spread biological incident. A relatively mild accident like the backflow of a dilute industrial chemical into Corpus Christi's distribution system in 2017 caused a ban on water use for much of the city's 300,000 residents for approximately 4 days, causing mass disruption to daily life and huge economic costs. A major incident, such as a highly toxic chemical warfare agent attack on a water system, would likely result in much greater impacts. Chemical warfare agents have been used multiple times recently in the Syrian civil war and in the United Kingdom, highlighting the threat and impact if used in the United States. Natural threats also continue, such as Hurricane Maria damaging much of Puerto Rico's drinking water systems, leading to a lack of safe water and increased waterborne disease incidents.

A disaster that results in wide-spread chemical, biological, radiological, and nuclear (CBRN) contamination over a large outdoor area, or throughout a water and wastewater system, presents a daunting challenge to EPA, state, tribal and local responders in carrying out their responsibilities. Once released into the environment, contaminants can spread via natural forces and human activities. The potential for cross-media spread of contamination is depicted in Figure 1 and represents a sample of the complex scenario that large-scale contamination incidents present to communities.

Figure 1: Schematic Overview of a Wide-Area and Water-System Contamination Incident for Scenario-Based Resilience Planning

Drinking water systems can become contaminated by several mechanisms causing direct threats to public health. Distribution systems can become contaminated when source water becomes polluted to such an extent that treatment plants cannot remove the contamiatnion. Such source water contamination can result from releases by industrial sources caused by accidents or natural disasters. Distrubtion systems can be directly contaminated by industiral accidents, pipe breaks, or intentionally.

There is also considerable uncertainy in the effectiveness of sampling methods and strategies to characterize wide-spread contamination, in decontamination methods to reduce or eliminate contamination in complex urban environments, and in the ability to manage the vast amount of waste that could be generated. Current methods used in previous, smaller-scale CBRN incidents are not readily suitable for deployment over large areas. The dynamic nature of the contaminant within the environment, coupled with the lack of readily-available tools, lead to considerable challenges in ensuring communities are resilient to disasters. The United States needs remediation methods that are rapidly deployable and scalable, with documented effectiveness. With readily-available approaches repurposed

from other sectors, responders can adapt methods to address different-sized incidents and unanticipated challenges within finite budget and time contraints.

As a real-world example, consider the release of asbestos-containing ash from a warehouse fire in 2017 that caused wide-area asbestos contamination of North Portland, Oregon. Asbestos-containing debris was thought to have spread as far as two miles on each side of the Willamette River. EPA provided support to the Oregon Department of Environmental Quality to clean up debris and assess the potential for public exposure. This incident presented the challenge of determining where asbestos fibers might have settled over a 13-square mile area and raised concerns for suspended particle (dust) transfer of asbestos into residences. Researchers and responders had to address many questions, such as how to determine which areas were contaminated (both indoors and outdoors); what type of sampling was both effective and technically feasible over the potentially contaminated, large area; and the impact of wind, rain, and human activity on the redistribution of asbestos and, hence, the value of sampling results from a previous day. This incident provided a vivid example of the challenges that would be faced if CBRN contaminants were spread over an urban area.

Science to support response decisions prior to and during a disaster should consider long-term recovery. The decisions and priorities set by an impacted community prior to a disaster (prevention and protection pillars in the National Disaster Recovery Framework (NDRF)) and during the mitigation and response phase of a disaster have a cascading effect on the overall recovery (U.S. DHS, 2016). The importance of community engagement highlights the need to understand the social-environmental system interactions as scienitific solutions to mitigation and response are developed. Contaminant movement, exposure, and human susceptibility are affected by social, as well as environmental systems. So too are decontamination actions and outcomes.

Considering the general widespread contamination scenario discussed above, HSRP focuses on supporting community resilience to disasters by supporting decision makers in addressing questions such as:

- What tools and strategies are available for sampling wide areas or water systems to determine the extent of the contamination?
- How can movement of contaminants in the environment be predicted, monitored, or suppressed in support of sampling, cleanup, and public health decisions?
- How can detection, surveying, monitoring, and sampling information be used to guide public health decisions, including mitigating human exposure potential?
- How can wide areas and water systems be rapidly and safely cleaned up and returned to normalcy?
- How can water systems be protected against contamination incidents?

This StRAP outlines priority research efforts for 2019-2022 intended to address the current highest priority needs with respect to EPA's Homeland Security responsibilities. HSRP also undertakes a systematic examination of potential threats and opportunities (i.e., horizon scanning) to identify scientific challenges that may rise in importance from emerging technologies. For example, recently-developed genome editing technologies are poised to revolutionize the use of biotechnology to benefit mankind. Yet, these technologies could also result in unintended consequences for public health and the environment or be used to develop novel threat agents. Demonstrated by the recent outbreaks of the Ebola, Zika, and avian flu viruses, we should expect unanticipated disease outbreaks to continue to

challenge public and animal health and the environment. The increasing capability of computational approaches will revolutionize the prediction of scientific properties (e.g., chemistry, toxicology), enhance decision-support tools, and help manage environmental systems (e.g., monitor whole watersheds, including water distribution systems). However, as such advances become more affordable/accessible, they could have unintended consequences, accentuating the importance of understanding how such effects could be detected and minimized. Finally, recent uses of chemical warfare agents in Syria and the United Kingdom warn of an increased use of these agents that can have impact beyond the intended targets.

HSRP serves as a foundation for anticipating and communicating scientific issues of which EPA and other stakeholders must be aware, and for ensuring that the research designed to address high priority needs related to existing threats can also support response to all hazards (anticipated and unforeseen).

Problem Statement

Disasters often result in contamination that can threaten public health and the environment. The United States is regularly affected by natural disasters, industrial accidents, and has been the target of intentional contamination incidents with a growing list of chemical, biological, and radiological agents. When scientifically-sound information is not readily available for the potential array of low-probability, high-consequence threats, communities cannot be resilient to these acute, environmental catastrophes.

Program Vision

Federal, state, tribal, and local decision makers have timely access to information and the tools they need to ensure community resilience to catastrophes involving environmental contamination that threatens public health and welfare.

Program Objectives

The HSRP StRAP is focused on addressing two primary research objectives. One primary research objective is to advance EPA capabilities to respond to wide-area contamination incidents. Terrorist-related incidents or natural disasters can result in wide-area contamination with hazardous materials, including oil spills or CBRN agents or materials. Wide-area contamination includes contamination of the built environment (both inside and outside of buildings and semi-enclosed infrastructures such as subways or arenas) and the natural environment. EPA needs effective and affordable cleanup strategies and methods so that affected communities can successfully and rapidly recover.

The second objective is to improve the ability of water utilities to prevent, prepare for, and respond to water contamination that threatens public health. Disasters, anthropogenic or naturally occurring, can impact the ability of water and wastewater utilities to function, including the potential disruption of drinking water supplies to municipalities. To support disaster preparedness, HSRP develops modeling tools that aid the design and operation of water and wastewater systems in a way that decreases their vulnerability to disasters. HSRP has developed tools, technologies, and data to support post-incident responses.

Research Topics

The research to address HSRP partner needs is organized into seven research areas that are categorically under three research topic areas (see Table 1). The research topics depict the research program design at higher level of organization. The research areas are more descriptive of the program; the research areas align with EPA's response decisions supporting recovery under the NRF, specifically with respect to

EPA's lead role under Emergency Support Function #10 - Oil and Hazardous Materials Response Annex (ESF-10). This general mapping of the ESF-10 response decisions (or planning categories) is also shown in Table 1 alongside the corresponding research topics and research areas. It is recognized that these response decisions are highly interdependent, one decision impacting other decisions. Thus, the research areas are designed to reflect and support this interdependent system of activities through coordination across the program in support of the HSRP's two primary objectives.

Table 1: List of Topics and Research Areas in HSRP

<table>
<tr><th colspan="2">HSRP Research Topics and Area</th><th>ESF-10 Response/Planning Categories</th></tr>
<tr><td>Research Topic 1</td><td>Contaminant characterization and consequence assessment</td><td rowspan="3">• Mitigation of Drinking Water and Waste Water Treatment Plant Operation
• Mitigation of Critical Infrastructure Operation
• Sampling, Monitoring, and Measurements</td></tr>
<tr><td rowspan="2">Research Areas</td><td>Contaminant Fate, Transport, and Exposure</td></tr>
<tr><td>Contaminant Detection/Environmental Sampling and Analysis</td></tr>
<tr><td>Research Topic 2</td><td>Environmental cleanup and infrastructure remediation</td><td rowspan="5">• Environmental Cleanup
• Treatment of Decontamination Water and Contaminated Water
• Waste Management</td></tr>
<tr><td rowspan="4">Research Areas</td><td>Wide-Area Decontamination</td></tr>
<tr><td>Water Treatment and Infrastructure Decontamination</td></tr>
<tr><td>Oil Spill Response</td></tr>
<tr><td>Waste Management</td></tr>
<tr><td>Research Topic 3</td><td>System approaches to preparedness and response</td><td rowspan="2">• Environmental Cleanup Sequencing
• ESF-10 Operations
• Cost Considerations</td></tr>
<tr><td>Research Areas</td><td>Tools to Support Systems-based Decision-Making</td></tr>
</table>

Topic 1: Contaminant Characterization and Consequence Assessment

Effective contaminant characterization provides for understanding the extent and nature of the environmental contamination. Information on contaminant characterization coupled with an understanding of exposure potential can be used to inform the potential consequences of the contamination on public health. Following a CBRN incident or oil spill, EPA may support or lead site characterization and remediation of contaminated water systems and wide areas. Additional characterization of the site may be required during cleanup operations to assess progress and determine waste streams, and to inform site re-occupancy and reuse decisions (sometimes referred to as clearance decisions). EPA's Office of Land and Emergency Management (OLEM) founded the EPA Environmental Response Laboratory Network (ERLN)[2], including the Water Laboratory Alliance (WLA)[3], to establish the capability and capacity for analyzing environmental samples for site characterization, clearance sampling, and remediation after national-scale incidents.

Remediation decisions are made to reduce the risk related to exposure to environmental contamination. However, using environmental characterization data in a risk assessment is not straightforward,

[2] https://www.epa.gov/emergency-response/environmental-response-laboratory-network
[3] https://www.epa.gov/waterlabnetwork

particularly for microbial contamination, due to the uncertainty and variability in the field data as well as uncertainty in how to estimate exposure to the contaminant in the environment. For effective response and remediation, decision makers must have capabilities to rapidly detect contamination, to determine the extent of the contamination, to understand the behavior of the contaminant in the environment, and to assess the impact of the contaminated environment on public health. Many decisions makers may not have ready access to such capabilities.

The research under this topic is planned and executed under two research areas. The first research area addresses how contaminants behave in water systems and the built and natural environment, including the development of capabilities to support decision makers in their assessment of the threat that the contamination poses to public health. The second research area is focused on developing contaminant detection, environmental sampling, and analytical capabilities. Combined, these two research areas provide essential information to support environmental response and remediation decision-making to protect public health and the environment.

Research Area 1: Contaminant Fate, Transport, and Exposure

Knowledge of the persistence, movement, and associated phenomena is closely linked to understanding the risk of exposure and informing the development of sampling, decontamination, and waste management strategies. During the Gotham Shield[4] exercise, impacted state and local decision makers sought information from EPA on the impact of impending rain on their response actions.

Exposure assessment information and models, including understanding the ability of a contaminant released into the environment to continue to pose an exposure threat, can inform public health and cleanup decisions. The persistence of a chemical or biological agent depends on environmental conditions (e.g., temperature, relative humidity, sunlight, etc.) and the material in or on which the chemical or biological agent is bound. For some contaminants, natural attenuation (where naturally-occurring degradation processes are used to reduce the concentration and subsequent exposure) is a viable cleanup option under some circumstances. The impacts of wind and precipitation events, and their ability to move contaminants within an outdoor area, may have a profound impact on subsequent public health risk and the ability of responders to contain and mitigate the contamination. These incidents can also spread contamination into venues that were previously uncontaminated, including storm and sewer collection systems, as well as drinking water sources.

The unintentional or intentional introduction of harmful contaminants into drinking water distribution systems can affect a relatively large area, and can impact the storage tanks, pipes, and pumps used in water distribution systems, service connections to buildings, and water-consuming appliances such as water heaters. Fate and transport information informs actions such as decontamination of water infrastructure, allowing reuse of the system. Additionally, to inform where physical security or other measures are needed to reduce vulnerability of water systems, information and models can help assess the consequences resulting from exposures to CBRN contaminants.

[4] Operation Gotham Shield was an exercise conducted by FEMA in 2017 testing civil response capabilities to a nuclear weapons attack in the New York City area.

This research area focuses on identifying and quantifying issues related to movement and persistence of contaminants over wide areas and in water and wastewater systems. Research is conducted at the bench- and pilot-scale to understand fate and transport, which will inform decisions regarding sampling, decontamination, waste management, and operational countermeasures. This research area also focuses on assessing exposure to contaminants, for example, through understanding the implications of the sampling results.

Program, regional, state, and/or tribal needs

The needs and corresponding research generally fall into the following categories:

- Persistence of contaminants in and on different types of infrastructure
- Movement of contaminants within and between different types of infrastructure
- Understanding how movement and persistence of contaminants can affect sampling strategies, decontamination, and risk assessment

An example of an output under this research area is a synthesis of information on the fate and persistence of radiological agents on surfaces, which will inform sampling and remediation decisions (Appendix 1, Output HS.1.5056). Research in this area, such as understanding the transport of *B. anthracis* spores will feed into outputs developed under other research areas (e.g., informing vehicle decontamination by understanding fate of contaminants within vehicles passing through contaminated areas) (Appendix 1, Output HS.3.5002). Figure 2 shows an example of research in the aerosol wind tunnel in EPA's facility in Research Triangle Park, NC to assess the re-aerosolization and spread of *B. anthracis* surrogate spores due to human activity, including responders' activities.

For water systems, it's critical to understand how contaminants may adhere to corrosion products or biofilms on pipe walls, which could prolong contamination by desorption, leaching, or otherwise detaching from the pipe surface and into the water over time. Contamination could also impact drinking water treatment plants, wastewater treatment facilities, and storm and sewer collection systems. To better understand the behavior of contaminants in water infrastructure, this research area develops innovative processes for prediction of the fate and transport. Researchers examine the fate and transport of contaminants in drinking water and wastewater systems at bench, pilot, and full-scale. Data on decontamination and contaminant persistence in drinking water and wastewater infrastructure will be included in the Water Contaminant Information Tool (WCIT)[5]. HSRP researchers are developing innovative methods for modeling contaminant fate and transport to enhance water utilities' ability to manage contaminated source water (e.g., water in rivers that is treated for drinking water) and contaminated overland flow. Researchers will develop a tool that predicts the fate and transport of biological contamination in stormwater in a wide-area urban setting (Appendix 1, Output HS.1.5050).

To support risk-based site-specific decisions during response incidents, decision makers must have methods to assess exposure pathways and exposure models for CBRN contaminants. Exposure-based modeling is a mature field for traditional chemical contaminants like conventional pesticides, but modeling efforts for exposure to biological agents are limited. Research conducted under this area

[5] https://www.epa.gov/waterdata/water-contaminant-information-tool-wcit

develops or modifies existing exposure models. For example, models for water-based exposures are being developed and incorporated into a tool that estimates consequences for entire water systems (Appendix 1, Output HS.1.5050). Another set of example outputs are Provisional Advisory Levels (PALs). PALs are quantitative risk values for short duration exposures that exceed safe levels, used to inform emergency actions like evacuation and cessation of water service (Appendix 1, Output HS.1.4424).

Figure 2: Assessment of reaerosolization of *B. anthracis* surrogate spores due to typical and response-related human activity (Aerosol Wind Tunnel at EPA's Facility in Research Triangle Park, NC)

Research Area 2: Contaminant Detection/Environmental Sampling and Analysis

Decisions regarding remediation are based largely on the results of infrastructure or site characterization sampling (to establish the extent of contamination) and on clearance sampling (to evaluate the efficacy of the cleanup). The recovery of contaminated areas and infrastructure will be hindered by a lack of consensus on contaminant detection capabilities, sampling strategies, sample collection procedures, and sample analysis methodologies.

HSRP, working with its partners, will address critical gaps related to this research area by evaluating current detection capabilities, developing and/or refining sampling strategies, developing innovative sample collection techniques, and providing sample processing and analysis methodologies. The goal of this research is to develop, synthesize, and compile the protocols into user-friendly and readily-available tools for the EPA response community and homeland security partners and stakeholders. Overall, HSRP provides the science needed to establish detection and sampling strategies for wide areas and water systems. This work will provide the maximum amount of information regarding the extent of contamination while minimizing the sampling and laboratory resources required.

Program, regional, state, and/or tribal needs

Advances have been made in environmental contaminant detection, sampling strategies, sample collection, and sample analysis. However, major gaps remain in these areas, especially as they apply to wide-area biological releases. The currently-accepted surface sampling methods are not practical for

wide-area responses because they are very time consuming, labor intensive, and require many samples. Strategies that significantly reduce the cost and time associated with site characterization and clearance sampling are needed to effectively respond to a wide-area incident. Surface sampling approaches that expand collection areas or pool samples collected using historic methods have demonstrated the potential to achieve effective sampling coverage of large areas while reducing the resources required. These "composite sampling" methods have considerable advantages over historical sampling methods that covered more discrete sample sizes.

New sampling methods will, therefore, be further developed to support decision makers during characterization of wide-area incidents. This will be accomplished through research to refine historical methods and develop new and innovative approaches. The focus will be on increasing the capability to sample and analyze complex environmental matrices, such as underground transit systems and outdoor urban areas. Examples of the research include developing field-deployable protocols using novel techniques that include pathogen concentration techniques, commercially available robotic cleaners, wet vacuum-sampling devices, native air filters (e.g., heating, ventilation and air conditioning filters), and activity-based air sampling. HSRP will develop outputs that describe sample collection methods for different environmental media (outdoor construction surfaces, soil and vegetation, air). This will be reported in an overall collection method summary (Appendix 1, Outputs HS.2.5030, and HS.2.3347) and added to the online sample collection information document that is part of the Environmental Sampling and Analytical Methods (ESAM) online tool (Appendix 1, Output HS.2.2269).

The ESAM program[6] continues to be a major focus for HSRP. ESAM is a website that supports the entire environmental characterization process. ESAM includes searchable method queries and downloadable documents for use by responders and the public. During an environmental response, ESAM provides responders and laboratories with the single best available sample collection and analysis method. When using ESAM, decision makers have confidence in the integrity of the data, can quickly interpret the data, and can readily communicate its meaning to the public. HSRP ensures that ESAM includes methods for the highest priority contaminants and is continually updated with the most recent methods. In addition to ESAM, HSRP will identify and develop indoor mapping technologies and data management tools to enhance site characterization capabilities. Collectively, the HSRP tools for characterization, mapping, and data management will help local, state, tribal, and federal emergency response field personnel and their supporting laboratories more efficiently respond to incidents, enabling smooth transitions of samples and data from the field to the laboratory to the decision makers (Appendix 1, Outputs HS.2.2269, HS.2.3346, and HS.2.4486).

HSRP is also looking to address sampling and analysis of bio-contaminated solid waste and wastewater (including water from the decontamination processes) in coordination with OLEM's Office of Resource Conservation and Recovery (ORCR) and the Office of Water's (OW) Office of Waste Management (OWM). Sampling and analysis of solid and liquid waste generated during remediation will be needed to determine if the waste requires treatment or has been adequately treated to allow for transportation as conventional solid or liquid waste. Currently, there is no federal regulatory framework for management of bio-contaminated waste, therefore each state regulates the requirements separately. Regardless of whether regulations specify sampling requirements, response personnel will need effective and feasible waste sampling strategies and methods so that waste treatment/disposal facilities can safely accept treated waste. HSRP will modify existing methods or create new ones, as needed, to characterize bio-contaminated solid waste and wastewater. Sampling protocols for these methods will be included in

[6] https://www.epa.gov/homeland-security-research/sam

ESAM (Appendix 1, Output HS.2.2269) and sampling strategies for water distribution systems will be summarized in a separate output (Appendix 1, Output HS.2.2268).

HSRP researchers are also developing sampling and analysis methods to address emerging chemical threats, including nation state-supported threats and illegal drug manufacture fueling the opioid (e.g., fentanyl) crisis in states and tribes. Local, tribal, state, and federal partners have expressed significant needs regarding characterization, cleanup, and waste management alternatives for these emerging threats, notably the risks posed by abandoned illegal drug manufacture sites or the evolution of chemical agents that do not lend themselves to current rapid detection methodologies. Without sampling and analysis methods, response personnel are very limited in making informed decisions on the extent of contamination, efficacy of cleanup, and proper waste disposal options. The chemical collection and sample analysis methods will be included in the ESAM. In addition, HSRP will develop an output that summarizes chemical sampling strategies for environmental media (Appendix 1, Output HS.2.5030). Existing modeling and mapping capabilities for sampling strategies will be identified and developed to utilize optimal locations and methods (Appendix 1, Outputs HS.2.5030 and HS.2.3346).

Topic 2: Environmental Cleanup and Infrastructure Remediation

After understanding the extent of the contamination and assessing its potential impact on public health, EPA may then be responsible for supporting the cleanup of oil or hazardous contaminants and mitigating their impact on human health and the environment. EPA has a long history and extensive expertise in cleaning up contamination associated with accidental spills and industrial accidents. However, remediating CBRN contamination released over wide areas, such as outdoor urban centers or impacted water systems, is a responsibility for which EPA lacks substantial operational experience. Such a release, including oil spills, can pose a continual challenge with long-standing consequences.

Cleanup includes having the capability to address contaminants in all media within the built and natural environment. Department of Defense (DOD) has expertise in the tactical decontamination of personnel and equipment, but this expertise is not directly applicable to the decontamination of public facilities and outdoor areas. These areas have a variety of porous surfaces and might require more stringent cleanup goals for public re-occupation. Furthermore, water systems pose considerable additional challenges.

HSRP activities in this topic aim to fill the most critical scientific gaps in the capabilities of EPA's response community (identified by HSRP's program office and regional partners) so that when needed, EPA can make the most informed mitigation and remediation decisions. Understanding social, cultural, behavioral, and economic factors is also important to inform effective response decisions that will ultimately lead to healthy community recovery. EPA's tools, methods, and technologies for disaster preparedness and response are designed to improve the ability of our communities, including water utilities, to rapidly recover from a disaster (or contamination incident). To support research needs related to cleanup, HSRP has four research areas under this topic. The first, wide-area decontamination research area, develops capabilities for addressing hazardous contaminants in the environment, including indoor and outdoor areas. The second research area focuses on addressing needs related specifically to water treatment and decontamination of water systems. Research to support response to oil spills is addressed under the third research area. The fourth research area addresses capabilities associated with waste management as part of the response and remediation efforts.

Research will continue to evolve to focus on scalability of cleanup methods and application of the research to additional hazards inside and outside of the traditional CBRN paradigm (as needs and threats emerge). Related to water systems, the focus will continue to move towards more field-scale assessments and improving the overall resilience of water systems to disasters.

Research Area 3: Wide-Area Decontamination

Wide-area contamination requires comprehensive remediation capabilities to help impacted communities recover rapidly and safely. Decision makers developing a remediation strategy seek to identify and secure the most applicable decontamination methods and resources (e.g., workers, equipment, materials, etc.) to execute the identified methods.

For example, critical infrastructure (e.g., government, health care, schools, transportation, energy, communication) in the contaminated area must be restored quickly to minimize both direct and indirect impacts. Wide-area contamination may pose a direct impact on the local community due to health impacts and disruption of services, including possible relocation. Surrounding communities may also be (secondarily) impacted, such as through people being unable to commute to work or disruption of services from the directly impacted area.

HSRP's decontamination research outputs can be used to support decision makers in selecting decontamination options with consideration for safety, resource demand, logistics, training, availability, and technology necessary to remediate a wide-area incident. Researchers will develop methods and critical information for response strategy development and to inform the decision-making process.

Program, regional, state, and/or tribal needs

Following a wide-area incident, local response authorities need access to decontamination methods that are effective, feasible, and versatile for various contamination situations. Since there is no universal decontamination method that is applicable for all combinations of environments and contaminants, decision makers seek information to help them decide on the most appropriate site-specific approaches. Information to assist decision makers includes understanding the effectiveness and impact of various decontamination approaches for contaminated areas depending on conditions and priorities (e.g., urgency, contamination level, surface/media types, etc.) for remediation.

Decontamination of public and residential areas is challenging due to the complexity of the material types and their different uses within communities. Common outdoor surfaces such as soil, concrete, brick, and asphalt pose significant decontamination challenges due to their porous and reactive nature. To meet the capability gap posed by outdoor surfaces, HSRP will continue to evaluate and develop decontamination methods that are effective for outdoor surfaces under various environmental conditions. Results will be summarized in summary outputs (Appendix 1, Outputs HS.3.5002, HS.3.5064, HS.3.641, and HS.3.5006), and will be used to inform the development of trade-off and strategic-consideration decision-support tools (Appendix 1, Output HS.7.5039).

Rapid decontamination methods are needed to clean up critical infrastructure and enable continuous operation. Examples of critical infrastructure include water and wastewater utilities (discussed in the next research area), hospitals, electrical power utilities, and transportation systems. Some critical infrastructure contains sensitive and valuable instruments/equipment; therefore, the decontamination process must be designed to protect this equipment from damage so that the infrastructure can be promptly returned to service. In addition to the summary outputs supporting biological and chemical

threat response, HSRP will produce specific outputs that describe decontamination methods for these threats that are compatible with sensitive and valuable items (Appendix 1, Outputs HS.3.5060 and HS.3.1165).

Response to contamination incidents affecting residential and commercial areas may be delayed until resources are available, as federal, state, tribal, and local government resources are devoted to critical infrastructure. Research is needed to develop feasible decontamination methods for residential and commercial areas that are widely available, user-friendly, economical, and safe. To meet this need, HSRP will identify widely-applicable decontamination methods by surveying: (1) CBRN decontamination methods previously used by national and international agencies; (2) equipment commonly available in municipalities (e.g., street sweepers, orchard sprayers, sanitation trucks, and snow plows) that could be repurposed to support remediation; and (3) household maintenance activities for indoor and outdoor decontamination (including social, cultural, behavioral, and economic factors).

The methods identified will be developed as field-usable decontamination options via laboratory and field studies. Figure 3 shows one example of this, depicting an orchard sprayer that could be used to rapidly spray liquid decontaminants over large areas. Decontamination methods using common municipal or commercial equipment and household maintenance activities are innovative approaches that will reduce contamination exposure to the public and decrease the need for decontamination resources that may be needed elsewhere. HSRP will also conduct research to develop gross decontamination methods that can be safely and rapidly deployable for remediation. While these methods may not ultimately achieve a cleanup goal, they can help to reduce exposure potential until additional decontamination methods can be deployed as necessary. An example output from this research is listed in Appendix 1 as Output HS.3.5006, providing decision makers information on widely-available and user-friendly decontamination options for wide-area radiological incident response.

Remediation of a CBRN wide-area incident requires an extensive number of decisions that span numerous areas of expertise. These decision points, and the tools and models that support them, are tightly intertwined and should employ a holistic solution. HSRP will produce user-friendly tools to assess numerous factors (e.g., efficacy, availability, logistics, worker training, diminishing returns) that can be considered when selecting the most appropriate decontamination options following a wide-area incident. Information regarding an array of decontamination methods will be incorporated into these decision-support tools (Appendix 1, Output HS.7.5039). To ensure the tools are relevant and easy to use, HSRP will request input from local, state, tribal, and federal governments as part of the output development process.

Figure 3: Demonstration of the use of an orchard air blast sprayer for the decontamination of a subway station during an operational technology demonstration

Research Area 4: Water Treatment and Infrastructure Decontamination

Resilient water infrastructure systems can facilitate quick and effective decision-making during emergency situations to ensure access to adequate water capacity and quality. Decontamination of drinking water systems following intentional contamination, or after a natural disaster (e.g., pipe breaks, storms, earthquakes) is critical for effectively resuming operation and restoring water distribution for drinking purposes, as well as other applications such as fire protection, hospital, and industrial use. For example, EPA Region 6 in Texas requested assistance to address contamination from an asphalt emulsifying agent, Indulin AA-86, that had contaminated Corpus Christi's water supply leading to a temporary suspension of use. ORD scientists provided data on flushing chemical contaminants to help with the cleanup. ORD also helped the region evaluate the toxicity and possible risks associated with ingesting water contaminated with Indulin AA-86 and the water-soluble salt from the product. The researchers established a health-based action level for the contaminant in support of an immediate need by the region, state, and the city to protect public health.

Drinking water distribution systems, household plumbing, and appliances are increasingly vulnerable to interruption in service from a terrorist attack, industrial accident, or extreme weather events. Water systems can also be impacted significantly if their source water is affected by natural disasters and/or spills of industrial chemicals and oils. This vulnerability presents operational challenges in maintaining good water quality to protect human health and ensure water availability for fire protection and other vital uses. Natural and man-made incidents further exacerbate the declining integrity of our aging water infrastructure. Regardless of the source of contamination, the ability to reliably and cost effectively decontaminate miles of distribution system pipes and plumbing is critical to rapidly returning the system

to service. Making swift and effective decisions will help minimize impacts to partners, the time to return to service, and associated costs.

Wastewater infrastructure is also vulnerable to contamination incidents. Depending on the contaminant, the incident may impact the operation of wastewater treatment (e.g., worker safety, sludge, aeration), which in turn can disrupt wastewater collection or result in the discharge of untreated waste to receiving waters. Contaminants in the wastewater treatment process may end up in the biosolids, which in turn may impact reuse (e.g., land application).

Program, regional, state, and/or tribal needs

To address the challenges mentioned above, an HSRP priority is to provide tools and methodologies to inform decontamination of water infrastructure, management of the contaminated water, and resumption of operations. Discussions with the drinking water management community and recommendations from Water Critical Infrastructure Protection Advisory Committee (CIPAC) emphasize the importance of water infrastructure decontamination and testing of methods and technologies on a large-scale system, representative of a real drinking water distribution system. To address this need, HSRP constructed the Water Security Test Bed (WSTB)[7] in at Idaho National Laboratory to conduct water infrastructure research at the full-scale (see Figure 4). Through operational technology demonstrations and exercises (e.g., tabletops, full-scale exercises), WSTB research can be used by emergency response and water-sector communities to fully understand the operation, application, and performance of these tools and techniques. In consultation with stakeholders, HSRP plans to expand current research to include additional contaminants, materials, and scenarios, such as:

- Decontamination methodologies (including automatic flushing) for various contaminants
- Consequences of a cyberattack on water distribution systems
- Effectiveness of in-line contaminant detectors
- Pipe materials in water distribution systems (e.g., iron, concrete, PVC, PEX, etc.)
- Wash-water treatment methodologies
- Water system modeling tools

Example outputs from this work include summarizing decontamination approaches and incident detection methods for water infrastructure (Appendix 1, Outputs HS.4.470, HS.4.663, and HS.4.662), including methods to extrapolate the research for contaminants not directly addressed and methods to support disinfection for *Legionella pneumophila.*

EPA also supports wastewater utilities by providing tools and data that help them respond to and recover from contamination incidents and other disasters. Data from HSRP's water infrastructure and decontamination research will be used in tools developed by OW and the response community, including state, tribal, and local responders. Contamination of source waters will be addressed through the Drinking Water Source Vulnerability and Emergency Management Tool, which identifies upstream hazards using geographic information system (GIS) databases and models to determine travel time to downstream drinking water intakes, as well as leading edge, peak, and trailing edge contaminant levels. The technical basis for a water/wastewater decontamination and treatment technology tool will be developed for integration into EPA Water Security Division's (WSD) Decontamination Preparedness and Assessment Strategy (DPAS).

[7] https://www.epa.gov/homeland-security-research/water-security-test-bed

The enhanced capability of water systems to predict future system behavior and evaluate the implications of response decisions will improve emergency response and shorten the time needed to resume operations. As such, real-time modeling tools can support accurate hydraulic and water quality predictions. Modeling tools can also enable rapid and effective decisions. HSRP has developed tools and technologies[8] to assist water infrastructure systems in identifying, evaluating, and improving their resilience to man-made or natural disasters, whether by changing operations or by redesigning and retrofitting the infrastructure. These system-specific tools need to be tested and adapted to be applicable for wastewater, stormwater, source water, and water reuse applications. In addition, a complete watershed system approach needs to be explored to examine the effects of one system's perturbation on another.

Initial HSRP research efforts have focused on developing prototype decision-support tools for drinking water systems. HSRP will focus on expanding these tools to "all hazards", validating their results with real-world data, and using the tools in case study applications with partner drinking water utilities.

Figure 4: Aerial view of the Water Security Test Bed

Research Area 5: Oil Spill Response Support

EPA is responsible for responding to and assessing environmental releases of oil that occur over land, on inland waters, and in the ocean (in conjunction with the U.S. Coast Guard). Oil spills can affect human and ecological health, as well as the economy, by impacting water (including drinking water supplies), air quality, ecosystem health, or by directly exposing humans and ecological life to toxic constituents. Atypical oil spills (e.g., deep sea and prolonged releases, such as the 2010 Deepwater Horizon spill) have highlighted the capabilities and limitations of current spill response methods and of the ecological and

[8] Information on existing EPA tools developed by HSRP can be found at https://www.epa.gov/homeland-security-research.

human health concerns associated with certain spill mitigation technologies. Federal, state, tribal, and local governments, especially those who rely on aquatic resources, are concerned regarding the toxicity of oil- and spill-treating agents on aquatic flora and fauna, their fate in the environment, and the effects on impacted shorelines and wetlands.

Program, regional, state, and/or tribal needs

The National Contingency Plan (NCP) includes a Product Schedule (NCPPS) for commercially available spill-treating agents (e.g., dispersants, surface washing agents, herders, solidifiers) (U.S. EPA, 2018b). The CWA and the Oil Pollution Act (OPA) give authority to EPA to prepare and maintain this schedule. The NCP also requires that EPA maintain reference oils for product testing. HSRP develops and refines the protocols for product effectiveness and toxicity that are used to inform regulatory actions. This research also provides guidance for emergency responders on product performance and trade-offs to potentially impacted communities and ecosystems. Research in support of this guidance is dedicated to:

- NCPPS efficacy protocol development: Currently, the focus includes developing efficacy tests for surface washing agents, solidifiers, and chemical herders, and evaluating product performance in fresh and salt waters (Appendix 1, Output HS.5.5048).
- Toxicity of oils and oil spill-treating agents: Developing toxicity procedures and threshold determinations for regulatory listing and establishing LC_{50} values (i.e., the lethal concentration required to kill 50% of the species population tested) for a range of crude oils (Appendix 1, Output HS.5.5047).
- NCP reference oil evaluation: Evaluating potential reference oils for dispersant effectiveness, chemical characterization, and toxicity to enable EPA's Office of Emergency Management (OEM) to select new reference oils (Appendix 1, Output HS.5.5047).

In addition, efficient oil spill response requires the ability to rapidly characterize the behavior, transport, fate, and effects of various oils and spill agents, including diluted bitumen, which is particularly difficult to remediate and exhibits unique chemical and physical behavior. To protect communities and ecosystems, further research is needed on the chemical characterization, biodegradation, weathering, and toxicity of a range of oils and spill agents. Studies at the bench-, laboratory-, and field-scale improve our ability to minimize environmental and human impacts from spills and serve to calibrate numerical models of oil tracking. Understanding environmental behavior informs predictions of oil fate and transport and helps establish appropriate response, remediation, and restoration methods, including Net Environmental Benefit Analysis (NEBA) Natural Resource Damage Assessment (NRDA).[9] Research supporting these needs includes:

- Degradation of oil- and spill- treating agents: Characterizing fate processes (e.g., biodegradation) and toxicity of oil exposed to NCPPS agents that are not intended to be recovered from the environment and evaluating degradation of oil encapsulated in ice or under sediments (Appendix 1, Output HS.5.5047).
- Oil toxicity and exposure pathways: Evaluating unconventional oils, including diluted bitumen, to determine the fate and transport when discharged to the aquatic ecosystem, and evaluating

[9] NEBA is used to balance trade-offs during oil spill response for considering the most appropriate options to minimize the impact of the spill. Additional information on NEBA can be found at http://www.oilspillprevention.org/oil-spill-cleanup/oil-spill-cleanup-toolkit/net-environmental-benefit-analysis-neba (last accessed July 24, 2018).

additional new species for toxicity testing beyond current test species for oil-agent mixtures (Appendix 1, Output HS.5.5048).

- Behavior of oil and spill-treating agents at laboratory-, tank-, and field-scale: Performing comparative analyses of spill detection sensors, determining oil behavior for validation of subsea blowout models, evaluating agent effectiveness as a function of oil weathering and environmental conditions, and assessing *in situ* burn efficiencies.

A portion of ORD oil spill research is reserved for emergency response technical support, spill exercises and area planning, interagency working groups, and emerging issues (e.g., Arctic spill planning and increased shipment of diluted bitumen via rail, barge, and pipeline). Focus topics are ever-evolving but current research is dedicated but not limited to:

- Oil tracking tools and emergency response technical support: Evaluating oil spill detection assays and establishing cutting-edge technologies for oil slick thickness estimates for decision-making in skimming and burning (Appendix 1, Output HS.5.5049).
- Spill planning and guidance formulation: Coordinating interagency activities, including research on International Maritime Organization (IMO) dispersant guidelines, updates to the National Response Team (NRT) science and technology factsheet, and formulation of the six-year Interagency Coordinating Committee for Oil Pollution Research (ICCOPR) plan.

ORD oil spill research includes experiments over large scales, such as spill simulations using wave tank facilities, like Ohmsett at the Naval Weapons Station Earle in New Jersey (Figure 5, left panel), and at small scales for evaluating the performance of spill-treating agents on the NCP Product Schedule (Figure 5, right panel).

Figure 5: Photo of spill simulations using the Ohmsett wave tank facility at the Naval Weapons Station Earle in New Jersey (left panel) and laboratory evaluation of the performance of spill-treating agents (right panel).

Research Area 6: Waste Management

Waste management presents considerable challenges during any large-scale disaster; additional challenges will exist during a wide-area CBRN incident. For example, there is currently no federal regulatory framework for bio-contaminated waste. The existing disposal capacity for radiologically-contaminated waste is likely only a fraction of what would be needed in a large-scale radiological or

nuclear incident. Environmental remediation after the Fukushima Daiichi accident is estimated to have generated over 37 million tons of waste, much of it soil.[10] Waste staging and on-site waste minimization and treatment will be critical to allow remediation efforts to proceed. The waste streams include materials impacted by the contamination incident, as well as waste generated through the decontamination process. As a marker of how challenging waste management can be for highly pathogenic or toxic contaminants, the single Ebola patient in New York City generated 352 drums of waste (335 drums from patient treatment, 17 drums from apartment cleanup) and the total cost for disposal was $1,120,000.[11]

In addition to solid waste, large volumes of contaminated water may be generated during flushing of contaminated infrastructure or decontamination operations. With the current goal of containing and treating much of the waste on-site (by discharging to surface water, a wastewater treatment plant, stormwater, or combined systems), these waste streams may be difficult to manage[12].

Program, regional, state, and/or tribal needs

Decision makers need sound science and tools to assist in planning for and conducting waste management activities effectively. Information is needed to:

- Support effective staging of waste and waste minimization and treatment, and assess the fate and transport of contaminants in disposal facilities.
- Prove the ability of existing treatment technologies (e.g., incineration) to destroy acutely toxic chemicals when they are associated with building materials and other materials that may be contaminated after an incident.
- Test and further develop scalable water treatment and containment methods (potentially recycling the water for further use) to support effective management of contaminated water.
- Predict the effectiveness of treatment methods for contaminants that lack treatment data in preparation for unknown water system contamination threats.

To support these needs, HSRP will develop an all hazards tool on EPA's Geoplatform[13] that analyzes GIS layers to determine optimal waste staging locations; estimate the cost, time, and logistical requirements associated with transporting large volumes of waste; and assist state, tribal, and local governments in determining optimal waste transport options and routes. HSRP will also continue to develop tools to support estimations of waste volumes that are needed to develop waste management plans, including evaluation of advanced technologies (e.g., aerial photography, remote sensing) for waste estimation post-incident. Ultimately, HSRP will develop synthesis documents that will be incorporated into decision-support tools that assist state, tribal, and local governments in developing and executing their

[10] This estimate was derived from materials presented by the Government of Japan, Ministry of the Environment. The presentation is titled "Environmental Remediation in Japan", dated March 2018, and accessed at http://josen.env.go.jp/en/pdf/progressseet_progress_on_cleanup_efforts.pdf (last accessed July 24, 2018).
[11] This information was provided by EPA Region 2 in a presentation that can be accessed at https://www.nrt.org/site/download.ashx?counter=3098 (last accessed July 24, 2018).
[12] Discharging to Hazardous Material Water Treatment Facilities is also an option in some areas of the country.
[13] https://epa.maps.arcgis.com/

waste management plans, pre- and/or post-incident[14]. Specifically, the program will integrate its tools into EPA's forthcoming pre-planning waste management and response tool (Appendix 1, Output HS.6.5008).

HSRP will continue to develop and test methods for the minimization and treatment of CBRN-contaminated waste (Appendix 1, Output HS.6.5009). Efforts range from developing field-usable treatment technologies for pathogen-contaminated waste (Appendix 1, Output HS.6.5010)—a key gap identified during the recent Underground Transit Restoration Operational Technology Demonstration[15] (see Figure 6)—to developing treatment technologies for chemical threat-contaminated building and outdoor materials. HSRP will also develop innovative approaches to manage niche waste streams, like vehicles, to overcome the limitation or prohibitions of using existing processes for recycling and salvage.

Chemical contaminants, biological agents, and radiological agents ending up in water and other complex matrices (e.g., wastewater collection systems) during emergency situations pose significant, and often unique, treatment challenges. Some of these contaminants (e.g., PFAS in firefighting foam) can be generated during initial response activities. HSRP is evaluating on-site water treatment technologies to address the need for treating chemically-contaminated water on-site or at the contamination source (Appendix 1, Output HS.6.5010). This research will inform a water treatment selection framework within the OW's DPAS tool.

Decision makers and waste treatment operators need information to facilitate their acceptance of waste for treatment or disposal. HSRP will examine the impact of contaminated water on wastewater infrastructure and support the development of management options, such as those needed for management of contaminated biosolids and membranes. HSRP will also work to understand the characteristics of the treated water and how it might impact wastewater, stormwater, or combined sewer systems (Appendix 1, Output HS.6.5010). HSRP will share information on difficult-to-treat perfluorooctanesulfonic acid (PFOS) and shorter chain perfluoroalkyl sulfonic acids in collected wash water with ORD's SSWR program, recognizing the cross-program interest, along with leveraging other research of mutual interest.

[14] EPA has developed guidance on how to construct pre-incident waste management plans and provided resources to support their development. Please see: https://www.epa.gov/homeland-security-waste/waste-management-benefits-planning-and-mitigation-activities-homeland#preincident

[15] The Underground Transport Restoration Project was a collaborative effort between U.S. DHS, U.S. EPA, and local stakeholders designed to develop capabilities for the rapid return to service of underground transportation systems after a biological incident.

Figure 6: Testing of on-site solid waste treatment approaches.

Topic 3: Systems Approaches to Preparedness and Response

Transitioning the research into fieldable capabilities involves ensuring that decision makers and responders have knowledge of and access to the latest information. Decision makers need access to tools and information built from a systems approach where each of the research areas are brought together through their interdependencies and relative impacts. This topic area addresses the development of systems-based tools by pulling together the connected elements of the previous two research topics (contaminant characterization and consequence assessment, environmental cleanup and infrastructure remediation) to provide technical support and decision-support tools. This topic focuses on ensuring that information is readily and easily accessible during an emergency.

Research Area 7: Tools to Support Systems-based Decision Making

During a wide-area incident, the response community needs tools to rapidly assess the incident, including access to emerging technologies capable of surveying, detecting, and monitoring the event. HSRP models and tools enhance the timeliness of disaster recovery by providing metrics and decision support, ensuring decision makers have access to information on technologies for characterizing or remediating environments after various CBRN agent-related incidents. The response community also needs tools that consider timeframes and costs to evaluating viable options from economic or social standpoints, as well as tools that retain flexibility in remediation activities due to the complexity, uncertainty, and dynamic nature of a wide-area incident. HSRP recognizes the need to develop a baseline model and simulation tools for comparing or measuring decisions against the true resiliency of a community.

Program, regional, state, and/or tribal needs

A great number of decision-support tools have already been developed under HSRP, covering a wide range of hazards. These support tools individually consume separate sources of data, making them susceptible to becoming obsolete and costly to update. The response community has sought EPA's assistance in developing a centralized and routinely-maintained database for monitoring and surveying the latest decontamination, mitigation, and waste treatment technologies/methods (Appendix 1, Output HS.7.5039). A database could store up-to-date data derived from HSRP literature reviews, studies, and tools in a web-based searchable platform, greatly enhancing response, planning, and preparedness capabilities and efficiencies. HSRP will also develop and integrate a cost model for predicting the economic and social survivability of urban areas according to a range of geographically-specific criteria (Appendix 1, Output HS.7.5039). The model could then connect to other HSRP tools (such as the Waste Estimation Support Tool[16]) to provide end-users with a tool to assess community viability based on selected technologies.

In addition to selecting the appropriate technologies and considering resource needs, the consequences of remediation activities and the impact to the follow-on activities must be carefully considered. The effectiveness of remediation activities is difficult to predict due to the complexity, uncertainty, and dynamic nature of a wide-area incident. HSRP plans to develop a tool that can simulate the remediation effectiveness of various response activities that will be helpful for a wide-area response (Appendix 1, Output HS.7.5039). This work will build on existing support tools and will provide quantitative estimations for the following items:

- The impact of selecting certain methods (decontamination, sampling, and waste treatment) on the overall remediation
- Bottlenecks in the remediation activities
- Resource availability and demand for remediation
- Testing of future decision-support-tool feasibility before development/deployment
- Testing of future methods/technologies before investment.

Another significant gap for a wide-area incident is the need to collect and communicate data effectively. Inefficiencies in this process can hamper recovery efforts and potentially put lives and the environment at risk. There is a need to develop a framework and identify potential technologies for collecting and synthesizing information to better inform situational awareness, decision-making, and management of data during a response. This includes communication of information to decision makers, ultimately to inform the public regarding exposure risks, risk management, and response activities at the federal, state, tribal, and local level. HSRP will address this gap by developing tools for community stakeholders to conduct self-assessments of their community environmental resilience to disasters (Appendix 1, Output HS.7.5041).

Program Design

The ORD StRAPs are guided by EPA's Strategic Plan and the ORD Strategic Plan. The StRAPs position ORD to contribute to EPA meeting its strategic measures. The HSRP StRAP provides a vision and blueprint for advancing homeland security research in ways that meet legislative and policy mandates and address the highest priority partner needs. HSRP supports EPA's responsibilities to prepare for and respond to

[16] https://www.epa.gov/homeland-security-research/waste-estimation-support-tool

acute disasters by conducting short-term, applied scientific research. The foundation of the program focuses on CBRN contamination resulting from intentional or unintentional incidents.

Program Components

HSRP research will continue to be conducted at EPA facilities (intramural) and off-site (extramural) at grantee or contractor laboratories. Extramural research, funded through interagency agreements, grants, and contracts, complements and expands the intramural research program by engaging the Agency with the nation's leading scientists and engineers. This broad engagement is particularly valuable where additional expertise and capabilities are needed from the scientific community to provide an expanded strategic response to an environmental challenge and to address important gaps in scientific expertise. EPA also participates in similarly focused Small Business Innovation Research (SBIR)[17] efforts established by the Small Business Innovation Development Act of 1982.

ORD recognizes that EPA program and regional, state, and tribal partners must respond to emerging, unforeseen needs that can benefit from ORD research and technical expertise. ORD works with partners to balance the relative importance of these emerging needs with other research activities and to ensure agreement in any changes in research direction with respect to available resources. HSRP promotes the development of innovative commercial technologies to address environmental challenges. HSRP does this through vehicles including SBIR, innovative incentive programs (e.g., citizen prizes/awards to drive crowd sourcing of inventive approaches), and ORD internal innovative challenges (e.g., Pathfinder Innovative Projects).

HSRP collaborates with other ORD research programs and with other federal departments/agencies to address the most pressing needs related to an "all hazards" approach to disasters. HSRP also finds multiple uses of its research by applying, when appropriate, its products to EPA's needs that are not otherwise met. One example is the Ebola Outbreak in 2014; although this was a natural outbreak with major response efforts led by the Centers for Disease Control (CDC), EPA's expertise was requested related to environmental cleanup and waste treatment and disposal. HSRP provided necessary expertise on environmental decontamination, personal protective equipment decontamination, and solid waste and wastewater management through adaptation of its work with other biological agents. An essential component of HSRP is the ability to adapt and apply its research to meet unforeseen challenges in a timely manner.

Developing resilience at the community level is a critical aspect of building sustainability, especially for communities that have greater exposure to disasters and are more vulnerable to their impacts. Communities that "prepare for, absorb and recover" (National Research Council, 2012) from disasters will, in turn, have more sustainable economic, environmental, and social systems. By developing and transitioning effective tools and guidance to community decision makers, including emergency management officials and water and wastewater utility owners and operators, HSRP is helping communities to prepare for and more rapidly recover from these incidents.

A significant and critical component of the HSRP is providing technical support to our partners and stakeholders. Technical support is provided to aid in the development of guidance (for example, supporting development of threat agent quick reference guides by the National Response Team), teaching end-users how to deploy HSRP-developed products, and supporting decision makers during incident response. A significant portion of staff time is devoted to providing such technical support, serving to effectively transition the research to developed solutions and capabilities.

[17] https://www.epa.gov/sbir

Solutions-Driven Research

ORD is renewing and expanding its commitment to producing research that addresses real-world problems and helps EPA program and regional offices, state and local agencies, as well as tribal organizations, to make timely decisions based on science. This commitment includes exploring ways to improve research processes through the application of a solutions-driven research framework.

This research framework emphasizes:

1) Planned partner and stakeholder engagement throughout the research process, starting with problem formulation and informing all elements of research planning, implementation, dissemination, transition, and evaluation
2) A focus on research outputs identified in collaboration with partners and stakeholders
3) Coordination, communication, and collaboration both among ORD researchers and between researchers and partners to develop integrated research that multiplies value to partners and stakeholders
4) Application of research outputs in cooperation with partners and stakeholders to solve complex environmental problems, and to test the feasibility, appropriateness, meaningfulness, and effectiveness of the solutions.

Risk communication is a central factor in this framework, allowing people to understand their risks and adopt protective behaviors, as well as informing risk management decisions. ORD will emphasize advances in the science of risk communication and apply best practices for communicating risk to different audiences across HSRP and the other national research programs.

EPA Partner and Stakeholder Involvement

In line with ORD's strategic measure to increase the percentage of research products that meet customer needs, the HSRP StRAP FY19-22 guides ORD research to address the high-priority needs of the Agency and its partners and stakeholders. Numerous EPA program offices and regions implement EPA's homeland security responsibilities. EPA's Office of Homeland Security, within the Administrator's Office, coordinates all EPA activities relating to homeland security. HSRP's primary partners include EPA's OW, OLEM, and each of the Agency's ten regional offices. Additional EPA partners include The Office of Chemical Safety and Pollution Prevention (OCSPP), the Office of Air and Radiation (OAR), the Office of Enforcement and Compliance Assurance (OECA), and the Office of Policy's Office of Sustainable Communities.

Much of the implementation and enforcement of homeland security responses is operationalized at local, state, and tribal levels. EPA serves mostly in a technical support role to these decision makers and first responders, as well as to water and wastewater utilities. Input from these partners is relayed to the EPA regional and program offices, who then incorporate this information into the programmatic needs that are transmitted to HSRP. The HSRP engages directly with the Association of State Drinking Water Administrators[18] and the Association of Clean Water Associations[19]; these stakeholders are on the front lines supporting water and wastewater systems in responding to operational and emergency response challenges. ORD will also seek additional state, tribal, and local input more directly during the

[18] https://www.asdwa.org/
[19] https://www.acwa-us.org/

implementation of the 2019-2022 StRAP. Engagements with ECOS and ERIS, as discussed previously, are coordinated across all six EPA National Research Programs, as their needs are broad and influence each program. The HSRP specifically engages with ASTHO, ASTWMO, and NEMA, coordinating across programs as appropriate; these associations have a more specifically focused relevance with respect to the mission of the HSRP.

HSRP's innovative oil spill research supports OEM, OW, and technical support to the regions, states, tribes, and other regulatory authorities. This research has fostered strong collaboration with the National Oceanic and Atmospheric Administration (NOAA), the U.S. Coast Guard, Department of Interior's Bureau of Safety and Environmental Enforcement, and the U.S. Geological Survey (USGS). Additionally, this research effort is in collaboration with Canada's Department of Fisheries and Oceans, the American Petroleum Institute, and other industry members. Needs related to this research area are developed in coordination with EPA and federal partners. EPA participates on the Interagency Coordinating Committee on Oil Pollution Research (ICCOPR)[20] with fifteen federal agencies. The committee focuses on providing updates on oil research, discussing collaboration plans, and developing ways for research to translate to response efforts.

As indicated in the Solutions-Driven Research section above, end-users of HSRP research will find scientific products most useful if they are closely involved with the research program from the outset. HSRP addresses prioritized needs based on specific problems identified through defined interactions with HSRP's partners. The process of understanding and prioritizing the needs of HSRP's partners is collaborative and involves discussion of current capabilities and desired end states and is informed by DHS-led threat assessments. EPA's mission and strategic direction further informs prioritization of needs. In addition, water utilities convey their needs through the water sector's Critical Infrastructure Protection Advisory Committee (CIPAC) (U.S. DHS, 2018), managed out of DHS and co-led by EPA's OW. This group periodically releases research priorities, such as the Roadmap to a Secure and Resilient Water and Wastewater Sector (Water and Wastewater Sector Strategic Roadmap Work Group, 2017), and these priorities inform HSRP research on this topic. For oil spill-specific needs, HSRP coordinates with EPA partners and other federal agencies, including NOAA, the U.S. Coast Guard, and the National Response Team (NRT).

HSRP collaborates extensively with other federal agencies whose missions support environmental disaster response, particularly those where there is overlapping or complementary mission space with EPA. HSRP works closely with the DHS, DOD, Department of Health and Human Services (HHS), USDA, and others to leverage their homeland security/environmental disaster science efforts. These interactions range from high-level strategic planning and coordination managed by the White House's National Science and Technology Council[21] to staff collaboration on individual research efforts.

[20] https://www.dco.uscg.mil/ICCOPR/Members/

[21] ORD HSRP participates on the National Science and Technology Council's (NSTC) Committee on Environment and the Committee on Homeland and National Security.

Anticipated Research Accomplishments and Projected Impacts

Some of the anticipated research accomplishments from across HSRP and their intended impacts or outcomes are highlighted below.

Advancing Resources for Characterization after a Wide-Area Contamination Incident

HSRP is developing ESAM[22] as a comprehensive online source for all information needed to conduct characterization activities after a CBRN incident. During a large environmental response, ESAM provides responders and laboratories with the single best available sample collection and analysis method. When a single method is used, decision makers can feel confident about data integrity and can more easily interpret and communicate the information. Over the period of the StRAP, the analytical methods and sample collection information contained in ESAM will be updated. Sampling procedures and information will be added to support the development of sampling strategies. New methods for sample collection will be developed and added for priority biological agents on urban and outdoor surfaces and in air, solid waste, and wastewater. Sample collection methods for chemical threats in water and on surfaces will be developed for inclusion in ESAM.

Developing a Decontamination and Water Treatment Technology Selection Tool

Water contamination incidents continue to threaten the delivery of clean water. To address this concern, HSRP will continue to conduct pilot to field-scale technology testing for water infrastructure decontamination and water treatment. Findings from this research, as well as previously completed research, will be used to construct a tool to assist water utilities in selecting decontamination and water treatment technologies. The tool will consider technology efficacy and operational considerations when providing the end-user options for the selection of an appropriate technology. The tool will be developed in collaboration with technology end-users and incorporated into OW's DPAS, a tool used directly by water utilities to prepare for and respond to water contamination incidents.

Improving Approaches for Response to Emerging Chemical Threats

Fentanyl and its analogs (e.g., carfentanil and 3-methyl fentanyl) are compounds of increasing concern to states, tribes, and local public health and environmental agencies due to their increased availability, extreme toxicity, and increasing misuse. HSRP will continue to address state, tribal, and local needs related to fentanyl and its analogs by developing sampling and analysis methods and proven decontamination options in environmental matrices (specifically, surfaces and water). To assist in interpreting these data and informing emergency response activities, HSRP will develop exposure values that describe health effects based on dosage. The ability of decontamination techniques to clean up fentanyl and its analogs on different types of surfaces (porous and non-porous) will be assessed initially at the lab-scale, prior to testing methods in the field for transition to responders. The development of sampling, analysis, and decontamination methods will provide an update to the recently released fentanyl fact sheet for responders, filling gaps in knowledge and capabilities that were recognized during the development of the fact sheet. Field demonstrations and updates to the fact sheet will provide an opportunity to transition the most effective sampling and decontamination methods to end-users. This

[22] https://www.epa.gov/homeland-security-research/environmental-sampling-analytical-methods-esam-program-home

research will allow EPA to make cleanup recommendations and offer solutions to first responders across the country.

Scalable Approaches for Remediation after a Wide-Area Radiological Incident

Federal government cleanup resources will be extremely stretched after a wide-area radiological incident, like the Fukushima Daiichi Nuclear Power Plant accident. Innovative decontamination approaches that can be safely employed by the public and state, tribal, and local government will be needed. HSRP is developing the technical information required for state, tribal, and local agencies to develop self-help decontamination instructions for owner/occupants or their contractors. HSRP is also developing radiological and nuclear response-specific "how-to" documents for operators on the use of municipal, construction, farm, and critical-infrastructure-specific equipment. These resources will greatly increase local communities' self-sufficiency after a wide-area radiological or nuclear incident and decrease the time needed to recover.

Field-scale Assessment and Demonstration of Wide-Area Biological Response Capabilities

HSRP partners often express the high priority need for capabilities and information to support response to a wide-area biological incident, specifically response to a large urban area intentionally contaminated with *B. anthracis* spores. Over the course of this 4-year StRAP, HSRP, in coordination with OLEM, and in close collaboration with other EPA partners and stakeholders, including states, regions, and other federal agencies, plans to work with the DHS Science and Technology Directorate and the U.S. Coast Guard to develop wide-area biological response capabilities and test them in the laboratory and in the field, resulting in generic guidance and tools to support a wide-area biological incident response. These efforts will then culminate in a field-scale (operational) wide-area biological response demonstration to assess and improve developed capabilities.

Conclusion

HSRP works with EPA program and regional, federal, state, tribal, and local partners, and other stakeholders, to improve the nation's resilience to "all hazards". HSRP works closely with these partners and stakeholders to understand the challenges posed by CBRN threats, including oil spills, regardless of the cause of the contaminant/threat release and to develop capabilities to aid in rapid response. This response includes capabilities to support pre-incident planning, detection of contamination, characterization of the environment to determine the extent of contamination and its potential threat to public health, hazard mitigation, cleanup of the contaminated environment including built infrastructure, and effective waste management.

An underlying principle of the program is to understand the capabilities of communities and residents as they address historical and emerging threats and how this experience factors into the current and future state of community environmental resilience. The program focuses on the many challenges associated with wide-area contamination, including improving the nation's water infrastructure protection and resilience. Proven characterization, risk assessment, and cleanup approaches provide a deterrence to terrorist activities because timely and effective responses serve to minimize the overall impact of an incident (Pavel, 2012).

References

National Research Council. (2012). *Disaster Resilience: A National Imperative*. Retrieved from Washington, D.C.:

Pavel, M. K. a. B. (2012). How to Deter Terrorism. *The Washington Quarterly, 35*(2), 21-36. doi:https://doi.org/10.1080/0163660X.2012.665339

U.S. DHS. (2016). *National Disaster Recovery Framework*. Washington, D.C. Retrieved from https://www.fema.gov/media-library-data/1466014998123-4bec8550930f774269e0c5968b120ba2/National_Disaster_Recovery_Framework2nd.pdf.

U.S. DHS. (2018, October 29, 2018). Critical Infrastructure Partnership Advisory Council. Retrieved from https://www.dhs.gov/critical-infrastructure-partnership-advisory-council

U.S. EPA. (2018a). *FY 2018-2022 EPA Strategic Plan*. Washington, D.C. Retrieved from https://www.epa.gov/planandbudget/strategicplan.

U.S. EPA. (2018b, October 9, 2018). NCP Product Schedule (Products Available for Use on Oil Spills). Retrieved from https://www.epa.gov/emergency-response/ncp-product-schedule-products-available-use-oil-spills

U.S. EPA. (2018c). *ORD Strategic Plan 2018-2022*. Washington, D.C. Retrieved from https://www.epa.gov/research/epa-office-research-and-development-strategic-plan-2018-2022

U.S. EPA. (2018d, February 14, 2018). Water System Security and Resilience in Homeland Security Research. Retrieved from https://www.epa.gov/homeland-security-research/water-system-security-and-resilience-homeland-security-research

Water and Wastewater Sector Strategic Roadmap Work Group. (2017). *Roadmap to a Secure and Resilient Water and Wastewater Sector*. Washington, D.C.: WaterISAC Retrieved from https://www.waterisac.org/sites/default/files/public/2017_CIPAC_Water_Sector_Roadmap_FINAL_051217.pdf.

Appendices

Appendix 1: Summary Table of Proposed Outputs for Homeland Security Research Program (FY2019 -2022)

The following table lists the expected Outputs from the Homeland Security Research Program, organized by topic. It should be noted that the Outputs may change as new scientific findings emerge. Outputs are also contingent on budget appropriations. The Research Need that the Output is addressing is provided in the table; these needs were defined through the HSRP's partner involvement process. Specific research Products to address these Outputs will be identified and implemented through continued engagement with partners.

Research Area	Program, Regional, State and/or Tribal Need	Output Title
Topic 1: Contaminant Characterization and Consequence Assessment		
1. Contaminant Fate, Transport, and Exposure	Fate of radiological contaminants in the environment after a wide-area release	HS.1.5056) FY22 - Fate, transport, and containment of rad contaminants in urban environments
	A process to determine a cleanup goal for chemical warfare agents and their degradates Understanding and applying fate and transport of chemical, biological, and radiological contaminants resulting from water infrastructure contamination to improve risk management decisions Develop and evaluate tools and methodologies to inform decontamination of water infrastructure (drinking water, premise plumbing, wastewater, stormwater, source water, and reuse), management of the contaminated water, and return to service	HS.1.5050) FY22 - Potential exposure pathway assessment to contaminants in water and wastewater systems
	Review, Clearance, and Dissemination of Provisional Advisory Levels (PALs) for high priority chemical contaminants	HS.1.4424) FY22 - PALs for hazardous chemicals and PALs User Guide
2. Contaminant Detection/ Environmental Sampling and Analysis	Need for continuance of systematic development of sampling and analytical methods for analysis of priority chemical agents (for example CWAs, precursors, degradates, TICs) and their degradation products for all environmental matrices (this includes waste matrices).	HS.2.5030) FY22 - Sampling strategies for chemical incidents
	Sampling methods and strategies are needed for outdoor urban surfaces	HS.2.3347) FY21 - Sampling strategies for wide-area biological incidents

Research Area	Program, Regional, State and/or Tribal Need	Output Title
	Strategies for sample collection, processing, and analysis methods for persistent biological agents or biotoxins in solid wastes, including decontaminated wastes Development of sample collection and analysis methods for drinking water contaminants of interest. (CBR contaminants and biotoxins)	
	Need for continuance of systematic development of sampling and analytical methods for analysis of priority chemical agents (for example CWAs, precursors, degradates, TICs) and their degradation products for all environmental matrices (this includes waste matrices) Development of Rapid and High-Throughput Methods for Analysis of Pathogens in Characterization and Post-Decontamination Samples	HS.2.2269) FY22 - Environmental Sampling and Analytical Methods (ESAM) Tool
	Development of methods and tools to identify sampling locations and strategies within water infrastructure	HS.2.2268) FY21 - Sampling strategies for water distribution systems
	Assessment of emerging technologies to enhance surveying/detection/monitoring capabilities for wide-area incident response application	HS.2.3346) FY21 - Indoor mapping technologies to support remediation decision making
	Need for an adaptive framework that encompasses a series of tools and systems for acquiring, storing, communicating, and visualizing data, and standardizes a process for evaluating new data management technologies	HS.2.4486) FY22 - Data management tools for wide-area biological incidents
Topic 2: Environmental Cleanup and Infrastructure Remediation		
3. Wide-Area Decontamination	Need data on wide-area, outdoor decontamination efficacy and application parameters for B. anthracis, including the effectiveness of various types of washdown and rain in reducing spore concentrations on surfaces, vegetation, and soil, and research supporting strategies for remediating urban environments including the exterior of high-rise buildings	HS.3.5002) FY22 - *B. anthracis* decontamination approaches for wide-area incidents

Research Area	Program, Regional, State and/or Tribal Need	Output Title
	Persistence, fate and transport, and methods to prevent the transport of spore-forming biological agents in natural environments (including waterways) and in/on built infrastructure Self-help and low-tech approaches applicable for indoor and outdoor areas, supporting remediation of multiple facilities Decontamination methods suitable for critical infrastructure	
	Decontamination methods for surfaces contaminated with biotoxins (e.g. ricin and abrin), including impacts on decontamination of sensitive equipment	HS.3.2284) FY22 - Summary of decontamination methods for biotoxins
	Need data on wide-area, outdoor decontamination efficacy and application parameters for non-anthrax biological agents, including the effectiveness of various types of washdown and rain in reducing concentrations on surfaces, vegetation, and soil, and research supporting strategies for remediating urban environments including the exterior of high-rise buildings	HS.3.5064) FY22 - Summary of methods and considerations for wide-area outdoor remediation involving non-spore-forming agent incidents
		HS.3.5060) FY22 - Decontamination methods for sensitive equipment and materials contaminated with biological agents
	Decontamination and Waste Volume Reduction Methods for Wide-Area Remediation Self-Help Decontamination and/or Risk Reduction Measures/Tools/Practices	HS.3.641) FY20 - Compendium of radiological decontamination methods for surfaces and environmental media
		HS.3.5006) FY22 - Best practices for gross decontamination and containment during radiological and nuclear incident response
	Effective decontamination methods for porous or permeable materials for CWA and other HS chemicals of concern. Nondestructive and operational decontamination methods for CWAs and TICs on sensitive equipment, rolling stock, valuable items, and records	HS.3.5004) FY22 - Decontamination technologies for indoor permeable surfaces contaminated with persistent chemicals
		HS.3.1165) FY22 - In-situ decontamination options for persistent chemicals on sensitive and valuable surfaces

Research Area	Program, Regional, State and/or Tribal Need	Output Title
4. Water Treatment and Infrastructure Decontamination	Develop and evaluate tools and methodologies to inform decontamination of water infrastructure (drinking water, premise plumbing, wastewater, stormwater, source water, and reuse), management of the contaminated water, and return to service Treatment and disposal options for large volumes of chemical agent-contaminated drinking water and wastewater – this includes decontamination of wash water Water infrastructure systems (drinking water, wastewater, stormwater, source water, and water reuse) need to be resilient to man-made and natural disasters, with the ability for rapid response	HS.4.470) FY22 - Compendium of water infrastructure decontamination research
	Application of tools and techniques in operational technology demonstrations and exercises	HS.4.663) FY21 - The effectiveness of automated and intelligent water meters, valves, and fire hydrants to flush contaminants
	Development of methods and tools for incident detection (including evaluation of on-line monitoring sensors, sensor placement and event detection) for water infrastructure (drinking water, wastewater, storm water and source water)	HS.4.662) FY21 - Update of sensors handbook for water security
5. Oil Spill Response Support	Emergency Response to Oil Spills: Some products on the NCPPS are not intended to be recovered from the environment (e.g., dispersants, herding agents). However, little information exists on certain fate processes (e.g., biodegradation) Emergency Response to Oil Spills: Evaluate additional new species for toxicity testing beyond M. beryllina and A. bahia for dispersants and dispersants mixed with oil	HS.5.5048) FY22 - Behavior, fate and effects of oil and spill-treating agents
	Develop efficacy test protocol for surface washing agents, solidifiers, and oil herding agents, as well as determine fate of these agents in salt and fresh waters	HS.5.5047) FY22 - National Contingency Plan regulatory support

Research Area	Program, Regional, State and/or Tribal Need	Output Title
	Subpart J Regulatory Support: Evaluate new reference oils testing for Dispersant Effectiveness, Chemical Characterization, and Toxicity Subpart J Regulatory Support: Need LC50s for crude oils.	
	Improving oil slick thickness estimates for decision making on skimming and burning. Emergency Response to Oil Spills: Evaluation of oil spill detection assets	HS.5.5049) FY22 - Oil Spill planning, response and technical support
6. Waste Management	Treatment and disposal options for large volumes of biological agent-contaminated water Treatment and disposal options for large volumes of chemical agent-contaminated drinking water and wastewater– this includes decontamination wash water	HS.6.5009) FY21 - Management of contaminated water and associated waste streams
	Develop and evaluate tools and methodologies to inform decontamination of water infrastructure (drinking water, premise plumbing, wastewater, stormwater, source water, and reuse), management of the contaminated water, and return to service	HS.6.5010) FY22 - On-site and portable treatment methods for chemical and biological waste streams
	Best management practices for staging, segregating, and transporting waste contaminated with biological agents Comprehensive resource which enables efficient, fast, and accurate decision making regarding sustainable waste and debris management	HS.6.5008) FY21 - Decision making tools to support waste management of chemical, biological, radiological contaminated waste

Research Area	Program, Regional, State and/or Tribal Need	Output Title
Topic 3: System Approaches to Preparedness and Response		
7. Tools to Support Systems-based Decision Making	Centralized and routinely maintained database for monitoring, surveying, decontamination, mitigation, and waste treatment technologies/methods Assessment of emerging technologies to enhance surveying/detection/monitoring capabilities for wide-area incident response application Need for a user-friendly decision-support tool that assists in the prioritization of remediation activities Water infrastructure systems (drinking water, wastewater, stormwater, source water and water reuse) need to be resilient to man-made and natural disasters with the ability to respond rapidly	HS.7.5039) FY22 - HSRP integrated decision-support tools to enhance resiliency, response and recovery
	Systems measures for communities to assess resilience as part of pre-incident planning or post-incident recovery	HS.7.5041) FY22 - Tools and training to assess community resilience and to understand social aspects of remediation

Appendix 2: Homeland Security Research Program Supports Decisions Mandated by Legislation and Executive Actions

Legislation	Acronym	Website
Clean Air Act (1970)	CAA	https://www.govinfo.gov/app/details/STATUTE-84/STATUTE-84-Pg1676
Clean Water Act (1972)	CWA	https://www.govinfo.gov/app/details/STATUTE-86/STATUTE-86-Pg816
Safe Drinking Water Act (1974)	SDWA	https://www.govinfo.gov/app/details/STATUTE-88/STATUTE-88-Pg1660-2
Resource Conservation and Recovery Act (1976)	RCRA	https://www.govinfo.gov/app/details/STATUTE-90/STATUTE-90-Pg2795
Comprehensive Environmental Response, Compensation and Liability Act (1980)	CERCLA	https://www.govinfo.gov/app/details/STATUTE-94/STATUTE-94-Pg2767
Emergency Planning and Community Right-to-Know Act (1986)	EPCRA	https://www.govinfo.gov/app/details/STATUTE-100/STATUTE-100-Pg1613
Robert T. Stafford Disaster Relief and Emergency Assistance Act (1988)		https://www.govinfo.gov/content/pkg/USCODE-2015-title42/pdf/USCODE-2015-title42-chap68.pdf
Oil Pollution Act (1990)	OPA	https://www.govinfo.gov/app/details/STATUTE-104/STATUTE-104-Pg484
Federal Insecticide, Fungicide, and Rodenticide Act (1996)	FIFRA	https://www.govinfo.gov/app/details/STATUTE-110/STATUTE-110-Pg1489
Homeland Security Act (2002)	HSA	https://www.govinfo.gov/app/details/PLAW-107publ296
Public Health Security and Bioterrorism Preparedness and Response Act (2002)		https://www.govinfo.gov/app/details/STATUTE-116/STATUTE-116-Pg594
Post-Katrina Emergency Management Reform Act (2006)		https://www.govinfo.gov/app/details/PLAW-109publ295
Food Safety Modernization Act (2011)	FSMA	https://www.govinfo.gov/app/details/PLAW-111publ353
Executive Action	**Acronym**	**Website**
Homeland Security Presidential Directive-4 *National Strategy to Combat Weapons of Mass Destruction* (2002)	HSPD-4	https://www.hsdl.org/?abstract&did=860
Homeland Security Presidential Directive-5 *Management of Domestic Incidents* (2003)	HSPD-5	https://www.govinfo.gov/app/details/PPP-2003-book1/PPP-2003-book1-doc-pg229
Homeland Security Presidential Directive-9 *Defense of United States Agriculture and Food* (2004)	HSPD-9	https://www.govinfo.gov/app/details/PPP-2004-book1/PPP-2004-book1-doc-pg173
Homeland Security Presidential Directive-18 *Medical Countermeasures Against Weapons of Mass Destruction* (2017)	HSPD-18	https://www.hsdl.org/?abstract&did=456436
Presidential Policy Directive-22 *Domestic Chemical Defense*	HSPD-22	Classified

Presidential Policy Directive-8 *National Preparedness* (2011)	PPD-8	https://www.hsdl.org/?abstract&did=7423
Presidential Policy Directive-21 *Critical Infrastructure Security and Resilience* (2013)	PPD-21	https://www.govinfo.gov/app/details/DCPD-201300092
National Security Presidential Memorandum-14 *Support for National Biodefense* (2018)	NSPM-14	https://www.whitehouse.gov/presidential-actions/presidential-memorandum-support-national-biodefense/
Executive Order-13636 *Improving Critical Infrastructure Cybersecurity* (2013)	EO-13636	https://www.govinfo.gov/app/details/DCPD-201300091

NATIONAL BIODEFENSE STRATEGY

2018

This page is intentionally blank

FOREWORD

It is a vital interest of the United States to manage the risk of biological incidents. In today's interconnected world, biological incidents have the potential to cost thousands of American lives, cause significant anxiety, and greatly impact travel and trade.

Biological threats—whether naturally occurring, accidental, or deliberate in origin—are among the most serious threats facing the United States and the international community. Outbreaks of disease can cause catastrophic harm to the United States. They can cause death, sicken, and disable on a massive scale, and they can also inflict psychological trauma and economic and social disruption. Natural or accidental outbreaks, as well as deliberate attacks, can originate in one country and spread to many others, with potentially far-reaching international consequences. Advances in science promise better and faster cures, economic advances, a cleaner environment, and improved quality of life, but they also bring new security risks. In this rapidly changing landscape, the United States must be prepared to manage the risks posed by natural outbreaks of disease, accidents with high consequence pathogens, or adversaries who wish to do harm with biological agents.

Health security means taking care of the American people in the face of biological threats to our homeland and to our interests abroad. The significant infectious disease outbreaks of recent decades, including Severe Acute Respiratory Syndrome (SARS), pandemic influenza, Ebola virus disease, and Zika virus disease, have revealed the extent to which individual countries and international communities need to improve their preparedness and biosurveillance systems to detect and respond to the next health crisis. The health of the American people depends on our ability to stem infectious disease outbreaks at their source, wherever and however they occur. America's biodefense enterprise needs to be nimble enough to address emerging infectious disease threats, the risks associated with the accelerating pace of biotechnology, and threats posed by terrorist groups or adversaries seeking to use biological weapons.

The *National Biodefense Strategy* is aligned with the 2018 *National Security Strategy* of the United States. Pillar One of the 2018 *National Security Strategy* explicitly calls for protecting "the American people, the homeland, and the American way of life." One component of this goal is achieved by detecting and containing biothreats at their source, supporting and promoting the responsible conduct of biomedical innovation, and improving emergency response. Pillar Two calls for "promot[ing] American prosperity," which increasingly will depend on a vibrant life sciences and biotechnology enterprise.

This *National Biodefense Strategy* highlights the President's commitment to protect the American people and our way of life, laying out a clear pathway and set of objectives to effectively counter threats from naturally occurring, accidental, and deliberate biological events. It is broader than a Federal Government strategy. It is a call to action for state, local, territorial, and tribal (SLTT) entities, other governments, practitioners, physicians, scientists, educators, and industry.

This page is intentionally blank

TABLE OF CONTENTS

FOREWORD i
VISION 1
PURPOSE 1
THREATS AND CONSEQUENCES 2
BIOLOGICAL RISK MANAGEMENT 2
ASSUMPTIONS 3
GOVERNANCE 4
GOALS AND OBJECTIVES 6
CONCLUSION 8
ANNEX I: NATIONAL BIODEFENSE STRATEGY IMPLEMENTATION PLAN 9
ANNEX II: DEFINITIONS 28
ANNEX III: SCOPE, STATUTORY REQUIREMENTS, AND AGENCIES 29

This page is intentionally blank

VISION

The United States actively and effectively prevents, prepares for, responds to, recovers from, and mitigates risk from natural, accidental, or deliberate biological threats.

PURPOSE

This *National Biodefense Strategy* brings together and puts in place for the first time, a single coordinated effort to orchestrate the full range of activity that is carried out across the United States Government to protect the American people from biological threats. With National Security Presidential Memorandum (NSPM)-14, this strategy explains how the United States Government will manage its activities more effectively to assess, prevent, detect, prepare for, respond to, and recover from biological threats, coordinating its biodefense efforts with those of international partners, industry, academia, non-governmental entities, and the private sector.

The mission of the Federal Government during a biological incident is to save lives, reduce human suffering, protect property and the environment, control the spread of disease, and support community efforts to overcome the physical, emotional, environmental, and economic impacts. This federal mission is contingent upon the coordination with and the success of the community response. This strategy describes the goals and objectives that will guide the United States in assessing, preventing, detecting, preparing for, responding to, and recovering from a biological incident, consistent with its international obligations, including those identified in the World Health Organization's International Health Regulations (2005).

Enhancing the national biodefense enterprise will help protect the United States and its partners abroad from biological incidents, whether deliberate, naturally occurring, or accidental in origin. It will simultaneously build the U.S. innovation base for cutting edge medical countermeasures (MCMs), biosensors and diagnostics, and biosurveillance information technologies, and advance the biomedical industry.

THREATS AND CONSEQUENCES

Naturally Occurring Biological Threats. Infectious disease threats do not respect borders. Urbanization, habitat encroachment, and increased and faster travel, coupled with weak health systems, increase the ability of infectious diseases to spread rapidly across the globe. Antimicrobial resistance, novel infectious diseases, and the resurgence and spread of once geographically limited infectious diseases can overwhelm response capacities and make outbreaks harder to control. An infectious disease outbreak—even in the most remote places of the world—could spread rapidly across oceans and continents, directly impacting the U.S. population and its health, security, and prosperity.

Deliberate and Accidental Biological Threats. The use of biological weapons or their proliferation by state or non-state actors presents a significant challenge to our national security, our population, our agriculture, and the environment. Multiple nations have pursued clandestine biological weapons programs and a number of terrorist groups have sought to acquire biological weapons. In many countries around the world, pathogens are stored in laboratories that lack appropriate biosecurity measures where they could be diverted by actors who wish to do harm. Similarly, some laboratories do not have appropriate biocontainment or biosafety protocols, which could lead to an outbreak through a laboratory acquired infection or if a pathogen is accidentally released into the environment. Biological material is ubiquitous and can self-propagate; pathogens are found all over the world—in the environment, animal reservoirs, humans, and laboratories. A natural outbreak can lead quickly to not only a public health crisis, but also a biosecurity vulnerability due to the thousands of clinical samples that are generated during an epidemic, which, if handled without appropriate biosecurity measures, could facilitate the development of a biological weapon.

BIOLOGICAL RISK MANAGEMENT

Biological risk management requires understanding and assessing biological risks, and taking steps to prepare for, prevent, and respond to them, regardless of whether they originate in the United States or abroad. It also requires shared international recognition that the risk is global to empower effective, collective mitigation. In our interconnected world, it is not if, but when, the next biological incident will occur.

As the biological threat continues to evolve, so must our biodefense capabilities. If all countries could prevent, detect, and respond to infectious disease outbreaks at the local level, we can minimize the risk of global health emergencies, saving both lives and resources. Preventing acquisition of dangerous pathogens, equipment, and expertise for nefarious purposes, and maintaining the capability to rapidly control outbreaks in the event of a biological attack, are strategic interests of the United States. These must be strategic interests for partners around the world as well. The United States cannot carry the burden alone. Finally, as we reap the benefits from biotechnologies, we must also understand and consider the risks they may pose. The United States will pursue an efficient and coordinated biodefense enterprise to protect the American people.

Domestic action alone is insufficient to protect America's health and security. The rapid globalization of science and technology and the interconnectedness of travel and trade necessitate

a strong biodefense enterprise that has global reach to effectively prevent, detect, and respond to biological incidents. The United States Government works at home and abroad to ensure that the United States and its partners are protected from natural, accidental, or deliberate biological threats. While the desired outcomes at home and abroad are the same, the conditions and avenues available to achieve these outcomes can be very different. Internationally, our efforts to protect the United States and our partners include direct investment in sustainable, context-appropriate capacity building that leads to self-reliance. We will work with multilateral organizations, partner nations, private donors, and civil society to control disease outbreaks at their source by supporting the development and implementation of biodefense and health security capabilities, policies, and standards.

The United States has long been an innovation leader. Whether augmenting our ability to provide health care and protect the environment, or expanding our capacity for energy and agricultural production towards global sustainability, continued research and development in life sciences is essential for a brighter future for the American people. To ensure that the United States is poised to meet the evolving biological risk landscape, at a time when unparalleled advancement and innovation in the life sciences globally continue to transform our way of life, we are committed to promoting innovation throughout the national biodefense enterprise. We will promote innovative technologies and systems; encourage innovative technology communities and industry leaders to meet our targeted biodefense and health capacity needs; link stakeholders with new ideas, tools, and products; and pursue innovative approaches and partnerships to achieve, at home and abroad, the desired goals articulated in this *National Biodefense Strategy*.

Through the *National Biodefense Strategy*, the United States will use all appropriate means to assess, understand, prevent, prepare for, respond to, and recover from biological incidents—whatever their origin—that threaten national or economic security. The *National Biodefense Strategy* recognizes that a collaborative, multi-sectoral, and trans-disciplinary approach to the national biodefense enterprise is necessary to counter biological threats effectively and efficiently.

ASSUMPTIONS

The evolving biological threat landscape requires a comprehensive approach, and the United States recognizes the following principles:

- **Biological Threats are Persistent**. Pathogens have emerged and spread throughout history, and as new naturally occurring threats develop, the risk from them grows more acute as the world becomes more urbanized, travel increases, and habitats change. Separately, nation-states and terrorist groups have found value in pursuing biological weapons, and there can be no confidence that will change in the future. Advances in the life sciences will both reduce the technological hurdles to such weapons and expand the number of individuals with relevant skills to effectuate threats.

- **Biological Threats Originate from Multiple Sources**. The United States will include, within the scope of biodefense, not just countering deliberate biological threats, but also the threats that stem from naturally occurring and accidental outbreaks. This approach will allow the United States Government to fully utilize, integrate, and coordinate the biodefense enterprise and ensure the most efficient use of all biodefense assets.

- **Infectious Diseases Do Not Respect Borders**. An interconnected world increases the opportunity for pathogens to emerge and spread so that a disease threat anywhere is a disease threat everywhere. Infectious diseases travel without visas and cross borders indiscriminately; infected travelers may not manifest any symptoms. The United States Government will mitigate biological incidents both here in the United States and work with partners abroad because the United States cannot counter biological threats nationally without addressing them internationally. We will also seek to improve our ability to prevent the spread of infectious diseases to the United States through inbound travelers and goods. The Ebola outbreaks of 2014 and 2018 demonstrated that the United States Government must be prepared to act swiftly, and unilaterally if necessary, to respond to public health emergencies abroad if multilateral institutions and partners are not prepared to do so.

- **Multi-sectoral Cooperation is Critical for Prevention and Response**. This strategy calls for engagement and cooperation across all levels of government, to include SLTT governments, as well as internationally. It involves partnership with multiple sectors, including the medical; public, animal, and plant health; emergency response; scientific and technical; law enforcement; industrial; academic; diplomatic; defense and security; intelligence; and nonproliferation and counterproliferation sectors, among others. Engagement with non-governmental organizations (NGOs) and the private sector is critical to prevent the spread of disease and respond to the next outbreak before it becomes an epidemic.

- **A Multidisciplinary Approach Will Help Prevent Disease Emergence**. The health of people, animals, plants, and the environment are linked, and diseases affecting one component can soon affect others. At least 75 percent of infectious disease threats to human health are of animal origin. Threats to animals and plants can cause economic disruption and physical harm to health and well-being. A coordinated, multidisciplinary approach, representing the collaborative efforts across local, national, and global jurisdictions, is a best practice for understanding, communicating, and mitigating biological threats swiftly and efficiently. Such an approach is necessary to prevent and detect early inter-species cross-over of infectious diseases.

- **Science and Technology Will Continue to Advance Globally**. The ongoing revolution in the life sciences and biotechnology will continue at an ever-increasing rate, offering solutions to many of the challenges of ensuring the health, prosperity, and security of a growing global population. These technologies, no longer confined to sophisticated research laboratories, are being developed and utilized all over the world and the necessary expertise, materials, and equipment are available widely. Advances in science and technology bring revolutionary cures and progress, but they also have the potential to facilitate intentional misuse. The United States has a responsibility to ensure our technology, development, and assistance programs do not exacerbate this risk unintentionally.

GOVERNANCE

The NSPM that accompanies the issuance of this *National Biodefense Strategy* creates a dedicated mechanism, housed within the U.S. Department of Health and Human Services, to coordinate federal biodefense activities and assess the effectiveness with which the *National Biodefense Strategy*'s goals and objectives are being met. Led by the President of the United States and coordinated by the National Security Council staff in the Executive Office of the President, with day-

to-day coordination and execution by the Secretary of Health and Human Services, this mechanism will continually assess how effectively the objectives of the *National Biodefense Strategy* are being met.

The Assistant to the President for National Security Affairs will, in acting through the process described in NSPM-4, *Organization of the National Security Council, the Homeland Security Council, and Subcommittees*, serve as the lead for policy coordination and review, providing strategic input and policy oversight for federal biodefense efforts.

The Biodefense Steering Committee, chaired by the Secretary of Health and Human Services, and comprising the Secretary of State, the Secretary of Defense, the Attorney General, the Secretary of Agriculture, the Secretary of Veterans Affairs, the Secretary of Homeland Security, and the Administrator of the Environmental Protection Agency, will be responsible for overseeing and coordinating the execution of the strategy and its implementation plan, and ensuring federal coordination with domestic and international government and non-governmental partners. The Chair of the Biodefense Steering Committee, the Secretary of Health and Human Services, will serve as the federal lead for implementation of the strategy. The heads of other agencies with responsibilities or capabilities pertaining to biodefense shall participate in the Biodefense Steering Committee, as appropriate. This coordination and oversight mechanism also has a mandate to reach beyond the Federal Government to engage with SLTT, non-federal, and non-governmental stakeholders. Further, the recommendations and feedback stemming from this governance mechanism will be communicated back to departments and agencies in synchronization with the annual budget cycle. Recognizing that threats, actors, and biodefense-related science and technology are constantly evolving, the governance mechanisms will be adaptive, reviewing and recommending changes, as appropriate, in the *National Biodefense Strategy* and its implementation plan.

GOALS AND OBJECTIVES

The *National Biodefense Strategy* has five goals with associated objectives for strengthening the biodefense enterprise, establishing a layered risk management approach to countering biological threats and incidents.

GOAL 1: ENABLE RISK AWARENESS TO INFORM DECISION-MAKING ACROSS THE BIODEFENSE ENTERPRISE. The United States will build risk awareness at the strategic level, through analyses and research efforts to characterize deliberate, accidental, and natural biological risks; and at the operational level, through surveillance and detection activities to detect and identify biological threats and anticipate biological incidents.	
OBJECTIVES:	
1.1: Ensure decision-making is informed by intelligence, forecasting, and risk assessment.	**1.2**: Ensure that domestic and international biosurveillance and information-sharing systems are coordinated and are capable of timely bioincident prevention, detection, assessment, response, and recovery.

GOAL 2: ENSURE BIODEFENSE ENTERPRISE CAPABILITIES TO PREVENT BIOINCIDENTS. The United States will work to prevent the outbreak and spread of naturally occurring disease, and minimize the chances of laboratory accidents. The United States will also strengthen biosecurity to prevent hostile actors from obtaining or using biological material, equipment, and expertise for nefarious purposes, consistent with the United States Govermenent's approach to countering weapons of mass destruction (WMD) terrorism. Goal 2 will ensure we have the capabilities necessary to disrupt plots, degrade technical capabilities, and deter support for terrorists seeking to use WMD. This goal also recognizes the "dual use" natures of the life sciences and biotechnology, in which the same science and technology base that improves health, promotes innovation, and protects the environment, can also be misused to facilitate a biological attack. The United States seeks to prevent the misuse of science and technology while promoting and enhancing legitimate use and innovation.	
OBJECTIVES:	
2.1: Promote measures to prevent or reduce the spread of naturally occurring infectious diseases.	**2.3**: Deter, detect, degrade, disrupt, deny, or otherwise prevent nation-state and non-state actors' attempts to pursue, acquire, or use biological weapons, related materials, or their means of delivery.
2.2: Strengthen global health security capacities to prevent local bioincidents from becoming epidemics.	**2.4**: Strengthen biosafety and biosecurity practices and oversight to mitigate risks of bioincidents.

GOAL 3: ENSURE BIODEFENSE ENTERPRISE PREPAREDNESS TO REDUCE THE IMPACTS OF BIOINCIDENTS. The United States will take measures to reduce the impacts of bioincidents, including maintaining a vibrant national science and technology base to support biodefense; ensuring a strong public health infrastructure; developing, updating, and exercising response capabilities; establishing risk communications; developing and effectively distributing and dispensing medical countermeasures; and preparing to collaborate across the country and internationally to support biodefense.

OBJECTIVES:

3.1: Ensure a vibrant and innovative national science and technology base to support biodefense.	**3.6**: Enhance preparedness to limit the spread of disease through Community Mitigation Measures (CMMs).
3.2: Ensure a strong public and veterinary health infrastructure.	**3.7**: Enhance preparedness to support decontamination.
3.3: Develop, exercise, and update prevention, response, and recovery plans and capabilities.	**3.8**: Strengthen preparedness to operate and collaborate across the United States, including the U.S. territories.
3.4: Develop, exercise, and update risk communication plans and promote consistent messaging to inform key audiences, expedite desired response actions, and address public uncertainty and fear.	**3.9**: Strengthen international preparedness to support international response and recovery capabilities.
3.5: Enhance preparedness to save lives through MCMs.	

GOAL 4: RAPIDLY RESPOND TO LIMIT THE IMPACTS OF BIOINCIDENTS. The United States will respond rapidly to limit the impacts of bioincidents through information-sharing and networking; coordinated response operations and investigations; and effective public messaging.

OBJECTIVES:

4.1: Compile and share biothreat and bioincident information to enable appropriate decision-making and response operations across all levels of government and with non-governmental, private sector, and international entities, as appropriate.	**4.3**: Conduct operations and investigations, and use all available tools to hold perpetrators accountable.
4.2: Conduct federal response operations and activities in coordination with relevant non-federal actors to contain, control, and rapidly mitigate impacts of biothreats or bioincidents.	**4.4**: Execute risk-informed, accurate, timely, and actionable public messaging.

GOAL 5: FACILITATE RECOVERY TO RESTORE THE COMMUNITY, THE ECONOMY, AND THE ENVIRONMENT AFTER A BIOINCIDENT. The United States will take actions to restore critical infrastructure services and capability; coordinate recovery activities; provide recovery support and long-term mitigation; and minimize cascading effects elsewhere in the world.

OBJECTIVES:

5.1: Promote restoration of critical infrastructure capability and capacity to enable the resumption of vital U.S. activities.	**5.3**: Provide recovery support and conduct long-term mitigation actions to promote resilience.
5.2: Ensure coordination of recovery activities across federal and SLTT governments and, as appropriate, international, non-governmental, and private sector partners to enable effective and efficient recovery operations.	**5.4**: Reduce the cascading effects of international biological incidents on the global economy, health, and security.

CONCLUSION

The risks from biological threats cannot be reduced to zero – but they can and must be managed. Wide-ranging threats require a comprehensive approach to minimizing the risks. Through this *National Biodefense Strategy*, the United States Government will optimize its own efforts, and harness the work of essential partners—inside government and outside, domestically and internationally—to understand, prevent, prepare for, respond to, and recover from the full range of biological threats that can harm the American people and our partners.

ANNEX I
NATIONAL BIODEFENSE STRATEGY IMPLEMENTATION PLAN

GOAL 1:
ENABLE RISK AWARENESS TO INFORM DECISION-MAKING ACROSS THE BIODEFENSE ENTERPRISE.

1.1 Ensure decision-making is informed by intelligence, forecasting, and risk assessment.

1.1.1 Enhance Intelligence and Analysis Activities.

- Provide timely intelligence analysis and information that identifies and assesses current and future biological threats posed by nation-state and non-state actors.
- Provide strategic warning for, and assess the potential impacts of, diseases with the potential to affect U.S. national security or interests abroad, including assessments of the potential cascading effects (e.g., economic, societal, and governmental impacts).
- Incorporate forecasting and modeling into intelligence products and processes, as appropriate.
- Routinely evaluate developments and advances in the life sciences, biotechnology, and related fields to identify emerging hazards and mitigation options.

1.1.2 Conduct Research and Modeling Activities.

- Conduct research to characterize biological hazards, production methods, and dissemination methods that could be used in deliberate threats, when:
  - The results of that research are critical to informing risk assessments and plans to prevent or respond to deliberate bioincidents; and
  - The responsible department or agency utilizes a process to ensure that the research complies with treaties, laws, and policies and follows applicable nationally recognized guidance for best practices.
- Improve the ability to model and forecast the likelihood and impact of bioincidents, including accidental releases.

1.1.3 Assess Risks and Capabilities.

- Conduct periodic national bioincident risk assessments to evaluate the risks, including relative risks, of deliberate, accidental, and naturally occurring bioincidents.
- Assess the security risks posed by the deliberate misuse of biotechnologies and life sciences research and training with dual-use potential.
- Assess the risks posed by research, such as with potential pandemic pathogens, where biosafety lapses could have very high consequences.
- Provide all levels of government with a common basis for understanding biological risks to support operational planning and preparedness actions.
- Develop risk-informed planning scenarios to facilitate capability and capacity assessments and identify gaps.

- Assess the potential impacts of bioincidents on critical infrastructure and supply chains, and how disruption of these systems might affect the ability to respond to bioincidents.

1.2 Ensure that domestic and international biosurveillance and information-sharing systems are coordinated and are capable of timely bioincident prevention, detection, assessment, response, and recovery.

1.2.1 Enhance the Integration and Evaluation of Biosurveillance Systems.

- Improve development, interoperability, integration, and evaluation processes for domestic biosurveillance systems, including opportunities to better-leverage multi-sectoral information.

1.2.2 Improve Information-sharing and Reporting.

- Using a multi-sectoral approach, promote timely sharing of biosurveillance information among federal and SLTT biosurveillance programs and other federal programs designed to investigate biothreats and bioincidents.
- Coordinate and exchange relevant information between environmental biological detection systems and biosurveillance networks.
- Strengthen foreign governments' and international bodies' capability and commitment to identify, characterize, and report biothreats and bioincidents rapidly and transparently.
- Integrate international disease reporting data with domestic biosurveillance systems to enable early action that limits potential impact.
- Create biosurveillance and situational awareness reports tailored to inform decision-makers, the public, partner nations, and other audiences routinely and during a bioincident response.
- Ensure that the Federal Government, SLTT governments, partner nations, and the private sector have appropriate access to relevant information and analysis.
- As appropriate, ensure rapid downgrade of classified or otherwise sensitive intelligence information and write intelligence products for release, as appropriate, to enable sharing with those who need to act on it.

1.2.3 Develop and Deploy Enhanced Biosurveillance and Bioincident Characterization Capabilities.

- Maintain and enhance public health, medical, animal, and plant surveillance systems for disease outbreaks that pose a risk to national security.
- Promote the sustainable development, maintenance, and improvement of SLTT, private sector, federal, regional, and international (United States Government and other national) surveillance systems and networks with reliable access to trained workforces and essential infrastructure for human, animal, and plant diseases.
- Identify and incorporate new technologies, data sources, analytic methods, and partnerships that include public, private sector, and non-traditional sources of data.
- Maintain and enhance biosurveillance capabilities for the identification of emerging biothreats, and monitor and assess short- and long-term post-bioincident health effects using traditional and non-traditional methods.
- Enhance capability to characterize bioincidents rapidly with respect to biohazards involved, populations and areas affected, and consequences (e.g., health, economic, societal, and environmental).

1.2.4 Develop and Deploy Enhanced Environmental Detection Systems, as Appropriate.

- Monitor and evaluate the capability and effectiveness of systems for the environmental identification and detection of human, animal, and plant biohazards, and disease vectors.

- Develop improved environmental identification and detection systems, ensuring that they:
  - Are aligned with assessments of evolving and emerging biothreats; and
  - Can provide information that is timely, accurate, and relevant for response decisions.
- Assess options to ensure the effectiveness of environmental biodetection systems deployed by governmental or non-governmental entities.

1.2.5 Enhance Biosurveillance Laboratory Operations.

- Promote the sustainable development, maintenance, and improvement of SLTT, private sector, federal, regional, and international (United States Government and partner nation) laboratory networks, with reliable access to trained workforces and essential infrastructure, for human, animal, and plant diseases.
- Promote interoperability of laboratory reporting systems at all levels of government.
- Strengthen capabilities and address appropriate needs for sharing—under both routine and crisis conditions—timely information (e.g., data and results), samples, and reagents among sectors including research; human, animal, and plant health; emergency services; and law enforcement.
- Address impediments to the timely sharing of information, samples, and reagents among countries and international organizations under both routine and crisis conditions.

GOAL 2:
ENSURE BIODEFENSE ENTERPRISE CAPABILITIES TO PREVENT BIOINCIDENTS.

2.1 Promote measures to prevent or reduce the spread of naturally occurring infectious diseases.

2.1.1 Strengthen Infection Prevention Measures Domestically and Internationally.

- Using a multidisciplinary approach, strengthen medical, public health, animal health, and plant health capacities to improve infection prevention and control.
- Strengthen vaccination and other health intervention activities.

2.1.2 Reduce the Emergence and Spread of Antimicrobial-resistant Pathogens Domestically and Internationally.

- Strengthen awareness of drug-resistant pathogens and their associated diseases, and improve stewardship of medically important drugs.
- Strengthen understanding of the drivers of drug resistance and improve the development and adoption of effective mitigation measures.
- Promote the use of preventive and therapeutic options other than antimicrobial drugs.
- Accelerate basic and applied research and development of new antimicrobials, novel preventatives and therapeutics, vaccines, and diagnostic tests.

2.1.3 Strengthen Multidisciplinary Efforts to Control Vector-borne Disease Domestically and Internationally.

- Identify the risk of the vectors transmitting disease to humans, animals, and plants.
- Develop and disseminate, as appropriate, measures that will safely limit the exposure of humans, animals, and plants to disease vectors and the ability of vectors to transmit disease to humans and animals.
- Address resistance of vectors to vector control or mitigation measures.

2.1.4 Limit Trans-border Introductions and Domestic Spread of Biohazards, Including Those Responsible for Food-borne Illness.

- Identify, locate, and destroy or contain contaminated/infected plant, animal, and food prior to entry into the United States, and within the United States, that:
  - Contain biohazards that could give rise to bioincidents, including food-borne illness; or
  - Harbor economically and environmentally significant pests.
- Improve capabilities and protocols for screening, isolation, and quarantine of humans, plants, and animals to reduce disease spread.
- Develop programs and policies to encourage plant and animal producers to report suspected or actual biohazards and encourage full compliance with response guidance to limit the spread of plant or animal diseases and reduce their impact on the overall industry.

2.1.5 Strengthen Animal Disease Detection and Prevention Capacity.

- Strengthen capacity to detect and prevent the spread of animal and zoonotic diseases.
- Support the development and deployment of diagnostics and countermeasures for use in animals as well as the development of disease-resistant animals.

- Strengthen international partnerships regarding awareness, detection and control, and eradication of animal diseases before they reach the United States.

2.1.6 Strengthen Plant Disease Prevention Capacity.

- Strengthen the capacity to prevent establishment and spread of plant pests.
- Support the development and deployment of new disease-resistant crops.
- Strengthen international partnerships regarding detection and management of plant diseases before they reach the United States.

2.1.7 Strengthen the Resilience of the Water Sector to Prevent or Contain Water-borne Disease Outbreaks.

- Identify water system vulnerabilities that increase the risk of drinking water contamination, and promote the development of engineering controls and best practices to reduce the risk.
- Develop plans and procedures to reduce the spread of contaminants in a compromised water system and reduce public exposure to contaminated water.
- Improve the ability to detect biohazardous agents in source and finished drinking water.

2.2 Strengthen global health security capacities to prevent local bioincidents from becoming epidemics.

2.2.1 Promote Global Health Security.

- Promote the development and implementation of national legal frameworks adequate to support and enable the implementation of the World Health Organization's International Health Regulations (2005) and the World Organisation for Animal Health reporting requirements.
- Promote transparent, independent, and objective assessments of country capacity to prevent, detect, and respond to bioincidents.
- Strengthen timely surveillance and monitoring for core syndromes and confirmed reportable infections as outlined by international bodies to ensure quick identification and reporting of bioincidents.

2.2.2 Strengthen Country Capacity to Prevent, Detect, and Respond to Bioincidents.

- Promote a prepared public health and animal health workforce appropriate for the population.
- Strengthen capacity and promote policies and best practices to minimize transmission of disease between humans and animals.
- Promote incident management systems capable of activating an emergency operations system in response to public health emergencies.
- Promote the development of a system for specimen referral and effective diagnostics to ensure timely testing of biological specimens, and work to remove barriers to the sharing of samples among countries and international organizations.
- Promote national laboratory systems capable of timely receipt and testing of biological specimens from all jurisdictions in a country.

2.3 Deter, detect, degrade, disrupt, deny, or otherwise prevent nation-state and non-state actors' attempts to pursue, acquire, or use biological weapons, related materials, or their means of delivery.

2.3.1 Deter Nation-state and Non-state Actors.

- Ensure accountability by increasing and communicating the political, economic, and other consequences for actors that develop, acquire, produce, or use biological weapons, or assist in such efforts.
- Ensure domestic and international capabilities to identify, investigate, and attribute development or use of biological weapons in order to hold accountable those who are responsible.
- Demonstrate reduced vulnerability through enhanced U.S. and partner-nation capacity to prevent, respond to, and recover from bioincidents.
- Reinforce the obligations in the Convention on the Prohibition of the Development, Production, and Stockpiling of Bacteriological and Toxin Weapons and on their Destruction (BWC) (1975) and United Nations (U.N.) Security Council Resolution 1540, as well as other standards and norms against nation-state or non-state development, acquisition, or use of biological weapons, related materials, or means of delivery.

2.3.2 Detect, Degrade, or Deny Acquisition, Development, or Transfer of Biological Weapons.

- Strengthen nations' commitment and support their efforts to implement their obligations under the BWC and U.N. Security Council Resolution 1540 to establish and enforce appropriate and effective laws prohibiting and preventing the acquisition, development, or transfer of biological weapon-related materials, equipment, and means of delivery for purposes proscribed by these instruments.
- Strengthen domestic and international capabilities to identify, deny, and disrupt biological weapon-related transfers, and to identify and disrupt adversary proliferation networks.
- Deny the acquisition of pathogenic material, equipment, knowledge, or expertise for illicit purposes, and promote appropriate measures to impede misuse of life sciences and biotechnology, while facilitating legitimate use and innovation.

2.3.3 Prevent, Disrupt, Degrade, or Deny Use of Biological Weapons.

- Identify and locate threat actors and proliferation networks, and preempt or disrupt deliberate biothreats and bioincidents.
- Ensure robust capabilities to interdict, disable, destroy, render safe, and attribute responsibility for biological weapons and weapons-related equipment, material, means of delivery, and facilities.
- Strengthen the engagement of the law enforcement and security communities with other stakeholders to facilitate recognition and mitigation of situations involving deliberate biothreats and bioincidents.

2.3.4 Develop, Exercise, and Update Prevention and Disruption Plans and Capabilities.

- Ensure prevention and disruption capabilities and plans are developed, routinely exercised, evaluated, and updated, as appropriate.

2.4 Strengthen biosafety and biosecurity practices and oversight to mitigate risks of bioincidents.

2.4.1 Strengthen Biosafety and Biosecurity.

- Maintain and continuously improve biosafety, biosecurity, and oversight programs and practices for laboratories and other facilities, and for the end-to-end management of samples and specimens (e.g., collection, transport, inactivation, disposal, and waste management).

- Promote appropriate national and facility-specific biosafety, biosecurity (including cybersecurity), and oversight programs, policies, practices, and legislation in partner nations while facilitating legitimate research and innovation.
- Coordinate and conduct basic and applied biosafety and biosecurity research to provide an evidence base for improving safety and security practices.
- Encourage facilities working with biohazards to engage in pre-incident response planning, training, and exercises, including with local responders, to minimize impacts from accidental releases.

2.4.2 Support and Promote the Responsible Conduct of the Life Science and Biotechnology Enterprise.

- Support and promote a culture of global biosafety, biosecurity, ethical, and responsible conduct in the life sciences.
- Promote effective global oversight of:
  - Dual-use research, to prevent misuse; and
  - Research for which biosafety lapses could have very high consequences, such as with potential pandemic pathogens.
- Encourage engagement among the health, scientific, biotechnology, enthusiast, and security communities in the United States, and with international partners, to reduce the risk of misuse.
- Promote the development and implementation of relevant national and international policies, guidance, training, and other resources across the health, scientific, biotechnology, enthusiast, and security communities to reduce the risk of misuse.

GOAL 3:
ENSURE BIODEFENSE ENTERPRISE PREPAREDNESS TO REDUCE THE IMPACTS OF BIOINCIDENTS.

3.1 Ensure a vibrant and innovative national science and technology base to support biodefense.

3.1.1 Enable U.S.-led Innovation for Biodefense Through Robust Scientific, Technical, and Industrial Bases.

- Support investments and U.S. leadership in emerging technologies.
- Maintain laboratory capabilities required for biodefense preparedness and response, including:
  - Assured United States Government access to laboratory infrastructure, including a trained workforce capable of supporting United States Government biodefense programs and decision-making; and
  - A secure and dedicated United States Government laboratory capability for conducting forensic analysis of biological agents and traditional forensic examinations of contaminated evidence up to the highest biosafety levels.
- Strengthen U.S. processes to prevent industrial espionage and other actions that would weaken the U.S. biodefense enterprise.

3.1.2 Integrate Research and Development (R&D) into Federal Planning.

- Identify and facilitate sharing of tools, practices, policies, and incentives across interagency response R&D efforts.
- Establish capabilities to conduct rapid-response, real-time R&D during bioincidents to inform ongoing response measures and to understand phenomena that only occur during bioincidents.
- Establish procedures for prioritizing, funding, and coordinating R&D efforts during bioincidents.

3.2 Ensure a strong public and veterinary health infrastructure.

3.2.1 Ensure Public and Veterinary Health Critical Capacities.

- Establish capability to provide surge staffing, resources, and supplies to SLTT public and veterinary health departments.
- Advance and sustain a highly-skilled public and veterinary health workforce.

3.2.2 Modernize Public and Veterinary Health Laboratories.

- Ensure core public and veterinary health laboratories have access to modern and updated diagnostic tests, methods, equipment, and technologies.

3.3 Develop, exercise, and update prevention, response, and recovery plans and capabilities.

3.3.1 Develop and Exercise Policies, Plans, Guidelines, and Recommendations to Support Prevention, Response, and Recovery Activities.

- Establish policies, plans, guidelines, and recommendations with multi-sectoral input (and

international stakeholder input, as appropriate) to inform appropriate and timely federal and SLTT response actions to biothreats and bioincidents.

- Develop plans that implement or support surge capabilities across response sectors in coordination with SLTT entities, health care coalitions, foreign governments, international organizations, NGOs, and private sector partners, to include the following:
  - Medical surge response, including to augment specialized clinical care, behavioral and mental health care, transition to crisis standards of care, and provision of mass care and mass fatality management;
  - Clinical guidance to assist with appropriate triage and medical management of illnesses;
  - Transport and reception system and capabilities for crossing borders and U.S. jurisdictions with highly infectious disease patients and materials related to incident response
  - Augmenting provision of human services, including shelters, housing, and commodity distribution;
  - Implementing enhanced surveillance and public health measures for disease control;
  - Clinical, environmental, food testing, and forensic surge laboratory operations;
  - Controlling, responding to, and recovering from animal and plant disease;
  - Engineering response for managing water, land, waste, and air systems; and
  - Routinely conducting and evaluating biothreat and bioincident response exercises for all incident management phases of the response at the federal and SLTT levels.

3.3.2 Ensure that Emergency Funding Mechanisms Exist to Support Urgent Responses to Bioincidents.

- Establish, as appropriate, dedicated funding processes and mechanisms to respond to an actual or imminent bioincident.
- Establish processes to access funds in a timely manner.

3.3.3 Support the Effective Deployment of the MCM Stockpiles.

- Conduct pre-incident planning for distribution and dispensing of the MCM stockpiles to ensure such activities can be accomplished in a timely manner, are informed by appropriate guidance, and can be supported operationally by federal and SLTT agencies during a bioincident.
- Ensure plans consider the provision of MCMs to personnel performing mission-essential functions to help ensure that mission-essential functions continue to be performed after a bioincident.
- Ensure the safety, security (including cybersecurity), and reliability of supply chains to provide necessary MCMs and other materiel support during bioincidents.
- Ensure the capability to monitor the safety and effectiveness of deployed MCMs.
- Integrate the access and functional needs of at-risk individuals in planning for MCM distribution and dispensing.
- Ensure that operational plans, clinical guidance, regulatory mechanisms, and operational capacity are in place to administer stockpiled MCMs effectively.

3.3.4 Support the Provision of Health Care and the Conduct of Clinical Research During Bioincidents.

- Establish procedures and guidelines for the use of MCMs, including personal protective equipment (PPE), and infection control strategies.
- Ensure plans address the needs of all populations, including at-risk individuals.
- Establish and identify medical centers capable of providing specialized care, including at the initial stages of bioincidents.
- Strengthen healthcare system preparedness to enhance hospital and health care facilities' ability to maintain health care operations and provide necessary care during bioincidents.

- Identify existing mechanisms to protect health care workers from financial liability during federally-led responses.
- Establish capabilities to conduct clinical research at the onset of a bioincident to inform optimal clinical care strategies for current and future bioincidents and to support MCM development.
- Establish and pre-position protocols for the conduct of ethical, efficient, and interpretable clinical trials to test promising investigational MCMs during domestic or international bioincidents.
- Establish mechanisms for the collection and sharing of clinical samples to support development of diagnostic tests.
- Establish a regional aid system that will improve national healthcare readiness and medical surge for bioincidents.

3.3.5 Support the Continuity of Operations.

- Further refine, exercise, and evaluate Continuity of Operations plans (including the mitigation of impacts on critical infrastructure located within and outside the United States) to ensure continuation of National Essential Functions during and after bioincidents.

3.3.6 Support Provision of Essential Services and Long-term Recovery.

- Protect the continuity of critical infrastructure, and restore infrastructure and services disrupted by the bioincident.
- Restore critical infrastructure to minimize cascading effects.
- Provide an environment in which essential businesses can continue to operate.
- Support or restore transportation pathways and infrastructure to facilitate supply chains and movement of people.
- Facilitate movement/delivery of supplies critical to response and recovery.

3.4 Develop, exercise, and update risk communication plans and promote consistent messaging to inform key audiences, expedite desired response actions, and address public uncertainty and fear.

3.4.1 Improve Federal Messaging Coordination for Biothreats and Bioincidents.

- Develop a government-wide strategy that institutionalizes the use of risk communication principles to provide clear, consistent, and coordinated information.
- Train spokespersons for federal departments and agencies on risk communications.
- Clarify roles of lead agencies for risk communication messaging to key sectors (e.g., public health, medical, animal, plant, and the environment).

3.4.2 Develop and Exercise Communications Plans.

- Develop and test messaging strategies, platforms, and materials for all sectors and stakeholders to synchronize messaging, address public fear and uncertainty, encourage appropriate response actions, and empower the public during biothreats and bioincidents.
- Develop messaging for non-English speaking populations and in formats that accommodate the access and functional needs of all individuals.
- Establish a national "brand" where stakeholders may routinely seek information on biodefense activities and response actions.
- Routinely exercise communication strategies during pre-incident planning to prepare for real-time biothreat and bioincident response communications.

3.4.3 Enhance Messaging Partnerships.

- Identify a cadre of academic and private sector experts who would be encouraged to interact with traditional and social media and provide accurate information on biothreats and bioincidents.
- Strengthen pre-incident relationships between government communication specialists and the media who specialize in bioincidents and related topics.
- Strengthen pre-incident relationships with private sector social media and other non-traditional media partners capable of broadly disseminating information.

3.5 Enhance preparedness to save lives through MCMs.

3.5.1 Improve Diagnostic Capabilities.

- Advance diagnostic capabilities, including for plants and animal diseases, to enable timely and accurate biohazard and disease detection.
- Maintain a core capability to develop, produce, and refine diagnostic tests rapidly to meet outbreak response needs.
- Develop instructions for public health and medical stakeholders regarding the use of Food and Drug Administration (FDA)-authorized or -cleared diagnostic tests, if available.
- Enhance capability to rapidly characterize bioincidents to help inform ongoing or future response to biothreats and bioincidents.
- Establish standardized Material Transfer Agreements for sample sharing.

3.5.2 Enhance MCM Development, Sustainment, and Availability.

- Use risk and intelligence assessments, epidemiologic analysis, and anticipated operational capacities to inform the life cycle of research, development, evaluation, manufacturing, acquisition, stockpiling, and sustainment of MCMs for humans and animals.
- Support and strengthen mechanisms to comprehensively evaluate and make changes, as needed, across the portfolio of MCMs.
- Prioritize the development and procurement of MCMs with the highest potential to reduce severe morbidity and mortality.
- Prioritize the development of modular platform and innovative technologies to support timely development, production, and availability of MCMs for bioincidents.
- Identify additional incentive mechanisms to engage MCM developers and stimulate private sector investment and innovation across the range of the MCM technology base.
- Improve or develop affordable, flexible, and multi-functional PPE for responders, health professionals, and the general population.
- Establish manufacturing surge capacity for MCMs, including diagnostic tests and PPE.

3.6 Enhance preparedness to limit the spread of disease through CMMs.

3.6.1 Enhance Development of and Capabilities for Implementing CMMs.

- Develop and assess the effectiveness of CMMs to mitigate the impact of bioincidents.
- Establish and promote best practices for implementing CMMs during bioincidents.

3.7 Enhance preparedness to support decontamination.

3.7.1 Conduct Research and Develop Verified Technologies.

- Conduct research to understand the persistence and potential for secondary transmission of biological contaminants in a variety of environments and the ability of various disinfection

technologies to inactivate or remove biological contaminants.

- Develop and verify technologies for all phases of environmental cleanup that address various types of infrastructure, equipment, and environments.
- Develop readily available and scalable technologies and software tools to support water and wastewater infrastructure decontamination and the treatment of contaminated water.

3.7.2 Develop and Exercise Decontamination Plans.

- Develop and verify plans for all phases of environmental cleanup for facilities, equipment, and the environment through drills and exercises that incorporate relevant partners and stakeholders.
- Establish pre-incident decontamination and waste management recommendations for:
  - Impacted community members, patients, and response personnel;
  - Contaminated drinking water;
  - Waste collection, handling, and packaging methods suitable for waste transport (including interstate transport), temporary storage, off-site treatment, and disposal;
  - Handling and disposition of human remains;
  - Disposition of animal remains; and
  - Environmental decontamination practices, as warranted.

3.8 Strengthen preparedness to operate and collaborate across the United States, including U.S. territories.

3.8.1 Establish Collaborative and Resource Sharing Policies and Operational Frameworks.

- Establish mechanisms to facilitate rapid deployment of federal and SLTT response personnel and response resources across jurisdictional boundaries.
- Establish and augment mechanisms by which the Federal Government can use assistance from non-federal and foreign sources with medical products, qualified public health, medical, or other personnel, or other resources during a bioincident.
- Establish protocols for timely sharing of samples, specimens, and related clinical information among federal departments and agencies and across public health, animal health, and environmental jurisdictions in the United States and U.S. territories.

3.9 Strengthen international preparedness to support international response and recovery capabilities.

3.9.1 Strengthen Foreign Governments and International Organizations' Commitment to, Preparedness for, and Capacity to Respond to Bioincidents.

- Promote global health security as a leadership priority and a national responsibility to accelerate bioincident detection, response, and recovery capacity-building.
- Support health emergency response teams of qualified personnel to respond rapidly to international health emergencies.
- Support workforce preparedness in emergency management principles, exercised on an Emergency Operation Center platform.
- Promote multi-sectoral and trans-disciplinary collaboration across diverse stakeholders to facilitate rapid and comprehensive response to bioincidents.
- Improve international access to and promote use of: best practices, model procedures, reporting templates, and training materials to facilitate rapid identification and notification of, and response to, potential biothreats or bioincidents.
- Promote and enhance mechanisms for sharing specimens, samples, and information.

- Ensure that international mechanisms are prepared fully for the unique challenges of responding to deliberate biothreats and bioincidents.
- Support transparent, independent, and objective assessments of the international community's capacity to respond to bioincidents.
- Coordinate with partner countries to develop and implement multi-sectoral plans to address identified gaps in health security and ensure adherence to standards outlined in the International Health Regulations (2005) and by the World Organisation for Animal Health.
- Support country and regional development and sustainment of public and veterinary core capacities and standards.

3.9.2 Enhance International Preparedness through MCMs.

- Promote increased global capacities for research, development, evaluation, manufacturing, acquisition, stockpiling, deployment, and distribution of MCMs, including through collaborative arrangements.
- Address legal, regulatory, administrative, and financing barriers for international sharing of MCMs, other medical products, and qualified personnel.
- Ensure that international coordination and planning for bioincidents include consideration of the constraints to the ability of the United States to provide MCMs to other countries to address international bioincidents.
- Expand the international deployment and utilization of FDA-authorized or -cleared diagnostic tests.
- Develop appropriate plans and agreements to facilitate the rapid international deployment and distribution of MCMs under the appropriate regulatory mechanisms, or for the rapid development, including clinical trials, of investigational MCMs during a crisis.
- Strengthen international protocols for the conduct of clinical trials in a crisis.

3.9.3 Enhance International Preparedness Through CMMs.

- Promote the implementation of CMMs that can prevent transmission of communicable disease (e.g., voluntary isolation, hand washing with soap, covering mouth when coughing or sneezing, voluntary home quarantine).
- Support international partners in developing the authority to invoke and the capacity to implement threat-appropriate travel and border health measures, such as travel warnings and restrictions.
- Enhance engagement with community leaders to promote understanding of CMMs.
- Strengthen whole of society approaches through promoting multi-sectoral civil society, government, and private sector partnerships to improve incident reporting, and early action and response, and to mitigate the impact within communities by expanding coordination and response networks.

3.9.4 Further Develop, Exercise, and Update United States Government Plans for Responding to and Recovering from International Bioincidents.

- Develop bioincident response plans for response and recovery at the international level with key international stakeholders as well as key SLTT, non-governmental, and private sector partners.
- Ensure that international coordination and planning for bioincidents consider the constraints to the ability of the United States to provide response capabilities to address international bioincidents.
- Prepare and exercise plans for repatriation of personnel and materiel during a bioincident.

GOAL 4:
RAPIDLY RESPOND TO LIMIT THE IMPACTS OF BIOINCIDENTS.

4.1 Compile and share biothreat and bioincident information to enable appropriate decision-making and response operations across all levels of government and with non-governmental, private sector, and international entities, as appropriate.

4.1.1 Ensure Access to Timely, Accurate, and Useful Information.

- Coordinate and exchange biothreat and bioincident information and analysis across multi-sectoral stakeholders nationally and internationally.

4.1.2 Coordinate Federal Decision-making to Augment and Support Response Operations.

- Coordinate and communicate decision-making during biothreat and bioincident prevention, response, and recovery operations.
- Rapidly identify and resolve at the federal level any resource and policy issues related to on-going response and recovery activities, both nationally and internationally.
- Utilize intelligence, biosurveillance, diplomacy, healthcare capacity and capability data, and modeling capabilities to maintain situational awareness and support decision-making across sectors and between local, national, and international organizations and partners throughout the response.
- Notify, share information, and coordinate with international organizations and partners in accordance with the International Health Regulations (2005) and World Organization for Animal Health reporting requirements, and relevant frameworks throughout the bioincident response.

4.1.3 Enhance Situational Awareness Through Real-time, Incident Information Sharing.

- Rapidly share modeling, detection, healthcare capacity and capability data, and diagnostic information with appropriate stakeholders to monitor the bioincident continually and support multi-sectoral decision-making throughout the response.
- Utilize all sources of data, as appropriate, including social media and intelligence feeds, electronic medical records/health information exchanges, and new data analytic technologies, such as artificial intelligence, to further support incident awareness.
- Provide timely information to domestic and international stakeholders regarding utilization of border measures, prioritization of MCM dispensing, epidemiological control measures, and re-occupation of decontaminated areas.

4.2 Conduct federal response operations and activities in coordination with relevant non-federal actors to contain, control, and to rapidly mitigate impacts of biothreats or bioincidents.

4.2.1 Ensure Appropriate Oversight and Coordination.

- Identify a lead federal department or agency to provide overall coordination for the United States Government response to a national or international bioincident and to ensure coordination of response at the national/international interface level.

- Provide federal bioincident coordination to improve incident management across sectors and with all key stakeholders.
- Coordinate support to international bioincident response operations through the Department of State, including Chiefs of Mission, to prevent the spread of bioincidents.
- Identify mechanisms for access to budgetary resources to support the rapid response to a large-scale bioincident.
- When necessary, integrate coordinated federal activities into SLTT response efforts.
- Coordinate domestic assistance from international entities and from the private sector.
- Plan to use the *Defense Production Act of 1950*, as amended (2009) (50 U.S.C. 2061-2071) to obtain and facilitate distribution of resources that are urgently needed to respond to biological threats and incidents.

4.2.2 Deploy MCMs and Implement CMMs.

- Rapidly identify potentially exposed populations to begin triage, preventive healthcare activities, and treatment.
- Ensure that access and functional needs of at-risk individuals are integrated into rapid deployment.
- Implement CMMs and other multidisciplinary bioincident control measures, to include addressing service animal and wildlife concerns, animal vaccination, and agricultural depopulation.
- Deploy MCMs and support SLTT and medical supply distribution systems in the dispensing of MCMs, PPE, and medical equipment, under the appropriate regulatory mechanisms.
- Monitor the safety and effectiveness of deployed MCMs.
- Supplement, as necessary, the capabilities of affected jurisdictions to rapidly deploy MCMs following a bioincident, via a rapid response capability.
- Ensure provision of MCMs, as appropriate, to personnel performing or supporting mission-essential functions following a bioincident.
- Ensure resources to maintain or develop clinical guidance and utilization policies to prepare for MCM deployment in crisis situations.
- Assess deficiencies in the health care system in the United States and U.S. territories to address these threats and coordinate *in extremis*.

4.2.3 Conduct Real-time Research.

- Conduct real-time research during response to characterize emerging biothreat agents and develop response tools in order to improve response and recovery capacity, capability, and future preparedness.
- Rapidly identify and disseminate guidelines and clinical approaches during a bioincident for the purpose of decreasing transmission, morbidity, and mortality; and rapidly identify and disseminate analogous approaches for animals and plants.
- Conduct real-time clinical research to evaluate promising investigational MCMs, and identify potential novel diagnostics, treatments, and vaccines.
- Establish processes to accelerate protocol development, clinical sites identification, and institutional review board and regulatory review.

4.2.4 Implement or Support Response Operations.

- Deliver and distribute response equipment and supplies, including healthcare resources and trained personnel, and provide for the availability of security capabilities to support response operations domestically and internationally.
- Facilitate implementation of crisis standards of care as needed and return to conventional care, as appropriate.
- Provide available federal medical, public health, and veterinary surge capacity and capabilities in a timely, coordinated manner to implement or support public and animal health, behavioral, and medical and veterinary services, including by augmenting SLTT capabilities.
- Provide mass fatality management including mortuary affairs, as appropriate.
- Augment transportation and reception systems and provide capabilities to support movement of highly infectious disease patients and response-generated materiels across borders and U.S. jurisdictions.
- Provide oversight and assistance for carcass management services, as appropriate.
- Conduct decontamination operations and the management of waste and contaminated materials in a manner that is protective of human, animal, and plant health, the environment, and the economy.
- Ensure the health and safety of federal, SLTT, private sector, and NGO responders involved in response operations.

4.2.5 Preserve the Continuity of Operations.

- Maintain comprehensive and effective continuity of operations, including appropriate devolution, to ensure the preservation of the United States Government's structure under the U.S. Constitution and the continuing performance of National Essential Functions under all conditions.
- Secure, protect, and restore, as needed, critical infrastructure assets that have the potential to impact or be impacted by the spread of the bioincident.
- Secure and protect critical information and communications systems necessary for biodefense.

4.3 Conduct operations and investigations, and use all available tools to hold perpetrators accountable.

4.3.1 Conduct Incident Operations and Investigations.

- Utilize secure advanced communications capabilities between specialized response assets, technical experts, and senior decision-makers.
- Strengthen federal and SLTT law enforcement, medical, public health, animal, and plant health stakeholder capacity and capabilities to conduct joint criminal-epidemiologic investigations for suspect and confirmed intentional biothreats or bioincidents.
- Rapidly assess interdicted biological materials contained within a weapon or dispersal device, disable it, and contain the materials to prevent further dissemination.
- Transport biological weapons, materials, and means of delivery to an appropriate location for further characterization.
- Draw from national and international tools, including applicable laws and agreements, where appropriate and consistent with prosecutorial discretion, to hold perpetrators of intentional bioincidents accountable.

4.3.2 Forensics and Attribution.

- Utilize forensic tools and investigation capabilities to conduct forensic examinations to support attribution of a biothreat or a bioincident.
- Use applicable protocols and memoranda of agreement to facilitate transport of potentially bio-contaminated evidence and classified materials to appropriate, predesignated facilities for analysis.

4.3.3 Support International Investigations.

- Provide appropriate technical and logistical support to investigations of alleged biological weapons, materials, and means of delivery under international auspices.

4.4 Execute risk-informed, accurate, timely, and actionable public messaging.

4.4.1 Deliver Public Messaging to Facilitate Public Understanding and Decision-making During a Bioincident.

- Provide timely, regular, coordinated, and consistent risk communication, including information on response and recovery procedures and personal protective measures, across a range of media for the public.
- Provide mechanisms for stakeholders and members of the public to ask questions and provide comments and feedback.
- Use accessible communication strategies to maximize participation in appropriate response measures that address the needs for messaging in multiple formats and languages to accommodate the access and functional needs of the entire population.
- Identify and combat misinformation, including information regarding movement restrictions and re-entry of health workers and other incident responders.

GOAL 5:
FACILITATE RECOVERY TO RESTORE THE COMMUNITY, THE ECONOMY, AND THE ENVIRONMENT AFTER A BIOINCIDENT.

5.1 Promote restoration of critical infrastructure capability and capacity to enable the resumption of vital U.S. activities.

5.1.1 Restore Capability and Capacity.

- Ensure that safety measures are in place to enable and help restore health, social, and economic activity.
- Address the loss of critical infrastructure capability and capacity as quickly as possible to limit cascading effects by working with owners and operators, SLTT entities, and international partners, as appropriate.
- Support restoration of critical infrastructure in addition to continued performance of National Essential Functions through recovery of the federal, military, local first responders, and other critical workforces.
- Facilitate health monitoring and surveillance for emergency responders, health care providers, federal personnel, and the public, including through the provision of post-exposure evaluations and medical monitoring.

5.2 Ensure coordination of recovery activities across federal and SLTT governments and, as appropriate, international, non-governmental, and private sector partners to enable effective and efficient recovery operations.

5.2.1 Coordinate and Oversee.

- Coordinate recovery planning and information-sharing among federal, SLTT, non-government, and health care coalition partners.
- Support SLTT officials in decision-making and implementation of services such as relocation, alternative housing, and re-occupancy strategies, and access to health and social services.
- Support SLTT officials in decision-making regarding re-habitation and re-introduction of wildlife, livestock, service animals, and pets in the environment, homes, or commercial market.
- Conduct impact assessments, develop recovery strategies, and implement operational capabilities.
- Restore public confidence in community and environmental safety through frequent strategic communications via various media and other messaging partners.

5.3 Provide recovery support and conduct long-term mitigation actions to promote resilience.

5.3.1 Conduct Recovery and Mitigation Activities.

- Support SLTT officials in decision-making about long-term recovery operations, including remediation of remaining contaminated areas, long-term environmental monitoring, and assessing and communicating the appropriateness for re-occupancy of impacted areas.

- Support provision of long-term medical and behavioral health services to affected populations, including for emergency responders.
- Support effective and timely risk communication to promote public awareness of recovery operations.
- Provide necessary support and augmentation of SLTT civilian capabilities to maintain and sustain public safety protection assurances.
- Assist recovery of private entities that cannot operate because of a bioincident, as funding and authorities permit.
- Support partner countries in decision-making about long-term recovery operations.
- Support SLTT officials and private-sector responders involved in determining how to integrate mitigation considerations into long-term recovery operations.
- Coordinate the activities of the Federal Government in support of SLTT officials to assess, restore, and initiate necessary interventions to re-establish critical capabilities in health and social services.

5.4 Reduce the cascading effects of international biological incidents on the global economy, health, and security.

5.4.1 Reduce International Economic, Health, and Security Impact.

- Promote the provision of recovery support and related activities to mitigate the second order impacts of a bioincident.
- Assess impacts—such as severe disruptions of health services, economic and social activity and the decline of essential governmental services—caused by an international bioincident.
- Support activities to strengthen host governments' ability to deliver critically needed services and to retain democracy and governance.
- Support households, communities, and agriculture markets to recover from the food safety impacts of the bioincident.

ANNEX II
DEFINITIONS

The terminology used throughout the strategy is consistent with the following definitions:

Biodefense: Actions to counter biological threats, reduce risks, and prepare for, respond to, and recover from bioincidents.

Biodefense enterprise: Stakeholders with a role in the prevention, preparedness for, detection, response, and recovery from bioincidents (e.g., federal and SLTT governments, non-governmental and private sector entities, and international partners).

Biological hazard (biohazard): A biological agent or biologically active substance—excluding toxic chemical substances that are considered solely as chemical weapons agents, regardless of origin (e.g., naturally occurring or bioengineered)—that represents an actual or potential danger to humans, animals, plants, or the environment.

Biological incident (bioincident):

- Any act of biological warfare or terrorism;
- A crime involving a biohazard consistent with the scope of this strategy; or
- Any natural or accidental occurrence in which a biohazard harms humans, animals, plants, or the environment consistent with the scope of this strategy.

Biological threat (biothreat): An entity involved with, or a situation involving, a biohazard that can potentially cause a bioincident.

Biosurveillance: The process of gathering, integrating, interpreting, and communicating essential information and indications related to all-hazard threats or disease activity affecting human, animal, plant, and environmental health to achieve early detection and provide early warning, contribute to overall situational awareness of the health aspects of the incident, and to enable better decision-making at all levels.

Bioweapons-related: Materials, equipment, information, or technology covered by relevant multilateral treaties and arrangements, or included on national or international control lists, which could be misused for the design, development, production, or use of biological weapons and their means of delivery.

Clinical Guidance: Recommendations that define prevention, triage, and medical management of individuals who are at-risk or affected by biothreats.

Community Mitigation Measures (CMMs): Behaviors or actions that people and communities can take to help slow the spread of a biological hazard, to include threat-appropriate travel and border health measures.

Delivery system: Any apparatus, equipment, device, or means of delivery used or intended to be used to deliver or disseminate biological material.

Dual–use: Intended for legitimate purposes but having the potential for both benevolent and malevolent applications.

Healthcare coalition: A collaborative network of healthcare organizations and their respective public and private sector emergency response partners, including, but not limited to, hospitals, emergency medical services, and emergency management and public health agencies, that serves as a multiagency coordinating group to assist with preparedness, detection, response, recovery, and mitigation activities related to healthcare service delivery during bioincidents.

Medical Countermeasures (MCMs): Pharmaceutical products, such as vaccines, antimicrobials, and antitoxins, and non-pharmaceutical products, such as ventilators, diagnostic tests, PPE, and patient decontamination materials, that may be used to prevent, mitigate, or treat the adverse health effects from a bioincident.

ANNEX III
SCOPE, STATUTORY REQUIREMENTS, AND AGENCIES

SCOPE

The *National Biodefense Strategy* addresses biothreats and bioincidents that have the potential to cause significant harm (as measured by injury or death, or damage to property, the environment, or the economy) to the United States or to U.S. interests; or that otherwise affect U.S. national security.

The *National Biodefense Strategy* is intended to inform the policy development process and is not a budget document. The commitment of federal resources to support activities associated with this document will be determined through the annual budget process, which will be informed by this strategy.

STATUTORY REQUIREMENTS

Section 1086 of the *National Defense Authorization Act for Fiscal Year 2017* (Pub. L. No. 114-328; enacted December 23, 2016), codified at 6 U.S.C. 104, provides:

> **SEC. 1086. NATIONAL BIODEFENSE STRATEGY.**
>
> (a) STRATEGY AND IMPLEMENTATION PLAN REQUIRED.—The Secretary of Defense, the Secretary of Health and Human Services, the Secretary of Homeland Security, and the Secretary of Agriculture shall jointly develop a national biodefense strategy and associated implementation plan, which shall include a review and assessment of biodefense policies, practices, programs and initiatives. Such Secretaries shall review and, as appropriate, revise the strategy biennially.
>
> (b) ELEMENTS. The strategy and associated implementation plan required under subsection (a) shall include each of the following:
>
> (1) An inventory and assessment of all existing strategies, plans, policies, laws, and interagency agreements related to biodefense, including prevention, deterrence, preparedness, detection, response, attribution, recovery, and mitigation.
>
> (2) A description of the biological threats, including biological warfare, bioterrorism, naturally occurring infectious diseases, and accidental exposures.
>
> (3) A description of the current programs, efforts, or activities of the United States Government with respect to preventing the acquisition, proliferation, and use of a biological weapon, preventing an accidental or naturally occurring biological outbreak, and mitigating the effects of a biological epidemic.
>
> (4) A description of the roles and responsibilities of the Executive Agencies, including internal and external coordination procedures, in identifying and sharing information related to, warning of, and protection against, acts of terrorism using biological agents and weapons and accidental or naturally occurring biological outbreaks.
>
> (5) An articulation of related or required interagency capabilities and whole-of-Government activities required to support the national biodefense strategy.
>
> (6) Recommendations for strengthening and improving the current biodefense

capabilities, authorities, and command structures of the United States Government.

(7) Recommendations for improving and formalizing interagency coordination and support mechanisms with respect to providing a robust national biodefense.

(8) Any other matters the Secretary of Defense, the Secretary of Health and Human Services, the Secretary of Homeland Security, and the Secretary of Agriculture determine necessary.

(c) SUBMITTAL TO CONGRESS.—Not later than 275 days after the date of the enactment of this Act, the Secretary of Defense, the Secretary of Health and Human Services, the Secretary of Homeland Security, and the Secretary of Agriculture shall submit to the appropriate congressional committees the strategy and associated implementation plan required by subsection (a). The strategy and implementation plan shall be submitted in unclassified form, but may include a classified annex.

(d) BRIEFINGS. Not later than March 1, 2017, and annually thereof ter until March 1, 2019, the Secretary of Defense, the Secretary of Health and Human Services, the Secretary of Homeland Security, and the Secretary of Agriculture shall provide to the Committee on Armed Services of the House of Representatives, the Committee on Energy and Commerce of the House of Representatives, the Committee on Homeland Security of the House of Representatives, and the Committee on Agriculture of the House of Representatives a joint briefing on the strategy developed under subsection (a) and the status of the implementation of such strategy.

(e) GAO REVIEW.—Not later than 180 days after the date of the submittal of the strategy and implementation plan under subsection (c), the Comptroller General of the United States shall conduct a review of the strategy and implementation plan to analyze gaps and resources mapped against the requirements of the National Biodefense Strategy and existing United States biodefense policy documents.

(f) APPROPRIATE CONGRESSIONAL COMMITTEES DEFINED. In this section, the term "appropriate congressional committees" means the following:

(1) The congressional defense committees.

(2) The Committee on Energy and Commerce of the House of Representatives and the Committee on Health, Education, Labor, and Pensions of the Senate.

(3) The Committee on Homeland Security of the House of Representatives and the Committee on Homeland Security and Governmental Affairs of the Senate.

(4) The Committee on Agriculture of the House of Representatives and the Committee on Agriculture, Nutrition, and Forestry of the Senate.

AGENCIES

Consistent with the requirements of the *National Defense Authorization Act for Fiscal Year 2017*, the primary drafters for the *National Biodefense Strategy* are the Departments of Defense, Health and Human Services, Homeland Security, and Agriculture. In addition, the National Security Council Staff coordinated the review and finalization of the *National Biodefense Strategy* with the Departments of State, Treasury, Justice, Interior, Commerce, Labor, Transportation, Energy, and Veterans Affairs, the Environmental Protection Agency, the Office of Management and Budget, the Office of the Director of National Intelligence, the Office of Science and Technology Policy, the U.S. Agency for International Development, and the Federal Bureau of Investigation.

DOI: 10.1002/rem.21629

RESEARCH ARTICLE

WILEY

Low-concentration hydrogen peroxide decontamination for *Bacillus* spore contamination in buildings

Ronald Leroy Mickelsen[1] | Joseph Wood[2] | Michael Worth Calfee[2] | Shannon Serre[1] | Shawn Ryan[2] | Abderrahmane Touati[3] | Francis Robbins Delafield[3] | Lola Denise Aslett[3]

[1]U.S. Environmental Protection Agency, Office of Land and Emergency Management, Durham, North Carolina

[2]U.S. Environmental Protection Agency, Office of Research and Development, Durham, North Carolina

[3]Homeland Security Department, Jacobs Technology Inc., Durham, North Carolina

Correspondence
Ronald Leroy Mickelsen, U.S. Environmental Protection Agency, 109 TW Alexander Dr., Durham, NC 27711.
Email: mickelsen.leroy@epa.gov

Abstract

Remediation and recovery efforts after a release of *Bacillus anthracis* (anthrax) spores may be difficult and costly. In addition, response and recovery technologies may be focused on critical resources, leaving the small business or homeowner without remediation options. This study evaluates the efficacy of relatively low levels of hydrogen peroxide vapor (HPV) delivered from off-the-shelf equipment for the inactivation of *Bacillus* spores within an indoor environment. Decontamination evaluations were conducted in a house using both *Bacillus atrophaeus* var. *globigii* (*Bg*; as surrogates for *B. anthracis*) inoculated on the carpet and galvanized metal as coupons and *Geobacillus stearothermophilus (Gs)* as biological indicators on steel. The total decontamination time ranged from 4 to 7 days. Using the longer exposure times, low concentrations of HPV (average levels below 20 parts per million) effectively inactivated *Bg* and *Gs* spores on the materials tested. The HPV was generated with commercial humidifiers and household-strength hydrogen peroxide solutions. The presence of home furnishings did not have a significant impact on HPV efficacy. This simple, inexpensive, and effective decontamination method could have significant utility for remediation following a *B. anthracis* spore release, such as following a terrorist attack.

KEYWORDS
Bacillus anthracis, commercial off-the-shelf, decontamination, hydrogen peroxide vapor, sporicide

1 | INTRODUCTION

The impact of a *Bacillus anthracis* release into the environment, the efficacy of low concentration hydrogen peroxide vapor (HPV) in the laboratory, and the applicability of surrogates for *B. anthracis* were described previously (Wood et al., 2016). Summarizing, numerous structures were intentionally contaminated with *B. anthracis* (Ames strain) spores through letters processed by the U.S. Postal Service in the fall of 2001. Several decontamination approaches, including HPV, were used on affected structures (Canter, 2005). Typically, HPV has been tested as a sterilant using high concentrations, 250 parts per million by volume (ppmv), 90 minutes (min) for nonporous hard surfaces (U.S. Environmental Protection Agency [US EPA], 2019), specialized equipment, and liquid HP at concentrations over 30%. High HPV concentrations pose an immediate threat to life and health and after aeration may result in off-gassing of HPV for extended periods from some materials (Baron, Estill, Beard, Hein, & Larsen, 2007; Meyer et al., 2014). In addition, the high HPV concentrations obtained in the laboratory have been difficult to attain in the field (US EPA, 2013). These results led to the laboratory investigation of the sporicidal effects of long-duration, low-concentration HPV. Results showed that laboratory experiments conducted with 4 to 7-day exposures to low levels of HPV (average levels as low as 5 ppm) effectively inactivated *B. anthracis* spores on several different materials (Wood et al., 2016). This present study extends those laboratory findings to a field-level evaluation using commercial off-the-shelf (COTS) humidifiers and 3% liquid HP.

 © 2019 Wiley Periodicals, Inc.

2 | MATERIALS AND METHODS

2.1 | Test organisms and inoculation procedures

Dried spores of *B. atrophaeus* var. *globigii* (*Bg*) were prepared as described previously (Brown et al., 2007). Using an aerosol deposition method (Lee, Ryan, & Snyder, 2011), spores blended with silicon dioxide particles were inoculated onto 18-millimeter (mm) diameter material surfaces (coupon) resulting in approximately 1×10^7 spores per coupon.

The commercial biological indicators (BIs) used for this study were purchased from Mesa Laboratories Inc. (Lakewood, CO; P/N HMV-091). Each BI was made of a 9-mm diameter by 0.2-mm-thick stainless steel (Grade 304) disc inoculated with a nominal 1×10^6 *Geobacillus stearothermophilus* (*Gs*) spores and placed in a Tyvek envelope.

2.2 | Test material coupons

Discs with an 18-mm diameter were cut to make coupons from carpet (Multiplicity 54594; Shaw Industries Group, Dalton, GA) and galvanized metal (26-gauge stock metal; East Coast Metal, Durham, NC), materials which were purposely selected because they were the materials that were the most difficult (excluding concrete) to completely decontaminate using HPV (Wood et al., 2016). All materials were mounted on 18-mm diameter aluminum stubs (P/N 16119; Ted Pella, Inc., Redding, CA) using double-sided adhesive tape (P/N 16073-2; Ted Pella, Inc.). All coupons with their stubs were sterilized before inoculation by exposure to ethylene oxide (Anderson EOGas AN333 Sterilization System, Haw River, NC). Coupon sterilization was performed to eliminate background contamination that could confound analysis and results.

2.3 | Field-scale test environment

The structure used in the test was a three-bedroom, ranch-style house with a crawl space; a natural gas, a central forced-air heating system; and an electric air-conditioning system (HVAC). The structure's total floor area was 110 m^2, and the total living-space volume was approximately 270 m^3. The structure was considered relatively airtight with an average air exchange rate between 0.3 and 0.4 air changes per hour for the ambient conditions experienced during testing.

Whole-house COTS humidifiers, Figure 1 (Model HCN-6009; Honeywell, Morris Plains, NJ) were charged with 3% HP solution. This type of humidifier uses a small fan to push air through a sponge that absorbs liquid from the reservoir. Humidifiers had a 12.9 L capacity. The location and number of humidifiers were varied across tests. The HVAC system maintained indoor temperatures at 21°C, and the circulation fan was set to run continuously. A real-time relative humidity (RH) and temperature meter (Model HMD53; Vaisala, Helsinki, Finland) was used to monitor indoor RH and temperature. The HP (Part No. 512021-1; Hi-Valley Chemical, Inc., Centerville, UT) was diluted to a concentration of 3% using deionized water.

Three ranges of electrochemical HP sensors were used during fumigation: one HP sensor capable of detecting 0–10 ppm HP (Model B12–34-1–0010-1, Analytical Technology Inc. [ATI], Collegeville, PA) for low concentrations and safety monitoring, one HP sensor capable of detecting 0–25 ppm HP (Model B12–34-5–0025-1; ATI), and five HP sensors capable of detecting 0–100 ppm HP (Model B120100-1; ATI). Sensors were connected to a data acquisition system and variable outputs were both stored and monitored in real-time. The HP sensor capable of detecting 0–25 ppm HP was placed in the center of the house during fumigation, along with one real-time RH and temperature probe (Model HMD53; Vaisala, Helsinki, Finland). The five 0- to 100-ppm sensors were distributed throughout the house and the 0- to 10-ppm sensor was placed in the garage where monitoring equipment and field personnel resided during testing.

Sets of coupons, BIs, and a temperature and RH monitor were placed in eight locations within the house (Figure 2). Each set of coupons consisted of three inoculated carpet coupons, three inoculated galvanized metal coupons, one uninoculated carpet coupon, one uninoculated galvanized metal coupon, and one BI. The inoculated coupons served as the test coupons for determination of log reduction (LR; as effectiveness) due to exposure to the test conditions. The uninoculated coupons served as controls for indicating any cross-contamination during coupon handling. Two additional BIs were placed near (in the same room) each coupon set but in more secluded locations, such as in a closet or taped to an exterior wall. In addition, RH and temperature sensors (HOBO® RH/T Onset Data Logger [Model U12]; Onset Computers, Bourne, MA)

FIGURE 1 Whole-house humidifier in the kitchen location. Coupons can be seen in the oven [Color figure can be viewed at wileyonlinelibrary.com]

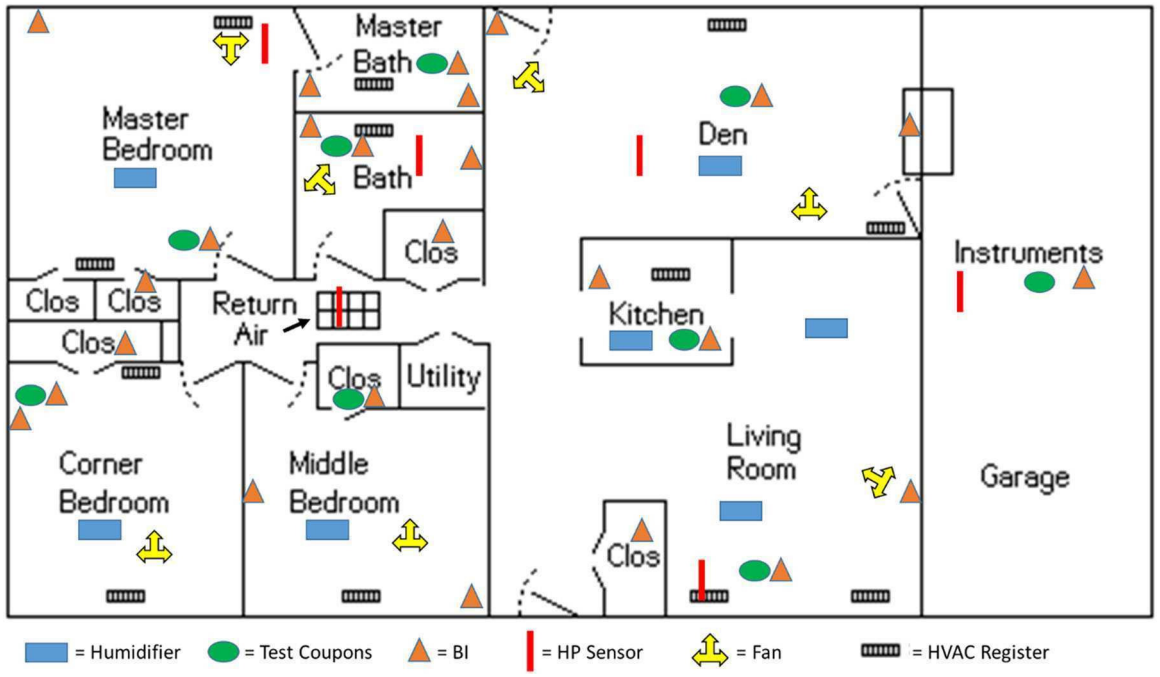

FIGURE 2 House floor plan with location of equipment, test coupons, and biological indicators for Test 1. BI, biological indicator; HP, hydrogen peroxide; HVAC, heating, ventilation, and air conditioning. [Color figure can be viewed at wileyonlinelibrary.com]

FIGURE 3 Biological indicators placed in buttoned pants pocket for testing, Test 4 [Color figure can be viewed at wileyonlinelibrary.com]

were placed with each set of coupons. Oscillating fans were also used to help circulate the air. During some of the tests, extra BIs were placed in strategic locations to gauge penetration and decontamination efficacy in those locations (Figure 3). Positive control coupons (inoculated, but unexposed to HPV) and blanks (uninoculated and unexposed to HPV) were covered with a lid and placed in the garage.

The humidifiers were filled with the prescribed amount of HP liquid and turned on (in one case humidifiers were refilled), the house was secured (locked), signage was posted, and parameters

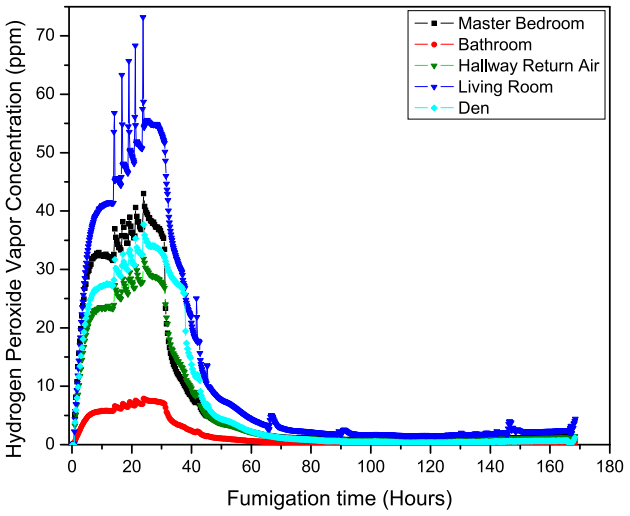

FIGURE 4 Test 1 hydrogen peroxide vapor concentration as a function of time at different locations in the house [Color figure can be viewed at wileyonlinelibrary.com]

TABLE 1 Test matrix

Test #	Number of humidifiers	Amount of HP (L)		Description
		Loaded	Used	
0	7	0	0	Water only, 53 L used
1	7	53	51.3	7.6 L 3% liquid HP each humidifier
2	7	53	51.8	Same as Test 1 plus furniture and clothing
3	2	26	25.1	Same as Test 2 two humidifiers, half the HP
4	2	46	43.8	Same as Test 3 two humidifiers with refill

Abbreviation: HP, hydrogen peroxide.

were monitored throughout the fumigation process. The HPV concentration at the five different locations as a function of time is shown in Figure 4 for Test 1 as an example. The oscillating peaks observed between 14 and 24 hour (hr) in Figure 4 are the HPV sensor reaction to the heat system cycling on and off in response to the lower ambient temperature. These short-duration peak values were not included in the maximum HPV concentration determination.

Following the decontamination process, a sampling team verified that the HPV concentration was below 1 ppm using Dräger HP tubes (Dräger™ Short-Term Detector Tubes—Hydrogen Peroxide; Cat. No 8101041; Dräger, Inc., Houston, TX), and then entered the house to collect coupon sets and BIs. The one set of positive control and blank coupons that remained outside of the living space (in the garage) were collected at the same time.

Coupons were placed aseptically into sterile 50-milliliters (ml) conical tubes and transported to the laboratory. To each 50-ml conical tube, 20-ml sterile phosphate-buffered saline with 0.05% Tween® 20 (PBST) was added. The tubes were sonicated for 10 min and subsequently vortexed continuously for 2 min. Aliquots were plated in triplicate using a spiral plater (Autoplate 5000; Advanced Instruments Inc., Norwood, MA). Plates were incubated at 35 ± 2°C for 16–19 hr. The colonies on each plate were enumerated using a QCount® colony counter (Advanced Instruments Inc.). Low count samples were related using a vacuum filtering system (Pall Corporation, Port Washington, NY) to improve the detection limit.

BI discs containing *Gs* were aseptically transferred to 15-ml polypropylene culture tubes (P/N 169897; USA Scientific Inc., Ocala, FL) containing 10 ml of tryptic soy broth (TSB). The tubes were statically incubated at 55 ± 2°C. After 7 days, the medium in each tube was visually inspected for turbidity, indicating growth. A 0.1-ml aliquot was plated to confirm that the colony morphology was consistent with that of the target organism. All sample tubes with no turbidity also were plated (0.1 ml) to confirm that there was no target organism growth.

2.4 | Test conditions

The test matrix for the field-scale experiments is shown in Table 1. To establish a baseline with humidity only, Test 0 was conducted with the seven humidifiers filled with water only. Humidifiers were placed in the living room (two), kitchen (one), den (one), and in each of the three bedrooms (one each). For Test 1 the same locations were used but each humidifier was filled with 7.6 liters (L) of 3% HP. Furniture was added for Test 2 and to increase HP vapor concentrations in the hall bathroom, one of the living room humidifiers was moved to the hallway near the hall bathroom. In addition, several coupons and BIs were added and placed in strategic locations. For Test 3 only two humidifiers were used.

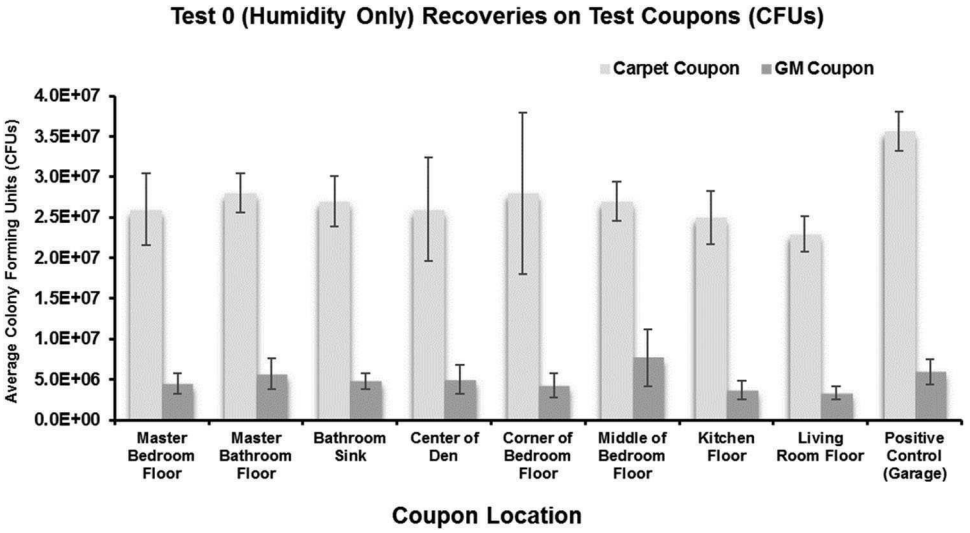

FIGURE 5 Test 0 spore recoveries on the carpet and galvanized metal coupons by location

TABLE 2 Test 1—Fumigation and relative humidity conditions by location

Location	HPV max (ppm)	CT (ppm-hour)	RH average (%)	RH max (%)
Master bedroom	38	1,300	72	86
Master bathroom	Not measured		74	85
Hall bathroom	7.5	270	72	86
Center of den	33	1,300	72	86
Corner bedroom	Not measured		69	85
Middle bedroom	Not measured		72	88
Kitchen	Not measured		69	86
Living room	55	2,000	71	88
Air return	28	1,100	65	82

Abbreviations: CT, concentration multiplied by time; HPV, hydrogen peroxide vapor; RH, relative humidity.

Both were placed in the hallway under the house ventilation system return air duct and both were filled to capacity, 12.9 L of 3% HP. One of those humidifiers was set to turn on 24-hr after the other had been started. Test 4 was a repeat of Test 3 with the addition of refilling the two humidifiers with 3% HP, one with 12.1 L and one with 7.6 L. The humidifier start times were staggered by 24 hr during this run. The volume of liquid 3% HP shown in the matrix is the amount charged into the humidifiers. Humidifiers ran until they automatically shut off when the reservoir was nearly empty. There were 27–37 ml of HP liquid remaining in each humidifier at the end of Tests 1–3 and almost 300 ml in each of the two humidifiers after Test 4. In addition, there were varying amounts 31–542 ml) of HP liquid remaining in the humidifier sponge. Loaded and used HP liquid amounts are shown in Table 1.

3 | RESULTS

For Test 0, water only was used in humidifiers. The RH went from 54% to 85% within an hour of turning on the humidifiers. After 2 days the RH started to decline slowly for the rest of the week-long experiment, ending at a low of 55%. The temperature was stable at 21°C (±2) throughout the house, over time, and between all tests; thus, temperature data are not reported beyond this result. Growth was observed for all BIs in all Test 0 locations. Recoveries for the test coupons are shown in Figure 5. The use of water only in the humidifiers had no significant effect on spore survivability for galvanized metal coupons (*t* test, metal: $p = .37$) as compared to the positive control coupons. And although the effect of humidity on the carpet coupons was statistically significant (*t* test, carpet: $p = .0027$), the average 25% reduction was less than one-LR and was of no practical significance.

Table 2 shows the fumigation conditions throughout the house for Test 1, including maximum HPV concentration, integrated HPV concentration, and average and maximum RH. The integrated HPV concentration multiplied by time (CT) has units of ppm-hours and is a cumulative measure of fumigation dose. The CT calculations are for the full week (168 hr) of exposure time. With two humidifiers in the living room, the maximum HPV concentration (55 ppm) approaches the immediately dangerous to life and health (IDLH) level for HPV (75 ppm; National Institute for Occupational Safety & Health, 2007). The HPV concentrations and CT in the hall bathroom were very low. Note that these HPV concentrations are values recorded at one location in each of the monitored rooms and do not represent every location within that room, especially where there are closets or other obstructions to vapor penetration.

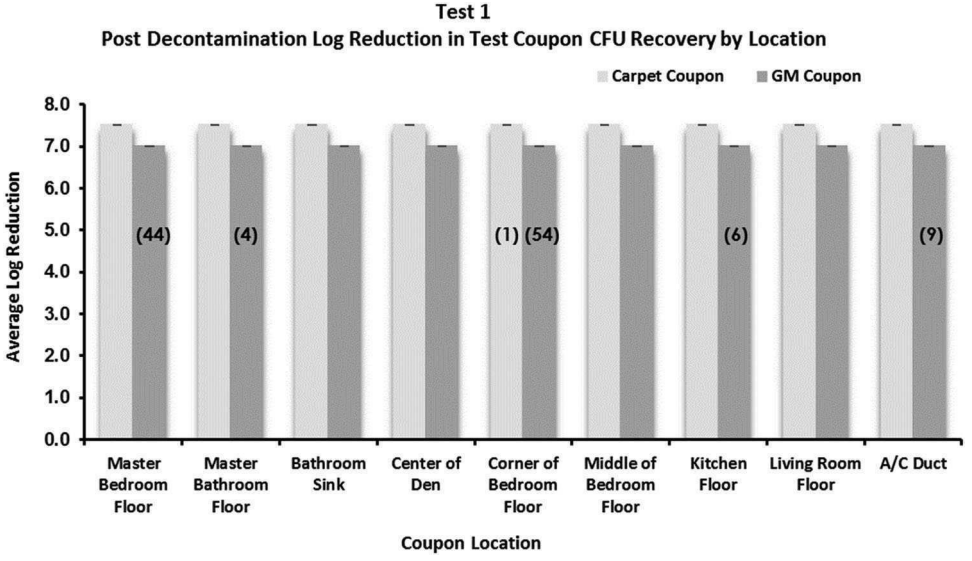

FIGURE 6 Test 1 LR in spore recoveries on the carpet and galvanized metal coupons by location. All samples were nondetect except where numbers in parentheses indicate the mean number of detectable spores in CFUs post decontamination. The average inoculated spore recovered (CFUs) from positive controls were 3.0×10^7 for carpet ($SD = 0$) and 1.5×10^7 for GM ($SD = 1.3 \times 10^7$). CFU, colony forming unit; LR, log reduction; GM, galvanized metal; *SD*, standard deviation

TABLE 3 Test 2 fumigation conditions with furniture in the house

Location	HPV max (ppm)	CT (ppm-hour)	RH average (%)	RH max (%)
Master bedroom	38	1,500	60	86
Master bathroom	Not measured		61	83
Hallway bathroom	14	660	55	81
Center of den	25	1,100	62	85
Corner bedroom	Not measured		59	85
Middle bedroom	Not measured		59	83
Kitchen	Not measured		61	89
Living room	65	2,800	58	84
Air return	30	1,200	50	78

Abbreviations: CT, concentration multiplied by time; HPV, hydrogen peroxide vapor; RH, relative humidity.

Test 1 efficacy results are shown in Figure 6. The LR is calculated by taking the average of the logs of the three positive control coupons and subtracting the average of the logs of the three test coupons for each material. Of the 54 coupons deployed, eight had detectible spores. Both materials averaged over a six-LR even though some spores remained on some coupons after fumigation. Of the 27 BIs exposed to HPV for 7 days in the living area, four were positive after fumigation: two on the master bathroom floor, one on the bathroom sink, and one in the kitchen.

With furniture in the house, Table 3 shows the maximum HPV concentration, the CT and the RH for Test 2. The HPV concentration in the hall bathroom was more than double that of Test 1. This is most likely a result of moving one humidifier from the living room to the hall near the bathroom. One humidifier remained in the living room, yet the maximum HPV concentration (65 ppm) in the living room increased from Test 1 and was nearer to the IDLH for HPV of 75 ppm.

Test 2 efficacy results are shown in Figure 7. Additional coupons and BIs were added to four rooms and designated by placing (b) after the location name. These additional coupons and BIs were removed from the house and processed after 3 days of exposure to the fumigant. The other coupons and BIs remained in the house for the full week. Of the 78 coupons deployed, nine had detectable spores. Of the 27 BIs exposed to HPV for 7 days in the living area, two were positive after fumigation: one on the corner bedroom floor and one on the living room floor. And of the 31 BIs placed in hard-to-reach places, just over half were positive for growth as shown in Table 4.

With furniture remaining in the house and a reduced amount of liquid HP delivered from only two humidifiers, Table 5 shows the maximum HPV concentration as well as the integrated concentration over the duration of Test 3. The highest maximum concentration was at the return duct, immediately over the humidifiers.

Test 3 efficacy results are shown in Figure 8. The LRs were much lower than previous runs most likely due to the reduced amount of liquid HP used for this test. Of the 72 coupons deployed, 68 had detectable spores. Of the 27 BIs exposed for 7 days in the living area, only four were positive after fumigation: one in the bathroom sink, one in the middle bedroom floor, one in the kitchen floor, and one in the living room floor. The number of no growth BIs was unexpected given the lower LR results for the coupons located in the living area. But the number of growth BIs located in hard-to-reach places increased in comparison to Test 2, as shown in Table 6.

With furniture in the house, using only two humidifiers and refilling those two humidifiers after 3 days, Table 7 shows the maximum HPV concentration, CT, and RH for Test 4. Note that the maximum concentrations were not much different from Test 3,

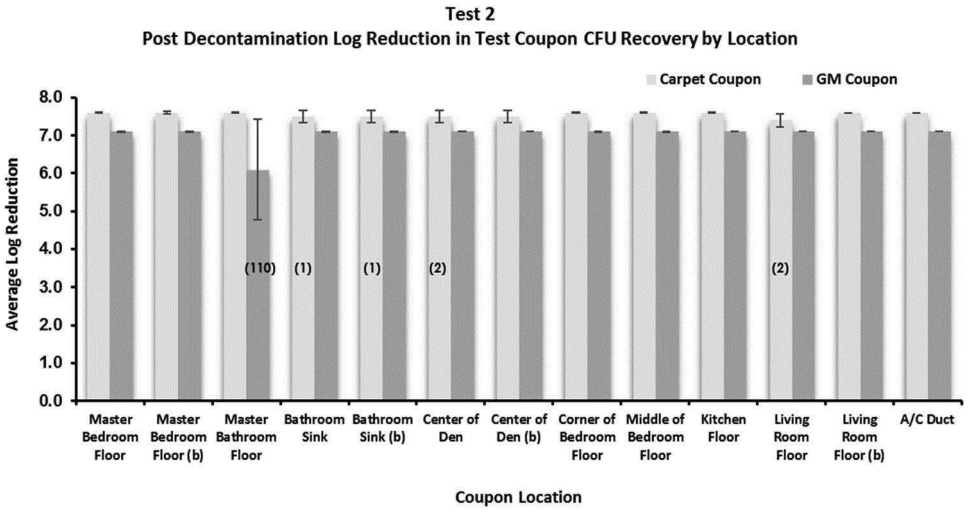

FIGURE 7 Test 2 LR in spore recoveries on the carpet and galvanized metal coupons by location, (b) location coupons were collected after 3 days of HPV exposure and all other locations after 7 days. All samples were nondetect except where numbers in parentheses indicate mean number of detectable spores in CFUs. CFUs were 2.8×10^7 for carpet ($SD = 4.4 \times 10^6$) and 9.2×10^6 for GM ($SD = 2.5 \times 10^6$). CFU, colony forming unit; LR, log reduction; GM, galvanized metal; *SD*, standard deviation

TABLE 4 Test 2 postdecontamination recoveries on BI discs placed in challenging locations

Location	Growth	No growth
Between couch cushions	7	3
Under rug	10	
Under one piece of paper		3
Under five pieces of paper		3
In bathroom drawer		5

TABLE 5 Test 3 fumigation conditions

Location	HPV max (ppm)	CT (ppm-hour)	RH average (%)	RH max (%)
Master bedroom	17	788	41	58
Master bathroom	Not measured		40	55
Hallway bathroom	12	525	31	46
Center of den	10	432	47	55
Corner bedroom	Not measured		38	50
Middle bedroom	Not measured		47	61
Kitchen	Not measured		43	56
Living room	15	873	45	55
Air return	34	1,320	44	55

Abbreviations: CT, concentration multiplied by time; HPV, hydrogen peroxide vapor; RH, relative humidity.

however, the integrated CT was significantly higher due to the refilling of the humidifiers after 3 days.

Test 4 efficacy results are shown in Figure 9. Of the 78 coupons deployed, 28 had detectable spores. Of the 27 BIs exposed for 7 days in the living area, one placed on the living room

Floor was positive after fumigation. Of those placed in challenging locations, about half of the 63 BIs resulted in growth, as shown in Table 8.

Table 9 shows a summary of results, which includes the amount of 3% HP liquid used, CT (dose) calculated, number of coupons (carpet and galvanized metal) with >6-LR, number of coupons with no detection of spores, and number of negative BIs used in the house (not inside furniture, under rugs, etc.). The CT data are correlated with the number of coupons sets >6-LR (0.95) and a number of coupons without detectable spores (0.96), but to a lesser degree with a number of negative BIs (0.38). The coupons correlate better with CT and may give a better indication of decontamination efficacy than the BIs.

4 | DISCUSSION AND CONCLUSIONS

This study shows that the efficacy of low-concentration HP, as seen in the laboratory (Wood et al., 2016), is transferable to the field scale. Results from the 165 carpet coupons, 165 galvanized metal coupons, and 250 BIs used in these test runs to support the conclusion that, at the conditions tested, 20 L of 3% HP liquid evenly dispersed within every 100 m^3 of indoor volume would be efficacious for inactivating *Bacillus* spores on most non-occluded surfaces. The noted exception may be for concrete surfaces. Previously, HPV was not efficacious against *Bacillus* spores on concrete (Rastogi, Wallace, Smith, Ryan, & Martin, 2009), but that condition was not specifically assessed in the current field-scale study.

A direct impact of adding furniture cannot be made using Test 1 and Test 2 data because one living room humidifier was moved to the hall before running Test 2. However, there was not a significant change in HP concentration or efficacy between those two tests. In fact, for the locations where measurements were taken, the CT was

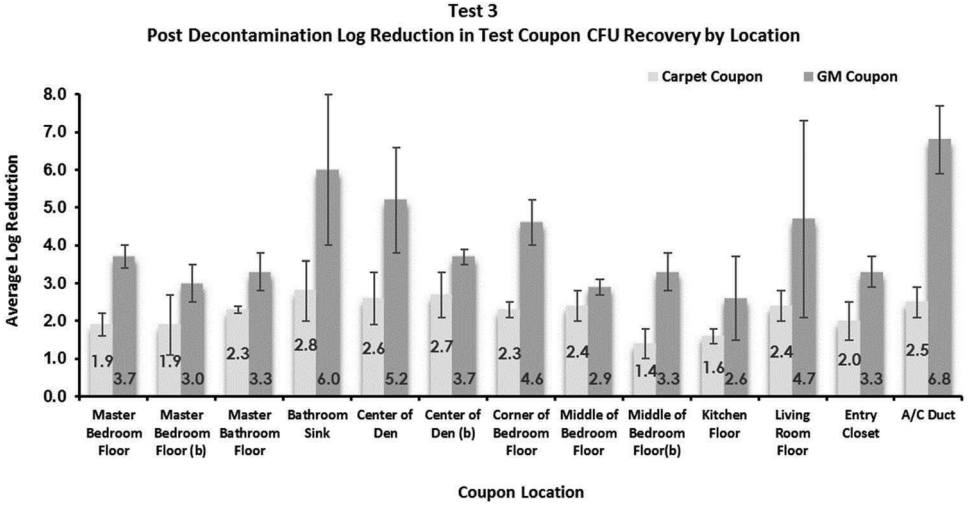

FIGURE 8 Test 3 LR in spore recoveries on the carpet and galvanized metal coupons by location, (b) location coupons were collected after 3 days of HPV exposure and all other locations after 7 days. CFUs were 3.8×10^7 for carpet ($SD = 8.9 \times 10^6$) and 1.8×10^7 for GM ($SD = 7.8 \times 10^6$). CFU, colony forming unit; LR, log reduction; GM, galvanized metal; *SD*, standard deviation

TABLE 6 Test 3 postdecontamination recoveries on BI discs placed in challenging locations

Location	Growth	No growth
Inside closed book	3	
Pants pocket	2	1
Coat pocket	3	
Behind light switch plate	6	
Window sill	1	2
Door jams	6	

TABLE 7 Test 4 fumigation conditions

Location	HPV max (ppm)	CT (ppm-hour)	RH average (%)	RH max (%)
Master bedroom	14	1,217	49	57
Master bathroom	Not measured		51	60
Hallway bathroom	8	767	52	61
Center of den	21	1,239	52	63
Corner bedroom	Not measured		49	57
Middle bedroom	Not measured		45	60
Kitchen	Not measured		52	63
Living room	33	2,274	50	61
Air return	27	2,053	51	64

Abbreviations: CT, concentration multiplied by time; HPV, hydrogen peroxide vapor; RH, relative humidity.

higher for Test 2 than Test 1. A reduction in efficacy did accompany the reduction of the total amount of HP delivered, comparing Test 2 and 3. Conducting the HPV fumigation with only two COTS humidifiers was effective when the two humidifiers were refilled at

TABLE 8 Test 4 postdecontamination recoveries on biological indicator discs in challenging locations

Location	Growth	No growth
Between couch cushions	3	
Under carpet or floor mat	6	
Under one piece of paper		3
Under five pieces of paper		3
Under ten pieces of paper	3	
Door jams	6	
Pants pocket		3
Coat pocket	3	
Inside book	3	
Inside light switch plates	6	
Inside pillowcase		3
Between bed sheets		3
Under bed comforter		3
Inside light fixture		3
Inside closed hall closet		3
Inside closed drawer	3	
In open drawer		3
Window sill		3
Totals	33	30

day three, Test 4. Staggering the two humidifiers to run sequentially rather than concurrently kept the maximum air concentration of hydrogen peroxide below 33 ppm but still achieved 1,370 ppm-hours CT. The carpet and galvanized metal coupons responded to fumigation with a better correlation with CT than the BIs. Material coupons may be a better predictor of decontamination efficacy than the BIs.

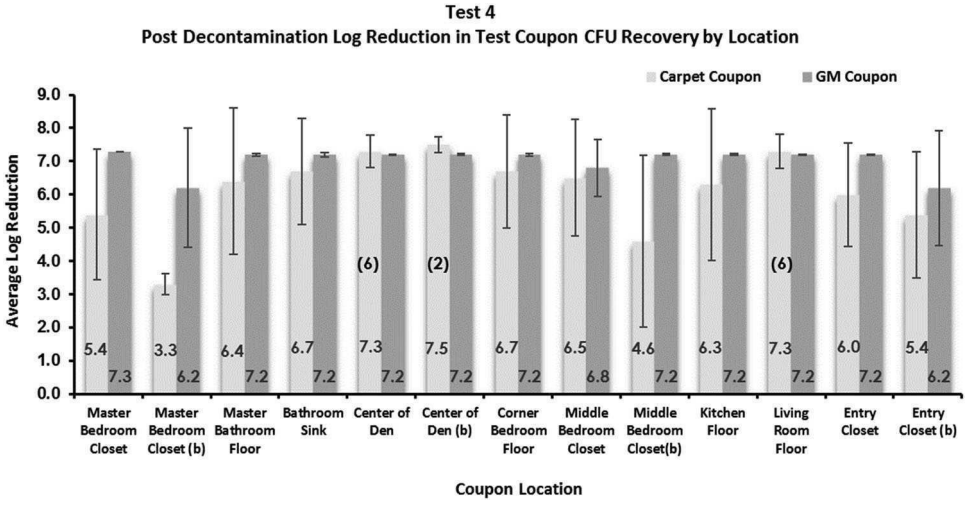

FIGURE 9 Test 4 LR in spore recoveries on the carpet and galvanized metal coupons by location, (b) location coupons were collected after 3 days of HPV exposure and all other locations after 7 days. Numbers in parentheses indicate the mean number of detectable spores in CFUs. CFUs were 3.4×10^7 for carpet ($SD = 5.5 \times 10^6$) and 1.2×10^7 for GM ($SD = 4.0 \times 10^6$). CFU, colony forming unit; LR, log reduction; GM, galvanized metal; *SD*, standard deviation

TABLE 9 Test results matrix

Test no.	Amount of HP (L)	CT (ppm-hrs)	No. coupon sets >6-LR		No. coupon w/out CFUs		No. negative BIs	
1	51.3	1,220	18/18	100%	46/54	85%	20/27	74%
2	51.8	1,520	18/18	100%	48/54	89%	25/27	93%
3	25.1	655	2/18	11%	7/54	13%	23/27	85%
4	43.8	1,370	17/18	94%	43/54	80%	26/27	96%

Abbreviations: BI, biological indicator; CFU, colony forming unit; CT, concentration multiplied by time; LR, log reduction.

An intriguing and critical aspect of this study was seen by the placement of BIs into difficult-to-reach locations, into and beneath objects. These results illustrate the penetrating potential of HPV. This method of fumigating with HPV was efficacious when BIs were placed under one or five pieces of paper, in pants pocket that was hanging in an open closet, under bedsheets, and under a comforter, in a light fixture, in a closed closet, in an open drawer, and on a window sill. However, this method of fumigating with HPV was not efficacious for BIs placed between couch cushions, under carpets or floor mats, under 10 pieces of paper, inside a winter coat pocket hanging in an open closet, inside a book, inside a light-switch box with the plate attached, in a closed drawer, and near leaky door weather stripping. Considering all these BI results gives a good indication of the HPV penetration potential. With respect to penetration into and through materials, it would be interesting to compare this low-concentration approach to the typical HPV fumigation parameters as well as comparing the difference in off-gassing of HP from materials after fumigation. Neither was performed in this current test.

The use of the method shown in this study has the potential to significantly reduce spore concentration along with the potential exposures and the health risks associated with those exposures. The current cleanup criteria with respect to a *B. anthracis* release is, "no detection of viable spores" as measured by current sampling methods (Center for Disease Control and US EPA, 2012). The scarcity of response and recovery resources including sampling will play a major role in a response strategy. The appropriate strategy for applying this method, along with many other remediation and sampling methods, to a wide-area release was not in the scope of this study; however, this method may increase our capacity to respond and positively impact future response strategies.

The threshold limit value (American Conference of Governmental Industrial Hygienists) and the permissible exposure limit (Occupational Safety and Health Administration) for HPV are both designated as 1 ppm, indicating that healthy workers may be exposed up to that level during typical work hours without expecting adverse health outcomes. When the humidifiers were dispensing HPV the resulting concentrations were lower than typical fumigations; however, the concentrations throughout the house were above this 1 ppm level. Thus, entering the house during that time would require appropriate respiratory protection. When entering the house after this fumigation cycle was complete the concentration of HPV was always below 1 ppm without the need for additional aeration at the end of the fumigation cycle. A closer look at the kinetics of desorption of HP from household materials and the concentration of HPV near those materials after fumigation may be warranted before the widespread application of this method.

The utility of using this method of decontaminating structures after a wide-area incident may be profound in that it would greatly increase the current response capacity. Allowing individuals to decontaminate their own properties without specialized equipment or workforce could have a significant impact on recovery times and costs. Effectively relaying this information, how to carry out the low-concentration fumigation with an understanding of potential health risks, to the general public for their personal use would have to be carried out in a thoughtful manner.

ACKNOWLEDGEMENTS

The authors gratefully acknowledge the contributions of William Nichols, John Archer, Kenneth Rhame, Benjamin Franco, Natalie Koch, and Elise Jakabhazy for test and document planning; and Timothy Boe, Jayson Griffin, Douglas Hamilton, Lee Brush, Ahmed Abdel-Hady, and Brian Sechrest for their help in conducting the tests; and to Dan Freeland and the Raleigh, North Carolina Marriott for providing the used beds and linens.

REFERENCES

Baron, P. A., Estill, C. F., Beard, J. K., Hein, M. J., & Larsen, L. (2007). Bacterial endospore inactivation caused by outgassing of vapourous hydrogen peroxide from polymethyl methacrylate (Plexiglas). *Letters in Applied Microbiology*, *45*, 485–490.

Brown, G. S., Betty, R. G., Brockmann, J. E., Lucero, V., Souza, C. A., Walsh, K. S., … Rudolph, T. (2007). Evaluation of a wipe surface sample method for collection of *Bacillus* spores from nonporous surfaces. *Applied Environmental Microbiology*, *73*(3), 706–710.

Canter, D. A. (2005). Remediating anthrax-contaminated sites: Learning from the past to protect the future. *Chemical Health and Safety*, *12*, 13–19.

Center for Disease Control & U.S. Environmental Protection Agency (US EPA). (2012). *Interim clearance strategy for environments contaminated with Bacillus anthracis* Retrieved from https://www.epa.gov/emergency-response/epacdc-interim-clearance-strategy-environments-contaminated-anthrax

Lee, S. D., Ryan, S. P., & Snyder, E. G. (2011). Development of an aerosol surface inoculation method for *Bacillus* spores. *Applied Environmental Microbiology*, *77*(5), 1638–1645.

Meyer, K. M., Calfee, M. W., Wood, J. P., Mickelsen, R. L., Attwood, B., Clayton, M., … Delafield, R. (2014). Fumigation of a laboratory-scale HVAC system with hydrogen peroxide for decontamination following a biological contamination incident. *Journal of Applied Microbiology*, *116*, 533–541.

National Institute of Occupational Safety and Health. (2007, September). *Pocket Guide to Chemical Hazards* (NIOSH Publication No. 2005-149). Cincinnati, OH: Author.

Rastogi, V. K., Wallace, L., Smith, L. S., Ryan, S. P., & Martin, B. (2009). Quantitative method to determine sporicidal decontamination of building surfaces by gaseous fumigants, and issues related to laboratory-scale studies. *Applied Environmental Microbiology*, *75*(11), 3688–3694.

U.S. Environmental Protection Agency (US EPA). (2013). *Bio-response operational testing and evaluation (BOTE) project—Phase 1: Decontamination assessment, EPA/600/R-13/168*. Washington, DC: Author.

U.S. Environmental Protection Agency (US EPA). (2019). *List A: Antimicrobial products registered with the EPA as sterilizers* (Registration number: 58779-4). Retrieved from https://www.epa.gov/pesticide-registration/list-antimicrobial-products-registered-epa-sterilizers

Wood, J. P., Calfee, M. W., Clayton, M., Griffin-Gatchalian, N., Touati, A., Ryan, S., … Rastogi, V. K. (2016). A simple decontamination approach using hydrogen peroxide vapor for *Bacillus anthracis* spore inactivation. *Journal of Applied Microbiology*, *121*(6), 1603–1615.

AUTHOR BIOGRAPHIES

Ronald Leroy Mickelsen, M.S., P.E., has worked for 12 years for the Chemical, Biological, Radiological, and Nuclear Consequence Management Advisory Division within the US EPA preparing and responding to chemical, biological, and radiological hazards. His position there allows him to work with laboratory researchers as well as in the field with responders. Areas of interest include recovery from a biological agent release, ventilation for controlling hazards, and general health and safety topics.

Joseph Wood, M.S., P.E., is a senior research engineer with US EPA's National Homeland Security Research Center (NHSRC). He has been with the US EPA since 1991 (previously doing air pollution engineering work), and with NHSRC's Decontamination and Consequence Management Division since 2004. Currently, his research focuses primarily on the development, testing, and evaluation of technologies for the decontamination and disposal of materials contaminated with biological agents and biotoxins. He is the primary author or coauthor for many peer-reviewed journal articles and US EPA published reports. He holds a master's degree in environmental engineering from the University of Illinois (Urbana-Champaign), and is a licensed professional engineer.

Michael Worth Calfee, Ph.D., is a research microbiologist within US EPA's NHSRC. He has over 20 years of microbiological research experience with 10 years at the US EPA in decontamination and consequence management of chemical, biological, radiological, and nuclear (CBRN) agents. His research foci include sampling, decontamination, and management of wastes from CBRN contamination incidents. Dr. Calfee received his Ph.D. in 2007 from East Carolina University, where he studied coastal and estuarine microbial communities. He also earned a B.S. in molecular biology from East Carolina University in 1999.

Shannon Serre, Ph.D., has worked for the US EPA for 21 years, six of those with the CBRN Consequence Management Advisory Division preparing and responding to chemical, biological, and radiological hazards.

Shawn Ryan, Ph.D., is a chemical engineer within US EPA's NHSRC. He has over 18 years of research experience at the US EPA in decontamination and consequence management of CBRN agents. His research outputs include publications on the decontamination of chemical and biological agents on surfaces and assessing the impact of decontamination processes on equipment and materials. Dr. Ryan received his Ph.D. in 2001 from Rensselaer Polytechnic Institute in Troy, New York. He also earned a B.S. in environmental engineering from Rensselaer Polytechnic Institute in 1995.

Abderrahmane Touati, Ph.D., is a Senior Research Engineer with Jacobs Technology Inc. Since 2015 he has been the Jacobs Homeland Security Research Department Manager where he leads a research program supporting the US EPA's NHSRC Decontamination and Consequence Management Division. He provides expertise in the selection and implementation of decontamination methods and leads projects designed to provide the scientific basis for significant reductions in decontamination time and cost.

Francis Robbins Delafield, has a B.A. in natural sciences and has been performing and supporting laboratory research at the US EPA for 27 years on a variety of projects.

Lola Denise Aslett, Ph.D., is a Senior Microbiologist at Jacobs Technology Inc. and has worked for 3 years supporting laboratory research for the US EPA. Areas of Bacillus research interest include remediation, cell metabolism, sporulation, spore architecture, germination, and detection of spores in complex matrices such as soil and water.

How to cite this article: Mickelsen RL, Wood J, Calfee MW, et al. Low-concentration hydrogen peroxide decontamination for *Bacillus* spore contamination in buildings. *Remediation*. 2019;30:47–56. https://doi.org/10.1002/rem.21629

EPA/600/R-18/215 | September 2018
www.epa.gov/homeland-security-research

United States
Environmental Protection
Agency

Decontamination of Materials Contaminated with Spores of *Bacillus anthracis* Ames and Vollum Strains Using Low Concentrations of Hydrogen Peroxide Vapor

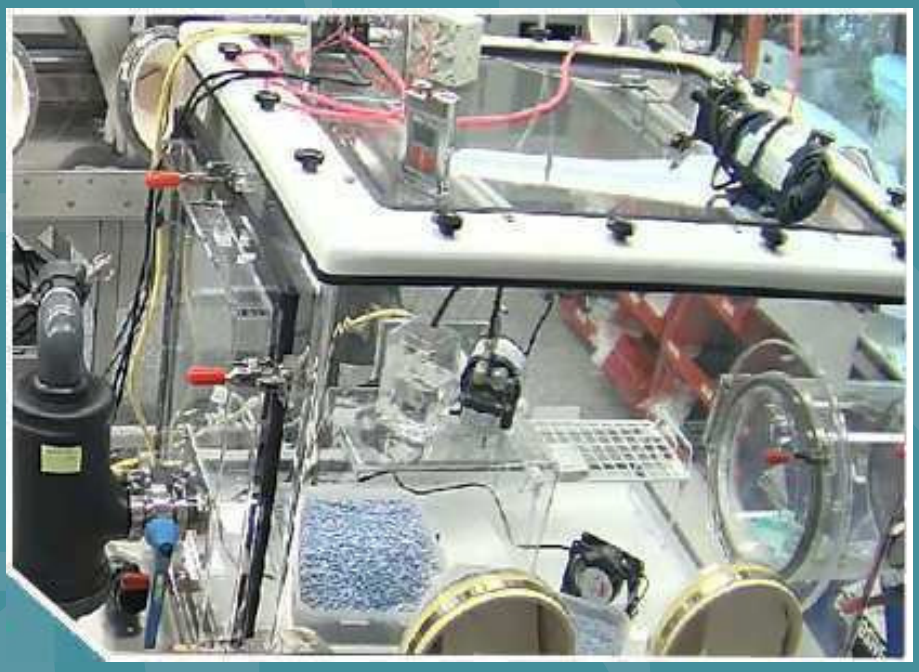

Office of Research and Development
Homeland Security Research Program

This page left intentionally blank

EPA/600/R-18/215
September 2018

REPORT

Decontamination of Materials Contaminated with Spores of *Bacillus anthracis* Ames and Vollum Strains Using Low Concentrations of Hydrogen Peroxide Vapor

U.S. Environmental Protection Agency
Research Triangle Park, NC 27711

Disclaimer

The U.S. Environmental Protection Agency (EPA), through its Office of Research and Development's (ORD's) National Homeland Security Research Center (NHSRC), funded, directed and managed this work through Contract Number EP-C-15-002, Task Order 0017, with Battelle. This report has been peer and administratively reviewed and has been approved for publication as an EPA document. The views expressed in this report are those of the authors and do not necessarily reflect the views or policies of the Agency. Mention of trade names or commercial products does not constitute endorsement or recommendation for use of a specific product.

Questions concerning this document or its application should be addressed to:

Mr. Joseph Wood
National Homeland Security Research Center
Office of Research and Development
U.S. Environmental Protection Agency
Mail Code E343-06
Research Triangle Park, NC 27711
919-541-5029

Acknowledgments

Contributions of the following individuals and organization to this report are gratefully acknowledged:

U.S. Environmental Protection Agency (EPA) Project Team
Joseph Wood (Principal Investigator)
Anne Mikelonis
Leroy Mickelsen

US EPA Technical Reviewers of Report
Lukas Oudejans
Doris Betancourt

US EPA Quality Assurance
Eletha Brady-Roberts

Battelle
William Richter
Michelle Sunderman
Zach Willenberg

The National Caucus and Center on Black Aging, Inc.
Joan Bursey (Technical editing and Quality Assurance review)

Executive Summary

The U.S. Environmental Protection Agency's (EPA's) Homeland Security Research Program (HSRP) is helping protect human health and the environment from adverse impacts resulting from the release of chemical, biological, or radiological agents. With an emphasis on decontamination and consequence management, water infrastructure protection, and threat and consequence assessment, the HSRP is working to develop technology and information that will help detect the intentional introduction of chemical, biological, or radiological contaminants in buildings or water systems; contain these contaminants; decontaminate buildings, water systems, other infrastructure and the outdoor environment; and facilitate the treatment and disposal of material resulting from restoration activities.

In the decontamination of buildings contaminated with *Bacillus anthracis* (*Ba*) spores using fumigation techniques, it may be challenging to reach the desired gas concentration without specialized equipment, modifications, or expertise. Thus, fumigating at relatively low levels may allow for contractors to provide decontamination services with less specialized equipment. This advantage may be critical to increasing the nation's decontamination capacity in the event of a wide area release of *Ba* spores.

In this study, the decontamination efficacy of low concentrations of hydrogen peroxide vapor (HPV) was evaluated on common building materials (glass, bare pine wood, carpet, painted wallboard paper, unpainted concrete, and ceiling tile) contaminated with *Ba* spores. All testing was conducted using both *Ba* Ames and Vollum strains concurrently to allow for direct comparison of the two strains. Decontamination efficacy was quantified based on the $\log_{10}$ reduction (LR) in viable spores, calculated from difference in spores recovered from positive controls and test materials.

Summary of Major Findings

Low concentrations (or levels) of HPV (e.g., 10-50 parts per million (ppm)) were effective in decontaminating all materials tested in the study except for unpainted concrete. Moreover, the glass, ceiling tile and painted wallboard paper materials were more amenable to decontamination by low concentrations of HPV compared to unpainted concrete, carpet, and wood. Even with using extended contact times (and hence higher dosages of HPV), the number of occurrences in which unpainted concrete, carpet, and wood were successfully decontaminated (complete inactivation of spore population or ≥6 log reduction) in the study was much less than the glass, ceiling tile, and painted wallboard materials. Although there were still several instances in which the carpet and wood materials were successfully decontaminated.

The results of the study may be summarized in terms of the minimum contact times needed to achieve effective decontamination of each material, for each experimental condition; refer to Tables ES-1 and ES-2. Contact times needed for effective decontamination generally decreased with increased HPV concentration. For example, at the higher concentration of 222 ppm (Test 1), only 15 minutes were required to decontaminate glass effectively; in contrast, at the 10-ppm level, 4-12 hours were required for effective decontamination of glass, depending on the strain and relative humidity (RH) level. With the Vollum strain of *Ba* on glass, ceiling tile, and painted wallboard paper, successful decontamination occurred in 2-16 hours for the 10-50 ppm HPV concentrations evaluated. In some experiments, however, effective decontamination may not have occurred for a material.

In terms of the HPV dosage requirements to achieve effective decontamination, again the results varied by material. For example, no more than 100-200 ppm*hours were required for effective decontamination in most of the tests for glass, painted wallboard, and ceiling tile. In some tests, the wood and carpet materials were successfully decontaminated with doses as low as 120-200 ppm*hours. However, there were a few tests in which successful decontamination was not achieved for wood and carpet when using the highest dose of 1200 ppm*hours.

While elevated RH has been shown to improve *Ba* spore inactivation with nearly all sporicidal fumigants, some debate still exists whether elevated RH is needed for HPV decontamination. From the statistical analysis of the study results, when assessed as a main effect, the RH level appeared to be a non-significant factor. However, when comparing the effect of RH by strain, significant differences were observed and varied by material type. As an example, for a given HPV concentration and strain, we found that the number of occurrences of successful decontamination always increased with increasing RH. In addition, the effect of increasing RH appears to have had more of an impact on the Ames strain.

Lastly, the data generated from this evaluation suggest that the resistance to inactivation by HPV is not significantly different for the two *Ba* strains that were used in the investigation.

Table ES-1. Minimum Time (Hours) Demonstrating Effective Decontamination for Ames Strain

	Test 1	Test 2	Test 3	Test 4	Test 5	Test 9	Test 6	Test 7	Test 8
Average HPV ppm	222	9-10		25-26			44-50		
average % RH	38	58	76	33	62	92	26	60	77
	Time (hours)								
Glass	0.25	12	8	8	4	6	6	1	2
PW* Paper	0.5	>20	8	>12	>12	2	>12	1	2
Ceiling Tile	2	12	8	>12	4	6	2	4	4
Pine Wood	3	12	>20	>24	>24	>48	>24	16	24
Carpet	0.25	>20	>20	>24	16	20	>24	20	8
Concrete	>3	>20	>20	>24	>24	>48	>24	>24	>24

*Painted wallboard.

A ">" denotes that effective decontamination was not achieved at any time point, with the longest contact time listed

Table ES-2. Minimum Time (Hours) Demonstrating Effective Decontamination for Vollum Strain

	Test 1	Test 2	Test 3	Test 4	Test 5	Test 9	Test 6	Test 7	Test 8
Average HPV ppm	222	9-10		25-26			44-50		
average % RH	38	58	76	33	62	92	26	60	77
	Time (hours)								
Glass	0.25	8	4	8	4	2	4	4	2
PW Paper	1	16	8	6	4	6	6	4	4
Ceiling Tile	1	8	8	8	6	6	2	4	4
Pine Wood	2	>20	>20	>24	>24	>48	24	16	24
Carpet	>3	>20	20	>24	24	20	24	20	12
Concrete	>3	>20	>20	>24	>24	>48	>24	>24	>24

A ">" denotes that effective decontamination was not achieved at any time point, with the longest contact time listed

Contents

Acknowledgments iii
Executive Summary iii
1.0 Introduction 1
2.0 Procedures 2
2.1 Test Matrix 2
2.2 Biological Agents 3
2.3 Test Materials 3
2.4 Inoculation of Coupons 5
2.5 Test Chamber and Procedures 6
2.6 Coupon Extraction and Biological Agent Quantification 9
2.7 Decontamination Efficacy 10
2.8 Statistical Analysis 11
2.9 Surface Damage 11
3.0 Quality Assurance/Quality Control 12
3.1 Equipment Calibration 12
3.2 QC Results 12
3.3 Operational Parameters 13
3.4 Audits 14
3.5 QA/QC Reporting 15
3.6 Data Review 15
4.0 Summary of Results and Discussion 16
4.1 Comparing the Effect of Material and Strain on Decontamination Efficacy 27
4.2 Effect of HPV Dose on Efficacy 30
4.3 Effects of Relative Humidity on Efficacy 30
4.4 Surface Damage to Materials 31
4.5 Summary 31
5.0 References 33

Figures

Figure 2-1. Coupon Types 4
Figure 2-2. Liquid Inoculation of Coupon Using a Micropipette 5
Figure 2-3. Bubbler Method 6
Figure 2-4. Generator Method, Configuration 1 7
Figure 2-5. Generator Method, Configuration 2 7
Figure 2-6. Generator Method, Configuration 3 8
Figure 2-7. Representative Graph of Temperature, RH, and Fumigant Stability (Test 7) 8

Tables

Table ES-1. Minimum Time (Hours) Demonstrating Effective Decontamination for Ames v
Table ES-2. Minimum Time (Hours) Demonstrating Effective Decontamination for Vollum ... v
Table 2-1 Decontamination Test Matrix 2
Table 2-2. Test Materials 4
Table 3-1. Summary of Average Recovery (Percent) of Spores from Positive Controls 143
Table 3-2. Actual Fumigant Conditions for Tests 144
Table 3-3. Performance Evaluation Audits 14
Table 4-1. Minimum Time (Hours) Demonstrating Effective Decontamination for Ames 27
Table 4-2. Minimum Time (Hours) Demonstrating Effective Decontamination for Vollum . 17
Table 4-3. Summary of Efficacy Results for Test 1 (222 ppm) 18
Table 4-4. Summary of Efficacy Results at 10 ppm and Medium RH 19
Table 4-5. Summary of Efficacy Results at 10 ppm and High RH 20
Table 4-6. Summary of Efficacy Results at 25 ppm and Low RH 21
Table 4-7. Summary of Efficacy Results at 25 ppm and Medium RH 22
Table 4-8. Summary of Efficacy Results at 50 ppm and Low RH 23
Table 4-9. Summary of Efficacy Results at 50 ppm and Medium RH 24
Table 4-10. Summary of Efficacy Results at 50 ppm and High RH 25
Table 4-11. Summary of Efficacy Results at 25 ppm and High RH 26
Table 4-12. Number of Succesful Decontamination Instances for *Ba* Ames 27
Table 4-13. Number of Succcesful Decontamination Instances for *Ba* Vollum 28
Table 4-14. Significant Effects Based on Logistic Regression Model 29
Table 4-15. Minimum HPV Dose Required for Effective Decontamination 30
Table 4-16. Number of Succesful Decontaminations by RH 31

Table A-1. Inactivation of *B. anthracis* Ames Spores using low level HPV[a] 1
Table A-2. Inactivation of *B. anthracis* Ames Spores using low level HPV[a] *(Continued)*..... 2
Table A-3. Inactivation of *B. anthracis* Ames Spores using low level HPV[a] *(Continued)*..... 3
Table A-4. Inactivation of *B. anthracis* Ames Spores using low level HPV[a] *(Continued)*..... 4
Table A-5. Inactivation of *B. anthracis* Ames Spores using low level HPV[a] *(Continued)*..... 5
Table A-6. Inactivation of *B. anthracis* Ames Spores using low level HPV[a] *(Continued)*..... 6
Table A-7. Inactivation of *B. anthracis* Ames Spores using low level HPV[a] *(Continued)*..... 7
Table A-8. Inactivation of *B. anthracis* Ames Spores using low level HPV[a] *(Continued)*..... 8
Table A-9. Inactivation of *B. anthracis* Ames Spores using low level HPV[a] *(Continued)*..... 9
Table A-10. Inactivation of *B. anthracis* Vollum Spores using low level HPV[a] *(Continued)*... 10
Table A-11. Inactivation of *B. anthracis* Vollum Spores using low level HPV[a] *(Continued)*... 11
Table A-12. Inactivation of *B. anthracis* Vollum Spores using low level HPV[a] *(Continued)*... 12
Table A-13. Inactivation of *B. anthracis* Vollum Spores using low level HPV[a] *(Continued)*... 13
Table A-14. Inactivation of *B. anthracis* Vollum Spores using low level HPV[a] *(Continued)*... 14
Table A-15. Inactivation of *B. anthracis* Vollum Spores using low level HPV[a] *(Continued)*... 15
Table A-16. Inactivation of *B. anthracis* Vollum Spores using low level HPV[a] *(Continued)*... 16
Table A-17. Inactivation of *B. anthracis* Vollum Spores using low level HPV[a] *(Continued)*... 17
Table A-18. Inactivation of *B. anthracis* Vollum Spores using low level HPV[a] *(Continued)*... 18

List of Appendices

Appendix A Detailed Test Results A1
Appendix B Efficacy Results Figures B1
Appendix C Details on HPV Dose Requirements for Effective Decontamination C1
Appendix D Detailed Statistical Analysis D1

Abbreviations/Acronyms

ASTM	American Society of Testing and Materials
Ba	*Bacillus anthracis* Ames or Vollum
BBRC	Battelle Biomedical Research Center
BSC	biological safety cabinet
CFU	colony forming unit(s)
CI	confidence interval
cm	centimeter(s)
°C	degree(s) Celsius
DNA	Deoxyribonucleic Acid
DF	degrees of freedom
E-beam	electron beam
EPA	U.S. Environmental Protection Agency
H_2O_2	hydrogen peroxide
HPV	hydrogen peroxide vapor
h	Hour
HCl	Hydrochloric acid
HSRP	Homeland Security Research Program
HVAC	heating, ventilation, and air conditioning
kGy	kilogray(s)
LAL	Limulus Amebocyte Lysate
LR	Log_{10} reduction
PE	performance evaluation
PW	painted wallboard
µg	microgram(s)
µL	microliter(s)
mg	milligram(s)
mL	milliliter(s)
mil	thousandth of an inch
min	minute(s)
mm	millimeter(s)
µm	micrometer(s)
L	liter
NA	not applicable
NHSRC	National Homeland Security Research Center
ORD	Office of Research and Development
PBS	phosphate buffered saline
PBST	PBS + 0.1% Triton X-100
PCR	polymerase chain reaction
ppm	part(s) per million
QA	quality assurance

QAPP	Quality Assurance Project Plan
QC	quality control
QMP	Quality Management Plan
RH	relative humidity
rpm	revolution(s) per minute
s	second(s)
SD	standard deviation
SE	standard error
SFW	sterile filtered water (cell-culture grade)
TSA	technical systems audit

1.0 Introduction

The U.S. Environmental Protection Agency's (EPA's) Homeland Security Research Program (HSRP) is helping protect human health and the environment from adverse impacts resulting from the release of chemical, biological, or radiological agents. With an emphasis on decontamination and consequence management, water infrastructure protection, and threat and consequence assessment, the HSRP is working to develop technology and information that will help detect and contain these contaminants; decontaminate buildings, water systems, or other infrastructure and outdoor environments; and facilitate the disposal of material resulting from said restoration activities.

In the decontamination of buildings contaminated with *Bacillus anthracis* (*Ba*) spores using fumigation techniques, it may be challenging to reach the desired gas concentration, temperature, or relative humidity (RH) targets without special equipment, modifications, and/or expertise. Thus, fumigating at or near ambient temperatures and RH levels, and the use of lower fumigant concentrations (or levels), may allow for less experienced personnel to provide decontamination services and with less specialized equipment. This advantage may be critical in increasing decontamination capacity in the event of a large release of *Ba* spores.

In this investigation, the decontamination efficacy of hydrogen peroxide vapor (HPV) was evaluated using common building materials: glass, bare pine wood, carpet, painted wallboard paper, unpainted concrete, and ceiling tile. While the first experiment in the study was conducted at a more typical HPV concentration (250 parts per million [ppm]) to allow for some comparison to previous literature (Rogers et al. 2005; Rastogi et al. 2009; US EPA 2010; US EPA 2011), the remainder of the nine experiments utilized relatively low concentrations of HPV (10-50 ppm). The present study builds on previous research (Wood et al. 2016) that initially demonstrated low concentrations of HPV were effective for *Ba* spore inactivation, with the present study focusing on the additional experimental elements described below.

Testing was conducted with spores of *Ba*, using both Ames and Vollum strains. All testing was conducted with both strains concurrently (inoculated separately on coupon materials, however) to allow for direct comparison. While there is a large body of research and data for the decontamination of materials contaminated with the Ames strain, few efficacy data are available for the Vollum strain. One of the objectives of this study was to fill that data gap and assess the importance of strain variation.

In addition to HPV concentration, building material type, and *Ba* spore strain, other test variables that were examined as part of this study included contact time and RH. Each experiment consisted of exposing inoculated coupons to a constant HPV concentration, with coupons withdrawn from the test chamber at five pre-determined time points. Having five contact times in each experiment allowed for determining the minimum contact time needed for effective decontamination for a given HPV concentration and RH level. In addition, as testing proceeded, it became clear that the glass, painted wallboard, and ceiling tile materials were being effectively decontaminated at shorter contact times compared to the unpainted concrete, wood, and carpet materials. Because of this difference, beginning with the fourth experiment, we segregated these materials into two groups, with each group having its own set of five contact times.

Further, while elevated RH has been shown to improve *Ba* spore inactivation with nearly all sporicidal fumigants, some debate still exists whether elevated RH is needed for HPV

decontamination. Thus, another objective of this study was to evaluate the effect of different RH levels on HPV decontamination efficacy.

Decontamination efficacy was determined based on the $\log_{10}$ reduction (LR) in viable spores recovered from the inoculated samples, with and without exposure to HPV. A decontaminant or fumigant technology is effective via AOAC 966.04 if a 6 LR or greater is achieved on the materials tested for a given set of fumigation conditions (fumigant concentration, temperature, contact time, and RH (US EPA, 2010).

2.0 Procedures

This section provides an overview of the procedures used for the bench-scale evaluation of low concentration HPV to inactivate *Ba* Ames and Vollum on six material types.

2.1 Test Matrix

The test matrix for the decontamination tests is shown in Table 2-1. Each test was performed using six material types inoculated with *Ba* Ames and another set of the same six material types inoculated with *Ba* Vollum. Testing was conducted at ambient temperature and low (26-38%) medium (59-62%), or high (76-92%) average RH levels. Note in each the first three tests, all materials shared the same contact times. After that, the materials that were harder to decontaminate (wood, carpet, unpainted concrete) were exposed to longer contact times. (Specifically, one of the aims was to see if we could achieve effective decontamination for unpainted concrete by extending the contact time.) Lastly, various equipment was used to generate the HPV; this is further discussed in Section 2.5.

The first test was meant to be conducted at a vendor's EPA antimicrobial label requirements for use as a sterilant for both porous and nonporous materials (US EPA, 2012), to tie back to previous testing. Following Test 1, all tests thereafter used a target HPV concentration of either 10, 25, or 50 ppm, paired with different RH levels.

Table 2-1 Decontamination Test Matrix

Test Number	Equipment	Target HPV Level (ppm)	Temp (°C)	RH	Easy[1] Material Contact Times (h)	Difficult[2] Material Contact Times (h)	Materials
1	Generator	250	23	Low	0.25,0.50,1,2,3		Glass, Painted Wallboard Paper, Ceiling Tile, Pine Wood, Carpet, Unpainted Concrete
2	Bubbler	10	23	Medium	4, 8, 12, 16, 20		
3	Bubbler	10	23	High	4, 8, 12, 16, 20		
4	Generator	25	23	Low	2,4,6,8,12	8,12,16,20,24	
5	Generator	25	23	Medium	2,4,6,8,12	8,12,16,20,24	
6	Generator	50	23	Low	2,4,6,8,12	8,12,16,20,24	
7	Generator	50	23	Medium	1,2,4,5,6	8,12,16,20,24	
8	Generator	50	23	High	1,2,4,5,6	8,12,16,20,24	
9	Bubbler	25	23	High	1,2,6,8,12	8,12,20,24, 48	

[1] Glass, Painted Wallboard Paper and Ceiling Tile

[2] Pine Wood, Carpet, Unpainted Concrete

2.2 Biological Agents

The virulent *Ba* Ames (Ames-Lot B21) and Vollum (Vollum-Lot BAV-1) spores used for this testing were prepared from qualified stocks at the Battelle Biomedical Research Center (BBRC, , West Jefferson, OH) using a BioFlo 3000 fermenter (New Brunswick Scientific Co., Inc., Edison, NJ). The spore lot was subjected to a stringent characterization and qualification process required by the Battelle standard operating procedure for spore production. Specifically, the spore lots were characterized prior to use by observation of colony morphology, direct microscopic observation of spore morphology, and size and determination of percent refractivity and percent encapsulation. In addition, the number of viable spores was determined by colony count and expressed as colony forming units per milliliter (CFU/mL). Theoretically, once plated onto bacterial growth media, each viable spore germinates and can yield one CFU. Variations in the expected colony phenotypes were recorded. Endotoxin concentration of each spore preparation was determined by the Limulus Amebocyte Lysate (LAL) assay to assess whether contamination from gram-negative bacteria occurred during the propagation and purification process of the spores. Genomic deoxyribonucleic acid (DNA) was extracted from the spores and DNA fingerprinting by polymerase chain reaction (PCR) was done to confirm the genotype. This work was confirmed by an independent third party. The virulence of the original spore lot was measured by challenging guinea pigs intradermally with a dilution series of spore suspensions, and virulence was expressed as the intradermal median lethal dose. In addition, testing of the original spore lot was conducted for robustness of the Ames strain spores via hydrochloric acid (HCl) resistance.

The *Ba* Ames and Vollum stock spore suspensions were prepared in sterile filtered water (SFW) at an approximate concentration of 1×10^9 CFU/mL and stored at 2 to 8 degrees Celsius (°C). This suspension medium was chosen to be consistent with previous work conducted with the U.S. EPA.

2.3 Test Materials

Decontamination testing was conducted using common building materials (glass, bare pine wood, carpet, painted wallboard paper, unpainted concrete, and ceiling tile). Information on these materials is presented in Table 2-2, and a picture of each is presented in Figure 2-1. Material coupons were cut to uniform length and width (Table 2-2) from larger pieces of stock material. Materials were prepared for testing by either sterilization via electron beam (E-beam) irradiation at ~200 kilograys (kGy; E-beam Services Inc., Lebanon, OH) or autoclaved at 121 °C for 15 minutes (min). E-beam-irradiated material coupons were sealed in 6 mil (0.006 inch) Uline Poly Tubing (Cat. No. S-2940, Uline, Chicago, IL), and autoclaved coupons were sealed in sterilization pouches (Cat. No. 01-812-50, Fisher, Pittsburgh, PA) to preserve sterility until the coupons were ready for use. Sterilization was intended to eliminate contamination by endogenous microorganisms.

Figure 2-1. Coupon Types from Left to Right: Glass, Painted Wallboard Paper, Ceiling Tile, Bare Pine Wood, Unpainted Concrete, and Carpet

Table 2-2. Test Materials

Material	Lot, Batch, or ASTM No., or Observation	Manufacturer/ Supplier Name Location	Approximate Coupon Size, Width x Length x Thickness	Sterilization Technique
Glass	C1036	Brooks Brothers, Columbus, OH	1.9 centimeters (cm) x 7.6 cm x 0.2 cm	Autoclave
Bare Pine Wood	Generic Molding	Commercial lumber retailer	1.9 cm x 3.8 cm x 0.2 cm	E-Beam
Carpet	Shaw Swizzle EcoWorx, Style: 10401 Color: Jacks	Shaw Industries, Dalton, GA	1.9 cm x 3.8 cm x 0.2 cm	E-Beam
Painted Wallboard Paper	Roller painted on one side using Martin Senour Paints. One primer (#71-1185) and two finish (flat, #70-1001) coats	United States Gypsum Company, Chicago, IL	1.9 cm x 3.8 cm x 0.2 cm	E-Beam
Unpainted Concrete	ASTM C90 cinder block	Wellnitz Columbus, OH	1.9 cm x 7.6 cm x 0.2 cm	E-Beam
Ceiling Tile	Armstrong® B513, classic fine textured	Armstrong, Columbus, OH	1.9 cm x 3.8 cm x 0.2 cm	E-Beam

2.4 Inoculation of Coupons

Test (exposed to HPV) and positive control (not exposed to HPV) coupons were placed on a flat surface within a Class II biological safety cabinet (BSC) and inoculated with approximately 1×10^8 CFU of viable *Ba* Ames or Vollum spores per coupon. A 100 microliter (µL) aliquot of a stock suspension of approximately 1×10^9 CFU/mL was dispensed using a micropipette applied as 10 µL droplets across the coupon surface (see Figure 2-2). This approach provided a more uniform distribution of spores across the coupon surface than would be obtained through a single drop of the suspension.

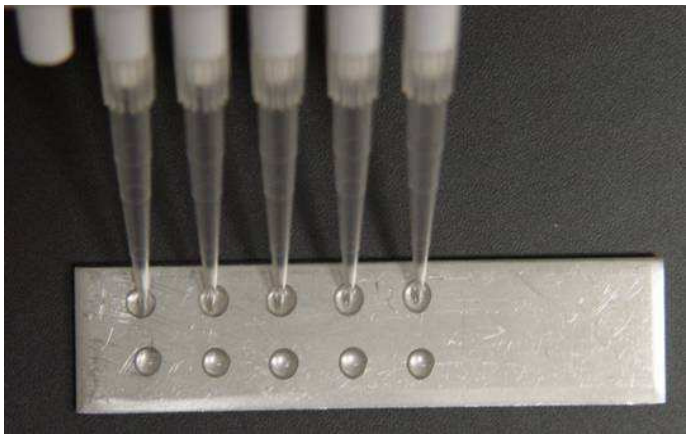

Figure 2-2. Liquid Inoculation of Coupon Using a Micropipette

Although application of the inoculum onto each material was uniform, the behavior of the inoculum droplets was not. Droplets beaded on the surface of the glass (nonporous material) while they soaked into the other porous materials after producing a liquid bead for a short period of time. The difference in the behavior of the inoculum droplets on each material could lead to a variance in microorganism distribution across coupons; however, this effect was not studied in this evaluation. After inoculation, the coupons were transferred to a Class III BSC and left undisturbed overnight to dry under ambient conditions, approximately 22 °C and 40% RH.

The number and type of replicate test coupons and positive controls used for each experiment, for each material and *Ba* strain is as follows:

- Three test coupons per material, timepoint, and strain
- Five positive controls for each material and strain (inoculated with *Ba* but not exposed to HPV)
- One laboratory blank (not inoculated and not exposed to HPV) for each material
- One procedural blank (not inoculated and exposed to HPV) for each material.

On the day following inoculation, coupons intended for decontamination (including blanks) were transferred into the test chamber and exposed to the HPV using the apparatus and application conditions specified in Section 2.5. Control coupons remained in the BSC III chamber where they were dried and collected for processing after the last contact time.

2.5 Test Chamber and Procedures

Decontamination testing was conducted inside a 498 liter (L) custom acrylic compact glove box (Plaslabs, Lansing, MI). The test chamber was outfitted with three low-speed mixing fans and two patch panels on the walls to allow for the required plumbing and electrical connections. All testing was conducted at ambient laboratory temperatures and was not controlled. Fixed humidity point salts or Drierite® were utilized to adjust RH prior to the initiation of an experiment. Temperature and RH inside the test chamber were measured using an MX1101 temperature and humidity data logger (Onset, Bourne, MA) and data were recorded every minute for the duration of the experiment. HPV concentration was measured using an ATI B12 2-wire gas transmitter (Analytical Technology, Inc., Collegeville, PA) and was connected to a CNI-822 process controller (Omega Engineering, Norwalk, CT) which allowed for automatic control of concentration within the test chamber, and data were recorded every minute during the experiment using the associated iLOG software. The test chamber was hard-ducted to the facility exhaust system, but during each test, valves on both the exhaust and supply were closed to create a sealed enclosure. Once the final contact time had concluded, the exhaust and supply valves were opened to allow for any residual fumigant to be removed.

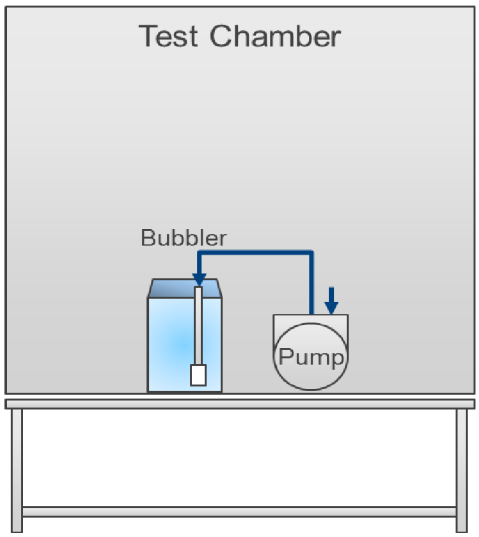

Figure 2-3. Bubbler Method

Generation of the HPV fumigant was achieved using either a bubbler method or with the use of a commercial generator, depending on the target concentration. A stock solution of 35% aqueous hydrogen peroxide (H_2O_2) Cat # HPV-AQ was used as the starting material for both methods (Bioquell, Horsham, PA). Figure 2-3 illustrates the bubbler method, which used a fritted impinger connected to a small air circulating pump. Test chamber air was circulated through the pump and supplied to the impinger which created bubbles when immersed into a 1 L bottle containing the H_2O_2 stock solution. This pump was controlled by the Omega CNI-822 using the ATI B12 ppm data. This method was used for fumigant concentrations up to 25 ppm. Higher concentrations were attempted using this method but resulted in excessive humidity and condensation on chamber walls, skewing the concentration data.

The commercial generator method utilized a STERIS 1000ED HPV generator (STERIS Corp., Mentor, OH). These types of commercial generators typically target much higher concentrations (e.g., 200-400 ppm) and use higher flow rates, resulting in the need for three separate configurations of the generator, test chamber, and a third class III BSC chamber, which were used to achieve lower targeted concentrations. These are discussed as follows. Figure 2-4 shows the generator configured in a daisy chain approach that allowed for increased chamber volume to be able to target concentrations at or above 200 ppm.

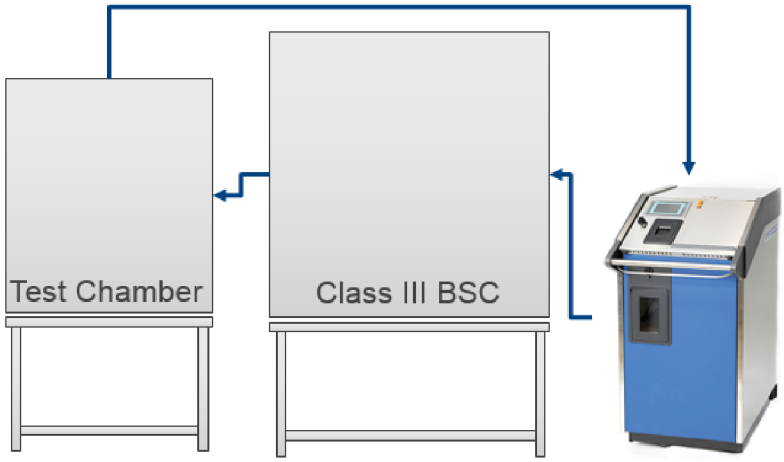

Figure 2-4. Generator Method, Configuration 1

Figure 2-5 shows the commercial generator, configuration 2, in which the generator was connected primarily to the class III BSC. A higher-than-target ppm was generated in this chamber. The test chamber used the Omega controller to turn the pump placed inside this BSC III on and off to draw HPV vapor from the primary BSC III chamber to the test chamber. This method allowed for concentrations ranging from 1 to 200 ppm and was used during testing for 25 and 50 ppm concentrations.

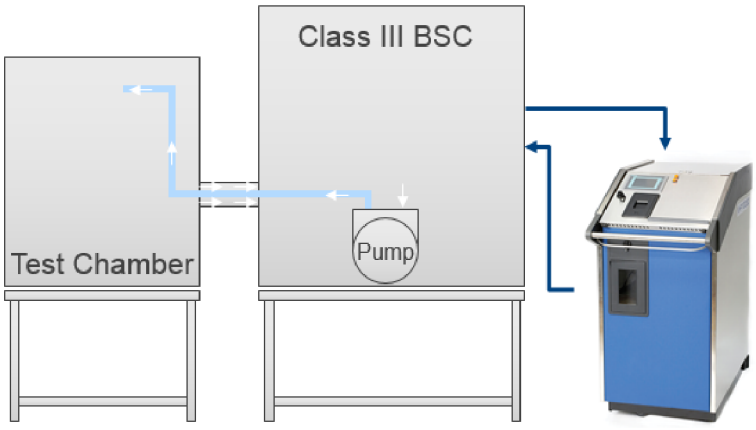

Figure 2-5. Generator Method, Configuration 2

A representative graph of the test chamber conditions (Test 7) data collection can be seen in Figure 2-6. The generator we used continually dries and catalytically breaks down the HPV atmosphere returning to the generator. This can be seen in the figure by the drying effect from approximately 79% RH down to the mid 50% range. Later in the run, as the desiccant within the

generator began to be saturated, the RH began to rise again. Test runs lasting longer than 24 hours were therefore run in a third configuration shown in Figure 2-7. In this approach, the HPV was supplied to the class III BSC but then it was exhausted through the facility heating, ventilation and air conditioning (HVAC) system. This approach allowed for laboratory air to be supplied to the STERIS generator so that the desiccant was not challenged by the high RH conditions.

The method for achieving the target RH varied by HPV generation method. As stated previously, the commercial generator continuously dried the returning atmosphere from the test chamber to avoid high humidity levels (which would potentially result in condensation on chamber walls). Test runs that utilized the commercial generator resulting in high RH levels required the use of saturated salts during the run to re-humidify the test chamber. The bubbler method increased RH whenever the pump was active. Tests using this method with low RH target levels utilized Drierite to pre-dehumidify the test chamber prior to initiation of testing. This pre-dehumidification step is also a standard procedure used by commercial generators. Tests were limited with this method in general to approximately 24 hours (h) before condensation would begin to form on the chamber walls. Once the condensation began to form, HPV concentrations decreased and caused the pump to run continuously.

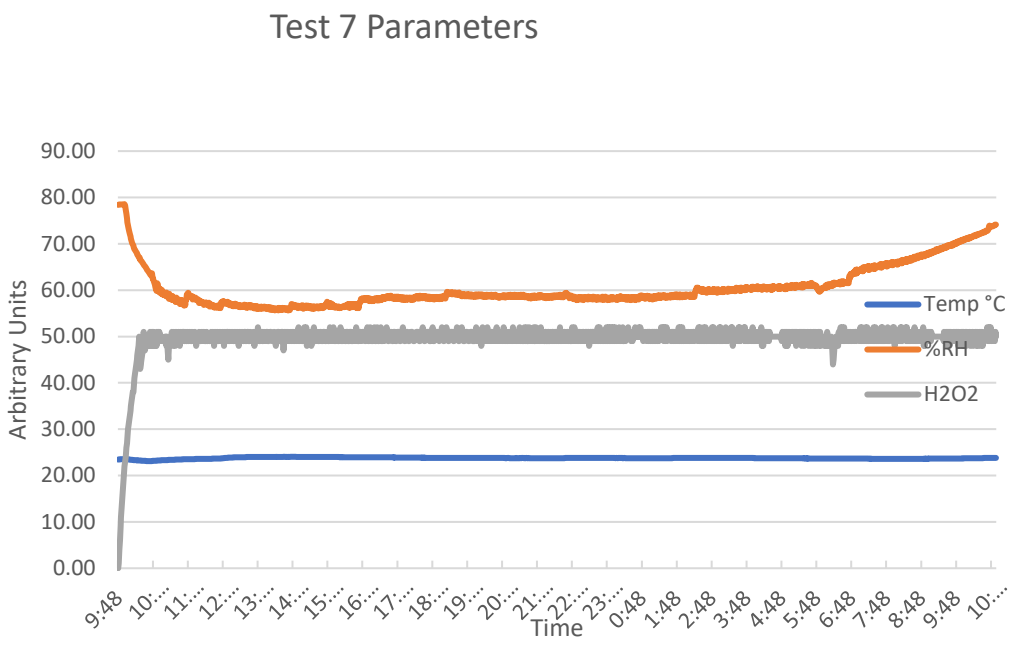

Figure 2-6. Representative Graph of Temperature, RH, and Fumigant Stability (Test 7)

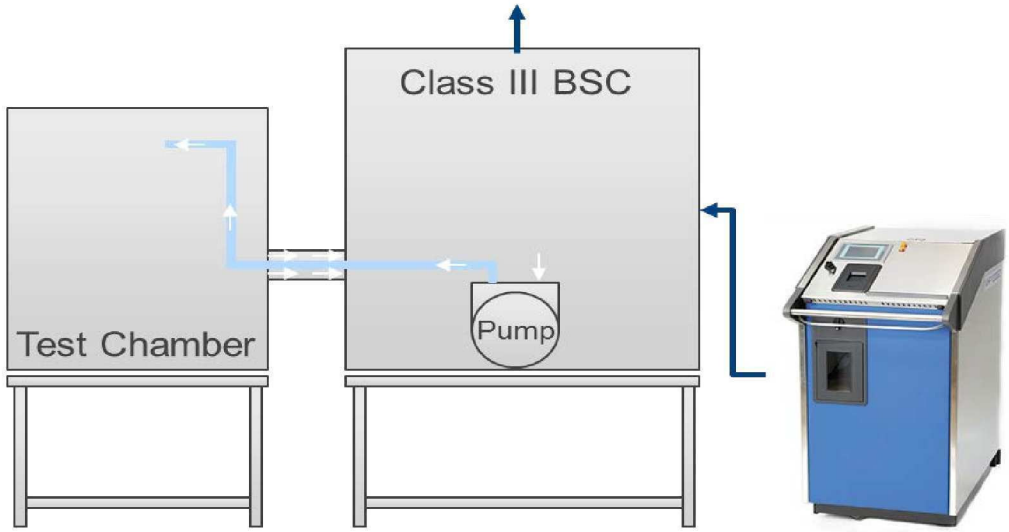

Figure 2-7. Generator Method, Configuration 3

2.6 Coupon Extraction and Biological Agent Quantification

Spore extraction from coupons was achieved by placing test, positive control, and blank coupons in 50 mL polypropylene conical tubes containing 10 mL of sterile phosphate buffered saline plus 0.1% Triton X-100 (PBST). The vials were capped, placed on their side and agitated on an orbital shaker for 15 min at approximately 200 revolutions per minute (rpm) at room temperature.

The number of residual viable spores was determined using a dilution plating approach. Following extraction, the extract was removed, and a series of tenfold dilutions was prepared in SFW. An aliquot (0.1 mL) of either the undiluted extract and/or each serial dilution was plated onto tryptic soy agar (TSA) in triplicate and incubated for 18 to 24 hours at 37 ± 2 ºC. Colonies were counted manually, and CFU/mL was determined by multiplying the average number of colonies per plate by the reciprocal of the dilution, for plates ranging between 25-250 CFU for diluted samples and 0-250 CFU for undiluted samples. Dilution data representing the greatest number of individually definable colonies were expressed as arithmetic mean ± standard deviation (SD) of the numbers of CFU observed. Laboratory blanks controlled for sterility and procedural blanks controlled for viable spores inadvertently introduced to test coupons. The target acceptance criterion for extracts of laboratory or procedural blanks was zero CFU.

After each decontamination test, the test and control chambers were thoroughly cleaned (using separate steps involving bleach, ethanol, water, then drying).

2.7 Decontamination Efficacy

The mean percent spore recovery from each coupon was calculated using results from positive control coupons (inoculated, not decontaminated), by means of the following equation:

$$\text{Mean \% Recovery} = [\text{Mean } CFU_{pc}/CFU_{spike}] \times 100 \quad (1)$$

where Mean CFU_{pc} is the mean number of CFU recovered from five replicate positive control coupons of a single material, and CFU_{spike} is the number of CFU spiked onto each of those coupons. The value of CFU_{spike} was known from enumeration of the stock spore suspension. One aliquot of the stock suspension was plated and enumerated on each day of testing to confirm CFU_{spike} concentration. Spore recovery was calculated for *Ba* Ames or Vollum on each coupon, and the results are included in Section 4 and Appendix A.

The performance or efficacy of the fumigant was assessed by determining the number of CFU remaining on each test coupon after decontamination. Those numbers were compared to the number of CFU extracted from the positive control coupons.

The number of viable spores of *Ba* Ames or Vollum in extracts of test and positive control coupons was determined to calculate efficacy of the decontaminant. Efficacy (in terms of LR) is defined as the extent to which viable spores extracted from test coupons after decontamination were less numerous than the viable spores extracted from positive control coupons. The logarithm of the CFU abundance from each coupon extract was determined, and the mean of those logarithm values was then determined for each set of control and associated test coupons, respectively. Efficacy of a decontaminant for a test organism/test condition on the ith coupon material was calculated as the difference between those mean log values, i.e.:

$$Efficacy\,(LR) = \overline{(\log_{10} CFUc_{ij})} - \overline{(\log_{10} CFUt_{ij})} \quad (2)$$

where $\log_{10} CFUc_{ij}$ refers to the j individual logarithm values obtained from the positive control coupons and $\log_{10} CFUt_{ij}$ refers to the j individual logarithm values obtained from the individual corresponding test coupons, and the overbar designates a mean value. In tests conducted under this plan, there were five positive controls (i.e., $j = 5$) and three corresponding test coupons for each coupon material. A decontaminant or fumigant technology is considered effective via AOAC 966.04 if a 6 LR or greater is achieved (US EPA 2016).

In the case where no viable spores were found in the extracts of any of the three test coupon replicates after decontamination, a CFU abundance of 1 was assigned, resulting in a $\log_{10}$ CFU of 0 for that material. This situation occurred when the decontaminant was highly effective, and no viable spores were found on the decontaminated test coupons. In such cases, the final efficacy on that material was reported as greater than or equal to (≥) the value calculated by Equation 2.

The variances (i.e., the square of the SD) of the $\log_{10} CFUc_{ij}$ and $\log_{10} CFUt_{ij}$ values were also calculated for both the control and test coupons (i.e., S^2c_{ij} and S^2t_{ij}), and were used to calculate the pooled standard error (SE) for the efficacy value calculated in Equation 2, as follows:

$$SE = \sqrt{\frac{S^2 c_{ij}}{5} + \frac{S^2 t_{ij}}{3}} \quad (3)$$

where the number 5 again represents the number j of coupons in the control and 3 in the test data sets. Each efficacy result is reported as an LR value with an associated 95% confidence interval (CI), calculated as follows:

$$95\ \%\ \text{CI} = \textit{Efficacy (LR)} \pm (1.96 \times \text{SE}) \quad (4)$$

In some cases, the significance of differences in efficacy across different test conditions and *Ba* strain was assessed based on the 95% CI of each efficacy result. Differences in efficacy were judged to be significant if the 95% CIs of the two efficacy results did not overlap. This comparison is not applicable when the two efficacy results being compared are both reported with LRs as ≥ some value (complete inactivation).

2.8 Statistical Analysis

A binary response based on LR in spores was the primary endpoint. For this endpoint, a trial was recorded as a success if either: 1) the LR was greater than or equal to 6, or 2) the $\log_{10}$ recovery was equal to or less than the average control recovery (complete inactivation). The proportion of tests that were successful and the 95 percent Clopper-Pearson confidence intervals (Clopper and Pearson, 1934) were computed by strain (Ames or Vollum), material, contact time, RH, and HPV concentration.

A logistic regression model was fitted to the full data set to test whether the proportions of successes were significantly associated with any effects included in the model. The logistic regression model included main effects for strain (Ames or Vollum), material, dose (defined as contact time times HPV concentration, i.e., ppm*hours), and RH; the model also included all two-factor interactions and the three-factor interaction for dose, strain, and material. An implicit assumption in the analysis was that the effect of dose is the same for any concentration and time used to achieve it.

For comparisons, results may be presented in terms of an odds ratio. The “odds ratio” is defined as the ratio of probability of successful decontamination (≥ 6 LR or complete kill) to the probability of unsuccessful decontamination. When the odds ratio is greater than one, a higher odds ratio implies greater odds of successful decontamination for the level 1 of the factor compared to level 2. For odds ratios less than one, there are greater odds of successful decontamination for level 2 of the factor compared to level 1. An odds ratio equal to one indicates the odds of successful decontamination are approximately the same for both levels of the factor. All statistical analyses were performed using SAS (version 9.4; Cary, NC). All results are reported at the 0.05 level of significance. Further details on the statistical analysis methods and results are found in Appendix D.

2.9 Surface Damage

The physical effect of the HPV on the materials was qualitatively monitored during the evaluation. This approach provided a visual assessment of whether the test condition changed the appearance of the test materials compared to positive controls. The procedural blank was visually compared to a laboratory blank coupon when testing was completed.

3.0 Quality Assurance/Quality Control

Quality assurance (QA)/quality control (QC) procedures were performed in accordance with the Testing and Evaluation (T&E II) Program Quality Management Plan (QMP), Version 1 and the TO14 quality assurance project plan. The QA/QC procedures and results are summarized below.

3.1 Equipment Calibration

All equipment (e.g., pipettes, incubators, biological safety cabinets) and monitoring devices (e.g., Vaisala thermometer/hygrometer and ATI HPV sensor) used at the time of the evaluation were verified as being certified, calibrated, or validated.

3.2 QC Results

QC efforts conducted during decontaminant testing included positive control samples, procedural blanks, laboratory blanks, and inoculation control samples.

All positive control results were within the target recovery range of 5 to 120% of the inoculated CFU amount for the *Ba* Ames strain. The *Ba* Vollum strain exhibited relatively lower recovery for most materials, for most of the tests (75% of Vollum positive control recoveries were < 5% of the inoculated level), with recoveries ranging from 3.4 to 13% on glass, 4.3 to 47.4% on painted wallboard paper, 0.1 to 1.5% on ceiling tile, 0.5 to 5.3% on pine wood, 0.7 to 13.4% on industrial carpet, and 0.8 to 10.5% on unpainted concrete. The positive control recovery results are summarized in Table 3-1.

While occasional low recoveries of bacterial spores from porous surfaces is not uncommon, the generally high percentage of low recoveries for Vollum was a new trend not seen before with the Ames strain. (Further research may be warranted to help explain this phenomenon.) Testing proceeded in these cases, with the implication that depending on the recovery, complete decontamination of a material may have occurred without achieving ≥ 6 LR. Finally, all procedural and laboratory blanks met the criterion of no observed CFU for both strains.

Table 3-1. Summary of Average Recovery (Percent) of Spores from Positive Controls

Average ± SD Ames % Recovery									
	Test 1	**Test 2**	**Test 3**	**Test 4**	**Test 5**	**Test 6**	**Test 7**	**Test 8**	**Test 9**
Glass	38±13	37±1	59±7	57±9	47±8	36±7	55±5	15±7	42±7
PW Paper	84±4	83±7	79±9	72±25	63±12	63±8	66±13	41±16	64±9
Ceiling Tile	43±11	30±12	31±4	38±7	37±6	26±6	40±5	25±12	14±2
Wood	28±10	27±9	18±12	22±11	23±11	10±2	24±12	15±4	21±21
Carpet	79±30	89±8	92±8	73±9	87±3	75±5	69±7	50±7	92±9
Concrete	15±9	100±27	39±25	19±24	14±4	12±8	25±14	11±4	27±15
Average ± SD Vollum % Recovery									
	Test 1	**Test 2**	**Test 3**	**Test 4**	**Test 5**	**Test 6**	**Test 7**	**Test 8**	**Test 9**
Glass	13±5	6±3	8±2	4±1	4±2	3±0.1	9±1	9±3	6±3
PW Paper	47±61	17±26	5±0.3	6±1	4±0.5	5±1	6±1	6±2	7±1
Ceiling Tile	2±2	0.3±0.1	0.1±0.0	0.7±0.4	0.4±0.2	0.4±0.3	0.3±0	0.4±0.1	0.9±1
Wood	5±2	2±1	0.5±0.1	4±2	4±3	4±0.4	1±1	5±1	3±2
Carpet	13±1	6±0	8±1	4±1	0.9±1.0	4±1	5±2	10±2	5±1
Concrete	2±3	0.8±1	10±5	2±1	0.01±0	1±0.8	2±2	3±3	6±4

Inoculation control samples were taken from the spore suspension on the day of testing and serially diluted, plated, and counted to establish the spore density used to inoculate the samples. The spore density levels met the QA target criterion of 1×10^9 CFU/mL (±1 log) for all tests.

3.3 Operational Parameters

The temperature, RH, and HPV concentration during each test were monitored as described in Section 2.0. For some tests, the RH was passively controlled by using Drierite or saturated salt solutions as described in Section 2.5. This method allowed for consistent targeted starting conditions for RH but ultimately the RH varied somewhat during a test due to the dynamic nature of constantly adding moisture to the system through use of 35% HPV or the continuous drying effect of the generator. Readings were taken once every minute for the duration of the contact time. The actual fumigation parameters for each test are shown in Table 3-2 and reported as the average value ± SD. Due to commercial equipment issues in Tests 1 and 8, the HPV concentrations temporarily dropped below the target range. Test 1 had a target concentration of 250 ppm but average actual measurement was 222 ppm due to a low flow alarm which caused the equipment to cease operation mid-testing. Upon finding this error, the system was reset and the run continued. Test 8 again used the commercial generator, but targeted high RH conditions. The target concentration was 50 ppm but an actual concentration of 44 ppm HPV resulted. As the desiccant in the commercial generator was approaching saturation level, the vaporization of HPV became less efficient causing the HPV concentrations to decrease. To remedy this issue, the generator return line was disconnected, which allowed for room air (lower RH) to be introduced into the system. Instead of returning to the generator, the excess HPV concentration was vented through the facility exhaust system to stabilize the HPV concentration in the Class III BSC and test chamber.

Table 3-2. Actual Fumigant Conditions for Tests

Test Number	Target HPV ppm	Avg. HPV ppm*	Temperature (°C)	RH (%)		Contact Time (hours)†	
				Target	Actual*	Easy[1] Materials	Hard[2] Materials
1	250	221.6 ± 30.9	23.0 ± 0.0	Low	38.1 ± 4.3	0.25,0.50,1,2,3	
2	10	10.4 ± 0.6	23.6 ± 0.3	Medium	58.5 ± 9.1	4, 8, 12, 16, 20	
3	10	9.3 ± 1.0	27.4 ± 0.8	High	76.1 ± 5.4	4, 8, 12, 16, 20	
4	25	25.7 ± 1.4	22.9 ± 0.1	Low	32.6 ± 22.4	2,4,6,8,12	8,12,16,20,24
5	25	25.5 ± 1.0	23.9 ± 0.1	Medium	62.4 ± 23.9	2,4,6,8,12	8,12,16,20,24
6	50	50.3 ± 1.51	23.5 ± 0.3	Low	25.9 ± 1.9	2,4,6,8,12	8,12,16,20,24
7	50	50.0 ± 1.1	23.8 ± 3.9	Medium	60.1 ± 3.9	1,2,4,5,6	8,12,16,20,24
8	50	43.5 ± 12.6	23.0 ± 0.4	High	76.9 ± 5.5	1,2,4,5,6	8,12,16,20,24
9	25	25.2 ± 1.6	23.8 ± 0.4	High	91.6 ± 6.3	1,2,6,8,12	8,12,20,24, 48

[1] Glass, Painted Wallboard Paper and Ceiling Tile
[2] Pine Wood, Carpet, Concrete
* Data reported as average ± SD.
† Contact time did not deviate from target during any test.

3.4 Audits

3.4.1 Performance Evaluation Audit

Performance evaluation (PE) audits were conducted to assess the quality of the results obtained during these experiments. Table 3-3 summarizes the PE audits that were performed.

No PE audits were performed for confirmation of the concentration and purity of *Ba* Ames or Vollum spores because quantitative standards do not exist for these organisms. The titer enumerations and the control and blank test coupons support the spore measurements.

Table 3-3. Performance Evaluation Audits

Measurement	Audit Procedure	Allowable Tolerance	Actual Tolerance
Volume of liquid from micropipettes	Gravimetric evaluation	± 10%	± 0.04% to 2.33%
Time	Compared to independent clock	± 2 s/h	0 s/h
Temperature	Compared to independent calibrated thermometer	± 2 °C	± 0.42 to 0.52 °C
Relative Humidity	Compare to independent calibrated hygrometer	± 10%	± 0.42 to 0.99%

3.4.2 Technical Systems Audit

Observations and findings from the TSA were documented and submitted to the laboratory technical lead for response. TSAs were conducted on July 11, 2017, to ensure that tests were being conducted in accordance with the appropriate QAPP and QMP. As part of the audit, test procedures were compared to those specified in the QAPP, and data acquisition and handling procedures were reviewed. None of the findings of the TSA required corrective action.

3.4.3 Data Quality Audit

At least 10 % of the data acquired during the evaluation were audited. Data were reviewed in 5 separate batches from May 2017 through Feb 2018. A QA auditor traced the data from the initial acquisition, through reduction and statistical analysis, to final reporting to ensure the integrity of the reported results. All calculations performed on the data undergoing the audit were verified. Only minor issues were noted with the data, mostly data transcription errors that were corrected.

3.5 QA/QC Reporting

Each assessment and audit was documented in accordance with the QAPP and QMP. For these tests, findings were noted (none significant) in the data quality audit, and no follow-up corrective action was necessary. The findings were mostly minor data transcription errors requiring some recalculation of efficacy results, but none were gross errors in recording. QA/QC procedures were performed in accordance with the QAPP.

3.6 Data Review

Records and data generated in the evaluation received a QC/technical review before they were utilized in calculating or evaluating results and prior to incorporation in this report.

4.0 Results and Discussion

The decontamination efficacy of HPV was assessed against virulent spores of *Ba* Ames and Vollum strains. A total of nine tests were conducted with contact times ranging from 0.25 to 48 hours. Each test was performed using six material types inoculated with *Ba* Ames and an additional set of coupons of the same materials were inoculated with *Ba* Vollum. Testing was conducted at ambient temperature (~ 23 °C) and low (26-38%), medium (59-62%), and high (76-92%) RH levels. The first test was conducted at an HPV-generation equipment vendor's label requirement (target of 250 ppm for 90 minutes) to tie back to previous testing using more typical levels of HPV. Following Test 1, all tests proceeded with using target HPV concentrations of either 10, 25, or 50 ppm, paired with different RH levels. All nine tests utilized five contact times.

Overall results of the study are summarized in Tables 4-1 and 4-2, which show the minimum contact times needed to achieve effective decontamination of each material for each experimental condition. Contact times for effective decontamination generally decreased with increased HPV concentration. For example, at the higher concentration of 222 ppm (Test 1), only 15 minutes were required to effectively decontaminate glass; in contrast, at the 10-ppm level, 4-12 hours were required for effective decontamination of glass, depending on the strain and RH level. With the Vollum strain on glass, ceiling tile, and painted wallboard paper, successful decontamination occurred in 2-16 hours for the 10-50 ppm HPV concentrations evaluated. In some experiments, effective decontamination may not have occurred for a specific material(s) at the longest contact time evaluated; these results are displayed in Tables 4-1 and 4-2 as greater than the longest contact time tested.

The results for each individual test are summarized via Tables 4-3 to 4-11. Additional detailed decontamination efficacy results, showing the average CFU recovery from each material for both positive controls and test coupons, for all tests, are found in Appendix A. Further, Appendix B provides graphical representations of the decontamination efficacy results (LR) for each test. This chapter also discusses decontamination efficacy as a function of some of the variables that were tested in the study. Statistical results are also presented when applicable to indicate whether test variables significantly affected efficacy.

Table 4-1. Minimum Time (Hours) Demonstrating Effective Decontamination for Ames Strain

	Test 1	Test 2	Test 3	Test 4	Test 5	Test 9	Test 6	Test 7	Test 8
Average HPV ppm	222	9-10		25-26			44-50		
Average % RH	38	58	76	33	62	92	26	60	77
	Time (hours)								
Glass	0.25	12	8	8	4	6	6	1	2
PW Paper	0.5	>20	8	>12	>12	2	>12	1	2
Ceiling Tile	2	12	8	>12	4	6	2	4	4
Pine Wood	3	12	>20	>24	>24	>48	>24	16	24
Carpet	0.25	>20	>20	>24	16	20	>24	20	8
Concrete	>3	>20	>20	>24	>24	>48	>24	>24	>24

A ">" denotes that effective decontamination was not achieved at any time point, with the longest contact time listed

Table 4-2. Minimum Time (Hours) Demonstrating Effective Decontamination for Vollum Strain

	Test 1	Test 2	Test 3	Test 4	Test 5	Test 9	Test 6	Test 7	Test 8
Average HPV ppm	222	9-10		25-26			44-50		
Average % RH	38	58	76	33	62	92	26	60	77
	Time (hours)								
Glass	0.25	8	4	8	4	2	4	4	2
PW Paper	1	16	8	6	4	6	6	4	4
Ceiling Tile	1	8	8	8	6	6	2	4	4
Pine Wood	2	>20	>20	>24	>24	>48	24	16	24
Carpet	>3	>20	20	>24	24	20	24	20	12
Concrete	>3	>20	>20	>24	>24	>48	>24	>24	>24

A ">" denotes that effective decontamination was not achieved at any time point, with the longest contact time listed

The efficacy results for Test 1 are shown in Table 4-3, in terms of the LR ± the 95% confidence interval (CI). Note that the actual average HPV concentration of 222 ppm was below the vendor's registered fumigation condition of 250 ppm, due to equipment malfunction. Nevertheless, for the glass, ceiling tile, and wallboard materials, effective decontamination occurred with contact times ~ 1-2 hours, in a range mostly consistent with the vendor's registration requirement of a 90-minute contact time. However, for the wood, carpet, and unpainted concrete, effective decontamination occurred in only three instances (out of 30) under

the Test 1 conditions. These results are generally consistent with a previous EPA study (US EPA, 2010).

Table 4-3. Summary of Efficacy Results (LR) for Test 1 (222 ppm HPV) and Low RH Against *B. anthracis* Ames and Vollum.

Test 1					
Material	**Contact Time (h)**	***Ba Ames Efficacy***	***95% CI***	***Ba Vollum Efficacy***	***95%CI***
Glass	0.25	7.02	1.20	6.52	1.02
	0.5	4.37	3.51	4.34	2.73
	1	6.74	1.75	7.03	0.21
	2	7.63	0.16	7.03	0.21
	3	7.63	0.16	5.36	1.68
Wallboard Paper	0.25	5.55	2.74	2.90	2.96
	0.5	8.00	0.02	2.55	0.71
	1	4.68	3.27	7.42	0.38
	2	8.00	0.02	7.42	0.38
	3	8.00	0.02	7.42	0.38
Ceiling Tile	0.25	1.84	0.39	5.44	1.07
	0.5	3.26	0.61	4.83	1.18
	1	6.99	1.39	5.95	0.40
	2	7.70	0.10	5.95	0.40
	3	7.70	0.10	5.95	0.40
Pine Wood	0.25	3.47	3.96	2.47	0.75
	0.5	2.05	0.29	3.05	0.99
	1	3.70	1.16	5.43	2.29
	2	4.40	1.69	6.08	1.02
	3	6.61	1.75	5.01	1.83
Industrial Carpet	0.25	7.23	1.40	1.02	0.18
	0.5	5.16	4.04	0.30	0.46
	1	4.03	3.85	2.32	0.07
	2	4.67	3.22	4.94	2.10
	3	4.74	3.14	4.55	0.27
Unpainted Concrete	0.25	0.32	0.59	1.06	1.07
	0.5	0.36	0.23	1.58	1.42
	1	0.35	0.43	2.92	0.65
	2	0.59	0.22	4.52	2.74
	3	0.58	0.26	2.59	0.68

Results highlighted in yellow represent effective decontamination but not complete inactivation. Results highlighted in green represent complete inactivation.

Table 4-4. Summary of Efficacy Results (LR) at 10 ppm and Medium RH against *B. anthracis* Ames and Vollum.

Test 2					
Material	**Contact Time (h)**	***Ba Ames Efficacy***	***95% CI***	***Ba Vollum Efficacy***	***95% CI***
Glass	4	2.68	0.43	3.47	3.85
	8	3.91	1.63	6.79	2.16
	12	7.62	0.01	6.79	0.19
	16	6.11	1.69	6.79	0.19
	20	7.62	0.01	6.79	0.19
Wallboard Paper	4	0.55	0.92	2.41	1.86
	8	2.89	1.46	5.83	1.25
	12	3.75	4.22	5.83	2.34
	16	5.91	4.02	7.00	0.42
	20	3.81	1.29	7.00	0.80
Ceiling Tile	4	0.86	0.23	2.38	0.47
	8	3.31	0.56	5.49	0.14
	12	6.89	1.56	5.49	0.14
	16	7.48	0.20	5.49	0.14
	20	7.48	0.20	5.49	0.14
Pine Wood	4	2.39	0.65	2.44	0.89
	8	4.32	3.07	3.69	2.58
	12	7.44	0.15	4.61	1.66
	16	7.44	0.15	5.56	1.22
	20	7.44	0.15	5.56	1.22
Industrial Carpet	4	0.04	0.05	0.23	0.07
	8	0.68	0.06	1.04	0.08
	12	1.65	0.24	4.06	0.64
	16	1.66	0.21	3.83	0.08
	20	2.09	0.16	5.51	1.39
Unpainted Concrete	4	1.18	0.25	0.95	0.80
	8	0.99	0.24	0.44	0.75
	12	1.26	0.49	1.36	0.63
	16	1.53	0.26	2.24	0.74
	20	1.49	0.13	1.29	0.73

Results highlighted in yellow represent effective decontamination but not complete inactivation.
Results highlighted in green represent complete inactivation.

Table 4-5. Summary of Efficacy Results (LR) at 10 ppm and High RH against *B. anthracis* Ames and Vollum.

Test 3					
Material	**Contact Time (h)**	***Ba Ames Efficacy***	***95%CI***	***Ba Vollum Efficacy***	***95%CI***
Glass	4	7.17	1.19	6.83	0.11
	8	7.78	0.05	6.83	0.11
	12	7.78	0.05	6.83	0.11
	16	7.78	0.05	6.83	0.11
	20	7.78	0.05	6.83	0.11
Wallboard Paper	4	3.43	2.67	5.33	2.62
	8	6.90	1.97	6.67	0.02
	12	7.90	0.05	6.67	0.02
	16	7.90	0.05	6.67	0.02
	20	7.90	0.05	6.67	0.02
Ceiling Tile	4	3.84	0.22	2.58	0.37
	8	6.99	1.00	4.89	0.11
	12	7.50	0.05	4.89	0.11
	16	7.50	0.05	4.89	0.11
	20	7.50	0.05	4.89	0.11
Pine Wood	4	2.24	0.53	2.36	1.54
	8	3.23	1.06	2.83	0.20
	12	3.12	1.76	5.61	0.10
	16	3.55	0.77	5.10	1.00
	20	3.42	0.78	4.34	1.26
Industrial Carpet	4	0.24	0.03	0.90	0.15
	8	1.45	0.32	2.18	0.05
	12	1.00	0.16	3.59	0.08
	16	2.32	0.22	5.15	1.65
	20	2.67	0.69	6.83	0.03
Unpainted Concrete	4	-0.02	0.47	1.30	0.29
	8	1.36	1.38	4.26	2.68
	12	1.06	0.55	2.68	0.51
	16	1.35	0.71	2.78	0.86
	20	1.36	0.66	5.26	1.70

Results highlighted in yellow represent effective decontamination but not complete inactivation.
Results highlighted in green represent complete inactivation.

Table 4-6. Summary of Efficacy Results (LR) at 25 ppm and Low RH against *B. anthracis* Ames and Vollum.

Test 4					
Material	**Contact Time (h)**	***Ba Ames Efficacy***	***95% CI***	***Ba Vollum Efficacy***	***95% CI***
Glass	2	1.82	0.63	5.85	1.39
	4	3.56	1.43	5.39	1.19
	6	4.64	1.09	5.82	1.46
	8	7.73	0.06	6.56	0.11
	12	5.58	2.31	6.56	0.11
Wallboard Paper	2	0.36	0.50	1.51	0.94
	4	0.86	0.27	4.90	1.74
	6	1.06	0.29	6.67	0.08
	8	2.20	0.57	6.67	0.08
	12	2.99	0.77	6.67	0.08
Ceiling Tile	2	1.94	0.15	2.32	0.33
	4	2.77	0.22	4.51	1.22
	6	2.63	0.10	5.17	1.04
	8	3.98	0.37	5.68	0.30
	12	3.94	0.09	5.68	0.30
Pine Wood	8	2.88	0.65	3.63	1.67
	12	3.03	0.45	4.26	0.82
	16	2.22	0.31	3.93	0.88
	20	2.98	0.71	5.38	1.19
	24	4.20	1.57	3.50	1.17
Industrial Carpet	8	1.21	0.12	2.02	0.61
	12	0.80	0.08	2.05	0.36
	16	2.11	0.26	2.60	0.18
	20	2.28	1.07	5.49	1.95
	24	2.34	1.07	4.94	1.62
Unpainted Concrete	8	0.47	0.57	2.01	0.56
	12	0.73	0.61	3.60	2.40
	16	1.10	1.58	2.22	0.80
	20	0.64	0.61	2.58	0.40
	24	0.57	0.45	2.30	0.28

Results highlighted in yellow represent effective decontamination but not complete inactivation.
Results highlighted in green represent complete inactivation.

Table 4-7. Summary of Efficacy Results (LR) at 25 ppm and Medium RH against *B. anthracis* Ames and Vollum.

Test 5					
Material	**Contact Time (h)**	***Ba Ames Efficacy***	***95%CI***	***Ba Vollum Efficacy***	***95%CI***
Glass	2	4.34	3.20	5.56	1.81
	4	7.60	0.07	6.48	0.19
	6	7.60	0.07	6.48	0.19
	8	7.09	1.00	6.48	0.19
	12	7.60	0.07	6.48	0.19
Wallboard Paper	2	2.87	1.79	2.35	0.55
	4	4.05	2.11	6.58	0.04
	6	3.85	1.15	6.58	0.04
	8	3.80	1.35	6.58	0.04
	12	5.18	0.26	6.58	0.04
Ceiling Tile	2	4.16	2.05	2.22	0.69
	4	6.88	1.19	4.95	1.02
	6	6.14	1.34	5.46	0.25
	8	6.78	1.39	5.46	0.25
	12	7.49	0.06	5.46	0.25
Pine Wood	8	2.92	1.30	4.94	1.65
	12	4.94	2.34	5.54	1.71
	16	3.95	0.28	4.86	1.63
	20	4.66	2.59	5.18	2.40
	24	3.07	1.33	5.29	2.20
Industrial Carpet	8	5.70	4.25	0.89	0.43
	12	2.34	0.57	2.53	0.36
	16	6.22	3.23	3.26	0.76
	20	7.87	0.01	4.42	1.40
	24	7.87	0.01	5.71	0.35
Unpainted Concrete	8	0.50	0.16	1.91	0.68
	12	0.65	0.25	3.06	2.58
	16	0.55	0.37	2.19	0.41
	20	0.64	0.17	2.03	0.46
	24	0.55	0.17	1.74	0.36

Results highlighted in yellow represent effective decontamination but not complete inactivation.
Results highlighted in green represent complete inactivation.

Table 4-8. Summary of Efficacy Results (LR) at 50 ppm and Low RH against *B. anthracis* Ames and Vollum.

Test 6					
Material	**Contact Time (h)**	***Ba Ames Efficacy***	***95%CI***	***Ba Vollum Efficacy***	***95%CI***
Glass	2	5.57	2.17	5.96	0.99
	4	5.94	1.63	6.47	0.01
	6	7.61	0.07	6.47	0.01
	8	7.61	0.07	5.47	1.96
	12	7.61	0.07	6.47	0.01
Wallboard Paper	2	1.51	0.41	3.20	0.11
	4	1.86	1.13	4.65	0.61
	6	1.90	0.92	6.62	0.10
	8	2.44	0.54	6.62	0.10
	12	4.01	0.92	6.62	0.10
Ceiling Tile	2	6.94	1.00	5.49	0.22
	4	5.71	1.76	5.49	0.22
	6	6.17	1.33	5.49	0.22
	8	7.45	0.11	5.49	0.22
	12	7.45	0.11	5.49	0.22
Pine Wood	8	2.89	0.82	4.34	2.11
	12	3.15	1.10	5.70	1.55
	16	1.83	0.37	5.89	1.19
	20	3.57	1.28	5.89	1.19
	24	2.95	2.20	6.49	0.04
Industrial Carpet	8	0.48	0.05	1.06	0.09
	12	1.53	0.30	3.30	0.24
	16	1.91	0.39	5.17	1.46
	20	2.01	0.13	5.22	1.30
	24	2.99	0.24	6.53	0.07
Unpainted Concrete	8	0.18	0.21	1.90	0.35
	12	0.47	0.29	3.51	2.43
	16	0.79	0.43	2.06	0.36
	20	0.74	0.56	2.74	0.53
	24	0.87	0.44	2.86	0.37

Results highlighted in yellow represent effective decontamination but not complete inactivation.
Results highlighted in green represent complete inactivation.

Table 4-9. Summary of Efficacy Results (LR) at 50 ppm and Medium RH against *B. anthracis* Ames and Vollum.

Test 7					
Material	**Contact Time (h)**	***Ba Ames Efficacy***	***95%CI***	***Ba Vollum Efficacy***	***95%CI***
Glass	1	7.71	0.04	2.12	0.13
	2	7.71	0.04	5.39	0.31
	4	7.71	0.04	7.08	0.04
	5	7.71	0.04	7.08	0.04
	6	7.71	0.04	7.08	0.04
Wallboard Paper	1	7.79	0.08	1.80	0.13
	2	7.79	0.08	5.71	2.25
	4	5.05	3.21	6.35	1.00
	5	5.71	0.69	6.86	0.05
	6	4.32	1.15	6.86	0.05
Ceiling Tile	1	3.63	0.94	2.38	0.16
	2	5.42	0.66	3.79	0.05
	4	7.58	0.05	5.61	0.05
	5	7.58	0.05	5.61	0.05
	6	7.58	0.05	5.61	0.05
Pine Wood	8	2.17	0.53	2.43	0.52
	12	4.10	3.26	3.66	1.22
	16	6.22	2.17	6.14	0.21
	20	4.24	3.04	6.14	0.21
	24	7.32	0.18	5.63	1.02
Industrial Carpet	8	1.49	0.17	3.54	0.71
	12	2.51	0.27	3.95	0.68
	16	4.96	2.83	5.50	0.67
	20	6.08	1.84	6.04	0.79
	24	5.67	2.18	6.78	0.74
Unpainted Concrete	8	0.83	0.35	1.78	0.38
	12	0.83	0.42	2.07	0.64
	16	0.62	0.22	1.96	1.26
	20	1.04	0.27	2.57	1.46
	24	0.78	0.34	2.23	0.12

Results highlighted in yellow represent effective decontamination but not complete inactivation.
Results highlighted in green represent complete inactivation.

Table 4-10. Summary of Efficacy Results (LR) at 50 ppm and High RH against *B. anthracis* Ames and Vollum.

Test 8					
Material	**Contact Time (h)**	***Ba Ames Efficacy***	***95% CI***	***Ba Vollum Efficacy***	***95% CI***
Glass	1	5.81	2.33	5.65	1.11
	2	7.00	0.16	6.77	0.13
	4	7.00	0.16	6.77	0.13
	5	7.00	0.16	6.77	0.13
	6	7.00	0.16	6.77	0.13
Wallboard Paper	1	2.65	1.90	1.14	0.35
	2	7.42	0.21	2.13	0.94
	4	6.55	1.73	6.59	0.10
	5	7.42	0.21	6.59	0.10
	6	7.42	0.21	6.59	0.10
Ceiling Tile	1	1.70	0.30	0.92	0.12
	2	4.98	2.22	1.83	0.12
	4	7.21	0.18	5.49	0.07
	5	7.21	0.18	5.49	0.07
	6	7.21	0.18	5.49	0.07
Pine Wood	8	2.81	0.44	5.96	1.19
	12	3.99	3.00	5.96	1.19
	16	3.64	1.81	4.31	0.72
	20	3.67	0.64	5.25	1.30
	24	7.00	0.11	6.57	0.08
Industrial Carpet	8	6.03	2.98	4.97	0.50
	12	7.55	0.05	6.83	0.66
	16	7.55	0.05	6.83	0.45
	20	7.55	0.05	6.83	0.49
	24	7.55	0.05	6.83	0.51
Unpainted Concrete	8	0.78	0.40	2.60	0.41
	12	0.77	0.20	2.58	0.08
	16	1.38	0.53	3.28	0.08
	20	0.85	0.25	2.90	0.08
	24	0.80	0.41	2.54	0.08

Results highlighted in yellow represent effective decontamination but not complete inactivation.
Results highlighted in green represent complete inactivation.

Table 4-11. Summary of Efficacy Results (LR) at 25 ppm and High RH against *B. anthracis* Ames and Vollum.

Test 9					
Material	**Contact Time (h)**	***Ba Ames Efficacy***	***95%CI***	***Ba Vollum Efficacy***	***95%CI***
Glass	1	0.97	0.10	1.67	0.39
	2	1.88	0.49	6.19	1.21
	6	7.56	0.07	6.79	0.21
	8	7.56	0.07	6.79	0.21
	12	7.56	0.07	6.79	0.21
Wallboard Paper	1	1.72	0.19	1.10	0.14
	2	6.08	3.28	1.76	0.33
	6	7.75	0.05	6.91	0.04
	8	7.75	0.05	6.91	0.04
	12	7.75	0.05	6.91	0.04
Ceiling Tile	1	0.34	0.25	1.02	0.39
	2	1.07	0.24	1.88	0.40
	6	7.09	0.06	5.82	0.38
	8	5.92	2.31	5.82	0.38
	12	7.09	0.06	5.82	0.38
Pine Wood	8	2.35	0.95	4.20	0.42
	12	2.27	0.49	2.91	1.81
	20	2.22	0.33	3.53	0.91
	24	2.76	1.24	4.09	1.14
	48	4.86	2.30	4.08	2.37
Industrial Carpet	8	2.04	0.28	4.07	0.24
	12	2.00	0.46	4.59	0.23
	20	7.91	0.52	6.78	0.42
	24	7.91	0.34	6.78	1.00
	48	7.91	0.90	6.78	0.30
Unpainted Concrete	8	1.45	0.16	2.23	0.32
	12	0.87	0.12	2.77	0.48
	20	1.26	0.04	4.36	0.10
	24	1.71	0.04	3.42	0.10
	48	1.83	0.04	4.53	0.10

Results highlighted in yellow represent effective decontamination but not complete inactivation.
Results highlighted in green represent complete inactivation.

4.1 Comparing the effect of material and strain on decontamination efficacy

Overall study results can also be summarized in terms of the number of instances (out of the five contact times) in which successful decontamination (complete inactivation or ≥6 LR) occurred for each experiment, material, and strain. These results are displayed in Tables 4-12 and 4-13. Decontamination results vary by material and strain, and so it is important to know which materials and strains are problematic to decontaminate or inactivate, respectively.

As these tables show, the number of successful decontaminations was highest for the glass, ceiling tile, and painted wallboard paper materials for both Ames and Vollum strains. These materials were effectively decontaminated in 63, 55, and 46 out of a potential 90 instances (2 strains X 5 contact times X 9 experiments), respectively. (Note that for ceiling tile, while there was routinely complete inactivation, the efficacy never exceeded 6.0 due to the lower recovery from positive controls.) After the first three tests, it was evident that the wood, carpet, and unpainted concrete materials were being decontaminated much less effectively. Therefore, these materials were exposed to the same HPV concentrations, but at longer contact times (compared with the other materials, in the same experiment) beginning with Test 4. Even with exposure to HPV at these longer contact times, the carpet, wood, and unpainted concrete were effectively decontaminated in only 28, 12, and 0 instances, respectively. The highest efficacy achieved for unpainted concrete during the study was 5.3 LR (Test 3 for Vollum). The results showing that unpainted concrete was difficult to decontaminate effectively is consistent with previous findings when testing peracetic acid and aqueous hydrogen peroxide fogging (Richter et al., 2018).

Comparing the two strains, out of a total of 270 efficacy results for each strain (9 tests X 6 materials X 5 contact times), there were 97 instances of successful decontamination for *Ba* Ames and 107 instances for the Vollum strain.

Table 4-12. Number of Successful Decontamination Instances for *Ba* Ames by Test and Material

	Test 1	Test 2	Test 3	Test 4	Test 5	Test 9	Test 6	Test 7	Test 8	Total
Average HPV ppm	222	10	9	26	26	25	50	50	44	
average % RH	38	58	76	33	62	92	26	60	77	
	Number of Successful Decontamination Instances									
Glass	4	3	5	1	4	3	3	5	4	31
PW Paper	3	0	4	0	0	4	0	2	4	17
Ceiling Tile	3	3	4	0	4	2	3	3	3	26
Pine Wood	1	3	0	0	0	0	3	2	1	7
Carpet	1	0	0	0	3	3	0	1	5	16
Concrete	0	0	0	0	0	0	0	0	0	0
Total	**12/30**	**9/30**	**13/30**	**1/30**	**11/30**	**12/30**	**9/30**	**13/30**	**17/30**	**97**

* Results shown are the number of effective decontamination instances (out of five time-points) for each test

Table 4-13. Number of Successful Decontamination Instances for *Ba* Vollum by Test and Material

	Test 1	Test 2	Test 3	Test 4	Test 5	Test 9	Test 6	Test 7	Test 8	Total
Average HPV ppm	222	10	9	26	26	25	50	50	44	
average % RH	38	58	76	33	62	92	26	60	77	
	Number of Successful Decontamination Instances									
Glass	3	3	5	2	4	4	3	3	4	32
PW Paper	3	2	4	3	4	3	3	3	3	29
Ceiling Tile	3	4	4	2	3	3	5	3	3	29
Pine Wood	1	0	1	0	0	0	1	2	1	5
Carpet	0	0	1	0	1	3	1	2	4	12
Concrete	0	0	0	0	0	0	0	0	0	0
Total	**10/30**	**9/30**	**15/30**	**7/30**	**12/30**	**13/30**	**13/30**	**13/30**	**15/30**	**107**

As discussed in Section 2.8, statistical analysis was performed by converting all LR data into a binary response with the endpoint being a success if LR $\geq$ 6.0 or if complete inactivation occurred. Table 4-14 shows results from the logistic regression model which was fitted to the full data set to test whether the proportion of success was significantly associated with the *Ba* strain, material, dose (concentration x time), and RH. The Wald test statistic, the degrees of freedom (DF), and the p-value are shown in the table; the Wald statistic is the appropriate statistic when using a logistic model. The presence of a statistically significant three-factor interaction complicated interpretation of the results, as all results for one of the three factors must be interpreted with respect to the levels of the other two factors. While the main effects for strain, average RH, and dose were not statistically significant, the two factor interactions involving these factors are statistically significant: these factors do impact the probability of a successful decontamination, but the successful decontamination is dependent on the strain, the material, and the dose.

Based on the parameters of the logistic model, the effect of material type was significant, but the significance varied compared against the other materials. With respect to the effect of strain, using the full logistical regression model, the results showed that *Ba* Ames and Vollum were not significantly different (p-value = 0.99) from each other relative to successful decontamination. When assessing the two-factor interactions of material and RH level, the odds ratio for Ames compared to Vollum showed significance and decreased with dose for all materials except glass (which increased) and concrete (slight increase). Refer to Appendix C for the full results of the statistical analyses.

Table 4-14. Significant Effects Based on Logistic Regression Model Fitted to Full Dataset

Effect	DF	Wald Test Statistic	p-value
Strain	1	0.0001	0.9943
Material	5	33.0119	<.0001*
Avg. RH	2	0.4301	0.8065
Strain*Material	5	22.6643	0.0004*
Strain*Avg. RH	2	12.0131	0.0025*
Material*Avg. RH	10	44.0611	<.0001*
Dose*Material	5	88.5148	<.0001*
Dose*Avg. RH	2	18.1219	0.0001*

* Effect is statistically significant at or below the 0.05 level; DF = degrees of freedom

4.2 Effect of HPV Dose on Efficacy

The overall results of the study may also be summarized and interpreted in terms of the minimum dose of HPV (in ppm*hours) demonstrating effective decontamination. These results are summarized by material and *Ba* strain in Table 4-15. More detailed individual dosage requirements for each test (per given HPV and RH level), material, and strain combination are found in Appendix C. The HPV dose was shown to have a significant effect on the odds of successful decontamination when material or RH was factored (refer to Table 4-14).

For the glass, painted wallboard, and ceiling tile materials, dosages as low as 100-200 ppm*hours were all that were needed for effective decontamination in most of the tests. In some tests, the wood and carpet materials were successfully decontaminated with doses as low as 120-200 ppm*hours, although there were a few tests that required > 1200 ppm*hours for successful decontamination. In general, successful decontamination using lower dosages of HPV were associated with higher RH levels, as well as with the Vollum strain, although there were exceptions. In an actual decontamination scenario using HPV, these results may be helpful to officials in determining target dosage levels based on the presence of materials.

Table 4-15. Minimum HPV Dose Required for Effective Decontamination

	Range in Minimum Dose Demonstrating Effective Decontamination for Ames Strain (ppm*Hours)	**Range in Minimum Dose Demonstrating Effective Decontamination for Vollum Strain (ppm*Hours)**
Glass	50-200	40-200
PW Paper	50 - >1200	80-300
Ceiling Tile	80 - >600	80-222
Pine Wood	120 - >1200	444- >1200
Carpet	>200 - >1200	200 - 1200
Unpainted Concrete	>200 - >1200	>200 - >1200

4.3 Effects of Relative Humidity on Efficacy

When assessed as a main effect by the statistical analyses, the RH level appeared to be a non-significant factor. However, when comparing average RH by strain, significant differences were observed, and the differences varied by material type. These effects are illustrated in Table 4-16. As Table 4-16 shows, the number of successful decontaminations always increased with increasing RH (for a given HPV concentration and strain). This effect was most pronounced when comparing Tests 4 and 5 (25 ppm HPV, RH increased from 33% to 62%). The effect of increasing RH appears to have more of an impact on the Ames strain.

Table 4-16. Number of Successful Decontaminations by RH

	Test 2	Test 3	Test 4	Test 5	Test 9	Test 6	Test 7	Test 8
average HPV (ppm)	10		25			50		
average RH %	58.5	76.1	32.6	62.4	91.6	25.9	60.1	76.9
	Number of Successful Decontaminations							
Ames Total	9	12	1	11	12	10	13	17
Vollum Total	9	14	7	12	13	13	14	15

* Results shown are the number of successful decontamination results per test.

4.4 Surface Damage to Materials

At the end of each decontamination test, the procedural blanks were visually compared to the laboratory blanks, and test coupons were visually compared to positive controls to qualitatively assess any aesthetic impact the low-concentration HPV may have had on each material type. Based on the visual appearance of the decontaminated coupons, there were no apparent changes in the color, reflectivity, or roughness of the six material surfaces after being exposed to the low concentrations of the sporicidal fumigant.

4.5 Summary

This investigation focused on finding efficacious conditions (e.g., minimum contact times) for inactivating *Ba* Ames and Vollum strains on a variety of building materials when using relatively low concentrations of HPV. In addition to *Ba* strain and material, other test variables included were HPV concentration, contact time, and RH level. These independent variables were adjusted to assess their effect on decontamination efficacy.

In general, fumigating at or near ambient temperatures and RH levels, with the use of lower fumigant concentrations, would allow for personnel and contractors to provide decontamination services with less specialized equipment. This advantage may be critical in increasing the decontamination capacity of the nation in the event of a large release of *Ba* spores, in which numerous buildings and other infrastructures may become contaminated.

The data generated from this evaluation suggest that the resistance to inactivation by HPV is not significantly different for the two *Ba* strains that were used in the investigation. The side-by-side

data with both strains provide evidence indicating that the Ames data may be representative of the Vollum strain when using HPV for decontamination.

Low concentrations of HPV (e.g., 10-50 ppm) were effective in decontaminating all materials tested in the study except for unpainted concrete. Moreover, the glass, ceiling tile and painted wallboard paper materials were more amenable to decontamination by low concentrations of HPV compared to unpainted concrete, carpet, and wood. Even using extended contact times (and hence higher dosages of HPV), the number of occurrences in which unpainted concrete, carpet, and wood were successfully decontaminated in the study was much less than the glass, ceiling tile, and painted wallboard materials. That said, there were in fact several instances when the carpet and wood materials were successfully decontaminated.

Contact times required for effective decontamination generally decreased with increased HPV concentration. For example, at the highest HPV concentration tested (222 ppm), only 15 minutes were required to effectively decontaminate glass; in contrast, at 10 ppm, 4-12 hours were required for effective decontamination of glass, depending on the strain and RH level. In terms of HPV dosage requirements, only 100-200 ppm*hours were required for effective decontamination in most of the tests for the glass, painted wallboard, and ceiling tile. In some tests, the wood and carpet materials were successfully decontaminated with doses as low as 120-200 ppm*hours, although there were a few tests that required > 1200 ppm*hours for successful decontamination of wood and carpet.

While elevated RH has been shown to improve *Ba* spore inactivation with nearly all sporicidal fumigants, some debate still exists whether elevated RH is needed for HPV decontamination. From the statistical analysis of the study results, when assessed as a main effect, the RH level appeared to be a non-significant factor. However, when comparing the effect of RH by strain, significant differences were observed and varied by material type. For example, the effect of increasing RH appears to generally have had more of an impact on the Ames strain. In addition, for a given HPV concentration and strain, it was found that the number of occurrences of successful decontamination always increased with increasing RH.

5.0 References

ASTM International. Standard Practice for Maintaining Constant Relative Humidity by Means of Aqueous Solutions, ASTM E104-02. October 2006.

Clopper CJ, Pearson E. The Use of Confidence or Fiducial Limits Illustrated in the Case of Binomial. *Biometrika* Vol. 26, 404-413. 1934.

Rastogi, VK, Wallace, L, Smith, LS., Ryan, SP, Martin, B. Quantitative Method to Determine Sporicidal Decontamination of Building Surfaces by Gaseous Fumigants, and Issues Related to Laboratory-Scale Studies. *Applied and Environmental Microbiology*, Vol. 75, 3688 – 3694. 2009. DOI:10.1128/AEM.02592-08.

Richter WR, Wood JP, Wendling MQS, Rogers JV Inactivation of *Bacillus anthracis* Spores to Decontaminate Subway Railcar and Related Materials via the Fogging of Peracetic Acid and Hydrogen Peroxide Sporicidal Liquids. *Journal of Environmental Management,* Vol. 206, 800 – 806. 2017. DOI: 10.1016/j.jenvman.2017.11.027.

Rogers JV, Sabourin, CL, Choi, YW, Richter, WR, Rudnicki, DC, Riggs, KB, Taylor, ML, Chang, J. Decontamination Assessment of *Bacillus anthracis*, *Bacillus subtilis*, and *Geobacillus stearothermophilus* Spores on Indoor Surfaces Using a Hydrogen Peroxide Gas Generator, *Journal of Applied Microbiology*, Vol. 99, 739-748. 2005. DOI: org/10.1111/j.1366-2672.2006.02686.x.

U.S. Environmental Protection Agency. Determining the Efficacy of Liquids and Fumigants in Systematic Decontamination Studies for *Bacillus anthracis* Using Multiple Test Methods. Report 600/R-10/088, December 2010.

U.S. Environmental Protection Agency. Systematic Investigation of Liquid and Fumigant Decontamination Efficacy against Biological Agents Deposited on Test Coupons of Common Indoor Materials. Report EPA/600/R-11/076, 2011.

U.S. Environmental Protection Agency. Vaprox Hydrogen Peroxide Sterilant - Amendment to Add Aseptic Food Processing Use. EPA Pesticide Label Reg. No. 58779-4, 2012.

U.S. Environmental Protection Agency. 2016 AOAC Use Dilution Method for Testing Disinfectants. Revised 08/11/2016.

U.S. Environmental Protection Agency. Quality Assurance Project Plan for the Determination of Effective Hydrogen Peroxide Vapor Fumigation Conditions, Version Final. January 2017. (Available upon request by contacting EPA).

Wood JP, Calfee MW, Clayton M, Griffin-Gatchalian N, Touati A, Ryan S, Mickelsen L, Smith L, Rastogi V. A Simple Decontamination Approach Using Hydrogen Peroxide Vapour for *Bacillus anthracis* Spore Inactivation. *Journal of Applied Microbiology*, Vol. 121, 1603-1615. 2016. doi:10.1111/jam.13284

Appendix A
Detailed Test Results

Efficacy results for low level HPV against *Ba* Ames and Vollum on six material types are shown in Tables A-1 through A-18. Zero CFU were observed on all laboratory and procedural blanks.

Table A-1. Inactivation of *B. anthracis* Ames Spores using low level HPV[a]

Test Number	Concentration (ppm)	Equipment	Temp (°C)	%RH	Inoculum (CFU/coupon)	Contact Time (hours)	Material	Mean Recovered *B. anthracis* (CFU/coupon)		Efficacy ± CI[d]
								Positive Control[b]	Test Coupon[c]	
1	250	STERIS 1000ED	23.0 ± 0.04	38.1 ± 4.3	1.19E+08	0.25	Glass	$4.55 \pm 1.61 \times 10^7$	$2.29 \pm 3.79 \times 10^1$	7.02 ± 1.20
						0.50			$4.98 \pm 8.59 \times 10^5$	4.37 ± 3.51
						1.00			$1.56 \pm 2.69 \times 10^2$	6.74 ± 1.75
						2.00			0.00 ± 0.00	≥7.63 ± 0.16
						3.00			0.00 ± 0.00	≥7.63 ± 0.16
						0.25	Pine Wood	$3.34 \pm 1.14 \times 10^7$	$7.53 \pm 6.54 \times 10^5$	3.47 ± 3.96
						0.50			$3.04 \pm 1.38 \times 10^5$	2.05 ± 0.29
						1.00			$3.32 \pm 5.46 \times 10^4$	3.70 ± 1.16
						2.00			$1.09 \pm 1.72 \times 10^4$	4.40 ± 1.69
						3.00			$1.56 \pm 2.69 \times 10^2$	6.61 ± 1.75
						0.25	Carpet	$9.38 \pm 3.57 \times 10^7$	$4.50 \pm 7.62 \times 10^1$	7.23 ± 1.40
						0.50			$2.06 \pm 3.56 \times 10^6$	5.17 ± 4.04
						1.00			$5.87 \pm 6.99 \times 10^5$	4.03 ± 3.85
						2.00			$5.76 \pm 5.80 \times 10^4$	4.67 ± 3.22
						3.00			$4.29 \pm 4.04 \times 10^4$	4.74 ± 3.14
						0.25	Painted Wallboard Paper	$1.00 \pm 0.05 \times 10^8$	$2.29 \pm 3.93 \times 10^4$	5.55 ± 2.74
						0.50			0.00 ± 0.00	≥8.00 ± 0.02
						1.00			$7.19 \pm 7.87 \times 10^4$	4.68 ± 3.30
						2.00			0.00 ± 0.00	≥8.00 ± 0.02
						3.00			0.00 ± 0.00	≥8.00 ± 0.02
						0.25	Unpainted Concrete	$1.79 \pm 1.09 \times 10^7$	$1.15 \pm 1.28 \times 10^7$	0.32 ± 0.59
						0.50			$6.92 \pm 1.26 \times 10^6$	0.36 ± 0.23
						1.00			$8.65 \pm 7.15 \times 10^6$	0.35 ± 0.43
						2.00			$4.11 \pm 0.49 \times 10^6$	0.59 ± 0.22
						3.00			$4.26 \pm 1.18 \times 10^6$	0.58 ± 0.26
						0.25	Ceiling Tile	$5.15 \pm 1.30 \times 10^7$	$8.75 \pm 6.57 \times 10^5$	1.84 ± 0.39
						0.50			$3.93 \pm 2.90 \times 10^4$	3.26 ± 0.61
						1.00			$4.50 \pm 7.62 \times 10^1$	6.99 ± 1.39
						2.00			0.00 ± 0.00	≥7.70 ± 0.10
						3.00			0.00 ± 0.00	≥7.70 ± 0.10

[a] Data expressed as the mean (± SD) of the logs of the number of spores (CFU) observed on individual samples and decontamination efficacy (log reduction).

[b] Positive Controls = samples inoculated, not decontaminated.

[c] Test Coupons = samples inoculated, decontaminated.

[d] CI = confidence interval (± 1.96 × SE). Results highlighted in yellow signify ≥ 6 LR, and green signifies complete inactivation.

Table A-2. Inactivation of *B. anthracis* Ames Spores using low level HPV[a] *(Continued)*

Test Number	Concentration (ppm)	Equipment	Temp (°C)	%RH	Inoculum (CFU/coupon)	Contact Time (hours)	Material	Mean Recovered *B. anthracis* (CFU/coupon)		Efficacy ± CI[d]
								Positive Control[b]	Test Coupon[c]	
2	10.42 ± 0.60	Bubbler	23.6 ± 0.26	58.5 ± 9.12	1.10E+08	0.25	Glass	4.14 ± 0.13 x 10^7	1.06 ± 0.65 x 10^5	2.68 ± 0.43
						0.50			4.47 ± 7.22 x 10^4	3.91 ± 1.63
						1.00			0.00 ± 0.00	≥7.62 ± 0.01
						2.00			3.34 ± 5.49 x 10^2	6.11 ± 1.69
						3.00			0.00 ± 0.00	≥7.62 ± 0.01
						0.25	Pine Wood	2.93 ± 0.94 x 10^7	1.74 ± 1.53 x 10^5	2.39 ± 0.65
						0.50			3.60 ± 3.93 x 10^4	4.32 ± 3.07
						1.00			0.00 ± 0.00	≥7.44 ± 0.15
						2.00			0.00 ± 0.00	≥7.44 ± 0.15
						3.00			0.00 ± 0.00	≥7.44 ± 0.15
						0.25	Carpet	9.77 ± 0.87 x 10^7	8.89 ± 0.72 x 10^7	0.04 ± 0.05
						0.50			2.04 ± 0.20 x 10^7	0.68 ± 0.06
						1.00			2.34 ± 0.95 x 10^6	1.65 ± 0.24
						2.00			2.28 ± 0.99 x 10^6	1.66 ± 0.21
						3.00			8.18 ± 2.62 x 10^5	2.09 ± 0.16
						0.25	Painted Wallboard Paper	9.13 ± 0.82 x 10^7	5.20 ± 4.58 x 10^7	0.55 ± 0.92
						0.50			1.02 ± 1.71 x 10^6	2.89 ± 1.46
						1.00			4.15 ± 6.89 x 10^6	3.75 ± 4.22
						2.00			4.67 ± 8.08 x 10^5	5.91 ± 4.01
						3.00			4.79 ± 5.55 x 10^4	3.81 ± 1.29
						0.25	Unpainted Concrete	1.10 ± 0.29 x 10^8	7.74 ± 4.03 x 10^6	1.18 ± 0.25
						0.50			1.18 ± 0.46 x 10^7	0.99 ± 0.24
						1.00			7.65 ± 4.97 x 10^6	1.26 ± 0.49
						2.00			3.51 ± 1.92 x 10^6	1.53 ± 0.27
						3.00			3.52 ± 0.62 x 10^6	1.49 ± 0.13
						0.25	Ceiling Tile	3.33 ± 1.31 x 10^7	4.26 ± 0.88 x 10^6	0.86 ± 0.23
						0.50			2.11 ± 2.01 x 10^4	3.31 ± 0.56
						1.00			7.83 ± 13.4 x 10^1	6.69 ± 1.56
						2.00			0.00 ± 0.00	≥7.48 ± 0.20
						3.00			0.00 ± 0.00	≥7.48 ± 0.20

[a] Data expressed as the mean (± SD) of the logs of the number of spores (CFU) observed on individual samples and decontamination efficacy (log reduction).

[b] Positive Controls = samples inoculated, not decontaminated.

[c] Test Coupons = samples inoculated, decontaminated.

[d] CI = confidence interval (± 1.96 × SE).). Results highlighted in yellow signify ≥ 6 LR, and green signifies complete inactivation.

Table A-3. Inactivation of *B. anthracis* Ames Spores using low level HPV[a] *(Continued)*

Test Number	Concentration (ppm)	Equipment	Temp (°C)	%RH	Inoculum (CFU/coupon)	Contact Time (hours)	Material	Mean Recovered *B. anthracis* (CFU/coupon)		Efficacy ± CI[d]
								Positive Control[b]	Test Coupon[c]	
3	9.29 ± 1.02	Bubbler	27.4 ± 0.84	76.1 ± 5.43	1.02E+08	4.00	Glass	6.06 ± 0.74 x 10^7	2.29 ± 3.79 x 10^1	7.17 ± 1.19
						8.00			0.00 ± 0.00	≥7.78 ± 0.05
						12.00			0.00 ± 0.00	≥7.78 ± 0.05
						16.00			0.00 ± 0.00	≥7.78 ± 0.05
						20.00			0.00 ± 0.00	≥7.78 ± 0.05
						4.00	Pine Wood	1.86 ± 1.20 x 10^7	7.33 ± 2.51 x 10^4	2.24 ± 0.53
						8.00			1.66 ± 1.90 x 10^4	3.23 ± 1.06
						12.00			5.84 ± 7.87 x 10^4	3.12 ± 1.76
						16.00			5.03 ± 4.90 x 10^3	3.55 ± 0.77
						20.00			7.35 ± 7.81 x 10^3	3.42 ± 0.78
						4.00	Carpet	9.35 ± 0.85 x 10^7	5.31 ± 0.03 x 10^7	0.24 ± 0.03
						8.00			3.85 ± 2.62 x 10^6	1.45 ± 0.32
						12.00			9.57 ± 2.78 x 10^6	1.00 ± 0.16
						16.00			4.70 ± 2.02 x 10^5	2.32 ± 0.22
						20.00			3.39 ± 3.41 x 10^5	2.67 ± 0.69
						4.00	Painted Wallboard Paper	8.04 ± 0.97 x 10^7	4.60 ± 7.97 x 10^6	3.43 ± 2.67
						8.00			3.44 ± 5.94 x 10^2	6.90 ± 1.97
						12.00			0.00 ± 0.00	≥7.90 ± 0.05
						16.00			0.00 ± 0.00	≥7.90 ± 0.05
						20.00			0.00 ± 0.00	≥7.90 ± 0.05
						4.00	Unpainted Concrete	3.94 ± 2.56 x 10^7	4.13 ± 2.54 x 10^7	-0.02 ± 0.47
						8.00			4.74 ± 4.09 x 10^6	1.36 ± 1.38
						12.00			3.78 ± 2.57 x 10^6	1.06 ± 0.56
						16.00			2.77 ± 3.60 x 10^6	1.35 ± 0.71
						20.00			2.51 ± 3.13 x 10^6	1.36 ± 0.67
						4.00	Ceiling Tile	3.19 ± 0.38 x 10^7	4.88 ± 2.28 x 10^3	3.84 ± 0.22
						8.00			1.18 ± 1.86 x 10^1	6.99 ± 1.00
						12.00			0.00 ± 0.00	≥7.50 ± 0.05
						16.00			0.00 ± 0.00	≥7.50 ± 0.05
						20.00			0.00 ± 0.00	≥7.50 ± 0.05

[a] Data expressed as the mean (± SD) of the logs of the number of spores (CFU) observed on individual samples and decontamination efficacy (log reduction).
[b] Positive Controls = samples inoculated, not decontaminated.
[c] Test Coupons = samples inoculated, decontaminated.
[d] CI = confidence interval (± 1.96 × SE).). Results highlighted in yellow signify ≥ 6 LR, and green signifies complete inactivation.

Table A-4. Inactivation of *B. anthracis* Ames Spores using low level HPV[a] *(Continued)*

Test Number	Concentration (ppm)	Equipment	Temp (°C)	%RH	Inoculum (CFU/coupon)	Contact Time (hours)	Material	Mean Recovered *B. anthracis* (CFU/coupon)		Efficacy ± CI[d]
								Positive Control[b]	Test Coupon[c]	
4	25.7 ± 1.41	STERIS 1000ED	22.9 ± 0.05	32.6 ± 22.4	9.50E+07	2.00	Glass	5.41 ± 0.81 x 10^6	1.42 ± 1.72 x 10^6	1.82 ± 0.63
						4.00			1.41 ± 2.39 x 10^5	3.56 ± 1.43
						6.00			3.23 ± 3.49 x 10^3	4.64 ± 1.09
						8.00			0.00 ± 0.00	≥7.73 ± 0.06
						12.00			3.98 ± 6.69 x 10^3	5.58 ± 2.31
						8.00	Pine Wood	2.05 ± 1.05 x 10^7	3.56 ± 2.60 x 10^4	2.88 ± 0.65
						12.00			2.10 ± 1.25 x 10^4	3.03 ± 0.45
						16.00			1.21 ± 0.63 x 10^4	2.22 ± 0.31
						20.00			3.01 ± 2.35 x 10^4	2.98 ± 0.71
						24.00			1.50 ± 2.57 x 10^4	4.20 ± 1.57
						8.00	Carpet	6.97 ± 0.83 x 10^7	4.38 ± 1.00 x 10^6	1.21 ± 0.12
						12.00			1.12 ± 0.15 x 10^7	0.80 ± 0.08
						16.00			5.81 ± 2.51 x 10^5	2.11 ± 0.26
						20.00			8.79 ± 8.40 x 10^5	2.28 ± 1.07
						24.00			8.03 ± 8.37 x 10^5	2.34 ± 1.07
						2.00	Painted Wallboard Paper	6.81 ± 2.34 x 10^7	3.73 ± 3.61 x 10^7	0.36 ± 0.50
						4.00			9.81 ± 3.33 x 10^6	0.86 ± 0.27
						6.00			5.92 ± 2.74 x 10^6	1.06 ± 0.29
						8.00			5.53 ± 4.33 x 10^5	2.20 ± 0.57
						12.00			1.24 ± 1.49 x 10^5	2.99 ± 0.77
						8.00	Unpainted Concrete	7.86 ± 5.14 x 10^7	4.26 ± 3.26 x 10^6	0.27 ± 0.44
						12.00			2.51 ± 2.20 x 10^6	0.53 ± 0.49
						16.00			3.29 ± 2.83 x 10^6	0.90 ± 1.54
						20.00			2.91 ± 1.85 x 10^6	0.44 ± 0.48
						24.00			2.84 ± 0.34 x 10^6	0.37 ± 0.26
						2.00	Ceiling Tile	3.58 ± 0.65 x 10^7	4.17 ± 1.14 x 10^5	1.94 ± 0.15
						4.00			6.35 ± 2.66 x 10^4	2.77 ± 0.22
						6.00			8.33 ± 1.17 x 10^4	2.63 ± 0.10
						8.00			4.48 ± 3.28 x 10^3	3.98 ± 0.37
						12.00			4.10 ± 0.46 x 10^2	3.94 ± 0.09

[a] Data expressed as the mean (± SD) of the logs of the number of spores (CFU) observed on individual samples and decontamination efficacy (log reduction).

[b] Positive Controls = samples inoculated, not decontaminated.

[c] Test Coupons = samples inoculated, decontaminated.

[d] CI = confidence interval (± 1.96 × SE).). Results highlighted in yellow signify ≥ 6 LR, and green signifies complete inactivation.

Table A-5. Inactivation of *B. anthracis* Ames Spores using low level HPV[a] *(Continued)*

Test Number	Concentration (ppm)	Equipment	Temp (°C)	%RH	Inoculum (CFU/coupon)	Contact Time (hours)	Material	Mean Recovered *B. anthracis* (CFU/coupon)		Efficacy ± CI[d]
								Positive Control[b]	Test Coupon[c]	
5	25.5 ± 0.98	STERIS 1000ED	23.9 ± 0.05	62.4 ± 23.9	8.50E+07	2.00	Glass	4.01 ± 0.65 x 10^7	5.38 ± 5.12 x 10^4	4.34 ± 3.20
						4.00			0.00 ± 0.00	≥7.60 ± 0.07
						6.00			0.00 ± 0.00	≥7.60 ± 0.07
						8.00			1.18 ± 1.86 x 101	7.09 ± 1.00
						12.00			0.00 ± 0.00	≥7.60 ± 0.07
						8.00	Pine Wood	1.99 ± 0.95 x 10^7	1.48 ± 2.47 x 10^5	2.92 ± 1.30
						12.00			3.20 ± 4.65 x 10^3	4.94 ± 2.34
						16.00			2.20 ± 0.85 x 10^3	3.95 ± 0.28
						20.00			7.16 ± 9.40 x 10^3	4.66 ± 2.59
						24.00			1.04 ± 1.72 x 10^5	3.07 ± 1.33
						8.00	Carpet	7.36 ± 2.14 x 10^7	1.07 ± 1.85 x 10^6	5.70 ± 4.25
						12.00			5.11 ± 5.36 x 10^5	2.34 ± 0.57
						16.00			2.94 ± 5.10 x 10^4	6.22 ± 3.23
						20.00			0.00 ± 0.00	≥7.87 ± 0.01
						24.00			0.00 ± 0.00	≥7.87 ± 0.01
						2.00	Painted Wallboard Paper	5.33 ± 1.05 x 10^7	4.23 ± 4.50 x 10^5	2.87 ± 1.79
						4.00			3.70 ± 3.22 x 10^4	4.05 ± 2.11
						6.00			3.73 ± 6.12 x 10^4	3.85 ± 1.15
						8.00			5.31 ± 8.66 x 10^4	3.80 ± 1.35
						12.00			3.78 ± 1.68 x 10^2	5.18 ± 0.26
						8.00	Unpainted Concrete	1.17 ± 0.38 x 10^7	3.56 ± 6.49 x 10^6	0.50 ± 0.16
						12.00			2.62 ± 0.99 x 10^6	0.65 ± 0.25
						16.00			3.57 ± 1.91 x 10^6	0.55 ± 0.37
						20.00			2.60 ± 0.53 x 10^6	0.64 ± 0.17
						24.00			3.20 ± 0.69 x 10^6	0.55 ± 0.17
						2.00	Ceiling Tile	3.11 ± 0.49 x 10^7	4.77 ± 8.08 x 10^4	4.16 ± 2.05
						4.00			2.29 ± 3.79 x 10^1	6.88 ± 1.19
						6.00			7.82 ± 8.36 x 10^1	6.14 ± 1.34
						8.00			4.50 ± 7.62 x 10^1	6.78 ± 1.39
						12.00			0.00 ± 0.00	≥7.49 ± 0.06

[a] Data expressed as the mean (± SD) of the logs of the number of spores (CFU) observed on individual samples and decontamination efficacy (log reduction).

[b] Positive Controls = samples inoculated, not decontaminated.

[c] Test Coupons = samples inoculated, decontaminated.

[d] CI = confidence interval (± 1.96 × SE).). Results highlighted in yellow signify ≥ 6 LR, and green signifies complete inactivation.

Table A-6. Inactivation of *B. anthracis* Ames Spores using low level HPV[a] *(Continued)*

Test Number	Concentration (ppm)	Equipment	Temp (°C)	%RH	Inoculum (CFU/coupon)	Contact Time (hours)	Material	Mean Recovered *B. anthracis* (CFU/coupon)		Efficacy ± CI[d]
								Positive Control[b]	Test Coupon[c]	
6	50.3 ± 1.51	STERIS 1000ED	23.5 ± 0.28	25.9 ± 1.93	1.13E+08	2.00	Glass	4.09 ± 0.75 x 10^7	2.21 ± 3.66 x 10^3	5.57 ± 2.17
						4.00			2.12 ± 1.89 x 10^2	5.94 ± 1.63
						6.00			0.00 ± 0.00	≥7.61 ± 0.07
						8.00			0.00 ± 0.00	≥7.61 ± 0.07
						12.00			0.00 ± 0.00	≥7.61 ± 0.07
						8.00	Pine Wood	1.10 ± 0.22 x 10^7	3.30 ± 4.68 x 10^4	2.89 ± 0.82
						12.00			3.25 ± 5.21 x 10^4	3.15 ± 1.10
						16.00			1.95 ± 1.55 x 10^5	1.83 ± 0.37
						20.00			1.49 ± 2.35 x 10^4	3.57 ± 1.28
						24.00			3.41 ± 5.79 x 10^5	2.95 ± 2.20
						8.00	Carpet	8.46 ± 0.58 x 10^7	2.81 ± 0.27 x 10^7	0.48 ± 0.05
						12.00			2.84 ± 1.89 x 10^6	1.53 ± 0.30
						16.00			1.24 ± 0.74 x 10^6	1.91 ± 0.39
						20.00			8.52 ± 2.33 x 10^5	2.01 ± 0.13
						24.00			9.31 ± 4.06 x 10^4	2.99 ± 0.24
						2.00	Painted Wallboard Paper	7.11 ± 0.94 x 10^7	2.61 ± 1.56 x 10^6	1.51 ± 0.41
						4.00			3.98 ± 6.18 x 10^6	1.86 ± 1.13
						6.00			2.20 ± 2.86 x 10^6	1.90 ± 0.92
						8.00			3.88 ± 4.22 x 10^5	2.44 ± 0.54
						12.00			1.57 ± 1.84 x 10^4	4.01 ± 0.92
						8.00	Unpainted Concrete	1.40 ± 0.91 x 10^7	8.27 ± 1.13 x 10^6	0.18 ± 0.21
						12.00			4.48 ± 2.08 x 10^6	0.47 ± 0.29
						16.00			2.51 ± 2.10 x 10^6	0.79 ± 0.43
						20.00			3.29 ± 3.51 x 10^6	0.74 ± 0.56
						24.00			2.06 ± 1.54 x 10^6	0.87 ± 0.44
						2.00	Ceiling Tile	2.89 ± 0.71 x 10^7	1.18 ± 1.86 x 10^1	6.94 ± 1.00
						4.00			3.78 ± 5.17 x 10^2	5.71 ± 1.76
						6.00			7.81 ± 10.70 x 10^2	6.17 ± 1.33
						8.00			0.00 ± 0.00	≥7.45 ± 0.11
						12.00			0.00 ± 0.00	≥7.45 ± 0.11

[a] Data expressed as the mean (± SD) of the logs of the number of spores (CFU) observed on individual samples and decontamination efficacy (log reduction).

[b] Positive Controls = samples inoculated, not decontaminated.

[c] Test Coupons = samples inoculated, decontaminated.

[d] CI = confidence interval (± 1.96 × SE).). Results highlighted in yellow signify ≥ 6 LR, and green signifies complete inactivation.

Table A-7. Inactivation of *B. anthracis* Ames Spores using low level HPV[a] *(Continued)*

Test Number	Concentration (ppm)	Equipment	Temp (°C)	%RH	Inoculum (CFU/coupon)	Contact Time (hours)	Material	Mean Recovered *B. anthracis* (CFU/coupon)		Efficacy ± CI[d]
								Positive Control[b]	Test Coupon[c]	
7	50.0 ± 1.10	STERIS 1000ED	23.77 ± 3.86	60.07 ± 3.86	9.53E+07	1.00	Glass	5.20 ± 0.47 x 10^7	0.00 ± 0.00	≥7.71 ± 0.04
						2.00			0.00 ± 0.00	≥7.71 ± 0.04
						4.00			0.00 ± 0.00	≥7.71 ± 0.04
						5.00			0.00 ± 0.00	≥7.71 ± 0.04
						6.00			0.00 ± 0.00	≥7.71 ± 0.04
						8.00	Pine Wood	2.31 ± 1.14 x 10^7	2.09 ± 2.24 x 10^5	2.17 ± 0.53
						12.00			1.16 ± 1.88 x 10^5	4.10 ± 3.26
						16.00			0.67 ± 1.17 x 10^3	6.22 ± 2.17
						20.00			3.19 ± 3.56 x 10^4	4.24 ± 3.04
						24.00			0.00 ± 0.00	≥7.32 ± 0.18
						8.00	Carpet	6.59 ± 0.70 x 10^7	2.19 ± 0.79 x 10^5	1.49 ± 0.17
						12.00			2.27 ± 1.31 x 10^5	2.51 ± 0.27
						16.00			1.66 ± 2.13 x 10^4	4.96 ± 2.83
						20.00			5.77 ± 9.13 x 10^2	6.08 ± 1.84
						24.00			1.95 ± 2.94 x 10^3	5.67 ± 2.18
						1.00	Painted Wallboard Paper	6.31 ± 1.24 x 10^7	0.00 ± 0.00	≥7.79 ± 0.08
						2.00			0.00 ± 0.00	≥7.79 ± 0.08
						4.00			1.53 ± 2.65 x 10^5	5.05 ± 3.21
						5.00			2.22 ± 2.71 x 10^2	5.71 ± 0.69
						6.00			1.43 ± 2.33 x 10^4	4.32 ± 1.15
						8.00	Unpainted Concrete	2.35 ± 1.32 x 10^7	3.38 ± 1.75 x 10^6	0.83 ± 0.35
						12.00			3.53 ± 1.47 x 10^6	0.83 ± 0.42
						16.00			4.96 ± 0.19 x 10^6	0.62 ± 0.22
						20.00			1.96 ± 0.67 x 10^6	1.04 ± 0.27
						24.00			3.78 ± 1.98 x 10^6	0.78 ± 0.34
						1.00	Ceiling Tile	3.83 ± 0.51 x 10^7	2.56 ± 3.74 x 10^4	3.63 ± 0.94
						2.00			2.33 ± 2.19 x 10^2	5.42 ± 0.67
						4.00			0.00 ± 0.00	≥7.58 ± 0.05
						5.00			0.00 ± 0.00	≥7.58 ± 0.05
						6.00			0.00 ± 0.00	≥7.58 ± 0.05

[a] Data expressed as the mean (± SD) of the logs of the number of spores (CFU) observed on individual samples and decontamination efficacy (log reduction).

[b] Positive Controls = samples inoculated, not decontaminated.

[c] Test Coupons = samples inoculated, decontaminated.

[d] CI = confidence interval (± 1.96 × SE).). Results highlighted in yellow signify ≥ 6 LR, and green signifies complete inactivation.

Table A-8. Inactivation of *B. anthracis* Ames Spores using low level HPV[a] *(Continued)*

Test Number	Concentration (ppm)	Equipment	Temp (°C)	%RH	Inoculum (CFU/coupon)	Contact Time (hours)	Material	Mean Recovered *B. anthracis* (CFU/coupon)		Efficacy ± CI[d]
								Positive Control[b]	Test Coupon[c]	
8	43.50 ± 12.61	STERIS 1000ED	22.98 ± 0.43	76.91 ± 5.45	7.17E+07	1.00	Glass	1.27 ± 0.47 x 10^7	1.21 ± 2.10 x 10^3	5.81 ± 2.33
						2.00			0.00 ± 0.00	≥7.00 ± 0.16
						4.00			0.00 ± 0.00	≥7.00 ± 0.16
						5.00			0.00 ± 0.00	≥7.00 ± 0.16
						6.00			0.00 ± 0.00	≥7.00 ± 0.16
						8.00	Pine Wood	1.04 ± 0.30 x 10^7	2.04 ± 1.88 x 10^4	2.81 ± 0.44
						12.00			3.66 ± 5.41 x 10^4	3.99 ± 3.00
						16.00			1.35 ± 1.33 x 10^4	3.64 ± 1.81
						20.00			3.68 ± 4.32 x 10^3	3.67 ± 0.64
						24.00			0.00 ± 0.00	≥7.00 ± 0.11
						8.00	Carpet	3.61 ± 0.50 x 10^7	1.21 ± 2.10 x 10^4	6.03 ± 2.98
						12.00			0.00 ± 0.00	7.55 ± 0.05
						16.00			0.00 ± 0.00	7.55 ± 0.05
						20.00			0.00 ± 0.00	7.55 ± 0.05
						24.00			0.00 ± 0.00	7.55 ± 0.05
						1.00	Painted Wallboard Paper	2.92 ± 1.15 x 10^7	3.96 ± 4.26 x 10^5	2.65 ± 1.90
						2.00			0.00 ± 0.00	≥7.42 ± 0.21
						4.00			1.45 ± 2.49 x 10^2	6.55 ± 1.74
						5.00			0.00 ± 0.00	≥7.42 ± 0.21
						6.00			0.00 ± 0.00	≥7.42 ± 0.21
						8.00	Unpainted Concrete	8.02 ± 2.60 x 10^6	1.58 ± 1.32 x 10^6	0.78 ± 0.41
						12.00			1.34 ± 0.35 x 10^6	0.77 ± 0.20
						16.00			4.67 ± 5.05 x 10^6	1.38 ± 0.53
						20.00			1.14 ± 0.51 x 10^6	0.85 ± 0.25
						24.00			1.50 ± 1.24 x 10^6	0.80 ± 0.41
						1.00	Ceiling Tile	1.76 ± 0.85 x 10^7	3.45 ± 1.46 x 10^5	1.70 ± 0.30
						2.00			1.90 ± 2.48 x 10^3	4.98 ± 2.22
						4.00			0.00 ± 0.00	≥7.21 ± 0.18
						5.00			0.00 ± 0.00	≥7.21 ± 0.18
						6.00			0.00 ± 0.00	≥7.21 ± 0.18

[a] Data expressed as the mean (± SD) of the logs of the number of spores (CFU) observed on individual samples and decontamination efficacy (log reduction).

[b] Positive Controls = samples inoculated, not decontaminated.

[c] Test Coupons = samples inoculated, decontaminated.

[d] CI = confidence interval (± 1.96 × SE). Results highlighted in yellow signify ≥ 6 LR, and green signifies complete inactivation.

Table A-9. Inactivation of *B. anthracis* Ames Spores using low level HPV[a] *(Continued)*

Test Number	Concentration (ppm)	Equipment	Temp (°C)	%RH	Inoculum (CFU/coupon)	Contact Time (hours)	Material	Mean Recovered *B. anthracis* (CFU/coupon)		Efficacy ± CI[d]
								Positive Control[b]	Test Coupon[c]	
9	25.22 ± 1.64	Bubbler	23.77 ± 0.40	91.64 ± 6.33	8.80E+07	1.00	Glass	3.67 ± 0.61 x 10^7	3.95 ± 0.52 x 10^6	0.97 ± 0.10
						2.00			6.18 ± 4.24 x 10^5	1.88 ± 0.49
						6.00			0.00 ± 0.00	≥7.56 ± 0.07
						8.00			0.00 ± 0.00	≥7.56 ± 0.07
						12.00			0.00 ± 0.00	≥7.56 ± 0.07
						8.00	Pine Wood	1.84 ± 1.82 x 10^7	1.42 ± 1.70 x 10^5	2.35 ± 0.95
						12.00			9.54 ± 6.01 x 10^4	2.25 ± 0.49
						16.00			8.68 ± 2.97 x 10^4	2.22 ± 0.33
						20.00			4.80 ± 7.97 x 10^4	3.23 ± 1.24
						24.00			2.66 ± 3.77 x 10^3	4.86 ± 2.30
						8.00	Carpet	8.07 ± 0.81 x 10^7	7.67 ± 2.23 x 105	2.04 ± 0.16
						12.00			8.19 ± 2.03 x 10^5	2.00 ± 0.12
						16.00			0.00 ± 0.00	7.91 ± 0.04
						20.00			0.00 ± 0.00	7.91 ± 0.04
						24.00			0.00 ± 0.00	7.91 ± 0.04
						1.00	Painted Wallboard Paper	5.65 ± 0.77 x 10^7	7.57 ± 3.07 x 10^5	1.89 ± 0.19
						2.00			3.50 ± 6.06 x 10^4	6.08 ± 3.28
						6.00			0.00 ± 0.00	≥7.75 ± 0.05
						8.00			0.00 ± 0.00	≥7.75 ± 0.05
						12.00			0.00 ± 0.00	≥7.75 ± 0.05
						8.00	Unpainted Concrete	2.36 ± 1.36 x 10^7	7.85 ± 3.16 x 10^5	1.45 ± 0.28
						12.00			3.42 ± 2.19 x 10^6	0.87 ± 0.46
						16.00			1.59 ± 1.58 x 10^6	1.26 ± 0.52
						20.00			4.55 ± 2.71 x 10^5	1.71 ± 0.34
						24.00			5.94 ± 5.06 x 10^5	1.83 ± 0.90
						1.00	Ceiling Tile	1.26 ± 0.22 x 10^7	6.07 ± 2.51 x 10^6	0.34 ± 0.25
						2.00			1.13 ± 0.46 x 10^5	1.07 ± 0.25
						6.00			0.00 ± 0.00	≥7.09 ± 0.06
						8.00			1.14 ± 1.98 x 10^3	5.92 ± 2.31
						12.00			0.00 ± 0.00	≥7.09 ± 0.06

[a] Data expressed as the mean (± SD) of the logs of the number of spores (CFU) observed on individual samples and decontamination efficacy (log reduction).

[b] Positive Controls = samples inoculated, not decontaminated.

[c] Test Coupons = samples inoculated, decontaminated.

[d] CI = confidence interval (± 1.96 × SE). Results highlighted in yellow signify ≥ 6 LR, and green signifies complete inactivation.

Table A-10. Inactivation of *B. anthracis* Vollum Spores using low level HPV[a] *(Continued)*

Test Number	Concentration (ppm)	Equipment	Temp (°C)	%RH	Inoculum (CFU/coupon)	Contact Time (hours)	Material	Mean Recovered *B. anthracis* (CFU/coupon)		Efficacy ± CI[d]
								Positive Control[b]	Test Coupon[c]	
1	250	STERIS 1000ED	23.0 ± 0.04	38.1 ± 4.3	8.97E+07	0.25	Glass	$1.17 \pm 0.48 \times 10^7$	$1.18 \pm 1.86 \times 10^1$	6.52 ± 1.02
						0.50			$1.54 \pm 2.45 \times 10^4$	4.34 ± 2.73
						1.00			0.00 ± 0.00	≥7.03 ± 0.21
						2.00			0.00 ± 0.00	≥7.03 ± 0.21
						3.00			$2.56 \pm 3.09 \times 10^2$	5.36 ± 1.68
						0.25	Pine Wood	$4.43 \pm 2.09 \times 10^6$	$2.71 \pm 3.69 \times 10^4$	2.47 ± 0.76
						0.50			$1.04 \pm 1.53 \times 10^4$	3.05 ± 0.99
						1.00			$1.03 \pm 1.79 \times 10^3$	5.43 ± 2.29
						2.00			$1.18 \pm 1.86 \times 10^1$	6.08 ± 1.02
						3.00			$5.45 \pm 9.14 \times 10^2$	5.01 ± 1.83
						0.25	Carpet	$1.20 \pm 0.12 \times 10^7$	$1.20 \pm 0.40 \times 10^6$	1.02 ± 0.18
						0.50			$7.69 \pm 5.32 \times 10^6$	0.30 ± 0.46
						1.00			$5.74 \pm 0.62 \times 10^4$	2.32 ± 0.07
						2.00			$1.09 \pm 0.95 \times 10^3$	4.94 ± 2.10
						3.00			$3.78 \pm 2.22 \times 10^2$	4.55 ± 0.27
						0.25	Painted Wallboard Paper	$4.25 \pm 5.44 \times 10^7$	$7.18 \pm 6.92 \times 10^5$	2.90 ± 2.96
						0.50			$1.22 \pm 1.48 \times 10^5$	2.55 ± 0.71
						1.00			0.00 ± 0.00	≥7.42 ± 0.38
						2.00			0.00 ± 0.00	≥7.42 ± 0.38
						3.00			0.00 ± 0.00	≥7.42 ± 0.38
						0.25	Unpainted Concrete	$1.92 \pm 2.78 \times 10^6$	$1.56 \pm 2.07 \times 10^5$	1.06 ± 1.07
						0.50			$1.33 \pm 2.23 \times 10^5$	1.58 ± 1.42
						1.00			$8.33 \pm 2.67 \times 10^2$	2.97 ± 0.65
						2.00			$4.00 \pm 6.93 \times 10^3$	4.52 ± 2.74
						3.00			$2.10 \pm 1.15 \times 10^3$	2.59 ± 0.68
						0.25	Ceiling Tile	$1.38 \pm 1.43 \times 10^6$	$1.18 \pm 1.86 \times 10^1$	5.44 ± 1.07
						0.50			$3.37 \pm 3.29 \times 10^1$	4.83 ± 1.18
						1.00			0.00 ± 0.00	≥5.95 ± 0.40
						2.00			0.00 ± 0.00	≥5.95 ± 0.40
						3.00			0.00 ± 0.00	≥5.95 ± 0.40

[a] Data expressed as the mean (± SD) of the logs of the number of spores (CFU) observed on individual samples and decontamination efficacy (log reduction).

[b] Positive Controls = samples inoculated, not decontaminated.

[c] Test Coupons = samples inoculated, decontaminated.

[d] CI = confidence interval (± 1.96 × SE). Results highlighted in yellow signify ≥ 6 LR, and green signifies complete inactivation.

Table A-11. Inactivation of *B. anthracis* Vollum Spores using low level HPV[a] *(Continued)*

Test Number	Concentration (ppm)	Equipment	Temp (°C)	%RH	Inoculum (CFU/coupon)	Contact Time (hours)	Material	Mean Recovered *B. anthracis* (CFU/coupon)		Efficacy ± CI[d]
								Positive Control[b]	Test Coupon[c]	
2	10.42 ± 0.60	Bubbler	23.6 ± 0.26	58.5 ± 9.12	1.15E+08	4.00	Glass	6.81 ± 3.03 x 10^6	2.06 ± 3.56 x 10^6	3.47 ± 3.85
						8.00			0.67 ± 1.15 x 10^3	5.69 ± 2.17
						12.00			0.00 ± 0.00	≥6.79 ± 0.19
						16.00			0.00 ± 0.00	≥6.79 ± 0.19
						20.00			0.00 ± 0.00	≥6.79 ± 0.19
						4.00	Pine Wood	1.84 ± 1.33 x 10^6	1.31 ± 1.84 x 10^4	2.44 ± 0.89
						8.00			0.97 ± 1.59 x 10^4	3.69 ± 2.58
						12.00			2.67 ± 4.05 x 10^2	4.61 ± 1.67
						16.00			2.29 ± 3.79 x 10^1	5.56 ± 1.22
						20.00			2.29 ± 3.79 x 10^1	5.56 ± 1.22
						4.00	Carpet	6.70 ± 0.28 x 10^6	3.93 ± 0.55 x 10^6	0.23 ± 0.07
						8.00			6.10 ± 0.94 x 10^5	1.04 ± 0.08
						12.00			8.78 ± 6.70 x 10^2	4.06 ± 0.64
						16.00			9.98 ± 1.51 x 10^2	3.83 ± 0.08
						20.00			1.00 ± 1.45 x 10^2	5.51 ± 1.39
						4.00	Painted Wallboard Paper	1.95 ± 2.99 x 10^7	0.93 ± 1.60 x 10^6	2.41 ± 1.86
						8.00			4.48 ± 5.01 x 10^1	5.83 ± 1.26
						12.00			1.11 ± 1.92 x 10^3	5.83 ± 2.34
						16.00			0.00 ± 0.00	≥7.00 ± 0.42
						20.00			0.00 ± 0.00	≥7.00 ± 0.42
						4.00	Unpainted Concrete	0.90 ± 1.47 x 10^6	4.62 ± 3.26 x 10^4	0.95 ± 0.80
						8.00			1.45 ± 1.20 x 10^5	0.44 ± 0.75
						12.00			1.39 ± 0.28 x 10^4	1.36 ± 0.63
						16.00			2.32 ± 2.06 x 10^3	2.24 ± 0.74
						20.00			1.91 ± 1.25 x 10^4	1.29 ± 0.73
						4.00	Ceiling Tile	3.25 ± 1.23 x 10^5	1.62 ± 1.18 x 10^3	2.38 ± 0.47
						8.00			0.00 ± 0.00	≥5.49 ± 0.14
						12.00			0.00 ± 0.00	≥5.49 ± 0.14
						16.00			0.00 ± 0.00	≥5.49 ± 0.14
						20.00			0.00 ± 0.00	≥5.49 ± 0.14

[a] Data expressed as the mean (± SD) of the logs of the number of spores (CFU) observed on individual samples and decontamination efficacy (log reduction).

[b] Positive Controls = samples inoculated, not decontaminated.

[c] Test Coupons = samples inoculated, decontaminated.

[d] CI = confidence interval (± 1.96 × SE). Results highlighted in yellow signify ≥ 6 LR, and green signifies complete inactivation.

Table A-12. Inactivation of *B. anthracis* Vollum Spores using low level HPV[a] *(Continued)*

Test Number	Concentration (ppm)	Equipment	Temp (°C)	%RH	Inoculum (CFU/coupon)	Contact Time (hours)	Material	Mean Recovered *B. anthracis* (CFU/coupon)		Efficacy ± CI[d]
								Positive Control[b]	Test Coupon[c]	
3	9.29 ± 1.02	Bubbler	27.4 ± 0.84	76.1 ± 5.43	9.13E+07	4.00	Glass	6.90 ± 1.99 x 10^6	0.00 ± 0.00	≥6.83 ± 0.11
						8.00			0.00 ± 0.00	≥6.83 ± 0.11
						12.00			0.00 ± 0.00	≥6.83 ± 0.11
						16.00			0.00 ± 0.00	≥6.83 ± 0.11
						20.00			0.00 ± 0.00	≥6.83 ± 0.11
						4.00	Pine Wood	4.19 ± 1.21 x 10^5	1.19 ± 1.83 x 10^4	2.36 ± 1.54
						8.00			6.33 ± 2.03 x 10^2	2.83 ± 0.20
						12.00			0.00 ± 0.00	≥5.61 ± 0.10
						16.00			1.18 ± 1.86 x 10^1	5.10 ± 1.00
						20.00			5.59 ± 5.04 x 10^1	4.34 ± 1.26
						4.00	Carpet	6.91 ± 6.16 x 10^6	8.69 ± 2.55 x 10^5	0.91 ± 0.15
						8.00			4.51 ± 0.32 x 10^4	2.18 ± 0.05
						12.00			1.73 ± 0.24 x 10^2	3.60 ± 0.08
						16.00			2.22 ± 1.92 x 10^2	5.16 ± 1.65
						20.00			0.00 ± 0.00	≥6.84 ± 0.03
						4.00	Painted Wallboard Paper	4.71 ± 0.31 x 10^6	3.47 ± 6.00 x 10^3	5.33 ± 2.63
						8.00			0.00 ± 0.00	≥6.67 ± 0.03
						12.00			0.00 ± 0.00	≥6.67 ± 0.03
						16.00			0.00 ± 0.00	≥6.67 ± 0.03
						20.00			0.00 ± 0.00	≥6.67 ± 0.03
						4.00	Unpainted Concrete	9.57 ± 4.80 x 10^6	4.39 ± 1.50 x 10^5	1.30 ± 0.29
						8.00			1.14 ± 1.70 x 10^4	4.26 ± 2.68
						12.00			2.39 ± 2.33 x 10^4	2.68 ± 0.51
						16.00			3.61 ± 5.33 x 10^4	2.78 ± 0.86
						20.00			2.89 ± 3.90 x 10^2	5.26 ± 1.70
						4.00	Ceiling Tile	8.02 ± 2.16 x 10^4	2.44 ± 1.93 x 10^2	2.58 ± 0.37
						8.00			0.00 ± 0.00	≥4.89 ± 0.11
						12.00			0.00 ± 0.00	≥4.89 ± 0.11
						16.00			0.00 ± 0.00	≥4.89 ± 0.11
						20.00			0.00 ± 0.00	≥4.89 ± 0.11

[a] Data expressed as the mean (± SD) of the logs of the number of spores (CFU) observed on individual samples and decontamination efficacy (log reduction).

[b] Positive Controls = samples inoculated, not decontaminated.

[c] Test Coupons = samples inoculated, decontaminated.

[d] CI = confidence interval (± 1.96 × SE). Results highlighted in yellow signify ≥ 6 LR, and green signifies complete inactivation.

Table A-13. Inactivation of *B. anthracis* Vollum Spores using low level HPV[a] *(Continued)*

Test Number	Concentration (ppm)	Equipment	Temp (°C)	%RH	Inoculum (CFU/coupon)	Contact Time (hours)	Material	Mean Recovered *B. anthracis* (CFU/coupon)		Efficacy ± CI[d]
								Positive Control[b]	Test Coupon[c]	
4	25.7 ± 1.41	STERIS 1000ED	22.9 ± 0.05	32.6 ± 22.4	8.63E+07	2.00	Glass	3.77 ± 1.10 x 10^6	4.50 ± 7.62 x 10^1	5.85 ± 1.39
						4.00			4.48 ± 5.05 x 10^1	5.39 ± 1.19
						6.00			5.63 ± 9.58 x 10^1	5.82 ± 1.46
						8.00			0.00 ± 0.00	≥6.56 ± 0.11
						12.00			0.00 ± 0.00	≥6.56 ± 0.11
						8.00	Pine Wood	3.83 ± 1.64 x 10^6	0.96 ± 1.60 x 10^4	3.63 ± 1.67
						12.00			3.78 ± 4.11 x 10^2	4.26 ± 0.82
						16.00			0.92 ± 1.13 x 10^3	3.93 ± 0.88
						20.00			4.48 ± 5.05 x 10^1	5.38 ± 1.19
						24.00			5.10 ± 8.06 x 10^3	3.50 ± 1.17
						8.00	Carpet	0.91 ± 1.22 x 10^7	4.22 ± 3.34 x 10^4	2.22 ± 0.74
						12.00			3.15 ± 1.90 x 10^4	2.25 ± 0.55
						16.00			7.78 ± 1.78 x 10^3	2.80 ± 0.45
						20.00			3.12 ± 5.38 x 10^2	5.69 ± 1.99
						24.00			2.34 ± 3.47 x 10^2	5.14 ± 1.62
						2.00	Painted Wallboard Paper	4.80 ± 0.95 x 10^6	4.64 ± 7.16 x 10^5	1.51 ± 0.94
						4.00			3.00 ± 2.60 x 10^2	4.90 ± 1.74
						6.00			0.00 ± 0.00	≥6.67 ± 0.08
						8.00			0.00 ± 0.00	≥6.67 ± 0.08
						12.00			0.00 ± 0.00	≥6.67 ± 0.08
						8.00	Unpainted Concrete	1.28 ± 0.75 x 10^6	1.50 ± 1.49 x 10^4	2.01 ± 0.56
						12.00			3.04 ± 2.80 x 10^3	3.60 ± 2.40
						16.00			1.45 ± 2.04 x 10^4	2.22 ± 0.80
						20.00			3.20 ± 1.58 x 10^3	2.58 ± 0.40
						24.00			5.50 ± 1.07 x 10^3	2.30 ± 0.28
						2.00	Ceiling Tile	5.84 ± 3.32 x 10^5	2.32 ± 0.58 x 10^3	2.32 ± 0.33
						4.00			4.48 ± 5.05 x 10^1	4.51 ± 1.22
						6.00			1.18 ± 1.86 x 10^1	5.17 ± 1.04
						8.00			0.00 ± 0.00	≥5.68 ± 0.30
						12.00			0.00 ± 0.00	≥5.68 ± 0.30

[a] Data expressed as the mean (± SD) of the logs of the number of spores (CFU) observed on individual samples and decontamination efficacy (log reduction).

[b] Positive Controls = samples inoculated, not decontaminated.

[c] Test Coupons = samples inoculated, decontaminated.

[d] CI = confidence interval (± 1.96 × SE). Results highlighted in yellow signify ≥ 6 LR, and green signifies complete inactivation.

Table A-14. Inactivation of *B. anthracis* Vollum Spores using low level HPV[a] *(Continued)*

Test Number	Concentration (ppm)	Equipment	Temp (°C)	%RH	Inoculum (CFU/coupon)	Contact Time (hours)	Material	Mean Recovered *B. anthracis* (CFU/coupon)		Efficacy ± CI[d]
								Positive Control[b]	Test Coupon[c]	
5	25.5 ± 0.98	STERIS 1000ED	23.9 ± 0.10	62.4 ± 23.9	9.03E+07	2.00	Glass	3.31 ± 1.42 x 10^6	1.90 ± 3.27 x 10^2	5.56 ± 1.81
						4.00			0.00 ± 0.00	≥6.48 ± 0.19
						6.00			0.00 ± 0.00	≥6.48 ± 0.19
						8.00			0.00 ± 0.00	≥6.48 ± 0.19
						12.00			0.00 ± 0.00	≥6.48 ± 0.19
						8.00	Pine Wood	3.30 ± 2.35 x 10^6	2.45 ± 3.95x 10^2	4.94 ± 1.65
						12.00			1.23 ± 2.11 x 10^2	5.54 ± 1.71
						16.00			2.23 ± 3.29 x 10^2	4.86 ± 1.63
						20.00			1.46 ± 2.52 x 10^3	5.18 ± 2.40
						24.00			0.71 ± 1.23 x 10^3	5.29 ± 2.20
						8.00	Carpet	0.80 ± 1.02 x 10^6	7.18 ± 3.10 x 10^4	0.89 ± 0.43
						12.00			1.54 ± 0.20 x 10^3	2.53 ± 0.35
						16.00			5.32 ± 6.92 x 10^2	3.26 ± 0.76
						20.00			0.89 ± 1.26 x 10^2	4.42 ± 1.40
						24.00			0.00 ± 0.00	≥5.71 ± 0.35
						8.00	Painted Wallboard Paper	3.84 ± 0.43 x 10^6	2.34 ± 1.71 x 10^4	2.35 ± 0.55
						12.00			0.00 ± 0.00	≥6.58 ± 0.04
						16.00			0.00 ± 0.00	≥6.58 ± 0.04
						20.00			0.00 ± 0.00	≥6.58 ± 0.04
						24.00			0.00 ± 0.00	≥6.58 ± 0.04
						8.00	Unpainted Concrete	6.00 ± 4.40 x 10^5	7.77 ± 5.53 x 10^3	1.91 ± 0.68
						12.00			5.87 ± 6.59 x 10^3	3.06 ± 2.58
						16.00			3.10 ± 1.47 x 10^3	2.19 ± 0.41
						20.00			4.75 ± 2.79 x 10^3	2.03 ± 0.46
						24.00			8.35 ± 1.69 x 10^3	1.74 ± 0.36
						8.00	Ceiling Tile	3.35 ± 1.85 x 10^5	3.18 ± 4.09 x 10^3	2.32 ± 0.33
						12.00			1.18 ± 1.86 x 10^1	4.65 ± 1.03
						16.00			0.00 ± 0.00	≥5.46 ± 0.25
						20.00			0.00 ± 0.00	≥5.46 ± 0.25
						24.00			0.00 ± 0.00	≥5.46 ± 0.25

[a] Data expressed as the mean (± SD) of the logs of the number of spores (CFU) observed on individual samples and decontamination efficacy (log reduction).

[b] Positive Controls = samples inoculated, not decontaminated.

[c] Test Coupons = samples inoculated, decontaminated.

[d] CI = confidence interval (± 1.96 × SE). Results highlighted in yellow signify ≥ 6 LR, and green signifies complete inactivation.

Table A-15. Inactivation of *B. anthracis* Vollum Spores using low level HPV[a] *(Continued)*

Test Number	Concentration (ppm)	Equipment	Temp (°C)	%RH	Inoculum (CFU/coupon)	Contact Time (hours)	Material	Mean Recovered *B. anthracis* (CFU/coupon)		Efficacy ± CI[d]
								Positive Control[b]	Test Coupon[c]	
6	50.3 ± 1.51	STERIS 1000ED	23.5 ± 0.28	25.9 ± 1.93	8.67E+07	2.00	Glass	2.96 ± 0.01 x 10^6	1.18 ± 1.86 x 10^1	5.96 ± 1.00
						4.00			0.00 ± 0.00	≥6.48 ± 0.01
						6.00			0.00 ± 0.00	≥6.48 ± 0.01
						8.00			3.34 ± 5.77 x 10^2	5.47 ± 1.96
						12.00			0.00 ± 0.00	≥6.48 ± 0.01
						8.00	Pine Wood	3.13 ± 0.35 x 10^6	1.13 ± 1.00 x 10^3	4.34 ± 2.11
						12.00			0.78 ± 1.34 x 10^2	5.70 ± 1.55
						16.00			2.29 ± 3.79 x 10^1	5.89 ± 1.19
						20.00			2.29 ± 3.79 x 10^3	5.89 ± 1.19
						24.00			0.00 ± 0.00	≥6.49 ± 0.04
						8.00	Carpet	3.47 ± 0.75 x 10^6	3.01 ± 0.29 x 10^4	1.06 ± 0.08
						12.00			1.84 ± 0.74 x 10^3	3.30 ± 0.24
						16.00			1.34 ± 2.03 x 10^2	5.17 ± 1.46
						20.00			6.69 ± 6.60 x 10^1	5.22 ± 1.30
						24.00			0.00 ± 0.00	≥6.53 ± 0.07
						8.00	Painted Wallboard Paper	4.28 ± 1.13 x 10^6	2.62 ± 0.24 x 10^3	3.20 ± 0.11
						12.00			1.56 ± 1.84 x 10^2	4.65 ± 0.62
						16.00			0.00 ± 0.00	≥6.62 ± 0.10
						20.00			0.00 ± 0.00	≥6.62 ± 0.10
						24.00			0.00 ± 0.00	≥6.62 ± 0.10
						8.00	Unpainted Concrete	1.12 ± 0.64 x 10^6	1.23 ± 0.50 x 10^4	1.90 ± 0.35
						12.00			3.29 ± 2.86 x 10^3	3.51 ± 2.43
						16.00			8.69 ± 3.41 x 10^3	2.06 ± 0.36
						20.00			2.12 ± 1.55x 10^3	2.74 ± 0.53
						24.00			1.37 ± 0.58 x 10^3	2.86 ± 0.37
						8.00	Ceiling Tile	3.59 ± 2.28 x 10^5	0.00 ± 0.00	≥5.49 ± 0.22
						12.00			0.00 ± 0.00	≥5.49 ± 0.22
						16.00			0.00 ± 0.00	≥5.49 ± 0.22
						20.00			0.00 ± 0.00	≥5.49 ± 0.22
						24.00			0.00 ± 0.00	≥5.49 ± 0.22

[a] Data expressed as the mean (± SD) of the logs of the number of spores (CFU) observed on individual samples and decontamination efficacy (log reduction).

[b] Positive Controls = samples inoculated, not decontaminated.

[c] Test Coupons = samples inoculated, decontaminated.

[d] CI = confidence interval (± 1.96 × SE). Results highlighted in yellow signify ≥ 6 LR, and green signifies complete inactivation.

Table A-16. Inactivation of *B. anthracis* Vollum Spores using low level HPV[a] *(Continued)*

Test Number	Concentration (ppm)	Equipment	Temp (°C)	%RH	Inoculum (CFU/coupon)	Contact Time (hours)	Material	Mean Recovered *B. anthracis* (CFU/coupon)		Efficacy ± CI[d]
								Positive Control[b]	Test Coupon[c]	
7	50.0 ± 1.10	STERIS 1000ED	23.77 ± 3.86	60.07 ± 3.86	1.29E+08	1.00	Glass	1.20 ± 0.11 x 10^7	9.31 ± 2.22 x 10^4	2.12 ± 0.13
						2.00			5.55 ± 3.85 x 10^1	5.39 ± 0.31
						4.00			0.00 ± 0.00	≥7.08 ± 0.04
						5.00			0.00 ± 0.00	≥7.08 ± 0.04
						6.00			0.00 ± 0.00	≥7.08 ± 0.04
						8.00	Pine Wood	1.59 ± 1.03 x 10^6	6.57 ± 4.30 x 10^3	2.43 ± 0.52
						12.00			1.48 ± 2.36 x 10^3	3.66 ± 1.22
						16.00			0.00 ± 0.00	≥6.14 ± 0.21
						20.00			0.00 ± 0.00	≥6.14 ± 0.21
						24.00			1.18 ± 1.86 x 10^1	5.63 ± 1.02
						8.00	Carpet	6.26 ± 2.34 x 10^6	2.07 ± 1.51 x 10^3	3.54 ± 0.38
						12.00			1.02 ± 0.92 x 10^3	3.95 ± 0.64
						16.00			5.59 ± 5.04 x 10^1	5.50 ± 1.26
						20.00			5.63 ± 9.58 x 10^1	6.04 ± 1.46
						24.00			0.00 ± 0.00	≥6.78 ± 0.12
						1.00	Painted Wallboard Paper	7.29 ± 1.03 x 10^6	1.18 ± 0.28 x 10^5	1.80 ± 0.13
						2.00			0.92 ± 1.60 x 10^3	5.71 ± 2.25
						4.00			1.18 ± 1.86 x 10^1	6.35 ± 1.00
						5.00			0.00 ± 0.00	≥6.86 ± 0.05
						6.00			0.00 ± 0.00	≥6.86 ± 0.05
						8.00	Unpainted Concrete	2.35 ± 2.74 x 10^6	1.59 ± 0.85 x 10^4	1.80 ± 0.71
						12.00			7.88 ± 2.32 x 10^3	2.07 ± 0.68
						16.00			1.02 ± 0.22 x 10^4	1.96 ± 0.67
						20.00			3.11 ± 2.56 x 10^3	2.57 ± 0.79
						24.00			5.96 ± 3.12 x 10^3	2.23 ± 0.74
						1.00	Ceiling Tile	4.14 ± 0.52 x 10^5	1.76 ± 0.55 x 10^3	2.38 ± 0.16
						2.00			6.67± 0.00 x 10^1	3.79 ± 0.05
						4.00			0.00 ± 0.00	≥5.61 ± 0.05
						5.00			0.00 ± 0.00	≥5.61 ± 0.05
						6.00			0.00 ± 0.00	≥5.61 ± 0.05

[a] Data expressed as the mean (± SD) of the logs of the number of spores (CFU) observed on individual samples and decontamination efficacy (log reduction).

[b] Positive Controls = samples inoculated, not decontaminated.

[c] Test Coupons = samples inoculated, decontaminated.

[d] CI = confidence interval (± 1.96 × SE). Results highlighted in yellow signify ≥ 6 LR, and green signifies complete inactivation.

Table A-17. Inactivation of *B. anthracis* Vollum Spores using low level HPV[a] *(Continued)*

Test Number	Concentration (ppm)	Equipment	Temp (°C)	%RH	Inoculum (CFU/coupon)	Contact Time (hours)	Material	Mean Recovered *B. anthracis* (CFU/coupon)		Efficacy ± CI[d]
								Positive Control[b]	Test Coupon[c]	
8	43.50 ± 12.61	STERIS 1000ED	22.98 ± 0.43	76.91 ± 5.45	7.07E+07	1.00	Glass	6.09 ± 1.90 x 10^6	3.37 ± 3.29 x 10^1	5.65 ± 1.11
						2.00			0.00 ± 0.00	≥6.77 ± 0.13
						4.00			0.00 ± 0.00	≥6.77 ± 0.13
						5.00			0.00 ± 0.00	≥6.77 ± 0.13
						6.00			0.00 ± 0.00	≥6.77 ± 0.13
						8.00	Pine Wood	3.75 ± 0.74 x 10^6	2.29 ± 3.79 x 10^1	5.96 ± 1.20
						12.00			2.29 ± 3.79 x 10^1	5.96 ± 1.20
						16.00			2.89 ± 2.22 x 10^2	4.31 ± 0.72
						20.00			6.69 ± 6.60 x 10^1	5.25 ± 1.30
						24.00			0.00 ± 0.00	≥6.57 ± 0.08
						8.00	Carpet	6.85 ± 1.66 x 10^6	8.90 ± 6.96 x 10^1	4.97 ± 0.41
						12.00			0.00 ± 0.00	≥6.83 ± 0.08
						16.00			0.00 ± 0.00	≥6.83 ± 0.08
						20.00			0.00 ± 0.00	≥6.83 ± 0.08
						24.00			0.00 ± 0.00	≥6.83 ± 0.08
						1.00	Painted Wallboard Paper	3.99 ± 1.15 x 10^6	3.25 ± 1.97 x 10^5	1.14 ± 0.35
						2.00			5.87 ± 4.82 x 10^4	2.13 ± 0.94
						4.00			0.00 ± 0.00	≥6.59 ± 0.10
						5.00			0.00 ± 0.00	≥6.59 ± 0.10
						6.00			0.00 ± 0.00	≥6.59 ± 0.10
						8.00	Unpainted Concrete	1.88 ± 1.90 x 10^6	3.05 ± 1.37 x 10^3	2.60 ± 0.50
						12.00			4.27 ± 4.47 x 10^3	2.58 ± 0.66
						16.00			6.11 ± 1.07 x 10^2	3.28 ± 0.45
						20.00			1.52 ± 0.62 x 10^3	2.90 ± 0.49
						24.00			3.55 ± 1.56 x 10^3	2.54 ± 0.51
						1.00	Ceiling Tile	3.11 ± 0.61 x 10^5	3.73 ± 0.75 x 10^4	0.92 ± 0.12
						2.00			4.54± 0.89 x 10^2	1.83 ± 0.12
						4.00			0.00 ± 0.00	≥5.49 ± 0.07
						5.00			0.00 ± 0.00	≥5.49 ± 0.07
						6.00			0.00 ± 0.00	≥5.49 ± 0.07

[a] Data expressed as the mean (± SD) of the logs of the number of spores (CFU) observed on individual samples and decontamination efficacy (log reduction).

[b] Positive Controls = samples inoculated, not decontaminated.

[c] Test Coupons = samples inoculated, decontaminated.

[d] CI = confidence interval (± 1.96 × SE). Results highlighted in yellow signify ≥ 6 LR, and green signifies complete inactivation.

Table A-18. Inactivation of *B. anthracis* Vollum Spores using low level HPV[a] *(Continued)*

Test Number	Concentration (ppm)	Equipment	Temp (°C)	%RH	Inoculum (CFU/coupon)	Contact Time (hours)	Material	Mean Recovered *B. anthracis* (CFU/coupon)		Efficacy ± CI[d]
								Positive Control[b]	Test Coupon[c]	
9	25.22 ± 1.64	Bubbler	23.77 ± 0.40	91.94 ± 14.52	1.24E+08	1.00	Glass	7.01 ± 3.80 x 10^6	1.54 ± 1.01 x 10^5	1.67 ± 0.39
						2.00			2.29 ± 3.79 x 10^1	6.19 ± 1.21
						6.00			0.00 ± 0.00	≥6.79 ± 0.21
						8.00			0.00 ± 0.00	≥6.79 ± 0.21
						12.00			0.00 ± 0.00	≥6.79 ± 0.21
						8.00	Pine Wood	3.69 ± 2.31 x 10^6	2.22 ± 1.35 x 10^2	4.20 ± 0.42
						12.00			3.01 ± 4.37 x 10^4	2.91 ± 1.81
						16.00			1.90 ± 2.13 x 10^3	3.53 ± 0.91
						20.00			1.00 ± 1.56 x 10^3	4.09 ± 1.14
						24.00			2.82 ± 2.81 x 10^3	4.08 ± 2.38
						8.00	Carpet	6.23 ± 1.59 x 10^6	5.78 ± 3.17 x 10^2	4.07 ± 0.32
						12.00			2.11 ± 1.95 x 10^2	4.59 ± 0.48
						16.00			0.00 ± 0.00	≥6.78 ± 0.10
						20.00			0.00 ± 0.00	≥6.78 ± 0.10
						24.00			0.00 ± 0.00	≥6.78 ± 0.10
						1.00	Painted Wallboard Paper	8.19 ± 0.78 x 10^6	6.64 ± 1.98 x 10^5	1.10 ± 0.14
						2.00			1.64 ± 1.12 x 10^5	1.76 ± 0.33
						6.00			0.00 ± 0.00	≥6.91 ± 0.04
						8.00			0.00 ± 0.00	≥6.91 ± 0.04
						12.00			0.00 ± 0.00	≥6.91 ± 0.04
						8.00	Unpainted Concrete	7.78 ± 4.42 x 10^6	4.04 ± 0.65 x 10^4	2.23 ± 0.24
						12.00			1.17 ± 0.15 x 10^4	2.77 ± 0.23
						16.00			3.56 ± 2.72 x 10^2	4.36 ± 0.42
						20.00			5.62 ± 4.90 x 10^3	3.42 ± 1.00
						24.00			2.11 ± 0.84 x 10^2	4.53 ± 0.30
						1.00	Ceiling Tile	1.09 ± 1.48 x 10^6	6.33 ± 1.34 x 10^4	1.02 ± 0.39
						2.00			8.89 ± 2.31 x 10^3	1.88 ± 0.40
						6.00			0.00 ± 0.00	≥5.82 ± 0.38
						8.00			0.00 ± 0.00	≥5.82 ± 0.38
						12.00			0.00 ± 0.00	≥5.82 ± 0.38

[a] Data expressed as the mean (± SD) of the logs of the number of spores (CFU) observed on individual samples and decontamination efficacy (log reduction).

[b] Positive Controls = samples inoculated, not decontaminated.

[c] Test Coupons = samples inoculated, decontaminated.

[d] CI = confidence interval (± 1.96 × SE). Results highlighted in yellow signify ≥ 6 LR, and green signifies complete inactivation.

Appendix B

Efficacy Results Figures

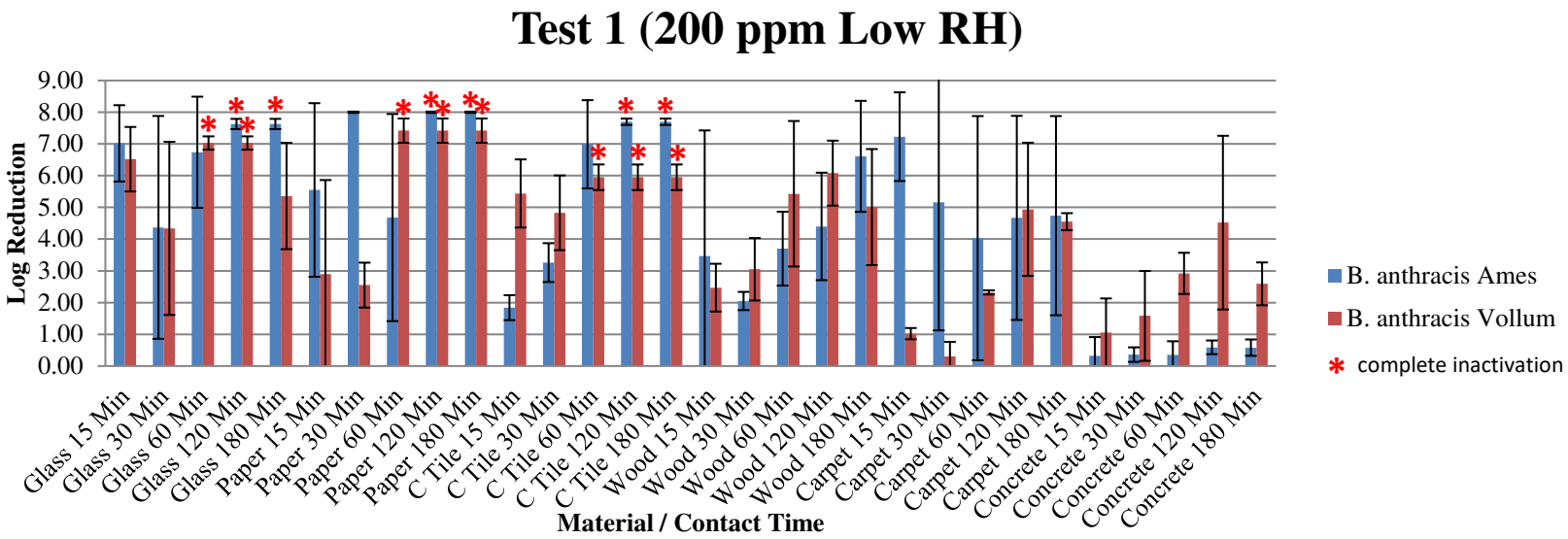

Figure B-1. Summary of efficacy results at 200 ppm and Low RH against *B. anthracis* Ames and Vollum.

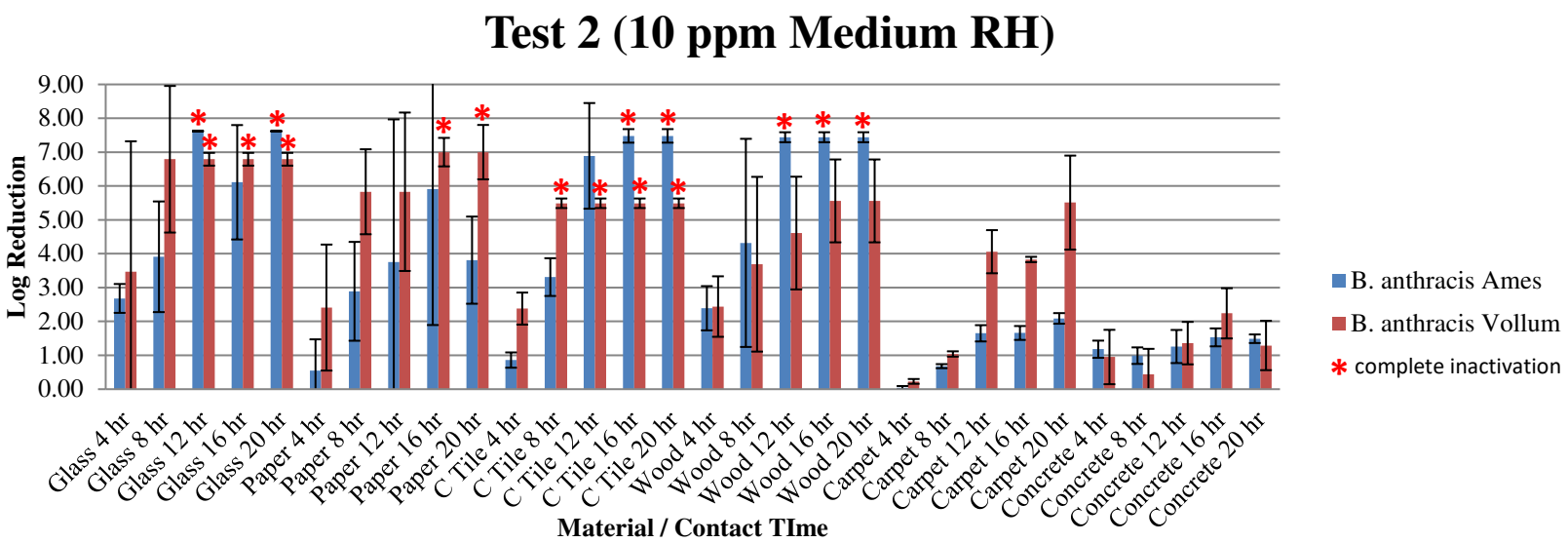

Figure B-2. Summary of efficacy results at 10 ppm and Medium RH against *B. anthracis* Ames and Vollum.

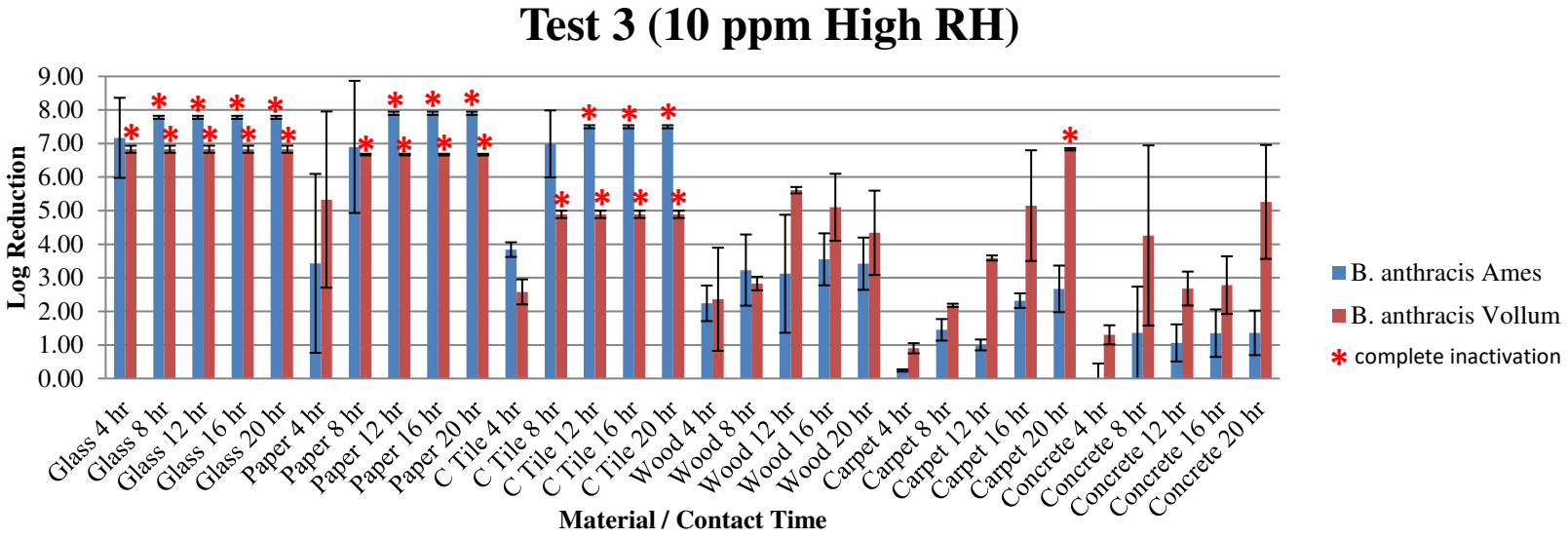

Figure B-3. Summary of efficacy results at 10 ppm and High RH against *B. anthracis* Ames and Vollum.

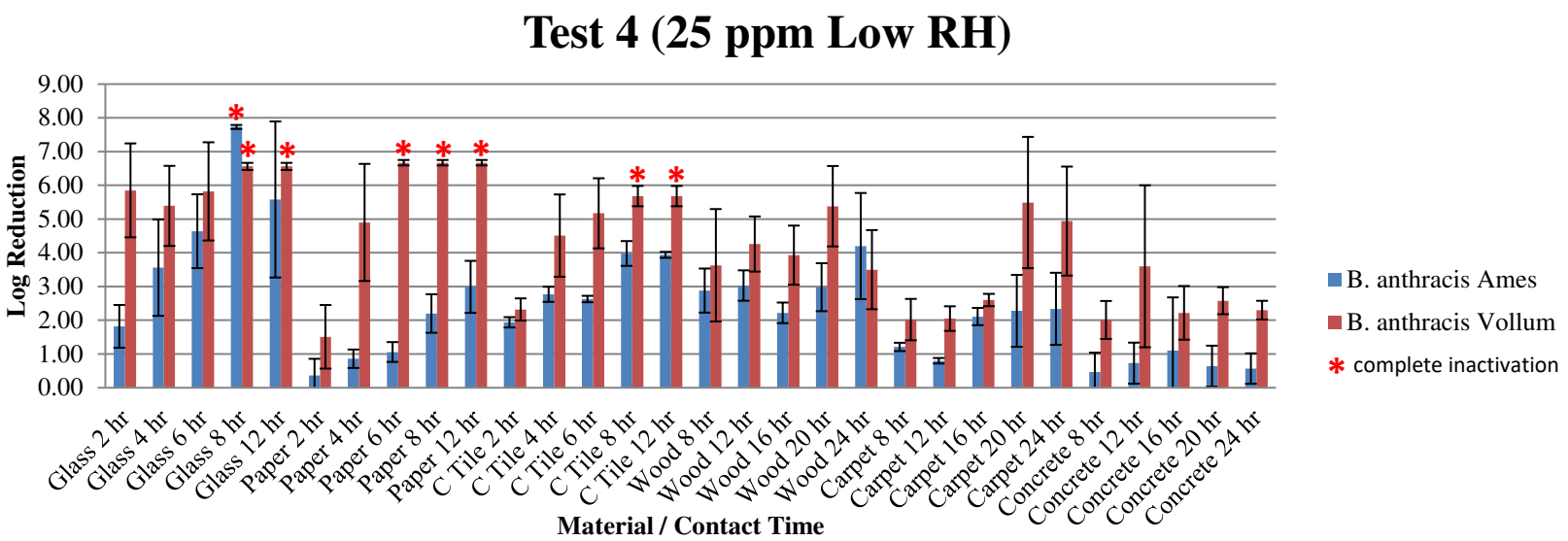

Figure B-4. Summary of efficacy results at 25 ppm and Low RH against *B. anthracis* Ames and Vollum.

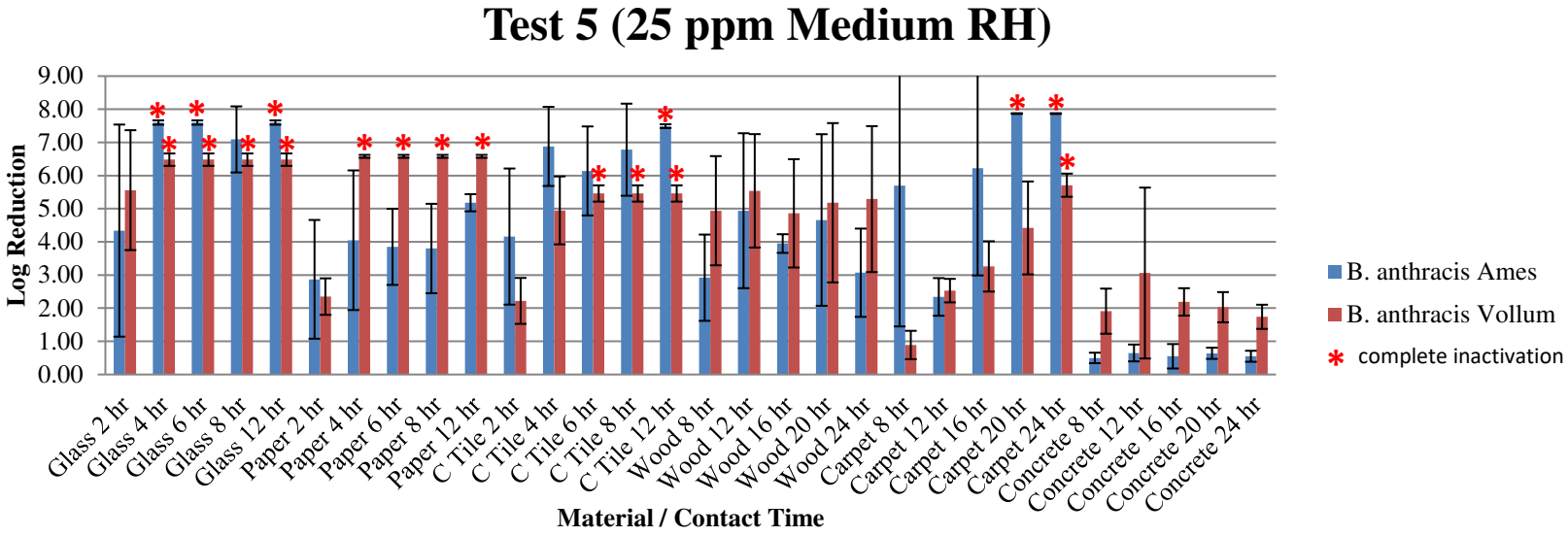

Figure B-5. Summary of efficacy results at 25 ppm and Medium RH against *B. anthracis* Ames and Vollum.

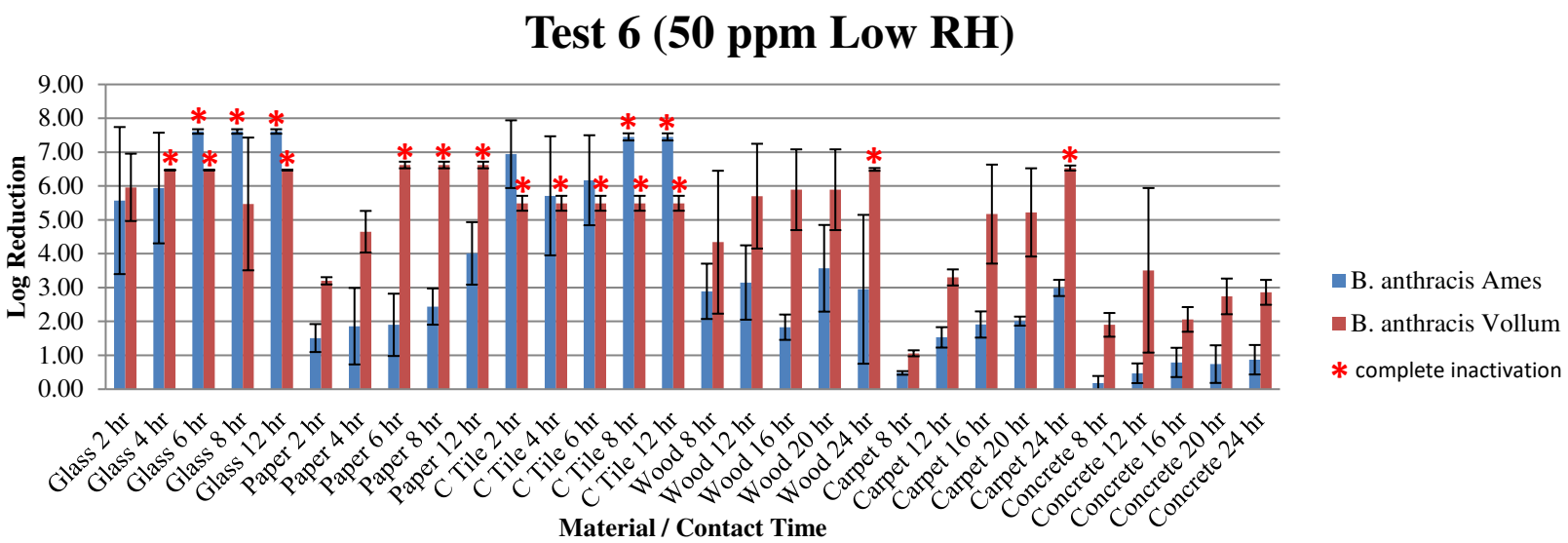

Figure B-6. Summary of efficacy results at 50 ppm and Low RH against *B. anthracis* Ames and Vollum.

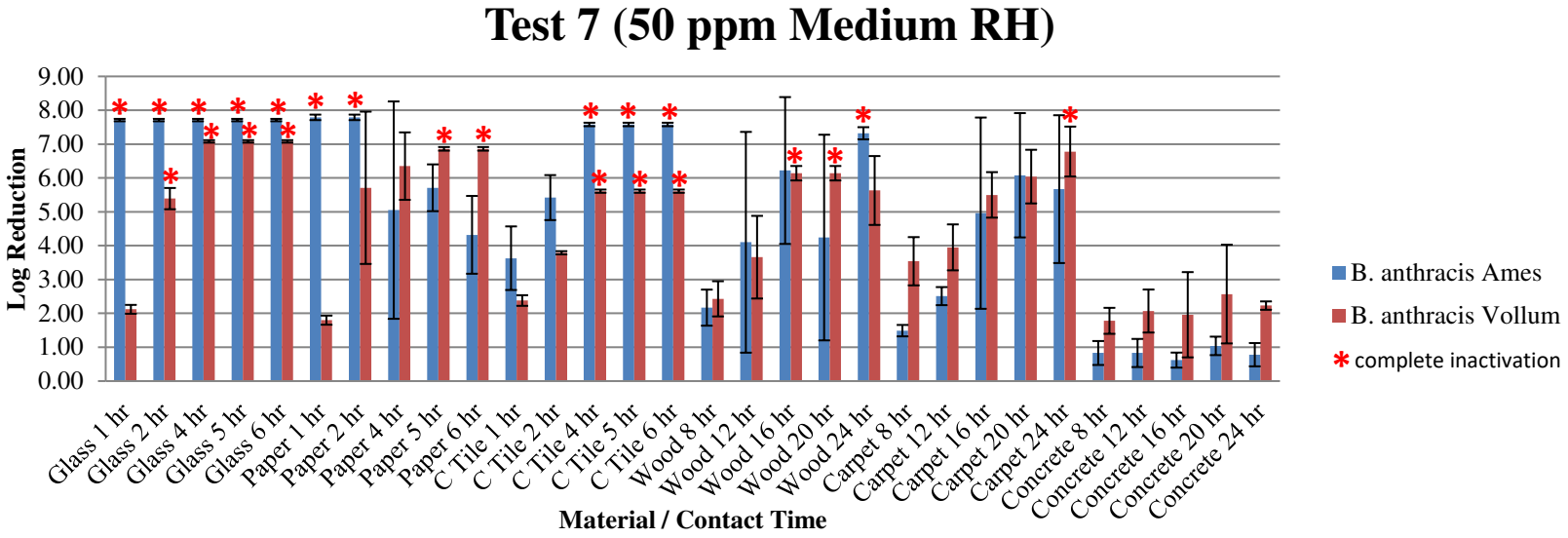

Figure B-7. Summary of efficacy results at 50 ppm and Medium RH against *B. anthracis* Ames and Vollum.

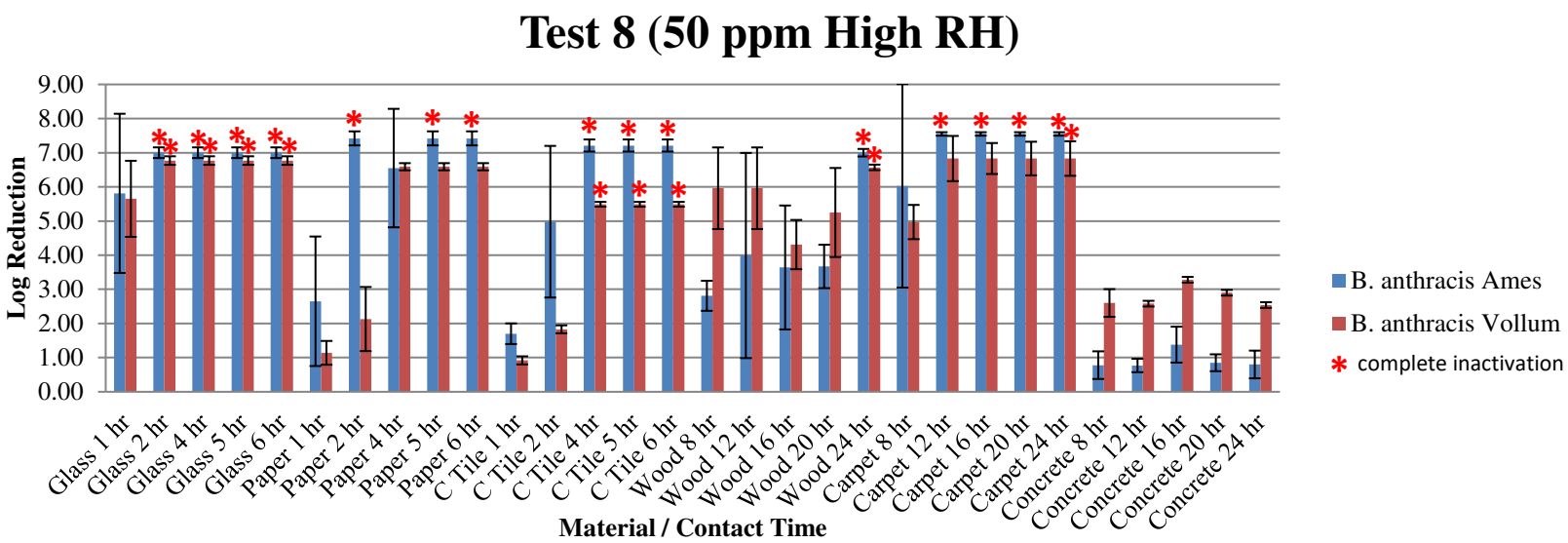

Figure B-8. Summary of efficacy results at 50 ppm and High RH against *B. anthracis* Ames and Vollum.

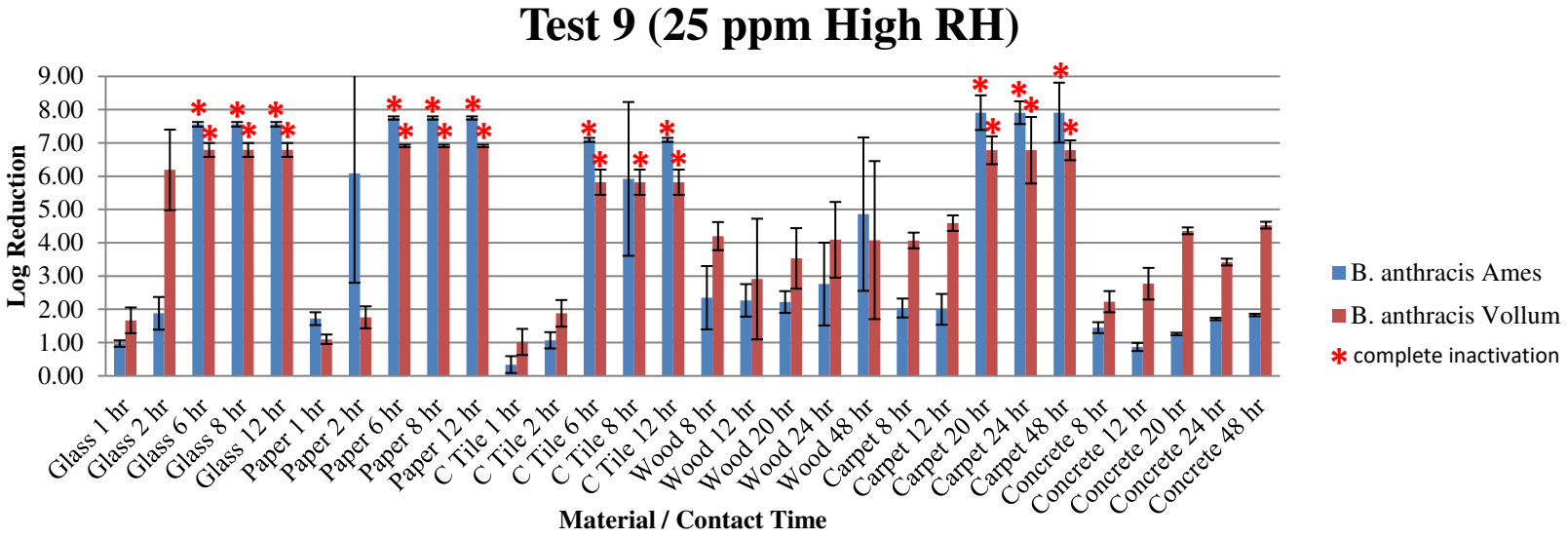

Figure B-9. Summary of efficacy results at 25 ppm and High RH against *B. anthracis* Ames and Vollum.

Appendix C
HPV Dose Requirements for Effective Decontamination

Table C-1. Minimum dose in ppm*hours demonstrating effective decontamination for Ames strain

	Test 1	Test 2	Test 3	Test 4	Test 5	Test 9	Test 6	Test 7	Test 8	Range
Average HPV ppm	222	9-10		25-26			44-50			
Average % RH	38	58	76	33	62	92	26	60	77	
	Minimum Dose in ppm*hours									
Glass	56	120	80	200	100	150	300	50	100	50-200
PW Paper	111	>200	80	>600	>600	50	>1200	100	100	50 - >1200
Ceiling Tile	444	120	80	>600	100	150	100	200	200	80 - >600
Pine Wood	666	120	>200	>600	>600	>1200	>1200	800	1200	120 - >1200
Carpet	56	>200	>200	>600	400	500	>1200	1000	400	>200 - >1200
Concrete	>666	>200	>200	>600	>600	>1200	>1200	>1200	>1200	>200 - >1200

Table C-2. Minimum dose in ppm*hours demonstrating effective decontamination for Vollum strain

	Test 1	Test 2	Test 3	Test 4	Test 5	Test 9	Test 6	Test 7	Test 8	Range
Average HPV ppm	222	9-10		25-26			44-50			
average % RH	38	58	76	33	62	92	26	60	77	
	Minimum Dose in ppm*hours									
Glass	56	80	40	200	100	50	200	200	100	40-200
PW Paper	222	160	80	150	100	150	300	200	200	80-300
Ceiling Tile	222	80	80	200	150	150	100	200	200	80-222
Pine Wood	444	>200	>200	>600	>600	>1200	1200	800	1200	444->1200
Carpet	>666	>200	200	>600	600	500	1200	1000	600	200 - 1200
Concrete	>666	>200	>200	>600	>600	>1200	>1200	>1200	>1200	>200 - >1200

Appendix D

Detailed Statistical Analysis

Introduction

This report contains the statistical analysis of *B. anthracis Ames* (*Ba*A) and *B. anthracis Vollum* (*Ba*V) decontamination data for different decontamination conditions (contact time, HPV concentration, Average RH) on a variety of materials. The study design is presented in Text Table 1. Data were collected in support of EPA Task Order 14 study conducted at the Battelle Biomedical Research Center (BBRC).

Text Table D1. Study Design

Test Number	Equipment	Test Organism	HPV ppm	Temp (ºC)	Average RH	Easy[1] Material Contact Times (h)	Difficult[2] Material Contact Time (h)	Material
1	STERIS (direct)	*Ba* Ames and vollum	200	23	Low	0.25,0.50,1,2,3		Glass, PW Paper, Ceiling Tile, Pine Wood, Carpet, Concrete
2	Bubbler		10	23	Medium	4, 8, 12, 16, 20		
3	Bubbler		10	23	High	4, 8, 12, 16, 20		
4	STERIS (dual chamber)		25	23	Low	2,4,6,8,12	8,12,16,20,24	
5	STERIS (dual chamber)		25	23	Medium	2,4,6,8,12	8,12,16,20,24	
6	STERIS (dual chamber)		50	23	Low	2,4,6,8,12	8,12,16,20,24	
7	STERIS (dual chamber)		50	23	Medium	1,2,4,5,6	8,12,16,20,24	
8	STERIS (single pass)		50	23	High	1,2,4,5,6	8,12,16,20,24	
9	Bubbler		25	23	High	1,2,6,8,12	8,12,20,24, 48	

[1] Glass, PW Paper and Ceiling Tile
[2] Pine Wood, Carpet, Concrete

Statistical Methods

A binary response based on log reduction in spores was the primary endpoint. For this endpoint, a trial was recorded as a success or pass if either: 1) the log10 reduction was greater than or equal to 6, or 2) the log10 recovery was equal to or less than the average control recovery (complete kill). The proportion of tests that pass and 95 percent Clopper-Pearson confidence

intervals were computed by strain (Ames or Vollum), material, contact time, relative humidity, and HPV concentration.
A logistic regression model was fitted to the full data to test whether the proportions of successes are significantly associated with any effects included in the model. The logistic regression model included main effects for strain (Ames or Vollum), material, dose (defined as contact time times HPV concentration), and relative humidity; the model also included all two-factor interactions and the three-factor interactions for dose, strain, and material. An implicit assumption in the analysis is that the effect of dose is the same for any concentration and time used to achieve it.

Results

Text Table 2 contains the proportions of tests that pass for each strain, material, contact time, relative humidity, and HPV concentration with 95 percent Clopper-Pearson confidence intervals.

The joint tests for all effects included in the logistic regression model are presented in Text Table 3. A joint test for an effect of interest is a test that the values of the parameters associated with that effect are zero. As can be seen in Text Table 3, the main effect for material was statistically significant; the two-factor interactions for strain and material, strain and average RH, material and average RH, dose and material, and dose and average RH were also statistically significant as well as the three-factor interaction for dose, strain, and material. Odds ratios were calculated for each effect conditional on the values of the other effects. Figure D1 through Figure D20 present plots of the odds ratios. In these figures, the lines extend to different doses based on the range of doses studied for a given condition; the lines are constrained so as not to extrapolate the odds ratio outside the studied ranges.

Conclusions

Presence of a statistically significant three-factor interaction complicates interpretation of the results, as all results for one of the three factors must be interpreted with respect to the levels of the other two factors. While the main effects for strain, average RH, and dose are not statistically significant, the two-factor interactions involving these factors are statistically significant. Therefore, these factors do impact the probability of a complete kill, but that impact is dependent on the level of another factor. For example, the effect of average RH is dependent on the strain, the material, and the dose.

For all conclusions, a higher odds ratio greater than one is indicative of greater odds of a complete kill for level 1 of the factor compared to level 2. For odds ratios less than one, there are greater odds of a complete kill for level 2 of the factor compared to level 1. An odds ratio equal to one indicates the odds of a complete kill are approximately the same for both levels of the factor. The odds are defined as the ratio of probability of complete kill to the probability of an incomplete kill.

From Figure D1, the odds ratio for bare pine wood is roughly constant at slightly less than one for all levels of dose; thus, the odds ratio does not depend on dose. For bare pine wood, the odds

of a complete kill are greater for Vollum than for Ames. The odds ratio for carpet decreases from approximately 10 to approximately 0.1, indicating that at low dose the odds of a complete kill are greater for Ames while at high dose the odds of a complete kill are greater for Vollum. The odds ratio for unpainted concrete is slightly increasing as dose increases but is always less than one, indicating for all levels of dose the odds of complete kill are greater for Vollum than for Ames. For ceiling tile and painted wallboard paper, the odds ratio is steeply decreasing from between 1 and 10 to between 10^{-2} and 10^{-10}, indicating that at low dose the odds of a complete kill are greater for Ames while at high dose the odds of a complete kill are greater for Vollum. The steep decrease indicates that the ratio between Ames and Vollum decreases as dose increases; the decreasing ratio results in increasing discrepancy between the two strains. Finally, for glass, the odds ratio increases from less than 1 to approximately 100. In this case, the odds of a complete kill are greater for Vollum at low dose but greater for Ames at high dose. The increasing slope indicates the ratio is greater at higher dose. For all materials, the odds ratio is greatest at the medium RH and least at the low RH. This ratio does not indicate that the probability of a complete kill is greatest for the medium RH, only that the ratio of the odds for Ames to Vollum is the greatest, showing the greatest discrepancy between the two odds.

The odds ratios comparing the different materials vary (Figure D2 - Figure D16). For most comparisons, the odds ratio decreases with increasing dose; increasing odds ratios can be transformed to decreasing by reversing the order of the levels and taking the reciprocal of the odds ratio. Thus, the discrepancy between the two materials increases as dose increases. For a few cases, the odds ratio is flat with respect to dose: for Ames on bare pine wood compared to unpainted concrete, for Ames on carpet compared to unpainted concrete, and for Ames on ceiling tile compared to glass. For one case, the odds ratio is increasing with increasing dose: Ames on glass compared to painted wallboard paper. For cases where the odds ratios decrease with increasing dose, the rate of decrease varies between Ames and Vollum. In most cases, the rate of decrease is faster for Vollum than for Ames, indicating the discrepancy between the two materials gets larger faster for Vollum.

The odds ratios for high RH compared to low RH (Figure D17), high RH compared to medium RH (Figure D18), and low RH compared to medium RH (Figure D19) increase with dose. Rate of increase is relatively constant for all strain and material combinations. For each material, the odds ratio is greater for Ames than it is for Vollum. For bare pine wood and unpainted concrete, the odds ratio for high RH to low RH increases from less than 1 to greater than 1 as dose increases, indicating that at low dose the odds of a complete kill are greater for low RH while at high dose the odds of a complete kill are greater for high RH. For all other materials, the odds ratio is always greater than 1, indicating greater odds of a complete kill at high RH compared to low RH. Again, comparing high RH to medium RH, for bare pine wood and unpainted concrete, the odds ratio increases from less than 1 to greater than 1; for all other materials, the odds ratio is always greater than 1. Comparing low RH to medium RH, the odds ratio decreases from greater than 1 to less than 1 for carpet and unpainted concrete. For these materials, the odds of a complete kill are greater for low RH at low dose and are greater for medium RH at high dose. The odds ratio is strictly less than 1 for all other materials, indicating greater odds of a complete kill at medium RH compared to low RH.

Figure D20 investigates the interactions between material, strain, and RH based on a fixed change in dose. The odds ratio for dose compared to a 100-unit increase is greater than 1 for all materials, strains, and RH levels. Thus, the odds of a complete kill are greater as dose increases. The largest odds ratios are observed for ceiling tile and painted wallboard paper, indicating the greatest effect of increasing dose on the odds of a complete kill for these materials. The odds ratio increases as average RH increases.

Text Table D2. Summary of Kill Proportions by Strain, Material, Contact Time, Average RH and HPV Concentration

Strain	Material	Contact Time	Average RH	HPV ppm	Kills/ Trials	Proportion of Kills (95 Percent Confidence Interval)
Ames	Bare Pine Wood	0.25 h	Low	200	1/3	0.33 (0.01, 0.91)
Ames	Bare Pine Wood	0.5 h	Low	200	0/3	0.00 (0.00, 0.71)
Ames	Bare Pine Wood	12 h	High	10	0/3	0.00 (0.00, 0.71)
Ames	Bare Pine Wood	12 h	High	25	0/3	0.00 (0.00, 0.71)
Ames	Bare Pine Wood	12 h	High	50	1/3	0.33 (0.01, 0.91)
Ames	Bare Pine Wood	12 h	Low	25	0/3	0.00 (0.00, 0.71)
Ames	Bare Pine Wood	12 h	Low	50	0/3	0.00 (0.00, 0.71)
Ames	Bare Pine Wood	12 h	Medium	10	3/3	1.00 (0.29, 1.00)
Ames	Bare Pine Wood	12 h	Medium	25	1/3	0.33 (0.01, 0.91)
Ames	Bare Pine Wood	12 h	Medium	50	1/3	0.33 (0.01, 0.91)
Ames	Bare Pine Wood	16 h	High	10	0/3	0.00 (0.00, 0.71)
Ames	Bare Pine Wood	16 h	High	50	0/3	0.00 (0.00, 0.71)
Ames	Bare Pine Wood	16 h	Low	25	0/3	0.00 (0.00, 0.71)
Ames	Bare Pine Wood	16 h	Low	50	0/3	0.00 (0.00, 0.71)
Ames	Bare Pine Wood	16 h	Medium	10	3/3	1.00 (0.29, 1.00)
Ames	Bare Pine Wood	16 h	Medium	25	0/3	0.00 (0.00, 0.71)
Ames	Bare Pine Wood	16 h	Medium	50	2/3	0.67 (0.09, 0.99)
Ames	Bare Pine Wood	1 h	Low	200	0/3	0.00 (0.00, 0.71)
Ames	Bare Pine Wood	20 h	High	10	0/3	0.00 (0.00, 0.71)
Ames	Bare Pine Wood	20 h	High	25	0/3	0.00 (0.00, 0.71)
Ames	Bare Pine Wood	20 h	High	50	0/3	0.00 (0.00, 0.71)
Ames	Bare Pine Wood	20 h	Low	25	0/3	0.00 (0.00, 0.71)

Text Table D2. Continued.

Strain	Material	Contact Time	Average RH	HPV ppm	Kills/ Trials	Proportion of Kills (95 Percent Confidence Interval)
Ames	Bare Pine Wood	20 h	Low	50	0/3	0.00 (0.00, 0.71)
Ames	Bare Pine Wood	20 h	Medium	10	3/3	1.00 (0.29, 1.00)
Ames	Bare Pine Wood	20 h	Medium	25	1/3	0.33 (0.01, 0.91)
Ames	Bare Pine Wood	20 h	Medium	50	1/3	0.33 (0.01, 0.91)
Ames	Bare Pine Wood	24 h	High	25	0/3	0.00 (0.00, 0.71)
Ames	Bare Pine Wood	24 h	High	50	3/3	1.00 (0.29, 1.00)
Ames	Bare Pine Wood	24 h	Low	25	0/3	0.00 (0.00, 0.71)
Ames	Bare Pine Wood	24 h	Low	50	0/3	0.00 (0.00, 0.71)
Ames	Bare Pine Wood	24 h	Medium	25	0/3	0.00 (0.00, 0.71)
Ames	Bare Pine Wood	24 h	Medium	50	3/3	1.00 (0.29, 1.00)
Ames	Bare Pine Wood	2 h	Low	200	0/3	0.00 (0.00, 0.71)
Ames	Bare Pine Wood	3 h	Low	200	2/3	0.67 (0.09, 0.99)
Ames	Bare Pine Wood	48 h	High	25	1/3	0.33 (0.01, 0.91)
Ames	Bare Pine Wood	4 h	High	10	0/3	0.00 (0.00, 0.71)
Ames	Bare Pine Wood	4 h	Medium	10	0/3	0.00 (0.00, 0.71)
Ames	Bare Pine Wood	8 h	High	10	0/3	0.00 (0.00, 0.71)
Ames	Bare Pine Wood	8 h	High	25	0/3	0.00 (0.00, 0.71)
Ames	Bare Pine Wood	8 h	High	50	0/3	0.00 (0.00, 0.71)
Ames	Bare Pine Wood	8 h	Low	25	0/3	0.00 (0.00, 0.71)
Ames	Bare Pine Wood	8 h	Low	50	0/3	0.00 (0.00, 0.71)
Ames	Bare Pine Wood	8 h	Medium	10	1/3	0.33 (0.01, 0.91)
Ames	Bare Pine Wood	8 h	Medium	25	0/3	0.00 (0.00, 0.71)

Text Table D2. Continued.

Strain	Material	Contact Time	Average RH	HPV ppm	Kills/ Trials	Proportion of Kills (95 Percent Confidence Interval)
Ames	Bare Pine Wood	8 h	Medium	50	0/3	0.00 (0.00, 0.71)
Ames	Carpet	0.25 h	Low	200	2/3	0.67 (0.09, 0.99)
Ames	Carpet	0.5 h	Low	200	2/3	0.67 (0.09, 0.99)
Ames	Carpet	12 h	High	10	0/3	0.00 (0.00, 0.71)
Ames	Carpet	12 h	High	25	0/3	0.00 (0.00, 0.71)
Ames	Carpet	12 h	High	50	3/3	1.00 (0.29, 1.00)
Ames	Carpet	12 h	Low	25	0/3	0.00 (0.00, 0.71)
Ames	Carpet	12 h	Low	50	0/3	0.00 (0.00, 0.71)
Ames	Carpet	12 h	Medium	10	0/3	0.00 (0.00, 0.71)
Ames	Carpet	12 h	Medium	25	0/3	0.00 (0.00, 0.71)
Ames	Carpet	12 h	Medium	50	0/3	0.00 (0.00, 0.71)
Ames	Carpet	16 h	High	10	0/3	0.00 (0.00, 0.71)
Ames	Carpet	16 h	High	50	3/3	1.00 (0.29, 1.00)
Ames	Carpet	16 h	Low	25	0/3	0.00 (0.00, 0.71)
Ames	Carpet	16 h	Low	50	0/3	0.00 (0.00, 0.71)
Ames	Carpet	16 h	Medium	10	0/3	0.00 (0.00, 0.71)
Ames	Carpet	16 h	Medium	25	2/3	0.67 (0.09, 0.99)
Ames	Carpet	16 h	Medium	50	1/3	0.33 (0.01, 0.91)
Ames	Carpet	1 h	Low	200	1/3	0.33 (0.01, 0.91)
Ames	Carpet	20 h	High	10	0/3	0.00 (0.00, 0.71)
Ames	Carpet	20 h	High	25	3/3	1.00 (0.29, 1.00)

Text Table D2. Continued.

Strain	Material	Contact Time	Average RH	HPV ppm	Kills/ Trials	Proportion of Kills (95 Percent Confidence Interval)
Ames	Carpet	20 h	Low	25	0/3	0.00 (0.00, 0.71)
Ames	Carpet	20 h	Low	50	0/3	0.00 (0.00, 0.71)
Ames	Carpet	20 h	Medium	10	0/3	0.00 (0.00, 0.71)
Ames	Carpet	20 h	Medium	25	3/3	1.00 (0.29, 1.00)
Ames	Carpet	20 h	Medium	50	1/3	0.33 (0.01, 0.91)
Ames	Carpet	24 h	High	25	3/3	1.00 (0.29, 1.00)
Ames	Carpet	24 h	High	50	3/3	1.00 (0.29, 1.00)
Ames	Carpet	24 h	Low	25	0/3	0.00 (0.00, 0.71)
Ames	Carpet	24 h	Low	50	0/3	0.00 (0.00, 0.71)
Ames	Carpet	24 h	Medium	25	3/3	1.00 (0.29, 1.00)
Ames	Carpet	24 h	Medium	50	1/3	0.33 (0.01, 0.91)
Ames	Carpet	2 h	Low	200	1/3	0.33 (0.01, 0.91)
Ames	Carpet	3 h	Low	200	1/3	0.33 (0.01, 0.91)
Ames	Carpet	48 h	High	25	3/3	1.00 (0.29, 1.00)
Ames	Carpet	4 h	High	10	0/3	0.00 (0.00, 0.71)
Ames	Carpet	4 h	Medium	10	0/3	0.00 (0.00, 0.71)
Ames	Carpet	8 h	High	10	0/3	0.00 (0.00, 0.71)
Ames	Carpet	8 h	High	25	0/3	0.00 (0.00, 0.71)
Ames	Carpet	8 h	High	50	2/3	0.67 (0.09, 0.99)
Ames	Carpet	8 h	Low	25	0/3	0.00 (0.00, 0.71)
Ames	Carpet	8 h	Low	50	0/3	0.00 (0.00, 0.71)

Text Table D2. Continued.

Strain	Material	Contact Time	Average RH	HPV ppm	Kills/ Trials	Proportion of Kills (95 Percent Confidence Interval)
Ames	Carpet	8 h	Medium	10	0/3	0.00 (0.00, 0.71)
Ames	Carpet	8 h	Medium	25	2/3	0.67 (0.09, 0.99)
Ames	Carpet	8 h	Medium	50	0/3	0.00 (0.00, 0.71)
Ames	Ceiling Tile	0.25 h	Low	200	0/3	0.00 (0.00, 0.71)
Ames	Ceiling Tile	0.5 h	Low	200	0/3	0.00 (0.00, 0.71)
Ames	Ceiling Tile	12 h	High	10	3/3	1.00 (0.29, 1.00)
Ames	Ceiling Tile	12 h	High	25	3/3	1.00 (0.29, 1.00)
Ames	Ceiling Tile	12 h	Low	25	0/3	0.00 (0.00, 0.71)
Ames	Ceiling Tile	12 h	Low	50	3/3	1.00 (0.29, 1.00)
Ames	Ceiling Tile	12 h	Medium	10	2/3	0.67 (0.09, 0.99)
Ames	Ceiling Tile	12 h	Medium	25	3/3	1.00 (0.29, 1.00)
Ames	Ceiling Tile	16 h	High	10	3/3	1.00 (0.29, 1.00)
Ames	Ceiling Tile	16 h	Medium	10	3/3	1.00 (0.29, 1.00)
Ames	Ceiling Tile	1 h	High	25	0/3	0.00 (0.00, 0.71)
Ames	Ceiling Tile	1 h	High	50	0/3	0.00 (0.00, 0.71)
Ames	Ceiling Tile	1 h	Low	200	2/3	0.67 (0.09, 0.99)
Ames	Ceiling Tile	1 h	Medium	50	0/3	0.00 (0.00, 0.71)
Ames	Ceiling Tile	20 h	High	10	3/3	1.00 (0.29, 1.00)
Ames	Ceiling Tile	20 h	Medium	10	3/3	1.00 (0.29, 1.00)
Ames	Ceiling Tile	2 h	High	25	0/3	0.00 (0.00, 0.71)
Ames	Ceiling Tile	2 h	High	50	1/3	0.33 (0.01, 0.91)

Text Table D2. Continued.

Strain	Material	Contact Time	Average RH	HPV ppm	Kills/ Trials	Proportion of Kills (95 Percent Confidence Interval)
Ames	Ceiling Tile	2 h	Low	25	0/3	0.00 (0.00, 0.71)
Ames	Ceiling Tile	2 h	Low	50	2/3	0.67 (0.09, 0.99)
Ames	Ceiling Tile	2 h	Low	200	3/3	1.00 (0.29, 1.00)
Ames	Ceiling Tile	2 h	Medium	25	0/3	0.00 (0.00, 0.71)
Ames	Ceiling Tile	2 h	Medium	50	1/3	0.33 (0.01, 0.91)
Ames	Ceiling Tile	3 h	Low	200	3/3	1.00 (0.29, 1.00)
Ames	Ceiling Tile	4 h	High	10	0/3	0.00 (0.00, 0.71)
Ames	Ceiling Tile	4 h	High	50	3/3	1.00 (0.29, 1.00)
Ames	Ceiling Tile	4 h	Low	25	0/3	0.00 (0.00, 0.71)
Ames	Ceiling Tile	4 h	Low	50	1/3	0.33 (0.01, 0.91)
Ames	Ceiling Tile	4 h	Medium	10	0/3	0.00 (0.00, 0.71)
Ames	Ceiling Tile	4 h	Medium	25	2/3	0.67 (0.09, 0.99)
Ames	Ceiling Tile	4 h	Medium	50	3/3	1.00 (0.29, 1.00)
Ames	Ceiling Tile	5 h	High	50	3/3	1.00 (0.29, 1.00)
Ames	Ceiling Tile	5 h	Medium	50	3/3	1.00 (0.29, 1.00)
Ames	Ceiling Tile	6 h	High	25	3/3	1.00 (0.29, 1.00)
Ames	Ceiling Tile	6 h	High	50	3/3	1.00 (0.29, 1.00)
Ames	Ceiling Tile	6 h	Low	25	0/3	0.00 (0.00, 0.71)
Ames	Ceiling Tile	6 h	Low	50	1/3	0.33 (0.01, 0.91)
Ames	Ceiling Tile	6 h	Medium	25	1/3	0.33 (0.01, 0.91)
Ames	Ceiling Tile	6 h	Medium	50	3/3	1.00 (0.29, 1.00)

Text Table D2. Continued.

Strain	Material	Contact Time	Average RH	HPV ppm	Kills/ Trials	Proportion of Kills (95 Percent Confidence Interval)
Ames	Ceiling Tile	8Hr	High	10	2/3	0.67 (0.09, 0.99)
Ames	Ceiling Tile	8Hr	High	25	2/3	0.67 (0.09, 0.99)
Ames	Ceiling Tile	8Hr	Low	25	0/3	0.00 (0.00, 0.71)
Ames	Ceiling Tile	8Hr	Low	50	3/3	1.00 (0.29, 1.00)
Ames	Ceiling Tile	8Hr	Medium	10	0/3	0.00 (0.00, 0.71)
Ames	Ceiling Tile	8Hr	Medium	25	2/3	0.67 (0.09, 0.99)
Ames	Glass	0.25Hr	Low	200	2/3	0.67 (0.09, 0.99)
Ames	Glass	0.5Hr	Low	200	1/3	0.33 (0.01, 0.91)
Ames	Glass	12Hr	High	10	3/3	1.00 (0.29, 1.00)
Ames	Glass	12Hr	High	25	3/3	1.00 (0.29, 1.00)
Ames	Glass	12Hr	Low	25	1/3	0.33 (0.01, 0.91)
Ames	Glass	12Hr	Low	50	3/3	1.00 (0.29, 1.00)
Ames	Glass	12Hr	Medium	10	3/3	1.00 (0.29, 1.00)
Ames	Glass	12Hr	Medium	25	3/3	1.00 (0.29, 1.00)
Ames	Glass	16Hr	High	10	3/3	1.00 (0.29, 1.00)
Ames	Glass	16Hr	Medium	10	2/3	0.67 (0.09, 0.99)
Ames	Glass	1Hr	High	25	0/3	0.00 (0.00, 0.71)
Ames	Glass	1Hr	High	50	2/3	0.67 (0.09, 0.99)
Ames	Glass	1Hr	Low	200	2/3	0.67 (0.09, 0.99)
Ames	Glass	1Hr	Medium	50	3/3	1.00 (0.29, 1.00)
Ames	Glass	20Hr	High	10	3/3	1.00 (0.29, 1.00)

Text Table D2. Continued.

Strain	Material	Contact Time	Average RH	HPV ppm	Kills/ Trials	Proportion of Kills (95 Percent Confidence Interval)
Ames	Glass	20 h	Medium	10	3/3	1.00 (0.29, 1.00)
Ames	Glass	2 h	High	25	0/3	0.00 (0.00, 0.71)
Ames	Glass	2 h	High	50	3/3	1.00 (0.29, 1.00)
Ames	Glass	2 h	Low	25	0/3	0.00 (0.00, 0.71)
Ames	Glass	2 h	Low	50	1/3	0.33 (0.01, 0.91)
Ames	Glass	2 h	Low	200	3/3	1.00 (0.29, 1.00)
Ames	Glass	2 h	Medium	25	1/3	0.33 (0.01, 0.91)
Ames	Glass	2 h	Medium	50	3/3	1.00 (0.29, 1.00)
Ames	Glass	3 h	Low	200	3/3	1.00 (0.29, 1.00)
Ames	Glass	4 h	High	10	2/3	0.67 (0.09, 0.99)
Ames	Glass	4 h	High	50	3/3	1.00 (0.29, 1.00)
Ames	Glass	4 h	Low	25	0/3	0.00 (0.00, 0.71)
Ames	Glass	4 h	Low	50	1/3	0.33 (0.01, 0.91)
Ames	Glass	4 h	Medium	10	0/3	0.00 (0.00, 0.71)
Ames	Glass	4 h	Medium	25	3/3	1.00 (0.29, 1.00)
Ames	Glass	4 h	Medium	50	3/3	1.00 (0.29, 1.00)
Ames	Glass	5Hr	High	50	3/3	1.00 (0.29, 1.00)
Ames	Glass	5Hr	Medium	50	3/3	1.00 (0.29, 1.00)
Ames	Glass	6Hr	High	25	3/3	1.00 (0.29, 1.00)
Ames	Glass	6Hr	High	50	3/3	1.00 (0.29, 1.00)
Ames	Glass	6Hr	Low	25	0/3	0.00 (0.00, 0.71)

Text Table D2. Continued.

Strain	Material	Contact Time	Average RH	HPV ppm	Kills/ Trials	Proportion of Kills (95 Percent Confidence Interval)
Ames	Glass	6 h	Low	50	3/3	1.00 (0.29, 1.00)
Ames	Glass	6 h	Medium	25	3/3	1.00 (0.29, 1.00)
Ames	Glass	6 h	Medium	50	3/3	1.00 (0.29, 1.00)
Ames	Glass	8 h	High	10	3/3	1.00 (0.29, 1.00)
Ames	Glass	8 h	High	25	3/3	1.00 (0.29, 1.00)
Ames	Glass	8 h	Low	25	3/3	1.00 (0.29, 1.00)
Ames	Glass	8 h	Low	50	3/3	1.00 (0.29, 1.00)
Ames	Glass	8 h	Medium	10	0/3	0.00 (0.00, 0.71)
Ames	Glass	8 h	Medium	25	3/3	1.00 (0.29, 1.00)
Ames	Painted Wallboard Paper	0.25 h	Low	200	1/3	0.33 (0.01, 0.91)
Ames	Painted Wallboard Paper	0.5 h	Low	200	3/3	1.00 (0.29, 1.00)
Ames	Painted Wallboard Paper	12 h	High	10	3/3	1.00 (0.29, 1.00)
Ames	Painted Wallboard Paper	12 h	High	25	3/3	1.00 (0.29, 1.00)
Ames	Painted Wallboard Paper	12 h	Low	25	0/3	0.00 (0.00, 0.71)
Ames	Painted Wallboard Paper	12 h	Low	50	0/3	0.00 (0.00, 0.71)
Ames	Painted Wallboard Paper	12 h	Medium	10	1/3	0.33 (0.01, 0.91)
Ames	Painted Wallboard Paper	12 h	Medium	25	0/3	0.00 (0.00, 0.71)
Ames	Painted Wallboard Paper	16 h	High	10	3/3	1.00 (0.29, 1.00)
Ames	Painted Wallboard Paper	16 h	Medium	10	2/3	0.67 (0.09, 0.99)
Ames	Painted Wallboard Paper	1 h	High	25	0/3	0.00 (0.00, 0.71)
Ames	Painted Wallboard Paper	1 h	High	50	0/3	0.00 (0.00, 0.71)

Text Table D2. Continued.

Strain	Material	Contact Time	Average RH	HPV ppm	Kills/ Trials	Proportion of Kills (95 Percent Confidence Interval)
Ames	Painted Wallboard Paper	1 h	Low	200	1/3	0.33 (0.01, 0.91)
Ames	Painted Wallboard Paper	1 h	Medium	50	3/3	1.00 (0.29, 1.00)
Ames	Painted Wallboard Paper	20 h	High	10	3/3	1.00 (0.29, 1.00)
Ames	Painted Wallboard Paper	20 h	Medium	10	0/3	0.00 (0.00, 0.71)
Ames	Painted Wallboard Paper	2 h	High	25	2/3	0.67 (0.09, 0.99)
Ames	Painted Wallboard Paper	2 h	High	50	3/3	1.00 (0.29, 1.00)
Ames	Painted Wallboard Paper	2 h	Low	25	0/3	0.00 (0.00, 0.71)
Ames	Painted Wallboard Paper	2 h	Low	50	0/3	0.00 (0.00, 0.71)
Ames	Painted Wallboard Paper	2 h	Low	200	3/3	1.00 (0.29, 1.00)
Ames	Painted Wallboard Paper	2 h	Medium	25	0/3	0.00 (0.00, 0.71)
Ames	Painted Wallboard Paper	2 h	Medium	50	3/3	1.00 (0.29, 1.00)
Ames	Painted Wallboard Paper	3 h	Low	200	3/3	1.00 (0.29, 1.00)
Ames	Painted Wallboard Paper	4 h	High	10	0/3	0.00 (0.00, 0.71)
Ames	Painted Wallboard Paper	4 h	High	50	2/3	0.67 (0.09, 0.99)
Ames	Painted Wallboard Paper	4 h	Low	25	0/3	0.00 (0.00, 0.71)
Ames	Painted Wallboard Paper	4 h	Low	50	0/3	0.00 (0.00, 0.71)
Ames	Painted Wallboard Paper	4 h	Medium	10	0/3	0.00 (0.00, 0.71)
Ames	Painted Wallboard Paper	4 h	Medium	25	1/3	0.33 (0.01, 0.91)
Ames	Painted Wallboard Paper	4 h	Medium	50	1/3	0.33 (0.01, 0.91)
Ames	Painted Wallboard Paper	5 h	High	50	3/3	1.00 (0.29, 1.00)
Ames	Painted Wallboard Paper	5 h	Medium	50	1/3	0.33 (0.01, 0.91)

Text Table D2. Continued.

Strain	Material	Contact Time	Average RH	HPV ppm	Kills/ Trials	Proportion of Kills (95 Percent Confidence Interval)
Ames	Painted Wallboard Paper	6 h	High	25	3/3	1.00 (0.29, 1.00)
Ames	Painted Wallboard Paper	6 h	High	50	3/3	1.00 (0.29, 1.00)
Ames	Painted Wallboard Paper	6 h	Low	25	0/3	0.00 (0.00, 0.71)
Ames	Painted Wallboard Paper	6 h	Low	50	0/3	0.00 (0.00, 0.71)
Ames	Painted Wallboard Paper	6 h	Medium	25	0/3	0.00 (0.00, 0.71)
Ames	Painted Wallboard Paper	6 h	Medium	50	0/3	0.00 (0.00, 0.71)
Ames	Painted Wallboard Paper	8 h	High	10	2/3	0.67 (0.09, 0.99)
Ames	Painted Wallboard Paper	8 h	High	25	3/3	1.00 (0.29, 1.00)
Ames	Painted Wallboard Paper	8 h	Low	25	0/3	0.00 (0.00, 0.71)
Ames	Painted Wallboard Paper	8 h	Low	50	0/3	0.00 (0.00, 0.71)
Ames	Painted Wallboard Paper	8 h	Medium	10	0/3	0.00 (0.00, 0.71)
Ames	Painted Wallboard Paper	8 h	Medium	25	0/3	0.00 (0.00, 0.71)
Ames	Unpainted Concrete	0.25 h	Low	200	0/3	0.00 (0.00, 0.71)
Ames	Unpainted Concrete	0.5 h	Low	200	0/3	0.00 (0.00, 0.71)
Ames	Unpainted Concrete	12 h	High	10	0/3	0.00 (0.00, 0.71)
Ames	Unpainted Concrete	12 h	High	25	0/3	0.00 (0.00, 0.71)
Ames	Unpainted Concrete	12 h	High	50	0/3	0.00 (0.00, 0.71)
Ames	Unpainted Concrete	12 h	Low	25	0/3	0.00 (0.00, 0.71)
Ames	Unpainted Concrete	12 h	Low	50	0/3	0.00 (0.00, 0.71)
Ames	Unpainted Concrete	12 h	Medium	10	0/3	0.00 (0.00, 0.71)
Ames	Unpainted Concrete	12 h	Medium	25	0/3	0.00 (0.00, 0.71)

Text Table D2. Continued.

Strain	Material	Contact Time	Average RH	HPV ppm	Kills/ Trials	Proportion of Kills (95 Percent Confidence Interval)
Ames	Unpainted Concrete	12 h	Medium	50	0/3	0.00 (0.00, 0.71)
Ames	Unpainted Concrete	16 h	High	10	0/3	0.00 (0.00, 0.71)
Ames	Unpainted Concrete	16 h	High	50	0/3	0.00 (0.00, 0.71)
Ames	Unpainted Concrete	16 h	Low	25	0/3	0.00 (0.00, 0.71)
Ames	Unpainted Concrete	16 h	Low	50	0/3	0.00 (0.00, 0.71)
Ames	Unpainted Concrete	16 h	Medium	10	0/3	0.00 (0.00, 0.71)
Ames	Unpainted Concrete	16 h	Medium	25	0/3	0.00 (0.00, 0.71)
Ames	Unpainted Concrete	16 h	Medium	50	0/3	0.00 (0.00, 0.71)
Ames	Unpainted Concrete	1 h	Low	200	0/3	0.00 (0.00, 0.71)
Ames	Unpainted Concrete	20 h	High	10	0/3	0.00 (0.00, 0.71)
Ames	Unpainted Concrete	20 h	High	25	0/3	0.00 (0.00, 0.71)
Ames	Unpainted Concrete	20 h	High	50	0/3	0.00 (0.00, 0.71)
Ames	Unpainted Concrete	20 h	Low	25	0/3	0.00 (0.00, 0.71)
Ames	Unpainted Concrete	20 h	Low	50	0/3	0.00 (0.00, 0.71)
Ames	Unpainted Concrete	20 h	Medium	10	0/3	0.00 (0.00, 0.71)
Ames	Unpainted Concrete	20 h	Medium	25	0/3	0.00 (0.00, 0.71)
Ames	Unpainted Concrete	20 h	Medium	50	0/3	0.00 (0.00, 0.71)
Ames	Unpainted Concrete	24 h	High	25	0/3	0.00 (0.00, 0.71)
Ames	Unpainted Concrete	24 h	High	50	0/3	0.00 (0.00, 0.71)
Ames	Unpainted Concrete	24 h	Low	25	0/3	0.00 (0.00, 0.71)
Ames	Unpainted Concrete	24 h	Low	50	0/3	0.00 (0.00, 0.71)

Text Table D2. Continued.

Strain	Material	Contact Time	Average RH	HPV ppm	Kills/ Trials	Proportion of Kills (95 Percent Confidence Interval)
Ames	Unpainted Concrete	24 h	Medium	25	0/3	0.00 (0.00, 0.71)
Ames	Unpainted Concrete	24 h	Medium	50	0/3	0.00 (0.00, 0.71)
Ames	Unpainted Concrete	2 h	Low	200	0/3	0.00 (0.00, 0.71)
Ames	Unpainted Concrete	3 h	Low	200	0/3	0.00 (0.00, 0.71)
Ames	Unpainted Concrete	48 h	High	25	0/3	0.00 (0.00, 0.71)
Ames	Unpainted Concrete	4 h	High	10	0/3	0.00 (0.00, 0.71)
Ames	Unpainted Concrete	4 h	Medium	10	0/3	0.00 (0.00, 0.71)
Ames	Unpainted Concrete	8 h	High	10	0/3	0.00 (0.00, 0.71)
Ames	Unpainted Concrete	8 h	High	25	0/3	0.00 (0.00, 0.71)
Ames	Unpainted Concrete	8 h	High	50	0/3	0.00 (0.00, 0.71)
Ames	Unpainted Concrete	8 h	Low	25	0/3	0.00 (0.00, 0.71)
Ames	Unpainted Concrete	8 h	Low	50	0/3	0.00 (0.00, 0.71)
Ames	Unpainted Concrete	8 h	Medium	10	0/3	0.00 (0.00, 0.71)
Ames	Unpainted Concrete	8 h	Medium	25	0/3	0.00 (0.00, 0.71)
Ames	Unpainted Concrete	8 h	Medium	50	0/3	0.00 (0.00, 0.71)
Voll	Bare Pine Wood	0.25 h	Low	200	0/3	0.00 (0.00, 0.71)
Voll	Bare Pine Wood	0.5 h	Low	200	0/3	0.00 (0.00, 0.71)
Voll	Bare Pine Wood	12 h	High	10	3/3	1.00 (0.29, 1.00)
Voll	Bare Pine Wood	12 h	High	25	0/3	0.00 (0.00, 0.71)
Voll	Bare Pine Wood	12 h	High	50	2/3	0.67 (0.09, 0.99)
Voll	Bare Pine Wood	12 h	Low	25	0/3	0.00 (0.00, 0.71)

Text Table D2. Continued.

Strain	Material	Contact Time	Average RH	HPV ppm	Kills/ Trials	Proportion of Kills (95 Percent Confidence Interval)
Voll	Bare Pine Wood	12 h	Low	50	2/3	0.67 (0.09, 0.99)
Voll	Bare Pine Wood	12 h	Medium	10	1/3	0.33 (0.01, 0.91)
Voll	Bare Pine Wood	12 h	Medium	25	2/3	0.67 (0.09, 0.99)
Voll	Bare Pine Wood	12 h	Medium	50	0/3	0.00 (0.00, 0.71)
Voll	Bare Pine Wood	16 h	High	10	2/3	0.67 (0.09, 0.99)
Voll	Bare Pine Wood	16 h	High	50	0/3	0.00 (0.00, 0.71)
Voll	Bare Pine Wood	16 h	Low	25	0/3	0.00 (0.00, 0.71)
Voll	Bare Pine Wood	16 h	Low	50	2/3	0.67 (0.09, 0.99)
Voll	Bare Pine Wood	16 h	Medium	10	2/3	0.67 (0.09, 0.99)
Voll	Bare Pine Wood	16 h	Medium	25	1/3	0.33 (0.01, 0.91)
Voll	Bare Pine Wood	16 h	Medium	50	3/3	1.00 (0.29, 1.00)
Voll	Bare Pine Wood	1 h	Low	200	2/3	0.67 (0.09, 0.99)
Voll	Bare Pine Wood	20 h	High	10	1/3	0.33 (0.01, 0.91)
Voll	Bare Pine Wood	20 h	High	25	0/3	0.00 (0.00, 0.71)
Voll	Bare Pine Wood	20 h	High	50	1/3	0.33 (0.01, 0.91)
Voll	Bare Pine Wood	20 h	Low	25	1/3	0.33 (0.01, 0.91)
Voll	Bare Pine Wood	20 h	Low	50	2/3	0.67 (0.09, 0.99)
Voll	Bare Pine Wood	20 h	Medium	10	2/3	0.67 (0.09, 0.99)
Voll	Bare Pine Wood	20 h	Medium	25	2/3	0.67 (0.09, 0.99)
Voll	Bare Pine Wood	20 h	Medium	50	3/3	1.00 (0.29, 1.00)
Voll	Bare Pine Wood	24 h	High	25	0/3	0.00 (0.00, 0.71)

Text Table D2. Continued.

Strain	Material	Contact Time	Average RH	HPV ppm	Kills/ Trials	Proportion of Kills (95 Percent Confidence Interval)
Voll	Bare Pine Wood	24 h	High	50	3/3	1.00 (0.29, 1.00)
Voll	Bare Pine Wood	24 h	Low	25	0/3	0.00 (0.00, 0.71)
Voll	Bare Pine Wood	24 h	Low	50	3/3	1.00 (0.29, 1.00)
Voll	Bare Pine Wood	24 h	Medium	25	2/3	0.67 (0.09, 0.99)
Voll	Bare Pine Wood	24 h	Medium	50	2/3	0.67 (0.09, 0.99)
Voll	Bare Pine Wood	2 h	Low	200	2/3	0.67 (0.09, 0.99)
Voll	Bare Pine Wood	3 h	Low	200	1/3	0.33 (0.01, 0.91)
Voll	Bare Pine Wood	48 h	High	25	1/3	0.33 (0.01, 0.91)
Voll	Bare Pine Wood	4 h	High	10	0/3	0.00 (0.00, 0.71)
Voll	Bare Pine Wood	4 h	Medium	10	0/3	0.00 (0.00, 0.71)
Voll	Bare Pine Wood	8 h	High	10	0/3	0.00 (0.00, 0.71)
Voll	Bare Pine Wood	8 h	High	25	0/3	0.00 (0.00, 0.71)
Voll	Bare Pine Wood	8 h	High	50	2/3	0.67 (0.09, 0.99)
Voll	Bare Pine Wood	8 h	Low	25	0/3	0.00 (0.00, 0.71)
Voll	Bare Pine Wood	8 h	Low	50	1/3	0.33 (0.01, 0.91)
Voll	Bare Pine Wood	8 h	Medium	10	1/3	0.33 (0.01, 0.91)
Voll	Bare Pine Wood	8 h	Medium	25	1/3	0.33 (0.01, 0.91)
Voll	Bare Pine Wood	8 h	Medium	50	0/3	0.00 (0.00, 0.71)
Voll	Carpet	0.25 h	Low	200	0/3	0.00 (0.00, 0.71)
Voll	Carpet	0.5 h	Low	200	0/3	0.00 (0.00, 0.71)
Voll	Carpet	12 h	High	10	0/3	0.00 (0.00, 0.71)

Text Table D2. Continued.

Strain	Material	Contact Time	Average RH	HPV ppm	Kills/ Trials	Proportion of Kills (95 Percent Confidence Interval)
Voll	Carpet	12 h	High	25	0/3	0.00 (0.00, 0.71)
Voll	Carpet	12 h	High	50	3/3	1.00 (0.29, 1.00)
Voll	Carpet	12 h	Low	25	0/3	0.00 (0.00, 0.71)
Voll	Carpet	12 h	Low	50	0/3	0.00 (0.00, 0.71)
Voll	Carpet	12 h	Medium	10	0/3	0.00 (0.00, 0.71)
Voll	Carpet	12 h	Medium	25	0/3	0.00 (0.00, 0.71)
Voll	Carpet	12 h	Medium	50	0/3	0.00 (0.00, 0.71)
Voll	Carpet	16 h	High	10	1/3	0.33 (0.01, 0.91)
Voll	Carpet	16 h	High	50	3/3	1.00 (0.29, 1.00)
Voll	Carpet	16 h	Low	25	0/3	0.00 (0.00, 0.71)
Voll	Carpet	16 h	Low	50	1/3	0.33 (0.01, 0.91)
Voll	Carpet	16 h	Medium	10	0/3	0.00 (0.00, 0.71)
Voll	Carpet	16 h	Medium	25	0/3	0.00 (0.00, 0.71)
Voll	Carpet	16 h	Medium	50	1/3	0.33 (0.01, 0.91)
Voll	Carpet	1 h	Low	200	0/3	0.00 (0.00, 0.71)
Voll	Carpet	20 h	High	10	3/3	1.00 (0.29, 1.00)
Voll	Carpet	20 h	High	25	3/3	1.00 (0.29, 1.00)
Voll	Carpet	20 h	High	50	3/3	1.00 (0.29, 1.00)
Voll	Carpet	20 h	Low	25	2/3	0.67 (0.09, 0.99)
Voll	Carpet	20 h	Low	50	1/3	0.33 (0.01, 0.91)
Voll	Carpet	20 h	Medium	10	1/3	0.33 (0.01, 0.91)

Text Table D2. Continued.

Strain	Material	Contact Time	Average RH	HPV ppm	Kills/ Trials	Proportion of Kills (95 Percent Confidence Interval)
Voll	Carpet	20 h	Medium	25	1/3	0.33 (0.01, 0.91)
Voll	Carpet	20 h	Medium	50	2/3	0.67 (0.09, 0.99)
Voll	Carpet	24 h	High	25	3/3	1.00 (0.29, 1.00)
Voll	Carpet	24 h	High	50	3/3	1.00 (0.29, 1.00)
Voll	Carpet	24	Low	25	1/3	0.33 (0.01, 0.91)
Voll	Carpet	24 h	Low	50	3/3	1.00 (0.29, 1.00)
Voll	Carpet	24 h	Medium	25	3/3	1.00 (0.29, 1.00)
Voll	Carpet	24 h	Medium	50	3/3	1.00 (0.29, 1.00)
Voll	Carpet	2 h	Low	200	1/3	0.33 (0.01, 0.91)
Voll	Carpet	3 h	Low	200	0/3	0.00 (0.00, 0.71)
Voll	Carpet	48 h	High	25	3/3	1.00 (0.29, 1.00)
Voll	Carpet	4 h	High	10	0/3	0.00 (0.00, 0.71)
Voll	Carpet	4 h	Medium	10	0/3	0.00 (0.00, 0.71)
Voll	Carpet	8 h	High	10	0/3	0.00 (0.00, 0.71)
Voll	Carpet	8 h	High	25	0/3	0.00 (0.00, 0.71)
Voll	Carpet	8 h	High	50	0/3	0.00 (0.00, 0.71)
Voll	Carpet	8 h	Low	25	0/3	0.00 (0.00, 0.71)
Voll	Carpet	8 h	Low	50	0/3	0.00 (0.00, 0.71)
Voll	Carpet	8 h	Medium	10	0/3	0.00 (0.00, 0.71)
Voll	Carpet	8 h	Medium	25	0/3	0.00 (0.00, 0.71)
Voll	Carpet	8 h	Medium	50	0/3	0.00 (0.00, 0.71)

Text Table D2. Continued.

Strain	Material	Contact Time	Average RH	HPV ppm	Kills/ Trials	Proportion of Kills (95 Percent Confidence Interval)
Voll	Ceiling Tile	0.25 h	Low	200	2/3	0.67 (0.09, 0.99)
Voll	Ceiling Tile	0.5 h	Low	200	1/3	0.33 (0.01, 0.91)
Voll	Ceiling Tile	12 h	High	10	3/3	1.00 (0.29, 1.00)
Voll	Ceiling Tile	12 h	High	25	3/3	1.00 (0.29, 1.00)
Voll	Ceiling Tile	12 h	Low	25	3/3	1.00 (0.29, 1.00)
Voll	Ceiling Tile	12 h	Low	50	3/3	1.00 (0.29, 1.00)
Voll	Ceiling Tile	12 h	Medium	10	3/3	1.00 (0.29, 1.00)
Voll	Ceiling Tile	12 h	Medium	25	3/3	1.00 (0.29, 1.00)
Voll	Ceiling Tile	16 h	High	10	3/3	1.00 (0.29, 1.00)
Voll	Ceiling Tile	16 h	Medium	10	3/3	1.00 (0.29, 1.00)
Voll	Ceiling Tile	1 h	High	25	0/3	0.00 (0.00, 0.71)
Voll	Ceiling Tile	1 h	High	50	0/3	0.00 (0.00, 0.71)
Voll	Ceiling Tile	1 h	Low	200	3/3	1.00 (0.29, 1.00)
Voll	Ceiling Tile	1 h	Medium	50	0/3	0.00 (0.00, 0.71)
Voll	Ceiling Tile	20 h	High	10	3/3	1.00 (0.29, 1.00)
Voll	Ceiling Tile	20 h	Medium	10	3/3	1.00 (0.29, 1.00)
Voll	Ceiling Tile	2 h	High	25	0/3	0.00 (0.00, 0.71)
Voll	Ceiling Tile	2 h	High	50	0/3	0.00 (0.00, 0.71)
Voll	Ceiling Tile	2 h	Low	25	0/3	0.00 (0.00, 0.71)
Voll	Ceiling Tile	2 h	Low	50	3/3	1.00 (0.29, 1.00)
Voll	Ceiling Tile	2 h	Low	200	3/3	1.00 (0.29, 1.00)

Text Table D2. Continued.

Strain	Material	Contact Time	Average RH	HPV ppm	Kills/ Trials	Proportion of Kills (95 Percent Confidence Interval)
Voll	Ceiling Tile	2 h	Medium	25	0/3	0.00 (0.00, 0.71)
Voll	Ceiling Tile	2 h	Medium	50	0/3	0.00 (0.00, 0.71)
Voll	Ceiling Tile	3 h	Low	200	3/3	1.00 (0.29, 1.00)
Voll	Ceiling Tile	4 h	High	10	0/3	0.00 (0.00, 0.71)
Voll	Ceiling Tile	4 h	High	50	3/3	1.00 (0.29, 1.00)
Voll	Ceiling Tile	4 h	Low	25	1/3	0.33 (0.01, 0.91)
Voll	Ceiling Tile	4 h	Low	50	3/3	1.00 (0.29, 1.00)
Voll	Ceiling Tile	4 h	Medium	10	0/3	0.00 (0.00, 0.71)
Voll	Ceiling Tile	4 h	Medium	25	2/3	0.67 (0.09, 0.99)
Voll	Ceiling Tile	4 h	Medium	50	3/3	1.00 (0.29, 1.00)
Voll	Ceiling Tile	5 h	High	50	3/3	1.00 (0.29, 1.00)
Voll	Ceiling Tile	5 h	Medium	50	3/3	1.00 (0.29, 1.00)
Voll	Ceiling Tile	6 h	High	25	3/3	1.00 (0.29, 1.00)
Voll	Ceiling Tile	6 h	High	50	3/3	1.00 (0.29, 1.00)
Voll	Ceiling Tile	6 h	Low	25	2/3	0.67 (0.09, 0.99)
Voll	Ceiling Tile	6 h	Low	50	3/3	1.00 (0.29, 1.00)
Voll	Ceiling Tile	6 h	Medium	25	3/3	1.00 (0.29, 1.00)
Voll	Ceiling Tile	6 h	Medium	50	3/3	1.00 (0.29, 1.00)
Voll	Ceiling Tile	8 h	High	10	3/3	1.00 (0.29, 1.00)
Voll	Ceiling Tile	8 h	High	25	3/3	1.00 (0.29, 1.00)
Voll	Ceiling Tile	8 h	Low	25	3/3	1.00 (0.29, 1.00)

Text Table D2. Continued.

Strain	Material	Contact Time	Average RH	HPV ppm	Kills/ Trials	Proportion of Kills (95 Percent Confidence Interval)
Voll	Ceiling Tile	8 h	Low	50	3/3	1.00 (0.29, 1.00)
Voll	Ceiling Tile	8 h	Medium	10	3/3	1.00 (0.29, 1.00)
Voll	Ceiling Tile	8 h	Medium	25	3/3	1.00 (0.29, 1.00)
Voll	Glass	0.25 h	Low	200	2/3	0.67 (0.09, 0.99)
Voll	Glass	0.5 h	Low	200	1/3	0.33 (0.01, 0.91)
Voll	Glass	12 h	High	10	3/3	1.00 (0.29, 1.00)
Voll	Glass	12 h	High	25	3/3	1.00 (0.29, 1.00)
Voll	Glass	12 h	Low	25	3/3	1.00 (0.29, 1.00)
Voll	Glass	12 h	Low	50	3/3	1.00 (0.29, 1.00)
Voll	Glass	12 h	Medium	10	3/3	1.00 (0.29, 1.00)
Voll	Glass	12 h	Medium	25	3/3	1.00 (0.29, 1.00)
Voll	Glass	16 h	High	10	3/3	1.00 (0.29, 1.00)
Voll	Glass	16 h	Medium	10	3/3	1.00 (0.29, 1.00)
Voll	Glass	1 h	High	25	0/3	0.00 (0.00, 0.71)
Voll	Glass	1 h	High	50	1/3	0.33 (0.01, 0.91)
Voll	Glass	1 h	Low	200	3/3	1.00 (0.29, 1.00)
Voll	Glass	1 h	Medium	50	0/3	0.00 (0.00, 0.71)
Voll	Glass	20 h	High	10	3/3	1.00 (0.29, 1.00)
Voll	Glass	20 h	Medium	10	3/3	1.00 (0.29, 1.00)
Voll	Glass	2 h	High	25	2/3	0.67 (0.09, 0.99)
Voll	Glass	2 h	High	50	3/3	1.00 (0.29, 1.00)

Text Table D2. Continued.

Strain	Material	Contact Time	Average RH	HPV ppm	Kills/ Trials	Proportion of Kills (95 Percent Confidence Interval)
Voll	Glass	2 h	Low	25	2/3	0.67 (0.09, 0.99)
Voll	Glass	2 h	Low	50	2/3	0.67 (0.09, 0.99)
Voll	Glass	2 h	Low	200	3/3	1.00 (0.29, 1.00)
Voll	Glass	2 h	Medium	25	2/3	0.67 (0.09, 0.99)
Voll	Glass	2 h	Medium	50	0/3	0.00 (0.00, 0.71)
Voll	Glass	3 h	Low	200	1/3	0.33 (0.01, 0.91)
Voll	Glass	4 h	High	10	3/3	1.00 (0.29, 1.00)
Voll	Glass	4 h	High	50	3/3	1.00 (0.29, 1.00)
Voll	Glass	4 h	Low	25	1/3	0.33 (0.01, 0.91)
Voll	Glass	4 h	Low	50	3/3	1.00 (0.29, 1.00)
Voll	Glass	4 h	Medium	10	1/3	0.33 (0.01, 0.91)
Voll	Glass	4 h	Medium	25	3/3	1.00 (0.29, 1.00)
Voll	Glass	4 h	Medium	50	3/3	1.00 (0.29, 1.00)
Voll	Glass	5 h	High	50	3/3	1.00 (0.29, 1.00)
Voll	Glass	5 h	Medium	50	3/3	1.00 (0.29, 1.00)
Voll	Glass	6 h	High	25	3/3	1.00 (0.29, 1.00)
Voll	Glass	6 h	High	50	3/3	1.00 (0.29, 1.00)
Voll	Glass	6 h	Low	25	2/3	0.67 (0.09, 0.99)
Voll	Glass	6 h	Low	50	3/3	1.00 (0.29, 1.00)
Voll	Glass	6 h	Medium	25	3/3	1.00 (0.29, 1.00)
Voll	Glass	6 h	Medium	50	3/3	1.00 (0.29, 1.00)

Text Table D2. Continued.

Strain	Material	Contact Time	Average RH	HPV ppm	Kills/ Trials	Proportion of Kills (95 Percent Confidence Interval)
Voll	Glass	8 h	High	10	3/3	1.00 (0.29, 1.00)
Voll	Glass	8 h	High	25	3/3	1.00 (0.29, 1.00)
Voll	Glass	8 h	Low	25	3/3	1.00 (0.29, 1.00)
Voll	Glass	8 h	Low	50	2/3	0.67 (0.09, 0.99)
Voll	Glass	8 h	Medium	10	2/3	0.67 (0.09, 0.99)
Voll	Glass	8 h	Medium	25	3/3	1.00 (0.29, 1.00)
Voll	Painted Wallboard Paper	0.25 h	Low	200	0/3	0.00 (0.00, 0.71)
Voll	Painted Wallboard Paper	0.5 h	Low	200	0/3	0.00 (0.00, 0.71)
Voll	Painted Wallboard Paper	12 h	High	10	3/3	1.00 (0.29, 1.00)
Voll	Painted Wallboard Paper	12 h	High	25	3/3	1.00 (0.29, 1.00)
Voll	Painted Wallboard Paper	12 h	Low	25	3/3	1.00 (0.29, 1.00)
Voll	Painted Wallboard Paper	12 h	Low	50	3/3	1.00 (0.29, 1.00)
Voll	Painted Wallboard Paper	12 h	Medium	10	2/3	0.67 (0.09, 0.99)
Voll	Painted Wallboard Paper	12 h	Medium	25	3/3	1.00 (0.29, 1.00)
Voll	Painted Wallboard Paper	16 h	High	10	3/3	1.00 (0.29, 1.00)
Voll	Painted Wallboard Paper	16 h	Medium	10	3/3	1.00 (0.29, 1.00)
Voll	Painted Wallboard Paper	1 h	High	25	0/3	0.00 (0.00, 0.71)
Voll	Painted Wallboard Paper	1 h	High	50	0/3	0.00 (0.00, 0.71)
Voll	Painted Wallboard Paper	1 h	Low	200	3/3	1.00 (0.29, 1.00)
Voll	Painted Wallboard Paper	1 h	Medium	50	0/3	0.00 (0.00, 0.71)
Voll	Painted Wallboard Paper	20 h	High	10	3/3	1.00 (0.29, 1.00)

Text Table D2. Continued.

Strain	Material	Contact Time	Average RH	HPV ppm	Kills/ Trials	Proportion of Kills (95 Percent Confidence Interval)
Voll	Painted Wallboard Paper	20 h	Medium	10	3/3	1.00 (0.29, 1.00)
Voll	Painted Wallboard Paper	2 h	High	25	0/3	0.00 (0.00, 0.71)
Voll	Painted Wallboard Paper	2 h	High	50	0/3	0.00 (0.00, 0.71)
Voll	Painted Wallboard Paper	2 h	Low	25	0/3	0.00 (0.00, 0.71)
Voll	Painted Wallboard Paper	2 h	Low	50	0/3	0.00 (0.00, 0.71)
Voll	Painted Wallboard Paper	2 h	Low	200	3/3	1.00 (0.29, 1.00)
Voll	Painted Wallboard Paper	2 h	Medium	25	0/3	0.00 (0.00, 0.71)
Voll	Painted Wallboard Paper	2 h	Medium	50	2/3	0.67 (0.09, 0.99)
Voll	Painted Wallboard Paper	3 h	Low	200	3/3	1.00 (0.29, 1.00)
Voll	Painted Wallboard Paper	4 h	High	10	2/3	0.67 (0.09, 0.99)
Voll	Painted Wallboard Paper	4 h	High	50	3/3	1.00 (0.29, 1.00)
Voll	Painted Wallboard Paper	4 h	Low	25	1/3	0.33 (0.01, 0.91)
Voll	Painted Wallboard Paper	4 h	Low	50	0/3	0.00 (0.00, 0.71)
Voll	Painted Wallboard Paper	4 h	Medium	10	0/3	0.00 (0.00, 0.71)
Voll	Painted Wallboard Paper	4 h	Medium	25	3/3	1.00 (0.29, 1.00)
Voll	Painted Wallboard Paper	4 h	Medium	50	2/3	0.67 (0.09, 0.99)
Voll	Painted Wallboard Paper	5 h	High	50	3/3	1.00 (0.29, 1.00)
Voll	Painted Wallboard Paper	5 h	Medium	50	3/3	1.00 (0.29, 1.00)
Voll	Painted Wallboard Paper	6 h	High	25	3/3	1.00 (0.29, 1.00)
Voll	Painted Wallboard Paper	6 h	High	50	3/3	1.00 (0.29, 1.00)
Voll	Painted Wallboard Paper	6 h	Low	25	3/3	1.00 (0.29, 1.00)

Text Table D2. Continued.

Strain	Material	Contact Time	Average RH	HPV ppm	Kills/ Trials	Proportion of Kills (95 Percent Confidence Interval)
Voll	Painted Wallboard Paper	6 h	Low	50	3/3	1.00 (0.29, 1.00)
Voll	Painted Wallboard Paper	6 h	Medium	25	3/3	1.00 (0.29, 1.00)
Voll	Painted Wallboard Paper	6 h	Medium	50	3/3	1.00 (0.29, 1.00)
Voll	Painted Wallboard Paper	8 h	High	10	3/3	1.00 (0.29, 1.00)
Voll	Painted Wallboard Paper	8 h	High	25	3/3	1.00 (0.29, 1.00)
Voll	Painted Wallboard Paper	8 h	Low	25	3/3	1.00 (0.29, 1.00)
Voll	Painted Wallboard Paper	8 h	Low	50	3/3	1.00 (0.29, 1.00)
Voll	Painted Wallboard Paper	8 h	Medium	10	1/3	0.33 (0.01, 0.91)
Voll	Painted Wallboard Paper	8 h	Medium	25	3/3	1.00 (0.29, 1.00)
Voll	Unpainted Concrete	0.25 h	Low	200	0/3	0.00 (0.00, 0.71)
Voll	Unpainted Concrete	0.5 h	Low	200	0/3	0.00 (0.00, 0.71)
Voll	Unpainted Concrete	12 h	High	10	0/3	0.00 (0.00, 0.71)
Voll	Unpainted Concrete	12 h	High	25	0/3	0.00 (0.00, 0.71)
Voll	Unpainted Concrete	12 h	High	50	0/3	0.00 (0.00, 0.71)
Voll	Unpainted Concrete	12 h	Low	25	1/3	0.33 (0.01, 0.91)
Voll	Unpainted Concrete	12 h	Low	50	1/3	0.33 (0.01, 0.91)
Voll	Unpainted Concrete	12 h	Medium	10	0/3	0.00 (0.00, 0.71)
Voll	Unpainted Concrete	12 h	Medium	25	1/3	0.33 (0.01, 0.91)
Voll	Unpainted Concrete	12 h	Medium	50	0/3	0.00 (0.00, 0.71)
Voll	Unpainted Concrete	16 h	High	10	0/3	0.00 (0.00, 0.71)
Voll	Unpainted Concrete	16 h	High	50	0/3	0.00 (0.00, 0.71)

Text Table D2. Continued.

Strain	Material	Contact Time	Average RH	HPV ppm	Kills/ Trials	Proportion of Kills (95 Percent Confidence Interval)
Voll	Unpainted Concrete	16 h	Low	25	0/3	0.00 (0.00, 0.71)
Voll	Unpainted Concrete	16 h	Low	50	0/3	0.00 (0.00, 0.71)
Voll	Unpainted Concrete	16 h	Medium	10	0/3	0.00 (0.00, 0.71)
Voll	Unpainted Concrete	16 h	Medium	25	0/3	0.00 (0.00, 0.71)
Voll	Unpainted Concrete	16 h	Medium	50	0/3	0.00 (0.00, 0.71)
Voll	Unpainted Concrete	1 h	Low	200	0/3	0.00 (0.00, 0.71)
Voll	Unpainted Concrete	20 h	High	10	1/3	0.33 (0.01, 0.91)
Voll	Unpainted Concrete	20 h	High	25	0/3	0.00 (0.00, 0.71)
Voll	Unpainted Concrete	20 h	High	50	0/3	0.00 (0.00, 0.71)
Voll	Unpainted Concrete	20 h	Low	25	0/3	0.00 (0.00, 0.71)
Voll	Unpainted Concrete	20 h	Low	50	0/3	0.00 (0.00, 0.71)
Voll	Unpainted Concrete	20 h	Medium	10	0/3	0.00 (0.00, 0.71)
Voll	Unpainted Concrete	20 h	Medium	25	0/3	0.00 (0.00, 0.71)
Voll	Unpainted Concrete	20 h	Medium	50	0/3	0.00 (0.00, 0.71)
Voll	Unpainted Concrete	24 h	High	25	0/3	0.00 (0.00, 0.71)
Voll	Unpainted Concrete	24 h	High	50	0/3	0.00 (0.00, 0.71)
Voll	Unpainted Concrete	24 h	Low	25	0/3	0.00 (0.00, 0.71)
Voll	Unpainted Concrete	24 h	Low	50	0/3	0.00 (0.00, 0.71)
Voll	Unpainted Concrete	24 h	Medium	25	0/3	0.00 (0.00, 0.71)
Voll	Unpainted Concrete	24 h	Medium	50	0/3	0.00 (0.00, 0.71)
Voll	Unpainted Concrete	2 h	Low	200	2/3	0.67 (0.09, 0.99)

Text Table D2. Continued.

Strain	Material	Contact Time	Average RH	HPV ppm	Kills/ Trials	Proportion of Kills (95 Percent Confidence Interval)
Voll	Unpainted Concrete	3 h	Low	200	0/3	0.00 (0.00, 0.71)
Voll	Unpainted Concrete	48 h	High	25	0/3	0.00 (0.00, 0.71)
Voll	Unpainted Concrete	4 h	High	10	0/3	0.00 (0.00, 0.71)
Voll	Unpainted Concrete	4 h	Medium	10	0/3	0.00 (0.00, 0.71)
Voll	Unpainted Concrete	8 h	High	10	1/3	0.33 (0.01, 0.91)
Voll	Unpainted Concrete	8 h	High	25	0/3	0.00 (0.00, 0.71)
Voll	Unpainted Concrete	8 h	High	50	0/3	0.00 (0.00, 0.71)
Voll	Unpainted Concrete	8 h	Low	25	0/3	0.00 (0.00, 0.71)
Voll	Unpainted Concrete	8 h	Low	50	0/3	0.00 (0.00, 0.71)
Voll	Unpainted Concrete	8 h	Medium	10	0/3	0.00 (0.00, 0.71)
Voll	Unpainted Concrete	8 h	Medium	25	0/3	0.00 (0.00, 0.71)
Voll	Unpainted Concrete	8 h	Medium	50	0/3	0.00 (0.00, 0.71)

Text Table D3. Joint Test for Logistic Regression Model Fit to Full Dataset

Effect	DF	Wald Test Statistic	p-value
Strain	1	0.0002	0.9878
Material	5	33.4403	<0.0001*
Average RH	2	1.3788	0.5019
Dose	1	0.0150	0.9025
Strain*Material	5	23.7072	0.0002*
Strain*Average RH	2	6.6379	0.0362*
Dose*Strain	1	0.0021	0.9631
Material*Average RH	10	55.1795	<0.0001*
Dose*Material	5	98.4537	<0.0001*
Dose*Average RH	2	18.6340	<0.0001*
Dose*Strain*Material	5	37.1099	<0.0001*

* Effect is statistically significant if the p-value is ≤ 0.05; DF = degrees of freedom

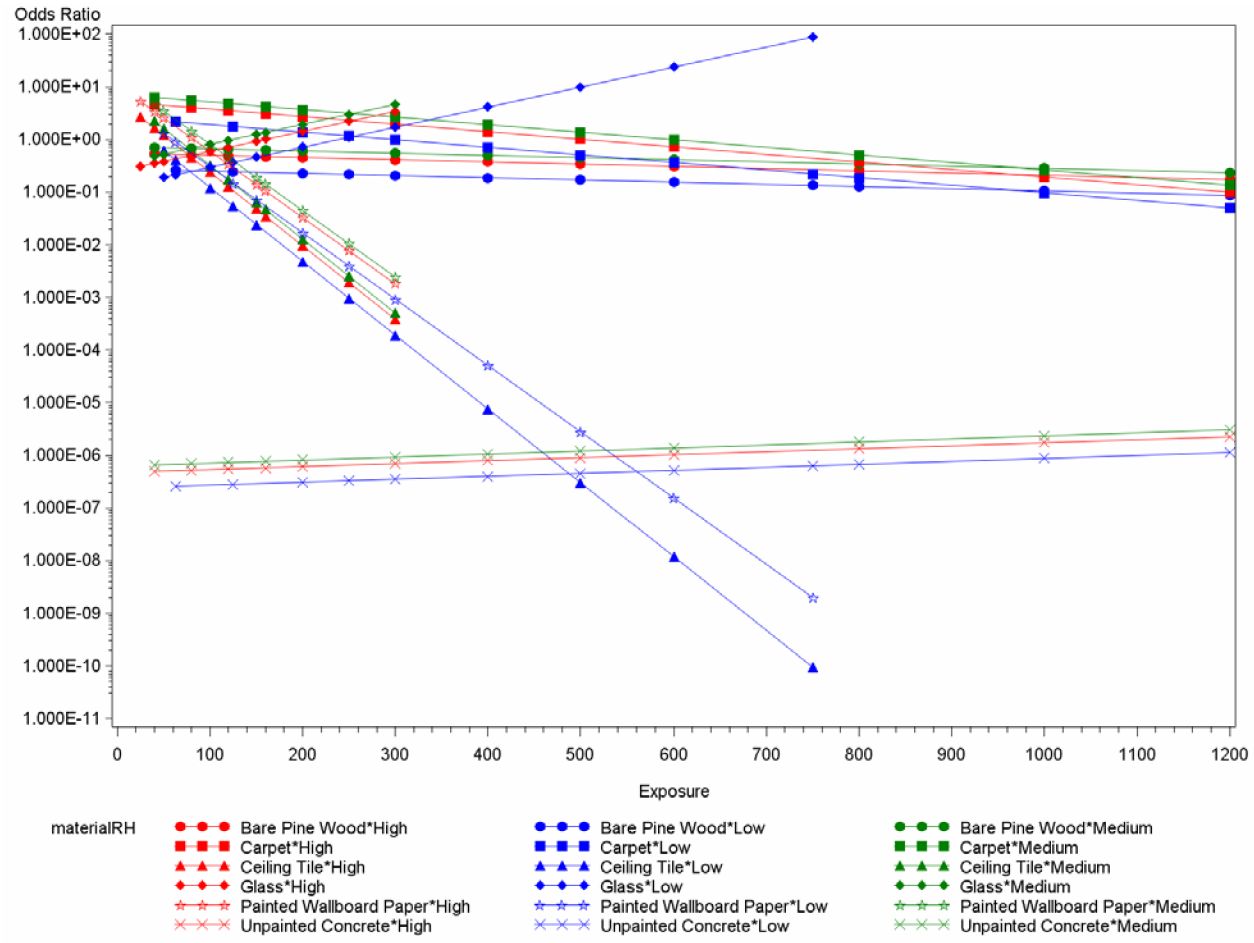

Figure D1. Odds Ratios Comparing Strains (Ames vs Vollum) which Varies by Material*RH

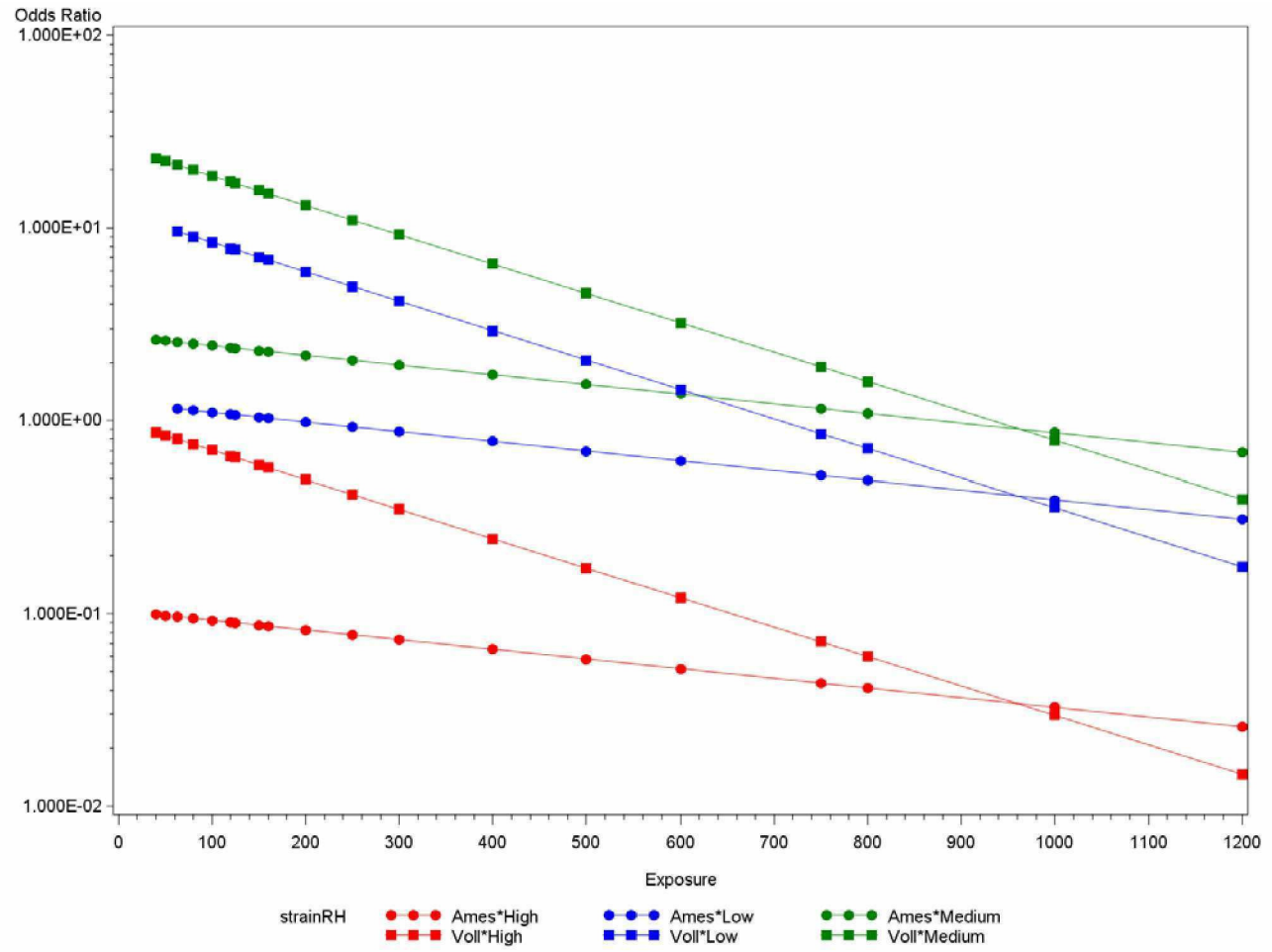

Figure D2. Odds Ratios Comparing Materials – Bare Pine Wood vs Carpet (Varying by Strain by RH)

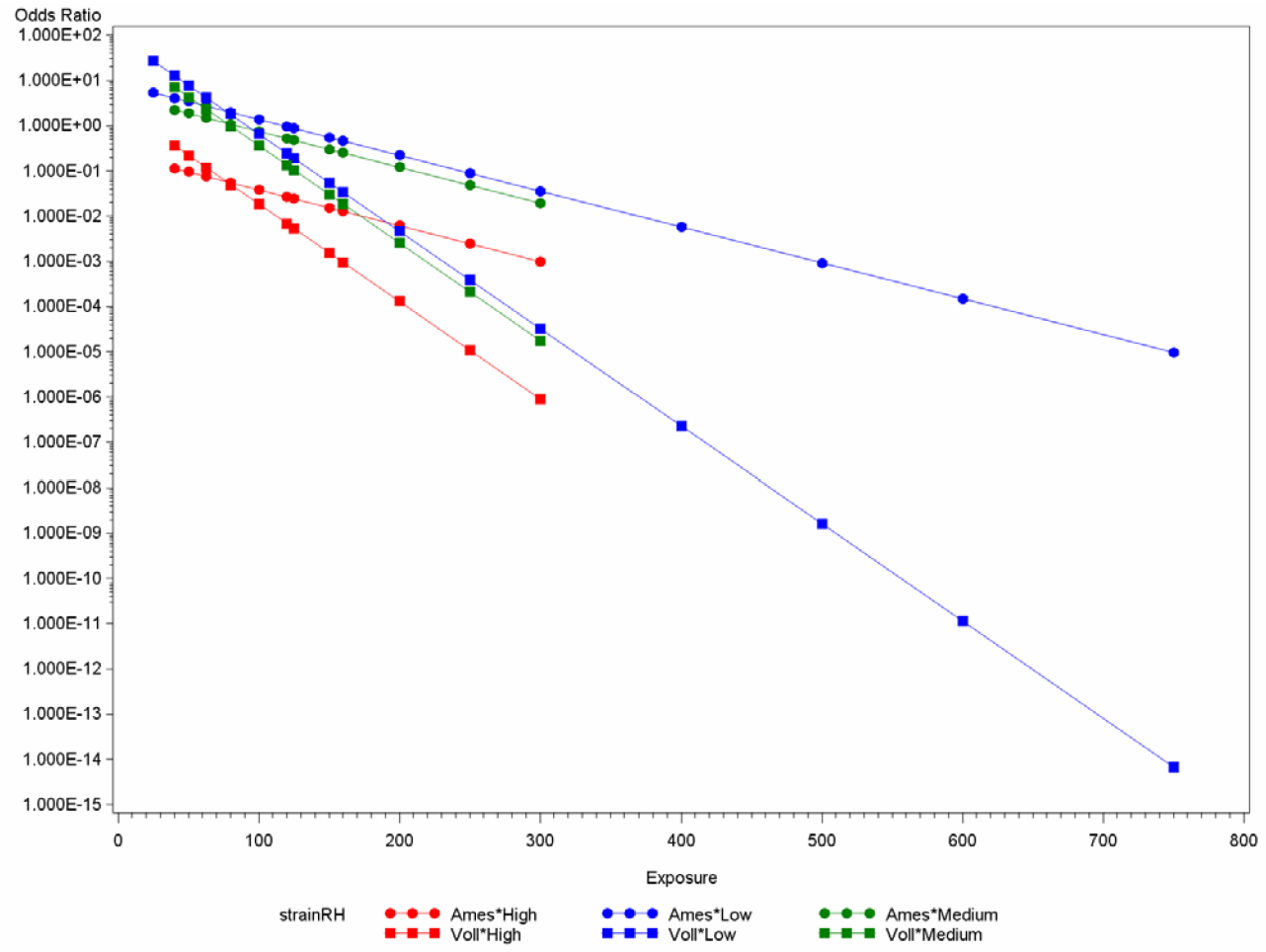

Figure D3. Odds Ratios Comparing Materials – Bare Pine Wood vs Ceiling Tile (Varying by Strain by RH)

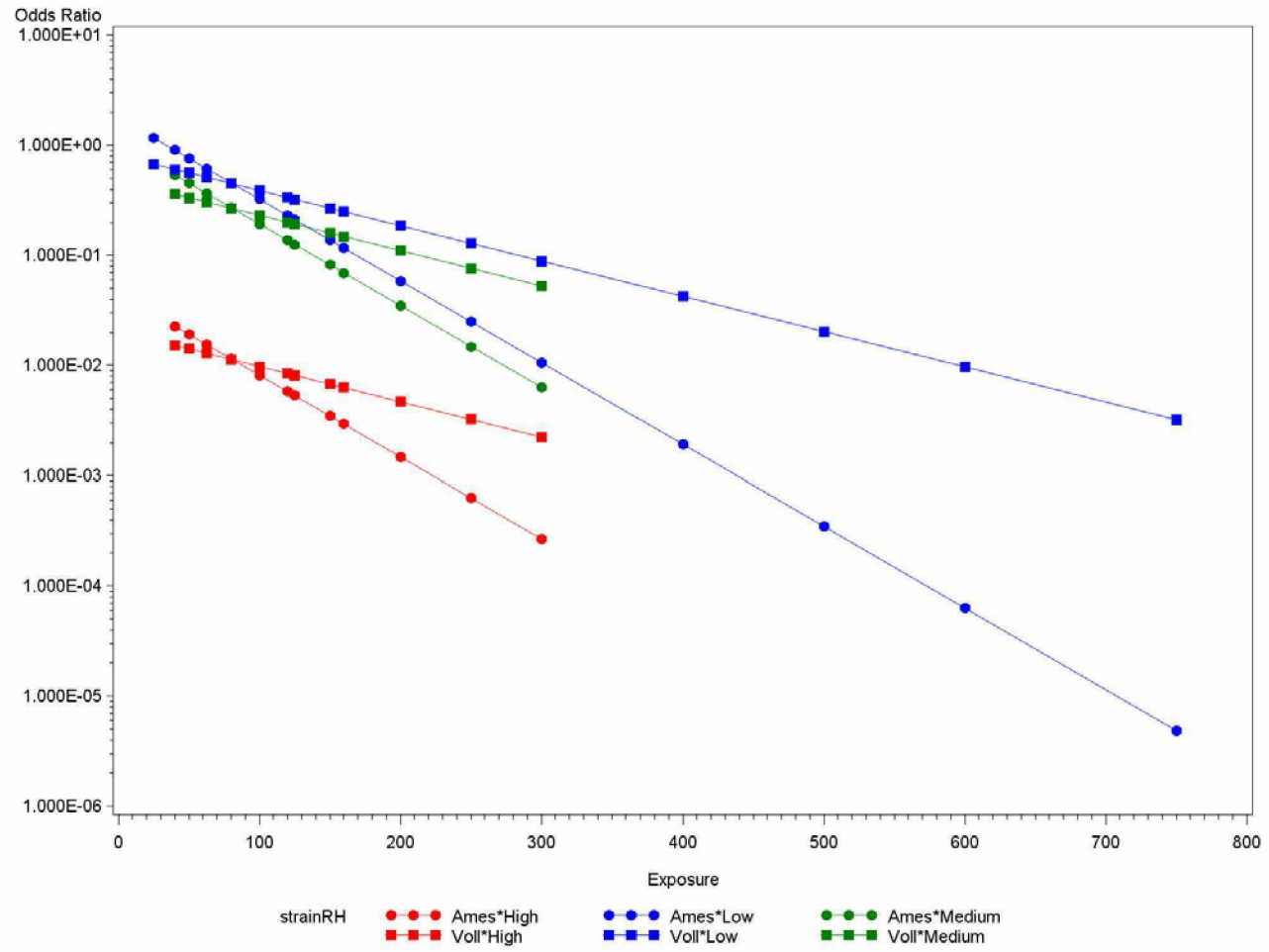

Figure D4. Odds Ratios Comparing Materials – Bare Pine Wood vs Glass (Varying by Strain by RH)

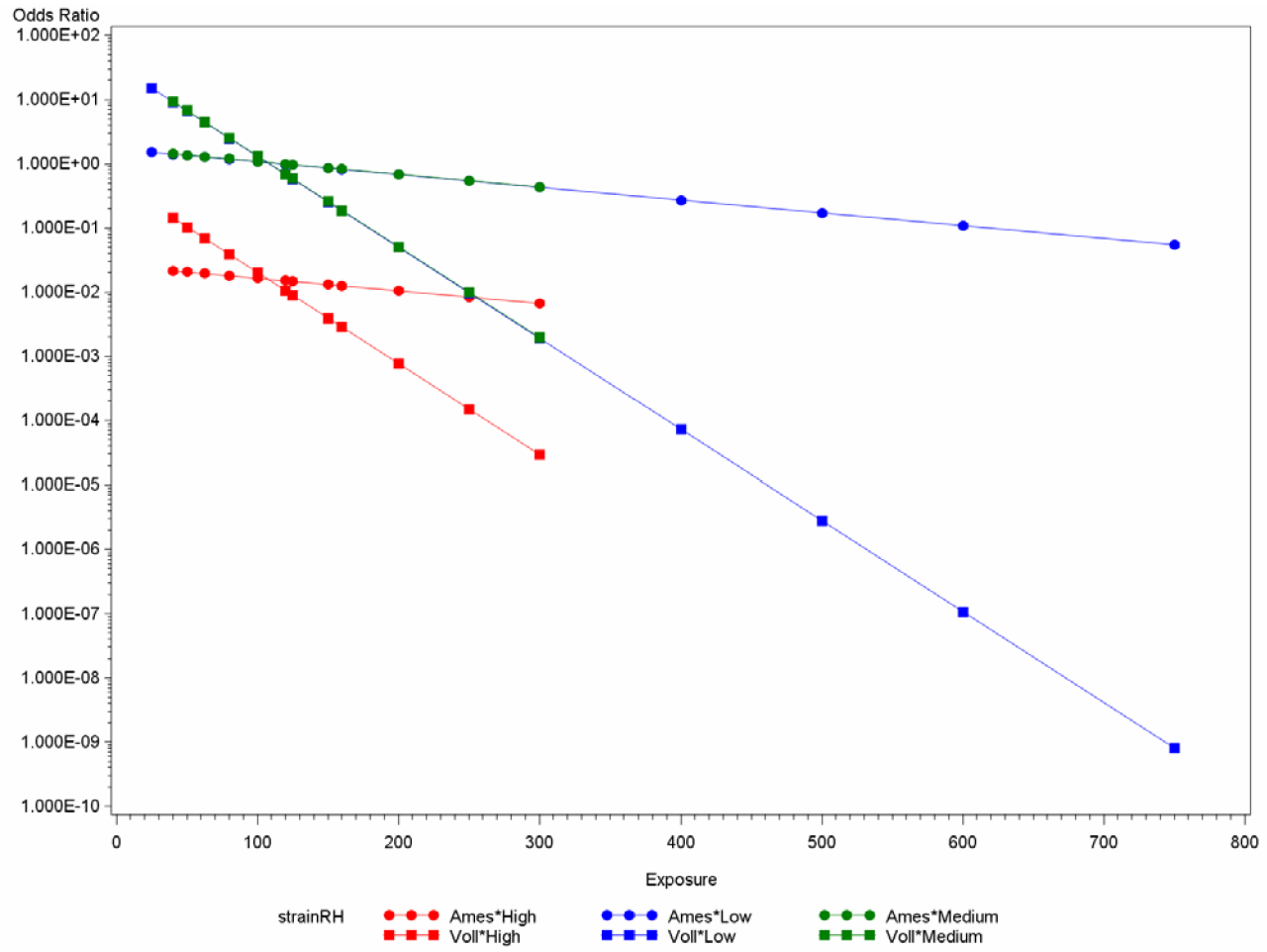

Figure D5. Odds Ratios Comparing Materials – Bare Pine Wood vs Painted Wallboard Paper (Varying by Strain by RH)

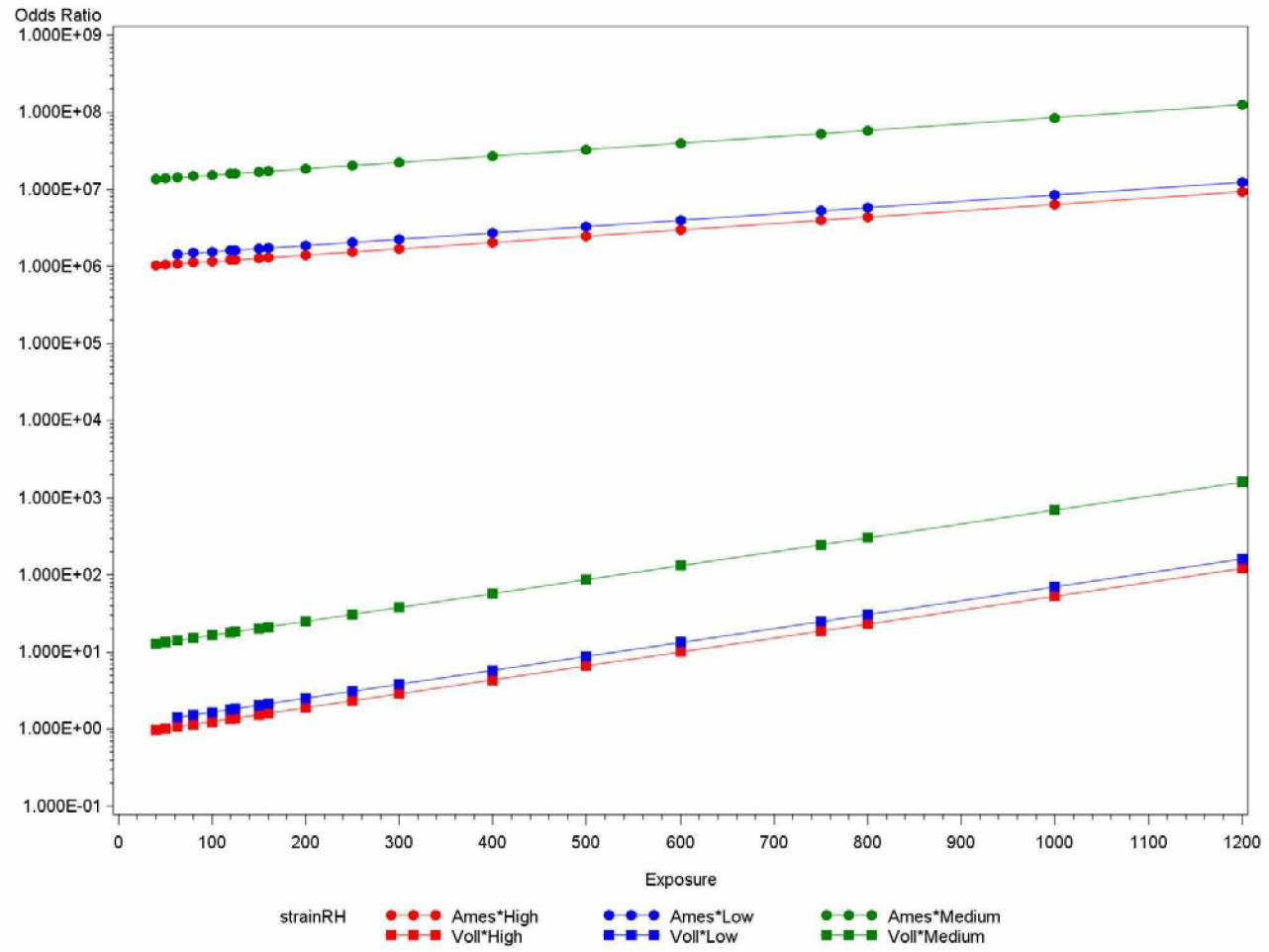

Figure D6. Odds Ratios Comparing Materials – Bare Pine Wood vs Unpainted Concrete (Varying by Strain by RH)

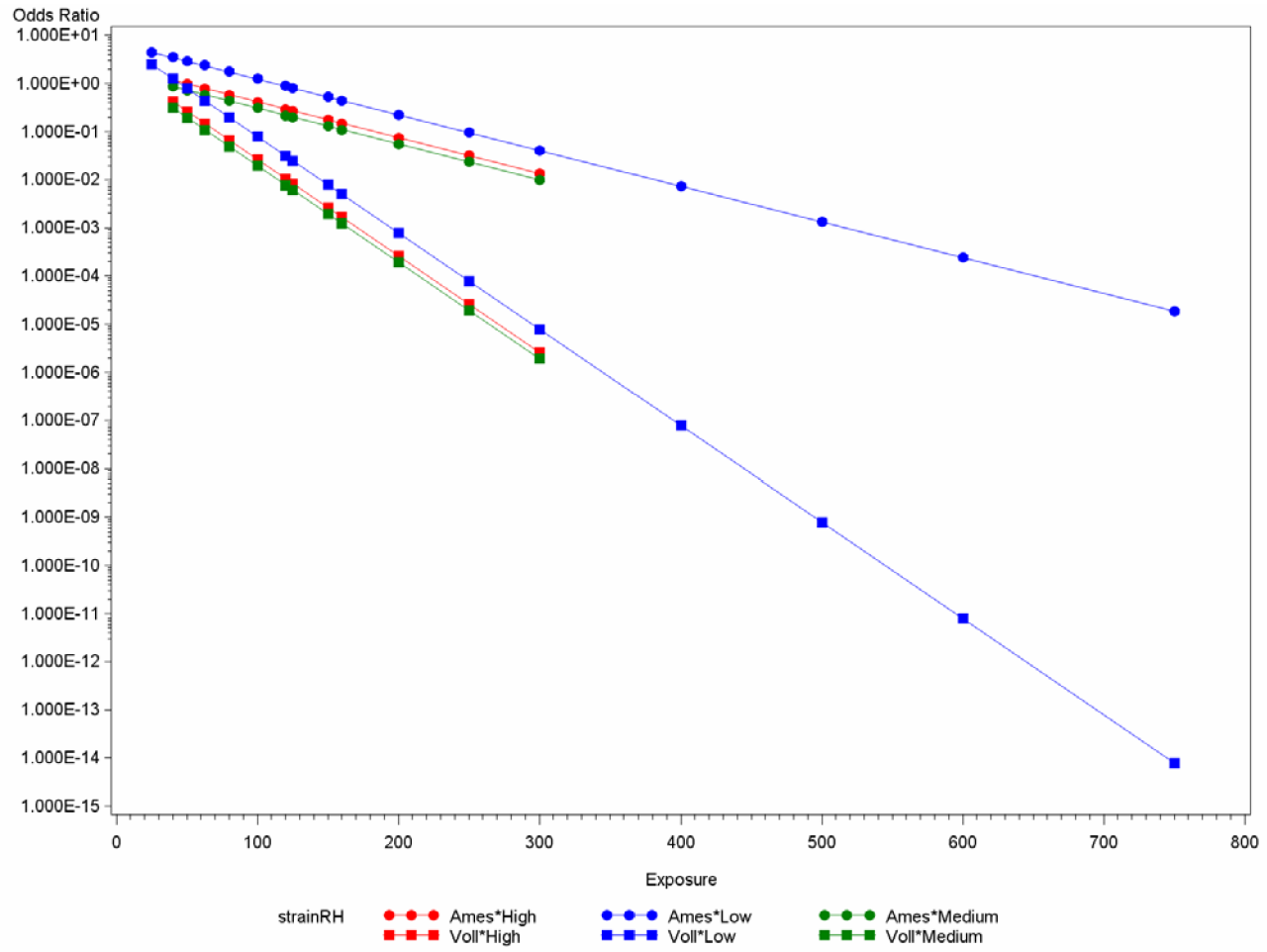

Figure D7. Odds Ratios Comparing Materials – Carpet vs Ceiling Tile (Varying by Strain by RH)

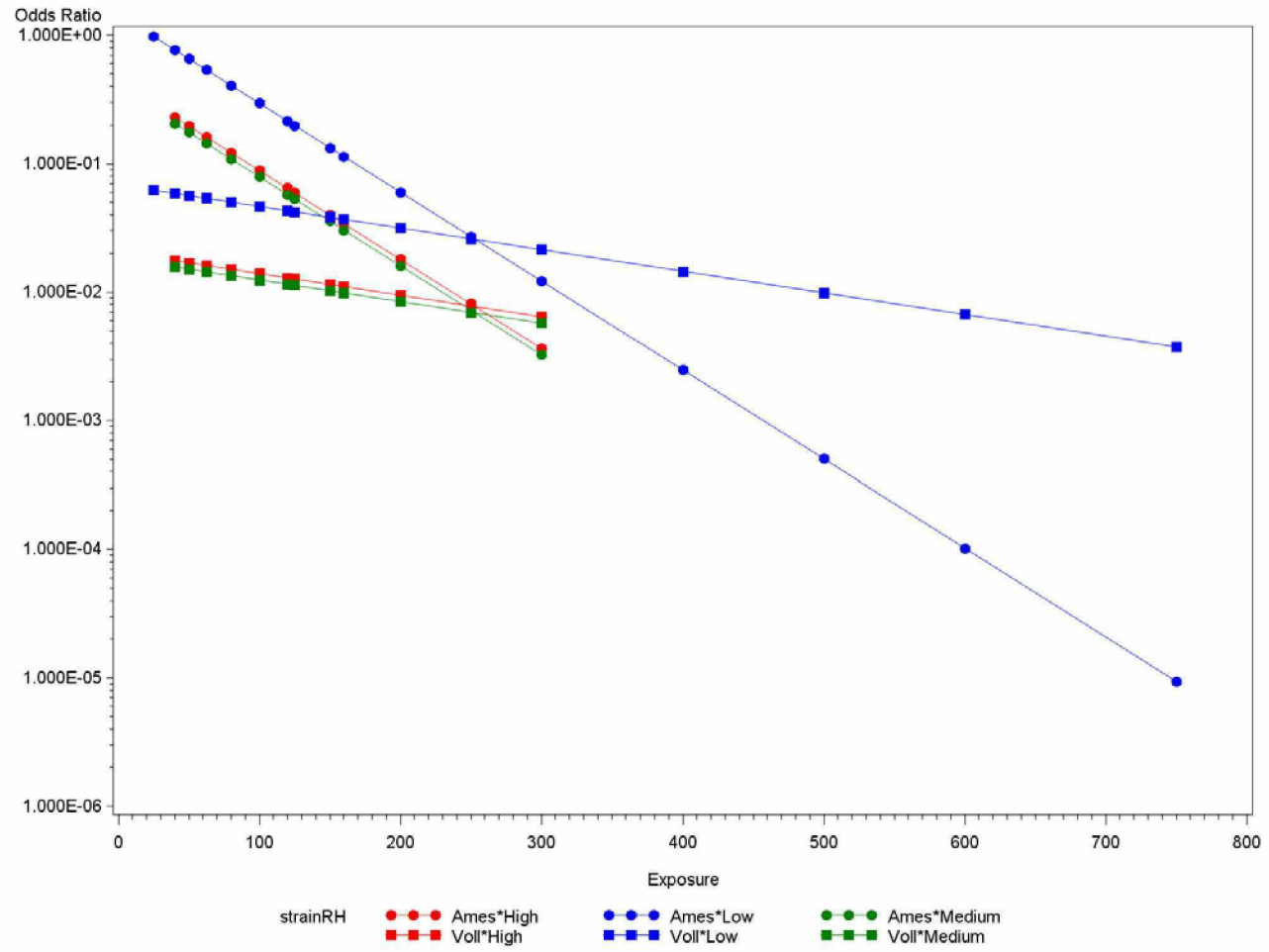

Figure D8. Odds Ratios Comparing Materials – Carpet vs Glass (Varying by Strain by RH)

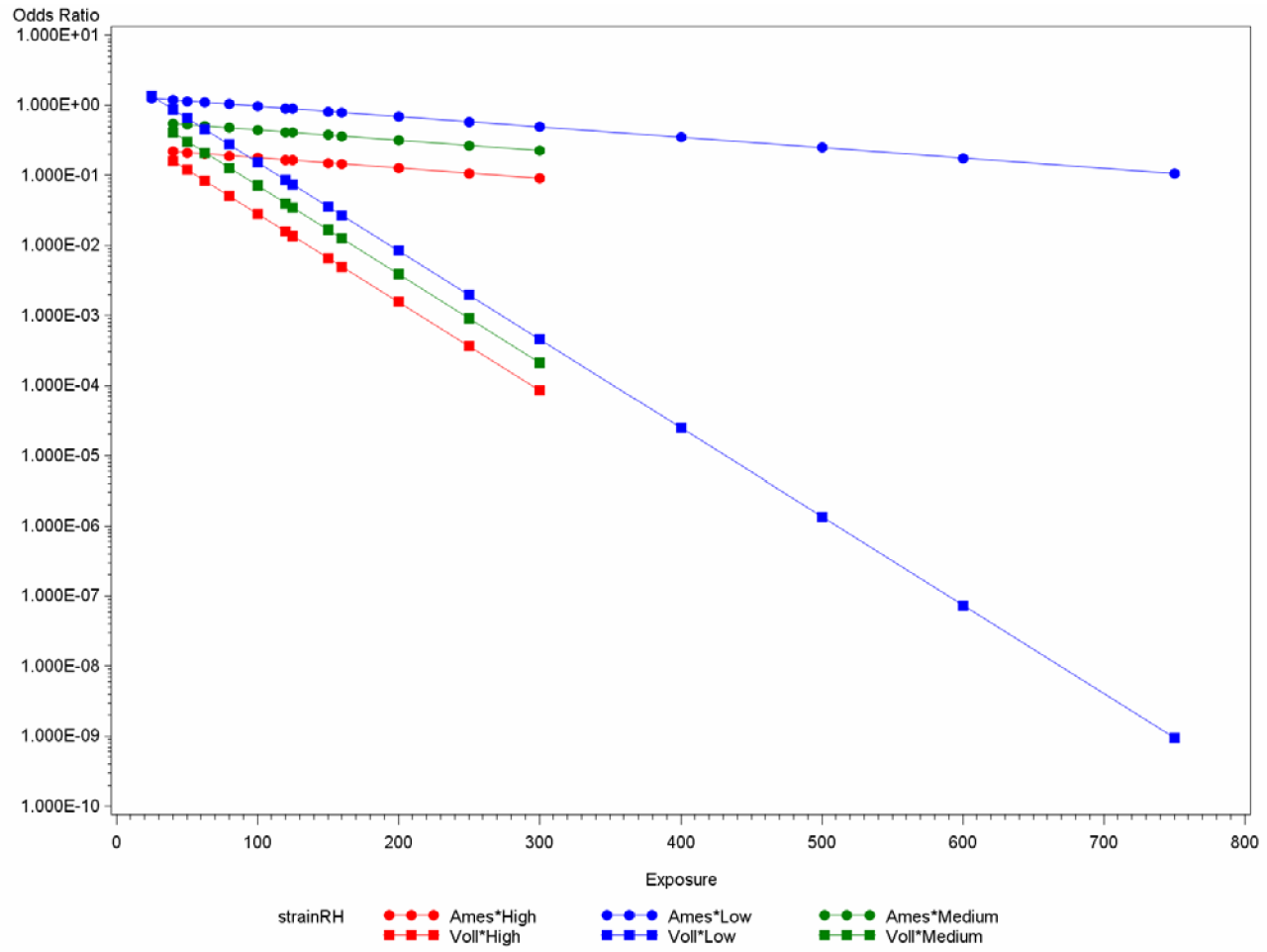

Figure D9. Odds Ratios Comparing Materials – Carpet vs Painted Wallboard Paper (Varying by Strain by RH)

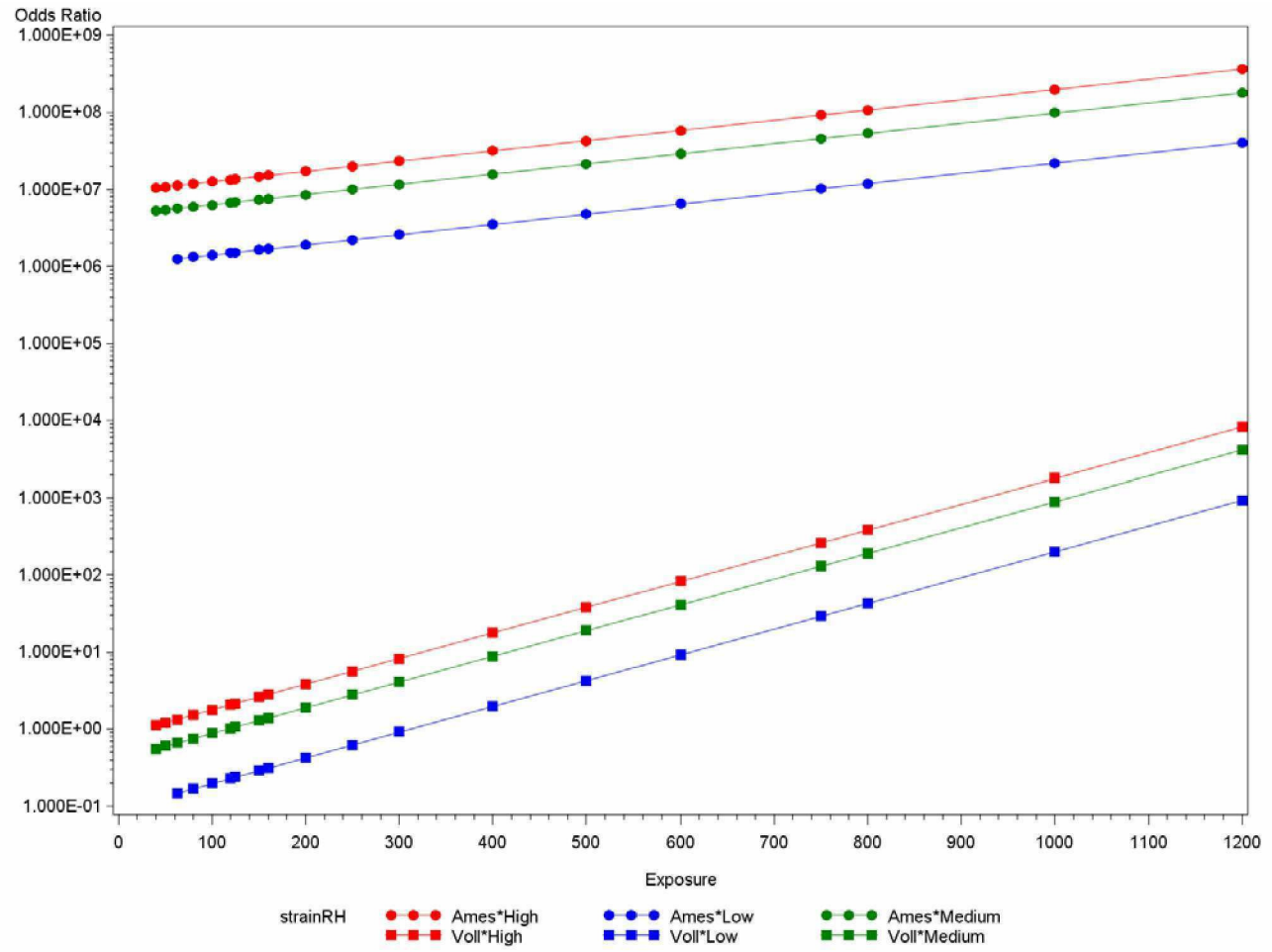

Figure D10. Odds Ratios Comparing Materials – Carpet vs Unpainted Concrete (Varying by Strain by RH)

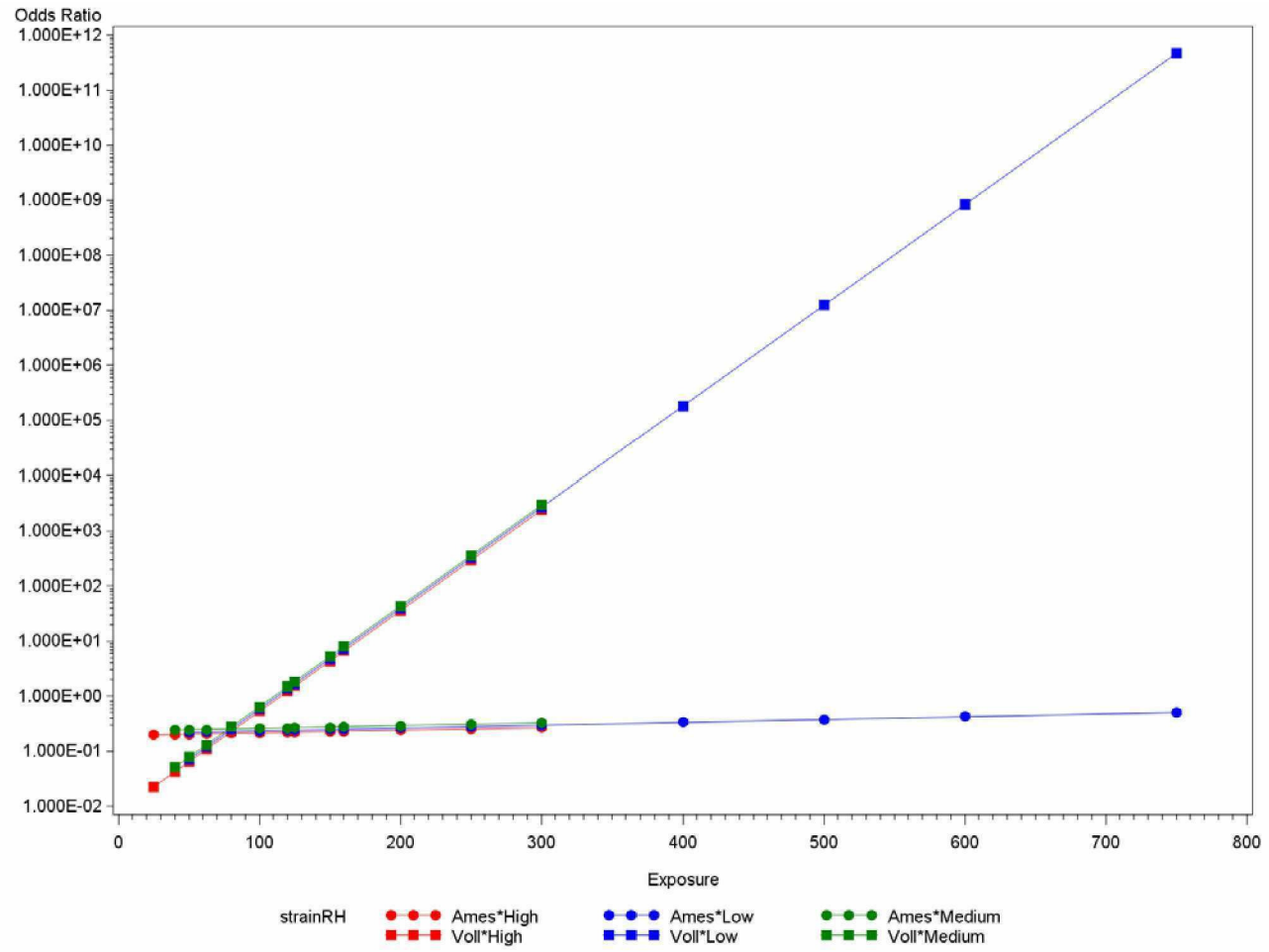

Figure D11. Odds Ratios Comparing Materials – Ceiling Tile vs Glass (Varying by Strain by RH)

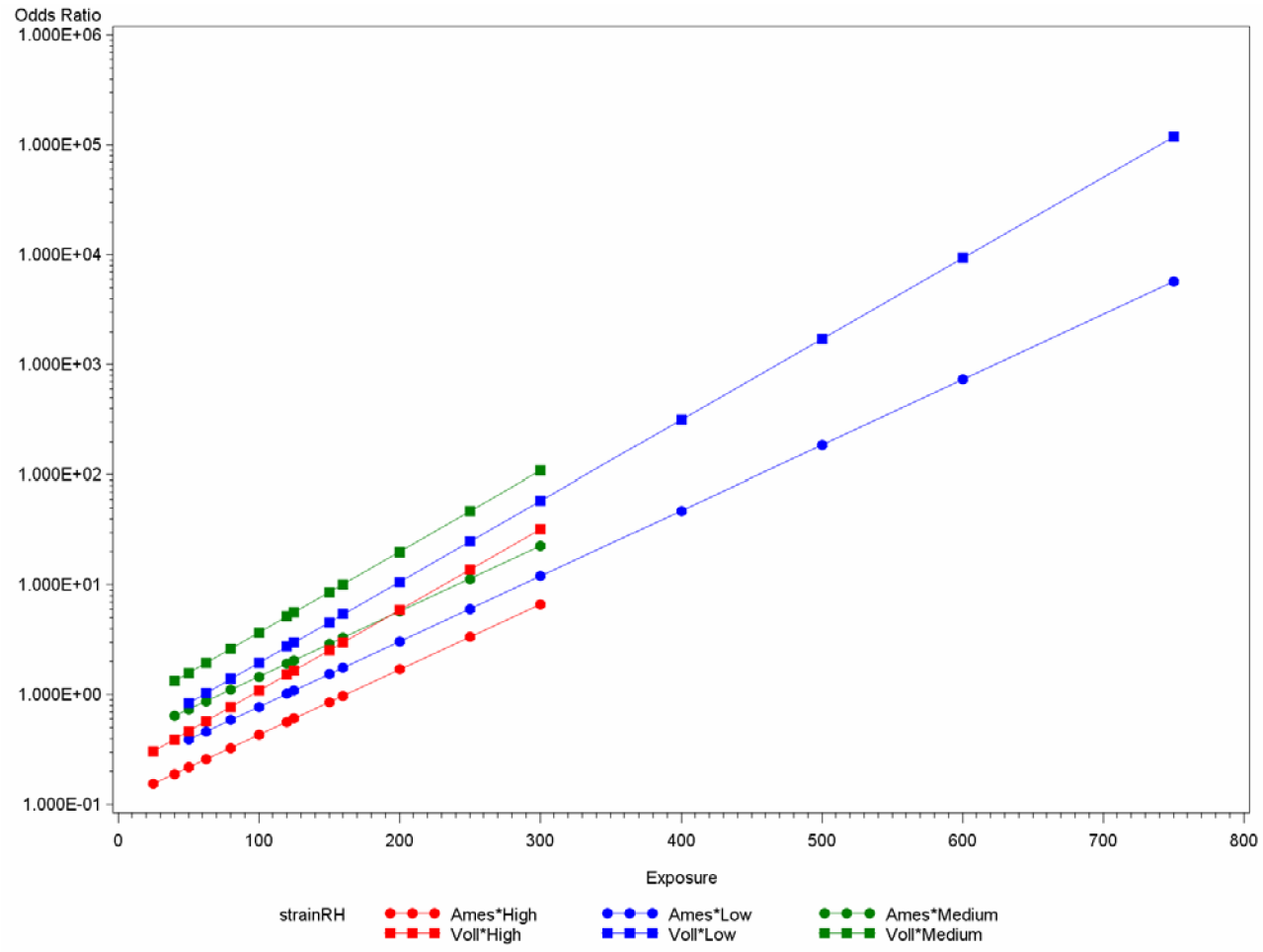

Figure D12. Odds Ratios Comparing Materials – Ceiling Tile vs Painted Wallboard Paper (Varying by Strain by RH)

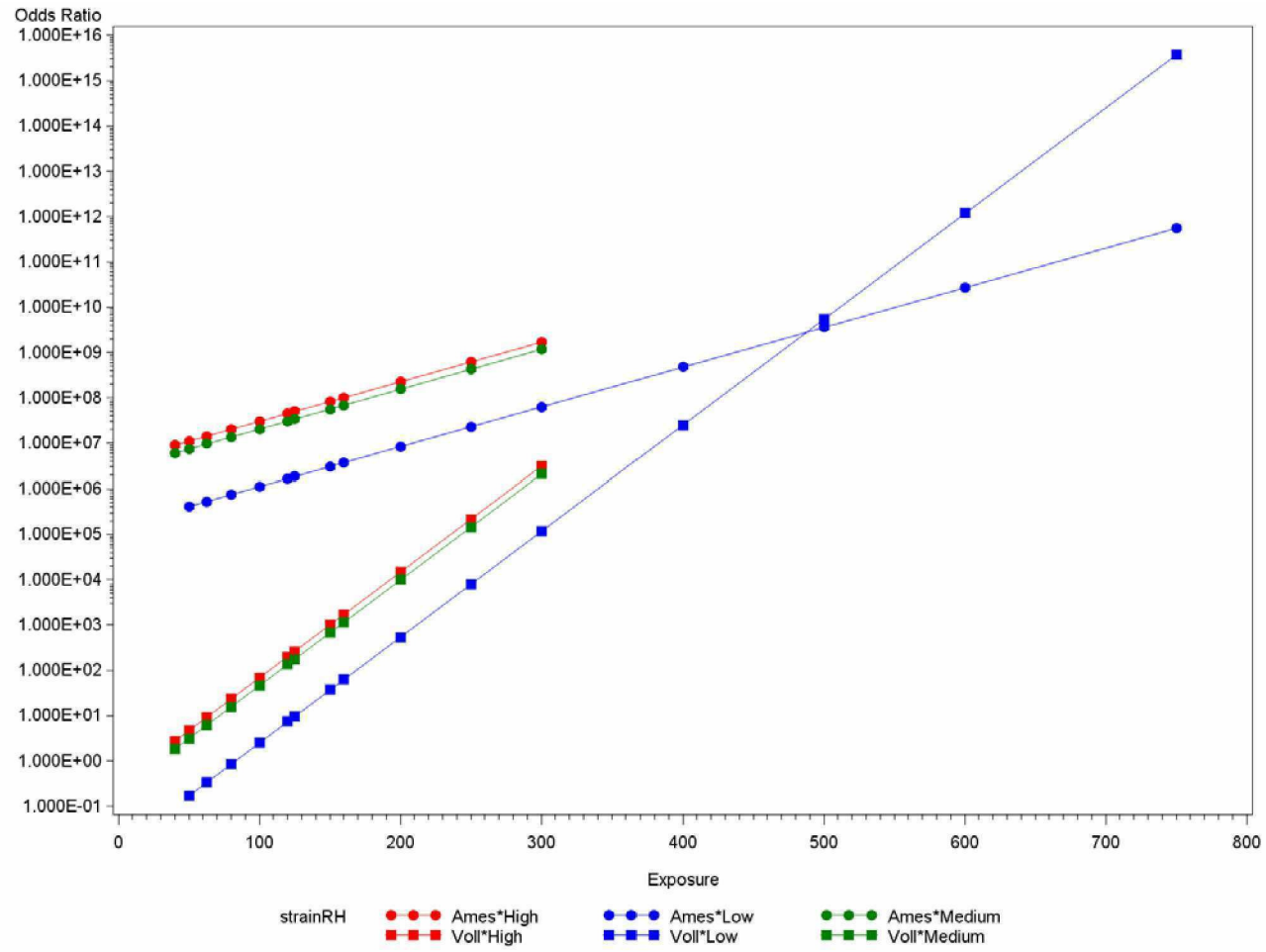

Figure D 13. Odds Ratios Comparing Materials – Ceiling Tile vs Unpainted Concrete (Varying by Strain by RH)

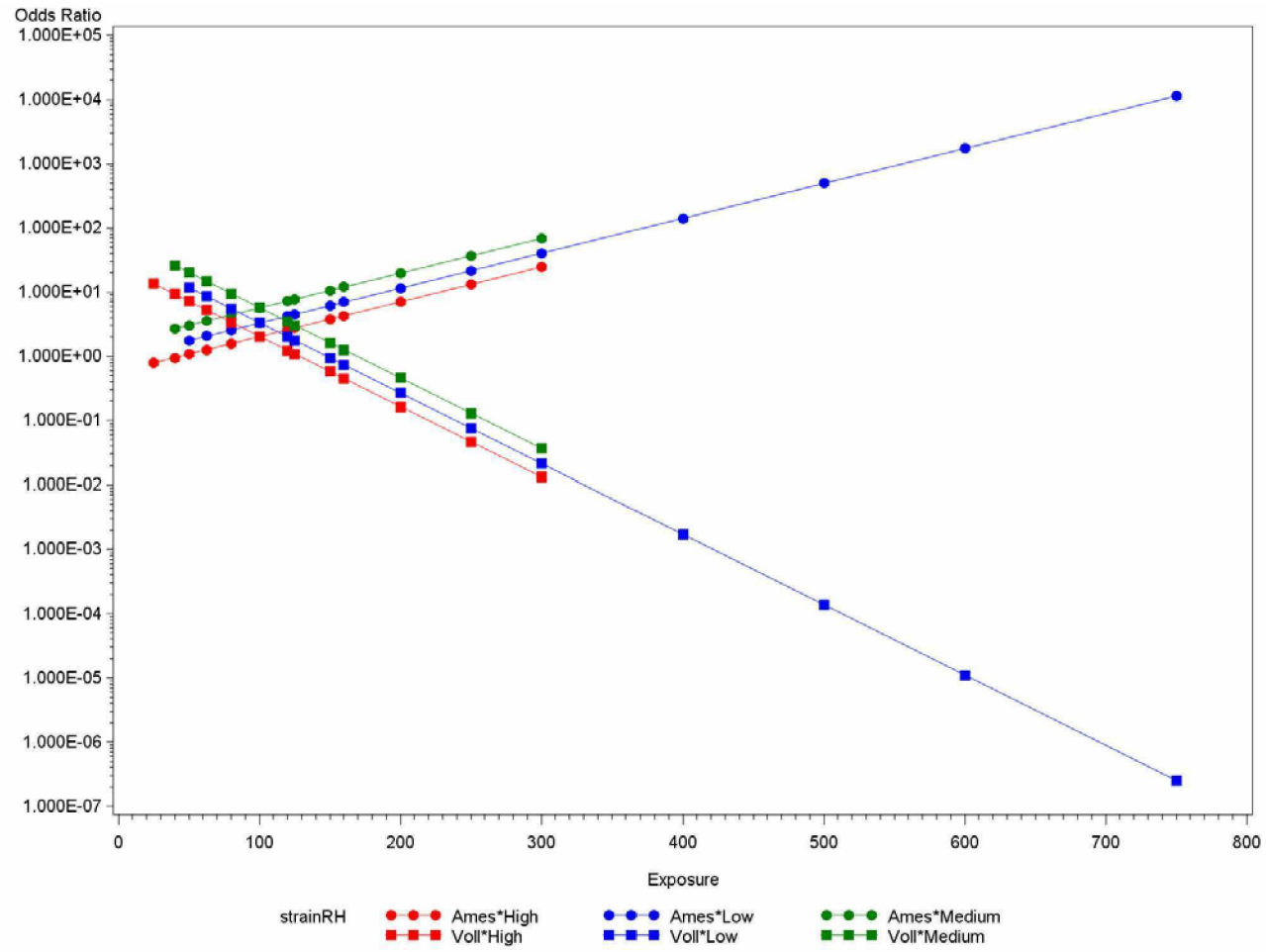

Figure D14. Odds Ratios Comparing Materials – Glass vs Painted Wallboard Paper (Varying by Strain by RH)

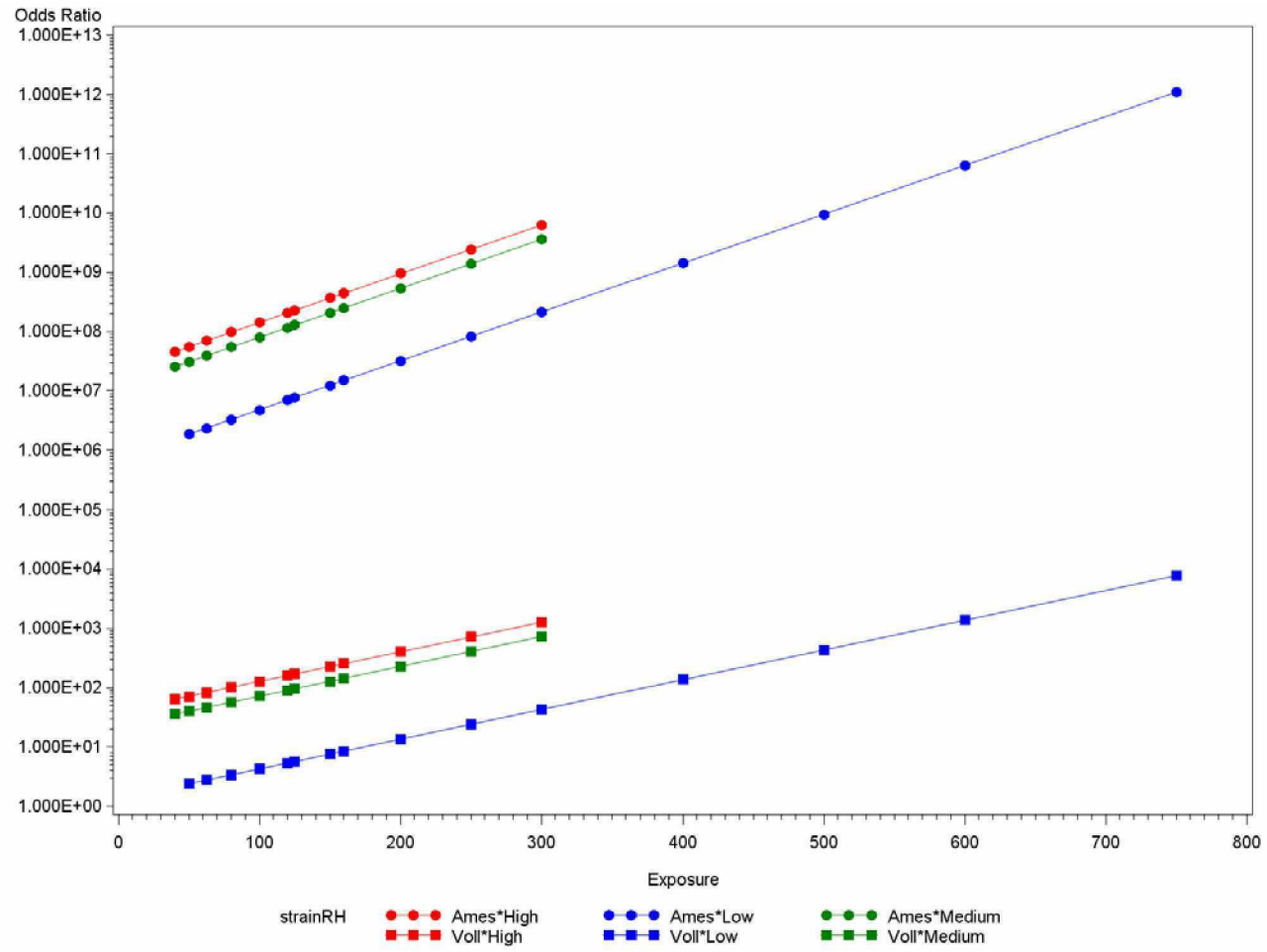

Figure D15. Odds Ratios Comparing Materials – Glass vs Unpainted Concrete (Varying by Strain by RH)

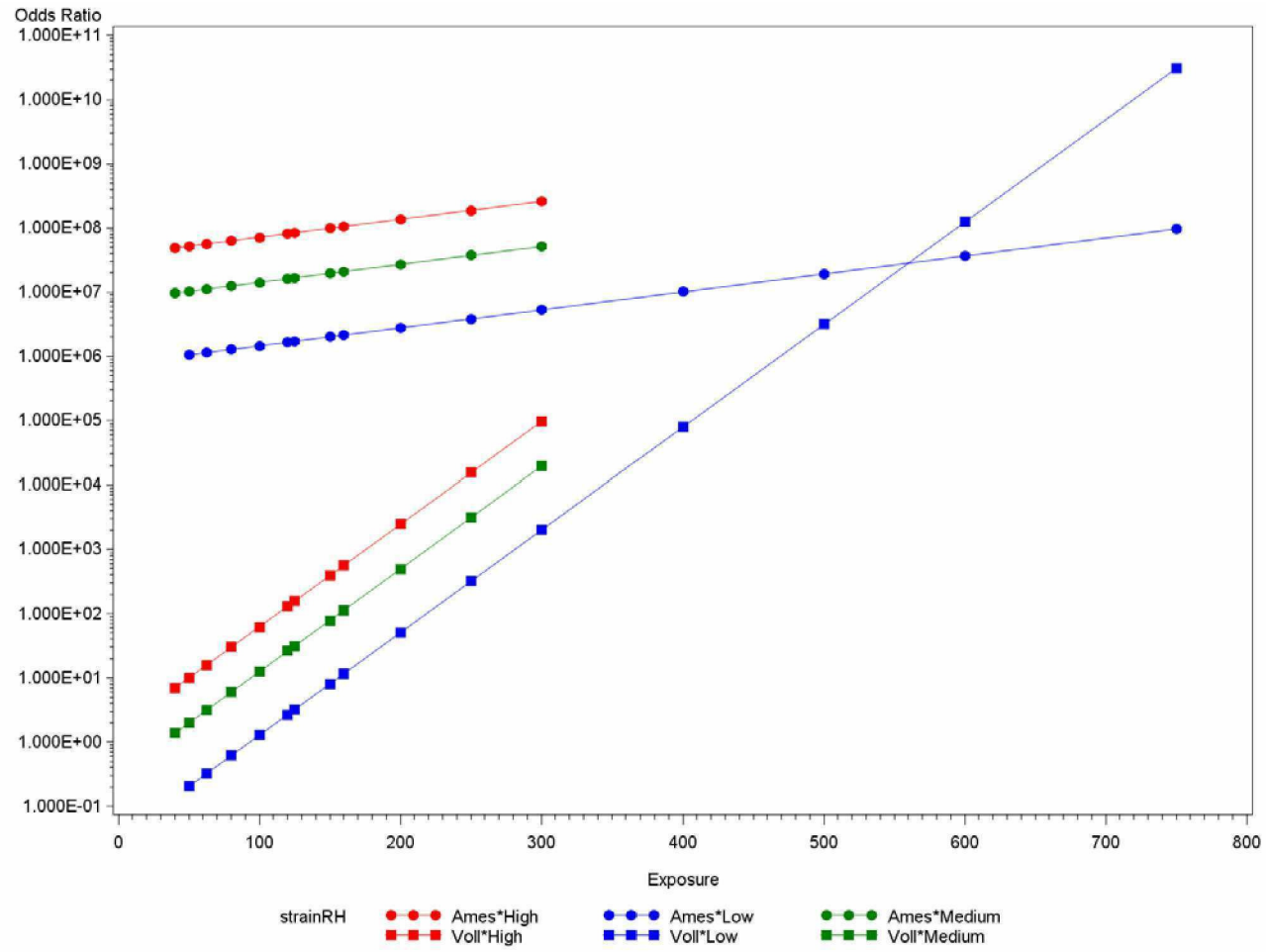

Figure D16. Odds Ratios Comparing Materials – Painted Wallboard Paper vs Unpainted Concrete (Varying by Strain by RH)

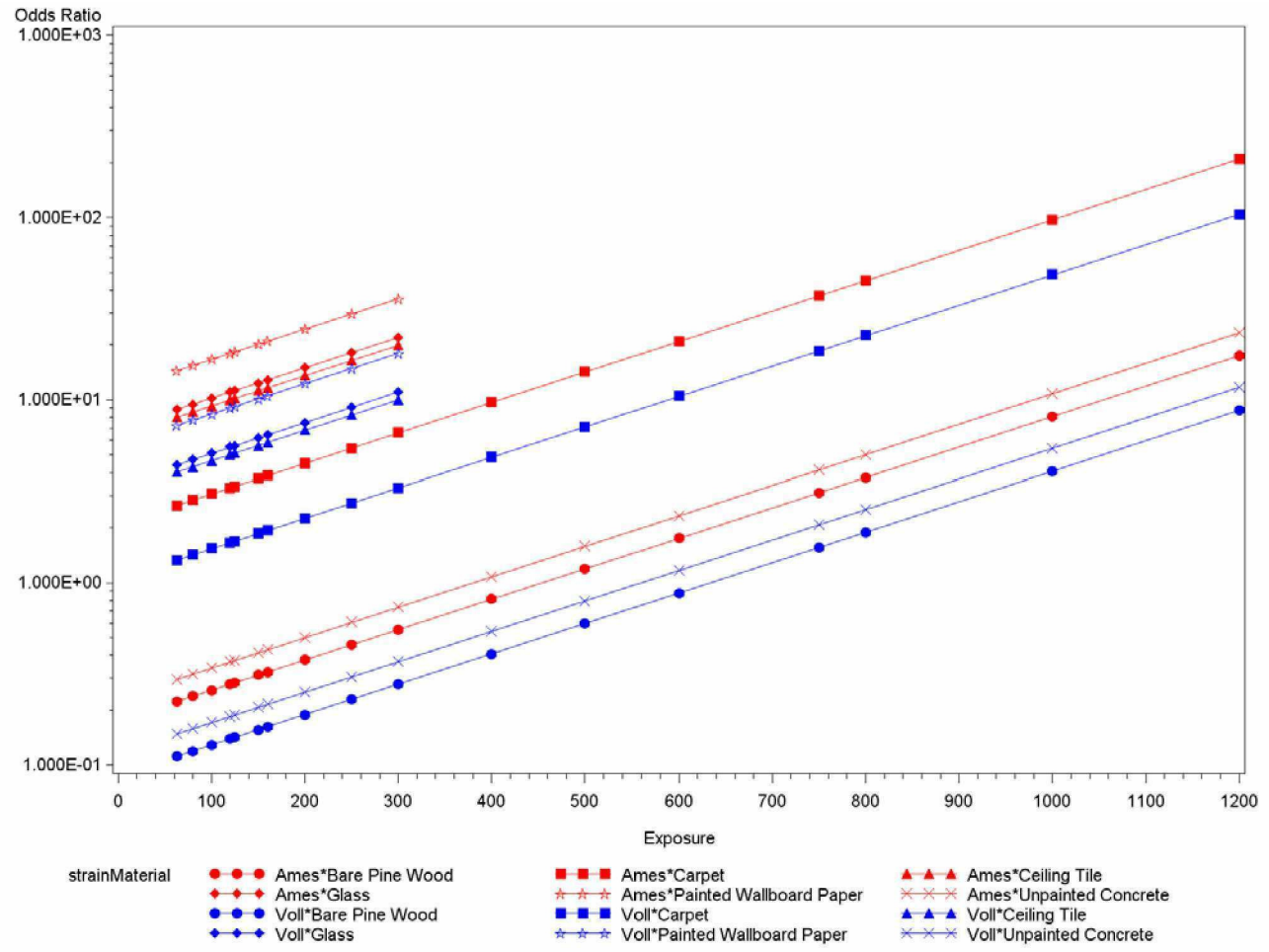

Figure D17. Odds Ratios Comparing RH – High vs Low (Varying by Strain by Material)

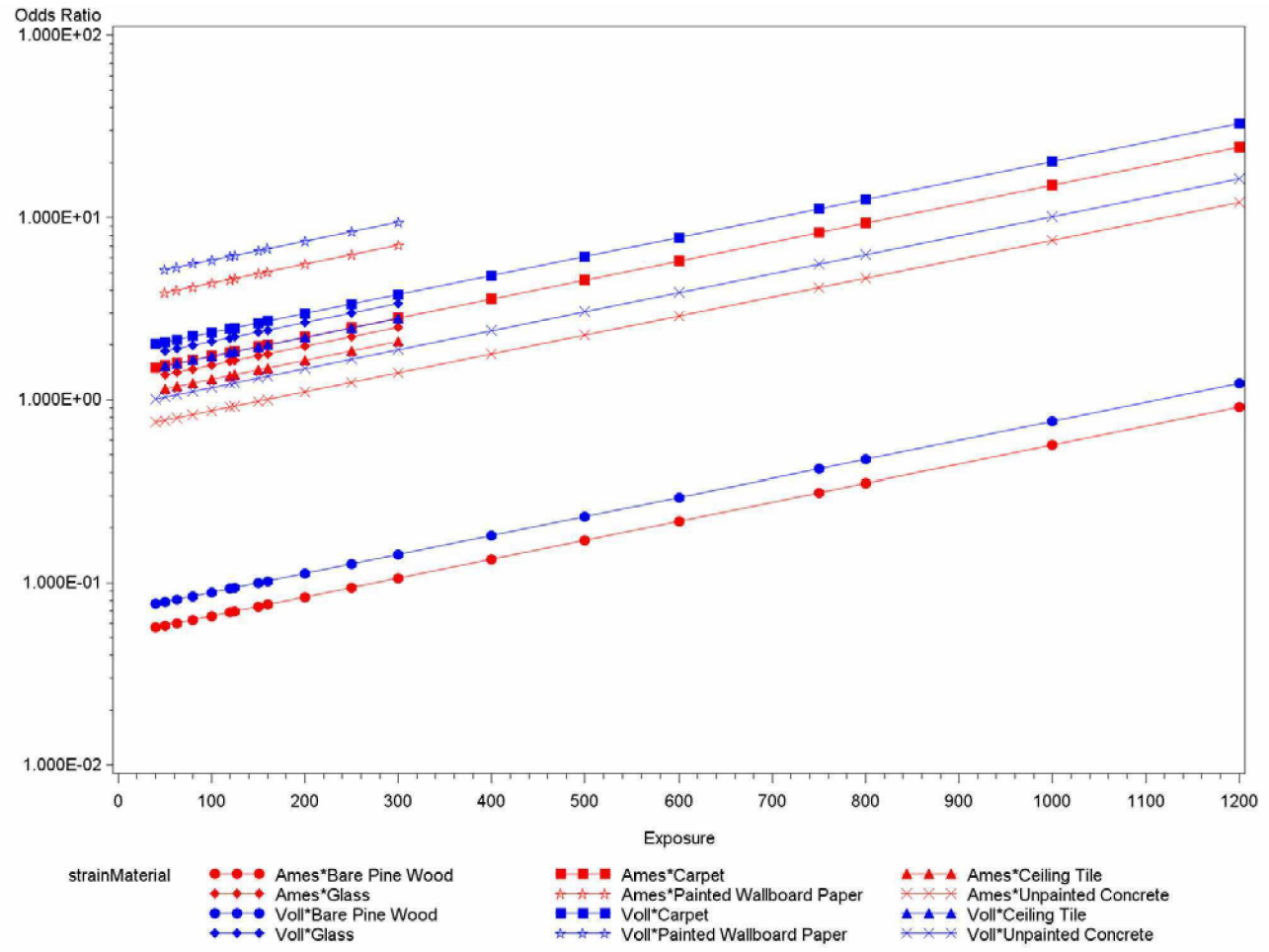

Figure D18. Odds Ratios Comparing RH – High vs Medium (Varying by Strain by Material)

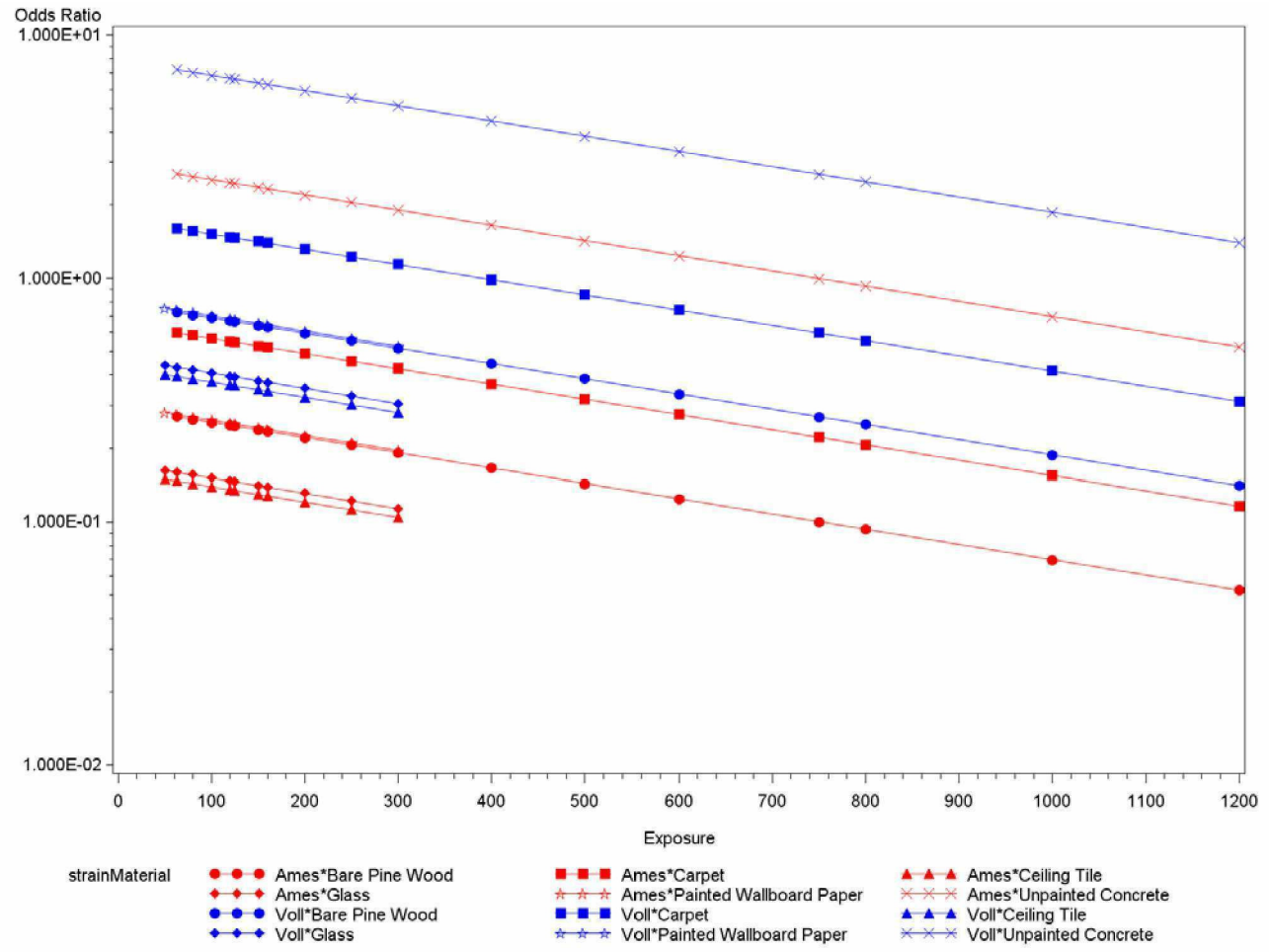

Figure D19. Odds Ratios Comparing RH – Low vs Medium (Varying by Strain by Material)

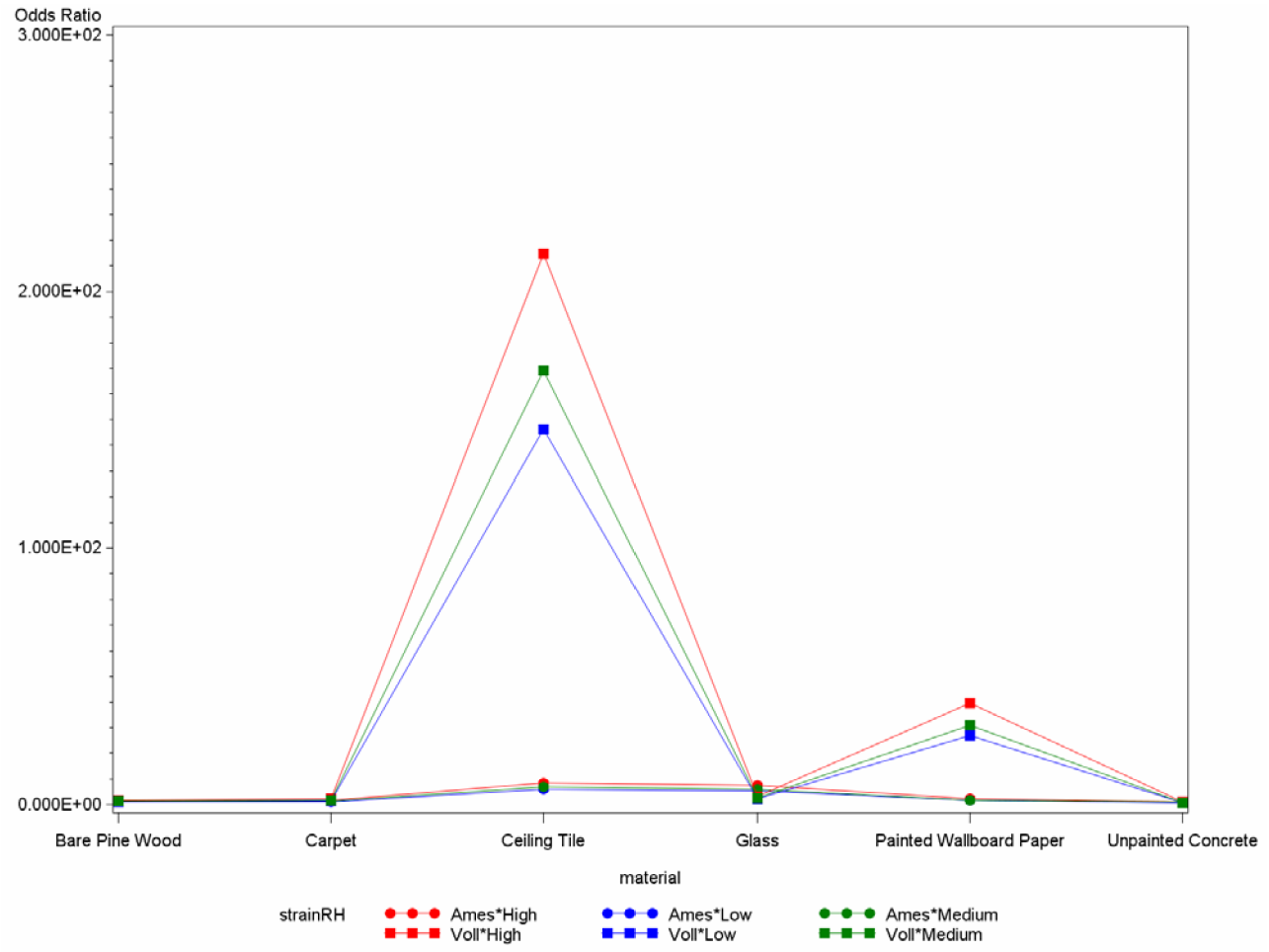

Figure D20. Odds Ratios per 100 Unit Increase in Dose

United States
Environmental Protection
Agency

PRESORTED STANDARD
POSTAGE & FEES PAID
EPA
PERMIT NO. G-35

Office of Research and Development (8101R)
Washington, DC 20460

Official Business
Penalty for Private Use
$300

Environmental Science & Technology

pubs.acs.org/est

Article

Evaluating the Environmental Persistence and Inactivation of MS2 Bacteriophage and the Presumed Ebola Virus Surrogate Phi6 Using Low Concentration Hydrogen Peroxide Vapor

Joseph P. Wood,* William Richter, Michelle Sunderman, M. Worth Calfee, Shannon Serre, and Leroy Mickelsen

Cite This: https://dx.doi.org/10.1021/acs.est.9b06034

Read Online

ACCESS | Metrics & More | Article Recommendations | Supporting Information

ABSTRACT: Ebola virus (EBOV) disease outbreaks, as well as the ability of EBOV to persist in the environment under certain conditions, highlight the need to develop effective decontamination techniques against the virus. We evaluated the efficacy of hydrogen peroxide vapor (HPV) to inactivate MS2 and Phi6 bacteriophages, the latter a recommended surrogate for EBOV. The phages were inoculated onto six material types with and without the presence of whole human blood. The inoculated materials were then exposed to either a high or low concentration of HPV for various elapsed times. The phages were also recovered from positive controls at these same elapsed times, to assess environmental persistence and decontamination efficacy. Low concentration hydrogen peroxide vapor (LCHP; 25 ppm) was effective against both phages on all materials without the presence of blood at 2 h. LCHP was ineffective against the phages in the presence of blood, on all materials, even with a 3-day contact time. Higher concentrations of HPV (>400 ppm) with contact times of 24−32 h achieved approximately 2−6 log reduction of the phages in the presence of blood.

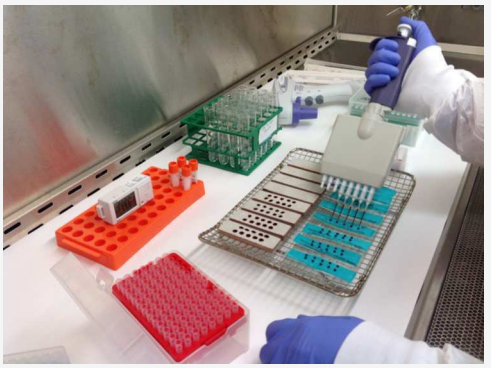

Downloaded via US EPA RESEARCH TRIANGLE PARK on March 3, 2020 at 13:29:54 (UTC).
See https://pubs.acs.org/sharingguidelines for options on how to legitimately share published articles.

INTRODUCTION

In the 2014−2016 Ebola virus (EBOV) disease outbreak in West Africa, there were 28 600 cases and over 11 000 fatalities.[1] The current EBOV disease outbreak in the Democratic Republic of the Congo has a fatality rate of approximately 67%[2] and highlights the concern of using the EBOV as a bioterrorism agent.[3] (Viruses producing hemorrhagic fever, such as EBOV, are considered Category A biological agents by the U.S. Centers for Disease Control and Prevention [CDC].) Moreover, environmental transmission of EBOV from fomites may be possible due to its persistence[4] and low infectious dose (10 viral particles).[5] EBOV may persist outside host cells for several days[6] or over a week,[7] depending on the environmental conditions and matrix (e.g., blood) with which the virus is associated.

Ebola virus is a filamentous, enveloped virus of the *Filoviridae* family.[8] Since EBOV is classified as a Risk Group 4 and Biosafety Level 4 agent,[9] relatively few laboratory disinfection studies using the actual EBOV[10−13] have been conducted. In lieu of evaluating EBOV, surrogate viruses have been proposed for disinfectant efficacy testing. In particular, the bacteriophage Phi6 has been recommended as an appropriate surrogate for EBOV for evaluating either environmental persistence or disinfection, based on having a similar viral structure (both EBOV and Phi6 are enveloped, RNA viruses) and empirical evidence.[8,14−19]

The presence of a lipid envelope in viruses is known to provide less resistance to disinfection compared to nonenveloped viruses.[9,20] Thus, as a precaution, the CDC recommends that disinfectants registered with the U.S. Environmental Protection Agency (EPA) for the more resistant nonenveloped viruses be used in environments where the enveloped EBOV may be present.[21] Accordingly, Sassi et al.[22] utilized the nonenveloped bacteriophage MS2 as a model virus for EBOV in their disinfection tests. In the present study we used the Phi6 bacteriophage as a surrogate for EBOV to evaluate disinfection via hydrogen peroxide vapor (HPV). But we also included MS2 as a test virus in our study, consistent with CDC recommendations and other research that included both bacteriophages to model EBOV.[23] Ideally, it would be preferable to conduct these tests alongside an actual EBOV strain to confirm the phage's suitability as a surrogate (to the best of our knowledge such tests have never been

Received: October 7, 2019
Revised: January 6, 2020
Accepted: February 19, 2020
Published: February 19, 2020

© XXXX American Chemical Society

Table 1. Study Test Matrix

virus	test materials	diluent	target decontamination conditions	time points assessed (h)
Phi6	glass, stainless steel, ceramic tile, N95 media, painted joint tape, wood	blood	25 ppm, 75% RH	2, 4, 24, 72
		PBS	25 ppm, 75% RH	2, 4, 6, 8
		blood	400 ppm, 75% RH	4, 8, 24, 32
MS2	glass, stainless steel, ceramic tile, N95 media, painted joint tape, wood	blood	25 ppm, 75% RH	2, 4, 8, 24, 32, 72
		PBS	25 ppm, 75% RH	2, 4, 6, 8
		blood	400 ppm, 75% RH	4, 8, 24, 32

undertaken), and this is suggested as further research to close this data gap.

While HPV has been demonstrated to be effective in the inactivation of viruses (e.g., refs 24−26), only a few studies evaluating HPV efficacy have included Phi6 or MS2,[27,28] and none with EBOV. Further, the present study focused on using a relatively low concentration of hydrogen peroxide vapor (LCHP; which, for the purpose of this study, we selected as ≤25 ppm [ppm]), based on previous research which was shown to be effective against influenza viruses[29] as well as for inactivating *Bacillus anthracis* spores,[30,31] provided sufficient contact time. The benefit to using LCHP is that it may be generated through inexpensive means such as off-the-shelf humidifiers using off-the-shelf 3 or 8% aqueous solutions of hydrogen peroxide, and be more compatible with materials.[30] This "low-tech" approach would be advantageous where specialized equipment and financial resources are limited. To assess the decontamination efficacy of HPV, the phages were recovered from positive controls (not exposed to HPV) at the same elapsed times as the decontaminated coupons; these data are also presented to provide an indication of the environmental stability of the phages.

MATERIALS AND METHODS

Bacteriophage Propagation. In general, the methods described here for inoculation and recovery of Phi6 and MS2 phage from material coupons are consistent with previous related research investigating environmental disinfection and persistence of viruses.[14,15,19,32,33]

The two bacteriophage viruses, MS2 (ATCC 15597-B1) and Phi6 (The EPA water treatment laboratory, Cincinnati, OH) were stored at −80 °C until testing. Working stocks of each phage were prepared using a top agar overlay technique.[15] Briefly, agar plates using Tryptic Soy Agar with Magnesium for Phi6 (Hardy Diagnostics, Santa Clara, CA; Model G341) and LB Agar (Hardy Diagnostics, G77) for MS2 were inoculated with 100 μL (μL) of stock phage, 100 μL of bacterial culture (*Pseudomonas syringae* LM2489 for Phi6 and *Escherichia coli* C-3000 [ATCC 15597] for MS2), and 5 mL (mL) of molten top agar (50 ± 5 °C) of the same media type. Following overnight incubation, top agar layers from plates with visible clearing of host bacteria were aseptically scraped into conical tubes containing 5 mL SM buffer (Teknova Inc., Hollister, CA; Model S0249) and centrifuged at 7000 rpm for 15 min. The supernatant was removed and filtered through a 0.2-μm syringe filter (Corning Inc., Corning, NY; model no. 431229).

Test Materials. Since decontamination efficacy is strongly dependent on the material with which the microorganism is associated,[34,35] five common indoor surface materials were used: glass (ASTM C1036, Brooks Brothers Glass & Mirror, Columbus, OH), painted joint tape (PJT; United States Gypsum Company, Chicago, IL; model no 382198), 304 stainless steel (SS; ASTM A240; McMaster Carr, Aurora, OH), glazed ceramic tile (Lowes, Hilliard, OH model PWHITW91L01), and bare pine wood (model 142−8PINE Lowes, Hilliard, OH). These materials were selected to include both porous and nonporous, organic and inorganic substrates, to provide a wide range of challenge to HPV. Additionally, due to its medical relevance, an N95 filter medium (used for respiratory protection; 3M, St. Paul, MN; model 1860) was included. Test coupons (1.9 × 7.5 cm^2) were cut from a larger piece of each representative material. The N95 filter medium was heat sealed along the edges to bind the three layers together, representative of the larger filtering facepiece respirator. Prior to testing, glass, SS, and ceramic tile coupons were sterilized by autoclaving at 121 °C for 15 min in sterilization pouches (Fisher Cat. No. NC9241087, Pittsburgh, PA). Painted joint tape, N95 filter media, and bare pine wood were sterilized by γ-irradiation with a dose of approximately 40 kilogray.

Environmental Conditions and Test Matrix. Overall, seven experiments were conducted in the study. Each experiment included all six test materials exposed to one HPV concentration, for up to four time points. While the focus of the study was on the use of LCHP (target of 25 ppm of HPV, based on an approximate average concentration that could be obtained using a humidifier in a large test chamber), we also conducted two experiments at a target of 400 ppmv HPV, since the higher concentration is more typical of what is used in medical or hospital environments,[36] or for decontamination of biocontainment laboratories.[37] The study design included the use of two bacteriophages (MS2 or Phi6), the stock solutions of which were diluted (1 in 10) with either phosphate buffered saline (PBS) or human whole blood, since blood has been shown to diminish efficacy.[12] When either phage was used with just the PBS diluent, we evaluated only the lower HPV concentration of 25 ppm, since the lower concentration was efficacious within a reasonable time. See Table 1, below, which provides an overview of the test matrix. An adaptive experimental test approach was taken in some cases, i.e., some time points were adjusted based on previous interim results, to better assess improvement in efficacy.

Sample Processing. Each day of testing, a 1:10 dilution of the stock solution of phage was prepared using either PBS (HyClone Laboratories, Cat. No. SH302560.2, Logan, UT) or human whole blood [BioIVT, Wesbury, NY; Cat. No. HUMANWBK2UZN]), to achieve a target titer of 5 × 10^7 plaque forming units (PFU)/mL. The actual inoculum titer was verified each day coupons were inoculated, using the phage quantification techniques discussed below. Sterile coupons were laid flat in a Class II Biological Safety Cabinet (BSC) and inoculated with approximately 5 × 10^6 PFU per coupon by dispensing 100 μL as 10 droplets (10 μL per droplet) across the surface of the test coupons. For each material type, three replicate coupons were used at each time point during decontamination. The maximum number of time

https://dx.doi.org/10.1021/acs.est.9b06034
Environ. Sci. Technol. XXXX, XXX, XXX−XXX

points that could be assessed in one experiment (test condition) was four, to allow 72 coupons in the test chamber. Three additional replicate coupons were used as positive controls (inoculated, exposed to ambient conditions, no exposure to HPV) for each time point and material. (The positive controls used for each time point allowed us to determine efficacy of the HPV treatment but also to assess persistence of the phage as well.) Following inoculation, all material coupons were dried for approximately 1 h in the BSC under ambient environmental conditions, prior to commencing exposure to HPV or the initial recovery of the phage at time zero. Additionally, two coupons of each material were used as blanks (not inoculated) and included for each time point tested. The blank coupons controlled for potential cross-contamination during testing as well as the sterility of the test coupons.

Decontaminant Testing. Decontamination testing was conducted inside a 498-L (L) acrylic glovebox (Plaslabs, Lansing, MI) at ambient temperatures. Fixed humidity point salts[38] were used to adjust relative humidity (RH) to a target of 75% for each experiment. Temperature and RH inside the test chamber were measured using a NIST-traceable temperature and humidity data logger (Onset, Bourne, MA; MX1101). Hydrogen peroxide vapor concentration was measured using a calibrated ATI B12 2-wire gas transmitter (Analytical Technology, Inc., Collegeville, PA) and was connected to a CNI-822 process controller (Omega Engineering, Norwalk, CT), which allowed for automatic control of HPV concentration within the test chamber; HPV data were recorded using the associated iLOG software (Omega Engineering, Norwalk, CT).

Generation of the HPV was achieved using a commercial generator (Bioquell Clarus C, Horsham, PA). Since commercial generators are typically used to target higher concentrations (>200 ppm), a two-chamber approach was required to achieve the lower 25 ppm target. For this lower target concentration, the generator supplied the HPV first to a mixing chamber to achieve a concentration of approximately 350 ppm, which then fed the test chamber as needed to maintain the target concentration of 25 ppm. Experiments targeting 400 ppm exposure level were achieved by connecting the HPV generator directly to the test chamber using a stock solution of 35% aqueous hydrogen peroxide. Once target RH and HPV were achieved and stable, the inoculated coupons were placed into a sealed container and transferred to the test chamber and opened, starting the exposure. With the direct connection between the HPV generator and the test chamber for the 400 ppm tests, the temperature within the test chamber was somewhat higher than in the LCHP tests, due to the flash evaporation of aqueous hydrogen peroxide. At the selected time points, a set of coupons was removed by placing them back into a sealed container and transferring them to a Class II BSC. Once in the BSC, the coupons were transferred to the extraction tubes.

Phage Recovery from Coupons and Quantification. At each time point, test and positive control coupons were collected and extracted for the phage by placing each individual coupon in a conical tube that contained 10 mL PBS. The tubes were agitated on their sides at room temperature on an orbital shaker for 15 min at 200 rpm. A series of 10-fold dilutions was prepared in PBS. An aliquot (0.1 mL) of the selected dilution and, when necessary, the undiluted extracts were plated onto the appropriate agar plates in triplicate by the overlay plaque assay method[15] as previously described. Each prepared tube of phage and host bacteria was then poured on a single plate and allowed to solidify under ambient conditions, then incubated at 26 ± 2 °C (Phi6) or 37 ± 2 °C (MS2) for 18−24 h. After incubation, plates were observed on light boxes, and visible plaques in the bacterial lawns were counted manually. The number of PFU/coupon was calculated by multiplying the mean number of plaques per plate by the reciprocal of the dilution, and then multiplying by 100 (0.1 mL aliquot was plated from the 10 mL sample used for each coupon extraction).

Decontamination Efficacy Calculations and D-values. For each test (coupons exposed to HPV, noted with subscript t) and positive control coupon (subscript pc), the number of PFU recovered was transformed to its $\log_{10}$ value. Then, the mean of the $\log_{10}$ values for each test coupon was subtracted from the mean of the $\log_{10}$ values from each positive control, for each time point assessed. This process is illustrated per the following equation, with efficacy reported in terms of $\log_{10}$ reduction (LR):

$$\text{efficacy} = \overline{(\log \text{PFUpc})} - \overline{(\log \text{PFUt})} \quad (1)$$

Test coupons in which there were no PFU recovered were assigned a PFU count of 1, resulting in a log PFU of zero. In such cases, the LR is reported as ≥ the value calculated by eq 1. For reference, we note that the US EPA requires that disinfectants with viricidal claims demonstrate ≥3 LR of the test virus on each surface.[39]

The LR results are reported with an associated 95% confidence interval (CI), calculated as follows:

$$95\%\text{CI} = \text{efficacy} \pm (1.96 \times \text{SE}) \quad (2)$$

The term SE is the pooled standard error, and was calculated as follows:

$$\text{SE} = \sqrt{\frac{S^2\text{pc}}{3} + \frac{S^2\text{t}}{3}} \quad (3)$$

where S is the standard deviation of the LR results for either the three positive controls (pc) or three test coupons (t) for each test condition.

In addition to calculating an LR value for each test condition and time point, we have determined inactivation rates (as D-values) for positive controls and the coupons exposed to HPV. D-values are commonly used to quantify the rate of inactivation of a microbial population, over several time points and are expressed as the time in h to reach 1 LR from the initially recovered PFU amount.[40,41] For brevity, these calculated D-values for each phage and test condition, as well as further information on the statistical methods and their detailed results, are found in the Supporting Information (SI). The D-values were calculated as the ratio of the shorter of the number of hours to achieve complete decontamination (i.e., when the phage was not detected) or the end of the decontamination test period; divided by the difference between the log recovery of the phage at the time point and the log recovery at time zero. To determine central values (e.g., median) and spread (e.g., 95% confidence interval) for D-value estimates at each condition, a resampling approach using R statistical computing software version 3.5.3 (https://www.r-project.org/) was used. From the distributions of D-values at each condition, several statistical comparisons were made to

https://dx.doi.org/10.1021/acs.est.9b06034
Environ. Sci. Technol. XXXX, XXX, XXX−XXX

Table 2. Experimental Test Conditions

test number	test bacteriophage	phage stock solution diluent	actual average ± SD concentration HPV ppm	actual average ± SD temperature ° C	actual average ± SD RH%	time points (h)
1.1	Phi6	blood	24.4 ± 1.23	22.8 ± 0.24	74.7 ± 0.20	2, 4
1.2	Phi6	PBS	24.6 ± 1.38	23.3 ± 0.07	72.5 ± 0.63	2, 4
1.2	Phi6	blood	25.0 ± 0.36	22.6 ± 0.57	73.5 ± 2.19	24, 72
2	Phi6	blood	429 ± 43.0	28.1 ± 0.52	63.4 ± 2.47	4, 8, 24, 32
3	MS2	PBS	24.9 ± 0.34	22.3 ± 0.10	71.6 ± 1.32	2, 4, 6, 8
4.1	MS2	blood	24.9 ± 0.42	22.2 ± 0.13	64.6 ± 2.8	4, 8
4.2	MS2	blood	25.0 ± 0.68	22.4 ± 0.11	63.5 ± 4.3	24, 32
5	MS2	blood	454 ± 49.3	27.4 ± 0.35	74.6 ± 3.28	4, 8, 24, 32
6.1	Phi6	PBS	25.2 ± 0.6	22.0 ± 0.14	69.7 ± 1.11	6, 8
6.2	MS2	blood	25.3 ± 0.51	22.3 ± 0.3	75.8 ± 2.32	2, 72

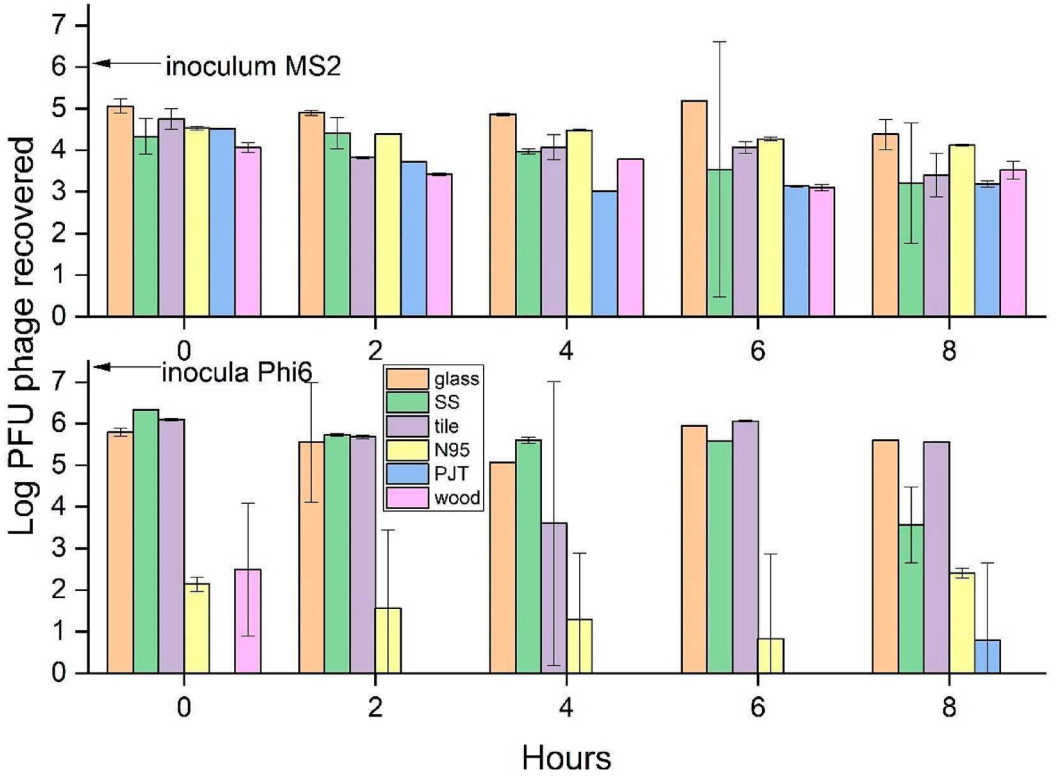

Figure 1. Inoculum and recovery of phages (average log plaque forming units ± SD) diluted in phosphate buffered saline from positive control materials, by elapsed time.

determine the significance of variables, and these are discussed along with efficacy results.

RESULTS AND DISCUSSION

Environmental Conditions. The measured air temperature, RH, and HPV concentration within the test chamber for each experiment of the study are summarized in Table 2. As Table 2 shows, some experiments such as Test 1.2 or Test 6 utilized both phages or both phage diluents (blood or PBS) concurrently in the test chamber. In Test 4, in which MS2 in blood was evaluated at 25 ppm of HPV, two subtrials were conducted because of the wide range in time points.

Air temperatures within the test chamber ranged between 22 and 28 °C, and average RH levels ranged from 63 to 76%. When fumigating at the LCHP target of 25 ppm (all tests except 2 and 5), actual concentrations were within 1 ppm of the target. In the two tests where we targeted a higher HPV concentration of 400 ppm, the actual average levels ranged from 429 to 454 ppm. While these HPV levels were somewhat higher (7−13%) than we had intended, the results are still valid and informative. The positive controls, which were kept outside the test chamber at ambient conditions, were exposed to average air temperatures ranging from 21.1−21.7 °C and average RH levels from 15−59%. A table summarizing these environmental conditions for the controls in terms of average ± standard deviation is found in the SI.

Inoculum and Recovery Levels for MS2 and Phi6 Phages from Positive Controls. The results for the inoculum titer quantification and the subsequent recoveries of the Phi6 and MS2 phages from the positive controls, presented as the average log PFU recovered from each material at each elapsed time, are shown in Figures 1 and 2. (For a more detailed listing of these results, including additional time points, refer to the corresponding tables found in the SI.) The positive control recoveries are aggregated in the figures as a function of phage and diluent and varied by several orders of

https://dx.doi.org/10.1021/acs.est.9b06034
Environ. Sci. Technol. XXXX, XXX, XXX−XXX

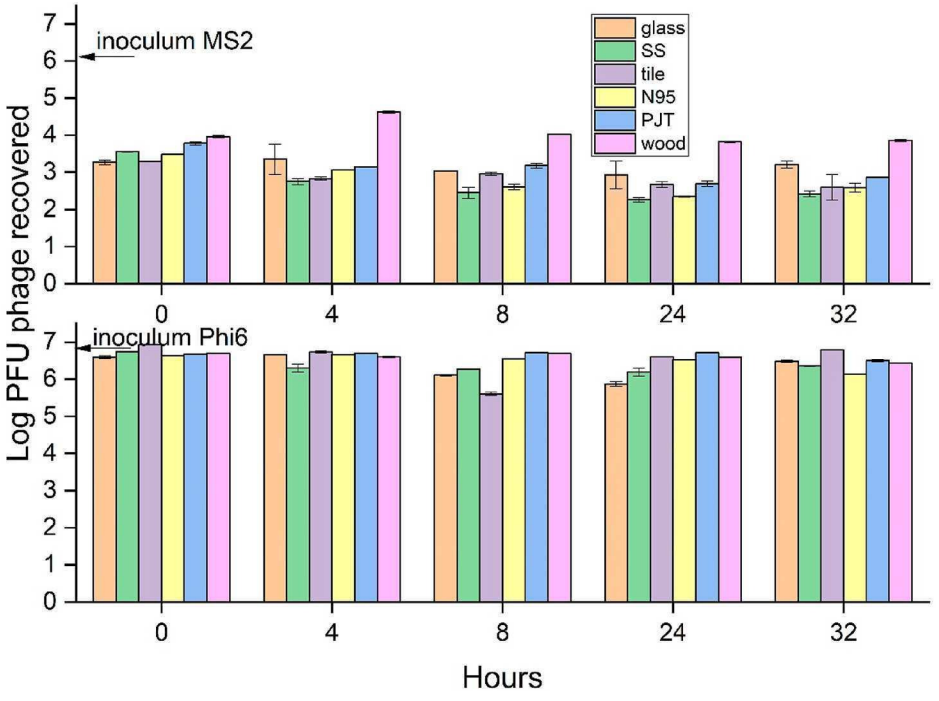

Figure 2. Inoculum and recovery of phages (average log plaque forming units ± SD) in blood diluent from positive control materials, by elapsed time.

magnitude. The inoculum levels of Phi6 averaged approximately 7.0 log PFU/coupon, whereas the MS2 inoculum levels averaged approximately a log lower, at 6.1 log PFU/coupon. While the results for the phage recoveries from positive controls are used primarily for the calculation of decontamination efficacy, the recoveries also provide insight into how the phages may persist over time outside their host cells on various materials, with or without the presence of human blood. In general, the loss in recovery or detection of a virus (or any other microorganism) from an inoculated material at ambient conditions may be due to the inability to physically extract the virus particle from the material (e.g., because of material porosity, adherence to the material) and/or that the virus was inactivated to some degree (possibly due to desiccation, chemical interaction with material).

In comparing the results for Figures 1 and 2, while the Phi6 phage was generally more persistent in blood than in PBS, the Phi6 phage in PBS was still recovered in appreciable quantities (>3.5 log PFU) from the nonporous glass, tile, and SS at the longest time point tested (8 h). With Phi6 in blood (Figure 2 and Table S9), nearly 6 log PFU was recovered from all materials at the longest time point tested of 72 h (Test 1.2), and >6 log PFU recovered at 32 h (Test 2) on all materials. The loss in recovery of the Phi6 phage in blood after 72 h was only 0.7−1.3 LR. The effect of material on the recovery of Phi6 was masked by the presence of blood. That is, the recovery of Phi6 in the PBS diluent (Figure 1, Table S8) from positive controls varied more by material than it did in blood, with generally poorer recoveries of the Phi6 phage occurring with the porous materials (PJT, N95 mask material, and wood). Further, in the PBS diluent, the Phi6 phage was not recovered from PJT at the initial "zero" time point, and was not recovered (not detected) from PJT or wood at the 2-h time point. The Phi6 phage in PBS did, however, demonstrate more stability on the nonporous materials (glass, SS, and tile), with over 5.5 log PFU recovered from glass and tile at 8 h, the longest time examined for the phages in PBS. That the Phi6 phage was generally more persistent (higher recoveries) in blood compared to PBS is generally consistent with their associated decay rates (refer to SI Table S4). Specifically, the *D*-values for Phi6 positive controls in blood ranged from 57 to 331 h, while the *D*-values for Phi6 in PBS were more variable (by material) and indeterminate, but generally lower.

In contrast to Phi6, the effect of diluent and material was not as pronounced for the MS2 phage.. When comparing the common 8-h time points for the two diluents, the range in average recovery of the MS2 phage in blood was ∼2.5−4.0 (Figure 2) and the range in recovery of the MS2 phage in PBS was 3.2−4.4 PFU. Further, the *D*-values for the MS2/blood positive controls were not significantly different from the *D*-values for the MS2/PBS positive controls, except for the N95 material (Table S4).

Thus, the presence of blood did not provide much additional protection to the MS2 phage, whereas the presence of blood does so for the enveloped Phi6 phage. This is an important finding as it contradicts the general thinking behind the disinfection hierarchy which indicates that the nonenveloped viruses (such as MS2) should be more resistant than the enveloped viruses. We were not able to locate data in the literature assessing the effect of blood on the persistence of MS2 or Phi6, to compare with our results. Research with EBOV did show that the virus was more stable in the presence of dried blood, although it depended on temperature and RH. Specifically, Schuitt et al.[7] showed that the decay rates of EBOV diluted in cell culture media and dried on materials were similar to the decay rates when EBOV was diluted in blood at room temperature (22 °C, 41% RH). However, at 28 °C and 90% RH, EBOV did persist longer in the blood matrix than in the cell culture media. Interestingly, for their 22 °C/41% RH test condition, which is comparable to our environmental condition for positive controls, Schuitt et al.[7] recovered approximately 0.8−1.5 log PFU EBOV/Mak-C05 in

https://dx.doi.org/10.1021/acs.est.9b06034
Environ. Sci. Technol. XXXX, XXX, XXX−XXX

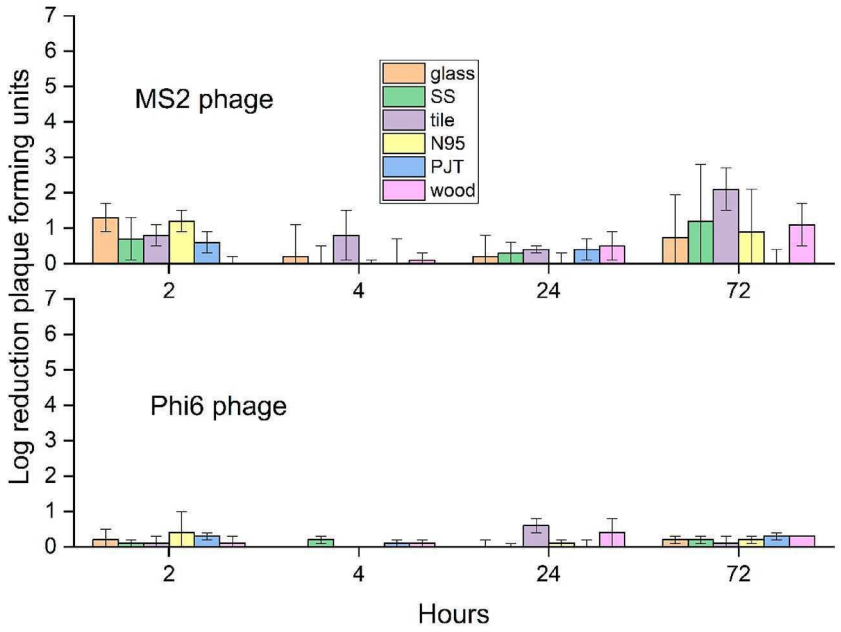

Figure 3. Decontamination efficacy results for Phi6 and MS2 diluted in blood, using low concentration hydrogen peroxide vapor (~25 ppm), as average log reduction ±95% confidence interval limits.

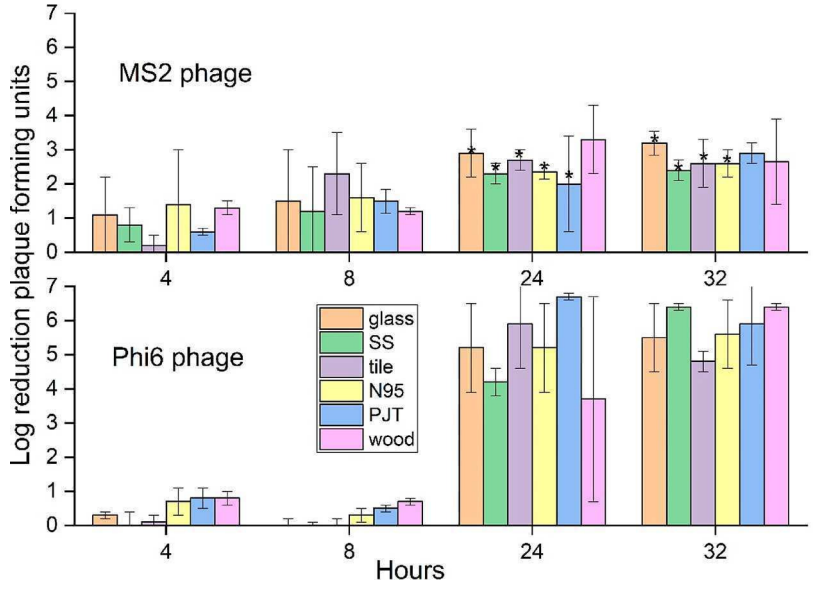

Figure 4. Decontamination efficacy results for Phi6 and MS2 diluted in blood, using hydrogen peroxide vapor >400 ppm, as average log reduction ±95% confidence interval limits. Bars with an asterisk indicate no phage were recovered from any test coupons, and thus efficacy results are determined based on recovery from positive controls.

dried blood from their four materials at 72 h (an approximately 2−3 LR). Under similar environmental conditions and elapsed time, our recovery of MS2 (1.9−3.6 log PFU) in the blood matrix was comparable to their EBOV recovery (the LR values for both were similar as well), but our recovery of the Phi6 phage was much higher (5.8−5.9 log PFU recovered; ~0.5 LR). In another study, EBOV showed greater persistence when maintained in liquid blood compared to water.[42]

In comparing the persistence of the two phages, the loss in recovery of MS2 in the presence of blood (Figure 2) was generally greater than the loss in recovery of Phi6 in blood. For example, at the common 72-h time point, only approximately 2−3 log PFU of MS2 in blood was recovered from the six positive control materials (refer to Table S11), which contrasts to the nearly 6 log PFU of the Phi6 in blood that was recovered for the same elapsed time, for every material. However, when comparing the two phages suspended in PBS (Figure 1), MS2 was recovered on all positive control materials, including PJT and wood, at 8 h, while the Phi6 in PBS was less persistent, at least on the porous materials (wood, PJT, N95). Thus, without the protection of the dried human blood, the nonenveloped MS2 phage shows more environmental persistence/stability on all materials than the enveloped Phi6, which is consistent with the general thinking that enveloped viruses are less resistant than nonenveloped viruses to disinfectants.[21,43] This finding is also consistent with a study

https://dx.doi.org/10.1021/acs.est.9b06034
Environ. Sci. Technol. XXXX, XXX, XXX−XXX

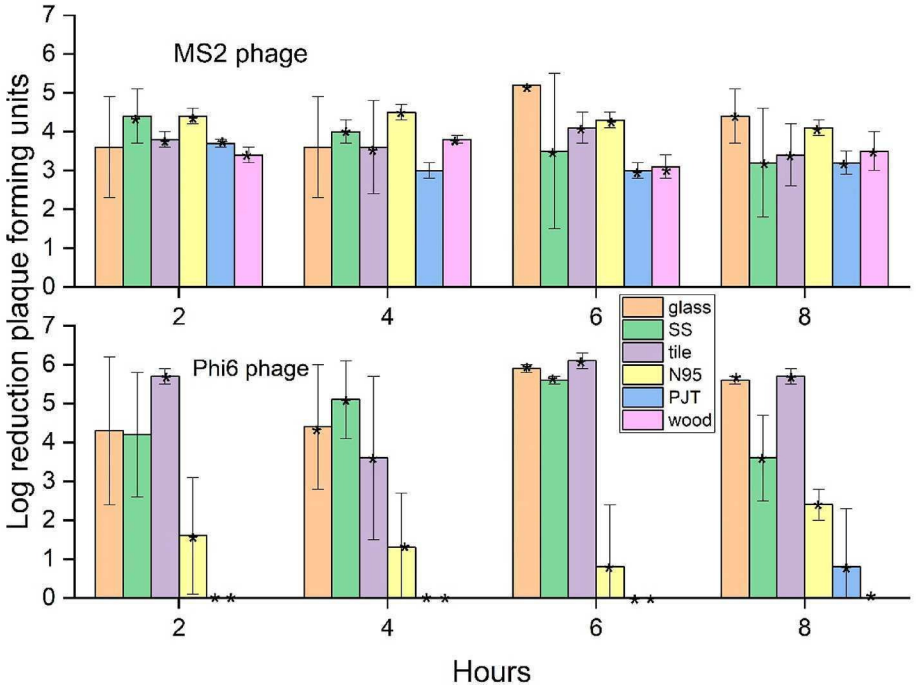

Figure 5. Decontamination efficacy results for Phi6 and MS2 diluted in phosphate buffered saline, using low concentration hydrogen peroxide vapor (~25 ppm), as average log reduction ±95% confidence interval limits. Bars with an asterisk indicate that no phages were recovered from any test coupons, and thus efficacy results are determined based on recovery from positive controls.

examining the persistence of MS2 and Phi6 (as potential surrogates for EBOV) in landfill leachate,[15] which found the enveloped Phi6 phage was much less stable than the MS2. In another study, the MS2 phage was also more stable (retained infectivity longer) than Phi6 when aerosolized and exposed to various RH levels and temperatures.[44]

Overall, the MS2 phage was recovered on all positive control materials at 8 h in the PBS diluent, and both phages were recovered at 72 h on all positive control materials in the presence of human blood. In the blood diluent, the persistence of both phages was prolonged and generally masked the effect of material, although this effect of blood was not as pronounced in the recovery of the nonenveloped MS2 phage. Relatively little decrease in the recovery of the Phi6 phage occurred at the longest time point evaluated (72 h) when dried in human whole blood, on all materials, corresponding to *D*-values up to hundreds of hours for a 1 LR.

HPV Decontamination Efficacy Results for MS2 and Phi6. The decontamination efficacy results for the study, presented in terms of the average LR of PFU, are summarized in Figures 3, 4, and 5. Select representative results are displayed for each material in each experiment, as a function of the HPV concentration (e.g., low or high level), diluent (PBS or human blood), and contact time. (All detailed decontamination efficacy results are also tabulated in the SI, Table S12.) There was minimal inactivation efficacy against both the MS2 and Phi6 phages when the phages were diluted in blood, dried onto various materials, and exposed to the LCHP of 25 ppm; refer to Figure 3. Over 90% of these average efficacy results from these test runs, for both phages, were <1 LR, while the maximum efficacy achieved overall at this condition was 2.09 LR (for MS2), which occurred at the 72-h time point on tile (Test 6.2). Although the decontamination efficacy of the LCHP was relatively low for both phages diluted in blood, statistical analysis (refer to SI) of the inactivation rates showed that the *D*-values for MS2 were generally significantly lower (approximately an order of magnitude) than for Phi6.

The presence of blood continued to preserve or shield both phages at the higher HPV concentrations (429 and 454 ppm) as well, albeit some inactivation (at least 3 to 4 LR) of both Phi6 and MS2 became evident at 24-h; refer to Figure 4. For example, at the 4- and 8-h time points for the tests >400 ppm of HPV, the LR values for the six materials were all less than 1.0 for the Phi6 phage, while the LR values for the MS2 phage were somewhat higher than the LR values for the Phi6 and ranged from 1.2 to 2.3 at the 8-h time point. At 24 h, the >400 ppm of HPV did effectively inactivate the Phi6 phage on all materials. For the MS2 phage at 24 h, none of the phage was recovered on any of the materials except wood, making decontamination efficacy values indeterminate but generally ≥2 LR. Overall, these efficacy values are still quite low compared to efficacy values achievable with similarly high HPV concentrations against other microorganisms, but without the presence of blood. For example, >6 LR was achieved against *Bacillus anthracis* spores on similar materials when using 290 ppm of HPV for 3 h.[45]

As expected, the LCHP decontamination approach (25 ppm) achieved higher efficacy with the phages inoculated in PBS (Figure 5) compared to when they were inoculated in blood. That is, without the presence of blood, the LCHP was effective (≥3 LR) for both phages on all materials at 2 h, for the materials in which phage were recovered/detected. In Test 3, with MS2/PBS at the 2-h time point, none of the materials had recoverable phage except for glass, which showed a LR of 3.58. The MS2 phage was inactivated at >5.2 LR on glass at the 6-h time point. In Test 6.1 with Phi6/PBS, decontamination at 25 ppm of HPV for 6 h resulted in no recoverable phage from all six materials. With the highest recovery of Phi6 on the nonporous material controls, this resulted in having >5.58 LR on glass, SS, and tile. The highest LR achieved against Phi6/

https://dx.doi.org/10.1021/acs.est.9b06034
Environ. Sci. Technol. XXXX, XXX, XXX−XXX

PBS was >6.06 on tile at 6 h. As also expected, the *D*-values for the LCHP (25 ppm) for both phages in PBS were all ≤1 h and were significantly lower than the *D*-values for the inactivation of phages in blood.

These results demonstrating the deleterious effect of blood on the efficacy of HPV are generally consistent with the literature.[46] For example, Heckert et al. showed minimal LR against Classical Swine Fever (hog cholera) virus in the presence of porcine whole blood.[24] Pottage et al. showed that increasing the blood diluent level from 10% to 50% decreased the inactivation against the MS2 phage several orders of magnitude when using HPV.[27] The presence of blood also diminishes the efficacy of other decontaminants against other microorganisms, one example being the use of chlorine dioxide gas for the inactivation of several species of bacteria.[47] In the evaluation of several liquid disinfectants (including chlorine bleach) to assess their ability to inactivate EBOV in the presence of blood, only 5% peracetic acid was effective.[12] We would agree with Smither et al.,[12] who suggest two reasons why the presence of blood diminishes inactivation of viruses and microorganisms: that the blood may be providing a physical barrier for the decontaminant to reach the virus; and/or that the blood, an organic material, reacts with the oxidant-based decontaminant and reduces its concentration prior to reaching the virus. HPV, bleach, chlorine dioxide, and many other decontaminants rely on oxidation as the mechanism for microbial inactivation.

We were not able to locate any literature related to the use of LCHP for the inactivation of MS2, Phi6, and/or EBOV, with which to compare our results. The best comparison we can make with the literature is a study evaluating LCHP for the inactivation of another enveloped virus, i.e., several influenza viruses,[29] and which reported nearly 3.5 LR of the virus on stainless steel, using a HPV concentration of 10 ppm for only 15 min.

Regarding the effect of material on decontamination efficacy in the presence of blood, for both phages, the results indicate a lack of difference in efficacy among the six materials, most likely due to the blood overriding or masking any underlying material effects. With the phages diluted in PBS, the majority of the LCHP decontamination tests resulted in no recovery of the phages, making it difficult to make valid comparisons among the materials.

In summary, without the presence of human blood, the LCHP was effective (≥3 LR) against both phages on all materials at two h contact time, for the phages that were recoverable from controls at that time. Additionally, both the Phi6 and MS2 phages in the PBS diluent were completely inactivated (none detected) by the LCHP on all materials by 6 h. But in the blood matrix, LCHP was ineffective against both phages for all materials, even with a 3-day contact time. Thus, extrapolating from these results for both an enveloped and nonenveloped virus, we would expect LCHP would be a viable decontamination option for EBOV for relatively clean surfaces. Although we caveat that having data for an EBOV would be preferred to that of a surrogate, the evidence we proffer here and, as noted in the literature,[10] suggest that the presence/absence of a viral envelope, protective organic matrix such as blood, and the material with which the microorganism is associated may be more of a factor in decontamination efficacy (as well as environmental persistence) than the actual virus genome/biochemistry. In the presence of blood, high levels of HPV (>400 ppm) were effective in inactivating the Phi6 phage on all materials with 1 day contact time, but results were indeterminant for MS2, due to the inability to recover the MS2 phage from positive control materials ≥3 log PFU at 24 h. Further investigation of decontamination techniques that would be effective in inactivating the EBOV in a blood matrix is recommended.

■ ASSOCIATED CONTENT

Supporting Information

The Supporting Information is available free of charge at https://pubs.acs.org/doi/10.1021/acs.est.9b06034.

> Inactivation/decay rates (as *D*-values) for phages, for positive controls and those exposed to HPV; statistical comparison of *D*-values; positive control recovery results in visual format (figures) and detailed results in tables; environmental conditions for positive controls; and detailed decontamination efficacy results in table format (PDF)

■ AUTHOR INFORMATION

Corresponding Author

Joseph P. Wood − *U.S. Environmental Protection Agency, Office of Research and Development, National Homeland Security Research Center, Research Triangle Park, North Carolina 27711, United States;* orcid.org/0000-0001-6316-9418; Email: wood.joe@epa.gov

Authors

William Richter − *Battelle Memorial Institute, Columbus, Ohio 43201, United States*

Michelle Sunderman − *Battelle Memorial Institute, Columbus, Ohio 43201, United States*

M. Worth Calfee − *U.S. Environmental Protection Agency, Office of Research and Development, National Homeland Security Research Center, Research Triangle Park, North Carolina 27711, United States*

Shannon Serre − *U.S. Environmental Protection Agency, Office of Land and Emergency Management, Chemical, Biological, Radiological, and Nuclear Consequence Management Advisory Division, Research Triangle Park, North Carolina 27711, United States*

Leroy Mickelsen − *U.S. Environmental Protection Agency, Office of Land and Emergency Management, Chemical, Biological, Radiological, and Nuclear Consequence Management Advisory Division, Research Triangle Park, North Carolina 27711, United States*

Complete contact information is available at: https://pubs.acs.org/10.1021/acs.est.9b06034

Funding

The EPA, through its Office of Research and Development, funded and directed the research described herein under contract EP-C-15-002-0019 with Battelle Memorial Institute. It has been subjected to the Agency's review and has been approved for publication. Mention of trade names, products, or services does not convey official EPA approval, endorsement, or recommendation.

Notes

The authors declare no competing financial interest.

■ ACKNOWLEDGMENTS

We acknowledge Robert Krile and William White for statistical analysis.

■ REFERENCES

(1) U.S. CDC. U.S. Centers for Disease Control and Prevention 2014−2016 Ebola Outbreak in West Africahttps://www.cdc.gov/vhf/ebola/history/2014-2016-outbreak/index.html (Accessed 4/8/19).
(2) World Health Organization (WHO). World Health Organization Ebola Situation Reports: Democratic Republic of the Congo. https://www.who.int/ebola/situation-reports/drc-2018/en/ (Accessed 9/16/19).
(3) Cenciarelli, O.; Gabbarini, V.; Pietropaoli, S.; Malizia, A.; Tamburrini, A.; Ludovici, G. M.; Carestia, M.; Di Giovanni, D.; Sassolini, A.; Palombi, L.; et al. Viral bioterrorism: Learning the lesson of Ebola virus in West Africa 2013−2015. *Virus Res.* **2015**, *210*, 318−326.
(4) Vetter, P.; Fischer, W. A., 2nd; Schibler, M.; Jacobs, M.; Bausch, D. G.; Kaiser, L. Ebola Virus Shedding and Transmission: Review of Current Evidence. *J. Infect. Dis.* **2016**, *214*, S177−S184.
(5) Osterholm, M. T.; Moore, K. A.; Kelley, N. S.; Brosseau, L. M.; Wong, G.; Murphy, F. A.; Peters, C. J.; LeDuc, J. W.; Russell, P. K.; Van Herp, M.; et al. Transmission of Ebola viruses: what we know and what we do not know. *mBio* **2015**, *6* (2), No. e00137-15.
(6) Nikiforuk, A. M.; Cutts, T. A.; Theriault, S. S.; Cook, B. W. M. Challenge of Liquid Stressed Protective Materials and Environmental Persistence of Ebola Virus. *Sci. Rep.* **2017**, *7* (1), 4388.
(7) Schuit, M.; Miller, D. M.; Reddick-Elick, M. S.; Wlazlowski, C. B.; Filone, C. M.; Herzog, A.; Colf, L. A.; Wahl-Jensen, V.; Hevey, M.; Noah, J. W. Differences in the Comparative Stability of Ebola Virus Makona-C05 and Yambuku-Mayinga in Blood. *PLoS One* **2016**, *11* (2), No. e0148476.
(8) Gallandat, K.; Lantagne, D. Selection of a Biosafety Level 1 (BSL-1) surrogate to evaluate surface disinfection efficacy in Ebola outbreaks: Comparison of four bacteriophages. *PLoS One* **2017**, *12* (5), No. e0177943.
(9) U.S. Department of Health and Human Services. *Biosafety in Microbiological and Biomedical Laboratories*, 5th ed.; CDC 21−1112, 2009.
(10) Cook, B. W.; Cutts, T. A.; Nikiforuk, A. M.; Poliquin, P. G.; Court, D. A.; Strong, J. E.; Theriault, S. S. Evaluating environmental persistence and disinfection of the Ebola virus Makona variant. *Viruses* **2015**, *7* (4), 1975−86.
(11) Cutts, T.; Cook, B.; Poliquin, G.; Strong, J.; Theriault, S. Inactivating Zaire Ebolavirus in Whole-Blood Thin Smears Used for Malaria Diagnosis. *J. Clin. Microbiol.* **2016**, *54* (4), 1157−9.
(12) Smither, S. J.; Eastaugh, L.; Filone, C. M.; Freeburger, D.; Herzog, A.; Lever, M. S.; Miller, D. M.; Mitzel, D.; Noah, J. W.; Reddick-Elick, M. S.; et al. Two-Center Evaluation of Disinfectant Efficacy against Ebola Virus in Clinical and Laboratory Matrices. *Emerging Infect. Dis.* **2018**, *24* (1), 135−139.
(13) Cook, B. W.; Cutts, T. A.; Nikiforuk, A. M.; Leung, A.; Kobasa, D.; Theriault, S. S. The Disinfection Characteristics of Ebola Virus Outbreak Variants. *Sci. Rep.* **2016**, *6* (1), 38293.
(14) Gallandat, K.; Wolfe, M. K.; Lantagne, D. Surface Cleaning and Disinfection: Efficacy Assessment of Four Chlorine Types Using Escherichia coli and the Ebola Surrogate Phi6. *Environ. Sci. Technol.* **2017**, *51* (8), 4624−4631.
(15) U.S. Environmental Protection Agency. *Viral Persistence in Landfill Leachate*; Washington, DC, 2018.
(16) Sassi, H. P.; Ikner, L. A.; Abd-Elmaksoud, S.; Gerba, C. P.; Pepper, I. L. Comparative survival of viruses during thermophilic and mesophilic anaerobic digestion. *Sci. Total Environ.* **2018**, *615*, 15−19.
(17) Bibby, K.; Casson, L. W.; Stachler, E.; Haas, C. N. Ebola virus persistence in the environment: state of the knowledge and research needs. *Environ. Sci. Technol. Lett.* **2015**, *2* (1), 2−6.
(18) Wolfe, M. K.; Gallandat, K.; Daniels, K.; Desmarais, A. M.; Scheinman, P.; Lantagne, D. Handwashing and Ebola virus disease outbreaks: A randomized comparison of soap, hand sanitizer, and 0.05% chlorine solutions on the inactivation and removal of model organisms Phi6 and E. coli from hands and persistence in rinse water. *PLoS One* **2017**, *12* (2), No. e0172734.
(19) Aquino de Carvalho, N.; Stachler, E. N.; Cimabue, N.; Bibby, K. Evaluation of Phi6 persistence and suitability as an enveloped virus surrogate. *Environ. Sci. Technol.* **2017**, *51* (15), 8692−8700.
(20) McDonnell, G. E. *Antisepsis, Disinfection, and Sterilization: Types, Action, and Resistance*, 2nd ed.. ASM Press: 2017.
(21) U.S. CDC. U.S. Centers for Disease Control and Prevention Interim Guidance for Environmental Infection Control in Hospitals for Ebola Virus. https://www.cdc.gov/vhf/ebola/clinicians/cleaning/hospitals.html (Accessed 4/8/2019),.
(22) Sassi, H. P.; Reynolds, K. A.; Pepper, I. L.; Gerba, C. P. Evaluation of hospital-grade disinfectants on viral deposition on surfaces after toilet flushing. *Am. J. Infect. Control* **2018**, *46* (5), 507−511.
(23) Lin, K.; Marr, L. C. Aerosolization of Ebola virus surrogates in wastewater systems. *Environ. Sci. Technol.* **2017**, *51* (5), 2669−2675.
(24) Heckert, R.; Best, M.; Jordan, L.; Dulac, G.; Eddington, D.; Sterritt, W. Efficacy of vaporized hydrogen peroxide against exotic animal viruses. *Appl. Environ. Microbiol.* **1997**, *63* (10), 3916−3918.
(25) Tuladhar, E.; Terpstra, P.; Koopmans, M.; Duizer, E. Virucidal efficacy of hydrogen peroxide vapour disinfection. *Journal of Hospital Infection* **2012**, *80* (2), 110−115.
(26) Goyal, S. M.; Chander, Y.; Yezli, S.; Otter, J. Evaluating the virucidal efficacy of hydrogen peroxide vapour. *Journal of hospital infection* **2014**, *86* (4), 255−259.
(27) Pottage, T.; Richardson, C.; Parks, S.; Walker, J. T.; Bennett, A. M. Evaluation of hydrogen peroxide gaseous disinfection systems to decontaminate viruses. *J. Hosp Infect* **2010**, *74* (1), 55−61.
(28) Turgeon, N.; Michel, K.; Ha, T. L.; Robine, E.; Moineau, S.; Duchaine, C. Resistance of Aerosolized Bacterial Viruses to Four Germicidal Products. *PLoS One* **2016**, *11* (12), No. e0168815.
(29) Rudnick, S. N.; McDevitt, J. J.; First, M. W.; Spengler, J. D. Inactivating influenza viruses on surfaces using hydrogen peroxide or triethylene glycol at low vapor concentrations. *Am. J. Infect. Control* **2009**, *37* (10), 813−819.
(30) Wood, J. P.; Calfee, M. W.; Clayton, M.; Griffin-Gatchalian, N.; Touati, A.; Ryan, S.; Mickelsen, L.; Smith, L.; Rastogi, V. A simple decontamination approach using hydrogen peroxide vapour for Bacillus anthracis spore inactivation. *J. Appl. Microbiol.* **2016**, *121* (6), 1603−1615.
(31) U.S. Environmental Protection Agency. Decontamination of Materials Contaminated with Spores of Bacillus anthracis Ames and Vollum Strains Using Low Concentrations of Hydrogen Peroxide Vapor; EPA/600/R-18/215; Washington, DC, 2018.
(32) Wood, J. P.; Choi, Y. W.; Chappie, D. J.; Rogers, J. V.; Kaye, J. Z. Environmental persistence of a highly pathogenic avian influenza (H5N1) virus. *Environ. Sci. Technol.* **2010**, *44* (19), 7515−7520.
(33) Wyrzykowska-Ceradini, B.; Calfee, M.W.; Touati, A.; Wood, J.; Mickelsen, R.L.; Miller, L.; Colby, M.; Slone, C.; Gatchalian, N.G.; Pongur, S.G.; Aslett, D. The use of bacteriophage MS2 for the development and application of a virucide decontamination test method for porous and heavily soiled surfaces. *J. Appl. Microbiol.* **2019**, *127* (5), 1315−1326.
(34) Calfee, M. W.; Wendling, M. Inactivation of vegetative bacterial threat agents on environmental surfaces. *Sci. Total Environ.* **2013**, *443*, 387−396.
(35) Wood, J. P.; Adrion, A. C. Review of Decontamination Techniques for the Inactivation of Bacillus anthracis and Other Spore-Forming Bacteria Associated with Building or Outdoor Materials. *Environ. Sci. Technol.* **2019**, *53* (8), 4045−4062.
(36) U.S. Environmental Protection Agency.. Vaprox Hydrogen Peroxide Sterilant—Amendment to Add Aseptic Food Processing Use. *EPA Pesticide Label Reg.* **2012**, 58779.
(37) Rogers, J. V.; Richter, W. R.; Shaw, M. Q.; Shesky, A. M. Large-scale inactivation of Bacillus anthracis Ames, Vollum, and Sterne

https://dx.doi.org/10.1021/acs.est.9b06034
Environ. Sci. Technol. XXXX, XXX, XXX−XXX

spores using vaporous hydrogen peroxide. *Applied Biosafety* **2009**, *14* (3), 127−134.
(38) ASTM International. Standard practice for maintaining constant relative humidity by means of aqueous solutions. West Conshohocken, PA, 2007.
(39) U.S. Environmental Protection Agency. Product Performance Test Guidelines, OCSPP 810.2200: Disinfectants for Use on Environmental Surfaces, Guidance for Efficacy Testing; EPA 712-C-17−004; Washington, DC, 2018.
(40) Wood, J. P.; Lemieux, P.; Betancourt, D.; Kariher, P.; Griffin, N. Pilot-scale experimental and theoretical investigations into the thermal destruction of a Bacillus anthracis surrogate embedded in building decontamination residue bundles. *Environ. Sci. Technol.* **2008**, *42* (15), 5712−5717.
(41) Richter, W.; Sunderman, M.; Wendling, M.; Serre, S.; Mickelsen, L.; Rupert, R.; Wood, J.; Choi, Y.; Willenberg, Z.; Calfee, M. Evaluation of Altered Environmental Conditions as a Decontamination Approach for Non-Spore-Forming Biological Agents. *J. Appl. Microbiol.* **2019** DOI: 10.1111/jam.14532.
(42) Fischer, R.; Judson, S.; Miazgowicz, K.; Bushmaker, T.; Prescott, J.; Munster, V. J. Ebola virus stability on surfaces and in fluids in simulated outbreak environments. *Emerging Infect. Dis.* **2015**, *21* (7), 1243.
(43) Weber, D. J.; Rutala, W. A.; Fischer, W. A.; Kanamori, H.; Sickbert-Bennett, E. E. Emerging infectious diseases: Focus on infection control issues for novel coronaviruses (Severe Acute Respiratory Syndrome-CoV and Middle East Respiratory Syndrome-CoV), hemorrhagic fever viruses (Lassa and Ebola), and highly pathogenic avian influenza viruses, A (H5N1) and A (H7N9). *Am. J. Infect. Control* **2016**, *44* (5), e91−e100.
(44) Verreault, D.; Marcoux-Voiselle, M.; Turgeon, N.; Moineau, S.; Duchaine, C. Resistance of aerosolized bacterial viruses to relative humidity and temperature. *Appl. Environ. Microbiol.* **2015**, *81* (20), 7305−7311.
(45) Rastogi, V. K.; Wallace, L.; Smith, L. S.; Ryan, S. P.; Martin, B. Quantitative method to determine sporicidal decontamination of building surfaces by gaseous fumigants, and issues related to laboratory-scale studies. *Appl. Environ. Microbiol.* **2009**, *75* (11), 3688−3694.
(46) Krug, P. W.; Davis, T.; O'Brien, C.; LaRocco, M.; Rodriguez, L. L. Disinfection of transboundary animal disease viruses on surfaces used in pork packing plants. *Vet. Microbiol.* **2018**, *219*, 219−225.
(47) Lowe, J. J.; Hewlett, A. L.; Iwen, P. C.; Smith, P. W.; Gibbs, S. G. Surrogate testing suggests that chlorine dioxide gas exposure would not inactivate Ebola virus contained in environmental blood contamination. *J. Occup. Environ. Hyg.* **2015**, *12* (9), D211−D215.

https://dx.doi.org/10.1021/acs.est.9b06034
Environ. Sci. Technol. XXXX, XXX, XXX−XXX

Decontamination Studies Related to Operation of Vehicles in an Area Contaminated with a Biological Agent

Presented at 2019 EPA International Decontamination Research and Development Conference

20 November 2019

William Richter
richterwr@battelle.org
614-424-4160

BATTELLE

Disclaimer

- The U.S. Environmental Protection Agency (EPA) through its Office of Research and Development (ORD) funded and managed the research described. It has been subjected to the Agency's review and has been approved for publication and distribution. Note that approval does not signify that the contents necessarily reflect the views of the Agency. Mention of trade names, products, or services does not convey official EPA approval, endorsement, or recommendation.
- Battelle is a contractor to EPA and provided technical support for the work described.

Background

- EPA is responsible for remediation following a wide area biological contamination event (including public infrastructure) involving *Bacillus anthracis* spores
- Following a wide area biological contamination event, many emergency or personal vehicles may become contaminated through direct event exposure or secondary exposure from cross-contamination.
- Following such an event many logistical challenges exist, including decontamination of large numbers of contaminated vehicles.
- Move contaminated vehicles to central processing area or decontaminate in-situ?
- EPA has developed a low-tech method of generating low concentration vapor phase hydrogen peroxide which offers benefits of rapid deployment and scalability.

Objective

- Evaluate the efficacy of low concentration vapor phase hydrogen peroxide generated by a common household humidifier against *Bacillus atrophaeus* spores (*B. anthracis* surrogate) within the interior of a mid sized sedan.

Technical Approach – Test Facility

- Testing conducted within Battelle's ambient breeze tunnel
  - 20'x20'x135'
  - Generates ~5 mph linear airflow
    - While interior contamination active
    - While pre-sterilization was active
    - With vehicle motor running
  - Breeze tunnel exhaust HEPA filtered
- Provided vehicle contamination mitigation and breathing air safety

Technical Approach – Vehicle

- Testing conducted using 2015 Chevrolet Malibu
  - Interior volume = 2840 L
  - Remote start capability
- Patch panels added into both rear window frames (Lexan)
  - Passenger side patch panel:
    - 2 - 6” exhaust fans
  - Drivers side patch panel:
    - 2 – 1.5” cam lock fittings for commercial HPV generator
    - 5 - ¼” tube fittings for aerosol generation and sampling
  - Various electrical connections made through trunk/rear seat

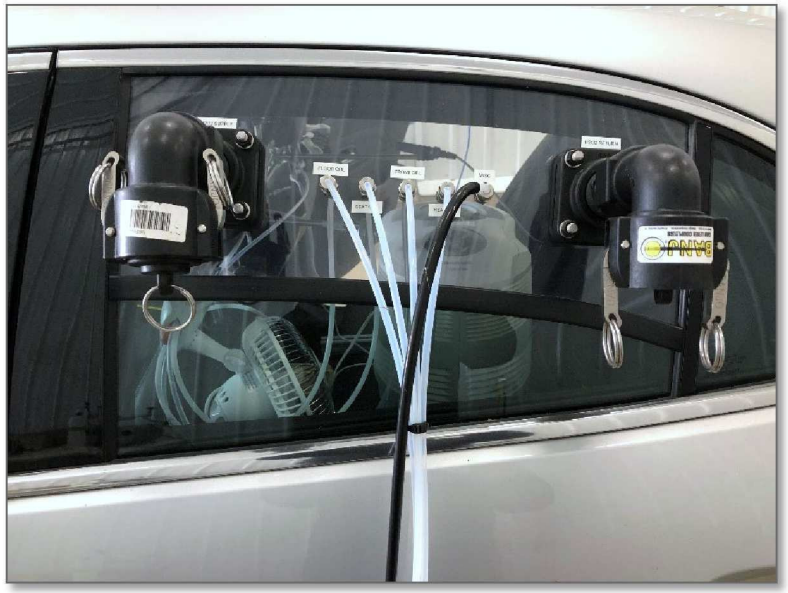

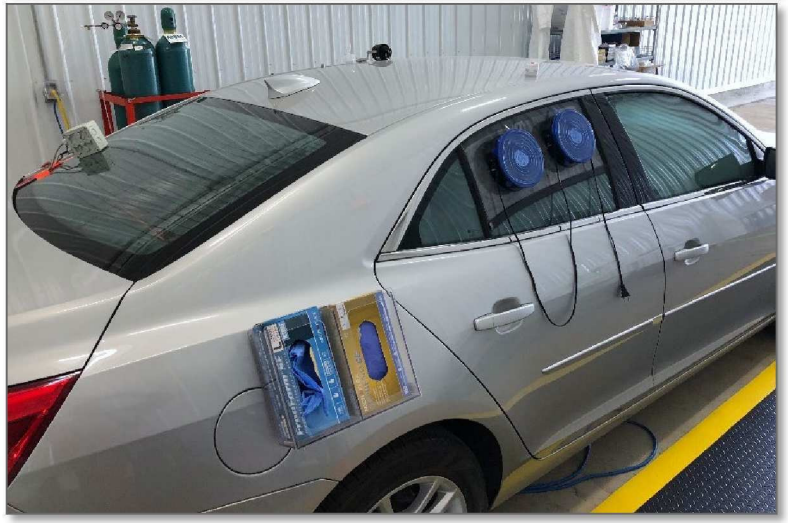

Technical Approach – Vehicle Operation

- Remote vehicle engine start operation (10 min x 2 = 20 min)
  - Pre-Test Sterilization
  - Contamination
  - Re-Contamination
- HVAC Settings
  - Fan on high
  - Temperature on cool
  - Recirculation mode
  - Face vent output selected

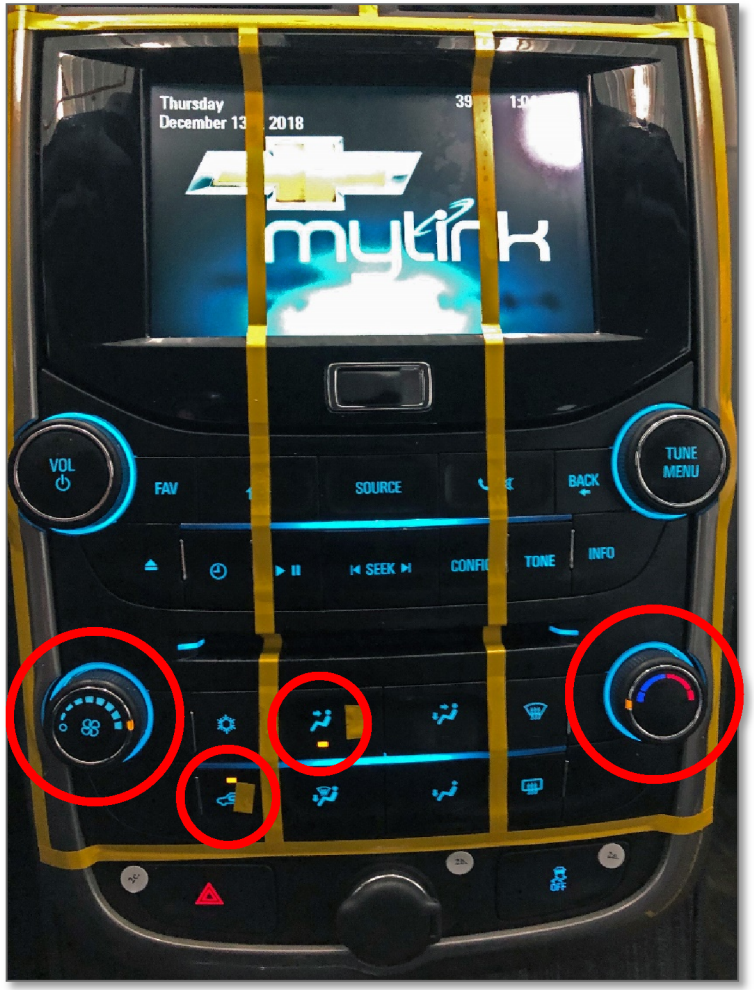

Technical Approach – Pre-Test Sterilization of Interior

- High level decontamination using commercial generator
  - Bioquell Clarus C cycle development

	Time (min)	Inj. Rate (g/min)
Conditioning	15	NA
Gassing	30	8
Dwell	120	2
Aeration	9999	NA

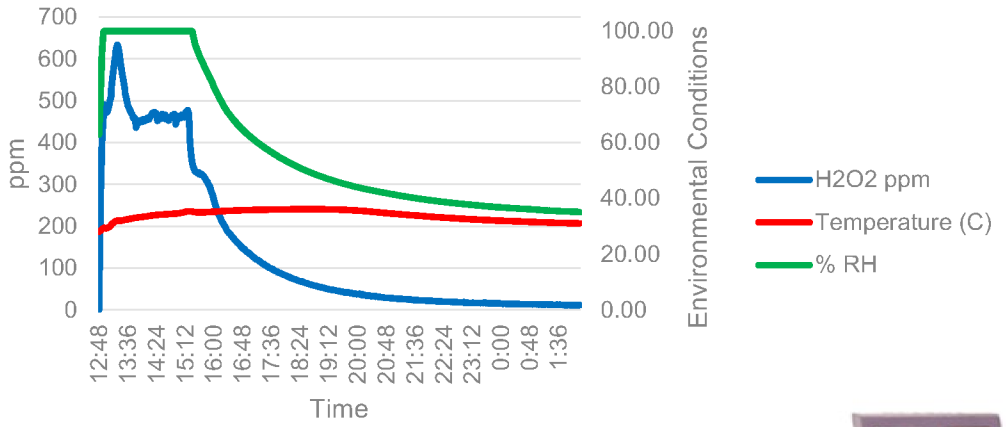

  - Vehicle remote start activated twice 10 min into gassing phase (total 20 min)
  - Achieved condensation and peak concentration of 600 to 800 ppm
  - Resulted in no BI growth after 48-hour incubation
- Low level clearance [0.0 ppm] required sampling at vent outlets

Technical Approach – Parameter Measurements

- High level H_2O_2 detector
  - ATI B12 gas transmitter w/ 0 -1000 ppm electrochemical sensor
  - Mounted in rear passenger side of vehicle
  - Data logged with Onset HOBO U12
- Low level H_2O_2 detector
  - Dräeger PAC III 0-20 ppm electrochemical sensor
- Temperature/Relative Humidity
  - Onset HOBO MX1101 Data logger
  - One inside and one outside vehicle

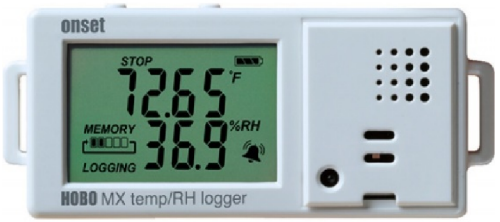

Technical Approach – Contamination

- Test organism *B. atrophaeus* (1 x 10^9 CFU/mL)
- Target load 10^3 CFU per cm^2
- Two 6-jet Collison nebulizers
  - Main cabin – located between front seat headrests
  - Cabin filter – located in passenger foot box area
- Operation parameters
  - Loaded with 20 mL spore suspension
  - 20 psi zero air (0.5 mL per min)
  - 20 min contamination time
  - Vehicle remote started
  - Mixing fans and cabin HVAC operated

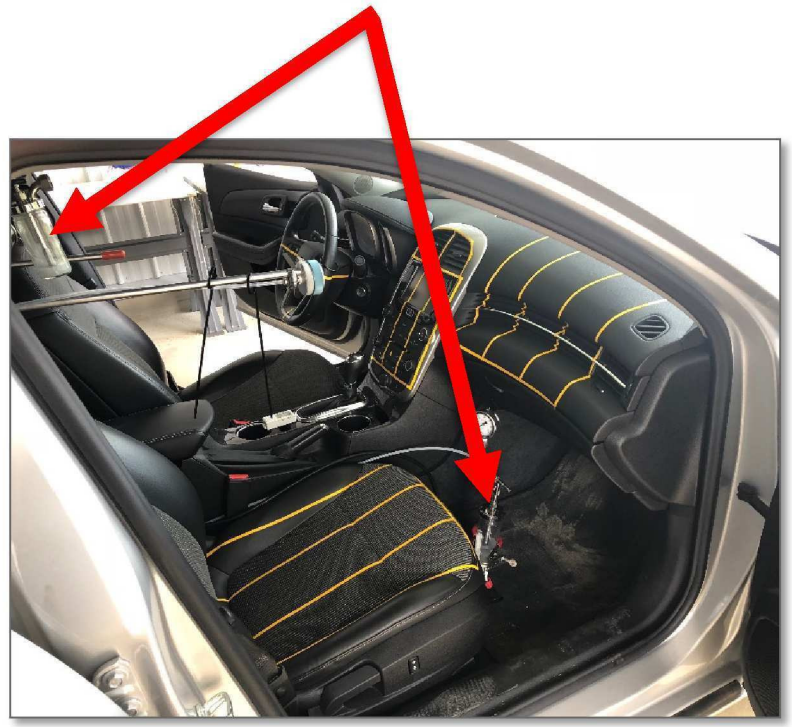

Technical Approach – Test Decontamination

- Test sporicide = 3% aqueous hydrogen peroxide
- Low-Tech H_2O_2 vapor generator
  - Honeywell QuietCare cool mist humidifier (HCM-6099)
  - Uses coarse filter to wick liquid and internal fan to circulate air through filter
  - Float switch to turn off automatically
  - Operated in back seat (level placement required)
- Two mixing fans circulated cabin air for duration of decontamination

Technical Approach – Test Process Overview

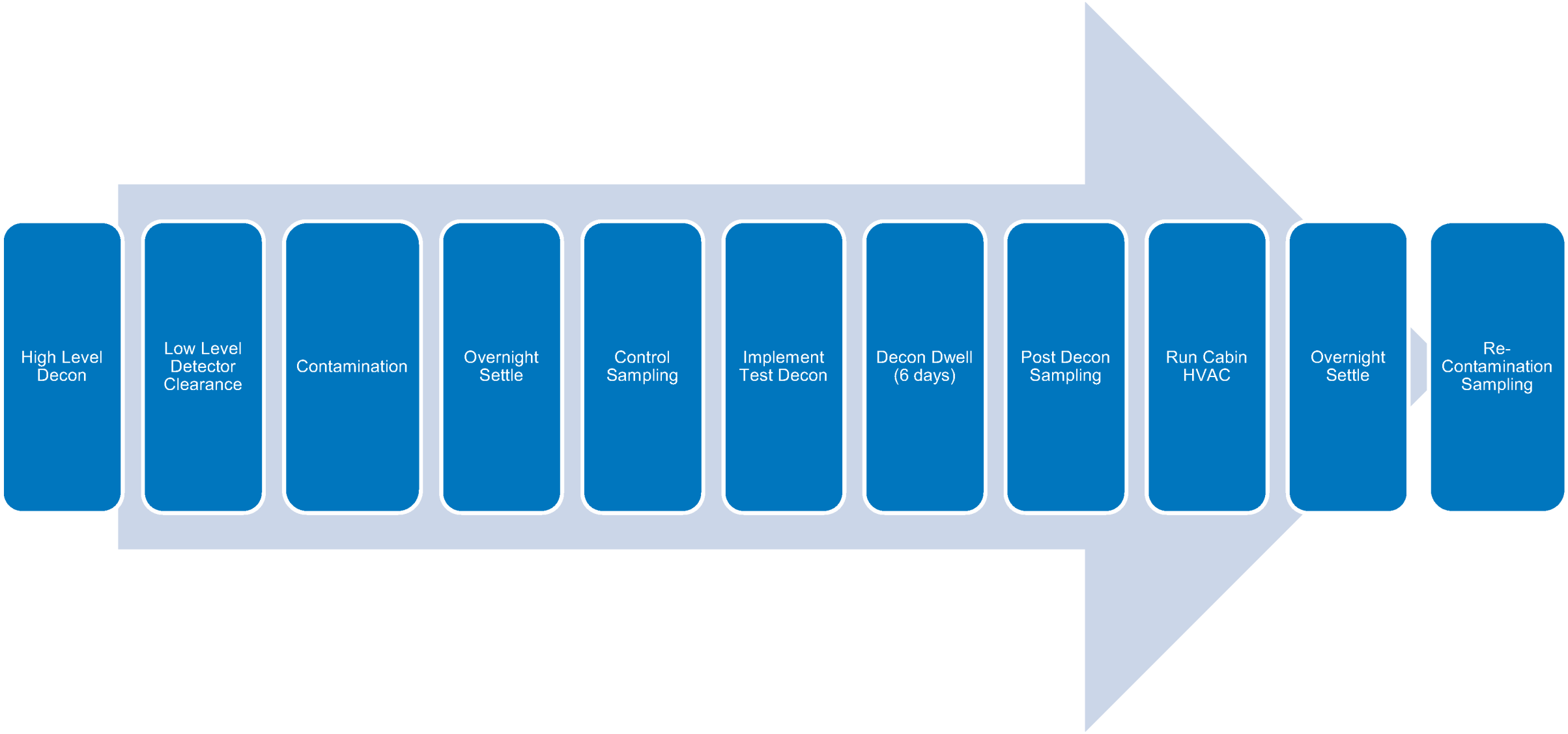

Technical Approach – Test Sample Type

- Vehicle blank (A)
- Positive control (A)
- Test sample (B)
- Recirculation test sample (C)

- Field blank
- Procedural blank

Technical Approach – Sample Processing

3M Sponge-Stick

Processed per EPA MOP*
Extracts plated on Tryptic Soy Agar (serial dilutions and filters)

Vacuum Filter Cassette

Processed per EPA MOP*
Extracts plated on Tryptic Soy Agar (serial dilutions and filters)

Direct Extraction

Extracted by orbital shaking at ambient temperature and 200 rpm for 15 minutes. Supernatant plated on Tryptic Soy Agar (serial dilutions and filters)

* Shah, S. Protocol for Detection of Bacillus anthracis in Environmental Samples During the Remediation Phase of an Anthrax Incident, 2nd Edition. U.S. Environmental Protection Agency, Washington, DC, 2017.

Technical Approach – Test Materials (locations)

Location	Surface	Approximate Coupon Size	Sampling Technique	Material Preparation
Referee Glass	C1036	1.9 cm x 7.5 cm (14.3 cm^2)	Direct Extraction	Autoclave
Cabin Filter	Cabin Filter (located behind glove box	1.9 cm x 7.5 cm (14.3 cm^2)	Direct Extraction	NA
1	Steering wheel	Steering wheel divided into three equal pie shaped areas (323 cm^2)	Sponge Stick	HPV
2	Radio/HVAC console	Radio console divided into three equal vertical columns (213 cm^2)	Sponge Stick	
3	Dashboard	Horizontal section of dashboard with three equal sections (645 cm^2)	Sponge Stick	
4	Passenger seat	Horizontal section of passenger seat with three equal sections (645 cm^2)	Sponge Stick	
5	Rear Carpet	Horizontal section of passenger carpet with three equal sections (929 cm^2)	Vacuum Cassette	
6	Rear Seat Back	Vertical section of rear seat material with three equal sections (645 cm^2)	Sponge Stick	
7	Vent outlets	1 vent per test location [control-driver side, test and post-test middle vents (100 cm^2)]	Sponge Stick	
8	Windshield	Driver side section of windshield with three equal sections (645 cm^2)	Sponge Stick	
9	Rear Deck	Horizontal section rear deck with three equal sections (929 cm^2)	Vacuum Cassette	
10	Headliner	Horizontal (inverted) section of headliner fabric with three equal sections (929 cm^2)	Vacuum Cassette	

Technical Approach – Test Matrix

Test Number	Liquid Volume (L)	Cabin HVAC	Cabin Filter	Temperature (°C)	RH (%)	H_2O_2 (ppm)	Contact Time (days)
1	1.5	Off	In Situ	24.85 ± 2.78	95.17 ± 2.89	1.12 ± 2.05	6
2	3.0	Off	In Situ	26.8 ± 3.02	99.99 ± 0.33	5.82 ± 6.45	6
3	3.0	On (20 min)	In Situ	23.42 ± 4.87	99.36 ± 1.52	16.41 ± 16.80	6
4	3.0	Off	Removed to Cabin	9.63 ± 3.41	99.97 ± 0.58	14.01 ± 7.42	6
5	3.0	Off	Removed to Cabin	5.24 ± 1.54	99.96 ± 0.67	11.07 ± 2.21	6

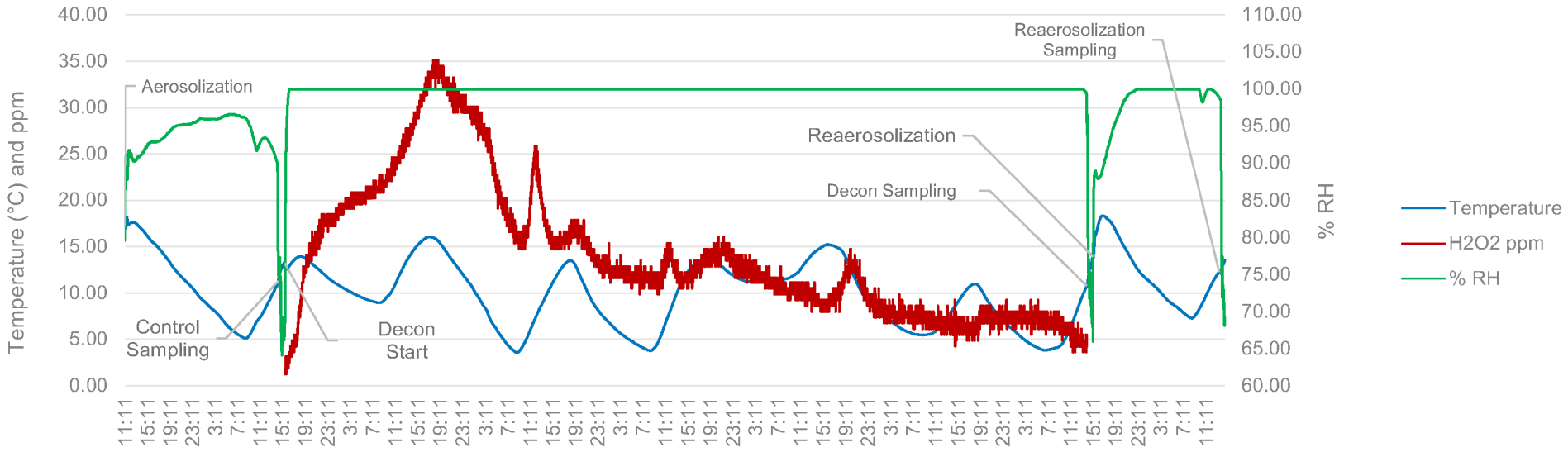

Results– Glass Contamination

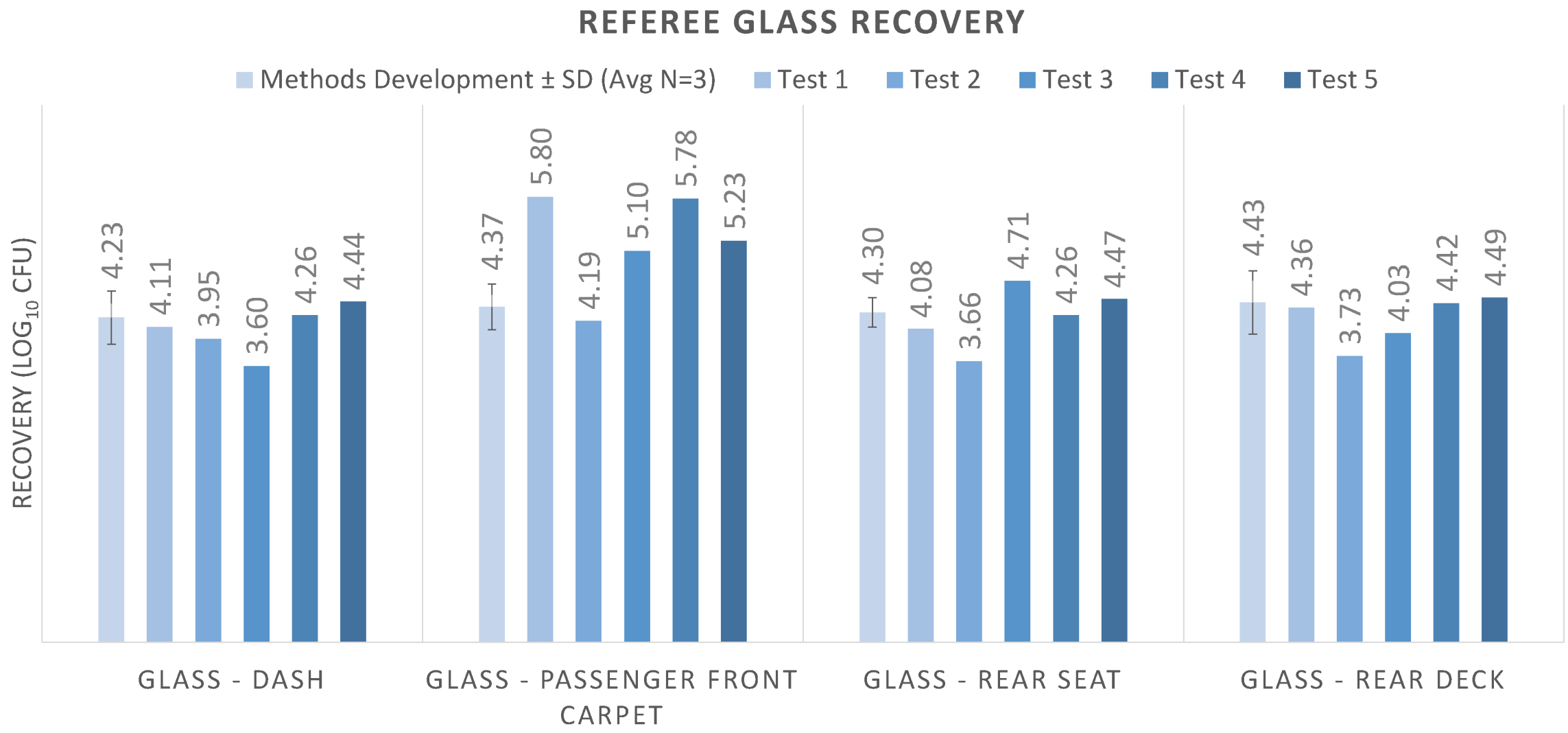

Results– Surface Contamination

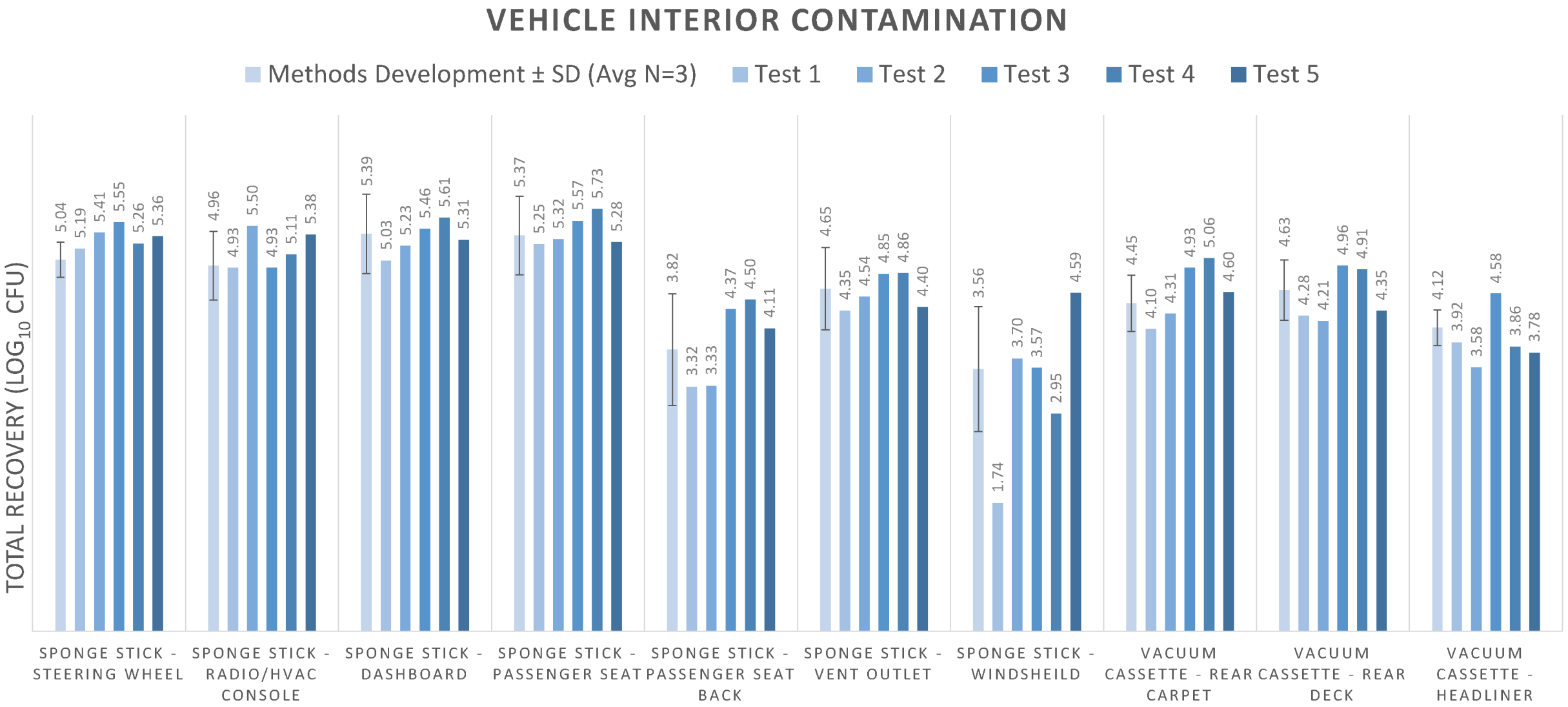

Results– Cabin Filter Contamination

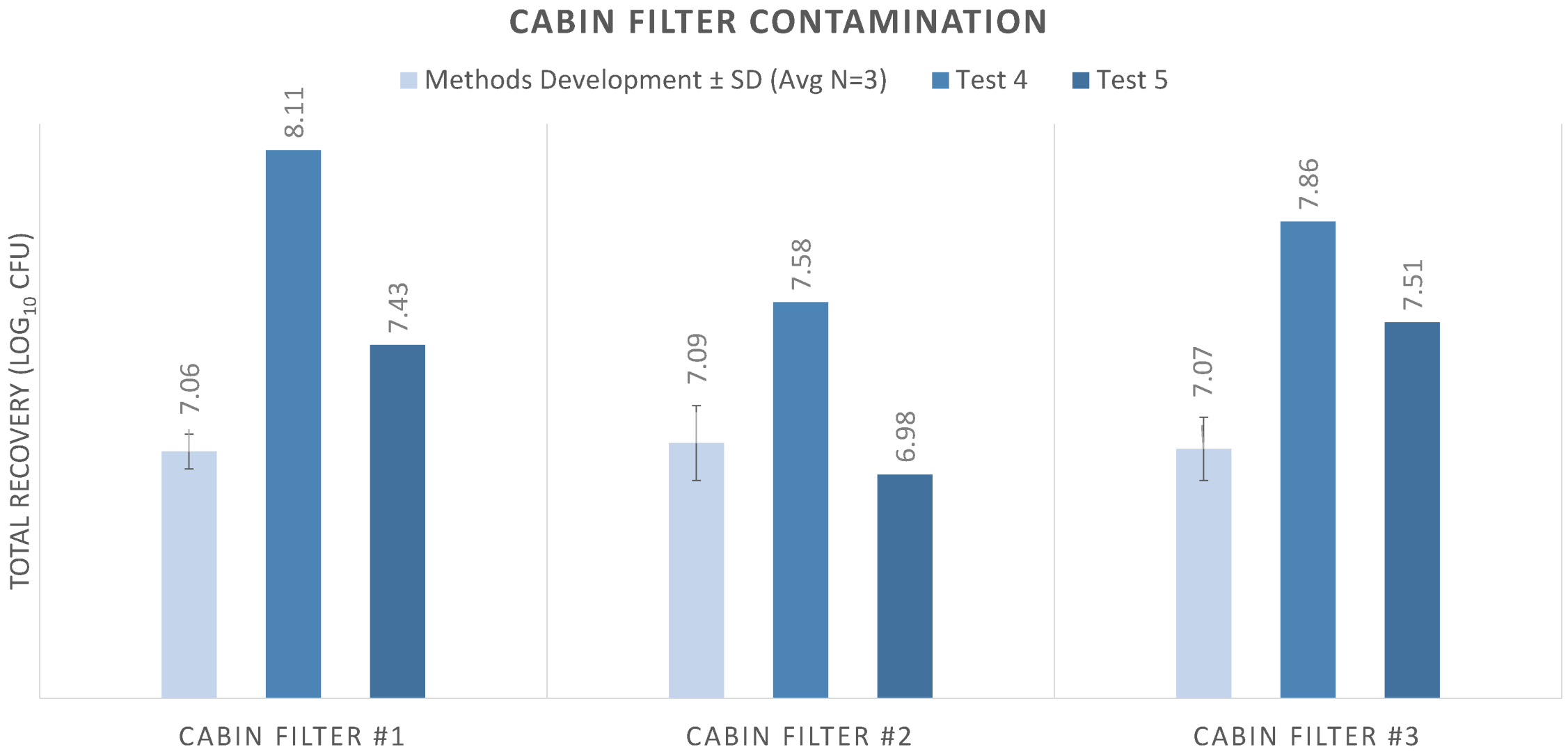

Results– Decontamination Efficacy

Coupon Type	Test 1			Test 2			Test 3			Test 4			Test 5		
	Control	Decon	Re-aerosol	Control	Decon	Re-aerosol	Control	Decon	Re-aerosol	Control	Decon	Re-aerosol	Control	Decon	Re-aerosol
Glass - Dash	4.11	0.00	0.00	3.95	0.00	1.28	3.60	0.00	0.00	4.26	0.00	0.00	4.44	1.08	0.00
Glass - Passenger front carpet	5.80	0.00	0.00	4.19	0.00	0.00	5.10	0.30	0.00	5.78	0.48	0.00	5.23	0.48	0.70
Glass - Rear seat	4.08	0.00	0.00	3.66	0.00	0.90	4.71	0.00	0.00	4.26	0.48	0.00	4.47	0.00	0.00
Glass - Rear deck	4.36	0.00	0.00	3.73	0.30	0.00	4.03	0.00	0.00	4.42	0.00	0.00	4.49	0.00	0.00
Sponge stick - Steering wheel	5.19	1.98	1.86	5.41	0.00	0.00	5.55	0.00	0.00	5.26	0.00	0.00	5.36	0.00	0.00
Sponge stick - Radio	4.93	0.48	0.48	5.50	0.00	0.60	4.93	0.00	0.00	5.11	1.51	0.00	5.38	0.00	0.00
Sponge stick - Dashboard	5.03	0.00	1.28	5.23	0.00	0.48	5.46	0.00	0.00	5.61	0.00	0.00	5.31	0.00	0.00
Sponge stick - Passenger seat	5.25	0.00	0.30	5.32	0.00	0.00	5.57	3.45	0.00	5.73	0.00	0.00	5.28	0.00	1.34
Sponge stick - Passenger seat back	3.32	2.21	0.60	3.33	0.00	0.00	4.37	0.00	0.00	4.50	0.00	0.00	4.11	0.00	0.00
Sponge stick - Vent outlet	4.35	1.92	1.38	4.54	0.00	1.23	4.85	0.00	0.00	4.86	0.00	0.48	4.40	0.00	0.48
Sponge stick - Windshield	1.74	0.00	1.00	3.70	0.00	0.00	3.57	0.00	0.00	2.95	0.00	0.30	4.59	0.00	0.00
Vacuum cassette - Rear carpet	4.10	1.23	1.86	4.31	0.00	1.30	4.93	0.30	0.00	5.06	0.00	1.87	4.60	0.30	0.70
Vacuum cassette - Rear deck	4.28	0.00	1.20	4.21	0.00	1.23	4.96	0.30	0.30	4.91	0.00	0.00	4.35	0.48	0.00
Vacuum cassette - Headliner	3.92	1.38	1.28	3.58	0.00	0.00	4.58	0.30	1.08	3.86	3.82	1.20	3.78	0.00	0.00
Cabin filter #1			7.58			6.81			7.03	8.11	1.58		7.43	0.00	
Cabin filter #2			7.68			6.95			6.97	7.58	1.46		6.98	0.30	
Cabin filter #3			7.07			6.96			7.68	7.86	1.71		7.51	1.53	

Results– Material Damage

- Visual assessment made after each round of testing.
  - Effects to stitching noted starting with Test 2
  - Combination effect of test decontamination as well as pre-sterilization

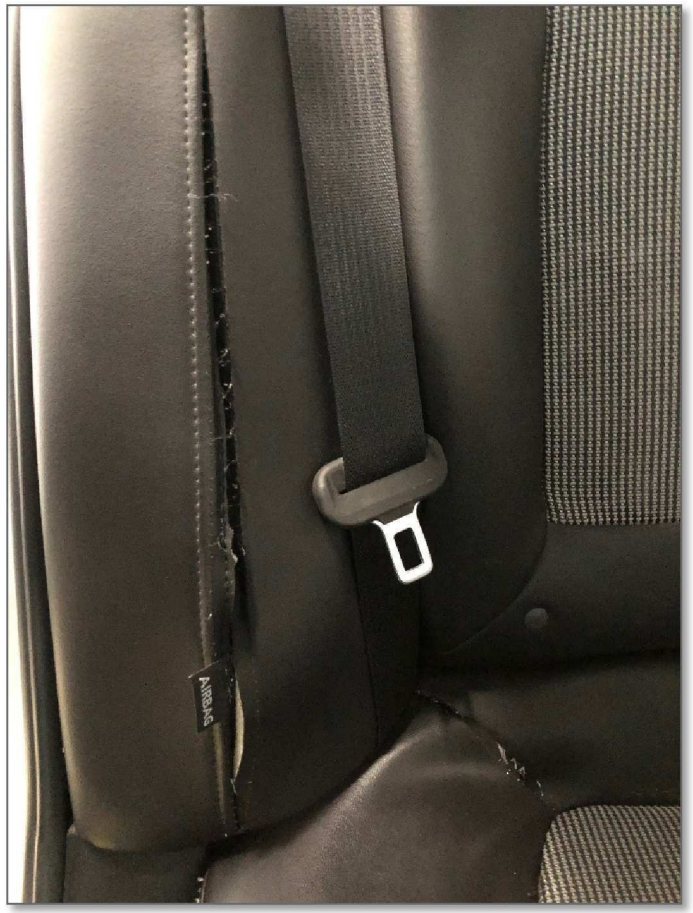

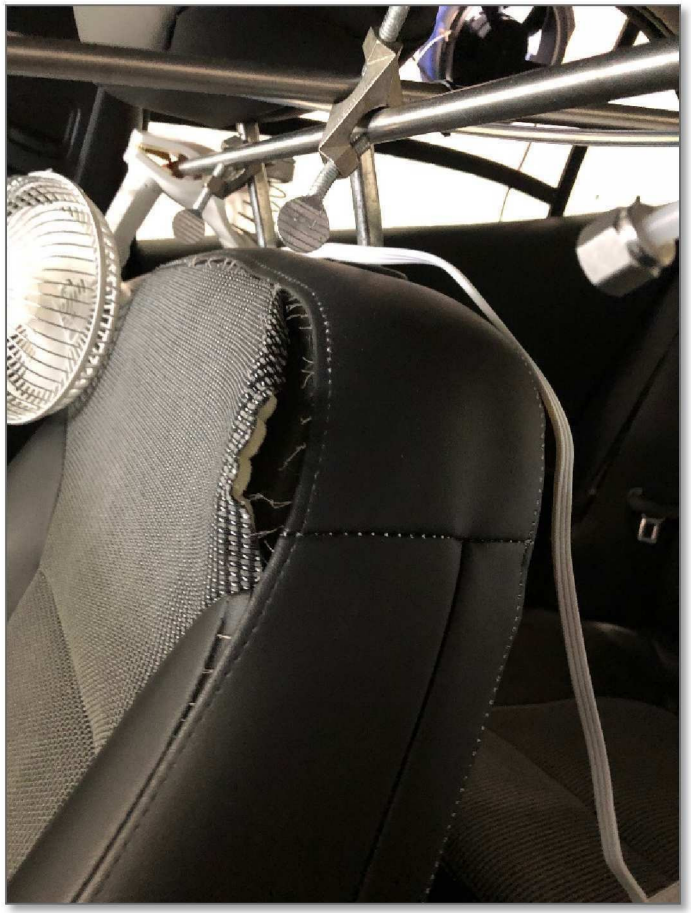

Summary of Key Findings

- Consistent interior contamination was achieved using 2-6 jet collision nebulizers.
- Decontamination efficacy increased when H_2O_2 volume increased from 1.5 to 3.0 L, resulting in 4 of 10 and 10 of 10 non-detects respectively.
- Re-contamination observed when no treatment of HVAC system attempted.
- Circulating cabin air through HVAC system did not appear to effect efficacy on cabin filter but did reduce the amount of re-contamination.
- 6 log reduction achieved on cabin filter by removing it to the cabin during decontamination process.
- Testing at lower temperatures (10 and 5°C) efficacy remained high with 8 of 10 locations resulting in non-detects for both temperatures.

Acknowledgements

- Research funded by U.S. EPA contract EP-C-16-014; TO-04

- Co-authors
  - EPA: Dr. Lukas Oudejans, Dr. Worth Calfee, Mr. Leroy Mickelsen, and Dr. Sang Don Lee
  - Battelle: Ms. Michelle Sunderman, Mr. Kent Hofacre and Mr. Patrick Keys

Low Concentration Hydrogen Peroxide Vapor (LCHPV) for Remediation of Indoor Environments Contaminated with Persistent Toxic Chemicals

Bill Williamson, Albert Zwiener, Yirgaalem Abrha, Ph.D, Michael Dammann - Southwest Research Institute
Sujoy Roy, Ph.D, - Tetra Tech, Inc. Lukas Oudejans, Ph.D, - U.S. EPA

Introduction

The imminent threat of a chemical warfare agent (CWA) release in a building or transportation hub is driving U.S. EPA's Homeland Security Research Program to systematically evaluate potential decontamination technologies for chemical agents. The use of low-concentration hydrogen peroxide vapor (LCHPV) fumigation has gained attention as hydrogen peroxide is a readily available, efficacious green technology, and relatively easy to implement as a decontamination approach using readily available equipment (e.g., humidifiers).

The goal of this research is to determine conditions under which LCHPV fumigation can be used to decontaminate permeable or porous interior structural materials contaminated with CWAs or selected pesticides that are hard to clean using traditional surface decontamination approaches. This poster describes the research approach; the study is ongoing.

Objectives

To assess conditions under which LCHPV fumigation can be used to effectively decontaminate CWAs from interior structures

- Identify representative material surfaces for fumigation testing
- Demonstrate control of chamber temperature and stability of LCHPV
- Develop analytical method for VX and EA-2192 residual on selected surface materials
- Perform LCHPV efficacy studies on materials contaminated with VX

Selected Test Surfaces

Coupons were approximately 1.375" x 1.375"

- Vinyl Tile (12"x12" Excelon VCT Flooring)
- Rubber (Black Rubber wall cove base)
- Painted wood (Douglas Fir, White Flat Zero VOC Interior Paint)
- Stainless steel (304 bar stock)

Environmental Chamber

Chamber Requirements:

- Capacity over 300 Liters with minimal air exchange
- Operational temperature range between 15 and 25 °C with tolerance of ±3 °C of set point
- Generate hydrogen peroxide concentration of 25 ± 5 ppmv
- Monitor and log chamber temperature, percent relative humidity (RH), and hydrogen peroxide concentration.
- Expected test duration is five days

Figure 1: Experimental Chamber with glove ports (no gloves present) and shelves

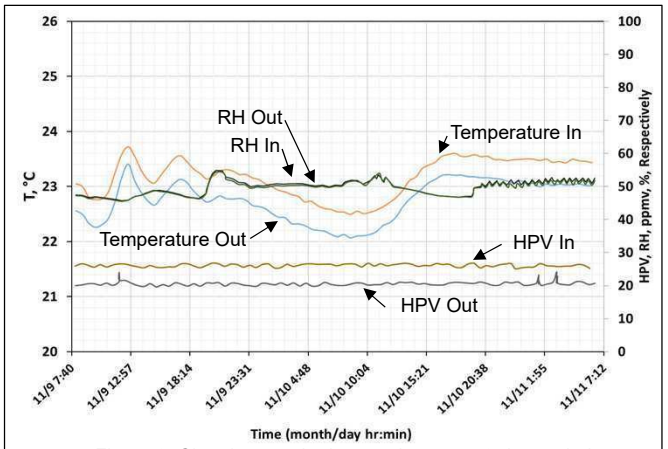

Figure 2: Chamber monitoring results over a 2-day period

Analytical Method

Extraction Method: The coupon will be placed into 2oz wide mouth jar filled with 20 mL of 10% acetone in methylene chloride, swirled for 30 seconds, and sonicated for 10 minutes. The extract will be removed, centrifuged, filtered, and stored in a freezer.

Analysis: Quantitative analysis will be performed on Liquid Chromatograph triple quadrupole mass spectrometer (LC-qqq) operating in multiple reaction monitoring (MRM) mode.

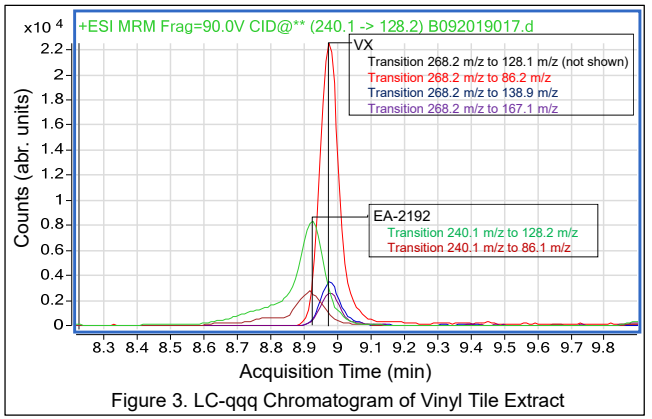

Figure 3. LC-qqq Chromatogram of Vinyl Tile Extract

Method Performance: Performance of each analyte was demonstrated in separate studies using seven replicate spikes and one method blank (MB) for each material type.

Material	VX Results			EA-2192 Results		
	MB	Replicate Spikes		MB	Replicate Spikes	
		Avg. Rec.	%RSD		Avg. Rec.	%RSD
Stainless Steel	ND	75%	8%	ND	57%	9%
Painted Wood	ND	100%	9%	ND	31%	14%
Rubber	ND	101%	16%	ND	46%	12%
Vinyl Tile	ND	91%	18%	ND	11%	28%
VX spike contact time was 5 minutes; EA-2192 spike contact time was 1 hour.						

Planned LCHPV Efficacy Study

#	Agent	Fumigant	Condition[1]	Materials	Coupons per Material per Time Point (TP)					Total Coupon
					TP-0[2]	TP-1[3]	TP-2[4]	TP-3[4]	TP-4[4]	
V1	VX	H_2O_2	#1 TBD	4 Types	3C[5]/1B[6]	3C/1B	3C/1B	3C/1B	3C/1B	80
V2	VX	H_2O_2	#2 TBD	4 Types	3C/1B	3C/1B	3C/1B	3C/1B	3C/1B	80
V3	VX	H_2O_2	#3 TBD	4 Types	3C/1B	3C/1B	3C/1B	3C/1B	3C/1B	80
V4	VX	Water	#1 TBD	4 Types	3C/1B	3C/1B			3C/1B	48
V5	VX	None	#1 TBD	4 Types	3C/1B	3C/1B			3C/1B	48

[1] Conditions will be determined by EPA. Parameters include: H_2O_2 conc., duration.
[2] TP-0 = Spike controls used to validate the amount of agent spiked and recovered from the coupons.
[3] TP-1 = Collected after 24 h weathering time and before start of fumigation.
[4] TP-2 thru 4 = Collected after 24 h weathering time and specified duration after start of fumigation. Durations determined by EPA
[5] 3C = three coupons for each material spiked with 2µL of chemical agent.
[6] B = 1 procedural blank coupon for each material not contaminated with chemical agent.

Disclaimer: The U.S. Environmental Protection Agency (EPA) through its Office of Research and Development (ORD) funded and managed the research described. It has been subjected to the Agency's review and has been approved for publication and distribution. Note that approval does not signify that the contents necessarily reflect the views of the Agency. Mention of trade names, products, or services does not convey official EPA approval, endorsement, or recommendation.

Laboratory Decontamination Using Low-Concentration Hydrogen Peroxide

National Decontamination Conference, November 2019

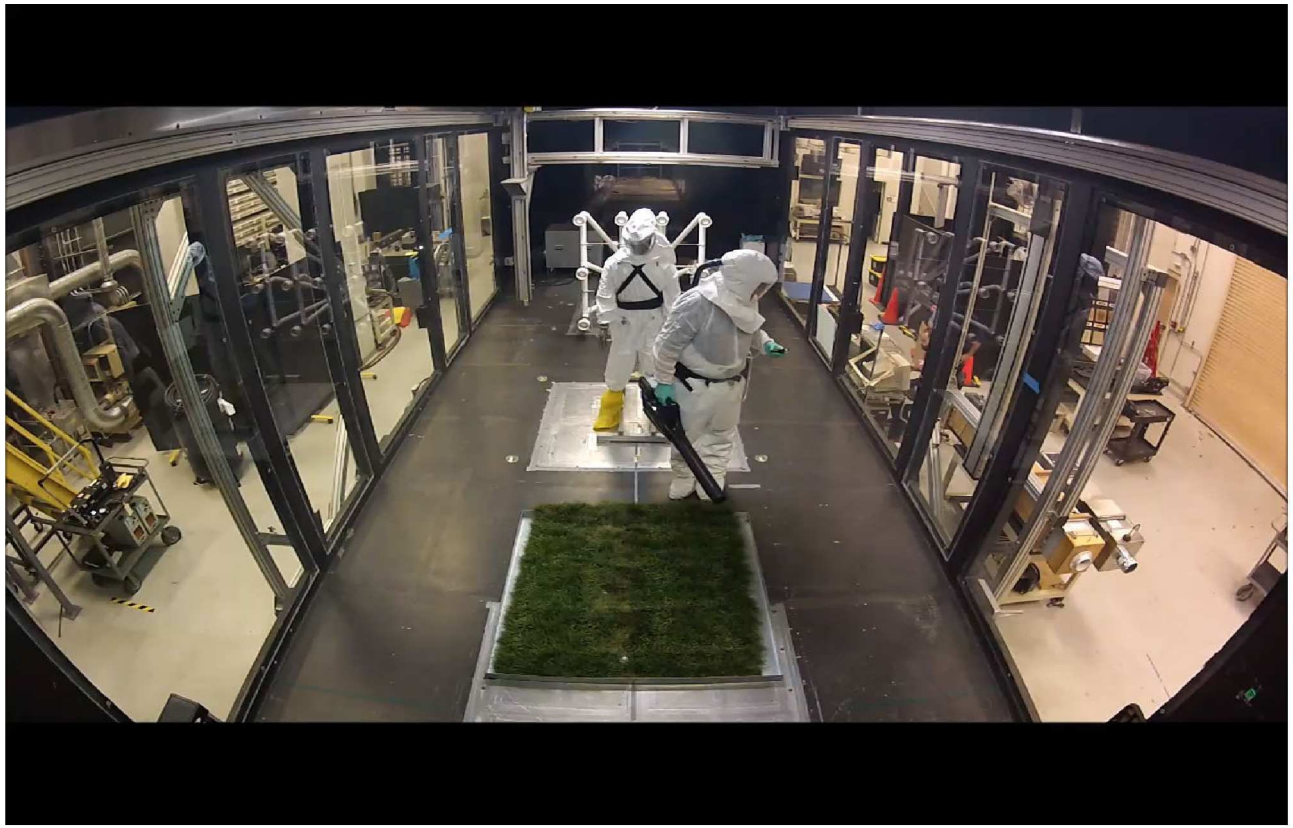

R. Leroy Mickelsen, EPA

CBRN Consequence Management Advisory Division

Contributors to Low-Concentration HP Study

EPA's CBRN Consequence Management Advisory Division /OLEM

- Shannon Serre

EPA's Center for Environmental Solutions & Emergency Response /ORD

- Joseph Wood
- M. Worth Calfee
- Shawn Ryan

Jacobs Technology, Inc.

- Abderrahmane Touati
- Rob Delafield
- Denise Aslett

Problem Statement

- Limited resources available to respond to a large *Bacillus anthracis* release.
- Many efficacious decontamination options have issues:
  - Produce highly toxic environments,
  - Require specialized equipment and expertise,
  - Have material compatibility issues, and
  - They are costly

Overview

Background

EPA laboratory study found:

- Hydrogen peroxide (HP) vapor at 5 ppm for four to seven days was efficacious for both *Bacillus anthracis* and surrogate spores
- The “low-concentration” HP vapor could be achieved using commercially available vaporizers or humidifiers

Health Frame of Reference:

- HP Immediately Dangerous to Life and Health (IDLH) = 75 ppm
- HP Threshold Limit Value (TLV®) = 1 ppm

Overview (continued)

Objective

- To test this methodology in full-scale laboratory settings

Methodology

- **Location:** EPA wind tunnel & High-bay laboratory
- **Equipment:** Commercially-available off-the-shelf humidifiers
- **Decon Agent:** Commercially-available liquid HP
- **Efficacy Evaluation:** Surrogate spores on structures & coupons

Concept

- Measure volume of contaminated space
- Purchase humidifiers & HP
- Fill humidifiers w HP liquid
- Turn on humidifiers
- Exit and secure space

- Return in several days.

EPA Wind Tunnel

- Plastic sealed off section
- 12’ x 30’ x 10’ +
- 6’ x 20’ x 5’ + Transition
- 4,500 sq ft
- No air flow
- Three humidifiers
- Total of 30 liters of 3% HP
- Surface samples (21)
- Measured HP vapor concentration, T, RH

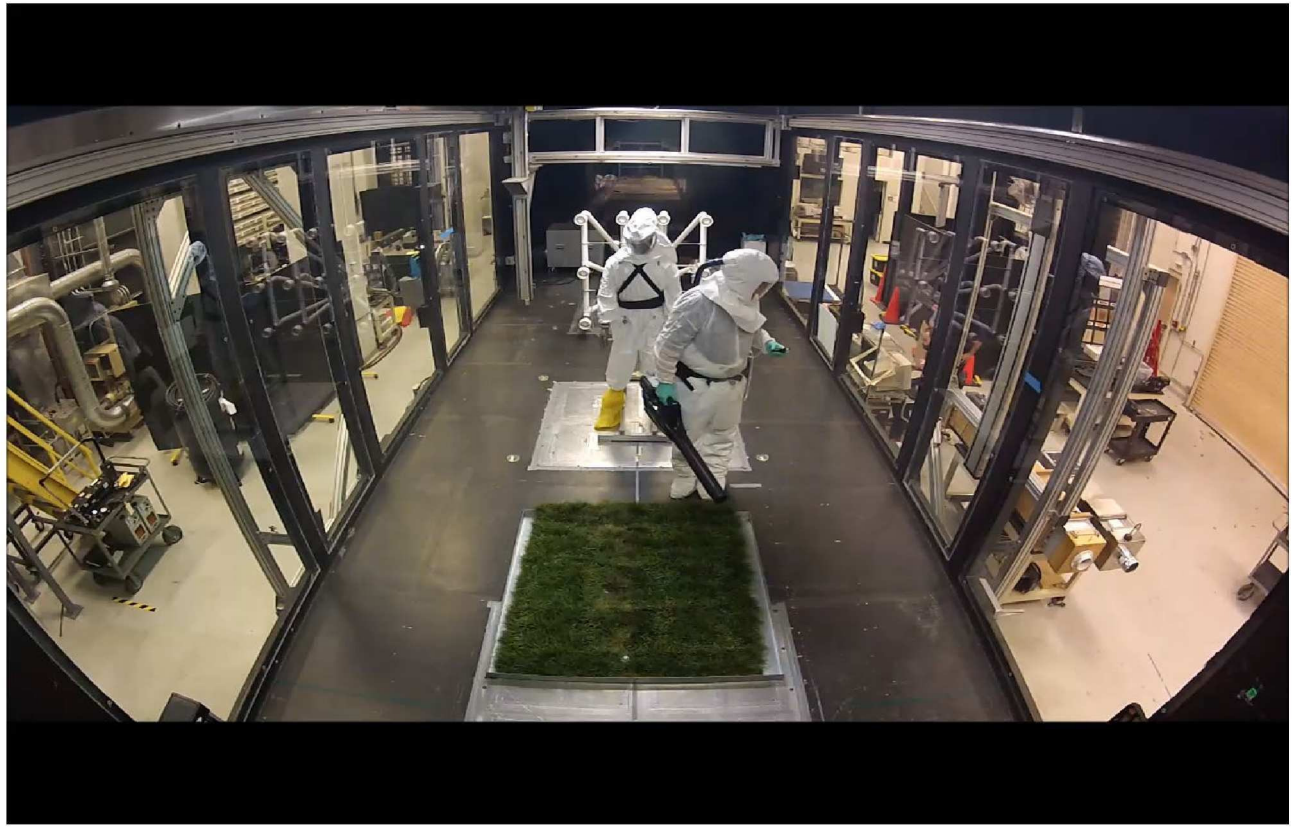

Section of EPA High-Bay Laboratory

- Plastic tarps
- 15’ x 25’ x 12’
- One humidifier
- 12 liters of 6% HP liquid
- Surface samples (12)
- Concrete coupons
- Estimated 1-ACH exhaust

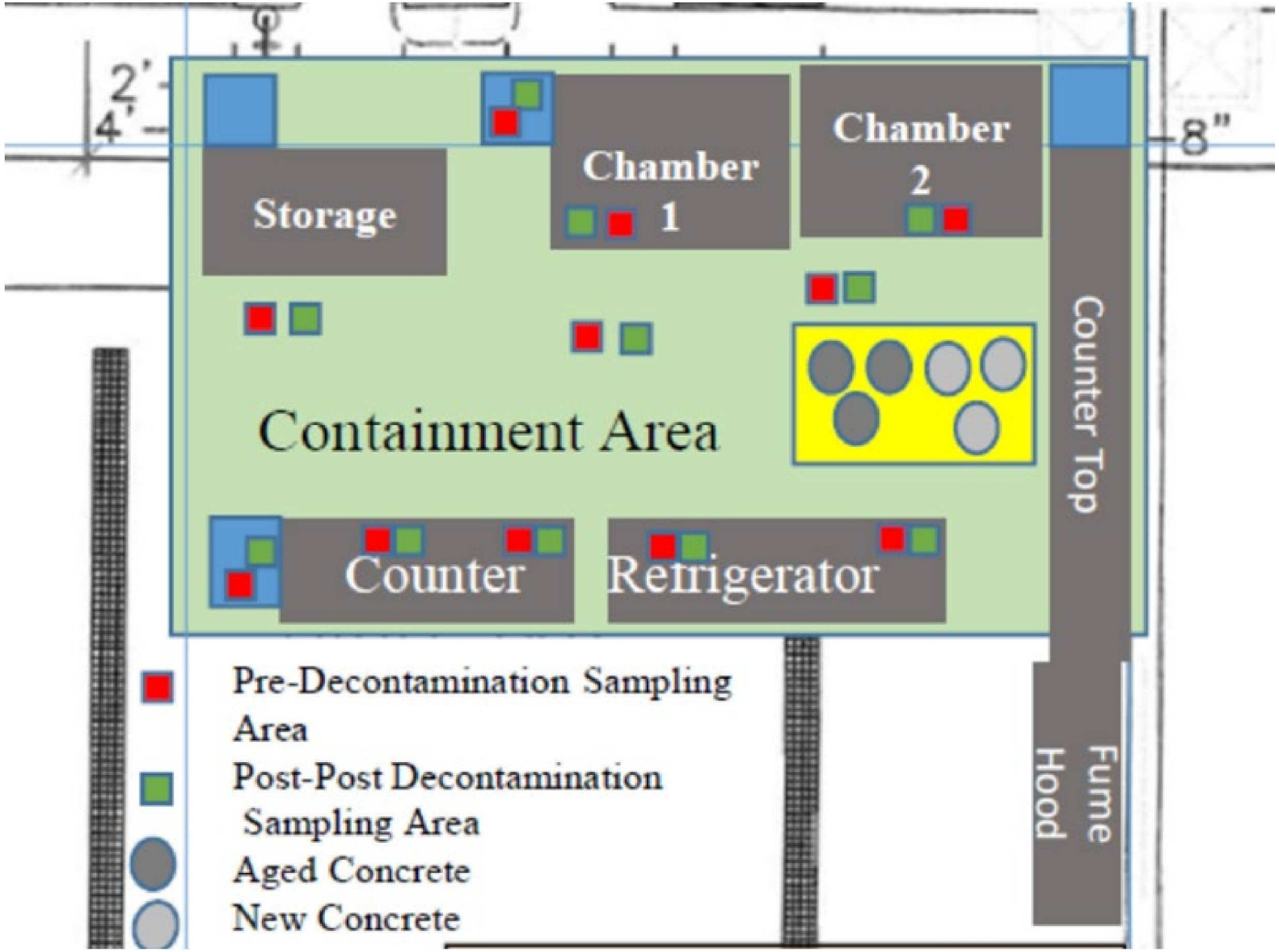

Efficacy Testing

Wind Tunnel

- Surface sampling pre- & post-decon
  - Glass, painted steel plate
  - Painted plywood, polyethylene trap
  - Aluminum plate, polypropylene table
  - Vinyl fabric covering table
- 21 biological indicators (BIs)
  - *Geobacillus stearothermophilus:*
  - Two million CFU/BI on steel disks
- Temperature & humidity sensors (HOBO)

High-Bay Laboratory

- Surface sampling pre- & post-decon
- Concrete test coupons old and new
  - *Bacillus atrophaeus:*
  - ten million colony-forming unit (CFU)/coupon
- Six biological indicators (BIs)
  - *Geobacillus stearothermophilus:*
  - Two million CFU/BI on steel disks
- Temperature & humidity sensors (HOBO)

EPA Wind Tunnel HPV Fumigation Concentrations

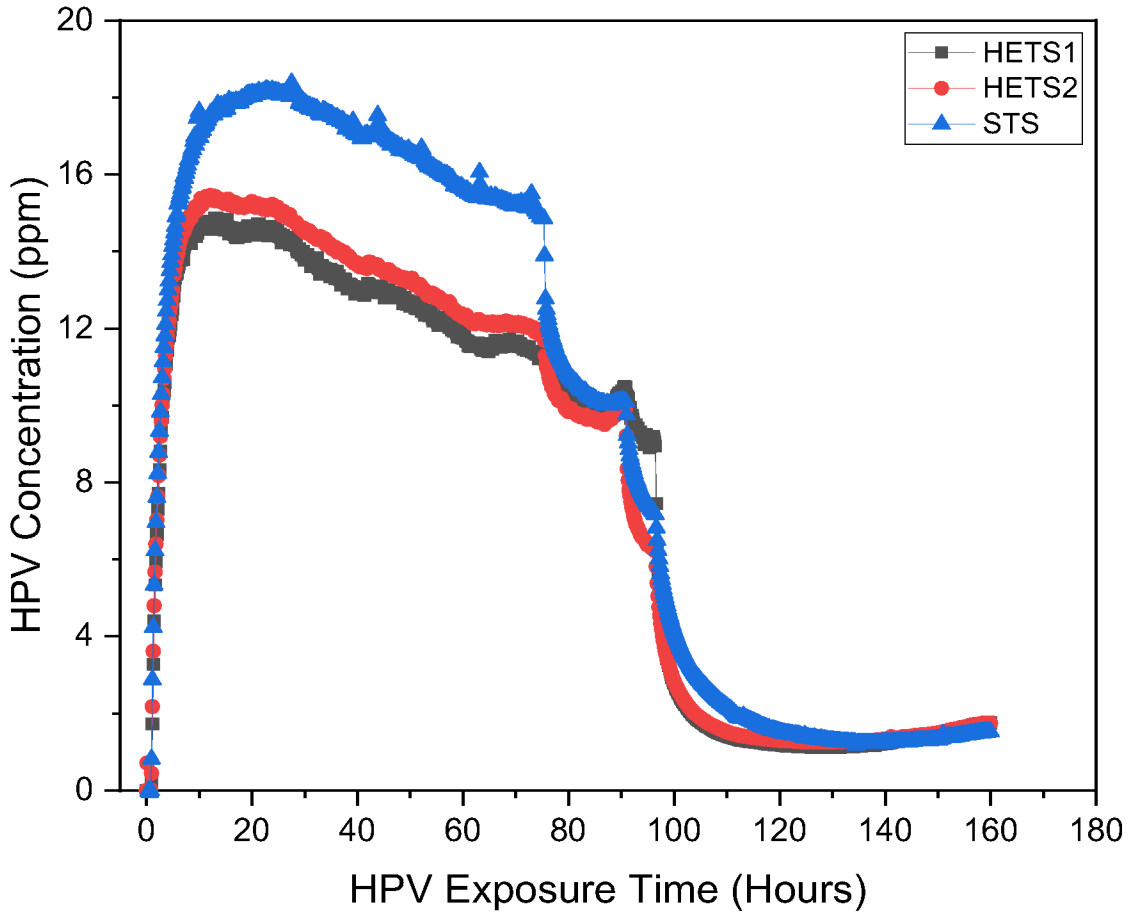

Wind Tunnel Surface Sample Results

Test Condition	Pre-Decontamination					Post-Decontamination
Spores Types		Btk		Bg		Btk/Bg
Material		CFU/ft^2	Log (CFU/ft^2)	CFU/ft^2	Log (CFU/ft^2)	CFU/ ft^2
Aluminum Plate	Average	9.6 10^4	4.9	3.1 10^2	2.5	Non-Detectable Spores
Polypropylene Folding Table	Average	6.4 10^7	7.4	1.9 10^2	2.3	
Painted plywood	Average	1.3 10^7	7.1	3.7 10^3	3.2	
Polyethylene Tarp	Average	3.0 10^5	5.2	3.1 10^2	2.2	
Painted Steel Plate	Average	7.3 10^5	5.5	9.9 10^2	2.9	
Vinyl Fabric	Average	4.6 10^5	5.7	1.9 10^2	2.1	
Glass	Average	2.0 10^4	4.0	1.9 10^2	2.1	

* BI Results: 19 of 21 no growth

High Bay Laboratory Surface Sample Results

Location	Material	Pre-decon	Pre-decon	Post -decon
		CFU/ft^2	Log	CFU/ft^2
Column base front	Painted concrete	2.65E+03	3.4	Non-Detectable for Spores
Column base back	Painted concrete	3.30E+03	3.5	
Floor (front)	Painted concrete	3.44E+03	3.5	
Floor (mid)	Painted concrete	2.79E+03	3.4	
Floor (back)	Painted concrete	8.73E+04	4.9	
Table	Plastic	1.49E+03	3.2	
Counter top	Soapstone	9.41E+02	3.0	
Computer monitor	Video screen	9.78E+01	2.0	
Small chamber front	Plexiglass	1.16E+01	1.1	
Small chamber back	Plexiglass	5.88E+01	1.8	
Refrigerator top	metal	9.50E+01	2.0	
Refrigerator kick plate	metal	1.25E+04	4.1	

High Bay Laboratory Concrete Coupon Surface Sample Results

Material	Pre-decon		Post -decon		Efficacy
	CFU/ft^2	Log	CFU/ft^2	Log	LR
Fresh concrete 1	5.36E+04	4.7	4.87E+03	3.7	1.0
Fresh concrete 2	1.52E+05	5.2	3.01E+03	3.5	1.7
Fresh concrete 3	5.26E+04	4.7	9.79E+03	4.0	0.7
Aged concrete 1	9.61E+05	6.0	3.81E+05	5.6	0.4
Aged concrete 2	6.91E+06	6.8	5.16E+04	4.7	2.1
Aged concrete 3	2.73E+06	6.4	1.45E+04	4.2	2.3

Summary: Improved Response Capabilities for EPA

- ✓ Scale up lab test to field study
- ✓ Affordable off-the-shelf equipment
  - $180 vs. $80,000
- ✓ Easy to use
- ✓ Low vapor concentrations
  - Below IDLH
- ✓ Longer exposure times
  - Days vs. 4 hours
- ✓ Green tech: By-products, water & oxygen
- ✓ 1.5-gal 3% HP liquid/1000 cubic feet, @ 70°F
- Conclusion: Effective &

  Increases Response Readiness

What Next?

- **Follow-on research:** Desorption: When is it safe to put your head to a pillow after an LCHP decontamination effort is conducted?
- **Legal:** How to provide self-help guidance for emergency responders and general public? Guidance vs. Standard Operating Procedures?

- Any other testing ideas? Let me know what you think.

Questions?

EPA
United States
Environmental Protection
Agency

Effective Decontamination Using Low Levels of Hydrogen Peroxide Vapor for *Bacillus Anthracis* Spore Inactivation

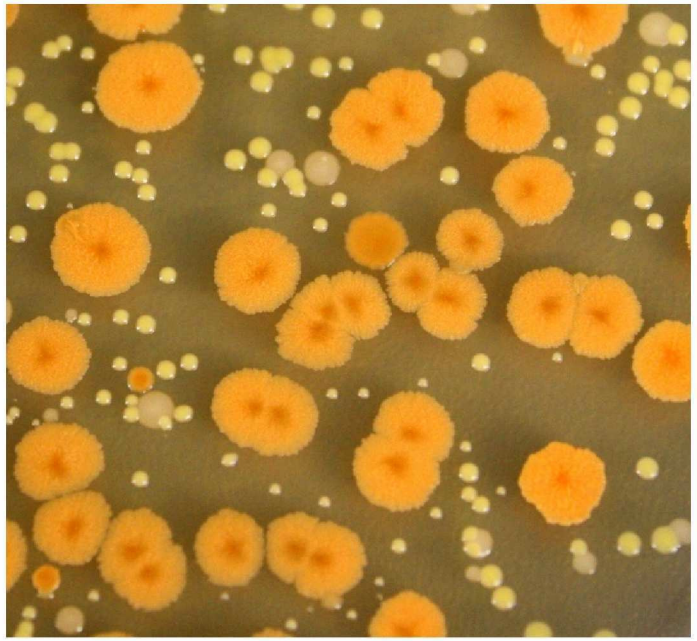

Joseph Wood
US EPA

Presented at 8th Singapore International Symposium on Protection Against Toxic Substances, March 22, 2017

Acknowledgements – Project Team Members and Co-Authors

- US EPA: Leroy Mickelsen, Shawn Ryan, Worth Calfee
- Arcadis: Matt Clayton, Nicole Griffin, Dahman Touati
- ECBC: Vipin Rastogi, Lisa Smith

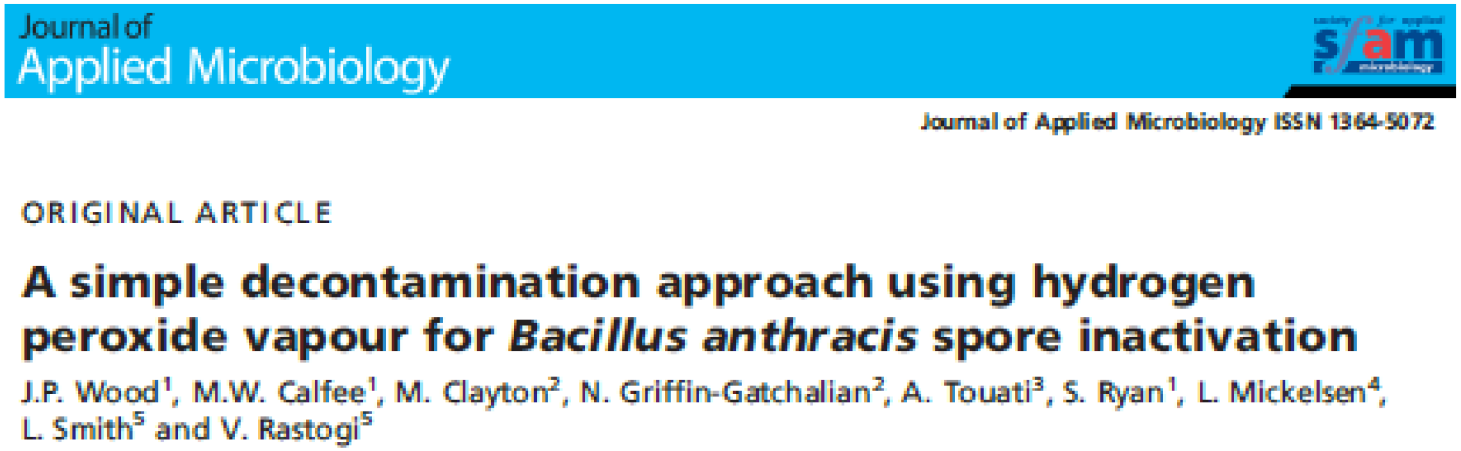

Disclaimer: The U.S. Environmental Protection Agency, through its Office of Research and Development, directed, funded, and managed the research described here under CONTRACT EP-C-09-027. It has been subjected to the Agency's review and has been approved for publication. Note that approval does not signify that the contents necessarily reflect the views of the Agency. Mention of trade names, products, or services does not convey official EPA approval, endorsement, or recommendation.

EPA
United States
Environmental Protection
Agency

Overview of Talk

- Background
- Methods
- Results
- Next steps
- Conclusions

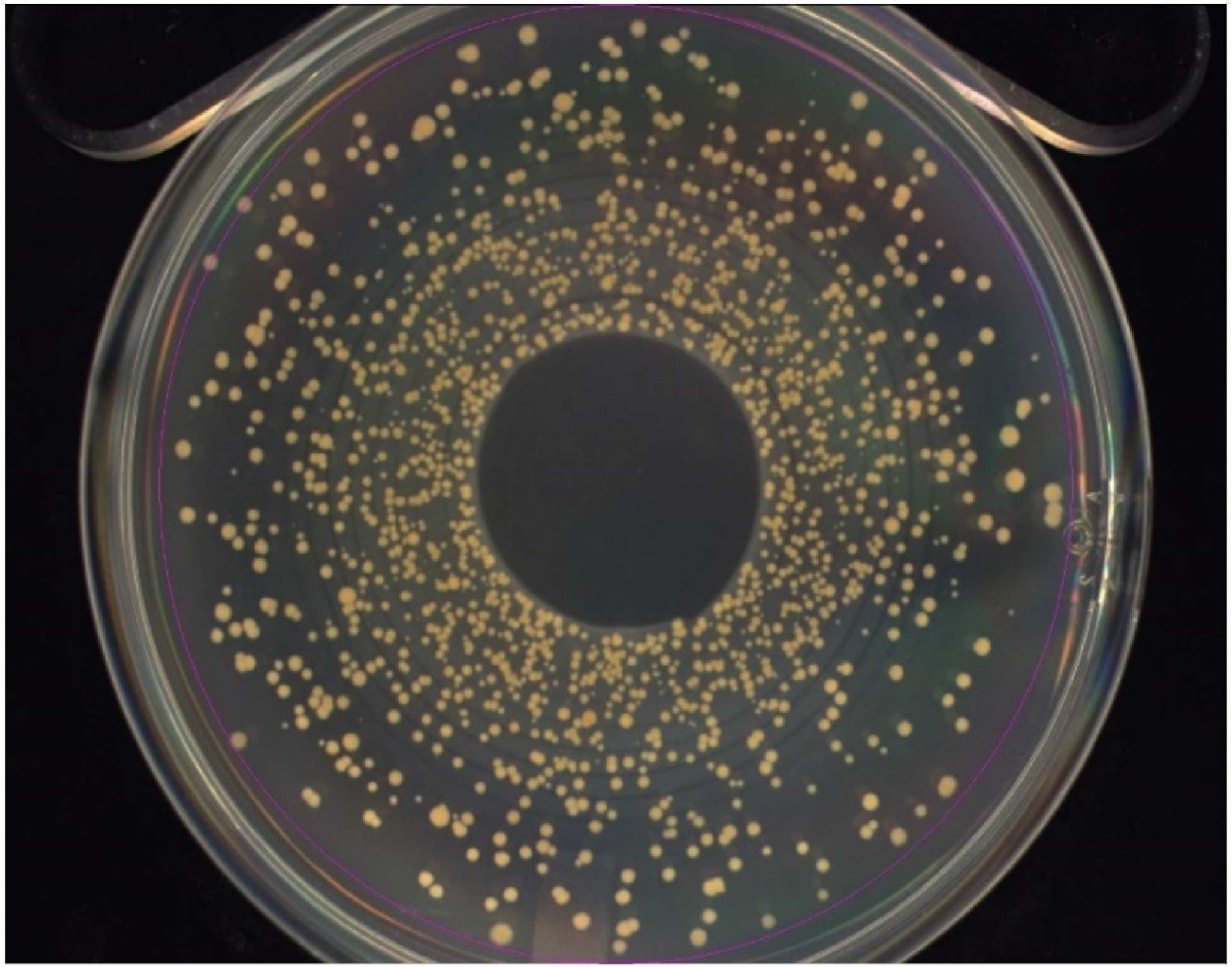

EPA United States Environmental Protection Agency

How did this decontamination method originate?

A. In resetting our pilot-scale test chamber (COMMANDER) with VHP® between tests, we found that recovery of spores inoculated onto surfaces was diminished and that low levels of H_2O_2 vapor remained for up to a week

B. Recovery of spores from our mock HVAC system exposed to hydrogen peroxide vapor (HPV) also diminished; HVAC system off-gassed HPV

C. Literature about off-gassing at low levels (< 20 parts per million [ppm])

EPA United States Environmental Protection Agency

Background on HPV for decon and sterilization

- Steris VHP® used to decontaminate State Department building after Amerithrax event, using 216 ppm for 4 hours
- VHP® typically used for disinfecting/sterilizing in healthcare, pharmaceutical, animal, and food industry using expensive generating equipment and at high levels of HPV (> 200 ppm)
- HPV shown to be effective in inactivating bacterial spores, viruses, vegetative bacteria, prions
- Use high concentration aqueous solutions (35%)

EPA United States Environmental Protection Agency

Benefits of using low levels of HPV

- Less hazardous
- More compatible with materials
- Inexpensive
- Simple to use; potentially used by lay personnel
- Widely available

EPA United States Environmental Protection Agency

Methods – where tests done

- Lab-scale chamber and COMMANDER tests done in EPA labs located in Research Triangle Park, using spores of *B. atrophaeus*
- Lab-scale tests with spores of *B. anthracis* (Ames strain) and *B. atrophaeus* done at US Army Edgewood Chemical and Biological Center in 0.23 m^3 stainless steel chamber

EPA United States Environmental Protection Agency

Methods – Coupon Materials and Biological Indicators

- 18 mm diameter coupons
- carpet, glass, ceiling tile, laminate, concrete, painted wallboard paper, galvanized metal

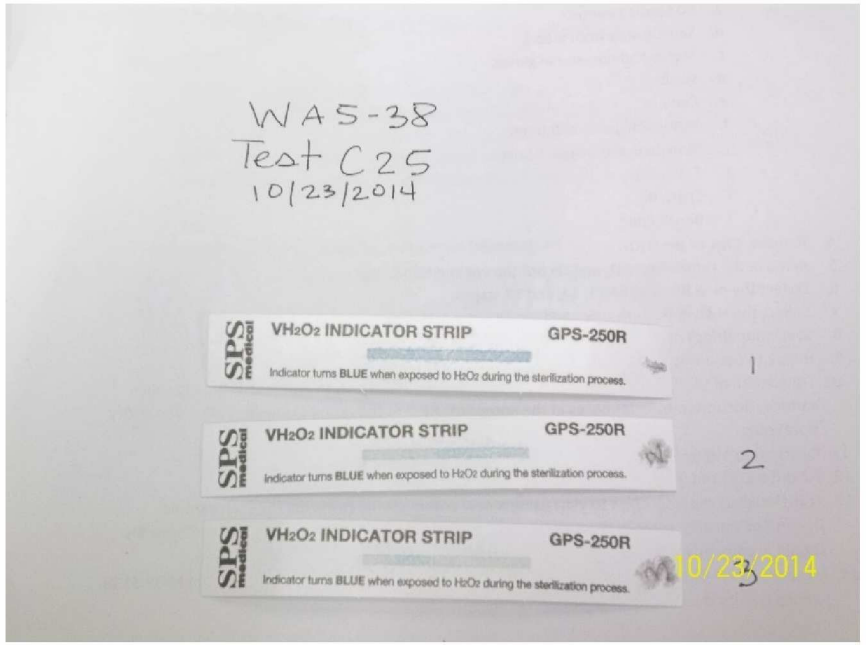

EPA United States Environmental Protection Agency

Methods – Inoculation

- Spores inoculated as an aerosol onto coupons using metered dose inhaler and custom made deposition apparatus

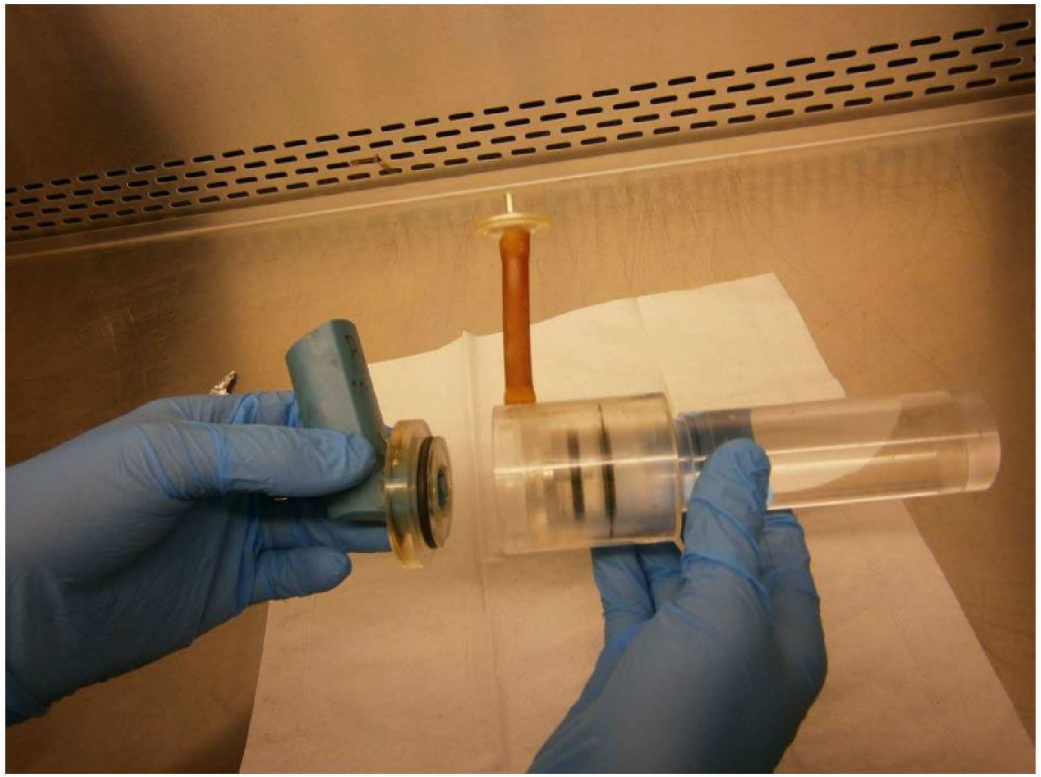

EPA United States Environmental Protection Agency

Methods – small chamber

- Small glove box
- Air sparged through small beaker of aqueous H_2O_2 solution

Methods – COMMANDER and office

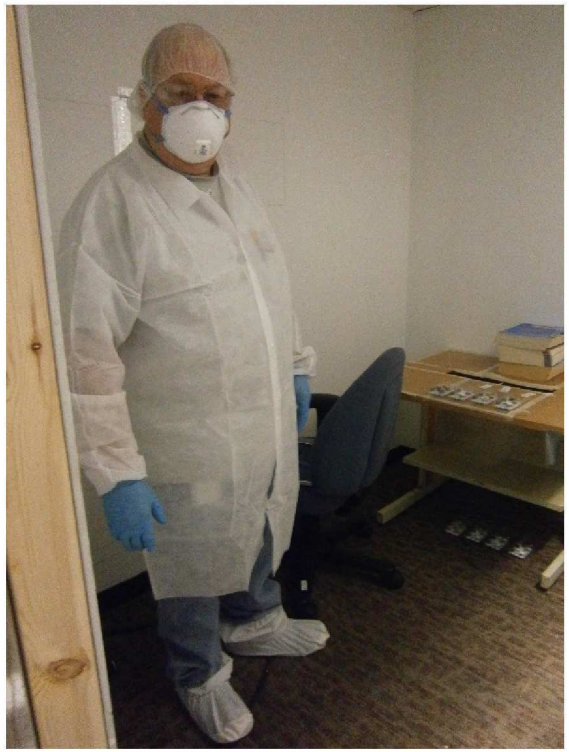

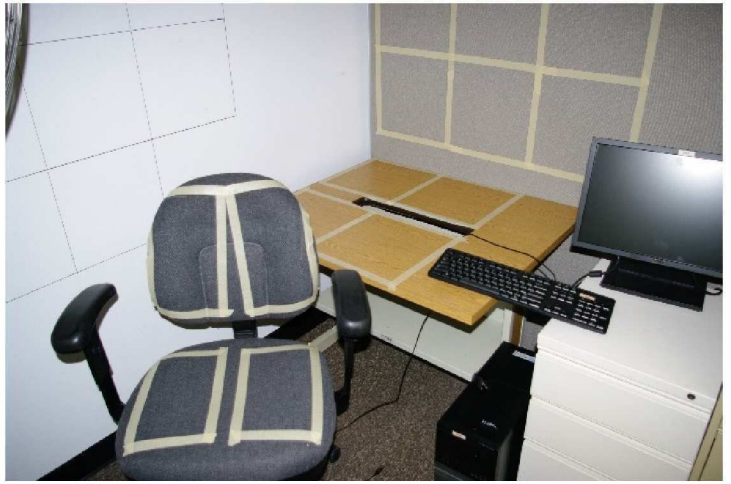

24 m^3 inner chamber set up as mock office

Methods – Measuring HPV, T, RH

- HPV measurement: Model B12, Analytical Technology Inc., Collegeville, PA, USA
- Temperature and RH measurement: Model HMD53, Vaisala, Helsinki, Finland
- Also used dosimeters to report levels in ppm*hours

EPA United States Environmental Protection Agency

Methods – Humidifiers used

EPA United States Environmental Protection Agency

Methods – Aqueous H_2O_2

Used either 3 or 8% solutions, purchased from drug store or on line

Pilot-scale test conditions

EPA United States Environmental Protection Agency

Test ID	Humidifier type	H_2O_2 conc. in aqueous solution (%)	H_2O_2 solution disseminated, ml/m^3	Air exchange	Average HPV conc. in air (ppm)	Max HPV conc. (ppm)	HPV dose (ppm * hours)	Avg RH (%)	Max RH (%)
Test C1*	Ultrasonic	8	128	None	5.5	7.3	889	74	81
Test C2	Ultrasonic	8	164	None	11	78	1900	75	93
Test C3	Sponge evaporation	8	154	None	9	43	1430	72	88
Test C4	Ultrasonic	8	173	0.3	11	59	1716	54	91
Test C5	Heated vaporizer	8	161	None	7.5	69	1224	77	94
Test C6	Sponge evaporation	3	148	None	2.2	10	362	78	93
Test C7	Sponge evaporation	3	148	None	2.5	11	428	72	85
Test C8	Sponge evaporation	3	200	None	3.2	11	543	82	89
Test C9	Sponge evaporation	3	224	0.3	6.4	24	1067	62	85
Test C10	Sponge evaporation	3	224	0.5	3.55	21	597	50	89

EPA United States Environmental Protection Agency

ECBC bench scale test conditions

Test Run	HPV set point conc. (ppm)	Average Actual HPV (ppm)	Contact time (days)	HPV Dose (ppm*hours)	Average RH (%)
1	5	5.87	7	986	41.7
2	5	5.6	4	538	47.3
3	5	6.18	1	148	44.9
4	10	8.46	1	203	56.7
5	10	11.32	0.33	91	49.4

EPA United States Environmental Protection Agency

Typical hydrogen peroxide vapor concentration profile

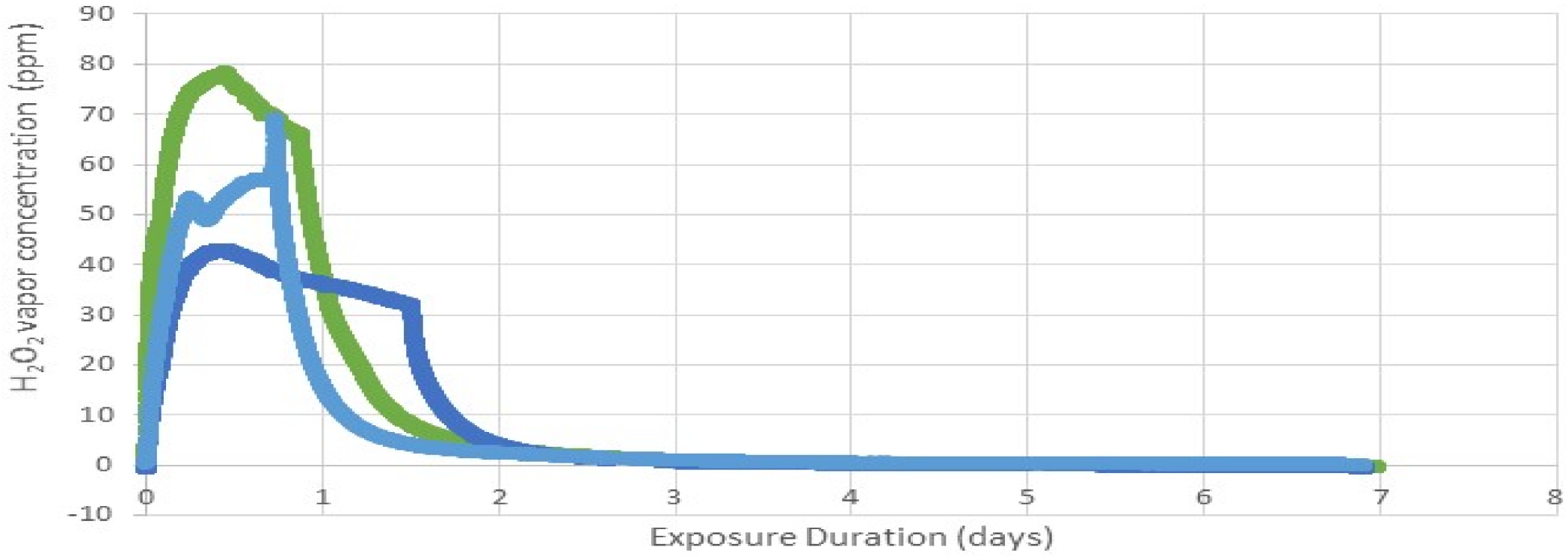

Humidifier type: Ultrasonic = green; sponge evaporation = dark blue; heated = light blue

Pilot-scale efficacy results (log reduction [LR])

Test ID	carpet	ceiling tile	glass	painted wallboard	laminate	wood	galvanized metal	Avg by test*
Test C1	7.04	6.46	6.45	5.90	6.82			6.53
Test C2	7.61	6.77	7.17	7.45	7.54	7.88	7.46	7.31
Test C3	7.61	6.66	7.29	7.63	7.80	7.78	7.35	7.40
Test C4	7.50	6.56	7.48	7.36	7.46	7.76	7.43	7.27
Test C5	7.25	6.62	7.28	7.19	7.54	7.36	7.47	7.18
Test C6	6.89	4.85	7.74	7.50	7.13	7.89	6.62	6.82
Test C7	5.83	5.71	6.70	5.53	7.02	7.62	4.04	6.16
Test C8	7.70	6.35	7.19	6.89	7.55	7.65	6.79	7.14
Test C9	6.08	6.64	6.16	6.59	7.30	7.31	6.12	6.55
Test C10	7.75	6.52	6.76	6.48	7.63	7.64	5.54	7.03
Avg by material	7.13	6.31	7.02	6.85	7.38	7.65	6.45	

- **Ineffective conditions (< 6 LR) shown in red**
- **Less than 2 LR for one test with concrete**

EPA United States Environmental Protection Agency

Bench-scale Findings

- A four-day exposure to 5 ppm HPV was effective in inactivating *B. anthracis* spores on all the materials tested in the lab-scale tests.
- A one-day exposure to 10 ppm HPV was effective for all materials except carpet.
- With the exception of one test/material, *B. atrophaeus* spores were equally or more resistant to HPV inactivation compared to those from *B. anthracis* Ames.

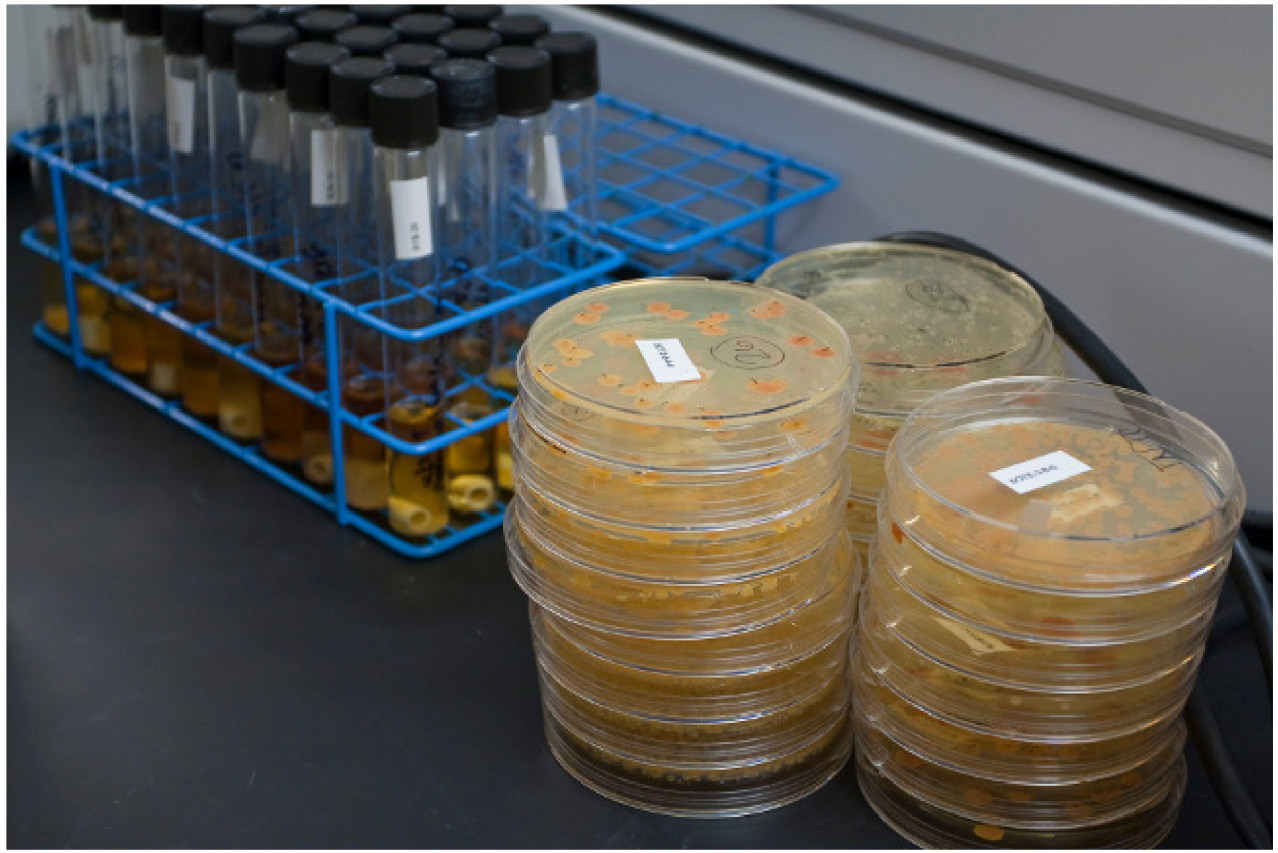

Pilot-scale Findings

- In the ten pilot scale tests, most of the materials were effectively decontaminated (≥ 6 LR), with a few exceptions:
  - In one test with unpainted concrete, less than 2 LR was achieved, and so tests with this material were discontinued.
  - The carpet and ceiling tile were also relatively more difficult to decontaminate compared to the other materials.
- Location may impact efficacy but that humidifier type may not be as important.
- A dose of at least 1000 ppm*hours HPV would be effective for a range of materials, under the conditions tested in our experiments.

Next steps

- Larger Scale
- Different contaminants

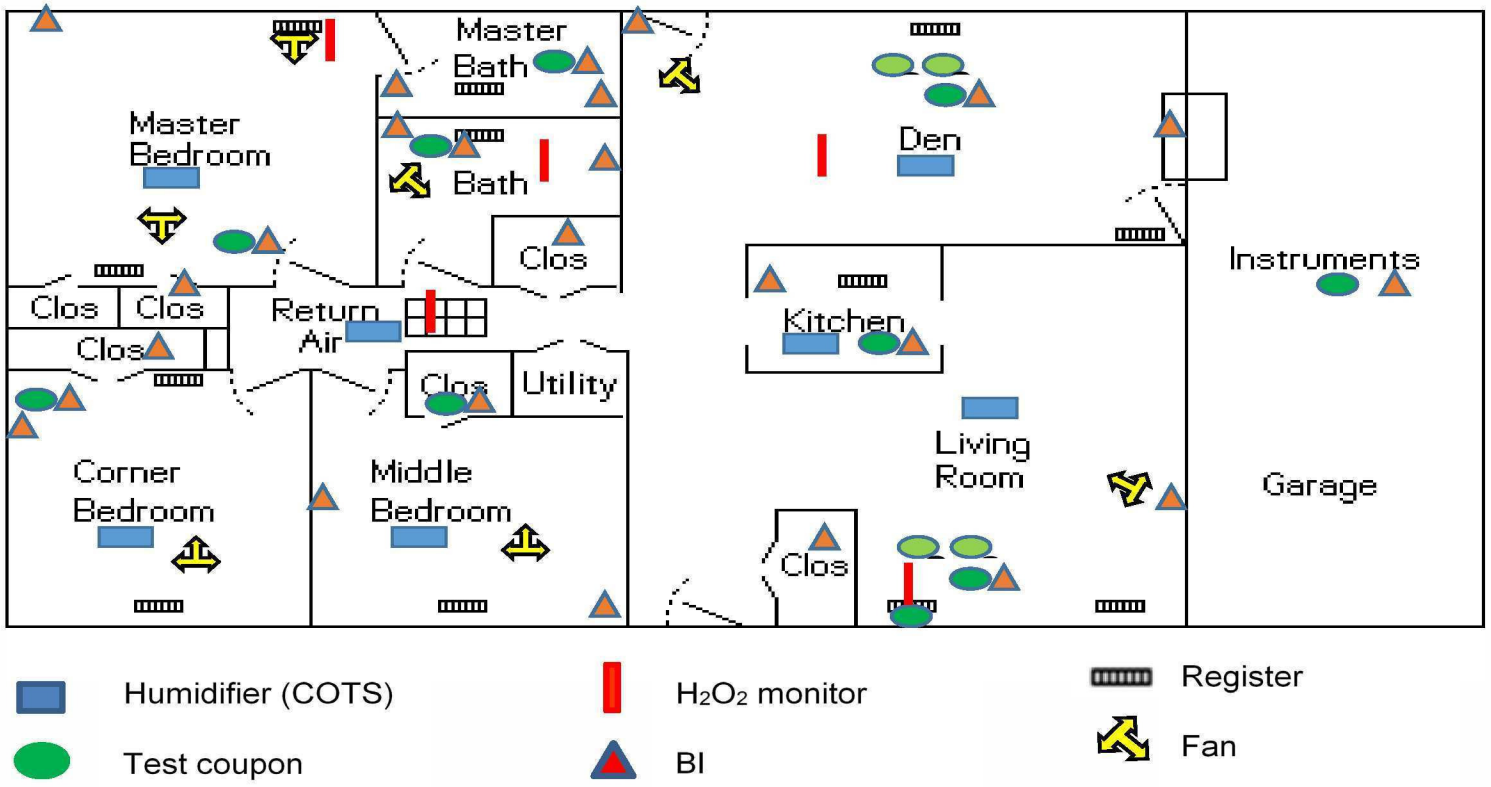

EPA United States Environmental Protection Agency

Conclusions

- HPV can be generated with commercial off the shelf (COTS) humidifiers and household H_2O_2 solutions, and is a simple and effective decontamination method that could be applied in the event of a *B. anthracis* spore release.

- The approach is an inexpensive and relatively safe way to decontaminate structures that can be left vacated for a few days, and may be less detrimental to materials.

- With the exception of concrete, our results show that 160 mL of 8% H_2O_2 per m^3 volume or 200 mL/m^3 of 3% H_2O_2 aqueous solution was the minimum amount of H_2O_2 solution needed to be an effective sporicidal decontaminant.

Table of Contents

General_Authors_Publications.....2
LI-264291_LI-264291.....16
LI-264296_LI-264296.....27
LI-264298_LI-264298.....33
Record_of_Agreement.....48

United States Environmental Protection Agency
Washington, DC 20460

STAA REPORT FOR THE SCIENTIST NOMINATIONS

General Information:

Nomination ID/App ID:	20-072
Research Category Primary:	Health Effects Research and Human Health Risk Assessment (HE)
Research Category Secondary:	Health Effects Research and Human Health Risk Assessment (HE);Monitoring and Measurement Methods (MM)
Laboratory/Office Name:	ORD
Nomination Entered By:	Marsha Morgan

Eligibility Checklist:

[Y] The nominated publication(s) has not been submitted to a previous STAA competition.

[Y] The nominated publication(s) was published on or before January 1, 2017 and on or after January 1,2012

[Y] The principal author was an EPA employee or a PHS employee assigned to EPA when the research was performed

[Y] The EPA authors (includes PHS employees assigned to EPA) contributed collectively a minimum of 50% toward the publication(s)

Nominating Official Name:	Marsha Morgan
Nominating Official Title:	PHYSICAL SCIENTIST
Nominating OfficialEmail:	morgan.marsha@epa.gov
STAA Coordinator Name:	Marsha Morgan
STAA Coordinator Email:	morgan.marsha@epa.gov

Justifications:

Justification 1:

EPA/ORD's "Pilot Study to Estimate Human Exposure to Pyrethroids using An Exposure Reconstruction Approach" (Ex-R study) was designed to collect critical exposure data and exposure modeling inputs that were needed by the Agency and lacking in the literature for pyrethroid insecticides and subsequently for bisphenol A (BPA). These critical exposure data and modeling inputs were identified using a new exposure reconstruction framework developed by our team of scientists in EPA/ORD's Chemical Safety for Sustainability (CSS) research program under task 3.1.1 Biomarkers of Exposure. Briefly, the Ex-R study was an observational exposure measurements study that concurrently collected environmental samples (duplicate-diet solid food, drinking water, carpet dust, kitchen surface floor wipes), biological samples (urine [first-morning, bedtime, and 24-h]), and diary data (food, activity, and pesticide-use) from 50 adults over a six-week monitoring period in North Carolina in 2009-2011. This was the first large-scale adult exposure/dose study to use an exposure reconstruction approach. The included manuscripts show that sampling all exposure sources in an exposure/dose measurement scheme is not necessary. These results provide the Agency with an exposure/dose design template that simplifies and reduces the costs of human studies. For this nomination, we are submitting the first three articles published in peer-reviewed journals from the Ex-R study (2016-2018) -- which have greatly advanced the field of exposure science by generating new, important data for adults on 1) the temporal variability of pyrethroid insecticides, pyrethroid degradates, and BPA in consumed diets, 2) temporal variability of BPA on household (kitchen) floor surfaces, 3) temporal dietary intake estimates to pyrethroids and BPA, 4) temporal variability of urinary pyrethroid metabolites and (total) BPA, and 5) longitudinal food, pesticide-use, and activity pattern data. The innovative Ex-R study directly supported the CSS research program under the Lifecycle and Human Exposure Modeling (LC-HEM) project by 1) providing Agency scientists, modelers, and risk assessors (i.e., EPA's Office of Pesticide Programs) with new published data on the cumulative and temporal adult exposures to pyrethroid insecticides and BPA, 2) identifying the major sources and routes of pyrethroid and BPA exposures, and 3) providing temporal pesticide-use patterns indoors and outdoors at residences. In addition, the Office of Pesticide Programs was provided these Ex-R pyrethroid data in 2018 to help assist in the interpretation of exposure data for their upcoming re-registration eligibility decisions (REDs) for several different pyrethroid insecticides. A brief description of the three nominated articles from the Ex-R study are below:

<u>Article 1</u> (Temporal variability of pyrethroid metabolite levels in bedtime, morning, and 24-hr urine samples for 50 adults in North Carolina).

Important Findings: Few studies exist on the temporal variability of urinary pyrethroid metabolites in humans, globally. This is the first US study to report the temporal variability (six-weeks) of several different pyrethroid metabolites in the urine samples of adults. The results showed that 3-PBA, *cis*-DCCA, *trans*-DCCA (non-specific metabolites of several pyrethroids) and MPA (specific metabolite of bifenthrin) were detected in 74%, 32%, 39%, and 2% of the 2500 urine samples of 50 Ex-R adults, respectively. **Scientific Impact:** For the frequently detected 3-PBA, the results indicated that a random spot urine sample did not provide a reliable estimate of the average 3-PBA level for the Ex-R adults. This above information questions the validity of using a single urinary 3-PBA measurement to quantitatively characterize the daily exposure and potential health risks of adults to non-specific pyrethroids (i.e., permethrin, cypermethrin) and can lead to exposure misclassification (e.g., epidemiological studies). These data were provided to the Office of Pesticide Programs to help assist in the interpretation of urinary biomonitoring data that are submitted by registrants in their upcoming re-registration of several different pyrethroid insecticides.

Article 2 (Pyrethroid insecticides and their environmental degradates in repeated duplicate-diet solid food samples of 50 adults).

Important Findings: Very limited published data are available on the co-occurrence of pyrethroid insecticides and pyrethroid degradates in food samples. Concerns have been raised about using these same pyrethroid degradates occurring in the diet as urinary biomarkers of exposures in people. The Ex-R study is the first published article to concurrently quantify the temporal levels of seven pyrethroids (bifenthrin, -cyhalothrin, cyfluthrin, cypermethrin, *cis*-deltamethrin, esfenvalerate, and *cis/trans*-permethrin) and six pyrethroid degradates (3-PBA, 4-F-3-PBA, *cis*-DBCA, *cis*-DCCA, and *trans*-DCCA) in duplicate-diet solid food samples of adults. The results showed that the measured pyrethroids (<22%) and pyrethroid degradates (<3%) were not frequently detected in the 782 food samples. **Scientific Impact:** This important information suggests that the measured pyrethroid degradates were likely not present in sufficient concentrations in the diet to substantially impact urinary biomarker concentrations in Ex-R adults. This research supported the Agency's mission (i.e., The Office of Pesticide Programs) as the results indicate urinary-based biomarker estimates for pyrethroids are likely not confounded by the presence of pyrethroid degradates in the diet.

Article 3 **(Distribution, variability, and predictors of urinary bisphenol A levels in 50 North Carolina adults over a six-week monitoring period).**

Important Findings: Previous research has quantified the levels of bisphenol A (BPA) mostly in food items purchased from grocery stores and supermarkets (i.e., Total Diet Studies), worldwide. These studies have reported that adults are likely mainly exposed to BPA (> 90%) through dietary ingestion. The Ex-R study was the first observational exposure measurements study to concurrently measure BPA levels in several different media (duplicate-diet solid food samples, drinking water, kitchen surface wipes, and urine [first-morning, bedtime, and 24-h]) from 50 adults in North Carolina in 2009-2011. BPA was detected in 4%, 38%, 99%, and 98% of the drinking water, duplicate-diet solid food, surface wipe, and urine samples, respectively. BPA concentrations in the surface wipe, drinking water, or solid food samples did not substantially contribute to the adults urinary (total) BPA levels. Specifically, dietary ingestion of BPA (via solid food) only accounted for ~20% of the total dietary intake dose of this chemical in Ex-R adults. **Scientific Impact:** This was the first study to quantify the levels of BPA in the actual consumed diets of adults in their everyday lives, globally. Our results were important as they suggest that the Ex-R adults were likely exposed to other major (unknown) non-dietary sources of BPA.

Justification 2A:

As part of the EPA/ORD's Chemical Safety for Sustainability (CSS) research program (under task 3.1.1. Biomarkers of Exposure), a team of ORD scientists developed a novel exposure reconstruction framework that provided a new and systematic, trans-disciplinary way to identify major data gaps and exposure modeling inputs that were likely needed to greatly improve the aggregate or cumulative exposure estimates for non-persistent chemicals (e.g., pesticides and phenols) using urinary biomarkers. Using this innovative framework, this team of scientists systematically identified the critical exposure data gaps and exposure modeling inputs for the Agency that would substantially improve pyrethroid insecticide and bisphenol A exposure estimates for adults – a significant change on how past observational exposure measurements studies were designed. Then, these scientists designed the novel "Pilot Study to Estimate Human Exposure to Pyrethroids using An Exposure Reconstruction Approach" (Ex-R study) to collect these specific needed exposure data and exposure modeling inputs for these chemicals identified in this framework. Directly supporting this exposure reconstruction framework, these three nominated articles have provided a wealth of new published data in peer-reviewed journals on 1) the temporal variability of pyrethroid insecticides, pyrethroid degradates, and

BPA in the diets of adults, 2) temporal variability of BPA on household (kitchen) surfaces, 3) temporal dietary intake estimates to pyrethroids and BPA for adults, 4) temporal variability of urinary pyrethroid metabolites and (total) BPA, and 5) longitudinal food, pesticide-use, and activity pattern data.

Justification 2B:

n/a

Justification 2C:

n/a

Justification 2D:

n/a

Justification 2E:

n/a

Justification 3A:

Articles 1, 2, and 3 (published between 2016-2018) have already been cited 26, 20, and 18 times in Google Scholar, respectively (assessed on April 21, 2020). In addition, article 2 was awarded the 2018 International Society of Exposure Science (ISES) Best Journal of Environmental Science and Environmental Epidemiology (JESEE) paper titled "*Pyrethroid insecticides and their environmental degradates in repeated duplicate-diet solid food samples of 50 adults.*" This prestigious ISES award "recognizes innovative and creative exposure science research and scholarship from the ISES membership published in the society's journal (JESEE)" each year.

Justification 3B:

The final Ex-R study database was extensively reviewed by an EPA/ORD Quality Assurance Officer and received final approval for publication. All EPA draft manuscripts were reviewed

by internal experts in exposure science before they were submitted to journals for publication. In addition, these EPA draft manuscripts were also rigorously peer-reviewed by external experts that were selected by journal editors before they were accepted for publication.

AUTHORS

Principal Author

Author Name:	Marsha K. Morgan		
Professional Title:		Salutation:	Dr.
Email:	morgan.marsha@epa.gov	Organization:	
Mailing Address:			
Street Line 1:	109 TW Alexander Drive		
City:			
Zip Code:	27711	State:	NC
At time of research was:	EPA Employee		
Separation Date:			
% of Effort:	30		

Contributing Author

Author Name:	Carry Croghan		
Professional Title:		Salutation:	Ms.
Email:	croghan.carry@epa.gov	Organization:	
Mailing Address:			
Street Line 1:	109 TW Alexander Drive		
City:	Research Triangle Park		

Zip Code:	27711	State:	NC
At time of research was:	EPA Employee		
Separation Date:			
% of Effort:	2		

Contributing Author

Author Name:	Jon Sobus		
Professional Title:		Salutation:	Dr.
Email:	sobus.jon@epa.gov	Organization:	
Mailing Address:			
Street Line 1:	109 TW Alexander Drive		
City:	Research Triangle Park		
Zip Code:	27711	State:	NC
At time of research was:	EPA Employee		
Separation Date:			
% of Effort:	20		

Contributing Author

Author Name:	Denise MacMillan		
Professional Title:		Salutation:	Dr.
Email:	macmillan@epa.gov	Organization:	
Mailing Address:			
Street Line 1:	109 TW Alexander Drive		
City:	Research Triangle Park		

Zip Code:	27711	State:	NC
At time of research was:	EPA Employee		
Separation Date:			
% of Effort:	10		

Contributing Author

Author Name:	Fu-Lin Chen		
Professional Title:		Salutation:	Mr.
Email:	fulinc100@gmail.com	Organization:	
Mailing Address:			
Street Line 1:			
City:			
Zip Code:		State:	
At time of research was:	EPA Employee		
Separation Date:	Sun Dec 31 00:00:00 GMT 2017		
% of Effort:	1		

Contributing Author

Author Name:	Maliha Nash		
Professional Title:		Salutation:	Dr.
Email:	nash.maliha@epa.gov	Organization:	
Mailing Address:			
Street Line 1:	2111 Southeast Marine Science Drive		
City:	Newport		

Zip Code:	97365	State:	OR
At time of research was:	EPA Employee		
Separation Date:			
% of Effort:	10		

Contributing Author

Author Name:	James Starr		
Professional Title:		Salutation:	Dr.
Email:	starr.james@epa.gov	Organization:	
Mailing Address:			
Street Line 1:	109 TW Alexander Drive		
City:	Research Triangle Park		
Zip Code:	27711	State:	NC
At time of research was:	EPA Employee		
Separation Date:			
% of Effort:	10		

Contributing Author

Author Name:	Matthew Clifton		
Professional Title:		Salutation:	Mr.
Email:	clifton.matthew@epa.gov	Organization:	
Mailing Address:			
Street Line 1:	109 TW Alexander Drive		
City:	Research Triangle Park		

Zip Code:	27711	State:	NC
At time of research was:	EPA Employee		
Separation Date:			
% of Effort:	3		

Contributing Author

Author Name:	Erik Andersen		
Professional Title:		Salutation:	Mr.
Email:	eanderse4@gmail.com	Organization:	
Mailing Address:			
Street Line 1:	314 Liberty Street		
City:	Pawcatuck		
Zip Code:	06379	State:	CT
At time of research was:	EPA Employee		
Separation Date:			
% of Effort:	1		

Contributing Author

Author Name:	Dana Boyd Barr		
Professional Title:		Salutation:	Dr.
Email:	dbbarr@emory.edu	Organization:	
Mailing Address:			
Street Line 1:	1518 Clifton Road		
City:	Atlanta		

Zip Code:	30322	State:	GA
At time of research was:	Non EPA Personnel		
Separation Date:			
% of Effort:	10		

Contributing Author

Author Name:	Lillian Alston		
Professional Title:		Salutation:	Ms.
Email:	alston.lillian@epa.gov	Organization:	
Mailing Address:			
Street Line 1:	109 TW Alexander Drive		
City:	Research Triangle Park		
Zip Code:	27711	State:	NC
At time of research was:	Non EPA Personnel		
Separation Date:			
% of Effort:	1		

Contributing Author

Author Name:	Richard Walker		
Professional Title:		Salutation:	Mr.
Email:	walker.richard@epa.gov	Organization:	
Mailing Address:			
Street Line 1:	109 TW Alexander Drive		
City:	Research Triangle Park		

Zip Code:	27711	State:	NC
At time of research was:	Non EPA Personnel		
Separation Date:			
% of Effort:	1		

Contributing Author

Author Name:	Dan Zehr (deceased)		
Professional Title:		Salutation:	Mr.
Email:	zehr.dan@epa.gov	Organization:	
Mailing Address:			
Street Line 1:	109 TW Alexander Drive		
City:	Research Triangle Park		
Zip Code:	27711	State:	NC
At time of research was:	Non EPA Personnel		
Separation Date:			
% of Effort:	1		

PUBLICATIONS

Publication 1:

Publication Title:	Temporal variability of pyrethroid metabolite levels in bedtime, morning, and 24-hr urine samples fo
Publication Date:	Fri Jan 01 00:00:00 GMT 2016
Journal/Publication Method:	Environmental Research
All Author(s):	

Volume:	144	Number:	0
Pages:	81-91	Immediately Index:	Immediately Index:
Citation ½ Life:	7.70	Impact Factor:	5.0

Publication 2:

Publication Title:	Pyrethroid insecticides and their environmental degradates in repeated duplicate-diet solid food sam
Publication Date:	Mon Jan 01 00:00:00 GMT 2018
Journal/Publication Method:	Journal of Exposure Science and Environmental Epidemiology
All Author(s):	

Volume:	28	Number:	0
Pages:	40-45	Immediately Index:	Immediately Index:
Citation ½ Life:	7.50	Impact Factor:	3.0

Publication 3:

Publication Title:	Distribution, variability, and predictors of urinary bisphenol-A levels in 50 North Carolina adults
Publication Date:	Mon Jan 01 00:00:00 GMT 2018
Journal/Publication Method:	Environment International
All Author(s):	

Volume:	112	Number:	0
Pages:	85-99	Immediately Index:	Immediately Index:

Citation ½ Life:	6.50	Impact Factor:	7.9

Environmental Research 144 (2016) 81–91

Contents lists available at ScienceDirect

Environmental Research

journal homepage: www.elsevier.com/locate/envres

Temporal variability of pyrethroid metabolite levels in bedtime, morning, and 24-h urine samples for 50 adults in North Carolina

Marsha K. Morgan [a,*], Jon R. Sobus [a], Dana Boyd Barr [b], Carry W. Croghan [a], Fu-Lin Chen [a], Richard Walker [a], Lillian Alston [a], Erik Andersen [a], Matthew S. Clifton [a]

[a] National Exposure Research Laboratory, US EPA, Research Triangle Park, NC, USA
[b] Department of Environmental Health, Rollins School of Public Health, Emory University, Atlanta, GA, USA

ARTICLE INFO

Article history:
Received 8 September 2015
Received in revised form
30 October 2015
Accepted 3 November 2015
Available online 14 November 2015

Keywords:
Pyrethroids
Adults
Urine
Homes
Biomonitoring
Variability

ABSTRACT

Pyrethroid insecticides are widely used to control insects in both agricultural and residential settings worldwide. Few data are available on the temporal variability of pyrethroid metabolites in the urine of non-occupationally exposed adults. In this work, we describe the study design and sampling methodology for the Pilot Study to Estimate Human Exposures to Pyrethroids using an Exposure Reconstruction Approach (Ex-R study). Two major objectives were to quantify the concentrations of several pyrethroid metabolites in bedtime, first morning void (FMV), and 24-h urine samples as concentration (wet weight), specific-gravity (SG) corrected, creatinine (CR) corrected, and excretion rate values for 50 Ex-R adults over a six-week monitoring period and to determine if these correction approaches for urine dilution reduced the variability of the biomarker levels. The Ex-R study was conducted at the United States Environmental Protection Agency's Human Studies Facility in Chapel Hill, North Carolina USA and at participants' homes within a 40-mile radius of this facility. Recruitment of participants and field activities occurred between October 2009 and May 2011. Participants, ages 19–50 years old, provided daily food, activity, and pesticide-use diaries and collected their own urine samples (bedtime, FMV, and 24-h) during weeks 1, 2, and 6 of a six-week monitoring period. A total of 2503 urine samples were collected from the study participants. These samples were analyzed for the pyrethroid metabolites 3-phenoxybenzoic acid (3-PBA), *cis/trans*-3-(2,2-dichlorovinyl)-2,2-dimethyl-cyclopropane carboxylic acid (*cis/trans*-DCCA), and 2-methyl-3-phenylbenzoic acid (MPA) using high performance liquid chromatography/tandem mass spectrometry. Only 3-PBA was frequently detected ($>50\%$) in the adult urine samples. Median urinary 3-PBA levels were 0.88 ng/mL, 0.96 ng/mL-SG, 1.04 ng/mg, and 1.04 ng/min for concentration, SG-corrected, CR-corrected, and excretion rate values, respectively, across all urine samples. The results showed that median urinary 3-PBA concentrations were consistently the lowest in FMV samples (0.77 ng/mL, 0.68 ng/mL-SG, 0.68 ng/mg, and 0.58 ng/min) and the highest in 24-h samples (0.92 ng/mL, 1.06 ng/mL-SG, 1.18 ng/mg, and 1.19 ng/min) across all four methods. Intraclass correlation coefficient (ICC) estimates for 3-PBA indicated poor reproducibility (<0.22) for all urine sample types and methods over a day, week, and six weeks. Correcting for urine sample dilution, based on either SG, CR or urine output, introduced additional measurement variability both between- and within-individuals. These results indicate that a single measure of urinary 3-PBA was not sufficient to characterize average exposure regardless of sample type, correction method, and time frame of collection. In addition, the study results can be used to inform the design of exposure characterization strategies in relevant environmental epidemiology studies in the future.

Published by Elsevier Inc.

1. Introduction

Pyrethroids are a class of insecticides that are widely and globally used to control a variety of insects at homes, on domestic pets, and on agricultural crops (US EPA, 2013; Saillenfait et al., 2015). These lipophilic insecticides have replaced many of the previous residential and some agricultural applications of the organophosphates because of

Abbreviations: 3-PBA, 3-phenoxybenzoic acid; CDC, Centers for Disease Control and Prevention; *cis/trans*-DCCA, *cis/trans*-3-(2,2-dichlorovinyl)-2,2-dimethylcyclopropane-1-carboxylic acid; EPA, Environmental Protection Agency; Ex-R study, Pilot Study to Estimate Human Exposures to Pyrethroids using an Exposure Reconstruction Approach; HSF, Human Studies Facility; FMV, first morning void; ICC, intraclass correlation coefficient; LOQ, limit of quantitation; NHANES, National Health and Nutritional Examination Survey; NC, North Carolina; MPA, 2-methyl-3-phenylbenzoic acid; RTP, Research Triangle Park; US, United States

* Corresponding author.
E-mail address: morgan.marsha@epa.gov (M.K. Morgan).

http://dx.doi.org/10.1016/j.envres.2015.11.003
0013-9351/Published by Elsevier Inc.

their lower volatility and lower mammalian toxicity due to faster enzymatic detoxification (Elliott, 1976; Barr et al., 2010). However, recent research has raised concerns about potential adverse health effects (i.e., developmental and male reproductive) occurring from human exposure to pyrethroids at environmental levels (Saillenfait et al., 2015).

In the United States (US), at least 20 different pyrethroids are registered for commercial use in residential or agricultural settings (US EPA, 2011). However, no published data are currently available on the national retail sales or usage patterns of pyrethroid insecticides in these settings (Kuivila et al., 2012; Palmquist et al., 2012; Xue et al., 2014). Several US studies have detected a number of current-use pyrethroids (i.e., bifenthrin, cyfluthrin, cypermethrin, cyhalothrin, deltamethrin, and esfenvalerate) in dust, food, and/or wipes in residential environments (Morgan et al., 2007; Julien et al., 2008; Starr et al., 2008; Stout et al., 2009; Tulve et al., 2008; Chuang and Wilson, 2011; Trunnelle et al., 2014). Research has suggested that dietary ingestion is likely the major route of exposure to pyrethroids in the general US adult population (Riederer et al., 2008; Barr et al., 2010).

After absorption into the body, pyrethroid insecticides are metabolized rapidly and primarily excreted in urine with an elimination half-life of less than 12-h (Leng et al., 1997; Kuhn et al., 1999; Ratelle et al., 2015). Several cross-sectional studies have reported measureable concentrations of pyrethroid metabolites, including 3-phenoxybenzoic acid (3-PBA) and *cis*/*trans*-3-(2,2-dichlorovinyl)-2,2-dimethylcyclopropane-1-carboxylic acid (*cis*/*trans*-DCCA), in the spot urine samples of adults recruited from the general population (referred to subsequently as non-occupationally exposed) in the US (Berkowitz et al., 2003; Barr et al., 2010; McKelvey et al., 2013; Young et al., 2013; Trunnelle et al., 2014; CDC, 2015; Morgan, 2015). In the US National Health and Nutritional Examination Survey (NHANES, 2001–2002 cycle), which was a population-based survey that included 1128 adults, ages 20–59 years, 3-PBA, *cis*-DCCA, and *trans*-DCCA were detected in 76%, 33%, and 25% of the urine samples, respectively (Barr et al., 2010). 3-PBA is a nonspecific urinary biomarker of at least 18 different pyrethroid insecticides including cyhalothrin, cypermethrin, deltamethrin, esfenvalerate, and permethrin (CDC, 2009; Barr et al., 2010). The isomers, *cis*-DCCA and *trans*-DCCA, are also the nonspecific urinary biomarkers of cyfluthrin, cypermethrin, and permethrin (CDC, 2009).

For spot urine measurements, a major concern is that volume-based concentrations (e.g., ng/mL) can be affected by variable urine dilutions in humans from factors such as fluid intake, perspiration, gender, age, and disease status (e.g., kidney and heart) (Boeniger et al., 1993; Mage et al., 2004; Barr et al., 2005; Fortin et al., 2008). To adjust for variable urine dilutions in spot samples, correction methods involving specific gravity (SG) and creatinine (CR) measurements or timed excretion rates (e.g., ng/min) have been used to normalize pesticide biomarker measurements across and within individuals (Hwang et al., 1997; Fortin et al., 2008; Christensen et al., 2012). CR-correction of urine sample volumes is the most widely used method in studies, and assumes that CR is eliminated at a constant rate by the kidneys into urine in humans (Hwang et al., 1997; Barr et al., 2005). But, this correction method may also bias study results because CR excretion can also vary due to many factors such as age, gender, dietary intake, muscle mass, physical activity, and diurnal patterns (Boeniger et al., 1993; Hwang et al., 1997; Mage et al., 2004). Further complicating interpretation of these data, concentrations in spot samples likely only reflect recent exposures because these chemicals have short elimination half-lives ($<$ 12-h). Continual exposures to pyrethroid insecticides would likely result in relatively constant urinary metabolite levels over time (e.g., day, week or month) (NRC, 2006; Wielgomas, 2013a). In contrast, episodic exposures to these insecticides would probably cause significant fluctuations in urinary biomarker levels over time (NRC, 2006). Little information, however, is currently known on the temporal variability of pyrethroid metabolites in non-occupationally exposed adults. Temporal variability is useful for understanding the patterns and magnitude of a person's exposures to pyrethroid insecticides over time using urinary biomonitoring. When relying on only one spot urine measurement, this unknown variability in an individual's biomarker level could lead to exposure misclassification in epidemiological studies (Lassen et al., 2013). Wielgomas (2013a) recently examined the temporal variability of 3-PBA concentrations in the urine samples of seven, non-occupationally exposed adults (ages 24–71 years old) over a week in an urban area of Poland in 2011. In this study, the intraclass correlation coefficient (ICC), which quantifies reliability, were estimated for 3-PBA levels by urine sample type (first morning void [FMV], spot, and 24-h) as concentration, CR-corrected, and excretion rate values. The ICCs were the highest for the CR-corrected spot urine samples (ICC = 0.846). Based on this ICC of 0.846, a single spot sample appeared representative of average exposure over a single week, and that these adults were likely continually exposed to similar levels of pyrethroids, likely from the same sources, in their urban environments (Wielgomas, 2013a).

The "Pilot Study to Estimate Human Exposures to Pyrethroids using an Exposure Reconstruction Approach" (Ex-R study) investigated longitudinal exposures (over six weeks) of adults to pyrethroid insecticides commonly found in residential settings. The first study objective was to assess the variability of 3-PBA, *cis*-DCCA, *trans*-DCCA, and 2-methyl-3-phenylbenzoic acid (MPA; specific metabolite of bifenthrin) in the urine samples of 50 adults at home over a six-week monitoring period. The second study objective was to estimate the dietary and non-dietary exposures of these adults to selected current-use pyrethroids and to their preformed metabolites (e.g., 3-PBA) in media using an exposure reconstruction approach. Here we report the study design and sampling methodology for the Ex-R study, and the study results related to objective 1 above. Specifically for objective 1, we quantified the distributions of 3-PBA, *cis*-DCCA, *trans*-DCCA, and MPA by urine sample type (bedtime, FMV, and 24-h) as concentration, SG-corrected, CR-corrected, and excretion rate values over a six-week monitoring period. We also determined if these three correction approaches for urine dilution reduced the variability of the observed biomarker levels (3-PBA, only). In addition, we calculated the number of urine samples needed to adequately assess the exposures of Ex-R adults to pyrethroids insecticides over a day, week, and six weeks.

2. Materials and methods

The design strategy, recruitment of participants, field sampling procedures, and analytical methodology (urine, only) for the Ex-R study are discussed below.

2.1. Study cohort

The Ex-R study investigated the longitudinal exposures of 50 adults to pyrethroid insecticides at their residences over a six-week monitoring period. The study was conducted at the US Environmental Protection Agency's (EPA's) Human Studies Facility (HSF) in Chapel Hill, North Carolina (NC) and at participants' homes within a 40-mile radius of the HSF. From October 2009 to March 2011, adults were recruited by an on-site US EPA contractor (WESTAT) at the HSF via their in-house database of volunteers or by word of mouth (i.e., US EPA researchers or prior participants). Interested individuals were asked several questions (e.g., "Are you

exposed at work to products that contain pyrethroid insecticides [yes or no]?)" over the phone by a WESTAT technician to determine their eligibility to participate. To be eligible, a participant had to be a healthy, non-pregnant adult (18–50 years old), had no pre-existing medical conditions (e.g., kidney disease) affecting urine output, was currently living in a residential home or apartment, had no occupational exposures to pyrethroids, could provide their own transportation to and from the HSF, and could speak, read, and use English fluently. A total of 56 adults who contacted WESTAT were eligible to participate in the study; only two of these adults declined to provide consent to participate (e.g., work conflict). Before beginning the study, the adult participants were trained individually (~2 h) by US EPA researchers at the HSF on the procedures for filling out diaries (activity, food, and pesticide-use), collecting their own samples (urine, solid food, drinking water, surface wipes, and vacuum dust), and storing the samples in portable thermoelectric coolers until collected by study personnel.

2.2. Human subjects protection

The study protocol and procedures to acquire informed consent from the adult participants followed EPA policies and the guidelines set forth by the Scientific and Ethical Approaches for Observational Exposure Studies report (US EPA, 2008) and were reviewed and approved by the US EPA's Human Subjects Research Review Official and by the University of North Carolina's Institutional Review Board (study number 09-0741). Adult volunteers read and signed informed consent documents prior to beginning the study.

2.3. Field sampling

Field activities were performed between November 2009 and May 2011. A total of 11 consecutive, six-week monitoring periods were performed in this study. During each monitoring period, up to six adult participants filled out diaries and collected their own samples during weeks 1, 2 and 6. Fig. 1 presents the sampling schedule that the participants followed for each sampling week. Each sampling week began in the morning of day 1 (Sunday) and ended in the morning of day 6 (Friday). There were two sampling intervals, days 1–3 (Sunday to Tuesday) and days 4–6 (Wednesday to Friday), per sampling week.

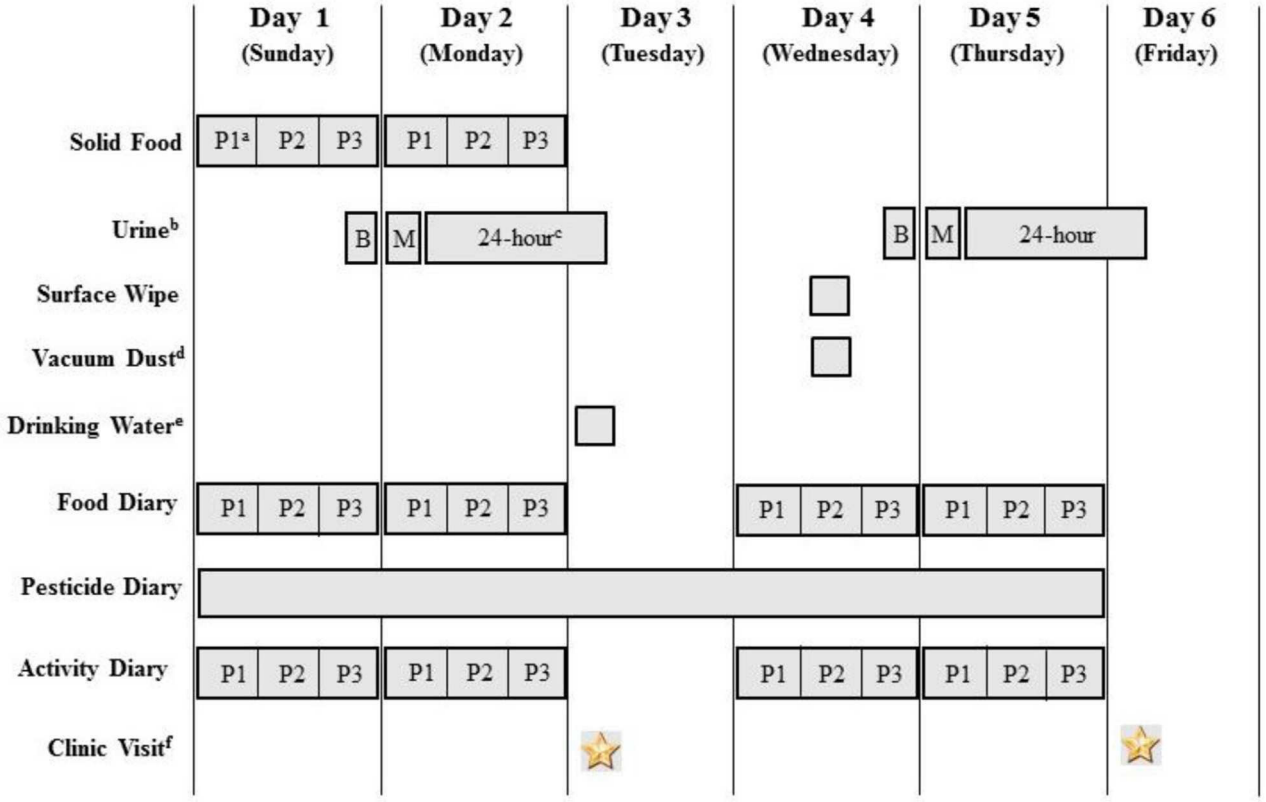

[a] Period 1 (P1) = 4:00 am–11:00 am; Period 2 (P2) = 11:00 am–5:00 pm; Period 3 (P3) = 5:00 pm–4:00 am

[b] Bedtime void (B), first morning void (M), and 24-hr sample

[c] Individual urine voids were collected over the 24-hr period and analyzed separately

[d] Vacuum dust sample was collected only on day 4 of week 6

[e] Drinking water sample was collected only on day 3 of week 6

[f] Study items were dropped off at the HSF between 8:00 am – 11:00 am

Fig. 1. Field sampling activities that the Ex-R adult participants performed during each sampling week (1, 2, or 6). [a]Period 1 (P1)=4:00 am–11:00 am; Period 2 (P2)=11:00 am–5:00 pm; Period 3 (P3)=5:00 pm–4:00 am. [b]Bedtime void (B), first morning void (M), and 24-h sample. [c]Individual urine voids were collected over the 24-h period and analyzed separately. [d]Vacuum dust sample was collected only on day 4 of week 6. [e]Drinking water sample was collected only on day 3 of week 6. [f]Study items were dropped off at the HSF between 8:00 am–11:00 am.

The participants used portable thermoelectric coolers (13.5″ Dx12″ Wx14.5″H Princess International or Vinotemp®) to store their samples and diaries (in an outside pocket) for each sampling interval. Each cooler contained a notebook with sampling instructions, calendar and schedule, a notebook containing food, activity, and/or pesticide-use diaries, sampling equipment and containers, gloves, ballpoint pens, and an electric power adapter (Koolatron® Model AC-15). Barcodes were attached to all diaries and sampling containers. Temperature data recorders (Easy Log EL-USB-LITE or EL-USB-1, Lascar Electronic, Ltd) were placed inside each cooler to record internal temperatures. The participants kept the coolers at reduced temperatures by plugging them into their vehicle (using a car adapter) or an electric wall outlet at home or other location (e.g., work).

The participants were provided with two coolers for the first sampling interval (days 1–3) on the Friday before each sampling week. These two coolers were returned by the participants to the HSF between 8:00 am–11:00 am on day 3 of each sampling week. After arriving at the HSF, US EPA researchers checked-in all study items in the two coolers with each participant. Afterwards, the participants were provided with two new coolers for the next sampling interval (days 4–6) of each sampling week. These two coolers were returned to the HSF between 8:00 am–11:00 am on day 6 of each sampling week, and all study items were checked-in by US EPA researchers. After each sampling interval, the used coolers containing collected study items with blue ice were then transported (~20 miles) by US EPA researchers in a van to the US EPA laboratory in Research Triangle Park (RTP), NC. The participants came to the HSF a total of eight times, including the training session, during the six-week monitoring period.

2.4. Collection of diaries

The participants filled out three different types of diaries (food, activity, and pesticide-use) during sampling weeks 1, 2, and 6 (Fig. 1). For the food and activity diaries, information was collected during three consecutive time periods on days 1–2 and days 4–5 of each sampling week. These time periods were period 1 (4:00 am–11:00 am), period 2 (11:00 am–5:00 pm), and period 3 (5:00 pm to 4:00 am). In the food diary, the participants recorded the types and amount of foods and beverages they consumed during each time period. In the activity diary, the participants recorded their primary location (i.e., inside home, outside home, away from home, or transit) and primary activity (i.e., sleeping, low activity [e.g., sitting], medium activity [e.g., walking] or high activity [e.g., running]) in 30-minute time intervals for each time period. They also recorded when they ate, drank, or urinated during these 30-minute time intervals. For the pesticide-use diary, information was collected on day 5 of each sampling week. In this diary, the participants recorded the types of insecticides that were used at their home over a period of 30 days prior to and during the six-week monitoring period. They also recorded their pesticide usage patterns including type, location, frequency, and day of insecticide application during each sampling week.

2.5. Collection of environmental samples

Environmental samples including solid food, drinking water, surface wipes, and vacuum dust were collected by the adult participants at their residences during sampling weeks 1, 2, and/or 6 (Fig. 1). Detailed information on the collection of these media by the participants can be found in the Supplemental Information section.

2.6. Collection of urine samples

Spot urine voids (bedtime and FMV) and 24-h urine samples were collected by the participants during each sampling week (Fig. 1). Bedtime voids were collected before going to sleep on days 1 and 4 of each sampling week. FMV's were collected after waking up on days 2 and 5 of each sampling week. For the 24-h samples, individual urine voids for a person were collected starting after the FMV on day 2 or 5 until collection of the FMV the next day (e.g., day 3 or 6) (Fig. 1). Up to 11 individual voids were collected by a participant over a 24-h sampling period.

All urine voids were collected by the participants in separate 1 L polypropylene containers. The entire amount of urine was collected for each type of urine void. The time of sample collection for each void was recorded on a label affixed to the lid of the container. At the HSF, US EPA researchers recorded the volume of each urine void using a transparent, graduated plastic cylinder that was placed over the container. A total of 2503 urine voids (includes bedtime, FMV, and 24-h) were collected by the participants during the study.

At the US EPA laboratory, up to eight, 8 mL aliquots of urine from each void were placed into separate 10 mL cryogenic vials with lids. All aliquots were stored in laboratory freezers (−80 °C) until analysis.

2.7. Analysis of urine samples

In 2010–2011, US EPA laboratory technicians shipped 2503 urine aliquots (8 mL each) in coolers containing dry ice overnight by UPS to Emory University's Rollins School of Public Health laboratory in Atlanta, Georgia. The urine aliquots were stored in −80 °C freezers until analyzed (2013–2014). For the 24-h urine samples, each void was analyzed separately. All urine samples were extracted and levels of 3-PBA, *cis*-DCCA, *trans*-DCCA, and MPA were measured using a slight modification of the method by Baker et al. (2004). Briefly, 0.5-mL aliquot of urine from each sample was hydrolyzed with β-glucuronidase/sulfatase for ~16 h. Next, the target analytes were extracted using solid phase extraction (3cc-60 mg OASIS HLB cartridge) and then evaporated to dryness using a TurboVap LV Evaporator set at 45 °C and 15 psi N_2. Finally, the extract was reconstituted with 100 μL of a 30% methanol/70% deionized water solution prior to chemical analysis. The urine extracts were quantified for the target pyrethroid metabolites using a high performance liquid chromatography/tandem mass spectrometer (Agilent Tech, Waldbronn, Germany) equipped with a negative mode jet-stream electrospray chemical ionization interface. Separation was performed using a Betasil C_{18}, 100x2.1 mm–3 μm particle size, column (Thermo Scientific, Waltham, MA, USA) with a gradient elution using 0.1% acetic acid in deionized water and 0.1% acetic acid in methanol. The column temperature was maintained at 45 °C, and the total run time was seven minutes. The estimated limits of quantitation (LOQ) were 0.25 ng/mL for 3-PBA, *cis*-DCCA, and *trans*-DCCA and 0.5 ng/mL for MPA.

All urine samples were also analyzed for SG and CR levels. At the US EPA laboratory in 2012, another identical set of urine aliquots (8 mL each) was thawed overnight in a refrigerator (~4 °C). Each aliquot of urine was vortex mixed (~5 s) and then transferred into a 50 mL vial and sonicated for 15 min. A 50 μL aliquot of urine was removed from each 50 mL vial and analyzed for CR levels using a spectrophotometer (Biotek® ELx800 or Elx808ui), equipped with a 96-well plate at a wavelength at 490 nm using a modified version of the Jaffé method (Andersen et al., 2014). SG was also measured by dipping the tip of a hand-held refractometer (Atago® model no. 3741) into each 50 mL vial of remaining urine (~7.9 mL) using water as a calibrant.

2.8. Quality assurance and quality control

A total of 150 field blanks and 150 field spikes were prepared prior to the onset of sampling activities by laboratory technicians at the Centers for Disease Control and Prevention (CDC) in Atlanta, Georgia in 2009. These quality control (QC) samples consisted of pooled urine samples that were collected from non-occupationally exposed adult volunteers at CDC. The pooled urine samples were prescreened for 3-PBA, *cis*-DCCA, and *trans*-DCCA and diluted, when necessary, to reduce background levels. Each field blank or field spike consisted of 8 mL of urine in a 10-mL polypropylene cryovial. For the field spikes, 3-PBA, *cis*-DCCA, and *trans*-DCCA standards (25 ng/mL) were individually added to each cryovial; the MPA standard was not obtained until after preparation of the field spikes at CDC. These QC samples were shipped in coolers on dry ice overnight by Fed-Ex from the CDC laboratory to the US EPA laboratory in 2009 and kept frozen in freezers ($-80\ ^{\circ}C$) until field sampling.

A single field blank and field spike were assigned to each study participant during days 4–6 of each sampling week. These QC samples were thawed overnight in an US EPA refrigerator and then placed unopened in a (plugged-in) portable thermoelectric cooler in a study room at the HSF. After each sampling interval, the field blanks and field spikes were transported in separate coolers along with study sample coolers to the US EPA laboratory and kept frozen ($-80\ ^{\circ}C$) in freezers.

In 2010–2011, 150 field blanks, 150 field spikes, and 150 duplicate urine samples were shipped in coolers on dry ice by UPS from the US EPA laboratory to the Emory University laboratory in Atlanta, GA. These QC samples were analyzed for the target pyrethroid metabolites following the same analytical procedures described in Section 2.7 above. For the field blanks and field spikes, a value of $LOQ/\sqrt{2}$ was first imputed for all target analyte measurements that were below the LOQ (Verbovsek, 2011). Precision estimates, expressed as percent relative standard deviations (RSDs), were then calculated for the field blanks and field spikes. Measures of field blanks were all below the LOQ for *cis*-DCCA, *trans*-DCCA, and MPA. However, all field blanks had low 3-PBA background levels (likely stemming from true background levels in the pooled urine samples, and not sample contamination), and yielded an RSD estimate of 2.5%. For the field spikes, estimates of percent relative standard deviation across the samples were between 6% and 7% for 3-PBA, *cis*-DCCA, and *trans*-DCCA. Precision across duplicate urine samples was evaluated using relative percent difference estimates at both the metabolite and sample levels. Not including zero values (where the initial and replicate measures were identical – generally a consequence of single value imputation for measurements $<$LOQ), median relative percent differences across duplicate sample measures were estimated to be 17% for 3-PBA (based on 129 samples), 26% for *cis*-DCCA (based on 64 samples), 18% for *trans*-DCCA (based on 80 samples), and 41% for MPA (based on 4 samples).

In addition to field QCs, laboratory QC samples ($\sim$15% of the samples tested) were used to evaluate the quality of each analytic run. A minimum of eight calibrants, 2 QC materials, 2 blank samples, and 1 replicate sample were analyzed concurrently with 30–40 unknown samples in each analytic run. QC samples had to be within 20% of the spiked concentration for the run to be considered valid. Replicate samples were not used to determine run validity but were rather used as a quality check. Replicate samples were generally within 20% of their respective duplicate.

2.9. Statistical analysis

All statistical analyses were performed using SAS version 9.4 (SAS Institute, Cary, NC, USA). For each pyrethroid metabolite, all urine data values below the LOQ were assigned the value of $LOQ/\sqrt{2}$ (Verbovsek, 2011). Descriptive statistics including geometric mean, range, and selected percentiles (25th, 50th, 75th, 95th, and 99th) were calculated for the concentrations of 3-PBA, *cis*-DCCA, and *trans*-DCCA by urine sample type (bedtime, FMV, 24-h, and overall) as concentration (ng/mL), SG-corrected (ng/mL-SG), CR-corrected (ng/mg), and excretion rate (ng/min) values. These descriptive statistics were not calculated for MPA as it was detected in only 2% of the urine samples. SG-corrected values were computed using the following equation (Morgan et al., 2008): SG-corrected value (ng/mL-SG) = urine concentration (ng/mL) $\times$ $(SG_{target}-1.000)/(SG_{urine\ sample}-1.000)$, where SG_{target} was selected to be the median SG value (1.014) across all study measurements. SG values ranged from 1.0018–1.0372 ng/mL-SG. CR-corrected values were calculated using the following equation (Morgan et al., 2008): CR-corrected values (ng/mg) = 100 mL/dL $\times$ urine concentration (ng/mL)/CR concentration (mg/dL). CR concentration values ranged from 7.0–442 mg/dL. The metabolite excretion rate was calculated as follows: Excretion rate (ng/min) = urine concentration (ng/mL) $\times$ volume of urine void (mL)/time since previous urine void (min). Urine void volumes ranged from 5 mL to 1000 mL (limited by container size of 1 L).

Pairwise associations between urinary 3-PBA, *cis*-DCCA, and *trans*-DCCA levels were evaluated using Spearman correlation coefficients. Since repeated measures from individuals are not independent, the results of these analyses were used only to screen for general trends between the urinary metabolites.

Urinary 3-PBA was the only frequently detected analyte ($>$50%), and therefore the only analyte on which parametric analyses were performed. Based on the Shapiro-Wilks normality test, the distribution of urinary 3-PBA was found to be log-normal, and therefore all urine values were log-transformed (ln) for further statistical analyses. For the frequently detected 3-PBA, one-way random effects models (Proc Mixed) were used to estimate within- and between-person variance components for ln-transformed 3-PBA. These estimates were then used to estimate ICCs and 95% fold-ranges ($R_{0.95}$) according to Rappaport and Kupper, 2008. The ICC represents the ratio of between-person variance to total variance. ICC values can range from 0 to 1; values nearer to 0 signify low reliability, and values nearer to 1 signify high reliability (Fleiss, 1985). ICCs values can be used to indicate poor reproducibility (<0.4), good reproducibility (0.4 to 0.75) or excellent reproducibility (>0.75) of a spot urine measurement (Rosner, 2006). Traditionally, an ICC value of 0.80 or greater indicates that a random spot urine measurement would accurately represent the average biomarker value over a defined period of time (Fleiss, 1985). The between-person fold-range ($_{b}R_{0.95}$) represents the fold-range containing the middle 95% of individual-specific mean biomarker levels. The within-person fold-range ($_{w}R_{0.95}$) represents the fold-range containing the middle 95% of biomarker levels for any individual. ICC and fold-range estimates for ln(urinary 3-PBA levels) were calculated separately by urine sample type as concentration, SG-corrected, CR-corrected, and excretion rate measures corresponding to a day, week, and six-weeks. Lastly, we estimated the number of random spot urine voids per adult that would be required to provide a reliable biomarker estimate (ICC = 0.80) by sample type and method for each time period using the following equation (Fleiss, 1985): $m=(p_{r,m}(1-p_r))\ /\ (p_r(1-p_{r,m}))$. In this equation, m is the number of random spot urine measurements per adult required to correctly rank individuals within a cohort, $p_{r,m}$ is the specified reliability of the mean (ICC = 0.80), and p_r is the ICC value for each urine sample type and method.

3. Results

Table 1 presents the physical characteristics including gender, age, weight, height, and race of the 50 adult participants in the Ex-R study. There were a total of 30 females and 20 males, and their ages ranged from 19–50 years old. All of the participants completed the six-week monitoring period, except for one female who dropped out of the study due to a family emergency during the last sampling interval (days 4–6) of week six (Fig. 1.). Four additional participants were dropped from the study before completing the six-week monitoring period because they did not properly follow sampling procedures (e.g., missed collection of several solid food and/or urine samples).

During sampling weeks 1, 2, and 6 a total of 12%, 14%, and 12% of the participants, respectively, reported that a product containing a pyrethroid was applied to kill insect pests at their residences. In addition, during non-sampling weeks, 10% of the participants reported that pyrethroid products had been used for insect control at their homes. Targeted

insects included ants, cockroaches, crickets, fleas, mosquitoes, silverfish, spiders, and/or ticks. Pyrethroids contained in these applied products at the homes were allethrin, bifenthrin, cyfluthrin, cyhalothrin, cypermethrin, cyphenothrin, deltamethrin, esfenvalerate, imiprothrin, metofluthrin, permethrin, phenothrin, prallethrin and tralomethrin. Based on this information, at least 70% of the applied pyrethroid insecticides at the participants' homes (within a month and during the six-week monitoring period) can be metabolized to form 3-PBA, *cis*-DCCA, *trans*-DCCA, and/or MPA in the body (Fig. 2).

The participants collected on average 8 urine voids (range = 3–11) per sampling day. The pyrethroid metabolites, 3-PBA, *cis*-DCCA, *trans*-DCCA, and MPA were detected in 74%, 32%, 39%, and 2% of the urine samples, respectively. Table 2 provides the descriptive statistics for the urinary levels of 3-PBA, *cis*-DCCA, and *trans*-DCCA by urine sample type and method. In all of the urine samples at the 75th and 95th percentiles, urinary levels of 3-PBA were consistently higher compared to urinary levels of *cis*-DCCA and *trans*-DCCA for all methods. For 3-PBA (the only metabolite with measurements $>$LOQ at the 50th percentile), median urinary levels were consistently the lowest in FMV samples

(0.77 ng/mL, 0.68 ng/mL-SG, 0.68 ng/mg, and 0.58 ng/min) and the highest in 24-h samples (0.92 ng/mL, 1.06 ng/mL-SG, 1.18 ng/mg, and 1.19 ng/min) across all four methods.

Based on Spearman correlation coefficients, *cis*-DCCA and *trans*-DCCA levels (ng/mL) were highly correlated ($r=0.86$, $p<0.0001$) with each other in the adult urine samples. In addition, levels of *cis*-DCCA ($r=0.64$, $p<0.0001$) and *trans*-DCCA ($r=0.69$, $p<0.0001$) were strongly correlated with 3-PBA levels.

Table 3 presents ICC and fold-range estimates for repeated 3-PBA measurements by urine sample type and method for the Ex-R adults over a day, week, and six weeks. ICCs indicated poor reproducibility (<0.22) for all urine sample types and methods over each time period. In general, ICCs for SG-corrected, CR-corrected, and excretion rate values were only slightly higher than those based on unadjusted concentration values (suggesting a larger proportion of between-person variance to total variance). All of the ICCs indicated a low level of reliability of repeated 3-PBA measurements in spot urine samples for each method over a day, week, or six weeks. The number of random spot urine samples required to provide a reliable 3-PBA biomarker estimate for an individual ranged from 15 to 800 samples depending on the sample type and method used. CR-corrected FMV urine samples had the lowest number of urine samples ($n=15$) needed to provide a reliable 3-PBA biomarker estimate (over a week). Regardless of the sample type and method, an unreasonably high number of spot urine samples would be required to provide a reliable estimate of the average 3-PBA concentration for the Ex-R participants over a day or longer.

Between- and within-person fold-range estimates in Table 3 support ICC estimates and further indicate that 3-PBA measurements were far more variable within individuals than between individuals. In addition to producing the smallest ICC estimates, 3-PBA concentration values also produced the smallest between- and within-person fold-ranges.

Results for 3-PBA concentrations suggest that the central 95% of individual-specific mean levels were observed across a 1 to 4–fold range, whereas the central 95% of individual measures for a given person were observed across a 182 to 360-fold range, depending on sample type and evaluation period. In contrast to the concentration values, 3-PBA excretion rate values had the highest within-person fold ranges, and the second highest between-person fold ranges. The highest between-person fold ranges were observed for CR-corrected values. As shown in Table 3, the central 95% of mean CR-corrected levels were observed across a 2.8 to 13.9-fold range, and the central 95% of individual excretion rate measures for a given person were observed across a 220 to 514–fold range. These results in Table 3 indicate that correcting for urine sample dilution, based on either SG, CR, or urine output, actually introduced measurement variability, both between- and within-individuals, when evaluating urinary 3-PBA levels.

Table 1
Physical characteristics of the adult participants in the Ex-R study.

Characteristic	All	Females	Males
Sex (number)	50	30	20
Age (years)	33.4 ± 9.1 (19–50)[a]	34.8 ± 9.4 (21–50)	31.3 ± 8.5 (19–48)
Weight (kilogram)	82.2 ± 18.9 (48.1–130)	75.6 ± 17.9 (48.1–130)	92.0 ± 16.2 (57.6–130)
Height (cm)	170 ± 8.5 (149–191)	165 ± 5.8 (149–191)	178 ± 5.3 (166–188)
race[b]			
Non-Hispanic White	25 (56%)[c]	14 (31%)	11 (25%)
Non-Hispanic black	11 (25%)	9 (20%)	2 (4%)
Hispanic	6 (13%)	3 (7%)	3 (7%)
Asian	2 (4%)	1 (2%)	1 (2%)
Native american	1 (2%)	0 (0%)	1 (2%)

[a] Mean ± standard deviation and range.
[b] Race data were collected ~ 4 months after the study was completed. These data were collected from 45 out of 50 of the participants.
[c] Number and percentage of total.

4. Discussion

The Ex-R study was designed to be a participatory-based, exposure measurements study that investigated the longitudinal exposures of 50 adults to pyrethroid insecticides and to their preformed metabolites in media at their homes in NC in 2009–2011. We found that participatory-based sampling was quite an effective way to engage and actively involve the adult volunteers in the Ex-R study. The 50 participants filled out a total of 299 (99%) food, 299 (99%) activity, and 149 (99%) pesticide-use diaries. They also collected a total of 783 (99%) solid food, 50 (100%) drinking water, 149 (99%) surface wipe, 48 (96%) vacuum dust, and 2502 (98%) urine samples during the study. The 100% and 98% completeness for the recruitment of 50 participants and field samples/diaries surpassed our study completeness goals of $\geq$85% and $\geq$95%, respectively. In addition, despite the subject burden (~10-h per person a week), participatory-based sampling resulted in few problems in the field. The most frequently encountered

Urinary Metabolite	3-PBA	*cis*/*trans*-DCCA	MPA
Chemical Structure	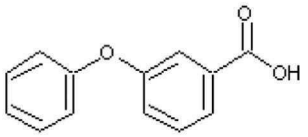	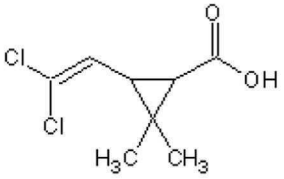	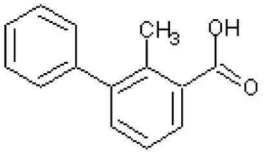
Corresponding Pyrethroid Insecticide			
Allethrin			
Bifenthrin			●
Cyfluthrin		●	
Cyhalothrin	●		
Cypermethrin	●	●	
Cyphenothrin	●		
Deltamethrin	●		
Esfenvalerate	●		
Imiprothrin			
Metofluthrin			
Permethrin	●	●	
Phenothrin	●		
Prallethrin			
Tralomethrin	●		

[a] 3-phenoxybenzoic acid (3-PBA), *cis/trans*-3-(2,2-dichlorovinyl)-2,2-dimethylcyclopropane-1-carboxylic acid (*cis*-DCCA), and 2-methyl-3-phenylbenzoic acid (MPA)

Fig. 2. Urinary metabolites measured in Ex-R adults and their corresponding parent pyrethroid(s) used at study homes one month before and during the six-week monitoring period. (3-phenoxybenzoic acid (3-PBA), *cis/trans*-3-(2,2-dichlorovinyl)-2,2-dimethylcyclopropane-1-carboxylic acid. (*cis*-DCCA), and 2-methyl-3-phenylbenzoic acid (MPA)).

problems by study participants included malfunctioning temperature data loggers due to low batteries, moisture occurring in the temperature data loggers due to cooler condensation, loose electric power adapter/cooler connections, broken cooler adapters, and broken cooler zippers. We quickly corrected the temperature data logger problems by purchasing a new model (EL-USB-1) that had a longer battery life and by placing the new loggers into 10 mL cryogenic vials with lids to eliminate condensation when inside the coolers. The loose power adapter problem was easily fixed by using an inexpensive ($5) Velco strap (Speedtech International Inc., Racine, Wisconsin) that snuggly connected the power adapter with the cooler plug.

We believe this is the first study in the literature to report the urinary levels of MPA, the specific metabolite of bifenthrin, in non-occupationally exposed adults in the US. Bifenthrin is currently registered by the US EPA for use in both agricultural and residential settings (NPIC, 2011). In our study, conducted in 2009–2011, MPA was detected in less than 3% of the Ex-R adult urine samples (maximum = 8.9 ng/mL). This information suggests that the majority of the participants were probably not exposed to measureable levels of bifenthrin residues in food or residential media during the six-week monitoring period in NC. These results are supported by a recent study (Tao et al., 2013) showing that MPA was not detected (<0.04 ng/mL) in the spot urine samples of 10 US children, ages 3–11 years old, in Massachusetts, USA.

Our biomonitoring results, however, did show that 3-PBA was frequently detected (74%) in the Ex-R adult urine samples. This is in agreement with other published US studies that have also found 3-PBA detected often ($\geq$55%) in the urine of non-occupationally exposed adults (Berkowitz et al., 2003; Barr et al., 2010; McKelvey et al., 2013; Young et al., 2013; Trunnelle et al., 2014; Morgan, 2015). Interestingly, the geometric mean 3-PBA levels (0.96 ng/mL) in Ex-R participants were twice as high compared to the geometric mean 3-PBA levels (0.42 ng/mL) in 2009-2010 NHANES adults (CDC, 2015). Trunnelle et al. (2014) also recently reported two times higher median urinary 3-PBA concentrations (0.82 ng/mL) in 90 Californian adults in 2007–2009 in comparison to the 2009–2010 NHANES adults (0.39 ng/mL). This information suggests that

Table 2
Urinary 3-PBA, *cis*-DCCA, and *trans*-DCCA levels in 50 Ex-R adults over a six-week monitoring period[a,b].

Type of Urine sample	N[c]	%[d]	Unit[e]	GM[h]	GSD[i]	Percentiles					Max.
						25th	50th	75th	95th	99th	
Bedtime											
3-PBA	291	77	ng/mL	0.96	4.02	0.35	0.82	2.15	16.3	37.6	101.9
	288		ng/mL-SG[f]	0.88	4.33	0.31	0.81	2.38	14.9	31.2	43.9
	288		ng/mg[f]	0.94	4.67	0.29	0.80	2.52	17.2	33.3	50.6
	285		ng/min[g]	0.90	5.13	0.25	0.83	2.87	19.3	46.4	46.8
cis-DCCA	291	27	ng/mL	–[j]	–	<	<	0.38	3.25	11.4	17.0
	288		ng/ml-SG	–	–	<	<	0.50	2.34	9.00	14.9
	288		ng/mg	–	–	<	<	0.59	3.51	8.85	17.0
	285		ng/min	–	–	<	<	0.59	3.47	13.7	22.8
trans-DCCA	290	33	ng/mL	–	–	<	<	0.74	5.90	26.7	36.6
	287		ng/ml-SG	–	–	<	<	0.67	4.87	22.4	27.4
	287		ng/mg	–	–	<	<	0.83	6.69	27.7	36.4
	284		ng/min	–	–	<	<	0.84	7.33	28.9	31.9
FMV											
3-PBA	296	70	ng/mL	0.83	3.99	<	0.77	2.34	7.54	92.3	180.6
	295		ng/mL-SG	0.76	4.13	<	0.68	2.16	8.35	56.1	115.1
	295		ng/mg	0.74	4.29	<	0.68	2.05	9.78	45.6	116.4
	293		ng/min	0.62	4.25	<	0.58	1.64	7.69	54.8	134.6
cis-DCCA	298	32	ng/mL	<	<	<	<	0.50	2.56	15.3	39.4
	297		ng/mL-SG	<	<	<	<	0.45	2.23	13.8	24.0
	297		ng/mg	<	<	<	<	0.46	2.71	13.5	19.5
	295		ng/min	<	<	<	<	0.37	2.09	12.4	23.4
trans-DCCA	297	38	ng/mL	<	<	<	<	0.99	5.62	17.8	67.1
	296		ng/mL-SG	<	<	<	<	0.84	4.71	14.9	40.8
	296		ng/mg	<	<	<	<	0.86	4.54	14.6	40.2
	294		ng/min	<	<	<	<	0.62	4.24	15.3	39.8
24-h											
3-PBA	1877	74	ng/mL	0.98	4.29	<	0.92	2.39	12.3	64.7	3154.9
	1856		ng/mL-SG	1.17	4.80	<	1.06	3.24	18.7	80.4	1983.9
	1856		ng/mg	1.30	5.28	<	1.18	3.75	24.3	115.5	1784.5
	1864		ng/min	1.32	5.38	<	1.19	3.95	23.7	106.1	2035.4
cis-DCCA	1888	33	ng/mL	<	<	<	<	0.54	3.28	18.2	702.5
	1866		ng/mL-SG	<	<	<	<	0.71	4.45	25.0	441.8
	1866		ng/mg	<	<	<	<	0.90	5.62	30.3	397.3
	1875		ng/min	<	<	<	<	0.95	5.33	35.0	453.2
trans-DCCA	1887	41	ng/mL	<	<	<	<	1.03	7.54	42.3	197.7
	1865		ng/mL-SG	<	<	<	<	1.20	9.73	39.6	291.4
	1865		ng/mg	<	<	<	<	1.40	12.3	48.2	516.1
	1874		ng/min	<	<	<	<	1.53	12.3	62.5	563.8
All											
3-PBA	2472	74	ng/mL	0.96	4.22	<	0.88	2.33	12.2	56.4	3154.9
	2446		ng/mL-SG	1.07	4.70	<	0.96	2.88	16.5	72.6	1983.9
	2446		ng/mg	1.17	5.13	<	1.04	3.30	20.6	93.2	1784.5
	2449		ng/min	1.15	5.31	<	1.04	3.47	21.3	93.9	2035.4
cis-DCCA	2485	32	ng/mL	<	<	<	<	0.50	3.16	16.9	702.5
	2458		ng/mL-SG	<	<	<	<	0.64	3.84	20.2	441.8
	2458		ng/mg	<	<	<	<	0.81	4.85	24.9	397.3
	2462		ng/min	<	<	<	<	0.84	4.61	30.7	453.2
trans-DCCA	2482	39	ng/mL	<	<	<	<	0.99	7.15	32.9	197.7
	2455		ng/mL-SG	<	<	<	<	1.08	8.66	35.4	291.4
	2455		ng/mg	<	<	<	<	1.19	10.3	43.2	516.1
	2459		ng/min	<	<	<	<	1.29	9.64	52.3	563.8

[k]Below the LOQ (< 0.25 ng/mL) for a pyrethroid metabolite in the urine samples.

[a] 3-Phenoxybenzoic acid (3-PBA), *cis*-3-(2,2-dichlorovinyl)-2,2-dimethylcyclopropane-1-carboxylic acid (*cis*-DCCA), and *trans*-3-(2,2-dichlorovinyl)-2,2-dimethylcyclopropane carboxylic acid (*trans*-DCCA).

[b] 2-methyl-3-phenylbenzoic acid (MPA) values are not reported because it was detected in 2% of the urine samples.

[c] Number of urine samples (note: not all 2503 samples could be analyzed due to limited sample volume).

[d] Percentage of urine samples at or above the limit of quantitation (LOQ).

[e] Data are provided as concentration (ng/mL), specific gravity-corrected (ng/mL-SG), creatinine-corrected (ng/mg), and excretion rate (ng/min) values.

[f] 26 urine samples were excluded because of missing creatinine and specific gravity data due to laboratory error.

[g] 17 urine samples were excluded due to missing or partial voids provided by the adult participants.

[h] Geometric mean.

[i] Geometric standard deviation (unitless).

[j] The geometric mean and geometric standard deviation are not reported for pyrethroid metabolites that were detected in less than 50% of the urine samples.

there is probably geographical differences in US adult exposures to pyrethroid insecticides that are metabolized to form 3-PBA in the body. Studies conducted outside the contiguous US have also reported 3-PBA being frequently detected ($\geq$ 70%) in the urine of the general adult population, except for one in Puerto Rico (46%) (Table 4). In these

available studies, geometric mean urinary 3-PBA concentrations were the lowest for Puerto Rico, Poland, and Japan (< 0.30 ng/mL) and the highest for China (0.97 ng/mL). Our study results (GM = 0.96 ng/mL) were similar to the reported geometric

Table 3
Variance components and other related statistics for 3-PBA levels in adults by urine sample type and method over a day, week, and six-weeks[a]

Urine sample type	ng/mL				ng/mL-SG				ng/mg				ng/min			
	${}_bR_{0.95}$ [b]	${}_wR_{0.95}$ [c]	ICC[d]	m[e]	${}_bR_{0.95}$	${}_wR_{0.95}$	ICC	m	${}_bR_{0.95}$	${}_wR_{0.95}$	ICC	m	${}_bR_{0.95}$	${}_wR_{0.95}$	ICC	m
One Day																
24-h[f]	2.1	182	0.02	204	4.9	243	0.08	47	9.6	325	0.13	26	7.9	341	0.11	32
One Week																
Bedtime	1.0	360	0.00	–[h]	1.0	441	0.00	–	2.8	500	0.03	144	6.8	514	0.09	43
FMV[g]	4.0	210	0.06	60	9.3	175	0.16	22	13.9	163	0.21	15	10.6	220	0.16	21
24-h	3.7	214	0.06	66	6.1	306	0.09	40	9.8	393	0.13	27	8.4	449	0.11	33
Six Weeks																
Bedtime	1.5	232	0.01	800	3.6	271	0.05	77	5.9	322	0.09	42	6.5	460	0.09	43
FMV	3.0	204	0.04	95	5.9	196	0.10	35	7.1	212	0.12	30	5.2	228	0.08	43
24-h	2.7	278	0.03	128	7.6	333	0.11	33	12.5	412	0.15	23	9.6	490	0.12	30

[a] Urine data (log-transformed) are provided as concentration (ng/mL), specific gravity-corrected (ng/mL-SG), creatinine-corrected (ng/mg), and excretion rate (ng/min) values.
[b] Between-person fold range.
[c] Within-person fold range.
[d] Intraclass correlation coefficient.
[e] Number of random spot urine samples per adult likely needed to have a reliable biomarker estimate (ICC=0.80) (Fleiss, 1985).
[f] Results are limited to the first 24-h interval of week one as the completion rates were the highest for this interval (88%) compared to all intervals (6 total).
[g] First morning void.
[h] The between-person variance was zero resulting in an ICC of 0.00, therefore, no sample size could be estimated.

Table 4
Comparison of urinary 3-PBA levels in non-occupationally exposed adults worldwide.

Country	Study year	N[a]	Age	%[b]	GM[c]	95th [d]	Reference
ng/mL							
Canada	2005	120	18–64	99	–[e]	4.23	Fortin et al. (2008)
Caribbean[f]	2008–2011	297	20–39	100	0.54	3.51	Dewailly et al. (2014)
China	2009–2010	1149	17–45	99	0.97	5.39	Qi et al. (2012)
Germany	2000[g]	46	17–61	70	–	0.67	Schettgen et al. (2002)
Japan	2005	448	39–85	98	0.29	1.96	Ueyama et al. (2009)
Poland	2010-2011	132	5–77[g]	80	0.26	1.15	Wielgomas et al. (2013b)
Puerto rico	2010–2012	54	18–40	46	0.20	2.30	Lewis et al. (2014)
USA (NHANES)[h]	2007–2008	1110	20–59	–	0.43	6.65	CDC (2015)
	2009–2010	1296	20–59	–	0.42	6.95	CDC (2015)
This study	2009–2011	50	19–50	74	0.96	12.2	–
ng/mg							
China	2009–2010	1149	17–45	99	1.53	8.11	Qi et al. (2012)
Japan	2005	448	39–85	98	0.40	2.33	Ueyama et al. (2009)
Poland	2010–2011	132	5–77	80	0.22	0.95	Wielgomas et al. (2013b)
USA (NHANES)	2007–2008	1110	20–59	–	0.44	6.29	CDC (2015)
	2009–2010	1296	20–59	–	0.42	4.72	CDC (2015)
This study	2009–2011	50	19–50	74	1.17	20.6	–

[a] Number of study participants.
[b] Percentage of urine samples with detectable levels of 3-PBA.
[c] Geometric mean.
[d] Percentile.
[e] Not provided.
[f] Includes ten different countries.
[g] Eight of the participants were children below the age of 14 years old.
[h] NHANES adults between 20–59 years old, only.

mean 3-PBA levels of 0.97 ng/mL reported in 1149 women from China in 2009–2010 (Qi et al., 2012). This likely reflects the increased usage of pyrethroid insecticides in residential settings and some agricultural settings in the US and China (Barr et al., 2010; Qi et al., 2012).

We found that urinary *cis*-DCCA and *trans*-DCCA levels were highly correlated with each other ($r=0.86$, $p<0.0001$) and with urinary 3-PBA levels (*cis*-DCCA: $r=0.64$, $p<0.0001$; *trans*-DCCA: $r=0.69$, $p<0.0001$) in the Ex-R adult urine samples. Similar results were observed by Barr et al. (2010) showing strong correlations occurring between the concentrations of these two isomers ($r=0.89$, $p<0.001$) and 3-PBA ($r=0.77$, $p=0.02$) in the urine samples of 1999–2002 NHANES adults. Only the current-use pyrethroids, permethrin and cypermethrin, are known to breakdown to form both 3-PBA and DCCA in the body (Tao et al., 2013; CDC, 2009). The strong correlations occurring between these urinary biomarkers suggest that the Ex-R adults were likely primarily exposed to these two pyrethroids in their residential environments (Barr et al., 2010). This is in agreement with recent research by Xue et al. (2014) indicating that permethrin and cypermethrin likely contributed to about 80% of the observed urinary levels of 3-PBA and DCCA in the general US population.

Our ICC results indicate poor reproducibility (<0.22) of repeated 3-PBA measurements in the spot urine samples of the Ex-R adults regardless of the sample type (bedtime, FMV, or 24-h) and method (non-corrected or corrected) over a day, week, and six weeks. This ICC information suggests that a random spot urine sample did not provide a reliable estimate of the average 3-PBA concentration for the adults in this study. In addition, we found regardless of sample type or method used an unreasonably high

number of random spot urine samples (15–800) would likely be required per person to provide a reliable biomarker estimate over a day or longer–which is unrealistic for most exposure and epidemiological studies due to budget constraints and participant burden. Our results also imply that the Ex-R adults were likely not continually exposed to low levels of pyrethroid residues in consumed foods and/or other residential media (i.e., dust and surfaces) over the six-week monitoring period. Our study results are in contrast to Wielgomas (2013a) that reported much higher ICCs for 3-PBA measurements in FMV, spot, and 24-h urine samples by concentration, CR-corrected, and excretion rate values for seven non-occupationally exposed adults over a week in an urban area of Poland in 2011. In that study, the highest ICCs occurred in the CR-corrected spot (ICC=0.846) and the CR-corrected 24-h urine samples (ICC=0.796). Based on these ICCs, the authors concluded that a random spot urine sample would adequately represent the average 3-PBA biomarker concentration for an individual over a week, and that the Polish adults were likely continually exposed to similar levels of pyrethroid residues in their urban environments. This above research suggests that the temporal usage patterns and/or exposure patterns of adults to pyrethroids may be quite different in Poland compared to the US and more research is needed worldwide.

In our current study, we found that comparisons of biomarker measurement variance and ICC estimates across concentration, SG-corrected, CR-corrected, and excretion rate measures yielded unexpected results. It is generally assumed that, for urinary biomarkers eliminated via renal filtration, measurement error will decrease after correcting for SG, CR, or urine output. However, the opposite trend was observed in the Ex-R study. Specifically, measurement variability was the lowest both between- and within-individuals for concentration-based measures. Correcting for CR, SG, and urine output increased fold-range estimates in most instances. Furthermore, these correction approaches increased between-person measurement variability more so than within-person measurement variability, leading to elevated ICC estimates for corrected values. While higher ICCs are beneficial from the standpoint of measurement reliability, they are meant to reflect true exposure differences between individuals. In this study, it is conceivable that the observed variability between subjects in urine output, CR excretion, and SG levels, generally resulting from differences in hydration status, diet, body mass, etc., are responsible for the heightened ICCs. Given these sources of measurement variation, (reflecting physiological and behavioral factors and not pyrethroid exposure) researchers are urged to use caution when selecting urinary biomarker-based exposure metrics for 3-PBA as part of exposure and epidemiology studies in the future.

At the moment, it is unclear whether preformed metabolites of pyrethroid insecticides (e.g., 3-PBA, *cis*-DCCA, and *trans*-DCCA) in media are substantially contributing to the measured urinary pesticide metabolite levels in humans. Few studies have measured for the concurrent levels of pyrethroids and their preformed metabolites in foods or other environmental media (Starr et al., 2008; Chen et al., 2012; Trunnelle et al., 2014). Starr et al. (2008) showed that permethrin, DCCA, and 3-PBA, were frequently detected ($\geq$67%) in 85 vacuum dust samples collected at homes and childcare centers in NC and Ohio in 2000–2001. Chen et al. (2012) also reported detectable levels of several different pyrethroids and 3-PBA in 23 different produce samples including blackberries, blueberries, cherries, strawberries, and green onions in California in 2010. More recently, Trunnelle et al. (2014) reported that permethrin and 3-PBA were both frequently detected ($>$97%) in 79 kitchen floor wipe samples collected at homes in California in 2007–2009. This above research suggests that humans can be exposed to measureable levels of preformed pyrethroid metabolites in several different media (i.e., food, dust, and surface wipes) at residences. Therefore, more research is necessary to determine if preformed metabolites in media are overinflating measured urinary pyrethroid biomarker levels in non-occupationally exposed adults. Future work is planned to quantify the distributions of the target pyrethroids and their preformed metabolites in solid food, drinking water, vacuum dust, and surface wipe samples collected at the participant's residences in the Ex-R study.

5. Conclusions

Based on the urinary biomonitoring data, the majority of the Ex-R adults were likely temporally exposed to one or more pyrethroid insecticides at their homes during the six-week monitoring period in NC in 2009–2011. For the frequently detected 3-PBA ($>$50%), there was poor reproducibility of repeated measurements of this metabolite in the urine samples of Ex-R adults regardless of sample type (bedtime, FMV, and 24-h) and method (concentration, SG-corrected, CR-corrected, and excretion rate) over a day, week, and six weeks. Correcting for urine sample dilution, based on either SG, CR, or urine output, was found to increase measurement variability between- and within-individuals. Given these findings, scientists should use caution when selecting urinary biomarker-based exposure metrics for 3-PBA in their future exposure and environmental epidemiology studies.

Acknowledgments

We sincerely thank the adult volunteers who participated in the Ex-R study. We also thank Ronald Williams, James Starr, Denise McMillian, Kent Thomas, and Daniel Stout II for their technical assistance during the study. We also gratefully acknowledge WESTAT (Andrea Ware and Bethany Bradford) for their valuable assistance in recruiting study participants. This work was funded in whole by the US EPA. *Disclaimer: "The US EPA through its Office of Research and Development has provided administrative review of this article and approved it for publication."*

Appendix A. Supplementary material

Supplementary data associated with this article can be found in the online version at http://dx.doi.org/10.1016/j.envres.2015.11.003.

References

Andersen, E.M., Sobus, J.R., Strynar, M.J., Pleil, J.D., Nakayama, S.F., 2014. Evaluating an alternative method for rapid urinary creatinine determination. J. Toxicol. Environ. Health A 77, 1114–1123.

Baker, S.E., Olsson, A.O., Barr, D.B., 2004. Isotope dilution high-performance liquid chromatography-tandem mass spectrometry method for quantifying urinary metabolites of synthetic pyrethroid insecticides. Arch. Environ. Contam. Toxicol. 46, 281–288.

Barr, D.B., Wilder, L.C., Caudill, S.P., Gonzalez, A.J., Needham, L.L., Pirkle, J.L., 2005. Urinary creatinine concentrations in the US population: implications for urinary biologic monitoring measurements. Environ. Health Perspect. 113, 192–200.

Barr, D.B., Olsson, A.O., Wong, L.Y., Udunka, S.O., Baker, S.E., Whitehead, R.D., et al., 2010. Urinary concentrations of metabolites of pyrethroid insecticides in the general US population: National Health and Nutrition Examination Survey 1999–2002. Environ. Health Perspect. 118, 742–748.

Berkowitz, G.S., Obel, J., Deych, E., Lapinski, R., Godbold, J., Liu, Z., et al., 2003. Exposure to indoor pesticides during pregnancy in a multiethnic, urban cohort. Environ. Health Perspect. 111, 79–84.

Boeniger, M.F., Lowry, L.K., Rosenberg, J., 1993. Interpretation of urine results used to assess chemical exposure with emphasis on creatinine adjustments: A review. Am. Ind. Hyg. Assoc. J. 54, 615–627.

CDC (Centers for Disease Control and Prevention). Fourth national report on human exposure to environmental chemicals. 2009. [⟨http://www.cdc.gov/exposurereport/⟩ (5 May 2015)].
CDC (Centers for Disease Control and Prevention). Fourth national report on human exposure to environmental chemicals; Updated tables. 2015. [⟨http://www.cdc.gov/biomonitoring/pdf/FourthReportUpdatedTables_Feb2015.pdf⟩ (11 May 2015)].
Chen, L., Zhao, T., Pan, C., Ross, J.H., Krieger, R.L., 2012. Preformed biomarkers including dialkylphosphate (DAPs) in produce may confound biomonitoring in pesticide exposure and risk assessment. J. Agric. Food Chem. 60, 9342–9351.
Christensen, K.L., Lorber, M., Koch, H.M., Kolossa-Gehring, M., Morgan, M.K., 2012. Population variability of phthalate metabolites and bisphenol a concentrations in spot urine samples versus 24-h or 48-h collections. J. Expo. Sci. Env. Epidemiol. 22, 632–640.
Chuang, J.C., Wilson, N.K., 2011. Multiresidue analysis of organophosphate and pyrethroid pesticides in duplicate-diet solid food by pressurized liquid extraction. J. Environ. Sci. Heal. B 46 41–40.
Dewailly, E., Forde, M., Robertson, L., Kaddar, N., Sidi, E.A., Cote, S., et al., 2014. Evaluation of pyrethroid exposure in pregnant women from 10 Caribbean countries. Environ. Int. 63 201–201.
Elliott, M., 1976. Properties and applications of pyrethroids. Env. Health Perspect. 14, 3–13.
Fleiss, J., 1985. The Design and Analysis of Clinical Experiments. John Wiley & Sons, New York, NY, USA.
Fortin, M.C., Bouchard, M., Carrier, G., Dumas, P., 2008. Biological monitoring of exposure to pyrethrins and pyrethroids in a metropolitan population of the Providence of Quebec, Canada. Environ. Res. 107, 343–350.
Hwang, Y.H., Bornschein, R.L., Grote, J., Menrath, W., Roda, S., 1997. Urinary arsenic excretion as biomarker of arsenic exposure in children. Arch. Env. Health 52, 139–147.
Julien, R., Adamkiewicz, G., Levy, J., Bennett, D.B., Nishioka, M., Spengler, J.D., 2008. Pesticide loadings of select organophosphate and pyrethroid pesticides in urban public housing. J. Expo. Sci. Environ. Epidemiol. 18, 167–174.
Kuhn, K.H., Wieseler, B., Leng, G., Idel, H., 1999. Toxicokinetics of pyrethroids in humans: Consequences for biological monitoring. Bull. Environ. Contam. Toxicol. 62, 101–108.
Kuivila, KM., Hladik, ML., Ingersoll, CG., Kemble, NE., Moran, PW., Valhoun, D.L., et al., 2012. Occurrence and potential sources of pyrethroid insecticides in stream sediments from seven U.S. Metropolitan Areas. Environ. Sci. Technol 46, 4297–4303.
Lassen, T.H., Frederiksen, H., Jensen, T.K., Peterssen, J.H., Main, K.M., Skakkebaek, N. E., et al., 2013. Temporal variability in urinary excretion of bisphenol A and seven other phenols in spot, morning, and 24-h urine samples. Environ. Res. 126, 64–170.
Leng, G., Kuhn, K.H., Idel, H., 1997. Biological monitoring of pyrethroids in blood and pyrethroid metabolites in urine; Applications and limitations. Sci. Total. Environ. 199, 173–181.
Lewis, R.C., Cantonwine, D.E., Anzalota Del Toro, L.V., Calafat, A.M., Valentin-Blasini, L., Davis, M.D., et al., 2014. Urinary biomarkers of exposure to insecticides, herbicides, and one insect repellent among pregnant women in Puerto Rico. Environ. Health 13, 97.
Mage, D.T., Allen, R.H., Gondy, G., Smith, W., Barr, D.B., Needham, L.L., 2004. Estimating pesticide dose from urinary pesticide concentration data by creatinine correction in the Third National Health and Nutritional Examination Survey. J. Expo. Sci. Environ. Epidemiol. 14, 457–465.
McKelvey, W., Jacobson, J.B., Kass, D., Barr, D.B., Davis, M., Calafat, A.M., et al., 2013. Population-based biomonitoring of exposure to organophosphate and pyrethroid pesticides in New York City. Environ. Health Perspect. 121, 1349–1356.
Morgan, M.K., Sheldon, L.S., Croghan, C.W., Jones, P.A., Chuang, J.C., Wilson, N.K., 2007. An observational study of 127 preschool children at their homes and daycare centers in Ohio: Environmental pathways to *cis*- and *trans*-permethrin exposure. Environ. Res. 104, 266–274.
Morgan, M.K., Sheldon, L.S., Thomas, K.W., Egeghy, P.P., Croghan, C.W., Jones, P.A., et al., 2008. Adult and children's exposure to 2,4-D from multiple sources and pathways. J. Expo. Sci. Environ. Epidemiol. 18, 486–494.
Morgan, M.K. Predictors of urinary levels of 2,4-dichlorophenoxyacetic acid, 3,5,6-trichloro-2-pyridinol, 3-phenoxybenzoic acid, and pentachlorophenol in 121 adults in Ohio. Int J Hyg Environ Health (*ePub Ahead of Print*, *7 April* 2015).
NPIC (National Pesticide Information Center). Bifenthrin: General fact sheet. 2011. [⟨http://npic.orst.edu/factsheets/bifgen.html⟩ (11 May 2015)].
NRC, 2006. (National Research Council of the National Academies of Sciences). Human Biomonitoring for Environmental Chemicals. The National Academies Press, Washington DC, p. 215.
Palmquist K., Salatas J., Fairbrother A. Chapter 11; Pyrethroid insecticides: Use, environmental fate, and ecotoxicology. In Insecticides - Advances in Integrated Pest Management. 2012. [⟨http://www.intechopen.com/books/insecticides-advances-in-integrated-pest-management/pyrethroidinsecticides-use-environmental-fate-and-ecotoxicology⟩ (4 November 2014)].
Qi, X., Zheng, M., Wu, C., Wang, G., Feng, C., Zhou, Z., 2012. Urinary pyrethroid metabolites among pregnant women in an agricultural area of the Province of Jiangsu, China. Int. J. Hyg. Environ. Health 215, 487–495.
S.M. Rappaport L.L. Kupper. Quantitative Exposure Assessment. Publisher: SM Rappaport El Cerrito 2008 168.
Ratelle, M., Cote, J., Bouchard, M., 2015. Toxicokinetics of permethrin biomarkers of exposure in orally exposed volunteers. Toxicol. Lett. 232, 369–375.
Riederer, A.M., Bartell, S.M., Barr, D.B., Ryan, P.B., 2008. Diet and nondiet predictors of urinary 3-phenoxybenzoic acid in NHANES 1999-2002. Environ. Health Perspect. 116, 1015–1022.
Rosner, B., 2006. Fundamentals of biostatistics, 6th edition. Duxbury Press, Pacific Grove, CA.
Saillenfait, A.M., Ndiaye, D., Sabate, J.P., 2015. Pyrethroids: Exposure and health effects – An update. Int. J. Hyg. Environ. Heal. 218, 281–292.
Schettgen, T., Koch, H., Drexler, H., Angerer, J., 2002. New gas chromatographic-mass spectrometric method for the determination of urinary pyrethroid metabolites in environmental medicine. J. Chromatogr. B 778, 121–131.
Starr, J., Graham, S., Stout, D., Andrews, K., Nishioka, M., 2008. Pyrethroid pesticides and their metabolites in vacuum cleaner dust collected from homes and daycare centers. Environ. Res. 108, 271–279.
Stout, D.M., Bradham, K.D., Egeghy, P.P., Jones, P.A., Croghan, C.W., Ashley, P.A., et al., 2009. American Healthy Homes Survey: A national study of residential pesticides measured from floor wipes. Env. Sci. Technol. 43, 4294–4300.
Tao, L., Chen, M., Collins, E., Lu, C., 2013. Simultaneous quantitation of seven pyrethroid metabolites in human urine by capillary gas chromatography–mass spectrometry. J. Sep. Sci. 36, 773–780.
Trunnelle, K.J., Bennett, D.H., Tulve, N.S., Clifton, M.S., Davis, M.D., Calafat, A.M., et al., 2014. Urinary Pyrethroid and Chlorpyrifos Metabolite Concentrations in Northern California Families and Their Relationship to Indoor Residential Insecticide Levels, Part of the Study of Use of Products and Exposure Related Behavior (SUPERB). Environ. Sci. Technol. 48, 1931–1939.
Tulve, N.S., Egeghy, P.P., Fortmann, R.C., Whitaker, D.A., Nishioka, M.G., Naeher, L.P., et al., 2008. Multimedia measurements and activity patterns in an observational pilot study of nine young children. J. Expo. Sci. Environ. Epidemiol. 18, 31–44.
Ueyama, J., Kimata, A., Kamijima, M., Hamajima, N., Ito, Y., Suzuki, K., et al., 2009. Urinary excretion of 3-phenoxybenzoic acid in middle-aged and elderly general population of Japan. Environ. Res. 109, 175–180.
US EPA (US Environmental Protection Agency). Scientific and Ethical Approaches for Observational Exposure Studies (SEAOS). 2008. EPA/600/R-08/062. [⟨http://www.epa.gov/nerl/sots/SEAOES_doc20080707.pdf⟩ (25 May 2015)].
US EPA (United States Environmental Protection Agency). Office of Pesticide Programs: Pyrethrins/Pyrethroid Cumulative Risk Assessment. 2011. [⟨http://www.regulations.gov/⟩ #!documentDetail;D=EPA-HQ-OPP-2011-0746-0003 (3 November 2014)].
US EPA (United States Environmental Protection Agency). Pyrethroids and Pyrethrins. 2013. [⟨http://www.epa.gov/oppsrrd1/reevaluation/pyrethroids-pyrethrins.html⟩ (19 March 2015)].
Verbovsek, T., 2011. A comparison of parameters below the limit of detection in geochemical analyses by substitution methods. Mater. Geoenviron. 58, 393–404.
Wielgomas, B., 2013. Variability of urinary excretion of pyrethroid metabolites in seven persons over seven consecutive days – Implications for observational studies. Toxicol. Lett. 221, 15–22.
Wielgomas, B., Nahorski, W., Czarnowski, W., 2013. Urinary concentrations of pyrethroid metabolites in the convenience sample of an urban population of Northern Poland. Int. J. Hyg. Environ. Heal. 216, 295–300.
Xue, J., Zartarian, V.G., Tornero-Velez, R., Tulve, N.S., 2014. EPA's SHEDs-multimedia model: Children's cumulative pyrethroid exposure estimates and evaluation against NHANES biomarker data. Environ. Int. 73, 304–311.
Young, H.A., Meeker, J.D., Martenies, S.E., Figueroa, Z.I., Boyd-Barr, D., Perry, M.J., 2013. Environmental exposure to pyrethroids and sperm sex chromosome disomy: A cross sectional study. Environ. Health 12, 111.

Journal of Exposure Science and Environmental Epidemiology (2018) 28, 40–45

www.nature.com/jes

OPEN

ORIGINAL ARTICLE

Pyrethroid insecticides and their environmental degradates in repeated duplicate-diet solid food samples of 50 adults

Marsha K. Morgan[1], Denise K. MacMillan[2], Dan Zehr[2] and Jon R. Sobus[1]

Previous research has reported concurrent levels of pyrethroid insecticides and their environmental degradates in foods. These data raise concerns about using these same pyrethroid degradates found in the diet as urinary biomarkers of exposures in humans. The primary objective was to quantify levels of selected pyrethroids and their environmental degradates in duplicate-diet solid food samples of 50 adults over a six-week monitoring period. The study was conducted at the US EPA's Human Studies Facility in North Carolina and at participants' residences in 2009–2011. Participants collected duplicate-diet solid food samples on days 1 and 2 during weeks 1, 2, and 6 of the monitoring period. These samples were collected over three consecutive time periods each sampling day. A total of 782 food samples were homogenized and analyzed by LC/MS/MS for seven pyrethroids (bifenthrin, λ-cyhalothrin, cyfluthrin, cypermethrin, *cis*-deltamethrin, esfenvalerate, and *cis/trans*-permethrin) and six pyrethroid degradates. Results showed that 49% and 2% of all the samples contained at least one target pyrethroid or pyrethroid degradate, respectively. *Cis/trans*-permethrin (20%) and bifenthrin (20%) were the most frequently detected pyrethroids. The results suggest that the pyrethroid degradates were likely not present in sufficient levels in the diet to substantially impact the adults' urinary biomarker concentrations.

Journal of Exposure Science and Environmental Epidemiology (2018) **28,** 40–45; doi:10.1038/jes.2016.69; published online 14 December 2016

Keywords: adults; degradates; dietary; food; pyrethroids; temporal

INTRODUCTION

Pyrethroids are a class of insecticides that are used for crop protection worldwide.[1,2] These lipophilic insecticides account for more than 17% of the global agrochemical market.[1] In the United States (US), at least 18 different pyrethroid insecticides are currently registered by the US Environmental Protection Agency (EPA) for use on domestic crops for human consumption.[3] However, no published data are currently available on the total amount of pyrethroid insecticides that are applied on US croplands, including residential gardens, each year.[3]

Research has shown that humans can be exposed to pyrethroids through the inhalation, ingestion, and dermal routes.[2,4,5] However, dietary ingestion is likely the major exposure route to these insecticides in the general US adult population.[4–5] This is supported by several studies reporting measureable residues of a number of different current-use pyrethroids in duplicate-diet samples or in individual food items (e.g., lettuce, blueberries, butter, and sour cream).[6–14] In these studies, pyrethroid insecticides were generally detected at much higher levels in solid foods compared to liquid foods (e.g. beverages).[6,10,13,14] Current-use pyrethroids detected in these solid food samples included bifenthrin, cyfluthrin, λ-cyhalothrin, cypermethrin, *cis*-deltamethrin, esfenvalerate, and *cis/trans*-permethrin.

Few published data are available on the concurrent levels of these pyrethroid insecticides and their environmental degradates in foods.[7,11] In a recent study by Chen et al.,[11] they reported measureable levels of cypermethrin, λ-cyhalothrin, *cis*-deltamethrin, esfenvalerate, and/or permethrin, and their common degradation product, 3-phenoxybenzoic acid (3-PBA), in eight different produce samples, collected in California between 2010 and 2011. This information raises concerns about using 3-PBA and perhaps other pyrethroid degradates found in the diet as urinary biomarkers of exposure in humans.

After oral ingestion, pyrethroids are metabolized quickly and are mainly renally eliminated as polar metabolites (e.g., 3-PBA) in humans with an urinary excretion half-life of less than 10h.[15–17] For the pyrethroid degradates, no published (oral) toxicokinetic data exist based on human exposure studies. Previous biomonitoring studies have found several different pyrethroid metabolites (i.e., 3-PBA and *cis/trans*-3-(2,2-dichlorovinyl)-2,2-dimethylcyclopropane carboxylic acid (*cis/trans*-DCCA)) in the urine of the general US adult population.[5,18–21] It is currently unknown whether pyrethroid degradates in the diet are substantially contributing to pyrethroid metabolite levels in the urine of adults in the general US population.

The Pilot Study to Estimate Human Exposures to Pyrethroids using an Exposure Reconstruction Approach (Ex-R study) investigated the temporal exposures (over 6 weeks) of 50 North Carolina (NC) adults to selected pyrethroid insecticides and their environmental degradates in several different media (e.g., food, drinking water, dust, and floor wipes) at homes in 2009–2011.[21] In this current work, we quantified the levels of seven current-use pyrethroids and six of their environmental degradates (Table 1) in 782 duplicate-diet solid food samples of 50 Ex-R adults over a six-

[1]National Exposure Research Laboratory, US EPA, Research Triangle Park, North Carolina, USA and [2]National Health and Environmental Effects Research Laboratory, US EPA, Research Triangle Park, North Carolina, USA. Correspondence: Dr Marsha Morgan, National Exposure Research Laboratory, US EPA, Research Triangle Park 27713, North Carolina, USA.
Tel.: +1 919 541 2598. Fax: +1 919 541 0905.
E-mail: morgan.marsha@epa.gov
Received 10 May 2016; accepted 25 October 2016; published online 14 December 2016

Table 1. Target pyrethroid insecticides and their environmental degradates measured in the duplicate-diet solid food samples.

Pyrethroid	*Environmental Degradate*[a]					
	3-PBA	*4-F-3-PBA*	*cis-DBCA*	*cis-DCCA*	*trans-DCCA*	*MPA*
Bifenthrin						○[b]
Cyfluthrin		○		●	●	
λ-Cyhalothrin	●[c]					
Cypermethrin	●			●	●	
cis-Deltamethrin	●		○			
Esfenvalerate	●					
cis-Permethrin	●			●		
trans-Permethrin	●				●	

Abbreviations: 3-PBA (3-phenoxybenzoic acid); 4-F-3-PBA (4-fluoro-3-phenoxybenzoic acid); *cis*-DBCA (*cis*-3-(2,2-dibromovinyl)-2,2-dimethylcyclopropane carboxylic acid); *cis*-DCCA (*cis*-3-(2,2-dichlorovinyl)-2,2-dimethylcyclopropane carboxylic acid); *trans*-DCCA (*trans*-3-(2,2-dichlorovinyl)-2,2-dimethylcyclo-propane carboxylic acid; MPA (2-methyl-3-phenylbenzoic acid). [a]The environmental degradates are also commonly used as urinary biomarkers of exposure in humans. [b]'○' equals specific metabolite of one pyrethroid insecticide. [c]'●' equals nonspecific metabolite of one or more pyrethroid insecticides.

week monitoring period. We also estimated the maximum daily dietary intake doses of the adults to each target pyrethroid.

MATERIALS AND METHODS

Study Cohort

A detailed description of the Ex-R study design and sampling methodology can be found in Morgan et al.[21] Briefly, this study was performed at the US EPA's Human Subjects Facility (HSF) located in Chapel Hill, NC and at the participants' residences within a 40 mile radius of the HSF.[21] Recruitment of adult participants began in October 2009 and ended in March 2011. Field sampling occurred at the participants' residences from November 2009 to May 2011. The adults, ages 19–50 years old, collected their own duplicate-diet solid food samples and completed daily food diaries over a 6-week monitoring period. All protocols and procedures for the Ex-R study were approved by the University of North Carolina's Institutional Review Board (study number: 09-0741).[21] In addition, the adults signed informed consent forms before participating.

Collection of Duplicate-Diet Solid Food Samples

The duplicate-diet solid food samples consisted of duplicate amounts of all the consumed solid foods (excluding beverages) that the participants' ate on day 1 (Sunday) and day 2 (Monday) during weeks 1, 2, and 6 of the six-week monitoring period.[21] These samples were collected by each participant over three, consecutive time periods (period 1 = 4:00 am - 11:00 am; period 2 = 11:00 am - 5:00 pm; and period 3 = 5:00 pm - 4:00 am) each sampling day. Up to 18 individual food samples (6 per sampling week) were collected by each participant over the monitoring period. Solid foods were defined as any edible items that were solid, semi-solid, or contained solids (e.g., hamburger, salad, vegetable soup, smoothie, and ice cream). Inedible parts of foods such as chicken bones, banana peels, and apple cores as well as medicines/vitamins were excluded from these samples. The participants also completed daily food diaries that listed the specific food items that they consumed during each sampling time period.

For each food sample, the participants placed duplicate amounts of their consumed solid food items into a re-sealable polyethylene bag (31 × 31 cm; Uline Shipping Supply Specialists, Pleasant Prairie, WI) and then into a larger re-sealable polyethylene bag (41 × 41 cm). The collection date of each food sample was written with a pen on the provided label on the outside polyethylene bag. The food samples were stored in portable thermoelectric coolers (Princess International, Brooklyn, NY, USA or Vinotemp, Irvine, CA, USA) until the participants returned the coolers to the HSF on day 3 (Tuesday) between 8:00 am–11:00 am of each sampling week.[21] At the HSF, US EPA researchers weighed each food sample. These researchers then transported the food samples in study coolers with blue ice to an US EPA laboratory in Research Triangle Park (RTP), NC, USA.

Food Sample Preparation, Extraction, and Analysis

Food samples were homogenized (for up to 1 min) using a vertical cutter mixer (Robot Coupe R4N-D or R10-Ultra) or a high-speed blender (Waring MBB518 Professional Food/Beverage). The blender was only used for a few types of food items (i.e., soups and purees). Samples containing a single food item with a smooth texture (i.e., peanut butter and ice cream) were not homogenized. Up to six replicates (12 g each) of each food sample were then transferred into separate, pre-cleaned amber glass jars (30 ml) with lids. All replicates were stored in US EPA laboratory freezers (⩽ −20 °C) until analysis.

The homogenized food samples were extracted using the QuEChERS (quick, easy, cheap, effective, rugged, and safe) technique that was modified for use in complex food mixtures.[22,23] For each study sample, a 12 g replicate was thawed, and a 2 g aliquot was removed and transferred to a vial. The 2 g aliquot was then spiked with internal standards ($^{13}C_6$-cypermethrin, $^{13}C_6$-λ-cyhalothrin, $^{13}C_6$-*cis*-permethrin, $^{13}C_6$-*trans*-permethrin, $^{13}C_6$-3-PBA, $^{13}C_6$-4-fluoro-3-phenoxybenzoic acid ($^{13}C_6$-4-F-3-PBA), and $^{13}C_6$-d_1-*cis*-DCCA [Cambridge Isotope Laboratories, Andover, MA, USA]) and 2 ml of acetonitrile was added. The sample was mechanically shaken for 1–2 min. to completely wet the contents, and then $MgSO_4$ (800 mg) and NaCl (200 mg) were added. The sample was vortexed to fully disperse the solids in the mixture, and then centrifuged at 4000 rpm (3220 × g) for 5 min. Next, an aliquot of the supernatant (1 ml) was added to a clean-up tube containing 150 mg $MgSO_4$/carbon black (Supelclean ENVI-carb 120/400 (Supelco, Sigma-Aldrich, Bellefonte, PA, USA, 30:1; w/w) and 300 mg bulk C-18 (Discovery DSC-C18, Supelco, Sigma-Aldrich). The clean-up tube was vortexed for 30 s. and then centrifuged at 15,000 rpm (26,000 *g*) for 10 min. An aliquot (300 µl) of the resulting extract was diluted 1:1 with 0.1% formic acid, filtered through a PTFE filter (0.2 µm), and stored at ~ 4 °C until analysis.

The extracts were analyzed to quantify levels of the target pyrethroids and their environmental degradates (Table 1) using electrospray ionization liquid chromatography/tandem mass spectrometry (LC/MS/MS) on a 4000 QTrap linear ion trap mass spectrometer (AB Sciex, Framingham, MA, USA) in positive (pyrethroids) or negative (degradates) ion modes. All analytical standards were purchased from Chem Services (West Chester, PA, USA) with the exception of 4-F-3-PBA (Cambridge Isotope Laboratories, Andover, MA, USA) and 2-methyl-3-phenylbenzoic acid (MPA) (FMC Agricultural Products Group, Philadelphia, PA, USA). Instrument parameters are given in Supplementary Table 1. Separation was performed using a Hypersil Gold 50 × 2.1 mm column (1.9 µ) (Thermo Fisher Scientific, Waltham, MA, USA) with gradient elution (Supplementary Table 2). The mobile phase used for the parent pyrethroids consisted of (A) 25:75 5 mM ammonium acetate:methanol with 0.1% formic acid, and (B) 5 mM ammonium acetate in methanol with 0.1% formic acid. For the pyrethroid degradates, the mobile phases were the same as mentioned above, except formic acid was not included. Multiple reaction monitoring with two characteristic transitions per target analyte was used for definitive identification (Supplementary Table 3). Quantitation was obtained by internal calibration using isotope dilution and matrix-matched curves made by spiking the control matrix with internal standards and target analytes prior to extraction. The limits of quantitation (LOQs) for the target analytes were set at the concentration of the lowest calibration standard. Estimated limits of detection (LODs) were set at concentrations that gave a signal-to-noise ratio of at least 3 and were ~ 2–5 times below LOQs. The LODs and LOQs for the target analytes are provided in Table 2. Calibration ranges were from the LOQ to 200 ng/g for all analytes. Curves were constructed using quadratic equations with 1/x weighting. Additional details of the method validation are included in the Supplementary Information section.

Quality Assurance and Quality Control Procedures

Field and laboratory quality control samples were used to determine the overall quality of food sample collection, processing, extraction, and analysis. A control food mixture was prepared in-house to be used as the medium for the field/laboratory blank and spike samples. Approximately 5 kg of the control food mixture (5% fat) was made using a slightly modified method by Rosenblum et al.[24] The food mixture contained applesauce, bread, cake, cereal, cheese, fruit cocktail, lunchmeat,

Table 2. Estimated limits of detection (LODs) and limits of quantitation (LOQs) for the target analytes in the duplicate-diet solid food samples.

Target analyte	*LOD (ng/g)*	*LOQ (ng/g)*
Pyrethroid insecticide		
Bifenthrin	0.05	0.10
Cyfluthrin	1.0	2.5
λ-Cyhalothrin	0.30	1.0
Cypermethrin	0.30	1.0
cis-Deltamethrin	0.05	0.25
Esfenvalerate	0.30	1.0
cis-Permethrin	0.10	0.25
trans-Permethrin	0.10	0.25
Pyrethroid degradate		
4-F-3-PBA	0.10	0.25
3-PBA	0.30	2.5
cis-DBCA	0.30	1.0
cis-DCCA	0.30	1.0
trans-DCCA	0.30	1.0
MPA	0.30	1.0

Abbreviations: 3-PBA (3-phenoxybenzoic acid); 4-F-3-PBA (4-fluoro-3-phenoxybenzoic acid); *cis*-DBCA (*cis*-3-(2,2-dibromovinyl)-2,2-dimethylcyclopropane carboxylic acid); *cis*-DCCA (*cis*-3-(2,2-dichlorovinyl)-2,2-dimethylcyclopropane carboxylic acid); *trans*-DCCA (*trans*-3-(2,2-dichlorovinyl)-2,2-dimethylcyclo-propane carboxylic acid; MPA (2-methyl-3-phenylbenzoic acid).

Table 3. Levels of pyrethroid insecticides and their environmental degradates (ng/g) in the duplicate-diet solid food samples.

Target analyte	N[a,b]	%[c]	*90th*[d]	*95th*[d]	*Maximum*
Pyrethroid insecticide					
Bifenthrin	774	20	0.63	1.8	13.9
Cyfluthrin	781	1	—	—	103
λ-Cyhalothrin	781	2	—	—	27.7
Cypermethrin	781	7	—	1.6	154
cis-Deltamethrin	778	17	0.82	1.9	16.3
Esfenvalerate	780	2	—	—	358
cis-Permethrin	780	19	0.84	5.2	111
trans-Permethrin	774	21	0.90	5.4	172
Pyrethroid degradate					
4-F-3-PBA	781	< 1	—	—	0.4
3-PBA	780	< 1	—	—	2.3
cis-DBCA	779	< 1	—	—	1.0
cis-DCCA	782	1	—	—	8.3
trans-DCCA	782	2	—	—	38.3
MPA	780	0	—	—	—

Abbreviations: 3-PBA (3-phenoxybenzoic acid); 4-F-3-PBA (4-fluoro-3-phenoxybenzoic acid); *cis*-DBCA (*cis*-3-(2,2-dibromovinyl)-2,2-dimethylcyclopropane carboxylic acid); *cis*-DCCA (*cis*-3-(2,2-dichlorovinyl)-2,2-dimethylcyclopropane carboxylic acid); *trans*-DCCA (*trans*-3-(2,2-dichlorovinyl)-2,2-dimethylcyclo-propane carboxylic acid; MPA (2-methyl-3-phenylbenzoic acid). [a]Number of samples ($n = 782$). [b]Missing data due to laboratory error. [c]Percentage of analytes at or above the limit of detection by analyte. [d]Percentile.

margarine, mayonnaise, pizza, potato chips, and vegetables that were purchased from local grocery stores. Organic food items were used (when available) to reduce background contamination of pyrethroid insecticides. The control food mixture was homogenized in 1 kg batches using a vertical cutter mixer (Robot Coupe R10-Ultra). Replicates of control food (12 g each) were placed into pre-cleaned amber glass jars (30 ml) and stored in ⩽ − 20 °C in freezers.

The field QC samples consisted of blanks and three spikes (low, medium, and high levels) that were assigned to 10% of the study participants during days 1–2 of each sampling week. A blank or spike sample contained 12 g of the control food mixture (above) that was spiked with internal standards by using 100 µl of a mixed standard (500 ng/ml in methanol) for a final concentration of 4.2 ng/g. For the field spike samples only, they were also spiked with 20, 100, or 200 µl of a solution (in methanol) of the target pyrethroids for a final concentration of 0.9, 4.5, or 8.9 ng/g and the pyrethroid degradates for a final concentration of 4.5, 22.5, or 45 ng/g, respectively. The concentration of the mixed standard used for spiking the field samples was 500 ng/ml for the pyrethroids and 2500 ng/ml for the degradates. Each field blank or field spike was stirred thoroughly with a spatula prior to being transferred into a re-sealable polyethylene bag (8 × 13 cm) and then into another polyethylene bag (8 × 13 cm). These field QC samples were placed into a portable thermoelectric cooler (plugged into an electric wall outlet) in a study room at the HSF during each sampling period (Sunday–Monday). The samples were stored in EPA laboratory freezers (⩽ −20 °C) until analysis. The field blanks ($n = 18$) were below the LODs for all pyrethroids and their environmental degradates in food, except for *cis*-permethrin and *trans*-permethrin that co-occurred in two samples. For the medium and high field spike samples, mean percent recoveries of the target analytes were within empirically determined percent recovery acceptance limits, except for λ-cyhalothrin, *cis*-permethrin, *trans*-permethrin, 3-PBA, and *cis*-DBCA (Supplementary Table 4). For the low field spike samples, the recovery results were inconsistent and highly variable for all analytes (data not shown) most likely due to the low spiked volume (20 µl) which caused incomplete mixing of the samples. A detailed discussion of the field spike results can be found in the Supplementary Information section.

The laboratory (batch) QC samples consisted of laboratory blanks, sample duplicates (duplicate extraction of a study sample), analytical duplicates (duplicate analysis of a study sample extract), laboratory control samples (LCS; spiked control mixture) and matrix spikes (MSS; spiked study samples). The LCS and MSS were spiked at 10 ng/g. The laboratory blanks ($n = 50$) were all below the LODs for the target analytes in food, except for *cis*-permethrin in one sample and *trans*-permethrin in three samples. Mean values for the laboratory blanks were below the LOD for each isomer, so no background correction was made. Mean relative percent differences between sample duplicates or analytical duplicates for the parent pyrethroids were less than 7% in the food samples. For the pyrethroid degradates, mean relative percent differences between the sample duplicates or analytical duplicates were less than 1%. Mean percent recoveries for the LCS and MSS were within the empirically determined percent recovery acceptance limits for all target analytes (Supplementary Table 4). In addition, the mean percent recoveries of the target analytes for the MSS were within 5% of the mean percent recoveries for the LCS, except for bifenthrin. For this analyte, the mean percent recovery for the MSS was 15% lower than the mean percent recovery for the LCS.

Statistical Analyses

For each target analyte, all data values below the LOD in the food samples were replaced by the $\mathrm{LOD}/\sqrt{2}$ as described in Verbovsek.[25] Descriptive statistics were calculated for the analytes in the food samples using JMP version 12.1 (SAS Institute, Cary, NC, USA).

The estimated maximum daily dietary intake doses (ng/kg/day) of the Ex-R adults to each target pyrethroid insecticide (D) was calculated using the following equation:

$$D = \frac{\sum_{t=1}^{3} (F_t \times M_t)}{B}$$

In this equation, Ft (concentration (ng/g) of each target pyrethroid in a food sample) was multiplied by M_t (mass of the same food sample (g)). The subscript t denotes whether the sample was the first, second, or third sample on a given sampling day. Then, the amount of each target pyrethroid in the participant's food samples (up to three) was summed over a sampling day (ng/d) and divided by B (body weight (kg)).

RESULTS

Table 3 provides the summary statistics for the target pyrethroids and their environmental degradates measured in the duplicate-diet solid food samples of 50 Ex-R participants over the six-week monitoring period. For the pyrethroids, *trans*-permethrin (21%),

Table 4. Levels of the four most frequently detected pyrethroids in the duplicate-diet solid food samples.[a,b]

Target analyte	N[c]	%[d]	Mean ± SD[e]	*Min.*	*50th*	*75th*[f]	*90th*[f]	*95th*[f]	*Max.*
Bifenthrin	156	100	1.8 ±2.8	0.06	0.63	1.7	4.7	8.2	13.9
cis-Deltamethrin	129	100	1.9 ± 2.4	0.12	1.0	2.4	4.1	6.2	16.3
cis-Permethrin	145	100	9.1 ± 20.0	0.10	1.1	5.6	28.7	52.5	111
trans-Permethrin	164	100	8.9 ± 22.2	0.10	0.80	4.9	25.8	48.6	172

[a]Includes pyrethroids that were detected in ⩾17% of the food samples (Table 3). For each analyte, only values at or above the LOD are presented in this table. [b]Units = ng/g. [c]Number of samples. [d]Percentage of samples. [e]Arithmetic mean and SD. [f]Percentile.

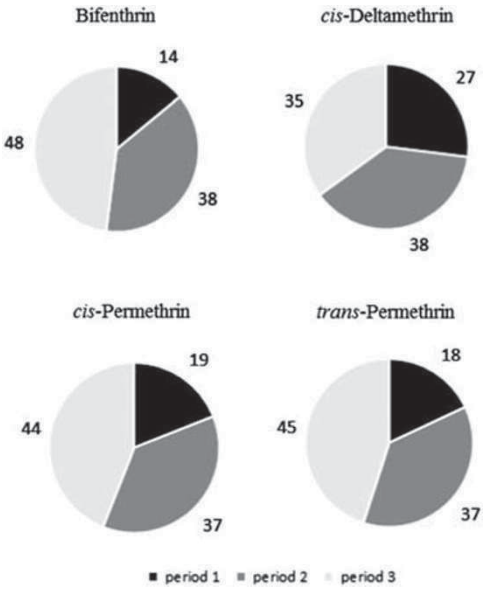

Figure 1. Percentage of duplicate-diet solid food samples with detectable levels of bifenthrin, *cis*-deltamethrin, *cis*-permethrin, and *trans*-permethrin by sampling time period.[a,b,c] [a]Includes the four most frequently detected (⩾17%) pyrethroids measured in the duplicate-diet solid food samples. [b]Data are shown for food samples that have detectable levels (⩾LOD) of each pyrethroid by time period (period 1 = 0400–1100 hours, period 2 = 1100–1700 hours, and period 3 = 1700–0400 hours). [c]Number of food samples: bifenthrin ($n = 156$), *cis*-deltamethrin ($n = 129$), *cis*-permethrin ($n = 145$), and *trans*-permethrin ($n = 164$).

bifenthrin (20%), *cis*-permethrin (19%), and *cis*-deltamethrin (17%) were detected the most often in the food samples. At the 95th percentile, the levels of *cis*-permethrin (5.2 ng/g) and *trans*-permethrin (5.4 ng/g) were at least two times greater compared to the levels of the other pyrethroids (⩽1.9 ng/g) in the samples. The highest maximum concentration of the pyrethroids occurred for esfenvalerate (358 ng/g) in one participant's food sample. In comparison to the parent pyrethroids, the degradates were not frequently detected (< 3%) in the food samples (Table 3). MPA (bifenthrin degradate) was not detected in any of these samples. The highest maximum levels of the degradates occurred for *trans*-DCCA (38.3 ng/g) and *cis*-DCCA (8.3 ng/g) in the same food sample of one participant.

Table 4 presents the summary statistics for the levels (⩾LOD) of the four most frequently detected pyrethroids (bifenthrin, *cis*-deltamethrin, *cis*-permethrin, and *trans*-permethrin) in the food samples. Mean levels of *cis*-permethrin (9.1 ±20.0 ng/g) and *trans*-permethrin (8.9 ± 22.2 ng/g) were at least four time greater compared to mean levels of bifenthrin (1.8 ± 2.8 ng/g) and *cis*-deltamethrin (1.9 ± 2.4 ng/g) in the food samples. At the 95th percentile, the levels of *cis*-permethrin (52.5 ng/g) and *trans*-permethrin (48.6 ng/g) were at least five times higher than the levels of the other two pyrethroids (⩽8.2 ng/g). Figure 1 presents the levels of these four pyrethroids in the participant's food samples by sampling time period (1, 2, or 3). The results show that these four pyrethroids were consistently detected the least often in the food samples during period 1 (4:00 am - 11:00 am) compared with period 2 (11:00 am - 5:00 pm) and period 3 (5:00 pm - 4.00 am). These pyrethroids were found the most often in the participants' food samples during period 3, except for *cis*-deltamethrin (period 2).

The co-occurrence of the target pyrethroids in the food samples of the Ex-R adults over the six-week monitoring period is presented in Figure 2. In this figure, the results show that 49% of all the food samples contained at least one or more target pyrethroids. In particular, 32% of the participants' food samples contained one target pyrethroid. In addition, 13% of the adult food samples contained at least two different target pyrethroids. Only 3% and 1% of the food samples had three or four different target pyrethroids, respectively.

Table 5 presents the estimated adults' maximum dietary exposures (ng/day) and maximum dietary intake doses (ng/kg/day) to the target pyrethroid insecticides and compares these estimates to available oral reference doses (RfDs) in the US EPA's Integrated Risk Information System (IRIS).[26] In IRIS, oral RfDs currently exist only for bifenthrin, λ-cyhalothrin, cypermethrin, and permethrin. The participants' maximum dietary intake doses were the highest for the combined isomers of *cis/trans*-permethrin (2,115 ng/kg/day), followed by esfenvalerate (1,784 ng/kg/day). The estimated adults' maximum dietary intake doses to bifenthrin, λ-cyhalothrin, cypermethrin, and permethrin were all well below the established oral RfDs in IRIS.

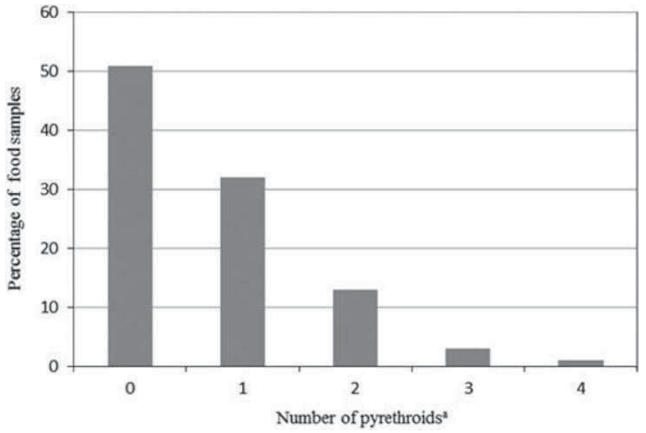

Figure 2. Co-occurrence of the target pyrethroid insecticides in the duplicate-diet solid food samples of Ex-R adults. [a]*cis*-and *trans*-permethrin were counted as one pyrethroid insecticide.

Table 5. The estimated adults' maximum dietary exposures and intake doses to the target pyrethroid insecticides.[a]

Pyrethroid	*Maximum dietary exposure (ng/day)*	*Maximum dietary dose (ng/kg/day)*	*Oral RfD*[b] *(ng/kg/day)*
Bifenthrin	6206	63.1	15,000
Cyfluthrin	31,153[c]	265	—[d]
λ-Cyhalothrin	7807	69.7	5000
Cypermethrin	46,207[c]	393	10,000
cis-Deltamethrin	205	2.93	—
Esfenvalerate	102,071	1784	—
Permethrin[e]	121,000	2115	50,000

[a]Estimates using 24-h duplicate-diet solid food samples (excludes beverages). [b]Oral reference dose (RfD), US EPA's Integrated Risk Information System (IRIS), http://www.epa.gov/iris/. [c]Missing food mass data from same study participant due to laboratory error; used average food mass data of all study adults by time period. [d]Not available in IRIS. [e]Combined *cis*- and *trans*-isomers.

DISCUSSION

Previous research has suggested that the diet is likely the major source of exposure to pyrethroids insecticides in the general adult population worldwide.[4,5,27] Few data exist on the temporal levels of current-use pyrethroid insecticides in the everyday diets of adults.[10,12] Our study results showed that the individual target pyrethroids were not detected often (1–21%) in the duplicate-diet solid food samples of 50 Ex-R adults over the 6-week monitoring period. However on a cumulative basis, 49% of the participants' food samples contained at least one of the target pyrethroids. Based on these data, 100% of the Ex-R participants were intermittently exposed to several different pyrethroids in their normal diets during the six-week monitoring period. Our study results are similar to Melnyk et al.[12,28] that also showed low detection frequencies (LOD range = 0.05–0.8 ng/g) for bifenthrin (30%), cyfluthrin (4%), cypermethrin (11%), *cis*-deltamethrin (1%), esfenvalerate (10%), and *cis/trans*-permethrin (33%) in 67 solid food samples composited by eating event (breakfast, lunch, dinner, and snack) over several days for nine Hispanic women in Florida USA in 2008. In an earlier study conducted by Riederer et al.,[10] the authors reported higher detection frequencies (LOD range = 0.4–0.8 ng/g) than our study for cyfluthrin (59%), cypermethrin (67%), *cis*-deltamethrin (28%), and *cis/trans*-permethrin (43%) in duplicate diet samples (composited by food group) of 12 adults collected over eight sampling days in Georgia USA in 2005–2006. Interestingly in that study, the authors reported that measureable levels of these pyrethroid residues were found in several different types of foods (i.e., fruits, vegetables, legumes, grains, meats, and dairy).[10] This information emphasize the importance of collecting total diet samples (i.e., not just produce) from adults to assess their daily dietary exposures to pyrethroids. As data are limited, more research is necessary to determine the cumulative and temporal dietary exposures of adults to current-use pyrethroid insecticides.

Another important study finding was that the detectable levels of the target pyrethroids substantially varied by sampling time frame (period 1, 2, or 3) over a day. The most frequently detected pyrethroids (bifenthrin, *cis*-deltamethrin, *cis*-permethrin, and *trans*-permethrin) were found less often in food consumed during period 1 compared to periods 2 and 3. In support of our study results, Melnyk et al.[12,28] also reported that the mean intake levels of several different pyrethroids were substantially different by type of adult meal sampled (breakfast, lunch, or dinner). In that study, the authors found that the mean intake levels of permethrin, cypermethrin, and esfenvalerate were the lowest in the participants breakfast meals compared to their lunch/dinner meals. This information suggests that people's eating patterns are likely an important factor influencing their dietary exposures to pyrethroid insecticides over a day.

Few data are available on the estimated dietary intake doses to single or multiple pyrethroid insecticides derived from the actual consumed diets of adults, globally.[10] Assuming 100% absorption, our estimated adults' maximum dietary intake doses to bifenthrin (63.1 ng/kg/day), λ-cyhalothrin (69.7 ng/kg/day), cypermethrin (393 ng/kg/day), and permethrin (2,115 ng/kg/day) were all well below the corresponding oral RfDs listed in IRIS (Table 5).[26] Since oral RfDs are not currently available for cyfluthrin, *cis*-deltamethrin, or esfenvalerate in IRIS,[26] we could not determine if the estimated adults' dietary intake doses to these insecticides (Table 5) were below a level of concern. Only one other smaller duplicate-diet study was found by Reiderer et al.[10] that reported estimated dietary intake doses to cypermethrin (1400 ng/kg/day), *cis*-deltamethrin (2700 ng/kg/day), and permethrin (1500 ng/kg/day) for 12 adults in Georgia USA in 2005–2006.

Few published studies have measured the concurrent levels of pyrethroids and their environmental degradates (commonly used as urinary biomarkers) in individual food items (i.e., produce)[7,11] and none in duplicate-diet samples. Our study results showed that 3-PBA, 4-F-3-PBA, *cis*-DBCA, *cis*-DCCA, *trans*-DCCA, and MPA were not frequently detected (< 3%) in the duplicate-diet solid food samples of 50 Ex-R participants over the six-week monitoring period. This information suggests that these pyrethroid degradates were probably not present in sufficient levels in the diet to substantially influence the Ex-R adults' urinary pyrethroid biomarker concentrations. Our results are in agreement with Li et al.[7] that recently reported measureable levels of several different pyrethroids in samples of apples, grapes, and lettuce purchase from local grocery stores in Durham NC, but only the pyrethroid degradates, *cis*-DCCA and *trans*-DCCA, occurring in one lettuce sample.

Our study had some limitations. Because of participant burden and budget constraints, the Ex-R study only collected duplicate-diet solid food samples (which excluded beverages). Therefore, it is possible that we may have underestimated the total daily dietary exposures and intake doses of the Ex-R adults to these individual pyrethroids. However, previous research has indicated that beverages were a minor contributor to the dietary exposure of adults to pyrethroid insecticides.[6,9,29] Another study limitation was that the Ex-R participants' solid food samples were collected over three, consecutive time frames each sampling day, so we were unable to determine the specific food items that had detectable levels of the pyrethroid residues.

CONCLUSIONS

On basis of the food sample data, our study results showed that the Ex-R adults were likely intermittently exposed to several different pyrethroid insecticides in their diets during the six-week monitoring period in NC in 2009–2011. In addition, the results suggests that the measured pyrethroid degradates (3-PBA, 4-F-3-PBA, *cis*-DBCA, *cis*-DCCA, and *trans*-DCCA) were likely not present in sufficient levels in the diet to substantially impact the adults' urinary biomarker concentrations.[30]

CONFLICT OF INTEREST

The authors declare no conflict of interest.

ACKNOWLEDGEMENTS

We thank Carry Croghan, Paul Jones, Fu-Lin Chen, Lillian Alston, Richard Walker, Erik Andersen, Jim Starr, Scott Clifton, and Scott Rhoney for their technical assistance in this study. We would also like to thank Joseph Evans (Alion) for homogenizing the food samples.

DISCLAIMER

This United States Environmental Protection Agency through its Office of Research and Development has provided administrative review of this article and approved it for publication.

REFERENCES

1 Elbert A, Haas M, Springer B, Thielert W, Nauen R. Applied aspects of neonicotinoid uses in crop protection. *Pest Manag Sci* 2008; **64**: 1099–1105.
2 Saillenfait AM, Ndiaye D, Sabate JP. Pyrethroids: exposure and health effects – an update. *Int J Hyg Envir Heal* 2015; **218**: 281–292.
3 USEPA (United States Environmental Protection Agency). *Pyrethrins/ Pyrethroids Cumulative Risk Assessment*. Available at: http://epa.gov/pesticides/cumulative/common mechgroups/htm#pyrethrins, 2011. Accessed on 29 July 2015.
4 Riederer AM, Bartell SM, Barr DB, Ryan PB. Diet and nondiet predictors of urinary 3-phenoxybenzoic acid in NHANES 1999-2002. *Environ Health Perspect* 2008; **116**: 1015–1022.
5 Barr DB, Olsson AO, Wong LY, Udunka SO, Baker SE, Whitehead RD *et al.* Urinary concentrations of metabolites of pyrethroid insecticides in the general US population: National Health and Nutrition Examination Survey 1999-2002. *Environ Health Perspect* 2010; **118**: 742–748.
6 Morgan MK, Sheldon LS, Croghan CW, Jones PA, Chuang JC, Wilson NK. An observational study of 127 preschool children at their homes and daycare centers in Ohio: Environmental pathways to *cis*- and *trans*-permethrin exposure. *Environ Res* 2007; **104**: 266–274.
7 Li W, Morgan MK, Graham S, Starr JM. Measurement of Pyrethroids and Their Environmental Degradates in Fresh Fruits and Vegetables using a Modification of the Quick Easy Cheap Effective Rugged Safe (QuEChERS) Method. *Talanta* 2016; **151**: 42–50.
8 Chuang JC, Wilson NK. Multiresidue analysis of organophosphate and pyrethroid pesticides in duplicate-diet solid food by pressurized liquid extraction. *J Environ Sci Health B* 2011; **46**: 41–40.
9 Lu C, Schenck FJ, Pearson MA, Wong JW. Assessing children's dietary pesticide exposure: Direct measurement of pesticide residues in 24-hr duplicate food samples. *Environ Health Perspect* 2010; **118**: 1625–1630.
10 Riederer AM, Hunter RE, Hayden SW, Ryan PB. Pyrethroid and organophosphorus pesticides in composite diet samples from Atlanta, USA adults. *Environ Sci Technol* 2010; **44**: 483–490.
11 Chen L, Zhao T, Pan C, Ross JH, Krieger RL. Preformed biomarkers including dialkylphosphate (DAPs) in produce may confound biomonitoring in pesticide exposure and risk assessment. *J Agric Food Chem* 2012; **60**: 9342–9351.
12 Melnyk LJ, McCombs M, Brown GG, Raymer JJ, Nishioka MG, Buehler S *et al.* Community duplicate diet methodology: A new tool for estimating dietary exposures to pesticides. *J Environ Monit* 2012; **14**: 85–93.
13 USDA (United States Department of Agriculture). *Pesticide Data Program*. Available at: http://www.ams.usda.gov/datasets/pdp. 2014. Accessed on 13 January 2016.
14 USFDA (United States Food and Drug Administration). *Total Diet Study*. 2004-2005. Available at: http://www.fda.gov/Food/FoodScienceResearch/TotalDietStudy/default.htm. Accessed on 13 January 2016.
15 Leng G, Kuhn KH, Idel H. Biological monitoring of pyrethroids in blood and pyrethroid metabolites in urine; Applications and limitations. *Sci Total Environ* 1997; **199**: 173–181.
16 Ratelle M, Cote J, Bouchard M. Toxicokinetics of permethrin biomarkers of exposure in orally exposed volunteers. *Toxicol Lett* 2015; **232**: 369–375.
17 Eadsforth CV, Bragt PC, Van Sittert NJ. Human dose-excretion studies with pyrethroid insecticides cypermethrin and alphacypermethrin: Relevance for biological monitoring. *Xenobiotica* 1988; **18**: 603–613.
18 CDC (Centers for Disease Control and Prevention). *Fourth national report on human exposure to environmental chemicals*. 2009. Available at: http://www.cdc.gov/ exposurereport/. Accessed on 11 August 2015.
19 McKelvey W, Jacobson JB, Kass D, Barr DB, Davis M, Calafat AM *et al.* Population-based biomonitoring of exposure to organophosphate and pyrethroid pesticides in New York City. *Environ Health Perspect* 2013; **121**: 1349–1356.
20 Trunnelle KJ, Bennett DH, Tulve NS, Clifton MS, Davis MD, Calafat AM *et al.* Urinary Pyrethroid and Chlorpyrifos Metabolite Concentrations in Northern California Families and Their Relationship to Indoor Residential Insecticide Levels, Part of the Study of Use of Products and Exposure Related Behavior (SUPERB). *Environ Sci Technol* 2014; **48**: 1931–1939.
21 Morgan MK, Sobus JR, Boyd-Barr D, Croghan CW, Chen F, Walker R *et al.* Temporal variability of pyrethroid metabolite levels in bedtime, morning, and 24-hr urine samples for 50 adults in North Carolina. *Environ Res* 2016; **144**: 81–91.
22 Anastassiades M, Lehotay SJ, Stajnbaher D, Schenck FJ. Fast and easy multiresidue method employing acetonitrile extraction partitioning and dispersive solid phase extraction for determination of pesticide residues in produce. *J AOAC Int* 2003; **86**: 412–431.
23 Lehotay SJ, Mastovska K, Yun SJ. Evaluation of two fast and easy methods for pesticide residue analysis in fatty food matrixes. *J AOAC Int* 2005; **88**: 630–638.
24 Rosenblum L, Hieber T, Morgan J. Determination of pesticides in composite dietary samples by gas chromatography/mass spectrometry in the selected ion monitoring mode by using a temperature-programmable large volume injector with preseparation column. *J AOAC Int* 2001; **84**: 891–900.
25 Verbovsek T. A comparison of parameters below the limit of detection in geochemical analyses by substitution methods. *Materials Geoenviron* 2011; **58**: 393–404.
26 IRIS (Integrated Risk Information System). 2015. Available at: http://www.epa.gov/iris/. Accessed on 21 August 2015.
27 Schettgen T, Heudorf U, Drexler H, Angerer J. Pyrethroid exposure of the general population – is this due to diet? *Toxicol Lett* 2002; **134**: 141–145.
28 Melnyk LJ, Xue J, Brown GG, McCombs M, Nishioka M, Michael LC. Dietary intakes of pesticides based on community duplicate diet samples. *Sci Total Environ* 2014; **468–469**: 785–790.
29 Morgan MK, Sheldon LS, Croghan CW, Chuang JC, Lordo R, Wilson NK *et al. A Pilot Study of Children's Total Exposure to Persistent Pesticides and Other Persistent Organic Pollutants (CTEPP)*. United States Environmental Protection Agency: Washington, DC, USA, 2004 EPA/600/R-041/193.
30 Matuszewski BK, Constanzer ML, Chavez-Eng CM. Strategies for the assessment of matrix effect in quantitative bioanalytical methods based on HPLC-MS/MS. *Anal Chem* 2003; **75**: 3019–3030.

This work is licensed under a Creative Commons Attribution 4.0 International License. The images or other third party material in this article are included in the article's Creative Commons license, unless indicated otherwise in the credit line; if the material is not included under the Creative Commons license, users will need to obtain permission from the license holder to reproduce the material. To view a copy of this license, visit http://creativecommons.org/licenses/by/4.0/

© The Author(s) 2018

Supplementary Information accompanies the paper on the Journal of Exposure Science and Environmental Epidemiology website (http://www.nature.com/jes)

Environment International 112 (2018) 85–99

Contents lists available at ScienceDirect

Environment International

journal homepage: www.elsevier.com/locate/envint

Distribution, variability, and predictors of urinary bisphenol A levels in 50 North Carolina adults over a six-week monitoring period

Marsha K. Morgan[a,*], Maliha Nash[b], Dana Boyd Barr[c], James M. Starr[a], M. Scott Clifton[a], Jon R. Sobus[a]

[a] United States Environmental Protection Agency, National Exposure Research Laboratory, Research Triangle Park, NC 27711, USA
[b] United States Environmental Protection Agency, National Exposure Research Laboratory, Las Vegas, NV 89154, USA
[c] Department of Environmental Health, Rollins School of Public Health, Emory University, Atlanta, GA 30322, USA

ARTICLE INFO

Keywords:
Bisphenol A (BPA)
Adults
Urine
Homes
Biomonitoring
Temporal
Determinants

ABSTRACT

Bisphenol A (BPA) is commonly manufactured to make polycarbonate plastics and epoxy resins for use in consumer products and packaged goods. BPA has been found in several different types of environmental media (e.g., food, dust, and air). Many cross-sectional studies have frequently detected BPA concentrations in adult urine samples. However, limited data are available on the temporal variability and important predictors of urinary BPA concentrations in adults. In this work, the major objectives were to: 1) quantify BPA levels in duplicate-diet solid food, drinking water, hard floor surface wipe, and urine samples (first-morning void [FMV], bedtime, and 24-h) collected from adults over a six-week monitoring period; 2) determine the temporal variability of urinary BPA levels using concentration, specific gravity (SG) adjusted, creatinine (CR) adjusted, and excretion rate values, and; 3) examine associations between available study factors and urinary BPA concentrations. In 2009–2011, a convenience sample of 50 adults was recruited from residential settings in North Carolina. The participants completed diaries and collected samples during weeks 1, 2, and/or 6 of a six-week monitoring period. BPA was detected in 38%, 4%, and 99% of the solid food (n = 775), drinking water (n = 50), and surface wipe samples (n = 138), respectively. Total BPA (free plus conjugated) was detected in 98% of the 2477 urine samples. Median urinary BPA levels were 2.07 ng/mL, 2.20 ng/mL-SG, 2.29 ng/mg, and 2.31 ng/min for concentration, SG-adjusted, CR-adjusted, and excretion rate values, respectively. The intraclass correlation coefficient (ICC) estimates for BPA showed poor reproducibility (≤ 0.35) for all urine sample types and methods over a day, week, and six weeks. CR-adjusted bedtime voids collected over six-weeks required the fewest, realistic number of samples (n = 11) to obtain a reliable biomarker estimate (ICC = 0.80). Results of linear mixed-effects models showed that sex, race, season, and CR-level were all significant predictors ($p < 0.05$) of the adults' urinary BPA concentrations. BPA levels in the solid food and surface wipe samples did not contribute significantly to the participants' urinary BPA concentrations. However, a significant positive relationship was observed between solid food intake and urine-based estimates of BPA dose, when aggregated over 24-h periods. Ingestion of BPA via solid food explained only about 20% of the total dose (at the median of the dose distribution), suggesting that these adults were likely exposed to other major unknown (non-dietary) sources of BPA in their everyday environments.

1. Introduction

Bisphenol A (4,4′-dihydroxy-2,2-diphenylpropane, [BPA]), is a synthetic chemical with over two billion pounds produced annually in the United States (US) (Geens et al., 2012; Loganathan and Kannan, 2011). BPA is commonly used to create polycarbonate plastics and epoxy resins for use in everyday consumer products and packaged goods (ACC, 2015). Several studies have found measurable levels of

Abbreviations: BPA, bisphenol-A; BMI, body mass index; CR, creatinine concentration; EPA, US Environmental Protection Agency; Ex-R study, A Pilot Study to Estimate Human Exposures to Pyrethroids using an Exposure Reconstruction Approach; LC/MS/MS, liquid chromatograph - tandem mass spectrometer; HSF, Human Studies Facility; FMV, first-morning void; GC/MSD, gas chromatograph-mass selective detector; GM, geometric mean; ICC, intraclass correlation coefficient; LOQ, limit of quantitation; NHANES, National Health and Nutritional Examination Survey; NC, North Carolina; QC, quality control; QuEChERS, quick, easy, cheap, effective, rugged, and safe method; RTP, Research Triangle Park; SG, specific gravity; SRS, surrogate recovery standard; UPS, United Parcel Service; US, United States

* Corresponding author at: US EPA, 109 T.W. Alexander Dr., MD E205-04, Research Triangle Park, NC 27709, USA.
E-mail address: morgan.marsha@epa.gov (M.K. Morgan).

https://doi.org/10.1016/j.envint.2017.12.014
Received 11 September 2017; Received in revised form 7 December 2017; Accepted 10 December 2017
Available online 18 December 2017
0160-4120/ Published by Elsevier Ltd. This is an open access article under the CC BY-NC-ND license (http://creativecommons.org/licenses/BY-NC-ND/4.0/).

BPA in many commonly used consumer items including food storage containers, food cans (liners), tableware, paper receipts, electronic equipment, magazines, paints, adhesives, shampoos, bar soaps, body lotions, sunscreens, nail polishes, and recycled paper towels, napkins and toilet papers (Dotson et al., 2012; Geens et al., 2012; Liao and Kannan, 2011; Vandenberg et al., 2007).

Due to its widespread use, BPA has been found in several different types of environmental media including foods, beverages, dust, surface wipes, and air at residences in the US (Loganathan and Kannan, 2011; Rudel et al., 2003; Schecter et al., 2010; Wilson et al., 2007). Although adults can be exposed to BPA though multiple routes, research has indicated that dietary ingestion is likely the dominant exposure route (> 90%) (Geens et al., 2012; Morgan et al., 2011; Von Goetz et al., 2017; Wang et al., 2015). Currently, the US Food and Drug Administration does not regulate the amount of BPA that can be present in foods or beverages for adult consumption (Schecter et al., 2010). Several recent studies have raised concerns that exposures to BPA at environmental concentrations may be adversely impacting human health (i.e., reproductive, developmental, and cardiovascular effects) (Rezg et al., 2014; Rochester, 2013; Schug and Birnbaum, 2014).

Once ingested, BPA undergoes rapid metabolism in the liver and is mainly excreted in the urine as conjugated BPA-glucuronide with an elimination half-life of < 7 h in adults (Dekant and Volkel, 2008; Thayer et al., 2015; Volkel et al., 2002). In recent cross-sectional studies (2009–2014), total BPA was frequently detected (> 73%) in the urine samples of adults recruited from the US general population (CDC, 2017; Cox et al., 2016; LaKind and Naiman, 2015; Ye et al., 2015). In these studies, median urinary BPA concentrations ranged from 0.36–2.4 ng/mL.

A number of US studies have examined the short- or long-term variability (1 week to 3 years) of total BPA concentrations in spot, first-morning void (FMV), and/or 24-h urine samples in adults in non-occupational settings (Braun et al., 2011, 2012; Cox et al., 2016; Meeker et al., 2013; Philippat et al., 2013; Pollack et al., 2016; Reeves et al., 2014; Townsend et al., 2013; Ye et al., 2011). In some of these studies, FMVs has been the preferred sample type collected based on the assumption that they provide the best weighted-average biomarker level over a day (Kissel et al., 2005). None of these prior studies have specifically examined the levels of BPA in bedtime voids. Across these various studies, poor reproducibility (ICC < 0.30) of repeated measurements of BPA occurred in adult urine samples regardless of urine sample type and method of adjustment (unadjusted, specific gravity [SG] adjusted, or creatinine [CR] adjusted). The observed high within-individual variability reported in these studies suggests that a single BPA urine measurement is probably not sufficient to characterize a person's average exposure over a day or longer. However, information is currently lacking on the actual type and number of urine samples that are likely needed to obtain a reliable BPA biomarker estimate for adults over a day or longer.

Several US studies of non-occupationally exposed adults have reported significant ($p < 0.05$) associations occurring between urinary BPA concentrations and various sociodemographic, lifestyle, and dietary factors including age, gender, and race/ethnicity (LaKind and Naiman, 2008, 2015), pre-pregnancy body mass index (BMI) (Meeker et al., 2013), contact with paper receipts (Gerona et al., 2016), and consumption frequency of canned vegetables (Braun et al., 2011), hamburgers (Quiros-Alcala et al., 2013), and soda (LaKind and Naiman, 2008; Quiros-Alcala et al., 2013). Currently, we are not aware of any published study that has quantitatively examined the association between measured BPA levels in the actual consumed diets of adults and their urinary BPA levels.

In previous work from the Pilot Study to Estimate Human Exposures to Pyrethroids using an Exposure Reconstruction Approach (Ex-R study), we quantified the levels of several pyrethroid insecticides and pyrethroid degradates in media (duplicate-diet solid food, drinking water, hard floor surface wipes, and urine) for 50 adults in residential settings over a six-week monitoring period in North Carolina (NC) in 2009–2011 (Clifton et al., 2015; Morgan et al., 2016a; Morgan et al., 2016b; Starr et al., 2017). In this present work, we have now quantified the concentrations of BPA in the same media (above) from the Ex-R study. The major objectives were to: 1) quantify the BPA levels in the duplicate-diet solid food, drinking water, hard floor surface wipe, and urine samples (spot and 24-h) collected from 50 Ex-R adults over a six-week monitoring period; 2) determine the temporal variability of BPA levels in the FMV, bedtime, and 24-h urine samples as concentration, SG-adjusted, CR-adjusted, and excretion rate values, and; 3) examine associations between available study factors and urinary levels of BPA.

2. Materials and methods

2.1. Study cohort

The Ex-R study design and sampling methodology has been described earlier in Morgan et al., 2016a. This study was designed to assess the short-term (over six-weeks) exposures of adults to pyrethroid insecticides and BPA in selected media at residences. Briefly, this observational exposure measurements study was conducted at the US Environmental Protection Agency's (EPA's) Human Studies Facility (HSF) in Chapel Hill, NC, and within a 40-mile radius of the HSF at the adult participants' homes. A total of 50 adults between the ages of 19 and 50 years old were recruited into the study. The participants filled out diaries (food and activity) and collected duplicate-diet solid food, drinking water, hard floor surface wipe, and urine samples (spot and 24-h) during weeks 1, 2, and 6 of a six-week monitoring period from November 2009 to May 2011 (Fig. 1). Each sampling week started on Sunday (day 1) and ended on Friday (day 6). The University of North Carolina's Institutional Review Board approved the Ex-R study protocol and procedures (study number 09–0741) in 2008. All study adults reviewed and signed informed consent forms before participating.

2.2. Collection of diaries and physical information

The Ex-R participants filled out the food and activity diaries during sampling weeks 1, 2, and 6 of the six-week monitoring period (Morgan et al., 2016a). Food diaries were complete on days 1–2 and days 4–5 of each sampling week. Each 24-h sampling day consisted of three consecutive time periods (period 1 = 4:00–11:00 am, period 2 = 11:00 am–5:00 pm, and period 3 = 5:00 pm–4:00 am). The food diary was used to record all of the solid and liquid foods (including estimated amounts) consumed by individual participants during each sampling time period. Activity diaries were completed on days 1–2 and days 4–5 of each sampling week. Each 24-h sampling day in this diary consisted of three consecutive time periods (as described above). The activity diary was used to record the participants' activity levels (sleeping, low [e.g., sitting/standing], medium [e.g., walking], or high [e.g., running]) in consecutive, 30-min time increments during each sampling time period. In addition, an EPA technician recorded specific physical information (weight, height, age, and sex) about each participant at the HSF at the beginning of sampling week 1.

2.3. Collection of samples

The participants were trained to collect their own duplicate-diet solid food, drinking water, hard floor surface wipe, and urine samples during weeks 1, 2, and/or 6 of a six-week monitoring period (Morgan et al., 2016a). Duplicate-diet liquid food samples (mainly beverages, excluding drinking water) were not collected in the Ex-R study because of participant burden and budget constraints. The adults collected duplicate amounts of all solid food samples (e.g., fruits, vegetables, meats, pastas, soups, crackers, cheeses, breads, cookies, and ice creams) they consumed on sampling days 1 and 2 during each sampling week. The solid food samples were collected over three consecutive time periods

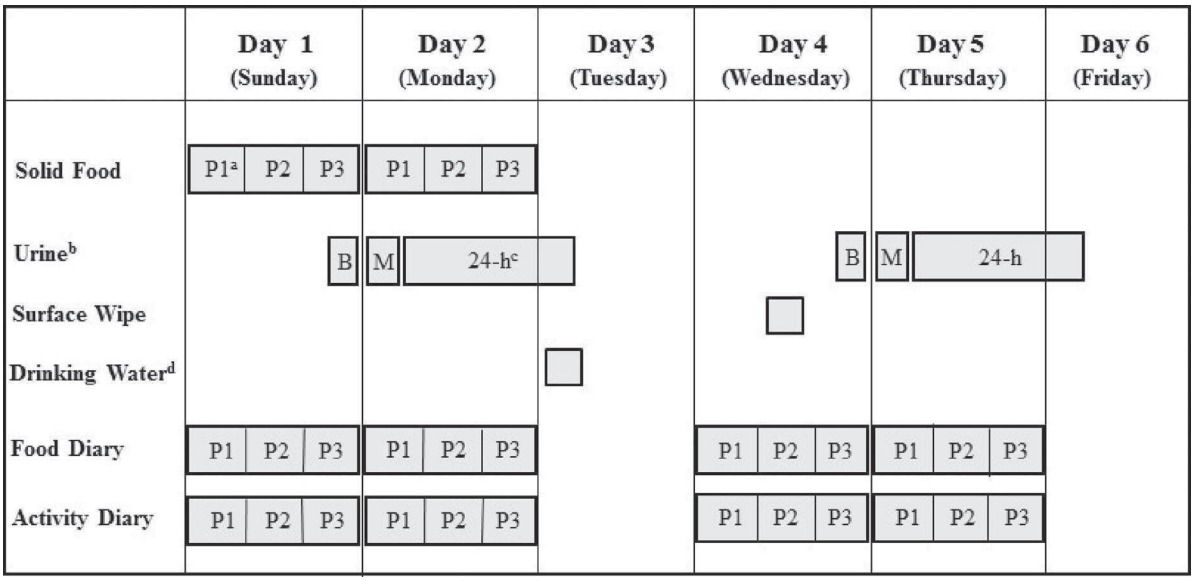

[a] Period 1 (P1) = 4:00 – 11:00 am, Period 2 (P2) = 11:00 am – 5:00 pm, and Period 3 (P3) = 5:00 pm – 4:00 am
[b] Bedtime void (B), first-morning void (M), and 24-h sample
[c] Individual urine voids were collected over the 24-h period, and each void was analyzed separately
[d] The drinking water sample was collected only on day 3 of sampling week 6
[e] This sampling schedule was modified from the one presented in Morgan et al., 2016a

Fig. 1. Sampling schedule for the Ex-R study field activities for each sampling week (1, 2, or 6).[e]

(1, 2, or 3) each sampling day (as mentioned above in Section 2.2). For each period, the participants placed their solid food items into a (BPA-free) re-sealable polyethylene bag (31 × 31 cm, Uline Shipping Supply Specialist). A drinking water sample was obtained from the participants' main source of water (i.e., municipal or well) on day 3 of the last sampling week, only. Drinking water samples (> 500 mL) were placed directly into a (BPA-free) 1 L polypropylene container (Government Scientific Source). Hard floor surface wipe samples (pre-cleaned 100% cotton pad wetted with 10 mL of isopropanol) were collected from two, separate high traffic areas (929 cm^2 each) of the participants' kitchens (e.g., sink, stove, or entryway) on day 4 of each sampling week. After sampling was completed, each cotton pad was put into a separate pre-cleaned (60 mL) amber glass jar (Government Scientific Source). Lastly, the participants collected several different types of urine samples (FMV, bedtime, and 24-h). Bedtime voids were collected before the participants went to sleep on day 1 and day 4 of each sampling week. FMV's were collected after the participants woke up on day 2 and day 5 of each sampling week. For the 24-h samples, the participants collected up to 11 consecutive, urine voids beginning after the FMV on day 2 or day 5 until the collection of the FMV the next morning (day 3 or day 6). Each urine sample was collected directly into a 1 L polypropylene container. All collected samples were immediately stored by the participants in provided portable thermoelectric coolers (Vinotemp or Princess International®).

The participants returned the coolers containing the study samples to the HSF between 8:00–11:00 am on days 3 or 6 of each sampling week. At the HSF, the mass (g) of each food sample was measured using an electronic weight scale. The samples were then transported in the portable coolers at reduced temperatures to the EPA laboratory in Research Triangle Park, NC.

At the laboratory, an EPA technician made up to eight aliquots (8 mL each) from each urine void; the individual urine aliquots were stored in 10 mL (BPA-free) cryovials (Simport polypropylene T310-10A). The urine samples, solid food, and surface wipes were all stored in laboratory freezers (≤ − 20 °C) until analysis. The drinking water samples were placed into a refrigerator (~4 °C) until chemical extraction (within 1–2 days).

2.4. Sample analysis

The separate analytical methods used to quantify BPA levels in the solid food, drinking water, surface wipe, and urine samples are described below. All chemical analyses of the sampled media were performed at the EPA laboratory in Research Triangle Park, NC, except for the urine samples (Emory University's Rollins School of Public Health environmental laboratory in Atlanta, Georgia). The quality assurance and quality control procedures, including results, for each medium are provided in Appendix A.

2.4.1. Duplicate-diet solid food

Each solid food sample (n = 775) was prepared using a modified QuEChERS (quick, easy, cheap, effective, rugged, and safe) method (Anastassiades et al., 2003; Clifton et al., 2015). Briefly, the samples were homogenized and 2 g amounts placed into 50 mL polypropylene centrifuge tubes. An internal standard solution and a ceramic homogenizer were added to each tube prior to vortex extraction with acetonitrile in combination with magnesium sulfate and sodium acetate extraction salt. The tubes were centrifuged at 4000 RPM for 5 min, and the acetonitrile extract was transferred to a 15-mL polypropylene tube containing graphitized carbon black. The tubes were vortexed to facilitate dispersive solid phase extraction and then centrifuged at 4000 rpm for 5 min. The extract was transferred to a 50-mL tapered glass centrifuge tube and evaporated just to dryness using a parallel evaporator. The extracts were reconstituted with 1 mL of acetonitrile and transferred to autosampler vials. Next, the extracts were silylated by adding 100 µL of Sylon BFT and mixed and heated at 80 °C for 15 min. After cooling, the extracts (1 mL) were mixed again, and BPA concentrations were determined using an Agilent 6890 gas chromatograph-mass selective detector (GC-MSD) equipped with an autosampler. Separation was achieved using a Varian VF-XMS column (20 m × 0.15 mm × 0.15 µm), with helium as the carrier gas. The initial temperature was 75 °C for 2 min., raised to 217 °C at 10 °C/min.

and then to 223 °C at 1 °C/min., and the final temperature of 330 °C was held for 5 min. The ions monitored for BPA were *m/z* 357 (quantifier) and m/z 372 (qualifier). The internal standard used for BPA was BPA $^{13}C_{12}$ with ions m/z 369 and 384 monitored. The estimated limit of quantitation (LOQ) was 1.1 ng/g for BPA in solid food.

2.4.2. Drinking water

Drinking water samples (n = 50) in 1 L polypropylene containers were removed from the refrigerator (within 1–2 days) and warmed to room temperature. The water volume was measured, and the surrogate recovery standard (fipronil des F3) added. After adjustment of the pH to pH = 3, sufficient methanol was added so that the ratio of water: methanol was 10:1 (v:v). BPA was extracted from the water/methanol mixture using a 500 mg C_{18} cartridge that was in-line with an active pump system. The samples were stirred continuously during this process to minimize adherence of BPA to the surface of the containers. After each sample was extracted, BPA was collected by flushing the system (pump lines, SPE cartridge, and polypropylene sample container) with methanol, followed by ethyl acetate, and then hexane. All solvents were combined, and the volume was reduced to approximately 100 µL by evaporation. To this, 3 mL of pH 3 water and 3 mL hexane:toluene 1:1 (v:v) were added. The extracts were partitioned, and the organic layer was collected. The extracts were partitioned two additional times, and each time fresh organic solvents were added, collected, and combined. The internal standard, ($^{13}C_{12}$ Bisphenol A) and 200 µL of pH 3 water were added, and the volume was reduced under nitrogen to 200 µL. Finally, 800 µL of methanol was added to the extracts, and the contents were transferred to autosampler vials. All extracts were stored in a freezer (− 20 °C) until analysis. BPA concentrations were determined using a high-performance liquid chromatograph coupled to a tandem mass spectrometer (LC-MS/MS). The mobile phase was 5 mM ammonium acetate:methanol, (2:8) at a flow rate of 400 µL/min, and the analytical column was C_{18} (3.0 × 150, 3.5 µm). The ions used for BPA were *m/z* 227 (Q1) and m/z 212 (Q3). The internal standard used for BPA was BPA $^{13}C_{12}$ using ions at m/z 239 (Q1) and 224 (Q3). The estimated LOQ for BPA was 0.032 ng/mL in drinking water.

2.4.3. Hard floor surface wipe

The method for the extraction and analysis of the surface wipes has been described in Starr et al., 2017. Briefly, for each participant, the two collected surface wipes (from two different areas of the kitchen) were combined into one sample per sampling week. BPA was extracted from the paired wipe samples (n = 138) using pressurized liquid extraction with hexane:acetone, 25:75 (v/v). The samples were cleaned using a C_{18} cartridge, and the volume reduced to 200 µL under nitrogen. The internal standard, ($^{13}C_{12}$ Bisphenol A), was added, followed by an additional amount of methanol and water such that the final volume was 1 mL with a ratio of aqueous:organic of 6:4. The samples were vortexed (~5 s.), transferred to autosampler vials and stored at -20° C until analysis. The extracts were analyzed by LC-MS/MS using the same settings, solvents, flow rate and column that was used for the analysis of BPA in drinking water described above. The ions used for BPA were *m/z* 227 (Q1) and m/z 212 (Q3). The internal standard used for BPA was BPA $^{13}C_{12}$ using ions at m/z 239 (Q1) and 224 (Q3). The estimated LOQ for BPA was 0.027 ng/cm^2 in the surface wipes.

2.4.4. Urine

One set of the participants' urine aliquots was shipped (8 mL each) in coolers with dry ice overnight to Emory University in Atlanta, Georgia (Morgan et al., 2016a). The urine aliquots were kept in laboratory freezers at ≤ − 20 °C until chemical analysis. For the 24-h urine samples, each urine void (aliquot) was analyzed separately. The urine aliquot was thawed overnight, then 1 mL was placed into a vial, and a labeled standard ($^{13}C_{12}$ bisphenol A) was added. The sample was hydrolyzed with a *β*- glucuronidase/sulfatase (*Helix pomatia*) mixture in 0.1 M acetate buffer for about 16-h at 37 °C. To each sample, 250 µL of a 1 M ammonium acetate and 1 mL of 33% formic acid. Next, the sample was subjected to solid phase extraction (3 cm^3/60 mg OASIS HLB cartridge), and eluted with 1.5 mL methanol (twice), then evaporated to dryness under nitrogen. The dried extract was reconstituted with 1 mL of dichloromethane. Then 0.5 mL of a 0.1 M tetrabutylammonium hydrogen sulfate, 0.05 mL of a 0.2 M sodium hydroxide, and 20 µL of pentafluorobenzyl bromide were added to the vial, and the mixture was vortexed (~ 5 s.). Next, the extract was incubated to form the pentafluorobenzyl ether of BPA, centrifuged, and the dichloromethane (bottom) layer was transferred to another vial, and evaporated to dryness. Finally, the extract was reconstituted with 50 µL of isooctane and transferred to a GC vial. The 2501 urine extracts (1 µL) were quantified for total BPA levels (free plus conjugated) using an Agilent 5977 series GC-MSD using negative chemical ionization (methane as the reagent gas) with a single quadrupole mass spectrometer (MS), equipped with an autosampler. Chromatographic separation was performed with a DB-5 capillary column (J&W Scientific, 30 m, 0.25 mm ID, 0.25 µ film thickness), and the carrier gas was helium. The temperature was initially set at 60 °C, raised to 200 °C at a rate of 20 °C/min, and then to 280 °C at a rate of 10 °C/min. The MS was run in the selected ion-monitoring mode, and the masses selected were *m/z* 407 for BPA and *m/z* 419 for its labeled standard. As an adequate confirmation ion was unavailable, we used tight limits (± 1%) on the relative retention time (BPA/labeled standard) for positive identification of BPA. The estimated LOQ was 0.10 ng/mL for BPA in urine. Quality control and assurance procedures were incorporated into the analyses. Two positive and two negative (blanks) samples were analyzed concurrently with unknown samples and calibrants for each run. Special care was take to avoid BPA contamination of reagents (e.g., use of BPA free water for reagents). NIST SRMs 3672 (smoker urine) and 3673 (nonsmoker urine) were analyzed periodically alongside samples. In general, one of each SRM was analyzed per 100 samples. Our quantified levels of BPA in SRMs 3672 (N = 36) and 3673 (N = 36) were 3.09 ± 0.17 and 1.94 ± 0.18 which were within the NIST tolerance ranges.

CR- and SG-levels were quantified in an identical set of the participants' urine aliquots (8 mL each) at the EPA laboratory (Morgan et al., 2016a). Individual urine aliquots were thawed overnight in a refrigerator (~4 °C). CR-levels were analyzed in each urine aliquot using a modified Jaffé method (Andersen et al., 2014). SG-levels were measured in the urine aliquots using a hand-held refractometer (Atago® model no. 3741) (Andersen et al., 2014).

2.5. Data and statistical analysis

For each type of matrix, sample data values below the LOQ for BPA were replaced with the value of LOQ/$\sqrt{2}$ (Verbovsek, 2011). Descriptive statistics were computed for BPA levels in the solid food, drinking water, and surface wipe samples. Descriptive statistics were also calculated for BPA by urine sample type (FMV, bedtime, 24-h and total) as concentration (ng/mL), SG-adjusted (ng/mL-SG), CR-adjusted (ng/mg), and excretion rate (ng/min) values. The volume of each urine void ranged from 5 mL to 1000 mL (an upper bound based on the size of the urine collection containers). The participants had an average of eight urine voids per sampling day (range = 3 to 11 [an upper bound based on the maximum number of provided collection containers]).

All data values were log-transformed (ln) prior to statistical analysis. Using a one-way random effects model, we estimated the within- and between-person variance components for BPA concentrations by each urine sample type and method (adjusted and unadjusted) over a day, week, and six-weeks. These variance component estimates were then used to calculate ICCs and 95% between and within-person fold-ranges ($_bR_{0.95}$ and $_wR_{0.95}$) for each urine sample type and method over each specified period of time (Morgan et al., 2016a; Rappaport and Kupper, 2008). The ICC is defined as the ratio of the between-person

variance to the total variance; ICCs values can range from 0 (low reliability) to 1 (high reliability). In exposure and epidemiology studies, ICC's are commonly used to signify either poor reproducibility (< 0.40), good reproducibility (0.40–0.75), or excellent reproducibility (> 0.75) of a spot urinary biomarker measurement (Fleiss, 1985; Rosner, 2006). Next, we calculated the number of random spot urine samples per participant that would likely be needed to obtain a reliable BPA concentration estimate (ICC = 0.80) by urine sample type and method for each time period using the following equation by Fleiss (1985):

$$m = (\rho_{r,m}(1-\rho_r))/(\rho_r(1-\rho_{r,m})) \quad (1)$$

where m is the estimated number of random spot BPA urine measurements per participant needed to accurately rank participants in this study cohort, $\rho_{r,m}$ is the specified reliability of the mean (0.80), and ρ_r is the ICC value by urine sample type and method for each specified time period.

Prior to building linear mixed effects models, multicollinearity between predictors (BMI, age and the ln of urinary CR-concentration) were measured using variance inflation factor (VIF). Our VIF values were < 1.3 which indicated there was not significant collinearity (Neter et al., 1996; Griffith and Amerhein, 1997).

SAS version 9.4 (SAS Institute, Cary NC, USA) was used for all linear mixed effects modeling (Proc Mixed, SAS®). We first developed a "urine" model to determine the effects of available (non-environmental matrix) predictors on urinary BPA concentrations (Morgan et al., 2016a). The 50 Ex-R participants were treated in the models as random subjects. Correlation among successive measurements from each subject was accounted for using an autoregressive [AR(1)] variance-covariance structure. This approach enables correlation among residuals to decay exponentially over distance/time. The likelihood ratio test was used to evaluate the relative improvement in model fit when error structure was added through the "repeated" statement (Proc Mixed, SAS®). Nine predictor variables (age, sex, race, BMI, activity level, season, urine sample type, sequence of the participant's voids over time, and ln(CR-level)) were used in the "urine" mixed model. Here, we treated the final urine samples on days 2 and 5 as bedtime voids, and the first sample on days 3 and 6 as FMVs. Initially, all predictors were regressed to ln(BPA) concentration. Manual backwards elimination of individual predictors was used to eliminate non-explanatory variables, and all predictors in the final model had a $p < 0.05$. All models converged with < 10 iterations. The equation for our final model was:

$$y_{ij} = \gamma_{00} + \beta_1\, Gender_j + \beta_2\, Race_j + \beta_3\, Season_j + \beta_4\, Creat_{ij} + \mu_{0j} + r_{ij} \quad (2)$$

The first five terms are fixed effects, γ_{00}, β_1, β_2, β_3, *and* β_4 are fixed coefficients, μ_{0j} is random intercept representing deviations from population intercept for each subject, and the residuals $r_{ij} \sim N(0, \sigma^2)$.

There were a limited number of food samples (n = 775) and surface wipes samples (n = 138) that were collected over the six-week monitoring period (in comparison to the urine samples n = 2501). As such, separate mixed models were developed to focus on the relationship between these environmental measures and urinary BPA values. For the "food" model, the participants' corresponding urinary sample data were averaged (arithmetic mean of natural-space values) over these same sampling time periods. Three types of food models were set to match the participants' ln(BPA food levels) with their ln(urinary BPA levels): 1) Food Model A = the same time period (e.g., BPA food level during period 1 [4:00–11:00 am] compared to the average urinary BPA level during period 1 [4:00–11:00 am]); 2) Food Model B = the next time period (e.g., BPA food level in period 1 [4:00–11:00 am] compared with the average urinary BPA level in period 2 [11:00 am–5:00 pm]); and, 3) Food Model C = two time periods later (e.g., BPA food level in period 1 [4:00–11:00 am] compared with the average urinary BPA level in period 3 [5:00 pm–4:00 am]). In each type of food model (A, B, and C), we also included significant predictors as determined for the aforementioned "urine" regression model. For the "surface wipe" model, the participants' ln(BPA surface wipe) data (day 4) were matched to their corresponding BPA bedtime urine data (day 4) by sampling week; again, significant predictors from the "urine" model were also included in this model. The goodness of model fit of each model was assessed by visualizing the residual diagnostic plots.

The adults' estimated daily dietary intake doses of BPA were calculated by sampling week and overall using the equation by Morgan et al. (2016b):

$$D_F = \frac{\sum_{t=1}^{3}(F_t \times M_t)}{B} \times A \quad (3)$$

where D_F is the estimated daily dose by food intake (ng/kg/day), F_t is the level of BPA measured in the participant's solid food sample (ng/g), M_t is the measured amount (g) of the solid food sample, A is the percent absorption of BPA (100%) in the gut (Volkel et al., 2002), and B is the participant's body weight (kg). The subscript t signifies whether the food sample was collected during sampling periods 1, 2, or 3 each sampling day.

Two reverse dosimetry approaches were also used to estimate body weight-adjusted dose. The first approach utilized urine concentration measures and urine void volumes, as described in Eq. (4). Here, D_{EM} is the estimated daily dose based on excreted mass (ng/kg/day), C_s is the measured concentration of BPA (ng/mL) in sample s, V_s is the total void volume (mL) of sample s, n is the total number of voids in a given 24-h period, E is the percent of BPA dose that is assumed excreted in urine (100%), and B is the participant's body weight (kg).

$$D_{EM} = \frac{\sum_{s=1}^{n}(C_s \times V_s)}{B \times E} \quad (4)$$

This approach (Eq. (4)) is likely not appropriate for calculating BPA dose on sampling days when one or more urine voids were missed by a participant. To overcome this challenge, a second approach (Eq. (5)) utilized the average BPA excretion rate over each 24-h sampling period. This approach relies on the product of the average excretion rate (R in ng/min) and the exact duration of the sampling window (T in min) for a given participant-day, and produces the estimated daily dose (ng/kg/day) based on BPA excretion rate (D_{ER}).

$$D_{ER} = \frac{R \times T}{B \times E} \quad (5)$$

Estimates of D_{EM} and D_{ER} were compared across complete and incomplete collection days via scatterplots, Spearman's rank-order correlations, the Wilcoxon rank-sum test, and the Wilcoxon signed-rank test. Estimates of D_F, D_{EM} (for complete collection days, only) and D_{ER} were compared using cumulative percentile plots and Spearman's rank-order correlations.

3. Results

3.1. Demographic characteristics

Table 1 presents the demographics of the 50 Ex-R participants. The ages ranged from 19 to 50 years old, and 60% of the participants were female. The racial backgrounds of the participants were reported as Hispanic (13%), non-Hispanic black (25%), non-Hispanic white (56%), and other (6%). The BMI data indicated that 34%, 26%, and 40% of the participants were underweight/normal, overweight, and obese, respectively.

3.2. Environmental concentrations of BPA

BPA was detected in 38%, 4%, and 99% of all of the participants'

Table 1
Demographics of the Ex-R adult participants.

Characteristic	N[a]	%[b]
Age		
19–29	22	44
30–39	14	28
40–50	14	28
Sex		
Male	20	40
Female	30	60
Race[c]		
Hispanic	6	13
Non-Hispanic black	11	25
Non-Hispanic white	25	56
Other[d]	3	6
BMI[e]		
Underweight/normal (< 25.0)	17	34
Overweight (25.0–29.9)	13	26
Obese (≥ 30)	20	40

[a] Number of adults.
[b] Percentage of adults.
[c] Race information was collected from 45 out of 50 of the participants (Morgan et al., 2016a).
[d] Other race category included one Native American and two Asians.
[e] BMI (body mass index).

duplicate-diet solid food, drinking water, and hard floor surface wipe samples, respectively. The maximum BPA level in the drinking water was 0.062 ng/mL. Table 2 presents the distributions of BPA concentrations in the solid food and surface wipe samples (by week and total) over the six-week monitoring period. At the 75th percentile, BPA levels in the solid food samples were 2.00 ng/g (week 1), 2.20 ng/g (week 2), and 1.80 ng/g (week 6). The maximum BPA concentration across all solid food samples was 138 ng/g. For the surface wipes collected on the participants' kitchen floors, median concentrations of BPA were 0.46 ng/cm^2 (week 1), 0.56 ng/cm^2 (week 2), and 0.46 ng/cm^2 (week 6). The maximum BPA level across all surface wipe samples was 21.3 ng/cm^2 – this maximum value was approximately two times higher than the next highest measured value (11.4 ng/cm^2).

3.3. Urinary concentrations of BPA

Table 3 presents the distributions of total BPA levels by urine sample type (FMV, bedtime, 24-h, and total) as concentration, SG-adjusted, CR-adjusted, and excretion rate values for 50 Ex-R adults over a six-week monitoring period. BPA was detected in 98% of the total urine samples. For all of the urine samples, median BPA levels were 2.07 ng/mL, 2.20 ng/mL-SG, 2.29 ng/mg, and 2.31 ng/min for concentration, SG-adjusted, CR-adjusted, and excretion rate values, respectively. Results showed that median BPA concentrations were consistently the lowest in FMV samples (1.75 ng/mL, 1.63 ng/mL-SG, 1.64 ng/mg-CR, and 1.38 ng/min) and the highest in 24-h samples (2.12 ng/mL, 2.41 ng/mL-SG, 2.57 ng/mg-CR, and 2.67 ng/min) across all four methods. Similarly, at the 95th percentile BPA levels were the lowest in the FMV urine samples (9.30 ng/mL, 14.3 ng/mL-SG, 15.2 ng/mg-CR, and 12.6 ng/mL) and the greatest in the 24-h samples (12.6 ng/mL, 24.8 ng/mL-SG, 31.3 ng/mg-CR, and 31.5 ng/mL).

3.4. ICC estimates for repeated urinary BPA measurements

Table 4 provides estimates of between and within-person fold ranges and ICCs for repeated measurements of total BPA by urine sample type and method for the 50 Ex-R adults over a day, week, and six weeks. The results showed poor reproducibility (ICC < 0.40) for all urine sample types and methods over all time periods. In general, the ICC estimates for SG-adjusted, CR-adjusted, and excretion rate values for BPA were slightly greater than the ICC estimates for unadjusted values for BPA. Also in Table 4, the highest ICC value of 0.35 occurred for CR-adjusted bedtime voids collected over a week. However, to obtain a reliable average biomarker estimate (ICC = 0.80) for BPA, the results indicated that a minimum of eight bedtime urine voids (an unattainable number) would be needed for each adult over a week. CR-adjusted bedtime voids collected over six weeks required the fewest, realistic number of samples (n = 11) to obtain a reliable biomarker estimate.

3.5. Predictors of urinary BPA concentrations

The results of our final mixed-effects “urine” model are presented in Table 5. Sex, race, season, and CR-level were all significant predictors ($p < 0.05$) of the participants' urinary BPA concentrations. The levels of urinary BPA were significantly higher ($p = 0.007$) in female participants compared to male participants. The urinary BPA concentrations were also significantly different ($p = 0.007$) among the races with the highest concentrations observed in the Hispanic adults. In addition, the participants' urinary BPA levels were significantly different

Table 2
BPA levels in collected environmental media over the six-week monitoring period[a].

Medium	N[b]	%[c]	GM (GSD)[d]	Percentiles					Maximum
				25th	50th	75th	95th	99th	
Duplicate-diet solid food (ng/g)									
Week 1	251[e]	37	–[f]	<	<	2.00	17.2	52.5	91.6
Week 2	263	38	–	<	<	2.20	22.3	104	138
Week 6	261	38	–	<	<	1.80	13.0	56.2	63.1
All	775	38	–	<	<	2.00	17.2	60.9	138
Hard floor surface wipes (ng/cm^2)									
Week 1	44[g]	100	0.54 (3.69)	0.23	0.46	1.23	4.68	21.3	21.3
Week 2	45[h]	100	0.60 (3.09)	0.24	0.56	1.49	4.14	8.19	8.19
Week 6	49[i]	98	0.51 (3.34)	0.22	0.46	1.26	3.67	11.4	11.4
All	138	99	0.55 (3.35)	0.22	0.54	1.28	4.14	11.4	21.3

[a] BPA was detected in 4% of the drinking water samples (maximum value = 0.062 ng/mL).
[b] Number of samples.
[c] Percentage of samples at or above the limit of quantitation (LOQ).
[d] Geometric mean and geometric standard deviation.
[e] Two samples were excluded due to participant collection error.
[f] Not reported because BPA was detected in < 50% of the solid food samples.
[g] Six samples were lost due to a laboratory equipment malfunction.
[h] Four samples were lost due to a laboratory equipment malfunction.
[i] One participant did not provide a surface wipe sample due to a family emergency on week 6.

Table 3
Urinary concentrations of BPA in 50 Ex-R adults over a six-week monitoring period[a].

Sample type[b,c,d]	N[f]	GM (GSD)[g]	Min.	Percentiles						Max.
				5th	25th	50th	75th	95th	99th	
FMV[e]										
ng/mL	294	1.83 (3.17)	<	0.22	0.98	1.75	3.88	9.30	44.0	81.5
ng/mL-SG	293	1.67 (3.40)	<	0.18	0.86	1.63	3.29	14.3	48.1	141
ng/mg	293	1.63 (3.62)	<	0.17	0.83	1.64	3.41	15.2	58.3	133
ng/min	291	1.35 (3.63)	<	0.13	0.63	1.38	2.81	12.6	56.6	134
Bedtime void										
ng/mL	289	1.79 (3.26)	<	0.18	0.96	2.04	3.66	10.2	20.5	38.2
ng/mL-SG	287	1.67 (4.11)	<	0.13	0.73	1.87	3.70	18.4	40.5	94.9
ng/mg	287	1.78 (4.53)	<	0.12	0.77	1.89	4.24	23.6	63.9	162
ng/min	284	1.71 (4.44)	<	0.12	0.73	1.72	4.53	19.4	75.3	96.7
24-h sample										
ng/mL	1886	2.00 (3.41)	<	0.23	1.00	2.12	4.20	12.6	35.9	1021
ng/mL-SG	1866	2.39 (4.06)	<	0.24	1.03	2.41	5.21	24.8	88.6	2100
ng/mg	1866	2.65 (4.56)	<	0.24	1.03	2.57	6.35	31.3	128	3262
ng/min	1875	2.70 (4.53)	<	0.24	1.03	2.67	6.66	31.5	122	2832
All										
ng/mL	2477	1.96 (3.36)	<	0.22	0.99	2.07	4.12	12.2	34.7	1021
ng/mL-SG	2453	2.19 (4.01)	<	0.21	0.99	2.20	4.73	23.3	73.6	2100
ng/mg	2453	2.38 (4.48)	<	0.20	0.97	2.29	5.70	28.0	102	3262
ng/min	2457	2.36 (4.49)	<	0.20	0.94	2.31	5.85	28.1	96.3	2832

[a] Urine data are presented as unadjusted (ng/mL) and as specific-gravity (ng/mL-SG), creatinine (ng/mg), and excretion rate (ng/min) adjusted values.
[b] BPA was detected in 98%, 97%, and 98% of the FMV, bedtime, and 24-h urine samples, respectively.
[c] 18 urine samples were excluded because they failed our quality control standards.
[d] 6 urine samples were not analyzed for BPA levels due to laboratory error.
[e] FMV (first-morning void).
[f] Number of urine samples.
[g] Geometric mean and geometric standard deviation.

Table 4
Components of variance and other associated statistics for BPA concentrations in Ex-R adults by urine sample type and method over a day, week, and six weeks.

Urine sample type[a]	Unadjusted (ng/mL)				SG-adjusted (ng/mL-SG)				CR-adjusted (ng/mg)				Excretion rate (ng/min)			
	${}_{b}R_{0.95}$[b]	${}_{W}R_{0.95}$[c]	ICC[d]	m[e]	${}_{b}R_{0.95}$	${}_{W}R_{0.95}$	ICC	m	${}_{b}R_{0.95}$	${}_{W}R_{0.95}$	ICC	m	${}_{b}R_{0.95}$	${}_{W}R_{0.95}$	ICC	m
One day																
24-h[f]	7.8	89.6	0.17	20	17.4	161	0.24	13	28.8	216	0.28	11	21.0	223	0.24	13
One week																
FMV	1.0	78.1	0.00	–[g]	1.0	133	0.00	–	1.0	166	0.00	–	1.0	142	0.00	–
Bedtime	10.5	68.0	0.24	13	25.6	90.4	0.34	8	33.6	122	0.35	8	18.3	176	0.24	13
24-h	8.7	81.7	0.19	17	17.3	145	0.25	13	24.6	200	0.27	11	18.5	218	0.23	14
Six weeks																
FMV	3.9	75.4	0.09	41	4.3	97.1	0.09	40	5.9	113	0.12	29	6.0	113	0.13	28
Bedtime	6.8	68.1	0.17	20	16.0	122	0.25	12	23.1	152	0.28	11	16.6	168	0.23	14
24-h	7.3	83.5	0.17	20	13.2	133	0.22	14	19.4	184	0.24	13	13.2	133	0.22	15

[a] Bedtime void, first morning void (FMV) or 24-h sample.
[b] Estimated between-person fold range.
[c] Estimated within-person fold range.
[d] Estimated ICC (intraclass correlation coefficient).
[e] Number of random spot urine samples per adult likely required to have a reliable biomarker estimate (ICC = 0.80) (Fleiss, 1985).
[f] Urine data values are limited to the first sampling period of week 1 as this interval had the highest participant completion rates over the six-week period.
[g] Between-person variance was zero resulting in an ICC of zero, so a sample size could not be determined.

($p < 0.0001$) across the four sampling seasons with the greatest levels occurring in the winter season followed by the spring season. Also in this model (Table 5), CR-concentration had a significant ($p = 0.0002$) negative effect (β-coefficient = −0.131) on the participants' urinary BPA concentrations. For the sake of comparison, we also re-ran the above "urine" model substituting the variable urine output (mL/min) for the variable CR-level. The final model had a similar outcome showing that sex, race, season, and urine output were all significant predictors ($p < 0.05$) of the adults' urinary levels of BPA (Appendix B). However, the variable, ln(urine output), had a significant positive effect ($p = 0.011$, β-coefficient = 0.080) on ln(urinary BPA concentrations) – (we note that the correlation between ln(urine output) and ln(CR-level) was 0.83). While significant effects of CR-level and urine output were observed on urinary BPA concentrations, the effect sizes were generally small. For example, considering the reference group, non-Hispanic white males (in the summer), we estimate a BPA concentration of 0.74 ng/mL given a urine output of 0.1 mL/min, and a BPA concentration of 1.07 ng/mL given a urine output of 10 mL/min. So, a 100 × change in urine output is expected to yield a < 2 × change in urinary BPA concentration. When using the same reference group, we estimate a urinary BPA concentration of 1.2 ng/mL given a CR-concentration of 10 mg/dL, and a BPA concentration of 0.66 ng/mL given a CR-concentration of 1000 mg/dL. Therefore, a 100 × change in CR-concentration is expected to yield a ~2 × change in urinary BPA concentration. These results underscore a somewhat limited sensitivity of urinary BPA concentration to changing urine output and CR-level.

As mentioned previously, since the solid food and surface wipe samples were collected on different sampling days, separate models

Table 5
The final regression model of factors (excluding environmental media) influencing the adults' urinary BPA levels.

Factor	β-Coefficient	Standard error	p-Value[a]
Intercept	0.484	0.204	0.019
Creatinine (mg/dL)[b]	− 0.131	0.035	0.0002
Sex[c]			0.007
Female	0.297	0.105	
Male	0	–	
Race[c]			0.007
Hispanic	0.526	0.163	
Other	0.311	0.144	
Non-Hispanic black	0.272	0.134	
Non-Hispanic white	0	–	
Season[c]			< 0.0001
Winter	0.596	0.135	
Spring	0.593	0.131	
Fall	0.253	0.130	
Summer	0	–	

[a] Statistically significant at $p < 0.05$.
[b] Continuous variable (natural log-transformed).
[c] Discrete variable.

were developed to examine relationships between these measures and urinary BPA levels. Three different types of food models (A, B and C) were used to examine the temporal influence of measured BPA levels in the solid food samples, and of other significant variables mentioned above (sex, race, season, and CR-level), on the variability of the adults urinary BPA concentrations (Appendix C). The results showed that BPA levels in the solid food samples did not contribute significantly to urinary BPA concentrations in all three models (p-values ranged from 0.458 to 0.841). Only the variable "CR-level" was a significant predictor ($p < 0.05$) of the adults' urinary BPA concentrations across all three models. In a separate surface wipe model, we examined the collective influence of the measured BPA levels in the surface wipes, along with sex, race, season, and CR-level, on the variability of the adults' urinary BPA concentrations (data not shown). The results showed that surface wipes collected in the participants' kitchens were not significantly associated with urinary BPA levels ($p = 0.233$); only season ($p = 0.012$) and CR-level ($p = 0.043$) were significant predictors of the adults' urinary BPA concentrations.

3.6. Forward and reverse dosimetry estimates for BPA

Table 6 provides the distributions of the estimated dietary intake doses (ng/kg/day) of BPA for the Ex-R adults by sampling week and overall. The participant's estimated median dietary intake doses of BPA were similar across the three sampling weeks (week 1 = 10.7 ng/kg/day, week 2 = 10.3 ng/kg/day (week 2), and week 6 = 10.0 ng/kg/day). However, at the 95th percentile, the participants' estimated dietary intake doses of BPA were at least two times higher for sampling week 2 (306 ng/kg/day) compared to sampling week 1 (107 ng/kg/day) and sampling week 6 (130 ng/kg/day).

In Appendix D, Fig. D.1(A) shows a scatterplot of D_{EM} (estimated dose based on excreted mass [ng/kg/day]) versus D_{ER} (estimated dose based on excretion rate [ng/kg/day]), with a differentiation made for complete and incomplete urine collection days. A strong linear relationship exists across estimates, regardless of completion status (Spearman's Rho = 0.948; $p < 0.0001$ for complete days, only). Yet, an offset is also apparent for measures made on incomplete collection days, indicating an underestimation of BPA dose based on excreted mass. This effect of underestimation is shown more clearly in Appendix D (Fig. D.1(B)), where the ratio of D_{EM} to D_{ER} is plotted separately for complete and incomplete collection days. Here, box-and-whiskers plots show a small but significant ($p < 0.0001$; Wilcoxon signed-rank test) underestimation of D_{ER} by D_{EM} even on complete collection days (median ratio = 0.86). The even spread of the interquartile range (25th percentile = 0.72; 75th percentile = 1.00) and overall range (minimum = 0.35; maximum = 2.09), however, suggest that D_{EM} may over- or underestimate D_{ER} to a similar degree, but often by no more than a factor of 2 in either direction. The box-and-whiskers plot for incomplete collection days (Fig. D.1(B)) shows a clear overall underestimation of D_{ER} by D_{EM} (median ratio = 0.64). Ratios determined for incomplete days were significantly lower than those determined for complete days ($p < 0.0001$; Wilcoxon rank-sum test). Furthermore, as indicated by the overall range (minimum = 0.17; maximum = 1.19), the magnitude of underestimation can be far greater ($> 5\times$) on incomplete collection days when compared to complete collection days. Based on these results, only values of D_{EM} for complete collection days are used for comparisons to D_F. In contrast, all values of D_{ER} are used for subsequent dose estimate comparisons. In Appendix E, Fig. E.1 shows a scatterplot of D_{ER} versus D_F (n = 119), and Fig. 2 (below) shows cumulative percentile plots of D_{ER} (n = 119), D_F (n = 119), and D_{EM} (n = 100). Measurements in each of these figures reflect only those participant-days during which solid food and urine samples were collected over a 24-h period. A significant positive correlation was observed between D_{ER} and D_F (Spearman's Rho = 0.25; p = 0.006). Yet, D_F levels across the cumulative percentile distribution were considerably lower than D_{ER} and D_{EM}. Whereas D_{ER} and D_{EM} tracked reasonably well across the distribution, D_F levels were generally about five times lower than either D_{ER} or D_{EM} between the 25th and 75th percentiles. This indicates that BPA intake via ingestion of solid food comprised only a portion of the total dose, as estimated by urinary BPA measures (assuming 100% urinary excretion).

4. Discussion

Previous research has indicated that dietary ingestion of BPA is a major route of exposure in non-occupationally exposed adults worldwide (Geens et al., 2012; Von Goetz et al., 2017; Wang et al., 2015). This is supported by several studies that have found measurable levels of BPA in total diet samples (typical diet of a population) or in specific food items (e.g., canned foods) purchased from grocery stores (Cao

Table 6
The adults' estimated dietary intake doses of BPA (ng/kg/day) by sampling week and overall.

Sampling interval	N[a]	GM[b]	SD[c]	Min.	Percentiles						Max.
					5th	25th	50th	75th	95th	99th	
Week 1	42	13.2	2.94	1.20	1.70	6.90	10.7	21.7	107	267	267
Week 2	42	15.0	3.79	0.80	3.30	7.00	10.3	30.5	306	774	774
Week 6	42	13.2	3.86	0.10	3.10	6.10	10.0	24.7	130	447	447
All	42	13.7	3.52	0.10	2.90	6.80	10.3	27.7	167	409	774

[a] Number of subjects. Dietary intake doses could not be estimated for 8 out of the 50 participants because their daily mass of food (g) eaten was not recorded in this study. A total of 238 individual solid food samples (representing 42 adults with up to six samples per person) were used for the dose estimates.
[b] Geometric mean.
[c] Geometric standard deviation.

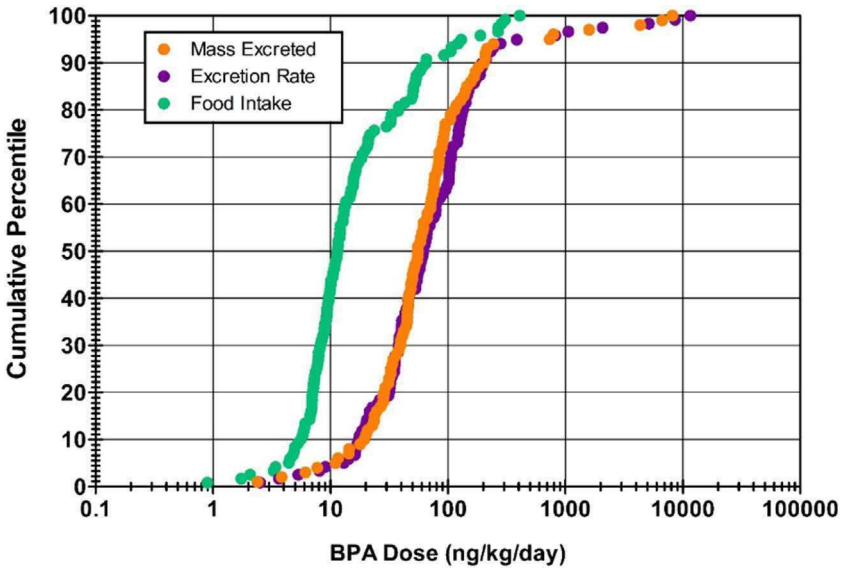

Fig. 2. Cumulative percentile plots for adult BPA dose based on food intake (D_F; n = 119), urinary excretion rate (D_{ER}; n = 119), and excreted mass in urine (D_{EM}; n = 100).

et al., 2011; Mariscal-Arcas et al., 2009; Noonan et al., 2011; Sajiki et al., 2007; Sakhi et al., 2014; Schecter et al., 2010). However, only a few published studies have measured BPA concentrations in the actual consumed diets (foods and beverages) of children (Wilson et al., 2001, 2003, 2007), and no studies have examined BPA in the consumed diets of adults. In our study, conducted in 2009–2011, drinking water and duplicate-diet solid food samples were collected from 50 adult participants in residential environments over a six-week monitoring period in NC (Table 2). BPA was not frequently detected (4%) in the drinking water samples (n = 50); therefore, this source was considered a minor contributor to the adults' total dietary intake of BPA. Our result agrees with Arnold et al. (2013) who reported BPA levels were detected in < 10% of the drinking water samples in 34 different studies conducted in the US between 1990 and 2010. For the Ex-R duplicate-diet solid food samples, BPA was detected (LOD = 1.1 ng/g) in 38% of the 775 samples. At the 95th percentile (Table 2), BPA levels in the solid food samples were 17.2 ng/g, 22.3 ng/g, and 13.0 ng/g for weeks 1, 2, and 6, respectively. The maximum BPA concentration of 138 ng/g occurred in a female participant's solid food sample during one sampling time period. This participant also had the highest maximum BPA level (288 ng/g) in her solid food samples over a 24-h sampling day. Based on this participant's 24-h solid food data, the Ex-R adults' maximum dietary intake dose of BPA (assuming 100% absorption) was 0.77 μg/kg/day. This maximum dietary intake dose was 65 times lower than the established oral reference dose of 50 μg/kg/day by the US EPA's Integrated Risk Information System (IRIS, 1988). However, the Ex-R adults' maximum dietary intake dose of BPA was only 5 times lower than the recently modified Tolerable Daily Intake of 4 μg/kg/day (based on aggregate intake doses) by the European Food Safety Authority (EFSA, 2015; LaKind and Naiman, 2015). Since duplicate-diet liquid food samples were not collected in the Ex-R study, we could not ascertain how much this source may have contributed to the participants' total dietary intake doses of BPA. As the most comparable study, Wilson et al. (2007) did show that median levels of BPA were approximately eight times lower in 48-h duplicate-diet liquid food samples (~0.5 ng/g) compared to 48-h duplicate-diet solid food samples (~4.0 ng/g) for 256 children in NC and Ohio in 2000–2001. As data are scant, more research is necessary to quantify the temporal levels of BPA in the actual consumed diets of adults.

Research has indicated that non-dietary ingestion of dust and/or residues from residential flooring is likely a minor source of adult exposures to BPA (Geens et al., 2012). Only two cross-sectional studies were found in the literature that have measured BPA concentrations in surface wipes collected from hard floors at homes (Clifton et al., 2013; Wilson et al., 2007). Wilson et al. (2007) reported median BPA levels of ~0.05 ng/cm^2 in surface wipes collected from various types of hard floors at 49 homes in NC and OH in 2000–2001. More recently, Clifton et al. (2013) showed slightly lower median BPA concentrations of 0.02 ng/cm^2 in surface wipes collected from kitchen floors at 130 residences in California in 2007–2009. In comparison to the Ex-R study, our median levels of BPA (0.54 ng/cm^2) in 138 hard floor surface wipe samples were an order of magnitude higher than median BPA levels reported in the two prior studies. This is likely attributed to differences in the amount of isopropanol used for the Ex-R wipes (10 mL each) compared to the two previous study wipes (≤ 3 mL each). For our study, using a one-way random effects mixed model, the estimated ICC was 0.79, indicating that a single surface wipe measurement was likely sufficient to characterize the average BPA level on kitchen floors at homes.

Many studies in the US have frequently detected total BPA in the urine of non-occupationally exposed adults in the last decade (Braun et al., 2011; Cantonwine et al., 2015; CDC, 2017; Cox et al., 2016; Philippat et al., 2013; Pollack et al., 2016; Quiros-Alcala et al., 2013; Ye et al., 2015). Our study also frequently detected total BPA (98%) in the urine of Ex-R adults, with a geometric mean (GM) level of 1.96 ng/mL. In comparison to our study, the 2009–2010 National Health and Nutritional Examination Survey (NHANES), a US population-based study, reported slightly lower GM BPA concentrations of 1.79 ng/mL for adults, 20 years of age or older (CDC, 2017). Recently, LaKind and Naiman (2015) showed that GM levels of urinary BPA have significantly decreased for NHANES adults over the past decade (2003–2004 survey, GM = 2.6 ng/mL versus 2011–2012 survey, GM = 1.5 ng/mL). Ye et al. (2015) also showed a significant decline in GM urinary BPA concentrations in a convenience sample of 616 adults in Georgia between 2010 (2.1 ng/mL) and 2014 (0.4 ng/mL). In other studies (2007–2014), conducted outside the contiguous US including Canada, China, Denmark, Germany, Israel, Korea, and Puerto Rico, median urinary BPA levels have ranged from 1.0–3.0 ng/mL in adults (Berman et al., 2014; Fisher et al., 2015; Huo et al., 2015; Kasper-Sonnenberg et al., 2012; Lassen et al., 2013; Meeker et al., 2013; Park et al., 2017). This information confirms there is still widespread exposure of adults to BPA worldwide.

In the Ex-R study, our ICC estimates showed poor reproducibility (< 0.40) of repeated measurements of BPA in the urine samples of adults for all urine sample types (FMV, bedtime, or 24-h) and methods (unadjusted and adjusted) over a day, week, and six weeks. Our results agree with other published studies (Table 7) that have also reported low ICC values for serial measurements of BPA in adults, globally. In the

Table 7
Comparison of ICC estimates of urinary BPA concentrations in non-occupationally exposed adults worldwide.

Country	Study year	Gender	N[a]	Sampling methodology	Sample type	ICC			Reference
						ng/mL	ng/mL-SG	ng/mg	
Belgium	2012	Men & women	8	All voids over four (baseline) days	Spot	0.15	–	0.26	Koch et al. (2014)
					24-h	0.15	–	0.28	
Canada	2009–2010	Women	80	Two spot & two 24-h samples during pregnancy & one spot post-partum	Spot	0.06	0.05	–	Fisher et al. (2015)
					24-h[b]	0.32	0.32	–	
China	1997–2006	Men & women	100	Three spot samples between 0 and 9 years apart	Spot (M)[c]	0.32	–	0.25	Engel et al. (2014)
					Spot (F)	0.07	–	0.13	
Denmark	2008	Men	33	Two spot, three FMV, & three 24-h samples over three months	FMV	0.10	–	–	Lassen et al. (2013)
					Spot	0.42	–	–	
					24-h	0.26	–	0.26	
Netherlands	2004–2006	Women	80	Three spot samples during pregnancy	Spot	0.32	–	0.31	Jusko et al. (2014)
Norway	2007–2008	Women	30	Three spot samples during pregnancy	Spot	0.36	–	0.13	Guidry et al. (2015)
Puerto Rico	2010–2012	Women	105	Three spot samples during pregnancy	Spot	0.27	0.24	–	Meeker et al. (2013)
United States	1996–2001	Women	80	Two FMVs between 1 and 3 yrs. apart	FMV	–	–	0.15	Townsend et al. (2013)
United States	2003–2006	Women	389	Two spot samples during pregnancy & one after birth	Spot	0.25	–	0.10	Braun et al. (2011)
United States	2004–2009	Women	137	Two or more spot samples before and during pregnancy	Spot	–	0.23[e]	–	Braun et al. (2012)
United States	2005–2007	Women	143	Three to five spot samples over two months	Spot	0.04	–	0.04	Pollack et al. (2016)
United States	2005–2008	Women	71	Three spot samples during pregnancy	Spot	0.23	0.11	0.14	Philippat et al. (2013)
United States	1992–2007[d]	Women	90	Two to three FMVs 1 and 3 yrs. apart	FMV	0.09	–	–[f]	Reeves et al. (2014)
United States	2012	Men & women	83	Seven FMVs for one week (males)	FMV	0.15	–	–	Cox et al. (2016)
				14–18 FMVs for two weeks (females)	FMV				
United States[g]	2009–2011	Men & women	50	Six spots (FMVs and bedtime) & six 24-h samples over a six-week period	FMV	0.09	0.09	0.12	This study
					Bedtime	0.17	0.25	0.28	
					24-h	0.17	0.22	0.24	

[a] Number of adults.
[b] Combined data for samples collected on both weekdays and weekends.
[c] Data for 50 males (M) and 50 female (F) reported separately.
[d] These data are from the Women Health Initiative conducted between 1992 and 2007. Data were taken on year 1 and 3 to compare urine data results.
[e] Before pregnancy samples, only.
[f] Authors reported similar ICCs estimates for creatinine-adjusted values as unadjusted values (ICC = 0.09) in this study, but actual data not provided.
[g] Data shown for only ICC estimates over six-weeks, only.

above studies, these low ICC estimates are likely attributed to the episodic exposures of adults to BPA (from various sources) and to its short biological half-life (< 6 h) in the body (Meeker et al., 2013; Volkel et al., 2002). In addition, these low ICC values provide substantial evidence that a single measure of urinary BPA is probably not sufficient to characterize the average short- or long-term exposures of adults in non-occupational settings. In our study, depending on the urine sample type and method used, the results (Table 4) indicated that between 8 and 41 samples would be necessary to obtain a reliable BPA biomarker estimate for an adult over a day, week, or six weeks. CR-adjusted bedtime voids collected over six weeks required the fewest, realistic number of samples (n = 11) to obtain a reliable biomarker estimate. This information suggests that bedtime voids may be the preferred sample type to collect in future studies to adequately assess the BPA exposures in adults.

At least three different mechanisms are believed to control renal elimination of xenobiotic compounds – namely, passive diffusion, filtration and active secretion (Boeniger et al., 1993). Research has indicated that CR is mainly eliminated by renal filtration, and that the rate of excretion (mass/time) is relatively constant (Boeniger et al., 1993). For this type of mechanism, as urine output decreases, CR concentration (mass/volume) increases. Similar elimination mechanisms are believed to govern renal removal of a number of organic chemicals. In the current investigation, however, we found that BPA excretion does not track with CR-excretion – that is, a positive association was not observed between urinary BPA and urinary CR-concentrations. Interestingly, it appears that BPA excretion is somewhat dependent on urine output – meaning as urine output decreases, BPA excretion decreases, or as urine output increases, BPA excretion increases. The consequence of this physiological behavior is less within-person variability in BPA concentration measures when compared to SG- or CR-adjusted levels, or BPA excretion rate levels (as shown in Table 4). By adding additional adjustments for CR, SG, or urine output, it appears that we are introducing variability into the measurements – variability that is likely independent of the actual BPA exposure in question. This variability may help "separate" individuals (in terms of biomarker "reliability"), but the separation is being driven by factors other than BPA exposure. According to Table 4, we observed more between- and within-person variability for urinary BPA when using SG-adjusted, CR-adjusted, and excretion rate values compared to unadjusted concentration values. We also observed a disproportionate increase in between-person variability, which causes larger ICC values and lower "m" values. It is likely that the elevated between-person variance in SG-adjusted, CR-adjusted, and excretion rate levels stems from real between-person differences in CR-elimination (differences based on diet, body mass, etc.) and/or urine output (differences based on fluid intake, activity level, etc.). These biological phenomena are independent of BPA exposure. Thus, inherent biases may exist when using any of these "adjusted" values, despite the benefit of higher ICC and lower "m" values. Therefore, fewer urine samples may be needed when using CR-adjusted, SG-adjusted, or excretion rate measures, but these measures may potentially yield less accurate information about adult exposures to BPA when compared to concentration measures. This information implies that CR-adjusted, SG-adjusted and excretion rate values may be more "reliable", but unadjusted BPA concentration measures may be more accurate. Additional research is needed to understand the factors and processes that govern renal elimination of environmental chemicals, including BPA, that are routinely monitored in human urine.

Results of our final "urine" model (excluding non-environmental matrices) showed that significant predictors ($p < 0.05$) of the Ex-R adults' urinary BPA concentrations were sex, race, season, and CR-level

(Table 5). Of these factors, season of collection was the strongest predictor ($p < 0.0001$) of urinary BPA levels in Ex-R adults. Interestingly, the participant's urinary BPA levels were the highest in the winter season and the lowest in the summer season, but the reason for this remains unclear. Further research is therefore needed to determine the reason(s) for the seasonality of urinary BPA levels. In addition, we found that female participants had significantly higher urinary levels of BPA than male participants in this study. LaKind and Naiman (2015) also reported that sex was a strong predictor of urinary BPA levels in NHANES participants (2003–2010 survey years). In our subsequent regression models, we showed that BPA levels in solid food or surface wipes were not significant predictors of the adults' individual urinary BPA levels. However, when considering measures aggregated over 24-h periods, a significant positive relationship was observed between solid food intake and urine-based estimates of BPA dose. This association was found to exist even though urine-based dose estimates were about five times larger than food-based estimates. As such, BPA in consumed solid food does appear to contribute to a portion of the aggregate urine measures. Specifically, dose estimates based on food intake (D_F median = 11.5 ng/kg/day) were about 20% of those based on urinary BPA measures (D_{EM} median = 55.4 and D_{ER} median = 61.8 ng/kg/day) (Fig. 2). This is an important finding as dietary ingestion is currently considered the dominant exposure route (> 90%) in adults (Geens et al., 2012; Von Goetz et al., 2017; Wang et al., 2015). In support of our finding, LaKind and Naiman (2015) recently reported, using urinary biomonitoring data, a significant decline in the estimated median BPA intakes of NHANES participants from the 2003–2004 survey (~50 ng/kg/day) to the 2011–2012 survey (~25 ng/kg/day). It is suspected that this observed decrease in the dietary intakes of BPA in US adults is partly attributed to the removal of BPA from some food packaging (e.g., can linings) by some US companies starting in the late 2000s (GCCM, 2010; Ye et al., 2015).

5. Conclusion

Based on the urinary biomonitoring data, the results showed that all the Ex-R adults were temporally exposed to BPA in residential settings over a six-week monitoring period in NC 2009–2011. Poor reproducibility (< 0.40) of repeated measurements of BPA occurred in the participants' urine samples for all sample types, methods and time frames. Specific factors (sex, race, season, and CR-level) were identified that significantly impacted the participants urinary BPA concentrations. We found that dietary ingestion of BPA via solid food only accounted for ~20% of the total intake dose of BPA (at the median of the dose distribution) in Ex-R adults. This above information suggests that these adults were likely exposed to other major unidentified (non-diet) sources of BPA.

Acknowledgements

We would like to thank Carry Croghan for her technical assistance with the Ex-R study database and associated datasets. We would also like to thank Lillian Alston, Fu-Lin Chen, Richard Walker, and Erik Andersen for their technical assistance during this study. This work was funded in whole by the US EPA. *Disclaimer*: "*The US EPA through its Office of Research and Development funded and managed the research described here. It has been subjected to Agency review and approved for publication. Although this work was reviewed by US EPA and approved for publication, it may not necessarily reflect official Agency policy. Mention of trade names or commercial products does not constitute endorsement or recommendation for use*."

Conflict of interest

None.

Appendix A

The quality assurance and quality control procedures (including results) used for the solid food, drinking water, surface wipe, and urine samples are described below.

Duplicate-diet solid food

Matrix blank, matrix spike and recovery spike samples were prepared using a previously made homogenized control food mixture (5% fat) that contained mainly organic food items to decrease background residues of the target pyrethroids (not BPA) (Rosenblum et al., 2001; Morgan et al., 2016a). Replicates of this control food mixture (12 g each) were stored in individual 30 mL amber glass jars and kept in laboratory freezers (− 20 °C) until needed. The three types of quality control (QC) samples (above) were prepared using the same jar of control food mixture (12 g). The BPA concentration in the spiked samples was determined by subtracting the background concentration found in the matrix blank. The matrix spikes in food (added before extraction) had a mean percent recovery of 99.5 ± 5.5 (one of 49 samples were excluded due a matrix effect). The mean percent recovery of the BPA spikes added after extraction- was 82.1 ± 6.8 (one of 50 samples were excluded because of an internal standard spiking error). In addition to the matrix-based QC samples, a reagent blank was prepared to assess background levels occurring in lab ware or during sample preparation procedures. Low background levels of BPA occurred in 21% of the reagent blank samples, so background correction in the field samples was necessary. The mean relative percent difference was 9.0 ± 11.4 in duplicate food samples (aliquots of the same field sample). For analytical duplicates (extracts of the same sample), the mean relative percent difference was 3.0 ± 4.1.

Drinking water

All field and laboratory blanks were below the LOQ for BPA. The field spikes had a mean percent recovery of 104 ± 3.8 for BPA (two of six samples were excluded due to spiking errors). For the matrix spikes, the mean percent recovery for BPA was 102 ± 9.0. The SRS results were variable with a mean percent recovery of 117 ± 32.0 (10 additional samples were excluded due to technician laboratory error).

Hard floor surface wipe

All field and laboratory blanks for BPA were below the LOQ. For the field spikes, the mean percent recovery for BPA was 114 ± 7.8 (one additional sample was excluded because no spike was added). The mean percent recovery for the matrix spikes was 99.8 ± 6.7, and the mean percent recovery for the SRS was 92.6 ± 16.3.

Urine

Field and laboratory blanks consisted of pooled urine samples from adult volunteers (Morgan et al., 2016a). Low background levels of BPA occurred in all field blanks (mean = 0.19 ± 0.05 ng/mL) and laboratory blanks (mean = 0.14 ± 0.08 ng/mL). This likely resulted from true background levels of BPA occurring in the pooled urine samples (not sample contamination), therefore, background correction was not made. For the field spikes, a percent relative standard deviation of 1% was observed for BPA. In addition, all reagent blanks were below the LOQ for BPA. For duplicate samples (aliquots of the same urine sample), the mean relative percent difference was 19.6 ± 14.9 for BPA. Lastly, all QC samples had to be within ± 20 of the spiked level for each analytical run to be acceptable (Morgan et al., 2016a).

Appendix B

Table B.1
The final regression model of factors (excluding environmental media) influencing the adults' urinary BPA levels.

Factor	β-Coefficient	Standard error	p-Value[a]
Intercept	− 0.117	0.138	0.397
Urine output (mL/min)[b]	0.080	0.031	**0.011**
Sex[c]			**0.004**
Female	0.324	0.107	
Male	0	–	
Race[c]			**0.017**
Hispanic	0.481	0.164	
Other	0.294	0.145	
Non-Hispanic black	0.226	0.135	
Non-Hispanic white	0	–	
Season[c]			< **0.0001**
Winter	0.610	0.136	
Spring	0.602	0.133	
Fall	0.274	0.130	
Summer	0	–	

[a] Statistically significant at $p < 0.05$.
[b] Continuous variable (natural log-transformed).
[c] Discrete variable.

Appendix C

Table C.1
The final linear mixed-effects models examining the impact of BPA levels in solid food and other selected variables on urinary BPA levels[a].

Factors	Food Model A			Food Model B			Food Model C		
	β-Coefficient	Standard error	p-Value	β-Coefficient	Standard error	p-Value	β-Coefficient	Standard error	p-Value
Intercept	1.877	0.538	**0.0006**[c]	1.623	0.614	**0.009**	2.002	0.717	**0.006**
Creatinine (mg/dL)[b]	− 0.370	0.107	**0.0007**	− 0.302	0.121	**0.013**	− 0.371	0.145	**0.012**
Solid food[b]	− 0.044	0.060	0.458	− 0.013	0.064	0.841	− 0.054	0.080	0.499
Sex[d]			0.063			**0.035**			**0.039**
Female	0.294	0.157		0.375	0.173		0.455	0.213	
Male	0	–		0	–		0	–	
Race[d]			**0.0008**			0.179			0.090
Hispanic	0.927	0.252		0.169	0.283		0.875	0.348	
Other	0.560	0.204		0.474	0.225		0.187	0.262	
Non-Hispanic black	0.352	0.191		0.311	0.212		0.360	0.266	
Non-Hispanic white	0	–		0	–		0	–	
Season[d]			**0.020**			0.219			**0.004**
Winter	0.452	0.193		0.293	0.225		0.352	0.259	
Spring	0.6260.139	0.229		0.490	0.259		0.850	0.304	
Fall	0.139	0.221		0.066	0.254		− 0.362	0.309	
Summer	0	–		0	–		0	–	

[a] The types of food models (A–C) were set to relate the participant's BPA solid food levels with their urinary BPA levels over time: Food Model A = the same time period (e.g., BPA food level during period 1 with average urinary BPA level during period 1); 2) ood odel B = the next time period (e.g., BPA food level in period 1 with urinary BPA level in period 2); and, ood odel C = two time periods later (e.g., BPA food level in period 1 with urinary BPA level in period 3). Urine was log-transformed.
[b] Continuous variable (log-transformed).
[c] Statistically significant variables ($p < 0.05$) are in bold text.
[d] Discrete variable.

Appendix D

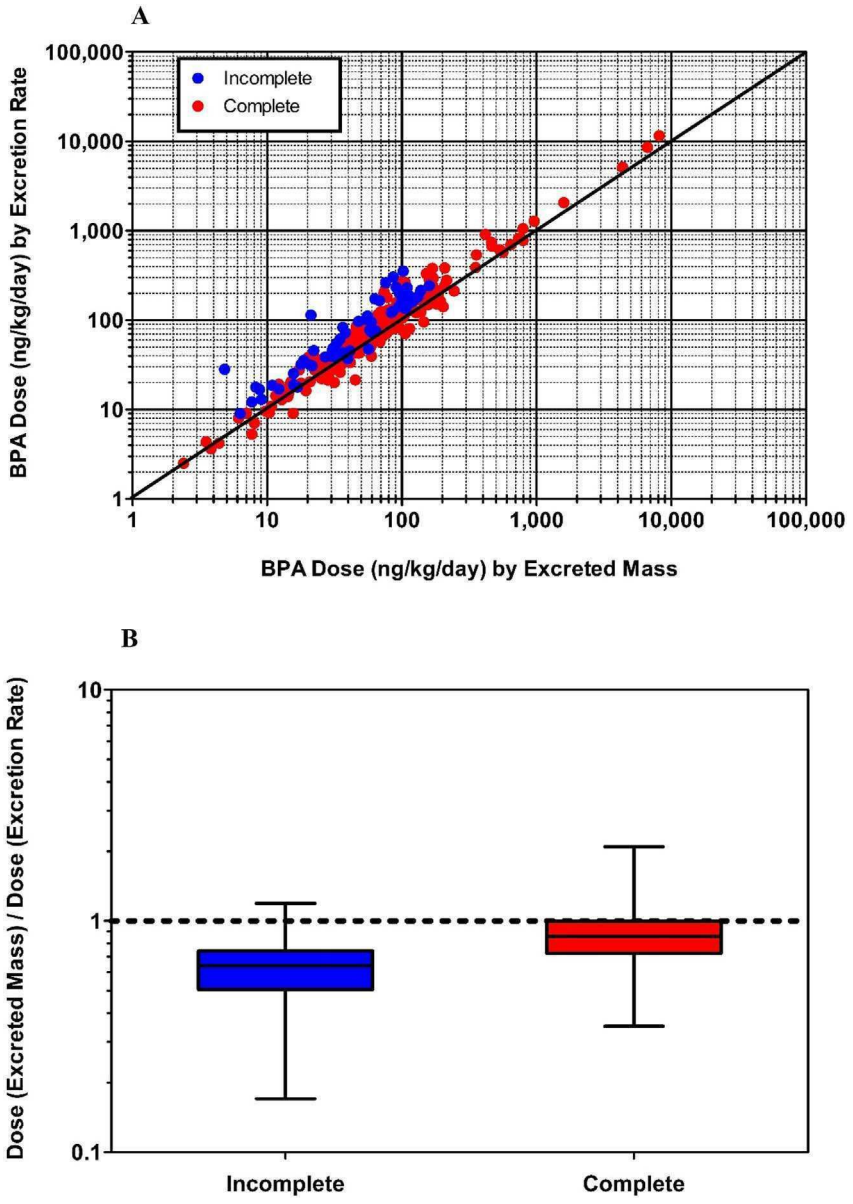

Fig. D.1. Comparison of urinary BPA dose estimates by excreted mass versus excretion rate (A). BPA dose ratio for complete and incomplete 24-h voids (B).

Appendix E

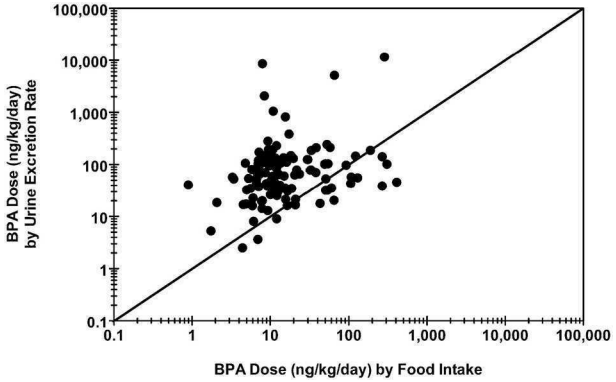

Fig. E.1. Comparison of BPA dose estimates by food intake versus urine excretion rate. Spearman's Rho = 0.25; p = 0.0064.

References

ACC (American Chemistry Council), 2015. About bisphenol A. http://www.bisphenol-a.org/about/ (accessed 09 May 2017).

Anastassiades, M., Lehotay, S.J., Stajnbaher, D., Schenck, F.J., 2003. Fast and easy multiresidue method employing acetonitrile extraction partitioning and dispersive solid phase extraction for determination of pesticide residues in produce. J. AOAC Int. 86, 412–431.

Andersen, E.M., Sobus, J.R., Strynar, M.J., Pleil, J.D., Nakayama, S.F., 2014. Evaluating an alternative method for rapid urinary creatinine determination. J. Toxicol. Environ. Health A 77, 1114–1123.

Arnold, S.M., Clark, K.E., Staples, C.A., Klecka, G.M., Dimond, S.S., Caspers, N., et al., 2013. Relevance of drinking water as a source of human exposure to bisphenol A. J. Expo. Sci. Environ. Epidemiol. 23, 137–144.

Berman, T., Goldsmith, R., Goen, T., Spungen, J., Novack, L., Levine, H., et al., 2014. Demographic and dietary predictors of urinary bisphenol A concentrations in adults in Israel. Int. J. Hyg. Environ. Health 217, 638–644.

Boeniger, M.K., Lowry, L.K., Rosenberg, J., 1993. Interpretation of urine results used to assess chemical exposure with emphasis on creatinine adjustments: a review. Am. Ind. Hyg. Assoc. 54, 615–627.

Braun, J.M., Kalkbrenner, A.E., Calafat, A.M., Bernert, J.T., Ye, X., Silva, M.J., et al., 2011. Variability and predictors of urinary bisphenol A concentrations during pregnancy. Environ. Health Perspect. 119, 131–137.

Braun, J.M., Smith, K.W., Williams, P.L., Calafat, A.M., Berry, K., Ehrlich, S., et al., 2012. Variability of urinary phthalate metabolite and bisphenol A concentrations before and during pregnancy. Environ. Health Perspect. 120, 739–745.

Cantonwine, D.E., Ferguson, K.K., Mukherjee, B., McElrath, T., Meeker, J.D., 2015. Urinary bisphenol A levels during pregnancy and risk of preterm birth. Environ. Health Perspect. 123, 895–901.

Cao, X.L., Perez-Locas, C., Dufresne, G., Clement, G., Popovic, S., Beraldrin, F., et al., 2011. Concentrations of bisphenol A in the composited food samples from the 2008 Canadian total diet study in Quebec City and dietary intake estimates. Food Addit. Contam. 28, 791–798.

CDC (Centers for Disease Control and Prevention), 2017. Fourth National Report on Human Exposure to Environmental Chemicals; Updated Tables. vol. 1 (https://www.cdc.gov/exposurereport/pdf/FourthReport_UpdatedTables_Volume1_Jan2017.pdf, accessed 09 May 2017).

Clifton, M.S., Wargo, J.P., Weathers, W.S., Colon, M., Bennett, D.H., Tulve, N.S., 2013. Quantitative analysis of organophosphate and pyrethroid insecticides, pyrethroid transformation products, polybrominated diphenyl ethers and bisphenol A in residential surface wipe samples. J. Chromatogr. A 273, 1–11.

Clifton, M.S., Wargo, J.P., Morgan, M.K., 2015. A robust, high throughput method for measurement of triclosan and bisphenol A residues in duplicate diet samples. In: Published Abstract at the 36th National Meeting of the Society of Environmental Toxicology and Chemistry, Salt Lake City, UT.

Cox, K.J., Porucznik, C.A., Andersen, D.J., Brozek, E.M., Szczotka, K.M., Bailey, N.M., et al., 2016. Exposure Classification and Temporal Variability in Urinary Bisphenol A Concentrations Among Couples in Utah – The HOPE Study. 124. pp. 498–506.

Dekant, W., Volkel, W., 2008. Human exposure to bisphenol A by biomonitoring; methods, results and assessment of environmental exposures. Toxicol. Appl. Pharmacol. 228, 114–134.

Dotson, R.E., Nishioka, M., Standley, L.J., Perovich, L.J., Brody, J.G., Rudel, R.A., 2012. Endocrine disruptors and asthma-associated chemicals in consumer products. Environ. Health Perspect. 120, 935–943.

EFSA (European Food Safety Authority), 2015. Scientific opinion on the risks to public health related to the presence of bisphenol A (BPA) in foodstuffs. EFSAJ 13, 3978.

Engel, L.S., Buckley, J.P., Yang, G., Liao, L.M., Satagopan, J., Calafat, A.M., et al., 2014. Predictors and variability of repeat measurements of urinary phenols and parabens in a cohort of Shanghai women and men. Environ. Health Perspect. 122, 733–740.

Fisher, M., Arbuckle, T.E., Mallick, R., LeBlanc, A., Hauser, R., Feeley, M., et al., 2015. Bisphenol A and phthalate metabolite urinary concentrations: daily and across pregnancy variability. J. Expo. Sci. Environ. Epidemiol. 25, 231–239.

Fleiss, J., 1985. The Design and Analysis of Clinical Experiments. John Wiley & Sons, New York, NY, USA.

GCCM (Green Century Capital Management), 2010. Safer packaging: ranking packaged food companies on BPA 2010. http://greencentury.com/wp-content/uploads/2013/05/bpareport2010.pdf (accessed 23 Aug 2017).

Geens, T., Aerts, D., Berthot, C., Bourguignon, J.P., Goeyens, L., Lecomte, P., et al., 2012. A review of dietary and non-dietary exposure to bisphenol A. Food Chem. Toxicol. 50, 3725–3740.

Gerona, R., Pan, J., Zota, A., Schwartz, J., Friesen, M., Taylor, J., et al., 2016. Direct measurement of Bisphenol A (BPA), BPA glucuronide and BPA sulfate in a diverse and low-income population of pregnant women reveals high exposure, with potential implications for previous exposure estimates: a cross-sectional study. Environ. Health 15 (1), 50.

Griffith, D.A., Amerhein, C.G., 1997. Multivariate Statistical Analysis for Geographers. Prentice Hall, New Jersey.

Guidry, V.T., Longnecker, M.P., Aase, H., Eggesbo, M.E., Zeiner, P., Reichborn-Kjennerud, T., et al., 2015. Measurement of total and free urinary phenol and paraben concentrations over the course of pregnancy: assessing reliability and contamination of specimens in the Norwegian mother and child cohort study. Environ. Health Perspect. 123, 705–711.

Huo, W., Xia, W., Wan, Y., Zhang, B., Zhou, A., Zhang, Y., et al., 2015. Maternal urinary Bisphenol A levels and infant low birth weight: a nested case–control study of the Healthy Baby Cohort in China. Environ. Int. 85, 96–103.

IRIS (Integrated Risk Information System), 1988. Bisphenol A (CASRN 80-5-7). https://www.epa.gov/iris (accessed 11 May 2017).

Jusko, T.A., Shaw, P.A., Snijder, C.A., Pierik, F.H., Koch, H.M., Hauser, R., et al., 2014. Reproducibility of urinary bisphenol A concentrations measured during pregnancy in the Generation R study. J. Expo. Sci. Environ. Epidemiol. 24, 532–536.

Kasper-Sonnenberg, M., Wittsiepe, J., Koch, H.M., Fromme, H., Wilhelm, M., 2012. Determination of bisphenol A in urine from mother-child pairs–results from the Duisburg Birth Cohort Study, Germany. J. Toxicol. Environ. Health A 75, 429–437.

Kissel, K.C., Curl, C.L., Kedan, G., Lu, C., Griffith, W., Barr, D.B., et al., 2005. Comparison of organophosphorus pesticide metabolite levels in single and multiple daily urine samples collected from preschool children in Washington State. J. Expo. Anal. Environ. Epidemiol. 15, 164–171.

Koch, H.M., Aylward, L.L., Hays, S.M., Smolders, R., Moos, R.K., Cocker, J., et al., 2014. Inter- and intra-individual variation in urinary biomarker concentrations over a 6-day sampling period. Part 2: personal care product ingredients. Toxicol. Lett. 231, 261–269.

LaKind, J.S., Naiman, D.Q., 2008. Bisphenol A (BPA) daily intakes in the United States: estimates from the 2003–2004 NHANES urinary BPA data. J. Expo. Sci. Environ. Epidemiol. 18, 608–615.

LaKind, J.S., Naiman, D.Q., 2015. Temporal trends in bisphenol A exposure in the United States from 2003–2012 and factors associated with BPA exposure: spot samples and urine dilution complicate data interpretation. Environ. Res. 142, 84–95.

Lassen, T.H., Frederiksen, H., Jensen, T.K., Peterssen, J.H., Main, K.M., Skakkebaek, N.E., et al., 2013. Temporal variability in urinary excretion of bisphenol A and seven other phenols in spot, morning, and 24-h urine samples. Environ. Res. 126, 64–170.

Liao, C., Kannan, K., 2011. Widespread occurrence of bisphenol A in paper and paper products implications for human exposure. Environ. Sci. Technol. 45, 9372–9379.

Loganathan, S.N., Kannan, K., 2011. Occurrence of bisphenol A in indoor dust from two locations in the Eastern United States and implications of human exposure. Arch. Environ. Contam. Toxicol. 61, 68–73.

Mariscal-Arcas, M., Rivas, A., Granada, A., Monteagudo, C., Murcia, M.A., Olea-Serrano, F., 2009. Dietary exposure assessment of pregnant women to bisphenol-A from cans and microwave containers in Southern Spain. Food Chem. Toxicol. 47, 506–510.

Meeker, J.D., Cantonwine, D.E., Rivera-Gonzalez, L.O., Ferguson, K.K., Mukherjee, B., Calafat, A.M., et al., 2013. Distribution, variability, and predictors of urinary concentrations of phenols and parabens among pregnant women in Puerto Rico. Environ. Sci. Technol. 47, 3439–3447.

Morgan, M.K., Jones, P.P., Calafat, A.M., Ye, X., Croghan, C.W., Chuang, J.C., et al., 2011. Assessing the quantitative relationships between preschool children's exposures to bisphenol A by route and urinary biomonitoring. Environ. Sci. Technol. 45, 5309–5316.

Morgan, M.K., Sobus, J.R., Boyd Barr, D., Croghan, C.W., Chen, F., Walker, R., et al., 2016a. Temporal variability of pyrethroid metabolite levels in bedtime, morning, and 24-hr urine samples for 50 adults in North Carolina. Environ. Res. 144, 81–91.

Morgan, M.K., MacMillan, D.K., Zehr, D., Sobus, J., 2016b. Pyrethroid insecticides and their environmental degradates in repeated duplicate-diet solid food samples of 50 adults. J. Expo. Sci. Environ. Epidemiol. 1–6. http://dx.doi.org/10.1038/jes.2016.69. (Epub ahead of print).

Neter, J., Kutner, M.H., Nachtsheim, C.J., Wasserman, W., 1996. Applied Linear Statistical Models. WCB McGraw-Hill, MA.

Noonan, G.O., Ackerman, L.K., Begley, T.H., 2011. Concentration of bisphenol A in highly consumed canned foods on the US Market. J. Agric. Food Chem. 59, 7178–7185.

Park, C., Choi, W., Hwang, M., Lee, Y., Kim, S., Yu, S., et al., 2017. Associations between urinary phthalate metabolites and bisphenol A levels, and serum thyroid hormones among the Korean adult population - Korean National Environmental Health Survey (KoNEHS) 2012–2014. Sci. Total Environ. 584-585, 950–957.

Philippat, C., Wolff, M.S., Calafat, A.M., Ye, X., Bausell, R., Meadows, M., et al., 2013. Prenatal exposures to environmental phenols: concentrations in amniotic fluid and variability in urinary concentrations during pregnancy. Environ. Health Perspect. 121, 1225–1231.

Pollack, A.Z., Perkins, N.J., Sjaarda, L., Mumford, S.L., Kannan, K., Philippat, C., et al., 2016. Variability and exposure classification of urinary phenol and paraben metabolite concentrations in reproductive-aged women. Environ. Res. 151, 513–520.

Quiros-Alcala, L., Eskenazi, B., Bradman, A., Ye, X., Calafat, A.M., Harley, K., 2013. Determinants of urinary bisphenol A concentrations in Mexican/Mexican American pregnant women. Environ. Int. 59, 152–160.

Rappaport, S.M., Kupper, L.L., 2008. Quantitative Exposure Assessment. Publisher: SM Rappaport El Cerrito, USA.

Reeves, K.W., Luo, J., Hankinson, S.E., Hendryx, M., Margolis, K.L., Manson, J.E., et al., 2014. Within-person variability of urinary bisphenol-A in postmenopausal women. Environ. Res. 135, 285–288.

Rezg, R., El-Fazaa, S., Gharbi, N., Mornagui, B., 2014. Bisphenol A and human chronic diseases: current evidences, possible mechanisms, and future perspectives. Environ. Int. 64, 83–90.

Rochester, J.R., 2013. Bisphenol A and human health: a review of the literature. Reprod. Toxicol. 42, 132–155.

Rosenblum, L., Hieber, T., Morgan, J., 2001. Determination of pesticides in composite dietary samples by gas chromatography/mass spectrometry in the selected ion monitoring mode by using a temperature-programmable large volume injector with preseparation column. J. AOAC Int. 84, 891–900.

Rosner, B., 2006. Fundamentals of Biostatistics, 6th edition. Duxbury Press, Pacific Grove, CA.

Rudel, R.A., Camann, D.E., Spengler, J.D., Korn, L.R., Brody, J.G., 2003. Phthalates, alkylphenols, pesticides, polybrominated diphenyl ethers, and other endocrine-

disrupting compounds in indoor air and dust. Environ. Sci. Technol. 37, 4643–4663.
Sajiki, J., Miyamoto, F., Fukata, H., Mori, C., Yonekubo, J., Hayakawa, K., 2007. Bisphenol A (BPA) and its source in foods in Japanese Markets. Food Addit. Contam. 24, 103–112.
Sakhi, A.K., Lillegaard, I.T., Voorspoels, S., Carlsen, M.H., Loken, E.B., Brantsæter, A.L., et al., 2014. Concentrations of phthalates and bisphenol A in Norwegian foods and beverages and estimated dietary exposure in adults. Environ. Int. 73, 259–269.
Schecter, A., Malik, N., Haffner, D., Smith, S., Harris, T.R., Paepke, O., et al., 2010. Bisphenol A (BPA) in US food. Environ. Technol. Sci. 44, 9425–9430.
Schug, T., Birnbaum, L.S., 2014. Human health effects of bisphenol A. In: Toxicants in Food Packaging and Household Plastics. Molecular and Integrative Toxicology. Springer-Verlag, London (Chapter 1).
Starr, J.M., Graham, S.E., Li, W., Gemma, A.A., Morgan, M.K., 2017. Variability of Pyrethroid Concentrations on Hard Surface Kitchen Flooring in Occupied Housing. (submitted).
Thayer, K.A., Doerge, D.R., Hunt, D., Schurman, S.H., Twaddle, N.C., Churchwell, M.I., et al., 2015. Pharmacokinetics of bisphenol A in humans following a single oral administration. Environ. Int. 83, 107–115.
Townsend, M.K., Franke, A.A., Li, X., Hu, F.B., Eliassen, A.H., 2013. Within-person reproducibility of urinary bisphenol A and phthalate metabolites over a 1 to 3-year period among women in the Nurses' Health Studies: a prospective cohort study. Environ. Health 12, 80.
Vandenberg, L.N., Hauser, R., Marcus, M., Olea, N., Welshons, W.V., 2007. Review: human exposure to bisphenol A (BPA). Reprod. Toxicol. 24 (139), 177.
Verbovsek, T., 2011. A comparison of parameters below the limit of detection in geochemical analyses by substitution methods. Mater. Geoenviron. 58, 393–404.
Volkel, W., Colnot, T., Csanady, G., Filser, J., Dekant, W., 2002. Metabolism and kinetics of bisphenol A in humans at low doses following oral administration. Chem. Res. Toxicol. 15, 1281–1287.
Von Goetz, N., Pirow, R., Hart, A., Bradley, E., Poças, F., Arcella, D., et al., 2017. Including non-dietary sources into an exposure assessment of the European Food Safety Authority: the challenge of multi-sector chemicals such as Bisphenol A. Regul. Toxicol. Pharmacol. 85, 70–78.
Wang, W., Abualnaja, K., Asimakopoulos, A., Covaci, A., Gevao, B., Johnson-Restrepo, B., et al., 2015. A comparative assessment of human exposure to tetrabromobisphenol A and eight bisphenols including bisphenol A via indoor dust ingestion in twelve countries. Environ. Int. 83, 183–191.
Wilson, N.K., Chuang, J.C., Lyu, C., 2001. Levels of persistent organic pollutants in several child daycare centers. J. Expo. Anal. Environ. Epidemiol. 1, 449–458.
Wilson, N.K., Chuang, J.C., Lyu, C., Menton, R., Morgan, M.K., 2003. Aggregate exposures of nine preschool children to persistent organic pollutants at day care and at home. J. Expo. Anal. Environ. Epidemiol. 13, 187–202.
Wilson, N.K., Chuang, J.C., Lordo, R., Morgan, M.K., Sheldon, L.S., 2007. An observation study of the potential exposures of preschool children to pentachlorophenol, bisphenol-A, and nonylphenol at home and daycare. Environ. Res. 103, 9–20.
Ye, X., Wong, L.Y., Bishop, A.M., Calafat, A.M., 2011. Variability of urinary concentrations of bisphenol A in spot samples, first morning voids, and 24-hour collections. Environ. Health Perspect. 119, 983–988.
Ye, X., Wong, L.Y., Kramer, J., Zhou, X., Jia, T., Calafat, A.M., 2015. Urinary concentrations of bisphenol A and three other bisphenols in convenience samples of U.S. adults during 2000–2014. Environ. Sci. Technol. 49, 11834–11839.

STAA Application: Record of Percentage of Agreement: Carry Croghan

3

Label: 10 years (Capstone approach) (10 years) Expires: Thu 4/11/2030 12:04 PM

Croghan, Carry
Mon 4/13/2020 12:04 PM
Morgan, Marsha

The author agrees with her designated percentage of 2% contribution

...

STAA Application: Record of Percentage of Agreement: Fu-Lin Chen

1

...

Label: 10 years (Capstone approach) (10 years) Expires: Mon 4/8/2030 4:22 PM

FC

Fu-Lin Chen <fulinc100@gmail.com>
Fri 4/10/2020 4:22 PM
Morgan, Marsha

> The author agrees with his designated percentage of 1% contribution.
> My contact information is "fulinc100@gmail.com"
> My last day to work in EPA is December 31, 2017.
>
> Fu-Lin chen

STAA Application: Record of Percentage of Agreement: Erik Andersen

1

From: Erik Andersen <eanderse4@gmail.com>
Sent: Thursday, April 9, 2020 2:07 PM
To: Morgan, Marsha <morgan.marsha@epa.gov>
Subject: Re: STAA Application: Record of Percentage of Agreement: Erik Andersen

Hey Marsha,

It is good to hear from you. I can only guess times at the EPA have been other than optimal based on the current political environment. I hope you are doing well and thank you for including me in the STAA award.

Consider this my confirmation email in regards to the publications annotated as well as the percentages assigned in this email from Dr Marsha Morgan.

STAA Application: Record of Percentage of Agreement: Erik Andersen

1

I have assigned your % of Total Effort = **1%**. Please reply with the following required statement: "The author agrees with his designated percentage of 1% contribution". Also, provide me with your full contact info and date (month and year) of EPA separation. **Provide this info by April 15, 2020.**

I have also attached an Excel file that provides the % of Total Effort that I have assigned to all co-authors and some pertinent STAA guidelines for authors (if you have questions).

Thank you,

Marsha

[External] EPA STAA Application: Record of Percentage of Agreement: Dana Boyd Barr

1

Label: 10 years (Capstone approach) (10 years) Expires: Sun 4/7/2030 1:43 PM

D

dbbarr@emory.edu
Thu 4/9/2020 1:43 PM
Morgan, Marsha

Thanks Marsha. I agree with my designated percentage of 10% contribution. My contact information is given below. I hope you are doing well and staying safe. Best of luck to you on the award.

Best,
Dana

STAA Application: Record of Percentage of Agreement: Richard Walker

1

Label: 10 years (Capstone approach) (10 years) Expires: Sun 4/7/2030 12:58 PM

WR

Walker, Richard
Thu 4/9/2020 12:58 PM
Morgan, Marsha

I coauthor Richard Walker agree with my designated percentage of 1% contribution.

My contact information is : **At work:**

Richard Walker
Environmental Health Scientist (SEE)
Environmental Protection Agency (EPA)
Office of Research and Development (ORD))
Center of Environmental Measurement and Modeling (CEMM)
Air Methods & Characterization Division (AMCD)

STAA Application: Record of Percentage of Agreement: James Starr

1

Label: 10 years (Capstone approach) (10 years) Expires: Sun 4/7/2030 12:48 PM

SJ

Starr, James
Thu 4/9/2020 12:48 PM
Morgan, Marsha

Marsha,

"The author agrees with his designated percentage of 10% contribution".

James Starr
ORD/CEMM/WECD/MMB
RTP, NC 27711
919-541-4608
Starr.james@epa.gov

STAA Application: Record of Percentage of Agreement: Matthew Scott Clifton

1

Label: 10 years (Capstone approach) (10 years) Expires: Sun 4/7/2030 12:45 PM

CM

Clifton, Matthew
Thu 4/9/2020 12:45 PM
Morgan, Marsha

Hi Marsha,

"The author agrees with his designated percentage of 3% contribution".

My full contact info is below.

Thanks!
Scott

M. Scott Clifton
Physical Scientist
Multimedia Methods Branch

STAA Application: Record of Percentage of Agreement: Lillian Alston

1

AM

Alston, Lillian M.
Thu 4/9/2020 12:28 PM
Morgan, Marsha

Hi Marsha:

It's good to hear from you! I hope you doing well. I have gone by your office several times to say "Hi", but saw you weren't in. It's hard to keep up with you.
Now we all know where we are "staying at home" and enjoying the teleworking.

Thanks for providing this information. Please let me know, if I need to include or exclude anything per your email request for the 2020 STAA.

Statement: - "The author agrees with her designated percentage of 1% contribution".

STAA Application: Record of Percentage of Agreement: Denise MacMillan

1

Label: 10 years (Capstone approach) (10 years) Expires: Sun 4/7/2030 11:40 AM

MD

MacMillan, Denise
Thu 4/9/2020 11:40 AM
Morgan, Marsha

Marsha,

I agree with my designated percentage of 10% contribution.

My contact information follows:
Denise MacMIllan, PhD
Research Chemist
ORD-CCTE-CCED-AACMB
109 TW Alexander Dr MD D305-02
Durham, NC 27711
O: 919-541-4128
M: 919-397-8038

STAA Application: Record of Percentage of Agreement: Maliha Nash

1

NM

Nash, Maliha
Thu 4/9/2020 11:33 AM
Morgan, Marsha

Good Morning Marsha,

Good to hear from you and hope all are OK in your side.

I am glad that you are putting the STAA.

I agree for the designated percentage of 10% contribution.

My contact is:

Research Statistcian
Pacific Coastal Ecology Branch
Western Ecology Division, National Health & Environmental Effects Laboratory
US Environmental Protection Agency

One of the co-authors Dan Zehr passed away a few years ago; he was given a 1% contribution.

Table of Contents

General_Authors_Publications.....2
LI-264101_GriffithMB2017-EnvironToxicolChem-final.....8
LI-264101_GriffithMB2017-EnvironToxicolChem-SupplTablesS1-S9.....33
LI-264101_MEMO-RecordPercentAgreement_mbgriffith.....75
Papers_that_Cite_GriffithMB2017-EnvironToxicolChem.....76
GriffithMB2014-FreshwSci.....80

United States Environmental Protection Agency
Washington, DC 20460

STAA REPORT FOR THE SCIENTIST NOMINATIONS

General Information:

Nomination ID/App ID:	20-073
Research Category Primary:	Review Articles (RA)
Research Category Secondary:	Ecological Research (ER)
Laboratory/Office Name:	ORD
Nomination Entered By:	Michael Griffith

Eligibility Checklist:

[Y] The nominated publication(s) has not been submitted to a previous STAA competition.

[Y] The nominated publication(s) was published on or before January 1, 2017 and on or after January 1,2012

[Y] The principal author was an EPA employee or a PHS employee assigned to EPA when the research was performed

[Y] The EPA authors (includes PHS employees assigned to EPA) contributed collectively a minimum of 50% toward the publication(s)

Nominating Official Name:	Kevin Oshima
Nominating Official Title:	BIOLOGIST
Nominating OfficialEmail:	oshima.kevin@epa.gov
STAA Coordinator Name:	Kathleen Wiser
STAA Coordinator Email:	wiser.kathi@epa.gov

Justifications:

Justification 1:

This literature review was completed to assist toxicologists and ecologists in the Office of Water and Office of Research and Development in interpreting their toxicological and biotic data in support of EPA's Strategic Goal 2: Protecting America's Waters. Increased salinity has become a widespread anthropogenic stressor in freshwater streams, rivers and lakes worldwide. It had been assumed that increased salinity effects were largely the result of osmotic effects, but standard toxicological studies have shown that the effects of salinity in freshwater animals are not that simple and can depend, in part, on the mixture of additional ions and the type of animal. Unlike xenobiotic chemicals, these major ions [i.e., hydrogen (H^+), sodium (Na^+), potassium (K^+), calcium (Ca^{2+}), magnesium (Mg^{2+}), chloride (Cl), bicarbonate (HCO_3), and sulfate (SO_4^{2})] have natural metabolic roles and functions in animals, and salinity is a natural gradient from freshwater to estuarine to marine environments along which evolution has occurred. Physiologists have recognized that most freshwater animals are hyper-regulators that maintain intercellular and blood or hemolymph ion concentrations that are greater than those found in most natural freshwaters. In addition, proteins called permeases help to maintain these internal concentrations by the active or passive transport, exchange, or cotransport of specific ions across otherwise, relatively impermeant or tight epithelial membranes, such as in the gills of fish, Crustacea or Mollusca; the anal papillae, chloride epithelia or other external structures of aquatic insect nymphs; intestinal systems or renal systems. Moreover, the mechanisms of other inorganic constituent effects, such as low pH, the effect of pH on the toxicity of ammonia (NH_3), and the bioavailability of nitrite and metals, are related to the transport of hydrogen, ammonia, chloride and calcium ions, respectively, by different ion transporters. However, as I recognized from a comment made by a colleague, many toxicologists have little training in physiology and less familiarity with the recent biochemical research on the identity and function of these ion transporter proteins. Conversely, most physiological research in ionoregulation is focused on single species and lacks the across taxa synthesis required for a full understanding the effects of increased salinity on freshwater communities and ecosystems. I conducted this literature survey to bring together the literature on osmoregulation and ionoregulation in a single resource and do so from the perspective of the four primary groups of freshwater animals, teleost fish, Crustacea, Mollusca and aquatic insects, to inform toxicologists and ecologists, help them interpret their laboratory and field data, and ultimately inform decisions on how to regulate increased salinity in freshwaters, such as streams, rivers, and lakes. In addition, the literature survey identified a data gap related to the transport of sulfate, which has been less studied by physiologists, but is an elevated ion in some freshwaters, which we pursued in more recent research.

Justification 2A:

n/a

Justification 2B:

2016 STAA:

Griffith, M.B. 2014. Natural variation and current reference for specific conductivity and major

ions in wadeable streams of the conterminous USA. Freshwater Science 33(1):1-17.

Honorable Mention

Justification 2C:

While both papers are related to salinity and major ions in freshwaters, Griffith (2014) was about the ranges of specific conductivity (i.e., a measure of salinity), pH, and the concentrations of individual ions (i.e., listed in Justification 1) measured in streams of different Level III ecoregions across the conterminous by EPA's biomonitoring surveys (i.e., the acid precipitation surveys through EMAP to the national stream surveys). The intent was to synthesize the current patterns of variation in salinity and specific ions in stream among the ecoregions and summarize current background levels. Conversely, Griffith (2016), the current review paper, synthesizes information on the physiology of osmoregulation and ionoregulation of these major ions in four different freshwater animal groups to support interpretation of laboratory data on specific ion toxicity.

Justification 2D:

I have attached a copy of Griffith (2014), which was previously nominated for a STAA Award, not as a nominated paper but as supplemental information for the presently nominated paper, "Toxicological perspective on the osmoregulation and ionoregulation physiology of major ions by freshwater animals: Teleost fish, Crustacea, aquatic insects and Mollusca", because the paper are broadly related. However, the two papers address different aspects of major

ions in freshwater ecosystems. The rather extensive supplemental tables and figures for Griffith (2014) that present the data by ecoregion are not included but are available.

Justification 2E:

n/a

Justification 3A:

I have not received any formal recognition for this paper, like an award, but I have received some more informal recognition. I was asked by Dr. Ben Kefford, a professor at the University of Canberra, Australia, whose laboratory works on the effects of salinity and other contaminants on freshwater ecosystems to be an outside reviewer for a student's dissertation. I did this on my own time and without renumeration.

At last count, this paper has been cited by 34 journal articles, 7 theses or dissertations and 1 book-chapter. A list of these papers may be found in the file, "Papers that Cite GriffithMB2017-EnvironToxicolChem.docx", that is appended to this nomination. On Research Gate, the paper has had 183 reads.

Justification 3B:

I am not a physiologist by training. My undergraduate training was in biology and included coursework in organismal physiology and cell biology. However, this training preceded most of the recent research on the biochemistry and molecular biology of the transporter proteins central to this literature review, and my other training and experience are in freshwater ecology. As a result, I chose to ask an established physiologist to review the manuscript prior to my submitting it to a journal. The intent was in part to have him check whether I missed anything or misunderstood the papers that I reviewed. Therefore, concurrent with the internal review and clearance of the manuscript, I had it reviewed by Dr. Andrew Donini, an associate professor at York University, Toronto, Canada, whose research is in aquatic invertebrate ionoregulation physiology. I had become familiar with his research during the literature review. He provided me with very positive comments.

After revision of the manuscript in response to Dr. Donini's and internal comments, I submitted the manuscript to the journal, *Environmental Toxicology and Chemistry*. There, the manuscript was reviewed and commented on by two anonymous peer reviewers along with an associate editor. I responded to the peer review comments and revised the manuscript accordingly. The manuscript was then accepted for publication in this journal.

AUTHORS

Principal Author

Author Name:	Michael B Griffith		
Professional Title:		Salutation:	
Email:	griffith.michael@epa.gov	Organization:	
Mailing Address:			
Street Line 1:	26 Martin Luther King Drive MS A-130		
City:	Cincinnati		
Zip Code:	45268	State:	Ohio
At time of research was:	EPA Employee		
Separation Date:			
% of Effort:	100		

PUBLICATIONS

Publication 1:

Publication Title:	Toxicological perspective on the osmoregulation and ionoregulation physiology of major ions by fresh

Publication Date:	Wed Mar 01 00:00:00 GMT 2017		
Journal/Publication Method:	Environmental Toxicology and Chemistry		
All Author(s):			
Volume:	36	Number:	3
Pages:	576-600	Immediately Index:	Immediately Index:
Citation ½ Life:	5.1	Impact Factor:	3.421

SETAC PRESS

Environmental Toxicology and Chemistry, Vol. 36, No. 3, pp. 576–600, 2017
© 2016 The Authors Published 2016 SETAC
Printed in the USA

Critical Review

TOXICOLOGICAL PERSPECTIVE ON THE OSMOREGULATION AND IONOREGULATION PHYSIOLOGY OF MAJOR IONS BY FRESHWATER ANIMALS: TELEOST FISH, CRUSTACEA, AQUATIC INSECTS, AND MOLLUSCA

MICHAEL B. GRIFFITH*
Office of Research and Development, National Center for Environmental Assessment, US Environmental Protection Agency, Cincinnati, Ohio, USA

(Submitted 21 January 2016; Returned for Revision 11 April 2016; Accepted 1 November 2016)

Abstract: Anthropogenic sources increase freshwater salinity and produce differences in constituent ions compared with natural waters. Moreover, ions differ in physiological roles and concentrations in intracellular and extracellular fluids. Four freshwater taxa groups are compared, to investigate similarities and differences in ion transport processes and what ion transport mechanisms suggest about the toxicity of these or other ions in freshwater. Although differences exist, many ion transporters are functionally similar and may belong to evolutionarily conserved protein families. For example, the Na^+/H^+-exchanger in teleost fish differs from the $H^+/2Na^+$ (or Ca^{2+})-exchanger in crustaceans. In osmoregulation, Na^+ and Cl^- predominate. Stenohaline freshwater animals hyperregulate until they are no longer able to maintain hypertonic extracellular Na^+ and Cl^- concentrations with increasing salinity and become isotonic. Toxic effects of K^+ are related to ionoregulation and volume regulation. The ionic balance between intracellular and extracellular fluids is maintained by Na^+/K^+-adenosine triphosphatase (ATPase), but details are lacking on apical K^+ transporters. Elevated H^+ affects the maintenance of internal Na^+ by Na^+/H^+ exchange; elevated HCO_3^- inhibits Cl^- uptake. The uptake of Mg^{2+} occurs by the gills or intestine, but details are lacking on Mg^{2+} transporters. In unionid gills, SO_4^{2-} is actively transported, but most epithelia are generally impermeant to SO_4^{2-}. Transporters of Ca^{2+} maintain homeostasis of dissolved Ca^{2+}. More integration of physiology with toxicology is needed to fully understand freshwater ion effects. *Environ Toxicol Chem* 2017;36:576–600. © 2016 The Authors. Published 2016 Wiley Periodicals Inc. on behalf of SETAC. This article is a US government work and, as such, is in the public domain in the United States of America.

Keywords: Ionoregulation Teleost fish Aquatic invertebrates Major ions Toxicity mechanisms Freshwater toxicity

INTRODUCTION

The salinity, ionic strength, or total concentration of mineral ions in freshwater has increased in many regions from anthropogenic sources such as road salt and effluents from wastewater treatment plants (Table 1). Total ion concentrations are easily measured by testing for specific conductivity or total dissolved solids [1]. However, anthropogenic sources differ in their constituent ions (Table 1). Thus, elevated concentrations of some ions may not be the same as those in Na^+- and Cl^--dominated marine waters or Ca^{2+}- and HCO_3^--dominated freshwaters [2]. Moreover, ions have differing physiological roles in freshwater organisms [3] and are required in different concentrations within cells.

Salinity is a primary environmental gradient differentiating freshwater, marine, or estuarine ecosystems. The evolution of the many freshwater groups, such as fish, Crustacea, and most Mollusca, involved invasion of freshwater simply by migration from at least estuarine waters [4–6]. The dual role of gills in gas exchange and ionoregulation in fish, Crustacea, and Mollusca reflect this evolution. Although some fish and Crustacea have diadromous life histories and ionoregulatory adaptations that facilitate movement among the extremes of this salinity gradient [7], many taxa have distinct lineages that are stenohaline and limited to freshwater [8]. Conversely, the evolutionary ancestors of insects and pulmonate gastropods migrated first to terrestrial environments and secondarily to freshwaters [5,9–12]. Insects adapted to terrestrial life partly by adding a lipid layer to their exoskeleton's epicuticle to minimize water loss [13], and this layer still makes the insect cuticle relatively impermeable.

Insect groups have migrated to freshwater multiple times [9,14,15]. Some aquatic insects have evolved mechanisms to continue to breathe air, including siphons, spiracles modified to pierce the aerenchyma of aquatic plants, or ways to carry air bubbles that act as temporary physical or compressible gills. Other aquatic insects use cutaneous respiration or tracheal gills to exchange O_2 and CO_2 with the water [16]. Tracheal gills in aquatic insects are unlike fish or crustacean gills because O_2 and CO_2 diffuse across a membrane into the gas-filled tracheal system rather than to the hemolymph [17,18]. Although ionocytes or chloride cells occur on the tracheal gills or other respiratory surfaces, such as the anal organ of dragonfly nymphs, ionocytes can occur on nonrespiratory body surfaces or be clustered in specialized ion-absorption organs, such as chloride epithelia and anal papillae [19,20].

Like the aquatic insects, fully aquatic Hygrophila (Gastropoda) include species that breathe air through a diffusional lung in their mantle cavity. Others rely on cutaneous diffusion of O_2 from the water [10]; some larger species in this group have developed neomorphic gills.

Hypo-osmotic freshwaters are very different environments in their ionoregulatory requirements from hyperosmotic marine waters [21]. Freshwaters expose all organisms inhabiting them to similar osmoregulatory and ionoregulatory requirements [21–23]. Most freshwater animals, including fish [21,23], unionid mussels [24,25], crayfish and other Crustacea [3,7], and aquatic insects [26,27], are hyperregulators that maintain greater ion concentrations in their blood or hemolymph than

This article includes online-only Supplemental Data.

This is an open access article under the terms of the Creative Commons Attribution License, which permits use, distribution and reproduction in any medium, provided the original work is properly cited.

* Address correspondence to griffith.michael@epa.gov

Published online 3 November 2016 in Wiley Online Library (wileyonlinelibrary.com).
DOI: 10.1002/etc.3676

Table 1. Dominant ions associated with different anthropogenic sources of salts

Source	Dominant ions	Reference
Use of salt to melt ice and snow	Na^+, Cl^-, Ca^{2+}, Mg^{2+}	Forman and Alexander [326], Kaushal et al. [327], Kelting et al. [328]
Weathering of concrete in urban drainage systems	K^+, Ca^{2+}, HCO_3^-	Davies et al. [329], [330]
Produced water from traditional oil and gas production	Na^+, Cl^-, SO_4^{2-}	Boelter et al. [331], Veil et al. [332]
Produced water from coalbed methane production	Na^+, HCO_3^-, Cl^-	Jackson and Reddy [333], Brinck et al. [334], Dahm et al. [335]
Flowback and produced water from shale gas production (i.e., hydraulic fracturing)	Na^+, Cl^-, Mg^{2+}, Ca^{2+}, Br^-	Entrekin et al. [336], Haluszczak et al. [337]
Runoff and effluents from traditional coal mining	SO_4^{2-}, Na^+, Cl^-, Ca^{2+}, Mg^{2+}, K^+	Kennedy et al. [338], Hopkins et al. [339]
Runoff from valley fills associated with mountaintop mining	Ca^{2+}, Mg^{2+}, HCO_3^-, SO_4^{2-}	Griffith et al. [322]
Coal combustion residue effluents	Ca^{2+}, Mg^{2+}, Cl^-, SO_4^{2-}	Ruhl et al. [340]
Irrigation runoff	Na^+, Mg^{2+}, Cl^-, F^-, SO_4^{2-}	Leland et al. [341], Scanlon et al. [342]
Anthropogenic increases in geochemical weathering	Ca^{2+}, HCO_3^-, SO_4^{2-}	Raymond and Oh [343], Kaushal et al. [344]
Industrial sources	Na^+, Cl^-	Echols et al. [345]
Wastewater treatment plants	Na^+, Cl^-, K^+, SO_4^{2-}	Andersen et al. [346], Hur et al. [347]

is found in freshwaters. Because the external medium is more dilute than body fluids, these species deal with continuous diffusional loss of salts and absorption of water across their permeable membranes. Water balance is accomplished by excretion of dilute waste fluids by their renal systems, whereas salt concentrations are maintained by various proteins on gill or renal-system membranes that actively transport ions against concentration gradients [23,24,28]. Most freshwater species, unlike saltwater species, drink little water, thereby limiting water absorption through the gastrointestinal system and dilution of the hemolymph or blood [28]. Even so, water turnover is generally greater in freshwater animals [29]. Freshwater animals reabsorb ions from their urine to produce urine that is more isotonic with the freshwater and reduce their energy expenditure for osmoregulation by 80% to 90% [30].

Taxa differ in how osmoregulation changes if the water salinity changes along a natural gradient from freshwater to saltwater. In most fish and amphibians, the ion concentrations or osmolality of intracellular (i.e., the cytosol or fluids within cells) and extracellular (i.e., the fluids outside of cells, particularly the blood or hemolymph) fluids remain relatively constant as the water osmolality increases. Most invertebrates, including unionid mussels [25] and freshwater Crustacea, are hyperregulators in freshwater and become isosmotic when placed in brackish or salt waters [3,31,32]. Hemolymph ion concentrations in freshwater molluscs are lower than in either fish or arthropods [24].

The present review assesses the current understanding of the ionoregulatory and osmoregulatory physiology of selected animal groups in freshwater ecosystems. The major ions considered include the cations H^+, Na^+, K^+, Ca^{2+}, and Mg^{2+} and the anions Cl^-, HCO_3^-, and SO_4^{2-}. The review focuses particularly on cellular membrane transport processes that regulate the concentrations of these ions both in the cytosol of epithelial cells and in the blood or hemolymph (i.e., ionoregulation). However, the review also touches on the interaction between ionoregulation and processes that regulate movement of water into and out of these compartments (i.e., osmoregulation). A comparative approach is taken to understand how these processes may be similar or different among freshwater fish and 2 major phyla of freshwater invertebrates, the Mollusca and Arthropoda. Within the Mollusca, the focus is on bivalves in the family Unionidae, but some data on the Corbiculidae and Dreissenidae and on freshwater Gastropoda is also included. Among the Arthropoda, the focus is on the Crustacea, particularly the Decapoda and Cladocera, and aquatic Insecta. Because of their dominance among the Decapoda in inland North American freshwaters, the crayfish (Astacidea) is the primary focus, but data are also included on freshwater shrimp (Caridea) when similar studies have not been done on crayfish. The ultimate intent is to use this physiological literature to investigate 2 ecological questions. How are the transport processes for specific major ions similar or different among these freshwater animal taxa (fish, crustaceans, aquatic insects, and molluscs)? What do the transport mechanisms for each of these ions suggest about the potential of these or other ions, such as metals, Br^-, and NO_2^-, to affect aquatic animal assemblages in freshwater ecosystems, when concentrations are greater than or less than concentrations normally occurring in freshwater habitats? As a shorthand, square brackets ([]) are used throughout the present review to indicate concentrations of ions or compounds.

The present review is particularly intended to benefit aquatic ecotoxicologists. An understanding of the mechanisms by which aquatic animals ionoregulate and osmoregulate is needed for ecotoxicologists to interpret the data from toxicity studies and to place the major ions, which are components of natural waters and of intracellular and extracellular fluids, into an adverse outcome pathways conceptual framework [33]. However, the review also highlights current gaps in this understanding—information that may be provided by environmental physiologists.

GENERAL OSMOREGULATION

For freshwater animals, physiological homeostasis is attained by limiting uptake of water and maintaining higher concentrations of ions in intracellular and extracellular fluids. Although ions, such as H^+, K^+, and HCO_3^-, can contribute to the osmolality of intracellular and extracellular fluids and are also important in movement of solutes between these compartments and the external environment, Na^+ and Cl^- are generally the 2 most dominant ions in terms of maintaining this hyperosmotic state in freshwater animals [21,22,34,35]. Because of their importance as primary osmolytes in intracellular and extracellular fluids, elevated Na^+ and Cl^- may not have adverse effects on many freshwater animals unless the water concentrations become hyperosmotic (Supplemental Data, Table S1). Experiments with bivalves model the process whereby many invertebrates shift from hyperregulation in the low salinities characteristic of freshwaters to iso-osmolality if exposed to higher salinities, such as those characteristic of estuarine or marine waters. Whether the higher salinity causes adverse effects, such as mortality, may depend on

species-specific tolerance to higher salinities and the relative concentrations of the various ions [36]. This tolerance to increased or variable salinity can be very species specific, varying among species within the same family or even genus (Supplemental Data, Table S1).

Although there is evidence for paracellular pathways, or mechanisms that allow diffusion (i.e., the random movement of molecules because of their kinetic energy causing them to intermingle and disperse from areas of higher concentrations in solutions where there are no barriers to such movement) of certain solutes through tight or septate junctions between cells [37], ionoregulation generally occurs by transport through the epithelial cells (i.e., transcellular pathways) using transporters that will be described in the following sections with water being transported along with the ions [38]. Infolding of the cell membranes helps this process by increasing the surface area across which transport occurs. Some channels across the basolateral membrane of ionocytes, such as the Cl^--channel and K^+-channel (KC), are pathways out of the cell for water [39]. These channels are involved in volume regulation [40] because they transport water along with the ions across the epithelial basolateral membrane cells and into the blood or hemolymph. The water is then transported to the renal system for excretion in dilute urine. Aquaporins are another channel that increases the permeability of membranes to water; limited available data indicate that aquaporins are up-regulated in freshwater animals [41,42], where the osmoregulatory problem is water influx (Supplemental Data, Table S1).

Septate junctions can be compromised if solute concentrations in the aquatic medium exceed those of the intracellular and extracellular fluids. This may be particularly important for freshwater bivalves because these molluscs maintain lower ion concentrations in intracellular and extracellular fluids than either fish or arthropods [43] (Supplemental Data, Table S1). *Dreissena polymorpha*, a relatively recent immigrant to freshwater, appears to be particularly susceptible to hyperosmotic effects of a sugar solution because it maintains lower hemolymph osmolarity, and its septate junctions have not been tightened to minimize paracellular diffusion of solutes, a characteristic of most freshwater hyperosmoregulators [44]. One strategy that is not available to all animals is the accumulation of organic osmolytes (Supplemental Data, Table S1).

Freshwater organisms balance a combination of ion uptake with ion reabsorption that appears to minimize energy expenditure for ionic regulation. Exposure of an organism to a different salinity may increase energy expenditures as the organism attempts to adjust to this stress (Supplemental Data, Table S1). However, in *Eurytemora affinis*, an estuarine and salt marsh copepod that has independently invaded freshwater habitats multiple times in the last century, Lee et al. [45] found that freshwater populations maintain greater hemolymph osmolality than do saline populations. Such maintenance of greater hemolymph osmolality seems to require greater energy expenditure.

ION-TRANSPORTING EPITHELIAL MEMBRANES AND ION TRANSPORT

Cell membranes contain transporter proteins that move specific solutes across the membrane [46]. Some proteins are permeases, which conserve energy by reducing the energy required for movement of ions across the membrane bilayer [47]. These proteins are similar to enzymes in that the flux of ions through the transporter follows Michaelis–Menten kinetics. Here, ion flux is related to the ion concentration by variables, V_{max} (i.e., maximal velocity) and K_m (i.e., Michaelis constant), which are the maximum flux rate when it is saturated by the ion concentration and the ion concentration that is half that at $V_{max,}$ respectively. The affinity of a transporter for an ion increases as K_m decreases, because the transporter can transport the ion from a solution with a lower ambient ion concentration. The capacity of a transporter for an ion increases as V_{max} increases, because the ion flux rate increases for a solution of a particular ambient ion concentration. These proteins differ between the apical plasma membranes in contact with the external environment (or the lumen of organs that open to the external environment, such as the renal or gastrointestinal systems) and basolateral plasma membranes that interface with the extracellular fluids. Ion transfers across epithelial membranes are 2-step processes. During ion uptake, the ion is transported first across the apical membrane into the intracellular fluids and then across the basolateral membrane into extracellular fluids.

Often ion transport occurs against a gradient of electrical charge (i.e., membrane potential), solute concentration, or both (i.e., an electrochemical gradient) [47] and requires energy (i.e., active transport). Exchangers trade 2 cations or 2 anions across a membrane whereby movement of 1 ion down its electrochemical gradient supplies energy to move the other ion up its electrochemical gradient [47]. Cotransporters move electroneutral combinations of cations and anions across a membrane with movement of 1 ion along its electrochemical gradient supplying energy for transport of the other ions. Transmembrane ATPases use energy supplied by hydrolysis of adenosine triphosphate to transport either single ions or exchange different ions. The energy demand is enough that glycogen-rich cells containing glycogen phosphorylase surround ionocytes in tilapia (*Oreochromis mossambicus*) gills [48]. Fish energy expenditure for ionoregulation and osmoregulation increases as environmental salinity varies from isotonicity, and more energy is required for up-regulation of ion transporters [49,50]. In cutthroat trout (*Oncorhynchus clarkii*), O_2 consumption decreased in isolated gills treated with 0.5 mM ouabain to inhibit Na^+/K^+-adenosine triphosphatase (ATPase; NKA) or 1 μM bafilomycin A_1 to inhibit vacuolar-type H^+-ATPase (VHA) [51]. Approximately 1.8% of resting metabolic rate was used for Na^+ transport by these 2 transporters. Also, O_2 consumption of cutthroat trout gills in freshwater was slightly greater than that in saltwater (3.9% vs 2.4% of resting metabolic rate, respectively).

Conversely, channels transport a single ion across a membrane, usually down its electrochemical gradient. This is a type of passive transport [47]. Because of their ion specificity, channels often create a difference in electrical potential across an epithelial membrane.

Although ion transporters are central to maintenance of hypertonic extracellular ion concentrations in freshwater, mechanisms that regulate ion loss from diffusive leakage across the gill epithelia are also important. Most aquatic animal epithelia, despite their permeability to water, gases, and some ions, are resistant (or tight) to penetration by nonelectrolytes [37], and this tightness allows these animals to hyperregulate in freshwater. This tightness involves maintaining septate junctions in invertebrates and tight junctions in vertebrates [52,53]. These intercellular junctions, although not homologous [54], are barriers to solute diffusion through the spaces between adjoining epithelial cells.

The tight junctions between fish gill epithelial cells are characterized by a cross-linked complex of multiple proteins, including transmembrane proteins, such as claudins and occludins, along with zona occludens and cingulin, plaque proteins that anchor the transmembrane proteins to the actin cytoskeleton [55]. Claudins and occludin are integral components of tight junctions between fish gill epithelial cells (Supplemental Data, Table S2).

Cells involved in transport have limited distributions on the epithelia of most organisms. Whereas cells in the gastrointestinal system absorb nutrients and energy from food and those in the renal system remove waste products and retain ions, the gills are a particularly important interface for ionoregulation. Because gill membranes are involved in gas exchange with the external environment, they are by necessity very thin. The membranes are also in direct contact with the surrounding water, which is a source of ions for aquatic organisms. In larval fish and some aquatic insects that lack gills, other epithelial membranes on the body surface are involved in ion transport.

TRANSPORTERS AND PHYSIOLOGY OF INDIVIDUAL IONS

Sodium (Na^+)

The primary cation involved in osmoregulation in animals is Na^+. Uptake of Na^+ across the apical plasma membrane is accomplished by exchange with H^+, a product of metabolism [56]. Research with fish and other freshwater organisms supports a model in which Na^+ is exchanged for H^+ across the apical membrane by 1 or both of 2 molecular systems [57,58]. Because Na^+ is exchanged for H^+, Na^+ also is involved in acid–base regulation in these animals [15,59–61].

Teleost fish. In fish, an electroneutral Na^+/H^+-exchanger (NHE) transports $1H^+$ across the apical membrane in exchange for $1Na^+$ [62,63]. The second system involves 2 transporters: 1) VHA transports H^+ out across the apical membrane [64,65], creating an electrochemical gradient for 2) Na^+ to diffuse across the apical membrane through an amiloride-sensitive apical Na^+-channel that may also be permeable to K^+ [23,66,67]. Molecular research has been unable to identify messenger ribonucleic acid (mRNA) or proteins associated with an epithelial Na^+-channel (ENaC) as described in mammals [68] in gill ionocytes of tilapia or zebrafish (*Danio rerio*) [69–71]. However, a related acid-sensing ion channel (ASIC), specifically ASIC 4, was recently identified on the ionocyte apical membranes of rainbow trout (*Oncorhynchus mykiss*) and zebrafish that appears to act as an Na^+-channel [72,73]. Parks et al. [74] questioned whether both types of molecular systems could function in freshwater, but their subsequent research has identified both systems in freshwater fish [75,76] (Supplemental Data, Table S3). Ionocytes have morphological characteristics that create localized microenvironments with low $[Na^+]$ or higher $[H^+]$ that facilitate operation of NHE [63] (Supplemental Data, Table S3). Carbonic anhydrase (CA) plays a role in Na^+ transport by catalyzing production of H^+ from the hydrolysis of CO_2 [77] (Figures 1 and 2 and Table 2).

Uptake of Na^+ from food occurs in the gastrointestinal system of freshwater fish. However, the relative importance of this source of Na^+ is not clear (Supplemental Data, Table S3).

The relative concentrations of Na^+ and K^+ differ between the intracellular and extracellular fluids of animal cells [47]: intracellular fluids contain greater $[K^+]$ compared with $[Na^+]$ whereas the reverse occurs in extracellular fluids. The difference can be as much as 10-fold. These opposing concentration gradients are maintained by active transport

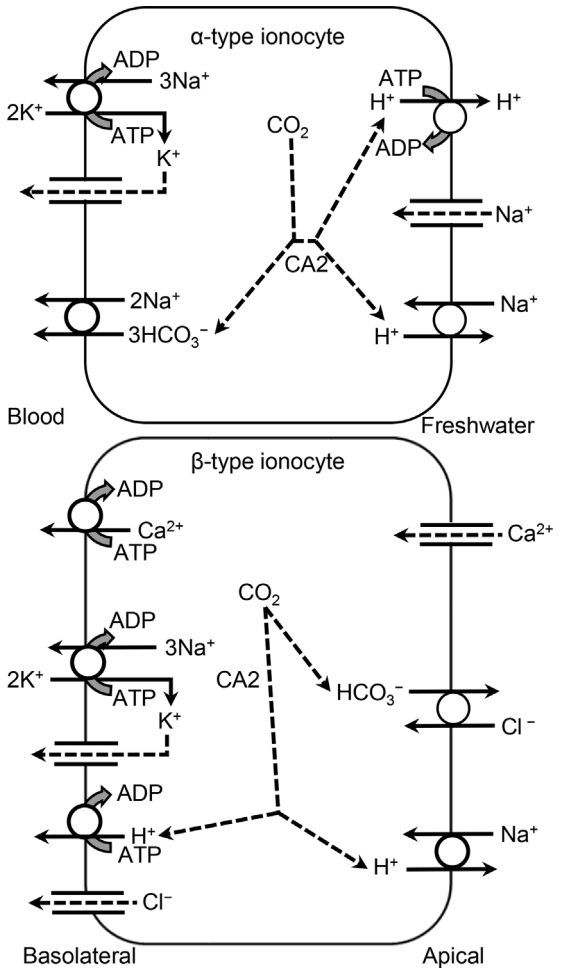

Figure 1. Current model for transporters on α-type and β-type ionocytes of fish such as salmonids. In the α-type ionocyte, along the apical membrane are vacuolar-type H^+-adenosine triphosphatase (ATPase; VHA), apical Na^+-channel, and Na^+/H^+-exchanger (NHE), whereas along the basolateral membrane are Na^+/K^+-ATPase (NKA), K^+-channel (KC), and Na^+/HCO_3^--cotransporter (NBC). In the β-type ionocyte, along the apical membrane are the epithelial Ca^{2+}-channel (ECaC), anion exchanger (AE), and NHE, whereas along the basolateral membrane are plasma membrane Ca^{2+}-ATPase (PMCA), NKA, KC, VHA, and Cl^--channel. The carbonic anhydrase type 2 enzyme is CA2. Dashed arrows indicate diffusion, whereas solid arrows indicate active transport. Arrows that split indicate reactions. Modified from Dymowska et al. [303]. ATP = adenosine triphosphate; ADP = adenosine diphosphate.

involving NKA on the basolateral membrane [66] (Supplemental Data, Table S3).

Fish gills have important roles in gas exchange, ionoregulation, and acid–base regulation [61]. The 2 apical Na^+ transport systems have different roles in these functions and are accordingly segregated among different ionocyte types (Figures 1 and 2 and Supplemental Data, Table S3). An NHE isoform, NHE3b, is expressed predominantly in the gills and is relevant to Na^+ uptake under low Na^+ or acidic conditions. Particularly under acidic conditions at least in larval zebrafish, zNHE3b appears to be tied to a metabolon that includes excretion of NH_3 by the Rhesus protein Rhcg1 [78] (Supplemental Data and Supplemental Data, Table S3).

Crustacea. Similar ion transporters (Figure 3 and Table 2) that exchange H^+ for Na^+ exist in crayfish [67,79], but while the paired VHA and apical Na^+-channel are potentially homologous to those in fish, Crustacea possess an electrogenic $H^+/2Na^+$- (or Ca^{2+}) exchanger [H2Na(Ca)E] [80–83] on gill

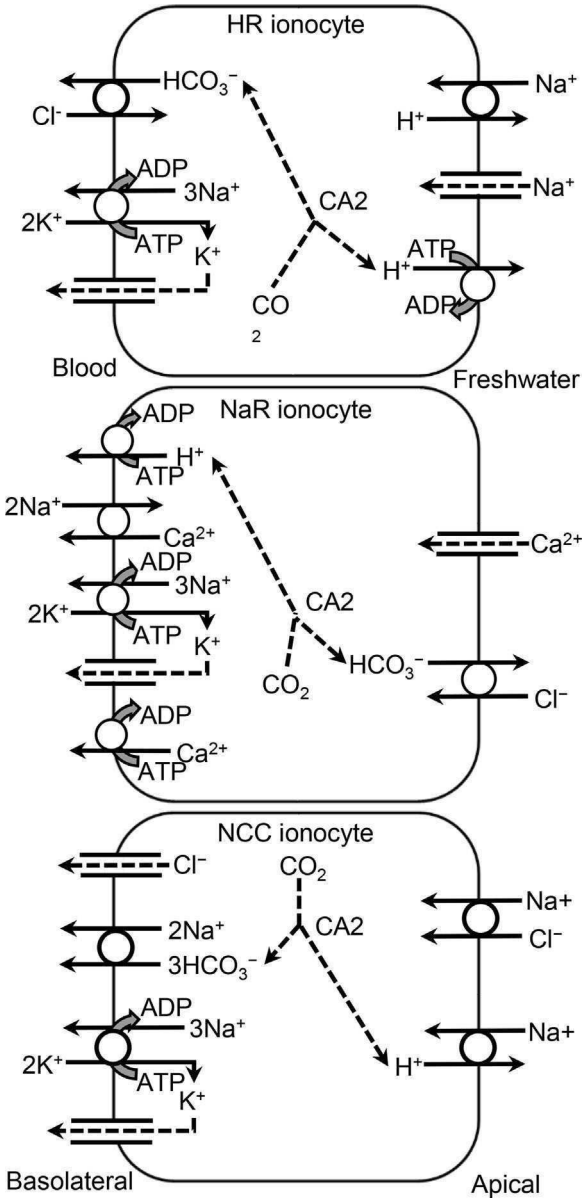

Figure 2. Current model for transporters on H^+-adenosine triphosphatase (ATPase)-rich (HR), Na^+/K^+-ATPase-rich (NaR), and Na^+/Cl^--cotransporter (NCC) ionocytes of fish, such as zebrafish. In the HR ionocyte along the apical membrane are Na^+/H^+-exchanger (NHE), apical Na^+-channel, and vacuolar-type H^+-ATPase (VHA), whereas along the basolateral membrane are the anion exchanger (AE), Na^+/K^+-ATPase (NKA) and K^+-channel (KC). In the NaR ionocyte, along the apical membrane are the epithelial Ca^{2+}-channel (ECaC) and anion exchanger, whereas along the basolateral membrane are VHA, Na^+/Ca^{2+}-exchanger (NCX), NKA, KC, and plasma membrane Ca^{2+}-ATPase (PMCA). In the NCC ionocyte, along the apical membrane are NCC and NHE, whereas along the basolateral membrane are the Cl^--channel, Na^+/HCO_3^--cotransporter (NBC), NKA, and KC. Dashed arrows indicate diffusion, whereas solid arrows indicate active transport. Arrows that split indicate reactions. Modified from Dymowska et al. [303]. CA2 = carbonic anhydrase type 2 enzyme; ATP = adenosine triphosphate; ADP = adenosine diphosphate.

epithelia apical membranes [84]. This exchanger also transports Ca^{2+}, and elevated external [Ca^{2+}] can competitively inhibit Na^+ uptake [80,81,85]. However, an electroneutral, amiloride-sensitive NHE was identified on the gill epithelium apical membrane of *Orconectes limosus* opposite from NKA on the basolateral membrane [86]. As in fish, Na^+ movement across the apical membrane of crayfish is facilitated by maintenance of intracellular [Na^+] that are lower than hemolymph [Na^+] by Na^+ transport across the basolateral membrane by NKA.

Aquatic insects. In freshwater mosquito (Culicidae) or midge (Chironomidae) larvae, 4 anal papillae on abdominal segment 10 are the primary sites of Cl^- and Na^+ absorption [87–89]. Vacuolar-type H^+-ATPase is found on the apical membrane of anal papillae epithelial ionocytes, whereas P-type NKA is found on the basolateral membrane [88] (Supplemental Data, Table S3).

Export of H^+ across the apical membrane creates a negative potential that favors counter, electrodiffusive movement of Na^+ possibly through an apical Na^+-channel [90] with NKA maintaining a lower concentration gradient across the apical membrane by transporting Na^+ across the basolateral membrane (Figure 4 and Table 2). Also present is NHE, but it differs at least pharmacologically from mammalian NHE [91] (Supplemental Data, Table S3).

In early experiments to elucidate interactions between different anions and cations and Na^+ influx in *Chironomus tentans*, Wright [92] observed inhibition of Na^+ uptake by elevated [NO_3^-], [SO_4^{2-}], [Li^+], [Rb^+], [NH_4^+], or [H^+] in the external medium. Based on current models of Na^+ transport, elevated [NH_4^+] or [H^+] affect the counter export of H^+ by VHA required for Na^+ influx by an apical Na^+-channel. Substitution of Li^+ for Na^+ in the apical Na^+-channel [93] appears to result in competitive inhibition of Na^+ uptake, whereas Rb^+ substitution for K^+ may affect NKA, which maintains the concentration gradients of Na^+ across both the apical and basolateral membranes. The effects of NO_3^- and SO_4^{2-} are not readily explained, but Wright [94] suggested that Na^+ transport between the water and hemolymph is coupled with independent Cl^--transport, such that a relatively impermeant anion, such as SO_4^{2-} or NO_3^-, cannot substitute for Cl^-. Data on Na^+-transport in other aquatic insect classes are more limited (Supplemental Data, Table S3).

Mollusca. In freshwater bivalves, Na^+ uptake across the apical epithelial membrane occurs by exchange for H^+ [35,95] and at least includes an NHE (Figure 5 and Table 2). In unionid mussels, maintenance of ionic homeostasis relies more on active uptake of Na^+ than uptake of Cl^-. However, whether the NHE is electroneutral, as in fish, or electrogenic, as in Crustacea, is unknown. In freshwater, NKA activity is greater in the unionid gills than in the gills of oligohaline bivalves [96], suggesting that this transporter plays a role in maintaining a [Na^+] gradient across the epithelial membrane [95,97], as in fish.

Other Na^+ transporters. A Na^+/HCO_3^--cotransporter (NBC) on the basolateral membrane of gill epithelia helps maintain very low [Na^+] in the cytosol and also removes HCO_3^- from cells that primarily export H^+ in some fish [21,69,70,98,99]. The NBC occurs in rainbow trout, zebrafish, and Osorezan dace (*Tribolodon hakonensis*) gill ionocytes [69,99] but not in American eel (*Anguilla rostrata*) [100].

In some fish, there is a transporter for both Na^+ and Cl^- on the apical membrane of specific epithelial cell types. This electroneutral Na^+/Cl^--cotransporter (NCC) has been detected in the apical membrane of type II ionocytes of tilapia embryos reared in freshwater [69] and in NCC ionocytes of zebrafish (Figure 2 and Table 2) [70,99,101].

In neonates of the crustacean *Daphnia magna*, an NCC has been detected by inhibition of Na^+-uptake with either bumetanide (NCC and $Na^+/K^+/Cl^-$-cotransporter [NKCC] inhibitor) and thiazide (NCC inhibitor) [102]. There is an ontogenic change between the neonates and adults, because NKCC was detected in adult *D. magna* by the inhibition of

Table 2. List of ion transporters identified by the present review in the physiological literature on freshwater fish, Crustacea, aquatic insects, and Mollusca

Transporter	Acronym	Function	Gene family
V-type H^+-ATPase	VHA	Transports H^+ across apical or basolateral membranes	ATPase H^+-transporting subunits
Apical Na^+-channel	—	Transports Na^+ across usually apical membranes	?
Acid sensing ion channel	ASIC	Possibly transports Na^+ across usually apical membranes	Acid sensing ion channel subunits
Na^+/H^+-exchanger	NHE	Exchanges Na^+ for H^+ across apical membranes	Solute carrier family 9
P-type Na^+/K^+-ATPase	NKA	Exchanges Na^+ and K^+ across basolateral membranes	ATPase Na^+/K^+-transporting subunits
K^+-channel	KC	Transports K^+ across basolateral membranes	K^+ voltage-gated channel
Na^+/HCO_3^--cotransporter	NBC	Transports Na^+ and HCO_3^- across basolateral membranes	Solute carrier family 4
Cl^-/HCO_3^--exchanger	AE	Exchanges Cl^- for HCO_3^- across apical membranes	Solute carrier family 4
Epithelial Ca^{2+}-channel	ECaC	Transports Ca^{2+} across apical membranes	Transient receptor potential cation channel
Ca^{2+}-ATPase	PMCA	Transports Ca^{2+} across basolateral membranes	ATPase Ca^{2+} transporting
Cl^--channel	—	Transports Cl^- across basolateral membranes	?
Carbonic anhydrase	CA	Catalyzes the hydrolysis of CO_2 to form H^+ and HCO_3^-	Carbonic anhydrase
Na^+/Ca^{2+}-exchanger	NCX	Exchanges Na^+ for Ca^{2+} across basolateral membranes	Solute carrier family 8
Na^+/Cl^--cotransporter	NCC	Transports Na^+ and Cl^- across apical membranes	Solute carrier family 12
$Na^+/K^+/Cl^-$-cotransporter	NKCC	Transports Na^+, K^+ and Cl^- across apical membranes	Solute carrier family 12
$H^+/2Na^+$(or Ca^{2+})-exchanger	H2Na(Ca)E	Exchanges $2Na^+$ or Ca^{2+} for H^+ across apical membranes	Solute carrier family 9
Anion/SO_4^{2-}-antiporter	—	Exchanges another anion for SO_4^{2-}across apical membranes	?

ATPase = adenosinetriphosphatase; V-type = vacuolar-type; P-type = Purkinje cells-type; ? = not sufficiently characterized to place in a gene family.

Na^+-uptake by bumetanide and not by thiazide. The function of NKCC in these cladoceran adults (i.e., ion uptake) differs from that in fish, where an NKCC is active in fish from more saline habitats and is involved in ion excretion [69,103–105].

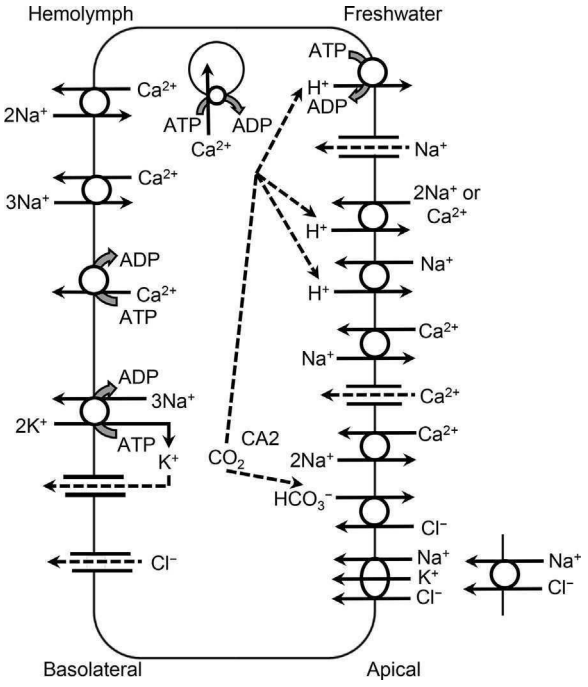

Figure 3. Generalized model for transporters on gill ionocytes of freshwater Crustacea based on transporters identified by the present review. A single cell is shown because no studies have identified different ionocyte types. Along the apical membrane are vacuolar-type H^+-adenosine triphosphatase (ATPase; VHA), apical Na^+-channel, electrogenic $H^+/2Na^+$ (or Ca^{2+})-exchanger [H2Na(Ca)E], electroneutral Na^+/H^+-exchanger (NHE), Na^+/Ca^{2+}-exchanger (NCX), epithelial Ca^{2+}-channel (ECaC), electroneutral NCX ($2Na^+/Ca^{2+}$), anion exchanger, and $Na^+/K^+/Cl^-$-cotransporter (NKCC; *Daphnia magna* adults) or Na^+/Cl^--cotransporter (NCC; *D. magna* neonates). On the basolateral membrane are the electroneutral NCX ($2Na^+/Ca^{2+}$), electrogenic NCX ($3Na^+/Ca^{2+}$), plasma membrane Ca^{2+}-ATPase (PMCA), Na^+/K^+-ATPase (NKA), K^+-channel (KC), and Cl^--channel. Plasma membrane Ca^{2+}-ATPase may also move Ca^{2+} into organelles within the cells. Dashed arrows indicate diffusion, whereas solid arrows indicate active transport. Arrows that split indicate reactions. CA2 = carbonic anhydrase type 2 enzyme; ATP = adenosine triphosphate; ADP = adenosine diphosphate.

Effects on Na^+ transport by other ions in the water. Low pH inhibits influx of Na^+ by increasing the $[H^+]$ gradient against which the NHE or VHA act [106–108]. Low pH also increases gill epithelial ion permeability, resulting in increased Na^+ efflux [109–112]. The result is a large decrease in blood $[Na^+]$ in fish, although sensitivity can vary significantly among species.

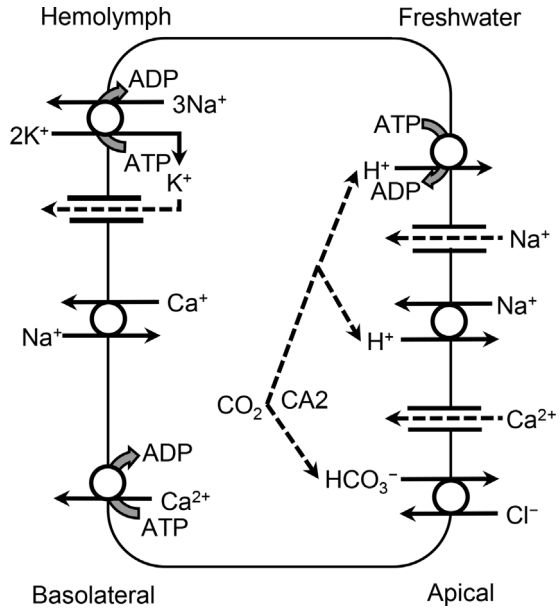

Figure 4. Generalized model for transporters on epithelial ionocytes of aquatic insects based on transporters identified by the present review. A single cell is shown because no studies have identified different ionocyte types, although research with mosquito larvae suggests that transporters for at least K^+ and Ca^{2+} are not collocated with those for Na^+ and Cl^- on the anal papillae. Also, the evidence suggests variation among aquatic insect orders. Along the apical membrane are vacuolar-type H^+-adenosine triphosphatase (ATPase; VHA), apical Na^+-channel, Na^+/H^+-exchanger (NHE), epithelial Ca^{2+}-channel (ECaC), and anion exchanger (AE). On the basolateral membrane are Na^+/K^+-ATPase (NKA). K^+-channel (KC), Na^+/Ca^{2+}-exchanger (NCX), and plasma membrane Ca^{2+}-ATPase (PMCA). Dashed arrows indicate diffusion, whereas solid arrows indicate active transport. Arrows that split indicate reactions. CA2 = carbonic anhydrase type 2 enzyme; ATP = adenosine triphosphate; ADP = adenosine diphosphate.

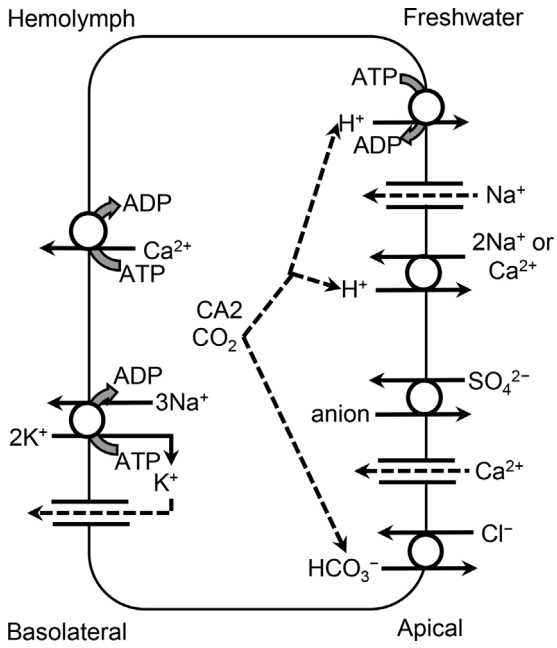

Figure 5. Generalized model for transporters on gill ionocytes of Unionidae (Mollusca) based on transporters identified by the present review. A single cell is shown because no studies have identified different ionocyte types. Along the apical membrane are vacuolar-type H^+-adenosine triphosphatase (ATPase; VHA), apical Na^+-channel, electrogenic $H^+/2Na^+$ (or Ca^{2+})-exchanger [H2Na(Ca)E], anion/SO_4^{2-}-exchanger, epithelial Ca^{2+}-channel (ECaC), and anion exchanger. On the basolateral membrane are plasma membrane Ca^{2+}-ATPase (PMCA), Na^+/K^+-ATPase (NKA), and K^+-channel (KC). Dashed arrows indicate diffusion, whereas solid arrows indicate active transport. Arrows that split indicate reactions. CA2 = carbonic anhydrase type 2 enzyme; ATP = adenosine triphosphate; ADP = adenosine diphosphate.

Similar loss of Na^+ has been observed in crayfish, various classes of aquatic insects, and unionid mussels (Supplemental Data, Table S3).

Elevated Ag^+ and Cu^{2+} are also associated with reductions in blood [Na^+] resulting from decreased Na^+ in fish [113]. Research on metal uptake indicates that the ENaC is involved in the uptake of Cu^{2+} and Ag^+ by fish, particularly in low [Na^+] freshwaters. Interactions between Na^+ and these 2 metals suggest noncompetitive inhibition at the apical Na^+-channel, through which these ions all can be transported [114,115] (Supplemental Data, Table S3). Copper is transported by the apical Na^+-channel, because the ion crosses as Cu^+ rather than Cu^{2+} [116,117]. Reduced Na^+ uptake is because of inhibition of NKA by Cu^{2+} or Ag^+ [118]. Also, acute Ag^+ exposure inhibits CA activity, which limits the availability of H^+ for exchange with Na^+. This is also observed in freshwater Crustacea and Mollusca (Supplemental Data, Table S3), although Cu^{2+} may also be transported through an electrogenic H2Na(Ca) E [119–121]. Other divalent metals are known to reduce Na^+ uptake by inhibiting basolateral NKA or CA activity (Supplemental Data, Table S3). *Chironomus* spp. have demonstrated a similar relationship between whole-body [Na^+] and NKA inhibition by metals (Supplemental Data, Table S3), but Na^+ uptake by *Maccaffertium pudicum* (Ephemeroptera), several Plecoptera, and another dipteran (*Atherix* sp.) showed variable effects with exposure to Ag^+ or Cu^{2+} [122], suggesting some differences in the Na^+ transporters between these insects and other freshwater animals.

Synthesis. Across both freshwater invertebrate and fish species, evidence exists for exchange of Na^+ for H^+ on the apical membrane of ionocytes either on gill or other epithelia involved in ion exchange between the organisms and water. There is also significant evidence that increasing [H^+] in the water inhibits Na^+ uptake, either by competition for external attachment sites on the NHE between these 2 cations [123] or by increasing the concentration gradient for export of H^+. However, there is much variability; 1 factor affecting species-specific sensitivity to acidification may be the epithelial membrane's permeability to Na^+ loss under low pH conditions [124]. This leads to 1 hypothesis that the reason Ephemeroptera, in particular, exhibit sensitivity to acidification, metals, and other ionoregulatory challenges is because of the high permeability of their larval integument. Unlike other aquatic insects, the ionocytes of Ephemeroptera are scattered as single cells or cell complexes not just located on the tracheal gills but also over the rest of the body integument [125]. Moreover, each ionocyte is separated from the external medium by only a thin porous plate ($\approx$0.1 μm). Therefore, epithelial membrane permeability might be greater than in other aquatic insects.

Among the species that have been studied, VHA and NKA are functionally very similar and may be biochemically similar enough to be classified in the same molecular families [126,127]. However, there has been minimal research with the aquatic insects, which because of their evolutionary history, could be the most divergent. In the case of the NHE, at least the Crustacea have evolved an electrogenic transporter that transports either Na^+ or Ca^{2+} owing to these animals' requirements for Ca^{2+} in their exoskeleton. However, there is uncertainty here because newer molecular methods used to study vertebrates have not yet been applied to invertebrates.

There have been no extensive comparisons even within phyla, but there is evidence that the affinity and capacity of these transporters as measured by K_m and V_{max} can be variable among species and even populations within a species. This can result in significant intraspecific variance in the tolerance of animals to low [Na^+].

In research that tried to assess the relative toxicity of various major ions for *Ceriodaphnia dubia*, *D. magna*, and fathead minnows (*Pimephales promelas*), Na^+ was not a significant variable in the resulting regressions [128]. A number of recent studies of the relationship between hardness and acute effects of Na^+ salts have found toxicity for a range of freshwater fish, crustaceans, aquatic insects, and molluscs at relatively high concentrations: 5.3 mM to 147.1 mM for Na_2SO_4 [129–133] and 3.7 mM to 170.1 mM for NaCl [134,135]. As the primary osmoregulatory cation in animals, Na^+ is regulated by the apical and basolateral membrane transporters and maintained at levels in the extracellular and intracellular fluids that exceed ambient [Na^+] of most natural freshwaters. In diadromous species that migrate between freshwater and brackish or saltwater as part of their life cycle, the arrangement and molecular isoforms of these transporters often change, in part to shift from hyper-regulation and uptake of Na^+ in hypotonic freshwaters to hyporegulation or isoregulation and excretion of Na^+ in hypertonic estuarine or marine waters [136–138]. Many stenohaline freshwater species are unable to make such changes and tolerate [Na^+] that is hypoionic but begin to exhibit adverse effects as the ambient [Na^+] approaches or exceeds that of intracellular fluids and blood or hemolymph [139–144] and the directions of water movement and ion diffusion change.

Potassium (K^+)

Potassium is important in Na^+ transport from the cytosol across the basolateral membrane to extracellular fluids by NKA.

Furthermore, the greater cytosol [K^+] allows diffusion of K^+ back across the basolateral membrane to the extracellular fluids through a KC. The primary transporter for Na^+ across the basolateral membrane is Na^+/K^+-ATPase [21,88].

The KC, which moves K^+ back across the basolateral membrane to the extracellular fluids, is structured so that it is also somewhat permeable to larger alkali metal ions, such as Rb^+ and Cs^+, but relatively impermeable to Na^+ and Li^+ [145]. This channel limits its permeability to K^+ but also positions ions attached to the transporter so that the repulsive force between pairs of K^+ ions enhances their conduction through the transporter [145].

Teleost fish. The flux of K^+ across the apical membrane of gill epithelia in freshwater fish, such as rainbow trout, occurs by active transport against a concentration gradient [146], which is maintained, in part, by the exchange of Na^+ for K^+ by NKA across the basolateral membrane (Figure 1 and Table 2). This has been shown in a few studies that have used either ^{42}K as a radiotracer or ^{86}Rb as an analog for K, although Rb^+ penetrated fish tissues much less than K^+ [146]. Some studies have suggested that the amiloride-sensitive apical Na^+-channel may also be permeable to K^+ [23,66,67,147], but no research has conclusively identified an apical transporter involved in K^+ uptake.

In zebrafish embryos, complementary deoxyribonucleic acid was identified as *kcnj1*, an ortholog of *Kir1.1b* that encodes the mammalian kidney K^+-channel (ROMK) [148]. Although expression of *kcnj1* occurred in the duct midsegment of the pronephros, the gene was also expressed in the ventrolateral integument and in a cell population in the gill primordia that also expressed the *a1a.4* subunit isoform of NKA. Abbas et al. [148] suggested that this cell population is a fourth ionocyte type in which the encoded protein, kcnj1, is located on the apical membrane and is involved in K^+ excretion, not uptake. Similarly, a ROMK is expressed in gill ionocytes of saltwater-acclimated tilapia, where it is also involved in K^+ excretion [149]. However, bands for ROMK were not detected by Western blot analysis in the gills of freshwater-acclimated tilapia, suggesting that this transporter is not active in freshwater. Because this evidence is equivocal for freshwater fish, this potential transporter or the potential ionocyte is not illustrated in Figure 2. Uptake of K^+ also occurs from food in the gastrointestinal tract (Supplemental Data, Table S4).

Crustacea. As with Na^+, uptake of K^+ increases in crayfish during the postmolt period to counteract the dilution of ion hemolymph concentrations that result from absorption of water to increase body volume following ecdysis [150,151]. However, no research has identified a mechanism for apical K^+ uptake.

An NKCC has been detected in adult *D. magna* [102]. This transporter is involved in Na^+ and presumably K^+ uptake.

Aquatic insects. Although influx of Na^+ and Cl^- and efflux of H^+ from the anal papillae of *Chironomus riparius* demonstrate that the papillae are a site of exchange for these ions, K^+ fluxes are near 0 [89,152], suggesting that the anal papillae are not the location of K^+ uptake. Conversely, when the anal papillae of *Aedes aegypti* larvae were removed there was less uptake of K^+ when the larvae were placed in 1.7 mM KCl for 12 h to 14 h [153].

Pullikuth et al. [154] identified a $K^+/2H^+$-exchanger, possibly energized by VHA [155], in the midgut of mosquito larvae, and maximum absorption of K^+ occurred in the midgut of the midge *C. riparius* [152]. A hypothesized relationship between the $K^+/2H^+$-exchanger and VHA was tested by inhibiting VHA with amiloride or increasing the luminal [K^+], but neither decreased the alkalization, suggesting that these 2 transporters are independent [156]. A similar $K^+/2H^+$-exchanger has been studied extensively in terrestrial larvae of *Manduca sexta* (Supplemental Data, Table S4).

The whole-animal [Na]:[K] ratio in *A. aegypti* larvae was approximately 2.5:1, whereas the ratio in the hemolymph was 25:1 [153]. Moreover, larvae survived for 3 wk or more in distilled water, suggesting that the tissues held a reserve of K^+ for maintaining the low hemolymph concentrations. Other information on K^+-transport in aquatic insects is limited (Supplemental Data, Table S4).

Mollusca. Freshwater mussels require a minimal [K^+] but also do not tolerate high concentrations [157,158]. Optimal [K^+] in artificial freshwater for *D. polymorpha* ranged from 0.5 mM to 1.0 mM, and survival times decreased when [K^+] exceeded 1.5 mM [36,159]. Peak survival of *D. polymorpha* was observed when the [K^+]:[Na^+] ratio ranged from 0.01 to 0.02, and this bivalve tolerated artificial saltwater with a [K^+]:[Na^+] ratio in this range [36]. A similar [K^+]:[Na^+] ratio in the blood is found for Mollusca from various salinities [160]. The requirement for K^+ is related to its role in internal ion transport (Supplemental Data, Table S4), particularly the transport of Na^+ across the basolateral membrane via the NKA (Figure 5 and Table 2) [95]. Potassium also plays a role in cell volume regulation (Supplemental Data, Table S4).

Effects on K^+ transport by other ions in the water. In trout exposed to water with some combination of low pH, low Ca^{2+}, and Al, either whole-body [K^+] decreased or net efflux of K^+ increased. Similar increases in efflux or decreases in hemolymph [K^+] have been observed in crayfish exposed to low pH (Supplemental Data, Table S4). If K^+ transport across the apical epithelial membrane is by exchange with H^+, as has been suggested for some fish [23,147], inhibition of this transport may explain these observations, although increased efflux through more permeable epithelial tight junctions are also likely involved.

Synthesis. K^+ is a dominant intracellular cation and plays a well-studied role in transporting Na^+ across the basolateral membrane between the intracellular fluids and hemolymph or blood by NKA. Nevertheless, few details are available on how freshwater organisms obtain K^+ from the external environment, other than a few conjectured pathways with little evidence that NHE may transport K^+ and the presence of NKCC in adult *Daphnia*. Of the major ions, K^+ generally has the lowest ambient concentrations in freshwaters [161], so the concentration gradient across the gill epithelial apical membrane may be relatively steep. For example, hemolymph [K^+] in *D. polymorpha* was 0.4 ± 0.0 mM K^+ compared with 0.05 mM K^+ in pond water [60], and intracellular [K^+] is expected to be greater. There is evidence for active transport of K^+ from ambient freshwater for fish, crustaceans, and molluscs. The data for active uptake, at least through the anal papillae of freshwater Diptera, is mixed. However, there may be some evidence for uptake through the gastrointestinal system in aquatic insects.

Molluscs are sensitive to elevated water [K^+] to the point that K^+ is used as a molluscicide for *D. polymorpha* in water intake structures [159,162]. The most toxic of the major ions for *C. dubia*, *D. magna,* and fathead minnow was K^+ [128]. The available research with Mollusca suggests that these effects may be related to ionoregulatory disturbances associated with the role of K^+ in Na^+ transport and homeostasis and in volume regulation.

Calcium (Ca^{2+})

In freshwater osmoregulators, extracellular free [Ca^{2+}] can range from 0.25 mM to 7.7 mM [163], whereas intracellular free [Ca^{2+}] is much lower, 0.1 mM to 1 μM [163,164]. Although more extracellular and intracellular Ca is present, most is bound chemically to organic molecules, such as proteins and phospholipids [164] because intracellular free [Ca^{2+}] beyond these limits has adverse neural, muscular, and cardiovascular effects [165]. Even low ionic strength freshwaters generally have minimum [Ca^{2+}] of 2 μM to 230 μM and many exceed 2 mM [161,163]. Therefore, the normal gradient across the apical membrane in freshwaters is down a concentration gradient, unlike most other ions.

Teleost fish. Because the electrochemical gradient across the apical membrane favors Ca^{2+} entry, Ca^{2+} uptake across the gill apical membrane can occur by diffusion through a selective epithelial Ca^{2+}-channel (ECaC) [23,70,163,166,167]. Such a channel has been identified on the gill apical membrane ionocytes in rainbow trout (Figure 1 and Table 2) [168] and zebrafish (Figure 2 and Table 2) [167,169]. The second step, Ca^{2+} transport across the basolateral membrane, occurs against an electrochemical gradient and requires active transport [163]. In freshwater fish, this occurs by the combined action of a plasma membrane Ca^{2+}-ATPase (PMCA) and a Na^+/Ca^{2+}-exchanger (NCX) [23,70,163,167,170]. The reverse concentration gradient for Na^+ across the basolateral membrane used by the NCX is in turn maintained by NKA, which is collocated in the same ionocyte type [171–174].

At the low levels of free intracellular Ca^{2+} in freshwater fish (0.1−1 μM), PMCA may be more important than the NCX because the PMCA activity exceeds that of NCX until the [Ca^{2+}] approaches 1 μM, but only by a factor of 1.8 at 0.1 μM [175]. Increased cortisol, either as a result of exposure to low Ca^{2+} waters or by injection, increases Ca^{2+} uptake, primarily by increasing ionocytes with PMCA [176]. However, the NCX alone can maintain relatively low intracellular [Ca^{2+}] (Supplemental Data, Table S5).

Increased NKA can be an adaption to low [Ca^{2+}]. The ECaC also can increase in response to low [Ca^{2+}]. In rainbow trout, the transporters for Ca^{2+} are located on β-type ionocytes (Supplemental Data, Table S5).

In addition to uptake through the gills, Ca^{2+} is absorbed from food through epithelia of the fish gastrointestinal system. This occurs by very similar transporters [177,178] (Supplemental Data, Table S5).

Crustacea. Crayfish have been used frequently to study Ca^{2+} ionoregulation [179–182]. Because Ca is lost with molted exoskeletons, the Ca^{2+} requirement for Crustacea is substantial, and its uptake occurs mainly during postmolt following ecdysis [150,151,183–185]. During intermolt, crustacean Ca^{2+} requirements are met by reabsorption of up to 95% of the Ca^{2+} in the primary urine [186]. At ecdysis in *Procambarus clarkii*, only 17% of Ca^{2+} was retained, mostly in gastroliths, 42% was shed with the exuviae, and 41% had been excreted during the premolt stage [34]. Gastrolith Ca^{2+} was used to harden essential body parts, such as mouthparts and gastric ossicles for feeding and cactyles of the walking legs.

Because the movement is down a concentration gradient across the apical membrane, Ca^{2+} uptake is by an ECaC, which may be inhibited by verapamil [182]. However, this Ca^{2+} uptake is supplemented by at least 1 of 2 other exchangers (Figure 3 and Table 2). One is the amiloride-sensitive electrogenic H2Na(Ca)E, which was also discussed in relation to Na^+, where Ca^{2+} competes with Na^+ for external binding sites. This exchanger can transport either 2 Na^+ or 1 Ca^{2+} because it has 2 external binding sites, and because of competition for these binding sites, these ions competitively and reciprocally inhibit the other's passage [80,81,182,183,187]. This shared electrogenic exchanger for Na^+ and Ca^{2+} is also affected by the interaction between pH and Na^+ or Ca^{2+} [187]. As pH decreases in the external medium, the increased [H^+] gradient across the apical cell membrane inhibits export of H^+ and reduces influx of Na^+ or Ca^{2+} [188]. There is also evidence that 1 Na^+ can be exported by this exchanger in exchange for 1 Ca^{2+} [34,183], but H^+ is the preferred substrate [189].

There is also an electroneutral $2Na^+/Ca^{2+}$-exchanger that has a lower binding affinity for Ca^{2+} but a greater V_{max} [183]. Unlike the electrogenic H2Na(Ca)E, Na^+ is the favored antiport substrate rather than H^+, but this transporter can act as an electroneutral $2H^+/Ca^{2+}$-exchanger, which is identifiable by the insensitivity to amiloride [183]. Because of the differences in the direction of movement of Ca^{2+} during different stages of molt, these transporters can move Ca^{2+} both ways across epithelial membranes [190].

On the basolateral or other internal membranes, Ca^{2+}-ATPase generally maintains cytosolic Ca^{2+} at lower concentrations than found either in the water or in extracellular fluids [47,183,191,192]. This active cation transporter system is part of the family of P-type ATPases that also includes NKA. Although PMCA appears adequate to meet the transport requirements for Ca^{2+} during intermolt, the transport requirements are much greater during premolt and postmolt [182]. First, during premolt, Ca^{2+} is solubilized from the exoskeleton, transported through the epithelium to the hemolymph, and transferred for temporary storage. Then, during postmolt, the Ca^{2+} is mobilized from temporary storage, transported back across the epithelium, and deposited into the new exoskeleton [182]. Much of this increased transport across the basolateral membrane is accomplished by either an electrogenic $3Na^+/Ca^{2+}$-exchanger or an electroneutral $2Na^+/Ca^{2+}$-exchanger, both of which have greater transport capacities than PMCA [182,183]. However, PMCA is also up-regulated during the premolt and postmolt stages of *P. clarkii,* both in the gill and particularly in the antennal gland [193]. The electroneutral $2Na^+/Ca^{2+}$-exchanger, the electrogenic $3Na^+/Ca^{2+}$-exchanger, the amiloride-sensitive electrogenic H2Na(Ca)E, and Ca^{2+}-ATPase, also occur in the labyrinth of the antennal gland, where they reabsorb Ca^{2+} from the primary urinary filtrate [186,189]. In *P. clarkii* during the postmolt period, a portion of this Ca^{2+} is stored in the antennal gland, in part as a source of Ca^{2+} to maintain extracellular and intracellular fluid homeostasis [194].

Aquatic insects. Insect cuticle is not calcified and is mostly chitin and proteins [15,195]. Therefore, the calcium requirements of aquatic insects are much less than either crustaceans or molluscs, and aquatic insects may not require very high water [Ca^{2+}]. Also, organic detritus, which is a common trophic resource for aquatic insects, may be a significant source of Ca^{2+} along with Mg^{2+} and K^+ [196].

Research with larvae of the mosquito *A. aegypti* found that uptake of Ca^{2+} followed Michaelis–Menten kinetics and was inhibited by Ruthenium red, a PMCA inhibitor, but unlike the transporters for Na^+ and Cl^-, PMCA does not appear to occur in cells of the anal papillae (Supplemental Data, Table S5). Therefore, the location of divalent cation absorption is unclear.

As in other animals, much of the Ca^{2+} in the hemolymph appears to be bound to organic molecules, and there is relatively little free Ca^{2+} [197].

Mollusca. The Ca^{2+} requirements for freshwater Mollusca can be substantial. In addition to needing Ca^{2+} for their shells, Unionidae form calcium concretions in their gills. These calcium concretions provide calcium for the shells of the glochidia, which develop from up to several hundred thousand eggs in a brooding chamber formed in the female's gill [198–200].

Dreissena polymorpha maintained greater hemolymph [Ca^{2+}] in pond water, which contained less Ca^{2+}, than in artificial saltwater [60] (Supplemental Data, Table S5). The same authors [60] suggested that increased hemolymph [SO_4^{2-}] could be affecting the solubility of Ca^{2+} (SO_4^{2-} and Ca^{2+} being the least soluble anion and cation, respectively).

Unionids also regulate ion concentrations in extrapallial fluids separately from the hemolymph (Supplemental Data, Table S5). In *Amblema plicata*, extrapallial fluid [Ca^{2+}] was maintained at 3 to 4 times the water concentration.

Lymnaea stagnalis embryos have sufficient maternally supplied Ca^{2+} in the perivitelline fluid and gelatinous matrix surrounding the eggs for initial shell formation. However, after metamorphosis, Ca^{2+} concentrations decrease to less than ambient water concentrations. Embryos raised in Ca^{2+}-free water exhibit reduced growth rates and longer times to hatch [201], suggesting that an external source of Ca^{2+} is needed for completion of embryonic development. Results with pharmacological agents (Supplemental Data, Table S5) [202] suggest that uptake of Ca^{2+} is accomplished both by an L-type ECaC and by Ca^{2+}exchange for H^+, with the H^+ being supplied by the action of CA.

Effects on Ca^{2+} transport by other ions in the water. Uptake of Ca^{2+} is inhibited by other divalent metals, because these divalent metals can also be transported by the ECaC across the apical membrane [203–206] and interact with PMCA on the basolateral membrane [207,208]. Competition between Ca^{2+} and other divalent metals results in inhibition of Ca^{2+} uptake by the divalent metals and vice versa [209–213] (Supplemental Data, Table S5). Variability in the relative affinity of PMCA for divalent metals versus Ca^{2+} among species explains, in part, the variation in these metals' toxicity.

The electrogenic H2Na(Ca)E also transports divalent ions, such as Zn^{2+} and Cd^{2+}, in addition to Ca^{2+} across the apical membrane [80] (Supplemental Data, Table S5). Therefore, competition for the external binding sites with Ca^{2+} explains the effect of water hardness on bioavailability and toxicity of these metals and Cu^{2+} in crustaceans [214]. This exchanger on vacuolar membranes is involved in metal sequestration into phosphate or sulfate concretions, a detoxification mechanism in crustaceans, and Ca^{2+} is sequestered into similar concretions until needed during molting [80]. In Crustacea, as in fish, Cd^{2+} and Ca^{2+} also compete for the ECaC (Supplemental Data, Table S5).

Although the location of Ca^{2+} transporters on *C. riparius* (midge) epithelia is unknown, Ca^{2+} uptake is inhibited by Cd^{2+} as in fish and Crustacea (Supplemental Data, Table S5). In Ephemeroptera and Trichoptera, which have tracheal gills, uptake mechanisms for divalent metals involve Ca^{2+} transporters associated with ionocytes (Supplemental Data, Table S5). Differences in the effect of verapamil, an inhibitor of ECaC, suggest differences in ECaC between these orders [215]. Also, differences in the relative affinity of the shared transporters for Ca^{2+} and Cd^{2+} or Zn^{2+} in these insects suggest that these transporters differ from those in Crustacea or fish (Supplemental Data, Table S5).

As in other freshwater animals, inhibition of divalent metal uptake by elevated ambient [Ca^{2+}] suggests the presence of at least an ECaC on the gill apical epithelial membrane of Mollusca (Figure 5 and Table 2). Divalent metal uptake was inhibited by elevated Ca^{2+} in freshwater bivalves, and Ca^{2+} uptake was inhibited by divalent metals in *L. stagnalis* (Supplemental Data, Table S5). Elevated [Ca^{2+}] in the hemolymph and extrapallial fluids occurs, because Cd^{2+} inhibits PMCA [216] and CA [217], which assist in movement of dissolved Ca^{2+} into the shell and into concretions in the soft tissues (Supplemental Data, Table S5).

As with Na^+ and K^+, inhibition of exchange of Ca^{2+} for H^+ may explain the observation that negative net Ca^{2+} flux occurred in crayfish, such as *Orconectes propinquus,* exposed to pH 4.0 [218]. However, the same authors [218] also suggest that $CaCO_3$ was demineralized from the crayfishes' exoskeletons. Other crayfish can vary in their sensitivity to low pH (Supplemental Data, Table S5).

Synthesis. It is clear that Ca^{2+} is required by aquatic organisms, and most Ca^{2+} uptake is from ambient water by epithelial ionocytes with a relatively common set of transporters, particularly the ECaC on the apical membrane and PMCA on the basolateral membrane. These similarities are evident from the similarities in uptake and competitive inhibition of Ca^{2+} uptake by a number of divalent metals. However, as with the transporters for Na^+, some uncertainties exist for the aquatic insects because there is less research on this group (the transporter locations of the epithelial ionocytes have not been identified).

Particularly, Crustacea, which harden their exoskeleton with Ca^{2+} and then lose a significant proportion of that Ca^{2+} during molting, have a number of both apical and basolateral transporters that contribute to the uptake of Ca^{2+}, particularly the potentially unique electrogenic H2Na(Ca)E, which has the shared potential for both Ca^{2+} and Na^+ uptake. Because of this transporter's role in Crustacea, there is potential for mutual competitive inhibition of Ca^{2+} and Na^+ uptake. This may explain at least in part the observed relationship between hardness (i.e., [Ca^{2+}]) and the toxicity of Na^+-salts, such as NaCl and Na_2SO_4, in bioassays particularly with Crustacea [129,131–135]. This also explains the inhibition of Ca^{2+}uptake by alterations in the concentration gradient for H^+, either by decreased ambient pH or inhibition of CA activity in Crustacea [182,183,187,218]. Although freshwater Mollusca also accumulate Ca^{2+} in their shells, the turnover is not as great as in Crustacea, and the process appears to be more gradual and involves formation of Ca concretions in their soft tissues. However, research on the evolutionary relationships among functionally similar ion transporters has not been conducted for these invertebrate groups.

It is clear that Ca^{2+} contributes to the osmolarity of freshwaters, and elevated dissolved Ca^{2+} in intracellular and extracellular fluids can cause adverse effects. However, animals have very efficient homeostatic mechanisms to move Ca^{2+} out of the dissolved form and into other forms, such as organic molecules or particulates, like $CaCO_3$ or $Ca_3(PO_4)_2$, which can be stored in bone, concretions, shells, or exoskeleton. Most toxicity associated with Ca salts in a study of 2 cladocerans and a fish could be attributed to the salt's associated anion; the Ca^{2+} cation itself was relatively nontoxic [128]. Conversely, there appears to be potential for the Michaelis–Menten uptake variables K_m and V_{max} for Ca^{2+} uptake to vary significantly

among families and species [219]. Such physiological variation might underlie the differences in tolerance to low [Ca^{2+}] and the resulting distribution of species along natural gradients, such as between soft and hard waters [220].

Magnesium (Mg^{2+})

In extracellular fluids, Ca^{2+} is predominant over Mg^{2+}, while within the cells, [Mg^{2+}] is generally greater, often being at least the third most abundant cation [221] and [Ca^{2+}] is relatively low [222]. Magnesium is a cofactor for enzymes that transfer phosphate groups, such as the ATPases, involved in energizing the pumps for H^+ and Ca^{2+} and the exchanger for Na^+ and K^+ [221,223], and most cellular Mg^{2+} is associated with ATP [224]. As a result, Mg^{2+} deficiency has been implicated in imbalances of Ca^{2+}, Na^+, and K^+, including shifts in the [K^+]:[Na^+] ratio in fish [225].

In its ionic geometry, Mg^{2+} is unusual among common cations, because it has a high hydrated radius but low ionic radius. Thus, Mg^{2+} requires a transporter protein with a large binding site and a dehydration mechanism to fit the cation through a relatively small pore [226]. In terrestrial vertebrate plasma membranes, Mg^{2+}-channels in the solute carrier (SLC) 41 family have been identified and are homologous to an Mg^{2+} transporter family identified from prokaryotes [227]. However, no similar transporters have yet been identified in fish or aquatic invertebrates.

Teleost fish. The freshwater fish absorb most required Mg^{2+} from their diet across the intestinal epithelia [228] (Supplemental Data, Table S6). Transport of Mg^{2+} across the apical membrane of the intestinal epithelia is by electrodiffusive transport along a negative potential gradient associated with K^+ across the membrane, and transport can be inhibited by some divalent metals, particularly Co^{2+} and Ni^{2+} [229]. Transport across the basolateral membrane is by an anion/Mg^{2+}-cotransport mechanism using membrane-permeable anions, such as Cl^-, SO_4^{2-}, or NO_3^- [230,231]. The amount of Mg^{2+} absorbed through the gill epithelia directly from the water is variable among fish species. Common carp (*Cyprinus carpio)*, for example, absorb at least 84% of Mg^{2+} from food through the intestinal tract, and the remainder is absorbed through the gills from the water [232]. Moreover, Mg^{2+} absorption by the gills can be insufficient to meet the need for Mg^{2+} (Supplemental Data, Table S6), particularly in quickly growing juvenile fish [233]. Conversely, tilapia fed a low Mg diet continued to grow (Supplemental Data, Table S6), which indicates that these fish absorb sufficient Mg^{2+} from the water through their gills [170]. Although 1.9 mM Mg^{2+} in water was sufficient to meet the requirements of juvenile rainbow trout fed a low Mg^{2+} diet, exposure to high [Mg^{2+}] caused mortality (Supplemental Data, Table S5). However, that study did not investigate a mechanism for these adverse effects [234]. Loss of Mg^{2+} is primarily by renal excretion [235], but Mg^{2+} retention is efficient because the element is reabsorbed by the renal epithelium [236].

Crustacea. In the freshwater prawn *Macrobrachium rosenbergii* hemolymph [Mg^{2+}] peaked at 1.56 mM Mg^{2+} at 2 d to 3 d premolt and decreased postmolt to a minimum during the intermolt period [237]. Similar patterns of variation in Mg^{2+} were observed in the exoskeleton, hepatopancreas, and whole body. Premolt [Mg^{2+}] was similar to the water [Mg^{2+}] (1.8 mM), suggesting that the increase resulted from movement of water and diffusion of Mg^{2+} across an increasingly permeable epithelial membrane and was perhaps associated with the role of Mg^{2+} as a cofactor in the ATPases involved in ion transport during the molt [237].

Aquatic insects. In *Aedes campestris*, a mosquito that lives in alkali ponds dominated by $NaHCO_3$ and, particularly in summer, Mg^{2+}, the larvae drank the water (as do most animals living in hypertonic waters), and most of the ingested Mg^{2+} was absorbed into the hemolymph from the midgut [238]. Hemolymph [Mg^{2+}] was maintained at <5 mM compared with a water [Mg^{2+}] of up to 100 mM. This difference was because of the Mg^{2+} being excreted by the Malpighian tubules and salt gland [239]. Urine [Mg^{2+}] exceeded the water [Mg^{2+}] [238].

Mollusca. Bivalves, possibly because they are filter feeders and are not as strong hyper-regulators in freshwaters, appear to depend more on absorption of Mg^{2+} through the gill epithelia from the water [240] (Supplemental Data, Table S6). When *D. polymorpha* were placed in different salt solutions, solutions lacking Mg^{2+} caused 100% mortality in less than 20 d, as did solutions lacking Na^+ or Cl^-. However, unionids and *Corbicula* appear to have ionoregulation mechanisms to avoid this depletion of Mg^{2+}, because these bivalves have been maintained in deionized water for much longer [240].

Effects on Mg^{2+} transport by other ions in the water. Toxicity testing in support of a biotic ligand model for acute Cu toxicity suggested that increased [Ca^{2+}], [Na^+], and [Mg^{2+}] all increase the 48-h 50% effects concentration values for Cu^{2+} [214]. Although both Na^+ and Ca^{2+} may competitively inhibit uptake of Cu^{2+} by the electrogenic H2Na(Ca)E, this transporter is not known to transport Mg^{2+}, and the interaction between Mg^{2+} and Cu^{2+} is unclear. Moreover, Ni^{2+}, which is known to move through Mg^{2+} transporters in prokaryotes [226], reduced Mg^{2+} influx and whole-body [Mg^{2+}] in *Daphnia* spp. exposed to 0.8 μM to 59 μM Ni^{2+} [241,242]. In *L. stagnalis*, soft tissue [Mg^{2+}] decreased after acute and chronic exposures to 8 μM and 0.29 μM Ni^{2+}, respectively [242,243]. These observations suggest the presence of an Mg^{2+} transporter similar to those found in prokaryotes.

Synthesis. Although the role of Mg^{2+} in cells, particularly as a cofactor for ATPases, is clear, relatively little has been published on the transepithelial transport of Mg^{2+} in aquatic animals. Much of the Mg^{2+} in juvenile and adult freshwater fish appears to be obtained from food, but there is interspecific variability. Studies of crustaceans suggest that transport of Mg^{2+} from ambient water across the gill epithelium may be down a concentration gradient, and some studies of Mollusca agree. However, the study of *D. polymorpha* in dilute pond water suggests a more active Mg^{2+} transport mechanism across the gill epithelium [240]. Several studies suggest that Mg^{2+} can cause mortality at greater concentrations [234], and the relative toxicity of Mg^{2+} has been ranked as similar to HCO_3^- but less than K^+ [128].

Several toxicological papers have suggested that Mg^{2+} has a role in the uptake and toxicity of metals, apparently based mostly on the protective effect of water hardness on some metals and experiments conducted with Ag^+ and Cu^{2+} [214,244,245]. However, no effects on accumulation of Ag^+ measured as total gill [Ag^+] were found for water [$MgSO_4$] of 0 mM to 210 mM or water [$CaSO_4$] of 0 mM to 8.6 mM in rainbow trout [244]. No relationship between [Ca^{2+}]:[Mg^{2+}] ratios and Cu^{2+} toxicity was found for fathead minnows *C. dubia*, or *Gammarus* spp. [245]. Other studies have shown that uptake of both Ag^+ and Cu^{2+} occurs by an Na^+ transporter and not the ECaC, unlike other divalent metals, and Mg^{2+} should have little effect on the uptake of these 2 metals, particularly if one assumes a relationship with Ca^{2+}. However, there is no evidence that Mg^{2+} is transported by a Ca^{2+} transporter. Moreover, it is unclear why Cu^{2+} toxicity, as measured by an acute median

lethal concentration (LC50), increases in fingerling rainbow trout and decreases in *D. magna* with increasing [Mg^{2+}] [245]. More research is needed on Mg^{2+} transporters in freshwater animals to better understand the ionoregulation of this ion.

Chloride (Cl^-)

Similar to uptake of Na^+ in exchange for H^+, uptake of Cl^- is in exchange for an ion that is a product of metabolism, HCO_3^-. Both vertebrate and invertebrate apical membranes possess a Cl^-/HCO_3^--exchanger (or anion exchanger) [3,23,75,166,246–249]. Although Cl^- uptake is clearly independent of the Na^+ uptake [246], VHA activity appears to enhance uptake of Cl^- by the anion exchanger, particularly when the [Cl^-] is very low [250].

Teleost fish. Research on fish [251] first suggested that HCO_3^- was exchanged for Cl^-. Moreover, inhibition of CA, which catalyzes formation of HCO_3^- and H^+, decreased the uptake of Cl^- in rainbow trout gills [252]. The uptake affinity and capacity for zebrafish of Cl^- was more than 3 times greater in soft water (43 μM Cl^-) than in hard water (1625 μM Cl^-) [250], and uptake was inhibited by bafilomycin, a VHA inhibitor. Inhibition of Cl^- uptake by ethoxzolamide, a CA inhibitor, in both hard and soft water, adds evidence that Cl^- uptake occurs by exchange for HCO_3^-. Moreover, in soft water this exchange appears to be inhibited by reduction of the concentration gradient for HCO_3^- across the apical membrane [250]. Molecular analyses of zebrafish implicate anion transporters of the SLC26 family as the anion exchanger most involved in Cl^- transport and located these transporters on the apical membrane of base-excreting ionocytes (Figure 2 and Table 2) [253] (Supplemental Data, Table S7). On the yolk-sac membrane of tilapia larvae, the proportion of active ionocytes (indicated by the presence of concanavalin-A), which also stained for NKA, increased in larvae acclimated for 48 h to low [Cl^-] artificial freshwater (2−7 μM) compared with larvae in high Cl^- artificial freshwater (7500−7900 μM) [254]. These ionocytes were inactivated at high Cl^- by being covered by pavement cells. This interaction, which also involves CA, occurs because of an ion-transport metabolon [255] (Supplemental Data, Table S7). However, variation in anion exchanger among fish species is suggested by pharmacological differences between goldfish (*Carassius auratus*) and neon tetra (*Paracheirodon innesi*) [256] (Supplemental Data, Table S7). In addition to the anion exchanger, NCC, which is discussed in relation to Na^+ uptake (*Sodium (Na^+) - Other Na^+ transporters*), uses the Na^+ gradient created by combined action of NKA and the NBC on the basolateral membrane to transport Cl^- against its concentration gradient across the apical membrane between freshwater and the cytosol [99,101,166].

Some Cl^- uptake can occur from food in the gastrointestinal system. Rainbow trout absorbed approximately 80% of the Cl^- in a single experimental meal that supplied 2.65 mmol Cl^- kg^{-1} fish body mass [257].

Cytosol [Cl^-] in epithelial ionocytes is maintained at higher levels than in extracellular fluids and allows Cl^- transport across the basolateral membrane by a Cl^--channel [3,166]. Limited research has been conducted to characterize such basolateral channels in fish gill ionocytes, and 2 types of Cl^--channels have been identified. One similar to the Cl^- channel 3 has been identified in spotted green pufferfish (*Tetraodon nigroviridis*) [258] and another is related to the cystic fibrosis transmembrane regulator [166,259]. In rainbow trout, a maxi Cl^--channel has been described in pavement cells that may fulfill this function [260]. Although most research has been conducted on terrestrial vertebrates, the SLC26 family includes diverse anion exchangers that couple exchange of Cl^- with other anions, including HCO_3^-. The family also includes several transporters that can act as either an obligatory coupled exchanger or as an ion channel [261].

Crustacea. As a major hemolymph osmolyte along with Na^+, Cl^- uptake increases ($J_{net}^{Cl} = 250–800\ \mu mol\ kg^{-1}\ h^{-1}$) during the postmolt period in crayfish, primarily to counteract the dilution of hemolymph ion concentrations by water absorption and the increase in body volume following ecdysis [150,151]. Uptake occurs in exchange for HCO_3^- and is reduced by acetazolamide, which inhibits CA [79]. As with Na^+, renal filtration and reabsorption of Cl^- in the antennal gland exceeds fluxes through the gills during intermolt because recycling of these ions is more energy efficient [34]. In addition to the anion exchanger, NCC and NKCC, which is discussed in relation to Na^+ uptake (*Sodium (Na^+) - Other Na^+ transporters*), have been detected pharmacologically in neonates and adults, respectively, of the cladoceran *D. magna* [102].

In freshwater Decapoda, gas and ion exchange is separated among different gill filaments and lamina on the branchiae [262,263] (Supplemental Materials, Table S6). This separation of functions between gill filaments and lamina also separates the 2 functions of CA [264,265], shifting the equilibrium toward HCO_3^- for exchange of Cl^- at the apical membranes of the lamina ionocytes, while shifting the equilibrium toward CO_2 at the basolateral membranes of the second filament type for excretion across the epithelia [266]. Most research with Decapoda indicates that inhibition of CA affects Cl^- uptake more than Na^+ uptake [267]. Similarly, in the cladoceran *D. magna, 2* types of gill epithelial cells, called dark and light cells, are hypothesized to be involved in ionoregulation and gas exchange, respectively [268].

Aquatic insects. Stobbart [269] provided evidence for exchange of Cl^- for HCO_3^- during uptake of Cl^- across the anal papillae by larvae of *A. aegypti* via active transport mechanisms [270]. Application of methazolamide (CA inhibitor), 4-acetamido-4′-isothiocyanatostilbene-2-2′-disulfonate (anion exchanger inhibitor), or 4,4′-diisothiocyanatostilbene-2,2′-disulfonic acid (DIDS; anion exchanger inhibitor) to the anal papillae of *A. aegypti* reduced Cl^- uptake by 79%, 80%, and 40%, respectively [271]. Bumetanide (NKCC) had no effect on Cl^- uptake, supporting the role of anion exchanger but not an NKCC in Cl^- uptake across the anal papillae (Figure 4 and Table 2). In *Anopheles albimanus*, an apical anion exchanger on dorsal anterior rectal cells in the rectum uses HCO_3^- produced by CA in either ventral anterior or posterior rectal cells to exchange for Cl^-, resorbing this ion from the insect's primary urine [272].

One factor in the sensitivity of freshwater-restricted mosquitoes such as *Culex quinquefasciatus* to increased NaCl salinity may lie in the permeability of their anal papillae to influx of Cl^- compared with euryhaline species such as *Culex tarsalis* [273] (Supplemental Data, Table S7). Similar variation in permeability was observed among euryhaline and freshwater of caddisflies (Supplemental Data, Table S7).

However, the Cl^- uptake process is clearly independent from that of Na^+. When *A. aegypti* larvae were transferred from freshwater to 30% saltwater and back [90], the K_m for Na^+ uptake was altered, whereas that for Cl^- remained relatively constant, and recovery of V_{max} for Na^+ was much slower than that for Cl^- (20 h vs 5 h) when the larvae were returned to freshwater.

In Ephemeroptera, autoradiography and histochemical precipitation showed active Cl^- absorption across a steep concentration gradient [274] by ionocytes on the tracheal gill epithelia [275]. The Cl^- uptake rate was directly related to the water hypotonicity, showing that the cells were involved in ionoregulation. Similar results were observed for ionocytes in aquatic Hemiptera nymphs in Notonectidae and Naucoridae [276].

As with Na^+, the anal papillae of the midge *C. riparius* are a site of Cl^- ion uptake [89]. The anal papillae of marsh beetle larvae, *Elodes minuta* and *Odeles marginata* (Coleoptera, Scirtidae), are also a site of active Cl^- uptake [277]. However, none of these authors measured HCO_3^- and did not demonstrate exchange of these anions. Similarly, chloride epithelia in the rectal chamber of dragonfly nymphs (*Uropetala carovei* and *Aeshna cyanea*) were involved in active uptake of Cl^- in addition to Na^+ [278–281], although the mechanisms for Cl^- uptake were not elucidated.

Mollusca. Although unionids have anion exchangers [95], these river mussels maintain approximately equal amounts of Cl^- and HCO_3^- in their extracellular fluids, and pH maintenance relies more on exchange of Na^+ and H^+ [282] (Figure 5 and Table 2). Transport of Cl^- in *Ligumia subrostrata* was inhibited by DIDS (anion exchanger inhibitor) and thiocyanate (Cl^- transporter inhibitor), but not furosemide (NKCC) [283]. As with other freshwater groups, exchange of HCO_3^- for Cl^- is independent of Na^+ in freshwater mussels (Supplemental Data, Table S7). Also, hemolymph [Cl^-] increases and become isoionic with increasing salinity (Supplemental Data, Table S7). It was hypothesized that HCO_3^--dependent ATPase is involved in this Cl^-/HCO_3^- exchange in 2 freshwater gastropods (Architaenioglossa), *Viviparus contectus* and *Pomacea canaliculata* [284], but reanalysis suggests the authors may have misinterpreted the activity of VHA, which in fish and decapods removes H^+ and maintains the supply of HCO_3^- from CA-catalyzed hydrolysis of CO_2 to the anion exchanger [250,285] (Supplemental Data, Table S7).

Effects on Cl^- transport by other ions in the water. In fish and crustaceans, exposure to pH of 4.0 to 4.3 causes net flux of Cl^- from the extracellular fluids along with decreased [HCO_3^-] and pH; P_{CO2} is unchanged or increased (Supplemental Data, Table S7). Current models suggest that inhibition of HCO_3^- production by decreased extracellular pH decreases the availability of HCO_3^- to exchange for Cl^-. At the same time, HCO_3^- is retained to maintain extracellular acid–base balance.

Uptake of NO_2^- can occur through the anion exchanger in both fish and Crustacea. This transporter has an affinity for several anions in addition to Cl^-, including Br^- but not SO_4^{2-} or PO_4^{3-} [286,287]. It competitively inhibits uptake of Cl^- and reduces blood [Cl^-] while blood [NO_2^-] increases [288,289]. Conversely, elevated Cl^- or Br^- can inhibit uptake of NO_2^- [287]. In crayfish, increased hemolymph [HCO_3^-] as a result of induced hypercapnia increased NO_2^- uptake because HCO_3^- is the counter ion for anion exchanger [286] (Supplemental Data, Table S7). In fish, NO_2^- has an added effect on respiration (Supplemental Data, Table S7).

In rainbow trout and several tetra species acutely exposed to Ag^+, Cl^- uptake decreased, as did Na^+ uptake [113,290]. There was also a decrease in CA activity, which would limit the supply of HCO_3^- for exchange with Cl^-.

Synthesis. The most important anion for osmoregulation in freshwater animals is Cl^-. Although its transport across gill epithelial membranes is independent of Na^+ transport, there are a number of parallels because the transporters for Cl^- and Na^+ exchange these ions for HCO_3^- and H^+, respectively. In turn, HCO_3^- and H^+ are produced by hydration of CO_2 by CA and have opposing roles in maintaining acid–base balance in intracellular and extracellular fluids. In most freshwater animals, an anion exchanger moves Cl^- across the apical epithelial membrane, while some type of Cl^--channel moves Cl^- across the basolateral epithelial membrane. As with H^+ and the NHE or VHA, elevation of ambient water [HCO_3^-] can inhibit Cl^- uptake by increasing the [HCO_3^-] gradient across the apical membrane.

Elevation of a number of other ions in the water has been shown to inhibit uptake of Cl^- by the anion exchanger: H^+ or low pH inhibit Cl^- uptake because they appear to inhibit VHA by increasing the H^+ gradient across the apical epithelial membrane. Also, removal of H^+ helps maintain the [HCO_3^-] gradient required for the anion exchanger [255]. Anions such as NO_2^- and Br^- inhibit uptake of Cl^- by competing for attachment sites on the exchanger.

Because of the importance of Cl^- in osmoregulation, any effects associated with elevated Cl^- appear to be related to osmotic imbalances. Particularly in stenohaline freshwater animals, extracellular [Cl^-] generally remains greater than that in increasingly saline water until the water becomes isotonic with the hemolymph. Then, at greater salinities, extracellular [Cl^-] either increases and remains approximately isotonic with the water (as in invertebrates) or becomes hypotonic with the water (as in fish). At this point mortality often becomes significant [139,140]. As a result, Cl^- ranks low in relative toxicity [128].

Bicarbonate (HCO_3^-)

As in all aerobic organisms, CO_2 is produced by respiration and eliminated from the bodies of freshwater animals. However, because CO_2 is more water soluble than O_2, the greater ventilation rates of gas-exchange surfaces in water-breathing organisms render changes in P_{CO2} relatively ineffective at controlling intracellular and extracellular pH [291]. Although a significant proportion of molecular CO_2 is still eliminated by passive diffusion across the epithelia [291], CA in the cytosol catalyzes the hydration of CO_2 and shifts the equilibrium to H^+ and HCO_3^-, making these ions available for exchange across the apical membrane and for regulation of the concentrations of Na^+ and Cl^-, respectively, [292]. This exchange of acid–base equivalents also regulates the acid–base balance of intracellular and extracellular fluids [15,292,293].

Teleost fish. In a 2-substrate enzyme model, the rate of ion transport is dependent on the availability of the internal substrate, which in this case is H^+ or HCO_3^-, as well as the external substrates, Na^+ and Cl^-, respectively [294,295]. If metabolic acidosis occurs, [H^+] increases while [HCO_3^-] decreases, which in turn increases exchange of H^+ for Na^+ and decreases exchange of HCO_3^- for Cl^-, thereby increasing acid excretion and decreasing hemolymph [Cl^-] (Supplemental Data, Table S8). The decreased exchange of HCO_3^- for Cl^- may occur because the anion exchanger on ionocyte apical membranes (Figure 1 and Table 2) are physically covered by adjacent pavement cells [296]. However, the decrease in blood [Cl^-] could result from a reversal of HCO_3^-(influx)/Cl^-(efflux) exchange by the apical anion exchanger based on observations that compensation for decreased pH from hypercapnia occurred more quickly in waters with greater [HCO_3^-] (5.3 mM) than in those with lower [HCO_3^-] (0.13 mM) [297]. If metabolic alkalosis occurs, H^+ is retained and HCO_3^- is exchanged for Cl^-, increasing base

excretion [298]. Together, this negative feedback system regulates acid–base balance [295]. Under balanced acid–base status, uptakes of Na^+ and Cl^- are equal to maintain these conditions [299].

However, at least among rainbow trout, American eel, and brown bullhead (*Ameiurus nebulosus*), there is variation in whether a decrease in pH (i.e., systemic acidosis) is countered by decreased excretion of HCO_3^- or increased H^+ excretion [291,292,299,300], and interspecies differences occur in the relative importance of Na^+/H^+ versus Cl^-/HCO_3^- exchange to maintaining acid–base balance (Supplemental Data, Table S8).

The transporters involved export of HCO_3^- or H^+ across the apical membrane and in acid–base regulation are also segregated among different epithelial cell types [21,66,70,71,249,255,292,301]. Depending on the fish species, various ion transporters may be segregated among 2 to 4 cell types [71,301–303] (Figures 1 and 2). This segregation allows these ions to be moved between the cytosol and hemolymph for maintaining acid–base balance and for use in transporters (e.g., NBC) on the basolateral membrane [99]. Moreover, this variation in the relative importance of Na^+/H^+ versus Cl^-/HCO_3^- may explain the variation in response to acidosis.

Although they did not investigate the physiological mechanisms, Harper et al. [304] assessed the toxic effects of $NaHCO_3$ as a major constituent of produced waters from coalbed natural gas wells. The 96-h LC50 values for the larval stages (1−22 d posthatch [dph]) of white sucker (*Catostomus commersonii*), fathead minnow, walleye (*Sander vitreus*), rainbow trout, and northern pike (*Esox lucius*), respectively, were estimated as 13.6 mM, 38.5 mM, 58.9 mM, 93.4 mM, and 131.1 mM $NaHCO_3$. For fathead minnows, the chronic LC50 for survival at 37 dph was 6.0 mM $NaHCO_3$, whereas a 7-d growth test that began with 2-dph larval fish had a 20% effect concentration of 8.2 mM $NaHCO_3$ [305]. The lower toxicity values appear to result from effects of HCO_3^- rather than Na^+.

Crustacea. During premolt in crayfish, excretion of CO_2 increases above intermolt rates. Immediately following ecdysis, CO_2 excretion decreases [306], probably reflecting accumulation of HCO_3^- with Ca^{2+} as $CaCO_3$ in the exoskeleton [150].

When tissue and hemolymph acidosis (i.e., decrease of 0.1–0.5 pH units by 3 h) was induced by exposing *Pacifastacus leniusculus* to hyperoxia ($P_{O2} = 67$ kPa), this acidosis was corrected by metabolic accumulation of $HCO_3^- + CO_3^{2-}$ by 48 h [59]. Consequent to this accumulation of $HCO_3^- + CO_3^{2-}$ was a small net loss of Cl^- (Supplemental Data, Table S8).

A number of studies have shown that HCO_3^- can cause adverse effects to Cladocera and freshwater shrimp (Table 3). The effects for $NaHCO_3$ occur at lower molar concentrations or specific conductivity than those for NaCl, showing that there were effects in excess of those resulting from Na^+ or Cl^-.

Aquatic insects. The role of HCO_3^- and H^+ in maintaining acid–base balance has not been directly investigated in aquatic insects. However, logically these ions likely play a role similar to that in other aquatic animals. One question that might be important in the case of aquatic insects is whether the CO_2 is supplied by respiration in the individual ionocytes or whether there is some other mechanism that moves CO_2 to the ionocytes, because gas exchange in most aquatic insects occurs separately via the tracheal system.

Studies of the adverse effects of HCO_3^- in water for aquatic insects are few. A 96-h LC50 for *Chironomus dilutus* was 58.9 mM $NaHCO_3$ [304]. An analysis was conducted of macroinvertebrates in streams of the central Appalachians, where the most abundant elevated anions were HCO_3^- and SO_4^{2-}, and showed a field-based species sensitivity distribution of 95% extirpation concentration values for specific conductivity (a measure of the total ion concentration), which for aquatic insects ranged from 150 μS/cm to >11 000 μS/cm. The results also showed a 5% hazardous concentration of 300 μS/cm [307].

Mollusca. In the unionid *Anodonta cygnea*, CA catalyzed hydration of CO_2 supplies HCO_3^- for transport of Cl^- [95]. Short-circuit current across the outer mantle epithelium of *A. cygnea* was inhibited by acetazolamide (CA inhibitor), DIDS (anion exchanger inhibitor), and dinitrophenol (VHA inhibitor), showing that the short-circuit current was affected by the $[CO_2]$ and $[HCO_3^-]$ as well as $[H^+]$ in the shell-side solution and that acid–base transport was inhibited [308]. Therefore, acid–base balance across this outer mantle epithelium was maintained by both anion exchanger and VHA (Figure 5 and Table 2). However, in *D. polymorpha*, HCO_3^- was not excreted to counter an increase in pH (Supplemental Data, Table S8).

Comparing an estuarine osmoconformer, *Rangia cuneata*, with 2 freshwater hyper-regulators, *L. subrostrata* and *Corbicula fluminea*, CA activity in the gills increased among these species to the extent that the animals' hemolymph $[Na^+]$ and $[Cl^-]$ were regulated above the ambient water concentrations. This reflected the increased Na^+/H^+ and Cl^-/HCO_3^- exchange to maintain these gradients [309] (Supplemental Data, Table S8).

In molluscs, CA plays a role in exchange of Ca^{2+} between the dissolved ion form and solid forms, such as in concretions and the shell, by affecting the equilibrium between CO_3^{2-} and

Table 3. Results of bioassays with Crustacea comparing $NaHCO_3$ and NaCl

Species	Endpoint	Effect	Concentration (mM)	Salt	Conductivity (μS cm^{-1})	Reference
Ceriodaphnia dubia	EC10	Reproduction	19.9 ± 1.5	$NaHCO_3$	1900	Lopez Vera et al. [348]
C. dubia	EC50	Reproduction	24.1 ± 0.3	$NaHCO_3$		
C. dubia	EC10	Reproduction	ND	NaCl	2800	
Daphnia magna	48-h LC50	Mortality	15.1 ± 2.2	$NaHCO_3$		Hoke et al. [349]
D. magna	48-h LC50	Mortality	81.3 ± 6.2	NaCl		
C. dubia	48-h LC50	Mortality	12.8 ± 1.5	$NaHCO_3$		
C. dubia	48-h LC50	Mortality	13.5 ± 2.2	NaCl		
C. dubia	48-h LC50	Mortality	11.5	$NaHCO_3$		Harper et al. [304]
C. dubia	EC20	Reproduction	4.5	$NaHCO_3$		Farag and Harper [305]
Paratya australiensis	10-d LC10	Mortality	10.1 ± 1.4	$NaHCO_3$		Lopez Vera et al. [348]
P. australiensis	10-d LC50	Mortality	15.2 ± 2.5	$NaHCO_3$		

C10 = 10% effects concentration; EC20 = 20% effects concentration; LC10 = 10% lethal concentration; LC50 = median lethal concentration; ND = not determined.

HCO_3^-. Inhibition of CA increased $[Ca^{2+}]$ in the hemolymph and extrapallial fluids (Supplemental Data, Table S8).

A study of the effects of $NaHCO_3$ as a constituent of produced water from coalbed natural gas wells included the unionid *Lampsilis siliquoidea*. Using absence of foot movement during a 5-min observation as the indicator of mortality, the 96-h LC50 and 7-d LC50 for juveniles were 13.8 mM and 12.6 mM $NaHCO_3$, respectively [304,305].

Synthesis. HCO_3^- and H^+ play a primary role in acid–base balance of extracellular and intracellular fluids in freshwater animals. Because elevated $[H^+]$ in ambient waters inhibits exchange of H^+ for Na^+ by increasing the $[H^+]$ gradient across the apical epithelial membrane, elevation of ambient water $[HCO_3^-]$ can also inhibit exchange of HCO_3^- for Cl^-, apparently in the same manner, by increasing the $[HCO_3^-]$ gradient against which the anion exchanger is excreting HCO_3^-. Inhibition of HCO_3^- excretion would have at least 2 direct effects. First, it could cause metabolic alkalosis, increasing hemolymph or blood pH. Second, it could, in particular, cause decreased hemolymph or blood $[Cl^-]$. Adverse effects, including impaired reproduction and mortality, have been identified in some fish, crustaceans, aquatic insects, and molluscs. In terms of its acute relative toxicity to standard bioassay species, HCO_3^- ranked only behind K^+ [128].

Sulfate (SO_4^{2-})

Sulfate appears to be an impermeant anion to the gills of freshwater fish [310,311], crustaceans [312,313], and unionid molluscs [25]. However, some research has identified SO_4^{2-} transporters, particularly in ionocytes of the gastrointestinal and renal systems.

Teleost fish. Although similar data are lacking for fish, active transport of SO_4^{2-} into *Bufo bufo* (European toad) has been localized to ionocytes in the skin [314] (Supplemental Data, Table S8). Larsen and Simonsen [314] suggested that SO_4^{2-} was transported in exchange for HCO_3^- via an exchanger similar to, if not the same as, the anion exchanger. Also, the transported ion is monovalent (i.e., XSO_4^-), and the antiporter is energized by movement of HCO_3^- down its concentration gradient as in the anion exchanger.

Several SO_4^{2-} transporters have been identified in the SLC26 and SLC13 families of anion transporters [315]. Although most research on these transporter families has been on terrestrial vertebrates [261], transporters that are homologs of the human anion exchanger SLC26a1 have been identified in the kidney of Japanese eel (*Anguilla japonica*) and rainbow trout [316,317]. In rainbow trout that were infused with solutions of $MgSO_4$ or Na_2SO_4, most of the SO_4^{2-} load was excreted by the renal tubules [235].

In Japanese eels in freshwater, most regulation of SO_4^{2-} occurs by resorption in the kidney's proximal tubule, the SO_4^{2-} possibly being derived from metabolism of sulfur-containing compounds [316]. In these epithelial cells, 2 transporters are involved in SO_4^{2-} transport. First, a $3Na^+/SO_4^{2-}$-cotransporter (SLC13s1) moves both Na^+ and SO_4^{2-} across the apical brush-border membrane driven by the Na^+ gradient produced by NKA on the basolateral membrane. Then, the SO_4^{2-} is moved across the basolateral membrane by an $SO_4^{2-}/2HCO_3^-$-exchanger (SLC26a1), which is energized by an SO_4^{2-} gradient across the basolateral membrane [316]. In Japanese eels, SO_4^{2-} may play a role in osmoregulation in freshwater because serum SO_4^{2-} is elevated in freshwater ($\sim$19 mM vs $\sim$1 mM in saltwater), whereas Cl^- is reduced compared with the Japanese eels in saltwater or other fish in freshwater [316,318].

Crustacea. In a study of Na^+ absorption from water by *Austropotamobius pallipes* using various anion salts, including Na_2SO_4 [312], there was no penetration of gill epithelial membranes by SO_4^{2-}. A review of a number of studies that used H_2SO_4 to study the physiological effects of acidification [313] found that, at most, SO_4^{2-} permeates very slowly across gill epithelial membranes.

Like a number of other ions, there was a negative net flux of SO_4^{2-} from the crayfish *O. propinquus* exposed to pH 4.0 [218]. In the absence of SO_4^{2-} transporters on the gill epithelia, increased efflux may be because of increased paracellular permeability at low pH.

Aquatic insects. In *A. campestris*, a mosquito that lives in hyperosmotic inland waters, including saline lakes dominated by Mg^{2+} and SO_4^{2-}, larvae maintained hemolymph $[SO_4^{2-}]$ at approximately 2 mM to 7 mM, despite water $[SO_4^{2-}]$ that was up to 80 mM. Ingestion of this water resulted in absorption of the SO_4^{2-} through the midgut [319]. This balance resulted from the excretion of fluids containing high $[SO_4^{2-}]$ (up to $\approx$95 mM) by the mosquito's Malpighian tubules, where active transport of SO_4^{2-} occurs.

Mollusca. In unionid mussels, SO_4^{2-} is accumulated rather slowly (e.g., 0.04 μmol g^{-1} dry wt h^{-1}) and is a relatively impermeant anion [25]. It occurs in the range of 0.23 mM to 0.30 mM in hemolymph of unionid mussels and is metabolized to form amino acids and mucopolysaccharides. The hemolymph $[SO_4^{2-}]$ of 0.23 mM, although relatively low for an anion, was approximately 8 times the $[SO_4^{2-}]$ in pond water [25].

Using the radioisotope $^{35}SO_4$ to measure transport of SO_4^{2-}, uptake of SO_4^{2-} by the unionid *Toxolasma texasiense* from pond water was inhibited by addition of DIDS, an anion exchanger inhibitor [25]. Furthermore, clearance of $^{35}SO_4$ injected into *T. texasiense* individuals was 16% of a simultaneously injected chemical, polyethylene glycol, used to measure renal filtration rates, indicating that SO_4^{2-} was reabsorbed by the kidney [25]. Similar results were obtained for pond water-acclimated *D. polymorpha* (Supplemental Data, Table S9). Although the transporter for SO_4^{2-} is still unclear, the inhibition of the ion's uptake by DIDS, an anion exchanger inhibitor, suggests an anion exchanger (Figure 5 and Table 2) [25,320].

Effects on SO_4^{2-} transport by other ions in the water. Hōbe [321] observed net influx of SO_4^{2-} in white sucker and rainbow trout exposed to natural soft water acidified to pH 4.0 by addition of H_2SO_4 but not in controls (pH 6.8). Based on current models, this influx appears to have resulted from passive movement of SO_4^{2-}down a concentration gradient created by the addition of H_2SO_4 to the soft water ($[SO_4^{2-}]$ was 0.20 mM to 0.40 mM in acidified soft water and 0.07 mM to 0.10 mM in control soft water) across tight junctions made more permeable by the low pH and low Ca^{2+} conditions, rather than the action of any transporter. As in other studies of acidic, soft waters, net effluxes of Na^+, K^+, Ca^{2+}, Mg^{2+}, and Cl^- were also observed.

Synthesis. Data for various animals suggest that SO_4^{2-} transporters may not be present on the gill epithelia of most freshwater animals because of the slow permeation of these epithelia. However, in the European toad, there is evidence for active transport of SO_4^{2-} across the skin epithelia, which are at least functionally equivalent to gill epithelia. There is also evidence for active transport of SO_4^{2-} from ambient water to the hemolymph in freshwater mussels, but the location of a transporter is not clear. In general, SO_4^{2-} has not been well studied in freshwater animals compared with other ions.

Soucek and Kennedy [133] and Soucek [132] attempted to assess the relationships among hardness, Cl^-, and acute effects

associated with SO_4^{2-} in bioassays with 2 crustaceans, although the dose consisted of solutions of the salt Na_2SO_4. Physiological research has generally suggested that gill epithelial membranes are impermeant to SO_4^{2-}, although SO_4^{2-} transporters may occur in the renal system. A possible mechanism is related to the cation Na^+. In the electrogenic H2Na(Ca)E on the crustacean gill, Ca^{2+} and Na^+ can compete for attachment sites on this transporter, which would result in the positive relationship between hardness and the LC50 values for *Hyalella azteca* and *C. dubia*.

It is clear, however, that SO_4^{2-} transporters are present in ionocytes of the renal system in fish where these transporters resorb SO_4^{2-}. The question remains whether there are SO_4^{2-} transporters in either the gill or gastrointestinal epithelia of any freshwater animals that might be affected by elevated [SO_4^{2-}] as a result of anthropogenic sources, such as those associated with mining [322]. Although elevated [SO_4^{2-}] is present in freshwaters associated with acidic precipitation or acid mine drainage, the effects of low pH have been more obvious and, consequently, well studied in both the physiological and toxicological literatures. Thus, the potential for any effects related directly to SO_4^{2-} has been overlooked.

DISCUSSION

In general, there appears to be a significant level of evolutionary conservatism in ion transporters among the 4 freshwater groups reviewed. Where there are physiological data, transporters, such as VHA, anion exchanger, NKA, PMCA, and NCX, appear to be functionally similar, and where there are genomic data, these transporters usually belong to identified protein families that occur in species across various phyla. However, there are also differences (e.g., the electroneutral NHE in teleost fish compared with the electrogenic H2Na(Ca)E in crustaceans that helps crustaceans to meet their greater requirements for Ca^{2+} uptake during molting). Also, when the apparent relative affinities of the Ca^+-channels of the groups are compared, it appears that the affinities for Cd^{2+} and Zn^{2+} in fish, crustaceans, and molluscs are greater than those for Ca^{2+}, whereas in aquatic insects, the affinities for divalent metals may be less than those for Ca^{2+}. There may also be differences between some aquatic insects and these other animal groups in the apical Na^+-channel that also transports metals like Ag^+ and Cu^{2+}.

The most widespread difference of these transporters among species, and 1 that is more subtle, is the affinity and capacity of each transporter for its ion as measured by K_m and V_{max}. These 2 variables seem to have the potential to describe the variation in the tolerance of different species particularly to low ion concentrations. However, few studies have compared these variables for an ion measured under the same conditions among more than 1 species in the same freshwater group (e.g., goldfish, zebrafish, and ayu [*Plecoglossus altivelis*]; [219]), and no studies have done this among fish and various invertebrate groups (e.g., rainbow trout with crayfish).

Among the individual major ions, K^+ appears to have the most potential for causing toxic effects to freshwater animals if water concentrations of this ion are elevated. The relative acute toxicity of K^+ was ranked as the highest of the major ions studied [128], and it has been used as a molluscicide. Survival of *D. polymorpha* was greatest when the [K^+]:[Na^+] ratio was very low (0.01−0.02) [36]. The counter ion for NKA is K^+, which is important to maintaining the relative [Na^+] in intracellular fluids and the blood or hemolymph, suggesting that this toxicity is related to an ionoregulatory imbalance. Lack of data on the identity of an apical membrane K^+ transporter makes the details of such an imbalance unclear. However, K^+ usually has the lowest concentrations in freshwaters of these major ions [161].

The toxic effects of H^+ have been well studied, particularly in relation to the effects of acid precipitation on stream and lake assemblages, but the mechanistic link to inhibition of Na^+ uptake by the NHE or VHA and apical Na^+-channel and decreases in intracellular and extracellular [Na^+] has seldom been mentioned in the toxicological literature. Similarly, elevated ambient HCO_3^- appears to inhibit uptake of Cl^- by the anion exchanger and decreases intracellular and extracellular [Cl^-]. Elucidation of the details of this mechanism are needed because HCO_3^- ranked relatively high among the major ions in terms of toxicity [128]. Moreover, HCO_3^- is a primary constituent of produced waters from coalbed natural gas development and effluents from mountaintop mines and valley fills [304,305,322].

Although the relative acute toxicity of Mg^{2+} was ranked as similar to that of HCO_3^- [128], much of the available literature emphasizes the effects of a lack of Mg^{2+} in ambient waters or diet, although at least 1 study found toxic effects from the highest tested [Mg^{2+}]. The bulk of toxicological research focuses on whether Mg^{2+} contributes to the ameliorative effects of water hardness on metal toxicity. Some fish appear to need Mg^{2+} in their diet, but there is also evidence for uptake of Mg^{2+} by ionocytes on the gill or other epithelial membranes from ambient waters. However, no studies have been found on the identity or nature of Mg^{2+} transporters on these epithelia, although there are some data on transporters in the epithelia of the intestine or in the renal system. Therefore, additional research is needed to understand the transport of Mg^{2+} in freshwater animals and fully understand its role in ionoregulation, especially in combination with other ions.

The literature is clear that Na^+ and Cl^- generally dominate osmoregulation of freshwater animals and of most living organisms in general, although all inorganic ions and organic osmolytes contribute to intracellular and extracellular osmolarity. Increasing water [Na^+] or [Cl^-], such as occurs along the gradient between freshwater and estuarine or marine waters, is generally accompanied by increasing blood or hemolymph [Na^+] or [Cl^-] as the animals maintain the hypertonicity of their extracellular fluids. Diadromous fish, such as salmon or eels, adapt to the increasing salinity by inactivating ionocytes with freshwater transporter arrangements designed for ion uptake and activating ionocytes with saltwater transporter arrangements designed for ion excretion [103,323]. Invertebrates generally iono-conform, and most fish hyporegulate in greater salinity waters. Many freshwater species often hyper-regulate with increasing salinity until the animals are no longer able to maintain blood or hemolymph [Na^+] or [Cl^-] greater than in the water, and the animals become isotonic to the water. It is then that mortality occurs in stenohaline species, and this is why Na^+ and Cl^- toxicity occurs at relatively greater concentrations compared with some other major ions. However, because Na^+ and Cl^- are exchanged for H^+ and HCO_3^-, respectively, the relative internal concentrations of these ions can reflect alterations of acid−base balance, which is often quantified as the difference between the equivalents of strongly disassociated cations (i.e., Na^+, K^+, Ca^{2+}, and Mg^{2+}) and of strongly disassociated anions (i.e., Cl^- and SO_4^{2-})—the strong ion difference [60,295] that may be the result of increases in water salinity.

There has been little research on the physiology of SO_4^{2-} in freshwater animals. Most available data suggest that SO_4^{2-} is at

most slowly permeable to gill epithelial ionocytes, and this appears to explain the ion's relatively low toxicity to daphnids or fathead minnows [128]. However, SO_4^{2-} transporters have been identified in skin ionocytes of European toads and active transport appears to occur in freshwater mussels. To fully understand SO_4^{2-} transport or the lack thereof in freshwater animals, research is needed to establish whether SO_4^{2-} transporters are present in gills or other external epithelial membranes or in the gastrointestinal system of these animals, and if present, to elucidate the roles of these transporters.

A statistically significant adverse effect could not be attributed to Ca^{2+} in toxicological studies of daphnids and fathead minnows [128]. The physiological literature suggests that the Ca^{2+} transporters help exert a strong homeostatic effect on dissolved Ca^{2+} in both the extracellular and intracellular fluids. Although there can be significant requirements for Ca^{2+}, much of this ion is stored either bound to proteins or phospholipids within cells or as inorganic salts in the endo- or exoskeleton as well as in gastroliths in Crustacea and concretions in Mollusca. As a result, intracellular free Ca^{2+}, the Ca species with the most potential for adverse effects, is maintained in the 0.1 μM to 1 μM range.

The availability of data on freshwater ionoregulation physiology is very uneven across the 4 taxonomic groups. The literature on teleost fish is the most extensive, and that for Crustacea is the second most extensive. Research on freshwater Mollusca and particularly bivalves is relatively limited; much of it was published before 2000, and does not include the genomic data that have become common in the fish literature.

The group most lacking in data is the aquatic insects, particularly the Ephemeroptera, Plecoptera, and Trichoptera, whose assemblages are important to the bioassessment of streams and rivers. Because aquatic insects migrated from terrestrial to freshwater environments, an unexplored potential exists that the mechanisms of ionoregulation differ from those in other freshwater animals that migrated from estuarine or marine to freshwater environments. Moreover, the separate migration of different orders of insects to freshwater suggests that there could be alternate evolutionary solutions to the problems of ionoregulation in freshwaters. This has been shown to be true of gas exchange in aquatic insects [16].

As evidenced by the literature reviewed, the 2 disciplines that meet at the nexus of freshwater ionoregulation and osmoregulation are physiology and toxicology. However, the questions usually asked by these 2 disciplines can be very different. The toxicologists want to know how much of an ion causes adverse effects to individuals and how that may be related to effects at higher levels of biological organization, such as populations and often communities. The physiologists want to know the mechanisms that allow maintenance of internal homeostasis for these ions, which have various functions in cells and the blood or hemolymph, particularly when these mechanisms are related to natural ionic gradients, such as from freshwater to saltwater or from soft to hard water. Both toxicologists and physiologists investigate when maintenance of internal homeostasis fails, such as in metal toxicity, where adverse effects occur after metal ions are inadvertently transported across apical ionocyte membranes by the ECaC or apical Na^+-channel because the specific metal ions have a similar charge and atomic radius to Ca^{2+} and Na^+, respectively. This is part of the physiological basis of the biotic ligand model, although this often has not been made clear in the toxicological literature.

Given the differing questions of freshwater toxicology and physiology, there are striking differences in the model organisms used by the 2 disciplines. Until recently, many common techniques in physiology either measured directly or sampled and measured ion or radioisotope concentrations in intracellular or extracellular fluids. A microprobe, cannula, or hypodermic needle, for example, would have been placed into the animal without disturbing normal functions. This often required larger, often adult species, such as rainbow trout or crayfish. In freshwater toxicology, there has been an advantage to using species that can be cultured in significant numbers and used when needed at a specific life stage (i.e., larval or neonate). As a result, daphnids and fathead minnows dominate the freshwater toxicological literature. The increasing use of zebrafish represents a change that is tied to the use of genomic data. The increasing use of molecular methods is slowly altering these size and natural history limitations on species used in toxicological studies.

Lack of understanding of ionoregulation in aquatic insects occurs, in part, because they do not meet the requirements for either physiology or toxicological studies. Aquatic insects are usually smaller than even crayfish. They also have complex life cycles in which the adult often does not live in water and is short-lived. Moreover, other large life stages, such as the penultimate and final instars, only persist for a short period and the entire life cycle is usually univoltine, although there are species with multivoltine life cycles that may persist for a month at warmer temperatures. Use of different model species, such as 1 of the Ephemeroptera, Plecoptera, or Trichoptera, may be required to close some gaps in our knowledge. A species of parthenogenic baetid mayfly, *Neocloeon triangulifer*, is currently being investigated for use in aquatic toxicology [324,325].

Finally, freshwater toxicology can gain a better understanding of the toxic mechanisms of major ions that may be elevated by anthropogenic sources from what is known about the physiology of ion transport. Although there is some interaction among those ions that share transporters, such as H^+ and Na^+ or HCO_3^- and Cl^-, it is not the type of interaction that has been assumed based on the example of divalent metals and hardness. For ions that have some biochemical or physiological role in animals, including nutrient metals, such as Cu and Zn, there are specific transporter proteins involved in their uptake across apical and basolateral membranes of ionocytes on the gills or other external epithelial surfaces or in the gastrointestinal systems of freshwater animals at normal concentrations. However, some ions have been incompletely studied, and we currently do not know the identity and characteristics of some of these transporters. This is particularly true of Mg^{2+} and SO_4^{2-} but is also true of an apical K^+ transporter. There are many more gaps in our knowledge of freshwater invertebrates, particularly aquatic insects. Finally, even in comparative physiological literature reviews, comparisons across phyla and classes of freshwater animals similar to what have been made in the present review do not exist.

CONCLUSIONS

Where there are physiological data to compare, there are functional similarities among ion transport processes, particularly for freshwater fish, crustaceans, and molluscs. The similarities are at least partially the result of evolutionary conservatism in ion transporter proteins. However, there are differences, such as the electroneutral NHE in teleost fish, the electrogenic H2Na(Ca)E in crustaceans, and a pharmacologically different NHE in aquatic insects. Also, there is some

evidence that the relative affinity of the ECaC for Ca^{2+} or the apical Na^+-channel for Na^+ differs between aquatic insects and fish, crustaceans, or molluscs compared with the metals that also can be transported by these channels.

Increased concentrations of ions in the water most directly affect ionoregulation or osmoregulation and cause adverse effects when they change osmotic or electrochemical gradients or otherwise interact with other ions. Increased external aqueous $[H^+]$ or $[HCO_3^-]$ change the electrochemical gradients across the apical epithelial membrane whereby the movement of these ions down their electrochemical gradient energizes uptake of Na^+ and Cl^-, respectively. Inhibition of CA also affects this concentration gradient by reducing the $[H^+]$ and $[HCO_3^-]$ within the cell. Anything affecting these 2 ion transport processes also affects the excretion of H^+ or HCO_3^- required for acid−base regulation. Along with K^+, Na^+ and Cl^- appear to be particularly important for osmoregulation, with K^+ being important in the movement of Na^+ from intracellular to extracellular fluids and for volume regulation. A large enough increase in the water $[Na^+]$ and $[Cl^-]$ or [total ions] can change the osmotic gradients maintained by freshwater animals. An ion that is not the primary ion transported, but that can pass through the transporter, may compete for attachment sites on the transporter and thereby inhibit uptake of the primary ion. This occurs in the ECaC with metals and the anion exchanger with NO_2^-. As a result, research to address the effects of increased salinity in freshwaters associated with different sources and compositions of ions needs to consider the interactions among individual ions along with the effect of total ion concentrations on the movement of water or ions across epithelial membranes.

Supplemental Data—The Supplemental Data are available on the Wiley Online Library at DOI: 10.1002/etc.3676.

Acknowledgment—Earlier drafts of the manuscript were reviewed and improved by comments from S. Cormier and G. Suter (US Environmental Protection Agency, Office of Research and Development [USEPA, ORD]), Cincinnati, OH), C. Penalva-Arana (USEPA, ORD, Washington, DC), J. Nichols and R. Erickson (USEPA, ORD, Duluth, MN), A. Donini (Department of Biology, University of York, Toronto, ON, Canada), and 3 anonymous reviewers.

Disclaimer—The present review was prepared at the US Environmental Protection Agency (USEPA), National Center for Environmental Assessment (NCEA), Cincinnati Division. It has been subjected to the agency's peer and administrative review and approved for publication. However, the views expressed are those of the author and do not necessarily represent the views or policies of the USEPA. The author declares that there are no conflicts of interest.

Data availability—Contact Michael B. Griffith at griffith.michael@epa.gov for an EndNote bibliography of the studies that were considered for this literature review.

REFERENCES

1. American Public Health Association. 1998. *Standard Methods for the Examination of Water and Wastewater*, 20th ed. Washington, DC.
2. Wetzel RG. 2001. *Limnology: Lake and River Ecosystems*, 3rd ed. Academic, San Diego, CA, USA.
3. Charmantier G, Charmantier-Daures M, Towle DW. 2009. Osmotic and ionic regulation in aquatic arthropods. In Evans DH, ed, *Osmotic and Ionic Regulation: Cells and Animals*. CRC, Boca Raton, FL, USA, pp 165–230.
4. Gray J. 1988. Evolution of the freshwater ecosystem: The fossil record. *Palaeogeogr Palaeocl* 62:1–214.
5. Miller MF, Labandeira CC. 2002. Slow crawl across the salinity divide: Delayed colonization of freshwater ecosystems by invertebrates. *GSA Today* 12:4–10.
6. Lee CE, Kiergaard M, Gelembiuk GW, Eads BD, Posavi M. 2011. Pumping ions: Rapid parallel evolution of ionic regulation following habitat invasions. *Evolution* 65:2229–2244.
7. Belli NM, Faleiros RO, Firmino KCS, Masui DC, Leone FA, McNamara JC, Furriel RPM. 2009. Na,K-ATPase activity and epithelial interfaces in gills of the freshwater shrimp *Macrobrachium amazonicum* (Decapoda, Palaemonidae). *Comp Biochem Phys A* 152:431–439.
8. Berra TM. 2007. *Freshwater Fish Distribution*. University of Chicago, Chicago, IL, USA.
9. Wootton RJ. 1972. The evolution of insects in freshwater ecosystems. In Clark RG, Wooten RJ, eds, *Essays in Hydrobiology*. University of Exeter, Exeter, UK, pp 69–82.
10. McMahon RF. 1983. Physiological ecology of freshwater pulmonates. In Russell-Hunter WD, ed, *The Mollusca Ecology*, Vol 6—The Mollusca. Academic, Orlando, FL, USA, pp 359–430.
11. Pritchard G, McKee MH, Pike EM, Scrimgeour GJ, Zloty J. 1993. Did the first insects live in water or in air? *Biol J Linn Soc* 49:31–44.
12. Mordan P, Wade C. 2008. Heterobranchia II. The Pulmonata. In Ponder WF, R. LD, eds, *Phylogeny and Evolution of the Mollusca*. University of California, Berkley, CA, USA, pp 409–426.
13. Beyenbach KW, Piermarini PM. 2009. Osmotic and ionic regulation in insects. In Evans DH, ed, *Osmotic and Ionic Regulation: Cells and Animals*. CRC, Boca Raton, FL, USA, pp 231–293.
14. Wootton RJ. 1988. The historical ecology of aquatic insects: An overview. *Palaeogeogr Palaeocl* 62:477–492.
15. Cooper PD. 1994. Mechanisms of hemolymph acid-base regulation in aquatic insects. *Physiol Zool* 67:29–53.
16. Eriksen CH, Resh VH, Lamberti GA. 1996. Aquatic insect respiration. In Merritt RW, Cummins KW, eds, *An Introduction to the Aquatic Insects of North America*, 3rd ed. Kendall/Hunt, Dubuque, IA, USA, pp 29–40.
17. Wichard W, Komnick H. 1974. Structure and function of the respiratory epithelium in the tracheal gills of stonefly larvae. *J Insect Physiol* 20:2397–2406.
18. Miller JR, Andelman JB. 1987. Speciation of aluminum in an acidic mountain stream. *Water Res* 21:999–1005.
19. Wichard W, Komnick H. 1974. Fine structure and function of the rectal chloride epithelia of damselfly larvae. *J Insect Physiol* 20:1611–1621.
20. Komnick H. 1977. Chloride cells and chloride epithelia of aquatic insects. *Int Rev Cytol* 49:285–328.
21. Evans DH. 2008. Teleost fish osmoregulation: What have we learned since August Krogh, Homer Smith, and Ancel Keys. *Am J Physiol-Reg I* 295:R704–R713.
22. Bradley TJ. 1987. Physiology of osmoregulation in mosquitos. *Annu Rev Entomol* 32:439–462.
23. Perry SF, Shahsavarani A, Georgalis T, Bayaa M, Furimsky M, Thomas SLY. 2003. Channels, pumps, and exchangers in the gill and kidney of freshwater fishes: Their role in ionic and acid-base regulation. *J Exp Zool* 300A:53–62.
24. Burton RF. 1983. Ionic regulation and water balance. In Saleuddin ASM, Wilbur KM, eds, *The Mollusca*, Vol 5: Physiology, Part 2. Academic, New York, NY, USA, pp 292–352.
25. Dietz TH, Udoetok AS, Cherry JS, Silverman H, Byrne RA. 2000. Kidney function and sulfate uptake and loss in the freshwater bivalve *Toxolasma texasensis*. *Biol Bull* 199:14–20.
26. Bradley TJ. 1994. The role of physiological capacity, morphology, and phylogeny in determining habitat use in mosquitoes. In Wainwright PC, Reilly SM, eds, *Ecological Morphology: Integrative Organismal Biology*. University of Chicago, Chicago, IL, USA, pp 303–315.
27. Bradley TJ. 2008. Hyper-regulators: Life in fresh water. In *Animal Osmoregulation*. Oxford University, Oxford, UK, pp 87–155.
28. Evans DH. 1980. Osmotic and ionic regulation by freshwater and marine fishes. In Ali MA, ed, *Environmental Physiology of Fishes*. Plenum, New York, NY, USA, pp 93–122.
29. Motais R, Isaia J, Rankin JC, Maetz J. 1969. Adaptive changes of the water permeability of the teleostean gill epithelium in relation to external salinity. *J Exp Biol* 51:529–546.
30. Potts WTW. 1954. The energetics of osmotic regulation in brackish- and fresh-water animals. *J Exp Biol* 31:618–630.
31. Teschner M. 1995. Effects of salinity on the life history and fitness of *Daphnia magna*: Variability within and between populations. *Hydrobiologia* 307:33–41.
32. Aladin NV, Potts WTW. 1995. Osmoregulatory capacity of the Cladocera. *J Comp Phys B* 164:671–683.

33. Ankley GT, Bennett RS, Erickson RJ, Hoff DJ, Hornung MW, Johnson RD, Mount DR, Nichols JW, Russom CL, Schmieder PK, Serrrano JA, Tietge JE, Villeneuve DL. 2010. Adverse outcome pathways: A conceptual framework to support ecotoxicology research and risk assessment. *Environ Toxicol Chem* 29:730–741.
34. Wheatly MG, Gannon AT. 1995. Ion regulation in crayfish: Freshwater adaptations and the problem of molting. *Am Zool* 35:49–59.
35. Dietz TH. 1979. Uptake of sodium and chloride by freshwater mussels. *Can J Zool* 57:156–160.
36. Dietz TH, Wilcox SJ, Silverman H, Byrne RA. 1997. Effects of hyperosmotic challenge on the freshwater bivalve *Dreissena polymorpha*: Importance of K^+. *Can J Zool* 75:697–705.
37. Zheng H, Dietz TH. 1998. Paracellular solute uptake in the freshwater bivalves *Corbicula fluminea* and *Toxolasma texasensis*. *Biol Bull* 194:170–177.
38. O'Donnell MJ, Maddrell SHP, Gardiner BOC. 1984. Passage of solutes through walls of Malpighian tubules of *Rhodnius* by paracellular and transcellular routes. *Am J Phys-Reg I* 246: R759–R769.
39. Choe KP, Strange K. 2009. Volume regulation and osmosensing in animal cells. In Evans DH, ed, *Osmotic and Ionic Regulation: Cells and Animals*. CRC, Boca Raton, FL, USA, pp 37–57.
40. Strange K, Emma F, Jackson PS. 1996. Cellular and molecular physiology of volume-sensitive anion channels. *Am J Physiol-Cell Ph* 270:C711–C730.
41. Lignot J-H, Cutler CP, Hazon N, Cramb G. 2002. Immunolocalisation of aquaporin 3 in the gill and the gastrointestinal tract of the European eel *Anguilla anguilla* (L.). *J Exp Biol* 205:2653–2663.
42. Cutler CP, Cramb G. 2002. Branchial expression of an aquaporin 3 (AQP-3) homologue is downregulated in the European eel *Anguilla anguilla* following seawater acclimation. *J Exp Biol* 205: 2643–2651.
43. Zheng H, Dietz TH. 1998. Ion transport in the freshwater bivalve *Corbicula fluminea*. *Biol Bull* 194:161–169.
44. Dietz TH, Byrne RA, Lynn JW, Silverman H. 1995. Paracellular solute uptake by the freshwater zebra mussel *Dreissena polymorpha*. *Am J Phys-Reg I* 269:R300–R307.
45. Lee CE, Posavi M, Charmantier G. 2012. Rapid evolution of body fluid regulation following independent invasions into freshwater habitats. *J Evol Biol* 25:625–633.
46. Gouaux E, MacKinnon R. 2005. Principles of selective ion transport in channels and pumps. *Science* 310:1461–1465.
47. Nelson DL, Cox MM. 2005. Biological membranes. In *Lehninger Principles of Biochemistry*, 4th ed. WH Freeman, New York, NY, USA, pp 369–420.
48. Tseng Y-C, Huang C-J, Chang JC-H, Teng W-Y, Baba O, Fann M-J, Hwang P-P. 2007. Glycogen phosphorylase in glycogen-rich cells is involved in the energy supply for ion regulation in fish gill epithelia. *Am J Phys-Reg I* 293:R482–R491.
49. Tseng Y-C, Hwang P-P. 2008. Some insights into energy metabolism for osmoregulation in fish. *Comp Biochem Physiol C* 148:419–429.
50. Bœuf G, Payan P. 2001. How should salinity influence fish growth? *Comp Biochem Physiol C Toxicol Pharmacol* 130:411–423.
51. Morgan JD, Iwama GK. 1999. Energy cost of NaCl transport in isolated gills of cutthroat trout. *Am J Phys-Reg I* 277:R631–R639.
52. Kukulies J, Komnick H. 1983. Plasma membranes, cell junctions and cuticle of the rectal chloride epithelia of the larval dragonfly *Aeshna cyanea*. *J Cell Sci* 59:159–182.
53. Skaer HlB, Maddrell SHP. 1987. Commentary: How are invertebrate epithelia made tight? *J Cell Sci* 88:139–141.
54. Lord BAP, DiBona DR. 1976. Role of the septate junction in the regulation of paracellular transepithelial flow. *J Cell Biol* 71:967–972.
55. Shen L, Weber CR, Turner JR. 2008. The tight junction protein complex undergoes rapid and continuous molecular remodeling at steady state. *J Cell Biol* 181:683–695.
56. Evans DH. 1986. The role of branchial and dermal epithelia in acid-base regulation in aquatic vertebrates. In Heisler N, ed, *Acid-Base Regulation in Animals*. Elsevier Sciences, Amsterdam, Netherlands, pp 139–172.
57. Weihrauch D, Donini A, O'Donnell MJ. 2012. Ammonia transport by terrestrial and aquatic insects. *J Insect Physiol* 58:473–487.
58. Sinha AK, Liew HJ, Nawata CM, Blust R, Wood CM, De Boeck G. 2013. Modulation of Rh glycoproteins, ammonia excretion and Na^+ fluxes in 3 freshwater teleosts when exposed chronically to high environmental ammonia. *J Exp Biol* 216:2917–2930.
59. Wheatly MG. 1989. Physiological responses of the crayfish *Pacifastacus leniusculus* to environmental hyperoxia: I. Extracellular acid-base and electrolyte status and transbranchial exchange. *J Exp Biol* 143:33–51.
60. Byrne RA, Dietz TH. 2006. Ionic and acid-base consequences of exposure to increased salinity in the zebra mussel, *Dreissena polymorpha*. *Biol Bull* 211:66–75.
61. Evans DH, Piermarini PM, Choe KP. 2005. The multifunctional fish gill: Dominant site of gas exchange, osmoregulation, acid-base regulation, and excretion of nitrogenous waste. *Physiol Rev* 85: 97–177.
62. Hirata T, Kaneko T, Ono T, Nakazato T, Furukawa N, Hasegawa S, Wakabayashi S, Shigekawa M, Chang M-H, Romero MF, Hirose S. 2003. Mechanism of acid adaptation of a fish living in a pH 3.5 lake. *Am J Phys-Reg I* 284:R1199–R1212.
63. Perry SF, Gilmour KM. 2006. Acid–base balance and CO_2 excretion in fish: Unanswered questions and emerging models. *Resp Physiol Neurobiol* 154:199–215.
64. Wieczorek H, Brown D, Grinstein S, Ehrenfeld J, Harvey WR. 1999. Animal plasma membrane energization by proton-motive V-ATPases. *Bioessays* 21:637–648.
65. Beyenbach KW, Wieczorek H. 2006. The V-type H^+ ATPase: Molecular structure and function, physiological roles and regulation. *J Exp Biol* 209:577–589.
66. Choe KP, O'Brien S, Evans DH, Toop T, Edwards SL. 2004. Immunolocalization of Na^+/K^+-ATPase, carbonic anhydrase II, and vacuolar H^+-ATPase in the gills of freshwater adult lampreys, *Geotria australis*. *J Exp Zool Part A* 301:654–665.
67. Kirschner LB. 2004. The mechanism of sodium chloride uptake in hyperregulating aquatic animals. *J Exp Biol* 207:1439–1452.
68. Kellenberger S, Schild L. 2002. Epithelial sodium channel/degenerin family of ion channels: A variety of functions for a shared structure. *Physiol Rev* 82:735–767.
69. Hiroi J, Yasumasu S, McCormick SD, Hwang P-P, Kaneko T. 2008. Evidence for an apical Na–Cl cotransporter involved in ion uptake in a teleost fish. *J Exp Biol* 211:2584–2599.
70. Hwang P-P, Perry SF. 2010. Ionic and acid–base regulation. In Perry SF, Ekker M, Farrell AP, Colin JB, eds, *Fish Physiology*, Vol 29. Academic, San Diego, CA, USA, pp 311–344.
71. Hwang P-P, Lee T-H, Lin L-Y. 2011. Ion regulation in fish gills: Recent progress in the cellular and molecular mechanisms. *Am J Phys-Reg I* 301:R28–R47.
72. Dymowska AK, Schultz AG, Blair SD, Chamot D, Goss GG. 2014. Acid-sensing ion channels are involved in epithelial Na+ uptake in the rainbow trout *Oncorhynchus mykiss*. *Am J Physiol-Cell Ph* 307: C255–C265.
73. Dymowska AK, Boyle D, Schultz AG, Goss GG. 2015. The role of acid-sensing ion channels in epithelial Na+ uptake in adult zebrafish (*Danio rerio*). *J Exp Biol* 218:1244–1251.
74. Parks SK, Tresguerres M, Goss GG. 2008. Theoretical considerations underlying Na^+ uptake mechanisms in freshwater fishes. *Comp Biochem Physiol C* 148:411–418.
75. Parks SK, Tresguerres M, Goss GG. 2009. Cellular mechanisms of Cl^- transport in trout gill mitochondrion-rich cells. *Am J Phys-Reg I* 296:R1161–R1169.
76. Parks SK, Tresguerres M, Galvez F, Goss GG. 2010. Intracellular pH regulation in isolated trout gill mitochondrion-rich (MR) cell subtypes: Evidence for Na^+/H^+ activity. *Comp Biochem Phys A* 155:139–145.
77. Esbaugh AJ, Perry SF, Bayaa M, Georgalis T, Nickerson J, Tufts BL, Gilmour KM. 2005. Cytoplasmic carbonic anhydrase isozymes in rainbow trout *Oncorhynchus mykiss*: Comparative physiology and molecular evolution. *J Exp Biol* 208:1951–1961.
78. Kumai Y, Perry SF. 2011. Ammonia excretion via Rhcg1 facilitates Na+ uptake in larval zebrafish, *Danio rerio,* in acidic water. *Am J Phys-Reg I* 301:R1517–R1528.
79. Ehrenfeld J. 1974. Aspects of ionic transport mechanisms in crayfish *Astacus leptodactylus*. *J Exp Biol* 61:57–70.
80. Ahearn GA. 1996. The invertebrate electrogenic $2Na^+/1H^+$ exchanger: Polyfunctional epithelial workstation. *News Physiol Sci* 11:31–35.
81. Ahearn GA, Mandal PK, Mandal A. 2001. Biology of the $2Na^+/1H^+$ antiporter in invertebrates. *J Exp Zool* 289:232–244.
82. Zetino AM, Kirschner LB, Harvey M. 2001. On the mechanism of sodium-proton exchange in crayfish. *Comp Biochem Phys A* 128:863–872.
83. Kirschner LB. 2002. Sodium–proton exchange in crayfish. *Biochim Biophys Acta* 1566:67–71.
84. Kimura C, Ahearn GA, Busquets-Turner L, Haley SR, Nagao C, Couet HG. 1994. Immunolocalization of an antigen associated with the

invertebrate electrogenic $2Na^+/1H^+$ antiporter. *J Exp Biol* 189: 85–104.
85. Shaw J. 1960. The absorption of sodium ions by the crayfish *Astacus pallipes* Lereboullet: III. The effect of other cations in the external solution. *J Exp Biol* 37:548–556.
86. Strauss O, Graszynski K. 1992. Isolation of plasma membrane vesicles from the gill epithelium of the crayfish, *Orconectes limosus* Rafinesque, and properties of the Na^+/H^+ exchanger. *Comp Biochem Phys A* 102:519–526.
87. Donini A, O'Donnell MJ. 2005. Analysis of Na^+, Cl^-, K^+, H^+ and NH_4^+ concentration gradients adjacent to the surface of anal papillae of the mosquito *Aedes aegypti*: Application of self-referencing ion-selective microelectrodes. *J Exp Biol* 208:603–610.
88. Patrick ML, Aimanova K, Sanders HR, Gill SS. 2006. P-type Na^+/K^+-ATPase and V-type H^+-ATPase expression patterns in the osmoregulatory organs of larval and adult mosquito *Aedes aegypti*. *J Exp Biol* 209:4638–4651.
89. Nguyen H, Donini A. 2010. Larvae of the midge *Chironomus riparius* possess two distinct mechanisms for ionoregulation in response to ion-poor conditions. *Am J Phys-Reg I* 299:R762–R773.
90. Donini A, Gaidhu MP, Strasberg DR, O'Donnell MJ. 2007. Changing salinity induces alterations in hemolymph ion concentrations and Na^+ and Cl^- transport kinetics of the anal papillae in the larval mosquito, *Aedes aegypti*. *J Exp Biol* 210:983–992.
91. Pullikuth AK, Aimanova K, Kang'ethe W, Sanders HR, Gill SS. 2006. Molecular characterization of sodium/proton exchanger 3 (NHE3) from the yellow fever vector, *Aedes aegypti*. *J Exp Biol* 209: 3529–3544.
92. Wright DA. 1975. The effect of external sodium concentration upon sodium fluxes in *Chironomus dorsalis* (Meig.) and *Camptochironomus tentans* (Fabr.), and the effect of other ions on sodium influx in *C. tentans*. *J Exp Biol* 62:141–155.
93. Timmer RT, Sands JM. 1999. Lithium intoxication. *J Am Soc Nephrol* 10:666–674.
94. Wright DA. 1975. The relationship between transepithelial sodium movement and potential difference in the larva of *Camptochironomus tentans* (Fabr.) and some observations on the accumulation of other ions. *J Exp Biol* 62:157–174.
95. Coimbra J, Machado J, Fernandes PL, Ferreira HG, Ferreira KG. 1988. Electrophysiology of the mantle of *Anodonta cygnea*. *J Exp Biol* 140:65–88.
96. Deaton LA. 2009. Osmotic and ionic regulation in molluscs. In Evans DH, ed, *Osmotic and Ionic Regulation: Cells and Animals*. CRC, Boca Raton, FL, USA, pp 37–57.
97. Deaton LE. 1982. Tissue (Na + K)-activiated adenosinetriphosphatase activities in freshwater and brackish water bivalve molluscs. *Mar Biol Lett* 3:107–112.
98. Parks SK, Tresguerres M, Goss GG. 2007. Interactions between Na^+ channels and Na^+-HCO_3^- cotransporters in the freshwater fish gill MR cell: A model for transepithelial Na^+ uptake. *Am J Physiol-Cell Ph* 292:C935–C944.
99. Lee Y-C, Yan J-J, Cruz SA, Horng J-L, Hwang P-P. 2011. Anion exchanger 1b, but not sodium-bicarbonate cotransporter 1b, plays a role in transport functions of zebrafish H^+-ATPase-rich cells. *Am J Physiol-Cell Ph* 300:C295–C307.
100. Perry SF, Furimsky M, Bayaa M, Georgalis T, Shahsavarani A, Nickerson JG, Moon TW. 2003. Integrated responses of Na^+/HCO_3^- cotransporters and V-type H^+-ATPases in the fish gill and kidney during respiratory acidosis. *Biochim Biophys Acta* 1618:175–184.
101. Wang Y-F, Tseng Y-C, Yan J-J, Hiroi J, Hwang P-P. 2009. Role of SLC12A10.2, a Na-Cl cotransporter-like protein, in a Cl uptake mechanism in zebrafish (*Danio rerio*). *Am J Phys-Reg I* 296: R1650–R1660.
102. Bianchini A, Wood CM. 2008. Sodium uptake in different life stages of crustaceans: The water flea *Daphnia magna* Strauss. *J Exp Biol* 211:539–547.
103. Hiroi J, McCormick SD. 2007. Variation in salinity tolerance, gill Na^+/K^+-ATPase, $Na^+/K^+/2Cl^-$ cotransporter and mitochondria-rich cell distribution in three salmonids *Salvelinus namaycush*, *Salvelinus fontinalis* and *Salmo salar*. *J Exp Biol* 210:1015–1024.
104. Inokuchi M, Hiroi J, Watanabe S, Lee KM, Kaneko T. 2008. Gene expression and morphological localization of NHE3, NCC and NKCC1a in branchial mitochondria-rich cells of Mozambique tilapia (*Oreochromis mossambicus*) acclimated to a wide range of salinities. *Comp Biochem Phys A* 151:151–158.
105. Tipsmark CK, Madsen SS, Seidelin M, Christensen AS, Cutler CP, Cramb G. 2002. Dynamics of Na^+,K^+,$2Cl^-$ cotransporter and Na^+, K^+-ATPase expression in the branchial epithelium of brown trout (*Salmo trutta*) and Atlantic salmon (*Salmo salar*). *J Exp Zool* 293: 106–118.
106. McWilliams PG. 1980. Effects of pH on sodium uptake in Norwegian brown trout (*Salmo trutta*) from an acid river. *J Exp Biol* 88: 259–268.
107. McDonald DG, Wood CM. 1981. Branchial and renal acid and ion fluxes in the rainbow trout, *Salmo gairdneri*, at low environmental pH. *J Exp Biol* 93:101–118.
108. McDonald DG, Milligan CL. 1988. Sodium transport In the brook trout, *Salvelinus fontinalis*: Effects of prolonged low pH exposure in the presence and absence of aluminum. *Can J Fish Aquat Sci* 45: 1606–1613.
109. McDonald DG. 1983. The interaction of environmental calcium and low pH on the physiology of the rainbow trout, *Salmo gairdneri*: I. Branchial and renal net ion and H^+ fluxes. *J Exp Biol* 102:123–140.
110. McDonald DG, Walker RL, Wilkes PRH. 1983. The interaction of environmental calcium and low pH on the physiology of the rainbow trout, *Salmo gairdneri*: II. Branchial ionoregulatory mechanisms. *J Exp Biol* 102:141–155.
111. Hõbe H, Wood CM, McMahon BR. 1984. Mechanisms of acid-base and ionoregulation in white suckers (*Catostomus commersoni*) in natural soft water. 1. Acute exposure to low ambient pH. *J Comp Phys B* 154:35–46.
112. Fraser GA, Harvey HH. 1984. Effects of environmental pH on the ionic composition of the white sucker (*Catostomus commersoni*) and pumpkinseed (*Lepomis gibbosus*). *Can J Zool* 62:249–259.
113. Morgan IJ, Henry RP, Wood CM. 1997. The mechanism of acute silver nitrate toxicity in freshwater rainbow trout (*Oncorhynchus mykiss*) is inhibition of gill Na^+ and Cl^- transport. *Aquat Toxicol* 38:145–163.
114. Bury NR, Wood CM. 1999. Mechanism of branchial apical silver uptake by rainbow trout is via the proton-coupled Na+channel. *Am J Phys-Reg I* 277:R1385–R1391.
115. Grosell M, Wood CM. 2002. Copper uptake across rainbow trout gills: Mechanisms of apical entry. *J Exp Biol* 205:1179–1188.
116. Bogdanova AY, Virkki LV, Gusev GP, Nikinmaa M. 1999. Copper effects on ion transport across lamprey erythrocyte membrane: Cl^-/OH^- exchange induced by cuprous ions. *Toxicol Appl Pharmacol* 159:204–213.
117. Niyogi S, Wood CM. 2004. Biotic ligand model, a flexible tool for developing site-specific water quality guidelines for metals. *Environ Sci Technol* 38:6177–6192.
118. Grosell M, Nielsen C, Bianchini A. 2002. Sodium turnover rate determines sensitivity to acute copper and silver exposure in freshwater animals. *Comp Biochem Physiol C* 133:287–303.
119. Brix KV, Esbaugh AJ, Grosell M. 2011. The toxicity and physiological effects of copper on the freshwater pulmonate snail, *Lymnaea stagnalis*. *Comp Biochem Physiol C* 154:261–267.
120. Bianchini A, Wood CM. 2003. Mechanism of acute silver toxicity in *Daphnia magna*. *Environ Toxicol Chem* 22:1361–1367.
121. Grosell M, Brauner CJ, Kelly SP, McGeer JC, Bianchini A, Wood CM. 2002. Physiological responses to acute silver exposure in the freshwater crayfish (*Cambarus diogenes diogenes*)—A model invertebrate? *Environ Toxicol Chem* 21:369–374.
122. Scheibener SA, Richardi VS, Buchwalter DB. 2016. Comparative sodium transport patterns provide clues for understanding salinity and metal responses in aquatic insects. *Aquat Toxicol* 171:20–29.
123. Avella M, Bornancin M. 1989. A new analysis of ammonia and sodium transport through the gills of the freshwater rainbow trout (*Salmo gairdneri*). *J Exp Biol* 142:155–175.
124. Havas M, Advokaat E. 1995. Can sodium regulation be used to predict the relative acid-sensitivity of various life-stages and different species of aquatic fauna? *Water Air Soil Pollut* 85:865–870.
125. Wichard W, Komnick H, Abel JH, Jr. 1972. Typology of ephemerid chloride cells. *Z Zellforsch Mikrosk Anat* 132:533–551.
126. Rheault MR, Okech BA, Keen SBW, Miller MM, Meleshkevitch EA, Linser PJ, Boudko DY, Harvey WR. 2007. Molecular cloning, phylogeny and localization of AgNHA1: The first Na^+/H^+ antiporter (NHA) from a metazoan, *Anopheles gambiae*. *J Exp Biol* 210: 3848–3861.
127. Iwabe N, Kuma K, Miyata T. 1996. Evolution of gene families and relationship with organismal evolution: Rapid divergence of tissue-specific genes in the early evolution of chordates. *Mol Biol Evol* 13:483–493.
128. Mount DR, Gulley DD, Hockett JR, Garrison TD, Evans JM. 1997. Statistical models to predict the toxicity of major ions to *Ceriodaphnia dubia*, *Daphnia magna*, and *Pimephales promelas* (fathead minnows). *Environ Toxicol Chem* 16:2009–2019.

129. Elphick JR, Davies M, Gilron G, Canaria extracellular, Lo B, Bailey HC. 2011. An aquatic toxicological evaluation of sulfate: The case for considering hardness as a modifying factor in setting water quality guidelines. *Environ Toxicol Chem* 30:247–253.
130. Wang N, Dorman RA, Ingersoll CG, Hardesty DK, Brumbaugh WG, Hammer EJ, Bauer CR, Mount DR. 2016. Acute and chronic toxicity of sodium sulfate to four freshwater organisms in water-only exposures. *Environ Toxicol Chem* 35:115–127.
131. Davies TD, Hall KJ. 2007. Importance of calcium in modifying the acute toxicity of sodium sulphate to *Hyalella azteca* and *Daphnia magna*. *Environ Toxicol Chem* 26:1243–1247.
132. Soucek DJ. 2007. Comparison of hardness- and chloride-regulated acute effects of sodium sulfate on two freshwater crustaceans. *Environ Toxicol Chem* 26:773–779.
133. Soucek DJ, Kennedy AJ. 2005. Effects of hardness, chloride, and acclimation on the acute toxicity of sulfate to freshwater invertebrates. *Environ Toxicol Chem* 24:1204–1210.
134. Elphick JRF, Bergh KD, Bailey HC. 2011. Chronic toxicity of chloride to freshwater species: Effects of hardness and implications for water quality guidelines. *Environ Toxicol Chem* 30:239–246.
135. Soucek DJ, Linton TK, Tarr CD, Dickinson A, Wickramanayake N, Delos CG, Cruz LA. 2011. Influence of water hardness and sulfate on the acute toxicity of chloride to sensitive freshwater invertebrates. *Environ Toxicol Chem* 30:930–938.
136. Uchida K, Kaneko T, Yamauchi K, Hirano T. 1996. Morphometrical analysis chloride cell activity in the gill filaments and lamellae and changes in Na^+, K^+-ATPase activity during seawater adaptation in chum salmon fry. *J Exp Zool* 276:193–200.
137. Hawkings GS, Galvez F, Goss GG. 2004. Seawater acclimation causes independent alterations in Na^+/K^+- and H^+-ATPase activity in isolated mitochondria-rich cell subtypes of the rainbow trout gill. *J Exp Biol* 207:905–912.
138. Bystriansky JS, Richards JG, Schulte PM, Ballantyne JS. 2006. Reciprocal expression of gill Na^+/K^+-ATPaseα -subunit isoforms α1a and α1b during seawater acclimation of three salmonid fishes that vary in their salinity tolerance. *J Exp Biol* 209:1848–1858.
139. Wilkes PRH, McMahon BR. 1986. Responses of a stenohaline freshwater teleost (*Catostomus commersoni*) to hypersaline exposure: I. The dependence of plasma pH and bicarbonate concentration on electrolyte regulation. *J Exp Biol* 121:77–94.
140. Wilkes PRH, McMahon BR. 1986. Responses of a stenohaline freshwater teleost (*Catostomus commersoni*) to hypersaline exposure: II. Transepithelial flux of sodium, chloride and 'acidic equivalents'. *J Exp Biol* 121:95–113.
141. Wichard W, Tsui PTP, Komnick H. 1973. Effect of different salinities on the coniform chloride cells of mayfly larvae. *J Insect Physiol* 19:1825–1835.
142. Sutcliffe DW. 1961. Studies on salt and water balance in caddis larvae (Trichoptera): II. Osmotic and ionic regulation of body fluids in *Limnephilus stigma* Curtis and *Anabolia nervosa* Leach. *J Exp Biol* 38:521–530.
143. Castille FL, Jr, Lawrence AL. 1981. The effect of salinity on the osmotic, sodium, and chloride concentrations in the hemolymph of the freshwater shrimps, *Macrobrachium ohione* Smith and *Macrobrachium rosenbergii* de Man. *Comp Biochem Physiol A* 70:47–52.
144. Horohov J, Silverman H, Lynn JW, Dietz TH. 1992. Ion transport in the freshwater zebra mussel, *Dreissena polymorpha*. *Biol Bull* 183:297–303.
145. Doyle DA, Cabral JM, Pfuetzner RA, Kuo A, Gulbis JM, Cohen SL, Chait BT, MacKinnon R. 1998. The structure of the potassium channel: Molecular basis of K^+ conduction and selectivity. *Science* 280:69–77.
146. Eddy FB. 1985. Uptake and loss of potassium by rainbow trout (*Salmo gairdneri*) in fresh water and dilute sea water. *J Exp Biol* 118:277–286.
147. Evans DH, Piermarini PM, Potts WTW. 1999. Ionic transport in the fish gill epithelium. *J Exp Zool* 283:641–652.
148. Abbas L, Hajihashemi S, Stead LF, Cooper GJ, Ware TL, Munsey TS, Whitfield TT, White SJ. 2011. Functional and developmental expression of a zebrafish Kir1.1 (ROMK) potassium channel homologue Kcnj1. *J Physiol* 589:1489–1503.
149. Furukawa F, Watanabe S, Kimura S, Kaneko T. 2012. Potassium excretion through ROMK potassium channel expressed in gill mitochondrion-rich cells of Mozambique tilapia. *Am J Physiol Regul Integr Comp Physiol* 302:R568–R576.
150. Wheatly MG, Ignaszewski LA. 1990. Electrolyte and gas exchange during the moulting cycle of a freshwater crayfish. *J Exp Biol* 151:469–483.
151. Zare S, Greenaway P. 1997. Ion transport and the effects of moulting in the freshwater crayfish *Cherax destructor* (Decapoda: Parastacidae). *Aust J Zool* 45:539–551.
152. Belowitz R, O'Donnell MJ. 2013. Ion-selective microelectrode measurements of Tl^+ and K^+ transport by the gut and associated epithelia in *Chironomus riparius*. *Aquat Toxicol* 138–139:70–80.
153. Ramsay JA. 1953. Exchanges of sodium and potassium in mosquito larvae. *J Exp Biol* 30:79–89.
154. Pullikuth AK, Filippov V, Gill SS. 2003. Phylogeny and cloning of ion transporters in mosquitoes. *J Exp Biol* 206:3857–3868.
155. Harvey WR, Wieczorek H. 1997. Animal plasma membrane energization by chemiosmotic H^+ V-ATPases. *J Exp Biol* 200: 203–216.
156. Onken H, Moffett DF. 2009. Revisiting the cellular mechanisms of strong luminal alkalinization in the anterior midgut of larval mosquitoes. *J Exp Biol* 212:373–377.
157. Ram JL, Walker JU. 1993. Effects of deionized water on viability of the zebra mussel, *Dreissena polymorpha*. *Comp Biochem Physiol C* 105:409–414.
158. Wilcox SJ, Dietz TH. 1995. Potassium transport in the freshwater bivalve *Dreissena polymorpha*. *J Exp Biol* 198:861–868.
159. Fisher SW, Stromberg P, Bruner KA, Boulet LD. 1991. Molluscicidal activity of potassium to the zebra mussel, *Dreissena polymorphia*: Toxicity and mode of action. *Aquat Toxicol* 20:219–234.
160. Shakhmatova EI, Berger VY, Natochin YV. 2006. Cations in molluscan tissues at sharply different hemolymph osmolality. *Biol Bull* 33:269–275.
161. Griffith MB. 2014. Natural variation and current reference for specific conductivity and major ions in wadeable streams of the conterminous USA. *Freshw Sci* 33:1–17.
162. Wildridge PJ, Werner RG, Doherty FG, Neuhauser EF. 1998. Acute toxicity of potassium to the adult zebra mussel *Dreissena polymorpha*. *Arch Environ Contam Toxicol* 34:265–270.
163. Fenwick JC. 1989. Calcium exchange across fish gills. In Pang PKT, Schreibman MP, eds, *Regulation of Calcium and Phosphate*, Vol 3—Vertebrate Endocrinology: Fundamentals and Biomedical Implications. Academic, San Diego, CA, USA, pp 319–342.
164. Cameron JN. 1990. Unusual aspects of calcium metabolism in aquatic animals. *Annu Rev Physiol* 52:77–95.
165. Flik G, Verbost PM, Bonga SEW. 1995. Calcium transport processes in fishes. In Chris MW, Trevor JS, eds, *Fish Physiology*, Vol 14. Academic, San Diego, CA, USA, pp 317–342.
166. Hwang P-P, Lee T-H. 2007. New insights into fish ion regulation and mitochondrion-rich cells. *Comp Biochem Physiol A* 148:479–497.
167. Liao B-K, Deng A-N, Chen S-C, Chou M-Y, Hwang P-P. 2007. Expression and water calcium dependence of calcium transporter isoforms in zebrafish gill mitochondrion-rich cells. *BMC Genomics* 8:354.
168. Shahsavarani A, McNeill B, Galvez F, Wood CM, Goss GG, Hwang P-P, Perry SF. 2006. Characterization of a branchial epithelial calcium channel (ECaC) in freshwater rainbow trout (*Oncorhynchus mykiss*). *J Exp Biol* 209:1928–1943.
169. Craig PM, Wood CM, McClelland GB. 2007. Gill membrane remodeling with soft-water acclimation in zebrafish (*Danio rerio*). *Physiol Genomics* 30:53–60.
170. Flik G, van der Velden JA, Dechering KJ, Verbost PM, Schoenmakers TJM, Kolar ZI, Bonga SEW. 1993. Ca^{2+} and Mg^{2+} transport in gills and gut of tilapia, *Oreochromis mossambicus*: A review. *J Exp Zool* 265:356–365.
171. Flik G, van Rijs JH, Wendelaar Bonga SE. 1985. Evidence for high-affinity Ca^{2+}-ATPase activity and ATP-driven Ca^{2+}-transport in membrane preparations of the gill epithelium of the cichlid fish *Oreochromis mossambicus*. *J Exp Biol* 119:335–347.
172. Flik G, Klaren PHM, Schoenmakers TJM, Bijvelds MJC, Verbost PM, Bonga SEW. 1996. Cellular calcium transport in fish: Unique and universal mechanisms. *Physiol Zool* 69:403–417.
173. Pan T-C, Liao B-K, Huang C-J, Lin L-Y, Hwang P-P. 2005. Epithelial Ca^{2+} channel expression and Ca^{2+} uptake in developing zebrafish. *Am J Phys-Reg I* 289:R1202–R1211.
174. Saito K, Nakamura N, Ito Y, Hoshijima K, Esaki M, Zhao B, Hirose S. 2010. Identification of zebrafish FXYD11a protein that is highly expressed in ion-transporting epithelium of the gill and skin and its possible role in ion homeostasis. *Front Physiol* 1:129.
175. Verbost PM, Schoenmakers TJM, Flik G, Wendelaar Bonga SE. 1994. Kinetics of ATP- and $Na(^+)$-gradient driven Ca^{2+} transport in basolateral membranes from gills of freshwater- and seawater-adapted tilapia. *J Exp Biol* 186:95–108.

176. Flik G, Perry SF. 1989. Cortisol stimulates whole body calcium uptake and the branchial calcium pump in freshwater rainbow trout. *J Endocrinol* 120:75–82.
177. Flik G, Schoenmakers TJM, Groot JA, Os CH, Wendelaar Bonga SE. 1990. Calcium absorption by fish intestine: The involvement of ATP- and sodium-dependent calcium extrusion mechanisms. *J Membr Biol* 113:13–22.
178. Baldisserotto B, Chowdhury MJ, Wood CM. 2005. Effects of dietary calcium and cadmium on cadmium accumulation, calcium and cadmium uptake from the water, and their interactions in juvenile rainbow trout. *Aquat Toxicol* 72:99–117.
179. Wheatly MG, Weil JR, Douglas PB. 1998. Isolation, visualization, characterization, and osmotic reactivity of crayfish BLMV. *Am J Phys-Reg I* 274:R725–R734.
180. Wheatly MG, Pence RC, Weil JR. 1999. ATP-dependent calcium uptake into basolateral vesicles from transporting epithelia of intermolt crayfish. *Am J Phys-Reg I* 276:R566–R574.
181. Ahearn GA, Duerr JM, Zhuang Z, Brown RJ, Aslamkhan A, Killebrew DA. 1999. Ion transport processes of crustacean epithelial cells. *Physiol Biochem Zool* 72:1–18.
182. Ahearn GA, Mandal PK, Mandal A. 2004. Calcium regulation in crustaceans during the molt cycle: A review and update. *Comp Biochem Physiol A* 137:247–257.
183. Wheatly MG, Zanotto FP, Hubbard MG. 2002. Calcium homeostasis in crustaceans: Subcellular Ca dynamics. *Comp Biochem Physiol B* 132:163–178.
184. Greenaway P. 1974. Calcium balance at the postmoult stage of the freshwater crayfish *Austropotamobius pallipes* (Lereboullet). *J Exp Biol* 61:35–45.
185. Neufeld DS, Cameron JN. 1993. Transepithelial movement of calcium in crustaceans. *J Exp Biol* 184:1–16.
186. Wheatly MG. 1999. Calcium homeostasis in crustacea: The evolving role of branchial, renal, digestive and hypodermal epithelia. *J Exp Zool* 283:620–640.
187. Glover CN, Wood CM. 2005. Physiological characterisation of a pH- and calcium-dependent sodium uptake mechanism in the freshwater crustacean, *Daphnia magna*. *J Exp Biol* 208:951–959.
188. Zanotto FP, Wheatly MG. 1993. The effect of ambient pH on electrolyte regulation during the postmolt period in freshwater crayfish *Procambarus clarkii*. *J Exp Biol* 178:1–19.
189. Ahearn GA, Franco P. 1993. Ca^{2+} transport pathways in brush-border membrane vesicles of crustacean antennal glands. *Am J Phys-Reg I* 264:R1206–R1213.
190. Wheatly MG. 1997. Crustacean models for studying calcium transport: The journey from whole organisms to molecular mechanisms. *J Mar Biol Assoc UK* 77:107–125.
191. Flik G, Fenwick JC, Kolar Z, Mayer-Gostan N, Wendelaar Bonga SE. 1986. Effects of low ambient calcium levels on wholebody Ca^{2+} flux rates and internal calcium pools in the freshwater cichlid teleost, *Oreochromis mossambicus*. *J Exp Biol* 120:249–264.
192. Flik G, Verbost PM, Atsma W, Lucu C. 1994. Calcium transport in gill plasma membranes of the crab *Carcinus maenas*: Evidence for carriers driven by ATP and a Na^+ gradient. *J Exp Biol* 195:109–122.
193. Gao Y, Wheatly MG. 2004. Characterization and expression of plasma membrane Ca^{2+} ATPase (PMCA3) in the crayfish *Procambarus clarkii* antennal gland during molting. *J Exp Biol* 207:2991–3002.
194. Rogers JV, Wheatly MG. 1997. Accumulation of calcium in the antennal gland during the molting cycle of the freshwater crayfish *Procambarus clarkii*. *Invertebr Biol* 116:248–254.
195. Willis JH. 1999. Cuticular proteins in insects and crustaceans. *Am Zool* 39:600–609.
196. Woodall WR, Jr, Wallace JB. 1975. Mineral pathways in small Appalachian streams. In Howell FG, Gentry JB, Smith MH, eds, *Mineral Cycling in Southeastern Ecosystems: Proceedings of a Symposium Held at Augusta, Georgia, May 1–3, 1974*. Energy Reseach and Development Symposium Series. Technical Information Center, Office of Public Affairs, US Energy and Development Administration, Oak Ridge, TN, USA, pp 408–422.
197. Barkai AI, Williams RW. 1983. The exchange of calcium in larvae of the mosquito *Aedes aegypti*. *J Exp Biol* 104:139–148.
198. Dietz TH. 1985. Ionic regulation in freshwater mussels: A brief review. *Am Malacol Bull* 3:233–242.
199. Silverman H, Kays WT, Dietz TH. 1987. Maternal calcium contribution to glochidial shells in freshwater mussels (Eulamellibranchia: Unionidae). *J Exp Zool* 242:137–146.
200. O'Donnell MJ. 1997. Mechanisms of excretion and ion transport in invertebrates. In Dantzler WH, ed, *Handbook of Physiology, Section 13: Comparative Physiology*, Vol II. Oxford University, New York, NY, USA, pp 1207–1289.
201. Ebanks SC, O'Donnell M, Grosell M. 2010. Acquisition of Ca^{2+}; and HCO_3^-/CO_3^{2-} for shell formation in embryos of the common pond snail *Lymnaea stagnalis*. *J Comp Phys B* 180:953–965.
202. Ebanks SC, O'Donnell MJ, Grosell M. 2010. Characterization of mechanisms for Ca^{2+} and HCO_3^-/CO_3^{2-} acquisition for shell formation in embryos of the freshwater common pond snail *Lymnaea stagnalis*. *J Exp Biol* 213:4092–4098.
203. Verbost PM, van Rooij J, Flik G, Lock RAC, Wendelaar Bonga SE. 1989. The movement of cadmium through freshwater trout branchial epithelium and its interference with calcium transport. *J Exp Biol* 145:185–197.
204. Hogstrand C, Webb N, Wood CM. 1998. Covariation in regulation of affinity for branchial zinc and calcium uptake in freshwater rainbow trout. *J Exp Biol* 201:1809–1815.
205. Rogers JT, Richards JG, Wood CM. 2003. Ionoregulatory disruption as the acute toxic mechanism for lead in the rainbow trout (*Oncorhynchus mykiss*). *Aquat Toxicol* 64:215–234.
206. Qiu A, Hogstrand C. 2004. Functional characterisation and genomic analysis of an epithelial calcium channel (ECaC) from pufferfish, *Fugu rubripes*. *Gene* 342:113–123.
207. Hogstrand C, Verbost PM, Bonga SE, Wood CM. 1996. Mechanisms of zinc uptake in gills of freshwater rainbow trout: Interplay with calcium transport. *Am J Phys-Reg I* 270:R1141–R1147.
208. Comhaire S, Blust R, Van Ginneken L, Verbost PM, Vanderborght OLJ. 1998. Branchial cobalt uptake in the carp, *Cyprinus carpio*: Effect of calcium channelblockers and calcium injection. *Fish Physiol Biochem* 18:1–13.
209. Verbost PM, Flik G, Lock RAC, Wendelaar Bonga SE. 1987. Cadmium inhibition of Ca^{2+} uptake in rainbow trout gills. *Am J Phys-Reg I* 253: R216–R221.
210. Schoenmakers TJM, Klaren PHM, Flik G, Lock RAC, Pang PKT, Wendelaar-Bonga SE. 1992. Actions of cadmium on basolateral plasma membrane proteins involved in calcium uptake by fish intestine. *J Membr Biol* 127:161–172.
211. Comhaire S, Blust R, Van Ginneken L, Vanderborght OLJ. 1994. Cobalt uptake across the gills of the common carp, *Cyprinus carpio*, as a function of calcium concentration in the water of acclimation and exposure. *Comp Biochem Physiol C* 109:63–76.
212. Hogstrand C, Wilson RW, Polgar D, Wood CM. 1994. Effects of zinc on the kinetics of branchial calcium uptake in freshwater rainbow trout during adaptation to waterborne zinc. *J Exp Biol* 186:55–73.
213. Rogers JT, Wood CM. 2004. Characterization of branchial lead-calcium interaction in the freshwater rainbow trout *Oncorhynchus mykiss*. *J Exp Biol* 207:813–825.
214. de Schamphelaere KAC, Janssen CR. 2001. A biotic ligand model predicting acute copper toxicity for *Daphnia magna*: The effects of calcium, magnesium, sodium, potassium, and pH. *Environ Sci Technol* 36:48–54.
215. Buchwalter DB, Luoma SN. 2004. Differences in dissolved cadmium and zinc uptake among stream insects: Mechanistic explanations. *Environ Sci Technol* 39:498–504.
216. Faubel D, Lopes-Lima M, Freitas S, Pereira L, Andrade J, Checa A, Frank H, Matsuda T, Machado J. 2008. Effects of Cd^{2+} on the calcium metabolism and shell mineralization of bivalve *Anodonta cygnea*. *Mar Freshwat Behav Physiol* 41:131–146.
217. Ngo HTT, Gerstmann S, Frank H. 2011. Subchronic effects of environment-like cadmium levels on the bivalve *Anodonta anatina* (Linnaeus 1758): III. Effects on carbonic anhydrase activity in relation to calcium metabolism. *Toxicol Environ Chem* 93:1815–1825.
218. Wood CM, Rogano MS. 1986. Physiological responses to acid stress in crayfish (*Orconectes*): Haemolymph ions, acid–base status, and exchanges with the environment. *Can J Fish Aquat Sci* 43:1017–1026.
219. Chen Y-Y, Lu F-I, Hwang P-P. 2003. Comparisons of calcium regulation in fish larvae. *J Exp Zool Part A* 295:127–135.
220. McKillop WB, Harrison AD. 1972. Distribution of aquatic gastropods across an interface between the Canadian Shield and limestone formations. *Can J Zool* 50:1433–1445.
221. Flatman PW. 1991. Mechanisms of magnesium transport. *Annu Rev Physiol* 53:259–271.
222. Morritt D, Spicer JI. 1993. A brief re-examination of the function and regulation of extracellular magnesium and its relationship to activity in crustacean arthropods. *Comp Biochem Physiol A* 106:19–23.
223. Klungsøyr L. 1987. Magnesium ion activated ATPase and proton transport in vesicles from the gill of rainbow trout (*Salmo gairdnerii*). *Comp Biochem Physiol B* 88:1125–1134.

224. Burton RF. 1980. Adenosine triphosphate as a determinant of magnesium levels in cytoplasm. *Comp Biochem Physiol A* 65:1–4.
225. Bijvelds MJC, Flik G, Wendelaar-Bonga SE. 1997. Mineral balance in *Oreochromis mossambicus*: Dependence on magnesium in diet and water. *Fish Physiol Biochem* 16:323–331.
226. Kehres DG, Maguire ME. 2002. Structure, properties and regulation of magnesium transport proteins. *BioMetals* 15:261–270.
227. Sahni J, Scharenberg AM. 2013. The SLC41 family of MgtE-like magnesium transporters. *Mol Aspects Med* 34:620–628.
228. van der Velden JA, Kolar ZI, Flik G. 1991. Intake of magnesium from water by freshwater tilapia fed on a low-Mg diet. *Comp Biochem Physiol A* 99:103–105.
229. Bijvelds MJC, Kolar ZI, Flik G. 2001. Electrodiffusive magnesium transport across the intestinal brush border membrane of tilapia (*Oreochromis mossambicus*). *Eur J Biochem* 268:2867–2872.
230. Bijvelds MJC, Kolar ZI, Wendelaar Bonga SE, Flik G. 1996. Magnesium transport across the basolateral plasma membrane of the fish enterocyte. *J Membr Biol* 154:217–225.
231. Bijvelds MJC, van der Velden JA, Kolar ZI, Flik G. 1998. Magnesium transport in freshwater teleosts. *J Exp Biol* 201:1981–1990.
232. van der Velden JA, Flik G, Spanings FAT, Verburg TG, Kolar ZI, Wendelaar Bonga SE. 1992. Physiological effects of low-magnesium feeding in the common carp, *Cyprinus carpio*. *J Exp Zool* 264: 237–244.
233. Dabrowska H, Meyer-Burgdorff K, Gunther K-D. 1991. Magnesium status in freshwater fish, common carp (*Cyprinus carpio*, L.) and the dietary protein-magnesium interaction. *Fish Physiol Biochem* 9:165–172.
234. Shearer KD, Åsgård T. 1992. The effect of water-borne magnesium on the dietary magnesium requirement of the rainbow trout (*Oncorhynchus mykiss*). *Fish Physiol Biochem* 9:387–392.
235. Oikari AOJ, Rankin JC. 1985. Renal excretion of magnesium in a freshwater teleost, *Salmo gairdneri*. *J Exp Biol* 117:319–333.
236. Freire CA, Kinne RK, Kinne-Saffran E, Beyenbach KW. 1996. Electrodiffusive transport of Mg across renal membrane vesicles of the rainbow trout *Oncorhynchus mykiss*. *Am J Physiol-Renal* 270: F739–F748.
237. Fieber LA, Lutz PL. 1985. Magnesium and calcium metabolism during molting in the freshwater prawn *Macrobrachium rosenbergii*. *Can J Zool* 63:1120–1124.
238. Kiceniuk J, Phillips JE. 1974. Magnesium regulation in mosquito larvae (*Aedes campestris*) living in waters of high $MgSO_4$ content. *J Exp Biol* 61:749–760.
239. Phillips JE, Maddrell SHP. 1974. Active transport of magnesium by the Malpighian tubules of the larvae of the mosquito, *Aedes campestris*. *J Exp Biol* 61:761–771.
240. Dietz TH, Lessard D, Silverman H, Lynn JW. 1994. Osmoregulation in *Dreissena polymorpha*: The importance of Na, Cl, K, and particularly Mg. *Biol Bull* 187:76–83.
241. Pane EF, Smith C, McGeer JC, Wood CM. 2003. Mechanisms of acute and chronic waterborne nickel toxicity in the freshwater cladoceran, *Daphnia magna*. *Environ Sci Technol* 37:4382–4389.
242. Leonard EM, Wood CM. 2013. Acute toxicity, critical body residues, Michaelis–Menten analysis of bioaccumulation, and ionoregulatory disturbance in response to waterborne nickel in four invertebrates: *Chironomus riparius*, *Lymnaea stagnalis*, *Lumbriculus variegatus* and *Daphnia pulex*. *Comp Biochem Physiol C* 158:10–21.
243. Niyogi S, Brix KV, Grosell M. 2014. Effects of chronic waterborne nickel exposure on growth, ion homeostasis, acid-base balance, and nickel uptake in the freshwater pulmonate snail, *Lymnaea stagnalis*. *Aquat Toxicol* 150:36–44.
244. Schwartz ML, Playle RC. 2001. Adding magnesium to the silver-gill binding model for rainbow trout (*Oncorhynchus mykiss*). *Environ Toxicol Chem* 20:467–472.
245. Naddy RB, Stubblefield WA, May JR, Tucker SA, Hockett JR. 2002. The effect of calcium and magnesium ratios on the toxicity of copper to five aquatic species in freshwater. *Environ Toxicol Chem* 21:347–352.
246. Maetz J, García-Romeu F. 1964. The mechanism of sodium and chloride uptake by the gills of a fresh-water fish, *Carassius auratus*. II. Evidence for NH_4^+/Na^+ and HCO_3^-/Cl^- exchanges. *J Gen Physiol* 47:1209–1229.
247. Evans DH. 1975. Ionic exchange mechanisms in fish gills. *Comp Biochem Physiol A* 51:491–495.
248. Dejours P, Armand J, Beekenkamp H. 1982. The effect of ambient chloride concentration changes on branchial chloride-bicarbonate exchanges and hemolymph acid-base balance of crayfish. *Respir Physiol* 48:375–386.
249. Wilson JM, Laurent P, Tufts BL, Benos DJ, Donowitz M, Vogl AW, Randall DJ. 2000. NaCl uptake by the branchial epithelium in freshwater teleost fish: An immunological approach to ion-transport protein localization. *J Exp Biol* 203:2279–2296.
250. Boisen AMZ, Amstrup J, Novak I, Grosell M. 2003. Sodium and chloride transport in soft water and hard water acclimated zebrafish (*Danio rerio*). *Biochim Biophys Acta* 1618:207–218.
251. Maetz J. 1971. Fish gills: Mechanisms of salt transfer in fresh water and sea water. *Philos Trans R Soc B* 262:209–249.
252. Kerstetter TH, Kirschner LB. 1972. Active chloride transport by the gills of rainbow trout (*Salmo gairdneri*). *J Exp Biol* 56:263–272.
253. Bayaa M, Vulesevic B, Esbaugh AJ, Braun M, Ekker ME, Grosell M, Perry SF. 2009. The involvement of SLC26 anion transporters in chloride uptake in zebrafish (*Danio rerio*) larvae. *J Exp Biol* 212:3283–3295.
254. Lin L-Y, Hwang P-P. 2004. Mitochondria-rich cell activity in the yolk-sac membrane of tilapia (*Oreochromis mossambicus*) larvae acclimatized to different ambient chloride levels. *J Exp Biol* 207:1335–1344.
255. Tresguerres M, Katoh F, Orr E, Parks SK, Goss Greg G. 2006. Chloride uptake and base secretion in freshwater fish: A transepithelial ion-transport metabolon? *Physiol Biochem Zool* 79:981–996.
256. Preest M, Gonzalez R, Wilson R. 2005. A pharmacological examination of Na^+ and Cl^- transport in two species of freshwater fish. *Physiol Biochem Zool* 78:259–272.
257. Bucking C, Wood CM. 2006. Gastrointestinal processing of Na^+, Cl^-, and K^+ during digestion: Implications for homeostatic balance in freshwater rainbow trout. *Am J Phys-Reg I* 291:R1764–R1772.
258. Tang CH, Lee TH. 2007. The effect of environmental salinity on the protein expression of Na^+/K^+-ATPase, $Na^+/K^+/2Cl^-$ cotransporter, cystic fibrosis transmembrane conductance regulator, anion exchanger 1, and chloride channel 3 in gills of a euryhaline teleost, *Tetraodon nigroviridis*. *Comp Biochem Physiol A* 147:521–528.
259. Marshall WS, Singer TD. 2002. Cystic fibrosis transmembrane conductance regulator in teleost fish. *Biochim Biophys Acta* 1566:16–27.
260. O'Donnell MJ, Kelly SP, Nurse CA, Wood CM. 2001. A maxi $Cl(^-)$ channel in cultured pavement cells from the gills of the freshwater rainbow trout *Oncorhynchus mykiss*. *J Exp Biol* 204:1783–1794.
261. Ohana E, Yang D, Shcheynikov N, Muallem S. 2009. Diverse transport modes by the solute carrier 26 family of anion transporters. *J Physiol* 587:2179–2185.
262. Dickson JS, Dillaman RM, Roer RD, Roye DB. 1991. Distribution and characterization of ion transporting and respiratory filaments in the gills of *Procambarus clarkii*. *Biol Bull* 180:154–166.
263. Dunel-Erb S, Barradas C, Lignon J. 1997. Morphological evidence for the existence of two distinct types of mitochondria rich cells in the gill of the crayfish *Astacus leptodactylus* Eschscholtz. *Acta Zool* 78: 195–203.
264. Burnett LE, Dunn TN, Infantino RL, Jr. 1985. The function of carbonic anhydrase in crustacean gills. In Gilles R, Gilles-Baillien M, eds, *Transport Processes, Iono- and Osmoregulation*. Springer-Verlag, Berlin, Germany, pp 159–168.
265. Henry RP. 1988. Multiple functions of carbonic anhydrase in the crustacean gill. *J Exp Zool* 248:19–24.
266. Burnett LE, McMahon BR. 1985. Facilitation of CO_2 excretion by carbonic anhydrase located on the surface of the basal membrane of crab gill epithelium. *Respir Physiol* 62:341–348.
267. Cameron JN. 1986. Acid-base equilibria in invertebrates. In Heisler N, ed, *Acid-base Regulation in Animals*. Elsevier Science, Amsterdam, The Netherlands, pp 357–394.
268. Kikuchi S. 1983. The fine structure of the gill epithelium of a freshwater flea, *Daphnia magna* (Crustacea: Phyllopoda) and changes associated with acclimation to various salinities. *Cell Tissue Res* 229:253–268.
269. Stobbart RH. 1971. Evidence for Na^+/H^+ and Cl^-/HCO_3^- exchanges during independent sodium and chloride uptake by the larva of the mosquito *Aedes aegypti* (L.). *J Exp Biol* 54:19–27.
270. Stobbart RH. 1974. Electrical potential differences and ionic transport in the larva of the mosquito *Aedes aegypti* (L.). *J Exp Biol* 60:493–533.
271. del Duca O, Nasirian A, Galperin V, Donini A. 2011. Pharmacological characterisation of apical Na+ and Cl– transport mechanisms of the anal papillae in the larval mosquito *Aedes aegypti*. *J Exp Biol* 214:3992–3999.
272. Smith KE, Raymond SL, Valenti ML, Smith PJS, Linser PJ. 2010. Physiological and pharmacological characterizations of the larval *Anopheles albimanus* rectum support a change in protein distribution

and/or function in varying salinities. *Comp Biochem Physiol A* 157: 55–62.
273. Patrick ML, Gonzalez RJ, Bradley TJ. 2001. Sodium and chloride regulation in freshwater and osmoconforming larvae of *Culex* mosquitoes. *J Exp Biol* 204:3345–3354.
274. Komnick H, Rhees RW, Abel JH, Jr. 1972. The function of ephemerid chloride cells: Histochemical, autoradiographic and physiological studies with radioactive chloride on *Callibaetis*. *Cytobiologie* 5: 65–82.
275. Wichard W, Komnick H. 1971. Electron microscopical and histochemical evidence of chloride cells in tracheal gills of mayfly larvae. *Cytobiologie* 3:215–228.
276. Komnick H, Wichard W. 1975. Chloride cells of larval *Notonecta glauca* and *Naucoris cimicoides* (Hemiptera, Hydrocorisae). *Cell Tissue Res* 156:539–549.
277. Treherne JE. 1954. Osmotic regulation in the larvae of *Helodes* (Coleoptera: Helodidae). *Trans R Ent Soc Lond* 105:117–130.
278. Moens J. 1975. Ionic regulation of the haemolymph in the larvae of the dragonfly *Aeshna cyanea* (Miiller) (Odonata, Anisoptera). *Arch Int Physiol Biochim* 83:443–451.
279. Leader JP, Green LB. 1978. Active transport of chloride and sodium by the rectal chamber of the larvae of the dragonfly, *Uropetala carovei*. *J Insect Physiol* 24:685–692.
280. Komnick H. 1978. Osmoregulatory role and transport ATPases of the rectum of dragonfly larvae. *Odonatologica* 7:247–262.
281. Komnick H, Achenbach U. 1979. Comparative biochemical, histochemical and autoradiographic studies of Na^+/K^+-ATPase in the rectum of dragonfly larvae (Odonata, Aeshnidae). *Eur J Cell Biol* 20:92–100.
282. Byrne RA, Dietz TH. 1997. Ion transport and acid-base balance in freshwater bivalves. *J Exp Biol* 200:457–465.
283. Dietz TH, Hagar AF. 1990. Chloride uptake in isolated gills of the freshwater mussel *Ligumia subrostrata*. *Can J Zool* 68:6–9.
284. Taylor PM, Andrews EB. 1987. Tissue adenosine-triphosphatase activities of the gill and excretory system in mesogastropod molluscs in relation to osmoregulatory capacity. *Comp Biochem Physiol A* 86:693–696.
285. Riestenpatt S, Petrausch G, Siebers D. 1995. Cl^- influx across posterior gills of the Chinese crab (*Eriocheir sinensis*): Potential energization by a V-type H^+-ATPase. *Comp Biochem Physiol A* 110:235–241.
286. Jensen FB. 1996. Uptake, elimination and effects of nitrite and nitrate in freshwater crayfish (*Astacus astacus*). *Aquat Toxicol* 34:95–104.
287. Stormer J, Jensen FB, Rankin JC. 1996. Uptake of nitrite, nitrate, and bromide in rainbow trout, (*Oncorhynchus mykiss*): Effects on ionic balance. *Can J Fish Aquat Sci* 53:1943–1950.
288. Williams EM, Eddy FB. 1986. Chloride uptake in freshwater teleosts and its relationship to nitrite uptake and toxicity. *J Comp Phys B* 156:867–872.
289. Harris RR, Coley S. 1991. The effects of nitrite on chloride regulation in the crayfish *Pacifastacus leniusculus* Dana (Crustacea: Decapoda). *J Comp Phys B* 161:199–206.
290. Wood CM, Robertson LM, Johannsson OE, Val AL. 2014. Mechanisms of Na^+ uptake, ammonia excretion, and their potential linkage in native Rio Negro tetras (*Paracheirodon axelrodi*, *Hemigrammus rhodostomus*, and *Moenkhausia diktyota*). *J Comp Phys B* 184:877–890.
291. Heisler N. 1986. Acid-base regulation in fishes. In Heisler N, ed, *Acid-Base Regulation in Animals*. Elsevier Science, Amsterdam, The Netherlands, pp 309–356.
292. Gilmour KM, Perry SF. 2009. Carbonic anhydrase and acid–base regulation in fish. *J Exp Biol* 212:1647–1661.
293. Wheatly MG, Henry RP. 1992. Extracellular and intracellular acid-base regulation in crustaceans. *J Exp Zool* 263:127–142.
294. Goss GG, Wood CM. 1991. Two-substrate kinetic analysis: A novel approach linking ion and acid-base transport at the gills of freshwater trout, (*Oncorhynchus mykiss*). *J Comp Phys B* 161: 635–646.
295. Goss GG, Perry SF, Wood CM, Laurent P. 1992. Mechanisms of ion and acid-base regulation at the gills of freshwater fish. *J Exp Zool* 263:143–159.
296. Goss GG, Perry SF, Fryer JN, Laurent P. 1998. Gill morphology and acid-base regulation in freshwater fishes. *Comp Biochem Physiol A* 119:107–115.
297. Jensen LJ, Sørensen JN, Larsen EH, Willumsen NJ. 1997. Proton pump activity of mitochondria-rich cells: The interpretation of external proton-concentration gradients. *J Gen Physiol* 109:73–91.
298. Perry SF, Goss GG. 1994. The effects of experimentally altered gill chloride cell surface area on acid-base regulation in rainbow trout during metabolic alkalosis. *J Comp Phys B* 164:327–336.
299. Goss GG, Laurent P, Perry SF. 1994. Gill morphology during hypercapnia in brown bullhead (*Ictalurus nebulosus*): Role of chloride cells and pavement cells in acid-base regulation. *J Fish Biol* 45: 705–718.
300. Perry SF, Malone S, Ewing D. 1987. Hypercapnic acidosis in the rainbow trout (*Salmo gairdneri*). I. Branchial ionic fluxes and blood acid–base status. *Can J Zool* 65:888–895.
301. Goss GG, Adamia S, Galvez F. 2001. Peanut lectin binds to a subpopulation of mitochondria-rich cells in the rainbow trout gill epithelium. *Am J Phys-Reg I* 281:R1718–R1725.
302. Galvez F, Reid SD, Hawkings GS, Goss GG. 2002. Isolation and characterization of mitochondria-rich cell types from the gill of freshwater rainbow trout. *Am J Phys-Reg I* 282:R658–R668.
303. Dymowska AK, Hwang P-P, Goss GG. 2012. Structure and function of ionocytes in the freshwater fish gill. *Resp Physiol Neurobiol* 184:282–292.
304. Harper DD, Farag AM, Skaar D. 2014. Acute toxicity of sodium bicarbonate, a major component of coal bed natural gas produced waters, to 13 aquatic species as defined in the laboratory. *Environ Toxicol Chem* 33:525–531.
305. Farag AM, Harper DD. 2014. The chronic toxicity of sodium bicarbonate, a major component of coal bed natural gas produced waters. *Environ Toxicol Chem* 33:532–540.
306. Whiteley NM. 1999. Acid-base regulation in crustaceans: The role of bicarbonate ions. In Eggington S, Taylor EW, Raven JA, eds, *Regulation of Tissue pH in Plants and Animals*. Cambridge University, Cambridge, UK, pp 233–255.
307. Cormier SM, Suter GW, Zheng L. 2013. Derivation of a benchmark for freshwater ionic strength. *Environ Toxicol Chem* 32:263–271.
308. Machado JP, Ferreira KG, Ferreira HG, Fernandes PL. 1990. The acid-base balance of the outer mantle epithelium of *Anodonta cygnea*. *J Exp Biol* 150:159–169.
309. Henry RP, Saintsing DG. 1983. Carbonic anhydrase activity and ion regulation in three species of osmoregulating bivalve molluscs. *Physiol Zool* 56:274–280.
310. García-Romeu F, Maetz JG. 1964. The mechanism of sodium and chloride uptake by the gills of a fresh-water fish, *Carassius auratus*: I. Evidence for an independent uptake of sodium and chloride ions. *J Gen Physiol* 47:1195–1207.
311. de Renzis G, Maetz J. 1973. Studies on the mechanism of chloride absorption by the goldfish gill: Relation with acid-base regulation. *J Exp Biol* 59:339–358.
312. Shaw J. 1960. The absorption of sodium ions by the crayfish, *Astacus pallipes* Lereboullet: II. The effect of the external anion. *J Exp Biol* 37:534–547.
313. McMahon BR, Stuart SA. 1989. The physiological problems of crayfish in acid waters. In Morris R, Taylor EW, Brown DJA, Brown JA, eds, *Acid Toxicity and Aquatic Animals*, Vol 34—Society for Experimental Biology Seminar Series. Cambridge University, Cambridge, UK, pp 171–199.
314. Larsen EH, Simonsen K. 1988. Sulfate transport in toad skin: Evidence for mitochondria-rich cell pathways in common with halide ions. *Comp Biochem Physiol A* 90:709–714.
315. Piłsyk S, Paszewski A. 2009. Sulfate permease—Phylogenetic diversity of sulfate transport. *Acta Biochim Pol* 56:375–384.
316. Nakada T, Zandi-Nejad K, Kurita Y, Kudo H, Broumand V, Kwon CY, Mercado A, Mount DB, Hirose S. 2005. Roles of Slc13a1 and Slc26a1 sulfate transporters of eel kidney in sulfate homeostasis and osmoregulation in freshwater. *Am J Phys-Reg I* 289:R575–R585.
317. Katoh F, Tresguerres M, Lee KM, Kaneko T, Aida K, Goss GG. 2006. Cloning of rainbow trout SLC26A1: Involvement in renal sulfate secretion. *Am J Phys-Reg I* 290:R1468–R1478.
318. Watanabe T, Takei Y. 2011. Environmental factors responsible for switching on the SO_4^{2-} excretory system in the kidney of seawater eels. *Am J Phys-Reg I* 301:R402–R411.
319. Maddrell SHP, Phillips JE. 1975. Active transport of sulphate ions by the Malpighian tubules of larvae of the mosquito *Aedes campestris*. *J Exp Biol* 62:367–378.
320. Dietz TH, Byrne RA. 1999. Measurement of sulfate uptake and loss in the freshwater bivalve *Dreissena polymorpha* using a semi-microassay. *Can J Zool* 77:331–336.
321. Hōbe H. 1987. Sulphate entry into soft-water fish (*Salmo gairdneri*, *Catostomus commersoni*) during low ambient pH exposure. *J Exp Biol* 133:87–109.

322. Griffith MB, Norton SB, Alexander LC, Pollard AI, LeDuc SD. 2012. The effects of mountaintop mines and valley fills on the physico-chemical quality of stream ecosystems in the central Appalachians: A review. *Sci Total Environ* 417–418:1–12.
323. Wilson JM, Antunes JC, Bouça PD, Coimbra J. 2004. Osmoregulatory plasticity of the glass eel of *Anguilla anguilla*: Freshwater entry and changes in branchial ion-transport protein expression. *Can J Fish Aquat Sci* 61:432–442.
324. Xie L, Buchwalter DB. 2011. Cadmium exposure route affects antioxidant responses in the mayfly *Centroptilum triangulifer*. *Aquat Toxicol* 105:199–205.
325. Struewing KA, Lazorchak JM, Weaver PC, Johnson BR, Funk DH, Buchwalter DB. 2014. Part 2: Sensitivity comparisons of the mayfly *Centroptilum triangulifer* to *Ceriodaphnia dubia* and *Daphnia magna* using standard reference toxicants; NaCl, KCl and $CuSO_4$. *Chemosphere* 139:597–603.
326. Forman RTT, Alexander LE. 1998. Roads and their major ecological effects. *Annu Rev Ecol Syst* 29:207–231.
327. Kaushal SS, Groffman PM, Likens GE, Belt KT, Stack WP, Kelly VR, Band LE, Fisher GT. 2005. Increased salinization of fresh water in the northeastern United States. *Proc Natl Acad Sci U S A* 102:13517–13520.
328. Kelting DL, Laxson CL, Yerger EC. 2012. Regional analysis of the effect of paved roads on sodium and chloride in lakes. *Water Res* 46:2749–2758.
329. Davies PJ, Wright IA, Jonasson OJ, Findlay SJ. 2010. Impact of concrete and PVC pipes on urban water chemistry. *Urban Water J* 7:233–241.
330. Wright IA, Davies PJ, Findlay SJ, Jonasson OJ. 2011. A new type of water pollution: Concrete drainage infrastructure and geochemical contamination of urban waters. *Mar Freshw Res* 62:1355–1361.
331. Boelter AM, Lamming FN, Farag AM, Bergman HL. 1992. Environmental effects of saline oil-field discharges on surface waters. *Environ Toxicol Chem* 11:1187–1195.
332. Veil JA, Puder MG, Elcock D, Redweik RJ, Jr. 2004. A white paper describing produced water from production of crude oil, natural gas, and coal bed methane. US Department of Energy, Argonne National Laboratory, Argonne, IL, USA.
333. Jackson R, Reddy K. 2007. Geochemistry of coalbed natural gas (CBNG) produced water in Powder River basin, Wyoming: Salinity and sodicity. *Water Air Soil Pollut* 184:49–61.
334. Brinck EL, Drever JI, Frost CD. 2008. The geochemical evolution of water coproduced with coalbed natural gas in the Powder River Basin, Wyoming. *Environ Geosci* 15:153–171.
335. Dahm KG, Guerra KL, Xu P, Drewes JrE. 2011. Composite geochemical database for coalbed methane produced water quality in the Rocky Mountain region. *Environ Sci Technol* 45:7655–7663.
336. Entrekin S, Evans-White M, Johnson B, Hagenbuch E. 2011. Rapid expansion of natural gas development poses a threat to surface waters. *Front Ecol Environ* 9:503–511.
337. Haluszczak LO, Rose AW, Kump LR. 2013. Geochemical evaluation of flowback brine from Marcellus gas wells in Pennsylvania, USA. *Appl Geochem* 28:55–61.
338. Kennedy AJ, Cherry DS, Currie RJ. 2003. Field and laboratory assessment of a coal processing effluent in the Leading Creek watershed, Meigs County, Ohio. *Arch Environ Contam Toxicol* 44:324–331.
339. Hopkins RL II, Altier BM, Haselman D, Merry AD, White JJ. 2013. Exploring the legacy effects of surface coal mining on stream chemistry. *Hydrobiologia* 713:87–95.
340. Ruhl L, Vengosh A, Dwyer GS, Hsu-Kim H, Schwartz G, Romanski A, Smith SD. 2012. The impact of coal combustion residue effluent on water resources: A North Carolina example. *Environ Sci Technol* 46:12226–12233.
341. Leland HV, Brown LR, Mueller DK. 2001. Distribution of algae in the San Joaquin River, California, in relation to nutrient supply, salinity and other environmental factors. *Freshw Biol* 46:1139–1167.
342. Scanlon BR, Stonestrom DA, Reedy RC, Leaney FW, Gates J, Cresswell RG. 2009. Inventories and mobilization of unsaturated zone sulfate, fluoride, and chloride related to land use change in semiarid regions, southwestern United States and Australia. *Water Resour Res* 45:W00A18.
343. Raymond PA, Oh N-H. 2009. Long term changes of chemical weathering products in rivers heavily impacted from acid mine drainage: Insights on the impact of coal mining on regional and global carbon and sulfur budgets. *Earth Planet Sci Lett* 284:50–56.
344. Kaushal SS, Likens GE, Utz RM, Pace ML, Grese M, Yepsen M. 2013. Increased river alkalinization in the eastern U.S. *Environ Sci Technol* 47:10302–10311.
345. Echols BS, Currie RJ, Cherry DS. 2009. Influence of conductivity dissipation on benthic macroinvertebrates in the North Fork Holston River, Virginia, downstream of a point source brine discharge during severe low-flow conditions. *Hum Ecol Risk Assess* 15:170–184.
346. Andersen CB, Lewis GP, Sargent KA. 2004. Influence of wastewater-treatment effluent on concentrations and fluxes of solutes in the Bush River, South Carolina, during extreme drought conditions. *Environ Geosci* 11:28–41.
347. Hur J, Schlautman M, Karanfil T, Smink J, Song H, Klaine S, Hayes J. 2007. Influence of drought and municipal sewage effluents on the baseflow water chemistry of an upper Piedmont river. *Environ Monit Assess* 132:171–187.
348. Lopez Vera C, Hyne RV, Patra R, Ramasamy S, Pablo F, Julli M, Kefford BJ. 2014. Bicarbonate toxicity to *Ceriodaphnia dubia* and the freshwater shrimp *Paratya australiensis* and its influence on zinc toxicity. *Environ Toxicol Chem* 33:1179–1186.
349. Hoke RA, Gala WR, Drake JB, Giesy JP, Flegler S. 1992. Bicarbonate as a potential confounding factor in cladoceran toxicity assessments of pore water from contaminated sediments. *Can J Fish Aquat Sci* 49:1633–1640.

Table S1. Detailed data on osmoregulation and water movement

Aspect of Transport	Evidence
Aquaporins	In European eel (*Anguilla anguilla*), a homolog of mammalian aquaporin 3 (AQP-3) occurs on the apical membrane of gill epithelial cells [1, 2]. AQP-3 mRNA expression in the gills of adult silver eels (i.e., SW adult stage) in FW was 3 times that in yellow eels (i.e., FW adult stage). Moreover, in silver and yellow eels acclimated to SW for 3 wks, gill AQP-3 mRNA expression was reduced 97 and 76%, respectively, of AQP-3 mRNA expression in eels acclimated to FW. In Atlantic salmon (*Salmo salar*), 3 aquaporin isoforms were found in the gills [3]. Expression of 2 aquaporins, AQP-1a and AQP-3, was greater in gills of FW-acclimated Atlantic salmon, while expression of the third, AQP-1b, was greater in gills of SW-acclimated Atlantic salmon, suggesting that the roles of these aquaporin isoforms in water transport differ.
Compromise of septate junctions by high ion concentrations in FW bivalves	When *Toxolasma texasiense* or *Corbicula fluminea* were exposed to AFW that was made hyperosmotic by addition of 100 mmol mannitol or glucose to avoid the confounding effects of elevated individual inorganic ion concentrations, some EC fluid ion concentrations increased initially (upto 36 h in *C. fluminea* and only up to 8 h in *T. texasiense*), probably as a result of water movement out of the animals along the altered osmotic gradient, because there were no changes in Na^+ or Cl^- flux. After this initial period, most IC fluid ion concentrations decreased, with K^+ decreasing below detection limits, and sugar concentrations increased despite the absence of sugar transporters. When lanthanum (as $LaCl_3$, which forms an insoluble precipitate, $La_2(CO_3)_3$, when it is exposed to endogenous HCO_3^-) was added to the hyperosmotic PW as an electron-dense diffusion tracer, La precipitates were observed in the IC space between the epithelial gill cells [4].
Tolerance of a stonefly nymph to increasing salinity	Many stenohaline FW species can tolerate elevated [Na^+] and [Cl^-] that are at most isotonic with their hemolymph. Nymphs of the stonefly *Paragnetina media* were tolerant (100% survival) of salinities ranging from DW up to 163 mM NaCl, which was approximately isotonic to their hemolymph [5]. However, at salinities of 188 and 205 mM NaCl, which were hypertonic to the nymphs' hemolymph, 15 and 80% of the nymphs died by 72 h, respectively.
Interspecific variation in sensitivity to increased salinity among centrarchids	While the centrarchids, spotted sunfish (*Lepomis punctatus*) and spotted bass (*Micropterus punctulatus*), took more than 12 h to acclimate to increased salinity of up to 8‰, a third species, redear sunfish (*Lepomis microlophus*), acclimated in less than 1 h [6]. The acclimation times for spotted sunfish and spotted bass were sufficiently long that these two species are unlikely to adapt to habitats where salinity varies with the diurnal tidal cycle [6].
Interspecific variation in sensitivity to increased salinity among *Daphnia* spp.	In *Daphnia*, a 48-h EC50 for immobilization (49.6 mM NaCl for *D. longispina* vs. 101 mM NaCl for *D. magna*) and a 21-d (chronic) EC50 for life history parameters (37.6 mM NaCl L^{-1} for *D. longispina* vs. 85.6 mM NaCl for *D. magna*) for *D. longispina* were nearly one-half those for *D. magna* [7].

Table S1. Detailed data on osmoregulation and water movement *(Continued)*.

Aspect of Transport	Evidence
Variation in sensitivity to increased salinity among clonal groups of the *Daphnia pulex* complex	Even within some species that are not necessarily euryhaline, there can be great variability in tolerance to salinity. In a survey of FW rock bluff and tundra ponds along a salinity gradient related to their proximity to the shore of Hudson Bay, Canada, as many as 7 parthenogenetic clonal groups of the *D. pulex* complex inhabited ponds ranging in specific conductivity from 236 to 1,162 μS cm^{-1} up to 1,204 to 16,955 μS cm^{-1} [8]. Similarly, there was great variability in the fitness of clones from a brackish water lake and a FW pond exposed to different salinities [9].
Ability of FW molluscs to use organic osmolytes to increase hemolymph osmolarity	Comparing two FW molluscs, the gastropod *Pomacea bridgesi* and unionid *Lampsilis teres* [10] were gradually acclimated to media ranging from FW to dilute SW with an osmolality of 400 mOsm (i.e., 200 mM NaCl) [10]. There was 100% survival in *L. teres* and 80−100% survival in *P. bridgesi* up to 200 mOsm (100 mM NaCl); survival decreased to 80 and 0%, respectively, in 400 mOsm. *P. bridgesi* remained hyperosmotic and maintained greater hemolymph [Na^+], [Cl^-], [K^+], and [Ca^{2+}] than the water up to 200 mOsm, whereas *L. teres* became isosmotic to the water at 50 mOsm (i.e., 25 mM NaCl) and maintained hemolymph concentrations of individual ions that were similar or slightly greater than the water. While amino acids that are osmolytes, such as alanine, glycine, and β-alanine, increased in the gills of both molluscs, the increase was greater in *L. teres* than in *P. bridgesi*, which has less capacity to increase these amino acids in response to increasing salinity. In another unionid, *Ligumia subrostrata*, these amino acids constitute only 1% of hemolymph solutes but 11% of the solutes in IC fluids and are important in regulating cell volume [11].
Shifts in the energy budget of juvenile common carp at near isotonic conditions	In stenohaline juvenile common carp, exposure to Na^+ and Cl^- at near isotonic concentrations (i.e., 171 mM NaCl) for 28 d resulted in increased blood osmolality and ion concentrations, which remained slightly hypertonic for total ions and Cl^- and slightly hypotonic for Na^+ [12]. Although, the strongest effect was reduced appetite (i.e., food ingestion decreased initially by 30% and later by 70%), juvenile growth rates were reduced to zero, which was a greater reduction than in reference fish placed in FW whose food ration was decreased to match the ingestion rates of the juveniles in isotonic water. Moreover, respiration rates were increased and glycogen stores in the liver were reduced in the juveniles reared in the isotonic water, suggesting a reallocation of energy to osmoregulation.
Mechanism for reducing energy expenditures for ion uptake by Amazonian oscar exposed to hypoxia	Amazonian oscar (*Astronotus ocellatus*), a fish of low-oxygen black waters, is able to reduce efflux of Na^+ and also K^+ when exposed to hypoxia [13]. The fish reduce transcellular permeability by closing channels in the ionocytes, in part by covering apical crypts in pavement cells, thereby reducing energy expenditure for ion uptake at a time when O_2 is not available for aerobic respiration.

AQP, aquaporin; AFW, artificial freshwater; DW, distilled water; EC, extracellular; EC50, median effect concentration; FW, freshwater; IC, intracellular; PW, pond water; SW, saltwater.

Table S1. Detailed data on osmoregulation and water movement *(Continued)*.

Table S2. Detailed data on structure of ion transporting epithelial membranes and ion transport processes.

Aspect of Transport	Evidence
Expression of claudin gene in fish in FW and SW	In green spotted pufferfish (*Tetraodon nigroviridis*), 2 of 4 claudin-3 genes, all 4 claudin-8 genes, and all 4 claudin-27 genes found in this species were expressed in the gills [14, 15]. Expression of claudin mRNAs, *Tncldn3a*, *Tncldn3c*, and *Tncldn8d*, was greater in FW compared to SW, while expression of *Tncldn27a* and *Tncldn27c* mRNA was less in FW. However, expression of the 5 genes was not statistically different between FW and SW. Similar differences in expression of gill claudin isoform mRNAs in FW and SW were observed in Atlantic salmon [16] and tilapia *(Oreochromis mossambicus)* [17].
Expression of occludin and claudins in goldfish (*Carassius auratus*) in ion-poor water	In goldfish, acute exposure to ion-poor water after acclimation to FW increased occludin expression by 10 to 20% only during the first 3 h, while longer acclimation to low-ion water (14 to 28 d) increased occludin expression by 400 to 500% compared to exposure to FW only [18]. Transcript abundance also increased for 6 of 8 claudins, and tight junction depth increased in goldfish acclimated to low-ion water [19] suggesting that occludin and most claudins play roles in decreasing ion loss across the tight junctions.
Role of cortisol in expression of occludin and claudins	In cultured rainbow trout (*Oncorhynchus mykiss*) gill epithelia, the glucocorticoid hormone cortisol increased mRNA expression of occludin and most claudins, while transepithelial resistance increased and paracellular permeability decreased [20, 21]. In cultured spotted green pufferfish gill epithelia, cortisol had variable effects on mRNA expression of various claudin isoforms [22], and the heterogeneous changes in claudin abundances appear to differentially affect paracellular permeability. Cultured goldfish gill epithelia showed a much smaller response of occludin, claudins, and ZO-1 mRNA to cortisol than did rainbow trout [23], which may explain goldfish stenohalinity, although the cultured gill epithelia included only pavement cells, not ionocytes.

FW, freshwater; SW, saltwater; Tncldn, *Tetraodon nigroviridis* claudin; ZO, zona occludins.

Table S3. Detailed data on Na^+ transport.

Subsection	Aspect of Transport	Evidence
Teleost fish	VHA with apical Na^+-channel	External treatments with bafilomycin, which inhibits VHA, have reduced Na^+ uptake as much as 90% in juvenile tilapia and common carp (*Cyprinus carpio*) [24].
	NHE	Parks et al. [25] argued against an operable NHE, particularly in low-ionic FW, for thermodynamic reasons. However, Parks et al. [26] provided evidence for a Cl^--dependent NHE in rainbow trout.
	NHE and apical Na^+-channel	Parks et al. [27] localized NHE to both α-type and β-type ionocytes, while also localizing the apical Na^+-channel to α-type ionocytes in rainbow trout.
	NHE and VHA with apical Na^+-channel	In FW-reared tilapia, both types of Na^+ transport mechanisms were identified [28].
	VHA	The β-subunit of VHA was cloned from both the gills and kidney of rainbow trout [29].
	NKA	In isolated tilapia gill MR ionocytes exposed to ouabain or copper (Cu^{2+}), both of which inhibit NKA activity, intracellular [Na^+] increased [30]. Addition of a membrane-permeant Cu^{2+} chelator to the Cu^{2+} treatment decreased intracellular [Na^+] because the chelator reversed the inhibition of NKA activity.
	NHE metabolon	Infolding the basolateral membrane brings that membrane near the apical membrane and allows the NKA to create areas of low [Na^+] near the NHE [31]. Production of H^+ by cytosolic CA also creates areas of greater [H^+] close to the NHE. Finally, mucus on external gill surfaces may concentrate Na^+ in the boundary layer outside the apical membrane [32].
	Regulation of intracellular [Na^+]	Whatever the transporters, though, Na^+ uptake rate across the apical membrane of ionocytes is regulated to match the extrusion rate of Na^+ across the basolateral membrane to maintain intracellular [Na^+] and cell volume [33].
	Uptake of Na^+ from food	When fed a meal that provided 6.4 mmol Na^+ kg^{-1} fish, rainbow trout absorbed ≈90% of the Na^+ content of ingested food in their stomach but then appeared to excrete a similar amount of Na^+ into the anterior intestine, resulting in net absorption of ≈9% [34]. Another study of rainbow trout observed similar absorption of dietary Na^+ loads of 0.5 to 70 mmol kg^{-1} fish, but did not measure [Na^+] in the intestine [35]. Gill epithelial Na^+ uptake decreased across the range of dietary Na^+ loads, and branchial Na^+ efflux increased particularly at greater dietary Na^+ loads (i.e., >18 mmol kg^{-1} fish), with little change in excretion via the kidneys [35]. Moreover, blood plasma [Na^+] did not increase substantially in either study when dietary Na^+ loads were similar. However, rainbow

Table S3. Detailed data on Na^+ transport (*Continued*).

Subsection	Aspect of Transport	Evidence
Subsection	Aspect of Transport	Evidence
Teleost fish (continued)	Uptake of Na^+ from food (continued)	trout appear to use Na^+ from their diet to replace losses associated with exposure to low pH [36].
	CA	CA plays a role in Na^+ transport by catalyzing production of H^+ from the hydrolysis of CO_2. A CA isoform identified in rainbow trout gills and involved in acid-base regulation [37], tCAc, is collocated on the apical membrane with NKA on the basolateral membrane of some gill ionocytes, although both were located separately in other ionocytes [38]. When respiratory acidosis was imposed on the trout by elevating the water P_{CO2}, tCAc levels and net H^+ excretion increased, while net H^+ excretion was inhibited by treatment with acetazolamide, which inhibits CA.
	Role of two apical Na^+ transport systems in ionoregulation vs. acid-base regulation	Sodium green, a Na^+-dependent fluorescent reagent, was used to collocate Na^+ accumulation in a mitochondria-rich ionocyte subpopulation that exhibited high VHA levels but only moderate NKA levels [39]. To elucidate the Na^+ uptake mechanisms of these cells, larval zebrafish (*Danio* rerio) were exposed to the ion transporter inhibitors, EIPA (inhibits NHE), amiloride (inhibits apical Na^+-channel at low concentration, apical Na^+-channel and NHE at high concentration), bafilomycin (inhibits VHA), metolazone (inhibits CA), ouabain (inhibits NKA) and ethoxzolamide (inhibits CA) [39]. Na^+ uptake was inhibited by EIPA, bafilomycin, ethoxzolamide, and higher concentrations of amiloride, suggesting that NHE and not the apical Na^+-channel was involved in the Na^+ uptake. As CA supplies the H^+ needed to exchange for Na^+, its inhibition would affect the NHE, while the inhibition of VHA suggests that the electrochemical gradient created by VHA may help energize the NHE [39, 40], particularly in soft, very low [Na^+] (35 μM) waters [41].
	Role of two apical Na^+ transport systems in low vs. higher [Na^+] waters	In soft, very low [Na^+] waters, both Na^+ uptake affinity and capacity were at least twice that in hard, higher [Na^+] (1480 μM) waters. Na^+ uptake in soft water was inhibited by a higher concentration of the VHA inhibitor bafilomycin (1 μM), but not in hard water [41]. At a lower concentration of bafilomycin (0.05 μM), Na^+ uptake increased in hard water but not soft water, providing evidence for both transport mechanisms (i.e., VHA and apical Na^+-channel in soft water and NHE in hard water). In such waters, both Na^+ uptake affinity and capacity were at least twice that in hard, higher [Na^+] (1480 μM) waters.

Table S3. Detailed data on Na^+ transport (*Continued*).

Subsection	Aspect of Transport	Evidence
Teleost fish (continued)	NHE3 under acidic conditions	Immunohistochemical methods have identified NHE3-type NHE in the gills of rainbow trout [42] and zebrafish. In zebrafish, at least 8 NHE isoforms were identified [43]. Two isoforms, zNHE2 and zNHE3b, were expressed predominately in the gills, and zNHE3b was relevant to acidic conditions. The isoform zNHE3b was not located on MR ionocytes with NKA but near the opening of the apical membrane in H^+-ATPase-rich ionocytes along with concanavalin A, an apical marker [44]. When the adult zebrafish were acclimatized to acidic water (pH 4.0−4.1), zNHE3b mRNA decreased to 94% of the control (pH 6.7−6.9), while *zatp6v0c* (subunit c of VHA) mRNA increased to 138% of the control. In zebrafish acclimatized to low [Na^+] FW (0.04−0.05 mM), zNHE3b mRNA was upregulated by 157% compared with the high [Na^+] control (10.0−10.5 mM), while *zatp6v0c* mRNA was downregulated to 58% of the control [43], showing that zNHE3b is involved in Na^+ uptake and not acid regulation, while the converse is true of *zatp6v0c*. Similarly, zNHE3b was upregulated and *zatp6v1a* (subunit a of VHA) was downregulated in low [Na^+] water (0.005 mM), and the reverse occurred in higher [Na^+] water (0.5 m) [45].
	NHE3 under acidic conditions and a NHE3/Rhcg1 metabolon	The role of zNHE3b in Na^+ uptake, particularly under acidic conditions (pH 3.9−4.0), at least in larval zebrafish, may be tied to a metabolon that also includes the excretion of NH_3 by the Rhesus protein, Rhcg1 [46]. Larvae exposed to acidified dechlorinated TW (pH 3.9−4.0) for 4 to 5 d after fertilization were compared with control fish exposed to unacidified water (pH 7.3−7.5). Pointing out that zebrafish along with the Osorezan dace (*Tribolodon hakonensis*) are among the few FW teleosts known to increase Na^+ uptake in acidic water, the authors compared both NH_3 excretion and Na^+ uptake in control and test fish. In some series, test fish were acutely exposed to water (pH 7.3−7.5) to separate the effect of the rearing pH from the effect of the testing pH. In two series, the water was manipulated to inhibit NH_3 excretion by maintaining high external [NH_3/NH_4^+] and highly buffered conditions. EIPA, a NHE inhibitor, was also added to the unacidified water or the buffered water, and the VHA inhibitor bafilomycin A_1 was added to the unacidified water in 3 series. A morpholino oligonucleotide designed to knockdown zebrafish Rhcg1 or a sham were injected into embryos used in two series. In these experiments, Na^+ uptake was always at least two to 4 times greater in larvae acclimated to pH 3.9−4.0 than to pH 7.3−7.5. Except for the treatment with high external NH_3/NH_4^+, which affected Na^+ uptake in both control and acid-acclimated larvae, the treatments reduced NH_3 excretion in both control and acid-acclimated larvae but reduced Na^+ uptake only in the acid-acclimated zebrafish larvae.

Table S3. Detailed data on Na^+ transport (*Continued*).

Subsection	Aspect of Transport	Evidence
Crustacea	Electrogenic $H^+/2Na^+$(or Ca^{2+})-exchanger [H2Na(Ca)E]	This exchanger is electrogenic rather than electroneutral because it exchanges 2 Na^+ for a 1 H^+, which may allow the thermodynamic capacity to move H^+ ions against a greater concentration gradient [47].
	Competitive inhibition of Na^+ uptake by elevated [Ca^{2+}]	Competitive inhibition of Na^+ uptake by elevated external [Ca^{2+}] has been observed in the crayfish *Austropotamobius pallipes* [48].
	Lack of homology with mammalian NHE	Use of a monoclonal antibody from mice putatively for the mammalian NHE suggests the crustacean H2Na(Ca)E differs structurally from the vertebrate NHE [49].
	H2Na(Ca)E transport in *Daphnia*	In *Daphnia* this electrogenic H2Na(Ca)E transports 1 Na^+ instead of 2 Na^+ at low [Na^+], following Michaelis-Menten kinetics. In this model, Na^+ and H^+ may interact cooperatively where H^+ binds to 1 binding site, thereby facilitating binding of Na^+ to the second binding site and promoting increased Na^+ flux [50].
	Noncompetitive inhibition of Na^+ uptake by humic substances	Humic substances noncompetitively affect Na^+ uptake in Cladocera by absorbing to the gill epithelial membranes where they change membrane permeability. This increases J_{max} but does not necessarily alter the K_m for Na^+ [51].
	Na^+ uptake during molt	During molt in FW, Crustacea absorb water and increase body volume, resulting in dilution of ions in the hemolymph [52, 53]. In the Australian crayfish *Cherax destructor* activities of both NKA and VHA increased 2−3 times during postmolt relative to normal intermolt periods, and increased ATPase activities were associated with increased J_{net} of Na^+ [52]. These ATPase activities were similar to those in intermolt crayfish that had Na^+ depleted by placing them in Na^+-free artificial TW. Therefore, these ATPases are involved in uptake of Na^+ across the apical gill membrane, particularly through the apical Na^+-channel but probably also through the NHE.
	Reabsorption of Na^+ by antennal gland	Renal filtration and reabsorption in the antennal gland can be several times greater than absorption through the gills probably because such ion recyling is more energy efficient [54].
	Maintenance of hypertonic hemolymph	The hypertonic hemolymph in FW crayfish is also maintained, in part, by reabsorption of Na^+ along with Cl^- by the antennal gland [55], and NKA activity can be much greater in the antennal gland than in the gills [56].
Aquatic insects	Pharmacological evidence of the presence of VHA and CA	Bafilomycin, a VHA inhibitor, reduced H^+ export and Na^+ import across the anal papillae by 55 and 41% respectively, while methazolamide, a CA inhibitor, reduced H^+ export by 74% in *Aedes aegypti* [57].

Table S3. Detailed data on Na^+ transport (*Continued*).

Subsection	Aspect of Transport	Evidence
Aquatic insects (continued)	Pharmacological evidence of the presence of an apical Na^+-channel and NHE on anal papillae	In whole *A. aegypti* larvae treated with 100 μM phenamil (Na^+-channel inhibitor), Na^+ import decreased and Na^+ was secreted across the anal papillae, while 5-(*N*,*N*-hexamethylene)amiloride (NHE inhibitor) had no effect on Na^+ import [57]. However, Pullikuth et al. [58] showed that amiloride and ethyl-isopropyl amiloride (other NHE inhibitors) only inhibited $^{22}Na^+$ uptake by 40% at concentrations that completely inhibited mammalian NHE. This suggests that AeNHE3, the NHE localized to the basolateral epithelial membrane of the Malpighian tubule, midgut, and gastric caeca of *A. aegypti*, is insensitive to the amiloride-type inhibitors used to distinguish NHEs [58]
	Cloning evidence for NHE on other epithelia	An NHE, AgNHE1, has been cloned from the alimentary canal of larval *Anophele[59]*. In *Anopheles albimanus*, an NHE has been localized to the apical membrane of nondorsal anterior rectal cells [60] that interacts with NKA on the basolateral membrane to reabsorb Na^+ from the primary urine.
	Na^+ transport in Ephemeroptera	In Ephemeroptera, ionocytes are associated with thin areas of cuticle called porous plates located particularly on the tracheal gills [61-63]. Histochemical methods have been used to localize Na^+ along with Cl^- to these cells in both *Rhithrogena semicolorata* and *Cloeon dipterum [62]*.
	Na^+ transport in Plecoptera	In Plecoptera, Kapoor [64] detected activity of NKA in the gills of *P. media* nymphs and showed the activity increased by 84% when the nymphs were moved from CW with 3.4 mM Na^+ to a more dilute mixture of half CW and half DW. NKA activity decreased by 21% when the nymphs were placed in a hypertonic solution (188 mM Na^+). This ion exchange was localized to ionocytes in the proximal wall of the tracheal gills that are separate from the tracheoles [65-67]. Colby [68] concluded simply that *Pteronarcys californica* actively transports Na^+ against a concentration gradient.
	Na+-homeostasis in Trichoptera	The body wall of *Limnephilus affinis*, a caddisfly known to inhabit both FW and estuarine (i.e., salt-marsh pools) habitats in Europe, was relatively impermeable to Na^+ and more permeable to water [69]. At lower external [Na^+] (< 100 mM), hemolymph Na^+ was maintained at greater concentrations (75−100 mM), while at higher external [Na^+] (up to 400 mM), hemolymph [Na^+] remained less than the external concentrations. Like some euryhaline mosquitos, the difference in osmolarity was equalized by liberation of unidentified organic osmolytes into the hemolymph, and the urine was hyperosmotic to both the hemolymph and to the water at greater external salt concentrations [70]. In contrast, two species that inhabit FW, *Limnephilus stigma* and *Anabolia*

Table S3. Detailed data on Na^+ transport (*Continued*).

Subsection	Aspect of Transport	Evidence
Aquatic insects (continued)	Na^+-homeostasis in Trichoptera (continued)	*nervosa*, maintain hemolymph [Na^+] that is greater than external [Na^+] (up to 220 mM), although the difference between the hemolymph and external [Na^+] narrows, particularly above 120 mM Na^+ [71]. These 2 species lacked the organic osmolytes in their hemolymph that were found in *L. affinis*, and their body walls were more permeable to Na^+. Note that this research preceded recognition that ion uptake occurred via the chloride epithelia in Trichoptera larvae [72]. In general, aquatic insects are thought to have lower ion permeability than other aquatic organisms [73].
	Na^+ transport in Odonata	In dragonflies (Odonata), ionocytes are found on chloride epithelia in the anal chamber [74], and Na^+ is actively transported into the hemolymph through the rectum of *Uropetala carovei* [75] and *Aeshna cyanea* larvae [76]. NKA was located on the basolateral membrane of chloride epithelial ionocytes, because Na^+ uptake was inhibited by ouabain, a NKA inhibitor, and a second unidentified ATPase was present [77, 78], likely VHA. Activity of both ATPases increased with decreasing ion concentrations.
	Na^+ transport in other classes.	Some air-breathing aquatic insects, such as the beetle *Dytiscus verticalis*, do not rely on Na^+ uptake from water but obtain Na^+ from their food [79, 80]. Shaw [81] concluded that the megalopteran *Sialis lutaria* absorbed Na^+, K^+, and Cl^- from ingested water through the gut.
Mollusca	Evidence for VHA and an apical Na^+-channel in Unionidae	There is minimal evidence for an apical Na^+-channel energized by VHA in Unionidae [82, 83], and amiloride, an apical Na^+-channel inhibitor at low concentrations, inhibits uptake of Na^+ in *T. texasiense* and *L. subrostrata* [84, 85]. Moreover, the VHA inhibitor bafilomycin inhibits H^+ excretion from the extrapallial fluid across the mantle in *Elliptio complanata*, demonstrating the role of VHA in acid excretion by the apical membrane of mantle epithelia [86].
	Lack of evidence for an apical Na^+-channel in other taxa	Na^+ import is not inhibited by amiloride, an apical Na^+-channel inhibitor, in either *C. fluminea* or *Dreissena polymorpha* [87].
Other Na^+ transporters	Occurrence and localization of NBC in rainbow trout	In rainbow trout, the NBC was localized to the basolateral membrane of ionocytes with an apical Na^+-channel and VHA on the apical membrane where its activity induced cytosol acidification [88].
	Function of NCC	The NCC is energized by movement of Na^+ down a concentration gradient [89]. There is some question whether the concentration gradient of Na^+ between FW and the cytosol is sufficient (i.e.,
Other Na^+	Function of NCC	currently no data exists on whether cytosol [Na^+] specifically in Type II cells or NCC cells is less

Table S3. Detailed data on Na^+ transport (*Continued*).

Subsection	Aspect of Transport	Evidence
transporters	(continued)	than FW [Na^+]) [90, 91]. However, these ionocytes also pair NKA with the NBC on the basolateral membrane [89, 92, 93], forming a transporter combination that may maintain very low cytosol [Na^+].
	Regulation of Na^+ transporters along a salinity gradient	In tilapia, NHE3 and an NCC were localized to the apical membrane and NKCC1a to the basolateral membrane of gill NaR ionocytes [94]. When tilapia were exposed to 4 different salinities: undiluted SW, 1/3-diluted SW, FW, and DI water [94], the NHE was upregulated in DI water, while the NCC was increasingly upregulated in FW and DI water. Both the NHE and NCC are involved in Na^+ uptake, while the NCC also is involved in Cl^- uptake. Conversely, NKCC1a was increasingly upregulated in 1/3-diluted SW and undiluted SW and is involved in Na^+, K^+ and Cl^- excretion. In these fish, VHA expression did not differ among the different salinities, suggesting it was less involved in Na^+ regulation.
Effects on Na^+ transport by other ions	Effect of low pH on rainbow trout	In rainbow trout exposed to pH 4.2 for 4 d, a large net H^+ influx across the gills was countered by excretion of one-third to one-half of the H^+ by the kidney [95], and there was a large Na^+ efflux, mostly through the gills.
	Effect of low pH on Osorezan dace	In Osorezan dace, which live in very low pH conditions (pH 3.4−3.8), the NBC is paired with NKA basolaterally on an ionocyte with an apical NHE [96]. Expression of mRNA for all 3 transporters along with that for CA increased when the fish were moved from neutral to acidic conditions, suggesting this arrangement is an adaptation for export of acid units (H^+), along with retention of base units (HCO_3^-) and Na^+ in response to external acidity [93].
	Adaptations to low [Ca^{2+}] and low pH in tetra	Fish tolerant of low [Ca^{2+}] and low pH waters possess adaptations that reduce Na^+ loss, maintain Na^+ uptake or both [97, 98]. In neon tetra (*Paracheirodon innesi*) exposed to pH 3.5, Na^+ uptake did not decrease, but only a small, temporary increase in Na^+ efflux occurred [99]. However, when the neon tetra were exposed to pH 3.25, Na^+ efflux increased substantially, while Na^+ uptake was maintained. In blackskirt tetra (*Gymnocorymbus ternetzi*) exposed to pH 4.5, Na^+ uptake increased and Na^+ efflux increased but to a greater amount resulting in net Na^+ loss [100]. Moreover, Na^+ uptake was only reduced 25% by amiloride, an apical Na^+-channel or NHE inhibitor depending on concentration, suggesting a difference in molecular structure of the Na^+ transporter. In 3 additional tetra species also native to low pH waters, Na^+ uptake was not inhibited by amiloride [101].
Effects on Na^+ transport by other ions (continued)	Adaptations to low [Ca^{2+}] and pH in Amazonian fish	Of the Amazonian species tested, members of the Cichlidae generally had greater Na^+ uptake at low pH and greater Na^+ efflux, while members of the Characidae had lower Na^+ uptake at low pH but also had lower Na^+ efflux [102]. However, by 24 h, both Na^+ uptake and efflux had decreased

Table S3. Detailed data on Na^+ transport (*Continued*).

Subsection	Aspect of Transport	Evidence
		again to near their original levels resulting in a net Na^+ flux near zero.
	Adaptations to low $[Ca^{2+}]$ and pH in temperate fish	In yellow perch (*Perca flavescens*), a temperate, acid-tolerant species, K_m for uptake of Na^+ was greater and Ca^{2+}-related paracellular permeability and Na^+ efflux were less than in less acid-tolerant species, such as rainbow trout [103]. In the acid-tolerant banded sunfish (*Enneacanthus obesus*), Na^+ uptake was nearly completely inhibited at pH 4.0 or less, but Na^+ efflux was 0 at pH 4.0 and reduced at pH 3.25 after acclimation at pH 4.0 [104].
	Dominant Na^+ transporter in zebrafish in acidic waters	Increased Na^+ uptake in acidic water by zebrafish changes the dominant Na^+ transporter to zNHE3b, which is not inhibited by $[H^+]$ partly due to a link to NH_3/NH_4^+ excretion [105].
	Role of claudins, occludins, and Ca^{2+} in low paracellular permeability and Na^+ loss	Although as many as 14 claudin and 2 occludin isoforms increased at some point during a 300-h experiment, Na^+ efflux did not decrease because $[Ca^{2+}]$ was low. Ca^{2+} interacts with these claudins and occludins to maintain low paracellular permeability across the tight junctions, and paracellular permeability increases at low $[Ca^{2+}]$. In mammalian kidney epithelial cells, Ca^{2+} is described as a critical component of tight junction formation [106, 107]. Increased Na^+ efflux has long been observed in low $[Ca^{2+}]$ water at low or more neutral pH in other fish, such as brown trout (*Salmo trutta*), rainbow trout, Eurasian minnow (*Phoxinus phoxinus*), and tambaqui (*Colossoma macropomum*) [97, 108-110].
	Loss of Na^+ at low pH by crayfish	Exposure of the crayfish *Orconectes propinquus* to pH 4.0 resulted in net retention of H^+, a decrease in pH of 0.5 units, and negative net Na^+ flux from the hemolymph relative to crayfish exposed to pH 7.5 [111]. The negative net Na^+ flux resulted from ≈ 50% inhibition of Na^+ uptake with little change in Na^+ efflux, pointing to inhibition of Na^+/H^+ exchange across the apical epithelial membranes.
	Variation in Na^+ loss among crayfish species	Similarly, net Na^+ uptake was inhibited at pH < 5.5 in *A. pallipes* [48], and hemolymph $[Na^+]$ decreased in *Astacus astacus* exposed to pH 4.0 [112]. The inhibition of Na^+ uptake results from competitive inhibition with the counter ion H^+, which is elevated in the water [113]. However, no differences in hemolymph $[Na^+]$ in adults or whole body $[Na^+]$ in juveniles were observed in *Cambarus robustus* exposed to pH ranging from 7.5 to 3.8, whereas in *Orconectes rusticus*, adult
Effects on Na^+ transport by other ions (continued)	Variation in Na^+ loss among crayfish species (continued)	hemolymph $[Na^+]$ and juvenile whole body $[Na^+]$ were reduced in pH 4.0 and 3.8, respectively, compared to crayfish in pH 7.5 to 5.0 [114].

Table S3. Detailed data on Na^+ transport (*Continued*).

Subsection	Aspect of Transport	Evidence
	Interaction of $[Ca^{2+}]$ and pH on Na^+ uptake in crayfish, *C. destructor*	In *C. destructor* exposed to pH 4.5 and high $[Ca^{2+}]$ (500 μM), hemolymph $[Na^+]$ decreased during the first 96 h but then recovered and was similar to that in control crayfish (pH 7.1, 500 μM Ca^{2+}) after 288 h [115]. In *C. destructor* exposed to lower $[Ca^{2+}]$ (50 μM), hemolymph $[Na^+]$ was less than that of the crayfish in high $[Ca^{2+}]$ even when exposed to pH 7.1. In crayfish exposed to pH 4.5 and low $[Ca^{2+}]$, hemolymph $[Na^+]$ exceeded that of those exposed to pH 7.1 and low $[Ca^{2+}]$ after 288 h, suggesting an interaction between Na^+ and Ca^{2+} in the H2Na(Ca)E.
	Variation in effects of low pH on mosquitos that inhabit phytotelmata	Among the larvae of 4 different mosquitos that inhabit phytotelmata with low ionic water, hemolymph $[Na^+]$ ranged from 75 to 115 mM and uptake rates ranged from 0.075 to 0.2 nmol Na^+ mg^{-1} h^{-1} when the larvae were placed in control media (0.02 mM Na^+, 0.03 mM K^+, 0.03 mM Ca^{2+}, and 0.05 mM Cl^-, pH 6.0−6.5) [116]. When placed in low pH water (pH 3.5 and other ions the same as in the control water), Na^+ uptake was reduced by 42 to 86% [116], suggesting increased external $[H^+]$ inhibited Na^+ uptake. Conversely, when three of the culicids were placed in more saline water (Na^+ and Cl^- both 6 mM and other ions the same as in the control water), Na^+ uptake increased by 6 to 28 times, suggesting differences in uptake affinity and capacity for Na^+ among the species.
	Effects of low pH on net loss of Na^+ in tundra pond aquatic insects	In a study of the effect of pH on invertebrates from tundra ponds in the Smoking Hills, Northwest Territories, Canada, *Orthocladius consobrinus* exhibited net loss of Na^+ along with Cl^- at pH 3.0 and not at pH 4.5 or 8.0, and mortality increased with decreasing pH [117]. In comparison, another chironomid, *Chironomus riparius*, did not exhibit a net loss of Na^+ or Cl^-, and there was no relationship between pH and mortality. The caddisfly *Limnephilus pallens* exhibited net loss of Na^+ only at pH 2.8 and not at pH 3.5, 4.5, or 8.0.
	Effects of low pH on whole-body $[Na^+]$ in Ephemeroptera	*Stenonema femoratum* nymphs exposed to pH 3.5 water for 96 h had lower whole-body $[Na^+]$ compared to nymphs exposed to pH 6.5 water [118]. A similar decrease in whole-body $[Na^+]$ was observed in *Leptophlebia cupida* nymphs exposed to pH 3.5 water at 96 h and 192 h but not to pH 4.5 water compared with nymphs exposed to pH 6.5 water [119].

Table S3. Detailed data on Na^+ transport (*Continued*).

Subsection	Aspect of Transport	Evidence
Effects on Na^+ transport by other ions (continued)	Effects of low pH Na^+ balance in acid-tolerant vs. acid-sensitive Plecoptera	A comparison of acid-tolerant (*Amphinemura sulcicollis*, *Protonemura meyeri*, and *Leuctra moselyi*) and acid-sensitive (*Perla bipunctata*, *Dinocras cephalotes*, and *Isoperla grammatica*) species of Plecoptera found that acid tolerance, including tolerance to elevated Al, was related to the effect on Na^+ balance [120]. In the acid-sensitive species, Na^+ uptake was depressed at low pH due to competitive inhibition of Na^+ attachment to the enzyme carrier (presumably the NHE) by H^+. The affinity constants of the enzyme carrier for Na^+ compared to H^+ were greater in the acid-tolerant species (Aff. Na^+/Aff. $H^+ > 4$), whereas in the acid-sensitive species, the ratio was less than 1, suggesting that at low pH, these enzyme carriers in acid-tolerant species have greater discrimination between Na^+ and H^+ resulting in less competitive inhibition of Na^+ by H^+ [120]. A similar whole-body [Na^+] decrease was observed in *Pteronarcys dorsata* nymphs placed in pH 3.0 water [121] and in *Acroneuria carolinensis* exposed to pH 4.0 water [122].
	Effect of low pH on [Na^+] in an acid-tolerant Odonata	In the acid-tolerant dragonfly *Ladona julia*, whole-body [Na^+] in nymphs exposed to pH 2.3 water (21.2 μmol Na^+ $nymph^{-1}$) for 96 h was not less than in those exposed to control water at pH 5.7 (21.2 μmol Na^+ $nymph^{-1}$) but was less in those exposed to pH 2.3 water with 1.0 mM total Al (8.2 μmol Na^+ $nymph^{-1}$) [123]. In a second study with the same species, hemolymph [Na^+] in nymphs exposed to pH 2.3 water (142 mM Na^+) for 96 h was also not less than in those exposed to control water at 5.9 (156 mM Na^+), but again, was less than in those exposed to pH 2.3 water with 37 μM total Al (104 mM Na^+) [124].
	Effect of low pH on hemolymph [Na^+] in unionid mussels	As with other aquatic animals, exposure of the unionids *Anodonta anatina*, *A. cygnea*, *Unio pictorum*, and *U. tumidus* to low pH (4.0−4.5) in either soft (0.11 mM Ca^{2+}) or hard (0.46 mM Ca^{2+}) water resulted in decreased hemolymph [Na^+] [125].
	Evidence that Ag^+ and Cu^{2+} interact with the apical Na^+-channel in rainbow trout	Uptake of either Cu^{2+} or Ag^+, as well as Na^+, was inhibited in rainbow trout gills by either bafilomycin (68%), a VHA inhibitor, or phenamil (39%), an apical Na^+-channel inhibitor [126, 127]. Moreover, uptake of either Cu^{2+} or Ag^+ was inhibited by greater external [Na^+] just as the uptake of Na^+ was inhibited at greater external [Cu^{2+}] or [Ag^+] [127]. This Na^+ transporter was confirmed to be an apical Na^+-channel in α-type MR ionocytes in rainbow trout by showing that increased Na^+ uptake stimulated by a 0.4 unit increase in the IC pH of isolated α-type MR ionocytes was inhibited by 50 nM bafilomycin (VHA inhibitor), 10 μM phenamil (apical Na^+-channel inhibitor), 1 or 10 μM Ag^+, or 1 or 10 μM Cu^{2+} [128]. Uptake of Cu^{2+} from water is also inhibited by increased dietary [Na^+] in rainbow trout because uptake activity by apical Na^+-channel is downregulated by increased internal [Na^+] [129]; this Cu^{2+} uptake was also reduced by

Table S3. Detailed data on Na^+ transport (*Continued*).

Subsection	Aspect of Transport	Evidence
Effects on Na^+ transport by other ions (continued)	Evidence that Ag^+ and Cu^{2+} interact with the apical Na^+-channel in rainbow trout (continued)	dietary exposure to Cu^{2+} [130]. At greater [Cu^{2+}] (≥ 0.79 μM) there was also loss of Na^+, particularly at low pH (5.0).
	Effects of [Ag^+] at sublethal concentrations are transient	However, at [Ag^+] less than the LC50, these effects are transient, and the decreases in blood [Na^+], Na^+ influx, and NKA activity returned to reference levels by 15 to 20 d as the fish acclimated to the sublethal exposures [131].
	Evidence that Cu^{2+} is not related to hardness but is related to pH	Cu^{2+} uptake was not related to hardness or alkalinity, but uptake was reduced when the water pH was decreased from 7.8 to 5.0 [132]. However, the 96-h LC50 for Cu in fathead minnow (*Pimephales promelas*) decreased as pH was decreased from 7.2 to 5.5 [133], probably because H^+ and Cu combined to competitively inhibit Na^+ uptake.
	Acute LC50s for Ag^{2+} are related to gill surface area in daphnids	Acute LC50s for Ag^+ was directly related to whole body Na^+ uptake rate and inversely related to body mass in daphnids because gill surface area, the site of Na^+ uptake, per gram of body mass decreased with increasing body mass [134].
	Effect of Pb^{2+} on whole-body [Na^+] in *Lymnaea. stagnalis*	In *L. stagnalis* exposed to dissolved lead (Pb^{2+}) (0.20−0.53 μM) in moderately hard water (1.4 mM $CaCO_3$ hardness), whole-body [Na^+] decreased from ~32 μmol g^{-1} in the control to 10−20 μmol g^{-1} [135].
	Effect of metals on EC [Na^+] in *A. cygnea*	Similarly, in *A. cygnea*, exposure to Cd^{2+}, Cu^{2+}, or Pb^{2+} decreased [Na^{2+}] in the hemolymph and extrapallial fluids [136, 137].
	Effect of Cu^{2+} on hemolymph osmolality in *L. stagnalis*	Both hemolymph osmolality, which is primarily related to the [Na^+], and net Ca^+ influx were reduced in *L. stagnalis* exposed to 0.76 μM Cu^{2+} [138].
	Mechanisms by which divalent metals affect Na^+ uptake	Both Cd^{2+} and Pb^{2+} are transported by the apical ECaC but inhibit the basolateral NKA by interference with dephosphorylation and cycling of the enzyme [139]. Pb^{2+} is known to inhibit CA activity, which produces H^+ that is exchanged for Na^+ [140].

Table S3. Detailed data on Na^+ transport (*Continued*).

Subsection	Aspect of Transport	Evidence
Effects on Na^+ transport by other ions (continued)	Effect of Cd^{2+} on whole-body [Na^+] in *Chironomus* spp.	In *C. riparius* exposed to Cd^{2+} (0.16−8.7 mM) in moderately hard water (1.4 mM $CaCO_3$ hardness), whole-body [Na^+] decreased from ~85 μmol g^{-1} in the control to 55−75 μmol g^{-1} [141]. In *Chironomus staegeri*, the bioaccumulation of Cd^{2+} is affected by the water [Ca^{2+}] or hardness because Cd^{2+} crosses the apical epithelial membrane by the ECaC but inhibits NKA, which transports Na^+ across the basolateral membrane [142].

CA, carbonic anhydrase; CW, creek water; DI, deionized; DW, distilled water; ECaC, epithelial Ca^{2+} channel; EIPA, 5-(*N*-ethyl-*N*-isopropyl)amiloride; EC, extracellular; FW, freshwater; H2Na(Ca)E, H^+/2Na^+(or Ca^{2+}) exchanger; IC, intracellular; J_{max}, maximum uptake rate; J_{net}, net uptake rate; K_m, ion concentration at which the uptake rate is half of J_{max}; LC50, median lethal concentration; MR, mitochondria-rich; NaR, Na^+/K^+-ATPase-rich; NBC, Na^+/HCO_3^--cotransporter; NCC, Na^+/Cl^--cotransporter; NHE, Na^+/H^+-exchanger; NKA, Na^+/K^+-ATPase; NKCC, Na^+/K^+/Cl^--cotransporter; P_{CO2}, partial pressure of CO_2; SW, saltwater; tCAc, trout cytosolic carbonic anhydrase isoform; TW, tap water; VHA, vacuolar-type H^+-ATPase

Table S4. Detailed data on K^+ transport.

Subsection	Aspect of Transport	Evidence
Teleost fish	K^+ uptake from food	Rainbow trout absorbed 90% of the K^+ from a single experimental meal that supplied 3.3 mmol K^+ kg^{-1} fish body mass [34].
Crustacea	Active transport of K^+	In an experiment with isolated gills of *A. pallipes*, the electrochemical potential of K^+ was greater than that in the perfusion medium, indicating that K^+ is actively transported across the gill epithelium into the hemolymph [143].
Aquatic insects	KHE in terrestrial *Manduca sexta* larvae	A KHE has been studied in larvae of terrestrial lepidopteran *M. sexta* [144, 145], but this exchange transports H^+ toward the hemolymph and K^+ toward the lumen of the anterior midgut, alkalinizing the lumen and not resulting in K^+ uptake [146]. Moreover, a CA, AgCA9, which was particularly localized to the gastric caeca and transitional zone between the anterior and posterior midgut, produces HCO_3^- that buffers the high luminal pH , particularly when removal of the H^+ from the lumen by VHA and a KHE further deprotonate the HCO_3^- to form CO_3^{2-} [147].
	Reabsorption of K^+	Reabsorption of K^+ in the lower Malpighian tubules of mosquito larvae appears to be a very efficient mechanism for retention of K^+ [148].
	Active transport of K^+ in Plecoptera	In a simple experiment that compared hemolymph [K^+] of starved Plecoptera nymphs in CW and DI water, Colby [68] concluded that *P. californica* actively transported K^+ from the water against a concentration gradient.
Mollusca	K^+ and maintenance of ion balance	When *D. polymorpha* was placed in solutions containing different combinations of salts, solutions lacking K^+ did not cause significant mortality (i.e., more than 2 of 20 individuals) in 51 d if the solutions contained Na^+, Mg^{2+}, and Cl^-, but these individuals were unable to maintain normal ion balance and had lower [Na^+] and [Cl^-] in their blood [149, 150].
	Role of K^+ in volume regulation by Unionidae	Gill filament lateral ciliated cells shrank (i.e., cell height decreased 20 to 30%) when gills of the FW mussel *T. texasiense* were superfused with a hypertonic solution containing 90 mM NaCl and did not reverse after 20 to 30 min [151]. When 2 mM KCl was also added to the hypertonic solution, the shrinkage recovered by 40−50%. *D. polymorpha* exposed to 45 mM NaCl with less than 0.05 mM K^+ lost cell volume, while elevated [K^+] (1 mM) resulted in excess cell volume [150]. FW mussels have reduced their IC solutes by balancing the solute concentrations in their blood. This includes organic osmolytes, leaving K^+ practically the sole IC osmolyte for regulating cell volume and maintaining electrochemical balance [151]. This type of regulation appears to make these bivalves much more sensitive to a balance of Na^+ and K^+ in ambient waters to maintain cell volumes.

Table S4. Detailed data on K^+-transporters (*Continued)*.

Subsection	Aspect of Transport	Evidence
Mollusca (continued)	K^+ transport in *Dreissena* vs. unionids	The uptake rate of K^+ was 0.7 μmol g^{-1} dry tissue h^{-1} for *C. fluminea* and 0.4 μmol g^{-1} dry tissue h^{-1} for the unionids *T. texasiense* and *L. subrostrata* placed in PW containing about 0.06 mM K^+ [152]. However, the transport mechanism is unclear. In *Dreissena*, uptake of K^+ is active and exhibits saturation kinetics [150, 153]. Efflux of K^+ was greater than uptake in *C. fluminea*, but less than uptake in the unionids [152]. Therefore, net flux was negative in *C. fluminea* and positive in the unionids, but net flux increased and was positive in both *C. fluminea* and *T. texasiense* when [K^+] was increased to 0.13 or 0.36 mM. When Rb^+, which can substitute for K^+ in this type of study at the low concentrations in AFW, was substituted, K_m increased in mussels that had been placed in DI water to deplete IC and EC salt concentrations and then returned to water with K^+ and Rb^+, suggesting that K^+ uptake is under endogenous control in the epithelia of these mussels [152]. Moreover, 17% of the mussels' K^+ was exchanged daily, suggesting high turnover of K^+ [154].
Effects on K^+ transport by other ions in the water	Effects of low pH on fish	In brook trout (*Salvelinus fontinalis*) larvae exposed to 4 40-h pulses of low pH, low Ca^{2+} water with or without Al over a 28-d test, whole-body K^+ was decreased relative to the control but did not consistently differ with decreasing treatment pH level. Whole-body K^+ increased in the presence of Al [155]. Rainbow trout exposed to pH 4.2 for 4 d lost 5.3 mmol K^+ kg^{-1}, three-quarters by efflux across the gills and one-quarter by excretion through the kidneys, but despite this, blood [K^+] remained relatively constant (2−3 mM).
	Effects of low pH on crayfish	When exposed to pH 4.0, the crayfish *O. propinquus* exhibited greater net efflux of K^+ compared to controls exposed to pH 7.5 [111]. Similarly, hemolymph [K^+] decreased in *A. astacus* exposed to pH 4.0 water compared to controls in pH 7.9 [112].

AFW, artificial freshwater; CA, carbonic anhydrase; CW, creek water; DI, deionized; EC, extracellular; FW, freshwater; IC, intracellular; KHE, K^+/H^+-exchanger; K_m, ion concentration at which the uptake rate is half of J_{max}; PW, pond water; VHA, vacuolar-type H^+-ATPase.

Table S5. Detailed data on Ca^{2+} transport.

Subsection	Aspect of Transport	Evidence
Teleost fish	NCX	In isolated tilapia gill MR ionocytes, replacement of EC Na^+ with the organic ion *N*-methyl-d-glucamine$^+$ increased IC [Ca^{2+}] because this replacement removed the counter ion for the NCX, Na^+ [30].
	Role of NKA in Ca^{2+} transport	An α-subunit isozyme of NKA (*zatp1a1a.1*), a FXYD protein believed to regulate the transport ability of NKA (zfxyd11) and ECaC were localized to NaR ionocytes of zebrafish and were upregulated in low [Ca^{2+}] water [156].
	Increase in ECaC at low [Ca^{2+}]	In a study that gradually decreased the exposure of zebrafish from hard water to soft water, the greatest change was the increase in both gene and protein expression for ECaC [157]. In rainbow trout, expression of mRNA and the ECaC protein increased after exposure to low [Ca^{2+}] water (0.02−0.03 μM) vs. normal FW (0.2−0.3 μM Ca^{2+}) or to hypercapnia (i.e., 1.0 kPa CO_2) [158].
	Location of Ca^{2+} transporters in specific ionocyte types	Research on the segregation of different transporters among different gill epithelial ionocyte types in rainbow trout [159] found that uptake of both Cd^{2+} and Ca^{2+} occurred preferentially in β-type ionocytes. Also, Cd^{2+} accumulation was inhibited when the experiment was conducted in Cl^--free, phosphate-buffered saline (i.e., Cl^- salts were replaced by gluconate salts) [159], and ECaC were collocated with an AE on the apical membrane of β-type ionocytes [160]. The ECaC was located on the apical membranes of both pavement ionocytes and to MR ionocytes that also expressed NKA, presumably the β-type ionocytes [158].
	Absorption of Ca^{2+} from food	Rainbow trout absorbed 28% of the Ca^{2+} in a single experimental meal that supplied 5.9 mmol Ca^{2+} kg^{-1} fish body mass [161]. Addition of Ca^{2+} to the diet of rainbow trout reduced accumulation of Cd, which had also been added to their diet [162]. Moreover, Ca^{2+} or Cd^{2+} added to the diet reduced the uptake of Ca^{2+} and Cd^{2+} by the gills [163, 164]. For Ca^{2+}, this occurs by the mechanisms that regulate uptake of Ca^{2+} in relation to plasma [Ca^{2+}], such as elevation of [Ca^{2+}] in the ionocytes or increased levels of the regulatory hormone, stanniocalcin [165]. Cd^{2+} entering the ionocytes across the basolateral membrane from the blood likely has a similar inhibitory effect on Ca^{2+}-ATPase [162].
Aquatic insects	Evidence that Ca^{2+} uptake does not occur by the anal papillae	Removal of the anal papillae from larvae of the mosquito, *A. aegypti*, resulted in increased Ca^{2+} uptake [166].

Table S5. Detailed data on Ca^{2+} transport (*Continued*)

Subsection	Aspect of Transport	Evidence
Aquatic insects (continued)	Evidence that Ca^{2+} uptake does not occur by the anal papillae	Donini and O'Donnell [167] did not measure net flux of Ca^{2+} across the anal papillae of *A. aegypti*, but much earl of the anal papillae.
Mollusca	Hemolymph [Ca^{2+}] relative to [Ca^{2+}] in PW vs. ASW	When *D. polymorpha* was transferred from PW (0.4 mM Ca^{2+}) to ASW (1.0 mM Ca^{2+}), hemolymph [Ca^{2+}] remai (4.0 ± 0.2−4.5 ± 0.2 mM Ca^{2+} in PW vs. 2.2 ± 0.1−2.8 ± 0.1 mM Ca^{2+} in ASW) [169]. As with other ions, this cha
	Ion regulation in extrapallial fluids of unionids.	In 5 species sampled from a single mussel bed in the Muskingum River, OH, mean extrapallial fluid [Ca^{2+}] range fluid [Ca^{2+}] was maintained at 3 to 4 times the water concentration when water [Ca^{2+}] and [Mg^{2+}] were similar.
	Evidence for the presence of an L-type ECaC and $Ca^{2+}/1H^{+}$-exchanger in *L. stagnalis*	Between the trochophore stage and hatching, the Ca^{2+} content of *L. stagnalis* embryos increased from 0.001 nmo 10 μM dihydropyridine nifedipine or 100 μM phenylalkylamine verapamil (L-type Ca^{+}-channel inhibitors), lanth inhibitor) [172]. In addition, ethoxzolamide and bafilomycin inhibited accumulation of titratable alkalinity, a mea inhibitor that is specific to cation/H^{+}-exchangers, could not be used with the ion-specific microelectrodes used to H^{+}-microelectrodes), [172] showed that EIPA inhibited uptake of Ca^{2+} and accumulation of titratable alkalinity by electrogenic $Ca^{2+}/1H^{+}$-exchanger similar to that used by crustaceans [47, 173].
Effects of Ca^{2+} transport by other ions in the water	Variation in affinity of PMCA for Ca^{2+} versus Cd^{2+} and Zn^{2+}	PMCA has about 100 times greater affinity for Cd^{2+} than it does for Ca^{2+} in rainbow trout, and inhibition of Ca^{2+} t 10 times greater affinity than it does for Ca^{2+}, and inhibition of Ca^{2+} transport in rainbow trout may occur at 15 μl
Effects of Ca^{2+} transport by other ions in the water (continued)	Variation in affinity and toxicity of divalent metals between yellow perch and rainbow trout	Comparing yellow perch (96-h LC50 = 72 μM Cd^{2+}) and rainbow trout (96-h LC50 = 0.168 μM Cd^{2+}) in moderat (0.54 ± 0.08 nmol Cd^{2+} g^{-1} wet weight h^{-1} in water with 100 μM Ca^{2+}) was less than the J_{max} for rainbow trout (0.8 yellow perch (276.4 ± 30.1 nmol Cd^{2+}) was greater than that for rainbow trout (155.2 ± 24.1 nmol Cd^{2+}) [176]. Th concentration to inhibit Ca^{2+} uptake in yellow perch. These variables are characteristics of the transporter protein,
	Variation in crayfish sensitivity to low pH	In *C. destructor* exposed to pH 4.5 and 500 μM Ca^{2+}, carapace [Ca^{2+}] decreased for up to 100 h but then increase pH-intolerant species, hemolymph [Na^{+}] decreased in adults exposed to pH 4.0 for 96 h, but there was no signific *C. robustus* exposed to pH 3.8 and pH 6.5 [114].
	Transport of divalent metals by the H2Na(Ca)E in Crustacea	The inhibition of Cd^{2+} uptake by increased [Ca^{2+}] and increased total salinity indicates that the electrogenic H2Na

Table S5. Detailed data on Ca^{2+} transport (*Continued*)

Subsection	Aspect of Transport	Evidence
	Transport of divalent metals by the ECaC in Crustacea	In *Carcinus maenas*, influx of both Ca^{2+} and Cd^{2+} decreased in the presence of lanthanum, another ECaC blocker by ECaC. Also, in *C. maenas*, hemolymph [Cd^{2+}] decreased with increasing water [Ca^{2+}] [180], and uptake rates experiment conducted to develop a biotic ligand model for Cd^{2+}, the 48-h LC50 for *D. pulex* increased with incre (0.03−1.6 mM) [181], suggesting the affinity of the ECaC for Cd^{2+} was greater than that for Ca^{2+}.
	Inhibition of Ca^{2+} uptake by Cd^{2+} in a midge, *C. riparius*	In *C. riparius* exposed to Cd^{2+} (0.89−8,700 μM) in moderately hard water (1.4 mM $CaCO_3$ hardness), whole-bod Whole-body [Ca^{2+}] recovered by 48 h at the lowest 2 [Cd^{2+}] (0.89 and 8.9 μM), but did not at the greater [Cd^{2+}] (relatively rapid removal and secretion of Cd^{2+} by the Malpighian tubules [182].
Effects of Ca^{2+} transport by other ions in the water (continued)	Transport of divalent metals by Ca^{2+} transporters on ionocytes in Ephemeroptera and Trichoptera	Rates of Cd^{2+} and Zn^{2+} uptake varied from 11.6 ± 0.8 pmol Cd^{2+} g^{-1} h^{-1} for *Drunella flavilinea* to 0.09 ± 0.00 pmo among all species tested, and neither gill size nor water permeability were related to metal uptake rates. However rates. Among mayflies, *Drunella* have greater uptake rates and more ionocytes on their tracheal gills compared to family, Ephemerellidae (6 species), or the caddisfly family, Hydropsychidae (5 species), Ca^{2+} uptake rates for the Ca^{2+} uptake rates were inversely related to body mass [184].
	Competitive inhibition of Cd^{2+} and Zn^{2+} uptake by Ca^{2+} and of Zn^{2+} uptake by Cd^{2+}	Cd^{2+} uptake was competitively inhibited when Ca^{2+} was increased from 0.18 to 0.71 mM in *Drunella*, while both 0.18 to 1.4 mM. In *Ceratopsyche sparna*, the presence of Cd^{2+} inhibited Zn^{2+} uptake by 35%, while uptake of Cd^{2} to 1.4 mM from 0.03 mM somewhat inhibited both Cd^{2+} and Zn^{2+} uptake, while ruthenium red, a PMCA inhibitor by these metals and Ca^{2+}.
	Effect of verapamil on Cd^{2+} uptake in Trichoptera and Ephemeroptera	Application of verapamil, an L-type Ca^{2+}-channel inhibitor, had variable effects ranging from no effect in *Hydrop* that ECaC differs in some way among these aquatic insects [183].
	Differences in the relative affinity of Ca^{2+} vs. Cd^{2+} or Zn^{2+} in Trichoptera and Ephemeroptera	Again looking at a number of species in the Ephemerellidae or Hydropsychidae, Poteat and Buchwalter [184] ob $P < 0.0001$), their respective correlations with Ca^{2+} uptake rates were weaker (Cd^{2+}: $r = 0.49$, $P = 0.10$; Zn^{2+}: $r =$ used in these analyses. Moreover, exposure to low [Cd^{2+}] (0.89, 8.9, or 89 nM) or [Zn^{2+}] (0.015, 0.15, or 1.5 μM) affinity of any shared transporters for Cd^{2+} or Zn^{2+} is not greater than that for Ca^{2+} and may differ from similar tra
	Inhibition of divalent metal uptake by elevated [Ca^{2+}] in FW bivalves	Uptake of Pb^{2+}, Mn^{2+}, Cd^{2+}, and Co^{2+} were each reduced in 2 bivalves, *Hyridella depressa* and *Velesunio ambigu* 0.111 mM); the decrease in the uptake rate for each metal was consistent with competitive

Table S5. Detailed data on Ca^{2+} transport (*Continued*)

Subsection	Aspect of Transport	Evidence
Effects of Ca^{2+} transport by other ions in the water (continued)	Inhibition of divalent metal uptake by elevated [Ca^{2+}] in FW bivalves (continued)	inhibition by Ca^{2+} in these transporters [186]. A similar effect was observed for Cd^{2+} in *E. complanata* [187].
	Inhibition of Ca^{2+} uptake by divalent metals in *L. stagnalis*	In *L. stagnalis*, uptake of Ca^{2+} was inhibited by exposure to 0.091 μM Pb^{2+} [188, 189], and hemolymph Ca^{2+} was
	Elevation of [Ca^{2+}] in hemolymph and extrapallial fluids of Mollusca by interaction between divalent metals and Ca^{2+}-transporters	In *A. anatina* exposed to 0.002 μM Cd^{2+} for 1 h to 35 d, [Ca^{2+}] increased from 3.94 ± 0.3 to 4.49 ± 0.7 mM in the hemolymph and from 3.92 ± 0.25 to 4.19 ± 0.32 mM in the extrapallial fluids, respectively, from control [Ca^{2+}] (i.e., in mussels not exposed to Cd^{2+}) of 3.14 ± 0.12 to 3.57 ± 0.32 mM in the hemolymph and 3.14 ± 0.35 to 3.59 ± 0.27 mM in the extrapallial fluids [191]. The [Ca^{2+}] decreased again as the Cd^{2+} was depurated from the mussels following the end of the exposure to Cd^{2+}. A similar increase in the hemolymph [Ca^{2+}] occurred in *A. cygnea* exposed to 1 mM Cd^{2+} [192], and PMCA has been specifically identified with immunolabeling on the outer mantle epithelium of this species [193]. Moreover, exposure to Cd^{2+} also reduced tissue [Zn^{2+}], another divalent metal, which can be transported by the ECaC and inhibits PMCA activity [191]. A similar decrease in tissue [Zn^{2+}] with exposure to Cd^{2+} has been observed in the pulmonate gastropod, *L. stagnalis* [194]. However, exposure to low pH (i.e., 4.0−4.5) also has been shown to elevate hemolymph [Ca^{2+}] in unionid mussels [125].

AE, Cl^-/HCO_3^--exchanger; ASW, artificial saltwater; CA, carbonic anhydrase; EC, extracellular; ECaC, epithelial Ca^{2+}-channel; EIPA, 5-(*N*-ethyl-*N*-isopropyl)amiloride; FW, freshwater; H2Na(Ca)E, $H^+/2Na^+$(or Ca^{2+})-exchanger; IC, intracellular; J_{max}, maximum uptake rate; LC50, median lethal concentration; MR, mitochondria-rich; NaR, Na^+/K^+-ATPase-rich; NCX, Na^+/Ca^{2+}-exchanger; NKA, Na^+/K^+-ATPase; PMCA, plasma membrane Ca^{2+}-ATPase; PW, pond water; VHA, vacuolar-type H^+-ATPase

Table S6. Detailed data on Mg^{2+} transport.

Subsection	Aspect of Transport	Evidence
Teleost fish	Absorption of Mg^{2+} from their diet	Rainbow trout absorbed 60% of a single experimental meal that supplied 3.3 mmol Mg^{2+} kg^{-1} fish body mass [161].
	Absorption of Mg^{2+} by the gills	Common carp fed a diet low in Mg^{2+} became hypomagnesemic, mobilized Mg^{2+} from their bone, and could not meet their needs by absorbing Mg^{2+} from the water, which contained 0.17−0.23 mM Mg^{2+} [195].
	Acclimation to a low Mg^{2+} diet by adult tilapia	Adult tilapia fed a low Mg^{2+} diet (1 mmol kg^{-1} vs. 30 mmol kg^{-1} in the control) grew at a reduced rate [196], while MR ionocyte density and NKA activity increased. Also, Na^+ uptake and loss both decreased. Therefore, the adult tilapia were able to acclimate to this diet and maintain blood ion homeostasis [197].
	Uptake of Mg^{2+} through the gills by tilapia	An uptake rate of 1 μmol Mg^{2+} d^{-1} through the gills was estimated for a 50 g tilapia fed a low Mg^{2+} diet in water with $[Mg^{2+}]$ = 0.2 mM, although the transporter is unknown [198].
	Exposure of juvenile rainbow trout to low Mg^{2+} diet and different water $[Mg^{2+}]$	For juvenile rainbow trout, 1.9 mM Mg^{2+} in water was sufficient to meet the fishes' Mg^{2+} requirement when fed a low-Mg diet [199]. A minimum diet was 3.2 μmol Mg^{2+} g^{-1} in fish that consumed 0.92−1.19 g dry weight of food over 28 d. The range in the diets tested was 3.2−30 μmol Mg^{2+} g^{-1}. Fish in a greater water $[Mg^{2+}]$ (41 mM, 20 times the greatest of the other 4 treatments [2.1 mM Mg^{2+}]) consumed less feed than fish in other treatments, exhibited greater whole-body $[Mg^{2+}]$, exhibited mortality after 2 d, and reached 48% mortality after 14 d.
Mollusca	Changes in hemolymph ion concentrations of *D. polymorpha* placed in Mg-free AFW	Hemolymph $[Mg^{2+}]$ in *D. polymorpha*, which is a weaker hyper-regulator than most other FW bivalves [87], decreased from 1.5 to 0.05 mM over 15 d when individuals were placed in Mg-free AFW, whereas $[Na^+]$ and $[K^+]$ did not change. Hemolymph $[Ca^{2+}]$ decreased slightly but then increased to near its original concentration by 15 d, whereas $[Cl^-]$ decreased from 16.9 to 14.0 mM, and HCO_3^- increased from approximately 1.0 to 4.1 mM [149].
	Mg^{2+} uptake in Mg-depleted *D. polymorpha*	When Mg-depleted *D. polymorpha* were placed in AFW with $[Mg^{2+}]$ of 0.05, 0.1, or 0.2 mM, net Mg^{2+} uptake increased in relation to the AFW $[Mg^{2+}]$, and hemolymph $[Mg^{2+}]$ exceeded the AFW $[Mg^{2+}]$ after 17 h by 0.1, 0.1, and 0.3 mM, respectively [149].

AFW, artificial freshwater; FW, freshwater; MR, mitochondria-rich; NKA, Na^+/K^+-ATPase.

Table S7. Detailed data on Cl^- transport.

Subsection	Aspect of Transport	Evidence
Teleost fish	Isoforms of SLC26a and their location on ionocytes of zebrafish gills	The most common isoforms in zebrafish gills are SLC26a3, SLC26a4 and SLC26a6, and at least SLC26a3 is located in ionocytes on gill filaments and at the base of the gill lamellae, which may or may not be enriched with NKA [200]. The NaR ionocytes have, at least, AE on the apical membrane and VHA on the basolateral membrane [200].
	Upregulation of SLC26 mRNA and Cl^- uptake	When zebrafish were placed in waters with low (0.02 mM) vs. high (2.0 mM), ambient [Cl^-], relative expression of gill SLC26 mRNA was substantially increased after 3 to 10 d [200]. Similarly, when zebrafish were exposed to elevated [$NaHCO_3$], relative expression of gill SLC26 mRNA increased and Cl^- uptake rates increased [200]. Studies have also observed increased expression of cytosolic CA mRNA or protein levels in fish placed in soft, low [Cl^-] waters [201, 202].
	Metabolon for Cl^- uptake	CA is localized close to AE on the apical membrane of an ionocyte specialized for Cl^- uptake, and base (i.e., HCO_3^-) excretion increases local [HCO_3^-] sufficiently to drive electroneutral exchange of Cl^- and HCO_3^- by the exchanger (Figure 1). At the same time, VHA on the basolateral membrane, which is invaginated to place it closer to the CA and AE on the apical membrane, removes H^+ produced by CA and transports it across the basolateral membrane out of the cell maintaining the shift in the reaction equilibrium to produce more HCO_3^- [203]. This ionoregulation activity is facilitated by separation of transporters among different ionocyte types, and Cl^- uptake along with greater levels of VHA occur in β-type MR ionocytes in rainbow trout [204].
	Interspecific differences in inhibition of Cl^- influx	In neon tetra, Cl^- influx was inhibited at least 60% by SITS, an AE inhibitor, or by thiocyanate (SCN^-), a Cl^--channel inhibitor. In goldfish, Cl^- influx was completely inhibited by SITS but was not inhibited by SCN^-.
Crustacea	Separation of gas and ion exchange among different gill filaments and lamina of *Pontastacus leptodactylus*	In *P. leptodactylus*, asymmetrical perfusion of one type of filament with artificial water containing 0.0001 to 1 mM Na^+ caused electrical potential differences across single filaments, while perfusion of a second type of filament did not cause electrical potential differences [205]. The first filament type was involved in ion uptake, as the epithelium was mitochondria-rich and had an invaginated basolateral membrane as is characteristic of ion-transporting epithelia. The second filament type was involved in gas exchange, as morphologically its epithelium was much thinner, lacked mitochondria, and was composed of squamous cells [206]. Moreover, the laminae were involved in Cl^- uptake [205, 207].

Table S7. Detailed data on Cl^- transport (*Continued*).

Subsection	Aspect of Transport	Evidence
Aquatic insects	Differences in Cl^- uptake among mosquito larvae	Among the larvae of 4 different mosquitos that inhabit phytotelmata with low ionic water, hemolymph [Cl^-] ranged from 58 to 78 mM and Cl^- uptake rates ranged from < 0.01 to 0.6 nmol g^{-1} h^{-1} [116]. When the mosquito larvae were placed in low pH (3.5) water, Cl^- uptake rates unexpectedly increased, possibly suggesting a different uptake mechanism, such as an NCC, although this hypothesis has not been tested with molecular studies. Like Na^+, Cl^- uptake increased by 4-7 times when the mosquitoes were placed in more saline water [116]. Among different populations of *A. aegypti* (a colony maintained by J. Shaw at University of Newcastle upon Tyne vs. one at Ohio State University), Stobbart [208] found that K_m differed for Cl^- (500 μM vs. 0.2 μM, respectively).
	Variation in body wall impermeability to Cl^- among a euryhaline and 2 FW species of caddisflies	As with Na^+, the body wall of the euryhaline caddisfly *L. affinis* was relatively impermeable to Cl^- [69], and hemolymph [Cl^-] was maintained at higher levels at lower external [Cl^-] (< 100 mM), while mean hemolymph [Cl^-] remained less than 150 mM at greater external [Cl^-] (up to 400 mM). Conversely, the FW caddisflies *L. stigma* and *A. nervosa* maintained hemolymph [Cl^-] at slightly greater levels at very low external [Cl^-] (< 15 mM), and hemolymph [Cl^-] increased but was less than the external concentrations at greater external concentrations (15 to 220 mM) [71]. These 2 species generally excreted urine with greater [Cl^-] than that in their hemolymph at these greater external [Cl^-]. As hemolymph [Na^+] and [Cl^-] were measured on the same larvae, this change to hypotonic hemolymph occurred coincident with high mortality at [NaCl] > 120 mM.
Mollusca	Evidence showing exchange of HCO_3^-/Cl^- exchange is independent of Na^+	In *L. subrostrata* maintained in 0.1 mM sodium sulfate (Na_2SO_4) solution for about 60 d (vs. a control of DI water), hemolymph HCO_3^- increased from 11.0 to 13.5 mM, while hemolymph Cl^- decreased by 89 to 94% (from 11.4 to 1.3 mM) [209]. When the Cl^--depleted, mussels were placed in 1.0 mM solutions of NaCl or the organic salt, choline Cl, net Cl^- influx was 0.5−1.0 μmol g^{-1} h^{-1} for the first 3 d compared to near 0 for mussels placed in 0.1 mM Na_2SO_4 solutions, while in undepleted mussels placed in a choline Cl solution, hemolymph [HCO_3^-] decreased from 12.9 to 8.6 mM.
	Changes in hemolymph [Cl^-] with changes in water NaCl salinity	When maintained in PW, hemolymph [Cl^-] (14.6−16.2 mM) of *D. polymorpha* was greater than that of the PW [Cl^-] (1.4 mM) [169], but when transferred to 10% ASW, the hemolymph [Cl^-] (44.3−46.9 mM) approached that of the 10% ASW (52.4 mM Cl^-). As with the other ions, the changes reversed when the mussels were returned to PW.

Table S7. Detailed data on Cl^- transport (*Continued*).

Subsection	Aspect of Transport	Evidence
Mollusca (continued)	Changes in hemolymph [Cl^-] with decreased pH	As in fish and decapods, unionid mussels exposed to low pH (i.e., 4.0−4.5) in either soft (0.11 mM Ca^{2+}) or hard (0.46 mM Ca^{2+}) water showed decreased hemolymph [Cl^-], possibly because the VHA activity is inhibited by elevated ambient [H^+] [125]. In turn, inhibition of VHA activity would affect the production of HCO_3^- from CO_2 by CA for exchange for Cl^- by the AE [203].
Effects of Cl^- transport by other ions in the water	Effects of decreased pH on blood [Cl^-] in fish	In rainbow trout exposed to pH 4.2 for 4 d, total Cl^- efflux was 9.4 mmol kg^{-1}, with slightly more than two-thirds by efflux across the gills and the remainder by excretion through the kidneys, resulting in a decrease in blood Cl^- of 21.6 mM over the 4 d [95]. Blood [HCO_3^-] was also depressed by the acid disturbance, although blood P_{CO2} was relatively unchanged, suggesting that acid stress (pH decreased from 7.8 to 7.2 during the 4 d) may have inhibited production of HCO_3^-, which in turn inhibited uptake of Cl^- by the AE. Similar changes in pH, HCO_3^- and Cl^- were observed in *Catostomus commersonii* (white sucker) exposed to pH 4.3 in low [Ca^{2+}] (82−92 μM) water [210].
	Effects of decreased pH on blood [Cl^-] in Crustacea	Exposure of the crayfish *O. propinquus* to pH 4.0 resulted in net efflux of Cl^- from the hemolymph that resulted from a decrease in Cl^- influx with little change in Cl^- efflux [111]. This was accompanied by a decrease in hemolymph pH and an increase in P_{CO2}, which decreased HCO_3^- that could be exchanged for Cl^-. Similarly in the amphipod *Gammarus fossarum*, hemolymph Cl^- as well as Na^+ decreased with decreasing pH [211]. Although the authors did not investigate any mechanisms, the current model suggests that inhibition of H^+ excretion, which reduces concomitant uptake of Na^+ and is the cause of the reduction in hemolymph Na^+ also decreases HCO_3^- production by the CA-catalyzed hydrolysis of CO^2 along with retention of the HCO_3^- to maintain hemolymph acid/base balance. As a result, there is a concomitant reduction in Cl^- uptake by the AE that reduces hemolymph [Cl^-] [203].
	Effects of increased pH on blood [Cl^-] in fish	Rainbow trout exposed to pH 9.5 (0.6 mM Na^+, 0.8 mM Cl^-) after acclimation to pH 8.0 exhibited a decrease in Cl^- influx (from ≈ 275 μmol kg^{-1} h^{-1} in control to < 50 μmol kg^{-1} h^{-1} after 4-h exposure to pH 9.5). The [Cl^-] then increased and was not less than the control after 72 h [212]. As in experiments with low-salinity water, MR ionocyte density and total apical surface increased on gill filaments of fish exposed to pH 9.5. However, in this case, the decreased uptake may also be caused, in part, by a decrease in the availability of HCO_3^- for exchange with Cl^- [213]. In addition to increased blood pH, decreased P_{CO2} and decreased [H^+], metabolic alkalosis in rainbow trout exposed to pH 9.5 decreased blood [HCO_3^-] from 7.50 mM in control fish at pH 8.0 to between 2.58 and 5.04 mM. In rainbow trout exposed to pH 10.5 with or without a glycine buffer,

Table S7. Detailed data on Cl^- transport (*Continued*).

Subsection	Aspect of Transport	Evidence
Effects of Cl^- transport by other ions in the water (continued)	Effects of increased pH on blood [Cl^-] in fish (continued)	effects of increased pH on blood [Cl^-] in fish blood [HCO_3^-] increased and [Cl^-] decreased because of inhibition of the AE [214], possibly associated with an increase in the alkalinity gradient across the apical membrane. As also observed by Wilkie and Wood [212], this ion perturbation was reversed after 1 to 2 d associated with an increase in the proportional exposure of MR ionocytes on the gills.
	NO_2^- uptake in crayfish	Uptake of NO_2^- in *A. astacus* or *Pacifastacus leniusculus* showed Michaelis-Menten kinetics, suggesting active transport, and NO_2^- competitively inhibited uptake of Cl^- [215] as well as Br^- [216]. Moreover, uptake rates of NO_2^- increased 24 h following induction of hypercapnia by bubbling the water with 1% CO_2 and 99% air when hemolymph [HCO_3^-] increased. In parallel with the accumulation of NO_2^-, NO_3^- also accumulated in the hemolymph but its concentrations were unrelated to any other ion concentration in the water, indicating that it was produced by processes that detoxify the NO_2^- by oxidizing it to NO_3^- [216]. However, there are no effects on respiration similar to those in fish because NO_2^- does not oxidize hemocyanin as it does hemoglobin. When the crayfish were returned to water without NO_2^-, hemolymph NO_2^- was eliminated by 7 d and [Cl^-] returned to control levels, but [NO_3^-] remained elevated, suggesting low gill-epithelial-membrane permeability for NO_3^- [216].
	Additional effect of NO_2^- on respiration in fish	In fish, NO_2^- has an added effect on respiration because it oxidizes oxyhemoglobin to methemoglobin converting Fe^{2+} to Fe^{3+} and forms NO_3^- [217].

AE, Cl^-/HCO_3^--exchanger; ASW, artificial saltwater; CA, carbonic anhydrase; DI, deionized; FW, freshwater; K_m, ion concentration at which the uptake rate is half of J_{max}; MR, mitochondria-rich; NaR, Na^+/K^+-ATPase-rich; NCC, Na^+/Cl^--cotransporter; NKA, Na^+/K^+-ATPase; P_{CO2}, partial pressure of CO_2; PW, pond water; SITS, disodium 4 acetamido-4′ isothiocyanatostilbene-2, 2′ disulfonate; SLC, solute carrier; VHA, vacuolar-type H^+-ATPase.

Table S8. Detailed data on HCO_3^- transport.

Subsection	Aspect of Transport	Evidence
Teleost fish	Fish where the described response to metabolic acidosis has been observed	Such a response to metabolic acidosis resulting from external hypercapnia has been described for common carp [218], *Ictalurus punctatus* (channel catfish) [219], and rainbow trout [220].
	Comparison of the response to metabolic acidosis by American eel (*Anguilla rostrata*) and rainbow trout	In a comparison of American eel and rainbow trout, fish were exposed to external hypercapnia which induced metabolic acidosis and reduced blood pH 0.4 and 0.35 units, respectively [221]. In American eels, Na^+/H^+ exchange occurred to compensate for the acidosis, exporting the H^+, as both branchial J_{in}^{Na+} and J_{net}^{Na+} increased relative to controls. In rainbow trout, J_{net}^{Cl-} was negative as HCO_3^- was accumulated to compensate for the acidosis. Following removal from external hypercapnia, blood pH increased to slightly greater than the original pH as a result of alkalosis. The rainbow trout rapidly recovered from this alkalosis by increasing J_{net}^{Cl-}, exporting HCO_3^-, but the American eels were unable to increase Cl^-/HCO_3^- exchange and had not recovered by 24 h [222].
	Response to increases in acid or base load by channel catfish	Channel catfish infused with either NH_4Cl or $NaHCO_3$ to increase their acid or base loads, respectively, excreted H^+ in response to acidosis and HCO_3^- in response to alkalosis, mostly through the gills [223].
Crustacea	Responses of Cl− and Na^+ to excretion of acid and base units following hemolymph acidosis in *P. leniusculus*	The small net loss of Cl^- occurred because of decreased Cl^- uptake in exchange for HCO_3^-. Na^+ was unchanged because excretion of acid units (H^+) maintained the uptake of Na^+. Upon return to normoxia, the levels of $HCO_3^- + CO_3^{2-}$ decreased and H^+ excretion decreased, while net Na^+ efflux and net Cl^- influx brought Na^+, Cl^-, and acid-base balance back to control levels. Part of these exchanges occurred via the antennal gland, and the urine was acidified, while HCO_3^- was reabsorbed. Urinary Na^+ efflux increased during hyperoxia, and Cl^- efflux decreased, particularly after 36 h [224, 225].
Mollusca	Response of hemolymph $[HCO_3^-]$ to increased hemolymph pH	Although total $[CO_3]$ were the same (0.2 mM) in PW and 10% ASW, hemolymph $[HCO_3^-]$ of *D. polymorpha* increased from 2.38−2.98 mM in PW to 5.31−6.37 mM when the mussels were moved to 10% ASW [169]. Hemolymph pH also increased from 7.74−7.96 in PW to 8.17−8.25 in 10% ASW, while P_{CO2} was variable but showed no trend (1.49−3.21 mm Hg). $[HCO_3^-]$ again decreased when the mussels were returned to PW. This sequence suggests that HCO_3^- was not excreted to counter the increase in pH.

Table S8. Detailed data on HCO_3^- transport (*Continued*).

Subsection	Aspect of Transport	Evidence
	Responses of CA activity in an estuarine and 2 FW bivalves to alterations in salinity	*Rangia cuneata* had greater gill CA activity in 1‰ salinity water, where these bivalves' blood $[Na^+]$ and $[Cl^-]$ were greater than those in the water, compared to 10‰ salinity water, where *Rangia*'s blood $[Na^+]$ and $[Cl^-]$ were approximately equal to those in the water [226]. Similarly, the 2 FW bivalves had greater gill CA activity in DI water than in AFW, although *C. fluminea* had greater gill CA activity in both waters because its blood $[Na^+]$ and $[Cl^-]$ were greater than those of *L. subrostrata*. Moreover, because the 2 FW bivalves both maintained greater ionic gradients than *R. cuneata*, their gill CA activities were greater than in *R. cuneata*. Conversely, lower hemolymph $[Na^+]$ and $[Cl^-]$ in *Anodonta* spp. exposed to Cd^{2+} appear likely to result from inhibition of CA, which reduces the availability of H^+ and HCO_3^- for exchange [192, 227].
	Responses of dissolved $[Ca^{2+}]$ and pH to inhibition of CA	The addition of acetazolamide, a CA inhibitor, decreased pH and dissolved Ca^{2+} in mantle homogenates of *A. cygnea [228]*. Similarly, inhibition of CA by Cd^{2+} increased $[Ca^{2+}]$ in the hemolymph and extrapallial fluids of *A. anatina* [191, 227].

AFW, artificial freshwater; ASW, artificial saltwater; CA, carbonic anhydrase; DI, deionized; FW, freshwater; J_{in}^{NA+}, uptake rate of sodium; J_{net}^{X}, net uptake rate of ion; P_{CO2}, partial pressure of CO_2; PW, pond water.

Table S9. Detailed data on sulfate transport

Subsection	Aspect of Transport	Evidence
Teleost fish (toad)	Characteristics of SO_4^{2-} transport in European toad (*Bufo bufo*)	When European toad skin was mounted in an Ussing chamber and clamped at −80 mV and with apical Na^+ conductance eliminated by treatment with amiloride (a Na^+-transporter inhibitor), transepithelial conductance of SO_4^{2-} was identical to voltage activated Cl^- conductance [229].
Mollusca	Characteristics of SO_4^{2-} transport in *D. polymorpha*	*D. polymorpha* maintained hemolymph [SO_4^{2-}] 4 to 24 times greater than PW [SO_4^{2-}] (0.2 mM), accumulated $^{35}SO_4$ in its hemolymph from the bathing medium, cleared $^{35}SO_4$ at a rate 19−21% of that of polyethylene glycol, and the $^{35}SO_4$ accumulation was inhibited by treatment with DIDS, an AE inhibitor [230]. However, *D. polymorpha* that had been acclimated to 10% ASW (2.8 mM SO_4^{2-}) cleared $^{35}SO_4$ at a similar rate to polyethylene glycol, suggesting that SO_4^{2-} was not reabsorbed by the kidney [230], as these mussels did not need to conserve this SO_4^{2-} because their hemolymph concentrations were greater [169].

AE, anion exchanger; ASW, artificial saltwater; DIDS, 4,4′-disorthiocyanato-stilbeen 2,2′-disulfonic acid; PW, pond water

REFERENCES

[1] Cutler CP, Cramb G. 2002. Branchial expression of an aquaporin 3 (AQP-3) homologue is downregulated in the European eel *Anguilla anguilla* following seawater acclimation. *J Exp Biol* 205:2643-2651.

[2] Lignot J-H, Cutler CP, Hazon N, Cramb G. 2002. Immunolocalisation of aquaporin 3 in the gill and the gastrointestinal tract of the European eel *Anguilla anguilla* (L.). *J Exp Biol* 205:2653-2663.

[3] Tipsmark CK, Sørensen KJ, Madsen SS. 2010. Aquaporin expression dynamics in osmoregulatory tissues of Atlantic salmon during smoltification and seawater acclimation. *J Exp Biol* 213:368-379.

[4] Zheng H, Dietz TH. 1998. Paracellular solute uptake in the freshwater bivalves *Corbicula fluminea* and *Toxolasma texasensis*. *Biol Bull* 194:170-177.

[5] Kapoor NN. 1979. Osmotic regulation and salinity tolerance of the stonefly nymph, *Paragnetina media*. *J Insect Physiol* 25:17-20.

[6] Peterson MS. 1988. Comparative physiological ecology of centrarchids in hyposaline environments. *Can J Fish Aquat Sci* 45:827-833.

[7] Gonçalves AMM, Castro BB, Pardal MA, Gonçalves F. 2007. Salinity effects on survival and life history of two freshwater cladocerans (*Daphnia magna* and *Daphnia longispina*). *Ann Limnol Internat J Limnol* 43:13-20.

[8] Weider LJ, Hebert PDN. 1987. Ecological and physiological differentiation among low-arctic clones of *Daphnia pulex*. *Ecology* 68:188-198.

[9] Teschner M. 1995. Effects of salinity on the life history and fitness of *Daphnia magna*: variability within and between populations. *Hydrobiologia* 307:33-41.

[10] Jordan PJ, Deaton LE. 1999. Osmotic regulation and salinity tolerance in the freshwater snail *Pomacea bridgesi* and the freshwater clam *Lampsilis teres*. *Comp Biochem Phys A* 122:199-205.

[11] Hanson JA, Dietz TH. 1976. The role of free amino acids in cellular osmoregulation in the freshwater bivalve *Ligumia subrostrata* (Say). *Can J Zool* 54:1927-1931.

[12] de Boeck G, Vlaeminck A, van der Linden A, Blust R. 2000. The energy metabolism of common carp (*Cyprinus carpio*) when exposed to salt stress: An increase in energy expenditure or effects of starvation? *Physiol Biochem Zool* 73:102-111.

[13] Wood CM, Iftikar FI, Scott GR, De Boeck G, Sloman KA, Matey V, Valdez Domingos FX, Duarte RM, Almeida-Val VMF, Val AL. 2009. Regulation of gill transcellular permeability and renal function during acute hypoxia in the Amazonian oscar (*Astronotus ocellatus*): new angles to the osmorespiratory compromise. *J Exp Biol* 212:1949-1964.

[14] Bagherie-Lachidan M, Wright SI, Kelly SP. 2008. Claudin-3 tight junction proteins in *Tetraodon nigroviridis:* cloning, tissue-specific expression, and a role in hydromineral balance. *Am J Phys-Reg I* 294:R1638-R1647.

[15] Bagherie-Lachidan M, Wright SI, Kelly SP. 2009. Claudin-8 and -27 tight junction proteins in puffer fish *Tetraodon nigroviridis* acclimated to freshwater and seawater. *J Comp Phys B* 179:419-431.

[16] Tipsmark CK, Kiilerich P, Nilsen TO, Ebbesson LOE, Stefansson SO, Madsen SS. 2008. Branchial expression patterns of claudin isoforms in Atlantic salmon during seawater acclimation and smoltification. *Am J Phys-Reg I* 294:R1563-R1574.

[17] Tipsmark CK, Baltzegar DA, Ozden O, Grubb BJ, Borski RJ. 2008. Salinity regulates claudin mRNA and protein expression in the teleost gill. *Am J Phys-Reg I* 294:R1004-R1014.

[18] Chasiotis H, Effendi JC, Kelly SP. 2009. Occludin expression in goldfish held in ion-poor water. *J Comp Phys B* 179:145-154.

[19] Chasiotis H, Kolosov D, Kelly SP. 2012. Permeability properties of the teleost gill epithelium under ion-poor conditions. *Am J Phys-Reg I* 302:R727-R739.

[20] Chasiotis H, Wood CM, Kelly SP. 2010. Cortisol reduces paracellular permeability and increases occludin abundance in cultured trout gill epithelia. *Mol Cell Endocrinol* 323:232-238.
[21] Kelly SP, Chasiotis H. 2011. Glucocorticoid and mineralocorticoid receptors regulate paracellular permeability in a primary cultured gill epithelium. *J Exp Biol* 214:2308-2318.
[22] Bui P, Bagherie-Lachidan M, Kelly SP. 2010. Cortisol differentially alters claudin isoforms in cultured puffer fish gill epithelia. *Mol Cell Endocrinol* 317:120-126.
[23] Chasiotis H, Kelly SP. 2011. Permeability properties and occludin expression in a primary cultured model gill epithelium from the stenohaline freshwater goldfish. *J Comp Phys B* 181:487-500.
[24] Fenwick JC, Wendelaar Bonga SE, Flik G. 1999. In vivo bafilomycin-sensitive Na^+ uptake in young freshwater fish. *J Exp Biol* 202:3659-3666.
[25] Parks SK, Tresguerres M, Goss GG. 2008. Theoretical considerations underlying Na^+ uptake mechanisms in freshwater fishes. *Comp Biochem Physiol C* 148:411-418.
[26] Parks SK, Tresguerres M, Galvez F, Goss GG. 2010. Intracellular pH regulation in isolated trout gill mitochondrion-rich (MR) cell subtypes: Evidence for Na^+/H^+ activity. *Comp Biochem Phys A* 155:139-145.
[27] Parks SK, Tresguerres M, Goss GG. 2009. Cellular mechanisms of Cl^- transport in trout gill mitochondrion-rich cells. *Am J Phys-Reg I* 296:R1161-R1169.
[28] Wilson JM, Laurent P, Tufts BL, Benos DJ, Donowitz M, Vogl AW, Randall DJ. 2000. NaCl uptake by the branchial epithelium in freshwater teleost fish: an immunological approach to ion-transport protein localization. *J Exp Biol* 203:2279-2296.
[29] Perry SF, Beyers ML, Johnson DA. 2000. Cloning and molecular characterisation of the trout (*Oncorhynchus mykiss*) vacuolar $H(^+)$-ATPase B subunit. *J Exp Biol* 203:459-470.
[30] Li J, Eygensteyn J, Lock RAC, Wendelaar Bonga SE, Flik G. 1997. Na^+ and Ca^{2+} homeostatic mechanisms in isolated chloride cells of the teleost *Oreochromis mossambicus* analysed by confocal laser scanning microscopy. *J Exp Biol* 200:1499-1508.
[31] Kumai Y, Perry SF. 2012. Mechanisms and regulation of Na+ uptake by freshwater fish. *Resp Physiol Neurobiol* 184:249-256.
[32] Perry SF, Gilmour KM. 2006. Acid–base balance and CO_2 excretion in fish: Unanswered questions and emerging models. *Resp Physiol Neurobiol* 154:199-215.
[33] Alvarez de la Rosa D, Canessa CM, Fyfe GK, Zhang P-P. 2000. Structure and regulation of amiloride-sensitive sodium channels. *Annu Rev Physiol* 62:573-594.
[34] Bucking C, Wood CM. 2006. Gastrointestinal processing of Na^+, Cl^-, and K^+ during digestion: implications for homeostatic balance in freshwater rainbow trout. *Am J Phys-Reg I* 291:R1764-R1772.
[35] Smith NF, Eddy FB, Talbot C. 1995. Effect of dietary salt load on transepithelial Na^+ exchange in freshwater rainbow trout (*Oncorhynchus mykiss*). *J Exp Biol* 198:2359-2364.
[36] D'Cruz Leela M, Wood Chris M. 1998. The influence of dietary salt and energy on the response to low pH in juvenile rainbow trout. *Physiol Zool* 71:642-657.
[37] Esbaugh AJ, Perry SF, Bayaa M, Georgalis T, Nickerson J, Tufts BL, Gilmour KM. 2005. Cytoplasmic carbonic anhydrase isozymes in rainbow trout *Oncorhynchus mykiss*: Comparative physiology and molecular evolution. *J Exp Biol* 208:1951-1961.
[38] Georgalis T, Perry SF, Gilmour KM. 2006. The role of branchial carbonic anhydrase in acid-base regulation in rainbow trout *(Oncorhynchus mykiss*). *J Exp Biol* 209:518-530.
[39] Esaki M, Hoshijima K, Kobayashi S, Fukuda H, Kawakami K, Hirose S. 2007. Visualization in zebrafish larvae of Na^+ uptake in mitochondria-rich cells whose differentiation is dependent on foxi3a. *Am J Phys-Reg I* 292:R470-R480.
[40] Wieczorek H, Brown D, Grinstein S, Ehrenfeld J, Harvey WR. 1999. Animal plasma membrane energization by proton-motive V-ATPases. *Bioessays* 21:637-648.
[41] Boisen AMZ, Amstrup J, Novak I, Grosell M. 2003. Sodium and chloride transport in soft water and hard water acclimated zebrafish (*Danio rerio*). *Biochim Biophys Acta* 1618:207-218.

[42] Edwards SL, Tse CM, Toop T. 1999. Immunolocalisation of NHE3-like immunoreactivity in the gills of the rainbow trout (*Oncorhynchus mykiss*) and the blue-throated wrasse (*Pseudolabrus tetrious*). *J Anat* 195:465-469.
[43] Yan J-J, Chou M-Y, Kaneko T, Hwang P-P. 2007. Gene expression of Na^+/H^+ exchanger in zebrafish H^+-ATPase-rich cells during acclimation to low-Na^+ and acidic environments. *Am J Physiol-Cell Ph* 293:C1814-C1823.
[44] Lin L-Y, Horng J-L, Kunkel JG, Hwang P-P. 2006. Proton pump-rich cell secretes acid in skin of zebrafish larvae. *Am J Physiol-Cell Ph* 290:C371-C378.
[45] Shih T-H, Horng J-L, Liu S-T, Hwang P-P, Lin L-Y. 2011. Rhcg1 and NHE3b are involved in ammonium-dependent sodium uptake by zebrafish larvae acclimated to low-sodium water. *Am J Phys-Reg I* 302:R84-R93.
[46] Kumai Y, Perry SF. 2011. Ammonia excretion via Rhcg1 facilitates Na+ uptake in larval zebrafish, *Danio rerio*, in acidic water. *Am J Phys-Reg I* 301:R1517-R1528.
[47] Ahearn GA. 1996. The invertebrate electrogenic $2Na^+/1H^+$ exchanger: Polyfunctional epithelial workstation. *News Physiol Sci* 11:31-35.
[48] Shaw J. 1960. The absorption of sodium ions by the crayfish *Astacus pallipes* Lereboullet : III. The effect of other cations in the external solution. *J Exp Biol* 37:548-556.
[49] de Couet HG, Busquets-Turner L, Gresham A, Ahearn GA. 1993. Electrogenic 2 Na/1 H antiport in crustacean epithelium is inhibited by a monoclonal antibody. *Am J Phys-Reg I* 264:R804-R810.
[50] Glover CN, Wood CM. 2005. Physiological characterisation of a pH- and calcium-dependent sodium uptake mechanism in the freshwater crustacean, *Daphnia magna*. *J Exp Biol* 208:951-959.
[51] Glover CN, Pane EF, Wood CM. 2005. Humic substances influence sodium metabolism in the freshwater crustacean *Daphnia magna*. *Physiol Biochem Zool* 78:405-416.
[52] Zare S, Greenaway P. 1997. Ion transport and the effects of moulting in the freshwater crayfish *Cherax destructor* (Decapoda : Parastacidae). *Aust J Zool* 45:539-551.
[53] Wheatly MG, Ignaszewski LA. 1990. Electrolyte and gas exchange during the moulting cycle of a freshwater crayfish. *J Exp Biol* 151:469-483.
[54] Wheatly MG, Gannon AT. 1995. Ion regulation in crayfish: Freshwater adaptations and the problem of molting. *Am Zool* 35:49-59.
[55] Lucu Č, Towle DW. 2003. Na^++K^+-ATPase in gills of aquatic crustacea. *Comp Biochem Phys A* 135:195-214.
[56] Sarver RG, Flynn MA, Holliday CW. 1994. Renal Na,K-ATPase and osmoregulation in the crayfish, *Procambarus clarkii*. *Comp Biochem Phys A* 107:349-356.
[57] del Duca O, Nasirian A, Galperin V, Donini A. 2011. Pharmacological characterisation of apical Na+ and Cl– transport mechanisms of the anal papillae in the larval mosquito *Aedes aegypti*. *J Exp Biol* 214:3992-3999.
[58] Pullikuth AK, Aimanova K, Kang'ethe W, Sanders HR, Gill SS. 2006. Molecular characterization of sodium/proton exchanger 3 (NHE3) from the yellow fever vector, *Aedes aegypti*. *J Exp Biol* 209:3529-3544.
[59] Rheault MR, Okech BA, Keen SBW, Miller MM, Meleshkevitch EA, Linser PJ, Boudko DY, Harvey WR. 2007. Molecular cloning, phylogeny and localization of AgNHA1: the first Na^+/H^+ antiporter (NHA) from a metazoan, *Anopheles gambiae*. *J Exp Biol* 210:3848-3861.
[60] Smith KE, Raymond SL, Valenti ML, Smith PJS, Linser PJ. 2010. Physiological and pharmacological characterizations of the larval *Anopheles albimanus* rectum support a change in protein distribution and/or function in varying salinities. *Comp Biochem Phys A* 157:55-62.
[61] Komnick H, Rhees RW, Abel JH, Jr. 1972. The function of ephemerid chloride cells: Histochemical, autoradiographic and physiological studies with radioactive chloride on *Callibaetis*. *Cytobiologie* 5:65-82.

[62] Wichard W, Komnick H. 1971. Electron microscopical and histochemical evidence of chloride cells in tracheal gills of mayfly larvae. *Cytobiologie* 3:215-228.
[63] Filshie BK, Campbell IC. 1984. Design of an insect cuticle associated with osmoregulation: The porous plates of chloride cells in a mayfly nymph. *Tissue Cell* 16:789-803.
[64] Kapoor NN. 1980. Relationship between gill Na^+,K^+-activated ATPase activity and osmotic stress in the plecopteran nymph, *Paragnetina media*. *J Exp Zool* 213:213-218.
[65] Wichard W, Komnick H. 1974. Structure and function of the respiratory epithelium in the tracheal gills of stonefly larvae. *J Insect Physiol* 20:2397-2406.
[66] Kapoor NN, Zachariah K. 1973. Presence of specialized cellular complexes in the tracheal gills of stonefly nymph, *Paragnetina media* (Walker). *Experientia* 29:848-850.
[67] Kapoor NN, Zachariah K. 1973. A study of specialized cells of the tracheal gills of *Paragnetina media* (Plecoptera). *Can J Zool* 51:983-986.
[68] Colby C. 1972. Salt and water balance in stonefly naiads, *Pteronarcys californica* Newport. *Comp Biochem Phys A* 41:851-860.
[69] Sutcliffe DW. 1961. Studies on salt and water balance in caddis larvae (Trichoptera): I. Osmotic and ionic regulation of body fluids in *Limnephilus affinis* Curtis. *J Exp Biol* 38:501-519.
[70] Sutcliffe DW. 1962. Studies on salt and water balance in caddis larvae (Trichoptera): III. Drinking and excretion. *J Exp Biol* 39:141-160.
[71] Sutcliffe DW. 1961. Studies on salt and water balance in caddis larvae (Trichoptera): II. Osmotic and ionic regulation of body fluids in *Limnephilus stigma* Curtis and *Anabolia nervosa* Leach. *J Exp Biol* 38:521-530.
[72] Wichard W, Komnick H. 1973. Fine structure and function of the abdominal chloride epithelia in caddisfly larvae. *Z Zefforsch Mikrosk Anat* 136:579-590.
[73] Leader JP. 1972. Osmoregulation in the larva of the marine caddis fly, *Philanisus plebeius* (Walk.) (Trichoptera). *J Exp Biol* 57:821-838.
[74] Komnick H. 1977. Chloride cells and chloride epithelia of aquatic insects. *Int Rev Cytol* 49:285-328.
[75] Leader JP, Green LB. 1978. Active transport of chloride and sodium by the rectal chamber of the larvae of the dragonfly, *Uropetala carovei*. *J Insect Physiol* 24:685-692.
[76] Moens J. 1975. Ionic regulation of the haemolymph in the larvae of the dragonfly *Aeshna cyanea* (Miiller) (Odonata, Anisoptera). *Arch Int Physiol Biochim* 83:443-451.
[77] Komnick H. 1978. Osmoregulatory role and transport ATPases of the rectum of dragonfly larvae. *Odonatologica* 7:247-262.
[78] Komnick H, Achenbach U. 1979. Comparative biochemical, histochemical and autoradiographic studies of Na^+/K^+-ATPase in the rectum of dragonfly larvae (Odonata, Aeshnidae). *Eur J Cell Biol* 20:92-100.
[79] Frisbie MP, Dunson WA. 1988a. Sodium and water balance in larvae of the predaceous diving beetle, *Dytiscus verticalis*: An air-breather resistant to acid-induced sodium loss. *Comp Biochem Phys A* 89:409-414.
[80] Frisbie MP, Dunson WA. 1988b. The effect of food consumption on sodium and water balance in the predaceous diving beetle, *Dytiscus verticalis*. *J Comp Phys B* 158:91-98.
[81] Shaw J. 1955. Ionic regulation and water balance in the aquatic larva of *Sialis lutaria*. *J Exp Biol* 32:353-382.
[82] Zheng H, Dietz TH. 1998. Ion transport in the freshwater bivalve *Corbicula fluminea*. *Biol Bull* 194:161-169.
[83] Coimbra J, Machado J, Fernandes PL, Ferreira HG, Ferreira KG. 1988. Electrophysiology of the mantle of *Anodonta cygnea*. *J Exp Biol* 140:65-88.

[84] Dietz TH. 1978. Sodium transport in the freshwater mussel, *Carunculina texasensis* (Lea). *Am J Phys-Reg I* 235:R35-R40.
[85] Dietz TH, Graves SY. 1981. Sodium influx in isolated gills of the freshwater mussel, *Ligumia subrostrata*. *J Comp Phys B* 143:185-190.
[86] Hudson RL. 1993. Bafilomycin-sensitive acid secretion by mantle epithelium of the freshwater clam, *Unio complanatus*. *Am J Phys-Reg I* 264:R946-R951.
[87] Horohov J, Silverman H, Lynn JW, Dietz TH. 1992. Ion transport in the freshwater zebra mussel, *Dreissena polymorpha*. *Biol Bull* 183:297-303.
[88] Parks SK, Tresguerres M, Goss GG. 2007. Interactions between Na^+ channels and Na^+-HCO_3^- cotransporters in the freshwater fish gill MR cell: a model for transepithelial Na^+ uptake. *Am J Physiol-Cell Ph* 292:C935-C944.
[89] Hiroi J, Yasumasu S, McCormick SD, Hwang P-P, Kaneko T. 2008. Evidence for an apical Na–Cl cotransporter involved in ion uptake in a teleost fish. *J Exp Biol* 211:2584-2599.
[90] Hwang P-P, Perry SF. 2010. 8 - Ionic and acid–base regulation. In Perry SF, Ekker M, Farrell AP, Colin JB, eds, *Fish Physiology*. Vol 29. Academic Press, San Diego, CA, pp 311-344.
[91] Wang Y-F, Tseng Y-C, Yan J-J, Hiroi J, Hwang P-P. 2009. Role of SLC12A10.2, a Na-Cl cotransporter-like protein, in a Cl uptake mechanism in zebrafish (*Danio rerio*). *Am J Phys-Reg I* 296:R1650-R1660.
[92] Hwang P-P, Lee T-H, Lin L-Y. 2011. Ion regulation in fish gills: Recent progress in the cellular and molecular mechanisms. *Am J Phys-Reg I* 301:R28-R47.
[93] Lee Y-C, Yan J-J, Cruz SA, Horng J-L, Hwang P-P. 2011. Anion exchanger 1b, but not sodium-bicarbonate cotransporter 1b, plays a role in transport functions of zebrafish H^+-ATPase-rich cells. *Am J Physiol-Cell Ph* 300:C295-C307.
[94] Inokuchi M, Hiroi J, Watanabe S, Lee KM, Kaneko T. 2008. Gene expression and morphological localization of NHE3, NCC and NKCC1a in branchial mitochondria-rich cells of Mozambique tilapia (*Oreochromis mossambicus*) acclimated to a wide range of salinities. *Comp Biochem Phys A* 151:151-158.
[95] McDonald DG, Wood CM. 1981. Branchial and renal acid and ion fluxes in the rainbow trout, *Salmo gairdneri*, at low environmental pH. *J Exp Biol* 93:101-118.
[96] Hirata T, Kaneko T, Ono T, Nakazato T, Furukawa N, Hasegawa S, Wakabayashi S, Shigekawa M, Chang M-H, Romero MF, Hirose S. 2003. Mechanism of acid adaptation of a fish living in a pH 3.5 lake. *Am J Phys-Reg I* 284:R1199-R1212.
[97] Gonzalez RJ, Wood CM, Wilson RW, Patrick ML, Bergman HL, Narahara A, Val Adalberto L. 1998. Effects of water pH and calcium concentration on ion balance in fish of the Rio Negro, Amazon. *Physiol Zool* 71:15-22.
[98] Wilson RW, Wood CM, Gonzalez RJ, Patrick ML, Bergman HL, Narahara A, Val AL. 1999. Ion and acid-base balance in three species of Amazonian fish during gradual acidification of extremely soft water. *Physiol Biochem Zool* 72:277-285.
[99] Gonzalez RJ, Preest MR. 1999. Ionoregulatory specializations for exceptional tolerance of ion-poor, acidic waters in the neon tetra (*Paracheirodon innesi*). *Physiol Biochem Zool* 72:156-163.
[100] Gonzalez Richard J, Dalton Valerie M, Patrick Marjorie L. 1997. Ion regulation in ion-poor acidic water by the blackskirt tetra (*Gymnocorymbus ternetzi*), a fish native to the Amazon River. *Physiol Zool* 70:428-435.
[101] Wood CM, Robertson LM, Johannsson OE, Val AL. 2014. Mechanisms of Na^+ uptake, ammonia excretion, and their potential linkage in native Rio Negro tetras (*Paracheirodon axelrodi*, *Hemigrammus rhodostomus*, and *Moenkhausia diktyota*). *J Comp Phys B* 184:877-890.
[102] Gonzalez RJ, Wilson RW, Wood CM, Patrick ML, Val AL. 2002. Diverse strategies for ion regulation in fish collected from the ion-poor, acidic Rio Negro. *Physiol Biochem Zool* 75:37-47.

[103] Freda J, McDonald DG. 1988. Physiological correlates of interspecific variation in acid tolerance in fish. *J Exp Biol* 136:243-258.
[104] Gonzalez RJ, Dunson WA. 1989. Acclimation of sodium regulation to low pH and the role of calcium in the acid-tolerant sunfish *Enneacanthus obesus*. *Physiol Zool* 62:977-992.
[105] Kumai Y, Bahubeshi A, Steele S, Perry SF. 2011. Strategies for maintaining Na^+ balance in zebrafish (Danio rerio) during prolonged exposure to acidic water. *Comp Biochem Phys A* 160:52-62.
[106] Gonzalez-Mariscal L, Contreras RG, Bolivar JJ, Ponce A, Chavez de Ramirez B, Cereijido M. 1990. Role of calcium in tight junction formation between epithelial cells. *Am J Physiol-Cell Ph* 259:C978-C986.
[107] Stuart RO, Sun A, Panichas M, Hebert SC, Brenner BM, Nigam SK. 1994. Critical role for intracellular calcium in tight junction biogenesis. *Journal of Cellular Physiology* 159:423-433.
[108] McWilliams PG. 1982. The effects of calcium on sodium fluxes in the brown trout, *Salmo trutta*, in neutral and acid water. *J Exp Biol* 96:439-442.
[109] McDonald DG. 1983. The interaction of environmental calcium and low pH on the physiology of the rainbow trout, *Salmo gairdneri*: I. Branchial and renal net ion and H^+ fluxes. *J Exp Biol* 102:123-140.
[110] Frain WJ. 1987. The Effect of external sodium and calcium concentrations on sodium fluxes by salt-depleted and non-depleted minnows, *Phoxinus phoxinus* (L.). *J Exp Biol* 131:417-425.
[111] Wood CM, Rogano MS. 1986. Physiological responses to acid stress in crayfish (*Orconectes*): Haemolymph ions, acid–base status, and exchanges with the environment. *Can J Fish Aquat Sci* 43:1017-1026.
[112] Jensen FB, Malte H. 1990. Acid-base and electrolyte regulation, and haemolymph gas transport in crayfish, *Astacus astacus*, exposed to soft, acid water with and without aluminium. *J Comp Phys B* 160:483-490.
[113] Potts WTW, Fryer G. 1979. The effects of pH and salt content on sodium balance in *Daphina magna* and *Acantholeberis curvirostris* (Crustacea: Cladocera). *J Comp Phys B* 129:289-294.
[114] Hollett L, Berrill M, Rowe L. 1986. Variation in major ion concentration of *Cambarus robustus* and *Orconectes rusticus* following exposure to low pH. *Can J Fish Aquat Sci* 43:2040-2044.
[115] Ellis BA, Morris S. 1995. Effects of extreme pH on the physiology of the Australian 'yabby' *Cherax destructor*: acute and chronic changes in haemolymph carbon dioxide, acid-base and ionic status. *J Exp Biol* 198:395-407.
[116] Patrick ML, Ferreira RL, Gonzalez RJ, Wood CM, Wilson RW, Bradley TJ, Val AL. 2002. Ion regulatory patterns of mosquito larvae collected from breeding sites in the Amazon rain forest. *Physiol Biochem Zool* 75:215-222.
[117] Havas M, Hutchinson TC. 1983. Effect of low pH on the chemical composition of aquatic invertebrates from tundra ponds at the Smoking Hills, N.W.T., Canada. *Can J Zool* 61:241-249.
[118] Rowe L, Berrill M, Hollett L. 1988. The influence of season and pH on mortality, molting and whole-body ion concentrations in nymphs of the mayfly *Stenonema femoratum*. *Comp Biochem Phys A* 90:405-408.
[119] Rowe L, Berrill M, Hollett L, Hall RJ. 1989. The effects of short-term laboratory pH depressions on molting, mortality and major ion concentrations in the mayflies *Stenonema femoratum* and *Leptophlebia cupida*. *Hydrobiologia* 184:89-97.
[120] Twitchen ID. 1990. The physiological bases of resistance to low pH among aquatic insect larvae. In Mason BJ, ed, *The Surface Waters Acidification Programme*. Press Syndicate of the University of Cambridge, Cambridge, U.K., pp 413-418.
[121] Lechleitner RA, Cherry DS, Cairns J, Jr., Stetler DA. 1985. Ionoregulatory and toxicological responses of stonefly nymphs (Plecoptera) to acidic and alkaline pH. *Arch Environ Contam Toxicol* 14:179-185.
[122] Whipple AV, Dunson WA. 1993. Amelioration of the toxicity of H^+ to larval stoneflies by metals found in coal mine effluent. *Arch Environ Contam Toxicol* 24:194-200.

[123] Rockwood JP, Coler RA, Chih-Ming Y. 1988. The effect of aluminum in soft water at low pH on osmoregulation and ionic balance in the dragonfly *Libellula julia* Uhler. *Comp Biochem Physiol C* 91:499-502.
[124] Rockwood JP, Coler RA. 1991. The effect of aluminum in soft water at low pH on water balance and hemolymph ionic and acid-base regulation in the dragonfly *Libellula julia* Uhler. *Hydrobiologia* 215:243-250.
[125] Pynnönen K. 1990. Physiological responses to severe acid stress in 4 species of freshwater clams (Unionidae). *Arch Environ Contam Toxicol* 19:471-478.
[126] Bury NR, Wood CM. 1999. Mechanism of branchial apical silver uptake by rainbow trout is via the proton-coupled Na+channel. *Am J Phys-Reg I* 277:R1385-R1391.
[127] Grosell M, Wood CM. 2002. Copper uptake across rainbow trout gills: Mechanisms of apical entry. *J Exp Biol* 205:1179-1188.
[128] Goss GG, Gilmour K, Hawkings G, Brumbach JH, Huynh M, Galvez F. 2011. Mechanism of sodium uptake in PNA negative MR cells from rainbow trout, *Oncorhynchus mykiss* as revealed by silver and copper inhibition. *Comp Biochem Phys A* 159:234-241.
[129] Pyle GG, Kamunde CN, McDonald DG, Wood CM. 2003. Dietary sodium inhibits aqueous copper uptake in rainbow trout (*Oncorhynchus mykiss*). *J Exp Biol* 206:609-618.
[130] Kamunde CN, Grosell M, Lott JNA, Wood CM. 2001. Copper metabolism and gut morphology in rainbow trout (*Oncorhynchus mykiss*) during chronic sublethal dietary copper exposure. *Can J Fish Aquat Sci* 58:293-305.
[131] Galvez F, Wood CM. 2002. The mechanisms and costs of physiological and toxicological acclimation to waterborne silver in juvenile rainbow trout (*Oncorhynchus mykiss*). *J Comp Physiol B Biochem System Environ Physiol* 172:587-597.
[132] Laurén DJ, McDonald DG. 1986. Influence of water hardness, pH, and alkalinity on the mechanisms of copper toxicity in juvenile rainbow trout, *Salmo gairdneri*. *Can J Fish Aquat Sci* 43:1488-1496.
[133] Welsh PG, Skidmore JF, Spry DJ, Dixon DG, Hodson PV, Hutchinson NJ, Hickie BE. 1993. Effect of pH and dissolved organic carbon on the toxicity of copper to larval fathead minnow (*Pimephales promelas*) in natural lake waters of low alkalinity. *Can J Fish Aquat Sci* 50:1356-1362.
[134] Bianchini A, Grosell M, Gregory SM, Wood CM. 2002. Acute silver toxicity in aquatic animals is a function of sodium uptake rate. *Environ Sci Technol* 36:1763-1766.
[135] Grosell M, Gerdes RM, Brix KV. 2006. Chronic toxicity of lead to three freshwater invertebrates—*Brachionus calyciflorus*, *Chironomus tentans*, and *Lymnaea stagnalis*. *Environ Toxicol Chem* 25:97-104.
[136] Hemelraad J, Holwerda DA, Wijnne HJA, Zandee DI. 1990. Effects of cadmium in freshwater clams. I. Interaction with essential elements in *Anodonta cygnea*. *Arch Environ Contam Toxicol* 19:686-690.
[137] Lopes-Lima M, Freitas S, Pereira L, Gouveia E, Hinzmann M, Checa A, Machado J. 2012. Ionic regulation and shell mineralization in the bivalve *Anodonta cygnea* (swan mussel) following heavy-metal exposure. *Can J Zool* 90:267-283.
[138] Brix KV, Esbaugh AJ, Grosell M. 2011. The toxicity and physiological effects of copper on the freshwater pulmonate snail, *Lymnaea stagnalis*. *Comp Biochem Physiol C* 154:261-267.
[139] Gramigni E, Tadini-Buoninsegni F, Bartolommei G, Santini G, Chelazzi G, Moncelli MR. 2009. Inhibitory effect of Pb^{2+} on the transport cycle of the Na^+,K^+-ATPase. *Chem Res Toxicol* 22:1699-1704.
[140] Rogers JT, Patel M, Gilmour KM, Wood CM. 2005. Mechanisms behind Pb-induced disruption of Na^+ and Cl^- balance in rainbow trout (*Oncorhynchus mykiss*). *Am J Phys-Reg I* 289:R463-R472.
[141] Gillis PL, Wood CM. 2008. The effect of extreme waterborne cadmium exposure on the internal concentrations of cadmium, calcium, and sodium in *Chrionomus riparius* larvae. *Ecotoxicol Environ Saf* 71:56-74.

[142] Craig A, Hare L, Tessier A. 1999. Experimental evidence for cadmium uptake via calcium channels in the aquatic insect *Chironomus staegeri*. *Aquat Toxicol* 44:255-262.
[143] Croghan PC, Curra RA, Lockwood APM. 1965. The electrical potential difference across the epithelium of isolated gills of the crayfish *Austropotamobius pallipes* (Lereboullet). *J Exp Biol* 42:463-474.
[144] Harvey WR. 1992. Physiology of V-ATPases. *J Exp Biol* 172:1-17.
[145] Wieczorek H. 1992. The insect V-ATPase, a plasma membrane proton pump energizing secondary active transport: molecular analysis of electrogenic potassium transport in the tobacco hornworm midgut. *J Exp Biol* 172:335-343.
[146] Boudko DY, Moroz LL, Linser PJ, Trimarchi JR, Smith PJ, Harvey WR. 2001. In situ analysis of pH gradients in mosquito larvae using non-invasive, self-referencing, pH-sensitive microelectrodes. *J Exp Biol* 204:691-699.
[147] Smith KE, VanEkeris LA, Linser PJ. 2007. Cloning and characterization of AgCA9, a novel α-carbonic anhydrase from *Anopheles gambiae* Giles sensu stricto (Diptera: Culicidae) larvae. *J Exp Biol* 210:3919-3930.
[148] O'Donnell MJ, Maddrell SHP. 1983. Paracellular and transcellular routes for water and solute movements across insect epithelia. *J Exp Biol* 106:231-253.
[149] Dietz TH, Lessard D, Silverman H, Lynn JW. 1994. Osmoregulation in *Dreissena polymorpha*: the importance of Na, Cl, K, and particularly Mg. *Biol Bull* 187:76-83.
[150] Dietz TH, Wilcox SJ, Byrne RA, Lynn JW, Silverman H. 1996. Osmotic and ionic regulation of North American zebra mussels (*Dreissena polymorpha*). *Am Zool* 36:364-372.
[151] Dietz TH, Neufeld DH, Silverman H, Wright SH. 1998. Cellular volume regulation in freshwater bivalves. *J Comp Phys B* 168:87-95.
[152] Dietz TH, Byrne RA. 1990. Potassium and rubidium uptake in freshwater bivalves. *J Exp Biol* 150:395-405.
[153] Wilcox SJ, Dietz TH. 1995. Potassium transport in the freshwater bivalve Dreissena polymorpha. *J Exp Biol* 198:861-868.
[154] Byrne RA, Dietz TH. 1997. Ion transport and acid-base balance in freshwater bivalves. *J Exp Biol* 200:457-465.
[155] Cleveland L, Little EE, Ingersoll CG, Wiedmeyer RH, Hunn JB. 1991. Sensitivity of brook trout to low pH, low and elevated aluminum concentrations during laboratory pulse exposures. *Aquat Toxicol* 19:303-317.
[156] Saito K, Nakamura N, Ito Y, Hoshijima K, Esaki M, Zhao B, Hirose S. 2010. Identification of zebrafish FXYD11a protein that is highly expressed in ion-transporting epithelium of the gill and skin and its possible role in ion homeostasis. *Front Physiol* 1:129.
[157] Craig PM, Wood CM, McClelland GB. 2007. Gill membrane remodeling with soft-water acclimation in zebrafish (*Danio rerio*). *Physiol Genomics* 30:53-60.
[158] Shahsavarani A, Perry SF. 2006. Hormonal and environmental regulation of epithelial calcium channel in gill of rainbow trout (*Oncorhynchus mykiss*). *Am J Phys-Reg I* 291:R1490-R1498.
[159] Galvez F, Wong D, Wood CM. 2006. Cadmium and calcium uptake in isolated mitochondria-rich cell populations from the gills of the freshwater rainbow trout. *Am J Phys-Reg I* 291:R170-R176.
[160] Perry SF, Shahsavarani A, Georgalis T, Bayaa M, Furimsky M, Thomas SLY. 2003. Channels, pumps, and exchangers in the gill and kidney of freshwater fishes: Their role in ionic and acid-base regulation. *J Exp Zool Part A* 300A:53-62.
[161] Bucking C, Wood CM. 2007. Gastrointestinal transport of Ca^{2+} and Mg^{2+} during the digestion of a single meal in the freshwater rainbow trout. *J Comp Phys B* 177:349-360.
[162] Baldisserotto B, Chowdhury MJ, Wood CM. 2005. Effects of dietary calcium and cadmium on cadmium accumulation, calcium and cadmium uptake from the water, and their interactions in juvenile rainbow trout. *Aquat Toxicol* 72:99-117.

[163] Baldisserotto B, Kamunde C, Matsuo AYO, Wood CM. 2004. Acute waterborne cadmium uptake in rainbow trout is reduced by dietary calcium carbonate. *Comp Biochem Physiol C Toxicol Pharmacol* 137:363-372.
[164] Baldisserotto B, Kamunde C, Matsuo AYO, Wood CM. 2004. A protective effect of dietary calcium against acute waterborne cadmium uptake in rainbow trout. *Aquat Toxicol* 67:57-73.
[165] Verbost PM, Flik G, Fenwick JC, Greco A-M, Pang PKT, Wendelaar Bonga SE. 1993. Branchial calcium uptake: Possible mechanisms of control by stanniocalcin. *Fish Physiol Biochem* 11:205-215.
[166] Barkai AI, Williams RW. 1983. The exchange of calcium in larvae of the mosquito *Aedes aegypti*. *J Exp Biol* 104:139-148.
[167] Donini A, O'Donnell MJ. 2005. Analysis of Na^+, Cl^-, K^+, H^+ and NH_4^+ concentration gradients adjacent to the surface of anal papillae of the mosquito *Aedes aegypti*: application of self-referencing ion-selective microelectrodes. *J Exp Biol* 208:603-610.
[168] Wigglesworth VB. 1933. The effect of salts on the anal gills of the mosquito larva. *J Exp Biol* 10:1-14.
[169] Byrne RA, Dietz TH. 2006. Ionic and acid-base consequences of exposure to increased salinity in the zebra mussel, *Dreissena polymorpha*. *Biol Bull* 211:66-75.
[170] Pietrzak JE, Bates JM, Scott RM. 1976. Constituents of unionid extrapallial fluid. II. pH and metal ion composition. *Hydrobiologia* 50:89-93.
[171] Taylor HH. 1977. The ionic and water relations of embryos of *Lymnaea stagnalis*, A feshwater pulmonate mollusc. *J Exp Biol* 69:143-172.
[172] Ebanks SC, O'Donnell MJ, Grosell M. 2010. Characterization of mechanisms for Ca^{2+} and HCO_3^-/CO_3^{2-} acquisition for shell formation in embryos of the freshwater common pond snail *Lymnaea stagnalis*. *J Exp Biol* 213:4092-4098.
[173] Ahearn GA, Mandal PK, Mandal A. 2001. Biology of the $2Na^+/1H^+$ antiporter in invertebrates. *J Exp Zool* 289:232-244.
[174] Verbost PM, Flik G, Lock RAC, Wendelaar Bonga SE. 1988. Cadmium inhibits plasma membrane calcium transport. *J Membr Biol* 102:97-104.
[175] Hogstrand C, Verbost PM, Bonga SE, Wood CM. 1996. Mechanisms of zinc uptake in gills of freshwater rainbow trout: Interplay with calcium transport. *Am J Phys-Reg I* 270:R1141-R1147.
[176] Niyogi S, Wood CM. 2004. Kinetic analyses of waterborne Ca and Cd transport and their interactions in the gills of rainbow trout (*Oncorhynchus mykiss*) and yellow perch (*Perca flavescens*), two species differing greatly in acute waterborne Cd sensitivity. *J Comp Phys B* 174:243-253.
[177] Bjerregaard P, Depledge MH. 1994. Cadmium accumulation in *Littorina littorea*, *Mytilus edulis* and *Carcinus maenas*: The influence of salinity and calcium ion concentrations. *Mar Biol* 119:385-395.
[178] Pedersen TV, Bjerregaard P. 1995. Calcium and cadmium fluxes across the gills of the shore crab, *Carcinus maenas*. *Mar Pollut Bull* 31:73-77.
[179] Bondgaard M, Bjerregaard P. 2005. Association between cadmium and calcium uptake and distribution during the moult cycle of female shore crabs, *Carcinus maenas*: An in vivo study. *Aquat Toxicol* 72:17-28.
[180] Wright DA. 1977. The effect of calcium on cadmium uptake by the shore crab *Carcinus maenas*. *J Exp Biol* 67:163-173.
[181] Clifford M, McGeer JC. 2010. Development of a biotic ligand model to predict the acute toxicity of cadmium to *Daphnia pulex*. *Aquat Toxicol* 98:1-7.
[182] Leonard EM, Pierce LM, Gillis PL, Wood CM, O'Donnell MJ. 2009. Cadmium transport by the gut and Malpighian tubules of *Chironomus riparius*. *Aquat Toxicol* 92:179-186.
[183] Buchwalter DB, Luoma SN. 2004. Differences in dissolved cadmium and zinc uptake among stream insects: Mechanistic explanations. *Environ Sci Technol* 39:498-504.

[184] Poteat MD, Buchwalter DB. 2014. Calcium uptake in aquatic insects: influences of phylogeny and metals (Cd and Zn). *J Exp Biol* 217:1180-1186.
[185] Poteat MD, Díaz-Jaramillo M, Buchwalter DB. 2012. Divalent metal (Ca, Cd, Mn, Zn) uptake and interactions in the aquatic insect *Hydropsyche sparna*. *J Exp Biol* 215:1575-1583.
[186] Markich SJ, Jeffree RA. 1994. Absorption of divalent trace metals as analogues of calcium by Australian freshwater bivalves: an explanation of how water hardness reduces metal toxicity. *Aquat Toxicol* 29:257-290.
[187] Wang Y, Evans RD. 1993. Influence of calcium concentrations on cadmium uptake by the freshwater mussel *Ellptio complanata*. *Can J Fish Aquat Sci* 50:2591-2596.
[188] Brix KV, Esbaugh AJ, Munley KM, Grosell M. 2012. Investigations into the mechanism of lead toxicity to the freshwater pulmonate snail, *Lymnaea stagnalis*. *Aquat Toxicol* 106–107:147-156.
[189] Grosell M, Brix KV. 2009. High net calcium uptake explains the hypersensitivity of the freshwater pulmonate snail, Lymnaea stagnalis, to chronic lead exposure. *Aquat Toxicol* 91:302-311.
[190] de Schamphelaere KAC, Koene JM, Heijerick DG, Janssen CR. 2008. Reduction of growth and haemolymph Ca levels in the freshwater snail *Lymnaea stagnalis* chronically exposed to cobalt. *Ecotoxicol Environ Saf* 71:65-70.
[191] Ngo HTT, Gerstmann S, Frank H. 2011. Subchronic effects of environment-like cadmium levels on the bivalve *Anodonta anatina* (Linnaeus 1758): I. Bioaccumulation, distribution and effects on calcium metabolism. *Toxicol Environ Chem* 93:1788-1801.
[192] Faubel D, Lopes-Lima M, Freitas S, Pereira L, Andrade J, Checa A, Frank H, Matsuda T, Machado J. 2008. Effects of Cd^{2+} on the calcium metabolism and shell mineralization of bivalve *Anodonta cygnea*. *Mar Freshwat Behav Physiol* 41:131-146.
[193] Lopes-Lima M, Bleher R, Forg T, Hafner M, Machado J. 2008. Studies on a PMCA-like protein in the outer mantle epithelium of *Anodonta cygnea*: insights on calcium transcellular dynamics. *J Comp Phys B* 178:17-25.
[194] Présing M, V.-Balogh K, Salánki J. 1993. Cadmium uptake and depuration in different organs of *Lymnaea stagnalis* L. and the effect of cadmium on the natural zinc level. *Arch Environ Contam Toxicol* 24:28-34.
[195] van der Velden JA, Flik G, Spanings FAT, Verburg TG, Kolar ZI, Wendelaar Bonga SE. 1992. Physiological effects of low-magnesium feeding in the common carp, *Cyprinus carpio*. *J Exp Zool* 264:237-244.
[196] van der Velden JA, Flik G, Wendelaar Bonga SE. 1992. Prolactin cell activity and ion regulation in tilapia, *Oreochromis mossambicus* (Peters): Effects of a low magnesium diet. *J Fish Biol* 40:875-885.
[197] van der Velden JA, Spanings FAT, Flik G, Zegers C, Kolar Z, Wendelaar Bonga SE. 1991. Growth rate and tissue magnesium concentration in adult freshwater tilapia, *Oreochromis mossambicus* (Peters), fed diets differing in magnesium content. *J Fish Biol* 39:83-91.
[198] Bijvelds MJC, Flik G, Kolar ZI, Wendelaar Bonga SE. 1996. Uptake, distribution and excretion of magnesium in *Oreochromis mossambicus*: Dependence on magnesium in diet and water. *Fish Physiol Biochem* 15:287-298.
[199] Shearer KD, Åsgård T. 1992. The effect of water-borne magnesium on the dietary magnesium requirement of the rainbow trout (*Oncorhynchus mykiss*). *Fish Physiol Biochem* 9:387-392.
[200] Perry SF, Vulesevic B, Grosell M, Bayaa M. 2009. Evidence that SLC26 anion transporters mediate branchial chloride uptake in adult zebrafish (*Danio rerio*). *Am J Phys-Reg I* 297:R988-R997.
[201] Gilmour KM, Perry SF. 2009. Carbonic anhydrase and acid–base regulation in fish. *J Exp Biol* 212:1647-1661.
[202] Lin T-Y, Liao B-K, Horng J-L, Yan J-J, Hsiao C-D, Hwang P-P. 2008. Carbonic anhydrase 2-like a and 15a are involved in acid-base regulation and Na^+ uptake in zebrafish H^+-ATPase-rich cells. *Am J Physiol-Cell Ph* 294:C1250-C1260.

[203] Tresguerres M, Katoh F, Orr E, Parks SK, Goss Greg G. 2006. Chloride uptake and base secretion in freshwater fish: A transepithelial ion-transport metabolon? *Physiol Biochem Zool* 79:981-996.
[204] Hawkings GS, Galvez F, Goss GG. 2004. Seawater acclimation causes independent alterations in Na^+/K^+- and H^+-ATPase activity in isolated mitochondria-rich cell subtypes of the rainbow trout gill. *J Exp Biol* 207:905-912.
[205] Barradas C, Dunel-Erb S, Lignon J, Péqueux A. 1999. Superimposed morphofunctional study of ion regulation and respiration in single gill filaments of the crayfish *Astacus leptodactylus*. *J Crust Biol* 19:14-25.
[206] Dunel-Erb S, Barradas C, Lignon J. 1997. Morphological evidence for the existence of two distinct types of mitochondria rich cells in the gill of the crayfish *Astacus leptodactylus* Eschscholtz. *Acta Zool* 78:195-203.
[207] Barradas C, Wilson JM, Dunel-Erb S. 1999. Na^+/K^+-ATPase activity and immunocytochemical labeling in podobranchial filament and lamina of the freshwater crayfish *Astacus leptodactylus* Eschscholtz: evidence for the existence of sodium transport in the filaments. *Tissue Cell* 31:523-528.
[208] Stobbart RH. 1967. The effect of some anions and cations upon the fluxes and net uptake of chloride in the larva of *Aedes aegypti* (L.), and the nature of the uptake mechanisms for sodium and chloride. *J Exp Biol* 47:35-57.
[209] Scheide JI, Dietz TH. 1982. The effects of independent sodium and chloride depletion on ion balance in freshwater mussels. *Can J Zool* 60:1676-1682.
[210] Höbe H, Wood CM, McMahon BR. 1984. Mechanisms of acid-base and ionoregulation in white suckers (*Catostomus commersoni*) in natural soft water. 1. Acute exposure to low ambient pH. *J Comp Phys B* 154:35-46.
[211] Felten V, Guerold F. 2004. Haemolymph Na^+ and Cl^- loss in *Gammarus fossarum* exposed in situ to a wide range of acidic streams. *Dis Aquat Org* 61:113-121.
[212] Wilkie MP, Wood CM. 1994. The effects of extremely alkaline water (pH 9·5) on rainbow trout gill function and morphology. *J Fish Biol* 45:87-98.
[213] Wilkie MP, Laurent P, Wood CM. 1999. The physiological basis for altered Na^+ and Cl^- movements across the gills of rainbow trout (*Oncorhynchus mykiss*) in alkaline (pH = 9.5) water. *Physiol Biochem Zool* 72:360-368.
[214] McGeer James C, Eddy FB. 1998. Ionic regulation and nitrogenous excretion in rainbow trout exposed to buffered and unbuffered freshwater of pH 10.5. *Physiol Zool* 71:179-190.
[215] Harris RR, Coley S. 1991. The effects of nitrite on chloride regulation in the crayfish *Pacifastacus leniusculus* Dana (Crustacea: Decapoda). *J Comp Phys B* 161:199-206.
[216] Jensen FB. 1996. Uptake, elimination and effects of nitrite and nitrate in freshwater crayfish (*Astacus astacus*). *Aquat Toxicol* 34:95-104.
[217] Stormer J, Jensen FB, Rankin JC. 1996. Uptake of nitrite, nitrate, and bromide in rainbow trout, (*Oncorhynchus mykiss*): effects on ionic balance. *Can J Fish Aquat Sci* 53:1943-1950.
[218] Claiborne JB, Heisler N. 1984. Acid-base regulation and ion transfers in the carp (*Cyprinus carpio*) during and after exposure to environmental hypercapnia. *J Exp Biol* 108:25-43.
[219] Cameron JN, Iwama GK. 1987. Compensation of progressive hypercapnia in channel catfish and blue crabs. *J Exp Biol* 133:183-197.
[220] Goss GG, Perry SF. 1993. Physiological and morphological regulation of acid–base status during hypercapnia in rainbow trout (*Oncorhynchus mykiss*). *Can J Zool* 71:1673-1680.
[221] Hyde DA, Perry SF. 1989. Differential approaches to blood acid-base regulation during exposure to prolonged hypercapnia in two freshwater teleosts: the rainbow trout (*Salmo gairdneri*) and the American eel (*Anguilla rostrata*). *Physiol Zool* 62:1164-1186.

[222] Goss GG, Perry SF. 1994. Different mechanisms of acid-base regulation in rainbow trout (*Oncorhynchus mykiss*) and American eel (*Anguilla rostrata*) during $NaHCO_2$ infusion. *Physiol Zool* 67:381-406.
[223] Cameron JN, Kormanik GA. 1982. The acid-base responses of gills and kidneys to infused acid and base loads in the channel catfish, *Ictalurus punctatus*. *J Exp Biol* 99:143-160.
[224] Wheatly MG, Toop T. 1989. Physiological responses of the crayfish *Pacifastacus leniusculus* to environmental hyperoxia: II. Role of the antennal gland in acid-base and ion regulation. *J Exp Biol* 143:53-70.
[225] Wheatly MG, Toop T, Morrison RJ, Yow LC. 1991. Physiological responses of the crayfish *Pacifastacus leniusculus* (Dana) to environmental hyperoxia. III. Intracellular acid-base balance. *Physiol Zool* 64:323-343.
[226] Henry RP, Saintsing DG. 1983. Carbonic anhydrase activity and ion regulation in three species of osmoregulating bivalve molluscs. *Physiol Zool* 56:274-280.
[227] Ngo HTT, Gerstmann S, Frank H. 2011. Subchronic effects of environment-like cadmium levels on the bivalve *Anodonta anatina* (Linnaeus 1758): III. Effects on carbonic anhydrase activity in relation to calcium metabolism. *Toxicol Environ Chem* 93:1815-1825.
[228] Istin M, Girard JP. 1970. Dynamic state of calcium reserves in freshwater clam mantle. *Calc Tiss Res* 5:196-205.
[229] Larsen EH, Simonsen K. 1988. Sulfate transport in toad skin: Evidence for mitochondria-rich cell pathways in common with halide ions. *Comp Biochem Phys A* 90:709-714.
[230] Dietz TH, Byrne RA. 1999. Measurement of sulfate uptake and loss in the freshwater bivalve *Dreissena polymorpha* using a semi-microassay. *Can J Zool* 77:331-336.

UNITED STATES ENVIRONMENTAL PROTECTION AGENCY
Center for Environmental Measurement & Modeling
Cincinnati, OH 45268

OFFICE OF
RESEARCH AND DEVELOPMENT

April 14, 2020

MEMORANDUM

SUBJECT: Record of Percentage Agreement - Michael B. Griffith

FROM: Michael B. Griffith, Ph.D.
Ecologist

With reference to the 2020 STAA nomination for the following publication:

Griffith M.B. 2017. Toxicological perspective on the osmoregulation and ionoregulation physiology of major ions by freshwater animals: Teleost fish, Crustacea, aquatic insects and Mollusca. *Environmental Toxicology and Chemistry* 36(3):576-600. DOI: 10.1002/etc.3676.

As the sole author of this publication, I agree to the 100% of Total Effort stated in the nomination.

Papers that cite Griffith, M. B. 2017. Toxicological perspective on the osmoregulation and ionoregulation physiology of major ions by freshwater animals: Teleost fish, Crustacea, aquatic insects and Mollusca. *Environmental Toxicology and Chemistry* 36(3):576-600. DOI: 10.1002/etc.3676.

34 journal articles, 1 book chapter, 7 theses or dissertations

Baker, M. E., M. L. Schley, and J. O. Sexton. 2019. Impacts of expanding impervious surface on specific conductance in urbanizing streams. *Water Resources Research* 55(8):6482-6498. DOI: 10.1029/2019WR025014.

Browne, A. A. 2018. Calcium transport by insect Malpighian tubules. Ph. D. Thesis, McMaster University, Hamilton, Ontario, Canada.

Calcino, A. D., A. L. de Oliveira, O. Simakov, T. Schwaha, E. Zieger, T. Wollesen, and A. Wanninger. 2019. The quagga mussel genome and the evolution of freshwater tolerance. *DNA Research* 26(5):411-411. DOI: 10.1093/dnares/dsz019

Cañedo-Argüelles Inglesias, M. A review of recent advances and future challenges in freshwater salinization. *Limnetica* 39(1):185-211. DOI: 10.23818/limn.39.13.

Carambelas, E. E. 2018. Monitoring the effectiveness of stormwater control measures on reversing deteriorated stream functions in an urban setting. M. S. Thesis, Villanova University, Villanova, Pennsylvania.

Carter, M. J., M. Flores, and R. Ramos-Jiliberto. 2020. Geographical origin determines responses to salinity of Mediterranean caddisflies. *PLoS One* 15(1): e0220275. DOI: 10.1371/journal.pone.0220275.

Ciparis, S., G. Rhyne, and T. Stephenson. 2019. Exposure to elevated concentrations of major ions decreases condition index of freshwater mussels: Comparison of metrics. *Freshwater Mollusk Biology and Conservation* 22(2):98-108.

Cormier, S. M., L. Zheng, and C. M. Flaherty. 2018. A field-based model of the relationship between extirpation of salt-intolerant benthic invertebrates and background conductivity. *Science of the Total Environment* 633:1629-1636. DOI: 10.1016/j.scitotenv.2018.02.044.

Cormier, S. M., L. Zheng, G. Hayslip, and C. M. Flaherty. 2018. A field-based characterization of conductivity in areas of minimal alteration. A case example in the Cascades of northwestern United States. *Science of the Total Environment* 633: 1657-1666. DOI: 10.1016/j.scitotenv.2018.02.018.

Cormier, S. M., L. Zheng, R. A. Hill, R. M. Novak, and C. M. Flaherty. 2018. A flow-chart for developing water quality criteria from two field-based methods. *Science and the Total Environment* 633:1647-1656. DOI: 10.1016/j.scitotenv.2018.10.137.

Dowse, R., C. G. Palmer, K. Hills, F. Torpy, and B. J. Kefford. 2017. The mayfly nymph *Austrophlebioides pusillus* Harker defies common osmoregulatory assumptions. *Royal Society Open Science* 4(1):160520. DOI: 10.1098/rsos.160520.

Drover, D. R. 2018. Benthic macroinvertebrate community structure responses to multiple stressors in mining-influenced streams of central Appalachia, U.S.A. Ph. D. Dissertation, Virginia Polytechnic Institute and State University, Blacksburg, Virginia.

Drover, D. R., S. H. Schoenholtz, D. J. Soucek, and C. E. Zipper. 2020. Multiple stressors influence benthic macroinvertebrate communities in central Appalachian coalfield streams. *Hydrobiologia* 847:191-205. DOI: 10.1007/s10750-019-04081-4.

Drover, D. R., C. E. Zipper, D. J. Soucek, and S. H. Schoenholtz. 2019. Using density, dissimilarity, and taxonomic replacement to characterize mining-influenced benthic macroinvertebrate community alterations in central Appalachia. *Ecological Indicators* 106:105535. DOI:10.1016/j.ecolind.2019.105535.

Edmunds, S. M. 2018. The effects of coal ash storage facilities on aquatic biota. M. S. Thesis, University of Maryland, College Park, Maryland

Entrekin, S. A., N. A. Clay, A. Mogilevski, B. Howard-Parker, and M. A. Evans-White. 2018. Multiple riparian–stream connections are predicted to change in response to salinization. *Philosophical Transactions of the Royal Society B. Biological Sciences* 374:20180042. DOI:10.1098/rstb.2018.0042.

Fair, H. L. 2017. Ecology of aquatic insects in monsoonal temperate glacier streams of Southeast Tibet: A departure from the conceptual model. Ph.D. Dissertation, Ohio State University, Columbus, Ohio.

Fanelli, R. M., K. L. Prestegaard and M.A. Palmer. 2019. Urban legacies: Aquatic stressors and low aquatic biodiversity persist despite implementation of regenerative stormwater conveyance systems. *Freshwater Science* 38(4):818-833. DOI: 10.1086/706072

Ferrer, M. L. N., C. López, D. C. M. Hernández, G. Pares, J. M. M. Marcano, M. S. M. Serpa, and R. Sánchez. 2018. Tolerancia máxima a la salinidad del gasterópodo *Pyrgophorus platyrachis* (Littorinimorpha: Cochliopidae) de la Laguna Las Peonías, Sistema de Maracaibo, Venezuela Afiliación actual. *Ecotropicos* 30(E0004):1-8.

Griffith, M. B., L. Zheng, and S. M. Cormier. 2018. Using extirpation to evaluate ionic tolerance of freshwater fish: Fish tolerance for freshwater ionic concentration. *Environmental Toxicology and Chemistry* 37(3):871-883. DOI: 10.1002/etc.4022.

Jeffree, R. A., S. J Markich, F. Oberhaensli and J.-L. Teyssie. 2017. Radionuclide biokinetics in the Russian sturgeon and phylogenetic consistencies with cartilaginous and bony marine fishes. *Journal of Environmental Radioactivity* 177:266-279. DOI: 10.1016/j.jenvrad.2017.06.007.

Jeffrey, J. D., K. D. Hannan, C. T. Hasler and C. D. Suski. 2018. Hot and bothered: The effects of elevated pCO_2 and temperature on juvenile freshwater mussels. *American Journal of Physiology. Regulatory Integrative and Comparative Physiology* 315(1):R115-R127. DOI: 10.1152/ajpregu.00238.2017.

Kefford, B.J. 2018. Why are mayflies (Ephemeroptera) lost following small increases in salinity? Three conceptual osmophysiological hypotheses. *Philosophical Transactions of the Royal Society B. Biological Sciences* 374:20180021. DOI: 10.1098/rstb.2018.0021.

Kleinhenz, L. S., D. Nugegoda, M. A. Threnfield, R. A. van Dam, C. L. Humphrey, T. J. Mooney and A. J. Harford. Acute and chronic toxicity of magnesium to the early life states of two trophic freshwater mussel species. *Ecotoxicology and Environmental Safety* 184:109638. DOI: 10.1016/j.ecoenv.2019.109638.

Koroiva, R. and M. Pepinelli. 2019. Distribution and habitats of aquatic insects. Pages 11-23. In: K. Del Claro and R. Guillermo, editors. Aquatic Insects: Behavior and Ecology. Springer Nature Switzerland AG, Basel, Switzerland. DOI: 10.1007/978-3-030-16327-3.

Larson, M. D., J. C. Dewey and A. C. Krist. 2019. Invasive Potamopyrgus antipodarum (New Zealand mud snails) and native snails differ in sensitivity to specific electrical conductivity and cations. *Aquatic Ecology* 54:103-117. 10.1007/s10452-019-09729-w.

Leite, T., J. M. Santo, M. T. Ferreira, C. Canhoto and P. Branco. 2019. Does short-term salinization of freshwater alter the behaviour of the Iberian barbel (*Luciobarbus bocagei*, Steindachner 1864)? *Science of the Total Environment* 651(1):648-655. DOI: 10.1016/j.scitotenv.2018.09.191.

Leppänen, J., T. P. Luoto and J. Weckström. 2019. Spatio-temporal impact of salinated mine water on Lake Jormasjärvi, Finland. *Environmental Pollution* 247:1078-1088. DOI: 10.1016/j.envpol.2019.01.111.

Mangahas, R. S., R. L. Murray, and S. Mccauley. 2019. Chronic exposure to high concentrations of road salt decreases the immune response of dragonfly larvae. *Frontiers in Ecology and Evolution* 7:376. DOI: 10.3389/fevo.2019.00376.

Meina, E. G., K. Raes and K. Liber. 2019. Models for the acute and chronic aqueous toxicity of vanadium to *Daphnia pulex* under a range of surface water chemistry conditions. *Ecotoxicology and Environmental Safety* 179:301-309. DOI: 10.1016/j.ecoenv.2019.04.052.

Mohindra, V., T. Dangi, R. K. Tripathi, R. Kumar, R. K. Singh, J. K. Jena and T. Mohapatra. 2019. Draft genome assembly of *Tenualosa ilisha*, Hilsa shad, provides resource for osmoregulation studies. Scientific Reports 9:16511. DOI: 10.1038/s41598-019-52603-w.

Nowghanij, F. , C. C. Chen, S. Jonusaite, T. Watson-Leung, S. P. Kelly and A. Donini. 2019. Impact of salt-contaminated freshwater on osmoregulation and tracheal gill function in nymphs of the mayfly *Hexagenia rigida*. *Aquatic Toxicology* 211:92-104. DOI: 10.1016/j.aquatox.2019.03.019.

Nutile, S. A. and M. E. Solan. 2019. Toxicity testing of “eco-friendly” de-icing formulations using *Chironomus dilustus*. *Environmental Pollution* 246: 408-413. DOI: 10.1016/j.envpol.2018.12.033.

Pallarés, S. 2017. Ecological and evolutionary physiology of aquatic beetles: Coping with multiple natural stressors in inland saline waters. Ph.D. Thesis, University of Murcia, Murcia, Spain.

Pallarés, S., P. Arribas, D. T. Bilton, A. Millán, and I. Ribera. 2017. The chicken or the egg? Adaptation to desiccation and salinity tolerance in a lineage of water beetles. *Molecular Ecology* 26(20):5614-5628. DOI: 10.1111/mec.14334.

Pfenninger, M. and Q. Foucault. 2020. Genomic processes underlying rapid adaptation of a natural *Chironomus riparius* population to unintendedly applied experimental selection pressures. *Molecular Ecology* 29(3):536-548. DOI: 10.1111/mec.15347.

Pilehvar, A., R. M. Town and R. Blust. 2019. The effect of thermal pre-incubation and exposure on sensitivity of zebrafish (*Danio rerio*) to copper and cadmium single and binary exposures. *Aquatic Toxicology* 10:105226. DOI: 10.1016/j.aquatox.2019.105226.

Samani, H. E.-Z., M. Banaee, P. Shoukat, A. Noori, and L. M. Dehmoredi. 2017. Protective effects of dietary *Spirulina platensis* against cadmium-Induced oxidative stress in gills of rainbow trout. *Iranian Journal of Toxicology* 11(4):5-12. DOI:10.29252/arakmu.11.4.5.

Scheibener, S. A. 2017. Osmoregulatory physiology in aquatic insects: Implications for major ion toxicity in a saltier world. M. S. Thesis, North Carolina State University, Raleigh, North Carolina.

Scheibener, S. A., J. M. Conley, and D. Buchwalter. 2017. Sulfate transport kinetics and toxicity are modulated by sodium in aquatic insects. *Aquatic Toxicology* 190:62-69. DOI: 10.1016/j.aquatox.2017.06.027.

Schuler, M. S., M. Cañedo-Argüelles, W. D. Hintz, B. Dyack, S. Birk, and R. A. Relyea. 2019. Regulations are needed to protect freshwater ecosystems from salinization. *Philosophical Transactions of the Royal Society. B. Biological Sciences* 374:20180019. DOI: 1-.1098/rstb.20180019.

Schulz, C.-J., M. Cañedo-Argüelles. 2019. Lost in translation: The German literature on freshwater salinization. *Philosophical Transactions of the Royal Society. B. Biological Sciences* 374:20180007. DOI: 10.1098/4stb.2018.0007.

Natural variation and current reference for specific conductivity and major ions in wadeable streams of the conterminous USA

Michael B. Griffith[1,2]

[1]Office of Research and Development, National Center for Environmental Assessment, US Environmental Protection Agency, MS A-130, 26 W. Martin Luther King Drive, Cincinnati, Ohio 45268 USA

Abstract: Variation in specific conductivity and major ions in streams must be understood to assess the effects of changes in ionic strength and salinity on stream biota. I compiled data for randomly selected sites from surveys conducted from 1985 to 2009 by the US Environmental Protection Agency (EPA). I followed EPA methods to estimate reference values for specific conductivity (60 ecoregions) and each major ion (34 ecoregions) as the 25th percentile of values in 1st- to 4th-order streams in Level III ecoregions with data from ≥25 sites (85 ecoregions). The 25th percentiles of specific conductivity were <200 µS/cm for most eastern and western montane ecoregions, except those dominated by limestone or calcareous till. Arid western ecoregions had higher specific conductivities. Ca^{2+} was generally the most abundant cation followed by Mg^{2+}, Na^{+}, and K^{+}. HCO_3^{-} was generally the most abundant anion followed by SO_4^{2-} and Cl^{-}. Ecoregions where SO_4^{2-} or Cl^{-} concentrations were greater than HCO_3^{-} concentration have been affected by acidic precipitation or are influenced by marine air masses, respectively, and have very low specific conductivities. Patterns of variation appear to be associated with 3 processes controlling total and relative concentrations of major ions in freshwaters. In many ecoregions, relative ionic concentrations reflect underlying geology, but in arid ecoregions, relative ionic concentrations show concentration by evaporation. Relative ionic concentrations in coastal ecoregions and those affected by acidic precipitation reflect the ionic content of precipitation. Verification of these factors awaits better quantification of the geological and climatic characteristics of each ecoregion.

Key words: specific conductivity, calcium, magnesium, sodium, potassium, bicarbonate, sulfate, chloride, ecoregions, geographic variation, current reference, wadeable streams

The ionic strength, salinity, or the total concentration of ions in freshwater ecosystems, such as streams, has increased in many regions of the USA because of increasing anthropogenic sources. Anthropogenic sources include rock salt used to melt ice and snow on roads, walks, and parking areas (Jackson and Jobbágy 2005, Kaushal et al. 2005, Kelly et al. 2008); weathering of concrete infrastructure associated with suburban and urban areas (Rose 2007, Wright et al. 2011); produced water and effluents from exploration and production of crude oil or natural gas (Meyer et al. 1985, Boelter et al. 1992, Veil et al. 2004) including coal-bed methane (Jackson and Reddy 2007, Dahm et al. 2011) and shale gas (Entrekin et al. 2011, Gregory et al. 2011); runoff and effluents from coal mining and processing (Zielinski et al. 2001, Kennedy et al. 2003, Kimmel and Argent 2010), particularly mountaintop mines and valley fills (Pond et al. 2008, Griffith et al. 2012); agricultural irrigation return waters (El-Ashry et al. 1985, Duncan et al. 2008); and effluent from wastewater treatment plants (Andersen et al. 2004) or industrial processes (Echols et al. 2009). In a few cases, natural sources may include inputs of saline water from deep groundwater (i.e., upper Rio Grande basin; Phillips et al. 2003) or saline springs (i.e., Delores River, tributary to the Colorado River; Blackman et al. 1973, Chafin 2003).

The natural range and variation of these ion concentrations in the absence of anthropogenic sources, particularly in wadeable streams, must be understood before we can fully understand the effects of these elevated ion concentrations on steam biota and ecosystems. Gibbs (1970) and others have described 3 general processes, or axes, that control the total and relative concentrations of major ions in surface waters: 1) the evaporation–crystallization or precipitation process (i.e., increasing ratio of evaporation to precipitation [e.g., rainfall] with differential loss [e.g., mineral precipitation, degassing] of ions), 2) rock dominance

E-mail address: [2]griffith.michael@epa.gov

DOI: 10.1086/674704. Received 29 January 2013; Accepted 22 September 2013; Published online 10 January 2014.

(the mineral composition of the geological strata), and 3) atmospheric precipitation dominance (the ionic content of the original precipitation) (Feth 1971, Gibbs 1971, Stallard and Edmond 1981, 1983, 1987, Kilham 1990). These 3 processes are not independent and interact to produce the natural levels of specific conductivity and concentrations of the individual ions in fresh waters. Concentrations of ions in precipitation are generally low and depend on the sources of aerosols, dusts, and other materials in the atmosphere (Gorham 1958, 1961). Contact to soils and rock increases ion concentrations as a result of weathering unless the geology is resistant to chemical weathering. Evaporation can concentrate these ions, but some ions may be lost by mineral precipitation or degassing.

No investigator has sought to characterize systematically the natural range and variation of ions, measured as total dissolved solids, salinity, or specific conductivity in surface waters of streams in different regions of the conterminous USA. Moreover, no investigator has examined the relative natural concentrations of the major constituent ions in these waters, including the cations: Ca^{2+}, Mg^{2+}, Na^{+}, and K^{+}, and the anions: HCO_3^{-}, SO_4^{2-}, and Cl^{-}. Specific conductivity is a simple way to measure total ion concentrations in fresh waters (Pawlowicz 2008), but the concentration of individual ions and the relative concentrations of constituent ions may be more important for understanding the adverse effects of elevated ion concentrations on aquatic assemblages (Mount et al. 1997, Tietge et al. 1997). The mechanisms described by Gibbs (1971) can lead to differing relative natural concentrations of constituent ions, whereas anthropogenic sources contribute differing ion mixtures to fresh waters (Andersen et al. 2004, Jackson and Reddy 2007, Duncan et al. 2008, Kelly et al. 2008, Echols et al. 2009, Entrekin et al. 2011, Wright et al. 2011, Griffith et al. 2012).

Many environmental factors, such as flow, nutrients, ion concentrations, bedded or suspended sediments, dissolved O_2, light, and heat, are natural parts of the physicochemical regimes that are fundamental to aquatic ecosystems (Petts 2000, Poole et al. 2004). Each factor has a natural range that is characteristic of particular streams but varies among regions because of differences in geology, climate, and other large-scale factors (Omernik 1995, Naiman and Anderson 1997). Estimates of reference values provide a baseline for assessing human alteration of ion concentrations relative to the regime to which native flora and fauna are adapted. The fauna are likely to be sensitive to this alteration and not to the natural conditions they typically encounter. Fresh waters are generally hypo-osmotic, and organisms inhabiting them are exposed to similar osmo- and iono-regulatory challenges (Perry et al. 2003, Evans 2008). Fish, unionid mussels, crayfish, and aquatic insects are hyperregulators that maintain greater internal ion concentrations than are found in fresh waters (Dietz et al. 2000, Bradley 2008, Evans 2008, Charmantier et al. 2009). They maintain ion balance by excreting dilute waste fluids via their renal systems, and maintain salt concentrations with various ion-transporting proteins in epithelial membranes, such as the gills, that allow active transport of ions against concentration gradients (Evans 1980, Burton 1983, Perry et al. 2003). Increased concentrations of different major ions may cause osmotic, ionic, or acid–base imbalances that can eliminate sensitive species from biotic assemblages (USEPA 2011a). Therefore, water-quality benchmarks or criteria are derived for the altered, nonbackground state (USEPA 2011a), and assessment of natural variation of environmental factors among regions and adjustment of benchmarks or criteria for any regional variation is appropriate (USEPA 2000, Smith et al. 2003, Paul and MacDonald 2006).

My goal was to answer the questions: 1) How do current reference specific conductivities and concentrations of major ions in streams vary among Level III ecoregions (Omernik 1987, 1995, USEPA 2011b) in the USA? 2) How do the relative concentrations of the major cations and anions vary among ecoregions? I hypothesized that if the 25th percentiles (used to describe reference conditions for criteria development) for specific conductivity and concentrations of major ions describe current reference conditions in streams within ecoregions, their patterns of variation should be consistent with the 3 processes described by Gibbs (1970).

METHODS

I approached these questions and estimated reference specific conductivity and concentrations of individual ions by compiling water-chemistry data from stream surveys in which selected sites were sampled randomly (Herlihy et al. 2000) by the EPA and cooperating agencies since 1985 (Table 1, Fig. 1). In the National Acid Precipitation Assessment Program (NAPAP) surveys, streams were sampled in selected nascent ecoregions (Omernik 1987), mostly in the eastern USA; in the Environmental Monitoring and Assessment Program (EMAP) and regional EMAP surveys, streams were sampled in selected states, ecoregions, groups of conterminous ecoregions, or river basins in different parts of the USA; and in the National Wadeable Streams Assessment (NWSA) and the National Rivers and Streams Assessment (NRSA) surveys, streams were sampled across the USA.

With the exception of the NRSA and some later EMAP surveys, these surveys were focused primarily on wadeable streams, and my analysis was limited to these streams, defined here as 1st- to 4th-order streams (Strahler 1957) as identified in the National Hydrography Dataset (USEPA 2005). Most sites were only visited once, but some sites

Table 1. Survey data sets included in this study. Years indicates the period during which the survey was conducted, and *n* is the number of unique sites included in the survey. Western Environmental Monitoring and Assessment Program (EMAP) survey sites are included in the count of sites from the National Wadeable Streams Assessment (NWSA).

Survey	Years	Sample frame	*n*
National Acid Precipitation Assessment Program (NAPAP)	1985–1986	Blue-line headwater segments or segments between confluences on 1 : 250,000-scale US Geological Survey topographic maps	950
EMAP and Regional EMAP	1993–2003	River Reach File Version 3 (RF3)	2382
NWSA	2000–2004	River Reach File Version 3 (RF3) Alpha	1359
National Rivers and Streams Assessment (NRSA)	2008–2009	National Hydrography Dataset Plus	949

were revisited either within 1 y or in consecutive years to assess between-visit variability. I used data from the 1st visit to a site.

I used Level III ecoregions (Omernik 1987, 1995, USEPA 2011b) to classify sites into groups with similar geology and climate, which are 2 of the mechanisms discussed by Gibbs (1970). Level III ecoregions, as defined by Omernik (1987, 1995), are generally similar to the classic physiographic provinces used by geologists to classify regions with similar geology and geomorphology (Fenneman 1928) but also are related to variations in climate (Carr et al. 2000). I used the hierarchical 6-digit code for the Level III ecoregions (e.g., 08.01.03) published by Wilken et al. (2011) because this approach enabled me to group Level III ecoregions at hierarchical Level II. I referenced the commonly used 2-digit codes in Table S1. I included an ecoregion in the analyses if data were available from ≥25 sites in the ecoregion. Individual ions were not analyzed in some surveys, particularly regional EMAP studies. Dissolved inorganic C (DIC) was not measured in the NRSA, in which only acid-neutralizing capacity was measured. Therefore, data for individual ions, particularly HCO_3^-, were not available for all sites. I ana-

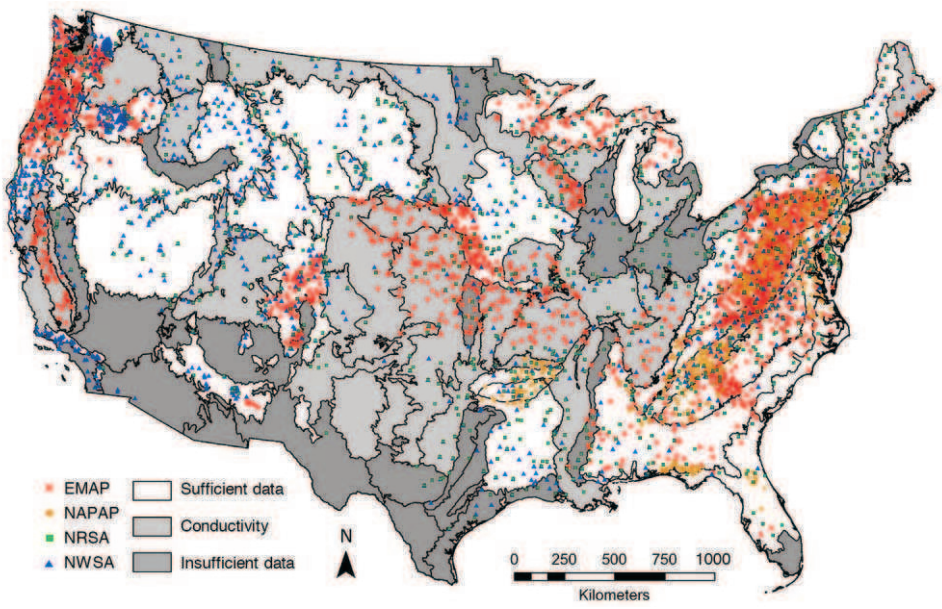

Figure 1. Map showing the sites in each survey and within each Level III ecoregion (outlines). The symbols and their colors differentiate the 4 different surveys: Environmental Monitoring and Assessment Program (EMAP) and regional EMAP, National Acid Precipitation Assessment Program (NAPAP), National Rivers and Streams Assessment (NRSA), and National Wadeable Streams Assessment (NWSA). *Sufficient data* indicates those ecoregions with data from ≥25 sites that were used to characterize specific conductivity and all the ions, *Conductivity* indicates those ecoregions with data from ≥25 sites at least for specific conductivity and often a subset of ions that was used to characterize those variables, and *Insufficient data* indicates those ecoregions with data from <25 sites that could not be used for analysis of either specific conductivity or ions.

lyzed data for each ion only if observations were available from ≥25 sites in an ecoregion. I selected the minimum of 25 sites as a compromise between characterizing as many Level III ecoregions as possible and the uncertainty of characterizing an ecoregion with few sites.

The Ridge and Valley ecoregion (08.03.01) is geologically heterogeneous (Pan et al. 1996, McCormick et al. 2000, Zheng et al. 2008), so I further subdivided the ecoregion into 2 subregions—the Limestone and Shale Valleys and the Ridges—to investigate the effect of this heterogeneity on specific conductivity and ion concentrations. I assigned level IV subdivisions of the Ridge and Valley to these 2 subregions based on descriptions by Woods et al. (1999, 2007).

In most of the surveys, samples were collected at baseflow during a spring (April) to summer (September) index period. Over the entire data set, 10, 10, 12, 22, 23, and 12% of sites were sampled during April, May, June, July, August, and September, respectively. Fewer sites were sampled in March (7%), October (4%), November (0.4%), and December (<0.1%). Preliminary analyses of data from the Central Appalachians (08.04.02) and Western Allegheny Plateau (08.04.03) in West Virginia showed seasonal variation in specific conductivity with higher levels during the April-to-September index period (USEPA 2011a). Therefore, sampling captured these higher levels of specific conductivity and individual ions.

Measured water-chemistry variables included specific conductivity (μS/cm) and the individual concentrations (μeq/L) of 4 major cations (Ca^{2+}, Mg^{2+}, Na^{+}, and K^{+}) and 3 major anions (HCO_3^{-}, SO_4^{2-}, and Cl^{-}). Collection and chemical analysis of water samples in these studies followed EPA procedural and quality-control protocols (Drousé et al. 1986, USEPA 1987, Lazorchak et al. 1998, USEPA 2004a, b, c, 2009a, b, 2010). Water samples generally were collected at midchannel at the lowermost transect of the sampling reach, placed in 4-L cubitainers, and stored on ice for transport to the laboratory. Water samples for analysis of pH and DIC were collected without contact with the atmosphere in 60-mL syringes with Luer-Lok® valves to minimize CO_2 exchange. The water samples for ions were filtered, and samples for cations were acidified with nitric acid (H_2NO_3) until analysis. The water samples for pH and DIC were not filtered. In the laboratory, Cl^{-} and SO_4^{2-} were analyzed with ion chromatography, and the cations were analyzed with atomic absorption spectroscopy. pH was measured with a calibrated pH meter with a glass electrode, and DIC was measured with a C analyzer equipped with a high sensitivity loop. Specific conductivity was measured with a calibrated conductivity meter, which standardized the measurement to 25°C or, in the case of 1 regional EMAP study of the Southern Rockies ecoregion (06.02.14), was calculated from the measurements of ion concentrations (USEPA 1987). HCO_3^{-} was calculated from the measurements of pH and DIC. In most studies, specific conductivity also was calculated from measurements of ion concentrations and compared to the meter specific conductivity measurements as part of quality assurance (USEPA 1987). No data presented an analytical problem that could not be corrected.

EPA (USEPA 2000) guidance has suggested 2 approaches to estimating reference concentrations from survey data. These studies produced probability-based data sets but reference sites frequently were not identified. Therefore, I estimated the upper limit of current reference-site specific conductivity and the concentrations of individual ions as the 25th percentile following EPA (USEPA 2000) guidance. However, I also plotted the maximum, 75th percentile, median, and minimum values for specific conductivity and have presented these data and the mean for specific conductivity, pH, and the individual ions in Table S1.

I calculated Pearson correlations between the 25th percentiles for specific conductivity and the individual ions for each ecoregion with sufficient data to assess the relationships among the different ions. I also plotted the 25th percentile for specific conductivity against the percentile ratio of Na^{+} to (Na^{+} + Ca^{2+}) for each ecoregion with sufficient data to compare them to the original model by Gibbs (1970). This model describes variation in total dissolved ions and dominance by Ca^{2+} and HCO_3^{-} vs Na^{+} and Cl^{-} in relation to 3 processes affecting the ionic composition of fresh waters: evaporation–crystallization, rock composition, and atmospheric precipitation composition. I used principal components analysis (PCA) of the $\log_{10}(x)$-transformed 25th-percentile concentrations of the individual ions for each ecoregion followed by cluster analysis of the ecoregion scores on the first 3 principal component axes to assess the similarities among sites. I used SAS® (SAS Institute, Cary, North Carolina) to manage the data and the UNIVARIATE, CORR, PRINCOMP, and FASTCLUS procedures for the analyses. The figures were made following the linked micromaps concept of Carr et al. (2000) in which geographically referenced data are presented by combining graphs that display measures of variation with maps (Symanzik and Carr 2008, Carr and Pickle 2010).

RESULTS

Specific conductivity

Specific conductivities ranged from 1.6 to 12,290 μS/cm (median = 132.7 μS/cm, mean = 312.4 μS/cm). Specific-conductivity data were available from ≥25 sites in 60 of 85 Level III ecoregions (Fig. 1). Sufficient data were lacking for all of the warm desert ecoregions in the southwestern USA (Omernik 1995). Among those ecoregions, the 25th percentile for specific conductivity ranged from 16.2 to 563 μS/cm.

For most ecoregions in the eastern USA, the 25th percentiles of specific conductivity were <200 μS/cm, and often the median and 75th percentiles were less than this level (Fig. 2). This level was used by the EPA to characterize

ecoregions with low specific conductivity and its constituent ions (USEPA 2011a). Ecoregions where the 25th percentile was >200 µS/cm included the Interior Plateau (08.03.03), Interior River Valleys and Hills (08.03.02), Ozark Highlands (08.04.05), Erie Drift Plain (08.01.10), Southern Michigan/Northern Indiana Drift Plains (08.01.06), and Driftless Area (08.01.05).

In the western USA, 25th percentiles of specific conductivity were <200 µS/cm for most montane ecoregions, such as those in the Rockies, the Pacific Northwest, and

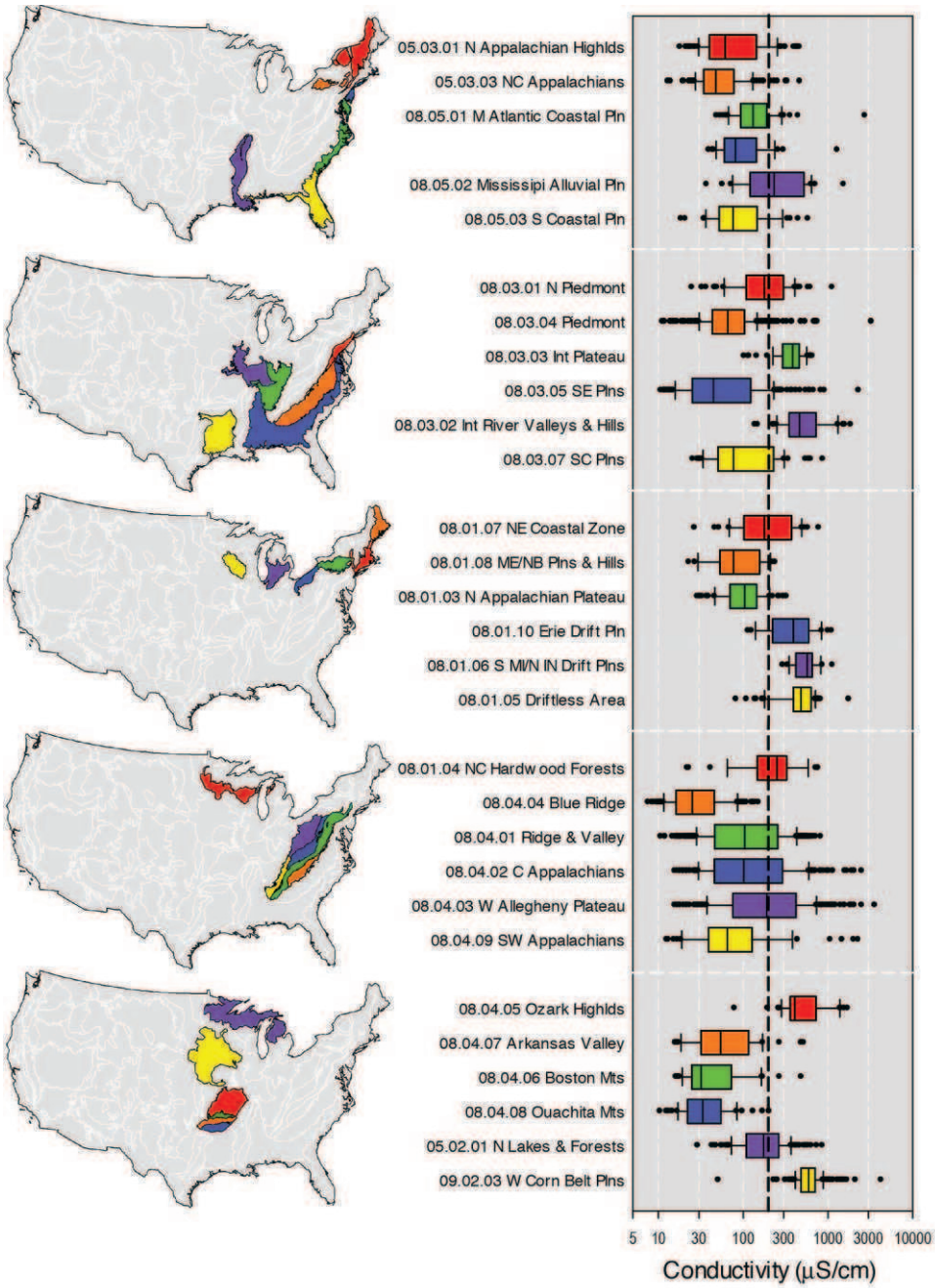

Figure 2. Box-and-whisker plots showing the 90th, 75th, 50th, 25th, and 10th percentiles of specific conductivity (µS/cm) for Level III ecoregions in the eastern conterminous USA and the Western Corn Belt Plains (09.02.03) with sufficient data. Dots represent sites with specific conductivity values >90th percentile or <10th percentile. The vertical dashed line on the graph represents 200 µS/cm. The maps show each plotted ecoregion. The color of the box in the graph (right) matches the color of the ecoregion in the map (left). The abbreviations of the ecoregions include the direction (C = Central, M = Middle, N = Northern, NC = North Central, NE = Northeastern, S = Southern, SC = South Central, SE = Southeastern, SW = Southwestern, W = Western), geographic name (Highlds = Highlands, Int = Interior, Mts = Mountains, Pln/Plns = Plain/Plains), and state or province (IN = Indiana, ME = Maine, MI = Michigan, NB = New Brunswick).

the Upper Gila Mountains (i.e., Arizona/New Mexico Mountains [13.01.01]; Fig. 3). However, for most of the prairie ecoregions and some of the Great Basin or Cold Desert (10.01) ecoregions, the 25th percentiles of specific conductivity were >200 µS/cm. For the ecoregions composing the more eastern Temperate Prairies (09.02, n = 3), the 25th percentiles ranged from 309 to 563 µS/cm, whereas those for the ecoregions composing the West-Central Semiarid Prairies (09.03, n = 3) ranged from 160 to 490 µS/cm, and the South-Central Semiarid Prairies (09.04, n = 4) ranged from 291 to 594 µS/cm. The 25th percentiles in the Cold Desert (10.01, n = 5) ecoregions ranged from 98.4 to 405 µS/cm. The Mediterranean California (11.01, n = 3) ecoregions also had 25th percentiles that ranged from 90.3 to 249 µS/cm. I lacked sufficient data to characterize the 25th percentiles of conductivities and ion concentra-

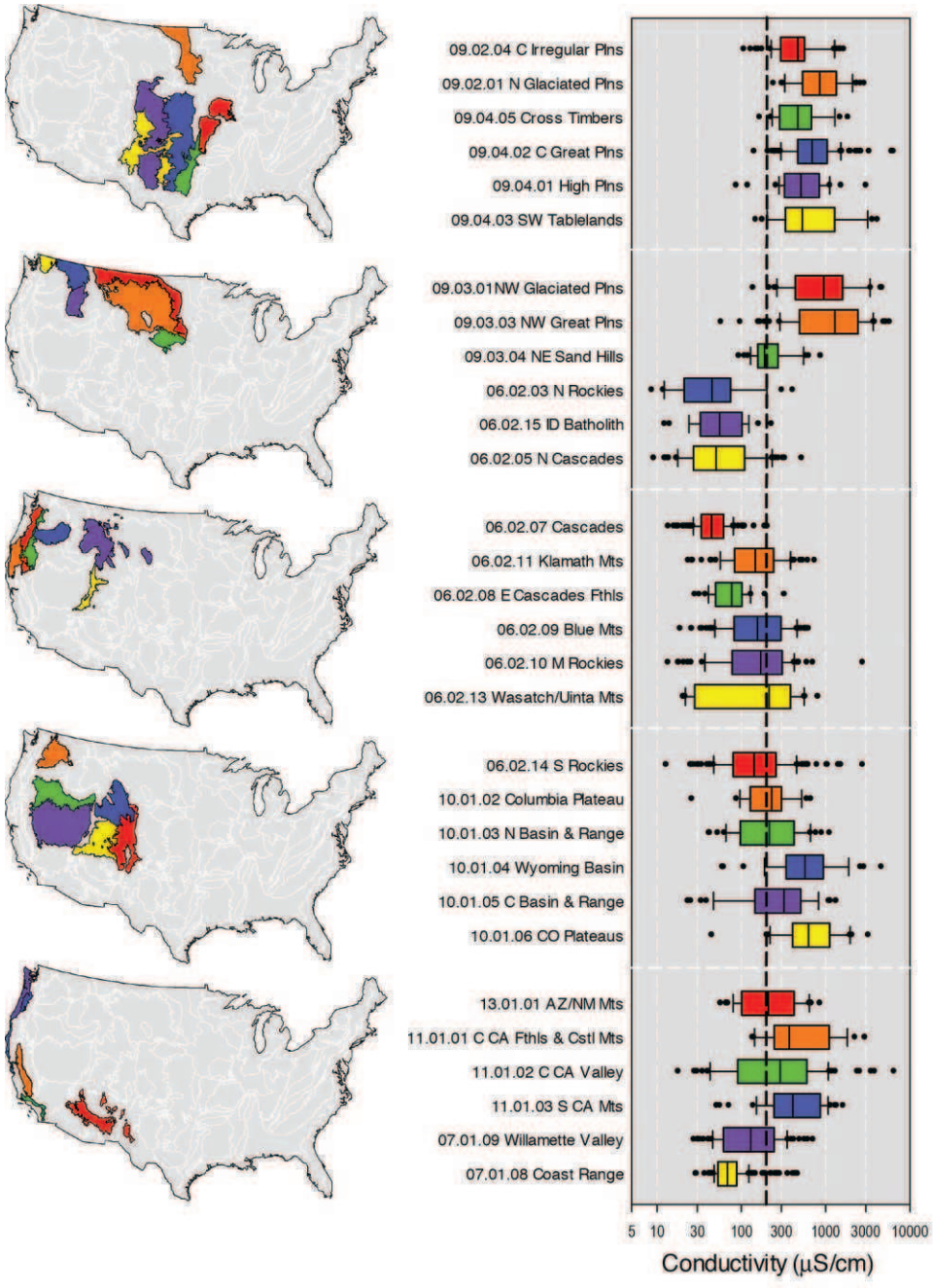

Figure 3. Box-and-whisker plots showing the 90th, 75th, 50th, 25th, and 10th percentiles of specific conductivity (µS/cm) for Level III ecoregions in the western conterminous USA with sufficient data. Figure symbols and abbreviations are as in Fig. 2 except for geographic names (Cstl = Coastal, Fthls = Foothills, Mts = Mountains, Plns = Plains), and states (AZ = Arizona, CA = California, CO = Colorado, NE = Nebraska, NM = New Mexico, ID = Idaho).

tions in streams in the Warm Desert (10.02) ecoregions, but the 8 observations in the data set from these 3 ecoregions ranged from 279 to 12,290 (median = 2622) µS/cm. Within the Ridge and Valley (08.04.01) ecoregion, the 25th percentile for specific conductivity at sites in the Limestone and Shale Valleys was generally greater than that in the Ridges (Fig. 4A).

Concentrations of individual ions

Concentrations of individual cations ranged from 1.9 to 25,694 µeq/L for Ca^{2+}, 2.6 to 44,444 µeq/L for Mg^{2+}, 3.7 to 108,851 µeq/L for Na^{+}, and 0 to 3406 µeq/L for K^{+}. Concentrations of individual anions ranged from 0.01 to 16,654 µeq/L for HCO_3^{-}, 0 to 75,568 µeq/L for SO_4^{2-}, and 0 to 74,750 µeq/L for Cl^{-}. I had sufficient data for all ions from 34 of 85 ecoregions, and sufficient data for a subset of ions from 24 more ecoregions (Fig. 1).

Among the cations, the 25th percentile concentration of Ca^{2+} either alone or in combination with Mg^{2+} generally exceeded the concentration of Na^{+} (Figs 5B, S1–S4), whereas in a few cases, the 25th percentile of Mg^{2+} exceeded that of Ca^{2+}. Exceptions to this pattern included several Eastern Coastal Plain ecoregions: Northeastern Coastal Zone (08.01.07), Atlantic Coastal Pine Barrens (08.05.04), and Southeastern Plains (08.03.05) (Figs 5B, S1, Table S2). The 25th percentiles of Ca^{2+} and Na^{+} were similar in several other ecoregions, such as the Middle Atlantic Coastal Plain (08.05.01; Fig. S1), Blue Ridge (08.04.04; Fig. S2), and Coast Range (07.01.08; Fig. S4). In the Arkansas Valley (08.04.07) and Ouachita Mountains (08.04.08) (Figs 5B, S2), the 25th percentiles of Na^{+} were greater than those of Ca^{2+} but were less than those of Mg^{2+}. The 25th percentile concentration of K^{+} was generally much less than each of the other 3 cations. The 25th percentile concentration of Mg^{2+} relative to that of Na^{+} was more variable. Within the Ridge and Valley (08.04.01) ecoregion, the 25th percentile for concentrations of both cations and anions at sites in the Limestone and Shale Valleys were generally greater than those in the Ridges (Fig. 4B).

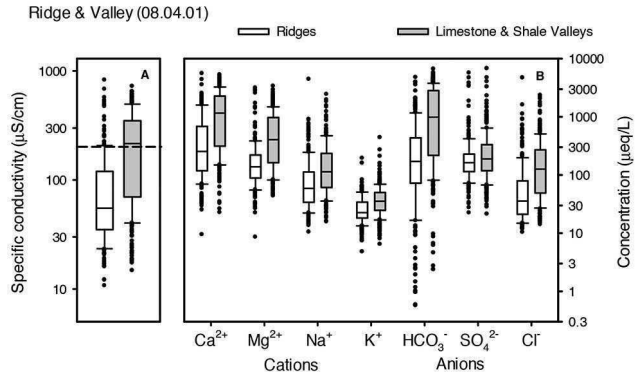

Figure 4. Box-and-whisker plots showing the 90th, 75th, 50th, 25th, and 10th percentiles of specific conductivity (A) and cation and anion concentrations (B). Dots indicate sites that exceeded the 90th and 10th percentiles in the Ridge (n = 222–225 depending on variable) and the Limestone and Shale Valleys (n = 286–295 depending on variable) subregions of the Ridge and Valley (08.04.01) ecoregion. The horizontal dashed line in panel A represents 200 µS/cm.

The 25th percentiles of the concentrations for the cations Ca^{2+}, Mg^{2+}, Na^{+}, and K^{+} ranged from 37.8 to 3089 µeq/L, 29.8 to 1974 µeq/L, 28.3 to 1316 µeq/L, and 0.0 to 195 µeq/L, respectively. The correlations among these cation concentrations were moderate (Table 2), and r ranged from 0.67 to 0.87. The correlations of the 25th percentiles for each cation and specific conductivity were moderate to strong (Table 2), and r ranged from 0.78 to 0.96.

Among the anions, the 25th percentile concentration of HCO_3^{-} exceeded the concentrations of either SO_4^{2-} or Cl^{-}, often by at least an order of magnitude (Figs 5C, S1–S4). Exceptions to this pattern occurred in the Southeastern Plains (08.03.05), Southern Coastal Plain (08.05.03), and Middle Atlantic Coastal Plain (08.05.01) (Fig. 5C, Table S2), where Cl^{-} concentration exceeded HCO_3^{-} concentration; the Central Appalachians (08.04.02, Fig. 5C), the ridges of the Ridge and Valley (08.04.01, Fig. 4), and North Central Appalachians (05.03.03, Fig. 5C) where SO_4^{2-} concentration exceeded HCO_3^{-} concentration; and Atlantic Coastal Pine Barrens (08.05.04, Figs 5C, S1), where both SO_4^{2-} and Cl^{-} concentrations exceeded HCO_3^{-} concentration. These ecoregions had low conductivities (25th percentile = 25.0–103 µS/cm; Fig. 5A) and the lowest 25th percentiles for pH (3.96–6.57; Table S1). For many of these ecoregions, the 25th percentile concentrations of Na^{+} and Cl^{-} were similar. Usually, the 25th percentile concentration of SO_4^{-} exceeded that of Cl^{-}. However, the reverse occurred in the Marine West Coast Forest (07.01, Fig. S4), Southeastern USA Plains (08.03, Fig. S1), and Mississippi Alluvial and Southeastern USA Coastal Plains (08.05, Fig. S1) ecoregions.

The 25th percentiles of the concentrations for HCO_3^{-}, SO_4^{2-}, and Cl^{-} ranged from 0.9 to 4010 µeq/L, 4.1 to 1487 µeq/L, and 5.1 to 441 µeq/L, respectively. The correlation between HCO_3^{-} and SO_4^{2-} was moderate (Table 2), whereas the correlations between these 2 anions and Cl^{-} were weaker (Table 2). The correlations of the 25th percentiles for SO_4^{2-} and HCO_3^{-} with specific conductivity were relatively strong, but the correlation between Cl^{-} and specific conductivity was weaker (Table 2). The correlations between HCO^{3-} or SO_4^{2-} and the 4 cations were moderate to strong, whereas the correlations between Cl^{-} and the 4 cations were weaker (Table 2).

When I plotted the ratio of the 25th percentile Na^{+} concentration to the summed 25th percentile concentrations of Na^{+} and Ca^{2+} (i.e., $Na^{+}:[Na^{+} + Ca^{2+}]$) against the 25th percentile of specific conductivity for each ecoregion (similar to the method used by Gibbs 1970), several ecoregions with high specific conductivities plotted on the upper part of the graph (Fig. 6), and some ecore-

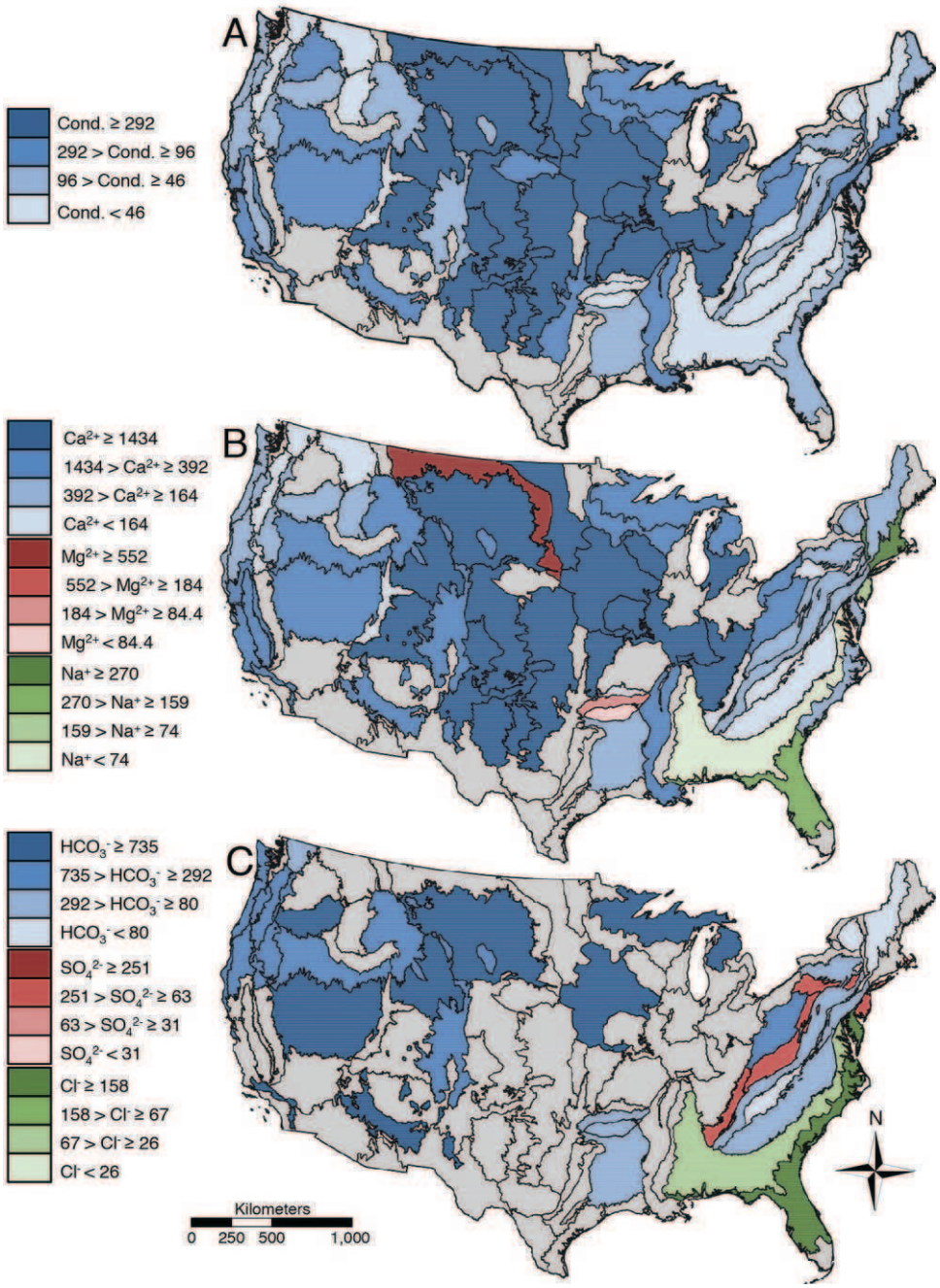

Figure 5. Maps showing the quartiles of the specific conductivity (Cond.) (A) reference values, cations with the greatest reference values (B), and anions with the greatest reference values (C) for each Level III ecoregion. Ecoregions shown in color have data from ≥25 sites for specific conductivity in panel A, all major cations (Ca^{2+}, Mg^{2+}, Na^{+}, K^{+}) in panel B, or all major anions (HCO_3^{-}, SO_4^{2-}, Cl^{-}) in panel C. Ecoregions shown in gray lack sufficient data. The quartile range for each variable is the quartile of the range of all reference values for that variable for ecoregions with sufficient data. See Table S2 for the Level III ecoregions in each group.

gions where Cl^{-} was greater than HCO_3^{-} plotted on the lower right part of the graph. However, most sites plotted toward the left center of the graph.

I did not include HCO_3^{-} in the PCA because the 25th percentiles for HCO_3^{-} were strongly correlated with those of Ca^{2+} and Mg^{2+} (Table 2). This decision allowed me to include more ecoregions in the analysis. Axes 1, 2, and 3 explained 75, 10, and 7% of the variance in the ionic concentrations, respectively (Table 3). All 6 ions were positively correlated with Axis 1 (Table 3, Fig. 7), whereas Cl^{-} was positively and Ca^{2+} and Mg^{2+} were inversely correlated with Axis 2.

Table 2. Pearson correlation (r and associated p-values) matrix of 25th-percentile concentrations of ions (μeq/L) and the 25th percentiles for specific conductivity (μS/cm). n = 55 to 57, except for HCO_3^-, where n = 34.

		Ions					
Ions	Specific conductivity (μS/cm)	Ca^{2+}	Mg^{2+}	Na^+	K^+	HCO_3^-	SO_4^{2-}
Ca^{2+}	0.96 ($p<0.001$)						
Mg^{2+}	0.90 ($p<0.001$)	0.86 ($p<0.001$)					
Na^+	0.81 ($p<0.001$)	0.67 ($p<0.001$)	0.67 ($p<0.001$)				
K^+	0.78 ($p<0.001$)	0.68 ($p<0.001$)	0.71 ($p<0.001$)	0.87 ($p<0.001$)			
HCO_3^-	0.97 ($p<0.001$)	0.96 ($p<0.001$)	0.93 ($p<0.001$)	0.80 ($p<0.001$)	0.69 ($p<0.001$)		
SO_4^{2-}	0.86 ($p<0.001$)	0.76 ($p<0.001$)	0.80 ($p<0.001$)	0.83 ($p<0.001$)	0.87 ($p<0.001$)	0.75 ($p<0.001$)	
Cl^-	0.59 ($p<0.001$)	0.59 ($p<0.001$)	0.49 ($p<0.001$)	0.46 ($p<0.001$)	0.43 ($p=0.001$)	0.23 ($p=0.18$)	0.43 ($p<0.001$)

I identified 7 groups of ecoregions in the cluster analysis (Fig. 7, Table S3). Cluster A included many of the eastern montane ecoregions, including the Appalachians and the Ozark–Ouachita Highlands, whereas cluster D, which overlapped cluster A along the first 2 axes, included several southeastern lowland ecoregions. Cluster B included a number of Great Plains ecoregions and some more eastern ecoregions influenced by either calcareous bedrock or tills. Cluster G included 7 western montane ecoregions, whereas cluster E included some western montane and Great Basin ecoregions, along with the Willamette (07.01.09) and Central California (11.01.02) valleys and the more eastern Northern Lakes and Forests (05.02.01). Cluster C included 3 eastern coastal or alluvial plain ecoregions, the adjacent Northern Piedmont (08.03.01) and South Central Plains (08.03.07) and the Northern Appalachian Plateau (08.01.03) and North Central Hardwood Forests (08.01.03). Cluster F included a mixture of ecoregions, including 3 eastern ecoregions influenced by calcareous bedrock or tills, 2 Great Plains ecoregions, and 2 basin and range ecoregions along with the Western Allegheny Plateau (08.04.03) and Central California Foothills and Coastal Mountains (11.01.01).

DISCUSSION

Specific conductivity and the concentrations of major ions characteristic of the natural factors originally described by Gibbs (1970) varied in wadeable streams among ecoregions. Such variation must be considered when setting water-quality expectations during stream assessments or when considering management options. Estimates of current reference conditions also are a baseline for future assessment of stream impairments associated with salinity from anthropogenic sources. The observations by Gibbs (1970) were made in larger rivers. However, within the more-limited range of conditions in wadeable streams and ecoregions sampled during the surveys, I also observed examples that exhibited ionic concentrations and compositions characteristic of rock dominance, evaporation–crystallization, and atmospheric precipitation dominance.

Most ecoregions (75%) appeared to be primarily rock dominant, and the ion signature of the streams was dominated by Ca^{2+}, Mg^{2+}, and HCO_3^- (Gibbs 1970, Stallard and Edmond 1987). In the eastern USA, specific conductivity is generally <200 μS/cm because precipitation is moderate (average annual precipitation = 100–250 cm), but some ecoregions with greater conductivities are generally characterized either by limestone karst (e.g., Interior Plateau [08.03.03], Ozark Highlands [08.04.05], Driftless Area [08.01.05]; Veni et al. 2001), or by calcareous tills (e.g., Southern Michigan/Northern Indiana Drift Plains [08.01.06], Erie Drift Plain [08.01.10]; Smeck and Wilding 1980, Szabo 2006).

The greater conductivities in ecoregions characterized by limestone karst prompted me to investigate whether specific conductivities in streams in the valleys of the Ridge and Valley (08.04.01) ecoregion, which are also characterized by areas of limestone karst, were greater than those of streams on the ridges. They were (Fig. 4), but the 25th percentile of specific conductivity for the limestone and shale valleys was not >200 μS/cm. Moreover, the greater conductivities were associated with greater concentrations of Ca^{2+}, Mg^{2+}, Cl^-, and HCO_3^-. Other investigators have recognized the effects of this heterogeneity in geology (Pan et al. 1996, McCormick et al. 2000, Zheng et al. 2008), and these differences are clearly related to the differences in the li-

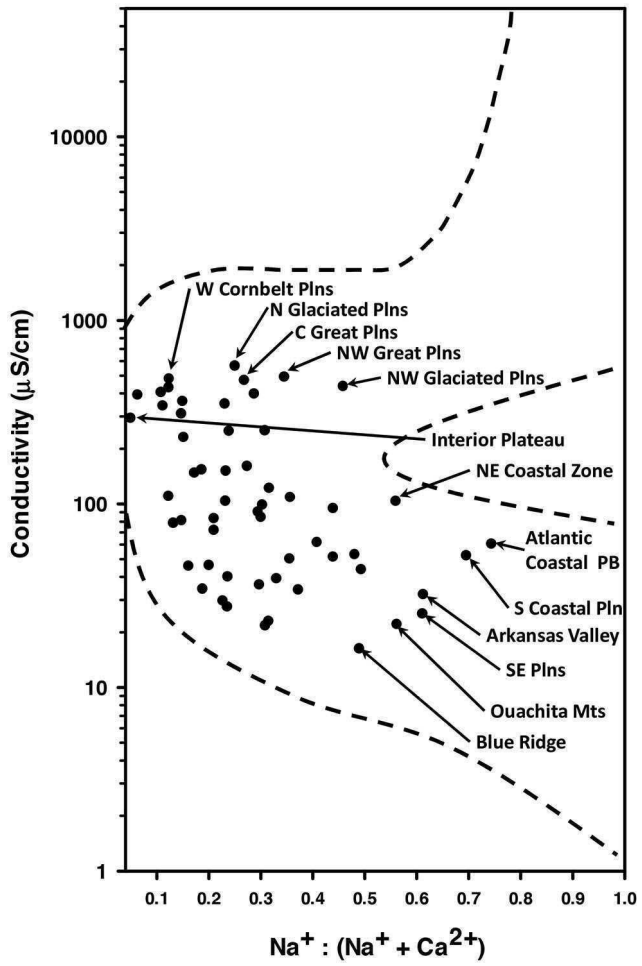

Figure 6. Plot of specific conductivity vs the ratio of Na^+ : (Na^+ + Ca^{2+}) (25th percentiles) for each Level III ecoregion with sufficient data. Ecoregions that plot to the upper right (sites with characteristics of the evaporation–crystallization process) or lower right (sites with characteristics of atmospheric precipitation dominance) of the plot are labeled. The dashed lines approximate the outline surrounding the plotted surface waters in fig. 1 by Gibbs (1970). See Figs 2, 3 for abbreviations.

thology. Therefore, geological heterogeneity within other ecoregions may affect variation of ambient specific conductivity and concentrations of individual ions. However, the small size and geomorphologic relationship between these Level IV ecoregions are such that many stream sites in the valleys have their headwaters on the ridges, and this relationship may limit variation in specific conductivity and ion concentrations. Level III ecoregions are generally much larger than level IV ecoregions, and I limited the analyses to wadeable streams (1st- to 4th-order). Thus, effects associated with stream sites with at least part of their headwaters in a different ecoregion appear to be uncommon.

In the western USA, particularly outside the montane ecoregions of the Rockies and the Pacific Northwest, where the climate is semiarid, the 25th percentiles of specific conductivity were often >200 µS/cm and ranged up to 563 µS/cm. Yet, the anions were still dominated by HCO_3^-, and Ca^{2+} was the most abundant cation. Some of these same ecoregions (Western Corn Belt Plains [09.02.03], Northern Glaciated Plains [09.02.01], Central Great Plains [09.04.02], Northwestern Great Plains [09.03.03], and Northwestern Glaciated Plains [09.03.01]) occur in the upper part of the graph of specific conductivity vs the Na^+ : (Na^+ + Ca^{2+}) ratio (Fig. 6), results suggesting that these increased ion concentrations reflected concentration of the ions by the evaporation–crystallization process (Gibbs 1970).

The eastern ecoregions, where specific conductivities were very low and either SO_4^{2-} or Cl^- were greater than HCO_3^-, are characteristic of dominance by atmospheric precipitation. The North Central Appalachians (05.03.03) and Central Appalachians (08.04.02) both have been affected by acidic precipitation (Herlihy et al. 1991, Kaufmann et al. 1991), which is a source of SO_4^{2-}. However, both ecoregions also have histories of coal mining (Herlihy et al. 1990), and coal-mine drainage is a source of SO_4^{2-}. The Atlantic Coastal Pine Barrens (08.05.04) receives precipitation both from continental air masses, which are a source of SO_4^{2-} as in the 2 Appalachian ecoregions, and marine air masses, which are the source of Na^+ and Cl^- (Raynor and Hayes 1982, Morgan and Good 1988). However, regulation of emissions from coal-fired power plants, the ultimate source of the SO_4^{2-}, has decreased atmospheric deposition of SO_4^{2-} in the northeastern USA (Stoddard et al. 2003).

Similar to the Atlantic Coastal Pine Barrens (08.05.04), the Southern Coastal Plain (08.05.03), Southeastern Plains (08.05.03), and Northeastern Coastal Zone (08.01.07) are influenced by marine air masses (Beck et al. 1974, Richter et al. 1983, Mattson et al. 1992), as is the Coast Range (07.01.08) in the Pacific Northwest (Wigington et al. 1998). Moreover, many of these marine-influenced ecoregions plot in the lower right part of the graph of specific conduc-

Table 3. Eigenvectors, eigenvalues, and cumulative proportion of variance for the first 3 axes of the principal components analysis for the 25th percentiles of Ca^{2+}, Mg^{2+}, Na^+, K^+, SO_4^{2-}, and Cl^- concentrations for ecoregions with sufficient data (n = 55).

Ion	Axis 1	Axis 2	Axis 3
Ca^{2+}	0.477	−0.523	0.163
Mg^{2+}	0.445	−0.321	0.155
Na^+	0.334	0.032	0.408
K^+	0.308	0.059	−0.053
SO_4^{2-}	0.487	0.179	−0.809
Cl^-	0.361	0.766	0.353
Eigenvalue	1.137	0.157	0.108
Cumulative proportion of variance	0.75	0.85	0.92

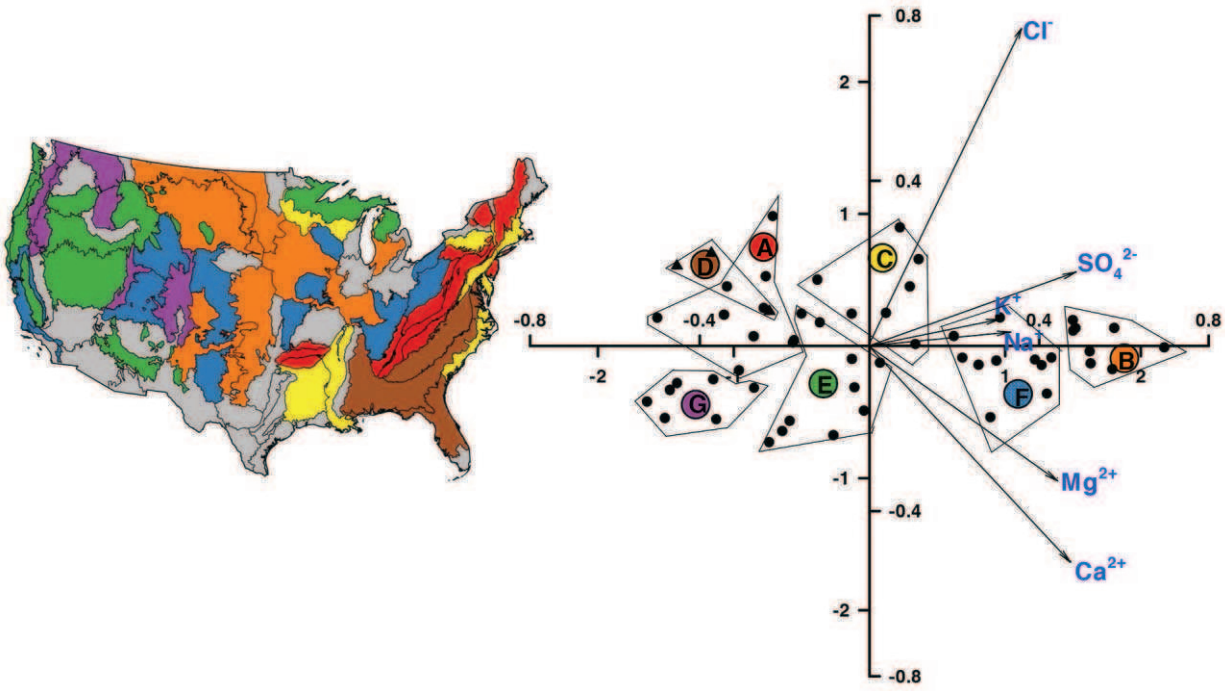

Figure 7. Biplot of principal components analysis (PCA) axes 1 and 2 for the ecoregions of the conterminous USA with data from ≥25 sites for the 25th percentiles of Ca^{2+}, Mg^{2+}, Na^{+}, K^{+}, SO_4^{2-}, and Cl^{-}. The scale in standard deviation units is −2 to 2 for the ecoregion scores and −0.8 to 0.8 for the ion eigenvectors. The clusters, A–G, are the groups of ecoregions identified by cluster analysis. The triangles are used to differentiate the ecoregions in cluster D where it overlaps with cluster A. The map shows the ecoregions in each cluster. The colors on the map match the colored dot behind each cluster letter. See Table S3 for lists of ecoregions in each cluster.

tivity vs the Na^{+} : (Na^{+} + Ca^{2+}) ratio (Fig. 6), supporting the model by Gibbs (1970) because specific conductivities are low, whereas relative concentrations of Na^{+} are greater.

Over all the ecoregions, the 25th percentiles for specific conductivity were most strongly correlated with those of HCO_3^{-} and Ca^{2+}, which were generally the most common anion and cation, respectively. The correlations of 25th percentiles of the other ions with that of specific conductivity decreased in relation to their general abundance (Table 2). All of these ions contribute to specific conductivity (Pawlowicz 2008), so this decrease is not necessarily surprising. The 25th percentiles of the Ca^{2+} and Mg^{2+} were more closely correlated with each other as were those of Na^{+} and K^{+}, but the correlations between these 2 pairs of cations were less strong. Similarly, the correlation between HCO_3^{-} and SO_4^{2-} was greater than the correlation of either anion with Cl^{-}. This result suggests the 3 processes differ in their importance for control of different ion concentrations because Ca^{2+}, Mg^{2+}, and HCO_3^{-} are associated with rock dominance, whereas Na^{+}, K^{+}, and Cl^{-} are associated with atmospheric precipitation (Gibbs 1970).

The PCA, followed by cluster analysis, identified many of these patterns. The ions were all positively correlated with the PCA axis 1, whereas the additional axes separated differences among the ions. Ecoregions that are often grouped together in higher-level classifications, such as those in the Appalachian and Ozark/Ouachita Mountains, the Rocky Mountains, the Great Plains, and Great Basin, were generally grouped by the cluster analysis, but differences exist that are not necessarily explained by geography.

Tests of hypotheses about the variation in specific conductivity and ions among ecoregions require further quantification of climate, geology, and precipitation chemistry for each ecoregion. Such data are not currently available for the entire conterminous USA, but geographic information system (GIS) modeling approaches do exist that could be used to estimate the ratio of evaporation to precipitation at the ecoregion scale (Vörösmarty et al. 1989) and variation in rock chemical and physical properties across map units (Smart et al. 2001). Olson and Hawkins (2012) used GIS modeling of rock chemical and physical properties to predict natural baseflow stream water chemistry in the western USA. This pathway warrants further investigation.

The EPA (USEPA 2000) suggested using either the 25th percentile of randomly selected samples or the 75th percentile of identified reference sites as an estimate of reference values. I chose the 1st approach to make maximum use of the data compiled from the various EPA surveys, which in some cases, did not identify reference sites. Much

discussion exists in the literature as to whether estimates like mine are true estimates of background or at least current reference conditions (Stoddard et al. 2006, Hawkins et al. 2010), but much of this discussion has focused on setting expectations for assessments when biotic assemblages are used to assess biotic integrity. Reference sites should "be stream sites at which biota are exposed to the lowest level of anthropogenic stressors" (Whittier et al. 2007, p. 370). However, professional judgment or the use of objective criteria can be biased. In an analysis of a survey data set from the Western EMAP pilot study, Whittier et al. (2007) found that ~35% of their handpicked reference sites, selected using primarily GIS and other mapped data, could be classified as in least-disturbed condition (75% of reference sites are generally expected to be representative of least-disturbed conditions) compared with 20% for their probability sites (25% of probability sites are generally expected to be in least-disturbed condition). In an analysis of the WSA data, Paulsen et al. (2008) established a condition class as being good based on the 25th percentile of the reference-site distribution of a Multimetric Index of Macroinvertebrate Integrity. This criterion means that 75% of the reference sites were assumed to be representative of least-disturbed conditions. When this threshold was applied to all randomly selected sites sampled nationally, 28% of the stream kilometers were classified as being in good condition, and 18 to 45% of the stream kilometers were classified as being in good condition in the 3 subregions used in their assessment. In many regions, minimally disturbed sites may not exist because of extensive anthropogenic disturbances (Whittier et al. 2007), and the 25th percentile would overestimate undisturbed conditions.

Several investigators have used national survey data for nutrients to compare these approaches (Herlihy and Sifneos 2008, Dodds et al. 2009). In an analysis of WSA data (Herlihy and Sifneos 2008), the 25th percentile of population data was lower for both total P (TP) and total N (TN) than the 75th percentile of reference sites for all national nutrient ecoregions with sufficient probability and reference sites for analysis. In an analysis of national nutrient ecoregions, Dodds et al. (2009) found that 53 to 96% of a probability sample of rivers had higher TP and 69 to 100% had higher TN than the median ecoregion-specific nutrient reference values. However, it seems unlikely that elemental cycles of the major ions have been altered to the extent to which P and N cycles have been altered. Identifying sites that truly represent natural background conditions is prohibitively difficult, so the 25th percentile probably does provide a reasonable estimate of current reference conditions.

The eastern ecoregions that have low specific conductivity, low total ion concentrations, and dominance by SO_4^{2-} have been affected by acidic deposition (Kaufmann et al. 1991, Herlihy et al. 1991). Since 1995, amendments to the Clean Air Act have reduced atmospheric deposition of acidity and SO_4^{2-}, with resultant increases in stream pH and decreases in SO_4^{2-} in most of these ecoregions, except the Blue Ridge (08.04.04), where accumulated SO_4^{2-} appears to be leaching more slowly from soils (Skjelkvåle et al. 2005, Chen and Lin 2009). In these same ecoregions, longer-term effects of acidic deposition may include decreased stream concentrations of some ions, like Ca^{2+}, because of depletion of exchangeable ions in soils (Jeziorski et al. 2008). Moreover, Likens et al. (1970) and others have shown that land disturbances, such as forest cutting, agriculture, and urbanization, may increase mineralization and export of many ions from catchments (Smart et al. 1985, Morgan and Good 1988, Webster et al. 1992, Zampella 1994, Johnson et al. 1997, Herlihy et al. 1998), and Carpenter et al. (2011) describe such landuse change as a pervasive driver of ongoing ecosystem change. Increases in evapotranspiration rates, one of the factors described by Gibbs (1970) that can increase ion concentrations, are occurring as part of climate change (Carpenter et al. 2011). All of these changes have occurred during the 25-y period during which these surveys were conducted (i.e., 1985–2009) and beyond (Drummond and Loveland 2010, Sleeter et al. 2012). However, many ecoregions were not sampled in all surveys, particularly in the earliest survey, NAPAP, in 1985–1986 (Fig. 1).

Based on the definitions proposed by Stoddard et al. (2006), my estimates should be described as "best attainable." They provide a reasonable estimate of current reference levels in these ecoregions in light of increasing anthropogenic sources of salinity to streams and other freshwater ecosystems. However, these estimates are not benchmarks or criteria, which are generally based on adverse effects to biota and would be greater than my estimates of best attainable conditions (USEPA 2011a).

Conclusions

The 25th percentiles of specific conductivity were <200 μS/cm for most ecoregions in the eastern USA and in montane ecoregions in the western USA. Exceptions were some ecoregions dominated by limestone karst or calcareous till. Greater 25th percentiles of conductivity (e.g., 98.4–563 μS/cm) were observed in arid ecoregions of the Great Plains, Great Basins and Ranges, and Mediterranean California. For most ecoregions, $Ca^{2+} > Mg^{2+} > Na^+$, and $HCO_3^- > SO_4^{2-} > Cl^-$. Ecoregions with greater SO_4^{2-} are affected by acidic precipitation and coal mining, whereas those with greater Cl^- are influenced by marine air masses, and streams in these ecoregions have very low specific conductivities.

The patterns of variation appear to be associated with the 3 general processes controlling total and relative concentrations of major ions in freshwaters described by Gibbs (1970). However, better quantification of these re-

lationships will require better quantification of the characteristics of ecoregions relative to these processes. For the 60 Level III ecoregions with sufficient data, the supplementary material (Table S1) provides current reference levels for specific conductivity, and for many of these ecoregions, current reference levels for individual ions. Moreover, I continue to seek additional data from randomly selected sites to characterize the ecoregions for which insufficient data currently exist. In a monitoring and assessment context, the levels are valuable because they estimate the baseline conditions in streams to which the native flora and fauna are adapted. These levels are generally lower than benchmarks or criteria, which are based on adverse effects to biota.

ACKNOWLEDGEMENTS

I thank my colleagues in the Regions, Office of Research and Development (ORD), and Office of Water (OW) of the EPA and with cooperating state agencies and universities for their work on the sampling and analyses that produced the data sets I used. I particularly thank L. Herger (Region 10), A. Herlihy (Oregon State University), Y. Pan (Portland State University), D. Peck (NHEERL), R. Hall (Region 9), P. Kalla (Region 4), M. Miller (Wisconsin DNR), E. Hammer (Region 5), K. Bazata (Nebraska DEQ), E. Baker (Michigan DNR), and E. Tarquinio (OW, OWOW), who answered questions about the individual studies and provided data from specific surveys. J. Prater (ECFlex, Inc.) produced the maps. S. Cormier and M. McManus (NCEA), B. Hill (NHEERL), C. Flaherty and R. Novak (OW, OST), S. Hagerthey (NCEA), C. Neitch (NRMRL), and 2 anonymous referees reviewed earlier drafts of this manuscript. This document was prepared at the EPA, ORD, National Center for Environmental Assessment, Cincinnati Division. It has been subjected to the agency's peer and administrative review and approved for publication. However, the views expressed in this article are those of the author and do not necessarily represent the views or policies of the EPA.

LITERATURE CITED

Andersen, C. B., G. P. Lewis, and K. A. Sargent. 2004. Influence of wastewater-treatment effluent on concentrations and fluxes of solutes in the Bush River, South Carolina, during extreme drought conditions. Environmental Geosciences 11:28–41.

Beck, K. C., J. H. Reuter, and E. M. Perdue. 1974. Organic and inorganic geochemistry of some coastal plain rivers of the southeastern United States. Geochimica et Cosmochimica Acta 38:341–364.

Blackman, W. C., J. V. Rouse, G. R. Schillinger, and W. H. Shafer. 1973. Mineral pollution in the Colorado River basin. Journal of the Water Pollution Control Federation 45:1517–1557.

Boelter, A. M., F. N. Lamming, A. M. Farag, and H. L. Bergman. 1992. Environmental effects of saline oil-field discharges on surface waters. Environmental Toxicology and Chemistry 11: 1187–1195.

Bradley, T. J. 2008. Hyper-regulators: life in fresh water. Pages 87–110 *in* Animal osmoregulation. Oxford University Press, Oxford, UK.

Burton, R. F. 1983. Ionic regulation and water balance. Pages 292–352 *in* A. S. M. Saleuddin and K. M. Wilbur (editors). The Mollusca. Volume 5: Physiology, Part 2. Academic Press, New York.

Carpenter, S. R., E. H. Stanley, and M. J. Vander Zanden. 2011. State of the world's freshwater ecosystems: physical, chemical, and biological changes. Annual Review of Environmental Resources 36:75–99.

Carr, D. B., A. R. Olsen, S. M. Pierson, and J.-Y. P. Courbois. 2000. Using linked micromap plots to characterize Omernik ecoregions. Data Mining and Knowledge Discovery 4:43–67.

Carr, D. B., and L. W. Pickle. 2010. Visualizing data patterns with micromaps. CRC Press, Boca Raton, Florida.

Chafin, D. T. 2003. Effect of the Paradox Valley unit on the dissolved-solids load of the Dolores River near Bedrock, Colorado, 1988–2001. Water Resources Investigation Report 02-4275. US Geological Survey, Grand Junction, Colorado.

Charmantier, G., M. Charmantier-Daures, and D. W. Towle. 2009. Osmotic and ionic regulation in aquatic arthropods. Pages 165–230 *in* D. H. Evans (editor). Osmotic and ionic regulation: cells and animals. CRC Press, Boca Raton, Florida.

Chen, Y., and L.-S. Lin. 2009. Responses of streams in central Appalachian Mountain region to reduced acidic deposition—comparisons with other regions in North America and Europe. Science of the Total Environment 407:2285–2295.

Dahm, K. G., K. L. Guerra, P. Xu, and J. E. Drewes. 2011. Composite geochemical database for coalbed methane produced water quality in the Rocky Mountain region. Environmental Science and Technology 45:7655–7663.

Dietz, T. H., A. S. Udoetok, J. S. Cherry, H. Silverman, and R. A. Byrne. 2000. Kidney function and sulfate uptake and loss in the freshwater bivalve *Toxolasma texasensis*. Biological Bulletin 199:14–20.

Dodds, W. K., W. W. Bouska, J. L. Eitzmann, T. J. Pilger, K. L. Pitts, A. J. Riley, J. T. Schloesser, and D. J. Thornbrugh. 2009. Eutrophication of U.S. freshwaters: analysis of potential economic damages. Environmental Science and Technology 43:12–19.

Drousé, S. K., D. C. Hillman, J. L. Engels, L. W. Creelman, and S. J. Simon. 1986. National Surface Water Survey, National Stream Survey (Phase I—Pilot, Mid-Atlantic Phase 1, Southeast Screening and Episodes Pilot) Quality Assurance Plan. EPA 600/4-86/044. US Environmental Protection Agency, Las Vegas, Nevada.

Drummond, M. A., and T. R. Loveland. 2010. Land-use pressure and a transition to forest-cover loss in the eastern United States. BioScience 60:286–298.

Duncan, R. A., M. G. Bethune, T. Thayalakumaran, E. W. Christen, and T. A. McMahon. 2008. Management of salt mobilization in the irrigated landscape – a review of selected irrigation regions. Journal of Hydrology 351:238–252.

Echols, B. S., R. J. Currie, and D. S. Cherry. 2009. Influence of conductivity dissipation on benthic macroinvertebrates in the North Fork Holston River, Virginia, downstream of a point-source brine discharge during severe low-flow conditions. Human and Ecological Risk Assessment 15:170–184.

El-Ashry, M. T., J. van Schilfgaarde, and S. Schiffman. 1985. Salinity pollution from irrigated agriculture. Journal of Soil and Water Conservation 40:48–52.

Entrekin, S., M. Evans-White, B. Johnson, and E. Hagenbuch. 2011. Rapid expansion of natural gas development poses a threat to surface waters. Frontiers of Ecology and the Environment 9:503–511.

Evans, D. H. 1980. Osmotic and ionic regulation by freshwater and marine fishes. Pages 93–122 *in* M. A. Ali (editor). Environmental physiology of fishes. Plenum Press, New York.

Evans, D. H. 2008. Teleost fish osmoregulation: what have we learned since August Krogh, Homer Smith, and Ancel Keys. American Journal of Physiology 295:R704–R713.

Fenneman, N. M. 1928. Physiographic divisions of the United States. Annals of the Association of American Geographers 18:261–353.

Feth, J. H. 1971. Mechanisms controlling world water chemistry: evaporation–crystallization process. [Comments on Gibbs (1970), "Mechanisms controlling world water chemistry." Science 170:1088–1090]. Science 172:870–871.

Gibbs, R. J. 1970. Mechanisms controlling world water chemistry. Science 170:1088–1090.

Gibbs, R. J. 1971. Reply to Feth (1971), "Mechanisms controlling world water chemistry: evaporation–crystallization process." Science 172:871–872.

Gorham, E. 1958. The influence and importance of daily weather conditions in the supply of chloride, sulphate and other ions to fresh waters from atmospheric precipitation. Philosophical Transactions of the Royal Society of London Series B: Biological Sciences 241:147–178.

Gorham, E. 1961. Factors influencing supply of major ions to inland waters, with special reference to the atmosphere. Geological Society of America Bulletin 72:795–840.

Gregory, K. B., R. D. Vidic, and D. A. Dzombak. 2011. Water management challenges associated with the production of shale gas by hydraulic fracturing. Elements 7:181–186.

Griffith, M. B., S. B. Norton, L. C. Alexander, A. I. Pollard, and S. D. LeDuc. 2012. The effects of mountaintop mines and valley fills on the physicochemical quality of stream ecosystems in the central Appalachians: a review. Science of the Total Environment 417–418:1–12.

Hawkins, C. P., J. R. Olson, and R. A. Hill. 2010. The reference condition: predicting benchmarks for ecological and water-quality assessments. Journal of the North American Benthological Society 29:312–343.

Herlihy, A. T., P. R. Kaufmann, and M. E. Mitch. 1991. Stream chemistry in the eastern United States. 2. Current sources of acidity in acidic and low acid-neutralizing capacity streams. Water Resources Research 27:629–642.

Herlihy, A. T., P. R. Kaufmann, M. E. Mitch, and D. D. Brown. 1990. Regional estimates of acid mine drainage impact on streams in the mid-Atlantic and southeastern United States. Water, Air, and Soil Pollution 50:91–107.

Herlihy, A. T., D. P. Larsen, S. G. Paulsen, N. S. Urquhart, and B. J. Rosenbaum. 2000. Designing a spatially balanced, randomized site selection process for regional stream surveys: the EMAP Mid-Atlantic pilot study. Environmental Monitoring and Assessment 63:95–113.

Herlihy, A. T., and J. C. Sifneos. 2008. Developing nutrient criteria and classification schemes for wadeable streams in the conterminous U.S. Journal of the North American Benthological Society 27:932–948.

Herlihy, A. T., J. L. Stoddard, and C. B. Johnson. 1998. The relationship between stream chemistry and watershed land cover data in the mid-Atlantic region, U.S. Water, Air, and Soil Pollution 106:377–386.

Jackson, R. B., and E. G. Jobbágy. 2005. From icy roads to salty streams. Proceedings of the National Academy of Sciences of the United States of America 102:14487–14488.

Jackson, R. E., and K. J. Reddy. 2007. Geochemistry of coalbed natural gas (CBNG) produced water in Powder River Basin, Wyoming: salinity and sodicity. Water, Air, and Soil Pollution 184:49–61.

Jeziorski, A., N. D. Yan, A. M. Paterson, A. M. DeSellas, M. A. Turner, D. S. Jeffries, B. Keller, R. C. Weeber, D. K. McNicol, M. E. Palmer, K. McIver, K. Arseneau, B. K. Ginn, B. F. Cumming, and J. P. Smol. 2008. The widespread threat of calcium decline in fresh waters. Science 322:1374–1377.

Johnson, L. B., C. Richards, G. E. Host, and J. W. Arthur. 1997. Landscape influences on water chemistry in Midwestern stream ecosystems. Freshwater Biology 37:193–208.

Kaufmann, P. R., A. T. Herlihy, M. E. Mitch, J. J. Messer, and W. S. Overton. 1991. Stream chemistry in the eastern United States. 1. Synoptic survey design, acid-base status, and regional patterns. Water Resources Research 27:611–627.

Kaushal, S. S., P. M. Groffman, G. E. Likens, K. T. Belt, W. P. Stack, V. R. Kelly, L. E. Band, and G. T. Fisher. 2005. Increased salinization of fresh water in the northeastern United States. Proceedings of the National Academy of Sciences of the United States of America 102:13517–13520.

Kelly, V. R., G. M. Lovett, K. C. Weathers, S. E. Findlay, D. L. Strayer, D. I. Burns, and G. E. Likens. 2008. Long-term sodium chloride retention in a rural watershed: legacy effects of road salt on streamwater concentration. Environmental Science and Technology 42:410–415.

Kennedy, A. J., D. S. Cherry, and R. J. Currie. 2003. Field and laboratory assessment of a coal processing effluent in the Leading Creek watershed, Meigs County, Ohio. Archives of Environmental Contamination and Toxicology 44:324–331.

Kilham, P. 1990. Mechanisms controlling the chemical composition of lakes and rivers: data from Africa. Limnology and Oceanography 35:80–83.

Kimmel, W. G., and D. G. Argent. 2010. Stream fish community responses to a gradient of specific conductance. Water, Air, and Soil Pollution 206:49–56.

Lazorchak, J. M., D. J. Klemm, and D. V. Peck (editors). 1998. Environmental Monitoring and Assessment Program—Surface Waters: field operations and methods for measuring the ecological conditions of wadeable streams. EPA 620/R-94/004F. National Exposure Research Laboratory and National Health and Environmental Effects Research Laboratory, Office of Research and Development, US Environmental Protection Agency, Research Triangle Park, North Carolina.

Likens, G. E., F. H. Bormann, N. M. Johnson, D. W. Fisher, and R. S. Pierce. 1970. Effects of forest cutting and herbicide treatment on nutrient budgets in the Hubbard Brook Watershed ecosystem. Ecological Monographs 40:23–47.

Mattson, M. D., P. J. Godfrey, M. F. Walk, P. A. Kerr, and O. T. Zajicek. 1992. Regional chemistry of lakes in Massachusetts. Water Resources Bulletin 28:1045–1056.

McCormick, F. H., D. V. Peck, and D. P. Larsen. 2000. Comparison of geographic classification schemes for Mid-Atlantic stream fish assemblages. Journal of the North American Benthological Society 19:385–404.

Meyer, J. S., D. A. Sanchez, J. A. Brookman, D. B. McWhorter, and H. L. Bergman. 1985. Chemistry and aquatic toxicity of raw oil shale leachates from Piceance Basin, Colorado. Environmental Toxicology and Chemistry 4:559–572.

Morgan, M. D., and R. E. Good. 1988. Stream chemistry in the New Jersey Pinelands: the influence of precipitation and watershed disturbance. Water Resources Research 24:1091–1100.

Mount, D. R., D. D. Gulley, J. R. Hockett, T. D. Garrison, and J. M. Evans. 1997. Statistical models to predict the toxicity of major ions to *Ceriodaphnia dubia*, *Daphnia magna* and *Pimephales promelas* (fathead minnows). Environmental Toxicology and Chemistry 16:2009–2019.

Naiman, R. J., and E. C. Anderson. 1997. Streams and rivers: their physical and biological variability. Pages 131–148 *in* P. K. Schoonmaker, B. von Hagen, and E. C. Wolf (editors). The rainforests of home: profile of a North American bioregion. Island Press, Washington, DC.

Olson, J. R., and C. P. Hawkins. 2012. Predicting natural baseflow stream water chemistry in the western United States. Water Resource Research 48:W02504.

Omernik, J. M. 1987. Ecoregions of the conterminous United States. Annals of the Association of American Geographers 77:118–125.

Omernik, J. M. 1995. Ecoregions: a spatial framework for environmental management. Pages 49–62 *in* W. S. Davis and T. P. Simon (editors). Biological assessment and criteria: tools for water resource planning and decision making. Lewis Publishers, Boca Raton, Florida.

Pan, Y., R. J. Stevenson, B. H. Hill, A. T. Herlihy, and G. B. Collins. 1996. Using diatoms as indicators of ecological conditions in lotic systems: a regional assessment. Journal of the North American Benthological Society 15:481–495.

Paul, J. F., and M. E. McDonald. 2006. Development of empirical, geographically specific water quality criteria: a conditional probability analysis approach. Journal of the American Water Resources Association 41:1211–1223.

Paulsen, S. G., A. Mayio, D. V. Peck, J. L. Stoddard, E. Tarquinio, S. M. Holdsworth, J. van Sickle, L. L. Yuan, C. P. Hawkins, A. T. Herlihy, P. R. Kaufmann, M. T. Barbour, D. P. Larsen, and A. R. Olsen. 2008. Condition of stream ecosystems in the US: an overview of the first national assessment. Journal of the North American Benthological Society 27:812–821.

Pawlowicz, R. 2008. Calculating the conductivity of natural waters. Limnology and Oceanography: Methods 6:489–501.

Perry, S. F., A. Shahsavarani, T. Georgalis, M. Bayaa, M. Furimsky, and S. L. Y. Thomas. 2003. Channels, pumps, and exchangers in the gill and kidney of freshwater fishes: their role in ionic and acid-base regulation. Journal of Experimental Zoology Part A: Comparative Experimental Biology 300A: 53–62.

Petts, G. E. 2000. A perspective of the abiotic processes sustaining the ecological integrity of running waters. Hydrobiologia 422/423:15–27.

Phillips, F. M., S. Mills, M. H. Hendrickx, and J. Hogan. 2003. Environmental tracers applied to quantifying causes of salinity in arid-region rivers: results from the Rio Grande basin, southwestern USA. Developments in Water Science 50:327–334.

Pond, G. J., M. E. Passmore, F. A. Borsuk, L. Reynolds, and C. J. Rose. 2008. Downstream effects of mountaintop coal mining: comparing biological conditions using family- and genus-level macroinvertebrate bioassessment tools. Journal of the North American Benthological Society 27:717–737.

Poole, G. C., J. B. Dunham, D. M. Keenan, S. T. Sauter, D. A. McCullough, C. Mebane, J. C. Lockwood, D. A. Essig, M. P. Hicks, D. J. Sturdevant, E. J. Materna, S. A. Spalding, J. Risley, and M. Deppman. 2004. The case for regime-based water quality standards. BioScience 54:155–161.

Raynor, G. S., and J. V. Hayes. 1982. Concentrations of some ionic species in central Long Island, New York, precipitation in relation to meteorological variables. Water, Air, and Soil Pollution 17:309–335.

Richter, D. D., C. W. Ralston, and W. R. Harms. 1983. Chemical composition and spatial variation of bulk precipitation at a Coastal Plain watershed in South Carolina. Water Resources Research 19:134–140.

Rose, S. 2007. The effects of urbanization on the hydrochemistry of base flow within the Chattahoochee River Basin (Georgia, USA). Journal of Hydrology 341:42–54.

Skjelkvåle, B. L., J. L. Stoddard, D. S. Jeffries, K. Tørseth, T. Høgåsen, J. Bowman, J. Mannio, D. T. Monteith, R. Mosello, M. Rogora, D. Rzychon, J. Vesely, J. Wieting, A. Wilander, and A. Worsztynowicz. 2005. Regional scale evidence for improvements in surface water chemistry 1990–2001. Environmental Pollution 137:165–176.

Sleeter, B. M., C. E. Soulard, T. S. Wilson, and D. G. Sorenson. 2012. Land-cover trends in the western United States—1973 to 2000. Pages 3–32 *in* B. M. Sleeter, T. S. Wilson, and W. Acevedo (editors). Status and trends of land change in the western United States: 1973–2000. Professional Paper 1794-A. US Geological Survey, Reston, Virginia.

Smart, M. M., J. R. Jones, and J. L. Sebaugh. 1985. Stream-watershed relations in the Missouri Ozark Plateau province. Journal of Environmental Quality 14:77–82.

Smart, R. P., C. Soulsby, M. S. Cresser, A. J. Wade, J. Townend, M. F. Billett, and S. Langan. 2001. Riparian zone influence on stream water chemistry at different spatial scales: a GIS-based modeling approach, an example for the Dee, NE Scotland. Science of the Total Environment 280:173–193.

Smeck, N. E., and L. P. Wilding. 1980. Quantitative evaluation of pedon formation in calcareous glacial deposits in Ohio. Geoderma 24:1–16.

Smith, R. A., R. B. Alexander, and G. E. Schwarz. 2003. Natural background concentrations of nutrients in streams and rivers of the conterminous United States. Environmental Science and Technology 37:3039–3047.

Stallard, R. F., and J. M. Edmond. 1981. Geochemistry of the Amazon. 1. Precipitation chemistry and the marine contribution to the dissolved load at the time of peak discharge. Journal of Geophysical Research 86:9844–9858.

Stallard, R. F., and J. M. Edmond. 1983. Geochemistry of the Amazon. 2. The influence of geology and weathering environment of the dissolved load. Journal of Geophysical Research 88:9671–9688.

Stallard, R. F., and J. M. Edmond. 1987. Geochemistry of the Amazon. 3. Weathering chemistry and limits to dissolved inputs. Journal of Geophysical Research 92:8293–8302.

Stoddard, J. L., J. S. Kahl, F. A. Deviney, D. R. DeWalle, C. T. Driscoll, A. T. Herlihy, J. H. Kellogg, P. S. Murdoch, J. R. Webb, and K. E. Webster. 2003. Response of surface water chemistry to the Clean Air Act Amendments of 1990. EPA 620/R-03/001. National Health and Environmental Effects Research Laboratory, Office of Research and Development, US Environmental Protection Agency, Research Triangle Park, North Carolina.

Stoddard, J. L., D. P. Larsen, C. P. Hawkins, R. K. Johnson, and R. H. Norris. 2006. Setting expectations for the ecological condition of streams: the concept of reference condition. Ecological Applications 16:1267–1276.

Strahler, A. H. 1957. Quantitative analysis of watershed geomorphology. Transactions of the American Geophysical Union 38:913–920.

Symanzik, J., and D. B. Carr. 2008. Interactive linked micromap plots for the display of geographically referenced statistical data. Pages 267–294 *in* C. Chen, W. Härdle, and A. Unwin (editors). Handbook of data visualization. Springer, Berlin, Germany.

Szabo, J. P. 2006. Textural and mineralogical characteristics of tills of northeastern and north-central Ohio. Ohio Journal of Science 106:9–16.

Tietge, J. E., J. R. Hockett, and J. M. Evans. 1997. Major ion toxicity of six produced waters to three freshwater species: application of ion toxicity models and TIE procedures. Environmental Toxicology and Chemistry 14:2002–2008.

USEPA (US Environmental Protection Agency). 1987. Handbook of methods for acid deposition studies: laboratory analysis for surface water chemistry. EPA 600/4-87/026. Office of Research and Development, Office of Acid Deposition, Environmental Monitoring, and Quality Assurance, US Environmental Protection Agency, Washington, DC.

USEPA (US Environmental Protection Agency). 2000. Nutrient criteria technical guidance manual: rivers and streams. EPA 822/B-00/002. Office of Water, Office of Science and Technology, US Environmental Protection Agency, Washington, DC.

USEPA (US Environmental Protection Agency). 2004a. Wadeable stream assessment: field operations manual. EPA 841/B-04/004. Office of Water, US Environmental Protection Agency, Washington, DC.

USEPA (US Environmental Protection Agency). 2004b. Wadeable stream assessment: quality assurance project plan. EPA 841/B-04/005. Office of Water, US Environmental Protection Agency, Washington, DC.

USEPA (US Environmental Protection Agency). 2004c. Wadeable stream assessment: water chemistry laboratory manual. EPA 841/B-04/008. Office of Water, US Environmental Protection Agency, Washington, DC.

USEPA (US Environmental Protection Agency). 2005. National hydrography dataset plus. Edition 1.0. Office of Water, US Environmental Protection Agency, Washington, DC.

USEPA (US Environmental Protection Agency). 2009a. National rivers and streams assessment: field operations manual. EPA 841/B-07/009. Office of Water, US Environmental Protection Agency, Washington, DC.

USEPA (US Environmental Protection Agency). 2009b. National rivers and streams assessment: laboratory methods manual. EPA 841/B-07/010. Office of Water, US Environmental Protection Agency, Washington, DC.

USEPA (US Environmental Protection Agency). 2010. National rivers and streams assessment: quality assurance project plan. EPA 841/B-07/007. Office of Water, US Environmental Protection Agency, Washington, DC.

USEPA (US Environmental Protection Agency). 2011a. A field-based aquatic life benchmark for conductivity in central Appalachian streams. EPA 600/R-10/023F. Office of Research and Development, National Center for Environmental Assessment, US Environmental Protection Agency, Washington, DC.

USEPA (US Environmental Protection Agency). 2011b. Level III ecoregions of the continental United States (revision of Omernik, 1987). Map M-1, various scales, and shapefiles. Office of Research and Development, National Health and Environmental Effects Research Laboratory, Corvallis, Oregon.

Veil, J. A., M. G. Puder, D. Elcock, and R. J. Redweik. 2004. A white paper describing produced water from production of crude oil, natural gas, and coal bed methane. Argonne National Laboratory, US Department of Energy, Argonne, Illinois. (Available from: http://s3.amazonaws.com/propublica/assets/natural_gas/doe_produced_water_2004.pdf)

Veni, G., H. DuChene, N. C. Crawford, C. G. Groves, G. H. Huppert, E. H. Kastning, R. Olson, and B. J. Wheeler. 2001. Living with karst: a fragile foundation. Environmental Awareness Series 4. American Geological Institute, Alexandria, Virginia. (Available from: http://www.agiweb.org/environment/publications/karst.pdf)

Vörösmarty, C. J., B. Moore, A. L. Grace, M. P. Gildea, J. M. Melillo, B. J. Peterson, E. B. Rastetter, and P. A. Steudler. 1989. Continental scale models of water balance and fluvial transport: an application to South America. Global Biogeochemical Cycles 3:241–265.

Webster, J. R., S. W. Golladay, E. F. Benfield, J. L. Meyer, W. T. Swank, and J. B. Wallace. 1992. Catchment disturbance and stream response: overview of stream research at Coweeta Hydrologic Laboratory. Pages 231–253 *in* P. J. Boon, P. Calow, and G. E. Petts (editors). River conservation and management. John Wiley and Sons, Chichester, UK.

Whittier, T. R., J. L. Stoddard, D. P. Larsen, and A. T. Herlihy. 2007. Selecting reference sites for stream biological assessments: best professional judgment or objective criteria. Journal of the North American Benthological Society 26:349–360.

Wigington, P. J., M. R. Church, T. C. Strickland, K. N. Eshleman, and J. van Sickle. 1998. Autumn chemistry of Oregon Coast Range streams. Journal of the American Water Resources Association 34:1035–1049.

Wilken, E., F. J. Nava, and G. Griffith. 2011. North American terrestrial ecoregions—Level III. Commission for Environmental Cooperation, Montreal, Quebec, Canada. (Available from: ftp://ftp.epa.gov/wed/ecoregions/pubs/NA_TerrestrialEcoregionsLevel3_Final-2june11_CEC.pdf)

Woods, A. J., J. M. Omernik, and D. D. Brown. 1999. Level III and IV ecoregions of EPA Region 3: Delaware, Maryland,

Pennsylvania, Virginia, and West Virginia. National Health and Environmental Effects Research Laboratory, US Environmental Protection Agency, Corvallis, Oregon.

Woods A. J., J. M. Omernik, and B. C. Moran. 2007. Level III and IV ecoregions of New Jersey. Map WO-1-07. National Health and Environmental Effects Research Laboratory, US Environmental Protection Agency, Corvallis, Oregon.

Wright, I. A., P. J. Davies, S. J. Findlay, and O. J. Jonasson. 2011. A new type of water pollution: concrete drainage infrastructure and geochemical contamination of urban waters. Marine and Freshwater Research 62:1355–1361.

Zampella, R. A. 1994. Characterization of surface water quality along a watershed disturbance gradient. Water Resources Bulletin 30:605–611.

Zheng, L., J. Gerritsen, J. Beckman, J. Ludwig, and S. Wilkes. 2008. Land use, geology, enrichment, and stream biota in the eastern Ridge and Valley ecoregion: implications for nutrient criteria development. Journal of the American Water Resources Association 44:1521–1536.

Zielinski, R. A., J. K. Otton, and C. A. Johnson. 2001. Sources of salinity near a coal mine spoil pile, north-central Colorado. Journal of Environmental Quality 30:1237–1248.

Table of Contents

General_Authors_Publications.....2
LI-266371_Rappold_et_al_2017.....14
LI-266372_Fann_et_al_2017.....23
Fann_et_al_2017.....31
Rappold_et_al_2017.....39
Rappold2017_AIR.....48
Fann2018_AIR.....53
Fann_2018_News.....58
Concur_emails.....69

United States Environmental Protection Agency
Washington, DC 20460

STAA REPORT FOR THE SCIENTIST NOMINATIONS

General Information:

Nomination ID/App ID:	20-075
Research Category Primary:	Health Effects Research and Human Health Risk Assessment (HE)
Research Category Secondary:	Risk Management and Ecosystem Restoration (RM);Environmental Policy and Decision-Making Studies (EP)
Laboratory/Office Name:	OAR
Nomination Entered By:	Neal Fann

Eligibility Checklist:

[Y] The nominated publication(s) has not been submitted to a previous STAA competition.

[Y] The nominated publication(s) was published on or before January 1, 2017 and on or after January 1,2012

[Y] The principal author was an EPA employee or a PHS employee assigned to EPA when the research was performed

[Y] The EPA authors (includes PHS employees assigned to EPA) contributed collectively a minimum of 50% toward the publication(s)

Nominating Official Name:	Erika Sasser
Nominating Official Title:	DIRECTOR
Nominating OfficialEmail:	sasser.erika@epa.gov
STAA Coordinator Name:	Kathleen Wiser
STAA Coordinator Email:	wiser.kathi@epa.gov

Justifications:

Justification 1:

These two manuscripts advance greatly the Agency's ability to: (1) understand the size and distribution of the burden to health of wildland fires in the U.S.; (2) describe the economic value of this burden; and (3) identify communities in the U.S. who are most vulnerable to wildland fire smoke. Taken together, this research provides further evidence that wildland fires represent a substantial burden to the U.S. population—in terms both of the number and dollar value of adverse health effects—and gives the EPA, state and local air agencies insight to who specifically is at greatest risk and where these individuals live.

The first manuscript, published in *Environmental Science and Technology* (Rappold et al. 2017) and authored by a multi-disciplinary team of biostatisticians, clinicians and air quality modelers, developed a new Community Health-Vulnerability Index; this identified the attributes and location of population subgroups at greatest risk of fine particles (particulate matter sized 2.5 microns and smaller, or $PM_{2.5}$) originating from wildfire events. Performing a principle components analysis, the team identified five population attributes that were the best predictors of vulnerability, including economic depravation, age of population, chronic pre-existing respiratory conditions, hypertension and pediatric asthma. The team next simulated daily wildland fire-attributable $PM_{2.5}$ concentrations for 2008 to 2012.

Synthesizing these data, the team identified approximately 10% of the U.S. population was both highly exposed to wildland fire $PM_{2.5}$ and also at greatest baseline risk to $PM_{2.5}$-related health impacts. Counties identified as most vulnerable tended to be located in southeastern states including South Carolina, Georgia, Alabama, Mississippi, Kentucky and Missouri. Such information may be used by federal, state and local agencies when developing air quality management plans and determining how best to manage prescribed burns as a forest management practice.

In the second manuscript, published in *Science of the Total Environment* (Fann et al. 2018), a U.S.-Australian research team comprised of biostatisticians, clinicians, public health officials, risk assessors and epidemiologists described the number and economic value of wildland fire episodes in the Continental U.S. Using the same time series of wildland fire-attributable $PM_{2.5}$ concentrations modeled for the period from 2008 to 2012, the team quantified the number and economic value of PM2.5-attributable premature deaths and illnesses over this 5-year period.

This manuscript is unique for having both quantified the national burden of wildland fires and the number and economic value of these impacts, finding that tens of thousands of wildland $PM_{2.5}$-related respiratory hospital admissions and premature deaths occurred over this period, carrying an economic value of between $76 and $120B (2010$). The team found that the greatest impacts occurred in the northwestern and southeastern portions of the U.S. and that black populations received relatively greater exposure than populations of other races. Finally, the team reported the greatest estimated burden from wildland fires occuring in 2008.

Each of the manuscripts above directly support the Agency's Strategic Plan. In particular, by detailing the air quality and health impacts posed by wildland fire $PM_{2.5}$, these papers support Goal 1.1 (Improve Air Quality). The manuscripts also support Goal 3.3 (Prioritize Robust Science) by informing policy decisions with more detailed information regarding the scope and magnitude of the wildland fire problem in the U.S.

Justification 2A:

These manuscripts use a common set of model parameters and demographic data to address two dimensions of a critical science-policy question—namely, who is most vulnerable to $PM_{2.5}$ originating from wildland fires and what is the overall burden? Rappold and co-authors applied CMAQ photochemical modeled concentrations jointly with health and socioeconomic data to characterize population vulnerability. Fann and co-authors employed these same CMAQ model predictions and many of the same demographic data to describe the burden to health of wildfire episodes.

Justification 2B:

George Pouliot

2017, EPA STAA award Honorable Mention, co-author of "Historical gaseous and primary aerosol emissions in the United States from 1990 to 2010" Xing, J., J. Pleim, R. Mathur, G. Pouliot, C. Hogrefe, C.-M. Gan, and C. Wei (2013), Historical gaseous and primary aerosol emissions in the United States from 1990 to 2010, *Atmospheric Chemistry and Physics*, *13*(15), 7531-7549. 2016, EPA STAA award Level 3, co-author of "WRF-CMAQ two-way coupled system with aerosol feedback: software development and preliminary results" Wong, D., J. Pleim, R. Mathur, F. Binkowski, T. Otte, R. Gilliam**,** G. Pouliot, A. Xiu, J. Young, and D. Kang (2012), WRF-CMAQ two-way coupled system with aerosol feedback: software development and preliminary results, *Geoscientific Model Development*, *5* (2), 299-312.

2016, EPA STAA award Level 3, co-author of "Predicting the effects of nano-scale cerium additives in diesel fuel on regional-scale air quality" Erdakos, G. B., P. V. Bhave, G. Pouliot, H. Simon, and R. Mathur (2014), Predicting the effects of nanoscale cerium additives in diesel fuel on regional-scale air quality, *Environmental Science & Technology*, *48*(21), 12775-12782.

Justification 2C:

This nomination is distinct from those proposed by Pouliot in 2016 and 2017. Where those proposals demonstrated improved techniques for modeling air quality concentrations, this nomination is focused instead on the air quality and health impacts attributable to wildland fire smoke.

Justification 2D:

N/A

Justification 2E:

Fann is included as a co-author on an STAA nomination for a 2015 paper characterizing climate-related changes in ozone concentrations and subsequent

health impacts. Where that project explored the relationship between changes in future climate, air quality and health, the present work focuses on the air quality and health impacts associated with recent wildfire activity.

Justification 3A:

Rappold et al. (2017) has accumulated 33 citations in the peer reviewed literature in the three years from which it was first published in *Environmental Science and Technology.* This paper has informed manuscripts describing best practices for adapting to the increased incidence of wildland fires (Schumann et al. 2020); those improving the reliability of wildfire photochemical forecasting (Liu et al. 2019); and, health impact assessments of wildfire effects in certain states (e.g. Stowell et al. 2019). Researchers citing this work are affiliated with the U.S. Forest Service, the U.S. Centers for Disease Control and Prevention and the Environment & Climate Change Canada. This manuscript was part of the record supporting the Agency's award of a Silver Medal in 2018 for Rappold (*for prescient research on wildfire smoke and for constructive tools used by public health officials, health care providers, and the public to protect human health*).The journal *Environmental Science and Technology* has a high impact factor (7.1) and a broad readership within the air quality and environmental health communities.

Fann et al. (2018) accumulated 62 citations in the peer reviewed literature in the two years from which it was first published. This paper was featured in 11 news outlets in three countries, including a Washington Post article titled “Smoke from Wildfires may be Surprisingly Deadly, scientists report,” describing the adverse human health effects attributable to wildfire events. Other publications including Wired.com, the Herald Tribune and the Denver Post. The American Thoracic Society and Marron Institute each cited this paper in an article proposing a lower, and the argued more health protective, $PM_{2.5}$ air quality standard. This paper also supported a broader research effort led by the author team that was funded in part by a Department of Interior-sponsored Joint Fire Science Program grant. Finally, elsewhere in the peer reviewed literature, this paper has supported studies characterizing the distribution of wildland fire $PM_{2.5}$ among non-white populations (Johnston Gautier et al. 2019); the influence of climate change on projected wildfire smoke impacts (Limaye et al. 2019); and, epidemiologic studies examining the cardiovascular effects of wildfire smoke (DeFlorio-Barker et al. 2019).

Justification 3B:

The article appearing in *Environmental Science and Technology* received critical feedback from anonymous referees in December of 2016. The authors revised the manuscript over a 5 month period. The journal accepted the manuscript for publication in May of 2017.

The article appearing in *State of the Total Environment* received critical feedback from two anonymous referees in April of 2017. Each identified weaknesses in the methodology—particularly the choice of epidemiologic study used to estimate risks from wildland fire episodes and the role of the quantitative meta-analysis in supporting the risk analysis. The co-authors addressed these weaknesses by more rigorously assessing the suitability of the wildfire epidemiologic studies to supporting a risk assessment and by clarifying the role of the quantitative meta-analysis. After revising the manuscript over a three month period, the journal accepted the article for publication in August of 2017.

AUTHORS

Contributing Author

Author Name:	Richard Broome		
Professional Title:		Salutation:	Dr.
Email:	richard.broome@sswahs.nsw.gov.au	Organization:	
Mailing Address:			
Street Line 1:			
City:			
Zip Code:		State:	
At time of research was:	Non EPA Personnel		
Separation Date:			
% of Effort:	5		

Contributing Author

Author Name:	Jeanette Reyes		
Professional Title:		Salutation:	Dr.
Email:	reyes.jeanette@epa.gov	Organization:	
Mailing Address:			
Street Line 1:			
City:			
Zip Code:		State:	
At time of research was:	EPA Employee		
Separation Date:			
% of Effort:	10		

Contributing Author

Author Name:	Ana Rappold		
Professional Title:		Salutation:	Dr.
Email:		Organization:	
Mailing Address:			
Street Line 1:			
City:			
Zip Code:		State:	
At time of research was:	EPA Employee		
Separation Date:			
% of Effort:	27		

Contributing Author

Author Name:	Breanna Alman		
Professional Title:		Salutation:	Ms.
Email:	pcq6@cdc.gov	Organization:	
Mailing Address:			
Street Line 1:			
City:			
Zip Code:		State:	
At time of research was:	Non EPA Personnel		
Separation Date:			
% of Effort:	10		

Contributing Author

Author Name:	Wayne Cascio		
Professional Title:		Salutation:	Dr.
Email:	cascio.wayn@epa.gov	Organization:	
Mailing Address:			
Street Line 1:			
City:			
Zip Code:		State:	
At time of research was:	EPA Employee		
Separation Date:			
% of Effort:	5		

Contributing Author

Author Name:	David Diaz-Sanchez		
Professional Title:		Salutation:	Dr.
Email:	diaz-sanchez.david@epa.gov	Organization:	
Mailing Address:			
Street Line 1:			
City:			
Zip Code:		State:	
At time of research was:	EPA Employee		
Separation Date:			
% of Effort:	5		

Contributing Author

Author Name:	Fay Johnston		
Professional Title:		Salutation:	Dr.
Email:	fay.johnston@utas.edu.au	Organization:	
Mailing Address:			
Street Line 1:			
City:			
Zip Code:		State:	
At time of research was:	Non EPA Personnel		
Separation Date:			
% of Effort:	5		

Contributing Author

Author Name:	Geoff Morgan		
Professional Title:		Salutation:	Dr.
Email:	geoffrey.morgan@sydney.edu.au	Organization:	
Mailing Address:			
Street Line 1:			
City:			
Zip Code:		State:	
At time of research was:	Non EPA Personnel		
Separation Date:			
% of Effort:	5		

Contributing Author

Author Name:	George Pouliot		
Professional Title:		Salutation:	Dr.
Email:	pouliot.george@epa.gov	Organization:	
Mailing Address:			
Street Line 1:			
City:			
Zip Code:		State:	
At time of research was:	EPA Employee		
Separation Date:			
% of Effort:	10		

Principal Author

Author Name:	Neal L. Fann		
Professional Title:		Salutation:	
Email:	fann.neal@epa.gov	Organization:	
Mailing Address:			
Street Line 1:			
City:			
Zip Code:		State:	
At time of research was:	EPA Employee		
Separation Date:			
% of Effort:	18		

PUBLICATIONS

Publication 1:

Publication Title:	Community Vulnerability to Health Impacts of Wildland Fire Smoke Exposure		
Publication Date:	Thu May 11 00:00:00 GMT 2017		
Journal/Publication Method:	Environmental Science & Technology		
All Author(s):			
Volume:	51	Number:	12
Pages:	6674-6682	Immediately Index:	Immediately Index:
Citation ½ Life:	7.8	Impact Factor:	7.149

Publication 2:

Publication Title:	Fann, N, et al. (2018). The Health Impacts and Economic Value of Wildland Fire Episodes in the US: 2		
Publication Date:	Fri Aug 18 00:00:00 GMT 2017		
Journal/Publication Method:	Science of the Total Environment		
All Author(s):			
Volume:	610	Number:	1
Pages:	802-809	Immediately Index:	Immediately Index:
Citation ½ Life:	4.4	Impact Factor:	5.589

Environmental Science & Technology

Policy Analysis

pubs.acs.org/est

Community Vulnerability to Health Impacts of Wildland Fire Smoke Exposure

Ana G. Rappold*

National Health and Environmental Effects Research Laboratory/Environmental Public Health Division, United States Environmental Protection Agency, Research Triangle Park, North Carolina 27709, United States

Jeanette Reyes

National Health and Environmental Effects Research Laboratory/Environmental Public Health Division, United States Environmental Protection Agency, Research Triangle Park, North Carolina 27709, United States

George Pouliot

National Exposure Research Laboratory/Computational Exposure Division, United States Environmental Protection Agency, Research Triangle Park, North Carolina 27709, United States

Wayne E. Cascio

National Health and Environmental Effects Research Laboratory/Environmental Public Health Division, United States Environmental Protection Agency, Research Triangle Park, North Carolina 27709, United States

David Diaz-Sanchez

National Health and Environmental Effects Research Laboratory/Environmental Public Health Division, United States Environmental Protection Agency, Research Triangle Park, North Carolina 27709, United States

Supporting Information

ABSTRACT: Identifying communities vulnerable to adverse health effects from exposure to wildfire smoke may help prepare responses, increase the resilience to smoke and improve public health outcomes during smoke days. We developed a Community Health-Vulnerability Index (CHVI) based on factors known to increase the risks of health effects from air pollution and wildfire smoke exposures. These factors included county prevalence rates for asthma in children and adults, chronic obstructive pulmonary disease, hypertension, diabetes, obesity, percent of population 65 years of age and older, and indicators of socioeconomic status including poverty, education, income and unemployment. Using air quality simulated for the period between 2008 and 2012 over the continental U.S. we also characterized the population size at risk with respect to the level and duration of exposure to fire-originated fine particulate matter (fire-$PM_{2.5}$) and CHVI. We estimate that 10% of the population (30.5 million) lived in the areas where the contribution of fire-$PM_{2.5}$ to annual average ambient $PM_{2.5}$ was high (>1.5 $\mu g/m^3$) and that 10.3 million individuals experienced unhealthy air quality levels for more than 10 days due to smoke. Using CHVI we identified the most vulnerable counties and determined that these communities experience more smoke exposures in comparison to less vulnerable communities.

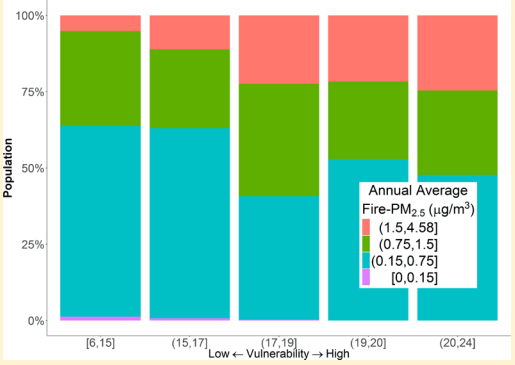

INTRODUCTION

Exposure to wildfire smoke is a serious health risk which can disproportionally impact sensitive groups. A number of studies have shown an association between smoke exposure and worsening of respiratory symptoms, increased rates of cardiorespiratory emergency visits, hospitalizations, and even

Received: December 8, 2016
Revised: May 4, 2017
Accepted: May 11, 2017
Published: May 11, 2017

ACS Publications © 2017 American Chemical Society

DOI: 10.1021/acs.est.6b06200
Environ. Sci. Technol. 2017, 51, 6674−6682

death.[1−12] Identifying communities vulnerable to adverse health outcomes during smoke days can provide valuable information for local, state, and federal governments and nongovernmental organizations to prioritize public health actions and improve public health outcomes on fire-smoke days.

Among the pollutants found in smoke, fine particulate matter ($PM_{2.5}$) is of the highest concern to health. In the most recent synthesis and evaluation of scientific literature on the health effects of air pollution, the Integrated Science Assessment (ISA), the U.S. Environmental Protection Agency[13] concluded that the weight of scientific evidence suggests a causal relationship between short- and long-term exposures and cardiovascular effects and mortality, and a likely causal relationship with respiratory effects. ISA is a comprehensive review of the health and ecological effects caused by air pollutants, mandated by the Clean Air Act, and provides the scientific basis for review of the National Ambient Air Quality Standards (NAAQS). Multiple studies demonstrate that the health impacts from $PM_{2.5}$ exposures are disproportionately shared by individuals in the sensitive groups.[14,15] The most sensitive groups include children, the aged, and pregnant women, as well as those with a pre-existing cardiopulmonary disease. Individuals and communities of lower socioeconomic status, and those with other pre-existing chronic inflammatory conditions are also considered at higher risk. Distribution of sensitive populations defines the vulnerability to adverse health effects across communities and reducing impacts among these populations is likely to bring the greatest public health burden benefit on smoke days.

Population vulnerability to various natural hazards has been studied for decades, however population vulnerability to smoke has not been well documented. Various aspects of population vulnerability have been examined in the context of heat waves,[16] famine, seismic events, coastal and inland floods, sea level rise, and drought.[17−20] Recent assessments have also focused on identifying communities vulnerable to environmental hazards exacerbated by climate change.[19,21,22] The purpose of assessing population vulnerability is to determine the population at greatest risk to environmental hazards, understand how communities respond and adapt and inform ways to mitigate the risk and negative impacts.[23] The communities that adapt to and recover after a disaster are those that can better plan, prepare and respond to environmental hazards. The alarming trends in the severity of wildland fires and growth of populations in the communities adjacent to wildlands call for an improved understanding of which communities are the most vulnerable to health impacts in order to improve public health response.

Here, we index community vulnerability to health effects of air pollution and wildfire smoke, based on previously studied clinical and social risk-factors that were found to modify the association between air pollution and adverse health outcomes. We then quantify population size at risk with respect to the levels of the index and the level and duration of smoke exposure in the recent past. To characterize smoke exposure in the recent past we simulated fire-originating fine particulate matter ($PM_{2.5}$) over a five-year period (2008−2012) using a chemical transport modeling system. The objective of this work is to demonstrate that community health vulnerability can be readily assessed using existing data and to provide motivation as to why it may be necessary. Understanding where the most vulnerable communities are found can be useful in developing outreach and education material.

MATERIALS AND METHODS

Development of Community Health-Vulnerability Index. To develop an index of community health-vulnerability to the adverse health effects of smoke exposures, we obtained specific socio-economic, demographic, and health outcome measures previously determined in the literature to modify the risk of air pollution related health outcomes.[13,24,25] More specifically, we obtained county prevalence for diabetes, hypertension, adult and pediatric asthma, chronic obstructive pulmonary disease (COPD); percent of population over 65 years of age, household income, education, rates of poverty, and unemployment. In the $PM_{2.5}$- Integrated Science Assessment,[13] both intrinsic (disease status) and extrinsic factors (poverty) are referred to as factors of susceptibility and vulnerability, respectively. However, because all of the factors are aggregated and not individual data, we use the term "vulnerability" throughout to define increased risk of adverse health outcomes related to exposure. In all cases we used county level indicators available across the continental U.S. because mitigation and adaptation plans are often planned and executed at the county level. The list of variables used to profile vulnerability is not intended to be exhaustive, but rather representative of the key clinical and social conditions known to or suspected to increase the risk of adverse health outcomes associated with fire- $PM_{2.5}$. Data sources and summary statistics are available in Supporting Information (SI) Table S1.

Prevalence and incidence estimates of pediatric asthma (in children <18 years of age), adult asthma (18+ years of age), and adult COPD (30+) which includes chronic bronchitis and emphysema, were obtained from the American Lung Association.[26] American Lung Association projected national and state prevalence of chronic lung disease to county levels using the Behavioral Risk Factor Surveillance System (BRFSS)[27] a phone based survey system that has been collecting data continuously since 2004, and statistical methods developed by the U.S. Census Bureau.

We used county level prevalence of hypertension to approximate prevalence of cardiovascular disease. We used sex specific and age adjusted hypertension prevalence data in adults over 30 years of age reported in Olives et al.[28] The study characterized the relationship between self-reported and physical measurements of hypertension reported in the National Health Examination and Nutrition Survey and used the relationship to adjust BRFSS 2009 self-reported responses on hypertension prevalence (among all respondents, percentage of those who reported systolic BP of at least 140 mmHg and/or self-reported taking medication) for self-reporting bias. Prevalence for county-level age, race, and sex adjusted estimates of diagnosed diabetes and obesity in adults (20 years of age and older) were obtained from BRFSS 2012 from http://www.cdc.gov/diabetes/atlas/countyrank/County_ListofIndicators.html.

Older adults and individuals of lower socio-economic status have been shown to be of increased risk of cardiovascular and respiratory effects in both short-term exposure studies and long-term exposure studies of air pollution.[13] Similarly, several studies found that socio-economic factors also modified health responses during the exposures to wildfire smoke.[29,30] Socio-economic and demographic profiles used in this study were taken from 2010 U.S. Census including population size by age group and gender, percent of individuals living in poverty, percent of families living in poverty, medium household income, and percent of unemployment.[31]

DOI: 10.1021/acs.est.6b06200
Environ. Sci. Technol. 2017, 51, 6674−6682

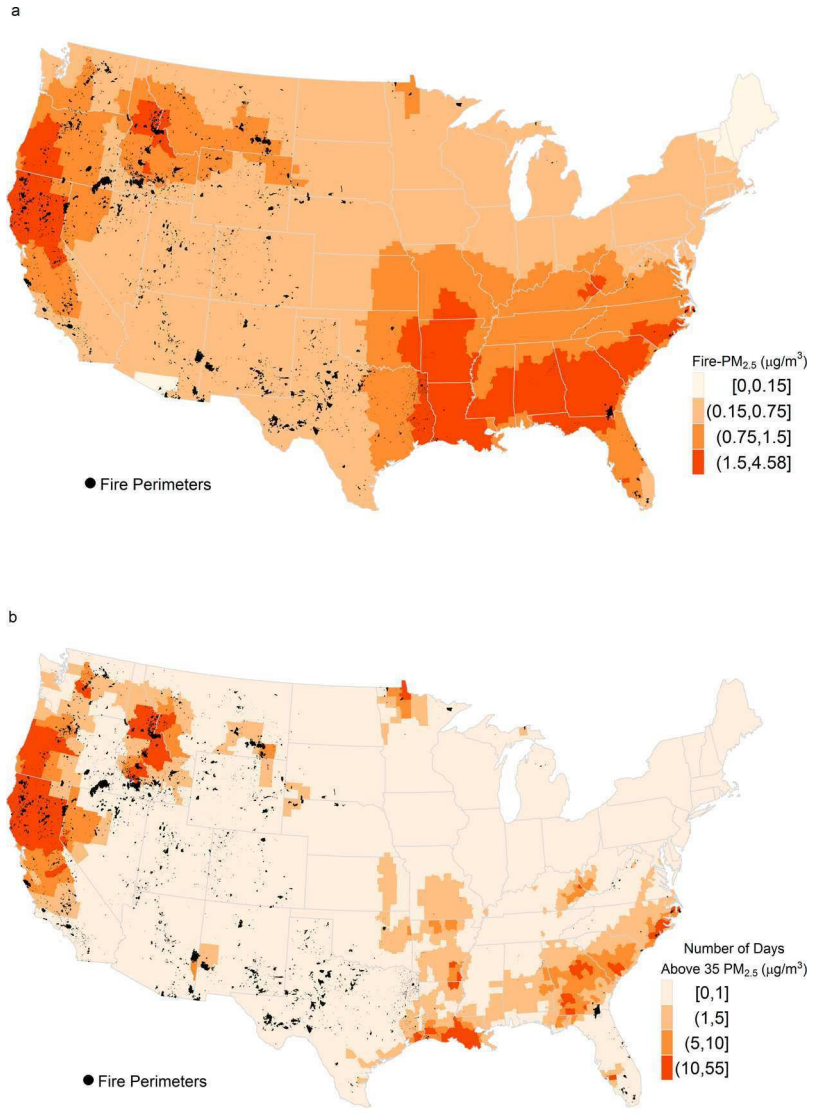

Figure 1. (a) Annual average daily fire-$PM_{2.5}$ footprint by counties of continental US and perimeters of area burned by large fires in black (GeoMAC) between 2008 and 2012. (b) Number of days with fire-$PM_{2.5}$ above 35 $\mu g/m^3$ by counties of continental US and perimeters of area burned by large fires in black (GeoMAC) between 2008 and 2012.

We used principal components analysis and varimax rotation to reduce the number of measures of vulnerability into a smaller number of independent components. All measures of vulnerability were standardized prior to analysis. The first five components explained 84% of variance and were highly loaded on (1) economic deprivation, (2) population of 65 years and older, (3) chronic adult respiratory conditions (COPD and asthma), (4) pre-existing conditions linked to hypertension, obesity and diabetes, and (5) pediatric asthma (SI Table S2). All five components were positively associated with primary measures, with the exception of median household income that was negatively loaded on the first component measuring economic deprivation (SI Figure S11). The higher scores of all five components described the more vulnerable state (more poverty, more individuals 65 years and older, more chronic respiratory and other conditions). The five components were individually assigned quintile scores (1 (the least vulnerable) to 5 (the most vulnerable)). Quintile ranks for each component were added together to create overall Community Health-Vulnerability Index (CHVI) with higher values defining more vulnerable states.

Air Quality Simulations. We simulated daily air quality from 2008 to 2012 using the Community Multiscale Air Quality (CMAQ) model with and without wildland and prescribed fires. The calculated difference between the two model runs represents the contribution of fire emissions to the ambient $PM_{2.5}$ levels (fire-$PM_{2.5}$). Inputs to the model included gridded meteorological fields, emissions data, and boundary conditions. For a regional or continental CMAQ model simulation, the meteorological fields were provided by annual CONUS Weather Research and Forecasting model (WRF) simulation that utilized 12 km horizontal grid spacing and 35 vertical layers of variable thickness extending up to 50 hPa, with the top of the lowest model layer at approximately 20 m above ground level. Initial and boundary conditions for WRF were provided by the North American Mesoscale Model available from the National Centers for Environmental Prediction. The input emissions were based on a 12 km national U.S. domain with speciation for the Carbon-Bond 05 chemical mechanism.[32]

DOI: 10.1021/acs.est.6b06200
Environ. Sci. Technol. 2017, 51, 6674−6682

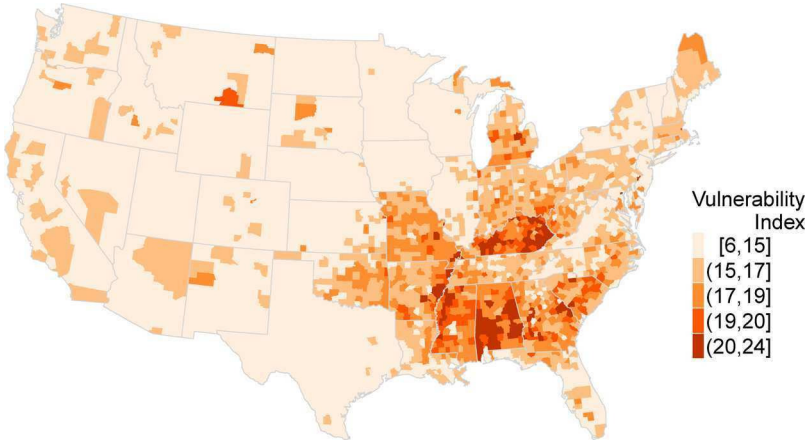

Figure 2. National map of the Community health-vulnerability Index (CHVI). The break points 15, 17, 19, and 20 correspond to the 50th, 75th, 90th, and 95th percentile of CHVI scores, respectively.

The emission inventory and ancillary files were based on the 2008 emissions modeling platform for 2008, 2009, and 2010 and on the 2011 emission modeling platform for 2011 and 2012. The fire emissions were based on year-specific daily fire estimates using the Hazard Mapping System fire detections and Sonoma Technology SMARTFIRE system (version 2) (http://www.getbluesky.org/smartfire/docs/Raffuse 2007.pdf). Plume rise was calculated within the CMAQ model (in-line). Biogenic emissions were processed in-line in CMAQ and are based on the Biogenic Emissions Inventory System v3.14 (http://www.cmascenter.org).

CMAQ hourly output was averaged to daily averages (midnight to midnight and adjusted for time zone) for each grid point. From the gridded output we calculated area weighted averages for daily and annual fire-$PM_{2.5}$ daily averages for each county. We characterize smoke exposure impacts with respect to the magnitude of exposure, frequency of days with moderate air quality (15−35 $\mu g/m^3$) and frequency of days with unhealthy levels of fire-$PM_{2.5}$ (>35 $\mu g/m^3$) according to 2006 $PM_{2.5}$ NAAQS. In terms of health risks, moderate air quality days are interpreted as "Unhealthy for Unusually Sensitive Groups"; while concentrations above 35.4 are interpreted as unhealthy for a broader population. More specifically, 35.5−55.4 $\mu g/m^3$ is considered "Unhealthy for Sensitive Individuals", 55.5−150.4 $\mu g/m^3$ is considered "Unhealthy" for all individuals, 150.5−250.4 is "Very Unhealthy", and ≥250.5 is "Hazardous".[33] The two concentrations used in this analysis also correspond to the annual (15 $\mu g/m^3$) and daily (35 $\mu g/m^3$) 2006 $PM_{2.5}$ NAAQS. Here we used the 2006 standard because it was the standard of the time period 2008 to 2012. In December, 2012 the NAAQS for $PM_{2.5}$ was revised, and the annual standard was reduced to 12 $\mu g/m^3$ while the daily standard 35 $\mu g/m^3$ was retained. We note that we use these thresholds to define moderate and unhealthy smoke days and not to define compliance to air quality regulations. Finally, to calculate population size at risk we used age and gender specific population size from 2010 U.S. Census.

Wildfire perimeters for each year in this five-year period used in the study were obtained from USGS Geospatial Multi-Agency Coordination Group (GeoMAC) Wildland Fire Support archives. The GeoMAC is an interactive mapping application that displays maps of current fire locations and perimeters in the 48 contiguous states plus Alaska. This tool gathers fire data from daily incidence reports and defines wildland fire perimeters based on incident intelligence sources, GPS data, fixed wing aircraft sources, and satellite data. Fires not reported to the incidence intelligence such as prescribed and agricultural fires are not represented in the GeoMAC. The shape files and metadata are available at http://rmgsc.cr.usgs.gov/outgoing/GeoMAC/historic_fire_data/.

RESULTS

Fire-$PM_{2.5}$ Patterns over the Continental U.S., 2008−2012. In Figure 1, we mapped a geographic distribution of the estimated fire-$PM_{2.5}$ daily average with respect to (a) the magnitude and (b) frequency of unhealthy smoke days. The maps of fire-$PM_{2.5}$ were also overlaid with the geocoded perimeters of large wildfires from GeoMAC archives. In combination with large fire parameters and with respect to the magnitude of impact, two distinct and large spatial footprints are observed for fire-$PM_{2.5}$. The first footprint was observed over the heavily forested, cold and temperate climates of Northern California and Pacific Northwest, where high concentrations were colocated with a dense distribution of fire perimeters. The second fire-$PM_{2.5}$ footprint was observed across the Southeast where vegetation includes hardwood, pine and southern mixed forests, and wetlands. According to the National Emissions Inventory used in our CMAQ simulations, a majority of the emissions in this region are attributed to smaller and more localized wildland fires, which include agricultural burning and prescribed burning, and a large number of smaller fires. Prescribed burning is done on an annual basis in early months of the year and with the exception of drought years, the smoke footprint is consistently present from year to year. Daily average fire-$PM_{2.5}$ on smoke days was substantially lower in the Southeast than in the Northwestern states with the exception of days when large wildfires occurred (wildfire impacts can be observed from hourly concentrations which are not shown here). Maps for individual years are given in the SI Figures S1−S10.

Figure 1 demonstrates a notable difference between the Northwest and Southeast regions in frequency by which estimated county-averaged fire-$PM_{2.5}$ was above the level considered "Unhealthy for Sensitive Individuals" (>35 $\mu g/m^3$). The largest impact was in the Northwest region where a number of communities experienced 10 or more days of high fire-$PM_{2.5}$ levels. With the exception of Louisiana during winter 2008, the Southeast region had a significantly lower number of

DOI: 10.1021/acs.est.6b06200
Environ. Sci. Technol. 2017, 51, 6674−6682

Table 1. Population Size at Risk Summarized by Annual Average Fire-$PM_{2.5}$ (2008−2012)[a]

$PM_{2.5}$ (μg/m3)	adult asthma	pediatric asthma	COPD	hyper- tensive	diabetes	obesity	poverty	under 18	65 and over	total population
	20.8	6.4	11.8	68.8	20.3	60.9	42.5	73.7	40.0	306.7
(0,0.15]	0.2	0.1	0.1	0.6	0.2	0.5	0.4	0.6	0.4	2.8
(0.15,0.75]	12.7	3.8	6.6	40.0	11.3	34.4	23.6	43.5	23.7	182.2
(0.75,1.5]	5.9	1.9	3.8	20.8	6.4	19.0	13.2	22.2	11.9	91.1
(1.5,4.58]	2.0	0.7	1.3	7.4	2.4	7.0	5.3	7.4	4.0	30.5

[a]We used outcome specific prevalence by county. Population size is given in millions.

Table 2. Population Size at Risk by Community Health-Vulnerability Index, Annual Average Fire-$PM_{2.5}$, and Frequency of Unhealthy Fire-$PM_{2.5}$ Days Between 2008 and 2012[a]

	CHVI bins	[6,15]	(15,17]	(17,19]	(19,20]	(20,24]	total
annual mean (μg/m^3)	[0,0.15]	2 (72.3%)[#]	0.7 (25.2%)	0.1 (2.6%)	0 (0%)	0 (0%)	2.8 (0.9%)*
	(0.15,0.75]	98.6 (54.1%)	61.4 (33.7%)	13.5 (7.4%)	5.6 (3.1%)	3.1 (1.7%)	182.2 (59.4%)
	(0.75,1.5]	49 (53.8%)	25.4 (27.8%)	12.3 (13.5%)	2.7 (3%)	1.8 (2%)	91.2 (29.7%)
	(1.5,4.58]	8.1 (26.6%)	11 (36.1%)	7.5 (24.6%)	2.3 (7.4%)	1.6 (5.3%)	30.5 (9.9%)
num. days with 15−35 μg/m^3	[1,5)	69.6 (63.1%)	29.9 (27.1%)	8 (7.3%)	2.1 (1.9%)	0.7 (0.6%)	110.4 (36%)
	[5,10)	16.6 (31.2%)	23.5 (44.2%)	8.8 (16.6%)	2.1 (4%)	2.1 (4%)	53.1 (17.3%)
	[10,76]	39.5 (47.9%)	22.9 (27.8%)	13.6 (16.4%)	3.8 (4.6%)	2.7 (3.3%)	82.4 (26.9%)
num. days with >35 μg/m^3	[1,5)	28.5 (49%)	14.4 (24.7%)	11 (18.9%)	2.8 (4.9%)	1.4 (2.5%)	58.2 (19%)
	[5,10)	9.9 (51.6%)	5.4 (28.2%)	2.2 (11.7%)	0.8 (4%)	0.9 (4.5%)	19.1 (6.2%)
	[10,55]	6.9 (67%)	2.8 (27.1%)	0.3 (2.9%)	0.2 (1.6%)	0.1 (1.3%)	10.3 (3.4%)
	Total	157.7 (51.4%)	98.5 (32.1%)	33.4 (10.9%)	10.6 (3.5%)	6.5 (2.1%)	306.7 (100%)

[a]Population size is given in millions ([#] % expressed conditional on the population in the right margin, * expressed as % of the total population).

unhealthy fire-$PM_{2.5}$ days. In summary, both footprints had a large number of moderate air quality days due to fire-$PM_{2.5}$, while days with fire-$PM_{2.5}$ exceeding the level considered unhealthy for wider population were mostly in the Northwest region.

Health-Vulnerability and Smoke Impacts. The CHVI score ranged from 6 to 25, with a median score of 15, and 75th, 90th, and 95th percentile of 17, 19, and 20, respectively. The highest vulnerability is observed in the counties along the western slope of the Appalachian Mountains, parts of the Midwest (Kentucky, Missouri, Oklahoma, and Kansas) and parts of the South (Arkansas, Mississippi, Alabama, and Georgia) (Figure 2). Although none of the five indices dominated CHVI overall, the regions of the highest vulnerability tend to have high index values on multiple factors, particularly the prevalence of preexisting cardiovascular, metabolic diseases, and childhood asthma as well as economic deprivation.

Table 1 shows the estimated population size at risk by factors of vulnerability. We estimate that 30.5 million (13%) individuals, including 7.4 million children under 18, and 4 million persons over 65 years of age lived in communities where the annual average of fire-$PM_{2.5}$ was estimated to be above 1.5 μg/m^3 (annual average). Among these communities, there were 7.4 million individuals over 30 years of age with known hypertension, 2 million adults with asthma and 0.7 million children with asthma, 1.3 million people with COPD, 7.0 million obese individuals, and 2.4 million individuals with diabetes. We note that population size at risk was calculated separately for each county level factor of vulnerability; thus individuals with comorbidities are counted for each health outcome.

Table 2 shows the population size at risk by CHVI, annual mean fire-$PM_{2.5}$ levels, and frequency of moderate and unhealthy fire-$PM_{2.5}$ days. We estimate that 82.4 million individuals lived in counties with moderate air quality due to fire-$PM_{2.5}$ (15−35 μg/m^3) and 10.3 million individuals lived in the counties with unhealthy air quality levels (>35 μg/m^3) for more than 10 days between 2008 and 2012. Among the communities with the highest annual fire-$PM_{2.5}$ means (>1.5 μg/m^3), 8.1 million (26.6%) lived in counties with vulnerability index below the median (CHVI 6−15) while 22.4 million lived in the counties with vulnerability above the median (73.4%, 36.1 + 24.6 + 7.4 + 5.3; CHVI (15−24] combined) and 12.7% lived in the counties with high vulnerability (7.4%+5.3%; CHVI > 19). In contrast, across the nation approximately half of population (51.4%) lived in counties where CHVI is below the median and half (49.6%) lived in the counties where CHVI was above the median.

Over the time period considered, areas with the highest vulnerability were more likely to experience unhealthy levels of fire-$PM_{2.5}$ annual average ([1.5,4.58]) than less vulnerable populations (1.6/6.5×100 = 25% for CVHI (20,24] compared to 8.1/157.7×100 = 5% for CVHI [6,15]). Similar was true for number of days with moderate fire-$PM_{2.5}$ (15−35 μg/m^3) for 10+ days and for number of days with fire-$PM_{2.5}$ above 35 μg/m^3 for 5+ days (Table 2). More specifically, among the counties with vulnerability index below the median, 25% (39.5/157.5×100%) lived in places that experienced an excess of 10 days of moderate air quality due to fire while among the counties with the highest vulnerability (CHVI 21−24), 41.5% (2.7/6.5*100%) of population experienced an excess of 10 days of moderate air quality due to fire. A substantially smaller population size was impacted by a large number of days with unhealthy air quality (>35 μg/m^3); 10.7% of the population in the counties with CHVI below the median and 15.2% of the population in the most vulnerable counties experienced more than 5 days of unhealthy air quality (>35 μg/m^3). However,

DOI: 10.1021/acs.est.6b06200
Environ. Sci. Technol. 2017, 51, 6674−6682

4.4% of the least vulnerable communities and only 2.1% of the most vulnerable communities were impacted by 10 or more days of fire-$PM_{2.5}$ above 35 $\mu g/m^3$.

DISCUSSION

In this study we constructed an index of population vulnerability to health impacts from smoke exposure based on clinical and social factors known to modify the risk of adverse health effects and estimated population size at risk with respect to the frequency and magnitude of smoke exposure in a recent period. The modeling methods used in the study estimate that between 2008 and 2012 population exposure to smoke in the continental U.S. was extensive; 29.7% of the population lived in areas with moderate exposure (annual average fire-$PM_{2.5}$ between 0.75 and 1.5 $\mu g/m^3$) and another 10% lived in areas where the contribution to annual ambient $PM_{2.5}$ was high (>1.5 $\mu g/m^3$). We identified the most vulnerable U.S. counties and determined that vulnerable communities were more likely to experience high and frequent smoke exposure in comparison to less vulnerable populations. The findings described in the study have potential implications for efficient and effective allocation of limited resources for dissemination of public health messaging, and land and fuel management to prevent large wildfires.

The constructed Community Health-Vulnerability Index incorporates disease prevalence, age and socio-economic status of individuals in the community. The specific factors were chosen based on published literature that demonstrates their role as risk factors for cardio-respiratory effects of particles or wildfire smoke. Published research describes multiple biological mechanisms by which air pollution causes cardio-respiratory effects including oxidative stress, pulmonary and systemic inflammation, activation of pulmonary nocioceptive receptors, and modulation of the autonomic nervous system (Brook et al. 2010). Therefore, individuals having chronic health conditions characterized in part by pro-inflammatory states (e.g., asthma, COPD, diabetes, cardiovascular disease) are considered at higher risk.[34] Among the risk factors, preexisting cardiovascular disease is one of the leading factors of increased health risks to air pollution effects.[35] We used hypertension to approximate prevalence of cardiovascular disease because it is well documented, the most prevalent cardiovascular condition, and is responsible for one in six deaths among adults. Chronic metabolic and inflammatory health conditions such as diabetes and obesity have been shown to increase the risk to air pollution impacts.[36−38] Children are considered more sensitive to impacts of air pollution because their lungs are smaller, and their dose per body weight and lung surface areas exceed those of the adult population.

The majority of evidence for wildfire smoke effects are based on studies of exposure to ambient air pollution[13] but there is also a growing number of fire-$PM_{2.5}$ studies that suggest consistency between respiratory effects within fire specific studies and in comparison to studies of urban air pollution.[9,39] The effects of air pollution and wildfire smoke exposure on adults with preexisting respiratory conditions such as asthma and COPD are extensively documented in literature. These effects have also been noted in both children with asthma and children without asthma[5,40] and have been noted to be stronger than in adults.[41] Additionally, older adults have been shown to have an increased risk of cardiovascular and respiratory effects in fire-$PM_{2.5}$ exposure studies.[3,7,42,43] Apart from the clinical characteristics discussed, low socioeconomic status has also been reported to modify the risk of respiratory outcomes in response to large wildland fire smoke events.[30] We have previously shown that when considering external factors influencing health (health behaviors, access and quality of clinical care, social and economic factors, and the physical environments) socio-economic factors are strong contributors of differences in risk for asthma and congestive heart failure resulting from exposure to wildfire smoke.[29]

In the development of the health-vulnerability index we restrict our attention to the key clinical and social conditions that have been identified by the Integrated Science Assessment as populations sensitive to adverse health effects following air pollution exposure. It is clear, however, that these are not the only risk factors involved at the individual level. Evidence for a role for genetics, epigenetics, diet, availability of green space and behavior is emerging and it is likely that some of these will ultimately prove to be strong predictors of $PM_{2.5}$ associated health outcomes. As new risk factors are identified the CHVI can be adapted to incorporate the new information. Additionally, a number of other extrinsic factors have been shown to identify social vulnerability to environmental hazards such as heat waves, including occupation, employment, housing, built environment, neighborhood deprivation, poor English skills and are likely to apply in wildfire smoke situations.[44−47] When constructing indicators at the regional, state or local levels, and particularly when considering decision making, it may be helpful and advantageous to incorporate determinants of social vulnerability along with the indicators of health vulnerability (e.g., built environment, landscape, social and physical connectivity, existing air quality, etc.) and examine sensitivity of the indicators.

Implications for Public Health Actions. Interventions and health-promoting behaviors can improve public health outcomes.[48,49] Many of the recommended measures including staying indoors during very unhealthy air quality days, running air conditioning on recirculation mode, creating a clean room, ensuring a supply of regular medication, etc. can reduce personal exposure and decrease the health risks. However, during wildfire episodes, individuals do not perceive risks to their health and become aware of them once smoke exposure is already occurring, when it may be too late to take many of the recommended preventative measures. Smoke impacts in the areas where wildfires are less common (e.g., Southeast) can be a special concern exactly because they are less frequent and the health risk awareness is not established at the individual or community level. Prior knowledge about community health vulnerability can help guide deliberate awareness building and outreach among the most sensitive populations. However, identifying communities at the greatest risk from wildfire smoke is currently based solely on the predicted risk of fire and we do not consider the composition of the communities. As such public health messaging and actions may not be appropriately scaled to communities with high numbers of sensitive individuals.

Increased frequency of large wildland fires is anticipated to continue and have effects on human health and environment.[50−52] Fuel management activities, such as prescribed burning, are a critically important component of the national strategy to improve ecological diversity and decrease wildfires harmful to human health and have been examined with respect to changes in frequency and area burned.[53−56] While such information provides important insights for a broad risk-based management system for wildfire, the framework does not

DOI: 10.1021/acs.est.6b06200
Environ. Sci. Technol. 2017, 51, 6674−6682

consider the potential public health burden of smoke emissions or disparities in sensitivity of the populations affected. Projecting community health-vulnerability under different fire mitigation strategies, climate change scenarios, and population growth projections may offer further refinement of such risk-based management approaches. In projecting community health-vulnerability for a specific future scenario we recommend using population-weighted exposures.

Limitations of the Study. We note some limitations to our analysis. To estimate smoke exposure at the national level we use CMAQ model simulated with and without fires and attribute the difference in estimated ambient $PM_{2.5}$ concentrations to large fires (mostly wild and prescribed). To assess model performance, we matched CMAQ grid locations to the locations of environmental monitors and compare predicted and observed values. We found the model has a high bias at low $PM_{2.5}$ concentrations suggesting that (1) plumes are too dispersive, and/or (2) small fires have too high emissions in the simulation. The model also over predicts $PM_{2.5}$ (mainly organic and elemental carbon) during all seasons for fire events. Another limitation is that only fire events that are part of the emission inventory have been evaluated. Any misspecification of emissions in the inventory is not included in our analysis. An important limitation to our simulation of fire-$PM_{2.5}$ that affects air quality is that our modeling system does not simulate the smoldering aspects of peat fires well which are common in the Southeast and emit large quantities of particles and gases. We note that as with all models CMAQ results should be interpreted with caution because any combination of these factors could lead to uncertainty and over or under prediction of estimated exposures. While various aspects of CMAQ performance have been published in the literature,[57] additional factors could play a role in the uncertainty specific to fire-$PM_{2.5}$.

Another limitation is the assumption that $PM_{2.5}$ from all sources is equally harmful to health. The composition and toxicity of these particles varies with respect to the type of fuel burned, conditions of burning and the age of the particles. Lower combustion efficiency yields more volatile and organic compounds in both particles and gases (polynuclear aromatic hydrocarbons, oxygenated organics, and various gases) which are harmful to human health. Toxicological studies also indicate that relative toxicity of particles varies when examined per unit mass or total mass, and by chemical composition of the particles. Fire-$PM_{2.5}$ and fire-PM_{10} collected during a peat fire in eastern North Carolina in 2008 had very different targets of cellular toxicity that depended on the particle mass of the smoke particles and the phase of the fire.[58] Cardiovascular toxicity was the dominant effect caused by ultrafine PM fraction collected during the active smoldering phase of the fire while in vitro pulmonary inflammatory responses were the dominant effects of coarse fraction of PM. Smoldering fires, as seen in the peat fires across Southeast U.S., Indonesia, and Boreal forest have also been hypothesized to carry higher risk for cardiovascular Emergency Department visits as well.[11,43] This could be due to lower combustion efficiency and vegetation type that define chemical composition of particles, such as the abundance polynuclear aromatic hydrocarbons which are carcinogenic and particularly harmful to health.[59] However, a systematic review of published literature suggests that there is no consistent relationship that identifies specific $PM_{2.5}$ components that may be unequivocally related to health outcomes.[60]

The most significant limitation to this assessment of human vulnerability to health impacts of smoke is the lack of a good measure of a community's ability to adapt. While the factors that define the vulnerability status certainly play a role, other less quantifiable measures including awareness, previous experience, outreach programs, engagement of public health, and proximity to health care providers or facilities can define human responses. Gaither et al. 2011 examined spatial association between fire prone areas in the Southeast and socially vulnerable "hot spots" using proximity to wildland fire mitigation programs as a measure of community's ability to adopt. However, we did not find equivalent measures of community responses specific to health responses.

Wildland fires have been an integral part of human history with clear benefit to the management of fire hazards and to the ecologic diversity of ecosystems. However, recent trends in very large wildfires, termed mega fires, have brought attention to the adverse health effects of smoke exposure, the high cost of wildfire suppression and management, and the need to establish community-based adaptation plans. Employing the same methodology used to determine social vulnerability to environmental hazards,[23] we provide a concept of mapping the vulnerability to health outcomes specific to smoke exposure. Such maps can be helpful tools for public officials in preparation of smoke adaptation plans for their communities and prioritization of communities for allocation of resources by the local, state and federal governments. In the U.S. there are over 70 000 wildfires annually, impacting communities and regional air quality with varying frequency and intensity and thus representing a challenge to building community resilience with respect to fire smoke and public health guidance. Therefore, as a proof of concept, the Community Health-Vulnerability Index offers a tool to help identify communities that have the potential to benefit the most from mitigation strategies to minimize smoke exposure for sensitive populations and to decrease the health and economic burden imposed on the population by fire-$PM_{2.5}$ The next step could include tailoring messages to community needs and development of exposure mitigation strategies.

■ ASSOCIATED CONTENT

Supporting Information

The Supporting Information is available free of charge on the ACS Publications website at DOI: 10.1021/acs.est.6b06200.

List of data sources (Table S1), figures of the annual average daily fire-PM2.5 footprint by year (Figures S1−S5), figures of number of days with fire-PM2.5 above 35 $\mu g/m^3$ (Figures S6−S10) and details of principal components analysis output (Table S2, Figure S11) (PDF).

■ AUTHOR INFORMATION

Corresponding Author

*Phone: 919 843 9504; e-mail: rappold.ana@epa.gov.

ORCID

Ana G. Rappold: 0000-0002-7696-0900

Funding

The research described in this article has been funded wholly by the U.S. Environmental Protection Agency intramural research funding.

DOI: 10.1021/acs.est.6b06200
Environ. Sci. Technol. 2017, 51, 6674−6682

Notes

Disclaimer: The research described in this article has been reviewed by the National Health and Environmental Effects Research Laboratory, U.S. Environmental Protection Agency, and approved for publication. Approval does not signify that the contents necessarily reflect the views and policies of the Agency, nor does the mention of trade names of commercial products constitute endorsement or recommendation for use. The authors declare no competing financial interest.

■ ACKNOWLEDGMENTS

The authors thank four anonymous reviewers, Pete Lahm (USFS), Jason Sacks (USEPA), Christina Baghdikian (USEPA), Ann Brown (USEPA) for their comments and careful review of the manuscript.

■ REFERENCES

(1) Dennekamp, M.; Abramson, M. J. The effects of bushfire smoke on respiratory health. *Respirology* **2011**, *16* (2), 198−209.
(2) Dennekamp, M.; Straney, L. D.; Erbas, B.; Abramson, M. J.; Keywood, M.; Smith, K.; Sim, M. R.; Glass, D. C.; Del Monaco, A.; Haikerwal, A.; Tonkin, A. M. Forest Fire Smoke Exposures and Out-of-Hospital Cardiac Arrests in Melbourne, Australia: A Case-Crossover Study. *Environ. Health Perspect* **2015**, *123* (10), 959−64.
(3) Haikerwal, A.; Akram, M.; Del Monaco, A.; Smith, K.; Sim, M. R.; Meyer, M.; Tonkin, A. M.; Abramson, M. J.; Dennekamp, M., Impact of Fine Particulate Matter (PM2.5) Exposure During Wildfires on Cardiovascular Health Outcomes. *J. Am. Heart Assoc.* **2015**, *4*, (7).e00165310.1161/JAHA.114.001653
(4) Haikerwal, A.; Akram, M.; Sim, M. R.; Meyer, M.; Abramson, M. J.; Dennekamp, M. Fine particulate matter (PM2.5) exposure during a prolonged wildfire period and emergency department visits for asthma. *Respirology* **2016**, *21* (1), 88−94.
(5) Jalaludin, B.; Smith, M.; O'Toole, B.; Leeder, S. Acute effects of bushfires on peak expiratory flow rates in children with wheeze: a time series analysis. *Aust N Z. J. Public Health* **2000**, *24* (2), 174−7.
(6) Johnston, F. H.; Henderson, S. B.; Chen, Y.; Randerson, J. T.; Marlier, M.; Defries, R. S.; Kinney, P.; Bowman, D. M.; Brauer, M. Estimated global mortality attributable to smoke from landscape fires. *Environ. Health Perspect* **2012**, *120* (5), 695−701.
(7) Johnston, F. H.; Purdie, S.; Jalaludin, B.; Martin, K. L.; Henderson, S. B.; Morgan, G. G. Air pollution events from forest fires and emergency department attendances in Sydney, Australia 1996−2007: a case-crossover analysis. *Environ. Health* **2014**, *13*, 105.
(8) Kunzli, N.; Avol, E.; Wu, J.; Gauderman, W. J.; Rappaport, E.; Millstein, J.; Bennion, J.; McConnell, R.; Gilliland, F. D.; Berhane, K. Health effects of the 2003 Southern California wildfires on children. *Am. J. Respir. Crit. Care Med.* **2006**, *174* (11), 1221−1228.
(9) Liu, J. C.; Pereira, G.; Uhl, S. A.; Bravo, M. A.; Bell, M. L. A systematic review of the physical health impacts from non-occupational exposure to wildfire smoke. *Environ. Res.* **2015**, *136*, 120−132.
(10) Morgan, G.; Sheppeard, V.; Khalaj, B.; Ayyar, A.; Lincoln, D.; Jalaludin, B.; Beard, J.; Corbett, S.; Lumley, T. Effects of bushfire smoke on daily mortality and hospital admissions in Sydney, Australia. *Epidemiology* **2010**, *21* (1), 47−55.
(11) Rappold, A. G.; Stone, S. L.; Cascio, W. E.; Neas, L. M.; Kilaru, V. J.; Carraway, M. S.; Szykman, J. J.; Ising, A.; Cleve, W. E.; Meredith, J. T.; Vaughan-Batten, H.; Deyneka, L.; Devlin, R. B. Peat bog wildfire smoke exposure in rural North Carolina is associated with cardiopulmonary emergency department visits assessed through syndromic surveillance. *Environ. Health Perspect* **2011**, *119* (10), 1415−20.
(12) Delfino, R. J.; Brummel, S.; Wu, J.; Stern, H.; Ostro, B.; Lipsett, M.; Winer, A.; Street, D. H.; Zhang, L.; Tjoa, T., The relationship of respiratory and cardiovascular hospital admissions to the southern California wildfires of 2003. *Occup. Environ. Med.* **2008**.6618910.1136/oem.2008.041376
(13) US EPA, *Integrated Science Assessment (ISA) for Particulate Matter (Final)*. In U.S. Environmental Protection Agency: Washington, DC, 2009.
(14) Bell, M. L.; Zanobetti, A.; Dominici, F. Evidence on vulnerability and susceptibility to health risks associated with short-term exposure to particulate matter: a systematic review and meta-analysis. *Am. J. Epidemiol.* **2013**, *178* (6), 865−76.
(15) Sacks, J. D.; Stanek, L. W.; Luben, T. J.; Johns, D. O.; Buckley, B. J.; Brown, J. S.; Ross, M. Particulate matter-induced health effects: who is susceptible? *Environ. Health Perspect* **2011**, *119* (4), 446−54.
(16) Reid, C. E.; O'Neill, M. S.; Gronlund, C. J.; Brines, S. J.; Brown, D. G.; Diez-Roux, A. V.; Schwartz, J. Mapping community determinants of heat vulnerability. *Environ. Health Perspect.* **2009**, *117* (11), 1730.
(17) Blaikie, P.; Cannon, T.; Davis, I.; Wisner, B. *At Risk: Natural Hazards, People'S Vulnerability and Disasters*; Routledge, 2014.
(18) Cutter, S. L.; Mitchell, J. T.; Scott, M. S. Revealing the vulnerability of people and places: a case study of Georgetown County, South Carolina. *Annals of the association of American Geographers* **2000**, *90* (4), 713−737.
(19) Wu, S.-Y.; Yarnal, B.; Fisher, A. Vulnerability of coastal communities to sea-level rise: a case study of Cape May County, New Jersey, USA. *Climate Research* **2002**, *22* (3), 255−270.
(20) Morrow, B. H. Identifying and mapping community vulnerability. *Disasters* **1999**, *23* (1), 1−18.
(21) Clougherty, J. E.; Kubzansky, L. D. A framework for examining social stress and susceptibility to air pollution in respiratory health. *Environ. Health Perspect* **2009**, *117* (9), 1351−8.
(22) Bradford, K.; Abrahams, L.; Hegglin, M.; Klima, K. A Heat Vulnerability Index and Adaptation Solutions for Pittsburgh, Pennsylvania. *Environ. Sci. Technol.* **2015**, *49* (19), 11303−11.
(23) Cutter, S. L.; Boruff, B. J.; Shirley, W. L. Social vulnerability to environmental hazards. *Social science quarterly* **2003**, *84* (2), 242−261.
(24) American Lung Association, State of the Air 2015. www.stateoftheair.org.
(25) Bateson, T. F.; Schwartz, J. Who is sensitive to the effects of particulate air pollution on mortality?: a case-crossover analysis of effect modifiers. *Epidemiology* **2004**, *15* (2), 143−149.
(26) American Lung Association. Estimated Prevalence and Incidence of Lung Disease. 2014.
(27) US CDC 2012 Behavioral Risk Factor Surveillance System (BRFSS). ftp://ftp.cdc.gov/pub/Data/Brfss/userguide.pdf.
(28) Olives, C.; Myerson, R.; Mokdad, A. H.; Murray, C. J.; Lim, S. S. Prevalence, awareness, treatment, and control of hypertension in United States counties, 2001−2009. *PLoS One* **2013**, *8* (4), e60308.
(29) Rappold, A. G.; Cascio, W. E.; Kilaru, V. J.; Stone, S. L.; Neas, L. M.; Devlin, R. B.; Diaz-Sanchez, D. Cardio-respiratory outcomes associated with exposure to wildfire smoke are modified by measures of community health. *Environ. Health* **2012**, *11* (1), 1.
(30) Reid, C. E.; Jerrett, M.; Tager, I. B.; Petersen, M. L.; Mann, J. K.; Balmes, J. R. Differential respiratory health effects from the 2008 northern California wildfires: A spatiotemporal approach. *Environ. Res.* **2016**, *150*, 227−235.
(31) Census, US Census Bureau. 2010. https://www2.census.gov/geo/tiger/TIGER2010DP1/County_2010Census_DP1.zip.
(32) Yarwood, G., R. S, T., Yocke, M., Whitten, G. Z. *Updates to the Carbon Bond Mechanism: CB05*. U.S. EPA 2005, *Final Report*.
(33) U.S. EPA, Technical Assistance Document for the Reporting of Daily Air Quality- the Air Quality Index (AQI). U.S. Environmental Protection Agency, Office of Air Quality Planning and Standards, Research Triangle Park, NC, 2013; Vol. EPA-454/B-13−001.
(34) Zanobetti, A.; Bind, M.-A. C.; Schwartz, J. Particulate air pollution and survival in a COPD cohort. *Environ. Health* **2008**, *7* (1), 1.
(35) Brook, R. D.; Rajagopalan, S.; Pope, C. A.; Brook, J. R.; Bhatnagar, A.; Diez-Roux, A. V.; Holguin, F.; Hong, Y.; Luepker, R. V.; Mittleman, M. A. Particulate matter air pollution and cardiovascular disease an update to the scientific statement from the American Heart Association. *Circulation* **2010**, *121* (21), 2331−2378.

DOI: 10.1021/acs.est.6b06200
Environ. Sci. Technol. 2017, 51, 6674−6682

(36) Devlin, R. B.; Smith, C. B.; Schmitt, M. T.; Rappold, A. G.; Hinderliter, A.; Graff, D.; Carraway, M. S. Controlled exposure of humans with metabolic syndrome to concentrated ultrafine ambient particulate matter causes cardiovascular effects. *Toxicol. Sci.* **2014**, *140* (1), 61−72.
(37) Ruckerl, R.; Hampel, R.; Breitner, S.; Cyrys, J.; Kraus, U.; Carter, J.; Dailey, L.; Devlin, R. B.; Diaz-Sanchez, D.; Koenig, W.; Phipps, R.; Silbajoris, R.; Soentgen, J.; Soukup, J.; Peters, A.; Schneider, A. Associations between ambient air pollution and blood markers of inflammation and coagulation/fibrinolysis in susceptible populations. *Environ. Int.* **2014**, *70*, 32−49.
(38) Schneider, A.; Neas, L.; Herbst, M. C.; Case, M.; Williams, R. W.; Cascio, W.; Hinderliter, A.; Holguin, F.; Buse, J. B.; Dungan, K. Endothelial dysfunction: associations with exposure to ambient fine particles in diabetic individuals. *Environ. Health Perspect.* **2008**, *116* (12), 1666.
(39) Reid, C. E.; Brauer, M.; Johnston, F.; Jerrett, M.; Balmes, J. R.; Elliott, C. T., Critical Review of Health Impacts of Wildfire Smoke Exposure. *Environ. Health Perspect.* **2016**.10.1289/ehp.1409277
(40) Kunzli, N.; Avol, E.; Wu, J.; Gauderman, W. J.; Rappaport, E.; Millstein, J.; Bennion, J.; McConnell, R.; Gilliland, F. D.; Berhane, K.; Lurmann, F.; Winer, A.; Peters, J. M. Health effects of the 2003 Southern California wildfires on children. *Am. J. Respir. Crit. Care Med.* **2006**, *174* (11), 1221−8.
(41) Ignotti, E.; Valente, J. G.; Longo, K. M.; Freitas, S. R.; Hacon, S. d. S.; Artaxo Netto, P. Impact on human health of particulate matter emitted from burnings in the Brazilian Amazon region. *Rev. Saude Publica* **2010**, *44* (1), 121−130.
(42) Morgan, G.; Corbett, S.; Wlodarczyk, J. Air pollution and hospital admissions in Sydney, Australia, 1990 to 1994. *Am. J. Public Health* **1998**, *88* (12), 1761−6.
(43) Tinling, M. A.; West, J. J.; Cascio, W. E.; Kilaru, V.; Rappold, A. G. Repeating cardiopulmonary health effects in rural North Carolina population during a second large peat wildfire. *Environ. Health* **2016**, *15*, 12.
(44) Harlan, S. L.; Declet-Barreto, J. H.; Stefanov, W. L.; Petitti, D. B. Neighborhood effects on heat deaths: social and environmental predictors of vulnerability in Maricopa County, Arizona. *Environ. Health Perspect* **2013**, *121* (2), 197−204.
(45) Messer, L. C.; Laraia, B. A.; Kaufman, J. S.; Eyster, J.; Holzman, C.; Culhane, J.; Elo, I.; Burke, J. G.; O'Campo, P. The development of a standardized neighborhood deprivation index. *J. Urban Health* **2006**, *83* (6), 1041−62.
(46) Petitti, D. B.; Harlan, S. L.; Chowell-Puente, G.; Ruddell, D. Occupation and environmental heat-associated deaths in Maricopa county, Arizona: a case-control study. *PLoS One* **2013**, *8* (5), e62596.
(47) Uejio, C. K.; Wilhelmi, O. V.; Golden, J. S.; Mills, D. M.; Gulino, S. P.; Samenow, J. P. Intra-urban societal vulnerability to extreme heat: the role of heat exposure and the built environment, socioeconomics, and neighborhood stability. *Health Place* **2011**, *17* (2), 498−507.
(48) Neidell, M. Air quality warnings and outdoor activities: evidence from Southern California using a regression discontinuity design. *J. Epidemiol Community Health* **2010**, *64* (10), 921−6.
(49) Mott, J. A.; Meyer, P.; Mannino, D.; Redd, S. C.; Smith, E. M.; Gotway-Crawford, C.; Chase, E. Wildland forest fire smoke: health effects and intervention evaluation, Hoopa, California, 1999. *West. J. Med.* **2002**, *176* (3), 157−62.
(50) Kinney, P. L. Climate change, air quality, and human health. *Am. J. Prev. Med.* **2008**, *35* (5), 459−67.
(51) Fann, N.; Fulcher, C. M.; Baker, K. The recent and future health burden of air pollution apportioned across U.S. sectors. *Environ. Sci. Technol.* **2013**, *47* (8), 3580−9.
(52) Liu, J. C.; Mickley, L. J.; Sulprizio, M. P.; Yue, X.; Peng, R. D.; Dominici, F.; Michelle L Bell, D. Future respiratory hospital admissions from wildfire smoke under climate change in the Western US. *Environ. Res. Lett.* **2016**, *11* (12), 124018.
(53) Prestemon, J.; Shankar, U.; Xiu, A.; Talgo, K.; Yang, D.; Dixon, IV, E.; McKenzie, D.; Abt, K. L., Projecting wildfire area burned in the south-eastern United States, 2011−60. 2016.
(54) Flannigan, M. D.; Van Wagner, C. E. Climate Change and wildfire in Canada. *Can. J. For. Res.* **1991**, *21*, 66−72.
(55) Bowman, D. M.; Balch, J. K.; Artaxo, P.; Bond, W. J.; Carlson, J. M.; Cochrane, M. A.; D'Antonio, C. M.; Defries, R. S.; Doyle, J. C.; Harrison, S. P.; Johnston, F. H.; Keeley, J. E.; Krawchuk, M. A.; Kull, C. A.; Marston, J. B.; Moritz, M. A.; Prentice, I. C.; Roos, C. I.; Scott, A. C.; Swetnam, T. W.; van der Werf, G. R.; Pyne, S. J. Fire in the Earth system. *Science* **2009**, *324* (5926), 481−4.
(56) Ager, A. A.; Day, M. A.; McHugh, C. W.; Short, K.; Gilbertson-Day, J.; Finney, M. A.; Calkin, D. E. Wildfire exposure and fuel management on western US national forests. *J. Environ. Manage.* **2014**, *145* (1), 54−70.
(57) Park, S.-K.; Cobb, C. E.; Wade, K.; Mulholland, J.; Hu, Y.; Russe, A. G. Uncertainty in air quality model evaluation for particulate matter due to spatial variations in pollutant concentrations. *Atmos. Environ.* **2006**, *40* (Supplement 2), 563−573.
(58) Kim, Y. H.; Tong, H.; Daniels, M.; Boykin, E.; Krantz, Q. T.; McGee, J.; Hays, M.; Kovalcik, K.; Dye, J. A.; Gilmour, M. I. Cardiopulmonary toxicity of peat wildfire particulate matter and the predictive utility of precision cut lung slices. *Part. Fibre Toxicol.* **2014**, *11*, 29.
(59) IARC. *Outdoor Air Pollution*; World Health Organization: International Agency for Research on Cancer, 2016.
(60) Stanek, L. W. S.; Jason, D.; Dutton; Steven, J.; Dubois; Jean-Jacques, B. Attributing health effects to apportioned components and sources of particulate matter: An evaluation of collective results. *Atmos. Environ.* **2011**, *45* (October), 5655−5663.

DOI: 10.1021/acs.est.6b06200
Environ. Sci. Technol. 2017, 51, 6674−6682

Science of the Total Environment 610–611 (2018) 802–809

Contents lists available at ScienceDirect

Science of the Total Environment

journal homepage: www.elsevier.com/locate/scitotenv

The health impacts and economic value of wildland fire episodes in the U.S.: 2008–2012

Neal Fann [a,*], Breanna Alman [a], Richard A. Broome [b], Geoffrey G. Morgan [c], Fay H. Johnston [d], George Pouliot [e], Ana G. Rappold [e]

[a] Office of Air Quality Planning and Standards, U.S. Environmental Protection Agency, 109 T.W. Alexander Drive, Research Triangle Park, NC 27711, USA
[b] Sydney South West Area Health Service, New South Wales, Australia
[c] University Center for Rural Health, University of Sydney, New South Wales, Australia
[d] Menzies Institute for Medical Research, University of Tasmania, Australia
[e] U.S. Environmental Protection Agency, Office of Research and Development, Research Triangle Park, NC, USA

HIGHLIGHTS

- Wildland fires adversely affect air quality and health in the U.S.
- Between 2008 and 2012, fires increased $PM_{2.5}$ levels in the Northwest and Southeast.
- We estimate thousands of premature deaths and illnesses from these episodes.
- The economic value of these impacts is in the tens to hundreds of billions of US$.

GRAPHICAL ABSTRACT

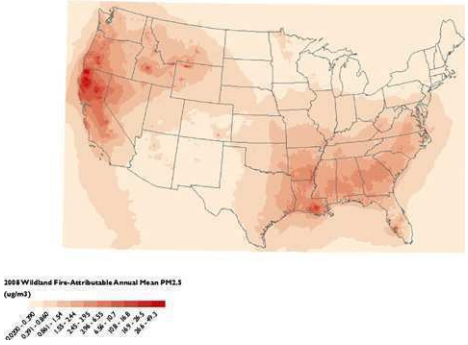

ARTICLE INFO

Article history:
Received 24 April 2017
Received in revised form 25 July 2017
Accepted 2 August 2017
Available online 18 August 2017

Keywords:
Health impact assessment
Source apportionment
$PM_{2.5}$
Ozone
CMAQ
Wildland fires
Wildfires

ABSTRACT

Introduction: Wildland fires degrade air quality and adversely affect human health. A growing body of epidemiology literature reports increased rates of emergency departments, hospital admissions and premature deaths from wildfire smoke exposure.
Objective: Our research aimed to characterize excess mortality and morbidity events, and the economic value of these impacts, from wildland fire smoke exposure in the U.S. over a multi-year period; to date no other burden assessment has done this.
Methods: We first completed a systematic review of the epidemiologic literature and then performed photochemical air quality modeling for the years 2008 to 2012 in the continental U.S. Finally, we estimated the morbidity, mortality, and economic burden of wildland fires.
Results: Our models suggest that areas including northern California, Oregon and Idaho in the West, and Florida, Louisiana and Georgia in the East were most affected by wildland fire events in the form of additional premature deaths and respiratory hospital admissions. We estimated the economic value of these cases due to short term exposures as being between $11 and $20B (2010$) per year, with a net present value of $63B (95% confidence intervals $6–$170); we estimate the value of long-term exposures as being between $76 and $130B (2010$) per year, with a net present value of $450B (95% confidence intervals $42–$1200).

Abbreviations: BenMAP-CE, environmental Benefits Mapping and Analysis Program—Community Edition; CMAQ, Community Multi-Scale Air Quality Model; U.S. EPA, United States Environmental Protection Agency; ICD, International Classification of Disease; NH_3, ammonia; NOx, nitrogen dioxide; O_3, ground-level ozone; $PM_{2.5}$, particulate matter, 2.5 μm or less in diameter; SO_2, sulfur dioxide; WHO, World Health Organization.

* Corresponding author.
E-mail address: Fann.Neal@epa.gov (N. Fann).

http://dx.doi.org/10.1016/j.scitotenv.2017.08.024
0048-9697/Published by Elsevier B.V.

Conclusion: The public health burden of wildland fires—in terms of the number and economic value of deaths and illnesses—is considerable.

Published by Elsevier B.V.

1. Introduction

The increasing frequency and intensity of large wildfires deteriorates air quality and adversely affects human health (Crimmins et al., 2016; Henderson et al., 2009; Liu et al., 2015, 2016; Westerling et al., 2006). These events in turn both promote, and are exacerbated by, long-term changes to the climate; current trends in these events are expected to continue (Crimmins et al., 2016; Stavros et al., 2014). While the level and type of pollutants emitted during wildfires vary according to region and fuel type, all fires release directly emitted particulate matter (PM) as well as precursors to fine particles ($PM_{2.5}$) and can contribute to downwind formation of ozone (Knorr et al., 2012).

While risks to human health from exposure to PM are especially well characterized in the epidemiological, toxicological and controlled human exposure literature (US EPA, 2009), health impacts from PM stemming from wildland fires have been less extensively studied, though epidemiological literature has consistently observed adverse human health impacts attributable to wildfire-related $PM_{2.5}$ (Liu et al., 2015). For example, Rappold et al. (2012, 2011) found that a peat fire episode in eastern North Carolina was associated with increasing numbers of Emergency Department visits for cardiopulmonary and respiratory outcomes. Similarly, Delfino et al. (2009) observed increasing rates of respiratory and cardiovascular hospital admissions resulting from a month-long wildland fire episode in southern California. Epidemiological studies conducted in other countries, including Australia, have observed similar affects (Johnston et al., 2007; Morgan et al., 2010). A systematic review of literature from the U.S., Australia and elsewhere by Liu et al. (2014) found that wildland fire-related coarse particles (PM_{10}) were most consistently associated with respiratory outcomes.

Despite the growing body of epidemiological studies, there are a relatively small number of air pollution risk assessments that attribute the number of premature deaths and illnesses and the economic value of health impacts to wildfire episodes. The risk assessments performed thus far have been limited in their temporal scope, using a single (2005) and projected (2016) year (Fann et al., 2013), or have been limited to examining one fire at a time (Jones et al., 2015; Kochi et al., 2012; Rappold et al., 2014; Rittmaster et al., 2006). This paper builds upon this literature to estimate the number and economic value of wildland fire $PM_{2.5}$-related premature deaths and illnesses in the contiguous United States using chemical transport model predictions of $PM_{2.5}$ from wildland fire episodes over a 5-year period beginning in 2008. Considering a national scope allows us to more fully capture the impact that wildland fires may have on human health.

2. Materials and methods

In this study we characterized the overall magnitude and distribution of adverse health impacts by age and race that were associated with exposure to fire-$PM_{2.5}$ during wildfire smoke episodes. We used health impact functions derived from epidemiological studies that assessed the relationship between fire-$PM_{2.5}$ and expected incidence of health outcomes. We also performed a systematic literature review and meta-analysis; however, using results from the meta-analysis in a health impact function would have introduced considerable uncertainty into the estimates, and thus were not used.

2.1. Health impact function

The risk assessment employs a health impact function to quantify the number of wildland fire-attributable premature deaths and illnesses in each of the five years we modeled. We estimated the number of $PM_{2.5}$-related deaths and hospital admissions (y_{ij}) during each year i (i = 2008, 2009, 2010, 2011, 2012) among individuals in each county j (j = 1,…,J where J is the total number of counties) as: $y_{ij} = \Sigma_a y_{ija}$

$$y_{ija} = m0_{ija} \times \left(e^{\beta \cdot C}{}_{ij} - 1\right) \times P_{ija},$$

where, β is the risk coefficient, $m0_{ija}$ is the baseline death rate or hospital admission rate for the population in county j in year i among individuals for 5-year age strata a, C_{ij} is annual mean wildfire-attributable $PM_{2.5}$ concentration in county j in year i, and P_{ija} is the number of residents in county j in year i for five-year age strata a.

To perform a health impact risk assessment we used baseline incidence rates, population counts, and health impact functions included in the environmental Benefits Mapping and Analysis Program—Community Edition (BenMAP-CE, v1.1) (U.S. Environmental Protection Agency, 2014) to estimate counts of $PM_{2.5}$ attributable deaths and respiratory hospital admissions in each of five years from 2008 to 2012. These inputs have previously been used to estimate health and economic impacts in the national ambient air quality standards reviews, and the methods have been validated in previous publications (Berman et al., 2012; Fann et al., 2011; Office of Air Quality Planning and Standards, 2011). Below we describe how we specify inputs and use the BenMAP-CE tool with the appropriate input data.

2.2. Air quality modeling predictions

We simulated daily air quality from 2008 to 2012 using the Community Multiscale Air Quality version 5.1 (CMAQ v5.1) model with and without emissions from wildland fires in the contiguous United States. Wildland fires in our study included wildfires, prescribed fires, and other significant fires but it excluded agricultural fires. The difference between the two model runs represents the contribution of fire-$PM_{2.5}$ and $PM_{2.5}$ precursor emissions. Inputs to the model included gridded meteorological fields, emissions data, and boundary conditions. Gridded meteorological fields were provided by annual CONUS Weather Research and Forecasting (WRF) model simulation. Meteorological fields were defined on a 12 × 12 km horizontal grid with 35 vertical layers of variable thickness extending up to 50 hPa. The lowest model layer, which extended to approximately 20 m above ground was used to calculate the annual mean concentration of $PM_{2.5}$ (Δx) in the health impact function.

The CMAQ input emissions were based on a 12 km national U.S. domain with speciation for the Carbon-Bond 05 chemical mechanism (Yarwood et al., 2005). The emission inventory and ancillary files were based on the 2008 emissions modeling platform for 2008, 2009, and 2010 (EPA, 2012) and on the 2011 emission modeling platform for 2011 and 2012 (US EPA, 2016). Since the focus of this study is wildland fires, any additional information about the non-fire emission sources is noted in the references. The fire emissions were based on year specific daily fire estimates using the Hazard Mapping System fire detections and Sonoma Technology SMARTFIRE system version 2 (Sonoma Technology, 2007). Smartfire2 is a framework for producing fire activity data and allows for the merging of multiple data sources. Some of the fires included in the fire inventory come from satellite based remote sensing sources which cannot distinguish large prescribed or debris burning fires from wildfires with certainty. After multiple sources of fire information are reconciled to create fire activity estimates, the fire emissions are estimated using fuel moistures (via the USFS Wildland Fire Assessment System), consumption estimates

from the Consume model (Ottmar, 2014; US Forest Service, 2015), emission factors from the Fire Emission Production Simulator (Ottmar, 2014; US Forest Service, 2015), and fuel loading from the United States Forest Service Fuel Characteristic Classification System (FCCS) database (McKenzie et al., 2012). Plume rise for all point sources including the wildland fires was calculated within the CMAQ model. Biogenic emissions were processed in CMAQ and are based on the Biogenic Emissions Inventory System v3.14 (Schwede et al., 2005; Carlton and Baker, 2011).

2.3. Effect coefficients

To identify $PM_{2.5}$ effect coefficients suitable for the health burden impact assessment, we consulted two sources of evidence. The first is the U.S. EPA's 2009 Integrated Science Assessment for Particulate Matter (PM ISA), which classified human health endpoints as having a "causal" or "likely to be causal" relationship with short-term and long-term exposure to $PM_{2.5}$. The PM ISA synthesizes the epidemiological, toxicological and controlled human exposure studies published to that point, and was peer reviewed by the independent Clean Air Scientific Advisory Committee (US EPA, 2009). The PM ISA indicated that mortality and cardiovascular outcomes were causally related, and respiratory outcomes were likely to be causally related, to short-term and long-term exposure to fine particle levels (US EPA, 2009). The ISA did not differentiate these effects by particle composition or source.

Next, we performed a systematic review and quantitative meta-analysis. We included epidemiological studies that looked at associations between $PM_{2.5}$ during smoke events and various health endpoints. Studies identified were conducted in the U.S., Australia, South America, and Asia, and were limited to health endpoints identified by the PM ISA as being causally related to $PM_{2.5}$ exposure. The systematic review employed a machine learning technique to identify relevant literature. We report detailed information regarding the search terms, our procedure for identifying and screening eligible literature, and a Preferred Reporting Items for Systematic Reviews and Meta-Analyses diagram in the Supplemental materials. The machine learning literature review identified a total of 276 epidemiological studies, of which we judged 21 to be suitable to be included in the quantitative meta-analysis (Supplemental Fig. 1). These 21 studies reported a total of 902 relative risks or odds ratios for respiratory ($n = 455$) or cardiovascular ($n = 308$) hospital or emergency department visits, or all-cause or non-accidental deaths ($n = 139$).

A subset of 4 studies reported risk estimates for respiratory hospital admissions that reported effect coefficients for a common endpoint, PM indicator (in this case, PM_{10}), lag structure and population age strata and so were suitable for pooling in a quantitative meta-analysis (Henderson et al., 2015; Johnston et al., 2007; Morgan et al., 2010; Tham et al., 2009). Using the Metafor library in the R statistical package, we perform a random effects meta-analysis (R Core Team, 2016; Viechtbauer, 2010). A forest plot illustrating the studies included in the meta-analysis, a random-effects pooled estimate, and additional information regarding tests for funnel plot asymmetry can be found in the Supplemental materials (Supplemental Figs. 2 and 3).

Ultimately, for the health impact assessment, we did not use this pooled estimate because the exposure of interest for our nationwide risk assessment was $PM_{2.5}$, not PM_{10}. Additionally, the risk coefficients may not be generalizable because all 4 studies were based on wildland fire events outside of the U.S. (Henderson et al., 2015; Johnston et al., 2007; Morgan et al., 2010; Tham et al., 2009). Populations in other countries may respond differently to wildland fire episodes to those in the U.S., have access to a different healthcare system, may be more or less susceptible to wildland fire smoke, and may differ in other ways that we cannot observe using the available data. For these reasons, we used a risk coefficients drawn Delfino et al. (2009), which reported risk estimates for both respiratory and cardiovascular hospital admissions during the wildland fire episodes in Southern California.

We also selected $PM_{2.5}$ epidemiological studies that reported short-term and long-term $PM_{2.5}$ effect coefficients that did not specifically report effect estimates for exposures to wildland fire $PM_{2.5}$. We used risk estimates U.S. EPA previously employed to evaluate the health benefits of alternative air quality standards (EPA, 2012), recognizing that these studies do not consider $PM_{2.5}$ particles originating from wildland fire events specifically and they generally consider $PM_{2.5}$ concentrations at levels significantly below those observed during wildland fire episodes. The short-term studies include Zanobetti et al. (2009), a multi-city time-series study that reported hospital admissions for respiratory outcomes, and Zanobetti and Schwartz (2009), a multi-city time series study of $PM_{2.5}$-related mortality. Because wildfire episodes can affect long-term levels of $PM_{2.5}$, we also employ effect coefficients from long-term epidemiological studies; these include an extended analysis of the American Cancer Society (Krewski et al., 2009) and an extended analysis of the Harvard Six Cities cohort (Lepeule et al., 2012).

2.4. Baseline rates of death and hospital admissions

The epidemiological studies noted above report estimates of risk that are expressed as being relative to a baseline rate. In this analysis we used effect coefficients to quantify cases of hospital admissions and premature deaths, and thus we applied baseline rates of all-cause mortality and hospital admissions. We selected county-level age-stratified all-cause death rates from the Centers for Disease Control (WONDER) database for the year 2010 (Centers for Disease Control and Prevention 2016). We selected hospital visit rates from the Healthcare Cost and Utilization Program (HCUP); these are a mixture of county, state and regional rates (see Supplemental Table 2).

2.5. Assigning $PM_{2.5}$ concentrations to the population

We quantified changes in population-level exposure by assigning the predicted $PM_{2.5}$ concentrations to the population in each 12 km by 12 km model grid cell. The BenMAP-CE tool contains 2010 U.S. Census reported population counts stratified by age, sex, race and ethnicity, assigned to each air quality grid. We used the census-reported population counts for the years 2010 and then projected these counts to the years 2011 and 2012 using the Woods and Poole forecast (Woods and Poole, 2012). Population data in each year are stratified by age, sex, race, and ethnicity.

To calculate a national wildland fire $PM_{2.5}$ concentrations for each of the five years that was weighted to the size of the population exposed to wildland fire $PM_{2.5}$ concentrations for all counties combined (C_i) in year i as

$$C_i = \frac{\sum_j C_{ij} \times P_{ij}}{P_i}$$

where C_{ij} is the wildfire-attributable annual mean $PM_{2.5}$ concentration in county j in year i, P_{ij} is the population in county j in year i, and P_i is the total population over all counties combined in year i.

2.6. Economic values

We estimated the value of avoided premature deaths using a Value of Statistical Life (VSL) recommended by the U.S. EPA's Guidelines for Preparing Economic Analyses (US EPA, 2010). Following U.S. EPA guidelines, we indexed this value to the inflation and income year of the analysis. Using a 2010 inflation year and assuming 2016 income levels, we calculated a VSL of $10.1M. To value changes in respiratory hospital admissions, we used a cost of illness estimate U.S. EPA employed in its Regulatory Impact Analysis for the $PM_{2.5}$ National Ambient Air Quality Standards (US EPA, 2012). This value of $36,000 reflects the direct medical costs associated with the hospital visit as well as lost earnings.

3. Results

3.1. Air quality

The median of the predicted annual mean wildland fire-attributable $PM_{2.5}$ concentrations across all model grid cells ranges from between 0.3 μg/m^3, in 2009 and 0.8 μg/m^3 in 2012, while the population-weighted annual mean $PM_{2.5}$ concentration ranges from between 0.6 μg/m^3 in 2009 to 1.1 μg/m^3 in 2008 (Table 1). In general, the distribution of wildfire attributable $PM_{2.5}$ concentrations are greatest in the year 2008 and lowest in the years 2009 and 2010 of the years included in this analysis.

A small number of states are most greatly affected by wildland fire events across the 5-year period (Fig. 1). In the western U.S., states including California, Oregon, Idaho and Montana experience wildland fires in each year. Among the Southeastern states, North Carolina, South Carolina, Georgia, Louisiana, Arkansas, Florida and eastern Texas are most impacted.

3.2. Estimated health impacts and economic values of wildland fire events

We estimate between 5200 and 8500 respiratory hospital admissions per year (Table 2) (from 2008 to 2012) from wildland fires when using the concentration-response relationship from the Delfino et al. (2009) study. This range is within the same order of magnitude as the values estimated using a concentration-response relationship from the Zanobetti et al. (2009) multi-city study that did not explicitly account for wildland fire episodes (3900 to 6300). Using an effect coefficient from the Delfino et al. (2009) study, we also estimate between 1500 and 2500 cardiovascular hospital admissions. As noted above, we could not identify a suitable wildland fire study that reported a mortality effect coefficient and so used a risk coefficient from a multi-city time-series study (Zanobetti & Schwartz). We quantified between 1500 and 2500 wildland-attributable $PM_{2.5}$-related deaths from short-term changes in $PM_{2.5}$ concentrations over the five-year period (Table 2). We estimate the largest number of excess deaths and hospital admissions for the year 2008, when wildland fire attributable $PM_{2.5}$ concentrations are the greatest out of the years included here.

To provide context for the estimates above, in the secondary analysis we also applied $PM_{2.5}$ concentration-response relationships recently employed in U.S. EPA health impact assessments, estimating thousands of non-fatal heart attacks, thousands of respiratory and cardiovascular hospital admissions, hundreds of thousands of cases of upper and lower respiratory symptoms and millions of cases of acute respiratory symptoms (Supplemental Table 4).

Summing the economic value of the short-term premature deaths and hospital admissions we estimated a total dollar value of between $11B and $20B per year (2010$) (Table 3). The present value of these economic values across the 5-year time period is $63B (3% discount rate, 2016$). We estimated the value of the long-term $PM_{2.5}$ related premature deaths and hospital admissions to fall between $76B and $130B per year (2010$). The present value of these economic values across the 5-year time period is $450B (3% discount rate, 2010$).

Table 1
Summary statistics of annual mean $PM_{2.5}$ (μg/m^3) predictions across 12 km grid cells attributable to wildfires (2008 to 2012).

	Year[a]				
	2008	2009	2010	2011	2012
10th %ile	0.26	0.14	0.14	0.26	0.33
25th %ile	0.37	0.18	0.23	0.40	0.52
50th %ile	0.61	0.33	0.43	0.60	0.81
Mean	1.1	0.56	0.70	0.80	0.92
75th %ile	1.4	0.79	0.96	1.1	1.2
90th %ile	2.3	1.3	1.7	1.7	1.6
Max	42	6.5	6.5	23	17
Population-weighted $PM_{2.5}$ level	1.1	0.61	0.68	0.73	0.75

[a] Values rounded to two significant figures.

3.3. The distribution of wildland fire-attributable health impacts among population subgroups

We next sought to better understand how the 5-year wildland fire episodes that we modeled in CMAQ were affecting populations across the U.S. For the 2008 to 2012 time period in which we modeled wildland fire episodes we mapped the cumulative CMAQ predicted wildland fire $PM_{2.5}$ concentrations as a distribution, and identified the upper 75th, 90th and 95th percentile. We then identified the portions of the CMAQ modeling domain at or above this level across the continental U.S. (Fig. 2). We next characterized the populations exposed to these elevated concentrations according to their race (Table 4).

When comparing the wildland fire-attributable $PM_{2.5}$ concentrations occurring among the highly affected and less affected areas, we found that: (1) in locations of the U.S. that are most affected by wildland fires, black populations represent a larger share of the individuals exposed to wildland fire $PM_{2.5}$ and a smaller share in those locations of the U.S. that are less affected by wildland fires; (2) by contrast, white populations experience a smaller share of the population in the highly affected areas and a larger share in the less affected areas (Table 4).

3.4. Sensitivity analysis

The estimated number of premature deaths and illnesses are sensitive to the predicted daily change in wildfire related $PM_{2.5}$ concentrations. Smoke plume height has been repeatedly identified as one of the critical sources of uncertainty in air quality modeling (Baker et al., 2016).

This parameter in turn affects the range in which particles disperse and therefore the predicted level of concentrations are most sensitive at both very short and far distances from fires. Examining model performance indicated that the model tends to over-predict at low concentrations, possibly over representing small fires, as well as at very high concentrations. Over-dispersion of particles in the model can yield an excess number of low impact days that can have a cumulative impact on the estimate of exposure.

To understand the sensitivity of our results to the high number of days with low concentrations we quantified the number of wildland fire-attributable deaths from daily changes in $PM_{2.5}$ that were at least 1, 3 and 5 μg/m^3 in size (Supplemental Table 3). We find that when quantifying $PM_{2.5}$-related deaths on days in which wildland $PM_{2.5}$ concentrations are at or above 1 μg/m^3, the estimated number of premature deaths is on average 17% lower than when we do not apply this threshold; when estimating premature deaths occurring on days when $PM_{2.5}$ levels at or above 5 μg/m^3, there are about 44% fewer premature deaths. These results suggest that our results were sensitive to low levels of model-predicted wildland $PM_{2.5}$ concentrations.

4. Discussion and conclusions

To our knowledge, this is the first manuscript to characterize the $PM_{2.5}$-related incidence and economic value of wildland fire impacts in the continental United States across an extended time period. The number of wildland fire-attributable $PM_{2.5}$-related hospital admissions, emergency department visits and other outcomes we estimated in this analysis are comparable to those reported in Fann, Fulcher and Baker (2013) for the year 2016. That analysis, like this one, employed photochemical modeling surfaces and used a similar array of health impact functions. However, Fann, Fulcher and Baker (2013) calibrated the air quality modeling predictions to monitored air quality data, which would affect the level and distribution of the wildland fire-attributable $PM_{2.5}$ concentrations. Here we do not calibrate model predictions with observed data because it has been noted that high concentrations of

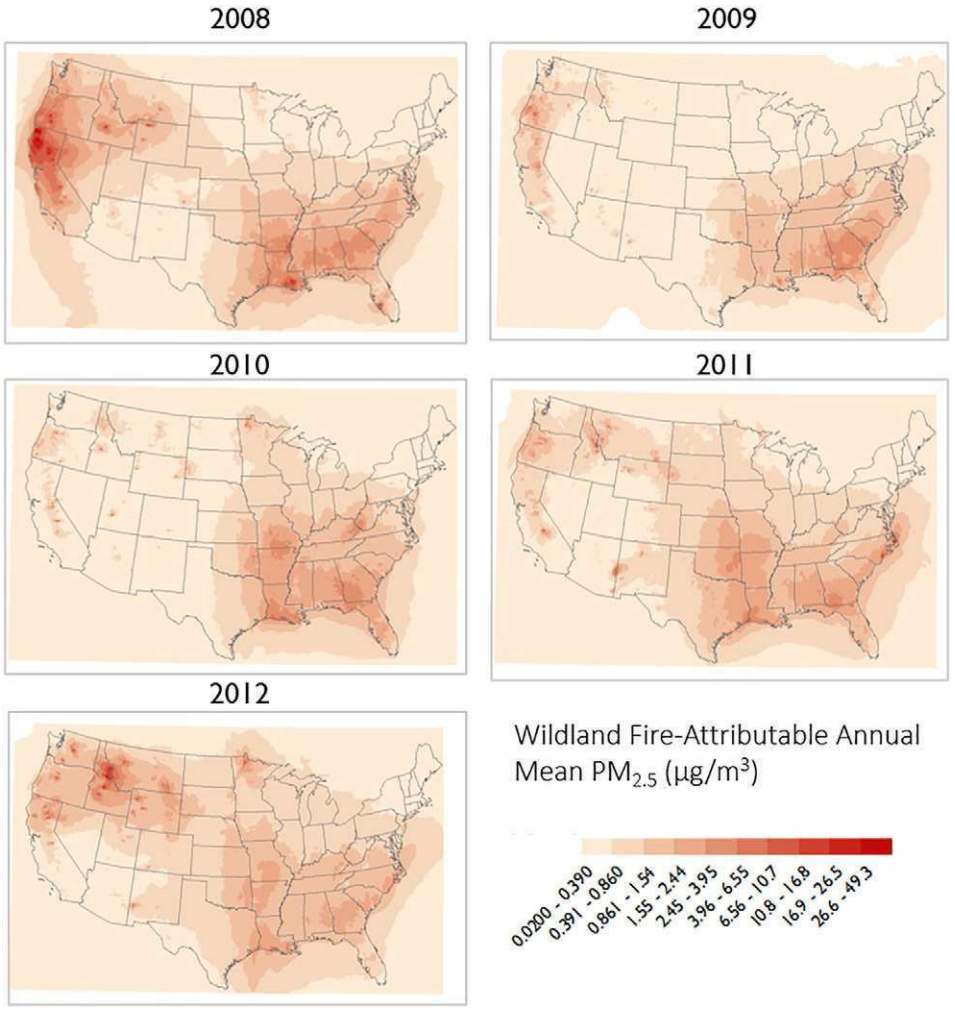

Fig. 1. Annual mean wildland fire-attributable $PM_{2.5}$ concentrations (2008–2012).

particles during wildfires restrict air flow to the pumps, shutting the monitors down and missing high concentration episodes, thus leading to potentially biased observed values. We also recognize the potential for CMAQ to overestimate wildland fire impacts (Baker et al., 2016). More complex calibration and data fusion models specific to the wildland fires are likely to become available with the increased usability of remote sensing in this area of research as well as improved parameterizations based on results from field campaigns such as the Fire and Smoke Model Evaluation Experiment (FASMEE) (http://www.fasmee.net).

Table 2
Premature deaths and illnesses attributable to wildfire-related $PM_{2.5}$ concentrations in each year calculated using alternative concentration-response functions (95% confidence intervals).

Endpoint	Year[a]				
	2008	2009	2010	2011	2012
Respiratory hospital admissions					
Delfino et al. (2009)	8500 (4400–12,000)	5200 (2700–7700)	6200 (3200–9100)	6300 (3300–9300)	6400 (3300–9400)
Zanobetti et al. (2009)	6300 (3600–9000)	3900 (2300–5500)	4600 (2600–6500)	4700 (2700–6700)	4800 (2800–6800)
Cardiovascular hospital admissions					
Delfino et al. (2009)	2800 (−500–6000)	1700 (−320–3700)	2100 (−380–4400)	2100 (−380–4500)	2100 (−390–4600)
Premature deaths from short-term exposure to $PM_{2.5}$					
Zanobetti and Schwartz (2009)	2500 (1900–3000)	1500 (1100–1800)	1700 (1300–2100)	1900 (1400–2200)	1800 (1400–2200)
Premature deaths from long-term exposure to $PM_{2.5}$					
Krewski et al. (2009)	14,000 (9700–19,000)	8700 (5800–11,000)	10,000 (6900–14,000)	11,000 (7300–14,000)	11,000 (7600–15,000)
Lepeule et al. (2012)	32,000 (16,000–48,000)	19,000 (9800–29,000)	23,000 (12,000–35,000)	24,000 (12,000–36,000)	25,000 (13,000–38,000)

[a] Values rounded to two significant figures; all functions estimated for populations ages 0–99.

Table 3
Estimated economic value of wildfire-attributable $PM_{2.5}$-related premature deaths and respiratory hospital admissions (2008 to 2012) (billions of 2010$, 95% confidence intervals).[a]

Health endpoints	Year					Present value
	2008	2009	2010	2011	2012	
Sum of mortality from short-term exposures and respiratory hospital admissions[a]	$20 ($2–$53)	$12 ($1–$31)	$14 ($1–$37)	$11 ($1–$30)	$12 ($1–$31)	$63 ($6–$170)
Sum of mortality from long-term exposures and respiratory hospital admissions[b]	$130 ($12–$340)	$76 ($7–$210)	$90 ($8–$250)	$96 ($9–$260)	$100 ($9–$270)	$450 ($42–$1000)

[a] Sum of Delfino et al. (2009) respiratory hospital admission estimates and Zanobetti and Schwartz (2009) mortality.
[b] Sum of Delfino et al. (2009) hospital admission estimates and Krewski et al. (2009) mortality.

The epidemiological literature reporting risks from wildland fire-related $PM_{2.5}$ is sparse; this makes quantifying wildland-attributable risks challenging. The epidemiology studies that the U.S. EPA and others commonly use to quantify PM-related mortality and morbidity impacts, and reported in the Supplemental materials to this article, were not explicitly designed to characterize risks from this emission source. However, it is reasonable to expect that many epidemiologic studies that did not explicitly address wildland fire impacts will have at least partially accounted for them, given that wildland fire particles tend to account for large portion of PM in the atmosphere (Verma et al., 2014). The National Emissions inventory of 2011 estimates that 41% of $PM_{2.5}$ emissions originate with wildland burning (U.S. EPA, 2011).

In light of this limitation, when we designed the health impact assessment, we took two steps to ensure that we were using effect coefficients that were well matched to the unique characteristics of wildland fire smoke events. First, we performed a random effects quantitative meta-analysis of respiratory hospital admission epidemiological studies of smoke events in the U.S. and elsewhere in the world. Second, we selected concentration-response relationships from epidemiological studies that we believe would better account for the episodic nature of smoke events and the corresponding elevated levels of particles (Zanobetti et al., 2009; Zanobetti and Schwartz, 2009).

The overall economic value of wildland fire-attributable premature deaths and respiratory hospital admissions is considerable. Depending on whether we quantify short-term $PM_{2.5}$-related premature deaths or long-term $PM_{2.5}$-realted deaths, the cumulative 5-year economic value is in the tens to hundreds of billions of dollars.

Nearly all states in the U.S. experienced elevated fine particle concentrations from wildland fire events over the 5-year period, according to our simulation of air quality. Certain states were affected by severe wildland fire events occurring across two or more years, including Louisiana (some of which may be due to debris burning after an active hurricane season because remote sensing of fires cannot distinguish between large debris burning from wildfires or prescribed fires), California, Idaho, and Georgia. Within these states, certain population subgroups were affected disproportionately. In particular, black populations, and to a lesser extent Asian populations, accounted for a greater share of wildland fire-attributable health impacts. State and local officials may wish to consider how best to communicate with subgroups that are most affected when deploying warning systems that alert the public to the health risks of wildland fire smoke. State and local officials deploying warning systems to alert the public to the health risks of wildland fire smoke may wish to consider how best to reach these subgroups.

This analysis is subject to certain limitations and uncertainties that shape the way in which the results may be interpreted. Considering first the air quality inputs, we assessed the performance of the chemical transport model by matching CMAQ grid locations to the locations of environmental monitors and comparing predicted and observed values. We found that the model is biased high when predicting low levels of

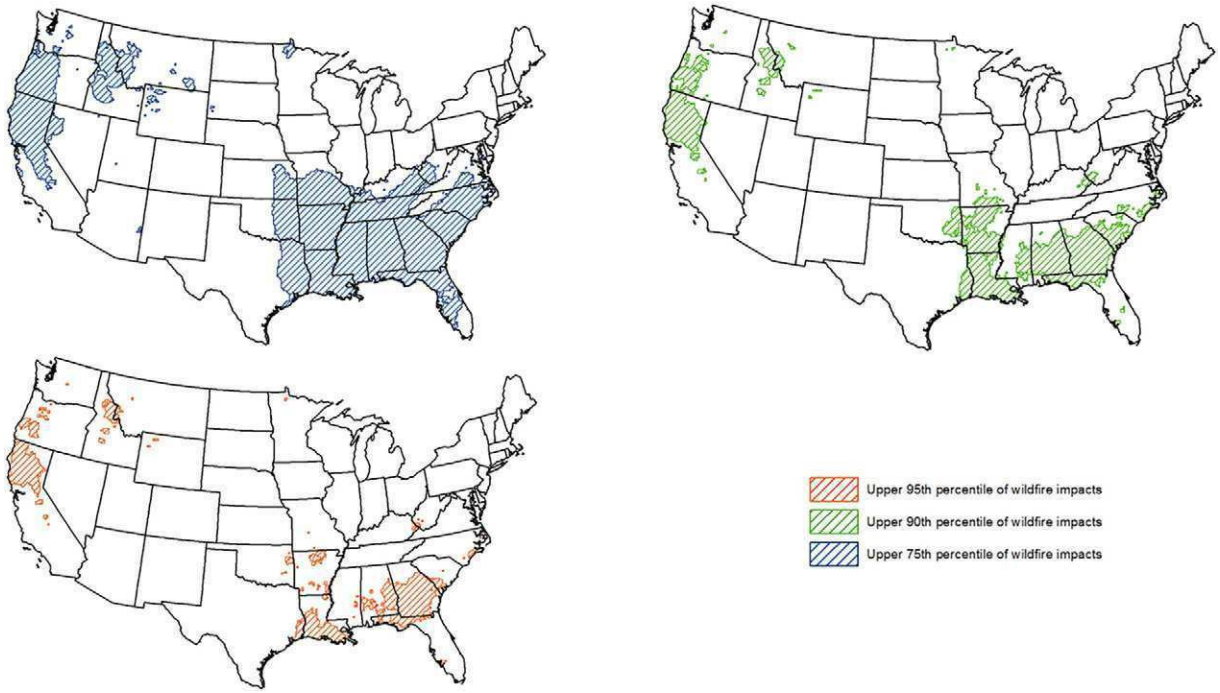

Fig. 2. Locations of the U.S. experiencing elevated wildfire-related $PM_{2.5}$ concentrations over a 5-year period.

Table 4
The percentage of individuals living in locations highly affected, and less affected, by wildland fires (2008 to 2012).[a]

Race	National average	Location of the U.S.[b]		Difference between highly and less affected
		Highly affected	Less affected	
Asian	5%	4%	5%	−1%
Black	13%	18%	13%	12%
Native American	1%	2%	1%	1%
White	81%	75%	81%	−6%
Total	100%	100%	100%	

[a] Highly affect subgroups are those individuals who have experienced cumulative levels of wildland fire attributable $PM_{2.5}$ concentrations that are at or above the 75th percentile, identified in Fig. 2 with blue hatched shading. Less affected subgroups are those not living in these areas.
[b] Estimates rounded to two significant figures.

$PM_{2.5}$ concentrations. The model also over predicts $PM_{2.5}$ (mainly Organic Carbon and Elemental Carbon) during all seasons for fire events. Baker et al. (2016) found the Flint Hills fire overestimated OC and EC but the Wallow fire did not overestimate to the same degree suggesting there is a lot of complexity in terms of how different fires are characterized in CMAQ. Another limitation is that only fire events that are part of the emission inventory have been evaluated. Any misspecification of emissions in the inventory fires is not included in our analysis. Further scientific advances and research efforts aimed to improve characterization of fire, fuel and emission inventories, and to improve measure characterization of differential toxicity of smoke emitted from different fuel types can potentially improve future health risk assessments.

The health impacts quantified using concentration-response relationships described in this paper are also subject to uncertainties. More specifically, questions remain regarding the extent to which certain species of fire-attributable PM may be more or less toxic than others (Sullivan et al., 2008). Thus, using effect coefficients from the epidemiological studies that did not specifically consider wildland fire episodes, may under- or over-estimate impacts. By contrast, the quantitative meta-analysis draws upon epidemiological studies of wildland fire events, but is limited to respiratory hospital admissions and PM_{10}. Several of these studies were conducted outside of the U.S.; differences between the health care system, wildland fire particle composition, behavioral responses to smoke events and other factors may bias the meta-analysis pooled risk coefficient. We also apply the effect coefficients from the Delfino et al. (2009) study of wildfires in Southern California nationwide; this may bias our estimates of risk high or low depending on the area that it is applied to. Finally, the present value calculation assumes that the wildland fire-related premature deaths estimated for each year are independent of those estimated in all other years. For example, individuals modeled as dying prematurely from wildland fire smoke exposure in year 1 cannot also die in year 2, but the net present value calculation introduces the possibility that deaths may have been counted more than once across years. However, given that the fraction of total deaths accounted for by air pollution episodes is relatively small (approximately 6% on a national basis), the potential for this approach to bias-high the number of wildland-attributable deaths is likely small (Fann et al., 2011).

Despite these uncertainties, this manuscript also exhibits a number of strengths and unique features. First, this analysis is, to our knowledge, the first to characterize the incidence and economic value of human health impacts attributable to wildland fire-emitted fine particles in the continental U.S. over a 5-year period. Second, while previous studies have incorporated a systematic review of wildland fire studies, none to our knowledge have performed a quantitative meta-analysis. Third, we characterize both the size, and distribution, of wildland fire-related premature deaths and hospital admissions across population subgroups. Taken together, the results in this analysis suggest that the number and value of wildland fire events is considerable and that these impacts are not shared equally across the U.S. population.

Disclaimer

The research described in this article has been reviewed by the National Health and Environmental Effects Research Laboratory, U.S. Environmental Protection Agency, and approved for publication. Approval does not signify that the contents necessarily reflect the views and policies of the Agency, nor does the mention of trade names of commercial products constitute endorsement or recommendation for use.

Competing financial interests

The authors declare no competing financial interests.

Acknowledgements

We gratefully acknowledge the comments received from Bryan Hubbell and Karen Wesson, who reviewed early versions of this manuscript.

Appendix A. Supplementary data

Supplementary data to this article can be found online at http://dx.doi.org/10.1016/j.scitotenv.2017.08.024.

References

Baker, K.R., Woody, M.C., Tonnesen, G.S., Hutzell, W., Pye, H.O.T., Beaver, M.R., et al., 2016. Contribution of regional-scale fire events to ozone and PM2.5 air quality estimated by photochemical modeling approaches. Atmos. Environ. 140:539–554. http://dx.doi.org/10.1016/j.atmosenv.2016.06.032.

Berman, J.D., Fann, N., Hollingsworth, J.W., Pinkerton, K.E., Rom, W.N., Szema, A.M., et al., 2012. Health benefits from large-scale ozone reduction in the United States. Environ. Health Perspect. 120:1404–1410. http://dx.doi.org/10.1289/ehp.1104851.

Carlton, A.G., Baker, K.R., 2011. Photochemical Modeling of the Ozark Isoprene Volcano: MEGAN, BEIS, and Their Impacts on Air Quality Predictions. Environmental Science & Technology 45, 4438–4445.

Crimmins, A., Balbus, J., Gamble, J.L., Beard, C.B., Bell, J.E., Dodgen, D., et al., 2016. Human health the impacts of climate change on in the United States the impacts of climate change on human health in the United States. U.S. Glob. Chang. Res. Progr.

Delfino, R.J., Brummel, S., Wu, J., Stern, H., Ostro, B., Lipsett, M., et al., 2009. The relationship of respiratory and cardiovascular hospital admissions to the southern California wildfires of 2003. Occup. Environ. Med. 66:189–197. http://dx.doi.org/10.1136/oem.2008.041376.

EPA, 2011. Regulatory Impact Assessment for Final Transport Rule.

Fann, N., Lamson, A.D., Anenberg, S.C., Wesson, K., Risley, D., Hubbell, B.J., 2011. Estimating the national public health burden associated with exposure to ambient PM(2.5) and ozone. Risk Anal. 32:81–95. http://dx.doi.org/10.1111/j.1539-6924.2011.01630.x.

Fann, Neal, Fulcher, Charles M., Baker, Kirk, 2013. The recent and future health burden of air pollution apportioned across US sectors. Environmental science & technology 47 (8), 3580–3589.

Henderson, S.B., Brauer, M., Kennedy, S., MacNab, Y., 2009. Three measures of forest fire smoke exposure and their association with respiratory and cardiovascular physician visits and hospital admissions. Epidemiology 20:S82. http://dx.doi.org/10.1097/01.ede.0000362956.02139.fd.

Henderson, S.B., Brauer, M., MacNab, Y.C., Kennedy, S.M., 2015. Three Measures of Forest Fire Smoke Exposure and Their Associations with Respiratory and Cardiovascular Health Outcomes in a Population-based Cohort. http://dx.doi.org/10.14288/1.0074714.

Johnston, F.H., Bailie, R.S., Pilotto, L.S., Hanigan, I.C., Samet, J., Zeger, S., et al., 2007. Ambient biomass smoke and cardio-respiratory hospital admissions in Darwin, Australia. BMC Public Health 7:240. http://dx.doi.org/10.1186/1471-2458-7-240.

Jones, R.R., Hogrefe, C., Fitzgerald, E.F., Hwang, S.A., Özkaynak, H., Garcia, V.C., et al., 2015. Respiratory hospitalizations in association with fine PM and its components in New York State. J. Air Waste Manage. Assoc. 65:559–569. http://dx.doi.org/10.1080/10962247.2014.1001500.

Knorr, W., Lehsten, V., Arneth, A., 2012. Determinants and predictability of global wildfire emissions. Atmos. Chem. Phys. 12:6845–6861. http://dx.doi.org/10.5194/acp-12-6845-2012.

Kochi, I., Champ, P.A., Loomis, J.B., Donovan, G.H., 2012. Valuing mortality impacts of smoke exposure from major southern California wildfires. J. For. Econ. 18:61–75. http://dx.doi.org/10.1016/j.jfe.2011.10.002.

Krewski, D., Jerrett, M., Burnett, R.T., Ma, R., Hughes, E., Shi, Y., et al., 2009. Extended follow-up and spatial analysis of the American Cancer Society study linking particulate air pollution and mortality. Res. Rep. Health Eff. Inst. 5, 114–136.

Krewski, Daniel, et al., 2009. Extended follow-up and spatial analysis of the American Cancer Society study linking particulate air pollution and mortality. No. 140. Health Effects Institute, Boston, MA.

Lepeule, J., Laden, F., Dockery, D., Schwartz, J., 2012. Chronic exposure to fine particles and mortality: an extended follow-up of the Harvard Six Cities study from 1974 to 2009. Environ. Health Perspect. 120:965–970. http://dx.doi.org/10.1289/ehp.1104660.

Liu, J.C., Pereira, G., Uhl S a, Bravo M a, Bell ML., 2014. A systematic review of the physical health impacts from non-occupational exposure to wildfire smoke. Environ. Res. 136: 120–132. http://dx.doi.org/10.1016/j.envres.2014.10.015.

Liu, J.C., Pereira, G., Uhl, S.A., Bravo, M.A., Bell, M.L., 2015. A systematic review of the physical health impacts from non-occupational exposure to wildfire smoke. Environ. Res. 136:120–132. http://dx.doi.org/10.1016/j.envres.2014.10.015.

Liu, J.C., Mickley, L.J., Sulprizio, M.P., Dominici, F., Yue, X., Ebisu, K., et al., 2016. Particulate air pollution from wildfires in the Western US under climate change. Clim. Chang.: 1–12 http://dx.doi.org/10.1007/s10584-016-1762-6.

McKenzie, D., French, N.H., Ottmar, R.D., 2012. National database for calculating fuel available to wildfires. EOS Trans. Am. Geophys. Union 93 (6), 57–58.

Morgan, G., Sheppeard, V., Khalaj, B., Ayyar, A., Lincoln, D., Jalaludin, B., et al., 2010. Effects of bushfire smoke on daily mortality and hospital admissions in Sydney, Australia. Epidemiology 21:47–55. http://dx.doi.org/10.1097/EDE.0b013e3181c15d5a.

Office of Air Quality Planning and Standards, 2011. Regulatory Impact Assessment for the Mercury and Air Toxics Standards.

Ottmar, R.D., 2014. Wildland fire emissions, carbon, and climate: modeling fuel consumption. For. Ecol. Manag. 317:41–50. http://dx.doi.org/10.1016/j.foreco.2013.06.010.

Rappold, A.G., et al., 2011. Peat bog wildfire smoke exposure in rural North Carolina is associated with cardiopulmonary emergency department visits assessed through syndromic surveillance. Environ. Health Perspect. 119, 1415.

Rappold, A.G., et al., 2012. Cardio-respiratory outcomes associated with exposure to wildfire smoke are modified by measures of community health. Environ. Health 11, 71.

R Core Team, 2016. R: A Language and Environment for Statistical Computing.

Rappold, A.G., Fann, N.L., Crooks, J., Huang, J., Cascio, W.E., Devlin, R.B., et al., 2014. Forecast-based interventions can reduce the health and economic burden of wildfires. Environ. Sci. Technol.

Rittmaster, R., Adamowicz, W.L., Amiro, B., Pelletier, R.T., 2006. Economic Analysis of Health Effects From Forest Fires. 877:pp. 868–877. http://dx.doi.org/10.1139/X05-293.

Schwede, Donna, Pouliot, George, Pierce, Thomas, 2005. Changes to the biogenic emissions inventory system version 3 (BEIS3)." 4th Annual CMAS Models-3 Users' Conference, September. Vol. 26.

Sonoma Technology, 2007. SMARTFIRE System Version 2.

Stavros, E.N., McKenzie, D., Larkin, N., 2014. The climate-wildfire-air quality system: interactions and feedbacks across spatial and temporal scales. Wiley Interdiscip. Rev. Clim. Chang. 5:719–733. http://dx.doi.org/10.1002/wcc.303.

Sullivan, A.P., Holden, A.S., Patterson, L.A., McMeeking, G.R., Kreidenweis, S.M., Malm, W.C., et al., 2008. A method for smoke marker measurements and its potential application for determining the contribution of biomass burning from wildfires and prescribed fires to ambient $PM_{2.5}$ organic carbon. J. Geophys. Res. 113, D22302. http://dx.doi.org/10.1029/2008JD010216.

Tham, R., Erbas, B., Akram, M., Dennekamp, M., Abramson, M.J., 2009. The impact of smoke on respiratory hospital outcomes during the 2002–2003 bushfire season, Victoria, Australia. Respirology 14:69–75. http://dx.doi.org/10.1111/j.1440-1843.2008.01416.x.

U.S. Environmental Protection Agency, 2014. Environmental Benefits Mapping and Analysis Program—Community Edition (BenMAP-CE).

U.S. Environmental Protection Agency, 2016. Technical Support Document Preparation of Emission Inventories for the Version 6.3, 2011 Emissions Modeling Platform. https://www.epa.gov/sites/production/files/2016-09/documents/2011v6_3_2017_emismod_tsd_aug2016_final.pdf.

U.S. EPA, 2011. National Emissions Inventory, 2011.

US EPA, 2009. Integrated Science Assessment for Particulate Matter (Final Report).

US EPA, 2010. Guidelines for Preparing Economic Analyses.

US EPA, 2012. Regulatory Impact Assessment for the PM NAAQS RIA.

US Forest Service, 2015. PNW - Fire and Environmental Research Applications Team (FERA) Research/Studies.Available:. https://www.fs.fed.us/pnw/fera/fft/consumemodule.shtml (accessed 13 March 2017).

Verma, V., Fang, T., Guo, H., King, L., Bates, J.T., Peltier, R.E., et al., 2014. Reactive oxygen species associated with water-soluble PM2.5 in the southeastern United States: spatiotemporal trends and source apportionment. Atmos. Chem. Phys. 14:12915–12930. http://dx.doi.org/10.5194/acp-14-12915-2014.

Viechtbauer, W., 2010. Conducting meta-analyses in *R* with the metafor package. J. Stat. Softw. 36:1–48. http://dx.doi.org/10.18637/jss.v036.i03.

Westerling, A.L., Hidalgo, H.G., Cayan, D.R., Swetnam, T.W., 2006. Warming and earlier spring increase western U.S. forest wildfire activity. Science 313:940–943. http://dx.doi.org/10.1126/science.1128834.

Woods and Poole, 2012. Woods & Poole.

Yarwood, G., Rao, S., Yocke, M., Whitten, G., 2005. Updates to the Carbon Bond Mechanism: CB05 (doi:RT-0400675 8).

Zanobetti, A., Schwartz, J., 2009. The effect of fine and coarse particulate air pollution on mortality: a national analysis. Environ. Health Perspect. 117:898–903. http://dx.doi.org/10.1289/ehp.0800108.

Zanobetti, A., Franklin, M., Koutrakis, P., Schwartz, J., 2009. Fine particulate air pollution and its components in association with cause-specific emergency admissions. Environ. Health 8:58. http://dx.doi.org/10.1186/1476-069X-8-58.

Science of the Total Environment 610–611 (2018) 802–809

Contents lists available at ScienceDirect

Science of the Total Environment

journal homepage: www.elsevier.com/locate/scitotenv

The health impacts and economic value of wildland fire episodes in the U.S.: 2008–2012

Neal Fann [a,*], Breanna Alman [a], Richard A. Broome [b], Geoffrey G. Morgan [c], Fay H. Johnston [d], George Pouliot [e], Ana G. Rappold [e]

[a] Office of Air Quality Planning and Standards, U.S. Environmental Protection Agency, 109 T.W. Alexander Drive, Research Triangle Park, NC 27711, USA
[b] Sydney South West Area Health Service, New South Wales, Australia
[c] University Center for Rural Health, University of Sydney, New South Wales, Australia
[d] Menzies Institute for Medical Research, University of Tasmania, Australia
[e] U.S. Environmental Protection Agency, Office of Research and Development, Research Triangle Park, NC, USA

HIGHLIGHTS

- Wildland fires adversely affect air quality and health in the U.S.
- Between 2008 and 2012, fires increased $PM_{2.5}$ levels in the Northwest and Southeast.
- We estimate thousands of premature deaths and illnesses from these episodes.
- The economic value of these impacts is in the tens to hundreds of billions of US$.

GRAPHICAL ABSTRACT

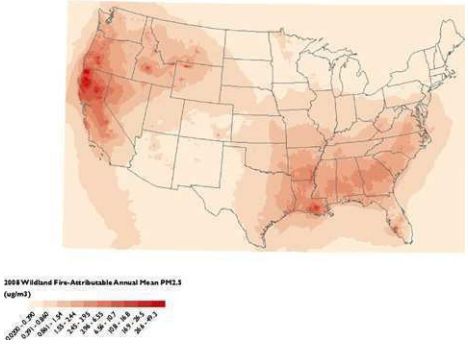

ARTICLE INFO

Article history:
Received 24 April 2017
Received in revised form 25 July 2017
Accepted 2 August 2017
Available online 18 August 2017

Keywords:
Health impact assessment
Source apportionment
$PM_{2.5}$
Ozone
CMAQ
Wildland fires
Wildfires

ABSTRACT

Introduction: Wildland fires degrade air quality and adversely affect human health. A growing body of epidemiology literature reports increased rates of emergency departments, hospital admissions and premature deaths from wildfire smoke exposure.
Objective: Our research aimed to characterize excess mortality and morbidity events, and the economic value of these impacts, from wildland fire smoke exposure in the U.S. over a multi-year period; to date no other burden assessment has done this.
Methods: We first completed a systematic review of the epidemiologic literature and then performed photochemical air quality modeling for the years 2008 to 2012 in the continental U.S. Finally, we estimated the morbidity, mortality, and economic burden of wildland fires.
Results: Our models suggest that areas including northern California, Oregon and Idaho in the West, and Florida, Louisiana and Georgia in the East were most affected by wildland fire events in the form of additional premature deaths and respiratory hospital admissions. We estimated the economic value of these cases due to short term exposures as being between $11 and $20B (2010$) per year, with a net present value of $63B (95% confidence intervals $6–$170); we estimate the value of long-term exposures as being between $76 and $130B (2010$) per year, with a net present value of $450B (95% confidence intervals $42–$1200).

Abbreviations: BenMAP-CE, environmental Benefits Mapping and Analysis Program—Community Edition; CMAQ, Community Multi-Scale Air Quality Model; U.S. EPA, United States Environmental Protection Agency; ICD, International Classification of Disease; NH_3, ammonia; NOx, nitrogen dioxide; O_3, ground-level ozone; $PM_{2.5}$, particulate matter, 2.5 μm or less in diameter; SO_2, sulfur dioxide; WHO, World Health Organization.

* Corresponding author.
E-mail address: Fann.Neal@epa.gov (N. Fann).

http://dx.doi.org/10.1016/j.scitotenv.2017.08.024
0048-9697/Published by Elsevier B.V.

Conclusion: The public health burden of wildland fires—in terms of the number and economic value of deaths and illnesses—is considerable.

Published by Elsevier B.V.

1. Introduction

The increasing frequency and intensity of large wildfires deteriorates air quality and adversely affects human health (Crimmins et al., 2016; Henderson et al., 2009; Liu et al., 2015, 2016; Westerling et al., 2006). These events in turn both promote, and are exacerbated by, long-term changes to the climate; current trends in these events are expected to continue (Crimmins et al., 2016; Stavros et al., 2014). While the level and type of pollutants emitted during wildfires vary according to region and fuel type, all fires release directly emitted particulate matter (PM) as well as precursors to fine particles ($PM_{2.5}$) and can contribute to downwind formation of ozone (Knorr et al., 2012).

While risks to human health from exposure to PM are especially well characterized in the epidemiological, toxicological and controlled human exposure literature (US EPA, 2009), health impacts from PM stemming from wildland fires have been less extensively studied, though epidemiological literature has consistently observed adverse human health impacts attributable to wildfire-related $PM_{2.5}$ (Liu et al., 2015). For example, Rappold et al. (2012, 2011) found that a peat fire episode in eastern North Carolina was associated with increasing numbers of Emergency Department visits for cardiopulmonary and respiratory outcomes. Similarly, Delfino et al. (2009) observed increasing rates of respiratory and cardiovascular hospital admissions resulting from a month-long wildland fire episode in southern California. Epidemiological studies conducted in other countries, including Australia, have observed similar affects (Johnston et al., 2007; Morgan et al., 2010). A systematic review of literature from the U.S., Australia and elsewhere by Liu et al. (2014) found that wildland fire-related coarse particles (PM_{10}) were most consistently associated with respiratory outcomes.

Despite the growing body of epidemiological studies, there are a relatively small number of air pollution risk assessments that attribute the number of premature deaths and illnesses and the economic value of health impacts to wildfire episodes. The risk assessments performed thus far have been limited in their temporal scope, using a single (2005) and projected (2016) year (Fann et al., 2013), or have been limited to examining one fire at a time (Jones et al., 2015; Kochi et al., 2012; Rappold et al., 2014; Rittmaster et al., 2006). This paper builds upon this literature to estimate the number and economic value of wildland fire $PM_{2.5}$-related premature deaths and illnesses in the contiguous United States using chemical transport model predictions of $PM_{2.5}$ from wildland fire episodes over a 5-year period beginning in 2008. Considering a national scope allows us to more fully capture the impact that wildland fires may have on human health.

2. Materials and methods

In this study we characterized the overall magnitude and distribution of adverse health impacts by age and race that were associated with exposure to fire-$PM_{2.5}$ during wildfire smoke episodes. We used health impact functions derived from epidemiological studies that assessed the relationship between fire-$PM_{2.5}$ and expected incidence of health outcomes. We also performed a systematic literature review and meta-analysis; however, using results from the meta-analysis in a health impact function would have introduced considerable uncertainty into the estimates, and thus were not used.

2.1. Health impact function

The risk assessment employs a health impact function to quantify the number of wildland fire-attributable premature deaths and illnesses in each of the five years we modeled. We estimated the number of $PM_{2.5}$-related deaths and hospital admissions (y_{ij}) during each year i (i = 2008, 2009, 2010, 2011, 2012) among individuals in each county j (j = 1,…,J where J is the total number of counties) as: $y_{ij} = \Sigma_a y_{ija}$

$$y_{ija} = m0_{ija} \times \left(e^{\beta \cdot C}{}_{ij} - 1\right) \times P_{ija},$$

where, β is the risk coefficient, $m0_{ija}$ is the baseline death rate or hospital admission rate for the population in county j in year i among individuals for 5-year age strata a, C_{ij} is annual mean wildfire-attributable $PM_{2.5}$ concentration in county j in year i, and P_{ija} is the number of residents in county j in year i for five-year age strata a.

To perform a health impact risk assessment we used baseline incidence rates, population counts, and health impact functions included in the environmental Benefits Mapping and Analysis Program—Community Edition (BenMAP-CE, v1.1) (U.S. Environmental Protection Agency, 2014) to estimate counts of $PM_{2.5}$ attributable deaths and respiratory hospital admissions in each of five years from 2008 to 2012. These inputs have previously been used to estimate health and economic impacts in the national ambient air quality standards reviews, and the methods have been validated in previous publications (Berman et al., 2012; Fann et al., 2011; Office of Air Quality Planning and Standards, 2011). Below we describe how we specify inputs and use the BenMAP-CE tool with the appropriate input data.

2.2. Air quality modeling predictions

We simulated daily air quality from 2008 to 2012 using the Community Multiscale Air Quality version 5.1 (CMAQ v5.1) model with and without emissions from wildland fires in the contiguous United States. Wildland fires in our study included wildfires, prescribed fires, and other significant fires but it excluded agricultural fires. The difference between the two model runs represents the contribution of fire-$PM_{2.5}$ and $PM_{2.5}$ precursor emissions. Inputs to the model included gridded meteorological fields, emissions data, and boundary conditions. Gridded meteorological fields were provided by annual CONUS Weather Research and Forecasting (WRF) model simulation. Meteorological fields were defined on a 12 × 12 km horizontal grid with 35 vertical layers of variable thickness extending up to 50 hPa. The lowest model layer, which extended to approximately 20 m above ground was used to calculate the annual mean concentration of $PM_{2.5}$ (Δx) in the health impact function.

The CMAQ input emissions were based on a 12 km national U.S. domain with speciation for the Carbon-Bond 05 chemical mechanism (Yarwood et al., 2005). The emission inventory and ancillary files were based on the 2008 emissions modeling platform for 2008, 2009, and 2010 (EPA, 2012) and on the 2011 emission modeling platform for 2011 and 2012 (US EPA, 2016). Since the focus of this study is wildland fires, any additional information about the non-fire emission sources is noted in the references. The fire emissions were based on year specific daily fire estimates using the Hazard Mapping System fire detections and Sonoma Technology SMARTFIRE system version 2 (Sonoma Technology, 2007). Smartfire2 is a framework for producing fire activity data and allows for the merging of multiple data sources. Some of the fires included in the fire inventory come from satellite based remote sensing sources which cannot distinguish large prescribed or debris burning fires from wildfires with certainty. After multiple sources of fire information are reconciled to create fire activity estimates, the fire emissions are estimated using fuel moistures (via the USFS Wildland Fire Assessment System), consumption estimates

from the Consume model (Ottmar, 2014; US Forest Service, 2015), emission factors from the Fire Emission Production Simulator (Ottmar, 2014; US Forest Service, 2015), and fuel loading from the United States Forest Service Fuel Characteristic Classification System (FCCS) database (McKenzie et al., 2012). Plume rise for all point sources including the wildland fires was calculated within the CMAQ model. Biogenic emissions were processed in CMAQ and are based on the Biogenic Emissions Inventory System v3.14 (Schwede et al., 2005; Carlton and Baker, 2011).

2.3. Effect coefficients

To identify $PM_{2.5}$ effect coefficients suitable for the health burden impact assessment, we consulted two sources of evidence. The first is the U.S. EPA's 2009 Integrated Science Assessment for Particulate Matter (PM ISA), which classified human health endpoints as having a "causal" or "likely to be causal" relationship with short-term and long-term exposure to $PM_{2.5}$. The PM ISA synthesizes the epidemiological, toxicological and controlled human exposure studies published to that point, and was peer reviewed by the independent Clean Air Scientific Advisory Committee (US EPA, 2009). The PM ISA indicated that mortality and cardiovascular outcomes were causally related, and respiratory outcomes were likely to be causally related, to short-term and long-term exposure to fine particle levels (US EPA, 2009). The ISA did not differentiate these effects by particle composition or source.

Next, we performed a systematic review and quantitative meta-analysis. We included epidemiological studies that looked at associations between $PM_{2.5}$ during smoke events and various health endpoints. Studies identified were conducted in the U.S., Australia, South America, and Asia, and were limited to health endpoints identified by the PM ISA as being causally related to $PM_{2.5}$ exposure. The systematic review employed a machine learning technique to identify relevant literature. We report detailed information regarding the search terms, our procedure for identifying and screening eligible literature, and a Preferred Reporting Items for Systematic Reviews and Meta-Analyses diagram in the Supplemental materials. The machine learning literature review identified a total of 276 epidemiological studies, of which we judged 21 to be suitable to be included in the quantitative meta-analysis (Supplemental Fig. 1). These 21 studies reported a total of 902 relative risks or odds ratios for respiratory ($n = 455$) or cardiovascular ($n = 308$) hospital or emergency department visits, or all-cause or non-accidental deaths ($n = 139$).

A subset of 4 studies reported risk estimates for respiratory hospital admissions that reported effect coefficients for a common endpoint, PM indicator (in this case, PM_{10}), lag structure and population age strata and so were suitable for pooling in a quantitative meta-analysis (Henderson et al., 2015; Johnston et al., 2007; Morgan et al., 2010; Tham et al., 2009). Using the Metafor library in the R statistical package, we perform a random effects meta-analysis (R Core Team, 2016; Viechtbauer, 2010). A forest plot illustrating the studies included in the meta-analysis, a random-effects pooled estimate, and additional information regarding tests for funnel plot asymmetry can be found in the Supplemental materials (Supplemental Figs. 2 and 3).

Ultimately, for the health impact assessment, we did not use this pooled estimate because the exposure of interest for our nationwide risk assessment was $PM_{2.5}$, not PM_{10}. Additionally, the risk coefficients may not be generalizable because all 4 studies were based on wildland fire events outside of the U.S. (Henderson et al., 2015; Johnston et al., 2007; Morgan et al., 2010; Tham et al., 2009). Populations in other countries may respond differently to wildland fire episodes to those in the U.S., have access to a different healthcare system, may be more or less susceptible to wildland fire smoke, and may differ in other ways that we cannot observe using the available data. For these reasons, we used a risk coefficients drawn Delfino et al. (2009), which reported risk estimates for both respiratory and cardiovascular hospital admissions during the wildland fire episodes in Southern California.

We also selected $PM_{2.5}$ epidemiological studies that reported short-term and long-term $PM_{2.5}$ effect coefficients that did not specifically report effect estimates for exposures to wildland fire $PM_{2.5}$. We used risk estimates U.S. EPA previously employed to evaluate the health benefits of alternative air quality standards (EPA, 2012), recognizing that these studies do not consider $PM_{2.5}$ particles originating from wildland fire events specifically and they generally consider $PM_{2.5}$ concentrations at levels significantly below those observed during wildland fire episodes. The short-term studies include Zanobetti et al. (2009), a multi-city time-series study that reported hospital admissions for respiratory outcomes, and Zanobetti and Schwartz (2009), a multi-city time series study of $PM_{2.5}$-related mortality. Because wildfire episodes can affect long-term levels of $PM_{2.5}$, we also employ effect coefficients from long-term epidemiological studies; these include an extended analysis of the American Cancer Society (Krewski et al., 2009) and an extended analysis of the Harvard Six Cities cohort (Lepeule et al., 2012).

2.4. Baseline rates of death and hospital admissions

The epidemiological studies noted above report estimates of risk that are expressed as being relative to a baseline rate. In this analysis we used effect coefficients to quantify cases of hospital admissions and premature deaths, and thus we applied baseline rates of all-cause mortality and hospital admissions. We selected county-level age-stratified all-cause death rates from the Centers for Disease Control (WONDER) database for the year 2010 (Centers for Disease Control and Prevention 2016). We selected hospital visit rates from the Healthcare Cost and Utilization Program (HCUP); these are a mixture of county, state and regional rates (see Supplemental Table 2).

2.5. Assigning $PM_{2.5}$ concentrations to the population

We quantified changes in population-level exposure by assigning the predicted $PM_{2.5}$ concentrations to the population in each 12 km by 12 km model grid cell. The BenMAP-CE tool contains 2010 U.S. Census reported population counts stratified by age, sex, race and ethnicity, assigned to each air quality grid. We used the census-reported population counts for the years 2010 and then projected these counts to the years 2011 and 2012 using the Woods and Poole forecast (Woods and Poole, 2012). Population data in each year are stratified by age, sex, race, and ethnicity.

To calculate a national wildland fire $PM_{2.5}$ concentrations for each of the five years that was weighted to the size of the population exposed to wildland fire $PM_{2.5}$ concentrations for all counties combined (C_i) in year i as

$$C_i = \frac{\sum_j C_{ij} \times P_{ij}}{P_i}$$

where C_{ij} is the wildfire-attributable annual mean $PM_{2.5}$ concentration in county j in year i, P_{ij} is the population in county j in year i, and P_i is the total population over all counties combined in year i.

2.6. Economic values

We estimated the value of avoided premature deaths using a Value of Statistical Life (VSL) recommended by the U.S. EPA's Guidelines for Preparing Economic Analyses (US EPA, 2010). Following U.S. EPA guidelines, we indexed this value to the inflation and income year of the analysis. Using a 2010 inflation year and assuming 2016 income levels, we calculated a VSL of $10.1M. To value changes in respiratory hospital admissions, we used a cost of illness estimate U.S. EPA employed in its Regulatory Impact Analysis for the $PM_{2.5}$ National Ambient Air Quality Standards (US EPA, 2012). This value of $36,000 reflects the direct medical costs associated with the hospital visit as well as lost earnings.

3. Results

3.1. Air quality

The median of the predicted annual mean wildland fire-attributable $PM_{2.5}$ concentrations across all model grid cells ranges from between 0.3 μg/m^3, in 2009 and 0.8 μg/m^3 in 2012, while the population-weighted annual mean $PM_{2.5}$ concentration ranges from between 0.6 μg/m^3 in 2009 to 1.1 μg/m^3 in 2008 (Table 1). In general, the distribution of wildfire attributable $PM_{2.5}$ concentrations are greatest in the year 2008 and lowest in the years 2009 and 2010 of the years included in this analysis.

A small number of states are most greatly affected by wildland fire events across the 5-year period (Fig. 1). In the western U.S., states including California, Oregon, Idaho and Montana experience wildland fires in each year. Among the Southeastern states, North Carolina, South Carolina, Georgia, Louisiana, Arkansas, Florida and eastern Texas are most impacted.

3.2. Estimated health impacts and economic values of wildland fire events

We estimate between 5200 and 8500 respiratory hospital admissions per year (Table 2) (from 2008 to 2012) from wildland fires when using the concentration-response relationship from the Delfino et al. (2009) study. This range is within the same order of magnitude as the values estimated using a concentration-response relationship from the Zanobetti et al. (2009) multi-city study that did not explicitly account for wildland fire episodes (3900 to 6300). Using an effect coefficient from the Delfino et al. (2009) study, we also estimate between 1500 and 2500 cardiovascular hospital admissions. As noted above, we could not identify a suitable wildland fire study that reported a mortality effect coefficient and so used a risk coefficient from a multi-city time-series study (Zanobetti & Schwartz). We quantified between 1500 and 2500 wildland-attributable $PM_{2.5}$-related deaths from short-term changes in $PM_{2.5}$ concentrations over the five-year period (Table 2). We estimate the largest number of excess deaths and hospital admissions for the year 2008, when wildland fire attributable $PM_{2.5}$ concentrations are the greatest out of the years included here.

To provide context for the estimates above, in the secondary analysis we also applied $PM_{2.5}$ concentration-response relationships recently employed in U.S. EPA health impact assessments, estimating thousands of non-fatal heart attacks, thousands of respiratory and cardiovascular hospital admissions, hundreds of thousands of cases of upper and lower respiratory symptoms and millions of cases of acute respiratory symptoms (Supplemental Table 4).

Summing the economic value of the short-term premature deaths and hospital admissions we estimated a total dollar value of between $11B and $20B per year (2010$) (Table 3). The present value of these economic values across the 5-year time period is $63B (3% discount rate, 2016$). We estimated the value of the long-term $PM_{2.5}$ related premature deaths and hospital admissions to fall between $76B and $130B per year (2010$). The present value of these economic values across the 5-year time period is $450B (3% discount rate, 2010$).

Table 1
Summary statistics of annual mean $PM_{2.5}$ (μg/m^3) predictions across 12 km grid cells attributable to wildfires (2008 to 2012).

	Year[a]				
	2008	2009	2010	2011	2012
10th %ile	0.26	0.14	0.14	0.26	0.33
25th %ile	0.37	0.18	0.23	0.40	0.52
50th %ile	0.61	0.33	0.43	0.60	0.81
Mean	1.1	0.56	0.70	0.80	0.92
75th %ile	1.4	0.79	0.96	1.1	1.2
90th %ile	2.3	1.3	1.7	1.7	1.6
Max	42	6.5	6.5	23	17
Population-weighted $PM_{2.5}$ level	1.1	0.61	0.68	0.73	0.75

[a] Values rounded to two significant figures.

3.3. The distribution of wildland fire-attributable health impacts among population subgroups

We next sought to better understand how the 5-year wildland fire episodes that we modeled in CMAQ were affecting populations across the U.S. For the 2008 to 2012 time period in which we modeled wildland fire episodes we mapped the cumulative CMAQ predicted wildland fire $PM_{2.5}$ concentrations as a distribution, and identified the upper 75th, 90th and 95th percentile. We then identified the portions of the CMAQ modeling domain at or above this level across the continental U.S. (Fig. 2). We next characterized the populations exposed to these elevated concentrations according to their race (Table 4).

When comparing the wildland fire-attributable $PM_{2.5}$ concentrations occurring among the highly affected and less affected areas, we found that: (1) in locations of the U.S. that are most affected by wildland fires, black populations represent a larger share of the individuals exposed to wildland fire $PM_{2.5}$ and a smaller share in those locations of the U.S. that are less affected by wildland fires; (2) by contrast, white populations experience a smaller share of the population in the highly affected areas and a larger share in the less affected areas (Table 4).

3.4. Sensitivity analysis

The estimated number of premature deaths and illnesses are sensitive to the predicted daily change in wildfire related $PM_{2.5}$ concentrations. Smoke plume height has been repeatedly identified as one of the critical sources of uncertainty in air quality modeling (Baker et al., 2016).

This parameter in turn affects the range in which particles disperse and therefore the predicted level of concentrations are most sensitive at both very short and far distances from fires. Examining model performance indicated that the model tends to over-predict at low concentrations, possibly over representing small fires, as well as at very high concentrations. Over-dispersion of particles in the model can yield an excess number of low impact days that can have a cumulative impact on the estimate of exposure.

To understand the sensitivity of our results to the high number of days with low concentrations we quantified the number of wildland fire-attributable deaths from daily changes in $PM_{2.5}$ that were at least 1, 3 and 5 μg/m^3 in size (Supplemental Table 3). We find that when quantifying $PM_{2.5}$-related deaths on days in which wildland $PM_{2.5}$ concentrations are at or above 1 μg/m^3, the estimated number of premature deaths is on average 17% lower than when we do not apply this threshold; when estimating premature deaths occurring on days when $PM_{2.5}$ levels at or above 5 μg/m^3, there are about 44% fewer premature deaths. These results suggest that our results were sensitive to low levels of model-predicted wildland $PM_{2.5}$ concentrations.

4. Discussion and conclusions

To our knowledge, this is the first manuscript to characterize the $PM_{2.5}$-related incidence and economic value of wildland fire impacts in the continental United States across an extended time period. The number of wildland fire-attributable $PM_{2.5}$-related hospital admissions, emergency department visits and other outcomes we estimated in this analysis are comparable to those reported in Fann, Fulcher and Baker (2013) for the year 2016. That analysis, like this one, employed photochemical modeling surfaces and used a similar array of health impact functions. However, Fann, Fulcher and Baker (2013) calibrated the air quality modeling predictions to monitored air quality data, which would affect the level and distribution of the wildland fire-attributable $PM_{2.5}$ concentrations. Here we do not calibrate model predictions with observed data because it has been noted that high concentrations of

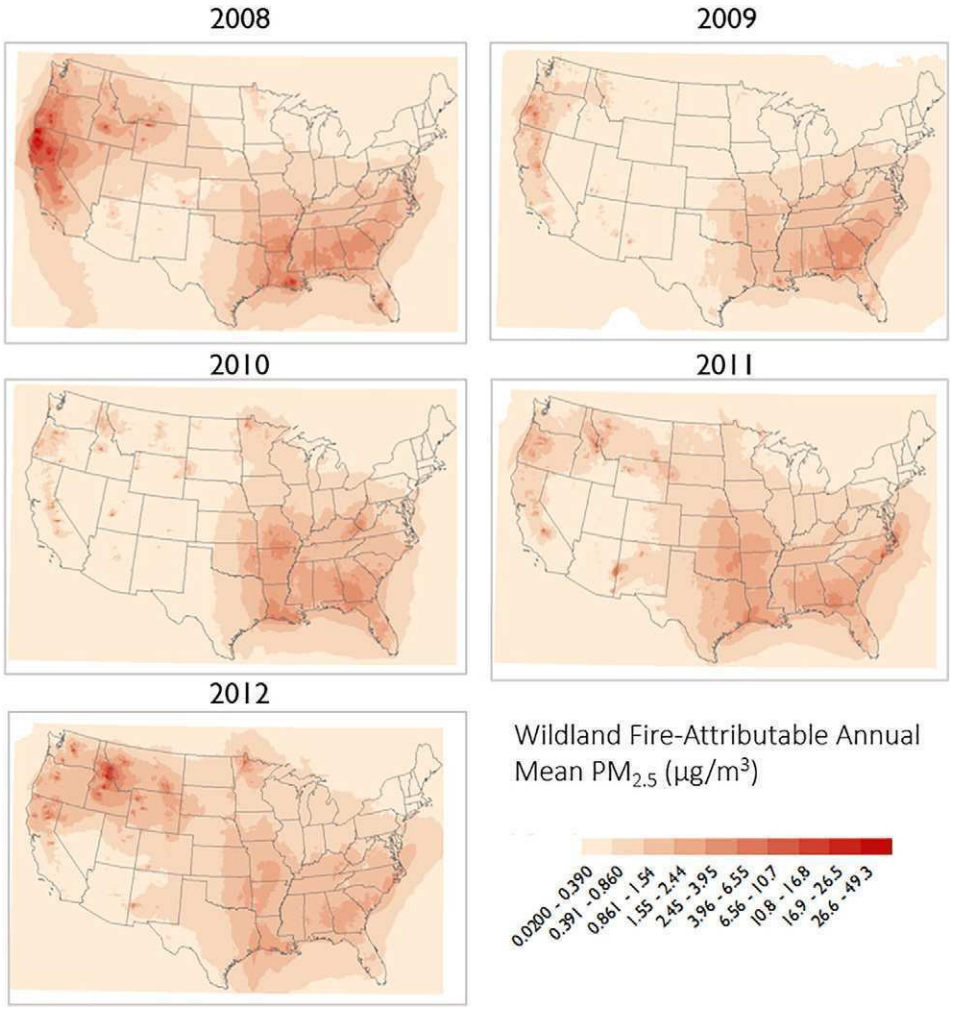

Fig. 1. Annual mean wildland fire-attributable $PM_{2.5}$ concentrations (2008–2012).

particles during wildfires restrict air flow to the pumps, shutting the monitors down and missing high concentration episodes, thus leading to potentially biased observed values. We also recognize the potential for CMAQ to overestimate wildland fire impacts (Baker et al., 2016). More complex calibration and data fusion models specific to the wildland fires are likely to become available with the increased usability of remote sensing in this area of research as well as improved parameterizations based on results from field campaigns such as the Fire and Smoke Model Evaluation Experiment (FASMEE) (http://www.fasmee.net).

Table 2
Premature deaths and illnesses attributable to wildfire-related $PM_{2.5}$ concentrations in each year calculated using alternative concentration-response functions (95% confidence intervals).

Endpoint	Year[a]				
	2008	2009	2010	2011	2012
Respiratory hospital admissions					
Delfino et al. (2009)	8500 (4400–12,000)	5200 (2700–7700)	6200 (3200–9100)	6300 (3300–9300)	6400 (3300–9400)
Zanobetti et al. (2009)	6300 (3600–9000)	3900 (2300–5500)	4600 (2600–6500)	4700 (2700–6700)	4800 (2800–6800)
Cardiovascular hospital admissions					
Delfino et al. (2009)	2800 (−500–6000)	1700 (−320–3700)	2100 (−380–4400)	2100 (−380–4500)	2100 (−390–4600)
Premature deaths from short-term exposure to $PM_{2.5}$					
Zanobetti and Schwartz (2009)	2500 (1900–3000)	1500 (1100–1800)	1700 (1300–2100)	1900 (1400–2200)	1800 (1400–2200)
Premature deaths from long-term exposure to $PM_{2.5}$					
Krewski et al. (2009)	14,000 (9700–19,000)	8700 (5800–11,000)	10,000 (6900–14,000)	11,000 (7300–14,000)	11,000 (7600–15,000)
Lepeule et al. (2012)	32,000 (16,000–48,000)	19,000 (9800–29,000)	23,000 (12,000–35,000)	24,000 (12,000–36,000)	25,000 (13,000–38,000)

[a] Values rounded to two significant figures; all functions estimated for populations ages 0–99.

Table 3
Estimated economic value of wildfire-attributable $PM_{2.5}$-related premature deaths and respiratory hospital admissions (2008 to 2012) (billions of 2010$, 95% confidence intervals).[a]

Health endpoints	Year					Present value
	2008	2009	2010	2011	2012	
Sum of mortality from short-term exposures and respiratory hospital admissions[a]	$20 ($2–$53)	$12 ($1–$31)	$14 ($1–$37)	$11 ($1–$30)	$12 ($1–$31)	$63 ($6–$170)
Sum of mortality from long-term exposures and respiratory hospital admissions[b]	$130 ($12–$340)	$76 ($7–$210)	$90 ($8–$250)	$96 ($9–$260)	$100 ($9–$270)	$450 ($42–$1000)

[a] Sum of Delfino et al. (2009) respiratory hospital admission estimates and Zanobetti and Schwartz (2009) mortality.
[b] Sum of Delfino et al. (2009) hospital admission estimates and Krewski et al. (2009) mortality.

The epidemiological literature reporting risks from wildland fire-related $PM_{2.5}$ is sparse; this makes quantifying wildland-attributable risks challenging. The epidemiology studies that the U.S. EPA and others commonly use to quantify PM-related mortality and morbidity impacts, and reported in the Supplemental materials to this article, were not explicitly designed to characterize risks from this emission source. However, it is reasonable to expect that many epidemiologic studies that did not explicitly address wildland fire impacts will have at least partially accounted for them, given that wildland fire particles tend to account for large portion of PM in the atmosphere (Verma et al., 2014). The National Emissions inventory of 2011 estimates that 41% of $PM_{2.5}$ emissions originate with wildland burning (U.S. EPA, 2011).

In light of this limitation, when we designed the health impact assessment, we took two steps to ensure that we were using effect coefficients that were well matched to the unique characteristics of wildland fire smoke events. First, we performed a random effects quantitative meta-analysis of respiratory hospital admission epidemiological studies of smoke events in the U.S. and elsewhere in the world. Second, we selected concentration-response relationships from epidemiological studies that we believe would better account for the episodic nature of smoke events and the corresponding elevated levels of particles (Zanobetti et al., 2009; Zanobetti and Schwartz, 2009).

The overall economic value of wildland fire-attributable premature deaths and respiratory hospital admissions is considerable. Depending on whether we quantify short-term $PM_{2.5}$-related premature deaths or long-term $PM_{2.5}$-realted deaths, the cumulative 5-year economic value is in the tens to hundreds of billions of dollars.

Nearly all states in the U.S. experienced elevated fine particle concentrations from wildland fire events over the 5-year period, according to our simulation of air quality. Certain states were affected by severe wildland fire events occurring across two or more years, including Louisiana (some of which may be due to debris burning after an active hurricane season because remote sensing of fires cannot distinguish between large debris burning from wildfires or prescribed fires), California, Idaho, and Georgia. Within these states, certain population subgroups were affected disproportionately. In particular, black populations, and to a lesser extent Asian populations, accounted for a greater share of wildland fire-attributable health impacts. State and local officials may wish to consider how best to communicate with subgroups that are most affected when deploying warning systems that alert the public to the health risks of wildland fire smoke. State and local officials deploying warning systems to alert the public to the health risks of wildland fire smoke may wish to consider how best to reach these subgroups.

This analysis is subject to certain limitations and uncertainties that shape the way in which the results may be interpreted. Considering first the air quality inputs, we assessed the performance of the chemical transport model by matching CMAQ grid locations to the locations of environmental monitors and comparing predicted and observed values. We found that the model is biased high when predicting low levels of

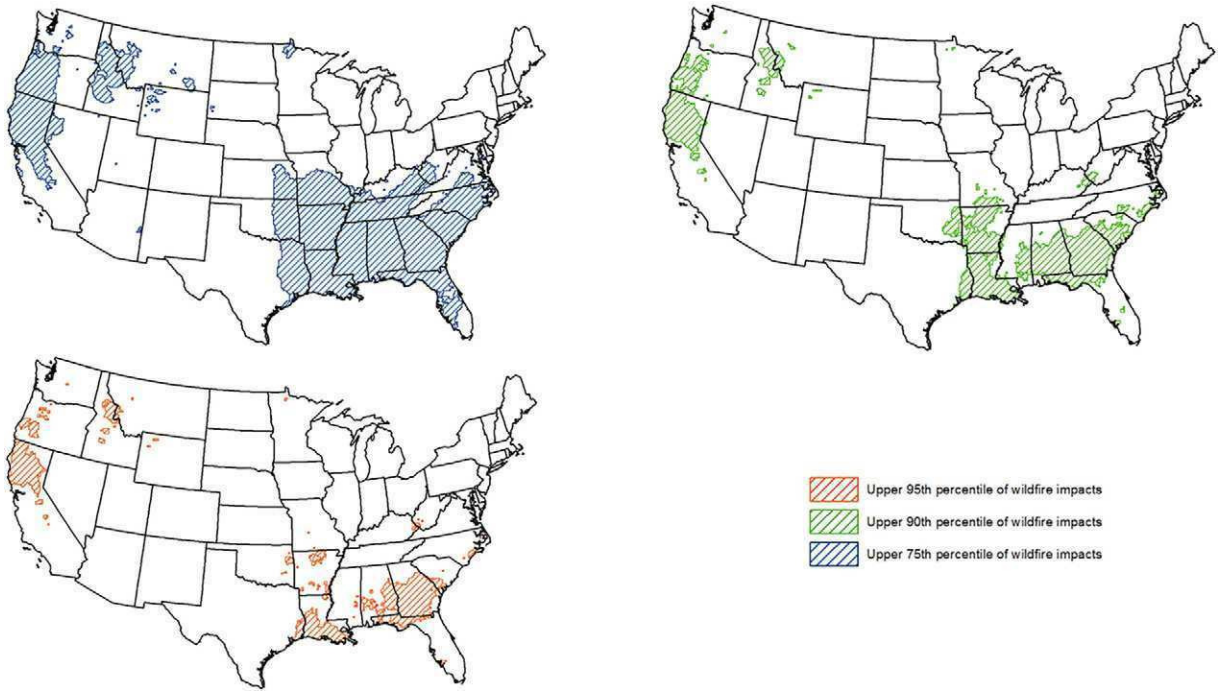

Fig. 2. Locations of the U.S. experiencing elevated wildfire-related $PM_{2.5}$ concentrations over a 5-year period.

Table 4
The percentage of individuals living in locations highly affected, and less affected, by wildland fires (2008 to 2012).[a]

Race	National average	Location of the U.S.[b]		Difference between highly and less affected
		Highly affected	Less affected	
Asian	5%	4%	5%	−1%
Black	13%	18%	13%	12%
Native American	1%	2%	1%	1%
White	81%	75%	81%	−6%
Total	100%	100%	100%	

[a] Highly affect subgroups are those individuals who have experienced cumulative levels of wildland fire attributable $PM_{2.5}$ concentrations that are at or above the 75th percentile, identified in Fig. 2 with blue hatched shading. Less affected subgroups are those not living in these areas.
[b] Estimates rounded to two significant figures.

$PM_{2.5}$ concentrations. The model also over predicts $PM_{2.5}$ (mainly Organic Carbon and Elemental Carbon) during all seasons for fire events. Baker et al. (2016) found the Flint Hills fire overestimated OC and EC but the Wallow fire did not overestimate to the same degree suggesting there is a lot of complexity in terms of how different fires are characterized in CMAQ. Another limitation is that only fire events that are part of the emission inventory have been evaluated. Any misspecification of emissions in the inventory fires is not included in our analysis. Further scientific advances and research efforts aimed to improve characterization of fire, fuel and emission inventories, and to improve measure characterization of differential toxicity of smoke emitted from different fuel types can potentially improve future health risk assessments.

The health impacts quantified using concentration-response relationships described in this paper are also subject to uncertainties. More specifically, questions remain regarding the extent to which certain species of fire-attributable PM may be more or less toxic than others (Sullivan et al., 2008). Thus, using effect coefficients from the epidemiological studies that did not specifically consider wildland fire episodes, may under- or over-estimate impacts. By contrast, the quantitative meta-analysis draws upon epidemiological studies of wildland fire events, but is limited to respiratory hospital admissions and PM_{10}. Several of these studies were conducted outside of the U.S.; differences between the health care system, wildland fire particle composition, behavioral responses to smoke events and other factors may bias the meta-analysis pooled risk coefficient. We also apply the effect coefficients from the Delfino et al. (2009) study of wildfires in Southern California nationwide; this may bias our estimates of risk high or low depending on the area that it is applied to. Finally, the present value calculation assumes that the wildland fire-related premature deaths estimated for each year are independent of those estimated in all other years. For example, individuals modeled as dying prematurely from wildland fire smoke exposure in year 1 cannot also die in year 2, but the net present value calculation introduces the possibility that deaths may have been counted more than once across years. However, given that the fraction of total deaths accounted for by air pollution episodes is relatively small (approximately 6% on a national basis), the potential for this approach to bias-high the number of wildland-attributable deaths is likely small (Fann et al., 2011).

Despite these uncertainties, this manuscript also exhibits a number of strengths and unique features. First, this analysis is, to our knowledge, the first to characterize the incidence and economic value of human health impacts attributable to wildland fire-emitted fine particles in the continental U.S. over a 5-year period. Second, while previous studies have incorporated a systematic review of wildland fire studies, none to our knowledge have performed a quantitative meta-analysis. Third, we characterize both the size, and distribution, of wildland fire-related premature deaths and hospital admissions across population subgroups. Taken together, the results in this analysis suggest that the number and value of wildland fire events is considerable and that these impacts are not shared equally across the U.S. population.

Disclaimer

The research described in this article has been reviewed by the National Health and Environmental Effects Research Laboratory, U.S. Environmental Protection Agency, and approved for publication. Approval does not signify that the contents necessarily reflect the views and policies of the Agency, nor does the mention of trade names of commercial products constitute endorsement or recommendation for use.

Competing financial interests

The authors declare no competing financial interests.

Acknowledgements

We gratefully acknowledge the comments received from Bryan Hubbell and Karen Wesson, who reviewed early versions of this manuscript.

Appendix A. Supplementary data

Supplementary data to this article can be found online at http://dx.doi.org/10.1016/j.scitotenv.2017.08.024.

References

Baker, K.R., Woody, M.C., Tonnesen, G.S., Hutzell, W., Pye, H.O.T., Beaver, M.R., et al., 2016. Contribution of regional-scale fire events to ozone and PM2.5 air quality estimated by photochemical modeling approaches. Atmos. Environ. 140:539–554. http://dx.doi.org/10.1016/j.atmosenv.2016.06.032.

Berman, J.D., Fann, N., Hollingsworth, J.W., Pinkerton, K.E., Rom, W.N., Szema, A.M., et al., 2012. Health benefits from large-scale ozone reduction in the United States. Environ. Health Perspect. 120:1404–1410. http://dx.doi.org/10.1289/ehp.1104851.

Carlton, A.G., Baker, K.R., 2011. Photochemical Modeling of the Ozark Isoprene Volcano: MEGAN, BEIS, and Their Impacts on Air Quality Predictions. Environmental Science & Technology 45, 4438–4445.

Crimmins, A., Balbus, J., Gamble, J.L., Beard, C.B., Bell, J.E., Dodgen, D., et al., 2016. Human health the impacts of climate change on in the United States the impacts of climate change on human health in the United States. U.S. Glob. Chang. Res. Progr.

Delfino, R.J., Brummel, S., Wu, J., Stern, H., Ostro, B., Lipsett, M., et al., 2009. The relationship of respiratory and cardiovascular hospital admissions to the southern California wildfires of 2003. Occup. Environ. Med. 66:189–197. http://dx.doi.org/10.1136/oem.2008.041376.

EPA, 2011. Regulatory Impact Assessment for Final Transport Rule.

Fann, N., Lamson, A.D., Anenberg, S.C., Wesson, K., Risley, D., Hubbell, B.J., 2011. Estimating the national public health burden associated with exposure to ambient PM(2.5) and ozone. Risk Anal. 32:81–95. http://dx.doi.org/10.1111/j.1539-6924.2011.01630.x.

Fann, Neal, Fulcher, Charles M., Baker, Kirk, 2013. The recent and future health burden of air pollution apportioned across US sectors. Environmental science & technology 47 (8), 3580–3589.

Henderson, S.B., Brauer, M., Kennedy, S., MacNab, Y., 2009. Three measures of forest fire smoke exposure and their association with respiratory and cardiovascular physician visits and hospital admissions. Epidemiology 20:S82. http://dx.doi.org/10.1097/01.ede.0000362956.02139.fd.

Henderson, S.B., Brauer, M., MacNab, Y.C., Kennedy, S.M., 2015. Three Measures of Forest Fire Smoke Exposure and Their Associations with Respiratory and Cardiovascular Health Outcomes in a Population-based Cohort. http://dx.doi.org/10.14288/1.0074714.

Johnston, F.H., Bailie, R.S., Pilotto, L.S., Hanigan, I.C., Samet, J., Zeger, S., et al., 2007. Ambient biomass smoke and cardio-respiratory hospital admissions in Darwin, Australia. BMC Public Health 7:240. http://dx.doi.org/10.1186/1471-2458-7-240.

Jones, R.R., Hogrefe, C., Fitzgerald, E.F., Hwang, S.A., Özkaynak, H., Garcia, V.C., et al., 2015. Respiratory hospitalizations in association with fine PM and its components in New York State. J. Air Waste Manage. Assoc. 65:559–569. http://dx.doi.org/10.1080/10962247.2014.1001500.

Knorr, W., Lehsten, V., Arneth, A., 2012. Determinants and predictability of global wildfire emissions. Atmos. Chem. Phys. 12:6845–6861. http://dx.doi.org/10.5194/acp-12-6845-2012.

Kochi, I., Champ, P.A., Loomis, J.B., Donovan, G.H., 2012. Valuing mortality impacts of smoke exposure from major southern California wildfires. J. For. Econ. 18:61–75. http://dx.doi.org/10.1016/j.jfe.2011.10.002.

Krewski, D., Jerrett, M., Burnett, R.T., Ma, R., Hughes, E., Shi, Y., et al., 2009. Extended follow-up and spatial analysis of the American Cancer Society study linking particulate air pollution and mortality. Res. Rep. Health Eff. Inst. 5, 114–136.

Krewski, Daniel, et al., 2009. Extended follow-up and spatial analysis of the American Cancer Society study linking particulate air pollution and mortality. No. 140. Health Effects Institute, Boston, MA.

Lepeule, J., Laden, F., Dockery, D., Schwartz, J., 2012. Chronic exposure to fine particles and mortality: an extended follow-up of the Harvard Six Cities study from 1974 to 2009. Environ. Health Perspect. 120:965–970. http://dx.doi.org/10.1289/ehp.1104660.

Liu, J.C., Pereira, G., Uhl S a, Bravo M a, Bell ML., 2014. A systematic review of the physical health impacts from non-occupational exposure to wildfire smoke. Environ. Res. 136: 120–132. http://dx.doi.org/10.1016/j.envres.2014.10.015.

Liu, J.C., Pereira, G., Uhl, S.A., Bravo, M.A., Bell, M.L., 2015. A systematic review of the physical health impacts from non-occupational exposure to wildfire smoke. Environ. Res. 136:120–132. http://dx.doi.org/10.1016/j.envres.2014.10.015.

Liu, J.C., Mickley, L.J., Sulprizio, M.P., Dominici, F., Yue, X., Ebisu, K., et al., 2016. Particulate air pollution from wildfires in the Western US under climate change. Clim. Chang.: 1–12 http://dx.doi.org/10.1007/s10584-016-1762-6.

McKenzie, D., French, N.H., Ottmar, R.D., 2012. National database for calculating fuel available to wildfires. EOS Trans. Am. Geophys. Union 93 (6), 57–58.

Morgan, G., Sheppeard, V., Khalaj, B., Ayyar, A., Lincoln, D., Jalaludin, B., et al., 2010. Effects of bushfire smoke on daily mortality and hospital admissions in Sydney, Australia. Epidemiology 21:47–55. http://dx.doi.org/10.1097/EDE.0b013e3181c15d5a.

Office of Air Quality Planning and Standards, 2011. Regulatory Impact Assessment for the Mercury and Air Toxics Standards.

Ottmar, R.D., 2014. Wildland fire emissions, carbon, and climate: modeling fuel consumption. For. Ecol. Manag. 317:41–50. http://dx.doi.org/10.1016/j.foreco.2013.06.010.

Rappold, A.G., et al., 2011. Peat bog wildfire smoke exposure in rural North Carolina is associated with cardiopulmonary emergency department visits assessed through syndromic surveillance. Environ. Health Perspect. 119, 1415.

Rappold, A.G., et al., 2012. Cardio-respiratory outcomes associated with exposure to wildfire smoke are modified by measures of community health. Environ. Health 11, 71.

R Core Team, 2016. R: A Language and Environment for Statistical Computing.

Rappold, A.G., Fann, N.L., Crooks, J., Huang, J., Cascio, W.E., Devlin, R.B., et al., 2014. Forecast-based interventions can reduce the health and economic burden of wildfires. Environ. Sci. Technol.

Rittmaster, R., Adamowicz, W.L., Amiro, B., Pelletier, R.T., 2006. Economic Analysis of Health Effects From Forest Fires. 877:pp. 868–877. http://dx.doi.org/10.1139/X05-293.

Schwede, Donna, Pouliot, George, Pierce, Thomas, 2005. Changes to the biogenic emissions inventory system version 3 (BEIS3)." 4th Annual CMAS Models-3 Users' Conference, September. Vol. 26.

Sonoma Technology, 2007. SMARTFIRE System Version 2.

Stavros, E.N., McKenzie, D., Larkin, N., 2014. The climate-wildfire-air quality system: interactions and feedbacks across spatial and temporal scales. Wiley Interdiscip. Rev. Clim. Chang. 5:719–733. http://dx.doi.org/10.1002/wcc.303.

Sullivan, A.P., Holden, A.S., Patterson, L.A., McMeeking, G.R., Kreidenweis, S.M., Malm, W.C., et al., 2008. A method for smoke marker measurements and its potential application for determining the contribution of biomass burning from wildfires and prescribed fires to ambient $PM_{2.5}$ organic carbon. J. Geophys. Res. 113, D22302. http://dx.doi.org/10.1029/2008JD010216.

Tham, R., Erbas, B., Akram, M., Dennekamp, M., Abramson, M.J., 2009. The impact of smoke on respiratory hospital outcomes during the 2002–2003 bushfire season, Victoria, Australia. Respirology 14:69–75. http://dx.doi.org/10.1111/j.1440-1843.2008.01416.x.

U.S. Environmental Protection Agency, 2014. Environmental Benefits Mapping and Analysis Program—Community Edition (BenMAP-CE).

U.S. Environmental Protection Agency, 2016. Technical Support Document Preparation of Emission Inventories for the Version 6.3, 2011 Emissions Modeling Platform. https://www.epa.gov/sites/production/files/2016-09/documents/2011v6_3_2017_emismod_tsd_aug2016_final.pdf.

U.S. EPA, 2011. National Emissions Inventory, 2011.

US EPA, 2009. Integrated Science Assessment for Particulate Matter (Final Report).

US EPA, 2010. Guidelines for Preparing Economic Analyses.

US EPA, 2012. Regulatory Impact Assessment for the PM NAAQS RIA.

US Forest Service, 2015. PNW - Fire and Environmental Research Applications Team (FERA) Research/Studies.Available:. https://www.fs.fed.us/pnw/fera/fft/consumemodule.shtml (accessed 13 March 2017).

Verma, V., Fang, T., Guo, H., King, L., Bates, J.T., Peltier, R.E., et al., 2014. Reactive oxygen species associated with water-soluble PM2.5 in the southeastern United States: spatiotemporal trends and source apportionment. Atmos. Chem. Phys. 14:12915–12930. http://dx.doi.org/10.5194/acp-14-12915-2014.

Viechtbauer, W., 2010. Conducting meta-analyses in *R* with the metafor package. J. Stat. Softw. 36:1–48. http://dx.doi.org/10.18637/jss.v036.i03.

Westerling, A.L., Hidalgo, H.G., Cayan, D.R., Swetnam, T.W., 2006. Warming and earlier spring increase western U.S. forest wildfire activity. Science 313:940–943. http://dx.doi.org/10.1126/science.1128834.

Woods and Poole, 2012. Woods & Poole.

Yarwood, G., Rao, S., Yocke, M., Whitten, G., 2005. Updates to the Carbon Bond Mechanism: CB05 (doi:RT-0400675 8).

Zanobetti, A., Schwartz, J., 2009. The effect of fine and coarse particulate air pollution on mortality: a national analysis. Environ. Health Perspect. 117:898–903. http://dx.doi.org/10.1289/ehp.0800108.

Zanobetti, A., Franklin, M., Koutrakis, P., Schwartz, J., 2009. Fine particulate air pollution and its components in association with cause-specific emergency admissions. Environ. Health 8:58. http://dx.doi.org/10.1186/1476-069X-8-58.

Environmental Science & Technology

Policy Analysis

pubs.acs.org/est

Community Vulnerability to Health Impacts of Wildland Fire Smoke Exposure

Ana G. Rappold*

National Health and Environmental Effects Research Laboratory/Environmental Public Health Division, United States Environmental Protection Agency, Research Triangle Park, North Carolina 27709, United States

Jeanette Reyes

National Health and Environmental Effects Research Laboratory/Environmental Public Health Division, United States Environmental Protection Agency, Research Triangle Park, North Carolina 27709, United States

George Pouliot

National Exposure Research Laboratory/Computational Exposure Division, United States Environmental Protection Agency, Research Triangle Park, North Carolina 27709, United States

Wayne E. Cascio

National Health and Environmental Effects Research Laboratory/Environmental Public Health Division, United States Environmental Protection Agency, Research Triangle Park, North Carolina 27709, United States

David Diaz-Sanchez

National Health and Environmental Effects Research Laboratory/Environmental Public Health Division, United States Environmental Protection Agency, Research Triangle Park, North Carolina 27709, United States

Supporting Information

ABSTRACT: Identifying communities vulnerable to adverse health effects from exposure to wildfire smoke may help prepare responses, increase the resilience to smoke and improve public health outcomes during smoke days. We developed a Community Health-Vulnerability Index (CHVI) based on factors known to increase the risks of health effects from air pollution and wildfire smoke exposures. These factors included county prevalence rates for asthma in children and adults, chronic obstructive pulmonary disease, hypertension, diabetes, obesity, percent of population 65 years of age and older, and indicators of socioeconomic status including poverty, education, income and unemployment. Using air quality simulated for the period between 2008 and 2012 over the continental U.S. we also characterized the population size at risk with respect to the level and duration of exposure to fire-originated fine particulate matter (fire-$PM_{2.5}$) and CHVI. We estimate that 10% of the population (30.5 million) lived in the areas where the contribution of fire-$PM_{2.5}$ to annual average ambient $PM_{2.5}$ was high (>1.5 $\mu g/m^3$) and that 10.3 million individuals experienced unhealthy air quality levels for more than 10 days due to smoke. Using CHVI we identified the most vulnerable counties and determined that these communities experience more smoke exposures in comparison to less vulnerable communities.

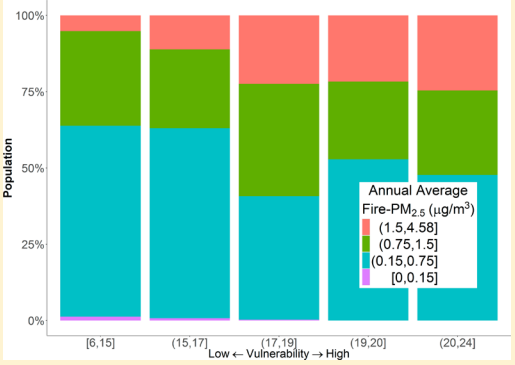

INTRODUCTION

Exposure to wildfire smoke is a serious health risk which can disproportionally impact sensitive groups. A number of studies have shown an association between smoke exposure and worsening of respiratory symptoms, increased rates of cardiorespiratory emergency visits, hospitalizations, and even

Received: December 8, 2016
Revised: May 4, 2017
Accepted: May 11, 2017
Published: May 11, 2017

ACS Publications © 2017 American Chemical Society

DOI: 10.1021/acs.est.6b06200
Environ. Sci. Technol. 2017, 51, 6674−6682

death.[1−12] Identifying communities vulnerable to adverse health outcomes during smoke days can provide valuable information for local, state, and federal governments and nongovernmental organizations to prioritize public health actions and improve public health outcomes on fire-smoke days.

Among the pollutants found in smoke, fine particulate matter ($PM_{2.5}$) is of the highest concern to health. In the most recent synthesis and evaluation of scientific literature on the health effects of air pollution, the Integrated Science Assessment (ISA), the U.S. Environmental Protection Agency[13] concluded that the weight of scientific evidence suggests a causal relationship between short- and long-term exposures and cardiovascular effects and mortality, and a likely causal relationship with respiratory effects. ISA is a comprehensive review of the health and ecological effects caused by air pollutants, mandated by the Clean Air Act, and provides the scientific basis for review of the National Ambient Air Quality Standards (NAAQS). Multiple studies demonstrate that the health impacts from $PM_{2.5}$ exposures are disproportionately shared by individuals in the sensitive groups.[14,15] The most sensitive groups include children, the aged, and pregnant women, as well as those with a pre-existing cardiopulmonary disease. Individuals and communities of lower socioeconomic status, and those with other pre-existing chronic inflammatory conditions are also considered at higher risk. Distribution of sensitive populations defines the vulnerability to adverse health effects across communities and reducing impacts among these populations is likely to bring the greatest public health burden benefit on smoke days.

Population vulnerability to various natural hazards has been studied for decades, however population vulnerability to smoke has not been well documented. Various aspects of population vulnerability have been examined in the context of heat waves,[16] famine, seismic events, coastal and inland floods, sea level rise, and drought.[17−20] Recent assessments have also focused on identifying communities vulnerable to environmental hazards exacerbated by climate change.[19,21,22] The purpose of assessing population vulnerability is to determine the population at greatest risk to environmental hazards, understand how communities respond and adapt and inform ways to mitigate the risk and negative impacts.[23] The communities that adapt to and recover after a disaster are those that can better plan, prepare and respond to environmental hazards. The alarming trends in the severity of wildland fires and growth of populations in the communities adjacent to wildlands call for an improved understanding of which communities are the most vulnerable to health impacts in order to improve public health response.

Here, we index community vulnerability to health effects of air pollution and wildfire smoke, based on previously studied clinical and social risk-factors that were found to modify the association between air pollution and adverse health outcomes. We then quantify population size at risk with respect to the levels of the index and the level and duration of smoke exposure in the recent past. To characterize smoke exposure in the recent past we simulated fire-originating fine particulate matter ($PM_{2.5}$) over a five-year period (2008−2012) using a chemical transport modeling system. The objective of this work is to demonstrate that community health vulnerability can be readily assessed using existing data and to provide motivation as to why it may be necessary. Understanding where the most vulnerable communities are found can be useful in developing outreach and education material.

MATERIALS AND METHODS

Development of Community Health-Vulnerability Index. To develop an index of community health-vulnerability to the adverse health effects of smoke exposures, we obtained specific socio-economic, demographic, and health outcome measures previously determined in the literature to modify the risk of air pollution related health outcomes.[13,24,25] More specifically, we obtained county prevalence for diabetes, hypertension, adult and pediatric asthma, chronic obstructive pulmonary disease (COPD); percent of population over 65 years of age, household income, education, rates of poverty, and unemployment. In the $PM_{2.5}$- Integrated Science Assessment,[13] both intrinsic (disease status) and extrinsic factors (poverty) are referred to as factors of susceptibility and vulnerability, respectively. However, because all of the factors are aggregated and not individual data, we use the term "vulnerability" throughout to define increased risk of adverse health outcomes related to exposure. In all cases we used county level indicators available across the continental U.S. because mitigation and adaptation plans are often planned and executed at the county level. The list of variables used to profile vulnerability is not intended to be exhaustive, but rather representative of the key clinical and social conditions known to or suspected to increase the risk of adverse health outcomes associated with fire- $PM_{2.5}$. Data sources and summary statistics are available in Supporting Information (SI) Table S1.

Prevalence and incidence estimates of pediatric asthma (in children <18 years of age), adult asthma (18+ years of age), and adult COPD (30+) which includes chronic bronchitis and emphysema, were obtained from the American Lung Association.[26] American Lung Association projected national and state prevalence of chronic lung disease to county levels using the Behavioral Risk Factor Surveillance System (BRFSS)[27] a phone based survey system that has been collecting data continuously since 2004, and statistical methods developed by the U.S. Census Bureau.

We used county level prevalence of hypertension to approximate prevalence of cardiovascular disease. We used sex specific and age adjusted hypertension prevalence data in adults over 30 years of age reported in Olives et al.[28] The study characterized the relationship between self-reported and physical measurements of hypertension reported in the National Health Examination and Nutrition Survey and used the relationship to adjust BRFSS 2009 self-reported responses on hypertension prevalence (among all respondents, percentage of those who reported systolic BP of at least 140 mmHg and/or self-reported taking medication) for self-reporting bias. Prevalence for county-level age, race, and sex adjusted estimates of diagnosed diabetes and obesity in adults (20 years of age and older) were obtained from BRFSS 2012 from http://www.cdc.gov/diabetes/atlas/countyrank/County_ListofIndicators.html.

Older adults and individuals of lower socio-economic status have been shown to be of increased risk of cardiovascular and respiratory effects in both short-term exposure studies and long-term exposure studies of air pollution.[13] Similarly, several studies found that socio-economic factors also modified health responses during the exposures to wildfire smoke.[29,30] Socio-economic and demographic profiles used in this study were taken from 2010 U.S. Census including population size by age group and gender, percent of individuals living in poverty, percent of families living in poverty, medium household income, and percent of unemployment.[31]

DOI: 10.1021/acs.est.6b06200
Environ. Sci. Technol. 2017, 51, 6674−6682

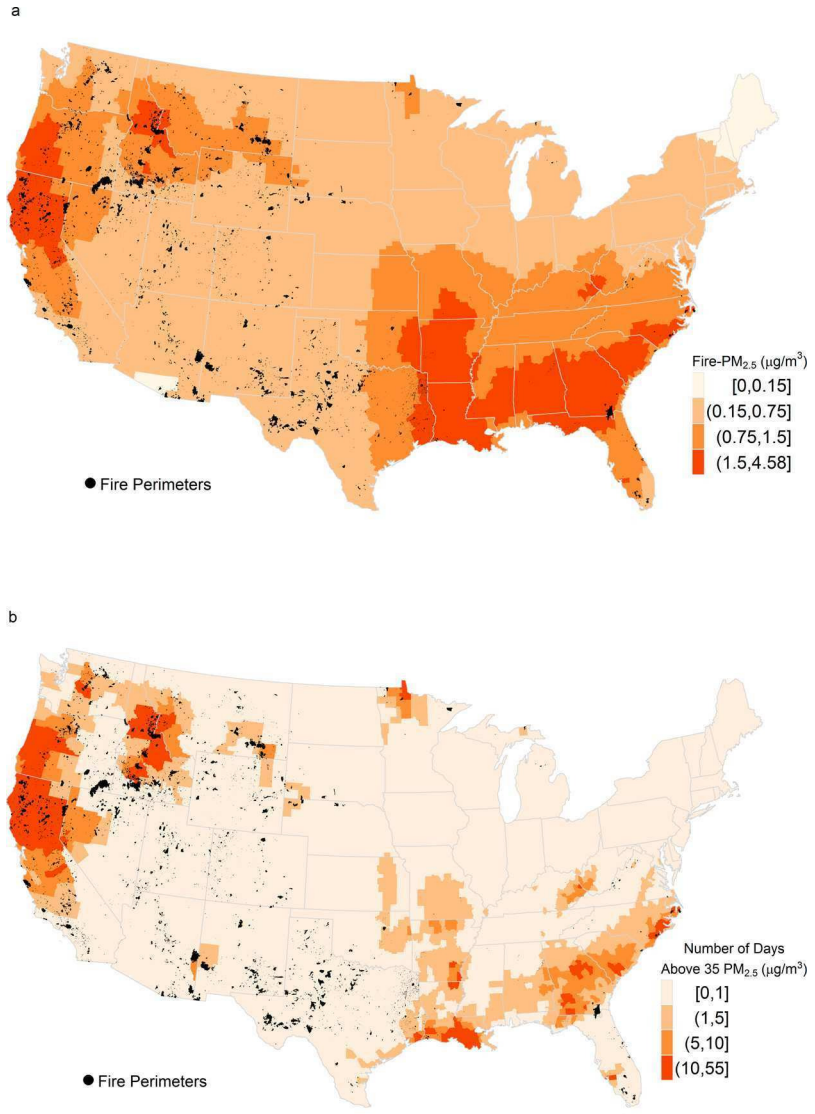

Figure 1. (a) Annual average daily fire-$PM_{2.5}$ footprint by counties of continental US and perimeters of area burned by large fires in black (GeoMAC) between 2008 and 2012. (b) Number of days with fire-$PM_{2.5}$ above 35 $\mu g/m^3$ by counties of continental US and perimeters of area burned by large fires in black (GeoMAC) between 2008 and 2012.

We used principal components analysis and varimax rotation to reduce the number of measures of vulnerability into a smaller number of independent components. All measures of vulnerability were standardized prior to analysis. The first five components explained 84% of variance and were highly loaded on (1) economic deprivation, (2) population of 65 years and older, (3) chronic adult respiratory conditions (COPD and asthma), (4) pre-existing conditions linked to hypertension, obesity and diabetes, and (5) pediatric asthma (SI Table S2). All five components were positively associated with primary measures, with the exception of median household income that was negatively loaded on the first component measuring economic deprivation (SI Figure S11). The higher scores of all five components described the more vulnerable state (more poverty, more individuals 65 years and older, more chronic respiratory and other conditions). The five components were individually assigned quintile scores (1 (the least vulnerable) to 5 (the most vulnerable)). Quintile ranks for each component were added together to create overall Community Health-Vulnerability Index (CHVI) with higher values defining more vulnerable states.

Air Quality Simulations. We simulated daily air quality from 2008 to 2012 using the Community Multiscale Air Quality (CMAQ) model with and without wildland and prescribed fires. The calculated difference between the two model runs represents the contribution of fire emissions to the ambient $PM_{2.5}$ levels (fire-$PM_{2.5}$). Inputs to the model included gridded meteorological fields, emissions data, and boundary conditions. For a regional or continental CMAQ model simulation, the meteorological fields were provided by annual CONUS Weather Research and Forecasting model (WRF) simulation that utilized 12 km horizontal grid spacing and 35 vertical layers of variable thickness extending up to 50 hPa, with the top of the lowest model layer at approximately 20 m above ground level. Initial and boundary conditions for WRF were provided by the North American Mesoscale Model available from the National Centers for Environmental Prediction. The input emissions were based on a 12 km national U.S. domain with speciation for the Carbon-Bond 05 chemical mechanism.[32]

DOI: 10.1021/acs.est.6b06200
Environ. Sci. Technol. 2017, 51, 6674−6682

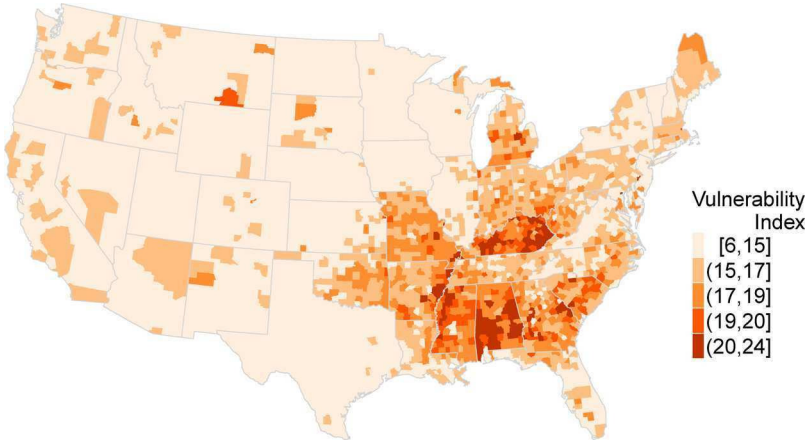

Figure 2. National map of the Community health-vulnerability Index (CHVI). The break points 15, 17, 19, and 20 correspond to the 50th, 75th, 90th, and 95th percentile of CHVI scores, respectively.

The emission inventory and ancillary files were based on the 2008 emissions modeling platform for 2008, 2009, and 2010 and on the 2011 emission modeling platform for 2011 and 2012. The fire emissions were based on year-specific daily fire estimates using the Hazard Mapping System fire detections and Sonoma Technology SMARTFIRE system (version 2) (http://www.getbluesky.org/smartfire/docs/Raffuse 2007.pdf). Plume rise was calculated within the CMAQ model (in-line). Biogenic emissions were processed in-line in CMAQ and are based on the Biogenic Emissions Inventory System v3.14 (http://www.cmascenter.org).

CMAQ hourly output was averaged to daily averages (midnight to midnight and adjusted for time zone) for each grid point. From the gridded output we calculated area weighted averages for daily and annual fire-$PM_{2.5}$ daily averages for each county. We characterize smoke exposure impacts with respect to the magnitude of exposure, frequency of days with moderate air quality (15−35 $\mu g/m^3$) and frequency of days with unhealthy levels of fire-$PM_{2.5}$ (>35 $\mu g/m^3$) according to 2006 $PM_{2.5}$ NAAQS. In terms of health risks, moderate air quality days are interpreted as "Unhealthy for Unusually Sensitive Groups"; while concentrations above 35.4 are interpreted as unhealthy for a broader population. More specifically, 35.5−55.4 $\mu g/m^3$ is considered "Unhealthy for Sensitive Individuals", 55.5−150.4 $\mu g/m^3$ is considered "Unhealthy" for all individuals, 150.5−250.4 is "Very Unhealthy", and ≥250.5 is "Hazardous".[33] The two concentrations used in this analysis also correspond to the annual (15 $\mu g/m^3$) and daily (35 $\mu g/m^3$) 2006 $PM_{2.5}$ NAAQS. Here we used the 2006 standard because it was the standard of the time period 2008 to 2012. In December, 2012 the NAAQS for $PM_{2.5}$ was revised, and the annual standard was reduced to 12 $\mu g/m^3$ while the daily standard 35 $\mu g/m^3$ was retained. We note that we use these thresholds to define moderate and unhealthy smoke days and not to define compliance to air quality regulations. Finally, to calculate population size at risk we used age and gender specific population size from 2010 U.S. Census.

Wildfire perimeters for each year in this five-year period used in the study were obtained from USGS Geospatial Multi-Agency Coordination Group (GeoMAC) Wildland Fire Support archives. The GeoMAC is an interactive mapping application that displays maps of current fire locations and perimeters in the 48 contiguous states plus Alaska. This tool gathers fire data from daily incidence reports and defines wildland fire perimeters based on incident intelligence sources, GPS data, fixed wing aircraft sources, and satellite data. Fires not reported to the incidence intelligence such as prescribed and agricultural fires are not represented in the GeoMAC. The shape files and metadata are available at http://rmgsc.cr.usgs.gov/outgoing/GeoMAC/historic_fire_data/.

RESULTS

Fire-$PM_{2.5}$ Patterns over the Continental U.S., 2008−2012. In Figure 1, we mapped a geographic distribution of the estimated fire-$PM_{2.5}$ daily average with respect to (a) the magnitude and (b) frequency of unhealthy smoke days. The maps of fire-$PM_{2.5}$ were also overlaid with the geocoded perimeters of large wildfires from GeoMAC archives. In combination with large fire parameters and with respect to the magnitude of impact, two distinct and large spatial footprints are observed for fire-$PM_{2.5}$. The first footprint was observed over the heavily forested, cold and temperate climates of Northern California and Pacific Northwest, where high concentrations were colocated with a dense distribution of fire perimeters. The second fire-$PM_{2.5}$ footprint was observed across the Southeast where vegetation includes hardwood, pine and southern mixed forests, and wetlands. According to the National Emissions Inventory used in our CMAQ simulations, a majority of the emissions in this region are attributed to smaller and more localized wildland fires, which include agricultural burning and prescribed burning, and a large number of smaller fires. Prescribed burning is done on an annual basis in early months of the year and with the exception of drought years, the smoke footprint is consistently present from year to year. Daily average fire-$PM_{2.5}$ on smoke days was substantially lower in the Southeast than in the Northwestern states with the exception of days when large wildfires occurred (wildfire impacts can be observed from hourly concentrations which are not shown here). Maps for individual years are given in the SI Figures S1−S10.

Figure 1 demonstrates a notable difference between the Northwest and Southeast regions in frequency by which estimated county-averaged fire-$PM_{2.5}$ was above the level considered "Unhealthy for Sensitive Individuals" (>35 $\mu g/m^3$). The largest impact was in the Northwest region where a number of communities experienced 10 or more days of high fire-$PM_{2.5}$ levels. With the exception of Louisiana during winter 2008, the Southeast region had a significantly lower number of

DOI: 10.1021/acs.est.6b06200
Environ. Sci. Technol. 2017, 51, 6674−6682

Table 1. Population Size at Risk Summarized by Annual Average Fire-$PM_{2.5}$ (2008−2012)[a]

$PM_{2.5}$ (μg/m3)	adult asthma	pediatric asthma	COPD	hyper- tensive	diabetes	obesity	poverty	under 18	65 and over	total population
	20.8	6.4	11.8	68.8	20.3	60.9	42.5	73.7	40.0	306.7
(0,0.15]	0.2	0.1	0.1	0.6	0.2	0.5	0.4	0.6	0.4	2.8
(0.15,0.75]	12.7	3.8	6.6	40.0	11.3	34.4	23.6	43.5	23.7	182.2
(0.75,1.5]	5.9	1.9	3.8	20.8	6.4	19.0	13.2	22.2	11.9	91.1
(1.5,4.58]	2.0	0.7	1.3	7.4	2.4	7.0	5.3	7.4	4.0	30.5

[a]We used outcome specific prevalence by county. Population size is given in millions.

Table 2. Population Size at Risk by Community Health-Vulnerability Index, Annual Average Fire-$PM_{2.5}$, and Frequency of Unhealthy Fire-$PM_{2.5}$ Days Between 2008 and 2012[a]

	CHVI bins	[6,15]	(15,17]	(17,19]	(19,20]	(20,24]	total
annual mean (μg/m^3)	[0,0.15]	2 (72.3%)[#]	0.7 (25.2%)	0.1 (2.6%)	0 (0%)	0 (0%)	2.8 (0.9%)*
	(0.15,0.75]	98.6 (54.1%)	61.4 (33.7%)	13.5 (7.4%)	5.6 (3.1%)	3.1 (1.7%)	182.2 (59.4%)
	(0.75,1.5]	49 (53.8%)	25.4 (27.8%)	12.3 (13.5%)	2.7 (3%)	1.8 (2%)	91.2 (29.7%)
	(1.5,4.58]	8.1 (26.6%)	11 (36.1%)	7.5 (24.6%)	2.3 (7.4%)	1.6 (5.3%)	30.5 (9.9%)
num. days with 15−35 μg/m^3	[1,5)	69.6 (63.1%)	29.9 (27.1%)	8 (7.3%)	2.1 (1.9%)	0.7 (0.6%)	110.4 (36%)
	[5,10)	16.6 (31.2%)	23.5 (44.2%)	8.8 (16.6%)	2.1 (4%)	2.1 (4%)	53.1 (17.3%)
	[10,76]	39.5 (47.9%)	22.9 (27.8%)	13.6 (16.4%)	3.8 (4.6%)	2.7 (3.3%)	82.4 (26.9%)
num. days with >35 μg/m^3	[1,5)	28.5 (49%)	14.4 (24.7%)	11 (18.9%)	2.8 (4.9%)	1.4 (2.5%)	58.2 (19%)
	[5,10)	9.9 (51.6%)	5.4 (28.2%)	2.2 (11.7%)	0.8 (4%)	0.9 (4.5%)	19.1 (6.2%)
	[10,55]	6.9 (67%)	2.8 (27.1%)	0.3 (2.9%)	0.2 (1.6%)	0.1 (1.3%)	10.3 (3.4%)
	Total	157.7 (51.4%)	98.5 (32.1%)	33.4 (10.9%)	10.6 (3.5%)	6.5 (2.1%)	306.7 (100%)

[a]Population size is given in millions ([#] % expressed conditional on the population in the right margin, * expressed as % of the total population).

unhealthy fire-$PM_{2.5}$ days. In summary, both footprints had a large number of moderate air quality days due to fire-$PM_{2.5}$, while days with fire-$PM_{2.5}$ exceeding the level considered unhealthy for wider population were mostly in the Northwest region.

Health-Vulnerability and Smoke Impacts. The CHVI score ranged from 6 to 25, with a median score of 15, and 75th, 90th, and 95th percentile of 17, 19, and 20, respectively. The highest vulnerability is observed in the counties along the western slope of the Appalachian Mountains, parts of the Midwest (Kentucky, Missouri, Oklahoma, and Kansas) and parts of the South (Arkansas, Mississippi, Alabama, and Georgia) (Figure 2). Although none of the five indices dominated CHVI overall, the regions of the highest vulnerability tend to have high index values on multiple factors, particularly the prevalence of preexisting cardiovascular, metabolic diseases, and childhood asthma as well as economic deprivation.

Table 1 shows the estimated population size at risk by factors of vulnerability. We estimate that 30.5 million (13%) individuals, including 7.4 million children under 18, and 4 million persons over 65 years of age lived in communities where the annual average of fire-$PM_{2.5}$ was estimated to be above 1.5 μg/m^3 (annual average). Among these communities, there were 7.4 million individuals over 30 years of age with known hypertension, 2 million adults with asthma and 0.7 million children with asthma, 1.3 million people with COPD, 7.0 million obese individuals, and 2.4 million individuals with diabetes. We note that population size at risk was calculated separately for each county level factor of vulnerability; thus individuals with comorbidities are counted for each health outcome.

Table 2 shows the population size at risk by CHVI, annual mean fire-$PM_{2.5}$ levels, and frequency of moderate and unhealthy fire-$PM_{2.5}$ days. We estimate that 82.4 million individuals lived in counties with moderate air quality due to fire-$PM_{2.5}$ (15−35 μg/m^3) and 10.3 million individuals lived in the counties with unhealthy air quality levels (>35 μg/m^3) for more than 10 days between 2008 and 2012. Among the communities with the highest annual fire-$PM_{2.5}$ means (>1.5 μg/m^3), 8.1 million (26.6%) lived in counties with vulnerability index below the median (CHVI 6−15) while 22.4 million lived in the counties with vulnerability above the median (73.4%, 36.1 + 24.6 + 7.4 + 5.3; CHVI (15−24] combined) and 12.7% lived in the counties with high vulnerability (7.4%+5.3%; CHVI > 19). In contrast, across the nation approximately half of population (51.4%) lived in counties where CHVI is below the median and half (49.6%) lived in the counties where CHVI was above the median.

Over the time period considered, areas with the highest vulnerability were more likely to experience unhealthy levels of fire-$PM_{2.5}$ annual average ([1.5,4.58]) than less vulnerable populations (1.6/6.5×100 = 25% for CVHI (20,24] compared to 8.1/157.7×100 = 5% for CVHI [6,15]). Similar was true for number of days with moderate fire-$PM_{2.5}$ (15−35 μg/m^3) for 10+ days and for number of days with fire-$PM_{2.5}$ above 35 μg/m^3 for 5+ days (Table 2). More specifically, among the counties with vulnerability index below the median, 25% (39.5/157.5×100%) lived in places that experienced an excess of 10 days of moderate air quality due to fire while among the counties with the highest vulnerability (CHVI 21−24), 41.5% (2.7/6.5*100%) of population experienced an excess of 10 days of moderate air quality due to fire. A substantially smaller population size was impacted by a large number of days with unhealthy air quality (>35 μg/m^3); 10.7% of the population in the counties with CHVI below the median and 15.2% of the population in the most vulnerable counties experienced more than 5 days of unhealthy air quality (>35 μg/m^3). However,

DOI: 10.1021/acs.est.6b06200
Environ. Sci. Technol. 2017, 51, 6674−6682

4.4% of the least vulnerable communities and only 2.1% of the most vulnerable communities were impacted by 10 or more days of fire-$PM_{2.5}$ above 35 $\mu g/m^3$.

DISCUSSION

In this study we constructed an index of population vulnerability to health impacts from smoke exposure based on clinical and social factors known to modify the risk of adverse health effects and estimated population size at risk with respect to the frequency and magnitude of smoke exposure in a recent period. The modeling methods used in the study estimate that between 2008 and 2012 population exposure to smoke in the continental U.S. was extensive; 29.7% of the population lived in areas with moderate exposure (annual average fire-$PM_{2.5}$ between 0.75 and 1.5 $\mu g/m^3$) and another 10% lived in areas where the contribution to annual ambient $PM_{2.5}$ was high (>1.5 $\mu g/m^3$). We identified the most vulnerable U.S. counties and determined that vulnerable communities were more likely to experience high and frequent smoke exposure in comparison to less vulnerable populations. The findings described in the study have potential implications for efficient and effective allocation of limited resources for dissemination of public health messaging, and land and fuel management to prevent large wildfires.

The constructed Community Health-Vulnerability Index incorporates disease prevalence, age and socio-economic status of individuals in the community. The specific factors were chosen based on published literature that demonstrates their role as risk factors for cardio-respiratory effects of particles or wildfire smoke. Published research describes multiple biological mechanisms by which air pollution causes cardio-respiratory effects including oxidative stress, pulmonary and systemic inflammation, activation of pulmonary nocioceptive receptors, and modulation of the autonomic nervous system (Brook et al. 2010). Therefore, individuals having chronic health conditions characterized in part by pro-inflammatory states (e.g., asthma, COPD, diabetes, cardiovascular disease) are considered at higher risk.[34] Among the risk factors, preexisting cardiovascular disease is one of the leading factors of increased health risks to air pollution effects.[35] We used hypertension to approximate prevalence of cardiovascular disease because it is well documented, the most prevalent cardiovascular condition, and is responsible for one in six deaths among adults. Chronic metabolic and inflammatory health conditions such as diabetes and obesity have been shown to increase the risk to air pollution impacts.[36−38] Children are considered more sensitive to impacts of air pollution because their lungs are smaller, and their dose per body weight and lung surface areas exceed those of the adult population.

The majority of evidence for wildfire smoke effects are based on studies of exposure to ambient air pollution[13] but there is also a growing number of fire-$PM_{2.5}$ studies that suggest consistency between respiratory effects within fire specific studies and in comparison to studies of urban air pollution.[9,39] The effects of air pollution and wildfire smoke exposure on adults with preexisting respiratory conditions such as asthma and COPD are extensively documented in literature. These effects have also been noted in both children with asthma and children without asthma[5,40] and have been noted to be stronger than in adults.[41] Additionally, older adults have been shown to have an increased risk of cardiovascular and respiratory effects in fire-$PM_{2.5}$ exposure studies.[3,7,42,43] Apart from the clinical characteristics discussed, low socioeconomic status has also been reported to modify the risk of respiratory outcomes in response to large wildland fire smoke events.[30] We have previously shown that when considering external factors influencing health (health behaviors, access and quality of clinical care, social and economic factors, and the physical environments) socio-economic factors are strong contributors of differences in risk for asthma and congestive heart failure resulting from exposure to wildfire smoke.[29]

In the development of the health-vulnerability index we restrict our attention to the key clinical and social conditions that have been identified by the Integrated Science Assessment as populations sensitive to adverse health effects following air pollution exposure. It is clear, however, that these are not the only risk factors involved at the individual level. Evidence for a role for genetics, epigenetics, diet, availability of green space and behavior is emerging and it is likely that some of these will ultimately prove to be strong predictors of $PM_{2.5}$ associated health outcomes. As new risk factors are identified the CHVI can be adapted to incorporate the new information. Additionally, a number of other extrinsic factors have been shown to identify social vulnerability to environmental hazards such as heat waves, including occupation, employment, housing, built environment, neighborhood deprivation, poor English skills and are likely to apply in wildfire smoke situations.[44−47] When constructing indicators at the regional, state or local levels, and particularly when considering decision making, it may be helpful and advantageous to incorporate determinants of social vulnerability along with the indicators of health vulnerability (e.g., built environment, landscape, social and physical connectivity, existing air quality, etc.) and examine sensitivity of the indicators.

Implications for Public Health Actions. Interventions and health-promoting behaviors can improve public health outcomes.[48,49] Many of the recommended measures including staying indoors during very unhealthy air quality days, running air conditioning on recirculation mode, creating a clean room, ensuring a supply of regular medication, etc. can reduce personal exposure and decrease the health risks. However, during wildfire episodes, individuals do not perceive risks to their health and become aware of them once smoke exposure is already occurring, when it may be too late to take many of the recommended preventative measures. Smoke impacts in the areas where wildfires are less common (e.g., Southeast) can be a special concern exactly because they are less frequent and the health risk awareness is not established at the individual or community level. Prior knowledge about community health vulnerability can help guide deliberate awareness building and outreach among the most sensitive populations. However, identifying communities at the greatest risk from wildfire smoke is currently based solely on the predicted risk of fire and we do not consider the composition of the communities. As such public health messaging and actions may not be appropriately scaled to communities with high numbers of sensitive individuals.

Increased frequency of large wildland fires is anticipated to continue and have effects on human health and environment.[50−52] Fuel management activities, such as prescribed burning, are a critically important component of the national strategy to improve ecological diversity and decrease wildfires harmful to human health and have been examined with respect to changes in frequency and area burned.[53−56] While such information provides important insights for a broad risk-based management system for wildfire, the framework does not

DOI: 10.1021/acs.est.6b06200
Environ. Sci. Technol. 2017, 51, 6674−6682

consider the potential public health burden of smoke emissions or disparities in sensitivity of the populations affected. Projecting community health-vulnerability under different fire mitigation strategies, climate change scenarios, and population growth projections may offer further refinement of such risk-based management approaches. In projecting community health-vulnerability for a specific future scenario we recommend using population-weighted exposures.

Limitations of the Study. We note some limitations to our analysis. To estimate smoke exposure at the national level we use CMAQ model simulated with and without fires and attribute the difference in estimated ambient $PM_{2.5}$ concentrations to large fires (mostly wild and prescribed). To assess model performance, we matched CMAQ grid locations to the locations of environmental monitors and compare predicted and observed values. We found the model has a high bias at low $PM_{2.5}$ concentrations suggesting that (1) plumes are too dispersive, and/or (2) small fires have too high emissions in the simulation. The model also over predicts $PM_{2.5}$ (mainly organic and elemental carbon) during all seasons for fire events. Another limitation is that only fire events that are part of the emission inventory have been evaluated. Any misspecification of emissions in the inventory is not included in our analysis. An important limitation to our simulation of fire-$PM_{2.5}$ that affects air quality is that our modeling system does not simulate the smoldering aspects of peat fires well which are common in the Southeast and emit large quantities of particles and gases. We note that as with all models CMAQ results should be interpreted with caution because any combination of these factors could lead to uncertainty and over or under prediction of estimated exposures. While various aspects of CMAQ performance have been published in the literature,[57] additional factors could play a role in the uncertainty specific to fire-$PM_{2.5}$.

Another limitation is the assumption that $PM_{2.5}$ from all sources is equally harmful to health. The composition and toxicity of these particles varies with respect to the type of fuel burned, conditions of burning and the age of the particles. Lower combustion efficiency yields more volatile and organic compounds in both particles and gases (polynuclear aromatic hydrocarbons, oxygenated organics, and various gases) which are harmful to human health. Toxicological studies also indicate that relative toxicity of particles varies when examined per unit mass or total mass, and by chemical composition of the particles. Fire-$PM_{2.5}$ and fire-PM_{10} collected during a peat fire in eastern North Carolina in 2008 had very different targets of cellular toxicity that depended on the particle mass of the smoke particles and the phase of the fire.[58] Cardiovascular toxicity was the dominant effect caused by ultrafine PM fraction collected during the active smoldering phase of the fire while in vitro pulmonary inflammatory responses were the dominant effects of coarse fraction of PM. Smoldering fires, as seen in the peat fires across Southeast U.S., Indonesia, and Boreal forest have also been hypothesized to carry higher risk for cardiovascular Emergency Department visits as well.[11,43] This could be due to lower combustion efficiency and vegetation type that define chemical composition of particles, such as the abundance polynuclear aromatic hydrocarbons which are carcinogenic and particularly harmful to health.[59] However, a systematic review of published literature suggests that there is no consistent relationship that identifies specific $PM_{2.5}$ components that may be unequivocally related to health outcomes.[60]

The most significant limitation to this assessment of human vulnerability to health impacts of smoke is the lack of a good measure of a community's ability to adapt. While the factors that define the vulnerability status certainly play a role, other less quantifiable measures including awareness, previous experience, outreach programs, engagement of public health, and proximity to health care providers or facilities can define human responses. Gaither et al. 2011 examined spatial association between fire prone areas in the Southeast and socially vulnerable "hot spots" using proximity to wildland fire mitigation programs as a measure of community's ability to adopt. However, we did not find equivalent measures of community responses specific to health responses.

Wildland fires have been an integral part of human history with clear benefit to the management of fire hazards and to the ecologic diversity of ecosystems. However, recent trends in very large wildfires, termed mega fires, have brought attention to the adverse health effects of smoke exposure, the high cost of wildfire suppression and management, and the need to establish community-based adaptation plans. Employing the same methodology used to determine social vulnerability to environmental hazards,[23] we provide a concept of mapping the vulnerability to health outcomes specific to smoke exposure. Such maps can be helpful tools for public officials in preparation of smoke adaptation plans for their communities and prioritization of communities for allocation of resources by the local, state and federal governments. In the U.S. there are over 70 000 wildfires annually, impacting communities and regional air quality with varying frequency and intensity and thus representing a challenge to building community resilience with respect to fire smoke and public health guidance. Therefore, as a proof of concept, the Community Health-Vulnerability Index offers a tool to help identify communities that have the potential to benefit the most from mitigation strategies to minimize smoke exposure for sensitive populations and to decrease the health and economic burden imposed on the population by fire-$PM_{2.5}$ The next step could include tailoring messages to community needs and development of exposure mitigation strategies.

■ ASSOCIATED CONTENT

Supporting Information

The Supporting Information is available free of charge on the ACS Publications website at DOI: 10.1021/acs.est.6b06200.

List of data sources (Table S1), figures of the annual average daily fire-PM2.5 footprint by year (Figures S1−S5), figures of number of days with fire-PM2.5 above 35 $\mu g/m^3$ (Figures S6−S10) and details of principal components analysis output (Table S2, Figure S11) (PDF).

■ AUTHOR INFORMATION

Corresponding Author

*Phone: 919 843 9504; e-mail: rappold.ana@epa.gov.

ORCID

Ana G. Rappold: 0000-0002-7696-0900

Funding

The research described in this article has been funded wholly by the U.S. Environmental Protection Agency intramural research funding.

DOI: 10.1021/acs.est.6b06200
Environ. Sci. Technol. 2017, 51, 6674−6682

Notes

Disclaimer: The research described in this article has been reviewed by the National Health and Environmental Effects Research Laboratory, U.S. Environmental Protection Agency, and approved for publication. Approval does not signify that the contents necessarily reflect the views and policies of the Agency, nor does the mention of trade names of commercial products constitute endorsement or recommendation for use. The authors declare no competing financial interest.

■ ACKNOWLEDGMENTS

The authors thank four anonymous reviewers, Pete Lahm (USFS), Jason Sacks (USEPA), Christina Baghdikian (USEPA), Ann Brown (USEPA) for their comments and careful review of the manuscript.

■ REFERENCES

(1) Dennekamp, M.; Abramson, M. J. The effects of bushfire smoke on respiratory health. *Respirology* **2011**, *16* (2), 198−209.
(2) Dennekamp, M.; Straney, L. D.; Erbas, B.; Abramson, M. J.; Keywood, M.; Smith, K.; Sim, M. R.; Glass, D. C.; Del Monaco, A.; Haikerwal, A.; Tonkin, A. M. Forest Fire Smoke Exposures and Out-of-Hospital Cardiac Arrests in Melbourne, Australia: A Case-Crossover Study. *Environ. Health Perspect* **2015**, *123* (10), 959−64.
(3) Haikerwal, A.; Akram, M.; Del Monaco, A.; Smith, K.; Sim, M. R.; Meyer, M.; Tonkin, A. M.; Abramson, M. J.; Dennekamp, M., Impact of Fine Particulate Matter (PM2.5) Exposure During Wildfires on Cardiovascular Health Outcomes. *J. Am. Heart Assoc.* **2015**, *4*, (7).e00165310.1161/JAHA.114.001653
(4) Haikerwal, A.; Akram, M.; Sim, M. R.; Meyer, M.; Abramson, M. J.; Dennekamp, M. Fine particulate matter (PM2.5) exposure during a prolonged wildfire period and emergency department visits for asthma. *Respirology* **2016**, *21* (1), 88−94.
(5) Jalaludin, B.; Smith, M.; O'Toole, B.; Leeder, S. Acute effects of bushfires on peak expiratory flow rates in children with wheeze: a time series analysis. *Aust N Z. J. Public Health* **2000**, *24* (2), 174−7.
(6) Johnston, F. H.; Henderson, S. B.; Chen, Y.; Randerson, J. T.; Marlier, M.; Defries, R. S.; Kinney, P.; Bowman, D. M.; Brauer, M. Estimated global mortality attributable to smoke from landscape fires. *Environ. Health Perspect* **2012**, *120* (5), 695−701.
(7) Johnston, F. H.; Purdie, S.; Jalaludin, B.; Martin, K. L.; Henderson, S. B.; Morgan, G. G. Air pollution events from forest fires and emergency department attendances in Sydney, Australia 1996−2007: a case-crossover analysis. *Environ. Health* **2014**, *13*, 105.
(8) Kunzli, N.; Avol, E.; Wu, J.; Gauderman, W. J.; Rappaport, E.; Millstein, J.; Bennion, J.; McConnell, R.; Gilliland, F. D.; Berhane, K. Health effects of the 2003 Southern California wildfires on children. *Am. J. Respir. Crit. Care Med.* **2006**, *174* (11), 1221−1228.
(9) Liu, J. C.; Pereira, G.; Uhl, S. A.; Bravo, M. A.; Bell, M. L. A systematic review of the physical health impacts from non-occupational exposure to wildfire smoke. *Environ. Res.* **2015**, *136*, 120−132.
(10) Morgan, G.; Sheppeard, V.; Khalaj, B.; Ayyar, A.; Lincoln, D.; Jalaludin, B.; Beard, J.; Corbett, S.; Lumley, T. Effects of bushfire smoke on daily mortality and hospital admissions in Sydney, Australia. *Epidemiology* **2010**, *21* (1), 47−55.
(11) Rappold, A. G.; Stone, S. L.; Cascio, W. E.; Neas, L. M.; Kilaru, V. J.; Carraway, M. S.; Szykman, J. J.; Ising, A.; Cleve, W. E.; Meredith, J. T.; Vaughan-Batten, H.; Deyneka, L.; Devlin, R. B. Peat bog wildfire smoke exposure in rural North Carolina is associated with cardiopulmonary emergency department visits assessed through syndromic surveillance. *Environ. Health Perspect* **2011**, *119* (10), 1415−20.
(12) Delfino, R. J.; Brummel, S.; Wu, J.; Stern, H.; Ostro, B.; Lipsett, M.; Winer, A.; Street, D. H.; Zhang, L.; Tjoa, T., The relationship of respiratory and cardiovascular hospital admissions to the southern California wildfires of 2003. *Occup. Environ. Med.* **2008**.6618910.1136/oem.2008.041376
(13) US EPA, *Integrated Science Assessment (ISA) for Particulate Matter (Final)*. In U.S. Environmental Protection Agency: Washington, DC, 2009.
(14) Bell, M. L.; Zanobetti, A.; Dominici, F. Evidence on vulnerability and susceptibility to health risks associated with short-term exposure to particulate matter: a systematic review and meta-analysis. *Am. J. Epidemiol.* **2013**, *178* (6), 865−76.
(15) Sacks, J. D.; Stanek, L. W.; Luben, T. J.; Johns, D. O.; Buckley, B. J.; Brown, J. S.; Ross, M. Particulate matter-induced health effects: who is susceptible? *Environ. Health Perspect* **2011**, *119* (4), 446−54.
(16) Reid, C. E.; O'Neill, M. S.; Gronlund, C. J.; Brines, S. J.; Brown, D. G.; Diez-Roux, A. V.; Schwartz, J. Mapping community determinants of heat vulnerability. *Environ. Health Perspect.* **2009**, *117* (11), 1730.
(17) Blaikie, P.; Cannon, T.; Davis, I.; Wisner, B. *At Risk: Natural Hazards, People'S Vulnerability and Disasters*; Routledge, 2014.
(18) Cutter, S. L.; Mitchell, J. T.; Scott, M. S. Revealing the vulnerability of people and places: a case study of Georgetown County, South Carolina. *Annals of the association of American Geographers* **2000**, *90* (4), 713−737.
(19) Wu, S.-Y.; Yarnal, B.; Fisher, A. Vulnerability of coastal communities to sea-level rise: a case study of Cape May County, New Jersey, USA. *Climate Research* **2002**, *22* (3), 255−270.
(20) Morrow, B. H. Identifying and mapping community vulnerability. *Disasters* **1999**, *23* (1), 1−18.
(21) Clougherty, J. E.; Kubzansky, L. D. A framework for examining social stress and susceptibility to air pollution in respiratory health. *Environ. Health Perspect* **2009**, *117* (9), 1351−8.
(22) Bradford, K.; Abrahams, L.; Hegglin, M.; Klima, K. A Heat Vulnerability Index and Adaptation Solutions for Pittsburgh, Pennsylvania. *Environ. Sci. Technol.* **2015**, *49* (19), 11303−11.
(23) Cutter, S. L.; Boruff, B. J.; Shirley, W. L. Social vulnerability to environmental hazards. *Social science quarterly* **2003**, *84* (2), 242−261.
(24) American Lung Association, State of the Air 2015. www.stateoftheair.org.
(25) Bateson, T. F.; Schwartz, J. Who is sensitive to the effects of particulate air pollution on mortality?: a case-crossover analysis of effect modifiers. *Epidemiology* **2004**, *15* (2), 143−149.
(26) American Lung Association. Estimated Prevalence and Incidence of Lung Disease. 2014.
(27) US CDC 2012 Behavioral Risk Factor Surveillance System (BRFSS). ftp://ftp.cdc.gov/pub/Data/Brfss/userguide.pdf.
(28) Olives, C.; Myerson, R.; Mokdad, A. H.; Murray, C. J.; Lim, S. S. Prevalence, awareness, treatment, and control of hypertension in United States counties, 2001−2009. *PLoS One* **2013**, *8* (4), e60308.
(29) Rappold, A. G.; Cascio, W. E.; Kilaru, V. J.; Stone, S. L.; Neas, L. M.; Devlin, R. B.; Diaz-Sanchez, D. Cardio-respiratory outcomes associated with exposure to wildfire smoke are modified by measures of community health. *Environ. Health* **2012**, *11* (1), 1.
(30) Reid, C. E.; Jerrett, M.; Tager, I. B.; Petersen, M. L.; Mann, J. K.; Balmes, J. R. Differential respiratory health effects from the 2008 northern California wildfires: A spatiotemporal approach. *Environ. Res.* **2016**, *150*, 227−235.
(31) Census, US Census Bureau. 2010. https://www2.census.gov/geo/tiger/TIGER2010DP1/County_2010Census_DP1.zip.
(32) Yarwood, G., R. S, T., Yocke, M., Whitten, G. Z. *Updates to the Carbon Bond Mechanism: CB05*. U.S. EPA 2005, *Final Report*.
(33) U.S. EPA, Technical Assistance Document for the Reporting of Daily Air Quality- the Air Quality Index (AQI). U.S. Environmental Protection Agency, Office of Air Quality Planning and Standards, Research Triangle Park, NC, 2013; Vol. EPA-454/B-13−001.
(34) Zanobetti, A.; Bind, M.-A. C.; Schwartz, J. Particulate air pollution and survival in a COPD cohort. *Environ. Health* **2008**, *7* (1), 1.
(35) Brook, R. D.; Rajagopalan, S.; Pope, C. A.; Brook, J. R.; Bhatnagar, A.; Diez-Roux, A. V.; Holguin, F.; Hong, Y.; Luepker, R. V.; Mittleman, M. A. Particulate matter air pollution and cardiovascular disease an update to the scientific statement from the American Heart Association. *Circulation* **2010**, *121* (21), 2331−2378.

DOI: 10.1021/acs.est.6b06200
Environ. Sci. Technol. 2017, 51, 6674−6682

(36) Devlin, R. B.; Smith, C. B.; Schmitt, M. T.; Rappold, A. G.; Hinderliter, A.; Graff, D.; Carraway, M. S. Controlled exposure of humans with metabolic syndrome to concentrated ultrafine ambient particulate matter causes cardiovascular effects. *Toxicol. Sci.* **2014**, *140* (1), 61−72.
(37) Ruckerl, R.; Hampel, R.; Breitner, S.; Cyrys, J.; Kraus, U.; Carter, J.; Dailey, L.; Devlin, R. B.; Diaz-Sanchez, D.; Koenig, W.; Phipps, R.; Silbajoris, R.; Soentgen, J.; Soukup, J.; Peters, A.; Schneider, A. Associations between ambient air pollution and blood markers of inflammation and coagulation/fibrinolysis in susceptible populations. *Environ. Int.* **2014**, *70*, 32−49.
(38) Schneider, A.; Neas, L.; Herbst, M. C.; Case, M.; Williams, R. W.; Cascio, W.; Hinderliter, A.; Holguin, F.; Buse, J. B.; Dungan, K. Endothelial dysfunction: associations with exposure to ambient fine particles in diabetic individuals. *Environ. Health Perspect.* **2008**, *116* (12), 1666.
(39) Reid, C. E.; Brauer, M.; Johnston, F.; Jerrett, M.; Balmes, J. R.; Elliott, C. T., Critical Review of Health Impacts of Wildfire Smoke Exposure. *Environ. Health Perspect.* **2016**.10.1289/ehp.1409277
(40) Kunzli, N.; Avol, E.; Wu, J.; Gauderman, W. J.; Rappaport, E.; Millstein, J.; Bennion, J.; McConnell, R.; Gilliland, F. D.; Berhane, K.; Lurmann, F.; Winer, A.; Peters, J. M. Health effects of the 2003 Southern California wildfires on children. *Am. J. Respir. Crit. Care Med.* **2006**, *174* (11), 1221−8.
(41) Ignotti, E.; Valente, J. G.; Longo, K. M.; Freitas, S. R.; Hacon, S. d. S.; Artaxo Netto, P. Impact on human health of particulate matter emitted from burnings in the Brazilian Amazon region. *Rev. Saude Publica* **2010**, *44* (1), 121−130.
(42) Morgan, G.; Corbett, S.; Wlodarczyk, J. Air pollution and hospital admissions in Sydney, Australia, 1990 to 1994. *Am. J. Public Health* **1998**, *88* (12), 1761−6.
(43) Tinling, M. A.; West, J. J.; Cascio, W. E.; Kilaru, V.; Rappold, A. G. Repeating cardiopulmonary health effects in rural North Carolina population during a second large peat wildfire. *Environ. Health* **2016**, *15*, 12.
(44) Harlan, S. L.; Declet-Barreto, J. H.; Stefanov, W. L.; Petitti, D. B. Neighborhood effects on heat deaths: social and environmental predictors of vulnerability in Maricopa County, Arizona. *Environ. Health Perspect* **2013**, *121* (2), 197−204.
(45) Messer, L. C.; Laraia, B. A.; Kaufman, J. S.; Eyster, J.; Holzman, C.; Culhane, J.; Elo, I.; Burke, J. G.; O'Campo, P. The development of a standardized neighborhood deprivation index. *J. Urban Health* **2006**, *83* (6), 1041−62.
(46) Petitti, D. B.; Harlan, S. L.; Chowell-Puente, G.; Ruddell, D. Occupation and environmental heat-associated deaths in Maricopa county, Arizona: a case-control study. *PLoS One* **2013**, *8* (5), e62596.
(47) Uejio, C. K.; Wilhelmi, O. V.; Golden, J. S.; Mills, D. M.; Gulino, S. P.; Samenow, J. P. Intra-urban societal vulnerability to extreme heat: the role of heat exposure and the built environment, socioeconomics, and neighborhood stability. *Health Place* **2011**, *17* (2), 498−507.
(48) Neidell, M. Air quality warnings and outdoor activities: evidence from Southern California using a regression discontinuity design. *J. Epidemiol Community Health* **2010**, *64* (10), 921−6.
(49) Mott, J. A.; Meyer, P.; Mannino, D.; Redd, S. C.; Smith, E. M.; Gotway-Crawford, C.; Chase, E. Wildland forest fire smoke: health effects and intervention evaluation, Hoopa, California, 1999. *West. J. Med.* **2002**, *176* (3), 157−62.
(50) Kinney, P. L. Climate change, air quality, and human health. *Am. J. Prev. Med.* **2008**, *35* (5), 459−67.
(51) Fann, N.; Fulcher, C. M.; Baker, K. The recent and future health burden of air pollution apportioned across U.S. sectors. *Environ. Sci. Technol.* **2013**, *47* (8), 3580−9.
(52) Liu, J. C.; Mickley, L. J.; Sulprizio, M. P.; Yue, X.; Peng, R. D.; Dominici, F.; Michelle L Bell, D. Future respiratory hospital admissions from wildfire smoke under climate change in the Western US. *Environ. Res. Lett.* **2016**, *11* (12), 124018.
(53) Prestemon, J.; Shankar, U.; Xiu, A.; Talgo, K.; Yang, D.; Dixon, IV, E.; McKenzie, D.; Abt, K. L., Projecting wildfire area burned in the south-eastern United States, 2011−60. 2016.
(54) Flannigan, M. D.; Van Wagner, C. E. Climate Change and wildfire in Canada. *Can. J. For. Res.* **1991**, *21*, 66−72.
(55) Bowman, D. M.; Balch, J. K.; Artaxo, P.; Bond, W. J.; Carlson, J. M.; Cochrane, M. A.; D'Antonio, C. M.; Defries, R. S.; Doyle, J. C.; Harrison, S. P.; Johnston, F. H.; Keeley, J. E.; Krawchuk, M. A.; Kull, C. A.; Marston, J. B.; Moritz, M. A.; Prentice, I. C.; Roos, C. I.; Scott, A. C.; Swetnam, T. W.; van der Werf, G. R.; Pyne, S. J. Fire in the Earth system. *Science* **2009**, *324* (5926), 481−4.
(56) Ager, A. A.; Day, M. A.; McHugh, C. W.; Short, K.; Gilbertson-Day, J.; Finney, M. A.; Calkin, D. E. Wildfire exposure and fuel management on western US national forests. *J. Environ. Manage.* **2014**, *145* (1), 54−70.
(57) Park, S.-K.; Cobb, C. E.; Wade, K.; Mulholland, J.; Hu, Y.; Russe, A. G. Uncertainty in air quality model evaluation for particulate matter due to spatial variations in pollutant concentrations. *Atmos. Environ.* **2006**, *40* (Supplement 2), 563−573.
(58) Kim, Y. H.; Tong, H.; Daniels, M.; Boykin, E.; Krantz, Q. T.; McGee, J.; Hays, M.; Kovalcik, K.; Dye, J. A.; Gilmour, M. I. Cardiopulmonary toxicity of peat wildfire particulate matter and the predictive utility of precision cut lung slices. *Part. Fibre Toxicol.* **2014**, *11*, 29.
(59) IARC. *Outdoor Air Pollution*; World Health Organization: International Agency for Research on Cancer, 2016.
(60) Stanek, L. W. S.; Jason, D.; Dutton; Steven, J.; Dubois; Jean-Jacques, B. Attributing health effects to apportioned components and sources of particulate matter: An evaluation of collective results. *Atmos. Environ.* **2011**, *45* (October), 5655−5663.

DOI: 10.1021/acs.est.6b06200
Environ. Sci. Technol. 2017, 51, 6674−6682

EPA-RTP LIBRARY

Article Impact Report

Community Vulnerability to Health Impacts of Wildland Fire Smoke Exposure

ENVIRONMENTAL SCIENCE & TECHNOLOGY

Rappold, AG; Reyes, J; Pouliot, G; Cascio, WE; Diaz-Sanchez, D

Rappold, AG, et al. (2017). Community Vulnerability to Health Impacts of Wildland Fire Smoke Exposure. *Environmental Science & Technology, 51*(12), 6674-6682. PMID: 28493694. DOI: 10.1021/acs.est.6b06200

Highlights

Citations

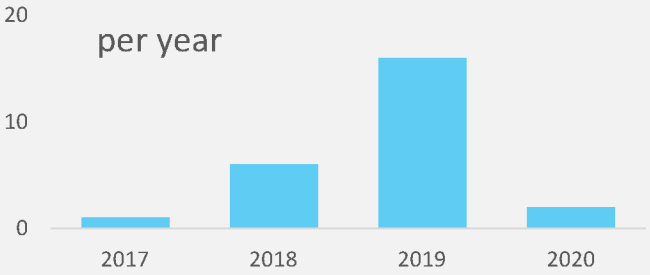

33 Google scholar

25 Web of Science

29 Dimensions

by authors from
53 organizations
across
13 publication titles

Environmental Science & Technology

7.149	Impact Factor
1.141	Immediacy Index
7.8	Cited Half-Life

Publisher Metrics

1596 views

Citations by Country

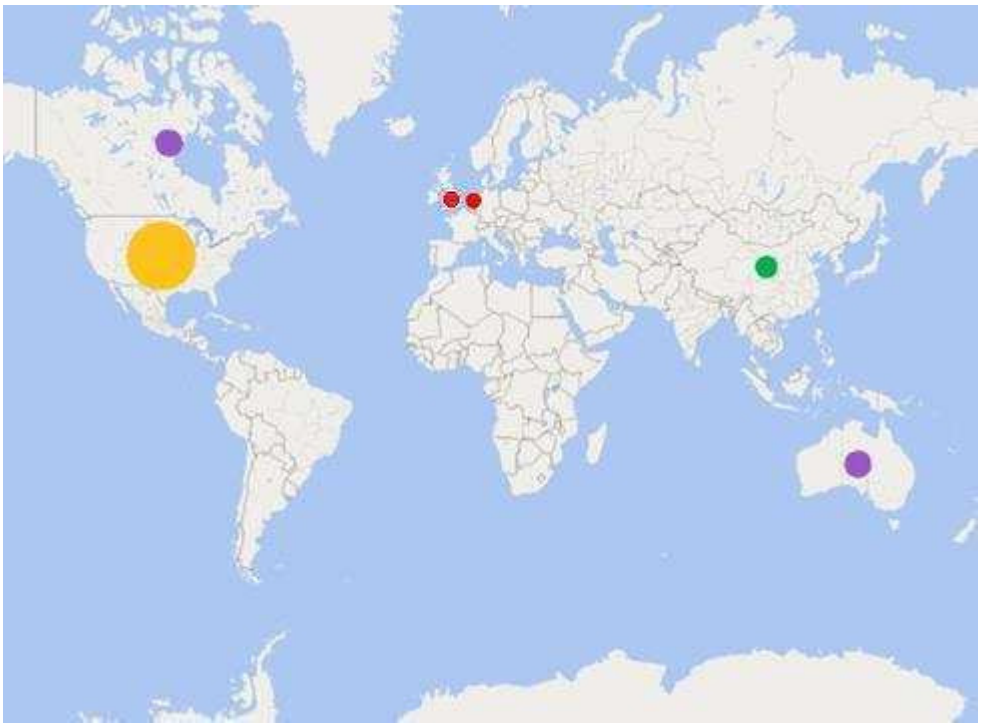

Countries	Papers
USA	19
AUSTRALIA	3
CANADA	3
CHINA	2
ENGLAND	1
NETHERLANDS	1

Top Citing Organizations

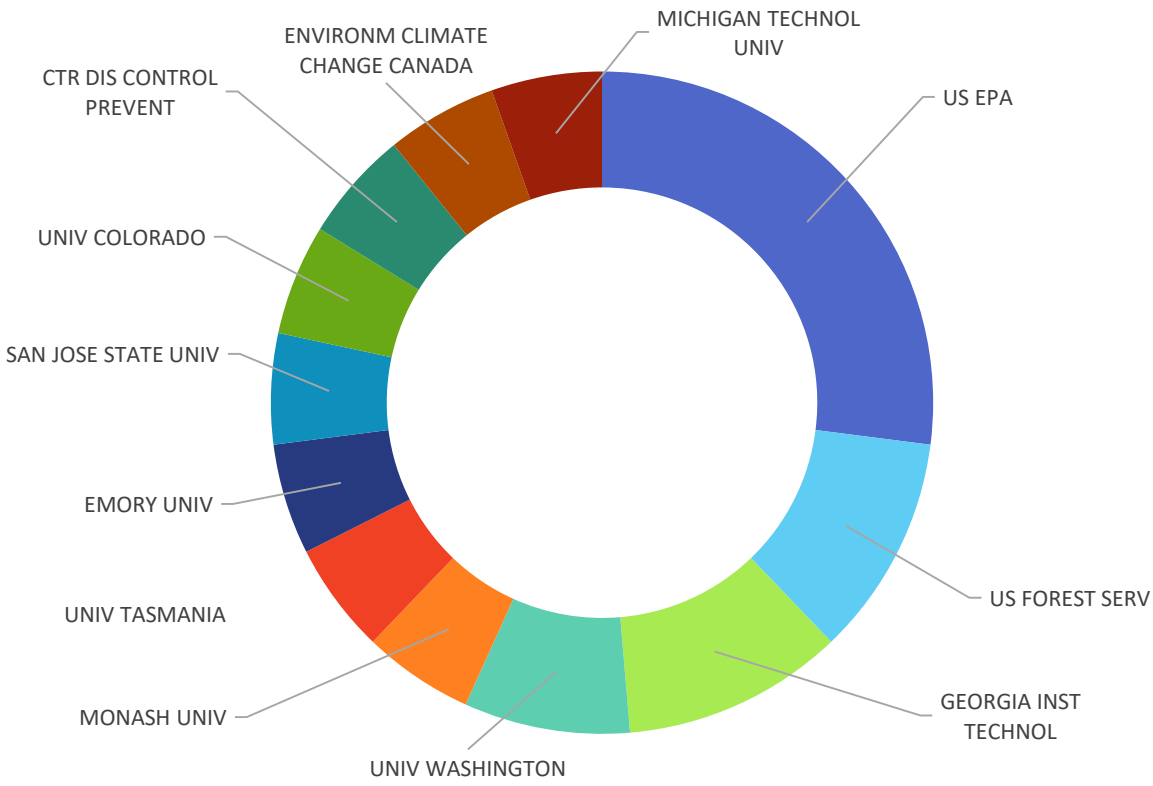

Citing Journals (Impact Factor)

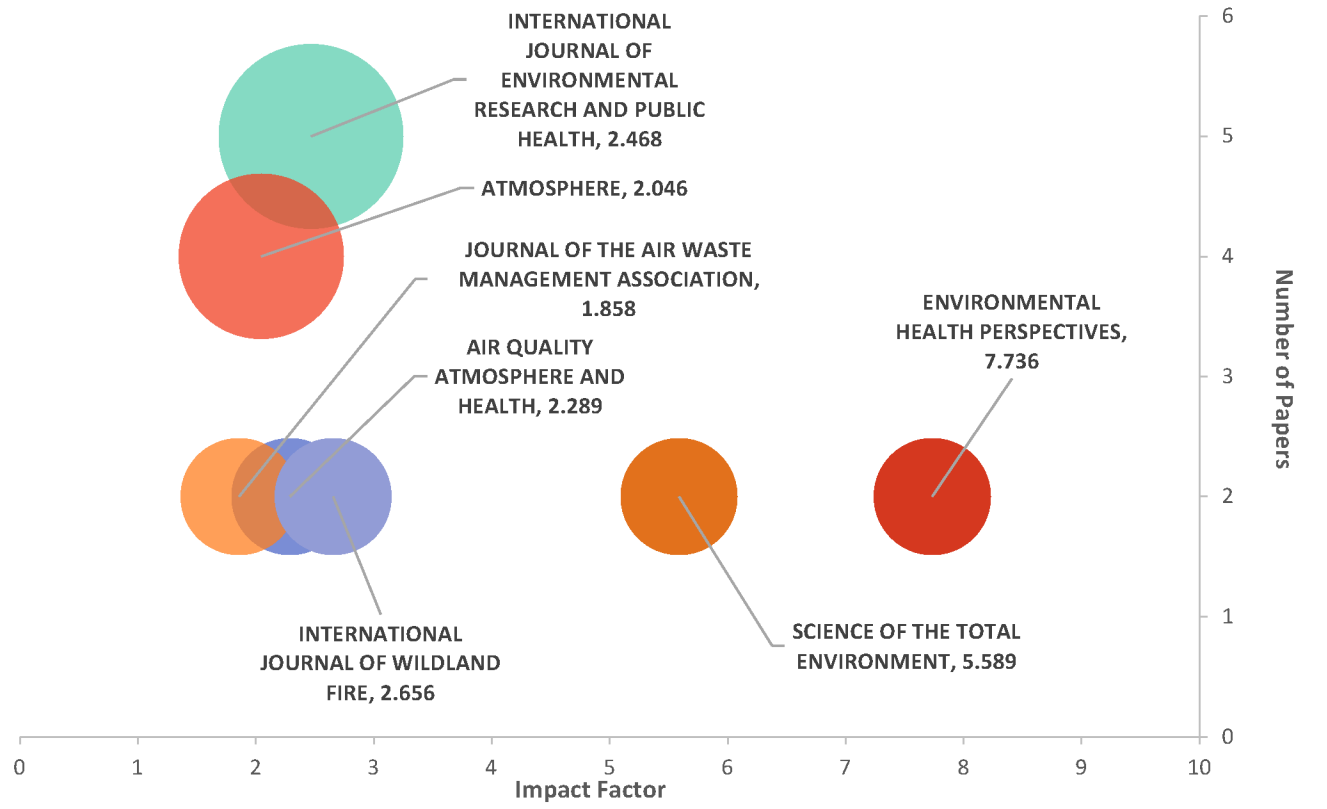

Research Areas

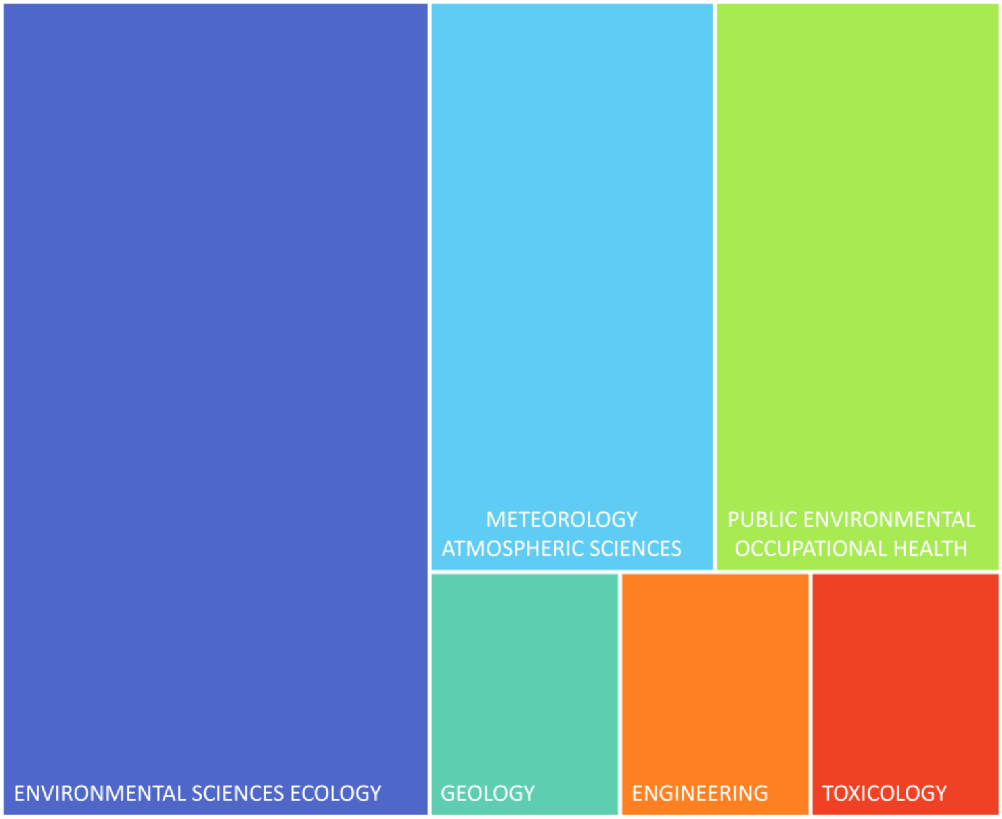

Research Areas	Papers
ENVIRONMENTAL SCIENCES ECOLOGY	15
METEOROLOGY ATMOSPHERIC SCIENCES	7
PUBLIC ENVIRONMENTAL OCCUPATIONAL HEALTH	7
GEOLOGY	2
ENGINEERING	2
TOXICOLOGY	2
FORESTRY	2

Alternative Metrics

Altmetric

Mentioned by

1 tweeter

Citations

29 Dimensions

Readers on

107 Mendeley

PLUMX Metrics

USAGE	442
Abstract Views	370
EBSCO	370
Link-outs	72
EBSCO	72
CAPTURES	**332**
Readers	305

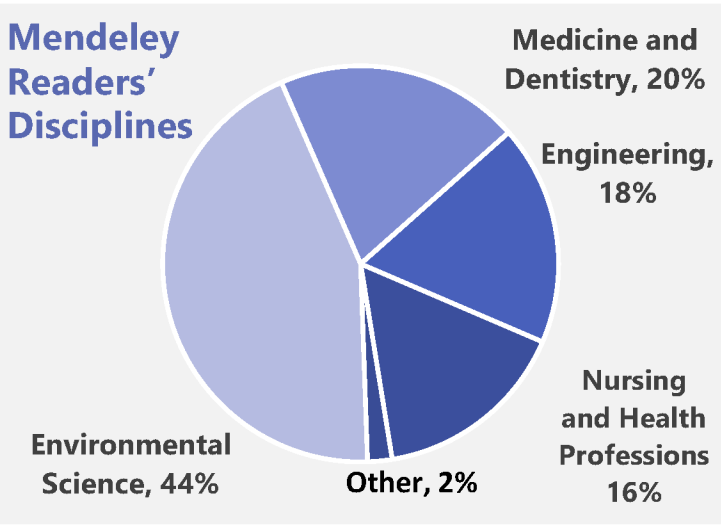

Dimensions

13

Field Citation Ratio

This article features relative citation performance **13 times higher**, on average, than similarly aged articles in its subject field.

2.95

Relative Citation Ratio

This article has been cited at a rate that is **almost 3 times higher** than the average rate of articles normally cited alongside it.

Top Citing Journal

Int'l Journal of Research & Public Health

5 Articles

2.47 Impact Factor

Data collected 22 April 2019.
Current data may differ.

About the Report

This report was compiled using data from Web of Science, Google Scholar, Altmetric, and other databases when necessary. It is a snapshot of a particular article where the impact has been determined through analyzing various information about the papers citing that article. By collecting and organizing these statistics, a picture of reach, popularity, and value is created.

Citations by Country

The origin of the citing papers as determined by author addresses. All records are shown on the graphic, and the logical threshold is displayed in the accompanying table.

Top Citing Organizations

The listed author affiliations of citing articles. Percentage is determined using a logical threshold where the remaining percent of the whole would be considered "other."

Citing Journals

The volume of citing papers per the top ten journal titles compared to other titles citing the paper, displayed along with the journal's impact factor for the report year. In the graphic:

- position along the x axis is determined by the journal impact factor
- position along the y axis is determined by the number of citing papers published in the source title
- size is determined by the percentage of citing papers published in the specific source title compared to all other titles

Research Areas

The scientific category for each citing paper. A logical threshold is displayed in the graphic, and an expansion is shown in the accompanying table.

Alternative Metrics

Metrics gathered using the Altmetric database, PlumX Analytics, publisher website data, and other sources including but not limited to those listed in the Altmetric doughnut:

Source name	Definition
Twitter	Collection of tweets, retweets, and quoted tweets with links to scholarly content
Facebook	Monitors Public Facebook Pages and posts
Google+	Mentions from public posts (Coverage ended Jan. 2019 but historical data still available)
Policy documents	Scans and text-mines policy document PDFs for references; connected to CrossRef and PubMed for DOIs
Patents	Using data from IIFI CLAIMS®, tracks references found in patents filed with nine international patents offices
News	Manually curated data provided from third-parties and RSS feeds
Blogs	Manually curated list, attempts to gather posts linking to scholarly articles
Wikipedia	Mentions located in References section
Mendeley	Number of readers with the content in their library
CiteULike	Online reference manager counted similar to Mendeley (Coverage ended Dec. 2014 but historical data still available)

EPA-RTP LIBRARY

Article Impact Report

The Health Impacts and Economic Value of Wildland Fire Episodes in the US: 2008-2012

SCIENCE OF THE TOTAL ENVIRONMENT

Fann, N; Alman, B; Broome, RA; Morgan, GG; Johnston, FH; Pouliot, G; et al.

Fann, N, et al. (2018). The Health Impacts and Economic Value of Wildland Fire Episodes in the US: 2008-2012. *Science Of The Total Environment, 610,* 802-809. PMID: 28826118. DOI: 10.1016/j.scitotenv.2017.08.024

Highlights

Citations

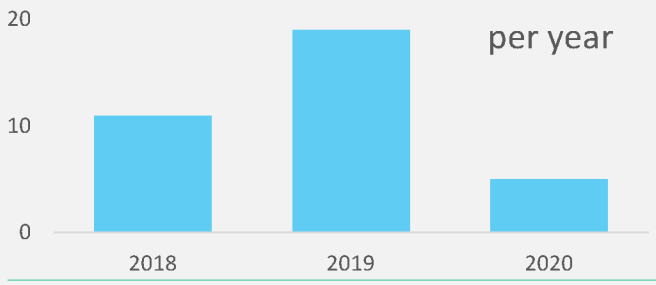

62 Google Scholar

35 Web of Science

44 Dimensions

by authors from
76 organizations
across
22 publication titles

Science of the Total Environment

5.589	Impact Factor
1.682	Immediacy Index
4.4	Cited Half-Life

Picked up in

news articles

Altmetric Attention Score

Citations by Country

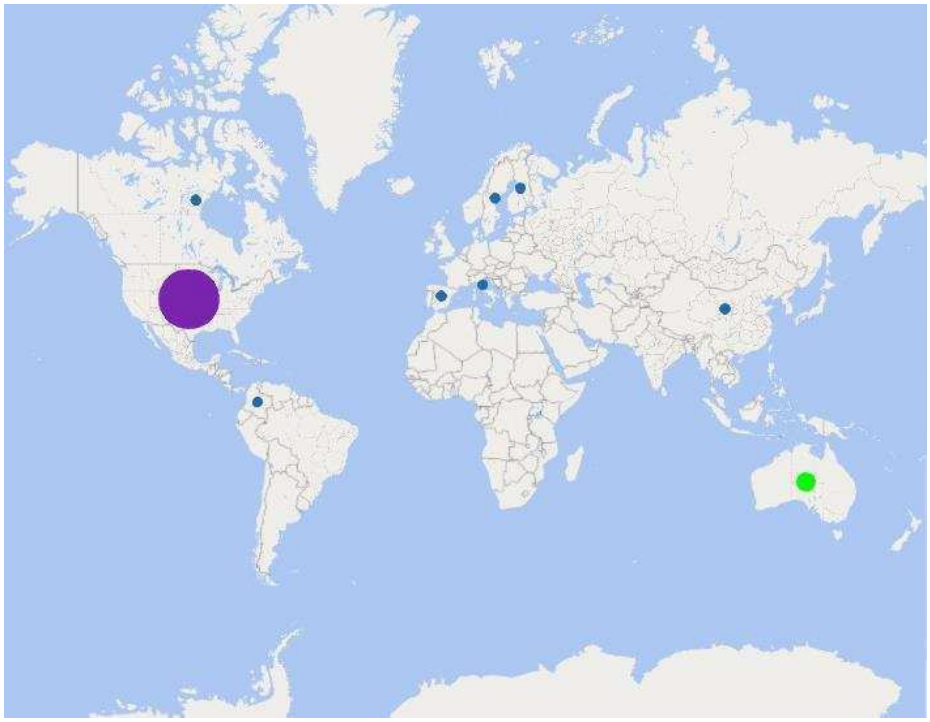

Countries	Papers
USA	31
AUSTRALIA	3
SPAIN	1
ITALY	1
FINLAND	1
SWEDEN	1
CANADA	1
COLOMBIA	1
CHINA	1

Top Citing Organizations

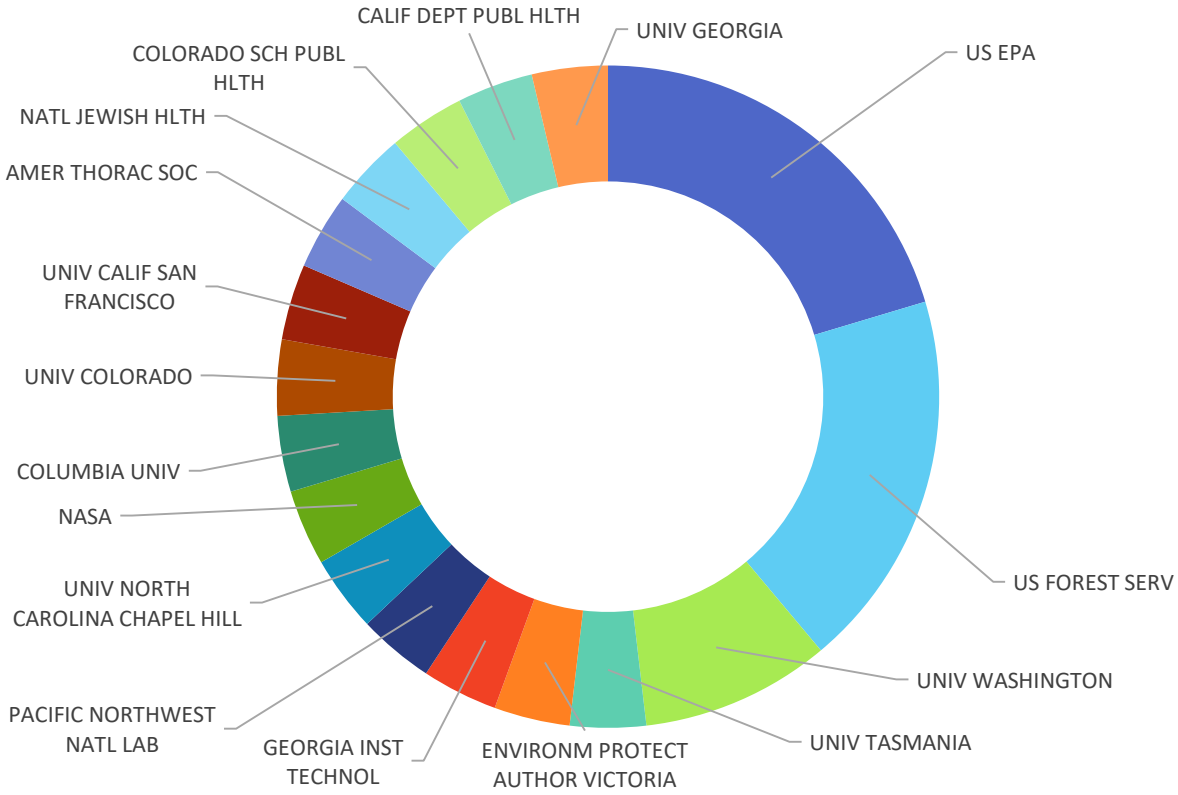

Citing Journals (Impact Factor)

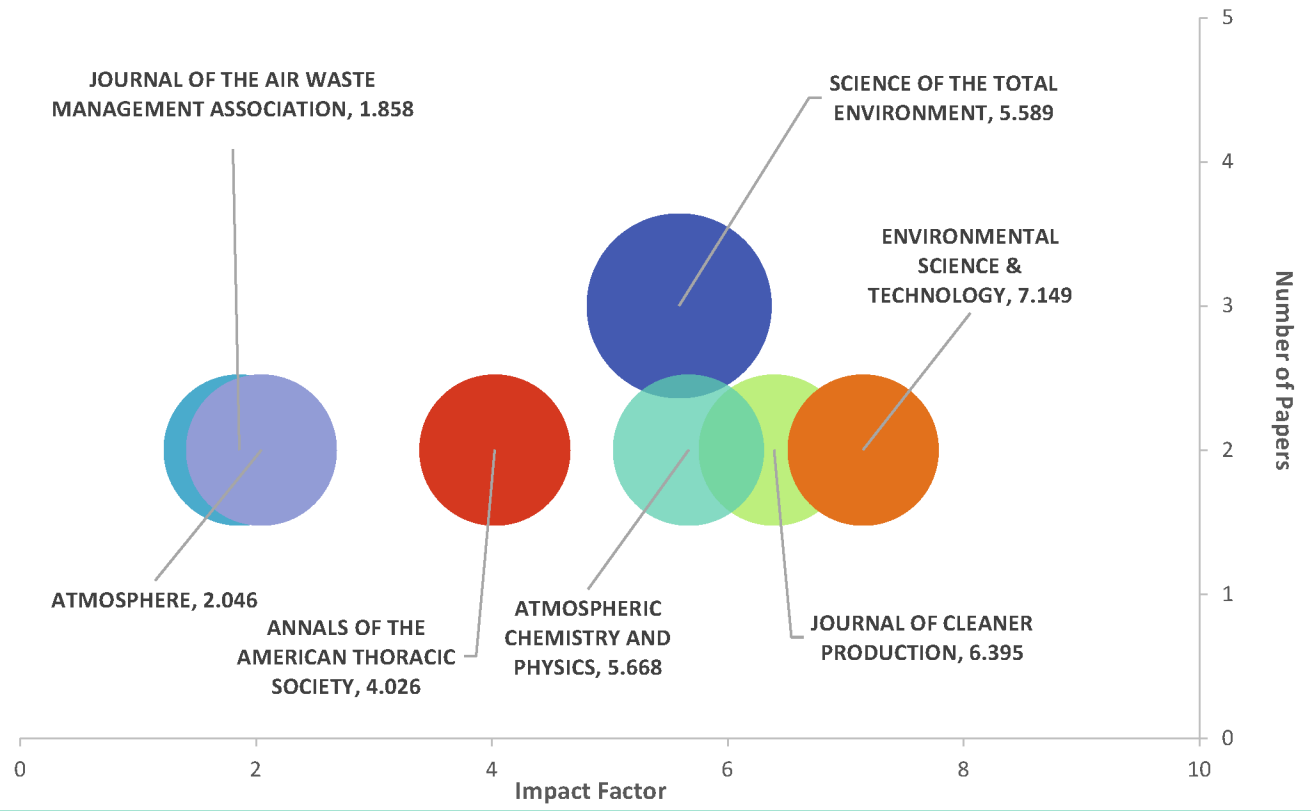

Research Areas

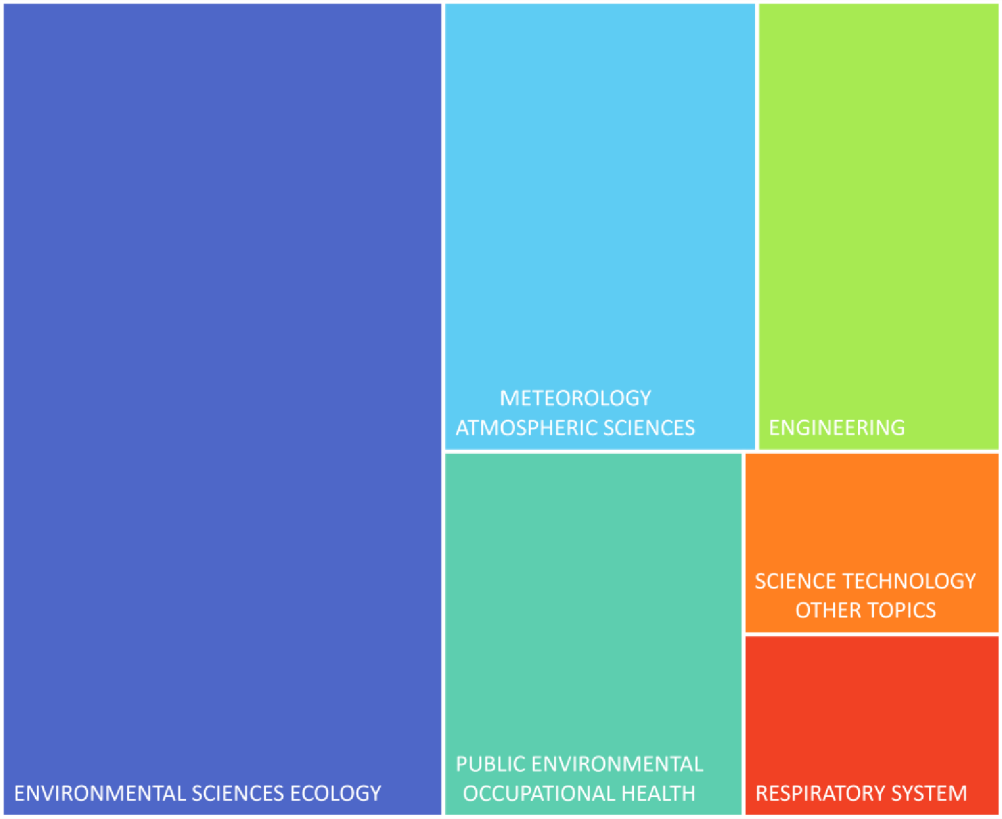

Research Areas	Papers
ENVIRONMENTAL SCIENCES ECOLOGY	23
METEOROLOGY ATMOSPHERIC SCIENCES	9
ENGINEERING	7
PUBLIC ENVIRONMENTAL OCCUPATIONAL HEALTH	7
SCIENCE TECHNOLOGY OTHER TOPICS	3
RESPIRATORY SYSTEM	3

Alternative Metrics

Altmetric

About this Attention Score

In the top 5% of all research outputs scored by Altmetric

High Attention Score compared to outputs of the same age (97th percentile)

High Attention Score compared to outputs of the same age and source (98th percentile)

Mentioned by

- **11** news outlets
- **2** blogs
- **5** tweeters
- **1** Google+ user

Citations

- **44** Dimensions

Readers on

- **136** Mendeley

Highly Cited Paper

As of November/December 2019, this highly cited paper received enough citations to place it in the **Top 1%** of the academic field of Environment/Ecology based on a highly cited threshold for the field and publication year.

Cited by **11 news outlets**, including:

The Washington Post

Medium

WIRED

Notable News Mention

"Smoke from wildfires may be surprisingly deadly, scientists report"

-*The Washington Post*, 12/15/17

Data collected 21 April 2020.
Current data may differ.

About the Report

This report was compiled using data from Web of Science, Google Scholar, Altmetric, and other databases when necessary. It is a snapshot of a particular article where the impact has been determined through analyzing various information about the papers citing that article. By collecting and organizing these statistics, a picture of reach, popularity, and value is created.

Citations by Country

The origin of the citing papers as determined by author addresses. All records are shown on the graphic, and the logical threshold is displayed in the accompanying table.

Top Citing Organizations

The listed author affiliations of citing articles. Percentage is determined using a logical threshold where the remaining percent of the whole would be considered "other."

Citing Journals

The volume of citing papers per the top ten journal titles compared to other titles citing the paper, displayed along with the journal's impact factor for the report year. In the graphic:

- position along the x axis is determined by the journal impact factor
- position along the y axis is determined by the number of citing papers published in the source title
- size is determined by the percentage of citing papers published in the specific source title compared to all other titles

Research Areas

The scientific category for each citing paper. A logical threshold is displayed in the graphic, and an expansion is shown in the accompanying table.

Alternative Metrics

Metrics gathered using the Altmetric database, PlumX Analytics, publisher website data, and other sources including but not limited to those listed in the Altmetric doughnut:

Source name	Definition
Twitter	Collection of tweets, retweets, and quoted tweets with links to scholarly content
Facebook	Monitors Public Facebook Pages and posts
Google+	Mentions from public posts (Coverage ended Jan. 2019 but historical data still available)
Policy documents	Scans and text-mines policy document PDFs for references; connected to CrossRef and PubMed for DOIs
Patents	Using data from IIFI CLAIMS®, tracks references found in patents filed with nine international patents offices
News	Manually curated data provided from third-parties and RSS feeds
Blogs	Manually curated list, attempts to gather posts linking to scholarly articles
Wikipedia	Mentions located in References section
Mendeley	Number of readers with the content in their library
CiteULike	Online reference manager counted similar to Mendeley (Coverage ended Dec. 2014 but historical data still available)

id_a0St0000002RyyJEAS__z_'042820142559'Fann_2018_News

Mention Type	Mention Date	Outlet or Author
News story	11/13/2019 18:09	Medium US
News story	10/9/2019 12:14	Earth & Space Science News
News story	9/11/2018 12:00	Wired.com
News story	8/20/2018 21:43	KUOW
News story	12/23/2017 6:38	Winnipeg Free Press
News story	12/15/2017 21:42	True Viral News
News story	12/15/2017 17:00	South Coast Today
News story	12/15/2017 17:00	Herald Tribune
News story	12/15/2017 16:00	The State Journal-Register
News story	12/15/2017 15:52	The Denver Post
News story	12/15/2017 14:03	Washington Post

Mention Title	Country
Wildfires?—?the perfect behavioral problem	United States
Putting a Price on the Costs of Climate Related Health Impacts	United States
We Know Exactly How to Stop Wildfires—With Money	United States
This smoke means smaller newborns and more ER visits	United States
wildfire smoke surprisingly deadly: data	Canada
Smoke from wildfires may be surprisingly deadly, scientists report	Russia
Smoke from wildfires may be surprisingly deadly, scientists report	United States
Smoke from wildfires may be surprisingly deadly, scientists report	United States
Smoke from wildfires may be surprisingly deadly, scientists report	United States
Smoke from wildfires may be surprisingly deadly, CSU researchers say	United States
Smoke from wildfires may be surprisingly deadly, scientists report	United States

id_a0St0000002RyyJEAS__z_'042820142559'Fann_2018_News

External Mention ID

Mention URL
http://ct.moreover.com/?a=40666515819&p=1pl&v=1&x=VTqpfodiwCSIOzBMbEumJA
http://ct.moreover.com/?a=40384651714&p=1pl&v=1&x=is2aMmnukaLlbNEDvzsspg
http://ct.moreover.com/?a=37069153711&p=1pl&v=1&x=Wmsa-x5ppEEy2clhREMHAw
http://ct.moreover.com/?a=34867740394&p=1pl&v=1&x=nFrTk2URLRDHbfNAGAXwJw
https://www.winnipegfreepress.com/world/wildfire-smoke-surprisingly-deadly-data-466063383.html
http://ct.moreover.com/?a=32792276602&p=1pl&v=1&x=qyK4f1EksZcTUzQ4YblKeQ
http://ct.moreover.com/?a=32791147254&p=1pl&v=1&x=3SgMJJc6jcJQsAB5DyRfIA
http://ct.moreover.com/?a=32790604122&p=1pl&v=1&x=tEDUFXGrLAMifY81vtam_Q
http://ct.moreover.com/?a=32791135007&p=1pl&v=1&x=wW989UJeYueyT_VNGE3YAQ
http://ct.moreover.com/?a=32790003232&p=1pl&v=1&x=ysPrsrTvQqHqyUFBmR41MA
https://www.washingtonpost.com/news/energy-environment/wp/2017/12/15/smoke-from-wildfires-may-be-surprisingly-dea

Research Output Title

The health impacts and economic value of wildland fire episodes in the U.S.: 2008–2012
The health impacts and economic value of wildland fire episodes in the U.S.: 2008–2012
The health impacts and economic value of wildland fire episodes in the U.S.: 2008–2012
The health impacts and economic value of wildland fire episodes in the U.S.: 2008–2012
The health impacts and economic value of wildland fire episodes in the U.S.: 2008–2012
The health impacts and economic value of wildland fire episodes in the U.S.: 2008–2012
The health impacts and economic value of wildland fire episodes in the U.S.: 2008–2012
The health impacts and economic value of wildland fire episodes in the U.S.: 2008–2012
The health impacts and economic value of wildland fire episodes in the U.S.: 2008–2012
The health impacts and economic value of wildland fire episodes in the U.S.: 2008–2012
The health impacts and economic value of wildland fire episodes in the U.S.: 2008–2012

id_a0St0000002RyyJEAS__z_'042820142559'Fann_2018_News

Journal/Collection Title	Authors at my Institution	Departments	Output Type
Science of the Total Environment			Article
Science of the Total Environment			Article
Science of the Total Environment			Article
Science of the Total Environment			Article
Science of the Total Environment			Article
Science of the Total Environment			Article
Science of the Total Environment			Article
Science of the Total Environment			Article
Science of the Total Environment			Article
Science of the Total Environment			Article
Science of the Total Environment			Article
Science of the Total Environment			Article

Subjects (FoR)

11 Medical and Health Sciences; 1117 Public Health and Health Services
11 Medical and Health Sciences; 1117 Public Health and Health Services
11 Medical and Health Sciences; 1117 Public Health and Health Services
11 Medical and Health Sciences; 1117 Public Health and Health Services
11 Medical and Health Sciences; 1117 Public Health and Health Services
11 Medical and Health Sciences; 1117 Public Health and Health Services
11 Medical and Health Sciences; 1117 Public Health and Health Services
11 Medical and Health Sciences; 1117 Public Health and Health Services
11 Medical and Health Sciences; 1117 Public Health and Health Services
11 Medical and Health Sciences; 1117 Public Health and Health Services
11 Medical and Health Sciences; 1117 Public Health and Health Services

Affiliations (GRID)

Environmental Protection Agency; Sydney South West Area Health Service; University of Sydney; University of Tasmania
Environmental Protection Agency; Sydney South West Area Health Service; University of Sydney; University of Tasmania
Environmental Protection Agency; Sydney South West Area Health Service; University of Sydney; University of Tasmania
Environmental Protection Agency; Sydney South West Area Health Service; University of Sydney; University of Tasmania
Environmental Protection Agency; Sydney South West Area Health Service; University of Sydney; University of Tasmania
Environmental Protection Agency; Sydney South West Area Health Service; University of Sydney; University of Tasmania
Environmental Protection Agency; Sydney South West Area Health Service; University of Sydney; University of Tasmania
Environmental Protection Agency; Sydney South West Area Health Service; University of Sydney; University of Tasmania
Environmental Protection Agency; Sydney South West Area Health Service; University of Sydney; University of Tasmania
Environmental Protection Agency; Sydney South West Area Health Service; University of Sydney; University of Tasmania
Environmental Protection Agency; Sydney South West Area Health Service; University of Sydney; University of Tasmania

id_a0St0000002RyyJEAS__z_'042820142559'Fann_2018_News

Publication Date	Altmetric Attention Score	Details Page URL
1/1/2018	106	https://www.altmetric.com/details/24167099
1/1/2018	106	https://www.altmetric.com/details/24167099
1/1/2018	106	https://www.altmetric.com/details/24167099
1/1/2018	106	https://www.altmetric.com/details/24167099
1/1/2018	106	https://www.altmetric.com/details/24167099
1/1/2018	106	https://www.altmetric.com/details/24167099
1/1/2018	106	https://www.altmetric.com/details/24167099
1/1/2018	106	https://www.altmetric.com/details/24167099
1/1/2018	106	https://www.altmetric.com/details/24167099
1/1/2018	106	https://www.altmetric.com/details/24167099
1/1/2018	106	https://www.altmetric.com/details/24167099

DOI	ISBN	National Clinical Trial ID	URI	PubMed ID	PubMedCentral ID
10.1016/j.scitotenv.2017.08.024				28826118	PMC6117838
10.1016/j.scitotenv.2017.08.024				28826118	PMC6117838
10.1016/j.scitotenv.2017.08.024				28826118	PMC6117838
10.1016/j.scitotenv.2017.08.024				28826118	PMC6117838
10.1016/j.scitotenv.2017.08.024				28826118	PMC6117838
10.1016/j.scitotenv.2017.08.024				28826118	PMC6117838
10.1016/j.scitotenv.2017.08.024				28826118	PMC6117838
10.1016/j.scitotenv.2017.08.024				28826118	PMC6117838
10.1016/j.scitotenv.2017.08.024				28826118	PMC6117838
10.1016/j.scitotenv.2017.08.024				28826118	PMC6117838
10.1016/j.scitotenv.2017.08.024				28826118	PMC6117838

id_a0St0000002RyyJEAS__z_'042820142559'Fann_2018_News

Handle.net IDs	ADS Bibcode	arXiv ID	RePEc ID	SSRN	URN
	2018ScTEn.610..802F				
	2018ScTEn.610..802F				
	2018ScTEn.610..802F				
	2018ScTEn.610..802F				
	2018ScTEn.610..802F				
	2018ScTEn.610..802F				
	2018ScTEn.610..802F				
	2018ScTEn.610..802F				
	2018ScTEn.610..802F				
	2018ScTEn.610..802F				
	2018ScTEn.610..802F				

Rappold, Ana

From: Alman, Breanna (ATSDR/DTHHS/ETB) <pcq6@cdc.gov>
Sent: Wednesday, April 15, 2020 11:35 AM
To: Rappold, Ana
Subject: RE: STAA Award Health Burden from Wildfire Smoke Exposure
Attachments: ATT00001.txt

Yes, I concur.

From: Rappold, Ana <Rappold.Ana@epa.gov>
Sent: Wednesday, April 15, 2020 11:17 AM
To: Alman, Breanna (ATSDR/DTHHS/ETB) <pcq6@cdc.gov>
Subject: STAA Award Health Burden from Wildfire Smoke Exposure

Dear Breanna

We estimate your participation level for the STAA award related to two papers mentioned below as 10%. Please reply to this email with your concurrence.

1. Rappold AG, Reyes J, Pouliot G, et al. Community Vulnerability to Health Impacts of Wildland Fire Smoke Exposure. 2017. doi:10.1021/acs.est.6b06200
2. Fann N, Alman B, Broome RA, et al. The health impacts and economic value of wildland fire episodes in the U.S.: 2008–2012. Sci Total Environ. 2018;610-611. doi:10.1016/j.scitotenv.2017.08.024

Ana

Sincerely,

Ana G. Rappold, Ph.D.
Statistician
919 843 9504

Join Smoke Sense today

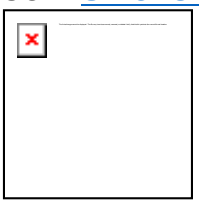

U.S. EPA
Office of Research and Development
Center for Public Health and Environmental Assessment
Clinical Research Branch

Rappold, Ana

From: Richard Broome <richardbroome2002@yahoo.co.uk>
Sent: Thursday, April 16, 2020 4:51 AM
To: Rappold, Ana
Subject: Re: STAA Award Health Burden from Wildfire Smoke Exposure

Yes

On 16 Apr 2020, at 1:15 am, Rappold, Ana <Rappold.Ana@epa.gov> wrote:

Dear Richard

We estimate your participation level for the STAA award related to two papers mentioned below as 5%. Please reply to this email with your concurrence.

1. Rappold AG, Reyes J, Pouliot G, et al. Community Vulnerability to Health Impacts of Wildland Fire Smoke Exposure. 2017. doi:10.1021/acs.est.6b06200
2. Fann N, Alman B, Broome RA, et al. The health impacts and economic value of wildland fire episodes in the U.S.: 2008–2012. Sci Total Environ. 2018;610-611. doi:10.1016/j.scitotenv.2017.08.024

Ana

Sincerely,

Ana G. Rappold, Ph.D.
Statistician
919 843 9504
Join Smoke Sense today
<image003.jpg>

U.S. EPA
Office of Research and Development
Center for Public Health and Environmental Assessment
Clinical Research Branch

Rappold, Ana

From: Cascio, Wayne
Sent: Wednesday, April 15, 2020 11:27 AM
To: Rappold, Ana
Subject: RE: STAA Award Health Burden from Wildfire Smoke Exposure

Ana – Thank you for your email. Yes, my contribution to these papers is as you say <5%. Wayne

Wayne E. Cascio, MD, FACC | Director | Center for Public Health and Environmental Assessment | Office of Research and Development | U.S. Environmental Protection Agency | Research Triangle Park, NC 27711 | Phone: 919.541.2508 | Cell: 919.627.3762|

From: Rappold, Ana <Rappold.Ana@epa.gov>
Sent: Wednesday, April 15, 2020 11:18 AM
To: Cascio, Wayne <Cascio.Wayne@epa.gov>
Subject: STAA Award Health Burden from Wildfire Smoke Exposure

Dear Wayne

We estimate your participation level for the STAA award related to two papers mentioned below as 5%. Please reply to this email with your concurrence.

1. Rappold AG, Reyes J, Pouliot G, et al. Community Vulnerability to Health Impacts of Wildland Fire Smoke Exposure. 2017. doi:10.1021/acs.est.6b06200
2. Fann N, Alman B, Broome RA, et al. The health impacts and economic value of wildland fire episodes in the U.S.: 2008–2012. Sci Total Environ. 2018;610-611. doi:10.1016/j.scitotenv.2017.08.024

Ana

Sincerely,

Ana G. Rappold, Ph.D.
Statistician
919 843 9504

Join Smoke Sense today

U.S. EPA
Office of Research and Development
Center for Public Health and Environmental Assessment
Clinical Research Branch

Rappold, Ana

From: Diaz-Sanchez, David
Sent: Wednesday, April 15, 2020 11:33 AM
To: Rappold, Ana
Subject: RE: STAA Award Health Burden from Wildfire Smoke Exposure

I concur.

From: Rappold, Ana <Rappold.Ana@epa.gov>
Sent: Wednesday, April 15, 2020 11:19 AM
To: Diaz-Sanchez, David <Diaz-Sanchez.David@epa.gov>
Subject: STAA Award Health Burden from Wildfire Smoke Exposure

Dear David

We estimate your participation level for the STAA award related to two papers mentioned below as 5%. Please reply to this email with your concurrence.

1. Rappold AG, Reyes J, Pouliot G, et al. Community Vulnerability to Health Impacts of Wildland Fire Smoke Exposure. 2017. doi:10.1021/acs.est.6b06200
2. Fann N, Alman B, Broome RA, et al. The health impacts and economic value of wildland fire episodes in the U.S.: 2008–2012. Sci Total Environ. 2018;610-611. doi:10.1016/j.scitotenv.2017.08.024

Ana

Sincerely,

Ana G. Rappold, Ph.D.
Statistician
919 843 9504

Join Smoke Sense today

U.S. EPA
Office of Research and Development
Center for Public Health and Environmental Assessment
Clinical Research Branch

Rappold, Ana

From: Fann, Neal
Sent: Wednesday, April 15, 2020 11:20 AM
To: Rappold, Ana
Subject: RE: STAA Award Health Burden from Wildfire Smoke Exposure

I concur

From: Rappold, Ana <Rappold.Ana@epa.gov>
Sent: Wednesday, April 15, 2020 11:20 AM
To: Fann, Neal <Fann.Neal@epa.gov>
Subject: STAA Award Health Burden from Wildfire Smoke Exposure

Dear Neal

We estimate your participation level for the STAA award related to two papers mentioned below as 18%. Please reply to this email with your concurrence.

1. Rappold AG, Reyes J, Pouliot G, et al. Community Vulnerability to Health Impacts of Wildland Fire Smoke Exposure. 2017. doi:10.1021/acs.est.6b06200
2. Fann N, Alman B, Broome RA, et al. The health impacts and economic value of wildland fire episodes in the U.S.: 2008–2012. Sci Total Environ. 2018;610-611. doi:10.1016/j.scitotenv.2017.08.024

Ana

Sincerely,

Ana G. Rappold, Ph.D.
Statistician
919 843 9504

Join Smoke Sense today

U.S. EPA
Office of Research and Development
Center for Public Health and Environmental Assessment
Clinical Research Branch

Rappold, Ana

From: Fay Johnston <fay.johnston@utas.edu.au>
Sent: Wednesday, April 15, 2020 1:47 PM
To: Rappold, Ana
Subject: Re: STAA Award Health Burden from Wildfire Smoke Exposure

Yes

From: Rappold, Ana <Rappold.Ana@epa.gov>
Sent: Thursday, April 16, 2020 1:13:35 AM
To: Fay Johnston <fay.johnston@utas.edu.au>; Fay Johnston <fay.johnston@utas.edu.au>
Subject: STAA Award Health Burden from Wildfire Smoke Exposure

Dear Fay

We estimate your participation level for the STAA award related to two papers mentioned below as 5%. Please reply to this email with your concurrence.

1. Rappold AG, Reyes J, Pouliot G, et al. Community Vulnerability to Health Impacts of Wildland Fire Smoke Exposure. 2017. doi:10.1021/acs.est.6b06200
2. Fann N, Alman B, Broome RA, et al. The health impacts and economic value of wildland fire episodes in the U.S.: 2008–2012. Sci Total Environ. 2018;610-611. doi:10.1016/j.scitotenv.2017.08.024

Ana

Sincerely,

Ana G. Rappold, Ph.D.
Statistician
919 843 9504
Join Smoke Sense today

U.S. EPA
Office of Research and Development
Center for Public Health and Environmental Assessment
Clinical Research Branch

University of Tasmania Electronic Communications Policy (December, 2014).
This email is confidential, and is for the intended recipient only. Access, disclosure, copying, distribution, or reliance on any of it by anyone outside the intended recipient organisation is prohibited and may be a criminal offence. Please delete if obtained in error and email confirmation to the sender. The views expressed in this email are not necessarily the views of the University of Tasmania, unless clearly intended otherwise.

Rappold, Ana

From: Geoffrey Morgan <geoffrey.morgan@sydney.edu.au>
Sent: Wednesday, April 15, 2020 6:27 PM
To: Rappold, Ana
Subject: RE: STAA Award Health Burden from Wildfire Smoke Exposure
Attachments: ATT00001.txt

Hi Ana

Thanks for all your work pulling the ML paper together and good luck with the STAA award nomination. I concur with your estimated of participation level in the papers.

Regards
Geoff

From: Rappold, Ana [mailto:Rappold.Ana@epa.gov]
Sent: Thursday, 16 April 2020 1:14 AM
To: Geoffrey Morgan <geoffrey.morgan@sydney.edu.au>
Subject: STAA Award Health Burden from Wildfire Smoke Exposure

Dear Geoffrey

We estimate your participation level for the STAA award related to two papers mentioned below as 5%. Please reply to this email with your concurrence.

1. Rappold AG, Reyes J, Pouliot G, et al. Community Vulnerability to Health Impacts of Wildland Fire Smoke Exposure. 2017. doi:10.1021/acs.est.6b06200
2. Fann N, Alman B, Broome RA, et al. The health impacts and economic value of wildland fire episodes in the U.S.: 2008–2012. Sci Total Environ. 2018;610-611. doi:10.1016/j.scitotenv.2017.08.024

Ana

Sincerely,

Ana G. Rappold, Ph.D.
Statistician
919 843 9504

Join Smoke Sense today

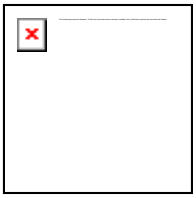

U.S. EPA

Rappold, Ana

From: Pouliot, George
Sent: Wednesday, April 15, 2020 3:12 PM
To: Rappold, Ana
Subject: RE: STAA Award Health Burden from Wildfire Smoke Exposure

I concur with 10% for the STAA award related to two papers noted here:

1. Rappold AG, Reyes J, Pouliot G, et al. Community Vulnerability to Health Impacts of Wildland Fire Smoke Exposure. 2017. doi:10.1021/acs.est.6b06200
2. Fann N, Alman B, Broome RA, et al. The health impacts and economic value of wildland fire episodes in the U.S.: 2008–2012. Sci Total Environ. 2018;610-611. doi:10.1016/j.scitotenv.2017.08.024

George Pouliot

George Pouliot
Physical Scientist
Emissions Systems Analysis Branch (ESAB)
Atmospheric and Environmental Systems Modeling Division (AESMD)
Center for Environmental Measurement and Modeling (CEMM)
US Environmental Protection Agency (US EPA)
Mail Drop E243-04
Research Triangle Park, North Carolina
VOICE: (919) 541-5475 Telework (919) 601-1827
pouliot.george@epa.gov

From: Rappold, Ana <Rappold.Ana@epa.gov>
Sent: Wednesday, April 15, 2020 11:19 AM
To: Pouliot, George <Pouliot.George@epa.gov>
Subject: STAA Award Health Burden from Wildfire Smoke Exposure

Dear George

We estimate your participation level for the STAA award related to two papers mentioned below as 10%. Please reply to this email with your concurrence.

1. Rappold AG, Reyes J, Pouliot G, et al. Community Vulnerability to Health Impacts of Wildland Fire Smoke Exposure. 2017. doi:10.1021/acs.est.6b06200
2. Fann N, Alman B, Broome RA, et al. The health impacts and economic value of wildland fire episodes in the U.S.: 2008–2012. Sci Total Environ. 2018;610-611. doi:10.1016/j.scitotenv.2017.08.024

Ana

Sincerely,

Ana G. Rappold, Ph.D.
Statistician
919 843 9504

Join Smoke Sense today

U.S. EPA
Office of Research and Development
Center for Public Health and Environmental Assessment
Clinical Research Branch

Rappold, Ana

From: Rappold, Ana
Sent: Wednesday, April 15, 2020 11:21 AM
To: Rappold, Ana
Subject: RE: STAA Award Health Burden from Wildfire Smoke Exposure

I concur

From: Rappold, Ana <Rappold.Ana@epa.gov>
Sent: Wednesday, April 15, 2020 11:20 AM
To: Rappold, Ana <Rappold.Ana@epa.gov>
Subject: STAA Award Health Burden from Wildfire Smoke Exposure

Ana
We estimate your participation level for the STAA award related to two papers mentioned below as 27%. Please reply to this email with your concurrence.

1. Rappold AG, Reyes J, Pouliot G, et al. Community Vulnerability to Health Impacts of Wildland Fire Smoke Exposure. 2017. doi:10.1021/acs.est.6b06200
2. Fann N, Alman B, Broome RA, et al. The health impacts and economic value of wildland fire episodes in the U.S.: 2008–2012. Sci Total Environ. 2018;610-611. doi:10.1016/j.scitotenv.2017.08.024

Ana

Sincerely,

Ana G. Rappold, Ph.D.
Statistician
919 843 9504
Join Smoke Sense today

U.S. EPA
Office of Research and Development
Center for Public Health and Environmental Assessment
Clinical Research Branch

From: Reyes, Jeanette
To: Rappold, Ana
Subject: RE: STAA Award Health Burden from Wildfire Smoke Exposure
Date: Wednesday, April 15, 2020 11:58:56 AM
Attachments: image001.jpg

Yes, I concur.

Jeanette

From: Rappold, Ana <Rappold.Ana@epa.gov>
Sent: Wednesday, April 15, 2020 11:20 AM
To: Reyes, Jeanette <Reyes.Jeanette@epa.gov>
Subject: STAA Award Health Burden from Wildfire Smoke Exposure

Dear Jeanette

We estimate your participation level for the STAA award related to two papers mentioned below as 10%. Please reply to this email with your concurrence.

1. Rappold AG, Reyes J, Pouliot G, et al. Community Vulnerability to Health Impacts of Wildland Fire Smoke Exposure. 2017. doi:10.1021/acs.est.6b06200
2. Fann N, Alman B, Broome RA, et al. The health impacts and economic value of wildland fire episodes in the U.S.: 2008–2012. Sci Total Environ. 2018;610-611. doi:10.1016/j.scitotenv.2017.08.024

Ana

Sincerely,

Ana G. Rappold, Ph.D.
Statistician
919 843 9504

Join Smoke Sense today

qr-code

U.S. EPA
Office of Research and Development
Center for Public Health and Environmental Assessment
Clinical Research Branch

Table of Contents

General_Authors_Publications.....2
LI-265069_Blackwell_et_al2019_EST_USGS_streams.....21
LI-265088_Blackwell_et_al2017EAR_Great_Lakes.....32
LI-265088_Supporting_document_Corsi_et_al_2019_Prioritizing_chemicals.....44
LI-265088_Supporting_documentation_DeCicco_et_al_2018_ToxEval_R_package.....59
Supporting_document_Corsi_et_al_2019_Prioritizing_chemicals.....64
Supporting_documentation_DeCicco_et_al_2018_ToxEval_R_package.....79

STAA REPORT FOR THE SCIENTIST NOMINATIONS

General Information:

Nomination ID/App ID:	20-082
Research Category Primary:	Ecological Research (ER)
Research Category Secondary:	Integrated Risk Assessment (IR)
Laboratory/Office Name:	ORD/CCTE/GLTED
Nomination Entered By:	Brett Blackwell

Eligibility Checklist:

[Y] The nominated publication(s) has not been submitted to a previous STAA competition.

[Y] The nominated publication(s) was published on or before January 1, 2017 and on or after January 1,2012

[Y] The principal author was an EPA employee or a PHS employee assigned to EPA when the research was performed

[Y] The EPA authors (includes PHS employees assigned to EPA) contributed collectively a minimum of 50% toward the publication(s)

Nominating Official Name:	Dale Hoff
Nominating Official Title:	DIRECTOR, MID-CONTINENT ECOLOGY DIV
Nominating OfficialEmail:	hoff.dale@epa.gov
STAA Coordinator Name:	Kathleen Wiser
STAA Coordinator Email:	wiser.kathi@epa.gov

Justifications:

Justification 1:

The nominated papers take the emerging tools and data sets of 21st century chemical safety assessment and apply them to the challenge of e hazards associated with complex mixtures of chemicals in the environment. In 2007, the U.S. National Research Council published its vision ar toxicity testing in the 21st century (Krewski et al. 2010). This vision advocated a shift away from the direct observation of final toxicity outcomes mortality; impaired growth, development or reproduction; target organ pathologies) in animal toxicity tests. Instead it recommended increased u of high throughput cell-based and cell-free assays that can detect the ability of chemicals to interact with biological targets (e.g., proteins, DNA, and perturb biological pathways and functions in ways that can lead to negative effects on health and/or ecological fitness. Consistent with that developed its ToxCast program and contributed to the interagency Tox21 consortium. These programs generated pathway-based high through data for thousands of individual chemicals. While some of the initial focus was on well-studied chemicals for which the high throughput screeni could be anchored to traditional toxicity test data, these programs also provided novel sources of dose-response data that could be used to bot potencies and to infer potential biological hazards of chemicals whose toxicity had not been well studied previously.

Chemicals and mixtures of contaminants for which toxicity information and benchmark biological effect concentrations, derived from dose-respo lacking have presented a long-standing challenge to environmental monitoring. With steady improvements in analytical instrumentation, enviro chemists can detect an increasing number and diversity of chemical contaminants in a wide range of samples (e.g., extracts of water, sedimen dust, etc.). However, without toxicity data it is difficult to understand whether the contaminants detected, at the concentrations detected, are like problematic for ecological or human health and how best to focus limited resources for more in depth monitoring, hypothesis testing, and/or reg mitigation. A major aim of the nominated papers was to show how data from the new approach methodologies being employed for chemical sa could be used to aid the assessment of complex mixtures in the environment that include many chemicals whose toxicity has not been well cha using traditional animal testing.

The first nominated paper (Blackwell et al. 2017) focused on the use of existing ToxCast and Tox21 data for individual chemicals to identify pri chemicals, sites, and/or biological effects of concern within six watersheds in the Laurentian Great Lakes basin. The approach is simple in conc on the traditional approach of calculating a hazard quotient. However, in this case, rather than calculating the ratio of the exposure concentratio the environment to a concentration at which no adverse effects are expected (hazard quotient), the concentration at which that chemical elicits activity in a specific high throughput screening assay is substituted. The latter ratio is termed an Exposure-Activity ratio (EAR) where the greate value, the greater potential for hazard mediated through that biological activity or pathway.

Although the calculation of EARs is simple in concept, implementation in the context of environmental monitoring studies is more challenging. F ToxCast data sets had to be quality checked and curated to remove artifacts, that could lead to erroneous conclusions. Methods to address po "double-counting" or over-counting of chemicals evaluated in multiple assays focused on the same target/functional endpoint had to be develop appropriate effect concentration measurement from the ToxCast datasets (activity concentration at cut-off) needed to be selected from a numb (e.g., 50% activity concentration, area under the curve). Likewise, chemical abstract service (CAS) numbers and chemical names had to be ha between the ToxCast database and the exposure datasets. Finally, although calculation of a single EAR is simple and can be done by hand, ap typical environmental monitoring dataset entails conducting the calculation for 10s to 100s of samples x 100s of relevant assays for thousands thousands of calculations. Thus, novel computer code (R scripts) was developed to facilitate computation as well as summary and visualizatior The efforts that went into the technical implementation of this method for nominated paper 1 formed the backbone of the publicly accessible To

tool (see supporting software tool) that was developed as a collaboration between US EPA and US Geological Survey. The ToxEval software h
been used in the development of over six peer-reviewed publications, including the supporting article by Corsi et al. 2019, and the list of users
grow.

An important aspect of applying EARs is appropriate use and interpretation. Because the effect concentration, measured in vitro in a high throu
screening assay, is not directly equivalent to a water concentration that aquatic wildlife would be exposed to (or exposure of wildlife or humans
sample media and/routes), the EAR does not provide a direct indication of risk. However, it does provide a risk-based screening approach that
both the relative concentrations of chemicals in the environmental samples being examined and the relative potencies of those chemicals to ac
biological targets. This risk based-screening approach was used to identify chemicals of greater or lesser concern at Great Lakes sites based o
likelihoods to perturb specific biological pathways. Importantly, because the high throughput screening assays are standardized and all chemic
given assay are acting on the same biological target (i.e., are evaluated for the same mode of action), EAR values for all the individual chemica
a mixture can be summed to estimate the integrated effect of those chemicals on the target. This summation approach is demonstrated in the r
paper and was used to both prioritize sites of concern among the watersheds evaluated and biological effects of interest. Given the anchoring t
pathway-specific biological potencies, the approach represents a significant leap forward compared to prioritization of chemicals based on thei
concentrations or summed concentrations alone.

A limitation to the EAR-based approach developed as part of nominated paper 1 is that it only considers the fraction of chemicals in a sample t
detected analytically and have been previously evaluated in ToxCast. In the case of the two nominated papers, ToxCast data were available fo
(Blackwell et al. 2017) and 73% (Blackwell et al. 2019), of chemicals detected in the respective studies. Thus, coverage of commonly monitore
contaminants is fairly good. However, it is recognized that there are additional chemicals in the samples (e.g., degradates, biotransformation pr
compounds for which analytical standards are unavailable, etc.) that may go unmeasured, but nonetheless contribute to the overall biological p
complex mixture. Consequently, nominated paper two (Blackwell et al. 2019) focused on a complementary approach that involved directly anal
mixtures using the same types of high throughput screening assays that the ToxCast program employs for the evaluation of individual chemica
a pair of Attagene multi-Factorial assays were used to screen surface water extracts from a nationwide survey of organic contaminants in US s
Activity of the chemical mixtures against 69 different pathway-based endpoints were evaluated. Because each extracted mixture, including all o
and unknown components, is tested the method can evaluate the collective potency of the mixture for each endpoint. The study identified 10 pr
activities (11 endpoints) that were observed with some frequency across the range of surface water samples surveyed. The adverse outcome p
knowledgebase (aopwiki.org) was used to link those activities to established toxicological hazards in wildlife or humans, or where existing AOP
lacking, identify priorities for further study. Additionally, the nominated paper demonstrated how the direct analysis of environmental mixtures u
assays can be coupled with EAR analyses to estimate how much the known chemical composition of the mixtures contributes to the overall me
activity. For example, the known estrogenic chemicals detected in the samples could largely account for the total estrogen receptor-mediated a
detected in the bioassay. In contrast, for at least four other endpoints, the measured chemicals did not explain the amount of activity induced b
suggesting that other bioactive contaminants are present in the samples.

Thus, in combination, nominated papers 1 and 2 demonstrate the complementary ways that both the assays and existing data associated with
and Tox21 programs can be applied to environmental monitoring of complex mixtures. This is of considerable interest to the Agency and its sta
Broadly, the methods contribute to EPA's strategic goal of "A Cleaner, Healthier Environment" by providing tools that can help to discriminate c
the environment that are fairly innocuous at the concentrations detected from those that are demonstrably bioactive. Depending on the media o
approaches are applied to, they can contribute to providing clean and safe water (Objective 1.2), revitalizing land (Objective 1.3), and/or ensuri
of chemicals in the marketplace and already present in our environment (Objective 1.4). The work was responsive to Objectives 2 and 3 of the
Safety for Sustainability research program by developing and providing tools for chemical evaluation and promoting complex systems understa

Beyond broad responsiveness to EPA's strategic goals, the approaches detailed in the nominated papers have addressed specific needs of EP stakeholders. Development and application of the EAR approach and associated ToxEval tool were directly responsive to needs identified by tl Lakes National Program office in Action Plans I and II of the Great Lakes Restoration Initiative. Goal 5 within Focus Area 1 of the GLRI action p protect the health and integrity of wildlife populations and habitat from adverse chemical and biological effects associated with the presence of substances in the Great Lake Basin. The EAR and bioactivity surveillance approaches described in the nominated papers have been used to ic significant sources and potential impacts of new toxics (contaminants of emerging concern) and are helping to inform identification of potential mutual concern under the binational agreement between the US and Canada. At another Great Lakes site, the bioactivity surveillance approac nominated paper 2 is being used to aid evaluation of remedy effectiveness by characterizing the biological activity profile of complex mixtures c site before and after remediation. At wastewater impacted sites in Region 8, multi-Factorial bioactivity surveillance identified estrogen receptor, receptor, and peroxisome-proliferator activated receptor-mediated activities downstream of wastewater impacted sites. In collaboration with EP Park Service, and USGS personnel the surveillance data led to a multi-year targeted monitoring effort that assessed the impact of wastewater upgrades on loading of bioactive contaminants to surface waters and evaluated the potential impacts on aquatic biota in the receiving water. Si EAR approaches have been employed not only for monitoring in the Great Lakes and a nation-wide stream survey, but also in reconnaissance contaminants in tapwaters (Bradley et al. 2018), US watersheds (Bradley et al. 2020), and in prioritizing contaminants for future research in bal populations (Elliott et al. 2019). Overall, the tools and concepts first described in the nominated papers provide a new range of tools and option characterization of complex mixtures. As such, they are expected to have broad utility and significant impacts on a wide range of decision-mak potential impacts of organic contaminants in the environment.

Bradley, P.M., et al. (2018). "Reconnaissance of Mixed Organic and Inorganic Chemicals in Private and Public Supply Tapwaters at Selected F Workplace Sites in the United States." Environ Sci Technol 52(23): 13972-13985.

Bradley, P.M., et al. (2020). "Multi-region assessment of pharmaceutical exposures and predicted effects in USA wadeable urban-gradient stre One **15**(1): e0228214.

Elliott, S.M., et al. (2019). "Contaminants in bald eagles of the upper Midwestern U.S.: A framework for prioritizing future research based on in- bioassays." Environ Pollut **244**: 861-870.

Krewski, D., et al. (2010). "Toxicity testing in the 21st century: a vision and a strategy." J Toxicol Environ Health B Crit Rev **13**(2-4): 51-138.

Justification 2A:

The two nominated papers describe highly complementary approaches for employing the data and tools of high throughput chemical safety scr evaluation of complex mixtures. Nominated paper 1 focused on the implementation and use of Exposure-Activity Ratios (EARs) calculated as t detected exposure concentration to its activity concentration at cut-off (ACC) in a pathway-based high throughput screening assay. The EAR a be used to prioritize known contaminants for research and monitoring in a manner that considers not only their concentration in a sample but a relative potency to interact with specific biological targets and pathways. The approach explicitly recognizes that some chemicals may be relati to organisms, even at high concentration, while others can be highly toxic even at minute levels. In the absence of toxicity data from traditional ability to consider potential pathway-based potency of various detected chemicals can mean the difference between wasting resources monito

abundance chemical that proves to have little or no biological impact and strategic investment in reducing sources and exposure to a less prom chemical that is a primary driver of biological impact. Thus, the approach represents a significant leap forward for screening and prioritization e be directly applied for risk assessment.

As noted, the EAR approach provides a basis to consider the integrated effect of multiple contaminants in a mixture since EARs for chemicals same biological target (high throughput screening assay endpoint) can be summed. However, what the EAR approach cannot do is account fo undetected chemicals in a sample. Nominated paper 2 addresses this gap. It takes advantage of the power of a multi-factorial assay, like the A assays employed by ToxCast, and directly analyzed complex mixtures extracted from environmental samples. As a result, the approach captur integrated potency of all components in the mixture, whether they are known/measured or not. Although in the case of nominated paper 2, the bioactivity surveillance approach was applied to samples for which there was extensive analytical characterization, unlike the EAR approach th be applied even if there a no chemical monitoring data available. It can still provide an integrated measure of biological potency and help to ide target(s)/pathway(s) impacted.

Given that each approach has limitations, they can best be used in a complementary fashion. Chemical monitoring can identify specific chemic a sample and their precise concentrations. Calculation of EARs using the ToxCast data can adjust those concentrations based on relative pote specific targets to estimate the collective biological impact of the known fraction of contaminants. Bioactivity surveillance applied to the mixture the integrated biological impact of the known and unknown components of a mixture. Finally, by comparing the observed biological activity of th the anticipated or predicted activity (based on summed EARs) one can determine whether the known fraction reasonably explains the respons or whether investments should be made in identifying additional bioactive contaminants that may be of environmental concern.

The supporting paper by Corsi et al. (2019) and the supporting ToxEval tool further build on the concepts, principles, and examples presented nominated papers. The ToxEval tool provides a user-friendly, publicly accessible implementation of the EAR calculation and visualization appro originally developed for nominated paper 1 (Blackwell et al. 2017). The effort that went into curation and quality assurance of the ToxCast data harmonization of chemical names and identifiers are implemented in the software in a way that eliminates the need for subsequent users to rep Likewise, the ability to link bioactivites identified via the EAR analysis to potential apical hazards, via the adverse outcome pathway (AOP) fram further elaborated in the Corsi et al. (2019) paper. The nominated papers discussed the results relative what was known and unknown concern potential apical effects associated with the bioactivities associated with samples surveyed. The Corsi et al. (2019) paper takes that a step furth extracting relevant AOP networks and demonstrating how those networks may be impacted by mixtures of different compositions that were pric EAR analysis. Overall, the two nominated papers, and additional collaborative work that has followed, continue to expand the technical sophist diversity of applications, and demonstrated utility of the methods and approaches pioneered in the nominated papers.

Nominated citations:

1. Blackwell BR, Ankley GT, Corsi SR, DeCicco LA, Houck KA, Judson RS, Li S, Martin MT, Murphy E, Schroeder AL, Smith ER, Swintek J, Villeneuve DL. 2017. An "I Environmental Surveillance and Monitoring: A Case Study on the Use of Exposure-Activity Ratios (EARs) to Prioritize Sites, Chemicals, and Bioactivities of Concern in Grea *Environ Sci Technol*, *51*, (15), 8713-8724. https://doi.org/10.1021/acs.est.7b01613

2. Blackwell BR, Ankley GT, Bradley PM, Houck KA, Makarov S, Makarov A, Swintek J, Villeneuve DL. 2019. Potential toxicity of complex mixtures in surface waters fr survey of United States streams: Identifying in vitro bioactivities and causative chemicals. *Environ Sci Technol*, 53, 2, 973-83. https://doi.org/10.1021/acs.est.8b05304

Supporting Citations:

1. Corsi SR, DeCicco LA, Villeneuve DL, Blackwell BR, Fay KA, Ankley GT, Baldwin AK. Prioritizing chemicals of ecological concern in Great Lakes tributaries using high screening data and adverse outcome pathways. *Sci Tot Environ* 2019, 686, 995-1009.

2. DeCicco LA, Corsi SR, Villeneuve DL, Blackwell BR, Ankley GT. toxEval: Evaluation of measured concentration data using the ToxCast high-throughput screening databa user-defined set of concentration benchmarks. 2018, R package version 1.1.0., https://code.usgs.gov/water/toxEval, doi:10.5066/P906UQ5I

Justification 2B:

Author(s)	Citation	Publication Title(s)	Year
Ankley, Gerald; Villeneuve, Daniel	Developing Biological Tools for Monitoring Impacted Surface Waters in Support of the Great Lakes Restoration Initiative	1. Field-Based Approach for Assessing the Impacts of Treated Pulp and Paper Mill Effluent on Endogenous Metabolites of Fathead Minnows (Pimephales promelas). 2. Biological Effects-Based Tools for Monitoring Impacted Surface Waters in the Great Lakes: A Multiagency Program in Support of the Great Lakes Restoration Initiative. 3. An Inexpensive, Temporally Integrated System for Monitoring Occurrence and Biological Effects of Aquatic Contaminants in the Field.	20
Ankley, Gerald; Villeneuve, Daniel	Development and Application of Innovative Species Extrapolation Methodology to Focus Toxicity Testing and Monitoring	1. Molecular Target Sequence Similarity as a Basis for Species Extrapolation to Assess the Ecological Risk of Chemicals with Known Modes of Action. 2. Cross-Species Sensitivity to a Novel Androgen Receptor Agonist of Potential Environmental Concern, Spironolactone. 3. Leveraging Existing Data for Prioritization of the Ecological Risks of Human and Veterinary Pharmaceuticals to Aquatic Organisms	20
Ankley, Gerald; Villeneuve, Daniel	Development of Guidance for Practical Use of the Fish Short Term Reproduction Assays for Endocrine Disruptor Screening and	1. Cross-Species Conservation of Endocrine Pathways: A Critical Analysis of Tier 1 Fish and Rat Screening Assays with 12 Model Chemicals. 2. A Novel Framework for Interpretation of Data from the Fish Short-Term Reproduction Assay	20

		Testing	(FSTRA) for the Detection of Endocrine-Disrupting Chemicals	
	Ankley, Gerald; Villeneuve, Daniel	Demonstrating the utility of the Seqapass tool for addressing 21st century challenges in species extrapolation	1. Addressing the Challenges of Species Extrapolation Associated with 21st Century Toxicology using the SeqAPASS Tool. 2. Demonstrating the utility of the SeqAPASS Tool for Addressing 21st Century Challenges in Species Extrapolation	20
	Ankley, Gerald; Blackwell, Brett; Villeneuve, Daniel	Applying biological effects prediction, surveillance, and monitoring approaches to complex mixture assessments	1. Pathway-based approaches for assessment of real-time exposure to an estrogenic wastewater treatment plant effluent on fathead minnow reproduction. 2. An integrated approach for identifying priority contaminant in the Great Lakes Basin -Investigations in the Lower Green Bay/Fox River and Milwaukee Estuary areas of concern. 3. Prior knowledge-based approach for associating contaminants with biological effects: A case study in the St. Croix river basin, MN, WI, USA.	20
	Ankley, Gerald; Villeneuve, Daniel	Temporal Changes in Biological Responses and Uncertainty in Assessing Risks of Endocrine-Disrupting Chemicals	Temporal Changes in Biological Responses and Uncertainty in Assessing Risks of Endocrine-Disrupting Chemicals: Insights from Intensive Time-Course Studies with Fish	20
	Houck, Keith; Judson, Richard	Development and deployment of a high-throughput assay to detect chemical disruptors of thyroid hormone synthesis.	1. Tiered High-Throughput Screening Approach to Identify Thyroperoxidase Inhibitors within the ToxCast Phase I and II Chemical Libraries. 2. Development of a Thyroperoxidase Inhibition Assay for High-Throughput Screening.	20
	Houck, Keith; Judson, Richard	A chemical and Cheminformatics foundation for ToxCast & Tox21 research programs	The ToxCast chemical landscape: Paving the road to 21st century toxicology.	20

Justification 2C:

The focus on a risk-based prioritization using 21st century toxicology tools, including high throughput databases for rapid screening of environ monitoring data, and the use of high throughput assays to screen both known and unknown components of environmental mixtures distinguish nomination from previous. Of the previously submitted nominations, the 2015 Level III award for developing biological tools for monitoring impa waters in support of the Great Lakes Restoration Initiative, and the 2017 Level III award for applying biological effects prediction, surveillance, a approaches to complex mixture assessments, addressed the challenges of complex mixture assessments. However, the 2015 nomination focu development and implementation of methods using targeted and "omics" endpoints in caged fish, cell-based bioassays, and composite water s monitor contaminant-impacted surface waters. The 2017 STAA used associations of chemical and gene interactions to attempt to predict poter effects, but a primary limitation of this approach was a lack of chemical potency to incorporate a risk-based prioritization, accounting for both ob chemical concentration and potency. The current nomination continues to build on foundational pieces developed from these previous submiss novel focus and development of risk-based approaches incorporating novel data from high throughput toxicology programs (i.e. ToxCast). The nomination also includes the direct use of the same high throughput assays for screening of water sampes, allowing for direct assessment of c mixtures and methods for assessing the effects of the "unknown" fraction of environmental contaminants. These methods and focus were not p previous nominations, and as such, do not overlap with previous nominations.

Justification 2D:

The listed supplemental information has not been previously submitted for STAA consideration.

Justification 2E:

Author name	STAA publications	Lead Author
Richard Judson	1) Rager JE, Strynar MJ, Liang S, McMahen RL, Richard AM, Grulke CM, Wambaugh JF, Isaacs KK, Judson R, Williams AJ, Sobus JR. Linking high resolution mass spectrometry data with exposure and toxicity forecasts to advance high-throughput environmental monitoring. Environ Int. 2016 Mar;88:269-280. 2) Sobus JR, Wambaugh JF, Isaacs KK, Williams AJ, McEachran AD, Richard AM, Grulke CM, Ulrich EM, Rager JE, Strynar MJ, Newton SR. Integrating tools for non-targeted analysis research and chemical safety evaluations at the US EPA. J Expo Sci Environ Epidemiol. 2018 Sep;28(5):411-426.	Jon Sobus
Daniel Villeneuve, Gerald Ankley	1) Wang RL, Biales AD, Garcia-Reyero N, Perkins EJ, Villeneuve DL, Ankley GT, Bencic DC. Fish connectivity mapping: linking chemical stressors by their mechanisms of action-driven transcriptomic profiles. BMC Genomics 2016, 17 (84), ttps://doi.org/10.1186/s12864-016-2406-y. 2) Wang RL, Edwards SW, Ives C. Ontology-based semantic mapping of chemical toxicities. Toxicology 2019, 412:89-100.	Rong-Lin Wang

Richard Judson is on another current nomination related to the use of high-resolution mass spectrometry to improve environmental monitoring safety. While one publication does relate to environmental monitoring, it is focused on the identification of unknown chemicals, distinctly differe current nomination.

Daniel Villeneuve and Gerald Ankley are on another nomination related to chemical toxicity and transcriptomic responses, and further linking to known ontologies. This nomination is related to chemical effects and rapid assessments of chemical toxicity, which is distinctly different than th nomination.

Justification 3A:

In addition to interest from EPA stakeholders, the nominated publications have gained external recognition from the broader scientific commun 2020, the first (Blackwell et al. 2017) and second (Blackwell et al. 2019) nominated papers have been cited 19 and 10 times, respectively. Of th there is an increasing number of citations from groups external to EPA. The Exposure-Activity Ratio (EAR) concept from nominated publication (Blackwell et al. 2017) has been incorporated into environmental mixture analyses by other US government agencies including US Geological S citations) and National Park Service (1 citation), and academics (2 citations) for screening of surface, tap, and ground waters across the US. O US, the approach has been used by researchers in the Netherlands (2 citations) for screening and prioritizing contaminants in drinking waters a

The direct bioassay screening approach demonstrated by nominated paper 2 (Blackwell et al. 2019) has also gained acceptance as an importa environmental monitoring. Nearly half of citing papers are from European groups, recognizing acknowledgment of the importance of this approa environmental monitoring not only in the US, but worldwide. In a recent Science publication entitled “Tracking complex mixtures of chemicals ir environment” (Escher et al. 2020), the nominated paper was identified as an example of the need to incorporate both analytical and bioanalytic to fully understand potential risks of environmental contaminant mixtures.

In addition to publications, multiple workshops have been held to teach the use of ToxEval, the publicly accessible tool that facilitates rapid EAI The first ToxEval workshop was held at the 2019 National Monitoring Conference in Denver, CO. The workshop was attended by stakeholders academia, government, and private sectors. At the 2019 SETAC North America meeting, ToxEval was presented during the invited session “Pu Accessible Data Analytic Tools”. This was a new format session incorporating a short, introductory presentation followed by an opportunity for p see a live demonstration of tool use. Lastly, a ToxEval workshop was held in December 2019 at the US Geological Survey Water Science Cen WI drawing attendees from academia and state and local government stakeholders.

Escher, B. I., H. M. Stapleton and E. L. Schymanski (2020). "Tracking complex mixtures of chemicals in our changing environmer **367**(6476): 388-392.

Justification 3B:

Both nominated publications went through a rigorous peer review process including internal EPA review, internal USGS review, and external pe through the publishing journal. Each paper went through ORD internal review by an ORD researcher prior to journal submission. Each paper in affiliated authors, requiring the papers to be reviewed by an internal USGS reviewer prior to submission to a journal. Nominated paper 2 (Black 2019) additionally went through ORD's "Advanced Notification" process. Office of Water (OW) received the manuscript and reviewed it prior to submission. Finally, both papers were submitted to Environmental Science and Technology (ES&T), a top journal in the field of environmental s Nominated papers were each reviewed by a panel of 3 anonymous reviewers prior to publication in the journal.

AUTHORS

Principal Author

Author Name:	Brett R. Blackwell		
Professional Title:		Salutation:	Dr.
Email:	blackwell.brett@epa.gov	Organization:	
Mailing Address:			
Street Line 1:			
City:			
Zip Code:		State:	
At time of research was:	EPA Employee		
Separation Date:			
% of Effort:	28		

Contributing Author

Author Name:	Matthew Martin		
Professional Title:		Salutation:	Dr.
Email:	martin.matt.184@gmail.com	Organization:	
Mailing Address:			

Street Line 1:	116 Farmholme Rd		
City:	Stonington		
Zip Code:		State:	CT
At time of research was:	EPA Employee		
Separation Date:	Sat Apr 01 00:00:00 GMT 2017		
% of Effort:	1		

Contributing Author

Author Name:	Gerald Ankley		
Professional Title:		Salutation:	Dr.
Email:	ankley.gerald@epa.gov	Organization:	
Mailing Address:			
Street Line 1:			
City:			
Zip Code:		State:	
At time of research was:	EPA Employee		
Separation Date:			
% of Effort:	12		

Contributing Author

Author Name:	Keith Houck		
Professional Title:		Salutation:	Dr.
Email:	houck.keith@epa.gov	Organization:	
Mailing Address:			

Street Line 1:			
City:			
Zip Code:		State:	
At time of research was:	EPA Employee		
Separation Date:			
% of Effort:	6		

Contributing Author

Author Name:	Elizabeth Murphy		
Professional Title:		Salutation:	
Email:	murphy.elizabeth@epa.gov	Organization:	
Mailing Address:			
Street Line 1:			
City:			
Zip Code:		State:	
At time of research was:	EPA Employee		
Separation Date:			
% of Effort:	1		

Contributing Author

Author Name:	Richard Judson		
Professional Title:		Salutation:	Dr.
Email:	judson.richard@epa.gov	Organization:	
Mailing Address:			

Street Line 1:			
City:			
Zip Code:		State:	
At time of research was:	EPA Employee		
Separation Date:			
% of Effort:	3		

Contributing Author

Author Name:	Edwin Smith		
Professional Title:		Salutation:	
Email:	smith.edwin@epa.gov	Organization:	
Mailing Address:			
Street Line 1:			
City:			
Zip Code:		State:	
At time of research was:	EPA Employee		
Separation Date:			
% of Effort:	1		

Contributing Author

Author Name:	Shibin Li		
Professional Title:		Salutation:	Dr.
Email:	shibin.li@syngenta.com	Organization:	
Mailing Address:			

Street Line 1:	401 S Swing road		
City:	Greensboro		
Zip Code:	27409	State:	NC
At time of research was:	Non EPA Personnel		
Separation Date:			
% of Effort:	1		

Contributing Author

Author Name:	Daniel Villeneuve		
Professional Title:		Salutation:	Dr.
Email:	villeneuve.dan@epa.gov	Organization:	
Mailing Address:			
Street Line 1:			
City:			
Zip Code:		State:	
At time of research was:	EPA Employee		
Separation Date:			
% of Effort:	12		

Contributing Author

Author Name:	Alex Medvedev		
Professional Title:		Salutation:	Dr.
Email:	amedvedev@attagene.com	Organization:	
Mailing Address:			

Street Line 1:	PO Box 12054		
City:	RTP		
Zip Code:	27709	State:	NC
At time of research was:	Non EPA Personnel		
Separation Date:			
% of Effort:	1		

Contributing Author

Author Name:	Paul Bradley		
Professional Title:		Salutation:	Dr.
Email:	pbradley@usgs.gov	Organization:	
Mailing Address:			
Street Line 1:	720 Gracern Rd, Suite 129		
City:	Columbia		
Zip Code:	29210	State:	SC
At time of research was:	Non EPA Personnel		
Separation Date:			
% of Effort:	3		

Contributing Author

Author Name:	Sergei Makarov		
Professional Title:		Salutation:	Dr.
Email:	smak@attagene.com	Organization:	
Mailing Address:			

Street Line 1:	PO Box 12054		
City:	RTP		
Zip Code:	27709	State:	NC
At time of research was:	Non EPA Personnel		
Separation Date:			
% of Effort:	1		

Contributing Author

Author Name:	Steven Corsi		
Professional Title:		Salutation:	
Email:	srcorsi@usgs.gov	Organization:	
Mailing Address:			
Street Line 1:	8505 Research Way		
City:	Middleton		
Zip Code:	53562	State:	WI
At time of research was:	Non EPA Personnel		
Separation Date:			
% of Effort:	6		

Contributing Author

Author Name:	Laura DeCicco		
Professional Title:		Salutation:	
Email:	ldecicco@usgs.gov	Organization:	
Mailing Address:			

Street Line 1:	8505 Research Way		
City:	Middleton		
Zip Code:	53562	State:	WI
At time of research was:	Non EPA Personnel		
Separation Date:			
% of Effort:	6		

Contributing Author

Author Name:	Anthony Schroeder		
Professional Title:		Salutation:	Dr.
Email:	aschroed@crk.umn.edu	Organization:	
Mailing Address:			
Street Line 1:	Dowell Hall 249 2900 University Ave		
City:	Crookston		
Zip Code:	56716	State:	MN
At time of research was:	Non EPA Personnel		
Separation Date:			
% of Effort:	3		

Contributing Author

Author Name:	Joseph Swintek		
Professional Title:		Salutation:	
Email:	swintek.joe@epa.gov	Organization:	
Mailing Address:			

Street Line 1:	6201 Congdon Blvd		
City:	Duluth		
Zip Code:	55804	State:	MN
At time of research was:	Non EPA Personnel		
Separation Date:			
% of Effort:	15		

PUBLICATIONS

Publication 1:

Publication Title:	Potential Toxicity of Complex Mixtures in Surface Waters from a Nationwide Survey of United States S		
Publication Date:	Tue Jan 15 00:00:00 GMT 2019		
Journal/Publication Method:	ENVIRONMENTAL SCIENCE & TECHNOLOGY		
All Author(s):			
Volume:	53	Number:	2
Pages:	973-983	Immediately Index:	Imn Inde
Citation ½ Life:	7.8	Impact Factor:	7.87

Publication 2:

Publication Title:	An "EAR" on Environmental Surveillance and Monitoring: A Case Study on the Use of Exposure Activity		
Publication Date:	Tue Aug 01 00:00:00 GMT 2017		
Journal/Publication Method:	ENVIRONMENTAL SCIENCE & TECHNOLOGY		

All Author(s):

Volume:	51	Number:	15
Pages:	8713-8724	Immediately Index:	Imr Ind
Citation ½ Life:	7.8	Impact Factor:	7.8

This is an open access article published under an ACS AuthorChoice License, which permits copying and redistribution of the article or any adaptations for non-commercial purposes.

Environmental Science & Technology

Article

Cite This: Environ. Sci. Technol. 2019, 53, 973−983

pubs.acs.org/est

Potential Toxicity of Complex Mixtures in Surface Waters from a Nationwide Survey of United States Streams: Identifying in Vitro Bioactivities and Causative Chemicals

Brett R. Blackwell,*[,†] Gerald T. Ankley,[†] Paul M. Bradley,[‡] Keith A. Houck,[§] Sergei S. Makarov,[∥] Alexander V. Medvedev,[∥] Joe Swintek,[⊥] and Daniel L. Villeneuve[†]

[†]U.S. EPA, Mid-Continent Ecology Division, 6201 Congdon Boulevard, Duluth, Minnesota 55804, United States

[‡]U.S. Geological Survey, South Atlantic Water Science Center, 720 Gracern Road, Columbia, South Carolina 29210, United States

[§]U.S. EPA, National Center for Computational Toxicology, 109 T.W. Alexander Drive, Research Triangle Park, North Carolina 27711, United States

[∥]Attagene, Inc., 7020 Kit Creek Road, Suite 260, Morrisville, North Carolina 27560, United States

[⊥]Badger Technical Services, 6201 Congdon Boulevard, Duluth, Minnesota 55804, United States

Supporting Information

ABSTRACT: While chemical analysis of contaminant mixtures remains an essential component of environmental monitoring, bioactivity-based assessments using in vitro systems increasingly are used in the detection of biological effects. Historically, in vitro assessments focused on a few biological pathways, for example, aryl hydrocarbon receptor (AhR) or estrogen receptor (ER) activities. High-throughput screening (HTS) technologies have greatly increased the number of biological targets and processes that can be rapidly assessed. Here we screened extracts of surface waters from a nationwide survey of United States streams for bioactivities associated with 69 different end points using two multiplexed HTS assays. Bioactivity of extracts from 38 streams was evaluated and compared with concentrations of over 700 analytes to identify chemicals contributing to observed effects. Eleven primary biological end points were detected. Pregnane X receptor (PXR) and AhR-mediated activities were the most commonly detected. Measured chemicals did not completely account for AhR and PXR responses. Surface waters with AhR and PXR effects were associated with low intensity, developed land cover. Likewise, elevated bioactivities frequently associated with wastewater discharges included endocrine-related end points ER and glucocorticoid receptor. These results underscore the value of bioassay-based monitoring of environmental mixtures for detecting biological effects that could not be ascertained solely through chemical analyses.

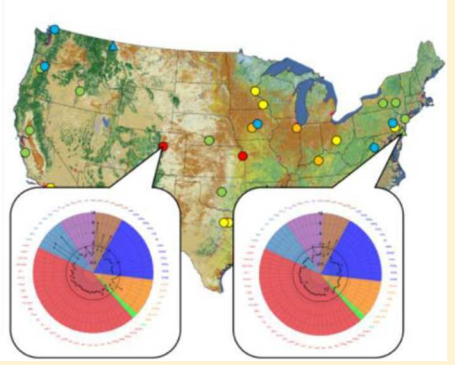

INTRODUCTION

Increased usage of organic chemicals in agricultural, industrial, and personal care applications has intensified concerns that aquatic organisms may be exposed to potentially hazardous mixtures of chemical contaminants. Compounds for which ecological or human health hazards are generally not well understood, which have recently been discovered in the environment, or for which public attention has greatly increased have been termed contaminants of emerging concern (CECs) and include pharmaceuticals, personal care products, natural and synthetic steroids, pesticide metabolites, persistent organics (polybrominated and perfluoro compounds), flame retardants, and plasticizers. Multiple studies since the early 2000s have demonstrated the complexity and near-ubiquitous presence of CEC mixtures in surface waters.[1−3] However, even recent, dramatically expanded chemical assessments provide only partial coverage of the presumptive surface water contaminant space.[4] Combined analytical chemistry methods and in vitro bioassay approaches support improved characterization of pathway-specific bioactivities and the potential hazard of complex mixtures of CECs to ecological receptors.[5−7] In vitro bioassays covering a range of processes (genotoxicity,[8,9] inflammation,[9] mutagenicity,[8,10] oxidative stress,[9−11] photosynthetic processes[10]) or individual receptor-based bioactivities (reflecting androgen,[9,12,13] aryl hydrocarbon,[8,9,14,15] estrogen,[9,16−18] glucocorticoid,[8,9,19] peroxisome-proliferator,[8,9,14] pregnane X,[14,15] progesterone,[8,9,20] retinoic acid,[9] retinoid X,[9] and thyroid[8,14] signaling pathways) have been used, at least to some extent, to assess surface waters.

Received: September 19, 2018
Revised: December 13, 2018
Accepted: December 14, 2018
Published: December 14, 2018

Downloaded via 67.3.46.120 on April 1, 2020 at 15:25:15 (UTC).
See https://pubs.acs.org/sharingguidelines for options on how to legitimately share published articles.

© 2018 American Chemical Society

DOI: 10.1021/acs.est.8b05304
Environ. Sci. Technol. 2019, 53, 973−983

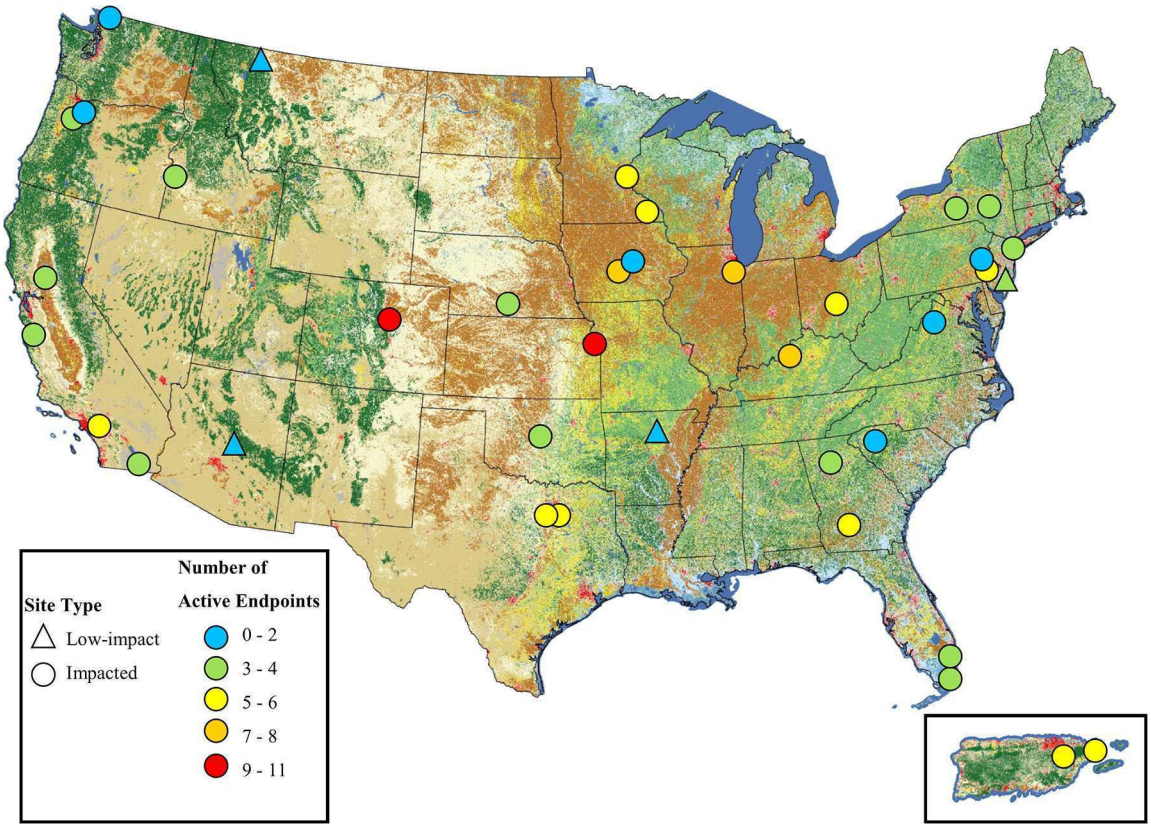

Figure 1. Site location, classification, and number of active (AUC ≥ 1.5-fold above extract blank) bioassay end points for each site sampled from 2012 to 2014. Only end points tested across all 38 sites are included. See SI Table S1 for site details and SI Table S4 for bioassay response values.

The Tox21 collaboration and the U.S. Environmental Protection Agency (USEPA) ToxCast programs began in 2007−2008 with the aim of advancing toxicity testing through use of in vitro high-throughput screening (HTS) assays that can rapidly measure chemical effects on hundreds of different biological pathways/processes.[21] These programs generated publicly available bioactivity data for over 9000 unique substances, including many CECs.[22,23] Recent approaches have leveraged ToxCast data to screen for potential pathway-specific effects of detected compounds in environmental samples using hazard quotients based on bioactivity.[9,24,25] Such computational approaches are readily applied to detected environmental contaminants but are likewise constrained by extant analytical chemistry techniques and poor understanding of complex, interactive effects. Alternatively, HTS assays can be applied directly to surface water samples or extracts to screen for net effects of contaminant mixtures on targeted biological end points.

The present study is among a growing number of studies to apply a subset of ToxCast HTS assays to directly assess the biological effects potential of environmental samples.[9,14,26,27] Specifically, the U.S. Geological Survey (USGS) and USEPA conducted a collaborative investigation of both chemical occurrence and bioactivity in streams across the continental U.S. and Puerto Rico.[28] The target-chemical coverage included over 700 unique organic analytes from many functional classes (pesticides, wastewater indicators, steroid hormones, volatile organics, pharmaceuticals, and halogenated organics).[29] Initial assessment of split-sample bioactivity targeted in vitro transcriptional reporter assays for the estrogen receptor (ER), androgen receptor (AR), and glucocorticoid receptor (GR).[30] Here, we expand the characterization of split-sample bioactivity using two multiplexed HTS assays (Attagene cis-Factorial and trans-Factorial assays)[31,32] that encompass 69 biological end points. The selected HTS assays had been used in the ToxCast program to screen over 3600 compounds, providing a robust data set to compare against known chemical composition of the samples.[31] Bioactivity results were compared with measured concentrations of compounds in the samples using existing HTS data for the individual chemicals to assess how well target-chemical analysis captured compounds responsible for observed bioactivities. Additional statistical analyses were then performed to identify potential relationships between bioactivity measures and chemicals detected in the test samples. Finally, ER, AR, and GR results from the HTS assays and from the previously reported in vitro assays[30] were compared to assess the performance of the HTS system for routine environmental monitoring. Results of this work intended to identify the most prevalent bioactivities (among the 69 end points monitored), important contaminant and land-use drivers of bioactivity, and potential adverse ecological effects of CECs in streams across the U.S.

MATERIALS AND METHODS

Sample Collection and Processing. Surface water samples were collected from a total of 38 sites (4 low-impact sites—those with minimal anthropogenic inputs; 34 impacted sites—those with increased anthropogenic inputs)[29] between December 2012 and June 2014 (Figure 1; Supporting Information (SI) Table S1). Sites were selected to cover a range of land use including largely undeveloped, agricultural, and heavily urban developed watersheds. Water from each site

DOI: 10.1021/acs.est.8b05304
Environ. Sci. Technol. 2019, 53, 973−983

was collected into a Teflon churn prior to splitting between prepared sample bottles according to established trace-level sampling methods.[29] Samples were shipped on ice to USGS and USEPA laboratories for chemical or bioassay analysis. Upon arrival at the USEPA-Duluth laboratory, samples in 1 L amber glass bottles were logged and stored at 4 °C for no more than 24 h prior to filtration and extraction.

Sample Preparation. All solvents were HPLC grade or better and purchased from Fisher Scientific (Waltham, MA). Dimethyl sulfoxide (DMSO) was >99.7% purity and purchased from Sigma-Aldrich (St. Louis, MO). Water samples were processed by solid-phase extraction (SPE) using Waters Oasis HLB cartridges (200 mg sorbent, 5 mL glass cartridge; Milford, MA). Field blanks were not received for this bioassay analysis, but an extraction method blank (HPLC grade water) was generated with each sample batch and used to assess background activity in the method. Cartridges were preconditioned sequentially using 5 mL each of ethyl acetate, 50:50 methanol (MeOH):dichloromethane (DCM), 100% MeOH, and, finally, ultrapure water. Prior to SPE, approximately 1 L of whole water was filtered through a baked 47 mm glass-fiber filter (0.7 μm porosity). After filtration, 0.5 L of each sample was loaded onto preconditioned cartridges. Cartridges were aspirated for approximately 30 min to remove residual water then eluted sequentially with 6 mL of MeOH followed by 6 mL of 50:50 MeOH:DCM. Extracts were evaporated to dryness under a gentle stream of nitrogen at 30 °C. Samples were reconstituted in 500 μL of DMSO for a final 1000-fold relative enrichment factor (REF). Samples were extracted as they were received and sent for analysis in three batches ranging 8−18 samples per batch. Extracts were frozen at −20 °C and shipped overnight on ice for bioassay analysis.

HTS Bioassays. Sample extracts were tested by Attagene, Inc. (Morrisville, NC) under contract to the USEPA, using the cis-Factorial and trans-Factorial assays.[31,32] Each assay uses HepG2 cells to assess transcription factor activity (cis-Factorial) or transfected nuclear receptor activity (trans-Factorial). Together, these multiplexed assays comprise a total of 69 target end points covering a range of biological pathways including xenobiotic metabolism (e.g., aryl hydrocarbon receptor [AhR], pregnane X receptor [PXR]), lipid metabolism (peroxisome proliferator-activated receptor [PPAR],) endocrine signaling (e.g., AR, ER, GR), and cellular stress (e.g., antioxidant response element [NRF2]; SI Table S2). Additionally, a subset of eight samples (the initial eight samples screened through the assays) was analyzed using a separate assay (trans-Factorial-2), which covers 24 additional nuclear receptors beyond the 69 targets from the cis-Factorial and trans-Factorial assays (SI Table S2). Sample extracts were tested at six dilutions from a maximum REF of 10 followed by five, 3-fold serial dilutions (i.e., 10, 3.3, 1.1, 0.37, 0.12, 0.04 REF). The highest REF was tested at 1% DMSO, while all remaining dilutions were at 0.33% DMSO. Positive control compounds for several of the targets (e.g., E2 for ER) were run in triplicate at a single concentration with each batch (see SI Table S2), and six replicates of DMSO solvent controls (both 1.0 and 0.33%) were run with each sample set. Positive controls inducing responses >2 fold passed quality assurance criteria

For the cis-Factorial assay, a set of cis-Factorial reporters as well as PXR and ER-alpha expression vectors were transiently transfected into HepG2 cells (12-well plates) using TransIT-LT1 (Mirus Bio; Madison, WI) transfection reagent and according to the manufacturer's protocol. The next day, the transfected cells were supplied with 1% charcoal-stripped HyClone FBS (GE Healthcare Life Sciences; Marlborough, MA) and incubated with sample extracts for 24 h. For the trans-Factorial assay, each of the trans-Factorial reporter GAL4-NR expression vector pairs were transiently transfected into separate pools of HepG2 cells using TransIT-LT1 transfection reagent and according to the manufacturer's protocol. The next day, the transfected cells were mixed and plated into 12-well plates for compound analysis. Twenty-four h after plating, the transfected cells were supplied with 1% charcoal-stripped HyClone FBS and incubated with evaluated compounds for 24 h. For both assays, cell viability was measured in parallel using XTT Cell Proliferation Assay Kit (ATCC; Manassas, CT) with cell viability >70% required to generate acceptable data quality. A standard set of six control reporters were used to normalize response of the transfected end points. To assess Factorial reporter activity, total RNA was isolated using the PureLink RNA isolation kit (Invitrogen; Carlsbad, CA). Total RNA from each well was reversely transcribed into cDNA, and reporter cDNA was amplified in a single PCR reaction using a pair of common primers. The PCR products were labeled using a 6-Fam-labeled primer and digested with *Hpa*I. The resulting labeled DNA fragments were separated using capillary electrophoresis (Genetic Analyzer 3130xl; Applied Biosystems; Waltham, MA). The relative activities of end points were calculated from the electropherogram peaks using proprietary software.[29]

Statistical Analysis. Bioassay responses were expressed as fold-change relative to DMSO control by dividing expression of treated cells by that of appropriate DMSO control. The use of fold-change relative to DMSO controls does influence the potential magnitude of response for each end point, so the relative magnitude of response across different end points should not be directly compared. Dose−response data were plotted and response calculated as the area under the curve (AUC) using GraphPad Prism (v5.02). Other metrics could have been used, such as a more traditional EC50. However, since many end points are lacking positive controls, AUC allowed for consideration of the full dose−response relative to extraction method blanks, which could be applied consistently for all end points regardless of a positive control. To further correct response across multiple assay batches, sample AUC was divided by the mean extraction method blank (n = 1−3 per batch) AUC within each sample batch. A cutoff of 1.5-fold response (50% increase) relative to the blank baseline was used to identify end points clearly responding to environmental extracts. Pearson correlation was used to assess relations between blank-corrected AUC responses, exposure-activity ratios (EARs),[25] or land use metrics. A nonparametric analysis of ranked, normalized AUC responses and bioanalytical equivalent concentrations (i.e., 17β-estradiol equivalents [E2eqs, ng L^{-1}]), previously reported by Conley et al.,[30] was performed using Spearman Rank correlation.

Exposure-activity ratio (EAR) analysis[25] was used to estimate whether bioactivity would be expected based on the measured concentrations of detected compounds[29] and their corresponding activity concentration at cutoff (ACC) values for Attagene assays, where available (i.e., for compounds previously tested in ToxCast).[22] The ACC was chosen as a metric of chemical potency as this value compares chemical response with a defined baseline and is independent of chemical efficacy, though other metrics of potency, such as the

DOI: 10.1021/acs.est.8b05304
Environ. Sci. Technol. 2019, 53, 973−983

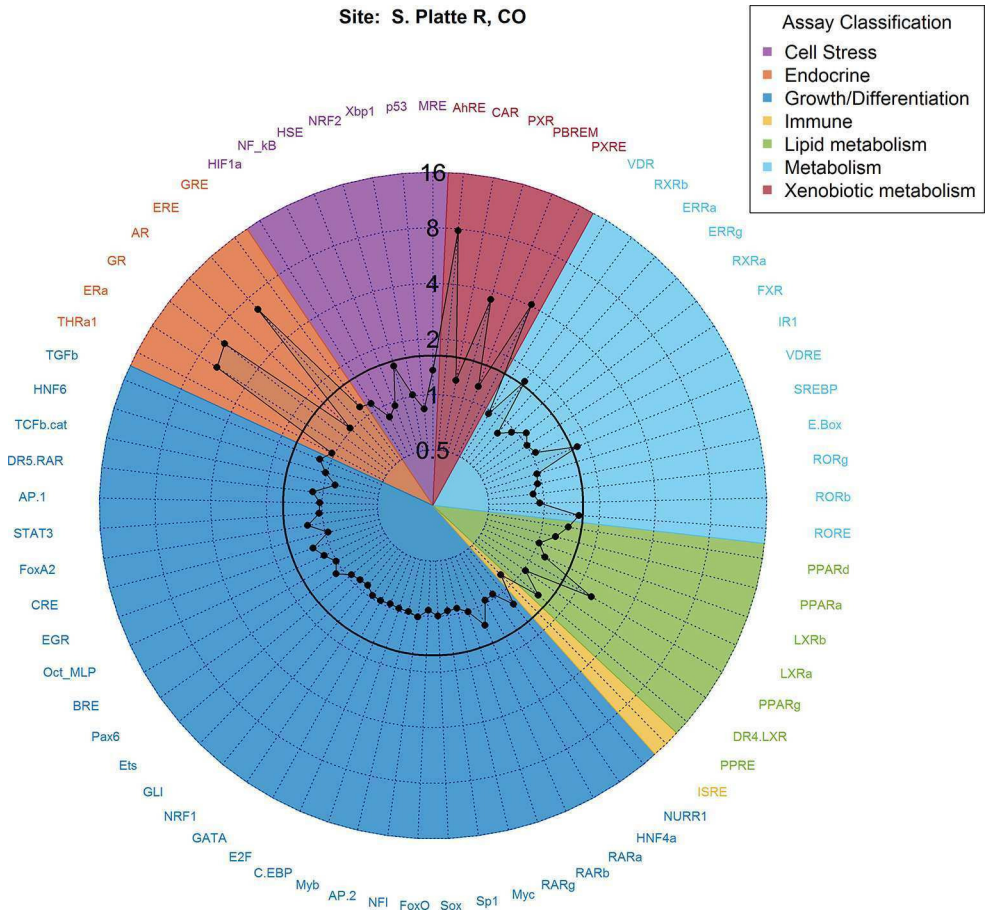

Figure 2. An example radar plot of blank-normalized area under the curve (AUC) values of both cis_Factorial and trans_Factorial end points for the South Platte River, CO site. Assay end point names correspond to those in Table S2 and are grouped in colors by general function. The radar axis represents AUC values for each measured end point. The activity cutoff value of 1.5 is shown in bold, and activities at or above this value were identified as active.

half-maximal activity concentration (AC50), could be used. An EAR value was calculated for each site and assay by summing EAR values of individual compounds (eq 1) detected in a given mixture, thus assuming noninteractive concentration addition. Theoretically, EAR values ≥1 indicate measured compounds are at a concentration expected to produce bioactivity for a given end point. Comparison of this predicted bioactivity with that observed in the Attagene bioassay can be used to infer whether the known composition of the sample likely accounts for the activity observed, or whether unidentified compounds may be contributing. Likewise, if observed bioactivity is less than predicted, the results may suggest nonadditive interactions are occurring between compounds present in the mixture.

$$\mathrm{EAR}_{\mathrm{mixture}} = \sum_{i=1}^{n} \frac{\mathrm{exposure}_i(\mathrm{chemical\ concentration};\ \mu\mathrm{M})}{\mathrm{activity}_i(\mathrm{ToxCastACC};\ \mu\mathrm{M})} \quad (1)$$

To identify other potential associations between chemical occurrence and bioassay responses, a sparse partial least-squares (SPLS) analysis[33] was performed to identify correlations between measured chemicals and bioassay response in order to identify potentially bioactive compounds. The SPLS analysis is a partial least-squares analysis with the addition of elastic net regulation, which allows for the removal of variables.[34] Analysis was performed using the SPLS package[35] in R version 3.3.3.[36] After SPLS analysis was performed, bootstrapped confidence intervals (also using the SPLS package[35]) were estimated for each chemical-assay combination, and those with intervals that contained zero were removed.

Prior to SPLS analysis, the full chemical data set[37] was filtered to remove chemicals with no detections above the reporting limit, chemicals with zero variance in concentration, or chemicals not reported at three or more sites. Both chemical concentration and assay AUC were then centered and scaled across sites. For analytes with missing values at two or fewer sites, Multiple Imputation by Chained Equations (MICE)[38] was used to generate missing values for SPLS analysis using the MICE R package.[39] Finally, based on prior knowledge of analyte loss during the evaporation step of extract preparation (see SI for more information; Figure S1, Table S3), chemicals with vapor pressure above 0.01 mmHg (as calculated using EpiSuite v4.11[40]) were removed from the SPLS data set. These more volatile compounds are lost during evaporation and solvent exchange and are not expected to be present in the final bioassay extract. A total of 386 analytes and 69 assay end points were used for SPLS analysis.

RESULTS AND DISCUSSION

Bioactivity in Surface Water Extracts. Activity ≥1.5-fold above baseline (hereafter referred to as "active") was detected

DOI: 10.1021/acs.est.8b05304
Environ. Sci. Technol. 2019, 53, 973−983

in the cis-Factorial and trans-Factorial assays at two or more sites for 11 end points (SI Table S4). The site with the greatest number of active end points of any sampled site (South Platte River, CO), is shown in Figure 2 while all remaining sites are provided in the SI (Figures S2−S38). The 11 active end points reflected nine different receptor-mediated pathways. In the subset of eight samples that were analyzed using the trans-Factorial-2 assay, three more end points (ERβ_TRANS2, PR_TRANS2, MR_TRANS2) were active (SI Figure S39, Table S4). Most active end points are associated with regulation of metabolism of xenobiotic (e.g., AhR_CIS, PXR_TRANS, PXRE_CIS) or endogenous compounds (PPARγ_TRANS, RORE_CIS, RXRβ_TRANS, VDRE_CIS) and one end point (NRF2_CIS) is indicative of oxidative stress. The remaining end points (ERα_TRANS, ERE_CIS, and GR_TRANS) and the end points active from the subset of samples analyzed through the trans-Factorial-2 assay (ERβ_-TRANS2, MR_TRANS2, PR_TRANS2) are associated with different endocrine pathways.

Several of these receptor-based pathways have well-defined ligands known to induce activity. For example, AhR ligands include polycyclic and halogenated hydrocarbons including many current use pesticides;[41] AhR activity has previously been observed in different studies with environmental samples (often through induction of CYP1A1).[9,10,42] PXR is a relatively promiscuous receptor with a large, hydrophobic binding pocket capable of interacting with a broad range of organic compounds.[43] PPARγ ligands include endogenous fatty acids, prostaglandins, and thiazolidinedione pharmaceuticals (e.g., rosiglitazone, pioglitazone). Comparatively few ligands have been identified for the retinoid X receptor (RXR), the RAR-related orphan receptor (ROR), or vitamin-D receptor (VDR) aside from the endogenous molecules such as retinoic acids or vitamin-D3. NRF2 activity is associated with oxidative stress and can be induced by a wide range of compounds, such as reactive oxygen species and electrophilic chemicals. Activation of NRF2 has been previously observed in environmental samples, but specific compounds responsible for activity were not identified.[11] Progesterone receptor (PR), GR and ER activation have previously been documented in environmental samples[26] and several known natural (e.g., estradiol, cortisol, progesterone) and synthetic (e.g., 17α-ethinylestradiol, dexamethasone, levonorgestrel) ligands detected in surface waters. Mineralocorticoid receptor (MR) activity, which was observed at one of eight tested sites, has not been commonly reported in surface waters. The MR is known to bind two endogenous classes of corticosteroid ligands; the mineralocorticoid aldosterone; and the glucocorticoids cortisol or corticosterone, in the human or rat, respectively.[44] The trans-Factorial-2 assay, which contains the MR end point, is not available in the ToxCast database;[22] however, another assay NVS_NR_rMR, which uses the rat MR, has been used to screen over 2700 chemicals. Twenty-one compounds were active, including 17 steroidal compounds. Those with the highest binding affinity include three glucocorticoids (corticosterone, dexamethasone, and 17α-hydroxyprogesterone), which are also active in GR-related assays. The single site with elevated MR activity induced the highest GR activity observed at any site, suggesting that the observed MR activity reflects glucocorticoids present at this site.

Distribution of Activity Across U.S. Streams. Biological activity varied widely across sites with the number of active end points ranging from zero to 11 (Figure 1) and the magnitude of response within individual active end points ranging from an AUC of 1.55 to 10.3 (Figure 3). Activation of end points

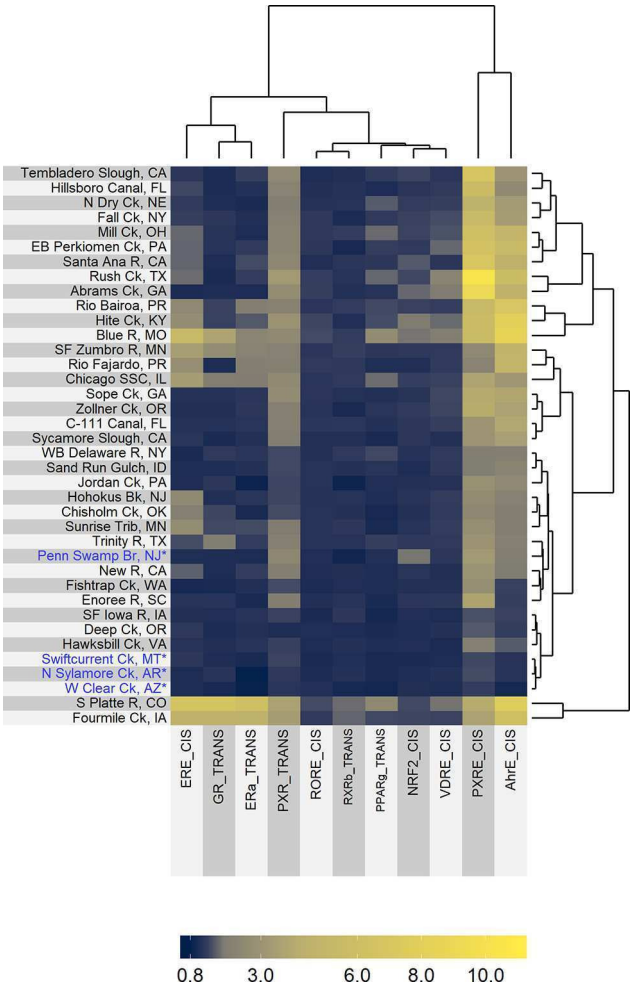

Figure 3. Hierarchical clustering of blank normalized area under the curve (AUC) of site extracts for individual assay end points. Only end points with AUC response ≥1.5 at one or more sites are included. Sites noted with an asterisk (*) and in blue are low-impact sites, with limited anthropogenic inputs compared to other sites. See SI Table S4 for bioassay response values.

associated with xenobiotic metabolism were the most frequently induced. Elevated PXRE_CIS, AhRE_CIS, and PXR_TRANS occurred at 36, 31, and 30 sites, respectively, demonstrating near-ubiquitous activity across surface waters. The remaining end points responded at fewer sites. For example, ERE_CIS was active at 17 sites, ERα_TRANS and PPARγ_TRANS at 10 sites, VDRE_CIS at eight sites, GR_TRANS at seven sites, NRF2_CIS at six sites, and RORE_CIS and RXRβ_TRANS at two sites. Among the eight samples tested using the trans-Factorial-2 assay, ERβ_-TRANS2 activity was detected at two sites, whereas MR_TRANS2 and PR_TRANS2 activity were detected at one (SI Figure S39).

Samples from two low-impact sites (West Clear Creek, AZ; Swiftcurrent Creek, MT) did not elicit any responses above baseline. Some responses associated with xenobiotic metabolism or cell stress were detected at the two other low-impact locations (PXRE_CIS at North Sylamore Creek, AR; PXRE_CIS, AhRE_CIS, PXR_TRANS, and NRF2_CIS at

DOI: 10.1021/acs.est.8b05304
Environ. Sci. Technol. 2019, 53, 973−983

Penn Swamp Branch, NJ), but neither induced any endocrine-related bioactivities, such as ER or GR (Figure 3). Penn Swamp Branch, NJ is noted as unique compared to other low-impact sites in that it drains a wetland area, is acidic (pH 4.18), and contains high dissolved organic carbon (15.9 mg L^{-1}; SI Table S1).[29] Natural humic acids, which would be expected to be present at high concentrations in an acidic, wetland-drained watershed, have been previously identified as activators of AhR, though at concentrations several orders of magnitude higher than TCDD, the prototypical ligand for AhR.[45] Many natural product ligands have been identified for PXR, a very promiscuous xenobiotic-sensing nuclear receptor.[46] Thus, the presence of natural dissolved organic compounds at the low-impact Penn Swamp Branch, NJ site (and possibly at other "impacted" sites) may contribute to increased activity observed in AhR and PXR related end points. If ubiquitous organic compounds are indeed a primary driving force for these end points, the utility of these end points for predicting potential adverse effects will be reduced.

Overall, most of the impacted sites cluster closely with low-impact sites and were characterized by low to moderate PXR and AhR bioactivity and little to no ER or GR bioactivity (Figure 3). Remaining sites show moderate to high ER and GR activity and generally elevated PXR and AhR activity. The wide occurrence of elevated PXR and AhR activity suggests somewhat nonspecific effects associated with a wide variety of natural and manmade ligands, which is consistent with a biological role of xenobiotic sensing and induction of metabolizing enzymes.[47] Both AhR and PXR can interact with a wide range of structurally diverse compounds, thus the wide occurrence of both bioactivities is not surprising and aligns with previous studies of environmental extracts.[15,48] The promiscuity of both receptors is also reflected in the ToxCast database as AhRE_CIS and PXRE_CIS are active in 13.8% and 46.7%, respectively, of 3860 compounds tested in the cis-Factorial assay. Elevated ER and GR activity can be due to a variety of natural or synthetic steroidal compounds, and elevated activity has been previously observed in water samples associated with wastewater treatment plant (WWTP) discharges.[9,16,49] Activation of GR_TRANS was highly correlated with ERE_CIS ($p < 0.0001$, $r = 0.90$; 95% CI [0.82, 0.95]) and ERα_TRANS end points ($p < 0.0001$, $r = 0.94$; 95% CI [0.90, 0.97]), and ERE_CIS was significantly correlated with PPARγ_TRANS ($p < 0.0001$, r = 0.74; 95% CI [0.54, 0.85]), consistent with a common point source of chemicals contributing to ER, GR, and PPARγ bioactivities across sampled streams (Figure 4). Because no individual detected compound was identified in the ToxCast database[22] as a strong agonist of more than one of these receptors (data not shown), the observed bioactivities may be due to a mixture of compounds (as would be expected from WWTP effluents). Anecdotally, the three sites showing the greatest ER, GR, and PPARγ activity (South Platte River, CO; Blue River, MO; Fourmile Creek, IA) are sites with documented WWTP effluent sources.

Lastly, the inclusion of end points for the same pathway across both Attagene assays allows for a comparison across assays. Both ER- (ERE_CIS, ERα_TRANS) and PXR-related (PXRE_CIS, PXR_TRANS) end points from the two separate assays were well correlated, demonstrating a similar response from each individual assay (Figure 4). These two sets of end points are the only paired end points that showed consistent activation across both assays. On the contrary, the PPAR- and

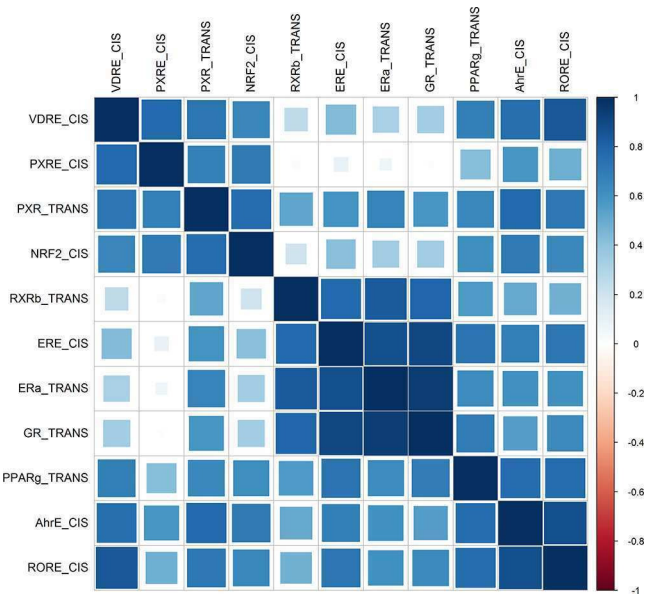

Figure 4. Correlation matrix of 11 end points with AUC response ≥1.5. Cell color and area of shading represent the correlation coefficient between end points.

GR-related end points (PPRE_CIS, GRE_CIS) were not active at any site, while their counterparts (PPARγ_TRANS, GR_TRANS) were active at 10 and 7 sites, respectively. This demonstrates that each end point may have differential response across both assays.

Exposure-Activity Ratio Analysis. An EAR analysis was performed to identify how well measured compounds explained the observed bioactivity of surface waters. Of the 406 unique compounds analytically detected at one or more sites,[29] 297 (73%) were tested in ToxCast, and 201 (49.5%) were tested in the Attagene HTS assays used in the current study. Where there were co-occurring chemical concentration and ToxCast bioactivity data, EAR values were calculated for each assay end point at each site (SI Table S5). An EAR value could be calculated for a total of 53 end points (one or more chemicals active for end point). Two end points, ERE_CIS and ERα_TRANS, had EAR values above 0.1 and ERE_CIS showed EAR values above 1.0. Four other end points (AhR_CIS, NRF2_CIS, PXRE_CIS, Sox_CIS) had a maximum EAR > 0.01, while the remaining 47 end points had maximum EARs < 0.006. For both ERα_TRANS and ERE_CIS, over 50 compounds contributed to some degree to the calculated EARs, but estrone, 17β-estradiol, bisphenol A, and 4-nonylphenol account for much of the EAR. At sites where it was detected above the reporting limit, estrone alone explained 55−100% and 80−100% of the total EAR for the ERα_TRANS and ERE_CIS assays, respectively. Observed bioactivity and EARs for both ERα_TRANS ($p < 0.0001$, $r = 0.83$; 95% CI [0.70, 0.91]) and ERE_CIS ($p < 0.0001$, r = 0.68; 95% CI [0.46, 0.82]) were also significantly correlated, indicating the measured chemicals largely account for observed ER activity. The remaining four end points with EARs > 0.01 were not significantly correlated with observed bioactivity, indicating that measured chemicals likely do not adequately explain any other observed bioactivities.

Sparse Partial Least Squares Analysis. Sparse partial least-squares (SPLS) analysis was performed to identify possible relationships between detected chemicals and bioassay

DOI: 10.1021/acs.est.8b05304
Environ. Sci. Technol. 2019, 53, 973−983

responses. Through this technique, it was possible to take more chemicals into account (386 chemicals) compared to EAR calculations (201 chemicals); however, results are inferred from statistical (correlative) relationships, not empirical assay data. Among the 386 chemicals in the data set, 48 unique compounds were identified by SPLS as predictors of bioassay responses (SI Table S6). Out of 70 total assay end points, 27 were related to observed chemical occurrence patterns. These included 10 of the 11 end points activated by the tested water samples (the exception was PXRE_CIS). Other than estrone, 17β-estradiol, and androstenedione, most of the compounds identified through SPLS analysis are not known to directly interact with receptors responsible for the commonly observed bioactivities (AhR, ER, GR, PXR, etc.). Many identified compounds are classified as pharmaceuticals or wastewater indicators, both of which can be broad indicators of anthropogenic waste. Two specific compounds, HHCB and triclosan, were previously shown to have a positive relationship between their concentrations and the total number of compounds detected across these same 38 sites.[29] Therefore, we hypothesize, that most compounds identified by SPLS are likely not causing observed bioactivities directly but rather covary with other bioactive compounds present in these systems. Regardless, the identification of multiple pharmaceuticals and other wastewater indicators as covariates of bioeffects does provide a reduced set of targeted analytical methods to monitor as a potential surrogate of effects.

Comparison of HTS and Targeted Reporter Assays. An important attribute of the current study was the use of split samples for all chemical and biological analyses, allowing for direct comparison of data produced at different laboratories. Conley et al. measured bioactivity in these same samples using targeted transcriptional reporter assays with ER, GR, and AR,[30] providing an opportunity to compare the performance of the HTS assays. Three samples were lost during shipment and were not analyzed by Conley et al.[30] but comparisons could be made for 35 of 38 sites presented in the current work.

Five samples analyzed by Conley et al. elicited AR-dependent responses in the MDA-kb2 assay,[30] but no samples induced AR activity above baseline in the HTS assay. The MDA-kb2 assay can detect both AR or GR agonists, although the assay is ∼100-fold more sensitive to AR agonists.[30] One site (Blue River, MO), had detectable androgenic compounds that potentially account for AR activity in the MDA-kb2 assay; however, four of five sites inducing MDA-kb2 activity also showed elevated GR activity in both the GR transcriptional assay employed by Conley et al. and the HTS assays described herein. Overall, while it appears that the HTS Attagene assay may be less sensitive to AR agonists than the MDA-kb2 system, it remains unclear whether MDA-kb2 activity observed at most sites was actually AR- or GR-dependent.

Elevated GR activity was identified at nine sites using CV-1 cells transduced with human GR.[26] Using the HTS assays, seven samples were identified as active, five of which were in common with the CV-1 assay results. Conley et al. reported relative GR-mediated potency in terms of an equivalent concentration of dexamethasone (dexamethasone equivalents; DexEq), a potent GR agonist, that produces the same magnitude of bioassay response. Three sites with reported Dexeq greater than 30 ng L^{-1} were active in the HTS assays. In contrast, for samples estimated to contain 6.0−30 ng Dexeq L^{-1}, only three of six samples were active. Overall, the HTS Attagene assays appear somewhat less sensitive to GR agonists compared to the CV-1 reporter assay, but the sites inducing the greatest activity were identified using both systems.

Measures of ER activity provide the most complete comparison between the Attagene HTS system and a targeted in vitro reporter assay. Using the T47D-KBluc assay,[26] Conley et al. detected elevated ER activity in 34 samples, whereas the HTS end points ERE_CIS and ERα_TRANS identified 17 and 10 active samples, respectively. This again indicates a lower sensitivity to ER agonists in the HTS assays compared to the T47D-KBluc reporter gene assay. Dose-dependent responses to a 17β-estradiol positive control in the T47D-KBluc assays allowed the determination of equivalent concentration (E2Eq) values for the test samples, but positive controls for the HTS assays were not run in concentration−response, so E2eq could not be calculated for the HTS results. However, the rank order of E2eq concentration in the T47D-KBluc assay and normalized AUC values for both ERE_CIS and ERα_TRANS were significantly correlated (r = 0.73; r = 0.69, respectively; SI Figure S40). Thirteen of 16 sites with >0.8 ng E2eq L^{-1} were active for one or both ER end points, demonstrating the ability of the HTS assay to identify sites with low ng L^{-1} E2eq activity.

As with any in vitro system, there are strengths and weaknesses of the presented approach using the Attagene assay systems. The HTS assays utilized in the current study appear to be less sensitive overall compared to the three individual targeted in vitro assays. The NRF2 pathway, which provides a measure of oxidative stress, has been commonly observed in rivers in Europe, but was observed less frequently using the multiplexed assays in the current study. This again may be indicative of lower sensitivity in the multiplexed assay relative to targeted in vitro assays. Nonetheless, sites with the greatest GR and ER bioactivities were identified by both targeted and multiplexed assay approaches. The multiplexed nature of the Attagene systems may partially explain the differential sensitivity between assay systems, but the multiplexed nature of the assays (one of the greatest strengths of this approach) does additionally provide for an integrated system response accounting for potential interactions between transcriptional pathways. Other disadvantages of the current approach include a lack of positive control compounds for all end points and the lack of dose−response data for positive controls. This ultimately limits the ability to quantitatively compare extract response to that of a reference compound. Finally, for this specific study, screening was limited to a single replicate due to cost constraints. While issues of positive controls and replication could be overcome, it would come at additional project costs. Taken together, we propose the use of these multiplexed assays as a screening and prioritization tool in environmental monitoring. Where warranted, further site-specific follow-up employing the more sensitive targeted assays could be performed at high priority sites to more quantitatively assess relevant bioactivities.

Associating Bioactivity with Land Use Land Cover. Another objective of the overall mixtures study was to identify potential associations between chemical occurrence or bioassay response and land use and land cover (LULC) attributes.[29] The National Land Cover Database (NLCD) classification of site watershed-scale LULC attributes (previously reported[29]) were compared with AUC values for the 11 active end points to better evaluate whether specific point sources or land use patterns were related to bioactivity. Of 38 watershed-scale LULC parameters evaluated, two showed weak but significant

DOI: 10.1021/acs.est.8b05304
Environ. Sci. Technol. 2019, 53, 973−983

correlation with bioactivity. Percent of watershed area classified as developed, low intensity (NLCD category 22) was significantly correlated with AhRE_CIS (p = 0.016, r = 0.39, 95% CI [0.080, 0.63]), ERE_CIS (p = 0.037, r = 0.34, 95% CI [0.021, 0.59]), PPARγ_TRANS (p = 0.027, r = 0.36, 95% CI [0.044, 0.61]), PXR_TRANS (p = 0.016, r = 0.39, 95% CI [0.077, 0.63]), PXRE_CIS (p = 0.026, r = 0.36, 95% CI [0.047, 0.61]), RORE_CIS (p = 0.009, r = 0.42, 95% CI [0.12, 0.65]), and VDRE_CIS (p = 0.001, r = 0.51, 95% CI [0.23, 0.71]). Additionally, the number of registered National Pollution Discharge Elimination System (NPDES) facilities was correlated with ERE_CIS (p = 0.020, r = 0.38, 95% CI [0.066, 0.63]), ERα_TRANS (p = 0.016, r = 0.39, 95% CI [0.078, 0.64]), GR_TRANS (p = 0.012, r = 0.41, 95% CI [0.096, 0.65]), PPARγ_TRANS (p = 0.020, r = 0.38, 95% CI [0.064, 0.63]), and RXRβ_TRANS (p = 0.048, r = 0.33, 95% CI [0.0045, 0.59]). Correlation of mainly xenobiotic metabolism related assays with low intensity development suggests nonpoint sources of bioactivity. Increased chemical burdens, either of natural organics (as seen at Penn Swamp Branch, NJ) or anthropogenic-related contaminants, may be a primary contributor to activity of xenobiotic-metabolism related end points such as AhR and PXR. AhR activity in surface water was previously identified at the highest levels in urban streams in Southern California,[27] suggesting anthropogenic related contaminants are likely the primary contributors of elevated AhR activity. Correlation of more specific, endocrine-related activity (ER and GR) with NPDES inputs suggests wastewater as a source of bioactive contaminants.

While significant, no single LULC showed a strong predictive relationship with bioactivity (R^2 ranging 0.108−0.262). Both significantly correlated features relate to urban use and wastewater inputs, which does strengthen the case that urban, anthropogenic inputs are the primary contributing factors of observed bioactivity. To supplement the watershed-scale analysis, catchment-scale LULC attributes were generated for each site to determine if increased resolution would provide better indicators of bioactivity, but similar relationships between catchment-scale LULC and bioactivity were observed. Catchment-scale medium and high intensity development were additionally correlated with metabolism and endocrine-related end points, further suggesting urban, anthropogenic inputs are the primary drivers of observed effects.

Linking Observed Bioactivities to Adverse Effects. The ultimate purpose of identifying pathway-based bioactivity in samples is to gain insights into potential hazards of exposure to contaminants present in surface waters. The adverse outcome pathway (AOP) framework[50] provides the means to link pathway-based activity, such as data from in vitro bioassays, with higher organismal responses and relevant adverse outcomes. Some molecular targets, such as AhR and ER, have been studied extensively and AOPs associated with their activation are well-defined for aquatic vertebrates.[51] However, clear and well supported associations with apical hazards are still lacking for a number of the active HTS end points identified in the present work. Efforts are being made to link all ToxCast assay targets, which includes those used in the current study, with existing AOP descriptions publicly available through the AOP-Wiki,[51] a repository for developed or in-progress AOPs. Relevant AOPs in terms of species (e.g., fish) and end points (growth, development, reproduction) are available only for pathways associated with the AhR and ER (SI Table S7).[51] Potential apical hazards associated with activation of those pathways include early life stage mortality and reproductive dysfunction. A search of the AOP-Wiki also identified existing AOPs for GR, NRF2, PPARγ, and PXR, although these have been primarily demonstrated in mammalian species and may not be applicable to aquatic species of concern (SI Table S7). As such, these four pathways represent targets for which AOP development should be prioritized. However, as with all in vitro based monitoring, in vitro bioactivity alone does not necessarily indicate adverse effects will occur in the environment. Much research has focused on establishing trigger values, or a value of bioactivity at which there is reasonable concern of adverse effects in the environment, for assays commonly used in environmental monitoring (e.g., ER reporter assays).[11,48] Additional characterization of the Factorial assays is needed before similar trigger values could be established.

No AOPs linking RXR, ROR, or VDR activation to apical outcomes have been described to date on the AOP-Wiki.[51] These three activities were not as frequently observed in the environment relative to other targets, but they could be prioritized for AOP development, particularly if they are detected for a growing number of samples. It is notable that VDR response element, which is monitored by the VDRE_CIS end point, has been previously identified as a binding target of PXR.[52] VDRE_CIS is significantly correlated with PXRE_CIS (p < 0.001, r = 0.77; 95% CI [0.60, 0.88]) and PXR_TRANS activity (p < 0.001, r = 0.73; 95% CI [0.53, 0.85]). The TRANS assay counterpart to VDRE_CIS, VDR_TRANS, which measures direct VDR-mediated activity, is not active at any site. This supports observed VDRE_CIS activity as an indicator of PXR-mediated activity and not indicative of specific VDR-mediated responses. As such, even if available, VDR-related AOPs are likely not relevant.

With regard to AOPs, for complex mixtures multiple relevant AOPs may be triggered simultaneously. Consequently, it has been proposed that consideration of AOP networks may be important for hazard prediction in these scenarios.[53,54] Knapen et al.[53] provided an example of how Attagene bioactivity screening data for a complex environmental sample could be linked to relevant AOPs, assembled into a relevant AOP network, refined based on problem formulation, and used to both identify potential hazards of concern and end points that could be employed in effects-based monitoring. Based upon activation of eight end points in the Attagene assays, all of which were active in the current study, Knapen et al. identified potential adverse outcomes of impaired reproduction, early life stage mortality, and cardiotoxicity.[53] The utility of this integrated approach will increase with continued linkage of Attagene end points and improved tools for assembling, filtering, and analyzing AOP networks.[53]

Finally, when considering in vitro assays in the context of AOPs for ecologically relevant species, the conservation of molecular targets must be considered. The Attagene assays used in the current work use only human-based receptors, which may or may not be representative of ecological species of concern. The AhR, for example, is broadly conserved in vertebrates, but AhR-mediated embryo toxicity can vary across teleost fish species by multiple orders of magnitude (see review by Doering et al.).[55] Techniques now exist to help assess the similarity of molecular targets across various taxa. The SeqaPASS tool was recently used to compare all targets present in the ToxCast database with currently known sequences for nonhuman taxa.[56] This data source could be

DOI: 10.1021/acs.est.8b05304
Environ. Sci. Technol. 2019, 53, 973−983

used to compare the targets identified through the current study with those of ecologically relevant species of concern and predict if human-based assay results are representative of the target species. Ultimately, as extrapolations move from the molecular level, as measured through in vitro cell-based techniques, to the apical-level, the information required to make confident assessments of potential effects will continue to grow.

The use of HTS assays to characterize bioactivity in U.S. streams, along with parallel chemical characterization, identified multiple bioactivities of concern, potential chemicals of concern, and sites with the greatest potential for adverse effects to ecological receptors. Further, comparison with more traditional, cell-based reporter assays aligned well with the HTS assay results, providing evidence supporting the use of these HTS assays for environmental surveillance efforts. Though coverage of the chemical space (>700 compounds monitored) and biological space (69 end points) was more extensive than many studies, the majority of bioactivity could not be explained by measured chemicals, and only estrogenic activity could be reasonably predicted. The expanded end point coverage of the HTS assays employed here revealed additional biological pathways that may be commonly impacted in the environment. Because these assays cover vertebrate-centric (especially mammalian) end points, other relevant targets (i.e., those pertaining to invertebrates and plants) should be examined to more realistically evaluate potential ecological effects of complex, environmental mixtures.

■ ASSOCIATED CONTENT

Supporting Information

The Supporting Information is available free of charge on the ACS Publications website at DOI: 10.1021/acs.est.8b05304.

Complete USGS water quality data are downloadable from USGS ScienceBase (https://doi.org/10.5066/F7GF0RPH)[37] and USGS National Water Information System (NWIS) (http://dx.doi.org/10.5066/F7P55KJN).[57] Additional details on analyte recovery following evaporation and 40 figures (PDF)

Seven tables (XLSX)

■ AUTHOR INFORMATION

Corresponding Author

*Phone: (218) 529-5078; fax: (218) 529-5003; e-mail: blackwell.brett@epa.gov.

ORCID

Brett R. Blackwell: 0000-0003-1296-4539

Gerald T. Ankley: 0000-0002-9937-615X

Paul M. Bradley: 0000-0001-7522-8606

Daniel L. Villeneuve: 0000-0003-2801-0203

Notes

The authors declare no competing financial interest.

■ ACKNOWLEDGMENTS

We thank Dr. Anthony Schroeder for early discussions of data processing and interpretation, and Dr. William Foreman for supplying analyte loss data for inclusion in data analysis. This research was performed as part of the Chemical Safety for Sustainability (CSS) research program of the U.S. Environmental Protection Agency (EPA) Office of Research and Development (ORD). This manuscript has been reviewed in accordance with the requirements of EPA ORD. The findings and conclusions in this article do not necessarily represent the views or policies of the EPA. Any use of trade, firm, or product names is for descriptive purposes only and does not imply endorsement by the U.S. Government.

■ REFERENCES

(1) Bradley, P. M.; Battaglin, W. A.; Clark, J. M.; Henning, F. P.; Hladik, M. L.; Iwanowicz, L. R.; Journey, C. A.; Riley, J. W.; Romanok, K. M. Widespread occurrence and potential for biodegradation of bioactive contaminants in Congaree National Park, USA. *Environ. Toxicol. Chem.* **2017**, *36* (11), 3045−3056.

(2) Kolpin, D. W.; Furlong, E. T.; Meyer, M. T.; Thurman, E. M.; Zaugg, S. D.; Barber, L. B.; Buxton, H. T. Pharmaceuticals, hormones, and other organic wastewater contaminants in U.S. streams, 1999−2000: a national reconnaissance. *Environ. Sci. Technol.* **2002**, *36* (6), 1202−11.

(3) Lee, K. E.; Langer, S. K.; Menheer, M. A.; Hansen, D. S.; Foreman, W. T.; Furlong, E. T.; Jorgenson, Z. G.; Choy, S. J.; Moore, J. N.; Banda, J.; Gefell, D. J. *Chemicals of Emerging Concern in Water and Bottom Sediment in the Great Lakes Basin, 2012: Collection Methods, Analytical Methods, Quality Assurance, And Study Data*; Reston, VA, 2015; *910*, p 14.

(4) Tang, J. Y.; McCarty, S.; Glenn, E.; Neale, P. A.; Warne, M. S.; Escher, B. I. Mixture effects of organic micropollutants present in water: towards the development of effect-based water quality trigger values for baseline toxicity. *Water Res.* **2013**, *47* (10), 3300−14.

(5) Altenburger, R.; Ait-Aissa, S.; Antczak, P.; Backhaus, T.; Barcelo, D.; Seiler, T. B.; Brion, F.; Busch, W.; Chipman, K.; Lopez de Alda, M.; Umbuzeiro Gde, A.; Escher, B. I.; Falciani, F.; Faust, M.; Focks, A.; Hilscherova, K.; Hollender, J.; Hollert, H.; Jager, F.; Jahnke, A.; Kortenkamp, A.; Krauss, M.; Lemkine, G. F.; Munthe, J.; Neumann, S.; Schymanski, E. L.; Scrimshaw, M.; Segner, H.; Slobodnik, J.; Smedes, F.; Kughathas, S.; Teodorovic, I.; Tindall, A. J.; Tollefsen, K. E.; Walz, K. H.; Williams, T. D.; Van den Brink, P. J.; van Gils, J.; Vrana, B.; Zhang, X.; Brack, W. Future water quality monitoring–adapting tools to deal with mixtures of pollutants in water resource management. *Sci. Total Environ.* **2015**, *512*−*513*, 540−51.

(6) Brack, W.; Altenburger, R.; Schuurmann, G.; Krauss, M.; Lopez Herraez, D.; van Gils, J.; Slobodnik, J.; Munthe, J.; Gawlik, B. M.; van Wezel, A.; Schriks, M.; Hollender, J.; Tollefsen, K. E.; Mekenyan, O.; Dimitrov, S.; Bunke, D.; Cousins, I.; Posthuma, L.; van den Brink, P. J.; Lopez de Alda, M.; Barcelo, D.; Faust, M.; Kortenkamp, A.; Scrimshaw, M.; Ignatova, S.; Engelen, G.; Massmann, G.; Lemkine, G.; Teodorovic, I.; Walz, K. H.; Dulio, V.; Jonker, M. T.; Jager, F.; Chipman, K.; Falciani, F.; Liska, I.; Rooke, D.; Zhang, X.; Hollert, H.; Vrana, B.; Hilscherova, K.; Kramer, K.; Neumann, S.; Hammerbacher, R.; Backhaus, T.; Mack, J.; Segner, H.; Escher, B.; de Aragao Umbuzeiro, G. The SOLUTIONS project: challenges and responses for present and future emerging pollutants in land and water resources management. *Sci. Total Environ.* **2015**, *503*−*504*, 22−31.

(7) Di Paolo, C.; Ottermanns, R.; Keiter, S.; Ait-Aissa, S.; Bluhm, K.; Brack, W.; Breitholtz, M.; Buchinger, S.; Carere, M.; Chalon, C.; Cousin, X.; Dulio, V.; Escher, B. I.; Hamers, T.; Hilscherova, K.; Jarque, S.; Jonas, A.; Maillot-Marechal, E.; Marneffe, Y.; Nguyen, M. T.; Pandard, P.; Schifferli, A.; Schulze, T.; Seidensticker, S.; Seiler, T. B.; Tang, J.; van der Oost, R.; Vermeirssen, E.; Zounkova, R.; Zwart, N.; Hollert, H. Bioassay battery interlaboratory investigation of emerging contaminants in spiked water extracts - Towards the implementation of bioanalytical monitoring tools in water quality assessment and monitoring. *Water Res.* **2016**, *104*, 473−484.

(8) Jia, A.; Escher, B. I.; Leusch, F. D.; Tang, J. Y.; Prochazka, E.; Dong, B.; Snyder, E. M.; Snyder, S. A. In vitro bioassays to evaluate complex chemical mixtures in recycled water. *Water Res.* **2015**, *80*, 1−11.

(9) Konig, M.; Escher, B. I.; Neale, P. A.; Krauss, M.; Hilscherova, K.; Novak, J.; Teodorovic, I.; Schulze, T.; Seidensticker, S.; Kamal

Hashmi, M. A.; Ahlheim, J.; Brack, W. Impact of untreated wastewater on a major European river evaluated with a combination of in vitro bioassays and chemical analysis. *Environ. Pollut.* **2017**, *220* (Pt B), 1220−1230.
(10) Neale, P. A.; Altenburger, R.; Ait-Aissa, S.; Brion, F.; Busch, W.; de Aragao Umbuzeiro, G.; Denison, M. S.; Du Pasquier, D.; Hilscherova, K.; Hollert, H.; Morales, D. A.; Novak, J.; Schlichting, R.; Seiler, T. B.; Serra, H.; Shao, Y.; Tindall, A. J.; Tollefsen, K. E.; Williams, T. D.; Escher, B. I. Development of a bioanalytical test battery for water quality monitoring: Fingerprinting identified micropollutants and their contribution to effects in surface water. *Water Res.* **2017**, *123*, 734−750.
(11) Escher, B. I.; van Daele, C.; Dutt, M.; Tang, J. Y.; Altenburger, R. Most oxidative stress response in water samples comes from unknown chemicals: the need for effect-based water quality trigger values. *Environ. Sci. Technol.* **2013**, *47* (13), 7002−11.
(12) Blake, L. S.; Martinovic, D.; Gray, L. E.; Wilson, V. S.; Regal, R. R.; Villeneuve, D. L.; Ankley, G. T. Characterization of the androgen-sensitive MDA-KB2 cell line for assessing complex environmental mixtures. *Environ. Toxicol. Chem.* **2010**, *29* (6), 1367−1376.
(13) Cavallin, J. E.; Durhan, E. J.; Evans, N.; Jensen, K. M.; Kahl, M. D.; Kolpin, D. W.; Kolodziej, E. P.; Foreman, W. T.; LaLone, C. A.; Makynen, E. A.; Seidl, S. M.; Thomas, L. M.; Villeneuve, D. L.; Weberg, M. A.; Wilson, V. S.; Ankley, G. T. Integrated assessment of runoff from livestock farming operations: Analytical chemistry, in vitro bioassays, and in vivo fish exposures. *Environ. Toxicol. Chem.* **2014**, *33* (8), 1849−57.
(14) Escher, B. I.; Allinson, M.; Altenburger, R.; Bain, P. A.; Balaguer, P.; Busch, W.; Crago, J.; Denslow, N. D.; Dopp, E.; Hilscherova, K.; Humpage, A. R.; Kumar, A.; Grimaldi, M.; Jayasinghe, B. S.; Jarosova, B.; Jia, A.; Makarov, S.; Maruya, K. A.; Medvedev, A.; Mehinto, A. C.; Mendez, J. E.; Poulsen, A.; Prochazka, E.; Richard, J.; Schifferli, A.; Schlenk, D.; Scholz, S.; Shiraishi, F.; Snyder, S.; Su, G.; Tang, J. Y.; van der Burg, B.; van der Linden, S. C.; Werner, I.; Westerheide, S. D.; Wong, C. K.; Yang, M.; Yeung, B. H.; Zhang, X.; Leusch, F. D. Benchmarking organic micropollutants in wastewater, recycled water and drinking water with in vitro bioassays. *Environ. Sci. Technol.* **2014**, *48* (3), 1940−56.
(15) Neale, P. A.; Ait-Aissa, S.; Brack, W.; Creusot, N.; Denison, M. S.; Deutschmann, B.; Hilscherová, K.; Hollert, H.; Krauss, M.; Novák, J.; Schulze, T.; Seiler, T.-B.; Serra, H.; Shao, Y.; Escher, B. I. Linking in Vitro Effects and Detected Organic Micropollutants in Surface Water Using Mixture-Toxicity Modeling. *Environ. Sci. Technol.* **2015**, *49* (24), 14614−14624.
(16) Cavallin, J. E.; Jensen, K. M.; Kahl, M. D.; Villeneuve, D. L.; Lee, K. E.; Schroeder, A. L.; Mayasich, J.; Eid, E. P.; Nelson, K. R.; Milsk, R. Y.; Blackwell, B. R.; Berninger, J. P.; LaLone, C. A.; Blanksma, C.; Jicha, T.; Elonen, C.; Johnson, R.; Ankley, G. T. Pathway-based approaches for assessment of real-time exposure to an estrogenic wastewater treatment plant effluent on fathead minnow reproduction. *Environ. Toxicol. Chem.* **2016**, *35* (3), 702−16.
(17) Conley, J. M.; Evans, N.; Mash, H.; Rosenblum, L.; Schenck, K.; Glassmeyer, S.; Furlong, E. T.; Kolpin, D. W.; Wilson, V. S. Comparison of in vitro estrogenic activity and estrogen concentrations in source and treated waters from 25 U.S. drinking water treatment plants. *Sci. Total Environ.* **2017**, *579*, 1610−1617.
(18) Wehmas, L. C.; Cavallin, J. E.; Durhan, E. J.; Kahl, M. D.; Martinovic, D.; Mayasich, J.; Tuominen, T.; Villeneuve, D. L.; Ankley, G. T. Screening complex effluents for estrogenic activity with the T47D-KBluc cell bioassay: assay optimization and comparison with in vivo responses in fish. *Environ. Toxicol. Chem.* **2011**, *30* (2), 439−45.
(19) Chen, Q.; Jia, A.; Snyder, S. A.; Gong, Z.; Lam, S. H. Glucocorticoid activity detected by in vivo zebrafish assay and in vitro glucocorticoid receptor bioassay at environmental relevant concentrations. *Chemosphere* **2016**, *144*, 1162−9.
(20) Scott, P. D.; Bartkow, M.; Blockwell, S. J.; Coleman, H. M.; Khan, S. J.; Lim, R.; McDonald, J. A.; Nice, H.; Nugegoda, D.; Pettigrove, V.; Tremblay, L. A.; Warne, M. S.; Leusch, F. D. An assessment of endocrine activity in Australian rivers using chemical and in vitro analyses. *Environ. Sci. Pollut. Res.* **2014**, *21* (22), 12951−67.
(21) Dix, D. J.; Houck, K. A.; Martin, M. T.; Richard, A. M.; Setzer, R. W.; Kavlock, R. J. The ToxCast program for prioritizing toxicity testing of environmental chemicals. *Toxicol. Sci.* **2007**, *95* (1), 5−12.
(22) USEPA, ToxCast & Tox21 Summary Files from invitrodb_v2. In October 2015 ed.; https://www.epa.gov/chemical-research/exploring-toxcast-data-downloadable-data (accessed April 9, 2018.
(23) Richard, A. M.; Judson, R. S.; Houck, K. A.; Grulke, C. M.; Volarath, P.; Thillainadarajah, I.; Yang, C.; Rathman, J.; Martin, M. T.; Wambaugh, J. F.; Knudsen, T. B.; Kancherla, J.; Mansouri, K.; Patlewicz, G.; Williams, A. J.; Little, S. B.; Crofton, K. M.; Thomas, R. S. ToxCast Chemical Landscape: Paving the Road to 21st Century Toxicology. *Chem. Res. Toxicol.* **2016**, *29* (8), 1225−51.
(24) Becker, R. A.; Friedman, K. P.; Simon, T. W.; Marty, M. S.; Patlewicz, G.; Rowlands, J. C. An exposure:activity profiling method for interpreting high-throughput screening data for estrogenic activity–proof of concept. *Regul. Toxicol. Pharmacol.* **2015**, *71* (3), 398−408.
(25) Blackwell, B. R.; Ankley, G. T.; Corsi, S. R.; DeCicco, L. A.; Houck, K. A.; Judson, R. S.; Li, S.; Martin, M. T.; Murphy, E.; Schroeder, A. L.; Smith, E. R.; Swintek, J.; Villeneuve, D. L. An ″EAR″ on Environmental Surveillance and Monitoring: A Case Study on the Use of Exposure-Activity Ratios (EARs) to Prioritize Sites, Chemicals, and Bioactivities of Concern in Great Lakes Waters. *Environ. Sci. Technol.* **2017**, *51* (15), 8713−8724.
(26) Mehinto, A. C.; Jia, A.; Snyder, S. A.; Jayasinghe, B. S.; Denslow, N. D.; Crago, J.; Schlenk, D.; Menzie, C.; Westerheide, S. D.; Leusch, F. D.; Maruya, K. A. Interlaboratory comparison of in vitro bioassays for screening of endocrine active chemicals in recycled water. *Water Res.* **2015**, *83*, 303−9.
(27) Mehinto, A. C.; VanDervort, D. R.; Lao, W.; He, G.; Denison, M. S.; Vliet, S. M.; Volz, D. C.; Mazor, R. D.; Maruya, K. A. High throughput in vitro and in vivo screening of inland waters of Southern California. *Environmental Science: Processes & Impacts* **2017**, *19* (9), 1142−1149.
(28) Buxton, H. T.; Reilly, T. J.; Kuivila, K. M.; Kolpin, D. W.; Bradley, P. M.; Villeneuve, D. L.; Mills, M. A. Chemical mixtures and environmental effects—A pilot study to assess ecological exposure and effects in streams. *U.S. Geological Survey Open-File Report* **2015**, 2015−1113.
(29) Bradley, P. M.; Journey, C. A.; Romanok, K. M.; Barber, L. B.; Buxton, H. T.; Foreman, W. T.; Furlong, E. T.; Glassmeyer, S. T.; Hladik, M. L.; Iwanowicz, L. R.; Jones, D. K.; Kolpin, D. W.; Kuivila, K. M.; Loftin, K. A.; Mills, M. A.; Meyer, M. T.; Orlando, J. L.; Reilly, T. J.; Smalling, K. L.; Villeneuve, D. L. Expanded Target-Chemical Analysis Reveals Extensive Mixed-Organic-Contaminant Exposure in U.S. Streams. *Environ. Sci. Technol.* **2017**, *51* (9), 4792−4802.
(30) Conley, J. M.; Evans, N.; Cardon, M. C.; Rosenblum, L.; Iwanowicz, L. R.; Hartig, P. C.; Schenck, K. M.; Bradley, P. M.; Wilson, V. S. Occurrence and In Vitro Bioactivity of Estrogen, Androgen, and Glucocorticoid Compounds in a Nationwide Screen of United States Stream Waters. *Environ. Sci. Technol.* **2017**, *51* (9), 4781−4791.
(31) Martin, M. T.; Dix, D. J.; Judson, R. S.; Kavlock, R. J.; Reif, D. M.; Richard, A. M.; Rotroff, D. M.; Romanov, S.; Medvedev, A.; Poltoratskaya, N.; Gambarian, M.; Moeser, M.; Makarov, S. S.; Houck, K. A. Impact of environmental chemicals on key transcription regulators and correlation to toxicity end points within EPA's ToxCast program. *Chem. Res. Toxicol.* **2010**, *23* (3), 578−90.
(32) Romanov, S.; Medvedev, A.; Gambarian, M.; Poltoratskaya, N.; Moeser, M.; Medvedeva, L.; Gambarian, M.; Diatchenko, L.; Makarov, S. Homogeneous reporter system enables quantitative functional assessment of multiple transcription factors. *Nat. Methods* **2008**, *5* (3), 253−60.
(33) Chun, H.; Keles, S. Sparse partial least squares regression for simultaneous dimension reduction and variable selection. *J. R Stat Soc. Series B Stat Methodol* **2010**, *72* (1), 3−25.

DOI: 10.1021/acs.est.8b05304
Environ. Sci. Technol. 2019, 53, 973−983

(34) Zou, H.; Hastie, T. Regularization and Variable Selection via the Elastic Net. *Journal of the Royal Statistical Society. Series B (Statistical Methodology)* **2005**, *67* (2), 301−320.
(35) Chung, D.; Chun, H.; Keles, S. spls: Sparse Partial Least Squares (SPLS) Regression and Classification, R package version 2.2−1; https://CRAN.R-project.org/package=spls, 2013.
(36) Team, R. D. C. *R: A Language and Environment for Statistical Computing*. In Vienna, Austria, 2008.
(37) Romanok, K. M.; Bradley, P. M.; Journey, C. A. *Inorganic and Organic Concentration Data Collected from 38 Streams in the United States, 2012−2014, with Supporting Data, As Part of the Chemical Mixtures and Environmental Effects Pilot Study*; U.S. Geological Survey Data Release, 2017. DOI: 10.5066/F7GF0RPH.
(38) Azur, M. J.; Stuart, E. A.; Frangakis, C.; Leaf, P. J. Multiple imputation by chained equations: what is it and how does it work? *Int. J. Methods Psychiatr Res.* **2011**, *20* (1), 40−9.
(39) van Buuren, S.; Groothuis-Oudshoorn, K., mice: Multivariate Imputation by Chained Equations in R. *Journal of Statistical Software*; Vol *1*, Issue 3 (2011) **2011**.
(40) EPA, U. *Estimations Program Interface Suite for Microsoft Windows*, v4.11. United States Environmental Protection Agency, Washington, DC, 2012.
(41) Long, M.; Laier, P.; Vinggaard, A. M.; Andersen, H. R.; Lynggaard, J.; Bonefeld-Jørgensen, E. C. Effects of currently used pesticides in the AhR-CALUX assay: comparison between the human TV101L and the rat H4IIE cell line. *Toxicology* **2003**, *194* (1), 77−93.
(42) Behnisch, P. A.; Hosoe, K.; Sakai, S. Bioanalytical screening methods for dioxins and dioxin-like compounds a review of bioassay/biomarker technology. *Environ. Int.* **2001**, *27* (5), 413−39.
(43) Ekins, S.; Chang, C.; Mani, S.; Krasowski, M. D.; Reschly, E. J.; Iyer, M.; Kholodovych, V.; Ai, N.; Welsh, W. J.; Sinz, M.; Swaan, P. W.; Patel, R.; Bachmann, K. Human pregnane X receptor antagonists and agonists define molecular requirements for different binding sites. *Mol. Pharmacol.* **2007**, *72* (3), 592−603.
(44) Fuller, P. J.; Yao, Y.; Yang, J.; Young, M. J. Mechanisms of ligand specificity of the mineralocorticoid receptor. *J. Endocrinol.* **2012**, *213* (1), 15−24.
(45) Bittner, M.; Janošek, J.; Hilscherová, K.; Giesy, J.; Holoubek, I.; Bláha, L. Activation of Ah receptor by pure humic acids. *Environ. Toxicol.* **2006**, *21* (4), 338−342.
(46) Staudinger, J. L.; Ding, X.; Lichti, K. Pregnane X receptor and natural products: beyond drug-drug interactions. *Expert Opin. Drug Metab. Toxicol.* **2006**, *2* (6), 847−57.
(47) Omiecinski, C. J.; Vanden Heuvel, J. P.; Perdew, G. H.; Peters, J. M. Xenobiotic metabolism, disposition, and regulation by receptors: from biochemical phenomenon to predictors of major toxicities. *Toxicol. Sci.* **2011**, *120* (Suppl 1), S49−75.
(48) Escher, B. I.; Neale, P. A.; Leusch, F. D. Effect-based trigger values for in vitro bioassays: Reading across from existing water quality guideline values. *Water Res.* **2015**, *81*, 137−48.
(49) Roberts, J.; Bain, P. A.; Kumar, A.; Hepplewhite, C.; Ellis, D. J.; Christy, A. G.; Beavis, S. G. Tracking multiple modes of endocrine activity in Australia's largest inland sewage treatment plant and effluent- receiving environment using a panel of in vitro bioassays. *Environ. Toxicol. Chem.* **2015**, *34* (10), 2271−81.
(50) Ankley, G. T.; Bennett, R. S.; Erickson, R. J.; Hoff, D. J.; Hornung, M. W.; Johnson, R. D.; Mount, D. R.; Nichols, J. W.; Russom, C. L.; Schmieder, P. K.; Serrrano, J. A.; Tietge, J. E.; Villeneuve, D. L. Adverse outcome pathways: a conceptual framework to support ecotoxicology research and risk assessment. *Environ. Toxicol. Chem.* **2010**, *29* (3), 730−41.
(51) Adverse Outcome Pathway Wiki (AOP-Wiki). https://aopwiki.org/) (accessed April 26, 2018).
(52) Echchgadda, I.; Song, C. S.; Roy, A. K.; Chatterjee, B. Dehydroepiandrosterone sulfotransferase is a target for transcriptional induction by the vitamin D receptor. *Mol. Pharmacol.* **2004**, *65* (3), 720−9.
(53) Knapen, D.; Angrish, M. M.; Fortin, M. C.; Katsiadaki, I.; Leonard, M.; Margiotta-Casaluci, L.; Munn, S.; O'Brien, J. M.; Pollesch, N.; Smith, L. C.; Zhang, X.; Villeneuve, D. L. Adverse outcome pathway networks I: Development and applications. *Environ. Toxicol. Chem.* **2018**, *37* (6), 1723−1733.
(54) Villeneuve, D. L.; Crump, D.; Garcia-Reyero, N.; Hecker, M.; Hutchinson, T. H.; LaLone, C. A.; Landesmann, B.; Lettieri, T.; Munn, S.; Nepelska, M.; Ottinger, M. A.; Vergauwen, L.; Whelan, M. Adverse outcome pathway (AOP) development I: strategies and principles. *Toxicol. Sci.* **2014**, *142* (2), 312−20.
(55) Doering, J. A.; Giesy, J. P.; Wiseman, S.; Hecker, M. Predicting the sensitivity of fishes to dioxin-like compounds: possible role of the aryl hydrocarbon receptor (AhR) ligand binding domain. *Environ. Sci. Pollut. Res.* **2013**, *20* (3), 1219−1224.
(56) LaLone, C. A.; Villeneuve, D. L.; Doering, J. A.; Blackwell, B. R.; Transue, T. R.; Simmons, C. W.; Swintek, J.; Degitz, S. J.; Williams, A. J.; Ankley, G. T. Evidence for Cross Species Extrapolation of Mammalian-Based High-Throughput Screening Assay Results. *Environ. Sci. Technol.* **2018**, *52* (23), 13960−13971.
(57) U.S. Geological Survey *National Water Information System—Web interface*. DOI: 10.5066/F7P55KJN (accessed February 27, 2018).

DOI: 10.1021/acs.est.8b05304
Environ. Sci. Technol. 2019, 53, 973−983

Environmental Science & Technology

Article

pubs.acs.org/est

An "EAR" on Environmental Surveillance and Monitoring: A Case Study on the Use of Exposure−Activity Ratios (EARs) to Prioritize Sites, Chemicals, and Bioactivities of Concern in Great Lakes Waters

Brett R. Blackwell,[*,†] Gerald T. Ankley,[†] Steven R. Corsi,[‡] Laura A. DeCicco,[‡] Keith A. Houck,[§] Richard S. Judson,[§] Shibin Li,[†,∥] Matthew T. Martin,[§] Elizabeth Murphy,[⊥] Anthony L. Schroeder,[#] Edwin R. Smith,[⊥] Joe Swintek,[▽] and Daniel L. Villeneuve[†]

[†]Mid-Continent Ecology Division, U.S. Environmental Protection Agency, 6201 Congdon Blvd., Duluth, Minnesota 55804, United States

[‡]Wisconsin Water Science Center, U.S. Geological Survey, 8505 Research Way, Middleton, Wisconsin 53562, United States

[§]National Center for Computational Toxicology, U.S. Environmental Protection Agency, 109 T.W. Alexander Drive, Research Triangle Park, North Carolina 27711, United States

[∥]National Research Council, U.S. Environmental Protection Agency, 6201 Congdon Blvd., Duluth, Minnesota 55804, United States

[⊥]Great Lakes National Program Office, U.S. Environmental Protection Agency, 77 West Jackson Blvd., Chicago, Illinois 60604, United States

[#]Math, Science, and Technology Department, University of Minnesota Crookston, 2900 University Avenue, Crookston, Minnesota 56716, United States

[▽]Badger Technical Services, 6201 Congdon Blvd., Duluth, Minnesota 55804, United States

Supporting Information

ABSTRACT: Current environmental monitoring approaches focus primarily on chemical occurrence. However, based on concentration alone, it can be difficult to identify which compounds may be of toxicological concern and should be prioritized for further monitoring, in-depth testing, or management. This can be problematic because toxicological characterization is lacking for many emerging contaminants. New sources of high-throughput screening (HTS) data, such as the ToxCast database, which contains information for over 9000 compounds screened through up to 1100 bioassays, are now available. Integrated analysis of chemical occurrence data with HTS data offers new opportunities to prioritize chemicals, sites, or biological effects for further investigation based on concentrations detected in the environment linked to relative potencies in pathway-based bioassays. As a case study, chemical occurrence data from a 2012 study in the Great Lakes Basin along with the ToxCast effects database were used to calculate exposure−activity ratios (EARs) as a prioritization tool. Technical considerations of data processing and use of the ToxCast database are presented and discussed. EAR prioritization identified multiple sites, biological pathways, and chemicals that warrant further investigation. Prioritized bioactivities from the EAR analysis were linked to discrete adverse outcome pathways to identify potential adverse outcomes and biomarkers for use in subsequent monitoring efforts.

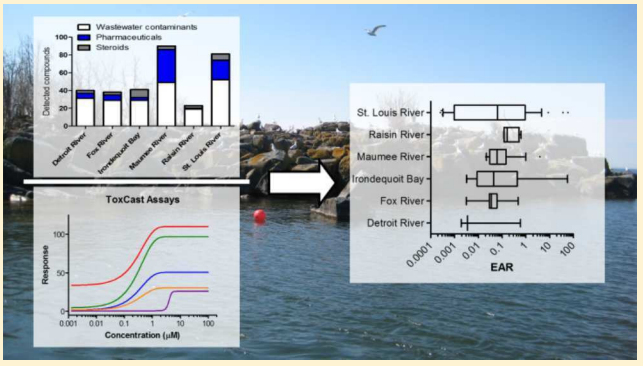

INTRODUCTION

Environmental monitoring has traditionally relied heavily upon analysis of different matrices (water, sediment, soil, etc.) for potential contaminants through targeted analytical methods. Advances in analytical instrumentation have increased the sensitivity of targeted methods, with compounds routinely measured in water at low part-per-trillion levels.[1,2] Additionally, the expansion of high-resolution instruments in environmental monitoring has led to nontargeted analytical methods being implemented, with hundreds to thousands of compounds detected and dozens to hundreds of compounds tentatively identified in some instances.[3−6] Despite advances in the ability to detect contaminants in the environment, understanding of the biological implications from exposure to these compounds has not kept pace. Thus, while chemicals can be identified and

Received: March 28, 2017
Revised: June 27, 2017
Accepted: July 3, 2017
Published: July 3, 2017

ACS Publications © 2017 American Chemical Society

DOI: 10.1021/acs.est.7b01613
Environ. Sci. Technol. 2017, 51, 8713−8724

quantified in the environment, the potential biological effects of hundreds to thousands of individual contaminants remain poorly defined.[7]

Advances of high-throughput toxicology have led to the development of biological effects data for a large number of chemicals. For example, the Tox21 program[8,9] and the Environmental Protection Agency (EPA) ToxCast program[10] together provide high-throughput screening (HTS) data for over 9 000 unique substances, including many industrial and environmentally relevant chemicals for which traditional human health or ecological effects data are lacking. Chemicals are prepared and screened in a standardized manner, and each chemical is tested using a consistent dose−response design across assays. This allows the derivation of point of departure estimates, such as the chemical-specific half-maximal activity concentration (AC50) or activity concentration at cutoff (ACC) for each chemical−assay combination, and chemicals can be subsequently ranked in terms of potency for a given assay target. Together the programs utilize a number of in vitro and in vivo HTS assays to identify a range of pathway-specific and nonspecific biological interactions providing a final database covering hundreds of specific biological pathways and processes.

To effectively leverage the breadth of biological and chemical space covered within these databases, new approaches and tools are being developed. A method for exposure−activity profiling using exposure−activity ratios (EARs) represents one approach for screening and prioritizing chemicals using both chemical occurrence and HTS data[11] and has been previously highlighted with potential for application to environmental monitoring.[12,13] Exposure−activity ratios, similar in concept to toxic units,[14] incorporate both the dose (i.e., environmental concentration) and the relative potency (i.e., point of departure estimate) for a given chemical−assay pair, allowing for the prioritization of chemicals or sites based on expected biological activity. Assays identified as higher priority based on EARs can be further linked through adverse outcome pathways (AOPs) to identify hazards to organisms or ecosystems,[15] and measurable end points associated with the perturbation of specific biological processes identified for the confirmation or monitoring of predicted site-specific hazards.

The EAR approach utilizing the ToxCast database offers a currently viable, standardized method of integrating chemical occurrence and biological effects for the prioritization of environmental monitoring data sets. The present work applies this approach to a study focused on identifying and characterizing emerging contaminants across tributaries and areas of concern (AOCs) within the Great Lakes,[1] specifically demonstrating the use of EAR analysis as a rapid, screening-level tool for the prioritization of existing chemical occurrence data sets. This study was part of an ongoing, multi-agency effort directed at effects-based tool development for application to monitoring and surveillance of contaminants of emerging concern and their potential impacts on resident biota and ecosystems in the Great Lakes.[16] The present case study demonstrates how EARs can be used to prioritize environmental sites, identify potential biological activity(ies) of concern, and highlight chemicals likely contributing to the biological activity. Furthermore, prioritized biological activities are linked to existing AOPs to identify potential adverse effects and strategies for monitoring predicted hazards in exposed organisms. Issues that may commonly be faced when using HTS databases for EAR calculations are detailed to focus on the application of this approach for utility in environmental monitoring.

EXPERIMENTAL SECTION

Study Locations and Sample Collection. Data presented in this study were obtained from a publicly available U.S. Geological Survey (USGS) report.[1] In 2012, surface water samples were collected at 66 sites across 6 watersheds in the Great Lakes Basin, including the Saint Louis River and Duluth Harbor, MN; Fox River and Green Bay, WI; Detroit River, MI; Raisin River, MI; Maumee River, OH; and Irondequoit Bay, NY. Sampling locations varied from those with low anticipated anthropogenic impact to sites in close proximity to municipal wastewater treatment plants (WWTPs). Samples were collected from all watersheds in spring (April−May), and additional samples were collected from the Maumee and Saint Louis Rivers in summer (September). A total of 140 water samples were collected for chemical analysis (excluding blanks and duplicates). Samples were collected as either 1 L depth-integrated grab samples or 96 h temporally integrated samples.[17] Site features including depth, flow, and water quality parameters were recorded at the time of sample collection.[1] Sample numbers varied across watersheds ranging from 3 to 76. The most-intensive efforts were focused at the Saint Louis River and Maumee River watersheds with collection of 76 and 37 samples, respectively. Full collection methods are detailed elsewhere.[1]

Analytical Chemistry. Surface water samples (both grab and composite) were submitted to the USGS National Water Quality Laboratory (Denver, CO) and analyzed for three broad suites of contaminants: wastewater indicators,[18] pharmaceuticals,[19] and steroids and sterols[20] (see Table S1 for a complete list of contaminants and methods). In total, 134 unique organic compounds were measured using these three gas chromatography−mass spectrometry (GC−MS)-based analytical methods. In the cases in which compounds were measured across multiple analytical methods (3β-coprostanol, bisphenol A [BPA], and cholesterol), only the result from the method with the lowest laboratory reporting limit (LRL) was retained for our analysis. Further details including complete analyte lists, quality-control procedures, and concentrations of analytes were reported previously.[1]

Chemical Concentration Data Set Processing. Analytical methods used in this study are reported by USGS as information-rich methods,[21] meaning additional qualifying information is included alongside analyte quantification. As such, reported concentrations of some compounds are below the given LRL. All reported values, including those below LRLs, were used for EAR calculations without adjustment. Nondetections (reported as <LRL) were assigned a value of zero to prevent highly bioactive compounds (i.e., from the HTS data set) from skewing EAR results.

In Vitro Bioassays. A limited number of water samples were further screened for total estrogenic activity using the T47D-KBluc cell line, which is stably transfected with an ERα-reporter gene construct.[22] Samples were tested in triplicate, independent wells. The full methodology for this bioassay is available in the Supporting Information.

ToxCast Database. The ToxCast database[23] (including both ToxCast and Tox21 information) contains HTS data for thousands of chemicals screened through multiple assay platforms. The database currently includes 12 platforms covering a variety of cell-based, cell-free, and whole-organism

DOI: 10.1021/acs.est.7b01613
Environ. Sci. Technol. 2017, 51, 8713−8724

HTS assays, encompassing over 300 unique signaling pathways (e.g., estrogen receptor [ER], aryl hydrocarbon receptor, glucocorticoid receptor, etc.) and nonspecific end points (oxidative stress, cytotoxicity, organelle conformation, etc.). ToxCast assay sources and operating procedures are described in detail elsewhere.[24−41] All ToxCast data used for this study were from the October 2015 data release and are publicly available online through the ToxCast Web site.[23]

Exposure−Activity Ratios. To support screening and prioritization, EARs comparing surface-water chemical concentration to ACC estimates for all chemicals available in the ToxCast database were calculated (eq 1). Assuming noninteractive concentration addition within assays, a summed EAR of environmental mixtures containing n number of chemicals can be calculated (eq 2). While the AC50 has previously been used as the point of departure estimate for EAR calculations,[11−13] we chose the ACC for the present analysis. ACC estimates the chemical concentration at which a defined threshold of response (the activity cutoff) is achieved within an assay[42] (see Figure S1). Unlike the AC50, in which the concentration estimate may align with different magnitudes of bioassay response for each chemical tested in an assay, the activity cutoff threshold is uniform for all chemicals tested in the same assay. Thus, the ACC is less prone to violating assumptions underlying relative potency estimation.[43] The activity cutoff for each assay is based on a multiplier of the baseline median absolute deviation (BMAD; 3×, 5×, 6×, or 10×), which is calculated as the median absolute deviation for each assay end point using data points from the two lowest tested concentrations of all chemicals within a given assay. The multiple of the BMAD was generally selected specific to assay platforms (sometimes individual assays) to account for the baseline variability and signal window with a goal of achieving a high sensitivity for true activity while minimizing false positives due to baseline variability to the extent possible. The two lowest concentrations were used for determining BMAD as they are below bioactive concentrations for the great majority of samples. The use of median over mean provides for protection from extreme values from highly potent chemicals. Also, the use of sample wells rather than solvent controls for background activity measurement has an advantage of being derived from wells treated identically to all other sample-treated wells. For assays that are normalized to a positive control, a cutoff threshold of 20% response may also be used to ensure the response is in a reasonable range of the response of a known, reference chemical to provide some test for biological significance in addition to statistical significance. Assay specific cutoff threshold criteria are given in Table S2.

While the EAR is a simple calculation conceptually, processing of the extensive chemical data set (154 samples × 134 chemicals) and even larger ToxCast database (1192 assays × 9076 chemicals) was expedited by development of a custom, R-based program to facilitate the processing, calculation, and visualization of the EAR data set (see details in the Supporting Information):

$$\mathrm{EAR} = \frac{\text{exposure (environmental concentration, μM)}}{\text{activity (ACC in μM)}} \quad (1)$$

$$\mathrm{EAR}_{\text{mixture}} = \sum_{i=1}^{n} \frac{\text{exposure (environmental concentration in μM)}}{\text{activity (ACC in μM)}} \quad (2)$$

Quality Assurance Considerations. During the process of generating EARs, multiple issues with chemical occurrence and ToxCast data sets were identified, which could lead to artifacts and errors in interpretation and use of the EARs. The first issue was the use of chemical salts for toxicity testing in ToxCast assays. Chemical occurrence data are reported as free compound (e.g., methadone, CAS no. 76-99-3), while some compounds, especially pharmaceuticals, are tested in ToxCast assays as ion pairs (e.g., methadone hydrochloride, CAS no. 1095-90-5). Compounds from the chemical occurrence data set that were not identified in the ToxCast database through a search for a matching CAS number were manually screened for tested chemical alternatives. Among 27 analyzed compounds initially identified as not present in the ToxCast database, a total of 9 were actually present as chemical analogs. In these cases, CAS numbers were updated to better align chemical occurrence data with the ToxCast database for EAR generation (Table S3). Additionally, within the ToxCast data, molecular weights for these CAS numbers were updated to match the measured compound and maintain correct μM calculations. For the purposes of EAR generation, free and salt forms were considered to be equipotent across the assays.

In the ToxCast database, assays are grouped by platform and target (as defined by annotation fields from the database).[23] Some of these assays were purposefully excluded from EAR consideration. Specifically, because a goal of this case study was to link EARs to potential adverse outcomes, most nonspecific cell-based or cell-free assay end points were excluded. For example, we excluded assays from the platforms Apredica (APR) and Bioseek (BSK), which largely target nonspecific end points[44] such as cell cycle status, cell proliferation, organelle conformation, DNA damage, and stress response and are difficult to interpret though specific pathway-based toxicity assessment. Assays categorized as "background measurement", "cell cycle", and "cell morphology" (based on "intended_target_family" annotation field) also were excluded from EAR calculations as these monitor baseline assay performance, not specific effects. The "intended_target_family" annotation was used for subsequent grouping of assay results, and several assays designated "NA" were manually assigned to an existing category (Table S2). For all zebrafish (*Danio rerio*)-related assays, a new category, "ZF", was included. Attagene (ATG) assays reporting in the "loss" direction and Novascreen (NVS) assays reporting in the "gain" direction (based on the "signal_direction" annotation field) also were removed from the final EAR results, as these platforms are not optimized or designed to report for the given assay direction.[23] Overall, 528 of 1192 assay end points were considered for the final EAR calculations (Table S2).

Chemical−assay pairs were further censored from the final data set using ToxCast data quality flags. These flags, explicitly noted in the ToxCast database, were implemented to identify potential false positive and false negative results based on dose−response irregularities.[42] Chemical−assay pairs indicating false positives were removed from the final results (specifically, data with flag identifications 7, 10, 11, 15, and 17 (Table S4). Employing these flags enabled the removal of the majority of

DOI: 10.1021/acs.est.7b01613
Environ. Sci. Technol. 2017, 51, 8713−8724

false-positive chemical−assay pairs from the final EAR results. A specific chemical−assay pair, fluoranthene in the "Tox21_p53_BLA_p3_ratio" assay, was observed to result in very high EAR values (>100). Upon closer examination, the dose response curve was found to be flat and was identified as an unflagged, false positive. This chemical−assay pair also was removed from the final data set. Other unflagged, false-positive chemical−assay pairs may be present in the data set, but no other individual pairs exhibited the very high EAR values that may greatly skew the final interpretation of results. No flagged, potential false negatives were identified after evaluating actual concentration−response curves, a typical finding given that the "hit-calling" algorithm is designed to be conservative (i.e., favoring false positives) in the interest of identifying all potential hazards.

A final observation was associated with generation of best-fit dose−response curves and corresponding ACC values using the automated ToxCast data analysis pipeline.[42] For a number of assays, ACCs of specific chemicals were reported below the minimum concentration tested within the assay. Closer examination of dose−response curves showed that the minimum tested concentration for many strong agonists was at or near saturation for receptor targets (e.g., 17β-estradiol and ER-related assays); thus, full dose−response curves are estimated from the upper "plateau" of the curve. For example, the lowest concentration of 17β-estradiol tested in the "ATG_ERE_CIS-up" assay (0.09 μM) induces approximately 98% of the maximum 17β-estradiol response, and an ACC value of 3.1×10^{-5} μM is extrapolated from the model fit. For compounds detected in the chemical occurrence data set, 85 chemical−assay pairs (composed of 14 chemicals and 34 assays) have ACCs below the minimum tested concentration (Table S5). A total of 11 of the identified chemicals are steroids or xenobiotics known to interact with nuclear receptors, and 27 of 38 assays are related to nuclear receptors. This suggests the dose range generally screened in ToxCast is insufficient to fully characterize strong agonists of some nuclear receptors. Moreover, ACC estimates extrapolated over orders of magnitude in concentration will inherently be less accurate or unreliable compared with those estimated from a full dose−response curve. No adjustments were made for these chemical−assay pairs, and consequently, EARs for these instances may be underestimated.

RESULTS AND DISCUSSION

Chemical Occurrence Summary. Of 134 contaminants analyzed across the three analytical methods, 109 were reported above LRLs in one or more surface water samples (Table S1). Grouped by analytical method, 60 of 67 (90%) wastewater contaminants, 39 of 48 (81%) pharmaceuticals, and 10 of 19 (53%) steroids and sterols were detected at one or more sites. By watershed, the greatest number of wastewater contaminants, pharmaceuticals, and steroids and sterols were detected within the Saint Louis River, Maumee River, and Irondequoit Bay watersheds, respectively (Figure 1). Of note, the Saint Louis River and Maumee River watersheds had more intensive sampling efforts centered on WWTPs, and as such, it could be reasonably expected to observe a greater number of compounds at these sites. Based on frequency and concentration alone, several chemicals can be highlighted from within the data set. Cholesterol, DEET, fluoranthene, and pyrene, which are all within the wastewater indicators method, were detected most frequently, in 98%, 93%, 71%, and 69% of all samples,

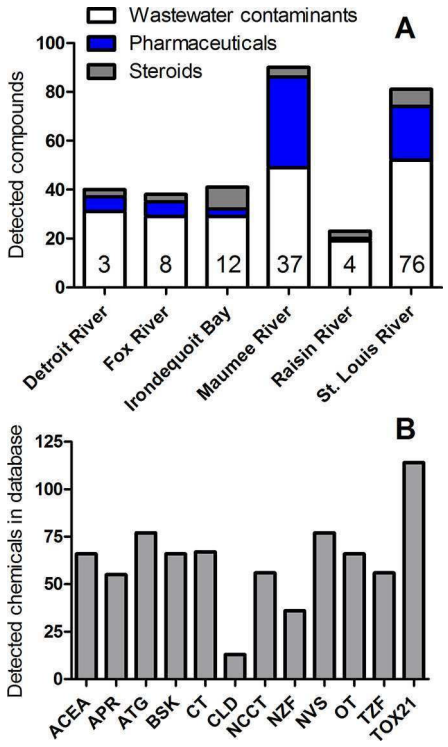

Figure 1. (A) Number of detected chemicals within each analytical method at each watershed reported in the chemical occurrence data set. The value within each column represents the total number of samples from a watershed. (B) Number of detected chemicals with available data in each ToxCast assay platform. See Figure S2 for more-detailed information on chemical coverage across assay platforms. ACEA, ACEA Biosciences; APR, Apredica; ATG, Attagene; BSK, BioSeek; CT, CeeTox; CLD, CellzDirect; NCCT, National Center for Computational Toxicology; NZF, NHEERL zebrafish; NVS, NovaScreen; OT, Odyssey Thera; TZF, Tanguay Lab zebrafish; Tox21, Tox21 Initiative.

respectively. Cholesterol, 3β-coprostanol, β-sitosterol, and BPA, again all within the wastewater indicators method, were detected at the highest single concentrations, with maximum concentrations of 120, 95.2, 64.4, and 60.5 μg/L, respectively. This abbreviated list again demonstrates the need to consider effects concentrations of compounds, as several chemicals present at high concentrations (e.g., the naturally derived sterols) would be expected to have limited biological effects.

ToxCast Coverage of Chemicals. Compounds in ToxCast were screened in multiple phases, with different batteries of assays used for some phases of the overall testing program (for an overview, see ref 45); thus, the assay coverage for all chemicals in ToxCast is not consistent. For chemicals measured within the current study, 116 of 134 (86%) analyzed chemicals and 96 of 109 (88%) detected chemicals had been evaluated in one or more assays (Tables S1 and S6). Tox21 had the greatest coverage of detected chemicals (87%), followed by ATG and NVS (61%) and then BSK and CEETOX (51%) (Figure 1). Considering assay coverage of detected chemicals, 48 (44%) have data in 10 or more batteries, 66 (61%) have data in 3 or more batteries, and 30 chemicals (28%) have data only for the Tox21 assay suite (Figure S2).

Exposure−Activity Ratio-Based Prioritization. *Site Prioritization.* As an initial screen of the chemical occurrence data set, $EAR_{mixture}$ values (eq 2) were calculated for all sites (Table S7). No active chemicals were detected for 299 of 528

DOI: 10.1021/acs.est.7b01613
Environ. Sci. Technol. 2017, 51, 8713−8724

assays, leaving 229 total ToxCast assays with calculated EAR values in one or more samples. Similarly, 3 of 140 water samples had no detected compounds that were active in ToxCast, leaving a total of 137 samples with calculated EAR values. To better summarize the EAR data set by watershed and individual sites, $EAR_{mixture}$ values across all 229 assays were summed for each site as a cumulative $EAR_{mixture}$. Because the data matrix of chemicals and assays is consistent for all samples, this provides a value of estimated activity at each site irrespective of individual assay target. Through this approach, the Saint Louis River watershed, which was most intensively sampled, showed the highest values and had the largest range of cumulative $EAR_{mixture}$ of any watershed (Figure 2A). The

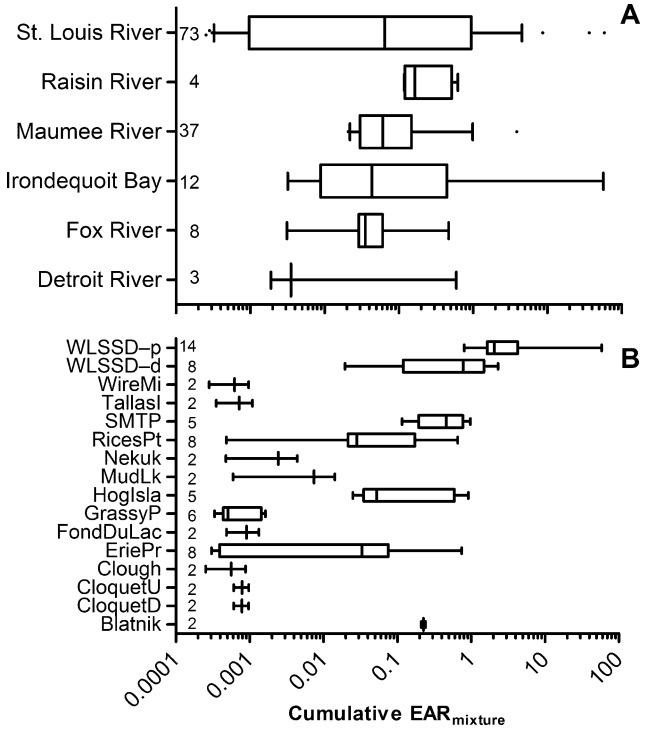

Figure 2. (A) Cumulative $EAR_{mixture}$ (i.e., sum of $EAR_{mixture}$ values across all assays) values within each watershed. The value within each row represents the total number of samples from a watershed. For graphical purposes, sites with $EAR_{mixture}$ equal to 0 (three samples; all from the Saint Louis River) were removed. (B) Cumulative $EAR_{mixture}$ values for each site within the Saint Louis River watershed. The value within each row represents the total number of samples from a site. For graphical purposes, sites with $EAR_{mixture}$ equal to 0 or with only one sample are not shown. Site information is available from the original data source.[1]

median EAR was highest at the Raisin River, followed by Maumee River, Fox River, and Saint Louis River watersheds. Focusing on the Saint Louis River (representing the watershed with the maximum EAR values and greatest sample coverage), three sites with the greatest potential impact, WLSSD-Proximal (WLSSD-P), WLSSD-Distal (WLSSD-D), and SMTP were identified (Figure 2B). These three sites all are notably in close proximity to two WWTPs and reasonably could be hypothesized as having a relatively greater potential for biological effects. WLSSD-P and WLSSD-D are impacted by a larger WWTP receiving both municipal and industrial waste, with WLSSD-P nearest to the WWTP outflow and WLSSD-D at a more distal location with a greater dilution of the effluent.[17] SMTP is impacted by a separate, smaller WWTP receiving exclusively municipal waste. Accordingly, the highest cumulative EARs are observed at WLSSD-P, followed by WLSSD-D and SMTP. Although details of specific chemicals and relevant biological pathways are not captured at this level of site prioritization, the ability to condense chemical occurrence and biological activity data sets into a single output allowed for the rapid comparison and prioritization of watersheds or individual sites from the data set.

As an alternative strategy for site prioritization, exceptionally high cumulative $EAR_{mixture}$ values were identified across watersheds to highlight unique sites or potential point sources of contamination. Only four sites in total, located in the Saint Louis River, Maumee River, and Irondequoit Bay watersheds, had cumulative $EAR_{mixture}$ values greater than 2 (Figure 2). As noted above, both sites within the Saint Louis River (WLSSD-P and WLSSD-D), as well as the single site in the Maumee River watershed (MX-WWTP), are in close proximity to WWTPs, which likely explains the elevated $EAR_{mixture}$ values from these sites. The single site in Irondequoit Bay (IB-06), however, has no obvious point sources of contamination. This site is unique in the composition of detected contaminants, with many steroidal compounds observed only at this site. Several naturally occurring androgenic and estrogenic steroids were detected, as well as two synthetic estrogens, mestranol and diethylstilbestrol, all of which contribute heavily to the high EAR values observed in this sample. The presence of many steroids in this single sample likely indicates an unknown contamination source upstream of the site. Mestranol is a component of some oral contraceptives,[46] indicating a possible human waste source; conversely, the presence of 17α-estradiol is generally associated with animal waste or animal production facilities.[47,48] Also, although diethylstilbestrol is no longer used as a human pharmaceutical, its environmental occurrence could be associated with illicit use in livestock operations,[49] again suggesting that agricultural sources may be contributing to the estrogenic signal. Further investigation would be required to identify potential sources of the observed contamination. Given the elevated EAR values and unique chemical signature at IB-06, further monitoring at this site is warranted.

Biological Activity Prioritization. To prioritize molecular targets and biological pathways most likely to be perturbed by chemicals broadly observed in the Great Lakes samples and at specific sites, mean $EAR_{mixture}$ values were calculated within each assay across all sites (Table S8). Assays were then grouped according to the ToxCast database "intended_target_family" annotation,[23] resulting in 15 assays groups containing 1 to 75 individual assays (Figure 3A). Of categories containing two or more assays, the greatest median mean $EAR_{mixture}$ values were observed for "transporter", "nuclear receptor", and "oxidoreductase" at 4.8×10^{-4}, 2.1×10^{-4}, and 1.8×10^{-4}, respectively. Maximum mean EARs of 0.50, 0.018, and 0.0097 were observed for the "nuclear receptor", "DNA binding", and "oxidoreductase" assay groupings. Other end-points including "cyp", "esterase", and "ZF" assay groupings are also elevated (and likely not statistically different) from assay groupings highlighted above, so these groupings could be further investigated. Because the "intended_target_family" level of assay organization does not inform as to specific molecular targets of the detected chemicals, broad categories such as "nuclear receptor" and "DNA binding" must be further "dissected" to reveal relevant biological pathways. For example, exploring "nuclear receptor" assays in more detail by using the

DOI: 10.1021/acs.est.7b01613
Environ. Sci. Technol. 2017, 51, 8713−8724

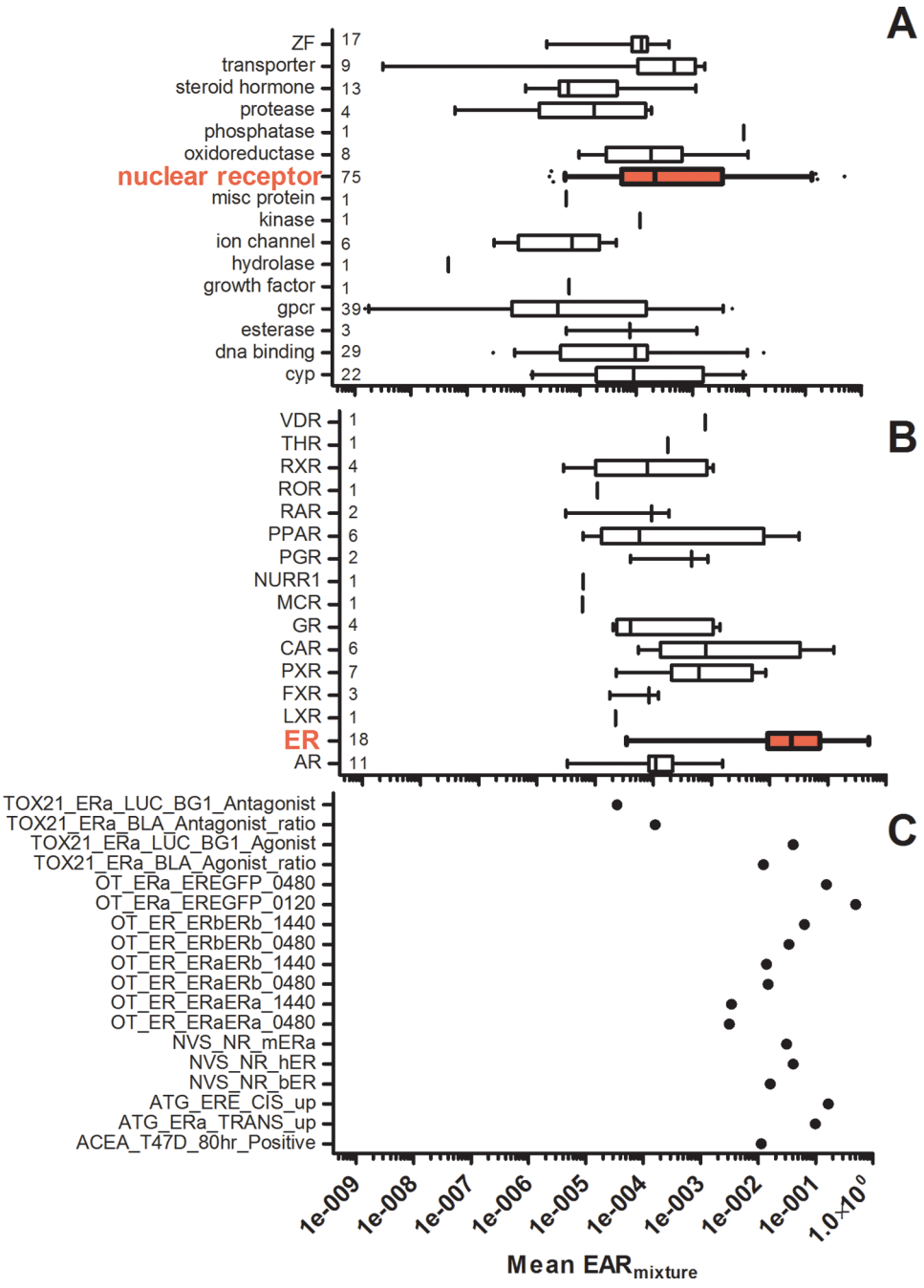

Figure 3. (A) Mean $EAR_{mixture}$ values within each assay category as defined by the "intended_target_family" annotation field (see Table S2). The number in each row is the number of assays in a category. (B) Mean $EAR_{mixture}$ values within the "nuclear receptor" assay category as defined by the "intended_target_gene_symbol" annotation field (see Table S2). The number in each row is the number of assays in a category. (C) Mean $EAR_{mixture}$ values for individual assays under the "ER" category.

"intended_target_gene_symbol" annotation field of the ToxCast database reveals assay gene targets, which would be most relevant for linking biological activity to adverse effects through AOP constructs (Figure 3B). The primary targets driving the high response in "nuclear receptor" assays are ER, constitutive androstane receptor (NR1I3; CAR), and peroxisome proliferator-activated receptor (PPAR) assays (Figure 3B). Elevated EARs observed in "oxidoreductase" and "DNA binding" are driven by assays measuring thyroid peroxidase (TPO) inhibition and increased SOX1 expression, respectively. Because both TPO inhibition and SOX1 expression are measured by only a single assay, it is not possible to evaluate the veracity of this response across multiple test systems.

For targets measured by multiple assays, such as ER (which is reflected in some manner in a total of 18 different assay end points), the range of $EAR_{mixture}$ values from individual assays can be dissected further to compare individual assay end points. For the ER-based assays, mean $EAR_{mixture}$ values across all sites ranged from 3.5×10^{-5} to 0.50 (Figure 3C). Aside from two antagonist assays, the bulk of the mean $EAR_{mixture}$ values for the various ER assays fall between 0.001 and 0.1. However, slightly greater EARs were detected for the Odyssey Thera (OT) "OT_ERE_GFP" assays and the ATG ER assays. The range of

DOI: 10.1021/acs.est.7b01613
Environ. Sci. Technol. 2017, 51, 8713−8724

EARs observed in the ER assays reinforces that not all assays are equivalent in performance and design. ER assay end points are measured at different points along the signaling pathway, including receptor binding (NVS), receptor dimer formation (OT), receptor−DNA interaction (OT), mRNA transcription (ATG), protein production (Tox21), and cell proliferation (ACEA). Additionally, possible errors from extrapolating ACC values below tested concentrations may be contributing to interassay variability. The use of aggregate or average values may eliminate much variability for targets with a rich assay coverage (e.g., ER), but for targets with few or only a single assay, caution should be exercised in establishing a predefined EAR screening threshold without first considering the range of responses observed in a data set.

Chemical Prioritization. Individual chemicals can also be prioritized by EAR calculations. Here, chemicals were prioritized based on EARs calculated using the maximum concentrations reported in the Great Lakes data set. The full matrix of chemical−assay pairs results in a total of 50 688 theoretically possible EARs (96 detected chemicals × 528 considered assays; Table S9). However, not all possible EARs can be calculated due to chemicals not being tested in all assay batteries or chemicals being inactive in tested assays. In total, EARs could be calculated for 1245 (2.5%) chemical−assay pairs, with values ranging from 3.5×10^{-8} to 44.9. It should be again noted that chemicals in the ToxCast database have been tested in multiple phases, using variable assay platforms across phases; thus, chemicals present in the database are not necessarily tested in all the same assays (see Figure S2 and Tables S1 and S6). Of detected chemicals that were present in the ToxCast database, 73 of 96 were active in one or more assay(s). Focusing on EARs ≥ 0.01, representing approximately the upper 10% of EARs, the chemical list can be narrowed to 20 compounds and 146 chemical−assay pairs (Table S9). BPA, at a maximum detected concentration of 60.5 μg/L, had the greatest number of nonzero EARs (89) and the greatest number of EARs >1 (9). BPA is known to be an estrogen receptor agonist,[50] and 8 of 9 EARs >1 are from ER related assays. Another assay yielding a high EAR for BPA is a CAR antagonist assay. The CAR is involved in xenobiotic metabolism and energy homeostasis and can increase expression of cytochrome P450 (CYP) enzymes.[51] In addition to BPA, five other chemicals (17α-estradiol, 17β-estradiol, diethylstilbestrol, estriol, and estrone) have EARs of >1; all are natural or synthetic estrogens. A total of 14 additional chemicals have one or more EARs of >0.01 (see Table S9), including androgenic steroids (androstenedione and epitestosterone), pesticides (atrazine and metolachlor), and several other common wastewater and urban contaminants (4-nonylphenol, methadone, triclosan, and triphenyl phosphate). Methadone shows the greatest activity in a NVS opiate receptor binding assay, which is consistent with the therapeutic use of methadone as an opiate pain reliever. Triphenyl phosphate shows the greatest activity in a PPARγ receptor binding assay and has been demonstrated to interact with the human PPARγ receptor.[52,53] The known androgen receptor (AR) agonist androstenedione surprisingly has a higher EAR value in the "ATG_ERa_trans_up" assay (EAR = 0.017) than in the AR responsive assay end points (maximum EAR = 0.007). In this case, ACC extrapolation error may explain the higher predicted ER activity because the extrapolated ACC within the "ATG_ERa_trans_up" is more than 50 times below the lowest tested concentration. Another possible reason for this elevated ER activity could relate to assay platform differences. A pair of other ER-responsive assays, "TOX21_ERa_LUC_BG1_Agonist" and "ACEA_T47D_80 h_Positive", predict androstenedione to have much lower ER activity, with EARs of 3.0×10^{-4} and 5.3×10^{-7}, respectively. Additionally, androstenedione is not active in two NVS ER assays, which directly measure competitive receptor-binding, suggesting that androstenedione has a low affinity for direct binding to the ER. Androstenedione is, however, a direct precursor to estrone, a potent ER agonist, and can be converted to such by CYP-aromatase (CYP19A1).[54] ATG assays use a modified HepG2 cell line,[36] which plausibly could be more metabolically active than other assay cell lines, leading to an elevated ER signal from androstenedione through direct formation of estrone. Taken together, this example highlights the value of considering chemical response across multiple assays (if available) when elevated EAR values are observed for a chemical.

Recently, computational models have been developed to aid in separating true positive and false positive chemicals for ER, AR, and TPO assays within the ToxCast database.[55−57] Development of such models requires multiple orthogonal assays, which are not currently available for many assay targets. Nevertheless, if chemicals for these select pathways are identified through EAR analysis, the developed models could be applied to confirm that compounds are predicted to be active in the given biological pathway, further increasing confidence in the EAR prioritization of select chemicals and biological pathways.

Exposure−Activity Prioritization Validation. As part of the development of methods for an effects-based monitoring program,[16] a set of 12 water samples from the Saint Louis River watershed for which we had generated EAR values were screened for estrogenic activity using the T47D-KBluc cell line (Table S10; see the Supporting Information for methods details). This provided an opportunity to directly compare measured ER-mediated activity and EAR prioritization in these samples. The samples were collected both in the spring and the fall of 2012 along a wastewater gradient with the EriePr site upstream, WLSSD-P at the WWTP outfall, WLSSD-D downstream of the outfall, and RicesPt farthest downstream. Derived 17α-ethinylestradiol equivalents (EEQs) from the T47D-KBluc assay were compared to the range of EARs generated from the 16 ER agonist assays present in the ToxCast database (Figure 4). Derived EEQs were above detection threshold at the two sites nearest the WWTP (WLSSD-P and WLSSD-D) in all three samples and below the detection threshold at the upstream and downstream site, aside from one sample (RicesPt 9/6/2012 1015). If a median EAR cutoff of 0.01 is applied to the data set, four samples are excluded, three of which had EEQs below detection. The remaining site (RicesPt 9/6/2012 1015) had no detection of compounds active in the ToxCast ER assays but had 0.4 ng/L EEQs. For the 8 sites with median EAR values above 0.01, 2 had estimated EEQs below detection. Overall, EAR prioritization identified all sites with EEQs of >0.5 ng/L and all but one site with detectable EEQs, demonstrating high sensitivity (0.86) for predicting positive results and thereby supporting EARs as a useful screening-level prioritization tool. Incidentally, the concordance of ER results also suggests that the most influential ER agonists are being captured by the targeted analytical methods. We note, however, that ER is the most well represented assay target in the ToxCast database and endocrine active compounds are also well-represented in the suite of

DOI: 10.1021/acs.est.7b01613
Environ. Sci. Technol. 2017, 51, 8713−8724

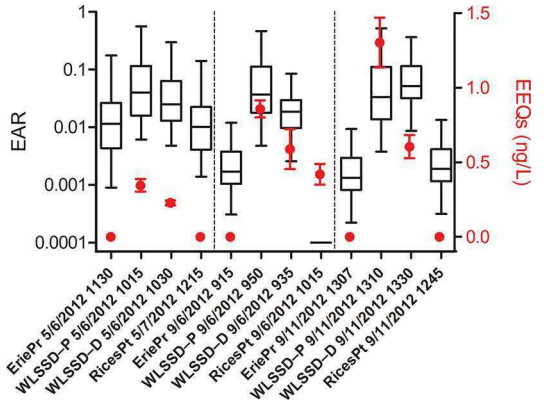

Figure 4. Comparison of exposure−activity ratios (EARs) generated from 16 estrogen receptor (ER)-related assays in the ToxCast database and in 17α-ethinylestradiol equivalents (EEQs; ng/L, in red) derived from in vitro screening with T47D-Kbluc cell line (mean ± SEM; n = 3). Samples are grouped by collection date and ordered (left to right) from upstream to downstream along the wastewater gradient. For graphical purposes, a site with no EAR calculated was assigned a value of 0.0001, and EEQs below the detection threshold were assigned a value of 0. Site information is available from the original data source.[1]

chemicals tested through the HTS assays. Biological targets with less assay and chemical coverage will need to be further investigated to verify the accuracy of other EAR estimates; nevertheless, chemical and assay coverage will only increase in the future.

Integrating EARs with Adverse Outcome Pathways. The AOP framework provides a means to link molecular level data (i.e., biological targets or pathways associated with high EARs generated from this study) to apical end points of regulatory concern (i.e., reproduction, growth, and survival). Assay targets can reflect defined molecular initiating events (MIEs) or key events (KEs) whose perturbation has been credibly linked to adverse outcomes (AOs). Key events downstream of identified assay targets can also serve as potential biomarkers for subsequent monitoring efforts. Biological pathways prioritized through EAR analysis, including ER, TPO, and PPARγ, are associated with established AOPs and were further investigated to explore potential AOs and to identify KEs, which could serve as verification of hazard in impacted ecosystems.

Assays associated with ER activation consistently showed the highest EARs across the data set. This is not unexpected for sites in close proximity to WWTPs; for example, several previous studies have demonstrated the estrogenic nature of WWTP effluent within the Saint Louis River.[17,58,59] An AOP for estrogen receptor activation leading to altered reproduction in adult fishes and subsequent declining population trajectory has been detailed by Ankley et al.[15] At the organismal level, multiple AOs are identified, including reduced fecundity in female fish, altered gamete ratio in spawning males, and impaired spawning behavior in both male and female fishes. Though data gaps exist in the full mechanistic linkage of ER activation to some KEs in the AOP, biomarkers of effect are identified and could be applied to follow-up monitoring efforts. For example, production of the egg yolk precursor protein, vitellogenin (VTG), is linked to ER activation, and measures of VTG mRNA or plasma VTG have historically been used as a biomarker of estrogenic activity in both laboratory and field studies.[59−61] In normal, unimpaired male fishes, VTG is not present or present only at very low concentrations, making this an ideal biomarker for identification of exposure to exogenous ER agonists in male fishes. The development of intersex male fish is another potential histological indicator of ER activation. Intersex in fishes has been reported at wastewater impacted sites and has previously been used as an indicator of estrogenicity of effluents.[62,63] Though the described ER activation AOP is specific to fish, aspects of it likely are applicable to other aquatic egg-laying animals as well (e.g., amphibian and avian species) because ER signaling pathways are highly conserved across vertebrate classes.[64] Conversely, a functional ER has not been identified in invertebrates, suggesting they would be of limited utility for biomonitoring for the occurrence of estrogens in the field.

Another assay end point that was identified by elevated EARs was TPO inhibition. TPO is an enzyme involved in the synthesis of thyroid hormone from mono- and di-iodotyrosines, so its inhibition leads directly to reduced thyroid hormone production.[65] TPO inhibition is a defined MIE in the publicly available AOPWiki (https://aopwiki.org) and linked to two ecologically relevant AOPs: TPO inhibition leading to reduced young of year survival via anterior swim bladder inflation (https://aopwiki.org/aops/159) and TPO inhibition leading to altered amphibian metamorphosis (https://aopwiki.org/aops/175). In both, the final AO from an ecosystem level would be population decline, an end point of regulatory importance. Thyroid hormone concentrations in the whole body[66] or specific tissues[65,67] of fish and amphibians have been used for verification of TPO inhibition in laboratory studies and could serve as a biomarker for follow-up monitoring at specific sites in wild populations[68−70] or in situ exposed organisms. Aquatic vertebrates would be considered the most susceptible class to TPO inhibition because the thyroid axis is well conserved across vertebrates.[71] Thyroid hormones have also been demonstrated to play a role in bivalves,[71] indicating that some invertebrate taxa could potentially be affected by TPO inhibition. However, it is not currently known how well invertebrate TPO orthologs relate to rat TPO, which is the target for the TPO assay in the ToxCast database.

One final biological response prioritized through the EAR analysis was PPARγ activation. At present, there is one AOP related to PPARγ activation in the AOPWiki: PPARγ activation leading to sarcomas in rodents (https://aopwiki.org/aops/163). Cancer is not generally considered an ecologically relevant end point, and other potential effects of PPARγ agonists in aquatic vertebrates are not well-defined. However, PPARγ is involved in energy metabolism, namely adipogenesis (fatty acid storage), and glucose metabolism,[72] so putative AOPs relevant to aquatic species such as fish could be proposed. Alterations to normal, homeostatic fatty acid storage or metabolism in aquatic vertebrates may adversely result in altered energy-resource storage or allocation, which could plausibly impact individual fitness, leading to decreased resources being available for survival or reproduction. For the purposes of possible follow-up environmental monitoring, an obvious, easily measured KE is not currently available for PPARγ activation, so the development of AOPs (and associated biomarkers) for PPAR activation is a research priority for our team.

The three highlighted biological targets (ER, TPO, and PPARγ) were prioritized because concentrations of one or more chemicals detected in the environment were near concentrations known to induce biological activity in vitro. This suggests the potential for observed effects in wildlife at

DOI: 10.1021/acs.est.7b01613
Environ. Sci. Technol. 2017, 51, 8713−8724

impacted sites; however, the study reporting environmental concentrations of compounds across the Great Lakes was designed as a surveillance study, capturing contaminant data from many locations but with little replication at most sites.[1] As such, it would be premature to interpret these results through the lens of risk assessment. The results do provide potential targeted end points that can be examined in more-detailed follow-up monitoring to identify whether specific biological activities are actually a concern in the prioritized sites. The EAR approach will always be limited by both occurrence and effects data; thus, the potential to underestimate the biological effects of complex mixtures remains. Incorporating other effects-based monitoring methods, such as targeted bioassays or "omics" approaches, in a tiered approach can provide a secondary means to confirm predicted effects or identify novel chemicals or biological pathways of concern that may not be captured through EAR analysis.[12]

To conclude, the presented case study highlights the potential of using HTS effects databases as a tool for environmental monitoring. Exposure−activity ratios provide a rapid, efficient tool for screening existing chemical monitoring data to prioritize sites, chemicals, and bioactivities of potential concern by leveraging HTS data sets to cast a wide-reaching net in terms of chemical availability and biological targets. While currently presented as a screening level assessment, the approach could be refined by including models to better characterize exposure of ecological receptors to environmental contaminants (e.g., bioaccumulation and metabolism) and to better characterize the dosimetry of in vitro HTS test systems. Further refinements, along with an expected increase in HTS data sources, should only continue to increase the future utility of EAR screening for environmental monitoring.

■ ASSOCIATED CONTENT

Supporting Information

The Supporting Information is available free of charge on the ACS Publications website at DOI: 10.1021/acs.est.7b01613.

Figures showing examples of point of departure estimates and a chemical−assay coverage heatmap. Details on T47D assay methods. (PDF)

Tables showing chemical occurrence and ACC values, assay categorization and activity cutoff values, alignment of CAS registry numbers, flag IDs and descriptions, chemical−assay combinations, coverage of analyzed chemicals, $EAR_{mixture}$ matrices and cumulative values, an EAR value matrix, and EEQs. (XLSX)

EAR calculation functions. (PDF)

■ AUTHOR INFORMATION

Corresponding Author

*Phone: (218)-529-5078; fax: (218)-529-5003; e-mail: blackwell.brett@epa.gov.

ORCID

Brett R. Blackwell: 0000-0003-1296-4539
Gerald T. Ankley: 0000-0002-9937-615X
Daniel L. Villeneuve: 0000-0003-2801-0203

Notes

The authors declare no competing financial interest.

■ ACKNOWLEDGMENTS

We thank Jon Doering for providing valuable comments on a previous draft of this paper. This research was performed as part of the Chemical Safety for Sustainability (CSS) research program of the U.S. Environmental Protection Agency (EPA) Office of Research and Development (ORD). Research was supported in part by the Great Lakes Restoration Initiative (GLRI). This manuscript has been reviewed in accordance with the requirements of EPA ORD. The views expressed in this work are those of the authors and do not necessarily reflect the views or policies of the U.S. EPA, nor does the mention of trade names or commercial products constitute endorsement or recommendation for use.

■ REFERENCES

(1) Lee, K. E.; Langer, S. K.; Menheer, M. A.; Hansen, D. S.; Foreman, W. T.; Furlong, E. T.; Jorgenson, Z. G.; Choy, S. J.; Moore, J. N.; Banda, J.; Gefell, D. J. Chemicals of emerging concern in water and bottom sediment in the Great Lakes Basin, 2012—Collection methods, analytical methods, quality assurance, and study data. *U.S. Geological Survey Data Series* **2015**, *910*, 14.

(2) Kolpin, D. W.; Furlong, E. T.; Meyer, M. T.; Thurman, E. M.; Zaugg, S. D.; Barber, L. B.; Buxton, H. T. Pharmaceuticals, hormones, and other organic wastewater contaminants in U.S. streams, 1999−2000: a national reconnaissance. *Environ. Sci. Technol.* **2002**, *36* (6), 1202−11.

(3) Hug, C.; Ulrich, N.; Schulze, T.; Brack, W.; Krauss, M. Identification of novel micropollutants in wastewater by a combination of suspect and nontarget screening. *Environ. Pollut.* **2014**, *184*, 25−32.

(4) Peng, H.; Chen, C.; Saunders, D. M.; Sun, J.; Tang, S.; Codling, G.; Hecker, M.; Wiseman, S.; Jones, P. D.; Li, A.; Rockne, K. J.; Giesy, J. P. Untargeted identification of organo-bromine compounds in lake sediments by ultrahigh-resolution mass spectrometry with the data-independent precursor isolation and characteristic fragment method. *Anal. Chem.* **2015**, *87* (20), 10237−46.

(5) Peng, H.; Chen, C.; Cantin, J.; Saunders, D. M.; Sun, J.; Tang, S.; Codling, G.; Hecker, M.; Wiseman, S.; Jones, P. D.; Li, A.; Rockne, K. J.; Sturchio, N. C.; Giesy, J. P. Untargeted screening and distribution of organo-bromine compounds in sediments of Lake Michigan. *Environ. Sci. Technol.* **2016**, *50* (1), 321−30.

(6) Schymanski, E. L.; Singer, H. P.; Longree, P.; Loos, M.; Ruff, M.; Stravs, M. A.; Ripolles Vidal, C.; Hollender, J. Strategies to characterize polar organic contamination in wastewater: exploring the capability of high resolution mass spectrometry. *Environ. Sci. Technol.* **2014**, *48* (3), 1811−8.

(7) Judson, R.; Richard, A.; Dix, D. J.; Houck, K.; Martin, M.; Kavlock, R.; Dellarco, V.; Henry, T.; Holderman, T.; Sayre, P.; Tan, S.; Carpenter, T.; Smith, E. The toxicity data landscape for environmental chemicals. *Environ. Health Perspec.t* **2009**, *117* (5), 685−95.

(8) Attene-Ramos, M. S.; Miller, N.; Huang, R.; Michael, S.; Itkin, M.; Kavlock, R. J.; Austin, C. P.; Shinn, P.; Simeonov, A.; Tice, R. R.; Xia, M. The Tox21 robotic platform for the assessment of environmental chemicals–from vision to reality. *Drug Discovery Today* **2013**, *18* (15−16), 716−23.

(9) Tice, R. R.; Austin, C. P.; Kavlock, R. J.; Bucher, J. R. Improving the human hazard characterization of chemicals: a Tox21 update. *Environ. Health Perspect.* **2013**, *121* (7), 756−65.

(10) Dix, D. J.; Houck, K. A.; Martin, M. T.; Richard, A. M.; Setzer, R. W.; Kavlock, R. J. The ToxCast program for prioritizing toxicity testing of environmental chemicals. *Toxicol. Sci.* **2007**, *95* (1), 5−12.

(11) Becker, R. A.; Friedman, K. P.; Simon, T. W.; Marty, M. S.; Patlewicz, G.; Rowlands, J. C. An exposure:activity profiling method for interpreting high-throughput screening data for estrogenic activity–proof of concept. *Regul. Toxicol. Pharmacol.* **2015**, *71* (3), 398−408.

(12) Schroeder, A. L.; Ankley, G. T.; Houck, K. A.; Villeneuve, D. L. Environmental surveillance and monitoring-The next frontiers for

DOI: 10.1021/acs.est.7b01613
Environ. Sci. Technol. 2017, 51, 8713−8724

high-throughput toxicology. *Environ. Toxicol. Chem.* **2016**, *35* (3), 513−25.
(13) Li, S.; Villeneuve, D. L.; Berninger, J. P.; Blackwell, B. R.; Cavallin, J. E.; Hughes, M. N.; Jensen, K. M.; Jorgenson, Z.; Kahl, M. D.; Schroeder, A. L.; Stevens, K. E.; Thomas, L. M.; Weberg, M. A.; Ankley, G. T. An integrated approach for identifying priority contaminant in the Great Lakes Basin - Investigations in the Lower Green Bay/Fox River and Milwaukee Estuary areas of concern. *Sci. Total Environ.* **2017**, *579*, 825−837.
(14) Sprague, J. B.; Ramsay, B. A. Lethal levels of mixed copper−zinc solutions for juvenile salmon. *J. Fish. Res. Board Can.* **1965**, *22* (2), 425−432.
(15) Ankley, G. T.; Bennett, R. S.; Erickson, R. J.; Hoff, D. J.; Hornung, M. W.; Johnson, R. D.; Mount, D. R.; Nichols, J. W.; Russom, C. L.; Schmieder, P. K.; Serrrano, J. A.; Tietge, J. E.; Villeneuve, D. L. Adverse outcome pathways: a conceptual framework to support ecotoxicology research and risk assessment. *Environ. Toxicol. Chem.* **2010**, *29* (3), 730−41.
(16) Ekman, D. R.; Ankley, G. T.; Blazer, V. S.; Collette, T. W.; Garcia-Reyero, N.; Iwanowicz, L. R.; Jorgenson, Z. G.; Lee, K. E.; Mazik, P. M.; Miller, D. H.; Perkins, E. J.; Smith, E. T.; Tietge, J. E.; Villeneuve, D. L. Environmental reviews and case studies: Biological effects−based tools for monitoring impacted surface waters in the Great Lakes: A multiagency program in support of the Great Lakes Restoration Initiative. *Environ. Pract.* **2013**, *15* (04), 409−426.
(17) Kahl, M. D.; Villeneuve, D. L.; Stevens, K.; Schroeder, A.; Makynen, E. A.; LaLone, C. A.; Jensen, K. M.; Hughes, M.; Holmen, B. A.; Eid, E.; Durhan, E. J.; Cavallin, J. E.; Berninger, J.; Ankley, G. T. An inexpensive, temporally integrated system for monitoring occurrence and biological effects of aquatic contaminants in the field. *Environ. Toxicol. Chem.* **2014**, *33* (7), 1584−95.
(18) Zaugg, S. D.; Smith, S. G.; Schroeder, M. P. Determination of wastewater compounds in whole water by continuous liquid−liquid extraction and capillary-column gas chromatography/mass spectrometry. *U.S. Geological Survey Techniques and Methods* **2006**, 30.
(19) Zaugg, S. D.; Phillips, P. J.; Smith, S. G. Analysis of pharmaceutical and other organic wastewater compounds in filtered and unfiltered water samples by gas chromatography/mass spectrometry. *U.S. Geological Survey Open-File Report 2013−1297* **2014**, 24.
(20) Foreman, W. T.; Gray, J. L.; ReVello, R. C.; Lindley, C. E.; Losche, S. A.; Barber, L. B. Determination of steroid hormones and related compounds in filtered and unfiltered water by solid-phase extraction, derivatization, and gas chromatography with tandem mass spectrometry. *U.S. Geological Survey Techniques and Methods* **2012**, 118.
(21) Childress, C.; Foreman, W.; Connor, B.; Maloney, T. New reporting procedures based on long-term method detection levels and some considerations for interpretations of water-quality data provided by the U.S. Geological Survey National Water Quality Laboratory. *U.S. Geological Survey Open-File Report 1999−193* **1999**, 1.
(22) Wilson, V. S.; Bobseine, K.; Gray, L. E., Jr. Development and characterization of a cell line that stably expresses an estrogen-responsive luciferase reporter for the detection of estrogen receptor agonist and antagonists. *Toxicol. Sci.* **2004**, *81* (1), 69−77.
(23) US EPA. ToxCast & Tox21 Summary Files from invitrodb_v2. https://www.epa.gov/chemical-research/toxicity-forecaster-toxcasttm-data (accessed Jan 20, 2016).
(24) Attene-Ramos, M. S.; Huang, R.; Michael, S.; Witt, K. L.; Richard, A.; Tice, R. R.; Simeonov, A.; Austin, C. P.; Xia, M. Profiling of the Tox21 chemical collection for mitochondrial function to identify compounds that acutely decrease mitochondrial membrane potential. *Environ. Health Perspect.* **2014**, *123* (1), 49−56.
(25) Giuliano, K. A.; Gough, A. H.; Taylor, D. L.; Vernetti, L. A.; Johnston, P. A. Early safety assessment using cellular systems biology yields insights into mechanisms of action. *J. Biomol. Screening* **2010**, *15* (7), 783−97.
(26) Houck, K. A.; Dix, D. J.; Judson, R. S.; Kavlock, R. J.; Yang, J.; Berg, E. L. Profiling bioactivity of the ToxCast chemical library using BioMAP primary human cell systems. *J. Biomol. Screening* **2009**, *14* (9), 1054−66.
(27) Huang, R.; Xia, M.; Cho, M. H.; Sakamuru, S.; Shinn, P.; Houck, K. A.; Dix, D. J.; Judson, R. S.; Witt, K. L.; Kavlock, R. J.; Tice, R. R.; Austin, C. P. Chemical genomics profiling of environmental chemical modulation of human nuclear receptors. *Environ. Health Perspect.* **2011**, *119* (8), 1142−8.
(28) Huang, R.; Sakamuru, S.; Martin, M. T.; Reif, D. M.; Judson, R. S.; Houck, K. A.; Casey, W.; Hsieh, J. H.; Shockley, K. R.; Ceger, P.; Fostel, J.; Witt, K. L.; Tong, W.; Rotroff, D. M.; Zhao, T.; Shinn, P.; Simeonov, A.; Dix, D. J.; Austin, C. P.; Kavlock, R. J.; Tice, R. R.; Xia, M. Profiling of the Tox21 10K compound library for agonists and antagonists of the estrogen receptor alpha signaling pathway. *Sci. Rep.* **2015**, *4*, 5664.
(29) Karmaus, A. L.; Toole, C. M.; Filer, D. L.; Lewis, K. C.; Martin, M. T. High-throughput screening of chemical effects on steroidogenesis using H295R human adrenocortical carcinoma cells. *Toxicol. Sci.* **2016**, *150* (2), 323−32.
(30) Kleinstreuer, N. C.; Yang, J.; Berg, E. L.; Knudsen, T. B.; Richard, A. M.; Martin, M. T.; Reif, D. M.; Judson, R. S.; Polokoff, M.; Dix, D. J.; Kavlock, R. J.; Houck, K. A. Phenotypic screening of the ToxCast chemical library to classify toxic and therapeutic mechanisms. *Nat. Biotechnol.* **2014**, *32* (6), 583−91.
(31) Knudsen, T. B.; Houck, K. A.; Sipes, N. S.; Singh, A. V.; Judson, R. S.; Martin, M. T.; Weissman, A.; Kleinstreuer, N. C.; Mortensen, H. M.; Reif, D. M.; Rabinowitz, J. R.; Setzer, R. W.; Richard, A. M.; Dix, D. J.; Kavlock, R. J. Activity profiles of 309 ToxCast chemicals evaluated across 292 biochemical targets. *Toxicology* **2011**, *282* (1−2), 1−15.
(32) MacDonald, M. L.; Lamerdin, J.; Owens, S.; Keon, B. H.; Bilter, G. K.; Shang, Z.; Huang, Z.; Yu, H.; Dias, J.; Minami, T.; Michnick, S. W.; Westwick, J. K. Identifying off-target effects and hidden phenotypes of drugs in human cells. *Nat. Chem. Biol.* **2006**, *2* (6), 329−37.
(33) Martin, M. T.; Dix, D. J.; Judson, R. S.; Kavlock, R. J.; Reif, D. M.; Richard, A. M.; Rotroff, D. M.; Romanov, S.; Medvedev, A.; Poltoratskaya, N.; Gambarian, M.; Moeser, M.; Makarov, S. S.; Houck, K. A. Impact of environmental chemicals on key transcription regulators and correlation to toxicity end points within EPA's ToxCast program. *Chem. Res. Toxicol.* **2010**, *23* (3), 578−90.
(34) Padilla, S.; Corum, D.; Padnos, B.; Hunter, D. L.; Beam, A.; Houck, K. A.; Sipes, N.; Kleinstreuer, N.; Knudsen, T.; Dix, D. J.; Reif, D. M. Zebrafish developmental screening of the ToxCast Phase I chemical library. *Reprod. Toxicol.* **2012**, *33* (2), 174−87.
(35) Paul, K. B.; Hedge, J. M.; Rotroff, D. M.; Hornung, M. W.; Crofton, K. M.; Simmons, S. O. Development of a thyroperoxidase inhibition assay for high-throughput screening. *Chem. Res. Toxicol.* **2014**, *27* (3), 387−99.
(36) Romanov, S.; Medvedev, A.; Gambarian, M.; Poltoratskaya, N.; Moeser, M.; Medvedeva, L.; Gambarian, M.; Diatchenko, L.; Makarov, S. Homogeneous reporter system enables quantitative functional assessment of multiple transcription factors. *Nat. Methods* **2008**, *5* (3), 253−60.
(37) Rotroff, D. M.; Beam, A. L.; Dix, D. J.; Farmer, A.; Freeman, K. M.; Houck, K. A.; Judson, R. S.; LeCluyse, E. L.; Martin, M. T.; Reif, D. M.; Ferguson, S. S. Xenobiotic-metabolizing enzyme and transporter gene expression in primary cultures of human hepatocytes modulated by ToxCast chemicals. *J. Toxicol. Environ. Health, Part B* **2010**, *13* (2−4), 329−46.
(38) Rotroff, D. M.; Dix, D. J.; Houck, K. A.; Kavlock, R. J.; Knudsen, T. B.; Martin, M. T.; Reif, D. M.; Richard, A. M.; Sipes, N. S.; Abassi, Y. A.; Jin, C.; Stampfl, M.; Judson, R. S. Real-time growth kinetics measuring hormone mimicry for ToxCast chemicals in T-47D human ductal carcinoma cells. *Chem. Res. Toxicol.* **2013**, *26* (7), 1097−107.
(39) Sipes, N. S.; Martin, M. T.; Kothiya, P.; Reif, D. M.; Judson, R. S.; Richard, A. M.; Houck, K. A.; Dix, D. J.; Kavlock, R. J.; Knudsen, T. B. Profiling 976 ToxCast chemicals across 331 enzymatic and receptor signaling assays. *Chem. Res. Toxicol.* **2013**, *26* (6), 878−95.

DOI: 10.1021/acs.est.7b01613
Environ. Sci. Technol. 2017, 51, 8713−8724

(40) Stossi, F.; Bolt, M. J.; Ashcroft, F. J.; Lamerdin, J. E.; Melnick, J. S.; Powell, R. T.; Dandekar, R. D.; Mancini, M. G.; Walker, C. L.; Westwick, J. K.; Mancini, M. A. Defining estrogenic mechanisms of bisphenol A analogs through high throughput microscopy-based contextual assays. *Chem. Biol.* **2014**, *21* (6), 743−53.
(41) Truong, L.; Reif, D. M.; Mary, L., St; Geier, M. C.; Truong, H. D.; Tanguay, R. L. Multidimensional in vivo hazard assessment using zebrafish. *Toxicol. Sci.* **2014**, *137* (1), 212−33.
(42) Filer, D. L.; Kothiya, P.; Setzer, R. W.; Judson, R. S.; Martin, M. T. tcpl: The ToxCast pipeline for high-throughput screening data. *Bioinformatics* **2016**, *33* (4), 618−20.
(43) Putzrath, R. M.; DABT. Estimating relative potency for receptor-mediated toxicity: reevaluating the toxicity equivalence factor (TEF) model. *Regul. Toxicol. Pharmacol.* **1997**, *25* (1), 68−78.
(44) Kavlock, R.; Chandler, K.; Houck, K.; Hunter, S.; Judson, R.; Kleinstreuer, N.; Knudsen, T.; Martin, M.; Padilla, S.; Reif, D.; Richard, A.; Rotroff, D.; Sipes, N.; Dix, D. Update on EPA's ToxCast program: providing high throughput decision support tools for chemical risk management. *Chem. Res. Toxicol.* **2012**, *25* (7), 1287−302.
(45) Richard, A. M.; Judson, R. S.; Houck, K. A.; Grulke, C. M.; Volarath, P.; Thillainadarajah, I.; Yang, C.; Rathman, J.; Martin, M. T.; Wambaugh, J. F.; Knudsen, T. B.; Kancherla, J.; Mansouri, K.; Patlewicz, G.; Williams, A. J.; Little, S. B.; Crofton, K. M.; Thomas, R. S. ToxCast chemical landscape: Paving the road to 21st Century toxicology. *Chem. Res. Toxicol.* **2016**, *29* (8), 1225−51.
(46) Dickinson, J. H.; Smith, G. G. A new and practical oral contraceptive agent: norethindrone with mestranol. *Can. Medi. Assoc. J.* **1963**, *89*, 242−5.
(47) Blackwell, B. R.; Brown, T. R.; Broadway, P. R.; Buser, M. D.; Brooks, J. C.; Johnson, B. J.; Cobb, G. P.; Smith, P. N. Characterization of trenbolone acetate and estradiol metabolite excretion profiles in implanted steers. *Environ. Toxicol. Chem.* **2014**, *33* (12), 2850−8.
(48) Hanselman, T. A.; Graetz, D. A.; Wilkie, A. C. Manure-borne estrogens as potential environmental contaminants: A review. *Environ. Sci. Technol.* **2003**, *37* (24), 5471−5478.
(49) Raun, A. P.; Preston, R. L. History of diethylstilbestrol use in cattle. *J. Anim. Sci.* **2002**, *80*, 1−7.
(50) Krishnan, A. V.; Stathis, P.; Permuth, S. F.; Tokes, L.; Feldman, D. Bisphenol-A: an estrogenic substance is released from polycarbonate flasks during autoclaving. *Endocrinology* **1993**, *132* (6), 2279−86.
(51) Kachaylo, E. M.; Pustylnyak, V. O.; Lyakhovich, V. V.; Gulyaeva, L. F. Constitutive androstane receptor (CAR) is a xenosensor and target for therapy. *Biochemistry (Moscow)* **2011**, *76* (10), 1087−97.
(52) Pillai, H. K.; Fang, M.; Beglov, D.; Kozakov, D.; Vajda, S.; Stapleton, H. M.; Webster, T. F.; Schlezinger, J. J. Ligand binding and activation of PPARgamma by Firemaster(R) 550: effects on adipogenesis and osteogenesis in vitro. *Environ. Health Perspect.* **2014**, *122* (11), 1225−32.
(53) Fang, M.; Webster, T. F.; Ferguson, P. L.; Stapleton, H. M. Characterizing the peroxisome proliferator-activated receptor (PPARgamma) ligand binding potential of several major flame retardants, their metabolites, and chemical mixtures in house dust. *Environ. Health Perspect.* **2014**, *123* (2), 166−72.
(54) Miller, W. L. Molecular biology of steroid hormone synthesis. *Endocr. Rev.* **1988**, *9* (3), 295−318.
(55) Judson, R. S.; Magpantay, F. M.; Chickarmane, V.; Haskell, C.; Tania, N.; Taylor, J.; Xia, M.; Huang, R.; Rotroff, D. M.; Filer, D. L.; Houck, K. A.; Martin, M. T.; Sipes, N.; Richard, A. M.; Mansouri, K.; Setzer, R. W.; Knudsen, T. B.; Crofton, K. M.; Thomas, R. S. Integrated model of chemical perturbations of a biological pathway using 18 in vitro high-throughput screening assays for the estrogen receptor. *Toxicol. Sci.* **2015**, *148* (1), 137−54.
(56) Kleinstreuer, N. C.; Ceger, P.; Watt, E. D.; Martin, M.; Houck, K.; Browne, P.; Thomas, R. S.; Casey, W. M.; Dix, D. J.; Allen, D.; Sakamuru, S.; Xia, M.; Huang, R.; Judson, R. Development and validation of a computational model for androgen receptor activity. *Chem. Res. Toxicol.* **2017**, *30* (4), 946−64.
(57) Paul Friedman, K.; Watt, E. D.; Hornung, M. W.; Hedge, J. M.; Judson, R. S.; Crofton, K. M.; Houck, K. A.; Simmons, S. O. Tiered high-throughput screening approach to identify thyroperoxidase inhibitors within the ToxCast Phase I and II chemical libraries. *Toxicol. Sci.* **2016**, *151* (1), 160−80.
(58) Davis, J. M.; Ekman, D. R.; Teng, Q.; Ankley, G. T.; Berninger, J. P.; Cavallin, J. E.; Jensen, K. M.; Kahl, M. D.; Schroeder, A. L.; Villeneuve, D. L.; Jorgenson, Z. G.; Lee, K. E.; Collette, T. W. Linking field-based metabolomics and chemical analyses to prioritize contaminants of emerging concern in the Great Lakes basin. *Environ. Toxicol. Chem.* **2016**, *35* (10), 2493−502.
(59) Cavallin, J. E.; Jensen, K. M.; Kahl, M. D.; Villeneuve, D. L.; Lee, K. E.; Schroeder, A. L.; Mayasich, J.; Eid, E. P.; Nelson, K. R.; Milsk, R. Y.; Blackwell, B. R.; Berninger, J. P.; LaLone, C. A.; Blanksma, C.; Jicha, T.; Elonen, C.; Johnson, R.; Ankley, G. T. Pathway-based approaches for assessment of real-time exposure to an estrogenic wastewater treatment plant effluent on fathead minnow reproduction. *Environ. Toxicol. Chem.* **2016**, *35* (3), 702−16.
(60) Kramer, V. J.; Miles-Richardson, S.; Pierens, S. L.; Giesy, J. P. Reproductive impairment and induction of alkaline-labile phosphate, a biomarker of estrogen exposure, in fathead minnows (Pimephales promelas) exposed to waterborne 17 beta-estradiol. *Aquat. Toxicol.* **1998**, *40* (4), 335−360.
(61) Routledge, E. J.; Sheahan, D.; Desbrow, C.; Brighty, G. C.; Waldock, M.; Sumpter, J. P. Identification of estrogenic chemicals in STW effluent. 2. In vivo responses in trout and roach. *Environ. Sci. Technol.* **1998**, *32* (11), 1559−1565.
(62) Woodling, J. D.; Lopez, E. M.; Maldonado, T. A.; Norris, D. O.; Vajda, A. M. Intersex and other reproductive disruption of fish in wastewater effluent dominated Colorado streams. *Comp. Biochem. Physiol., Part C: Toxicol. Pharmacol.* **2006**, *144* (1), 10−5.
(63) Vajda, A. M.; Barber, L. B.; Gray, J. L.; Lopez, E. M.; Woodling, J. D.; Norris, D. O. Reproductive disruption in fish downstream from an estrogenic wastewater effluent. *Environ. Sci. Technol.* **2008**, *42* (9), 3407−14.
(64) Eick, G. N.; Thornton, J. W. Evolution of steroid receptors from an estrogen-sensitive ancestral receptor. *Mol. Cell. Endocrinol.* **2011**, *334* (1−2), 31−8.
(65) Tietge, J. E.; Degitz, S. J.; Haselman, J. T.; Butterworth, B. C.; Korte, J. J.; Kosian, P. A.; Lindberg-Livingston, A. J.; Burgess, E. M.; Blackshear, P. E.; Hornung, M. W. Inhibition of the thyroid hormone pathway in Xenopus laevis by 2-mercaptobenzothiazole. *Aquat. Toxicol.* **2013**, *126*, 128−36.
(66) Nelson, K. R.; Schroeder, A. L.; Ankley, G. T.; Blackwell, B. R.; Blanksma, C.; Degitz, S. J.; Flynn, K. M.; Jensen, K. M.; Johnson, R. D.; Kahl, M. D.; Knapen, D.; Kosian, P. A.; Milsk, R. Y.; Randolph, E. C.; Saari, T.; Stinckens, E.; Vergauwen, L.; Villeneuve, D. L. Impaired anterior swim bladder inflation following exposure to the thyroid peroxidase inhibitor 2-mercaptobenzothiazole part I: Fathead minnow. *Aquat. Toxicol.* **2016**, *173*, 192−203.
(67) Hornung, M. W.; Kosian, P. A.; Haselman, J. T.; Korte, J. J.; Challis, K.; Macherla, C.; Nevalainen, E.; Degitz, S. J. In Vitro, Ex Vivo, and In Vivo determination of thyroid hormone modulating activity of benzothiazoles. *Toxicol. Sci.* **2015**, *146* (2), 254−64.
(68) Brar, N. K.; Waggoner, C.; Reyes, J. A.; Fairey, R.; Kelley, K. M. Evidence for thyroid endocrine disruption in wild fish in San Francisco Bay, California, USA. Relationships to contaminant exposures. *Aquat. Toxicol.* **2010**, *96* (3), 203−15.
(69) Simmons, D. B.; McMaster, M. E.; Reiner, E. J.; Hewitt, L. M.; Parrott, J. L.; Park, B. J.; Brown, S. B.; Sherry, J. P. Wild fish from the Bay of Quinte Area of Concern contain elevated tissue concentrations of PCBs and exhibit evidence of endocrine-related health effects. *Environ. Int.* **2014**, *66*, 124−37.
(70) Couderc, M.; Marchand, J.; Zalouk-Vergnoux, A.; Kamari, A.; Moreau, B.; Blanchet-Letrouve, I.; Le Bizec, B.; Mouneyrac, C.; Poirier, L. Thyroid endocrine status of wild European eels (Anguilla

DOI: 10.1021/acs.est.7b01613
Environ. Sci. Technol. 2017, 51, 8713−8724

anguilla) in the Loire (France). Relationships with organic contaminant body burdens. *Sci. Total Environ.* **2016**, *550*, 391−405.
(71) Bonett, R. M. Analyzing endocrine system conservation and evolution. *Gen. Comp. Endocrinol.* **2016**, *234*, 3−9.
(72) Kersten, S.; Desvergne, B.; Wahli, W. Roles of PPARs in health and disease. *Nature* **2000**, *405* (6785), 421−4.

DOI: 10.1021/acs.est.7b01613
Environ. Sci. Technol. 2017, 51, 8713−8724

Science of the Total Environment 686 (2019) 995–1009

Contents lists available at ScienceDirect

Science of the Total Environment

journal homepage: www.elsevier.com/locate/scitotenv

Prioritizing chemicals of ecological concern in Great Lakes tributaries using high-throughput screening data and adverse outcome pathways

Steven R. Corsi [a,*], Laura A. De Cicco [a], Daniel L. Villeneuve [b], Brett R. Blackwell [b], Kellie A. Fay [c,1], Gerald T. Ankley [b], Austin K. Baldwin [d]

[a] U.S. Geological Survey, Middleton, WI 53562, United States
[b] U.S. Environmental Protection Agency, Office of Research and Development, Duluth, MN 55804, United States
[c] General Dynamics Information Technology, Duluth, MN 55804, United States
[d] U.S. Geological Survey, Boise, ID 83702, United States

HIGHLIGHTS

- Potential for ecological impacts of 67 organic contaminants was evaluated.
- Use of ToxCast data increased the number for which bioeffects could be assessed.
- Chemicals and sites with greatest potential for adverse bioeffects were identified.
- Adverse outcome pathways linked ToxCast responses to potential adverse outcomes.
- Mixture effects were predicted using ToxCast exposure-activity-ratios and AOPs.

GRAPHICAL ABSTRACT

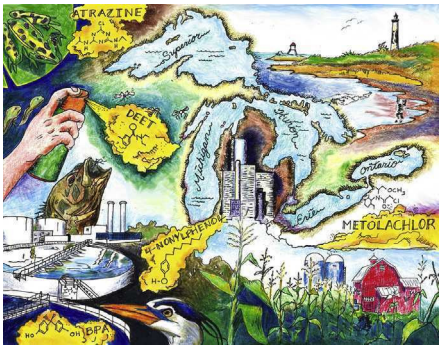

ARTICLE INFO

Article history:
Received 2 May 2019
Received in revised form 28 May 2019
Accepted 30 May 2019
Available online 5 June 2019

Editor: Damia Barcelo

Keywords:
Surface water
Organic contaminants
Chemical mixtures
Bioeffects
High-throughput screening
Adverse outcome pathways

ABSTRACT

Chemical monitoring data were collected in surface waters from 57 Great Lakes tributaries from 2010 to 13 to identify chemicals of potential biological relevance and sites at which these chemicals occur. Traditional water-quality benchmarks for aquatic life based on in vivo toxicity data were available for 34 of 67 evaluated chemicals. To expand evaluation of potential biological effects, measured chemical concentrations were compared to chemical-specific biological activities determined in high-throughput (ToxCast) in vitro assays. Resulting exposure-activity ratios (EARs) were used to prioritize the chemicals of greatest potential concern: 4 nonylphenol, bisphenol A, metolachlor, atrazine, DEET, caffeine, tris(2 butoxyethyl) phosphate, tributyl phosphate, triphenyl phosphate, benzo(a)pyrene, fluoranthene, and benzophenone. Water-quality benchmarks were unavailable for five of these chemicals, but for the remaining seven, EAR-based prioritization was consistent with that based on toxicity quotients calculated from benchmarks. Water-quality benchmarks identified three additional PAHs (anthracene, phenanthrene, and pyrene) not prioritized using EARs. Through this analysis, an EAR of 10^{-3} was identified as a reasonable threshold above which a chemical might be of potential concern. To better understand apical hazards potentially associated with biological activities captured in ToxCast assays, in vitro bioactivity data were matched with available adverse outcome pathway (AOP) information. The 49 ToxCast assays prioritized via EAR analysis aligned with 23 potentially-relevant AOPs present in the AOP-Wiki. Mixture effects at monitored sites were estimated by summation of EAR values for multiple chemicals by

* Corresponding author.
E-mail address: srcorsi@usgs.gov (S.R. Corsi).
[1] Current affiliation, U.S. Environmental Protection Agency.

https://doi.org/10.1016/j.scitotenv.2019.05.457
0048-9697/Published by Elsevier B.V. This is an open access article under the CC BY-NC-ND license (http://creativecommons.org/licenses/by-nc-nd/4.0/).

individual assay or individual AOP. Commonly predicted adverse outcomes included impacts on reproduction and mitochondrial function. The EAR approach provided a screening-level assessment for evidence-based prioritization of chemicals and sites with potential for adverse biological effects. The approach aids prioritization of future monitoring activities and provides testable hypotheses to help focus those efforts. This also expands the fraction of detected chemicals for which biologically-based benchmark concentrations are available to help contextualize chemical monitoring results.

Published by Elsevier B.V. This is an open access article under the CC BY-NC-ND license (http://creativecommons.org/licenses/by-nc-nd/4.0/).

1. Introduction

Tributaries of the Great Lakes are influenced by a diverse set of stressors that may cause adverse ecological effects. Consequently, deciding how to most effectively allocate limited resources for management and monitoring activities can be a challenge. When mixtures of contaminants are detected, it can be difficult to determine which contaminants are of greatest concern and in turn what potential source mitigation or remediation strategies could most effectively lower risk. For example, in addition to legacy contamination with compounds such as polychlorinated biphenyls (PCBs) and dichlorodiphenyltrichloroethane (DDT), Great Lakes tributary ecosystems are influenced by current-use contaminants from sources such as urban and agricultural runoff, treated and untreated wastewater, and atmospheric deposition (Custer et al., 2016; Furdui et al., 2007; Guo et al., 2017a, 2017b; Lepak et al., 2015). Contaminants from these sources include polycyclic aromatic hydrocarbons (PAHs), pesticides, pharmaceutical and personal care products, flame retardants, plasticizers, detergents, and degradation products of these contaminants, among others (Baldwin et al., 2016; Elliott et al., 2017, 2018a).

During 2010–13, 709 surface-water samples were collected in 57 Great Lakes tributaries and analyzed for 67 organic compounds that represent 15 classes of chemicals based on their functional use or chemical properties (Baldwin et al., 2016). Watersheds included in this effort represent a broad range of urban, agricultural, forested, and water and wetland land cover attributes (Table SI-1), and samples were collected to capture spatial, seasonal, and hydrologic variability. Understanding the potential significance of these contaminants on aquatic ecosystem health can be a challenge. For example, a comprehensive search for US and Canadian water-quality benchmarks for acute and chronic exposure to aquatic life for the 67 target analytes resulted in information for only 34 of them from 10 chemical classes (Baldwin et al., 2016). Considering the limited number of traditional, in vivo-based water-quality benchmarks available for the diverse range of contaminants, we aimed to expand the scope of our screening-level characterization of potential biological significance by leveraging the growing database of chemical-specific high throughput in vitro biological activity data generated via the ToxCast and Tox21 (hereafter referred to as ToxCast) programs (Dix et al., 2007; Kavlock et al., 2012; Tice et al., 2013).

The ToxCast database contains information on biological activities of thousands of chemicals. The information comes from several hundred high-throughput assays that cover a range of cell responses and approximately 300 signaling pathways (Kavlock et al., 2012; Tice et al., 2013). A number of other sources of potential chemical-biological interaction data also exists, including PubChem (Kim et al., 2016), ChEMBL (Gaulton et al., 2017), ToxNet (Fonger et al., 2000), TG-GATEs (Igarashi et al., 2015), the Comparative Toxicogenomics Database (Davis et al., 2013), and the Connectivity Map (Lamb et al., 2006; Subramanian et al., 2017). However, most of these sources aggregate chemical-biological interactions from the peer-reviewed literature where the use of different experimental designs, assay systems, testing conditions, and analytical/statistical approaches can confound quantitative comparisons of potency. In contrast, ToxCast chemicals were tested in a consistent and standardized set of assays and resultant data were analyzed with a uniform analysis pipeline (Filer et al., 2016). This allows for more reliable comparison of the relative potency of the tested chemicals thereby supporting the type of comparative prioritization analysis that was the aim of the present study.

Using in vitro bioeffects data in this manner is consistent with the long-range vision for toxicity-testing described in the National Research Council (NRC) report "Toxicity Testing in the 21st Century—a vision and strategy" (Krewski et al., 2010). This NRC report envisioned more efficient and effective strategies for toxicity-testing given advances in our understanding of biology and the emergence of modern testing technologies. Considering the complex mixture of chemicals that often occur in environmental waters impacted by multiple different sources and land uses, evaluation of potential biological effects could benefit from this 21st century approach to toxicity evaluation. While information from these techniques is commonly targeted at human health impacts, recent studies have explored it for use in evaluation of potential adverse impacts in nonmammalian species as well including evaluation of potential impact on aquatic life (Blackwell et al., 2017, 2019; Heiger-Bernays et al., 2018; Schroeder et al., 2016) and avian species (Elliott et al., 2018b). For this type of prioritization, exposure-activity ratios (EARs = sample concentration/bioactivity effect concentration) have been identified as a valuable calculation (Blackwell et al., 2017; Elliott et al., 2018b); however, it is currently unclear what EAR threshold to consider as a level of concern and whether the threshold is relatively constant or changes substantially as different chemicals are evaluated, and an evaluation is needed to determine which ToxCast assays and related adverse outcome pathways are ecologically relevant.

The objectives of the current study were to couple the contaminant surveillance data from 57 monitored Great Lakes tributaries with high-throughput assay results from ToxCast to (1) assess whether the EAR approach appears to be valuable in this context, (2) if so, determine what EAR level(s) warrant concern based on comparison with evaluations using traditional water quality benchmarks, (3) identify chemicals of concern, (4) screen for potential adverse biological effects that may be associated with those chemicals, through linking bioactivity data to adverse outcome pathways (AOPs) for ecologically-relevant species, and (5) prioritize tributaries with respect to potential biological effects.

2. Methods

2.1. Sampling design

The Great Lakes tributaries were sampled from September 2010 through September 2013 and included sites draining to each of the five Great Lakes (Fig. SI-1, Table SI-1). A total of 709 water samples were collected. The study was designed to provide a general indication of contaminants in Great Lakes tributaries on spatial, temporal, and seasonal scales. Thirty-eight of the sites were sampled only one or two times to provide background information on a large spatial scale and identify potential concern for future studies. These sites were thought to be less likely to have large numbers of contaminants present than sites sampled more frequently given their history and land use composition. The remaining 19 sites were sampled more frequently with 7–64 samples that added to the spatial extent of the study and served to represent temporal and seasonal variability. Drainage areas ranged from 101 to 16,400 km^2, with mean annual flows from 2.58 to 219 cubic meters per second (October 2010–September 2013). Watershed land cover varied from dominantly urban (up to 92% of watershed) to agricultural

(up to 84%) to forest and wetland (up to 93%). Watershed population densities ranged from 1.3 to 964 people/km^2 with 0% to 47% mean annual streamflow contributions from wastewater treatment plants. Details of the site selection, sampling design, sampling protocols, and quality assurance sample results have been previously published (Baldwin et al., 2016).

Whole water samples were analyzed for 67 organic waste compounds at the U.S. Geological Survey National Water Quality Laboratory in Denver, CO. Compounds were extracted using continuous liquid-liquid extraction and methylene chloride solvent, then determined by capillary-column gas chromatography/mass spectrometry (Zaugg et al., 2006). Four analytes were omitted from the final data set due to contamination in blank sample results (phenol, bis(2 ethylhexyl) phthalate (DEHP), acetophenone, and triethyl citrate). Analytes were categorized into 15 chemical classes based on their functional use or chemical properties (Table SI-2) and all analytical data have been previously published (Baldwin et al., 2016).

2.2. Screening values

2.2.1. ToxCast

Results from the ToxCast database (US EPA, 2015) were used to evaluate potential biological activities that may be associated with chemicals detected in the water samples. The ToxCast program evaluates individual chemicals for interactions with, or effects on, cells, proteins, DNA, RNA, mitochondria, receptors, and enzymes, etc. (Judson et al., 2016). For most of the ToxCast assays, annotations describing the intended biological targets are available in the database download (https://www.epa.gov/chemical-research/toxicity-forecaster-toxcasttm-data) or the U.S. Environmental Protection Agency (US EPA) CompTox dashboard (https://comptox.epa.gov/dashboard). The ToxCast data analysis pipeline provides several summary metrics modeled from chemical dose-assay response curves: the activity concentration at cutoff (ACC), the half maximal activity concentration (AC50), and the top value (T), or efficacy (Filer et al., 2016). The ACC is an assay-specific metric determined as a multiplier of the baseline median absolute deviation of measured activity in the assay that provides an indication of the concentration at which the bioactivity measured first exceeds the baseline concentration. More thorough descriptions of its derivation are provided elsewhere (Filer et al., 2016; Judson et al., 2009). Because this metric is indexed to a standard response threshold and is not dependent on chemical-specific activity, its use has been favored in recent applications of the ToxCast data over the other metrics (Blackwell et al., 2017; Fay et al., 2018). Thus, the ACC (parameter name modl acc in the ToxCast database) was used as the final endpoint for comparison with water quality data.

For this study, data from all assay platforms (Kavlock et al., 2012) available in the ToxCast database were considered, with the exception of BioSeek, which had several endpoint values that were anomalously low compared to those from other sources. Considering the nature of the assays and the associated reliability/quality for detecting gain or loss of signal, Attagene "gain" endpoints and Novascreen "loss" endpoints were used, while Attagene "loss" endpoints and Novascreen "gain" endpoints were removed because these assays were not optimized or designed to report for the given assay direction (Blackwell et al., 2017). Chemical/assay combinations that did not result in a significant test response (a "hit call") were also removed from consideration.

Data quality remarks were included with the reported metrics for the ToxCast test data. Results with the following data quality flags were removed from consideration for the present study: "Borderline active", "Only highest conc above baseline, active", "Gain AC50 < lowest conc & loss AC50 < mean conc", and "Biochemical assay with <50% efficacy". All results from in vivo zebrafish embryo assays (NHEERL_PADILLA) matched at least one of these filtering criteria, and so were removed. Dose-response curves for chemical-assay combinations remaining after this selection process were also examined manually. Eleven of these dose-response curves were found to be of questionable quality based on anomalous values or lack of response and removed from analysis: NVS_ENZ_hPTEN for nonylphenol, NVS_ENZ_rMAOBP for Diethyl phthalate, TOX21_p53_BLA_p3_viability for Cotinine, TOX21_p53_BLA_p5_ratio for Metolachlor, TOX21_p53_BLA_p3_ratio for Carbazole, TOX21_p53_BLA_p3_ratio for Triphenyl phosphate, TOX21_p53_BLA_p3_ratio for Tris(2 chloroethyl) phosphate, TOX21_p53_BLA_p3_ratio for Fluoranthene, NVS_NR_hPPARg for Triphenyl phosphate, CLD_CYP1A1_6hr for bisphenol A (BPA), CLD_CYP1A2_6hr for BPA. In addition, the Tanguay_ZF_120hpf_ActivityScores were removed since this endpoint is an aggregation of activity from other zebrafish assays that are all represented separately in the ToxCast data set. With these various exclusions, 255 total ToxCast assays were suitable for computations for the chemical data set in the present study (Table SI-3).

Of the 65 chemicals detected from the tributary samples, 54 (83%) were represented in ToxCast (i.e., tested in at least one ToxCast assay). Among those 54, 48 had measurable effects (i.e., at least one active hit call) within the range of concentrations tested. The number of active hits per chemical ranged from 1 to 92 assays (Table SI-4).

2.3. Data analysis procedures

2.3.1. Screening for potential pathway-based effects

To screen the water chemistry data for potential bioactivity, chemical concentrations were compared to effect concentrations in ToxCast assays by computing EAR values as the quotient of the measured concentration and the ACC for each assay-chemical combination. The EAR is analogous to a hazard quotient, but rather than relying on a concentration at which adverse health effects like impaired survival, growth, or reproduction are detected, one instead uses the concentration required to elicit a response in a pathway-based assay. An EAR of 1 or higher indicates that the measured concentration in a water sample was greater than the ACC in the assay medium. Extrapolating this information for application to environmental concentrations is complex. For example, current information does not include correction for chemical partitioning in the assay system (e.g., free versus bound chemical in a test well), so actual biological activity in vitro or in situ may differ from this. However, it does provide a value that effectively normalizes for relative concentration detected in the environment and relative potency to elicit a specific biological effect. Thus, the EAR value is suitable for relative ranking and prioritization. Still, it is recognized that not all ToxCast assays used in this analysis are likely to be relevant to ecological species even though many of them target biological activities that are conserved among species. A complete evaluation of ToxCast assays for ecological relevance is currently not available, so the EAR approach used here is conservative in this respect. The AOP analysis described below does include evaluation of ecological relevance but is not considered to be comprehensive, since AOP information is not yet defined for all biological targets represented in ToxCast.

For chemical concentrations reported as below the level of detection, EAR values were assumed to be zero for this analysis. To test the impact of this, EAR values were computed as a ratio of the detection limit for each compound and all available ACC values (Fig. SI-2). Results indicated that there was potential for pathway-based bioactivity at the detection limit for some chemical-assay pairs. EAR values from the minimum ACC for each compound ranged from $<10^{-4}$ (multiple compounds) to 0.19 (assay = OT_ERa_EREGFP_0120 for 4 Nonylphenol, Branched). This suggests that methods used in the current study could result in underestimation of EAR values in cases where concentrations below the analytical detection limits could still elicit a significant biological effect (i.e., near the ACC). Hence, further evaluation may be needed to determine whether these chemicals may be of concern.

Results were examined using several different EAR summations (Table 1a), and different combinations of chemical occurrence and EAR magnitudes (Table 1b). Each summation has value for addressing

Table 1a
Definition of several different EAR summations used for analysis and interpretation of results.

Summation	Abbreviation	Description
Exposure-activity ratio	EAR	The quotient of the measured concentration of a chemical in a sample and the activity concentration at cut-off (ACC) for a given assay-chemical combination. $EAR = \frac{measured\ concentration\ in\ sample\ (\mu M)}{ACC\ for\ chemical-assay\ pair\ (\mu M)}$
EAR by chemical	EAR_{Chem} $EAR_{SiteChem}$	The sum of EAR values from all assays for an individual chemical in a given sample. The number of active assays and magnitude of individual assay-chemical EAR values combine to provide a means to prioritize chemicals by potential for effect: $EAR_{Chem} = \sum EAR_{[i]}$, where i = assays relevant for each individual chemical. Maximum EAR_{Chem} for an individual site
EAR by assay endpoint	$EAR_{Mixture}$ $EAR_{SiteMixture}$	The sum of EAR values for each individual assay endpoint across all chemicals for a given sample. $EAR_{Mixture}$ provides an estimate of cumulative bioactivity for an individual assay from a mixture of chemicals, assuming additivity of effects. This is consistent with previous use of $EAR_{Mixture}$ for individual assays (Blackwell et al., 2017), and is analogous to a "toxic unit" approach for summing adverse effects for similar-acting chemicals present in complex mixtures (Nirmalakhandan et al., 1994). $EAR_{Mixture} = \sum EAR_{[i]}$, where i = chemicals associated with an individual assay endpoint. Maximum $EAR_{Mixture}$ for an individual site
EAR by adverse outcome pathway (AOP)	EAR_{AOP} $EAR_{SiteAOP}$	The sum of EAR values for each assay—chemical combination associated with an individual AOP. Using the subset of assays that are currently associated with AOPs, this summation accounts for the fact that more than one ToxCast assay may align with key events along a specific AOP. If all relevant EARs for each chemical were included, the effect of an individual chemical might essentially be "double counted". To avoid this, the summation considers only the maximum EAR for each individual chemical that is associated with an AOP: $EAR_{AOP} = \sum \max(EAR_{[i]})_{[j]}$, where i = chemical, j = an assay relevant to a given AOP. Maximum EAR_{AOP} for an individual site
Toxicity quotient	TQ TQ_{max}	The quotient of the measured concentration of a chemical in a sample and the water quality benchmark for a given chemical. $TQ = \frac{measured\ concentration\ in\ sample\ (\mu g/L)}{Water\ quality\ benchmark\ for\ chemical\ (\mu g/L)}$ Maximum TQ at a site for all water quality benchmarks available for a given chemical. 1

different questions. For example, the EAR-by-chemical (EAR_{Chem}) is useful for ranking and prioritizing among chemicals for a given sample with regard to their potential to elicit a biological effect. The EAR-by-assay endpoint ($EAR_{Mixture}$) is used to estimate the potential cumulative impact of a mixture of chemicals on a given assay response assuming additivity. Yet another summation, the EAR_{AOP} is used to consider the potential for a group of chemicals to contribute to a common adverse pathway/outcome (detailed further below). The frequency of occurrence of chemicals and exceedance of EAR or TQ thresholds were then used to help prioritize chemicals, ToxCast assays, and chemical mixtures to identify a manageable number of situations for which there is potential for adverse impacts (Table 1b). Similarly, identification of chemicals of concern and EAR and TQ levels of concern are defined for use with the intention to compare among the different chemicals, chemical mixtures, assays, and sites within the current study. Results are not intended for regulatory actions, but for consideration by stakeholders for further investigation and validation at specific sites.

Where appropriate, these different EAR summations were calculated for each of the 709 individual samples. The number of samples collected per site was variable, so the maximum EAR value per site was determined to provide a means to weight each site equally. This resulted in three additional EAR variables that were ultimately used in the current study: $EAR_{SiteChem}$, $EAR_{SiteMixture}$, $EAR_{SiteAOP}$ (Tables 1a and 1b).

Computations and analyses were primarily carried out using functionality of the R package *toxEval* (De Cicco et al., 2018) with additional custom calculations and visualizations developed using the R packages *dplyr* (Wickham et al., 2018), *ggplot2* (Wickham, 2016), and base R functionality (R Core Team, 2017). The *toxEval* package was developed within the current study to facilitate analysis and visualization of EAR and toxicity quotient (TQ) values for complex chemical concentration data sets that represent multiple chemicals, sampling locations, and samples per location. Version 2 of the ToxCast database was included as the default set of benchmark concentrations within *toxEval* with EAR values as the default evaluation parameters. Additionally, user-selected chemical-biological interaction benchmark data, such as the water quality benchmarks used in the current study, can be used for computation and analysis of TQs within *toxEval*.

2.3.2. Water quality benchmarks

Water quality benchmarks for 27 of the measured chemicals were reported by (Baldwin et al., 2016). For the present analysis, water quality benchmarks for an additional seven chemicals were added to the list. These include a broad range of toxicity benchmarks from regulatory and non-regulatory entities that are not necessarily enforceable limits but provide guidance on concentrations that represent a potential hazard for aquatic organisms (Table SI-2). The benchmark values were used to assess how the EAR-based approach compared with more traditional methods focused on apical adverse effects. Chemical-specific TQs were computed as the ratio of the measured concentration and the associated water quality benchmark. The minimum water quality benchmark and

Table 1b
Description of methods used for prioritization of chemicals, ToxCast assays, and chemical mixtures using EAR and TQ values.

Type of Prioritization	Parameter	Description
Chemical prioritization	TQ_{Max}	Chemical occurrence at ten or more sites and $TQ_{max} > 10^{-3}$ for five or more sites
Chemical prioritization	$EAR_{ChemSite}$	Chemical occurrence at ten or more sites and $EAR_{max} > 10^{-3}$ for five or more sites
ToxCast assay prioritization	$EAR_{SiteMixture}$	$EAR_{SiteMixture} > 10^{-3}$ for ten or more sites
Chemical mixture prioritization	$EAR_{SiteAOP}$	Samples that had chemical mixture combinations with $EAR_{SiteAOP} > 10^{-3}$ and chemicals that contributed at least 1% of $EAR_{SiteAOP}$ in samples from 5 or more sites

the maximum concentration per sampling location were used to compute the maximum toxicity quotient at each of the sampling locations (TQ_{max}).

In addition to traditional water quality benchmarks, 17β estradiol equivalency quotients (EEQ) were determined to estimate potential for estrogenic activity of the measured chemicals. The EEQs were obtained by multiplying the measured concentrations of estrogenic compounds by their respective estradiol equivalency factor (EEF) derived from published intersex and vitellogenin induction values in fish (Vajda et al., 2008). The EEQ values were then compared to EAR values for chemicals where both were available to better understand how EARs from ToxCast compare to a more traditional approach for evaluating estrogenic potential.

2.3.3. Linking to adverse effects

Most of molecular/biochemical responses associated with the ToxCast assays do not directly translate to endpoints typically considered in ecological risk assessments (i.e., impacts on survival, growth, reproduction, etc.). However, the adverse outcome pathway framework has been developed as a systematic and transparent means to describe the plausible and empirically supported linkages between the molecular, biochemical, and/or cellular biological activities typically evaluated in ToxCast assays and adverse outcomes that are more relevant to protection goals, management decisions, and risk assessment (Ankley et al., 2010). To help interpret the significance of ToxCast endpoints with regard to potential apical hazards, efforts have been made to map ToxCast assays to corresponding key events in AOPs described in the AOP-Wiki (Fay et al., 2018; Pittman et al., 2018; Society for the Advancement of Adverse Outcome Pathways, 2018). In the present study, cross-mapping of ToxCast endpoints to key events in AOPs (Fay et al., 2018) was updated here and used to help contextualize the significance of the EAR-based analyses relative to potential ecologically-relevant hazards.

Briefly, as of February 8, 2018 there were approximately 250 user-defined AOPs in the AOP-Wiki. Key events (including molecular initiating events) in these AOPs were manually curated for relevance to response from the ToxCast assays. Key event names were considered foremost for mapping to assays, although additional text included on the event pages also were considered. Some AOP key events are not molecular in nature, but describe general or higher-level responses (e.g., mitochondrial disruption, production of reactive oxygen species, cytokine suppression), which also is the case for some ToxCast assays which measure outcomes like cell proliferation, cell death, and mitochondrial dysfunction. In these cases, a panel of ToxCast assays relevant to a generalized response was identified and corresponding AOP events were mapped to each of the assays within the panel. Applicability of ToxCast assays considered not only the intended target but also the direction of measurement (e.g., agonism or antagonism of a given receptor). Mappings were also informed by the AOP event ontology annotations in the AOP wiki (Ives et al., 2017; Table SI-5).

Once the global mapping of ToxCast assays to key events and associated AOPs was developed, the subset of AOPs relevant to ToxCast assays prioritized in the current analysis ($n = 49$) were identified. Each assay—AOP pair was further evaluated for relevance to taxa in the Great Lakes ecosystem (Table SI-6). For example, AOPs establishing links to human health outcomes/endpoints that would typically not be considered as an assessment endpoint in ecological risk contexts (e.g., fatty liver disease) were not considered. This resulted in identification of 23 ecologically relevant AOPs associated with assays that were prioritized based on the EAR analysis.

An EAR summation approach (EAR_{AOP}) that considered potential cumulative impacts along specific AOPs was developed to aid interpretation of EAR results in an ecological hazard context (Tables 1a and 1b). An important consideration in calculating this EAR summation is that there can be more than one ToxCast assay that maps to a given key event in an AOP. For example, there are multiple ToxCast assays that measure estrogen receptor activation (Browne et al., 2015) even though estrogen receptor activation is a single key event in an AOP. Likewise, since AOPs are composed of multiple key events, ToxCast assays related to multiple different biological targets may map to a single AOP (e.g., assays 1 and 2 in Fig. 1 map to different key events along the same AOP). Consequently, to control for the fact that multiple assays and thus different numbers of EAR values may map to different AOPs, EAR_{AOP} considers the maximum EAR for any chemical-assay pair relevant to that AOP.

2.3.4. Chemical mixtures

EARs and AOP networks have each been recognized as tools for evaluating the potential significance and effects of chemical mixtures (Blackwell et al., 2017; Knapen et al., 2018). Consequently, we explored how these two approaches might be combined to better understand potential hazards associated with chemical mixtures detected in Great

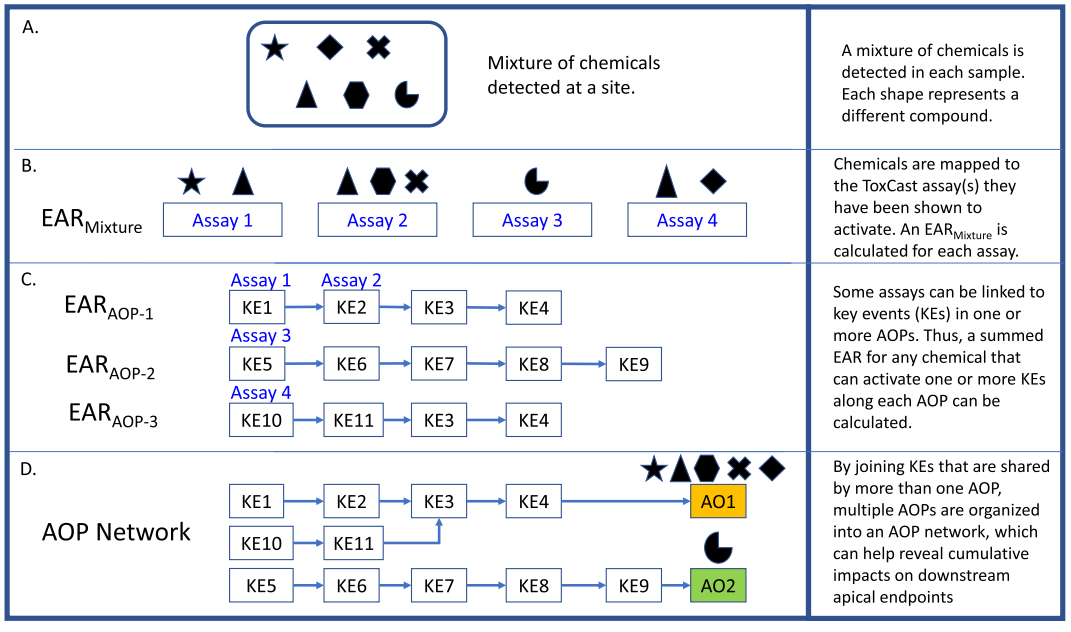

Fig. 1. Diagram of chemical mixture analysis using exposure-activity ratios for chemical-ToxCast assay pairs, adverse outcome pathways, and adverse outcome pathway networks.

Lakes tributaries. First, the number and identity of chemicals detected at each individual site was determined to establish the nature of the mixtures present (Fig. 1.A). Next, summations of EAR values for individual ToxCast assays ($EAR_{SiteMixture}$) were used to estimate potential cumulative biological activity from multiple co-occurring chemicals at a given site (Fig. 1.B). This allowed for prioritization of site-specific bioactivities, providing information on potential biological functions that may be influenced by these chemical mixtures. Third, summations of EAR values for AOPs ($EAR_{SiteAOP}$) that aligned with the biological activities detected at various sites were calculated (Fig. 1.C). After $EAR_{SiteAOP}$ values were calculated, samples that exceeded a given $EAR_{SiteAOP}$ threshold for AOPs that were designated as possibly environmentally relevant were identified. From this list of samples, chemicals that contributed at least 1% of the EAR at 5 or more sites were retained. From this list of chemicals and samples, mixtures of 2–12 co-occurring chemicals were identified.

Each AOP represents a unique sequence of biological events (key events) that link a molecular initiating event to an adverse outcome. However, AOPs employ a modular construct (Villeneuve et al., 2014). That means any given key event may be part of more than one AOP. This makes sense biologically. For example, the key event "agonism, estrogen receptor" (https://aopwiki.org/events/111) can have different biological consequences depending on the life stage exposed: altered larval development during an embryo-larval stage, impaired development of reproductive organs during sexual differentiation, or altered reproductive behaviors during adult life stages. Likewise, an apical endpoint like reproductive failure, also a key event, can have a diversity of causes. For this reason, in most real-world situations (i.e., exposure to multiple chemicals; chemicals having more than one biological activity), more than one AOP is likely to be triggered and because there are shared biological nodes among those AOPs, interactions can be expected (Knapen et al., 2018; Villeneuve et al., 2014). Based on these principles, AOP networks are defined as an assembly of two or more AOPs that share one or more key events. By linking together any shared key events, a group of individual AOPs can be assembled into an AOP network (Fig. 1.D; (Knapen et al., 2018)).

To derive an AOP network relevant to the present study, the AOP-Wiki was queried using the AOP identification number of each of the 23 ecologically-relevant AOPs of interest. Each AOP description page contains a table (relationship table) that defines the sequence of key events that make up a given AOP as a series of pairs: key event 1 leads to key event 2; key event 2 leads to key event 3; and so on. Two of the 23 AOPs did not include complete key event relationship information, and thus were not used in development of AOP networks (AOPs 52 and 53; Table SI-6). The relationship table was extracted from each of the remaining 21 AOP pages, and each pairwise key event relationship was parsed into a from-to matrix (Table SI-7). The from-to matrix was then loaded into Cytoscape (v.3.5.1; www.cytoscape.org; (Shannon et al., 2003)) to visualize the resulting network. The 21 AOPs yielded a network of seven disconnected components. The network was manually arranged for easier visualization. Three mixtures were chosen that represented different AOPs to highlight as examples, and the median $EAR_{SiteAOP}$ values for each of these three chemical mixtures was loaded as edge attributes and used to visualize the paths through the overall network that one would expect to be impacted by the mixture in question.

3. Results

Computed EAR values for individual compounds were first aggregated over the study sites for an overall assessment and examined in three primary ways: (1) by individual chemical and chemical class, (2) by monitoring location, and (3) by potential biological relevance. This sequence of analyses provided information to screen for pathway-based bioactivity and prioritize potential impacts by chemicals, watersheds, and biological functions. A goal was to enable future investigations of these tributaries to focus on a reduced set of influences at a limited number of watersheds and more efficiently identify and/or verify the potential impacts.

3.1. Prioritization of chemicals, EAR-versus TQ-based approaches

Exposure-activity ratios based on in vitro effect concentrations do not necessarily translate directly to in vivo apical responses. This is because of toxicodynamic considerations (i.e., the endpoints measured in ToxCast assays do not equate to definitive impacts on survival, development and growth, or reproduction) and toxicokinetic considerations (i.e., nominal concentrations in a test well do not necessarily translate to free chemical concentrations in plasma or environmental media). Consequently, the magnitude of EAR that is environmentally relevant for predicting adverse biological effects is not as easily defined as a TQ of concern (i.e., TQ > 0.1). To gain insight into the question of what EAR value would serve as a reasonable cut-off for prioritization purposes, EARs were compared with more traditional prioritization methods using water quality benchmarks and EEQ calculations (Fig. 2, B and D). Recognizing that water quality benchmarks are largely based on in vivo effects and EAR values are based on in vitro testing, this is not a perfect comparison. Nonetheless, it provided an empirical basis to start identifying what EAR levels may be of concern from a screening and prioritization standpoint.

The comparison of TQs based on water-quality benchmarks to $EAR_{SiteChem}$ levels indicated that the relation is chemical-specific. Considering $TQ_{max} = 10^{-1}$ as the benchmark for this analysis, corresponding $EAR_{SiteChem}$ levels that correspond to $TQ = 10^{-1}$ varied from approximately 10^{-4} to 10^{-1} (Fig. 2). Consequently, for the sake of screening and prioritizing the chemicals with the greatest potential for pathway-based bioactivity from a spatial distribution perspective, chemicals that were present at a minimum of 10 sites and had $EAR_{SiteChem} > 10^{-3}$ at a minimum of five sites were considered (Fig. SI-3). These chemicals included 4 nonylphenol (a detergent degradate and industrial chemical), BPA (used in plastics and epoxy resins), metolachlor and atrazine (herbicides), DEET (insect repellant), caffeine, tris(2 butoxyethyl) phosphate and tributyl phosphate (TBEP, TBP; flame retardants), benzo(a)pyrene and fluoranthene (PAHs with multiple origins), benzophenone (ultraviolet radiation protection in soaps, fragrances, plastics), and triphenyl phosphate (TPhP; plasticizer, flame retardant) (Fig. 2).

For water quality benchmarks, considering the number of sites with detections and the magnitude of the TQ_{max} for each site (detected at a minimum of 10 sites with $TQ_{max} \geq 10^{-1}$ at a minimum of five sites), the detected chemicals with the greatest potential for adverse impact were 4-nonylphenol, BPA, metolachlor, atrazine, and several PAHs (anthracene, benzo (a) pyrene, fluoranthene, phenanthrene, pyrene). Water quality benchmarks could not be identified for 23 of the detected chemicals that were present in the ToxCast database (i.e., for which EARs could be calculated); these included all chemicals within several broad usage classes (human nonprescription drugs, flame retardants, flavors and fragrances).

When endpoints for ToxCast and water quality benchmarks were both available, all chemical classes identified as a concern were consistent. There were differences when considering individual chemicals. For example, water quality benchmarks identified five PAHs as a potential concern while the ToxCast assessment identified only two, and DEET was identified as a potential concern using the EAR approach, but available water quality benchmarks for DEET did not indicate a substantial concern. While different $EAR_{SiteChem}$ levels of concern could be chosen depending on the circumstances, the choice of $EAR_{SiteChem} = 10^{-3}$ appeared to provide a reasonable level for comparison with water quality benchmarks.

Estradiol equivalency factors were available for eight compounds, four of which were not represented in the ToxCast database, and two that were not detected in samples (Fig. 2-C, D). For the compounds

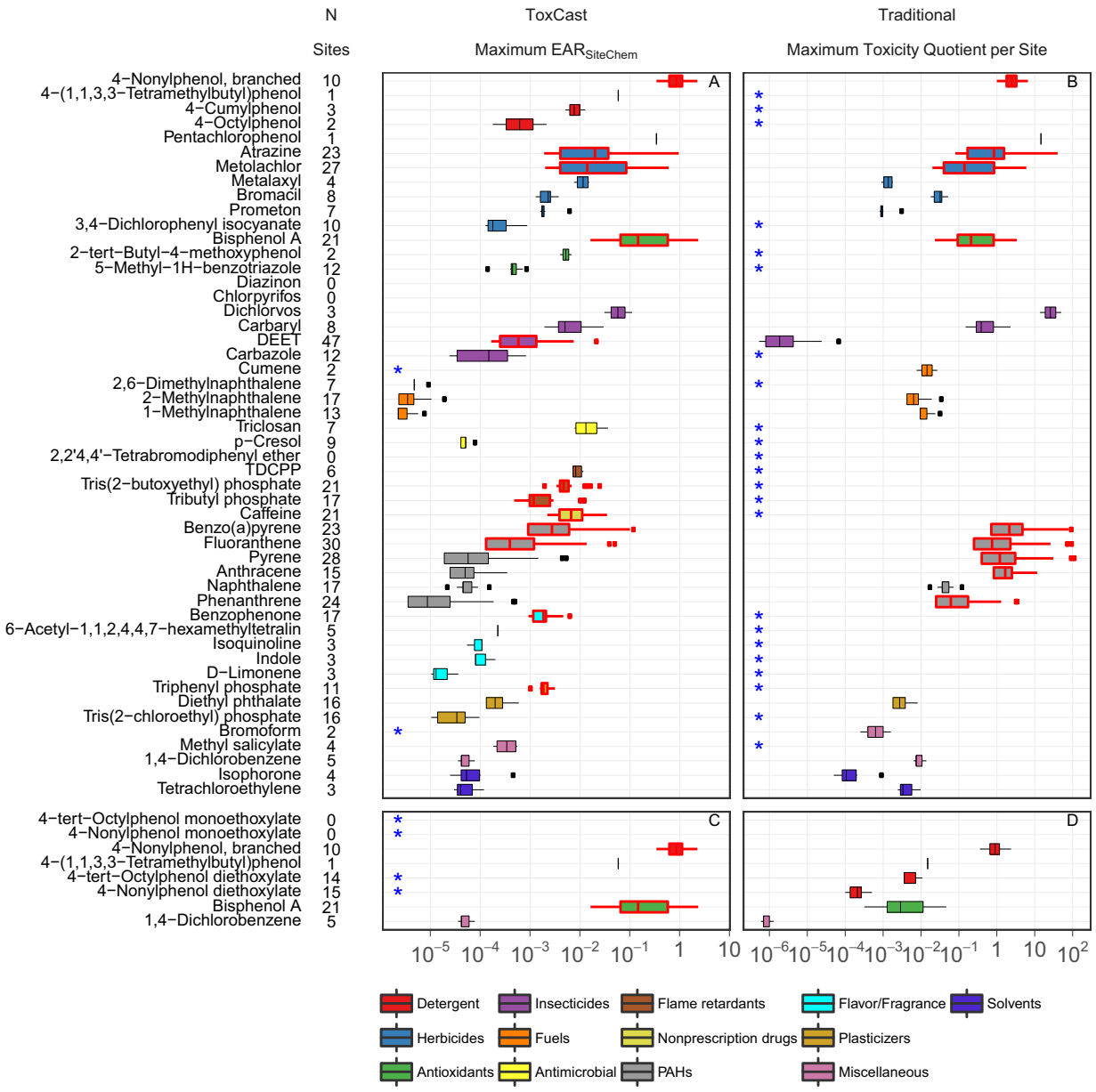

Fig. 2. Exposure activity ratios (EARs) using ToxCast endpoints for screening of potential pathway-based bioactivity from chemicals detected in water samples from 57 tributaries of the Great Lakes, 2010–2013 (A and C), toxicity quotients comparing established water quality benchmarks to sample results (B), and 17 β estradiol equivalency quotients (ng/L) for compounds with established estradiol equivalency factors (D). Compounds are grouped by chemical class and ordered by largest to smallest median EAR. Compounds where either water quality benchmarks or ToxCast information were unavailable are indicated with "*", and compounds where both were unavailable are not included in the graph. Boxplots with red borders designate chemicals that were present at 10 or more sites with EAR > 10^{-3} at 5 or more sites (panel A) or TQ > 0.1 at 5 or more sites (panel B). [N, number of sampling locations with detections of each chemical. Boxes, 25th to 75th percentiles; dark line, median; whiskers, data within 1.5× the interquartile range (IQR); circles, values outside 1.5× the IQR.]

with EEFs that were in the ToxCast database, results indicated similar priority rankings: 4 nonylphenol had the greatest potential effects and 1,4 dichlorobenzene had the least, with potential effects from 4 tert octylphenol between these two compounds. EAR values for BPA were not as comparable to EEQ results, with EAR calculations indicating greater potential effects relative to other compounds. This is because $EAR_{SiteChem}$ is computed using a summation of EAR values from all assays in which a given chemical is active. Bisphenol A is flagged not only in multiple assays related to estrogen receptors, but in several other ToxCast assays not related to estrogen signaling. Consequently, it is reasonable that the predicted impacts of a chemical that effects multiple types of biological activities, such as BPA, would deviate from a calculation considering only estrogenic activity. Nonetheless, EAR = 10^{-3} appeared to be a reasonable threshold from a prioritization perspective.

3.2. Prioritization of sites, EAR-based

Sites for potential follow-up monitoring were prioritized based on the number of chemicals detected at each with an associated $EAR_{SiteChem}$ > 10^{-3} (Fig. 3, Figs. SI-4 and SI-5 A-M). Sites with at least one chemical exceeding the $EAR_{SiteChem} > 10^{-3}$ value included four of nine Lake Superior tributaries monitored, 11 of 19 Lake Michigan tributaries, five of seven Lake Huron tributaries, all 15 Lake Erie tributaries (including the Detroit River and Lake St. Claire tributaries), and three of seven Lake Ontario tributaries. Sampling locations that had >15 chemicals with $EAR_{SiteChem} > 10^{-3}$ included River Rouge, the Clinton River, and the St. Louis River. These would be a high priority for future investigation. There were an additional eight sampling locations with at least 10 chemicals and 10 more sampling locations with at least five

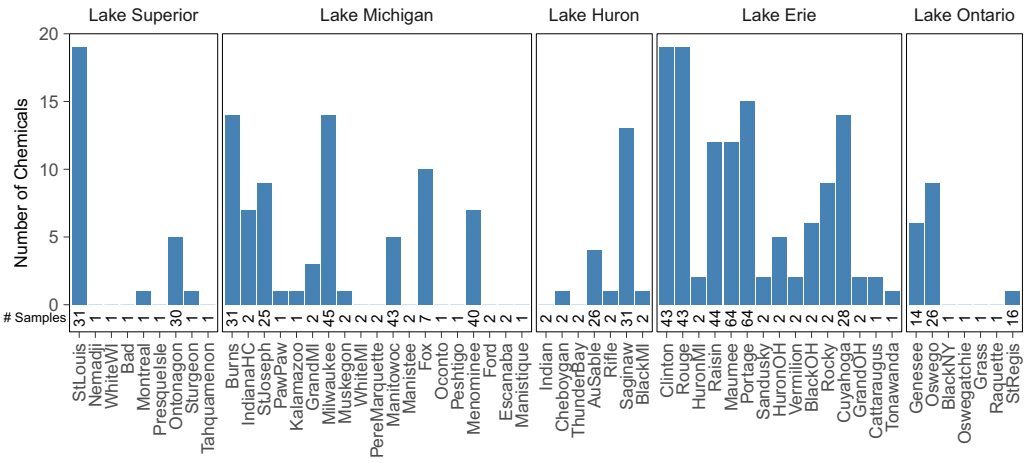

Fig. 3. Number of individual chemicals with at least one sample that resulted in a maximum exposure—activity ratio ($EAR_{SiteChem}$) > 10^{-3} for each site.

chemicals with $EAR_{SiteChem} > 10^{-3}$ (Fig. 3). Given that the number of samples collected from each site was variable (one to 64 samples) and that chemistry results varied temporally, the number of samples and timing of collection likely influenced the number of chemicals detected at each site. Nonetheless, the EARs provide an approach for differentiating sites with greater probability for biological effects from those with lesser probability.

Several sites had elevated EARs for multiple chemicals and/or chemical classes (Fig. SI-5 A-M). The EAR patterns throughout the study sites typically reflected the nature of land use within the watershed. Sites with urban influence most commonly had elevated EARs for PAHs and nonprescription drugs (Fig. SI-5 B and D). Agricultural sites were most likely to have higher EAR incidence of herbicides, primarily atrazine and metolachlor (Fig. SI-5 A). One exception to this was the St. Louis River where pentachlorophenol had an $EAR_{SiteChem} > 0.3$. The St. Louis River does not have a high percentage of either urban or agricultural land cover but does include wood and paper product industries that sometimes use pentachlorophenol in preservation processes (Karn et al., 2010). A mix of sites with differing dominant land covers had elevated $EAR_{SiteChem}$ values for insecticides, flavors/fragrances (benzophenone), plasticizers, flame retardants, antimicrobial disinfectants, and detergent degradates (Fig. SI-5 E, G, J, K, L, and M).

3.3. Prioritization by biological relevance, assay endpoints and adverse outcomes

A third approach to applying the EARs involves hypothesizing or inferring potential biological effects of concern at a given site, based on the known composition of chemical mixtures present. In this case, ToxCast assays were used to screen chemicals for biological activities (Fig. 1.A). The biological activities from those assays were aligned with key events in AOPs described in the AOP-Wiki (Fig. 1.B). Exposure activity ratios reflecting the potential effect of chemicals in a mixture on one or more key events along an AOP help to relate the potential biological activities to outcomes of concern (typically effects on survival, growth, reproduction; Fig. 1.C). In turn, recognizing that chemical-induced biological activities in vivo are occurring concurrently and can interact with one another in additive, antagonistic, and/or synergistic manners (Knapen et al., 2018), the group of AOPs potentially impacted by components of a mixture may in turn be considered in a network context (Fig. 1.D; (Villeneuve et al., 2018)).

To identify and prioritize biological activities most likely to be modulated in organisms resident to the Great Lakes tributaries surveyed, ToxCast assays with $EAR_{SiteMixture} > 10^{-3}$ at 10 or more sites were identified, resulting in a list of 46 assays (Fig. 4). For individual assays, the number of chemicals that contributed to the $EAR_{SiteMixture}$ varied from 1 to 33, further supporting the hypothesis that mixtures of chemicals are a necessary consideration for screening potential biological effects. Twenty seven of these 46 assays have been associated with AOP key events from the AOP Wiki (Fig. 4, Table SI-5; aopwiki.org). Some key events may occur in more than one AOP, and in this case the 27 assays were associated with a total of 49 AOPs (Fig. 5A and SI-6). Evaluation of the potential for effects on individual AOPs from multiple co-occurring chemicals was explored by computing summations of EAR values from all assays associated with individual AOPs ($EAR_{SiteAOP}$; Fig. 1; Tables 1a and 1b; Fig. 5A). For example, AOPs 52 and 53 are influenced by 6 of the ToxCast assays displayed in Fig. 5B. To estimate the cumulative EAR ($EAR_{SiteAOP}$) for these AOPs, the sum of EARs from all related assay-chemical combinations was computed. For any given AOP, the number of contributing assays varied from 1 to 35 (Table SI-5). Considering the ToxCast assays prioritized in Fig. 4 (i.e., those for which maximum $EAR_{SiteMixture} > 10^{-3}$ was calculated for at least 10 sites), the number of contributing assays per AOP varied from 1 to 17 (Fig. 5B).

Up to this point in the analysis, all ToxCast assays and associated AOPs potentially affected by chemicals measured in this study have been considered. However, not all ToxCast assays or associated AOPs are necessarily relevant in the context of ecological effects. Consequently, relevance of the 49 associated AOPs (Fig. 4) was evaluated. Based on this evaluation, 23 were classified as “relevant” or “potentially relevant” to resident Great Lakes tributary species (Fig. 5A, Table SI-6). Of these 23 AOPs, $EAR_{SiteAOP}$ varied from $<10^{-5}$ to 0.8.

To further understand the potential collective impacts of various mixtures detected in the Great Lakes tributaries on organisms, 21 of the 23 AOPs were assembled into an AOP network (Fig. 6). Two of the AOPs did not include sufficient information to include. The network was composed of 97 key event nodes (circles, squares, or diamonds in Fig. 6) organized into seven disconnected components (subnetworks). Overall, potential pathway-based bioactivity indicated by these AOPs includes various influences on reproduction and energy metabolism, specifically mitochondrial function (Table SI-6; Fig. 6). Detection of chemicals known to bind to and activate the estrogen receptor, produce excessive reactive oxygen species (ROS), activate peroxisome proliferator-activated receptor, inhibit histone deacetylase, or inhibit cyclooxygenase (molecular initiating events and/or “upstream” key events in Fig. 6) suggested potential for effects on reproduction and/or the reproductive system (adverse outcomes in Fig. 6). Additionally, available AOPs suggest that chemicals impacting mitochondrial function in vitro have potential to cause mortality and potential population-level impacts, including honeybee colony collapse (LaLone et al., 2017). In this case, the ToxCast assay hits did not necessarily align with the molecular initiating events of a corresponding AOP, but

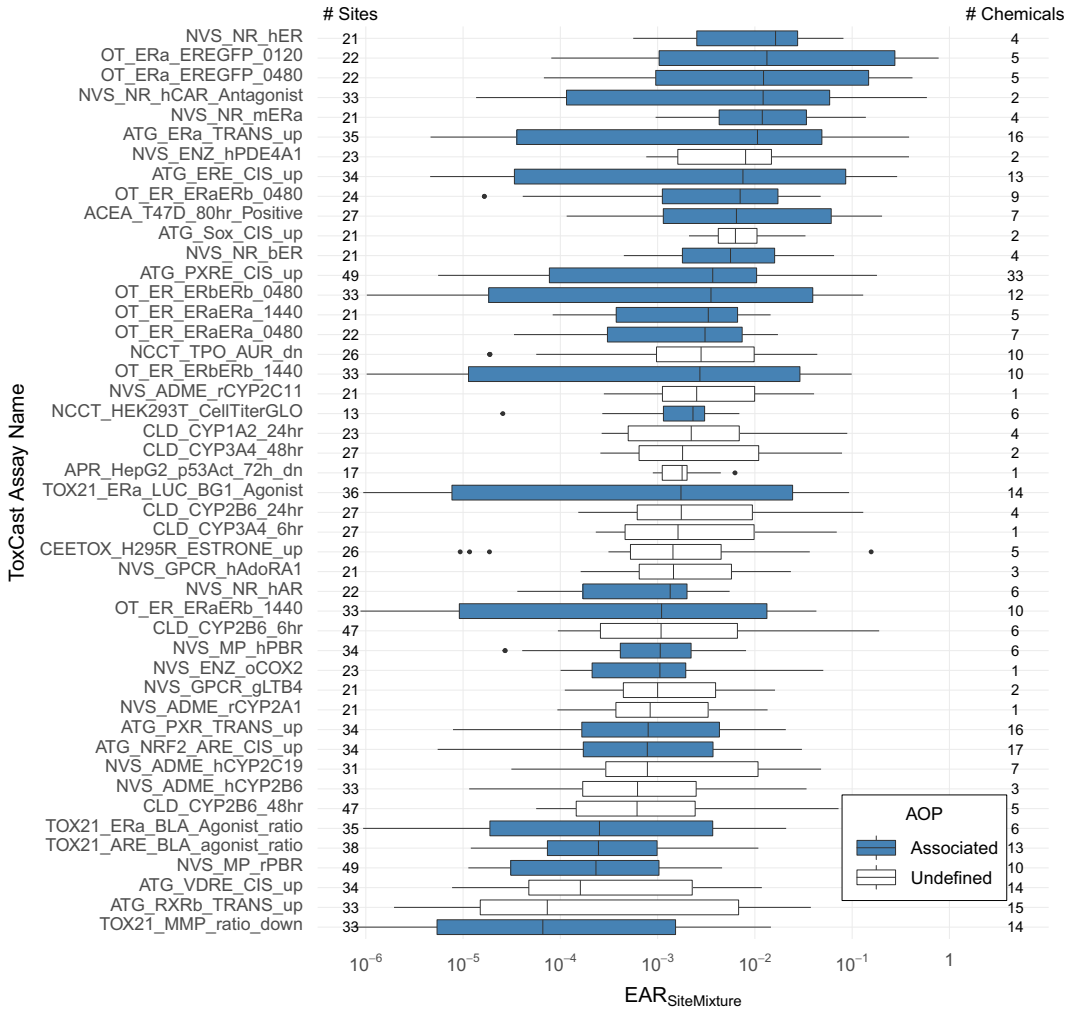

Fig. 4. Boxplots of maximum exposure-activity ratios (EARs) across sites for ToxCast assays with EARs $>10^{-3}$ from at least 10 sites. Assays with and without currently associated adverse outcome pathways (AOPs) are differentiated by color. [Boxes, 25th to 75th percentiles; dark line, median; whiskers, data within 1.5× the interquartile range (IQR); circles, values outside 1.5× the IQR. $EAR_{Mixture}$,the sum of EAR values for each individual assay endpoint across all chemicals for a given sample.]

rather the mitochondrial effects aligned with intermediate key events along an AOP (not all labeled in Fig. 6).

To illustrate how the AOP networks, along with EAR summations, can be used to hypothesize or infer potential effects of different mixtures, further consideration was given to chemical mixtures with high $EAR_{SiteAOP}$ values that occurred frequently. The list of detected chemicals was first reduced to those that contributed at least 1% of $EAR_{SiteAOP}$ in samples with $EAR_{SiteAOP} > 10^{-3}$. This identified twelve chemicals (Table SI-8). Instances when 2–12-compound mixtures occurred in samples were identified, resulting in1848 different combinations of mixtures of 2–12 compounds that occurred at between 5 and 21 sites with $EAR_{SiteAOP} > 0.001$ (Table SI-8).

Three of these mixtures were chosen as examples to illustrate how different mixture compositions (Fig. SI-7) may shift the patterns of biological responses across the network of 21 relevant AOPs (Fig. 6). To visualize this, the arrows depicting key event relationships along each AOP were weighted by their relative $EAR_{SiteAOP}$ values. Using this approach, one can see that at sites dominated by a mixture of TBP and caffeine, toxicities associated with mitochondrial function, activation of nicotinic acetylcholine receptors, activation of peroxisome proliferator activated receptor (PPAR), or inhibition of vitamin K epoxide reductase (VKOR) were predicted to be the most sensitive effects. Potential adverse outcomes linked with estrogen receptor agonism are less probable (Fig. 6A). In contrast, for mixtures containing BPA and DEET, estrogenic and anti-androgenic responses were predicted to be most likely, with mitochondrial-related toxicity potentially exacerbating some of the reproductive effects and potential impacts related with PPAR activation or VKOR inhibition a lower priority (Fig. 6B). A combination of 4 nonylphenol, atrazine, and metolachlor was predicted to have the most diverse range of potential effects on the overall network of AOPs (Fig. 6C). In particular, a series of AOPs associated with inhibition of cyclooxygenase activity, not prioritized for the other mixtures, are now identified as highly relevant, while potential estrogen receptor agonism-mediated pathways appearing less relevant for this mixture. While none of these examples are definitive, they illustrate how an EAR-based approach may be combined with an AOP network analysis (Knapen et al., 2018; Villeneuve et al., 2018) to infer potential biological hazards at different sites, and guide a hypothesis-driven approach to subsequent monitoring.

4. Discussion

A challenge for contaminant monitoring studies is to place results in the context of potential biological effects of concern to support resource management decision making. In the present study, an EAR-based application of high throughput screening data from ToxCast was explored along with AOP knowledge to provide an evidence-based approach for linking chemical occurrence with potential effects. This was done within the context of meeting the primary study objectives to prioritize chemicals and Great Lakes tributaries with the greatest likelihood for

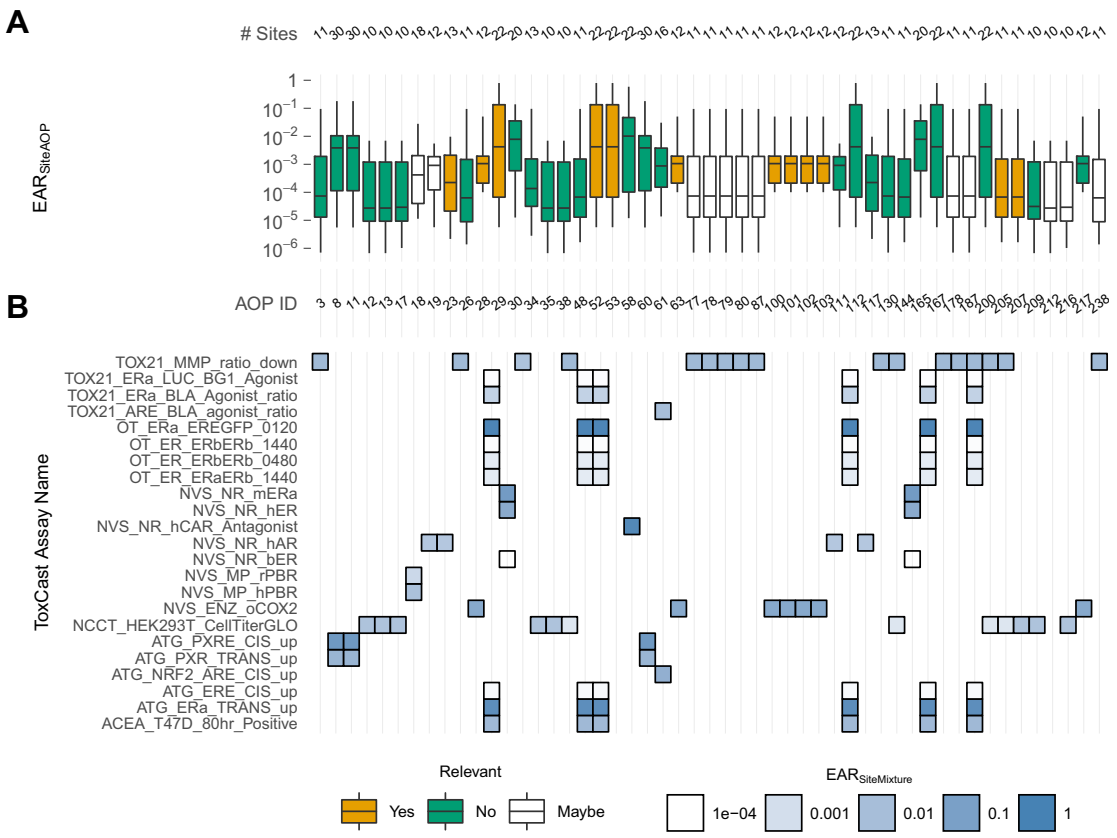

Fig. 5. Maximum exposure-activity ratios (EAR) by site for adverse- outcome pathway (AOP; A) and for ToxCast assay-AOP combinations (B) from chemicals detected in samples collected from Great Lakes tributaries, 2010–2013. Assays displayed include those that had EAR >10^{-3} for at least 10 sites. [Boxes, 25th to 75th percentiles; dark line, median; whiskers, data within 1.5× the interquartile range.]

potential ecological effects. To fully understand the effectiveness of this approach, there are several questions that need to be addressed, including: (a) Can an EAR-based screening and prioritization approach provide results comparable to those obtained with traditional water quality benchmarks?; (b) What magnitude of EAR warrants concern?; (c) Are there specific chemical properties that may lead to poor representation of some chemicals using high-throughput screening results?; and (d) Are there ecologically-relevant adverse outcomes that might be anticipated using these results? It was the aim of the current analysis to examine these questions in detail.

4.1. Prioritization of chemicals

4.1.1. Individual chemicals

Among the 65 chemicals detected in the present study, traditional in vivo water quality benchmarks were available for 34 compounds, and ToxCast data were available for 54, substantially increasing the number of compounds for which comparison with biological effects data was feasible. Using a threshold of 10^{-3} as an $EAR_{SiteChem}$ level of concern, the EAR-based approach yielded a priority list of chemicals similar to that obtained using available water quality benchmarks using a TQ threshold of 10^{-1} (Fig. 2). Chemicals flagged as contaminants of potential concern by both approaches also have been identified in previous studies: 4-nonylphenol (Careghini et al., 2015), BPA (Corrales et al., 2015), metolachlor and atrazine (Busch et al., 2016; Graymore et al., 2001; Love et al., 2011; Pérez et al., 2011), and PAHs (Ankley et al., 1994; Logan, 2007; Ohe et al., 2004; Simcik and Offenberg, 2006). DEET was flagged by the EAR approach but was not identified to be of concern using TQ_{max} values from the available water quality benchmark information. The list was expanded further using the EAR approach to include several compounds for which water quality benchmarks were unavailable. These additional chemicals included caffeine, TBEP, TBP, benzophenone, and TPhP.

DEET is a commonly used insect repellant that is detected regularly in environmental waters (Weeks et al., 2012). Most traditional in vivo benchmarks for DEET (i.e., those related to mortality, growth, or reproduction) exceed 20 mg/L (US EPA, 1996); https://cfpub.epa.gov/ecotox/search.cfm).The most sensitive reported in vivo effects of DEET include a decline in hepatosomatic index and altered expression of several endocrine-related genes in fathead minnows following exposure to concentrations as low as 0.6 μg/L (Zenobio et al., 2014). Concentrations in samples for the current study exceeded 0.6 μg/L and 0.06 μg/L (10-fold safety factor) at three and 25 sites respectively. EAR analysis identified DEET as a potential concern because it was present in samples from 47 of 57 sites and 17 of those sites had samples with $EAR_{SiteChem}$ > 10^{-3}. The greatest $EAR_{SiteChem}$ values for DEET corresponded to ToxCast assay activity measuring increased transcription of cytochrome P4502B6 (cyp2b6). Notably, previous studies have shown that cyp2b6 is one of the predominant cytochrome P450s involved in DEET metabolism (Usmani et al., 2002), so this chemical-biological interaction is not unexpected. Since this activity is directly linked with the metabolism of DEET, one cannot necessarily assume that induction of the protein would result in toxicity. In the case of DEET, the EAR approach may be conservative relative to traditional ecotoxicological benchmarks.

Caffeine is also detected regularly in environmental waters (Bradley et al., 2017). EAR analysis identified caffeine as a potential concern because it was present in samples from 21 sites, all of which had $EAR_{SiteChem} > 10^{-3}$. The greatest EARs for caffeine were due to its activation of Sox transcription factor (Sry-related high mobility group box) in the Attagene Cis-Factorial assay (Medvedev et al., 2018). However, given the diversity of genes regulated by this class of transcription

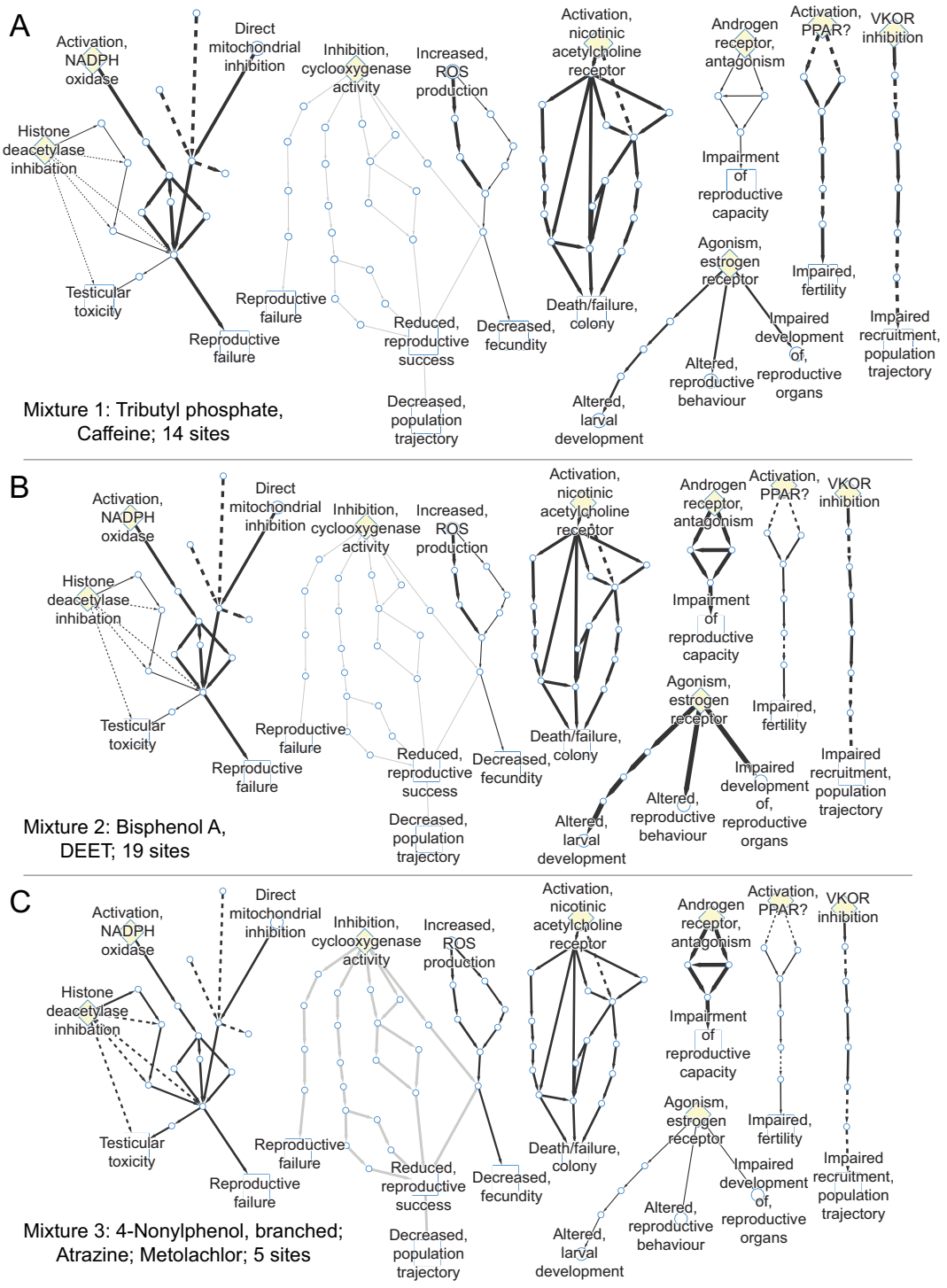

Fig. 6. Adverse outcome pathway network associated with 21 AOPs identified as relevant to the biological activities (assays) that had $EAR_{siteMixture} > 10^{-3}$. Panels represent potential relative influence for three example mixtures on the network, where arrows (key event relationships) linking the key events along a given AOP are weighted based on median $EAR_{siteAOP}$ for the mixture (thicker arrows indicate greater $EAR_{siteAOP}$ values). Biological key event nodes are represented as shapes: molecular initiating events as diamonds, adverse outcomes as squares, and intermediate key events as circles.

factors, it is difficult to infer the potential toxicological significance of the response. The second highest EARs for caffeine derive from its interaction with the human adenosine receptor a2a (assay ID NVS_GPCR_hAdoRA2a). This activity is consistent with caffeine's well-established activity as a non-selective blocker of adenosine receptors (Rivera-Oliver and Díaz-Ríos, 2014) and plays a role in many of the biological effects that caffeine is known for, including influences on sleep, cognition, heart rate, etc. However, these biological activities would not necessarily be linked to adverse effects on survival, growth, or reproduction in non-target aquatic species.

Two in vivo studies on aquatic species with TBP resulted in apical effect endpoints at 600 μg/L for regeneration of flatworms (Yoshioka et al., 1986) and between 1000 and 5000 μg/L for mortality of fathead minnows, *Daphnia magna*, and rainbow trout (Dave et al., 1979, 1981; Mayer and Ellersieck, 1986). In a study with zebrafish, TBEP caused significant early developmental toxicity by inhibiting the degradation and

utilization of maternally-derived nutrients, thereby inducing apoptosis. Effects were observed at a concentration as low as 150 μg TBEP/L (Han et al., 2014). TPhP was acutely toxic to *D. magna* with a lethal concentration required to kill 50% of the population (LC_{50}) of 89 μg/L (Lin, 2009), and in zebrafish larvae, whole-body thyroid hormones and related gene expression were influenced at 40 μg TPhP/L, the lowest concentration tested (Kim et al., 2015). TBP and TPhP have been shown to display additive effects during concurrent exposures (Lin, 2009). Compared to concentrations measured in the current study, these effect concentrations for TBP and TBEP are relatively high, and substantial adverse effects might not be expected. More detailed consideration of biological responses associated with EARs $>10^{-3}$ for TBP, TPhP, and TBEP suggest relatively sensitive interactions with peripheral benzodiazepine receptor (PBR; TBP; assay IDs NVS_MP_hPBR, NVS_MP_rPBR) or the pregnane × receptor (PXR; TBP, TBEP; assay IDs ATG_PXRE_CIS_up, NVS_NR_hPXR) as well as the estrogen receptor (TBEP; assay ACEA_T47D_80hr_Positive). Activation of PXR is caused by many different types of chemicals, and generally is indicative of potential to induce xenobiotic metabolism (Kliewer et al., 2002). The significance of the interaction with PBR is less clear, but the estrogenic responses establish a clear link to one or more AOPs. While estrogenic activity would not necessarily be expected to result in lethality in either short- or long-term aquatic toxicity tests, potential effects on reproduction and/or development in vertebrate species are possible (Ankley et al., 2016).

Collectively, these examples highlight some of the differences between the application of traditional in vivo toxicity benchmarks and pathway-based activities that may flag a chemical as a potential priority. While the high throughput screening assays are detecting "real" biological activities, those activities are not necessarily directly translatable into in vivo effects in aquatic species. At the level of $EAR_{SiteChem}$ the approach serves as a practical first tier prioritization tool. A lack of EARs exceeding the prioritization threshold is a reasonable, evidence-based indicator of lower likelihood for biological effects. However, although an EAR exceeding the threshold does suggest potential for biological activity, it does not necessarily indicate that activity will result in toxicity. This points to the potential value of further alignment of ToxCast endpoints with AOP knowledge as a potential means to refine the analysis in a way that helps to better differentiate indicators of probable hazard from indicators of potentially more benign effects like induction of hepatic metabolism or of sublethal physiological effects.

Just as there are activities captured in the high throughput screening battery that would not necessarily contribute to, or drive, conventional in vivo benchmarks, there are also cases where in vivo toxicity tests may detect biological effects that would go undetected using in vitro systems. For example, even though PAHs were identified as a potential concern using both $EAR_{SiteChem}$ and TQ_{max} values, results were notably different between the two methods (Fig. 2). $EAR_{SiteChem}$ values indicated less potential for pathway-based bioactivity than those from TQ_{max} values. This difference could be attributed to the different nature of information represented in high throughput assays as compared to that used to determine water quality benchmarks. PAH water quality benchmarks used in the present study included those published by US EPA as well as the Canadian Council of Ministers of the Environment (Table SI-2). These water quality benchmarks take into consideration multiple forms of toxicity, including two that are not accounted for in ToxCast assays: metabolic- and photo-activation. Some PAHs are known to be metabolically activated to more toxic forms (Incardona et al., 2006; Stegeman and Lech, 1991), and it has been acknowledged that ToxCast in vitro assays underestimate toxicity resulting from metabolic activation (DeGroot et al., 2018; Jacobs, 2013). The more stringent Canadian water quality benchmarks for PAHs included mortality in assays from post-test ultraviolet (UV) radiation (Canadian Council of Ministers of the Environment, 2015). UV radiation exposure can induce photo-activation of PAHs, thereby decreasing concentrations of concern by several orders of magnitude over those without UV exposure (US EPA, 1996, 2003). Given that high-throughput assay results used in the present study do not account for photo-activation, this could, at least partially, explain the differences in EAR_{max} and TQ_{max} values for PAHs.

Overall, these results suggest that the EAR-based evaluation is indeed useful for hypothesis formulation to prioritize individual chemicals of concern. An EAR threshold of 10^{-3} appeared to provide conservative results tending toward inclusion of chemicals in question except for PAHs where some mechanisms to influence biological activity (e.g., metabolic- or photo-activation) are not well represented by the current assays included in ToxCast. The parameters chosen for inclusion of priority chemicals, however, are somewhat arbitrary, and may change based on study objectives. In this case, chemicals that were detected at 10 or more sites with $EAR_{SiteChem} > 10^{-3}$ were selected as a priority. Revising these parameters could result in a different list of chemicals. For example, if the threshold for the number of sites detected was reduced to five, bromacil, prometon, carbaryl, triclosan, and tris (dichloroisopropyl) phosphate (TDCPP) would have been added to the priority list using the EAR-based approach, while only carbaryl would have been added using water quality benchmarks.

4.1.2. Chemical mixtures

The first approach employed in the present study compared detected concentrations of individual chemicals in water samples to the concentrations eliciting in vitro activity across the ToxCast suite of assays (EAR_{Chem}). This type of information was useful for highlighting chemicals and sites of concern where chemical concentrations may be approaching those that elicit pathway-based biological activity (in vitro). However, another significant advantage of the EAR approach is the ability to sum the potential effects of chemicals acting on either the same biological target/pathway captured by an individual ToxCast assay (i.e., the $EAR_{Mixture}$) or chemicals acting on the set of assays that align with one or more key events along an AOP (EAR_{AOP}). In these instances, additivity of EAR values is a reasonable conservative assumption for estimation of cumulative effects. Specifically, it is plausible that each individual chemical detected in a mixture may be present at concentrations that would not, alone, exceed the EAR_{Chem} threshold of 10^{-3} selected for this study; however, collectively, multiple chemicals acting on the same target or AOP could yield an $EAR_{Mixture}$ or EAR_{AOP} $>10^{-3}$. This concept has been verified, for example, for estrogenic compounds (Thrupp et al., 2018).

In the present study, there were two additional ToxCast assays identified when $EAR_{Mixture}$ was $>10^{-3}$ at 10 or more sites as compared to those identified from individual EAR_{Chem} values. The AOPs identified when EAR_{AOP} was $>10^{-3}$ did not change from those when EAR_{Chem} was $>10^{-3}$, but EAR_{Chem} alone often underestimated the potential for impact. The mean EAR_{Chem} contribution from the individual chemical with the greatest contribution to any given $EAR_{SiteMixture}$ and EAR_{AOPMix} was 69% and 31% respectively. In addition, there were 23 chemicals that had $EAR_{Chem} > 10^{-3}$, but 29 different chemicals contributed at least 5% to EAR_{AOP} values when EAR_{AOP} was $>10^{-3}$. Thus, while some chemicals acting alone may not warrant concern, when acting in concert with other chemicals present in the mixtures, they may exacerbate the impact of one of the individually prioritized compounds.

4.2. Prioritization of potential biological effects

A primary goal of this type of analysis is to link the contaminants detected, in their relative concentrations, to apical adverse outcomes that might be of greatest concern at a given site. Recognizing that these mixtures of chemicals will interact with more than one biological pathway, and as a result, likely trigger multiple AOPs, the consideration of AOP networks is viewed as one approach to try to understand the possible cumulative effects of the chemicals (Knapen et al., 2018). Examination of an EAR-weighted network (e.g., Fig. 6) demonstrates how cumulative EARs ($EAR_{SiteAOP}$) might be used to identify what key events and outcomes may dominate at one site versus another. However, the analysis of AOP networks is in its infancy (Knapen et al., 2018; Villeneuve et al.,

2018) and it must be recognized that only a small fraction of potentially relevant pathways is currently represented in the AOP Wiki. As many as 47 sites had chemicals associated with individual assays for which the target biological activity has not yet been linked with AOPs (Fig. 4).

As a first evaluation of the adverse outcomes predicted in the current study, comparison to previous research indicates that reproductive dysfunction has been documented in multiple field studies with fish. These have included phenotypic alterations in sexual characteristics associated with exposure to substances present in wastewater discharge (Jobling et al., 1998, 2002), reduced sperm abundance and motility in resident fish from rivers receiving wastewater effluent (Blazer et al., 2012), reduced fecundity in fish downstream from or directly exposed to a wastewater effluent discharge (Cavallin et al., 2016; Prado et al., 2014), and multiple effects on male and female reproductive organs of fish exposed to wastewater effluent (Vajda et al., 2008) among others. It is recognized that neither the EAR-based identification of priority AOPs within an overall AOP network, nor previous field studies reporting effects consistent with some of these AOPs, causally implicate that concentrations of these contaminants detected in Great Lakes tributaries are having ecological effects. However, they do provide evidence to hypothesize that this may be the case when considering further monitoring and evaluation.

4.3. Limitations of the EAR approach

There are some important limitations to the EAR screening approach that need to be highlighted: (1) comparison of water chemistry results to assay results for individual chemicals does not allow for true evaluation of the integrated effect of mixtures. Assumptions (such as EAR additivity) must be made to evaluate the full sample matrix; (2) this type of evaluation is limited to those chemicals that are analyzed in samples that intersect with those chemicals that are currently represented in the ToxCast database (i.e., not all chemicals have been tested); (3) ToxCast data are limited to a specific set of assays–there are effects and some major modes of action that are not represented, including effects that are unique to non-mammalian species; (4) many of the assays lack the ability to metabolize the parent compounds being tested, which can under-and over-estimate the in vivo toxicity of some chemicals, and (5) not all ToxCast assays are currently linked to AOPs. Even with these limitations, high-throughput screening data can serve as a valuable tool for screening for potential adverse biological effects particularly where traditional in vivo toxicity data required to calculate water quality benchmarks are lacking. In addition, applying the ToxCast data in this manner could further inform and improve the ToxCast data curation and the AOP knowledgebase. For example, as hypotheses emerging from such analyses are tested, anomalous activities in the ToxCast data set can be identified and flagged, leading to more reliable pathway-based prioritization in the future. Additionally, priorities for AOP development may be identified.

4.4. Application of findings

Ultimately, the current study findings can be used to focus available resources. For example, results can help identify which of the monitored chemicals and chemical mixtures are a priority at each of the sites evaluated (Fig. SI-4, Table SI-8) and which AOPs are most likely to be relevant for the identified chemicals and mixtures at any given site (Fig. SI-6, Tables SI-8 and SI-9). Predicted bioactivities can then be confirmed through laboratory- or field-based investigation or through observations of resident organisms. However, for confirmation studies to be representative of the greatest potential hazard from chemical exposures, testing conditions must reflect the circumstances under which these chemical mixtures are most likely to be present at any given site. The contaminants present, the concentrations, and the exact mixtures vary spatially (urban vs agricultural, commercial vs residential, crops vs pasture), seasonally, and hydrologically (base flow, snowmelt, rainfall) (Baldwin et al., 2016). Well-chosen investigations that reflect the setting for which the greatest potential hazard exists based on these factors would provide substantial value and additional confidence in verifying results. After confirmation of the hypothesized bioactivities, reduction strategies for sources of these chemicals can then be investigated and implemented.

5. Conclusions

When adequate data existed for a comparative analysis, chemicals of greatest concern identified using the ToxCast database with an EAR threshold of 10^{-3} were very similar to those identified using water quality benchmarks with a TQ threshold of 10^{-1}. However, the ability to use the ToxCast database allowed for evaluation of twice as many chemicals in terms of possible biological impacts, as compared to water quality benchmarks. Several PAHs identified as a concern using water quality benchmarks were not similarly flagged using the EAR approach, perhaps due to mechanisms that can enhance their in vivo toxicity but would not be captured using in vitro systems. Several additional chemicals were identified as a potential concern through evaluation of putative bioactivity from chemical mixtures. Results from this work will enable resource managers to examine information pertinent to individual sites and identify individual chemicals and chemical mixtures of potential concern. Hypothesis-driven studies may then be designed to verify results, and if confirmed, mitigation strategies may be formulated and implemented.

Acknowledgements

The authors gratefully acknowledge the many individuals from the U.S. Geological Survey involved in sample collection, processing, and analysis. We thank Anthony L. Schroeder and Keith A. Houck for technical input and Edwin Smith and Elizabeth Murphy for program coordination. Support for this project was provided by the Great Lakes Restoration Initiative through the U.S. Environmental Protection Agency's Great Lakes National Program Office under agreement number DW-014-92453901. The views expressed in this work are those of the authors and do not necessarily reflect the views or policies of the U.S. EPA. Any use of trade, product, or firm names is for descriptive purposes only and does not imply endorsement by the U.S. Government.

Appendix A. Supplementary data

Supplementary data to this article can be found online at https://doi.org/10.1016/j.scitotenv.2019.05.457.

References

Krewski Jr, D., D.A Jr., Andersen, M., Anderson, H., J.C.B III, Boekelheide, K., Brent, R., Charnley, G., Cheung, V.G., S.G Jr, Kelsey, K.T., Kerkvliet, N.I., Li, A.A., McCray, L., Meyer, O., Patterson, R.D., Pennie, W., Scala, R.A., Solomon, G.M., Stephens, M., Yager, J., Zeise, L., Testing, S. of C. on T., Agents, A. of E., 2010. Toxicity testing in the 21st century: a vision and a strategy. J. Toxicol. Environ. Health Part B 13, 51–138. doi:https://doi.org/10.1080/10937404.2010.483176.

Ankley, G.T., Collyard, S.A., Monson, P.D., Kosian, P.A., 1994. Influence of ultraviolet light on the toxicity of sediments contaminated with polycyclic aromatic hydrocarbons. Environ. Toxicol. Chem. Int. J. 13, 1791–1796.

Ankley, G.T., Bennett, R.S., Erickson, R.J., Hoff, D.J., Hornung, M.W., Johnson, R.D., Mount, D.R., Nichols, J.W., Russom, C.L., Schmieder, P.K., Serrrano, J.A., Tietge, J.E., Villeneuve, D.L., 2010. Adverse outcome pathways: a conceptual framework to support ecotoxicology research and risk assessment. Environ. Toxicol. Chem. 29, 730–741. https://doi.org/10.1002/etc.34.

Ankley, G.T., LaLone, C.A., Gray, L.E., Villeneuve, D.L., Hornung, M.W., 2016. Evaluation of the scientific underpinnings for identifying estrogenic chemicals in nonmammalian taxa using mammalian test systems. Environ. Toxicol. Chem. 35, 2806–2816. https://doi.org/10.1002/etc.3456.

Baldwin, A.K., Corsi, S.R., De Cicco, L.A., Lenaker, P.L., Lutz, M.A., Sullivan, D.J., Richards, K.D., 2016. Organic contaminants in Great Lakes tributaries: prevalence and potential aquatic toxicity. Sci. Total Environ. 554–555, 42–52. https://doi.org/10.1016/j.scitotenv.2016.02.137.

Blackwell, B.R., Ankley, G.T., Corsi, S.R., DeCicco, L.A., Houck, K.A., Judson, R.S., Li, S., Martin, M.T., Murphy, E., Schroeder, A.L., Smith, E.R., Swintek, J., Villeneuve, D.L., 2017. An "EAR" on environmental surveillance and monitoring: a case study on the use of exposure–activity ratios (EARs) to prioritize sites, chemicals, and bioactivities of concern in Great Lakes waters. Environ. Sci. Technol. 51, 8713–8724. https://doi.org/10.1021/acs.est.7b01613.

Blackwell, B.R., Ankley, G.T., Bradley, P.M., Houck, K.A., Makarov, S.S., Medvedev, A.V., Swintek, J., Villeneuve, D.L., 2019. Potential toxicity of complex mixtures in surface waters from a nationwide survey of United States streams: identifying in vitro bioactivities and causative chemicals. Environ. Sci. Technol. 53, 973–983. https://doi.org/10.1021/acs.est.8b05304.

Blazer, V.S., Iwanowicz, L.R., Henderson, H., Mazik, P.M., Jenkins, J.A., Alvarez, D.A., Young, J.A., 2012. Reproductive endocrine disruption in smallmouth bass (Micropterus dolomieu) in the Potomac River basin: spatial and temporal comparisons of biological effects. Environ. Monit. Assess. 184, 4309–4334. https://doi.org/10.1007/s10661-011-2266-5.

Bradley, P.M., Journey, C.A., Romanok, K.M., Barber, L.B., Buxton, H.T., Foreman, W.T., Furlong, E.T., Glassmeyer, S.T., Hladik, M.L., Iwanowicz, L.R., Jones, D.K., Kolpin, D.W., Kuivila, K.M., Loftin, K.A., Mills, M.A., Meyer, M.T., Orlando, J.L., Reilly, T.J., Smalling, K.L., Villeneuve, D.L., 2017. Expanded target-chemical analysis reveals extensive mixed-organic-contaminant exposure in U.S. streams. Environ. Sci. Technol. 51, 4792–4802. https://doi.org/10.1021/acs.est.7b00012.

Browne, P., Judson, R.S., Casey, W.M., Kleinstreuer, N.C., Thomas, R.S., 2015. Screening chemicals for estrogen receptor bioactivity using a computational model. Environ. Sci. Technol. 49, 8804–8814. https://doi.org/10.1021/acs.est.5b02641.

Busch, W., Schmidt, S., Kühne, R., Schulze, T., Krauss, M., Altenburger, R., 2016. Micropollutants in European rivers: a mode of action survey to support the development of effect-based tools for water monitoring: micropollutants in European rivers: a mode-of-action. Environ. Toxicol. Chem. 35, 1887–1899. https://doi.org/10.1002/etc.3460.

Canadian Council of Ministers of the Environment, 2015. Canadian environmental quality guidelines, water quality guidelines for the protection of aquatic life [WWW document]. URL. http://ceqg-rcqe.ccme.ca/, Accessed date: 20 November 2012.

Careghini, A., Mastorgio, A.F., Saponaro, S., Sezenna, E., 2015. Bisphenol A, nonylphenols, benzophenones, and benzotriazoles in soils, groundwater, surface water, sediments, and food: a review. Environ. Sci. Pollut. Res. 22, 5711–5741. https://doi.org/10.1007/s11356-014-3974-5.

Cavallin, J.E., Jensen, K.M., Kahl, M.D., Villeneuve, D.L., Lee, K.E., Schroeder, A.L., Mayasich, J., Eid, E.P., Nelson, K.R., Milsk, R.Y., Blackwell, B.R., Berninger, J.P., LaLone, C.A., Blanksma, C., Jicha, T., Elonen, C., Johnson, R., Ankley, G.T., 2016. Pathway-based approaches for assessment of real-time exposure to an estrogenic wastewater treatment plant effluent on fathead minnow reproduction. Environ. Toxicol. Chem. 35, 702–716. https://doi.org/10.1002/etc.3228.

Corrales, J., Kristofco, L.A., Steele, W.B., Yates, B.S., Breed, C.S., Williams, E.S., Brooks, B.W., 2015. Global assessment of bisphenol a in the environment: review and analysis of its occurrence and bioaccumulation. Dose-Response 13, 155932581559830. https://doi.org/10.1177/1559325815598308.

Custer, C.M., Custer, T.W., Dummer, P.M., Goldberg, D., Franson, J.C., 2016. Concentrations and spatial patterns of organic contaminants in tree swallow (Tachycineta bicolor) eggs at United States and binational Great Lakes areas of concern, 2010–2015. Environ. Toxicol. Chem. 35, 3071–3092. https://doi.org/10.1002/etc.3496.

Dave, Gör, Blanck, H., Gustafsson, K., 1979. Biological effects of solvent extraction chemicals on aquatic organisms. J. Chem. Technol. Biotechnol. 29, 249–257. https://doi.org/10.1002/jctb.503290406.

Dave, G., Andersson, K., Berglind, R., Hasselrot, B., 1981. Toxicity of eight solvent extraction chemicals and of cadmium to water fleas, Daphnia Magna, rainbow trout, Salmo Gairdneri, and Zebrafish, Brachydanio Rerio. Comp. Biochem. Physiol. Part C Comp. Pharmacol. 69, 83–98. https://doi.org/10.1016/0306-4492(81)90105-2.

Davis, A.P., Murphy, C.G., Johnson, R., Lay, J.M., Lennon-Hopkins, K., Saraceni-Richards, C., Sciaky, D., King, B.L., Rosenstein, M.C., Wiegers, T.C., Mattingly, C.J., 2013. The comparative Toxicogenomics database: update 2013. Nucleic Acids Res. 41, D1104–D1114. https://doi.org/10.1093/nar/gks994.

De Cicco, L.A., Corsi, S.R., Villeneuve, D.L., Blackwell, B.R., Ankley, G.T., 2018. toxEval: Evaluation of measured concentration data using the ToxCast high-throughput screening database or a user-defined set of concentration benchmarks. R Package version 1.0.0 [WWW Document]. URL https://code.usgs.gov/water/toxEval, doi:https://doi.org/10.5066/P906UQ5I.

DeGroot, D.E., Swank, A., Thomas, R.S., Strynar, M., Lee, M.-Y., Carmichael, P.L., Simmons, S.O., 2018. mRNA transfection retrofits cell-based assays with xenobiotic metabolism. J. Pharmacol. Toxicol. Methods 92, 77–94. https://doi.org/10.1016/j.vascn.2018.03.002.

Dix, D.J., Houck, K.A., Martin, M.T., Richard, A.M., Setzer, R.W., Kavlock, R.J., 2007. The ToxCast program for prioritizing toxicity testing of environmental chemicals. Toxicol. Sci. 95, 5–12. https://doi.org/10.1093/toxsci/kfl103.

Elliott, S.M., Brigham, M.E., Lee, K.E., Banda, J.A., Choy, S.J., Gefell, D.J., Minarik, T.A., Moore, J.N., Jorgenson, Z.G., 2017. Contaminants of emerging concern in tributaries to the Laurentian Great Lakes: I. patterns of occurrence. PLoS One 12, e0182868. https://doi.org/10.1371/journal.pone.0182868.

Elliott, S.M., Brigham, M.E., Kiesling, R.L., Schoenfuss, H.L., 2018a. Environmentally relevant chemical mixtures of concern in waters of United States tributaries to the Great Lakes. Intergrated Environ. Assess. Manag. 14, 509–518. https://doi.org/10.1002/ieam.4041.

Elliott, S.M., Route, W.T., DeCicco, L.A., VanderMeulen, D.D., Corsi, S.R., Blackwell, B.R., 2018b. Contaminants in bald eagles of the upper Midwestern U.S.: a framework for prioritizing future research based on in-vitro bioassays. Environ. Pollut. https://doi.org/10.1016/j.envpol.2018.10.093.

Fay, K.A., Villeneuve, D.L., Swintek, J., Edwards, S.W., Nelms, M.D., Blackwell, B.R., Ankley, G.T., 2018. Differentiating pathway-specific from nonspecific effects in high-throughput toxicity data: a foundation for prioritizing adverse outcome pathway development. Toxicol. Sci. 163, 500–515. https://doi.org/10.1093/toxsci/kfy049.

Filer, D.L., Kothiya, P., Setzer, R.W., Judson, R.S., Martin, M.T., 2016. tcpl: the ToxCast pipeline for high-throughput screening data. Bioinformatics, btw680 https://doi.org/10.1093/bioinformatics/btw680.

Fonger, G.C., Stroup, D., Thomas, P.L., Wexler, P., 2000. Toxnet: a computerized collection of toxicological and environmental health information. Toxicol. Ind. Health 16, 4–6. https://doi.org/10.1177/074823370001600101.

Furdui, V.I., Stock, N.L., Ellis, D.A., Butt, C.M., Whittle, D.M., Crozier, P.W., Reiner, E.J., Muir, D.C.G., Mabury, S.A., 2007. Spatial distribution of perfluoroalkyl contaminants in Lake Trout from the Great Lakes. Environ. Sci. Technol. 41, 1554–1559. https://doi.org/10.1021/es0620484.

Gaulton, A., Hersey, A., Nowotka, M., Bento, A.P., Chambers, J., Mendez, D., Mutowo, P., Atkinson, F., Bellis, L.J., Cibrián-Uhalte, E., Davies, M., Dedman, N., Karlsson, A., Magariños, M.P., Overington, J.P., Papadatos, G., Smit, I., Leach, A.R., 2017. The ChEMBL database in 2017. Nucleic Acids Res. 45, D945–D954. https://doi.org/10.1093/nar/gkw1074.

Graymore, M., Stagnitti, F., Allinson, G., 2001. Impacts of atrazine in aquatic ecosystems. Environ. Int. 26, 483–495. https://doi.org/10.1016/S0160-4120(01)00031-9.

Guo, J., Romanak, K., Westenbroek, S., Hites, R.A., Venier, M., 2017a. Current-use flame retardants in the water of Lake Michigan tributaries. Environ. Sci. Technol. 51, 9960–9969. https://doi.org/10.1021/acs.est.7b01294.

Guo, J., Romanak, K., Westenbroek, S., Li, A., Kreis, R.G., Hites, R.A., Venier, M., 2017b. Updated polychlorinated biphenyl mass budget for Lake Michigan. Environ. Sci. Technol. 51, 12455–12465. https://doi.org/10.1021/acs.est.7b02904.

Han, Z., Wang, Q., Fu, J., Chen, H., Zhao, Y., Zhou, B., Gong, Z., Wei, S., Li, J., Liu, H., Zhang, X., Liu, C., Yu, H., 2014. Multiple bio-analytical methods to reveal possible molecular mechanisms of developmental toxicity in zebrafish embryos/larvae exposed to tris (2 butoxyethyl) phosphate. Aquat. Toxicol. 150, 175–181. https://doi.org/10.1016/j.aquatox.2014.03.013.

Heiger-Bernays, W.J., Wegner, S., Dix, D.J., 2018. High-throughput in vitro data to inform prioritization of ambient water monitoring and testing for endocrine active chemicals. Environ. Sci. Technol. 52, 783–793. https://doi.org/10.1021/acs.est.7b00014.

Igarashi, Y., Nakatsu, N., Yamashita, T., Ono, A., Ohno, Y., Urushidani, T., Yamada, H., 2015. Open TG-GATEs: a large-scale toxicogenomics database. Nucleic Acids Res. 43, D921–D927. https://doi.org/10.1093/nar/gku955.

Incardona, J.P., Day, H.L., Collier, T.K., Scholz, N.L., 2006. Developmental toxicity of 4 ring polycyclic aromatic hydrocarbons in zebrafish is differentially dependent on AH receptor isoforms and hepatic cytochrome P4501A metabolism. Toxicol. Appl. Pharmacol. 217, 308–321. https://doi.org/10.1016/j.taap.2006.09.018.

Ives, C., Campia, I., Wang, R.-L., Wittwehr, C., Edwards, S., 2017. Creating a structured adverse outcome pathway knowledgebase via ontology-based annotations. Appl. Vitro Toxicol. 3, 298–311. https://doi.org/10.1089/aivt.2017.0017.

Jacobs, M., 2013. In vitro metabolism and bioavailability tests for endocrine active substances: what is needed next for regulatory purposes? ALTEX 30, 331–351. https://doi.org/10.14573/altex.2013.3.331.

Jobling, S., Nolan, M., Tyler, C.R., Brighty, G., Sumpter, J.P., 1998. Widespread sexual disruption in wild fish. Environ. Sci. Technol. 32, 2498–2506. https://doi.org/10.1021/es9710870.

Jobling, S., Beresford, N., Nolan, M., Rodgers-Gray, T., Brighty, G.C., Sumpter, J.P., Tyler, C.R., 2002. Altered sexual maturation and gamete production in wild roach (Rutilus rutilus) living in rivers that receive treated sewage effluents. Biol. Reprod. 66, 272–281. https://doi.org/10.1095/biolreprod66.2.272.

Judson, R.S., Houck, K.A., Kavlock, R.J., Knudsen, T.B., Martin, M.T., Mortensen, H.M., Reif, D.M., Rotroff, D.M., Shah, I., Richard, A.M., Dix, D.J., 2009. In vitro screening of environmental chemicals for targeted testing prioritization: the ToxCast project. Environ. Health Perspect. 118, 485–492. https://doi.org/10.1289/ehp.0901392.

Judson, R., Houck, K., Martin, M., Richard, A.M., Knudsen, T.B., Shah, I., Little, S., Wambaugh, J., Woodrow Setzer, R., Kothya, P., Phuong, J., Filer, D., Smith, D., Reif, D., Rotroff, D., Kleinstreuer, N., Sipes, N., Xia, M., Huang, R., Crofton, K., Thomas, R.S., 2016. Editor's highlight: analysis of the effects of cell stress and cytotoxicity on *in vitro* assay activity across a diverse chemical and assay space. Toxicol. Sci. 152, 323–339. https://doi.org/10.1093/toxsci/kfw092.

Karn, S.K., Chakrabarty, S.K., Sudhakara Reddy, M., 2010. Characterization of pentachlorophenol degrading Bacillus strains from secondary pulp-and-paper-industry sludge. Int. Biodeterior. Biodegrad. 64, 609–613. https://doi.org/10.1016/j.ibiod.2010.05.017.

Kavlock, R., Chandler, K., Houck, K., Hunter, S., Judson, R., Kleinstreuer, N., Knudsen, T., Martin, M., Padilla, S., Reif, D., Richard, A., Rotroff, D., Sipes, N., Dix, D., 2012. Update on EPA's ToxCast program: providing high throughput decision support tools for chemical risk management. Chem. Res. Toxicol. 25, 1287–1302. https://doi.org/10.1021/tx3000939.

Kim, S., Jung, J., Lee, I., Jung, D., Youn, H., Choi, K., 2015. Thyroid disruption by triphenyl phosphate, an organophosphate flame retardant, in zebrafish (Danio rerio) embryos/larvae, and in GH3 and FRTL-5 cell lines. Aquat. Toxicol. 160, 188–196. https://doi.org/10.1016/j.aquatox.2015.01.016.

Kim, S., Thiessen, P.A., Bolton, E.E., Chen, J., Fu, G., Gindulyte, A., Han, L., He, J., He, S., Shoemaker, B.A., Wang, J., Yu, B., Zhang, J., Bryant, S.H., 2016. PubChem substance and compound databases. Nucleic Acids Res. 44, D1202–D1213. https://doi.org/10.1093/nar/gkv951.

Kliewer, S.A., Goodwin, B., Willson, T.M., 2002. The nuclear pregnane × receptor: a key regulator of xenobiotic metabolism. Endocr. Rev. 23, 687–702. https://doi.org/10.1210/er.2001-0038.

Knapen, D., Angrish, M.M., Fortin, M.C., Katsiadaki, I., Leonard, M., Margiotta-Casaluci, L., Munn, S., O'Brien, J.M., Pollesch, N., Smith, L.C., Zhang, X., Villeneuve, D.L., 2018.

Adverse outcome pathway networks I: development and applications: advancing adverse outcome pathway networks. Environ. Toxicol. Chem. 37, 1723–1733. https://doi.org/10.1002/etc.4125.
LaLone, C.A., Villeneuve, D.L., Wu-Smart, J., Milsk, R.Y., Sappington, K., Garber, K.V., Housenger, J., Ankley, G.T., 2017. Weight of evidence evaluation of a network of adverse outcome pathways linking activation of the nicotinic acetylcholine receptor in honey bees to colony death. Sci. Total Environ. 584–585, 751–775. https://doi.org/10.1016/j.scitotenv.2017.01.113.
Lamb, J., Crawford, E.D., Peck, D., Modell, J.W., Blat, I.C., Wrobel, M.J., Lerner, J., Brunet, J.-P., Subramanian, A., Ross, K.N., Reich, M., Hieronymus, H., Wei, G., Armstrong, S.A., Haggarty, S.J., Clemons, P.A., Wei, R., Carr, S.A., Lander, E.S., Golub, T.R., 2006. The connectivity map: using gene-expression signatures to connect small molecules, genes, and disease. Science 313, 1929–1935. https://doi.org/10.1126/science.1132939.
Lepak, R.F., Yin, R., Krabbenhoft, D.P., Ogorek, J.M., DeWild, J.F., Holsen, T.M., Hurley, J.P., 2015. Use of stable isotope signatures to determine mercury sources in the Great Lakes. Environ. Sci. Technol. Lett. 2, 335–341. https://doi.org/10.1021/acs.estlett.5b00277.
Lin, K., 2009. Joint acute toxicity of tributyl phosphate and triphenyl phosphate to Daphnia magna. Environ. Chem. Lett. 7, 309–312. https://doi.org/10.1007/s10311-008-0170-1.
Logan, D.T., 2007. Perspective on ecotoxicology of PAHs to fish. Hum. Ecol. Risk Assess. Int. J. 13, 302–316. https://doi.org/10.1080/10807030701226749.
Love, B.J., Einheuser, M.D., Nejadhashemi, A.P., 2011. Effects on aquatic and human health due to large scale bioenergy crop expansion. Sci. Total Environ. 409, 3215–3229. https://doi.org/10.1016/j.scitotenv.2011.05.007.
Mayer, F., Ellersieck, M.R., 1986. Manual of Acute Toxicity:Interpretation and Data Base for 410 Chemicals and 66 Species of Freshwater Animals.
Medvedev, A., Moeser, M., Medvedeva, L., Martsen, E., Granick, A., Raines, L., Zeng, M., Makarov, S., Houck, K.A., Makarov, S.S., 2018. Evaluating biological activity of compounds by transcription factor activity profiling. Sci. Adv. 4, eaar4666. https://doi.org/10.1126/sciadv.aar4666.
Nirmalakhandan, N., Arulgnanendran, V., Mohsin, M., Sun, B., Cadena, F., 1994. Toxicity of mixtures of organic chemicals to microorganisms. Water Res. 28, 543–551. https://doi.org/10.1016/0043-1354(94)90005-1.
Ohe, T., Watanabe, T., Wakabayashi, K., 2004. Mutagens in surface waters: a review. Mutat. Res. Mutat. Res. 567, 109–149. https://doi.org/10.1016/j.mrrev.2004.08.003.
Pérez, J., Domingues, I., Soares, A.M.V.M., Loureiro, S., 2011. Growth rate of Pseudokirchneriella subcapitata exposed to herbicides found in surface waters in the Alqueva reservoir (Portugal): a bottom-up approach using binary mixtures. Ecotoxicology 20, 1167–1175. https://doi.org/10.1007/s10646-011-0661-x.
Pittman, M.E., Edwards, S.W., Ives, C., Mortensen, H.M., 2018. AOP-DB: a database resource for the exploration of adverse outcome pathways through integrated association networks. Toxicol. Appl. Pharmacol. 343, 71–83. https://doi.org/10.1016/j.taap.2018.02.006.
Prado, P.S., Pinheiro, A.P.B., Bazzoli, N., Rizzo, E., 2014. Reproductive biomarkers responses induced by xenoestrogens in the characid fish Astyanax fasciatus inhabiting a South American reservoir: an integrated field and laboratory approach. Environ. Res. 131, 165–173. https://doi.org/10.1016/j.envres.2014.03.002.
R Core Team, 2017. R: A Language and Environment for Statistical Computing. R Foundation for Statistical Computing, Vienna, Austria.
Rivera-Oliver, M., Díaz-Ríos, M., 2014. Using caffeine and other adenosine receptor antagonists and agonists as therapeutic tools against neurodegenerative diseases: a review. Life Sci. 101, 1–9. https://doi.org/10.1016/j.lfs.2014.01.083.
Schroeder, A.L., Ankley, G.T., Houck, K.A., Villeneuve, D.L., 2016. Environmental surveillance and monitoring-the next frontiers for high-throughput toxicology: surveillance and monitoring and high-throughput toxicology. Environ. Toxicol. Chem. 35, 513–525. https://doi.org/10.1002/etc.3309.
Shannon, P., Markiel, A., Ozier, O., Baliga, N.S., Wang, J.T., Ramage, D., Amin, N., Schwikowski, B., Ideker, T., 2003. Cytoscape: a software environment for integrated models of biomolecular interaction networks. Genome Res. 13, 2498–2504. https://doi.org/10.1101/gr.1239303.
Simcik, M.F., Offenberg, J.H., 2006. Polycyclic aromatic hydrocarbons in the Great Lakes. In: Hites, R.A. (Ed.), Persistent Organic Pollutants in the Great Lakes. Springer, Berlin Heidelberg, pp. 307–353 https://doi.org/10.1007/698_5_044.
Society for the Advancement of Adverse Outcome Pathways, 2018. Aopwiki [WWW Document]. URL. https://aopwiki.org/, Accessed date: 21 September 2018.
Stegeman, J.J., Lech, J.J., 1991. Cytochrome P-450 monooxygenase systems in aquatic species: carcinogen metabolism and biomarkers for carcinogen and pollutant exposure. Environ. Health Perspect. 90, 101. https://doi.org/10.2307/3430851.
Subramanian, A., Narayan, R., Corsello, S.M., Peck, D.D., Natoli, T.E., Lu, X., Gould, J., Davis, J.F., Tubelli, A.A., Asiedu, J.K., Lahr, D.L., Hirschman, J.E., Liu, Z., Donahue, M., Julian, B., Khan, M., Wadden, D., Smith, I.C., Lam, D., Liberzon, A., Toder, C., Bagul, M., Orzechowski, M., Enache, O.M., Piccioni, F., Johnson, S.A., Lyons, N.J., Berger, A.H., Shamji, A.F., Brooks, A.N., Vrcic, A., Flynn, C., Rosains, J., Takeda, D.Y., Hu, R., Davison, D., Lamb, J., Ardlie, K., Hogstrom, L., Greenside, P., Gray, N.S., Clemons, P.A., Silver, S., Wu, Xiaoyun, Zhao, W.-N., Read-Button, W., Wu, Xiaohua, Haggarty, S.J., Ronco, L.V., Boehm, J.S., Schreiber, S.L., Doench, J.G., Bittker, J.A., Root, D.E., Wong, B., Golub, T.R., 2017. A next generation connectivity map: L1000 platform and the first 1,000,000 profiles. Cell 171, 1437–1452.e17. https://doi.org/10.1016/j.cell.2017.10.049.
Thrupp, T.J., Runnalls, T.J., Scholze, M., Kugathas, S., Kortenkamp, A., Sumpter, J.P., 2018. The consequences of exposure to mixtures of chemicals: something from 'nothing' and 'a lot from a little' when fish are exposed to steroid hormones. Sci. Total Environ. 619–620, 1482–1492. https://doi.org/10.1016/j.scitotenv.2017.11.081.
Tice, R.R., Austin, C.P., Kavlock, R.J., Bucher, J.R., 2013. Improving the human Hazard characterization of chemicals: a Tox21 update. Environ. Health Perspect. 121, 756–765. https://doi.org/10.1289/ehp.1205784.
US EPA, 1996. Ecotox thresholds, EPA 540/F-95/038 [WWW document]. URL. http://www.epa.gov/sites/production/files/2015-09/documents/v3no2.pdf.
US EPA, 2003. Procedures for the Derivation of Equilibrium Partitioning Sediment Benchmarks (ESBs) for the Protection of Benthic Organisms. PAH Mixtures.
US EPA, 2015. US EPA. ToxCast & Tox21 summary files from invitrodb_v2. [WWW document]. URL. http://www2.epa.gov/chemical-research/toxicity-forecaster-toxcasttm-data, Accessed date: 22 February 2016.
Usmani, K.A., Rose, R.L., Goldstein, J.A., Taylor, W.G., Brimfield, A.A., Hodgson, E., 2002. In vitro human metabolism and interactions of repellent N,N diethyl m toluamide. Drug Metab. Dispos. 30, 289–294. https://doi.org/10.1124/dmd.30.3.289.
Vajda, A.M., Barber, L.B., Gray, J.L., Lopez, E.M., Woodling, J.D., Norris, D.O., 2008. Reproductive disruption in fish downstream from an estrogenic wastewater effluent. Environ. Sci. Technol. 42, 3407–3414. https://doi.org/10.1021/es0720661.
Villeneuve, D.L., Crump, D., Garcia-Reyero, N., Hecker, M., Hutchinson, T.H., LaLone, C.A., Landesmann, B., Lettieri, T., Munn, S., Nepelska, M., Ottinger, M.A., Vergauwen, L., Whelan, M., 2014. Adverse outcome pathway (AOP) development I: strategies and principles. Toxicol. Sci. 142, 312–320. https://doi.org/10.1093/toxsci/kfu199.
Villeneuve, D.L., Angrish, M.M., Fortin, M.C., Katsiadaki, I., Leonard, M., Margiotta-Casaluci, L., Munn, S., O'Brien, J.M., Pollesch, N.L., Smith, L.C., Zhang, X., Knapen, D., 2018. Adverse outcome pathway networks II: network analytics: adverse outcome pathway network analytics. Environ. Toxicol. Chem. 37, 1734–1748. https://doi.org/10.1002/etc.4124.
Weeks, J., Guiney, P., Nikiforov, A., 2012. Assessment of the environmental fate and ecotoxicity of N,N diethyl m toluamide (DEET). Integr. Environ. Assess. Manag. 8, 120–134. https://doi.org/10.1002/ieam.1246.
Wickham, H., 2016. ggplot2: Elegant Graphics for Data Analysis. Springer-Verlag, New York.
Wickham, H., François, R., Henry, L., Müller, K., 2018. dplyr: A Grammar of Data Manipulation.
Yoshioka, Y., Ose, Y., Sato, T., 1986. Correlation of the five test methods to assess chemical toxicity and relation to physical properties. Ecotoxicol. Environ. Saf. 12, 15–21. https://doi.org/10.1016/0147-6513(86)90003-5.
Zaugg, S.D., Smith, S.G., Schroeder, M.P., 2006. Determination of Wastewater Compounds in Whole Water by Continuous Liquid-Liquid Extraction and Capillary-Column Gas Chromatography/Mass Spectrometry (No. TM-5-B4). United States Geological Survey.
Zenobio, J.E., Sanchez, B.C., Archuleta, L.C., Sepulveda, M.S., 2014. Effects of triclocarban, N,N diethyl meta toluamide, and a mixture of pharmaceuticals and personal care products on fathead minnows (*Pimephales promelas*): effects of pharmaceuticals on fish. Environ. Toxicol. Chem. 33, 910–919. https://doi.org/10.1002/etc.2511.

Introduction to toxEval

15 April, 2020

Source: `vignettes/Introduction.Rmd` (https://github.com/USGS-R/toxEval/blob/master/vignettes/Introduction.Rmd)

Introduction

The `toxEval` R-package includes a set of functions to analyze, visualize, and organize measured concentration data as it relates to ToxCast data (https://www.epa.gov/chemical-research/toxicity-forecasting) (default) or other user-selected chemical-biological interaction benchmark data such as water quality criteria. The intent of these analyses is to develop a better understanding of the potential biological relevance of environmental chemistry data. Results can be used to prioritize which chemicals at which sites may be of greatest concern. These methods are meant to be used as a screening technique to predict potential for biological influence from chemicals that ultimately need to be validated with direct biological assays.

The functions within this package allow great flexibly for exploring the potential biological affects of measured chemicals. Also included in the package is a browser-based application made from the `Shiny` R-package (the app). The app is based on functions within the R-package and includes many convenient analyses and visualization options for users to choose. Use of the functions within the R-package allows for additional flexibility within the functions beyond what the app offers and provides options for the user to interact more directly with the data. The overview in this document focuses on the R-package. Documentation for the app is provided in the ShinyApp vignette (shinyApp.html).

This vignette provides a general overview of the concepts within `toxEval`, definitions of common terminology used throughout the package, and links to information to help understand fundamentals of the ToxCast database used within `toxEval`. In addition, instructions are provided for installing and updating the package from the Geological Survey R Archive Network (GRAN).

What is ToxCast?

The U.S. EPA's Toxicity Forecaster ToxCast (https://www.epa.gov/chemical-research/toxicity-forecasting) includes a database of chemical-biological interactions that contains information from hundreds of assays on thousands of chemicals, providing a means to assess biological relevance to measured concentrations. The `toxEval` package attempts to simplify the workflow for exploring data as it relates to these assay endpoints (benchmark data). The workflow uses ToxCast as a default for evaluation of chemical:biological interactions, but the user may also define alternative benchmarks for a custom or more traditional approach to biological relevance evaluation. This is also a useful capability for efficient comparison of ToxCast evaluation results with those from other toxicity benchmark databases.

When using the ToxCast endPoints for analysis, it is important to have at least a minimal understanding of what ToxCast data is, and which ToxCast data is relevant to any given study. There are many useful resources here (https://www.epa.gov/chemical-research/toxicity-forecasting). There is also a tool called the Comptox Dashboard (https://comptox.epa.gov/dashboard/) that has a wealth of information on ToxCast data.

So what are we doing with the user input data and ToxCast? First, we calculate an Exposure-Activity Ratio (EAR) for each measurement. Then we can explore the EARs based on a wide variety of groupings to view the data in many dimensions.

Exposure-Activity Ratio

An Exposure-Activity Ratio (EAR) is defined as the ratio of a measured concentration and a concentration that was determined to cause some activity in a specified ToxCast assay ("endPoint" concentration). An EAR > 1.0 would indicate that the measured concentration is greater than the endpoint concentration. The ToxCast database (as provided in the current version of `toxEval`) provides as many as several hundred endPoints for more than 7000 chemicals. Each endPoint is a single test that was done to detect some form of biological activity.

In order to get appropriate EAR results, it is important to use the correct units. The `toxEval` package assumes all measured concentrations are reported in micrograms per liter (μg/L). ToxCast data is reported in log(μM), so the `toxEval` package automatically performs the unit conversion.

A secondary option within `toxEval` is for the user to provide a set of "benchmark concentrations" to define custom biological responses to meet specific study objectives (e.g. water quality criteria). In this case, EAR values are replaced with toxicity quotients. Similar to EAR values, toxicity quotients are defined as the ratio of a measured concentration to the benchmark concentration.

EAR is basically synonymous with bioanalytical equivalent concentrations (BEQ). EAR is a ratio, and BEQ is a measure of concentration, but both convey the same information.

What is an "endPoint"?

ToxCast uses high-throughput assays to create concentration-response curves for each of these chemical:endPoint combinations. An endPoint is "associated with the perturbation of specific biological processes identified for the confirmation or monitoring of predicted site-specific hazards" Blackwell 2017 (https://doi.org/10.1021/acs.est.7b01613). That means a specific biological action was tested, and the concentration at which activity was observed was determined. Of several endpoint values provided within the ToxCast database, the activity concentration at cutoff (ACC) was chosen to compute EAR values within the `toxEval` package, consistent with the description in Blackwell, 2017 (https://doi.org/10.1021/acs.est.7b01613). ACC values from the ToxCast database are provided within the `toxEval` package.

What is a "group"?

Often, it is valuable to consider aggregations of single endPoints in evaluation efforts. ToxCast has provided tables that group individual endPoints into generalized categories for functional use. The grouping summary table is included in `toxEval` and can be explored via the `end_point_info` data:

```
library (https://rdrr.io/r/base/library.html)(toxEval)
end_point_info <- end_point_info
```

See the help file `?end_point_info` for specifics on how the table was downloaded.

Throughout the `toxEval` analysis, there are graphing and table functions that will summarize EARs based on either "Biological" groupings (as defined by a group of endPoints) or "Chemical Class" groupings (as defined by a group of chemicals).

The default grouping of ToxCast endPoints is “intended_target_family”, but depending on the analysis, it may be more appropriate to use other grouping categories. To change the default, specify a grouping in the `groupCol` argument of the `filter_groups` function. For example:

```
filtered_ep <- filter_groups (../reference/filter_groups.html)(end_point_info,
              groupCol = "intended_target_family",
              assays = c (https://rdrr.io/r/base/c.html)("ATG","NVS", "OT", "TOX21",
                         "CEETOX", "APR", "CLD", "TANGUAY",
                         "NHEERL_PADILLA","NCCT_SIMMONS", "ACEA"),
              remove_groups = c (https://rdrr.io/r/base/c.html)("Background Measurement",
                                 "Undefined"))
```

What is happening here is that the supplied data frame `end_point_info` is filtered to just the “intended_target_family” group. Additionally, the assay BioSeek is removed (it is the only one not included in the possible list of assays). Finally, of all the groups within intended_target_family, the end points designated “Undefined” and “Background Measurement” are removed.

Summarizing the data

The functions in `toxEval` summarize the data as follows:

First, individual EAR values are calculated for each chemical:endPoint combination. Then, the EAR values are summed together by samples (a sample is defined as a unique site/date) based on the grouping picked in the “category” argument. Categories include “Biological”, “Chemical Class”, or “Chemical”. “Biological” refers to the chosen ToxCast annotation as defined in the `groupCol` argument of the `filter_groups` function. “Chemical Class” refers to the groupings of chemicals as defined in the “Class” column of the “Chemicals” sheet of the input file. “Chemical” refers to the individual chemical as defined by a unique CAS value. Finally, the maximum or mean EAR is calculated per site (based on the `mean_logic` option). This ensures that each site is represented equally regardless of how many samples are available per site.

Some functions will also include a calculation for a “hit”. A threshold is defined by the user, and if the mean or maximum EAR (calculated as described above) is greater than the threshold, that is considered a “hit”.

Package logistics

Installation of toxEval

`toxEval` is available on any CRAN mirror.

```
install.packages (https://rdrr.io/r/utils/install.packages.html)("toxEval")
```

Update toxEval

`toxEval` does require a fair number of additional packages to run properly. These dependencies offer many benefits, such as a smooth running intuitive Shiny app. The drawbacks however are that there becomes more risk that those dependencies could change their output/workflow over time. `toxEval` developers will try to stay on top of those changes, but it is a challenge. It is important to always update *all* of your packages therefore…..not just `toxEval` .

`toxEval` may push out a new version to keep up with a critical change in a dependent package, and if you only update `toxEval`, the update could cause bugs (we will attempt to mandate the package version of each package, but it still is best to stay on top of new package versions).

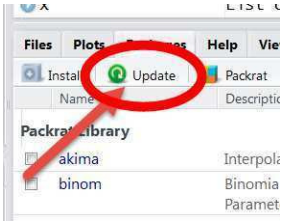

Regularly, it is a good idea to update *ALL* of installed packages in R. If using RStudio, this is done by using the Update button in the “Packages” tab in RStudio. Selecting this option checks CRAN for updates. Within the R-console, packages can be updated with the command:

```
update.packages (https://rdrr.io/r/utils/update.packages.html)()
```

Reporting bugs

If you discover an issue that you feel is a bug in the package or have a question on functionality, please consider reporting bugs and asking questions on the Issues page: https://github.com/USGS-R/toxEval/issues (https://github.com/USGS-R/toxEval/issues)

Citing toxEval

This package has not been reviewed and approved as a USGS-product. The implication is that `toxEval` cannot be cited in a publication. Once the software has been reviewed and approved, basic citation information will be available using the function:

```
citation (https://rdrr.io/r/utils/citation.html)(package = "toxEval")
```

```
##
## To cite toxEval in publications, please use:
##
##   De Cicco, L.A., Corsi, S.R., Villeneuve D.L, Blackwell, and B.R,
##   Ankley, G.T., 2018, toxEval: Evaluation of measured concentration
##   data using the ToxCast high-throughput screening database or a
##   user-defined set of concentration benchmarks. R package version
##   1.1.0., https://code.usgs.gov/water/toxEval, doi:10.5066/P906UQ5I
##
## A BibTeX entry for LaTeX users is
##
##   @Manual{,
##     author = {Laura A. {De Cicco} and Steven R. Corsi and Daniel L. Villeneuve and Brett R. Blackwe
##     title = {toxEval: Evaluation of measured concentration data using the ToxCast high-throughput s
##     publisher = {U.S. Geological Survey},
##     version = {1.1.0},
##     address = {Reston, VA},
##     institution = {U.S. Geological Survey},
##     year = {2019},
##     doi = {10.5066/P906UQ5I},
##     url = {https://code.usgs.gov/water/toxEval},
##   }
```

Disclaimer

This software has been approved for release by the U.S. Geological Survey (USGS). Although the software has been subjected to rigorous review, the USGS reserves the right to update the software as needed pursuant to further analysis and review. No warranty, expressed or implied, is made by the USGS or the U.S. Government as to the functionality of the software and related material nor shall the fact of release constitute any such warranty. Furthermore, the software is released on condition that neither the USGS nor the U.S. Government shall be held liable for any damages resulting from its authorized or unauthorized use.

Science of the Total Environment 686 (2019) 995–1009

Contents lists available at ScienceDirect

Science of the Total Environment

journal homepage: www.elsevier.com/locate/scitotenv

Prioritizing chemicals of ecological concern in Great Lakes tributaries using high-throughput screening data and adverse outcome pathways

Steven R. Corsi [a,*], Laura A. De Cicco [a], Daniel L. Villeneuve [b], Brett R. Blackwell [b], Kellie A. Fay [c,1], Gerald T. Ankley [b], Austin K. Baldwin [d]

[a] U.S. Geological Survey, Middleton, WI 53562, United States
[b] U.S. Environmental Protection Agency, Office of Research and Development, Duluth, MN 55804, United States
[c] General Dynamics Information Technology, Duluth, MN 55804, United States
[d] U.S. Geological Survey, Boise, ID 83702, United States

HIGHLIGHTS

- Potential for ecological impacts of 67 organic contaminants was evaluated.
- Use of ToxCast data increased the number for which bioeffects could be assessed.
- Chemicals and sites with greatest potential for adverse bioeffects were identified.
- Adverse outcome pathways linked ToxCast responses to potential adverse outcomes.
- Mixture effects were predicted using ToxCast exposure-activity-ratios and AOPs.

GRAPHICAL ABSTRACT

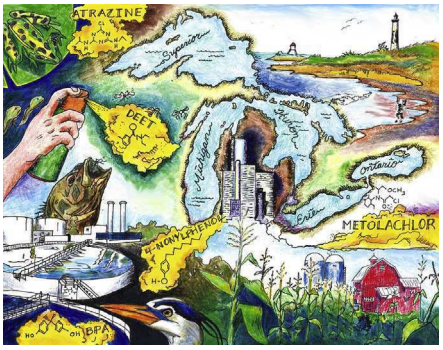

ARTICLE INFO

Article history:
Received 2 May 2019
Received in revised form 28 May 2019
Accepted 30 May 2019
Available online 5 June 2019

Editor: Damia Barcelo

Keywords:
Surface water
Organic contaminants
Chemical mixtures
Bioeffects
High-throughput screening
Adverse outcome pathways

ABSTRACT

Chemical monitoring data were collected in surface waters from 57 Great Lakes tributaries from 2010 to 13 to identify chemicals of potential biological relevance and sites at which these chemicals occur. Traditional water-quality benchmarks for aquatic life based on in vivo toxicity data were available for 34 of 67 evaluated chemicals. To expand evaluation of potential biological effects, measured chemical concentrations were compared to chemical-specific biological activities determined in high-throughput (ToxCast) in vitro assays. Resulting exposure-activity ratios (EARs) were used to prioritize the chemicals of greatest potential concern: 4 nonylphenol, bisphenol A, metolachlor, atrazine, DEET, caffeine, tris(2 butoxyethyl) phosphate, tributyl phosphate, triphenyl phosphate, benzo(a)pyrene, fluoranthene, and benzophenone. Water-quality benchmarks were unavailable for five of these chemicals, but for the remaining seven, EAR-based prioritization was consistent with that based on toxicity quotients calculated from benchmarks. Water-quality benchmarks identified three additional PAHs (anthracene, phenanthrene, and pyrene) not prioritized using EARs. Through this analysis, an EAR of 10^{-3} was identified as a reasonable threshold above which a chemical might be of potential concern. To better understand apical hazards potentially associated with biological activities captured in ToxCast assays, in vitro bioactivity data were matched with available adverse outcome pathway (AOP) information. The 49 ToxCast assays prioritized via EAR analysis aligned with 23 potentially-relevant AOPs present in the AOP-Wiki. Mixture effects at monitored sites were estimated by summation of EAR values for multiple chemicals by

* Corresponding author.
E-mail address: srcorsi@usgs.gov (S.R. Corsi).
[1] Current affiliation, U.S. Environmental Protection Agency.

https://doi.org/10.1016/j.scitotenv.2019.05.457
0048-9697/Published by Elsevier B.V. This is an open access article under the CC BY-NC-ND license (http://creativecommons.org/licenses/by-nc-nd/4.0/).

individual assay or individual AOP. Commonly predicted adverse outcomes included impacts on reproduction and mitochondrial function. The EAR approach provided a screening-level assessment for evidence-based prioritization of chemicals and sites with potential for adverse biological effects. The approach aids prioritization of future monitoring activities and provides testable hypotheses to help focus those efforts. This also expands the fraction of detected chemicals for which biologically-based benchmark concentrations are available to help contextualize chemical monitoring results.

Published by Elsevier B.V. This is an open access article under the CC BY-NC-ND license (http://creativecommons.org/licenses/by-nc-nd/4.0/).

1. Introduction

Tributaries of the Great Lakes are influenced by a diverse set of stressors that may cause adverse ecological effects. Consequently, deciding how to most effectively allocate limited resources for management and monitoring activities can be a challenge. When mixtures of contaminants are detected, it can be difficult to determine which contaminants are of greatest concern and in turn what potential source mitigation or remediation strategies could most effectively lower risk. For example, in addition to legacy contamination with compounds such as polychlorinated biphenyls (PCBs) and dichlorodiphenyltrichloroethane (DDT), Great Lakes tributary ecosystems are influenced by current-use contaminants from sources such as urban and agricultural runoff, treated and untreated wastewater, and atmospheric deposition (Custer et al., 2016; Furdui et al., 2007; Guo et al., 2017a, 2017b; Lepak et al., 2015). Contaminants from these sources include polycyclic aromatic hydrocarbons (PAHs), pesticides, pharmaceutical and personal care products, flame retardants, plasticizers, detergents, and degradation products of these contaminants, among others (Baldwin et al., 2016; Elliott et al., 2017, 2018a).

During 2010–13, 709 surface-water samples were collected in 57 Great Lakes tributaries and analyzed for 67 organic compounds that represent 15 classes of chemicals based on their functional use or chemical properties (Baldwin et al., 2016). Watersheds included in this effort represent a broad range of urban, agricultural, forested, and water and wetland land cover attributes (Table SI-1), and samples were collected to capture spatial, seasonal, and hydrologic variability. Understanding the potential significance of these contaminants on aquatic ecosystem health can be a challenge. For example, a comprehensive search for US and Canadian water-quality benchmarks for acute and chronic exposure to aquatic life for the 67 target analytes resulted in information for only 34 of them from 10 chemical classes (Baldwin et al., 2016). Considering the limited number of traditional, in vivo-based water-quality benchmarks available for the diverse range of contaminants, we aimed to expand the scope of our screening-level characterization of potential biological significance by leveraging the growing database of chemical-specific high throughput in vitro biological activity data generated via the ToxCast and Tox21 (hereafter referred to as ToxCast) programs (Dix et al., 2007; Kavlock et al., 2012; Tice et al., 2013).

The ToxCast database contains information on biological activities of thousands of chemicals. The information comes from several hundred high-throughput assays that cover a range of cell responses and approximately 300 signaling pathways (Kavlock et al., 2012; Tice et al., 2013). A number of other sources of potential chemical-biological interaction data also exists, including PubChem (Kim et al., 2016), ChEMBL (Gaulton et al., 2017), ToxNet (Fonger et al., 2000), TG-GATEs (Igarashi et al., 2015), the Comparative Toxicogenomics Database (Davis et al., 2013), and the Connectivity Map (Lamb et al., 2006; Subramanian et al., 2017). However, most of these sources aggregate chemical-biological interactions from the peer-reviewed literature where the use of different experimental designs, assay systems, testing conditions, and analytical/statistical approaches can confound quantitative comparisons of potency. In contrast, ToxCast chemicals were tested in a consistent and standardized set of assays and resultant data were analyzed with a uniform analysis pipeline (Filer et al., 2016). This allows for more reliable comparison of the relative potency of the tested chemicals thereby supporting the type of comparative prioritization analysis that was the aim of the present study.

Using in vitro bioeffects data in this manner is consistent with the long-range vision for toxicity-testing described in the National Research Council (NRC) report "Toxicity Testing in the 21st Century—a vision and strategy" (Krewski et al., 2010). This NRC report envisioned more efficient and effective strategies for toxicity-testing given advances in our understanding of biology and the emergence of modern testing technologies. Considering the complex mixture of chemicals that often occur in environmental waters impacted by multiple different sources and land uses, evaluation of potential biological effects could benefit from this 21st century approach to toxicity evaluation. While information from these techniques is commonly targeted at human health impacts, recent studies have explored it for use in evaluation of potential adverse impacts in nonmammalian species as well including evaluation of potential impact on aquatic life (Blackwell et al., 2017, 2019; Heiger-Bernays et al., 2018; Schroeder et al., 2016) and avian species (Elliott et al., 2018b). For this type of prioritization, exposure-activity ratios (EARs = sample concentration/bioactivity effect concentration) have been identified as a valuable calculation (Blackwell et al., 2017; Elliott et al., 2018b); however, it is currently unclear what EAR threshold to consider as a level of concern and whether the threshold is relatively constant or changes substantially as different chemicals are evaluated, and an evaluation is needed to determine which ToxCast assays and related adverse outcome pathways are ecologically relevant.

The objectives of the current study were to couple the contaminant surveillance data from 57 monitored Great Lakes tributaries with high-throughput assay results from ToxCast to (1) assess whether the EAR approach appears to be valuable in this context, (2) if so, determine what EAR level(s) warrant concern based on comparison with evaluations using traditional water quality benchmarks, (3) identify chemicals of concern, (4) screen for potential adverse biological effects that may be associated with those chemicals, through linking bioactivity data to adverse outcome pathways (AOPs) for ecologically-relevant species, and (5) prioritize tributaries with respect to potential biological effects.

2. Methods

2.1. Sampling design

The Great Lakes tributaries were sampled from September 2010 through September 2013 and included sites draining to each of the five Great Lakes (Fig. SI-1, Table SI-1). A total of 709 water samples were collected. The study was designed to provide a general indication of contaminants in Great Lakes tributaries on spatial, temporal, and seasonal scales. Thirty-eight of the sites were sampled only one or two times to provide background information on a large spatial scale and identify potential concern for future studies. These sites were thought to be less likely to have large numbers of contaminants present than sites sampled more frequently given their history and land use composition. The remaining 19 sites were sampled more frequently with 7–64 samples that added to the spatial extent of the study and served to represent temporal and seasonal variability. Drainage areas ranged from 101 to 16,400 km^2, with mean annual flows from 2.58 to 219 cubic meters per second (October 2010–September 2013). Watershed land cover varied from dominantly urban (up to 92% of watershed) to agricultural

(up to 84%) to forest and wetland (up to 93%). Watershed population densities ranged from 1.3 to 964 people/km^2 with 0% to 47% mean annual streamflow contributions from wastewater treatment plants. Details of the site selection, sampling design, sampling protocols, and quality assurance sample results have been previously published (Baldwin et al., 2016).

Whole water samples were analyzed for 67 organic waste compounds at the U.S. Geological Survey National Water Quality Laboratory in Denver, CO. Compounds were extracted using continuous liquid-liquid extraction and methylene chloride solvent, then determined by capillary-column gas chromatography/mass spectrometry (Zaugg et al., 2006). Four analytes were omitted from the final data set due to contamination in blank sample results (phenol, bis(2 ethylhexyl) phthalate (DEHP), acetophenone, and triethyl citrate). Analytes were categorized into 15 chemical classes based on their functional use or chemical properties (Table SI-2) and all analytical data have been previously published (Baldwin et al., 2016).

2.2. Screening values

2.2.1. ToxCast

Results from the ToxCast database (US EPA, 2015) were used to evaluate potential biological activities that may be associated with chemicals detected in the water samples. The ToxCast program evaluates individual chemicals for interactions with, or effects on, cells, proteins, DNA, RNA, mitochondria, receptors, and enzymes, etc. (Judson et al., 2016). For most of the ToxCast assays, annotations describing the intended biological targets are available in the database download (https://www.epa.gov/chemical-research/toxicity-forecaster-toxcasttm-data) or the U.S. Environmental Protection Agency (US EPA) CompTox dashboard (https://comptox.epa.gov/dashboard). The ToxCast data analysis pipeline provides several summary metrics modeled from chemical dose-assay response curves: the activity concentration at cutoff (ACC), the half maximal activity concentration (AC50), and the top value (T), or efficacy (Filer et al., 2016). The ACC is an assay-specific metric determined as a multiplier of the baseline median absolute deviation of measured activity in the assay that provides an indication of the concentration at which the bioactivity measured first exceeds the baseline concentration. More thorough descriptions of its derivation are provided elsewhere (Filer et al., 2016; Judson et al., 2009). Because this metric is indexed to a standard response threshold and is not dependent on chemical-specific activity, its use has been favored in recent applications of the ToxCast data over the other metrics (Blackwell et al., 2017; Fay et al., 2018). Thus, the ACC (parameter name modl acc in the ToxCast database) was used as the final endpoint for comparison with water quality data.

For this study, data from all assay platforms (Kavlock et al., 2012) available in the ToxCast database were considered, with the exception of BioSeek, which had several endpoint values that were anomalously low compared to those from other sources. Considering the nature of the assays and the associated reliability/quality for detecting gain or loss of signal, Attagene "gain" endpoints and Novascreen "loss" endpoints were used, while Attagene "loss" endpoints and Novascreen "gain" endpoints were removed because these assays were not optimized or designed to report for the given assay direction (Blackwell et al., 2017). Chemical/assay combinations that did not result in a significant test response (a "hit call") were also removed from consideration.

Data quality remarks were included with the reported metrics for the ToxCast test data. Results with the following data quality flags were removed from consideration for the present study: "Borderline active", "Only highest conc above baseline, active", "Gain AC50 < lowest conc & loss AC50 < mean conc", and "Biochemical assay with <50% efficacy". All results from in vivo zebrafish embryo assays (NHEERL_PADILLA) matched at least one of these filtering criteria, and so were removed. Dose-response curves for chemical-assay combinations remaining after this selection process were also examined manually. Eleven of these dose-response curves were found to be of questionable quality based on anomalous values or lack of response and removed from analysis: NVS_ENZ_hPTEN for nonylphenol, NVS_ENZ_rMAOBP for Diethyl phthalate, TOX21_p53_BLA_p3_viability for Cotinine, TOX21_p53_BLA_p5_ratio for Metolachlor, TOX21_p53_BLA_p3_ratio for Carbazole, TOX21_p53_BLA_p3_ratio for Triphenyl phosphate, TOX21_p53_BLA_p3_ratio for Tris(2 chloroethyl) phosphate, TOX21_p53_BLA_p3_ratio for Fluoranthene, NVS_NR_hPPARg for Triphenyl phosphate, CLD_CYP1A1_6hr for bisphenol A (BPA), CLD_CYP1A2_6hr for BPA. In addition, the Tanguay_ZF_120hpf_ActivityScores were removed since this endpoint is an aggregation of activity from other zebrafish assays that are all represented separately in the ToxCast data set. With these various exclusions, 255 total ToxCast assays were suitable for computations for the chemical data set in the present study (Table SI-3).

Of the 65 chemicals detected from the tributary samples, 54 (83%) were represented in ToxCast (i.e., tested in at least one ToxCast assay). Among those 54, 48 had measurable effects (i.e., at least one active hit call) within the range of concentrations tested. The number of active hits per chemical ranged from 1 to 92 assays (Table SI-4).

2.3. Data analysis procedures

2.3.1. Screening for potential pathway-based effects

To screen the water chemistry data for potential bioactivity, chemical concentrations were compared to effect concentrations in ToxCast assays by computing EAR values as the quotient of the measured concentration and the ACC for each assay-chemical combination. The EAR is analogous to a hazard quotient, but rather than relying on a concentration at which adverse health effects like impaired survival, growth, or reproduction are detected, one instead uses the concentration required to elicit a response in a pathway-based assay. An EAR of 1 or higher indicates that the measured concentration in a water sample was greater than the ACC in the assay medium. Extrapolating this information for application to environmental concentrations is complex. For example, current information does not include correction for chemical partitioning in the assay system (e.g., free versus bound chemical in a test well), so actual biological activity in vitro or in situ may differ from this. However, it does provide a value that effectively normalizes for relative concentration detected in the environment and relative potency to elicit a specific biological effect. Thus, the EAR value is suitable for relative ranking and prioritization. Still, it is recognized that not all ToxCast assays used in this analysis are likely to be relevant to ecological species even though many of them target biological activities that are conserved among species. A complete evaluation of ToxCast assays for ecological relevance is currently not available, so the EAR approach used here is conservative in this respect. The AOP analysis described below does include evaluation of ecological relevance but is not considered to be comprehensive, since AOP information is not yet defined for all biological targets represented in ToxCast.

For chemical concentrations reported as below the level of detection, EAR values were assumed to be zero for this analysis. To test the impact of this, EAR values were computed as a ratio of the detection limit for each compound and all available ACC values (Fig. SI-2). Results indicated that there was potential for pathway-based bioactivity at the detection limit for some chemical-assay pairs. EAR values from the minimum ACC for each compound ranged from $<10^{-4}$ (multiple compounds) to 0.19 (assay = OT_ERa_EREGFP_0120 for 4 Nonylphenol, Branched). This suggests that methods used in the current study could result in underestimation of EAR values in cases where concentrations below the analytical detection limits could still elicit a significant biological effect (i.e., near the ACC). Hence, further evaluation may be needed to determine whether these chemicals may be of concern.

Results were examined using several different EAR summations (Table 1a), and different combinations of chemical occurrence and EAR magnitudes (Table 1b). Each summation has value for addressing

Table 1a
Definition of several different EAR summations used for analysis and interpretation of results.

Summation	Abbreviation	Description
Exposure-activity ratio	EAR	The quotient of the measured concentration of a chemical in a sample and the activity concentration at cut-off (ACC) for a given assay-chemical combination. $EAR = \frac{measured\ concentration\ in\ sample\ (\mu M)}{ACC\ for\ chemical-assay\ pair\ (\mu M)}$
EAR by chemical	EAR_{Chem} $EAR_{SiteChem}$	The sum of EAR values from all assays for an individual chemical in a given sample. The number of active assays and magnitude of individual assay-chemical EAR values combine to provide a means to prioritize chemicals by potential for effect: $EAR_{Chem} = \sum EAR_{[i]}$, where i = assays relevant for each individual chemical. Maximum EAR_{Chem} for an individual site
EAR by assay endpoint	$EAR_{Mixture}$ $EAR_{SiteMixture}$	The sum of EAR values for each individual assay endpoint across all chemicals for a given sample. $EAR_{Mixture}$ provides an estimate of cumulative bioactivity for an individual assay from a mixture of chemicals, assuming additivity of effects. This is consistent with previous use of $EAR_{Mixture}$ for individual assays (Blackwell et al., 2017), and is analogous to a "toxic unit" approach for summing adverse effects for similar-acting chemicals present in complex mixtures (Nirmalakhandan et al., 1994). $EAR_{Mixture} = \sum EAR_{[i]}$, where i = chemicals associated with an individual assay endpoint. Maximum $EAR_{Mixture}$ for an individual site
EAR by adverse outcome pathway (AOP)	EAR_{AOP} $EAR_{SiteAOP}$	The sum of EAR values for each assay—chemical combination associated with an individual AOP. Using the subset of assays that are currently associated with AOPs, this summation accounts for the fact that more than one ToxCast assay may align with key events along a specific AOP. If all relevant EARs for each chemical were included, the effect of an individual chemical might essentially be "double counted". To avoid this, the summation considers only the maximum EAR for each individual chemical that is associated with an AOP: $EAR_{AOP} = \sum \max(EAR_{[i]})_{[j]}$, where i = chemical, j = an assay relevant to a given AOP. Maximum EAR_{AOP} for an individual site
Toxicity quotient	TQ TQ_{max}	The quotient of the measured concentration of a chemical in a sample and the water quality benchmark for a given chemical. $TQ = \frac{measured\ concentration\ in\ sample\ (\mu g/L)}{Water\ quality\ benchmark\ for\ chemical\ (\mu g/L)}$ Maximum TQ at a site for all water quality benchmarks available for a given chemical. 1

different questions. For example, the EAR-by-chemical (EAR_{Chem}) is useful for ranking and prioritizing among chemicals for a given sample with regard to their potential to elicit a biological effect. The EAR-by-assay endpoint ($EAR_{Mixture}$) is used to estimate the potential cumulative impact of a mixture of chemicals on a given assay response assuming additivity. Yet another summation, the EAR_{AOP} is used to consider the potential for a group of chemicals to contribute to a common adverse pathway/outcome (detailed further below). The frequency of occurrence of chemicals and exceedance of EAR or TQ thresholds were then used to help prioritize chemicals, ToxCast assays, and chemical mixtures to identify a manageable number of situations for which there is potential for adverse impacts (Table 1b). Similarly, identification of chemicals of concern and EAR and TQ levels of concern are defined for use with the intention to compare among the different chemicals, chemical mixtures, assays, and sites within the current study. Results are not intended for regulatory actions, but for consideration by stakeholders for further investigation and validation at specific sites.

Where appropriate, these different EAR summations were calculated for each of the 709 individual samples. The number of samples collected per site was variable, so the maximum EAR value per site was determined to provide a means to weight each site equally. This resulted in three additional EAR variables that were ultimately used in the current study: $EAR_{SiteChem}$, $EAR_{SiteMixture}$, $EAR_{SiteAOP}$ (Tables 1a and 1b).

Computations and analyses were primarily carried out using functionality of the R package *toxEval* (De Cicco et al., 2018) with additional custom calculations and visualizations developed using the R packages *dplyr* (Wickham et al., 2018), *ggplot2* (Wickham, 2016), and base R functionality (R Core Team, 2017). The *toxEval* package was developed within the current study to facilitate analysis and visualization of EAR and toxicity quotient (TQ) values for complex chemical concentration data sets that represent multiple chemicals, sampling locations, and samples per location. Version 2 of the ToxCast database was included as the default set of benchmark concentrations within *toxEval* with EAR values as the default evaluation parameters. Additionally, user-selected chemical-biological interaction benchmark data, such as the water quality benchmarks used in the current study, can be used for computation and analysis of TQs within *toxEval*.

2.3.2. Water quality benchmarks

Water quality benchmarks for 27 of the measured chemicals were reported by (Baldwin et al., 2016). For the present analysis, water quality benchmarks for an additional seven chemicals were added to the list. These include a broad range of toxicity benchmarks from regulatory and non-regulatory entities that are not necessarily enforceable limits but provide guidance on concentrations that represent a potential hazard for aquatic organisms (Table SI-2). The benchmark values were used to assess how the EAR-based approach compared with more traditional methods focused on apical adverse effects. Chemical-specific TQs were computed as the ratio of the measured concentration and the associated water quality benchmark. The minimum water quality benchmark and

Table 1b
Description of methods used for prioritization of chemicals, ToxCast assays, and chemical mixtures using EAR and TQ values.

Type of Prioritization	Parameter	Description
Chemical prioritization	TQ_{Max}	Chemical occurrence at ten or more sites and $TQ_{max} > 10^{-3}$ for five or more sites
Chemical prioritization	$EAR_{ChemSite}$	Chemical occurrence at ten or more sites and $EAR_{max} > 10^{-3}$ for five or more sites
ToxCast assay prioritization	$EAR_{SiteMixture}$	$EAR_{SiteMixture} > 10^{-3}$ for ten or more sites
Chemical mixture prioritization	$EAR_{SiteAOP}$	Samples that had chemical mixture combinations with $EAR_{SiteAOP} > 10^{-3}$ and chemicals that contributed at least 1% of $EAR_{SiteAOP}$ in samples from 5 or more sites

the maximum concentration per sampling location were used to compute the maximum toxicity quotient at each of the sampling locations (TQ_{max}).

In addition to traditional water quality benchmarks, 17β estradiol equivalency quotients (EEQ) were determined to estimate potential for estrogenic activity of the measured chemicals. The EEQs were obtained by multiplying the measured concentrations of estrogenic compounds by their respective estradiol equivalency factor (EEF) derived from published intersex and vitellogenin induction values in fish (Vajda et al., 2008). The EEQ values were then compared to EAR values for chemicals where both were available to better understand how EARs from ToxCast compare to a more traditional approach for evaluating estrogenic potential.

2.3.3. Linking to adverse effects

Most of molecular/biochemical responses associated with the ToxCast assays do not directly translate to endpoints typically considered in ecological risk assessments (i.e., impacts on survival, growth, reproduction, etc.). However, the adverse outcome pathway framework has been developed as a systematic and transparent means to describe the plausible and empirically supported linkages between the molecular, biochemical, and/or cellular biological activities typically evaluated in ToxCast assays and adverse outcomes that are more relevant to protection goals, management decisions, and risk assessment (Ankley et al., 2010). To help interpret the significance of ToxCast endpoints with regard to potential apical hazards, efforts have been made to map ToxCast assays to corresponding key events in AOPs described in the AOP-Wiki (Fay et al., 2018; Pittman et al., 2018; Society for the Advancement of Adverse Outcome Pathways, 2018). In the present study, cross-mapping of ToxCast endpoints to key events in AOPs (Fay et al., 2018) was updated here and used to help contextualize the significance of the EAR-based analyses relative to potential ecologically-relevant hazards.

Briefly, as of February 8, 2018 there were approximately 250 user-defined AOPs in the AOP-Wiki. Key events (including molecular initiating events) in these AOPs were manually curated for relevance to response from the ToxCast assays. Key event names were considered foremost for mapping to assays, although additional text included on the event pages also were considered. Some AOP key events are not molecular in nature, but describe general or higher-level responses (e.g., mitochondrial disruption, production of reactive oxygen species, cytokine suppression), which also is the case for some ToxCast assays which measure outcomes like cell proliferation, cell death, and mitochondrial dysfunction. In these cases, a panel of ToxCast assays relevant to a generalized response was identified and corresponding AOP events were mapped to each of the assays within the panel. Applicability of ToxCast assays considered not only the intended target but also the direction of measurement (e.g., agonism or antagonism of a given receptor). Mappings were also informed by the AOP event ontology annotations in the AOP wiki (Ives et al., 2017; Table SI-5).

Once the global mapping of ToxCast assays to key events and associated AOPs was developed, the subset of AOPs relevant to ToxCast assays prioritized in the current analysis ($n = 49$) were identified. Each assay—AOP pair was further evaluated for relevance to taxa in the Great Lakes ecosystem (Table SI-6). For example, AOPs establishing links to human health outcomes/endpoints that would typically not be considered as an assessment endpoint in ecological risk contexts (e.g., fatty liver disease) were not considered. This resulted in identification of 23 ecologically relevant AOPs associated with assays that were prioritized based on the EAR analysis.

An EAR summation approach (EAR_{AOP}) that considered potential cumulative impacts along specific AOPs was developed to aid interpretation of EAR results in an ecological hazard context (Tables 1a and 1b). An important consideration in calculating this EAR summation is that there can be more than one ToxCast assay that maps to a given key event in an AOP. For example, there are multiple ToxCast assays that measure estrogen receptor activation (Browne et al., 2015) even though estrogen receptor activation is a single key event in an AOP. Likewise, since AOPs are composed of multiple key events, ToxCast assays related to multiple different biological targets may map to a single AOP (e.g., assays 1 and 2 in Fig. 1 map to different key events along the same AOP). Consequently, to control for the fact that multiple assays and thus different numbers of EAR values may map to different AOPs, EAR_{AOP} considers the maximum EAR for any chemical-assay pair relevant to that AOP.

2.3.4. Chemical mixtures

EARs and AOP networks have each been recognized as tools for evaluating the potential significance and effects of chemical mixtures (Blackwell et al., 2017; Knapen et al., 2018). Consequently, we explored how these two approaches might be combined to better understand potential hazards associated with chemical mixtures detected in Great

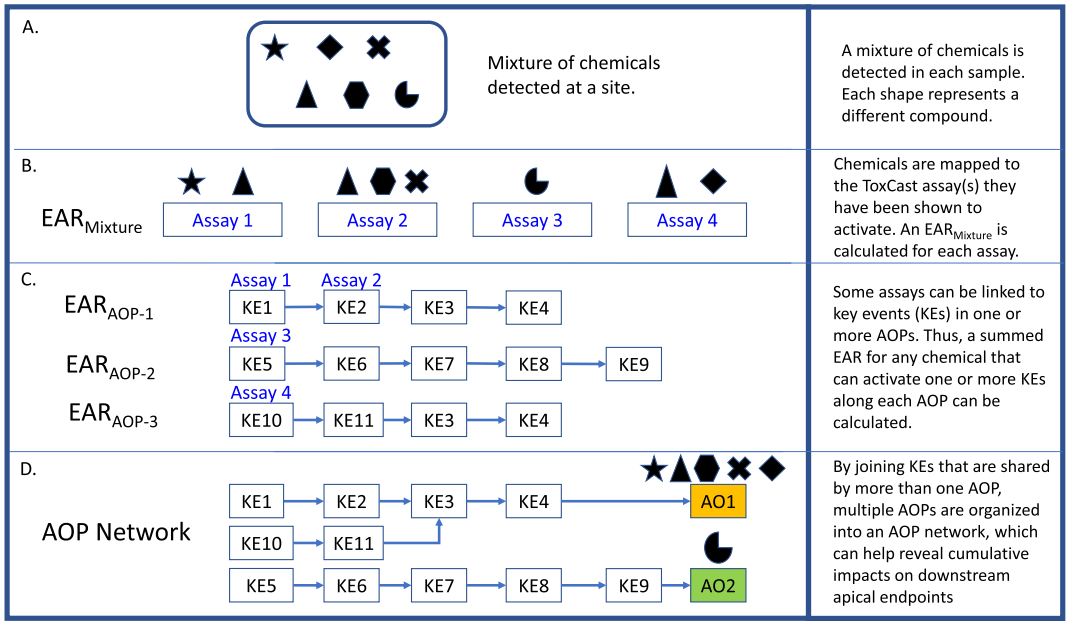

Fig. 1. Diagram of chemical mixture analysis using exposure-activity ratios for chemical-ToxCast assay pairs, adverse outcome pathways, and adverse outcome pathway networks.

Lakes tributaries. First, the number and identity of chemicals detected at each individual site was determined to establish the nature of the mixtures present (Fig. 1.A). Next, summations of EAR values for individual ToxCast assays ($EAR_{SiteMixture}$) were used to estimate potential cumulative biological activity from multiple co-occurring chemicals at a given site (Fig. 1.B). This allowed for prioritization of site-specific bioactivities, providing information on potential biological functions that may be influenced by these chemical mixtures. Third, summations of EAR values for AOPs ($EAR_{SiteAOP}$) that aligned with the biological activities detected at various sites were calculated (Fig. 1.C). After $EAR_{SiteAOP}$ values were calculated, samples that exceeded a given $EAR_{SiteAOP}$ threshold for AOPs that were designated as possibly environmentally relevant were identified. From this list of samples, chemicals that contributed at least 1% of the EAR at 5 or more sites were retained. From this list of chemicals and samples, mixtures of 2–12 co-occurring chemicals were identified.

Each AOP represents a unique sequence of biological events (key events) that link a molecular initiating event to an adverse outcome. However, AOPs employ a modular construct (Villeneuve et al., 2014). That means any given key event may be part of more than one AOP. This makes sense biologically. For example, the key event "agonism, estrogen receptor" (https://aopwiki.org/events/111) can have different biological consequences depending on the life stage exposed: altered larval development during an embryo-larval stage, impaired development of reproductive organs during sexual differentiation, or altered reproductive behaviors during adult life stages. Likewise, an apical endpoint like reproductive failure, also a key event, can have a diversity of causes. For this reason, in most real-world situations (i.e., exposure to multiple chemicals; chemicals having more than one biological activity), more than one AOP is likely to be triggered and because there are shared biological nodes among those AOPs, interactions can be expected (Knapen et al., 2018; Villeneuve et al., 2014). Based on these principles, AOP networks are defined as an assembly of two or more AOPs that share one or more key events. By linking together any shared key events, a group of individual AOPs can be assembled into an AOP network (Fig. 1.D; (Knapen et al., 2018)).

To derive an AOP network relevant to the present study, the AOP-Wiki was queried using the AOP identification number of each of the 23 ecologically-relevant AOPs of interest. Each AOP description page contains a table (relationship table) that defines the sequence of key events that make up a given AOP as a series of pairs: key event 1 leads to key event 2; key event 2 leads to key event 3; and so on. Two of the 23 AOPs did not include complete key event relationship information, and thus were not used in development of AOP networks (AOPs 52 and 53; Table SI-6). The relationship table was extracted from each of the remaining 21 AOP pages, and each pairwise key event relationship was parsed into a from-to matrix (Table SI-7). The from-to matrix was then loaded into Cytoscape (v.3.5.1; www.cytoscape.org; (Shannon et al., 2003)) to visualize the resulting network. The 21 AOPs yielded a network of seven disconnected components. The network was manually arranged for easier visualization. Three mixtures were chosen that represented different AOPs to highlight as examples, and the median $EAR_{SiteAOP}$ values for each of these three chemical mixtures was loaded as edge attributes and used to visualize the paths through the overall network that one would expect to be impacted by the mixture in question.

3. Results

Computed EAR values for individual compounds were first aggregated over the study sites for an overall assessment and examined in three primary ways: (1) by individual chemical and chemical class, (2) by monitoring location, and (3) by potential biological relevance. This sequence of analyses provided information to screen for pathway-based bioactivity and prioritize potential impacts by chemicals, watersheds, and biological functions. A goal was to enable future investigations of these tributaries to focus on a reduced set of influences at a limited number of watersheds and more efficiently identify and/or verify the potential impacts.

3.1. Prioritization of chemicals, EAR-versus TQ-based approaches

Exposure-activity ratios based on in vitro effect concentrations do not necessarily translate directly to in vivo apical responses. This is because of toxicodynamic considerations (i.e., the endpoints measured in ToxCast assays do not equate to definitive impacts on survival, development and growth, or reproduction) and toxicokinetic considerations (i.e., nominal concentrations in a test well do not necessarily translate to free chemical concentrations in plasma or environmental media). Consequently, the magnitude of EAR that is environmentally relevant for predicting adverse biological effects is not as easily defined as a TQ of concern (i.e., TQ > 0.1). To gain insight into the question of what EAR value would serve as a reasonable cut-off for prioritization purposes, EARs were compared with more traditional prioritization methods using water quality benchmarks and EEQ calculations (Fig. 2, B and D). Recognizing that water quality benchmarks are largely based on in vivo effects and EAR values are based on in vitro testing, this is not a perfect comparison. Nonetheless, it provided an empirical basis to start identifying what EAR levels may be of concern from a screening and prioritization standpoint.

The comparison of TQs based on water-quality benchmarks to $EAR_{SiteChem}$ levels indicated that the relation is chemical-specific. Considering $TQ_{max} = 10^{-1}$ as the benchmark for this analysis, corresponding $EAR_{SiteChem}$ levels that correspond to $TQ = 10^{-1}$ varied from approximately 10^{-4} to 10^{-1} (Fig. 2). Consequently, for the sake of screening and prioritizing the chemicals with the greatest potential for pathway-based bioactivity from a spatial distribution perspective, chemicals that were present at a minimum of 10 sites and had $EAR_{SiteChem} > 10^{-3}$ at a minimum of five sites were considered (Fig. SI-3). These chemicals included 4 nonylphenol (a detergent degradate and industrial chemical), BPA (used in plastics and epoxy resins), metolachlor and atrazine (herbicides), DEET (insect repellant), caffeine, tris(2 butoxyethyl) phosphate and tributyl phosphate (TBEP, TBP; flame retardants), benzo(a)pyrene and fluoranthene (PAHs with multiple origins), benzophenone (ultraviolet radiation protection in soaps, fragrances, plastics), and triphenyl phosphate (TPhP; plasticizer, flame retardant) (Fig. 2).

For water quality benchmarks, considering the number of sites with detections and the magnitude of the TQ_{max} for each site (detected at a minimum of 10 sites with $TQ_{max} \geq 10^{-1}$ at a minimum of five sites), the detected chemicals with the greatest potential for adverse impact were 4-nonylphenol, BPA, metolachlor, atrazine, and several PAHs (anthracene, benzo (a) pyrene, fluoranthene, phenanthrene, pyrene). Water quality benchmarks could not be identified for 23 of the detected chemicals that were present in the ToxCast database (i.e., for which EARs could be calculated); these included all chemicals within several broad usage classes (human nonprescription drugs, flame retardants, flavors and fragrances).

When endpoints for ToxCast and water quality benchmarks were both available, all chemical classes identified as a concern were consistent. There were differences when considering individual chemicals. For example, water quality benchmarks identified five PAHs as a potential concern while the ToxCast assessment identified only two, and DEET was identified as a potential concern using the EAR approach, but available water quality benchmarks for DEET did not indicate a substantial concern. While different $EAR_{SiteChem}$ levels of concern could be chosen depending on the circumstances, the choice of $EAR_{SiteChem} = 10^{-3}$ appeared to provide a reasonable level for comparison with water quality benchmarks.

Estradiol equivalency factors were available for eight compounds, four of which were not represented in the ToxCast database, and two that were not detected in samples (Fig. 2-C, D). For the compounds

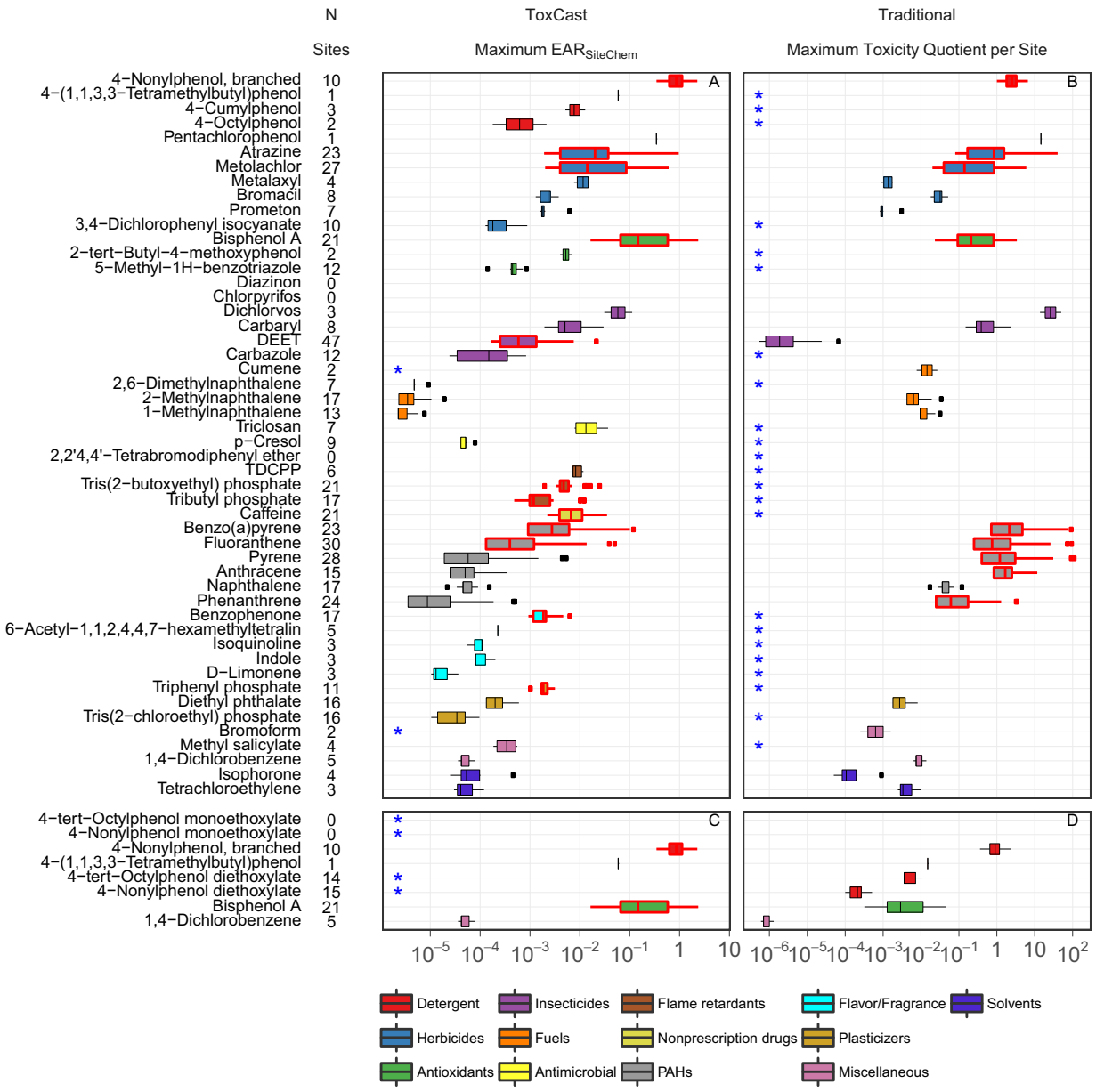

Fig. 2. Exposure activity ratios (EARs) using ToxCast endpoints for screening of potential pathway-based bioactivity from chemicals detected in water samples from 57 tributaries of the Great Lakes, 2010–2013 (A and C), toxicity quotients comparing established water quality benchmarks to sample results (B), and 17 β estradiol equivalency quotients (ng/L) for compounds with established estradiol equivalency factors (D). Compounds are grouped by chemical class and ordered by largest to smallest median EAR. Compounds where either water quality benchmarks or ToxCast information were unavailable are indicated with "*", and compounds where both were unavailable are not included in the graph. Boxplots with red borders designate chemicals that were present at 10 or more sites with EAR > 10^{-3} at 5 or more sites (panel A) or TQ > 0.1 at 5 or more sites (panel B). [N, number of sampling locations with detections of each chemical. Boxes, 25th to 75th percentiles; dark line, median; whiskers, data within 1.5× the interquartile range (IQR); circles, values outside 1.5× the IQR.]

with EEFs that were in the ToxCast database, results indicated similar priority rankings: 4 nonylphenol had the greatest potential effects and 1,4 dichlorobenzene had the least, with potential effects from 4 tert octylphenol between these two compounds. EAR values for BPA were not as comparable to EEQ results, with EAR calculations indicating greater potential effects relative to other compounds. This is because $EAR_{SiteChem}$ is computed using a summation of EAR values from all assays in which a given chemical is active. Bisphenol A is flagged not only in multiple assays related to estrogen receptors, but in several other ToxCast assays not related to estrogen signaling. Consequently, it is reasonable that the predicted impacts of a chemical that effects multiple types of biological activities, such as BPA, would deviate from a calculation considering only estrogenic activity. Nonetheless, EAR = 10^{-3} appeared to be a reasonable threshold from a prioritization perspective.

3.2. Prioritization of sites, EAR-based

Sites for potential follow-up monitoring were prioritized based on the number of chemicals detected at each with an associated $EAR_{SiteChem}$ > 10^{-3} (Fig. 3, Figs. SI-4 and SI-5 A-M). Sites with at least one chemical exceeding the $EAR_{SiteChem} > 10^{-3}$ value included four of nine Lake Superior tributaries monitored, 11 of 19 Lake Michigan tributaries, five of seven Lake Huron tributaries, all 15 Lake Erie tributaries (including the Detroit River and Lake St. Claire tributaries), and three of seven Lake Ontario tributaries. Sampling locations that had >15 chemicals with $EAR_{SiteChem} > 10^{-3}$ included River Rouge, the Clinton River, and the St. Louis River. These would be a high priority for future investigation. There were an additional eight sampling locations with at least 10 chemicals and 10 more sampling locations with at least five

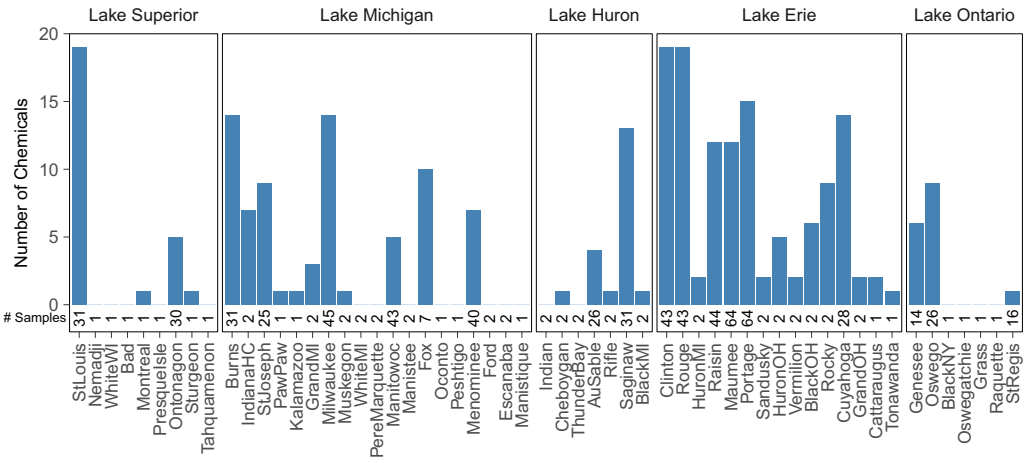

Fig. 3. Number of individual chemicals with at least one sample that resulted in a maximum exposure—activity ratio ($EAR_{SiteChem}$) > 10^{-3} for each site.

chemicals with $EAR_{SiteChem} > 10^{-3}$ (Fig. 3). Given that the number of samples collected from each site was variable (one to 64 samples) and that chemistry results varied temporally, the number of samples and timing of collection likely influenced the number of chemicals detected at each site. Nonetheless, the EARs provide an approach for differentiating sites with greater probability for biological effects from those with lesser probability.

Several sites had elevated EARs for multiple chemicals and/or chemical classes (Fig. SI-5 A-M). The EAR patterns throughout the study sites typically reflected the nature of land use within the watershed. Sites with urban influence most commonly had elevated EARs for PAHs and nonprescription drugs (Fig. SI-5 B and D). Agricultural sites were most likely to have higher EAR incidence of herbicides, primarily atrazine and metolachlor (Fig. SI-5 A). One exception to this was the St. Louis River where pentachlorophenol had an $EAR_{SiteChem} > 0.3$. The St. Louis River does not have a high percentage of either urban or agricultural land cover but does include wood and paper product industries that sometimes use pentachlorophenol in preservation processes (Karn et al., 2010). A mix of sites with differing dominant land covers had elevated $EAR_{SiteChem}$ values for insecticides, flavors/fragrances (benzophenone), plasticizers, flame retardants, antimicrobial disinfectants, and detergent degradates (Fig. SI-5 E, G, J, K, L, and M).

3.3. Prioritization by biological relevance, assay endpoints and adverse outcomes

A third approach to applying the EARs involves hypothesizing or inferring potential biological effects of concern at a given site, based on the known composition of chemical mixtures present. In this case, ToxCast assays were used to screen chemicals for biological activities (Fig. 1.A). The biological activities from those assays were aligned with key events in AOPs described in the AOP-Wiki (Fig. 1.B). Exposure activity ratios reflecting the potential effect of chemicals in a mixture on one or more key events along an AOP help to relate the potential biological activities to outcomes of concern (typically effects on survival, growth, reproduction; Fig. 1.C). In turn, recognizing that chemical-induced biological activities in vivo are occurring concurrently and can interact with one another in additive, antagonistic, and/or synergistic manners (Knapen et al., 2018), the group of AOPs potentially impacted by components of a mixture may in turn be considered in a network context (Fig. 1.D; (Villeneuve et al., 2018)).

To identify and prioritize biological activities most likely to be modulated in organisms resident to the Great Lakes tributaries surveyed, ToxCast assays with $EAR_{SiteMixture} > 10^{-3}$ at 10 or more sites were identified, resulting in a list of 46 assays (Fig. 4). For individual assays, the number of chemicals that contributed to the $EAR_{SiteMixture}$ varied from 1 to 33, further supporting the hypothesis that mixtures of chemicals are a necessary consideration for screening potential biological effects. Twenty seven of these 46 assays have been associated with AOP key events from the AOP Wiki (Fig. 4, Table SI-5; aopwiki.org). Some key events may occur in more than one AOP, and in this case the 27 assays were associated with a total of 49 AOPs (Fig. 5A and SI-6). Evaluation of the potential for effects on individual AOPs from multiple co-occurring chemicals was explored by computing summations of EAR values from all assays associated with individual AOPs ($EAR_{SiteAOP}$; Fig. 1; Tables 1a and 1b; Fig. 5A). For example, AOPs 52 and 53 are influenced by 6 of the ToxCast assays displayed in Fig. 5B. To estimate the cumulative EAR ($EAR_{SiteAOP}$) for these AOPs, the sum of EARs from all related assay-chemical combinations was computed. For any given AOP, the number of contributing assays varied from 1 to 35 (Table SI-5). Considering the ToxCast assays prioritized in Fig. 4 (i.e., those for which maximum $EAR_{SiteMixture} > 10^{-3}$ was calculated for at least 10 sites), the number of contributing assays per AOP varied from 1 to 17 (Fig. 5B).

Up to this point in the analysis, all ToxCast assays and associated AOPs potentially affected by chemicals measured in this study have been considered. However, not all ToxCast assays or associated AOPs are necessarily relevant in the context of ecological effects. Consequently, relevance of the 49 associated AOPs (Fig. 4) was evaluated. Based on this evaluation, 23 were classified as “relevant” or “potentially relevant” to resident Great Lakes tributary species (Fig. 5A, Table SI-6). Of these 23 AOPs, $EAR_{SiteAOP}$ varied from $<10^{-5}$ to 0.8.

To further understand the potential collective impacts of various mixtures detected in the Great Lakes tributaries on organisms, 21 of the 23 AOPs were assembled into an AOP network (Fig. 6). Two of the AOPs did not include sufficient information to include. The network was composed of 97 key event nodes (circles, squares, or diamonds in Fig. 6) organized into seven disconnected components (subnetworks). Overall, potential pathway-based bioactivity indicated by these AOPs includes various influences on reproduction and energy metabolism, specifically mitochondrial function (Table SI-6; Fig. 6). Detection of chemicals known to bind to and activate the estrogen receptor, produce excessive reactive oxygen species (ROS), activate peroxisome proliferator-activated receptor, inhibit histone deacetylase, or inhibit cyclooxygenase (molecular initiating events and/or “upstream” key events in Fig. 6) suggested potential for effects on reproduction and/or the reproductive system (adverse outcomes in Fig. 6). Additionally, available AOPs suggest that chemicals impacting mitochondrial function in vitro have potential to cause mortality and potential population-level impacts, including honeybee colony collapse (LaLone et al., 2017). In this case, the ToxCast assay hits did not necessarily align with the molecular initiating events of a corresponding AOP, but

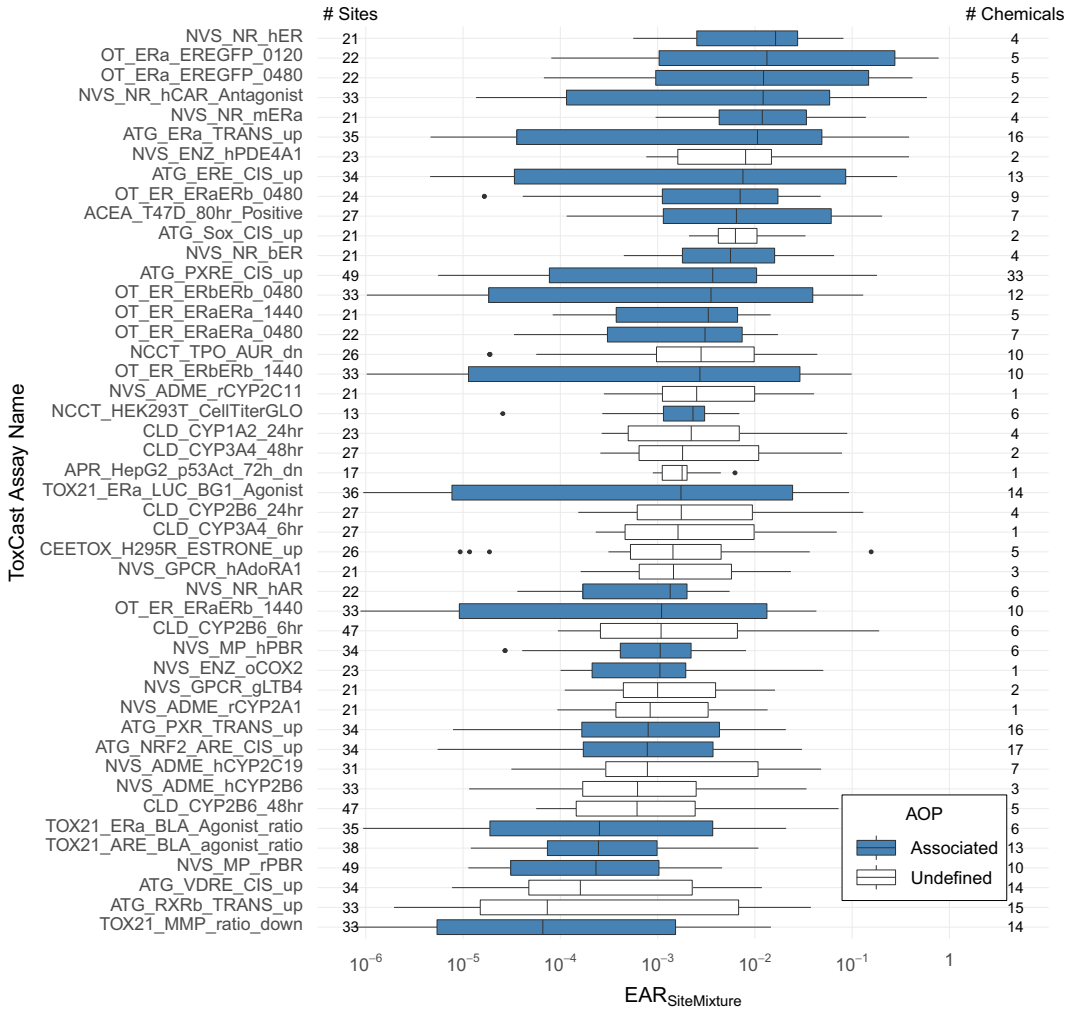

Fig. 4. Boxplots of maximum exposure-activity ratios (EARs) across sites for ToxCast assays with EARs $>10^{-3}$ from at least 10 sites. Assays with and without currently associated adverse outcome pathways (AOPs) are differentiated by color. [Boxes, 25th to 75th percentiles; dark line, median; whiskers, data within 1.5× the interquartile range (IQR); circles, values outside 1.5× the IQR. $EAR_{Mixture}$,the sum of EAR values for each individual assay endpoint across all chemicals for a given sample.]

rather the mitochondrial effects aligned with intermediate key events along an AOP (not all labeled in Fig. 6).

To illustrate how the AOP networks, along with EAR summations, can be used to hypothesize or infer potential effects of different mixtures, further consideration was given to chemical mixtures with high $EAR_{SiteAOP}$ values that occurred frequently. The list of detected chemicals was first reduced to those that contributed at least 1% of $EAR_{SiteAOP}$ in samples with $EAR_{SiteAOP} > 10^{-3}$. This identified twelve chemicals (Table SI-8). Instances when 2–12-compound mixtures occurred in samples were identified, resulting in1848 different combinations of mixtures of 2–12 compounds that occurred at between 5 and 21 sites with $EAR_{SiteAOP} > 0.001$ (Table SI-8).

Three of these mixtures were chosen as examples to illustrate how different mixture compositions (Fig. SI-7) may shift the patterns of biological responses across the network of 21 relevant AOPs (Fig. 6). To visualize this, the arrows depicting key event relationships along each AOP were weighted by their relative $EAR_{SiteAOP}$ values. Using this approach, one can see that at sites dominated by a mixture of TBP and caffeine, toxicities associated with mitochondrial function, activation of nicotinic acetylcholine receptors, activation of peroxisome proliferator activated receptor (PPAR), or inhibition of vitamin K epoxide reductase (VKOR) were predicted to be the most sensitive effects. Potential adverse outcomes linked with estrogen receptor agonism are less probable (Fig. 6A). In contrast, for mixtures containing BPA and DEET, estrogenic and anti-androgenic responses were predicted to be most likely, with mitochondrial-related toxicity potentially exacerbating some of the reproductive effects and potential impacts related with PPAR activation or VKOR inhibition a lower priority (Fig. 6B). A combination of 4 nonylphenol, atrazine, and metolachlor was predicted to have the most diverse range of potential effects on the overall network of AOPs (Fig. 6C). In particular, a series of AOPs associated with inhibition of cyclooxygenase activity, not prioritized for the other mixtures, are now identified as highly relevant, while potential estrogen receptor agonism-mediated pathways appearing less relevant for this mixture. While none of these examples are definitive, they illustrate how an EAR-based approach may be combined with an AOP network analysis (Knapen et al., 2018; Villeneuve et al., 2018) to infer potential biological hazards at different sites, and guide a hypothesis-driven approach to subsequent monitoring.

4. Discussion

A challenge for contaminant monitoring studies is to place results in the context of potential biological effects of concern to support resource management decision making. In the present study, an EAR-based application of high throughput screening data from ToxCast was explored along with AOP knowledge to provide an evidence-based approach for linking chemical occurrence with potential effects. This was done within the context of meeting the primary study objectives to prioritize chemicals and Great Lakes tributaries with the greatest likelihood for

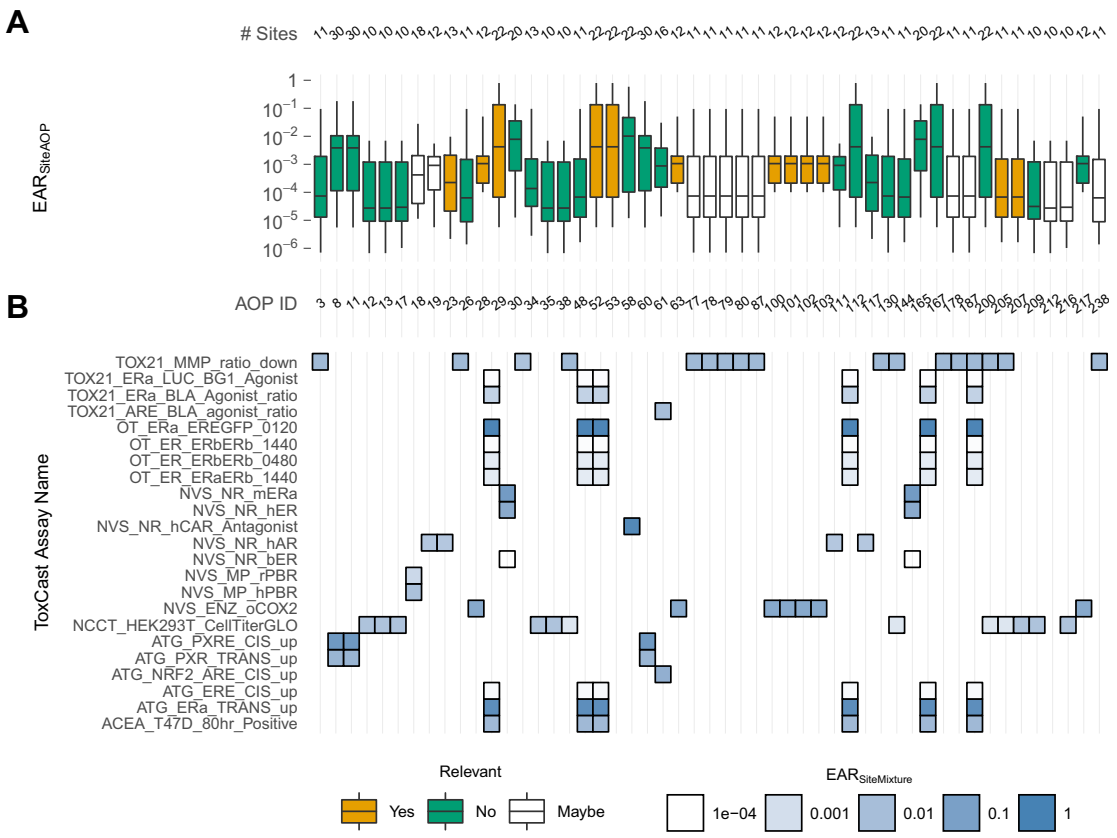

Fig. 5. Maximum exposure-activity ratios (EAR) by site for adverse- outcome pathway (AOP; A) and for ToxCast assay-AOP combinations (B) from chemicals detected in samples collected from Great Lakes tributaries, 2010–2013. Assays displayed include those that had EAR >10^{-3} for at least 10 sites. [Boxes, 25th to 75th percentiles; dark line, median; whiskers, data within 1.5× the interquartile range.]

potential ecological effects. To fully understand the effectiveness of this approach, there are several questions that need to be addressed, including: (a) Can an EAR-based screening and prioritization approach provide results comparable to those obtained with traditional water quality benchmarks?; (b) What magnitude of EAR warrants concern?; (c) Are there specific chemical properties that may lead to poor representation of some chemicals using high-throughput screening results?; and (d) Are there ecologically-relevant adverse outcomes that might be anticipated using these results? It was the aim of the current analysis to examine these questions in detail.

4.1. Prioritization of chemicals

4.1.1. Individual chemicals

Among the 65 chemicals detected in the present study, traditional in vivo water quality benchmarks were available for 34 compounds, and ToxCast data were available for 54, substantially increasing the number of compounds for which comparison with biological effects data was feasible. Using a threshold of 10^{-3} as an $EAR_{SiteChem}$ level of concern, the EAR-based approach yielded a priority list of chemicals similar to that obtained using available water quality benchmarks using a TQ threshold of 10^{-1} (Fig. 2). Chemicals flagged as contaminants of potential concern by both approaches also have been identified in previous studies: 4-nonylphenol (Careghini et al., 2015), BPA (Corrales et al., 2015), metolachlor and atrazine (Busch et al., 2016; Graymore et al., 2001; Love et al., 2011; Pérez et al., 2011), and PAHs (Ankley et al., 1994; Logan, 2007; Ohe et al., 2004; Simcik and Offenberg, 2006). DEET was flagged by the EAR approach but was not identified to be of concern using TQ_{max} values from the available water quality benchmark information. The list was expanded further using the EAR approach to include several compounds for which water quality benchmarks were unavailable. These additional chemicals included caffeine, TBEP, TBP, benzophenone, and TPhP.

DEET is a commonly used insect repellant that is detected regularly in environmental waters (Weeks et al., 2012). Most traditional in vivo benchmarks for DEET (i.e., those related to mortality, growth, or reproduction) exceed 20 mg/L (US EPA, 1996); https://cfpub.epa.gov/ecotox/search.cfm).The most sensitive reported in vivo effects of DEET include a decline in hepatosomatic index and altered expression of several endocrine-related genes in fathead minnows following exposure to concentrations as low as 0.6 μg/L (Zenobio et al., 2014). Concentrations in samples for the current study exceeded 0.6 μg/L and 0.06 μg/L (10-fold safety factor) at three and 25 sites respectively. EAR analysis identified DEET as a potential concern because it was present in samples from 47 of 57 sites and 17 of those sites had samples with $EAR_{SiteChem}$ > 10^{-3}. The greatest $EAR_{SiteChem}$ values for DEET corresponded to ToxCast assay activity measuring increased transcription of cytochrome P4502B6 (cyp2b6). Notably, previous studies have shown that cyp2b6 is one of the predominant cytochrome P450s involved in DEET metabolism (Usmani et al., 2002), so this chemical-biological interaction is not unexpected. Since this activity is directly linked with the metabolism of DEET, one cannot necessarily assume that induction of the protein would result in toxicity. In the case of DEET, the EAR approach may be conservative relative to traditional ecotoxicological benchmarks.

Caffeine is also detected regularly in environmental waters (Bradley et al., 2017). EAR analysis identified caffeine as a potential concern because it was present in samples from 21 sites, all of which had $EAR_{SiteChem} > 10^{-3}$. The greatest EARs for caffeine were due to its activation of Sox transcription factor (Sry-related high mobility group box) in the Attagene Cis-Factorial assay (Medvedev et al., 2018). However, given the diversity of genes regulated by this class of transcription

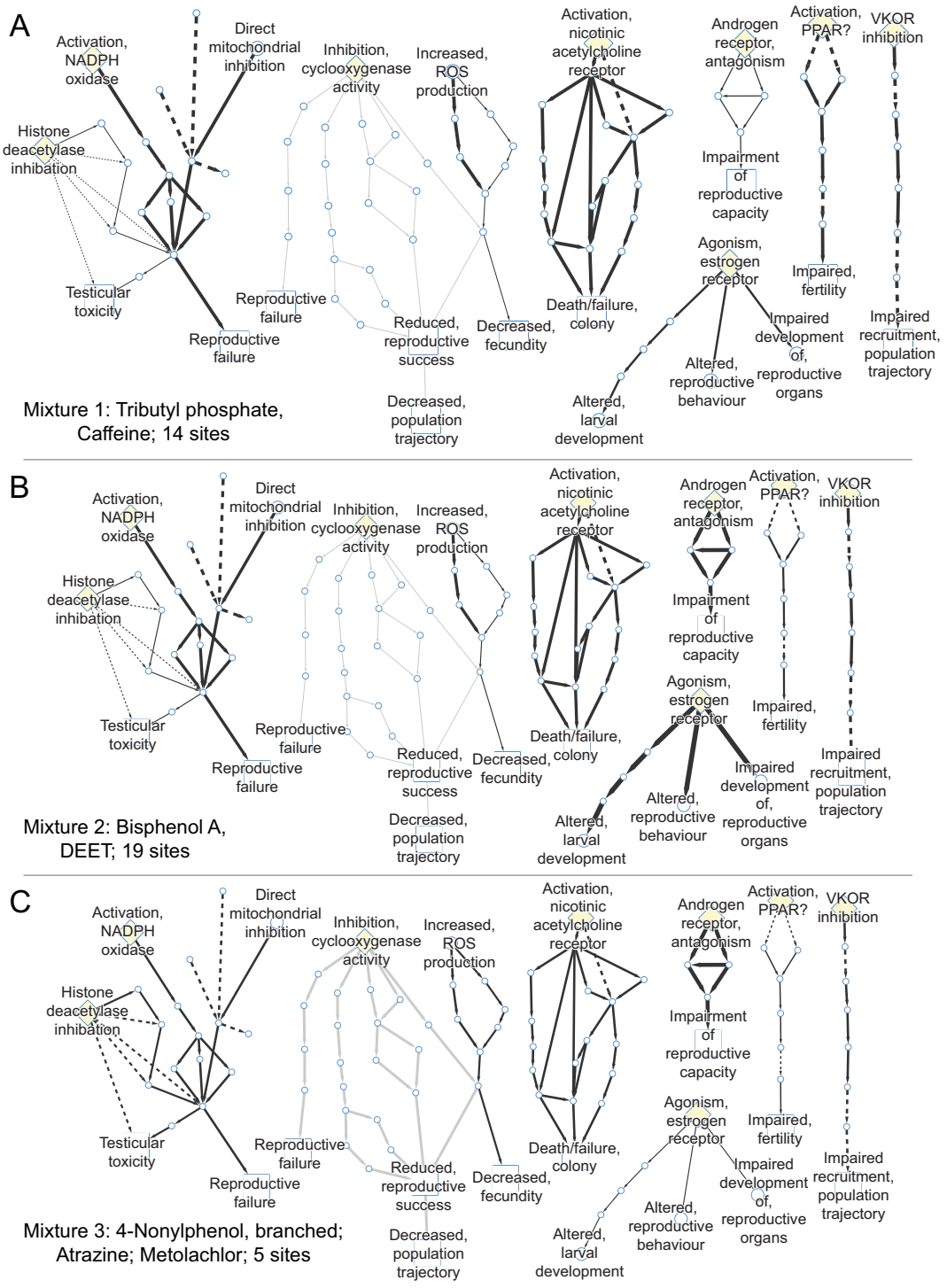

Fig. 6. Adverse outcome pathway network associated with 21 AOPs identified as relevant to the biological activities (assays) that had $EAR_{siteMixture} > 10^{-3}$. Panels represent potential relative influence for three example mixtures on the network, where arrows (key event relationships) linking the key events along a given AOP are weighted based on median $EAR_{siteAOP}$ for the mixture (thicker arrows indicate greater $EAR_{siteAOP}$ values). Biological key event nodes are represented as shapes: molecular initiating events as diamonds, adverse outcomes as squares, and intermediate key events as circles.

factors, it is difficult to infer the potential toxicological significance of the response. The second highest EARs for caffeine derive from its interaction with the human adenosine receptor a2a (assay ID NVS_GPCR_hAdoRA2a). This activity is consistent with caffeine's well-established activity as a non-selective blocker of adenosine receptors (Rivera-Oliver and Díaz-Ríos, 2014) and plays a role in many of the biological effects that caffeine is known for, including influences on sleep, cognition, heart rate, etc. However, these biological activities would not necessarily be linked to adverse effects on survival, growth, or reproduction in non-target aquatic species.

Two in vivo studies on aquatic species with TBP resulted in apical effect endpoints at 600 μg/L for regeneration of flatworms (Yoshioka et al., 1986) and between 1000 and 5000 μg/L for mortality of fathead minnows, *Daphnia magna*, and rainbow trout (Dave et al., 1979, 1981; Mayer and Ellersieck, 1986). In a study with zebrafish, TBEP caused significant early developmental toxicity by inhibiting the degradation and

utilization of maternally-derived nutrients, thereby inducing apoptosis. Effects were observed at a concentration as low as 150 μg TBEP/L (Han et al., 2014). TPhP was acutely toxic to *D. magna* with a lethal concentration required to kill 50% of the population (LC_{50}) of 89 μg/L (Lin, 2009), and in zebrafish larvae, whole-body thyroid hormones and related gene expression were influenced at 40 μg TPhP/L, the lowest concentration tested (Kim et al., 2015). TBP and TPhP have been shown to display additive effects during concurrent exposures (Lin, 2009). Compared to concentrations measured in the current study, these effect concentrations for TBP and TBEP are relatively high, and substantial adverse effects might not be expected. More detailed consideration of biological responses associated with EARs $>10^{-3}$ for TBP, TPhP, and TBEP suggest relatively sensitive interactions with peripheral benzodiazepine receptor (PBR; TBP; assay IDs NVS_MP_hPBR, NVS_MP_rPBR) or the pregnane × receptor (PXR; TBP, TBEP; assay IDs ATG_PXRE_CIS_up, NVS_NR_hPXR) as well as the estrogen receptor (TBEP; assay ACEA_T47D_80hr_Positive). Activation of PXR is caused by many different types of chemicals, and generally is indicative of potential to induce xenobiotic metabolism (Kliewer et al., 2002). The significance of the interaction with PBR is less clear, but the estrogenic responses establish a clear link to one or more AOPs. While estrogenic activity would not necessarily be expected to result in lethality in either short- or long-term aquatic toxicity tests, potential effects on reproduction and/or development in vertebrate species are possible (Ankley et al., 2016).

Collectively, these examples highlight some of the differences between the application of traditional in vivo toxicity benchmarks and pathway-based activities that may flag a chemical as a potential priority. While the high throughput screening assays are detecting "real" biological activities, those activities are not necessarily directly translatable into in vivo effects in aquatic species. At the level of $EAR_{SiteChem}$ the approach serves as a practical first tier prioritization tool. A lack of EARs exceeding the prioritization threshold is a reasonable, evidence-based indicator of lower likelihood for biological effects. However, although an EAR exceeding the threshold does suggest potential for biological activity, it does not necessarily indicate that activity will result in toxicity. This points to the potential value of further alignment of ToxCast endpoints with AOP knowledge as a potential means to refine the analysis in a way that helps to better differentiate indicators of probable hazard from indicators of potentially more benign effects like induction of hepatic metabolism or of sublethal physiological effects.

Just as there are activities captured in the high throughput screening battery that would not necessarily contribute to, or drive, conventional in vivo benchmarks, there are also cases where in vivo toxicity tests may detect biological effects that would go undetected using in vitro systems. For example, even though PAHs were identified as a potential concern using both $EAR_{SiteChem}$ and TQ_{max} values, results were notably different between the two methods (Fig. 2). $EAR_{SiteChem}$ values indicated less potential for pathway-based bioactivity than those from TQ_{max} values. This difference could be attributed to the different nature of information represented in high throughput assays as compared to that used to determine water quality benchmarks. PAH water quality benchmarks used in the present study included those published by US EPA as well as the Canadian Council of Ministers of the Environment (Table SI-2). These water quality benchmarks take into consideration multiple forms of toxicity, including two that are not accounted for in ToxCast assays: metabolic- and photo-activation. Some PAHs are known to be metabolically activated to more toxic forms (Incardona et al., 2006; Stegeman and Lech, 1991), and it has been acknowledged that ToxCast in vitro assays underestimate toxicity resulting from metabolic activation (DeGroot et al., 2018; Jacobs, 2013). The more stringent Canadian water quality benchmarks for PAHs included mortality in assays from post-test ultraviolet (UV) radiation (Canadian Council of Ministers of the Environment, 2015). UV radiation exposure can induce photo-activation of PAHs, thereby decreasing concentrations of concern by several orders of magnitude over those without UV exposure (US EPA, 1996, 2003). Given that high-throughput assay results used in the present study do not account for photo-activation, this could, at least partially, explain the differences in EAR_{max} and TQ_{max} values for PAHs.

Overall, these results suggest that the EAR-based evaluation is indeed useful for hypothesis formulation to prioritize individual chemicals of concern. An EAR threshold of 10^{-3} appeared to provide conservative results tending toward inclusion of chemicals in question except for PAHs where some mechanisms to influence biological activity (e.g., metabolic- or photo-activation) are not well represented by the current assays included in ToxCast. The parameters chosen for inclusion of priority chemicals, however, are somewhat arbitrary, and may change based on study objectives. In this case, chemicals that were detected at 10 or more sites with $EAR_{SiteChem} > 10^{-3}$ were selected as a priority. Revising these parameters could result in a different list of chemicals. For example, if the threshold for the number of sites detected was reduced to five, bromacil, prometon, carbaryl, triclosan, and tris (dichloroisopropyl) phosphate (TDCPP) would have been added to the priority list using the EAR-based approach, while only carbaryl would have been added using water quality benchmarks.

4.1.2. Chemical mixtures

The first approach employed in the present study compared detected concentrations of individual chemicals in water samples to the concentrations eliciting in vitro activity across the ToxCast suite of assays (EAR_{Chem}). This type of information was useful for highlighting chemicals and sites of concern where chemical concentrations may be approaching those that elicit pathway-based biological activity (in vitro). However, another significant advantage of the EAR approach is the ability to sum the potential effects of chemicals acting on either the same biological target/pathway captured by an individual ToxCast assay (i.e., the $EAR_{Mixture}$) or chemicals acting on the set of assays that align with one or more key events along an AOP (EAR_{AOP}). In these instances, additivity of EAR values is a reasonable conservative assumption for estimation of cumulative effects. Specifically, it is plausible that each individual chemical detected in a mixture may be present at concentrations that would not, alone, exceed the EAR_{Chem} threshold of 10^{-3} selected for this study; however, collectively, multiple chemicals acting on the same target or AOP could yield an $EAR_{Mixture}$ or EAR_{AOP} $>10^{-3}$. This concept has been verified, for example, for estrogenic compounds (Thrupp et al., 2018).

In the present study, there were two additional ToxCast assays identified when $EAR_{Mixture}$ was $>10^{-3}$ at 10 or more sites as compared to those identified from individual EAR_{Chem} values. The AOPs identified when EAR_{AOP} was $>10^{-3}$ did not change from those when EAR_{Chem} was $>10^{-3}$, but EAR_{Chem} alone often underestimated the potential for impact. The mean EAR_{Chem} contribution from the individual chemical with the greatest contribution to any given $EAR_{SiteMixture}$ and EAR_{AOPMix} was 69% and 31% respectively. In addition, there were 23 chemicals that had $EAR_{Chem} > 10^{-3}$, but 29 different chemicals contributed at least 5% to EAR_{AOP} values when EAR_{AOP} was $>10^{-3}$. Thus, while some chemicals acting alone may not warrant concern, when acting in concert with other chemicals present in the mixtures, they may exacerbate the impact of one of the individually prioritized compounds.

4.2. Prioritization of potential biological effects

A primary goal of this type of analysis is to link the contaminants detected, in their relative concentrations, to apical adverse outcomes that might be of greatest concern at a given site. Recognizing that these mixtures of chemicals will interact with more than one biological pathway, and as a result, likely trigger multiple AOPs, the consideration of AOP networks is viewed as one approach to try to understand the possible cumulative effects of the chemicals (Knapen et al., 2018). Examination of an EAR-weighted network (e.g., Fig. 6) demonstrates how cumulative EARs ($EAR_{SiteAOP}$) might be used to identify what key events and outcomes may dominate at one site versus another. However, the analysis of AOP networks is in its infancy (Knapen et al., 2018; Villeneuve et al.,

2018) and it must be recognized that only a small fraction of potentially relevant pathways is currently represented in the AOP Wiki. As many as 47 sites had chemicals associated with individual assays for which the target biological activity has not yet been linked with AOPs (Fig. 4).

As a first evaluation of the adverse outcomes predicted in the current study, comparison to previous research indicates that reproductive dysfunction has been documented in multiple field studies with fish. These have included phenotypic alterations in sexual characteristics associated with exposure to substances present in wastewater discharge (Jobling et al., 1998, 2002), reduced sperm abundance and motility in resident fish from rivers receiving wastewater effluent (Blazer et al., 2012), reduced fecundity in fish downstream from or directly exposed to a wastewater effluent discharge (Cavallin et al., 2016; Prado et al., 2014), and multiple effects on male and female reproductive organs of fish exposed to wastewater effluent (Vajda et al., 2008) among others. It is recognized that neither the EAR-based identification of priority AOPs within an overall AOP network, nor previous field studies reporting effects consistent with some of these AOPs, causally implicate that concentrations of these contaminants detected in Great Lakes tributaries are having ecological effects. However, they do provide evidence to hypothesize that this may be the case when considering further monitoring and evaluation.

4.3. Limitations of the EAR approach

There are some important limitations to the EAR screening approach that need to be highlighted: (1) comparison of water chemistry results to assay results for individual chemicals does not allow for true evaluation of the integrated effect of mixtures. Assumptions (such as EAR additivity) must be made to evaluate the full sample matrix; (2) this type of evaluation is limited to those chemicals that are analyzed in samples that intersect with those chemicals that are currently represented in the ToxCast database (i.e., not all chemicals have been tested); (3) ToxCast data are limited to a specific set of assays–there are effects and some major modes of action that are not represented, including effects that are unique to non-mammalian species; (4) many of the assays lack the ability to metabolize the parent compounds being tested, which can under-and over-estimate the in vivo toxicity of some chemicals, and (5) not all ToxCast assays are currently linked to AOPs. Even with these limitations, high-throughput screening data can serve as a valuable tool for screening for potential adverse biological effects particularly where traditional in vivo toxicity data required to calculate water quality benchmarks are lacking. In addition, applying the ToxCast data in this manner could further inform and improve the ToxCast data curation and the AOP knowledgebase. For example, as hypotheses emerging from such analyses are tested, anomalous activities in the ToxCast data set can be identified and flagged, leading to more reliable pathway-based prioritization in the future. Additionally, priorities for AOP development may be identified.

4.4. Application of findings

Ultimately, the current study findings can be used to focus available resources. For example, results can help identify which of the monitored chemicals and chemical mixtures are a priority at each of the sites evaluated (Fig. SI-4, Table SI-8) and which AOPs are most likely to be relevant for the identified chemicals and mixtures at any given site (Fig. SI-6, Tables SI-8 and SI-9). Predicted bioactivities can then be confirmed through laboratory- or field-based investigation or through observations of resident organisms. However, for confirmation studies to be representative of the greatest potential hazard from chemical exposures, testing conditions must reflect the circumstances under which these chemical mixtures are most likely to be present at any given site. The contaminants present, the concentrations, and the exact mixtures vary spatially (urban vs agricultural, commercial vs residential, crops vs pasture), seasonally, and hydrologically (base flow, snowmelt, rainfall) (Baldwin et al., 2016). Well-chosen investigations that reflect the setting for which the greatest potential hazard exists based on these factors would provide substantial value and additional confidence in verifying results. After confirmation of the hypothesized bioactivities, reduction strategies for sources of these chemicals can then be investigated and implemented.

5. Conclusions

When adequate data existed for a comparative analysis, chemicals of greatest concern identified using the ToxCast database with an EAR threshold of 10^{-3} were very similar to those identified using water quality benchmarks with a TQ threshold of 10^{-1}. However, the ability to use the ToxCast database allowed for evaluation of twice as many chemicals in terms of possible biological impacts, as compared to water quality benchmarks. Several PAHs identified as a concern using water quality benchmarks were not similarly flagged using the EAR approach, perhaps due to mechanisms that can enhance their in vivo toxicity but would not be captured using in vitro systems. Several additional chemicals were identified as a potential concern through evaluation of putative bioactivity from chemical mixtures. Results from this work will enable resource managers to examine information pertinent to individual sites and identify individual chemicals and chemical mixtures of potential concern. Hypothesis-driven studies may then be designed to verify results, and if confirmed, mitigation strategies may be formulated and implemented.

Acknowledgements

The authors gratefully acknowledge the many individuals from the U.S. Geological Survey involved in sample collection, processing, and analysis. We thank Anthony L. Schroeder and Keith A. Houck for technical input and Edwin Smith and Elizabeth Murphy for program coordination. Support for this project was provided by the Great Lakes Restoration Initiative through the U.S. Environmental Protection Agency's Great Lakes National Program Office under agreement number DW-014-92453901. The views expressed in this work are those of the authors and do not necessarily reflect the views or policies of the U.S. EPA. Any use of trade, product, or firm names is for descriptive purposes only and does not imply endorsement by the U.S. Government.

Appendix A. Supplementary data

Supplementary data to this article can be found online at https://doi.org/10.1016/j.scitotenv.2019.05.457.

References

Krewski Jr, D., D.A Jr., Andersen, M., Anderson, H., J.C.B III, Boekelheide, K., Brent, R., Charnley, G., Cheung, V.G., S.G Jr, Kelsey, K.T., Kerkvliet, N.I., Li, A.A., McCray, L., Meyer, O., Patterson, R.D., Pennie, W., Scala, R.A., Solomon, G.M., Stephens, M., Yager, J., Zeise, L., Testing, S. of C. on T., Agents, A. of E., 2010. Toxicity testing in the 21st century: a vision and a strategy. J. Toxicol. Environ. Health Part B 13, 51–138. doi:https://doi.org/10.1080/10937404.2010.483176.

Ankley, G.T., Collyard, S.A., Monson, P.D., Kosian, P.A., 1994. Influence of ultraviolet light on the toxicity of sediments contaminated with polycyclic aromatic hydrocarbons. Environ. Toxicol. Chem. Int. J. 13, 1791–1796.

Ankley, G.T., Bennett, R.S., Erickson, R.J., Hoff, D.J., Hornung, M.W., Johnson, R.D., Mount, D.R., Nichols, J.W., Russom, C.L., Schmieder, P.K., Serrrano, J.A., Tietge, J.E., Villeneuve, D.L., 2010. Adverse outcome pathways: a conceptual framework to support ecotoxicology research and risk assessment. Environ. Toxicol. Chem. 29, 730–741. https://doi.org/10.1002/etc.34.

Ankley, G.T., LaLone, C.A., Gray, L.E., Villeneuve, D.L., Hornung, M.W., 2016. Evaluation of the scientific underpinnings for identifying estrogenic chemicals in nonmammalian taxa using mammalian test systems. Environ. Toxicol. Chem. 35, 2806–2816. https://doi.org/10.1002/etc.3456.

Baldwin, A.K., Corsi, S.R., De Cicco, L.A., Lenaker, P.L., Lutz, M.A., Sullivan, D.J., Richards, K.D., 2016. Organic contaminants in Great Lakes tributaries: prevalence and potential aquatic toxicity. Sci. Total Environ. 554–555, 42–52. https://doi.org/10.1016/j.scitotenv.2016.02.137.

Blackwell, B.R., Ankley, G.T., Corsi, S.R., DeCicco, L.A., Houck, K.A., Judson, R.S., Li, S., Martin, M.T., Murphy, E., Schroeder, A.L., Smith, E.R., Swintek, J., Villeneuve, D.L., 2017. An "EAR" on environmental surveillance and monitoring: a case study on the use of exposure–activity ratios (EARs) to prioritize sites, chemicals, and bioactivities of concern in Great Lakes waters. Environ. Sci. Technol. 51, 8713–8724. https://doi.org/10.1021/acs.est.7b01613.

Blackwell, B.R., Ankley, G.T., Bradley, P.M., Houck, K.A., Makarov, S.S., Medvedev, A.V., Swintek, J., Villeneuve, D.L., 2019. Potential toxicity of complex mixtures in surface waters from a nationwide survey of United States streams: identifying in vitro bioactivities and causative chemicals. Environ. Sci. Technol. 53, 973–983. https://doi.org/10.1021/acs.est.8b05304.

Blazer, V.S., Iwanowicz, L.R., Henderson, H., Mazik, P.M., Jenkins, J.A., Alvarez, D.A., Young, J.A., 2012. Reproductive endocrine disruption in smallmouth bass (Micropterus dolomieu) in the Potomac River basin: spatial and temporal comparisons of biological effects. Environ. Monit. Assess. 184, 4309–4334. https://doi.org/10.1007/s10661-011-2266-5.

Bradley, P.M., Journey, C.A., Romanok, K.M., Barber, L.B., Buxton, H.T., Foreman, W.T., Furlong, E.T., Glassmeyer, S.T., Hladik, M.L., Iwanowicz, L.R., Jones, D.K., Kolpin, D.W., Kuivila, K.M., Loftin, K.A., Mills, M.A., Meyer, M.T., Orlando, J.L., Reilly, T.J., Smalling, K.L., Villeneuve, D.L., 2017. Expanded target-chemical analysis reveals extensive mixed-organic-contaminant exposure in U.S. streams. Environ. Sci. Technol. 51, 4792–4802. https://doi.org/10.1021/acs.est.7b00012.

Browne, P., Judson, R.S., Casey, W.M., Kleinstreuer, N.C., Thomas, R.S., 2015. Screening chemicals for estrogen receptor bioactivity using a computational model. Environ. Sci. Technol. 49, 8804–8814. https://doi.org/10.1021/acs.est.5b02641.

Busch, W., Schmidt, S., Kühne, R., Schulze, T., Krauss, M., Altenburger, R., 2016. Micropollutants in European rivers: a mode of action survey to support the development of effect-based tools for water monitoring: micropollutants in European rivers: a mode-of-action. Environ. Toxicol. Chem. 35, 1887–1899. https://doi.org/10.1002/etc.3460.

Canadian Council of Ministers of the Environment, 2015. Canadian environmental quality guidelines, water quality guidelines for the protection of aquatic life [WWW document]. URL. http://ceqg-rcqe.ccme.ca/, Accessed date: 20 November 2012.

Careghini, A., Mastorgio, A.F., Saponaro, S., Sezenna, E., 2015. Bisphenol A, nonylphenols, benzophenones, and benzotriazoles in soils, groundwater, surface water, sediments, and food: a review. Environ. Sci. Pollut. Res. 22, 5711–5741. https://doi.org/10.1007/s11356-014-3974-5.

Cavallin, J.E., Jensen, K.M., Kahl, M.D., Villeneuve, D.L., Lee, K.E., Schroeder, A.L., Mayasich, J., Eid, E.P., Nelson, K.R., Milsk, R.Y., Blackwell, B.R., Berninger, J.P., LaLone, C.A., Blanksma, C., Jicha, T., Elonen, C., Johnson, R., Ankley, G.T., 2016. Pathway-based approaches for assessment of real-time exposure to an estrogenic wastewater treatment plant effluent on fathead minnow reproduction. Environ. Toxicol. Chem. 35, 702–716. https://doi.org/10.1002/etc.3228.

Corrales, J., Kristofco, L.A., Steele, W.B., Yates, B.S., Breed, C.S., Williams, E.S., Brooks, B.W., 2015. Global assessment of bisphenol a in the environment: review and analysis of its occurrence and bioaccumulation. Dose-Response 13, 155932581559830. https://doi.org/10.1177/1559325815598308.

Custer, C.M., Custer, T.W., Dummer, P.M., Goldberg, D., Franson, J.C., 2016. Concentrations and spatial patterns of organic contaminants in tree swallow (Tachycineta bicolor) eggs at United States and binational Great Lakes areas of concern, 2010–2015. Environ. Toxicol. Chem. 35, 3071–3092. https://doi.org/10.1002/etc.3496.

Dave, Gör, Blanck, H., Gustafsson, K., 1979. Biological effects of solvent extraction chemicals on aquatic organisms. J. Chem. Technol. Biotechnol. 29, 249–257. https://doi.org/10.1002/jctb.503290406.

Dave, G., Andersson, K., Berglind, R., Hasselrot, B., 1981. Toxicity of eight solvent extraction chemicals and of cadmium to water fleas, Daphnia Magna, rainbow trout, Salmo Gairdneri, and Zebrafish, Brachydanio Rerio. Comp. Biochem. Physiol. Part C Comp. Pharmacol. 69, 83–98. https://doi.org/10.1016/0306-4492(81)90105-2.

Davis, A.P., Murphy, C.G., Johnson, R., Lay, J.M., Lennon-Hopkins, K., Saraceni-Richards, C., Sciaky, D., King, B.L., Rosenstein, M.C., Wiegers, T.C., Mattingly, C.J., 2013. The comparative Toxicogenomics database: update 2013. Nucleic Acids Res. 41, D1104–D1114. https://doi.org/10.1093/nar/gks994.

De Cicco, L.A., Corsi, S.R., Villeneuve, D.L., Blackwell, B.R., Ankley, G.T., 2018. toxEval: Evaluation of measured concentration data using the ToxCast high-throughput screening database or a user-defined set of concentration benchmarks. R Package version 1.0.0 [WWW Document]. URL https://code.usgs.gov/water/toxEval, doi:https://doi.org/10.5066/P906UQ5I.

DeGroot, D.E., Swank, A., Thomas, R.S., Strynar, M., Lee, M.-Y., Carmichael, P.L., Simmons, S.O., 2018. mRNA transfection retrofits cell-based assays with xenobiotic metabolism. J. Pharmacol. Toxicol. Methods 92, 77–94. https://doi.org/10.1016/j.vascn.2018.03.002.

Dix, D.J., Houck, K.A., Martin, M.T., Richard, A.M., Setzer, R.W., Kavlock, R.J., 2007. The ToxCast program for prioritizing toxicity testing of environmental chemicals. Toxicol. Sci. 95, 5–12. https://doi.org/10.1093/toxsci/kfl103.

Elliott, S.M., Brigham, M.E., Lee, K.E., Banda, J.A., Choy, S.J., Gefell, D.J., Minarik, T.A., Moore, J.N., Jorgenson, Z.G., 2017. Contaminants of emerging concern in tributaries to the Laurentian Great Lakes: I. patterns of occurrence. PLoS One 12, e0182868. https://doi.org/10.1371/journal.pone.0182868.

Elliott, S.M., Brigham, M.E., Kiesling, R.L., Schoenfuss, H.L., 2018a. Environmentally relevant chemical mixtures of concern in waters of United States tributaries to the Great Lakes. Intergrated Environ. Assess. Manag. 14, 509–518. https://doi.org/10.1002/ieam.4041.

Elliott, S.M., Route, W.T., DeCicco, L.A., VanderMeulen, D.D., Corsi, S.R., Blackwell, B.R., 2018b. Contaminants in bald eagles of the upper Midwestern U.S.: a framework for prioritizing future research based on in-vitro bioassays. Environ. Pollut. https://doi.org/10.1016/j.envpol.2018.10.093.

Fay, K.A., Villeneuve, D.L., Swintek, J., Edwards, S.W., Nelms, M.D., Blackwell, B.R., Ankley, G.T., 2018. Differentiating pathway-specific from nonspecific effects in high-throughput toxicity data: a foundation for prioritizing adverse outcome pathway development. Toxicol. Sci. 163, 500–515. https://doi.org/10.1093/toxsci/kfy049.

Filer, D.L., Kothiya, P., Setzer, R.W., Judson, R.S., Martin, M.T., 2016. tcpl: the ToxCast pipeline for high-throughput screening data. Bioinformatics, btw680 https://doi.org/10.1093/bioinformatics/btw680.

Fonger, G.C., Stroup, D., Thomas, P.L., Wexler, P., 2000. Toxnet: a computerized collection of toxicological and environmental health information. Toxicol. Ind. Health 16, 4–6. https://doi.org/10.1177/074823370001600101.

Furdui, V.I., Stock, N.L., Ellis, D.A., Butt, C.M., Whittle, D.M., Crozier, P.W., Reiner, E.J., Muir, D.C.G., Mabury, S.A., 2007. Spatial distribution of perfluoroalkyl contaminants in Lake Trout from the Great Lakes. Environ. Sci. Technol. 41, 1554–1559. https://doi.org/10.1021/es0620484.

Gaulton, A., Hersey, A., Nowotka, M., Bento, A.P., Chambers, J., Mendez, D., Mutowo, P., Atkinson, F., Bellis, L.J., Cibrián-Uhalte, E., Davies, M., Dedman, N., Karlsson, A., Magariños, M.P., Overington, J.P., Papadatos, G., Smit, I., Leach, A.R., 2017. The ChEMBL database in 2017. Nucleic Acids Res. 45, D945–D954. https://doi.org/10.1093/nar/gkw1074.

Graymore, M., Stagnitti, F., Allinson, G., 2001. Impacts of atrazine in aquatic ecosystems. Environ. Int. 26, 483–495. https://doi.org/10.1016/S0160-4120(01)00031-9.

Guo, J., Romanak, K., Westenbroek, S., Hites, R.A., Venier, M., 2017a. Current-use flame retardants in the water of Lake Michigan tributaries. Environ. Sci. Technol. 51, 9960–9969. https://doi.org/10.1021/acs.est.7b01294.

Guo, J., Romanak, K., Westenbroek, S., Li, A., Kreis, R.G., Hites, R.A., Venier, M., 2017b. Updated polychlorinated biphenyl mass budget for Lake Michigan. Environ. Sci. Technol. 51, 12455–12465. https://doi.org/10.1021/acs.est.7b02904.

Han, Z., Wang, Q., Fu, J., Chen, H., Zhao, Y., Zhou, B., Gong, Z., Wei, S., Li, J., Liu, H., Zhang, X., Liu, C., Yu, H., 2014. Multiple bio-analytical methods to reveal possible molecular mechanisms of developmental toxicity in zebrafish embryos/larvae exposed to tris (2 butoxyethyl) phosphate. Aquat. Toxicol. 150, 175–181. https://doi.org/10.1016/j.aquatox.2014.03.013.

Heiger-Bernays, W.J., Wegner, S., Dix, D.J., 2018. High-throughput in vitro data to inform prioritization of ambient water monitoring and testing for endocrine active chemicals. Environ. Sci. Technol. 52, 783–793. https://doi.org/10.1021/acs.est.7b00014.

Igarashi, Y., Nakatsu, N., Yamashita, T., Ono, A., Ohno, Y., Urushidani, T., Yamada, H., 2015. Open TG-GATEs: a large-scale toxicogenomics database. Nucleic Acids Res. 43, D921–D927. https://doi.org/10.1093/nar/gku955.

Incardona, J.P., Day, H.L., Collier, T.K., Scholz, N.L., 2006. Developmental toxicity of 4 ring polycyclic aromatic hydrocarbons in zebrafish is differentially dependent on AH receptor isoforms and hepatic cytochrome P4501A metabolism. Toxicol. Appl. Pharmacol. 217, 308–321. https://doi.org/10.1016/j.taap.2006.09.018.

Ives, C., Campia, I., Wang, R.-L., Wittwehr, C., Edwards, S., 2017. Creating a structured adverse outcome pathway knowledgebase via ontology-based annotations. Appl. Vitro Toxicol. 3, 298–311. https://doi.org/10.1089/aivt.2017.0017.

Jacobs, M., 2013. In vitro metabolism and bioavailability tests for endocrine active substances: what is needed next for regulatory purposes? ALTEX 30, 331–351. https://doi.org/10.14573/altex.2013.3.331.

Jobling, S., Nolan, M., Tyler, C.R., Brighty, G., Sumpter, J.P., 1998. Widespread sexual disruption in wild fish. Environ. Sci. Technol. 32, 2498–2506. https://doi.org/10.1021/es9710870.

Jobling, S., Beresford, N., Nolan, M., Rodgers-Gray, T., Brighty, G.C., Sumpter, J.P., Tyler, C.R., 2002. Altered sexual maturation and gamete production in wild roach (Rutilus rutilus) living in rivers that receive treated sewage effluents. Biol. Reprod. 66, 272–281. https://doi.org/10.1095/biolreprod66.2.272.

Judson, R.S., Houck, K.A., Kavlock, R.J., Knudsen, T.B., Martin, M.T., Mortensen, H.M., Reif, D.M., Rotroff, D.M., Shah, I., Richard, A.M., Dix, D.J., 2009. In vitro screening of environmental chemicals for targeted testing prioritization: the ToxCast project. Environ. Health Perspect. 118, 485–492. https://doi.org/10.1289/ehp.0901392.

Judson, R., Houck, K., Martin, M., Richard, A.M., Knudsen, T.B., Shah, I., Little, S., Wambaugh, J., Woodrow Setzer, R., Kothya, P., Phuong, J., Filer, D., Smith, D., Reif, D., Rotroff, D., Kleinstreuer, N., Sipes, N., Xia, M., Huang, R., Crofton, K., Thomas, R.S., 2016. Editor's highlight: analysis of the effects of cell stress and cytotoxicity on *in vitro* assay activity across a diverse chemical and assay space. Toxicol. Sci. 152, 323–339. https://doi.org/10.1093/toxsci/kfw092.

Karn, S.K., Chakrabarty, S.K., Sudhakara Reddy, M., 2010. Characterization of pentachlorophenol degrading Bacillus strains from secondary pulp-and-paper-industry sludge. Int. Biodeterior. Biodegrad. 64, 609–613. https://doi.org/10.1016/j.ibiod.2010.05.017.

Kavlock, R., Chandler, K., Houck, K., Hunter, S., Judson, R., Kleinstreuer, N., Knudsen, T., Martin, M., Padilla, S., Reif, D., Richard, A., Rotroff, D., Sipes, N., Dix, D., 2012. Update on EPA's ToxCast program: providing high throughput decision support tools for chemical risk management. Chem. Res. Toxicol. 25, 1287–1302. https://doi.org/10.1021/tx3000939.

Kim, S., Jung, J., Lee, I., Jung, D., Youn, H., Choi, K., 2015. Thyroid disruption by triphenyl phosphate, an organophosphate flame retardant, in zebrafish (Danio rerio) embryos/larvae, and in GH3 and FRTL-5 cell lines. Aquat. Toxicol. 160, 188–196. https://doi.org/10.1016/j.aquatox.2015.01.016.

Kim, S., Thiessen, P.A., Bolton, E.E., Chen, J., Fu, G., Gindulyte, A., Han, L., He, J., He, S., Shoemaker, B.A., Wang, J., Yu, B., Zhang, J., Bryant, S.H., 2016. PubChem substance and compound databases. Nucleic Acids Res. 44, D1202–D1213. https://doi.org/10.1093/nar/gkv951.

Kliewer, S.A., Goodwin, B., Willson, T.M., 2002. The nuclear pregnane × receptor: a key regulator of xenobiotic metabolism. Endocr. Rev. 23, 687–702. https://doi.org/10.1210/er.2001-0038.

Knapen, D., Angrish, M.M., Fortin, M.C., Katsiadaki, I., Leonard, M., Margiotta-Casaluci, L., Munn, S., O'Brien, J.M., Pollesch, N., Smith, L.C., Zhang, X., Villeneuve, D.L., 2018.

Adverse outcome pathway networks I: development and applications: advancing adverse outcome pathway networks. Environ. Toxicol. Chem. 37, 1723–1733. https://doi.org/10.1002/etc.4125.
LaLone, C.A., Villeneuve, D.L., Wu-Smart, J., Milsk, R.Y., Sappington, K., Garber, K.V., Housenger, J., Ankley, G.T., 2017. Weight of evidence evaluation of a network of adverse outcome pathways linking activation of the nicotinic acetylcholine receptor in honey bees to colony death. Sci. Total Environ. 584–585, 751–775. https://doi.org/10.1016/j.scitotenv.2017.01.113.
Lamb, J., Crawford, E.D., Peck, D., Modell, J.W., Blat, I.C., Wrobel, M.J., Lerner, J., Brunet, J.-P., Subramanian, A., Ross, K.N., Reich, M., Hieronymus, H., Wei, G., Armstrong, S.A., Haggarty, S.J., Clemons, P.A., Wei, R., Carr, S.A., Lander, E.S., Golub, T.R., 2006. The connectivity map: using gene-expression signatures to connect small molecules, genes, and disease. Science 313, 1929–1935. https://doi.org/10.1126/science.1132939.
Lepak, R.F., Yin, R., Krabbenhoft, D.P., Ogorek, J.M., DeWild, J.F., Holsen, T.M., Hurley, J.P., 2015. Use of stable isotope signatures to determine mercury sources in the Great Lakes. Environ. Sci. Technol. Lett. 2, 335–341. https://doi.org/10.1021/acs.estlett.5b00277.
Lin, K., 2009. Joint acute toxicity of tributyl phosphate and triphenyl phosphate to Daphnia magna. Environ. Chem. Lett. 7, 309–312. https://doi.org/10.1007/s10311-008-0170-1.
Logan, D.T., 2007. Perspective on ecotoxicology of PAHs to fish. Hum. Ecol. Risk Assess. Int. J. 13, 302–316. https://doi.org/10.1080/10807030701226749.
Love, B.J., Einheuser, M.D., Nejadhashemi, A.P., 2011. Effects on aquatic and human health due to large scale bioenergy crop expansion. Sci. Total Environ. 409, 3215–3229. https://doi.org/10.1016/j.scitotenv.2011.05.007.
Mayer, F., Ellersieck, M.R., 1986. Manual of Acute Toxicity:Interpretation and Data Base for 410 Chemicals and 66 Species of Freshwater Animals.
Medvedev, A., Moeser, M., Medvedeva, L., Martsen, E., Granick, A., Raines, L., Zeng, M., Makarov, S., Houck, K.A., Makarov, S.S., 2018. Evaluating biological activity of compounds by transcription factor activity profiling. Sci. Adv. 4, eaar4666. https://doi.org/10.1126/sciadv.aar4666.
Nirmalakhandan, N., Arulgnanendran, V., Mohsin, M., Sun, B., Cadena, F., 1994. Toxicity of mixtures of organic chemicals to microorganisms. Water Res. 28, 543–551. https://doi.org/10.1016/0043-1354(94)90005-1.
Ohe, T., Watanabe, T., Wakabayashi, K., 2004. Mutagens in surface waters: a review. Mutat. Res. Mutat. Res. 567, 109–149. https://doi.org/10.1016/j.mrrev.2004.08.003.
Pérez, J., Domingues, I., Soares, A.M.V.M., Loureiro, S., 2011. Growth rate of Pseudokirchneriella subcapitata exposed to herbicides found in surface waters in the Alqueva reservoir (Portugal): a bottom-up approach using binary mixtures. Ecotoxicology 20, 1167–1175. https://doi.org/10.1007/s10646-011-0661-x.
Pittman, M.E., Edwards, S.W., Ives, C., Mortensen, H.M., 2018. AOP-DB: a database resource for the exploration of adverse outcome pathways through integrated association networks. Toxicol. Appl. Pharmacol. 343, 71–83. https://doi.org/10.1016/j.taap.2018.02.006.
Prado, P.S., Pinheiro, A.P.B., Bazzoli, N., Rizzo, E., 2014. Reproductive biomarkers responses induced by xenoestrogens in the characid fish Astyanax fasciatus inhabiting a South American reservoir: an integrated field and laboratory approach. Environ. Res. 131, 165–173. https://doi.org/10.1016/j.envres.2014.03.002.
R Core Team, 2017. R: A Language and Environment for Statistical Computing. R Foundation for Statistical Computing, Vienna, Austria.
Rivera-Oliver, M., Díaz-Ríos, M., 2014. Using caffeine and other adenosine receptor antagonists and agonists as therapeutic tools against neurodegenerative diseases: a review. Life Sci. 101, 1–9. https://doi.org/10.1016/j.lfs.2014.01.083.
Schroeder, A.L., Ankley, G.T., Houck, K.A., Villeneuve, D.L., 2016. Environmental surveillance and monitoring-the next frontiers for high-throughput toxicology: surveillance and monitoring and high-throughput toxicology. Environ. Toxicol. Chem. 35, 513–525. https://doi.org/10.1002/etc.3309.
Shannon, P., Markiel, A., Ozier, O., Baliga, N.S., Wang, J.T., Ramage, D., Amin, N., Schwikowski, B., Ideker, T., 2003. Cytoscape: a software environment for integrated models of biomolecular interaction networks. Genome Res. 13, 2498–2504. https://doi.org/10.1101/gr.1239303.
Simcik, M.F., Offenberg, J.H., 2006. Polycyclic aromatic hydrocarbons in the Great Lakes. In: Hites, R.A. (Ed.), Persistent Organic Pollutants in the Great Lakes. Springer, Berlin Heidelberg, pp. 307–353 https://doi.org/10.1007/698_5_044.
Society for the Advancement of Adverse Outcome Pathways, 2018. Aopwiki [WWW Document]. URL. https://aopwiki.org/, Accessed date: 21 September 2018.
Stegeman, J.J., Lech, J.J., 1991. Cytochrome P-450 monooxygenase systems in aquatic species: carcinogen metabolism and biomarkers for carcinogen and pollutant exposure. Environ. Health Perspect. 90, 101. https://doi.org/10.2307/3430851.
Subramanian, A., Narayan, R., Corsello, S.M., Peck, D.D., Natoli, T.E., Lu, X., Gould, J., Davis, J.F., Tubelli, A.A., Asiedu, J.K., Lahr, D.L., Hirschman, J.E., Liu, Z., Donahue, M., Julian, B., Khan, M., Wadden, D., Smith, I.C., Lam, D., Liberzon, A., Toder, C., Bagul, M., Orzechowski, M., Enache, O.M., Piccioni, F., Johnson, S.A., Lyons, N.J., Berger, A.H., Shamji, A.F., Brooks, A.N., Vrcic, A., Flynn, C., Rosains, J., Takeda, D.Y., Hu, R., Davison, D., Lamb, J., Ardlie, K., Hogstrom, L., Greenside, P., Gray, N.S., Clemons, P.A., Silver, S., Wu, Xiaoyun, Zhao, W.-N., Read-Button, W., Wu, Xiaohua, Haggarty, S.J., Ronco, L.V., Boehm, J.S., Schreiber, S.L., Doench, J.G., Bittker, J.A., Root, D.E., Wong, B., Golub, T.R., 2017. A next generation connectivity map: L1000 platform and the first 1,000,000 profiles. Cell 171, 1437–1452.e17. https://doi.org/10.1016/j.cell.2017.10.049.
Thrupp, T.J., Runnalls, T.J., Scholze, M., Kugathas, S., Kortenkamp, A., Sumpter, J.P., 2018. The consequences of exposure to mixtures of chemicals: something from 'nothing' and 'a lot from a little' when fish are exposed to steroid hormones. Sci. Total Environ. 619–620, 1482–1492. https://doi.org/10.1016/j.scitotenv.2017.11.081.
Tice, R.R., Austin, C.P., Kavlock, R.J., Bucher, J.R., 2013. Improving the human Hazard characterization of chemicals: a Tox21 update. Environ. Health Perspect. 121, 756–765. https://doi.org/10.1289/ehp.1205784.
US EPA, 1996. Ecotox thresholds, EPA 540/F-95/038 [WWW document]. URL. http://www.epa.gov/sites/production/files/2015-09/documents/v3no2.pdf.
US EPA, 2003. Procedures for the Derivation of Equilibrium Partitioning Sediment Benchmarks (ESBs) for the Protection of Benthic Organisms. PAH Mixtures.
US EPA, 2015. US EPA. ToxCast & Tox21 summary files from invitrodb_v2. [WWW document]. URL. http://www2.epa.gov/chemical-research/toxicity-forecaster-toxcasttm-data, Accessed date: 22 February 2016.
Usmani, K.A., Rose, R.L., Goldstein, J.A., Taylor, W.G., Brimfield, A.A., Hodgson, E., 2002. In vitro human metabolism and interactions of repellent N,N diethyl m toluamide. Drug Metab. Dispos. 30, 289–294. https://doi.org/10.1124/dmd.30.3.289.
Vajda, A.M., Barber, L.B., Gray, J.L., Lopez, E.M., Woodling, J.D., Norris, D.O., 2008. Reproductive disruption in fish downstream from an estrogenic wastewater effluent. Environ. Sci. Technol. 42, 3407–3414. https://doi.org/10.1021/es0720661.
Villeneuve, D.L., Crump, D., Garcia-Reyero, N., Hecker, M., Hutchinson, T.H., LaLone, C.A., Landesmann, B., Lettieri, T., Munn, S., Nepelska, M., Ottinger, M.A., Vergauwen, L., Whelan, M., 2014. Adverse outcome pathway (AOP) development I: strategies and principles. Toxicol. Sci. 142, 312–320. https://doi.org/10.1093/toxsci/kfu199.
Villeneuve, D.L., Angrish, M.M., Fortin, M.C., Katsiadaki, I., Leonard, M., Margiotta-Casaluci, L., Munn, S., O'Brien, J.M., Pollesch, N.L., Smith, L.C., Zhang, X., Knapen, D., 2018. Adverse outcome pathway networks II: network analytics: adverse outcome pathway network analytics. Environ. Toxicol. Chem. 37, 1734–1748. https://doi.org/10.1002/etc.4124.
Weeks, J., Guiney, P., Nikiforov, A., 2012. Assessment of the environmental fate and ecotoxicity of N,N diethyl m toluamide (DEET). Integr. Environ. Assess. Manag. 8, 120–134. https://doi.org/10.1002/ieam.1246.
Wickham, H., 2016. ggplot2: Elegant Graphics for Data Analysis. Springer-Verlag, New York.
Wickham, H., François, R., Henry, L., Müller, K., 2018. dplyr: A Grammar of Data Manipulation.
Yoshioka, Y., Ose, Y., Sato, T., 1986. Correlation of the five test methods to assess chemical toxicity and relation to physical properties. Ecotoxicol. Environ. Saf. 12, 15–21. https://doi.org/10.1016/0147-6513(86)90003-5.
Zaugg, S.D., Smith, S.G., Schroeder, M.P., 2006. Determination of Wastewater Compounds in Whole Water by Continuous Liquid-Liquid Extraction and Capillary-Column Gas Chromatography/Mass Spectrometry (No. TM-5-B4). United States Geological Survey.
Zenobio, J.E., Sanchez, B.C., Archuleta, L.C., Sepulveda, M.S., 2014. Effects of triclocarban, N,N diethyl meta toluamide, and a mixture of pharmaceuticals and personal care products on fathead minnows (*Pimephales promelas*): effects of pharmaceuticals on fish. Environ. Toxicol. Chem. 33, 910–919. https://doi.org/10.1002/etc.2511.

Introduction to toxEval

15 April, 2020

Source: `vignettes/Introduction.Rmd` (https://github.com/USGS-R/toxEval/blob/master/vignettes/Introduction.Rmd)

Introduction

The `toxEval` R-package includes a set of functions to analyze, visualize, and organize measured concentration data as it relates to ToxCast data (https://www.epa.gov/chemical-research/toxicity-forecasting) (default) or other user-selected chemical-biological interaction benchmark data such as water quality criteria. The intent of these analyses is to develop a better understanding of the potential biological relevance of environmental chemistry data. Results can be used to prioritize which chemicals at which sites may be of greatest concern. These methods are meant to be used as a screening technique to predict potential for biological influence from chemicals that ultimately need to be validated with direct biological assays.

The functions within this package allow great flexibly for exploring the potential biological affects of measured chemicals. Also included in the package is a browser-based application made from the `Shiny` R-package (the app). The app is based on functions within the R-package and includes many convenient analyses and visualization options for users to choose. Use of the functions within the R-package allows for additional flexibility within the functions beyond what the app offers and provides options for the user to interact more directly with the data. The overview in this document focuses on the R-package. Documentation for the app is provided in the ShinyApp vignette (shinyApp.html).

This vignette provides a general overview of the concepts within `toxEval`, definitions of common terminology used throughout the package, and links to information to help understand fundamentals of the ToxCast database used within `toxEval`. In addition, instructions are provided for installing and updating the package from the Geological Survey R Archive Network (GRAN).

What is ToxCast?

The U.S. EPA's Toxicity Forecaster ToxCast (https://www.epa.gov/chemical-research/toxicity-forecasting) includes a database of chemical-biological interactions that contains information from hundreds of assays on thousands of chemicals, providing a means to assess biological relevance to measured concentrations. The `toxEval` package attempts to simplify the workflow for exploring data as it relates to these assay endpoints (benchmark data). The workflow uses ToxCast as a default for evaluation of chemical:biological interactions, but the user may also define alternative benchmarks for a custom or more traditional approach to biological relevance evaluation. This is also a useful capability for efficient comparison of ToxCast evaluation results with those from other toxicity benchmark databases.

When using the ToxCast endPoints for analysis, it is important to have at least a minimal understanding of what ToxCast data is, and which ToxCast data is relevant to any given study. There are many useful resources here (https://www.epa.gov/chemical-research/toxicity-forecasting). There is also a tool called the Comptox Dashboard (https://comptox.epa.gov/dashboard/) that has a wealth of information on ToxCast data.

So what are we doing with the user input data and ToxCast? First, we calculate an Exposure-Activity Ratio (EAR) for each measurement. Then we can explore the EARs based on a wide variety of groupings to view the data in many dimensions.

Exposure-Activity Ratio

An Exposure-Activity Ratio (EAR) is defined as the ratio of a measured concentration and a concentration that was determined to cause some activity in a specified ToxCast assay ("endPoint" concentration). An EAR > 1.0 would indicate that the measured concentration is greater than the endpoint concentration. The ToxCast database (as provided in the current version of `toxEval`) provides as many as several hundred endPoints for more than 7000 chemicals. Each endPoint is a single test that was done to detect some form of biological activity.

In order to get appropriate EAR results, it is important to use the correct units. The `toxEval` package assumes all measured concentrations are reported in micrograms per liter (μg/L). ToxCast data is reported in log(μM), so the `toxEval` package automatically performs the unit conversion.

A secondary option within `toxEval` is for the user to provide a set of "benchmark concentrations" to define custom biological responses to meet specific study objectives (e.g. water quality criteria). In this case, EAR values are replaced with toxicity quotients. Similar to EAR values, toxicity quotients are defined as the ratio of a measured concentration to the benchmark concentration.

EAR is basically synonymous with bioanalytical equivalent concentrations (BEQ). EAR is a ratio, and BEQ is a measure of concentration, but both convey the same information.

What is an "endPoint"?

ToxCast uses high-throughput assays to create concentration-response curves for each of these chemical:endPoint combinations. An endPoint is "associated with the perturbation of specific biological processes identified for the confirmation or monitoring of predicted site-specific hazards" Blackwell 2017 (https://doi.org/10.1021/acs.est.7b01613). That means a specific biological action was tested, and the concentration at which activity was observed was determined. Of several endpoint values provided within the ToxCast database, the activity concentration at cutoff (ACC) was chosen to compute EAR values within the `toxEval` package, consistent with the description in Blackwell, 2017 (https://doi.org/10.1021/acs.est.7b01613). ACC values from the ToxCast database are provided within the `toxEval` package.

What is a "group"?

Often, it is valuable to consider aggregations of single endPoints in evaluation efforts. ToxCast has provided tables that group individual endPoints into generalized categories for functional use. The grouping summary table is included in `toxEval` and can be explored via the `end_point_info` data:

```
library (https://rdrr.io/r/base/library.html)(toxEval)
end_point_info <- end_point_info
```

See the help file `?end_point_info` for specifics on how the table was downloaded.

Throughout the `toxEval` analysis, there are graphing and table functions that will summarize EARs based on either "Biological" groupings (as defined by a group of endPoints) or "Chemical Class" groupings (as defined by a group of chemicals).

The default grouping of ToxCast endPoints is “intended_target_family”, but depending on the analysis, it may be more appropriate to use other grouping categories. To change the default, specify a grouping in the `groupCol` argument of the `filter_groups` function. For example:

```
filtered_ep <- filter_groups (../reference/filter_groups.html)(end_point_info,
              groupCol = "intended_target_family",
              assays = c (https://rdrr.io/r/base/c.html)("ATG","NVS", "OT", "TOX21",
                         "CEETOX", "APR", "CLD", "TANGUAY",
                         "NHEERL_PADILLA","NCCT_SIMMONS", "ACEA"),
              remove_groups = c (https://rdrr.io/r/base/c.html)("Background Measurement",
                                 "Undefined"))
```

What is happening here is that the supplied data frame `end_point_info` is filtered to just the “intended_target_family” group. Additionally, the assay BioSeek is removed (it is the only one not included in the possible list of assays). Finally, of all the groups within intended_target_family, the end points designated “Undefined” and “Background Measurement” are removed.

Summarizing the data

The functions in `toxEval` summarize the data as follows:

First, individual EAR values are calculated for each chemical:endPoint combination. Then, the EAR values are summed together by samples (a sample is defined as a unique site/date) based on the grouping picked in the “category” argument. Categories include “Biological”, “Chemical Class”, or “Chemical”. “Biological” refers to the chosen ToxCast annotation as defined in the `groupCol` argument of the `filter_groups` function. “Chemical Class” refers to the groupings of chemicals as defined in the “Class” column of the “Chemicals” sheet of the input file. “Chemical” refers to the individual chemical as defined by a unique CAS value. Finally, the maximum or mean EAR is calculated per site (based on the `mean_logic` option). This ensures that each site is represented equally regardless of how many samples are available per site.

Some functions will also include a calculation for a “hit”. A threshold is defined by the user, and if the mean or maximum EAR (calculated as described above) is greater than the threshold, that is considered a “hit”.

Package logistics

Installation of toxEval

`toxEval` is available on any CRAN mirror.

```
install.packages (https://rdrr.io/r/utils/install.packages.html)("toxEval")
```

Update toxEval

`toxEval` does require a fair number of additional packages to run properly. These dependencies offer many benefits, such as a smooth running intuitive Shiny app. The drawbacks however are that there becomes more risk that those dependencies could change their output/workflow over time. `toxEval` developers will try to stay on top of those changes, but it is a challenge. It is important to always update *all* of your packages therefore…..not just `toxEval` .

`toxEval` may push out a new version to keep up with a critical change in a dependent package, and if you only update `toxEval`, the update could cause bugs (we will attempt to mandate the package version of each package, but it still is best to stay on top of new package versions).

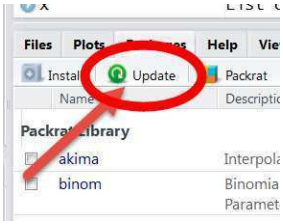

Regularly, it is a good idea to update *ALL* of installed packages in R. If using RStudio, this is done by using the Update button in the “Packages” tab in RStudio. Selecting this option checks CRAN for updates. Within the R-console, packages can be updated with the command:

```
update.packages (https://rdrr.io/r/utils/update.packages.html)()
```

Reporting bugs

If you discover an issue that you feel is a bug in the package or have a question on functionality, please consider reporting bugs and asking questions on the Issues page: https://github.com/USGS-R/toxEval/issues (https://github.com/USGS-R/toxEval/issues)

Citing toxEval

This package has not been reviewed and approved as a USGS-product. The implication is that `toxEval` cannot be cited in a publication. Once the software has been reviewed and approved, basic citation information will be available using the function:

```
citation (https://rdrr.io/r/utils/citation.html)(package = "toxEval")
```

```
##
## To cite toxEval in publications, please use:
##
##   De Cicco, L.A., Corsi, S.R., Villeneuve D.L, Blackwell, and B.R,
##   Ankley, G.T., 2018, toxEval: Evaluation of measured concentration
##   data using the ToxCast high-throughput screening database or a
##   user-defined set of concentration benchmarks. R package version
##   1.1.0., https://code.usgs.gov/water/toxEval, doi:10.5066/P906UQ5I
##
## A BibTeX entry for LaTeX users is
##
##   @Manual{,
##     author = {Laura A. {De Cicco} and Steven R. Corsi and Daniel L. Villeneuve and Brett R. Blackwe
##     title = {toxEval: Evaluation of measured concentration data using the ToxCast high-throughput s
##     publisher = {U.S. Geological Survey},
##     version = {1.1.0},
##     address = {Reston, VA},
##     institution = {U.S. Geological Survey},
##     year = {2019},
##     doi = {10.5066/P906UQ5I},
##     url = {https://code.usgs.gov/water/toxEval},
##   }
```

Disclaimer

This software has been approved for release by the U.S. Geological Survey (USGS). Although the software has been subjected to rigorous review, the USGS reserves the right to update the software as needed pursuant to further analysis and review. No warranty, expressed or implied, is made by the USGS or the U.S. Government as to the functionality of the software and related material nor shall the fact of release constitute any such warranty. Furthermore, the software is released on condition that neither the USGS nor the U.S. Government shall be held liable for any damages resulting from its authorized or unauthorized use.

Table of Contents

General_Authors_Publications.....2
LI-265105_Haselman_et_al_2016a_JAT.....19
LI-265105_Haselman_et_al_2016a_JAT_Supplementary_data.....31
LI-265105_InCites_Journal_Citation_Reports_JAT.....33
LI-265106_Haselman_et_al_2018_AqTox.....52
LI-265106_Haselman_et_al_2018_AqTox_Supplementary_data.....64
LI-265106_InCites_Journal_Citation_Reports_AqTox.....68
Record_of_Percentage_Agreement_Allen_Olmstead.....87
Record_of_Percentage_Agreement_Joseph_Korte.....89
Record_of_Percentage_Agreement_Patricia_Kosian.....91
Record_of_Percentage_Agreement_Rodney_Johnson.....93
Record_of_Percentage_Agreement_Sigmund_Degitz.....95
Record_of_Percentage_Agreement_Taisen_Iguchi.....97
Supporting_Automated_dilution_system.....99
Supporting_Exposure_unit.....100
Supporting_Haselman_et_al_2015_G&CE.....101
Supporting_Haselman_et_al_2015_G&CE_Supplementary_data1.....112
Supporting_Haselman_et_al_2015_G&CE_Supplementary_data2.....134
Supporting_Haselman_et_al_2016b_JAT.....136
Supporting_Haselman_et_al_2016b_JAT_Supplementary_data.....147
Supporting_OCSPP_890-2300_(LAGDA).....149
20-084_Complete_citations.....238

STAA REPORT FOR THE SCIENTIST NOMINATIONS

General Information:

Nomination ID/App ID:	20-084
Research Category Primary:	Environmental Policy and Decision-Making Studies (EP)
Research Category Secondary:	
Laboratory/Office Name:	ORD
Nomination Entered By:	Jonathan Haselman

Eligibility Checklist:

[Y] The nominated publication(s) has not been submitted to a previous STAA competition.

[Y] The nominated publication(s) was published on or before January 1, 2017 and on or after January 1,2012

[Y] The principal author was an EPA employee or a PHS employee assigned to EPA when the research was performed

[Y] The EPA authors (includes PHS employees assigned to EPA) contributed collectively a minimum of 50% toward the publication(s)

Nominating Official Name:	Dale Hoff
Nominating Official Title:	DIRECTOR, MID-CONTINENT ECOLOGY DIV
Nominating OfficialEmail:	hoff.dale@epa.gov
STAA Coordinator Name:	Kathleen Wiser
STAA Coordinator Email:	wiser.kathi@epa.gov

Justifications:

Justification 1:

The U.S. EPA's Endocrine Disruptor Screening Program (EDSP) was established in the late 1990's as a result of the Federal Food, Drug and Cosmetic Act and an amendment to the Safe Drinking Water Act which mandate EPA to use validated methods to evaluate the endocrine disrupting potential of chemicals. The Endocrine Disruptor Screening and Testing Advisory Committee (EDSTAC), chartered by EPA in response to the legislation, provided guidance to the Agency on the design and implementation of the EDSP. EDSTAC's recommendations included development of a tiered testing approach to evaluate a chemical's potential to interact with estrogen, androgen and thyroid endocrine systems in both humans and wildlife. The EDSP would consist of tier 1 screening and prioritization to determine a chemical's potential to interact with endocrine systems and tier 2 testing to characterize adverse organismal effects and define exposure levels at which those effects occur.

The Office of Chemical Safety and Pollution Prevention (OCSPP) oversees the battery of test guidelines including tier 1 (890.1000 series) and tier 2 (890.2300) guidelines. The tier 1 battery is a series of short-term in vivo bioassays spanning taxonomic classes representing rodents (mammalian model), birds, fish and amphibians. More recently, in vitro assays for estrogen receptor binding and steroidogenesis have been validated for inclusion in the tier 1 battery of assays. The tier 2 battery of test guidelines consist of long-term in vivo bioassays in birds, fish and amphibians and span multiple life-stages to better assess developmental sensitivities to both endocrine disruption and generalized toxicity. Many of the tier 1 and tier 2 assays were designed by ORD scientists who also participated in interlaboratory validation studies to establish standardized test protocols that would not only be used by the U.S. EPA but also move forward for global harmonization and adoption into the Organization for Economic Cooperation and Development's (OECD) Guidelines for the Testing of Chemicals.

The work nominated here involved the design, development, validation and global harmonization of the tier 2 test guideline, OCSPP 890.2300 Larval Amphibian Growth and Development Assay (LAGDA). The official test guideline is provided as supporting material. Prior to the establishment of this test guideline, there was no

existing standard for evaluating chronic chemical toxicity in an amphibian, let alone a standard that includes evaluations of both endocrine disruption and population-relevant endpoints important to ecological risk assessment such as growth, somatic development and reproductive development. This test guideline specifies recommended methods to generate data required by EPA for pesticide registration, setting tolerances of pesticide residues and supporting decision making

on regulation of industrial chemicals under various statutory authorities including the Federal Insecticide, Fungicide and Rodenticide Act (FIFRA), the FFDCA and the Toxic Substances Control Act (TSCA).

Development and validation of the test guideline required expertise in amphibian biology, endocrinology, toxicology, histopathology, statistics, analytical chemistry, engineering, collegiality and perseverance. The first challenge was to build a constant flow-through exposure system that could deliver consistent chemical concentrations from an automated dilution system for more than five months (>20 weeks) per study. The system also needed to have integrated monitoring and control so any failures or malfunctions occurring day or night that interrupted tank chemical concentrations or environmental conditions could effectively be communicated to appropriate staff for immediate response and correction. The exposure and automated dilution systems built by our team for the development of this test guideline remain to be some of the most sophisticated automated diluters in existence and have been the subject of numerous visits by contract lab staff outfitting their own facilities in preparation for running this test guideline. The engineering and innovation that went into the exposure and automated dilution systems capable of remaining stable and robust through a five-month long exposure must be considered when realizing the full impact and innovation of this work (images provided as supporting documents).

A key feature of this test guideline, which poses a unique challenge, is that the exposure spans multiple amphibian life stages. Exposure is initiated during embryonic development, continues post-hatch, through thyroid-mediated metamorphosis and into the juvenile life stage when the reproductive organs are fully differentiated and undergoing maturation. Experience with amphibian developmental biology was required for the ability to identify and carefully handle hundreds of fertilized, healthy and developmentally staged embryos to initiate exposure. This is followed by the need for a keen eye to count miniscule hatched larvae to evaluate hatching success and then rearing of the larvae through metamorphosis. Normally, rearing *Xenopus* larvae is not an exceptional challenge; however, every individual in the test is evaluated for their metamorphic rate as one indicator of thyroid axis function, so they are separated from one another within the same tank when they reach a developmental milestone (metamorphic climax). Some larvae were subsampled at metamorphic climax while others continued exposure. Following the completion of metamorphosis, all remaining individuals were

genetically tested to determine their gender and equal amounts of genotypic males and females were identified per tank to continue exposure to the end of the test whereas the rest were culled. These organism handling and accounting procedures were logistically and technically complicated but resulted in extremely robust evaluations of thyroid-mediated metamorphosis and reproductive development through comparisons of genotypic versus phenotypic sex.

Chemical stock preparation, dilution and delivery, and analytical verification of exposure concentrations were additional key components of this work. Some chemicals required preparation of solid-liquid saturator columns whereas others required carboy “shell-coating” in order to attain proper working stock concentrations. These techniques represent innovations passed down from the historical staff at the Great Lakes Toxicology and Ecology Division. Another significant challenge that our team overcame was the degradation of test chemical due to biofilm growth in the wetted components of the system – a challenge only posed by bioassays generally running longer than three weeks. Weekly comprehensive analytical verification of chemical concentrations was critical to track this phenomenon. Implementation of periodic system sterilization during the test was critical to maintaining stable chemical concentrations and “staying ahead” of biological growth that was naturally selected for consuming the test chemical. Performing system sterilization in situ without negatively impacting the developing organisms was a highly technical, high stakes procedure that our team executed routinely. This is the type of unforeseen phenomena that could incur extremely high costs in future testing had this not been identified by our experience and articulated within the test guidance.

Other efforts to provide comprehensive guidance included gathering of internal and external experts in statistics and histopathology to participate in workshops aimed at building consensus around recommended approaches. The LAGDA generates apical-level data useful for ecological risk assessment, which includes histopathology to evaluate morphological effects on endocrine glands/tissues that indicate active compensation, intersex/sex reversal or dysmorphogenesis. Development of many histological procedures resulted from the workshops including tissue collection, processing, sectioning, section sampling, definition of pathological diagnoses in various tissues and statistical analyses of incidence and severity scores. These procedures described in the LAGDA guideline are the most detailed and comprehensive histopathology methods for this commonly used model

organism to date. A similar level of effort went into the recommended statistical approaches for analyzing LAGDA data.

Finally, although many other details of this work could be discussed with regard to their scientific contribution and impact, a significant effort and Agency investment worth considering was our contribution to the interlaboratory validation study. Our team participated as the lead laboratory in the validation study which required a substantial amount of collaboration and collegiality. Following our drafting of the proposed guideline, we worked with a series of other groups including multiple U.S. contract laboratories, the U.S. Army, the Japanese Ministry of the Environment and a Japanese contract lab. In some cases, we were in weekly contact with labs to help them troubleshoot issues from embryo screening to rearing larvae to analytical chemistry to genetic testing. The overall coordination of this interlaboratory validation study resulted in submission of participant data to our team for assembly of an Integrated Summary Report to be used as the basis for a FIFRA Scientific Advisory Panel review and determination on whether the guideline was sufficiently validated. Following this exercise, the guideline went on to be globally harmonized and adopted by the OECD.

Justification 2A:

Haselman et al. (2016a) is the first presentation of the LAGDA study design in the peer reviewed literature. This manuscript consists of two validation studies, one that demonstrates the effects of a weak estrogenic compound, 4-*tert*-octylphenol, and the other study demonstrates the effects of a potent androgen, 17-trenbolone. Although these compounds had already been studied in the context of endocrine disruption across species, these compounds were treated as reference chemicals for causing specific modes of toxicity so the LAGDA endpoints could be evaluated. Aside from the breadth of data generated, there were two notable findings that came out of these studies. First, given the fact that organisms need to survive through embryonic exposure in order to provide chronic effect data through the rest of the test, this life stage becomes a driver of chemical concentration ranges. Effectively, this helps determine whether the predominant driver of the risk assessment is either survival or endocrine-related effects. In cases where a chemical may cause clear endocrine effects at concentrations tolerated by a larva, juvenile or adult, these concentrations may not be tolerated by an embryo undergoing gastrulation. The second notable finding resulting from these studies is that *Xenopus* oviducts are the most sensitive tissue to alterations in estrogen and androgen signaling. The mechanisms by which

the oviducts mature in females and resorb in males require estrogen and androgen signaling, respectively. The agonism of these chemicals was clearly demonstrated by the precocious maturation of oviducts in females and retention of oviducts in males exposed to 4-*tert*-octylphenol while exposure to 17-trenbolone caused complete resorption of oviducts in a portion of females, rendering them incapable of reproduction. This finding provided precedent for oviduct histopathology being

leveraged as an indicator of either estrogenic or androgenic modes of action when the gonads themselves appear to be less sensitive to dysmorphogenesis in the same exposure conditions.

Haselman et al. (2018) consisted of another LAGDA validation study that served multiple purposes. In addition to providing validation data, this study included more mechanistic endpoints to characterize effects of a chemical exhibiting an antiandrogenic mode of toxicity, the fungicide prochloraz. Haselman et al. (2015) is provided as a supporting publication which identifies a novel gene expression biomarker of normal testis development via microarray analysis in *Xenopus tropicalis* gonads. The relaxin family locus C type II (*rflcii*) gene in *Xenopus tropicalis* is orthologous to the human insulin-like 3 (*INSL3*) gene. *INSL3* had been shown to code for a Leydig cell specific protein and was being implemented as a biomarker of Leydig cell function in humans and rodents. As part of the prochloraz exposure, we implemented a gene expression measurement of the *Xenopus* ortholog, *rflcii*, to evaluate its utility as a biomarker of testis development and/or dysmorphogenesis. This was a novel application of this biomarker in a toxicological study using *Xenopus* and showed strong correlation with testis dysmorphogenesis caused by prochloraz exposure. Further, this study corroborated the finding in the previous LAGDA validation studies that oviducts are sensitive to hormonal alterations during development.

The two primary publications nominated here embody a significant amount of effort in the development and validation of the LAGDA guideline within our laboratory. Haselman et al. (2016b) is provided as a supporting publication because this study was run by a Japanese contract lab involved in the interlaboratory validation study and was published by us as a collaboration in support of globally harmonizing the test guideline. This study demonstrates the effectiveness of the LAGDA for characterizing the effects of chronic exposure to benzophenone-2, a chemical with multiple endocrine modes of action. The full extent of the LAGDA development and validation cannot be fully understood without considering the global efforts and collaborations highlighted by this publication.

Justification 2B:

The following four authors were co-authors on the same nomination in 2016, which included two publications in a single nomination that received Honorable Mention.

Jonathan Haselman; (1) In vitro, ex vivo, and in vivo determination of thyroid hormone modulating activity of benzothiazoles, (2) Inhibition of the thyroid hormone pathway in Xenopus laevis by 2-mercaptobenzothiazole; 2016; Honorable Mention

Patricia Kosian; (1) In vitro, ex vivo, and in vivo determination of thyroid hormone modulating activity of benzothiazoles, (2) Inhibition of the thyroid hormone pathway in Xenopus laevis by 2-mercaptobenzothiazole; 2016; Honorable Mention

Joseph Korte; (1) In vitro, ex vivo, and in vivo determination of thyroid hormone modulating activity of benzothiazoles, (2) Inhibition of the thyroid hormone pathway in Xenopus laevis by 2-mercaptobenzothiazole; 2016; Honorable Mention

Sigmund Degitz; (1) In vitro, ex vivo, and in vivo determination of thyroid hormone modulating activity of benzothiazoles, (2) Inhibition of the thyroid hormone pathway in Xenopus laevis by 2-mercaptobenzothiazole; 2016; Honorable Mention

Justification 2C:

The current nomination represents a completely different research effort. Specifically, this nomination encompasses the development and validation of a standardized, globally harmonized chronic toxicity test guideline needed by OCSPP for implementing policy. The 2016 nomination was focused on demonstrating a molecular pathway-based evaluation of benzothiazole thyroid toxicity using a series of experimental approaches including in vitro, ex vivo and short-term in vivo assays.

Justification 2D:

n/a

Justification 2E:

n/a

Justification 3A:

Recognition of this overall contribution from outside our division included Agency awards, an invitation to lead a short course at the Society of Environmental Toxicology and Chemistry national meeting, an invitation to write a book chapter and invitations to numerous U.S.-Japan Bilateral meetings to collaborate on global harmonization of endocrine disruptor testing methods. Additionally, we were invited to participate in the OECD Validation Management Group's review and adoption of the test guideline. The evidence of these activities and awards are listed below.

OECD (2015), Test No. 241: The Larval Amphibian Growth and Development Assay (LAGDA), OECD Guidelines for the Testing of Chemicals, Section 2, OECD Publishing, Paris, https://doi.org/10.1787/9789264242340-en.

U.S.-Japan Bilateral Collaboration on Ecotoxicity Assays for Endocrine Disruption Meeting. Washington DC. October 2013.

Bronze Medal for Commendable Service (2013) Office of Chemical Safety and Pollution Prevention. For significant accomplishments in development of Tier 2 test supporting EPA's science needs within the Endocrine Disruptor Screening Program (EDSP).

US-Japan Bilateral Collaboration on Ecotoxicity Assays for Endocrine Disruption 8th Meeting March 2012, Washington DC, USA.

Silver metal for Commendable Service (2011) Environmental Protection Agency. In recognition of exceptional leadership and meritorious service demonstrated in advancing the science of endocrine disruptors through translation and peer review of key topics related to screening and testing the universe of EDSP chemicals.

US-Japan Bilateral Collaboration on Ecotoxicity Assays for Endocrine Disruption 6th Meeting January 2010, Washington DC, USA.

US-Japan Bilateral Collaboration on Ecotoxicity Assays for Endocrine Disruption 5th Meeting. January 2009 Tokyo, Japan.

Ankley, G.T., G. Cripe, S.J. Degitz, M.L. Haasch, K.M. Jensen, R.D. Johnson, A.W. Olmstead, and J.E. Tietge. 2009. Chapter 4: Overview of USEPA tests with aquatic vertebrates for detecting and assessing endocrine disrupting chemicals. Endocrine Toxicology, Third Edition, Taylor & Francis, Boca Raton, FL, pp. 102-130.

US-Japan Bilateral Collaboration on Ecotoxicity Assays for Endocrine Disruption 4th Meeting. December 2008, San Fancisco CA, USA.

Short Course. *Endocrine Disruption Chemicals Tier I and Tier II Testing Protocols for Small Fish and Amphibians.* SETAC North America 29th Annual Meeting, November 16-17, 2008, Tampa, FL.

Justification 3B:

The peer review process for the nominated publications included standard peer review as directed by each of the journals. Each manuscript was reviewed by two anonymous external reviewers solicited by the journal editorial staff and/or their automated systems with the final decisions of acceptance made by either the Managing Editor or Editor-in-Chief.

An initial draft of the OCSPP 890.2300 guideline and associated interlaboratory validation studies were reviewed by a Scientific Advisory Panel (SAP) in June 2013 under the authority of the Federal Insecticide, Fungicide and Rodenticide Act. The panel consisted of members invited by EPA from academia, other U.S. governmental organizations and private industry. As part of the SAP review process, the draft 890.2300 guideline and integrated summary report (ISR) of the interlaboratory validation studies were posted on the public facing federal docket for additional public comment. Among these validation studies included in the ISR were the studies published and nominated here, so these studies have been uniquely externally peer reviewed multiple times at multiple levels and were even opened to the general public for review.

Toward the end of 2014 the test guideline was globally harmonized through further review by the Validation Management Group for Ecotoxicity Testing within the Organization for Economic Cooperation and Development (OECD). This process acted as yet another external review of the interlaboratory studies conducted to validate the test guideline. This review process resulted in the adoption of the test guideline and inclusion in their Guidelines for the Testing of Chemicals, which is described by the OECD as,

"*a collection of about 150 of the most relevant internationally agreed testing methods used by government, industry and independent laboratories to identify and characterise potential hazards of chemicals. They are a set of tools for professionals, used primarily in regulatory safety testing and subsequent chemical and chemical product notification, chemical registration and in chemical evaluation. They can also be used for the selection and ranking of candidate chemicals during the development of new chemicals and products and in toxicology research. This group of tests covers effects on biotic systems.*"

AUTHORS

Principal Author

Author Name:	Jonathan Haselman		
Professional Title:		Salutation:	
Email:	haselman.jon@epa.gov	Organization:	
Mailing Address:			
Street Line 1:	6201 Congdon Blvd.		
City:	Duluth		
Zip Code:	55804	State:	Minnesota
At time of research was:	EPA Employee		
Separation Date:			
% of Effort:	22		

Contributing Author

Author Name:	Allen Olmstead		
Professional Title:		Salutation:	Dr.
Email:	allen.olmstead@basf.com	Organization:	
Mailing Address:			
Street Line 1:			
City:			
Zip Code:		State:	
At time of research was:	Non EPA Personnel		

Separation Date:			
% of Effort:	22		

Contributing Author

Author Name:	Rodney Johnson		
Professional Title:		Salutation:	Dr.
Email:	julnrod@gmail.com	Organization:	
Mailing Address:			
Street Line 1:			
City:			
Zip Code:		State:	
At time of research was:	EPA Employee		
Separation Date:			
% of Effort:	5		

Contributing Author

Author Name:	Sigmund Degitz		
Professional Title:		Salutation:	Dr.
Email:	degitz.sigmund@epa.gov	Organization:	
Mailing Address:			
Street Line 1:	6201 Congdon Blvd.		
City:	Duluth		
Zip Code:	55804	State:	Minnesota
At time of research was:	EPA Employee		

Separation Date:		
% of Effort:	22	

Contributing Author

Author Name:	Joseph Korte	
Professional Title:		Salutation:
Email:	jkorte@charter.net	Organization:
Mailing Address:		
Street Line 1:		
City:		
Zip Code:		State:
At time of research was:	EPA Employee	
Separation Date:	Fri Apr 26 00:00:00 GMT 2019	
% of Effort:	12	

Contributing Author

Author Name:	Patricia Kosian	
Professional Title:		Salutation:
Email:	2patriciakosian@gmail.com	Organization:
Mailing Address:		
Street Line 1:		
City:		
Zip Code:		State:
At time of research was:	EPA Employee	

Separation Date:	Fri Feb 28 00:00:00 GMT 2020
% of Effort:	12

Contributing Author

Author Name:	Taisen Iguchi		
Professional Title:		Salutation:	Dr.
Email:	taiseni@hotmail.co.jp	Organization:	
Mailing Address:			
Street Line 1:			
City:			
Zip Code:		State:	
At time of research was:	Non EPA Personnel		
Separation Date:			
% of Effort:	5		

PUBLICATIONS

Publication 1:

Publication Title:	Development of the Larval Amphibian Growth and Development Assay: effects of chronic 4tertoctylphe		
Publication Date:	Mon May 23 00:00:00 GMT 2016		
Journal/Publication Method:	Journal of Applied Toxicology		
All Author(s):			
Volume:	36	Number:	12
		Immediately	Immediately

Pages:	1639-1650	Index:	Index:
Citation ½ Life:	6.4	Impact Factor:	3.065

Publication 2:

Publication Title:	Effects of multiple life stage exposure to the fungicide prochloraz in Xenopus laevis: Manifestation
Publication Date:	Tue Apr 03 00:00:00 GMT 2018
Journal/Publication Method:	Aquatic Toxicology
All Author(s):	

Volume:	199	Number:	n/a
Pages:	240-251	Immediately Index:	Immediately Index:
Citation ½ Life:	7.6	Impact Factor:	3.794

Research article

Journal of Applied Toxicology

Received: 16 November 2015, Revised: 25 February 2016, Accepted: 14 March 2016 Published online in Wiley Online Library: 3 May 2016

(wileyonlinelibrary.com) DOI 10.1002/jat.3330

Development of the Larval Amphibian Growth and Development Assay: effects of chronic 4-*tert*-octylphenol or 17β-trenbolone exposure in *Xenopus laevis* from embryo to juvenile

Jonathan T. Haselman[a]*, Patricia A. Kosian[a], Joseph J. Korte[a], Allen W. Olmstead[a], Taisen Iguchi[b], Rodney D. Johnson[a] and Sigmund J. Degitz[a]

ABSTRACT: The Larval Amphibian Growth and Development Assay (LAGDA) is a globally harmonized test guideline developed by the U.S. Environmental Protection Agency in collaboration with Japan's Ministry of the Environment. The LAGDA was designed to evaluate apical effects of chronic chemical exposure on growth, thyroid-mediated amphibian metamorphosis and reproductive development. During the validation phase, two well-characterized endocrine-disrupting chemicals were tested to evaluate the performance of the initial assay design: xenoestrogen 4-*tert*-octylphenol (*t*OP) and xenoandrogen 17β-trenbolone (TB). *Xenopus laevis* embryos were exposed, in flow-through conditions, to *t*OP (nominal concentrations: 0.0, 6.25, 12.5, 25 and 50 μg l^{-1}) or TB (nominal concentrations: 0.0, 12.5, 25, 50 and 100 ng l^{-1}) until 8 weeks post-metamorphosis, at which time growth measurements were taken, and histopathology assessments were made of the gonads, reproductive ducts, liver and kidneys. There were no effects on growth in either study and no signs of overt toxicity, sex reversal or gonad dysgenesis. Exposure to *t*OP caused a treatment-related decrease in circulating thyroxine and an increase in thyroid follicular cell hypertrophy and hyperplasia (25 and 50 μg l^{-1}) during metamorphosis. Müllerian duct development was affected after exposure to both chemicals; *t*OP exposure caused dose-dependent maturation of oviducts in both male and female frogs, whereas TB exposure caused accelerated Müllerian duct regression in males and complete regression in >50% of the females in the 100 ng l^{-1} treatment. Based on these results, the LAGDA performed adequately to evaluate apical effects of chronic exposure to two endocrine-active compounds and is the first standardized amphibian multiple life stage toxicity test to date. Published 2016. This article is a U.S. Government work and is in the public domain in the USA.

Additional supporting information may be found in the online version of this article at the publisher's web-site.

Keywords: *Xenopus laevis*; 17β-trenbolone; 4-*tert*-octylphenol; OECD Test 241; OCSPP 890.2300; thyroid; reproductive development; endocrine-disrupting chemicals

Introduction

The 1996 U.S. Food Quality Protection Act and an amendment to the Safe Drinking Water Act mandate the U.S. EPA to develop a screening program to determine whether certain substances have the potential to interact with human endocrine systems causing adverse hormonal effects. The EPA responded to this legislation by chartering the Endocrine Disruptor Screening and Testing Advisory Committee (EDSTAC) made up of representative scientists who recommended a tiered approach to endocrine disruptor testing that addresses effects in both humans and wildlife. EDSTAC also recommended that screening and testing should include estrogen-, androgen- and thyroid-related processes. The U.S. EPA's Endocrine Disruptor Screening Program (EDSP) has been actively developing assays to identify endocrine-disrupting chemicals (EDC) using the recommended tiered approach (EDSP Website). Tier 1 screening assays are designed to identify whether a chemical will interact with some aspect of the endocrine system. Early in 2015, EPA released Tier 1 screening results for 52 pesticide chemicals, of which a subset have been recommended for Tier 2 testing (US EPA, 2015a). Tier 2 tests are designed to assess Tier 1-active chemicals for endocrine-related effects *in vivo* and generate concentration-response information suitable for ecological risk assessment. Japan's Ministry of the Environment uses a similar approach to chemical testing and risk assessment (MOE, 2010) and collaborated with the U.S. EPA over the last decade to develop a standardized multiple life stage toxicity test guideline for amphibians. The Larval Amphibian Growth and Development Assay (LAGDA) guideline has been globally harmonized and recently adopted by the Organization for Economic Cooperation and Development

*Correspondence to: Jonathan T. Haselman, US EPA Mid-Continent Ecology Division, 6201 Congdon Blvd, Duluth, MN, 55804, USA.
E-mail: haselman.jon@epa.gov

[a]US EPA Mid-Continent Ecology Division, 6201 Congdon Blvd, Duluth, MN 55804, USA

[b]Okazaki Institute for Integrative Bioscience, National Institute for Basic Biology, National Institutes of Natural Sciences, 5-1 Higashiyama, Myodaiji, Okazaki, Aichi 444-8787, Japan

 Published 2016. This article is a U.S. Government work and is in the public domain in the USA.

(OECD, 2015) under Level 4 of their conceptual framework on endocrine-disruptor testing and assessment (OECD, 2012). The U.S. EPA has also published the test guideline under their EDSP 890 series of harmonized test guidelines (US EPA, 2015b). The work described herein contributed to the basis for the current assay design and methodology.

The LAGDA is a chronic toxicity testing procedure with an amphibian model that considers growth and development from shortly after fertilization through the early juvenile period. Specifically, the assay involves a water-borne exposure of early life stage *Xenopus laevis* embryos with the continuation of exposure until approximately 2 months after completion of metamorphosis, when the gonads are fully differentiated in control organisms. This design enables the collection of hormone-regulated endpoint data (e.g. metamorphosis, gonadal development) and information concerning various aspects of the reproductive biology and life stage viability. The suite of endpoints assessed throughout the assay are intended to characterize adverse apical outcomes of chronic exposure to endocrine disruptors or other types of developmental and reproductive toxicants.

As metamorphosis is a thyroid hormone-mediated process, developmental assessments at the pro-metamorphic Nieuwkoop and Faber (NF; 1994) stage 62, including growth, circulating thyroxine and thyroid gland histopathology, allow the assay to identify perturbations to the hypothalamic–pituitary thyroid (HPT) axis. Continuation of the assay post-metamorphosis allows further evaluations of growth and reproductive organ development to help identify a substance's potential to cause gonad dysgenesis or adverse effects on reproductive ducts. Histopathological assessments of liver and kidney are also made at test termination as measures of metabolic or overt toxicity. As an initial step towards evaluating this test protocol, the assay was performed using two well-characterized model chemicals representing two different modes of action within the hypothalamus–pituitary–gonadal (HPG) axis: 17β-trenbolone (TB), an androgen receptor agonist and 4-*tert*-octylphenol (*t*OP), an estrogen receptor agonist. The goal of this work was to test well-characterized endocrine disruptors as a means to evaluate the proposed assay's effectiveness for characterizing adverse apical outcomes after chronic exposure in an amphibian model.

Trenbolone acetate is a growth promoter used in cattle production and the excreted metabolite, 17β-trenbolone, has been measured in aquatic systems near concentrated animal-feeding operations (CAFOs) (Durhan *et al.*, 2006). The effects of TB exposure in aquatic life have been studied with respect to those physiological processes regulated via the HPG axis including gonad differentiation and development in fish and amphibian species (Orn *et al.*, 2006; Holbech *et al.*, 2006; Morthorst *et al.*, 2010; Olmstead *et al.*, 2012). TB has been tested previously in the closely related amphibian species *X. tropicalis* (Olmstead *et al.*, 2012). In that study, the authors characterized the effects of aqueous exposure to TB during larval *X. tropicalis* development using an exposure protocol similar to the one described herein. Concentrations $\geq 100\ ng\ l^{-1}$ resulted in a spectrum of androgenic responses which included hypertrophy of the larynx resulting in late larval mortality, development of nuptial pads, a mixed-sex phenotype in the ovaries of females and hypertrophy of the Wolffian ducts.

4-*tert*-Octylphenol is a degradation product of octylphenol polyethoxylate which is used as a non-ionic surfactant in industrial and household settings (Ahel *et al.*, 1994; Ying *et al.*, 2002) and has been shown to interact with the estrogen receptor in reporter cell lines, transactivation assays (Routledge and Sumpter, 1997; Kuiper *et al.*, 1998; Paris *et al.*, 2002) and trout primary hepatocytes (Jobling and Sumpter, 1993). Vitellogenin (Vtg), an estrogen-responsive biomarker, has been shown to be elevated in male zebrafish (Ortiz-Zarragoitia and Cajaraville, 2005), male eelpout (Rasmussen *et al.*, 2005), male and female medaka (Seki *et al.*, 2003) and in *X. laevis* primary cultured hepatocytes (Mitsui *et al.*, 2007) exposed to *t*OP. Additionally, exposure to *t*OP has been shown to cause decreased sperm count and the presence of testis-ova in medaka (Seki *et al.* 2003), decreased the gonadosomatic index and increased testis-ova in eelpout (Rasmussen *et al.*, 2005), decreased spermatozoa and increased testis anomalies in male sheepshead minnows (Karels *et al.*, 2003) and decreased percent of viable eggs in female sheepshead minnows (Karels *et al.*, 2003). Kloas *et al.* (1999) reported that exposure of larval *X. laevis* to 4-octylphenol resulted in a significant shift in the sex ratio towards females. However, when Porter *et al.* (2011) exposed *X. tropicalis* to *t*OP, sex ratios were unaffected, but significant induction of Vtg and advanced oviduct development in adult males were reported. Based on these previously published studies, *t*OP was used as a representative environmental estrogen and TB was used as a representative environmental androgen for evaluating the utility of the initial test design.

Materials and methods

Experimental design

Xenopus laevis embryos (≤ NF stage 15) were exposed to four different chemical concentrations and control water in each separate study until 10 weeks after the median time to NF stage 62 in the control (See Nieuwkoop and Faber, 1994 for staging details). For each study, there were five replicate tanks in each test concentration with eight replicate tanks for the control ($n = 26$ organisms/tank). Interim sub-samples ($n = 5$ per replicate tank) were collected at NF62 to assess growth, somatic development, circulating thyroxine and thyroid histopathology. Other endpoints evaluated during exposure included those indicative of generalized and metabolic toxicity: mortality, abnormal behavior, growth determinations (length and weight) and histopathology of the juvenile liver and kidney at test termination. Also, endpoints indicative of impacts on the HPG axis were evaluated including juvenile plasma Vtg and histopathology of the gonads and reproductive ducts. Genotypic/phenotypic sex ratios were also evaluated.

Test concentrations

Test concentrations were chosen to perturb the endocrine system and cause measurable effects on organ morphology and levels of endocrine-mediated biochemical indicators. Given the observed mortality in the studies of Olmstead *et al.* (2012), the highest target test concentration for TB was set at $100\ ng\ l^{-1}$ with a 0.5 dilution factor resulting in nominal test concentrations of 100, 50, 25 and $12.5\ ng\ l^{-1}$. In the case of *t*OP, test concentrations were set based on earlier collaborative studies performed by Porter *et al.* (2011) with *X. tropicalis*. From their short-term range-finding exposure, it was found that concentrations above $60\ \mu g\ l^{-1}$ resulted in significant mortality in embryos and early stage larvae (unpublished data). Therefore, the high test concentration was set at $50\ \mu g\ l^{-1}$ with a 0.5 dilution factor resulting in nominal test concentrations of 50, 25, 12.5 and $6.25\ \mu g\ l^{-1}$.

Published 2016. This article is a U.S. Government work and is in the public domain in the USA.

Journal of Applied Toxicology

Table 1. The mean (± SD) of all water quality measurements throughout the exposures

Study	Temperature (°C)	D.O. (% sat.)	pH	Alkalinity (mg l^{-1} $CaCO_3$)	Hardness (mg l^{-1} CaCO3)	Conductivity (μS)
17β-trenbolone	21.1 ± 0.4	63.0 ± 14.9	7.34 ± 0.20	47.4 ± 0.9	44.6 ± 1.1	111 ± 5
4-*tert*-octylphenol	21.1 ± 0.2	80.8 ± 4.8	7.64 ± 0.09	47.4 ± 0.7	47.3 ± 0.7	107 ± 1

The means and standard deviations include all replicate tanks throughout all treatments and control within each study.

Environmental conditions

Organisms were cultured in Lake Superior Water (LSW) initially filtered through sand, UV sterilized and filtered again to 5 μm before entering the in-house culture or exposure aquaria. Larvae were held at 21 °C throughout the duration of the exposure. Dissolved oxygen, pH and conductivity were measured in all-exposure tanks once per week throughout the duration of each test whereas alkalinity and hardness were measured once per month in one replicate tank per treatment (Table 1). There were no treatment-related effects on any water quality parameters, so Table 1 represents all measurements across all treatments and control within each study. A 12:12 light:dark cycle was used with fluorescent lighting at intensities between 600 and 2000 lux (lumens/m^2) at the water surface. Exposure tanks were randomly assigned to positions within each exposure system.

Exposure systems

For the TB study, a flow-through electronically controlled dilution system consisted of four metering pumps (Fluid Metering Inc., Syosset, NY, USA) that each pressurized a single manifold equipped with 12 solenoid valves. Two manifolds were supplied with LSW that had a subset of channels assigned to control tanks whereas the other two manifolds were supplied with toxicant concentrations of 100 and 25 ng l^{-1} TB. Systematic pairing of manifold channels and calibration of solenoid firing times allowed real-time formulation of the 50 and 12.5 ng l^{-1} concentrations upon delivery to the tanks. The flow rate of all treatments and controls provided nine tank turnovers per day to 4-l tanks. Wetted surfaces were strictly glass, Teflon® or stainless steel. All biomass, flow rates and water quality were essentially the same across all treatment and control tanks except the TB concentrations and slight variation in the number of individuals per tank owing to inherent hatch and mortality rates throughout the test period.

For the *t*OP study, a different exposure system was used because of laboratory logistics. The dilution system consisted of a series of single drive/dual head metering pumps (Fluid Metering Inc., Syosset, NY, USA) through which both diluent and toxicant flowed to make a single concentration in a stainless steel mixing cell. Flow-through conditions were maintained by delivering toxicant and control LSW solutions with multichannel peristaltic pumps to achieve 9.5 tank turnovers per day in 6.5-l tanks. Wetted surfaces were strictly glass, Teflon®, Pharmed® tubing, or stainless steel. All biomass, flow rates and water quality were essentially the same across all treatment and control tanks except the *t*OP concentrations and slight variation in the number of individuals per tank owing to inherent hatch and mortality rates throughout the test period.

To reduce chemical degradation by biofilms on the wetted surfaces of the test systems, prophylaxis treatments were performed at least every 3 weeks by sterilizing the wetted surfaces with a 2% solution of Minncare® Cold Sterilant, which consists of hydrogen peroxide and peroxyacetic acid (Mar Cor Purification, Plymouth, MN, USA). Also, animals were transferred to clean tanks on the same schedule to avoid biofilm overgrowth within the tanks.

Chemical stock preparation

17β-Trenbolone

A 2.5 mg ml^{-1} super stock was prepared by adding the neat material (Sigma-Aldrich, St. Louis, MO, USA, CAS 10161-33-8; purity ≥ 93%) to 100% ethanol. Aliquots of the super stock were prepared in air-tight liquid chromatography vials and stored at –20°C until stock preparation. To prepare the weekly stock, a 200-μl aliquot of the super stock was allowed to warm to room temperature and 114 μl was added to approximately 5 ml of high-purity acetone. The solution was mixed and quantitatively transferred to a 1-l glass bottle. The side walls of the bottle were rinsed with acetone, and it was carefully tipped onto its side and placed on a roller. Filtered and desiccated compressed air was gently blown into the bottle as it was rolled to evaporate the acetone and 'shell coat' the bottle with TB. Once the acetone was completely evaporated, the bottle was filled with reverse osmosis (RO) water and stirred overnight to dissolve. The concentrated 1-l stock was quantitatively transferred to a 19-l carboy and diluted with RO water to 15 μg l^{-1}.

4-*tert*-Octylphenol

As a result of the low solubility of *t*OP in water, saturator columns were constructed according to methods described by Kahl *et al.* (1999) to produce chemical stocks. Briefly, 1.2-m medium walled glass tubing (Kimble 80400, 25 mm o.d., 0.24 cm walls) was thoroughly cleaned and bent into a 'U' shape using a torch. Each leg was packed firmly with Pyrex® 3950 glass wool using an unbreakable rod. The glass wool columns were cleaned by flushing three pulses of 150 ml high purity acetone using positive and negative air pressure generated by a motorized pump. The clean columns were allowed to dry completely overnight under vacuum. To load chemical onto the columns, 5 g of *t*OP (CAS 140-66-9; purity 97%; Sigma-Aldrich) was dissolved in 150 ml of high purity acetone and half was used to coat each leg of the column. Next, 75 ml was poured into one leg while a vacuum was applied to the other leg. When the chemical solution interface reached the bottom of the leg, the vacuum was switched to draw the solution back up for even coating. After the acetone was evaporated, the other leg was coated using the same technique. Coated columns were then dried overnight under vacuum. Before columns were used to generate stocks, they were flushed at 40 ml min^{-1} for 8–12 h with RO water. Stocks were generated at 4 ml min^{-1} using RO

Published 2016. This article is a U.S. Government work and is in the public domain in the USA.

water and were measured to confirm concentrations of approximately 11 mg l^{-1} before being delivered to the test system.

Test initiation

Adult in-house breeding pairs were induced to spawn by injection of 750 IU human chorionic gonadotropin (hCG) (CAS 9002-61-3; Sigma-Aldrich) into the dorsal lymph sac of each male and female and were allowed to enter amplexus in static 10-l tanks filled with 6 l of culture water. Eggs were collected, and jelly coats were removed by L-cysteine treatment approximately 14–16 h after pairing. A 2% L-cysteine solution was prepared and pH adjusted to 8.1 with 1 N NaOH. This 21 °C solution was added to a 500-ml Erlenmeyer flask containing the eggs from a single spawn and swirled gently for 1–2 min and then rinsed thoroughly 6–8 times with 21 °C culture water. The spawn was transferred to a crystallizing dish and determined to be > 70% viable with minimal abnormalities in embryos exhibiting cell division. Embryos were carefully screened for any cellular or superficial abnormalities and then NF stage 10 through NF stage 15 embryos were distributed evenly into each of 28 glass beakers (250 ml) containing approximately 20 ml of culture water. Each beaker contained 26 embryos to be added to each exposure tank. Initiation of exposure occurred no later than NF stage 15. At test initiation, beakers containing the embryos were carefully submerged in the exposure tank solution and set on the bottom of the tank. This technique kept the embryos localized within the beaker until they were able to swim out into the tank on their own and allowed for simple observations of embryonic development. The beakers were positioned directly under the test solution delivery line to facilitate solution renewal and flow through the beaker. When all of the organisms had left the beakers, the beakers were removed from the exposure tanks. Observations of arrested embryonic development were recorded before hatch; mortality and abnormal behavior was recorded daily throughout the duration of the exposures.

Feeding

Tadpoles were fed a liquid diet three times per day on weekdays and once per day on weekends starting on day 4 post-fertilization. The diet consisted of Silver Cup Trout Starter (Nelson and Sons, Murray, UT, USA), *Spirulina* algae discs (Wardley, Secaucus, NJ, USA) and TetraFin® flakes (Tetra Sales, Blacksburg, VA, USA) blended in culture water. Tadpoles were also fed 24-h-old live brine shrimp (Bio-Marine® Brand; Bio-Marine, Hawthorne, CA, USA) twice daily on weekdays and once daily on the weekends starting on day 8 post-fertilization. Feeding was increased weekly until the majority of individuals in any given tank developed to NF stage 62, at which time food was systematically decreased based on a number of individuals still filter feeding (<NF62). When individuals completed metamorphosis (NF66), the diet was changed to 3/32″ premium sinking frog food pellets (Xenopus Express, Plant City, FL, USA) for the duration of the test.

Larval sub-sampling

Larval NF stage 62 sub-sampling was performed by dividing the exposure tank and separating individuals that reached NF62 from individuals < NF62 and recording the day on which each individual reached NF62. For measurements of weight, snout-to-vent length, serum thyroxine levels and thyroid histopathology, one out of each group of five consecutive individuals reaching NF62 in any given tank was randomly sampled (total sample: $n = 5$). For example, of the first five tadpoles in a particular replicate tank to reach NF62, one was randomly chosen (*a priori*) to be sampled. Blocking each consecutive five tadpoles reaching NF62 and randomly choosing one for sampling (*a priori*) was repeated until all individuals in the tank had reached NF62. The remaining larvae that had all developed past NF62 remained in the tank for continued exposure.

Sub-sampled tadpoles were euthanized by submersion in 200 mg l^{-1} tricaine methanesulfonate (MS-222; Argent Chemical Laboratories, Redmond, WA, USA) buffered with 400 mg l^{-1} sodium bicarbonate. Blood was immediately collected by exposing the heart, severing the aorta and allowing the pumping heart to fill a 25-µl non-heparinized capillary tube. Blood was allowed to clot on ice for approximately 4 h, centrifuged to separate the serum from the clot, and the serum was transferred to individual vials and stored at –80 °C until further analyses. After blood collection, a transverse cut was made at the posterior margin of the arms for decapitation, and the head was fixed in Davidson's solution for thyroid histopathology. Individuals not sampled were left in the divided tank until all individuals had reached NF62 or test day 70, at which time the tank dividers were removed, and any larvae that had not reached NF62 were documented and euthanized by immersion in MS-222.

Cull

Two to three weeks after all individuals completed metamorphosis (NF66), a cull was performed to reduce the tank density and resulted in five males and five females remaining in each tank until test termination (*t*OP resulted in four males and four females). Toe clips were taken from every individual in a manner where they could be uniquely identified based on tank ID and toe clip scheme. These toe clips were analyzed for the presence or absence of a W chromosome-linked gene, DM-W, to determine genetic sex (described in the section below). Equal numbers of males and females were randomly selected to remain in each replicate tank, and all other juveniles were euthanized by submersion in 500 mg l^{-1} MS-222 buffered with sodium bicarbonate.

Juvenile sampling (test termination)

The studies were terminated 10 weeks after the median time to NF62 in controls (i.e. approximately 8 weeks post-metamorphosis in controls). Endpoints were collected on all juveniles immediately after euthanasia by intraperitoneal injection of buffered MS-222. Juveniles were weighed and measured for snout-to-vent length; then the chest was opened to expose the heart for blood collection. The aorta was severed and blood was collected into a heparinized capillary tube (~50 µl). The heparinized blood was expelled into a microcentrifuge tube coated with aprotinin and placed on ice until centrifugation to separate the red blood cells from the plasma. Plasma was transferred to a new vial and stored at –80 °C until further analyses. After blood collection, the abdomen was opened and the liver was carefully removed intact, weighed, placed in a labeled cassette and transferred into Davidson's fixative. Subsequently, the remaining internal viscera was removed and discarded with care to leave the gonads, kidneys and reproductive ducts undamaged and *in situ* for fixation. Gonad phenotype was recorded, and a foot was removed and frozen for genetic sex determination. The torsos containing gonads, kidneys

Published 2016. This article is a U.S. Government work and is in the public domain in the USA.

Journal of AppliedToxicology

and reproductive ducts were placed in individually labeled cassettes and transferred to Davidson's fixative.

Histological procedures

All tissues preserved for histological analyses were fixed in Davidson's fluid for 48 h and then processed into paraffin for H&E staining and sectioning. Histopathologic findings were scored for severity according to the following grading system: NR = not remarkable, Grade 1 = minimal (less than 10% of tissue affected), Grade 2 = mild/slight (≥10% but less than 40% of tissue affected), Grade 3 = moderate (≥40% but less than 80% of tissue affected) and Grade 4 = severe (≥80% of tissue affected).

The larval thyroid glands were step sectioned transversely from caudal to rostral at approximately 50-μm intervals. Two step-sections containing bilateral gland tissue were obtained per larval sample. Both left and right glands of the selected sections were evaluated for pathology by brightfield microscopy according to previously reported criteria (Grim *et al*., 2009).

The juvenile livers were embedded in their entirety, and 200-μm step sections were taken until the largest possible cross-sectional area was reached, at which time two sections were evaluated.

The juvenile gonad, kidney and reproductive ducts were left *in situ* and were processed, sectioned and evaluated within the same sections. Torsos were trimmed transversely first at the anterior and posterior margins of the gonads, then the gonads were measured on the anterior–posterior axis and bisected transversely in the exact middle to yield two equally sized sections – one anterior and one posterior. Each section was embedded in a separate mold to efficiently obtain sections representative of the anterior, middle and posterior regions of the gonad. One section from each region was scored for pathologies and the most severe score from any of the three sections was used for subsequent analyses. This was done given the precedent that *X. tropicalis* gonads differentiate and mature along an anterior–posterior gradient (El Jamil *et al*., 2008) and that different regions could be affected differently by chemical exposure during differentiation.

Genetic sexing

A hind limb was kept from each individual and frozen at −20 °C until DNA could be isolated using DNeasy kits (Qiagen, Valencia, CA, USA) according to manufacturer's instructions. Testing for the presence or absence of the *X. laevis* W-linked marker (DM-W) was performed by PCR based on the method described by Yoshimoto *et al*. (2008). DMRT1 was also amplified in duplexed PCR reactions as a reference gene.

Serum thyroxine

Serum thyroxine (T4) was measured using the high-performance liquid chromatography with inductively coupled plasma mass spectrometry (HPLC/ICP-MS) method previously described by Tietge *et al*. (2010). Equal amounts of serum from five larvae per tank were pooled and diluted 1:10 with mobile phase before analysis. After HPLC/ICP-MS analysis, all remaining serum (from between 2 and 5 larvae) was pooled by replicate tank and another more transferrable method, enzyme-linked immunosorbent assay (ELISA), was used to evaluate the level of consistency between the two methods despite the differing pooling techniques. Each method analyzed slightly different numbers of sample pools per treatment owing to serum availability (see Fig. 1 for details). A

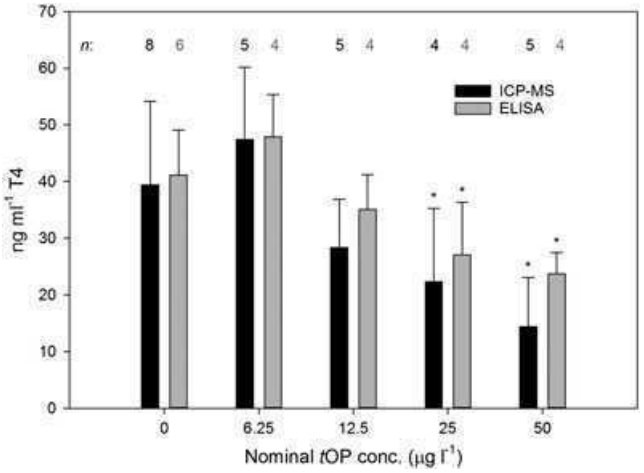

Figure 1. The mean serum T4 concentrations in NF62 tadpoles after exposure to xenoestrogen 4-*tert*-octylphenol (*t*OP) determined by high-performance liquid chromatography with inductively coupled plasma mass spectrometry (HPLC/ICP-MS) or enzyme-linked immunosorbent assay (ELISA) methods (error bars: ± 1 SD). Measurements and statistical results were in agreement between methods. Asterisks (*) indicate treatments that were statistically different than the control at $P < 0.05$ (Jonckheere–Terpstra). Statistical tests were run on data from each method independently. The corresponding number (*n*) of sample pools (by replicate tank independent of gender) are aligned across the top of the graph.

commercially available ELISA kit designed for measuring T4 in human serum (MP Biomedicals, Santa Ana, CA, USA, Cat # 07BC1007) was adapted for use in *X. laevis*. The kit instructions were followed with three exceptions: (i) a stock T4 standard at 154 μg ml^{-1} was prepared in 0.05 M Na_2CO_3 and subsequently diluted to desired concentrations (2.5 to 100 ng ml^{-1}) in Tris-methanol buffer (0.1 M Tris-Cl, pH 7.3, 1% methanol) and underwent the same extraction process as the samples to avoid matrix effects; (ii) T4 was liberated from binding proteins in samples using an ethanol extraction; and (iii) samples/standards were combined with T4-HRP conjugate before loading onto the ELISA plate. For deproteination of T4, 180 μl of 95 % ethanol was added to 60 μl of serum or serum diluted in Tris-methanol buffer. This solution was mixed several times by vortexing within a 10-min period then centrifuged for 10 min at 20 000 *g*. The supernatant was transferred to a different tube, and another 180 μl of ethanol was added to the remaining pellet for a second extraction. The second extraction was centrifuged for 5 min at 20 000 *g* and the supernatant was combined with the first extraction supernatant. The combined extracts were brought to dryness in a vacuum centrifuge concentrator, thoroughly resuspended in 60 μl of Tris-methanol buffer and then centrifuged for 10 min at 20 000 *g*. A 55-μl aliquot of the supernatant was transferred to a new tube, and 220 μl of diluted T4-conjugate was added. From this, a 125 μl aliquot was added to duplicate wells of the ELISA plate.

Plasma Vtg ELISA

Plasma Vtg was measured in juveniles from the *t*OP study using a competitive ELISA. The method was essentially the same as one previously described for use in *X. tropicalis* (Olmstead *et al*., 2009a), except that purified *X. laevis* Vtg was used as a standard and for coating the plates. The purified Vtg was prepared from

Published 2016. This article is a U.S. Government work and is in the public domain in the USA.

plasma collected from adult frogs fed 17α-ethinyl estradiol-coated food for approximately 2 weeks. Using standard concentrations of *X. laevis* Vtg from 12 760 to 50 ng ml^{-1}, standard curves were obtained that closely resembled the range of binding seen in the *X. tropicalis* ELISA. Plasma samples were diluted 1:30 in assay buffer before being assayed.

Exposure verification

17β-Trenbolone

Weekly water samples (50 to 110 ml) were collected from the TB exposure tanks (0, 12.5, 25, 50 and 100 ng l^{-1}), placed into clean amber bottles and immediately processed through solid phase extraction (SPE) columns using a Gilson GX-271 Liquid Handler (Gilson Incorporated, Middleton, WI, USA). Briefly, 3 -ml (200 mg) Strata X C-18 SPE columns (Phenomenex, Torrance, CA, USA) were pre-cleaned with 4 ml of acetonitrile, activated with 10 ml of methanol and then equilibrated with 10 ml of Burdick & Jackson (B&J) HPLC grade water. Water samples (15, 25, 50 or 100 ml) were processed through the columns at 5 ml min^{-1}. After sample addition, the columns were rinsed with 2 ml of water and then dried using a 3-ml air push. TB was eluted from the columns with 4 ml of methanol at 2.5 ml min^{-1}. Residual methanol was removed from the columns using a 3-ml air push. The eluates were collected in clean glass culture tubes and then placed in the refrigerator overnight. The next day the eluates were evaporated to dryness using nitrogen and a heated water bath (40 °C). During the evaporation process, the inside of the culture tubes were rinsed with methanol. Upon reaching dryness the culture tubes were immediately removed from the water bath and allowed to reach room temperature. The residue was reconstituted to 1.0 or 1.25 ml with 10% methanol and 90% B&J water and then vortexed to mix. The reconstituted extracts were immediately analyzed for TB concentrations. Quality assurance samples were conducted with each SPE sample set and consisted of an LSW blank, duplicate samples and matrix-spiked samples at each of the TB treatment levels.

TB concentrations were determined by reverse phase liquid chromatography-tandem mass spectrometry (LC-MS/MS). Aliquots of the SPE reconstituted extracts were placed into amber HPLC vials. An internal standard (allyl trenbolone, CAS 850-52-2) was added to each vial. The samples were then analyzed using an Agilent 1200 HPLC with a 6410 triple quadrupole mass spectrometer (LC-MS/MS). Next, 50 µl of sample was injected into an Agilent Zorbax Extend C-18 column (3.5-µ particle, 2.1 × 100 mm) that was maintained at 30 °C. The column was eluted under isocratic conditions (31%A:69%B) at a flow rate of 0.2 ml min^{-1}. Mobile phase A consisted of 2% ethanol:2% methanol:96% ammonium acetate (2.5 mM) containing 0.01% ammonium hydroxide. Mobile phase B consisted of 2% ethanol:96% methanol:2% ammonium acetate (2.5 mM) containing 0.01% ammonium hydroxide. The HPLC effluent was introduced into the mass spectrometer using electrospray ionization (ESI) in the positive mode. Nitrogen was used as nebulizing and collision gas and was obtained from a nitrogen generator. The source parameters were set at 350 °C (gas temperature), 10 l min^{-1} (gas flow), 30 psi (nebulizer pressure) and 1700 V (capillary voltage). Multiple reaction monitoring (MRM) was used during the MS/MS analysis of TB and the internal standard allyl trenbolone. The optimized MRM parameters for TB were collision energy (20 V), fragmentor (150 V), precursor ion (271 m/z), quantifier ion (199 m/z) and qualifier ion (157 m/z). The optimized MRM parameters for allyl trenbolone were collision energy (22 V), fragmentor (150 V), precursor ion (311 m/z), quantifier ion (227 m/z) and qualifier ion (199 m/z). Concentrations of TB were determined by the internal standard method of quantification using Agilent Mass Hunter software.

For the exposure water samples, the mean ± SD (n = 40) measured concentrations of the 12.5, 25, 50 and 100 ng l^{-1} TB treatments were 9.0 ± 2.8, 19.2 ± 5.8, 41.4 ± 9.7 and 79.9 ± 24.1 ng l^{-1}, respectively, over the duration of the experiment. Among-tank variability was ≤ 32% with the coefficient of variation (averaged over the duration of the exposure) of 31.4, 29.9, 23.3 and 30.2%, respectively, for the 12.5, 25, 50 and 100 ng l^{-1} treatments. No TB was detected in the control water treatments. For quality control samples, no TB was detected in the Lake Superior water blanks (n = 16). The mean ± SD (n = 16) recoveries of spiked samples were 64.5 ± 6.5%, 77.3 ± 6.1%, 81.4 ± 7.6% and 84.8 ± 4.0% at the 12.5, 25, 50 and 100 ng l^{-1} spiked levels, respectively. The mean ± SD agreement among duplicate samples were 98.7 ± 7.4% (n = 16), 101.7 ± 4.1% (n = 7), 102.4 ± 7% (n = 8) and 98.8 ± 5% (n = 15) for the 12.5, 25, 50 and 100 ng l^{-1} treatments, respectively. The method limit of quantification was 1.5 ng l^{-1}.

4-*tert*-Octylphenol

Water samples (1 ml) were collected weekly from the *t*OP exposure tanks (0, 6.25, 12.5, 25 and 50 µg l^{-1}) and placed into amber sample vials. The water samples were amended with 0.25 ml of acetonitrile, vortexed to mix and immediately analyzed using an Agilent 1260 series high-performance liquid chromatograph (HPLC) with diode array detection (λ = 194 nm). An aliquot (75 µl) of sample was injected directly into a Poroshell 120 EC-C18, 2.7 µm particle, 3 × 50 mm column (Agilent, Wilmington, DE, USA, PN# 699975-302) that was maintained at 23 °C. *t*OP eluted from the column under isocratic conditions with 20% Burdick & Jackson (B&J) HPLC grade water and 80% acetonitrile at 0.5 ml min^{-1}. Concentrations of *t*OP were determined by the external standard method of quantification using linear regression. Calibration standards ranged from 2.54 to 101.7 µg l^{-1} and were prepared in 75% B&J water and 25% acetonitrile.

For the exposure water samples, the mean ± SD measured concentrations of the 6.25, 12.5, 25 and 50 µg l^{-1} *t*OP treatments were 6.3 ± 0.5 (n = 80), 12.6 ± 1.2 (n = 73), 25.0 ± 2.0 (n = 79) and 54.2 ± 4.6 µg l^{-1} (n = 65), respectively, over the duration of the experiment. Among-tank variability was ≤ 10% with the coefficient of variation (averaged across the duration of the experiment) of 8.3, 9.4, 8.1 and 8.5%, respectively, for the 6.25, 12.5, 25 and 50 µg l^{-1} treatments. No *t*OP was detected in the control water treatment. Quality control samples were conducted with each sample set and included LSW blanks, duplicate samples and matrix-spiked samples at each of the *t*OP treatment levels. No *t*OP was detected in the LSW blanks (n = 16). The mean ± SD (n = 16) recoveries of spiked samples were 90.2 ± 6.5%, 95.6 ± 3.9%, 95.3 ± 4.2% and 96.6 ± 3.2% at the 6.25, 12.5, 25 and 50 µg l^{-1} spiked levels, respectively. The mean ± SD (n = 16) agreement among duplicate samples was 102.2 ± 4.0%, 98.9 ± 3.7%, 100.2 ± 1.7% and 100.2 ± 5.0% for the 6.25, 12.5, 25 and 50 µg l^{-1} treatments, respectively. The detection limit was 2.5 µg l^{-1}.

Published 2016. This article is a U.S. Government work and is in the public domain in the USA.

Journal of Applied Toxicology

Statistical analyses

All NF62 sub-sample data were analyzed independently of gender whereas all juvenile data were analyzed separately according to genetic sex. All quantitative data (weight, length, LSI, T4, mortality) was verified to be monotonic by fitting it to an ANOVA model and comparing linear and quadratic contrasts of normalized rank statistics. Treatment effects were determined using the Jonckheere–Terpstra trend test. Transformations were not applied to any of the data except for percent mortality, which was arcsine-square root transformed before analysis. For all statistical approaches described in this section, $P < 0.05$ was considered statistically significant.

Time-to-NF62 data were analyzed using a Cox mixed-effects proportional hazard model (Therneau, 2015). This model accounted for within tank and between tank variance in addition to mortalities. Individuals that did not reach NF62 before test day 70, including mortalities, were right-censored.

Incidence rates and severity scores from histopathological evaluations were analyzed using the Rao-Scott Cochran-Armitage by slices (RSCABS) test (Green *et al*., 2014). This test accounts for differential replication and takes the expected monotone dose-response relationship into account. RSCABS not only tests for differences between treatments and control but also tests for significant differences at each represented severity level resulting in outputs of significant treatments along with their corresponding significant severity level(s). This method was also used to determine the treatment effects on gonad and reproductive duct development by considering developmental stages as equivalent to 'severity' scores.

Results

Survival and growth

Mortality data were analyzed as the percent that either did not hatch or died post-hatch in any particular replicate tank, not due to a technical error, sampling or culling. All control tanks in both studies had ≤20% mortality and there were no treatment-related effects on survival in either study. However, technical difficulties (drain obstruction and tank overflow) late in the *t*OP study caused one 12.5 $\mu g\,l^{-1}$ replicate and two 50 $\mu g\,l^{-1}$ replicates to be lost after the post-NF stage 62 cull. There were no treatment-related effects on growth (weight and snout-to-vent length) or larval development (time to NF62) in either study and no effects on growth of juveniles at test termination in either study (Supporting Information Tables 1–3). Juvenile liver-somatic indices were also unaffected by chemical treatment in both studies (Supporting Information Tables 2, 3).

Larval serum T4 and thyroid histopathology

Two different methods were used to measure serum T4 from the *t*OP study, as described in the methods section. There was a treatment-related reduction in serum T4 concentrations in the 25 and 50 $\mu g\,l^{-1}$ *t*OP treatments (Fig. 1), which corresponds to increased incidence and severity of thyroid follicular cell hypertrophy observed in these two treatments and the increased incidence of moderate thyroid follicular cell hyperplasia observed in the 50 $\mu g\,l^{-1}$ treatment (Table 2). The measured serum T4 levels were consistent between the two methods (Fig. 1). There were no treatment-related effects on larval serum T4 concentrations or thyroid histopathology in the TB study (data not shown).

Table 2. The prevalance (% of *n*) and severity of larval thyroid gland histopathological observations after exposure to *t*OP

Nominal *t*OP concentration ($\mu g\,l^{-1}$)	0	6.25	12.5	25	50
Total *n*	39	24	25	25	24
Replicate tanks	8	5	5	5	5
Follicular Cell Hypertrophy					
NR	3	0	0	0	4
Mild	46	21	36	16	4
Moderate	51	75	56	(68)	(71)
Severe	0	4	(8)	(16)	(21)
Follicular Cell Hyperplasia					
NR	74	58	56	76	58
Mild	26	42	44	24	33
Moderate	0	0	0	0	(8)
Severe	0	0	0	0	0
Decreased Colloid					
NR	36	46	28	72	71
Mild	62	50	72	(28)	(29)
Moderate	3	4	0	0	0
Severe	0	0	0	0	0

NR, not remarkable, numbers in parentheses are significantly different from control based on RSCABS analysis.

Juvenile plasma Vtg

Overall, the majority of plasma Vtg levels were not quantifiable. The few samples that were quantifiable were slightly above the minimum detection limit of the ELISA method. Because Vtg was not detected in most of the samples, statistical analyses were deemed inappropriate, and the data are not presented.

Juvenile gonad histopathology

All of the individual genotypic sexes matched the corresponding histological gonad phenotypes in both studies, so there was no evidence of sex reversal or gonad dysgenesis in either study. Moreover, the developmental rates of the gonads were not affected by chemical treatment in either study. The only two treatment-related findings in the testes of males exposed to TB were increased spermatogonia (minimal) and germ cell vacuolation (minimal to mild) in frogs of the 100 $ng\,l^{-1}$ treatment (Table 3). Germ cell vacuolation was characterized by clear cytoplasmic ballooning in small clusters of pachytene phase spermatocytes. There were no effects on the pathology of the juvenile testes in the *t*OP study (data not shown), nor were there any apparent effects of TB exposure on the ovaries of juvenile females (data not shown). In the *t*OP study, ovaries experienced increased incidences and severity of mononuclear cellular infiltrate (minimal to mild) in the 12.5, 25 and 50 $\mu g\,l^{-1}$ treatments (Supporting Information Table 4).

Juvenile reproductive duct histopathology

There were treatment-related effects on oviduct development in both genders and in both studies. In the TB study, males exhibited accelerated regression of oviducts in the 100 $ng\,l^{-1}$ treatment as compared to the control whereas females experienced prodigious oviduct regression in the 50 and 100 $ng\,l^{-1}$ treatments (Table 4).

Published 2016. This article is a U.S. Government work and is in the public domain in the USA.

Table 3. The prevalence (% of *n*) and severity of juvenile male gonad histopathological observations after 17β-trenbolone (TB) exposure

Nominal TB concentration (ng l^{-1})	0	12.5	25	50	100
Total *n*	39	21	20	25	25
Replicate tanks	8	5	5	5	5
Increased spermatogonia					
NR	97	100	100	100	76
Minimal	3	0	0	0	(24)
Mild	0	0	0	0	0
Moderate	0	0	0	0	0
Severe	0	0	0	0	0
Germ cell vacuolation					
NR	100	95	95	96	76
Minimal	0	5	5	4	(20)
Mild	0	0	0	0	4
Moderate	0	0	0	0	0
Severe	0	0	0	0	0

NR, not remarkable; numbers in parentheses are significantly different than control based on RSCABS analysis.

The opposite effect occurred in the *t*OP study; there were significant delays in male oviduct regression (6.25, 12.5, 25 and 50 μg l^{-1}) and female oviduct maturation was significantly advanced with *t*OP exposure (Table 4). Given the importance of the oviduct as a female reproductive organ necessary for the application of the jelly coat to the oocyte and release of the oocyte to the external environment, effects observed as a result of TB exposure is expected to have a considerable consequence on reproductive capacity (Fig. 2). There were no treatment-related effects on Wolffian duct development or pathology in either gender in either study.

Juvenile kidney and liver histopathology

Two common findings in the juvenile kidneys of all individuals in both studies were renal tubule mineralization/casts (minimal to moderate) and renal tubule dilation (minimal to mild). Prevalence and severity were comparable between treatments and control in most cases; females showed a slight increase in incidences of mild tubule dilation in the 50 μg l^{-1} *t*OP treatment (data not shown). The livers of most individuals in both studies also had common occurrence of granulomatous inflammation, which was comparable between treated and control frogs although the severity was minimal. However, the prevalence of minimal cellular hypertrophy of hepatocytes was increased in the 50 and 100 ng l^{-1} TB treatments (data not shown). No treatment-related effects were present in any livers of the *t*OP-exposed frogs.

Discussion

Standardized toxicity tests utilizing the representative amphibian model species *X. laevis* currently exist only for specific life stages of development. The Frog Embryo Teratogenesis Assay-*Xenopus* (ASTM Standard E1439, 2012) is intended to evaluate a chemical's teratogenic properties only during embryonic development. The Amphibian Metamorphosis Assay is a Tier 1 assay utilized by the U.S. EPA's EDSP (US EPA, 2009) and has also been adopted globally by the OECD (OECD, 2009). This assay is intended to evaluate a chemical's impact on thyroid hormone-mediated metamorphosis; it begins just before pro-metamorphosis and ends before completion of metamorphosis, encompassing only a window of larval development. The LAGDA is the first standardized and globally harmonized test guideline that encompasses all of embryonic, larval and juvenile development and is designed to evaluate adverse apical effects that may manifest over multiple life stages of chronic exposure. The assay endpoints were intentionally designed to assess apical outcomes that could have population-level implications, which is most useful to risk assessors. Molecular markers were omitted from the test guideline because they do not provide risk assessors definitive information regarding the true adverse outcomes at the tissue or organismal level. However, independent of chemical testing for risk assessment, the LAGDA serves as a foundation on which specific molecular endpoints can easily be added to investigate other research questions.

Table 4. Histological staging of juvenile oviducts after either 17β-trenbolone (TB) or 4-*tert*-octylphenol (*t*OP) exposure

	Male					Female				
Nominal TB concentration (ng l^{-1})	0	12.5	25	50	100	0	12.5	25	50	100
Total *n*	39	21	20	25	25	38	25	29	24	25
Replicate tanks	8	5	5	5	5	8	5	5	5	5
Oviduct Stage										
1	54	29	40	64	(100)	0	0	0	(8)	(52)
2	46	71	60	36	0	100	100	100	92	48
3	0	0	0	0	0	0	0	0	0	0
Nominal *t*OP concentration (μg l^{-1})	0	6.25	12.5	25	50	0	6.25	12.5	25	50
Total *n*	32	20	16	16	9	30	20	16	21	12
Replicate tanks	8	5	4	5	3	8	5	4	5	3
Oviduct Stage										
1	88	60	44	31	67	0	0	0	0	0
2	12	(40)	(56)	(69)	(33)	87	80	75	67	25
3	0	0	0	0	0	13	20	25	33	(75)

Table values are percentages of *n*; numbers in parentheses are significantly different than control based on RSCABS analysis.

Published 2016. This article is a U.S. Government work and is in the public domain in the USA.

Journal of AppliedToxicology

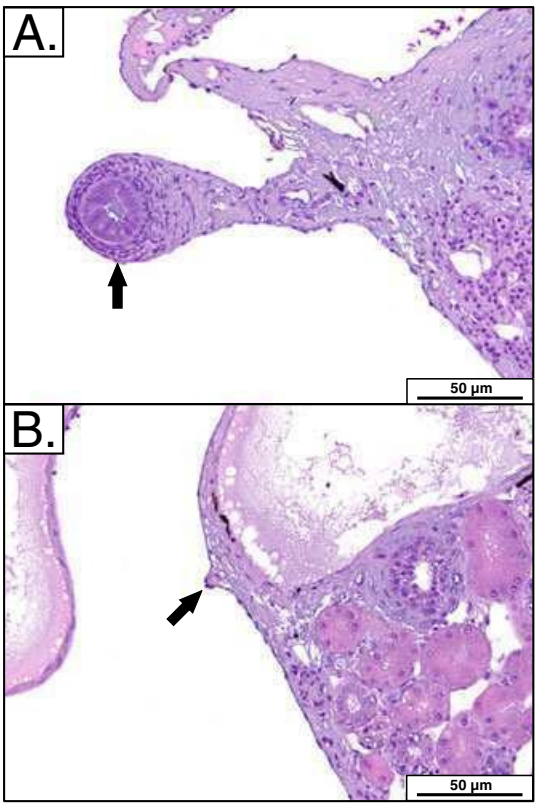

Figure 2. (A) Stage 2 oviduct (arrow) observed in control females. (B) Stage 1 oviduct (arrow) from a female exposed to 100 ng l^{-1} 17β-trenbolone (TB). Stage 1 oviducts, such as this, were not observed in any control females. Scale bar: 50 µm.

Initial considerations regarding the standardized assay design required that it be (i) feasible and reasonable to perform successfully on a semi-routine basis, (ii) reproducible and (iii) transferable. Early proposed assay designs and supporting work utilized *X. tropicalis* owing to the shorter time to sexual maturity (Olmstead *et al*., 2009a, 2009b, 2012; Porter *et al*., 2011), in addition to the availability of genetic information for that species (i.e. fully sequenced diploid genome). Unfortunately, the sex determination strategy of *X. tropicalis* has been shown to be rather complex, with the coexistence of Y, W and Z sex chromosomes within the laboratory population (Roco *et al*., 2015). The presence of three sex chromosomes leads to a departure from the normal 50/50 sex ratio in some instances requiring that all breeding animals be screened to ensure only ZZ males are bred. Further, a sex-linked gene has not been identified for *X. tropicalis* as has been identified for *X. laevis*, which allows for simple and routine genetic sexing (Yoshimoto *et al*., 2008). However, a sex-linked polymorphism has been established in a sub-population of *X. tropicalis*, although the source of the marker is a single female animal (Olmstead *et al*., 2010). Populations derived from that particular female are very limited, and efforts to increase the numbers have proven problematic leading to a strain that lacks the necessary robustness to be used for routine testing. Therefore, the assay design moved forward with *X. laevis* as the model amphibian species.

Xenopus laevis does not reach sexual maturity until at least 1-year post-hatch. A test of that length would present logistical, technical, and other challenges compromising reproducibility of the results and/or transferability of the approach. Aside from complications imposed by time to sexual maturity, classic reproductive assessments (fertility and fecundity) are not possible to make in *X. laevis* because they do not naturally mate in the laboratory, unlike other model species. Although mating behavior and calling have been shown to be affected by EDCs (Behrends *et al*., 2010), these assessments are also not feasible to include because they would require the test to be carried out, at least, a full year, presenting the same challenges mentioned above. Additionally, mate calling behavior and fertility/fecundity evaluations in *X. laevis* both require induction by hCG injections, which makes interpretation of results challenging in the context of environmental risk assessment. Taken together, the most feasible, reproducible and transferable assay design was determined to encompass embryonic, larval and juvenile development until the gonads are fully differentiated in control organisms, which takes approximately 16 weeks.

The studies presented here were conducted to evaluate the initial assay design and to generate validation data from two model EDCs targeting different points within the HPG axis. Demonstration of different modes of endocrine disruption with the LAGDA protocol would confirm its diagnostic capabilities and demonstrate the assay's utility for use within the U.S. EPA's EDSP and the OECD's Endocrine Disruptor Testing and Assessment framework. To that end, 4-*tert*-octylphenol was chosen as a model xenoestrogen and 17β-trenbolone was chosen as a model xenoandrogen, both of which have been well-characterized endocrine-active chemicals in other species.

The high test concentrations in the current studies were set as high as possible without causing embryo or larval lethality. This was based on previous studies performed with closely related amphibian species *X. tropicalis* using range-finder experiments and long-term exposure protocols similar to the LAGDA (Porter *et al*., 2011; Olmstead *et al*., 2012). Chronic exposure to *t*OP or TB at concentrations used in the current studies did not affect survival or growth. Liver and kidney histopathological evaluations for both studies identified only a minimal treatment-related increase in hepatocyte hypertrophy in the TB study (50, 100 ng l^{-1} TB) with no other treatment-related effects on these organs. These data support the notion that the concentrations tested were not overtly toxic and emphasizes the specificity of the endocrine modes of action observed.

Chronic exposure to higher levels of *t*OP appeared to negatively impact thyroid homeostasis during larval development. Amphibian metamorphosis is a thyroid hormone-mediated process and NF stage 62 represents metamorphic climax, when circulating thyroid hormone levels peak. The larval subsampling takes place at NF stage 62 for this reason, as opposed to NF stage 66 when circulating thyroid hormone levels have decreased toward adult baseline levels. NF stage 62 can also be easily identified visually without manipulation or handling of the organisms, similar to NF stage 66, making it an equally suitable stage to sample in that regard. As observed in the *t*OP study, the decrease in circulating T4, together with increased severity of thyroid follicular cell hypertrophy and hyperplasia are indicative of thyroid axis disruption. Croteau *et al*. (2009) exposed *Rana pipiens* to *t*OP (0.01 and 10 nM) and reported developmental delays in larvae that they attributed to disruptions in the thyroid axis. The authors suggest that alterations in deiodinase enzyme concentrations in peripheral tissues could be the mechanism through which *t*OP causes a decrease in circulating T4 concentrations. While not providing direct evidence for this mode of action, the effects seen in the current *t*OP study do seem to corroborate the observations seen

Published 2016. This article is a U.S. Government work and is in the public domain in the USA.

in *Rana pipiens*, suggesting the potential for extrapolation of LAGDA results to other amphibian species.

Vitellogenin levels were measured in juvenile plasma but proved to be very low in the *t*OP study. Vtg is an egg yolk precursor protein synthesized in the liver of oviparous vertebrates and is positively regulated by estrogen receptor agonists. This relationship is well characterized across species, and Vtg induction has been utilized extensively as an *in vivo* and *in vitro* assessment of xenoestrogen exposure. However, termination of the LAGDA study takes place several months before the appearance of measurable endogenous estradiol and Vtg in female *X. laevis* serum (Kelley, 1996). Although the liver is capable of producing Vtg after exogenous estradiol stimulation at developmental stages ≥ NF62 (May and Knowland, 1980), the levels of estradiol required to induce Vtg are relatively high given the potency of estradiol concerning the estrogen receptor. Additionally, Mitsui *et al.* (2003) demonstrated that Vtg induction in smaller, more immature juveniles is less sensitive to estradiol stimulation in both males and females as compared to sexually mature animals. Taken together, this indicates that *t*OP was too weak of a xenoestrogen to elicit a Vtg response in juvenile frogs and brings into question whether this endpoint is useful to include in this test guideline. Subsequent experimentation will help define the utility of this endpoint as it pertains to the LAGDA protocol, which may be strictly limited to potent xenoestrogens.

Interestingly, there were no pronounced treatment-related abnormalities observed in the gonads in either study. All genotypes matched the histologically determined phenotypes indicating no cases of gonad dysgenesis or sex reversal due to exposure. Although this was expected in the *t*OP study based on the results of Porter *et al.* (2011), ovary abnormalities were generally expected in the high treatment of our TB study based on the results reported by Olmstead *et al.* (2012), but did not occur. This could be related to differential androgen sensitivity across the closely related species tested (*X. laevis* vs. *X. tropicalis*) or that the mean measured exposure concentration in our high treatment was 80 ng l^{-1} as compared to the mean measured exposure concentration of 104 ng l^{-1} reported by Olmstead *et al.* (2012). Impaired gonadal development and function is a major focus in the area of ecological EDC testing due to the potential for population-level effects. However, most studies showing impairment of gonad morphogenesis and/or reproductive function generally initiate exposure during life stages that are better able to survive high exposure levels. In the case of the LAGDA protocol, survival through embryonic and larval development precludes observing effects on gonadal development at those higher concentrations, making embryo-larval survival the driver of test concentration ranges in this chronic exposure paradigm. This, in turn, emphasizes the specificity and significance of a chemical's endocrine disrupting potential as it pertains to chronic exposure during amphibian early life stage growth and development.

While gonad differentiation and development was generally unaffected in the current studies with *X. laevis,* oviduct development turned out to be the most sensitive indicator of HPG axis disruption by these two chemicals. Müllerian ducts are present in both genders during larval development until they are thought to be signaled either by an anti-Müllerian hormone in the males to regress, or estradiol in the females to mature (Kelley, 1996; Ogielska, 2009). The oviducts are one hallmark of secondary sexual differentiation that are influenced directly by hormonal control from the gonads. However, the true mechanisms and pathway interactions influencing *Xenopus* oviduct fate are not well understood. Consistent with this *t*OP study, Porter *et al.* (2011) reported occurrences of adult *X. tropicalis* males having oviducts following *t*OP exposure (1, 3.3, 11 and 36 μg l^{-1}) and a significant increase in oviduct weight in males exposed to 36 μg l^{-1} *t*OP. Conversely, when *X. tropicalis* were exposed to the anti-estrogen fadrozole (aromatase inhibitor) at concentrations of 16 and 64 μg l^{-1}, all females in those treatments were sex reversed into phenotypic males that did not have oviducts (Olmstead *et al.*, 2009b). Qin *et al.* (2007) demonstrated that polychlorinated biphenyl exposure in *X. laevis* inhibited Müllerian duct regression in juvenile males, likely resulting from observed decreases in serum testosterone levels. Taken together, all of these studies appear to support that estrogen is necessary, but not sufficient to cause oviduct maturation in *Xenopus,* and androgen-mediated Müllerian duct regression appears to trump endogenous estrogenic influence on the oviduct.

These mechanisms through which hormones and EDCs influence the oviduct are important when considering molecular initiating events that lead to adverse outcomes (Ankley *et al.*, 2010). The occurrence of oviducts in mature males is atypical but is questionable as to whether or not this occurrence is adverse. Males require alternative ducts, Wolffian ducts, for sperm to pass from the testes to the external environment, which appeared to be unaffected in the current studies. In contrast, females having no oviducts leaves no question as to whether or not this effect is adverse. Without oviducts, there is simply no way for the oocytes to pass to the external environment for fertilization. This effect is likely irreversible and renders these individuals incapable of reproduction, suggesting potential population-level impacts. This is a good example of an apical outcome generated by the LAGDA that would be given consideration in the risk assessment process for this compound. To date, the LAGDA is the only validated test that adequately evaluates amphibian reproductive duct and gonad development following chronic chemical exposure. Although this study design does not employ traditional apical reproductive assessments (fertility and fecundity), the TB concentration showing oviductal dysgenesis in females here is similar to the concentration range showing significantly reduced fecundity in reproductively competent fathead minnows exposed to TB for 21 days (Ankley *et al.,* 2003). Therefore, cross-species sensitivity to this androgenic compound, with regard to reproductive dysfunction, appears to be consistent. This supports that reproductive impairment can be evaluated through observations of gross organ morphology, albeit when profoundly impacted, rather than making fertility and fecundity assessments, of which are not feasible in this species or this particular testing paradigm. This study also emphasizes the importance of androgenic effects on reproductive duct development in amphibians and may also be a relevant mode of reproductive impairment worth investigating in other oviparous vertebrate species.

The LAGDA test guideline provides a foundation for standardized amphibian chronic toxicity testing, which has not existed thus far. There are many challenges associated with not only amphibian toxicity testing but also with chronic toxicity testing over multiple life stages; these studies demonstrate a feasible approach to meet these challenges. These studies have also demonstrated endocrine-specific effects at concentrations not eliciting overt toxicity and serve to support the use of this assay for its intended purpose. This assay has the potential to support ecological risk assessments based on apical outcomes, in addition to providing a basis from which other specific endpoints can be examined to support ongoing research efforts including

Published 2016. This article is a U.S. Government work and is in the public domain in the USA.

Journal of AppliedToxicology

elucidation of adverse outcome pathways and biological systems modeling.

Acknowledgments

The authors would like to thank Chad Blanksma (Oak Ridge Institute for Science and Education) and Dr Jeffrey Wolf (Experimental Pathology Laboratories, Inc.) for histotechnical support and histopathology assessments, respectively, and Joe Swintek (Badger Technical Services) for extensive statistical support and advice. Lindsey Blake, Shane Zavodnik, Kathryn Lillegard, Ben Heggested, Erica Nevalainen, Evan Eid, Luke Dahlin and Stephanie Hall (Student Contract Services) provided laboratory technical support with husbandry, exposure systems, sampling and sample analyses. The authors would also like to thank Kevin Flynn for thoughtful comments and suggestions to improve this manuscript. This work was funded by the U.S. EPA; this paper has been reviewed according to ORD guidelines, but the statements made do not represent views of the U.S. EPA, nor does mention of trade names indicate endorsement by the federal government.

Conflicts of interest

The authors declare no conflicts of interest.

References

Ahel M, Giger W, Koch M. 1994. Behavior of alkylphenol polyethoxylate surfactants in the aquatic environment—I. Occurrence and transformation in sewage treatment. *Water Res.* **28**(5): 1131–1142.

Ankley GT, Jensen KM, Makynen EA, Kahl MD, Korte JJ, Hornung MW, Henry TR, Denny JS, Leino RL, Wilson VS, Cardon MC, Hartig PC, Gray LE. 2003. Effects of the androgenic growth promoter 17β-trenbolone on fecundity and reproductive endocrinology of the fathead minnow. *Environ. Toxicol. Chem.* **22**(6): 1350–1360.

Ankley GT, Bennett RS, Erickson RJ, Hoff DJ, Hornung MW, Johnson RD, Mount DR, Nichols JW, Russom CL, Schmieder PK, Serrano JA, Tietge JE, Villeneuve DL. 2010. Adverse outcome pathways: a conceptual framework to support ecotoxicology research and risk assessment. *Environ. Toxicol. Chem.* **29**(3): 730–741.

ASTM Standard E1439. 2012. *Standard Guide for Conducting the Frog Embryo Teratogenesis Assay-Xenopus (FETAX)*. ASTM International: West Conshohocken.

Behrends T, Urbatzka R, Krackow S, Elepfandt A, Kloas W. 2010. Mate calling behavior of male South African clawed frogs (*Xenopus laevis*) is suppressed by the antiandrogenic endocrine disrupting compound flutamide. *Gen. Comp. Endocrinol.* **168**(2): 269–274.

Croteau MC, Davidson M, Duarte-Guterman P, Wade M, Popesku JT, Wiens S, Lean DRS, Trudeau VL. 2009. Assessment of thyroid system disruption in *Rana pipiens* tadpoles chronically exposed to UVB radiation and 4-*tert*-octylphenol. *Aquat. Toxicol.* **95**(2): 81–92.

Durhan EJ, Lambright CS, Makymen EA, Lazorchak J, Hartig PC, Wilson VS, Gray LE, Ankley GT. 2006. Identification of metabolites of trenbolone acetate in androgenic runoff from a beef feedlot. *Environ. Health Perspect.* **114**: 65.

EDSP Website. http://www.epa.gov/endo/ [24 September 2015]

El Jamil A, Magre S, Mazabraud A, Penrad-Mobayed M. 2008. Early aspects of gonadal sex differentiation in *Xenopus tropicalis* with reference to an antero-posterior gradient. *J. Exp. Zool. A Ecol. Genet. Physiol.* **309**(3): 127–137.

Green JW, Springer TA, Saulnier AN, Swintek J. 2014. Statistical analysis of histopathological endpoints. *Environ. Toxicol. Chem.* **33**(5): 1108–1116.

Grim KC, Wolfe M, Braunbeck T, Iguchi T, Ohta Y, Tooi O, Touart L, Wolf DC, Tietge J. 2009. Thyroid histopathology assessments for the amphibian metamorphosis assay to detect thyroid-active substances. *Toxicol. Pathol.* **37**(4): 415–424.

Holbech H, Kinnberg K, Petersen GI, Jackson P, Hylland K, Norrgren L, Bjerregaard P. 2006. Detection of endocrine disrupters: evaluation of a Fish Sexual Development Test (FSDT). *Comp. Biochem. Physiol. C Toxicol. Pharmacol.* **144**(1): 57–66.

Jobling S, Sumpter JP. 1993. Detergent components in sewage effluent are weakly oestrogenic to fish: An *in vitro* study using rainbow trout (*Oncorhynchus mykiss*) hepatocytes. *Aquat. Toxicol.* **27**(3): 361–372.

Kahl MD, Russom CL, DeFoe DL, Hammermeister DE. 1999. Saturation units for use in aquatic bioassays. *Chemosphere* **39**(3): 539–551.

Karels AA, Manning S, Brouwer TH, Brouwer M. 2003. Reproductive effects of estrogenic and antiestrogenic chemicals on sheepshead minnows (*Cyprinodon variegatus*). *Environ. Toxicol. Chem.* **22**(4): 855–865.

Kelley DB. 1996. 9 Sexual differentiation in *Xenopus laevis*. In *Symposia of the Zoological Society of London* (No. 68). The Society: London.

Kloas W, Lutz I, Einspanier R. 1999. Amphibians as a model to study endocrine disruptors: II. Estrogenic activity of environmental chemicals *in vitro* and *in vivo*. *Sci. Total Environ.* **225**(1): 59–68.

Kuiper GG, Lemmen JG, Carlsson BO, Corton JC, Safe SH, van der Saag PT, van der Berg B, Gustafsson JÅ. 1998. Interaction of estrogenic chemicals and phytoestrogens with estrogen receptor β. *Endocrinology* **139**(10): 4252–4263.

May FE, Knowland J. 1980. The role of thyroxine in the transition of vitellogenin synthesis from noninducibility to inducibility during metamorphosis in *Xenopus laevis*. *Dev. Biol.* **77**(2): 419–430.

Ministry of the Environment, Japan. 2010. Further Actions to Endocrine Disrupting Effects of Chemical Substances -EXTEND 2010. http://www.env.go.jp/en/chemi/ed/extend2010_full.pdf [accessed on 16 October 2015].

Mitsui N, Tooi O, Kawahara A. 2003. Sandwich ELISAs for quantification of *Xenopus laevis* vitellogenin and albumin and their application to measurement of estradiol-17β effects on whole animals and primary-cultured hepatocytes. *Comp. Biochem. Physiol. C Toxicol. Pharmacol.* **135**(3): 305–313.

Mitsui N, Tooi O, Kawahara A. 2007. Vitellogenin-inducing activities of natural, synthetic, and environmental estrogens in primary cultured *Xenopus laevis* hepatocytes. *Comp. Biochem. Physiol. C Toxicol. Pharmacol.* **146**(4): 581–587.

Morthorst JE, Holbech H, Bjerregaard P. 2010. Trenbolone causes irreversible masculinization of zebrafish at environmentally relevant concentrations. *Aquat. Toxicol.* **98**(4): 336–343.

Nieuwkoop PD, Faber J. 1994. *Normal Table of, Xenopus laevis, 1967*. Daudin: Amsterdam.

OECD. 2009. *Test No. 231: Amphibian Metamorphosis Assay, OECD Guidelines for the Testing of Chemicals, Section 2*, OECD Publishing: Paris. DOI: 10.1787/9789264076242-en.

OECD. 2012. Guidance document on standardized test guidelines for evaluating endocrine disrupters. In *Environment, Health and Safety Publications, Series on Testing and Assessment (No. 150)*. OECD Publishing: Paris.

OECD. 2015. *Test No.* 241: The Larval Amphibian Growth and Development Assay (LAGDA), OECD Guidelines for the Testing of Chemicals, Section 2, OECD Publishing: Paris.DOI: 10.1787/9789264242340-en.

Ogielska M. 2009. *Reproduction of Amphibians*. Science Pub Inc.: Enfield.

Olmstead AW, Korte JJ, Woodis KK, Bennett BA, Ostazeski S, Degitz SJ. 2009a. Reproductive maturation of the tropical clawed frog: *Xenopus tropicalis*. *Gen. Comp. Endocrinol.* **160**(2): 117–123.

Olmstead AW, Kosian PA, Korte JJ, Holcombe GW, Woodis KK, Degitz SJ. 2009b. Sex reversal of the amphibian, *Xenopus tropicalis*, following larval exposure to an aromatase inhibitor. *Aquat. Toxicol.* **91**(2): 143–150.

Olmstead AW, Lindberg-Livingston A, Degitz SJ. 2010. Genotyping sex in the amphibian, *Xenopus (Silurana) tropicalis*, for endocrine disruptor bioassays. *Aquat. Toxicol.* **98**(1): 60–66.

Olmstead AW, Kosian PA, Johnson R, Blackshear PE, Haselman JT, Blanksma C, Korte JJ, Holcombe GW, Burgess E, Lindberg-Livingston A, Bennett BA, Woodis KK, Degitz SJ. 2012. Trenbolone causes mortality and altered sexual differentiation in *Xenopus tropicalis* during larval development. *Environ. Toxicol. Chem.* **31**(10): 2391–2398.

Ortiz-Zarragoitia M, Cajaraville MP. 2005. Effects of selected xenoestrogens on liver peroxisomes, vitellogenin levels and spermatogenic cell proliferation in male zebrafish. *Comp. Biochem. Physiol. C Toxicol. Pharmacol.* **141**(2): 133–144.

Orn S, Yamani S, Norrgren L. 2006. Comparison of vitellogenin induction, sex ratio, and gonad morphology between zebrafish and Japanese medaka after exposure to 17α-ethinylestradiol and 17β-trenbolone. *Arch. Environ. Contam. Toxicol.* **51**(2): 237–243.

Paris F, Balaguer P, Térouanne B, Servant N, Lacoste C, Cravedi JP, Nicolas JC, Sultan C. 2002. Phenylphenols, biphenols, bisphenol-A and 4-*tert*-octylphenol exhibit α and β estrogen activities and

Published 2016. This article is a U.S. Government work and is in the public domain in the USA.

antiandrogen activity in reporter cell lines. *Mol. Cell. Endocrinol.* **193**(1): 43–49.

Porter KL, Olmstead AW, Kumsher DM, Dennis WE, Sprando RL, Holcombe GW, Korte JJ, Lindberg-Livingston A, Degitz SJ. 2011. Effects of 4-*tert*-octylphenol on *Xenopus tropicalis* in a long term exposure. *Aquat. Toxicol.* **103**(3): 159–169.

Qin ZF, Qin XF, Yang L, Li HT, Zhao XR, Xu XB. 2007. Feminizing/demasculinizing effects of polychlorinated biphenyls on the secondary sexual development of *Xenopus laevis*. *Aquat. Toxicol.* **84**(3): 321–327.

Rasmussen TH, Teh SJ, Bjerregaard P, Korsgaard B. 2005. Anti-estrogen prevents xenoestrogen-induced testicular pathology of eelpout (*Zoarces viviparus*). *Aquat. Toxicol.* **72**(3): 177–194.

Roco ÁS, Olmstead AW, Degitz SJ, Amano T, Zimmerman LB, Bullejos M. 2015. Coexistence of Y, W, and Z sex chromosomes in *Xenopus tropicalis*. *Proc. Natl. Acad. Sci. U. S. A.* **112**(34): E4752–E4761.

Routledge EJ, Sumpter JP. 1997. Structural features of alkylphenolic chemicals associated with estrogenic activity. *J. Biol. Chem.* **272**(6): 3280–3288.

Seki M, Yokota H, Maeda M, Tadokoro H, Kobayashi K. 2003. Effects of 4-nonylphenol and 4-*tert*-octylphenol on sex differentiation and vitellogenin induction in medaka (*Oryzias latipes*). *Environ. Toxicol. Chem.* **22**(7): 1507–1516.

Therneau TM. 2015. Mixed effects cox models. Available from: http://cran.r-project.org/web/packages/coxme/coxme.pdf [accessed on 16 October 2015].

Tietge JE, Butterworth BC, Haselman JT, Holcombe GW, Hornung MW, Korte JJ, Kosian PA, Wolfe M, Degitz SJ. 2010. Early temporal effects of three thyroid hormone synthesis inhibitors in *Xenopus laevis*. *Aquat. Toxicol.* **98**(1): 44–50.

US EPA. 2009. OPPTS 890.1100: Amphibian Metamorphosis Assay (AMA), Endocrine Disruptor Screening Program Test Guidelines, 890 series, http://www.regulations.gov, ID: EPA-HQ-OPPT-2009-0576-0002 [accessed on 7 April 2016].

US EPA. 2015a. EPA Releases Screening Results of Endocrine Disruptor Screening for 52 Pesticide Chemicals. http://www.epa.gov/oppfead1/cb/csb_page/updates/2015/endocrine-disruptor.html [accessed on 24 September 2015]

US EPA. 2015b. OCSPP 890.2300: Larval Amphibian Growth and Development Assay (LAGDA), Endocrine Disruptor Screening Program Test Guidelines, 890 series, http://www.regulations.gov, ID: EPA-HQ-OPPT-2014-0766-0020 [accessed on 7 April 2016].

Ying GG, Williams B, Kookana R. 2002. Environmental fate of alkylphenols and alkylphenol ethoxylates—a review. *Environ. Int.* **28**(3): 215–226.

Yoshimoto S, Okada E, Umemoto H, Tamura K, Uno Y, Nishida-Umehara C, Matsuda Y, Takamatsu N, Shiba T, Ito M. 2008. A W-linked DM-domain gene, DM-W, participates in primary ovary development in *Xenopus laevis*. *Proc. Natl. Acad. Sci. U. S. A.* **105**(7): 2469–2474.

Supporting information

Additional supporting information may be found in the online version of this article at the publisher's web-site.

Published 2016. This article is a U.S. Government work and is in the public domain in the USA.

Supporting information

Table S1. Larval growth and development following exposure to either TB or *t*OP (mean ± SD). Time to NF62 data are presented as means of tank medians ± SD.

		NF62 larvae		
Nominal concentration	*n*	Weight (g)	Length (mm)	Time to NF62 (d)
0 ng/L	8	0.818 ± 0.140	18.7 ± 1.1	40 ± 1
TB 12.5 ng/L	5	0.835 ± 0.146	18.7 ± 1.0	40 ± 2
TB 25 ng/L	5	0.853 ± 0.154	18.8 ± 1.2	39 ± 1
TB 50 ng/L	5	0.913 ± 0.193	19.2 ± 1.3	39 ± 1
TB 100 ng/L	5	0.867 ± 0.166	18.8 ± 1.2	38 ± 1
0 µg/L	8	0.96 ± 0.15	19.2 ± 1.0	42 ± 2
*t*OP 6.25 µg/L	5	1.05 ± 0.14	19.9 ± 0.9	41 ± 1
*t*OP 12.5 µg/L	5	0.90 ± 0.15	19.0 ± 1.0	42 ± 1
*t*OP 25 µg/L	5	1.00 ± 0.16	19.8 ± 1.1	42 ± 1
*t*OP 50 µg/L	5	0.93 ± 0.19	18.9 ± 1.4	43 ± 1

Table S2. Juvenile growth and liver-somatic indices following TB exposure (mean ± SD).

	n	Weight (g)	Length (mm)	LSI
Nominal TB concentration			Female	
0 ng/L	8	12.9 ± 3.7	47.5 ± 5.1	0.059 ± 0.006
12.5 ng/L	5	13.3 ± 2.6	47.3 ± 3.3	0.058 ± 0.010
25 ng/L	5	12.5 ± 3.2	46.4 ± 4.4	0.061 ± 0.006
50 ng/L	5	12.3 ± 3.0	46.6 ± 4.7	0.058 ± 0.008
100 ng/L	5	13.7 ± 3.6	49.0 ± 4.8	0.058 ± 0.009
			Male	
0 ng/L	8	12.3 ± 3.3	46.2 ± 4.1	0.060 ± 0.010
12.5 ng/L	5	11.4 ± 2.4	45.4 ± 3.2	0.058 ± 0.009
25 ng/L	5	11.9 ± 2.7	46.3 ± 4.0	0.057 ± 0.006
50 ng/L	5	13.2 ± 2.6	47.6 ± 4.0	0.057 ± 0.008
100 ng/L	5	11.7 ± 2.7	46.4 ± 3.6	0.058 ± 0.007

Table S3. Juvenile growth and liver-somatic indices following *t*OP exposure (mean ± SD).

	n	Weight (g)	Length (mm)	LSI
Nominal *t*OP concentration			Female	
0 µg/L	8	12.0 ± 2.7	44.7 ± 4.0	0.059 ± 0.012
6.25 µg/L	5	12.4 ± 3.1	46.1 ± 3.7	0.059 ± 0.008
12.5 µg/L	4	11.7 ± 2.9	44.3 ± 4.0	0.058 ± 0.004
25 µg/L	5	12.1 ± 2.4	44.5 ± 3.2	0.061 ± 0.008
50 µg/L	3	11.6 ± 3.0	43.9 ± 4.3	0.062 ± 0.013
			Male	
0 µg/L	8	10.9 ± 2.7	43.1 ± 3.3	0.058 ± 0.008
6.25 µg/L	5	11.1 ± 2.0	44.1 ± 2.8	0.060 ± 0.010
12.5 µg/L	4	11.5 ± 3.0	43.1 ± 4.1	0.058 ± 0.007
25 µg/L	5	11.3 ± 3.0	43.5 ± 3.6	0.062 ± 0.010
50 µg/L	3	10.9 ± 1.5	43.3 ± 2.2	0.066 ± 0.011

Table S4. Prevalence (% of *n*) and severity of juvenile gonad mononuclear cellular infiltrate following exposure to *t*OP (NR: not remarkable; numbers in parentheses are significantly different than control based on RSCABS analysis).

	Female				
Nominal *t*OP concentration (µg/L)	0	6.25	12.5	25	50
Total *n*	30	20	16	21	12
Replicate tanks	8	5	4	5	3
Mononuclear Cellular Infiltrate					
NR	63	40	25	38	42
Minimal	33	60	(56)	(57)	(50)
Mild	3	0	19	5	8
Moderate	0	0	0	0	0
Severe	0	0	0	0	0

InCites Journal Citation Reports

Clarivate Analytics

2018 Journal Performance Data for: JOURNAL OF APPLIED TOXICOLOGY

ISSN: 0260-437X
eISSN: 1099-1263
WILEY
111 RIVER ST, HOBOKEN 07030-5774, NJ
ENGLAND

TITLES
ISO: J. Appl. Toxicol.
JCR Abbrev: J APPL TOXICOL

LANGUAGES
English

CATEGORIES
TOXICOLOGY -- SCIE

PUBLICATION FREQUENCY
12 issues/year

Downloaded on 4/17/2020, 8:33:04 AM from Journal Citation Reports (©2020 Clarivate Analytics)

InCites Journal Citation Reports

Clarivate Analytics

The data in the two graphs below and in the Journal Impact Factor calculation panels represent citation activity in 2018 to items published in the journal in the prior two years. They detail the components of the Journal Impact Factor. Use the "All Years" tab to access key metrics and additional data for the current year and all prior years for this journal.

2018 Journal Impact Factor & percentile rank in category for: JOURNAL OF APPLIED TOXICOLOGY

3.065

2018 Journal Impact Factor

2018 JIF Citation Distribution for: JOURNAL OF APPLIED TOXICOLOGY

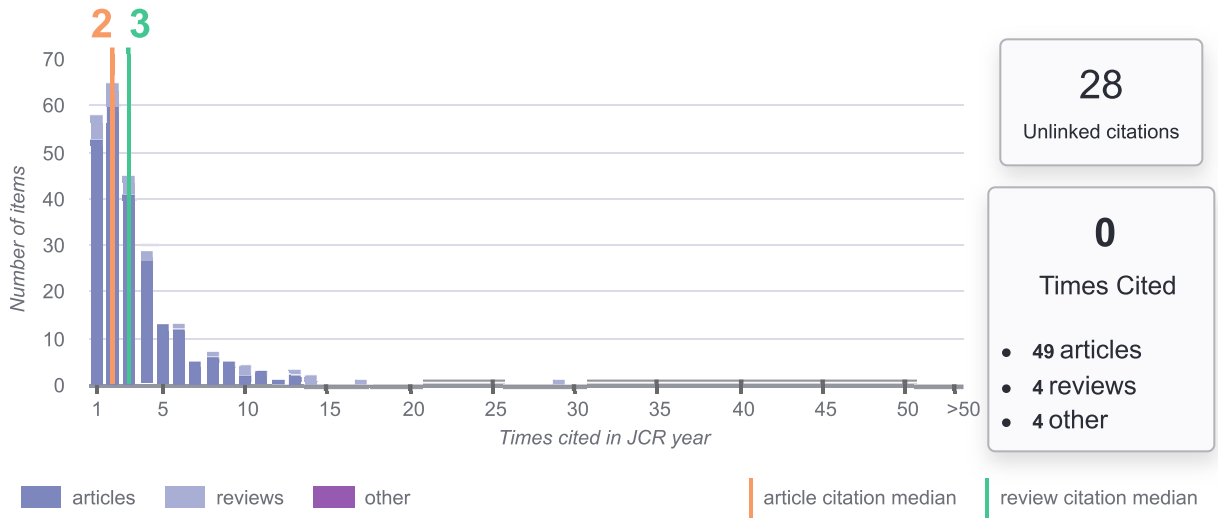

28
Unlinked citations

0
Times Cited

- **49** articles
- **4** reviews
- **4** other

Downloaded on 4/17/2020, 8:33:04 AM from Journal Citation Reports (©2020 Clarivate Analytics)

InCites Journal Citation Reports

Clarivate Analytics

Journal Impact Factor Calculation

$$\text{2018 Journal Impact Factor} = \frac{944}{308} = 3.065$$

How is Journal Impact Factor Calculated?

$$\text{JIF} = \frac{\text{Citations in 2018 to items published in } \mathbf{2016\ (489) + 2017\ (455)}}{\text{Number of citable items in } \mathbf{2016\ (157) + 2017\ (151)}} = \frac{944}{308}$$

Downloaded on 4/17/2020, 8:33:04 AM from Journal Citation Reports (©2020 Clarivate Analytics)

Journal Impact Factor contributing items

Citable items in 2017 and 2016 (308)

TITLE	CITATIONS COUNTED TOWARDS JIF
The C-elegans model in toxicity testing By: Hunt, Piper Reid **Volume: 37 Page: 50-59 Accession number: WOS:000388295300005** **Document Type: Review**	**29**
Mitochondrial oxidative stress and dysfunction in arsenic neurotoxicity: A review By: Prakash, Chandra; Soni, Manisha; Kumar, Vijay **Volume: 36 Page: 179-188 Accession number: WOS:000368144500001** **Document Type: Review**	**17**
Toxicity of inhaled particulate matter on the central nervous system: neuroinflammation, neuropsychological effects and neurodegenerative disease By: Wang, Yan; Xiong, Lilin; Tang, Meng **Volume: 37 Page: 644-667 Accession number: WOS:000399890400001** **Document Type: Review**	**14**
The use of human umbilical vein endothelial cells (HUVECs) as an in vitro model to assess the toxicity of nanoparticles to endothelium: a review By: Cao, Yi; Gong, Yu; Liu, Liangliang; Zhou, Yiwei; Fang, Xin et al. **Volume: 37 Page: 1359-1369 Accession number: WOS:000413314000001** **Document Type: Review**	**14**
Metabolic activation and drug-induced liver injury: in vitro approaches for the safety risk assessment of new drugs By: Gomez-Lechon, M. Jose; Tolosa, Laia; Donato, M. Teresa **Volume: 36 Page: 752-768 Accession number: WOS:000374382700001** **Document Type: Review**	**13**
PM2.5-induced lung inflammation in mice: Differences of inflammatory response in macrophages and type II alveolar cells By: He, Miao; Shibamoto, Takayuki; Ichinose, Takamichi; Yoshida, Seiichi; Ito, Tomohiro et al. **Volume: 37 Page: 1203-1218 Accession number: WOS:000409913500008** **Document Type: Article**	**13**
PM2.5-induced oxidative stress increases adhesion molecules expression in human endothelial cells through the ERK/AKT/NF-kappa B-dependent pathway By: Rui, Wei; Guan, Longfei; Zhang, Fang; Zhang, Wei; Ding, Wenjun **Volume: 36 Page: 48-59 Accession number: WOS:000365795900005** **Document Type: Article**	**13**

Downloaded on 4/17/2020, 8:33:04 AM from Journal Citation Reports (©2020 Clarivate Analytics)

Citations in 2018 (944)

TITLE	CITATIONS COUNTED TOWARDS JIF
JOURNAL OF APPLIED TOXICOLOGY	38
CHEMOSPHERE	24
FOOD AND CHEMICAL TOXICOLOGY	24
SCIENTIFIC REPORTS	18
ENVIRONMENTAL POLLUTION	17
SCIENCE OF THE TOTAL ENVIRONMENT	17
TOXICOLOGY LETTERS	16
ARCHIVES OF TOXICOLOGY	14
TOXICOLOGY AND APPLIED PHARMACOLOGY	14
INTERNATIONAL JOURNAL OF NANOMEDICINE	13

Downloaded on 4/17/2020, 8:33:04 AM from Journal Citation Reports (©2020 Clarivate Analytics)

InCites Journal Citation Reports

Clarivate Analytics

Source data

Journal source data 2018

	Articles	Reviews	Combined(C)	Other(O)	Percentage(C/(C+O))
Number in JCR Year 2018 (A)	119	18	137	3	98%
Number of References (B)	5,756	2,156	7,912	5	100%
Ratio (B/A)	48.4	119.8	57.8	1.7	

Downloaded on 4/17/2020, 8:33:04 AM from Journal Citation Reports (©2020 Clarivate Analytics)

InCites Journal Citation Reports

Clarivate Analytics

Box plot

Category Box Plot 2018

Category Box Plot

The category box plot depicts the distribution of Impact Factors for all journals in the category. The horizontal line that forms the top of the box is the 75th percentile (Q1). The horizontal line that forms the bottom is the 25th percentile (Q3). The horizontal line that intersects the box is the median Impact Factor for the category.
Horizontal lines above and below the box, called whiskers, represent maximum and minimum values.
The top whisker is the smaller of the following two values:
the maximum Impact Factor (IF)
Q1 IF + 3.5(Q1 IF - Q3 IF)
The bottom whisker is the larger of the following two values:
the minimum Impact Factor (IF)
Q1 IF - 3.5(Q1 IF - Q3 IF)
Box Plots are provided for the current JCR year for each of the categories in which the journal is indexed.

J APPL TOXICOL, IF: 3.065

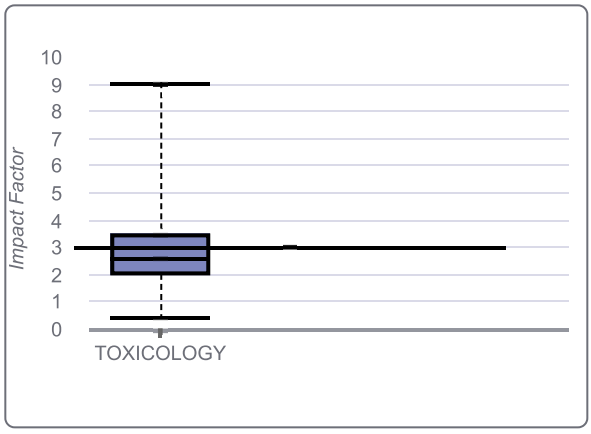

Downloaded on 4/17/2020, 8:33:04 AM from Journal Citation Reports (©2020 Clarivate Analytics)

InCites Journal Citation Reports

Clarivate Analytics

Rank

Rank

JCR Impact Factor

JCR Year	TOXICOLOGY		
	Rank	Quartile	JIF Percentile
2018	37/93	Q2	60.753
2017	36/94	Q2	62.234
2016	26/92	Q2	72.283
2015	33/90	Q2	63.889
2014	27/88	Q2	69.886
2013	24/87	Q2	72.989
2012	37/85	Q2	57.059
2011	38/83	Q2	54.819
2010	40/83	Q2	52.410
2009	43/77	Q3	44.805
2008	41/75	Q3	46.000
2007	37/73	Q3	50.000
2006	46/76	Q3	40.132
2005	31/75	Q2	59.333
2004	48/75	Q3	36.667
2003	49/77	Q3	37.013
2002	43/76	Q3	44.079
2001	48/78	Q3	39.103
2000	63/77	Q4	18.831
1999	40/74	Q3	46.622
1998	48/71	Q3	33.099
1997	54/63	Q4	15.079

Downloaded on 4/17/2020, 8:33:04 AM from Journal Citation Reports (©2020 Clarivate Analytics)

InCites Journal Citation Reports

Clarivate Analytics

ESI Total Citations

Rank

JCR Year	PHARMACOLOGY & TOXICOLOGY
2018	88/276-Q2
2017	86/274-Q2
2016	87/270-Q2
2015	89/266-Q2
2014	94/264-Q2
2013	100/267-Q2

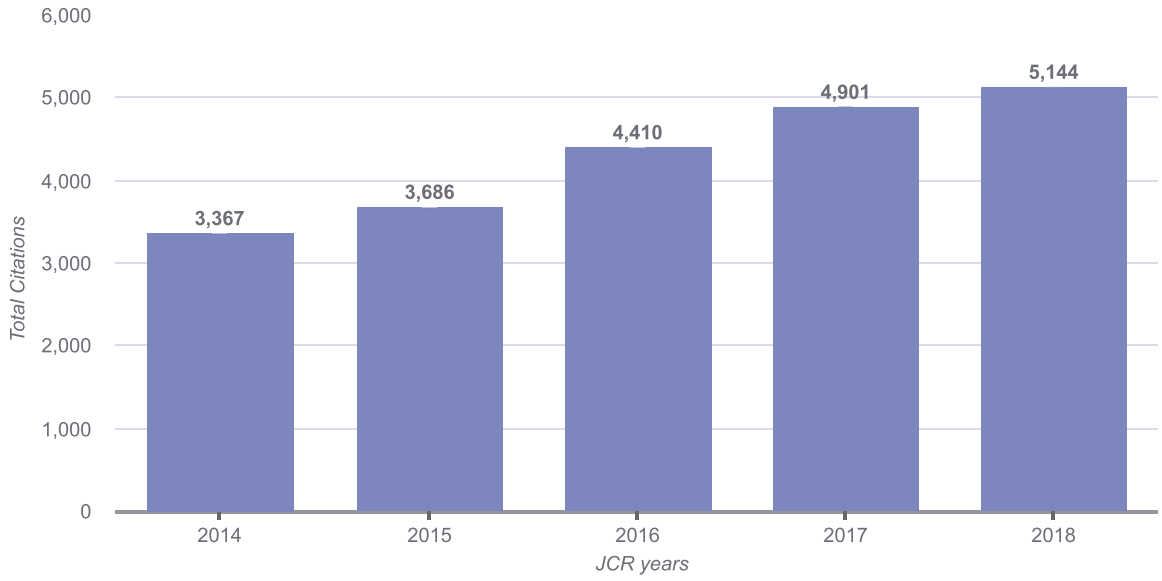

Downloaded on 4/17/2020, 8:33:04 AM from Journal Citation Reports (©2020 Clarivate Analytics)

InCites Journal Citation Reports

Clarivate Analytics

Cited Journal Data

Cited Half-Life Data

Cited Year	2018	2017	2016	2015	2014	2013	2012	2011	2010	2009	2008-All
#Cites from 2018	130	455	489	488	491	412	280	290	214	232	1,663
Cumulative %	2.53%	11.37%	20.88%	30.37%	39.91%	47.92%	53.36%	59.00%	63.16%	67.67%	100.00%

Cited Journal Graph 2018

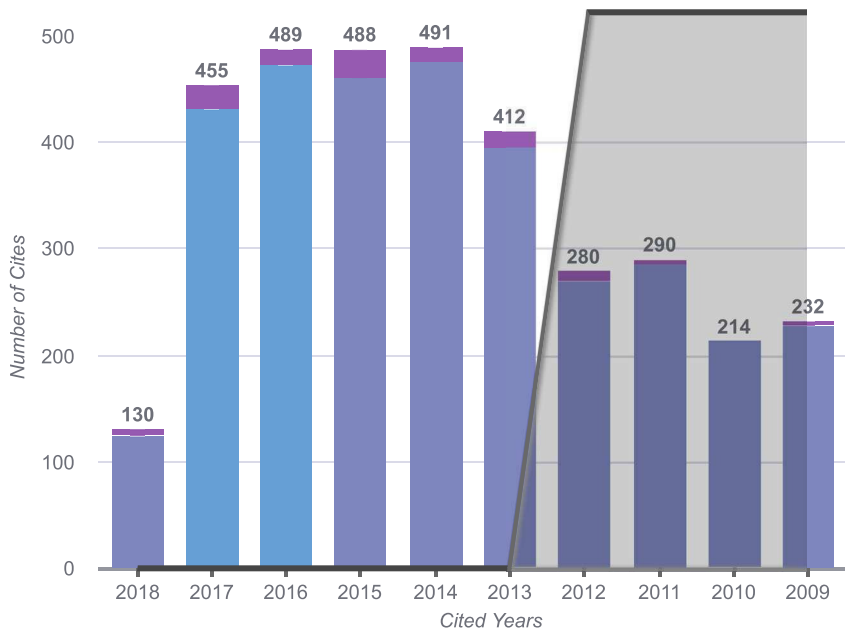

Non-self-citations: citations from the journal to articles in other journals.

Journal self - citations: citations from articles in the journal to articles in the same journal.

CITED JOURNAL GRAPH

The Cited Journal Graph shows the distribution (by cited year) of citations published in journals during the JCR year to items published in the Journal during the last 10 years.

The white/grey division indicates the cited half-life (if < 10.0). Half of the citations are to items that were published more recently than the cited half-life.

The two light-blue columns indicate citations used to calculate the Impact Factor (always the 2nd and 3rd columns).

Downloaded on 4/17/2020, 8:33:04 AM from Journal Citation Reports (©2020 Clarivate Analytics)

InCites Journal Citation Reports

Clarivate Analytics

Cited Journal Data 2018

Export

	Impact	Citing Journal	All Yrs	2018	2017	2016	2015	2014	2013	2012	2011	2010	2009	Res
		ALL Journals	5,144	130	455	489	488	491	412	280	290	214	232	1,66
		ALL OTHERS (731)	731	15	51	45	72	63	51	40	47	30	30	28
1	3.065	J APPL TOXICOL	148	6	23	15	26	13	15	10	3	0	4	3
2	3.499	TOXICOL LETT	104	6	2	14	4	3	4	8	6	5	1	5
3	5.108	CHEMOSPHERE	96	2	13	11	13	14	11	2	5	3	3	1
4	5.589	SCI TOTAL ENVIRON	86	2	10	7	8	10	5	3	11	5	6	1
5	3.775	FOOD CHEM TOXICOL	83	0	14	10	7	6	6	3	2	4	2	2
6	5.714	ENVIRON POLLUT	76	2	8	9	9	9	12	2	12	3	4	
7	5.741	ARCH TOXICOL	67	2	6	8	13	6	11	0	1	4	4	1
8	4.011	SCI REP-UK	66	2	12	6	6	8	5	3	5	1	3	1
9	4.183	INT J MOL SCI	65	7	2	9	10	6	2	4	3	4	4	1
10	3.564	TOXICOL SCI	64	2	7	5	11	9	7	7	1	0	2	1
11	2.996	REGUL TOXICOL PHARM	63	4	5	4	2	13	4	3	0	1	2	2
12	2.914	ENVIRON SCI POLLUT R	62	0	2	3	3	5	5	9	5	4	5	2
13	4.527	ECOTOX ENVIRON SAFE	55	2	6	5	6	2	1	2	7	4	2	1
14	3.585	TOXICOL APPL PHARM	47	0	9	5	2	2	5	3	5	3	0	1
15	3.067	TOXICOL IN VITRO	46	2	1	8	7	5	6	1	2	0	2	1
16	4.771	CRIT REV TOXICOL	37	2	7	3	8	4	5	0	1	0	2	
17	3.407	CHEM-BIOL INTERACT	35	1	3	4	2	3	4	1	0	5	2	1
18	7.943	ENVIRON INT	34	3	1	2	2	2	0	2	7	1	1	1
19	3.547	TOXICOLOGY	34	1	3	7	3	1	0	0	1	1	0	1
20	2.776	PLOS ONE	33	0	5	0	2	4	5	1	2	3	3	
21	3.845	FRONT PHARMACOL	32	1	2	3	6	4	2	3	0	1	4	
22	3.200	REPROD TOXICOL	32	1	7	2	8	2	3	3	1	0	0	
23	2.431	BIOL TRACE ELEM RES	30	0	2	4	2	0	4	3	4	2	0	
24	4.471	INT J NANOMED	30	2	8	5	1	4	4	2	0	1	2	
25	3.049	RSC ADV	29	1	6	0	1	5	0	3	2	0	1	1
26	1.593	TOXICOL RES-UK	29	1	3	4	2	3	2	0	3	2	1	
27	3.743	BIOMED PHARMACOTHER	28	0	1	3	1	2	1	1	1	2	0	1
28	5.026	ENVIRON RES	28	0	1	3	3	3	1	1	6	1	1	

Showing 1 - 30 rows of 636 total *(use export to download the full table)*

Downloaded on 4/17/2020, 8:33:04 AM from Journal Citation Reports (©2020 Clarivate Analytics)

InCites Journal Citation Reports

Clarivate Analytics

Citing Journal Data

Citing Half-Life Data

Citing Year	2018	2017	2016	2015	2014	2013	2012	2011	2010	2009	2008-All
#Cites from 2018	29	377	627	644	559	560	514	461	418	405	3,323
Cumulative %	0.37%	5.13%	13.05%	21.18%	28.24%	35.32%	41.81%	47.63%	52.91%	58.03%	100.00%

Citing Journal Graph 2018

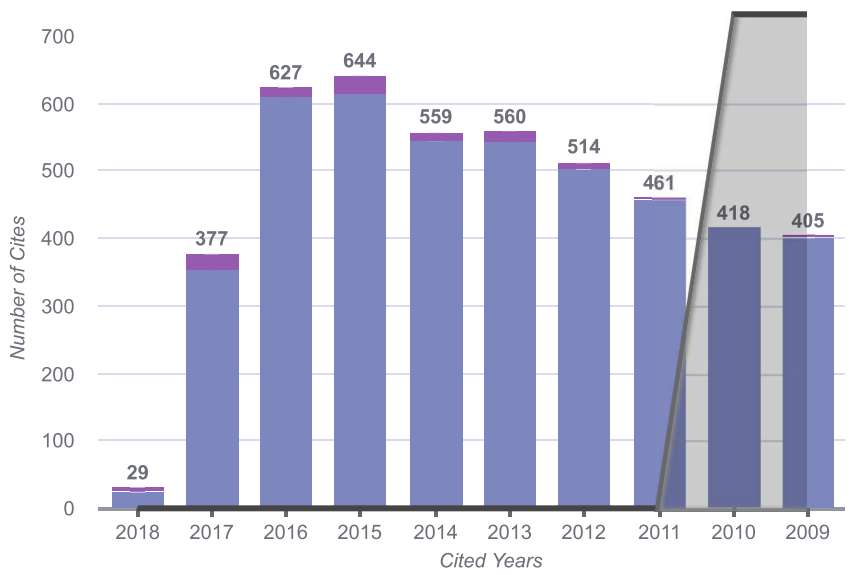

CITING JOURNAL GRAPH

The Citing Journal Graph shows the distribution (by cited year) of citations published in the Journal during the JCR year to items published in journals during the last 10 years.

The white/grey division indicates the citing half-life (if < 10.0). Half of the citations are to items that were published more recently than the citing half-life.

Non-self-citations: citations from the journal to articles in other journals.

Journal self - citations: citations from articles in the journal to articles in the same journal.

Downloaded on 4/17/2020, 8:33:04 AM from Journal Citation Reports (©2020 Clarivate Analytics)

InCites Journal Citation Reports

Clarivate Analytics

Citing Journal Data 2018

Export

	Impact	Citing Journal	All Yrs	2018	2017	2016	2015	2014	2013	2012	2011	2010	2009	Rest
		ALL Journals	7,917	29	377	627	644	559	560	514	461	418	405	3,32
		ALL OTHERS (1292)	1,292	3	67	109	95	92	98	78	65	60	62	56
1	3.564	TOXICOL SCI	156	0	11	5	14	9	8	13	10	12	9	6
2	3.065	J APPL TOXICOL	148	6	23	15	26	13	15	10	3	0	4	3
3	7.736	ENVIRON HEALTH PERSP	145	0	6	3	8	3	7	10	6	12	8	8
4	3.585	TOXICOL APPL PHARM	134	0	8	12	5	8	13	13	4	10	13	4
5	3.499	TOXICOL LETT	113	1	4	6	6	11	11	6	8	8	8	4
6	4.471	INT J NANOMED	102	0	1	11	15	29	10	10	9	8	1	
7	2.776	PLOS ONE	99	0	6	8	15	22	19	11	9	5	2	
8	7.149	ENVIRON SCI TECHNOL	93	0	0	7	9	10	9	13	9	4	5	2
9	3.547	TOXICOLOGY	90	1	1	2	7	3	7	3	6	4	5	5
10	4.106	J BIOL CHEM	85	0	0	1	2	2	3	4	4	2	7	6
11	3.067	TOXICOL IN VITRO	80	0	7	8	14	9	10	3	6	4	4	1
12	2.256	MUTAT RES-GEN TOX EN	77	0	1	1	3	2	2	2	3	3	3	5
13	3.200	REPROD TOXICOL	66	0	4	4	7	5	4	6	8	6	4	1
14	3.775	FOOD CHEM TOXICOL	65	0	4	9	3	6	8	4	3	2	2	2
15	3.794	AQUAT TOXICOL	63	0	4	11	3	9	6	7	5	3	3	1
16	5.108	CHEMOSPHERE	63	3	9	8	8	1	4	5	4	4	4	1
17	9.580	P NATL ACAD SCI USA	58	0	0	2	2	1	2	2	1	4	4	4
18	5.741	ARCH TOXICOL	57	0	6	6	7	6	5	5	6	1	2	1
19	2.996	REGUL TOXICOL PHARM	48	0	6	9	11	2	2	2	0	1	2	1
20	5.589	SCI TOTAL ENVIRON	46	0	5	6	4	5	1	2	5	5	0	1
21	43.070	NATURE	44	0	0	0	1	1	3	1	3	2	2	3
22	6.561	PART FIBRE TOXICOL	42	0	2	10	1	11	6	3	4	1	2	
23	3.274	CHEM RES TOXICOL	40	0	1	3	3	5	1	2	2	3	5	1
24	3.407	CHEM-BIOL INTERACT	40	0	2	5	1	3	4	2	1	4	3	1
25	36.216	CELL	38	0	0	1	0	1	4	2	4	3	2	2
26	7.943	ENVIRON INT	38	0	3	10	5	4	3	3	3	1	2	
27	4.011	SCI REP-UK	38	0	8	19	8	0	2	0	1	0	0	
28	41.063	SCIENCE	38	0	0	0	1	1	2	3	0	0	0	3

Showing 1 - 30 rows of 885 total *(use export to download the full table)*

Downloaded on 4/17/2020, 8:33:04 AM from Journal Citation Reports (©2020 Clarivate Analytics)

InCites Journal Citation Reports

Clarivate Analytics

Journal Relationships

Journal Relationships 2018

Citing Data

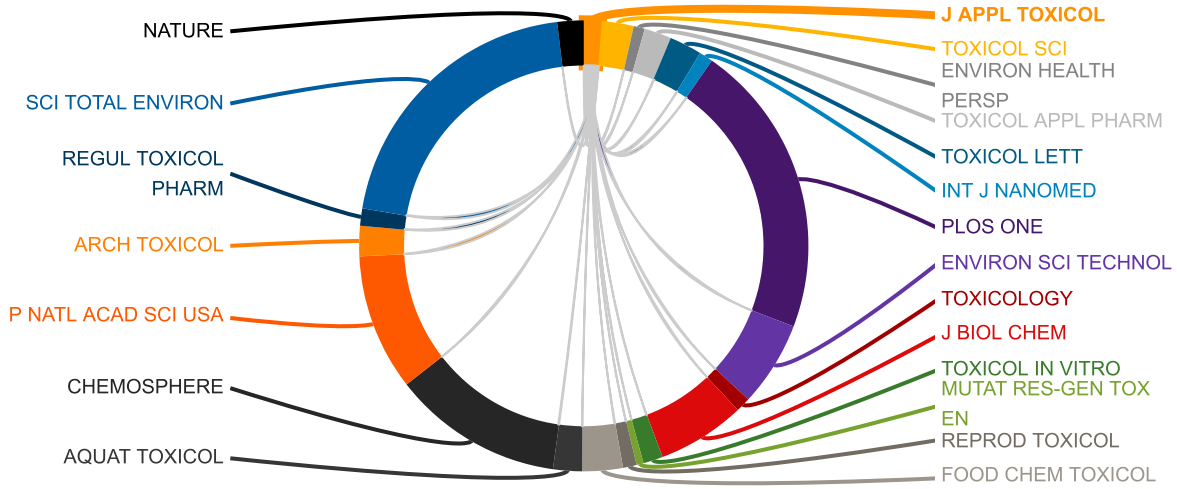

Cited Data

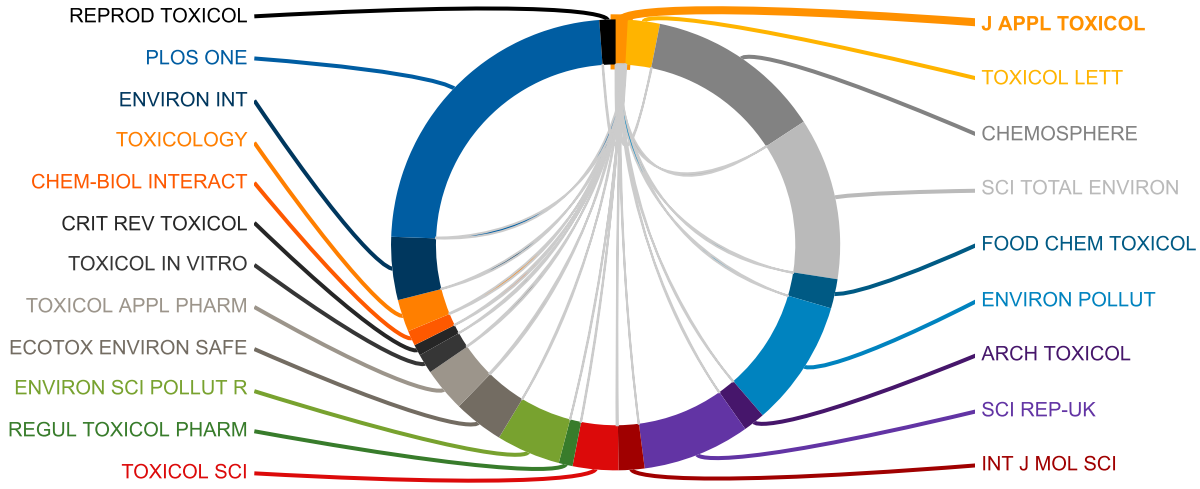

Downloaded on 4/17/2020, 8:33:04 AM from Journal Citation Reports (©2020 Clarivate Analytics)

InCites Journal Citation Reports

Clarivate Analytics

Key Indicators 2018

IMPACT METRICS	
Total Cites	5,144
Journal Impact Factor	3.065
5 Year Impact Factor	2.975
Immediacy Index	0.949
Impact Factor without Journal Self Cites	2.942

INFLUENCE METRICS	
Eigenfactor Score	0.00644
Article Influence Score	0.622
Normalized Eigenfactor	0.76678

SOURCE METRICS	
Citable Items	137
% Articles in Citable Items	86.86
Average JIF Percentile	60.753
Cited Half-Life	6.4
Citing Half-Life	8.4

Downloaded on 4/17/2020, 8:33:04 AM from Journal Citation Reports (©2020 Clarivate Analytics)

InCites Journal Citation Reports

Clarivate Analytics

Metric Trend Total Cites

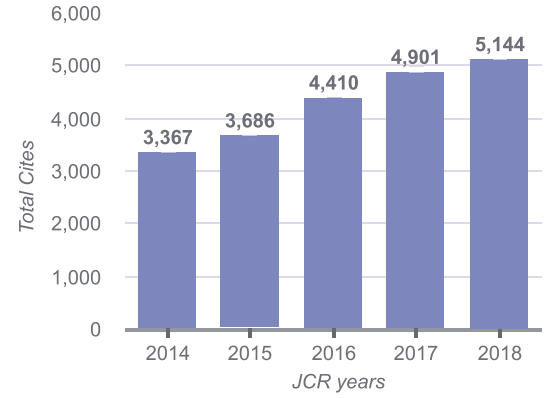

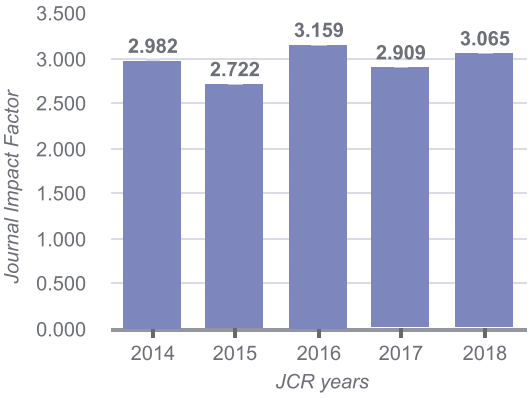

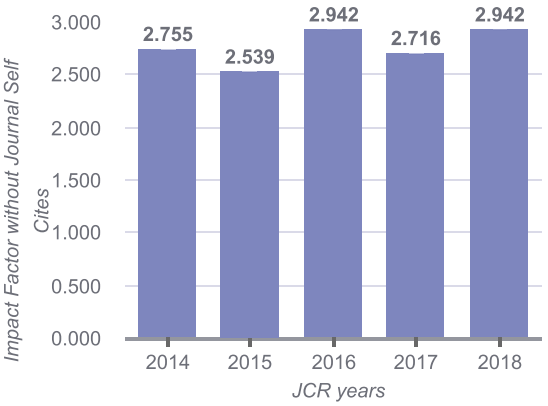

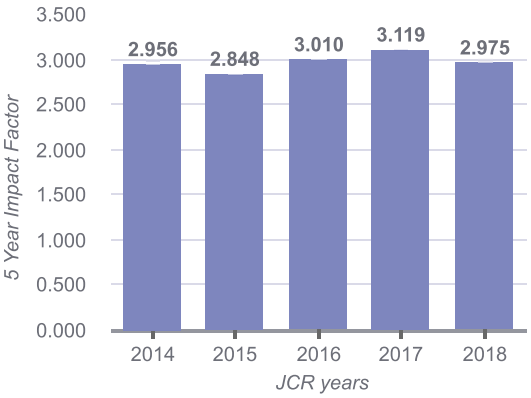

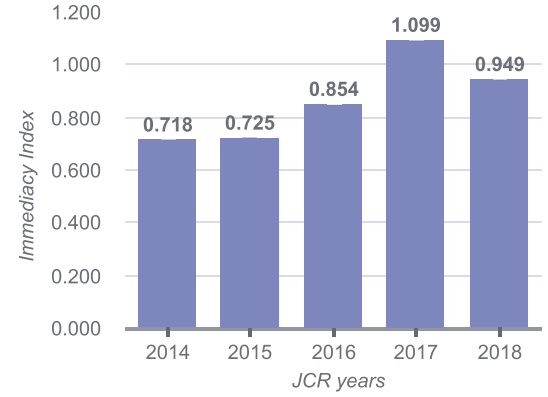

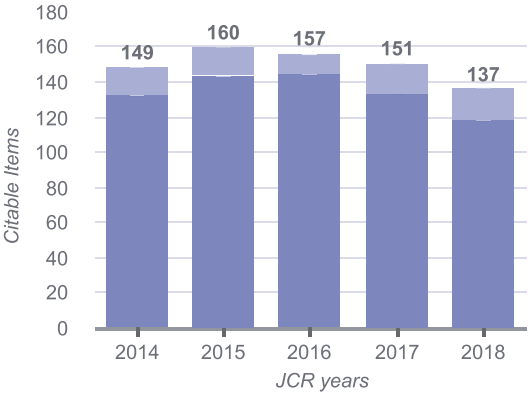

Downloaded on 4/17/2020, 8:33:04 AM from Journal Citation Reports (©2020 Clarivate Analytics)

InCites Journal Citation Reports

Clarivate Analytics

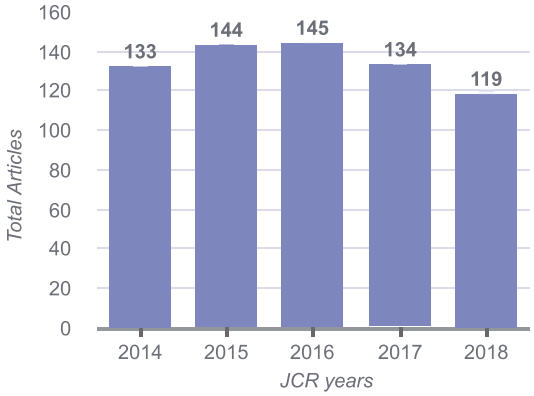

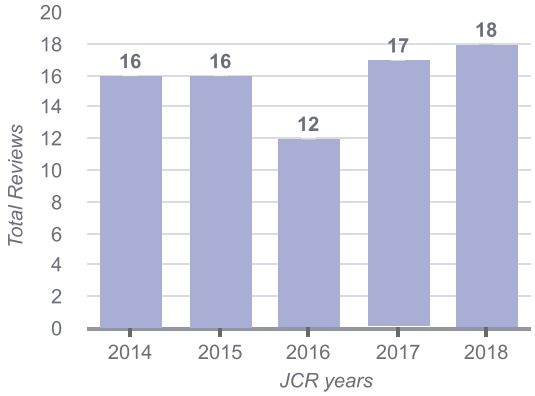

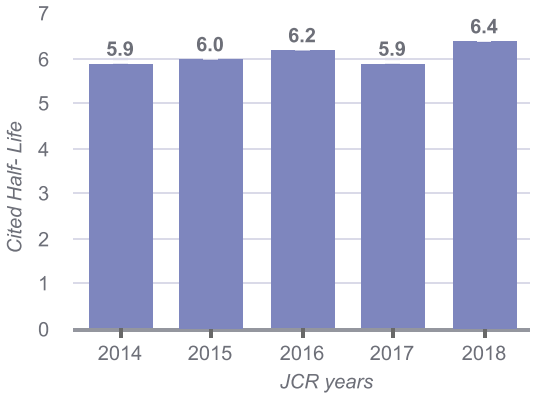

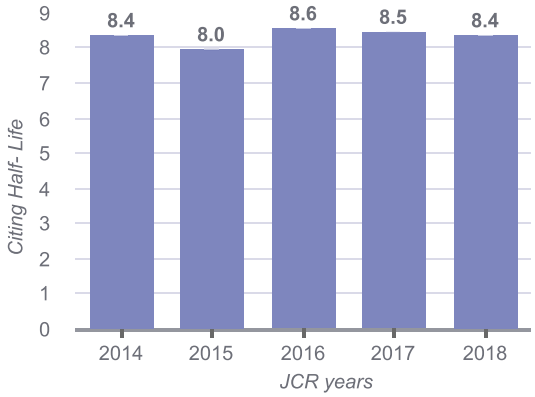

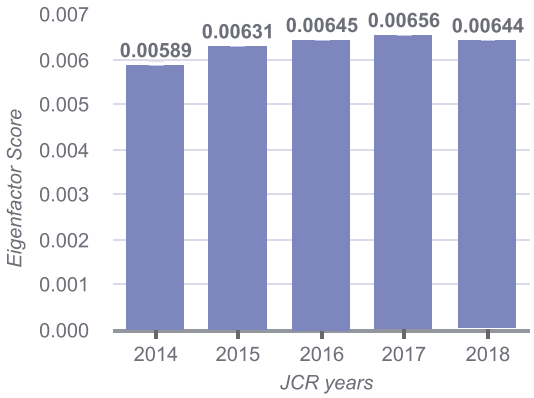

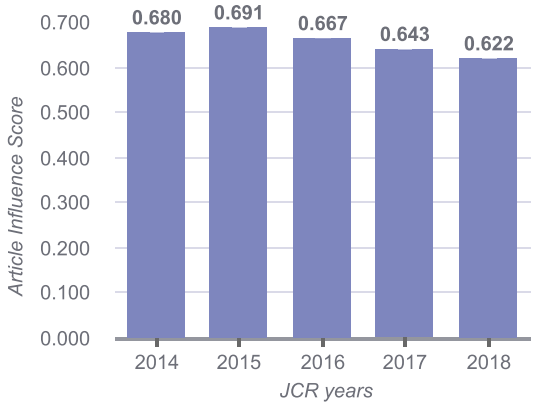

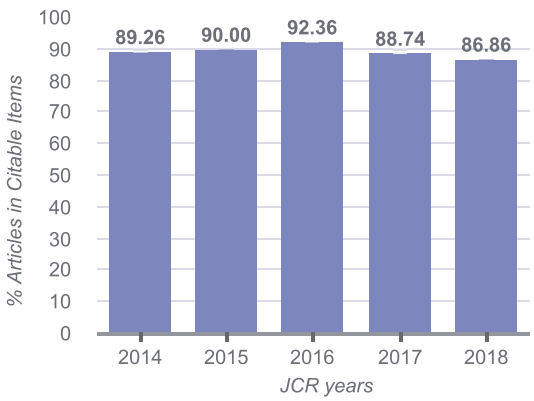

Downloaded on 4/17/2020, 8:33:04 AM from Journal Citation Reports (©2020 Clarivate Analytics)

InCites Journal Citation Reports

Clarivate Analytics

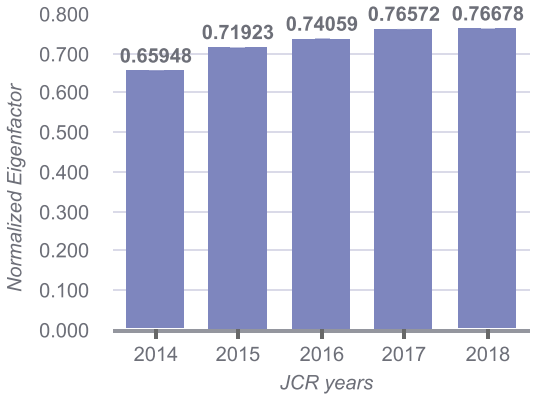

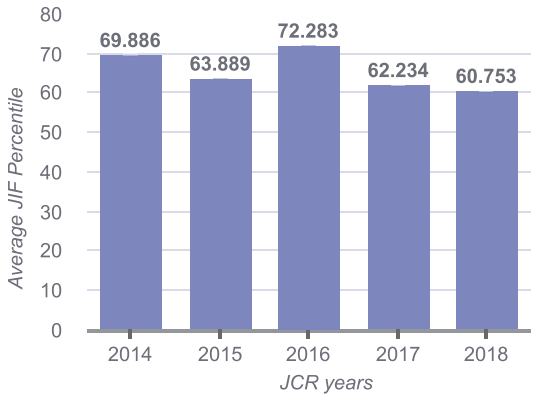

Downloaded on 4/17/2020, 8:33:04 AM from Journal Citation Reports (©2020 Clarivate Analytics)

InCites Journal Citation Reports

Clarivate Analytics

Journal profile [2016 - 2018]

Contributions by country/region

	country	count
1	USA	133
2	CHINA MAINLAND	106
3	Japan	80
4	England	29
5	South Korea	22
6	France	20
7	India	19
8	Canada	18
-	GERMANY (FED REP GER)	18
10	Italy	15

Contributions by organizations

	organization	count
1	US FOOD & DRUG ADMINISTRATION (FDA)	16
2	UNITED STATES ENVIRONMENTAL PROTECTION AGENCY	14
-	UNIVERSITY OF CALIFORNIA SYSTEM	14
4	UNIVERSITY OF ARKANSAS SYSTEM	12
5	NATIONAL INSTITUTE FOR ENVIRONMENTAL STUDIES - JAPAN	11
6	CHINESE ACADEMY OF SCIENCES	10
-	HUAZHONG UNIVERSITY OF SCIENCE & TECHNOLOGY	10
-	NATIONAL INSTITUTE OF HEALTH SCIENCES - JAPAN	10
9	KAROLINSKA INSTITUTET	9
10	INSTITUT NATIONAL DE LA SANTE ET DE LA RECHERCHE MEDICALE (INSERM)	8
-	NATIONAL INSTITUTES OF NATURAL SCIENCES (NINS) - JAPAN	8

Downloaded on 4/17/2020, 8:33:04 AM from Journal Citation Reports (©2020 Clarivate Analytics)

Aquatic Toxicology 199 (2018) 240–251

Contents lists available at ScienceDirect

Aquatic Toxicology

journal homepage: www.elsevier.com/locate/aqtox

Effects of multiple life stage exposure to the fungicide prochloraz in *Xenopus laevis*: Manifestations of antiandrogenic and other modes of toxicity

Jonathan T. Haselman*, Patricia A. Kosian, Joseph J. Korte, Allen W. Olmstead[1], Sigmund J. Degitz

US EPA Mid-Continent Ecology Division, 6201 Congdon Blvd, Duluth, MN, 55804, USA

ARTICLE INFO

Keywords:
Xenopus laevis
Prochloraz
LAGDA
Endocrine disruption
Insl3
Rflcii
Cyp17

ABSTRACT

The Larval Amphibian Growth and Development Assay (LAGDA) is an internationally harmonized testing guideline for evaluating effects of chronic chemical exposure in amphibians. In order to evaluate the effects of chronic exposure to an antiandrogenic chemical in an amphibian model, prochloraz was tested using a variation of the LAGDA design. Exposure was initiated with < 1d post-fertilization embryos at nominal concentrations of 0, 6.7, 20, 60 and 180 µg/L (0, 18, 53, 159, 478 nM) and continued in flow-through conditions until two months following the median time that controls completed metamorphosis. Growth, developmental rate, circulating thyroid hormone and thyroid gland histopathology were evaluated in a subsample at completion of metamorphosis. There were no effects on growth or development at this stage, but circulating thyroid hormone was elevated in the 20, 60 and 180 µg/L treatments and minimal to mild thyroid follicular cell hypertrophy was observed histologically in the 180 µg/L treatment. Growth, overt toxicity, and reproductive development were evaluated at test termination. There were no effects on growth in either gender, but livers and kidneys exhibited treatment-related pathologies consistent with organ toxicity related to metabolism and presumably impaired excretion of prochloraz metabolites. Histological assessments of female ovaries resulted in minimal pathologies only in the 180 µg/L treatment while male testes exhibited numerous treatment-related pathologies that are consistent with previously reported antiandrogenic effects of prochloraz in other species. The most severe testis pathologies occurred in the 180 µg/L treatment; however, incidences of treatment-related pathologies occurred in all prochloraz treatments. Müllerian duct regression in males was inhibited by prochloraz exposure while Müllerian duct maturation in females was accelerated, characteristic of a feminizing effect. Gene expression levels of potential biomarkers of testis function were also measured. Relative abundance of *cyp17a1* transcripts was generally unaffected by prochloraz exposure whereas the Insl3 orthologue, *rflcii*, was elevated by 3 and > 5-fold in the 60 and 180 µg/L treatments, respectively, indicating impaired Leydig cell maturation and testosterone signaling. Overall, prochloraz exposure caused effects characteristic of an antiandrogenic mode of action, which is consistent with previously reported results in other species and supports the utility of the LAGDA design for chemical testing.

1. Introduction

The Larval Amphibian Growth and Development Assay (LAGDA) is a second tier, multiple life stage, chemical testing guideline that was developed and globally harmonized under the Endocrine Disruptor Screening Program of the U.S. Environmental Protection Agency (https://www.epa.gov/endocrine-disruption) in collaboration with members of the Organization for Economic Cooperation and Development (OECD) to support ecological risk assessment (OECD, 2015; US EPA, 2015). The LAGDA is intended to be a definitive test that identifies apical effects following chronic chemical exposure in the model amphibian species *Xenopus laevis* and establishes a quantitative relationship between exposure concentrations and any adverse effects. During the development of the assay guideline, it was necessary to validate the assay design using chemicals with known modes of action within the endocrine system. Previous reports of LAGDA validation studies include exposures to 4-*tert*-octylphenol and 17β-trenbolone, a weak estrogen receptor agonist and potent androgen receptor agonist,

* Corresponding author.
E-mail addresses: haselman.jon@epa.gov (J.T. Haselman), kosian.pat@epa.gov (P.A. Kosian), korte.joe@epa.gov (J.J. Korte), allen.olmstead@bayer.com (A.W. Olmstead), degitz.sigmund@epa.gov (S.J. Degitz).
[1] Present address: Environmental Toxicology and Risk Assessment, Development North America, Bayer CropScience LP, Research Triangle Park, NC, 27709, USA

https://doi.org/10.1016/j.aquatox.2018.03.013
Received 14 December 2017; Received in revised form 8 March 2018; Accepted 12 March 2018
Available online 03 April 2018
0166-445X/ Published by Elsevier B.V.

respectively (Haselman et al., 2016a) and exposure to benzophenone-2, a chemical having estrogenic and thyroid disrupting properties (Haselman et al., 2016b). The objectives of the current study were to test a model chemical with antiandrogenic properties in order to further validate the diagnostic capabilities of the LAGDA design and to develop gene expression markers that could provide mechanistic insight into the antiandrogenic mode of action.

Prochloraz is an imidazole fungicide that disrupts ergosterol synthesis by inhibiting cytochrome P450 (CYP) 14α-demethylase (CYP51) through an interaction with iron in the heme cofactor, effectively weakening fungal cell membranes (Henry and Sisler, 1984; Bossche, 1985). Prochloraz has been implicated as an endocrine disrupting compound because it is an antagonist of the androgen receptor (Andersen et al., 2002; Ankley et al., 2005; Birkhøj et al., 2004; Kojima et al., 2004; Noriega et al., 2005; Vinggaard et al., 2002, 2006) and also inhibits steroidogenesis enzymes CYP19 aromatase (Andersen et al., 2002; Ankley et al., 2005; Sanderson et al., 2002; Vinggaard et al., 2000, 2006) and CYP 17α-hydroxylase/17,20-lyase (CYP17) (Blystone et al., 2007a, 2007b; Laier et al., 2006). The timing and life stage of in vivo prochloraz exposure likely influences the predominant toxic mode of action as evidenced by a series of studies in rodents and fish. Exposure to prochloraz in utero and in immature male rats caused reproductive malformations in androgen-dependent tissues, whereas effects on female reproductive development were minimal (Noriega et al., 2005; Laier et al., 2006; Vinggaard et al., 2002, 2005). Exposure to prochloraz in reproductively active fathead minnows caused decreased circulating estradiol in females with a corresponding decrease in circulating vitellogenin (estrogen-regulated egg yolk protein) in addition to oocyte atresia, while males exhibited decreased circulating testosterone and increased spermatogonia (Ankley et al., 2005). These studies support a consistent series of mechanisms by which prochloraz elicits antiandrogenic effects; however, the timing of exposure in relation to the ontogeny of the endocrine targets during reproductive development and maturation appears to have a substantial influence on the gender-specific phenotypes following exposure. The LAGDA prescribes chemical exposure throughout embryonic, larval and juvenile development, so it was expected that developmental effects in the current study would occur more consistent with the rodent studies that resulted in malformations of the male reproductive system. Following this hypothesis, a parallel investigation was conducted to evaluate potential gene expression biomarkers of chemical-induced testis dysfunction in this amphibian model.

Insulin-like 3 protein (INSL3) is a Leydig cell-specific peptide hormone necessary for testis descent and gubernacular development in mammals and plays a role in follicle selection in the adult ovary (Bathgate et al., 2013). Recently, INSL3 has been increasingly employed as a biomarker of Leydig cell function in mammals (Roth et al., 2013; Ivell et al., 2013). Relaxin family locus C type II (Rflcii) in *Xenopus* sp. is orthologous to the mammalian INSL3 protein. Global gene expression analysis in *Xenopus tropicalis* gonads during differentiation indicated that *rflcii* was the transcript showing the highest normalized expression level overall and was the most differentially expressed transcript between ovary and testis tissues (testis-enriched by ~300-fold) (Haselman et al., 2015). This profound difference in expression between tissues provided evidence of this gene's importance in *Xenopus* testis development and is consistent with mammalian testis *Insl3* expression exclusively in Leydig cells (Adham et al., 1993). However, the mechanistic function of INSL3 orthologues has not been well-characterized across species, nor has its response to chemical perturbation been investigated in amphibians. The results presented herein provide precedent for *rflcii* being a testis-specific biomarker for impaired androgen production and/or signaling in *Xenopus laevis*.

Another key protein closely associated with the androgen axis and male reproductive development is CYP17. This enzyme is active within the steroidogenesis pathway and is necessary for synthesis of testosterone and consequently affects downstream estradiol synthesis due to the required aromatization of testosterone to produce estradiol. A growing body of evidence supports that prochloraz inhibits CYP17 (Ankley et al., 2009; Blystone et al., 2007a, 2007b; Hecker et al., 2006; Laier et al., 2006; Villeneuve et al., 2007) and other CYPs due to the imidazole interaction with iron in the heme cofactor required by all CYPs, which could be a major contribution to the antiandrogenic mode of action of prochloraz. *Cyp17* gene expression has been shown to be upregulated in the testis of fathead minnows (Ankley et al., 2009) and medaka (Zhang et al., 2008) exposed to prochloraz, while rodents exposed to prochloraz upregulate CYP17 protein production in the testis without upregulating gene transcription (Blystone et al., 2007b; Laier et al., 2006). These CYP17-related responses to prochloraz exposure across species appear to be adaptive responses to compensate for impaired androgen signaling. Altogether, the current study provided a sensible means to evaluate gene expression of *rflcii* as a potential biomarker of testis dysfuntion and *cyp17* as a bioindicator of compensation due to chemical stress in an amphibian model.

2. Materials and methods

2.1. Experimental design

The experimental design of this study was similar to the previously described studies contributing to the development of the LAGDA (Haselman et al., 2016a) and the final published guidelines (OECD, 2015; US EPA, 2015). However, due to slight differences in execution of this study during guideline development, much of the methods will be described. *Xenopus laevis* embryos (< 1d post-fertilization) were exposed to four different chemical concentrations and control water until two months after the median time to Nieuwkoop and Faber ([NF], 1994) stage 66 (completion of metamorphosis) in the control. There were five replicate tanks in each test concentration with eight replicate tanks for the control. Generalized toxicity was evaluated by mortality rates, abnormal behavior and growth (weight and snout-vent length) while toxicity affecting metabolism and excretion was evaluated via histopathology of the juvenile liver and kidney at test termination. Thyroid-specific toxicity was evaluated by rates of larval development (time to NF stage 66) and NF stage 66 thyroid histopathology assessments. Histopathology assessments of the juvenile gonads and reproductive ducts at test termination were also performed to evaluate effects on reproductive development. Additionally, gene expression of *rflcii* and *cyp17a1* in testis tissues was evaluated by randomly choosing either the left or right testis from each male for gene expression while the contralateral testis was left in situ for histopathology assessments. Sex ratios and possible sex reversal were also determined by comparing individual genotypes to phenotypes.

2.2. Test concentrations

The high test concentration was set based on range finding experiments (data not shown). In those studies, conducted with *Xenopus tropicalis*, concentrations in excess of 200 µg/L resulted in mortality in early larval organisms. Therefore, the high test concentration was set at 180 µg/L with a 0.33 dilution factor resulting in nominal test concentrations of 180, 60, 20 and 6.7 µg/L (478, 159, 53, 18 nM).

2.3. Environmental conditions

The source water used for the study was from Lake Superior (LSW), which was initially filtered through sand, UV sterilized and filtered again to 5 µm before entering the in-house culture or exposure aquaria. The incoming culture water is tested on a yearly basis for contaminants including copper, chlorine, chloramine, estrogenic or androgenic chemicals, fluoride, perchlorate and chlorate as measurable levels of any of these compounds could confound results of the bioassay. Flow-through conditions were maintained by delivering toxicant solutions and control

LSW to 6.5 L glass exposure tanks at a constant rate of 44 ml/min, achieving approximately 9.5 tank replacements per day. The pump-driven dilution system was the same system as was used for the 4-*tert*-octylphenol study described in Haselman et al. (2016a). Exposure tanks were held at 21 °C throughout the duration of the exposure by controlling the temperature of the delivery/dilution water and also by a water bath in which the exposure tanks were partially submerged. Water quality measurements including dissolved oxygen, pH and conductivity were taken in all exposure tanks once per week throughout the duration of the test (Supplemental Table 1). Alkalinity and hardness were measured once per month in one replicate tank per treatment. There were no treatment-related effects on water quality. A 12-h light and 12-h dark cycle was used with fluorescent lighting at intensities between 600 and 2000 lx (lumens/m^2) at the water surface. Exposure tanks were randomly assigned to positions within the exposure system to reduce potential effects from systematic environmental differences in temperature or light.

2.4. Chemical stock preparation

18 mg/L prochloraz stock solutions were prepared by dissolving the neat material (Sigma-Aldrich, St. Louis, MO, USA; CAS 67747-09-5, purity: 99.1%) in 20 ml of high purity acetone and quantitatively transferring to a 19 L carboy. The side walls of the carboy were rinsed with acetone and it was carefully tipped onto its side and placed on a roller. Filtered and desiccated compressed air was gently blown into the bottle as it was rolled to evaporate the acetone and shell-coat the carboy with prochloraz. Once the acetone was completely evaporated, the carboy was filled with reverse osmosis water and stirred overnight to dissolve the prochloraz.

2.5. Test initiation and feeding

All animal care and use procedures for these experiments were reviewed and cleared by the Mid-Continent Ecology Division's Animal Care and Use Committee. Procedures for test initiation and feeding are the same as described by Haselman et al. (2016a) except that embryos were transferred to the test chambers at approximately NF stage 20 for initiation of exposure.

2.6. Sub-sampling at completion of metamorphosis (NF stage 66)

Sub-sampling was performed by dividing the exposure tank and separating individuals that completed metamorphosis (NF stage 66) from actively metamorphosing larvae and recording the date on which each individual reached NF stage 66. One out of each group of four consecutive individuals completing metamorphosis in any given tank was randomly sampled for growth metrics including weight and snout-vent length, serum for circulating thyroid hormone and thyroid gland histopathology. At any given time during metamorphosis, developmental stages of organisms within an experimental unit are generally normally distributed. This larval sub-sampling method was intended to reduce bias toward sampling individuals on the leading or trailing edges of development in a particular tank and ensure all individuals in a tank had equal likelihood of being sampled upon reaching NF stage 66. Sub-sampled individuals were euthanized by submersion in LSW with 200 mg/L tricaine methanesulfonate ([MS-222], Argent Chemical Laboratories, Redmond, WA, USA) buffered with 400 mg/L sodium bicarbonate. Following growth measurements, blood was collected directly from the aorta using a 25 µl capillary tube and then a transverse cut was made at the posterior margin of the arms for decapitation; the head was fixed in Davidson's solution for thyroid histopathology. Individuals not sampled were left in the divided tank until all individuals had reached NF stage 66, at which time the tank dividers were removed.

2.7. Cull and test termination

Two to three weeks following the time at which all individuals completed metamorphosis (NF stage 66), gender genotyping was conducted and a cull was performed to reduce tank density to five males and five females in each tank until test termination. The cull and associated genotyping were performed according to the procedures previously described by Haselman et al. (2016a). Briefly, non-invasive unique toe clips were taken from each individual in each tank resulting in both an identification scheme and DNA samples that were analyzed by PCR for the presence/absence of a W chromosome-linked gene (DM-W) that effectively identified genotypic females, a method previously described by Yoshimoto et al. (2008). Juvenile sampling at test termination was also performed according to procedures previously described by Haselman et al. (2016a). Briefly, following euthanasia by injection of buffered MS-222, frogs were laid in dorsal recumbency, chest cavities were opened and blood was collected by severing the aorta. Next, livers were removed, weighed, transferred to individual cassettes and fixed in Davidson's solution for 48 h. Finally, internal viscera were removed leaving the gonads, kidneys and Müllerian ducts in situ except that one of the juvenile testes per male was randomly chosen to be processed for total RNA purification and subsequent quantitative PCR analyses. Removed testes were homogenized in lysis buffer from an RNeasy Plus kit (Qiagen Inc., Valencia, CA, USA), and immediately frozen on dry ice until samples could be moved to storage at −80 °C. Abdomens containing the kidneys, Müllerian ducts and gonad(s) were trimmed at the anterior and posterior margins of the kidneys, transferred to individual cassettes and fixed in Davidson's fixative for 48 h. Tissue from the lower leg was kept for subsequent DNA purification and genotypic sex determination.

2.8. Histological procedures

All tissues preserved for histological analyses were fixed, processed and evaluated according to the procedures previously described by Haselman et al. (2016a). Following fixation in Davidson's fluid for 48 h and subsequent storage in 10% neutral buffered formalin, liver, kidney, gonad and reproductive duct tissues were shipped to Integrated Laboratory Systems, Inc. ([ILS®], Research Triangle Park, NC, USA) where they were processed, embedded, sectioned, mounted and stained with H&E using typical histological procedures. Histopathologic findings were scored for severity by an ILS® pathologist according to the grading system previously described by Haselman et al. (2016a) for all tissues except for thyroid. Thyroid tissues were shipped to Experimental Pathology Laboratories, Inc. ([EPL], Sterling, VA, USA) where they were processed as described above and histologic findings scored for severity by a pathologist using the grading system for thyroid histopathology developed and described by Grim et al. (2009).

2.9. Serum thyroid hormone

Following blood collection from NF stage 66 organisms, the capillary tubes were placed on ice and allowed to clot over a period of 4 h. They were subsequently spun at 13,700 × *g* for 2 min in a serological centrifuge and serum was transferred to vials and stored at −80 °C until they were pooled, diluted and analyzed. To quantify serum thyroxine (T4) and triiodothyronine (T3) levels, serum samples were initially pooled by combining equal volumes across individuals within a replicate tank (n = 4 or 5/pool), they were then diluted 1:8 in mobile phase A (1% methanol with 25 mM formic acid) and analyzed using high performance liquid chromatography (HPLC) interfaced with an inductively coupled plasma mass spectrometer (ICP-MS) as described previously by Tietge et al. (2010, 2013).

2.10. Plasma vitellogenin

Plasma vitellogenin concentrations were measured by ELISA using samples taken from frogs at test termination. Blood samples were processed and evaluated for vitellogenin concentrations according to methods previously described by Haselman et al. (2016a).

2.11. Testis RNA processing

Total RNA was isolated from testis homogenates using RNeasy Plus mini kits according to kit instructions. RNA concentrations were measured in three samples randomly chosen per tank using a fluorescence-based RNA quantitation assay (Quant-iT™ Ribo-green®, Life Technologies, Grand Island, NY, USA). One tank from the 20 µg/L prochloraz treatment was excluded from subsequent analyses due to extremely low yields from all testis samples. RNA quality was checked on all chosen samples using a 2100 Bioanalyzer with an RNA 6000 pico assay (Agilent, Santa Clara, CA, USA). If sample integrity was compromised based on the electropherogram generated by the Bioanalyzer, a new sample was randomly chosen from that tank and its concentration and integrity were measured prior to pooling. The three samples per tank were then diluted to between 0.5 and 1 ng/µl (depending on the lowest concentration of the three samples to be pooled) and combined in equal amounts to create one pool per tank (n = 3 per pool; 1 pool/tank). A new total RNA concentration was determined for each pool using the same fluorescence method previously described and then divided into multiple aliquots to avoid freeze/thaw cycles. All subsequent gene expression levels were normalized to the total RNA concentration in each respective pool (Control: n = 8; 6.7 µg/L: n = 5; 20 µg/L: n = 4; 60 µg/L: n = 5; 180 µg/L: n = 5).

2.12. Quantitative PCR

Xenopus tropicalis accession numbers for *rflcii* and *cyp17a1* were aligned with the National Center for Biotechnology Information (NCBI) Expressed Sequence Tag (EST) database for *Xenopus laevis* using the nucleotide Basic Local Alignment Search Tool (http://blast.ncbi.nlm.nih.gov/Blast.cgi). The highest scoring sequences were used to design primers and probes for a quantitative real-time PCR (qPCR) assay using a TaqMan® EZ RT-PCR assay (Applied Biosystems®, Foster City, CA, USA) (Table 1). Primers and probes were designed using Primer Express version 3.0 (Applied Biosystems®, Foster City, CA, USA). Standard RNA templates were generated by first cloning the cDNA target sequence using a total RNA sample extracted as described in Section 2.11 above and specifically designed "outer" primers with a one-step reverse-transcription PCR kit (Sigma-Aldrich, St. Louis, MO, USA; Enhanced Avian HS RT-PCR kit). Next, target cDNA was amplified using separate "middle" primers that flanked the "inner" qPCR primer sequences and contained the T7 promoter region for subsequent in vitro transcription using a MEGAScript kit (Ambion®|Thermo Fisher Scientific, USA) according to kit instructions. The resulting transcribed RNA template was purified using an RNeasy Plus mini kit according to kit instructions. Purified RNA standard template concentrations were determined using the mean of three measurements from a NanoDrop ND-1000 Spectrophotometer (NanoDrop Technologies, Inc., http://www.nanodrop.com); the mean concentration and calculated molecular mass was used to derive estimated copy numbers. Standard RNA templates were $\log_{10}$ serially diluted and each concentration was run in duplicate with each sample set to serve as a standard curve. Additionally, no template controls (NTC) were run in duplicate on each plate; no amplification occurred in any NTC well. Pooled samples were also run in duplicate in 96-well plates according to TaqMan® kit instructions on an Agilent Strategene Mx3005P qPCR instrument. Standard curves and data were processed using MxPro −Mx3005P9® software version 4.10 Build 389, Schema 85 (Stratagene, San Diego, CA, USA). Amplification efficiency was 99% for *rflcii* (standard curve slope = −3.341; R^2 = 0.998) and 97% for *cyp17a1* (standard curve slope = −3.385; R^2 = 1).

2.13. Exposure verification

Water samples (1 ml) were collected weekly from the prochloraz exposure tanks (0, 6.7, 20, 60 and 180 µg/L) and placed into amber sample vials. The water samples were amended with 0.1 ml methanol, vortex mixed and immediately analyzed using an Agilent 1100 series HPLC with diode array detection (λ = 205 nm). An aliquot (150 µl) of sample was injected directly into a Zorbax SB-C18, 2.1 × 75 mm column (Agilent, Wilmington, DE, USA) that was maintained at 25 °C. The auto sampler temperature was maintained at 5 °C. Prochloraz eluted from the column under isocratic conditions with 22% Burdick & Jackson (B&J) HPLC grade water and 78% methanol at 0.3 ml/min. Prochloraz concentrations were determined by the external standard method of quantification using linear regression. Prochloraz standards range from 5 to 200 µg/L and were prepared in 90% B&J water and 10% methanol. Quality assurance samples were conducted with each sample set and included LSW blanks, duplicate samples and matrix spiked samples at each of the prochloraz treatment levels. No prochloraz was detected in the LSW blanks (n = 15). Mean ± SD (n = 15) recoveries of spiked samples were 102.2 ± 3%, 99.5 ± 2.5%, 99.3 ± 2.5% and 100.7 ± 2.2% at the 6.5, 20, 60 and 180 µg/L spiked levels, respectively. Mean ± SD (n = 15) agreement among duplicate samples were 99.8 ± 1.9%, 99.3 ± 3.3%, 99.4 ± 1.5% and 100.3 ± 1.5% for the 6.7, 20, 60 and 180 µg/L treatments, respectively. The detection limit was 2.5 µg/L. Mean ± SD (n = 75) measured concentrations of the 6.7, 20, 60 and 180 µg/L treatment tanks were 6.10 ± 0.69, 18.11 ± 2.14, 52.83 ± 5.90 and 169.76 ± 14 µg/L, respectively, over the duration of the experiment. Among-tank variability was ≤ 12% with the coefficient of variation (averaged across the duration of the experiment) of 11.4%, 11.8%, 11.2% and 8.2%, respectively for the 6.7, 20, 60 and 180 µg/L treatments. No prochloraz was detected in the control water treatments.

2.14. Statistical analyses

Statistical analyses were performed according to methods previously described by Haselman et al. (2016a). All data from the NF stage 66 subsample were analyzed independent of genetic sex while all data from juveniles were analyzed separately according to genetic sex. Continuous data (e.g., weight, length, liver-somatic index [LSI], mortality, serum T4/T3, gene expression) were checked for monotonicity by rank transforming the data, fitting to an ANOVA model and comparing linear and quadratic contrasts. All data was monotonic with the exception of female weight at the final sample. A step-down

Table 1
Accession numbers, primer and probe sequences used for qPCR of selected gene transcripts.

Gene symbol	*X. tropicalis accession*	*X. laevis accession*	Primers (5′ − > 3′)	Probe (5′ − > 3′)
cyp17a1	NM_001127045.1	NM_001097071.2	For: CCACGTGCTGTGACAACAGATA Rev: GCACTACCTTGCGGTGAAACT	ACATTGCTTTCGCCAACTACAGCCCA
rflcii	NM_001126835.1	CV081081.1	For: TGACACCATGGAACAGTTGCA Rev: CCGCACTCCTCCTCATCCT	TAGGTCAAGAACCACGGAGCACCAGC

Jonckheere-Terpstra trend test was performed on replicate medians for endpoints meeting the monotonicity assumptions whereas female weight was analyzed using an ANOVA followed by Dunnett's multiple comparison procedure. Mortality data were analyzed for the time period encompassing the full test and was expressed as percent that died in any particular tank. Tadpoles that did not complete metamorphosis in the given time frame, those tadpoles that were randomly selected for the larval sub-sample or that were culled, and any animal that died due to experimenter error were censored within the mortality analysis. Prior to any statistical analyses, mortality ratios were arcsine-square root transformed and analyzed as described above. Time to NF stage 66 data were analyzed using a mixed effects Cox proportional hazard model (Therneau, 2015). Gene expression data were expressed and analyzed as copies mRNA per ng of total RNA. Histopathology data (both incidence and severity scores) were analyzed using the Rao-Scott Cochran-Armitage by slices (RSCABS) test (Green et al., 2014) implemented in R (R Core Team, 2017) using the StatCharrms package (Swintek et al., 2017).

3. Results

3.1. Generalized toxicity

Prochloraz treatment did not affect survival (data not shown) or growth in the larval phase (Supplemental Table 2) nor in either gender in the juvenile phase (Table 2). Liver-somatic indices were significantly lower in the 60 and 180 µg/L treatments in both genders at two months post-metamorphosis ($p < 0.05$, Jonckheere-Terpstra; Table 2). Histopathological evaluations identified a concentration-dependent increase in incidence and severity of hepatocellular degeneration (Supplemental Table 3; Fig. 1) and is consistent with the concentration-dependent decrease in liver-somatic indices (Table 2). In kidneys of 30 (60%) animals from the 180 µg/L treatment, large numbers of renal tubules contained ~12 µm, irregularly oval, amphophilic intracytoplasmic bodies (inclusions) (Supplemental Table 4; Fig. 2C). Minimal (infrequent) accumulations of protein within the Bowman's capsule were observed in all study groups with a slightly higher percentage of animals affected in the 180 µg/L treatment (Supplemental Table 4; Fig. 2D). The prevalence of liver and kidney pathologies was generally not gender-specific.

3.2. Endocrine toxicity

3.2.1. Thyroid

The purpose of the NF stage 66 subsample was to evaluate thyroid-related effects. Prochloraz exposure had no effect on thyroid-mediated metamorphic rates as measured by days to NF stage 66 (Supplemental Table 5). Thyroid histopathology evaluations showed a significant increase in incidences and severity of follicular cell hypertrophy in the 180 µg/L treatment ($p < 0.05$, RSCABS), but there were no other corresponding treatment-related pathologies observed (Supplemental Table 5). Circulating T4 increased with increasing exposure concentrations of prochloraz and was significantly different than control in the 20, 60 and 180 µg/L treatments ($p < 0.05$, Jonckheere-Terpstra; Fig. 3A). Circulating T3 was unaffected by prochlroaz treatment (Fig. 3B).

3.2.2. Gonad and Müllerian duct histopathology

Evaluations of gonad and Müllerian duct development were performed on the final sampling at two months post-metamorphosis. Prochloraz did not cause any incidences of sex reversal or gonadal intersex, as assessed by comparing the individual histological gonad phenotype to the genotype, which was determined by the presence/absence of the sex-specific gene DM-W on the W chromosome. Histopathological observations of female ovaries included increased incidences of mononuclear cellular infiltrate, granulomatous inflammation and ovarian hypoplasia, all of minimal severity in only the 180 µg/L treatment (Supplemental Table 6). Testis histopathology evaluations revealed a series of effects from prochloraz exposure mainly in the 180 µg/L treatment (Table 3). Gonadal degeneration that presented as germinal epithelial thinning/loss without apoptosis or necrosis was differentiated by the pathologist from gonadal degeneration with evidence of apoptosis and necrosis. Although incidences of these diagnoses occurred across all treatments and control, a higher percentage of individuals were affected in the higher treatments (Table 3; Fig. 4). During normal testis development, all germ cells associated with a single spermatocyst mature at the same rate and the spermatocyst generally maintains a circular or ovoid shape. Prochloraz treatment caused asynchronous development of germ cells within a spermatocyst and caused some spermatocysts to become irregular in shape (Table 3; Fig. 5); this occurred in a concentration-dependent manner. The 180 µg/L treatment experienced increased incidences of interstitial fibrosis, interstitial cell hypertrophy and hyperplasia, and mononuclear cellular infiltrate indicating inflammatory and compensatory responses from prochloraz insult in the testis.

By two months post-metamorphosis in *Xenopus laevis*, Müllerian ducts are typically resorbed to a fibrous tag in males and are actively maturing to become oviducts in females. Both male and female Müllerian duct development were affected by prochloraz exposure. Male Müllerian duct regression was generally inhibited in a concentration-dependent manner, and in some cases, the ducts partially matured to be characteristic of early female oviducts (Table 4). Female Müllerian ducts exhibited accelerated development with prochloraz exposure. The majority (88–100% among treatments) of prochloraz-exposed females had partially matured oviducts while only 56% of control females had oviducts at this same stage of development.

3.2.3. Circulating vitellogenin

Overall, constitutive vitellogenin levels in the blood of *Xenopus* sp. are very low to absent at two months post-metamorphosis (test termination) and are not significantly elevated unless exposed to potent estrogens (Haselman et al., 2016a, 2016b; Olmstead et al., 2009). In the current study, there was a slight, but significant, concentration-dependent increase in circulating vitellogenin in females exposed to 20,

Table 2
Mean ± SD for growth, LSI and plasma vitellogenin concentrations in control and prochloraz-exposed *Xenopus laevis* at two months post-metamorphosis. Asterisks (*) represent measurements that are statistically different than control ($p < 0.05$; Jonckheere-Terpstra).

PZ conc. (µg/L)	0		6.7		20		60		180	
Gender	♂	♀	♂	♀	♂	♀	♂	♀	♂	♀
n	8	8	5	4	5	5	5	5	5	5
Weight (g)	13.2 ± 1.0	13.0 ± 0.6	12.5 ± 1.4	13.6 ± 1.3	11.8 ± 0.6	14.1 ± 0.6	12.5 ± 0.7	13.9 ± 0.4	12.5 ± 0.8	13.3 ± 1.4
Snout-to-vent length (mm)	47.4 ± 1.5	47.3 ± 0.7	46.4 ± 1.9	47.9 ± 1.8	45.1 ± 0.9	47.9 ± 0.8	46.7 ± 1.0	47.9 ± 0.9	46.4 ± 1.6	48.1 ± 1.4
Liver-somatic index (%)	5.9 ± 0.7	6.1 ± 0.3	5.6 ± 0.5	5.6 ± 1.0	5.6 ± 0.5	6.0 ± 0.4	5.1 ± 0.4*	5.2 ± 0.2*	5.0 ± 0.2*	5.2 ± 0.2*
Vitellogenin (ng/ml)	0.03 ± 0.01	0.03 ± 0.02	0.05 ± 0.03	0.04 ± 0.01	0.05 ± 0.02	0.08 ± 0.06*	0.11 ± 0.06*	0.13 ± 0.03*	0.10 ± 0.05*	0.25 ± 0.17*

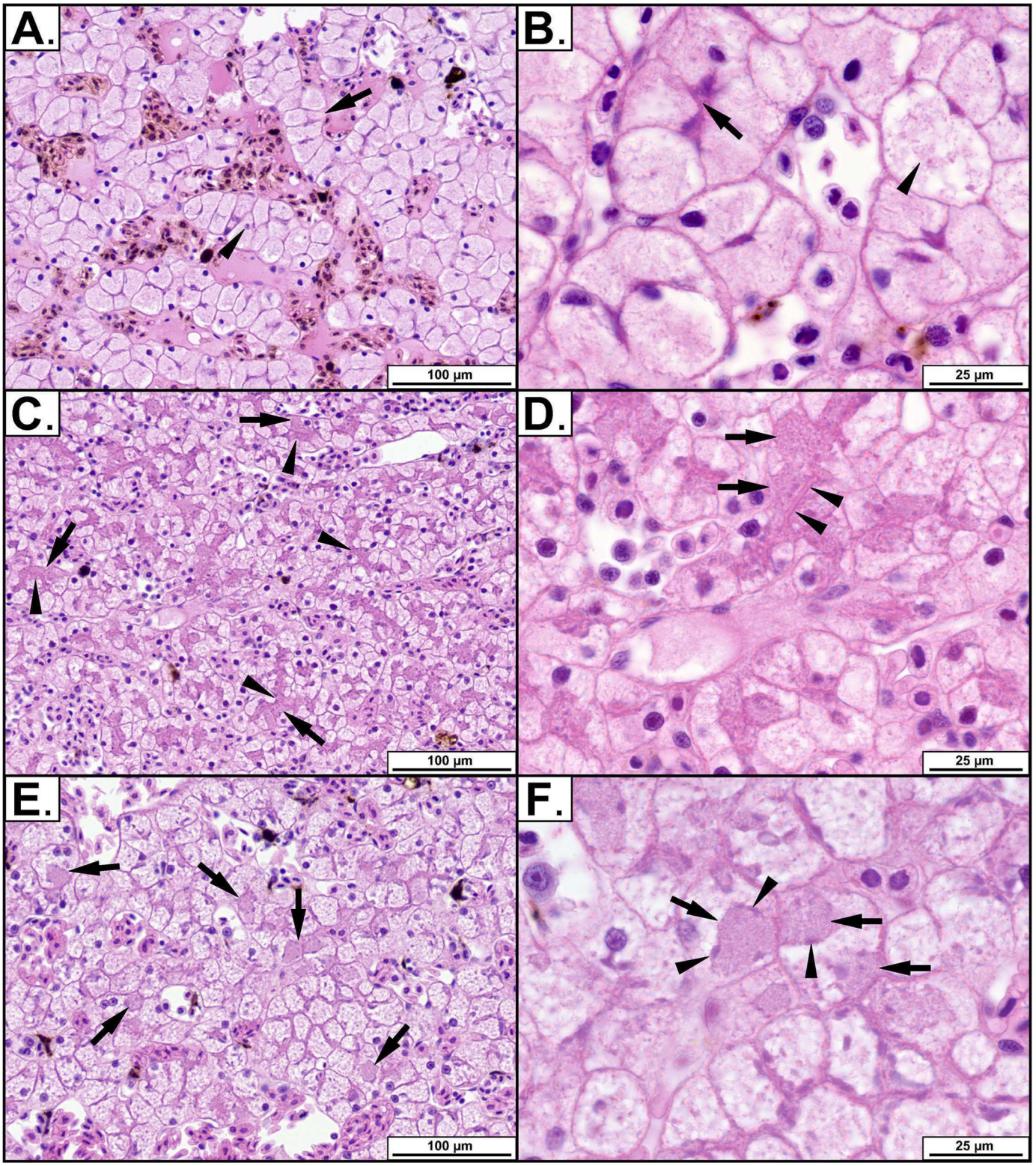

Fig. 1. Histological sections of control and prochloraz-exposed liver tissue at two months post-metamorphosis. Normal control liver (A). Hepatic cords are two cells thick (arrow) separated by bile canaliculus; hepatocyte cytoplasm is wispy and eosinophilic (arrowhead). Higher magnification of normal control liver (B). Note wispy eosinophilic cytoplasm (arrowhead) and condensed (basophilic) cytoplasm adjacent to bile canaliculus (arrow). 180 µg/L treated liver exhibiting moderate hepatocellular degeneration (C). Cytoplasmic inclusions are present within many hepatocytes (arrows); inclusion location is often pericanalicular (arrowheads). Panel D is higher magnification of panel C. Degenerative hepatocytes are smaller and contain pericanalicular inclusions (arrows); note prominent bile canaliculus (arrowhead). Another example of a 180 µg/L treated liver exhibiting moderate hepatocellular degeneration (E). Degenerative hepatocytes containing cytoplasmic inclusions may be swollen (arrows); hepatic cords appear jumbled. Panel F is higher magnification of panel E. Inclusions often consist of punctate granular material (arrow); note smudgy basophilic material at periphery of inclusion (arrowhead). Scale bars represent 100 µm in panels A, C and E; 25 µm for panels B, D and F.

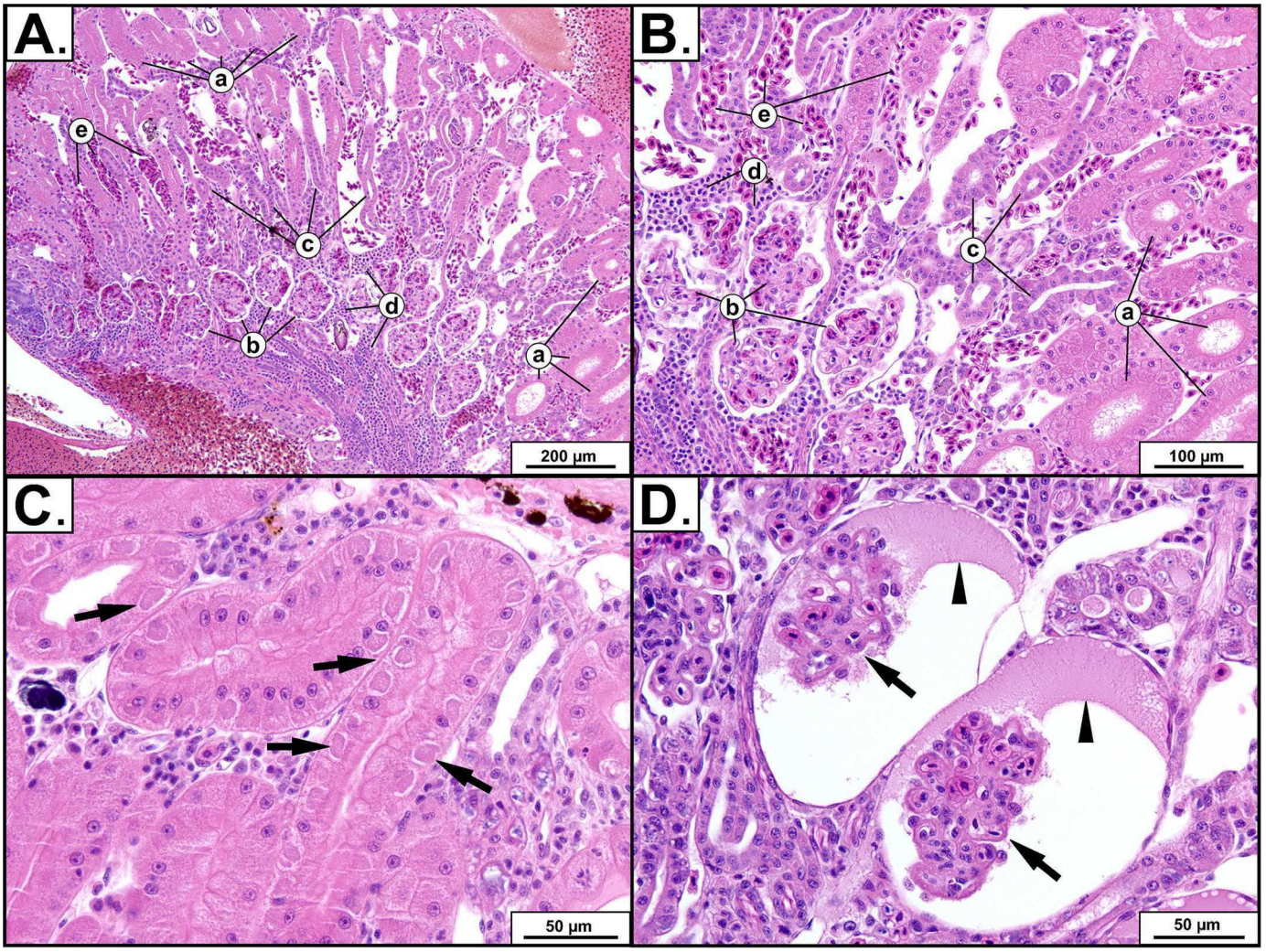

Fig. 2. Histology sections of control and prochloraz-treated kidneys at two months post-metamorphosis. Control kidney (A) and higher magnification control kidney (B). Profiles of the thick limb of the loop of Henle (a) fill the cortex; glomeruli (b) and collecting tubules (c) are largely confined to the cortex. Small clusters of myeloid cells are present (d) and large numbers of red blood cells (e) fill the interstitium. Intracytoplasmic amphophilic inclusions in the 180 µg/L study group (C). Renal tubular cells contain large, irregular, intracytoplasmic, amphophilic inclusions (arrows). 60 µg/L study group (D). The Bowman's capsule of several glomeruli contains small accumulations of pale, eosinophilic material (arrowheads) diagnosed as grade 1 glomerular protein. Scale bars represent 200, 100, 50 and 50 µm for panels A, B, C and D, respectively. (For interpretation of the references to colour in this figure legend, the reader is referred to the web version of this article.)

60, and 180 µg/L prochloraz with a maximum increase of approximately seven-fold above the control ($p < 0.05$, Jonckheere-Terpstra; Table 2). Circulating vitellogenin was also significantly increased in males exposed to 60 and 180 µg/L prochloraz with a maximum increase of approximately three-fold above the control ($p < 0.05$, Jonckheere-Terpstra; Table 2). Although the maximum increases were approximately seven- and three-fold above the control for females and males respectively, these vitellogenin concentrations are sub-ng/ml whereas mature female *Xenopus* sp. have circulating vitellogenin levels six to seven orders of magnitude higher in the mg/ml range (Olmstead et al., 2009), providing context for the lack of biological significance of these increases due to prochloraz exposure.

3.2.4. Testis gene expression

Gene expression was measured in testis tissue of frogs at test termination. *Rflcii* gene expression in the testis exhibited a significant increase in the 60 and 180 µg/L treatments ($p < 0.05$, Jonckheere-Terpstra) and showed three and greater than five-fold increases respectively (Fig. 6A). *Cyp17a1* was constitutively expressed at fairly high levels in all treatments and control in the testis at this stage of development (Fig. 6B); however, the 180 µg/L treatment was slightly increased as compared to the control ($p < 0.05$, Jonckheere-Terpstra). Additionally, two control ovary samples were analyzed for each *rflcii* and *cyp17a1* expression levels in separate analyses. In these ovaries, the mean normalized *rflcii* transcript level was less than one and the mean *cyp17a1* transcript level was approximately 54% of the mean control testis level (Fig. 6A & B).

4. Discussion

Prochloraz exposure throughout *Xenopus laevis* late embryonic, larval and juvenile development resulted in a range of toxicological effects characteristic of multiple modes of toxicity. The observed hepatocellular degeneration, together with measured decreases in liver-somatic indices and intracytoplasmic inclusions in renal tubular cells are all indicative of overt toxicity in the 60 and 180 µg/L treatments (159 and 478 nM, respectively). The histologic appearance of the hepatic inclusions is suggestive of excess protein and ribonucleic acid aggregations, presumably related to metabolism of prochloraz and/or impaired clearance of endogenous metabolites. A study by Needham and Challis (1991) reported that one of the major prochloraz metabolites in rats was a glucuronide conjugate and high concentrations of

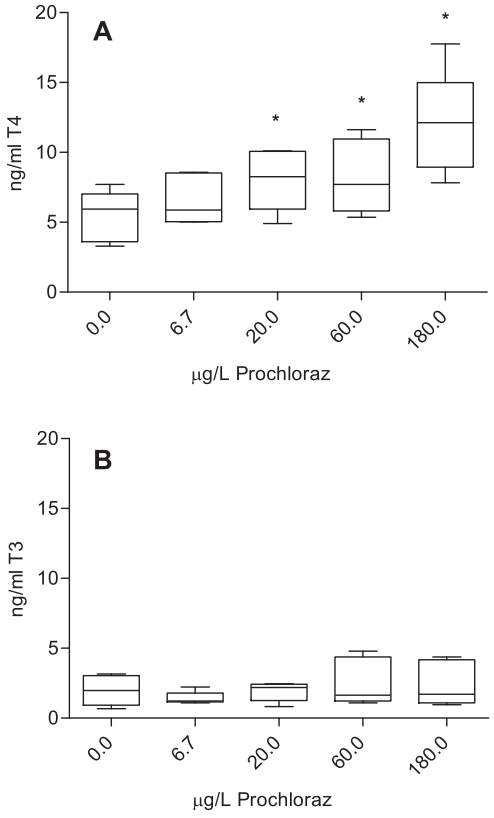

Fig. 3. Serum T4 (A) and T3 (B) levels from control and prochloraz-exposed NF stage 66 *X. laevis* (n = 8, 5, 5, 5, 5 for the 0.0, 6.7, 20, 60, 180 µg/L treatments, respectively). Horizontal lines represent medians, boxes represent the 25th-75th percentile and whiskers represent minimum and maximum values. Asterisks (*) indicate treatments that were statistically different than control ($p < 0.05$; Jonckheere-Terpstra).

prochloraz metabolites were found in liver tissue. In the same study, high concentrations of prochloraz metabolites were also found in kidneys. The similar appearance of hepatic and renal tubular cell inclusions in the current study is suggestive of metabolism, aggregation and excretion of prochloraz metabolites consistent with observations in rats (Needham and Challis, 1991). Despite the treatment-related pathologies in these organs, there were no measurable treatment-related effects on growth or developmental rates.

Rates of metamorphic development through the larval phase can be affected by thyroid disrupting chemicals. In the current study, thyroid-related effects from prochloraz exposure included thyroid follicular cell hypertrophy and increased circulating T4 levels at NF stage 66 (completion of metamorphosis). These effects occurred without concurrent differences in metamorphic rates or circulating T3 across treatments. One explanation for the concentration-dependent increase in circulating T4 levels is that following NF stage 62 (metamorphic climax and peak circulating TH levels), there is a rapid decrease in circulating TH levels (Sternberg et al., 2011) that is mediated by enhanced metabolism and excretion of TH. Given the compromised state of the liver and kidneys due to prochloraz exposure, T4 clearance could have also been compromised resulting in retention of higher blood concentrations at NF stage 66. This impaired clearance could also explain the slight elevation in plasma vitellogenin protein levels seen in juveniles of primarily the 60 and 180 µg/L treatments (159 and 478 nM, respectively). The difference between T4 and T3 profiles seen here is likely due to T3 having a much shorter half-life than T4 (hours vs. days) and being tightly regulated at a fraction of the circulating T4 concentrations. Another possibility for the increased T4 levels could be that prochloraz caused TH resistance by impacting one or more processes necessary to affirm negative feedback in the hypothalamus-pituitary (e.g., TH membrane transport, deiodination and/or transcription). Taken together, these data suggest that the compensatory capacity of the thyroid axis in *X. laevis* is sufficiently robust to have supported apparently normal metamorphic development during prochloraz exposure.

Table 3
Prevalence (%) and severity of juvenile male gonad histopathological observations showing significant treatment-related effects. Values in parentheses are significantly different than control based on RSCABS analysis ($p < 0.05$). NR = Not Remarkable.

PZ conc. (µg/L)	0	6.7	20	60	180
Replicate tanks	8	5	5	5	5
n	36	25	24	24	25
Testicular interstitial cell hyperplasia/hypertrophy					
NR	83	68	96	50	16
Minimal	17	32	4	(46)	(52)
Mild	0	0	0	4	(32)
Moderate	0	0	0	0	0
Increased spermatogonia					
NR	94	96	92	88	76
Minimal	6	4	4	8	(12)
Mild	0	0	0	0	(8)
Moderate	0	0	4	4	4
Germinal epithelium, thinning					
NR	92	84	92	54	12
Minimal	0	8	4	(38)	(40)
Mild	6	4	4	8	(16)
Moderate	3	4	0	0	(28)
Severe	0	0	0	0	4
Gonadal degeneration (necrosis / apoptosis)					
NR	92	64	96	83	32
Minimal	8	32	4	17	(64)
Mild	0	4	0	0	4
Moderate	0	0	0	0	0
Mononuclear cellular infiltrate					
NR	92	92	79	88	56
Minimal	8	8	21	12	40
Mild	0	0	0	0	4
Moderate	0	0	0	0	0
Asynchronous development within cysts					
NR	100	80	75	67	40
Minimal	0	(16)	(17)	(25)	(44)
Mild	0	(4)	(8)	(8)	(12)
Moderate	0	0	0	0	4
Interstitial fibrosis					
NR	75	52	71	75	12
Minimal	19	40	29	21	(36)
Mild	6	8	0	0	(52)
Moderate	0	0	0	4	0
Intratubular eosoniphilic droplets					
NR	94	96	100	96	76
Minimal	3	4	0	4	(24)
Mild	3	0	0	0	0
Moderate	0	0	0	0	0

Assessments of reproductive development took place at two months post-metamorphosis when the gonads are fully differentiated and actively maturing. At this stage of development, Müllerian duct regression in males is actively occurring and is mediated by testosterone and anti-Müllerian hormone (Kelley, 1996; Piprek et al., 2014). In females, Müllerian ducts are actively maturing to become oviducts, which is estrogen-mediated (Kelley, 1996). Prochloraz exposure caused concentration-dependent effects in all of these tissues with the most remarkable effects occurring in male reproductive organs. Histopathological evaluations of testes revealed degeneration of the germinal epithelium from the high test concentrations of prochloraz. Although the severities of the degenerative effects were quite variable within the high treatments, one individual exhibited such severe thinning of the germinal epithelium that the tissue presented with many large voids throughout the sections. Germinal epithelial thinning was generally accompanied by several other testicular lesions (e.g., interstitial cell hyperplasia, interstitial fibrosis, asynchronous spermatocyst

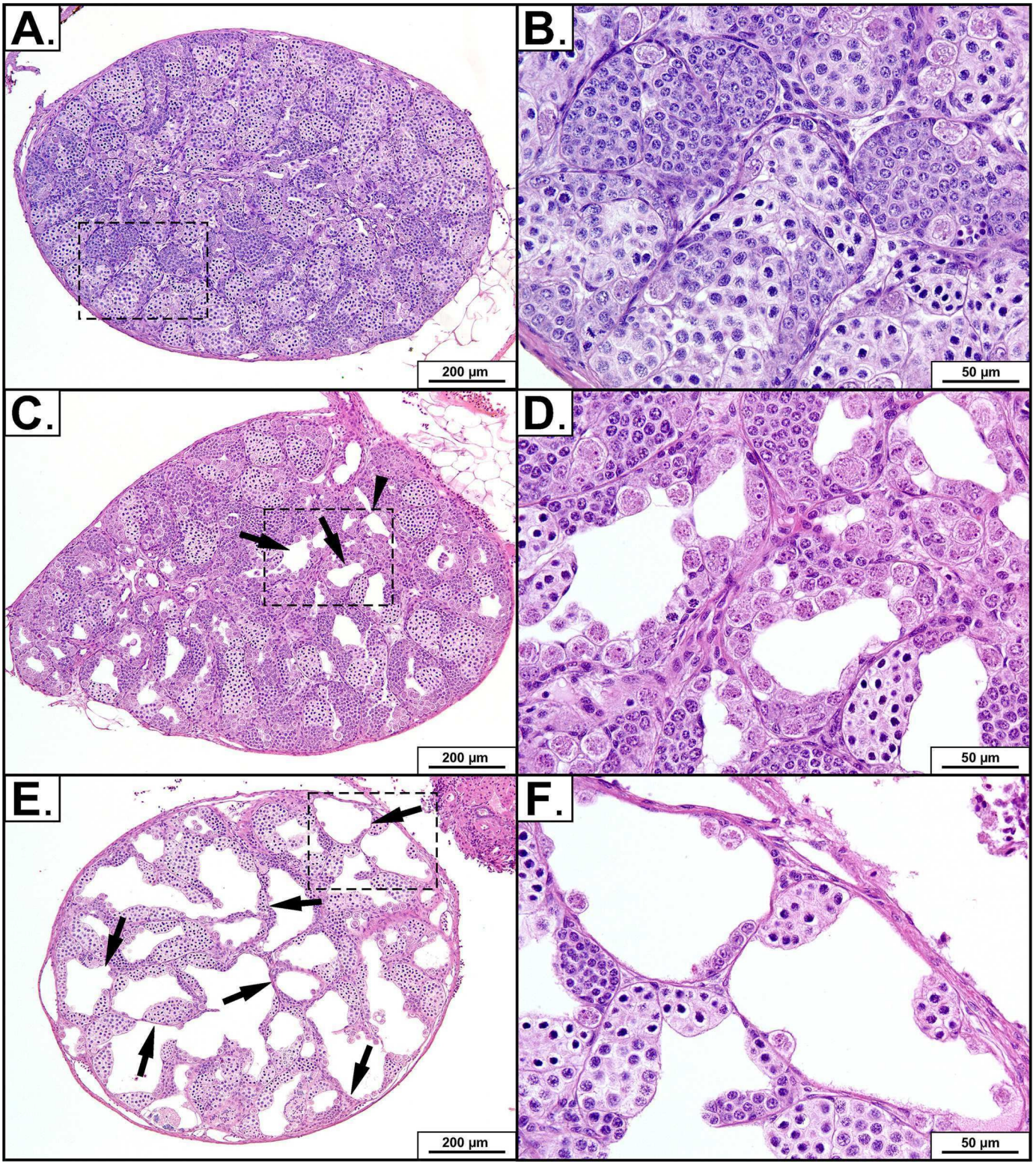

Fig. 4. Histology sections of control and prochloraz-exposed testis tissues at two months post-metamorphosis. Control group male provided for reference (A). The dashed boxes in panels A, C, and E are represented in higher magnification in corresponding panels B, D and F. 180 µg/L treatment group male showing mild gonadal degeneration thinning/loss (C and D). The germinal epithelium lining of numerous spermatic tubules is thin to absent (black arrows) with occasional exposure of the underlying basement membrane (arrowhead). 180 µg/L treatment group male exhibiting severe gonadal degeneration thinning/loss (E and F). Diffusely, the germinal epithelium is missing or thin with frequent exposure of the underlying basement membranes (arrows). Scale bars represent 200 µm in panels A, C and E; 50 µm in panels B, D and F.

development) in the higher treatments. This was in contrast to the lower treatments that, more often, presented with one or very few different lesions of minimal to mild severity. These antiandrogenic effects of prochloraz are consistent with what has been reported in fathead minnows (Ankley et al., 2005) and rats (Blystone et al., 2007a, 2007b; Noriega et al., 2005). Interestingly, the appearance of the testis

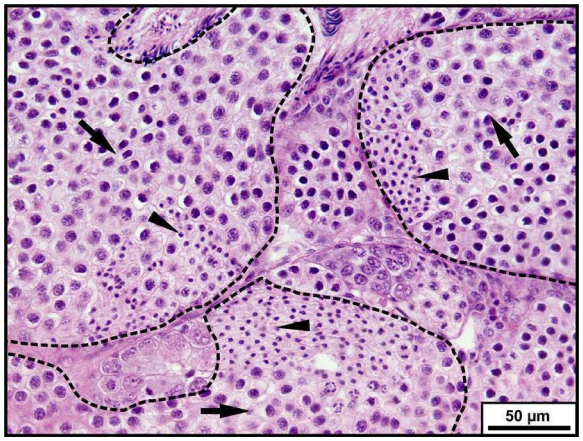

Fig. 5. Histological section of asynchronous cyst development in testis tissue of prochloraz-exposed male in the 180 µg/L study group. Asynchronous development within cysts, Grade 3. The normal architecture is distorted by large, irregular spermatocysts (outlined in black dashed lines) which contain cells of asynchronous maturity. Spermatocytes are indicated by arrows, and spermatids are shown by arrowheads. Scale bar represents 50 µm.

Table 4
Müllerian duct staging at two months post-metamorphosis following exposure to prochloraz. Values are expressed as percentages of total n.

PZ conc. (µg/L)	0	6.7	20	60	180	0	6.7	20	60	180
Replicate tanks	8	5	5	5	5	8	5	5	5	5
Müllerian duct stage	Male					Female				
n	37	25	24	26	25	43	26	22	24	25
Fibrous tag	84	88	50	31	4	0	0	0	0	0
Rudimentary	16	8	(42)	(58)	(92)	44	0	9	4	12
Partial oviduct	0	4	8	12	4	56	100	91	96	88

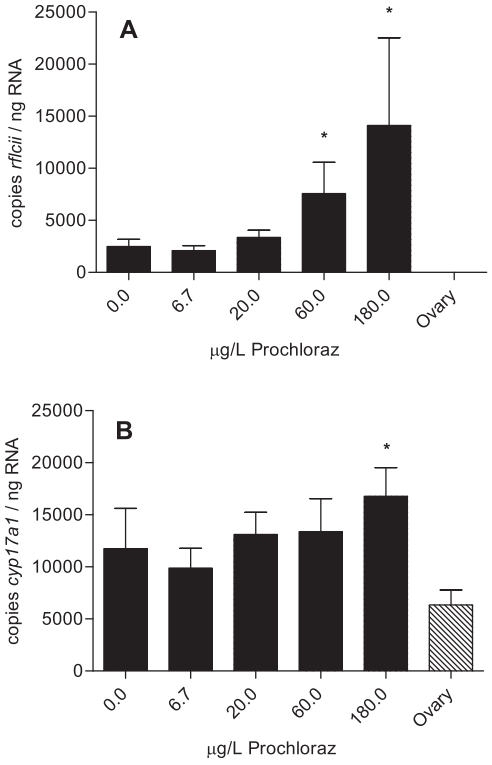

Fig. 6. Gene expression levels in testis tissue of two months post-metamorphosis control and prochloraz-exposed *X. laevis* (levels from control ovaries are included for comparison; n = 2). Means ± SD (error bars) are expressed as copies mRNA per ng total RNA (n = 8, 5, 4, 5, 5 for the 0.0, 6.7, 20, 60, 180 µg/L treatments, respectively). Asterisks (*) indicate treatments statistically different than control ($p < 0.05$, Jonckheere-Terpstra). Ovary values were not included in statistical analyses.

sections suggest that normal morphogenesis was not initially inhibited by prochloraz, as the macrostructure was completely formed – overall sizes of testes in the high prochloraz treatment were similar to control. Also, testis cords and spermatocysts were formed and appeared to be progressing through spermatogenesis, albeit atypically. The degenerative process caused by prohcloraz exposure appears to have occurred either concurrently with unabated testicular growth and structural formation, or was manifested following the completion of testis morphogenesis. The most plausible cause for the appearance of these testis pathologies was antagonism of the androgen-mediated phase of spermatogenesis that is initiated in the later stages of testis morphogenesis.

Our previous work indicates that the transcriptional activity in the testis around completion of metamorphosis is primarily associated with morphogenesis including organization of the seminiferous tubules, differentiation of interstitial cells and production of connective tissue (Haselman et al., 2015). Once testis cords are formed, pre-spermatogenesis takes place during late larval development and the early juvenile period. In two species of *Rana*, pre-spermatogenesis has been shown to occur at different points in the mating season independent of hormonal activity in interstitial tissue (reviewed by Ogielska, 2009). Androgens become essential for the second meiotic division of germ cells, which convert secondary spermatocytes to spermatids. Control testes in this study exhibited spermatocysts often containing spermatids and in some cases containing spermatozoa, indicating androgen-mediated spermatogenesis is taking place at two months post-metamorphosis. Therefore, critical levels of androgens are produced by steroidogenesis enzymes in the Leydig cells beginning at some point between the completion of metamorphosis and two months post-metamorphosis, presumably mediated by gonadotropins released by the pituitary. This late metamorphic climax period has been described as the onset of the functional hypothalamus-pituitary-gonadal (HPG) axis, before which larval gonad development occurs independent of gonadotropins from the pituitary (reviewed by Ogielska, 2009). We postulate that the point at which the testis becomes sensitive to the anti-androgenic action of prochloraz is when androgens become necessary to support spermatogenesis. In effect, prochloraz arrests meiosis and results in degeneration of the already formed germinal epithelium.

Cyp17a1 gene expression levels in testes also support the notion that steroidogenesis is active and prochloraz treatment may cause weak compensatory induction of the enzyme's transcript. This was not a strong response and suggests that *cyp17a1* gene expression may not be a primary mode of compensation in this particular system when androgen production and/or signaling is impaired. There appears to be reasonably high constitutive levels of the *cyp17a1* transcript already present in all treatments and control, which may act as an available reserve for compensatory activation of translation and protein production. Reports of *cyp17* gene regulation following prochloraz exposure have been varied. In a study by Ankley et al. (2009), male fathead minnows exposed to 300 µg/L (796 nM) for eight days exhibited significantly reduced circulating testosterone levels with a corresponding significant increase in testis *cyp17* mRNA. Laier et al. (2006) exposed fetal rats perinatally to 150 mg/kg/day prochloraz and reported upregulation of CYP17 protein by immunohistostaining whereas *Cyp17* gene expression was unchanged in gestational day 21 fetal testes. This provides precedent that compensatory action to increase testosterone levels in the developing testis via CYP17 could be occurring more at the translational level. Although testosterone levels in the testis are not known in this study, the weak *cyp17a1* expression increase seen in the 180 µg/L (478 nM) treatment could be an indication of a compensatory response caused by decreased testosterone levels and/or impaired androgen receptor signaling, but generally lacks usefulness as a biomarker in this

particular system.

Transcript expression levels of *rflcii* in the testis showed a marked increase in the 60 and 180 µg/L treatments (159 and 478 nM, respectively) where the majority of treatment-related pathologies were observed in testis tissues. *Xenopus rflcii* is orthologous to mammalian *INSL3* Leydig cell-specific growth factor peptide hormone. INSL3 has been well-characterized in mammalian reproductive development; however, this peptide has only recently been considered in teleosts and is essentially uncharacterized in amphibians (Bathgate et al., 2013; Good-Avila et al., 2009). The relaxin family of genes within and between species shares very little sequence similarity, but the resulting peptides share structural similarity with insulin and confer similar functionality (Wilkinson et al., 2005). INSL3 during early mammalian reproductive development is highly expressed in fetal Leydig cells and is responsible for testis decent by acting on the gubernaculum (Zimmermann et al., 1999; Nef and Parada, 1999). Prevention of germ cell apoptosis by paracrine signaling has also been a suggested role of INSL3 in the adult rat testis (Anand-Ivell et al., 2006; Kawamura et al., 2004). Unlike acute testosterone regulation by luteinizing hormone (LH), INSL3 is not acutely regulated (Ivell et al., 2013). Instead, its constitutive expression is correlated with Leydig cell number, function and differentiation status, which is regulated by long-term stimulation by LH from the pituitary. Previous studies in rat dams exposed to prochloraz for several days have shown that *Insl3* expression is unchanged in fetal testes, supporting the lack of acute regulation (Wilson et al., 2004). If the relationship between LH and *Insl3* regulation is conserved, chronic exposure to antiandrogen prochloraz in the current study may have caused prolonged LH stimulation as evidenced by *rflcii* expression levels. This would be indicative of a lack of either Leydig cell competence or mature differentiation status, perhaps due to reduced testosterone levels and/or impaired androgen signaling, either of which would reduce negative feedback on the hypothalamus-pituitary causing sustained LH release (from late metamorphic climax to two months post-metamorphosis). Although we did not measure circulating LH, sustained elevation of LH could be causing the elevated expression of *rflcii* in the prochloraz-exposed testes, whereas control *rflcii* expression levels are more representative of the mature status of Leydig cells and fully functional status of the HPG axis. With regard to *rflcii* expression in the testis of *X. laevis*, it appears to be an exceptional biomarker of impaired testis development when evaluated in this chronic exposure paradigm. However, further investigations are necessary to understand the predictive utility of this biomarker in relation to apical reproductive success.

Another notable antiandrogenic effect of prochloraz exposure occurred in both male and female Müllerian ducts. Müllerian duct regression was attenuated in prochloraz-treated males and Müllerian duct maturation was accelerated in prochloraz-treated females. The effects on the Müllerian ducts in both genders with prochloraz treatment is indicative of a feminizing effect similar to the feminization of secondary sex characteristics of male rats during perinatal prochloraz exposure (Noriega et al., 2005; Vinggaard et al., 2005). In the testes of fetal male rats, testosterone has been shown to increase post-translational processing of anti-Müllerian hormone that results in cleavage of the full length protein to N- and C-terminus peptides, of which the C-terminus peptide is bioactive toward Müllerian duct regression (Kuroda et al., 1991; Lee and Donahoe, 1993). If these processes are conserved across rodents and anurans, the results from the current study suggest that testosterone-mediated post-translational bioactivation of anti-Müllerian hormone was impaired by prochloraz treatment via reduced testosterone availability and/or inhibition of androgen receptor signaling. The acceleration of oviduct development in females could be viewed as an estrogenic response resulting from prochloraz exposure. However, anti-Müllerian hormone is present at some level in both testes and ovaries during *X. laevis* development (Piprek et al., 2014), suggesting that there may be competing biochemical pathways in both sexes that results in a developmental trajectory of the Müllerian duct characteristic of the predominant hormone action. In this case, we suggest that females exposed to an antiandrogen experience no influence of the constitutive anti-Müllerian hormone due to the lack of testosterone signaling and undergo unabated growth of the oviduct. This study, in addition to our previous studies (Haselman et al., 2016a, 2016b; Porter et al., 2011), emphasize that Müllerian duct fate is highly sensitive to xenobiotics that affect androgen and estrogen signaling.

5. Conclusion

Chronic prochloraz exposure throughout multiple life stages in model amphibian species *Xenopus laevis* caused developmental and apical effects characteristic of multiple modes of toxicity. Liver and kidney pathologies suggested rate-limited metabolism and clearance of prochloraz which may have impacted proper thyroid hormone homeostasis during the late stages of metamorphosis. Reproductive development was also impacted by prochloraz exposure as evidenced by testicular lesions including abnormal germ cell patterning and degeneration with corresponding effects on *rflcii* and *cyp17a1* gene expression suggestive of reduced testosterone production and/or androgen signaling. The feminization of the Müllerian ducts in both juvenile males and females is consistent with previous reports of feminized reproductive development in rodents following perinatal exposure to prochloraz. Overall, the effects on reproductive development caused by prochloraz exposure are consistent with an antiandrogenic mode of action and are in agreement with a number of studies implicating prochloraz as an antiandrogenic endocrine disruptor. This study further supports the diagnostic utility of the LAGDA for chemical testing in a chronic exposure paradigm.

Acknowledgements

The authors would like to thank Lindsey Blake, Erica Nevalainin, Kathryn Lillegaard, Ben Heggestad and Shane Zavodnik for helping with logistics, animal husbandry, sampling and data collection. Liver, gonad, kidney and duct histopathology samples were processed by Integrated Laboratory Systems, Inc. (Research Triangle Park, NC, USA). Liver tissues were evaluated and diagnoses scored by pathologist Kristen R. Hobbie (DVM, PhD). Pathologist Brigid V. Troan (DVM, DACVP) evaluated and scored diagnoses for gonad, kidney, and duct samples. Thyroid histopathology samples were processed by Experimental Pathology Laboratories, Inc. (Sterling, VA, USA); they were evaluated and scored by pathologist Jeffrey C. Wolf (PhD). Special thanks to Chad Blanksma for histotechnical support and preparation of high-quality digital micrographs. Many thanks to Kevin Flynn for helpful comments and suggestions to improve the content of this manuscript.

The research described in this article has been funded by the U.S. Environmental Protection Agency. The views expressed in this article are those of the authors and do not necessarily reflect the views or policies of the U.S. EPA.

Appendix A. Supplementary data

Supplementary data associated with this article can be found, in the online version, at https://doi.org/10.1016/j.aquatox.2018.03.013.

References

Adham, I.M., Burkhardt, E., Benahmed, M., Engel, W., 1993. Cloning of a cDNA for a novel insulin-like peptide of the testicular Leydig cells. J. Biol. Chem. 268 (35), 26668–26672.

Anand-Ivell, R.J., Relan, V., Balvers, M., Coiffec-Dorval, I., Fritsch, M., Bathgate, R.A., Ivell, R., 2006. Expression of the insulin-like peptide 3 (INSL3) hormone-receptor (LGR8) system in the testis. Biol. Reprod. 74 (5), 945–953.

Andersen, H.R., Vinggaard, A.M., Rasmussen, T.H., Gjermandsen, I.M., Bonefeld-Jørgensen, E.C., 2002. Effects of currently used pesticides in assays for estrogenicity,

androgenicity, and aromatase activity in vitro. Toxicol. Appl. Pharmacol. 179 (1), 1–12.
Ankley, G.T., Jensen, K.M., Durhan, E.J., Makynen, E.A., Butterworth, B.C., Kahl, M.D., Villeneuve, D.L., Linnum, A., Gray, L.E., Cardon, M., Wilson, V.S., 2005. Effects of two fungicides with multiple modes of action on reproductive endocrine function in the fathead minnow (*Pimephales promelas*). Toxicol. Sci. 86 (2), 300–308.
Ankley, G.T., Bencic, D.C., Cavallin, J.E., Jensen, K.M., Kahl, M.D., Makynen, E.A., Martinović, D., Mueller, N.D., Wehmas, L.C., Villeneuve, D.L., 2009. Dynamic nature of alterations in the endocrine system of fathead minnows exposed to the fungicide prochloraz. Toxicol. Sci. 112 (2), 344–353.
Bathgate, R.A.D., Halls, M.L., Van Der Westhuizen, E.T., Callander, G.E., Kocan, M., Summers, R.J., 2013. Relaxin family peptides and their receptors. Physiol. Rev. 93 (1), 405–480.
Birkhøj, M., Nellemann, C., Jarfelt, K., Jacobsen, H., Andersen, H.R., Dalgaard, M., Vinggaard, A.M., 2004. The combined antiandrogenic effects of five commonly used pesticides. Toxicol. Appl. Pharmacol. 201 (1), 10–20.
Blystone, C.R., Furr, J., Lambright, C.S., Howdeshell, K.L., Ryan, B.C., Wilson, V.S., LeBlanc, G.A., Gray Jr, L.E., 2007a. Prochloraz inhibits testosterone production at dosages below those that affect androgen-dependent organ weights or the onset of puberty in the male Sprague Dawley rat. Toxicol. Sci. 97 (1), 65–74.
Blystone, C.R., Lambright, C.S., Howdeshell, K.L., Furr, J., Sternberg, R.M., Butterworth, B.C., Durhan, E.J., Makynen, E.A., Ankley, G.T., Wilson, V.S., LeBlanc, G.A., 2007b. Sensitivity of fetal rat testicular steroidogenesis to maternal prochloraz exposure and the underlying mechanism of inhibition. Toxicol. Sci. 97 (2), 512–519.
Bossche, H.V., 1985. Biochemical targets for antifungal azole derivatives: hypothesis on the mode of action. Current Topics in Medical Mycology. Springer, New York, pp. 313–351.
Good-Avila, S.V., Yegorov, S., Harron, S., Bogerd, J., Glen, P., Ozon, J., Wilson, B.C., 2009. Relaxin gene family in teleosts: phylogeny, syntenic mapping, selective constraint, andexpression analysis. BMC Evol. Biol. 9 (1), 293.
Green, J.W., Springer, T.A., Saulnier, A.N., Swintek, J., 2014. Statistical analysis of histopathological endpoints. Environ. Toxicol. Chem. 33 (5), 1108–1116.
Grim, K.C., Wolfe, M., Braunbeck, T., Iguchi, T., Ohta, Y., Tooi, O., Touart, L., Wolf, D.C., Tietge, J., 2009. Thyroid histopathology assessments for the amphibian metamorphosis assay to detect thyroid-active substances. Toxicol. Pathol. 37 (4), 415–424.
Haselman, J.T., Olmstead, A.W., Degitz, S.J., 2015. Global gene expression during early differentiation of *Xenopus* (*Silurana*) *tropicalis* gonad tissues. Gen. Comp. Endocrinol. 214, 103–113.
Haselman, J.T., Kosian, P.A., Korte, J.J., Olmstead, A.W., Iguchi, T., Johnson, R.D., Degitz, S.J., 2016a. Development of the Larval Amphibian Growth and Development Assay: effects of chronic 4-*tert*-octylphenol or 17β-trenbolone exposure in *Xenopus laevis* from embryo to juvenile. J. Appl. Toxicol. 36 (12), 1639–1650.
Haselman, J.T., Sakurai, M., Watanabe, N., Goto, Y., Onishi, Y., Ito, Y., Onoda, Y., Kosian, P.A., Korte, J.J., Johnson, R.D., Iguchi, T., 2016b. Development of the Larval Amphibian Growth and Development Assay: effects of benzophenone-2 exposure in *Xenopus laevis* from embryo to juvenile. J. Appl. Toxicol. 36 (12), 1651–1661.
Hecker, M., Newsted, J.L., Murphy, M.B., Higley, E.B., Jones, P.D., Wu, R., Giesy, J.P., 2006. Human adrenocarcinoma (H295R) cells for rapid in vitro determination of effects on steroidogenesis: hormone production. Toxicol. Appl. Pharmacol. 217 (1), 114–124.
Henry, M.J., Sisler, H.D., 1984. Effects of sterol biosynthesis-inhibiting (SBI) fungicides on cytochrome P-450 oxygenations in fungi. Pestic. Biochem. Physiol. 22 (3), 262–275.
Ivell, R., Wade, J.D., Anand-Ivell, R., 2013. INSL3 as a biomarker of Leydig cell functionality. Biol. Reprod. 88 (6), 141–147.
Kawamura, K., Kumagai, J., Sudo, S., Chun, S.Y., Pisarska, M., Morita, H., Toppari, J., Fu, P., Wade, J.D., Bathgate, R.A., Hsueh, A.J., 2004. Paracrine regulation of mammalian oocyte maturation and male germ cell survival. Proc. Natl. Acad. Sci. U. S. A. 101 (19), 7323–7328.
Kelley, D.B., 1996. 9 sexual differentiation in xenopus laevis. Symposia of the Zoological Society of London. London, The Society, pp. 1960–1999 (No. 68, pp. 1960–1999).
Kojima, H., Katsura, E., Takeuchi, S., Niiyama, K., Kobayashi, K., 2004. Screening for estrogen and androgen receptor activities in 200 pesticides by in vitro reporter gene assays using Chinese hamster ovary cells. Environ. Health Perspect. 112 (5), 524.
Kuroda, T., Lee, M.M., Ragin, R.C., Hirobe, S., Donahoe, P.K., 1991. Müllerian inhibiting substance production and cleavage is modulated by gonadotropins and steroids. Endocrinology 129 (6), 2985–2992.
Laier, P., Metzdorff, S.B., Borch, J., Hagen, M.L., Hass, U., Christiansen, S., Axelstad, M., Kledal, T., Dalgaard, M., McKinnell, C., Brokken, L.J., 2006. Mechanisms of action underlying the antiandrogenic effects of the fungicide prochloraz. Toxicol. Appl. Pharmacol. 213 (2), 160–171.
Lee, M.M., Donahoe, P.K., 1993. Müllerian inhibiting substance: a gonadal hormone with multiple functions. Endocr. Rev. 14 (2), 152–164.
Needham, D., Challis, I.R., 1991. The metabolism and excretion of prochloraz, an imidazole-based fungicide, in the rat. Xenobiotica 21 (11), 1473–1482.
Nef, S., Parada, L.F., 1999. Cryptorchidism in mice mutant for Insl3. Nat. Genet. 22 (3), 295–299.
Nieuwkoop, P.D., Faber, J., 1994. Normal Table of Xenopus Laevis (Daudin): A Systematical and Chronological Survey of the Development from the Fertilized Egg Till the End of Metamorphosis.
Noriega, N.C., Ostby, J., Lambright, C., Wilson, V.S., Gray Jr, L.E., 2005. Late gestational exposure to the fungicide prochloraz delays the onset of parturition and causes reproductive malformations in male but not female rat offspring. Biol. Reprod. 72 (6), 1324–1335.
OECD, 2015. Test No. 241: The Larval Amphibian Growth and Development Assay (LAGDA), OECD Guidelines for the Testing of Chemicals, Section 2. OECD Publishing, Paris. http://dx.doi.org/10.1787/9789264242340-en.
Ogielska, M., 2009. Reproduction of Amphibians. Science Publishers.
Olmstead, A.W., Korte, J.J., Woodis, K.K., Bennett, B.A., Ostazeski, S., Degitz, S.J., 2009. Reproductive maturation of the tropical clawed frog: *Xenopus tropicalis*. Gen. Comp. Endocrinol. 160 (2), 117–123.
Piprek, R.P., Pecio, A., Laskowska-Kaszub, K., Kubiak, J.Z., Szymura, J.M., 2014. Sexual dimorphism of AMH, DMRT1 and RSPO1 localization in the developing gonads of six anuran species. Int. J. Dev. Biol. 57 (11–12), 891–895.
Porter, K.L., Olmstead, A.W., Kumsher, D.M., Dennis, W.E., Sprando, R.L., Holcombe, G.W., Korte, J.J., Lindberg-Livingston, A., Degitz, S.J., 2011. Effects of 4-*tert*-octylphenol on *Xenopus tropicalis* in a long term exposure. Aquat. Toxicol. 103 (3), 159–169.
R Core Team, 2017. R: A Language and Environment for Statistical Computing. R Foundation for Statistical Computing, Vienna, Austria. https://www.R-project.org/.
Roth, M.Y., Lin, K., Bay, K., Amory, J.K., Anawalt, B.D., Matsumoto, A.M., Marck, B.T., Bremner, W.J., Page, S.T., 2013. Serum insulin-like factor 3 is highly correlated with intratesticular testosterone in normal men with acute, experimental gonadotropin deficiency stimulated with low-dose human chorionic gonadotropin: a randomized, controlled trial. Fertil. Steril. 99 (1), 132–139.
Sanderson, J.T., Boerma, J., Lansbergen, G.W., van den Berg, M., 2002. Induction and inhibition of aromatase (CYP19) activity by various classes of pesticides in H295R human adrenocortical carcinoma cells. Toxicol. Appl. Pharmacol. 182 (1), 44–54.
Sternberg, R.M., Thoemke, K.R., Korte, J.J., Moen, S.M., Olson, J.M., Korte, L., Tietge, J.E., Degitz Jr, S.J., 2011. Control of pituitary thyroid-stimulating hormone synthesis and secretion by thyroid hormones during Xenopus metamorphosis. Gen. Comp. Endocrinol. 173 (3), 428–437.
Swintek, J., Flynn, K., Haselman, J., 2017. StatCharrms: Statistical Analysis of Chemistry, Histopathology, and Reproduction Endpoints Including Repeated Measures and Multi-Generation Studies. https://CRAN.R-project.org/package=StatCharrms.
Therneau, T.M., 2015. Mixed Effects Cox Models. (Available from: http://cran.r-project.org/web/packages/coxme/coxme.pdf [Accessed on 31 August 2017]).
Tietge, J.E., Butterworth, B.C., Haselman, J.T., Holcombe, G.W., Hornung, M.W., Korte, J.J., Kosian, P.A., Wolfe, M., Degitz, S.J., 2010. Early temporal effects of three thyroid hormone synthesis inhibitors in *Xenopus laevis*. Aquat. Toxicol. 98 (1), 44–50.
Tietge, J.E., Degitz, S.J., Haselman, J.T., Butterworth, B.C., Korte, J.J., Kosian, P.A., Lindberg-Livingston, A.J., Burgess, E.M., Blackshear, P.E., Hornung, M.W., 2013. Inhibition of the thyroid hormone pathway in *Xenopus laevis* by 2-mercaptobenzothiazole. Aquat. Toxicol. 126, 128–136.
US EPA, 2015. OCSPP 890.2300: Larval Amphibian Growth and Development Assay (LAGDA), Endocrine Disruptor Screening Program Test Guidelines, 890 Series. (ID: EPA-HQ-OPPT-2014-0766-0020). www.regulations.gov.
Villeneuve, D.L., Ankley, G.T., Makynen, E.A., Blake, L.S., Greene, K.J., Higley, E.B., Newsted, J.L., Giesy, J.P., Hecker, M., 2007. Comparison of fathead minnow ovary explant and H295R cell-based steroidogenesis assays for identifying endocrine-active chemicals. Ecotoxicol. Environ. Saf. 68 (1), 20–32.
Vinggaard, A.M., Hnida, C., Breinholt, V., Larsen, J.C., 2000. Screening of selected pesticides for inhibition of CYP19 aromatase activity in vitro. Toxicol. In Vitro 14 (3), 227–234.
Vinggaard, A.M., Nellemann, C., Dalgaard, M., Jørgensen, E.B., Andersen, H.R., 2002. Antiandrogenic effects in vitro and in vivo of the fungicide prochloraz. Toxicol. Sci. 69 (2), 344–353.
Vinggaard, A.M., Christiansen, S., Laier, P., Poulsen, M.E., Breinholt, V., Jarfelt, K., Jacobsen, H., Dalgaard, M., Nellemann, C., Hass, U., 2005. Perinatal exposure to the fungicide prochloraz feminizes the male rat offspring. Toxicol. Sci. 85 (2), 886–897.
Vinggaard, A., Hass, U., Dalgaard, M., Andersen, H.R., Bonefeld-Jørgensen, E.V.A., Christiansen, S., Laier, P., Poulsen, M.E., 2006. Prochloraz: an imidazole fungicide with multiple mechanisms of action. Int. J. Androl. 29 (1), 186–192.
Wilkinson, T.N., Speed, T.P., Tregear, G.W., Bathgate, R.A., 2005. Evolution of the relaxin-like peptide family. BMC Evol. Biol. 5, 14.
Wilson, V.S., Lambright, C., Furr, J., Ostby, J., Wood, C., Held, G., Gray, L.E., 2004. Phthalate ester-induced gubernacular lesions are associated with reduced insl3 gene expression in the fetal rat testis. Toxicol. Lett. 146 (3), 207–215.
Yoshimoto, S., Okada, E., Umemoto, H., Tamura, K., Uno, Y., Nishida-Umehara, C., Matsuda, Y., Takamatsu, N., Shiba, T., Ito, M., 2008. A W-linked DM-domain gene, DM-W, participates in primary ovary development in *Xenopus laevis*. Proc. Natl. Acad. Sci. U. S. A. 105 (7), 2469–2474.
Zhang, X., Hecker, M., Jones, P.D., Newsted, J., Au, D., Kong, R., Wu, R.S., Giesy, J.P., 2008. Responses of the medaka HPG axis PCR array and reproduction to prochloraz and ketoconazole. Environ. Sci. Technol. 42 (17), 6762–6769.
Zimmermann, S., Steding, G., Emmen, J.M., Brinkmann, A.O., Nayernia, K., Holstein, A.F., Engel, W., Adham, I.M., 1999. Targeted disruption of the Insl3 gene causes bilateral cryptorchidism. Mol. Endocrinol. 13 (5), 681–691.

Supplemental Material (Haselman et al., 2018)

S.Table 1.
Measured water quality parameters throughout the duration of prochloraz exposure (mean ± SD). All water quality parameters were within the same range across all treatments and control, so all data across treatments and control, and over time, are combined.

Temperature (ºC)	D.O. (% sat.)	pH	Alkalinity (mg/L $CaCO_3$)	Hardness (mg/L $CaCO_3$)	Conductivity (µS)
21.0 ± 0.4	76.9 ± 15.2	7.45 ± 0.44	42.4 ± 1.7	47.0 ± 0.8	98 ± 2

S.Table 2.
Larval growth and development (NF stage 66) following prochloraz exposure (mean ± SD).

PZ conc.	Weight (g)	Length (mm)	Time to NF66 (d)
0 µg/L	0.98 ± 0.11	20.9 ± 0.69	44.1 ± 1.2
6.7 µg/L	1.07 ± 0.09	21.5 ± 0.61	43.7 ± 2.0
20 µg/L	0.98 ± 0.03	20.9 ± 0.35	43.8 ± 1.6
60 µg/L	1.01 ± 0.06	20.6 ± 0.22	45 ± 2.2
180 µg/L	1.01 ± 0.04	20.7 ± 0.43	45.7 ± 0.7

S.Table 3.
Prevalence (%) and severity of juvenile liver hepatocellular degeneration. Values in parentheses are significantly different than control based on RSCABS analysis ($p < 0.05$). NR = Not Remarkable.

PZ conc. (µg/L)	0	6.7	20	60	180	0	6.7	20	60	180
Replicate tanks	8	5	5	5	5	8	5	5	5	5
	Male					Female				
n	16	10	10	10	10	16	10	10	10	10
Hepatocellular degeneration										
NR	100	100	90	70	0	100	100	90	60	0
Minimal	0	0	10	(30)	(10)	0	0	10	(40)	(60)
Mild	0	0	0	0	(70)	0	0	0	0	(10)
Moderate	0	0	0	0	(20)	0	0	0	0	(30)
Severe	0	0	0	0	0	0	0	0	0	0

S.Table 4.
Prevalence (%) and severity of juvenile kidney histopathological observations. Values in parentheses are significantly different than control based on RSCABS analysis ($p < 0.05$). NR = Not Remarkable.

PZ conc. (µg/L)	0	6.7	20	60	180	0	6.7	20	60	180
Replicate tanks	8	5	5	5	5	8	5	5	5	5
	Male					Female				
n	37	25	24	26	25	43	26	22	24	25
Glomerular protein										
NR	97	92	96	100	84	100	100	95	92	84
Minimal	3	8	4	0	16	0	0	5	(8)	(16)
Mild	0	0	0	0	0	0	0	0	0	0
Moderate	0	0	0	0	0	0	0	0	0	0
Severe	0	0	0	0	0	0	0	0	0	0
Tubules, protein										
NR	92	88	96	96	92	100	96	95	100	96
Minimal	8	12	4	4	8	0	4	5	0	0
Mild	0	0	0	0	0	0	0	0	0	4
Moderate	0	0	0	0	0	0	0	0	0	0
Severe	0	0	0	0	0	0	0	0	0	0
Interstitial fluid (proteinaceous)										
NR	100	100	96	100	92	100	100	95	92	96
Minimal	0	0	4	0	(8)	0	0	5	(4)	(4)
Mild	0	0	0	0	0	0	0	0	4	0
Moderate	0	0	0	0	0	0	0	0	0	0
Severe	0	0	0	0	0	0	0	0	0	0
Amphophilic intracytoplasmic bodies in tubule epithelium										
NR	100	100	100	100	44	100	100	100	100	36
Minimal	0	0	0	0	(56)	0	0	0	0	(64)
Mild	0	0	0	0	0	0	0	0	0	0
Moderate	0	0	0	0	0	0	0	0	0	0
Severe	0	0	0	0	0	0	0	0	0	0

S.Table 5.
Prevalence (%) and severity of NF stage 66 thyroid histopathology observations. Values in parentheses are significantly different than control based on RSCABS analysis ($p < 0.05$). NR = Not Remarkable.

PZ conc. (µg/L)	0	6.7	20	60	180
Replicate tanks	8	5	5	5	5
n	40	23	25	25	24
Follicular Cell Hypertrophy					
NR	38	65	28	28	8
Minimal	57	35	68	60	(75)
Mild	5	0	4	12	(17)
Moderate	0	0	0	0	0
Follicular Cell Hyperplasia					
NR	78	87	80	76	67
Minimal	22	13	20	24	33
Mild	0	0	0	0	0
Moderate	0	0	0	0	0

S.Table 6.
Prevalence (%) and severity of female ovary histopathology observations at two months post-metamorphosis following exposure to prochloraz. Values in parentheses are significantly different than control based on RSCABS analysis ($p < 0.05$). NR = Not Remarkable.

PZ conc. (µg/L)	0	6.7	20	60	180
Replicate tanks	8	5	5	5	5
n	43	26	22	24	25
Mononuclear cellular infiltrate					
NR	72	77	77	50	44
Minimal	26	15	18	50	(48)
Mild	2	8	5	0	8
Moderate	0	0	0	0	0
Granulomatous inflammation					
NR	100	100	91	100	92
Minimal	0	0	9	0	(4)
Mild	0	0	0	0	0
Moderate	0	0	0	0	4
Ovarian hypoplasia					
NR	95	92	95	96	72
Minimal	5	8	5	4	(28)
Mild	0	0	0	0	0
Moderate	0	0	0	0	0
Interstitial fibrosis					
NR	93	96	86	92	80
Minimal	7	0	14	8	12
Mild	0	4	0	0	8
Moderate	0	0	0	0	0

InCites Journal Citation Reports

Clarivate Analytics

2018 Journal Performance Data for: AQUATIC TOXICOLOGY

ISSN: 0166-445X
eISSN: 1879-1514
ELSEVIER SCIENCE BV
PO BOX 211, 1000 AE AMSTERDAM, NETHERLANDS
NETHERLANDS

TITLES
ISO: Aquat. Toxicol.
JCR Abbrev: AQUAT TOXICOL

LANGUAGES
English

CATEGORIES
MARINE & FRESHWATER BIOLOGY -- SCIE

TOXICOLOGY -- SCIE

PUBLICATION FREQUENCY
20 issues/year

Downloaded on 4/17/2020, 8:35:23 AM from Journal Citation Reports (©2020 Clarivate Analytics)

InCites Journal Citation Reports

Clarivate Analytics

The data in the two graphs below and in the Journal Impact Factor calculation panels represent citation activity in 2018 to items published in the journal in the prior two years. They detail the components of the Journal Impact Factor. Use the "All Years" tab to access key metrics and additional data for the current year and all prior years for this journal.

2018 Journal Impact Factor & percentile rank in category for: AQUATIC TOXICOLOGY

3.794

2018 Journal Impact Factor

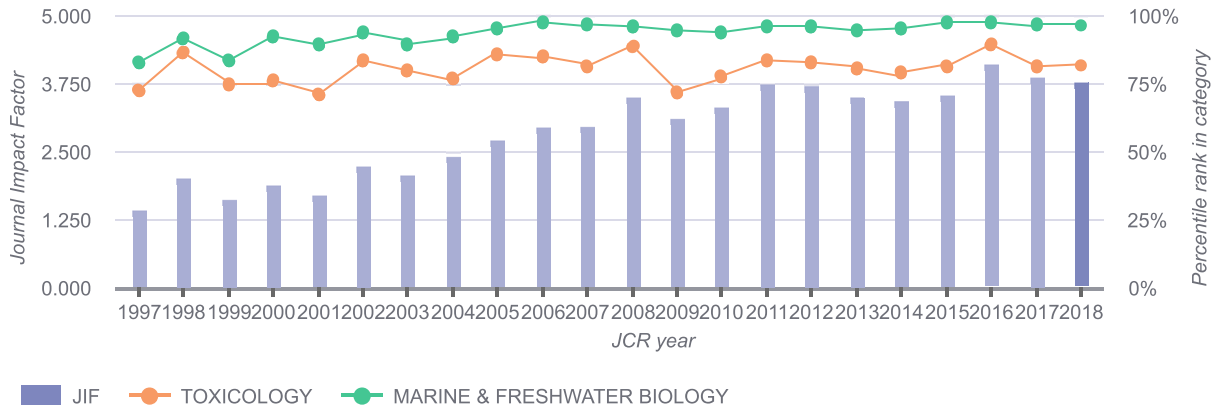

2018 JIF Citation Distribution for: AQUATIC TOXICOLOGY

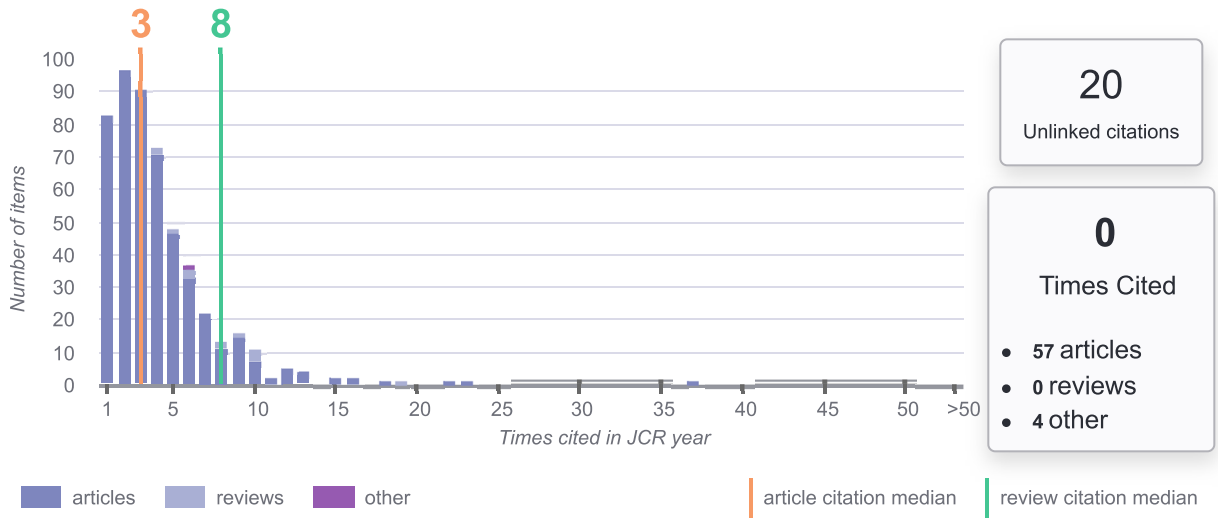

20
Unlinked citations

0
Times Cited

- **57** articles
- **0** reviews
- **4** other

Downloaded on 4/17/2020, 8:35:23 AM from Journal Citation Reports (©2020 Clarivate Analytics)

InCites Journal Citation Reports

Clarivate Analytics

Journal Impact Factor Calculation

$$\text{2018 Journal Impact Factor} = \frac{2{,}151}{567} = 3.794$$

How is Journal Impact Factor Calculated?

$$\text{JIF} = \frac{\text{Citations in 2018 to items published in } \textbf{2016 (1,272) + 2017 (879)}}{\text{Number of citable items in } \textbf{2016 (304) + 2017 (263)}} = \frac{2{,}151}{567}$$

Downloaded on 4/17/2020, 8:35:23 AM from Journal Citation Reports (©2020 Clarivate Analytics)

Journal Impact Factor contributing items

Citable items in 2017 and 2016 (567)

TITLE	CITATIONS COUNTED TOWARDS JIF
Cytotoxicity, haemolymphatic parameters, and oxidative stress following exposure to sub-lethal concentrations of quaternium-15 in Mytilus galloprovincialis	37
By: Faggio, Caterina; Pagano, Maria; Alampi, Roberto; Vazzana, Irene; Felice, Maria Rosa **Volume: 180 Page: 258-265 Accession number: WOS:000388777600026** **Document Type: Article**	
Oxidative stress and immunotoxicity induced by graphene oxide in zebrafish	23
By: Chen, Minjie; Yin, Junfa; Liang, Yong; Yuan, Shaopeng; Wang, Fengbang et al. **Volume: 174 Page: 54-60 Accession number: WOS:000374604100007** **Document Type: Article**	
Effects of multi-stressors on juveniles of the marine fish Pomatoschistus microps: Gold nanoparticles, microplastics and temperature	22
By: Ferreira, Pedro; Fonte, Elsa; Soares, M. Elisa; Carvalho, Felix; Guilhermino, Lucia **Volume: 170 Page: 89-103 Accession number: WOS:000368564500010** **Document Type: Article**	
Manufactured nanoparticles in the aquatic environment-biochemical responses on freshwater organisms: A critical overview	19
By: Vale, Goncalo; Mehennaoui, Kahina; Cambier, Sebastien; Libralato, Giovanni; Jomini, Stephane et al. **Volume: 170 Page: 162-174 Accession number: WOS:000368564500017** **Document Type: Review**	
Zinc oxide nanoparticles induce oxidative DNA damage and ROS-triggered mitochondria-mediated apoptosis in zebrafish embryos	18
By: Zhao, Xuesong; Ren, Xin; Zhu, Rong; Luo, Zhouying; Ren, Baixiang **Volume: 180 Page: 56-70 Accession number: WOS:000388777600006** **Document Type: Article**	
6:2 Chlorinated polyfluorinated ether sulfonate, a PFOS alternative, induces embryotoxicity and disrupts cardiac development in zebrafish embryos	16
By: Shi, Guohui; Cui, Qianqian; Pan, Yitao; Sheng, Nan; Sun, Sujie et al. **Volume: 185 Page: 67-75 Accession number: WOS:000398651300008** **Document Type: Article**	
Dietary administration of EDC mixtures: A focus on fish lipid metabolism	16
By: Carnevali, O.; Maradonna, F.; Notarstefano, V.; Olivotto, I.; Graziano, M. et al. **Volume: 185 Page: 95-104 Accession number: WOS:000398651300011** **Document Type: Article**	

Downloaded on 4/17/2020, 8:35:23 AM from Journal Citation Reports (©2020 Clarivate Analytics)

Citations in 2018 (2,151)

TITLE	CITATIONS COUNTED TOWARDS JIF
AQUATIC TOXICOLOGY	210
CHEMOSPHERE	185
SCIENCE OF THE TOTAL ENVIRONMENT	171
ECOTOXICOLOGY AND ENVIRONMENTAL SAFETY	134
ENVIRONMENTAL POLLUTION	129
ENVIRONMENTAL SCIENCE AND POLLUTION RESEARCH	70
ENVIRONMENTAL SCIENCE & TECHNOLOGY	65
ENVIRONMENTAL TOXICOLOGY AND CHEMISTRY	54
MARINE ENVIRONMENTAL RESEARCH	33
FISH & SHELLFISH IMMUNOLOGY	31

Downloaded on 4/17/2020, 8:35:23 AM from Journal Citation Reports (©2020 Clarivate Analytics)

InCites Journal Citation Reports

Clarivate Analytics

Source data

Journal source data 2018

	Articles	Reviews	Combined(C)	Other(O)	Percentage(C/(C+O))
Number in JCR Year 2018 (A)	256	4	260	1	100%
Number of References (B)	16,722	586	17,308	19	100%
Ratio (B/A)	65.3	146.5	66.6	19.0	

Downloaded on 4/17/2020, 8:35:23 AM from Journal Citation Reports (©2020 Clarivate Analytics)

InCites Journal Citation Reports

Clarivate Analytics

Box plot

Category Box Plot 2018

Category Box Plot

The category box plot depicts the distribution of Impact Factors for all journals in the category. The horizontal line that forms the top of the box is the 75th percentile (Q1). The horizontal line that forms the bottom is the 25th percentile (Q3). The horizontal line that intersects the box is the median Impact Factor for the category.
Horizontal lines above and below the box, called whiskers, represent maximum and minimum values.
The top whisker is the smaller of the following two values:
the maximum Impact Factor (IF)
Q1 IF + 3.5(Q1 IF - Q3 IF)
The bottom whisker is the larger of the following two values:
the minimum Impact Factor (IF)
Q1 IF - 3.5(Q1 IF - Q3 IF)
Box Plots are provided for the current JCR year for each of the categories in which the journal is indexed.

AQUAT TOXICOL, IF: 3.794

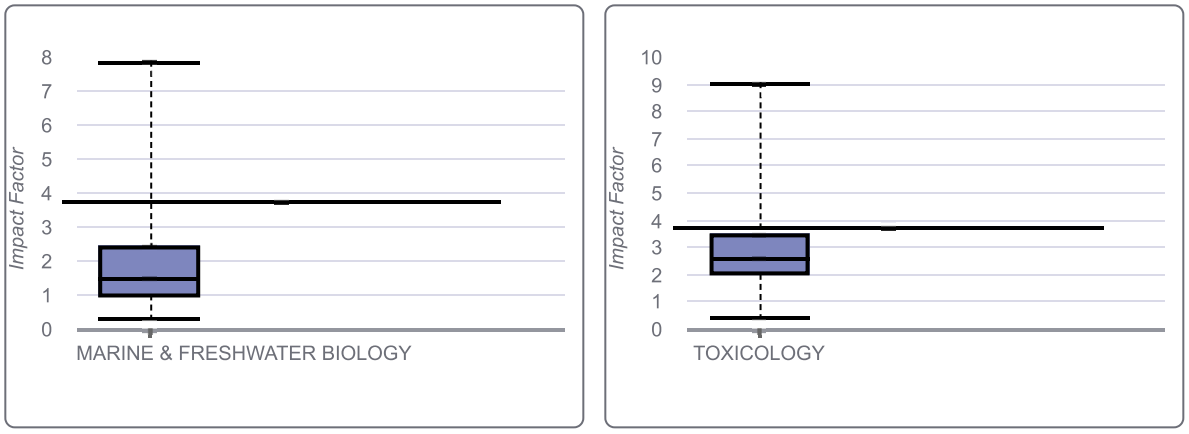

Downloaded on 4/17/2020, 8:35:23 AM from Journal Citation Reports (©2020 Clarivate Analytics)

InCites Journal Citation Reports

Clarivate Analytics

Rank

Rank

JCR Impact Factor

JCR Year	MARINE & FRESHWATER BIOLOGY			TOXICOLOGY		
	Rank	Quartile	JIF Percentile	Rank	Quartile	JIF Percentile
2018	4/108	Q1	96.759	17/93	Q1	82.258
2017	4/106	Q1	96.698	18/94	Q1	81.383
2016	3/105	Q1	97.619	10/92	Q1	89.674
2015	3/104	Q1	97.596	17/90	Q1	81.667
2014	5/103	Q1	95.631	19/88	Q1	78.977
2013	6/103	Q1	94.660	17/87	Q1	81.034
2012	4/100	Q1	96.500	15/85	Q1	82.941
2011	4/97	Q1	96.392	14/83	Q1	83.735
2010	6/93	Q1	94.086	19/83	Q1	77.711
2009	5/88	Q1	94.886	22/77	Q2	72.078
2008	4/87	Q1	95.977	9/75	Q1	88.667
2007	3/86	Q1	97.093	14/73	Q1	81.507
2006	2/79	Q1	98.101	12/76	Q1	84.868
2005	4/77	Q1	95.455	11/75	Q1	86.000
2004	6/75	Q1	92.667	18/75	Q1	76.667
2003	8/74	Q1	89.865	16/77	Q1	79.870
2002	5/73	Q1	93.836	13/76	Q1	83.553
2001	8/71	Q1	89.437	23/78	Q2	71.154
2000	6/71	Q1	92.254	19/77	Q1	75.974
1999	12/70	Q1	83.571	19/74	Q2	75.000
1998	6/68	Q1	91.912	10/71	Q1	86.620
1997	12/68	Q1	83.088	18/63	Q2	72.222

Downloaded on 4/17/2020, 8:35:23 AM from Journal Citation Reports (©2020 Clarivate Analytics)

InCites Journal Citation Reports

Clarivate Analytics

ESI Total Citations

Rank

JCR Year	PLANT & ANIMAL SCIENCE
2018	35/804-Q1
2017	32/791-Q1
2016	30/773-Q1
2015	35/774-Q1
2014	35/754-Q1
2013	43/741-Q1

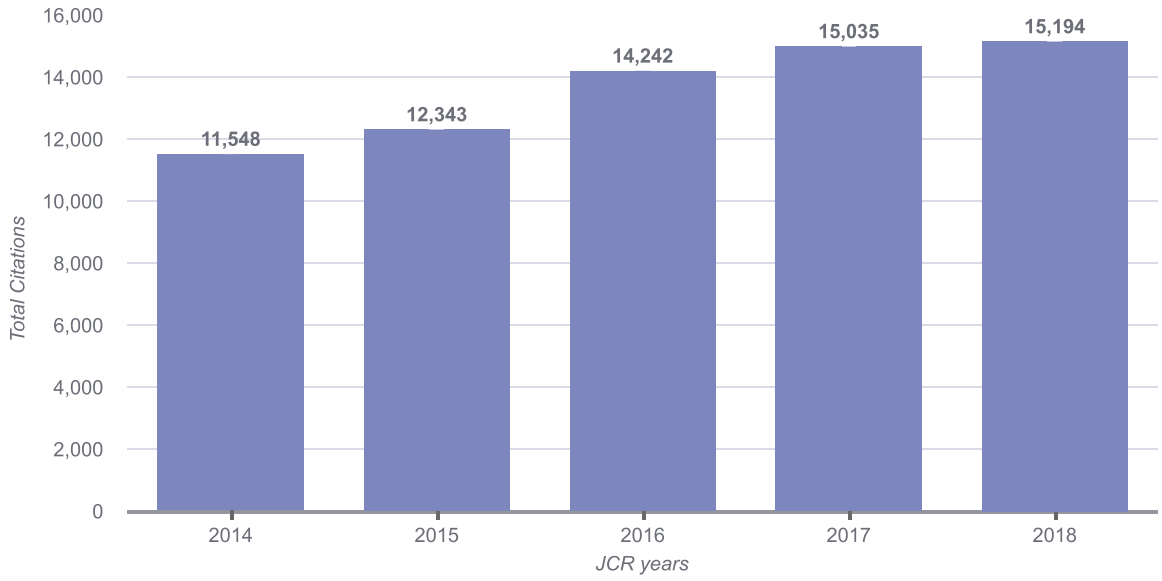

Downloaded on 4/17/2020, 8:35:23 AM from Journal Citation Reports (©2020 Clarivate Analytics)

InCites Journal Citation Reports

Clarivate Analytics

Cited Journal Data

Cited Half-Life Data

Cited Year	2018	2017	2016	2015	2014	2013	2012	2011	2010	2009	2008-All
#Cites from 2018	205	879	1,272	1,209	1,351	1,214	797	1,065	981	670	5,551
Cumulative %	1.35%	7.13%	15.51%	23.46%	32.35%	40.34%	45.59%	52.60%	59.06%	63.47%	100.00%

Cited Journal Graph 2018

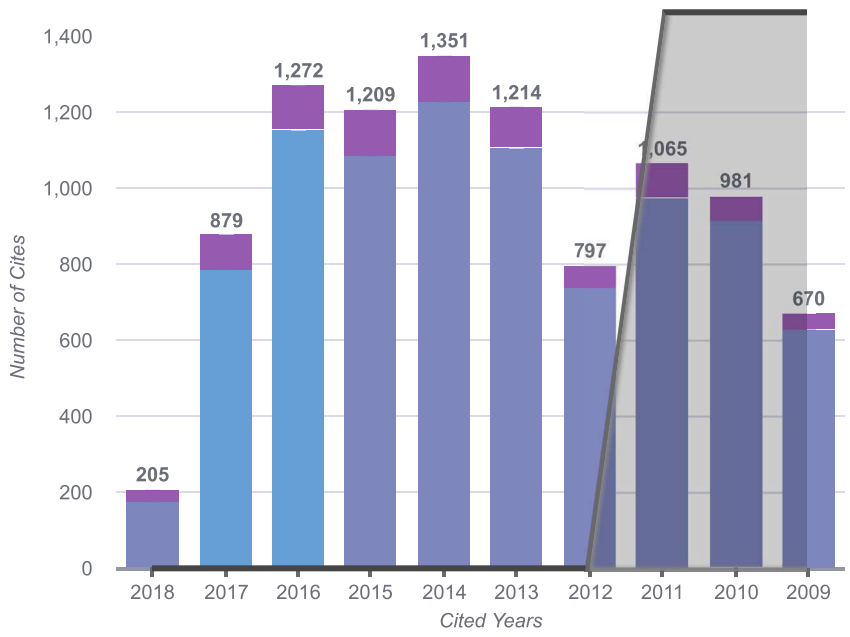

CITED JOURNAL GRAPH

The Cited Journal Graph shows the distribution (by cited year) of citations published in journals during the JCR year to items published in the Journal during the last 10 years.

The white/grey division indicates the cited half-life (if < 10.0). Half of the citations are to items that were published more recently than the cited half-life.

The two light-blue columns indicate citations used to calculate the Impact Factor (always the 2nd and 3rd columns).

Non-self-citations: citations from the journal to articles in other journals.

Journal self - citations: citations from articles in the journal to articles in the same journal.

Downloaded on 4/17/2020, 8:35:23 AM from Journal Citation Reports (©2020 Clarivate Analytics)

InCites Journal Citation Reports

Clarivate Analytics

Cited Journal Data 2018

Export

	Impact	Citing Journal	All Yrs	2018	2017	2016	2015	2014	2013	2012	2011	2010	2009	F
		ALL Journals	15,194	205	879	1,272	1,209	1,351	1,214	797	1,065	981	670	5
		ALL OTHERS (623)	623	8	39	35	54	39	45	18	45	34	39	
1	3.794	AQUAT TOXICOL	1,234	31	93	117	121	121	107	57	90	65	42	
2	5.589	SCI TOTAL ENVIRON	985	13	69	102	96	95	76	44	80	66	44	
3	4.527	ECOTOX ENVIRON SAFE	983	10	42	92	70	97	76	65	65	56	44	
4	5.108	CHEMOSPHERE	934	14	75	110	79	74	85	36	56	63	49	
5	5.714	ENVIRON POLLUT	876	15	51	78	81	103	76	56	61	44	36	
6	2.914	ENVIRON SCI POLLUT R	581	2	25	45	40	49	51	36	49	31	30	
7	3.421	ENVIRON TOXICOL CHEM	477	3	14	40	38	46	42	30	30	36	15	
8	7.149	ENVIRON SCI TECHNOL	411	12	31	34	35	36	38	28	33	37	9	
9	3.782	MAR POLLUT BULL	272	7	8	17	25	20	13	12	13	16	8	
10	2.697	COMP BIOCHEM PHYS C	232	1	6	13	20	23	12	16	14	21	5	
11	3.298	FISH SHELLFISH IMMUN	210	2	10	21	31	23	21	6	17	7	4	
12	3.445	MAR ENVIRON RES	204	5	16	17	13	21	13	10	17	14	8	
13	4.011	SCI REP-UK	197	4	7	19	16	19	17	13	11	23	16	
14	2.460	ECOTOXICOLOGY	178	0	5	13	11	29	20	7	13	13	11	
15	3.061	ENVIRON TOXICOL PHAR	159	1	3	10	9	14	17	6	18	14	5	
16	4.490	ECOL INDIC	137	0	5	15	7	8	12	9	8	8	6	
17	2.776	PLOS ONE	123	1	10	9	10	11	9	7	7	5	8	
18	7.704	ENVIRON SCI-NANO	98	2	11	8	14	14	5	8	4	7	7	
19	1.650	B ENVIRON CONTAM TOX	96	1	1	9	11	9	8	4	4	9	4	
20	3.022	AQUACULTURE	94	0	6	9	3	6	7	5	8	1	2	
21	3.201	FRONT PHYSIOL	92	1	13	6	3	6	12	5	17	5	2	
22	2.445	GEN COMP ENDOCR	91	0	3	6	7	8	7	10	5	7	2	
23	1.729	FISH PHYSIOL BIOCHEM	89	0	5	9	9	5	10	6	7	5	1	
24	7.913	WATER RES	89	0	6	4	5	15	6	4	12	8	4	
25	7.650	J HAZARD MATER	86	0	5	7	6	14	8	5	8	4	1	
26	2.135	ARCH ENVIRON CON TOX	72	0	3	3	2	5	4	2	5	3	4	
27	5.026	ENVIRON RES	68	0	2	4	11	9	4	3	5	2	3	
28	1.774	WATER AIR SOIL POLL	67	0	1	2	2	2	7	4	6	3	4	

Showing 1 - 30 rows of 727 total *(use export to download the full table)*

Downloaded on 4/17/2020, 8:35:23 AM from Journal Citation Reports (©2020 Clarivate Analytics)

InCites Journal Citation Reports

Clarivate Analytics

Citing Journal Data

Citing Half-Life Data

Citing Year	2018	2017	2016	2015	2014	2013	2012	2011	2010	2009	2008-All
#Cites from 2018	274	975	1,209	1,194	1,166	1,088	1,009	980	857	793	7,782
Cumulative %	1.58%	7.21%	14.19%	21.08%	27.81%	34.09%	39.91%	45.56%	50.51%	55.09%	100.00%

Citing Journal Graph 2018

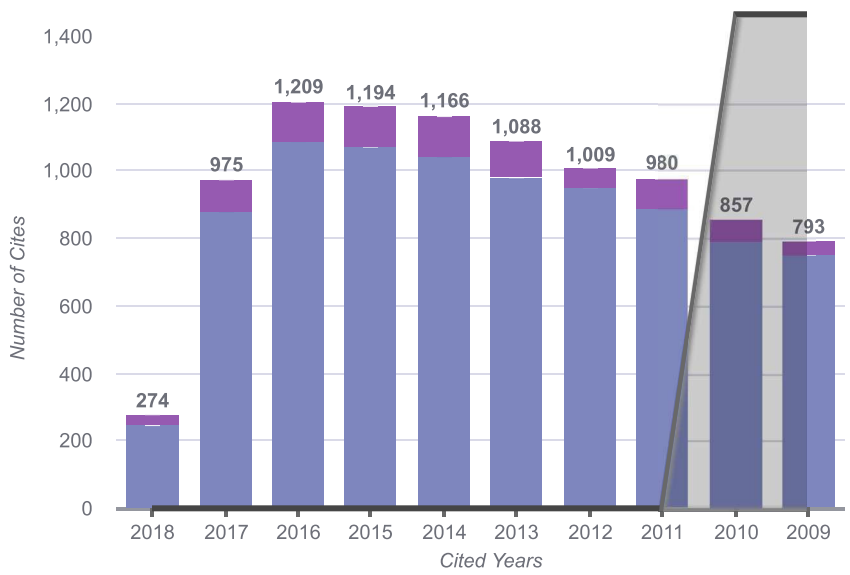

Non-self-citations: citations from the journal to articles in other journals.

Journal self - citations: citations from articles in the journal to articles in the same journal.

CITING JOURNAL GRAPH

The Citing Journal Graph shows the distribution (by cited year) of citations published in the Journal during the JCR year to items published in journals during the last 10 years.

The white/grey division indicates the citing half-life (if < 10.0). Half of the citations are to items that were published more recently than the citing half-life.

Downloaded on 4/17/2020, 8:35:23 AM from Journal Citation Reports (©2020 Clarivate Analytics)

InCites Journal Citation Reports

Clarivate Analytics

Citing Journal Data 2018

Export

	Impact	Citing Journal	All Yrs	2018	2017	2016	2015	2014	2013	2012	2011	2010	2009	F
		ALL Journals	17,327	274	975	1,209	1,194	1,166	1,088	1,009	980	857	793	7
		ALL OTHERS (1973)	1,973	31	114	136	117	109	106	110	95	104	80	
1	3.794	AQUAT TOXICOL	1,234	31	93	117	121	121	107	57	90	65	42	
2	3.421	ENVIRON TOXICOL CHEM	512	11	27	30	32	22	19	28	32	24	23	
3	7.149	ENVIRON SCI TECHNOL	505	5	25	54	47	57	57	31	32	15	29	
4	5.108	CHEMOSPHERE	504	17	75	38	39	30	42	31	44	26	31	
5	4.527	ECOTOX ENVIRON SAFE	379	15	28	24	31	35	27	36	24	21	17	
6	5.589	SCI TOTAL ENVIRON	361	20	48	50	27	41	22	26	12	8	17	
7	5.714	ENVIRON POLLUT	308	17	38	54	34	27	25	8	18	11	10	
8	3.782	MAR POLLUT BULL	274	2	23	21	21	26	16	11	29	9	8	
9	2.697	COMP BIOCHEM PHYS C	270	3	19	11	21	8	13	20	18	15	15	
10	2.776	PLOS ONE	256	1	16	21	42	37	55	44	18	11	4	
11	3.445	MAR ENVIRON RES	233	3	18	15	21	26	16	23	3	9	4	
12	3.564	TOXICOL SCI	158	2	2	1	16	13	7	8	15	9	14	
13	2.914	ENVIRON SCI POLLUT R	152	10	7	33	34	21	12	13	6	4	3	
14	3.298	FISH SHELLFISH IMMUN	144	0	15	20	23	13	8	8	13	6	3	
15	7.913	WATER RES	140	1	12	6	10	19	15	15	6	7	1	
16	3.585	TOXICOL APPL PHARM	136	0	5	6	5	7	7	5	14	6	10	
17	9.580	P NATL ACAD SCI USA	134	0	1	3	5	15	4	11	9	6	5	
18	3.017	J EXP BIOL	132	1	4	6	3	7	5	3	11	4	8	
19	4.106	J BIOL CHEM	124	0	1	1	4	2	1	4	2	0	6	
20	2.135	ARCH ENVIRON CON TOX	121	2	5	2	4	4	4	4	8	4	4	
21	7.736	ENVIRON HEALTH PERSP	118	0	2	2	7	1	2	6	5	11	5	
22	2.359	MAR ECOL PROG SER	112	1	0	3	1	1	2	4	3	2	4	
23	41.063	SCIENCE	109	0	1	4	2	8	4	3	5	2	3	
24	2.460	ECOTOXICOLOGY	107	1	6	3	8	11	14	15	13	11	6	
25	2.445	GEN COMP ENDOCR	107	0	4	9	7	7	5	5	9	10	4	
26	43.070	NATURE	103	0	2	2	3	2	3	6	4	4	4	
27	4.011	SCI REP-UK	96	6	25	35	19	4	6	0	0	0	0	
28	3.022	AQUACULTURE	91	0	4	4	1	3	3	3	5	10	3	

Showing 1 - 30 rows of 1,182 total *(use export to download the full table)*

Downloaded on 4/17/2020, 8:35:23 AM from Journal Citation Reports (©2020 Clarivate Analytics)

InCites Journal Citation Reports

Clarivate Analytics

Journal Relationships

Journal Relationships 2018

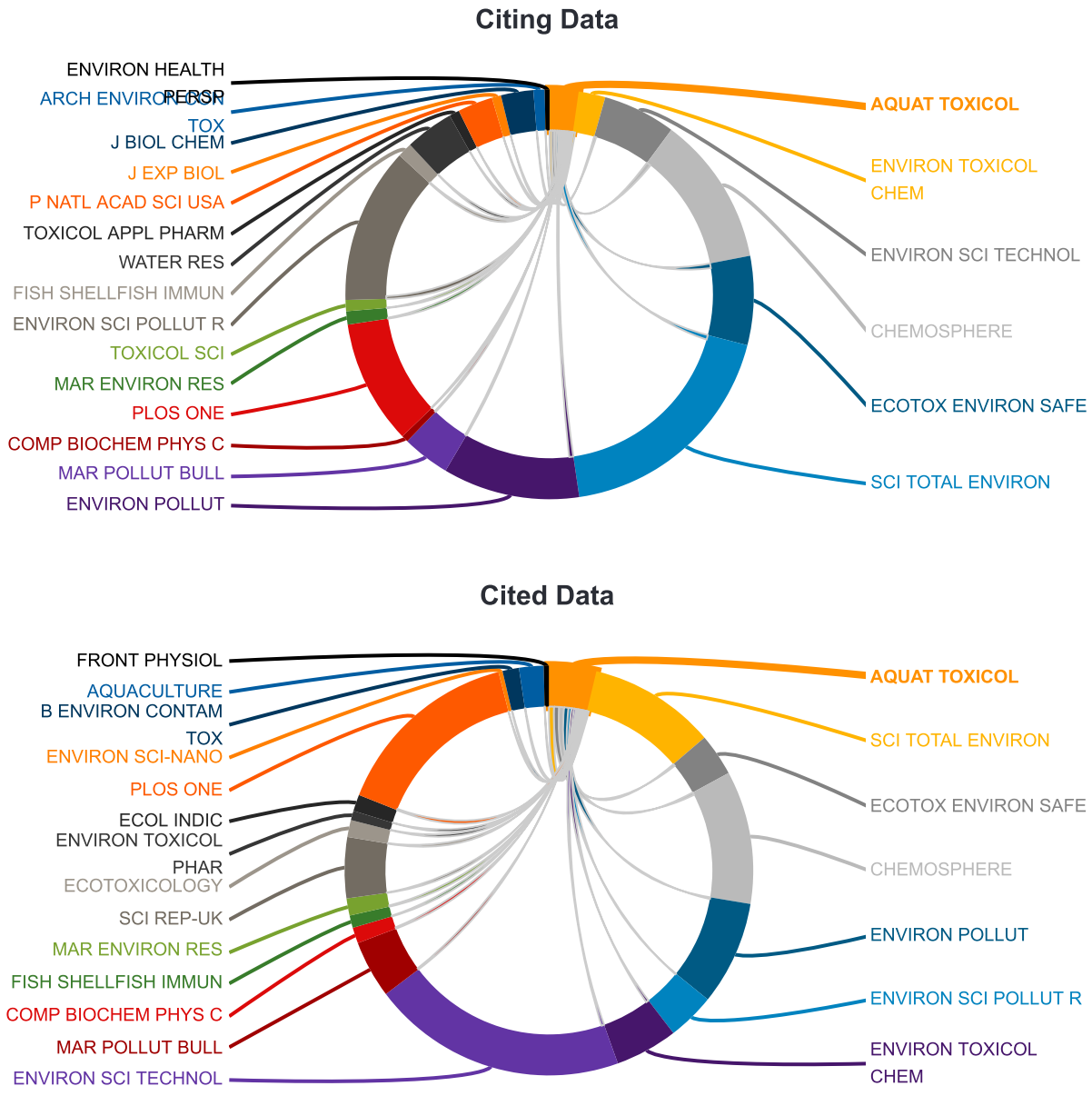

Downloaded on 4/17/2020, 8:35:23 AM from Journal Citation Reports (©2020 Clarivate Analytics)

InCites Journal Citation Reports

Clarivate Analytics

Key Indicators 2018

IMPACT METRICS	
Total Cites	15,194
Journal Impact Factor	3.794
5 Year Impact Factor	4.167
Immediacy Index	0.788
Impact Factor without Journal Self Cites	3.423

INFLUENCE METRICS	
Eigenfactor Score	0.01441
Article Influence Score	0.767
Normalized Eigenfactor	1.71421

SOURCE METRICS	
Citable Items	260
% Articles in Citable Items	98.46
Average JIF Percentile	89.509
Cited Half-Life	7.6
Citing Half-Life	8.9

Downloaded on 4/17/2020, 8:35:23 AM from Journal Citation Reports (©2020 Clarivate Analytics)

InCites Journal Citation Reports

Clarivate Analytics

Metric Trend Total Cites

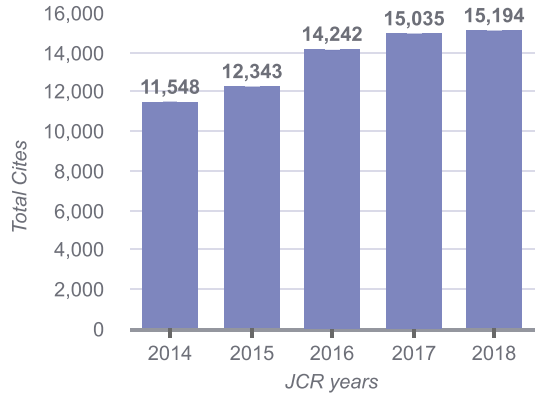

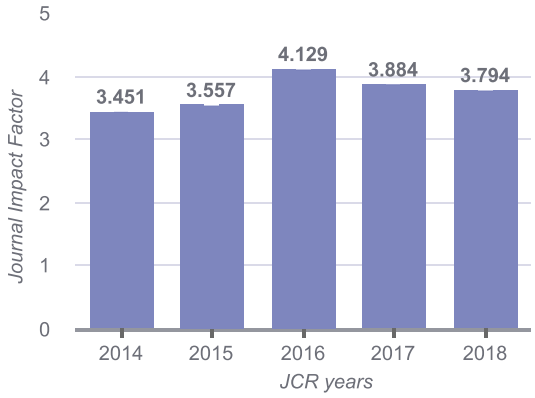

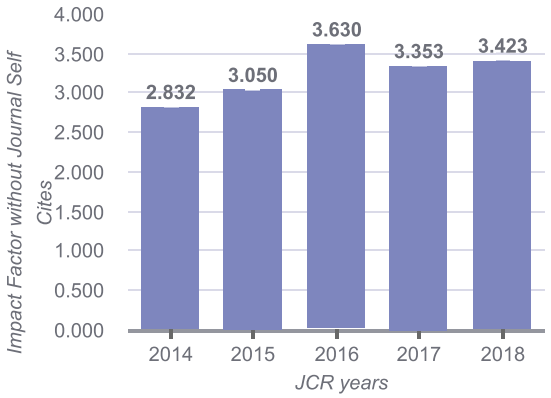

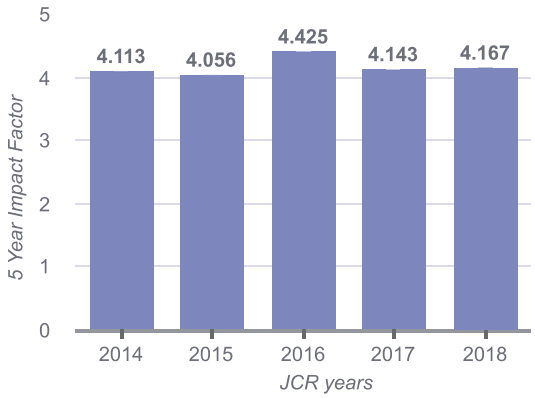

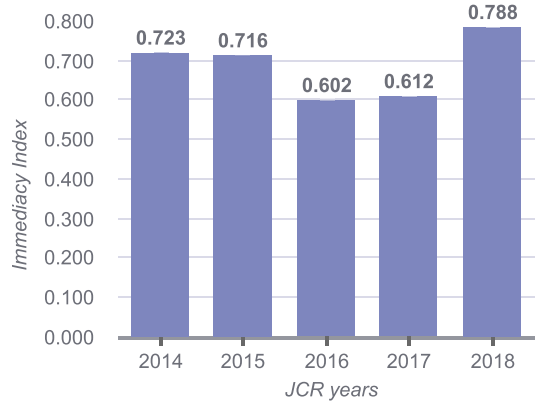

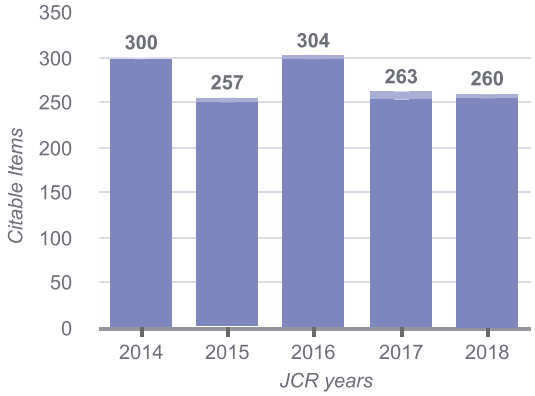

Downloaded on 4/17/2020, 8:35:23 AM from Journal Citation Reports (©2020 Clarivate Analytics)

InCites Journal Citation Reports

Clarivate Analytics

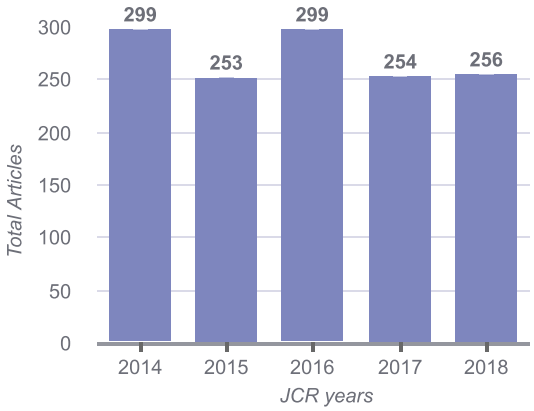

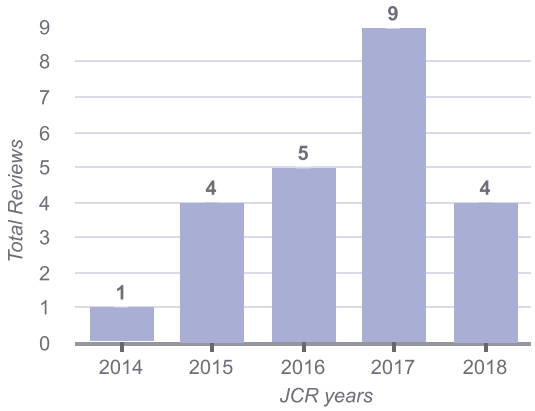

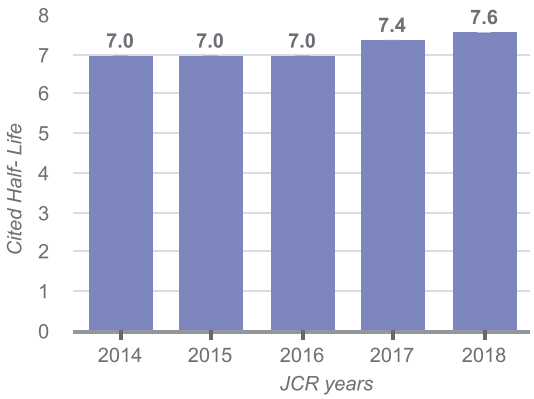

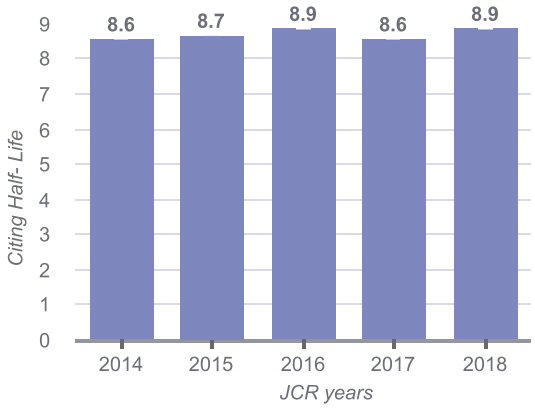

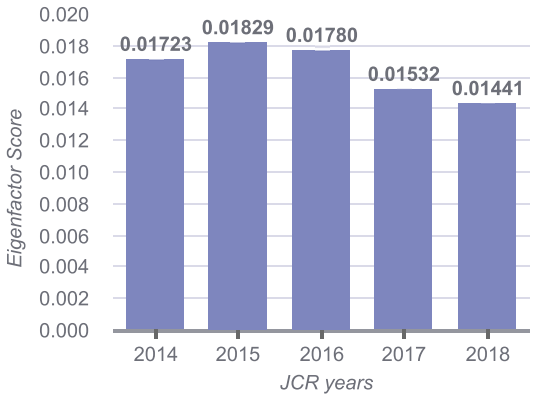

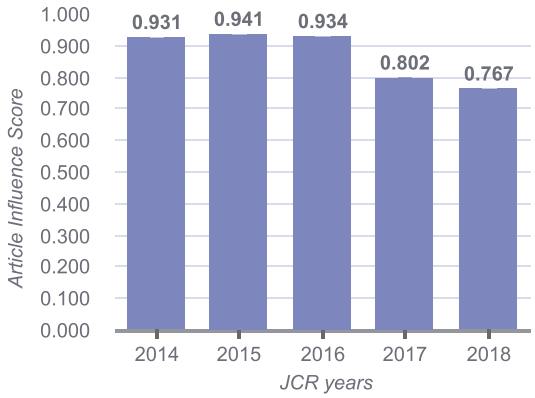

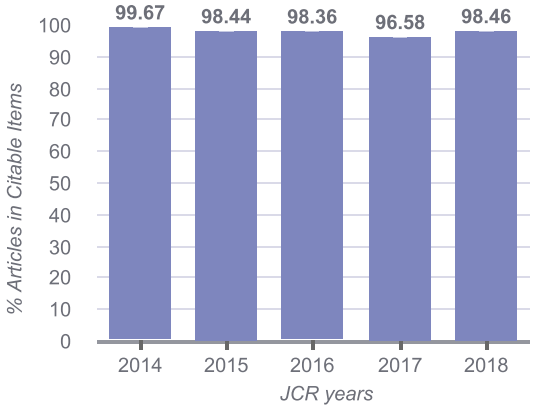

Downloaded on 4/17/2020, 8:35:23 AM from Journal Citation Reports (©2020 Clarivate Analytics)

InCites Journal Citation Reports

Clarivate Analytics

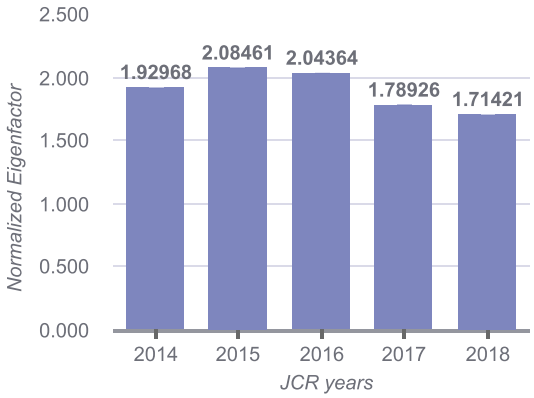

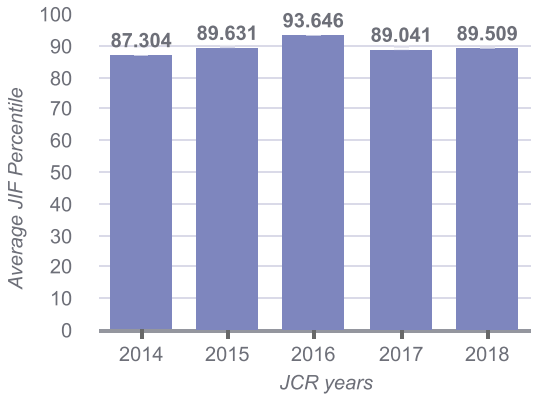

Downloaded on 4/17/2020, 8:35:23 AM from Journal Citation Reports (©2020 Clarivate Analytics)

InCites Journal Citation Reports

Clarivate Analytics

Journal profile [2016 - 2018]

Contributions by country/region

	country	count
1	CHINA MAINLAND	223
2	USA	153
3	Canada	85
4	France	64
5	Portugal	59
6	Brazil	55
7	Italy	42
8	Australia	41
-	South Korea	41
10	GERMANY (FED REP GER)	38
-	Spain	38

Contributions by organizations

	organization	count
1	CHINESE ACADEMY OF SCIENCES	56
2	CENTRE NATIONAL DE LA RECHERCHE SCIENTIFIQUE (CNRS)	39
3	UNIVERSIDADE DE AVEIRO	32
4	SUNGKYUNKWAN UNIVERSITY (SKKU)	26
5	HUAZHONG AGRICULTURAL UNIVERSITY	23
6	UNIVERSITY OF CALIFORNIA SYSTEM	22
7	IFREMER	20
8	UNIVERSIDADE DO PORTO	19
9	STATE UNIVERSITY SYSTEM OF FLORIDA	17
10	CITY UNIVERSITY OF HONG KONG	15
-	COLLABORAT INNOVAT CTR EFFICIENT & HLTH PROD FISH	15
-	XIAMEN UNIVERSITY	15

Downloaded on 4/17/2020, 8:35:23 AM from Journal Citation Reports (©2020 Clarivate Analytics)

Haselman, Jon

From: Allen Olmstead <allen.olmstead@basf.com>
Sent: Friday, April 17, 2020 1:42 PM
To: Haselman, Jon
Subject: RE: Record of Percentage Agreement - Allen Olmstead

Hello Jon,

I agree with the designated percentage of contributions in the table from your email below. If you need anything else from me, just let me know.

Sincerely,
Allen

Allen Olmstead
Ecotoxicology

Phone: +1 919 5472644, Mobile: +1 919 2706081, Email: allen.olmstead@basf.com
Postal Address: BASF Corporation - Agricultural Solutions, , 26 Davis Drive, 27709-3528 Research Triangle Park, United States

---

From: Haselman, Jon <Haselman.Jon@epa.gov>
Sent: Wednesday, April 15, 2020 4:00 PM
To: Allen Olmstead <allen.olmstead@basf.com>
Subject: Record of Percentage Agreement - Allen Olmstead

Hi Allen,

The following papers will be nominated for an EPA Scientific and Technical Achievement Award this year.

Haselman, J. T., Kosian, P. A., Korte, J. J., Olmstead, A. W., Iguchi, T., Johnson, R. D., & Degitz, S. J. (2016). Development of the Larval Amphibian Growth and Development Assay: effects of chronic 4-tert-octylphenol or 17β-trenbolone exposure in Xenopus laevis from embryo to juvenile. Journal of Applied Toxicology, 36(12), 1639-1650.

Haselman, J. T., Kosian, P. A., Korte, J. J., Olmstead, A. W., & Degitz, S. J. (2018). Effects of multiple life stage exposure to the fungicide prochloraz in Xenopus laevis: Manifestations of antiandrogenic and other modes of toxicity. Aquatic Toxicology, 199, 240-251.

In order to nominate these publications, the designated percentage contribution to the work represented by these manuscripts needs to be agreed upon by all authors. Please reply to this email with a brief statement indicating that you agree with your designated percentage of contribution shown in the table below. If you do not agree with this designation, please reply to this email ASAP with your concerns and suggestions. **Your reply must be received by Friday, April 24th** for this nomination to be submitted on time.

Authorship	Name	Organization	% contribution
Nominee (1st author)	Jonathan Haselman	EPA-ORD	22
Co-author	Patricia Kosian	EPA-ORD (retired)	12
Co-author	Joseph Korte	EPA-ORD (retired)	12
Co-author	Rodney Johnson	EPA-ORD (retired)	5
Co-author	Sigmund Degitz	EPA-ORD	22
Co-author	Allen Olmstead	Non-EPA	22
Co-author	Taisen Iguchi	Non-EPA	5

Thank you,

Jon Haselman
Great Lakes Toxicology and Ecology Division
Center for Computational Toxicology & Exposure
Office of Research and Development
U.S. Environmental Protection Agency
6201 Congdon Blvd.
Duluth, MN 55804
T: 218-529-5244
E: Haselman.jon@epa.gov

Haselman, Jon

From: jkorte@charter.net
Sent: Thursday, April 16, 2020 10:27 AM
To: Haselman, Jon
Subject: RE: Record of Percentage Agreement - Joseph Korte

Hi Jon,

Yes, I agree with the percentages.

I hope you are doing well. I imagine this is a very difficult time to get any work done in the lab. Hope it doesn't last too long.
Joe

From: "Haselman, Jon"
To: "jkorte@charter.net"
Cc:
Sent: Wednesday April 15 2020 2:54:58PM
Subject: Record of Percentage Agreement - Joseph Korte

Hi Joe,

The following papers will be nominated for an EPA Scientific and Technical Achievement Award this year.

Haselman, J. T., Kosian, P. A., Korte, J. J., Olmstead, A. W., Iguchi, T., Johnson, R. D., & Degitz, S. J. (2016). Development of the Larval Amphibian Growth and Development Assay: effects of chronic 4-tert-octylphenol or 17β-trenbolone exposure in Xenopus laevis from embryo to juvenile. Journal of Applied Toxicology, 36(12), 1639-1650.

Haselman, J. T., Kosian, P. A., Korte, J. J., Olmstead, A. W., & Degitz, S. J. (2018). Effects of multiple life stage exposure to the fungicide prochloraz in Xenopus laevis: Manifestations of antiandrogenic and other modes of toxicity. Aquatic Toxicology, 199, 240-251.

In order to nominate these publications, the designated percentage contribution to the work represented by these manuscripts needs to be agreed upon by all authors. Please reply to this email with a brief statement indicating that you agree with your designated percentage of contribution shown in the table below. If you do not agree with this designation, please reply to this email ASAP with your concerns and suggestions. **Your reply must be received by Friday, April 24th** for this nomination to be submitted on time.

Authorship	Name	Organization	% contribution
Nominee (1st author)	Jonathan Haselman	EPA-ORD	22
Co-author	Patricia Kosian	EPA-ORD (retired)	12
Co-author	Joseph Korte	EPA-ORD (retired)	12
Co-author	Rodney Johnson	EPA-ORD (retired)	5
Co-author	Sigmund Degitz	EPA-ORD	22

Co-author	Allen Olmstead	Non-EPA	22
Co-author	Taisen Iguchi	Non-EPA	5

Thank you,

Jon Haselman
Great Lakes Toxicology and Ecology Division
Center for Computational Toxicology & Exposure
Office of Research and Development
U.S. Environmental Protection Agency
6201 Congdon Blvd.
Duluth, MN 55804
T: 218-529-5244
E: Haselman.jon@epa.gov

Haselman, Jon

From: Patricia Kosian <2patriciakosian@gmail.com>
Sent: Wednesday, April 15, 2020 3:16 PM
To: Haselman, Jon
Subject: Re: Record of Percentage Agreement - Patricia Kosian

Hi Jon
I agree with my designated percentage. Good to hear from you. Hope you doing well and staying healthy!
Pat

Pat

On Wed, Apr 15, 2020 at 2:51 PM Haselman, Jon <Haselman.Jon@epa.gov> wrote:

> Hi Pat,
>
> The following papers will be nominated for an EPA Scientific and Technical Achievement Award this year.
>
> Haselman, J. T., Kosian, P. A., Korte, J. J., Olmstead, A. W., Iguchi, T., Johnson, R. D., & Degitz, S. J. (2016). Development of the Larval Amphibian Growth and Development Assay: effects of chronic 4-tert-octylphenol or 17β-trenbolone exposure in Xenopus laevis from embryo to juvenile. Journal of Applied Toxicology, 36(12), 1639-1650.
>
> Haselman, J. T., Kosian, P. A., Korte, J. J., Olmstead, A. W., & Degitz, S. J. (2018). Effects of multiple life stage exposure to the fungicide prochloraz in Xenopus laevis: Manifestations of antiandrogenic and other modes of toxicity. Aquatic Toxicology, 199, 240-251.
>
> In order to nominate these publications, the designated percentage contribution to the work represented by these manuscripts needs to be agreed upon by all authors. Please reply to this email with a brief statement indicating that you agree with your designated percentage of contribution shown in the table below. If you do not agree with this designation, please reply to this email ASAP with your concerns and suggestions. **Your reply must be received by Friday, April 24th** for this nomination to be submitted on time.

Authorship	Name	Organization	% contribution
Nominee (1st author)	Jonathan Haselman	EPA-ORD	22
Co-author	Patricia Kosian	EPA-ORD (retired)	12
Co-author	Joseph Korte	EPA-ORD (retired)	12

Co-author	Rodney Johnson	EPA-ORD (retired)	5
Co-author	Sigmund Degitz	EPA-ORD	22
Co-author	Allen Olmstead	Non-EPA	22
Co-author	Taisen Iguchi	Non-EPA	5

Thank you,

Jon Haselman

Great Lakes Toxicology and Ecology Division

Center for Computational Toxicology & Exposure

Office of Research and Development

U.S. Environmental Protection Agency

6201 Congdon Blvd.

Duluth, MN 55804

T: 218-529-5244

E: Haselman.jon@epa.gov

Haselman, Jon

From: Rodney Johnson <julnrod@gmail.com>
Sent: Wednesday, April 15, 2020 7:54 PM
To: Haselman, Jon
Subject: Re: Record of Percentage Agreement - Rodney Johnson

Hi Jon,
Thanks for including me in this nomination. I feel honored! And, yes I agree with the percentage you have allocated for my contribution. Thanks again, Rodney.

On Wed, Apr 15, 2020, 2:56 PM Haselman, Jon <Haselman.Jon@epa.gov> wrote:

> Hi Rodney,
>
> The following papers will be nominated for an EPA Scientific and Technical Achievement Award this year.
>
> Haselman, J. T., Kosian, P. A., Korte, J. J., Olmstead, A. W., Iguchi, T., Johnson, R. D., & Degitz, S. J. (2016). Development of the Larval Amphibian Growth and Development Assay: effects of chronic 4-tert-octylphenol or 17β-trenbolone exposure in Xenopus laevis from embryo to juvenile. Journal of Applied Toxicology, 36(12), 1639-1650.
>
> Haselman, J. T., Kosian, P. A., Korte, J. J., Olmstead, A. W., & Degitz, S. J. (2018). Effects of multiple life stage exposure to the fungicide prochloraz in Xenopus laevis: Manifestations of antiandrogenic and other modes of toxicity. Aquatic Toxicology, 199, 240-251.
>
> In order to nominate these publications, the designated percentage contribution to the work represented by these manuscripts needs to be agreed upon by all authors. Please reply to this email with a brief statement indicating that you agree with your designated percentage of contribution shown in the table below. If you do not agree with this designation, please reply to this email ASAP with your concerns and suggestions. **Your reply must be received by Friday, April 24th** for this nomination to be submitted on time.

Authorship	Name	Organization	% contribution
Nominee (1st author)	Jonathan Haselman	EPA-ORD	22
Co-author	Patricia Kosian	EPA-ORD (retired)	12
Co-author	Joseph Korte	EPA-ORD (retired)	12
Co-author	Rodney Johnson	EPA-ORD (retired)	5
Co-author	Sigmund Degitz	EPA-ORD	22

Co-author	Allen Olmstead	Non-EPA	22
Co-author	Taisen Iguchi	Non-EPA	5

Thank you,

Jon Haselman

Great Lakes Toxicology and Ecology Division

Center for Computational Toxicology & Exposure

Office of Research and Development

U.S. Environmental Protection Agency

6201 Congdon Blvd.

Duluth, MN 55804

T: 218-529-5244

E: Haselman.jon@epa.gov

Haselman, Jon

From: Degitz, Sigmund
Sent: Wednesday, April 15, 2020 2:59 PM
To: Haselman, Jon
Subject: RE: Record of Percentage Agreement - Sigmund Degitz

I agree.

From: Haselman, Jon <Haselman.Jon@epa.gov>
Sent: Wednesday, April 15, 2020 2:58 PM
To: Degitz, Sigmund <Degitz.Sigmund@epa.gov>
Subject: Record of Percentage Agreement - Sigmund Degitz

Hi Sig,

The following papers will be nominated for an EPA Scientific and Technical Achievement Award this year.

Haselman, J. T., Kosian, P. A., Korte, J. J., Olmstead, A. W., Iguchi, T., Johnson, R. D., & Degitz, S. J. (2016). Development of the Larval Amphibian Growth and Development Assay: effects of chronic 4-tert-octylphenol or 17β-trenbolone exposure in Xenopus laevis from embryo to juvenile. Journal of Applied Toxicology, 36(12), 1639-1650.

Haselman, J. T., Kosian, P. A., Korte, J. J., Olmstead, A. W., & Degitz, S. J. (2018). Effects of multiple life stage exposure to the fungicide prochloraz in Xenopus laevis: Manifestations of antiandrogenic and other modes of toxicity. Aquatic Toxicology, 199, 240-251.

In order to nominate these publications, the designated percentage contribution to the work represented by these manuscripts needs to be agreed upon by all authors. Please reply to this email with a brief statement indicating that you agree with your designated percentage of contribution shown in the table below. If you do not agree with this designation, please reply to this email ASAP with your concerns and suggestions. **Your reply must be received by Friday, April 24th** for this nomination to be submitted on time.

Authorship	Name	Organization	% contribution
Nominee (1st author)	Jonathan Haselman	EPA-ORD	22
Co-author	Patricia Kosian	EPA-ORD (retired)	12
Co-author	Joseph Korte	EPA-ORD (retired)	12
Co-author	Rodney Johnson	EPA-ORD (retired)	5
Co-author	Sigmund Degitz	EPA-ORD	22
Co-author	Allen Olmstead	Non-EPA	22
Co-author	Taisen Iguchi	Non-EPA	5

Thank you,

Jon Haselman
Great Lakes Toxicology and Ecology Division
Center for Computational Toxicology & Exposure
Office of Research and Development

U.S. Environmental Protection Agency
6201 Congdon Blvd.
Duluth, MN 55804
T: 218-529-5244
E: Haselman.jon@epa.gov

Haselman, Jon

From: Iguchi Taisen <taiseni@hotmail.co.jp>
Sent: Wednesday, April 15, 2020 7:24 PM
To: Haselman, Jon
Subject: RE: Record of Percentage Agreement - Taisen Iguchi

Dear Jon:

I hope you and your all colleagues in the Duluth Mid-Continent Ecology Division are safe from the COVID-19. In Japan, all universities and schools are closed until May 6. Our US-Japan members including Yuta Onishi and Tetsurou Okamura at Idea Co. are all fine.

I totally agree with the percentage of my contribution to the work.
Good luck for the Award!

Taisen Iguchi

Windows 10 版のメールから送信

差出人: Haselman, Jon
送信日時: 2020 年 4 月 16 日 5:02
宛先: Taisen
件名: Record of Percentage Agreement - Taisen Iguchi

Hello Taisen,

The following papers will be nominated for an EPA Scientific and Technical Achievement Award this year.

Haselman, J. T., Kosian, P. A., Korte, J. J., Olmstead, A. W., Iguchi, T., Johnson, R. D., & Degitz, S. J. (2016). Development of the Larval Amphibian Growth and Development Assay: effects of chronic 4-tert-octylphenol or 17β-trenbolone exposure in Xenopus laevis from embryo to juvenile. Journal of Applied Toxicology, 36(12), 1639-1650.

Haselman, J. T., Kosian, P. A., Korte, J. J., Olmstead, A. W., & Degitz, S. J. (2018). Effects of multiple life stage exposure to the fungicide prochloraz in Xenopus laevis: Manifestations of antiandrogenic and other modes of toxicity. Aquatic Toxicology, 199, 240-251.

In order to nominate these publications, the designated percentage contribution to the work represented by these manuscripts needs to be agreed upon by all authors. Please reply to this email with a brief statement indicating that you agree with your designated percentage of contribution shown in the table below. If you do not agree with this designation, please reply to this email ASAP with your concerns and suggestions. **Your reply must be received by Friday, April 24th** for this nomination to be submitted on time.

Authorship	Name	Organization	% contribution

Nominee (1st author)	Jonathan Haselman	EPA-ORD	22
Co-author	Patricia Kosian	EPA-ORD (retired)	12
Co-author	Joseph Korte	EPA-ORD (retired)	12
Co-author	Rodney Johnson	EPA-ORD (retired)	5
Co-author	Sigmund Degitz	EPA-ORD	22
Co-author	Allen Olmstead	Non-EPA	22
Co-author	Taisen Iguchi	Non-EPA	5

Thank you,

Jon Haselman
Great Lakes Toxicology and Ecology Division
Center for Computational Toxicology & Exposure
Office of Research and Development
U.S. Environmental Protection Agency
6201 Congdon Blvd.
Duluth, MN 55804
T: 218-529-5244
E: Haselman.jon@epa.gov

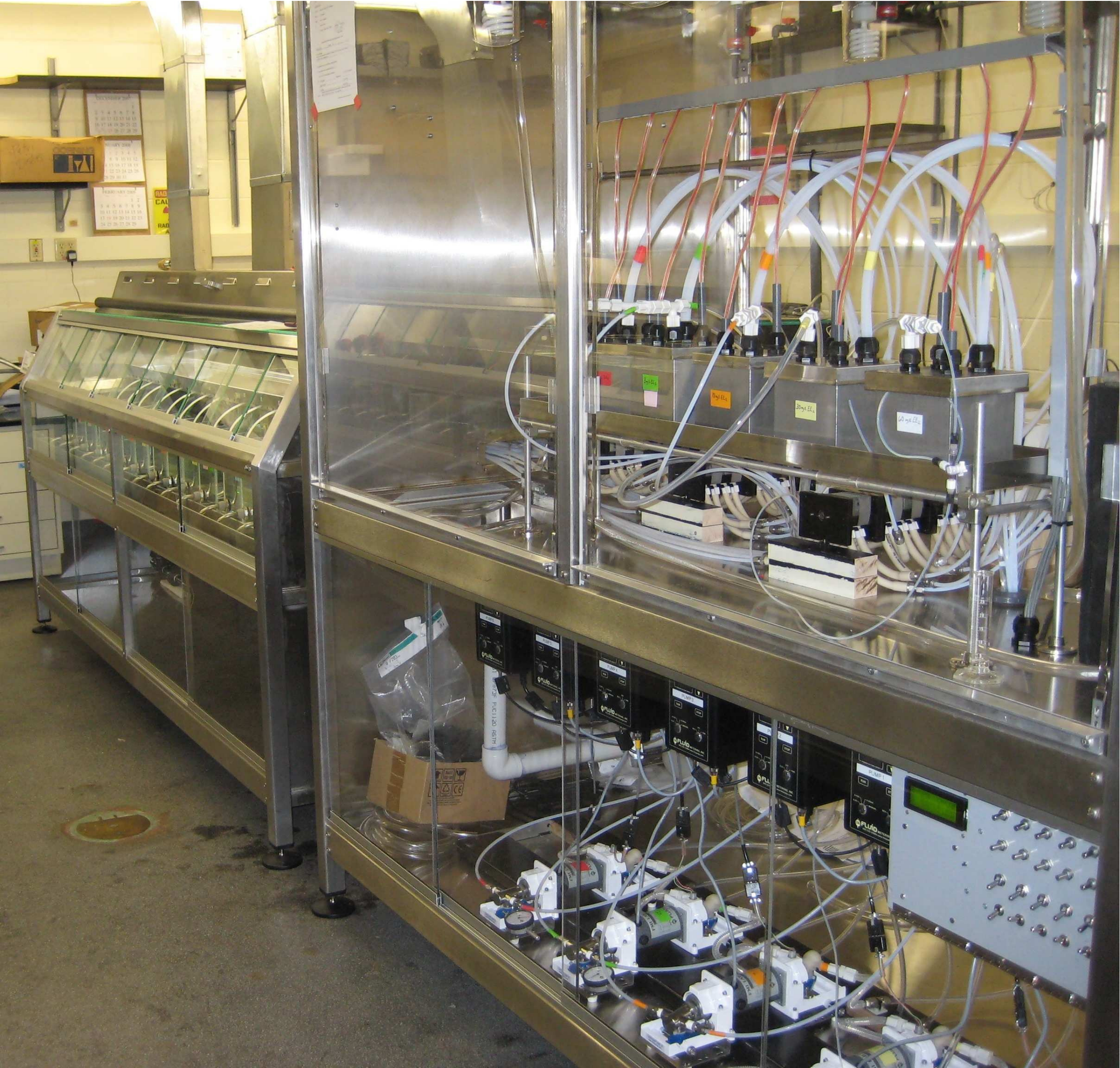

General and Comparative Endocrinology 214 (2015) 103–113

Contents lists available at ScienceDirect

General and Comparative Endocrinology

journal homepage: www.elsevier.com/locate/ygcen

Global gene expression during early differentiation of *Xenopus* (*Silurana*) *tropicalis* gonad tissues

Jonathan T. Haselman *, Allen W. Olmstead [1], Sigmund J. Degitz

US Environmental Protection Agency, Office of Research and Development, National Health and Environmental Effects Research Laboratory, Mid-Continent Ecology Division, 6201 Congdon Blvd., Duluth, MN 55804, USA

ARTICLE INFO

Article history:
Available online 21 June 2014

Keywords:
Xenopus tropicalis
Amphibian
Microarray
Gonad differentiation
Reproductive development
Gene expression

ABSTRACT

African clawed frog *Xenopus* sp. is used extensively for developmental biology and toxicology research. Amid concerns of environmental pollutants disrupting endocrine systems and causing altered reproductive development in wildlife, eco-toxicology research has led to a focus on linking molecular initiating events to population-level effects. As such, efforts to better understand reproductive development at the molecular level in these model species are warranted. To that end, transcriptomes were characterized in differentiating *Xenopus tropicalis* gonad tissues at Nieuwkoop and Faber (NF) stage 58 (pro-metamorphosis), NF66 (completion of metamorphosis), 1 week post-metamorphosis (1WPM), and 2 weeks post-metamorphosis (2WPM). Differential expression analysis between tissue types at each developmental stage revealed a substantial divergence of ovary and testis transcriptomes starting between NF58 and NF66; transcriptomes continued to diverge through 2WPM. Generally, testis-enriched transcripts were expressed at relatively constant levels, while ovary-enriched transcripts were up-regulated within this developmental period. Functional analyses of differentially expressed transcripts allowed linkages to be made between their putative human orthologues and specific cellular processes associated with differentiating gonad tissues. In ovary tissue, genetic programs direct germ cells through meiosis to the diplotene stage when maternal mRNAs are transcribed and trafficked to oocytes for translation following fertilization. In the testis, gene expression is consistent with connective tissue development, tubule formation, and germ cell support (Leydig and Sertoli cells). This dataset exhibited remarkable consistency with transcript profiles previously described in gonad tissues across species, and emphasizes the universal importance of certain transcripts for germ cell development and preparation of these tissues for reproduction.

Published by Elsevier Inc.

1. Introduction

African clawed frog *Xenopus* sp. has been used extensively for developmental biology and toxicology research. With mounting concerns about wildlife exposure to environmental pollutants and potential endocrine disrupting compounds (reviewed by Kloas, 2002), efforts to better understand the mechanisms by which xenobiotics cause reproductive harm are warranted. Many studies have demonstrated the susceptibility of amphibians to altered gonadal development due to xenobiotic or exogenous hormone exposure resulting in sex reversal or altered sex ratios (Bögi et al., 2002; Olmstead et al., 2009a; Ohtani et al., 2000; Pettersson et al., 2006; Reeder et al., 1998; Villalpando and Merchant-Larios, 1990). The molecular processes of sex determination in amphibians vary by species, but many of the downstream molecular processes driving differentiation (*e.g.*, steroid hormones) are similar even across taxa (reviewed by Hayes, 1998; reviewed by Ogielska 2009a,b,c; reviewed by Nakamura, 2010). Recent studies of gene expression related to gonad differentiation in *Xenopus* sp. focus on small subsets of genes in the gonad–mesonephric complex and lack anchoring to a genotypic sex (Duarte-Guterman and Trudeau, 2011; Flood and Langlois, 2014; Navarro-Martín et al., 2012). We are now able to identify genotypic sex in individual *Xenopus* larvae (Olmstead et al., 2010; Yoshimoto et al., 2008) and have the ability to excise pure gonad tissue as early as Nieuwkoop and Faber ([NF] 1994) stage 58. These advances allow clear comparisons of gene expression profiles in ovary and testis tissues for identification of gender-biased molecular networks specific to each tissue. With the latest technological advances in global gene expression analysis, it is now possible to characterize the genetic

* Corresponding author. Fax: +1 218 529 5003.
E-mail addresses: haselman.jon@epa.gov (J.T. Haselman), allen.olmstead@bayer.com (A.W. Olmstead), degitz.sigmund@epa.gov (S.J. Degitz).
[1] Present address: Environmental Toxicology and Risk Assessment, Development North America, Bayer CropScience LP, Research Triangle Park, NC 27709, USA.

http://dx.doi.org/10.1016/j.ygcen.2014.06.009
0016-6480/Published by Elsevier Inc.

programs responsible for active gonad differentiation. This foundational information can then be utilized in subsequent toxicological research to better understand how molecular perturbations in gonad tissues cause abnormal phenotypes.

Three sequential events are operative in determining the sex of most vertebrates: fusing of the gametes at conception (*e.g.*, XX/XY or ZZ/ZW sex chromosomes), sex determination by a molecular switch during embryonic or larval development, and finally, the cascading molecular expression patterns initiated by the sex determination switch. Prior to sex determination in anurans, the undifferentiated, bipotential gonad consists of a cortex and medulla (Merchant-Larios and Villalpando, 1981). In *Xenopus tropicalis*, the first signs of testicular differentiation at the histological level occur around NF stage 48, while the first evidence of ovarian differentiation occurs around NF stage 51 based on differences in laminin localization patterns (El Jamil et al., 2008). The primordial germ cells (PGC) reside in the cortex of the bipotential gonad and continue to remain in the cortex of the female gonad while the medulla recedes to an inner epithelial layer forming a lumen (Ogielska, 2009a). In the testis, the PGCs migrate from the cortex to the medulla; the cortex eventually disappears in lieu of the peritoneal epithelium. These processes are initiated and orchestrated by genetic control, but the exact mechanisms have not been elucidated in anuran species (Hayes, 1998; Ogielska 2009a,b,c; Nakamura, 2010). By NF58, the gonad is fully distinguishable histologically as either an ovary or a testis based on the presence or absence of the cortex and medulla (Fig. 1). Following NF58, many noticeable changes take place histologically that indicate substantial up-regulation of differentiation processes. In the ovary, primary oogonia are actively dividing mitotically and form germ cell nests of secondary oogonia (Ogielska, 2009b). These germ cell nests are surrounded by somatic pre-follicular cells that will eventually support development of the diplotene oocytes. Blood vessels and mesenchyme cells migrate into the cortex through the thin space between the cortex and what was previously the medulla. These blood vessels will eventually deliver yolk precursors to the oocytes from the liver where they are synthesized. Secondary oogonia become primary oocytes and proceed through meiosis to the diplotene stage, when follicular cells proliferate and envelop each oocyte to form follicles. Within each follicle, oocytes begin to protrude microvilli that interlace with follicular cell macrovilli, and gap junctions are formed between the oocyte and follicular cell villi which allow more surface area for passage of hormones and signaling molecules between cells to direct oocyte meiosis and maturation. The microvilli of the oocyte begin to branch out at their tips, running parallel with the oocyte surface creating an envelope (zona pellucida) where glycoproteins are localized to mediate the acrosome reaction and resist polyspermy. An extensive network of cytoskeletal components are assembled in the diplotene oocyte to traffic molecules and prepare for resumption of meiosis when triggered by progesterone much later in development. By 2 weeks following the completion of metamorphosis, the ovary contains premeiotic germ cells and meiocytes representing every stage of meiosis up to the arrested diplotene stage.

The histological hallmarks of testis differentiation throughout this period of development are mainly cellular organization and proliferation, as spermatogenesis does not commence until seminiferous tubules are fully developed closer to sexual maturity. However, notable activities include invasion of blood vessels and mesenchyme cells into the testis between the cortex and medulla (as in the ovary), primary spermatocytes become encapsulated by somatic cells and organize into primordial seminiferous cords that eventually become tubules, and mesenchyme cells differentiate into Leydig cells that will produce steroid hormones (Ogielska, 2009c). Overall, the ovary undergoes more activity in germ cell development while the testis experiences more cellular movement and organization for duct formation.

The objective of this study was to characterize the gene expression patterns associated with *X. tropicalis* early gonad differentiation and to identify candidate genes having robust associations with gonad maturation during this period of development. A secondary objective was to broaden the understanding of functional significance in a cross-species context by comparing the candidate gene expression profiles to existing knowledge of orthologous gene expression in other species during gonadal development. To that end, temporal global expression profiles were measured in four different stages of differentiating *X. tropicalis* ovary and testis tissues by microarray. Resulting expression profiles were compared between tissues at each developmental stage and enriched gene sets were analyzed further for functional associations. As part of the analysis process, human orthologues were identified for as many gene transcripts as possible so the extensive mammalian molecular

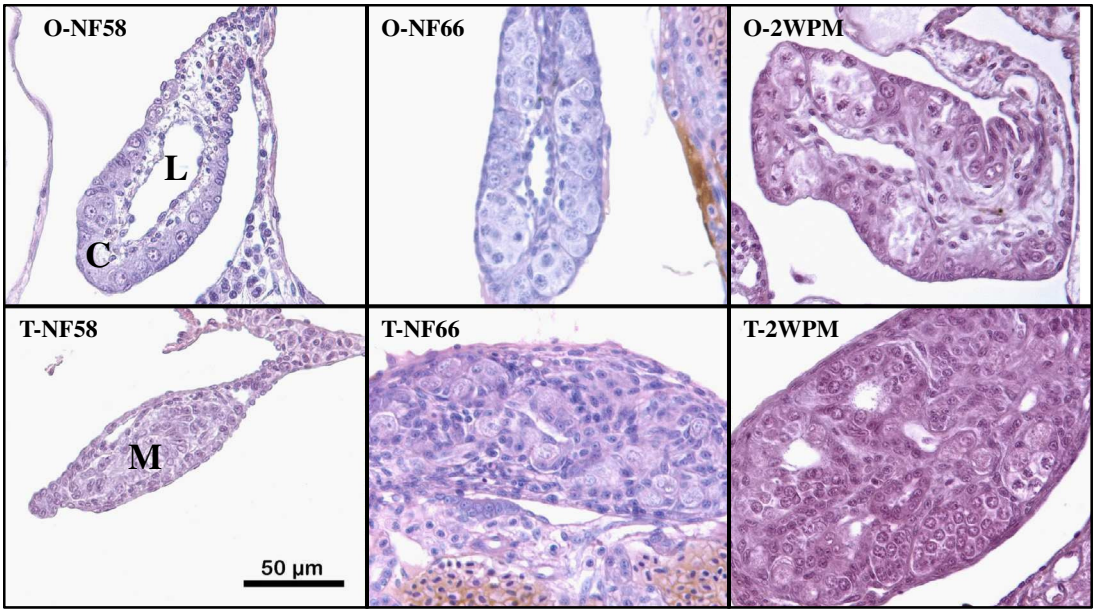

Fig. 1. Histological sections of ovary (O) and testis (T) tissues at NF58, NF66, and 2 weeks post-metamorphosis (2WPM). Stained with H&E. C: cortex; M: medulla; L: lumen.

interaction databases could be used for functional analyses and discussion of cross-species comparisons.

2. Materials and methods

2.1. Animal care and culture

The in-house *X. tropicalis* breeders used to generate animals for this study were of the "golden strain" and the female was confirmed to have the W-linked polymorphism identified by Olmstead et al. (2010). This sex-linked marker and a reference marker were used to determine the genetic sexes of the individual offspring following sampling (described later). The animal care and culture conditions were the same as described by Olmstead et al. (2009b) and were as follows. Adult breeding pairs were maintained on a 12:12 light:dark photoperiod at 25 °C in 7 L glass aquaria with 50 ml/min flow-through conditions and were fed 3/32″ premium sinking frog food pellets (Xenopus Express, Plant City, FL, USA). Water was from nearby Lake Superior (Duluth, MN, USA) and was ozone treated and filtered prior to use. Mating of breeding pairs was induced by injections of hCG (Sigma Aldrich, St. Louis, MO, USA). An initial injection of 20 IU hCG followed by a second injection of 100 IU hCG 5 h later were administered to both the male and female breeder. Following mating, the adult breeders were moved to another tank and embryos were allowed to hatch in flow-through conditions. A single spawn was disbanded to a density of 40/tank (12:12 photoperiod, 25 °C, 7 L tank, 25 ml/min flow) and fed a diet consisting of homogenized cooked carrot and spinach, Sera Micron (Sera North America, Toronto, Canada), and brine shrimp three times daily until removed for sampling.

2.2. Experimental design

Four developmental time-points were considered for global expression analysis: NF58 (pro-metamorphosis), NF66 (completion of metamorphosis), 1 week post-metamorphosis (1WPM), and 2 weeks post-metamorphosis (2WPM). Gonad tissues were time-matched and stage-matched, so collection occurred on a single day for each developmental time-point and all animals used were from the same spawn. For the 1WPM and 2WPM time-points, all animals reached NF66 on the same day and were separated from the rest of the spawn until sample collection 1 and 2 weeks later respectively. On the day of tissue collection, animals were developmentally staged (Nieuwkoop and Faber, 1994) and euthanized by submersion in a lethal concentration of tricaine methanesulfonate ([MS-222], Argent Chemical Laboratories, Redmond, WA, USA) buffered with sodium bicarbonate. Gonad tissues were then excised independently of any other tissues (*i.e.* "pure" gonad tissue) and transferred to a separate vial for each individual, homogenized in lysis buffer from an RNeasy micro kit (Qiagen Inc., Valencia, CA, USA), and immediately frozen on dry ice until samples could be moved to −80 °C storage. Tail or toe tissue was also collected from each individual for genetic sex determination using methods previously described by Olmstead et al. (2010). Once genetic sex was determined for each individual, testes and ovaries were randomly assigned to pools of four individuals (eight gonads per pool) to make a total of five pools of testis tissue and five pools of ovary tissue at each developmental time-point, with the exception of NF58 which had four pools of testis tissue and four pools of ovary tissue (38 total sample pools).

2.3. Total RNA target preparation and hybridization

Homogenates corresponding to the four individuals to be pooled were combined and then total RNA was extracted from each pool according to RNeasy kit instructions (Qiagen Inc., Valencia, CA, USA). RNA concentrations were measured on a NanoDrop ND-1000 Spectrophotometer (NanoDrop Technologies, Inc., http://www.nanodrop.com) and quality was checked using a 2100 Bioanalyzer with an RNA 6000 pico assay (Agilent, Santa Clara, CA, USA). Samples were then frozen at −80 °C and shipped on dry ice to the US EPA Genomics Research Core in Research Triangle Park, NC, where each RNA pool was amplified and labeled using the 3′ IVT Express kit (Affymetrix, Santa Clara, CA, USA) according to kit instructions. Subsequent hybridizations, washes, staining, and scanning of the 38 Affymetrix GeneChip® *X. tropicalis* Genome Arrays (http://www.affymetrix.com/) were performed according to the Expression Analysis instructions provided with the chips. The probe results files (.CEL) containing feature intensities were generated using Affymetrix GeneChip® Command Console® software. These data files can be found in the Gene Expression Omnibus repository (GEO: GSE58612).

2.4. Data analysis

2.4.1. Data summarization

The .CEL files were imported into GeneSpring GX 12.6 (Agilent) software where they were summarized using the PLIER16 algorithm including a baseline adjustment to the median of all samples. The PLIER16 algorithm assumes multiple-array analysis, uses quantile normalization and a weighted approach to background correction using perfect match and mismatch probe pairs (Hubbell, 2004, 2005). Quality control was performed on all arrays using principle component analysis and hybridization control comparisons. The series of biotin-labeled hybridization control levels for one sample replicate (NF58 testis) were indicative of faulty hybridization (Supplemental Fig. 1). This sample was determined to be compromised based on these hybridization controls and was removed from subsequent analyses. As a result, the NF58 testis sample set consisted of three replicates while there were four replicate NF58 ovary samples. The single NF58 testis sample was the only sample showing faulty hybridization; all other hybridizations were successful based on the biotin-labeled hybridization control levels and Pearson's correlation coefficients. The correlation plot including all chips compared to each other is also provided as evidence of this sample's faulty hybridization, but emphasizes the quality of the remaining biological replicates (Supplemental Fig. 2).

2.4.2. Differential expression analysis and clustering

T-tests assuming unequal variance (Welch) were performed to compare the testis versus ovary tissues at each of the developmental stages (Table 1). *P*-values were computed asymptotically and the Benjamini–Hochberg FDR multiple testing correction was applied (corrected p-value cutoff = 0.01). This analysis generated a gene list for each developmental stage which exhibited ⩾2-fold, ⩾5-fold, and ⩾10-fold differential expression between tissues. The 2WPM, ⩾5-fold gene list was chosen for functional analyses due to the 2WPM gonadal tissues being most differentiated and

Table 1
Numbers of transcripts differentially expressed between tissues at each developmental stage (Welch's *t*-test; Benjamini–Hochberg FDR corrected $p < 0.01$). Format of each cell: Testis-enriched/Ovary-enriched.

	Fold difference		
Dev. Stage	⩾2-fold	⩾5-fold	⩾10-fold
NF58	7/0	7/0	7/0
NF66	588/1079	88/91	27/19
1WPM	692/1626	95/196	41/54
2WPM	1487/2617	143/292	53/111

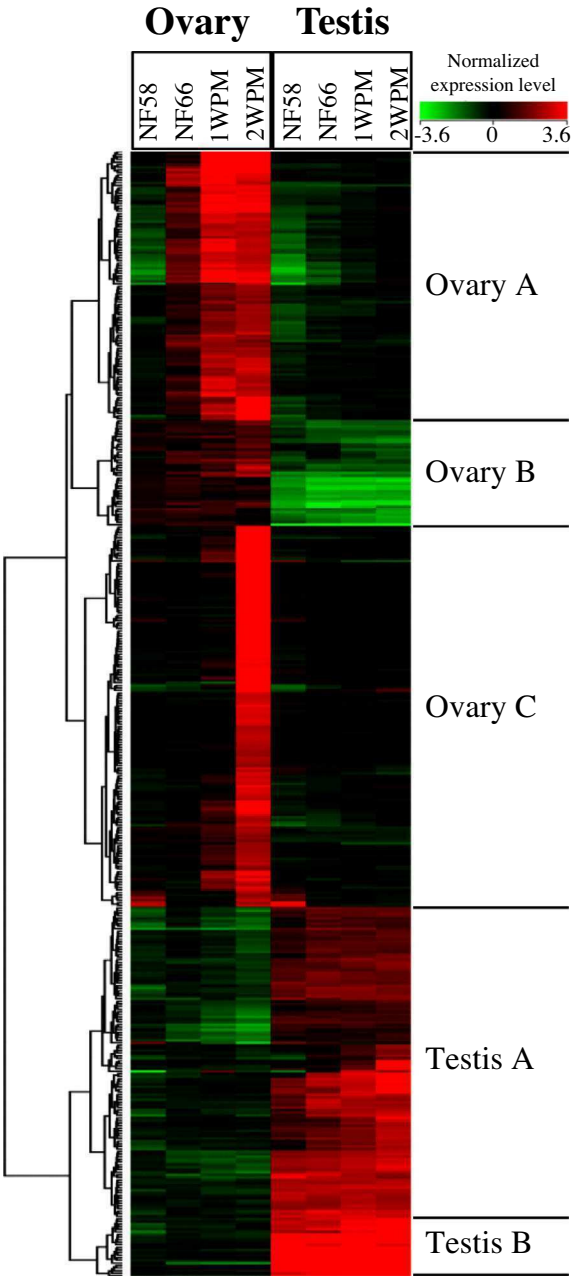

Fig. 2. Hierarchical clustering of the 2WPM, ⩾5-fold transcript list using Euclidian similarity measure and Ward's linkage rule. On the heatmap, red indicates the highest normalized expression level, green indicates the lowest normalized expression level and black indicates expression levels close to the median of all samples. Cluster designations are listed down the right side and correspond to specific clades within the dendrogram on the left side of the heatmap.

exhibiting the most differentially expressed transcripts. Additionally, using the ⩾5-fold cutoff as opposed to the ⩾2-fold cutoff was meant to target transcripts with more robust differences, but to also remain more inclusive than the ⩾10-fold cutoff. Hierarchical clustering was performed on the 2WPM, ⩾5-fold transcript list using Euclidian similarity measure and Ward's linkage rule. Similarity was determined using the transcript profile across all eight conditions (each gender and developmental stage) (Fig. 2).

2.4.3. Affymetrix GeneChip® Genome Arrays and approach to minimize false discovery

Current Affymetrix GeneChip® Genome Arrays utilize multiple oligonucleotide sequences from a single transcript in order to determine an expression level (http://www.affymetrix.com). There are approximately 11 perfect match oligonucleotide probes and 11 mismatch probes per probe set. These multiple perfect match and mismatch probes together provide more accurate determinations of true signal compared to background. Our approach to minimize false discovery was several-fold. First, normalization of the array intensities was performed using the PLIER algorithm. The PLIER normalization algorithm (described earlier), as opposed to several other commonly used normalization algorithms, has been shown to be most conservative in terms of showing false positives (Seo and Hoffman, 2006). A power analysis performed by Seo and Hoffman on various normalization algorithms suggested that PLIER shows no false positives due to its lack of statistical power for poorly performing probe sets. Next, the Benjamini–Hochberg FDR correction was applied to the *t*-test results in addition to applying a corrected *p*-value cutoff of 0.01 instead of the generally accepted cutoff of $p < 0.05$. Finally, for functional analyses and biological interpretation, only transcripts that were ⩾5-fold different between tissues (and statistically significant at corrected *p*-value <0.01) were considered.

2.4.4. Enhanced annotation

In order to utilize Ingenuity Pathway Analysis (IPA) software (Ingenuity Systems, Inc., Redwood City, CA, USA) developed for mammalian gene network, pathway and functional analysis, putative human orthologs were identified for as many probe sets as possible. This was performed by using Python programming language (version 2.7) to search the UniGene database (National Center for Biotechnology Information, http://www.ncbi.nlm.nih.gov/unigene) with each UniGene ID provided in the *X. tropicalis* GeneChip® annotation file. If a human alignment was present for a particular *X. tropicalis* UniGene ID, the human protein accession number was appended to the annotation file for the associated probe set ID. Some probe sets had multiple associated UniGene clusters and therefore had multiple UniGene IDs. For cases where multiple human orthologs were found for a single probe set, the human ortholog with the highest alignment score was used for any subsequent analyses. For details on UniGene cluster assignments and protein similarity criterion, see UniGene FAQ (http://www.ncbi.nlm.nih.gov/UniGene/help.cgi?item=FAQ). The updated annotation file was then imported into GeneSpring so post-analysis gene lists including human ortholog accession numbers for IPA recognition could be exported.

2.4.5. Functional analyses

Five clades from the hierarchical dendrogram were chosen for functional analyses based on the similarity of their expression profiles. The testis-enriched transcripts represented two clades while the ovary-enriched transcripts represented three clades. Each of these five clades were exported from GeneSpring as individual gene lists including human orthologs and were then imported into IPA separately for functional analyses. Transcripts not having a human ortholog were filtered out during the import by default. Also, not all of the recognized ortholog accessions were considered for analyses because interaction data is not yet available for every molecule in the IPA database. Therefore, the resulting number of molecules considered in each analysis was always less than the number of transcripts in the original lists.

3. Results

X. tropicalis ovary and testis transcriptomes were analyzed at four different developmental stages during active tissue differentiation using Affymetrix GeneChip® technology. Each of the arrays contained 59,021 probe sets representing approximately 51,000

unique transcripts. The objective of this study was not only to identify transcripts differentially expressed between the two tissue types, but to identify transcripts showing robust differences between the tissues attributable to the genetic programs associated with gonad differentiation processes. Therefore, stringent cutoffs were applied including a corrected *p*-value cutoff of 0.01 (Benjamini–Hochberg FDR) and fold difference cutoff of ⩾5-fold for functional analyses.

3.1. Differential expression and clustering

According to the corrected *p*-value cutoff of 0.01, there were very few differentially expressed transcripts between tissue types at NF58 and all were testis-enriched (*i.e.*, elevated expression levels in the NF58 testis as compared to the NF58 ovary) (Table 1). Between NF58 and the completion of metamorphosis (NF66), there was an appreciable increase in the number of differentially expressed transcripts, with subsequent increases throughout the remaining developmental stages. In most cases, aside from NF58, the testis-enriched transcripts make up approximately 1/3 of the total differentially expressed transcripts regardless of fold-differences.

As explained in methods Section 2.4.2, a decision had to be made regarding which transcript list to carry forward for functional analysis in order to set limits on the scope of the analysis. Gonad tissues at 2WPM are most differentiated histologically as compared to the earlier developmental stages and the differential expression data in Table 1 corroborates this fact. With regard to the fold-change cutoff, use of transcripts ⩾5-fold different between tissues was intended to include only those transcripts showing robust differences between tissues, but at the same time, remain more inclusive than the ⩾10-fold cutoff. Therefore, clustering and functional analyses were performed on the 2WPM, ⩾5-fold differentially expressed transcript list.

Hierarchical clustering revealed a distinct separation between ovary and testis expression profiles (Fig. 2). For interpretation, a coarse threshold was set to divide the dendrogram into five clusters, which were each later analyzed for function using IPA software. Generally, testis-enriched transcripts in both clades are already being expressed at NF58 and continue to be highly expressed throughout the developmental periods examined. Transcript profiles in the ovary, particularly clade A, indicate that expression is initiated for many genes starting between NF58 and NF66 and levels of expression increase throughout this period of development, whereas many other ovary-enriched genes, most notably clade C, are induced sometime between 1 and 2 weeks post-metamorphosis.

3.2. Functional analyses

3.2.1. Ovary clade A

Transcript expression profiles in this cluster are increasing substantially in the ovary throughout this period of development starting sometime between NF58 and NF66 (Fig. 2 and Supplemental Table 2). Each of the three ovary clusters show different timing of general transcript up-regulation. Ovary A generally shows up-regulation following Ovary B and prior to Ovary C. Many transcripts in the Ovary A cluster are functionally associated with gonadogenesis, gametogenesis, meiosis, and fertility including *FIGLA*, *BRDT*, *TDRD5*, *PABPC1L*, *HORMAD1*, *TEX11*, and *MSH5*. Interestingly, *BRDT*, *TDRD5*, *HORMAD1* and *TEX11* are associated with testis development in mammals and are being highly expressed in differentiating ovary tissue of *X. tropicalis*. Several other transcripts are functionally associated with ovary development and oocyte maturation (*LHX8*, *NPM2*, *GTSF1*, *CGA*, *ZGLP1*). Additionally, many transcripts are associated with DNA replication, recombination, and repair, of which some are also associated with cell cycle and meiosis of germ cells (*DMC1*, *HORMAD1*, *MSH5*, *BRDT*, *TEX11*,

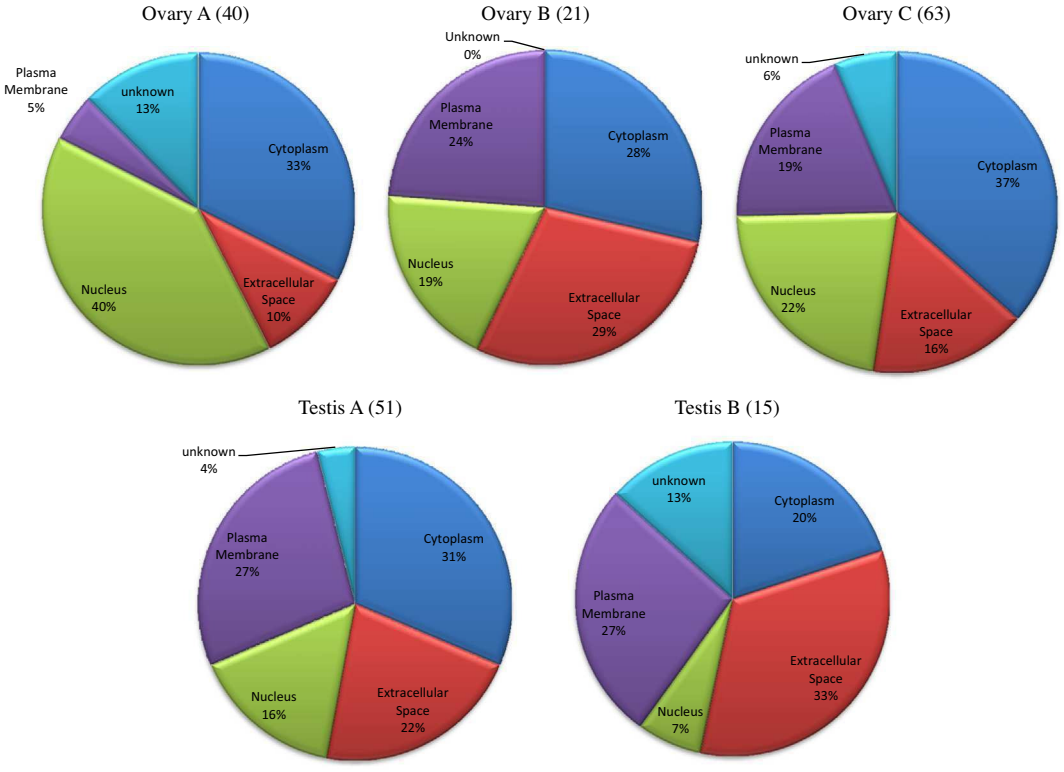

Fig. 3. Cellular distributions of gene products by cluster. Total numbers of unique gene products per cluster are in parentheses next to cluster ID. Cellular location information was derived from IPA output.

NPM2, *TBP*, *SASS6*, *BANF1*, *SYCE2*). Another interesting result from this cluster is that many transcripts are functionally associated with cancer, but lack information about more specific functions (see Supplemental Table 2). This is likely an artifact of the context in which these genes have been studied and the metadata associated with them in the IPA database. Nonetheless, these genes are likely associated with regulation of cell proliferation. The majority of gene products in this cluster reside in the nucleus (40%) and cytoplasm (32%) indicating an emphasis on intracellular processes (Fig. 3).

3.2.2. Ovary clade B

This cluster shows the earliest differential expression of the three ovary clusters starting at NF58 and remaining differentially expressed throughout this period of development, with some profiles showing increasing expression throughout this period of development (Fig. 2 and Supplemental Table 2). Transcripts in this cluster are mainly associated with gonad morphology (*CHST8*, *EMX2*, *CYP26A1*, *GGT1*, *IRX5*), cell proliferation (*OLFML2A*, *LUM*, *NPPC*, *ESRP1*, *CLDN6*, *CLDN7*, *TACSTD2*) and primary sex determination (*EMX2*, *CYP19A1*). Several transcripts are also associated with nervous system development (*NTN1*, *KAL1*, *IRX5*, *A2M*, *IRX3*). Interestingly, several of the upstream regulators predicted to be controlling expression in this cluster are being expressed in testis tissue throughout this period of development (Testis Clade A: *FGF10*, *RARRES1*, *DAX-1*). Other predicted upstream regulators of genes in this cluster include β-estradiol, progesterone, and FSHβ. Gene products in this cluster primarily reside in the extracellular space (29%) and plasma membrane (24%) indicating an emphasis on intercellular signaling/activity (Fig. 3).

3.2.3. Ovary clade C

Transcripts in this cluster are substantially up-regulated between 1WPM and 2WPM. Many of them have very similar temporal expression profiles and similar magnitudes of up-regulation at 2WPM. Functionally, these genes are associated with reproductive system development and gametogenesis (*BMP15*, *CCNA1*, *COMT*, *GJA4*, *H2AFX*, *NANOS2*, *OCA2*, *SOX2*, *ZP3*), cell cycle and meiosis (*BMP15*, *BTG3*, *BTG4*, *CCNA1*, *CCNB1*, *EIF4E*, *LGALS3*, *MAD1L1*, *SOX2*, *WEE2*), transcription (*BMP15*, *BTG3*, *CAPRIN2*, *FOXH1*, *GSTP1*, *GTF3A*, *H2AFX*, *MAD1L1*, *SALL4*, *SOX2*, *TDGF1*, *ZFP36*, *ZFP36L2*, *ZIC2*, *ZP3*), and RNA binding, stabilization and trafficking (*CCNB1*, *EIF4E*, *ZFP36*, *ZFP36L2*). Possible upstream regulators of genes in this cluster are *NOBOX*, *MYBL2*, *SALL4* and *FIGLA*. *FIGLA* is present in the Ovary A cluster and shows a substantial increase in expression starting between NF66 and 1WPM, which precedes up-regulation of many genes in this cluster making it a particularly strong candidate transcriptional regulator. Gene products in this cluster mainly reside in the cytoplasm (37%) and nucleus (22%) indicating an emphasis on intracellular processes and is consistent with cell cycle regulation, transcription, and RNA binding, stabilization, and trafficking occurring for developing meiotic oocytes (Fig. 3).

3.2.4. Testis clade A

Gene expression profiles in this cluster generally show less differential expression between tissue types overall as compared to the Testis B cluster (Supplemental Table 2). Additionally, most of the transcripts in this cluster become more testis-biased between NF66 and 2WPM. This is due in part to general decreases in ovary transcript expression while testis expression remains constant (upper half of cluster) and general increases in testis transcript expression while ovary expression remains constant (lower half of cluster) (Fig. 2). Many transcripts in this cluster are involved in cardiovascular system development (*TPM2*, *GAS6*, *CNN1*, *FBLN5*, *KCNJ8*, *MYH11*), vasculogenesis (*FHL2*, *COL13A1*, *ENPP2*, *SEMA3B*, *COL8A1*, *TGM2*), and connective tissue development (*INHA*, *INHBA*, *DHH*, *NLK*, *COL9A1*, *FHL2*, *FGF10*) (Supplemental Table 2). There are also many transcripts involved in reproductive system development and testis morphology (*NKX3-1*, *SRD5A2*, *INHA*, *INHBA*, *DHH*, *CYP26B1*, *FGF10*, *DAX-1*, *SNAI2*). Some of the same genes associated with testis morphology are also associated with sex determination (*SRD5A2*, *INHA*, *DHH*, *DAX-1*). In addition, there was significant enrichment of transcripts associated with steroidogenesis and androgen biosynthesis in this cluster (*AKR1C3*, *CYP17A1*, *SRD5A2*, *DKK3*, *INHBA*, *KITLG*). Upstream regulation analysis identified TGFβ and androgen receptor as potential activators based on enrichment of transcripts involved in those pathways. Gene products in this cluster show fairly even representation of possible cellular locations with a slight majority occurring in the cytoplasm (31%) (Fig. 3).

3.2.5. Testis clade B

Gene expression profiles in this cluster exhibit substantial expression levels in the testis throughout this period of development and are markedly higher than ovary expression levels, which are ostensibly absent (Fig. 2 and Supplemental Table 2). Functional analysis of this cluster indicates significant contributions to cardiovascular, connective tissue, and nervous system development as in the Testis A cluster. Specifically, transcripts are associated with blood vessel development (*ACTA2*, *MYL4*, *AQP1*, *FGFBP3*), angiogenesis (*AQP1*, *GPC1*, *NPTX1*), collagen development (*BMP1*), and cell signaling and nervous system development (*NPTX1*, *SLITRK4*, *HTR2C*, *CLEC4M*). Three transcripts in this cluster are functionally associated with reproductive system development (*INSL3*, *ASTL*, *AQP1*) with the first two being associated with fertility. Functional analysis of this cluster also identified laminin as a potential upstream regulator. Laminin is localized to the basal membrane surrounding seminiferous tubules in *X. tropicalis* testis tissue (El Jamil et al., 2008) and is known to influence cell migration, differentiation, and tissue organization (Hadley et al., 1990; Sasaki et al., 2004). The majority of gene products in this cluster are located in the extracellular space (33%) and plasma membrane (27%) indicating an emphasis on intercellular signaling and tissue development.

4. Discussion

Gonad tissues are unique from other vertebrate tissues in that the indifferent gonad is triggered, through genetic programs, to differentiate into one of two morphologically distinct mature tissues both supporting germ cells and reproduction. Gonad phenotype is determined genetically in some vertebrate species and by environmental triggers in others (*e.g.*, temperature). However, the sequence of events following sex determination and the molecular factors responsible for developing these tissues are similarly orchestrated in gonads across many vertebrate species, all in support of germ cells. Since gonad differentiation is susceptible to chemical perturbations leading to infertility or sex reversal at the individual level, efforts are necessary to understand the vulnerable targets and pathways leading to aberrant gonad development potentially causing adverse effects at the population level (Ankley et al., 2010).

To contribute to the knowledge base at the molecular level, we employed microarray technology to identify gender differences in the genetic programs associated with gonadal development and differentiation in model Anuran species *X. tropicalis*. To date, global gene expression analysis has not been performed strictly on ovary and testis tissues this early in *Xenopus* development, as they are difficult to excise and close to impossible to differentiate visually. Recent advances in *Xenopus* research allows for the genetic determination of gender in individual animals (Olmstead et al., 2010; Yoshimoto et al., 2008) making it possible to extract ovary and tes-

tis tissues from larvae prior to these tissues becoming visibly dimorphic. By collecting tissues at four different time-points through development, temporal profiles of gonad gene expression specific to each sex were acquired.

Differentially expressed transcripts were clustered by their temporal profiles, and bioinformatic analyses of gene function and pathway enrichment were performed to associate transcripts with tissue processes and to identify potential upstream regulators. Performing these types of analyses with molecular interaction, pathway, and functional annotations specific to *Xenopus* proved to be both bioinformatically cumbersome and not easily interpreted. In contrast, the mammalian-based Ingenuity Pathway Analysis software provided a reasonably comprehensive analysis that facilitated more meaningful interpretation of results. However, human orthologues had to be acquired from the NCBI UniGene database in an automated fashion using Python scripting language. The assumption underlying our analysis is that orthologous genes play similar roles in frogs and humans. While it is recognized that there may be exceptions, the expression profiles of well-characterized gender-biased genes in gonad tissue including *CYP19A1* and *SRD5A2* provided confidence that this assumption was generally valid.

4.1. Ovary

At larval somatic stage NF58, the ovary (stage IV according to Ogielska and Kotusz' (2004) staging criteria for Anuran ovary development) exhibits a cortex containing germ cells and germ cell nests separated by a layer of prefollicular cells. At this stage of ovarian differentiation, the germ cells are dividing mitotically while blood vessels and mesenchyme cells invade the cortex (Ogielska, 2009b). The suite of genes being expressed at this time are in Ovary Clade B which includes, most notably, those coding for enzymes CYP19A1 (aromatase) and CYP26A1. Aromatase catalyzes the production of 17β-estradiol, which has been studied extensively for its role in sex determination and sexual differentiation. It is no surprise aromatase is being expressed in the ovary as it is widely accepted to be a determining factor for whether the bipotential gonad becomes a testis or ovary; its expression profile supports the quality of these results. CYP26A1 is primarily involved in retinoic acid regulation and has been shown to be estrogen-responsive in human endometrium (Deng et al., 2003). Retinoic acid has also been identified as the key factor for initiating sex-specific timing of germ cell entry into meiosis in mammals (reviewed by Bowles and Koopman, 2007). Based on the timing of expression of other meiosis-specific transcripts in this dataset, it is highly plausible that retinoic acid, and regulator CYP26A1, are responsible for initiating *X. tropicalis* oocyte meiosis in a similar fashion.

Oocyte meiosis begins during ovary stage V which is approximately concomitant with the completion of metamorphosis (NF66). Many transcripts in Ovary Clade A are associated with meiosis and are up-regulated around NF66 including *HORMAD1*, *SPDYA*, *MSH5*, *SYCE1*, *BRDT*, *TEX11*, *DMC1*, *TDRD5*, and others. Interestingly, *HORMAD1*, *BRDT*, *TEX11*, and *TDRD5* have been primarily associated with testis tissue in mammals and were found to be playing roles in male germ cell meiosis (Chen et al., 2005; Gaucher et al., 2012; Jones et al., 1997; Wang et al., 2001a; Yabuta et al., 2011), but it is suggestive here that these genes also play significant roles in *X. tropicalis* oocyte meiosis. Further investigation identified that *HORMAD1*, *BRDT*, and *TEX11* have been found to play roles in both spermatocyte and oocyte meiosis (Houmard et al., 2009; Kogo et al., 2012; Paillisson et al., 2007). In mouse spermatogonial cell lines *TEX11* has been shown to modulate effects of estrogen receptor-β, and overexpression resulted in enhanced transcription of an estrogen-responsive reporter gene (Yu et al., 2012). Given the importance of estrogenic influence on gonadal development, *TEX11* could be a critical factor in *Xenopus* ovary and germ cell development ultimately affecting fertility.

Prior to the appearance of diplotene oocytes, which occurs during ovary stage VI, mRNAs coding for notable transcription factors including *TBP*, *LHX8*, and *FIGLA* are ovary-enriched. During this time, early folliculogenesis takes place and is orchestrated by signaling between the oocyte and cumulous, or granulosa cells. *FIGLA* has been shown to directly regulate transcription of a series of glycoproteins localized to the oocyte zona pellucida (Soyal et al., 2000). Notably, *ZP3* and *ZP4* are up-regulated subsequent to the up-regulation of *FIGLA* in the current dataset. A recent study by Hirakawa et al. (2013), using an alternate microarray platform to measure gene expression in juvenile *Xenopus* (*Silurana*) *tropicalis* gonad tissues, also found that *FIGLA*, *ZP4* and other transcripts represented by our current data set are highly ovary-biased. In mouse oocytes *FIGLA* appears to repress expression of testis-associated genes including *CYP17A1*, *DKKL1*, *TDRD1*, *TDRD6*, *TDRD7*, and others, while activating factors associated with oocyte development (Hu et al., 2010). Expression profiles of *CYP17A1* and *DKKL1* isoform *DKK3* in the present dataset are consistent with the findings of Hu et al. (2010) whereas the tudor-domain isoform *TDRD5* expression profile is ovary-enriched. This difference could be species related, temporally related, or isoform related, all of which would require further investigation. However, *FIGLA* has been well-characterized in mammalian reproductive development and plays a critical role in ovary development and fertility. These data support the structural and functional conservation of this transcription factor and its importance to ovary development across species.

Transcription factor *LHX8* has also been implicated in mammalian ovary development and fertility (Choi et al., 2008). Deficiencies in *LHX8* cause misexpression of *GDF9*, *POU5F1*, *NOBOX*, *KIT*, and *KITL*. *NOBOX* and paralogue *POU4F1* were both predicted upstream regulators of ovary-enriched genes in clades B and C. *NOBOX* has been shown to regulate germ-cell specific genes such as *BMP15* and *ZAR1* (Rajkovic et al., 2004), both of which are highly ovary-enriched here at 2WPM. *BMP15* and *GDF9* are close homologues in the TGF-β superfamily of growth factors and are both responsible for activation of primordial follicle development in the human ovary *in vitro* (Kedem et al., 2011). Although *GDF9* was not represented in Supplemental Table 2, it was ovary-enriched at 2WPM by over 2-fold (corrected $p < 0.01$) supporting its role in follicle development across species. In *X. tropicalis*, *KITL* message is continually increasing in testis tissue over this period of development. While in the ovary, expression of this transcript continually decreases. This appears inconsistent with what is reported in mammalian primordial follicle development (Driancourt et al., 2000), as KIT (receptor) together with KITL (ligand) control oocyte growth and theca cell differentiation, and protects preantral follicles from apoptosis. However, *KITL* has been well-characterized as an essential factor for mammalian spermatogenesis and male fertility (Vincent et al., 1998) consistent with expression levels in *X. tropicalis* testis tissues here. Furthermore, this emphasizes the potential importance of its proper expression and uninhibited function for reproductive success in mammals and amphibians alike.

In addition to transcription factor signaling during early folliculogenesis, maternal mRNAs begin to be transcribed in maternal cells and are localized to the developing germ cells. In *Xenopus laevis* embryos, maternal stores of *TBP* mRNA become translated leading up to the mid-blastula transition of embryogenesis and are translationally masked by association with a repressive protein prior to this event (Veenstra et al., 1999). This increase in *TBP* protein coincides with an increase in RNA polymerase I protein to which *TBP* associates in order for active translation to take place during embryogenesis (Bell and Scheer, 1999). *TBP* appears to be

one of many maternal mRNAs that begin to be localized to the soon diplotene oocytes. However, *TBP* expression is up-regulated here around NF66, which is well before many of the other maternal mRNAs are up-regulated indicating a possible role in translation both in primordial follicle development and embryogenesis.

During ovary stage VI and around 2WPM, oocytes reach the diplotene stage of meiosis, and oocyte maturation processes begin including maternal RNA transport and localization within the oocyte, arrangement of the cytoskeleton and microvilli in the oocyte cortex, and incorporation of sperm receptor glycoproteins in the zona pellucida (Ogielska, 2009b). Components of these processes are evident in this data set, especially in Ovary Clade C, as most of these gene profiles show substantial expression levels starting at the 2WPM time-point. Notable maternal mRNAs in this dataset previously identified as oocyte-specific are *ZAR1*, *NANOS1*, *FOXI2*, *H1FOO*, and *VEGT* to name a few that play key roles in embryogenesis following fertilization (Cha et al., 2012; Furuya et al., 2007; Lai et al., 2012; Wu et al., 2003). Translational control of mRNAs is evident by several regulators that are highly ovary-enriched here (*ZFP36*, *ZFP36L2*, *EIF4E*, *PABPCL1*). These may play roles in maternal mRNA translational regulation and/or regulate translation of factors involved in follicle development, but in either case show strong gender-biased expression profiles.

Oocyte meiosis is arrested at the diplotene stage and awaits resumption of meiosis during the later stages of progesterone-mediated oocyte maturation. *CCNB1*, *CCNB2*, and *CCNA1* all show robust expression around 2WPM when more oocytes are reaching the diplotene stage. *CCNB* complexed with a serine/threonine kinase (*CDC2*) mediates the G2/M transition when triggered upstream by progesterone (Nebreda and Ferby, 2000). Other genes involved in resumption of meiosis are *MAPK* and *WEE1*. Both of these genes are represented in this data set by putative homologues showing robust expression levels in the ovary starting around 1WPM and 2WPM respectively (*MAPK13* and *WEE2*). All of these transcripts are presumably being localized within the diplotene oocytes and inactivated prior to the events triggering resumption of meiosis.

4.2. Testis

Stage IV of Ogielska and Kotusz (2004) staging criteria for anuran gonad development is the point at which the undifferentiated gonad becomes either an early ovary or early testis. Therefore, similar to the ovary at somatic stage NF58, the testis is also at stage IV. This stage of testis development exhibits migration of germ cells and mesenchyme cells to the medullar space while the cortex recedes and eventually disappears (Ogielska, 2009a). The mesenchyme cells subsequently differentiate to become connective tissue and Leydig cells. Much uncertainty exists about what factor(s) signal germ cell migration toward the medullar space in anurans ultimately differentiating into spermatogonia. Experimentation with parabiosis, transplanted gonad grafts, and steroid hormone exposure brought about a theory that the anuran testis produces substance(s) other than steroid hormones that induce medullary development and is also capable of transforming ovaries of genetic females into testes (reviewed by Hayes, 1998). Furthermore, the putative inducer substance(s) were later suggested to be blood-bound. This theoretical substance, termed "medullarin" by Chang and Witschi (1956), has not yet been identified nor has the mechanism been elucidated. Interestingly, the gene showing the greatest magnitude of differential expression in the entire data set is a testis-biased relaxin family protein (rflcii) (Supplemental Table 2). The putative human ortholog for this gene is *INSL3*, which is a Leydig cell-specific insulin-like protein. Both of these proteins belong to the relaxin family of peptide hormones. This family of peptide hormones and their receptors have been implicated in various reproductive functions in humans and mice (Bathgate et al., 2013), but their roles in other vertebrates have not been well-studied. We propose that this *X. tropicalis* relaxin peptide hormone is a potential candidate for the unidentified "medullarin" substance promoting anuran testis development; however, further experimentation is necessary to support this suggestion.

Given that *INSL3* is Leydig cell-specific in mammals, it is likely that Leydig cells are present in the testis as early as NF58 despite being in the pre-spermatogenesis phase. Although fetal Leydig cells have been identified in 7-day-old rat testis tissues by immunohistochemical analyses (Svechnikov et al., 2010), histological studies in amphibians have not yet specifically identified how early Leydig cells differentiate and become influential in testis development. Our results now provide a precedent for "larval" Leydig cells being the amphibian equivalent to mammalian fetal Leydig cells. Also supporting the presence of Leydig cells at NF58 is the expression of genes coding for androgen-producing enzymes including *CYP17A1* and *SRD5A2*. Expression of these genes becomes more testis-enriched throughout this period of development. Another notable testis-enriched transcript codes for the *CYP26B1* enzyme. As discussed in relation to ovary-enriched *CYP26A1* during this period of development, CYP26 enzymes are responsible for retinoic acid regulation, which ultimately affects timing of germ cell meiosis (reviewed by Bowles and Koopman, 2007). *CYP26B1* expressed in Sertoli cells has been found to delay retinoic acid-mediated germ cell meiosis in mice testis tissue leading to development of spermatogonia later in reproductive maturation whereas Cyp26b1-knockouts exhibited precocious meiosis of germ cells similar to the timing of oocyte meiosis (Bowles et al., 2006). The observed patterns of CYP26 expression in *X. tropicalis* are consistent with what has been found in mammalian embryonic development research, emphasizing the conserved critical role of retinoic acid-mediated germ cell development.

In a general sense, the testis-enriched transcripts are expressed at relatively constant levels as compared to the ovary-enriched transcripts that show time-dependent increases in expression throughout this period of differentiation. This can be attributed to the cellular organization and tissue morphology processes initiated prior to NF58, and continuing until sex cords and ductules of *rete testis* are fully formed in the weeks and months following this period of differentiation. Orchestration of the various morphological changes in the differentiating testis involves signaling within and between cells involving extracellular proteins and growth factors (*FBLN5*, *DHH*, *FGFBP3*, *BMP1*, *ASTL*, *DKK3*, *NPTX1*, *FGF10*, *GAS6*, *INHA*, *INHBA*, *KITLG*), plasma membrane proteins (*ADCYAP1*, *COL13A1*, *RARRES1*, *INTGA2B*), and transcription factors (*DAX-1*, *FHL2*, *OSR2*, *SNAI2*).

Among the aggregation of primary spermatogonia into clusters that eventually become sex cords, mesenchymal cells begin to form connective tissue. Transcripts showing some of the highest magnitude of differential expression between testis and ovary tissue are *BMP1* and a similar gene *ASTL*, which are both pro-collagen metalloproteases (reviewed by Muir and Greenspan, 2011). Evidence of collagen production is further supported by the expression of various collagen isoforms *COL8A1*, *COL9A1*, and *COL13A1*. The recruitment of mesenchymal cells for the formation of connective tissue and Leydig cells involves the epithelial–mesenchymal transition (EMT) (reviewed by Thiery and Sleeman, 2006). This process has been shown to involve a complex network of signaling involving a series of genes well-represented by this data set's testis-enriched transcripts including a transcription repressor of E-cadherin *SNAI2*, an integrin cell surface receptor *INTGA2B*, fibroblast growth factor *FGF10*, and its putative activator *FGFBP3*. One component of the EMT is Wnt signaling, which is regulated in part by three members of the Dickkopf gene family (Krupnik et al., 1999). *DKK3* is testis-enriched here but has been shown not to

function like the other Wnt antagonist Dkk isoforms. Instead, *DKK3* is related to a novel secreted protein *SGY* (*DKKL1*) that has been shown to localize to the acrosome in mammalian spermatocytes (Kohn et al., 2005). However, upon reviewing the original data, *DKK1* was testis-enriched by approximately 2-fold (corrected $p < 0.01$), supporting antagonist action on the Wnt pathway allowing the EMT to take place in the testis. During the EMT, mesenchymal cells migrate and differentiate into the cells they are fated to become. This cell migration requires cytoskeletal components actin, myosin, and tropomyosin, which are all testis-enriched during this period of development (*MYH11*, *TPM2*, *ACTA2*, *MYL4*). However, whether the cells differentiate into connective tissue or support cells for spermatogenesis depends on other signaling factors.

One essential signaling factor being expressed in the testis is the desert hedgehog gene (*DHH*). This gene is expressed in Sertoli cells and is required for proper formation of sex cords by interacting with the peritubular myoid cells and inducing Leydig cell differentiation (Clark et al., 2000; reviewed by Franco and Yao, 2012). In fetal mice, Leydig cell differentiation is suggested to be triggered by Dhh-mediated steroidogenic factor 1 (*SF1*) up-regulation in cells outside the sex cords (Yao et al., 2002). A lack of Dhh protein in male Dhh-null mice has been shown to cause sterility, while having no effect on reproduction in females (Bitgood et al., 1996). This severity of response emphasizes the importance of *DHH* and associated signaling pathway to testis development; its expression pattern in *X. tropicalis* appears to be consistent with what is observed in mammals. Further investigation into modulation of *DHH* expression in anurans is necessary as inhibition of this pathway could have major implications on successful reproduction.

Other notable testis-enriched transcripts in *X. tropicalis* that have been well-characterized in mammalian reproductive development include inhibin subunits *INHA* and *INHBA*, and also *DAX-1* (*NR0B1*). Inhibins belong to the TGF-β protein superfamily and are multifunctional hormones involved in control of FSH secretion from the pituitary and also paracrine/autocrine signaling within the human testis (Luisi et al., 2005). In the fetal human testis, *INHA* is expressed in Sertoli cells and both *INHA* and *INHBA* are expressed in Leydig cells. However, inhibin B is the subunit expressed later in development that is used clinically as a diagnostic indicator of Sertoli cell function, spermatogenesis, and fertility (Pierik et al., 1998). Therefore, it is clear *INHA* and *INHBA* are playing roles in early gonadogenesis, presumably consistent with mammalian testis development, but currently lack correlation with fertility.

Finally, *DAX-1* is a multifunctional orphan nuclear receptor protein that, with duplication, is capable of causing male to female sex reversal in mammals with a normal *SRY* gene (Lalli and Sassone-Corsi, 2003). It has been shown to play many regulatory functions within steroidogenic tissues through various mechanisms including DNA binding to transcription activation sites, recruitment of co-repressors, and interaction with the androgen receptor and estrogen receptors α and β. DAX-1 has been shown to directly interact with steroidogenic factor 1 (SF1) negatively regulating transcription of steroidogenic enzymes including CYP17, CYP19, and others (Gurates et al., 2002; Hanley et al., 2001; Wang et al., 2001b). Inhibin α (*INHA*) discussed previously has also been shown to be negatively regulated either directly or indirectly by *DAX-1* (Achermann et al., 2001). Therefore, the expression pattern of *DAX-1* in *X. tropicalis* testis tissue during these stages of development is very curious, as the sex determining gene has not been found in this species (it is not known to have functional *SRY*) and expression levels of *CYP17* and inhibin α appear to be uninhibited. However, *CYP19* expression in the testis is low to absent suggesting a plausible mechanism for maintaining a masculine tissue during this period of development. The *DAX-1* expression pattern in *X. tropicalis* testis tissue is consistent with *DAX-1* expression patterns in *Rana rugosa* (Sugita et al., 2001) indicating the importance of this transcript in frog testis development despite it being an "anti-testis" gene in mammals. This gene's key activities and diverse mechanisms, within and between species, make it a particularly interesting candidate for further investigations regarding cross-species differences in reproductive development.

5. Conclusion

While we focused our analysis and discussion on transcripts with greater than 5-fold (corrected $p < 0.01$) differential expression between tissues, many other transcripts showing gender-biased expression remain to be explored. Robust expression profiles of key transcripts previously characterized in gonad development and the comprehensive representation of the various well-known developmental processes involved in gonad differentiation emphasize the quality of this data set, which remains freely available from the GEO repository for public investigations. This work has generated numerous testable hypotheses and provides a foundation for subsequent investigations of chemical-induced perturbations of pathways proximal to molecular initiating events. Linking these molecular initiating events to adverse effects on the reproductive organs will identify vulnerable targets of environmental pollutants, aid in elucidation of adverse outcome pathways, and have potential for cross-species extrapolation and population modeling.

Acknowledgments

The authors would like to thank Dr. Rodney Johnson and Chad Blanksma for providing micrographs of *Xenopus tropicalis* ovary and testis tissues, Hongzu Ren for processing and imaging the microarrays, and Dr. Marshall Hampton for guidance with writing Python code. The authors would also like to thank Dr. Daniel Villeneuve for thoughtful comments and suggestions to improve this manuscript. This paper has been reviewed according to ORD guidelines, but the statements made do not represent views of the USEPA, nor does mention of trade names indicate endorsement by the Federal government.

Appendix A. Supplementary data

Supplementary data associated with this article can be found, in the online version, at http://dx.doi.org/10.1016/j.ygcen.2014.06.009.

References

Achermann, J.C., Ito, M., Silverman, B.L., Habiby, R.L., Pang, S., Rosler, A., Jameson, J.L., 2001. Missense mutations cluster within the carboxyl-terminal region of DAX-1 and impair transcriptional repression. J. Clin. Endocrinol. Metab. 86 (7), 3171–3175.

Ankley, G.T., Bennett, R.S., Erickson, R.J., Hoff, D.J., Hornung, M.W., Johnson, R.D., Mount, D.R., Nichols, J.W., Russom, C.L., Schmieder, P.K., Serrano, J.A., Tietge, J.E., Villeneuve, D.L., 2010. Adverse outcome pathways: a conceptual framework to support ecotoxicology research and risk assessment. Env. Toxicol. Chem. 29 (3), 730–741.

Bathgate, R.A.D., Halls, M.L., van der Westhuizen, E.T., Callander, G.E., Kocan, M., Summers, R.J., 2013. Relaxin family peptides and their receptors. Phys. Rev. 93 (1), 405–480.

Bell, P., Scheer, U., 1999. Developmental changes in RNA polymerase I and TATA box-binding protein during early *Xenopus* embryogenesis. Exp. Cell Res. 248 (1), 122–135.

Bitgood, M.J., Shen, L., McMahon, A.P., 1996. Sertoli cell signaling by Desert hedgehog regulates the male germline. Curr. Biol. 6 (3), 298–304.

Bögi, C., Levy, G., Lutz, I., Kloas, W., 2002. Functional genomics and sexual differentiation in amphibians. Comp. Biochem. Phys. B 133 (4), 559–570.

Bowles, J., Koopman, P., 2007. Retinoic acid, meiosis and germ cell fate in mammals. Development 134 (19), 3401–3411.

Bowles, J., Knight, D., Smith, C., Wilhelm, D., Richman, J., Mamiya, S., Yashiro, K., Chawengsaksophak, K., Wilson, M.J., Rossant, J., Hamada, H., Koopman, P., 2006. Retinoid signaling determines germ cell fate in mice. Science 312 (5773), 596–600.

Cha, S.W., McAdams, M., Kormish, J., Wylie, C., Kofron, M., 2012. Foxi2 is an animally localized maternal mRNA in *Xenopus*, and an activator of the zygotic ectoderm activator foxi1e. PLoS One 7 (7), e41782.

Chang, C.Y., Witschi, E., 1956. Genic control and hormonal reversal of sex differentiation in Xenopus. Proc. Soc. Exp. Biol. Med. 93 (1), 140–144.

Chen, Y.T., Venditti, C.A., Theiler, G., Stevenson, B.J., Iseli, C., Gure, A.O., Jongeneel, C.V., Old, L.J., Simpson, A.J., 2005. Identification of CT46/HORMAD1, an immunogenic cancer/testis antigen encoding a putative meiosis-related protein. Cancer Immun. 5 (9).

Choi, Y., Ballow, D.J., Xin, Y., Rajkovic, A., 2008. Lim homeobox gene, lhx8, is essential for mouse oocyte differentiation and survival. Biol. Reprod. 79 (3), 442–449.

Clark, A.M., Garland, K.K., Russell, L.D., 2000. Desert hedgehog (Dhh) gene is required in the mouse testis for formation of adult-type Leydig cells and normal development of peritubular cells and seminiferous tubules. Biol. Reprod. 63 (6), 1825–1838.

Deng, L., Shipley, G.L., Loose-Mitchell, D.S., Stancel, G.M., Broaddus, R., Pickar, J.H., Davies, P.J., 2003. Coordinate regulation of the production and signaling of retinoic acid by estrogen in the human endometrium. J. Clin. Endocr. Metab. 88 (5), 2157–2163.

Driancourt, M.A., Reynaud, K., Cortvrindt, R., Smitz, J., 2000. Roles of KIT and KIT LIGAND in ovarian function. Rev. Reprod. 5 (3), 143–152.

Duarte-Guterman, P., Trudeau, V.L., 2011. Transcript profiles and triiodothyronine regulation of sex steroid-and thyroid hormone-related genes in the gonad–mesonephros complex of *Silurana tropicalis*. Mol. Cell. Endocrinol. 331 (1), 143–149.

El Jamil, A., Magre, S., Mazabraud, A., Penrad-Mobayed, M., 2008. Early aspects of gonadal sex differentiation in *Xenopus tropicalis* with reference to an antero-posterior gradient. J. Exp. Zool. A Ecol. Genet. Physiol. 309 (3), 127–137.

Flood, D.E., Langlois, V.S., 2014. Crosstalk between the thyroid hormone and androgen axes during reproductive development in *Silurana tropicalis*. Gen. Comp. Endocrinol. 203, 244–252.

Franco, H.L., Yao, H.H.C., 2012. Sex and hedgehog: roles of genes in the hedgehog signaling pathway in mammalian sexual differentiation. Chromosome Res. 20 (1), 247–258.

Furuya, M., Tanaka, M., Teranishi, T., Matsumoto, K., Hosoi, Y., Saeki, K., Ishimoto, H., Minegishi, K., Iritani, A., Yoshimura, Y., 2007. H1foo is indispensable for meiotic maturation of the mouse oocyte. J. Reprod. Dev. 53 (4), 895–902.

Gaucher, J., Boussouar, F., Montellier, E., Curtet, S., Buchou, T., Bertrand, S., Hery, P., Jounier, S., Depaux, A., Vitte, A.L., Guardiola, P., Pernet, K., Debernardi, A., Lopez, F., Holota, H., Imbert, J., Wolgemuth, D.J., Gérard, M., Rousseaux, S., Khochbin, S., 2012. Bromodomain-dependent stage-specific male genome programming by Brdt. EMBO J. 31 (19), 3809–3820.

Gurates, B., Sebastian, S., Yang, S., Zhou, J., Tamura, M., Fang, Z., Suzuki, T., Sasano, H., Bulun, S.E., 2002. WT1 and DAX-1 inhibit aromatase P450 expression in human endometrial and endometriotic stromal cells. J. Clin. Endocr. Metab. 87 (9), 4369–4377.

Hadley, M.A., Weeks, B.S., Kleinman, H.K., Dym, M., 1990. Laminin promotes formation of cord-like structures by sertoli cells *in vitro*. Dev. Biol. 140 (2), 318–327.

Hanley, N.A., Rainey, W.E., Wilson, D.I., Ball, S.G., Parker, K.L., 2001. Expression profiles of SF-1, DAX1, and CYP17 in the human fetal adrenal gland: potential interactions in gene regulation. Mol. Endocrinol. 15 (1), 57–68.

Hayes, T.B., 1998. Sex determination and primary sex differentiation in amphibians: genetic and developmental mechanisms. J. Exp. Zool. 281 (5), 373–399.

Hirakawa, I., Miyagawa, S., Mitsui, N., Miyahara, M., Onishi, Y., Kagami, Y., Kusano, T., Takeuchi, T., Ohta, Y., Iguchi, T., 2013. Developmental disorders and altered gene expression in the tropical clawed frog (*Silurana tropicalis*) exposed to 17α-ethinylestradiol. J. Appl. Toxicol. 33 (9), 1001–1010.

Houmard, B., Small, C., Yang, L., Naluai-Cecchini, T., Cheng, E., Hassold, T., Griswold, M., 2009. Global gene expression in the human fetal testis and ovary. Biol. Reprod. 81 (2), 438–443.

Hu, W., Gauthier, L., Baibakov, B., Jimenez-Movilla, M., Dean, J., 2010. FIGLA, a basic helix-loop-helix transcription factor, balances sexually dimorphic gene expression in postnatal oocytes. Mol. Cell. Biol. 30 (14), 3661–3671.

Hubbell, E. 2004. Designing Estimators for Low Level Expression Analysis. <http://mbi.osu.edu/2004/ws1abstracts.html>.

Hubbell, E., 2005. PLIER White Paper. Affymetrix, Santa Clara, California.

Jones, M.H., Numata, M., Shimane, M., 1997. Identification and Characterization of BRDT: a testis-specific gene related to the bromodomain genes RING3 and *Drosophila* fsh. Genomics 45 (3), 529–534.

Kedem, A., Fisch, B., Garor, R., Ben-Zaken, A., Gizunterman, T., Felz, C., Ben-Haroush, A., Kravarusic, D., Abir, R., 2011. Growth differentiating factor 9 (GDF9) and bone morphogenetic protein 15 both activate development of human primordial follicles in vitro, with seemingly more beneficial effects of GDF9. J. Clin. Endocr. Metab. 96 (8), E1246–E1254.

Kloas, W., 2002. Amphibians as a model for the study of endocrine disruptors. Int. Rev. Cytol. 216, 1–57.

Kogo, H., Tsutsumi, M., Ohye, T., Inagaki, H., Abe, T., Kurahashi, H., 2012. HORMAD1-dependent checkpoint/surveillance mechanism eliminates asynaptic oocytes. Genes Cells 17 (6), 439–454.

Kohn, M.J., Kaneko, K.J., DePamphilis, M.L., 2005. DkkL1 (Soggy), a Dickkopf family member, localizes to the acrosome during mammalian spermatogenesis. Mol. Reprod. Dev. 71 (4), 516–522.

Krupnik, V.E., Sharp, J.D., Jiang, C., Robison, K., Chickering, T.W., Amaravadi, L., Brown, D.E., Guyot, D., Mays, G., Leiby, K., Chang, B., Duong, T., Goodearl, A.D.J., Gearing, D.P., Sokol, S.Y., McCarthy, S.A., 1999. Functional and structural diversity of the human Dickkopf gene family. Gene 238 (2), 301–313.

Lai, F., Singh, A., King, M.L., 2012. *Xenopus* Nanos1 is required to prevent endoderm gene expression and apoptosis in primordial germ cells. Development 139 (8), 1476–1486.

Lalli, E., Sassone-Corsi, P., 2003. DAX-1, an unusual orphan receptor at the crossroads of steroidogenic function and sexual differentiation. Mol. Endocrinol. 17 (8), 1445–1453.

Luisi, S., Florio, P., Reis, F.M., Petraglia, F., 2005. Inhibins in female and male reproductive physiology: role in gametogenesis, conception, implantation and early pregnancy. Hum. Reprod. Update 11 (2), 123–135.

Merchant-Larios, H., Villalpando, I., 1981. Ultrastructural events during early gonadal development in *Rana pipiens* and *Xenopus laevis*. Anat. Rec. 199 (3), 349–360.

Muir, A., Greenspan, D.S., 2011. Metalloproteinases in *Drosophila* to humans that are central players in developmental processes. J. Biol. Chem. 286 (49), 41905–41911.

Nakamura, M., 2010. The mechanism of sex determination in vertebrates—are sex steroids the key-factor? J. Exp. Zool. A. 313 (7), 381–398.

Navarro-Martín, L., Velasco-Santamaría, Y.M., Duarte-Guterman, P., Robertson, C., Lanctôt, C., Pauli, B., Trudeau, V.L., 2012. Sexing frogs by real-time PCR: using aromatase (cyp19) as an early ovarian differentiation marker. Sex Dev. 6 (6), 303–315.

Nebreda, A.R., Ferby, I., 2000. Regulation of the meiotic cell cycle in oocytes. Curr. Opin. Cell Biol. 12 (6), 666–675.

Nieuwkoop, P.D., Faber, J., 1994. Normal Table of *Xenopus laevis* (Daudin): A Systematical and Chronological Survey of the Development from the Fertilized Egg till the End of Metamorphosis. Garland Publishing Inc, New York, NY, USA.

Ogielska, M., 2009a. Reproduction of amphibians. In: Ogielska, M. (Ed.), The Undifferentiated Amphibian Gonad. Science Pub Inc., Enfield, NH, USA, pp. 1–33.

Ogielska, M., 2009b. Reproduction of amphibians. In: Ogielska, M., Bartmańska, J. (Eds.), Oogenesis and Female Reproductive System in Amphibia-Anura. Science Pub Inc., Enfield, NH, USA, pp. 153–272.

Ogielska, M., 2009c. Reproduction of amphibians. In: Ogielska, M., Bartmańska, J. (Eds.), Spermatogenesis and Male Reproductive System in Amphibia-Anura. Science Pub Inc., Enfield, NH, USA, pp. 34–99.

Ogielska, M., Kotusz, A., 2004. Pattern and rate of ovary differentiation with reference to somatic development in anuran amphibians. J. Morphol. (Warszawa) 57, 46.

Ohtani, H., Miura, I., Ichikawa, Y., 2000. Effects of dibutyl phthalate as an environmental endocrine disruptor on gonadal sex differentiation of genetic males of the frog *Rana rugosa*. Environ. Health Persp. 108 (12), 1189.

Olmstead, A.W., Kosian, P.A., Korte, J.J., Holcombe, G.W., Woodis, K.K., Degitz, S.J., 2009a. Sex reversal of the amphibian, *Xenopus tropicalis*, following larval exposure to an aromatase inhibitor. Aquat. Toxicol. 91 (2), 143–150.

Olmstead, A.W., Korte, J.J., Woodis, K.K., Bennett, B.A., Ostazeski, S., Degitz, S.J., 2009b. Reproductive maturation of the tropical clawed frog: *Xenopus tropicalis*. Gen. Comp. Endocrinol. 160 (2), 117–123.

Olmstead, A.W., Lindberg-Livingston, A., Degitz, S.J., 2010. Genotyping sex in the amphibian, *Xenopus* (*Silurana*) *tropicalis*, for endocrine disruptor bioassays. Aquat. Toxicol. 98 (1), 60–66.

Paillisson, A., Levasseur, A., Gouret, P., Callebaut, I., Bontoux, M., Pontarotti, P., Monget, P., 2007. Bromodomain testis-specific protein is expressed in mouse oocyte and evolves faster than its ubiquitously expressed paralogs *BRD2*,*-3*, and *-4*. Genomics 89 (2), 215–223.

Pettersson, I., Arukwe, A., Lundstedt-Enkel, K., Mortensen, A.S., Berg, C., 2006. Persistent sex-reversal and oviducal agenesis in adult *Xenopus* (*Silurana*) *tropicalis* frogs following larval exposure to the environmental pollutant ethynylestradiol. Aquat. Toxicol. 79 (4), 356–365.

Pierik, F.H., Vreeburg, J.T., Stijnen, T., de Jong, F.H., Weber, R.F., 1998. Serum inhibin B as a marker of spermatogenesis. J. Clin. Endocrinol. Metab. 83 (9), 3110–3114.

Rajkovic, A., Pangas, S.A., Ballow, D., Suzumori, N., Matzuk, M.M., 2004. NOBOX deficiency disrupts early folliculogenesis and oocyte-specific gene expression. Science 305 (5687), 1157–1159.

Reeder, A.L., Foley, G.L., Nichols, D.K., Hansen, L.G., Wikoff, B., Faeh, S., Eisold, J., Wheeler, M.B., Warner, R., Murphy, J.E., Beasley, V.R., 1998. Forms and prevalence of intersexuality and effects of environmental contaminants on sexuality in cricket frogs (*Acris crepitans*). Environ. Health Persp. 106 (5), 261.

Sasaki, T., Fässler, R., Hohenester, E., 2004. Laminin the crux of basement membrane assembly. J. Cell Biol. 164 (7), 959–963.

Seo, J., Hoffman, E.P., 2006. Probe set algorithms: is there a rational best bet? BMC Bioinformatics 7 (1), 395.

Soyal, S.M., Amleh, A., Dean, J., 2000. FIGalpha, a germ cell-specific transcription factor required for ovarian follicle formation. Development 127 (21), 4645–4654.

Sugita, J., Takase, M., Nakamura, M., 2001. Expression of Dax-1 during gonadal development of the frog. Gene 280 (1), 67–74.

Svechnikov, K., Landreh, L., Weisser, J., Izzo, G., Colón, E., Svechnikova, I., Söder, O., 2010. Origin, development and regulation of human Leydig cells. Horm. Res. Paediatr. 73 (2), 93–101.

Thiery, J.P., Sleeman, J.P., 2006. Complex networks orchestrate epithelial–mesenchymal transitions. Nat. Rev. Mol. Cell Biol. 7 (2), 131–142.
Veenstra, G.J.C., Destrée, O.H., Wolffe, A.P., 1999. Translation of maternal TATA-binding protein mRNA potentiates basal but not activated transcription in *Xenopus* embryos at the midblastula transition. Mol. Cell. Biol. 19 (12), 7972–7982.
Villalpando, I., Merchant-Larios, H., 1990. Determination of the sensitive stages for gonadal sex-reversal in *Xenopus laevis* tadpoles. Int. J. Dev. Biol. 34 (2), 281–285.
Vincent, S., Segretain, D., Nishikawa, S., Nishikawa, S.I., Sage, J., Cuzin, F., Rassoulzadegan, M., 1998. Stage-specific expression of the Kit receptor and its ligand (KL) during male gametogenesis in the mouse: a Kit-KL interaction critical for meiosis. Development 125 (22), 4585–4593.
Wang, P.J., McCarrey, J.R., Yang, F., Page, D.C., 2001a. An abundance of X-linked genes expressed in spermatogonia. Nat. Genet. 27 (4), 422–426.
Wang, Z.J., Jeffs, B., Ito, M., Achermann, J.C., Richard, N.Y., Hales, D.B., Jameson, J.L., 2001b. Aromatase (Cyp19) expression is up-regulated by targeted disruption of Dax1. Proc. Natl. Acad. Sci. 98 (14), 7988–7993.
Wu, X., Viveiros, M.M., Eppig, J.J., Bai, Y., Fitzpatrick, S.L., Matzuk, M.M., 2003. Zygote arrest 1 (Zar1) is a novel maternal-effect gene critical for the oocyte-to-embryo transition. Nat. Genet. 33 (2), 187–191.
Yabuta, Y., Ohta, H., Abe, T., Kurimoto, K., Chuma, S., Saitou, M., 2011. TDRD5 is required for retrotransposon silencing, chromatoid body assembly, and spermiogenesis in mice. J. Cell Biol. 192 (5), 781–795.
Yao, H.H.C., Whoriskey, W., Capel, B., 2002. Desert Hedgehog/Patched 1 signaling specifies fetal Leydig cell fate in testis organogenesis. Gene. Dev. 16 (11), 1433–1440.
Yoshimoto, S., Okada, E., Umemoto, H., Tamura, K., Uno, Y., Nishida-Umehara, C., Matsuda, Y., Takamatsu, N., Shiba, T., Ito, M., 2008. A W-linked DM-domain gene, DM-W, participates in primary ovary development in *Xenopus laevis*. Proc. Natl. Acad. Sci. 105 (7), 2469–2474.
Yu, Y.H., Siao, F.P., Hsu, L.C.L., Yen, P.H., 2012. TEX11 modulates germ cell proliferation by competing with estrogen receptor β for the binding to HPIP. Mol. Endocrinol. 26 (4), 630–642.

Further reading

Loeber, J., Claußen, M., Jahn, O., Pieler, T., 2010. Interaction of 42Sp50 with the vegetal RNA localization machinery in *Xenopus laevis* oocytes. FEBS J. 277 (22), 4722–4731.

			|Fold-difference|							
Probe Set ID	Cluster	Position	NF58	NF66	1WPM	2WPM	Gene Symbol	Entrez Gene Name	Entrez Gene	Human Ortholog Ac	Function
Str.24477.2.S1_at	Testis-A	1	222	302	314	289	rflcii	insulin-like 3 (Leydig cell)	100145369	NM_001265587.1	Testis development, fertility
Str.34508.1.S1_s_at	Testis-A	2	8	12	27	161	LOC100492493 (bmp1)	bone morphogenetic protein 1	100492493	NP_001190.1	Collagen development, protein synthesis
Str.2374.2.A1_at	Testis-A	3	19	38	107	930	LOC100492493 (bmp1)	bone morphogenetic protein 2	100492493	NP_001190.1	Collagen development, protein synthesis
Str.12662.1.S1_at	Testis-A	4	37	98	110	151	fgfbp3///LOC100495029	fibroblast growth factor binding protein 3	100495029	///7NP_689642.3	Growth factor regulation, angiogenesis
Str.38523.1.S1_at	Testis-A	5	26	59	68	186	LOC100492324 (astl)	astacin-like metallo-endopeptidase (M12 family)	100492324	NP_001002036.3	Protein synthesis, fertility
Str.7898.1.S1_at	Testis-A	6	17	88	97	98	myl4	myosin, light chain 4, alkali; atrial, embryonic	100124786	NP_002467.1	Vascular development, muscle contraction
Str.21273.1.A1_at	Testis-A	7	70	36	53	47	nptx1	neuronal pentraxin I	100158577	NP_002513.2	Angiogenesis, cellular movement, nervous system development
Str.21365.1.S1_at	Testis-A	8	33	23	42	23					
Str.28021.1.A1_at	Testis-A	9	17	17	22	19	slitrk4	SLIT and NTRK-like family, member 4	100497316	NP_775101.1	Formation of cellular protrusions, nervous system development
Str.33400.1.S1_at	Testis-A	10	22	25	21	21	(rad50)	RAD50 homolog (S. cerevisiae)		NP_005723.2	DNA repair
Str.16705.1.A1_at	Testis-A	11	26	30	41	65	LOC100497586 (opa1)	optic atrophy 1 (autosomal dominant)	100497586	NP_570844.1	Mitochondrial organization, synthesis of pregnenolone
Str.28004.1.A1_at	Testis-A	12	16	24	25	36	LOC100496012 (htr2c)	5-hydroxytryptamine (serotonin) receptor 2C, G protein-coupled	100496012	NP_000859.1	Cell-to-cell signaling and interaction
Str.lgi.4087.1.S1_at	Testis-A	13	18	9	20	9	LOC100485995		100485995		
Str.38708.1.A1_at	Testis-A	14	19	14	12	20	LOC100485458 (clec4m)	C-type lectin domain family 4, member M	100485458	NP_001138378.1	Cell-to-cell signaling and interaction
Str.21971.1.A1_at	Testis-A	15	15	16	17	13					
Str.22031.1.S1_at	Testis-A	16	22	18	21	21	cryba4	crystallin, beta A4	100125109	NP_001877.1	
Str.38881.1.A1_at	Testis-A	17	21	16	20	21				XP_002347599.1	
Str.20614.1.S1_at	Testis-A	18	17	5	12	19	aqp1	aquaporin 1 (Colton blood group)	448309	NP_932766.1	Vascular development, permeability of blood vessel, molecular transport
Str.21784.1.A2_at	Testis-A	19	12	12	16	19	gpc1	glypican 1	779769	NP_002072.2	Vascular development, cellular movement
Str.21784.1.A1_s_at	Testis-A	20	13	11	17	22	gpc1	glypican 2	779769	NP_002072.2	Vascular development, cellular movement
Str.32323.1.A1_at	Testis-A	21	17	9	13	22					
StrEns.9382.1.S1_at	Testis-A	22	8	7	12	24	LOC100486396		100486396		
Str.5014.1.S1_at	Testis-A	23	9	12	12	23	acta2	actin, alpha 2, smooth muscle, aorta	496696	NP_001135417.1	Vascular development, muscle contraction
Str.14470.1.A1_at	Testis-B	24	9	9	10	6					
Str.11990.1.S1_at	Testis-B	25	13	9	10	11	rarres1	retinoic acid receptor responder (tazarotene induced) 1	100158540	NP_996846.1	Cellular movement
Str.31384.1.A1_at	Testis-B	26	13	11	11	12					
Str.19735.1.S1_at	Testis-B	27	6	5	7	7	tpst2	tyrosylprotein sulfotransferase 2	549785	NP_003586.3	Cellular movement, fertility
Str.5765.1.A1_at	Testis-B	28	6	6	8	7	LOC100488502		100488502	NP_689603.2	
Str.lgi.5073.1.S1_s_at	Testis-B	29	6	6	6	7	akr1cl1///LOC100490783	aldo-keto reductase family 1, member C3	100490783	///4NP_003730.4	Steroidogenesis
Str.52145.1.S1_at	Testis-B	30	6	6	7	8	akr1cl1	aldo-keto reductase family 1, member C4	448368	NP_003730.4	Steroidogenesis
Str.lgi.5074.1.S1_at	Testis-B	31	7	5	7	5	LOC100490956		100490956		
Str.21742.1.S1_at	Testis-B	32	8	6	8	6	adcyap1r1	adenylate cyclase activating polypeptide 1 (pituitary) receptor ty	780260	NP_001109.2	Cellular proliferation, concentration of hormone, fertility
Str.11952.1.S1_at	Testis-B	33	10	7	9	10	LOC100490204 (cadm3)	cell adhesion molecule 3	100490204	NP_001120645.1	
Str.38466.1.S1_at	Testis-B	34	11	8	9	11	cyp17a1	cytochrome P450, family 17, subfamily A, polypeptide 1	100145650	NP_000093.1	Steroidogenesis, fertility, sex determination
Str.7705.5.S1_at	Testis-B	35	7	9	13	11	osr2	odd-skipped related 2 (Drosophila)	100038196	NP_001135934.1	Cellular proliferation, growth
Str.14864.1.S1_at	Testis-B	36	7	7	10	9					
Str.38286.1.A1_at	Testis-B	37	8	7	7	7	kcnf1	potassium voltage-gated channel, subfamily F, member 1	100124998	NP_002227.2	
Str.48995.1.S1_at	Testis-B	38	7	7	10	8					
Str.21954.1.S1_at	Testis-B	39	14	12	14	8	LOC100494188		100494188		
Str.8998.1.S1_at	Testis-B	40	15	23	10	8	acbd7	acyl-CoA binding domain containing 7	779685	NP_001034933.1	
Str.33702.1.A1_at	Testis-B	41	9	8	15	22					
Str.49032.1.A1_at	Testis-B	42	5	6	12	19					
Str.5526.1.S1_at	Testis-B	43	6	10	12	22	tpm2	tropomyosin 2 (beta)	594975	NP_003280.2	Vascular development, muscle contraction
Str.1178.1.S1_at	Testis-B	44	7	7	12	22					
Str.37326.1.A1_s_at	Testis-B	45	6	12	15	15	LOC100485176 (nkx3-1)	NK3 homeobox 1	100485176	NP_006158.2	Morphogenesis of testis
Str.lgi.3167.1.S1_x_at	Testis-B	46	6	12	16	16	LOC100485176 (nkx3-1)	NK3 homeobox 2	100485176	NP_006158.3	Morphogenesis of testis
Str.17189.1.S1_at	Testis-B	47	5	8	11	16	srd5a2	steroid-5-alpha-reductase, alpha polypeptide 2 (3-oxo-5 alpha-s	549867	NP_000339.2	Steroidogenesis, fertility, sex determination, morphology of testis
Str.lgi.3167.1.S1_at	Testis-B	48	5	10	12	14	LOC100485176		100485176		
Str.37326.1.A1_x_at	Testis-B	49	4	10	12	14	LOC100485176 (nkx3-1)	NK3 homeobox 1	100485176	NP_006158.2	Morphogenesis of testis
Str.39201.1.S1_at	Testis-B	50	3	3	3	6	inha	inhibin, alpha	613114	NP_002182.1	Morphology of testis, fertility, steroidogenesis, sex determination
Str.51373.1.A1_at	Testis-B	51	3	5	7	7	(gas6)	growth arrest-specific 6		NP_001137417.1	Vascular development, cellular movement
Str.43407.1.A1_at	Testis-B	52	3	3	5	9				XP_002347599.1	
Str.33412.1.A1_at	Testis-B	53	2	3	4	7					
Str.8537.1.S1_at	Testis-B	54	3	6	6	9	cnn2 (cnn1)	calponin 1, basic, smo	548513	NP_001290.2	Vascular development, cellular movement, morphology of testis
Str.51661.1.S1_at	Testis-B	55	2	3	4	8	cxadr	coxsackie virus and adenovirus receptor	496497	NP_001329.1	Vascular development, cellular movement
Str.38097.1.A1_at	Testis-B	56	3	4	4	6	(dhh)	desert hedgehog		NP_066382.1	Gonadogenesis, morphology of testis, sex determination, steroid synthesis
Str.21927.1.S1_at	Testis-B	57	4	3	5	10	dkk3	dickkopf 3 homolog (Xenopus laevis)	100144724	NP_056965.3	Steroid hormone synthesis, cellular movement, cellular organization
Str.15475.1.S1_at	Testis-B	58	3	4	5	7	fam123a (amer2)	APC membrane recruitment protein 2	100038269	NP_689917.2	
Str.24498.1.S1_at	Testis-B	59	2	2	3	6	cadm2	cell adhesion molecule	448238	NP_001161146.1	
Str.28935.1.A1_at	Testis-B	60	2	2	5	6				XP_002347599.1	
Str.26721.1.S1_at	Testis-B	61	2	2	4	10	inhba	inhibin, beta A	100038114	NP_002183.1	Morphology of testis, fertility, steroidogenesis, cellular movement
Str.44307.1.S1_at	Testis-B	62	2	3	5	12					
Str.39202.1.S1_at	Testis-B	63	6	7	8	17	fbln5	fibulin 5	595007	NP_006320.2	Vascular development, cellular movement
Str.21675.1.A1_at	Testis-B	64	6	5	9	11	mpz	myelin protein zero	780198	NP_000521.2	Nervous system development, cellular movement
Str.21129.1.S1_at	Testis-B	65	3	5	8	10					
Str.32860.1.A1_at	Testis-B	66	4	9	7	8				XP_002347599.1	
Str.21184.1.S1_at	Testis-B	67	3	8	7	6					
Str.28079.1.S1_a_at	Testis-B	68	3	10	8	9	LOC100497842		100497842		
Str.33806.1.A1_at	Testis-B	69	6	9	6	6					
Str.lgi.1014.1.S1_s_at	Testis-B	70	3	5	7	6					
Str.25076.1.A1_at	Testis-B	71	5	8	10	8	(stx3)	syntaxin 3		NP_004168.1	Cellular organization of cytoskeleton, microtubule dynamics
StrEns.5047.1.S1_at	Testis-B	72	5	4	9	18	LOC100485437		100485437		
Str.30927.1.S1_at	Testis-B	73	5	4	7	17	LOC100493356		100493356		
Str.13088.1.S1_at	Testis-B	74	5	6	7	14	dclk2 (dclk1)	doublecortin-like kinase 1	733926	NP_004725.1	Cellular organization of cytoskeleton, microtubule dynamics
StrEns.3102.1.S1_at	Testis-B	75	5	7	7	11	LOC100491213		100491213		
Str.39178.1.S1_a_at	Testis-B	76	5	6	8	14	fmo5	flavin containing monooxygenase 5	548500	NP_001452.2	
Str.39178.2.A1_at	Testis-B	77	5	7	10	15	fmo5	flavin containing monooxygenase 5		NP_001452.2	
Str.11958.1.A1_at	Testis-B	78	2	9	11	17					
Str.12190.1.S1_at	Testis-B	79	2	8	11	17	fstl5 (elf4g3)	eukaryotic translation initiation factor 4 gamma, 3	100493709	NP_003751.2	Cellular organization of cytoskeleton, microtubule dynamics
Str.27613.3.S1_at	Testis-B	80	3	2	2	8	hba-l2 (hbz)	hemoglobin, zeta	100135125	NP_005323.1	Morphology of vascular system
Str.11255.1.S1_at	Testis-B	81	2	2	4	19	LOC100496483		100496483	XP_002347226.1	
Str.17054.1.S1_at	Testis-B	82	1	2	4	24	fabp7	fatty acid binding protein 7, brain	548661	NP_001437.1	Cellular proliferation, cellular movement
Str.29212.1.A1_at	Testis-B	83	1	1	2	13				XP_002347599.1	
Str.29212.1.A1_x_at	Testis-B	84	1	1	2	13				XP_002347599.1	
Str.38324.1.S1_at	Testis-B	85	1	2	2	5	nlk	nemo-like kinase	100144638	NP_057315.3	Morphology of vascular system
Str.32699.1.A1_at	Testis-B	86	1	2	2	7					
Str.1843.2.S1_at	Testis-B	87	1	1	3	6	slco2a1	solute carrier organic anion transporter family, member 2A1	100216228	NP_005621.2	Morphology of vascular system, molecular transport
Str.23487.1.S1_at	Testis-B	88	2	1	2	6					
Str.5759.1.S1_at	Testis-B	89	1	1	2	7	crip2	cysteine-rich protein 2	780192	NP_001303.1	Cellular proliferation, cellular differentiation
Str.22906.1.S1_at	Testis-B	90	1	2	2	5	col9a1	collagen, type IX, alpha 1	100145133	NP_511040.2	Connective tissue development
Str.lgi.5767.1.S1_at	Testis-B	91	1	2	2	5					
Str.40175.1.S1_at	Testis-B	92	2	5	5	7	LOC100487516		100487516		
Str.28002.1.S1_at	Testis-B	93	1	3	5	7	MGC107853 (slc29a1)	solute carrier family 29 (nucleoside transporters), member 1	548435	NP_001071642.1	Cellular proliferation
Str.5047.1.S2_at	Testis-B	94	2	3	4	6	des.1	desmin	394739	NP_001918.3	Morphology of vascular system
Str.35139.1.A1_at	Testis-B	95	2	3	4	6					
Str.lgi.3475.1.S1_at	Testis-B	96	2	3	6	7	LOC100497848		100497848		
Str.32447.1.S1_at	Testis-B	97	3	5	6	8	fhl5///LOC100485255 (fhl2)	four and a half LIM domains 2	100144736	///1NP_963849.1	Angiogenesis, cellular movement, muscle cell development
Str.28323.1.A1_at	Testis-B	98	3	5	9	9					
Str.15616.1.S1_at	Testis-B	99	3	4	6	7	rgs2	regulator of G-protein signaling 2, 24kDa	595010	NP_002914.1	Vascular development, development of muscle
Str.5581.1.S1_at	Testis-B	100	3	3	4	6	cfl2	cofilin 2 (muscle)	496574	NP_068733.1	
Str.25601.1.A1_at	Testis-B	101	3	3	6	9	(gabra2)	gamma-aminobutyric acid (GABA) A receptor, alpha 2		NP_000798.2	
Str.10824.1.S1_at	Testis-B	102	2	3	5	8	kitlg	KIT ligand	733847	NP_000890.1	Gonadogenesis, development of testis, steroid synthesis
Str.33801.1.A1_at	Testis-B	103	2	3	4	6					
Str.24395.1.A1_at	Testis-B	104	1	2	4	7	cyp26b1	cytochrome P450, family 26, subfamily B, polypeptide 1	780112	NP_063938.1	Gonadogenesis, morphology of testis
Str.33336.1.A1_at	Testis-B	105	1	3	3	5	itga2b.1	integrin, alpha 2b (platelet glycoprotein IIb of IIb/IIIa complex,	100158580	NP_000410.2	Morphology of vascular system, cellular movement
Str.15223.6.S1_at	Testis-B	106	2	3	4	5	klhl31	kelch-like family member 31	100495906	NP_001003760.2	
Str.31895.1.S1_at	Testis-B	107	1	3	4	5	LOC100488115///LOC100488265	(collagen, type XIII, alpha 1	100488115	///1NP_542988.3	Vasculogenesis, angiogenesis
Str.52251.1.S1_at	Testis-B	108	10	6	5	10	akr1c2 (akr1c3)	aldo-keto reductase family 1, member C3	779650	NP_003730.4	Steroid synthesis and metabolism
Str.9038.1.A1_at	Testis-B	109	4	5	5	6					
Str.50570.1.A1_at	Testis-B	110	5	4	6	6					
Str.51450.1.S1_at	Testis-B	111	6	6	7	6	spink2		100127184		
Str.6594.1.S1_at	Testis-B	112	11	6	7	6	enpp2	ectonucleotide pyrophosphatase/phosphodiesterase 2	548690	NP_001035181.1	Vasculogenesis, cellular movement
Str.15388.1.A2_at	Testis-B	113	8	4	4	5	psph	phosphoserine phosphatase	549747	NP_004568.2	
Str.lgi.3117.1.S1_s_at	Testis-B	114	5	5	5	5	tmem26	transmembrane protein 26	100145269	NP_848600.2	

Str.44746.1.A1_at	Testis-B	115	3	4	5	6				XP_002344577.1	
Str.15379.1.S1_at	Testis-B	116	3	4	5	5	fgf10	fibroblast growth factor 10	548923	NP_004456.1	Gonadogenesis, morphology of testis
Str.26230.1.S1_at	Testis-B	117	4	4	4	6				XP_002347599.1	
Str.30807.1.A1_at	Testis-B	118	4	5	5	5					
Str.15452.1.S1_at	Testis-B	119	4	4	3	5	sema3b	sema domain, immunoglobulin domain (Ig), short basic domain,	100151737	NP_004627.1	Vasculogenesis, cellular movement, cell signalling
Str.37100.1.A1_at	Testis-B	120	4	3	4	8	(enpp6)	ectonucleotide pyrophosphatase/phosphodiesterase 6		NP_699174.1	Hydrolysis
Str.50954.1.S1_at	Testis-B	121	3	3	5	8					
Str.31923.1.S1_at	Testis-B	122	3	5	6	9	LOC100037917 (col8a1)	collagen, type VIII, alpha 1	100037917	NP_001841.2	Vasculogenesis, angiogenesis
Str.44816.1.A1_at	Testis-B	123	4	6	9	6	LOC100487043 (nr0b1/dax-1)	nuclear receptor subfamily 0, group B, member 1	100487043	NP_000466.2	Gonadogenesis, morphology of testis, sex determination, fertility
Str.22594.1.A1_at	Testis-B	124	2	3	4	7	LOC100486154 (il17rc)	interleukin 17 receptor C	100486154	NP_116121.2	
Str.26739.1.S1_at	Testis-B	125	2	2	3	5	gpr146	G protein-coupled receptor 146	100125164	NP_612454.1	
Str.22685.1.S1_at	Testis-B	126	3	3	4	6					
Str.28107.1.S1_at	Testis-B	127	3	4	4	6	snai1 (snai2)	snail homolog 2 (Drosophila)	394880	NP_003059.1	Gonadogenesis, morphology of testis, cell movement
Str.33117.1.A1_at	Testis-B	128	3	3	4	6					
Str.31333.1.S1_a_at	Testis-B	129	3	3	3	6	pkdcc.2	protein kinase domain containing, cytoplasmic	100145744	NP_612379.2	Connective tissue development
Str.28835.1.A1_at	Testis-B	130	2	3	4	6					
Str.6049.1.A1_at	Testis-B	131	2	2	3	6	tgm2	transglutaminase 2 (C polypeptide, protein	100170618	NP_004604.2	Vasculogenesis, angiogenesis, concentration of hormone
Str.37641.1.S1_at	Testis-B	132	3	3	4	5	kcnj8	potassium inwardly-rectifying channel, subfamily J, member 8	100124909	NP_004973.1	Vascular development
Str.1924.1.S1_at	Testis-B	133	2	3	3	5					
Str.31088.1.A1_at	Testis-B	134	3	3	3	5					
Str.31855.1.S1_at	Testis-B	135	10	12	16	9	LOC100498168 (litaf)	lipopolysaccharide-induced TNF factor	100498168	NP_001129944.1	Cellular movement
Str.28269.1.S1_at	Testis-B	136	3	3	5	6					
Str.38882.1.S1_at	Testis-B	137	3	3	5	5	LOC100494767		100494767		
Str.29149.1.A1_at	Testis-B	138	3	3	5	6	LOC100490639 (myh11)	myosin, heavy chain 11, smooth muscle	100490639	NP_074035.1	Vascular development, muscle contraction
Str.39414.2.A1_at	Testis-B	139	2	4	5	6					
Str.21054.1.A1_at	Testis-B	140	5	3	4	6					
Str.31614.1.S1_at	Testis-B	141	4	3	5	7	(marco)	macrophage receptor with collagenous structure		NP_006761.1	Cellular organization of cytoskeleton, microtubule dynamics
Str.12245.1.S1_at	Testis-B	142	6	3	5	10	kazald1	Kazal-type serine peptidase inhibitor domain 1	100101767	NP_112191.2	
Str.51637.8.A1_at	Testis-B	143	6	5	6	7					
Str.5687.1.S1_s_at	Ovary-A	144	1	1	1	9	myl1		394551	NP_055625.4	
Str.44292.1.A1_x_at	Ovary-A	145	1	1	1	6					
Str.3249.1.S1_s_at	Ovary-A	146	1	1	1	9	cldn4	claudin 4	549417	NP_001296.1	Cell proliferation, cellular movement
Str.10989.1.S1_a_at	Ovary-A	147	2	1	1	6	agr2	anterior gradient 2 homolog (Xenopus laevis)	549381	NP_006399.1	Cell proliferation, cellular movement
Str.20226.1.S1_at	Ovary-A	148	1	1	1	5	hebp2	heme binding protein 2	548365	NP_055135.1	
Str.6678.1.S2_at	Ovary-A	149	1	1	1	5	upk1b	uroplakin 1B	733711	NP_088883.2	
StrEns.11770.1.S1_s_at	Ovary-A	150	1	1	2	9	LOC100486362///LOC100492826///LOC100492990///LOC100493160		100486362///100492826///100492990///100493160		
Str.48992.1.A1_at	Ovary-A	151	1	1	5	12	LOC100491528 (mfap4)	microfibrillar-associated protein 4	100491528	NP_002395.1	
Str.9495.1.S1_at	Ovary-A	152	1	1	4	6	ramp1	receptor (G protein-coupled) activity modifying protein 1	780274	NP_005846.1	
Str.49.1.S1_at	Ovary-A	153	1	1	3	7					
Str.27291.1.S1_at	Ovary-A	154	1	1	4	16	tspan1	tetraspanin 1	548861	NP_005718.2	
Str.31112.1.A1_at	Ovary-A	155	1	1	6	8	wdr72	WD repeat domain 72	100494443	NP_877435.2	Cell death and survival
Str.19439.1.S1_at	Ovary-A	156	1	1	5	13	tmem171	transmembrane protein 171	448384	NP_775761.4	
Str.37939.1.A1_at	Ovary-A	157	1	1	5	11	LOC100486197		100486197		
Str.31970.1.S1_at	Ovary-A	158	1	1	2	5	c3orf52		100500921		
Str.33670.1.S1_at	Ovary-A	159	1	1	1	6	LOC100485955 (cel)	carboxyl ester lipase	100485955	NP_001798.2	Lipid metabolism
Str.20358.1.S1_at	Ovary-A	160	1	1	2	7					
Str.116.1.S1_at	Ovary-A	161	1	1	2	6	LOC100496111///zpax (zp4)	zona pellucida glycoprotein 4	100496111///3NP_067009.1		Cell proliferation, cell signaling, activation of protein kinase
Str.1304.1.S1_at	Ovary-A	162	2	1	3	6	tmem51	transmembrane protein 51	734037	NP_001129688.1	
Str.13533.1.A1_at	Ovary-A	163	1	1	3	6	chrna5	cholinergic receptor, nicotinic, alpha 5 (neuronal)	100379824	NP_000736.2	Cell signaling, nervous system development
Str.31947.1.A1_at	Ovary-A	164	1	1	2	5	cntd2	cyclin N-terminal domain containing 2	779739	NP_001137501.1	
Str.36648.1.A1_s_at	Ovary-A	165	1	1	2	5					
Str.31340.2.S1_at	Ovary-A	166	1	1	2	5	grasp	GRP1 (general receptor for phosphoinositides 1)-associated scaff	100145424	NP_859062.1	Cell proliferation, localization, sprouting of mossy fibers
Str.29571.1.A1_at	Ovary-A	167	1	1	2	6					
StrAffx.141.1.S1_at	Ovary-A	168	1	1	3	10	gpnmb	glycoprotein (transmembrane) nmb	100124325	NP_001005340.1	Cell proliferation
Str.50260.1.A1_at	Ovary-A	169	2	2	3	5					
Str.15225.1.S1_at	Ovary-A	170	2	2	2	6	tmem184a	transmembrane protein 184A	549153	NP_001091089.1	Protein localization
Str.287.1.S1_at	Ovary-A	171	2	2	3	5	lgals3	lectin, galactoside-binding, soluble, 3	394583	NP_002297.2	Cell proliferation, expansion of mesangium
Str.4336.1.A1_at	Ovary-A	172	1	2	2	7	LOC100488374		100488374		
Str.5962.1.S2_at	Ovary-A	173	1	2	3	8	esrp1	epithelial splicing regulatory protein 1	448608	NP_060167.2	
Str.28193.1.A1_at	Ovary-A	174	2	2	4	8	LOC100487559 (oca2)	oculocutaneous albinism II	100487559	NP_000266.2	Reproductive system development, gametogenesis
Str.11491.1.A1_at	Ovary-A	175	2	4	3	7	armc4	armadillo repeat containing 4	779949	NP_060546.2	
Str.8000.1.S1_a_at	Ovary-A	176	3	3	2	6	ccnb2	cyclin B2	100270772	NP_004692.1	Cell proliferation, fecundity
Str.27817.1.S1_at	Ovary-A	177	1	2	2	5	fam46c	family with sequence similarity 46, member C	100379867	NP_060179.2	
Str.6542.1.S1_at	Ovary-A	178	2	2	2	6					
Str.4776.1.S1_at	Ovary-A	179	1	2	3	8	elovl7	ELOVL fatty acid elongase 7	448054	NP_079206.2	Cell proliferation, synthesis of hormone
Str.28063.1.S1_a_at	Ovary-A	180	1	2	3	10	LOC100494751		100494751		
StrEns.410.1.S1_at	Ovary-A	181	1	2	3	12	vegt	T-box protein VegT	394452	NP_542449.1	Oogenesis, germ layer specification of embryo
Str.16450.1.S1_at	Ovary-A	182	1	1	3	12	LOC100494176		100494176		
Str.3944.1.S1_at	Ovary-A	183	1	1	2	12	LOC733539		733539		
Str.7388.1.S1_at	Ovary-A	184	1	1	2	15	eif4e	eukaryotic translation initiation factor 4E	100127761	NP_001959.1	Cell proliferation, cell death and survival, RNA trafficking
Str.5899.1.S2_at	Ovary-A	185	1	1	2	8	rhebl1	Ras homolog enriched in brain like 1	394534	NP_653194.1	Regulation of cell growth and proliferation
Str.27867.1.A1_at	Ovary-A	186	1	1	2	7	LOC100485800		100485800		
Str.6496.1.S1_at	Ovary-A	187	2	1	2	9	sall4	sal-like 4 (Drosophila)	407860	NP_065169.1	Cell proliferation, growth
Str.37482.1.S1_at	Ovary-A	188	1	1	1	8	pnpla3	patatin-like phospholipase domain containing 2	548410	NP_065109.1	Lipid metabolism
StrEns.5801.1.S1_s_at	Ovary-A	189	1	1	1	7	proca1	protein interacting with cyclin A1	100145034	NP_056530.2	Lipid metabolism
Str.15996.2.S1_at	Ovary-A	190	1	1	1	8	proca1	protein interacting with cyclin A2	100145034	NP_056530.2	Lipid metabolism
Str.8371.1.S1_a_at	Ovary-A	191	1	1	1	6	LOC734032 (zar1l)	zygote arrest 1-like	734032	NP_001130043.1	Oogenesis, RNA regulation
Str.9274.1.S2_at	Ovary-A	192	1	1	2	7	sptssb	serine palmitoyltransferase, small subunit B	549969	NP_001035189.1	
Str.27229.1.S1_at	Ovary-A	193	1	1	2	7	ppp1r3c.2	protein phosphatase 1, regulatory subunit 3C	448158	NP_005389.1	Insulin regulation, glycogen homeostasis
Str.46745.1.A1_s_at	Ovary-A	194	1	1	2	7	ppp1r3c.2	protein phosphatase 1, regulatory subunit 3C	448158	NP_005389.1	Insulin regulation, glycogen homeostasis
Str.21882.1.S1_a_at	Ovary-A	195	1	1	2	16					
Str.21882.1.S1_at	Ovary-A	196	1	1	1	8					
Str.21882.1.S1_x_at	Ovary-A	197	1	1	1	11					
Str.33548.1.S1_at	Ovary-A	198	1	1	1	6	LOC100127750 (cox4i1)	cytochrome c oxidase subunit IV isoform 1	100127750	NP_001852.1	Cell cycle progression
Str.49374.1.A1_at	Ovary-A	199	1	1	1	5	(gstp1)	glutathione S-transferase pi 1		NP_000843.1	Cell proliferation, conversion of beta-estradiol
Str.39248.1.A1_at	Ovary-A	200	1	1	1	5	LOC100492681		100492681		
Str.29857.1.A1_at	Ovary-A	201	1	1	1	5	patl2 (patl1)	protein associated with topoisomerase II homolog 1 (yeast)	100216240	NP_689929.2	
Str.4026.1.S1_a_at	Ovary-A	202	1	1	1	5	foxh1	forkhead box H1	549838	NP_003914.1	Embryonic development, patterning
Str.6084.1.S2_at	Ovary-A	203	1	1	1	5	ly6g6c		100038197		
Str.19585.1.S1_at	Ovary-A	204	1	1	1	5	mcm6	minichromosome maintenance complex component 6	548975	NP_005906.2	Confirmational DNA modification
Str.15798.1.S1_at	Ovary-A	205	1	1	1	6	LOC100498579 (apba2)	amyloid beta (A4) precursor protein-binding, family A, member	100498579	NP_001123886.1	Exocytosis of vesicles
Str.36153.1.A1_at	Ovary-A	206	1	1	1	6					
Str.22168.2.S1_at	Ovary-A	207	1	1	1	6	LOC100490651 (rhcg)	Rh family, C glycoprotein	100490651	NP_057405.1	Morphology of gonad, molecular transport
Str.51683.1.S1_at	Ovary-A	208	1	1	1	6	(ctdspl2)	CTD (carboxy-terminal domain, RNA polymerase II, polypeptide A) small phosph	NP_057480.2		Phosphatase activity
Str.2712.1.S1_at	Ovary-A	209	1	1	1	7	LOC733553 (casp7)	caspase 7, apoptosis-related cysteine peptidase	733553	NP_203125.1	Cell death and survival, tissue morphology
Str.40962.1.A1_at	Ovary-A	210	1	1	1	6	LOC779566		779566		
Str.24662.1.S1_a_at	Ovary-A	211	1	1	1	6	zic2	Zic family member 2	549779	NP_009060.2	Nervous system development
Str.51964.1.S1_s_at	Ovary-A	212	1	1	1	6	map1lc3c	microtubule-associated protein 1 light chain 3 gamma	733779	NP_001004343.1	
Str.51435.1.S1_at	Ovary-A	213	1	1	1	5					
StrEns.5654.1.S1_at	Ovary-A	214	1	1	1	9					
Str.9274.1.S1_at	Ovary-A	215	1	1	1	9	sptssb	serine palmitoyltransferase, small subunit B	549969	NP_001035189.1	
Str.Igi.2341.1.S1_at	Ovary-A	216	1	1	1	8	LOC100494811		100494811		
Str.6626.1.S1_at	Ovary-A	217	1	1	1	7					
Str.5899.1.S1_at	Ovary-A	218	1	1	1	8	rhebl1	Ras homolog enriched in brain like 1	394534	NP_653194.1	Regulation of cell growth and proliferation
Str.6432.1.S1_at	Ovary-A	219	1	1	1	9	cdca9		779847		
Str.Igi.8914.1.S1_s_at	Ovary-A	220	1	1	1	7	LOC100492053///LOC394441 (itln2;intelectin 2		100492053///3NP_543154.1		
Str.6366.1.S1_at	Ovary-A	221	1	1	1	9	LOC100495756		100495756		
StrEns.6994.1.S1_s_at	Ovary-A	222	1	1	1	8					
Str.15673.1.S1_at	Ovary-A	223	1	1	1	9	comt.2 (comt)	catechol-O-methyltransferase	549911	NP_009294.1	Reproductive system development, metabolism, regulation of neurotransmitter
StrEns.9654.1.S1_s_at	Ovary-A	224	1	1	1	7	caprin2	caprin family member 2	100145510	NP_001002259.1	Cell proliferation, transcription
Str.10709.1.S1_at	Ovary-A	225	1	1	1	7	btbd17	BTB (POZ) domain containing 17	493324	NP_001073935.1	
Str.27710.1.S1_at	Ovary-A	226	1	1	1	8	parp12	poly (ADP-ribose) polymerase family, member 12	100327239	NP_073587.1	
Str.1153.1.S1_at	Ovary-A	227	1	0	0	11	tmprss4	transmembrane protease, serine 4	733869	NP_001167022.1	Oocyte vegetal mRNA transport (FEBS J. 2010 Nov;277(22):4722-31. doi: 10.1111/j.1742-4658.2010.07878.x. Epub 2010 Oct 6.)
Str.7206.1.S1_at	Ovary-A	228	1	1	1	18	42Sp50 (eef1a2)	eukaryotic translation elongation factor 1 alpha 2	496924	NP_001949.1	
Str.19423.1.S1_at	Ovary-A	229	1	1	1	10				NP_001025032.1	
Str.15730.1.A1_at	Ovary-A	230	1	0	0	14					

Str.51662.1.A1_at	Ovary-A	231	1	1	2	22	LOC100036665 (ssx2ip)	synovial sarcoma, X breakpoint 2 interacting protein	100036665	NP_001159766.1	Cell proliferation
Str.10367.1.S1_at	Ovary-A	232	1	1	2	17	slmo1	slowmo homolog 1 (Drosophila)	100145262	NP_001135877.1	
Str.49354.2.A1_a_at	Ovary-A	233	1	1	1	17	LOC100496955		100496955		
StrEns.5653.1.S1_s_at	Ovary-A	234	1	1	1	22	LOC100498162		100498162		
Str.52198.1.S1_at	Ovary-A	235	1	1	1	21	LOC100498162		100498162		
Str.4708.1.S1_at	Ovary-A	236	1	1	2	11	MGC147172		780305		
Str.31989.1.A1_at	Ovary-A	237	1	1	2	9	caprin2	caprin family member 2	100145510	NP_001002259.1	Cell proliferation, transcription
Str.39270.1.A1_at	Ovary-A	238	1	1	1	13	LOC100485893 (bmp15)	bone morphogenetic protein 15	100485893	NP_005439.2	Reproductive system development, gametogenesis, fertility
Str.15793.1.S1_at	Ovary-A	239	1	1	1	9					
Str.10825.1.S1_at	Ovary-A	240	1	1	1	12					
Str.20631.1.S1_at	Ovary-A	241	1	1	1	12	zp3.2		100135754		
Str.31783.1.A1_at	Ovary-A	242	1	1	1	10					
Str.30386.1.S1_at	Ovary-A	243	1	1	1	13					
Str.27268.1.S1_at	Ovary-A	244	1	1	1	12	sox3	SRY (sex determining region Y)-box 2	493228	NP_003097.1	Reproductive system development, cell proliferation
Str.17082.1.S1_s_at	Ovary-A	245	1	1	1	11	LOC549413///xk81a1 (krt12)	keratin 12	100145042	///5NP_000214.1	Disruption of keratin filaments
Str.Jgi.3075.1.S1_s_at	Ovary-A	246	1	1	1	12					
Str.6507.1.S1_at	Ovary-A	247	1	1	1	12	h1foo	H1 histone family, member O, oocyte-specific	549145	NP_722575.1	Oocyte-specific maternal mRNA
Str.3569.1.S1_at	Ovary-A	248	1	1	1	14	aldh3b1	aldehyde dehydrogenase 3 family, member B1	548883	NP_001154945.1	
StrEns.4910.1.S1_at	Ovary-A	249	1	1	1	14	LOC100170463 (gja4)	gap junction protein, alpha 4, 37kDa	100170463	NP_002051.2	Reproductive system development, gametogenesis, fertility
Str.52147.2.S1_x_at	Ovary-A	250	1	1	1	15	LOC549413 (has1)	hyaluronan synthase 1	549413	NP_001514.2	Cell proliferation, cellular movement
Str.3467.1.S1_at	Ovary-A	251	1	1	1	250	LOC733731 (btg3)	BTG family, member 3	733731	NP_006797.3	Cell cycle progression, cell proliferation, transcription
Str.21536.1.S1_at	Ovary-A	252	1	1	1	495	zfp36l2.2	ZFP36 ring finger protein-like 2	733887	NP_008818.3	Cell proliferation, mRNA stabilization, transcription
Str.4819.1.S1_at	Ovary-A	253	1	1	1	342					
Str.8649.1.S1_at	Ovary-A	254	1	1	2	91	cldn6.1	claudin 6	394468	NP_067018.2	Cell proliferation, differentiation
Str.117.1.S1_at	Ovary-A	255	1	1	1	120	LOC394444 (zp3)	zona pellucida glycoprotein 3 (sperm receptor)	394444	NP_009086.4	Oocyte development, gametogenesis, fertility
Str.3366.1.S1_at	Ovary-A	256	1	1	1	167	LOC100488960 (mt1f)	metallothionein 1F	100488960	NP_005940.1	Cell death and survival
Str.30111.1.S1_at	Ovary-A	257	1	1	1	48	(spire1)	spire homolog 1 (Drosophila)		NP_001122098.1	
Str.1668.2.S1_at	Ovary-A	258	1	1	1	49	LOC100489197 (heatr5b)	HEAT repeat containing 5B	100489197	NP_061897.1	
Str.31329.1.S1_at	Ovary-A	259	1	1	1	38	LOC100496019		100496019		
Str.754.1.S1_at	Ovary-A	260	1	1	1	40	LOC548809 (prss33)	protease, serine, 33	548809	NP_690851.2	
Str.5859.1.S1_a_at	Ovary-A	261	1	1	1	41	wee2	WEE1 homolog 2 (S. pombe)	100125126	NP_001099028.1	Cell cycle, meiosis I, prophase I
Str.27898.1.S1_at	Ovary-A	262	1	1	1	36	zfp36l2.1	ZFP36 ring finger protein	549576	NP_003398.1	Cell proliferation, mRNA stabilization, transcription
Str.2115.1.S1_at	Ovary-A	263	1	1	1	60	rnf138		549183	NP_057355.2	
Str.10913.1.S1_at	Ovary-A	264	1	1	1	37	LOC100487958		100487958		
Str.5107.1.S1_at	Ovary-A	265	1	1	1	36	zp4	zona pellucida glycoprotein 4	394445	NP_067009.1	Oocyte-specific, cell signaling, activation of protein kinase
Str.20406.1.S1_at	Ovary-A	266	1	1	1	33	LOC100486817 (zar1l)	zygote arrest 1-like	100486817	NP_001130043.1	Oocyte-specific maternal mRNA, RNA regulation embryogenesis
Str.7302.1.S1_at	Ovary-A	267	1	1	1	28					Oocyte maternal mRNA activator of embryonic development, Cha S-W, McAdams M, Kormish J, Wylie C, Kofron M (2012) Foxi2 Is an Animally Localized Maternal mRNA in Xenopus, and an Activator of the Zygotic Ectoderm Activator Foxi1e. PLoS ONE 7(7): e41782. doi:10.1371/journal.pone.0041782
Str.6457.1.S1_at	Ovary-A	268	1	1	1	31	foxi2	forkhead box I2	549298	NP_997309.2	
Str.3.1.S1_a_at	Ovary-A	269	1	1	1	32	nanos1		394451		Oocyte maternal mRNA regulation of embryonic development
Str.1617.1.S1_at	Ovary-A	270	1	1	1	30	zp4.2	zona pellucida glycoprotein 4	100142690	NP_067009.1	Oocyte-specific, cell signaling, activation of protein kinase
Str.17082.2.S1_x_at	Ovary-A	271	1	1	2	29	LOC549413 (mad1l1)	MAD1 mitotic arrest deficient-like 1 (yeast)	549413	NP_003541.2	Cell cycle progression, cell proliferation, transcription
Str.3682.1.S1_at	Ovary-A	272	1	1	2	28	btg4	B-cell translocation gene 4	549151	NP_060059.1	Cell cycle progression, cell proliferation, mitosis
Str.51979.1.S1_a_at	Ovary-A	273	1	1	1	31	velo1		100270674		
Str.32186.1.A1_at	Ovary-A	274	1	1	1	18	(znf80)	zinc finger protein 80		NP_009067.2	
Str.26862.1.S1_at	Ovary-A	275	1	1	1	25	zar1	zygote arrest 1	549701	NP_783318.1	Oocyte-specific maternal mRNA, embryogenesis
Str.39279.1.S1_at	Ovary-A	276	1	1	1	23	LOC100145154		100145154		
Str.6084.1.S1_at	Ovary-A	277	1	1	8	171	ly6g6c		100038197		
Str.51977.1.S1_at	Ovary-A	278	1	1	3	120	LOC733561		733561		
Str.8156.1.S1_at	Ovary-A	279	1	1	2	63	LOC100487709///tuba4 (tuba1b)	tubulin, alpha 1b	100487709	///4NP_006073.2	
Str.6468.4.S1_at	Ovary-A	280	1	1	3	101	mkrn3 (mkrn2)	makorin ring finger protein 2	100216134	NP_054879.3	
StrEns.9022.1.S1_s_at	Ovary-A	281	1	1	2	36	mkrn3 (mkrn2)	makorin ring finger protein 2	100216134	NP_054879.3	
Str.6258.1.S1_at	Ovary-A	282	1	1	2	50	cfc1 (tdgf1)	teratocarcinoma-derived growth factor 1	779849	NP_001167607.1	Embryonic development, mesoderm development
Str.3994.1.S1_a_at	Ovary-A	283	1	1	1	45	ccnb1	cyclin B1	100101736	NP_114172.1	Cell cycle progression, mitosis
Str.1760.2.S2_at	Ovary-A	284	1	1	2	42	cdca7	cell division cycle associated 7	100170427	NP_071370.2	Regulation of cell proliferation and transcription
Str.27228.1.S1_at	Ovary-A	285	1	1	2	34	LOC394448 (ccnb2)	cyclin B2	394448	NP_004692.1	Cell proliferation, fecundity
Str.4034.1.S1_at	Ovary-A	286	1	2	3	71	ccna1	cyclin A1	548993	NP_001104516.1	Gametogenesis, cell cycle progression
Str.7712.1.S1_a_at	Ovary-A	287	1	1	1	56	hist1h2aa///hist1h2am (h2afx)	H2A histone family, member X	100127770	///5NP_002096.1	Gametogenesis, meiosis, DNA repair
Str.1894.1.S1_at	Ovary-A	288	1	1	1	83	LOC100493862		100493862		
Str.6910.1.S1_at	Ovary-A	289	1	1	2	85	42Sp43 (gtf3a)	general transcription factor IIIA	548848	NP_002088.2	Confirmational DNA modification, transcription
Str.4820.2.A1_at	Ovary-A	290	1	1	1	96	LOC100488874		100488874		
StrAffx.70.1.S1_s_at	Ovary-B	291	21	61	43	64	ntn1	netrin 1	779839	NP_004813.2	Nervous system development, cellular movement
Str.13722.1.S1_at	Ovary-B	292	3	6	8	6	tyrp1	tyrosinase-related protein 1	549230	NP_000541.1	
Str.38277.1.A1_at	Ovary-B	293	5	4	5	5	chst8	carbohydrate (N-acetylgalactosamine 4-0) s	779984	NP_001121367.1	Morphology of gonad, concentration of hormone
StrEns.9618.1.S1_a_at	Ovary-B	294	4	7	6	6	olfml2a	olfactomedin-like 2A	100125057	NP_872293.2	Endometrial cell proliferation
Str.28084.1.S1_at	Ovary-B	295	5	7	9	6	emx2	empty spiracles homeobox 2	100038069	NP_004089.1	Morphology of gonad, primary sex determination
Str.15551.1.S1_at	Ovary-B	296	7	7	7	6	lum	lumican	496415	NP_002336.1	Cell proliferation, morphology, fertility
Str.15551.1.S2_at	Ovary-B	297	6	7	6	5	lum	lumican	496415	NP_002336.1	Cell proliferation, morphology, fertility
Str.12223.1.S1_at	Ovary-B	298	7	11	13	7	chrnd	cholinergic receptor, nicotinic, delta (muscle)	548531	NP_000742.1	Muscle growth
Str.24572.1.A1_s_at	Ovary-B	299	8	22	15	27	cyp26a1	cytochrome P450, family 26, subfamily A, polypeptide 1	548901	NP_000774.2	Organ development, morphology, metabolism
Str.28022.1.A1_at	Ovary-B	300	8	13	17	17	fibcd1	fibrinogen C domain containing 1	779974	NP_001138578.1	
Str.19828.1.S1_at	Ovary-B	301	6	5	5	6	amdhd1	amidohydrolase domain containing 1	493273	NP_689648.2	
Str.50546.1.S1_x_at	Ovary-B	302	6	10	6	6				XP_002347599.1	
Str.52013.1.S1_at	Ovary-B	303	5	8	5	6	cyp19a1	cytochrome P450, family 19, subfamily A, polypeptide 1	100036594	NP_000094.2	Morphology of gonad, primary sex determination
Str.50546.1.S1_at	Ovary-B	304	5	10	7	6				XP_002347599.1	
Str.8337.1.S1_at	Ovary-B	305	5	13	12	14	hal.2	histidine ammonia-lyase	448568	NP_002099.1	Amino acid metabolism
Str.34732.1.A1_at	Ovary-B	306	7	12	8	11	cyp19a1	cytochrome P450, family 19, subfamily A, polypeptide 1	100036594	NP_000094.2	Morphology of gonad, primary sex determination
Str.34778.1.A1_at	Ovary-B	307	7	11	10	6					
Str.33523.1.A1_at	Ovary-B	308	6	12	10	9	LOC100488372		100488372		
Str.41205.1.A1_at	Ovary-B	309	6	13	9	8	kal1	Kallmann syndrome 1 sequence	100135017	NP_000207.2	Guidance of axons, cell movement, gonad development
Str.34852.1.A1_at	Ovary-B	310	5	5	11	21	nppc	natriuretic peptide C	100127545	NP_077720.1	Reproductive system development, cell signaling, cell proliferation
Str.50262.1.S1_at	Ovary-B	311	5	11	18	14	LOC100490365		100490365		
Str.10951.1.S1_at	Ovary-B	312	3	3	3	12	LOC100488479 (kiaa1324)	KIAA1324	100488479	NP_065826.2	
Str.5962.1.S1_at	Ovary-B	313	2	3	6	20	esrp1	epithelial splicing regulatory protein 1	448608	NP_060167.2	Ovarian cell proliferation, RNA splicing
Str.5962.2.A1_at	Ovary-B	314	2	4	5	15	esrp2	epithelial splicing regulatory protein 2		NP_060167.2	Ovarian cell proliferation, RNA splicing
Str.13287.1.S1_at	Ovary-B	315	2	5	5	6	fam189a1	family with sequence similarity 189, member A1	779825	NP_056122.1	
Str.45620.1.A1_at	Ovary-B	316	3	5	9	10					
Str.37609.1.A1_at	Ovary-B	317	2	2	3	5	LOC100491685		100491685		
Str.51702.1.A1_at	Ovary-B	318	2	2	3	6					
Str.37609.2.S1_a_at	Ovary-B	319	2	3	4	7	LOC100491685		100491685		
Str.16327.1.S1_at	Ovary-B	320	2	1	4	5	ggt1	gamma-glutamyltransferase 1	448376	NP_005256.2	Morphology of gonad, fertility, cell proliferation
StrEns.4336.1.S1_a_at	Ovary-B	321	2	1	4	6					
Str.34769.1.A1_at	Ovary-B	322	2	1	4	7					
Str.8649.2.S1_at	Ovary-B	323	3	3	5	11	LOC100493413 (cldn6)	claudin 6	100493413	NP_067018.2	Cell proliferation, differentiation
Str.8649.2.S1_x_at	Ovary-B	324	3	3	5	11	LOC100493413 (cldn6)	claudin 6	100493413	NP_067018.2	Cell proliferation, differentiation
Str.15863.1.S1_at	Ovary-B	325	2	5	7	5	mlana		100379726		
Str.Jgi.3092.1.S1_at	Ovary-B	326	3	3	3	5	msc	musculin	100124790	NP_005089.2	Muscle development
Str.21092.1.S1_at	Ovary-B	327	2	4	4	5	irx5	iroquois homeobox 5	100038201	NP_005844.4	Organ development, morphology, nervous system development
Str.39298.2.S1_a_at	Ovary-B	328	2	5	5	6	LOC100489060 (a2m)	alpha-2-macroglobulin	100489060	NP_000005.2	Nervous system development, cellular movement
Str.51982.1.A1_s_at	Ovary-B	329	3	6	5	7	irx3	iroquois homeobox 3	407888	NP_077312.2	Organ development, nervous system development
Str.27610.1.S1_at	Ovary-B	330	3	4	4	8	epcam (tacstd2)	tumor-associated calcium signal transducer	496567	NP_002344.2	Ovarian cell proliferation, cellular movement
Str.4078.1.S1_a_at	Ovary-B	331	4	5	5	10	cldn7	claudin 7	394674	NP_001298.3	Ovarian cell proliferation, quantity of steroid hormone
Str.27686.1.S1_at	Ovary-C	332	1	1	5	14	lhx8	LIM homeobox 8	548653	NP_001001933.1	Gonadogenesis, ovary development, nervous system development
Str.38460.2.A1_at	Ovary-C	333	1	1	4	13	otud4		100145625	NP_001093392.1	Cancer-related
StrEns.2716.1.S1_at	Ovary-C	334	2	2	10	12	LOC100497989		100497989		
Str.11490.1.S1_at	Ovary-C	335	2	2	7	14	myc1	v-myc myelocytomatosis viral oncogene homolog 1, lung carcino	496561	NP_001028253.1	Cancer-related
Str.11490.1.S2_at	Ovary-C	336	2	2	7	14	myc1	v-myc myelocytomatosis viral oncogene homolog 1, lung carcino	496561	NP_001028253.1	Cancer-related
Str.19394.1.S1_at	Ovary-C	337	2	3	9	27	figla	folliculogenesis specific basic helix-loop-helix	549096	NP_001004311.2	Gonadogenesis, ovary development, meiosis of germ cells, fertility
Str.7111.1.S1_at	Ovary-C	338	1	2	5	21	npm2	nucleophosmin/nucleoplasmin 2	549692	NP_877724.1	Morphology of ovary, morphology of oocytes, fertility
Str.32445.1.S1_at	Ovary-C	339	2	3	3	12	LOC100487867///MGC97820 (tuba	tubulin, alpha 1a	100487867	///5NP_006000.2	Nervous system development, microtubule dynamics
Str.32445.1.S1_s_at	Ovary-C	340	2	3	4	18	LOC100487709///LOC100487867///	tubulin, alpha 1a	100487709	///1NP_006000.2	Nervous system development, microtubule dynamics
Str.37576.1.S1_s_at	Ovary-C	341	1	4	12	8	LOC100488825 (ccdc170)	coiled-coil domain containing 170	100488825	NP_079335.2	Cancer-related
Str.30824.1.A1_s_at	Ovary-C	342	1	4	10	7	LOC100496920///zg16	zymogen granule protein 16	100170438	///1NP_689551.1	Cancer-related
StrEns.8880.1.S1_a_at	Ovary-C	343	1	2	7	7	LOC100496967		100496967		
Str.28818.1.S1_at	Ovary-C	344	1	2	10	6					
Str.Jgi.2383.1.S1_at	Ovary-C	345	1	2	9	6	LOC100489575		100489575		
Str.34311.1.S1_at	Ovary-C	346	1	2	9	6	fbxo47	F-box protein 47	100158537	NP_001008777.2	Cancer-related

Str.lgi.1156.1.S1_at	Ovary-C	347	1	3	10	5	LOC100488611		100488611			
Str.8311.1.S1_at	Ovary-C	348	1	3	9	5	LOC100493022 (tldc2)	TBC/LysM-associated domain containing 2	100493022	NP_542195.1		
Str.38699.1.S1_a_at	Ovary-C	349	1	2	5	6	cccdc62		100127606	NP_115962.2		
Str.4536.1.S1_at	Ovary-C	350	1	1	6	7	(stk35)	serine/threonine kinase 35		NP_543026.1	Cancer-related, organization of actin stress fibers	
Str.710.2.S1_at	Ovary-C	351	1	1	5	8	c17orf39 (gid4)	GID complex subunit 4, VID24 homolog (S. cerevisiae)	100145021	NP_076957.3		
Str.1727.2.A1_at	Ovary-C	352	1	2	7	7	brdt	bromodomain, testis-specific	100144959	NP_001717.2	Gonadogenesis, chromatin remodeling (male?)	
Str.10181.1.S1_at	Ovary-C	353	1	2	8	8						
Str.27067.1.S1_at	Ovary-C	354	1	2	6	7	ripply2.1		100151713			
Str.27191.2.S1_at	Ovary-C	355	1	2	6	8	LOC100489839 (frrs1)	ferric-chelate reductase 1	100489839	NP_001013682.2		
StrEns.5301.1.S1_at	Ovary-C	356	1	2	8	6						
Str.38933.1.A1_a_at	Ovary-C	357	1	2	7	5						
Str.lgi.2280.1.S1_at	Ovary-C	358	1	2	4	5	LOC100491948		100491948			
Str.4267.1.S1_at	Ovary-C	359	2	2	6	6	sass6	spindle assembly 6 homolog (C. elegans)	733966	NP_919268.1	DNA replication	
Str.5073.1.S1_at	Ovary-C	360	2	4	6	5	c20orf3 (apmap)	adipocyte plasma membrane associated protein	548386	NP_065392.1	Cancer-related	
Str.38810.1.S1_at	Ovary-C	361	1	5	5	5	sel1l3	sel-1 suppressor of lin-12-like 3 (C. elegans)	100492622	NP_056002.2	Cancer-related	
Str.6726.1.S1_at	Ovary-C	362	3	6	6	5	gtsf1	gametocyte specific factor 1	100036720	NP_653195.2	Germ cell development	
Str.19341.2.S1_at	Ovary-C	363	2	3	5	6	LOC100036702		100036702	XP_002342913.1		
Str.49275.1.S1_at	Ovary-C	364	2	5	7	5	tdrd5	tudor domain containing 5	780220	NP_775804.2	Gonadogenesis, gametogenesis, meiosis, fertility (male?)	
Str.38422.2.A1_a_at	Ovary-C	365	2	2	6	8	LOC100486129 (asrgl1)	asparaginase like 1	100486129	NP_079356.3	Cancer-related	
Str.19341.1.A1_at	Ovary-C	366	2	2	4	6	LOC100036702		100036702	XP_002342913.1		
Str.1623.1.S1_at	Ovary-C	367	2	3	5	5	stk35 (pdlk1l)	PDLIM1 interacting kinase 1 like	447998	NP_690048.1	Organization of actin stress fibers	
Str.15950.1.S1_s_at	Ovary-C	368	2	2	4	5	reep6 (reep5)	receptor accessory protein 5	548805	NP_005660.4		
Str.47632.1.S1_x_at	Ovary-C	369	2	1	3	5	baf-l (banf1)	barrier to autointegration factor 1	100135163	NP_001137457.1	DNA recombination	
Str.lgi.1981.1.S1_s_at	Ovary-C	370	1	2	4	6	abcb9		100490138			
Str.32359.1.A1_at	Ovary-C	371	1	2	5	5	LOC100491097 (ggh)	gamma-glutamyl hydrolase (conjugase, folylpolygammaglutamyl	100491097	NP_003869.1	Amino acid metabolism	
Str.1988.1.S1_at	Ovary-C	372	2	3	6	5						
Str.1988.1.S2_a_at	Ovary-C	373	2	3	6	6						
Str.19885.1.S1_at	Ovary-C	374	3	3	4	5	gtf2a1///ston1	general transcription factor IIA, 1-like	100493990	///7NP_006863.2		
Str.26910.1.S1_at	Ovary-C	375	3	3	4	6	elavl2	ELAV (embryonic lethal, abnormal vision, Drosophila)-like 2 (Hu a	594913	NP_001164666.1	Cancer-related	
Str.52229.1.S1_at	Ovary-C	376	3	3	4	5	LOC100487055 (rpl17)	ribosomal protein L17	100487055	NP_000976.1	Cancer-related	
Str.967.1.S1_at	Ovary-C	377	1	2	9	6						
Str.8393.1.S1_at	Ovary-C	378	2	2	3	5	pabpc1l	poly(A) binding protein, cytoplasmic 1-like	448615	NP_001118228.1	Gonadogenesis, gametogenesis, oogenesis, meiosis, fertility	
Str.15244.2.S1_a_at	Ovary-C	379	2	2	4	5	pof1b	premature ovarian failure, 1B	733573	NP_079197.3	Cancer-related, premature ovarian failure	
Str.30634.1.A1_at	Ovary-C	380	1	2	4	5	LOC100485001 (akap13)	A kinase (PRKA) anchor protein 13	100485001	NP_009131.2	Cancer-related, decondensation of chromatin	
Str.32672.1.A1_at	Ovary-C	381	1	2	4	5	(nkiras2)	NFKB inhibitor interacting Ras-like 2		NP_001138400.1	Cancer-related	
Str.26977.1.S1_at	Ovary-C	382	1	2	4	5	dpepe		549202			
Str.20782.1.S1_a_at	Ovary-C	383	1	2	4	5	tesc	tescalcin	779877	NP_060369.3	Neurological disease, Na+ homeostasis	
Str.51692.1.S1_at	Ovary-C	384	2	5	3	7	LOC733728 (rplp0)	ribosomal protein, large, P0	733728	NP_444505.1	Cancer-related	
Str.49258.1.A1_at	Ovary-C	385	2	13	27	9	(dmc1)	DMC1 dosage suppressor of mck1 homolog, meiosis-specific homologous recon	NP_008999.2		Gonadogenesis, gametogenesis, oogenesis, meiosis, fertility	
Str.lgi.4569.1.S1_at	Ovary-C	386	1	9	20	7	LOC100496399		100496399			
Str.42327.1.A1_at	Ovary-C	387	1	7	19	11	LOC100486907 (syce2)	synaptonemal complex central element protein 2	100486907	NP_001099048.1	DNA recombination, synapsis	
Str.lgi.6590.1.S1_s_at	Ovary-C	388	1	8	19	11	LOC100486762		100486762			
Str.34301.1.S1_at	Ovary-C	389	1	11	18	7	LOC100489965 (hormad1)	HORMA domain containing 1	100489965	NP_115508.2	Gonadogenesis, gametogenesis, meiosis, fertility (male?)	
Str.38725.1.A1_a_at	Ovary-C	390	2	6	11	6	LOC100498554		100498554			
Str.34301.1.S1_a_at	Ovary-C	391	1	8	16	8	LOC100489965 (hormad1)	HORMA domain containing 1	100489965	NP_115508.2	Gonadogenesis, gametogenesis, meiosis, fertility (male?)	
Str.34301.3.A1_x_at	Ovary-C	392	1	8	13	6	LOC100489965 (hormad1)	HORMA domain containing 1	100489965	NP_115508.2	Gonadogenesis, gametogenesis, meiosis, fertility (male?)	
Str.49889.1.S1_at	Ovary-C	393	1	3	7	7	LOC100488112		100488112	NP_001032302.1		
Str.38725.1.A1_at	Ovary-C	394	1	4	10	5	LOC100498554		100498554			
Str.34311.2.A1_at	Ovary-C	395	2	4	9	6	fbxo47	F-box protein 47	100158537	NP_001008777.2	Cancer-related	
Str.lgi.3518.1.S1_at	Ovary-C	396	1	7	9	6	LOC100491502		100491502			
Str.50639.1.S1_at	Ovary-C	397	1	7	15	6						
Str.34278.1.A1_at	Ovary-C	398	1	5	11	7	LOC100494809 (tex11)	testis expressed 11	100494809	NP_001003811.1	Gonadogenesis, gametogenesis, meiosis, fertility (male?)	
Str.34280.1.A1_a_at	Ovary-C	399	2	4	12	6						
Str.lgi.1793.1.S1_s_at	Ovary-C	400	1	4	11	7	LOC100494809		100494809			
Str.33738.1.A1_at	Ovary-C	401	2	4	11	7	hfm1	HFM1, ATP-dependent DNA helicase homolog (S. cerevisiae)	779837	NP_001017975.3	Cancer-related	
Str.34837.1.S1_at	Ovary-C	402	1	3	4	6	rflb		779943			
Str.38593.1.S1_at	Ovary-C	403	1	2	9	5	LOC100170619 (c12orf40)	chromosome 12 open reading frame 40	100170619	NP_001026918.2		
StrEns.2278.1.S1_s_at	Ovary-C	404	1	2	8	5	LOC100496417		100496417			
Str.32350.2.A1_at	Ovary-C	405	1	2	7	6						
Str.31912.1.A1_at	Ovary-C	406	2	4	7	6	LOC100491026 (c1orf177)	chromosome 1 open reading frame 177	100491026	NP_689820.2		
Str.37820.1.S1_at	Ovary-C	407	2	3	7	6	LOC100127812 (fam47e)	family with sequence similarity 47, member E	100127812	NP_001130042.1		
Str.33483.1.A1_at	Ovary-C	408	1	4	12	7	LOC100486762		100486762			
Str.21686.1.S1_at	Ovary-C	409	1	3	9	9	LOC100488153 (cga)	glycoprotein hormones, alpha polypeptide	100488153	NP_000726.1	Gonadogenesis, morphology of ovary, quantity of hormone, fertility	
Str.33833.1.A1_at	Ovary-C	410	1	2	10	7	(ccdc170)	coiled-coil domain containing 170		NP_079335.2	Cancer-related	
Str.46899.1.S1_at	Ovary-C	411	1	3	9	7						
StrEns.2738.1.S1_at	Ovary-C	412	1	6	17	9	LOC100489156		100489156			
Str.38722.1.S1_at	Ovary-C	413	1	6	23	10	tmprss12	transmembrane (C-terminal) protease, serine 12	100127698	NP_872365.1	Cancer-related	
Str.34020.1.A1_at	Ovary-C	414	1	4	25	12						
StrAffx.106.1.S1_s_at	Ovary-C	415	2	4	13	12	mamdc2	MAM domain containing 2	780302	NP_694999.3		
Str.33708.1.A1_at	Ovary-C	416	1	3	17	9	LOC100491771 (ccdc152)	coiled-coil domain containing 152	100491771	NM_001128320.1		
Str.32425.1.A1_at	Ovary-C	417	1	3	16	9	LOC100485050 (syce1)	synaptonemal complex central element protein 1	100485050	NP_570140.1		
Str.34382.1.A1_at	Ovary-C	418	1	4	15	8	msh5	mutS homolog 5 (E. coli)	100489595	NP_751898.1	Gonadogenesis, gametogenesis, meiosis, fertility	
Str.27519.1.S1_at	Ovary-C	419	1	4	9	11	tbpl2 (tbp)	TATA box binding protein	550063	NP_003185.1	Transcription, embryonic development	
Str.1727.3.A1_at	Ovary-C	420	1	3	13	8	brdt	bromodomain, testis-specific	100144959	NP_001717.2	Gonadogenesis, chromatin remodeling (male?)	
Str.34567.1.S1_at	Ovary-C	421	1	3	16	8						
Str.37447.1.S1_at	Ovary-C	422	3	11	18	18	LOC100487171		100487171			
Str.34301.2.S1_at	Ovary-C	423	1	14	29	6	LOC100489965 (hormad1)	HORMA domain containing 1	100489965	NP_115508.2	Gonadogenesis, gametogenesis, meiosis, fertility (male?)	
Str.lgi.2328.1.S1_at	Ovary-C	424	1	6	28	10						
Str.49266.1.S1_at	Ovary-C	425	1	5	12	10				XP_002347599.1		
Str.38737.1.S1_at	Ovary-C	426	1	8	15	10	LOC100485446		100485446	XP_002342056.1		
StrEns.9191.1.S1_a_at	Ovary-C	427	1	5	28	18	LOC100487907		100487907			
Str.32211.1.A1_at	Ovary-C	428	1	7	30	26	LOC100488683 (zglp1)	zinc finger, GATA-like protein 1	100488683	NP_001096637.1	Gonadogenesis, gametogenesis, oogenesis, ovary development	
Str.7244.1.S1_at	Ovary-C	429	1	5	29	57	LOC100488624 (spdya)	speedy homolog A (Xenopus laevis)	100488624	NP_001008779.1	Oocyte maturation	
Str.31845.1.S1_at	Ovary-C	430	1	4	25	57	npy	neuropeptide Y	779985	NP_000896.1	Vascularization, secretion of hormone, fertility	
Str.1727.3.A2_a_at	Ovary-C	431	1	1	65	47	brdt (brd3)	bromodomain containing 3	100144959	NP_031397.1		
Str.50399.1.S1_at	Ovary-C	432	1	2	13	16	mapk13	mitogen-activated protein kinase 13	100144715	NP_002745.1	Cancer-related, cell proliferation	
Str.34008.1.A1_at	Ovary-C	433	1	1	12	16						
Str.10336.1.S1_at	Ovary-C	434	1	2	17	34	tmed6	transmembrane emp24 protein transport domain containing 6	496652	NP_653277.2		
Str.24079.1.A1_at	Ovary-C	435	1	1	14	40	(iws1)	IWS1 homolog (S. cerevisiae)		NP_060439.2	Cancer-related	

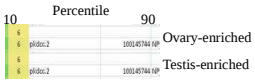

Cluster	NF58	NF66	1WPM	2WPM	Gene Symbol	Entrez Gene Name	Human Accession	Mammalian Function
Testis-A	222	302	314	289	rflcii	insulin-like 3 (Leydig cell)	NM_001265587.1	Testis development, fertility
Testis-A	8	12	27	161	LOC100492493 (bmp1)	bone morphogenetic protein 1	NP_001190.1	Collagen development, protein synthesis
Testis-A	19	38	107	930	LOC100492493 (bmp1)	bone morphogenetic protein 2	NP_001190.1	Collagen development, protein synthesis
Testis-A	37	98	110	151	fgfbp3///LOC100495029	fibroblast growth factor binding protein 3	NP_689642.3	Growth factor regulation, angiogenesis
Testis-A	26	59	68	186	LOC100492324 (astl)	astacin-like metallo-endopeptidase (M12 family)	NP_001002036.3	Protein synthesis, fertility
Testis-A	17	88	97	98	myl4	myosin, light chain 4, alkali; atrial, embryonic	NP_002467.1	Vascular development, muscle contraction
Testis-A	70	36	53	47	nptx1	neuronal pentraxin I	NP_002513.2	Angiogenesis, cellular movement, nervous system development
Testis-A	33	23	42	23				
Testis-A	17	17	22	19	slitrk4	SLIT and NTRK-like family, member 4	NP_775101.1	Formation of cellular protrusions, nervous system development
Testis-A	22	25	21	21	(rad50)	RAD50 homolog (S. cerevisiae)	NP_005723.2	DNA repair
Testis-A	26	30	41	65	LOC100497586 (opa1)	optic atrophy 1 (autosomal dominant)	NP_570844.1	Mitochondrial organization, synthesis of pregnenolone
Testis-A	16	24	25	36	LOC100496012 (htr2c)	5-hydroxytryptamine (serotonin) receptor 2C, G protein-coupled	NP_000859.1	Cell-to-cell signaling and interaction
Testis-A	18	9	20	9	LOC100485995			
Testis-A	19	14	12	20	LOC100485458 (clec4m)	C-type lectin domain family 4, member M	NP_001138378.1	Cell-to-cell signaling and interaction
Testis-A	15	16	17	13				
Testis-A	22	18	21	21	cryba4	crystallin, beta A4	NP_001877.1	
Testis-A	21	16	20	21			XP_002347599.1	
Testis-A	17	5	12	19	aqp1	aquaporin 1 (Colton blood group)	NP_932766.1	Vascular development, permeability of blood vessel, molecular transport
Testis-A	12	12	16	19	gpc1	glypican 1	NP_002072.2	Vascular development, cellular movement
Testis-A	13	11	17	22	gpc1	glypican 2	NP_002072.2	Vascular development, cellular movement
Testis-A	17	9	13	22				
Testis-A	8	7	12	24	LOC100486396			
Testis-A	9	12	12	23	acta2	actin, alpha 2, smooth muscle, aorta	NP_001135417.1	Vascular development, muscle contraction
Testis-B	9	9	10	6				
Testis-B	13	9	10	11	rarres1	retinoic acid receptor responder (tazarotene induced) 1	NP_996846.1	Cellular movement
Testis-B	13	11	11	12				
Testis-B	6	5	7	7	tpst2	tyrosylprotein sulfotransferase 2	NP_003586.3	Cellular movement, fertility
Testis-B	6	6	8	7	LOC100488502		NP_689603.2	
Testis-B	6	6	6	7	akr1cl1///LOC100490783	aldo-keto reductase family 1, member C3	NP_003730.4	Steroidogenesis
Testis-B	6	6	7	8	akr1cl1	aldo-keto reductase family 1, member C4	NP_003730.4	Steroidogenesis
Testis-B	7	5	7	5	LOC100490956			
Testis-B	8	6	8	6	adcyap1r1	adenylate cyclase activating polypeptide 1 (pituitary) receptor type I	NP_001109.2	Cellular proliferation, concentration of hormone, fertility
Testis-B	10	7	9	10	LOC100490204 (cadm3)	cell adhesion molecule 3	NP_001120645.1	
Testis-B	11	8	9	11	cyp17a1	cytochrome P450, family 17, subfamily A, polypeptide 1	NP_000093.1	Steroidogenesis, fertility, sex determination
Testis-B	7	9	13	11	osr2	odd-skipped related 2 (Drosophila)	NP_001135934.1	Cellular proliferation, growth
Testis-B	7	7	10	9				
Testis-B	8	7	7	7	kcnf1	potassium voltage-gated channel, subfamily F, member 1	NP_002227.2	
Testis-B	7	7	10	8				
Testis-B	14	12	14	8	LOC100494188			
Testis-B	15	23	10	8	acbd7	acyl-CoA binding domain containing 7	NP_001034933.1	
Testis-B	9	8	15	22				
Testis-B	5	6	12	19				
Testis-B	6	10	12	22	tpm2	tropomyosin 2 (beta)	NP_003280.2	Vascular development, muscle contraction
Testis-B	7	7	12	22				
Testis-B	6	12	15	15	LOC100485176 (nkx3-1)	NK3 homeobox 1	NP_006158.2	Morphogenesis of testis
Testis-B	6	12	16	16	LOC100485176 (nkx3-1)	NK3 homeobox 2	NP_006158.3	Morphogenesis of testis
Testis-B	5	8	11	16	srd5a2	steroid-5-alpha-reductase, alpha polypeptide 2 (3-oxo-5 alpha-steroid delta 4-dehydrogenase alpha 2)	NP_000339.2	Steroidogenesis, fertility, sex determination, morphology of testis
Testis-B	5	10	12	14	LOC100485176			
Testis-B	4	10	12	14	LOC100485176 (nkx3-1)	NK3 homeobox 1	NP_006158.2	Morphogenesis of testis
Testis-B	3	3	3	6	inha	inhibin, alpha	NP_002182.1	Morphology of testis, fertility, steroidogenesis, sex determination
Testis-B	3	5	7	7	(gas6)	growth arrest-specific 6	NP_001137417.1	Vascular development, cellular movement
Testis-B	3	3	5	9			XP_002347599.1	
Testis-B	2	3	4	7				
Testis-B	3	6	6	9	cnn2 (cnn1)	calponin 1, basic, smo	NP_001290.2	Vascular development, cellular movement, morphology of testis
Testis-B	2	3	4	8	cxadr	coxsackie virus and adenovirus receptor	NP_001329.1	Vascular development, cellular movement

Testis-B	3	4	4	6	(dhh)	desert hedgehog	NP_066382.1	Gonadogenesis, morphology of testis, sex determination, steroid synthesis
Testis-B	4	3	5	10	dkk3	dickkopf 3 homolog (Xenopus laevis)	NP_056965.3	Steroid hormone synthesis, cellular movement, cellular organization
Testis-B	3	4	5	7	fam123a (amer2)	APC membrane recruitment protein 2	NP_689917.2	
Testis-B	2	2	3	6	cadm2	cell adhesion molecule	NP_001161146.1	
Testis-B	2	2	5	6			XP_002347599.1	
Testis-B	2	2	4	10	inhba	inhibin, beta A	NP_002183.1	Morphology of testis, fertility, steroidogenesis, cellular movement
Testis-B	2	3	5	12				
Testis-B	6	7	8	17	fbln5	fibulin 5	NP_006320.2	Vascular development, cellular movement
Testis-B	6	5	9	11	mpz	myelin protein zero	NP_000521.2	Nervous system development, cellular movement
Testis-B	3	5	8	10				
Testis-B	4	9	7	8			XP_002347599.1	
Testis-B	3	8	7	6				
Testis-B	3	10	8	9	LOC100497842			
Testis-B	6	9	6	6				
Testis-B	3	5	7	6				
Testis-B	5	8	10	8	(stx3)	syntaxin 3	NP_004168.1	Cellular organization of cytoskeleton, microtubule dynamics
Testis-B	5	4	9	18	LOC100485437			
Testis-B	5	4	7	17	LOC100493356			
Testis-B	5	6	7	14	dclk2 (dclk1)	doublecortin-like kinase 1	NP_004725.1	Cellular organization of cytoskeleton, microtubule dynamics
Testis-B	5	7	7	11	LOC100491213			
Testis-B	5	6	8	14	fmo5	flavin containing monooxygenase 5	NP_001452.2	
Testis-B	5	7	10	15	fmo5	flavin containing monooxygenase 5	NP_001452.2	
Testis-B	2	9	11	17				
Testis-B	2	8	11	17	fstl5 (eif4g3)	eukaryotic translation initiation factor 4 gamma, 3	NP_003751.2	Cellular organization of cytoskeleton, microtubule dynamics
Testis-B	3	2	2	8	hba-l2 (hbz)	hemoglobin, zeta	NP_005323.1	Morphology of vascular system
Testis-B	2	2	4	19	LOC100496483		XP_002347226.1	
Testis-B	1	2	4	24	fabp7	fatty acid binding protein 7, brain	NP_001437.1	Cellular proliferation, cellular movement
Testis-B	1	1	2	13			XP_002347599.1	
Testis-B	1	1	2	13			XP_002347599.1	
Testis-B	1	2	2	5	nlk	nemo-like kinase	NP_057315.3	Morphology of vascular system
Testis-B	1	2	2	7				
Testis-B	1	1	3	6	slco2a1	solute carrier organic anion transporter family, member 2A1	NP_005621.2	Morphology of vascular system, molecular transport
Testis-B	2	1	2	6				
Testis-B	1	1	2	7	crip2	cysteine-rich protein 2	NP_001303.1	Cellular proliferation, cellular differentiation
Testis-B	1	2	2	5	col9a1	collagen, type IX, alpha 1	NP_511040.2	Connective tissue development
Testis-B	1	2	2	5				
Testis-B	2	5	5	7	LOC100487516			
Testis-B	1	3	5	7	MGC107853 (slc29a1)	solute carrier family 29 (nucleoside transporters), member 1	NP_001071642.1	Cellular proliferation
Testis-B	2	3	4	6	des.1	desmin	NP_001918.3	Morphology of vascular system
Testis-B	2	3	4	6				
Testis-B	2	3	6	7	LOC100497848			
Testis-B	3	5	6	8	fhl5///LOC100485255 (fhl2)	four and a half LIM domains 2	NP_963849.1	Angiogenesis, cellular movement, muscle cell development
Testis-B	3	5	9	9				
Testis-B	3	4	6	7	rgs2	regulator of G-protein signaling 2, 24kDa	NP_002914.1	Vascular development, development of muscle
Testis-B	3	3	4	6	cfl2	cofilin 2 (muscle)	NP_068733.1	
Testis-B	3	3	6	9	(gabra2)	gamma-aminobutyric acid (GABA) A receptor, alpha 2	NP_000798.2	
Testis-B	2	3	5	8	kitlg	KIT ligand	NP_000890.1	Gonadogenesis, development of testis, steroid synthesis
Testis-B	2	3	4	6				
Testis-B	1	2	4	7	cyp26b1	cytochrome P450, family 26, subfamily B, polypeptide 1	NP_063938.1	Gonadogenesis, morphology of testis
Testis-B	1	3	3	5	itga2b.1	integrin, alpha 2b (platelet glycoprotein IIb of IIb/IIIa complex, antigen CD41)	NP_000410.2	Morphology of vascular system, cellular movement
Testis-B	2	3	4	5	klhl31	kelch-like family member 31	NP_001003760.2	
Testis-B	1	3	4	5	(col13a1) LOC100488115///LOC	collagen, type XIII, alpha 1	NP_542988.3	Vasculogenesis, angiogenesis
Testis-B	10	6	5	10	akr1c2 (akr1c3)	aldo-keto reductase family 1, member C3	NP_003730.4	Steroid synthesis and metabolism
Testis-B	4	5	5	6				
Testis-B	5	4	6	6				
Testis-B	6	6	7	6	spink2			
Testis-B	11	6	7	6	enpp2	ectonucleotide pyrophosphatase/phosphodiesterase 2	NP_001035181.1	Vasculogenesis, cellular movement
Testis-B	8	4	4	5	psph	phosphoserine phosphatase	NP_004568.2	
Testis-B	5	5	5	5	tmem26	transmembrane protein 26	NP_848600.2	
Testis-B	3	4	5	6			XP_002344577.1	
Testis-B	3	4	5	5	fgf10	fibroblast growth factor 10	NP_004456.1	Gonadogenesis, morphology of testis
Testis-B	4	4	4	6			XP_002347599.1	
Testis-B	4	5	5	5				
Testis-B	4	4	3	5	sema3b	sema domain, immunoglobulin domain (Ig), short basic domain, secreted, (semaphorin) 3B	NP_004627.1	Vasculogenesis, cellular movement, cell signalling
Testis-B	4	3	4	8	(enpp6)	ectonucleotide pyrophosphatase/phosphodiesterase 6	NP_699174.1	Hydrolysis

Testis-B	3	3	5	8				
Testis-B	3	5	6	9	LOC100037917 (col8a1)	collagen, type VIII, alpha 1	NP_001841.2	Vasculogenesis, angiogenesis
Testis-B	4	6	9	6	LOC100487043 (nr0b1/dax-1)	nuclear receptor subfamily 0, group B, member 1	NP_000466.2	Gonadogenesis, morphology of testis, sex determination, fertility
Testis-B	2	3	4	7	LOC100486154 (il17rc)	interleukin 17 receptor C	NP_116121.2	
Testis-B	2	2	3	5	gpr146	G protein-coupled receptor 146	NP_612454.1	
Testis-B	3	3	4	6				
Testis-B	3	4	4	6	snai1 (snai2)	snail homolog 2 (Drosophila)	NP_003059.1	Gonadogenesis, morphology of testis, cell movement
Testis-B	3	3	4	6				
Testis-B	3	3	3	6	pkdcc.2	protein kinase domain containing, cytoplasmic	NP_612379.2	Connective tissue development
Testis-B	2	3	4	6				
Testis-B	2	2	3	6	tgm2	transglutaminase 2 (C polypeptide, protein	NP_004604.2	Vasculogenesis, angiogenesis, concentration of hormone
Testis-B	3	3	4	5	kcnj8	potassium inwardly-rectifying channel, subfamily J, member 8	NP_004973.1	Vascular development
Testis-B	2	3	3	5				
Testis-B	3	3	3	5				
Testis-B	10	12	16	9	LOC100498168 (litaf)	lipopolysaccharide-induced TNF factor	NP_001129944.1	Cellular movement
Testis-B	3	3	5	6				
Testis-B	3	3	5	5	LOC100494767			
Testis-B	3	3	5	6	LOC100490639 (myh11)	myosin, heavy chain 11, smooth muscle	NP_074035.1	Vascular development, muscle contraction
Testis-B	2	4	5	6				
Testis-B	5	3	4	6				
Testis-B	4	3	5	7	(marco)	macrophage receptor with collagenous structure	NP_006761.1	Cellular organization of cytoskeleton, microtubule dynamics
Testis-B	6	3	5	10	kazald1	Kazal-type serine peptidase inhibitor domain 1	NP_112191.2	
Testis-B	6	5	6	7				
Ovary-A	1	1	1	9	myl1		NP_055625.4	
Ovary-A	1	1	1	6				
Ovary-A	1	1	1	9	cldn4	claudin 4	NP_001296.1	Cell proliferation, cellular movement
Ovary-A	2	1	1	6	agr2	anterior gradient 2 homolog (Xenopus laevis)	NP_006399.1	Cell proliferation, cellular movement
Ovary-A	1	1	1	5	hebp2	heme binding protein 2	NP_055135.1	
Ovary-A	1	1	1	5	upk1b	uroplakin 1B	NP_008883.2	
Ovary-A	1	1	2	9	LOC100486362///LOC100492826///LOC100492990///LOC100493160			
Ovary-A	1	1	5	12	LOC100491528 (mfap4)	microfibrillar-associated protein 4	NP_002395.1	
Ovary-A	1	1	4	6	ramp1	receptor (G protein-coupled) activity modifying protein 1	NP_005846.1	
Ovary-A	1	1	3	7				
Ovary-A	1	1	4	16	tspan1	tetraspanin 1	NP_005718.2	
Ovary-A	1	1	6	8	wdr72	WD repeat domain 72	NP_877435.2	Cell death and survival
Ovary-A	1	1	5	13	tmem171	transmembrane protein 171	NP_775761.4	
Ovary-A	1	1	5	11	LOC100486197			
Ovary-A	1	1	2	5	c3orf52			
Ovary-A	1	1	1	6	LOC100485955 (cel)	carboxyl ester lipase	NP_001798.2	Lipid metabolism
Ovary-A	1	1	2	7				
Ovary-A	1	1	2	6	(zp4) LOC100496111///zpax	zona pellucida glycoprotein 4	NP_067009.1	Cell proliferation, cell signaling, activation of protein kinase
Ovary-A	2	1	3	6	tmem51	transmembrane protein 51	NP_001129688.1	
Ovary-A	1	1	3	6	chrna5	cholinergic receptor, nicotinic, alpha 5 (neuronal)	NP_000736.2	Cell signaling, nervous system development
Ovary-A	1	1	2	5	cntd2	cyclin N-terminal domain containing 2	NP_001137501.1	
Ovary-A	1	1	2	5				
Ovary-A	1	1	2	5	grasp	GRP1 (general receptor for phosphoinositides 1)-associated scaffold protein	NP_859062.1	Cell proliferation, localization, sprouting of mossy fibers
Ovary-A	1	1	2	6				
Ovary-A	1	1	3	10	gpnmb	glycoprotein (transmembrane) nmb	NP_001005340.1	Cell proliferation
Ovary-A	2	2	3	5				
Ovary-A	2	2	2	6	tmem184a	transmembrane protein 184A	NP_001091089.1	Protein localization
Ovary-A	2	2	3	5	lgals3	lectin, galactoside-binding, soluble, 3	NP_002297.2	Cell proliferation, expansion of mesangium
Ovary-A	1	2	2	7	LOC100488374			
Ovary-A	1	2	3	8	esrp1	epithelial splicing regulatory protein 1	NP_060167.2	
Ovary-A	2	2	4	8	LOC100487559 (oca2)	oculocutaneous albinism II	NP_000266.2	Reproductive system development, gametogenesis
Ovary-A	2	4	3	7	armc4	armadillo repeat containing 4	NP_060546.2	
Ovary-A	3	3	2	6	ccnb2	cyclin B2	NP_004692.1	Cell proliferation, fecundity
Ovary-A	1	2	2	5	fam46c	family with sequence similarity 46, member C	NP_060179.2	
Ovary-A	2	2	2	6				
Ovary-A	1	2	3	8	elovl7	ELOVL fatty acid elongase 7	NP_079206.2	Cell proliferation, synthesis of hormone
Ovary-A	1	2	3	10	LOC100494751			
Ovary-A	1	2	3	12	vegt	T-box protein VegT	NP_542449.1	Oogenesis, germ layer specification of embryo
Ovary-A	1	1	3	12	LOC100494176			
Ovary-A	1	1	2	12	LOC733539			
Ovary-A	1	1	2	15	eif4e	eukaryotic translation initiation factor 4E	NP_001959.1	Cell proliferation, cell death and survival, RNA trafficking
Ovary-A	1	1	2	8	rhebl1	Ras homolog enriched in brain like 1	NP_653194.1	Regulation of cell growth and proliferation

Ovary-A	1	1	2	7	LOC100485800			
Ovary-A	2	1	2	9	sall4	sal-like 4 (Drosophila)	NP_065169.1	Cell proliferation, growth
Ovary-A	1	1	1	8	pnpla3	patatin-like phospholipase domain containing 2	NP_065109.1	Lipid metabolism
Ovary-A	1	1	1	7	proca1	protein interacting with cyclin A1	NP_056530.2	Lipid metabolism
Ovary-A	1	1	1	8	proca1	protein interacting with cyclin A2	NP_056530.2	Lipid metabolism
Ovary-A	1	1	1	6	LOC734032 (zar1l)	zygote arrest 1-like	NP_001130043.1	Oogenesis, RNA regulation
Ovary-A	1	1	2	7	sptssb	serine palmitoyltransferase, small subunit B	NP_001035189.1	
Ovary-A	1	1	2	7	ppp1r3c.2	protein phosphatase 1, regulatory subunit 3C	NP_005389.1	Insulin regulation, glycogen homeostasis
Ovary-A	1	1	2	7	ppp1r3c.2	protein phosphatase 1, regulatory subunit 3C	NP_005389.1	Insulin regulation, glycogen homeostasis
Ovary-A	1	1	2	16				
Ovary-A	1	1	1	8				
Ovary-A	1	1	1	11				
Ovary-A	1	1	1	6	LOC100127750 (cox4i1)	cytochrome c oxidase subunit IV isoform 1	NP_001852.1	Cell cycle progression
Ovary-A	1	1	1	5	(gstp1)	glutathione S-transferase pi 1	NP_000843.1	Cell proliferation, conversion of beta-estradiol
Ovary-A	1	1	1	5	LOC100492681			
Ovary-A	1	1	1	5	patl2 (patl1)	protein associated with topoisomerase II homolog 1 (yeast)	NP_689929.2	
Ovary-A	1	1	1	5	foxh1	forkhead box H1	NP_003914.1	Embryonic development, patterning
Ovary-A	1	1	1	5	ly6g6c			
Ovary-A	1	1	1	5	mcm6	minichromosome maintenance complex component 6	NP_005906.2	Confirmational DNA modification
Ovary-A	1	1	1	6	LOC100498579 (apba2)	amyloid beta (A4) precursor protein-binding, family A, member 2	NP_001123886.1	Exocytosis of vesicles
Ovary-A	1	1	1	6				
Ovary-A	1	1	1	6	LOC100490651 (rhcg)	Rh family, C glycoprotein	NP_057405.1	Morphology of gonad, molecular transport
Ovary-A	1	1	1	6	(ctdspl2)	CTD (carboxy-terminal domain, RNA polymerase II, polypeptide A) small phosphatase like 2	NP_057480.2	Phosphatase activity
Ovary-A	1	1	1	7	LOC733553 (casp7)	caspase 7, apoptosis-related cysteine peptidase	NP_203125.1	Cell death and survival, tissue morphology
Ovary-A	1	1	1	6	LOC779566			
Ovary-A	1	1	1	6	zic2	Zic family member 2	NP_009060.2	Nervous system development
Ovary-A	1	1	1	6	map1lc3c	microtubule-associated protein 1 light chain 3 gamma	NP_001004343.1	
Ovary-A	1	1	1	5				
Ovary-A	1	1	1	9				
Ovary-A	1	1	1	9	sptssb	serine palmitoyltransferase, small subunit B	NP_001035189.1	
Ovary-A	1	1	1	8	LOC100494811			
Ovary-A	1	1	1	7				
Ovary-A	1	1	1	8	rhebl1	Ras homolog enriched in brain like 1	NP_653194.1	Regulation of cell growth and proliferation
Ovary-A	1	1	1	9	cdca9			
Ovary-A	1	1	1	7	(itln2) LOC100492053///LOC39	intelectin 2	NP_543154.1	
Ovary-A	1	1	1	9	LOC100495756			
Ovary-A	1	1	1	8				
Ovary-A	1	1	1	9	comt.2 (comt)	catechol-O-methyltransferase	NP_009294.1	Reproductive system development, metabolism, regulation of neurotransmitter
Ovary-A	1	1	1	7	caprin2	caprin family member 2	NP_001002259.1	Cell proliferation, transcription
Ovary-A	1	1	1	7	btbd17	BTB (POZ) domain containing 17	NP_001073935.1	
Ovary-A	1	1	1	8	parp12	poly (ADP-ribose) polymerase family, member 12	NP_073587.1	
Ovary-A	1	0	0	11	tmprss4	transmembrane protease, serine 4	NP_001167022.1	
Ovary-A	1	1	1	18	42Sp50 (eef1a2)	eukaryotic translation elongation factor 1 alpha 2	NP_001949.1	Oocyte vegetal mRNA transport (FEBS J. 2010 Nov;277(22):4722-31. doi: 10.1111/j.1742-4658.2010.07878.x. Epub 2010 Oct 6.)
Ovary-A	1	1	1	10			NP_001025032.1	
Ovary-A	1	0	0	14				
Ovary-A	1	1	2	22	LOC100036665 (ssx2ip)	synovial sarcoma, X breakpoint 2 interacting protein	NP_001159766.1	Cell proliferation
Ovary-A	1	1	2	17	slmo1	slowmo homolog 1 (Drosophila)	NP_001135877.1	
Ovary-A	1	1	1	17	LOC100496955			
Ovary-A	1	1	1	22	LOC100498162			
Ovary-A	1	1	1	21	LOC100498162			
Ovary-A	1	1	2	11	MGC147172			
Ovary-A	1	1	2	9	caprin2	caprin family member 2	NP_001002259.1	Cell proliferation, transcription
Ovary-A	1	1	1	13	LOC100485893 (bmp15)	bone morphogenetic protein 15	NP_005439.2	Reproductive system development, gametogenesis, fertility
Ovary-A	1	1	1	9				
Ovary-A	1	1	1	12				
Ovary-A	1	1	1	12	zp3.2			
Ovary-A	1	1	1	10				
Ovary-A	1	1	1	13				
Ovary-A	1	1	1	12	sox3	SRY (sex determining region Y)-box 2	NP_003097.1	Reproductive system development, cell proliferation
Ovary-A	1	1	1	11	LOC549413///xk81a1 (krt12)	keratin 12	NP_000214.1	Disruption of keratin filaments
Ovary-A	1	1	1	12				
Ovary-A	1	1	1	12	h1foo	H1 histone family, member O, oocyte-specific	NP_722575.1	Oocyte-specific maternal mRNA
Ovary-A	1	1	1	14	aldh3b1	aldehyde dehydrogenase 3 family, member B1	NP_001154945.1	
Ovary-A	1	1	1	14	LOC100170463 (gja4)	gap junction protein, alpha 4, 37kDa	NP_002051.2	Reproductive system development, gametogenesis, fertility

Ovary-A	1	1	1	15	LOC549413 (has1)	hyaluronan synthase 1	NP_001514.2	Cell proliferation, cellular movement
Ovary-A	1	1	1	250	LOC733731 (btg3)	BTG family, member 3	NP_006797.3	Cell cycle progression, cell proliferation, transcription
Ovary-A	1	1	1	495	zfp36l2.2	ZFP36 ring finger protein-like 2	NP_008818.3	Cell proliferation, mRNA stabilization, transcription
Ovary-A	1	1	1	342				
Ovary-A	1	1	2	91	cldn6.1	claudin 6	NP_067018.2	Cell proliferation, differentiation
Ovary-A	1	1	1	120	LOC394444 (zp3)	zona pellucida glycoprotein 3 (sperm receptor)	NP_009086.4	Oocyte development, gametogenesis, fertility
Ovary-A	1	1	1	167	LOC100488960 (mt1f)	metallothionein 1F	NP_005940.1	Cell death and survival
Ovary-A	1	1	1	48	(spire1)	spire homolog 1 (Drosophila)	NP_001122098.1	
Ovary-A	1	1	1	49	LOC100489197 (heatr5b)	HEAT repeat containing 5B	NP_061897.1	
Ovary-A	1	1	1	38	LOC100496019			
Ovary-A	1	1	1	40	LOC548809 (prss33)	protease, serine, 33	NP_690851.2	
Ovary-A	1	1	1	41	wee2	WEE1 homolog 2 (S. pombe)	NP_001099028.1	Cell cycle, meiosis I, prophase I
Ovary-A	1	1	1	36	zfp36l2.1	ZFP36 ring finger protein	NP_003398.1	Cell proliferation, mRNA stabilization, transcription
Ovary-A	1	1	1	60	rnf138		NP_057355.2	
Ovary-A	1	1	1	37	LOC100487958			
Ovary-A	1	1	1	36	zp4	zona pellucida glycoprotein 4	NP_067009.1	Oocyte-specific, cell signaling, activation of protein kinase
Ovary-A	1	1	1	33	LOC100486817 (zar1l)	zygote arrest 1-like	NP_001130043.1	Oocyte-specific maternal mRNA, RNA regulation embryogenesis
Ovary-A	1	1	1	28				
Ovary-A	1	1	1	31	foxi2	forkhead box I2	NP_997309.2	Oocyte maternal mRNA activator of embryonic development, Cha S-W, McAdams M, Kormish J, Wylie C, Kofron M (2012) Foxi2 Is an Animally Localized Maternal mRNA in Xenopus, and an Activator of the Zygotic Ectoderm Activator Foxi1e. PLoS ONE 7(7): e41782. doi:10.1371/journal.pone.0041782
Ovary-A	1	1	1	32	nanos1			Oocyte maternal mRNA regulation of embryonic development
Ovary-A	1	1	1	30	zp4.2	zona pellucida glycoprotein 4	NP_067009.1	Oocyte-specific, cell signaling, activation of protein kinase
Ovary-A	1	1	2	29	LOC549413 (mad1l1)	MAD1 mitotic arrest deficient-like 1 (yeast)	NP_003541.2	Cell cycle progression, cell proliferation, transcription
Ovary-A	1	1	2	28	btg4	B-cell translocation gene 4	NP_060059.1	Cell cycle progression, cell proliferation, mitosis
Ovary-A	1	1	1	31	velo1			
Ovary-A	1	1	1	18	(znf80)	zinc finger protein 80	NP_009067.2	
Ovary-A	1	1	1	25	zar1	zygote arrest 1	NP_783318.1	Oocyte-specific maternal mRNA, embryogenesis
Ovary-A	1	1	1	23	LOC100145154			
Ovary-A	1	1	8	171	ly6g6c			
Ovary-A	1	1	3	120	LOC733561			
Ovary-A	1	1	2	63	(tuba1b) LOC100487709///tuba	tubulin, alpha 1b	NP_006073.2	
Ovary-A	1	1	3	101	mkrn3 (mkrn2)	makorin ring finger protein 2	NP_054879.3	
Ovary-A	1	1	2	36	mkrn3 (mkrn2)	makorin ring finger protein 2	NP_054879.3	
Ovary-A	1	1	2	50	cfc1 (tdgf1)	teratocarcinoma-derived growth factor 1	NP_001167607.1	Embryonic development, mesoderm development
Ovary-A	1	1	1	45	ccnb1	cyclin B1	NP_114172.1	Cell cycle progression, mitosis
Ovary-A	1	1	2	42	cdca7	cell division cycle associated 7	NP_071370.2	Regulation of cell proliferation and transcription
Ovary-A	1	1	2	34	LOC394448 (ccnb2)	cyclin B2	NP_004692.1	Cell proliferation, fecundity
Ovary-A	1	2	3	71	ccna1	cyclin A1	NP_001104516.1	Gametogenesis, cell cycle progression
Ovary-A	1	1	1	56	(h2afx) hist1h2aa///hist1h2am	H2A histone family, member X	NP_002096.1	Gametogenesis, meiosis, DNA repair
Ovary-A	1	1	1	83	LOC100493862			
Ovary-A	1	1	2	85	42Sp43 (gtf3a)	general transcription factor IIIA	NP_002088.2	Confirmational DNA modification, transcription
Ovary-A	1	1	1	96	LOC100488874			
Ovary-B	21	61	43	64	ntn1	netrin 1	NP_004813.2	Nervous system development, cellular movement
Ovary-B	3	6	8	6	tyrp1	tyrosinase-related protein 1	NP_000541.1	
Ovary-B	5	4	5	5	chst8	carbohydrate (N-acetylgalactosamine 4-0) s	NP_001121367.1	Morphology of gonad, concentration of hormone
Ovary-B	4	7	6	6	olfml2a	olfactomedin-like 2A	NP_872293.2	Endometrial cell proliferation
Ovary-B	5	7	9	6	emx2	empty spiracles homeobox 2	NP_004089.1	Morphology of gonad, primary sex determination
Ovary-B	7	7	7	6	lum	lumican	NP_002336.1	Cell proliferation, morphology, fertility
Ovary-B	6	7	6	5	lum	lumican	NP_002336.1	Cell proliferation, morphology, fertility
Ovary-B	7	11	13	7	chrnd	cholinergic receptor, nicotinic, delta (muscle)	NP_000742.1	Muscle growth
Ovary-B	8	22	15	27	cyp26a1	cytochrome P450, family 26, subfamily A, polypeptide 1	NP_000774.2	Organ development, morphology, metabolism
Ovary-B	8	13	17	17	fibcd1	fibrinogen C domain containing 1	NP_001138578.1	
Ovary-B	6	5	5	6	amdhd1	amidohydrolase domain containing 1	NP_689648.2	
Ovary-B	6	10	6	6			XP_002347599.1	
Ovary-B	5	8	5	6	cyp19a1	cytochrome P450, family 19, subfamily A, polypeptide 1	NP_000094.2	Morphology of gonad, primary sex determination
Ovary-B	5	10	7	6			XP_002347599.1	
Ovary-B	5	13	12	14	hal.2	histidine ammonia-lyase	NP_002099.1	Amino acid metabolism
Ovary-B	7	12	8	11	cyp19a1	cytochrome P450, family 19, subfamily A, polypeptide 1	NP_000094.2	Morphology of gonad, primary sex determination
Ovary-B	7	11	10	6				
Ovary-B	6	12	10	9	LOC100488372			
Ovary-B	6	13	9	8	kal1	Kallmann syndrome 1 sequence	NP_000207.2	Guidance of axons, cell movement, gonad development
Ovary-B	5	5	11	21	nppc	natriuretic peptide C	NP_077720.1	Reproductive system development, cell signaling, cell proliferation

Ovary-B	5	11	18	14	LOC100490365			
Ovary-B	3	3	3	12	LOC100488479 (kiaa1324)	KIAA1324	NP_065826.2	
Ovary-B	2	3	6	20	esrp1	epithelial splicing regulatory protein 1	NP_060167.2	Ovarian cell proliferation, RNA splicing
Ovary-B	2	4	5	15	esrp2	epithelial splicing regulatory protein 2	NP_060167.2	Ovarian cell proliferation, RNA splicing
Ovary-B	2	5	5	6	fam189a1	family with sequence similarity 189, member A1	NP_056122.1	
Ovary-B	3	5	9	10				
Ovary-B	2	2	3	5	LOC100491685			
Ovary-B	2	2	3	6				
Ovary-B	2	3	4	7	LOC100491685			
Ovary-B	2	1	4	5	ggt1	gamma-glutamyltransferase 1	NP_005256.2	Morphology of gonad, fertility, cell proliferation
Ovary-B	2	1	4	6				
Ovary-B	2	1	4	7				
Ovary-B	3	3	5	11	LOC100493413 (cldn6)	claudin 6	NP_067018.2	Cell proliferation, differentiation
Ovary-B	3	3	5	11	LOC100493413 (cldn6)	claudin 6	NP_067018.2	Cell proliferation, differentiation
Ovary-B	2	5	7	5	mlana			
Ovary-B	3	3	3	5	msc	musculin	NP_005089.2	Muscle development
Ovary-B	2	4	4	5	irx5	iroquois homeobox 5	NP_005844.4	Organ development, morphology, nervous system development
Ovary-B	2	5	5	6	LOC100489060 (a2m)	alpha-2-macroglobulin	NP_000005.2	Nervous system development, cellular movement
Ovary-B	3	6	5	7	irx3	iroquois homeobox 3	NP_077312.2	Organ development, nervous system development
Ovary-B	3	4	4	8	epcam (tacstd2)	tumor-associated calcium signal transducer	NP_002344.2	Ovarian cell proliferation, cellular movement
Ovary-B	4	5	5	10	cldn7	claudin 7	NP_001298.3	Ovarian cell proliferation, quantity of steroid hormone
Ovary-C	1	1	5	14	lhx8	LIM homeobox 8	NP_001001933.1	Gonadogenesis, ovary development, nervous system development
Ovary-C	1	1	4	13	otud4		NP_001093392.1	Cancer-related
Ovary-C	2	2	10	12	LOC100497989			
Ovary-C	2	2	7	14	mycl1	v-myc myelocytomatosis viral oncogene homolog 1, lung carcinoma derived (avian)	NP_001028253.1	Cancer-related
Ovary-C	2	2	7	14	mycl1	v-myc myelocytomatosis viral oncogene homolog 1, lung carcinoma derived (avian)	NP_001028253.1	Cancer-related
Ovary-C	2	3	9	27	figla	folliculogenesis specific basic helix-loop-helix	NP_001004311.2	Gonadogenesis, ovary development, meiosis of germ cells, fertility
Ovary-C	1	2	5	21	npm2	nucleophosmin/nucleoplasmin 2	NP_877724.1	Morphology of ovary, morphology of oocytes, fertility
Ovary-C	2	3	3	12	(tuba1a) LOC100487867///MG(	tubulin, alpha 1a	NP_006000.2	Nervous system development, microtubule dynamics
Ovary-C	2	3	4	18	(tuba1a) LOC100487709///LOC	tubulin, alpha 1a	NP_006000.2	Nervous system development, microtubule dynamics
Ovary-C	1	4	12	8	LOC100488825 (ccdc170)	coiled-coil domain containing 170	NP_079335.2	Cancer-related
Ovary-C	1	4	10	7	LOC100496920///zg16	zymogen granule protein 16	NP_689551.1	Cancer-related
Ovary-C	1	2	7	7	LOC100496967			
Ovary-C	1	2	10	6				
Ovary-C	1	2	9	6	LOC100489575			
Ovary-C	1	2	9	6	fbxo47	F-box protein 47	NP_001008777.2	Cancer-related
Ovary-C	1	3	10	5	LOC100488611			
Ovary-C	1	3	9	5	LOC100493022 (tldc2)	TBC/LysM-associated domain containing 2	NP_542195.1	
Ovary-C	1	2	5	6	ccdc62		NP_115962.2	
Ovary-C	1	1	6	7	(stk35)	serine/threonine kinase 35	NP_543026.1	Cancer-related, organization of actin stress fibers
Ovary-C	1	1	5	8	c17orf39 (gid4)	GID complex subunit 4, VID24 homolog (S. cerevisiae)	NP_076957.3	
Ovary-C	1	2	7	7	brdt	bromodomain, testis-specific	NP_001717.2	Gonadogenesis, chromatin remodeling (male?)
Ovary-C	1	2	8	8				
Ovary-C	1	2	6	7	ripply2.1			
Ovary-C	1	2	6	8	LOC100489839 (frrs1)	ferric-chelate reductase 1	NP_001013682.2	
Ovary-C	1	2	8	6				
Ovary-C	1	2	7	5				
Ovary-C	1	2	4	5	LOC100491948			
Ovary-C	2	2	6	6	sass6	spindle assembly 6 homolog (C. elegans)	NP_919268.1	DNA replication
Ovary-C	2	4	6	5	c20orf3 (apmap)	adipocyte plasma membrane associated protein	NP_065392.1	Cancer-related
Ovary-C	1	5	5	5	sel1l3	sel-1 suppressor of lin-12-like 3 (C. elegans)	NP_056002.2	Cancer-related
Ovary-C	3	6	6	5	gtsf1	gametocyte specific factor 1	NP_653195.2	Germ cell development
Ovary-C	2	3	5	6	LOC100036702		XP_002342913.1	
Ovary-C	2	5	7	5	tdrd5	tudor domain containing 5	NP_775804.2	Gonadogenesis, gametogenesis, meiosis, fertility (male?)
Ovary-C	2	2	6	8	LOC100486129 (asrgl1)	asparaginase like 1	NP_079356.3	Cancer-related
Ovary-C	2	2	4	6	LOC100036702		XP_002342913.1	
Ovary-C	2	3	5	5	stk35 (pdik1l)	PDLIM1 interacting kinase 1 like	NP_690048.1	Organization of actin stress fibers
Ovary-C	2	2	4	5	reep6 (reep5)	receptor accessory protein 5	NP_005660.4	
Ovary-C	2	1	3	5	baf-l (banf1)	barrier to autointegration factor 1	NP_001137457.1	DNA recombination
Ovary-C	1	2	4	6	abcb9			
Ovary-C	1	2	5	5	LOC100491097 (ggh)	gamma-glutamyl hydrolase (conjugase, folylpolygammaglutamyl hydrolase)	NP_003869.1	Amino acid metabolism
Ovary-C	2	3	6	5				
Ovary-C	2	3	6	6				
Ovary-C	3	3	4	5	gtf2a1l///ston1	general transcription factor IIA, 1-like	NP_006863.2	
Ovary-C	3	3	4	6	elavl2	ELAV (embryonic lethal, abnormal vision, Drosophila)-like 2 (Hu antigen B)	NP_001164666.1	Cancer-related

Ovary-C	3	3	4	5	LOC100487055 (rpl17)	ribosomal protein L17	NP_000976.1	Cancer-related
Ovary-C	1	2	9	6				
Ovary-C	2	2	3	5	pabpc1l	poly(A) binding protein, cytoplasmic 1-like	NP_001118228.1	Gonadogenesis, gametogenesis, oogenesis, meiosis, fertility
Ovary-C	2	2	4	5	pof1b	premature ovarian failure, 1B	NP_079197.3	Cancer-related, premature ovarian failure
Ovary-C	1	2	4	5	LOC100485001 (akap13)	A kinase (PRKA) anchor protein 13	NP_009131.2	Cancer-related, decondensation of chromatin
Ovary-C	1	2	4	5	(nkiras2)	NFKB inhibitor interacting Ras-like 2	NP_001138400.1	Cancer-related
Ovary-C	1	2	4	5	dpepe			
Ovary-C	1	2	4	5	tesc	tescalcin	NP_060369.3	Neurological disease, Na+ homeostasis
Ovary-C	2	5	3	7	LOC733728 (rplp0)	ribosomal protein, large, P0	NP_444505.1	Cancer-related
Ovary-C	2	13	27	9	(dmc1)	DMC1 dosage suppressor of mck1 homolog, meiosis-specific homologous recombination (yeast)	NP_008999.2	Gonadogenesis, gametogenesis, oogenesis, meiosis, fertility
Ovary-C	1	9	20	7	LOC100496399			
Ovary-C	1	7	19	11	LOC100486907 (syce2)	synaptonemal complex central element protein 2	NP_001099048.1	DNA recombination, synapsis
Ovary-C	1	8	19	11	LOC100486762			
Ovary-C	1	11	18	7	LOC100489965 (hormad1)	HORMA domain containing 1	NP_115508.2	Gonadogenesis, gametogenesis, meiosis, fertility (male?)
Ovary-C	2	6	11	6	LOC100498554			
Ovary-C	1	8	16	8	LOC100489965 (hormad1)	HORMA domain containing 1	NP_115508.2	Gonadogenesis, gametogenesis, meiosis, fertility (male?)
Ovary-C	1	8	13	6	LOC100489965 (hormad1)	HORMA domain containing 1	NP_115508.2	Gonadogenesis, gametogenesis, meiosis, fertility (male?)
Ovary-C	1	3	7	7	LOC100488112		NP_001032302.1	
Ovary-C	1	4	10	5	LOC100498554			
Ovary-C	2	4	9	6	fbxo47	F-box protein 47	NP_001008777.2	Cancer-related
Ovary-C	1	7	9	6	LOC100491502			
Ovary-C	1	7	15	6				
Ovary-C	1	5	11	7	LOC100494809 (tex11)	testis expressed 11	NP_001003811.1	Gonadogenesis, gametogenesis, meiosis, fertility (male?)
Ovary-C	2	4	12	6				
Ovary-C	1	4	11	7	LOC100494809			
Ovary-C	2	4	11	7	hfm1	HFM1, ATP-dependent DNA helicase homolog (S. cerevisiae)	NP_001017975.3	Cancer-related
Ovary-C	1	3	4	6	rflb			
Ovary-C	1	2	9	5	LOC100170619 (c12orf40)	chromosome 12 open reading frame 40	NP_001026918.2	
Ovary-C	1	2	8	5	LOC100496417			
Ovary-C	1	2	7	6				
Ovary-C	2	4	7	6	LOC100491026 (c1orf177)	chromosome 1 open reading frame 177	NP_689820.2	
Ovary-C	2	3	7	6	LOC100127812 (fam47e)	family with sequence similarity 47, member E	NP_001130042.1	
Ovary-C	1	4	12	7	LOC100486762			
Ovary-C	1	3	9	9	LOC100488153 (cga)	glycoprotein hormones, alpha polypeptide	NP_000726.1	Gonadogenesis, morphology of ovary, quantity of hormone, fertility
Ovary-C	1	2	10	7	(ccdc170)	coiled-coil domain containing 170	NP_079335.2	Cancer-related
Ovary-C	1	3	9	7				
Ovary-C	1	6	17	9	LOC100489156			
Ovary-C	1	6	23	10	tmprss12	transmembrane (C-terminal) protease, serine 12	NP_872365.1	Cancer-related
Ovary-C	1	4	25	12				
Ovary-C	2	4	13	12	mamdc2	MAM domain containing 2	NP_694999.3	
Ovary-C	1	3	17	9	LOC100491771 (ccdc152)	coiled-coil domain containing 152	NP_001128320.1	
Ovary-C	1	3	16	9	LOC100485050 (syce1)	synaptonemal complex central element protein 1	NP_570140.1	
Ovary-C	1	4	15	8	msh5	mutS homolog 5 (E. coli)	NP_751898.1	Gonadogenesis, gametogenesis, meiosis, fertility
Ovary-C	1	4	9	11	tbpl2 (tbp)	TATA box binding protein	NP_003185.1	Transcription, embryonic development
Ovary-C	1	3	13	8	brdt	bromodomain, testis-specific	NP_001717.2	Gonadogenesis, chromatin remodeling (male?)
Ovary-C	1	3	16	8				
Ovary-C	3	11	18	18	LOC100487171			
Ovary-C	1	14	29	6	LOC100489965 (hormad1)	HORMA domain containing 1	NP_115508.2	Gonadogenesis, gametogenesis, meiosis, fertility (male?)
Ovary-C	1	6	28	10				
Ovary-C	1	5	12	10			XP_002347599.1	
Ovary-C	1	8	15	10	LOC100485446		XP_002342056.1	
Ovary-C	1	5	28	18	LOC100487907			
Ovary-C	1	7	30	26	LOC100488683 (zglp1)	zinc finger, GATA-like protein 1	NP_001096637.1	Gonadogenesis, gametogenesis, oogenesis, ovary development
Ovary-C	1	5	29	57	LOC100488624 (spdya)	speedy homolog A (Xenopus laevis)	NP_001008779.1	Oocyte maturation
Ovary-C	1	4	25	57	npy	neuropeptide Y	NP_000896.1	Vascularization, secretion of hormone, fertility
Ovary-C	1	1	65	47	brdt (brd3)	bromodomain containing 3	NP_031397.1	
Ovary-C	1	2	13	16	mapk13	mitogen-activated protein kinase 13	NP_002745.1	Cancer-related, cell proliferation
Ovary-C	1	1	12	16				
Ovary-C	1	2	17	34	tmed6	transmembrane emp24 protein transport domain containing 6	NP_653277.2	
Ovary-C	1	1	14	40	(iws1)	IWS1 homolog (S. cerevisiae)	NP_060439.2	Cancer-related

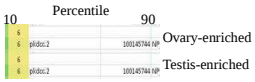

Cluster	NF58	NF66	1WPM	2WPM	Gene Symbol	Entrez Gene Name	Human Accession	Mammalian Function
Testis-A	222	302	314	289	rflcii	insulin-like 3 (Leydig cell)	NM_001265587.1	Testis development, fertility
Testis-A	8	12	27	161	LOC100492493 (bmp1)	bone morphogenetic protein 1	NP_001190.1	Collagen development, protein synthesis
Testis-A	19	38	107	930	LOC100492493 (bmp1)	bone morphogenetic protein 2	NP_001190.1	Collagen development, protein synthesis
Testis-A	37	98	110	151	fgfbp3///LOC100495029	fibroblast growth factor binding protein 3	NP_689642.3	Growth factor regulation, angiogenesis
Testis-A	26	59	68	186	LOC100492324 (astl)	astacin-like metallo-endopeptidase (M12 family)	NP_001002036.3	Protein synthesis, fertility
Testis-A	17	88	97	98	myl4	myosin, light chain 4, alkali; atrial, embryonic	NP_002467.1	Vascular development, muscle contraction
Testis-A	70	36	53	47	nptx1	neuronal pentraxin I	NP_002513.2	Angiogenesis, cellular movement, nervous system development
Testis-A	17	17	22	19	slitrk4	SLIT and NTRK-like family, member 4	NP_775101.1	Formation of cellular protrusions, nervous system development
Testis-A	22	25	21	21	(rad50)	RAD50 homolog (S. cerevisiae)	NP_005723.2	DNA repair
Testis-A	26	30	41	65	LOC100497586 (opa1)	optic atrophy 1 (autosomal dominant)	NP_570844.1	Mitochondrial organization, synthesis of pregnenolone
Testis-A	16	24	25	36	LOC100496012 (htr2c)	5-hydroxytryptamine (serotonin) receptor 2C, G protein-coupled	NP_000859.1	Cell-to-cell signaling and interaction
Testis-A	19	14	12	20	LOC100485458 (clec4m)	C-type lectin domain family 4, member M	NP_001138378.1	Cell-to-cell signaling and interaction
Testis-A	22	18	21	21	cryba4	crystallin, beta A4	NP_001877.1	
Testis-A	17	5	12	19	aqp1	aquaporin 1 (Colton blood group)	NP_932766.1	Vascular development, permeability of blood vessel, molecular transport
Testis-A	12	12	16	19	gpc1	glypican 1	NP_002072.2	Vascular development, cellular movement
Testis-A	13	11	17	22	gpc1	glypican 2	NP_002072.2	Vascular development, cellular movement
Testis-A	9	12	12	23	acta2	actin, alpha 2, smooth muscle, aorta	NP_001135417.1	Vascular development, muscle contraction
Testis-B	13	9	10	11	rarres1	retinoic acid receptor responder (tazarotene induced) 1	NP_996846.1	Cellular movement
Testis-B	6	5	7	7	tpst2	tyrosylprotein sulfotransferase 2	NP_003586.3	Cellular movement, fertility
Testis-B	6	6	6	7	akr1cl1///LOC100490783	aldo-keto reductase family 1, member C3	NP_003730.4	Steroidogenesis
Testis-B	6	6	7	8	akr1cl1	aldo-keto reductase family 1, member C4	NP_003730.4	Steroidogenesis
Testis-B	8	6	8	6	adcyap1r1	adenylate cyclase activating polypeptide 1 (pituitary) receptor type I	NP_001109.2	Cellular proliferation, concentration of hormone, fertility
Testis-B	10	7	9	10	LOC100490204 (cadm3)	cell adhesion molecule 3	NP_001120645.1	
Testis-B	11	8	9	11	cyp17a1	cytochrome P450, family 17, subfamily A, polypeptide 1	NP_000093.1	Steroidogenesis, fertility, sex determination
Testis-B	7	9	13	11	osr2	odd-skipped related 2 (Drosophila)	NP_001135934.1	Cellular proliferation, growth
Testis-B	8	7	7	7	kcnf1	potassium voltage-gated channel, subfamily F, member 1	NP_002227.2	
Testis-B	15	23	10	8	acbd7	acyl-CoA binding domain containing 7	NP_001034933.1	
Testis-B	6	10	12	22	tpm2	tropomyosin 2 (beta)	NP_003280.2	Vascular development, muscle contraction
Testis-B	6	12	15	15	LOC100485176 (nkx3-1)	NK3 homeobox 1	NP_006158.2	Morphogenesis of testis
Testis-B	6	12	16	16	LOC100485176 (nkx3-1)	NK3 homeobox 2	NP_006158.3	Morphogenesis of testis
Testis-B	5	8	11	16	srd5a2	steroid-5-alpha-reductase, alpha polypeptide 2 (3-oxo-5 alpha-steroid delta 4-dehydrogenase alpha 2)	NP_000339.2	Steroidogenesis, fertility, sex determination, morphology of testis
Testis-B	4	10	12	14	LOC100485176 (nkx3-1)	NK3 homeobox 1	NP_006158.2	Morphogenesis of testis
Testis-B	3	3	3	6	inha	inhibin, alpha	NP_002182.1	Morphology of testis, fertility, steroidogenesis, sex determination
Testis-B	3	5	7	7	(gas6)	growth arrest-specific 6	NP_001137417.1	Vascular development, cellular movement
Testis-B	3	6	6	9	cnn2 (cnn1)	calponin 1, basic, smo	NP_001290.2	Vascular development, cellular movement, morphology of testis
Testis-B	2	3	4	8	cxadr	coxsackie virus and adenovirus receptor	NP_001329.1	Vascular development, cellular movement
Testis-B	3	4	4	6	(dhh)	desert hedgehog	NP_066382.1	Gonadogenesis, morphology of testis, sex determination, steroid synthesis
Testis-B	4	3	5	10	dkk3	dickkopf 3 homolog (Xenopus laevis)	NP_056965.3	Steroid hormone synthesis, cellular movement, cellular organization
Testis-B	3	4	5	7	fam123a (amer2)	APC membrane recruitment protein 2	NP_689917.2	
Testis-B	2	2	3	6	cadm2	cell adhesion molecule	NP_001161146.1	
Testis-B	2	2	4	10	inhba	inhibin, beta A	NP_002183.1	Morphology of testis, fertility, steroidogenesis, cellular movement
Testis-B	6	7	8	17	fbln5	fibulin 5	NP_006320.2	Vascular development, cellular movement
Testis-B	6	5	9	11	mpz	myelin protein zero	NP_000521.2	Nervous system development, cellular movement
Testis-B	5	8	10	8	(stx3)	syntaxin 3	NP_004168.1	Cellular organization of cytoskeleton, microtubule dynamics
Testis-B	5	6	7	14	dclk2 (dclk1)	doublecortin-like kinase 1	NP_004725.1	Cellular organization of cytoskeleton, microtubule dynamics
Testis-B	5	6	8	14	fmo5	flavin containing monooxygenase 5	NP_001452.2	
Testis-B	5	7	10	15	fmo5	flavin containing monooxygenase 5	NP_001452.2	
Testis-B	2	8	11	17	fstl5 (eif4g3)	eukaryotic translation initiation factor 4 gamma, 3	NP_003751.2	Cellular organization of cytoskeleton, microtubule dynamics
Testis-B	3	2	2	8	hba-l2 (hbz)	hemoglobin, zeta	NP_005323.1	Morphology of vascular system
Testis-B	1	2	4	24	fabp7	fatty acid binding protein 7, brain	NP_001437.1	Cellular proliferation, cellular movement
Testis-B	1	2	2	5	nlk	nemo-like kinase	NP_057315.3	Morphology of vascular system
Testis-B	1	1	3	6	slco2a1	solute carrier organic anion transporter family, member 2A1	NP_005621.2	Morphology of vascular system, molecular transport
Testis-B	1	1	2	7	crip2	cysteine-rich protein 2	NP_001303.1	Cellular proliferation, cellular differentiation
Testis-B	1	2	2	5	col9a1	collagen, type IX, alpha 1	NP_511040.2	Connective tissue development
Testis-B	1	3	5	7	MGC107853 (slc29a1)	solute carrier family 29 (nucleoside transporters), member 1	NP_001071642.1	Cellular proliferation

Testis-B	2	3	4	6	des.1	desmin	NP_001918.3	Morphology of vascular system
Testis-B	3	5	6	8	fhl5///LOC100485255 (fhl2)	four and a half LIM domains 2	NP_963849.1	Angiogenesis, cellular movement, muscle cell development
Testis-B	3	4	6	7	rgs2	regulator of G-protein signaling 2, 24kDa	NP_002914.1	Vascular development, development of muscle
Testis-B	3	3	4	6	cfl2	cofilin 2 (muscle)	NP_068733.1	
Testis-B	3	3	6	9	(gabra2)	gamma-aminobutyric acid (GABA) A receptor, alpha 2	NP_000798.2	
Testis-B	2	3	5	8	kitlg	KIT ligand	NP_000890.1	Gonadogenesis, development of testis, steroid synthesis
Testis-B	1	2	4	7	cyp26b1	cytochrome P450, family 26, subfamily B, polypeptide 1	NP_063938.1	Gonadogenesis, morphology of testis
Testis-B	1	3	3	5	itga2b.1	integrin, alpha 2b (platelet glycoprotein IIb of IIb/IIIa complex, antigen CD41)	NP_000410.2	Morphology of vascular system, cellular movement
Testis-B	2	3	4	5	klhl31	kelch-like family member 31	NP_001003760.2	
Testis-B	1	3	4	5	(col13a1) LOC100488115///LOC	collagen, type XIII, alpha 1	NP_542988.3	Vasculogenesis, angiogenesis
Testis-B	10	6	5	10	akr1c2 (akr1c3)	aldo-keto reductase family 1, member C3	NP_003730.4	Steroid synthesis and metabolism
Testis-B	11	6	7	6	enpp2	ectonucleotide pyrophosphatase/phosphodiesterase 2	NP_001035181.1	Vasculogenesis, cellular movement
Testis-B	8	4	4	5	psph	phosphoserine phosphatase	NP_004568.2	
Testis-B	5	5	5	5	tmem26	transmembrane protein 26	NP_848600.2	
Testis-B	3	4	5	5	fgf10	fibroblast growth factor 10	NP_004456.1	Gonadogenesis, morphology of testis
Testis-B	4	4	3	5	sema3b	sema domain, immunoglobulin domain (Ig), short basic domain, secreted, (semaphorin) 3B	NP_004627.1	Vasculogenesis, cellular movement, cell signalling
Testis-B	4	3	4	8	(enpp6)	ectonucleotide pyrophosphatase/phosphodiesterase 6	NP_699174.1	Hydrolysis
Testis-B	3	5	6	9	LOC100037917 (col8a1)	collagen, type VIII, alpha 1	NP_001841.2	Vasculogenesis, angiogenesis
Testis-B	4	6	9	6	LOC100487043 (nr0b1/dax-1)	nuclear receptor subfamily 0, group B, member 1	NP_000466.2	Gonadogenesis, morphology of testis, sex determination, fertility
Testis-B	2	3	4	7	LOC100486154 (il17rc)	interleukin 17 receptor C	NP_116121.2	
Testis-B	2	2	3	5	gpr146	G protein-coupled receptor 146	NP_612454.1	
Testis-B	3	4	4	6	snai1 (snai2)	snail homolog 2 (Drosophila)	NP_003059.1	Gonadogenesis, morphology of testis, cell movement
Testis-B	3	3	3	6	pkdcc.2	protein kinase domain containing, cytoplasmic	NP_612379.2	Connective tissue development
Testis-B	2	2	3	6	tgm2	transglutaminase 2 (C polypeptide, protein	NP_004604.2	Vasculogenesis, angiogenesis, concentration of hormone
Testis-B	3	3	4	5	kcnj8	potassium inwardly-rectifying channel, subfamily J, member 8	NP_004973.1	Vascular development
Testis-B	10	12	16	9	LOC100498168 (litaf)	lipopolysaccharide-induced TNF factor	NP_001129944.1	Cellular movement
Testis-B	3	3	5	6	LOC100490639 (myh11)	myosin, heavy chain 11, smooth muscle	NP_074035.1	Vascular development, muscle contraction
Testis-B	4	3	5	7	(marco)	macrophage receptor with collagenous structure	NP_006761.1	Cellular organization of cytoskeleton, microtubule dynamics
Testis-B	6	3	5	10	kazald1	Kazal-type serine peptidase inhibitor domain 1	NP_112191.2	
Ovary-A	1	1	1	9	cldn4	claudin 4	NP_001296.1	Cell proliferation, cellular movement
Ovary-A	2	1	1	6	agr2	anterior gradient 2 homolog (Xenopus laevis)	NP_006399.1	Cell proliferation, cellular movement
Ovary-A	1	1	1	5	hebp2	heme binding protein 2	NP_055135.1	
Ovary-A	1	1	1	5	upk1b	uroplakin 1B	NP_008883.2	
Ovary-A	1	1	5	12	LOC100491528 (mfap4)	microfibrillar-associated protein 4	NP_002395.1	
Ovary-A	1	1	4	6	ramp1	receptor (G protein-coupled) activity modifying protein 1	NP_005846.1	
Ovary-A	1	1	4	16	tspan1	tetraspanin 1	NP_005718.2	
Ovary-A	1	1	6	8	wdr72	WD repeat domain 72	NP_877435.2	Cell death and survival
Ovary-A	1	1	5	13	tmem171	transmembrane protein 171	NP_775761.4	
Ovary-A	1	1	1	6	LOC100485955 (cel)	carboxyl ester lipase	NP_001798.2	Lipid metabolism
Ovary-A	1	1	2	6	(zp4) LOC100496111///zpax	zona pellucida glycoprotein 4	NP_067009.1	Cell proliferation, cell signaling, activation of protein kinase
Ovary-A	2	1	3	6	tmem51	transmembrane protein 51	NP_001129688.1	
Ovary-A	1	1	3	6	chrna5	cholinergic receptor, nicotinic, alpha 5 (neuronal)	NP_000736.2	Cell signaling, nervous system development
Ovary-A	1	1	2	5	cntd2	cyclin N-terminal domain containing 2	NP_001137501.1	
Ovary-A	1	1	2	5	grasp	GRP1 (general receptor for phosphoinositides 1)-associated scaffold protein	NP_859062.1	Cell proliferation, localization, sprouting of mossy fibers
Ovary-A	1	1	3	10	gpnmb	glycoprotein (transmembrane) nmb	NP_001005340.1	Cell proliferation
Ovary-A	2	2	2	6	tmem184a	transmembrane protein 184A	NP_001091089.1	Protein localization
Ovary-A	2	2	3	5	lgals3	lectin, galactoside-binding, soluble, 3	NP_002297.2	Cell proliferation, expansion of mesangium
Ovary-A	1	2	3	8	esrp1	epithelial splicing regulatory protein 1	NP_060167.2	
Ovary-A	2	2	4	8	LOC100487559 (oca2)	oculocutaneous albinism II	NP_000266.2	Reproductive system development, gametogenesis
Ovary-A	2	4	3	7	armc4	armadillo repeat containing 4	NP_060546.2	
Ovary-A	3	3	2	6	ccnb2	cyclin B2	NP_004692.1	Cell proliferation, fecundity
Ovary-A	1	2	2	5	fam46c	family with sequence similarity 46, member C	NP_060179.2	
Ovary-A	1	2	3	8	elovl7	ELOVL fatty acid elongase 7	NP_079206.2	Cell proliferation, synthesis of hormone
Ovary-A	1	2	3	12	vegt	T-box protein VegT	NP_542449.1	Oogenesis, germ layer specification of embryo
Ovary-A	1	1	2	15	eif4e	eukaryotic translation initiation factor 4E	NP_001959.1	Cell proliferation, cell death and survival, RNA trafficking
Ovary-A	1	1	2	8	rhebl1	Ras homolog enriched in brain like 1	NP_653194.1	Regulation of cell growth and proliferation
Ovary-A	2	1	2	9	sall4	sal-like 4 (Drosophila)	NP_065169.1	Cell proliferation, growth
Ovary-A	1	1	1	8	pnpla3	patatin-like phospholipase domain containing 2	NP_065109.1	Lipid metabolism
Ovary-A	1	1	1	7	proca1	protein interacting with cyclin A1	NP_056530.2	Lipid metabolism
Ovary-A	1	1	1	8	proca1	protein interacting with cyclin A2	NP_056530.2	Lipid metabolism
Ovary-A	1	1	1	6	LOC734032 (zar1l)	zygote arrest 1-like	NP_001130043.1	Oogenesis, RNA regulation
Ovary-A	1	1	2	7	sptssb	serine palmitoyltransferase, small subunit B	NP_001035189.1	
Ovary-A	1	1	2	7	ppp1r3c.2	protein phosphatase 1, regulatory subunit 3C	NP_005389.1	Insulin regulation, glycogen homeostasis
Ovary-A	1	1	2	7	ppp1r3c.2	protein phosphatase 1, regulatory subunit 3C	NP_005389.1	Insulin regulation, glycogen homeostasis
Ovary-A	1	1	1	6	LOC100127750 (cox4i1)	cytochrome c oxidase subunit IV isoform 1	NP_001852.1	Cell cycle progression

Ovary-A	1	1	1	5	(gstp1)	glutathione S-transferase pi 1	NP_000843.1	Cell proliferation, conversion of beta-estradiol
Ovary-A	1	1	1	5	patl2 (patl1)	protein associated with topoisomerase II homolog 1 (yeast)	NP_689929.2	
Ovary-A	1	1	1	5	foxh1	forkhead box H1	NP_003914.1	Embryonic development, patterning
Ovary-A	1	1	1	5	mcm6	minichromosome maintenance complex component 6	NP_005906.2	Confirmational DNA modification
Ovary-A	1	1	1	6	LOC100498579 (apba2)	amyloid beta (A4) precursor protein-binding, family A, member 2	NP_001123886.1	Exocytosis of vesicles
Ovary-A	1	1	1	6	LOC100490651 (rhcg)	Rh family, C glycoprotein	NP_057405.1	Morphology of gonad, molecular transport
Ovary-A	1	1	1	6	(ctdspl2)	CTD (carboxy-terminal domain, RNA polymerase II, polypeptide A) small phosphatase like 2	NP_057480.2	Phosphatase activity
Ovary-A	1	1	1	7	LOC733553 (casp7)	caspase 7, apoptosis-related cysteine peptidase	NP_203125.1	Cell death and survival, tissue morphology
Ovary-A	1	1	1	6	zic2	Zic family member 2	NP_009060.2	Nervous system development
Ovary-A	1	1	1	6	map1lc3c	microtubule-associated protein 1 light chain 3 gamma	NP_001004343.1	
Ovary-A	1	1	1	9	sptssb	serine palmitoyltransferase, small subunit B	NP_001035189.1	
Ovary-A	1	1	1	8	rhebl1	Ras homolog enriched in brain like 1	NP_653194.1	Regulation of cell growth and proliferation
Ovary-A	1	1	1	7	(itln2) LOC100492053///LOC39	intelectin 2	NP_543154.1	
Ovary-A	1	1	1	9	comt.2 (comt)	catechol-O-methyltransferase	NP_009294.1	Reproductive system development, metabolism, regulation of neurotransmitter
Ovary-A	1	1	1	7	caprin2	caprin family member 2	NP_001002259.1	Cell proliferation, transcription
Ovary-A	1	1	1	7	btbd17	BTB (POZ) domain containing 17	NP_001073935.1	
Ovary-A	1	1	1	8	parp12	poly (ADP-ribose) polymerase family, member 12	NP_073587.1	
Ovary-A	1	0	0	11	tmprss4	transmembrane protease, serine 4	NP_001167022.1	
Ovary-A	1	1	1	18	42Sp50 (eef1a2)	eukaryotic translation elongation factor 1 alpha 2	NP_001949.1	Oocyte vegetal mRNA transport (FEBS J. 2010 Nov;277(22):4722-31. doi: 10.1111/j.1742-4658.2010.07878.x. Epub 2010 Oct 6.)
Ovary-A	1	1	2	22	LOC100036665 (ssx2ip)	synovial sarcoma, X breakpoint 2 interacting protein	NP_001159766.1	Cell proliferation
Ovary-A	1	1	2	17	slmo1	slowmo homolog 1 (Drosophila)	NP_001135877.1	
Ovary-A	1	1	2	9	caprin2	caprin family member 2	NP_001002259.1	Cell proliferation, transcription
Ovary-A	1	1	1	13	LOC100485893 (bmp15)	bone morphogenetic protein 15	NP_005439.2	Reproductive system development, gametogenesis, fertility
Ovary-A	1	1	1	12	sox3	SRY (sex determining region Y)-box 2	NP_003097.1	Reproductive system development, cell proliferation
Ovary-A	1	1	1	11	LOC549413///xk81a1 (krt12)	keratin 12	NP_000214.1	Disruption of keratin filaments
Ovary-A	1	1	1	12	h1foo	H1 histone family, member O, oocyte-specific	NP_722575.1	Oocyte-specific maternal mRNA
Ovary-A	1	1	1	14	aldh3b1	aldehyde dehydrogenase 3 family, member B1	NP_001154945.1	
Ovary-A	1	1	1	14	LOC100170463 (gja4)	gap junction protein, alpha 4, 37kDa	NP_002051.2	Reproductive system development, gametogenesis, fertility
Ovary-A	1	1	1	15	LOC549413 (has1)	hyaluronan synthase 1	NP_001514.2	Cell proliferation, cellular movement
Ovary-A	1	1	1	250	LOC733731 (btg3)	BTG family, member 3	NP_006797.3	Cell cycle progression, cell proliferation, transcription
Ovary-A	1	1	1	495	zfp36l2.2	ZFP36 ring finger protein-like 2	NP_008818.3	Cell proliferation, mRNA stabilization, transcription
Ovary-A	1	1	2	91	cldn6.1	claudin 6	NP_067018.2	Cell proliferation, differentiation
Ovary-A	1	1	1	120	LOC394444 (zp3)	zona pellucida glycoprotein 3 (sperm receptor)	NP_009086.4	Oocyte development, gametogenesis, fertility
Ovary-A	1	1	1	167	LOC100488960 (mt1f)	metallothionein 1F	NP_005940.1	Cell death and survival
Ovary-A	1	1	1	48	(spire1)	spire homolog 1 (Drosophila)	NP_001122098.1	
Ovary-A	1	1	1	49	LOC100489197 (heatr5b)	HEAT repeat containing 5B	NP_061897.1	
Ovary-A	1	1	1	40	LOC548809 (prss33)	protease, serine, 33	NP_690851.2	
Ovary-A	1	1	1	41	wee2	WEE1 homolog 2 (S. pombe)	NP_001099028.1	Cell cycle, meiosis I, prophase I
Ovary-A	1	1	1	36	zfp36l2.1	ZFP36 ring finger protein	NP_003398.1	Cell proliferation, mRNA stabilization, transcription
Ovary-A	1	1	1	36	zp4	zona pellucida glycoprotein 4	NP_067009.1	Oocyte-specific, cell signaling, activation of protein kinase
Ovary-A	1	1	1	33	LOC100486817 (zar1l)	zygote arrest 1-like	NP_001130043.1	Oocyte-specific maternal mRNA, RNA regulation embryogenesis
Ovary-A	1	1	1	31	foxi2	forkhead box I2	NP_997309.2	Oocyte maternal mRNA activator of embryonic development, Cha S-W, McAdams M, Kormish J, Wylie C, Kofron M (2012) Foxi2 Is an Animally Localized Maternal mRNA in Xenopus, and an Activator of the Zygotic Ectoderm Activator Foxi1e. PLoS ONE 7(7): e41782. doi:10.1371/journal.pone.0041782
Ovary-A	1	1	1	32	nanos1			Oocyte maternal mRNA regulation of embryonic development
Ovary-A	1	1	1	30	zp4.2	zona pellucida glycoprotein 4	NP_067009.1	Oocyte-specific, cell signaling, activation of protein kinase
Ovary-A	1	1	2	29	LOC549413 (mad1l1)	MAD1 mitotic arrest deficient-like 1 (yeast)	NP_003541.2	Cell cycle progression, cell proliferation, transcription
Ovary-A	1	1	2	28	btg4	B-cell translocation gene 4	NP_060059.1	Cell cycle progression, cell proliferation, mitosis
Ovary-A	1	1	1	18	(znf80)	zinc finger protein 80	NP_009067.2	
Ovary-A	1	1	1	25	zar1	zygote arrest 1	NP_783318.1	Oocyte-specific maternal mRNA, embryogenesis
Ovary-A	1	1	2	63	(tuba1b) LOC100487709///tuba	tubulin, alpha 1b	NP_006073.2	
Ovary-A	1	1	3	101	mkrn3 (mkrn2)	makorin ring finger protein 2	NP_054879.3	
Ovary-A	1	1	2	36	mkrn3 (mkrn2)	makorin ring finger protein 2	NP_054879.3	
Ovary-A	1	1	2	50	cfc1 (tdgf1)	teratocarcinoma-derived growth factor 1	NP_001167607.1	Embryonic development, mesoderm development
Ovary-A	1	1	1	45	ccnb1	cyclin B1	NP_114172.1	Cell cycle progression, mitosis
Ovary-A	1	1	2	42	cdca7	cell division cycle associated 7	NP_071370.2	Regulation of cell proliferation and transcription
Ovary-A	1	1	2	34	LOC394448 (ccnb2)	cyclin B2	NP_004692.1	Cell proliferation, fecundity
Ovary-A	1	2	3	71	ccna1	cyclin A1	NP_001104516.1	Gametogenesis, cell cycle progression
Ovary-A	1	1	1	56	(h2afx) hist1h2aa///hist1h2am	H2A histone family, member X	NP_002096.1	Gametogenesis, meiosis, DNA repair
Ovary-A	1	1	2	85	42Sp43 (gtf3a)	general transcription factor IIIA	NP_002088.2	Confirmational DNA modification, transcription
Ovary-B	21	61	43	64	ntn1	netrin 1	NP_004813.2	Nervous system development, cellular movement
Ovary-B	3	6	8	6	tyrp1	tyrosinase-related protein 1	NP_000541.1	

Ovary-B	5	4	5	5	chst8	carbohydrate (N-acetylgalactosamine 4-0) s	NP_001121367.1	Morphology of gonad, concentration of hormone
Ovary-B	4	7	6	6	olfml2a	olfactomedin-like 2A	NP_872293.2	Endometrial cell proliferation
Ovary-B	5	7	9	6	emx2	empty spiracles homeobox 2	NP_004089.1	Morphology of gonad, primary sex determination
Ovary-B	7	7	7	6	lum	lumican	NP_002336.1	Cell proliferation, morphology, fertility
Ovary-B	6	7	6	5	lum	lumican	NP_002336.1	Cell proliferation, morphology, fertility
Ovary-B	7	11	13	7	chrnd	cholinergic receptor, nicotinic, delta (muscle)	NP_000742.1	Muscle growth
Ovary-B	8	22	15	27	cyp26a1	cytochrome P450, family 26, subfamily A, polypeptide 1	NP_000774.2	Organ development, morphology, metabolism
Ovary-B	8	13	17	17	fibcd1	fibrinogen C domain containing 1	NP_001138578.1	
Ovary-B	6	5	5	6	amdhd1	amidohydrolase domain containing 1	NP_689648.2	
Ovary-B	5	8	5	6	cyp19a1	cytochrome P450, family 19, subfamily A, polypeptide 1	NP_000094.2	Morphology of gonad, primary sex determination
Ovary-B	5	13	12	14	hal.2	histidine ammonia-lyase	NP_002099.1	Amino acid metabolism
Ovary-B	7	12	8	11	cyp19a1	cytochrome P450, family 19, subfamily A, polypeptide 1	NP_000094.2	Morphology of gonad, primary sex determination
Ovary-B	6	13	9	8	kal1	Kallmann syndrome 1 sequence	NP_000207.2	Guidance of axons, cell movement, gonad development
Ovary-B	5	5	11	21	nppc	natriuretic peptide C	NP_077720.1	Reproductive system development, cell signaling, cell proliferation
Ovary-B	3	3	3	12	LOC100488479 (kiaa1324)	KIAA1324	NP_065826.2	
Ovary-B	2	3	6	20	esrp1	epithelial splicing regulatory protein 1	NP_060167.2	Ovarian cell proliferation, RNA splicing
Ovary-B	2	4	5	15	esrp2	epithelial splicing regulatory protein 2	NP_060167.2	Ovarian cell proliferation, RNA splicing
Ovary-B	2	5	5	6	fam189a1	family with sequence similarity 189, member A1	NP_056122.1	
Ovary-B	2	1	4	5	ggt1	gamma-glutamyltransferase 1	NP_005256.2	Morphology of gonad, fertility, cell proliferation
Ovary-B	3	3	5	11	LOC100493413 (cldn6)	claudin 6	NP_067018.2	Cell proliferation, differentiation
Ovary-B	3	3	5	11	LOC100493413 (cldn6)	claudin 6	NP_067018.2	Cell proliferation, differentiation
Ovary-B	3	3	3	5	msc	musculin	NP_005089.2	Muscle development
Ovary-B	2	4	4	5	irx5	iroquois homeobox 5	NP_005844.4	Organ development, morphology, nervous system development
Ovary-B	2	5	5	6	LOC100489060 (a2m)	alpha-2-macroglobulin	NP_000005.2	Nervous system development, cellular movement
Ovary-B	3	6	5	7	irx3	iroquois homeobox 3	NP_077312.2	Organ development, nervous system development
Ovary-B	3	4	4	8	epcam (tacstd2)	tumor-associated calcium signal transducer	NP_002344.2	Ovarian cell proliferation, cellular movement
Ovary-B	4	5	5	10	cldn7	claudin 7	NP_001298.3	Ovarian cell proliferation, quantity of steroid hormone
Ovary-C	1	1	5	14	lhx8	LIM homeobox 8	NP_001001933.1	Gonadogenesis, ovary development, nervous system development
Ovary-C	1	1	4	13	otud4		NP_001093392.1	Cancer-related
Ovary-C	2	2	7	14	mycl1	v-myc myelocytomatosis viral oncogene homolog 1, lung carcinoma derived (avian)	NP_001028253.1	Cancer-related
Ovary-C	2	2	7	14	mycl1	v-myc myelocytomatosis viral oncogene homolog 1, lung carcinoma derived (avian)	NP_001028253.1	Cancer-related
Ovary-C	2	3	9	27	figla	folliculogenesis specific basic helix-loop-helix	NP_001004311.2	Gonadogenesis, ovary development, meiosis of germ cells, fertility
Ovary-C	1	2	5	21	npm2	nucleophosmin/nucleoplasmin 2	NP_877724.1	Morphology of ovary, morphology of oocytes, fertility
Ovary-C	2	3	3	12	(tuba1a) LOC100487867///MG	tubulin, alpha 1a	NP_006000.2	Nervous system development, microtubule dynamics
Ovary-C	2	3	4	18	(tuba1a) LOC100487709///LOC	tubulin, alpha 1a	NP_006000.2	Nervous system development, microtubule dynamics
Ovary-C	1	4	12	8	LOC100488825 (ccdc170)	coiled-coil domain containing 170	NP_079335.2	Cancer-related
Ovary-C	1	4	10	7	LOC100496920///zg16	zymogen granule protein 16	NP_689551.1	Cancer-related
Ovary-C	1	2	9	6	fbxo47	F-box protein 47	NP_001008777.2	Cancer-related
Ovary-C	1	3	9	5	LOC100493022 (tldc2)	TBC/LysM-associated domain containing 2	NP_542195.1	
Ovary-C	1	1	6	7	(stk35)	serine/threonine kinase 35	NP_543026.1	Cancer-related, organization of actin stress fibers
Ovary-C	1	1	5	8	c17orf39 (gid4)	GID complex subunit 4, VID24 homolog (S. cerevisiae)	NP_076957.3	
Ovary-C	1	2	7	7	brdt	bromodomain, testis-specific	NP_001717.2	Gonadogenesis, chromatin remodeling (male?)
Ovary-C	1	2	6	8	LOC100489839 (frrs1)	ferric-chelate reductase 1	NP_001013682.2	
Ovary-C	2	2	6	6	sass6	spindle assembly 6 homolog (C. elegans)	NP_919268.1	DNA replication
Ovary-C	2	4	6	5	c20orf3 (apmap)	adipocyte plasma membrane associated protein	NP_065392.1	Cancer-related
Ovary-C	1	5	5	5	sel1l3	sel-1 suppressor of lin-12-like 3 (C. elegans)	NP_056002.2	Cancer-related
Ovary-C	3	6	6	5	gtsf1	gametocyte specific factor 1	NP_653195.2	Germ cell development
Ovary-C	2	5	7	5	tdrd5	tudor domain containing 5	NP_775804.2	Gonadogenesis, gametogenesis, meiosis, fertility (male?)
Ovary-C	2	2	6	8	LOC100486129 (asrgl1)	asparaginase like 1	NP_079356.3	Cancer-related
Ovary-C	2	3	5	5	stk35 (pdik1l)	PDLIM1 interacting kinase 1 like	NP_690048.1	Organization of actin stress fibers
Ovary-C	2	2	4	5	reep6 (reep5)	receptor accessory protein 5	NP_005660.4	
Ovary-C	2	1	3	5	baf-l (banf1)	barrier to autointegration factor 1	NP_001137457.1	DNA recombination
Ovary-C	1	2	5	5	LOC100491097 (ggh)	gamma-glutamyl hydrolase (conjugase, folylpolygammaglutamyl hydrolase)	NP_003869.1	Amino acid metabolism
Ovary-C	3	3	4	5	gtf2a1l///ston1	general transcription factor IIA, 1-like	NP_006863.2	
Ovary-C	3	3	4	6	elavl2	ELAV (embryonic lethal, abnormal vision, Drosophila)-like 2 (Hu antigen B)	NP_001164666.1	Cancer-related
Ovary-C	3	3	4	5	LOC100487055 (rpl17)	ribosomal protein L17	NP_000976.1	Cancer-related
Ovary-C	2	2	3	5	pabpc1l	poly(A) binding protein, cytoplasmic 1-like	NP_001118228.1	Gonadogenesis, gametogenesis, oogenesis, meiosis, fertility
Ovary-C	2	2	4	5	pof1b	premature ovarian failure, 1B	NP_079197.3	Cancer-related, premature ovarian failure
Ovary-C	1	2	4	5	LOC100485001 (akap13)	A kinase (PRKA) anchor protein 13	NP_009131.2	Cancer-related, decondensation of chromatin
Ovary-C	1	2	4	5	(nkiras2)	NFKB inhibitor interacting Ras-like 2	NP_001138400.1	Cancer-related
Ovary-C	1	2	4	5	tesc	tescalcin	NP_060369.3	Neurological disease, Na+ homeostasis
Ovary-C	2	5	3	7	LOC733728 (rplp0)	ribosomal protein, large, P0	NP_444505.1	Cancer-related
Ovary-C	2	13	27	9	(dmc1)	DMC1 dosage suppressor of mck1 homolog, meiosis-specific homologous recombination (yeast)	NP_008999.2	Gonadogenesis, gametogenesis, oogenesis, meiosis, fertility
Ovary-C	1	7	19	11	LOC100486907 (syce2)	synaptonemal complex central element protein 2	NP_001099048.1	DNA recombination, synapsis
Ovary-C	1	11	18	7	LOC100489965 (hormad1)	HORMA domain containing 1	NP_115508.2	Gonadogenesis, gametogenesis, meiosis, fertility (male?)

Ovary-C	1	8	16	8	LOC100489965 (hormad1)	HORMA domain containing 1	NP_115508.2	Gonadogenesis, gametogenesis, meiosis, fertility (male?)
Ovary-C	1	8	13	6	LOC100489965 (hormad1)	HORMA domain containing 1	NP_115508.2	Gonadogenesis, gametogenesis, meiosis, fertility (male?)
Ovary-C	2	4	9	6	fbxo47	F-box protein 47	NP_001008777.2	Cancer-related
Ovary-C	1	5	11	7	LOC100494809 (tex11)	testis expressed 11	NP_001003811.1	Gonadogenesis, gametogenesis, meiosis, fertility (male?)
Ovary-C	2	4	11	7	hfm1	HFM1, ATP-dependent DNA helicase homolog (S. cerevisiae)	NP_001017975.3	Cancer-related
Ovary-C	1	2	9	5	LOC100170619 (c12orf40)	chromosome 12 open reading frame 40	NP_001026918.2	
Ovary-C	2	4	7	6	LOC100491026 (c1orf177)	chromosome 1 open reading frame 177	NP_689820.2	
Ovary-C	2	3	7	6	LOC100127812 (fam47e)	family with sequence similarity 47, member E	NP_001130042.1	
Ovary-C	1	3	9	9	LOC100488153 (cga)	glycoprotein hormones, alpha polypeptide	NP_000726.1	Gonadogenesis, morphology of ovary, quantity of hormone, fertility
Ovary-C	1	2	10	7	(ccdc170)	coiled-coil domain containing 170	NP_079335.2	Cancer-related
Ovary-C	1	6	23	10	tmprss12	transmembrane (C-terminal) protease, serine 12	NP_872365.1	Cancer-related
Ovary-C	2	4	13	12	mamdc2	MAM domain containing 2	NP_694999.3	
Ovary-C	1	3	17	9	LOC100491771 (ccdc152)	coiled-coil domain containing 152	NP_001128320.1	
Ovary-C	1	3	16	9	LOC100485050 (syce1)	synaptonemal complex central element protein 1	NP_570140.1	
Ovary-C	1	4	15	8	msh5	mutS homolog 5 (E. coli)	NP_751898.1	Gonadogenesis, gametogenesis, meiosis, fertility
Ovary-C	1	4	9	11	tbpl2 (tbp)	TATA box binding protein	NP_003185.1	Transcription, embryonic development
Ovary-C	1	3	13	8	brdt	bromodomain, testis-specific	NP_001717.2	Gonadogenesis, chromatin remodeling (male?)
Ovary-C	1	14	29	6	LOC100489965 (hormad1)	HORMA domain containing 1	NP_115508.2	Gonadogenesis, gametogenesis, meiosis, fertility (male?)
Ovary-C	1	7	30	26	LOC100488683 (zglp1)	zinc finger, GATA-like protein 1	NP_001096637.1	Gonadogenesis, gametogenesis, oogenesis, ovary development
Ovary-C	1	5	29	57	LOC100488624 (spdya)	speedy homolog A (Xenopus laevis)	NP_001008779.1	Oocyte maturation
Ovary-C	1	4	25	57	npy	neuropeptide Y	NP_000896.1	Vascularization, secretion of hormone, fertility
Ovary-C	1	1	65	47	brdt (brd3)	bromodomain containing 3	NP_031397.1	
Ovary-C	1	2	13	16	mapk13	mitogen-activated protein kinase 13	NP_002745.1	Cancer-related, cell proliferation
Ovary-C	1	2	17	34	tmed6	transmembrane emp24 protein transport domain containing 6	NP_653277.2	
Ovary-C	1	1	14	40	(iws1)	IWS1 homolog (S. cerevisiae)	NP_060439.2	Cancer-related

Table 2. Transcript IDs and functional information in cluster order corresponding to Figure 2. Fold difference in expression between tissues was calculated based on raw expression values and is colored according to magnitude of difference. Red indicates ovary-enriched, blue indicates testis-enriched, yellow indicates moderate difference and green indicates no difference. Gene symbols in parenthases are human gene symbols.

			|Fold-difference|					
Probe ID	Human Accession	Cluster	NF58	NF66	1WPM	2WPM	Gene Symbol (Human)	Entrez Human Gene Name	Mammalian Function
Str.24079.1.A1_at	NP_060439.2	Ovary-A	1	1	14	40	(iws1)	IWS1 homolog (S. cerevisiae)	Cancer-related
Str.10336.1.S1_at	NP_653277.2	Ovary-A	1	2	17	34	tmed6	transmembrane emp24 protein transport domain containing 6	
Str.50399.1.S1_at	NP_002745.1	Ovary-A	1	2	13	16	mapk13	mitogen-activated protein kinase 13	Cancer-related, cell proliferation
Str.1727.3.A2_a_at	NP_031397.1	Ovary-A	1	1	65	47	brdt (brd3)	bromodomain containing 3	
Str.31845.1.S1_at	NP_000896.1	Ovary-A	1	4	25	57	npy	neuropeptide Y	Vascularization, secretion of hormone, fertility
Str.7244.1.S1_at	NP_001008779.1	Ovary-A	1	5	29	57	(spdya)	speedy homolog A (Xenopus laevis)	Oocyte maturation
Str.32211.1.A1_at	NP_001096637.1	Ovary-A	1	7	30	26	(zglp1)	zinc finger, GATA-like protein 1	Gonadogenesis, gametogenesis, oogenesis, ovary development
Str.34301.2.S1_at	NP_115508.2	Ovary-A	1	14	29	6	(hormad1)	HORMA domain containing 1	Gonadogenesis, gametogenesis, meiosis, fertility (male)
Str.1727.3.A1_at	NP_001717.2	Ovary-A	1	3	13	8	brdt	bromodomain, testis-specific	Gonadogenesis, chromatin remodeling (male)
Str.27519.1.S1_at	NP_003185.1	Ovary-A	1	4	9	11	tbpl2 (tbp)	TATA box binding protein	Transcription, embryonic development
Str.34382.1.A1_at	NP_751898.1	Ovary-A	1	4	15	8	msh5	mutS homolog 5 (E. coli)	Gonadogenesis, gametogenesis, meiosis, fertility
Str.32425.1.A1_at	NP_570140.1	Ovary-A	1	3	16	9	(syce1)	synaptonemal complex central element protein 1	Meiosis
Str.33708.1.A1_at	NP_001128320.1	Ovary-A	1	3	17	9	(ccdc152)	coiled-coil domain containing 152	
StrAffx.106.1.S1_s_at	NP_694999.3	Ovary-A	2	4	13	12	mamdc2	MAM domain containing 2	
Str.38722.1.S1_at	NP_872365.1	Ovary-A	1	6	23	10	tmprss12	transmembrane (C-terminal) protease, serine 12	Cancer-related
Str.33833.1.A1_at	NP_079335.2	Ovary-A	1	2	10	7	(ccdc170)	coiled-coil domain containing 170	Cancer-related
Str.21686.1.S1_at	NP_000726.1	Ovary-A	1	3	9	9	(cga)	glycoprotein hormones, alpha polypeptide	Gonadogenesis, morphology of ovary, quantity of hormone, fertility
Str.37820.1.S1_at	NP_001130042.1	Ovary-A	2	3	7	6	(fam47e)	family with sequence similarity 47, member E	
Str.31912.1.A1_at	NP_689820.2	Ovary-A	2	4	7	6	(c1orf177)	chromosome 1 open reading frame 177	
Str.38593.1.S1_at	NP_001026918.2	Ovary-A	1	2	9	5	(c12orf40)	chromosome 12 open reading frame 40	
Str.33738.1.A1_at	NP_001017975.3	Ovary-A	2	4	11	7	hfm1	HFM1, ATP-dependent DNA helicase homolog (S. cerevisiae)	Cancer-related
Str.34278.1.A1_at	NP_001003811.1	Ovary-A	1	5	11	7	(tex11)	testis expressed 11	Gonadogenesis, gametogenesis, meiosis, fertility (male)
Str.34311.2.A1_at	NP_001008777.2	Ovary-A	2	4	9	6	fbxo47	F-box protein 47	Cancer-related
Str.34301.3.A1_x_at	NP_115508.2	Ovary-A	1	8	13	6	(hormad1)	HORMA domain containing 1	Gonadogenesis, gametogenesis, meiosis, fertility (male)
Str.34301.1.S1_a_at	NP_115508.2	Ovary-A	1	8	16	8	(hormad1)	HORMA domain containing 1	Gonadogenesis, gametogenesis, meiosis, fertility (male)
Str.34301.1.S1_at	NP_115508.2	Ovary-A	1	11	18	7	(hormad1)	HORMA domain containing 1	Gonadogenesis, gametogenesis, meiosis, fertility (male)
Str.42327.1.A1_at	NP_001099048.1	Ovary-A	1	7	19	11	(syce2)	synaptonemal complex central element protein 2	DNA recombination, synapsis, meiosis
Str.49258.1.A1_at	NP_008999.2	Ovary-A	2	13	27	9	(dmc1)	DMC1 dosage suppressor of mck1 homolog, meiosis-specific homologous recombination (yeast)	Gonadogenesis, gametogenesis, oogenesis, meiosis, fertility
Str.51692.1.S1_at	NP_444505.1	Ovary-A	2	5	3	7	(rplp0)	ribosomal protein, large, P0	Cancer-related
Str.20782.1.S1_a_at	NP_060369.3	Ovary-A	1	2	4	5	tesc	tescalcin	Neurological disease, Na+ homeostasis
Str.32672.1.A1_at	NP_001138400.1	Ovary-A	1	2	4	5	(nkiras2)	NFKB inhibitor interacting Ras-like 2	Cancer-related
Str.30634.1.A1_at	NP_009131.2	Ovary-A	1	2	4	5	(akap13)	A kinase (PRKA) anchor protein 13	Cancer-related, decondensation of chromatin
Str.15244.2.S1_a_at	NP_079197.3	Ovary-A	2	2	4	5	pof1b	premature ovarian failure, 1B	Cancer-related, premature ovarian failure
Str.8393.1.S1_at	NP_001118228.1	Ovary-A	2	2	3	5	pabpc1l	poly(A) binding protein, cytoplasmic 1-like	Gonadogenesis, gametogenesis, oogenesis, meiosis, fertility
Str.52229.1.S1_at	NP_000976.1	Ovary-A	3	3	4	5	(rpl17)	ribosomal protein L17	Cancer-related
Str.26910.1.S1_at	NP_001164666.1	Ovary-A	3	3	4	6	elavl2	ELAV (embryonic lethal, abnormal vision, Drosophila)-like 2 (Hu antigen B)	Cancer-related
Str.19885.1.S1_at	NP_006863.2	Ovary-A	3	3	4	5	gtf2a1l///ston1	general transcription factor IIA, 1-like	
Str.32359.1.A1_at	NP_003869.1	Ovary-A	1	2	5	5	(ggh)	gamma-glutamyl hydrolase (conjugase, folylpolygammaglutamyl hydrolase)	Amino acid metabolism
Str.47632.1.S1_x_at	NP_001137457.1	Ovary-A	2	1	3	5	baf-l (banf1)	barrier to autointegration factor 1	DNA recombination
Str.15950.1.S1_s_at	NP_005660.4	Ovary-A	2	2	4	5	reep6 (reep5)	receptor accessory protein 5	
Str.1623.1.S1_at	NP_690048.1	Ovary-A	2	3	5	5	stk35 (pdik1l)	PDLIM1 interacting kinase 1 like	Organization of actin stress fibers
Str.38422.2.A1_a_at	NP_079356.3	Ovary-A	2	2	6	8	(asrgl1)	asparaginase like 1	Cancer-related
Str.49275.1.S1_at	NP_775804.2	Ovary-A	2	5	7	5	tdrd5	tudor domain containing 5	Gonadogenesis, gametogenesis, meiosis, fertility (male)
Str.6726.1.S1_at	NP_653195.2	Ovary-A	3	6	6	5	gtsf1	gametocyte specific factor 1	Germ cell development
Str.38810.1.S1_at	NP_056002.2	Ovary-A	1	5	5	5	sel1l3	sel-1 suppressor of lin-12-like 3 (C. elegans)	Cancer-related
Str.5073.1.S1_at	NP_065392.1	Ovary-A	2	4	6	5	c20orf3 (apmap)	adipocyte plasma membrane associated protein	Cancer-related
Str.4267.1.S1_at	NP_919268.1	Ovary-A	2	2	6	6	sass6	spindle assembly 6 homolog (C. elegans)	DNA replication
Str.27191.2.S1_at	NP_001013682.2	Ovary-A	1	2	6	8	(frrs1)	ferric-chelate reductase 1	

			|Fold-difference|					
Probe ID	Human Accession	Cluster	NF58	NF66	1WPM	2WPM	Gene Symbol (Human)	Entrez Human Gene Name	Mammalian Function
Str.1727.2.A1_at	NP_001717.2	Ovary-A	1	2	7	7	brdt	bromodomain, testis-specific	Gonadogenesis, chromatin remodeling (male)
Str.710.2.S1_at	NP_076957.3	Ovary-A	1	1	5	8	c17orf39 (gid4)	GID complex subunit 4, VID24 homolog (S. cerevisiae)	
Str.4536.1.S1_at	NP_543026.1	Ovary-A	1	1	6	7	(stk35)	serine/threonine kinase 35	Cancer-related, organization of actin stress fibers
Str.8311.1.S1_at	NP_542195.1	Ovary-A	1	3	9	5	(tldc2)	TBC/LysM-associated domain containing 2	
Str.34311.1.S1_at	NP_001008777.2	Ovary-A	1	2	9	6	fbxo47	F-box protein 47	Cancer-related
Str.30824.1.A1_s_at	NP_689551.1	Ovary-A	1	4	10	7	zg16	zymogen granule protein 16	Cancer-related
Str.37576.1.S1_s_at	NP_079335.2	Ovary-A	1	4	12	8	(ccdc170)	coiled-coil domain containing 170	Cancer-related
Str.32445.1.S1_s_at	NP_006000.2	Ovary-A	2	3	4	18	tuba4 (tuba1a)	tubulin, alpha 1a	Nervous system development, microtubule dynamics
Str.32445.1.S1_at	NP_006000.2	Ovary-A	2	3	3	12	(tuba1a)	tubulin, alpha 1a	Nervous system development, microtubule dynamics
Str.7111.1.S1_at	NP_877724.1	Ovary-A	1	2	5	21	npm2	nucleophosmin/nucleoplasmin 2	Morphology of ovary, morphology of oocytes, fertility
Str.19394.1.S1_at	NP_001004311.2	Ovary-A	2	3	9	27	figla	folliculogenesis specific basic helix-loop-helix	Gonadogenesis, ovary development, meiosis of germ cells, fertility
Str.11490.1.S2_at	NP_001028253.1	Ovary-A	2	2	7	14	mycl1	v-myc myelocytomatosis viral oncogene homolog 1	Cancer-related
Str.11490.1.S1_at	NP_001028253.1	Ovary-A	2	2	7	14	mycl1	v-myc myelocytomatosis viral oncogene homolog 1	Cancer-related
Str.38460.2.A1_at	NP_001093392.1	Ovary-A	1	1	4	13	otud4		Cancer-related
Str.27686.1.S1_at	NP_001001933.1	Ovary-A	1	1	5	14	lhx8	LIM homeobox 8	Gonadogenesis, ovary development, nervous system development
Str.4078.1.S1_a_at	NP_001298.3	Ovary-B	4	5	5	10	cldn7	claudin 7	Ovarian cell proliferation, quantity of steroid hormone
Str.27610.1.S1_at	NP_002344.2	Ovary-B	3	4	4	8	epcam (tacstd2)	tumor-associated calcium signal transducer	Ovarian cell proliferation, cellular movement
Str.51982.1.A1_s_at	NP_077312.2	Ovary-B	3	6	5	7	irx3	iroquois homeobox 3	Organ development, nervous system development
Str.39298.2.S1_a_at	NP_000005.2	Ovary-B	2	5	5	6	(a2m)	alpha-2-macroglobulin	Nervous system development, cellular movement
Str.21092.1.S1_at	NP_005844.4	Ovary-B	2	4	4	5	irx5	iroquois homeobox 5	Organ development, morphology, nervous system development
StrJgi.3092.1.S1_at	NP_005089.2	Ovary-B	3	3	3	5	msc	musculin	Muscle development
Str.8649.2.S1_x_at	NP_067018.2	Ovary-B	3	3	5	11	(cldn6)	claudin 6	Cell proliferation, differentiation
Str.8649.2.S1_at	NP_067018.2	Ovary-B	3	3	5	11	(cldn6)	claudin 6	Cell proliferation, differentiation
Str.16327.1.S1_at	NP_005256.2	Ovary-B	2	1	4	5	ggt1	gamma-glutamyltransferase 1	Morphology of gonad, fertility, cell proliferation
Str.13287.1.S1_at	NP_056122.1	Ovary-B	2	5	5	6	fam189a1	family with sequence similarity 189, member A1	
Str.5962.2.A1_at	NP_060167.2	Ovary-B	2	4	5	15	esrp1	epithelial splicing regulatory protein 1	Ovarian cell proliferation, RNA splicing
Str.5962.1.S1_at	NP_060167.2	Ovary-B	2	3	6	20	esrp1	epithelial splicing regulatory protein 1	Ovarian cell proliferation, RNA splicing
Str.10951.1.S1_at	NP_065826.2	Ovary-B	3	3	3	12	(kiaa1324)	KIAA1324	
Str.34852.1.A1_at	NP_077720.1	Ovary-B	5	5	11	21	nppc	natriuretic peptide C	Reproductive system development, cell signaling, cell proliferation
Str.41205.1.A1_at	NP_000207.2	Ovary-B	6	13	9	8	kal1	Kallmann syndrome 1 sequence	Guidance of axons, cell movement, gonad development
Str.34732.1.A1_at	NP_000094.2	Ovary-B	7	12	8	11	cyp19a1	cytochrome P450, family 19, subfamily A, polypeptide 1	Morphology of gonad, primary sex determination
Str.8337.1.S1_at	NP_002099.1	Ovary-B	5	13	12	14	hal.2	histidine ammonia-lyase	Amino acid metabolism
Str.52013.1.S1_at	NP_000094.2	Ovary-B	5	8	5	6	cyp19a1	cytochrome P450, family 19, subfamily A, polypeptide 1	Morphology of gonad, primary sex determination
Str.19828.1.S1_at	NP_689648.2	Ovary-B	6	5	5	6	amdhd1	amidohydrolase domain containing 1	
Str.28022.1.A1_at	NP_001138578.1	Ovary-B	8	13	17	17	fibcd1	fibrinogen C domain containing 1	
Str.24572.1.A1_s_at	NP_000774.2	Ovary-B	8	22	15	27	cyp26a1	cytochrome P450, family 26, subfamily A, polypeptide 1	Organ development, morphology, metabolism
Str.12223.1.S1_at	NP_000742.1	Ovary-B	7	11	13	7	chrnd	cholinergic receptor, nicotinic, delta (muscle)	Muscle growth
Str.15551.1.S2_at	NP_002336.1	Ovary-B	6	7	6	5	lum	lumican	Cell proliferation, morphology, fertility
Str.15551.1.S1_at	NP_002336.1	Ovary-B	7	7	7	6	lum	lumican	Cell proliferation, morphology, fertility
Str.28084.1.S1_at	NP_004089.1	Ovary-B	5	7	9	6	emx2	empty spiracles homeobox 2	Morphology of gonad, primary sex determination
StrEns.9618.1.S1_a_at	NP_872293.2	Ovary-B	4	7	6	6	olfml2a	olfactomedin-like 2A	Endometrial cell proliferation
Str.38277.1.A1_at	NP_001121367.1	Ovary-B	5	4	5	5	chst8	carbohydrate (N-acetylgalactosamine 4-0) s	Morphology of gonad, concentration of hormone
Str.13722.1.S1_at	NP_000541.1	Ovary-B	3	6	8	6	tyrp1	tyrosinase-related protein 1	
StrAffx.70.1.S1_s_at	NP_004813.2	Ovary-B	21	61	43	64	ntn1	netrin 1	Nervous system development, cellular movement
Str.6910.1.S1_at	NP_002088.2	Ovary-C	1	1	2	85	42Sp43 (gtf3a)	general transcription factor IIIA	Confirmational DNA modification, transcription
Str.7712.1.S1_a_at	NP_002096.1	Ovary-C	1	1	1	56	hist1h2aa (h2afx)	H2A histone family, member X	Gametogenesis, meiosis, DNA repair
Str.4034.1.S1_at	NP_001104516.1	Ovary-C	1	2	3	71	ccna1	cyclin A1	Gametogenesis, cell cycle progression
Str.27228.1.S1_at	NP_004692.1	Ovary-C	1	1	2	34	(ccnb2)	cyclin B2	Cell proliferation, fecundity
Str.1760.2.S2_at	NP_071370.2	Ovary-C	1	1	2	42	cdca7	cell division cycle associated 7	Regulation of cell proliferation and transcription
Str.3994.1.S1_a_at	NP_114172.1	Ovary-C	1	1	1	45	ccnb1	cyclin B1	Cell cycle progression, mitosis
Str.6258.1.S1_at	NP_001167607.1	Ovary-C	1	1	2	50	cfc1 (tdgf1)	teratocarcinoma-derived growth factor 1	Embryonic development, mesoderm development
StrEns.9022.1.S1_s_at	NP_054879.3	Ovary-C	1	1	2	36	mkrn3 (mkrn2)	makorin ring finger protein 2	

			|Fold-difference|					
Probe ID	Human Accession	Cluster	NF58	NF66	1WPM	2WPM	Gene Symbol (Human)	Entrez Human Gene Name	Mammalian Function
Str.6468.4.S1_at	NP_054879.3	Ovary-C	1	1	3	101	mkrn3 (mkrn2)	makorin ring finger protein 2	
Str.8156.1.S1_at	NP_006073.2	Ovary-C	1	1	2	63	tuba4 (tuba1b)	tubulin, alpha 1b	
Str.26862.1.S1_at	NP_783318.1	Ovary-C	1	1	1	25	zar1	zygote arrest 1	Oocyte-specific maternal mRNA, embryogenesis
Str.32186.1.A1_at	NP_009067.2	Ovary-C	1	1	1	18	(znf80)	zinc finger protein 80	
Str.3682.1.S1_at	NP_060059.1	Ovary-C	1	1	2	28	btg4	B-cell translocation gene 4	Cell cycle progression, cell proliferation, mitosis
Str.17082.2.S1_x_at	NP_003541.2	Ovary-C	1	1	2	29	(mad1l1)	MAD1 mitotic arrest deficient-like 1 (yeast)	Cell cycle progression, cell proliferation, transcription
Str.1617.1.S1_at	NP_067009.1	Ovary-C	1	1	1	30	zp4.2	zona pellucida glycoprotein 4	Oocyte-specific, cell signaling, activation of protein kinase
Str.3.1.S1_a_at		Ovary-C	1	1	1	32	nanos1		Oocyte maternal mRNA regulation of embryonic development
Str.6457.1.S1_at	NP_997309.2	Ovary-C	1	1	1	31	foxi2	forkhead box I2	Oocyte maternal mRNA activator of embryonic development (Cha et al.,1 2012)
Str.20406.1.S1_at	NP_001130043.1	Ovary-C	1	1	1	33	(zar1l)	zygote arrest 1-like	Oocyte-specific maternal mRNA, RNA regulation embryogenesis
Str.5107.1.S1_at	NP_067009.1	Ovary-C	1	1	1	36	zp4	zona pellucida glycoprotein 4	Oocyte-specific, cell signaling, activation of protein kinase
Str.27898.1.S1_at	NP_003398.1	Ovary-C	1	1	1	36	zfp36l2.1 (zfp36)	ZFP36 ring finger protein	Cell proliferation, mRNA stabilization, transcription
Str.5859.1.S1_a_at	NP_001099028.1	Ovary-C	1	1	1	41	wee2	WEE1 homolog 2 (S. pombe)	Cell cycle, meiosis I, prophase I
Str.754.1.S1_at	NP_690851.2	Ovary-C	1	1	1	40	(prss33)	protease, serine, 33	
Str.1668.2.S1_at	NP_061897.1	Ovary-C	1	1	1	49	(heatr5b)	HEAT repeat containing 5B	
Str.30111.1.S1_at	NP_001122098.1	Ovary-C	1	1	1	48	(spire1)	spire homolog 1 (Drosophila)	
Str.3366.1.S1_at	NP_005940.1	Ovary-C	1	1	1	167	(mt1f)	metallothionein 1F	Cell death and survival
Str.117.1.S1_at	NP_009086.4	Ovary-C	1	1	1	120	(zp3)	zona pellucida glycoprotein 3 (sperm receptor)	Oocyte development, gametogenesis, fertility
Str.8649.1.S1_at	NP_067018.2	Ovary-C	1	1	2	91	cldn6.1	claudin 6	Cell proliferation, differentiation
Str.21536.1.S1_at	NP_008818.3	Ovary-C	1	1	1	495	zfp36l2.2	ZFP36 ring finger protein-like 2	Cell proliferation, mRNA stabilization, transcription
Str.3467.1.S1_at	NP_006797.3	Ovary-C	1	1	1	250	(btg3)	BTG family, member 3	Cell cycle progression, cell proliferation, transcription
Str.52147.2.S1_x_at	NP_001514.2	Ovary-C	1	1	1	15	(has1)	hyaluronan synthase 1	Cell proliferation, cellular movement
StrEns.4910.1.S1_at	NP_002051.2	Ovary-C	1	1	1	14	(gja4)	gap junction protein, alpha 4, 37kDa	Reproductive system development, gametogenesis, fertility
Str.3569.1.S1_at	NP_001154945.1	Ovary-C	1	1	1	14	aldh3b1	aldehyde dehydrogenase 3 family, member B1	
Str.6507.1.S1_at	NP_722575.1	Ovary-C	1	1	1	12	h1foo	H1 histone family, member O, oocyte-specific	Oocyte-specific maternal mRNA
Str.17082.1.S1_s_at	NP_000214.1	Ovary-C	1	1	1	11	xk81a1 (krt12)	keratin 12	Disruption of keratin filaments
Str.27268.1.S1_at	NP_003097.1	Ovary-C	1	1	1	12	sox3 (sox2)	SRY (sex determining region Y)-box 2	Reproductive system development, cell proliferation
Str.39270.1.A1_at	NP_005439.2	Ovary-C	1	1	1	13	(bmp15)	bone morphogenetic protein 15	Reproductive system development, gametogenesis, fertility
Str.31989.1.A1_at	NP_001002259.1	Ovary-C	1	1	2	9	caprin2	caprin family member 2	Cell proliferation, transcription
Str.10367.1.S1_at	NP_001135877.1	Ovary-C	1	1	2	17	slmo1	slowmo homolog 1 (Drosophila)	
Str.51662.1.A1_at	NP_001159766.1	Ovary-C	1	1	2	22	(ssx2ip)	synovial sarcoma, X breakpoint 2 interacting protein	Cell proliferation
Str.7206.1.S1_at	NP_001949.1	Ovary-C	1	1	1	18	42Sp50 (eef1a2)	eukaryotic translation elongation factor 1 alpha 2	Oocyte vegetal mRNA transport (Loeber et al. 2010)
Str.1153.1.S1_at	NP_001167022.1	Ovary-C	1	1	1	11	tmprss4	transmembrane protease, serine 4	
Str.27710.1.S1_at	NP_073587.1	Ovary-C	1	1	1	8	parp12	poly (ADP-ribose) polymerase family, member 12	
Str.10709.1.S1_at	NP_001073935.1	Ovary-C	1	1	1	7	btbd17	BTB (POZ) domain containing 17	
StrEns.9654.1.S1_s_at	NP_001002259.1	Ovary-C	1	1	1	7	caprin2	caprin family member 2	Cell proliferation, transcription
Str.15673.1.S1_at	NP_009294.1	Ovary-C	1	1	1	9	comt.2 (comt)	catechol-O-methyltransferase	Reproductive system development, metabolism, regulation of neurotransmitter
StrJgi.8914.1.S1_s_at	NP_543154.1	Ovary-C	1	1	1	7	(itln2)	intelectin 2	
Str.5899.1.S1_at	NP_653194.1	Ovary-C	1	1	1	8	rhebl1	Ras homolog enriched in brain like 1	Regulation of cell growth and proliferation
Str.9274.1.S1_at	NP_001035189.1	Ovary-C	1	1	1	9	sptssb	serine palmitoyltransferase, small subunit B	
Str.51964.1.S1_s_at	NP_001004343.1	Ovary-C	1	1	1	6	map1lc3c	microtubule-associated protein 1 light chain 3 gamma	
Str.24662.1.S1_a_at	NP_009060.2	Ovary-C	1	1	1	6	zic2	Zic family member 2	Nervous system development
Str.2712.1.S1_at	NP_203125.1	Ovary-C	1	1	1	7	(casp7)	caspase 7, apoptosis-related cysteine peptidase	Cell death and survival, tissue morphology
Str.51683.1.S1_at	NP_057480.2	Ovary-C	1	1	1	6	(ctdspl2)	CTD (carboxy-terminal domain, RNA pol. II, polypep. A) small phosphatase like 2	Phosphatase activity
Str.22168.2.S1_at	NP_057405.1	Ovary-C	1	1	1	6	(rhcg)	Rh family, C glycoprotein	Morphology of gonad, molecular transport
Str.15798.1.S1_at	NP_001123886.1	Ovary-C	1	1	1	6	(apba2)	amyloid beta (A4) precursor protein-binding, family A, member 2	Exocytosis of vesicles
Str.19585.1.S1_at	NP_005906.2	Ovary-C	1	1	1	5	mcm6	minichromosome maintenance complex component 6	Confirmational DNA modification
Str.4026.1.S1_a_at	NP_003914.1	Ovary-C	1	1	1	5	foxh1	forkhead box H1	Embryonic development, patterning
Str.29857.1.A1_at	NP_689929.2	Ovary-C	1	1	1	5	patl2 (patl1)	protein associated with topoisomerase II homolog 1 (yeast)	
Str.49374.1.A1_at	NP_000843.1	Ovary-C	1	1	1	5	(gstp1)	glutathione S-transferase pi 1	Cell proliferation, conversion of beta-estradiol
Str.33548.1.S1_at	NP_001852.1	Ovary-C	1	1	1	6	(cox4i1)	cytochrome c oxidase subunit IV isoform 1	Cell cycle progression

			|Fold-difference|					
Probe ID	Human Accession	Cluster	NF58	NF66	1WPM	2WPM	Gene Symbol (Human)	Entrez Human Gene Name	Mammalian Function
Str.46745.1.A1_s_at	NP_005389.1	Ovary-C	1	1	2	7	ppp1r3c.2	protein phosphatase 1, regulatory subunit 3C	Insulin regulation, glycogen homeostasis
Str.27229.1.S1_at	NP_005389.1	Ovary-C	1	1	2	7	ppp1r3c.2	protein phosphatase 1, regulatory subunit 3C	Insulin regulation, glycogen homeostasis
Str.9274.1.S2_at	NP_001035189.1	Ovary-C	1	1	2	7	sptssb	serine palmitoyltransferase, small subunit B	
Str.8371.1.S1_a_at	NP_001130043.1	Ovary-C	1	1	1	6	(zar1l)	zygote arrest 1-like	Oocyte-specific maternal mRNA, RNA regulation embryogenesis
Str.15996.2.S1_at	NP_056530.2	Ovary-C	1	1	1	8	proca1	protein interacting with cyclin A2	Lipid metabolism
StrEns.5801.1.S1_s_at	NP_056530.2	Ovary-C	1	1	1	7	proca1	protein interacting with cyclin A1	Lipid metabolism
Str.37482.1.S1_at	NP_065109.1	Ovary-C	1	1	1	8	pnpla3	patatin-like phospholipase domain containing 2	Lipid metabolism
Str.6496.1.S1_at	NP_065169.1	Ovary-C	2	1	2	9	sall4	sal-like 4 (Drosophila)	Cell proliferation, growth
Str.5899.1.S2_at	NP_653194.1	Ovary-C	1	1	2	8	rhebl1	Ras homolog enriched in brain like 1	Regulation of cell growth and proliferation
Str.7388.1.S1_at	NP_001959.1	Ovary-C	1	1	2	15	eif4e	eukaryotic translation initiation factor 4E	Cell proliferation, cell death and survival, RNA trafficking
StrEns.410.1.S1_at	NP_542449.1	Ovary-C	1	2	3	12	vegt	T-box protein VegT	Oogenesis, germ layer specification of embryo
Str.4776.1.S1_at	NP_079206.2	Ovary-C	1	2	3	8	elovl7	ELOVL fatty acid elongase 7	Cell proliferation, synthesis of hormone
Str.27817.1.S1_at	NP_060179.2	Ovary-C	1	2	2	5	fam46c	family with sequence similarity 46, member C	
Str.8000.1.S1_a_at	NP_004692.1	Ovary-C	3	3	2	6	ccnb2	cyclin B2	Cell proliferation, fecundity
Str.11491.1.A1_at	NP_060546.2	Ovary-C	2	4	3	7	armc4	armadillo repeat containing 4	
Str.28193.1.A1_at	NP_000266.2	Ovary-C	2	2	4	8	(oca2)	oculocutaneous albinism II	Reproductive system development, gametogenesis
Str.5962.1.S2_at	NP_060167.2	Ovary-C	1	2	3	8	esrp1	epithelial splicing regulatory protein 1	
Str.287.1.S1_at	NP_002297.2	Ovary-C	2	2	3	5	lgals3	lectin, galactoside-binding, soluble, 3	Cell proliferation, expansion of mesangium
Str.15225.1.S1_at	NP_001091089.1	Ovary-C	2	2	2	6	tmem184a	transmembrane protein 184A	Protein localization
StrAffx.141.1.S1_at	NP_001005340.1	Ovary-C	1	1	3	10	gpnmb	glycoprotein (transmembrane) nmb	Cell proliferation
Str.31340.2.S1_at	NP_859062.1	Ovary-C	1	1	2	5	grasp	GRP1 (general receptor for phosphoinositides 1)-assoc. scaffold prot.	Cell proliferation, localization, sprouting of mossy fibers
Str.31947.1.A1_at	NP_001137501.1	Ovary-C	1	1	2	5	cntd2	cyclin N-terminal domain containing 2	
Str.13533.1.A1_at	NP_000736.2	Ovary-C	1	1	3	6	chrna5	cholinergic receptor, nicotinic, alpha 5 (neuronal)	Cell signaling, nervous system development
Str.1304.1.S1_at	NP_001129688.1	Ovary-C	2	1	3	6	tmem51	transmembrane protein 51	
Str.116.1.S1_at	NP_067009.1	Ovary-C	1	1	2	6	zpax (zp4)	zona pellucida glycoprotein 4	Cell proliferation, cell signaling, activation of protein kinase
Str.33670.1.S1_at	NP_001798.2	Ovary-C	1	1	1	6	(cel)	carboxyl ester lipase	Lipid metabolism
Str.19439.1.S1_at	NP_775761.4	Ovary-C	1	1	5	13	tmem171	transmembrane protein 171	
Str.31112.1.A1_at	NP_877435.2	Ovary-C	1	1	6	8	wdr72	WD repeat domain 72	Cell death and survival
Str.27291.1.S1_at	NP_005718.2	Ovary-C	1	1	4	16	tspan1	tetraspanin 1	
Str.9495.1.S1_at	NP_005846.1	Ovary-C	1	1	4	6	ramp1	receptor (G protein-coupled) activity modifying protein 1	
Str.48992.1.A1_at	NP_002395.1	Ovary-C	1	1	5	12	(mfap4)	microfibrillar-associated protein 4	
Str.6678.1.S2_at	NP_008883.2	Ovary-C	1	1	1	5	upk1b	uroplakin 1B	
Str.20226.1.S1_at	NP_055135.1	Ovary-C	1	1	1	5	hebp2	heme binding protein 2	
Str.10989.1.S1_a_at	NP_006399.1	Ovary-C	2	1	1	6	agr2	anterior gradient 2 homolog (Xenopus laevis)	Cell proliferation, cellular movement
Str.3249.1.S1_s_at	NP_001296.1	Ovary-C	1	1	1	9	cldn4	claudin 4	Cell proliferation, cellular movement
Str.12245.1.S1_at	NP_112191.2	Testis-A	6	3	5	10	kazald1	Kazal-type serine peptidase inhibitor domain 1	
Str.31614.1.S1_at	NP_006761.1	Testis-A	4	3	5	7	(marco)	macrophage receptor with collagenous structure	Cellular organization of cytoskeleton, microtubule dynamics
Str.29149.1.A1_at	NP_074035.1	Testis-A	3	3	5	6	(myh11)	myosin, heavy chain 11, smooth muscle	Vascular development, muscle contraction
Str.31855.1.S1_at	NP_001129944.1	Testis-A	10	12	16	9	(litaf)	lipopolysaccharide-induced TNF factor	Cellular movement
Str.37641.1.S1_at	NP_004973.1	Testis-A	3	3	4	5	kcnj8	potassium inwardly-rectifying channel, subfamily J, member 8	Vascular development
Str.6049.1.A1_at	NP_004604.2	Testis-A	2	2	3	6	tgm2	transglutaminase 2 (C polypeptide, protein	Vasculogenesis, angiogenesis, concentration of hormone
Str.31333.1.S1_a_at	NP_612379.2	Testis-A	3	3	3	6	pkdcc.2	protein kinase domain containing, cytoplasmic	Connective tissue development
Str.28107.1.S1_at	NP_003059.1	Testis-A	3	4	4	6	snai1 (snai2)	snail homolog 2 (Drosophila)	Gonadogenesis, morphology of testis, cell movement
Str.26739.1.S1_at	NP_612454.1	Testis-A	2	2	3	5	gpr146	G protein-coupled receptor 146	
Str.22594.1.A1_at	NP_116121.2	Testis-A	2	3	4	7	(il17rc)	interleukin 17 receptor C	
Str.44816.1.A1_at	NP_000466.2	Testis-A	4	6	9	6	(nr0b1/dax-1)	nuclear receptor subfamily 0, group B, member 1	Gonadogenesis, morphology of testis, sex determination, fertility
Str.31923.1.S1_at	NP_001841.2	Testis-A	3	5	6	9	(col8a1)	collagen, type VIII, alpha 1	Vasculogenesis, angiogenesis
Str.37100.1.A1_at	NP_699174.1	Testis-A	4	3	4	8	(enpp6)	ectonucleotide pyrophosphatase/phosphodiesterase 6	Hydrolysis
Str.15452.1.S1_at	NP_004627.1	Testis-A	4	4	3	5	sema3b	sema domain (semaphorin), immunoglobulin domain (Ig) 3B	Vasculogenesis, cellular movement, cell signalling
Str.15379.1.S1_at	NP_004456.1	Testis-A	3	4	5	5	fgf10	fibroblast growth factor 10	Gonadogenesis, morphology of testis
StrJgi.3117.1.S1_s_at	NP_848600.2	Testis-A	5	5	5	5	tmem26	transmembrane protein 26	
Str.15388.1.A2_at	NP_004568.2	Testis-A	8	4	4	5	psph	phosphoserine phosphatase	

			|Fold-difference|					
Probe ID	Human Accession	Cluster	NF58	NF66	1WPM	2WPM	Gene Symbol (Human)	Entrez Human Gene Name	Mammalian Function
Str.6594.1.S1_at	NP_001035181.1	Testis-A	11	6	7	6	enpp2	ectonucleotide pyrophosphatase/phosphodiesterase 2	Vasculogenesis, cellular movement
Str.52251.1.S1_at	NP_003730.4	Testis-A	10	6	5	10	akr1c2 (akr1c3)	aldo-keto reductase family 1, member C3	Steroid synthesis and metabolism
Str.31895.1.S1_at	NP_542988.3	Testis-A	1	3	4	5	(col13a1)	collagen, type XIII, alpha 1	Vasculogenesis, angiogenesis
Str.15223.6.S1_at	NP_001003760.2	Testis-A	2	3	4	5	klhl31	kelch-like family member 31	
Str.33336.1.A1_at	NP_000410.2	Testis-A	1	3	3	5	itga2b.1	integrin, alpha 2b	Morphology of vascular system, cellular movement
Str.24395.1.A1_at	NP_063938.1	Testis-A	1	2	4	7	cyp26b1	cytochrome P450, family 26, subfamily B, polypeptide 1	Gonadogenesis, morphology of testis
Str.10824.1.S1_at	NP_000890.1	Testis-A	2	3	5	8	kitlg	KIT ligand	Gonadogenesis, development of testis, steroid synthesis
Str.25601.1.A1_at	NP_000798.2	Testis-A	3	3	6	9	(gabra2)	gamma-aminobutyric acid (GABA) A receptor, alpha 2	
Str.5581.1.S1_at	NP_068733.1	Testis-A	3	3	4	6	cfl2	cofilin 2 (muscle)	
Str.15616.1.S1_at	NP_002914.1	Testis-A	3	4	6	7	rgs2	regulator of G-protein signaling 2, 24kDa	Vascular development, development of muscle
Str.32447.1.S1_at	NP_963849.1	Testis-A	3	5	6	8	fhl5 (fhl2)	four and a half LIM domains 2	Angiogenesis, cellular movement, muscle cell development
Str.5047.1.S2_at	NP_001918.3	Testis-A	2	3	4	6	des.1	desmin	Morphology of vascular system
Str.28002.1.S1_at	NP_001071642.1	Testis-A	1	3	5	7	(slc29a1)	solute carrier family 29 (nucleoside transporters), member 1	Cellular proliferation
Str.22906.1.S1_at	NP_511040.2	Testis-A	1	2	2	5	col9a1	collagen, type IX, alpha 1	Connective tissue development
Str.5759.1.S1_at	NP_001303.1	Testis-A	1	1	2	7	crip2	cysteine-rich protein 2	Cellular proliferation, cellular differentiation
Str.1843.2.S1_at	NP_005621.2	Testis-A	1	1	3	6	slco2a1	solute carrier organic anion transporter family, member 2A1	Morphology of vascular system, molecular transport
Str.38324.1.S1_at	NP_057315.3	Testis-A	1	2	2	5	nlk	nemo-like kinase	Morphology of vascular system
Str.17054.1.S1_at	NP_001437.1	Testis-A	1	2	4	24	fabp7	fatty acid binding protein 7, brain	Cellular proliferation, cellular movement
Str.27613.3.S1_at	NP_005323.1	Testis-A	3	2	2	8	hba-l2 (hbz)	hemoglobin, zeta	Morphology of vascular system
Str.12190.1.S1_at	NP_003751.2	Testis-A	2	8	11	17	fstl5 (eif4g3)	eukaryotic translation initiation factor 4 gamma, 3	Cellular organization of cytoskeleton, microtubule dynamics
Str.39178.2.A1_at	NP_001452.2	Testis-A	5	7	10	15	fmo5	flavin containing monooxygenase 5	
Str.39178.1.S1_a_at	NP_001452.2	Testis-A	5	6	8	14	fmo5	flavin containing monooxygenase 5	
Str.13088.1.S1_at	NP_004725.1	Testis-A	5	6	7	14	dclk2 (dclk1)	doublecortin-like kinase 1	Cellular organization of cytoskeleton, microtubule dynamics
Str.25076.1.A1_at	NP_004168.1	Testis-A	5	8	10	8	(stx3)	syntaxin 3	Cellular organization of cytoskeleton, microtubule dynamics
Str.21675.1.A1_at	NP_000521.2	Testis-A	6	5	9	11	mpz	myelin protein zero	Nervous system development, cellular movement
Str.39202.1.S1_at	NP_006320.2	Testis-A	6	7	8	17	fbln5	fibulin 5	Vascular development, cellular movement
Str.26721.1.S1_at	NP_002183.1	Testis-A	2	2	4	10	inhba	inhibin, beta A	Morphology of testis, fertility, steroidogenesis, cellular movement
Str.24498.1.S1_at	NP_001161146.1	Testis-A	2	2	3	6	cadm2	cell adhesion molecule	
Str.15475.1.S1_at	NP_689917.2	Testis-A	3	4	5	7	fam123a (amer2)	APC membrane recruitment protein 2	
Str.21927.1.S1_at	NP_056965.3	Testis-A	4	3	5	10	dkk3	dickkopf 3 homolog (Xenopus laevis)	Steroid hormone synthesis, cellular movement, cellular organization
Str.38097.1.A1_at	NP_066382.1	Testis-A	3	4	4	6	(dhh)	desert hedgehog	Gonadogenesis, morphology of testis, sex determination, steroid synthesis
Str.51661.1.S1_at	NP_001329.1	Testis-A	2	3	4	8	cxadr	coxsackie virus and adenovirus receptor	Vascular development, cellular movement
Str.8537.1.S1_at	NP_001290.2	Testis-A	3	6	6	9	cnn2 (cnn1)	calponin 1, basic, smo	Vascular development, cellular movement, morphology of testis
Str.51373.1.A1_at	NP_001137417.1	Testis-A	3	5	7	7	(gas6)	growth arrest-specific 6	Vascular development, cellular movement
Str.39201.1.S1_at	NP_002182.1	Testis-A	3	3	3	6	inha	inhibin, alpha	Morphology of testis, fertility, steroidogenesis, sex determination
Str.37326.1.A1_x_at	NP_006158.2	Testis-A	4	10	12	14	(nkx3-1)	NK3 homeobox 1	Morphogenesis of testis
Str.17189.1.S1_at	NP_000339.2	Testis-A	5	8	11	16	srd5a2	steroid-5-alpha-reductase, alpha polypeptide 2	Steroidogenesis, fertility, sex determination, morphology of testis
StrJgi.3167.1.S1_x_at	NP_006158.3	Testis-A	6	12	16	16	(nkx3-1)	NK3 homeobox 1	Morphogenesis of testis
Str.37326.1.A1_s_at	NP_006158.2	Testis-A	6	12	15	15	(nkx3-1)	NK3 homeobox 1	Morphogenesis of testis
Str.5526.1.S1_at	NP_003280.2	Testis-A	6	10	12	22	tpm2	tropomyosin 2 (beta)	Vascular development, muscle contraction
Str.8998.1.S1_at	NP_001034933.1	Testis-A	15	23	10	8	acbd7	acyl-CoA binding domain containing 7	
Str.38286.1.A1_at	NP_002227.2	Testis-A	8	7	7	7	kcnf1	potassium voltage-gated channel, subfamily F, member 1	
Str.7705.5.S1_at	NP_001135934.1	Testis-A	7	9	13	11	osr2	odd-skipped related 2 (Drosophila)	Cellular proliferation, growth
Str.38466.1.S1_at	NP_000093.1	Testis-A	11	8	9	11	cyp17a1	cytochrome P450, family 17, subfamily A, polypeptide 1	Steroidogenesis, fertility, sex determination
Str.11952.1.S1_at	NP_001120645.1	Testis-A	10	7	9	10	(cadm3)	cell adhesion molecule 3	
Str.21742.1.S1_at	NP_001109.2	Testis-A	8	6	8	6	adcyap1r1	adenylate cyclase activating polypeptide 1 (pituitary) receptor type I	Cellular proliferation, concentration of hormone, fertility
Str.52145.1.S1_at	NP_003730.4	Testis-A	6	6	7	8	akr1cl1 (akr1c3)	aldo-keto reductase family 1, member C3	Steroidogenesis
StrJgi.5073.1.S1_s_at	NP_003730.4	Testis-A	6	6	6	7	akr1cl1 (akr1c3)	aldo-keto reductase family 1, member C3	Steroidogenesis
Str.19735.1.S1_at	NP_003586.3	Testis-A	6	5	7	7	tpst2	tyrosylprotein sulfotransferase 2	Cellular movement, fertility
Str.11990.1.S1_at	NP_996846.1	Testis-A	13	9	10	11	rarres1	retinoic acid receptor responder (tazarotene induced) 1	Cellular movement
Str.5014.1.S1_at	NP_001135417.1	Testis-B	9	12	12	23	acta2	actin, alpha 2, smooth muscle, aorta	Vascular development, muscle contraction
Str.21784.1.A1_s_at	NP_002072.2	Testis-B	13	11	17	22	gpc1	glypican 1	Vascular development, cellular movement

			|Fold-difference|					
Probe ID	Human Accession	Cluster	NF58	NF66	1WPM	2WPM	Gene Symbol (Human)	Entrez Human Gene Name	Mammalian Function
Str.21784.1.A2_at	NP_002072.2	Testis-B	12	12	16	19	gpc1	glypican 1	Vascular development, cellular movement
Str.20614.1.S1_at	NP_932766.1	Testis-B	17	5	12	19	aqp1	aquaporin 1 (Colton blood group)	Vascular development, permeability of blood vessel, molecular transport
Str.22031.1.S1_at	NP_001877.1	Testis-B	22	18	21	21	cryba4	crystallin, beta A4	
Str.38708.1.A1_at	NP_001138378.1	Testis-B	19	14	12	20	(clec4m)	C-type lectin domain family 4, member M	Cell-to-cell signaling and interaction
Str.28004.1.A1_at	NP_000859.1	Testis-B	16	24	25	36	(htr2c)	5-hydroxytryptamine (serotonin) receptor 2C, G protein-coupled	Cell-to-cell signaling and interaction
Str.16705.1.A1_at	NP_570844.1	Testis-B	26	30	41	65	(opa1)	optic atrophy 1 (autosomal dominant)	Mitochondrial organization, synthesis of pregnenolone
Str.33400.1.S1_at	NP_005723.2	Testis-B	22	25	21	21	(rad50)	RAD50 homolog (S. cerevisiae)	Cell death of embryonic stem cells, DNA repair
Str.28021.1.A1_at	NP_775101.1	Testis-B	17	17	22	19	slitrk4	SLIT and NTRK-like family, member 4	Formation of cellular protrusions, nervous system development
Str.21273.1.A1_at	NP_002513.2	Testis-B	70	36	53	47	nptx1	neuronal pentraxin I	Angiogenesis, cellular movement, nervous system development
Str.7898.1.S1_at	NP_002467.1	Testis-B	17	88	97	98	myl4	myosin, light chain 4, alkali; atrial, embryonic	Vascular development, muscle contraction
Str.38523.1.S1_at	NP_001002036.3	Testis-B	26	59	68	186	(astl)	astacin-like metallo-endopeptidase (M12 family)	Protein synthesis, fertility
Str.12662.1.S1_at	NP_689642.3	Testis-B	37	98	110	151	fgfbp3	fibroblast growth factor binding protein 3	Growth factor regulation, angiogenesis
Str.2374.2.A1_at	NP_001190.1	Testis-B	19	38	107	930	(bmp1)	bone morphogenetic protein 1	Collagen development, protein synthesis
Str.34508.1.S1_s_at	NP_001190.1	Testis-B	8	12	27	161	(bmp1)	bone morphogenetic protein 1	Collagen development, protein synthesis
Str.24477.2.S1_at	NM_001265587.1	Testis-B	222	302	314	289	rflcii (insl3)	insulin-like 3 (Leydig cell)	Testis development, fertility

Supplemental Figure 1

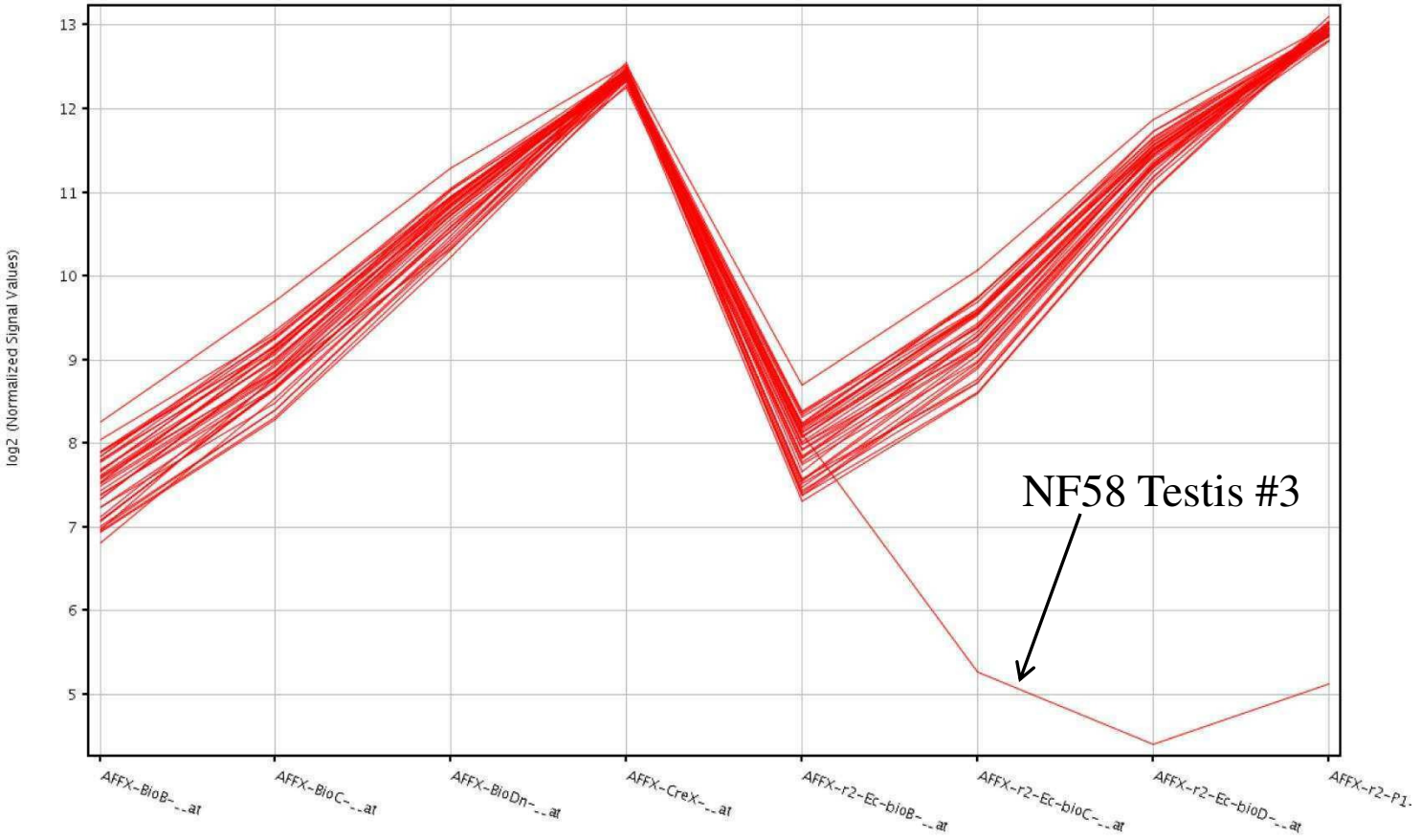

Supplemental Figure 2.

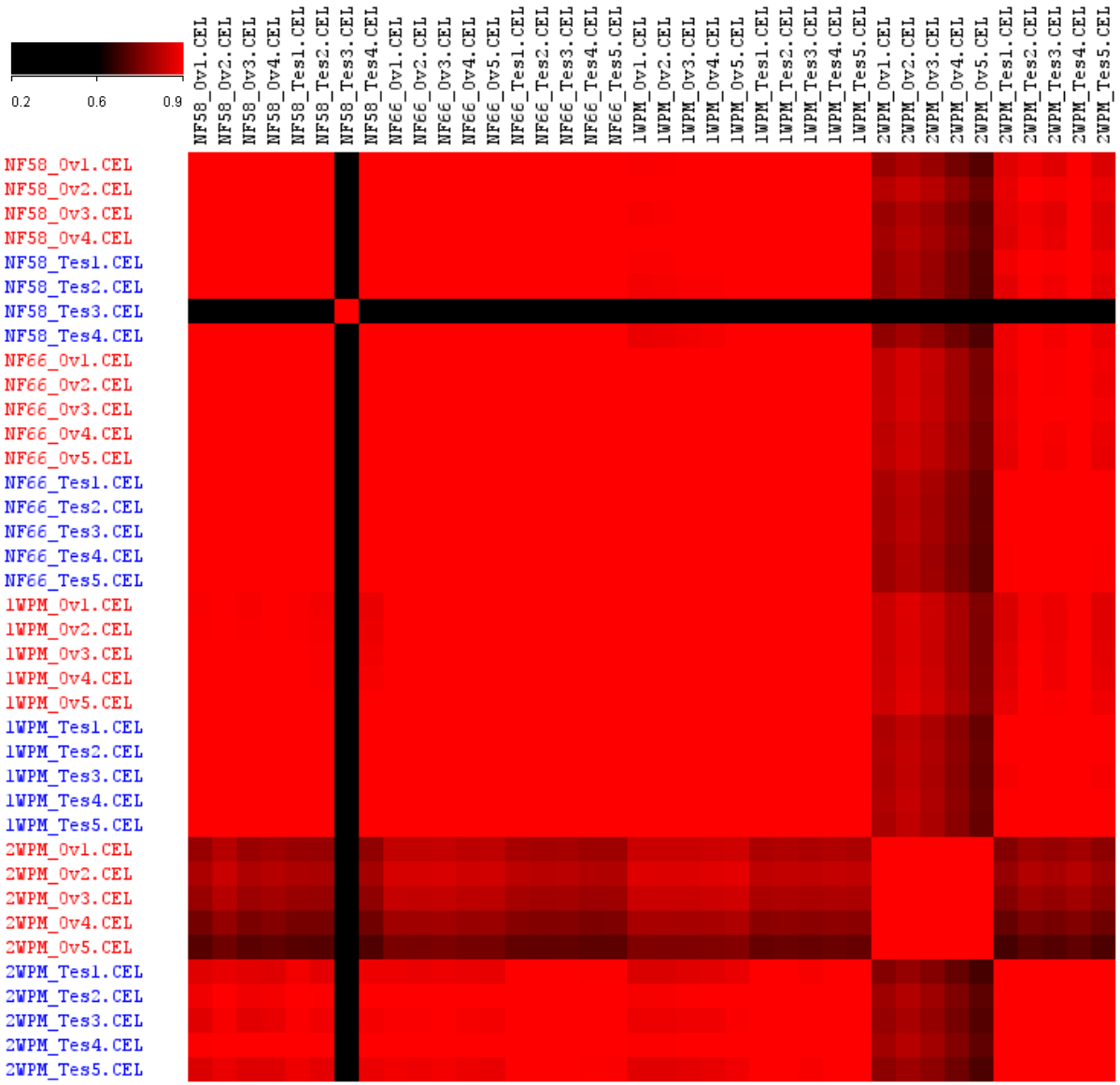

Research article

Journal of Applied Toxicology

Received: 16 November 2015, Revised: 22 March 2016, Accepted: 22 March 2016 Published online in Wiley Online Library: 30 May 2016

(wileyonlinelibrary.com) DOI 10.1002/jat.3336

Development of the Larval Amphibian Growth and Development Assay: Effects of benzophenone-2 exposure in *Xenopus laevis* from embryo to juvenile

Jonathan T. Haselman[a]*, Maki Sakurai[b], Naoko Watanabe[b], Yasushi Goto[b], Yuta Onishi[b], Yuki Ito[b], Yu Onoda[b], Patricia A. Kosian[a], Joseph J. Korte[a], Rodney D. Johnson[a], Taisen Iguchi[c] and Sigmund J. Degitz[a]

ABSTRACT: The Larval Amphibian Growth and Development Assay (LAGDA) is a globally harmonized chemical testing guideline developed by the U.S. Environmental Protection Agency in collaboration with Japan's Ministry of Environment to support risk assessment. The assay is employed as a higher tiered approach to evaluate effects of chronic chemical exposure throughout multiple life stages in a model amphibian species, *Xenopus laevis*. To evaluate the utility of the initial LAGDA design, the assay was performed using a mixed mode of action endocrine disrupting chemical, benzophenone-2 (BP-2). *X. laevis* embryos were exposed in flow-through conditions to 0, 1.5, 3.0 or 6.0 mg l^{-1} BP-2 until 2 months post-metamorphosis. Overt toxicity was evident throughout the exposure period in the 6.0 mg l^{-1} treatment due to elevated mortality rates and observed liver and kidney pathologies. Concentration-dependent increases in severity of thyroid follicular cell hypertrophy and hyperplasia occurred in larval tadpoles indicating BP-2-induced impacts on the thyroid axis. Additionally, gonads were impacted in all treatments with some genetic males showing both testis and ovary tissues (1.5 mg l^{-1}) and 100% of the genetic males in the 3.0 and 6.0 mg l^{-1} treatments experiencing complete male-to-female sex reversal. Concentration-dependent vitellogenin induction occurred in both genders with associated accumulations of protein in the livers, kidneys and gonads, which was likely vitellogenin and other estrogen-responsive yolk proteins. This is the first study that demonstrates the endocrine effects of this mixed mode of action chemical in an amphibian species and demonstrates the utility of the LAGDA design for supporting chemical risk assessment.
Copyright © 2016 John Wiley & Sons, Ltd.

Additional supporting information may be found in the online version of this article at the publisher's web site.

Keywords: *Xenopus laevis*; benzophenone-2; thyroid; gonad dysgenesis; LAGDA; OECD Test 241; OCSPP 890.2300

Introduction

The Ministry of the Environment (MOE), Government of Japan, uses a tiered system for risk assessment of chemicals having endocrine activities (MOE, 2010). The U.S. Environmental Protection Agency's Endocrine Disruptor Screening Program (EDSP) uses a similar tiered approach for prioritizing the testing of chemicals for risk assessment (EDSP Website). Tier 1 screening consists of a battery of *in vitro* and short-term *in vivo* tests to identify whether a chemical has the potential to interact with some aspect of the endocrine system. Over the last decade, Japan's MOE collaborated with the US EPA to develop Tier 2 *in vivo* tests that are longer-term chronic exposures meant to evaluate chemical effects across a range of exposure levels throughout multiple life stages in fish and amphibians (Organization for Economic Cooperation and Development [OECD], 2015a,b; US EPA, 2015a,b).

The Larval Amphibian Growth and Development Assay (LAGDA) is a multiple life-stage aqueous exposure beginning with embryos and proceeding to the juvenile stage in model amphibian species, *Xenopus laevis*. It was designed to evaluate adverse effects of chronic chemical exposure on thyroid-mediated amphibian metamorphosis, reproductive development, generalized organ toxicity, in addition to apical outcomes such as survival and growth. The LAGDA guideline was recently reviewed and approved by the Validation Management Group for Ecotoxicity Testing within the OECD (2015b) setting the stage for this assay to be used globally for generating data suitable for ecological risk assessment. The US EPA has also published the LAGDA under the EDSP 890 series of test guidelines (US EPA, 2015b). The work presented here was performed to aid validation efforts for the initial assay design and contribute to the refinement of the final test guideline. Two other studies contributing to the validation effort are presented in a companion paper (Haselman *et al.*, 2016) along with results

*Correspondence to: Jonathan T. Haselman, US EPA ORD/NHEERL/Mid-Continent Ecology Division, 6201 Congdon Blvd., Duluth, MN 55804, USA.
E-mail: haselman.jon@epa.gov

[a]US EPA ORD/NHEERL/Mid-Continent Ecology Division, 6201 Congdon Blvd, Duluth, MN 55804, USA

[b]Institute of Environmental Ecology, IDEA Consultants Inc., 1334-5 Riemon, Yaizu, Shizuoka 421-0212, Japan

[c]Okazaki Institute for Integrative Bioscience, National Institute for Basic Biology, National Institutes of Natural Sciences, 5-1 Higashiyama, Myodaiji, Okazaki, Aichi 444-8787, Japan

Copyright © 2016 John Wiley & Sons, Ltd.

demonstrating the apical effects of exposure to either 4-*tert*-octylphenol or 17β-trenbolone.

In this case, the utility of the LAGDA approach was evaluated by testing an environmentally relevant suspected endocrine disrupting compound, benzophenone-2 (BP-2). Benzophenones, are used as ultraviolet (UV) filters in personal care products such as cosmetics and sunscreens and in many other products for UV protection. Benzophenones have been found in aquatic and terrestrial environments (Balmer *et al*., 2005; Jeon *et al*., 2006; Kim & Choi, 2014, review [BP-3]; Schlenk *et al*., 2005) and drinking water (Loraine & Pettigrove, 2006). BP-2 has been found to be estrogenic (Kunz & Fent, 2006; Molina-Molina *et al*., 2008), androgenic and anti-androgenic *in vitro* (Kunz & Fent, 2006) and estrogenic in fish *in vivo* (Kunz *et al*., 2006). BP-2 is capable of impacting reproduction in fish by inhibiting germ cell development, inducing vitellogenin (Vtg) production in both genders and feminizing secondary sex characteristics in males (Weisbrod *et al*., 2007). In addition to this documented estrogenic activity, BP-2 has been shown to be a thyroid peroxidase (TPO) inhibitor (Paul *et al*., 2014; Schmutzler *et al*., 2007), and exposure to BP-2 can result in disruption of the thyroid axis in aquatic (Thienpont *et al*., 2011) and mammalian species (Jarry *et al*., 2004). Based on these putative modes of action, it was hypothesized that this chemical would elicit multiple measurable endocrine-related effects in *X. laevis* and provide significant value in terms of organism response and utility of the approach. In addition, testing of BP-2 using the LAGDA provided a unique study of a mixed mode of action chemical that has not been previously tested in amphibian species.

Materials and methods

Experimental design

The experimental design and other details of the LAGDA protocol are presented in a companion paper (Haselman *et al*., 2016). The current study was conducted by the Institute of Environmental Ecology, Japan by following the LAGDA protocol with the exception of using three test concentrations and a control, each with four replicates instead of running four test concentrations, each with four replicates and a control with eight replicates. To describe briefly the experimental details, *X. laevis* embryos (approximately stage 8 Nieuwkoop & Faber [NF], 1994) were exposed to three different chemical concentrations and control water until 10 weeks after the median time to NF stage 62 (NF62) in controls, at which time the test was terminated and juvenile samples were collected and evaluated. Interim subsamples were collected at larval NF62 to assess growth, somatic development, circulating thyroxine and thyroid gland histopathology. Endpoints evaluated in juveniles at the end of the exposure included those indicative of generalized and metabolic toxicity: growth determinations (length and weight) and histopathology of the liver and kidney. In addition, juvenile endpoints specific to reproductive development were evaluated including plasma Vtg and histopathology of the gonads and reproductive ducts. Genotypic/phenotypic sex ratios were also evaluated.

Environmental conditions

The range of environmental conditions is outlined in Table 1. The differences in test tank temperatures were generally within 1 °C for the duration of the exposure with the exception of 1 day. The differences in pH across a single treatment were within 0.5 pH units for the duration of the exposure, although there was a slight increase in pH in the 6.0 mg l^{-1} BP-2 treatment compared to the other treatments due to the pH of the stock solution.

Exposure system

A modified version of the continuous-flow mini-diluter exposure system, as explained by Benoit *et al*. (1982), was used. The system was composed of dilution water cells, mixing/flow-splitter cells and metering pumps with wetted surfaces consisting of glass, stainless steel and Teflon®. Glass tanks were used as test chambers that could hold 7 liters of test solution or control water at a water depth of 18 cm with flow rates of 25 ml min^{-1} throughout the exposure. Stock solutions of test chemical were accurately injected into the mixing cells with metering pumps (NP-KX-105; Nihon Seimitsu Kagaku Co. Ltd., Tokyo, Japan) where they were diluted with water to achieve the various test concentrations. The dilution water came from a groundwater well, was filtered through activated charcoal and then supplemented with potassium iodide to achieve an iodide (I^-) concentration of 0.5 μg l^{-1}.

Chemical stock preparation

A BP-2 reagent (i.e., 2,2′,4,4′-tetrahydroxybenzophenone; CAS: 131-55-5; lot number: KWP4417; purity: ≥ 95%) was obtained from Wako Pure Chemical Industries, Ltd. (Osaka, Japan). To prepare stock solutions, 16 g of BP-2 was dissolved in 160 ml of 1 M NaOH (JIS Special Grade; Wako) and then 240 ml deionized (DI) water was added before being quantitatively transferred to a 5 liter bottle. The volume was brought up to 3.5 liters with DI water and then, while stirring constantly, the pH was slowly adjusted to 8.5–8.8 with 1 M HCl (JIS Special Grade; Wako). The final volume was brought up to 4 liters with DI water and resulted in a stock solution of 4 g l^{-1}. This stock was further diluted with DI water to prepare

Table 1. Measured ranges of water quality parameters and environmental conditions

Environmental condition	Range	Frequency tested	Source water
Water temperature	20.0–21.9 °C	Daily	All tanks
pH	6.79–8.06	2 × per week	All tanks
Dissolved oxygen	4.29–8.02 mg l^{-1}	2 × per week	All tanks
Alkalinity	40–55 mg $CaCO_3$ l^{-1}	1 × per month	Dilution water
Hardness	61–66 mg $CaCO_3$ l^{-1}	1 × per month	Dilution water
Conductivity	173–230 μS cm^{-1}	1 × per month	All tanks
Photoperiod	12 h/12 h (light/dark)	N/A	N/A
Light intensity at water surface	630–1020 lux	1 × per month	All tanks

Copyright © 2016 John Wiley & Sons, Ltd.

stocks at 2 and 1 g l^{-1}. The 4, 2 and 1 g l^{-1} stocks were delivered to the test system mixing cells as previously described.

Test animals

Parental animals, adult *X. laevis* purchased from Hamamatsu Seibutsu Kyozai (Shizuoka, Japan), were injected with human chorionic gonadotropin (hCG; Sigma–Aldrich Co, St. Louis, MO, USA) the day before test initiation. Males received a priming injection of 400 IU of hCG in the dorsal lymph sac, followed by a boosting injection of 400 IU hCG 10 h after the priming injection. Females received a boosting injection of 1000 IU hCG. The following day, eggs were collected, cysteine treated to remove the jelly coats and transferred to crystallizing dishes to screen for viable embryos and identify developmental stage.

Test initiation and procedures

The test was initiated by randomly distributing 30 NF8–9 embryos to each tank. On day 4, the number of larvae in all tanks was balanced based on the lowest number left in any particular tank (29 larvae per tank). All test methods including feeding, NF62 larval subsampling, larval blood thyroxine (T4) analyses, the post-metamorphosis cull, juvenile sampling and somatic growth measurements were performed as described by Haselman *et al.* (2016); genetic sexing of juveniles was performed using methods described by Yoshimoto *et al.* (2008). The goal in this study was to randomly sample seven NF62 larvae per replicate to evaluate growth and thyroid-related endpoints. Owing to excessive mortality in the 6.0 mg l^{-1} treatment, NF62 sample numbers averaged four per replicate in that treatment, whereas NF62 sample numbers for the other treatments averaged seven per replicate. For the juvenile sampling, the goal was to sample even numbers of genetic males and females with a maximum of 10 individuals per replicate following the post-metamorphosis cull. Owing to excessive mortality in the 6.0 mg l^{-1} treatment, sample numbers ranged from six to nine per replicate in that treatment with generally even numbers of genetic males and females, whereas the other treatments averaged 10 per replicate with even numbers of genetic males and females per replicate.

Histological procedures

All tissues preserved for histological analyses were initially fixed in Davidson's fluid for 48 h and tissues were processed into paraffin for hematoxylin and eosin staining and sectioning. Histopathologic findings were scored for severity according to the following grading system: NR = not remarkable; grade 1 = minimal ($<$ 10% of tissue affected); grade 2 = mild/slight ($\geq$ 10% but $<$ 40% of tissue affected); grade 3 = moderate ($\geq$ 40% but $<$ 80% of tissue affected); and grade 4 = severe ($\geq$ 80% of tissue affected).

Of the seven NF62 larvae sampled per replicate, five were randomly chosen to be evaluated for thyroid pathology, with the exception of the 6.0 mg l^{-1} treatment where all samples were evaluated. The larval thyroid glands were step-sectioned transversely from caudal to rostral at approximately 60 μm intervals. Two sections containing bilateral gland tissue with approximately the largest cross-sectional area were evaluated for pathology by light microscopy according to previously reported criteria (Grim *et al.*, 2009).

The juvenile livers were embedded in paraffin and oriented to produce the largest two-dimensional area of section. Two 4 μm thick sections were acquired at 200 μm intervals and mounted on a single slide per individual and evaluated by light microscopy for pathology.

The juvenile gonad, kidney and reproductive ducts were processed, sectioned and evaluated within the same sections. Tissues were step-sectioned transversely at 200 μm (testis) or 400 μm (ovary) intervals and all serial sections were mounted on one or more slides per individual. Sections representing anterior, middle and posterior regions of the gonad were selected and examined for pathology by light microscopy. For a given pathology, the most severe score among the three sections was used for subsequent analyses.

Plasma vitellogenin enzyme-linked immunosorbent assay

Plasma Vtg was measured by a sandwich enzyme-linked immunosorbent assay (ELISA) method previously developed by Mitsui *et al.* (2003, 2007). The Vtg standard used by the ELISA was purified from serum of an adult male *X. laevis* stimulated by estradiol. The purified Vtg was then used to produce the polyclonal antibodies used in the ELISA.

Exposure verification

Analyses of BP-2 concentrations in the test chambers were conducted weekly throughout the exposure period. Each week, water samples from two of the four replicate tanks were collected and subjected to chemical analysis for all BP-2 treatments and control resulting in all four replicate tanks per treatment being analyzed every 2 weeks. BP-2 concentrations were determined using liquid chromatography (LC, ACQUITY UPLC; Waters Corporation, Milford, MA, USA) tandem mass spectrometry (MS/MS, Micromass Quattro Ultima; Waters Corporation). Water samples containing BP-2 were diluted with acetonitrile (ACN) to final ACN concentrations of 99.50% (1.5 mg l^{-1}), 99.75% (3 mg l^{-1}) and 99.88% (6 mg l^{-1}). Five microliters of sample was injected into an LC-MS/MS containing a BEH C18 column (2.1 mm × 100 mm, 1.7 μm; Waters Corporation) maintained at 40 °C. Mobile phase A was 10 mM ammonium acetate and mobile phase B was 100% ACN. The column was eluted under the following gradient conditions at a flow rate of 0.3 ml min^{-1}: 5% B (0–1 min), 5% → 80% B (1–3 min), 80% B (3–6 min), 80% → 5% B (6–6.1 min), 5% B (6.1–10 min). The MS/MS was equipped with an electrospray ionization source and was operated in negative ionization mode. Multiple reaction monitoring was used; the precursor to product ion transition was 245 *m/z* to 135 *m/z* (quantifier ion). The collision energy was 15 V and the collision gas was nitrogen. BP-2 concentrations in the water samples were calculated based on the peak area response of the quantifier ion. For these measurement conditions, the detection limit of BP-2 was 0.5 ng ml^{-1}. For the exposure water samples, the mean ± SD (n = 36) measured concentrations were 1.6 ± 0.1, 3.5 ± 0.2 and 6.1 ± 0.1 mg l^{-1} over the duration of the experiment for the 1.5, 3.0 and 6.0 mg l^{-1} nominal BP-2 treatments, respectively. CVs (averaged across the duration of the exposure) were 4, 6 and 1% for the 1.5, 3.0 and 6.0 mg l^{-1} treatments, respectively. No BP-2 was detected in control water.

Statistical analyses

Statistical procedures were followed as described by Haselman *et al.* (2016). Briefly, continuous data were tested for monotonicity by fitting to an ANOVA model and comparing linear and quadratic contrasts of normalized rank statistics. If the data were monotonic,

Copyright © 2016 John Wiley & Sons, Ltd.

a Jonckheere–Terpstra test was used to determine significant treatment effects. If the data were non-monotonic, significant treatment effects were determined using a mixed-effects ANOVA followed by Dunnett's test. Time-to-NF62 data were analyzed using a Cox mixed-effects proportional hazard model (http://cran.r-project.org/web/packages/coxme/coxme.pdf). Ordinal data (e.g., histopathology incidence rates and severity scores) were analyzed using the Rao–Scott Cochran–Armitage by slices test (RSCABS) (Green *et al.*, 2014). For all statistical approaches, $P < 0.05$ was considered statistically significant. When calculating treatment means and SDs, the replicate tank was considered the experimental unit, so there were four biological replicates per treatment and control.

Results

Survival, growth and development

There appeared to be no effect on survival (Fig. 1), growth or development (Table 2) in the 1.5 or 3.0 mg l^{-1} treatments. However, the 6.0 mg l^{-1} experienced significantly increased mortality rates throughout the exposure period and also experienced a significant delay in development with an associated significant increase in growth at NF62 (Table 2). This increase in tadpole size is consistent with previous reports following exposure to thyroid axis disruptors, which produce a significant developmental delay (Degitz *et al.*, 2005; Tietge *et al.*, 2005); delayed larval development allows more time for organisms to feed and grow. Another potential contributor to increased growth in the 6 mg l^{-1} treatment could be the significant mortality experienced in that treatment allowing the survivors more access to food.

Juvenile growth rates were unaffected in the 1.5 mg l^{-1} treatment, whereas juvenile growth was decreased by exposure to 3.0 mg l^{-1} BP-2, although this was not statistically significant (Fig. 2). The 6.0 mg l^{-1} treatment caused a significant decrease in juvenile growth rates as compared to control. Juvenile liver-somatic index showed a hormetic response in both genders (Fig. 2). In genetic females, the 1.5 mg l^{-1} treatment exhibited a moderate, but insignificant, increase in the mean liver-somatic index compared to the control while the 3 mg l^{-1} treatment was significantly higher than the control and the 6.0 mg l^{-1} treatment was significantly lower than the control. Genetic males showed the same trend but were not statistically different than the control. This hormetic response

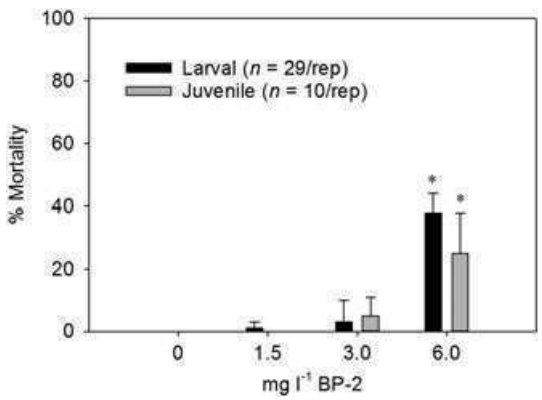

Figure 1. Mean (error bars: SD; $n = 4$ reps/treatment) percentage mortality during larval development and in juveniles post-cull. *Treatments significantly different than control as determined by Jonckheere–Terpstra test ($P < 0.05$). BP-2, benzophenone 2.

was likely due to the combination of increased Vtg production and BP-2 clearance in the livers exposed to 1.5 and 3.0 mg l^{-1} BP-2, then overt toxicity in the 6.0 mg l^{-1} treatment caused a transitional decrease in this measure.

Larval plasma thyroxine and thyroid histopathology

There were significant concentration-dependent effects on thyroid tissue due to BP-2 exposure. All treatments exhibited some level of follicular cell hypertrophy, hyperplasia and glandular hypertrophy (Fig. 3, Table 3). However, the 1.5 mg l^{-1} treatment presented with mild cases of these pathologies while the 3.0 and 6.0 mg l^{-1} treatments exhibited both increased incidences and severity of these diagnoses. The 6.0 mg l^{-1} treatment was most severely impacted with all three pathologies occurring in 100% of the surviving individuals. As noted above, there was also a significant delay in the rate of metamorphosis of these individuals exposed to 6.0 mg l^{-1} BP-2 (Table 2). Attempts were made to measure T4 levels in plasma using both the optimized ELISA described in Haselman *et al.* (2016) and the high-performance liquid chromatography/inductively coupled plasma-MS method described in Tietge *et al.* (2010). Significant interference by Vtg and other estrogen-responsive yolk proteins was suspected as the cause of erratic and inconsistent data that compromised the analyses (data not shown).

Juvenile plasma vitellogenin

There was a significant concentration-dependent induction of Vtg in all treatments compared to the control and the response was very consistent between genders (Fig. 2). The overall response was a > 5000-fold induction in the 6.0 mg l^{-1} treatment in both genetic males and females compared to the control. This illustrates the estrogenic properties of BP-2 and emphasizes the potential magnitude of response of this endpoint.

Juvenile gonad histopathology

In the 1.5 mg l^{-1} treatment, genetic males experienced feminization of the gonad resulting in both intersex gonads (e.g., presence of testicular oocytes and partial ovarian cavity) and sex-reversed gonads (Fig. 4, Table 4). Thinning of the germinal epithelium is specific to testis tissue, and significant increases in prevalence and severity of this pathology were observed in the 1.5 mg l^{-1} treatment (Table 4). In the 3.0 and 6.0 mg l^{-1} treatments, 100% of the genetic males had been completely sex-reversed exhibiting only ovarian tissue (i.e., phenotypic females). In genetic females, there was a significant treatment-related delay in ovary development based on differences in developmental stages of ovaries in control versus treated samples (Table 4). Similarly, there was a treatment-related delay in ovary development in sex-reversed genetic males. Mononuclear cellular infiltrate was observed in gonads of genetic males and females across all treatments and the control, but prevalence and severity were significantly attenuated in the 3.0 and 6.0 mg l^{-1} treatments for genetic females (Table 4). Prevalence and severity of proteinaceous fluid infiltrate were significantly increased in both genders in the 3.0 and 6.0 mg l^{-1} treatments (Table 4).

Juvenile reproductive duct histopathology

Müllerian ducts in control males at this stage of juvenile development are actively regressing (stage 1; Fig. 5A), which is thought to be induced by hormonal control from the gonad. In general,

Copyright © 2016 John Wiley & Sons, Ltd.

Table 2. NF62 growth and development following BP-2 exposure (mean ± SD; $n = 4$)

BP-2 conc. (mg l^{-1})	Weight (g)	Snout-vent length (mm)	Time to NF62 (d)
0	1.18 ± 0.09	22.2 ± 0.5	37 ± 2
1.5	1.05 ± 0.08	21.5 ± 0.4	36 ± 1
3.0	1.18 ± 0.10	22.2 ± 0.8	37 ± 1
6.0	1.92 ± 0.15*	25.3 ± 0.8*	47 ± 1*

* Significantly different than control as determined by Jonckheere–Terpstra test ($P < 0.05$).

effects of BP-2 exposure on this process in the majority of genetic males were equivocal (Table 5). However, there were a few individuals in the 1.5 and 3.0 mg l^{-1} treatments that exhibited oviducts two stages more advanced than the majority of the other genetic males (stage 4; Fig. 5C). In control juvenile females, Müllerian ducts are maturing into oviducts (stage 2; Fig. 5B), which is a process thought to be estrogen-mediated. Interestingly, BP-2 exposure generally inhibited oviduct maturation in the majority of genetic females across all treatments (Table 5), but there were a series of individuals in the 1.5 and 3.0 mg l^{-1} treatments that were two stages more advanced than the other genetic females in the same treatment, a notable pattern similar to genetic males exposed to 1.5 or 3.0 mg l^{-1} BP-2. Wolffian duct development appeared to

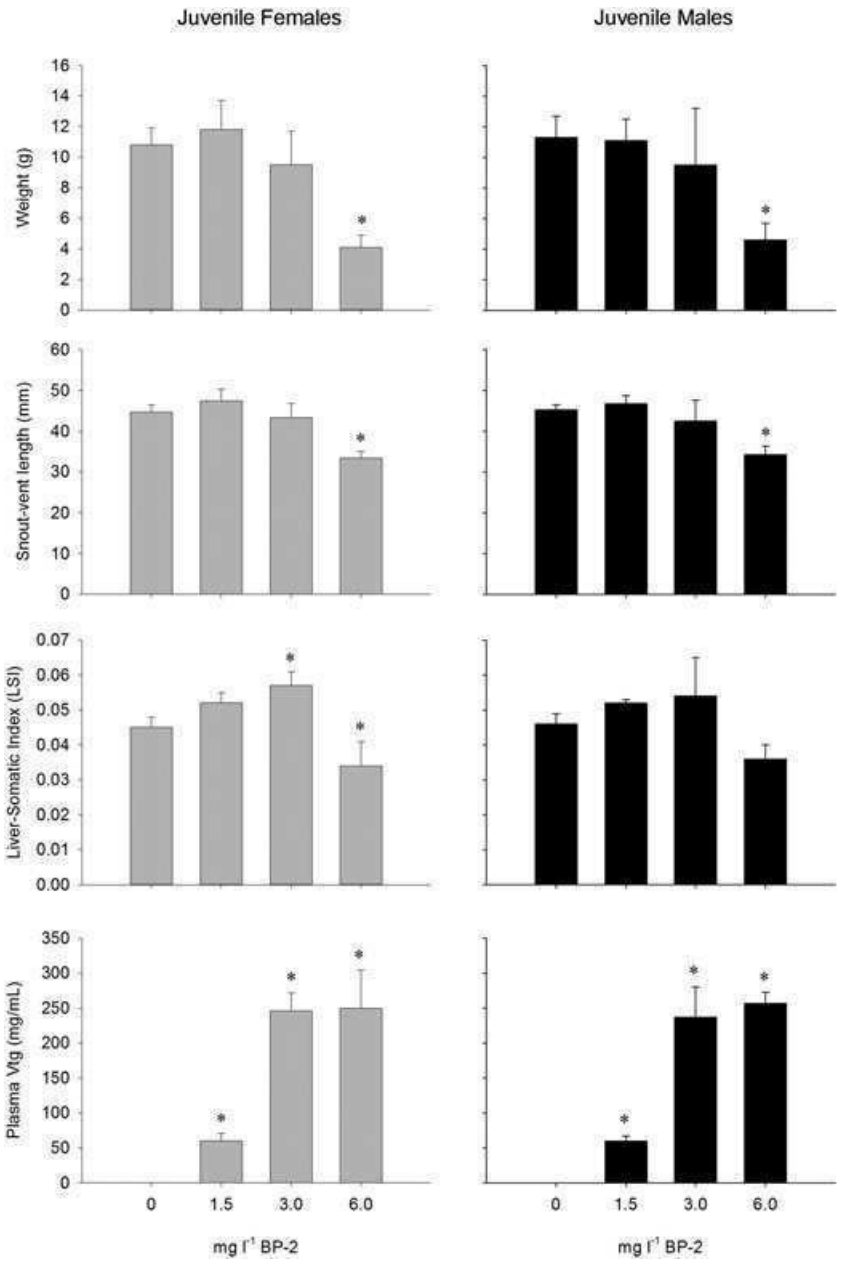

Figure 2. Mean (error bars: SD; $n = 4$) juvenile growth, liver-somatic index and plasma Vtg titers following BP-2 exposure. Left-hand column of graphs (gray bars) are data from genetic females; right-hand column of graphs (black bars) are data from genetic males. *Treatments statistically different than control as determined by Jonckheere–Terpstra test ($P < 0.05$), with the exception of the juvenile female liver-somatic index endpoint, which was determined by a mixed-effects ANOVA followed by Dunnett's test ($P < 0.05$) due to the non-monotonic response. BP-2, benzophenone 2; Vtg, vitellogenin.

Copyright © 2016 John Wiley & Sons, Ltd.

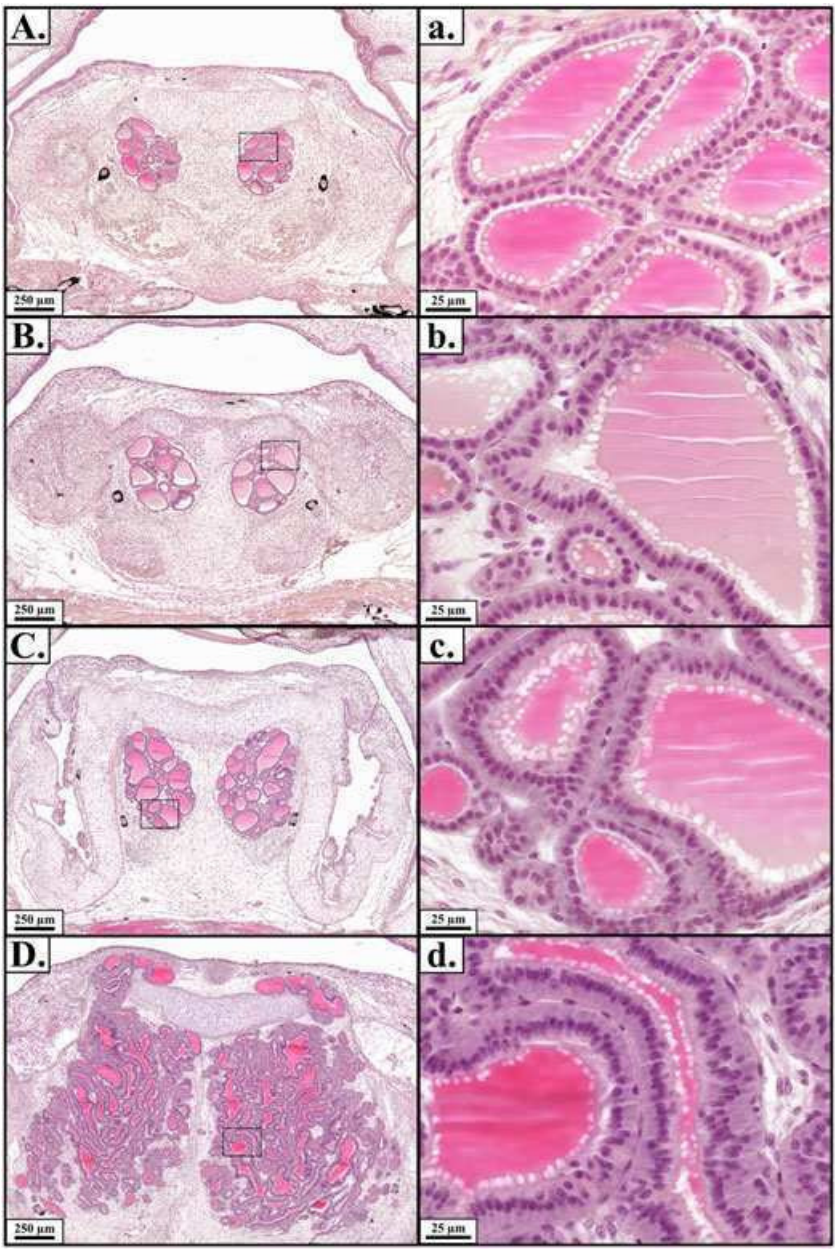

Figure 3. Transverse sections of NF62 thyroid glands from control (A, a) and BP-2 treatments of 1.5 mg l^{-1} (B, b), 3.0 mg l^{-1} (C, c) and 6 mg l^{-1} (D, d). Glands from BP-2-treated larvae show a dose-dependent increase in severity of follicular cell hypertrophy and hyperplasia and glandular hypertrophy. Control gland exhibits cuboidal follicular cells with evenly spaced nuclei. Increasing BP-2 exposure concentrations cause follicular cells to become progressively columnar with crowding and piling up of nuclei, characteristic of cellular hyperplasia. Black boxes in the left-hand column of images demarcate the areas depicted in the corresponding images to the right. (A–D) Scale bar = 250 µm; (a–d) scale bar = 25 µm. BP-2, benzophenone 2.

be unaffected in the 1.5 mg l^{-1} treatment compared to control whereas exposure to 3.0 and 6.0 mg l^{-1} BP-2 appeared to advance Wolffian duct development in both genders (Table 5).

Juvenile liver and kidney histopathology

There were no treatment-related findings in livers of individuals exposed to 1.5 mg l^{-1} BP-2, whereas all individuals (phenotypic females) in the 3.0 and 6.0 mg l^{-1} treatments exhibited a number of liver pathologies. These included concentration-dependent increases in the prevalence and severity of basophilia, decreased hepatocellular vacuolation, and intravascular proteinaceous fluid (Table S1). Individuals of the 3.0 and 6.0 mg l^{-1} treatment groups additionally had a higher prevalence of increased pigment as compared to controls, which also tended to be concentration-dependent. The few findings of individual hepatocyte necrosis were restricted to individuals in the 3.0 and 6.0 mg l^{-1} treatment groups and foci of hepatocellular alterations were only found in the 6.0 mg l^{-1} treatment group. Overall, these liver changes are likely related to estrogenic activity of BP-2 and significant upregulation of Vtg synthesis (i.e., vitellogenesis).

In the kidneys of juvenile genetic females, 1.5 mg l^{-1} BP-2 exposure caused minimal accumulation of protein in the glomerulus and interstitial fluid (Table S2). This was not observed in genetic males in the 1.5 mg l^{-1} treatment, nor were any other pathologies observed in genetic males exposed to 1.5 mg l^{-1} BP-2. However,

Copyright © 2016 John Wiley & Sons, Ltd.

Table 3. Prevalence (% of *n*) and severity of larval thyroid gland histopathological observations in BP-2-exposed larvae

	NF62 larvae			
BP-2 conc. (mg l^{-1})	0	1.5	3.0	6.0
Total *n*	20	20	20	18
Replicate tanks	4	4	4	4
Thyroid gland, hypertrophy				
NR	100	95	25	0
Mild	0	5	(75)	(0)
Moderate	0	0	0	(67)
Severe	0	0	0	(33)
Follicular cells, hypertrophy				
NR	50	30	5	0
Mild	50	70	(50)	(0)
Moderate	0	0	(45)	(33)
Severe	0	0	0	(67)
Follicular cells, hyperplasia				
NR	80	50	15	0
Mild	20	(50)	(65)	(0)
Moderate	0	0	(20)	(11)
Severe	0	0	0	(89)

NR, not remarkable.
Numbers in parentheses are significantly different than control as determined by RSCABS analysis.

exposure to BP-2 at 3.0 and 6.0 mg l^{-1} (100% female phenotypes) caused a suite of kidney pathologies in both genetic males and females (Table S2). Most notable is the accumulation of protein in the glomerulus, interstitial fluid and tubules, which is likely Vtg and other egg yolk proteins based on the observed accumulation of protein in the liver where Vtg is synthesized, and the associated high levels of circulating Vtg measured in plasma.

Discussion

Profound apical effects were observed in tissues specific to the suspected modes of action of BP-2, i.e., putative TPO inhibition causing thyroid axis disruption and estrogen receptor agonism causing Vtg induction and gonad dysgenesis. Further, this was the first study to characterize the effects of chronic, multiple life-stage exposure to BP-2 in amphibian model species, *X. laevis*, and supports the utility of the LAGDA design and approach developed through the collaborative effort between the US EPA and Japan's MOE.

Overt toxicity was evident in the 3.0 and 6.0 mg l^{-1} treatments observed as increased larval and juvenile mortality, in addition to the suite of observed liver and kidney pathologies. The profound effects observed in the livers and kidneys are likely due to the accumulation of Vtg and other estrogen-responsive yolk precursor proteins in these organs, which is consistent with estrogenic exposure in fish (Folmar *et al*., 2001; Pawlowski *et al*., 2004; Weber *et al*., 2003). Folmar *et al*. (2001) suggested that accumulation of Vtg and other estrogen-responsive proteins in the kidney led to acute renal failure in male summer flounder injected with 10 mg kg^{-1} 17β-estradiol. Although definitive identification of the accumulated protein in the current study was not performed, the weight of evidence suggests that renal failure was a likely cause of increased mortality rates in the 3.0 and 6.0 mg l^{-1} BP-2 treatments.

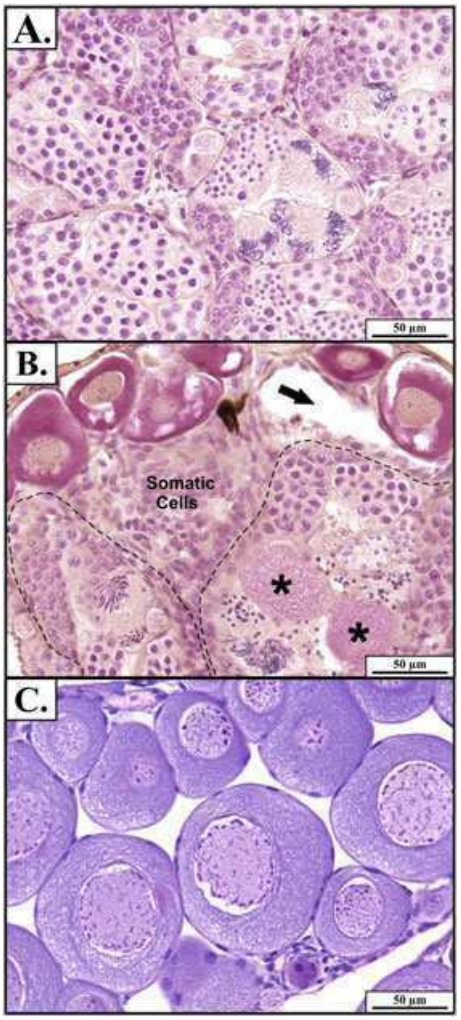

Figure 4. (A) Testis from control juvenile male exhibiting seminiferous tubules containing multiple germ cell nests. Each nest contains a population of synchronously-developing germ cells. Progressive stages of germ cell spermatogenesis can be observed, along with spermatozoa in the tubule lumen. (B) Intersex gonad of genetic male exposed to 1.5 mg l^{-1} BP-2 consists primarily of testicular tissue exhibiting seminiferous tubules (outlined) with germ cell nests, but also contains perinucleolar oocytes (*) occurring in the medulla, in addition to several oocytes occurring in the cortex (top of image). Arrow points to a putative epithelial-lined lumen characteristic of an ovarian cavity. (C) Ovary from control juvenile female containing perinucleolar oocytes. Scale bar = 50 µm.

The thyroid axis was clearly impacted by BP-2 exposure; significant treatment-related effects on thyroid tissue included increased prevalence and severity of follicular cell hypertrophy and hyperplasia and gland hypertrophy. These pathologies are indicative of thyroid axis disruption as demonstrated previously when larval *X. laevis* are exposed to various thyroid hormone synthesis inhibitors (Degitz *et al*., 2005; Tietge *et al*., 2005, 2010, 2013). Although the incidences and severity of these pathologies increased with increasing concentrations of BP-2, the 1.5 and 3.0 mg l^{-1} treatments did not exhibit an associated measurable delay in development, which would occur due to depleted circulating T4 levels. This emphasizes the compensatory capacity of the thyroid axis to maintain critical circulating T4 levels to support metamorphic development. Unfortunately, blood T4 levels in NF62 larvae could not be confirmed due to interference from high levels of serum protein, which were

Copyright © 2016 John Wiley & Sons, Ltd.

Table 4. Prevalence (% of *n*) and severity of juvenile gonad histopathological observations showing significant treatment-related effects following BP-2 exposure

	Genetic male				Genetic female			
BP-2 conc. (mg l^{-1})	0	1.5	3.0	6.0	0	1.5	3.0	6.0
Total *n*	20	19	12	14	17	17	16	9
Replicate tanks	4	4	4	4	4	4	4	4
Gonad phenotype								
1 (Testis)	100	37	0	0	0	0	0	0
2	0	(32)	0	0	0	0	0	0
3	0	0	0	0	0	0	0	0
4	0	0	0	0	0	0	0	0
5 (Ovary)	0	(32)	(100)	(100)	100	100	100	100
Gonad stage								
1	0	0	0	0	0	6	6	0
2	5	5	0	0	0	6	0	0
3	0	16	42	100	0	12	44	89
4	45	58	(58)	(0)	100	(76)	(50)	(11)
5	50	(21)	(0)	(0)	0	0	0	0
Testicular oocytes								
NR	100	53	0	0	–	–	–	–
Minimal	0	(11)	0	0	–	–	–	–
Mild	0	5	0	0	–	–	–	–
Moderate	0	0	0	0	–	–	–	–
Severe	0	0	0	0	–	–	–	–
Germinal epithelium, thinning								
NR	100	47	0	0	–	–	–	–
Minimal	0	(11)	0	0	–	–	–	–
Mild	0	(5)	0	0	–	–	–	–
Moderate	0	5	0	0	–	–	–	–
Severe	0	0	0	0	–	–	–	–
Mononuclear cellular infiltrate								
NR	90	79	83	86	47	35	88	100
Minimal	10	21	17	14	41	35	(13)	(0)
Mild	0	0	0	0	12	29	0	0
Moderate	0	0	0	0	0	0	0	0
Severe	0	0	0	0	0	0	0	0
Proteinaceous fluid Infiltrate								
NR	100	100	8	0	100	94	0	0
Minimal	0	0	(67)	(21)	0	6	(63)	(33)
Mild	0	0	(25)	(79)	0	0	(31)	(44)
Moderate	0	0	0	0	0	0	6	(22)
Severe	0	0	0	0	0	0	0	0

NR, not remarkable.
Numbers in parentheses are significantly different than control based on RSCABS analysis.

presumably estrogen-responsive yolk proteins, including Vtg. The 6 mg l^{-1} treatment did, however, experience a significant delay in development and exhibited remarkable thyroid pathologies in 100% of the subjects, suggesting a point of departure where T4 homeostasis could no longer be maintained. It is acknowledged that this observed delay in metamorphosis could have also been due to overt toxicity. However, the thyroid histopathology assessment confirmed substantial compensatory responses in that tissue, suggesting thyroid-stimulating hormone stimulation was occurring due to depleted blood T4 levels. Schmutzler *et al.* (2007) has shown that BP-2 is a mammalian TPO inhibitor *in vitro* and *in vivo*. When *X. laevis* larvae are exposed to known TPO inhibitors methimazole, propylthiouracil (Degitz *et al.*, 2005; Tietge *et al.*, 2010) or mercaptobenzothiazole (Tietge *et al.*, 2013), thyroid glands exhibit the same severe pathologies observed in this study, supporting that BP-2 is a TPO inhibitor in this species also.

With regard to thyroid-related outcomes from the LAGDA, it must be acknowledged that an alteration in metamorphic development is not the only adverse effect of hypothyroidism that could have population-level implications. Typically, metamorphic development, coupled with thyroid histopathology, has served as a robust evaluation of a chemical's potential to impact the thyroid axis and/or overwhelm thyroid axis compensation resulting in a clear adverse developmental outcome. Given the regulatory context for which the LAGDA was developed, a clear assessment of this thyroid-mediated apical effect was necessary to include in the assay design. However, a drawback of this approach is that thyroid-related outcomes falling short of an apical

Copyright © 2016 John Wiley & Sons, Ltd.

Journal of Applied Toxicology

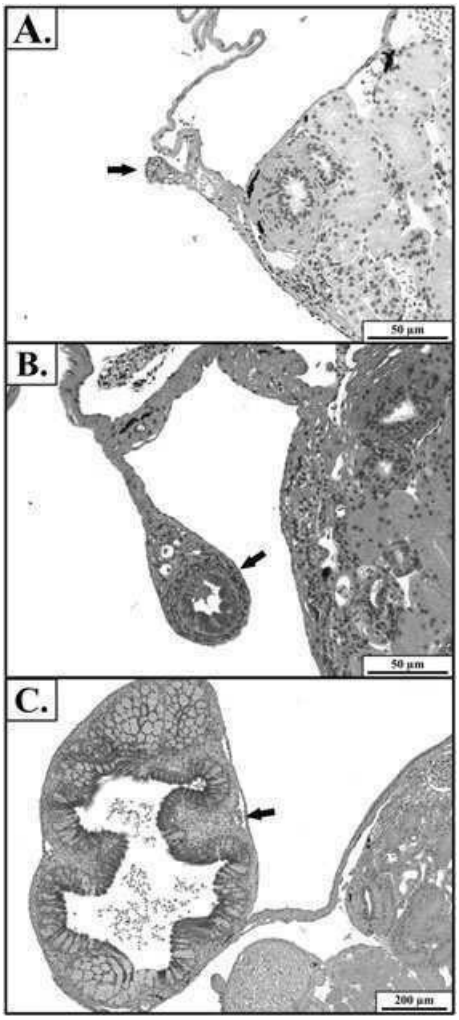

Figure 5. (A) Müllerian duct from control juvenile male has regressed to a fibrous tag (stage 1). (B) Immature oviduct from control juvenile female exhibits an epithelial-lined lumen (stage 2). (C) Mature oviduct from a juvenile genetic male/phenotypic female exposed to 3.0 mg l^{-1} benzophenone-2 with mature oviduct cells and a well-defined lumen (stage 4). (A,B) Scale bar = 50 µm; (C) scale bar = 200 µm.

effect on development makes interpretation difficult and inconclusive, depending on one's definition of adversity. As an example of other hypothyroid-related adverse outcomes, recent studies have shown that developmental exposure to propylthiouracil in rats caused only minor reductions in circulating T4 and minor changes in thyroid morphology, but caused permanent neurodevelopmental damage (Gilbert *et al*., 2016; Johnstone *et al*., 2013). Given the state of the science during the development of the LAGDA, evaluations of neurological effects were not pursued. However, much progress has been made in recent years utilizing *Xenopus* as a model for studying neurodevelopmental disorders by means of organismal swimming behavior, whole brain immunostaining, Ca^{2+} imaging, neuronal cell imaging and synapse electrophysiology (reviewed by Pratt & Khakhalin, 2013). When these diagnostic techniques prove to be predictive of adverse apical outcomes having population-level implications in amphibians, definitive neurological evaluations could be integrated into the LAGDA procedure. However, as the LAGDA design currently stands, it is recommended that subapical-level hypothyroid effects be interpreted with caution; these effect levels warrant a weight-of-evidence approach for environmental risk assessment.

Despite the thyroid-related effects observed in this study, most individuals exposed to BP-2 successfully completed metamorphosis and experienced further endocrine effects on reproductive development. Every genetic male in the 3.0 and 6.0 mg l^{-1} treatments experienced sex reversal exhibiting generally normal ovaries, albeit less mature compared to control ovaries. Typically, interpretation of endocrine disruption is confounded by overt toxicity, but in this case, overt toxicity and endocrine disruption appear to have substantial overlap. This is also evidenced by the concentration-dependent nature of gonad dysgenesis, as there were examples of normal testes, intersexed gonads and sex-reversed gonads all in the lowest BP-2 treatment of 1.5 mg l^{-1}, an exposure concentration that did not produce overt toxicity. The occurrence of 100% sex reversal at concentrations exceeding the 1.5 mg l^{-1} threshold cannot be discounted due to the co-occurrence of overt toxicity. This study supports the notion that endocrine-specific effects can indeed be evaluated in concert with overt toxicity. Furthermore, the endocrine-related effect of Vtg induction has the potential to be a main contributor to overt toxicity as the organisms are unable to excrete this protein, resulting in toxic accumulations. This would be a case where the endocrine effect actually causes the transition to overt toxicity and death.

In the current study, gonad development and induction of Vtg were profoundly affected due to apparent estrogenicity of BP-2, but impacts on oviducts in both males and females were erratic. Advanced oviduct maturation in both genetic males and females was induced by the weak estrogen 4-*tert*-octylphenol in our companion study (Haselman *et al*., 2016), leading us to believe that the estrogenic properties of BP-2 would induce similar effects on oviduct development here. However, many genetic females showed concentration-dependent delays in oviduct development while some females in the 1.5 and 3.0 mg l^{-1} treatments presented with oviducts that were two stages more advanced than the majority of controls, appearing as a binary response. Genetic males showed a similar pattern with a select few individuals in the 1.5 and 3.0 mg l^{-1} treatments also having stage 4 oviducts. While the effective concentrations of the two xenoestrogens differed by several orders of magnitude, the differences in reproductive effects observed in the two studies suggests that BP-2 acts through multiple modes of action within the hypothalamic–pituitary–gonadal axis. Oviduct regression in males is understood to be regulated by anti-Müllerian hormone (Kelley, 1996) and oviduct regression can be induced by the androgen 17β-trenbolone in *X. laevis* (Haselman *et al*., 2016). BP-2 has been shown to have both estrogenic and androgenic activity *in vitro* in recombinant yeast systems (Kunz & Fent, 2006), so it is possible that the delay in oviduct maturation observed in genetic females in this study is actually due to the androgenic properties of BP-2. The binary nature of the BP-2-induced oviduct response suggests that interesting toxicodynamics are at work in this concentration range that cannot be explained by these data. In any case, proper oviduct development is critical for successful reproduction and these studies demonstrate that oviducts are sensitive to hormonal perturbations during reproductive development. Therefore, further research would help to elucidate these mechanisms of oviduct maturation and regression to better interpret the apical effects and distinguish between classes of putative (anti-)estrogenic and (anti-)androgenic endocrine disrupting chemicals.

BP-2 exposure, at the relatively high concentrations tested, had profound effects on multiple facets of the *X. laevis* endocrine

 Copyright © 2016 John Wiley & Sons, Ltd.

Table 5. Histological staging of juvenile reproductive ducts following BP-2 exposure

	Genetic male				Genetic female			
BP-2 conc. (mg l^{-1})	0	1.5	3.0	6.0	0	1.5	3.0	6.0
Total *n*	20	19	12	14	17	17	16	9*
Replicate tanks	4	4	4	4	4	4	4	4
Oviduct stage								
Not present	5	0	0	0	0	0	0	0
1	95	89	92	93	6	(35)	(81)	(89)
2	0	0	0	7	88	0	0	0
3	0	0	0	0	6	0	0	0
4	0	11	8	0	0	65	19	0
Wolffian duct stage								
1	30	37	33	36	18	41	6	33
2	70	58	17	43	76	59	38	33
3	0	5	(50)	(21)	6	0	(50)	(11)
4	0	0	0	0	0	0	6	(11)

Numbers are expressed as percentages of *n* and numbers in parentheses are significantly different than control based on RSCABS analysis.

* One individual was unable to be evaluated due to missing tissue.

system. Although it is not likely that these levels of BP-2 would be encountered in the natural environment, this study successfully demonstrated the potential for this chemical to impact multiple endocrine targets and lead to adverse apical outcomes. These adverse apical outcomes occurred at exposure concentrations that also impair reproduction in fish (Weisbrod *et al*., 2007), supporting the potential for cross-species susceptibility to similar reproductive effects and highlighting the cross-species extrapolation potential of LAGDA results. This study has not only demonstrated the utility of the LAGDA approach to amphibian chronic toxicity testing, but has also characterized apical effects of exposure to a UV filtering compound that is common to everyday use.

Acknowledgments

This work was partially supported by the Ministry of the Environment, Japan. The authors would like to thank Chad Blanksma for histotechnical support and Dr. Michael Hornung for thoughtful comments and suggestions to improve this manuscript. This paper has been reviewed according to ORD guidelines, but the statements made do not represent views of the US EPA, nor does mention of trade names indicate endorsement by the federal government.

Conflict of interest

The authors did not report any conflict of interest.

References

Balmer ME, Buser HR, Müller MD, Poiger T. 2005. Occurrence of some organic UV filters in wastewater, in surface waters, and in fish from Swiss lakes. *Environ. Sci. Technol.* **39**(4): 953–962.

Benoit DA, Mattson VR, Olson DL. 1982. A continuous-flow mini-diluter system for toxicity testing. *Water Res.* **16**(4): 457–464.

Degitz SJ, Holcombe GW, Flynn KM, Kosian PA, Korte JJ, Tietge JE. 2005. Progress towards development of an amphibian-based thyroid screening assay using *Xenopus laevis*. Organismal and thyroidal responses to the model compounds 6-propylthiouracil, methimazole, and thyroxine. *Toxicol. Sci.* **87**(2): 353–364.

EDSP Website. http://www.epa.gov/endo/ [24 September 2015].

Folmar LC, Gardner GR, Schreibman MP, Magliulo-Cepriano L, Mills LJ, Zaroogian G, Gutjahr-Gobellb R, Haeblerb R, Horowitz DB, Denslow ND. 2001. Vitellogenin-induced pathology in male summer flounder (*Paralichthys dentatus*). *Aquat. Toxicol.* **51**(4): 431–441.

Gilbert ME, Sanchez-Huerta K, Wood C. 2016. Mild thyroid hormone insufficiency during development compromises activity-dependent neuroplasticity in the hippocampus of adult male rats. *Endocrinology* **157**(2): 774–787.

Green JW, Springer TA, Saulnier AN, Swintek J. 2014. Statistical analysis of histopathological endpoints. *Environ. Toxicol. Chem.* **33**(5): 1108–1116.

Grim KC, Wolfe M, Braunbeck T, Iguchi T, Ohta Y, Tooi O, Touart L, Wolf DC, Tietge J. 2009. Thyroid histopathology assessments for the amphibian metamorphosis assay to detect thyroid-active substances. *Toxicol. Pathol.* **37**(4): 415–424.

Haselman JT, Kosian PA, Korte JJ, Olmstead AW, Iguchi T, Johnson RD, Degitz SJ. 2016. Development of the larval amphibian growth and development assay: Effects of chronic 4-*tert*-octylphenol or 17β-trenbolone exposure in *Xenopus laevis* from embryo to juvenile. *J. Appl. Toxicol.* DOI: 10.1002/jat.3330

Jarry H, Christoffel J, Rimoldi G, Koch L, Wuttke W. 2004. Multi-organic endocrine disrupting activity of the UV screen benzophenone 2 (BP2) in ovariectomized adult rats after 5 days treatment. *Toxicology* **205**: 87–93.

Jeon HK, Chung Y, Ryu JC. 2006. Simultaneous determination of benzophenone-type UV filters in water and soil by gas chromatography–mass spectrometry. *J. Chromatogr. A* **1131**: 192–202.

Johnstone AF, Gilbert ME, Aydin C, Grace CE, Hasegawa M, Gordon CJ. 2013. Thermoregulatory deficits in adult Long Evans rat exposed perinatally to the antithyroidal drug, propylthiouracil. *Neurotoxicol. Teratol.* **39**: 1–8.

Kelley DB. 1996. Sexual differentiation in *Xenopus laevis*. In *Symposia of the Zoological Society of London* (No. 68). The Society: London; 1960–1999.

Kim S, Choi K. 2014. Occurrences, toxicities, and ecological risks of benzophenone-3, a common component of organic sunscreen products: a mini-review. *Environ. Int.* **70**: 143–157.

Kunz PY, Fent K. 2006. Multiple hormonal activities of UV filters and comparison of *in vivo* and *in vitro* estrogenic activity of ethyl-4-aminobenzoate in fish. *Aquat. Toxicol.* **79**(4): 305–324.

Kunz PY, Galicia HF, Fent K. 2006. Comparison of *in vitro* and *in vivo* estrogenic activity of UV filters in fish. *Toxicol. Sci.* **90**(2): 349–361.

Loraine GA, Pettigrove ME. 2006. Seasonal variations in concentrations of pharmaceuticals and personal care products in drinking water and

Copyright © 2016 John Wiley & Sons, Ltd.

reclaimed wastewater in southern California. *Environ. Sci. Technol.* **40**(3): 687–695.

Ministry of the Environment, Japan. 2010. Further Actions to Endocrine Disrupting Effects of Chemical Substances: EXTEND 2010. http://www.env.go.jp/en/chemi/ed/extend2010_full.pdf. [27 April 2016]

Mitsui N, Tooi O, Kawahara A. 2003. Sandwich ELISAs for quantification of *Xenopus laevis* vitellogenin and albumin and their application to measurement of estradiol-17β effects on whole animals and primary-cultured hepatocytes. *Comp. Biochem. Physiol. C Toxicol Pharmacol.* **135**(3): 305–313.

Mitsui N, Tooi O, Kawahara A. 2007. Vitellogenin-inducing activities of natural, synthetic, and environmental estrogens in primary cultured *Xenopus laevis* hepatocytes. *Comp. Biochem. Physiol. C Toxicol. Pharmacol.* **146**(4): 581–587.

Molina-Molina JM, Escande A, Pillon A, Gomez E, Pakdel F, Cavaillès V, Oleae N, Aït-Aïssah S, Balaguer P. 2008. Profiling of benzophenone derivatives using fish and human estrogen receptor-specific *in vitro* bioassays. *Toxicol. Appl. Pharmacol.* **232**(3): 384–395.

Nieuwkoop P, Faber J. 1994. *Normal Table of Xenopus Laevis* (Daudin). Garland: New York.

OECD. 2015a. *Test No. 240*: *Medaka Extended One Generation Reproduction Test* (*MEOGRT*). , OECD Guidelines for the Testing of Chemicals, Section 2OECD Publishing: Paris.

OECD. 2015b. *Test No. 241*: *The Larval Amphibian Growth and Development Assay* (*LAGDA*). , OECD Guidelines for the Testing of Chemicals, Section 2OECD Publishing: Paris.

Paul KB, Hedge JM, Rotroff DM, Hornung MW, Crofton KM, Simmons SO. 2014. Development of a thyroperoxidase inhibition assay for high-throughput screening. *Chem. Res. Toxicol.* **27**(3): 387–399.

Pawlowski S, Van Aerle R, Tyler CR, Braunbeck T. 2004. Effects of 17α-ethinylestradiol in a fathead minnow (*Pimephales promelas*) gonadal recrudescence assay. *Ecotoxicol. Environ. Saf.* **57**(3): 330–345.

Pratt KG, Khakhalin AS. 2013. Modeling human neurodevelopmental disorders in the *Xenopus* tadpole: from mechanisms to therapeutic targets. *Dis. Model. Mech.* **6**(5): 1057–1065.

Schlenk D, Sapozhnikova Y, Irwin MA, Xie L, Hwang W, Reddy S, Brownawell BJ, Armstrong J, Kelly M, Montagne DE, Kolodziej EP, Sedlak D, Snyder S. 2005. *In vivo* bioassay-guided fractionation of marine sediment extracts from the Southern California Bight, USA, for estrogenic activity. *Environ. Toxicol. Chem.* **24**(11): 2820–2826.

Schmutzler C, Bacinski A, Gotthardt I, Huhne K, Ambrugger P, Klammer H, Schlecht C, Hoang-Vu C, Grüters A, Wuttke W, Jarry H, Köhrle J. 2007. The ultraviolet filter benzophenone 2 interferes with the thyroid hormone axis in rats and is a potent *in vitro* inhibitor of human recombinant thyroid peroxidase. *Endocrinology* **148**(6): 2835–2844.

Thienpont B, Tingaud-Sequeira A, Prats E, Barata C, Babin PJ, Raldúa D. 2011. Zebrafish eleutheroembryos provide a suitable vertebrate model for screening chemicals that impair thyroid hormone synthesis. *Environ. Sci. Technol.* **45**(17): 7525–7532.

Tietge JE, Holcombe GW, Flynn KM, Kosian PA, Korte JJ, Anderson LE, Wolf DC, Degitz SJ. 2005. Metamorphic inhibition of *Xenopus laevis* by sodium perchlorate: effects on development and thyroid histology. *Environ. Toxicol. Chem.* **24**(4): 926–933.

Tietge JE, Butterworth BC, Haselman JT, Holcombe GW, Hornung MW, Korte JJ, Kosian PA, Wolfe M, Degitz SJ. 2010. Early temporal effects of three thyroid hormone synthesis inhibitors in *Xenopus laevis*. *Aquat. Toxicol.* **98**: 44–50.

Tietge JE, Degitz SJ, Haselman JT, Butterworth BC, Korte JJ, Kosian PA, Lindberg-Livingston AJ, Burgess EM, Blackshear PE, Hornung MW. 2013. Inhibition of the thyroid hormone pathway in *Xenopus laevis* by 2-mercaptobenzothiazole. *Aquat. Toxicol.* **126**: 128–136.

US EPA. 2015a. *OCSPP 890.2200*: *Medaka Extended One-Generation Reproduction Test* (*MEOGRT*), Endocrine Disruptor Screening Program Test Guidelines, 890 series, www.regulations.gov, ID: EPA-HQ-OPPT-2014-0766-0021.

US EPA. 2015b. *OCSPP 890.2300*: *Larval Amphibian Growth and Development Assay* (*LAGDA*), Endocrine Disruptor Screening Program Test Guidelines, 890 series, www.regulations.gov, ID: EPA-HQ-OPPT-2014-0766-0020.

Weber LP, Hill RL, Janz DM. 2003. Developmental estrogenic exposure in zebrafish (Danio rerio): II. Histological evaluation of gametogenesis and organ toxicity. *Aquat. Toxicol.* **63**(4): 431–446.

Weisbrod CJ, Kunz PY, Zenker AK, Fent K. 2007. Effects of the UV filter benzophenone-2 on reproduction in fish. *Toxicol. Appl. Pharmacol.* **225**(3): 255–266.

Yoshimoto S, Okada E, Umemoto H, Tamura K, Uno Y, Nishida-Umehara C, Matsuda Y, Takamatsu N, Shiba T, Ito M. 2008. A W-linked DM-domain gene, DM-W, participates in primary ovary development in *Xenopus laevis*. *Proc. Natl. Acad. Sci. U. S. A.* **105**(7): 2469–2474.

Supporting information

Additional supporting information may be found in the online version of this article at the publisher's web site.

Table S1. Prevalence (% of *n*) and severity of juvenile liver histopathological observations following BP-2 exposure (NR: not remarkable; numbers in parentheses are significantly different than control based on RSCABS analysis).

Table S2 Prevalence (% of *n*) and severity of juvenile kidney histopathological observations showing significant treatment-related effects following BP-2 exposure (NR: not remarkable; dash: not observed; numbers in parentheses are significantly different than control based on RSCABS analysis).

Copyright © 2016 John Wiley & Sons, Ltd.

Supporting information

Table S1. Prevalence (% of *n*) and severity of juvenile liver histopathological observations following BP-2 exposure (NR: not remarkable; numbers in parentheses are significantly different than control based on RSCABS analysis).

	Genotypic Male				Genotypic Female			
Nominal BP2 concentration (mg/L)	0	1.5	3.0	6.0	0	1.5	3.0	6.0
Total *n*	20	20	18	14	20	20	20	16
Replicate tanks	4	4	4	4	4	4	4	4
Basophilia								
NR	100	100	0	0	100	90	0	0
Minimal	0	0	(28)	(0)	0	10	(25)	(0)
Mild	0	0	(33)	(0)	0	0	(45)	(25)
Moderate	0	0	(28)	(86)	0	0	(30)	(50)
Severe	0	0	(11)	(14)	0	0	0	(25)
Decreased Hepatocellular Vacuolation								
NR	100	100	0	0	100	90	0	0
Minimal	0	0	(28)	(0)	0	10	(25)	(0)
Mild	0	0	(33)	(0)	0	0	(45)	(25)
Moderate	0	0	(28)	(86)	0	0	(30)	(50)
Severe	0	0	(11)	(14)	0	0	0	(25)
Proteinaceous Fluid Intravascular								
NR	100	100	6	0	100	100	5	6
Minimal	0	0	(28)	(0)	0	0	(30)	(0)
Mild	0	0	(22)	(0)	0	0	(30)	(19)
Moderate	0	0	(28)	(79)	0	0	(10)	(69)
Severe	0	0	(17)	(21)	0	0	(25)	(6)
Individual Hepatocyte Necrosis / Apoptosis								
NR	100	100	94	93	100	100	100	88
Minimal	0	0	6	7	0	0	0	(13)
Mild	0	0	0	0	0	0	0	0
Moderate	0	0	0	0	0	0	0	0
Severe	0	0	0	0	0	0	0	0
Increased Pigment								
NR	100	100	50	0	100	100	45	0
Minimal	0	0	(50)	(100)	0	0	(55)	(100)
Mild	0	0	0	0	0	0	0	0
Moderate	0	0	0	0	0	0	0	0
Severe	0	0	0	0	0	0	0	0
Focus of Hepatocellular Alteration								
NR	100	100	100	79	100	100	100	88
Minimal	0	0	0	(21)	0	0	0	(6)
Mild	0	0	0	0	0	0	0	0
Moderate	0	0	0	0	0	0	0	6
Severe	0	0	0	0	0	0	0	0

Table S2. Prevalence (% of *n*) and severity of juvenile kidney histopathological observations showing significant treatment-related effects following BP-2 exposure (NR: not remarkable; dash: not observed; numbers in parentheses are significantly different than control based on RSCABS analysis).

	Genotypic Male				Genotypic Female			
Nominal BP2 concentration (mg/L)	0	1.5	3.0	6.0	0	1.5	3.0	6.0
Total *n*	20	19	12	14	17	17	16	9
Replicate tanks	4	4	4	4	4	4	4	4
Glomerulomegaly								
NR	100	100	0	0	100	88	6	22
Minimal	0	0	(42)	(21)	0	12	(0)	(0)
Mild	0	0	(58)	(79)	0	0	(6)	(56)
Moderate	0	0	0	0	0	0	(38)	(22)
Severe	0	0	0	0	0	0	(50)	(0)
Glomerular Protein								
NR	100	100	17	0	100	82	0	0
Minimal	0	0	(50)	(7)	0	(18)	(0)	(22)
Mild	0	0	(33)	(93)	0	0	(56)	(22)
Moderate	0	0	0	0	0	0	(31)	(56)
Severe	0	0	0	0	0	0	13	0
Glomerulus, hypercellularity								
NR	100	100	8	100	100	94	0	56
Minimal	0	0	(67)	0	0	6	(13)	(33)
Mild	0	0	25	0	0	0	(25)	(11)
Moderate	0	0	0	0	0	0	(56)	(0)
Severe	0	0	0	0	0	0	6	0
Tubules, Protein								
NR	100	100	0	43	100	100	6	11
Minimal	0	0	(8)	(0)	0	0	(6)	(22)
Mild	0	0	(75)	(36)	0	0	(75)	(44)
Moderate	0	0	(17)	(21)	0	0	(13)	(0)
Severe	0	0	0	0	0	0	0	(22)
Interstitial Fluid (Proteinaceous)								
NR	100	100	0	0	100	71	0	0
Minimal	0	0	(8)	(14)	0	(29)	(13)	(0)
Mild	0	0	(92)	(86)	0	0	(56)	(44)
Moderate	0	0	0	0	0	0	(19)	(56)
Severe	0	0	0	0	0	0	13	0
Interstitial Fibrosis								
NR	100	100	8	100	100	100	25	89
Minimal	0	0	(33)	0	0	0	(19)	(11)
Mild	0	0	50	0	0	0	(50)	(0)
Moderate	0	0	8	0	0	0	6	0
Severe	0	0	0	0	0	0	0	0
Regenerative blast cell hyperplasia								
NR	-	-	-	-	100	100	25	44
Minimal	-	-	-	-	0	0	(31)	(56)
Mild	-	-	-	-	0	0	31	0
Moderate	-	-	-	-	0	0	13	0
Severe	-	-	-	-	0	0	0	0
Tubules, Dilation								
NR	25	11	0	7	18	12	0	56
Minimal	55	79	(0)	(36)	71	47	13	22
Mild	20	11	(92)	(50)	12	(41)	(50)	(0)
Moderate	0	0	8	7	0	0	(38)	(22)
Severe	0	0	0	0	0	0	0	0
Tubules, Mineralization / Casts								
NR	5	0	58	64	6	24	13	100
Minimal	30	42	(8)	(29)	35	24	25	(0)
Mild	65	53	33	(7)	59	53	63	(0)
Moderate	0	5	0	0	0	0	0	0
Severe	0	0	0	0	0	0	0	0

United States Environmental Protection Agency
Office of Chemical Safety and Pollution Prevention (7101)
EPA Pub No. 740-C-15-001
July 2015

Endocrine Disruptor Screening Program Test Guideline

OCSPP 890.2300: Larval Amphibian Growth and Development Assay (LAGDA)

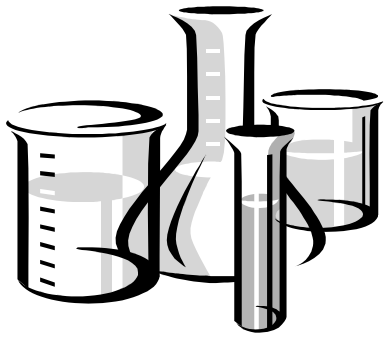

NOTICE

This guideline is one of a series of test guidelines established by the United States Environmental Protection Agency's Office of Chemical Safety and Pollution Prevention (OCSPP) for use in testing pesticides and chemical substances to develop data for submission to the Agency under the Toxic Substances Control Act (TSCA) (15 U.S.C. 2601, *et seq.*), the Federal Insecticide, Fungicide and Rodenticide Act (FIFRA) (7 U.S.C. 136, *et seq.*), and section 408 of the Federal Food, Drug and Cosmetic Act (FFDCA) (21 U.S.C. 346a). Prior to April 22, 2010, OCSPP was known as the Office of Prevention, Pesticides and Toxic Substances (OPPTS). To distinguish these guidelines from guidelines issued by other organizations, the numbering convention adopted in 1994 specifically included OPPTS as part of the guideline's number. Any test guidelines developed after April 22, 2010 will use the new acronym (OCSPP) in their title.

The OCSPP test guidelines serve as a compendium of accepted scientific methodologies and protocols that are intended to provide data to inform regulatory decisions under TSCA, FIFRA and/or FFDCA. This document provides guidance for conducting the test, and is also used by EPA, the public and the companies that are subject to data submission requirements under TSCA, FIFRA and/or the FFDCA. As a guidance document, these guidelines are not binding on either EPA or any outside parties, and the EPA may depart from the guidelines where circumstances warrant and without prior notice. At places in this guidance, the Agency uses the word "should." In this guidance, the use of "should" with regard to an action means that the action is recommended rather than mandatory. The procedures contained in this guideline are strongly recommended for generating the data that are the subject of the guideline, but EPA recognizes that departures may be appropriate in specific situations. You may propose alternatives to the recommendations described in these guidelines, and the Agency will assess them for appropriateness on a case-by-case basis.

For additional information about these test guidelines and to access these guidelines electronically, please go to http://www.epa.gov/ocspp and select "Test Methods & Guidelines" on the left side navigation menu. You may also access the guidelines in *http://www.regulations.gov* grouped by Series under Docket ID #s: EPA-HQ-OPPT-2009-0150 through EPA-HQ-OPPT-2009-0159, and EPA-HQ-OPPT-2009-0576.

OCSPP 890.2300: Larval Amphibian Growth and Development Assay (LAGDA)

(a) Scope.

(1) Applicability. This guideline is intended to be used to help develop data to submit to EPA under the Toxic Substances Control Act (TSCA) (15 U.S.C. 2601, et seq.), the Federal Insecticide, Fungicide, and Rodenticide Act (FIFRA) (7 U.S.C. 136, et seq.), and the Federal Food, Drug, and Cosmetic Act (FFDCA) (21 U.S.C. 346a).

(2) Background. The Endocrine Disruptor Screening Program (EDSP) reflects a two-tiered approach to implement the statutory testing requirements of FFDCA section 408(p) (21 U.S.C. 346a). In general, EPA intends to use the data collected under the EDSP, along with other information, to determine if a pesticide chemical, or other substances, may pose a risk to human health or the environment due to disruption of the endocrine system.

Tier 2 testing is designed to identify any adverse apical effects caused by the substance which may be attributable to possible endocrine interaction, and establish a quantitative relationship between the dose and that adverse effect. The determination whether to require additional Tier 2 testing is made on a weight-of-evidence basis taking into account data from the Tier 1 assays and other scientifically relevant information available. The fact that a substance may interact with a hormone system, however, does not necessarily mean that when the substance is used, it will cause adverse effects in humans or ecological systems. The EPA guidance document "Weight-of-Evidence: Evaluating Results of EDSP Tier 1 Screening to Identify the Need for Tier 2 Testing" (**Ref. 1**) explains this process.

The Larval Amphibian Growth and Development Assay (LAGDA) is a definitive Tier 2 test in the EDSP designed to characterize adverse apical effects on the development, growth and reproductive organ development in amphibians and to establish a quantitative relationship between the exposure concentration and that adverse effect. Adverse effects identified by the LAGDA may be caused by endocrine interaction of a chemical in amphibians, especially those active within the hypothalamic-pituitary-thyroid (HPT) and hypothalamic-pituitary-gonadal (HPG) systems. The method described in this guideline is derived from validation work on African clawed frog (*Xenopus laevis*) by the EPA with supporting work in Japan. The LAGDA test guideline would follow other guidelines in the OCSPP 890 series for the Endocrine Disruptor Screening Program.

(3) Source. This OCSPP harmonized test guideline was developed through a process of harmonization with Test Guideline 241 published by the Organization for Economic Cooperation and Development (**Ref. 2**).

(b) Purpose.

This guideline is intended for use in developing data, specifically characterizing any adverse apical effect(s) which may be caused by endocrine interaction of a chemical in amphibians and establish a quantitative relationship between the dose and that adverse effect(s). The LAGDA test guideline uses the African clawed frog (*Xenpous laevis*) as a surrogate to identify and characterize the adverse consequences of exposure to substances which interfere with the normal development and growth of amphibians from embryo-larval development, through metamorphosis and early juvenile development. The assay is intended to evaluate effects from exposure to pesticides and other chemicals, both through

endocrine and non-endocrine mechanisms, during the larval and juvenile stages that may adversely affect populations.

(c) Introduction.

Much of our current understanding of amphibian biology has been obtained using the laboratory model species *X. laevis.* This species can be routinely cultured in the laboratory, ovulation can be induced using human chorionic gonadotropin (hCG) and animal stocks are readily available from commercial breeders.

Like all vertebrates, reproduction in amphibians is under the control of the hypothalamic pituitary gonadal (HPG) axis (**Ref. 3**), while development and growth is regulated by the hypothalamic pituitary thyroid (HPT) axis. Estrogens and androgens are mediators of this endocrine system, directing the development and physiology of sexually-dimorphic tissues. There are three distinct phases in the life cycle of amphibians when this axis is especially active: (1) gonadal differentiation during larval development, (2) development of secondary sex characteristics and gonadal maturation during the juvenile phase and (3) functional reproduction of adults. Each of these three developmental windows are likely susceptible to endocrine perturbation by certain chemicals, ultimately affecting growth and reproductive fitness by the organisms.

The gonads begin development at NF stage 43, when the bipotential genital ridge first develops. Differentiation of the gonads begins at NF stage 52 when primordial germ cells either migrate to medullary tissue (males) or remain in the cortical region (females) of the developing gonads (**Ref. 4)**. This process of sexual differentiation of the gonads was first reported to be susceptible to chemical alteration in *Xenopus* in the 1950's (**Ref. 5; Ref. 6**). Exposure of tadpoles to estradiol during this period of gonad differentiation results in sex reversal of males that when raised to adulthood are fully functional females (**Ref. 7**; **Ref. 8**). Functional sex reversal of females into males is also possible and has been reported following implantation of testis tissue in tadpoles (**Ref. 9**). However, exposure to an aromatase inhibitor also causes functional sex reversal in *X. tropicalis* (**Ref. 10**), this has not yet been shown to occur in *X. laevis*. Historically, toxicant effects on gonadal differentiation have been assessed by histological examination of the gonads at metamorphosis and sex reversal could only be determined by analysis of sex ratios. Until recently, there had been no means to directly determine the genetic sex of *Xenopus*. However, recent establishment of sex linked markers in *X. laevis* make it possible to determine genetic sex and allows for the direct identification of sex reversed animals (**Ref. 11**).

In males, juvenile development proceeds as blood levels of testosterone increase corresponding with the development of secondary sex characteristics as well as testis development. In females, estradiol is produced by the ovaries resulting in the appearance of vitellogenin (Vtg) in the plasma, vitellogenic oocytes in the ovary and the development of oviducts (**Ref. 12**). Oviducts are female secondary sex characteristics that function in oocyte maturation during reproduction (**Ref. 13**). Jelly coats are applied to the outside of oocytes as they pass through the oviduct and collect in the ovisac, ready for fertilization. Oviduct development appears to be regulated by estrogens as development correlates with blood estradiol levels in *X. laevis* (**Ref. 14**) and *X. tropicalis* (**Ref. 12**). The development of oviducts in males following exposure to polychlorinated biphenyl compounds (**Ref. 15**) and 4-*tert*-octylphenol (**Ref. 16**) has been reported.

Though capable of detecting perturbations of normal reproductive development through HPG axis interference, the LAGDA is also designed to detect substances that interfere with normal function of the HPT axis. Amphibian metamorphosis from larval to adult life stages is a well-studied thyroid-dependent

process (**Ref. 17**), which responds to substances that are active within the HPT axis (**Ref. 3**). Metamorphosis occurs in all major chordate groups with the exception of amniotes (**Ref. 18; Ref. 19**) and is developmentally comparable to post-embryonic organogenesis in mammals (**Ref. 20**). Three primary physiological processes define amphibian metamorphosis: (1) reabsorption or regression of tissue/organs that are primarily functional during the larval life stage (*e.g.*, gills), (2) remodeling larval organ systems to their adult forms (*e.g.*, lungs, gut, liver), and (3) development of new tissues (*e.g.*, limbs) for the adult life stage that are not present in the early larval life stage. These changes allow adult amphibians to occupy an ecological niche distinct from that occupied by larvae. The LAGDA is intended to characterize the adverse consequences of exposure to substances which interfere with these metamorphic and developmental processes that may affect populations.

(d) General Experimental Design.

The general experimental design entails exposing *X. laevis* embryos at Nieuwkoop and Faber (NF) stage 8-10 to a minimum of four different concentrations of test chemical and control(s) until 10 weeks after the median time to reach NF stage 62 in the control, with one interim sub-sample at NF stage 62 (See **Ref. 4** for staging details). There are four replicates in each test concentration with eight replicates in the control. Endpoints evaluated during the course of the exposure include those indicative of generalized toxicity: mortality, abnormal behavior, abnormal morphological features, and growth determinations (length and weight), as well as endpoints designed to characterize potential apical consequences of endocrine toxicity acting through estrogen, androgen or thyroid-mediated physiological processes.

(e) Description of the Method.

(1) Test Species. The representative amphibian test species is *X. laevis*, because this species is routinely cultured in laboratories worldwide, is easily obtainable through commercial suppliers, and is capable of having its genetic sex determined. Reproduction can be induced in this species throughout the year using human chorionic gonadotropin (hCG) injections and the resultant embryos can be routinely reared in large numbers for use in this test protocol. It is preferred that larvae used in the assay are derived from in-house cultures of adults.

(2) Equipment and Supplies. The following equipment and supplies are recommended for the LAGDA:

- exposure system (described below);
- glass or stainless steel aquaria (described below);
- breeding tanks;
- temperature controlling apparatus (*e.g.*, heaters or coolers adjustable to 21±1ºC);
- thermometer;
- binocular dissection microscope and dissection tools;
- digital camera with at least 4 megapixel resolution and micro function;
- analytical balance capable of measuring to 0.001 mg or 1 µg;
- dissolved oxygen meter;
- pH meter;
- light intensity meter capable of measuring in lux units;
- miscellaneous laboratory glassware and tools;

- adjustable pipettes (10 to 5,000 µl) or assorted pipettes of equivalent sizes;
- the test chemical should be available in sufficient quantities, preferably from one lot, to conduct the study; and
- analytical instrumentation appropriate for the chemical on test or contracted analytical services.

(3) Chemical Testability. The LAGDA uses an aqueous exposure methodology whereby the test chemical is introduced into the test chambers via a flow-through system. Flow-through methods however, introduce constraints on the types of chemicals that can be tested, as determined by the physicochemical properties of the compound. Therefore, prior to using this protocol, baseline information about the chemical that is relevant to determining its testability should be obtained. Both the Organization for Economic Cooperation and Development (OECD) Guidance Document on Aquatic Toxicity Testing of Difficult Substances and Mixtures (**Ref. 21)** and the USEPA Guidance Document on Special Considerations for Conducting Aquatic Laboratory Studies should be consulted (OCSPP 850.1000; **Ref. 22**). Characteristics which indicate that the chemical may be difficult to test in aquatic systems include: high octanol-water partitioning coefficients (Log K_{ow}), high volatility, susceptibility to hydrolysis, and susceptibility to photolysis under ambient laboratory lighting conditions. Other factors may also be relevant to determining testability and should be determined on a case by case basis. If it has been demonstrated through range-finding or other preliminary trials that quantitation of the test substance cannot be conducted because the test substance concentration cannot be kept constant, or because there are other analytical difficulties, a successful test for the chemical is unlikely using a flow-through test system. Should this be the case, it is recommended that the chemical not be tested using this protocol.

(4) Exposure System. This test was developed using a flow-through diluter system. The system components should have water-contact components of glass, stainless steel, and/or chemically inert materials (*e.g.*, Teflon®). Plastics may be used if they have been demonstrated to be suitable for testing with amphibians. Exposure tanks should be glass or stainless steel aquaria, equipped with standpipes that result in an approximate tank volume between 4.0 and 10.0 L and a minimum water depth of 10 cm. The system should be capable of supporting all exposure concentrations, a control, and a solvent control, if necessary, with four replicates per treatment (eight in the control). The flow rate to each tank should be constant in consideration of both the maintenance of biological conditions and chemical exposure. It is recommended that flow rates accommodate at least 10 tank turnovers per day to avoid chemical concentration declines due to metabolism by both the test organisms and aquatic microorganisms present in the aquaria or abiotic routes of degradation (hydrolysis, photolysis) or dissipation (volatilization, sorption). The treatment tanks should be randomly assigned to a position in the exposure system to reduce potential positional effects, including slight variations in environmental conditions (*e.g.*, temperature and light intensity). Specific experimental conditions under which the protocol should be conducted are discussed below (Section (e)(7)(ii)). Further information on setting up flow-through exposure systems can be obtained from the ASTM Standard Guide for Conducting Acute Toxicity Tests on Test Materials with Fishes, Macroinvertebrates, and Amphibians (**Ref. 23**).

(5) Water Quality. Any dilution water that is locally available (*e.g.*, spring water or charcoal-filtered tap water) and permits normal growth and development of *X. laevis* can be used; evidence of normal growth in this water should be available. Because local water quality can differ substantially from one area to another, analysis of water quality should be undertaken, particularly if historical data on the utility of the water for raising amphibian larvae is not available. Special attention should be given that the water is reasonably free of copper, chlorine, and chloramines, all of which can be toxic to amphibians. Measurements of heavy metals (e.g. Cu, Pb, Zn, Hg, Cd, Ni), major anions and cations (*e.g.*, Ca, Mg, Na, K, Cl, SO_4), pesticides, total organic carbon, fluoride, perchlorate, and

chlorate (a by-product of drinking water disinfection) and suspended solids should be made before testing begins and/or, for example, every six months where a dilution water is known to be relatively constant in quality. Some chemical characteristics of acceptable dilution water are listed in Table 1.

Table 1. Some chemical characteristics of acceptable dilution water.

Substance	Limit concentration
Particulate matter	5 mg/L
Total organic carbon	2 mg/L
Un-ionized ammonia	1 µg/L
Residual chlorine	10 µg/L
Total organophosphorous pesticides	50 ng/L
Total organochlorine pesticides plus polychlorinated biphenyls	50 ng/L
Total organic chlorine	25 ng/L
Aluminium	1 µg/L
Arsenic	1 µg/L
Chromium	1 µg/L
Cobalt	1 µg/L
Copper	1 µg/L
Iron	1 µg/L
Lead	1 µg/L
Nickel	1 µg/L
Zinc	1 µg/L
Cadmium	100 ng/L
Mercury	100 ng/L
Silver	100 ng/L

(6) Iodide Concentration in Test Water. In order for the thyroid gland to synthesize thyroid hormones to support normal metamorphosis, sufficient iodide should be available to the larvae through a combination of aqueous and dietary sources. Currently, there are no empirically derived guidelines for minimum iodide concentrations in either food or water to ensure proper development. However, iodide availability may affect the responsiveness of the thyroid system to thyroid active agents and is known to modulate the basal activity of the thyroid gland, which deserves attention when interpreting the results from thyroid histopathology. Based on previous work, successful performance of the assay has been demonstrated when dilution water iodide (I^-) concentrations ranged between 0.5 and 10 µg/L. Ideally, the minimum iodide concentration in the dilution water throughout the test should be 0.5 µg/L. If the test water is iodine-deficient or is reconstituted from deionized water, iodine should be added at a minimum concentration of 0.5 µg/L (added as the sodium or potassium salt). The measured iodide concentrations from the dilution water and the supplementation of the test water with iodine or other salts (if used) should be reported. Iodine content may also be measured in food(s) in addition to test water.

(7) Animal Care.

(i) Adult Care and Breeding. Appropriate care and breeding of *X. laevis* is conducted using a standardized guideline, Frog Embryo Teratogenesis Assay Xenopus (FETAX) in ASTM (**Ref. 24**). Housing and care of *X. laevis* are also described by Read (**Ref. 25**). To induce breeding, three to five pairs of adult females and males are injected intraperitoneally with human chorionic gonadotropin (hCG). Female and male specimens are injected with approximately 800-1000 IU and 500-800 IU, respectively, of hCG dissolved in 0.6-0.9% saline solution (or frog Ringer's solution, an isotonic saline for use with amphibians; www.hermes.mbl.edu/biologicalbulletin/compendium/comp-RGR.html). Injection volumes should be about 10 µl/g body weight (~1000 µl). Afterwards, induced breeding pairs are held in large tanks, undisturbed and under static conditions to promote amplexus. The bottom of each breeding tank should have a false bottom of plastic or stainless steel mesh (*e.g.*, 1.25 cm openings) which permits the eggs to fall to the bottom of the tank. Frogs injected with hCG in the late afternoon will usually deposit most of their eggs by mid-morning of the next day. After a sufficient quantity of eggs are released and fertilized, adults should be removed from the breeding tanks.

Eggs are then collected and jelly coats are removed by L-cysteine treatment (**Ref. 24**). A 2% L-cysteine solution should be prepared and pH adjusted to 8.1 with 1M NaOH. This 21°C solution is added to a 500 mL Erlenmeyer flask containing the eggs from a single spawn and swirled gently for one to two minutes and then rinsed thoroughly 6-8 times with 21°C culture water. The eggs are then transferred to a crystallizing dish and determined to be >70% viable with minimal abnormalities in embryos exhibiting cell division.

(ii) Environmental Conditions. A summary of exposure conditions and frequency of monitoring is presented in Table 2. During the exposure period, temperature of test solutions should be measured daily and dissolved oxygen and pH of the test solutions measured twice per week. Conductivity, alkalinity, and hardness are measured once per month. For the water temperature of test solutions, the inter-replicate and inter-treatment differentials (within one day) should not exceed 1.0°C. Also, for pH of test solutions, the inter-replicate and inter-treatment differentials should not exceed 0.5.

Table 2. Environmental conditions and frequency of monitoring.

Environmental condition	Targeted range	Frequency tested	Source water

Water temperature	21±1°C	Daily	All tanks
Photoperiod	12:12 (hrs light:hrs dark)	n/a	n/a
Light intensity at water surface	600 to 2,000 lux (lumens/m^2)	Once	n/a
Test water dissolved oxygen (% saturation)	≥ 3.5 mg/L (>40%; however, ≥60% preferred)	2x per week	All tanks by end of week
Test water pH	6.5-8.5	2x per week	All tanks by end of week
Test water conductivity (µS)	n/a	1x per month (rotate through replicates)	One replicate from each treatment and control
Test water hardness (mg/L of $CaCO_3$)	10 – 250 mg $CaCO_3$/L	1x per month (rotate through replicates)	One replicate from each treatment and control
Test water alkalinity (mg/L of $CaCO_3$)	10 – 250 mg $CaCO_3$/L	1x per month (rotate through replicates)	One replicate from each treatment and control
Relative humidity inside test system enclosure	>30%	1x per month post-metamorphosis	n/a

(iii) Husbandry. The exposure tanks should be siphoned on a daily basis to remove uneaten food and waste products, being careful to avoid cross-contamination of tanks. Care should be used to minimize stress and trauma to the animals, especially during movement of animals or aquaria, cleaning of aquaria, and manipulation of equipment adjacent to aquaria. Stressful conditions/activities should be avoided such as loud and/or incessant noise, tapping on aquaria, vibrations in the aquaria, excessive activity in the laboratory, and rapid changes in environmental media (*e.g.*, light availability, temperature, pH, dissolved oxygen, and water flow rates).

(iv) Feeding Regime. Feed and feeding rates change during different life stages of *X. laevis* and are a very important aspect of the LAGDA. Excessive feeding during the larval phase typically results in increased incidences and severity of scoliosis (bent tail) and should be avoided. Conversely, inadequate feeding during the larval phase results in highly variable developmental rates among controls potentially compromising statistical power or confounding test results. Therefore, use of the outlined feeding regime for larval and juvenile *X. laevis* in flow-through conditions is recommended (see Appendix 2). Alternative feeding regimes are permissible providing the test organisms grow and develop satisfactorily according to the following performance criteria for control organisms (also outlined in Section (g)).

- The median time to NF stage 62 is ≤45 days.
- The mean weight at NF stage 62 is 1.0±0.2 grams.
- The mean juvenile weight at test termination is 11.5±3 grams.

(A) Larval feeding. A recommended larval diet is provided in Appendix 2. This diet consists of trout starter (*e.g.*, Skretting USA, Tooele, UT), *Spirulina* algae discs (*e.g.*, Wardley, Secaucus, NJ) and goldfish crisps (*e.g.*, TetraFin® flakes from Tetra Sales, Blacksburg, VA) homogenized in culture (or dilution) water (see Appendix 2 for guidance). This mixture is administered three times daily on weekdays and once daily on weekends. Tadpoles are also fed 24-hour-old live brine shrimp nauplii (*Artemia* spp.) (*e.g.*, Bio-Marine® Brand, Bio-Marine, Hawthorne, CA) twice daily on weekdays and once daily on the weekends starting on day 8 post-fertilization. The larval feeding, which should be

consistent in each test vessel, should allow appropriate growth and development of test animals in order to ensure reproducibility and transferability of the assay results: (1) the median time to NF stage 62 in controls should be ≤45 days and (2) a mean weight of 1.0±0.2 g at NF stage 62 in controls.

(B) Post-NF stage 62 and juvenile feeding. A recommended juvenile diet is provided in Appendix 2. Once tadpoles have reached NF stage 62, the feeding regime consists of premium sinking frog food (*e.g.*, Sinking Frog Food -3/32"; Xenopus Express, FL). For larvae post-NF stage 62 and froglets (early juveniles), the pellets are briefly run in a coffee grinder, blender or crushed with a mortar and pestle in order to reduce their size. Once juveniles are large enough to consume full pellets, grinding or crushing is no longer necessary. The animals should be fed once per day. The juvenile feeding should allow appropriate growth and development of the organisms to reach a mean weight of 11.5±3 g in control juveniles at the termination of the assay.

(8) Analytical Chemistry. Prior to initiating the study, the stability of the test compound (*e.g.*, solubility, degradability, and volatility) and all analytical methods needed should be established using existing information or knowledge. When dosing via the dilution water, it is recommended that test solutions from each replicate tank concentration be analyzed prior to test initiation to verify system performance. During the exposure period, the concentrations of the test chemical are determined at appropriate intervals, preferably every week in all replicate tanks in each treatment group. It is recommended that results be based on measured concentrations. Also, the coefficient of variation (CV) of the measured test concentrations over the entire test period within a treatment should be maintained at 20% or less in each concentration. When the measured concentrations do not remain within 80-120% of the nominal concentration (for example, when testing highly biodegradable or adsorptive chemicals), the effect concentrations should be determined and expressed relative to the arithmetic mean concentration for flow-through tests.

The flow rates of dilution water and stock solution should be checked at appropriate intervals (*e.g.*, three times a week) throughout the exposure duration. In the case of chemicals which cannot be detected at some or all of the nominal concentrations (*e.g.*, due to rapid degradation or adsorption in the test vessels, or by marked chemical accumulation in the bodies of exposed animals), it is recommended that the renewal rate of the test solution in each chamber be adapted to maintain test concentrations as constant as possible.

(9) Chemical Delivery: Preparation of Test Solutions. To make test solutions in the exposure system, stock solution of the test chemical should be dosed into the exposure system by an appropriate pump or other apparatus. The flow rate of the stock solution should be calibrated in accordance with analytical confirmation of the test solutions before the initiation of exposure, and checked volumetrically periodically during the test. It is recommended that the test solution in each chamber be renewed at a minimum of 10 volume renewals/day.

The method used to introduce the test chemical to the system can vary depending on its physicochemical properties. Therefore, prior to the test, baseline information about the chemical that is relevant to determining its testability should be obtained. Useful information about test chemical-specific properties include the structural formula, molecular weight, purity, stability in water and light, pKa and Log K_{ow}, water solubility (preferably in the test medium) and vapor pressure as well as results of a test for ready biodegradability (OECD TG 301, **Ref. 26**; TG 310, **Ref. 27**). Solubility and vapor pressure can be used to calculate Henry's law constant, which will indicate whether losses due to evaporation of the test chemical may occur. Conduct of this test without the information listed above should be carefully considered as the study design will be dependent on the physicochemical properties of the test chemical and, without these data, test results may be difficult to interpret or meaningless. A reliable analytical

method for the quantification of the test chemical in the test solutions with known and reported accuracy and limit of detection should be available.

Water soluble test chemicals can be dissolved in aliquots of dilution water at a concentration which allows delivery at the target test concentration in a flow-through system. Chemicals which are liquid or solid at room temperature and moderately soluble in water may require liquid:liquid or liquid:solid (*e.g*., glass wool column) saturators (**Ref. 28**). While it may also be possible to dose very hydrophobic test chemicals via the feed, there has been no experience using that exposure route in this assay.

Test solutions of the chosen concentrations are prepared by dilution of a stock solution. The stock solution should preferably be prepared by simply mixing or agitating the test chemical in dilution water by mechanical means (e.g. stirring and/or ultrasonication). Saturation columns/systems or passive dosing methods (**Ref. 29**) can be used for achieving a suitably concentrated stock solution. The preference is to use a co-solvent-free test system; however, different test chemicals will possess varied physicochemical properties that will likely require different approaches for preparation of stock solutions.

If possible, solvents or carriers should be avoided because: (1) certain solvents themselves may result in toxicity and/or undesirable or unexpected responses, (2) testing chemicals above their water solubility (as can frequently occur through the use of solvents) can result in inaccurate determinations of effective concentrations, (3) the use of solvents in longer-term tests can result in a significant degree of "biofilming" associated with microbial activity which may impact environmental conditions as well as the ability to maintain exposure concentrations and (4) the absence of historical data that demonstrate that the solvent does not influence the outcome of the study, (5) use of solvents requires a solvent control treatment which has significant animal welfare implications, as additional animals are required to conduct the test. For difficult to test chemicals, a solvent may be employed as a last resort, and the OECD Guidance Document on Aquatic Toxicity Testing of Difficult Substances and Mixtures should be consulted (**Ref. 21**) to determine the best method. The choice of solvent will be determined by the chemical properties of the test chemical and the availability of historical control data on the solvent. In the absence of historical data, the suitability of a solvent should be determined prior to conducting the definitive study. In the event that use of a solvent is unavoidable, and microbial activity (biofilming) occurs, recording/reporting of the biofilming per tank (at least weekly) throughout the test is recommended. Ideally, the solvent concentration should be kept constant in the solvent control and all test treatments. If the concentration of solvent is not kept constant, the highest concentration of solvent in the test treatment should be used in the solvent control. In cases where a solvent carrier is used, maximum solvent concentrations should not exceed 100 µl/L or 100 mg/L (**Ref. 21**), and it is recommended to keep the solvent concentration as low as possible (*e.g*, ≤20 µl/L) to avoid potential effects of the solvent on endpoints measured (**Ref. 30**).

(10) Exposure System Cleaning. The exposure systems used for the LAGDA prepare and deliver treatment solutions over long periods of time. A biofilm will invariably form on most wetted surfaces. The microbiological community that establishes itself will often be able to metabolize the compound being assessed. Detectable decreases in treatment concentration have been observed within three weeks of the start of the assay. Routine cleaning and disinfection of all wetted components in the diluter/delivery system, including the aquaria themselves, is strongly recommended (approximately every three weeks). As a precautionary note, the materials used in the construction of the diluter system may not be compatible with a specific sterilant. Before disinfecting any dilution system, an evaluation as to whether the system is compatible with the sterilant solution should be performed prior to use. Analysis of chemical concentrations should be made before and after any cleaning of the exposure system.

An example protocol for cleaning would be to divert the exposure tank delivery lines to drain. The exposure tanks can usually be left static without flow for the necessary time. The system components that can be removed should be cleaned with detergent and scrubbed with an abrasive pad. The delivery lines should be sanitized using a cold sterilant (*e.g.*, Minncare® Cold Sterilant, a solution of 22% hydrogen peroxide and 4.5% peroxyacetic acid). The cold sterilant solution should be mixed with water to a solution of 50X (2% concentration), and used to fill the toxicant delivery line circuit. Allow the lines to soak without flow for a minimum of 20 minutes. Rinse the delivery lines immediately with diluent water and check for residuals of the sterilant solution (*e.g.*, with Minncare® Residual Test Strips). Flush the lines until the cold sterilant concentration is below detection. Reassemble the system and return the delivery lines to the exposure tanks.

(11) Randomization. At all stages of the LAGDA and during daily tasks it is important to include randomization. This includes, but is not limited to the following procedures:

- The order in which food is delivered to the aquaria should be randomized in some fashion to mitigate potential changes in food quantity or quality during the course of feeding.
- It is essential to randomize the selection of embryos when distributing them into the replicates at test initiation.
- When larvae at NF stage 62 or juveniles are sampled or netted, the order in which the replicate aquaria are sampled or manipulated should be random.
- Cleaning and siphoning of tanks should not be performed in the same order on a daily basis. A separate set of tank cleaning supplies (*e.g.*, siphons) per treatment and control to avoid cross-contamination of chemical and/or disease is recommended.

(12) Selection of Test Concentrations.

(i) Establishing the High Test Concentration. For the purposes of this test, results from Tier I amphibian studies (*i.e.*, Amphibian Metamorphosis Assay, **Ref. 31;** OECD 231, **Ref. 32**) should be used to the extent possible in determining the highest test concentration so as to avoid concentrations that are overtly toxic. Other sources of information include: quantitative structure-activity relationships, read across and data from other existing amphibian studies such as the Frog Embryo Teratogenesis Assay - *Xenopus* (**Ref. 24**) and/or fish tests such as OECD TG229 (**Ref. 33**), TG234 (**Ref. 34)** and TG236 **(Ref. 35)** may contribute toward setting this concentration.

Prior to running the LAGDA, it is recommended that a range finding experiment be conducted. The range-finding exposure is initiated within 24 hours of fertilization and continued for 7-14 days (or more, if needed). Note that if a solvent has to be used, then the suitability of the solvent (*i.e.*, whether it may have an impact on the outcome of the study) could be determined as part of the range finding study. The range finding test concentrations are set such that the intervals between test concentrations are no greater than a factor of 10. The results of the range finding experiment should serve to set the highest test concentration in the LAGDA.

(ii) Test Concentration Range. For the definitive test, a minimum of four concentrations of the test substance, plus a dilution water control are tested (and a solvent control, if used). The results of the range finding experiment should serve to set the highest test concentration in the LAGDA. The recommended concentration separation (spacing factor) between adjacent test concentrations should generally be no less than 2-fold and no greater than 3.2-fold (half-log). The test concentration differential between the highest and lowest should be approximately a factor of 10. Determination of the spacing factor should be made based on concentration-response relationships characterized in previous

studies (*e.g.*, Tier 1 Amphibian Metamorphosis Assay, **Ref. 31** or OECD 231, **Ref. 32** and/or range-finding experiments), if available, in order to permit the highest likelihood of determining both a lowest observed effect concentration (LOEC) and no observed effect concentration (NOEC).

(f) Procedure.

(1) Assay Overview. The exposure is initiated with newly spawned embryos (NF stage 8-10) and continued until ten weeks after the median time to NF stage 62 (≤45 days from the assay initiation) in control group (Figure 1). Generally, the duration of the LAGDA is 16 weeks (maximum 17 weeks). Animals are examined daily for mortality and any sign of abnormal behavior. As larvae reach NF stage 62, a larval sub-sample (5 animals per replicate) is collected and various endpoints are examined (Table 4). Subsequently, a cull is performed to reduce tank density after all animals in the test have completed metamorphosis (*i.e.*, reached NF stage 66) or after 70 days from the assay initiation, whichever comes first. The cull is carried out at random (but without sub-sampling) and the remaining animals (10 per tank) continue exposure until 10 weeks after the median time to NF stage 62 in the control. At test termination (juvenile sampling), additional measurements are made (see Table 4). Illustrations of each stage of *X. laevis* development (from **Ref. 4**) are available on-line at http://www.xenbase.org/anatomy/alldev.do.

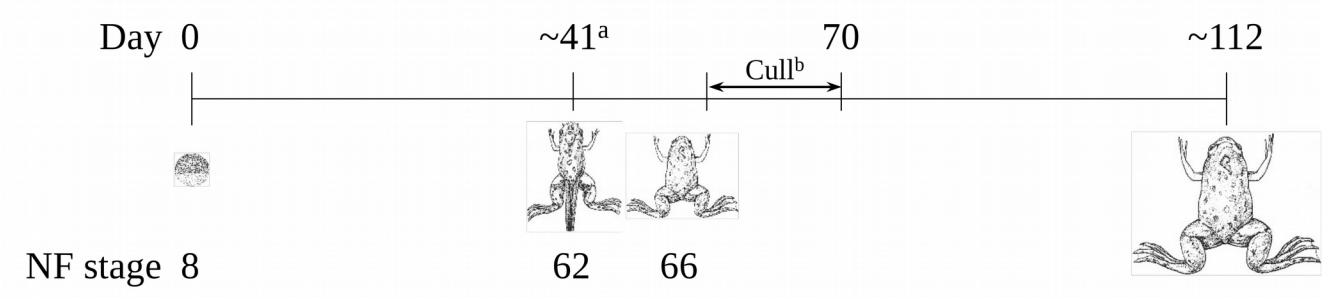

Figure 1. Timeline for the LAGDA. Images are adapted from Nieuwkoop and Faber (1994; **Ref. 4**).
[a] 41 days is the approximate median time to NF stage 62 in the controls; all control larvae will generally reach NF stage 62 over a 2 week period of time.
[b] The cull takes place after all animals on test reach NF stage 66, or at 70 days, whichever comes first.

A minimum of four replicate tanks per test concentration and a minimum of eight replicates for the controls (and solvent control, if needed) should be used (*i.e.*, the number of replicates in the control and any solvent control should be twice as large as the number of replicates of each treatment group to ensure appropriate statistical power). Each replicate should contain the same number of animals; 20 animals per replicate is recommended, but replicates should contain no more than 30 animals. While using the test method in this guideline, the minimum number of animals processed would be 15 (5 for NF stage 62 subsample and 10 juveniles). However, additional animals are added to each replicate to factor in the possibility for unsuccessful hatch and/or mortality while maintaining the critical number of 15.

The test conditions for LAGDA are summarized in Table 3.

Table 3. Test Conditions for LAGDA.

Test animal	***Xenopus laevis***

Initial larval stage		Nieuwkoop and Faber (NF) stage 8-10
Exposure period		Until 10 weeks after the median time to NF stage 62 in the clean water control
Test concentrations		Minimum of 4 different concentrations
Dilution water / laboratory control		Any water that permits normal growth and development of *X. laevis* (*e.g.*, spring water or charcoal-filtered tap water)
Replication		4 replicate test vessels / test concentration 8 replicate test vessels / control
Exposure regime		Flow-through
Test system flow-rate		Constant, in consideration of both the maintenance of biological conditions and chemical exposure (*e.g.*, flow rate sufficient to provide 10 tank volume additions/day)
Test solution / test vessel		4 – 10 L (10 cm minimum water depth) / glass or stainless steel
Initial larval density		~20 larvae / test vessel
Larval density after NF stage 66 cull		10 juveniles / test vessel (chosen randomly)
Feeding regime		See Appendix 2
Lighting	Photoperiod	12 hr light : 12 hr dark
	Intensity	600 to 2000 lux (lumens/m^2) at the water surface
Mean water temperature		21º ± 1°C (and the inter-replicate and -treatment differentials should be <1.0 ºC)
pH		6.5 to 8.5
Dissolved oxygen (DO) concentration		≥3.5 mg/L (>40% air saturation value, however, ≥60% preferred)
Analytical chemistry schedule		initiation (Day 0), and weekly thereafter for each replicate tank at each concentration
Control mortality		≤ 20% in each replicate
Median time to NF stage 62 (controls)		≤45 days
Mean weight (controls)		NF stage 62 = 1.0±0.2; At termination of assay = 11.5±3 g
Concentrations of the test chemical in solution throughout the test		Maintain within ±20% of the mean measured values

As shown in Table 4, the endpoints evaluated during the course of the exposure are those indicative of toxicity including mortality, abnormal behavior such as clinical signs of disease and/or general toxicities, and growth determinations (length and weight), as well as pathology endpoints which may respond to both general toxicity and endocrine toxicity acting through estrogen-, androgen-, or thyroid-mediated pathways.

Table 4. Timing of endpoint measurements over the course of the LAGDA.

Endpoints*	**Daily**	**Interim Sampling**	**Test Termination**

		(Larval Sampling at NF stage 62)	**(Juvenile Sampling)**
Mortality	X		
Abnormal appearances - Clinical signs of disease and/or general toxicities	X		
Time to NF stage 62		X	
Histopathology – thyroid gland		X	
Morphometrics (growth in weight and length)		X	X
Liver-somatic index (LSI)			X
Genetic/phenotypic sex ratios			X
Histopathology for gonads, reproductive ducts, kidney and liver			X

* All endpoints are analyzed statistically.

(2) Test Initiation. Parent animals used for the initiation of the assay should have previously been shown to produce offspring that can be genetically sexed (Appendix 3). After spawning of adults, embryos are collected, cysteine-treated to remove the jelly coat and screened for viability (**Ref. 24**). Cysteine treatment allows the embryos to be handled during screening without sticking to surfaces. Screening takes place under a dissecting microscope using an appropriately sized eye dropper to remove non-viable embryos. It is preferred that a single spawn resulting in greater than 70% viability be used for the test. Embryos at NF stage 8-10 are randomly distributed into exposure treatment tanks containing an appropriate volume of dilution water until each tank contains an equal number of embryos (20-30 embryos). Embryos can be constrained to a similar location in the tank in a submerged beaker or glass petri dish that is later removed when larvae are free-swimming. This method helps account for embryos and helps with observations of hatching success. An appropriately sized container would be no less than 6 cm in diameter and would allow adequate test solution replacement, enough to avoid areas of stagnant test solution. Embryos should be carefully handled during this transfer in order to minimize handling stress and to avoid any injury. At 96 hours post fertilization, the tadpoles should have moved up the water column and begun clinging to the sides of the tank.

(3) Mortality and Morbidity. All test tanks should be checked daily for dead animals and mortalities recorded for each tank. Dead animals should be removed from the test tank as soon as observed. The date, concentration, tank number and developmental stage of dead animals should be recorded as accurately as possible. If the NF stage is not discernable, it should be categorized as either pre-NF stage 58 (pre-forelimb emergence), NF stage 58-NF stage 62, NF stage 63-NF stage 66 (between NF stage 62 and complete tail absorption), or post-NF stage 66 (post-larval). Consistency in the NF stage at which death occurs may indicate a specific chemical mode of action and is important information for the study record. Mortality rates exceeding 20% may indicate inappropriate test conditions or overtly toxic effects of the test chemical. The animals tend to be most sensitive to non-chemical induced mortality events during the first few days of development after the spawning event and during metamorphic climax. If an organism is euthanized due to morbidity (possibly determined by observing abnormal behaviors listed in the next section), this should be noted and reported. Depending on when the individual is euthanized during the study, the carcass may need to be retained for possible histopathology analysis. Procedures for euthanasia and fixation of tissues for histology are described below and should be followed according to the appropriate life-stage-specific procedures.

(4) Additional Observations. In addition, any observation of abnormal behavior, grossly visible malformations (*e.g*., scoliosis, also described as bent tail in tadpoles), or lesions should be

recorded (include treatment and tank number). Normal behavior for larval animals is characterized by suspension in the water column with tail elevated above the head, regular rhythmic tail fin beating, periodic surfacing, operculating, and being responsive to stimuli. Abnormal behaviors would include, for example, floating on the surface, lying on the bottom of the tank, inverted or irregular swimming, lack of surfacing activity, and being nonresponsive to stimuli. For post-metamorphic animals, in addition to the above abnormal behaviors, gross differences in food consumption between treatments should be recorded. Gross malformations and lesions could include morphological abnormalities (*e.g.*, limb deformities), hemorrhagic lesions, abdominal edema, and bacterial or fungal infections, to name a few. The occurrences of lesions on the head of juveniles, just posterior to the nostrils, may be indications of insufficient humidity levels. These determinations are qualitative and should be considered akin to clinical signs of disease/stress and made in comparison to control animals. If the rate of occurrence is greater in exposed tanks than in the controls, then these should be considered as evidence for overt toxicity.

Observations of scoliosis should be counted (incidence) and graded with respect to severity (*e.g.*, not remarkable – NR, minimal – 1, moderate – 2, severe – 3). Guidance for grading and minimizing scoliosis is found in Appendix 4. Efforts should be made to ensure that the prevalence of moderate and severe scoliosis is limited (*e.g.*, below 10% in controls) throughout the study, although greater prevalence of control abnormalities would not necessarily mean the test should be ended. Differences in food consumption may be determined by how quickly the tanks clear after feeding, how much uneaten food accumulates on the bottom of the tank, and the amount of feces that accumulates between daily tank cleaning.

(5) Larval Sub-sample. Those tadpoles that have reached NF stage 62 should be removed from the exposure tanks and either sampled or moved to the next part of the exposure in a new tank, or physically separated from the remaining tadpoles in the same tank with a divider. Tadpoles are checked daily and the study day on which an individual tadpole reaches NF stage 62 is recorded. The defining characteristic for use in this assessment is the shape of the head shown in Figure 2a. Once the head has become reduced in size such that it is visually approximately the same width as the trunk of the tadpole, the olfactory nerve length is shorter than the diameter of the olfactory bulb and the forelimbs are at the level of the middle of the heart, then that individual would be counted as having attained NF stage 62. This determination can generally be made without netting or handling the individual by observing the dorsal characteristics of NF stage 62. The goal is to sample a total of five NF stage 62 tadpoles per replicate tank. This should be performed entirely at random, but decided *a priori* (explained below).

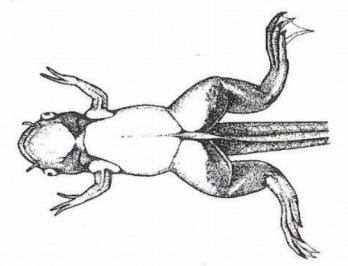

a. Larval sub-sampling (NF stage 62) b. Juvenile sampling

Ventral

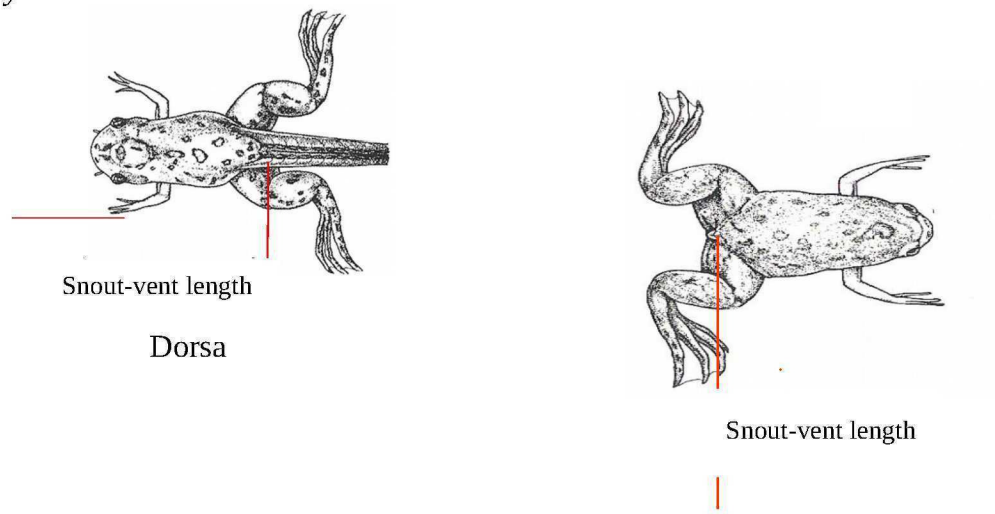

Figure 2. Landmarks for measuring snout-vent length for the LAGDA in NF Stage 62 (a) and juvenile frogs (b). The defining characteristics of NF stage 62 (a): the head is the same width as the trunk, the olfactory nerve length is shorter than the diameter of the olfactory bulb (dorsal view), and the forelimbs are at the level of the heart (ventral view). Images adapted from Nieuwkoop and Faber (1994¸**Ref. 4**).

A hypothetical example of a replicate tank is provided in Figure 3. Should there be 20 surviving tadpoles in a particular tank when the first individual reaches NF stage 62, five random numbers should be chosen from 1-20. Tadpole #1 is the first individual to reach NF stage 62 and tadpole #20 is the last individual in a tank to reach NF stage 62. Likewise, if there are 18 surviving larvae in a tank, five random numbers should be chosen from 1-18. This should be performed for every replicate tank when the first individual on test reaches NF stage 62. If there are mortalities during the NF stage 62 sampling, the remaining samples need to be re-randomized based on how many larvae are left less than NF stage 62 and how many more samples are needed to reach a total of five samples from that replicate.
On the day a tadpole reaches NF stage 62, reference to the prepared sampling chart is made to determine whether that individual is sampled or physically separated from the remaining tadpoles for continued exposure. In the example provided below (Figure 3), the first individual to reach NF stage 62 (*i.e.*, box #1) is physically separated from the other larvae, continues exposure and the study day on which that individual reached NF stage 62 is recorded. Subsequently, individuals #2 and #3 are treated the same way as #1 and then individual #4 is sampled for growth and thyroid histology (according to this example). This procedure continues until the 20th individual either joins the rest of the post-NF stage 62 individuals or is sampled. The random procedure used should give each organism on test equal probability of being selected. This can be achieved by using any randomizing method, but also requires that each tadpole be netted at some point throughout the NF stage 62 sub-sampling period.

Time (duration ~2 weeks) →

Single replicate tank – no mortalities

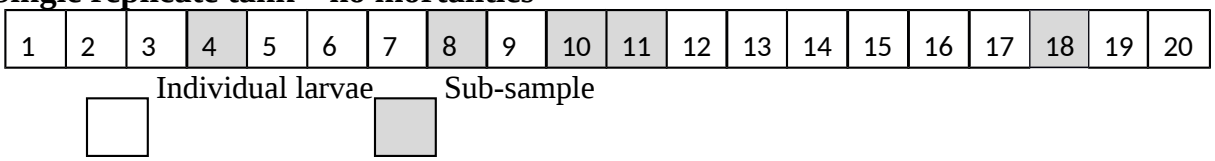

Figure 3. Hypothetical example of NF stage 62 sampling regime for a single replicate tank.

(i) Larval Sub-Sample Endpoints. For the larval sub-sampling, the endpoints obtained are:

- time to NF stage 62 (*i.e.*, number of days between fertilization and NF stage 62; n ≈ 20),
- external abnormalities (n ≈ 20),
- morphometrics (*i.e.*, weight and snout-to-vent length; n = 5),
- thyroid histology (n = 5).

(ii) Larval Sampling Procedure. The following steps are in the larval sub-sampling procedure:

- euthanize tadpole,
- rinse and blot dry,
- weigh tadpole (mg) and measure snout-vent length (mm),
- note any gross morphologic abnormalities and/or clinical signs of toxicity,
- remove and discard the lower torso posterior to the forelimbs (see Appendix 5 for guidance),
- fix the upper torso for 48 hours in Davidson's solution, rinse, and store tissues in 10% neutral buffered formalin (NBF) (see Appendix 5 for guidance).

(A) Tadpole Euthanasia. The sub-sample of NF stage 62 tadpoles (5 individuals per replicate) should be euthanized by immersion in a 0.03% (w/v) MS-222, tricaine methane sulfonate (CAS.886-86-2), solution (*e.g.*, 500 ml). The MS-222 solution should be buffered with sodium bicarbonate to a pH of approximately 7.0 because unbuffered MS-222 solution is acidic and irritating to frog skin resulting in poor absorption and unnecessary additional stress to the organisms. The characteristics of the water used to make this solution may impact the pH and the amount of sodium bicarbonate needed to neutralize this solution. In general, however, one part MS-222 to two parts of sodium bicarbonate should be used as a starting point.

Using a mesh dip net, a tadpole is removed from the experimental chamber and transported to the necropsy area in a suitable transport container. The tadpole is then placed into the euthanasia solution. The animal is properly euthanized and is ready for necropsy when it is unresponsive to external stimuli such as pinching the hind limb with a pair of forceps (approximately 5-8 minutes).

(B) Morphometrics (Weight and Length). Measurements of wet weight (nearest mg) and snout-to-vent length (SVL) to the nearest 0.1 mm for each tadpole (see Figure 2a) should be made immediately after it becomes non-responsive by anesthesia. These measurements are included in the test protocol to assess possible effects of a test chemical on the growth rate of organisms and are useful for detecting generalized toxicity. Tadpoles should be blotted dry before weighing to remove excess adherent water. Image analysis software may be used to measure SVL from a photograph. After measurements of body size (SVL and weight) are made, any gross morphological abnormalities such as scoliosis (see Appendix 4) and/or clinical signs of toxicity, petechiae and hemorrhage should be

recorded or noted, and digital documentation is recommended. Note: Petechiae are small red or purple hemorrhages in skin capillaries.

(C) Larval Sub-Sample Tissue Preparation for Histopathology. Each larval sample (NF stage 62) is evaluated histologically for pathology in the thyroid glands. The lower torso posterior to the forelimbs is removed and discarded (see Appendix 5, Figure 1 for trimming details and approximate gland locations). The trimmed carcass is placed into individually labelled histological cassettes and fixed in Davidson's fixative (recipe below).

Care should be taken not to compress tissues in cassettes as this will cause histological artifacts and could compromise pathology assessments. The volume of fixative in the container should be at least 10 times the approximate volume of the tissues. Appropriate circulation of the fixative should be achieved to adequately fix the tissues of interest. All tissues remain in Davidson's fixative for at least 48 hours, but no longer than 96 hours, at which time they are rinsed in deionized water and stored in 10% neutral buffered formalin (recipe below).

Histopathology guidance (Appendix 5) provides procedural information on trimming and processing tissues for histological examination as well as detailed information regarding pathologic effect evaluations and interpretation of diagnostic criteria.

Davidson's Fixative
Glacial acetic acid……115 ml
Formaldehyde (35-40%)……..220 ml
95% Ethyl Alcohol……...330 ml
Distilled water……..335 ml

10% Neutral Buffered Formalin (NBF)
100 ml formalin, full strength (37-40% formaldehyde)
6.5 g sodium phosphate dibasic (anhydrous)
4.0 g sodium phosphate monobasic
900 ml distilled water

(6) End of Larval Exposure. Given the initial number of tadpoles, it is expected that there will likely be a small percentage of individuals that do not develop normally and do not reach NF stage 66 in less than 70 days (a treatment-related delay in development could also cause individuals to not reach NF stage 66 in 70 days). Because of this situation, larval exposure ends after all animals have reached NF stage 66 or after 70 days, whichever comes first. Any tadpoles remaining at the end of larval exposure should be euthanized by immersion in 0.03% (w/v) buffered MS-222 (pH 7.0). Their wet weight and SVL should be measured, the developmental stage recorded (**Ref. 4**), and any developmental abnormalities noted.

(7) Cull After NF Stage 66. After all juvenile animals have reached NF stage 66 or after 70 days (whichever occurs first), a cull should be conducted. Post NF 66 animals that will continue the exposure should be selected at random. Following the culling process, only 10 individuals (maximum) per tank should continue exposure until termination of the test. Animals that are not selected to continue exposure are euthanized by immersion in a 0.05% (w/v) MS-222 solution buffered with sodium bicarbonate to a pH of approximately 7.0. Measurements of wet weight and snout-to-vent length (see Figure 2b), and a gross necropsy are conducted for each animal. The phenotypic sex (based on gonad morphology) is noted as female, male, or indeterminate.

(8) Juvenile Sampling. The remaining animals continue exposure until 10 weeks after the median time to NF stage 62 in the dilution water (and/or solvent control if relevant) control. At the end of the exposure period, the remaining animals (maximum 10 frogs per replicate) are euthanized, and the various endpoints listed below are measured or evaluated, and recorded. Final sample numbers will depend on genetic sex ratios.

(i) Juvenile Sample Endpoints. For the juvenile sampling, the endpoints obtained are:

- morphometrics (weight and length);
- phenotypic/genotypic sex ratios;
- gonad histopathology;
- reproductive duct histopathology;
- liver histopathology;
- liver weight (Liver-Somatic Index [LSI]); and
- kidney histopathology.

(ii) Juvenile Sampling Procedure. The juvenile sampling procedure has the following steps:

- euthanize frogs by immersion in buffered MS-222 solution (0.05% w/v) until subdued, followed by an intraperitoneal (IP) injection (*e.g.*, 0.02 ml per g of frog) of buffered 2.5% (w/v) MS-222 in physiological buffer;
- measure whole body weight (g) and snout-vent length (mm);
- record any developmental abnormalities and obvious signs of disease (*e.g.*, scoliosis, hemorrhage);
- place the frog in dorsal recumbence;
- open the abdominal cavity - excise, weigh, and fix the liver;
- carefully remove the digestive organs (*e.g.*, stomach, intestines) from the lower abdomen;
- assess gross morphological abnormalities in gonads (see Appendix 5, Figures 2a & 2b);
- remove a foot for a DNA sample and snap freeze in liquid nitrogen or dry ice; and,
- trim and fix abdominal section according to Appendix 5, Figures 2a & 2b depending on the gonadal phenotype.

(A) Juvenile Frog Euthanasia. The juvenile frogs are euthanized by immersion in a neutral buffered 0.05% (w/v) MS-222 solution until subdued, followed by an IP injection of 2.5% (w/v) MS-222 in a physiological buffer solution (*e.g.*, 0.1M phosphate buffered saline, pH 7.4). Dosage for frogs is approximately 0.02 ml per gram of frog. Injection provides efficient, fast euthanasia prior to sampling. Using this procedure, frogs may be sampled after becoming unresponsive, usually around 2 minutes after injection, but can take longer. Increasing the time of initial immersion and/or increasing the concentration of the immersion solution and/or increasing the volume of IP injection may be necessary depending on the effectiveness of the euthanasia procedure. Care should be taken not to damage internal organs during the IP injection.

(B) Morphometrics (Weight and Length). Measurements of wet weight and SVL (Figure 2b) are identical to those outlined for the larval sub-sampling.

(C) Juvenile Sample Tissue Preparation for Histopathology. Each juvenile sample is evaluated histologically for pathology in the gonads, reproductive ducts, kidneys and liver tissue. The abdominal cavity is opened and the entire liver is carefully dissected out and weighed. Next, the digestive organs (*e.g.*, stomach, intestines) and fat bodies are carefully removed from the lower abdomen to reveal the gonads, kidneys and reproductive ducts. Any gross morphological abnormalities in the gonads should be noted. Finally, the abdomen should be trimmed according to Appendix 5, Figures 2a & 2b depending on the phenotypic sex, and a hind limb (or appropriate tissue sample) should be retained (frozen) for genetic sex determination. Collected livers and the carcass with the gonads left *in situ* should be immediately placed into separate labelled histological cassettes and fixed in Davidson's fixative (for recipe, see section (f)(5)(ii)(*C*)). Care should be taken not to compress tissues in cassettes as this will cause histological artifacts and could compromise pathology assessments. The volume of fixative in the container should be at least 10 times the approximated volume of the tissues. The same fixatives used in the larval sub-sampling, as described previously, are used with adult samples. All tissues should remain in Davidson's fixative for at least 48 hours, but no longer than 96 hours, at which time they are rinsed in de-ionized or tap water and stored in 10% NBF (for recipe, see section (f)(5)(ii)(*C*)). Histopathology guidance is provided in Appendix 5 and contains procedural information on trimming and processing tissues for histological examinations. It also contains detailed information regarding pathologic effect evaluations and interpretation of diagnostic criteria.

***(D) Genetic Sex Determination*.** To determine genetic sex, DNA samples from frogs can be obtained from any tissues; however, one hind limb removed during dissection (or a portion of a hind limb) is easy to collect and store in a microfuge tube. Tissue should be snap frozen in liquid nitrogen or dry ice and can be stored at -20°C until DNA isolation. The isolation of DNA from tissues can be performed with commercially available kits and analysis for presence or absence of the marker is done by a polymerase chain reaction (PCR) method (see example protocol in Appendix 3). Development of the markers used for genetic sex determination of *X. laevis* is described by Yoshimoto et al. (**Ref. 11**). Generally, the concordance between juvenile histological sex (gonad phenotype) and genotype across control animals should be >95% (if the concordance is not 100% in control samples, there was likely a technical error). It would be prudent to test the primers for genetic sexing on the adult breeders using toe clips prior to running the LAGDA with their offspring.

(g) Performance Criteria and Test Acceptability/Validity.

(1) Performance Criteria. The performance criteria in Table 5 have been developed as guidance for determining the quality of the test performed and the general performance of the control organisms. When deviations from the test validity criteria are observed, the consequences should be considered in relation to the reliability of the test results, and these deviations and considerations should be included in the test report.

Table 5. Performance criteria for the LAGDA.

Parameter	Criteria
Test concentrations	Maintain concentrations of the test chemical in solution within 20% of the mean measured value over the entire test period.

Parameter	**Criteria**
Viability of spawn	≥70% viability in the spawn chosen to start the study
Mortality in controls	≤ 20% mortality in each replicate in the controls.
Median time to NF stage 62 in controls.	The median time to NF stage 62 is ≤45 days.
Mean weight of test organisms in controls	The mean weight of test organisms at NF stage 62 and at the termination of the assay in controls and solvent controls (if used) should be 1.0±0.2 and 11.5±3 g, respectively.
Dissolved Oxygen	The dissolved oxygen concentration should be ≥40% of air saturation value throughout the test.
pH	pH should be maintained between 6.5-8.5. The inter-replicate/inter-treatment differentials should not exceed 0.5.
Water temperature	21 ± 1ºC - the inter-replicate/inter-treatment differentials should not exceed 1.0 ºC.
Test concentrations without overt toxicity[a]	At least three treatment levels without obvious overt toxicity should be available for analysis. Excessive mortality, which compromises a treatment, is defined as >20% in 2 or more replicates that cannot be explained by technical error.
Replicate performance	1 replicate within a treatment can be compromised (see below for conditions for a compromised replicate). An increase beyond this results in loss of that treatment level.
Idiopathic scoliosis (“Bent tail”) in tadpoles	Prevalence of moderate and severe scoliosis should be limited to <10% to improve confidence that the test can detect treatment-related developmental effects in otherwise healthy amphibian larvae. See Appendix 4 for guidance.
Special conditions for use of a solvent (use of a solvent is strongly discouraged)	If a carrier solvent is used, both a solvent control and clean water control should be used. Statistically significant differences between solvent control and clean water control groups are treated specially. See below for more information.
Genotypic/phenotypic sex concordance in control juveniles	>95% concordance (if concordance is less than 100% in control juveniles, there was likely a technical error).
[a] Signs of overt toxicity may include, but are not limited to, floating on the surface, larvae lying on the bottom of the tank, inverted or irregular swimming, lack of surfacing activity, and being nonresponsive to stimuli, morphological abnormalities (*e.g.*, limb deformities), hemorrhagic lesions, and abdominal edema.	

(2) Test Validity. For a test to be considered valid, the following criteria should be met:

- At least three treatment levels with three uncompromised replicates are available for analysis. Excessive mortality, which compromises a treatment, is defined as >20% mortality in 2 or more replicates that cannot be explained by technical error.
- At least three treatment levels without obvious overt toxicity are available for analysis. Signs of overt toxicity may include, but are not limited to, floating on the surface, lying on the bottom of the tank, inverted or irregular swimming, lack of surfacing activity, and being nonresponsive to stimuli, morphological abnormalities (*e.g.*, limb deformities), hemorrhagic lesions, and abdominal edema.

- A NOEC and LOEC should be determined.

(h) Statistical Analyses.

The LAGDA generates three forms of data to be statistically analyzed:

- Quantitative continuous data including growth (weight, SVL, and LSI);
- Time-to-event data for developmental rates (*i.e.*, days to NF stage 62 from assay initiation);
- Ordinal data in the form of severity scores or developmental stages from histopathology evaluations.

Data are typically collected in spreadsheets and then transferred to and analyzed with a statistical software package. Statistical analyses of the data should preferably follow procedures described in the document, *Current Approaches in the Statistical Analysis of Ecotoxicity Data: A Guidance to Application* (**Ref. 36**). Figure 4 illustrates the recommended statistical analysis decision tree and guidance for the treatment of data from the LAGDA.

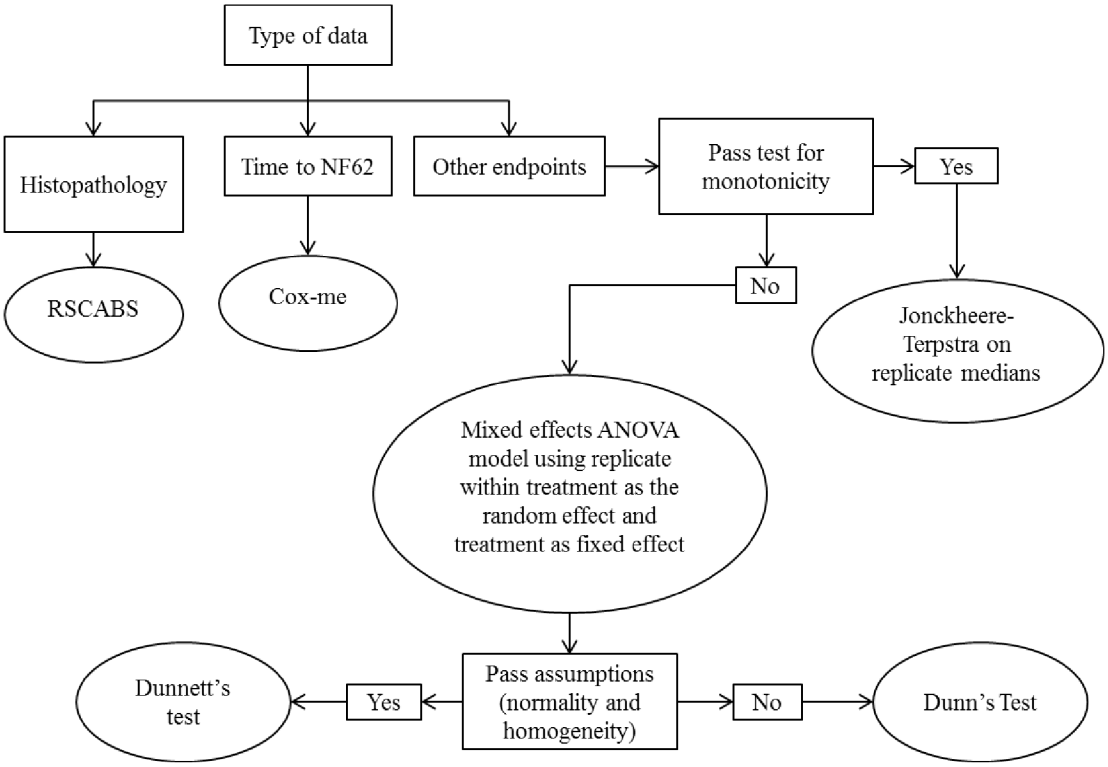

Figure 4. Statistical analysis decision tree for LAGDA data.

(1) Continuous Data. Data for continuous endpoints should first be checked for monotonicity by rank transforming the data, fitting to an ANOVA model and comparing linear and quadratic contrasts. If the data are monotonic, a step-down Jonckheere-Terpstra trend test should be performed on replicate medians and no subsequent analyses should be applied. If the data are non-monotonic (quadratic contrast is significant and linear is not significant), it should be analyzed using a mixed effects ANOVA model. The data should then be assessed for normality (preferably using the Shapiro-Wilk or Anderson-Darling test) and variance homogeneity (preferably using Levene's test). Both tests are performed on the residuals from the mixed effects ANOVA model. Expert judgment can be used in lieu of these formal tests for normality and variance homogeneity, though formal tests are preferred. If the

data are normally distributed with homogeneous variance, then the assumptions of a mixed effect ANOVA are met and a significant treatment effect is determined from Dunnett's test. Where non-normality or variance heterogeneity is found, then the assumptions of the mixed effect ANOVA model are violated and a significant treatment effect is determined with a Dunn's test. Whenever possible, a one-tailed test should be performed as opposed to a two-tailed test, but it requires expert judgment to determine which is appropriate for a given endpoint.

(2) Mortality. Mortality data should be analyzed for the time period encompassing the full test and should be expressed as percent that died in any particular tank. Tadpoles that do not complete metamorphosis in the given time frame, those tadpoles that are in the larval sub-sample cohort, those juvenile frogs that are culled, and any animal that dies due to experimenter error should be treated as censored data and not included in the denominator of the percent calculation. Prior to any statistical analyses, mortality ratios should be arcsin-square root transformed and analyzed according to the "Other endpoints" branch of the decision tree (Figure 4).

(3) Time to NF stage 62. Time to NF stage 62 data should be treated as time-to-event data. Mortalities or individuals not reaching NF stage 62 in 70 days are treated as right-censored data. Median time to NF stage 62 in clean water controls should be used to determine the test termination date. This endpoint should be analyzed using a mixed-effects Cox proportional hazard model that can be implemented in SAS or the free open source statistical program "R".

(4) Growth: Weight and Length. Males and females are not sexually-dimorphic during metamorphosis so larval sub-sampling growth data should be analyzed independent of gender. However, juvenile growth data should be analyzed separately based on genetic sex. These data should be analyzed according to the "Other endpoints" branch of the decision tree (Figure 4). Transformations are not recommended for these endpoints, unless deemed necessary by professional judgment.

(5) Liver-somatic-index (LSI). Liver weights should be normalized as proportions of whole body weights (LSI) and analyzed separately based on genetic sex. These data should be analyzed according to the "Other endpoints" branch of the decision tree (Figure 4). Transformations are not recommended for this endpoint, unless deemed necessary by professional judgment.

(6) Histopathology (severity scores and developmental stages). Histopathology data are in the form of severity scores or developmental stages. A test termed RSCABS (Rao-Scott Cochran-Armitage by Slices) uses a step-down Rao-Scott adjusted Cochran-Armitage trend test on each level of severity in a histopathology response (**Ref. 37**). The Rao-Scott adjustment incorporates the replicate vessel experimental design into the test. The "by slices" procedure incorporates the biological expectation that severity of effect tends to increase with increasing doses or concentrations, while retaining the individual subject scores and revealing the severity of any effect found. The RSCABS procedure not only determines which treatments are statistically different than controls (*i.e.*, have more severe pathology than controls), but it also determines at which severity score the difference occurs thereby providing much needed context to the analysis. In the case of developmental staging of gonads and reproductive ducts, an additional manipulation should be applied to the data since an assumption of RSCABS is that severity of effect increases with concentration. The effect observed could be a delay OR acceleration of development. Therefore, developmental staging data (gonad and reproductive ducts) should be analyzed as reported to detect acceleration in development and then manually inverted prior to a second analysis to detect a delay in development.

(7) Use of Compromised Replicates and Treatments. Replicates and treatments may become compromised due to excess mortality from overt toxicity, disease, or technical error (see Section (g) for performance criteria). If a treatment is compromised from disease or technical error, there should be at least three uncompromised treatments with three uncompromised replicates available for analysis. In the case that a single replicate in a treatment is compromised due to excess mortality, that replicate should be removed from statistical analysis. If overt toxicity occurs in the high treatment(s), it is preferable that at least three treatment levels with three uncompromised replicates are available for analysis (consistent with the Maximum Tolerated Concentration approach in Hutchinson *et al.* (**Ref. 30**). In addition to mortality, signs of overt toxicity may include behavioral effects (*e.g.*, floating on the surface, lying on the bottom of the tank, inverted or irregular swimming, lack of surfacing activity), morphological lesions (*e.g.*, hemorrhagic lesions, abdominal edema) or inhibition of normal feeding responses when compared qualitatively to control animals. A determination of test continuation should be made in consultation with the EPA.

(8) Solvent controls. The use of a solvent should only be considered as a last resort, when all other chemical delivery options have been considered. If a solvent is used, then a dilution water (negative) control should be run in concert with a solvent control. At the termination of the test, a statistical comparison of the solvent control group and the dilution water control group should be performed to determine any potential effects of the solvent. The most relevant endpoints for consideration in this analysis are growth determinants (weight and length), as these can be affected through generalized toxicities. If statistically significant differences are detected in these endpoints between the dilution water control and solvent control groups, best professional judgment should be used to determine if the validity of the test is compromised. If the two controls differ, then all test level comparisons should be made to the solvent control unless it is known that comparison to the dilution water control is preferred. If there is additional evidence that there is no solvent interference then statistical comparisons with the dilution water control may be appropriate. If there are no statistically significant differences between the two control groups, it is recommended that the treatments exposed to the test chemical are compared with the pooled solvent and dilution water control groups, unless it is known that comparison to either the dilution water or solvent control group only is preferred (see discussion in **Ref. 36**; **Ref. 37; Ref. 38**).

(i) Data Reporting.

All data should be collected using electronic or manual systems which conform to good laboratory practices (GLP). The test report should include the following information:

(1) Test Substance. The report should include a complete characterization of the test substance.

- Physical nature and, where relevant, physicochemical properties.
- Mono-constituent substance: physical appearance, water solubility, and additional relevant physicochemical properties; chemical identification, such as IUPAC (International Union of Pure and Applied Chemistry) or CAS name, CAS number, SMILES (Simplified Molecular Input Line Entry Specification) or InChI (IUPAC International Chemical Identifier code), structural formula, purity, chemical identity of impurities as appropriate and practically feasible, etc. (including the organic carbon content, if appropriate).
- Multi-constituent substance, UVBCs (substances of unknown or variable composition, complex reaction products or biological materials and mixtures) characterized as far as possible by chemical identity (see above), quantitative occurrence and relevant physicochemical properties of the constituents.

(2) Test Species. Include: scientific name, strain if available, source and method of collection of the fertilized eggs and subsequent handling; incidence of scoliosis in historical controls for the stock culture used.

(3) Test Conditions.

- Photoperiod(s);
- Test design (*e.g*., chamber size, material and water volume, number of test chambers and replicates, number of test organisms per replicate);
- Method of preparation of stock solutions and frequency of renewal (the solubilizing agent and its concentration should be given, when used);
- Method of dosing the test chemical (*e.g*., pumps, diluting systems);
- The recovery efficiency of the method and the nominal test concentrations, the limit of quantification, the means of the measured values and their standard deviations in the test vessels and the method by which these were attained and evidence that the measurements refer to the concentrations of the test chemical in true solution;
- Dilution water characteristics: pH, hardness, temperature, dissolved oxygen concentration, residual chlorine levels (if measured), total iodine, total organic carbon (if measured), suspended solids (if measured), salinity of the test medium (if measured) and any other measurements made;
- Solvent (if other than water). Justification of the choice of solvent, and characterization of solvent (nature, concentration used).
- The nominal test concentrations, the means of the measured values and their standard deviations;
- Water quality within test vessels, pH, temperature (daily) and dissolved oxygen concentration;
- Detailed information on feeding (*e.g*., type of foods, source, amount given and frequency).

(4) Biological Observations and Data.

- Daily observations of mortality, food consumption, abnormal swimming behavior, lethargy, loss of equilibrium, malformations (*e.g.*, scoliosis), lesions, *etc*.
- Observations and data collected at predetermined intervals include: growth (weight and SVL), clinical signs of disease or general toxicities, time to NF stage 62, and phenotypic as well as genetic sex.

(5) Histological Data. The report should include narrative descriptions, as well as graded severity and incidence scores of specific observations.

(6) Statistical Analyses. It is recommended that statistical analytical techniques outlined in this test guideline be used for analyses of LAGDA data. If there are deviations from these techniques to determine statistically significant effects, justification of alternative techniques should be provided. Results of the statistical analyses should be provided in tabular form.

(7) *Ad hoc* Observations. The report should include narrative descriptions of observations that do not fit into the previously described categories.

(8) Results.

- Evidence that controls met the performance criteria;

- Data for the control (plus solvent control when used) and the treatment groups as follows: mortality and abnormalities observed, time to NF stage 62, thyroid histology assessment (larval sample only), growth (weight and length), LSI (juvenile sample only), genetic/phenotypic sex ratios (juvenile sample only), and histopathology assessment results for gonads, reproductive ducts, kidney and liver (juvenile sample only).

- Approach for and results of the statistical analysis and treatment of data (statistical test or model used);

- No observed effect concentration (NOEC) for each response assessed;

- Lowest observed effect concentration (LOEC) for each response assessed (at $\alpha = 0.05$); ECx for each response assessed, if applicable, and confidence intervals (*e.g.*, 95%) and a graph of the fitted model used for its calculation, the slope of the concentration-response curve, the formula of the regression model, the estimated model parameters and their standard errors.

- Any deviation from the guideline and deviations from the acceptance criteria, and considerations of potential consequences on the outcome of the test.

- For the results of endpoint measurements, mean values and their standard deviations (on both replicate and concentration basis, if possible) should be presented. Results of the statistical analyses should be provided in tabular form.

- Median time to NF stage 62 in controls should be calculated and presented as the mean of replicate medians and their standard deviation. Likewise, for treatments, a treatment median should be calculated and presented as the mean of replicate medians and their standard deviation.

(j) References.

1) US EPA. 2011. Endocrine Disruptor Screening Program. Weight-of-Evidence: Evaluating Results of the EDSP Tier 1 Screening to Identify the Need for Tier 2 Testing. US EPA, Washington, DC.

2) OECD. 2015. Larvae Amphibian Growth and Development Assay (LAGDA). OECD Guidelines for the Testing of Chemicals No. 241; new TG, publication expected July 2015

3) Kloas W, Lutz I. 2006. Amphibians as model to study endocrine disrupters. Journal of Chromatography A 1130: 16-27.

4) Nieuwkoop, P.D. and Faber, J. (1994). Normal Table of *Xenopus laevis* (*Daudin*). Garland Publishing, Inc, New York, NY.

5) Chang C, Witschi E. 1956. Genic control and hormonal reversal of sex differentiation in Xenopus. Journal of the Royal Society of Medicine 93: 140-144.

6) Gallien L, 1953. Total inversion of sex in Xenopus laevis Daud, following treatment with estradiol benzoate administered during larval stage. Comptes Rendus Hebdomadaires des Séances de l'Académie des Sciences 237: 1565.

7) Villalpando I, Merchant-Larios H. 1990. Determination of the sensitive stages for gonadal sex reversal in *Xenopus laevis* tadpoles. International Journal of Developmental Biology 34: 281-285.

8) Miyata S, Koike S, Kubo T. 1999. Hormonal reversal and the genetic control of sex differentiation in Xenopus. Zoological Science 16: 335-340.

9) Mikamo K, Witschi E. 1963. Functional sex-reversal in genetic females of Xenopus laevis, induced by implanted testes. Genetics 48: 1411.

10) Olmstead AW, Kosian PA, Korte JJ, Holcombe GW, Woodis KK, Degitz SJ. 2009a. Sex reversal of the amphibian, *Xenopus tropicalis*, following larval exposure to an aromatase inhibitor. Aquatic Toxicology 91: 143-150.

11) Yoshimoto, S., Okada, E., Umemoto, H., Tamura, K., Uno, Y., Nishida-Umehara, C., Matsuda, Y., Takamatsu, N., Shiba, T., Ito, M. (2008). A W-linked DM-domain gene, DM-W, participates in primary ovary development in *Xenopus laevis*. *Proc Natl Acad Sci USA* 105(7):2469-2474.

12) Olmstead AW, Korte JJ, Woodis KK, Bennett BA, Ostazeski S, Degitz SJ. 2009b, Reproductive maturation of the tropical clawed frog: *Xenopus tropicalis*. General and Comparative Endocrinology 160: 117-123.

13) Wake, MH, Dickie, R. 1998. Oviduct structure and function and reproductive modes in amphibians. J. Exp. Zool., 282: 477-506.

14) Tobias ML, Tomasson J, Kelley DB. 1998. Attaining and maintaining strong vocal synapses in female *Xenopus laevis*. Journal of Neurobiology 37: 441-448.

15) Qin ZF, Qin XF, Yang L, Li HT, Zhao XR, Xu XB. 2007. Feminizing/demasculinizing effects of polychlorinated biphenyls on the secondary sexual development of *Xenopus laevis*. Aquatic Toxicology 84: 321-327.

16) Porter KL, Olmstead AW, Kumsher DM, Dennis WE, Sprando RL, Holcombe GW, Korte JJ, Lindberg-Livingston A, Degitz SJ. 2011. Effects of 4-*tert*-octylphenol on *Xenopus tropicalis* in a long term exposure. Aquatic Toxicology 103: 159-169.

17) Tata, J. R. 2006. Amphibian metamorphosis as a model for the developmental actions of thyroid hormone. Molecular and cellular endocrinology, 246(1), 10-20.

18) Dent, J. N. 1968. Survey of amphibian metamorphosis. In W. Etkin and L I. Gilbert (eds), Metamorphosis. A Problem in Developmental Biology, New York: Appleton-Century Crofts, pg. 271-311.

19) Just, J. J., Kraus-Just, J., & Check, D. A. 1981. Survey of chordate metamorphosis. In Metamorphosis (pp. 265-326). Springer US.

20) Tata, J. R. 1993. Gene expression during metamorphosis: an ideal model for post-embryonic development. Biossays, 15(4), 239-248.

21) OECD. 2002. *Guidance Document on Aquatic Toxicity Testing of Difficult Substances and Mixtures*, OECD Series on Testing and Assessment, No. 23, OECD Publishing, Paris. DOI: 10.1787/9789264078406-en.

22) United States EPA. 1996. OCSPP Harmonized Test Guidelines, Ecological Effects Test Guidelines, OCSPP 850.1000: Special Considerations for Conducting Aquatic Laboratory Studies. EPA 712-C-96-113. April 1996. Available on-line at 32.

23) American Society for Testing and Materials (ASTM). 2002. Standard Guide for Conducting Acute Toxicity Tests on Test Materials with Fishes, Macroinvertebrates, and Amphibians. American Society for Testing and Materials, ed., Philadelphia, PA.

24) American Society for Testing and Materials (ASTM). 2004. Standard Guide for Conducting the Frog Embryo Teratogenesis Assay - *Xenopus* (FETAX). American Society for Testing and Materials, ed., Philadelphia, PA.

25) Read BT. 2005. Guidance on the housing and care of the African clawed frog *Xenopus laevis*. Royal Society for the Prevention of Cruelty to Animals (RSPCA), Horsham, Sussex, U.K., 84 pp.

26) OECD. 1992. Ready Biodegradability. OECD Guidelines for Testing Chemicals. No. 301. OECD, Paris.

27) OCED. 2006. Ready Biodegrabability – CO2 in sealed vessels (headspace test). OECD Guidelines for Testing Chemicals. OECD, Paris.

28) Kahl, M.D., Russom, C.L., DeFoe, D.L., and Hammermeister, D.E. (1999). Saturation units for use in aquatic bioassays. Chemosphere 39, 539-551.

29) Adolfsson-Erici M, Åkerman G, Jahnke A, Mayer P, McLachlan M. 2012. A flow-through

passive dosing system for continuously supplying aqueous solutions of hydrophobic chemicals to bioconcentration and aquatic toxicity tests. Chemosphere 86: 593-599.

30) Hutchinson, T.H., Shillabeer, N., Winter, M.J., and Pickford, D.B. 2006. Acute and chronic effects of carrier solvents in aquatic organisms: a critical review. *Aquat Toxicol* **76**, 69-92.

31) US EPA. 2009. Endocrine Disruptor Screening Program Test Guidelines. OCSPP 890:1100: Amphibian Metamorphosis (Frog). US EPA, Washington, DC.

32) OECD. 2009. The Amphibian Metamorphosis Assay. OECD Guidelines for the Testing of Chemicals No. 231. OECD, Paris.

33) OECD. 2012b. Fish Short Term Reproduction Assay. OECD Guidelines for the Testing of Chemicals No. 229. OECD, Paris.

34) OECD. 2011. Fish Sexual Development Test. OECD Guidelines for the Testing of Chemicals no. 234, OECD, Paris.

35) OECD. 2013b. Fish Embryo Acute Toxicity (FET) Test. OECD Guidelines for the Testing of Chemicals No. 236. OECD, Paris.

36) OECD. 2006. *Guidance Document on Current Approaches in the Statistical Analysis of Ecotoxicity Data*, OECD Series on Testing and Assessment, No. 54. ENV/JM/MONO(2006)18. OECD Publishing, Paris.

37) Green J.W., Springer T.A., Saulnier A.N., Swintek J. 2014. Statistical analysis of histopathology endpoints. Environmental Toxicology and Chemistry. 33(5):1108-1116.

38) Green, J.W. Wheeler, J. 2013. The use of carrier solvents in regulatory aquatic toxicology testing: Practical, statistical and regulatory considerations. Aquatic Toxicology. 144-145C: 242-249.

(k) List of LAGDA Appendices. **Page**

(1) Definitions…… 32
(2) Larval and Juvenile Diet Protocols……. 33
(3) Genetic Sex Determination…….. 36
(4) Considerations for Tracking and Minimizing the Occurrence of Scoliosis……. 39
(5) Histopathology Guidance for LAGDA…….. 41

APPENDIX 1: Definitions

Apical endpoint: Causing effect at population level.

ELISA: Enzyme-Linked Immunosorbent Assay

dpf: days post fertilization

Flow-through test: is a test with continued flow of test solutions through the test system during the duration of exposure.

HPG axis: hypothalamic-pituitary-gonadal axis

HPT axis: hypothalamic-pituitary-thyroid axis

InChI: The IUPAC International Chemical Identifier is a textual identifier for chemical substances, designed to provide a standard and human-readable way to encode molecular information and to facilitate the search for such information in databases and on the web.

IUPAC: International Union of Pure and Applied Chemistry

Median Lethal Concentration (LC50): is the concentration of a test chemical that is estimated to be lethal to 50% of the test organisms within the test duration.

Liver-somatic index: Liver-somatic index

Lowest observed effect concentration (LOEC) is the lowest tested concentration of a test chemical at which the chemical is observed to have a statistically significant effect (at $p < 0.05$) when compared with the control. However, all test concentrations above the LOEC should have a harmful effect equal to or greater than those observed at the LOEC. When these two conditions cannot be satisfied, a full explanation should be given for how the LOEC (and hence the NOEC) has been selected.

No observed effect concentration (NOEC) is the test concentration immediately below the LOEC, which when compared with the control, has no statistically significant effect ($p < 0.05$), within a stated exposure period.

SMILES: Simplified Molecular Input Line Entry Specification

SVL: snout-to-vent length

UVCB: substances of unknown or variable composition, complex reaction products or biological materials

VTG: vitellogenin is a phospholipoglycoprotein precursor to egg yolk protein that normally occurs in sexually active females of all oviparous species.

APPENDIX 2: Larval and Juvenile Diet Protocol

The protocol described below is the recommended larval and juvenile diet protocol. This protocol is based on procedures used at the U.S. Environmental Protection Agency laboratory in Duluth, MN. Specific products and/or equipment listed can be substituted with comparable materials. Alternative diets are acceptable as long as the organisms meet the growth and development criteria.

(a) Larval Diet.

This diet, consisting of Trout Starter, algae/TetraFin®, and brine shrimp, allows control organisms to meet both of the following criteria:

Median time to NF stage 62 is ≤ 45 days, and
Mean weight at NF stage 62 is 1.0 ± 0.2 g.

(1) Larval Food Preparation.

(i) 1:1 (v/v) Trout Starter: algae/TetraFin®:

- Trout Starter: blend 50 grams of Trout Starter (fine granules or powder) and 300 mL of suitable filtered water on a high blender setting for 20 seconds.
- Algae/TetraFin® mixture: blend 12 g spirulina algae disks and 500 ml filtered water on high for 40 seconds, blend 12 g Tetrafin® with 500 ml filtered water and then combine these to make up one L of 12 g/L spirulina algae and 12 g/L Tetrafin.®
- Combine equal volumes of the blended Trout Starter and the algae/TetraFin® mixture.

(ii) Brine Shrimp. 15 ml brine shrimp eggs are hatched in 1 L of salt water (prepared by adding 20 mL of NaCl to 1 L deionized water). After aerating 24 hours at room temperature under constant light, the brine shrimp are harvested. Briefly, the brine shrimp are allowed to settle for 30 min by stopping aeration. Cysts that float to the top of the canister are poured off and discarded, and the shrimp are poured through the appropriate filters and brought up to 30 ml with filtered water.

(2) Larval Feeding Protocol. Table 1 summarizes the type and amount of feed used during the larval stages of the exposure. The animals are fed three times per day Monday through Friday and once per day on the weekends.

(b) Larval to Juvenile Diet Transition.

At NF stage 62, the tadpole opercula close and they no longer filter feed on suspended food. However, it is unclear when exactly the organisms begin bottom feeding. Therefore, pellet food is provided per post-NF stage 62 regardless of whether they consume it or not. To aid the transition over to pellet food, crushed pellets are provided at a rate per post-NF stage 62 larvae. Due to this diet transition, and to avoid overfeeding pre-NF stage 62 larvae (should all organisms be kept in the same divided tank), a decrease in larval feed concurrent with an increase in juvenile feed is recommended during this period of the test. This can be accomplished by feeding post-NF stage 62 at the rate specified in Table 2 while decreasing the larval feeding volume proportionally when each group of five (5) individuals in a particular tank develops past NF stage 62.

Table 1. Feeding regime for *X. laevis* larvae in flow-through conditions (Trout Starter, Algae/TetraFin® diet, and brine shrimp quantities for 20 tadpoles).

	Trout Starter: algae/TetraFin®		**Brine Shrimp**	
Time* Post-Fertilization (pf)	**Weekday Feeding Volume (3 times per day)**	**Weekend Feeding Volume (once per day)**	**Weekday (twice per day)**	**Weekend (once per day)**
4-14 days (Weeks 0-1)	0.33 ml	1.2 ml	0.5 ml (from Day 8 to 15 pf)	0.5 ml (from Day 8 to 15 pf)
Week 2	0.67 ml	2.4 ml	1 ml **(day 16)**	1 ml **(day 16)**
Week 3	1.3 ml	4.0 ml	1 ml	1 ml
Week 4	1.5 ml	4.0 ml	1 ml	1 ml
Week 5	1.6 ml	4.4 ml	1 ml	1 ml
Week 6	1.6 ml	4.6 ml	1 ml	1 ml
Week 7	1.7 ml	4.6 ml	1 ml	1 ml
Weeks 8-10	1.7 ml	4.6 ml	1 ml	1 ml

* Day 0 is defined as the day hCG injection is done.

(c) Post-NF stage 62 and Juvenile Diet.

After larvae reach NF stage 62, the feeding regime changes to 3/32 inch premium sinking frog food alone (Xenopus Express., FL) or equivalent.

(1) Food Preparation for Larval to Juvenile Transition. Sinking frog food pellets are briefly run in a coffee grinder, blender or mortar and pestle in order to reduce the size of the pellets by approximately 1/3. Processing too long results in powder and is discouraged.

(2) Post-NF stage 62 and Juvenile Feeding Protocol. Table 2 provides a reference regarding the type and amount of feed used during the post-NF stage 62 and juvenile life stages. The animals should be fed once per day. It should be noted that as animals metamorphose, they continue receiving a portion of the brine shrimp until >95% animals have completed metamorphosis (NF stage 66). The animals should not be fed on the day of test termination so feed does not confound weight measurements.

Table 2. Feeding regime for *X. laevis* juveniles in flow-through conditions. It should be noted that un-metamorphosed animals, including those whose metamorphosis has been delayed by the chemical treatment, cannot eat uncrushed pellets.

Weeks post-median NF stage 62 date in controls*	**Crushed pellet volume (mg per organism)**	**Whole pellet volume (mg per organism)**
As larvae reach NF stage 62	25	0
Weeks 0-1	25	28
Weeks 2-3	0	110
Weeks 4-5	0	165
Weeks 6-9	0	220

*The first day of week 0 is the median NF stage 62 date in control animals.

APPENDIX 3: Genetic Sex Determination.

The example protocol for genetic sex determination using PCR and gel electrophoresis is based on procedures used at the U.S. Environmental Protection Agency laboratory in Duluth, MN. Alternative methods, such as Q-RT-PCR, can be developed. Additionally, alternative supplies such as specific products and/or equipment listed below can be substituted with comparable materials.

(a) *Xenopus laevis* primers (see Ref.)

DM-W marker: Gene ID: 100137717
Forward: 5'-CCACACCCAGCTCATGTAAAG-3'
Reverse: 5'-GGGCAGAGTCACATATACTG-3'
Positive Control (DMRT1): Gene ID: 735040
Forward: 5'-AACAGGAGCCCAATTCTGAG-3'
Reverse: 5'-AACTGCTTGACCTCTAATGC-3'

(b) DNA purification.

Purify DNA from muscle or skin tissue using a commercially available kit according to kit instructions. If using spin columns, DNA can be eluted using less buffer to yield more concentrated samples if deemed necessary for PCR. The final DNA concentration for purified samples should be ~4 ng/µl.

(c) PCR.

Sample protocol using JumpStart™ Taq (Sigma-Aldrich) is outlined below:

Master Mix	**1x (µL)**	**[Final]**
NFW	11	-
10X Buffer	2.0	-
$MgCl_2$ (25mM)	2.0	2.5 mM
dNTP's (10mM ea)	0.4	200 µM
Marker for. primer (8 µM)	0.8	0.3 µM
Marker rev. primer (8 µM)	0.8	0.3 µM
Control for. primer (8 µM)	0.8	0.3 µM
Control rev. primer (8 µM)	0.8	0.3 µM
JumpStart™ Taq	0.4	0.05 units/µl
DNA template	1.0	~200 pg/µl

Note: When preparing Master Mixes, prepare extra to account for any loss that may occur while pipetting (*e.g.*, 25x Master Mix will only yield approximately 23 reactions).

Reaction:

Master Mix	19.0 µl
Template	1.0 µl
Total	20.0 µl

Thermocycler Profile:

Step 1. 94 ºC 1 min
Step 2. 94 ºC 30 sec
Step 3. 60 ºC 30 sec
Step 4. 72 ºC 1 min
Step 5. Go to step 2. 35 cycles
Step 6. 72 ºC 1 min
Step 7. 4 ºC hold

PCR products can be run immediately in an agarose gel or stored at 4ºC.

(d) Agarose Gel Electrophoresis (3%)

<u>50X TAE (Tris-acetate-EDTA)</u>
24.2 g Tris
5.71 ml Glacial acetic acid
3.72 g $Na_2(EDTA)\cdot 2H_2O$
Add water to 100 ml

<u>1X TAE</u>
392 ml H_2O
8 ml 50X TAE

<u>3:1 Agarose</u>
3 parts NuSieve™ GTG™ agarose
1 part Fisher agarose low electroendosmosis (EEO)

Electrophoresis Method

- Prepare a 3% gel by adding, *e.g.*, 1.2 g agarose mix to 43 ml 1X TAE. Swirl to disassociate large clumps.
- Microwave agarose mixture until completely dissolved (avoid boiling over). Let cool slightly.
- Add 1.0µl ethidium bromide (10 mg/mL). Swirl flask.
- Pour gel into mold with comb. Cool completely.
- Add gel to apparatus. Cover gel with 1X TAE.
- Add 1µl of 6x loading dye to each 10µl PCR product.
- Pipette samples into wells.
- Run at 160 constant volts for ~20 minutes.

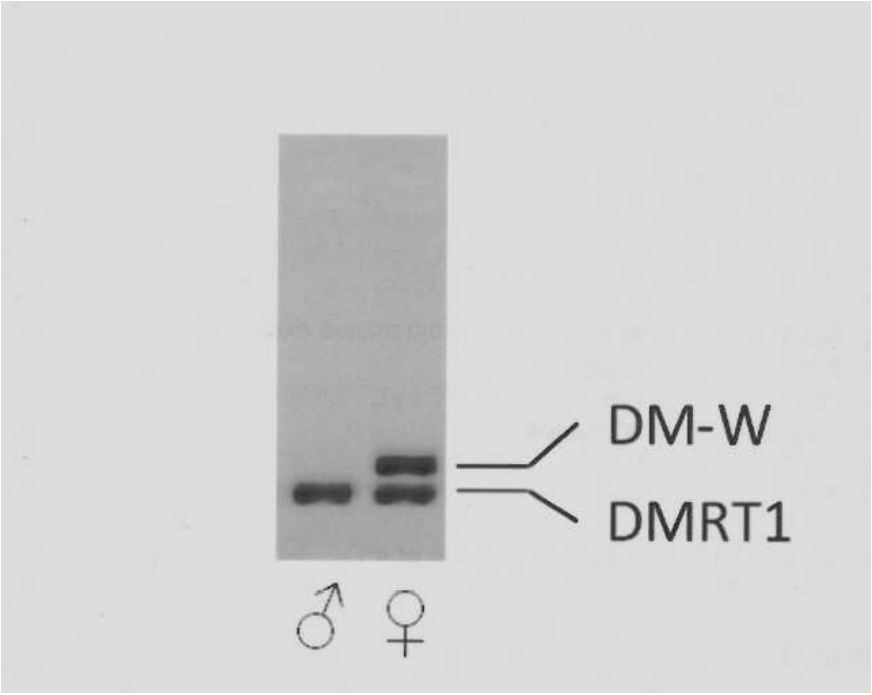

Figure 1. Agarose gel image showing the band pattern indicative of a male (♂) individual (single band ~203 bp: DMRT1) and of a female (♀) individual (two bands at ~259 bp: DM-W and 203 bp: DMRT1).

(e) Reference

Yoshimoto, S., Okada, E., Umemoto, H., Tamura, K., Uno, Y., Nishida-Umehara, C., Matsuda, Y., Takamatsu, N., Shiba, T., Ito, M. (2008). A W-linked DM-domain gene, DM-W, participates in primary ovary development in *Xenopus laevis*. *Proc Natl Acad Sci USA* 105(7):2469-2474.

APPENDIX 4: Considerations for Tracking and Minimizing the Occurrence of Scoliosis

(a) Recognition and Grading the Severity of Idiopathic Scoliosis.

Idiopathic scoliosis, usually manifesting as "bent tail" in *Xenopus laevis* tadpoles, may complicate morphological and behavioral observations in test populations. Efforts should be made to minimize or eliminate the incidence of scoliosis, both in stock and under test conditions. In the definitive test, it is recommended that the prevalence of moderate and severe scoliosis be less than 10%, to improve confidence that the test can detect treatment-related developmental effects in otherwise healthy amphibian larvae.

Daily observations during the definitive test should record both the incidence (individual count) and severity of scoliosis, when present. The nature of the abnormality should be described with respect to location (*e.g*., anterior or posterior to the vent) and direction of curvature (*e.g*., lateral or dorsal-to-ventral). Severity may be graded as follows:

- (NR) Not remarkable: no curvature present
- Minimal: slight, lateral curvature posterior to the vent; apparent only at rest
- Moderate: lateral curvature posterior to the vent; visible at all times but does not inhibit movement
- Severe: lateral curvature anterior to the vent; OR any curvature that inhibits movement; OR any dorsal-to-ventral curvature

(b) Recommendations for Reducing Idiopathic Scoliosis.

The EPA FIFRA Scientific Advisory Panel reviewed summary data for scoliosis in fifteen Amphibian Metamorphosis Assays (OCSPP 890.1100) with *X. laevis* (NF stage 51 through 60+) and provided general recommendations for reducing the prevalence of this abnormality in test populations (FIFRA SAP, 2013). These recommendations are summarized below.

(1) Historical Spawning Performance. Generally, high quality, healthy adults should be used as breeding pairs; eliminating breeding pairs that produce offspring with scoliosis may minimize its occurrence over time. Specifically, minimizing the use of wild-caught breeding stock may be beneficial. The LAGDA exposure period begins with NF stage 8-10 embryos, and it is not feasible to determine at the test outset whether given individuals will exhibit scoliosis. Thus, in addition to tracking the incidence of scoliosis in animals that are placed on test, historical clutch performance (including the prevalence of scoliosis in any larvae allowed to develop) should be documented. It may be useful to further monitor the portion of each clutch not used in a given study and to report these observations.

(2) Water Quality. It is important to ensure adequate water quality, both in laboratory stock and during the test. In addition to water quality criteria routinely evaluated for aquatic toxicity tests, it may be useful to monitor for and to correct any nutrient deficiencies (*e.g.*, deficiency of vitamin C, calcium, phosphorus) or excess levels of selenium and copper, which are reported to cause scoliosis to varying degrees in laboratory-reared *Rana* sp. and *Xenopus* sp. (Marshall *et al.* 1980; Leibovitz *et al*. 1992; Martinez *et al*. 1992; as stated in the FIFRA SAP report (FIFRA SAP, 2013)). The use of an appropriate dietary regimen (see Appendix 2), and regular tank cleaning, will generally improve water quality and health of the test specimens (FIFRA SAP, 2013).

(3) Diet. Specific recommendations for a dietary regimen, found to be successful in the LAGDA, are detailed in Appendix 2. It is recommended that feed sources be screened for biological toxins, herbicides, and other pesticides which are known to cause scoliosis in *X. laevis* or other aquatic animals (FIFRA SAP, 2013). For example, exposure to certain cholinesterase inhibitors has been associated with scoliosis in fish (Schultz *et al*. 1985) and frogs (Bacchetta *et al*. 2008).

(c) References

Bacchetta, R., P. Mantecca, M. Andrioletti, C. Vismara, and G. Vailati. 2008. Axial-skeletal defects caused by carbaryl in *Xenopus laevis* embryos. Science of the Total Environment 392: 110 – 118.

FIFRA Scientific Advisory Panel (SAP). 2013. Minutes of US EPA FIFRA SAP No. 2013-03. Endocrine Disruptor Screening Program (EDSP) Tier 1 Screening Assays and Battery Performance. May 21-23, 2013. Washington, DC.

Schultz, T.W., J.N. Dumont, and R.G. Epler. 1985. The embryotoxic and osteolathyrogenic effects of semicarbazide. Toxicology 36: 185-198.

Leibovitz, H.E., D.D. Culley, and J.P. Geaghan. 1982. Effects of vitamin C and sodium benzoate on survival, growth and skeletal deformities of intensively culture bullfrog larvae (*Rana catesbeiana*) reared at two pH levels. Journal of the World Aquaculture Society 13: 322-328.

Marshall, G.A., R.L. Amborski, and D.D. Culley. 1980. Calcium and pH requirements in the culture of bullfrog (*Rana catesbeiana*) larvae. Journal of the World Aquaculture Society 11: 445-453.

Martinez, I., R. Alvarez, I. Herraez, and P. Herraez. 1992. Skeletal malformations in hatchery reared *Rana perezi* tadpoles. Anatomical Records 233(2): 314-320.

APPENDIX 5: Histopathology Guidance for LAGDA

(a) Introduction.

This Appendix describes the collection, histological preparation, and pathological evaluation of thyroid glands, gonads and gonadal ducts, kidney, and liver specimens from African clawed frogs (*Xenopus laevis*) in support of the Larval Amphibian Growth and Development Assay (LAGDA), a Tier 2 assay in the EDSP. This guidance is provided to help ensure that histological procedures and pathological evaluations are performed accurately and consistently. The guidance provided is based on procedures developed by the U.S. Environmental Protection Agency in consultation with other scientific experts. Specific products and/or equipment listed can be substituted with comparable materials. Laboratories may depart from some aspects of this guidance due to variability in some standard laboratory practices (*e.g.*, how much information is included on slide labels, *etc.*).
This Appendix is divided into three sections: Necropsy Procedures, Histology Procedures and Pathology Evaluation. The Pathology Evaluation section includes written descriptions and illustrations of normal tissues and abnormal changes, with special emphasis on findings that are likely related to endocrine disruption, and specific examples of lesion severity grades as applicable. Additional guidance is provided on the topics of severity grading (in general), data recording, statistical analysis, data interpretation, and report formatting.

(b) Necropsy and Gross Trimming Procedures.

At study termination, each frog selected for sampling is euthanized via injection of a 10% solution (w/v) of MS-222 dissolved in a physiological buffer (e.g., 0.1M phosphate buffered saline pH 7.4) at a dose of 0.2 mL per 50 g body weight into the dorsal lymph sac.
Three different types of samples are collected for histopathology: 1) larval head and neck region for evaluation of the thyroid glands, 2) juvenile liver, and 3) juvenile dorsal trunk region for evaluation of the gonads, gonadal ducts, and kidneys.

(1) Larval Thyroid Glands (NF stage 62 sample). A transverse cut is made at the posterior margin of the arms prior to fixation (solid line; Figure 1). The head / neck samples are placed in appropriately sized cassettes and fixed in Davidson's solution for 48 hours, and are then rinsed thoroughly in tap water, after which they may be maintained in 10% neutral buffered formalin prior to shipment or processing. At any time following fixation, two transverse cuts are made through the head and neck region at the anterior margin of the eyes and anterior margin of the forelimbs, respectively (dashed lines; Figure 1). Care should be taken to ensure that the cut made anterior to the forelimbs is as square to the axial midline as possible and includes as much of the neck region as possible. This ensures that the thyroid glands will be included in the head / neck sample.

(2) Juvenile Liver (Test termination). The ventral abdominal wall is removed; the liver is carefully excised, weighed, transferred to an appropriately sized cassette that does not compress the tissue and fixed in Davidson's solution for 48 hours. The liver is then rinsed with tap water and maintained in 10% neutral buffered formalin prior to shipment or processing.

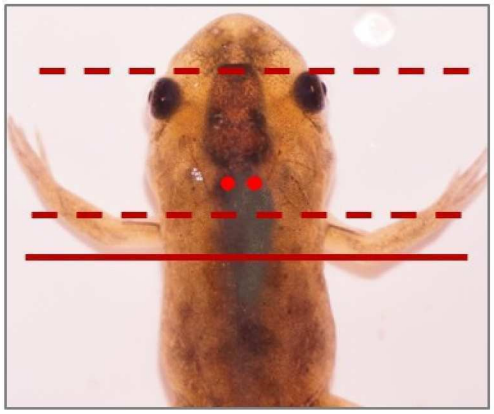

Figure 1. Dorsal view of a larval (NF stage 62) *X. laevis* specimen to be evaluated for thyroid histopathology with solid red line indicating trimming plane prior to fixation, dashed red lines indicating trimming planes following fixation and red dots indicating approximate location of glands in relation to posterior trim plane.

(3) Juvenile Gonads, Gonadal Ducts, and Kidneys. Following removal of the liver, the gastrointestinal tract is excised and discarded. When manipulating the abdominal viscera, care should be taken not to disrupt the dorsally positioned gonads and fragile gonadal ducts. One transverse cut is made through the trunk at the anterior margin of the hips (posterior margin of the kidneys) (Figure 2). Another transverse cut is made through the middle of the spleen or several millimeters rostral from the anterior margin of the gonad. The resulting trunk segment contains the intact gonads, gonadal ducts and kidneys. The head, legs and other residual excised tissues are discarded. The trunk is transferred to an appropriately sized cassette or container that does not compress the tissue and fixed in Davidson's solution for 48 hours. The fixed tissues are then rinsed with tap water and maintained in 10% neutral buffered formalin prior to shipment or processing.

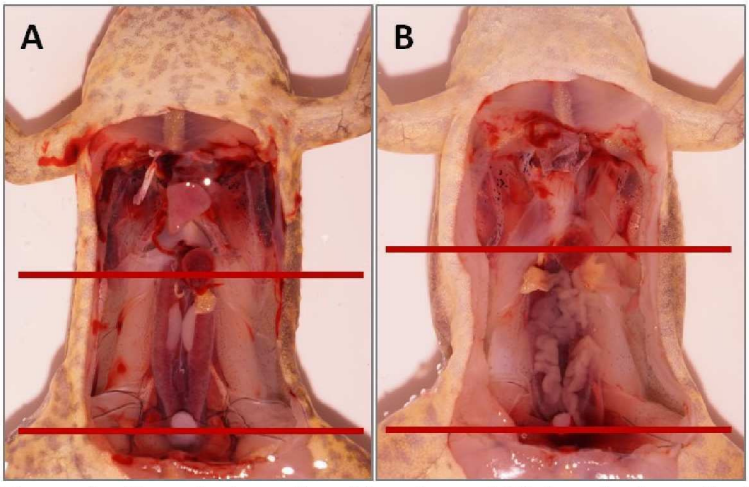

Figure 2. Ventral view of a: A) male; and B) female; juvenile (10 weeks post-NF62) *X. laevis* specimens with lines approximately indicating the tissue trimming to be performed before fixation, processing and evaluation for gonad and duct histopathology.

Prior to processing and embedment, the dorsal trunk segment is transected (bisected) at the axial midpoint of the gonads to create one anterior and one posterior segment. The trunk is also transected at the posterior margin of the gonad which will be the plane microtomed for the posterior sections (dashed lines in Figure 3).

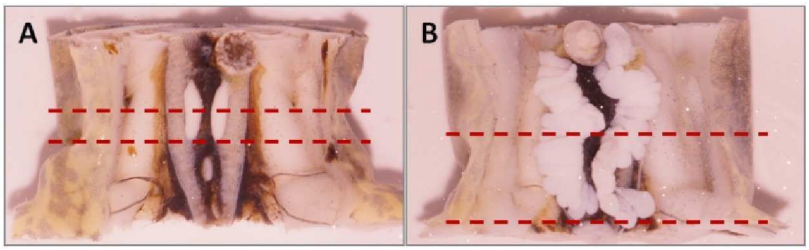

Figure 3. Dorsal trunk segments of A) male; and B) female juvenile (10 week post-NF62) *X. laevis* specimens which have been trimmed for evaluation of gonad and gonadal duct histopathology. The anterior margins of the gonads are positioned toward the tops of the images. The dashed lines represent the cuts used to bisect the specimens into anterior and posterior segments and to provide a sectioning plane for the posterior margin of the gonad.

(c) Histologic Procedures.

(1) Larval Thyroid Glands

(i) Decalcification. The acetic acid in modified Davidson's solution will soften bone and cartilage; therefore, decalcification prior to processing may or may not be required. The study tissues can be tested by processing and microtoming a few control frogs prior to the other study animals. If decalcification is found to be necessary, commercial preparations that contain a mixture of formic acid and EDTA are preferred, because they provide the optimum combination of gentleness and speed. Decalcification times can often be 24 hours or less.

(ii) Processing and embedding. Each head / neck specimen is processed in an automated tissue processor and infiltrated with paraffin according to routine methods. Samples are embedded in the paraffin block so that the cut surface of the posterior margin (the neck side) is sectioned first.

(iii) Microtomy. Each block is faced (excess paraffin trimmed away) until at least one of the thyroid glands has been reached (approximately 500 microns into the tissue). Step sections (4-5 microns thickness) are then taken at 50-micron intervals until the maximum diameter of at least one gland has been reached. Two additional step sections are then cut at an interval of 50 microns, and these two sections are placed on a single glass slide. Following microtomy, each paraffin block is sealed with paraffin.

(iv) Staining and coverslipping. The thyroid gland sections are stained with hematoxylin and eosin (H&E) and are mounted with a glass coverslip using an appropriate permanent mounting medium.

(v) Labeling. Slides are labeled with at least the following information:

- Study number
- Exposure Laboratory
- Name of the test chemical
- Individual animal identification number.

(vi) Quality control. The bilateral thyroid glands in the two step sections should contain the maximum number of follicles. If inadequate numbers of follicles are represented, and it is apparent that further thyroid tissue remains in the block, additional step sections are cut at 50 micron intervals until the appropriate sections are captured or until it is determined that additional recuts will not yield the

required tissue. The pathologist ultimately selects the sections to be evaluated. Following microtomy, each paraffin block is re-sealed with paraffin.

(2) Juvenile Liver.

(i) Processing and embedding. Each liver specimen is processed in an automated tissue processor and infiltrated with paraffin according to routine methods. Samples are embedded in the paraffin block so that the area of liver to be examined is maximized.

(ii) Microtomy. Each block is faced (excess paraffin trimmed away) until the liver surface is reached. Step sections (4-5 microns thickness) are then taken at 50-micron intervals until the maximum diameter of the liver samples is attained. Two additional step sections are then microtomed at an interval of 50 microns, and these two sections are placed on a single glass slide. Following microtomy, each paraffin block is sealed with paraffin.

(iii) Staining and coverslipping. The liver sections are stained with hematoxylin and eosin (H&E) and are mounted with a glass coverslip using an appropriate permanent mounting medium.

(iv) Labeling. Slides are labeled with at least the following information:

- Study number
- Exposure Laboratory
- Name of the test chemical
- Individual animal identification number

(3) Juvenile Gonads, Gonadal Ducts, and Kidneys

(i) Decalcification. The acetic acid in modified Davidson's solution will soften bone and cartilage; therefore, decalcification prior to processing may or may not be required. The study tissues can be tested by processing and microtoming a few control frogs prior to the other study animals. If decalcification is found to be necessary, commercial preparations that contain a mixture of formic acid and EDTA are preferred, because they provide the optimum combination of gentleness and speed. Decalcification times can often be 24 hours or less.

(ii) Processing and embedding. The trunk segments are processed in an automated tissue processor and infiltrated with paraffin according to routine methods. The anterior and posterior trunk segments are embedded in separate blocks. Blocks should be labeled as anterior (a) or posterior (p). Each sample is embedded in the paraffin block so that the middle gonad surface of the anterior segment and the posterior gonad surface of the posterior segment are microtomed first.

(iii) Microtomy. For blocks containing anterior segments, two serial sections (each 5 microns thick) are acquired as soon as the block is faced (excess paraffin trimmed away), and placed on a single slide; these will be the middle sections. Each anterior segment block is then microtomed 500 microns for males, or 1000 microns for females, and then a second pair of serial sections is taken and placed on a single slide; these will be the anterior sections. Finally each posterior section block is faced and then microtomed 1000 microns for males and females, and two serial sections are taken which are placed on a single slide; these will be the posterior sections. If the gonads are much larger or smaller than anticipated, adjustments may be made in the depths at which anterior and posterior sections are

acquired. Such adjustments should be documented in the methods section of the pathology report. Following microtomy, each paraffin block is re-sealed with paraffin.

(iv) Staining and coverslipping. The gonad/kidney/duct sections are stained with hematoxylin and eosin (H&E) and are mounted with a glass coverslip using an appropriate permanent mounting medium.

(v) Labeling. Slides should be labeled with the following information:

- Study number
- Exposure Laboratory
- Name of the test chemical
- Individual animal identification number
- Lower case letters are used to indicate the anatomic locations of the sections as follows: a = anterior; m = middle; p = posterior to indicate the gonad region for the slide (e.g. 141a = slide 141 anterior gonad sections).

(d) Pathologic Evaluation.

(1) General Approach to Pathologic Evaluations. Slides are to be read by individuals experienced in reading toxicologic pathology slides, and who are familiar with normal, amphibian thyroid and gonad histology, physiology, and general responses of these organs to toxicologic insult. Pathologists may be board certified (*e.g.*, American College of Veterinary Pathologists, The European Centre of Toxicologic Pathology, or other certifying organizations); however, certification is not a requirement as long as the pathologist has obtained sufficient experience with, and knowledge of, amphibian histology and toxicologic pathology.

It is recognized that there is a limited pool of pathologists with the necessary training and experience that are available to evaluate the histopathology endpoint for the LAGDA assay. If an individual has toxicologic pathology experience and is familiar with thyroid, liver, and gonadal histology in amphibian species, he/she may be trained to evaluate the LAGDA assay. If pathologists with little experience are used to conduct the histopathological analysis, informal peer review may be necessary.

Pathologists generally read slides unblinded (*i.e.*, with knowledge of the treatment group status of individual organisms) first and then they should be read blinded. This is because endocrinological effects on histomorphology tend to be incremental, and subtle differences between exposed and unexposed animals may not be recognizable unless tissue sections from high dose animals can be knowingly compared to those from controls. Thus the aim of the initial evaluation is to ensure that diagnoses are not missed (*i.e.*, to avoid false-negative results). Re-evaluating the treatment-finding by a pathologist in a blinded manner will prevent the reporting of false-positive results. As general practice, the control and high concentration samples are read first and then others are read using a step-down procedure.

Pathologists should specifically evaluate the target tissues identified in the guidelines; however, changes observed in other tissue types may also be recorded. This especially pertains to findings suspected to be treatment-related, or findings that might otherwise impact the study results (e.g., systemic inflammation or neoplasia).

It is suggested that the pathologist be provided with all available information related to the study. Information regarding gross morphologic abnormalities, mortality rates, and general test population performance and health are useful for pathologists to provide comprehensive reports and to aid in the interpretation of findings. For a more comprehensive discussion of standard reading approaches for toxicologic pathology studies, please refer to the Society of Toxicologic Pathology Best Practices for reading toxicologic histopathology studies (Crissman *et al.*, 2004).

(2) Severity Grading. In toxicologic pathology, it is recognized that compounds may exert subtle effects on tissues that are not adequately represented by simple binary (positive or negative) responses. Severity grading involves a semi-quantitative estimation of the degree to which a particular histomorphologic change is present in a tissue section (Shackelford *et al.*, 2002). The purpose of severity grading is to provide an efficient, semi-objective mechanism for comparing changes (including potential compound-related effects) among animals, treatment groups, and studies.
Severity grading should usually use the following system:

- 0 (not remarkable)
- Grade 1 (minimal)
- Grade 2 (mild)
- Grade 3 (moderate)
- Grade 4 (severe)

Findings that are not present are not graded and assigned a zero (0) to represent that the tissue section is not remarkable. This is not to mean "Grade 0." This practice provides continuity with subsequent statistical analyses.

It is recognized that this severity grading scheme differs from that of Grim et al., 2009, which advocated the following scale for the assessment of thyroid gland changes in *X. laevis*: Grade 1 = mild, Grade 2 = moderate, and Grade 3 = severe. However, for consistency, all Tier 2 tests should use the Grade 1-Grade 4 system.

A grading system needs to be flexible enough to encompass a variety of different tissue changes. In theory, there are three broad categories of changes based on the intuitive manner in which people tend to quantify observations in tissue sections:

Discrete: These are changes that could be readily counted. Examples include atretic follicles, oocytes in the testis, and clusters of apoptotic cells.
Spatial: These are changes that could be quantified by area measurements. Includes lesions that are typically classified as focal, multifocal, coalescing, or diffuse. Specific examples include granulomatous inflammation and tissue necrosis.
Global: These are generalized changes that would usually require more sophisticated measurement techniques for quantification. Examples include increased hepatocyte basophilia, thyroid follicular cell hypertrophy, or quantitative alterations in cell populations.

Listed below are general guidelines for the use of a severity grading system, with examples of how the system could be applied to each of the above categories. Please understand that the terms Discrete, Spatial, and Global are used for illustrative purposes only; it is not intended that these terms be incorporated into any diagnosis or grade. It should be stressed that the examples below should be modified as needed for each particular type of change (diagnosis).

Grade 1:

Discrete change example: 0 to 2 occurrences per microscopic field, or 1 to 2 occurrences per tissue section.
Spatial change example: The change occupies a miniscule area of either a specific tissue type or the entire tissue section.
Global change example: The least perceptible alteration relative to control animals or prior experience.

Grade 2:

Discrete change example: 3 to 5 occurrences per microscopic field or tissue section.
Spatial change example: The change occupies a larger area than Grade 1, but still less than or equal to 25% of either a specific tissue type or the tissue section.
Global change example: The alteration is easily appreciated, but still not dramatic.

Grade 3:

Discrete change example: 6 to 8 occurrences per microscopic field or tissue section.
Spatial change example: The change occupies more than 25% but less than or equal to 50% of either a specific tissue type or the entire tissue section.
Global change example: The alteration is dramatic, but a more pronounced alteration can be envisioned.

Grade 4:

Discrete change example: 9 or more occurrences per microscopic field or tissue section.
Spatial change example: The change occupies more than 50% of either a specific tissue type or the entire tissue section.
Global change example: Essentially, the most pronounced imaginable alteration.

At least some of the histomorphologic changes that have been associated with endocrine disrupting chemicals in wildlife are considered to be exacerbations of “normal”, physiologic findings. Whenever possible, the severity of a given change should be scored relative to the severity of the same change in concurrent control animals. For each important (*i.e.*, treatment-associated) finding, the severity scoring criteria should be stated in the Materials and Methods section of the pathology narrative report. By convention, it is recommended that severity grading should not be influenced by the estimated physiologic importance of the change. For example, the presence of two oocytes in the testis should not be graded as “severe”, even if the pathologist considers this finding to be highly significant in terms of endocrine modulation. The reason is that estimating the physiologic importance adds a further layer of subjectivity to the findings that complicates inter-laboratory results comparisons.

(3) Data Recording. The pathologist records the results in an appropriate record-keeping manner in keeping with GLP. Example spreadsheet templates for recording data are available on the EDSP website: http://www.epa.gov/endo/. For each frog, the pathologist records the presence of a diagnosis by indicating the severity grade. In rare instances (*e.g.*, tumor diagnoses), severity grading may not be applicable. If there are no findings for a particular frog, this should be recorded specifically. It is also important to record a notation if the target tissue is missing or if the amount of tissue present is insufficient to make a diagnosis. Adding modifiers to a diagnosis may help to further describe or categorize a finding in terms of chronicity, spatial distribution, color, etc. In many instances, modifiers are superfluous or redundant (*e.g.*, fibrosis is always chronic); therefore, the use of modifiers should be

kept to a minimum. An occasionally important modifier for evaluating paired organs is unilateral; unless specified in this manner, all diagnoses for paired organs are assumed to be bilateral. Other modifiers can be created sparingly as needed by the pathologist.

(4) Statistical Analysis. Histopathology data are in the form of severity scores or developmental stages. A test termed RSCABS (Rao-Scott Cochran-Armitage by Slices) uses a step-down Rao-Scott adjusted Cochran-Armitage trend test on each level of severity in a histopathology response (Greene *et al.*, 2014). The Rao-Scott adjustment incorporates the replicate vessel experimental design into the test. The "by slices" procedure incorporates the biological expectation that severity of effect tends to increase with increasing doses or concentrations, while retaining the individual subject scores and revealing the severity of any effect found. The RSCABS procedure not only determines which treatments are statistically different than controls (*i.e.*, have more severe pathology than controls), but it also determines at which severity score the difference occurs thereby providing much needed context to the analysis. In the case of developmental staging of gonads and reproductive ducts, an additional manipulation should be applied to the data since an assumption of RSCABS is that severity of effect increases with dose or concentration. The effect observed could be a delay OR acceleration of development. Therefore, developmental staging data should be analyzed as reported to detect acceleration in development and then manually inverted prior to a second analysis to detect a delay in development.
Advantages of using RSCABS as a statistical method for analyzing histopathology data include the ability to account for: 1) experimental designs with multiple replicates, 2) lesion severity scores of individual animals in addition to group-wise lesion prevalence, and 3) dose-response relationships. Additionally, the RSCABS test is relatively easy to perform and interpret.

(5) Data Interpretation. Once the microscopic examinations have been completed and statistical analyses have been performed on the resulting data, the pathologist interprets the histopathologic findings. The initial task is to determine which, if any, of the recorded findings are related to administration of the test article, and which are not. The goal is to classify each type of recorded finding (i.e., diagnosis) into one of three categories: 1) *Treatment-related*, 2) *Potentially treatment-related*, and 3) *Non-treatment-related*. Criteria for these determinations are listed below.

(i) Determining Relationship to Treatment. A weight-of-evidence (WOE) approach is used to determine if a particular finding should be considered treatment-related. Such evidence may include any or all of the following as available:
Differences between groups of control and treated animals in terms of lesion prevalence and severity, utilizing statistical analytical results to test for significance as warranted.
Ancillary data from the current study, involving information such as behavioral observations, liver and body weights, genotypic sex, time-to-metamorphosis, and age at sacrifice.
Results from other submitted or pending agency studies. The at-large scientific literature, giving greater weight to studies in which the quality of the research can be established and is considered superior.
Overall biological, physiological, and toxicological plausibility.

Findings that are considered potentially treatment-related may be those that have borderline statistical significance, or those in which the relationship to treatment is considered equivocal for other reasons (e.g., lack of corroborating evidence from other sacrifices or other studies, biological or toxicological implausibility, or commonality of the diagnosis as a background finding).
There are several points to be made regarding the determination of treatment-relatedness. First, it is possible for a finding to be treatment-related but not be caused by the test chemical. This can include situations in which group-wise differences may be associated with an uncontrolled (and possibly

unrecognized) variable involving conduct of the in-life assay, specimen preparation, or some other non-systemic bias. Second, not all statistically significant differences are real, as a p-value significance level of 0.05 allows for the probability that in 5% of cases the result occurred by chance. Third, a finding may be statistically significant and not necessarily biologically or toxicologically important. Fourth, in some instances, treatment-related findings may not be statistically significant. For example, this can occur when treatment induces a low frequency of a lesion type that rarely occurs spontaneously.

(ii) Determining Relationship to Endocrine Disruption. A similar weight-of-evidence (WOE) approach can be used to determine if a particular finding is likely to be endocrine-related; however, in this case the WOE will more heavily depend on ancillary data, results of other assays, and the published literature, including mechanistic studies where available.

(6) Report Format. The pathologist is responsible for deliverables that include: 1) Pathology Narrative Report, 2) Spreadsheet with recorded data, and 3) TIFF image files of figures.

(i) Pathology Narrative. Each histopathology narrative report should contain at least the first five of the following sections: Introduction, Materials and Methods, Results, Discussion, Summary / Conclusions, References, Tables, and Figures. The ***Introduction*** section briefly outlines the experimental design. The ***Materials and Methods*** section briefly describes procedures used during the slide preparation and examination phases of the study. If specific severity grading criteria were created for a particular finding, they should also be listed in this section. The ***Results*** section should report findings that are: 1) treatment-related; 2) potentially treatment-related; and 3) non-treatment-related findings that are novel or unusual. Detailed histomorphologic descriptions need only be included for findings that differ substantially from diagnoses presented the Histopathology Atlas. It is intended that the Results section should be as objective as possible (*i.e.*, opinions and hypotheses should be reserved for the Discussion section). The ***Discussion*** section, which contains subjective information, should address relevant findings that were reported in the Results section. Opinions and hypotheses can be included in this section, preferably backed by references from peer-reviewed sources, but unsupported speculation should be avoided. The ***Summary / Conclusions*** section should encapsulate the most important information from the Results and Discussion sections. The ***References*** section should include only material that is cited specifically in the narrative report. A separate ***Tables*** section may not be necessary if tables are embedded in the Results section. The ***Figures*** section should include photomicrographic examples of treatment-related findings, plus unusual or noteworthy lesions. The Figures section should include normal tissues for comparison, and digital images should be taken at magnifications that clearly illustrate the salient features of the findings. Figures embedded in the narrative should be in a universally readable compressed file format such as JPEG.

(ii) Spreadsheet. In addition to the recorded histopathology findings, the completed spreadsheet should indicate the animals from which figure images were photographed, and the number of images obtained per photographed organism. An example spreadsheet is provided on the EDSP website: http://www.epa.gov/endo/.

(iii) Figures. For record-keeping purposes, a complete set of unannotated photomicrographic figures should be submitted electronically on portable media as uncompressed TIFF files.

(7) Pathology Peer Review. Following the initial slide evaluation and creation of a draft report by the study pathologist (SP), it is encouraged that at least a subset of the original histologic sections be assessed by a second reviewing pathologist (RP). Known as pathology peer review, the purpose of this exercise is to increase confidence in the histopathology data by ensuring diagnostic accuracy and

consistency. Commonly, this procedure involves the targeted examination of one or more tissue types in which treatment-related findings were initially detected (this helps to guard against false positive results), plus all tissues from a randomly selected percentage (*e.g.*, 10-20%) of animals from the control and high-dose groups (this helps guard against false negatives). The RP is tasked with determining the accuracy and consistency of diagnostic criteria, diagnostic terminology, severity grading, and the interpretation of findings. The peer review can be performed in-house or (preferably) by an external pathologist, and frequently the reviewing pathologist has at least equal or greater expertise than the SP. Following the peer review, the SP and RP typically meet to resolve diagnostic differences. In unusual cases in which such differences cannot be resolved, a panel of experts (Pathology Working Group) may be convened to determine the final diagnoses. In addition to enhancing confidence in the histopathology results, benefits of peer review may include decreased inter-laboratory variability, and cross-training of pathologists (i.e., the initial study pathologist may not always need to be an avian expert). Examples of recommended procedures for conducting pathology peer reviews have been described (*e.g.*, Morton *et al.*, 2010; The Society of Toxicologic Pathologists, 1991; 1997).

(8) Summary of Diagnostic Criteria for Selected Histopathologic Findings. Table 1 lists diagnostic criteria for selected findings in LAGDA studies according to tissue type.

Table 1. Diagnostic Criteria for Potential Histopathological Findings in LAGDA Studies

Tissue	**Diagnostic Criteria**		
Thyroid	Criteria for thyroid gland assessment are available in Grim *et al.* (2009).		
Liver	Decreased (Glycogen) Vacuolation	1	Hepatocellular vacuolation is decreased slightly relative to controls, but at least 75% of the cytoplasm is vacuolated.
		2	50-75% of the cytoplasm is vacuolated.
		3	25-50% of the cytoplasm is vacuolated.
		4	Less than 25% of the cytoplasm is vacuolated.
Gonad	Testis Stage	1	Undifferentiated gonad
		2	Individual primary spermatogonia and undifferentiated somatic cells populate the medullary region
		3	Seminiferous tubules with primary spermatogonia and cysts of secondary spermatogonia
		4	Primary spermatocytes with rete testis formation; may have occasional spermatocysts that contain round or elongated spermatids
		5	All stages of spermatogenesis evident
	Tubule Development Score	1	Less than 50% of seminiferous tubules have visible lumens
		2	50% or greater seminiferous tubules have visible lumens
	Ovary Stage	1	Undifferentiated gonad
		2	Gonad identifiable as an ovary based on the presence of a discontinuously open lumen lined with epithelial cells; germ cells within the cortex consist of primary oogonia, cysts of primary mitotic oogonia, secondary oogonia, and very early meiotic oocytes

Tissue	**Diagnostic Criteria**		
Thyroid	Criteria for thyroid gland assessment are available in Grim *et al.* (2009).		
		3	First appearance of diplotene oocytes in cortex; the most prevalent germ cell types at this stage are cysts of secondary oogonia and cysts of leptotene-pachytene primary meiocytes
		4	Pre-vitellogenic (Dumont Stage I) diplotene oocytes are the most prevalent germ cell type observed by area and absolute cell counts; the central lumen is proportionately smaller while the whole ovary grows greatly in size and volume due to the growth of the oocytes; cysts in earlier stages of oogenesis become fewer in number and are located along the periphery of ovary
		5	Ovary consists almost entirely of vitellogenic oocytes (Dumont Stage IV); pre-vitellogenic diplotene oocytes can be found along the periphery of the ovary and germ patches of primary and secondary oogonia are difficult to locate
	Gonad Phenotype Score	0	Gonad phenotype matches genotype
		1	Gonad phenotype primarily matches genotype, with a relatively smaller portion of opposite sex gonad tissue
		2	Gonad is approximately equal parts testis and ovary
		3	Gonad phenotype primarily matches opposite genotype, with a relatively smaller portion of genotypic sex gonad tissue
		4	Gonad phenotype matches opposite genotype (sex reversed)
	Germ Cell Degeneration	1	A single degenerating germ cell to less than three clusters of degenerating germ cells per gonad
		2	Three or more clusters of degenerating germ cells, but less than 25% of gonad affected
		3	Gonad consists of greater than 25% but less than 50% of degenerating germ cells
		4	Gonad consists of 50% or more of degenerating germ cells
	Mononuclear Cell Infiltrates	1	Small, focal infiltrates in one gonad
		2	Small focal infiltrates in both gonads, or large area of infiltrates in one gonad
		3	Large areas of infiltrates in both gonads
		4	Gonads contain greater than 50% of infiltrates by area
Oviduct	Oviduct Stage	1	The oviduct is either a fibrous connective tissue tag, or is essentially non-existent
		2	The oviduct has an epithelial cell lining (1-3 cell layers), and is comparable in size to the Wolffian duct
		3	The oviduct has convoluted, multilayered epithelial cell lining, and is substantially larger (1.5x or greater) than the size of the Wolffian duct
		4	The oviduct is dwarfs the size of the Wolffian duct. Epithelial cells have formed large, basophilic glandular structures
Wolffian Duct	Wolffian Duct Stage	1	Epithelial lining of Wolffian duct is completely or focally less than two cell layers thick

Tissue	Diagnostic Criteria		
Thyroid	Criteria for thyroid gland assessment are available in Grim *et al.* (2009).		
		2	Epithelial lining of Wolffian duct is two cell layers thick or greater, but clear apical portion of cell (if present) is less than half the cell height
		3	Epithelial lining of Wolffian duct is two cell layers thick or greater, and clear apical portion of the columnar cells is at least half the cell height but less than 2/3 of the cell height
		4	The clear apical portion of the columnar cells represents 2/3 or greater of the total cell height
Kidney	Mineralization	1	Less than three small foci of mineralization per kidney
		2	Three or more small foci of mineralization per kidney, or less than three large foci
		3	Three or more large foci of mineralization per kidney
		4	Mineralized deposits in 50% or more tubules
	Tubule Dilation	1	Minimal to mild dilation of less than three tubule clusters
		2	Mild to moderate dilation of three or more tubule clusters
		3	Moderate dilation affecting 50% or more tubules
		4	Massive dilation of one or more tubules

(9) Atlas of Histopathologic Findings (Figures 4-39). The purpose of this section is to provide: 1) a common technical "language" for describing findings and 2) a reference atlas of both normal microanatomical structures and potential pathological findings. This atlas is organized first by organ type, followed by an alphabetical list of terms, then working definitions, and finally photomicrographic examples. The information in this section is derived from a number of sources including scientific articles, conference proceedings, related guidelines, toxicologic pathology textbooks, medical dictionaries, and the personal experience of various pathologists.

(i) Thyroid Glands

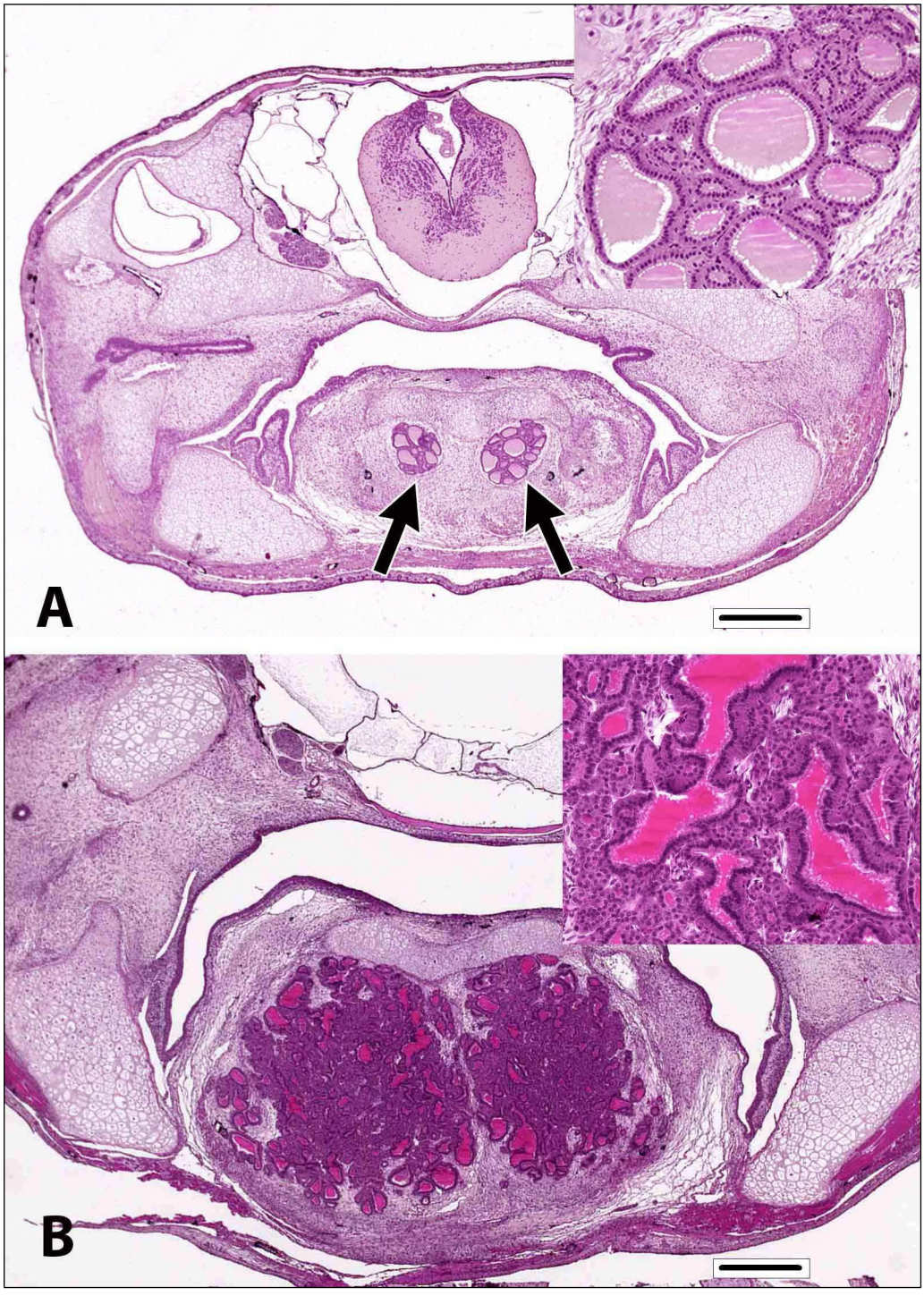

Figure 4. Normal versus Hypertrophic Thyroid Glands. A. Transverse section through the neck region to demonstrate thyroid glands (arrows and inset) in control frog. B. Severely hypertrophic thyroid glands. Morphologic criteria for the histopathologic evaluation of the thyroid glands are described and illustrated in Grim et al., 2009. Bar = 500 microns.

(ii) Liver

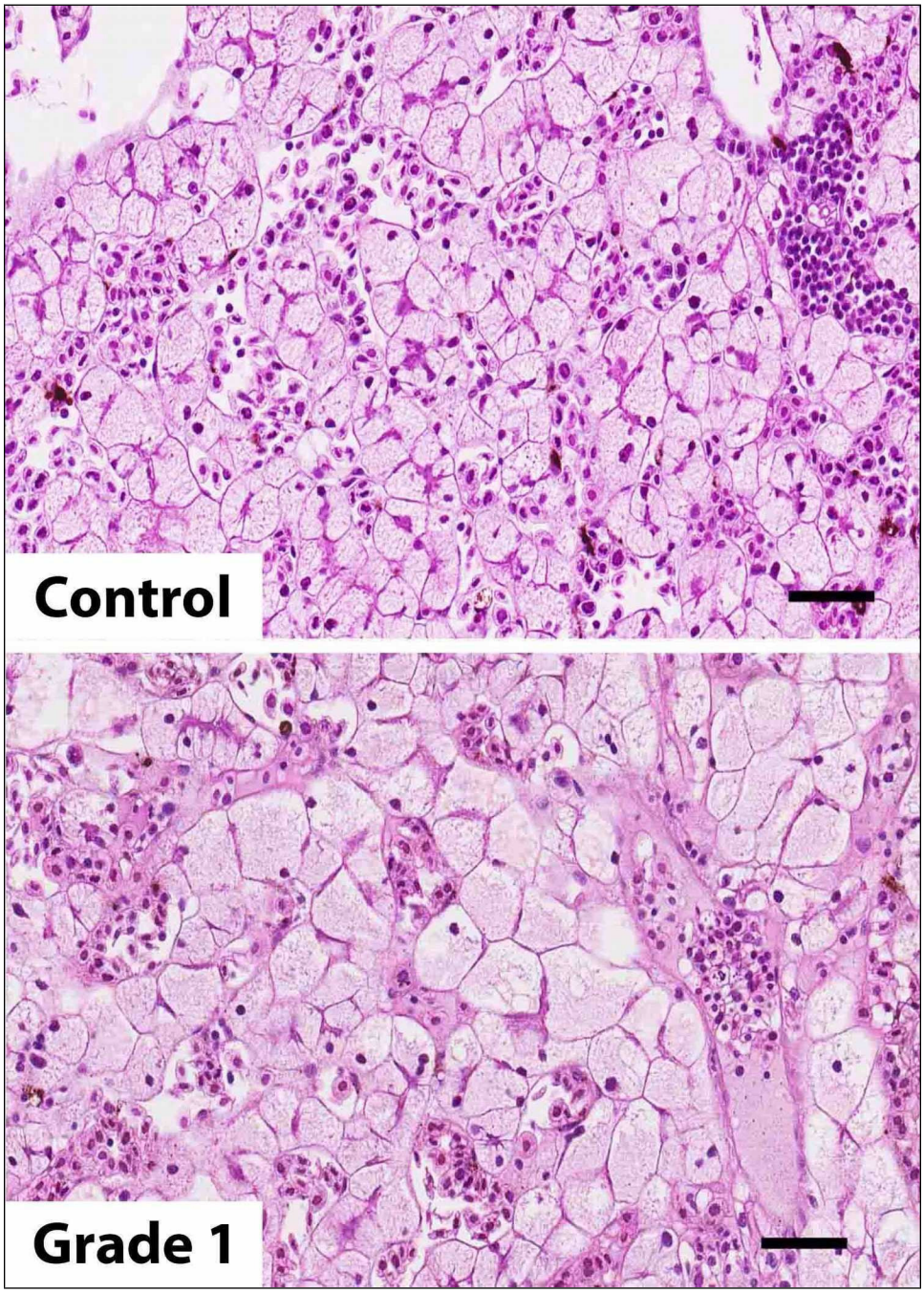

Figure 5. Hepatocellular Vacuolation, Increased. Relative to the control liver, affected hepatocytes in the treated frog liver contain greater amounts of pale granular cytoplasm, the contents of which are morphologically consistent with glycogen. Alterations in cell size can only be made by careful comparison of the treated frog livers to those of the concurrent controls. Bar = 50 microns.

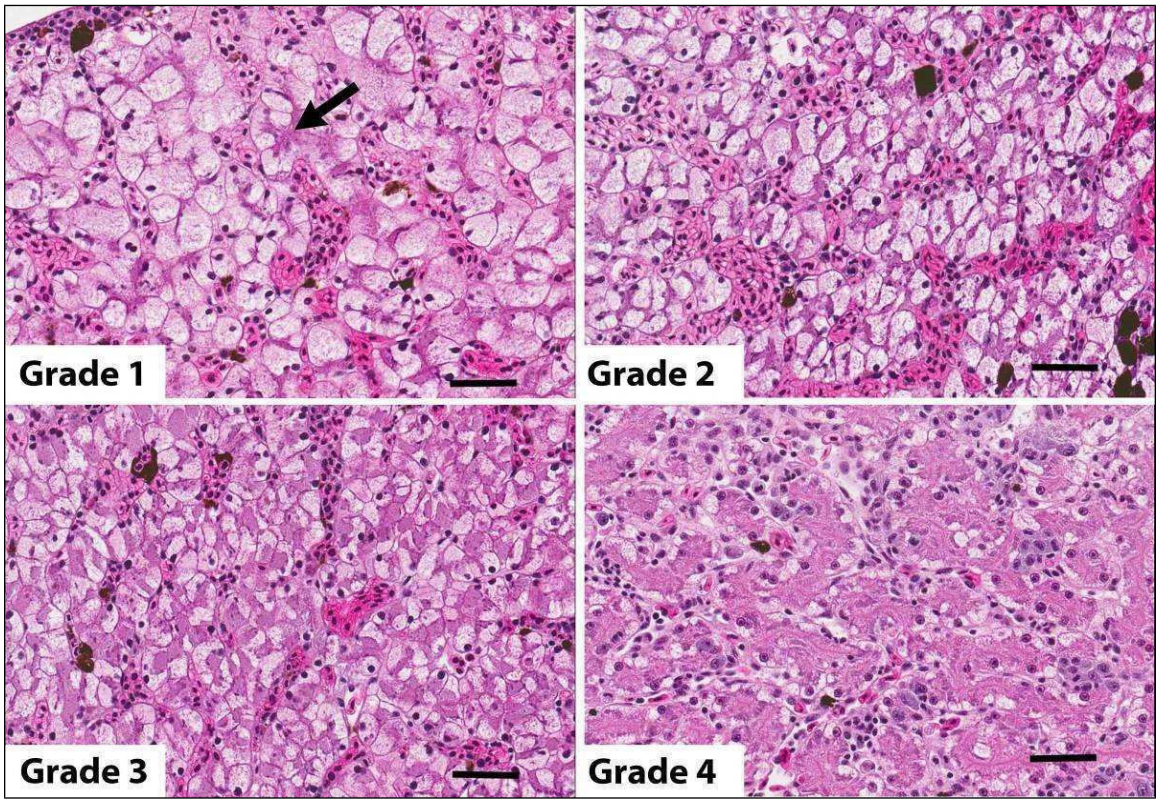

Figure 6. Hepatocellular Vacuolation, Decreased. Relative to the livers of control frogs (see previous figure), affected hepatocytes contain lesser amounts of cytoplasmic glycogen. This loss of glycogen vacuolation tends to occur preferentially in the basal (avascular) region of the cells, in the area adjacent to the biliary canals of Hering (arrow). As vacuolation decreases, the liver progressively acquires a more basophilic overall appearance. Bar = 50 microns.

(iii) Gonads.

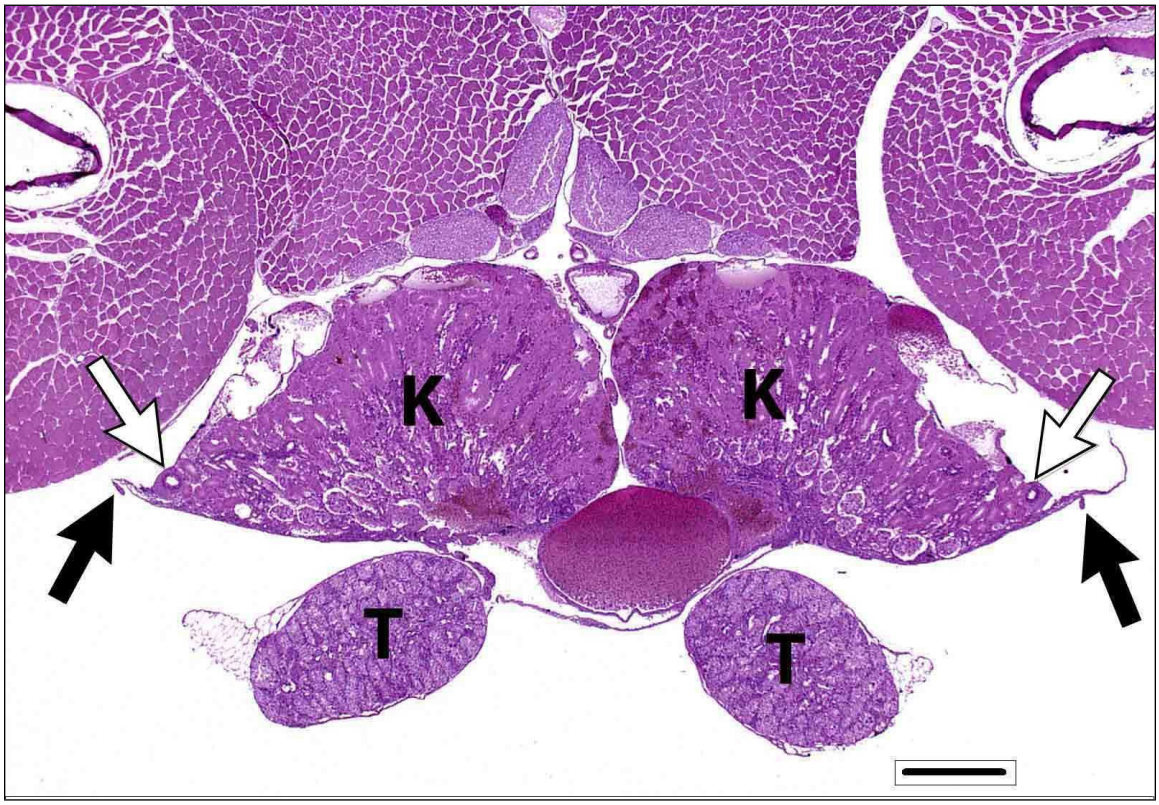

Figure 7. Normal Testes, Oviducts and Wolffian Ducts. The testes (T) are attached to the peritoneal surface of the kidneys (K) by suspensory ligaments. The black arrows indicate the oviduct (Müllerian duct) remnants (Stage 1 oviducts in this case), whereas the white arrows indicate the Wolffian ducts.
Bar = 500 microns.

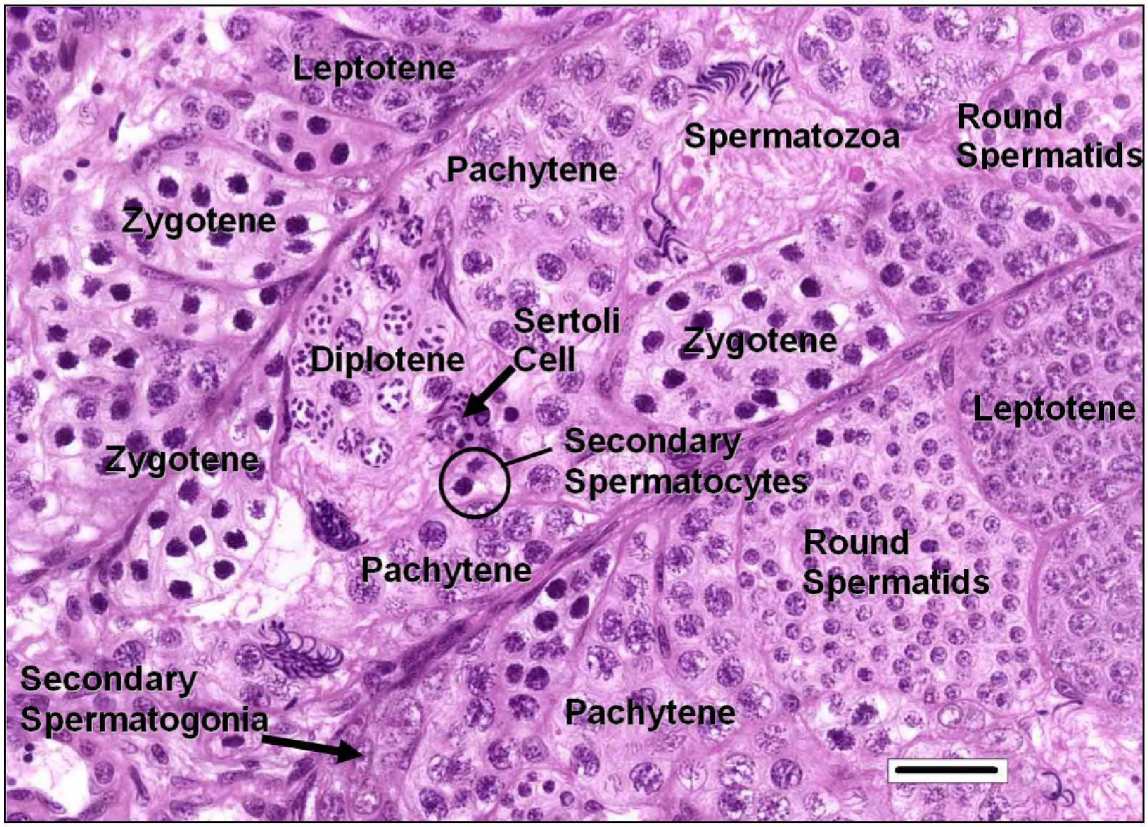

Figure 8. Normal Testis, Spermatogenic Stages. Germ cell maturation occurs as follows: primary spermatogonia secondary spermatogonia primary spermatocytes secondary spermatocytes round spermatids elongated spermatids spermatozoa. The majority of visible spermatocytes, which are primary spermatocytes, represent only prophase I of meiosis. These include leptotene zygotene pachytene diplotene phases. Secondary spermatocytes, which are haploid representatives of meiosis II, are comparatively rare. Sertoli cells are sparse, and those that are visible are usually surrounded by elongating spermatids. Interstitial areas contain low numbers of Leydig cells (not indicated).
Bar = 25 microns.

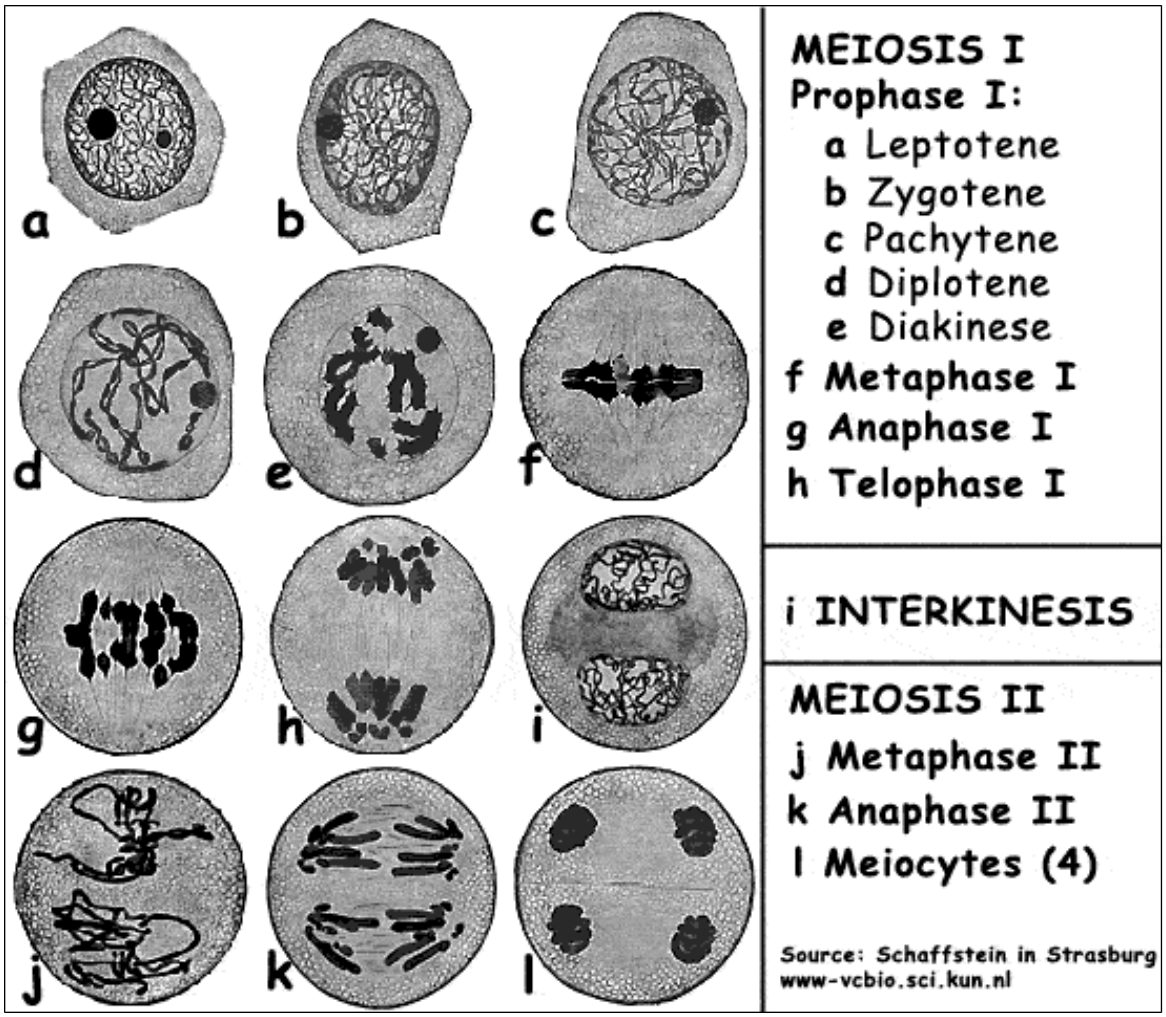

Figure 9. Meiotic Phases in the Vertebrate Testis. Schematic diagram included for reference.

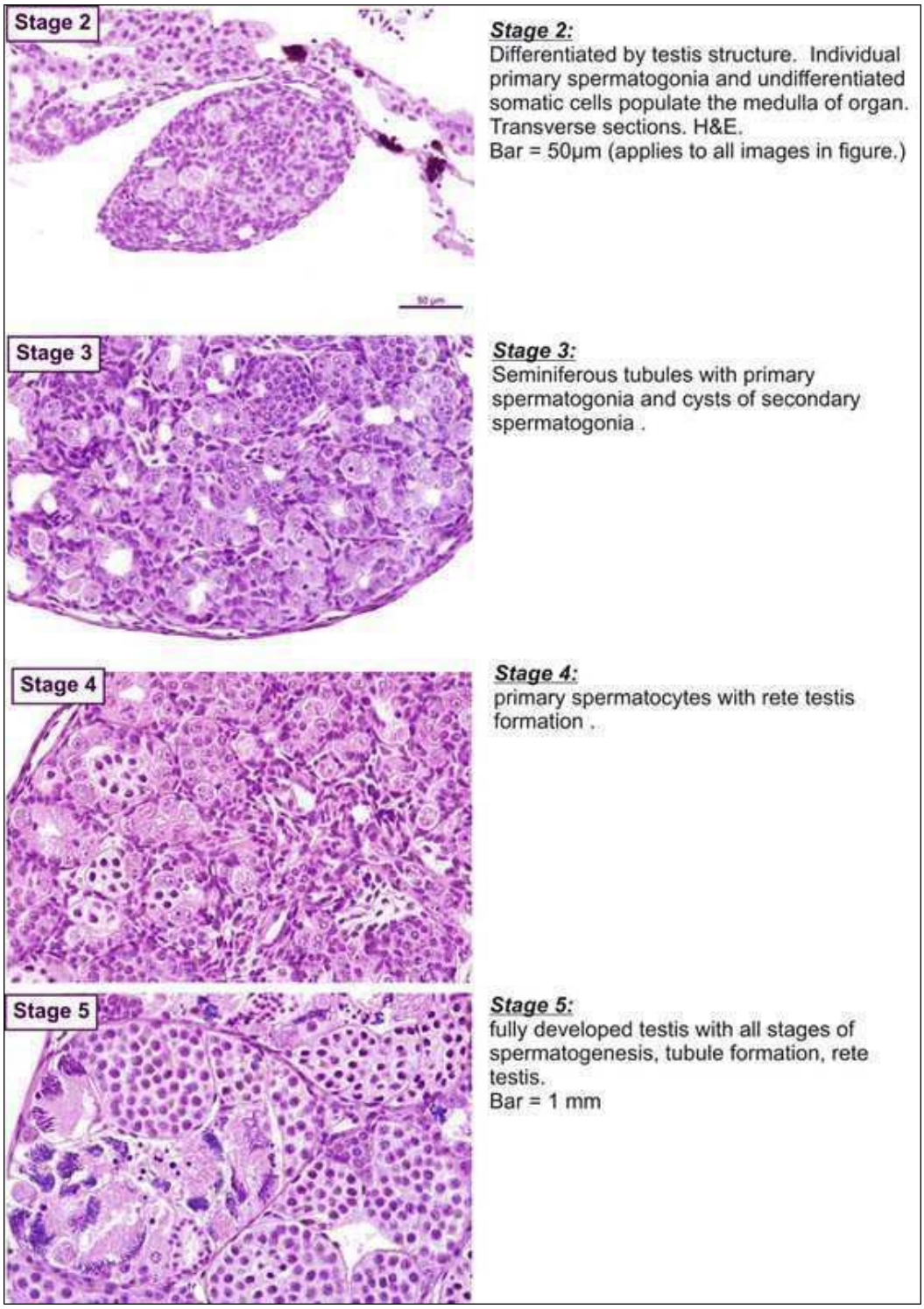

Figure 10. Staging of the Testis. Stage numbers increase with increasing maturity of the testis. Control males 10 weeks post NF stage 62 (LAGDA termination) typically have Stage 4 or 5 testes.

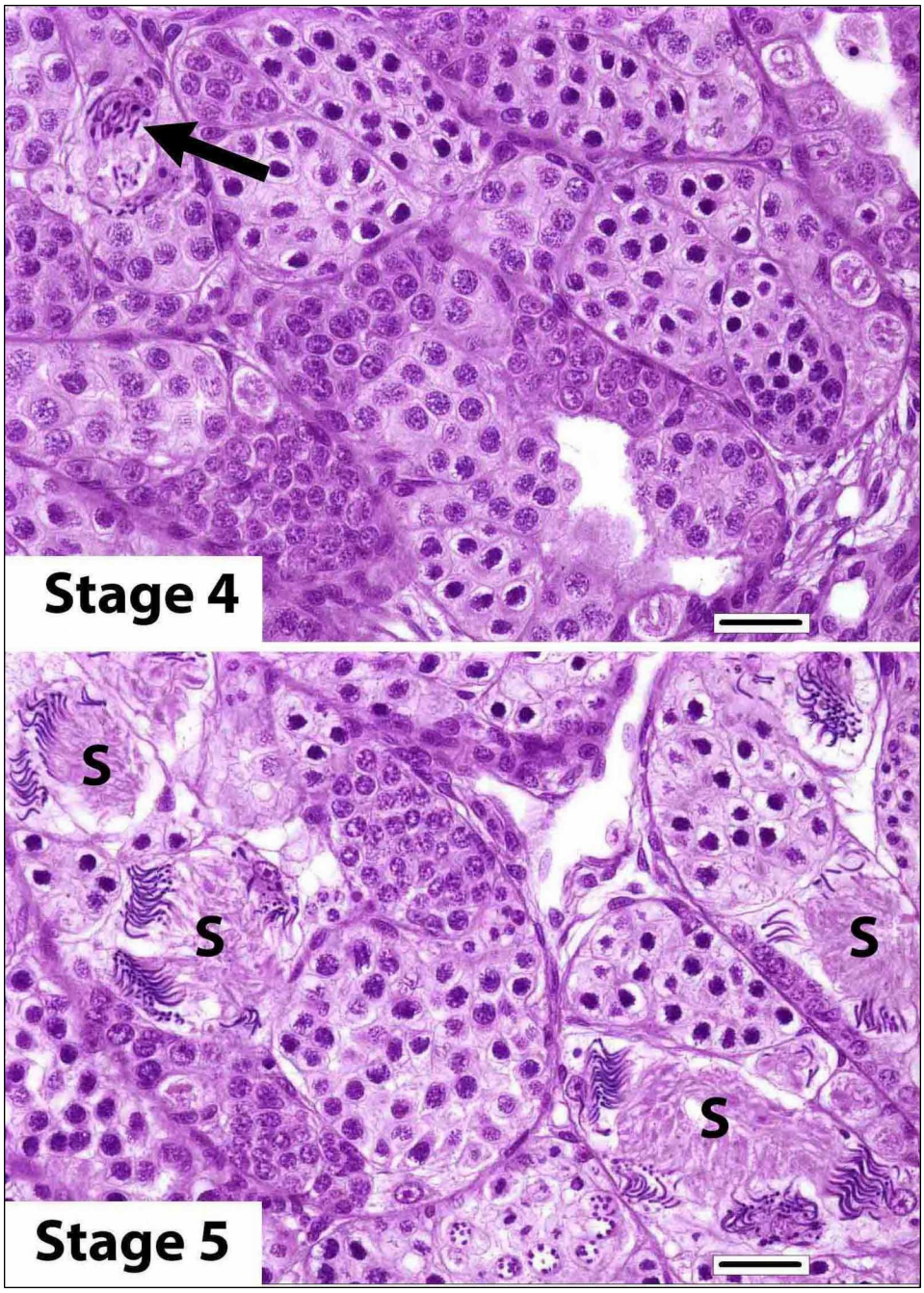

Figure 11. Stage 4 Versus 5 Testes, Higher Magnification. Stage 4 testes can have elongating spermatids (arrow), but spermatocysts that contain spermatozoa are rare or not apparent. Conversely, spermatozoa (S) are abundant in Stage 5 testes. Bar = 25 microns.

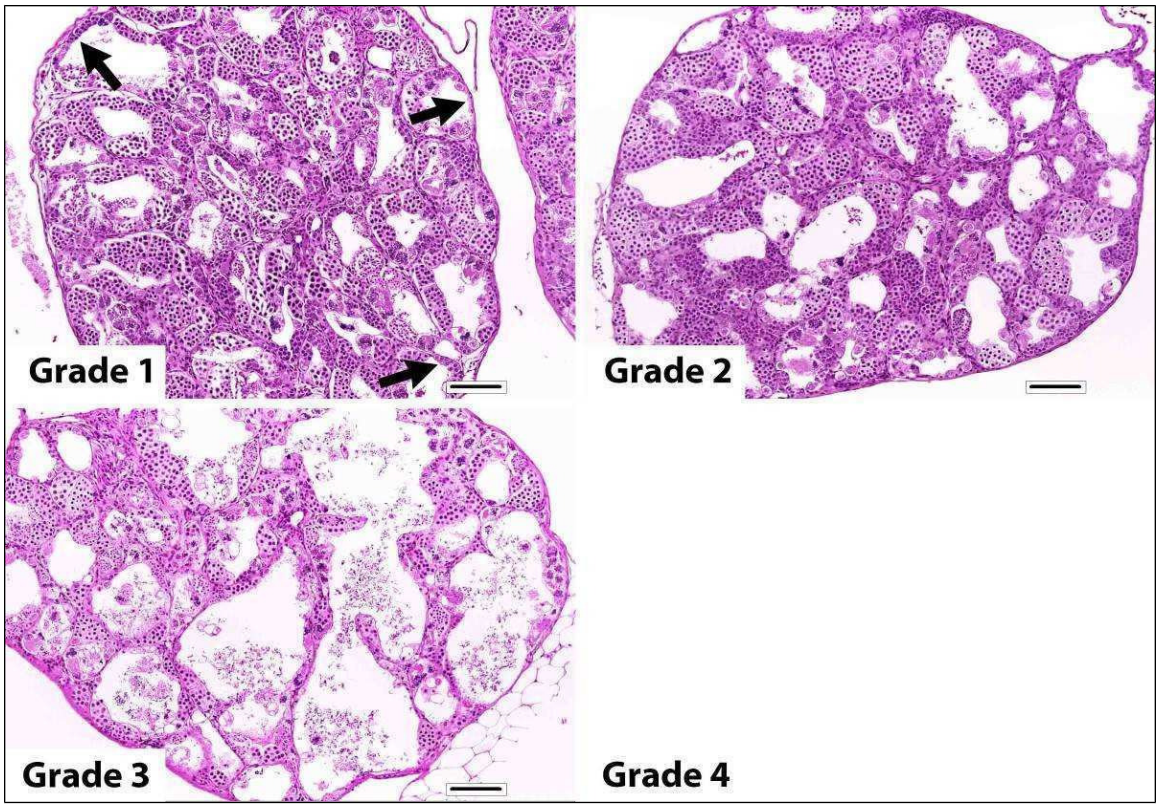

Figure 12. Germinal Epithelium Thinning and Dilation. This finding is characterized by focal to diffuse attenuation of the testicular germinal epithelium (arrows), with expansion of the adjacent tubular lumen. Germ cell degeneration is also evident. In a previous report, similar changes were termed “dilated testis tubules” (Wolf et al., 2010). Bar = 100 microns. Grade 4 is left intentionally blank.

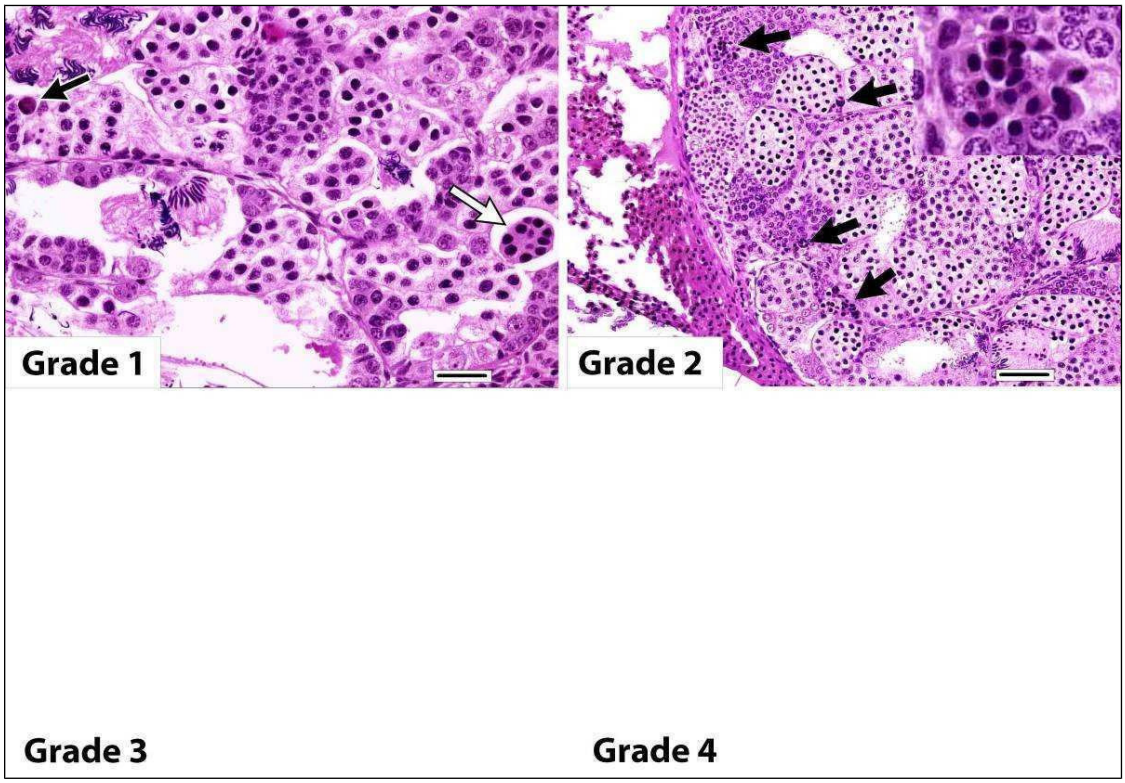

Figure 13. Testis, Germ Cell Degeneration. This finding is characterized by the scattered presence of individual or clustered apoptotic germ cells (black arrows and inset), or germ cell syncytia (white arrow), within the germinal epithelium. Affected testes may also have increased numbers of exfoliated cells and cellular debris in tubular lumina. Bar = 25 microns (Grade 1), 50 microns (Grade 2). Grades 3-4 are left intentionally blank.

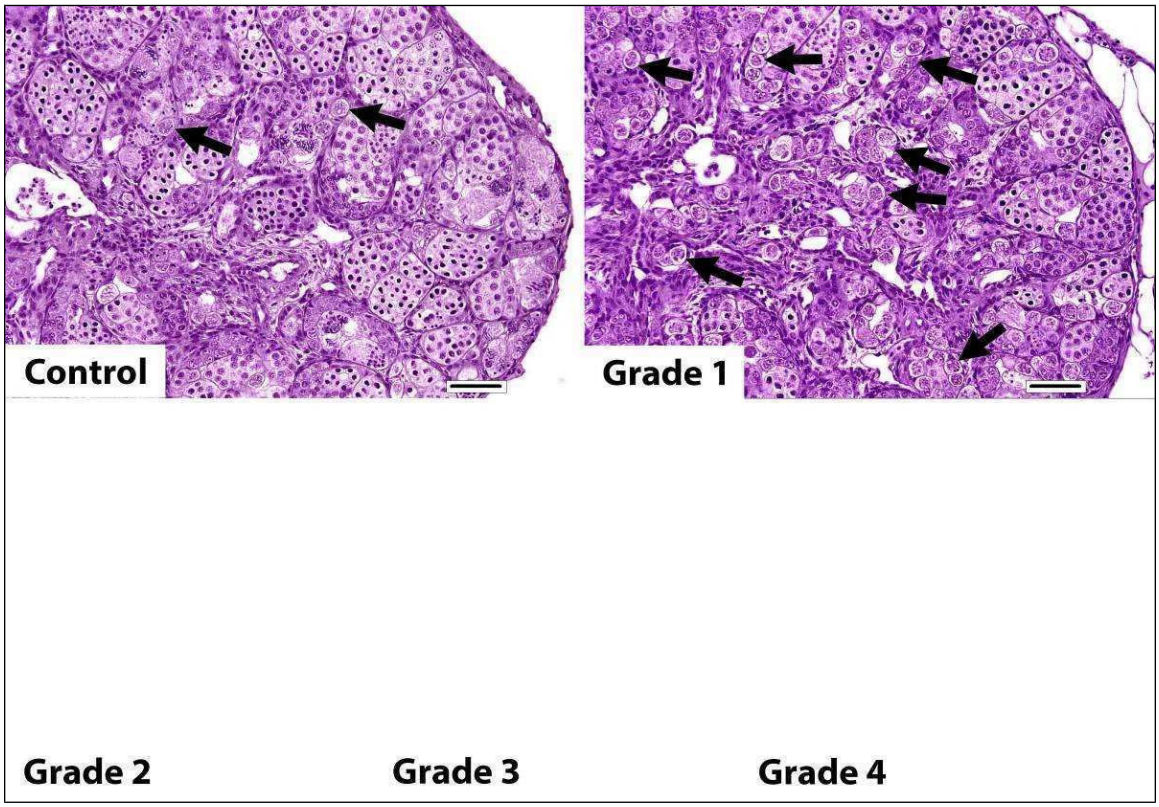

Figure 14. Spermatogonia, Increased. This finding is characterized by a greater frequency of spermatogonia (arrows) in the testes of affected frogs as compared to those of the average control frog. Bar = 50 microns. Grades 2-4 are left intentionally blank.

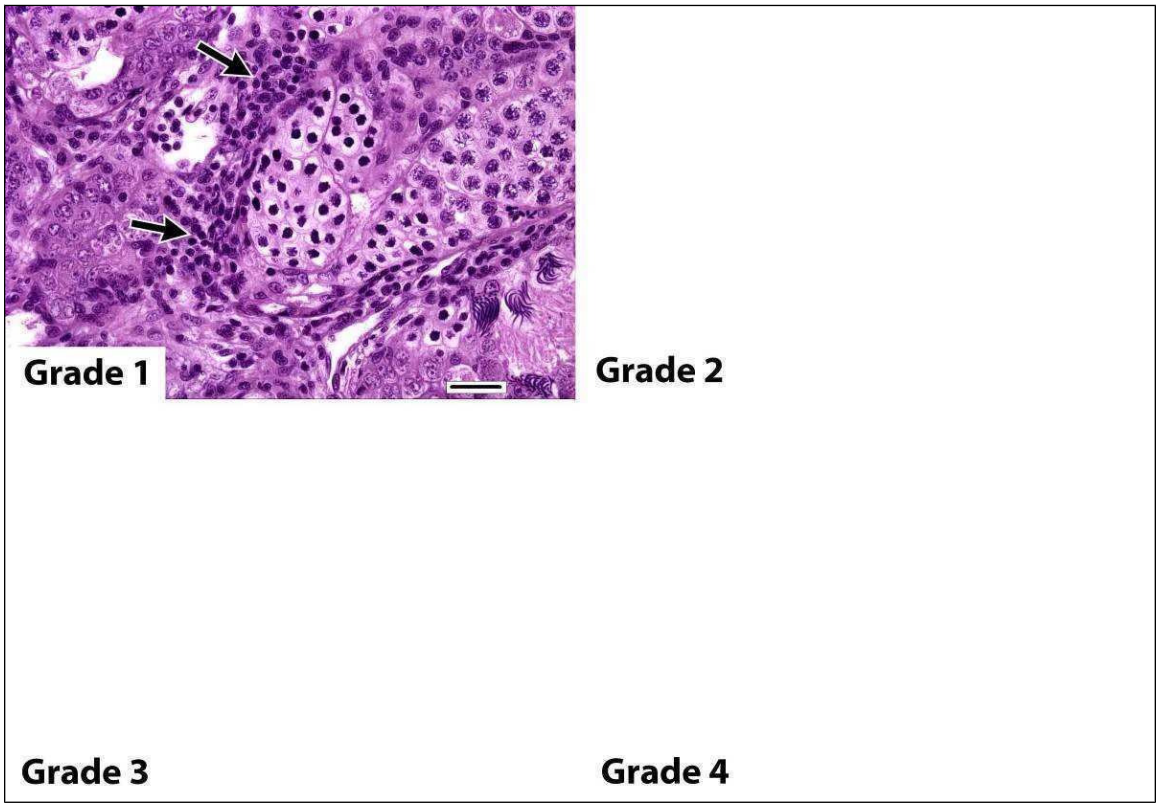

Figure 15. Mononuclear Cell Infiltrates. Mononuclear cell infiltrates (arrows), which appear to consist primarily of lymphocytes, are relatively common in the testes. Bar = 25 microns. Histogram provided for Grade 1 only. Grades 2-4 are intentionally left blank.

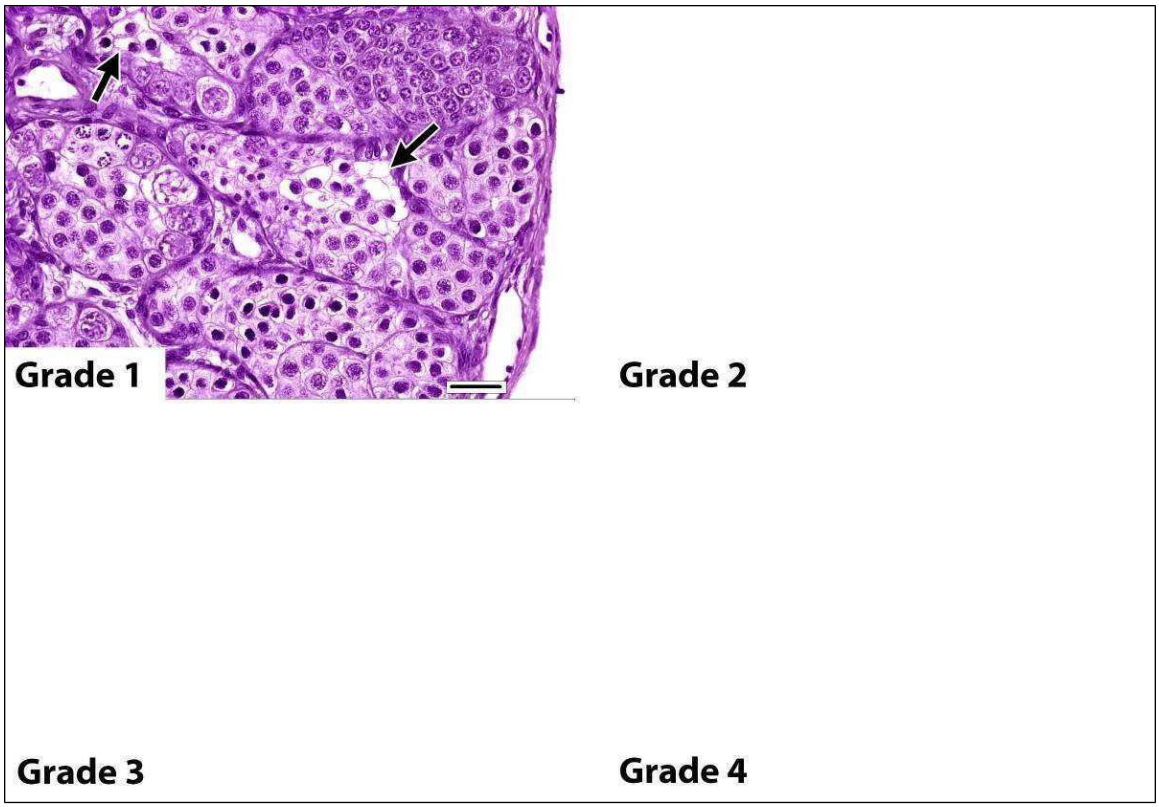

Figure 16. Germ Cell Vacuolation. This finding is characterized by increased amounts of clear cytoplasm in clusters of zygotene-phase primary spermatocytes. Bar = 25 microns. Illustration for Grade 1 only. Grades 2-4 are left intentionally blank.

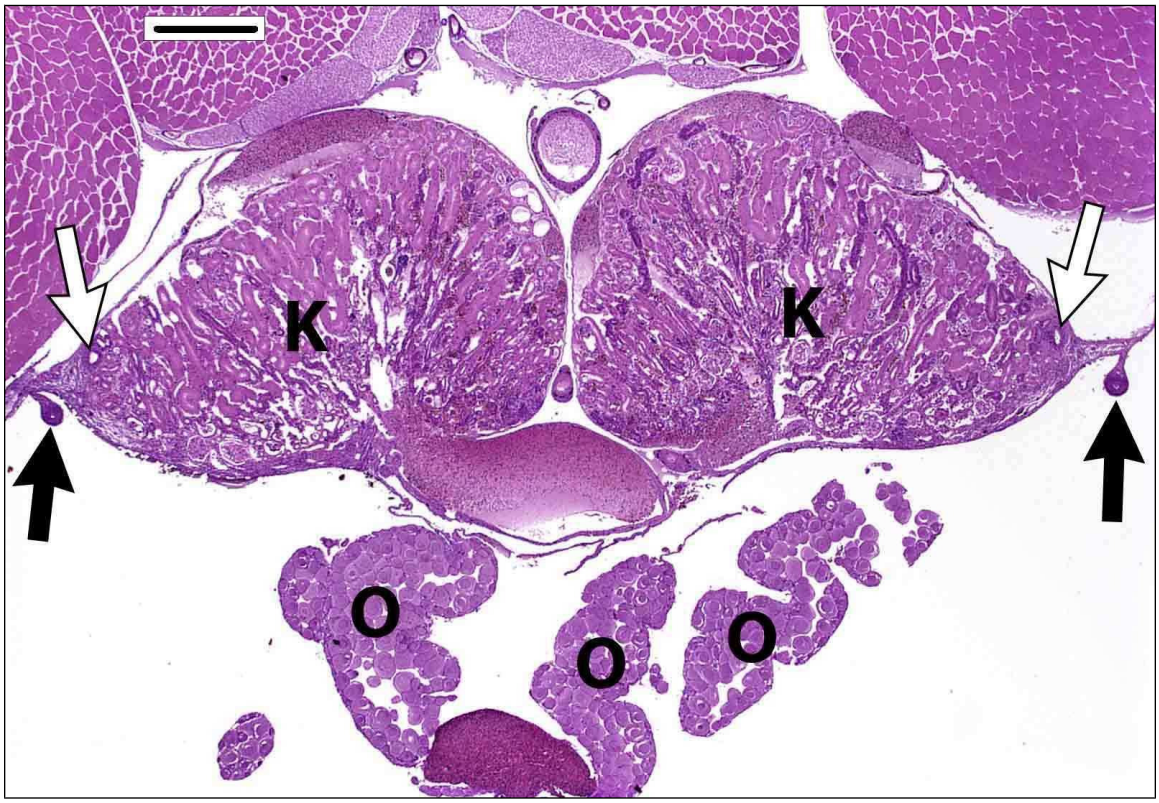

Figure 17. Normal Ovaries, Oviducts and Wolffian Ducts. The ovaries (O) are attached to the peritoneal surface of the kidneys (K) by suspensory ligaments. The black arrows indicate the oviduct (Müllerian duct) remnants (Stage 2 oviducts in this case), whereas the white arrows indicate the Wolffian ducts. Bar = 500 microns.

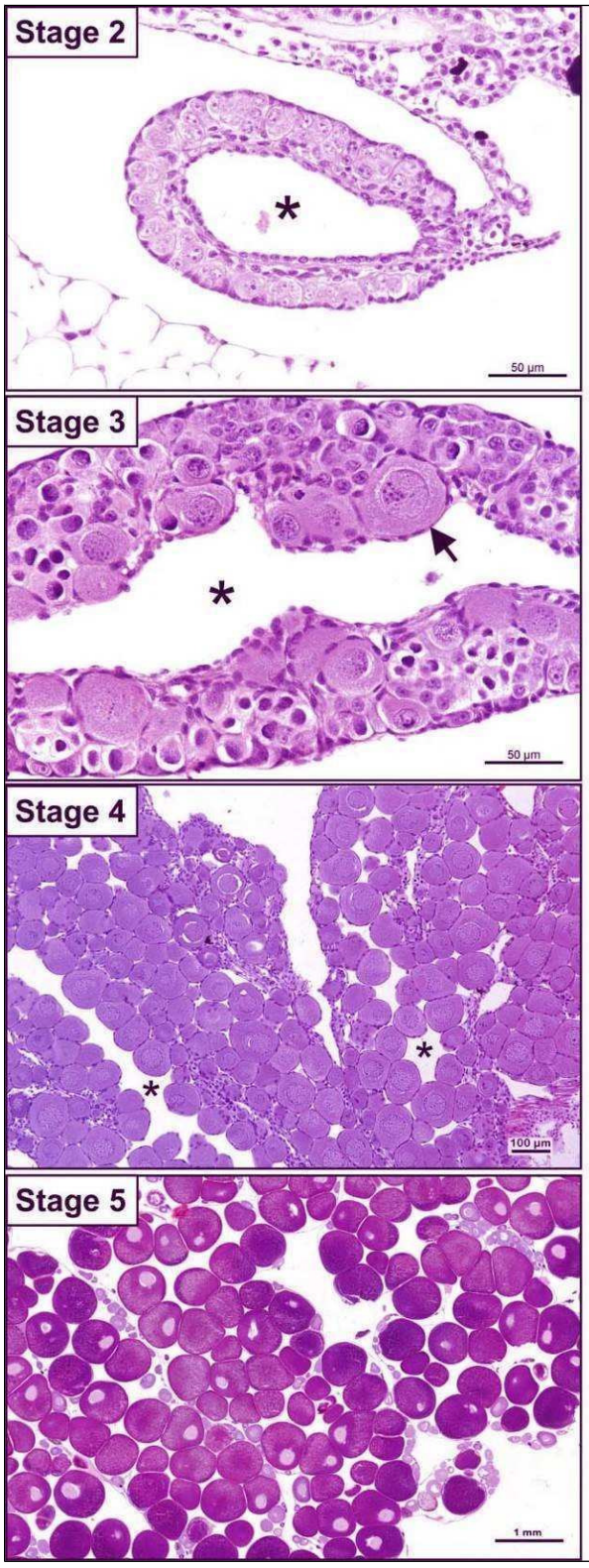

Stage 2:
Gonad identifiable as an ovary based on the presence of a discontinuously open lumen lined with epithelial cells. The germ cells within the cortex (the region outside the epithelial layer) consist of primary oogonia, cysts of primary mitotic oogonia, secondary oogonia, and very early meiotic oocytes.
Transverse sections. H&E.
Bar = 50µm
Asterisk*= Ovarian lumen/Ovarian cavity

Stage 3:
First appearance of diplotene oocytes in cortex. Structure and shape of the ovary similar to stage 1, but the appearance of diplotene oocytes is the first morphological difference between male and female germ cells. The most prevalent germ cell types at this stage are cysts of secondary oogonia and cysts of leptotene-pachytene primary meiocytes.
Bar = 50µm
Asterisk*= Ovarian lumen/Ovarian cavity
Arrow = Diplotene oocyte

Stage 4:
Pre-vitellogenic (Dumont Stage I) diplotene oocytes are the most prevalent germ cell type observed by area and absolute cell counts. The central lumen is proportionately smaller while the whole ovary grows greatly in size and volume due to the growth of the oocytes. Cysts in earlier stages of oogenesis become fewer in number and are located along the periphery of ovary.
Bar = 100µm
Asterisk*= Ovarian lumen/Ovarian cavity

Stage 5:
Ovary consists almost entirely of vitellogenic oocytes (Dumont Stage IV). Pre-vitellogenic diplotene oocytes can be found along the periphery of the ovary and germ patches of primary and secondary oogonia are difficult to locate.
Bar = 1 mm

Figure 18. Staging of the Ovary. Control females 10 weeks post NF stage 62 (LAGDA termination) typically have Stage 3 or 4 ovaries.

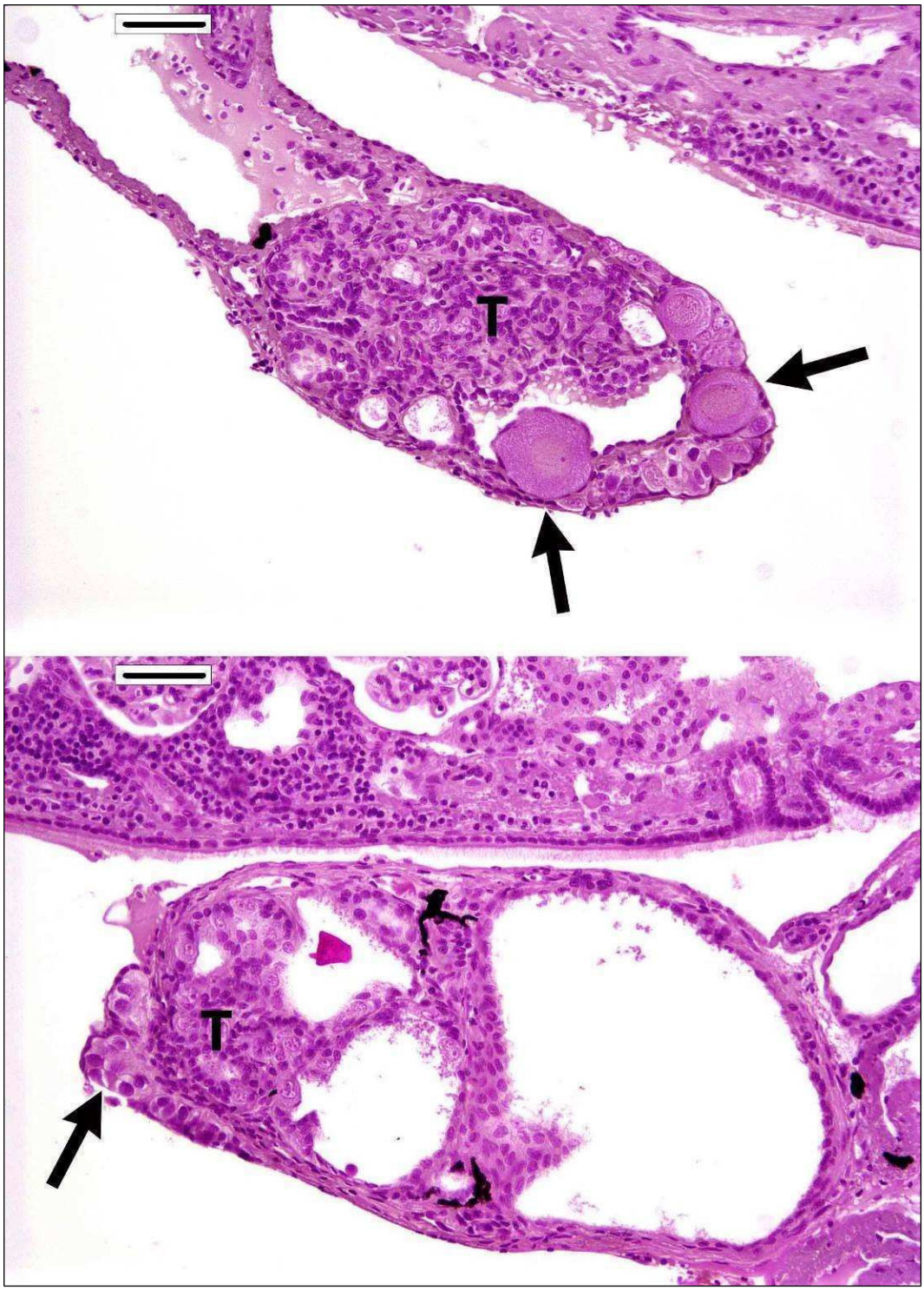

Figure 19. Mixed Sex Gonads. The gonads contain both testicular (T) and ovarian (arrows) components. Each of these gonads received a Phenotype Score of 2. Bar = 50 microns.

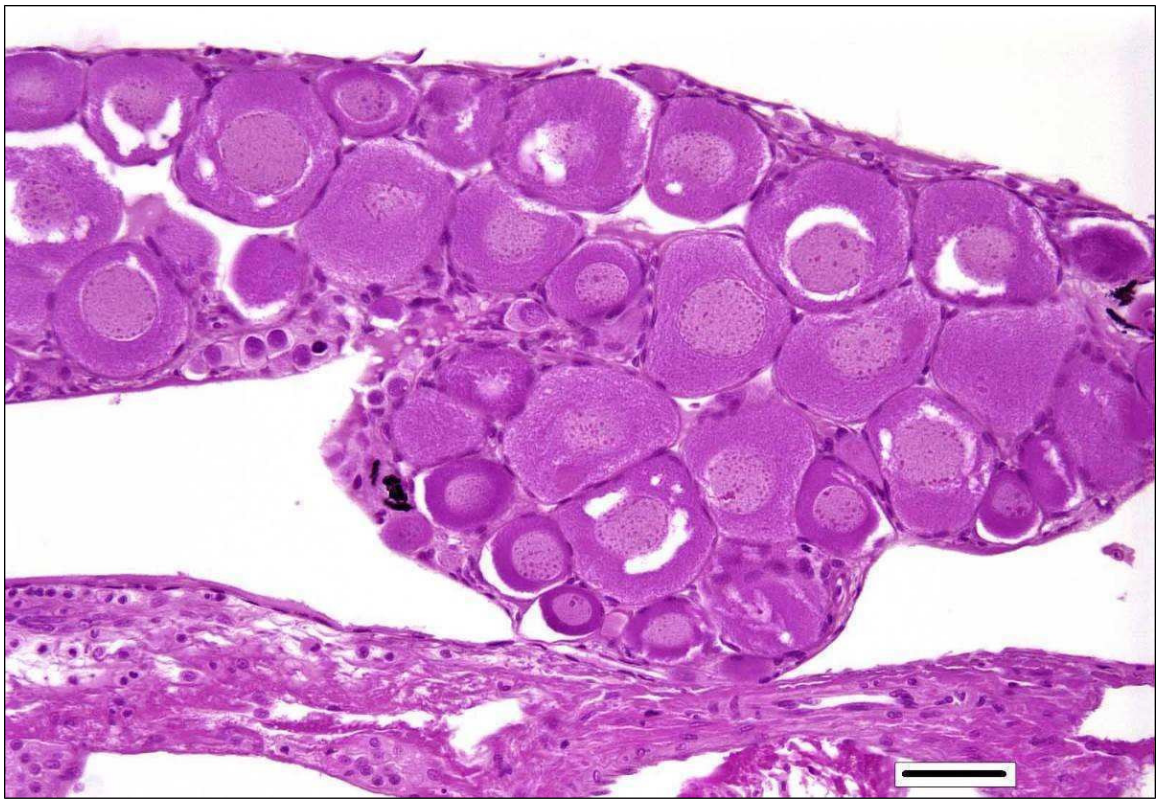

Figure 20. Complete Sex Reversal. This normal appearing ovary was a treatment-related phenotypic finding in a genetic male frog. This ovary would receive a Gonad Phenotype Score of 5. Bar = 50 microns.

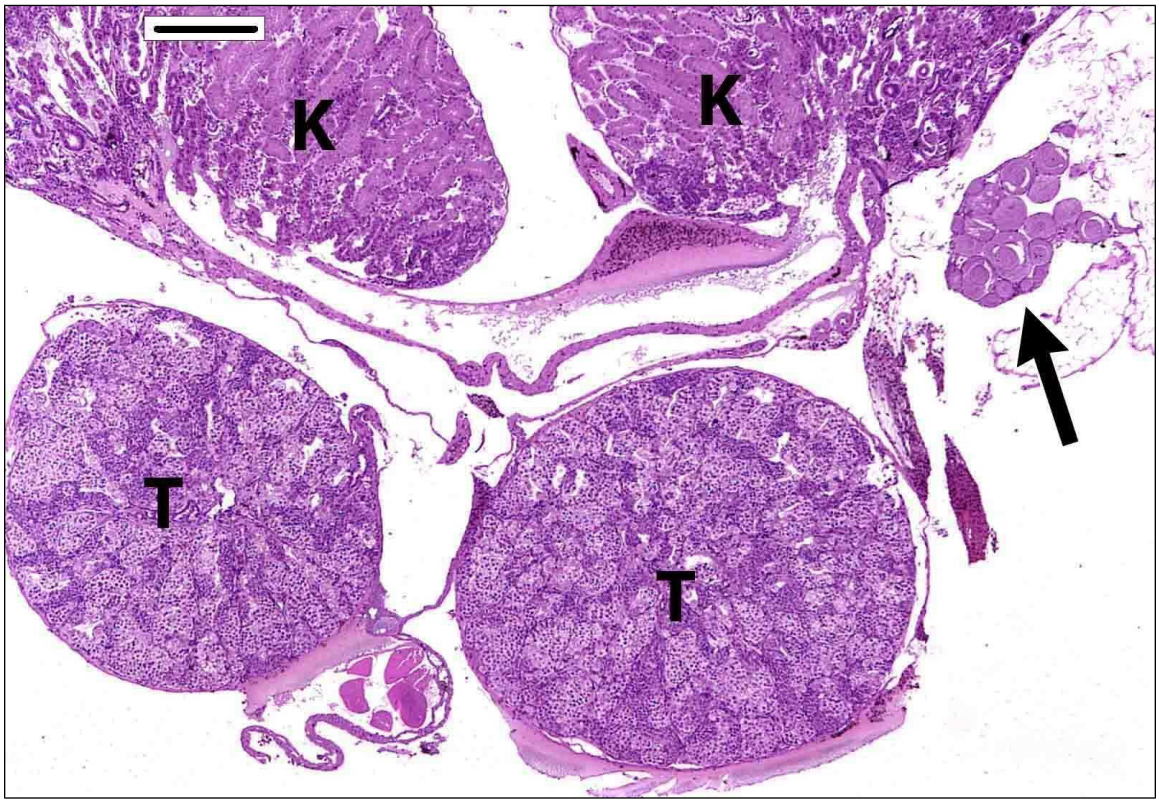

Figure 21. Hermaphroditism. In addition to left and right testes (T), this animal had a small amount of ovarian tissue (arrow) within the abdominal mesentery. K = kidney. Bar = 250 microns.

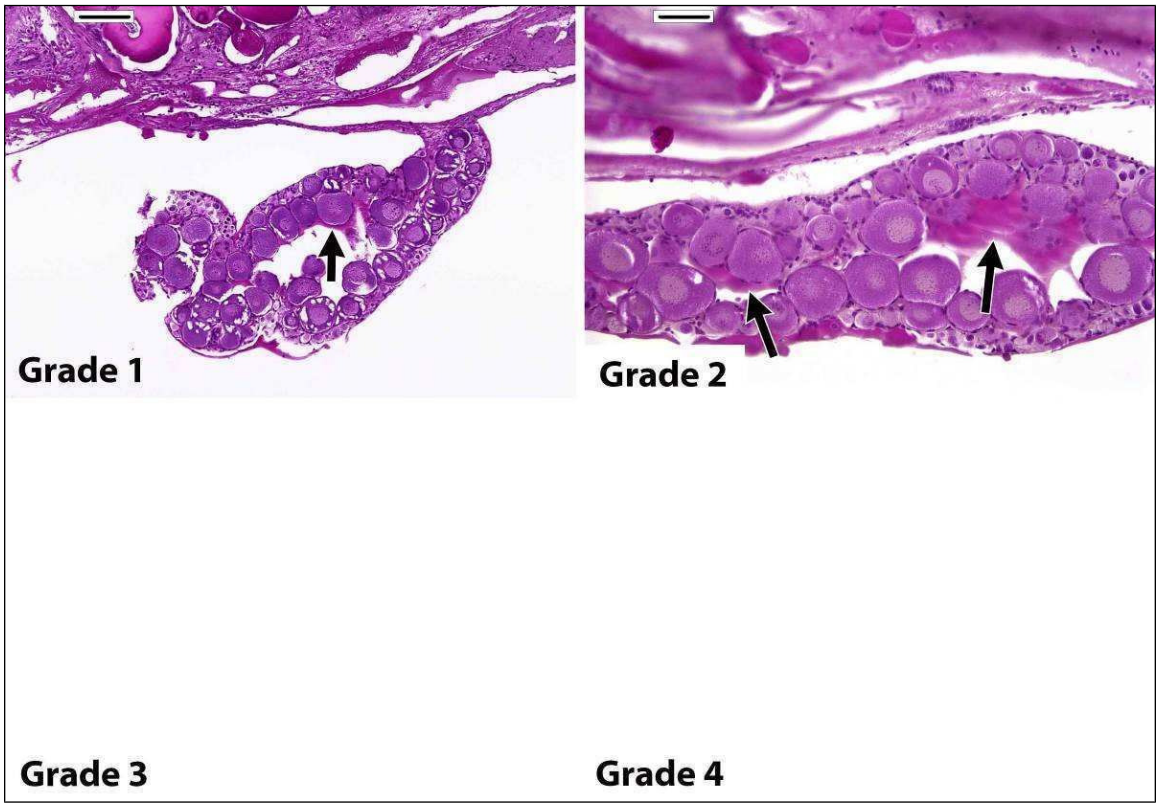

Figure 22. Proteinaceous Fluid. Proteinaceous fluid (arrows) appears as homogenous dark pink material within the central and subcapsular regions of the ovarian interstitium. Bar = 100 microns (Grade 1), 50 microns (Grade 2). Grades 2-4 are left intentionally blank.

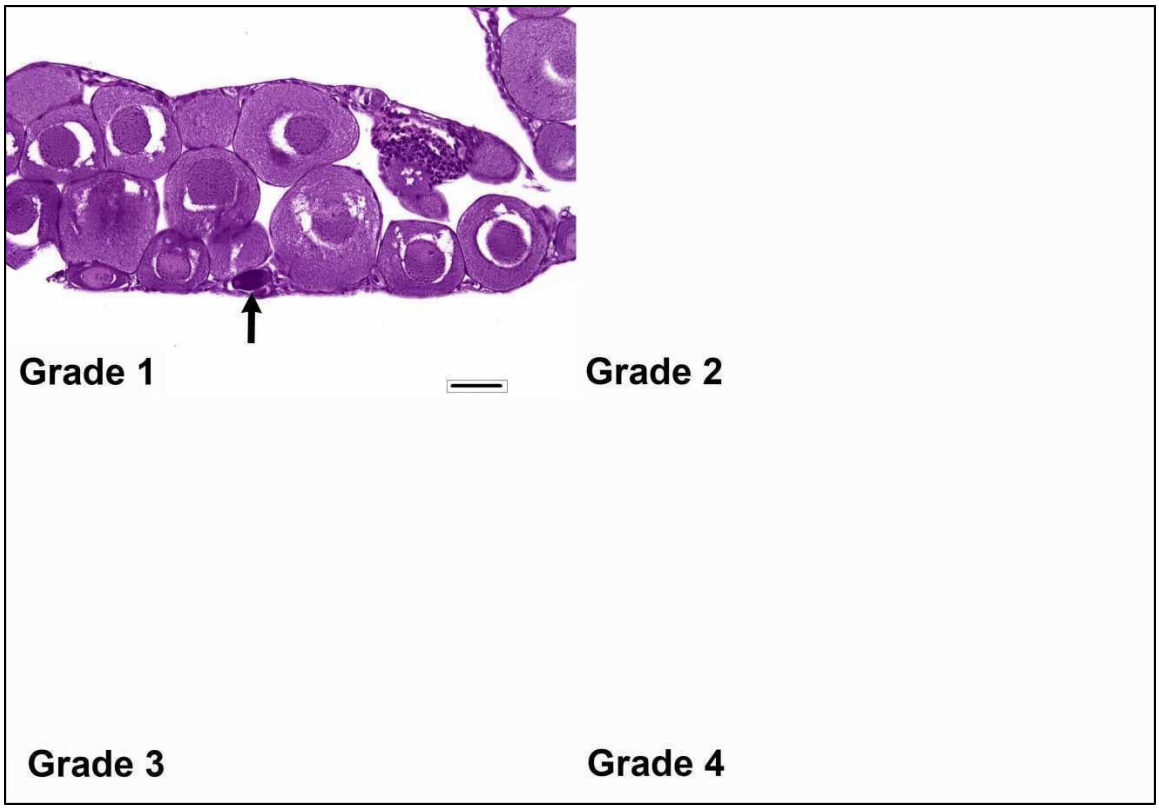

Figure 23. Oocyte atresia. Spontaneous oocyte atresia appears to be relatively uncommon in the Stage 3 or 4 ovaries of most untreated control frogs. Bar = 50 microns. Grades 2-4 are left intentionally blank.

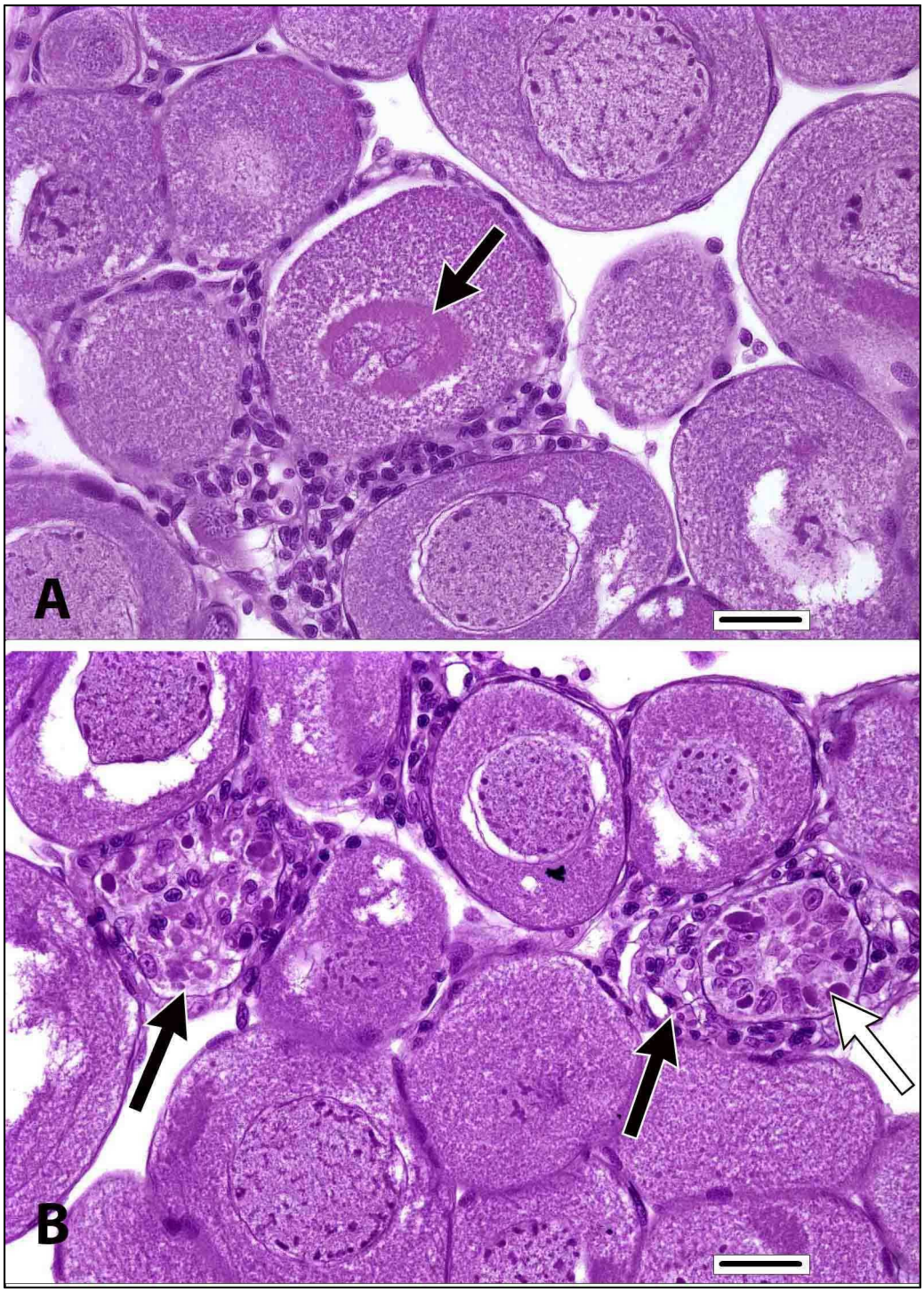

Figure 24. Oocyte atresia, Additional Examples. A. In this example, early oocyte degeneration is characterized by a loss of nuclear detail and increased nuclear density. B. In this later stage of atresia, oocyte remnants are being scavenged by nests of macrophages (black arrows). The white arrow indicates what appear to be hypertrophic granulosa cells from an atretic follicle. Bar = 25 microns.

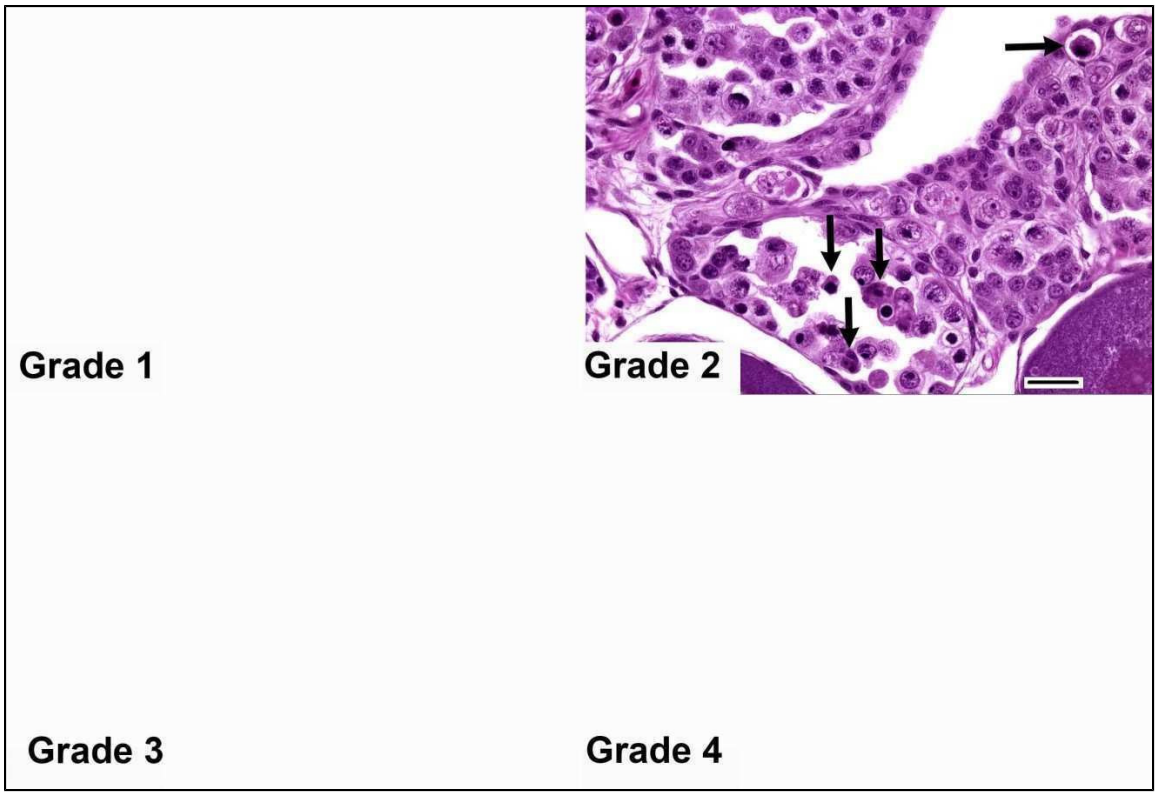

Figure 25. Ovary, Germ Cell Degeneration. The term "germ cell degeneration" is used rather than "atresia" to characterize the *in vivo* deterioration of stem cells or oogonia, or the deterioration of phenotypically undifferentiated cells in early stage gonads. Ovarian germ cell degeneration in the form of apoptotic-like cells (arrows) was observed as a treatment-related response in the Grade 2 image. Bar = 25 microns. Grade 1, 3, and 4 are left intentionally blank.

(iv) Gonadal Ducts.

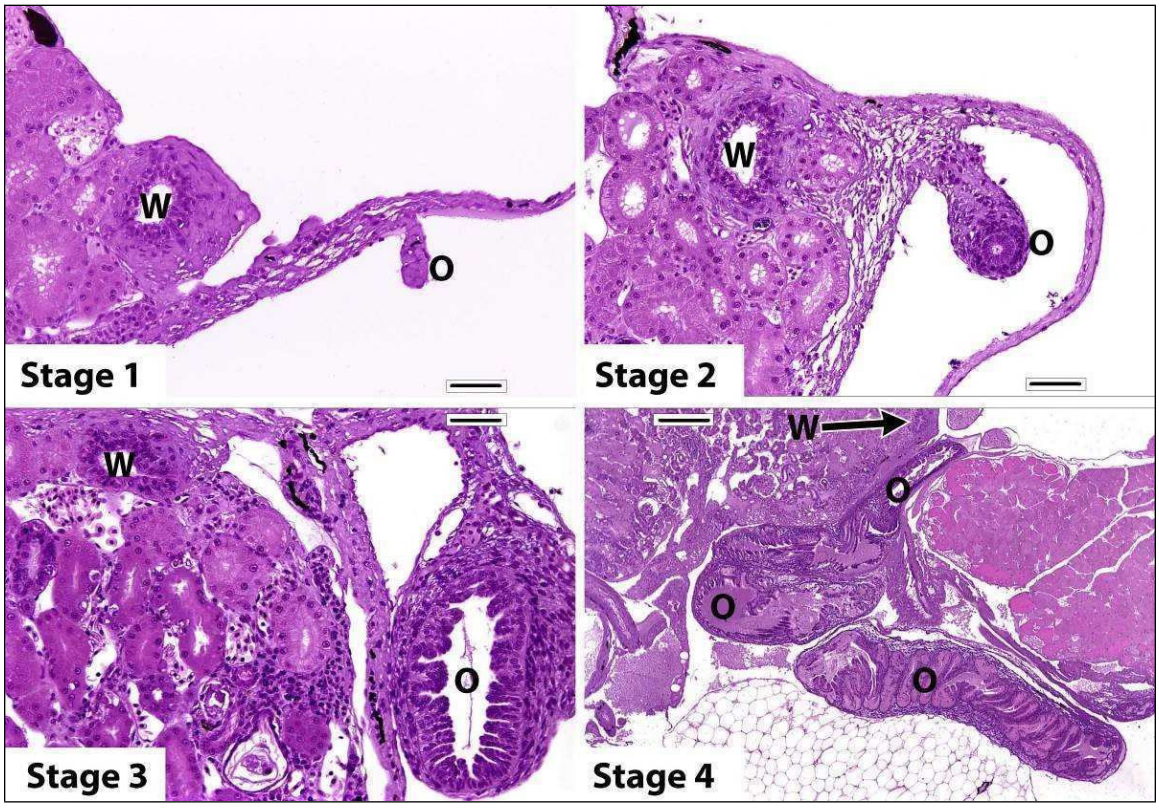

Figure 26. Oviduct Staging. As the oviduct (Müllerian duct) matures in the female, it becomes progressively larger, with an expanded lumen and a more convoluted mucosal lining. Conversely, oviducts regress over time in male frogs. Control male frogs typically have Stage 1 or 2 oviducts 10 weeks post NF stage 62 (LAGDA termination), and the average stage in males is usually less than the average stage in same-aged females of the same study. In borderline cases, the size of the oviduct relative to the Wolffian duct is a useful criterion for differentiating between Stage 2 and Stage 3 oviducts. Bar = 50 microns (Stages 1, 2, and 3), 100 microns (Stage 4).

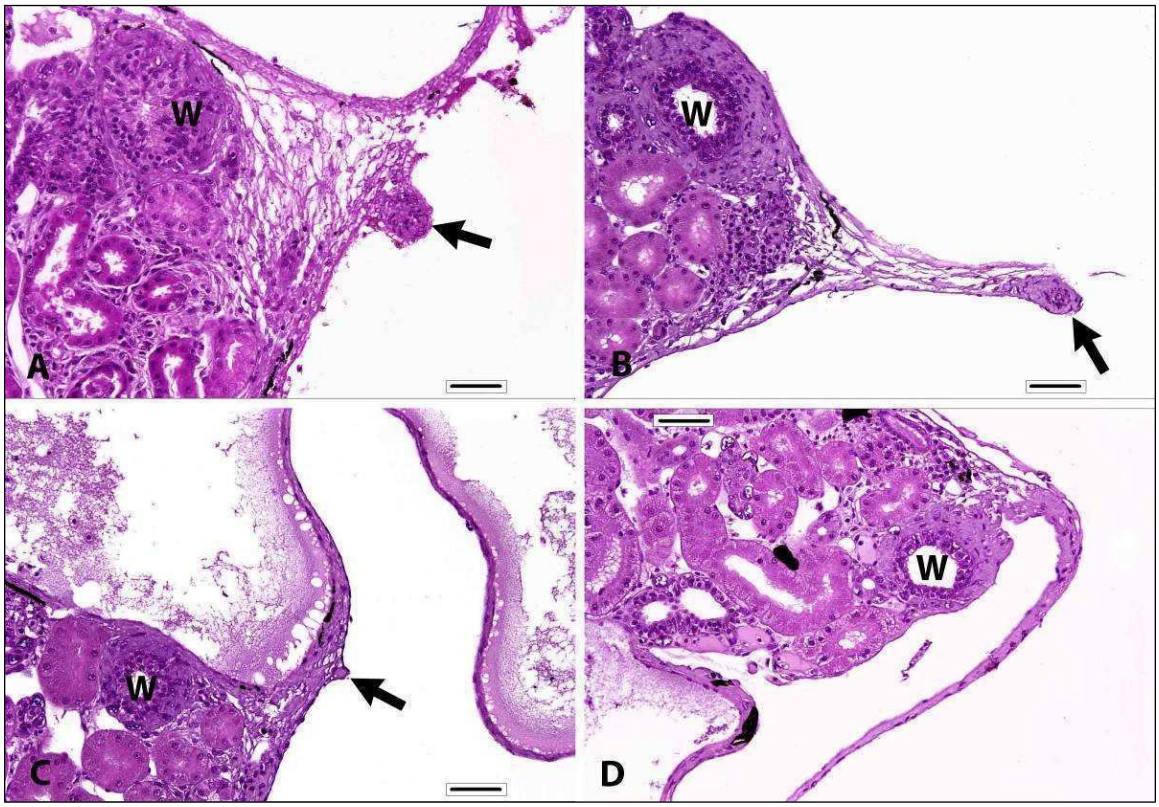

Figure 27. Oviduct Staging, Additional Examples of Stage 1 Oviducts. Stage 1 oviducts (arrows) range from small fibrous protuberances, to suspensory ligaments in which there is no apparent residual oviduct (e.g., Fig. D). These oviducts do not have lumens or mucosal linings. Bar = 50 microns.

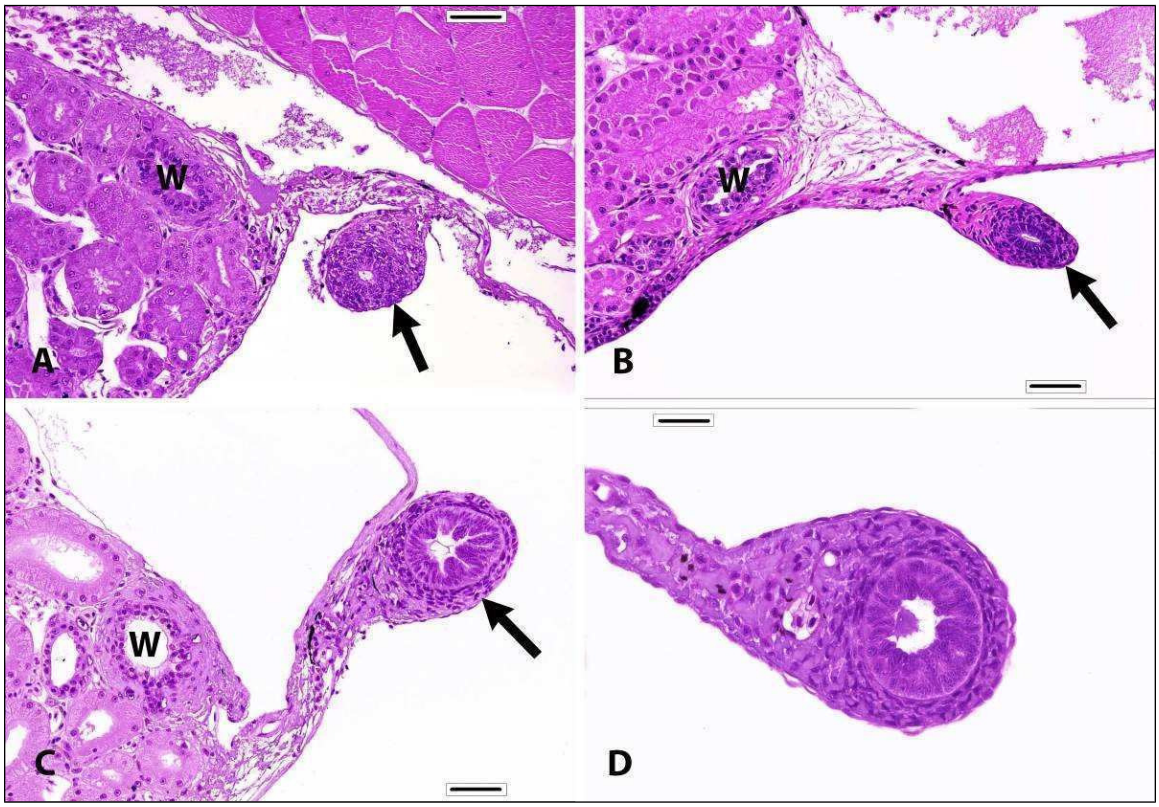

Figure 28. Oviduct Staging, Additional Examples of Stage 2 Oviducts. Stage 2 oviducts (arrows), which are comparable in size to the Wolffian ducts, all have a visible lumen and are lined by one to a few layers of mucosal epithelial cells, with or without slight mucosal folding. Bar = 50 microns (Figures 28A-C), 25 microns (Figure 28D).

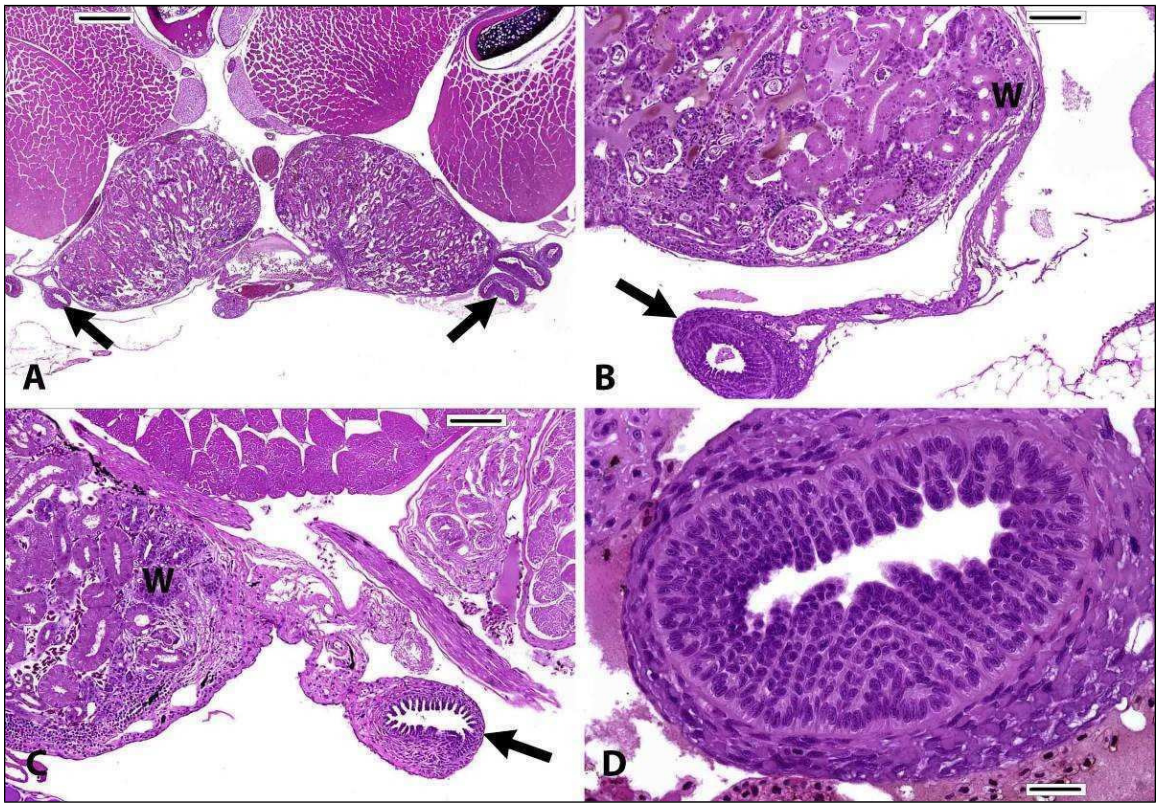

Figure 29. Oviduct Staging, Additional Examples of Stage 3 Oviducts. Stage 3 oviducts (arrows), which greater than 1.5 times the size of Wolffian ducts, have intricate mucosal folding. Bar = 500 microns (Figure 29A), 100 microns (Figures 29B-C), 25 microns (Figure 29D).

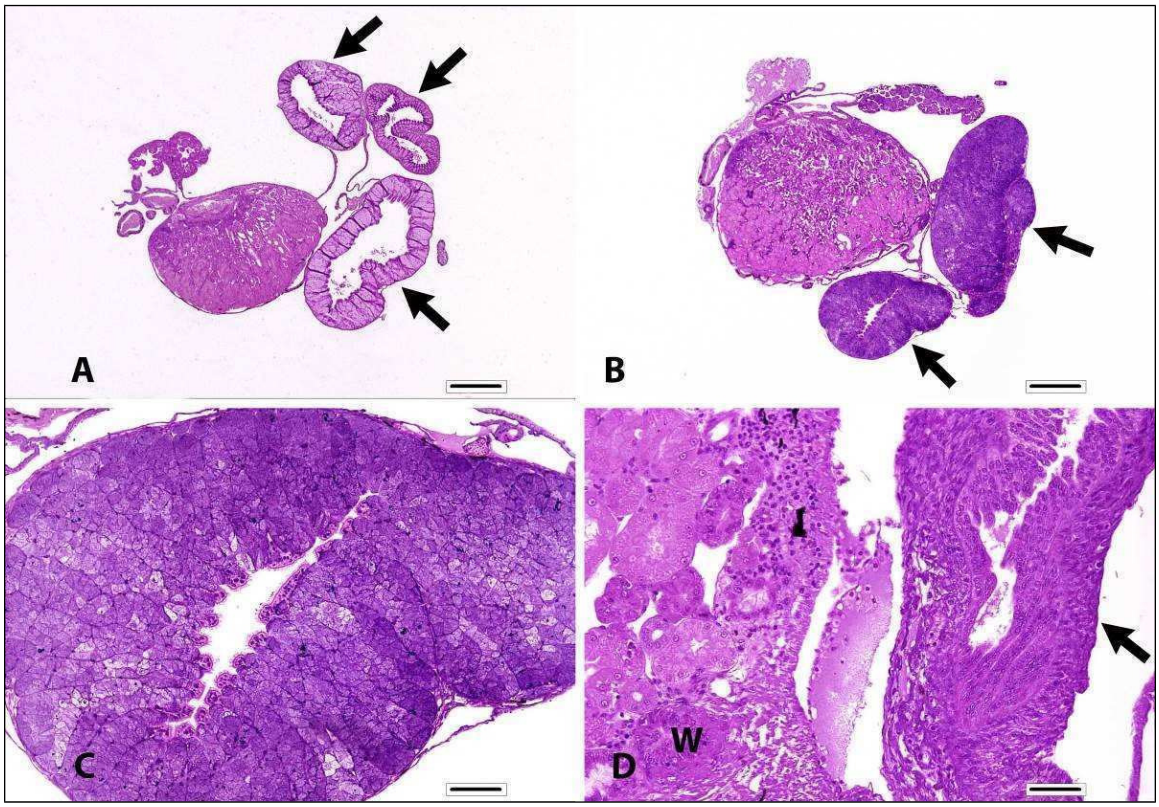

Figure 30. Oviduct Staging, Additional Examples of Stage 4 Oviducts. Stage 4 oviducts (arrows) are markedly larger than Wolffian ducts, and the mucosal epithelium is forming, or has formed, large glandular structures. Fig. D is enlarged relative to the other figures. The oviduct in Fig. D represents the borderline between Stages 3 and 4. Bar = 500 microns (Figure 30A- B), 100 microns (Figure 30C), 50 microns (Figure 30D).

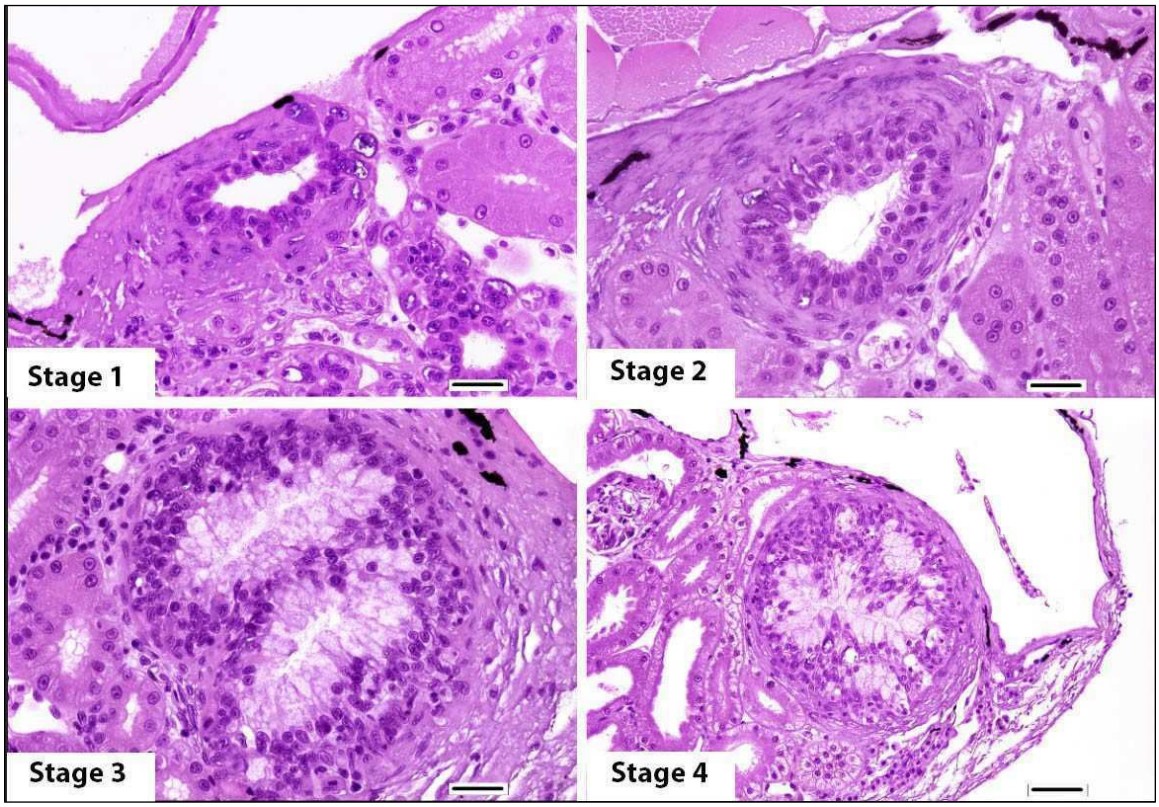

Figure 31. Wolffian Duct Staging. The Wolffian ducts, which are located within the lateral extremities of the right and left kidneys, also function as ureters in *Xenopus* spp. With maturity, the Wolffian ducts become progressively larger, although not to the extent of oviducts in female frogs. The mucosal lining of the ducts also becomes thicker and contains more mucous cells with age. Generally, mean Wolffian duct scores are slightly higher in control males than in control females of the same study. Bar = 25 microns (Stages 1-3), 50 microns (Stage 4).

(v) Kidneys.

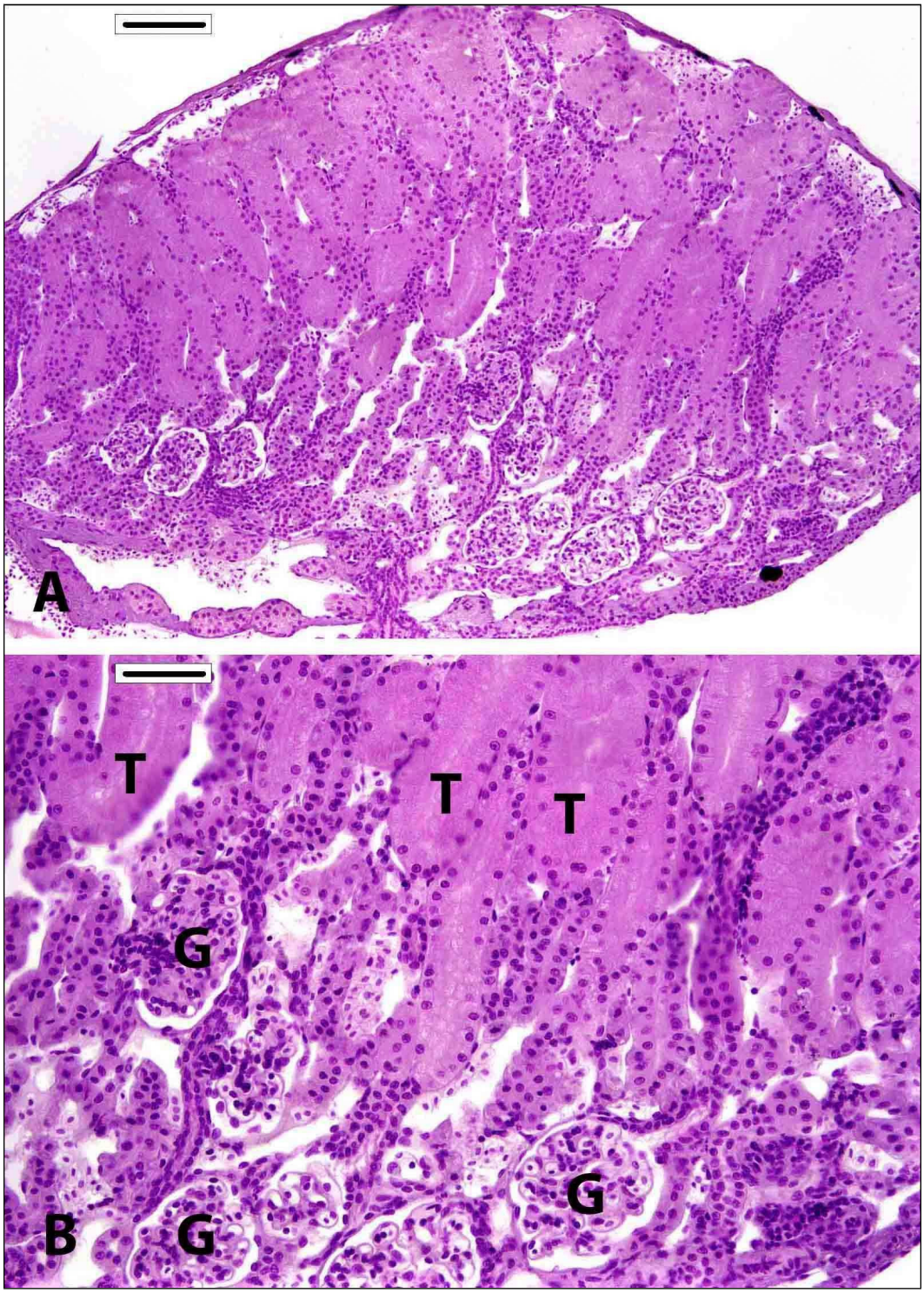

Figure 32. Normal Kidney from a Control Frog. Glomeruli (G) are located in the ventral third of the kidneys, whereas proximal tubules (T) occupy the dorsal portions. Bar = 100 microns (Figure 32A), 50 microns (Figure 32B).

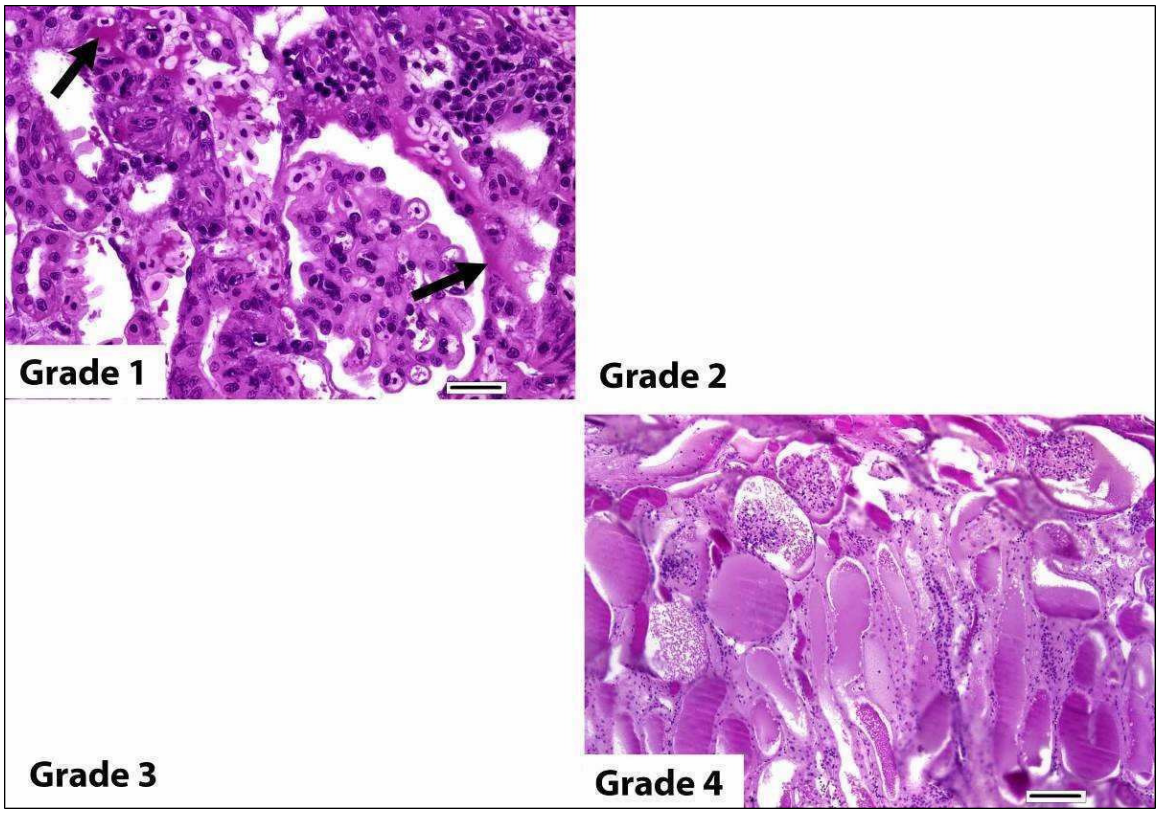

Figure 33. Proteinaceous Fluid. Proteinaceous fluid (arrows) appears as homogenous dark pink material within the renal interstitium, blood vessels, tubules, and/or Bowman's spaces. Bar = 25 microns (Grade 1), 100 microns (Grade 4). Grades 2-3 are left intentionally blank.

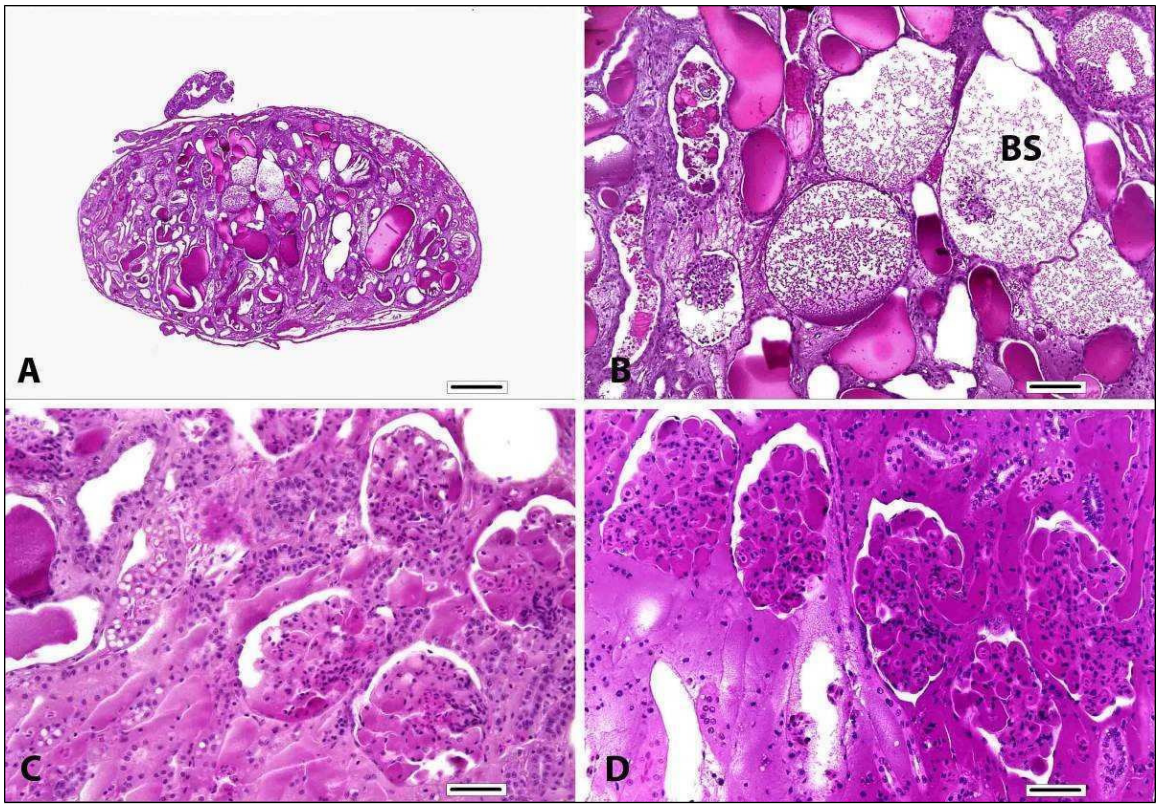

Figure 34. Proteinaceous Fluid, Grade 4, Additional Examples. Tubules, glomeruli, and the renal interstitium are flooded by proteinaceous fluid in these examples. BS = dilated Bowman's space. Bar = 500 microns (Figure 34A), 100 microns (Figure 34B), 50 microns (Figures 34C-D).

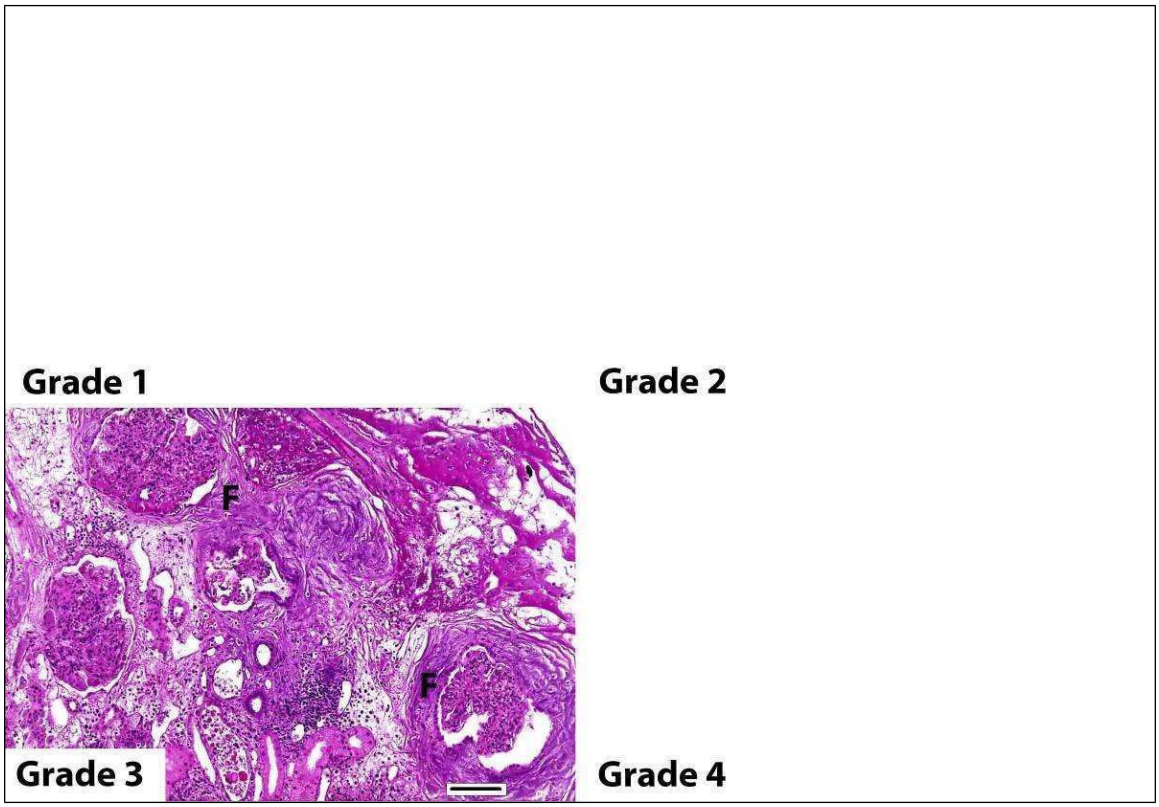

Figure 35. Fibrosis. This finding, which is characterized by excessive amounts of fibrous connective tissue (F) within the renal interstitium, usually occurs as a sequel to chronic inflammation or other long standing parenchymal damage. Bar = 100 microns (Grade 3). Grades 1, 2, and 4 are left intentionally blank.

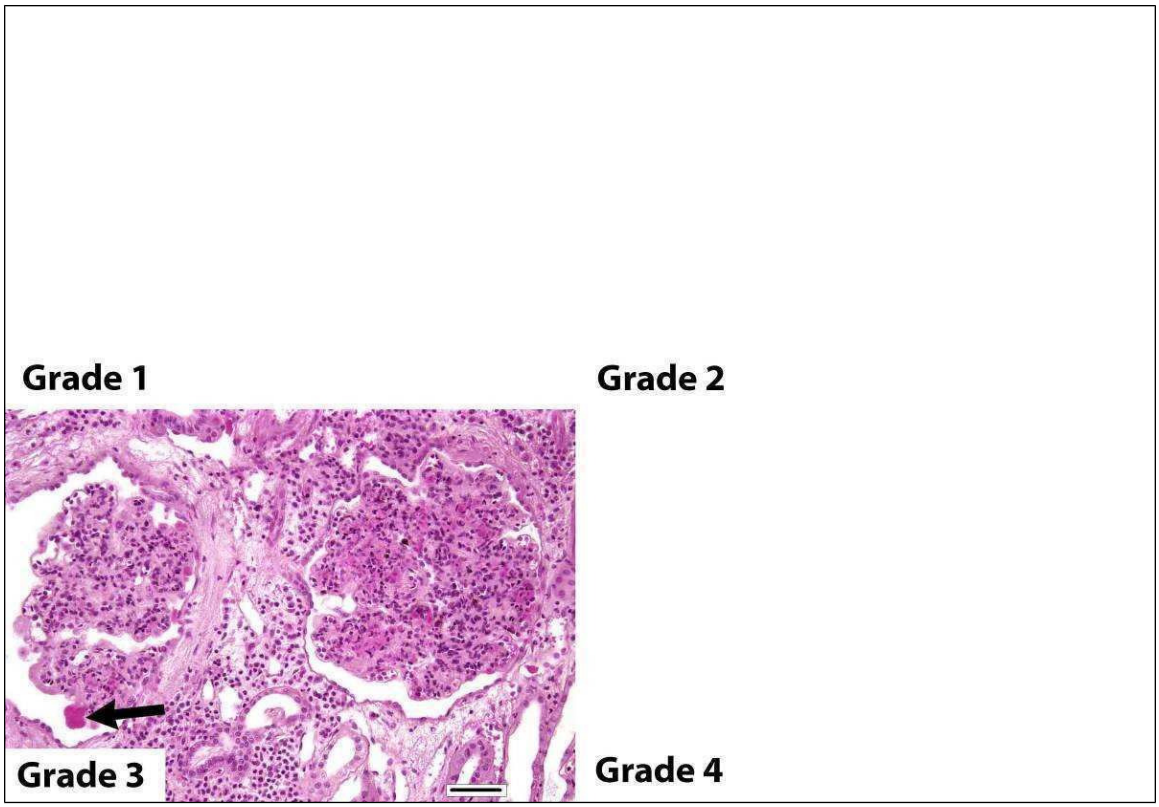

Figure 36. Glomerulomegaly and Glomerular Hypercellularity. This finding can be a consequence of low level chronic glomerular damage. The arrow indicates a small deposit of proteinaceous material within a glomerular capillary. Bar = 20 microns (Grade 3). Grades 1, 2, and 4 are left intentionally blank.

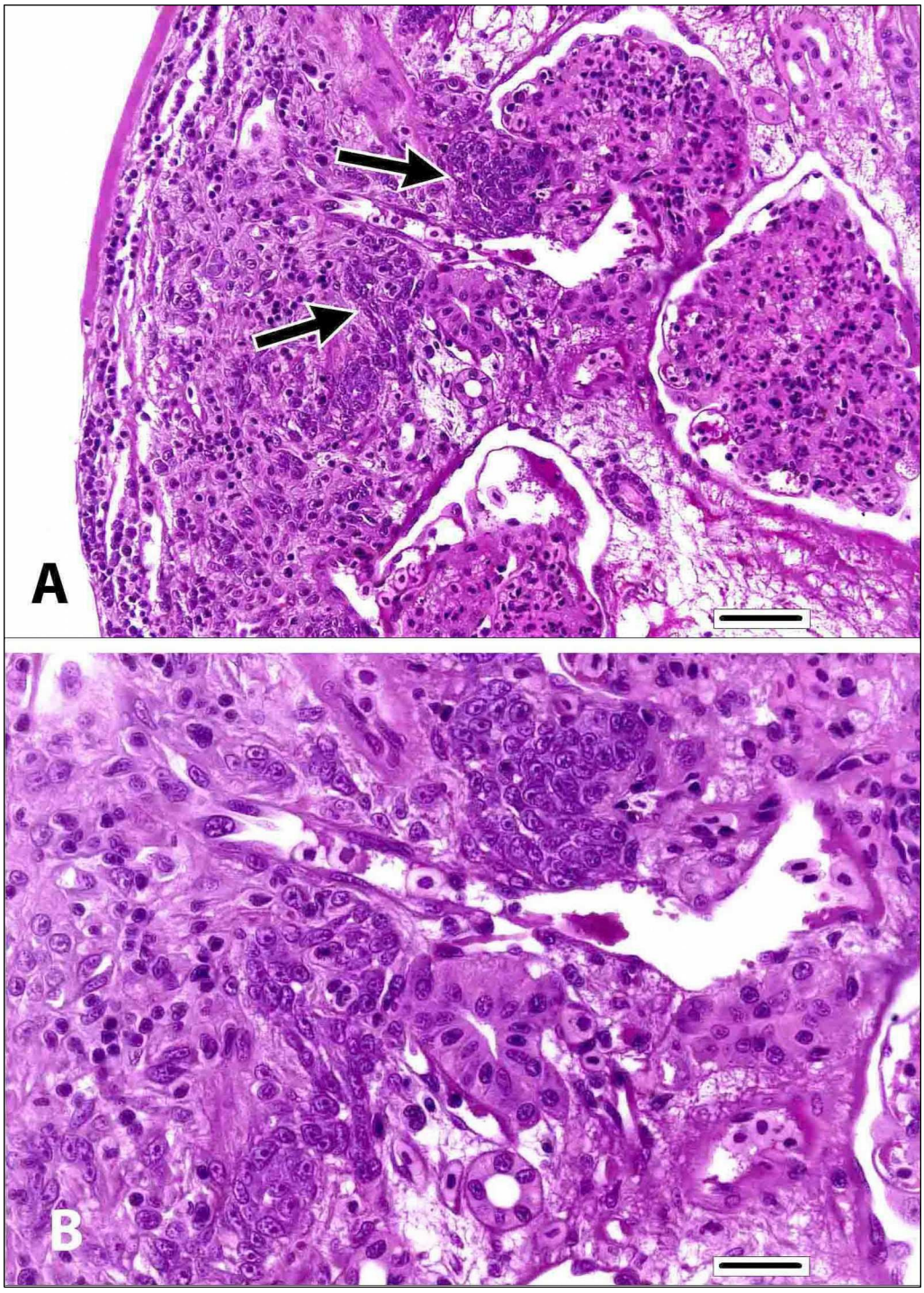

Figure 37. Regenerative Blast Cell Hyperplasia. This finding, which is another consequence of chronic renal damage and tubular loss, is characterized by streaming proliferations of cells with large, hyperchromatic (dark) nuclei (arrows). Figure 37B is a higher magnification of Figure 37A. This particular case was assigned a severity score of Grade 2 (mild). Bar = 50 microns (Figure 37A), 25 microns (Figure 37B).

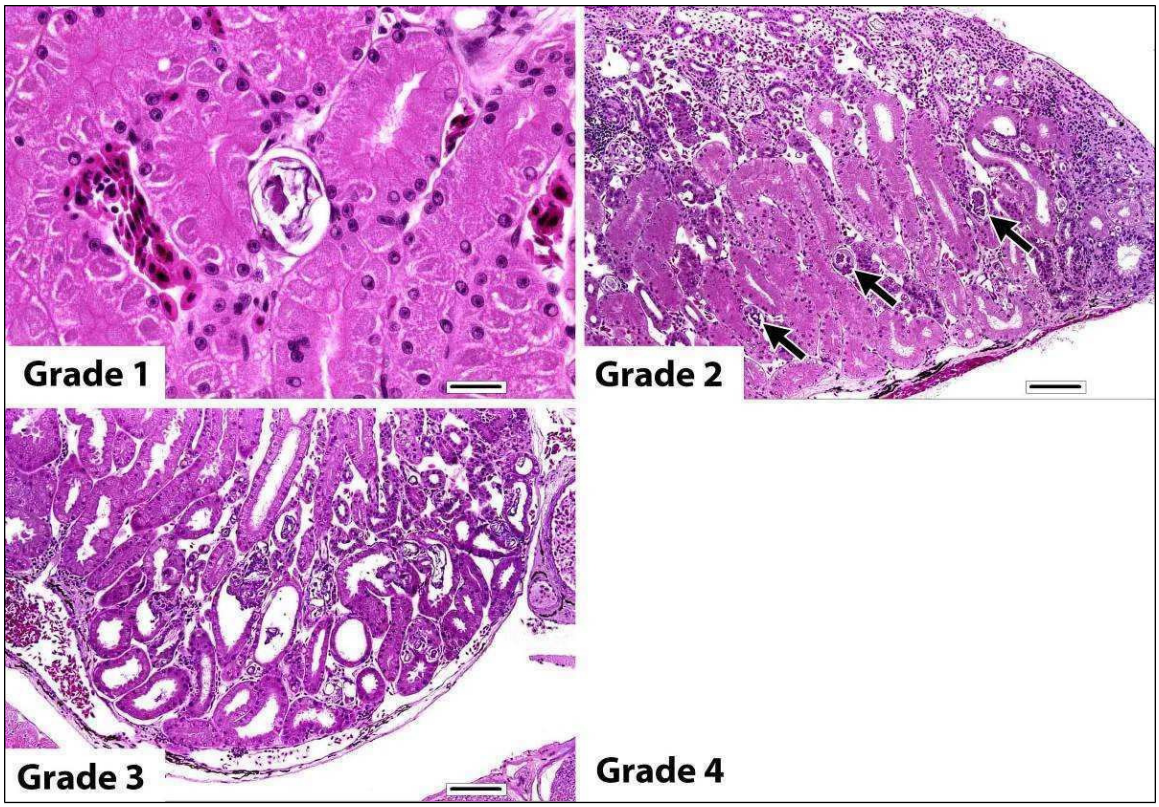

Figure 38. Mineralization with Tubular Dilation. Mineralization appears to be a common background finding in laboratory reared *X. laevis*, and the severity of this finding appears to vary from facility to facility. Husbandry factors (e.g., issues involving feed and/or water composition) are suspected causes. The occurrence of mineralization is associated with focal to diffuse renal tubular dilation, presumably due to obstruction of urine flow. Tubular dilation and mineralization are usually graded separately. In a given frog, the severity grade for tubular dilation is typically one grade less than that of mineralization (see example below). Bar = 25 microns (Grade 1), 100 microns (Grades 2 and 3). Grade 4 is left intentionally blank.

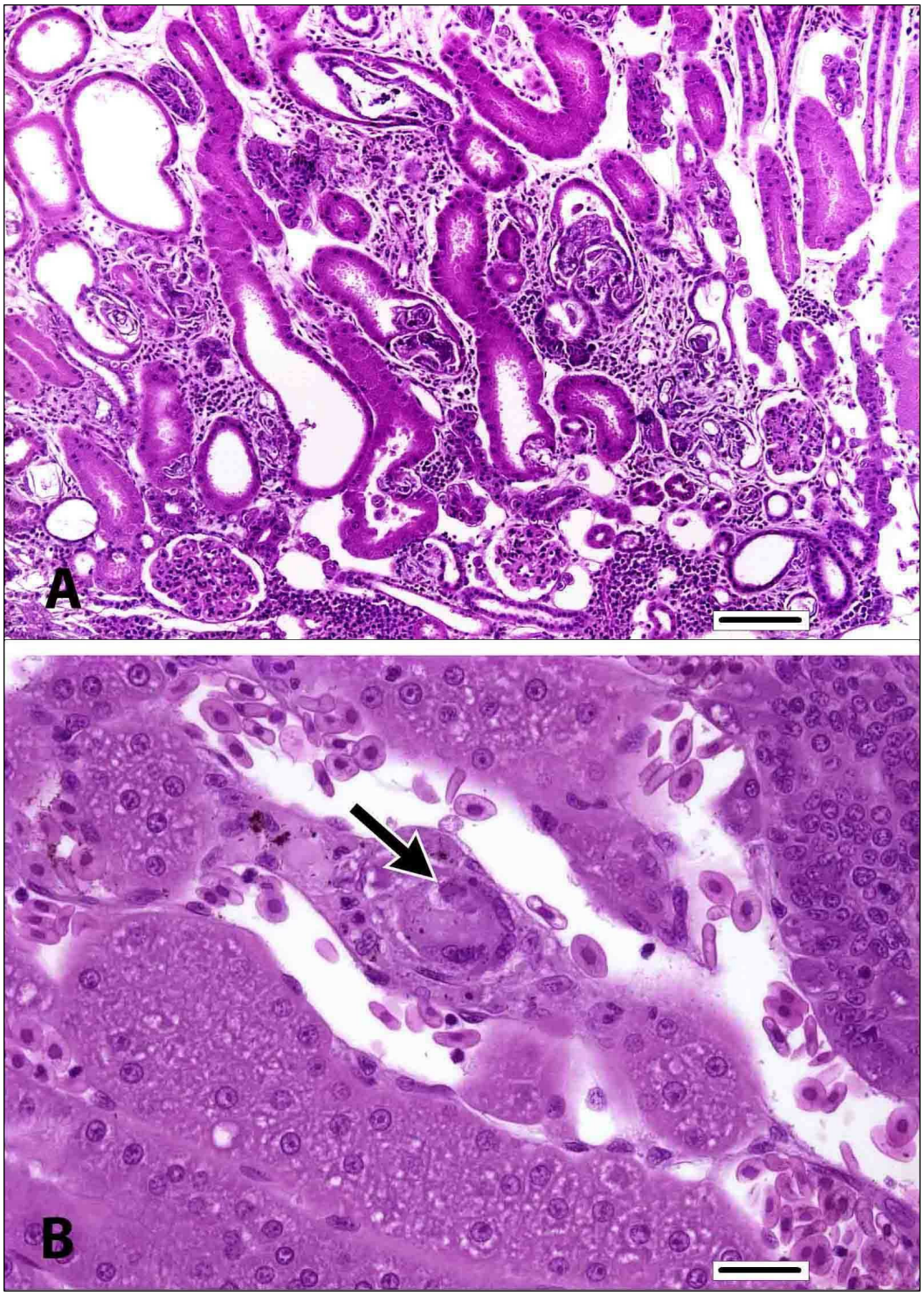

Figure 39. Mineralization, Additional Examples. Figure A represents another case of Grade 3 mineralization and Grade 2 tubular dilation. Figure B illustrates a small amount of mineral (arrow) within a multinucleated giant cell macrophage. Bar = 100 microns (Figure 39A), 25 microns (Figure 39B).

(e) References.

(1) Green J.W., Springer T.A., Saulnier A.N., Swintek J. (2014). Statistical analysis of histopathology endpoints. *Environ Toxicol Chem.* 33(5):1108-1116.

(2) Grim K.C., Wolfe M., Braunbeck T., Iguchi T., Ohta Y., Tooi O., Touart L., Wolf D.C., Tiege J. (2009). Thyroid histopathology assessments for the amphibian metamorphosis assay to detect thyroid-active substances. *Toxicol Pathol*. 37:415-424.

(3) Morton D., Sellers R.S., Barale-Thomas E., Bolon B., George C., Hardisty J.F., Irizarry A., McKay J.S., Odin M., Teranishi M. (2010). Recommendations for pathology peer review. *Toxicol Pathol*. 38(7):1118-1127.

(4) Nieuwkoop P.D., Faber J. (1994). Normal Table of *Xenopus laevis* (Daudin). Garland Publishing, Inc. New York and London.

(5) The Society of Toxicologic Pathologists. (1991). Peer review in toxicologic pathology: some recommendations. *Toxicol Pathol*. 19:290-292.

(6) The Society of Toxicologic Pathologists. (1997). Documentation of pathology peer review. Position of the Society of Toxicologic Pathologists. *Toxicol Pathol*. 25(6):655.

(7) Wolf J.C., Lutz I., Kloas W., Springer T.A., Holden L.R., Krueger H.O., Hosmer A.J. (2010). Effects of 17 beta-estradiol exposure on *Xenopus laevis* gonadal histopathology. *Environ Toxicol Chem*. 29(5):1091-1105.

STAA Citation

Development and validation of the OCSPP 890.2300 Larval Amphibian Growth and Development Assay

Primary Nominated Publications

(1) Haselman, J. T., Kosian, P. A., Korte, J. J., Olmstead, A. W., Iguchi, T., Johnson, R. D., & Degitz, S. J. (2016a). Development of the Larval Amphibian Growth and Development Assay: effects of chronic 4-tert-octylphenol or 17β-trenbolone exposure in *Xenopus laevis* from embryo to juvenile. *Journal of Applied Toxicology*, *36*(12), 1639-1650. (JAT impact factor: 3.065) (Cited by 10)

(2) Haselman, J. T., Kosian, P. A., Korte, J. J., Olmstead, A. W., & Degitz, S. J. (2018). Effects of multiple life stage exposure to the fungicide prochloraz in *Xenopus laevis*: Manifestations of antiandrogenic and other modes of toxicity. *Aquatic Toxicology*, *199*, 240-251. (Aq. Tox. Impact factor: 3.794)

Supporting Items

(1) Haselman, J. T., Sakurai, M., Watanabe, N., Goto, Y., Onishi, Y., Ito, Y., Onoda, Y., Kosian, P.A., Korte, J.J., Johnson, R.D. & Iguchi, T. (2016b). Development of the Larval Amphibian Growth and Development Assay: Effects of benzophenone-2 exposure in *Xenopus laevis* from embryo to juvenile. *Journal of Applied Toxicology*, *36*(12), 1651-1661. (Cited by 6)

(2) Haselman, J. T., Olmstead, A. W., & Degitz, S. J. (2015). Global gene expression during early differentiation of *Xenopus* (*Silurana*) *tropicalis* gonad tissues. *General and comparative endocrinology*, *214*, 103-113. (Gen. & Comp. Endocr. Impact factor: 2.445) (Cited by 11)

(3) US EPA (2015), OCSPP 890.2300: Larval Amphibian Growth and Development Assay (LAGDA), Endocrine Disruptor Screening Program Test Guidelines, 890 series, http://www.regulations.gov, ID: EPA-HQ-OPPT-2009-0576-0018 [accessed on 27 April 2020].

(4) OECD (2015), Test No. 241: The Larval Amphibian Growth and Development Assay (LAGDA), OECD Guidelines for the Testing of Chemicals, Section 2, OECD Publishing, Paris, https://doi.org/10.1787/9789264242340-en.

(5) Images of exposure unit and automated dilution system

Table of Contents

General_Authors_Publications.....2
LI-265143_Melnyk_etal_2019_Sr_paper.....8
RPA_Donohue_J.....13
RPA_Donohue_M.....14
RPA_Pham.....16

United States Environmental Protection Agency
Washington, DC 20460

STAA REPORT FOR THE SCIENTIST NOMINATIONS

General Information:

Nomination ID/App ID:	20-085
Research Category Primary:	Health Effects Research and Human Health Risk Assessment (HE)
Research Category Secondary:	Monitoring and Measurement Methods (MM)
Laboratory/Office Name:	ORD
Nomination Entered By:	Lisa Melnyk

Eligibility Checklist:

[Y] The nominated publication(s) has not been submitted to a previous STAA competition.

[Y] The nominated publication(s) was published on or before January 1, 2017 and on or after January 1,2012

[Y] The principal author was an EPA employee or a PHS employee assigned to EPA when the research was performed

[Y] The EPA authors (includes PHS employees assigned to EPA) contributed collectively a minimum of 50% toward the publication(s)

Nominating Official Name:	Lisa Baxter
Nominating Official Title:	BIOLOGIST
Nominating OfficialEmail:	baxter.lisa@epa.gov
STAA Coordinator Name:	Kathleen Wiser
STAA Coordinator Email:	wiser.kathi@epa.gov

Justifications:

Justification 1:

As part of the Safe and Sustainable Water Research Program, it is ORD's goal to meet clients' needs with regard to safe drinking water. The Office of Water (OW) requested assistance with their evaluation of the health advisory for strontium in drinking water given that some communities were experiencing levels that far exceeded the national average by a significant amount, as measured during the third Unregulated Contaminant Monitoring Rule (UCMR3) where around 60 mg/L of strontium was measured in water from the Great Lakes region, the southwest, and in Florida. The adverse effect of strontium is to cause a form of rickets in growing children with low calcium intakes. The study described in the publication on transfer of strontium from water to different foods during preparation provides data that informed the evaluation of exposure sources in the determination of the relative source contribution. The results indicated that 40-66% of the strontium in the water transferred to the varies foods tested which, in turn, provided a more accurate estimation of potential intakes of strontium that originate from a local public water supply. This enabled OW to evaluate total exposure from all exposure media compared to that of drinking water at the 90th percentile intake level to determine if regulation or health advisories were appropriate. This also assisted public water systems that identified high strontium levels during UCMR3 when developing appropriate communication materials for customers to reduce their exposure. The findings were used by OW for the Contaminant Candidate List Preliminary Regulatory Determination, draft 4, notice and technical support documents (https://www.epa.gov/ccl/regulatory-determination-4). Administrator Wheeler signed the Preliminary Determinations on 2/24/20 which provided updates on strontium and will be published in the Federal Registry.

Justification 2A:

NA

Justification 2B:

Maura Donohue

"Nationwide study on the prevalence and potential health effects of contaminants of emerging concern in drinking water" 2019, Level II

"Widespread Molecular Detection of Legionella pneumophila Serogroup 1 in Cold Water Taps across the United States" and "Increased Frequency of Nontuberculous Mycobacteria Detection at Potable Water Taps within the United States" 2016, Level III

Joyce Donohue

"Nationwide study on the prevalence and potential health effects of contaminants of emerging concern in drinking water" 2019, Level II

"Widespread Molecular Detection of Legionella pneumophila Serogroup 1 in Cold Water Taps across the United States" and "Increased Frequency of Nontuberculous Mycobacteria Detection at Potable Water Taps within the United States" 2016, Level III

Justification 2C:

Previous nominations were different by subject matter (microorganisms) and emphasis of the project (detection and prevalence of microorganisms). This nomination presents a study on strontium in drinking water and measures the amount of strontium that transfers from drinking water into various food items during preparation. There are no similarities between recently submitted nominations from any of the authors.

Justification 2D:

NA

Justification 2E:

NA

Justification 3A:

On 2/24/20, Administrator Wheeler signed the Preliminary Determinations which provided updates on strontium using the information published in the nominating paper.

Justification 3B:

The Journal of Trace Elements in Medicine and Biology is an internationally recognized publication that provides an independent external peer review process by leaders in the field who served as reviewers and have published in this journal. Internal review was conducted through the established clearance process consisting of multiple supervisory reviews.

AUTHORS

Principal Author

Author Name:	Lisa Jo Melnyk		
Professional Title:		Salutation:	Dr.
Email:	melnyk.lisa@epa.gov	Organization:	
Mailing Address:			
Street Line 1:	26 West Martin Luther King Drive		
City:	Cincinnati		
Zip Code:	45268	State:	OH
At time of research was:	EPA Employee		
Separation Date:			
% of Effort:	50		

Contributing Author

Author Name:	Maura Donohue		
Professional Title:		Salutation:	Dr.
Email:	donohue.maura@epa.gov	Organization:	
Mailing Address:			
Street Line 1:	26 West Martin Luther King Drive		
City:	Cincinnati		
Zip Code:	45268	State:	OH
At time of research was:	EPA Employee		
Separation Date:			
% of Effort:	10		

Contributing Author

Author Name:	Maily Pham		
Professional Title:		Salutation:	Ms.
Email:	pham.maily@epa.gov	Organization:	
Mailing Address:			
Street Line 1:	26 West Martin Luther King Drive		
City:	Cincinnati		
Zip Code:	45268	State:	OH
At time of research was:	EPA Employee		
Separation Date:			
% of Effort:	10		

Contributing Author

Author Name:	Joyce Donohue		
Professional Title:		Salutation:	Dr.
Email:	donohue.joyce@epa.gov	Organization:	
Mailing Address:			
Street Line 1:	1200 Pennsylvania Avenue NW		
City:	Washington DC		
Zip Code:	20460	State:	
At time of research was:	EPA Employee		
Separation Date:			
% of Effort:	30		

PUBLICATIONS

Publication 1:

Publication Title:	Absorption of strontium by foods prepared in drinking water		
Publication Date:	Thu Jan 03 00:00:00 GMT 2019		
Journal/Publication Method:	Journal of Trace Elements in Medicine and Biology		
All Author(s):			
Volume:	53	Number:	NA
Pages:	5	Immediately Index:	Immediately Index:
Citation ½ Life:	4.7	Impact Factor:	2.895

Journal of Trace Elements in Medicine and Biology 53 (2019) 22–26

Contents lists available at ScienceDirect

Journal of Trace Elements in Medicine and Biology

journal homepage: www.elsevier.com/locate/jtemb

Food chain

Absorption of strontium by foods prepared in drinking water

Lisa Jo Melnyk[a,*], Maura J. Donohue[a], Maily Pham[b], Joyce Donohue[c]

[a] National Exposure Research Laboratory, Office of Research and Development, U.S., Environmental Protection Agency, 26 West Martin Luther King Drive, Cincinnati, OH, 45268, USA

[b] National Risk Management Research Laboratory, Office of Research and Development, U.S. Environmental Protection Agency, 26 West Martin Luther King Drive, Cincinnati, OH, 45268, USA

[c] Office of Science and Technology, Office of Water, U.S. Environmental Protection Agency, 1200 Pennsylvania Avenue, Mail Code 4304T, Washington, DC, 20460, USA

ARTICLE INFO

Keywords:
Strontium
Transfer
Water
Foods
Relative source contribution

ABSTRACT

Strontium (Sr) is a natural element, ubiquitous in the environment and known to occur in water, food, air, and soils. Strontium is present in media as a salt or an ionized divalent cation. The Sr ion (dissociated) is toxicokinetically important because it is easily absorbed into systemic circulation when inhaled with particulates or ingested with water or foods. Dietary exposure can be influenced by using tap water containing dissolved Sr in food preparation. Research was conducted to determine the amount of Sr transferred from water to individual foods during preparation. Strontium transferred to broccoli, lentils, and spaghetti at all levels tested (1.5, 10, and 50 mg/L) as evidenced by the residual Sr in the pour-off water following food preparation (33–64%). The data from the cooking study support the hypothesis that cooking of foods with water containing Sr adds to total dietary exposure. This information can inform the determination of the relative source contribution (RSC) that is typically used in developing drinking water advisory guidelines. These cooking study results indicate that food prepared in water containing Sr should be considered as part of the food in a dietary exposure assessment.

1. Introduction

The natural element, Strontium (Sr), is ubiquitous in the environment and can be found in water, food, air, and soils. Strontium is present in all relevant media as a salt or an ionized divalent cation. Some Sr salts are more soluble than others. The Sr ion (dissociated) is toxicokinetically important because it is easily absorbed into systemic circulation when inhaled with air particulates or ingested with water or foods.

Strontium is an element of potential toxicological concern, because of its ability to substitute for calcium in bone, thereby possibly impacting bone density [1]. The potential for strontium to have an adverse effect on bone is strongly impacted by the calcium: strontium ratio [2]. The risk increases when the ratio decreases and is diminished when calcium intakes increase. The likelihood for strontium to have a detrimental impact on bone is greatest during periods of active bone growth in children and adolescents where it can contribute to a condition sometimes referred to as strontium rickets [3,4]. An increased fracture risk among children with low calcium intakes has been determined [5]. The risk can be increased through competition when high intakes of strontium is combined with lower dietary calcium uptake. In addition to strontium's impact on bone, it also can substitute for calcium in teeth during their formation causing permanent visible staining of the tooth surface [6].

Strontium ions carry a 2+ charge and can bind to the biopolymers (polysaccharides, proteins) in foods with areas of negative or partially negative charge. Thus, cooking foods in the presence of water containing Sr may increase the strontium content of the food as served for meats (slow cooked with water), cooked grains (e.g. rice), vegetables (e.g. broccoli), legumes (e.g. lentils), and fruits (e.g., applesauce). Preparation of foods (handling, washing, and rinsing) can also influence residue levels that become part of the diet [7–10]. This is more likely to occur with dissolved minerals in water than volatile compounds, such as alcohols that volatilize during cooking or baking [11].

Development of drinking water guidelines such as a Maximum Contaminant Level Goal (MCLG) used to support a regulation or non-

Abbreviations: ACS, American Chemical Standard; EPA–U.S, Environmental Protection Agency; FDA–U.S, Food and Drug Administration; ICP-AES, inductively coupled plasma atomic emission spectroscopy; ICP-OES, inductively coupled plasma optical emission spectrometry; MCLG, maximum contaminant level goal; QC, quality control; RSC, relative source contribution; Sr, strontium; TDS, total diet study; UCMR3, unregulated contaminant monitoring rule

* Corresponding author.
E-mail addresses: melnyk.lisa@epa.gov (L.J. Melnyk), Donohue.maura@epa.gov (M.J. Donohue), Pham.maily@epa.gov (M. Pham), Donohue.joyce@epa.gov (J. Donohue).

https://doi.org/10.1016/j.jtemb.2019.01.001
Received 19 October 2018; Received in revised form 20 December 2018; Accepted 3 January 2019
0946-672X/ Published by Elsevier GmbH.

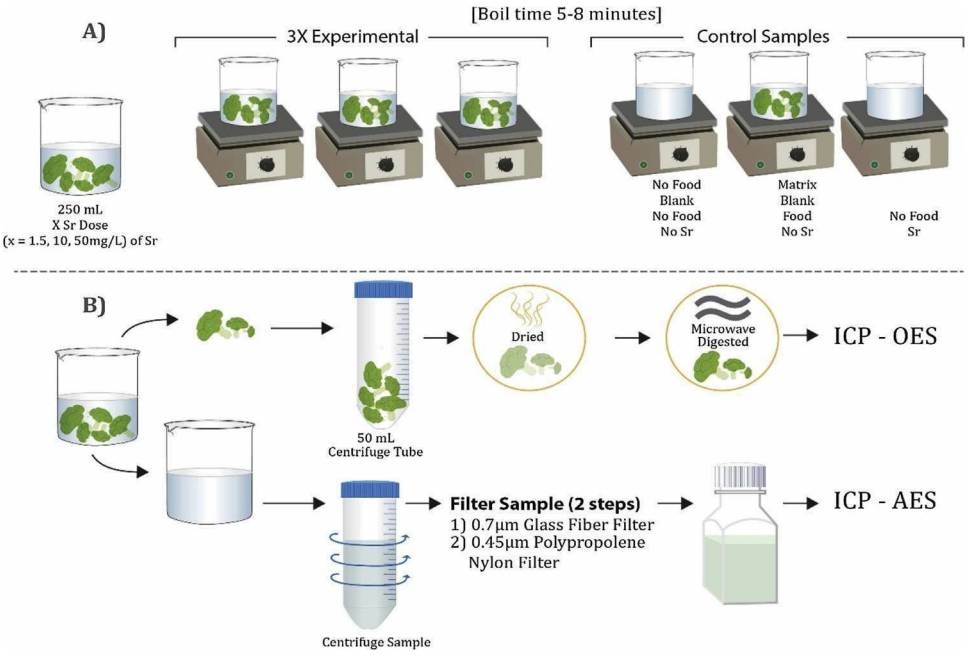

Fig. 1. Sample preparation Scheme.

regulatory Drinking Water Health Advisory considers exposures from ingestion of drinking water as it compares to other sources, such as, diet, ambient air and incidental ingestion from soils and dusts when developing a guideline value [12,13]. The latter are important considerations for crawling infants and toddlers [7,8].

Identifying all routes of exposure to Sr can provide important information when determining the relative source contribution (RSC). The dietary data for strontium collected by the U.S. Food and Drug Administration as part of their Total Diet Study (TDS) program were provided to the U.S. EPA to use in the RSC analysis. However, TDS foods that require water for cooking or during preparation prior to analysis are prepared with deionized water, so chemicals in the preparation water will not be incorporated in the food prior to analysis [14–16].

It is also important to realize that the Sr in the local tap water impacts not only the foods prepared at home with water, but those commercially prepared and packaged with water, e.g., products canned with water or syrup when the local tap water without additional treatment at the processing facility is used for preparation. However, in most of those cases the chemicals added during commercial preparation will be reflected in the TDS results. The exception would be foods prepared at local food establishments that use the water directly from the public water system (e.g. restaurants, school lunch programs, hospitals).

The amount of Sr transferred from drinking water (in tap) to the food items during preparation could be complete, none, or somewhere in between. Research to determine the amount of Sr transferred from water to individual foods during preparation was conducted. The results can provide a more complete estimation of potential intakes of Sr that originate from a local public water supply.

2. Methods and materials

2.1. Reagents and solutions

All reagents were ACS reagent grade. All sample preparation solutions were created with ultrapure water at 18.2 Ω obtained from a Millipore water purification system (Milli Q Plus, Millipore, Bedford, MA). The working solution was prepared by diluting 10,000 mg/L certified stock solution of Sr (GFS Chemicals, Columbus, OH) to the desired concentrations to use as the Sr containing water for the experiments.

2.2. Samples

Three food items were purchased at a local market to boil in ultrapure water containing three levels of Sr. The food items were a fresh vegetable (broccoli), dried pasta (spaghetti), and dried lentils which were chosen to represent a range of types of foods that are commonly boiled during preparation. Three Sr concentrations were tested in water; approximately 1.5 mg/L (reference level used in the Third Unregulated Contaminant Monitoring Rule (UCMR3) as a value established as protective for skeletal effects) [17], 10 mg/L, and 50 mg/L (representing high concentrations found in the UCMR3 [17]). Exact concentrations were determined by direct measurement (see Analysis section below). Blanks were generated by boiling Sr containing water with no foods and boiling food samples in ultrapure water containing no Sr. Samples were generated in triplicate for each Sr concentration level.

2.3. Preparation of samples

A measured amount of each food item was weighed (top-load balance, AND Electronic Balance, FX-4000, Denver, CO) to obtain the four separate, 30–50 g weighed samples (depending on the amount that would fit in the water) that were needed for each set of experiments. Six beakers were weighed dry with 15 glass beads (to aid in boiling), received approximately 250 mL of water (either with or without Sr, as needed), weighed again, then were set on hot plates (Corning, New York, USA) and allowed to boil, separately (see Fig. 1). Two beakers contained no food. The other four beakers contained the weighed amount of food. Two beakers contained Sr free water; one with no food (designated as no food blank), the other with food (designated as a matrix blank). Four beakers contained Sr contaminated water at the designated level; one had no food and was used to obtain the actual concentration of Sr in the water, three beakers contained the weighed food item to allow for replicate analysis.

After reaching a boiling state, the food item was placed into the beaker, allowed to return to boiling, then boiled for at least 5 min. The spaghetti required a longer boiling time of 8 min to allow for complete

preparation. Following completion of the boiling, the beakers were removed from the hot plates and allowed to cool for 2 min. The water containing food was separated into a new, clean, and weighed beaker and allowed to cool completely. The final weight of water was returned to the original, pre-boiled weight using ultrapure water.

Because of boiling the food items, the water contained particles of food, starch, and lentil husks. To obtain a clear sample amenable to analysis, the water was poured into centrifuge tubes (VWR.com, Brooklyn, NY) and centrifuged (Sorvall Super T 21, Newtown, CT) at 10,000 rpm at 20 °C for 10 min, filtered first through a 0.7 µm glass fiber filter (Whatman, Maidstone, England), and then filtered through a 0.45 µm polypropylene nylon disc (Millipore, Darmstadt, Germany). Water samples were stored at room temperature in labeled 60 mL plastic sampling containers (Thermo Scientific, Waltham, MA) and acidified with concentrated nitric acid (0.15% v/v). Food samples were placed into plastic tubes (FisherBrand, Waltham, MA) and frozen at −80 °C until preparation for analysis.

2.4. Analysis of samples

a) Pour-off Water –

The pour-off waters were preserved with analytical grade ultrapure nitric acid (0.15% v/v) and were analyzed for Sr on an Inductively coupled plasma atomic emission spectroscopy (ICP-AES) (Thermo Elemental model 7600 Duo, Waltham, MA) using U.S. EPA Method 200.7 [18]. A peristaltic pump delivers the sample into a nebulizer and the sample is injected directly into the plasma. The sample collides with electrons and charged ions in the plasma, breaking itself down into charged ions. Samples are modified with a 1:1 matrix modifier (10% HNO_3/HCl) solution. Strontium is measured at wavelength 421.552 nm with no interferences. Results were expressed as the concentration of Sr recovered (mg/L).

- Boiled Food Samples –

The boiled food samples were dried at 60 °C in a drying oven. One half of a gram of dried food item was microwave digested using a digester (CEM MARS Xpress, Mathews, NC), following U.S. EPA Method 3051 A [19]. The samples were digested in nitric acid and hydrochloric acid (9 mL: 3 mL) under pressure of 12 atm. The contents were heated to 175 °C within 5 min and 30 s, held for 4 min 30 s for a tray of samples (24 samples in a tray). The moisture content of the food samples was measured using Method CLC-MOI.03 from the U.S. Department of Agriculture Food Safety and Inspection Service, Office of Public Health Science [20]. Food sample digests were analyzed by inductively coupled plasma optical emission spectrometry (ICP/OES) Optima 2100 (Perkin Elmer, Waltham, MA) for Sr and reported as mg Sr/kg food using U.S. EPA Methods 200.7 and 6010C [18,19], as stated above. Food results were converted to wet weight.

- Mass Balance Calculation

The concentrations determined from the analysis of the pour-off water and the boiled foods were converted into milligram weights to evaluate the mass balance. The concentration (mg/L or mg/kg) was multiplied by the amount of water or food used (g) and divided by the conversion factor (1 L/1000 g or 1 kg/1000 g) to reach the amount of Sr in each sample for water or food item. The sum of the mass from the pour-off water and food item should be equivalent to the initial amount of Sr in the water. Differences between the total available Sr and the amount in the pour-off water and food items could be attributed to volatilization of the Sr that may occur during the boiling process.

2.5. Quality assurance

Quality control (QC) was strictly adhered to and all sample results were within the appropriate specified criteria. For the pour-off water samples, laboratory controls and blanks were analyzed simultaneously with each analysis for each batch of samples. Laboratory reagent blanks were analyzed every 10 samples, with QC limits of less than the method detection limit and continuous calibration checks were within 90–110% recovery. Fortified Sr water samples were all within an acceptable percent recovery of 85–115% of the true value. This included both laboratory fortified blanks and laboratory fortified matrices. Analytical water duplicates were also conducted with results within 10% of the original samples.

For food samples, laboratory controls and blanks were analyzed simultaneously with each analysis batch of 10 samples. All QC samples fell within the specified criteria of +25% for fortified matrix, +15% for fortified blanks, +10% for standard checks, < 20% difference for duplicates, and < 0.025 ppm for reagent blanks. Several samples failed the QC criteria when analyzing the broccoli samples, therefore, the broccoli data are not used or reported.

3. Results and discussion

The results from the analysis of the pour-off water varied by food item and initial Sr concentration (mg/L) in the water (Table 1). No food type tested absorbed the entire amount of Sr from the water. The concentration of Sr remaining in the pour-off water rose as the concentration increased. Broccoli and spaghetti had similar Sr absorption. Unexpectedly, the replicate pour-off water from the cooking of lentils consistently contained around 32%, regardless of the initial concentration.

The amount of Sr in the pour-off water from each food type was statistically different from that of the other food types ($p < 0.0001$) using the Student *t*-test [21], except for the broccoli and spaghetti samples cooked in water with 50 mg Sr/L. At the 50 mg/L concentration, the p values for Sr left in the pour off water were the same ($p = 0.492$) for the broccoli and spaghetti. The concentration of Sr in each food type differed for each concentration level ($p < 0.0028$). Based on the results of the pour off water, it appears that broccoli and spaghetti reached a saturation point and could no longer absorb the Sr from the water as the concentration increased. Lentils, on the other hand, continued to absorb more Sr from the water as the concentration

Table 1
Residual Strontium in Pour-off Water following Food Preparation, mg/L + standard deviation (percent recovery).

Theoretical water mg/L	1.5	2	10	50
Actual water mg/L	1.2 – 2.1	2.4	9.3 – 12	44 - 49
Blank	0.020	[a]	0.022	0.033
Broccoli	0.87 + 0.39 (41)	[a]	5.8 + 0.36 (47)	28 + 1.2 (64)
Blank	0.021	0.020	0.026	0.020
Lentils	0.44 + 0.04 (36)	0.77 + 0.02 (32)	3.7 + 0.02 (38)	14 + 0.44 (32)
Blank	0.021	[a]	0.13	0.007
Spaghetti	0.62 + 0.08 (33)	[a]	4.0 + 0.11 (44)	27 + 1.1 (56)

[a] Indicates no sample.

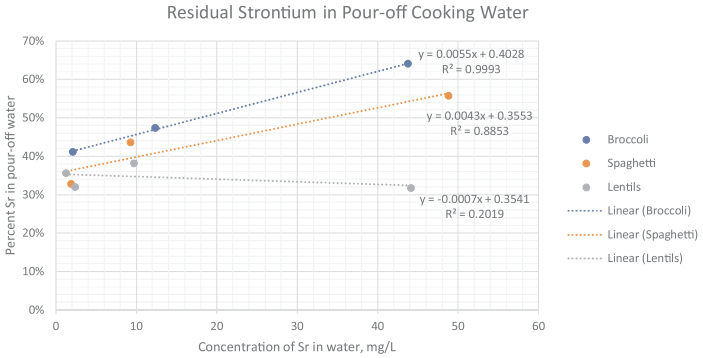

Fig. 2. Residual Strontium in Pour-off Cooking Water.

increased, as evidenced by the sequentially lower recoveries in the pour-off water. For broccoli and spaghetti, Sr absorption was dependent on the initial concentration available, broccoli – $r^2 = 0.9993$; spaghetti – $r^2 = 0.8853$ (Fig. 2), whereas, for lentils, Sr absorption was not dependent on the initial concentration, $r^2 = 0.2019$. Strontium was always absorbed at 57 ± 1%, resulting in a flat line across all concentrations (Fig. 2).

From the results of the analysis of the pour-off cooking water, Sr appeared to be absorbed by the foods. To ensure that the Sr transferred to the food items during cooking, the post preparation foods were analyzed. Table 2 summarizes the analytical results for Sr in lentils and spaghetti. As explained earlier issues arose with the broccoli samples and the results did not meet the QC requirements. Broccoli data are not reported.

Strontium did not volatilize as demonstrated by a mass balance calculation. Taking into consideration the actual weight of the amount of water used, amount of food used, and the analytical concentration, the mass of Sr (mg) in the pour-off water and food items accounted for most of the available Sr. The difference between the total amount of Sr measured and the amount of Sr in the pour-off water and food item combined falls well within the analytical error so would not be considered volatilized. These results are summarized in Table 3.

The strontium in the food items retained increasing amounts as the concentration in the cooking water increased. The blanks did contain some Sr, but the foods contained additional amounts indicating that the Sr from the water was absorbed by the food items. It is clear that Sr in the cooking water could become incorporated in the food as served adding to the total intake from the diet because of the use of the local tap water during cooking. This is a far greater concern when the water contains > 50 mg/L than it is for the 1.5 mg/L concentration of Sr, the current health reference level [17].

4. Conclusions

The data from the cooking study support the hypothesis that cooking of foods with water containing Sr that is poured off before serving adds to the total dietary Sr. Food groups where this needs to be considered include vegetables, grains, legumes and probably some mixed foods (e.g., soups) that are cooked or prepared using tap water. As shown in this study, intake through foods may be higher than what would be predicted from analysis of FDA's TDS data.

The RSC calculation uses the mean national concentration from public water systems (if known), not the high-end concentrations. In the case of Sr, the mean concentration observed during the monitoring under UCMR3 was less than 1 mg/L, while the concentrations at some systems exceeded 50 mg/L [17]. Accordingly, uptake of Sr from foods is a greater concern for some locations than others, such as, the parts of the country with elevated strontium concentrations including the states that surround the Great Lakes, Texas, New Mexico, Arizona and Florida [22]. Cooking studies, such as this one, assist toxicologists to quantify the contribution of the local tap water to total exposure, especially in cases where parts of the country receive concentrations in their tap water that are considerably higher than the average. Under the 1996 amendments to the Safe Drinking Water Act, consideration of sensitive populations during decision making is required [23]. Populations can be classified as sensitive based on their exposure potential, age (e.g. infants and children), life stage (e.g. women of childbearing age) and health status (e.g. those with autoimmune diseases). Some drinking water regulations require public notification for sensitive populations because of exposure concerns, most notably copper (Wilson's disease), fluoride (dental fluorosis) [24], sodium (salt-sensitive hypertension) [25,26]. Thus, when some populations that are highly exposed through drinking water from their public system, public notification can be considered as a regulatory option.

Table 2
Concentration of Strontium in Boiled Food, mg/kg (wet weight) + standard deviation.

Theoretical water mg/L	1.5	2	10	50
Actual water mg/L	1.2 – 2.1	2.4	9.3 – 12	44 - 49
Blank	1.1	1.1	0.83	1.0
Lentils	3.6 + 0.36	6.4 + 0.29	18 + 1.4	100 + 8.8
Blank	0.81	[a]	0.79	0.83
Spaghetti	5.2 + 0.25	[a]	16 + 0.74	55 + 2.0

[a] Indicates no sample.

Table 3
Mass Balance Calculations.

Theoretical Concentration, mg/L	Total Sr Available, mg	Sr in Pour-off Water, mg	Sr in Lentils, mg	Difference
1.5	0.31	0.11	0.26	−0.06
2	0.60	0.19	0.44	−0.03
10	2.4	0.92	1.6	−0.07
50	11	3.5	7.4	0.14

	Total Sr Available, mg	Sr in Pour-off Water, mg	Sr in Spaghetti, mg	
1.5	0.47	0.16	0.32	0.00
10	2.3	1.0	1.5	−0.17
50	12	6.8	8.5	−3.04

Disclaimer

The research described in this article was funded by the U.S. Environmental Protection Agency through its Office of Research and Development. It has been subjected to Agency's administrative review and approved for publication. The views expressed in this paper are those of the author[s] and do not necessarily reflect the views or

policies of the U.S. Environmental Protection Agency. Mention of trade names or commercial products does not constitute an endorsement or recommendation for use.

Conflict interest

The authors have no conflicts of interest.

References

[1] P.J. Marie, M.T. Garba, M. Holt, L. Miravel, Effects of low doses of stable strontium on bone metabolism in rates, Miner. Electrolyte Metab. 11 (1) (1985) 5–13.
[2] M.D. Grynpas, E. Hamilton, R. Cheung, Y. Tsouderos, P. Deloffre, M. Hott, P.J. Marie, Strontium increases vertebral bone volume in rats at a low dose that does not induce detectable mineralization defect, Bone 18 (3) (1996) 253–259.
[3] S. Özgür, H. Sümner, G. Kocoglu, Rickets and soil strontium, Arch. Dis. Child. 75 (1996) 524–526.
[4] E. Storey, Strontium "rickets": bone, calcium and strontium changes, Australas. Ann. Med. 10 (1961) 213–222.
[5] J.E. Rockell, S.M. Williams, R.W. Taylor, A.M. Grant, I.E. Jones, A. Goulding, Two-year changes in bone and body composition in young children with a history of prolonged milk avoidance, Osteoporos. Int. 16 (2005) 1016–1023.
[6] M.E.J. Curzon, P.C. Spector, Enamel mottling in a high strontium area of the USA, Community Dent. Oral Epidemiol. 5 (1977) 243–247.
[7] L.J. Melnyk, M. Byron, G. Brown, A. Clayton, L. Michael, Pesticides on household surfaces may influence dietary intake of children, Environ. Sci. Technol. 45 (2011) 4594–4601.
[8] L.J. Melnyk, T.E. Hieber, T. Turbeville, A.P. Vonderheide, J.N. Morgan, Influences on transfer of selected synthetic pyrethroids from treated Formica® to foods, J. Expo. Sci. Environ. Epidemiol. 21 (2) (2011) 186–196.
[9] M. Asami, N. Yoshida, K. Kosaka, K. Ohno, Y. Matsui, Contribution of tap water to chlorate and perchlorate intake: a market basket study, Sci. Total Environ. 463–464 (2013) 199–208.
[10] M.A. Rahman, H. Hasegawa, M.A. Rahman, M.M. Rahman, M.A. Majid Miah, Influence of cooking method on arsenic retention in cooked rice related to dietary exposure, Sci. Total Environ. 370 (2006) 51–60.
[11] J. Augustin, E. Augustin, R.L. Cutrufelli, S.R. Hagen, C. Teitzel, Alcohol retention in food preparation, Res. Prof. Briefs 92 (4) (1992) 486–488.
[12] U.S. EPA, National primary and secondary drinking water regulations. Proposed Rule, Fed. Regist. 54 (97) (1989) 22062 January 30, 1991.
[13] U.S. EPA, Methodology for Deriving Ambient Water Quality Criteria for the Protection of Human Health (2000). EPA-822-B-00-004, (2000).
[14] U.S. Food and Drug Administration, TDS Results, (2017) (Accessed 26 January 2018), www.fda.gov.
[15] S.K. Egan, P.M. Bolger, C.D. Carrington, Update of US FDA's total diet study food list and diets, J. Expo. Sci. Environ. Epidemiol. 17 (2007) 573–582.
[16] J. Pennington, J. Jones, Molybdenum, nickel, cobalt, vanadium and strontium in total diets, J. Am. Dietet. Assoc. 87 (1987) 1644–1650.
[17] U.S.EPA, UCMR3 Monitoring Results, (2017) (Accessed 3 October 2017), https://www.epa.gov/sites/production/files/2017-02/documents/ucmr3-data-summary-january-2017.pdf.
[18] U.S. EPA, Method 200.7: Determination of Metals and Trace Elements in Water and Wastes by Inductively Coupled Plasma-Atomic Emission Spectrometry, Revision 4.4, (1994) (Accessed 31 January 18), www.epa.gov/homeland-security-research/method-2007-determination-metals-and-trace-elements-water-and-wastes.
[19] U.S. EPA, SW-846 Methods, (2018) (Accessed 31 January 18), https://www.epa.gov/hw-sw846/sw-846-compendium.
[20] U.S.DA, Chemical Laboratory Guidebook, (2018) (Accessed 2 July 18), https://www.fsis.usda.gov/wps/portal/fsis/topics/science/laboratories-and-procedures/guidebooks-and-methods/chemistry-laboratory-guidebook.
[21] U.S. EPA, ProUCL, (2017) (Accessed 13 October 2017), https://www.epa.gov.
[22] U.S. EPA, Occurrence Data for the Unregulated Contaminant Monitoring Rule, (2017) (Accessed 18 December 18), https://www.epa.gov/dwucmr/occurrence-data-unregulated-contaminant-monitoring-rule#3.
[23] U.S. EPA, Save Drinking Water Act Amendments of 1996: General Guide to Provisions, Office of Water (EPA 810-S-96-001), 1996 p.7.
[24] U.S. EPA, Questions and Answers on Fluoride, (2011) https://www.epa.gov/sites/production/files/2015-0/documents/2011_fluoride_questionsanswers.pdf.
[25] U.S. EPA, Code of Federal Regulations: Protection of the Environment. Parts 126-149. Section 141.41. Office of the Federal Register, National Archives and Records Administration, Washington DC, 1996, pp. 352–353.
[26] U.S. EPA, Drinking Water Advisory: Consumer Acceptability Advice and Health Effects on Sodium, (2003) https://www.epa.gov/sites/production/files/2014-09/documents/support_cc1_sodium_dwreport.pdf.

Melnyk, Lisa

From: Donohue, Joyce
Sent: Tuesday, April 2, 2019 11:30 AM
To: Melnyk, Lisa
Subject: RE: Record of Percentage Agreement - Joyce Donohue

Dear Lisa:

I think your attribution on time is fine and generous when compared to your efforts.

Joyce

From: Melnyk, Lisa
Sent: Tuesday, April 02, 2019 11:28 AM
To: Donohue, Joyce <Donohue.Joyce@epa.gov>
Subject: Record of Percentage Agreement - Joyce Donohue

Joyce Donohue
Health Scientist
US Environmental Protection Agency
Office of Water – Office of Science and Technology
Health and Ecological Criteria Division
William Jefferson Clinton Building
1200 Pennsylvania Avenue, N. W.
Washington, DC 20460
202-566-1098
Donohue.joyce@epa.gov

I'm submitting our paper entitled "Absorption of strontium by foods prepared in drinking water" for a Scientific and Technological Achievement Award. As a co-author, I need your concurrence on the percentage of time that I have for your contribution to the paper.

The contribution for the submission will be:
Lisa Jo Melnyk – 50%
Maura J. Donohue – 10%
Maily Pham – 10%
Joyce Donohue – 30%

If you concur with your percentage, please E-mail me by reply, as I need to include it as part of the package. If you disagree with the percentage as presented, please forward your suggested change. Thanks.

Lisa Jo Melnyk, Ph.D.
US Environmental Protection Agency
National Exposure Research Laboratory
26 W. Martin Luther King Drive
Cincinnati, OH 45268
(513)569-7494

Melnyk, Lisa

From: Donohue, Maura
Sent: Tuesday, April 2, 2019 11:14 AM
To: Melnyk, Lisa
Subject: RE: Record of Percentage Agreement - Maura Donohue

I, Maura Donohue, concur with the percentage of contribution of 10%.

Sincerely,
Maura J. Donohue

Maura J. Donohue, Ph.D
Research Chemist
US Environmental Protection Agency
National Exposure Research Laboratory
Environmental Methods and Measurements Division
26 W. Martin Luther King Drive
Cincinnati, OH 45268
513-569-7634
Donohue.maura@epa.gov

From: Melnyk, Lisa
Sent: Tuesday, April 2, 2019 11:05 AM
To: Donohue, Maura <Donohue.Maura@epa.gov>
Subject: Record of Percentage Agreement - Maura Donohue

Maura J. Donohue
Research Chemist
US Environmental Protection Agency
National Exposure Research Laboratory
Environmental Methods and Measurements Division
26 W. Martin Luther King Drive
Cincinnati, OH 45268
513-569-7634
Donohue.maura@epa.gov

I'm submitting our paper entitled "Absorption of strontium by foods prepared in drinking water" for a Scientific and Technological Achievement Award. As a co-author, I need your concurrence on the percentage of time that I have for your contribution to the paper.

The contribution for the submission will be:
Lisa Jo Melnyk – 50%
Maura J. Donohue – 10%
Maily Pham – 10%
Joyce Donohue – 30%

If you concur with your percentage, please E-mail me by reply, as I need to include it as part of the package. If you disagree with the percentage as presented, please forward your suggested change. Thanks.

Lisa Jo Melnyk, Ph.D.
US Environmental Protection Agency
National Exposure Research Laboratory
26 W. Martin Luther King Drive
Cincinnati, OH 45268
(513)569-7494

Melnyk, Lisa

From: Pham, Maily
Sent: Tuesday, April 2, 2019 11:16 AM
To: Melnyk, Lisa
Subject: RE: Record of Percentage Agreement - Maily Pham

Looks good to me. Thanks Lisa.

Maily

From: Melnyk, Lisa
Sent: Tuesday, April 02, 2019 11:15 AM
To: Pham, Maily <Pham.Maily@epa.gov>
Subject: Record of Percentage Agreement - Maily Pham

Maily Pham
Chemist
US Environmental Protection Agency
National Risk Management Research Laboratory
Water Systems Division
26 W. Martin Luther King Drive
Cincinnati, OH 45268
513-569-7212
Pham.maily@epa.gov

I'm submitting our paper entitled "Absorption of strontium by foods prepared in drinking water" for a Scientific and Technological Achievement Award. As a co-author, I need your concurrence on the percentage of time that I have for your contribution to the paper.

The contribution for the submission will be:
Lisa Jo Melnyk – 50%
Maura J. Donohue – 10%
Maily Pham – 10%
Joyce Donohue – 30%

If you concur with your percentage, please E-mail me by reply, as I need to include it as part of the package. If you disagree with the percentage as presented, please forward your suggested change. Thanks.

Lisa Jo Melnyk, Ph.D.
US Environmental Protection Agency
National Exposure Research Laboratory
26 W. Martin Luther King Drive
Cincinnati, OH 45268
(513)569-7494

Table of Contents

General_Authors_Publications.....2
LI-266007_Ma_et_al_2015.....9
Alejandra_Gonz?lez-Mej?a.....44
Record_of_Percentage_Agreement_COT_xx_jc_xm_signed.....45
Record_of_Percentage_Agreement_COT_xx_jg_signed.....46

United States Environmental Protection Agency
Washington, DC 20460

STAA REPORT FOR THE SCIENTIST NOMINATIONS

General Information:

Nomination ID/App ID:	20-086
Research Category Primary:	Review Articles (RA)
Research Category Secondary:	Review Articles (RA);Integrated Risk Assessment (IR);Sustainability and Innovation (SI)
Laboratory/Office Name:	ORD
Nomination Entered By:	Xin Ma

Eligibility Checklist:

[Y] The nominated publication(s) has not been submitted to a previous STAA competition.

[Y] The nominated publication(s) was published on or before January 1, 2017 and on or after January 1,2012

[Y] The principal author was an EPA employee or a PHS employee assigned to EPA when the research was performed

[Y] The EPA authors (includes PHS employees assigned to EPA) contributed collectively a minimum of 50% toward the publication(s)

Nominating Official Name:	Regan Murray
Nominating Official Title:	SUPERVISORY INTERDISCIPLINARY SCIENTIST
Nominating OfficialEmail:	murray.regan@epa.gov
STAA Coordinator Name:	Kathleen Wiser
STAA Coordinator Email:	wiser.kathi@epa.gov

Justifications:

Justification 1:

We as a society gradually realize the previous siloed water management approaches cannot sustain quality water services at all fronts. The cities around the world are facing enormous challenges in urban water systems. A paradigm shift based on holistic management is absolutely needed to address these challenges. Sustainable solutions to protect the environment, strengthen the communities and foster long-term prosperity require scientifically based sustainability metrics to assess environmental, economic, and social components of sustainability. It is important to understand the historical background of current urban water systems, analyze their various issues as components of a larger system, and lay out the argument for a conceptual framework and potential tools for such comprehensive analysis. Our manuscript not only lists the issues with existing centralized water systems and the alternative approaches, but also present a design of urban water system for the future of cities to emphasize how different water system services can be organized in an organic whole. When the system dynamics and its underlying forces are better understood, it would be possible to provide more insights on the tradeoffs and a sustainable system design. Our intent is to catalyze and accelerate such paradigm shift and encourage decision makers to start thinking more systematically based on principles of sustainability when deal with issues unique to their cities or communities.

Justification 2A:

N/A

Justification 2B:

N/A

Justification 2C:

N/A

Justification 2D:

N/A

Justification 2E:

This research is nominated in the category of Review Articles (RA). It includes not only critical analyses of every major subsystem in the existing centralized water systems, providing potential transformative alternatives, but also a conceptual holistic framework of One Water concept and potential tools for such comprehensive analysis. Together, the research provides new insight into sustainable integrated water system management.

A concurrent nomination is submitted in Integrated Risk Assessment (IR). The research focuses on the metrics and tools used to quantify risk to the sustainability in urban water systems and vulnerability of ecosystems from multiple stressors at multiple scales.

Justification 3A:

N/A

Justification 3B:

Sustainability is one of the most advanced forums for studies related to sustainability and sustainable development in the world. The external peer review process of *Sustainability* operates a rigorous peer-review process and uses the criteria of quality, creativity, originality, accuracy and contribution to the field to evaluate the scientific merit of the publication. In most cases this is a single-blind assessment with at least two independent reviewers, followed by a final acceptance/rejection decision by the Editor-in-Chief, or another academic editor approved by the Editor-in-Chief. The Editor-in-Chief is responsible for the academic quality of the publication process, including acceptance decisions, approval of Guest Editors and special issue topics, and new Editorial Board members.

AUTHORS

Contributing Author

Author Name:	Xiaobo Xue	
Professional Title:		Salutation:
Email:	xxue@albany.edu	Organization:
Mailing Address:		
Street Line 1:		
City:		
Zip Code:		State:
At time of research was:	Non EPA Personnel	
Separation Date:		
% of Effort:	2	

Contributing Author

Author Name:	Jennifer Cashdollar	
Professional Title:		Salutation:
Email:	cashdollar.jennifer@epa.gov	Organization:
Mailing Address:		
Street Line 1:		
City:		
Zip Code:		State:
At time of research was:	EPA Employee	
Separation Date:		

% of Effort:	10		

Contributing Author

Author Name:	Jay Garland		
Professional Title:		Salutation:	
Email:	garland.jay@epa.gov	Organization:	
Mailing Address:			
Street Line 1:			
City:			
Zip Code:		State:	
At time of research was:	EPA Employee		
Separation Date:			
% of Effort:	2		

Contributing Author

Author Name:	Alejandra González-Mejía		
Professional Title:		Salutation:	
Email:	a.g.mejia@bangor.ac.uk	Organization:	
Mailing Address:			
Street Line 1:			
City:			
Zip Code:		State:	
At time of research was:	Non EPA Personnel		
Separation Date:			

% of Effort:	2

Principal Author

Author Name:	Xin (Cissy) Ma		
Professional Title:		Salutation:	
Email:	ma.cissy@epa.gov	Organization:	
Mailing Address:			
Street Line 1:			
City:			
Zip Code:		State:	
At time of research was:	EPA Employee		
Separation Date:			
% of Effort:	84		

PUBLICATIONS

Publication 1:

Publication Title:	Sustainable Water Systems for the City of Tomorrow—A Conceptual Framework		
Publication Date:	Tue Sep 01 00:00:00 GMT 2015		
Journal/Publication Method:	Sustainability		
All Author(s):			
Volume:	7	Number:	9
Pages:	12071-1210	Immediately Index:	Immediately Index:

Citation ½ Life:	3.10	Impact Factor:	2.592

Sustainability **2015**, *7*, 12071-12105; doi:10.3390/su70912071

OPEN ACCESS

sustainability

ISSN 2071-1050

www.mdpi.com/journal/sustainability

Review

Sustainable Water Systems for the City of Tomorrow—A Conceptual Framework

Xin (Cissy) Ma [1,*], Xiaobo Xue [2,†], Alejandra González-Mejía [2], Jay Garland [3] and Jennifer Cashdollar [3]

[1] National Risk Management Research Laboratory, US Environmental Protection Agency, 26 W Martin Luther King Drive, Cincinnati, OH 45268, USA

[2] Oak Ridge Institute for Science and Engineering (ORISE) Post Doctoral Research Participant, National Risk Management Research Laboratory, US Environmental Protection Agency, 26 W Martin Luther King Drive, Cincinnati, OH 45268, USA; E-Mails: xue.xiaobo@epa.gov (X.X.); gonzalez.alejandra@epa.gov (A.G.-M.)

[3] National Exposure Research Laboratory, US Environmental Protection Agency, 26 W Martin Luther King Drive, Cincinnati, OH 45268, USA; E-Mails: garland.jay@epa.gov (J.G.); cashdollar.jennifer@epa.gov (J.C.)

† Current address: Department of Environmental Health Sciences, School of Public Health, University at Albany, State University of New York, 1 University Place, Rensselaer, NY 12144, USA; E-Mail: xxue@albany.edu.

* Author to whom correspondence should be addressed; E-Mail: ma.cissy@epa.gov; Tel.: +1-513-569-7828; Fax: +1-513-569-7111.

Academic Editor: Marc A. Rosen

Received: 19 December 2014 / Accepted: 24 August 2015 / Published: 1 September 2015

Abstract: Urban water systems are an example of complex, dynamic human–environment coupled systems which exhibit emergent behaviors that transcend individual scientific disciplines. While previous siloed approaches to water services (*i.e.*, water resources, drinking water, wastewater, and stormwater) have led to great improvements in public health protection, sustainable solutions for a growing global population facing increased resource constraints demand a paradigm shift based on holistic management to maximize the use and recovery of water, energy, nutrients, and materials. The objective of this review paper is to highlight the issues in traditional water systems including water demand and use, centralized configuration, sewer collection systems, characteristics of mixed wastewater, and to explore alternative solutions such as decentralized water systems, fit for purpose and water reuse,

natural/green infrastructure, vacuum sewer collection systems, and nutrient/energy recovery. This review also emphasizes a system thinking approach for evaluating alternatives that should include sustainability indicators and metrics such as emergy to assess global system efficiency. An example paradigm shift design for urban water system is presented, not as the recommended solution for all environments, but to emphasize the framework of system-level analysis and the need to visualize water services as an organic whole. When water systems are designed to maximize the resources and optimum efficiency, they are more prevailing and sustainable than siloed management because a system is more than the sum of its parts.

Keywords: urban water systems; paradigm shift; system-based analysis; resource recovery; energy recovery; nutrient recovery; fit-for-purpose; dual water quality; system efficiency; emergy synthesis

1. Introduction

In the words of Ecologist Eugene Odum: "Water is more critical than energy. We have alternative sources of energy. But with water, there is no other choice." [1]. Water usage is growing at twice the rate of population increase in the last century [2]. The rapidly accelerating pressures on this resource arising from constant changing quality and availability of freshwater exposes mankind to significant risk expected to worsen with climate change-induced intensification of the global hydrological cycle [3–6].

Traditional water management approaches categorize water into four types: water resource (surface water/groundwater), drinking water, wastewater and stormwater. Different engineering designs and management instruments are used to target specific "water" issues with an open-ended approach; for example, all domestic water uses are treated to drinking water standards and water is used only once and then disposed of. The wastewater is treated as waste to be eliminated with the investment of large amount of energy and materials, regardless of the potential value of wastewater constituents. For instance, even though phosphorus fertilizer production from easily accessible phosphate rock could be depleted in 50–100 years and cause global food security issues [7,8], expensive treatment technologies are used to remove phosphorus as waste from wastewater to reduce eutrophication in receiving water [9–13]. Emerging chemical and biological contaminants from wastewater and eroded sediments penetrate into the source water, making the treatment of drinking water more technically and financially challenging [14–16]. These vicious cycles worsen with the growth of cities, the concentration of agricultural practices, and intensifying material flows. Water-related infrastructure in some cities is at a breaking point, costing trillions of dollars (euros, *etc.*) just to fix it. Even so under the current paradigm, the ecological goals of the Clean Water Act in US will still not be met [17].

Many current developments are still piecemeal efforts rather than an integrated effort of the entire system which can provide interconnected functioning ecosystem and engineering services to urban populations [18,19]. The complex water issues are intertwined and cannot be sustainably solved by the traditional siloed water management approaches. Changes on the edge do not reach the center of the issues. Only when all of these players are evaluated inclusively will the sustainability of any whole water system with balanced economic activities and ecological services be possible.

Although the ultimate goals are to integrate the monitoring, modeling, assessment and management of water resources, drinking water, wastewater, and stormwater using a systems approach and watershed perspective, as an initial effort, it is important to understand the historical background of current urban water systems, analyze their various issues as components of a larger system, and lay out the argument for a conceptual framework and potential tools for such comprehensive analysis. Urban water systems have been studied extensively regarding separate issues such as pollution degradation [20–22], nutrient removal [23–25], disinfection by-product and emerging contaminants' detection and removal [26–28], microbial risk [29–31], water scarcity [32,33], stormwater management [34,35], and financial issues [36–38] among others. However, it is worth re-examining them in the context of holistic analysis and explore new integrated solutions that break the traditional barriers. For proposed future systems for the City of Tomorrow, many technological components such as resource recovery [39], green infrastructure [40], wetlands [41], and dual-water [42] quality concepts have not been studied with a system thinking approach or they are in their nascent phases of application. Without better understanding of these alternative technologies, it is difficult to confidently design and assess entire future sustainable systems. There are also knowledge gaps about advantages, disadvantages, and opportunities to manage centralized (traditional) and decentralized (alternative) water systems in a sustainability context (*i.e.*, integrates social, economic, and environmental components).

Here, we review the historical context of current urban water systems and major issues such as, water quantity, quality, energy use, wastewater contamination, system configuration, costs, and some cultural aspects. Further, we present a conceptual framework of transformative alternatives, as well as a potential tool used for a system analysis. When the system dynamics and its underlying forces are better understood, it would be possible to provide more insights on the tradeoffs and a sustainable system design.

2. Traditional Water Systems

2.1. Water Demand and Water Use

The issues and concerns surrounding the urban water systems like water quality, energy use, water scarcity, and wastewater contamination may trace back to initial water demand and water use by customers.

Of the 3.4×10^{10} gallons of drinking water produced annually by public water systems in the US, approximately 63% is used for residential purposes (indoor and outdoor) [43]. Of that, 42% of annual residential use was for indoor purposes and 58% for outdoor purposes (without taking into account firefighting allocation) based on the evaluation of 1188 homes from 14 cities across six regions of the US. Of the indoor use, 17% is for human consumption or related use (faucet use and dishwasher); 19% is for human contact (shower and bath); 64% is for non-human ingestion or contact uses (toilet, clothes washers, leaks and other) [43,44]. Although there are regional differences, one fact that remains is that potable water is only a minor portion of the total demand.

Activities other than human consumption and contact such as outdoor non-potable landscape irrigation and firefighting (58%) still require the entire water infrastructure to provide water of a quality acceptable for human consumption [44] (Figure 1, Table 1). The standby fire flow provision requires adequate capacity and pressure [44,45]. The standards governed by the National Fire Protection Association require fire-flows to sustain from three to eight hours [46]. In order to satisfy this need for

adequate standby capacity and pressure, most distribution systems use standpipes, elevated tanks, and large storage reservoirs. Generally, up to 75% of the capacity of a typical drinking water distribution system is devoted to firefighting [47] (Figure 1, Table 1). Treating this large amount of water and moving it over long distances is energy- and material-intensive, mostly fossil fuel-driven. Additionally, there is a growing concern that such designs in most urban areas result in water quality degradation during transmission due to long water residence time which provide optimum conditions for the formation of disinfection by-products (DBPs) and the regrowth of microorganisms, a trade-off between public health and public safety [48,49]. The current flushing programs are costly and largely ineffective, resulting in wasted treated drinking water.

Table 1. Total residential drinking water demand of study.

Assumptions:		
Population (P)	100,000	Inhabitants
	gal/year	fraction
U.S. Drinking water provision [44]	3.40×10^{10}	
Residential	2.14×10^{10}	1
Residential indoor use		0.42
Human consumption or related use (faucet, dishwasher)		0.07
Human contact (shower and bath)		0.08
Nonhuman ingestion or contact (toilet, clothes, leaks)		0.27
Residential outdoor use		0.58
Water demands [50]	gpcd min	gpcd max
Residential	75	130
Firefighting demand based on population [50]		
The American Insurance Association recommends:	(P in thousands)	
$Q(gpm) = 1020\sqrt{P}(1 - 0.01\sqrt{P})$		
Calculated Q =	9.68×10^3	qpm
	13.93	mgd
Calculations:		
Total drinking water demand of study (average residential per capita)	102.5	gpcd
	10.25	mgd
According U.S. drinking water provision fractions:		
Consumption for 100,000 inhabitants	mgd	
Residential indoor use	**4.31**	18%
Human consumption or related use (faucet, dishwasher)	0.74	3%
Human contact (shower and bath)	0.80	3%
Nonhuman ingestion or contact (toilet, clothes, leaks)	2.77	11%
Residential outdoor use	**5.95**	25%
Firefighting demand	**13.93**	58%
Total residential demand	**24.18**	100%

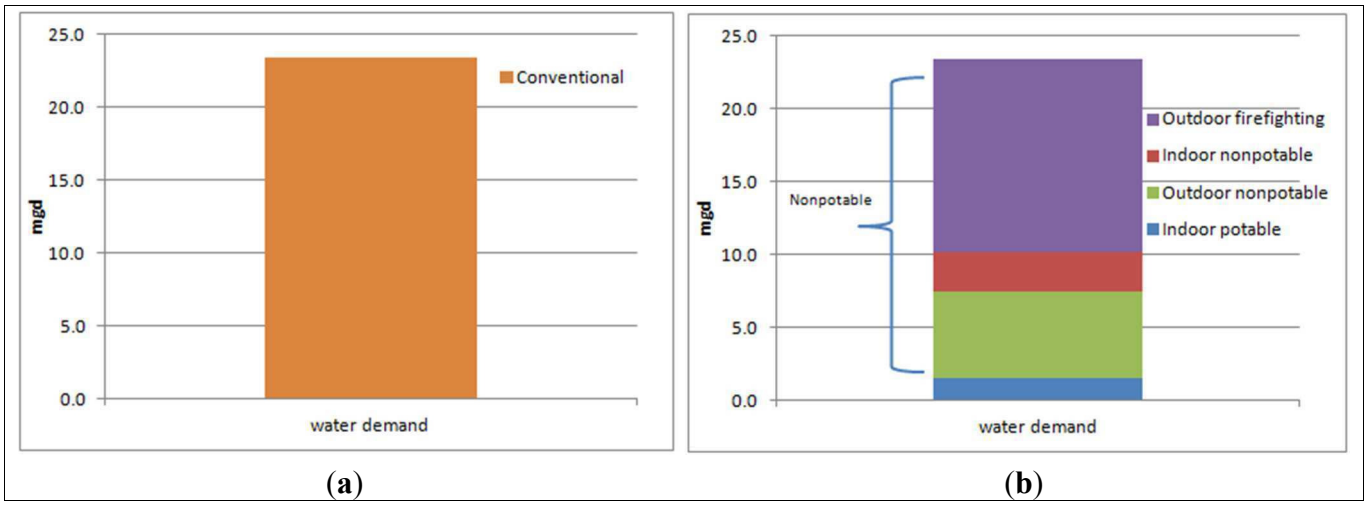

Figure 1. The demonstration of water demand and water use in a city with a population of 100,000. (**a**) Conventional water system with centralized water and wastewater facilities. All water demands are satisfied by potable water; (**b**) Dual water supply systems with potable from drinking water and non-potable from clean water, which accounts for 93% of the demand (see detail below).

2.2. Centralized Water Systems

Ancient Rome represents an example in the history of urban freshwater supply, hygiene and sanitation on a large scale [51]. However, with the rapid urban growth of early industrialization, the sanitary and freshwater-supply condition worsened in the early nineteenth century. The mid-nineteenth century sanitary crisis was an early sign of an inherent dilemma in the industrial market economy: it had no automatic, internal mechanism to restore a healthy equilibrium to natural ecosystems polluted by the unwanted by-products of growth, even though such environmental sustainability was a necessary condition of its continued productive expansion. The Great Stink in England in 1858 and the two cholera pandemics with the death of 25,000 Londoners in the previous decade was the final trigger to the sanitation revolution. A sophisticated network of intercepting sewers was built under London to reroute the waste far downstream from central London [51]. The Sanitary Awakening and acceptance of the germ theory of disease spurred England to take important actions to ensure water supply was both ample and clean. London was never again afflicted with cholera. England's sanitary revolution triggered a virtuous cycle of competition among industrial countries to improve water supplies and public health. By 1920, residents of almost all the world's rich industrial cities in Europe and North America enjoyed abundant and clean freshwater. At the beginning of the twentieth century, most of the largest American cities had municipality-run water supply systems [52]. Chicago achieved a most ambitious civil engineering project—the reversal of the flow of the Chicago River. The river no longer evacuated sewage into the city's Lake Michigan drinking supply; instead it was carried downstream to be diluted in the Illinois and Mississippi Rivers. The sanitary revolution played a pivotal role in sustaining the urban ecosystems at the heart of industrial civilization [51].

Currently, there are about 2 million miles of pipelines in US. These systems of engineering marvels, with some in the ground for over 100 years provide a critical public health function and are essential for economic development and growth. However, the "hard path" with massive infrastructure in the forms

of dams, aqueducts, pipelines, and centralized treatment plants have substantial unexpected social, economic, and environmental cost [53]. Many of the systems were installed at the turn of the 20th century. Due to age, wear, and tear, many are not functioning well. The U.S. EPA 2002 gap analysis shows there is a $540 billion infrastructure needs and funding gap for clean water and drinking water alone for the next 20 years [54]. In 2013, the American Society of Civil Engineers rated both drinking water and wastewater infrastructures as D, indicating a significant backlog of overdue maintenance and a pressing need for modernization [55]. There are 240,000 water main breaks per year and 75% of wastewater capital needs are for pipe repair. The capital investment needs for the wastewater and stormwater systems alone are estimated to total $298 billion over the next 20 years.

The topology of the centralized infrastructure was a result of the strong economies of scale: large centralized infrastructures may still be found to be cost-effective to a certain degree, due to efficiency-boosting features that can be cost effectively added only when the utilities become very large [44,56]. Infrastructures were located strategically to be close to water resource or water receiving bodies. Currently, 35% of a typical U.S. municipal energy budget is associated with water and wastewater utilities [57]. Electricity use accounts for approximately 80% of drinking water treatment and distribution cost and 25%–40% of the operating budgets for wastewater facilities. However, when cities grow bigger, the longer the distance to transport water, the higher the energy demand.

2.3. Current Wastewater Collection Infrastructure

One of the features in urban development is the land use shift from vegetated surfaces to impervious surfaces, creating more frequent and higher peak flows of stormwater. According to the U.S. EPA, over 700 cities in the US with early infrastructure have combined sewer systems (CSS) collecting stormwater in sewer systems that occasionally discharge overflow wastewater directly into water bodies [58]. The untreated sewage from these overflows can contaminate our waters, causing serious water quality problems.

Besides the potential health risk, the current sewer system is designed to accommodate the infiltration from groundwater due to cracks and poor joints (e.g., 10% of the average domestic rate) and inflow from stormwater sources. The sewer systems should be sized to carry peak flow as a gravity flow according to Recommended Standards for Sewage Works ("Ten States' Standards") [59]. Although pumping is not as significant a portion of the load for wastewater as for drinking water in transporting water because of reliance upon gravity, the large-piping system, deep trench and extensive lift stations inherently consume a lot of labor and material in construction and energy in operation. About 150 kWh/million gallons of electricity on average are required to collect sewer [60]. In smaller communities, it was found that the cost of conventional gravity collection systems was up to four times higher than the cost of treatment and disposal because of the lift stations required to service less densely populated areas [61].

2.4. Mixed Wastewater

Human excreta in pre-industrial societies such as the Chinese, Indian, Egyptian, and Amazonian Indians have been used in agriculture and soil enrichment for over 2000 years [51,62]. Not until the industrial revolution, with its urban population explosions, did human waste in cities become a serious problem and health hazard, and so was considered as waste. The engineering infrastructures of sewer

networks have been used to effectively convey the waste to water bodies like rivers or the sea in early times, and much later to the municipality-controlled wastewater treatment facilities [51,63]. Although the sanitary revolution made the rapid immigration from the countryside to the industrial cities possible and sustained the urban ecosystem, the one-directional waste transport and treatment solutions have given rise to new and more complex problems like eutrophication, loss of aqueous habitat, and increased financial burden. The technologies for meeting low levels of the key nutrients are very expensive to install and dramatically increase costs for the utility [64]. The "waste" transported away from urban areas actually removes valuable elements. Not until recent times when water pollution has become prevalent, energy costs have increased, and finite mineral resources are depleting, has wastewater begun to be reconsidered as a resource [65–69]. In fact, there is no such thing as waste in nature, only wasted resources [70]. To be more efficient and sustainable in the long run, human society should mimic natural processes.

Human waste comes from the metabolites of food digestion. The main compositions in wastewater are carbon, nitrogen, phosphorus and potassium. Currently, the primary and secondary treatments in the municipal wastewater treatment plants (WWTPs) effectively remove carbon as measured by biochemical oxygen demand and chemical oxygen demand (COD). Additional biological nutrient removal (BNR) treatments are needed to further remove nitrogen and phosphorus before discharging to the receiving body to avoid eutrophication. The removing processes are highly energy intensive even though many "free" microbes are employed along the treatment train. The in-plant pumping and aeration in common primary and secondary treatment often consists of more than 60% of the total plant electricity use [64]. The further sludge treatment and disposal is also energy-intensive because of dewatering, although the biosolids produced can be turned into fertilizer or soil amendment. If not treated effectively, the effluents from WWTPs are often the major sources contributing to eutrophication due to the excess carbon and nutrient release.

3. Alternative Solutions

3.1. Decentralized Water Systems

When populations in cities grow bigger, it is not only expensive to aggregate the services over a large region and size the systems to accommodate future demand, but also requires considerable pumping energy to transport water over longer distances and the systems are more vulnerable to contaminant transport like salt loads, drought or legal constraints [71]. A decentralized system, on the other hand, is a distributed control where localized, networked interactions between components (such as stormwater management, drinking water supply, firefighting water demand, and energy recovery) establish order and coordination based on local specific information. Decentralized wastewater management systems are stand-alone systems in which small wastewater flows are collected, treated and dispersed at or near the point of generation [72]. The U.S. EPA has formed the National Decentralized Water Resources Capacity Development Project (www.ndwrcdp.org) to support research and development in this area. It was found that the primary drivers for the uptake of decentralized systems in Australia were identified as (1) Overcoming limitations of local water and wastewater services; (2) Deferring infrastructure upgrade; (3) Environmental Protection; (4) Showcasing sustainability; (5) Water conservation;

(6) Enhancement of local amenity; (7) Technology showcase [73]. Decentralized water systems have less conveyance energy and more integrated resource management such as local system-wide reuse opportunities [38]. There is more flexibility, more utility optimization and community independence. Decentralized systems allow the communities to phase-in added sewer capacity as growth occurs, for example, and avoid the upfront financial burden of long-term demand projections in centralized systems where the current users bear the cost of future use [61]. The "soft path" approaches of small-scale decentralized facilities improve the productivity of water use and whole system efficiency, resulting in lower cost community-scale systems [53,74]. The investment risks are also far fewer than those of the "hard path" approaches found in centralized facilities [3]. In addition, the networks of decentralized subsystems provide the necessary redundancy and flexibility responsive to potential weather changes or other system disruptions. When one decentralized system fails, the other ones provide the auxiliary connections and can redirect resources in the event of an emergency. This will increase resource exchange among systems, optimal resource throughput and minimization of wastes. It is also easier to reach an equilibrium point between water, energy, and land use where improvements in one aspect does not signify cost in others [75]. The tradeoff of decentralized systems is the increased complexity within the clusters of independent, yet interconnected networks. In centralized systems, the system configuration and operations are much simpler, but costly. The efficiency of decentralized systems is achieved through complex information management that allows system exchange, and more diverse technology to achieve resource recovery and sharing, instead of extensive energy-driven technologies. The modern development of digital and communications technology can provide systematic communication between decentralized water systems like smart grid technology in electricity networks. Networks such as the Smart Water System use the automated and integrated remote sensing network to provide better efficiency, reliability and security, resulting in a more resilient system [76,77]. For example in an extreme weather event, the watershed management teams can automatically share stormwater modeling information with potential flooding zones and times based on predictive precipitation intelligence and develop corresponding timely emergency responses [78]. The emergence of localized systems will encourage more innovations and new market opportunities resembling those seen in the clean energy initiative such as nitrogen trading programs in nutrient management or "centralized operations of decentralized units" contracting business model [79]. This in turn can provide significant social, economic, and environmental benefits. As the high risk of the total system failure from critical centralized infrastructure is alleviated, so does the financial burden decrease.

Compared with a wealth of knowledge about conventional systems, decentralized systems have been shown conceptually promising. Although significant progress has been made [52,56,73,80–83], the decentralization concept is still in its relative infancy [72,84]. It is not a simple downscale of the centralized version, otherwise the economy of scale in microeconomics would determine that the cost generally decreases with increasing scale [38]. It should be effectively linked to other alternative options such as dual water quality, energy and material recovery, fit-for-purpose, *etc.* In reality, new system architectures can be configured in different designs, including hybrid systems which "tweak" the current systems and incorporate centralized and decentralized elements [72,84–86] and transformative systems that overcome the system inertia with new system designs [87]. The focus of system optimization certainly involves a general matter of scale that deserves more research [52,56].

3.2. Fit for Purpose and Greywater/Rainwater Reuse

The current distribution systems were designed for fire protection centuries ago and driven entirely by the need for large flows througout systems. Few structural standards are concerned with drinking water quality. The drinking water problems now inherent in all systems will not be addressed by continuing the same design practice [45]. Alternatively, dual systems in which separate pipe networks can be constructed for potable and non-potable water have the potential to improve water safety and reduce cost of drinking water distribution infrastructure, ultimately achieving maximum resource recovery from wastewater [88]. Dual water systems for dual water quality are not new. AWWA published the first edition of its *Manual of Practice: Dual Water Systems* in 1983 [89]. The original intention was to conserve high-quality natural waters for drinking and use reclaimed wastewater for nonpotable purposes. Dual systems in a new community/system would be built simultaneously. Such dual systems have been developed and are operating in a large suburb of Sydney, Australia serving 250,000 since the 1990s [90]. All houses are provided with reclaimed water lines inside for toilet flushing and with potable lines. For existing systems, dual systems can be retrofitted a new drinking water system (smaller pipes) and rely on the existing system (larger pipes) to serve as the non-potable supply [45].

If the majority of the domestic water use (e.g., 93% as in the case in Figure 1) is for non-potable purposes, the treatment strategy should adopt "fit-for-purpose" practice, in which the treated water, called "clean water", is for non-potable use, like toilet flush, clothes washing, firefighting and landscape irrigation. The City of St. Petersburg, FL develped the first major dual system in 1969 in US [90,91]. There are approximately 335 dual distribution systems in the U.S., mainly in Florida, California, Arizona, and Texas with reclaimed water [88]. The national mileage of pipes in dual systems is between 10,000 and 20,000 miles. However, most current dual systems do not serve residential users and the reclaimed water is only 1% to up to 60% of total water delivery. The survey of current dual water systems showed no major public health problems from the use of reclaimed water in US [88]. U.S. EPA's 2012 manual includes water reuse projects, state standards, regulations, and recommendations [92].

The source of clean water can be treated greywater and rainwater, in which the water quality standard is not as high as drinking water, but safe for its purpose. Unlike blackwater, *i.e.*, feces without urine, which is rich in organic matter, greywater is domestic non-sewage water which generates larger volumes with lower concentrations of contaminants, such as that from showers, sinks, and laundry.

Due to the evaporation and condensation processes as parts of the water cycle, rainwater is generally considered clean and the quality is better than surface water. It is when rainwater comes in to contact with the catchment area such as roof and road surfaces, contaminants like pathogens, VOC and road salts are introduced. The harvested rainwater can serve as an independent water source for clean water as well as for storage and other purposes such as landscape irrigation [93].

The treatment of combined greywater and stormwater can employ less energy-intensive technology and with lower capital expenditure [94]. Constructed wetlands can serve as one such option. The natural wetland system is one of the most productive primary production systems on terrestrial biomes. Although wetlands occupy only about 2% of the global surface area, they contain 10%–14% of the carbon [95]. Wetland soils, such as histosols, may contain up to 20% carbon by weight. The peats are even more carboniferous. The aerobic-anaerobic stratification of wetland sediment columns involving vegetation, microbial and soil community is uniquely important in the global cycling of sulfur, nitrogen, and

phosphorus as well as carbon [96]. An open-water wetland with land area of 6×10^4 m^2 (15 ha) can achieve 90% removal of most compounds in nitrified wastewater effluent receiving 3.8×10^3 m^3/d (1 million gallon per day (mgd) flow) [97]. The treatment efficiency would be higher for lower strength greywater and stormwater. This efficient ecological and evolutionary machinery from natural systems provides enormous natural capitals that often are not appreciated by market capitals. Moreover, the benefits beyond water purification can be food chain support, biodiversity conservation, stormwater and erosion control, flood conveyance, water storage and buffering, local climate control, reduction of wild fire, and downstream ecosystem improvement. Constructed wetlands are designed to simulate natural wetlands and use renewable energy to replace fossil fuel energy used in conventional treatment technologies to achieve the same water purification purpose.

The carbon sequestration of wetlands is not limited to simply carbon fixation by photosynthesis within the wetland. It is also the sinks of carbon from inflow water such as greywater from domestic use. The aquatic vegetation and organisms in wetlands also play an active role in taking up nitrogen, phosphorus and other compounds from inflow water. Over time, the peat production from the wetland can be used for soil conditioning and potting soil. Twenty-three states produced about 900,000 tons of peat worth about $20 million in 1988 [98].

The rising temperature and imbalanced water cycle has been and will continue to result in more severe climatological events [3,5]. It has been estimated that the frequency of such severe events has increased by 20% in the US since the beginning of the century [98]. In the areas with decreased precipitation, constructed wetland and its storage function will provide additional supply during summer months or drought periods because of its relative constant flow from domestic water use. In the areas with increased precipitation, the constructed wetland will provide water quality buffering, stormwater runoff treatment and erosion control. The integration of constructed wetland with urban living as a part of aesthetic co-design of water functioning services and urban landscape will not only provide a financially viable option (because the water purification is done by natural capital instead of market capital), but also offers numerous ecological services as mentioned above and additional urban design function such as more public spaces to promote social interactions, physical health and fitness, diminished crime and increased wellness, resulting in improving the quality of life within the livable, regenerative community (rather than the conventional mentality NIMBY-Not In My Back Yard) [99]. For example, hiking trails, and nature parks around the wetlands can offer public recreational space and increase aesthetic and property values [100].

Although the wetland treatment efficiency for lower strength greywater and stormwater would be higher than for traditional wastewater, the technology still requires extensive land occupation that captures renewable energy in the form of vegetation, soil and microbes to treat wastewater. In areas where land is not available such as in the densely populated communities, the treatment can instead employ technologies with smaller footprint, but driven by purchased inputs and fossil fuels to treat greywater and stormwater. Even so, the overall system efficiency may still outweigh the ones in centralized systems.

3.3. Natural/Green Infrastructure

To develop effective stormwater management and build cost-effective solutions with physical and operational resilience, it is suggested that hard urban surfaces are replaced by vegetated or permeable surfaces to retain runoff and natural shoreline features such as wetlands and sand dunes to mitigate the effects of storm surges [101]. Green infrastructure incorporates natural capitals like vegetation and soil to manage rainwater near where it falls [102]. Instead of diverting stormwater outside the watershed as much and as fast as possible with extensive piping system and transport energy, the available potential energy from the rain should be used to encourage maximum productivity and native biodiversity within the watershed [103].

Water system management should also collaborate with city zoning and land use management. Most metropolitan cities in US and around the world have experienced the massive flooding in severe storm and urban heat island (UHI) effects in hot summer due to the replacement of natural open and vegetated land surfaces with artificial concrete infrastructure and impermeable, dry surfaces [104,105]. Solar energy is converted to more sensible heat, rather than latent heat. Excess water is disposed as quick as possible before it returns to its natural cycle through evapotranspiration (ET) and infiltration. To overcome these issues, cities should implement strategies that encourage more ET and infiltration with urban forests, urban agriculture, trees and vegetation, green roof and cool roof, and cool and permeable pavements and surfaces [102]. The study of ecohydrologic effects of urbanization on ET showed that loamy soils can sustain vegetation transpiration more than sandy soils; mature tree covers with deep root structures have higher annual ET rates than shallow rooted covers such as grass, which may reduce runoff and mitigate against UHI effects [106]. Although urbanization necessarily comes with a certain degree of impervious surface at the expense of vegetated cover, it was shown that impacts to annual ET fluxes can be mitigated by strategies like eliminating directly connected impervious area [34]. The natural ground cover would only have 10% runoff with 40% via ET and 50% through infiltration while the impervious cover would have 55% runoff with 30% ET and 15% infiltration [107]. The basic principle of low-impact development (LID) practices as stormwater management alternative is to mimic pre-development hydrologic regime and detain runoff close to its source [108]. At the watershed level, if the efforts are focused on targeting the fundamental problem by making acyclic hydrologic process become more cyclic and restoring natural hydrologic cycle [109], the stormwater runoff will be alleviated and the more balanced natural hydrologic cycle will in turn provide resilient support for urban water systems in the long run.

Constructed wetlands will also increase ET and potentially infiltration. Large bodies of water greatly moderate land climates because of the high latent heat of evaporation and melting characteristic of water [109]. If possible and necessary, other underground and above-ground water storage bodies, like quarry reservoirs, can serve as water bank and environmental buffer to store excess water for later use, flood control, energy storage of potential hydroelectric power, emergency water supply and groundwater recharge, *etc.* [71]. For example, the Stone Quarry Reservoir in Carrboro, North Carolina stores up to 200 million gallons of water [110]. Regionally, Southern Nevada Water Bank program has stored over 104 billion gallons of water in the local hydrographical basins [111].

3.4. Vacuum Sewer Collection Systems

Unless there are onsite collection and treatment units like composting toilets or septic systems, the sewage generated must be connected to a common collection system and transferred to a treatment facility. The conventional gravity sewer is considered as the standard operation. However, one of the alternative systems, vacuum sewer, may provide an option for decentralized urban sewer transport replacement when blackwater transport is considered (see Section 3.5).

Vacuum sewer systems collect wastewater in a valve pit where sewage is drained from the house by gravity and then conveys the sewage by vacuum. When a pneumatically controlled valve on a service line is opened to atmospheric pressure, wastewater and air are "pulled" into the system. The vacuum valves do not need an onsite electricity source to operate. Therefore, a single vacuum valve pit can serve two or three equivalent dwelling units (EDUs) with no electricity sharing issues. The wastewater that enters with the air forms a "plug" in the line, and air pressure pushes the wastes toward the vacuum station. When the vacuum valves closes, atmospheric pressure is restored inside the valve pit by a central vacuum station. Cumulative kinetic energy moves the sewage toward the central vacuum station and break up the larger suspended solids during transport. This energy from the air pressure difference offsets the fossil fuel-driven energy needed to achieve the same sewage flow transport. However, due to the reference atmosphere pressure, vacuum sewers have a limited capacity to pull water uphill. The maximum expected lift is between 4.5 and 6 m (15–20 ft) under flat terrain [61]. Otherwise, lifts are needed to bring the vacuum line to a shallow elevation. Each vacuum station can serve approximately 1200 EDUs with a length of 3000 m (10,000 ft) service radius in a modest housing density and flat terrain. Vacuum stations are the centers of the vacuum sewer system. When sewage arrives in vacuum stations, it is stored in a large vacuum collection tank and then conveyed by sewage pump through a force main to the treatment facility.

The periodic air influx through valve openings encourages the aeration process so there are less anaerobic conditions in sewage flow. Vacuum sewers are "closed" systems and inherently watertight since any air leakage into the system reduces the available vacuum and the pipe breakage leads to the operation failure. This immediate "alert" feature will prevent any prolonged leakage without notice, unlike in a gravity system where the leak detection may take days to run a camera in the sewer main to locate the leak. The sewage in a vacuum line remains in the pipe if a break does occur due to the negative pressure in the piping system. Exfiltration rarely occurs and the impact of sewage contamination is greatly reduced. Another benefit is odor containment. Unlike gravity sewers with many places where odors can escape, vacuum mains tend to self-clean due to the scouring ability of the high speed of the wastewater in the line.

The pipe size for a vacuum sewer is smaller than those used in gravity sewers due to less infiltration. There is no need for large, deep trench installations, which reduces the excavation cost and community disruption. The shallow burial depth also simplifies the finding and repairing of leaks which reduces the long-term operational and maintenance cost. To convey more viscous blackwater, which is not mixed with urine and greywater and is mainly "dry" feces, vacuum sewer systems will work better than gravity sewer because of the negative pressure in the line. It has been proven to be 24% cheaper than gravity sewer [112].

3.5. Resource Recovery

In municipal solid waste management, source separation has been long advocated, in which compostable organic wastes, recyclable materials such as paper, glass and metal are diverted from other waste streams at the source for separate collection [113]. The view that the organic fraction of the waste stream is a resource to produce renewable energy and compost should apply in wastewater management. Instead of the extensive energy and chemical expenditures required to separate carbon and other nutrients in wastewater treatment processes, source separation at the user phase has been regarded as resource efficient to treat concentrated, unmixed solutions [114,115].

The challenge for source separation has prompted researchers to design urine diversion toilets, in which urine and feces are separately collected [63,116]. The toilet bowl has two openings, one toward the front for urine and one toward the back for feces. Since 2010, the Bill & Melinda Gates Foundation has awarded more than 50 grants for designing "next-generation sanitation" to maximize the recovery of nutrients and energy [116].

3.5.1. Nutrient Recovery

In the nitrification process in traditional BNR treatment, ammonia is converted to nitrate, followed by denitrification, reducing nitrate to nitrogen gas. Nitrogen gas is then released to the atmosphere as a part of the nitrogen biogeochemical cycle. To sustain all forms of life, nitrogen fixation is essential to convert nitrogen gas in the atmosphere into ammonium and nitrate forms which are the most readily used by plants. Nitrogen fixation is especially energy expensive because so much energy is required to break the triple bond of molecular N≡N so that it can be converted (with addition of hydrogen from water) to two molecules of ammonia. Free living biofixers are less efficient and may require up to 100 g of glucose to fix 1 g of nitrogen (1% efficiency) [117]. In the fertilizer industry, the most common nitrogen fixation process, the Haber-Bosch process requires a lot of fossil fuel energy in industrial fixation. In fact, 3%–5% of the world's natural gas production is used in the Haber-Bosch process [118]. This is the reason that nitrogen fertilizer is more expensive than most other fertilizers [109].

Phosphorus removal during BNR treatment may involve biological accumulation in biomass and chemical precipitation. The phosphate-rich sludge can be resold as fertilizers or soil conditioner. The great reservoir of phosphorus is not the air, however, but the rocks and other deposits formed in past geological ages. Much of the eroding and dissolved phosphate ends up in the sea. The returned phosphorus to the land (like extensive uplifting of sediments) is inadequate to compensate the loss [109]. Human activities have hastened the rate of phosphorus loss [119]. Phosphorus is one of the scarcest minerals in terms of its relative abundance in the available pools on the earth's surface [109]. Phosphate rock is predicted to be depleted in 50–100 years which puts global food security at risk [7,8]. Ultimately, phosphorus will have to be recycled on a large scale to avoid the collapse of agriculture [120].

Urine is an important source of minerals, especially nitrogen, phosphorus, and potassium. These minerals are also the feedstock ingredients for commercial fertilizer. Nitrogen in urine is already in the forms of ammonia and urea. If the two industrial processes are connected and minerals in urine are used directly, the high energy spent to nitrify ammonia and denitrify nitrate in wastewater, and fix the nitrogen gas in synthetic fertilizer can be offset. Technologies such as struvite crystallization (magnesium ammonium

phosphate hexahydrate, $MgNH_4PO_4 \cdot 6H_2O$) provide such promising potential. The struvite process occurs spontaneously in wastewater processes and it often clogs the pipes. The crystallization process can selectively extract phosphate and ammonia-nitrogen from the mixed wastewater stream and produce slow release pellets for fertilizer use [121–123]. The struvite product is thought to be more bioavailable. Therefore, less quantity is needed than the commercial one to achieve the same nutrient needs for plants and less unused nutrients will end up in the water ways. The same technology can be used in urine where the target constituents are more pure and concentrated. Therefore, higher efficiency would be expected for the crystallization from urine than from mixed wastewater. The theoretical potential has been estimated to be 67,000 tons of P_2O_5 fertilizer per year from the UK alone and 270,000 tons from Western Europe [124]. The nutrient recovery from urine will, at larger scale, make material acyclic processes become more cyclic, which is what natural biogeochemical cycles do.

3.5.2. Energy Recovery

When nutrients are diverted from the feces (and since greywater is also diverted) at the source, the more concentrated organic materials (mostly carbon) that are left, named blackwater, can be further processed to more efficiently recover embedded energy. In conventional wastewater, the suspended solids are settled in the form of sludge which is further digested to methane (CH_4). The soluble organic fraction has been treated with aerobic processes effectively, but with relatively high energy input and little financial advantage. One promising technology to capture the energy potential of the dissolved organic fraction is microbial fuel cells (MFCs) [125]. MFCs convert direct biological energy to electricity. Currently, only 30%–40% of the CH_4 energy is converted. More improvements such as less voltage loss and higher transfer efficiency are needed for this process to be competitive with complete anaerobic biological conversion to biogas, a renewable fuel used in electricity generation [68,125].

Anaerobic treatment has been considered as the core technology for energy recovery [126]. Anaerobic digestion is the biological degradation of organic matters in the absence of oxgen and converts the embedded chemical energy in organic carbon to biogas. The biogas can further be tranformed into other forms of energy such as electricity, heat, or compressed fuel. Anaerobic biological processes involve facultative hydrolysis and acidogenesis and strictly anaerobic acetogenesis and methanogenesis. Anaerobic organisms particularly methanogens are slow growers and respond slowly to changes. The common method for anaerobic processes in wastewater systems uses continuous feed with a single-stage system, resulting in lower capital costs. The temperature-phased digester has two reactors to separate microbial processes to optimize parameters with higher biogas and CH_4 production, although the cost of construction and materials increase with the separation of these processes [127].

Anaerobic digestion has been used for wastewater sludge treatment and reduction, agricultural manure management, and food waste management. In all cases, the organic carbon embeded in the waste is anaerobically converted into biogas. The higher the organic content, the more biogas. For blackwater stream where the organic concentration is at least 10 times higher than conventional mixed wastewater [128,129], up to 97% of total COD can be removed and 60% converted to CH_4 [127,129,130]. The diversion of urine prevents the inhibition of methanogensis from high levels of ammonium and improves the efficiency of digestion and energy recovery. Other configurations are being investigated to improve the efficiency of the biodegration of the organics, reduce the hydraulic and solid retention

time and recover the dissolved methane loss to the effluent in processes such as ananerobic membrane bioreactors [68,129,130], anaerobic fludized bed reactors [68,131,132], upflow anaerobic sludge blankets [129,133,134], and the combination of MFCs and anaerobic membrane bioreactor [135]. In addition, since organics in human feces are mostly metabolized low molecular weight carbons, co-digestion with food waste which contains higher molecular weight carbons can double the biogas production [127,129]. In response to a European Union Directive requiring diversion of 65% of the 1995 levels of organic wastes from landfills, there were 127 operational food waste anaerobic digesters, with a capacity of 4.6 million tons, installed as of 2006 in Europe [127]. Among the 16,000 municipal wasteater treatment facilities operating in the US, only 544 facilities employ anaerobic digestion, and only 106 of these now utilize the biogas produced to generate eletricitiy and/or thermal energy [136]. The potential of co-digestion to maximize the biogas production is huge.

Biogas is comprised of 60%–70% CH_4 and 30%–40% CO_2 and other trace gasses. Common applications for utilizing biogas include heat, power or combined heat and power (CHP). A portion of the generated biogas (approximately 10%) is the feedback of self-maintaining temperature and energy demands for the digestion process [127]. Remaining energy is available for electricity generation or direct combustion for heating purposes. Biogas can also provide space heating and compressing biogas for fleet vehicles [127]. An eco-village in Jenfelder Au, Germany with 2000 residents developed by HAMBURG WASSER intends to provide renewable energy supplies from locally CHP generated biogas from blackwater and organic waste (30%), geothermal energy (40%) and solar heat (10%) to achieve decentralized, energy self-sufficient cities of the future [128].

Besides the chemical energy embeded in organics, the thermal energy in the form of heat in wastewater is at least 2.5 time higher assuming 6 °C change in water temperature [68]. Heat pumps can use sewage water as heat source and extract heat for building heating [137]. Other technologies like hybrid pressure retarded osmosis-membrane distillation (PRO-MD) are being developed to capture the enoumous low-grade waste heat (<80 °C) for electricity generation, although technology gaps still exist [138]. Such energy recovery from blackwater, together with energy consumption reduction from other alternative strategies would greatly contribute to overall low carbon urban development [39,139].

4. The Sustainable Urban Water Systems Case Study: The City of Tomorrow

Each city has its unique socio-political and bio-physical characteristics [140]. There are no one-size-fits-all solutions. Many institutions and organizations around the world have been part of the efforts of promoting paradigm shift. The International Water Association (IWA) Cities of the Future program (http://www.iwa-network.org/) aspires to help cities create robust and resilient responses to various changes cities are facing and promote rethinking water management. Numerous cases under Global Water Partnership have applied different toolbox in dealing with various water challenges around the world [141]. While it is critical to gain experience of how a tool has worked in a given situation and with local context, the details from real world often not only focus on one aspect of water issues that specific community faces but also may mask or distract the higher level of understanding and core questions: how do different parts of water system interact and how can urban water system as a whole be more efficient and sustainable? Similar to the studies of process mechanisms under laboratory controlled environment before the field experiments, with the understanding of the potential alternative

options for each sector within the water system and its complex intertwined nature, a specific urban development setting is required to clearly explore how these players can be evaluated inclusively and the system reorganization can achieve global system efficiency.

Thus, it is indispensable to combine system thinking approaches with sustainability indicators or metrics for assessing holistically this global system efficiency. Some examples of these tools are metrics that evaluate particular dimensions such as: human health with risk assessment [31], and economic and environmental dimensions with footprints (e.g., ecological, water, and carbon), life cycle impact assessments, triple bottom line reporting, and benefit-cost analysis [142,143]. There is a plethora of publications about footprints (89,976 approximately) and life cycle assessment of water systems (21,316 approximately), but less about studies about integrated water systems such as: sustainability indicators (1434 approximately), benefit-cost analysis (531 approximately) and triple bottom (166 approximately), which indicates a gap of knowledge needed for holistic analysis of water systems (number of citations obtained from [144]).

One of these system tools is emergy, which incorporates all dimensions into one for a complete sustainability analysis. There have been attempts to evaluate separately each unit of the water system with emergy, *i.e.*, drinking water [145,146] and wastewater systems [147]. However, a more comprehensive study that assesses the current system configuration and sustainable alternatives is still needed.

4.1. System-Based Tool: Emergy Synthesis

While integrated measures are needed to provide a holistic view of sustainability, they require a "common currency" to compare different units and scales [148]. One such system-based method is emergy synthesis, a process previously used for various systems at multiple scales to incorporate environmental, social, and economic aspects into a common unit of nonmonetary measure (equivalent solar energy joule, sej). Emergy is defined as the available energy of one kind previously used up directly and indirectly to make a service or product [149]. It is based on the observation of the energy flow patterns in ecosystems and economic systems during self-organization. The theory states that the functions of all systems (ecological, social and economic) are derived from the transformation of available energy. Such transformation also defines the relative energy quality in a hierarchical order. For example, the transformity values for wind energy, electricity and phosphate fertilizer are 1.5×10^3, 2.0×10^5, and 1.0×10^7 sej/J [149]. It means that the processes for generating phosphate fertilizer require a lot more upstream energy investment than what it takes to regenerate wind energy, due to the geological sedimentary cycle for phosphorus rock to regenerate and the fossil fuels needed in mining and concentrating into the appropriate form as fertilizer. In other words, phosphate fertilizer has higher "energy quality". The unique concept of energy quality in emergy analysis has the capability to value natural resources such as rain or soil that are often considered as "free" in the economic market. Many other integrated tools including life cycle analysis or "footprint" analysis often limit the analyses within technosphere from unit processes and overlook the biophysical supports from natural capitals. Instead, emergy analysis can provide a more inclusive evaluation of water systems that not only satisfy the urban water services, but also serve as driving forces in shaping the landscape and sustaining the ecological services.

Such energy quality term can be easily used to clarify the misunderstanding that upstream reduction in demand does not produce *new* water because non-consumptive water used inefficiently will be used

by downstream users [150]. It is not just water quantity, but also energy quality of water that matters. With such a conversion factor to a common measuring unit, all energy, material, and information flows with completely different qualities in a system can be holistically assessed. Therefore, the behavior of a system as a whole and the interactions between subcomponents can be observed and optimized and its sustainability can be assessed. This applies to water systems with components like wastewater, stormwater, drinking water, surface/groundwater, water in natural systems and associated infrastructures.

Emergy theory asserts that prevailing systems are those whose designs maximize available energy by reinforcing resource intake at the optimum efficiency. This includes maximizing the resource intake *and* the operation at the optimum efficiency for maximum power. In other words, both *intake* and its best *use* are maximized [149]. The beneficial organization increases intake energy (first priority) and its efficient use (second priority) on all scales (not just maximizing levels with more energy, and not maximizing some levels at the expense of others) [151]. The same holds for water systems, particularly for urban water services. It is not a self-contained unit, economically or ecologically. Its future depends as much on the external life-support environment as on the activities within the city limits ([109,152,153]). If the hydrological cycle can be maintained and repaired, and if the acyclic processes driven by human activities become more cyclic, enabling a feedback loop, there is a better chance for sustainably managing urban water systems.

Emergy analysis of the urban water system finds that the drinking water and wastewater treatment processes are high energy-, chemical-, intensive processes. For example, it was found 5.87×10^{11} sej/m^3 for potable water [146] and 3.15×10^{11} sej/m^3 for activated sludge-treated wastewater [147] (global baseline adjusted to 15.2×10^{24} sej/year [154]). The high emergy values for drinking water come from chemicals and electricity for supreme quality of water and for wastewater come from the embedded emergy in raw materials in food (such as fertilizers, soil organic matter, *etc.*) and from modern agricultural processing and food distribution system inputs. This is why when the urbanization of the modern community creates large population centers that generate concentrated wastewater, a large expenditure on wastewater treatment has to be invested to make a modern city function without human and environmental health problems. Society relies on systems with technological energies rather than on systems with natural energies resulting in "systems being energy intensive rather than land-intensive" [155]. There is a reciprocity between the amount of resources used in the concentration of nutrients (the food support system) and the resources that have to be spent on dispersion (the WWTP system) [149,155,156]. The resources for treating the wastewater could either be drawn from local resources by the expropriation of large land areas (or less land for longer period time), or by the use of high technologies and large amounts of purchased inputs from other places or other time periods such as importing chemicals and materials from outside systems, or utilizing the higher emergy quality products like electricity driven by fossil fuels concentrated through prior geological times. Since concentrated wastewater is inherent to a modern city and requires certain emergy expenditure to disperse it, the more sustainable water system would maximize its available energy by reinforcing resource intake such as water, energy and nutrient recovery, and operating at the optimum efficiency by using more renewable emergy intake such as natural/green infrastructure to provide the same services.

4.2. The Alternative System for the City of Tomorrow

In order to become a more sustainable city, and to overcome the numerous drawbacks in the base-case scenario, the City of Tomorrow could employ various alternative approaches and design a more integrated system that breaks the invisible boundaries. Non-traditional strategies like fit-for-purpose treatment and source separation could be adopted, in which water services and qualities are delivered to match users' needs, less wasteful energy expenditure is spent and productivity of water use is maximized, rather than continuing to seek sources of new supply [53]. In the decentralized setting proposed herein (Figure 2), a dual water supply system is exploited at the community level. The drinking water supplies only for potable water needs. Only 2.07×10^6 m^3/year (1.5 mgd) is withdrawn from groundwater, a 93% reduction from the conventional practice (Figure 1). If only 7% of the potable water demand is supplied by high quality groundwater, the treatment and distribution cost will be greatly reduced. Shorter residence time is also expected. Smaller size piping, possibly stainless steel, requires fewer joints [88]. It will greatly decrease, if not eliminate, DBPs and pathogen risks. The high potable water quality is easier to achieve to protect public health and secure public safety, even with future population growth, and ensure long-term water resource sustainablity.

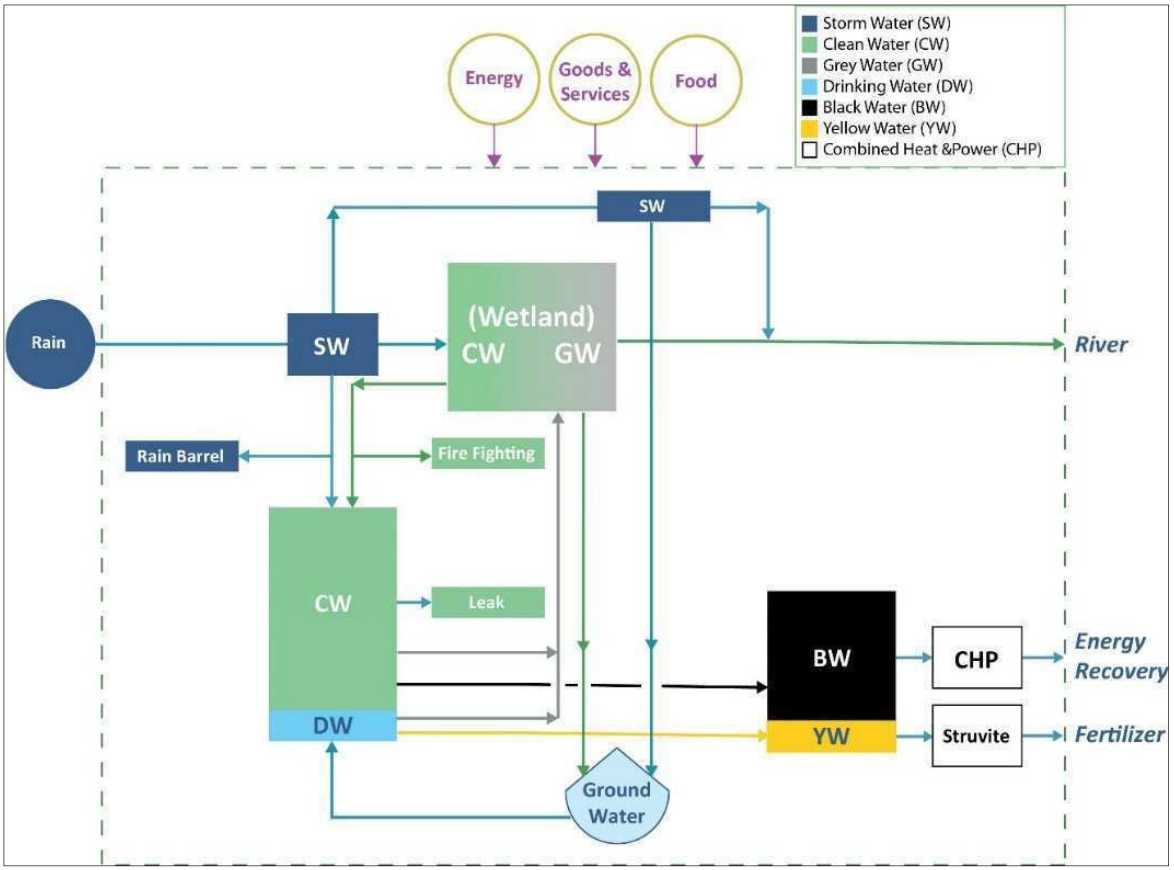

Figure 2. Sustainable alternative urban water system.

The non-potable demand cannot be solely satisfied from greywater generated. Rainwater/stormwater serves as an additional supply. The non-potable water sources (clean water from wetland-treated greywater and rainwater) provide water for non-potable demands (Figure 2). Smart land use strategies are used to further reduce stormwater runoff and encourage more evapotranspiration (40%) and water

storage and recharge (50%) [107], for example, promote the growth of more mature tree with deep root structures [106]. With the same precipitation, the water intake from natural resources in the alternative system is only 7% of the conventional practices. Most of the water is retained and recycled within the system. Only 20% of the water coming into the system is discharged. In a conventional system, the efficiency is much less with over 77% discharged (Figure 3). Instead of being lost as runoff, the flow of geopotential energy and chemical potential energy of water is dispersed in the watersheds and maximizes the biological productivity and other contributions [149].

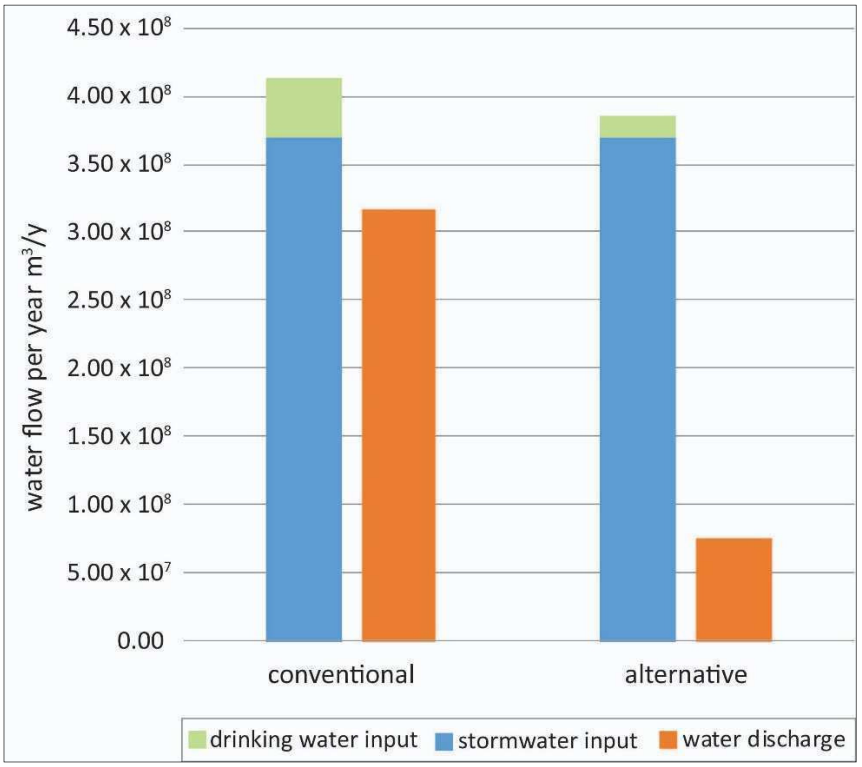

Figure 3. Whole system water flow balance for a city of 100,000 population. With the same rain precipitation (blue part), the difference in water inputs between two systems is the reduction of water withdrawal from groundwater (green part). Water input from natural resources in the alternative system is only 7% of the conventional system since most of the water is retained and recycled within the system. Only 20% of the water coming in the system is discharged in the alternative system. In the conventional system, the system efficiency is much less, with over 77% discharged.

Greywater, blackwater and yellow water are collected separately and treated at the neighborhood level for maximum energy and nutrient recovery. The greywater and blackwater are collected by separate vacuum sewer systems. Rainwater from roof and domestic greywater is drained into constructed wetland and treated for clean water use. Additional treatments such as filtration, and disinfection may be used for final polishing. Clean water is reused for non-potable indoor domestic uses (toilet flushing and clothes washing) and firefighting needs (68% of total demand). On-site containment of rainwater like rain barrels satisfies the outdoor needs (25% of total demand).

Since greywater (~57% of total) is diverted from the wastewater mixture, the volume of the waste stream is greatly reduced, so is the energy needed to convey the wastewater. The concentrated blackwater

is anaerobically digested and the biogas generated undergoes further energy recovery through CHP. The energy generated will not only self-sustain the anaerobic digestion and CHP processes, but will also aid in production of struvite fertilizer. The remaining energy can feed back to the smart grid and generate revenue for the city. Another revenue source is the struvite fertilizer through yellowwater processing. Instead of transporting all the fertilizer outside the city and losing potential local productivity, the community should encourage networks of urban or peri-urban agriculture, urban forestry, community gardens, local horticulture, *etc.* to support urban self-sufficiency in food production, improve food security, food safety and local employment.

Due to the internal looping, the majority of the water (greywater and rainwater/stormwater) is mainly treated with wetland systems. The energy thermodynamically needed to disperse organics and minerals is derived from renewable energy synergistically provided by plants, the microbial community and the soil matrix, instead of the fossil fuel-driven intensive centralized treatment. Less dependence on fossil fuel means more energy independence and more resiliency for the community. Additionally, the smart land use and green infrastructure applications will support the restoration of the natural hydrologic cycle by encouraging ET and infiltration. This will have long-term buffer effects on the imminent climate change of the local region and will alleviate impacts like Urban Heat Island (UHI), drought and flooding. It will provide a more sustainable external life-support environment for the urban community.

Further study needs to be done to characterize the performance and emergy expenditure in the alternative system with the non-traditional strategies, although some technologies might be still in the nascent phase and the integration of different new technologies may present the sizeable challenges at the beginning.

4.3. Centralized and Decentralized Water Systems Challenges

Centralized systems are inherently large and experience inertia in making any big changes. Nonetheless, they reduce opportunities for innovation development and implementation because of perceived financial, organizational, system operations and technical risks. If a community wants to implement alternative technologies and practices such as: collection and storage of rainwater in existing ponds or wetlands, rainwater reuse, anaerobic digesters for generating energy that can supply homes and business; it would be more likely implemented in smaller systems. While such innovative options might not be easily carried out in the scale of centralized system; the advantage of these systems is its uniformity that assures meeting the water demand and quality standards in an economy of scale (Table 1). Nonetheless, smaller systems can only become competitive if they can meet the demand and standards in terms of the cost–benefit relations that must be controlled by experts [77].

The advantage of decentralized systems is diversity, choosing the technologies to achieve maximum system efficiency such as the system described in Section 4.2. In the event of interruption, energy blackout or water outbreak, decentralized systems are more insulated from the events because of their relative independence. It is true that decentralized systems need more community participation and management. This is the stakeholder involvement process. Whenever there are stakeholder involvements, the communities will be more likely develop the objectives suitable for their own interests and collectively find more balanced solutions. This rootedness option is better than a one-size-fit-for-all centralized system. Nevertheless, the research and the demonstration of various decentralized systems is still not sufficient. More is needed to fill the gap (Table 2).

Table 2. Comparison of the traditional and the alternative water systems.

	Traditional Water Systems		References	Alternative Solutions		References
	Advantages	**Disadvantages/Opportunities**		**Advantages**	**Disadvantages/ Opportunities**	
Water quantity	Centralized control and assurance to meet demand and standards.	Drinking standard applied to potable and non-potable increases demand. Vulnerable to failures in service that will impact the whole system.	[43,44,48,49,71,150]	Decrease in demand of potable water for non-potable uses (fit for purpose). More resilient system.	Paradigm shift towards a new revenue model not based on water consumption.	[45,52,72,90,91]
Water quality		A critical event (e.g., algae bloom or spill) can impact the whole system. For larger systems is difficult to attain at the end of the distribution.		New methods are needed for monitoring, modeling, assessing, and managing water resources using a systems approach, and watershed perspective.		
Energy use	More research is needed Energy recovery	Intensive, mostly fossil fuel-driven	[61,64,157,158]	Potential use of renewable sources Energy recovery	More research is needed	[66,68]
Wastewater contamination	Centralized control and assurance to meet standards Resource recovery	CSS that discharge overflow directly into water bodies Infiltration to groundwater due to cracks and poor joints	[58,59,101]	Mimic natural processes Resource recovery	More research is needed	[69,115,159]

Table 2. *Cont.*

	Traditional Water Systems		References	Alternative Solutions		References
	Advantages	**Disadvantages/Opportunities**		**Advantages**	**Disadvantages/ Opportunities**	
Direct cost	Economies of scale	Huge infrastructure needs to modernize systems Intensive labor and material in construction and operation	[53–55]	Lower cost community-scale systems New markets for nutrients and energy generated in the system	More research is needed	[38,56,63,64,67,75]
Indirect cost	More research is needed	Water scarcity, eutrophication, loss of aqueous habitat		Watershed and ecosystem conservation	More research is needed	
Cultural	More research is need. Less community engagement.		[77,87]	More research is need. High community engagement.		[73,79,99,100]

The research of decentralization is still in its relative infancy. Decentralization is not solely referring to downscaling to the degree of individual homes. It should be effectively linked to other alternative options such as dual water quality, energy and material recovery, and fit-for-purpose. This is exactly why we need more in depth research and demonstration in this area. Nevertheless, more needs to be done to demonstrate reliable performances and gain more experiences in its applications. Theoretical modeling and calculations provide bases for such explorations. Without trial and error, we will not be able to confidently know if it is better or worst. However, one thing we know for sure is that the current centralized system is not sustainable. One example of a non-sustainable condition of a centralized approach is the high initial investment, maintenance and update, which is a burden on the local economy [77].

Future-oriented neighborhood should be built not only considering environmental sustainability which is characterized by a water-energy self-sufficient community, but also social sustainability in terms of public spaces (e.g., central park with water feature, communal garden with locally generated fertilizer and walkable green space with more mature trees) that promote social wellness and stability for a resilient community.

5. Moving Forward

The water system for the City of Tomorrow is fundamentally different from the conventional water systems. It may represent an ideal scenario for an urban water system, however, it by no means is the best or the only alternative. It also does not discredit other means that are not included here such as water conservation or efficiency improvement. In reality, a variety of factors affect the selection of the optimum configuration for a particular urban area, including local hydrology, water resource availability, water demands, local energy and nutrient-management situations, existing infrastructure, and utility governance structure [160]. There is no one-size-fits-all solution. The effort here is to demonstrate a holistic method that potentially resolves trade-offs across spatial, temporal scales based on thermodynamic principles to address various issues facing urban systems, no matter how the system designs would be. The example design of a future system here reveals how system thinking can be realized in transformative water systems and how the sub-components can be integrated based on system optimization. Nevertheless, such a paradigm shift is no easy task. The current standards, practices, codes, and municipal requirements that guide engineering practice result in the institutional inertia [88].

There are no test models, policy playbooks or historical data to confidently guide investors and decision-makers. The transformative changes may initially seem to be unrealistic or mission impossible. What is clear, however, is that even with plenty of evidence demonstrating the ineffectiveness of the conventional systems, more evidences of the effectiveness of new, alternative options are needed before abandoning faith in an institutional belief that has significantly supported markets and practices in the past centuries. Most importantly, it has to demonstrate that holistic analysis is not just an environmental, sustainable practice, but also has substantial economic gains for the community in the long run [3]. Prevailing systems are those whose designs maximize the productivity at the optimum efficiency [161].

The new water system will also require a new operating structure and governance framework to accommodate complexity and uncertainty [162]. Drinking water, wastewater and stormwater professionals are no longer separated in different institutions or departments. A truly integrated collaboration and management is required to achieve holistic system-wide planning and operation. A new revenue model

is needed that is not solely based on the flow and water usage, but rather on whole system efficiency such as energy and nutrient recovery. The economic appeal to those public utilities that struggle financially may be the main driving force for transformative changes [3,17]. More research and testing are needed for the new technologies, such as scale-up anaerobic digestion of blackwater, membrane reactors, struvite crystallization, constructed wetland and green infrastructure practices and to validate whether the new technologies provide the same protection for the public health and the ecosystem. New integrated tool and metrics such as emergy accounting are needed to explore the holistic analysis in water systems [148,149,163,164].

Finally, public perception and acceptance will be a critical factor to roll out these new ideas. The public may not be receptive to new ideas such as dual water quality, urine diversion toilets, or reclaimed water. Risk perception for most people is not from a scientific, mathematical calculation, but a gut feeling [165]. To win people over involves the delicate work of overcoming deep-rooted psychological barriers and cultural taboos surrounding water use [165]. The "yuck factor" has scuttled proposed wastewater recycling projects in San Diego, Los Angeles and elsewhere [165]. However, from a psychological perspective, when the public is being educated and communicated and the ideas are reframed differently such as reuse projects in the context of the urban water cycle and water as a reusable resource, the public is more willing to accept the ideas. In Singapore, the government has been successfully educating the public and 98% of the people now believe that reclaimed water is safe to drink [166,167].

It is encouraging to find that many communities around the world are taking steps towards more sustainable solutions [141,168]. Jenfelder Au in Hamburg, Germany is rethinking wastewater management by implementing an integrated concept for decentralized wastewater treatment, stormwater/greywater treatment, and energy recovery [169]. The city of San Francisco's non-potable water program currently aims to expand the recycled water reuse on the district-scale. The city of San Jose in northern California has been operating a dual distribution network since 1997 over 1.6 km (100 miles) and 1.4×10^6 m^3/year (10 mgd) serving over 690 customers [90]. Their current goal is to recycle 1.4×10^7 m^3/year (100 mgd) wastewater by 2022. In 2013, the city of Chicago announced the construction of the world's largest nutrient recovery facility with the potential capacity of 10,000–15,000 tons of fertilizer per year. To increase public acceptance, communities, government agencies, academics and other stakeholders should all work together and carry out more real world applications like "test beds" and "demo villages" such as those to help implement the needed changes at a faster pace. A thousand mile journey begins by taking the first step. As communities are taking incremental steps towards a more sustainable future, the City of Tomorrow will soon become the City of Today.

Acknowledgments

This research was part of the Safe and Sustainable Water Resources National Research Program in the EPA's Office of Research and Development and was supported in part by the appointments of Xiaobo Xue and Alejandra González-Mejía to the ORISE participant research program.

Author Contributions

Xin (Cissy) Ma conceptualized the design of urban water systems for the City of Tomorrow, conducted the emergy calculations and conceived the need for this review paper. Xin (Cissy) Ma drafted the earlier versions of the manuscript. Xiaobo Xue contributed to the discussions and literature review of the conventional systems. Alejandra González-Mejía contributed to the review of resource recovery, critical review and edition of the manuscript. Jay Garland and Jennifer Cashdollar provided constructive suggestions for the reorganization of the manuscript and critically reviewed the draft. All authors have read and approved the final manuscript.

Conflicts of Interest

The views expressed in this article are those of the authors and do not necessarily reflect the views or policies of the Environmental Protection Agency.

References

1. Miller, R.W.; Donahue, R.L. *Soils in Our Environment*, 7th ed.; Prentice-Hall Inc.: Eaglewood Cliffs, NJ, USA, 1990; p. 649.
2. United Nations Environment Programme. *Status Report on the Application of Integrated Approaches to Water Resources Management*; United Nations Environment Programme: Nairobi, Kenya, 2012; p. 119.
3. Bloomberg, M.; Paulson, H.; Steyer, T. Risky Business: The Economic Risks of Climate Change in the United States. Available online: http://riskybusiness.org/ (accessed on 26 June 2014).
4. Bates, B.C.; Kundzewicz, Z.W.; Wu, S.; Palutikof, J.P. *Climate Change and Water*; Intergovernmental Panel on Climate Change: Geneva, Switzerland, 2008; p. 210.
5. Melillo, J.M.; Richmond, T.C.; Yohe, G.W. *Climate Change Impacts in the United States: The Third National Climate Assessment*; U.S. Global Change Research Program: Washington, DC, USA, 2014; p. 841.
6. Schnoor, J.L. When the well runs dry. *Environ. Sci. Technol.* **2014**, *48*, 5351–5351.
7. Cordell, D.; Drangert, J.-O.; White, S. The story of phosphorus: Global food security and food for thought. *Global Environ. Chang.* **2009**, *19*, 292–305.
8. Jasinski, S.M. Phosphate rock. Mineral Commodity Summaries. U.S. Geological Survey. Available online: http://minerals.usgs.gov/minerals/pubs/commodity/phosphate_rock/index.html (accessed on 17 December 2012).
9. Mino, T.; van Loosdrecht, M.C.M.; Heijnen, J.J. Review paper: Microbiology and biochemistry of the enhanced biological phosphate removal process. *Water Res.* **1998**, *32*, 3193–3207.
10. Britton, A.; Koch, F.A.; Mavinic, D.S.; Adnan, A.; Oldham, W.K.; Udala, B. Pilot-scale struvite recovery from anaerobic digester supernatant at an enhanced biological phosphorus removal wastewater treatment plant. *J. Environ. Eng. Sci.* **2005**, *4*, 265–277.
11. Oguz, E.; Gurses, A.; Canpolat, N. Removal of phosphate from wastewaters. *Cement Concr. Res.* **2003**, *33*, 1109–1113.

12. Zeng, L.; Li, X.; Liu, J. Adsorptive removal of phosphate from aqueous solutions using iron oxide tailings. *Water Res.* **2004**, *38*, 1318–1327.
13. Metson, G.S.; Iwaniec, D.M.; Baker, L.A.; Bennett, E.M.; Childers, D.L.; Cordell, D.; Grimm, N.B.; Grove, J.M.; Nidzgorski, D.A.; White, S. Urban phosphorus sustainability: Systemically incorporating social, ecological, and technological factors into phosphorus flow analysis. *Environ. Sci. Policy* **2015**, *47*, 1–11.
14. Da Silva, A.K.; Amador, J.; Cherchi, C.; Miller, S.M.; Morse, A.N.; Pellegrin, M.L.; Wells, M.J.M. Emerging pollutants—Part i: Occurrence, fate and transport. *Water Environ. Res.* **2013**, *85*, 1978–2021.
15. Bell, K.Y.; Bandy, J.; Beck, S.; Keen, O.; Kolankowsky, N.; Parker, A.M.; Linden, K. Emerging pollutants—Part ii: Treatment. *Water Environ. Res.* **2012**, *84*, 1909–1940.
16. Brookes, J.D.; Carey, C.C.; Hamilton, D.P.; Ho, L.; van der Linden, L.; Renner, R.; Rigosi, A. Emerging challenges for the drinking water industry. *Environ. Sci. Technol.* **2014**, *48*, 2099–2101.
17. Novotny, V.; Ahern, J.; Brown, P. *Water Centric Sustainable Communities*; John Wiley & Sons, Inc.: Hoboken, NJ, USA, 2010.
18. Sedlak, D.L.; Schnoor, J.L. The challenge of water sustainability. *Environ. Sci. Technol.* **2013**, *47*, 5517.
19. Hill, K. Urban ecological design and urban ecology: An assessment of the state of current knowledge and a suggested research agenda. In *Cities of the Future: Towards Integrated Sustainable Water and Landscape Management*; Novotny, V., Brown, P., Eds.; IWA Publishing: London, UK, 2007; pp. 251–266.
20. Arceivala, S.J. *Wastewater Treatment and Disposal: Engineering and Ecology in Pollution Control*; Marcel Dekker, Inc.: New York, NY, USA, 1981.
21. Walsh, C. Urban impacts on the ecology of receiving waters: A framework for assessment, conservation and restoration. *Hydrobiologia* **2000**, *431*, 107–114.
22. Sirés, I.; Brillas, E. Remediation of water pollution caused by pharmaceutical residues based on electrochemical separation and degradation technologies: A review. *Environ. Int.* **2012**, *40*, 212–229.
23. Kishida, N.; Kim, J.; Tsuneda, S.; Sudo, R. Anaerobic/oxic/anoxic granular sludge process as an effective nutrient removal process utilizing denitrifying polyphosphate-accumulating organisms. *Water Res.* **2006**, *40*, 2303–2310.
24. Sakadevan, K.; Bavor, H.J. Nutrient removal mechanisms in constructed wetlands and sustainable water management. *Water Sci. Technol.* **1999**, *40*, 121–128.
25. Van Loosdrecht, M.C.M.; Brandse, F.A.; de Vries, A.C. Upgrading of waste water treatment processes for integrated nutrient removal—The BCFS® process. *Water Sci. Technol.* **1998**, *37*, 209–217.
26. Boyer, T.H.; Singer, P.C. Bench-scale testing of a magnetic ion exchange resin for removal of disinfection by-product precursors. *Water Res.* **2005**, *39*, 1265–1276.
27. Petrović, M.; Gonzalez, S.; Barceló, D. Analysis and removal of emerging contaminants in wastewater and drinking water. *TrAC Trends Anal. Chem.* **2003**, *22*, 685–696.
28. Bolong, N.; Ismail, A.F.; Salim, M.R.; Matsuura, T. A review of the effects of emerging contaminants in wastewater and options for their removal. *Desalination* **2009**, *239*, 229–246.

29. Macler, B.A.; Regli, S. Use of microbial risk assessment in setting us drinking water standards. *Int. J. Food Microbiol.* **1993**, *18*, 245–256.
30. Ashbolt, N.J.; Schoen, M.E.; Soller, J.A.; Roser, D.J. Predicting pathogen risks to aid beach management: The real value of quantitative microbial risk assessment (QMRA). *Water Res.* **2010**, *44*, 4692–4703.
31. Schoen, M.E.; Xue, X.; Hawkins, T.R.; Ashbolt, N.J. Comparative human health risk analysis of coastal community water and waste service options. *Environ. Sci. Technol.* **2014**, *48*, 9728–9736.
32. Brown, A.; Matlock, M.D. *A Review of Water Scarcity Indices and Methodologies*; White Paper #106; The Sustainability Consortium: Fayetteville, AR, USA, 2011; p. 19.
33. Schewe, J.; Heinke, J.; Gerten, D.; Haddeland, I.; Arnell, N.W.; Clark, D.B.; Dankers, R.; Eisner, S.; Fekete, B.M.; Colón-González, F.J.; *et al.* Multimodel assessment of water scarcity under climate change. *Proc. Natl. Acad. Sci. USA* **2014**, *111*, 3245–3250.
34. Lubick, N. Using nature's design to stem urban storm-water problems. *Environ. Sci. Technol.* **2006**, *40*, 5832–5833.
35. Jang, S.; Cho, M.; Yoon, J.; Yoon, Y.; Kim, S.; Kim, G.; Kim, L.; Aksoy, H. Using swmm as a tool for hydrologic impact assessment. *Desalination* **2007**, *212*, 344–356.
36. Bos, J.J.; Gijzen, H.J.; Hilderink, H.B.M.; Moussa, M.; de Ruyter van Steveninck, E.D. *Quick Scan Health Benefits and Costs of Water Supply and Sanitation*; National Institute for Public Health and the Environment: Bilthoven, The Netherlands, 2004.
37. Brown, M.T.; Martínez, A.; Uche, J. Emergy analysis applied to the estimation of the recovery of costs for water services under the european water framework directive. *Ecol. Model.* **2010**, *221*, 2123–2132.
38. Maurer, M. Full costs, (dis-)economies of scale and the price of uncertainty. In *Source Separation and Decentralization for Wastewater Management*; Larsent, T.A., Udert, K.M., Lienert, J., Eds.; IWA Publishing: London, UK, 2013; pp. 85–100.
39. Guest, J.; Skerlos, S.; Barnard, J.; Beck, M.; Daigger, G.; Hilger, H.; Jackson, S.; Karvazy, K.; Kelly, L.; Macpherson, L.; *et al.* A new planning and design paradigm to achieve sustainable resource recovery from wastewater. *Environ. Sci. Technol.* **2009**, *43*, 6126–6130.
40. Tzoulas, K.; Korpela, K.; Venn, S.; Yli-Pelkonen, V.; Kaźmierczak, A.; Niemela, J.; James, P. Promoting ecosystem and human health in urban areas using green infrastructure: A literature review. *Landsc. Urban Plan.* **2007**, *81*, 167–178.
41. Solano, M.L.; Soriano, P.; Ciria, M.P. Constructed wetlands as a sustainable solution for wastewater treatment in small villages. *Biosyst. Eng.* **2004**, *87*, 109–118.
42. Hurlimann, A.C.; McKay, J.M. What attributes of recycled water make it fit for residential purposes? The mawson lakes experience. *Desalination* **2006**, *187*, 167–177.
43. Mayer, P.; DeOreo, W.B.; Opitz, E.M.; Kiefer, J.C.; Davis, W.Y.; Dziegielewski, B.; Nelson, J.O. *Resiential end Uses of Water*; American Water Works Association Research Foundation: Denver, CO, USA, 1999.
44. National Research Council of the National Academies. *Drinking Water Distribution Systems: Assessing and Reducing Risks*; National Academies Press: Washington, DC, USA, 2006; p. 404.
45. Okun, D.A. Letter to the editor: Designing future water distribution systems. *J. Amer. Water Works Assoc.* **2005**, *6*, 99–101.

46. National Fire Protection Association (NFPA). *Fire Protection Handbook*; National Fire Protection Association (NFPA): Batterymarch Park Quincy, MA, USA, 1986.
47. Walski, T.M.; Chase, D.V.; Savic, D.A. *Water Distribution Modeling*, 1st ed.; Haestad Press: Waterbury, CT, USA, 2001.
48. Clark, R.M.; Grayman, W.M. Distribution system quality: A trade-off between public health and public safety. *J. Am. Water Works Assoc.* **1992**, *84*, 18.
49. Brandt, M.J. *Managing Distribution Retention Time to Improve Water Quality—Phase ii: Guidance Manual*; AWWRF Report 91121F; American Water Works Association Research Foundation: London, UK, 2007.
50. Lindeburg, M.R. Water supply treatment and distribution. In *Environmental Engineering Reference Manual for the PE Exam*, 2nd ed.; Professional Publications Inc.: Belmont, CA, USA, 2003; pp. 2418–2419.
51. Solomon, S. *Water: The Epic Struggle for Wealth, Power, and Civilization*; HarperCollins Publishers: New York, NY, USA, 2010.
52. Gikas, P.; Tchobanoglous, G. The role of satellite and decentralized strategies in water resources management. *J. Environ. Manag.* **2009**, *90*, 144–152.
53. Gleick, P.H. Global freshwater resources: Soft-path solutions for the 21st century. *Science* **2003**, *302*, 1524–1528.
54. U.S. Environmental Protection Agency. The Clean Water and Drinking Water Infrastructure Gap Analysis. Available online: http://www.epa.gov/ogwdw/gapreport.pdf (accessed on 9 April 2014).
55. American Society of Civil Engineers. *2013 Report Card for America's Infrastructure*; American Society of Civil Engineers: Reston, VA, USA, 2013.
56. Libralato, G.; Ghirardini, A.V.; Avezzu, F. To centralize or to decentralize: An overview of the most recent trends in wastewater treatment management. *J. Environ. Manag.* **2012**, *94*, 61–68.
57. U.S. Environmental Protection Agency. Energy Efficiency in Water and Wastewater Facilities. A Guide to Developing and Implementing Greenhouse Gas Reduction Programs. Local Government Climate and Energy Strategy Guides. Available online: www.epa.gov/statelocalclimate/resources/strategy-guides.html (accessed on 10 February 2015).
58. U.S. Environmental Protection Agency. Combined Sewer Overflows. Available online: http://cfpub.epa.gov/npdes/home.cfm (Accessed on 9 April 2014).
59. The Great Lakes—Upper Mississippi River Board of State and Provincial Public Health and Environmental Managers. *Recommended Standards for Water Works*; The Great Lakes—Upper Mississippi River Board of State and Provincial Public Health and Environmental Managers: Albany, NY, USA, 2012.
60. Klein, G. *California's Water–Energy Relationship*; California Energy Commission: Sacramento, CA, USA, 2005; p. 174.
61. Water Environment Federation. *Alternative Sewer Systems: Manual of Practice No. Fd-12*, 2nd ed.; WEF Press: Alexandria, VA, USA, 2008.
62. Factura, H.; Bettendorf, T.; Buzie, C.; Pieplow, H.; Reckin, J.; Otterpohl, R. Terra preta sanitation: Re-discovered from an ancient amazonian civilisation—Integrating sanitation, bio-waste management and agriculture. *Water Sci. Technol.* **2010**, *61*, 2673–2679.

63. Stichting Toegepas t Onder zoek Waterbeheer (STOWA). *Separate Urine Collection and Treatment: Options for Sustainable Wastewater Systems and Mineral Recovery*; STOWA: Amersfoort, The Netherlands, 2001.
64. The National Association of Clean Water Agencies (NACWA). *2008 Nacwa Financial Survey Summary: Highlighting Challenges in Utility Financing and Management*; NACWA: Washington, DC, USA, 2008.
65. Hering, J.G.; Waite, T.D.; Luthy, R.G.; Drewes, J.E.; Sedlak, D.L. A changing framework for urban water systems. *Environ. Sci. Technol.* **2013**, *47*, 10721–10726.
66. Heidrich, E.S.; Curtis, T.P.; Dolfing, J. Determination of the internal chemical energy of wastewater. *Environ. Sci. Technol.* **2011**, *45*, 827–832.
67. Grant, S.B.; Saphores, J.-D.; Feldman, D.L.; Hamilton, A.J.; Fletcher, T.D.; Cook, P.L.M.; Stewardson, M.; Sanders, B.F.; Levin, L.A.; Ambrose, R.F.; *et al.* Taking the "waste" out of "wastewater" for human water security and ecosystem sustainability. *Science* **2012**, *337*, 681–686.
68. McCarty, P.L.; Bae, J.; Kim, J. Domestic wastewater treatment as a net energy producer—Can this be achieved? *Environ. Sci. Technol.* **2011**, *45*, 7100–7106.
69. Otterpohl, R.; Grottker, M.; Lange, J. Sustainable water and waste management in urban areas. *Water Sci. Technol.* **1997**, *35*, 121–133.
70. Pennisi, E. Water reclamation going green. *Science* **2012**, *337*, 674–676.
71. Raucher, R.; Tchobanoglous, G. *The Opportunities and Economics of Direct Potable Reuse*; WaterReuse Research Foundation: Alexandria, VA, USA, 2014.
72. Tchobanoglous, G.; Leverenz, H. The rationale for decentralization of wastewater infrastructure. In *Source Separation and Decentralization for Wastewater Management*; Larsen, T.A., Udert, K.M., Lienert, J., Eds.; IWA Publishing: London, UK, 2013; pp. 101–115.
73. Gardner, T.; Sharma, A. Development of decentralized systems in Australia. In *Source Separation and Decentralization for Wastewater Management*; Larsen, T.A., Udert, K.M., Lienert, J., Eds.; IWA Publishing: London, UK, 2013; pp. 511–520.
74. Lee, E.J.; Criddle, C.S.; Bobel, P.; Freyberg, D.L. Assessing the scale of resource recovery for centralized and satellite wastewater treatment. *Environ. Sci. Technol.* **2013**, *47*, 10762–10770.
75. Makropoulos, C.; Butler, D. Distributed water infrastructure for sustainable communities. *Water Resour. Manag.* **2010**, *24*, 2795–2816.
76. Strother, N. Smart Water Making Gains beyond the U.S. Available online: http://www.smartgridnews.com/artman/publish/Technologies_Smart_Water/Smart-water-making-gains-beyond-the-U-S-6155.html (accessed on 3 June 2014).
77. Wilderer, P.A.; Schreff, D. Decentralised and centralised wastewater management: A challenge for developers. *Water Sci. Technol.* **2000**, *41*, 1–8.
78. Anderson, J.; Leinmiller, M. Why Smart Grid and Smart Water are Essential to A Smart City. Available online: http://www.smartgridnews.com/artman/publish/Technologies_Smart_Water/Why-smart-grid-and-smart-water-are-essential-to-a-smart-city-6365.html (accessed on 3 June 2014).
79. Hiessl, H. Alternative Scenarios of Urban Water Infrasturcture Systems. In Proceedings of the OECD Expert Meeting on "Sustainable Financing for Affordable Water Services: From Theory to Practice", Paris, France, 14–15 November 2007.

80. Larsen, T.A.; Gujer, W. Implementation of source separation and decentralization in cities. In *Source Separation and Decentralization for Wastewater Management*; Larsen, T.A., Udert, K.M., Lienert, J., Eds.; IWA Publishing: London, UK, 2013; pp. 135–150.
81. Boller, M. Source control and source separation: The Swiss experience. In *Source Separation and Decentralization for Wastewater Management*; Larsen, T.A., Udert, K.M., Lienert, J., Eds.; IWA Publishing: London, UK, 2013; pp. 439–446.
82. Londong, J. Practical experience with source separation in Germany. In *Source Separation and Decentralization for Wastewater Management*; Larsen, T.A., Udert, K.M., Lienert, J., Eds.; IWA Publishing: London, UK, 2013; pp. 423–430.
83. Sharma, A.; Grant, A.; Tjandraatmadja, G.; Grant, T.; Opray, L.; Pamminger, F. Towards sustainable water and sewerage servicing options for a multi-story infill development. In *Water Management Challenges in Global Change: Proceedings of the 9th Computing and Control for the Water Industry (CCWI 2007) and the Sustainable Urban Water Management (SUWM 2007) Conferences*; Ulanicki, B., Vairavamoorthy, K., Butler, D., Bounds, P., Memon, F., Eds.; Taylor & Francis: London, UK, 2007; pp. 507–513.
84. Weber, J.W. Optimal uses of advanced technologies for water and wastewater treatment in urban environments. *Water Supply* **2004**, *4*, 7–12.
85. Weber, J.W. Distributed optimal technology networks: A concept and strategy for potable water sustainability. *Water Sci. Technol.* **2002**, *46*, 241–246.
86. Davis, C.; Nikolic, I.; Dijkema, G.P.J. Integration of life cycle assessment into agent-based modeling. *J. Ind. Ecol.* **2009**, *13*, 306–325.
87. Childers, D.L.; Pickett, S.T.A.; Grove, J.M.; Ogden, L.; Whitmer, A. Advancing urban sustainability theory and action: Challenges and opportunities. *Landsc. Urban Plan.* **2014**, *125*, 320–328.
88. Grigg, N.; Rogers, P.; Edmiston, S. *Dual Water Systems: Characterization and Performance for Distribution of Reclaimed Water*; Web Report #4333; Water Research Foundation: Denver, CO, USA, 2013.
89. American Water Works Association (AWWA). *Planning for the Distribution of Reclaimed Water*; AWWA: Denver, CO, USA, 2009.
90. Okun, D.A. Distribuing reclaimed water through dual systems. *J. Amer. Water Works Assoc.* **1997**, *89*, 52–64.
91. National Research Council. *Water Conservation, Reuse, and Recycling: Proceedings of an Iranian-American Workshop*; The National Academies Press: Washington, DC, USA, 2005.
92. U.S. Environmental Protection Agency. *Guidelines for Water Reuse*; EPA/600/R-12/618; U.S. Environmental Protection Agency: Washington, DC, USA, 2012.
93. Grant, S.B.; Fletcher, T.D.; Feldman, D.; Saphores, J.-D.; Cook, P.L.M.; Stewardson, M.; Low, K.; Burry, K.; Hamilton, A.J. Adapting urban water systems to a changing climate: Lessons from the millennium drought in southeast Australia. *Environ. Sci. Technol.* **2013**, *47*, 10727–10734.
94. Mohanty, S.K.; Torkelson, A.A.; Dodd, H.; Nelson, K.L.; Boehm, A.B. Engineering solutions to improve the removal of fecal indicator bacteria by bioinfiltration systems during intermittent flow of stormwater. *Environ. Sci. Technol.* **2013**, *47*, 10791–10798.

95. Armentano, T.V. Drainage of organic soils as a factor in the world carbon cycle. *BioScience* **1980**, *30*, 825–830.
96. Odum, E.P.; Barrett, G.W. *Fundamental of Ecology*, 5th ed.; Brooks/Cole: Belmont, CA, USA, 2005.
97. Jasper, J.T.; Sedlak, D.L. Phototransformation of wastewater-derived trace organic contaminants in open-water unit process treatment wetlands. *Environ. Sci. Technol.* **2013**, *47*, 10781–10790.
98. Kusler, J. Common questions: Wetlands, climate change, and carbon sequestering. Available online: http://aswm.org/pdf_lib/11_carbon_6_26_06.pdf (accessed on 9 April 2014).
99. Wendel, H.E.W.; Downs, J.A.; Mihelcic, J.R. Assessing equitable access to urban green space: The role of engineered water infrastructure. *Environ. Sci. Technol.* **2011**, *45*, 6728–6734.
100. Mazzotta, M.J.; Besedin, E.; Speers, A.E. A meta-analysis of hedonic studies to assess the property value effects of low impact development. *Resources* **2014**, *3*, 31–61.
101. The National Association of Clean Water Agencies (NACWA); The Water Environment Research Foundation (WERF); The Water Environment Federation (WEF). *The Water Resources Utility of the Future: A Blueprint for Action*; NACWA: Washington, DC, USA; WERF: Washington, DC, USA; WEF: Washington, DC, USA, 2013; p. 48.
102. U.S. Environmental Protection Agency. Reducing urban heat islands: Compendium of strategies. Available online: http://www.epa.gov/heatisland/resources/compendium.htm (accessed on 30 May 2014).
103. Romitelli, M.S. *Energy Analysis of Watersheds*; University of Florida: Gainsville, FL, USA, 1997.
104. Peng, S.; Piao, S.; Ciais, P.; Friedlingstein, P.; Ottle, C.; Bréon, F.-M.; Nan, H.; Zhou, L.; Myneni, R.B. Surface urban heat island across 419 global big cities. *Environ. Sci. Technol.* **2011**, *46*, 696–703.
105. Shepherd, J.M. A review of current investigations of urban-induced rainfall and recommendations for the future. *Earth Interact.* **2005**, *9*, 1–27.
106. Arden, S.; Ma, X.; Brown, M. Ecohydrologic effects of urbanization on evapotranspiration in shallow groundwater table environments. *Water Sci. Technol.* **2014**, *70*, 1789–1797.
107. U.S. Environmental Protection Agency. *Protecting Water Quality from Urban Runoff*; EPA 841-F-03-003; U.S. Environmental Protection Agency: Washington, DC, USA, 2003.
108. Coffman, L. Low-impact development design strategies, an integrated design approach. Prince George's County, Maryand. Available online: http://water.epa.gov/polwaste/green/upload/lidnatl.pdf (accessed on 25 June 2014).
109. Odum, E.P. *Basic Ecology*; Saunders College Pub.: Philadelphia, PA, USA, 1983.
110. Saddleback Educational Publishing. *Water Conservation*; Saddleback Educational Publishing: Costa Mesa, CA, USA, 2009.
111. Southern Nevada Water Authority. Water Banking. Available online: http://www.snwa.com/ws/future_banking.html (accessed on 25 June 2014).
112. Panfil, C.; Mirel, I.; Szigyarto, I.; Isacu, M. Technical, economical, social and ecological characteristics of vacuum sewage system. *Environ. Eng. Manag. J.* **2013**, *12*, 1017–1022.
113. U.S. Environmental Protection Agency. *Composting Yard Trimmings and Municipal Solid Waste*; EPA530-R-94-003; U.S. Environmental Protection Agency: Washington, DC, USA, 1994.

114. Larsen, T.A.; Alder, A.C.; Eggen, R.I.L.; Maurer, M.; Lienert, J. Source separation: Will we see a paradigm shift in wastewater handling? *Environ. Sci. Technol.* **2009**, *43*, 6121–6125.
115. Otterpohl, R. Options for alternative types of sewerage and treatment systems directed to improvement of the overall performance. *Water Sci. Technol.* **2002**, *45*, 149–158.
116. Vogel, G. Finding a new way to go. *Science* **2012**, *337*, 673.
117. Gutschick, V. Energy and nitrogen fixation. *BioScience* **1978**, *28*, 571–575.
118. Smil, V. Enriching the Earth: Fritz Haber, Carl Bosch, and the Transformation of World Food Production; The MIT Press: Cambridge, MA, USA, 2004.
119. Metson, G.S.; Hale, R.L.; Iwaniec, D.; Cook, E.M.; Gorman, J.R.; Galletti, C.S.; Childers, D.L. Phosphorus in phoenix: A budget and spatial representation of phosphorus in an urban ecosystem. *Ecol. Appl.* **2012**, *22*, 705–721.
120. Childers, D.L.; Corman, J.; Edwards, M.; Elser, J.J. Sustainability challenges of phosphorus and food: Solutions from closing the human phosphorus cycle. *BioScience* **2011**, *61*, 117–124.
121. Rahman, M.M.; Salleh, M.A.M.; Rashid, U.; Ahsan, A.; Hossain, M.M.; Ra, C.S. Production of slow release crystal fertilizer from wastewaters through struvite crystallization—A review. *Arab. J. Chem.* **2014**, *7*, 139–155.
122. Mo, W.W.; Zhang, Q. Energy-nutrients-water nexus: Integrated resource recovery in municipal wastewater treatment plants. *J. Environ. Manag.* **2013**, *127*, 255–267.
123. De-Bashan, L.; Bashan, Y. Recent advances in removing phosphorus from wastewater and its future use as fertilizer (1997–2003). *Water Res.* **2004**, *38*, 4222–4246.
124. Gaterell, M.R.; Gay, R.; Wilson, R.; Gochin, R.J.; Lester, J.N. An economic and environmental evaluation of the opportunities for substituting phosphorus recovered from wastewater treatment works in existing UK fertiliser markets. *Environ. Technol.* **2000**, *21*, 1067–1084.
125. Logan, B.E.; Rabaey, K. Conversion of wastes into bioelectricity and chemicals by using microbial electrochemical technologies. *Science* **2012**, *337*, 686–690.
126. U.S. Environmental Protection Agency. Case study primer for participant discussion: Biodigesters and biogas. Available online: http://www.epa.gov/agstar/documents/biogas_primer.pdf (accessed on 9 April 2014).
127. Moriarty, K. Feasibility study of anaerobic digestion of food waste in st. Bernard, Louisiana. National Renewable Energy Laboratory. Available online: http://www.nrel.gov/docs/fy13osti/57082.pdf (accessed on 11 April 2014).
128. Augustin, K.; Skambraks, A.-K.; Li, Z.; Giese, T.; Rakelmann, U.; Meinzinger, F.; Schonlau, H.; Günner, C. Towards sustainable sanitation—The hamburg water cycle in the settlement jenfelder Au. *Water Sci. Technol.: Water Supply* **2014**, *14*, 13–21.
129. De Graaff, M.; Temmink, H.; Zeeman, G.; Buisman, C. Anaerobic treatment of concentrated black water in a uasb reactor at a short HRT. *Water* **2010**, *2*, 101–119.
130. Xu, S.N.; Wu, D.L.; Hu, Z.Q. Impact of hydraulic retention time on organic and nutrient removal in a membrane coupled sequencing batch reactor. *Water Res.* **2014**, *55*, 12–20.
131. Kim, J.; Kim, K.; Ye, H.; Lee, E.; Shin, C.; McCarty, P.L.; Bae, J. Anaerobic fluidized bed membrane bioreactor for wastewater treatment. *Environ. Sci. Technol.* **2010**, *45*, 576–581.

132. Shin, C.; McCarty, P.L.; Kim, J.; Bae, J. Pilot-scale temperate-climate treatment of domestic wastewater with a staged anaerobic fluidized membrane bioreactor (SAF-MBR). *Bioresour. Technol.* **2014**, *159*, 95–103.
133. Zeeman, G.; Kujawa, K.; de Mes, T.; Hernandez, L.; de Graaff, M.; Abu-Ghunmi, L.; Mels, A.; Meulman, B.; Temmink, H.; Buisman, C.; *et al.* Anaerobic treatment as a core technology for energy, nutrients and water recovery from source-separated domestic waste(water). *Water Sci. Technol.* **2008**, *57*, 1207–1212
134. Lettinga, G.; Roersma, R.; Grin, P. Anaerobic treatment of raw domestic sewage at ambient-temperatures using a granular bed UASB reactor. *Biotechnol. Bioeng.* **1983**, *25*, 1701–1723.
135. Ren, L.J.; Ahn, Y.; Logan, B.E. A two-stage microbial fuel cell and anaerobic fluidized bed membrane bioreactor (MFC-AFMBR) system for effective domestic wastewater treatment. *Environ. Sci. Technol.* **2014**, *48*, 4199–4206.
136. U.S. Environmental Protection Agency. *Opportunites for and Benefits of Combined Heat and Power at Wastewater Treatment Facilities*; EPA-430-R-07-003; U.S. Environmental Protection Agency: Washington, DC, USA, 2007.
137. Lindtrom, H.O. Experiences with a 3.3 MW heat pump using sewage water as heat source. *Heat Recovery Systems* **1985**, *5*, 33–38.
138. Lin, S.; Yip, N.Y.; Cath, T.Y.; Osuji, C.O.; Elimelech, M. Hybrid pressure retarded osmosis–membrane distillation system for power generation from low-grade heat: Thermodynamic analysis and energy efficiency. *Environ. Sci. Technol.* **2014**, *48*, 5306–5313.
139. Lehmann, S. *The Principles of Green Urbanism-Transforming the City for Sustainability*; Routledge: New York, NY, USA, 2010.
140. Brown, R.R.; Keath, N.; Wong, T.H.F. Urban water management in cities: Historical, current and future regimes. *Water Sci. Technol.* **2009**, *59*, 847–855.
141. Global Water Partnership. Toolbox: Case Studies. Available online: http://www.gwp.org/en/ToolBox/CASE-STUDIES/ (accessed on 8 October 2014).
142. Xue, X.; Schoen, M.E.; Ma, X.; Hawkins, T.R.; Ashbolt, N.J.; Cashdollar, J.; Garland, J. Critical insights for a sustainability framework to address integrated community water services: Technical metrics and approaches. *Water Res.* **2015**, *77*, 155–169.
143. Wood, A.; Blackhurst, M.; Hawkins, T.; Xue, X.; Ashbolt, N.; Garland, J. Cost-effectiveness of nitrogen mitigation by alternative household wastewater management technologies. *J. Environ. Manag.* **2015**, *150*, 344–354.
144. Thomson Reuters. Web of science [v.5.18] (search engine). Available online: http://thomsonreuters.com/en/products-services/scholarly-scientific-research/scholarly-search-and-discovery/web-of-science.html (accessed on 10 August 2015).
145. Fugaro, L.; Picchi, M.P.; Principi, I. *Application of Emergy Analysis to Sustainable Management of Water Resources*; A. A. Balkema Publishers: Leiden, The Netherlands, 2004; pp. 37–43.
146. Arbault, D.; Rugani, B.; Tiruta-Barna, L.; Benetto, E. Emergy evaluation of water treatment processes. *Ecol. Eng.* **2013**, *60*, 172–182.
147. Zhou, J.B.; Jiang, M.M.; Chen, B.; Chen, G.Q. Emergy evaluations for constructed wetland andconventional wastewater treatments. *Communications in Nonlinear Science and Numerical Simulation* **2009**, *14*, 1781–1789.

148. Hester, E.T.; Little, J.C. Measuring environmental sustainability of water in watersheds. *Environ. Sci. Technol.* **2013**, *47*, 8083–8090.
149. Odum, H.T. *Environmental Accounting*; John Wiley & Sons: New York, NY, USA, 1996.
150. Gleick, P. Water Use. *Annu. Rev. Environ. Resour* **2003**, *28*, 275–314.
151. Odum, H.T. Emergy evaluation. In *International Workshop on Advances in Energy Studies: Energy Flows in Ecology and Economy*; Biennial International Workshop Advances in Energy Studies: Porto Venere, Italy, 1998.
152. Prigogine, I.; Nicolis, G.; Babloyants, A. Thermodynamics of evolution (part i). *Phys. Today* **1972**, *25*, 23–28.
153. Prigogine, I.; Nicolis, G.; Babloyants, A. Thermodynamics of evolution (part ii). *Phys. Today* **1972**, *25*, 38–44.
154. Brown, M.T.; Ulgiati, S. Updated evaluation of exergy and emergy driving the geobiosphere: A review and refinement of the emergy baseline. *Ecol. Model.* **2010**, *221*, 2501–2508.
155. Björklund, J.; Geber, U.; Rydberg, T. Emergy analysis of municipal wastewater treatment and generation of electricity by digestion of sewage sludge. *Resour. Conserv. Recycl.* **2001**, *31*, 293–316.
156. Geber, U.; Bjo¨rklund, J. The relationship between ecosystem services and purchased input in swedish wastewater treatment systems—A case study. *Ecol. Eng.* **2002**, *19*, 97–117.
157. Griffiths-Sattenspiel, B.; Wilson, W. *The Carbon Footprint of Water*; River Network: Portland, OR, USA, 2009.
158. California Energy Commission. California's Water–Energy Relationship. Available online: http://www.energy.ca.gov/2005publications/CEC-700-2005-011/CEC-700-2005-011-SF.PDF (accessed on 24 August 2015).
159. Otterpohl, R.; Braun, U.; Oldenburg, M. Innovative technologies for decentralised water-, wastewater and biowaste management in urban and peri-urban areas. *Water Sci. Technol.* **2003**, *48*, 23–32.
160. Daigger, G.T. Evolving urban water and residuals management paradigms: Water reclamation and reuse, decentralization, resource recovery. *Wat. Env. Res* **2009**, *81*, 809–823.
161. Ulgiati, S.; Bargigli, S.; Raugei, M. An emergy evaluation of complexity, information and technology, towards maximum power and zero emissions. *J. Clean. Prod.* **2007**, *15*, 1359–1372.
162. Farrelly, M.; Brown, R. Rethinking urban water management: Experimentation as a way forward? *Global Environ. Chang.* **2011**, *21*, 721–732.
163. National Research Council. *Sustainability Concepts in Decision-Making: Tools and Approaches for the US Environmental Protection Agency*; National Research Council of the National Academies: Washington, DC, USA, 2014.
164. U.S. Environmental Protection Agency. *Sustainability Analytics: Assessment Tools & Approaches*; U.S. Environmental Protection Agency: Cincinnati, OH, USA, 2013; p. 166.
165. Miller, G. Getting minds out of the sewer. *Science* **2012**, *337*, 679–680.
166. Schnoor, J.L. Newater future? *Environ. Sci. Technol.* **2009**, *43*, 6441–6442.
167. Asian Development Bank (ADB). *Every Drop Counts: Learning from Good Practices in Eight Asian Cities*; ADB: Mandaluyong City, Philippines, 2010.

168. Bahri, A. *Integrated Urban Water Management*; Global Water Partnership: Stockholm, Sweden, 2012.
169. Skambraks, A.-K.; Augustin, K.; Meinzinger, F. Key Factors and Challenges for Implementing the Large-Scale Integrated Wastewater and Energy Generation Concept HAMBURG WATER Cycle® in the Settlement Jenfelder Au in Hamburg. In Proceedings of the International Water Week Conference, Amsterdam, The Netherland, 4–8 November 2013.

© 2015 by the authors; licensee MDPI, Basel, Switzerland. This article is an open access article distributed under the terms and conditions of the Creative Commons Attribution license (http://creativecommons.org/licenses/by/4.0/).

Ma, Cissy

To: a.g.mejia@bangor.ac.uk
Subject: RE: STAA application Record of Percentage Agreement_City of Tomorrow paper

Did not respond. Out of country

Xin (Cissy) Ma, Ph.D., P.E., Environmental Engineer

US EPA ORD
Center for Environmental Solutions and Emergency Response
Water Infrastructure Division
26 West Martin Luther King Drive, Mail Stop 483
Cincinnati, Ohio 45268
Phone: (513)-569-7828
Fax: (513)-569-7111
Ma.cissy@epa.gov

From: Ma, Cissy
Sent: Tuesday, April 28, 2020 6:35 PM
To: a.g.mejia@bangor.ac.uk
Subject: STAA application Record of Percentage Agreement_City of Tomorrow paper

Hi Ale,

Long time no contact. How have you been? Hope everything goes well with you and the family.

I am going to apply the EPA internal STAA award for the City of Tomorrow paper. It was published in 2015. This is the last year it will be eligible to be nominated since STAA only applies to the last 5 years of publications. Would you please sign the percentage agreement and send it back to me as soon as possible? The deadline of the nomination submission from the division is this Thursday (4/30). I will keep you informed if the paper gets any award.

Thanks!

Cissy

Xin (Cissy) Ma, Ph.D., P.E., Environmental Engineer

US EPA ORD
Center for Environmental Solutions and Emergency Response
Water Infrastructure Division
26 West Martin Luther King Drive, Mail Stop 483
Cincinnati, Ohio 45268
Phone: (513)-569-7828
Fax: (513)-569-7111
Ma.cissy@epa.gov

Record of Percentage Agreement on the following paper submitted for the 2020 STAA award

Sustainable Water Systems for the City of Tomorrow—A Conceptual Framework

Ma, X.C.; Xue, X.; González-Mejía, A.; Garland, J.; Cashdollar, J. Sustainable Water Systems for the City of Tomorrow—A Conceptual Framework. *Sustainability* **2015**, *7*, 12071-12105

Xin (Cissy) Ma	**84%**	XIN MA Digitally signed by XIN MA Date: 2020.04.28 21:02:57 -04'00'
Xiaobo Xue	**2%**	
Alejandra González-Mejía	**2%**	
Jay Garland	**2%**	
Jennifer Cashdollar	**10%**	JENNIFER CASHDOLLAR Digitally signed by JENNIFER CASHDOLLAR Date: 2020.04.28 08:57:47 -04'00'

Record of Percentage Agreement on the following paper submitted for the 2020 STAA award

Sustainable Water Systems for the City of Tomorrow—A Conceptual Framework

Ma, X.C.; Xue, X.; González-Mejía, A.; Garland, J.; Cashdollar, J. Sustainable Water Systems for the City of Tomorrow—A Conceptual Framework. *Sustainability* **2015**, *7*, 12071-12105

Xin (Cissy) Ma	**84%**	
Xiaobo Xue	**2%**	Xiaobo Xue Lovetko
Alejandra González-Mejía	**2%**	
Jay Garland	**2%**	Jay L Garland
Jennifer Cashdollar	**10%**	

Table of Contents

General_Authors_Publications.....2
LI-266151_BMC_genomics_2016.....17
LI-266152_Toxicology2018.....37
RecordOfAgreementRLW2020.....61

United States Environmental Protection Agency
Washington, DC 20460

STAA REPORT FOR THE SCIENTIST NOMINATIONS

General Information:

Nomination ID/App ID:	20-087
Research Category Primary:	Ecological Research (ER)
Research Category Secondary:	Health Effects Research and Human Health Risk Assessment (HE);Integrated Risk Assessment (IR)
Laboratory/Office Name:	ORD
Nomination Entered By:	Ronglin Wang

Eligibility Checklist:

[Y] The nominated publication(s) has not been submitted to a previous STAA competition.

[Y] The nominated publication(s) was published on or before January 1, 2017 and on or after January 1,2012

[Y] The principal author was an EPA employee or a PHS employee assigned to EPA when the research was performed

[Y] The EPA authors (includes PHS employees assigned to EPA) contributed collectively a minimum of 50% toward the publication(s)

Nominating Official Name:	Dale Hoff
Nominating Official Title:	DIRECTOR, MID-CONTINENT ECOLOGY DIV
Nominating OfficialEmail:	hoff.dale@epa.gov
STAA Coordinator Name:	Kathleen Wiser
STAA Coordinator Email:	wiser.kathi@epa.gov

Justifications:

Justification 1:

Ensuring chemical safety in terms of human health and the environment is an Agency core mission. Biological toxicities induced by chemical exposures range from endpoints of a molecular nature, such as gene expression, to those manifested at the higher levels of biological organization of cells, tissues/organs, organisms, and populations. Chemical toxicities can also be classified according to the domains of effects: biochemistry, physiology, molecular pathways, anatomy, morphology, behavior, and more. To capture, integrate, and assess toxicities across biological organization levels and knowledge domains is a significant challenge, yet a prerequisite for a holistic understanding of chemical safety. Such an understanding is essential to meeting the Agency goal of ultimately shifting away from animal testing towards *in vitro*, *in silico*, and short-term *in vivo* assays of a vast and ever-increasing number of chemicals in marketplace.

Many advances first pioneered in human biomedical sciences have potential applications in chemical toxicity assessment, particularly in the context of innovative scientific breakthroughs and a wide range of resources developed. For example, a landmark study of Connectivity Map (Cmap) linking human diseases, genetic perturbations, and small molecule drugs via whole genome expression profiles (WGEPs) of cell lines was first reported over a decade ago (Lamb et al., 2006). Since then, it has evolved into a NIH-funded national program with multiple partnering institutions (http://www.lincsproject.org/). The human Cmap library to date has also grown to more than a million WGEPs covering nearly 20,000 small molecule compounds (https://clue.io/). Similarly, early studies on mapping genotype-phenotype in human diseases (e.g., Washington et al., 2009) and concerted efforts to develop ontologies for biological knowledge representation (Smith et al., 2007) have led to a major initiative in disease research (McMurry et al., 2016) and the development of over 160 ontologies covering an array of biological knowledge domains.

These advances, coupled with years of toxicogenomics research and decades of chemical toxicity studies, inspired the work behind the two publications in this nomination. The first study (Wang et al., 2016) explored the utilities of Cmap in the assessment of chemical exposures and inferring mechanisms of action (MOAs), while the second study (Wang et al., 2019) developed an ontology-based semantic mapping method for chemical toxicity assessment. Specifically, the objectives of this work were to evaluate: 1) if chemical toxicities could be assessed, not just by individual genes or pathways, but at a whole transcriptome level similar to what had been done for human disease through Cmap; 2) if such toxicities manifested as diverse phenotypes across biological levels of organization could be integrated, and assessed beyond the boundaries of species and chemicals based on biological ontologies. Both studies represent collective bioinformatic endeavors by a group of ORD researchers, in collaboration with external scientists,

to develop novel computational approaches for toxicity assessment by leveraging the abundant

omics resources available in public domains. As such, for brevity and ease of discussion, the first journal article and its bioinformatic approach will be referred as Fish Cmap from here on, and the second article and its approach as OS-Mapping.

The Fish Cmap study demonstrated successfully that the chemical exposure history of a lab or field sample can be rapidly determined by using a small number of gene signatures, especially within a species. The MOAs of a lesser known chemical could also be inferred by its transcriptomic similarities to other well characterized chemicals. At the core of Fish Cmap was the curation, analysis, and assembly of a library of over 3500 WGEPs, each characterizing a single treated sample from one of two small fish model species, fathead minnow and zebrafish. The data originated from both public sources (https://www.ncbi.nlm.nih.gov/geo/) and from in-house experiments with a variety of test chemicals. Several innovative features stand out in this approach. First, instead of focusing on only a small number of genes/pathways after statistical filtering, the entire transcriptome of a fish species is considered—no information is omitted. Second, the greater the chemical and biological coverage a library of WGEPs has, the more powerful and informative Fish Cmap will be. Third, connections could be tiered/prioritized by fish species and/or technology platforms. Fourth, chemical "read-across" can be achieved biologically, i.e., grouping chemicals based on their MOAs. And lastly, no lengthy process of biomarker development and validation is necessary. Among the limitations of Fish Cmap, however, is its reliance on the molecular phenotypes of gene expression alone, which is somewhat removed from the types of apical endpoints (e.g., survival, growth, reproduction) commonly employed for ecological assessments of chemical risk.

The OS-Mapping study essentially extended the Fish Cmap by using knowledge representation and computing. It demonstrated successfully that by having biological responses (termed phenotypes) annotated into computable logical definitions and analyzed in conjunction with a universal cross-species, cross-domain phenotype ontology (Köhler et al., 2014), the toxicities of chemicals can be assessed by their semantic similarities to the phenotypes of other chemicals, genes, biological pathways, and diseases. The study involved the creation of 19 phenotypic profiles for 10 chemicals in six vertebrate species based on more than 700 published studies. While OS-Mapping is applicable to all phenotypes, it centers on those at the higher levels of biological organization with generally greater regulatory relevance, many of which are not intrinsically amenable to numeric representation for standard bioinformatic analyses. Such phenotypes are most commonly reported in scientific literature as unstructured text. Due to the concerted efforts in recent years by scientific communities to capture and represent biological knowledge into computable ontologies, these free-text phenotypes, once annotated, become accessible for machine inferencing. The OS-Mapping study is innovative in several aspects. First, a wide variety of textually described toxicities for a chemical in the extant literature can now be analyzed computationally because of their logical definitions. Second, once incorporated into a cross-species, cross-domains vertebrate (or metazoan) phenotype ontology, these logical definitions of chemical toxicities across the levels of biological organization become effectively

integrated with a comprehensive knowledge base of animal biology. They can be organized collectively as a phenotypic profile for a chemical and compared therein to targets across the boundaries of chemicals and diverse species, such as human, mouse, and zebrafish. Third, the implicit/hidden information (connections) in the knowledge base could be uncovered by using a sophisticated computer inferencing tool called reasoner, effectively expanding our knowledge of these chemicals beyond what is originally known. And lastly, OS-Mapping is flexible. It could be applied to any biological entities of interest that have been or could be characterized phenotypically. For instance, an adverse outcome pathway comprising multiple member events can be annotated into their respective logical definitions and semantically mapped to chemicals, genes, pathways, and diseases.

In part because of these two studies, two separate new ORD research efforts are either in planning or already underway. One is to scale up and build a comprehensive collection of WGEPs of fathead minnow, zebrafish, and human from both NCBI-GEO and in-house data to enable an expansion of Fish Cmap. The other is to develop an application ontology to serve as the foundation for semanticizing the USEPA/ORD ECOTOX Knowledgebase, an open-access repository of curated toxicity data for more than 13000 species and 11000 chemicals. This latter task with a proposed ontology construct has been endorsed and supported by the USEPA Office of Chemical Safety and Pollution Prevention, whose responsibilities involve the implementation of TSCA, pesticide registration, and evaluation of endocrine-disrupting chemicals. A semanticized ECOTOX Knowledgebase, as a triplestore graph database, will allow machine inferencing on its vast amount of annotated chemical toxicity information to uncover additional hidden knowledge and enable complex semantic queries no longer limited by its existing database schema. It will also be easily linkable to other triplestore databases such as the PubChemRDF (https://pubchemdocs.ncbi.nlm.nih.gov/rdf). The semantic analysis software powering OS-Mapping is also being developed as a web application allowing easy access by government, academic and industry researchers in the future.

Köhler et al., 2014: Construction and accessibility of a cross-species phenotype ontology along with gene annotations for biomedical research. F1000Research 2014, 2:30 (doi:

10.12688/f1000research.2-30.v2)

Lamb et al., 2006. The Connectivity Map: using gene-expression signatures to connect small molecules, genes, and disease. Science. 313(5795):1929-35.

McMurry et al., 2016. Navigating the Phenotype Frontier: The Monarch Initiative. Genetics. 2016 Aug;203(4):1491-5. doi: 10.1534/genetics.116.188870.

Smith et al. The OBO Foundry: coordinated evolution of ontologies to support biomedical data integration. Nat Biotechnol 25, 1251–1255 (2007). https://doi.org/10.1038/nbt1346.

Washington et al., 2009. Linking human diseases to animal models using ontology-based phenotype annotation. PLoS Biol. 2009 Nov;7(11):e1000247. doi:0.1371/journal.pbio.1000247.

Justification 2A:

Both Fish Cmap and OS-Mapping assess the toxicities of chemicals by constructing biological linkages among chemicals, genes, pathways, diseases, or other entities of interest based on their phenotypic profiles. Both approaches are big data-oriented, leveraging a vast and ever-increasing amount of public omics resources available including phenotypic data, pathway information, and ontologies. Fish Cmap works with molecular phenotypes alone, currently in the form of gene expression but potentially extendable to metabolomic and proteomic data as well. OS-Mapping extends the capabilities of Cmap even further, by representing textually described phenotypes across all levels of biological organization as computable logical definitions and incorporating them into biological ontologies covering a wide range of knowledge domains. At the core of this technology is human knowledge representation and machine inferencing, a component of artificial intelligence. As such, OS-Mapping greatly expands the scope of phenotypic coverage by Fish Cmap and enables more effective extrapolation of toxicities among chemicals and biological species.

Justification 2B:

Author(s)	Publication Title(s)	Year	Award
	1. Field-Based Approach for Assessing the Impacts of Treated Pulp and Paper Mill Effluent on Endogenous Metabolites of Fathead Minnows (Pimephales promelas).		
	2. Biological Effects-Based Tools for Monitoring Impacted Surface Waters in the Great Lakes: A Multiagency Program in Support of the Great Lakes Restoration Initiative.		

Ankley, Gerald; Villeneuve, Daniel	3. An Inexpensive, Temporally Integrated System for Monitoring Occurrence and Biological Effects of Aquatic Contaminants in the Field.	2015	Level 3
Ankley, Gerald; Villeneuve, Daniel	1. Molecular Target Sequence Similarity as a Basis for Species Extrapolation to Assess the Ecological Risk of Chemicals with Known Modes of Action. 2. Cross-Species Sensitivity to a Novel Androgen Receptor Agonist of Potential Environmental Concern, Spironolactone. 3. Leveraging Existing Data for Prioritization of the Ecological Risks of Human and Veterinary Pharmaceuticals to Aquatic Organisms	2015	Level 3
Ankley, Gerald; Villeneuve, Daniel	1. Cross-Species Conservation of Endocrine Pathways: A Critical Analysis of Tier 1 Fish and Rat Screening Assays with 12 Model Chemicals. 2. A Novel Framework for Interpretation of Data from the Fish Short-Term Reproduction Assay (FSTRA) for the Detection of Endocrine-Disrupting Chemicals	2015	Level 3
Ankley, Gerald; Villeneuve, Daniel	1. Addressing the Challenges of Species Extrapolation Associated with 21st Century Toxicology using the SeqAPASS Tool. 2. Demonstrating the utility of the SeqAPASS Tool for Addressing 21st Century Challenges in Species Extrapolation	2017	Level 2

Ankley, Gerald; Blackwell, Brett; Villeneuve, Daniel	1. Pathway-based approaches for assessment of real-time exposure to an estrogenic wastewater treatment plant effluent on fathead minnow reproduction. 2. An integrated approach for identifying priority contaminant in the Great Lakes Basin -Investigations in the Lower Green Bay/Fox River and Milwaukee Estuary areas of concern. 3. Prior knowledge-based approach for associating contaminants with biological effects: A case study in the St. Croix river basin, MN, WI, USA.	2017	Level 3
Ankley, Gerald; Villeneuve, Daniel	Temporal Changes in Biological Responses and Uncertainty in Assessing Risks of Endocrine-Disrupting Chemicals: Insights from Intensive Time-Course Studies with Fish	2017	HM

Justification 2C:

The publications in this nomination are bioinformatics- and data-driven in nature. The methodologies, software tools, and computational analyses therein were conceptualized, implemented, and executed by the primary author. So were the drafting and revision of the manuscripts. They have never been submitted to STAA until now. As such, there is no overlap in scope and content between this nomination and the previous nominations involving some of us. Another nomination for this STAA cycle from Brett Blackwell along with two contributors to this nomination (Gerald Ankley, Dan Villeneuve) and others, titled “Risk based prioritization of environmental contaminants, mixtures, and biological effects using 21st century toxicity tools and data”, is oriented towards field and experimental studies and thus unrelated.

Justification 2D:

n/a

Justification 2E:

n/a

Justification 3A:

The work underlying both publications was presented at various stages of research and well received in the annual conferences of the Society of Environmental Toxicology and Chemistry (Salt Lake City, 2015; Minneapolis, 2017). Since its publication in 2016, Fish Cmap has been accessed online over 2000 times (Publisher) and cited ten times (Google Scholar) or six times (Web of Science, Publisher) externally. OS-Mapping has been cited three times (Google Scholar, Publisher) or twice (Web of Science) since 2019.

Justification 3B:

Both publications cleared internal reviews prior to their submissions to the publishing journals for peer reviews. They were well received. One reviewer commented on Fish Cmap that, " *Interestingly and informatively was the demonstrated ability of this method to recognise estrogenic, polyaromatic and neurotoxin chemical types in the low-level mixture in the waste water effluent*". He/she further stated that, *"One of the best ways to investigate and elucidate mechanisms is to examine the gene expression profiles between connected chemicals. This is an informative approach"*. The second reviewer stated that, "A well written manuscript that convincingly demonstrates the utility of a Cmap approach in fish ecotoxicology". On OS-Mapping, one reviewer stated that, *"This manuscript builds an impressive integration of biological and toxicological information into what is referred to as an ontologybased semantic mapping of toxicity from information in the literature and various databases"*.

AUTHORS

Contributing Author

Author Name: Cataia Ives

Professional Title: Salutation:

Email:	cives@rti.org	Organization:
Mailing Address:		
Street Line 1:	Research Computing Division RTI International RTP, NC	
City:		
Zip Code:		State:
At time of research was:	Non EPA Personnel	
Separation Date:		
% of Effort:	8	

Contributing Author

Author Name:	Stephen Edwards	
Professional Title:		Salutation:
Email:	swedwards@rti.org	Organization:
Mailing Address:		
Street Line 1:	Research Computing Division RTI International RTP, NC	
City:		
Zip Code:		State:
At time of research was:	Non EPA Personnel	
Separation Date:		
% of Effort:	8	

Principal Author

Author Name:	Ronglin Wang

Professional Title:		Salutation:	
Email:	wang.rong-lin@epa.gov	Organization:	
Mailing Address:			
Street Line 1:	26 W Martin Luther King Dr Cincinnati, OH 45268		
City:			
Zip Code:		State:	
At time of research was:	EPA Employee		
Separation Date:			
% of Effort:	48		

Contributing Author

Author Name:	Adam Biales		
Professional Title:		Salutation:	
Email:	biales.adam@epa.gov	Organization:	
Mailing Address:			
Street Line 1:			
City:			
Zip Code:		State:	
At time of research was:	EPA Employee		
Separation Date:			
% of Effort:	6		

Contributing Author

Author Name:	Natalia Garcia-Reyero		
Professional Title:		Salutation:	
Email:	natalia.g.vinas@erdc.dren.mil	Organization:	
Mailing Address:			
Street Line 1:	U.S. Army Corps of Engineers Engineer Research and Development Center 3909 Halls Ferry Road Vicksburg, MS 39180-6199		
City:			
Zip Code:		State:	
At time of research was:	Non EPA Personnel		
Separation Date:			
% of Effort:	6		

Contributing Author

Author Name:	Edward Perkins		
Professional Title:		Salutation:	
Email:	edward.j.perkins@usace.army.mil	Organization:	
Mailing Address:			
Street Line 1:	Environmental Laboratory U.S. Army Engineer Research and Development Center Waterways Experiment Station 3909 Halls Ferry Road Vicksburg, MS 39180-6199		
City:			
Zip Code:		State:	
At time of research was:	Non EPA Personnel		

Separation Date:		
% of Effort:	6	

Contributing Author

Author Name:	Daniel Villeneuve	
Professional Title:		Salutation:
Email:	villeneuve.dan@epa.gov	Organization:
Mailing Address:		
Street Line 1:	6201 Congdon Blvd, Duluth, MN 55804	
City:		
Zip Code:		State:
At time of research was:	EPA Employee	
Separation Date:		
% of Effort:	6	

Contributing Author

Author Name:	Gerald T Ankley	
Professional Title:		Salutation:
Email:	ankley.gerald@epa.gov	Organization:
Mailing Address:		
Street Line 1:	6201 Congdon Blvd, Duluth, MN 55804	
City:		
Zip Code:		State:
At time of research was:	EPA Employee	

Separation Date:			
% of Effort:	6		

Contributing Author

Author Name:	David Bencic		
Professional Title:		Salutation:	
Email:	bencic.david@epa.gov	Organization:	
Mailing Address:			
Street Line 1:	26 W Martin Luther King Dr Cincinnati OH 45268		
City:			
Zip Code:		State:	
At time of research was:	EPA Employee		
Separation Date:			
% of Effort:	6		

PUBLICATIONS

Publication 1:

Publication Title:	Fish connectivity mapping: linking chemical stressors by their mechanisms of action-driven transcrip		
Publication Date:	Thu Jan 28 00:00:00 GMT 2016		
Journal/Publication Method:	BMC Genomics		
All Author(s):			
Volume:	17	Number:	84

Pages:	NA	Immediately Index:	Immediately Index:
Citation ½ Life:	5.2	Impact Factor:	3.501

Publication 2:

Publication Title:	Ontology-based semantic mapping of chemical toxicities		
Publication Date:	Tue Jan 15 00:00:00 GMT 2019		
Journal/Publication Method:	Toxicology		
All Author(s):			
Volume:	412	Number:	NA
Pages:	89-100	Immediately Index:	Immediately Index:
Citation ½ Life:	10.9	Impact Factor:	3.547

Wang et al. BMC Genomics (2016) 17:84
DOI 10.1186/s12864-016-2406-y

BMC Genomics

RESEARCH ARTICLE Open Access

Fish connectivity mapping: linking chemical stressors by their mechanisms of action-driven transcriptomic profiles

Rong-Lin Wang[1*], Adam D. Biales[1], Natalia Garcia-Reyero[2], Edward J. Perkins[2], Daniel L. Villeneuve[3], Gerald T. Ankley[3] and David C. Bencic[1]

Abstract

Background: A very large and rapidly growing collection of transcriptomic profiles in public repositories is potentially of great value to developing data-driven bioinformatics applications for toxicology/ecotoxicology. Modeled on human connectivity mapping (Cmap) in biomedical research, this study was undertaken to investigate the utility of an analogous Cmap approach in ecotoxicology. Over 3500 zebrafish (*Danio rerio*) and fathead minnow (*Pimephales promelas*) transcriptomic profiles, each associated with one of several dozen chemical treatment conditions, were compiled into three distinct collections of rank-ordered gene lists (ROGLs) by species and microarray platforms. Individual query signatures, each consisting of multiple gene probes differentially expressed in a chemical condition, were used to interrogate the reference ROGLs.

Results: Informative connections were established at high success rates within species when, as defined by their mechanisms of action (MOAs), both query signatures and ROGLs were associated with the same or similar chemicals. Thus, a simple query signature functioned effectively as an exposure biomarker without need for a time-consuming process of development and validation. More importantly, a large reference database of ROGLs also enabled a query signature to cross-interrogate other chemical conditions with overlapping MOAs, leading to novel groupings and subgroupings of seemingly unrelated chemicals at a finer resolution. This approach confirmed the identities of several estrogenic chemicals, as well as a polycyclic aromatic hydrocarbon and a neuro-toxin, in the largely uncharacterized water samples near several waste water treatment plants, and thus demonstrates its future potential utility in real world applications.

Conclusions: The power of Cmap should grow as chemical coverages of ROGLs increase, making it a framework easily scalable in the future. The feasibility of toxicity extrapolation across fish species using Cmap needs more study, however, as more gene expression profiles linked to chemical conditions common to multiple fish species are needed.

Keywords: Fish, Gene expression profiles, Connectivity mapping

Background

There are an estimated 80,000 chemicals in legal use today, with hundreds more added to the inventory each year [1]. A current lack of toxicological information for most of them poses a serious challenge to safeguarding human health and the environment from potentially harmful exposures. Given that traditional toxicity testing of chemicals based on whole animals is resource-intensive, time-consuming, and at times challenging in terms of cross-species and –chemical extrapolation, a general consensus has emerged across the environmental science community that alternative practices are needed for evaluation and management of chemical inventories. In recognition of rapid scientific advancements in "-omics" technologies, robotics, computational chemistry, systems biology, and high performance computing, the US National Academy of Sciences has put forth several reports since the turn of the century [2–5]

* Correspondence: Wang.Rong-Lin@epa.gov
[1]Exposure Methods & Measurements Division, National Exposure Research Laboratory, US Environmental Protection Agency, 26 W Martin Luther King Dr., MS 587, Cincinnati, OH 45268, USA
Full list of author information is available at the end of the article

BioMed Central

© 2016 Wang et al. **Open Access** This article is distributed under the terms of the Creative Commons Attribution 4.0 International License (http://creativecommons.org/licenses/by/4.0/), which permits unrestricted use, distribution, and reproduction in any medium, provided you give appropriate credit to the original author(s) and the source, provide a link to the Creative Commons license, and indicate if changes were made. The Creative Commons Public Domain Dedication waiver (http://creativecommons.org/publicdomain/zero/1.0/) applies to the data made available in this article, unless otherwise stated.

recommending broader utilization of *in vitro, in silico*, and short term *in vivo* assays with a greater focus on mechanistic pathways in testing of chemicals and assessing their toxicological risks.

Concurrent with this emerging paradigm of toxicology is the ongoing "big data" revolution across scientific disciplines and technological fields. Accelerated by technical advances, there has been an exponential growth in data generation. In biology, for example, the number of DNA sequence bases in GenBank has increased nearly 300,000 fold over the last 30 years, from 0.7 megabases in 1982 to 187 gigabases in 2015. As of May, 2015, the NCBI GEO (National Center for Biotechnology Information Gene Expression Omnibus) hosted well over 1.4 million gene expression profiles (GEPs), including ~20,000 for fish, ~70,000 for rats, and ~700,000 for humans. Each GEP represents the collective expression states of all genes, as measured by a given microarray, for a sample under study. Many of these GEPs are linked to chemical treatment or other biological conditions of potential relevance to toxicology. These abundant transcriptomic data contain a wealth of information and present opportunities for toxicologists to explore computational assessment of chemical toxicity by a data-driven approach. In contrast to individual studies with a narrowly defined scope and limited data, substantial novel insights may be gained from data mining across a large number of independent studies conducted within the same species or even across species. Yet, to date, there has been little research effort in this area in the field of toxicology.

Connectivity mapping (Cmap) represents an *in silico* and data-driven approach with potentially broad applications in biomonitoring, chemical exposure assessment, toxicity evaluation and extrapolation across species, and grouping of chemicals. Originally proposed for human biomedical research [6], Cmap connects chemicals and disease based on similarities in transcriptomic profiles, driven largely by the underlying mechanisms of action (MOA). Such similarities are revealed by interrogating a database of rank-ordered gene lists (ROGLs) with a query signature. The ROGLs are generated individually from GEPs of treated samples relative to those of the corresponding controls, based on gene probes sorted by their logarithmic fold-changes (LogFCs), and are inclusive of all gene probes on a given microarray. A query signature, on the other hand, contains only a small number of gene probes differentially expressed under a chemical or biological condition of interest. A non-random distribution of gene probes from a query signature on ROGLs suggests a similarity in their transcriptomic profiles, and therefore, a connectivity of the underlying chemical or biological conditions. This Cmap determination of the chemical identity associated with a biological sample is thus analogous to forensic database searches by human or DNA fingerprints. Since its inception, Cmap has made a significant impact on drug discovery research and development [7], and is now becoming part of much more ambitious public effort of profiling cell signatures [8]. A similar data-driven approach for pharmaceutical research has also been launched using commercial platforms [9]. For toxicogenomic research with chemicals, the principle of Cmap is equally applicable: those toxicants sharing the same or similar MOAs should yield comparable transcriptomic profiles, and connect with one another [10–12].

Compared to other computational approaches with similar toxicological applications, Cmap has several advantages. First, it is algorithmically simple. Connectivity between two chemical conditions is established simply based on a non-random distribution of multiple gene probes on ROGLs. Second, the information in each GEP is fully preserved, as there is no statistical filtering with regard to generating ROGLs: the entire set of gene probes in the GEP of a treated sample is ranked from top to bottom by their LogFCs relative to the corresponding control(s). Third, Cmap is easily scalable. As more GEPs become available, ROGLs can be simply added individually to an existing reference database without any restructuring or reanalysis. With more ROGLs in the database, there is a greater coverage of chemicals and biological conditions, so the power and applicability of Cmap also increase. Lastly, Cmap is cost-effective and user-flexible. As publicly-available GEPs continue to grow, they can be included in a database to expand chemical coverage. An end user can derive a query signature for a sample/condition of interest from a variety of sources such as literature, microarrays, RT-PCRs (reverse transcription polymerase chain reaction), or a public "-omics" data repository.

However, adopting a big data approach such as Cmap for toxicogenomics applications faces many challenges. Unlike human Cmap where GEPs originated from relatively homogeneous cell cultures from a single species, the development of Cmap for fish must take into account data heterogeneity as a result of differences in experimental designs and lab practices among independent studies. Technical factors such as choice of expression profiling platforms (e.g., microarrays vs RNA sequencing) and evolving designs within a platform (e.g., microarrays) may further complicate data integration. Lastly and perhaps most challenging of all, conducting interspecific Cmap introduces further evolutionary complexity.

Interspecific Cmap requires a signature derived from one species to interrogate ROGLs of one or more other species. If successful, this allows the broadest possible inclusion of GEPs available in public repositories, and

can inform toxicity extrapolation from model to non-model species. Interspecific Cmap depends on the conservation of both genomes and transcriptomes. In the presence of such conservation, genome annotations become the most limiting factor for interspecific Cmap. Given these considerations, zebrafish and fathead minnow appear to be the two very suitable fish species for a preliminary test of Cmap across species. As a common biological model with extensive genome-level knowledge, zebrafish is a species of choice for many studies, particularly in developmental biology [13]. As such, zebrafish has the largest number of public GEPs available among all fish species. The fathead minnow, on the other hand, has been the dominant aquatic vertebrate test organism in regulatory toxicity testing for decades [14]. Estimated to have shared a last common ancestor 31 million years ago [15], both the zebrafish and fathead minnow are members of the family Cyprinidae, with well-conserved genomes and transcriptomes [16].

This study was undertaken to explore the applications of Cmap in ecotoxicology. The goals were three-fold. First, Cmap was evaluated for connecting the same chemicals within species. In other words, both a query signature and ROGLs under consideration were selected from a single species and associated with an identical chemical. Second, Cmap was tested on related chemicals of the same MOA class within species, for example, by interrogating ROGLs linked to the natural estrogen 17β-estradiol (E2) with a signature linked to the synthetic estrogen 17α-ethinylestradiol (EE2). If successful, Cmap would not only simplify the development of exposure biomarkers, but also provide an alternative way to characterize the extent of overlap among MOAs of related chemicals and inform as to their relative toxicity. Lastly, based on a small number of chemical conditions shared between species, a preliminary trial of interspecific Cmap was conducted to identify issues critical to a more thorough feasibility study in the future.

Methods

Chemicals and field water samples

The data employed in the present study were derived from experiments with a number of chemicals (Table 1). The use or source of these chemicals ranges from pesticides, medicine, industrial chemicals or by products, personal care products, and fossil fuel contaminants. In the context of adverse outcome pathways, these chemicals could be grouped by their molecular initiating events (MIEs) [17]. A MIE is defined here as a molecular interaction between a xenobiotic and a specific biomolecule. Since many of these MIEs involve various receptors and enzymes commonly considered as part of the hypothalamic pituitary gonadal (HPG) axis [18], a large portion of chemicals under this study, for example E2 and EE2, are effectively HPG-active toxicants. Also included, among others, were several pyrethroid insecticides (bifenthrin, permethrin, esfenvalerate, cypermethrin) targeting neuro-transmission, and polycyclic aromatic hydrocarbons (PAHs).

In addition to experiments with individual chemicals, the data also include exposures to field water conditions (Table 1) sampled near several waste water treatment plants (WWTPs). The water samples were characterized for a limited number of chemicals (generally around 140 analytes) by their original investigators using traditional chemical analysis methods. For the purpose of evaluating Cmap performance, only those chemicals both positively identified therein and also present in the data of current study are listed in the table. Almost all of the water samples had detectable concentrations of estrogens and bisphenol A. Some of them also contained PAHs.

Microarray data

Microarray data for this investigation came from a series of US Environmental Protection Agency (USEPA) studies with zebrafish and fathead minnow [18] and US Army Corps of Engineers (USACE) studies with fathead minnow, as well as a number of datasets downloaded from NCBI GEO as of August 2014 (Table 2, Additional file 1: Table S1). There were a total of 3516 microarrays associated with 55 experimental conditions, as defined by chemical, dose, tissue type, and exposure duration. This dataset encompassed many independent studies carried out over years, with a wide range of differences in their original project objectives, experimental designs, and chemical treatment conditions and measured effects, using three microarray platforms in zebrafish and fathead minnow. Given the complex and heterogeneous nature of this dataset, it is difficult to describe in general terms all underlying experimental protocols. Instead, only a brief overview of this dataset is outlined below. Greater experimental details about various studies have been previously published [16, 18–20], are available from the summaries of individual data series available at NCBI GEO (Additional file 1: Table S1), or will be published elsewhere.

USEPA and USACE studies

A number of experiments were conducted with chemicals targeting HPG-axis [18] and neuro-transmission of zebrafish and fathead minnow. Over the course of these studies, microarray platforms evolved, leading to multiple platforms being used, including Agilent 013223, 015064, 019161 for zebrafish, and Agilent 019597 and 036574 for fathead minnow. Since these platforms had probes duplicated to various extent by design, only unique probes were considered in their cross-mapping. Agilent 013223 and 015064 shared the same 21495

Table 1 Chemicals and field mixtures associated with the exposure experiments considered in the current study

Chemicals/field mixtures	Use/source	Putative MIE	References
1,4-dimethoxybenzene (DMB)	Ingredient in consumer products	—	—
2,3,7,8-tetrachlorodibenzo-p-dioxin (TCDD)	Industrial byproduct	aromatic hydrocarbon (Ah) receptor agonist	[48]
2,4-dinitrophenol (DNP)	Antiseptic agent, pesticide, industrial chemical	Uncoupling oxidative phosphorylation	—
benz(a)anthracene (BAA)	Fossil fuels	DNA mutagen and Ah receptor agonist (PAH)	[49]
perfluorinated chemicals (PFC)	Industrial chemical	—	—
tert-Butylhydroquinone (TBHQ)	Ingredient in consumer products	—	—
Phenanthrene (PHE)	Fossil fuels	DNA mutagen and Ah receptor agonist (PAH)	[49]
Pyrene (PYR)	Fossil fuels	DNA mutagen and Ah receptor agonist (PAH)	[49]
decabromodiphenyl ether (BDE)	Flame retardant		—
dibenzothiophene (DBT)	Fossil fuels	DNA mutagen and Ah receptor agonist (PAH)	[49]
17ß-estradiol (E2)	Endogenous estrogen	ER agonist	[18]
Diethylstilbestrol (DES)	medicine	ER agonist	—
ethniyl estradiol (EE2)	medicine	ER agonist	[18]
fadrozol (FAD)	medicine	CYP19 inhibitor	[18]
fipronil (FIP)	insecticide	GABA receptor antagonist	[18]
flutamide (FLU)	medicine	Androgen receptor antagonist	[18]
genistein (GEN)	phytoestrogen	ER and PPAR agonist	[50]
ketochonazole (KET)	medicine	CYP11A/CYP17 inhibitor	[18]
trenbolone (TRB)	Beef production	AR agonist	[18]
trilostane (TRI)	Veterinary medicine	3βHSD inhibitor	[18]
vinclozolin (VIN)	fungicide	AR antagonist (fungicide)	[18]
prochloraz (PRO)	fungicide	CYP17/19 inhibitor	[18]
muscimol (MUS)	research	GABA receptor agonist	[18]
bisphenol A (BPA)	Industrial chemical	ER agonist	[51]
Progesterone (PGST)	Endogenous hormone, medicine	PR agonist	[52]
Dihydrotestosterone (DHT)	Endogenous hormone	AR agonist	[53]
Haloperidol (HAL)	medicine	Dopamine D2 receptor antagonist	[54]
Diazepam (DIA)	medicine	GABA-A receptor modulator	[55]
bifenthrin (BIF)	insecticide	voltage-gated sodium channels disruption	[56]
cypermethrin (CYP)	insecticide	voltage-gated sodium channels disruption	[56]
esfenvalerate (ESF)	Insecticide	voltage-gated sodium channels disruption	[56]
Linuron (LIN)	Herbicide	photosynthesis inhibitor	[57]
Terbufos (TER)	Insecticide	acetylcholine esterase inhibitor	[58]
methylparaben (MPA)	Anti-fungal agent	Uncoupling oxidative phosphorylation	[59]

Table 1 Chemicals and field mixtures associated with the exposure experiments considered in the current study *(Continued)*

permethrin (PER)	Insecticide	voltage-gated sodium channels disruption	[56]
Propanil (PPL)	Herbicide	photosynthesis inhibitor	[60]
azinphos-methyl (APM)	Insecticide	acetylcholine esterase inhibitor	[61]
Propranolol (PPLL)	Medicine	β-adrenergic receptor antagonist	[62]
protein kinase C inhibitor 412 (PKC412)	Pharmaceutical compound	tyrosine kinase inhibitor	[63]
Triclocarban (TCC)	Anti-bacterial agent	—	—
Gemfibrozil (GEM)	Medicine	PPAR binding and activation	[64]
cyclotrimethylenetrinitramine (RDX)	Explosive	Neuro-toxin?	—
TNT	Explosive	—	—
Water samples near WWTPs			
Effluent; WWTP, San Diego, California (EFFLa, EFFHa)	Positive for GEM, DIA, E2, PGST	—	[29]
Effluent; WWTP, Los Angeles, California (EFFHb)	Positive for GEM, PGST	—	[29]
Effluent; WWTP, Duluth Minnesota (WLSSD)	Positive for various estrogens, BPA	—	Unpublished observations (Jenna Cavallin US EPA)
Upstream, effluent, downstream, WWTP, Ely Minnesota (ElyUS, ElyEFF, ElyDS)	At least one site positive for various estrogens, BPA, TCC, PAHs, chlorpyrifos	—	[30]
Upstream, effluent, downstream, WWTP, Hutchinson Minnesota (HutUS, HutEFF, HutDS)	At least one site positive for various estrogens, DES, BPA, TCC, PAHs, chlorpyrifos	—	[30]
Upstream, effluent, downstream, WWTP, Rochester Minnesota (RochUS, RochEFF, RochDS)	At least one site positive for various estrogens, BPA, TCC,	—	[30]
storm, stream, waste water; WWTP, Gainesville, Florida (stormH2O, strH2O, wasteH2O)	wasteH2O seasonally positive for BPA, DIA, PFCs	—	[65]

AR androgen receptor, *ER* estrogen receptor, *GABA* gamma-aminobutyric acid, *HSD* hydroxysteroid dehydrogenase, *MIE* molecular initiating event, *PAH* polycyclic aromatic hydrocarbons, *PR* progesterone receptor, *PPAR* peroxisome proliferators-activated receptor–α, *WWTP* waste water treatment plant

probes but with different layouts (hereafter referred to as ZF 21K). Agilent 019161 had 43603 probes (ZF 43K), but only 37 % (16083) of them could be mapped to Agilent 015064. For fathead minnow, Agilent 019597 had 15208 probes (FHM 15K), which formed a subset of 49849 unique probes found in Agilent 036574 (FHM 60K). The experimental conditions in this study for fathead minnow overlapped considerably between these two platforms. In order to keep their ROGLs as a single collection for maximum comparability, only the 15000 common probes were retained. The entire microarray dataset from these studies is available at NCBI-GEO as the accessions GSE38070, GSE60202, GSE70807, and GSE70936.

Animal usage

Fish were treated humanely, and all laboratory procedures involving animals were reviewed and approved by the USEPA Animal Care and Use Committee in accordance with Animal Welfare Act regulations and Interagency Research Animal Committee guidelines.

Zebrafish experiments

Reproductively mature zebrafish (ab wild-type strain, 5–7 months old) were exposed to a continuous flow of sand filtered, UV-sterilized, Lake Superior water (LSW; controls) or test chemicals dissolved in LSW for 24, 48, or 96 h at the USEPA laboratory in Duluth, MN. At the end of each exposure period, fish were anesthetized in a buffered solution of tricaine methanesulfonate (MS-222; Finquel, Argent, Redmond WA, USA) and various tissues were collected and shipped overnight on dry ice to the USEPA laboratory in Cincinnati, OH. Total RNA isolated from selected tissue samples was then sent to Cogenics Corporation, an Agilent certified contract laboratory (Morrisville, North Carolina 27560, USA). Hybridization was conducted using a two-color protocol on ZF 15K and ZF 43K microarrays (Agilent Technologies, Santa Clara, CA, USA), followed by high-resolution

Table 2 A summary of 3516 microarray samples and their chemical treatment conditions

Zebrafish microarray design, sample size, and chemicals	Fathead minnow microarray design, sample size, and chemicals
ZF 21K (Agilent 013223, 15064): USEPA (290)	FHM 15K (Agilent 019597,_036574): USEPA (580)
ethniyl estradiol (**EE2**)[a]	bifenthrin (BIF)[a]
fadrozol (FAD)[a]	cypermethrin (CYP)[a]
fipronil (FIP)[a]	permethrin (PER)[a]
flutamide (**FLU**)[a]	esfenvalerate (ESF)
ketochonazole (KET)[a]	EE2[a]
muscimol (MUS)[a]	Terbufos (TER)[a]
prochloraz (**PRO**)[a]	
trenbolone (TRB)[a]	FHM 15K (Agilent 019597): USACE (1711)
trilostane (TRI)[a]	BPA
vinclozolin (VIN)[a]	FAD[a]
	FLU[a]
ZF 21K (Agilent 013223, 15064): NCBI (154)	Gemfibrozil (GEM)[a]
tert-Butylhydroquinone (TBHQ)[a]	KET[a]
2,3,7,8-tetrachlorodibenzo-p-dioxin (TCDD)[a]	KET_TNT_KET
oxygen (O2)[a]	KET_TNT_TNT
2,4-dinitrophenol (DNP)	PRO
1,4-dimethoxybenzene (DMB)	RDX
azinphos-methyl (APM)[a]	Effluent of Western Lake Superior Sanitary District (WLSSD)
Haloperidol (HAL)	**TRB**[a]
	TRB_BPA_TRB_BPA
ZF 43K (Agilent 019161): USEPA (24)	TRB_BPA_BPA
FLU[a]	TRB_BPA_TRB
PRO[a]	TRB_EE2_EE2
	TRB_EE2_TRB
ZF 43K (Agilent 019161): NCBI (270)	TRB_EE2_TRB_EE2
benz(a)anthracene (BAA)[a]	TRB_TCC_TCC (triclocarban)
decabromodiphenyl ether (BDE)[a]	TRB_TCC_TRB
bisphenol A (BPA)[a]	TRB_TCC_TRB_TCC
dibenzothiophene (DBT)	TRI[a]
Diazepam (DIA)[a]	VIN[a]
17ß-estradiol (E2)[a]	
E2[a]	FHM 15K (Agilent 019597_036574): NCBI (487)
EE2[a]	Diethylstilbestrol (**DES**)[a]
FLU	Dihydrotestosterone (DHT)
genistein (**GEN**)[a]	E2[a]
Linuron (LIN)[a]	Field exposure (EFFLa, EFFHa[a]; effluent, WWTP San Diego; EFFHb[a]; effluent, WWTP Los Angeles)
methylparaben (MPA)[a]	Field exposure (surface, stream, waste water[a])
protein kinase C inhibitor 412 (PKC412)[a]	Field exposure (liver: ElyUS[a], ElyEFF[a], ElyDS[a], HutUS, HutEFF[a], HutDS[a], RochUS[a], RochEFF[a], RochDS[a])
Propanil (PPL)[a]	Field exposure (ovary: ELYeff, ELYds, HUTeff, HUTds, ROCHds, ROCHeff)
PRO[a]	FLU
Pyrene (PYR)	Linuron

Table 2 A summary of 3516 microarray samples and their chemical treatment conditions *(Continued)*

cyclotrimethylenetrinitramine (RDX)[a]	perflorinated chemicals (PFC)
	Phenanthrene (PHE)[a]
	Progesterone (PGST)
	Propranolol (PPLL)
	RDX

Zebrafish: ZF 21K (Agilent 013223, 21495 probes unique; Agilent 015064, 21495 probes), ZF 43K (Agilent 019161, 43603 probes unique). Fathead minnow: FHM 15K (Agilent 019597, 15208 unique probes; Agilent 036574, 15208 of 49849 unique probes). Chemicals with at least one experiment condition (different exposure durations either in single or combinations) with DEGs ≥ 4 are marked by "[a]", and those shared across platforms or species are highlighted once in bold

scanning and image processing by Agilent Feature Extraction software.

Fathead minnow experiments

Fish exposures were conducted in the USEPA laboratories in Duluth, MN and Cincinnati, OH; and the USACE laboratories in Vicksburg, MS. For exposures to HPG-active toxicants, reproductively mature fathead minnows (5–7 months old) were tested using LSW as the control and carrier of the test chemicals. All exposures conducted at EPA Duluth laboratories were continuous, flow-through experiments. Representative experimental designs for these experiments are detailed elsewhere [18–20]. Exposures to pyrethroids were conducted in Cincinnati. Fathead minnow fry (48 hours post hatch) and adults (5–7 months old) were exposed to the selected chemicals for 24, 48, or 72 hours in a static or flow-through system. Exposures to TNT, RDX, and mixture of TNT and KET were conducted at USACE Vicksburg laboratories under static renewal conditions using adult fathead minnow (5–7 months old) that will be described elsewhere. At the end of each exposure period, whole fry or tissues from adult fish used for transcriptomic analyses were snap-frozen in liquid nitrogen and stored at −80 ° C until RNA was extracted, using either Qiagen RNeasy mini kits (Qiagen, Valencia, CA, USA) or Tri-Reagent (Sigma, St. Louis, MO, USA). Expression profiling was carried out using a single-color protocol on either a FHM 15K (GEO accession GPL9248, designed by Dr. Nancy Denslow, University of Florida, Gainesville, FL, USA) or a FHM 60K microarray (GPL17098, designed by Dr. Natalia Garcia-Reyero) [21], in the Environmental Laboratory of the US Army Engineer Research and Development Center in Vicksburg, MS (1711 arrays) or in EPA Cincinnati (580 arrays). One hundred to 1000 ng of total RNA was used for all hybridizations. Probe labeling, amplification, and hybridization were performed using Agilent Quick Amp Labeling Kit following the manufacturer's One-Color Microarray Hybridization Protocol. Microarrays were scanned with a high-resolution scanner and the images were processed with Agilent Feature Extraction software.

Public data from NCBI GEO

A total of 911 text output files from Agilent Feature Extraction software, representing 33 GEO data series sharing a common microarray platform with those of the USEPA and USACE studies as described above, were assembled and curated (Additional file 1: Table S1). Each sample file was annotated according to chemical exposure, dose, tissue type, and exposure duration.

Cmap development and analysis

Fish Cmap consists of three components: construction of query signatures from microarray samples of chemical and biological interest, construction of a reference database of ROGLs tagged with chemical or biological conditions, and computational query of the database using the prepared signatures. Each of the three components is outlined below.

Query signatures

A query signature for a treatment condition contained multiple differentially expressed gene probes (DEGs) relative to an appropriate control. The DEGs were determined by a modified *t*-test implemented in the R package limma [22]. A number of R scripts [23] were developed for this purpose to accommodate different microarray designs such as one-color, two-color direct comparison of treatment and control, two-color with a common reference, and two-color with dye-swaps. Greater detail about DEG determination is available elsewhere [16]. The number of top DEGs selected as a signature and ranked by false discovery rate depended on the types of Cmap query. The Cmap query minimum was lowered from the recommended value of 10 [24], to four DEGs in order to encompass more experimental conditions. On average, though, a signature contained 57 to 88 DEGs for queries made within platforms/species, and 110 to 181 DEGs for Cmap across platforms/species. Intuitively, a larger number of DEGs per signature in the latter case might help to compensate for the possible inconsistencies in GEPs from different microarray platforms within a species, and the possible divergence of chemical MOAs across species. Each DEG in a signature was accompanied by its own value of

logarithmic fold-change. In total, 109 unique signatures were prepared for within-platform queries and 61 signatures for queries across platforms/species (Additional file 2: Table S2). These signatures were named after fish sample treatment conditions by the order of chemical, dose, gender, tissue, and exposure duration.

ROGLs

A ROGL of a treated sample was prepared from appropriate GEPs in several ways depending on study design. For one-color data, gene probe intensities of each treated sample were compared to the corresponding average intensities derived from its specific group of control samples. As a result, each gene probe was given a LogFC of treated over control. Gene probes were then sorted by the absolute values of their LogFC from the smallest to the greatest, and assigned either a positive or negative rank from 1 to N based on the signs of LogFC, with N being number of probes in a given microarray. For two-color direct comparison of a pair of treated over control samples on the same microarray, a ROGL was generated similarly for the treated but within the pair only. For two-color with a common reference design, gene probe intensities of each treated sample were again compared to those averaged over the corresponding reference group. In total, there were 2387 ROGLs in the constructed fish reference database: 386, 203, and 1798 respectively for ZF 21K, ZF 43K, and FHM 15K. For maximum flexibility, the ROGLs from these three platforms were maintained as three distinct collections. Cmap across-platform or across-species was implemented by substituting the probe identifications (IDs) from a source query signature with their equivalent/orthologous probe IDs in its target platform or species.

Cmap

Interrogation of the fish reference database was conducted using software sscMap [24], containing an algorithm based on the principles of the original Cmap [6]. Basically, Cmap measures the strength of connectivity between a query signature and a ROGL by a connectivity score of their summed ranks. To assess its associated p-value, the default value of 10,000 simulated signatures, each containing the same number of gene probes as the original query signature, are randomly generated from the ROGL. From them connectivity scores are calculated. The p-value for the original query is the proportion of simulated query signatures with their connectivity scores greater than or equal to the observed score. In practice, related ROGLs are typically organized by sscMap into various sets, each defined by some common experimental parameters such as chemical, dosage, and tissue types, and then interrogated by query signatures. Both connectivity score and p-value are slightly modified to account for the variation in the size of individual ROGL sets. With a parameter S denoting the number of ROGL sets contained in a database collection and interrogated by a query signature, the number of false connections was controlled by a critical p-value of 1/S. Each signature was set as "unordered" in the analysis so all up-regulated genes had the same weight of +1, and down-regulated genes had a weight of −1 in contributing to the connectivity score. The highest-scored, statistically significant, and unique pairs of signature-ROGL (excluding those originated from the same experiment) were identified across queries within each platform, and visualized in Cytoscape [25].

To fully evaluate the effectiveness of Cmap, query signatures and ROGLs were arranged into three configurations: within the same platforms and species, across zebrafish platforms, and across species. Because of the differences in coverage of chemicals and their varying transcriptomic impact as measured by the number of DEGs/average LogFC among treatment conditions, queries across platforms and across species were conducted in both directions in order to identify all potential chemical-chemical connections. To enable queries across platforms and species, however, their corresponding probes or orthologs had to be mapped first. This was implemented through several successive steps of ID mapping among ZF 21K, ZF 43K, and FHM 15K microarrays. For example, to identify orthologs between FHM 15K and ZF 21K, the probe sequences from FHM 15K were mapped to their corresponding fathead minnow EST (Expressed Sequence Tag) target sequences (courtesy of Dr. Nancy Denslow, University of Florida) first by TBLASTX. These EST sequences were then mapped to the NCBI nucleotide (NT, as of July, 2013) and protein (NR, as of July 2013) databases by TBLASTX and BLASTX respectively, effectively associating fathead minnow probe IDs to their corresponding NCBI accession IDs. With their greater sequence length, ESTs are presumably more likely than shorter probe sequences to capture orthologs across species. All three rounds of BLAST mapping had a minimum E-value cutoff of E^{-06}. These fathead minnow IDs were then joined to a variety of zebrafish accession IDs prepared by the NCBI [26], and finally to Agilent probe annotations [27]. In the end, a total of 9304 probes (43 %) from ZF 21K were linked to 6899 probes (45 %) from FHM 15K through 6573 common Entrez GeneIDs in NCBI. Similarly, 16376 probes (38 %) from ZF 43K were mapped to 9861 probes (65 %) of FHM 15K based on a common set of 10353 Entrez GeneIDs. In addition, 13273 probes (62 %) from ZF 21K mapped to 16083 probes (37 %) of ZF 43K were

based entirely on the NCBI "gene2accession" file without using any BLAST programs.

Results

The performance of Cmap was evaluated by examining the ROGL hits with connectivity scores ranked highest either by individual query signatures or across signatures, based on fish samples profiled on each of the three microarray platforms: ZF 21K, ZF 43K, and FHM 15K. The primary purpose of examining queries individually was to evaluate whether a query signature can indeed connect with its intended ROGL targets when they had commonly associated chemical conditions. This evaluation was carried out both within and across microarray platforms, as well as across fish species. These connections essentially establish the chemical identity of a query signature based on the degree to which chemicals involved have shared MOAs. High-scoring pairs of query signature-ROGL across-queries, on the other hand, could reveal additional novel insights about the MOA similarity of related chemicals. For better clarity in their visualization in a chemical network, each connected pair of chemical conditions was treated as directionless, regardless of which node in the pair represented a signature or a set of ROGLs.

Validation of Cmap algorithm

Overall Cmap performance was variable, as measured by the percentage of query signatures producing informative connections. An informative connection is arbitrarily defined as a signature and one of its top five ROGL hits sharing the same or similar class of chemicals. Cmap was very effective when both query signatures and ROGLs were from the same microarray platform/species (Table 3). The relatively lower performance in fathead minnow was probably because many treatment conditions had no or very few DEGs (Table 2, Additional file 3: Figure S1). When query signatures and ROGLs were from different platforms and species, the gene probe IDs in a query signature had to be cross-mapped to those in the targeted ROGLs. With the configuration of target probe IDs coupled with source LogFC, an average success rate of 61 % was observed based on a small number of treatment conditions in common across the platforms/species.

Table 3 Summary of Cmap by the percentage of query signatures producing informative connections

Microarray platforms	ZF 21K	ZF 43K	FHM 15K
ZF 21K	35/36 (97 %)	11/13 (85 %)	4/8 (50 %)
ZF 43K	6/12 (50 %)	36/36 (100 %)	5/10 (50 %)
FHM 15K	6/12 (50 %)	5/6 (83 %)	35/46 (76 %)

An informative connection was established when a query signature shared the same or similar class of chemicals with at least one of the top five ROGL hits, as ranked by an adjusted connectivity score with a p-value ≤ 1/(S sets of ROGLs). All cross-platform/species Cmap were based on target probe IDs + source gene log-fold changes on shared chemical conditions. Only unique query signatures were considered in calculations

A more detailed examination of connectivity between query signatures and ROGLs provided additional insights into the performance of Cmap. As expected, a query signature almost always connected with ROGLs of its originating treatment condition as the best hit when both came from the same platform (Table 4). In many instances, this connectivity of the same or similar class of chemicals extended across independent experiments, different tissue types, and chemical mixtures as well. For example, a signature from the brain tissue of zebrafish treated with EE2 (EE2_30ngL_M_Brain_48hr) connected with the ROGLs of both EE2_testis and EE2_ovary, overriding the strong impact of tissue types typically observed on fish transcriptomes [28]. Significantly, this strong connectivity among chemical treatment conditions based on their shared MOAs was not limited to HPG-active toxicants. Similarly strong connections were observed in chemicals targeting other biological pathways/processes such as neurotransmission (BIF_0.15ugL_larvae_48hr), regulation of xenobiotic metabolism (TCDD_2nM_embryo_6h), signal transduction (PKC412_40ugL_fish_6dpf), and photosynthesis (linuron_1.2mgL_embryo_48hr).

Beyond single chemical exposures, Cmap was also effective in discriminating chemical mixtures. For example, when fish were exposed to a mixture of two different chemicals (Mixture_M_Brain; containing terbufos and permethrin), this mixture had barely detectable effects on gene expression, so no signature could be constructed. Still, its ROGLs were informative, connecting to the signatures of both terbufos and bifenthrin from other independent experiments. Bifenthrin is another pyrethroid insecticide similar to permethrin. Notable was the fact that the bifenthrin signature here originated from whole fish larvae while the ROGLs of terbufos/permethrin mixture came from adult brain tissue. At the concentrations used in the exposure, permethrin had very little effect on gene expression, resulting in a relatively uninformative signature consisting of only six gene probes. As ROGLs, however, permethrin also formed strong connection with terbufos and bifenthrin.

The microarray data from previous studies of water conditions near several municipal WWTPs across the USA provided a "real world" assessment of Cmap performance (Table 5). Several observations were notable. There were considerable similarities among the water conditions near these WWTPs as reflected in their fish ROGLs. These similarities were observed both within locations (e.g., upstream, effluent, downstream) and across geographic locations. Second, there were high agreements between Cmap and chemical analyses from those studies with regard to

Table 4 Top five significant hits, if any, of selected Cmap queries within microarray platforms

Signatures	1st match	2nd match	3rd match	4th match	5th match
	Within ZF 21K (p-value cutoff 1/45 = 0.022)				
EE2_30ngL_Ovary_96hr	Self	FAD_Ovary	TRB_F_Brain	**EE2_Testis**	FAD_M_Brain
EE2_30ngL_M_Brain_48hr	Self	**EE2_Testis**	FAD_M_Brain	TRB_F_Brain	**EE2_Ovary**
EE2_30ngL_M_Liver_48hr	Self	TRB_F_Liver	**EE2_Testis**	O2_Testis	KET_M_Liver
EE2_30ngL_Testis_48hr	Self	**EE2_Ovary**	**EE2_M_Brain**	FIP_F_Brain	TRI_TestisLow
FAD_25ugL_F_Brain_48hr	Self	TRB_F_Brain	**FAD_M_Brain**	**FAD_Ovary**	EE2_Testis
FAD_25ugL_Ovary_96hr	Self	EE2_Ovary	**FAD_M_Brain**	TRI_TestisLow	TRB_F_Brain
FIP_5ugL_Testis_48hr	Self	**FIP_Ovary**	TRI_Testis	**FIP_M_Brain**	FLU_Testis
FLU_1700ugL_Ovary_48hr	Self	**FLU_Testis**	PRO_Testis	VIN_Ovary	KET_Ovary
MUS_500ugL_F_Brain_48hr	Self	VIN_Ovary	**MUS_M_Brain**	KET_M_Brain	VIN_Testis
MUS_500ugL_M_Brain_48hr	Self	**MUS_F_Brain**	VIN_Ovary	KET_M_Brain	KET_Ovary
O2_1mgL_Testis_4d	Self	**O2_Ovary**	EE2_M_Liver	**O2_Ovary**	VIN_Testis
PRO_500ugL_F_Brain_48hr	FLU_Testis	self	**PRO_Testis**	VIN_Ovary	KET_Ovary
PRO_500ugL_Ovary_48hr	Self	FLU_Ovary	FLU_Testis	KET_Ovary	**PRO_Testis**
TCDD_2nM_Embryo_6h	Self	**TCDD_Embryo**	TRI_Ovary	O2_Ovary	PRO_Testis
TRI_2500ugL_Testis_24hr	Self	VIN_Testis	VIN_Ovary	KET_Ovary	**TRI_TestisLow**
VIN_1000ugL_Ovary_48hr	Self	KET_Ovary	TRI_Testis	**VIN_Testis**	FIP_Ovary
VIN_1000ugL_Testis_48hr	Self	FLU_Testis	PRO_Testis	TRI_Testis	**VIN_Ovary**
	Within ZF 43K (p-value cutoff 1/39 = 0.026)				
BPA_0.01ugL_Ovary_96hr	Self	**BPA_Ovary**	**BPA_Ovary**	**BPA_Ovary**	**BPA_Embryo**
E2_1uM_Embryo_4dpf	self	**E2_M_Liver**	**GEN_Embryo**	**GEN_Embryo**	FLU_Embryo
EE2_0.65mgL_Embryo_48hr	**EE2_Embryo**	**EE2_Embryo**	**GEN_Embryo**	PARAB_Embryo	PYR_Embryo
E2_5ugL_M_Liver_48hrs	self	**E2_Embryo**	PARAB_Embryo	PARAB_Embryo	**GEN_Embryo**
GEN_2.4mgL_Embryo_48hr	self	**GEN_Embryo**	PARAB_Embryo	DBT_Embryo	diazepam_Brain
PKC412_40ugL_fish_6dpf	**PKC412_fish**	self	RDX_fry	diazepam_Brain	RDX_fry
PRO_500ugL_F_Brain_48hr	**PRO_Ovary**	linuron_Embryo	FLU_Ovary	**PRO_F_Brain**	linuron_Embryo
PRO_500ugL_Ovary_48hr	self	FLU_Ovary	linuron_Embryo	**PRO_F_Brain**	linuron_Embryo
RDX_7.5mgL_fry_96hr	self	**RDX_fry**	**RDX_fry**	**RDX_fry**	**RDX_fry**
BPA_8mgL_Embryo_48hr	self	**BPA_Embryo**	EE2_Embryo	BAA_Embryo	PRO_Embryo
diazepam_273ngL_brain_14d	self	**diazepam_Brain**	PKC412_fish	RDX_fry	RDX_fry
linuron_1.2mgL_Embryo_48hr	self	**linuron_Embryo**	PKC412_fish	BPA_Embryo	diazepam_Brain
PARAB_19.8mgL_Embryo_48hr	self	**PARAB_Embryo**	linuron_Embryo	linuron_Embryo	PYR_Embryo
PRO_1.7mgL_Embryo_48hr	self	**PRO_Embryo**	E2_Embryo	BPA_Embryo	PARAB_Embryo
	Within FHM 15K (p-value cutoff 1/132 = 0.0076)				
BIF_0.15ugL_Larvae_48hr	**BIF_Larvae**	self	TER_M_Brain	**Mixture_M_Brain**	KETTNTKET_Ovary
BIF_0.3ugL_Larvae_48hr	self	**CYP_Larvae**	**ESF_Larvae**	**ESF_Larvae**	**PER_Larvae**
CYP_1ugL_Larvae_48hr	self	VZ_Ovary	**PER_Larvae**	**CYP_larva**	RDX_Ovary
DES_1ngL_Liver_96h	**EE2_Liver**	self	PHE_High_Liver	**E2_X_M_Liver**	**DES_Liver**
E2_4ugL_M_Liver_14d	self	**E2_M_Liver**	**EE2_Liver**	**DES_Liver**	**ElyEFF_Liver**
EE2_25ngL_Liver_72h	**E2_M_Liver**	self	**E2_X_M_Liver**	**DES_Liver**	**ElyEFF_Liver**

Table 4 Top five significant hits, if any, of selected Cmap queries within microarray platforms *(Continued)*

GEM_600ugL_Ovary_8d	self	**GEM_Ovary**	TrbEE2TrbEE2_Ovary	RochDS_Ovary	TrbEE2TRB_Ovary
PHE_High_Liver_48hr	self	**PHE_Med_Liver**	ElyEFF_Liver	ElyUS_Liver	PFCs_Low_Liver
TRB_30ngL_Ovary_24h	self	FLU_Ovary	TrbTCCTCC_Ovary	GEM_Ovary	GEM_Ovary
TER_57.5ugL_M_Brain_72h	self	**Mixture_M_Brain**	PER_M_Brain	BIF_Larvae	KET_Ovary

Only signatures connected to multiple conditions are included. Where similar signatures exist for a condition, only one is listed. ROGL hits are ranked by their adjusted connectivity scores and filtered by a p-value cutoff of 1/(number of sets of ROGLs). Informative connections, defined as a signature and one of its top five ROGL hits sharing the same or similar class of chemicals, are highlighted in bold. Self: a query signature and the connected ROGLs originated from the same experiment

the occurrence of known estrogenical chemicals, such as E2 and EE2 [29, 30]. For example, the water samples near WWTPs of San Diego (EFFHa, EFFLa) and Los Angeles (EFFHb), California were both reported to be estrogen-positive [29]. Their estrogenic identities were confirmed by Cmap when they were examined either as query signatures (Table 5) or ROGLs (not shown). Various types of estrogenic chemicals were also found near the WWTPs of Ely, Hutchinson, and Rochester, MN [30]. By Cmap, estrogen-associated ROGLs were also connected to the signatures of these water samples, with connectivity scores ranked at 10th (Ely effluent, Ely downstream), 16th (Ely upstream, Hutchinson effluent), 13th (Hutchinson downstream), 18th (Rochester downstream), 11th (Rochester effluent), and 12th (Rochester upstream). Measured against a p-value cutoff of 1/132 = 0.0076, all these estrogen connections were statistically highly significant. Finally, the sediment samples, and presumably the surrounding water, near the WWTPs in Ely and Hutchinson were positive for a number of PAHs (e.g. anthracene, phenanthrene, pyrene) and an organophosphate insecticide (chlorpyrifos) [31]. The query signatures from both locations ranked

Table 5 Cmap performance under "real world" conditions

Signatures (NCBI GEO accession)	1st – 2nd match	3rd-4th match	5th-6th match	7th-8th match	9th-10th match
EFFHa_5Perc_MaleLiver_14d (GSE29350)	self	BIF_Larvae	BIF_Larvae	Wastewater_Liver	FLU_50_Ovary
	EFFLa_M_Liver	HutDS_Liver	EFFHb_M_Liver	HutUS_Liver	PFCs_Mix_Liver
EFFHb_5Perc_MaleLiver_14d (GSE29350)	self	Wastewater_Liver	FAD_Ovary	TRI_Ovary	RDX_Liver
	E2_M_Liver	HutEFF_Ovary	VIN_Ovary	KET_Ovary	RDX_fry
ElyDS_999_Liver_4d (GSE49098)	self	HutEFF_Liver	RochUS_Liver	RochDS_Liver	PHE_Liver
	ElyEFF_Liver	ElyUS_Liver	HutUS_Liver	HutDS_Liver	E2_M_Liver
ElyEFF_999_Liver_4d (GSE49098)	self	ElyUS_Liver	PHE_Liver	RochDS_Liver	RochUS_Liver
	ElyDS_Liver	HutEFF_Liver	HutUS_Liver	PHE_Liver	E2_M_Liver
ElyUS_999_Liver_4d (GSE49098)	self	ElyDS_Liver	HutEFF_Liver	HutUS_Liver	BIF_Larvae
	ElyEFF_Liver	PFCs_Liver	EFFHa_M_Liver	RochDS_Liver	PFCs_Mix_Liver
HutchinsonDS_999_Liver_4d (GSE49098)	self	RochDS_Liver	HutEFF_Liver	ElyEFF_Liver	PFCs_Mix_Liver
	RochUS_Liver	ElyDS_Liver	HutUS_Liver	KET_Ovary	KET_Ovary
HutchinsonEFF_999_Liver_4d (GSE49098)	self	ElyDS_Liver	HutUS_Liver	HutDS_Liver	PHE_Liver
	ElyEFF_Liver	ElyUS_Liver	RochUS_Liver	RochDS_Liver	KET_Ovary
RochesterDS_999_Liver_4d (GSE49098)	self	HutUS_Liver	HutDS_Liver	ElyEFF_Liver	RochEFF_Liver
	RochUS_Liver	ElyDS_Liver	ElyUS_Liver	HutEFF_Liver	BIF_Larvae
RochesterEFF_999_Liver_4d (GSE49098)	HutUS_Liver	self	HutEFF_Liver	BIF_Larvae	PFCs_Mix_Liver
	ElyUS_Liver	RochDS_Liver	ElyDS_Liver	RochUS_Liver	PFCs_Liver
RochesterUS_999_Liver_4d (GSE49098)	self	RochDS_Liver	HutEFF_Liver	HutUS_Liver	ElyUS_Liver
	ElyDS_Liver	ElyEFF_Liver	HutDS_Liver	RochEFF_Liver	PFCs_Mix_Liver
Wastewater_999_Liver_48h (GSE37550)	self	CYP_Larvae	NA	NA	NA
	E2_M_Liver	surfaceH2O_Testis	NA	NA	NA

Fathead minnow samples were exposed to various water conditions near several waste water treatment plants in the USA either by field deployment or in a laboratory setting. Only those exposures generating a significant number of DEGs thus having query signatures available are listed. The top ten matched ROGLs are listed to provide a broad list of candidate chemicals. Waste water treatment plant locations: Ely, Hutchinson (Hut), Rochester (Roch), Minnesota; San Diego (Ha), Los Angeles (Hb), California; Gainesville (GSE37550), Florida. Abbreviations: EFF, effluent; US, upstream; DS, downstream. P-value cutoff 1/132 = 0.0076. Self: a query signature and the connected ROGLs originated from the same experiment

phenanthrene with high connectivity scores. With the same MIE (acetylcholinesterase inhibitor) shared between terbufos and chlorpyrifos, a strong connectivity was also found between a terbufos signature and the ROGLs of Ely downstream (6th), Ely effluent (8th), Hutchinson downstream (14th), and Hutchinson effluent (16th).

Cmap had a more limited success, ranging from 50 % to 85 %, across platforms and species based on a small number of conditions common to them (Table 2). In spite of varying performance between ZF 21K and ZF 43K in either direction, Cmap was able to connect query signatures to target ROGLs for all the conditions common to these two platforms: EE2/E2/genistein, flutamide, and prochloraz (Table 6, Additional file 4: Table S3). There was little difference in cross-platform performance between maximum signature size set at 100 and 500. Similar variation in the performance of Cmap was also observed across species. Among the conditions shared between FHM 15K and ZF 21K, and between FHM 15K and ZF 43K, were EE2/E2/DES/genistein, trenbolone, and RDX. With the exception of RDX and trenbolone, successful connections were made between query signatures and ROGLs for all other conditions.

Discovery of novel chemical connections

While the chemical identities of individual query signatures and their connected high-scored ROGLs enable an evaluation of Cmap performance, those connections that ranked high across query signatures also could provide novel insights into possibly shared MOAs and toxicity pathways among seemingly different chemicals. By individual platforms of ZF 21K, ZF 43K, and FHM 15K, the

Table 6 Top five significant hits, if any, of selected Cmap queries across microarray platforms and species

Signatures	1st match	2nd match	3rd match	4th match	5th match
	From ZF 21K to ZF 43K (p-value = 0.026; signature size average = 181, min = 15, max = 375)				
EE2_30ngL_M_Brain_48hr.sig.500.IDswap	LIN_Embryo	PRO_F_Brain	LIN_Embryo	**E2_M_Liver**	FLU_Ovary
EE2_30ngL_M_Liver_48hr.sig.500.IDswap	**E2_M_Liver**	RDX_fry	RDX_fry	RDX_fry	PKC412_fish
EE2_30ngL_M_Testis_48hr.sig.500.IDswap	**GEN_Embryo**	BPA_Ovary	BPA_Embryo	BPA_Ovary	DBT_Embryo
FLU_Ovary_48hr.sig.500.IDswap	**FLU_Embryo**	PKC412_fish	BPA_Ovary	PPL_Embryo	RDX_fry
FLU_Testis_48hr.sig.500.IDswap	LIN_Embryo	LIN_Embryo	**FLU_F_Ovary**	PKC412_fish	**FLU_Embryo**
PRO_F_Brain_48hr.sig.500.IDswap	E2_M_Liver	**PRO_F_Brain**	GEN_Embryo	FLU_Embryo	**PRO_Ovary**
PRO_Ovary_48hr.sig.500.IDswap	**PRO_Ovary**	FLU_Ovary	**PRO_F_Brain**		
PRO_Testis_48hr.sig.500.IDswap	E2_M_Liver	**PRO_Ovary***	**PRO_F_Brain***		
	From ZF 43K to ZF 21K (p-value = 0.022; signature size average = 134, min = 5, max = 310)				
E2_1uM_Embryo_4dpf.sig.500.IDswap	**EE2_Testis**	**EE2_M_Liver**	TRB_F_Liver	O2_Testis	O2_Ovary
E2_5ugL_M_Liver_4hrs.sig.500.IDswap	**EE2_M_Liver**	TRB_F_Liver	O2_Testis	O2_Testis	TCDD_Embryo
PRO_2mgL_Embryo_48hr.sig.500.IDswap	DMB_Embryo	tBHQ_Embryo	TRB_F_Brain	**PRO_F_Brain**	EE2_M_Liver
	From ZF 21K to FHM 15K (p-value = 0.0076; signature size average = 124, min = 9, max = 257)				
EE2_30ngL_Ovary_96hr.sig.500.IDswap	FAD_Ovary	**EE2_M_Brain**	**EE2_M_Brain***		
EE2_30ngL_M_Liver_48hr.sig.500.IDswap	**EE2_Liver**	RochDS_liver	PHE_Liver	RochUS_liver	Stream_Liver
EE2_30ngL_Testis_48hr.sig.500.IDswap	PFCs_Liver	KTC_Ovary	PFCs_High_Liver	**RochEFF_liver**	
	From FHM 15K to ZF 21K (p- value = 0.022; signature size average = 110, min = 5, max = 272)				
DES_100ngL_Liver_96h.sig.500.IDswap	**EE2_M_Liver**	DNP_Embryo	DMB_Embryo	TCDD_Embryo	APM_Embryo
E2a_4ugL_M_Liver_14d.sig.500.IDswap	**EE2_M_Liver**	KET_F_Liver	DNP_Embryo	KET_M_Liver	TRI_Ovary
EE2_25ngL_Liver_72h.sig.500.IDswap	**EE2_M_Liver**	KET_M_Liver	KET_F_Liver	TRB_F_Liver	FLU_M_Testis
	From ZF 43K to FHM 15K (p-value = 0.0076; signature size average = 120, min = 6, max = 274)				
E2_M_Liver_4hrs.sig.500.IDswap	**ElyEFF_liver**	ElyDS_liver	PHE_Liver	**E2_M_Liver**	**DES_Liver**
GEN_Embryo_48hr.sig.500.IDswap	PFCs_Blood	KTC_Ovary	BIF_Larvae	**E2_M_Liver**	PER_Larvae
	From FHM 15K to ZF 43K (p-value = 0.026; signature size average = 139, min = 5, max = 363)				
DES_1ngL_Liver_96h.sig.500.IDswap	**E2_M_Liver**				
E2_4ugL_M_Liver_14d.sig.500.IDswap	**E2_M_Liver**	PKC412_fish	BPA_Embryo	**GEN_Embryo**	BPA_Embryo
EE2_25ngL_Liver_72h.sig.500.IDswap	**E2_M_Liver**	PKC412_fish	LIN_Embryo	BPA_Embryo	BDE_Embryo

Where similar signatures exist for a condition, only one of them is listed. ROGL hits are ranked by their adjusted connectivity scores and filtered by a p-value cutoff of 1/(number of sets of ROGLs). Informative connections, defined as a signature and one of its top five ROGL hits sharing the same or similar class of chemicals, are highlighted in bold. "*", *p*-values slightly greater than the cutoffs

highest-scored connection was selected from all the significant ones for each distinct pair of chemicals, regardless of direction (i.e., two conditions linked to each other as either a signature or ROGLs), tissue type, dose, exposure duration or data origin, and visualized collectively in Cytoscape as a chemical network. With the recognition of likely confounding contributions from such factors as tissue type, this network provided a composite or "average" view of how chemicals relate to one another. Each chemical in this network became a node, with the connection between two nodes forming an edge. An edge was weighted by the connectivity score between the two connected chemicals. Such a network essentially provides a glimpse of chemical "neighborhood" as arranged by the similarities in the transcriptomic profiles among its chemical members.

In ZF 21K where a total of 17 chemicals were linked, 10 confirmed HPG-active toxicants formed a tight

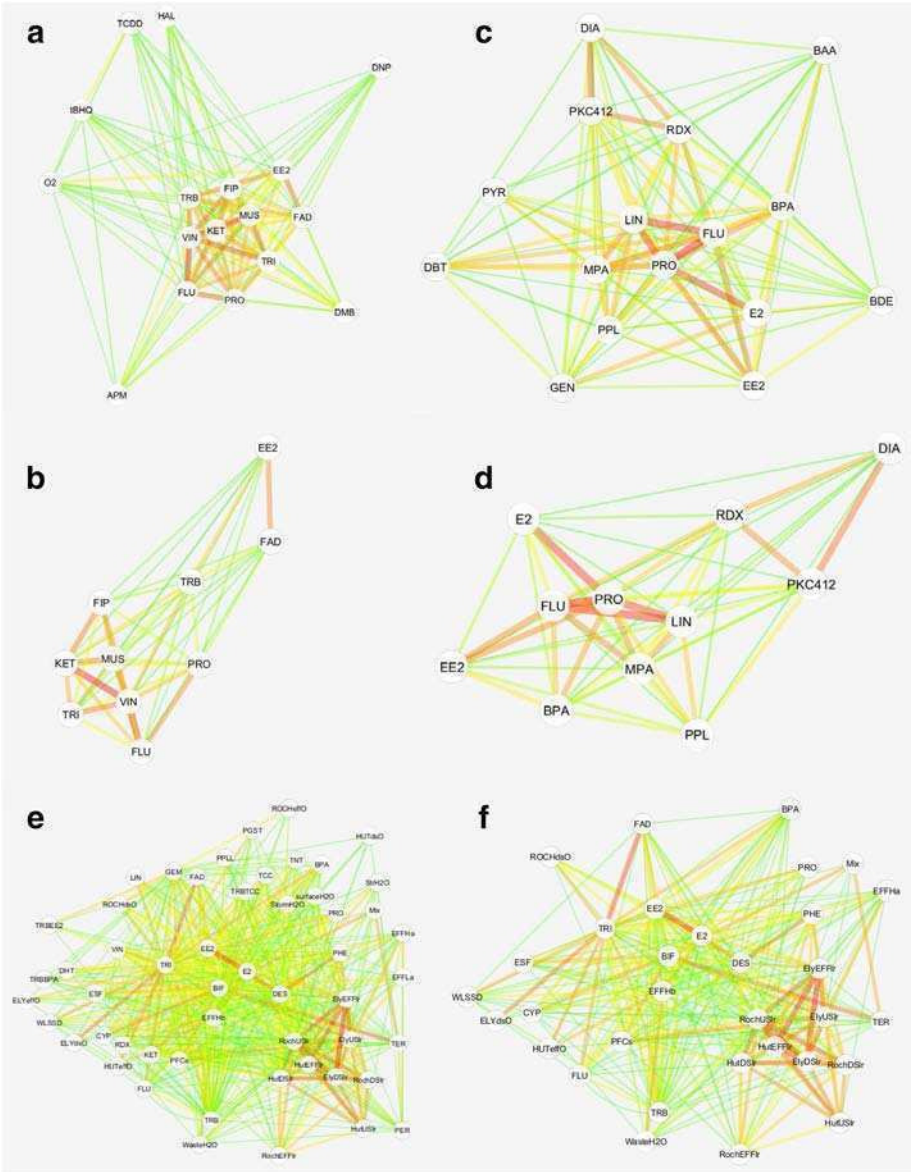

Fig. 1 A network view of chemical-chemical connectivity based on fish samples profiled on various microarray platforms. Each treatment condition is represented as a node. Two nodes are connected by an edge weighted by their connectivity score. A shorter, darker, and wider edge between two nodes denotes a higher connectivity score. All connections shown are statistically significant. **a** ZF 21K: 117 connections among 17 treatment conditions; **b** ZF 21K: 45 connections among 10 nodes with each node containing a connectivity score of ≥ 10 in at least one connection; **c** ZF 43K: 110 connections among 16 treatment conditions; **d** ZF 43K: 54 connections among 11 nodes with each node containing a connectivity score of ≥ 10 in at least one connection; E) FHM 15K: 541 connections among 53 treatment conditions; F) FHM 15K: 293 connections among 32 nodes with each node containing a connectivity score of ≥ 10 in at least one connection

cluster in the network while other chemicals that likely were not HPG-active spread out as distant outliers (Fig. 1a). A further differentiation of the 10 HPG-active toxicants could be made when they were selected to form their own sub-network based on achieving a minimum connectivity score (Fig. 1b). Under this scenario, there appeared to be two distinct groups: one made up of vinclozolin, ketoconazole, flutamide, trilostane, fipronil, muscimol, and prochloraz; and the other of EE2 and fadrozole. Trenbolone seemed to be unique as it shared substantial similarity to both groups. These observed clustering patterns were still clearly visible when both chemical and tissue type were considered together (Additional file 5: Figure S2). Beyond the contributions from chemical and sometimes tissue type, the structure of this network did not appear to coincide with other experimental conditions such as the lab origins of data.

In ZF 43K, there was also a distinct pattern in chemical connectivity (Fig. 1c, d). Prochloraz, flutamide, linuron, E2, and to the lesser extent, EE2, methylparaben, bisphenol A, formed a group of similar chemicals while RDX, PKC412, and diazepam formed another. Interestingly, the three confirmed estrogens; genistein, EE2, and E2; had relatively weak connections among themselves.

In FHM 15K, a number of interesting observations could also be made. Consistent with the earlier analysis by individual query signatures (Table 5), the water conditions near the three Minnesota WWTPs, as reflected in the transcriptomic profiles of deployed male fish, were indeed highly similar to one another not only across sites within a location, but also across locations (Fig. 1e, f; liver tissue of male fish exposed to water from Ely effluent, downstream, upstream: ElyEFFlr, ElyDSlr, ElyUSlr; Hutchinson effluent, downstream, upstream: HutEFFlr, HutDSlr, HutUSlr; Rochester effluent, downstream, upstream: RochEFFlr, RochDSlr, RochUSlr). These sites, all of which had detectable estrogens present [30], showed relatively strong connectivity with diethylstilbestrol (DES), E2, and EE2. However, in female fish samples exposed to these same sites (ELYeffO, ELYdsO, HUTdsO, HUTeffO, ROCHeffO, ROCHdsO), no detectable impact was found on gene expression, and perhaps not surprisingly, no obvious pattern in the connectivity among these conditions was observed. In a similar but independent study of WWTPs in San Diego (EFFHa, EFFLa) and Los Angeles (EFFHb), California [29], potential estrogenic properties as determined by chemistry were revealed in the current study by their significant connectivity to DES, E2, and EE2. Also notable is the fact that, probably due to the San Diego WWTP being a primary treatment plant and the Los Angeles WWTP a secondary treatment plant, their ROGLs were quite distinct. Finally, several pyrethroid insecticides (bifenthrin, BIF; cypermethrin, CYP; esfenvalerate, ESF), though seemingly far apart, also shared strong connectivity among themselves as indicated by their edge size and color. In the case of a mixture (Mix) of terbufos (TER) and permethrin (PER), the mixture was strongly connected to both terbufos and bifenthrin, but not to permethrin directly. Interestingly, permethrin was significantly linked to both terbufos and bifenthrin (Fig. 1e, Table 4).

Connectivity among chemicals appeared to be modulated by the intensity of their elicited transcriptomic responses, which are dependent on chemical dose, treatment duration, fish tissue type, and life stage. When only fathead minnow treatments with multiple doses of the same tissue type were considered, the nodes of the same chemical but with various doses were scattered throughout the network, with different numbers of neighbors (directly connected nodes) at different connectivity strength (Fig. 2). For a given node, the number of its neighbors measures its connectivity in a network. For instance, the two nodes representing two independent but concurrent bifenthrin exposure experiments with larvae (BIF_0.148ugL, BIF_0.593ugL) had 7 and 4 neighbors respectively, as determined by Cytoscape. Their closest neighbors by connectivity score, bifenthrin (BIF_0.15ugL, 7.2) and trilostane (TRI_1500ugL, 4.8) respectively, were also different. In other words, depending on dosage, the network neighborhood of a chemical could be altered to some extent. Similar observations were also made in other conditions such as bisphenol A with ovary (BPA_0.01ugL, BPA_0.1ugL, BPA_1.0ugL, BPA_10ugL, and BPA_100ugL; 9, 4, 7, 9, 11 neighbors), DES with liver (DES_1ngL, DES_10ngL, DES_100ngL; 10, 8, and 47 neighbors), and fadrozole with ovary (FAD_3ugL, FAD_5ugL, FAD_30ugL, FAD_50ugL; 8, 10, 8, 11 neighbors).

Discussion

Fish Cmap provides a data-driven approach for applying transcriptome profiling technology to the assessment of exposure, relative toxicity, and grouping of chemicals. The findings in this study have demonstrated the effectiveness of this approach to make connections among chemical conditions associated with a query signature and a set of ROGLs from independent experiments, especially when both are from the same microarray platform/species. Like any other query-database applications, its power is a function of coverage: the more chemical/biological conditions ROGLs in a database are linked to, the more likely a query signature will make an informative connection. Along with the rapid increase of transcriptomics data in public repositories and the expansion of this fish reference database in the future, fish Cmap should find increasing applications in ecotoxicology.

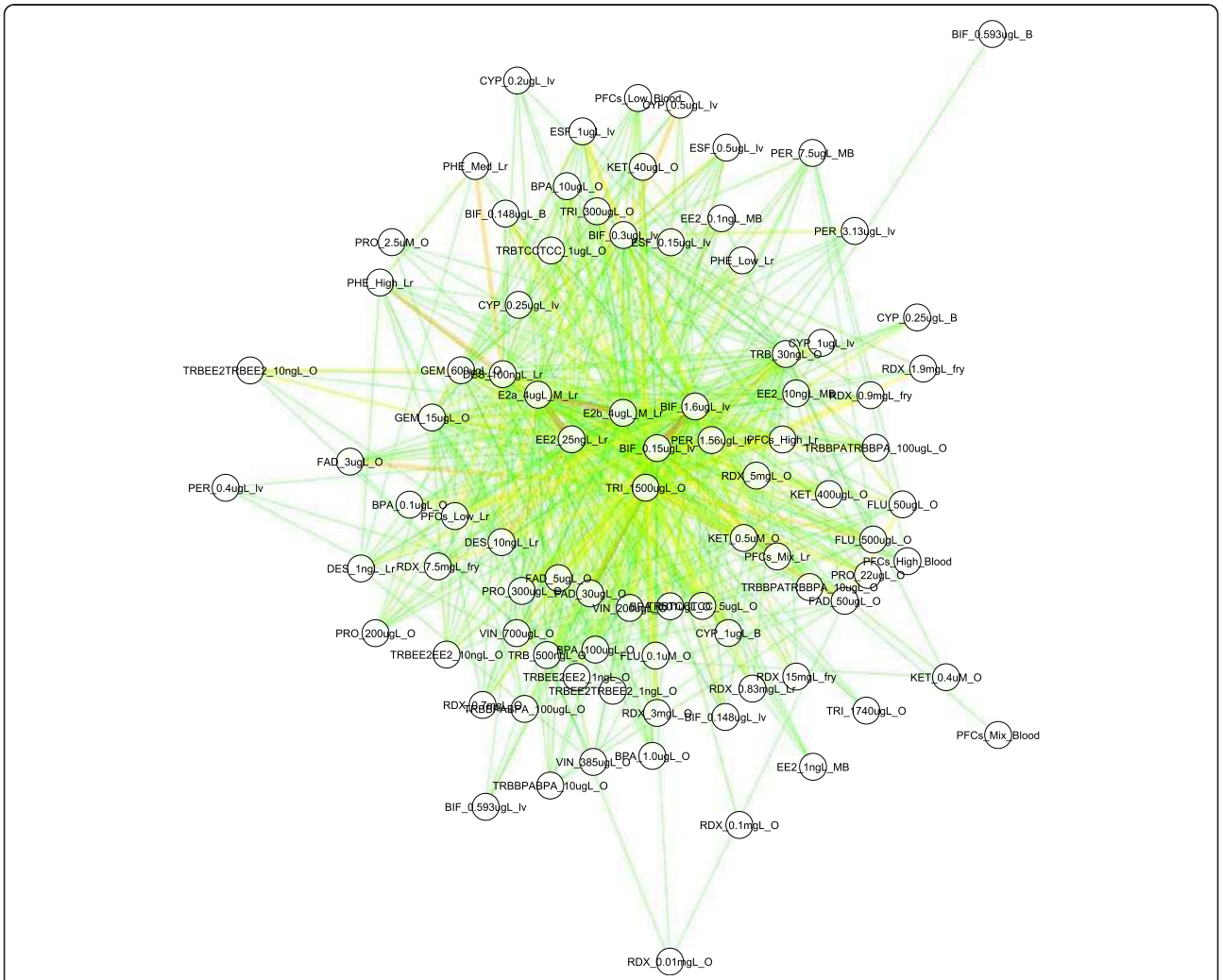

Fig. 2 A network view of chemical-chemical connectivity based on fish samples profiled on FHM 15K. Only treatments with multiple doses are included. Each treatment condition containing the information of both dosage and tissue type is represented as a node. Two nodes are connected by an edge weighted by their connectivity score. A shorter, darker, and wider edge between two nodes denote a higher connectivity score. All connections shown are statistically significant. Tissue types and gender: T, testis; O, ovary; B, brain; Lr, liver; lv, larvae; M, male

The performance of fish Cmap ultimately depends on MOAs/toxicity pathways shared among chemicals. For a given query signature and its target ROGLs, the connectivity strength is determined by both the direction in change (up, + or down, –) and ranking in magnitude of the selected DEGs therein (typically 10 to 100). In the current study, the direction of DEGs was considered in both signatures and ROGLs, but the ranking was considered only in ROGLs. In this configuration, a connectivity score is maximized when the signs of DEGs in a query signature perfectly match their counterparts in the target ROGLs, and these DEGs are ranked high in the latter [24]. Arguably, the direction of change of a DEG and its relative rank are not as sensitive as magnitude to extraneous factors such as exposure intensity (chemical dosage and duration) and "random" noise (natural variation; Wang et al. [16]), thus are more reflective of the underlying chemical MOA. In theory, a treatment condition must be of sufficient intensity to have a significant impact on fish transcriptome and enable subsequent Cmap. The relationship between connectivity strength and the magnitude of treatment effect as indicated by DEGs was examined in the current study by several measures of individual chemical conditions: relative transcriptome impact (RTI, the percentage of a transcriptome determined as DEGs), the average LogFC in absolute values over all DEGs, and total number of DEGs. There were no clear relationships for connectivity score (normalized to signature size), RTI, and average LogFC (Additional file 6: Figure S3A, S3B, S3C) among 106 chemical conditions with a RTI ≥ 0.001. However, a further examination within FHM 15K, which has 13 signatures each

containing less than 10 probes, revealed that connectivity scores (un-normalized) tended to increase as a function of total number of DEGs (Additional file 7: Table S4). All 11 unsuccessful queries (measured by p-value of 0.0076 in top five hits) occurred in conditions in which each had less than 100 DEGs in total. On the other hand, many chemical conditions with very few detectable DEGs were actually still able to yield informative ROGLs to allow appropriate connections with relevant query signatures. These pieces of evidence thus reinforce the importance of DEGs' directions of change and rankings to chemical connectivity in comparison to their LogFC, and the importance of guarding against false positives when a treatment condition has only minimal effects. Furthermore, Cmap connectivity should, in theory, be largely driven by chemical MOAs because both signatures and ROGLs were generated within the same tissue type between a treatment condition and corresponding experimental controls. Indeed, Cmap performed very well in connecting query signatures to their target ROGLs, especially within platforms/species. These connections were often made across experimental origins, chemical classes, complexity of exposures, and tissue types. As illustrated by fish samples from ZF 21K, when the connections of associated chemicals and tissue types were visualized simultaneously in a network, many nodes were distributed based on chemical conditions, not tissue types (Additional file 5: Figure S2A, S2B). However, it is evident that, in some cases, tissue type did contribute significantly to chemical connectivity. Such a confounding effect is probably a function of chemical, dosage, and tissue type.

Besides making a greater amount of public fish transcriptomic data available for Cmap, the primary significance in attempting interspecific Cmap lies in the prospect of extrapolating chemical toxicity across fish species. This is critical because it is impossible to test the toxicity of all chemicals of possible concern in all fish species. There are two potential limiting factors affecting the success of inter-specific (inter-platform) Cmap. One is genome annotation and probe mapping to identify orthologous/equivalent probes. The other is the conservation of toxicity pathways/MOAs between species. Given a very small number of conditions common across platforms and species in this study, it is difficult to assess Cmap performance across platforms/species reliably. However, generally low percentages of cross-mapped probes (62 % of ZF 21K vs 37 % of ZF 43K; 43 % of ZF 21K vs 45 % of FHM 15K; 38 % of ZF 43K vs 65 % of FHM 15K) suggest that a substantial loss of information was probably responsible in part for the relatively poor performance in the preliminary Cmap across platforms/species. With the relatively recent divergence between zebrafish and fathead minnow [15], broad conservation of molecular pathways among animal species [32–38], and high degree of genome conservation even between zebrafish and human [39], it seems reasonable to hypothesize that toxicity pathways are well conserved between these two small fish species. Indeed, a recent study of their transcriptomes provided strong evidence in this regard [16]. If this is the case, conservation of toxicity pathways should not be the primary issue in the performance of interspecific Cmap in the current study.

In addition to being able to connect the same chemicals underlying a query signature and its target ROGLs, Cmap also provided novel insights into some seemingly different chemicals that may possess similar MOAs. For those studies based on ZF 21K, Cmap grouped several well-characterized HPG-active toxicants together (Fig. 1a) [18], and further differentiated them into two sub-groups (Fig. 1b). One subgroup consisted of EE2 and fadrozole only; the other included vinclozolin, ketoconazole, flutamide, trilostane, fipronil, muscimol, and prochloraz. Trenbolone appeared to be an intermediate between the two subgroups. These clustering patterns did not correlate with extraneous factors such as tissue type or lab origins of data. For example, four different research groups produced data behind these nodes: oxygen, haloperidol and 10 other HPG-active toxicants; tetrachlorodibenzo-p-dioxin (TCDD); TCDD, tert-butylhydroquinone; dinitrophenol, dimethoxybenzene, and azinphosmethyl. Rather, the distribution patterns of these chemicals are more in line with their MOAs, some of which involve multiple MIEs. As an aromatase inhibitor, fadrozole blocks the transformation of testosterone to E2, the primary endogenous ligand for the estrogen receptor (ER), so it is reasonable that EE2 and fadrozole would cluster together. Further, since testosterone is a ligand for the androgen receptor (AR), it is quite conceivable to envision the same genes being activated by EE2, fadrozole, and trenbolone, a synthetic AR agonist [40, 41]. A similar argument could also be invoked to explain the shared MOAs of vinclozolin, flutamide, ketozonazole, and to a lesser extent, prochloraz, because of their common impact again on AR and aromatase: vinclozolin, flutamide, prochloraz are all AR antagonists, while ketoconazole and prochloraz are both aromatase inhibitors [18]. Note that fadrozole also shared strong connectivity with ketoconazole and prochloraz. There are other examples, as well, of the Cmap analysis highlighting chemicals that impact the same molecular target. For example, although fipronil and muscimol have opposite effects on gamma-aminobutyric acid (GABA) receptor, one being an antagonist while the other an agonist, they are identified as substantially similar. Between muscimol (MUS_500ugL_femaleBrain) as a signature and fipronil (FIP_5ugL_femaleOvary) as ROGLs, they reached a high connectivity score of 16.8 (ranged 2.5-23.6 in ZF 21K), with the corresponding average LogFC of only

0.42 and 0.33. In other words, these DEGs changed largely in the same direction and ranked high in both muscimol and fipronil-treated fish, despite the differences in tissue being examined.

Novel insights on chemical MOAs were gained as well from studies based on ZF 43K and FHM 15K. For ZF 43K-based studies, chemicals acting as AR antagonists, prochloraz and flutamide, had MOAs similar to those of ER agonists, E2 and EE2 (Fig. 1c, d), suggesting that, at some level, anti-androgens and ER agonists are somewhat functionally equivalent biologically. Indeed, bisphenol A, a compound known to exhibit both estrogenic and anti-androgenic effects [42, 43], showed substantial connectivity with prochloraz (score 12.0), flutamide (10.8), EE2 (8.9), and E2 (6.8). The strength of these connections represents 37-65 % of the maximum connectivity score observed in the ZF 43K-based studies. Linuron, a phenylurea herbicide and a confirmed anti-androgen [44], also formed strong connections to prochloraz and flutamide. Methylparaben, a common preservative in cosmetic products, has been shown to possess both estrogenic and anti-androgenic activities [45].

For FHM 15K-based studies (Fig. 1e, f), Cmap demonstrated its effectiveness in discriminating chemical exposures across a range of complexities. For single chemical exposures, strong connectivity was found among several MOA-based classes of chemicals including ER agonists (EE2, E2, DES), neuro-toxins (bifenthrin, permethrin, cypermethrin, esfenvalerate, terbufos), and inhibitors of steroidgenic enzymes 3β-HSD and aromatase (trilostane, fadrozole). Phenanthrene, a PAH, was also linked to DES, suggesting its possible estrogenicity.

Also notable is the fact that when a chemical condition has little detectable transcriptomic effect perhaps due to issues such as effective dosage, sample size, and statistical stringency, its ROGLs still could be informative and capable of connecting with appropriate query signatures. This was the case in a mixture of permethrin and terbufos, where, in the absence of its own signature and a sizeable signature from permethrin alone, its ROGLs could still connect with bifenthrin and terbufos. And so did the ROGLs from permethrin. Other than both being neurotoxins but with different MIEs, bifenthrin and terbufos are not known to share any other mechanisms underlying their connectivity. Perhaps a more striking revelation came from male fathead minnow liver samples exposed to the effluents near several WWTPs in Minnesota, which contained a complex array of chemicals including several known estrogens, PAHs, and a neuro-toxin [30, 31]. In spite of being located in very different ecological environment (non-agricultural, agricultural, urban), the effluents of these plants were remarkably similar to one another as measured by their common impact on fish transcriptomes. Quite possibly, the main drivers behind such a similarity include PAHs, natural and synthetic ER agonists, as well as other pollutants, rather than agricultural chemicals. There was, in fact, substantial connectivity between the effluent samples and several single chemical studies with known PAHs (maximum score 10.5) and estrogens (maximum score of 9.4) as compared to the observed score range of 2.6 to 19.9 for FHM 15K (Fig. 1e, f). These same effluents, however, had hardly any effect on the ovaries of female fish samples treated in the same study; some of their representative nodes present in the network were widely scattered. Thus, across the research based on the three platforms, ZF 21K, ZF 43K, and FHM 15K, Cmap has demonstrated its effectiveness in not only connecting the same chemical conditions underlying query signatures and ROGLs, but also establishing novel connectivity among seemingly different chemicals based on shared MOAs.

Connectivity among chemicals is a function of their shared transcriptomic profiles, which in turn are likely modulated by the dose and duration of a treatment on the targeted fish tissue at a given life stage. Conceivably, a varying number of genes and pathways could become perturbed by the same chemical under different conditions, leading to a different degree of overlap among MOAs. This hypothesis is supported by the findings in the current study, where the same chemical tested at multiple doses had different number of neighbors in a network of chemicals. Similar observations of dose-dependent, differential transcriptomic responses were also reported recently for chemicals in human cell cultures and fish [46, 47]. Such a dependency between chemical dose and transcriptomic response have both scientific and practical implications for applying Cmap in ecotoxicology. Scientifically, a chemical MOA could then be considered as consisting of both core and peripheral toxicity pathways, which may be defined by their responsiveness as a function of exposure intensity (dosage and duration), the specificity to a given chemical or tissue type, or the importance to the integrity of their larger biological network. The earliest responders at the lowest exposure intensity may not be necessarily those most critical to an organism's biological integrity. A better delineation of toxicity pathways in this regard should help to inform the assessment of relative toxicity among chemicals and their risks to ecosystems. For more practical application of Cmap in exposure assessment, however, those chemical-specific, earliest responsive pathways at the lowest exposure intensity are likely to be diagnostically useful in biomonitoring.

Conclusions

In summary, fish Cmap built on a very large collection of public and private GEPs from zebrafish and fathead minnow performed well in this study, particularly when conducted within the same platforms/species. When a query signature from samples of interest was made

against a reference database of ROGLs, informative connections were established at high success rates when both shared the same chemical conditions. In other words, Cmap provides an easily scalable framework for a simple query signature selected from DEGs to function as an exposure biomarker, without going through a typical time-consuming process of development and validation. More importantly, as demonstrated in this study, a large reference database of ROGLs also enables a query signature to cross interrogate other chemical conditions with overlapping MOAs, leading to novel groupings and subgroupings of seemingly unrelated chemicals at a finer resolution. By this approach, for example, the estrogenic and PAH identities of largely uncharacterized water samples near several WWTPs were confirmed, suggesting its future potential in real world applications. For toxicity extrapolation across fish species, however, a sufficient number of GEPs linked to chemical conditions common to multiple fish species are needed in the future in order to conduct a more thorough feasibility study of interspecific Cmap.

Availability of supporting data

The data sets supporting the results of this article are available in the NCBI GEO repository, with the accession numbers GSE38070, GSE60202, GSE70807, and GSE70936. Additional datasets downloaded from GEO are listed in Additional file 1: Table S1.

Additional files

Additional file 1: Table S1. A complete list of microarray data used in the current study. (XLSX 111 kb)

Additional file 2: Table S2. A complete list of query signatures constructed in the current study. Signatures were named after fish sample treatment conditions by the order of chemical, dose, gender, tissue, and exposure duration. Some conditions may each have multiple signatures generated because of either repeated experiments or different parameters in analysis. (XLSX 19 kb)

Additional file 3: Figure S1. Relative transcriptomic impact of various treatment conditions in fathead minnow. Effects are measured by the percentages of transcriptome determined to be DEGs. (PPTX 39 kb)

Additional file 4: Table S3. Cmap across ZF 21K and ZF 43K with the maximum signature size of 100 probes. (DOCX 14 kb)

Additional file 5: Figure S2. A network view of chemicals and tissue types based on samples profiled on ZF 21K. Each chemical treatment condition and the tissue profiled is represented as a node. Two nodes are connected by an edge weighted by their connectivity score. A shorter, darker, and wider edge between two nodes denote a higher connectivity score. All connections shown are statistically significant. A) 40 nodes with 573 connections; B) 30 nodes with 380 connections with each node having a minimum connectivity score of 10 in at least one of its connections. Tissue types: T, testis; O, ovary; B, brain; Lr, liver. (PDF 37 kb)

Additional file 6: Figure S3. Relationships between connectivity strength and DEGs. A total of 106 chemical conditions with relative transcriptomic impact ≥ 0.001 were considered. Connectivity scores were normalized to the size of respective query signatures. A) average LogFC vs connectivity scores; B) average logFC vs relative transcriptomic impact (RTI, percentage of transcriptome as DEGs); C) connectivity scores vs RTIs. (PPTX 49 kb)

Additional file 7: Table S4. Relationship between total number of DEGs and connectivity score among treatment conditions within FHM 15K. (XLSX 24 kb)

Abbreviations

Agilent 013223: ZF 21K; Agilent 015064: ZF 21K; Agilent 019161: ZF 43K; Agilent 019597_036574: FHM 15K; APM: azinphos-methyl; BAA: benz(a)anthracene; BDE: decabromodiphenyl ether; BIF: bifenthrin; BPA: bisphenol A; CYP: cypermethrin; DBT: dibenzothiophene; DES: Diethylstilbestrol; DHT: Dihydrotestosterone; DIA: Diazepam; DMB: 1,4-dimethoxybenzene; DNP: 2,4-dinitrophenol; E2: 17ß-estradiol; EE2: ethniyl estradiol; EFFHa: Effluent of WWTP in San Diego, California; EFFHb: Effluent of WWTP in Los Angeles, California; EFFLa: Effluent of WWTP in San Diego, California; ELYds: Downstream of WWTP in Ely, Minnesota (ovary tissue sampled); ElyDS: Downstream of WWTP in Ely, Minnesota (liver tissue sampled); ELYeff: Effluent of WWTP in Ely, Minnesota (ovary tissue sampled); ElyEFF: Effluent of WWTP in Ely, Minnesota (liver tissue sampled); ElyUS: Upstream of WWTP in Ely, Minnesota (liver tissue sampled); ESF: esfenvalerate; FAD: fadrozol; FIP: fipronil; FLU: flutamide; GEM: Gemfibrozil; GEN: genistein; HAL: Haloperidol; HUTds: Downstream of WWTP in Hutchinson, Minnesota (ovary tissue sampled); HutDS: Downstream of WWTP in Hutchinson, Minnesota (liver tissue sampled); HUTeff: Effluent of WWTP in Hutchinson, Minnesota (ovary tissue sampled); HutEFF: Effluent of WWTP in Hutchinson, Minnesota (liver tissue sampled); HutUS: Upstream of WWTP in Hutchinson, Minnesota (liver tissue sampled); KET: ketochonazole; LIN: Linuron; LSW: Lake Superior water; MPA: methylparaben; MUS: muscimol; O2: oxygen; PER: permethrin; PFC: perflorinated chemicals; PGST: Progesterone; PHE: Phenanthrene; PKC412: protein kinase C inhibitor 412; PPL: Propanil; PPLL: Propranolol; PRO: prochloraz; PYR: Pyrene; RDX: cyclotrimethylenetrinitramine; ROCHds: Downstream of WWTP in Rochester, Minnesota (ovary tissue sampled); RochDS: Downstream of WWTP in Rochester, Minnesota (liver tissue sampled); ROCHeff: Effluent of WWTP in Rochester, Minnesota (ovary tissue sampled); RochEFF: Effluent of WWTP in Rochester, Minnesota (liver tissue sampled); RochUS: Upstream of WWTP in Rochester, Minnesota (liver tissue sampled); stormH2O: storm water; strH2O: stream water; TBHQ: tert-Butylhydroquinone; TCC: Triclocarban; TCDD: 2,3,7,8-tetrachlorodibenzo-p-dioxin; TER: Terbufos; TNT: 2,4,6-trinitrotoluene; TRB: trenbolone; TRI: trilostane; VIN: vinclozolin; wasteH2O: waste water; WLSSD: Effluent, Western Lake Superior Sanitary District, Duluth, Minnesota; WWTP: waste water treatment plant.

Competing interests

The authors declare that there are no competing interests.

Authors' contributions

RLW, ADB, and DCB conceptualized and proposed this study. DLV, GTA, DCB, ADB, NG-R, and EJP conducted fish exposures to various chemicals. NG-R, EJP, DCB, and ADB contributed microarray work. RLW conducted all the bioinformatic analyses and prepared the manuscript. All coauthors contributed to the manuscript revisions and approved the final version for submission.

Acknowledgements

Funding for zebrafish exposures and microarray analysis was provided by US Environmental Protection Agency (USEPA). The U.S. Army Environmental Quality and Installations program and U.S. Army (grant BAA 11–4838) provided funding for fathead minnow microarrays analysis. The funders had no role in study design, data collection and analysis, or preparation of the manuscript. We thank Lynn Escalon and Xin Guan in the Environmental Laboratory, US Army Engineer Research and Development Center for microarray data generation. The internal technical review was conducted by Mark Nelms at the National Health and Environmental Effects Research Laboratory, USEPA. The views expressed in this article are those of the authors and do not necessarily represent the views or policies of the USEPA. The manuscript has been approved for publication by USEPA and US Army Corps Chief of Engineers.

Author details
[1]Exposure Methods & Measurements Division, National Exposure Research Laboratory, US Environmental Protection Agency, 26 W Martin Luther King Dr., MS 587, Cincinnati, OH 45268, USA. [2]Environmental Laboratory, US Army Engineer Research and Development Center, US Army Corps of Engineers, 3909 Halls Ferry Rd, Vicksburg, MS 39180, USA. [3]Mid-Continent Ecology Division, National Health and Environmental Effects Research Laboratory, US Environmental Protection Agency, 6201 Congdon Boulevard, Duluth, MN 55804, USA.

Received: 27 July 2015 Accepted: 19 January 2016

References

1. US EPA. 2015. TSCA chemical substance inventory. http://www.epa.gov/tsca-inventory. Accessed July 7 2015.
2. National Research Council. Scientific Frontiers in Developmental Toxicology and Risk Assessment. Washington: The National Academies Press; 2000.
3. National Research Council. Toxicity Testing in the 21st Century: A Vision and a Strategy. Washington: The National Academies Press; 2007.
4. National Research Council. Science and Decisions: Advancing Risk Assessment. Washington: The National Academies Press; 2009.
5. National Research Council. Exposure Science in the 21st Century: A Vision and a Strategy. Washington: The National Academies Press; 2012.
6. Lamb J, Crawford ED, Peck D, Modell JW, Blat IC, Wrobel MJ, et al. The Connectivity Map: Using Gene-Expression Signatures to Connect Small Molecules, Genes, and Disease. Science. 2006;313:1929–35.
7. Qu X, Rajpal DK. Applications of Connectivity Map in drug discovery and development. Drug Discov Today. 2012;17:1289–98.
8. Lincscloud. http://www.lincscloud.org/. Accessed July 8, 2015.
9. Kupershmidt I, Su QJ, Grewal A, Sundaresh S, Halperin I, Flynn J, et al. Ontology-based meta-analysis of global collections of high-throughput public data. PLoS One. 2010. doi:10.1371/journal.pone.0013066.
10. Smalley JL, Gant TW, Zhang SD. Application of connectivity mapping in predictive toxicology based on gene-expression similarity. Toxicology. 2010; 268:143–6.
11. Caiment F, Tsamou M, Jennen D, Kleinjans J. Assessing compound carcinogenicity in vitro using connectivity mapping. Carcinogenesis. 2014; 35:201–7.
12. Wang K, Weng Z, Sun L, Sun J, Zhou S-F, He L. Systematic drug safety evaluation based on public genomic expression (Connectivity Map) data: Myocardial and infectious adverse reactions as application cases. Biochem Biophys Res Commun. 2015;457:249–55.
13. Grunwald DJ, Eisen JS. Headwaters of the zebrafish — emergence of a new model vertebrate. Nat Rev Genet. 2002;3:717–24.
14. Ankley GT, Villeneuve DL. The fathead minnow in aquatic toxicology: past, present and future. Aquat Toxicol. 2006;78:91–102.
15. Wang XZ, Li JB, He SP. Molecular evidence for the monophyly of East Asian groups of Cyprinidae (Teleostei: Cypriniformes) derived from the nuclear recombination activating gene 2 sequences. Mol Phylogenet Evol. 2007;42: 157–70.
16. Wang R-L, Bencic DC, Garcia-Reyero N, Perkins EJ, Villeneuve DL, Ankley GT, et al. Natural Variation in Fish Transcriptomes: Comparative Analysis of the Fathead Minnow (Pimephales promelas) and Zebrafish (Danio rerio). PLoS One. 2014. doi:10.1371/journal.pone.0114178.
17. Ankley GT, Bennett RS, Erickson RJ, Hoff DJ, Hornung MW, Johnson RD, et al. Adverse outcome pathways: a conceptual framework to support ecotoxicology research and risk assessment. Environ Toxicol Chem. 2010;29: 730–41.
18. Ankley GT, Bencic DC, Breen MS, Collette TW, Conolly RB, Denslow ND, et al. Endocrine disrupting chemicals in fish: developing exposure indicators and predictive models of effects based on mechanism of action. Aquat Toxicol. 2009;92:168–78.
19. Skolness SY, Durhan EJ, Garcia-Reyero N, Jensen KM, Kahl MD, Makynen EA, et al. Effects of a short-term exposure to the fungicide prochloraz on endocrine function and gene expression in female fathead minnows (Pimephales promelas). Aquat Toxicol. 2011;103:170–8.
20. Villeneuve DL, Garcia-Reyero N, Lynn E, Jensen KM, Cavallin JE, Makynen EA, et al. Ecotoxicogenomics to Support Ecological Risk Assessment: A Case Study with Bisphenol A in Fish. Environ Sci Technol. 2012;46:51–9.
21. Garcia-Reyero N, Ekman DR, Habib T, Villeneuve DL, Collette TW, Bencic DC, et al. Integrated approach to explore the mechanisms of aromatase inhibition and recovery in fathead minnows (Pimephales promelas). Gen Comp Endocrinol. 2014;203:193–202.
22. Smyth GK. Limma: linear models for microarray data. In: Gentleman R, Carey V, Dudoit S, Irizarry R, Huber W, editors. Bioinformatics and Computational Biology Solutions using R and Bioconductor. New York: Springer; 2005. p. 397–420.
23. The R Project for Statistical Computing. http://www.r-project.org. Accessed July 8, 2015.
24. Zhang S-D, Gant TW. A simple and robust method for connecting small-molecule drugs using gene-expression signatures. BMC Bioinformatics. 2008;9:258.
25. Lopes CT, Franz M, Kazi F, Donaldson SL, Morris Q, Bader GD. Cytoscape Web: an interactive web-based network browser. Bioinformatics. 2010;26:2347–8.
26. NCBI-gene. ftp://ftp.ncbi.nlm.nih.gov/gene/DATA/gene2accession.gz. Accessed November 15, 2014.
27. Agilent-earray. https://earray.chem.agilent.com/earray/015064_D_AA_20140627.txt. Accessed Novembler 15, 2014.
28. Wang R-L, Biales A, Bencic B, Lattier D, Kostich M, Villeneuve D, et al. DNA Microarray Application In Ecotoxicology: Experimental Design, Microarray Scanning, And Factors Affecting Transcriptional Profiles In A Small Fish Species. Environ Toxicol Chem. 2008;27:652–63.
29. Vidal-Dorsch D, Colli-Dula RC, Bay SM, Greenstein DJ, Wiborg L, Petschauer D, et al. Gene Expression of Fathead Minnows (Pimephales promelas) Exposed to Two Types of Treated Municipal Wastewater Effluents. Environ Sci Technol. 2013;47:11268–77.
30. Martinovi -Weigelt D, Mehinto AC, Ankley GT, Denslow ND, Barber LB, Lee KE, et al. Transcriptomic Effects-Based Monitoring for Endocrine Active Chemicals: Assessing Relative contribution of Treated Wastewater to Downstream Pollution. Environ Sci Technol. 2014;48:2385–94.
31. Lee KE, Langer SK, Barber LB, Writer JH, Ferrey ML, Schoenfuss HL et al. Endocrine active chemicals, pharmaceuticals, and other chemicals of concern in surface water, wastewater-treatment plant effluent, and bed sediment, and biological characteristics in selected streams, Minnesota design, methods, and data, 2009. USGS Data Series 575. 2011; U.S. Geological Survey, Reston, VA
32. Adamska M, Degnan SM, Green KM, Adamski M, Craigie A, Larroux C, et al. Wnt and TGF-β expression in the sponge Amphimedon queenslandica and the origin of metazoan embryonic patterning. PLoS One. 2007. doi:10.1371/journal.pone.0001031.
33. Martindale MQ. The evolution of metazoan axial properties. Nat Rev Genet. 2005;6:917–27.
34. Vallée M, Aiba K, Piao Y, Palin MF, Ko MS, Sirard MA. Comparative analysis of oocyte transcript profiles reveals a high degree of conservation among species. Reproduction. 2008;135:439–48.
35. Ankley GT, Johnson RD. Small fish models for identifying and assessing the effects of endocrine-disrupting chemicals. Institute Laboratory Animal Res J. 2004;45:469–83.
36. Simmons SO, Fan CY, Ramabhadran R. Cellular stress response pathway system as a sentinel ensemble in toxicological screening. Toxicol Sci. 2009; 111:202–25.
37. LaLone CA, Villeneuve DL, Burgoon LD, Russom CL, Helgen HW, Berninger JP, et al. Molecular target sequence similarity as a basis for species extrapolation to assess the ecological risk of chemicals with known modes of action. Aquat Toxicol. 2013;144–145:141–54.
38. Perkins EJ, Ankley GT, Crofton KM, Garcia-Reyero N, LaLone CA, Johnson MS, et al. Current Perspectives on the Use of Alternative Species in Human Health and Ecological Hazard Assessments. Environ Health Perspect. 2013; 121:1002–10.
39. Howe K, Clark MD, Torroja CF, Torrance J, Berthelot C, Muffato M, et al. The zebrafish reference genome sequence and its relationship to the human genome. Nature. 2013;496:498–503.
40. Chang C, Saltzman A, Yeh S, Young W, Keller E, Lee H-J, et al. Androgen Receptor: An Overview. Crit Rev Eukaryot Gene Expr. 1995;5:97–125.
41. Hall JM, Couse JF, Korach KS. The Multifaceted Mechanisms of Estradiol and Estrogen Receptor Signaling. J Biol Chem. 2001;276:36869–72.
42. Paris F, Balaguer P, Térouanne B, Servant N, Lacoste C, Cravedi JP, et al. Phenylphenols, biphenols, bisphenol-A and 4-tert-octylphenol exhibit alpha and beta estrogen activities and antiandrogen activity in reporter cell lines. Mol Cell Endocrinol. 2002;193:43–9.

43. Ekman DR, Hartig PC, Cardon M, Skelton DM, Teng Q, Durhan EJ, et al. Metabolite Profiling and a Transcriptional Activation Assay Provide Direct Evidence of Androgen Receptor Antagonism by Bisphenol A in Fish. Environ Sci Technol. 2012;46:9673–80.
44. Wilson VS, Cardon MC, Gray Jr LE, Hartig PC. Competitive binding comparison of endocrine-disrupting compounds to recombinant androgen receptor from fathead minnow, rainbow trout, and human. Environ Toxicol Chem. 2007;26:1793–802.
45. Boberg J, Taxvig C, Christiansen S, Hass U. Possible endocrine disrupting effects of parabens and their metabolites. Reprod Toxicol. 2010;30:301–12.
46. Shioda T, Rosenthal NF, Coser KR, Suto M, Phatak M, Medvedovic M, et al. Expressomal approach for comprehensive analysis and visualization of ligand sensitivities of xenoestrogen responsive genes. Proc Natl Acad Sci U S A. 2013;110:16508–13.
47. Uren Webster TM, Santos EM. Global transcriptomic profiling demonstrates induction of oxidative stress and of compensatory cellular stress responses in brown trout exposed to glyphosate and Roundup. BMC Genomics. 2015;16:32.
48. Carney SA, Peterson RE, Heideman W. 2,3,7,8-Tetrachlorodibenzo-p-dioxin activation of the aryl hydrocarbon receptor/aryl hydrocarbon receptor nuclear translocator pathway causes developmental toxicity through a CYP1A-independent mechanism in zebrafish. Mol Pharmacol. 2004;66:512–21.
49. Andrysík Z, Vondráček J, Marvanová S, Ciganek M, Neča J, Pěnčíková K, et al. Activation of the aryl hydrocarbon receptor is the major toxic mode of action of an organic extract of a reference urban dust particulate matter mixture: the role of polycyclic aromatic hydrocarbons. Mutat Res. 2011;714:53–62.
50. Dang ZC, Audinot V, Papapoulos SE, Boutin JA, Löwik CW. Peroxisome proliferator-activated receptor gamma (PPARgamma) as a molecular target for the soy phytoestrogen genistein. J Biol Chem. 2003;278:962–7.
51. Sengupta S, Obiorah I, Maximov PY, Curpan R, Jordan VC. Molecular mechanism of action of bisphenol and bisphenol A mediated by oestrogen receptor alpha in growth and apoptosis of breast cancer cells. Br J Pharmacol. 2013;169:167–78.
52. DeMayo FJ, Zhao B, Takamoto N, Tsai SY. Mechanisms of action of estrogen and progesterone. Ann N Y Acad Sci. 2002;955:48–59.
53. Werner R, Holterhus PM. Androgen action. Endocr Dev. 2014;27:28–40.
54. Creese I, Burt D, Snyder SH. Dopamine receptor binding predicts clinical and pharmocological potencies of antischizophrenic drugs. Science. 1976; 192:481–3.
55. Griffin CE, Kaye AM, Pharm D, Bueno FR, Kaye AD. Benzodiazepine Pharmacology and Central Nervous System–Mediated Effects. Ochsner J. 2013;13:214–23.
56. Soderlund DM, Clark JM, Sheets LP, Mullin LS, Piccirillo VJ, Sargent D, et al. Mechanisms of pyrethroid neurotoxicity: implications for cumulative risk assessment. Toxicology. 2002;171:3–59.
57. Arnaud L, Taillandier G, Kaouadji M, Ravanel P, Tissut M. Photosynthesis inhibition by phenylureas: A QSAR approach. Ecotoxicol Environ Saf. 1994; 28:121–33.
58. Kim JR, Kim HJ, Kwon OS. Acetylcholinesterase and neuropathy target esterase activity in female and male rats exposed to pesticide terbufos. Environ Toxicol Pharmacol. 2005;20:149–56.
59. Soni MG, Taylor SL, Greenberg NA, Burdock GA. Evaluation of the health aspects of methyl paraben: a review of the published literature. Food Chem Toxicol. 2002;40:1335–73.
60. Matsunaka S. Activation and inactivation of herbicides by higher plants. Residue Rev. 1969;25:45–58.
61. Carrier G, Brunet RC. A toxicokinetic model to assess the risk of azinphosmethyl exposure in humans through measures of urinary elimination of alkylphosphates. Toxicol Sci. 1999;47:23–32.
62. Wang DW, Mistry AM, Kahlig KM, Kearney JA, Xiang J, George AL. Propranolol blocks cardiac and neuronal voltage-gated sodium channels. Front Pharmacol. 2010;1:144.
63. Oggier DM, Lenard A, Ku¨ry M, Hoeger B, Affolter M, Fent K. Effects of the Protein Kinase Inhibitor PKC412 on Gene Expression and Link to Physiological Effects in Zebrafish Danio rerio Eleuthero-Embryos. Toxicol Sci. 2011;119:104–15.
64. Roy A, Pahan K. Gemfibrozil, stretching arms beyond lipid lowering. Immunopharmacol Immunotoxicol. 2009;31:339–51.
65. Rodriguez-Jorquera IA, Kroll KJ, Toor GS, Denslow ND. Transcriptional and physiological response of fathead minnows (Pimephales promelas) exposed to urban waters entering into wildlife protected areas. Environ Pollut. 2015; 199:155–65.

Submit your next manuscript to BioMed Central and we will help you at every step:

- We accept pre-submission inquiries
- Our selector tool helps you to find the most relevant journal
- We provide round the clock customer support
- Convenient online submission
- Thorough peer review
- Inclusion in PubMed and all major indexing services
- Maximum visibility for your research

Submit your manuscript at
www.biomedcentral.com/submit

Toxicology 412 (2019) 89–100

Contents lists available at ScienceDirect

Toxicology

journal homepage: www.elsevier.com/locate/toxicol

Ontology-based semantic mapping of chemical toxicities

Rong-Lin Wang[a,*], Stephen Edwards[b], Cataia Ives[b]

[a] Exposure Methods and Measurements Division, National Exposure Research Laboratory, US EPA, Cincinnati, OH 45268, USA
[b] Research Computing Division, RTI International, Research Triangle Park, NC 27709, USA

ARTICLE INFO

Keywords:
Chemical toxicity
Ontology
Phenotype
Phenomics
Semantic analysis

ABSTRACT

This study was undertaken to evaluate the use of ontology-based semantic mapping (OS-Mapping) in chemical toxicity assessment. Nineteen chemical-species phenotypic profiles (CSPPs) were constructed by ontologically annotating the toxicity responses reported in more than seven hundred published studies of ten chemicals on six vertebrate species. The CSPPs were semantically compared to more than 29,000 publicly available phenotypic profiles of genes, KEGG (Kyoto Encyclopedia of Genes and Genomes) pathways, and diseases based on a cross-species phenotype ontology. OS-Mapping was shown to differentiate chemical toxicities among themselves as well as within and across species. It also revealed cases of chemical by species interactions. In addition to confirming similar MOAs (mechanisms of action) for a few chemicals, OS-Mapping also generated novel insights into the MOAs underlying some seemingly different, yet phenotypically similar, classes of chemicals. The nature of a unified cross-species phenotype ontology and its representation of diverse knowledge domains allowed the construction of a complete phenotypic continuum for the 17α-ethynylestradiol_fathead minnow across the biological levels of organization, which complemented a similar one derived from the Comparative Toxicogenomics Database but based primarily on 17α-ethynylestradiol-induced molecular phenotypes. Overall, OS-Mapping has been demonstrated to offer a powerful approach to help bridge the gap between the molecular and non-molecular phenotypes of chemicals characterized by using high throughput or traditional omics methods and their apical endpoints of greater regulatory relevance, which are typically phenotypes found at the higher levels of biological organization. OS-Mapping also enables comparative toxicity assessment among chemicals, both within and across species. Furthermore, the semantic analysis of phenotypes can reveal additional novel MOAs for some well-known chemicals and discover candidate MOAs for chemicals that are less molecularly characterized. A full phenotypic continuum based on OS-Mapping will also be conducive to the future development of adverse outcome pathways. As phenomics continues to advance and the ontological annotation of literature becomes more automated, the power of OS-Mapping will be further enhanced.

1. Introduction

A shift toward a new paradigm in toxicology is well underway, one that is moving away from animal testing and toward an approach with a greater focus on *in vitro*, short term *in vivo*, and *in silico* tests; high-throughput screening; and toxicity pathways (NRC, 2007). Contemporary advances in omics, systems biology, robotics, computational chemistry, and bioinformatics have been instrumental in the evident progress that has been made under this new paradigm. Programs such as the US Tox21 and EPA's ToxCast (Merrick, 2015; Richard et al., 2016) have screened thousands of chemicals for biological effects using biochemical- or cell-based assays and identified numerous molecular targets of potential interest. Transcriptomics, proteomics, and metabolomics-based studies of chemical exposures in both laboratory and field settings have also proliferated, resulting in the determination of many impacted genes, proteins, metabolic pathways, other non-molecular phenotypes, and the subsequent discovery of some novel molecular mechanisms of action (MOAs) for these chemicals and the

Abbreviations: CSPP, chemical-species phenotypic profile; CTD, Comparative Toxicogenomics Database; EPA, Environmental Protection Agency; EQ, Entity-Quality; ECOTOX, ECOTOXicology Knowledgebase; GO, Gene Ontology; HP, Human Phenotype Ontology; IC, information content; ID, identification; KEGG, Kyoto Encyclopedia of Genes and Genomes; MICA, most informative common ancestor; MOA, mechanism of action; MP, Mammalian Phenotype Ontology; OBO, Open Biological and biomedical Ontology; OMIM, Online Mendelian Inheritance in Man; OWL, Web Ontology Language; OWLAPI, OWL Application Programming Interface; PATO, Phenotype And Trait Ontology; RDF/XML, Resource Description Framework/Extensible Markup Language; RO, Relations Ontology; SML, Semantic Measure Library; TDCPP, Tris(1,3-dichloroisopropyl) phosphate; ZP, Zebrafish Phenotype Ontology

* Corresponding author at 26W Martin Luther King Dr, Cincinnati, OH, 45268, USA
E-mail address: wang.rong-lin@epa.gov (R.-L. Wang).

https://doi.org/10.1016/j.tox.2018.11.005
Received 24 August 2018; Received in revised form 11 November 2018; Accepted 19 November 2018
Available online 20 November 2018
0300-483X/ Published by Elsevier B.V.

development of their biomarkers. From these efforts, many powerful bioinformatic approaches for mining high-dimensional omics data in large volumes have also emerged.

Several daunting challenges remain during this paradigm shift. First, high-throughput screenings and omics studies of chemicals focus primarily on molecular phenotypes. Due to the enormous complexity of the phenotypic space and the many-to-many relationships commonly found in genotype-phenotype mapping (Houle et al., 2010), it is difficult to connect molecular phenotypes with their higher level apical endpoints such as anomalies in development, mating behavior, organ size/histopathology, reproduction, and mortality. Second, although some of these non-molecular phenotypes are characterized and recorded as descriptive texts in such studies, they are not readily computable for integrated analysis with molecular data. Third, toxicological studies are most likely conducted on a few model species; it is generally difficult to map and integrate phenotypes from a test species to other species of greater environmental and health concerns. Clearly, to realize the full potential of the new toxicology paradigm, a strategy to address these barrier issues needs to be developed.

Phenomics is the systematic study of the phenotypic responses of an organism on a genome-wide scale, which are determined by the complex interactions of its genotypes and environmental conditions. Phenomics adds a new dimension to the discipline of systems biology, which is largely founded on traditional omics. The term is sometimes used interchangeably with high-throughput phenotyping. Among the most high-profile phenomics projects to date is perhaps the one led by the International Mouse Phenotyping Consortium (Brown et al., 2018), in which mouse genes are systematically mutated and phenotyped by using a wide range of technologies. These phenotypes are described as free text and are then made computable by annotating them with the appropriate ontology terms. With numerous domain ontologies developed in recent years, phenomics coupled with ontology-based knowledge representation is increasingly being adopted by the scientific community as an approach to dissect complex traits, to better understand genetic variations, and to integrate phenotypes across biological levels of organization and species boundaries (Washington et al., 2009; Houle et al., 2010; Mungall et al., 2010; McMurry et al., 2016; Brown et al., 2018). As such, it should also help to fill the gap between the molecular and non-molecular phenotypes generated from traditional omics platforms and the apical endpoints of greater regulatory significance. The numerous phenomics projects underway are responsible for the abundant and increasing amount of phenotypic information now available across a wide range of species and knowledge domains (Smith et al., 2007; http://www.obofoundry.org; http://www.informatics.jax.org).

The emergence and widespread application of biological ontologies over the last two decades largely coincided with the omics revolution because of the growing necessity to conceptualize, represent, share, and compute this enormous amount of biological knowledge, including phenotypes, across domains and species (Gruber, 1995; Ashburner et al., 2000). An ontology represents a knowledge domain, such as those of omics, anatomies, behavior, disease etc., by a set of predefined web ontology language (OWL) constructs and standard vocabulary (Bard and Rhee, 2004). Such a representation standardizes knowledge and makes it accessible to both human and machine inferencing. In addition to pre-composed ontology classes, that is, sets of objects with common attributes originally created by ontology developers, complex phenotypes from phenomics projects can be post-composed into custom ontology classes during annotation by selecting terms from reference domain ontologies using Entity-Quality (EQ) syntax (Washington et al., 2009; Mungall et al., 2010; Hoehndorf et al., 2011; Gkoutos et al., 2017).

Ontologies covering a wide variety of biological domains have many applications, including genome annotation, interpretation of omics findings, knowledge integration across species and biological levels of organization, information retrieval, and semantic computing (Bard and Rhee, 2004; Hoehndorf et al., 2015). An ontology is intrinsically a directed acyclic graph, one in which nodes represent ontology classes and edges denote their subsuming relationships. The information content (IC) of a node is determined by its relative position in the graph: a node with more parent nodes and fewer leaf nodes (i.e., farther away from the root node) has higher IC, thus being more specific and informative. Two nodes are semantically more similar to each other when they share more information, as reflected by the greater IC of their most informative common ancestor (MICA). Subgraphs of an ontology, each representing the phenotypic profile of a chemical, a gene, a pathway, a disease, or other entities of interest by a group of ontology nodes, can be compared to one another for semantic similarities based on various arithmetic manipulations of their underlying ICs. An implicit assumption of this approach of ontology-based semantic mapping (OS-Mapping; Washington et al., 2009) is that, when two such subgraphs are similar, their associated chemicals, genes, pathways, or diseases must share convergent biological mechanisms (Gkoutos et al., 2017).

Although originated from and largely driven by applications in biomedical sciences (McMurry et al., 2016), OS-Mapping could potentially facilitate chemical toxicity assessment as well. To date, one of the most pressing issues in this area continues to be the need to efficiently evaluate the toxicities of numerous chemicals. Bridging the gap between molecular and non-molecular phenotypes from high-throughput screening/omics studies and the apical endpoints of relevance should facilitate that effort. Comparative assessments of multiple chemicals of their toxicity responses both within and across species will further advance model species-based toxicology as well. In many ways, OS-Mapping appears to represent an ideal approach to implement these types of integrated analysis of toxicological data, as a unified, multi-domain, multi-species ontology can be formed by merging a wide range of public bio-ontologies relevant to toxicology. These include ontologies of gene, protein, chemical, cell, disease, behavior, phenotypes, and importantly, both species-specific and universal anatomies (http://obofoundry.org). After subsuming relationships are established among various classes in the unified ontology by using a reasoner, a type of software tool for inferencing, a semantic analysis can be conducted among individual nodes, or subgraphs of multiple nodes associated with the biological entities of interest. The nature of this unified multi-domain, multi-species ontology allows chemical toxicities and their biology to be dissected both within and across species.

The goals of this pilot study were to evaluate OS-Mapping for its potential applications in chemical toxicity assessment and to demonstrate its value as a computational approach to complement current omics technologies widely used in studying chemical exposures. If proven successful, OS-Mapping would allow a vast amount of non-molecular phenotypes from phenomics projects across several species to inform chemical toxicity assessment in the future. The specific aims of this study were to: 1) build a number of custom chemical-species phenotypic profiles (CSPPs), each of which would summarize multiple published exposure studies for a specific chemical and vertebrate species using post-composed ontology classes; 2) assemble a comprehensive collection of publicly available phenotypic profiles (hereafter referred to as “profiles”) for human, mouse, and zebrafish, with each profile associated with a gene, a biological pathway, or a disease; 3) develop a Java application for the semantic analysis of ontology classes and profiles via OS-Mapping; and 4) assess the performance of OS-Mapping in dissecting chemical toxicities by comparing CSPPs against themselves, and against the assembled public target profiles. During semantic analysis, each CSPP or profile containing multiple ontology classes is effectively an equivalent of an ontology subgraph.

2. Material and methods

2.1. Ontological annotation of literature and preparation of CSPPs

The US EPA’s ECOTOXicology Knowledgebase (ECOTOX; https://

cfpub.epa.gov/ecotox/) and its predecessors were created in the early 1980s to collect, compile, and annotate literature on single chemical exposure studies on a variety of ecological species, including both aquatic and terrestrial animals and plants. The manual annotations of literature by ECOTOX curators were made with predefined codes covering various aspects of an exposure study, including the life stages of experimental organisms, effect types (genetics, morphology, growth, etc.), sites and trends of responses, measurements taken, and the statistical significance of findings (S. File 1, S. File 2). As of September 2016, ECOTOX had covered over 1600 vertebrate taxa involving more than 7000 chemicals.

The first step in the preparation of CSPPs was selection of the chemicals and species. To ensure that each CSPP would contain a sizeable number of ontology classes, the chemicals and species that ranked high in the number of exposure test results in ECOTOX (S. File 1) were reviewed and selections were made from those remaining after filtering out statistically insignificant and/or phenotypically uninformative mortality-related results. Where possible, preferences were also given to those chemicals studied in more than one species to facilitate the interspecific comparison of toxicity responses of the same chemicals. Ultimately, ten chemicals that had been tested in six vertebrate species that met these criteria were selected for ontological annotations: atrazine, bisphenol A, cadmium chloride, chlorpyrifos, copper sulfate, cypermethrin, dioxin, 17α-ethynylestradiol, malathion, and Tris(1,3-dichloroisopropyl) phosphate (TDCPP; Table 1). The six vertebrate species were: carp (*Cyprinus carpio*), zebrafish (*Danio rerio*), fathead minnow (*Pimephales promelas*), mouse (*Mus musculus*), rat (*Rattus norvegicus*), and trout (*Onchorhynchus mykiss*).

The next step of CSPP preparation was to export and preprocess the annotations of selected combinations of chemical and species from ECOTOX (Fig. 1A). A text file was exported for each chemical and species containing information about the response site, measurements, response trend, effect types, statistical significance of test results, organism life stages, and the references of original source publications (S. File 2). Statistically insignificant and/or mortality-related results were filtered out. A few publications with obvious quality issues or without annotatable phenotypes were excluded. After these steps, a non-redundant set of 726 publications spanning the last several decades was identified for subsequent manual annotations using EQ syntax (Fig. 1B and C). These publications were deemed acceptable because they originated largely from peer-reviewed journals and had been previously screened by ECOTOX curators. The original annotations in ECOTOX by its predefined codes were retained for reference purposes only. These annotations were not used directly in the EQ statements because of several considerations: a wide range of granularity in the coded responses, frequent omissions of histological details and other findings reported in the original publications, and occasional errors. These issues existed primarily because ECOTOX was not originally designed for ontological annotations and because ECOTOX had evolved over almost four decades under the likely curation of many different individuals over its annotation history. Nevertheless, these issues made it difficult to directly incorporate ECOTOX annotation codes into EQ statements with high specificity and accuracy.

In its most basic form, EQ syntax describes how an entity (E) such as an anatomical part, a biological process, or a biological function, is altered in its quality (Q; Fig. 1C; Washington et al., 2009; Hoehndorf et al., 2011; Gkoutos et al., 2017). The ontology term for an entity is selected from reference domain ontologies such as the Gene Ontology, Cell Ontology, and various anatomy ontologies. The quality term comes from the Phenotype And Trait Ontology (PATO; http://purl.obolibrary.org/obo/pato.owl). An entity and a quality are related to each other by an object property (R) from the Relations Ontology (RO; http://purl.obolibrary.org/obo/ro.owl). At times, EQ syntax needs to be expanded to include a secondary entity, as in E_1-Q-E_2, where Q denotes a relational quality. For example, "blood_serum(E_1) has_quality(R) increased_concentration (Q) towards (R) glucose (E_2)" denotes phenotype "raised blood glucose level". For a more complex phenotype, an entity can also be further post-composed, giving rise to a more generalized syntax in the form of [E_{1a}-R-E_{1b}]-[Q-QL]-[E_{2a}-R-E_{2b}], where QL is a quality modifier (e.g., PATO_0000460, "abnormal"). The post-composition of

Table 1
Summary of semantic mapping hits by chemical-species phenotypic profiles (CSPPs; P-value ≤ 0.05). Significant hits are the row sums of mapped CSPPs, genes, pathways, and diseases for individual CSPPs. Pearson correlation: r (profile size, significant hits) = 0.41, r (phenotypic coverage, significant hits) = 0.56.

CSPP (No. publications)	Profile size[a]	Phenotypic coverage[b]	CSPP[c]	Mouse Genes	Human Genes	Zebrafish Genes	KEGG pathways	Disease accessions[d]	Significant hits
cypermethrin _rat (40)	200	1.00	19	2059	201	102	50	549	2980
malathion _mouse (49)	182	0.96	18	1901	127	138	66	440	2690
atrazine _mouse (28)	187	0.96	18	1564	126	82	61	478	2329
atrazine _rat (94)	477	1.00	19	1275	110	55	31	337	1827
malathion _rat (93)	480	1.00	19	1248	85	73	39	289	1753
cadmium chloride_trout (30)	130	0.96	19	885	89	51	8	258	1310
cadmium chloride_rat (76)	404	1.00	19	898	47	7	18	169	1158
17α-ethynylestradiol _fathead minnow (34)	156	0.96	17	800	66	49	1	155	1088
17α-ethynylestradiol _zebrafish (66)	269	1.00	18	757	73	52	1	165	1066
copper sulfate_rat (28)	193	0.93	19	596	54	8	2	169	848
dioxin_trout (26)	139	0.96	19	375	84	45	4	226	753
chlorpyrifos _carp (27)	216	0.96	19	414	35	17	0	175	660
atrazine _carp (31)	244	0.93	19	354	21	17	0	120	531
cypermethrin _carp (12)	96	0.78	17	199	21	21	0	57	315
chlorpyrifos _mouse (42)	187	0.93	19	220	4	3	1	25	272
bisphenol A_zebrafish (26)	132	0.96	16	40	0	30	0	0	86
Copper sulfate_fathead minnow (23)	58	0.93	13	52	0	8	0	0	73
atrazine _zebrafish (22)	105	0.93	15	18	0	5	0	0	38
Tris(1,3-dichloroisopropyl) phosphate _zebrafish (8)	144	0.81	9	15	0	2	0	0	26
Total unique (726)	3999	—	19	3702	422	338	94	1181	5756

[a] The number of post-composed OWL classes included in a CSPP.
[b] Percentage (×100) of the 27 categories of high level phenotypes represented (http://www.informatics.jax.org).
[c] Including self-hits.
[d] Including human diseases (OMIM; https://www.omim.org) annotated by either HP or MP terms, and rare diseases (Orphanet; https://www.orpha.net/consor/cgi-bin/index.php).

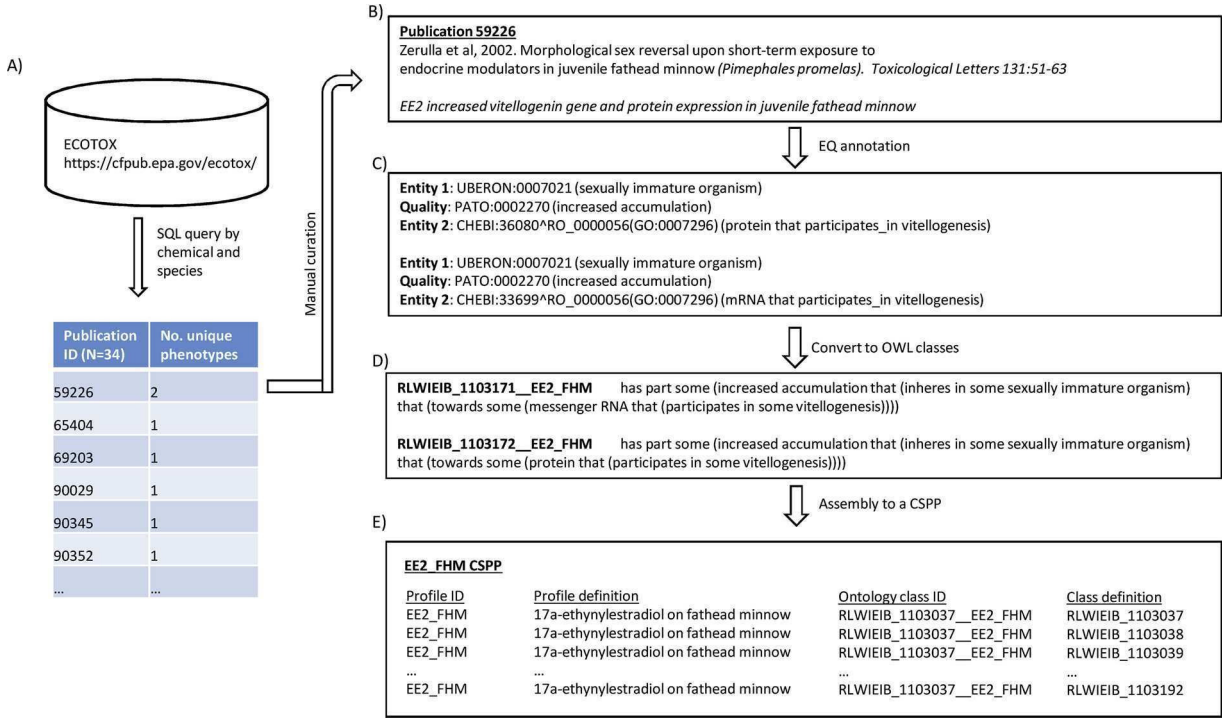

Fig. 1. The workflow to build a chemical-species phenotypic profile (CSPP) as illustrated by the 17α-ethynylestradiol_fathead minnow (EE2_FHM). A) Relevant publications were first identified from ECOTOX; B) two 17α-ethynylestradiol-induced phenotypes reported in the publication 59,226 were curated manually; C) the phenotypes were annotated in Entity-Quality (EQ) syntax; D) EQ annotations were converted to their respective ontology classes in Manchester syntax; E) all annotated ontology classes for the 17α-ethynylestradiol _fathead minnow were organized into its CSPP.

an entity may extend over multiple levels, which may either be nested or parallel to one another. To provide a more accurate annotation, an entity term could also be modified by another quality term, as in [E-R-Q]-[Q].

The chemical toxicity responses in the 726 publications selected were manually curated and annotated with EQ syntax by using Phenote software (Phenote_1_8_13_windows-x64_install4j.exe, released 11-29-2012; http://www.berkeleybop.org/index.html). Phenote was custom configured, and all user-designated ontologies in Open Biomedical Ontology (OBO) format were preloaded into memory during each session to expedite the selection of specific and appropriate ontology terms for a given phenotype. Once the annotation work was complete for all the selected chemicals/species, their tab-delimited outputs were manually checked to ensure that the order of terms in a post-composed entity remained unchanged (S. File 3). This step was necessary because Phenote occasionally rearranged those terms upon saving and re-opening an annotation file. EQ annotations were then converted into ontology classes in Manchester syntax (https://www.w3.org/TR/owl2-manchester-syntax) by using a custom Perl script (Fig. 1D, S. File 4), and further into RDF/XML format (https://www.w3.org/TR/rdf-syntax-grammar/) by using Protégé (http://protege.stanford.edu). Each result reported in a publication was in effect annotated into a custom ontology class with a distinct ID. All ontology classes constructed for each chemical and species were syntactically unique. A CSPP was then prepared consisting of all the relevant class IDs associated with a given combination of chemical and species (Fig. 1E). A total of 19 CSPPs was created from annotating the 726 publications.

2.2. Assembly of profiles from public phenomics data

Profiles were prepared for human, mouse, and zebrafish, the three vertebrate species for which public omics data, including phenotypes, is likely the most abundant. All data were downloaded on September 15, 2017. For the human profiles, two files were acquired from the Human Phenotype Ontology (HP) site (http://human-phenotype-ontology.github.io/downloads.html, redirected to http://compbio.charite.de/jenkins/job/hpo.annotations.monthly/lastStableBuild).

The first file, "ALL_SOURCES_ALL_FREQUENCIES_genes_to_phenotype.txt", contained human genes, each of which was annotated with multiple HP terms. A second file, "ALL_SOURCES_ALL_FREQUENCIES_diseases_to_genes_to_phenotypes.txt", linked human diseases to both human genes and HP terms. The human diseases were coded with either OMIM (Online Mendelian Inheritance in Man) IDs or Orphanet IDs (http://www.orpha.net/consor/cgi-bin/index.php?lng=EN). The mouse data file, "MGI_GenePheno.rpt", was downloaded from the Jackson Laboratory (http://www.informatics.jax.org/downloads/reports/index.html#pheno). Each mouse gene in the file was linked to multiple Mammalian Phenotype Ontology (MP) terms. The second mouse data file, "MGI_Geno_DiseaseDO.rpt", linked the OMIM disease IDs to MP terms. For the zebrafish profiles, genes linked to Zebrafish Phenotype Ontology (ZP) terms were downloaded (https://github.com/Phenomics/zebrafish-phenotype-ontology-build/blob/master/annot_gene_pos.txt). In addition to the profiles anchored by genes and diseases, profiles were also prepared for mouse KEGG (Kyoto Encyclopedia of Genes and Genomes; http://www.genome.jp/kegg) pathways by replacing the gene members in each pathway with their associated MP terms. A total of 29,154 profiles was assembled, including 3498 by human genes in HP terms, 12,009 by mouse genes in MP terms, 5892 by zebrafish genes in ZP terms, 1987 by OMIMs in MP terms (denoted as M_OMIM_digits), 4164 by human diseases and disorders in HP terms (denoted as OMIM_digits), 1272 by rare diseases in HP terms (Orpha_digits), 313 by KEGGs in MP terms, and 19 CSPPs.

2.3. Development of an OS-Mapping Java application

After evaluating a few existing applications available for ontology-based semantic analysis (e.g., OwlSim, http://www.berkeleybop.org/software/owlsim; SML Toolkit, http://www.semantic-measures-

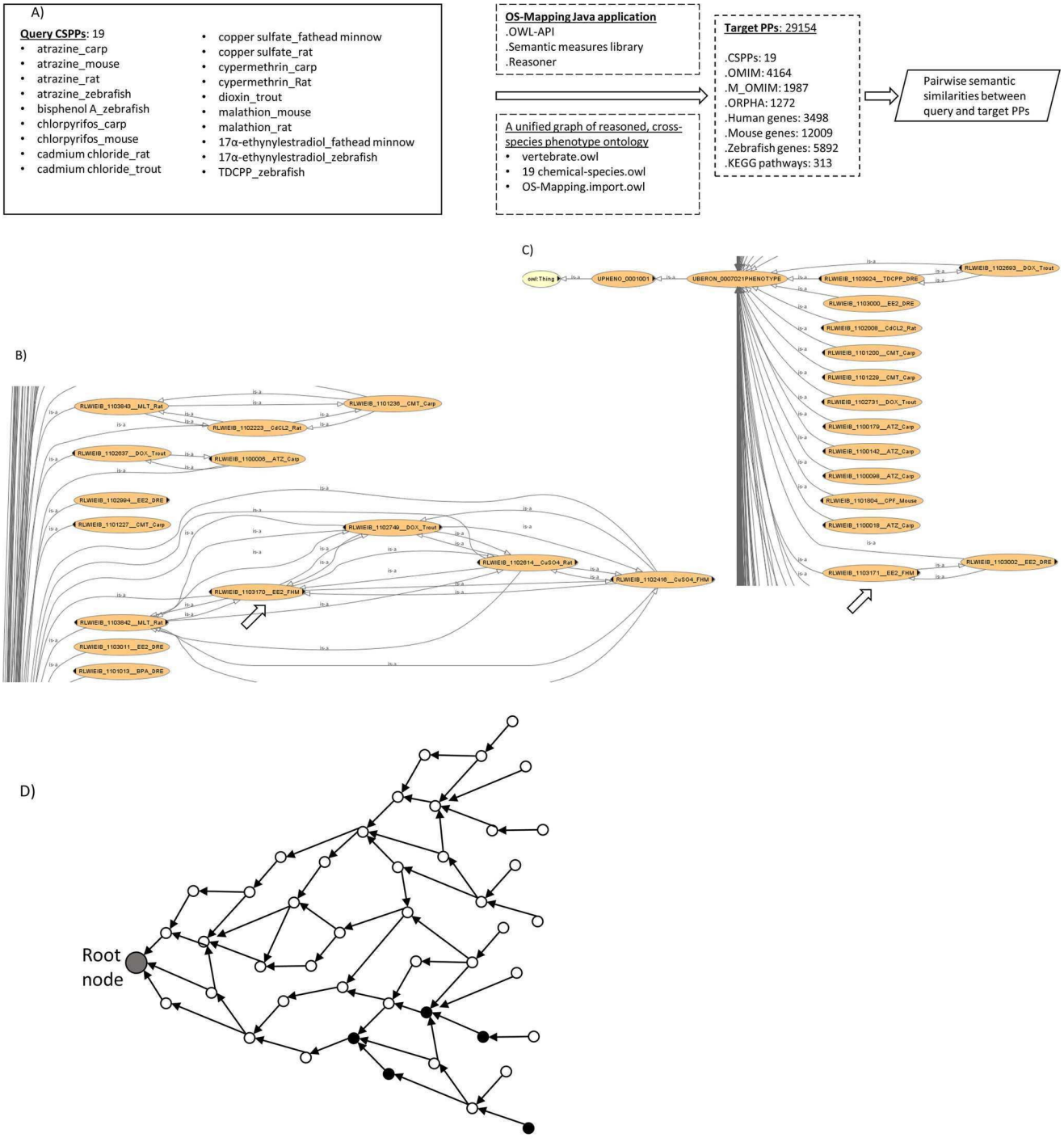

E)

query PP	target PP	similarity	query PP size	target PP size	target PP definition	cutoff P0.05	cutoff P0.01
EE2_FHM	EE2_FHM	1.000	156	156	17a-ethynylestradiol on fathead minnow	0.500	0.512
EE2_FHM	M_Ccnb1ip1	0.704	156	14	cyclin B1 interacting protein 1	0.569	0.590
EE2_FHM	M_repro15	0.698	156	4	reproductive mutant 15	0.571	0.590
EE2_FHM	M_Dms	0.696	156	7	dominant male sterility	0.588	0.604
EE2_FHM	M_Cdk16	0.695	156	8	cyclin-dependent kinase 16	0.597	0.609
EE2_FHM	M_Cnot7	0.694	156	20	CCR4-NOT transcription complex, subunit 7	0.593	0.610
EE2_FHM	EE2_DRE	0.694	156	269	17a-ethynylestradiol on zebrafish	0.522	0.538
...	...	...	...	...	...	...	...

(caption on next page)

Fig. 2. OS-Mapping analysis workflow. A) OS-Mapping java application compared the query against target phenotypic profiles semantically based on vertebrate.owl, a cross-species phenotype ontology. Prior to the analysis, vertebrate.owl first imported many other domain ontologies, and then merged them with both the custom OWL (Web Ontology Language) classes constructed from the Entity-Quality annotations of various chemical-species ('19 chemical-species.owl') and the external ontology terms contained therein (OS-Mapping.import.owl). The merged ontology was subsequently reasoned into a unified ontology graph, based on which CSPPs were analyzed; B, C) two sample subgraphs containing two of the 156 ontology classes of 17α-ethynylestradiol_fathead minnow from the merged and reasoned ontology as extracted by the robot tool (http://robot.obolibrary.org); D) an illustrative ontology graph with classes represented by nodes and their subsumption relationships by edges. A query profile (solid black nodes) and target profiles (various combinations of nodes in the entire graph) are compared semantically; E) part of a simplified 17α-ethynylestradiol_fathead minnow query output.

library.org/sml/index.php?q= toolkit; GOSemSim, Yu et al., 2010), a more streamlined and flexible application, called OS-Mapping.java, was developed in-house to better meet our needs in analyzing chemical toxicities. As a command line tool, OS-Mapping.java relies on several Java packages including OWLAPI (version 4.2.5; Horridge and Bechhofer, 2011), Semantic Measure Library (SML, version 0.9.4d; Harispe, 2014), and various reasoners (Dentler et al., 2011; Kazakov et al., 2011; Mendez, 2012; Ceylan et al., 2015). The OWLAPI is a well-known and widely adopted application programming interface that provides various functionalities to the creation and manipulation of OWL ontologies. The SML works with a preexisting reasoned ontology and provides multiple semantic measures for both pairwise and group-wise analyses of ontology classes. A reasoner examines ontology axioms (statements about classes, individuals, or properties) for their logical validity (consistency and satisfiability), and then infers subsumption relationships among classes. The development of OS-Mapping.java was conducted within NetBeans, an integrated development environment (version 8.2; https://netbeans.org).

To evaluate the statistical significance of the semantic similarity scores between a query and its target profiles, OS-Mapping.java generates a user-specified number of random profiles of the same size as the original query and calculates their similarities against target profiles individually. A random profile is formed by sampling all the classes present in a merged ontology, which, in the current version of cross-species phenotype ontology (http://purl.obolibrary.org/obo/upheno/vertebrate.owl; Köhler, 2013), number more than 151,000. In effect, a distribution of semantic similarity scores is generated for this query against each of the respective target profiles using the same group of random profiles. The scores at the top 5% and top 1% maximum range in each ascendingly sorted distribution are then selected as the cutoffs for the corresponding pair of query and target profiles. For the next query profile, a new set of random profiles is generated based on its size, which is then compared against all the target profiles again. The process repeats until similarity score cutoffs have been generated for all possible comparisons of query-target profiles. A pair of query and target profiles would be declared significantly similar to each other if its similarity was greater than its associated cutoffs. Although informative, this procedure is computationally expensive, particularly when a query has a large size and the number of random profiles grows. In addition, there is a possibility, depending on the query size and number of random profiles generated, that some sampled classes in a random profile may be correlated to various extents due to the nature of an

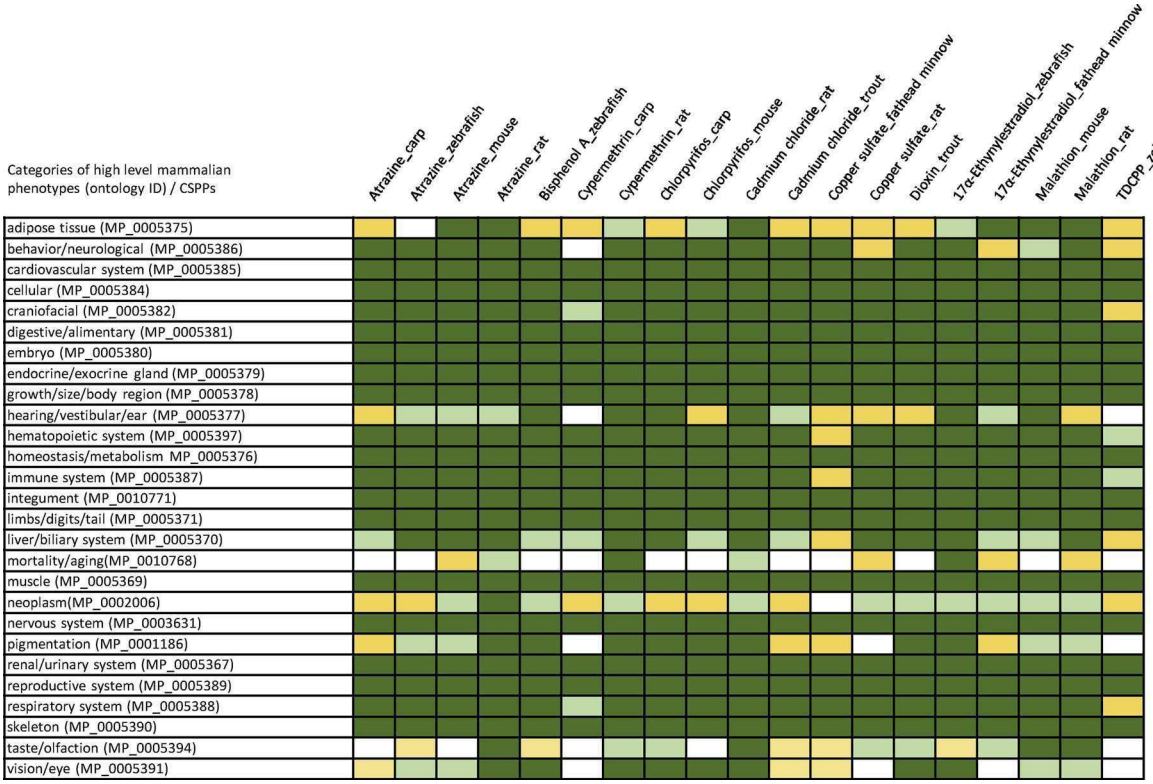

Fig. 3. The scope of coverage of mammalian phenotypes by chemical-species phenotypic profiles (CSPPs). The Mammalian Phenotype Ontology (MP) terms with pairwise similarities to the custom ontology classes from individual CSPPs ≥ 0.9, 0.8, or 0.7 were retained for extracting their respective superclasses in mp.owl using the Robot tool (http://robot.obolibrary.org). The 27 categories of high level MP terms (http://www.informatics.jax.org) present in each CSPP-associated MP superclasses based on the minimum similarity scores of 0.9, 0.8, or 0.7 are marked as dark green, light green, or yellow respectively. The categories absent at ≥ 0.7 are marked as white. The phenotypic coverages at these minimum scores are 77% (393/27 × 19), 85% (438/27 × 19), and 95% (485/27 × 19). TDCPP, Tris(1,3-dichloroisopropyl) phosphate (For interpretation of the references to colour in this figure legend, the reader is referred to the web version of this article).

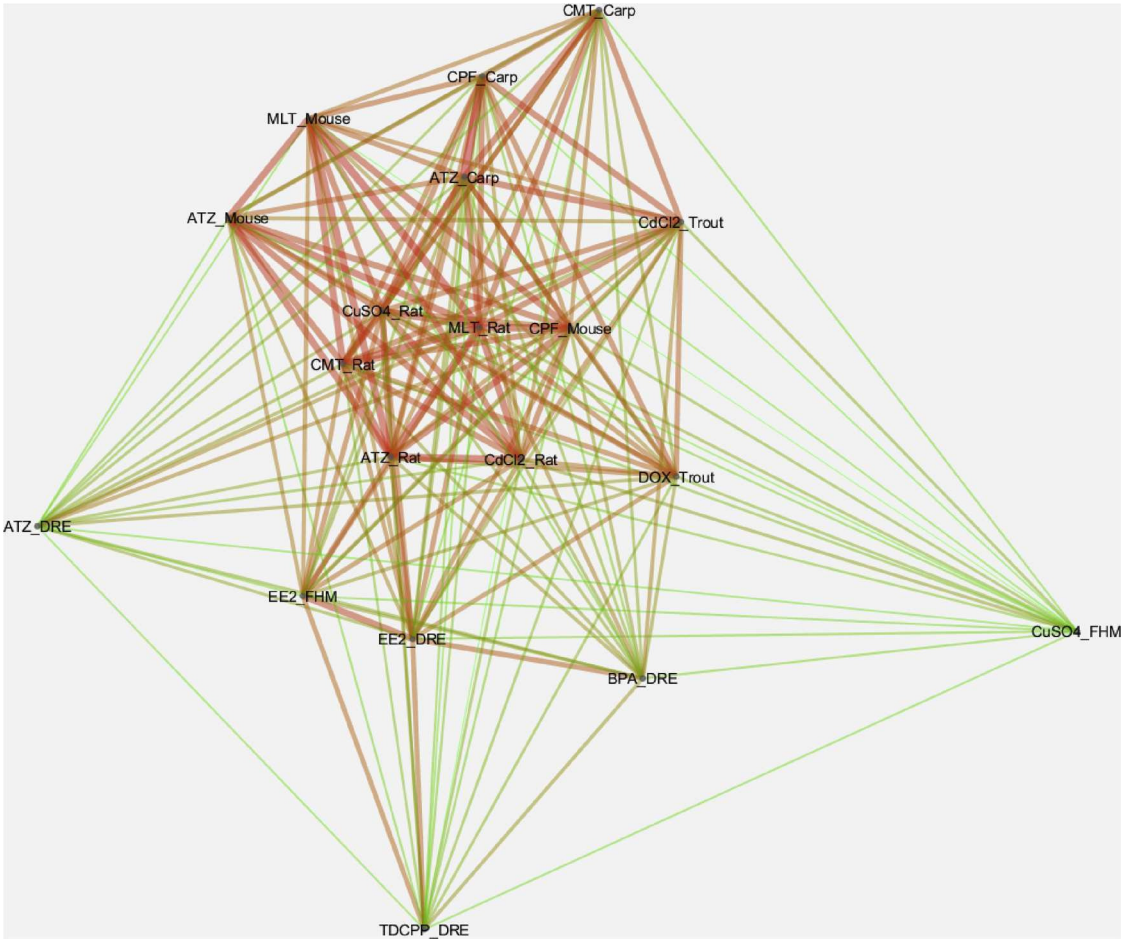

Fig. 4. Semantic similarity network of chemical-species phenotypic profiles (CSPPs). Edges are weighted by indirect group-wise similarity scores ranging between 0 and 1, in "prefuse force directed layout" at 3X scale in Cytoscape (http://www.cytoscape.org), with shorter and wider edges in darker red color indicating a greater similarity between the two connected nodes. Abbreviations: ATZ, atrazine; BPA, bisphenol A; CdCl2, cadmium chloride; CMT, cypermethrin; CPF, chlorpyrifos; CuSO4, copper sulfate; DOX, dioxin; DRE, zebrafish; EE2, 17α-Ethynylestradiol; FHM, fathead minnow; MLT, malathion; TDCPP, Tris(1,3-dichloroisopropyl) phosphate (For interpretation of the references to colour in this figure legend, the reader is referred to the web version of this article).

ontology graph. Such a correlation, when it occurs, would violate one of the assumptions of resampling that all individuals in a population should have an equal probability to be sampled.

When conducting an analysis, OS-Mapping.java takes a single configuration file (S. File 5) at the command line as the input argument to specify such analysis parameters as a starting root ontology, a set of query and target profiles, and the choices among seven reasoners, ten information content measures, 22 pairwise, and 13 group-wise semantic similarity measures. A preexisting reasoned ontology could be provided in lieu of the root ontology. Each profile contains four required fields, in the following order: a profile ID, a profile definition, an ontology class ID, and an ontology class definition (Fig. 1E). Additional fields in a profile are ignored. A profile could be anchored by a gene, disease, biological pathway, chemical, or any other biological entities of interest. Common reasoners supported include Hermit, Pellet, Elk, Jfact, Snorocket, Jcel, and Born (Dentler et al., 2011; Kazakov et al., 2011; Mendez, 2012; Ceylan et al., 2015).

2.4. Semantic similarity measures

The following four measures implemented in SML were selected for this study based on the previous evaluation of their performance on comparing gene products (Pesquita et al., 2009): 1) information content, "ICI_SANCHEZ_2011" (Sanchez et al., 2011); 2) pairwise similarity between two OWL classes, "SIM_PAIRWISE_DAG_NODE_LIN_1998" (Lin, 1998); 3) direct group-wise measure, "SIM_GROUPWISE_DAG_GIC" (Pesquita et al., 2007); and 4) indirect group-wise measure, "SIM_GROUPWISE_BMA" (Pesquita et al., 2008). They are defined as follows:

(1) "ICI_SANCHEZ_2011"

$$IC(\mu) = -\log\left(\frac{\frac{|leaves(\mu)|}{|A(\mu)|}+1}{max\_leaves+1}\right)$$

Where *IC* (μ) denotes information content for class node μ; *leaves* (μ), the number of leaf nodes below μ; A (μ), the number of parental nodes above μ; and *max_leaves*, the number of leaf nodes below the root. A class with more parental nodes and fewer leaf nodes has a greater *IC*.

(2) "SIM_PAIRWISE_DAG_NODE_LIN_1998"

$$sim(\mu, v) = \frac{2 \times IC(MICA_{\mu,v})}{IC(\mu) + IC(v)}$$

Where $MICA_{\mu,v}$ denotes the most informative common ancestor of the two nodes. The numerator measures the commonality between the two nodes, while the denominator measures their respective distances from *MICA*.

(3) "SIM_GROUPWISE_DAG_GIC"

$$simGIC(A, B) = \frac{\sum_{i=1}^{N} IC(t_i)}{\sum_{j=1}^{M} IC(t_j)}$$

Where $t_{i=1\text{-}N}$ and $t_{j=1\text{-}M}$ are the terms in the intersection and union of

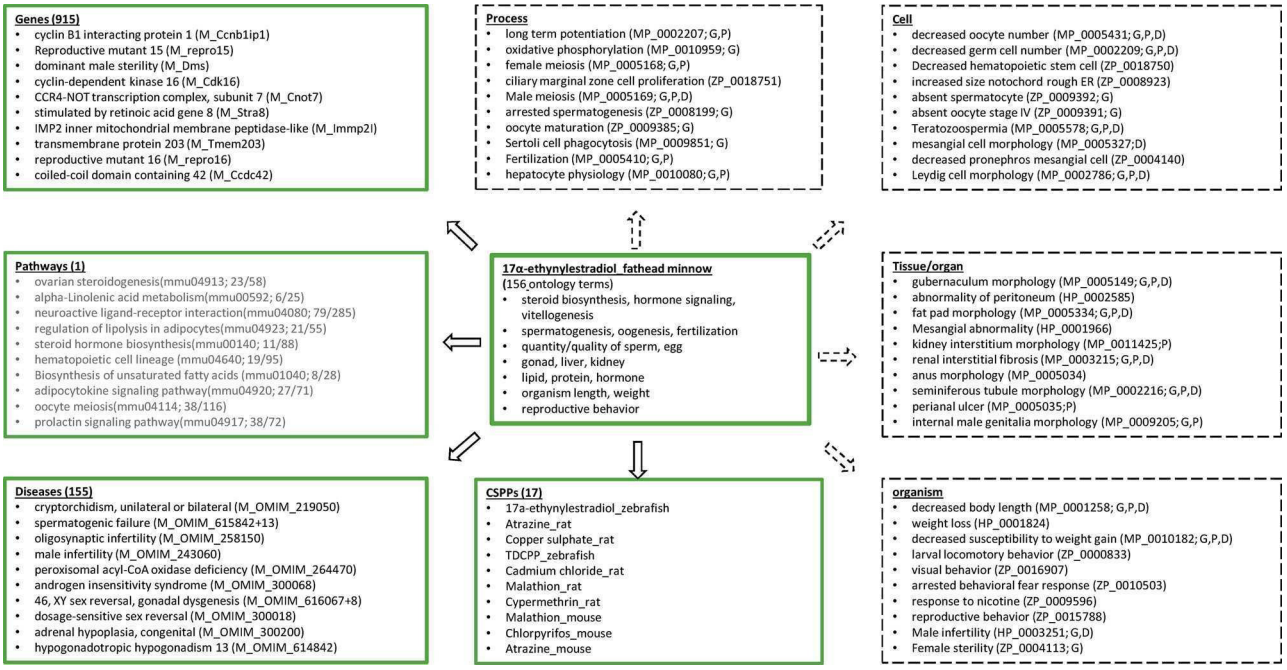

Fig. 5. A phenotypic continuum anchored by the 17α-ethynylestradiol_fathead minnow. Top ten mapped phenotypic profiles of genes ($P_{0.01}$), pathways, CSPPs ($P_{0.01}$), and disease ($P_{0.01}$) are listed. The total counts of genes, pathways, and diseases are based on $P_{0.05}$. The top ten KEGG pathways listed by OS-Mapping are not significant at $P_{0.05}$ (text in gray). Each pathway is denoted in a parenthesis by its KEGG ID, number of genes whose mutation/alleles directly caused phenotypes in reproductive systems (MP_0005389), and total number of genes in the pathway. The phenotypes at the levels of biological process, cell, tissue/organ, and organism (boxes in dash lines) were selected from the top five HP/MP/ZP terms present in the target phenotypic profiles, based on their semantic similarities to individual terms in the 17α-ethynylestradiol_fathead minnow. The terms overlapping with the phenotypic profiles of 915 genes, the top ten pathways, and 155 diseases are marked by G, P, and D in parentheses. A disease with multiple variants are denoted by its OMIM ID + the number of variants, for example, M_OMIM_615842 + 13. M_OMIM, an OMIM disease annotated by MP terms. Abbreviations: KEGG, Kyoto Encyclopedia of Genes and Genomes (https://www.genome.jp/kegg); OMIM, Online Mendelian Inheritance in Man (https://www.omim.org).

group A and B.

(4) "SIM_GROUPWISE_BMA"

$$simBMA(A, B) = \frac{1}{2}\left(\frac{1}{N}\sum_{i=1}^{N} maxS_{ij} + \frac{1}{M}\sum_{j=1}^{M} maxS_{ij}\right),\ 1 \le j \le M;\ 1 \le i \le N$$

Where groups A and B have size N and M, *respectively*, and S_{ij} is a pairwise similarity matrix with N rows and M columns for all possible class pairs between A and B based on a semantic measure, in this case, "SIM_PAIRWISE_DAG_NODE_LIN_1998". *simBMA* represents the average of the best row scores (A compared to B) and best column scores (B compared to A) in the similarity matrix for groups A and B.

2.5. OS-Mapping analysis

A merged and reasoned ontology was prepared during the semantic analysis of the 19 CSPPs against a total of 29,154 target profiles (Fig. 2A). The beginning root ontology was set as the vertebrate.owl (as of February 5, 2018), a cross-species phenotype ontology encompassing HP, MP, and ZP. It, in turn, imported many other domain ontologies in anatomy, behavior, cell, chemical, disease, gene, pathology, phenotypes, protein, relations etc. These domain ontologies had different release dates; for example, the imported ro.owl was released on April 12, 2015 while the hp.owl was released on January 26, 2018. Also imported were the custom ontology classes constructed from the EQ annotations of toxicity phenotypes ("19 chemical-species.owl") and the external reference ontology terms contained therein ("OS-Mapping.import.owl"). The latter was generated online by using OntoFox (Xiang et al., 2010) with appropriate terms from individual reference ontologies as top-level sources and additional import options of "includeAllIntermediates" and "includeAllAxiomsRecursively". Once all the ontologies were imported and merged into a single ontology, it was reasoned with Elk reasoner, a widely recognized high performer on large ontologies (Kazakov et al., 2012). The resultant ontology graph (sampled in Fig. 2B, 2C), containing over 151,000 classes and 1.7 million logical axioms, enabled the SML Engine to conduct semantic analysis. In this graph, multiple classes contained in a CSPP query are represented by a set of nodes (Fig. 2D, solid circles), while target profiles are various combinations of selected nodes in different sizes. In effect, when OS-Mapping compares a CSPP to target profiles, semantic similarities are calculated for groups of nodes of interest pairwise, as shown in a simplified sample output (Fig. 2E).

To determine if a pair of query and target profiles was statistically similar to each other, the parameter "GENERATE_SIM_SCORE_DISTRIBUTION" was turned on along with "NUM_SIMULATED_GRPS" set at 500 (S. File 5). In other words, for each such pair, $P_{0.05}$ and $P_{0.01}$ cutoffs (i.e., P-value $\le$ 0.05, $\le$ 0.01) were determined based on its unique distribution of 500 ascendingly sorted similarity values, which were calculated from 500 random profiles against the target profile under analysis. Those query-target profiles with similarities greater than their respective $P_{0.05}$ cutoffs were retained for further consideration. All analyses were conducted on the US EPA ATMOS Linux cluster (Intel E5-2697 A 2.6 GHz processors), taking a combined total of 3158 CPU hours.

Several follow-up analyses were also conducted. The scope of coverage of mammalian phenotypes by the CSPPs was estimated as follows. First, the MP terms having pairwise similarities to the custom ontology classes in each CSPP $\ge$ 0.7, 0.8, or 0.9 were identified. Each set of MP terms was then treated as seeds to extract their superclasses (i.e., parental classes) in mp.owl using the Robot tool (http://robot.obolibrary.org). The phenotypic coverage of each CSPP was measured by the number of the 27 categories of high level MP phenotypes (http://www.informatics.jax.org) present in its associated superclasses. To determine

the relationships of the CSPPs, their similarities were evaluated in the software Cytoscape (http://cytoscape.org). A complete phenotypic continuum across biological levels of organization was constructed for the 17α-ethynylestradiol_fathead minnow by organizing its top ten matched chemicals, genes, KEGG pathways, and diseases. Additional best matched phenotypes at the levels of biological processes, cell, tissue/organ, and organism were also identified from the five highest scoring HP/MP/ZP terms based on the pairwise similarity between the individual classes in the 17α-ethynylestradiol_fathead minnow and all the classes present in the target profiles. For comparison, a similar phenotypic continuum was also constructed for 17α-ethynylestradiol based on the information available as of July 2018 in the Comparative Toxicogenomics Database (CTD; http://ctdbase.org/).

3. Results

In this study, we assembled a total of 19 CSPPs containing nearly 4000 ontology classes that were manually annotated and constructed from chemical toxicity responses (Fig. 1). These CSPPs were semantically compared to each other to identify chemicals that showed similar toxicities, as well as compared against a broad array of over 29,000 target profiles corresponding to genes, KEGG pathways, and diseases to highlight potential MOAs (Fig. 2A, S. File 6). To evaluate the performance of OS-Mapping as a phenotype-oriented approach to dissect chemical toxicities, we will first focus on the relationships revealed by the CSPPs in general. We will then examine the CSPP corresponding to 17α-ethynylestradiol phenotypes observed in the fathead minnow in more detail to evaluate the mechanistic information provided by OS-Mapping. Unless specified otherwise, a statement about genes, pathways, chemicals, diseases, and their mutual similarities refers to their respective profiles.

The CSPPs appeared to have a good coverage of the 27 categories of high level mammalian phenotypes (Fig. 3). As expected, the lower threshold of minimum similarities between the MP terms and the custom ontology classes in each CSPP resulted in a greater coverage of the phenotypes, as the effect of retaining more MP terms initially was the extraction of more superclasses/phenotypic categories. The coverages were 95%, 85%, and 77%, respectively, when the minimum similarities were set at 0.7, 0.8, and 0.9. The coverage reached 100% when the minimum similarity was lowered to 0.5. The evaluation of individual MP terms mapped to the custom ontology classes from the CSPPs at various similarities suggested that the minimum threshold of 0.7 was sufficiently high for assessing the mammalian phenotypic categories covered by the CSPPs. It is notable that the category of mortality/aging was the least covered here because mortality responses were deemed uninformative and omitted during the ontological annotations of the published studies. The rat-based CSPPs tended to have a better coverage overall. The CSPPs representing the fewest phenotypic categories were cypermethrin_carp (21) and TDCPP_zebrafish (22).

The CSPPs mapped to a wide range of target profiles, with their specificities varying by more than 100-fold as measured by the number of hits (Table 1). Most of the CSPPs resembled one another to some degrees, as indicated by the number of other similar CSPPs mapped. A majority (3702/4462 = 83%) of the CSPP-mapped genes was from mouse, with the remainder split between human and zebrafish genes. Ultimately, the CSPPs were mapped to approximately 21% (4462/21399) of the genes under study. By species, these percentages were 31% (3702/12009) for mouse, 12% (422/3498) for human, and 6% (338/5892) for zebrafish, respectively. The CSPPs also matched to approximately 16% (1181/7423) of the diseases. Individually, cypermethrin_rat, malathion_mouse, and atrazine_mouse had the highest number of hits, whereas TDCPP_zebrafish, atrazine_zebrafish, copper sulfate_fathead minnow, and bisphenol A_zebrafish had the fewest hits. This trend was observed across species in genes, pathways, and diseases. The size of a CSPP did not appear to be correlated with its number of mapped targets (r = 0.41).

The relationships among CSPPs were complex, as shown in their network with individual CSPPs as nodes and edges weighted by their

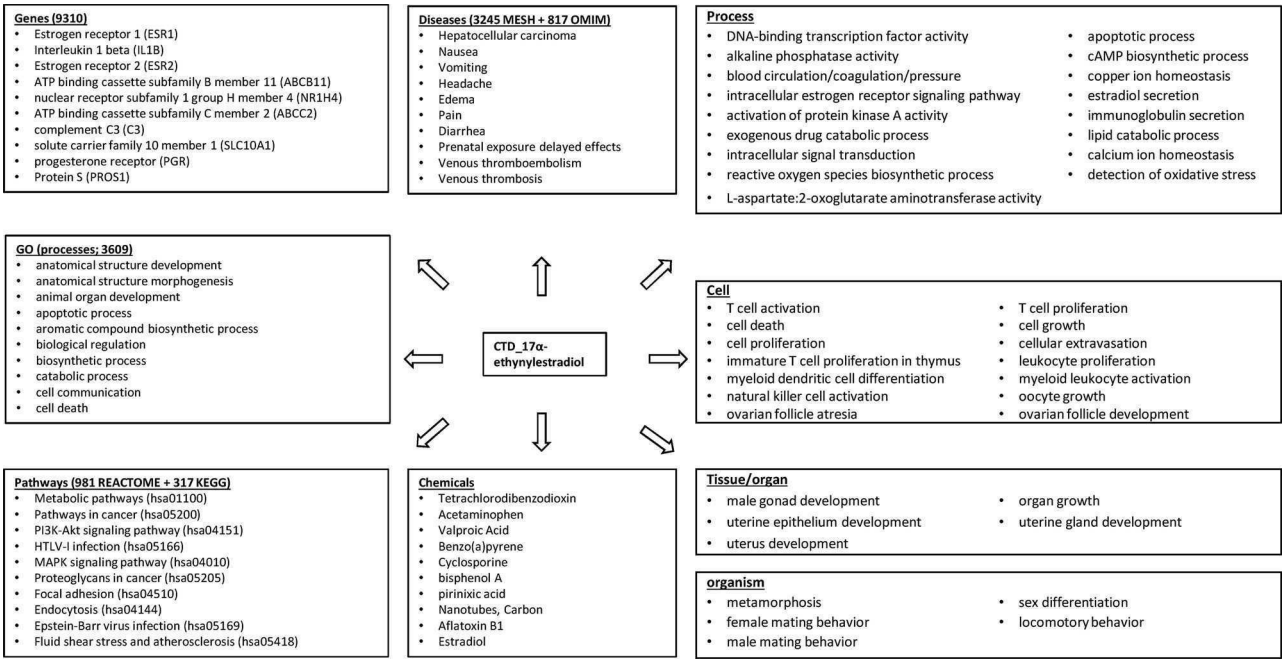

Fig. 6. Mappings of 17α-ethynylestradiol according to the Comparative Toxicogenomics Database (http://ctdbase.org; as of July 2018). The mappings were constructed as follows: chemical-genes, literature curation; chemical-pathways, human KEGG (hsa) and REACTOME pathways enriched in chemical-genes; chemical-Gene Ontology (GO) terms, GO terms enriched in chemical-genes; chemical-disease, direct curation from the literature (4.5%) or indirect inference from transitive chemical-gene-disease associations (99%), with a slight overlap between the two methods; chemical-phenotypes (delineated by process, cellular, tissue/organ, and organism), literature curation; chemical-chemical linkages, shared gene interactions. Except for phenotypes, only top ten mappings are listed for each category. For pathways, only human KEGGs are listed.

indirect group-wise similarity scores (value range 0.0–1.0; Fig. 4). The same chemicals in different species, for example, malathion_mouse vs malathion_rat (0.74), atrazine_rat vs atrazine_mouse (0.71), and 17α-ethynylestradiol_fathead minnow vs 17α-ethynylestradiol_zebrafish (0.69), were highly similar, as expected. In addition, different chemicals, such as chlorpyrifos_carp vs atrazine_carp (0.77), atrazine_rat vs malathion_rat (0.74), and malathion_rat vs cypermethrin_rat (0.72), mapped to each other very well too. In fact, chlorpyrifos_carp vs atrazine_carp achieved the highest similarity score among the CSPPs other than those self-hits. Overall, these CSPPs tended to segregate into two distinct groups. Atrazine_zebrafish, copper sulfate_fathead minnow, bisphenol A_zebrafish, and TDCPP_zebrafish belonged to the group with relatively low similarities to others, and the remainder of the CSPPs appeared to share much greater similarities among themselves. Zebrafish appeared to be less sensitive to the chemicals relative to the other species except when evaluating estrogenic compounds (Table 1, Fig. 4). Interestingly, atrazine and copper sulfate were present in both groups, a strong indication of chemical by species interaction in their toxicity responses. The lowest yet still statistically significant similarity was found between malathion_mouse and copper sulfate_fathead minnow, at 0.46.

Given the complexity of chemical-induced toxicity responses, it would be instructive to organize them according to their intrinsic biological hierarchy. As a well-studied semisynthetic estrogen and endocrine disrupting chemical, 17α-ethynylestradiol provided a good sample for this exercise (Fig. 5). This CSPP contained 156 custom-constructed ontology classes covering phenotypes across multiple biological levels from 34 studies. As expected, its semantically mapped targets were also diverse. All the top ten genes were involved, to various extents, in some aspects of reproductive biology: gonad development, male and female meiosis, endocrine glands, sperm and oocyte production, or infertility, as demonstrated by their mutant/allelic analyses (repro15 and repro16, JAX, 2004; Ccnb1ip1, Dms, Cdk16, Cnot7, Stra8, Immp2l, Tmem203, Ccdc42, http://www.informatics.jax.org). In contrast, across the mouse genome overall, this value was only 21% (2411/11409). At the pathway level, although none of the top ten pathways were significant ($P_{0.05}$), all were involved in reproductive processes and functions as well, according to mutant/allelic analyses of their gene members (http://www.informatics.jax.org). The sole significant pathway, mmu00440 (Phosphonate and phosphinate metabolism), was ranked low by similarity scores (263th out of 313), but three of its six gene members were also associated with reproductive system phenotypes. Moreover, the top phenotypes mapped by the 17α-ethynylestradiol_fathead minnow were also examined at the levels of biological process, cell, tissue/organ, and organism by identifying the HP, MP, and ZP terms of the target profiles most semantically similar to the individual terms of the 17α-ethynylestradiol_fathead minnow. Not surprisingly, almost all those terms related to reproduction overlapped with the profiles of genes, pathways, and diseases linked to the 17α-ethynylestradiol_fathead minnow. Among the notable biological processes mapped to the 17α-ethynylestradiol_fathead minnow were female and male meiosis, spermatogenesis, oocyte maturation, and fertilization. Regarding disease, most of the top matches were reproductive disorders. As to the relationships to the other CSPPs, in addition to the expected mapping to the 17α-ethynylestradiol _zebrafish (0.69), the 17α-ethynylestradiol_fathead minnow also shared substantial similarities to several chemicals with seemingly different MOAs, such as atrazine_rat (0.65) and copper sulfate_rat (0.63).

A phenotypic continuum for 17α-ethynylestradiol was also constructed by extracting the data curated and compiled by the CTD (Fig. 6). The CTD mappings of 17α-ethynylestradiol to GO processes, pathways, most of the diseases, and other chemicals were derived from the 17α-ethynylestradiol-gene interactions curated from the literature. The 17α-ethynylestradiol to phenotypes, as delineated by biological process, cell, tissue/organ, and organism, and to the remaining diseases came directly from the literature curation. Almost all 17α-ethynylestradiol-gene interactions (98%) in the CTD were based on the chemical-induced changes in gene expressions. Overall, many 17α-ethynylestradiol phenotypes from the CTD at the levels of cell, tissue/organ, and organism were related to immune functions and reproductive biology. This trend was somewhat aligned with the top matched 17α-ethynylestradiol genes (e.g., ESR1, ESR2, PGR) and chemicals (e.g., bisphenol A, estradiol), but less clear in the top GO processes, pathways, diseases, and phenotypes at the process level.

4. Discussion

OS-Mapping represents a unique approach to the study of chemical toxicities. It complements a typical omics study by providing a new perspective of semantically similar phenotypes at multiple levels of biological organization. It can also provide information about the underlying genotypes and molecular mechanisms of a biological target previously characterized only phenotypically. This pilot study explored the toxicological applications of OS-Mapping by converting previously published toxicity responses to chemicals into CSPPs of multiple ontology classes, and then comparing them semantically to the numerous profiles of genes, pathways, and diseases, and to one another, leading to a better understanding of the underlying MOAs.

OS-Mapping can differentiate chemical toxicities both within and across species. Given the 95% average coverage rate of the 27 categories of high level mammalian phenotypes (Fig. 3), the CSPPs should be quite comparable. The fact that CSPPs mapped to more mouse genes than human and zebrafish genes is likely just a reflection of the mouse phenome that is better characterized. The CSPPs appear to contain both shared and specific toxicity responses. The shared responses are indicated by the fact that most of these CSPPs were similar to one another to some degree (Table 1, Fig. 4). The specificity of CSPPs is evident in the wide variation in the number of genes, pathways, and diseases mapped by each CSPP. Conceivably, the toxicity responses of a chemical are determined by both its MOAs and target species. Perturbations at the higher levels of biological organization and in later life stages, on the other hand, may have a homogenizing effect on chemical toxicities, making some CSPPs more similar to one another. As to the degree of toxicity, it may be reasonable to assume that the more targets a chemical maps to, the more toxic it is. Under this assumption, therefore, 17α-ethynylestradiol would be considered more toxic to fish (i.e., wider impact) than copper sulfate, atrazine, or TDCPP; malathion would be more toxic to mouse than chlorpyrifos. In the meantime, there appear to be interactions between chemicals and species as well. Atrazine, thus, appears to be more toxic to rodents than it is to fish. The same conclusion could also be made for cypermethrin and copper sulfate. Chlorpyrifos, on the other hand, may be more toxic to fish than it is to rodents. And, the difference in toxicity to cadmium chloride between fish and rodents appears to be minimal. Overall, these findings are largely consistent with the current knowledge of differential species sensitivity to chemicals (Belanger et al., 2017).

OS-Mapping can yield novel insights into chemical MOAs. There are several notable pairs of highly similar CSPPs: atrazine_carp/chlorpyrifos_carp, atrazine_rat/malathion_rat, malathion_rat/malathion_mouse, atrazine_rat/atrazine_mouse, and 17α-ethynylestradiol_fathead minnow/17α-ethynylestradiol_zebrafish (Fig. 4). Although it is not surprising to observe similar interspecific toxicity responses for the same chemicals (malathion, atrazine, 17α-ethynylestradiol), the apparent MOAs of atrazine (a photosystem II inhibitor; Shimabukuro and Swanson, 1969) and chlorpyrifos/malathion (acetylcholinesterase inhibitors; Colovic et al., 2013) offer few clues about what underlies their shared toxicity phenotypes. The top contributing phenotypes to the similarity between atrazine_carp and chlorpyrifos_carp are acetylcholinesterase activity (brain) and a few key indicators of stress and immune physiology (antioxidant activity, alkaline phosphatase activity in head kidney/kidney; erythrocyte quantity, nitric-oxide synthase activity, nitric oxide level, gene and protein expressions of heat shock

protein 70 in spleen). The top KEGG pathways mapped to these two CSPPs, although not significant at $P_{0.05}$, are dominated by those related to immune responses (e.g., mmu05340, primary immunodeficiency; mmu05332, graft-versus-host disease; mmu05330, allograft rejection; S. File 6). In rodents, besides immune responses, the top KEGG pathways mapped to atrazine_rat and malathion_rat also include those involved in reproductive systems (e.g., mmu00592, mmu04913, mmu00140, $P_{0.05}$; Fig. 5, S. File 6). Therefore, the MOAs underlying atrazine toxicity in animals appear to resemble those of organophosphates, a hypothesis at least partially supported by the observed synergism between atrazine with both malathion and chlorpyrifos in a mixture (Pape-lindstrom and Lydy, 1997).

OS-Mapping enables the construction of a phenotypic continuum for chemical toxicity assessment. Two such continuums (Fig. 5,6) for 17α-ethynylestradiol offer contrasting views of its toxicities from different perspectives: one based on semantically similar phenotypes across biological levels of organization, and the other largely derived from molecular phenotypes alone (genes with expressions impacted by 17α-ethynylestradiol), except for a small number of higher level phenotypes directly curated from relevant literature. In both continuums, higher level phenotypes (cell, tissue/organ, organism) indicate a significant impact of 17α-ethynylestradiol on reproductive biology. Although this pattern is consistently observed throughout the 17α-ethynylestradiol_fathead minnow continuum, it is not as obvious in the CTD-17α-ethynylestradiol continuum among all its top mappings. Overall, the CTD-17α-ethynylestradiol continuum contained many more genes and their derived pathways/diseases than its counterpart. At the gene level, only 29 mapped genes are shared in both continuums. Noticeably absent in the top ten genes of the 17α-ethynylestradiol_fathead minnow continuum are two estrogen receptors (ESR1, ESR2), which, with similarity scores of 0.62 and 0.57, were deemed insignificant at $P_{0.05}$. Given the well-established functions of these receptors in estrogen signaling, their absence appears to indicate that OS-Mapping is less sensitive than the direct omics assays of gene expression for establishing chemical-gene linkages. This interpretation is also supported by the more than ten-fold difference between the two continuums in the number of genes mapped to 17α-ethynylestradiol. At the pathway level, the top ten in the 17α-ethynylestradiol_fathead minnow continuum contain a substantial number of gene members whose mutations/alleles directly led to phenotypes in reproductive systems (i.e., mapped to MP_0005389; http://www.informatics.jax.org). Nine out of these ten pathways are also found in the CTD-17α-ethynylestradiol continuum, but ranked hundreds below. For diseases, only two of the top ten from the 17α-ethynylestradiol_fathead minnow continuum, OMIM_616067 (gonadal dysgenesis) and OMIM_614842 (hypogonadism), are present in CTD-17α-ethynylestradiol disease mappings, but again, with very low rankings. Overall, these comparisons suggest that OS-Mapping appears to perform better for mapping toxicities of a chemical at the higher levels of biological organization, whereas the CTD provides a more comprehensive coverage of genes by relying on the data from omics-based gene expression assays directly.

The validity of OS-Mapping and its values for chemical toxicity assessment are strongly supported and demonstrated in this pilot study by the finding that the 17α-ethynylestradiol_fathead minnow continuum is dominated by reproductive phenotypes throughout. This finding is consistent with the established estrogen MOAs (Nilsson et al., 2001; Hess, 2003). Perhaps one of the most exciting prospects is that, due to the development of many reference ontologies over diverse knowledge domains, modeling chemical toxicities by incorporating a vast and growing amount of computable phenomics data throughout biological levels of organization has been made possible both within and across species. To fully realize this potential, however, efficient curation of toxicity responses into computable ontology classes must be attained. Manual curation of toxicity responses by EQ syntax is not only slow, but also subjective at times. In the current study, the curation of more than 700 publications took one individual several months to complete. Moreover, the phenotypes encountered during post composition were sometimes open to interpretation, leading to possible variations in the final annotations in terms of specificity and accuracy. A preferred solution to these issues would be found in the automated curation of free text, which is an area under active research. Considerable progress has been made for various aspects of this process, including mapping free text to ontology terms (e.g., https://www.ebi.ac.uk/spot/zooma), generating ontology classes en masse by adopting design patterns (Osumi-Sutherland et al., 2017), and even the completely automated construction of full EQ statements with binding relations (Cui et al., 2015). More efforts are needed, however, before the performance of an automated curation tool will be as accurate as that of human curators.

5. Conclusions

This study demonstrated that OS-Mapping offers a powerful approach to help bridge the gap between the molecular/non-molecular phenotypes of chemicals characterized by using traditional omics methods and their apical endpoints of greater regulatory relevance. OS-Mapping also enables the comparative toxicity assessment among chemicals, both within and across species. Furthermore, the semantic analysis of phenotypes can reveal additional novel MOAs for some of the well-known chemicals and assist in the discovery of candidate MOAs for chemicals that are less molecularly characterized. A full phenotypic continuum delineating chemical toxicities will also be conducive to the future development of adverse outcome pathways, a framework increasingly adopted under the new toxicology paradigm (Ankley et al., 2010). Continued advances in phenomics and more automation of the ontological annotation of the literature will further enhance the power of OS-Mapping.

Conflict of interest

The authors declare that there are no conflicts of interest.

Acknowledgements

The authors thank many members of the ontology community for their valuable advice on reasoners, OWLAPI, and OBO ontologies. Special thanks are due to Stephen Erickson for assistance on setting up a local copy of ECOTOX Database, Colleen Elonen for providing numerous journal articles, Yvonne Bradford and James Balhoff for advice on annotating chemical-induced toxicity responses, and Sébastien Harispe for guidance on the Semantic Measure Library. We also thank Nancy Baker and Kellie Fay for critical reviews of this manuscript. The information in this document has been funded wholly (or in part) by the US Environmental Protection Agency. It has been subjected to review by the National Exposure Research Laboratory and approved for publication. Approval does not signify that the contents reflect the views of the Agency, nor does mention of trade names or commercial products constitute endorsement or recommendation for use.

Appendix A. Supplementary data

Supplementary material related to this article can be found, in the online version, at doi:https://doi.org/10.1016/j.tox.2018.11.005.

References

Ankley, G.T., et al., 2010. Adverse outcome pathways: a conceptual framework to support ecotoxicology research and risk assessment. Environ. Toxicol. Chem. 29 (3), 730–741. https://doi.org/10.1002/etc.34.

Ashburner, M., et al., 2000. Gene ontology: tool for the unification of biology. Nat. Genet. 25 (1), 25–29.

Bard, J.B.L., Rhee, S.Y., 2004. Ontologies in biology: design, applications and future challenges. Nat. Rev. Genet. 5, 213–222.

Belanger, S., et al., 2017. Future needs and recommendations in the development of species sensitivity distributions: estimating toxicity thresholds for aquatic ecological communities and assessing impacts of chemical exposures. Integr. Environ. Assess. Manag. 13 (4), 664–674. https://doi.org/10.1002/ieam.1841.
Brown, S., et al., 2018. High-throughput mouse phenomics for characterizing mammalian gene function. Nat. Rev. Genet. 19, 357–370. https://doi.org/10.1038/s41576-018-0005-2.
Ceylan, İ.İ., et al., 2015. The Bayesian Ontology reasoner is BORN! In Dumontier, M., et al., Proceedings of the 4th International Workshop on OWL Reasoner Evaluation (ORE 2015) 1387:8-14, 2015. CEUR Workshop Proceedings.
Colovic, M.B., et al., 2013. Acetylcholinesterase inhibitors: pharmacology and toxicology. Curr. Neuropharmacol. 11 (3), 315–335. https://doi.org/10.2174/1570159X11311030006.
Cui, H., et al., 2015. Charaparser + EQ: performance evaluation without gold standard. Proceedings of the Association for Information Science and Technology 52 (1), 1–10. https://doi.org/10.1002/pra2.2015.145052010020.
Dentler, K., et al., 2011. Comparison of reasoners for large ontologies in the OWL 2 EL profile. Semant. Web 2 (2), 71–87. https://doi.org/10.3233/SW-2011-0034.
Gkoutos, G.V., et al., 2017. The anatomy of phenotype ontologies: principles, properties and applications. Brief. Bioinform. https://doi.org/10.1093/bib/bbx035.
Gruber, T.R., 1995. Toward principles for the design of ontologies used for knowledge sharing? Int. J. Hum. Stud. 43 (5–6), 907–928. https://doi.org/10.1006/ijhc.1995.1081.
Harispe, S., 2014. The semantic measures library and toolkit: fast computation of semantic similarity and relatedness using biomedical ontologies. Bioinformatics 30 (5), 740–742. https://doi.org/10.1093/bioinformatics/btt581.
Hess, R.A., 2003. Estrogen in the adult male reproductive tract: a review. Reprod. Biol. Endocrinol. 1, 52.
Hoehndorf, R., et al., 2011. PhenomeNET: a whole-phenome approach to disease gene discovery. Nucleic Acids Res. 39 (18). https://doi.org/10.1093/nar/gkr538. e119.
Hoehndorf, R., et al., 2015. The role of ontologies in biological and biomedical research: a functional perspective. Brief. Bioinform. 16 (6), 1069–1080. https://doi.org/10.1093/bib/bbv011.
Horridge, M., Bechhofer, S., 2011. The OWL API: a java API for OWL ontologies. Semantic Web J. 2 (1), 11–21. https://doi.org/10.3233/SW-2011-0025.
Houle, D., et al., 2010. Phenomics: the next challenge. Nat. Rev. Genet. 11, 855–866.
JAX reproductive mutagenesis program. Heritable Mouse Mutants from the Jackson Laboratory Reproductive Genomics Mutagenesis Program. MGI Direct Data Submission. J:92463. URL: http://reprogenomics.jax.org.
Kazakov, Y., et al., 2011. Concurrent Classification of EL Ontologies. Technical Report. University of Oxford 2011.
Kazakov, Y., et al., 2012. ELK reasoner: architecture and evaluation. In: Horrocks, I. (Ed.), Proceedings of the OWL Reasoner Evaluation Workshop 2012 (ORE'12), vol. 858. CEUR Workshop Proceedings, CEUR-WS.org.
Köhler, S., 2013. Construction and accessibility of a cross-species phenotype ontology along with gene annotations for biomedical research. F1000Res. https://doi.org/10.12688/f1000research.2-30.v2.
Lin, D., 1998. An information-theoretic definition of similarity. 15th International Conference of Machine Learning 296–304 1998.
McMurry, J.A., et al., 2016. Navigating the phenotype frontier: the monarch initiative. Genetics 203, 1491–1495.
Mendez, J., 2012. jcel: A Modular Rule-based Reasoner. In Proceedings of the 1st International Workshop on OWL Reasoner Evaluation (ORE 2012). pp. 858.
Merrick, B., 2015. Intersection of toxicogenomics and high throughput screening in the Tox21 program: an NIEHS perspective. Int. J. Biotechnol. 14 (1), 7–27.
Mungall, C.J., et al., 2010. Integrating phenotype ontologies across multiple species. Genome Biol. 11 (1), R2. https://doi.org/10.1186/gb-2010-11-1-r2.
National Research Council, 2007. Toxicity Testing in the 21st Century: A Vision and a Strategy. The National Academies Press, Washington.
Nilsson, S., et al., 2001. Mechanisms of estrogen action. Physiol. Rev. 81, 1536–1565.
Osumi-Sutherland, D., et al., 2017. Dead simple OWL design patterns. J. Biomed. Semantics 8, 18.
Pape-lindstrom, P.A., Lydy, M.J., 1997. Synergistic toxicity of atrazine and organophosphate insecticides contravenes the response addition mixture model. Environ. Toxicol. Chem. 16 (11), 2415–2420.
Pesquita, C., et al., 2007. Evaluating GO-based semantic similarity measures. Proc. 10th Annual Bio- 2007. pp. 1–4.
Pesquita, C., et al., 2008. Metrics for GO based protein semantic similarity: a systematic evaluation. BMC Bioinform. 9 (Suppl. 5), S4. https://doi.org/10.1186/1471-2105-9-S5-S4.
Pesquita, C., et al., 2009. Semantic similarity in biomedical ontologies. PLoS Comput. Biol. 5 (7), e1000443. https://doi.org/10.1371/journal.pcbi.1000443.
Richard, A., et al., 2016. ToxCast chemical landscape: paving the Road to 21st century toxicology. Chem. Res. Toxicol. 29 (8), 1225–1251. https://doi.org/10.1021/acs.chemrestox.6b00135.
Sanchez, D., et al., 2011. Ontology-based information content computation. Knowl. Based Syst. 24, 297–303.
Shimabukuro, R.H., Swanson, H.R., 1969. Atrazine metabolism, selectivity, and mode of action. J. Agric. Food Chem. 17 (2), 199–205. https://doi.org/10.1021/jf60162a044.
Smith, B., et al., 2007. The OBO Foundry: coordinated evolution of ontologies to support biomedical data integration. Nat. Biotechnol. 25 (11), 1251–1255. https://doi.org/10.1038/nbt1346.
Washington, N.L., et al., 2009. Linking human diseases to animal models using ontology-based phenotype annotation. PLoS Biol. 7 (11). https://doi.org/10.1371/journal.pbio.1000247. e1000247.
Xiang, Z., et al., 2010. OntoFox: web-based support for ontology reuse. BMC Res. Notes 3, 175.
Yu, G., et al., 2010. GOSemSim: a R package for measuring semantic similarity among GO terms and gene products. Bioinformatics 26 (7), 976–978. https://doi.org/10.1093/bioinformatics/btq064.

From: Ankley, Gerald
To: Wang, Rong-Lin
Subject: RE: STAA2020 Record of Percentage Agreement
Date: Monday, April 20, 2020 9:10:51 AM

Yes

From: Wang, Rong-Lin <Wang.Rong-Lin@epa.gov>
Sent: Monday, April 20, 2020 8:07 AM
To: Biales, Adam <Biales.Adam@epa.gov>; Bencic, David <Bencic.David@epa.gov>; Ankley, Gerald <Ankley.Gerald@epa.gov>; Villeneuve, Dan <Villeneuve.Dan@epa.gov>; Perkins, Edward J SES ERDC-RDE-EL-MS <Edward.J.Perkins@erdc.dren.mil>; natalia.g.vinas@erdc.dren.mil; Edwards, Steve <swedwards@rti.org>; Ives, Cataia <cives@rti.org>
Subject: FW: STAA2020 Record of Percentage Agreement

Hello again Everybody,

I am putting together the application. Apparently there is supposed to be only one agreement of contributions covering both publications. The simplest thing to do is to count each paper as having 50% of the total and merge them. In other words, individual contributions to each paper previously listed are divided by 2. Please respond by checking off your answer and initialize it in the table below. My apologies for the rehash. Thanks much again!

Rong-Lin Wang, Adam D. Biales, Natalia Garcia-Reyero, Edward J. Perkins, Daniel L. Villeneuve, Gerald T. Ankley & David C. Bencic. 2016. Fish connectivity mapping: linking chemical stressors by their mechanisms of action-driven transcriptomic profiles. BMC Genomics volume 17, Article number: 84

Rong-Lin Wang, Stephen Edwards, Cataia Ives. 2019. Ontology-based semantic mapping of chemical toxicities. Toxicology, Volume 412, Pages 89-100

The author agrees with his or her designated percentage of contribution as listed below

Authors	Organization	Percentage of contribution	Yes / No	Author initials
Rong-Lin Wang	US EPA	47.5%	Yes ☐/No ☐	
Adam Biales	US EPA	6.25%	Yes ☐/No ☐	
Natalia Garcia-Reyero	US Army Corps	6.25%	Yes ☐/No ☐	
Edward J. Perkins	US Army Corps	6.25%	Yes ☐/No ☐	
Daniel L. Villeneuve	US EPA	6.25%	Yes ☐/No ☐	
Gerald T. Ankley	US EPA	6.25%	Yes ☒/No ☐	
David C. Bencic	US EPA	6.25%	Yes ☐/No ☐	

Steve Edwards	RTI International	7.5%	Yes ☐/No ☐	
Cataia Ives	RTI International	7.5%	Yes ☐/No ☐	
		100.00%		

Rong-Lin Wang, Ph.D
Great Lakes Toxicology & Ecology Division / Center for Computational Toxicology & Exposure
Office of Research & Development / US EPA
26 W Martin Luther King Dr., Cincinnati, OH 45268
AWL: 513-426-6468, Cell: 858-414-1021
Office: 513-569-7862, Fax: 513-569-7757

From: Wang, Rong-Lin
Sent: Thursday, April 16, 2020 5:10 PM
To: Biales, Adam <Biales.Adam@epa.gov>; Bencic, David <Bencic.David@epa.gov>; Villeneuve, Dan (Villeneuve.Dan@epa.gov) <Villeneuve.Dan@epa.gov>; Ankley, Gerald <Ankley.Gerald@epa.gov>; Perkins, Edward J SES ERDC-RDE-EL-MS <Edward.J.Perkins@erdc.dren.mil>; natalia.g.vinas@erdc.dren.mil; Edwards, Steve <swedwards@rti.org>; Ives, Cataia <cives@rti.org>
Subject: STAA2020 Record of Percentage Agreement

Hello Everyone,

I would like to submit the two publications as a joint package for STAA 2020, one on fish connectivity mapping from 2016 and the other on semantic mapping from 2019. They fit nicely together under the theme of mapping chemical toxicities by phenotypic profiles. Another driver is that the Cmap paper is going to be timed out next year for STAA. You are all coauthors on either one of the two papers. As required, I need your consent with regard to author contributions before I can apply.

Could you take a quick look at the attached table, check off the box and put in your initials beside your name? The percentages I put down are quite arbitrary and hopefully agreeable with everybody. The only constraint is that EPA folks have to account for more than 50% for a paper to be eligible. Please send me your response soon. The final deadline is April 30.

Thanks much and best regards,

Rong-Lin Wang, Ph.D
Great Lakes Toxicology & Ecology Division / Center for Computational Toxicology & Exposure
Office of Research & Development / US EPA
26 W Martin Luther King Dr., Cincinnati, OH 45268
AWL: 513-426-6468, Cell: 858-414-1021
Office: 513-569-7862, Fax: 513-569-7757

From:	Bencic, David
To:	Biales, Adam; Wang, Rong-Lin; Ankley, Gerald; Villeneuve, Dan; Perkins, Edward J SES ERDC-RDE-EL-MS; natalia.g.vinas@erdc.dren.mil; Edwards, Steve; Ives, Cataia
Subject:	RE: STAA2020 Record of Percentage Agreement
Date:	Monday, April 20, 2020 10:16:05 AM

From: Biales, Adam <Biales.Adam@epa.gov>
Sent: Monday, April 20, 2020 9:27 AM
To: Wang, Rong-Lin <Wang.Rong-Lin@epa.gov>; Bencic, David <Bencic.David@epa.gov>; Ankley, Gerald <Ankley.Gerald@epa.gov>; Villeneuve, Dan <Villeneuve.Dan@epa.gov>; Perkins, Edward J SES ERDC-RDE-EL-MS <Edward.J.Perkins@erdc.dren.mil>; natalia.g.vinas@erdc.dren.mil; Edwards, Steve <swedwards@rti.org>; Ives, Cataia <cives@rti.org>
Subject: RE: STAA2020 Record of Percentage Agreement

Adam Biales, Ph.D.
Chief, Molecular Indicators Branch (MIB)
Center for Computational Toxicology and Exposure
Office of Research and Development
United States Environmental Protection Agency
26 W. Martin Luther King Dr.
Mail Stop 587
Cincinnati, OH 45268
Office: 513-569-7094
Mobile: 513-658-6071

From: Wang, Rong-Lin <Wang.Rong-Lin@epa.gov>
Sent: Monday, April 20, 2020 9:07 AM
To: Biales, Adam <Biales.Adam@epa.gov>; Bencic, David <Bencic.David@epa.gov>; Ankley, Gerald <Ankley.Gerald@epa.gov>; Villeneuve, Dan <Villeneuve.Dan@epa.gov>; Perkins, Edward J SES ERDC-RDE-EL-MS <Edward.J.Perkins@erdc.dren.mil>; natalia.g.vinas@erdc.dren.mil; Edwards, Steve <swedwards@rti.org>; Ives, Cataia <cives@rti.org>
Subject: FW: STAA2020 Record of Percentage Agreement

Hello again Everybody,

I am putting together the application. Apparently there is supposed to be only one agreement of contributions covering both publications. The simplest thing to do is to count each paper as having 50% of the total and merge them. In other words, individual contributions to each paper previously listed are divided by 2. Please respond by checking off your answer and initialize it in the

table below. My apologies for the rehash. Thanks much again!

Rong-Lin Wang, Adam D. Biales, Natalia Garcia-Reyero, Edward J. Perkins, Daniel L. Villeneuve, Gerald T. Ankley & David C. Bencic. 2016. Fish connectivity mapping: linking chemical stressors by their mechanisms of action-driven transcriptomic profiles. BMC Genomics volume 17, Article number: 84

Rong-Lin Wang, Stephen Edwards, Cataia Ives. 2019. Ontology-based semantic mapping of chemical toxicities. Toxicology, Volume 412, Pages 89-100

The author agrees with his or her designated percentage of contribution as listed below

Authors	Organization	Percentage of contribution	Yes / No	Author initials
Rong-Lin Wang	US EPA	47.5%	Yes ☐/No ☐	
Adam Biales	US EPA	6.25%	Yes ☒/No ☐	ADB
Natalia Garcia-Reyero	US Army Corps	6.25%	Yes ☐/No ☐	
Edward J. Perkins	US Army Corps	6.25%	Yes ☐/No ☐	
Daniel L. Villeneuve	US EPA	6.25%	Yes ☐/No ☐	
Gerald T. Ankley	US EPA	6.25%	Yes ☐/No ☐	
David C. Bencic	US EPA	6.25%	Yes ☒/No ☐	DCB
Steve Edwards	RTI International	7.5%	Yes ☐/No ☐	
Cataia Ives	RTI International	7.5%	Yes ☐/No ☐	
		100.00%		

Rong-Lin Wang, Ph.D
Great Lakes Toxicology & Ecology Division / Center for Computational Toxicology & Exposure
Office of Research & Development / US EPA
26 W Martin Luther King Dr., Cincinnati, OH 45268
AWL: 513-426-6468, Cell: 858-414-1021
Office: 513-569-7862, Fax: 513-569-7757

From: Wang, Rong-Lin
Sent: Thursday, April 16, 2020 5:10 PM
To: Biales, Adam <Biales.Adam@epa.gov>; Bencic, David <Bencic.David@epa.gov>; Villeneuve, Dan (Villeneuve.Dan@epa.gov) <Villeneuve.Dan@epa.gov>; Ankley, Gerald <Ankley.Gerald@epa.gov>; Perkins, Edward J SES ERDC-RDE-EL-MS <Edward.J.Perkins@erdc.dren.mil>; natalia.g.vinas@erdc.dren.mil; Edwards, Steve <swedwards@rti.org>; Ives, Cataia <cives@rti.org>
Subject: STAA2020 Record of Percentage Agreement

Hello Everyone,

I would like to submit the two publications as a joint package for STAA 2020, one on fish connectivity mapping from 2016 and the other on semantic mapping from 2019. They fit nicely together under the theme of mapping chemical toxicities by phenotypic profiles. Another driver is that the Cmap paper is going to be timed out next year for STAA. You are all coauthors on either one of the two papers. As required, I need your consent with regard to author contributions before I can apply.

Could you take a quick look at the attached table, check off the box and put in your initials beside your name? The percentages I put down are quite arbitrary and hopefully agreeable with everybody. The only constraint is that EPA folks have to account for more than 50% for a paper to be eligible. Please send me your response soon. The final deadline is April 30.

Thanks much and best regards,

Rong-Lin Wang, Ph.D
Great Lakes Toxicology & Ecology Division / Center for Computational Toxicology & Exposure
Office of Research & Development / US EPA
26 W Martin Luther King Dr., Cincinnati, OH 45268
AWL: 513-426-6468, Cell: 858-414-1021
Office: 513-569-7862, Fax: 513-569-7757

From:	Biales, Adam
To:	Wang, Rong-Lin; Bencic, David; Ankley, Gerald; Villeneuve, Dan; Perkins, Edward J SES ERDC-RDE-EL-MS; natalia.g.vinas@erdc.dren.mil; Edwards, Steve; Ives, Cataia
Subject:	RE: STAA2020 Record of Percentage Agreement
Date:	Monday, April 20, 2020 9:26:43 AM

Adam Biales, Ph.D.
Chief, Molecular Indicators Branch (MIB)
Center for Computational Toxicology and Exposure
Office of Research and Development
United States Environmental Protection Agency
26 W. Martin Luther King Dr.
Mail Stop 587
Cincinnati, OH 45268
Office: 513-569-7094
Mobile: 513-658-6071

From: Wang, Rong-Lin <Wang.Rong-Lin@epa.gov>
Sent: Monday, April 20, 2020 9:07 AM
To: Biales, Adam <Biales.Adam@epa.gov>; Bencic, David <Bencic.David@epa.gov>; Ankley, Gerald <Ankley.Gerald@epa.gov>; Villeneuve, Dan <Villeneuve.Dan@epa.gov>; Perkins, Edward J SES ERDC-RDE-EL-MS <Edward.J.Perkins@erdc.dren.mil>; natalia.g.vinas@erdc.dren.mil; Edwards, Steve <swedwards@rti.org>; Ives, Cataia <cives@rti.org>
Subject: FW: STAA2020 Record of Percentage Agreement

Hello again Everybody,

I am putting together the application. Apparently there is supposed to be only one agreement of contributions covering both publications. The simplest thing to do is to count each paper as having 50% of the total and merge them. In other words, individual contributions to each paper previously listed are divided by 2. Please respond by checking off your answer and initialize it in the table below. My apologies for the rehash. Thanks much again!

Rong-Lin Wang, Adam D. Biales, Natalia Garcia-Reyero, Edward J. Perkins, Daniel L. Villeneuve, Gerald T. Ankley & David C. Bencic. 2016. Fish connectivity mapping: linking chemical stressors by their mechanisms of action-driven transcriptomic profiles. BMC Genomics volume 17, Article number: 84

Rong-Lin Wang, Stephen Edwards, Cataia Ives. 2019. Ontology-based semantic mapping of chemical toxicities. Toxicology, Volume 412, Pages 89-100

The author agrees with his or her designated percentage of contribution as listed below

Authors	Organization	Percentage of contribution	Yes / No	Author initials
Rong-Lin Wang	US EPA	47.5%	Yes ☐/No ☐	
Adam Biales	US EPA	6.25%	Yes ☒/No ☐	ADB
Natalia Garcia-Reyero	US Army Corps	6.25%	Yes ☐/No ☐	
Edward J. Perkins	US Army Corps	6.25%	Yes ☐/No ☐	
Daniel L. Villeneuve	US EPA	6.25%	Yes ☐/No ☐	
Gerald T. Ankley	US EPA	6.25%	Yes ☐/No ☐	
David C. Bencic	US EPA	6.25%	Yes ☐/No ☐	
Steve Edwards	RTI International	7.5%	Yes ☐/No ☐	
Cataia Ives	RTI International	7.5%	Yes ☐/No ☐	
		100.00%		

Rong-Lin Wang, Ph.D
Great Lakes Toxicology & Ecology Division / Center for Computational Toxicology & Exposure
Office of Research & Development / US EPA
26 W Martin Luther King Dr., Cincinnati, OH 45268
AWL: 513-426-6468, Cell: 858-414-1021
Office: 513-569-7862, Fax: 513-569-7757

From: Wang, Rong-Lin
Sent: Thursday, April 16, 2020 5:10 PM
To: Biales, Adam <Biales.Adam@epa.gov>; Bencic, David <Bencic.David@epa.gov>; Villeneuve, Dan (Villeneuve.Dan@epa.gov) <Villeneuve.Dan@epa.gov>; Ankley, Gerald <Ankley.Gerald@epa.gov>; Perkins, Edward J SES ERDC-RDE-EL-MS <Edward.J.Perkins@erdc.dren.mil>; natalia.g.vinas@erdc.dren.mil; Edwards, Steve <swedwards@rti.org>; Ives, Cataia <cives@rti.org>
Subject: STAA2020 Record of Percentage Agreement

Hello Everyone,

I would like to submit the two publications as a joint package for STAA 2020, one on fish connectivity mapping from 2016 and the other on semantic mapping from 2019. They fit nicely together under the theme of mapping chemical toxicities by phenotypic profiles. Another driver is that the Cmap paper is going to be timed out next year for STAA. You are all coauthors on either one of the two papers. As required, I need your consent with regard to author contributions before I can apply.

Could you take a quick look at the attached table, check off the box and put in your initials beside your name? The percentages I put down are quite arbitrary and hopefully agreeable with everybody. The only constraint is that EPA folks have to account for more than 50% for a paper to be eligible. Please send me your response soon. The final deadline is April 30.

Thanks much and best regards,

Rong-Lin Wang, Ph.D
Great Lakes Toxicology & Ecology Division / Center for Computational Toxicology & Exposure
Office of Research & Development / US EPA
26 W Martin Luther King Dr., Cincinnati, OH 45268
AWL: 513-426-6468, Cell: 858-414-1021
Office: 513-569-7862, Fax: 513-569-7757

From: Edwards, Steve
To: Wang, Rong-Lin
Subject: RE: STAA2020 Record of Percentage Agreement
Date: Thursday, April 16, 2020 8:34:57 PM
Attachments: STAA2020 contribution.docx

HI Rong-Lin,

Happy to be included. Good luck!

Stephen (Steve) Edwards
Research Computing Division
RTI International
swedwards@rti.org
919-541-6841

From: Wang, Rong-Lin <Wang.Rong-Lin@epa.gov>
Sent: Thursday, April 16, 2020 5:10 PM
To: Biales, Adam <Biales.Adam@epa.gov>; Bencic, David <Bencic.David@epa.gov>; Villeneuve, Dan <Villeneuve.Dan@epa.gov>; Ankley, Gerald <Ankley.Gerald@epa.gov>; Perkins, Edward J SES ERDC-RDE-EL-MS <Edward.J.Perkins@erdc.dren.mil>; natalia.g.vinas@erdc.dren.mil; Edwards, Steve <swedwards@rti.org>; Ives, Cataia <cives@rti.org>
Subject: STAA2020 Record of Percentage Agreement

EXTERNAL: This email originated from outside of the organization. Do not click links or open attachments unless you recognize the sender and know the content is safe.

Hello Everyone,

I would like to submit the two publications as a joint package for STAA 2020, one on fish connectivity mapping from 2016 and the other on semantic mapping from 2019. They fit nicely together under the theme of mapping chemical toxicities by phenotypic profiles. Another driver is that the Cmap paper is going to be timed out next year for STAA. You are all coauthors on either one of the two papers. As required, I need your consent with regard to author contributions before I can apply.

Could you take a quick look at the attached table, check off the box and put in your initials beside your name? The percentages I put down are quite arbitrary and hopefully agreeable with everybody. The only constraint is that EPA folks have to account for more than 50% for a paper to be eligible. Please send me

your response soon. The final deadline is April 30.

Thanks much and best regards,

Rong-Lin Wang, Ph.D
Great Lakes Toxicology & Ecology Division / Center for Computational Toxicology & Exposure
Office of Research & Development / US EPA
26 W Martin Luther King Dr., Cincinnati, OH 45268
AWL: 513-426-6468, Cell: 858-414-1021
Office: 513-569-7862, Fax: 513-569-7757

From: Vinas, Natalia G ERDC-RDE-EL-MS CIV
To: Wang, Rong-Lin
Subject: Re: STAA2020 Record of Percentage Agreement
Date: Wednesday, April 22, 2020 12:04:18 PM

Hi Rong-Lin,

this is great! do you mind resending me the latest? or you can just add my initials yourself, that would be easier

thanks so much and hope you are staying well!
n

From: Wang, Rong-Lin <Wang.Rong-Lin@epa.gov>
Sent: Monday, April 20, 2020 8:07:21 AM
To: Biales, Adam; Bencic, David; Ankley, Gerald; Villeneuve, Dan; Perkins, Edward J SES ERDC-RDE-EL-MS CIV; Vinas, Natalia G ERDC-RDE-EL-MS CIV; Edwards, Steve; Ives, Cataia
Subject: FW: STAA2020 Record of Percentage Agreement

Hello again Everybody,

I am putting together the application. Apparently there is supposed to be only one agreement of contributions covering both publications. The simplest thing to do is to count each paper as having 50% of the total and merge them. In other words, individual contributions to each paper previously listed are divided by 2. Please respond by checking off your answer and initialize it in the table below. My apologies for the rehash. Thanks much again!

Rong-Lin Wang, Adam D. Biales, Natalia Garcia-Reyero, Edward J. Perkins, Daniel L. Villeneuve, Gerald T. Ankley & David C. Bencic. 2016. Fish connectivity mapping: linking chemical stressors by their mechanisms of action-driven transcriptomic profiles. BMC Genomics volume 17, Article number: 84

Rong-Lin Wang, Stephen Edwards, Cataia Ives. 2019. Ontology-based semantic mapping of chemical toxicities. Toxicology, Volume 412, Pages 89-100

The author agrees with his or her designated percentage of contribution as listed below

Authors	Organization	Percentage of contribution	Yes / No	Author initials
Rong-Lin Wang	US EPA	47.5%	Yes ☐/No ☐	

Adam Biales	US EPA	6.25%	Yes ☐/No ☐	
Natalia Garcia-Reyero	US Army Corps	6.25%	Yes ☐/No ☐	
Edward J. Perkins	US Army Corps	6.25%	Yes ☐/No ☐	
Daniel L. Villeneuve	US EPA	6.25%	Yes ☐/No ☐	
Gerald T. Ankley	US EPA	6.25%	Yes ☐/No ☐	
David C. Bencic	US EPA	6.25%	Yes ☐/No ☐	
Steve Edwards	RTI International	7.5%	Yes ☐/No ☐	
Cataia Ives	RTI International	7.5%	Yes ☐/No ☐	
		100.00%		

Rong-Lin Wang, Ph.D
Great Lakes Toxicology & Ecology Division / Center for Computational Toxicology & Exposure
Office of Research & Development / US EPA
26 W Martin Luther King Dr., Cincinnati, OH 45268
AWL: 513-426-6468, Cell: 858-414-1021
Office: 513-569-7862, Fax: 513-569-7757

From: Wang, Rong-Lin
Sent: Thursday, April 16, 2020 5:10 PM
To: Biales, Adam <Biales.Adam@epa.gov>; Bencic, David <Bencic.David@epa.gov>; Villeneuve, Dan (Villeneuve.Dan@epa.gov) <Villeneuve.Dan@epa.gov>; Ankley, Gerald <Ankley.Gerald@epa.gov>; Perkins, Edward J SES ERDC-RDE-EL-MS <Edward.J.Perkins@erdc.dren.mil>; natalia.g.vinas@erdc.dren.mil; Edwards, Steve <swedwards@rti.org>; Ives, Cataia <cives@rti.org>
Subject: STAA2020 Record of Percentage Agreement

Hello Everyone,

I would like to submit the two publications as a joint package for STAA 2020, one on fish connectivity mapping from 2016 and the other on semantic mapping from 2019. They fit nicely together under the theme of mapping chemical toxicities by phenotypic profiles. Another driver is that the Cmap paper is going to be timed out next year for STAA. You are all coauthors on either one of the two papers. As required, I need your consent with regard to author contributions before I can apply.

Could you take a quick look at the attached table, check off the box and put in your initials beside your name? The percentages I put down are quite arbitrary and hopefully agreeable with everybody. The only constraint is that EPA folks

have to account for more than 50% for a paper to be eligible. Please send me your response soon. The final deadline is April 30.

Thanks much and best regards,

Rong-Lin Wang, Ph.D
Great Lakes Toxicology & Ecology Division / Center for Computational Toxicology & Exposure
Office of Research & Development / US EPA
26 W Martin Luther King Dr., Cincinnati, OH 45268
AWL: 513-426-6468, Cell: 858-414-1021
Office: 513-569-7862, Fax: 513-569-7757

From: Perkins, Edward J SES ERDC-RDE-EL-MS CIV
To: Wang, Rong-Lin
Subject: Re: STAA2020 Record of Percentage Agreement
Date: Monday, April 20, 2020 10:18:57 AM

Here you go.

Ed

From: "Wang, Rong-Lin" <Wang.Rong-Lin@epa.gov>
Date: Monday, April 20, 2020 at 9:09 AM
To: "Biales, Adam" <Biales.Adam@epa.gov>, "Bencic, David" <Bencic.David@epa.gov>, "Ankley, Gerald" <Ankley.Gerald@epa.gov>, "Villeneuve, Dan" <Villeneuve.Dan@epa.gov>, "Perkins, Edward J SES ERDC-RDE-EL-MS CIV" <Edward.J.Perkins@erdc.dren.mil>, "Vinas, Natalia G ERDC-RDE-EL-MS CIV" <Natalia.G.Vinas@erdc.dren.mil>, steve edwards <swedwards@rti.org>, "Ives, Cataia" <cives@rti.org>
Subject: FW: STAA2020 Record of Percentage Agreement

Hello again Everybody,

I am putting together the application. Apparently there is supposed to be only one agreement of contributions covering both publications. The simplest thing to do is to count each paper as having 50% of the total and merge them. In other words, individual contributions to each paper previously listed are divided by 2. Please respond by checking off your answer and initialize it in the table below. My apologies for the rehash. Thanks much again!

Rong-Lin Wang, Adam D. Biales, Natalia Garcia-Reyero, Edward J. Perkins, Daniel L. Villeneuve, Gerald T. Ankley & David C. Bencic. 2016. Fish connectivity mapping: linking chemical stressors by their mechanisms of action-driven transcriptomic profiles. BMC Genomics volume 17, Article number: 84

Rong-Lin Wang, Stephen Edwards, Cataia Ives. 2019. Ontology-based semantic mapping of chemical toxicities. Toxicology, Volume 412, Pages 89-100

The author agrees with his or her designated percentage of contribution as listed below

Authors	Organization	Percentage of contribution	Yes / No	Author initials
Rong-Lin Wang	US EPA	47.5%	Yes ☐/No ☐	
Adam Biales	US EPA	6.25%	Yes ☐/No ☐	
Natalia Garcia-	US Army Corps	6.25%	Yes ☐/No ☐	

Reyero				
Edward J. Perkins	US Army Corps	6.25%	Yes X/No ☐	EJP
Daniel L. Villeneuve	US EPA	6.25%	Yes ☐/No ☐	
Gerald T. Ankley	US EPA	6.25%	Yes ☐/No ☐	
David C. Bencic	US EPA	6.25%	Yes ☐/No ☐	
Steve Edwards	RTI International	7.5%	Yes ☐/No ☐	
Cataia Ives	RTI International	7.5%	Yes ☐/No ☐	
		100.00%		

Rong-Lin Wang, Ph.D
Great Lakes Toxicology & Ecology Division / Center for Computational Toxicology & Exposure
Office of Research & Development / US EPA
26 W Martin Luther King Dr., Cincinnati, OH 45268
AWL: 513-426-6468, Cell: 858-414-1021
Office: 513-569-7862, Fax: 513-569-7757

From: Wang, Rong-Lin
Sent: Thursday, April 16, 2020 5:10 PM
To: Biales, Adam <Biales.Adam@epa.gov>; Bencic, David <Bencic.David@epa.gov>; Villeneuve, Dan (Villeneuve.Dan@epa.gov) <Villeneuve.Dan@epa.gov>; Ankley, Gerald <Ankley.Gerald@epa.gov>; Perkins, Edward J SES ERDC-RDE-EL-MS <Edward.J.Perkins@erdc.dren.mil>; natalia.g.vinas@erdc.dren.mil; Edwards, Steve <swedwards@rti.org>; Ives, Cataia <cives@rti.org>
Subject: STAA2020 Record of Percentage Agreement

Hello Everyone,

I would like to submit the two publications as a joint package for STAA 2020, one on fish connectivity mapping from 2016 and the other on semantic mapping from 2019. They fit nicely together under the theme of mapping chemical toxicities by phenotypic profiles. Another driver is that the Cmap paper is going to be timed out next year for STAA. You are all coauthors on either one of the two papers. As required, I need your consent with regard to author contributions before I can apply.

Could you take a quick look at the attached table, check off the box and put in your initials beside your name? The percentages I put down are quite arbitrary and hopefully agreeable with everybody. The only constraint is that EPA folks have to account for more than 50% for a paper to be eligible. Please send me

your response soon. The final deadline is April 30.

Thanks much and best regards,

Rong-Lin Wang, Ph.D
Great Lakes Toxicology & Ecology Division / Center for Computational Toxicology & Exposure
Office of Research & Development / US EPA
26 W Martin Luther King Dr., Cincinnati, OH 45268
AWL: 513-426-6468, Cell: 858-414-1021
Office: 513-569-7862, Fax: 513-569-7757

From: Villeneuve, Dan
To: Wang, Rong-Lin
Cc: Blackwell, Brett
Subject: RE: STAA2020 Record of Percentage Agreement
Date: Monday, April 20, 2020 10:08:02 AM
Attachments: RL Wang STAA2020 contribution(2)-DLV.docx

Here you go Rong-Lin,

Also, Brett has been working on an STAA package. He probably has the last 5 years of nomination information for Gary and I already assembled.

Dan V.

From: Wang, Rong-Lin <Wang.Rong-Lin@epa.gov>
Sent: Monday, April 20, 2020 8:07 AM
To: Biales, Adam <Biales.Adam@epa.gov>; Bencic, David <Bencic.David@epa.gov>; Ankley, Gerald <Ankley.Gerald@epa.gov>; Villeneuve, Dan <Villeneuve.Dan@epa.gov>; Perkins, Edward J SES ERDC-RDE-EL-MS <Edward.J.Perkins@erdc.dren.mil>; natalia.g.vinas@erdc.dren.mil; Edwards, Steve <swedwards@rti.org>; Ives, Cataia <cives@rti.org>
Subject: FW: STAA2020 Record of Percentage Agreement

Hello again Everybody,

I am putting together the application. Apparently there is supposed to be only one agreement of contributions covering both publications. The simplest thing to do is to count each paper as having 50% of the total and merge them. In other words, individual contributions to each paper previously listed are divided by 2. Please respond by checking off your answer and initialize it in the table below. My apologies for the rehash. Thanks much again!

Rong-Lin Wang, Adam D. Biales, Natalia Garcia-Reyero, Edward J. Perkins, Daniel L. Villeneuve, Gerald T. Ankley & David C. Bencic. 2016. Fish connectivity mapping: linking chemical stressors by their mechanisms of action-driven transcriptomic profiles. BMC Genomics volume 17, Article number: 84

Rong-Lin Wang, Stephen Edwards, Cataia Ives. 2019. Ontology-based semantic mapping of chemical toxicities. Toxicology, Volume 412, Pages 89-100

The author agrees with his or her designated percentage of contribution as listed below

Authors	Organization	Percentage of contribution	Yes / No	Author initials

Rong-Lin Wang	US EPA	47.5%	Yes ☐/No ☐	
Adam Biales	US EPA	6.25%	Yes ☐/No ☐	
Natalia Garcia-Reyero	US Army Corps	6.25%	Yes ☐/No ☐	
Edward J. Perkins	US Army Corps	6.25%	Yes ☐/No ☐	
Daniel L. Villeneuve	US EPA	6.25%	Yes ☐/No ☐	
Gerald T. Ankley	US EPA	6.25%	Yes ☐/No ☐	
David C. Bencic	US EPA	6.25%	Yes ☐/No ☐	
Steve Edwards	RTI International	7.5%	Yes ☐/No ☐	
Cataia Ives	RTI International	7.5%	Yes ☐/No ☐	
		100.00%		

Rong-Lin Wang, Ph.D
Great Lakes Toxicology & Ecology Division / Center for Computational Toxicology & Exposure
Office of Research & Development / US EPA
26 W Martin Luther King Dr., Cincinnati, OH 45268
AWL: 513-426-6468, Cell: 858-414-1021
Office: 513-569-7862, Fax: 513-569-7757

From: Wang, Rong-Lin
Sent: Thursday, April 16, 2020 5:10 PM
To: Biales, Adam <Biales.Adam@epa.gov>; Bencic, David <Bencic.David@epa.gov>; Villeneuve, Dan (Villeneuve.Dan@epa.gov) <Villeneuve.Dan@epa.gov>; Ankley, Gerald <Ankley.Gerald@epa.gov>; Perkins, Edward J SES ERDC-RDE-EL-MS <Edward.J.Perkins@erdc.dren.mil>; natalia.g.vinas@erdc.dren.mil; Edwards, Steve <swedwards@rti.org>; Ives, Cataia <cives@rti.org>
Subject: STAA2020 Record of Percentage Agreement

Hello Everyone,

I would like to submit the two publications as a joint package for STAA 2020, one on fish connectivity mapping from 2016 and the other on semantic mapping from 2019. They fit nicely together under the theme of mapping chemical toxicities by phenotypic profiles. Another driver is that the Cmap paper is going to be timed out next year for STAA. You are all coauthors on either one of the two papers. As required, I need your consent with regard to author contributions before I can apply.

Could you take a quick look at the attached table, check off the box and put in your initials beside your name? The percentages I put down are quite arbitrary

and hopefully agreeable with everybody. The only constraint is that EPA folks have to account for more than 50% for a paper to be eligible. Please send me your response soon. The final deadline is April 30.

Thanks much and best regards,

Rong-Lin Wang, Ph.D
Great Lakes Toxicology & Ecology Division / Center for Computational Toxicology & Exposure
Office of Research & Development / US EPA
26 W Martin Luther King Dr., Cincinnati, OH 45268
AWL: 513-426-6468, Cell: 858-414-1021
Office: 513-569-7862, Fax: 513-569-7757

Table of Contents

General_Authors_Publications.....2
LI-266322_Wambaugh-2015-TKTriage.....16
Wambaugh-2015-TKTriage.....29
Triage-2020-Thomas-STAA.....42
Triage-2020-Tropsha-STAA.....43
Triage-2020-Bosgra-STAA.....44
Triage-2020-Wetmore-STAA.....45
Triage-2020-Setzer-STAA.....46
Triage-2020-Shah-STAA.....47
Triage-2020-Strope-STAA.....48
Triage-2020-Pearce-STAA.....49
Triage-2020-Goldsmith-STAA.....50
Triage-2020-Judson-STAA.....51
Triage-2020-Sluka-STAA.....52
Triage-2020-Sedykh-STAA.....53
Triage-2020-Wambaugh-STAA.....54

United States Environmental Protection Agency
Washington, DC 20460

STAA REPORT FOR THE SCIENTIST NOMINATIONS

General Information:

Nomination ID/App ID:	20-090
Research Category Primary:	Health Effects Research and Human Health Risk Assessment (HE)
Research Category Secondary:	
Laboratory/Office Name:	CCTE/ORD
Nomination Entered By:	John Wambaugh

Eligibility Checklist:

[Y] The nominated publication(s) has not been submitted to a previous STAA competition.

[Y] The nominated publication(s) was published on or before January 1, 2017 and on or after January 1,2012

[Y] The principal author was an EPA employee or a PHS employee assigned to EPA when the research was performed

[Y] The EPA authors (includes PHS employees assigned to EPA) contributed collectively a minimum of 50% toward the publication(s)

Nominating Official Name:	Michael Devito
Nominating Official Title:	
Nominating OfficialEmail:	devito.michael@epa.gov
STAA Coordinator Name:	Kathleen Wiser
STAA Coordinator Email:	wiser.kathi@epa.gov

Justifications:

Justification 1:

Toxicokinetics describes the absorption, distribution, metabolism, and excretion of chemicals by the body. Toxicokinetics provides critical information for connecting chemical exposures to potential toxicities to characterize potential chemical risk to the public health. *In vitro* methods for toxicokinetics were developed by the pharmaceutical industry to help design more successful clinical trials and typically produce results within a factor of three of what is observed in subsequent clinical trials. *In vitro* toxicokinetic methods have been adapted by EPA and collaborators for non-pharmaceutical chemicals occurring in commerce and the environment. They offer animal-free new approach methodologies (NAMs) for rapidly and inexpensively determining toxicokinetics. However, since non-pharmaceutical chemicals will never be evaluated in a clinical trial, we must carefully assess the certainty in the predictions of these *in vitro* toxicokinetic NAMs.

The late Kenny Rogers famously sang “You've got to know when to hold 'em, Know when to fold 'em, Know when to walk away, And know when to run.” Traditional, *in vivo* methods are resource-intensive and often involve many laboratory animals. *In vitro* methods for toxicokinetics present a tantalizing opportunity to replace and/or augment traditional methods; however, you must know when they are likely to work, and when they may fail.

In this manuscript the authors describe the use of a machine learning technique (the method of random forests) to classify chemicals in the ToxCast screening program into categories based on the accuracy of toxicokinetic NAMs. This is accomplished by comparing predictions based on toxicokinetic NAMs with quantities from *in vivo* toxicokinetic studies. Machine learning was used to associate the size of error in the predictions with chemical features including physico-chemical properties, predictions of affinity for key cellular transporters, and the *in vitro* measured values themselves. Effectively this analysis predicted the “domain of applicability” of toxicokinetic NAMs. This domain of applicability separates those chemicals for which toxicokinetic NAMs are expected to be successful from those chemicals for which these methods are likely to fail. The analysis showed that the errors were expected to be like pharmaceuticals (within a factor of three) for roughly half of the ToxCast chemicals. For most of the remaining chemicals, errors were predicted to be conservative (over-stating risk). However, two important classes of chemicals – chemicals with long half-lives in general, and perfluoroalkyl substances (PFAS) in particular – were shown to have larger errors.

This manuscript deserves Agency-wide recognition because it characterized the uncertainty of toxicokinetic NAMs and placed them into an overall workflow ("toxicokinetic triage") for integrating NAMs with traditional toxicokinetic approaches. From a technological perspective, this manuscript is one of the first at the Agency to use machine learning to solve a public health problem by providing clear criteria for making scientifically sound decisions regarding when toxicokinetic NAMs are sufficient and when animal testing still may be warranted. The factors that were associated with unreliable results also provided guidance for ongoing Agency research to improve toxicokinetic NAMs. The Agency has relied upon the results published in this manuscript as justification to continue to develop and use NAMs for toxicokinetics, as indicated in the planned or proposed activities for the Toxic Substances Control Act, Endocrine Disruptor Screening Program, Office of Pesticide Programs, and Office of Land and Emergency Management, Moreover, based largely on the credibility provided by the Agency's work, *in vitro* toxicokinetic NAMs are now used by regulatory agencies in state governments and around the world, including Canada and the European Union.

First century philosopher Seneca wrote that "Luck Is what happens when preparation meets opportunity" – by using machine learning to predict when toxicokinetic NAMs are likely to succeed this research allows the Agency to make more rapid and accurate assessments of chemical toxicokinetics.

Justification 2A:

n/a

Justification 2B:

John Wambaugh

"Linking high resolution mass spectrometry data with exposure and toxicity forecasts to advance high-throughput environmental monitoring" and "Integrating tools for non-targeted analysis research and chemical safety evaluations at the US EPA", 2020, submitted

“Characterization and prediction of chemical functions and weight fractions in consumer products” and "High-throughput screening of chemicals as functional substitutes using structure-based classification models”, 2019, Level III award

"ToxCast chemical landscape: paving the road to 21st century toxicology”, 2019, Level III award

"SHEDS-HT: an integrated probabilistic exposure model for prioritizing exposures to chemicals with near-field and dietary sources” and "High-throughput dietary exposure predictions for chemical migrants from food contact substances for use in chemical prioritization", 2019, Level III award

"Comparison of modeling approaches to prioritize chemicals based on estimates of exposure an exposure potential", "A decision analytic approach to exposure-based chemical prioritization", and "Advances on a Decision Analytic Approach to ExposureBased Chemical Prioritization", 2019, Honorable Mention

"High throughput heuristics for prioritizing human exposure to environmental chemicals.", 2015, Level III award

Richard Judson

“Linking high resolution mass spectrometry data with exposure and toxicity forecasts to advance high-throughput environmental monitoring.” and “Integrating tools for non-targeted analysis research and chemical safety evaluations at the US EPA”, 2020, submitted

“An "EAR" on Environmental Surveillance and Monitoring: A Case Study on the Use of Exposure-Activity Ratios (EARs) to Prioritize Sites, Chemicals, and Bioactivities of Concern in Great Lakes Waters” and “Potential toxicity of complex mixtures in surface waters from a nationwide survey of United States streams: Identifying in vitro bioactivities and causative chemical”, 2020, submitted

“Development and deployment of a high-throughput assay to detect chemical disruptors of thyroid hormone synthesis”, 2019, Level I award

"ToxCast chemical landscape: paving the road to 21st century toxicology”, 2019, Level III award

Russell Thomas

"ToxCast chemical landscape: paving the road to 21st century toxicology”, 2019, Level III award

Woodrow Setzer

"High throughput heuristics for prioritizing human exposure to environmental chemicals.", 2015, Level III

Justification 2C:

This submission focuses on the application of machine learning to predict uncertainty in high throughput toxicokinetics. None of the previous and current

nominations involve high throughput toxicokinetics. Only one, the 2019 nomination on predicting chemical functions, involved machine learning, but with a different focus -- predicting how chemicals might be used from structure (previous nomination) instead of predicting confidence in high throughput toxicokinetic predictions (this nomination). Only one previous nomination focused on uncertainty analysis, but for a very different problem: the 2015 nomination developed high throughput predictions for chemical exposure (intake rates). The methods, problem, and impact on decision making of this nomination are distinct from all previous and current nominations.

Justification 2D:

n/a

Justification 2E:

Two authors on this submission are included on other submissions. The first of the other submissions describe work on analysis of features in mass spectrometry data and has no relation to this submission. The second of the other submissions involves aquatic toxicity and effects-driven analysis and has no relation to this submission.

Justification 3A:

The Society of Toxicology Board of Publications selected this manuscript as one of four Honorable Mention winners for 2017 Paper of the Year.

The manuscript was also discussed in the "The impact of novel assessment methodologies in toxicology on green chemistry and chemical alternatives" by Rusyn, Ivan, and Nigel Greene.

(Toxicological Sciences 161.2 (2018): 276-284):

“The following are examples of approaches that make use of in vitro data in human health assessments that also are useful with respect to assessments of alternatives:

4. The use of toxicokinetic information as a sufficient consideration in and of itself to enable rapid decisions on the risk of chemicals has been extended by Wambaugh et al. (2015) through the proposal for high-throughput physiologically based toxicokinetic model that predicts nonsteady-state chemical concentration time-courses for a variety of exposure scenarios. The authors used this model to propose a 4-element framework for chemical toxicokinetic triage that can group chemicals into categories based on varying levels of confidence in predictions of exposure, an approach that may be useful for triaging chemicals for which high-throughput toxicokinetic predictions may be sufficient, and identifying those that may require additional experiments to collect appropriate data."

Justification 3B:

Prior to submission to a journal, the methods presented in the publication were examined by a Federal Insecticide, Fungicide, and Rodenticide Act Scientific Advisory Panel as part of the topic "New High Throughput Methods to Estimate Chemical Exposure".

The manuscript was then submitted to the journal Toxicological Sciences where it was peer-reviewed by three anonymous reviewers. A revision was requested and created and re-reviewed by the same peer reviewers prior to acceptance for publication in Toxicological Sciences.

The Society of Toxicology Board of Publications reviewed papers published in Toxicological Sciences, nominated them for consideration, and then chose award recipients. This publication was selected as one of four Honorable Mention winners for 2017 Paper of the Year.

AUTHORS

Contributing Author

Author Name:	Barbara Wetmore		
Professional Title:		Salutation:	Dr.
Email:	wetmore.barbara@epa.gov	Organization:	
Mailing Address:			
Street Line 1:			
City:			
Zip Code:		State:	
At time of research was:	EPA Employee		
Separation Date:			
% of Effort:	5		

Contributing Author

Author Name:	Robert Pearce		
Professional Title:		Salutation:	Mr.
Email:	robertgraftonpearce@gmail.com	Organization:	
Mailing Address:			
Street Line 1:			
City:			
Zip Code:		State:	
At time of research was:	Non EPA Personnel		
Separation Date:			
% of Effort:	10		

Contributing Author

Author Name:	Cory Strope		
Professional Title:		Salutation:	Dr.
Email:	strope.cory@epa.gov	Organization:	
Mailing Address:			
Street Line 1:			
City:			
Zip Code:		State:	
At time of research was:	Non EPA Personnel		
Separation Date:			
% of Effort:	4		

Contributing Author

Author Name:	Rocky Goldsmith		
Professional Title:		Salutation:	Dr.
Email:	rocky.goldsmith@gmail.com	Organization:	
Mailing Address:			
Street Line 1:			
City:			
Zip Code:		State:	
At time of research was:	EPA Employee		
Separation Date:	Tue Apr 01 00:00:00 GMT 2014		
% of Effort:	4		

Contributing Author

Author Name:	Alexander Sedykh		
Professional Title:		Salutation:	Dr.
Email:	sunirks@gmail.com	Organization:	
Mailing Address:			
Street Line 1:			
City:			
Zip Code:		State:	
At time of research was:	Non EPA Personnel		
Separation Date:			
% of Effort:	10		

Contributing Author

Author Name:	James Sluka		
Professional Title:		Salutation:	Dr.
Email:	jsluka@indiana.edu	Organization:	
Mailing Address:			
Street Line 1:			
City:			
Zip Code:		State:	
At time of research was:	Non EPA Personnel		
Separation Date:			
% of Effort:	4		

Contributing Author

Author Name:	Alex Tropsha		
Professional Title:		Salutation:	Prof.
Email:	alex_tropsha@unc.edu	Organization:	
Mailing Address:			
Street Line 1:			
City:			
Zip Code:		State:	
At time of research was:	Non EPA Personnel		
Separation Date:			
% of Effort:	4		

Contributing Author

Author Name:	Sieto Bosgra		
Professional Title:		Salutation:	Dr.
Email:	sietobosgra@gmail.com	Organization:	
Mailing Address:			
Street Line 1:			
City:			
Zip Code:		State:	
At time of research was:	Non EPA Personnel		
Separation Date:			
% of Effort:	10		

Contributing Author

Author Name:	Richard Judson		
Professional Title:		Salutation:	Dr.
Email:	judson.richard@epa.gov	Organization:	
Mailing Address:			
Street Line 1:			
City:			
Zip Code:		State:	
At time of research was:	EPA Employee		
Separation Date:			
% of Effort:	5		

Contributing Author

Author Name:	Russell Thomas		
Professional Title:		Salutation:	Dr.
Email:	thomas.russell@epa.gov	Organization:	
Mailing Address:			
Street Line 1:			
City:			
Zip Code:		State:	
At time of research was:	EPA Employee		
Separation Date:			
% of Effort:	10		

Contributing Author

Author Name:	Woodrow Setzer		
Professional Title:		Salutation:	Dr.
Email:	setzer.woodrow@epa.gov	Organization:	
Mailing Address:			
Street Line 1:			
City:			
Zip Code:		State:	
At time of research was:	EPA Employee		
Separation Date:			
% of Effort:	10		

Contributing Author

Author Name:	Imran Shah		
Professional Title:		Salutation:	Dr.
Email:	shah.imran@epa.gov	Organization:	
Mailing Address:			
Street Line 1:			
City:			
Zip Code:		State:	
At time of research was:	EPA Employee		
Separation Date:			
% of Effort:	4		

Principal Author

Author Name:	John F. Wambaugh		
Professional Title:		Salutation:	
Email:	wambaugh.john@epa.gov	Organization:	
Mailing Address:			
Street Line 1:			
City:			
Zip Code:		State:	
At time of research was:	EPA Employee		
Separation Date:			
% of Effort:	20		

PUBLICATIONS

Publication 1:

Publication Title:	Toxicokinetic Triage for Environmental Chemicals		
Publication Date:	Tue Jun 16 00:00:00 GMT 2015		
Journal/Publication Method:	Toxicological Sciences		
All Author(s):			
Volume:	147	Number:	1
Pages:	55-67	Immediately Index:	Immediately Index:
Citation ½ Life:	8.9	Impact Factor:	3.564

OXFORD

SOT | Society of Toxicology
www.toxsci.oxfordjournals.org

TOXICOLOGICAL SCIENCES, 147(1), 2015, 55–67

doi: 10.1093/toxsci/kfv118
Advance Access Publication Date: June 16, 2015
Research Article

Toxicokinetic Triage for Environmental Chemicals

John F. Wambaugh*,[1], Barbara A. Wetmore†, Robert Pearce*, Cory Strope*,‡, Rocky Goldsmith§, James P. Sluka¶, Alexander Sedykh||, Alex Tropsha||, Sieto Bosgra|||, Imran Shah*, Richard Judson*, Russell S. Thomas*, R. Woodrow Setzer*

*National Center for Computational Toxicology and §National Exposure Research Laboratory, Office of Research and Development, US EPA, Research Triangle Park, North Carolina 27711; †The Hamner Institutes for Health Sciences, Research Triangle Park, North Carolina 27709-2137; ‡Oak Ridge Institute for Science and Education Grantee P.O. Box 117, Oak Ridge, Tennessee 37831-0117, United States; ¶Biocomplexity Institute, Indiana University, Bloomington, Indiana 47405-7105; ||Department of Chemical Biology and Medicinal Chemistry, University of North Carolina, Chapel Hill, North Carolina 27955-7568; and |||The Netherlands Organisation for Applied Scientific Research (TNO), 3700 AJ Zeist, The Netherlands

[1]To whom correspondence should be addressed at National Center for Computational Toxicology, Office of Research and Development, US EPA, 109 T.W Alexander Dr., Research Triangle Park, North Carolina 27711. Fax: (919) 541-1194. E-mail: Wambaugh.john@epa.gov.

Disclaimer: The views expressed in this publication are those of the authors and do not necessarily represent the views for policies of the U.S. Environmental Protection Agency. Reference to commercial products or services does not constitute endorsement.

Downloaded from http://toxsci.oxfordjournals.org/ at Environmental Protection Agency Library on September 23, 2015

ABSTRACT

Toxicokinetic (TK) models link administered doses to plasma, blood, and tissue concentrations. High-throughput TK (HTTK) performs *in vitro* to *in vivo* extrapolation to predict TK from rapid *in vitro* measurements and chemical structure-based properties. A significant toxicological application of HTTK has been "reverse dosimetry," in which bioactive concentrations from *in vitro* screening studies are converted into *in vivo* doses (mg/kg BW/day). These doses are predicted to produce steady-state plasma concentrations that are equivalent to *in vitro* bioactive concentrations. In this study, we evaluate the impact of the approximations and assumptions necessary for reverse dosimetry and develop methods to determine whether HTTK tools are appropriate or may lead to false conclusions for a particular chemical. Based on literature *in vivo* data for 87 chemicals, we identified specific properties (*eg, in vitro* HTTK data, physico-chemical descriptors, and predicted transporter affinities) that correlate with poor HTTK predictive ability. For 271 chemicals we developed a generic HT physiologically based TK (HTPBTK) model that predicts non-steady-state chemical concentration time-courses for a variety of exposure scenarios. We used this HTPBTK model to find that assumptions previously used for reverse dosimetry are usually appropriate, except most notably for highly bioaccumulative compounds. For the thousands of man-made chemicals in the environment that currently have no TK data, we propose a 4-element framework for chemical TK triage that can group chemicals into 7 different categories associated with varying levels of confidence in HTTK predictions. For 349 chemicals with literature HTTK data, we differentiated those chemicals for which HTTK approaches are likely to be sufficient, from those that may require additional data.

Key words: toxicokinetics; high throughput; environmental chemicals; IVIVE

Of the 30 000 chemicals that are estimated to be in wide commercial use, only a small subset has been characterized as to their potential toxicological effects in humans or wildlife (Judson *et al.*, 2008; National Research Council, 1984; USGAO, 2013). High-throughput screening (HTS) using *in vitro* assays, eg, the ToxCast and Tox21 programs, has been proposed as one

Published by Oxford University Press on behalf of Society of Toxicology 2015. This work is written by US Government employees and is in the public domain in the US.

approach to fill these data gaps by analyzing the activity of these chemicals across a broad range of potential biological targets (Bucher, 2008; Judson *et al.*, 2010). One challenge associated with the interpretation of the HTS data has been relating *in vitro* bioactive concentrations with relevant *in vivo* dose values, and doing so on a scale and throughput required to address the large number of chemicals (Judson *et al.*, 2011; Rotroff *et al.*, 2010; Thomas *et al.*, 2013; Tonnelier *et al.*, 2012; Wambaugh *et al.*, 2013, 2014; Wetmore *et al.*, 2012).

For pharmaceutical compounds, *in vitro* to *in vivo* extrapolation (IVIVE) methods have been developed to parameterize toxicokinetic (TK) models that relate blood and tissue concentrations to therapeutic doses for clinical studies. The IVIVE methods typically include limited *in vitro* measurements of hepatic clearance, plasma protein binding, and chemical structure-derived predictions of tissue partitioning (Jamei *et al.*, 2009; Lukacova *et al.*, 2009). The IVIVE methods and resulting TK models are considered effective since the predicted concentrations are often (Wang, 2010) within ~3-fold of the *in vivo* observations (we describe predictions as being "on the order of magnitude" if they are within $\sqrt{10} \approx 3.2$–fold). Ultimately, the human TK of a pharmaceutical compound may be fully characterized in follow-on human clinical trials (Jamei *et al.*, 2009), which is vastly different from the data available for environmental and industrial chemicals where both ethical and cost considerations preclude human testing.

The IVIVE methods developed for pharmaceuticals have been used to parameterize high-throughput TK (HTTK) models for hundreds of environmental and industrial chemicals (Rotroff *et al.*, 2010; Tonnelier *et al.*, 2012; Wetmore *et al.*, 2012, 2013, 2014). The primary example of the application of HTTK models has been to estimate the doses (mg/kg BW/day) needed to produce steady-state plasma concentrations (C_{ss}, in units of μM) equivalent to concentrations that produce bioactivity in *in vitro* assays—this process is often described as "reverse dosimetry" (Rotroff *et al.*, 2010; Tonnelier *et al.*, 2012; Wetmore *et al.*, 2012, 2013, 2014). Reverse dosimetry with HTTK models can provide estimated doses for environmental and industrial chemicals below which significant *in vitro* bioactivity is not expected to occur (Judson *et al.*, 2011; Wetmore *et al.*, 2012). The ratio between the lowest bioactive dose and the maximal expected exposure provides risk-based context to HTS data and is one metric for prioritization of additional chemical testing (Judson *et al.*, 2011; Thomas *et al.*, 2013; Wetmore *et al.*, 2012).

When benchmarked against a limited number of environmental, pesticidal, and industrial chemicals with *in vivo* TK data, HTTK models have demonstrated mixed success, but have generally provided health-protective estimates of bioactive doses (Wetmore *et al.*, 2012; Yoon *et al.*, 2014). The reasons for the discrepancies between steady-state concentrations predicted using HTTK and the concentrations from *in vivo* TK data are not clear. There may be extrapolation issues for environmental chemicals that are not present with pharmaceuticals.

This study evaluated the accuracy of HTTK predictions that were made using the same physiologically motivated, 3-compartment mathematical TK model previously used in reverse dosimetry studies (Rotroff *et al.*, 2010; Tonnelier *et al.*, 2012; Wetmore *et al.*, 2012, 2013, 2014). This assessment was conducted across the 349 chemicals for which the appropriate inputs and data were available. Of these, ~80% of the chemicals (ie, 271), possessed required inputs to parameterize a generic high-throughput physiologically based toxicokinetic (HTPBTK) mathematical model that we employed to test some of the assumptions used in the HTTK-based reverse dosimetry approach for environmental chemicals. HTTK model predictions were further evaluated using available human and rat *in vivo* measurements curated from TK literature.

We found that some properties of pharmaceutical and environmental chemicals correlated with either small or large discrepancies between HTTK predictions and *in vivo*-derived values. Those properties define a "domain of applicability" of chemical property space within which HTTK models may be expected to provide an adequate alternative to more traditional TK methods for reverse dosimetry and other applications. The results of our analyses were integrated into a multi-element TK triage system that organizes chemicals into different categories based on varying degrees of accuracy (eg, on the order, 10× over-estimated, 10× underestimated) of the HTTK predictions with additional categories for situations where more data or alternative approaches are needed to develop suitable TK models. Depending on the accuracy needed for a specific application and the degree of confidence for a particular prediction, this triage system separates those chemicals with which HTTK may be used with confidence from those chemicals that may benefit from specific types of analyses and/or additional experimental data collection.

MATERIALS AND METHODS

In this study, we first replicated the steady-state TK model used in previous studies and developed a new model allowing exploration of the impact of the steady-state assumption. We used these models to analyze the soundness of assumptions used in previous reverse dosimetry HTTK applications as exemplified by the Wetmore *et al.* (2012) study. We then applied statistical methods to determine the chemical-specific properties that correlate with HTTK predictive ability. Among the chemical-specific properties examined, we investigated xenobiotic transporter affinities predicted using quantitative structure–activity relationships (QSAR). The methods and data used for our analysis of HTTK have been made available as a package for the open source R statistical analysis software platform (R Development Core Team, 2013). The package, "httk," can be accessed from the Comprehensive R Archive Network (CRAN) repository (http://cran.r-roject.org/web/packages/httk/, last accessed 22 June 2015). All chemical-specific parameters are listed in Supplementary Table 1 with references.

TK models used. Two general (ie, chemical independent) TK models were used. The first model was intended to replicate the model used in previous reverse dosimetry analyses (Rotroff *et al.*, 2010; Wetmore *et al.*, 2012, 2013). Those analyses were performed using the SimCyp software (Jamei *et al.*, 2009). The first model (illustrated in Supplementary Fig. 1) was a physiologically motivated "3-compartment" model for determining plasma concentrations that assumed no tissue partitioning, elimination due to metabolism of the parent compound in the liver, renal elimination by passive glomerular filtration (GF), and is adjusted for plasma protein binding [ie, GF rate (GFR) × fraction of chemical unbound in plasma]. Metabolism in this model is comparable to the "well-stirred" approximation for hepatic metabolism (Wilkinson and Shand, 1975).

The second general TK model (illustrated in Supplementary Fig. 2) was physiologically based (PBTK) with separate tissue compartments for the gut, liver, lung (unused for dosing in this research, since the inhalation route was not simulated), kidneys, and arterial and venous blood. The rest of the tissues in the body were aggregated. Tissue volumes and blood flows were

Downloaded from http://toxsci.oxfordjournals.org/ at Environmental Protection Agency Library on September 23, 2015

taken from Birnbaum *et al.* (1994). Tissue flows and volumes were scaled to cardiac output and body weights from Davies and Morris (1993), which also provided values for GFR and hematocrit. Absorption from the gut lumen into gut tissue was modeled as a first-order process with an arbitrary, "fast" rate of 1/h. Venous blood from the gut and arterial blood fed separately into the liver, where metabolism was again modeled with the "well-stirred" approximation.

Physico-chemical and partitioning information were collated from various sources. Molecular weight and structure were determined from the DSStox database (http://www.epa.gov/ncct/dsstox, last accessed 22 June 2015) and hydrophobicity was drawn for all compounds from EPI Suite (http://www.epa.gov/opptintr/exposure/pubs/episuite.htm (last accessed 22 June 2015)—measured values used if available, predicted otherwise). Where available, ionization association/dissociation equilibrium constants were curated from the literature; otherwise predictions were based on chemical structure using the SPARC (SPARC Performs Automated Reasoning in Chemistry) model (Hilal *et al.*, 1995). Experimental values for membrane affinities (ie, lipid-bilayer to water concentration ratios) were used where available (Endo *et al.*, 2011) or predicted using a regression of the Endo *et al.* (2011) data based on hydrophobicity and temperature:

$$\log_{10}(K_{npl:water}) = 0.999831 - 0.016578 \times T + 0.881721 \times \log_{10}(K_{octanol:water}),$$

where T is the temperature (°C), $K_{npl:water}$ is the neutral phospholipid-to-water concentration ratio, and $K_{octanol:water}$ is the octanol-to-water concentration ratio.

Chemical-specific tissue to free fraction in plasma partition coefficients were predicted using Schmitt's method (2008a). Tissue-specificity was based upon the cellular fraction of total volume; water, lipid and protein fraction of cellular volume; and distribution of types of lipid (Schmitt, 2008b). Chemical-specificity was based upon plasma protein binding (fup), the hydrophobicity, and any ionization association/dissociation constants. Because we do not have a method for estimating the rate at which chemicals diffuse into tissues, we assumed that all tissues were perfusion-limited; ie, chemical concentrations in tissue, red blood cells, and plasma come to equilibrium instantaneously relative to the flow of blood.

Determination of steady state. We use the term "steady-state" to describe the situation where the chemical concentration in plasma caused by the assumed exposure scenario is unchanging in time. With the assumption of constant infusion dosing, as in Wetmore *et al.* (2012), this is a true steady-state. With constant infusion dosing the flow of chemical into the body is matched perfectly by clearance from the body. For dynamic exposure scenarios (such as exposures separated by time intervals), a quasi-steady-state is determined to occur if the plasma concentration effectively no longer increases across a fixed time interval. For example, if plasma concentration is the same just before the next dose as it was before the current dose, this is quasi-steady-state.

In order to determine if steady-state conditions were achieved, 2 analytic equations were derived from the differential equations of the 3-compartment TK and PBTK models by assuming constant infusion dosing. The analytic solution to the 3-compartment TK model is the equation used for steady-state plasma concentrations (C_{ss}) in previous work (Rotroff *et al.*, 2010; Wetmore *et al.*, 2012, 2013; Wilkinson and Shand, 1975). For the PBTK model, equations were solved numerically to simulate a series of repeated, every 8-h oral doses until the daily averaged venous concentration, just before re-dosing, was within a small tolerance (1%) of the concentration predicted with the analytical solution of the PBTK model. The PBTK simulations assume an initial body burden of no chemical, even though this may not be the case for certain persistent, bioaccumulating, or endogenous chemicals. The equations for the analytic solutions are given in the captions to Supplementary Figures 1 and 2.

In vitro chemical data. *In vitro* data used in this study was extracted from published literature. For environmental, pesticidal, and industrial chemicals, *in vitro* experimental data were obtained primarily from Wetmore *et al.* (2012) and Tonnelier *et al.* (2012). For pharmaceutical compounds these values were compiled from Obach (1999), Jones *et al.* (2002), Shibata *et al.* (2002), Lau *et al.* (2002), Naritomi *et al.* (2003), Ito and Houston (2004), McGinnity *et al.* (2004), Schmitt (2008a), and Obach *et al.* (2008).

Two types of *in vitro* data were extracted in order to parameterize the TK models—intrinsic hepatic clearance and plasma protein binding. The intrinsic metabolic clearance of the parent compound (CL_{int}) by primary hepatocytes (substrate depletion approach) was measured in wells on a multi-compound plate (Shibata *et al.*, 2002). Since only the unbound chemical in the hepatic clearance assay is available for metabolism, CL_{int} was determined from the observed clearance (CL_{uint}) which was divided by the estimated fraction of chemical unbound in the hepatocyte intrinsic clearance assay (f_{uhep}), as estimated using the method of Kilford *et al.* (2008). The Kilford *et al.* (2008) method includes a distribution coefficient estimated from hydrophobicity and ionization. In Wetmore *et al.* (2012), 2 chemical concentrations (1 and 10 μM) were tested, in part to test for saturation of metabolism. We have used only the 1 μM values. Fraction of chemical unbound in the presence of plasma protein (f_{up}) was assessed using rapid equilibrium dialysis (RED) in which 2 wells are separated by a membrane that is permeable to smaller molecules but prevents the plasma protein from migrating from one well to the other (ie, the relative chemical concentration in the 2 linked wells gives the free fraction of chemical) (Waters *et al.*, 2008).

Monte Carlo simulation and parameter distributions. Previous reverse dosimetry analyses (Rotroff *et al.*, 2010; Wetmore *et al.*, 2012) used the SimCYP software (Jamei *et al.*, 2009) to perform a Monte Carlo (MC) simulation of human variability and we have implemented a similar MC simulation ability. To match the assumptions used by SimCYP, normal distributions that were truncated to ensure positive values were used with mean values drawn from the references above and a coefficient of variation of 0.3. Body weight, liver volume, hepatic blood flow, glomerular filtration rate, and CL_{uint} were all varied in this manner. In a change from previous MC simulations, the values for protein binding, f_{up}, were drawn from a censored normal distribution: values were sampled from a uniform distribution between 0% and the limit of detection (LOD) (default of 1% unbound) at a rate proportional to the number of samples from the truncated normal distribution below the LOD. For each chemical, 1000 different combinations of parameters were used to determine C_{ss}, allowing estimation of the 5th, median, and 95th percentiles.

In vivo chemical data. In Wetmore *et al.* (2012), *in vivo* TK and PBTK modeling data for the environmental, pesticidal, and industrial chemicals were collected from the literature and used

Downloaded from http://toxsci.oxfordjournals.org/ at Environmental Protection Agency Library on September 23, 2015

to assess the predictive ability of the human *in vivo* C_{ss} estimation, assuming a 1 mg/kg/day daily oral administration. For pharmaceutical compounds, the measured human clearance (l/day) and volume of distribution (l) in Obach *et al.* (2008) was used to determine C_{ss} for the same dose.

Model compounds for rat IVIVE were chosen based on the availability of HTTK input parameters CL_{uint} and f_{up}. A list was constructed from Ito and Houston (2004), complemented by a group of compounds to which reverse dosimetry was applied in earlier studies (Krug *et al.*, 2013; Piersma *et al.*, 2013). For these compounds, we searched public sources for studies reporting plasma concentration time course data in rat following oral or intravenous administration. Pharmacokinetic data were retrieved from those studies (Supplementary Table 2) by digitizing published figures using TechDig v2.0.

In silico transporter predictions. We used the method of Random Forest (Breiman, 2001) to develop QSAR predictions of transporter affinity (Sedykh *et al.*, 2013). We used the R package "randomForest" by Liaw and Weiner (2002). Experimental data characterizing interaction of chemicals with membrane transporters were compiled from multiple available public sources (Sedykh *et al.*, 2013). The chemicals were represented using Chemistry Development Kit descriptors (Steinbeck *et al.*, 2003) determined from Simplified Molecular-Input Line Entry System strings (Weininger, 1988). Chembench (Walker *et al.*, 2010) was used to standardize chemical structures as well as normalize chemical descriptors to range between 0 and 1. Inhibitors were defined based on a potency threshold of 10 μM except for peptide transporter 1 (PepT1), organic cation transporter 1 (OCT1), and organic anion-transporting polypeptide 2B1 (OATP2B1), for which 100 μM threshold was used due to lower levels of affinity of reported inhibitors. Scores equal to 0 or 1 imply high-confidence predictions that a chemical is a non-substrate or a substrate, respectively, whereas a score of 0.5 indicates an ambiguous prediction (Sedykh *et al.*, 2013). The full list of transporters modeled is identified in Supplementary Table 1, which also contains the QSAR predictions for each compound.

A second model, based upon Bayesian classification, was used to predict interactions of the compounds with organic anion transporter protein (OATP) 1B1 (Van de Steeg *et al.*, 2015). The classification model is based on a database recording the inhibitory potential of 640 FDA-approved drugs from a commercial library (10 μM) on the uptake of [3H]-estradiol-17beta-D-glucuronide (1 μM) in Human Embryonic Kidney 293 cells stably transfected with human OATP1B1. The structural similarity (feature-connectivity bit string 4) to the nearest similar chemical in this training set is used as a measure for potential interaction with OATP1B1. Although this model predicts inhibition of OATP1B1-mediated uptake rather than uptake itself, we assume here that the inhibition is mostly competitive and therefore identifies potential transporter substrates.

HTTK-in vivo discrepancy analysis. The Random Forest algorithm was used to analyze the correlation of chemical descriptors with the discrepancy between HTTK predictions and results based on *in vivo* data. The Random Forest method is cross validated (Breiman, 2001), performing multiple analyses based on different subsets of chemicals and different subsets of chemical descriptors. Fifty thousand regression trees were constructed using random subsets of the data, with a subset of 17 factors considered at each split in the tree, and a minimum terminal node size of 5. Performance of each regression tree was evaluated against the chemicals not used to build that tree. The most important factors in the random forest model were calculated using the method of decrease in node impurities (essentially, a leave 1 factor out method) (Archer and Kimes, 2008). We used the R package "rpart" by Therneau *et al.* (2014) to perform the method of recursive partitioning (Breiman *et al.*, 1984) to develop a regression tree for the full dataset (ie, not cross-validated). Finally, a random forests approach was used to construct a classifier tree for 5 exclusive categories ("on the order," "3.2× under-predicted," "10× under-predicted," "3.2×over-predicted," "10× over-predicted"), with a subset of 17 factors considered at each split, and a minimum terminal node size of 1.

RESULTS

Our HTTK models require chemical-specific data on CL_{int} and f_{up} to predict human C_{ss}. We obtained data from the peer-reviewed literature for a total of 349 chemicals. These chemicals include (non-uniquely) 312 Tox21 chemicals, 248 ToxCast chemicals, 74 pharmaceuticals, and 35 chemicals for which human exposure is monitored by the Centers for Disease Control National Health and Nutrition Examination Survey (CDC, 2012). The distribution of the non-zero values of the CL_{int} and f_{up} data is roughly log-normal and is similar across the curated literature (Supplementary Figs. 3 and 4).

Figure 1 illustrates our ability to reproduce the Wetmore *et al.* (2012) results. As in Wetmore *et al.* (2012), we simulated population variability to determine the median, lower 5th, and upper 95th percentile of plasma concentrations for individuals exposed to the same, fixed dose (1 mg/kg BW/day). Since the upper 95th percentile individuals have higher plasma concentrations for the same exposure, they are considered to be an example of a sensitive population. Any 1 chemical in Figure 1 is indicated by 3 plot points connected by a line. The 3 points correspond to the median, lower 5th, and upper 95th percentiles of

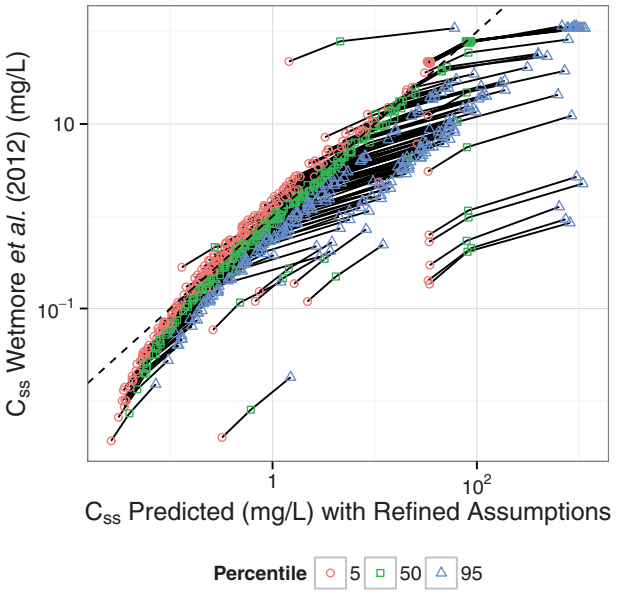

FIG. 1. Comparison of the median, upper, and lower 95th healthy adult human percentiles of steady-state plasma concentration (C_{ss}) predicted on the *y*-axis using SimCyp (Wetmore *et al.*, 2012) and on the *x*-axis using assumptions refined to better reflect screening for environmental chemicals. The C_{ss} values were estimated assuming a steady-state infusion of 1 mg/kg BW/day. Each chemical's median and upper and lower 95th percentiles are connected by a line. The dashed line indicates the identity (perfect predictor) line.

Downloaded from http://toxsci.oxfordjournals.org/ at Environmental Protection Agency Library on September 23, 2015

the C_{ss}. The dashed line indicates the identity (perfect predictor) line—the further a prediction is from the identity line the greater the discrepancy. We describe predictions with large discrepancies as "outliers."

There was good agreement ($R^2 = 0.84$) between our simulations and those in Wetmore *et al.* (2012) for all 3 percentiles. However, this comparison did identify 2 groups of outliers for which the predictions differ due to differing assumptions.

The first group of chemicals in Figure 1 with differing predictions is those that have an upper 95th percentile C_{ss} that was significantly higher than previously estimated, though the median and lower percentile values were unchanged. These chemicals are indicated in Figure 1 by a bent line connecting the 3 quantiles. This predicted difference indicates greater risk for the most sensitive individuals. This difference was due to replacing a default value with a censored distribution for chemicals with a failed RED assay for measuring f_{up} (protein binding). Among other reasons (eg, binding to membrane), the RED assay can fail because the amount of free chemical is below the LOD. In Wetmore *et al.* (2012), the RED assay failed for ~38% of the chemicals. For these chemicals, Wetmore *et al.* (2012) assumed a default value of 0.5% free (roughly half the average LODs). For the analysis shown in Figure 1, we have replaced this default value with a censored distribution in our MC variability simulation (essentially, simulating many different values between 0 and 1%).

There was a second group of chemicals in Figure 1 where the current modeling provided plasma concentration estimates different from Wetmore *et al.* (2012) due to a change in assumptions. This group contained chemicals where differences in the analysis of the hepatic clearance assay results led to different concentrations predicted for all 3 population percentiles in Figure 1 (ie, 3 quantiles connected by a line that are all distant from the identity line). Due to measurement variability and other factors, a linear model may not describe the decrease in parent chemical concentration as a function of time. Previously, a *P*-value threshold of .10 (probability of the null hypothesis of no disappearance of chemical was <10%) was used to determine if the chemical showed significant intrinsic clearance over the time examined. For the results shown in Figure 1, we have required that *P*-values be <.05. For those with a *P*-value >.05, we use a default value of 0 (ie, no hepatic clearance) which acts to increase the estimated plasma concentration for a fixed dose.

Most discrepancies between our predictions and Wetmore *et al.* (2012) disappear ($R^2 \sim 0.90$, Supplementary Fig. 5) if we replace our revised assumptions with the original assumptions of Wetmore *et al.* (2012). However, 8 discrepant chemicals remain due to issues such as the only C_{ss} available in Wetmore *et al.* (2012) was calculated using the 10 μM clearance data. The lone chemical for which we under-predict the value from Wetmore *et al.* (2012) for all 3 population percentiles is Chlorpyrifos-methyl, for which the 10 μM clearance assay was not statistically significant, leading Wetmore *et al.* (2012) to use 0 clearance. Since the clearance assays conducted at 1 μM was statistically significant, we used that value, leading to a larger predicted clearance.

Once we were satisfied that we could reproduce previous results for the majority of chemicals, and understood those cases where we differed, we proceeded to evaluate 3 key assumptions for the calculation of C_{ss}. Previously, chemical partitioning into tissues (eg, volume of distribution) was not determined from HTTK data, necessitating the use of C_{ss} as a dose metric because the concentration at steady-state does not depend on the amount of chemical in tissues. This means that we assume that humans reach steady state with respect to environmental exposures. Using the analytic solution for C_{ss} requires the further assumption of constant infusion dosing. Constant infusion dosing requires that we assume that steady-state plasma concentrations are a reasonable surrogate for peak concentrations which would be caused by other exposure scenarios (eg, exposure at meal times only). Further, constant infusion dosing requires either the assumption that 100% of the chemical is absorbed or the use of additional models to predict absorption. Wetmore *et al.* (2012) selected 100% absorption as being conservative (causing overestimated plasma concentration). By constructing non-steady-state, PBTK models, we can assess the plausibility of these 3 assumptions.

We developed HTPBTK models using Schmitt's method for tissue partitioning (Schmitt, 2008a). We used a generic PBTK model structure that could be parameterized for any chemical using CL_{int} and f_{up} and experimental or QSAR-derived physicochemical properties. Schmitt's method requires a value for protein binding in order to make predictions; therefore, we could only build HTPBTK models for 271 chemicals. Further assumptions about chemical absorption and bioavailability (ie, rapid absorption and 100% bioavailability) were required in order to parameterize the HTPBTK models.

Figure 2 illustrates our evaluation of the HTPBTK model predictions by comparison to literature *in vivo* time course data in rats for 22 chemicals. For a given chemical, the specific TK properties, dose, and route of administration result in different plasma concentration kinetics that we have summarized by the time-integrated plasma concentration (Area Under the Curve, AUC). Neglecting route of administration, we find that HTPBTK is predictive ($R^2 = 0.68$) of *in vivo* data (Fig. 2A). When we estimate a difference between oral exposures (which are subject to absorption and bioavailability) and intravenous and subcutaneous dose routes (which are not), we find slightly greater predictive ability ($R^2 = 0.73$). We systematically over-predict AUC for chemicals administered orally. The average difference between oral and intravenous doses is 6.4 (95% confidence interval 2.3–18), ie, on average AUCs from oral doses are roughly 6 times lower than predicted. This result indicates that the absorption assumptions we used for HTPBPTK are conservative and health protective since they produce higher predicted exposures. In Figure 2B, we show that peak plasma concentration (C_{max}) also appears to be well described by the HTPBTK model ($R^2 \sim 0.68$) and that there is a systematic bias toward over-prediction. The treatments that are over-estimated are predominantly for intravenous doses while predictions for oral doses are more evenly scattered about the identity line. The handful of cases where HTPBTK under-predicts C_{max} are all for oral administration.

Having established that our HTPBTK model predictions are consistent with the *in vivo* data that was available for 22 chemicals (Fig. 2), we conducted a simulation study to evaluate the assumptions used to calculate C_{ss} in previous HTTK reverse dosimetry analyses. In the simulation study, we replaced the infusion dose assumption with a dosing scenario of 3 daily doses totaling 1 mg/kg BW/day (eg, exposure at meal times or from consumer product use), to better reflect the near field sources of exposure that appear to be dominant for environmental chemicals (Wambaugh *et al.*, 2013). As illustrated in Figure 3A, 70% of chemicals (182 of 271) reach steady-state within 28 days, and 90% of chemicals (252 of 271) reach steady-state within 1000 days. However, there were 19 chemicals that required more than 1000 days to reach steady-state (Table 1). TK analyses based upon C_{ss} are inappropriate for these chemicals, suggesting a need for alternative approaches. Approaches based on dynamic TK simulation of the tissue concentrations

Downloaded from http://toxsci.oxfordjournals.org/ at Environmental Protection Agency Library on September 23, 2015

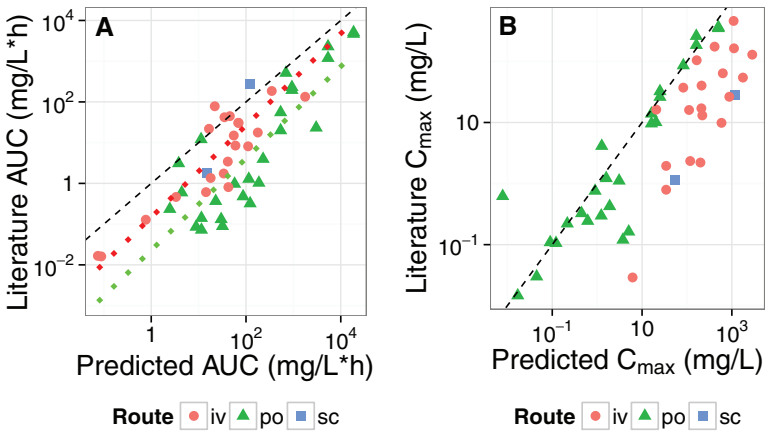

FIG. 2. Evaluation of the predictive ability of HTPBTK models by comparing predictions with *in vivo* measurements in the rat for the AUC (A) and C_{max} (B). Each chemical may have more than one study with potentially different doses and routes. Dose route is indicated by symbols (oral, po—triangle; intravenous, iv—circle; subcutaneous, sc – square). The upper dotted line is the linear regression for intravenous doses, while the lower dotted line is for the oral doses. The dashed line indicates the identity (perfect predictor) line.

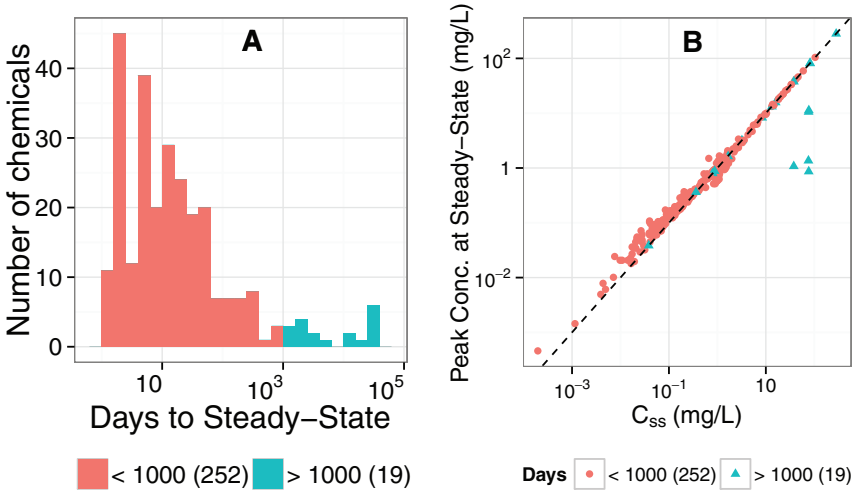

FIG. 3. HTPBTK simulation results evaluating the steady-state infusion assumption to predict C_{ss}. A, Histogram of number of chemicals versus the days needed to effectively reach steady-state assuming 3 daily doses (every 8 h). B, Comparison of peak plasma concentrations due to 3 daily does predicted with the HTPBTK model with the C_{ss} due to a constant infusion exposure as used in Figure 1 and previous reverse dosimetry studies. The dashed line indicates the identity (perfect predictor) line.

likely to be caused over a life-time of exposure may be more appropriate. The 5 chemicals that never reach steady-state (ie, the ratio of the simulated average daily concentration to the analytic C_{ss} never approaches 1) are polychlorinated biphenyls (PCBs), which are known to have long human half-lives (Ritter *et al.*, 2010) and are no longer deliberately in commerce.

With the HTPBTK models and more realistic exposure simulation, we then compared predicted peak concentrations with the C_{ss} derived from the analytical solution to the 3-compartment TK model (Fig. 1). As shown in Figure 3B, the peak concentration for repeated dosing is not different ($R^2 \sim 0.95$) from the C_{ss} predictions under the assumption of constant infusion dosing. Similarly, the average daily concentration at steady-state was nearly identical ($R^2 \sim 0.96$) to the analytical result for C_{ss} used in Wetmore *et al.* (2012) and elsewhere (Supplementary Fig. 6). For rapidly cleared compounds, the peak concentrations from 3 daily doses were within an order of magnitude of C_{ss}.

We then compared HTTK predictions of C_{ss} based on *in vitro* data with C_{ss} values inferred for humans from *in vivo* studies for 11 environmental chemicals (Wetmore *et al.*, 2012) and 74 pharmaceuticals (Obach *et al.*, 2008). Figure 4A illustrates that there is a weak predictive ability ($R^2 \sim 0.34$), but that the errors are mostly conservative (ie, the predicted plasma concentrations based on *in* vitro data are higher than the *in vivo* data indicates). When the perfluorinated chemicals (PFCs) are removed, the R^2 drops to ~0.23. We note that the correlation between the HTTK C_{ss} versus the C_{ss} inferred for humans from *in vivo* studies is lower than observed for AUC and C_{max} predictions in Figure 2. At steady-state, all C_{ss} values are compared for the same fixed dose rate of 1 mg/kg/day. When the HTPBTK predictions are normalized for administered dose, the R^2 for AUC and C_{max} drop to ~0.48 for both, indicating that a portion of the predictive ability of the HTPBTK might be due to the data varying linearly with dose for those chemicals.

Downloaded from http://toxsci.oxfordjournals.org/ at Environmental Protection Agency Library on September 23, 2015

TABLE 1. Chemicals Predicted to Require Long Time Periods to Reach Steady-State

Compound	CAS	Analytic C_{ss} (mg/l)	HTPBTK Average Daily Conc. (mg/l)	Ratio of HTPBTK to Analytic After 100 Years	Years to Steady-State	V_d (l)	K_{el} (h)
Fenpropathrin	39515-41-8	0.36	0.36	0.99	3.0	651.3	0.000162
Perfluorooctanoic acid	335-67-1	81.55	81.39	0.99	3.5	3.4	0.00015
Imazalil	35554-44-0	13.37	13.17	0.99	4.1	24.8	0.000128
Maprotinline	10262-69-8	0.8	0.8	0.99	4.9	480.9	0.000106
Tetraconazole	112281-77-3	15.92	15.67	0.99	5.7	28.9	9.22E−05
Perfluorooctane sulfonic acid	1763-23-1	81.83	81.66	0.99	6.6	6.4	7.92E−05
Isoxaben	82558-50-7	8.4	8.25	0.99	6.8	65.5	7.71E−05
Ddt	50-29-3	0.04	0.04	0.99	7.3	15127.0	3.84E−05
S-bioallethrin	28434-00-6	1.66	1.63	0.99	9.0	434.5	5.85E−05
Fenvalerate	51630-58-1	0.88	0.88	0.99	13.7	1235.3	3.71E−05
Zoxamide	156052-68-5	37.87	37.69	0.99	34.0	71.3	1.55E−05
Oxyfluorfen	42874-03-3	3.21	3.18	0.99	41.7	1033.9	1.26E−05
D-*cis*, *trans*-allethrin	584-79-2	1.35	1.33	0.99	46.7	2763.0	1.13E−05
Emamectin benzoate	155569-91-8	282.45	281.50	0.99	77.7	21.8	6.77E−06
PCB136	38411-22-2	37.68	1.08	0.03	>100	34485.6	3.21E−08
PCB153	35065-27-1	76.7	0.86	0.01	>100	43391.9	1.25E−08
PCB155	33979-03-2	75.67	1.36	0.02	>100	27407.8	2.01E−08
PCB77	32598-13-3	76.21	10.56	0.13	>100	3314.2	1.65E−07
PCB80	33284-52-5	77.06	11.26	0.14	>100	3093.6	1.75E−07

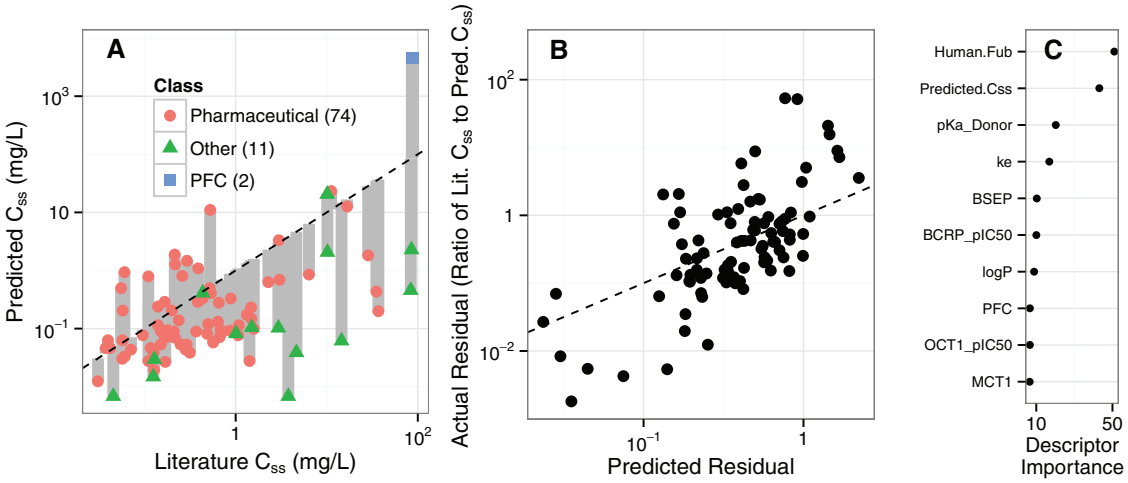

FIG. 4. A, Comparison of HTTK predicted C_{ss} values with measured *in vivo* C_{ss} values from literature studies. Two PFCs are plotted on top of each other. The dashed line indicates the identity (perfect predictor) line. Chemicals plotted below the identity line have predictions greater than literature values, and vice versa. The thick grey lines indicate the discrepancy between measured and predicted values (ie, the residuals). Comparison of the actual residuals calculated from (A) and the residuals predicted using a random forest analysis based on chemical descriptors is shown in (B). The most important factors in the random forest model, as calculated using the method of decrease in node impurities, are shown in (C). These factors are described in detail in Tables 2 and 3.

To identify chemical-specific properties that correlate with reduced HTTK predictive ability, we analyzed the difference between *in vivo* measurements and HTTK predictions (ie, the residuals), shown by thick grey lines in Figure 4A. The method of random forests was used to predict the residual for each chemical with *in vivo* data, as shown in Figure 4B. Chemical properties included chemical-specific physico-chemical properties, *in vitro* intrinsic hepatic clearance, *in vitro* plasma protein binding, and QSAR predictions of transporter affinity. Transporters were included because predictors were available (Sedykh *et al.*, 2013) and they constitute an often important driver of TK (Giacomini *et al.*, 2010; Shugarts and Benet, 2009) that is not included in the steady-state model. A large predicted residual for a specific chemical corresponds to a large expected error. The random forest approach ensures cross-validated predictive ability by averaging the predictions of many models constructed from random subsets of the chemicals and chemical descriptors. The relative importance of the top 10 chemical properties for predicting HTTK residuals (errors) is illustrated in Figure 4C. These factors are described in detail in Tables 2 and 3. Note that all transporters that were included as potential predictors of error were anticipated to be relevant to TK. The relative rankings of specific transporters in Table 2 may reflect the chemical evaluation set that was used.

Downloaded from http://toxsci.oxfordjournals.org/ at Environmental Protection Agency Library on September 23, 2015

TABLE 2. Transporters Associated With Differences Between HTTK Model Predictions and Human *in vivo* C_{ss}

Abbreviation (Gene)	Full Name	Transporter	References	Random Forest Importance[a]	Included in Tree Made From All Data
BSEP (ABCB11)	Bile Salt Export Pump	Hepatocyte bile secretion efflux transporter	Faber *et al.* (2003) and Giacomini *et al.* (2010)	10.3	
BCRP (ABCG2)	Breast cancer resistance protein	Hepatocyte bile and intestinal secretion efflux transporter	Giacomini *et al.* (2010)	9.97	
OCT1 (SLC22A1)	Organic Cation Transporter 1	Hepatocyte influx and intestinal secretion influx transporter	Faber *et al.* (2003) and Giacomini *et al.* (2010)	6.64	
MCT1 (SLC16A1)	Monocarboxylate Transporter 1	Ubiquitous Transporter	Halestrap and Meredith (2004)	6.6	Y
OATP2B1 (SLCO2B1)	Solute carrier organic anion transporter family member 2B1	Hepatocyte and blood-brain barrier influx transporter	Giacomini *et al.* (2010)	5.77	Y
PEPT1 (SLC15A1)	Peptide transporter 1	Intestinal and kidney secretion influx transporter	Giacomini *et al.* (2010)	5.54	Y

[a]Larger value indicates greater relative importance. When multiple predictors for same transporter were available, only the highest reported importance is reported.

TABLE 3. Other Factors Associated With Difference Between HTTK Model Predictions and Human *in vivo* C_{ss}

Factor	Description	Random Forest Importance[a]	Included in Tree Made From All Data
f_{up}	Fraction unbound to plasma protein as measured *in vitro*	51.0	Y
Predicted C_{ss}	Steady-state concentration predicted from *in vitro* measured f_{ub} and C_{lint}	43.1	Y
Ionization (pKa_Donor)	Acid dissociation equilibrium constant	20.2	
Elimination rate (k_e)	Elimination rate as calculated from total clearance (renal + hepatic) predicted from *in vitro* data, divided by V_d	16.9	
Log K_{ow}	Log transformed hydrophobicity (ratio of concentration in octanol to water)	8.86	
Perfluorinated compound (PFC) (yes/no)		6.65	

[a]Larger value indicates greater relative importance.

Although the random forest method produces a cross-validated predictor, the interpretation of how those predictions are achieved can be difficult since the predictions are the average of many different models. A single regression tree for predicting C_{ss} residuals based on all chemicals and all available chemical properties can be created for descriptive purposes (Fig. 5). Error in the HTTK models (ie, large residuals) appears to be driven by predicted C_{ss}, f_{up}, chemical ionization, and 2 of the transporters described in Table 2. We note 2 broad classes of chemicals—those chemicals where HTTK predictions are *on the order* (ie, within ~3.2× or $10^{1/2}$×) of the observed *in vivo* values (~65% of the chemicals), and those chemicals where the errors can be several orders of magnitude (28% of the chemicals were ~6× overestimated, and 8% of chemicals 120× overestimated on average). For this final group of chemicals, the large overestimation by the HTTK models leads to conservative reverse dosimetry predictions (ie, errors that would lead to lower predicted ratios between bioactive doses and the maximal expected exposures, thus leading to a higher predicted risk).

Motivated by the regression tree analysis in Figure 5, which classified all the data but was not suitable for prediction, a second random forest (ie, predictive, rather than descriptive) analysis was conducted. The analysis used the same descriptors as before to classify chemicals into 5 categories based on residual: those chemicals with predictions on the order of the *in vivo* C_{ss} (within ~3.2×), those that were between ~3.2× and 10× over or underestimated, and those that were >10× over or underestimated. The cross-validated classifier had a sensitivity of 79%, a specificity of 54%, and a balanced accuracy of 64% when predicting whether or not a HTTK C_{ss} prediction will be on the order of the *in vivo* measured C_{ss}. Chemicals for which the residuals are predicted to be on the order or overestimated are within the domain of applicability of our HTTK approach; ie, we expect to have either small or conservative errors for reverse dosimetry. Along with identifying those chemicals that never reach steady-state (Table 1) and those chemicals for which the plasma protein binding assay failed, the 5 categories from this random forest classifier allow each chemical to be placed into 1 of 7 categories, as illustrated in Figure 6.

By integrating the various analyses in this study, we developed a TK triage framework that provides guidance on the degree of confidence for a particular prediction and indicates which chemicals may benefit from specific types of analyses or experimental data collection (Table 4). The first step is the collection of basic *in vitro* TK data that allows a prediction to be made for C_{ss}. Second, the parameterization of HTPBTK models using physico-chemical properties and predicted partition coefficients, if possible, allows a determination of the plausibility of reaching steady state. Third, chemical properties that are correlated with large deviations between predicted and observed

Downloaded from http://toxsci.oxfordjournals.org/ at Environmental Protection Agency Library on September 23, 2015

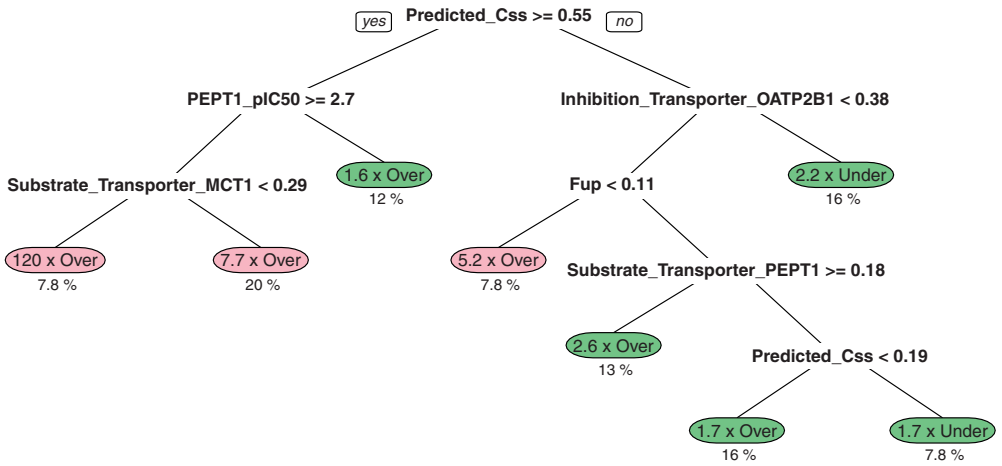

FIG. 5. A recursive partitioning regression tree was used to classify the discrepancy between the C_{ss} predicted from *in vitro* data and the *in vivo* C_{ss} (Obach *et al.*, 2008; Wetmore *et al.*, 2012). Each "leaf" of the tree shows a group of chemicals for which HTTK either overestimates C_{ss} (making conservative predictions) or underestimates C_{ss}. For all but 3 groups, the predictions are on the order of the observed C_{ss} (approximately within a factor of 3.2× greater or lesser). For the other 3 groups, the C_{ss} is 5.2×, 7.7×, and 120× overestimated. The dashed line indicates the identity (perfect predictor) line.

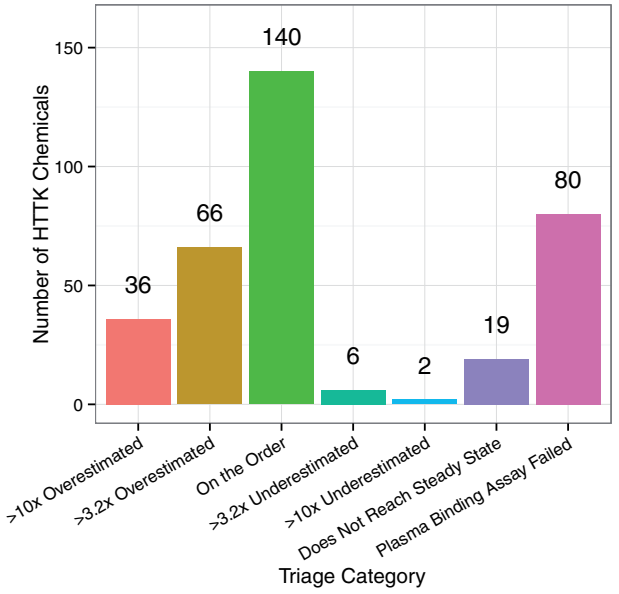

FIG. 6. Distribution of the 349 chemicals with IVIVE data among the triage elements in Table 4. C_{ss} is not meaningful for the chemicals that do not reach steady-state. Chemicals where the protein binding assay failed cannot easily be categorized since f_{up} is an important predictor (Table 3) of discrepancy between HTTK C_{ss} predictions and literature values for C_{ss}. The remaining chemicals are categorized as likely having HTTK predictions for C_{ss} that would be overestimated, underestimated, or on the order (±3.2× the *in vivo* value).

behavior can be used to screen out those chemicals for which HTTK is not expected to perform well. The 4th element of triage addresses those remaining chemicals in greatest need of alternative, perhaps traditional approaches. Different elements of triage may be applied concurrently, depending on the information that is available.

We applied the TK triage (Table 4) to the entire 349 chemical set in Figure 6. We find that a plurality (140) of the chemicals are estimated to be "on the order," ie, the HTTK predicted C_{ss} will be within ~3.2× of the literature value. The third largest category is chemicals for which the protein binding assay failed (80), precluding analysis of time to reach steady-state. However, only 7% of chemicals analyzed for time to reach steady-state did not do so within 1000 days, and we might assume this figure to be similar for these 80 chemicals. Of the remaining 110 chemicals, most (102) are predicted to be overestimated, leading to conservative errors when conducting reverse dosimetry. In total, we predict that the reverse dosimetry assumptions will be appropriate for 89% of the chemicals where the protein binding assay was successful.

DISCUSSION

Efforts to implement the vision outlined in Toxicity Testing in the 21st Century (National Research Council, 2007) include *in vitro* assays to identify potential biological targets of environmental and industrial chemicals (eg, ToxCast, Judson *et al.*, 2010). IVIVE methods are then needed to translate *in vitro* bioactive concentrations into administered doses (Blaauboer *et al.*, 2012; Wetmore *et al.*, 2012). HTS data might then be used in a risk-based context through the comparison of estimated bioactive doses to estimated exposures (Judson *et al.*, 2011; Thomas *et al.*, 2013; Wetmore *et al.*, 2012). Herein, we develop a method for identifying the degree of confidence with which we may apply HTTK in order translate HTS data for chemicals without other TK data. We have formalized this process in a triage system that has categorized 349 chemicals into 7 categories, 5 of which indicate varying degrees of confidence in the HTTK approach and 2 indicate a need for additional data or alternative approaches.

We examined 3 key assumptions in the previous HTTK research: that humans can reach a steady-state with respect to environmental exposures, that steady-state concentration is a reasonable surrogate when exposure is more episodic, and that 100% absorption is reasonable. These assumptions were tested using both simulation studies and direct comparison to *in vivo* data for both pharmaceuticals and environmental chemicals. Based on our analysis we organize HTTK testing into a TK triage framework for environmental chemicals (Table 4). Each element of the framework depends on data collection and/or analysis, and distinguishes those chemicals for which that sort of data is useful from those chemicals for which the approach does not apply. Based on this approach we expect the *in vivo* values to be within ~3.2× of predictions for ~59% the 246 chemicals that both had a successful plasma protein binding estimate and we

Downloaded from http://toxsci.oxfordjournals.org/ at Environmental Protection Agency Library on September 23, 2015

TABLE 4. Elements of HTTK Triage for Environmental Chemicals

	TK Data	Targeted Chemicals	TK Prediction/Consequence	Confidence	Domain of Applicability
1	*In vitro* clearance of parent compound by hepatocytes and binding to plasma protein	HTS compounds	Plasma C_{ss} from constant infusion exposure	If comparison with predicted exposure indicates large AER then infusion C_{ss} should be sufficient	Soluble low volatility (HTS appropriate) compounds
1a	CYP-specific *in vitro* data (Wetmore *et al.*, 2014)	Chemicals with AER near one for general population	Population variability, life-stage variability	Human variations in CYP expression are well characterized	Same as in 1
2	Physico-chemical properties (measured or QSAR)	All chemicals with successful binding *in vitro* assay	Prediction of partition coefficients allows HTPBTK steady-state predictions (including time to steady state) for more realistic exposure modeling	If comparison with predicted exposure indicates large AER then HTPBTK should be sufficient (ie, conservative due to 100% absorption)	QSAR-defined (eg, training set, extrapolation methodology)
3	QSARs for likely transporter substrates	All chemicals with successful binding *in vitro* assay	Assumptions of perfusion-limited tissue partitioning and passive renal excretion by glomerular filtration may be questionable	Can identify those chemicals where the impact is negligible (Fig. 4b)	Chemicals predicted to reach steady state in Tier 2 (Fig. 3a)
3b	Transporter-specific *in vitro* data	Chemicals indicated by QSAR	Tissue-specific accumulation, active secretion/resorption in kidney	Well characterized for non high-throughput applications	Same as in 3
4	*In vivo* oral and iv dose TK study, plasma only	Chemicals with large predicted residuals (Fig. 4b) and those that cannot be tested *in vitro*	Oral bioavailability, absorption rate, volume of distribution, and clearance (refined PBTK model)	If volume of distribution from HTPBTK model and *in vitro* estimate of clearance hold, then refined PBTK model should be excellent	Any compound

AER is the Activity to Exposure Ratio between HTS bioactive reverse dosimetry predictions and exposure.

predict will reach steady-state. We expect conservative errors for an additional ~37% of these 246 chemicals.

The final element of triage incorporates additional *in vitro* or *in vivo* testing for those chemicals that are most in need of additional attention. Admittedly, the domain of applicability for this approach is limited by the domain of chemicals used to conduct this analysis. Since there may be chemical properties that drive HTTK error that may be underrepresented by these chemicals, it will also be important to study at least a few members of diverse and novel classes of environmental and industrial chemicals.

The application of *in vitro* methods to TK is different in the pharmaceutical versus environmental chemical screening domains. For instance, it is expected that some samples of some compounds will be below the LOD of the cost-effective analytical chemistry that is required for the rapid TK screening of thousands of environmental and industrial chemicals (Rousu *et al.*, 2010; Wetmore *et al.*, 2012). When screening environmental and industrial chemicals, resources may not exist for follow-up work and the data must be used as is. This study found that typical assumptions such as half the LOD for protein binding (f_{up}) (Wetmore *et al.*, 2012) may result in an underestimation of C_{ss} values, which may not be health protective. However, this may be offset by other assumptions in the HTTK modeling that tend to produce an overestimate of C_{ss}.

For the metabolic clearance assay, stricter statistical limits are more conservative since they lead to overestimated C_{ss} values (ie, setting metabolic elimination to 0 for P-value $<.05$ instead of P-value $<.1$). However, many of the chemicals that we estimate to have 0 or non-significant clearance in the *in vitro* assays analyzed here may yield significant clearance in more physiological conditions, such as plated hepatocytes over a longer time period. Follow-up measurement of clearance rates using a plated hepatocytes system (Smith *et al.*, 2012) and/or longer times may ensure a more accurate hepatic clearance estimate.

For most environmental and industrial chemicals it is unlikely that there will ever be controlled human TK data. As evaluated by comparison to *in vivo* data, the predictive ability of the HTPBTK methods based on both IVIVE and QSAR-related methods was considerably greater than the HTTK models that assumed steady-state conditions. One possible explanation is that although the evaluation data for the HTPBPTK model predictions (*in vivo* AUCs and C_{max} values) were drawn from diverse literature, the *in vitro* data for this comparison were from a single source (Wetmore *et al.*, 2013). For the steady-state HTTK model evaluation, both the *in vivo* and the *in vitro* data were drawn from diverse literature sources.

Pharmaceuticals are typically small and well-absorbed molecules that are designed for specific biological targets (Lipinski, 2004). In contrast, environmental and industrial chemicals are structurally heterogeneous and may have multiple biological targets (Richard, 2006). Given the diversity of intended applications for environmental and industrial chemicals, their properties can vary greatly from those of pharmaceuticals. Unfortunately, though *in vitro* TK data have been collected for many of the 309 ToxCast Phase I chemicals, only 13 *in vivo* C_{ss} values were available for those chemicals (Wetmore *et al.*, 2012).

Although the HTPBTK models appear promising for predicting AUC and C_{max}, the *in vivo* evaluation data in Figure 2 are drawn from various treatments of only 15 pharmaceutical chemicals and 7 environmental chemicals, thus final

Downloaded from http://toxsci.oxfordjournals.org/ at Environmental Protection Agency Library on September 23, 2015

assessments of the HTPBTK methodology is not yet possible. An effort is needed to collect and organize additional *in vivo* data on environmental and industrial chemicals to confirm the usefulness of HTTK approaches. Generating the data necessary to evaluate HTTK methods does not necessarily require large resources: small, short term, *in vivo* studies—perhaps added to routine toxicological studies—could provide essential information for chemicals and chemical classes that are currently not well modeled. In addition, making existing TK-related data more accessible by creating databases and curating literature or legacy studies could inexpensively expand the available TK information. These *in vivo* TK data can inform important processes that are currently not assayed by HTTK.

The HTTK models analyzed here may omit or inaccurately estimate drivers of TK including: extra-hepatic metabolism; secretion in bile and enterohepatic recirculation; active transport in renal, hepatic, and other tissues; and absorption/bioavailability (Rotroff *et al.*, 2010). Until rapid and cost-effective *in vitro* assays are developed for these processes, QSAR models would seem to provide one-way forward. Unfortunately, QSAR is not yet capable of providing reliable rate constants (eg, transporter velocity); rather, QSAR can estimate how likely or unlikely it is that a process will occur (Sedykh *et al.*, 2013). By integrating the available QSAR predictions into a model to predict when the difference between HTTK predictions and *in vivo* data will be large, we can better identify those compounds in need of follow-up study. However, those chemical properties found to increase predictive error in this current analysis (and therefore indicate that we may be outside the domain of applicability for our methods) apply only to the chemical space we have analyzed thus far. As the approach is applied to new chemicals, additional properties might be identified that play a more significant role in the TK prediction of some of these other chemicals. We must target for further study those chemicals most likely to be subject to transport processes or other drivers of uncertainty as indicated by large errors in HTTK model predictions.

HTTK is intended to complement HTS assays that identify bioactivity of chemicals *in vitro*. As with most HTS assays, we so far have only the means to deal with the parent compound, and do not yet have the tools to deal with any metabolites in a high throughput manner. If these tools were to become available, they would become an important tier in TK triage.

We have shown that HTTK models can be developed from *in vitro* data for many environmental chemicals. The steady-state predictions of these models allow concentrations showing biological activity in HTS assays to be converted into administered dose values. We have evaluated the predictions of these models using comparison to *in vivo* values and HTPBTK simulation studies to identify when HTTK may be used with confidence and when additional, targeted measurements may be necessary.

SUPPLEMENTARY DATA

Supplementary data are available online at http://toxsci.oxfordjournals.org/.

FUNDING

The United States Environmental Protection Agency through its Office of Research and Development funded and managed the research described here. James Sluka was funded by the US EPA (R835001), the NIH (GM077138) and the Biocomplexity Institute at Indiana University. Barbara Wetmore was funded by the American Chemistry Council's Long-Range Research IniInitiative. Sieto Bosgra was funded by the European Commission 7th Framework Program project ChemScreen (GA244236). Alex Tropsha and Alex Sedykh were supported by grants from NIH (GM66940 and R21GM076059), The Johns Hopkins Center for Alternatives to Animal Testing (20011-21) and Boehringer Ingelheim (Canada) Ltd.

ACKNOWLEDGMENTS

We appreciate feedback from Kevin Crofton, Marina Evans, and William Jordan in preparation of this manuscript.

REFERENCES

Archer, K. J., and Kimes, R. V. (2008). Empirical characterization of random forest variable importance measures. *Comput. Stat. Data Anal.* **52**, 2249–2260.

Birnbaum, L., Brown, R., Bischoff, K., Foran, J., Blancato, J., Clewell, H., and Dedrick, R. (1994). *Physiological Parameter Values for PBPK Models*. International Life Sciences Institute, Risk Science Institute, Washington, DC.

Blaauboer, B. J., Boekelheide, K., Clewell, H. J., Daneshian, M., Dingemans, M. M., Goldberg, A. M., Heneweer, M., Jaworska, J., Kramer, N. I., Leist, M., *et al.* (2012). The use of biomarkers of toxicity for integrating in vitro hazard estimates into risk assessment for humans. *Altex* **29**, 411–425.

Breiman, L. (2001). Random forests. *Mach. Learn.* **45**, 5–32.

Breiman, L., Friedman, J., Stone, C. J., and Olshen, R. A. (1984). *Classification and Regression Trees*. CRC Press, Boca Raton.

Bucher, J. R. (2008). Guest editorial: NTP: new initiatives, new alignment. *Environ. Health Perspect.* **116**, A14–A15.

CDC (2012). *National Health and Nutrition Examination Survey*. Available at: http://www.cdc.gov/nchs/nhanes.htm, last accessed 22 June 2015.

Davies, B., and Morris, T. (1993). Physiological parameters in laboratory animals and humans. *Pharm. Res.* **10**, 1093–1095.

Endo, S., Escher, B. I., and Goss, K.-U. (2011). Capacities of membrane lipids to accumulate neutral organic chemicals. *Environ. Sci. Technol.* **45**, 5912–5921.

Faber, K. N., Müller, M., and Jansen, P. L. M. (2003). Drug transport proteins in the liver. *Adv. Drug Deliv. Rev.* **55**, 107–124.

Giacomini, K. M., Huang, S.-M., Tweedie, D. J., Benet, L. Z., Brouwer, K. L., Chu, X., Dahlin, A., Evers, R., Fischer, V., and Hillgren, K. M. (2010). Membrane transporters in drug development. *Nat. Rev. Drug Discov.* **9**, 215–236.

Halestrap, A., and Meredith, D. (2004). The SLC16 gene family—from monocarboxylate transporters (MCTs) to aromatic amino acid transporters and beyond. *Pflugers Arch. Eur. J. Physiol.* **447**, 619–628.

Hilal, S., Karickhoff, S., and Carreira, L. (1995). A rigorous test for SPARC's chemical reactivity models: estimation of more than 4300 ionization pKas. *Quant. Struct. -Act. Relat.* **14**, 348–355.

Ito, K., and Houston, J. B. (2004). Comparison of the use of liver models for predicting drug clearance using in vitro kinetic data from hepatic microsomes and isolated hepatocytes. *Pharm. Res.* **21**, 785–792.

Jamei, M., Marciniak, S., Feng, K., Barnett, A., Tucker, G., and Rostami-Hodjegan, A. (2009). The Simcyp population-based ADME simulator. *Expert Opin. Drug Metab. Toxicol.* **5**, 211–223.

Downloaded from http://toxsci.oxfordjournals.org/ at Environmental Protection Agency Library on September 23, 2015

Jones, O. A., Voulvoulis, N., and Lester, J. N. (2002). Aquatic environmental assessment of the top 25 English prescription pharmaceuticals. *Water Res.* **36**, 5013–5022.

Judson, R. S., Houck, K. A., Kavlock, R. J., Knudsen, T. B., Martin, M. T., Mortensen, H. M., Reif, D. M., Rotroff, D. M., Shah, I., Richard, A. M., *et al.* (2010). In vitro screening of environmental chemicals for targeted testing prioritization: the ToxCast Project. *Environ. Health Perspect.* **118**, 485–492.

Judson, R. S., Kavlock, R. J., Setzer, R. W., Cohen-Hubal, E. A., Martin, M. T., Knudsen, T. B., Houck, K. A., Thomas, R. S., Wetmore, B. A., and Dix, D. J. (2011). Estimating toxicity-related biological pathway altering doses for high-throughput chemical risk assessment. *Chem. Res. Toxicol.* **24**, 451–462.

Judson, R., Richard, A., Dix, D. J., Houck, K., Martin, M., Kavlock, R., Dellarco, V., Henry, T., Holderman, T., Sayre, P., *et al.* (2008). The toxicity data landscape for environmental chemicals. *Environ. Health Perspect.* **117**, 685–695.

Kilford, P. J., Gertz, M., Houston, J. B., and Galetin, A. (2008). Hepatocellular binding of drugs: correction for unbound fraction in hepatocyte incubations using microsomal binding or drug lipophilicity data. *Drug Metab. Dispos.* **36**, 1194–1197.

Krug, A. K., Kolde, R., Gaspar, J. A., Rempel, E., Balmer, N. V., Meganathan, K., Vojnits, K., Baquié, M., Waldmann, T. and Ensenat-Waser, R. (2013). Human embryonic stem cell-derived test systems for developmental neurotoxicity: a transcriptomics approach. *Archives of toxicology* **87**(1), 123–143.

Lau, Y. Y., Sapidou, E., Cui, X., White, R. E., and Cheng, K. C. (2002). Development of a novel in vitro model to predict hepatic clearance using fresh, cryopreserved, and sandwich-cultured hepatocytes. *Drug Metab. Dispos.* **30**, 1446–1454.

Liaw, A., and Wiener, M. (2002). Classification and regression by randomforest. *R News* **2**, 18–22.

Lipinski, C. A., (2004). Lead- and drug-like compounds: the rule-of-five revolution. *Drug Discovery Today: Technologies* **1**(4), 337–341, http://dx.doi.org/10.1016/j.ddtec.2004.11.007.

Lukacova, V., Woltosz, W., and Bolger, M. (2009). Prediction of modified release pharmacokinetics and pharmacodynamics from in vitro, immediate release, and intravenous data. *AAPS J.* **11**, 323–334.

McGinnity, D. F., Soars, M. G., Urbanowicz, R. A., and Riley, R. J. (2004). Evaluation of fresh and cryopreserved hepatocytes as in vitro drug metabolism tools for the prediction of metabolic clearance. *Drug Metab. Dispos.* **32**, 1247–1253.

Naritomi, Y., Terashita, S., Kagayama, A., and Sugiyama, Y. (2003). Utility of hepatocytes in predicting drug metabolism: comparison of hepatic intrinsic clearance in rats and humans in vivo and in vitro. *Drug Metab. Dispos.* **31**, 580–588.

National Research Council (1984). *Toxicity Testing: Strategies to Determine Needs and Priorities*. National Academy Press, Washington, DC.

National Research Council (2007). *Toxicity Testing in the 21st Century: A Vision and a Strategy*. The National Academies Press, Washington, DC.

Obach, R. S. (1999). Prediction of human clearance of twenty-nine drugs from hepatic microsomal intrinsic clearance data: an examination of in vitro half-life approach and nonspecific binding to microsomes. *Drug Metab. Dispos.* **27**, 1350–1359.

Obach, R. S., Lombardo, F., and Waters, N. J. (2008). Trend analysis of a database of intravenous pharmacokinetic parameters in humans for 670 drug compounds. *Drug Metab. Dispos.* **36**, 1385–1405.

Piersma, A., Bosgra, S., Van Duursen, M., Hermsen, S., Jonker, L., Kroese, E., Van der Linden, S., Man, H., Roelofs, M. and Schulpen, S. (2013). Evaluation of an alternative in vitro test battery for detecting reproductive toxicants. *Reproductive Toxicology* **38**, 53–64.

R Development Core Team. (2013). R: A Language and Environment for Statistical Computing, *Version* 3.0.2. R Foundation for Statistical Computing, Vienna, Austria.

Ritter, R., Scheringer, M., MacLeod, M., Moeckel, C., Jones, K. C., and Hungerbühler, K. (2010). Intrinsic human elimination half-lives of polychlorinated biphenyls derived from the temporal evolution of cross-sectional biomonitoring data from the United Kingdom. *Environ. Health Perspect.* **119**, 225–231.

Richard, A. M. (2006). Future of ToxicologyPredictive Toxicology: An Expanded View of "Chemical Toxicity". *Chemical Research in Toxicology* **19**(10), 1257–1262, 10.1021/tx060116u.

Rotroff, D. M., Wetmore, B. A., Dix, D. J., Ferguson, S. S., Clewell, H. J., Houck, K. A., Lecluyse, E. L., Andersen, M. E., Judson, R. S., Smith, C. M., *et al.* (2010). Incorporating human dosimetry and exposure into high-throughput in vitro toxicity screening. *Toxicol. Sci.* **117**, 348–358.

Rousu, T., Hokkanen, J., Pelkonen, O. R., and Tolonen, A. (2010). Applicability of generic assays based on liquid chromatography–electrospray mass spectrometry to study in vitro metabolism of 55 structurally diverse compounds. *Front. Pharmacol.* **1**, 10.

Schmitt, W. (2008a). General approach for the calculation of tissue to plasma partition coefficients. *Toxicol. in vitro* **22**, 457–467.

Schmitt, W. (2008b). Corrigendum to: "General approach for the calculation of tissue to plasma partition coefficients". [Toxicol. in vitro **22** (2008) 457–467]. *Toxicol. in vitro* **22**, 1666.

Sedykh, A., Fourches, D., Duan, J., Hucke, O., Garneau, M., Zhu, H., Bonneau, P., and Tropsha, A. (2013). Human intestinal transporter database: QSAR modeling and virtual profiling of drug uptake, efflux and interactions. *Pharm. Res.* **30**, 996–1007.

Shibata, Y., Takahashi, H., Chiba, M., and Ishii, Y. (2002). Prediction of hepatic clearance and availability by cryopreserved human hepatocytes: an application of serum incubation method. *Drug Metab. Dispos.* **30**, 892–896.

Shugarts, S., and Benet, L. Z. (2009). The role of transporters in the pharmacokinetics of orally administered drugs. *Pharm. Res.* **26**, 2039–2054.

Smith, C. M., Nolan, C. K., Edwards, M. A., Hatfield, J. B., Stewart, T. W., Ferguson, S. S., Lecluyse, E. L., and Sahi, J. (2012). A comprehensive evaluation of metabolic activity and intrinsic clearance in suspensions and monolayer cultures of cryopreserved primary human hepatocytes. *J. Pharm. Sci.* **101**, 3989–4002.

Steinbeck, C., Han, Y., Kuhn, S., Horlacher, O., Luttmann, E., and Willighagen, E. (2003). The Chemistry Development Kit (CDK): an open-source Java library for Chemo- and Bioinformatics. *J. Chem. Inf. Comput. Sci.* **43**, 493–500.

Therneau, T. M., Atkinson, B., and Ripley, B. (2014). *rpart: Recursive partitioning*. R Package Version 4.1(8).

Thomas, R. S., Philbert, M. A., Auerbach, S. S., Wetmore, B. A., Devito, M. J., Cote, I., Rowlands, J. C., Whelan, M. P., Hays, S. M., Andersen, M. E., *et al.* (2013). Incorporating new technologies into toxicity testing and risk assessment: moving from 21st century vision to a data-driven framework. *Toxicol. Sci.* **136**, 4–18.

Tonnelier, A., Coecke, S., and Zaldívar, J.-M. (2012). Screening of chemicals for human bioaccumulative potential with a physiologically based toxicokinetic model. *Arch. Toxicol.* **86**, 393–403.

Downloaded from http://toxsci.oxfordjournals.org/ at Environmental Protection Agency Library on September 23, 2015

USGAO (2013). Toxic substances: EPA has increased efforts to assess and control chemicals but could strengthen its approach. United States Government Accountability Office, Report to Congressional Requesters, GAO-13-249. Published: Mar 22, 2013. Publicly Released: Apr 29, 2013.

van de Steeg, E., Venhorst, J., Jansen, H., Nooijen, I., DeGroot, J., Wortelboer, H., and Vlaming, M. (2015). Generation of Bayesian prediction models for OATP-mediated drug-drug interactions based on inhibition screen of OATP1B1, OATP1B1 15 and OATP1B3. *European Journal of Pharmaceutical Sciences* **70**, 29–36.

Walker, T., Grulke, C. M., Pozefsky, D., and Tropsha, A. (2010). Chembench: a cheminformatics workbench. *Bioinformatics* **26**, 3000–3001.

Wambaugh, J. F., Setzer, R. W., Reif, D. M., Gangwal, S., Mitchell-Blackwood, J., Arnot, J. A., Jolliet, O., Frame, A., Rabinowitz, J., Knudsen, T. B., *et al.* (2013). High throughput models for exposure-based chemical prioritization in the ExpoCast Project. *Environ. Sci. Technol.* **47**, 8479–8488.

Wambaugh, J. F., Wang, A., Dionisio, K. L., Frame, A., Egeghy, P., Judson, R., and Setzer, R. W. (2014). High throughput heuristics for prioritizing human exposure to environmental chemicals. *Environ. Sci. Technol.* **48**, 12760–12767.

Wang, Y.-H. (2010). Confidence assessment of the Simcyp time-based approach and a static mathematical model in predicting clinical drug–drug interactions for mechanism-based CYP3A inhibitors. *Drug Metab. Dispos.* **38**, 1094–1104.

Waters, N. J., Jones, R., Williams, G., and Sohal, B. (2008). Validation of a rapid equilibrium dialysis approach for the measurement of plasma protein binding. *J. Pharm. Sci.* **97**, 4586–4595.

Weininger, D. (1988). SMILES, a chemical language and information system. 1. Introduction to methodology and encoding rules. *J. Chem. Inf. Comput. Sci.* **28**, 31–36.

Wetmore, B. A., Wambaugh, J. F., Ferguson, S. S., Sochaski, M. A., Rotroff, D. M., Freeman, K., Clewell, H. J., III, Dix, D. J., Andersen, M. E., Houck, K. A., *et al.* (2012). Integration of dosimetry, exposure, and high-throughput screening data in chemical toxicity assessment. *Toxicol. Sci.* **125**, 157–174.

Wetmore, B. A., Wambaugh, J. F., Ferguson, S. S., Li, L., Clewell, H. J., Judson, R. S., Freeman, K., Bao, W., Sochaski, M. A., Chu, T.-M., *et al.* (2013). Relative impact of incorporating pharmacokinetics on predicting in vivo hazard and mode of action from high-throughput in vitro toxicity assays. *Toxicol. Sci.* **132**,327–346.

Wetmore, B. A., Allen, B., Clewell, H. J., Parker, T., Wambaugh, J. F., Almond, L. M., Sochaski, M. A., and Thomas, R. S. (2014). Incorporating population variability and susceptible subpopulations into dosimetry for high-throughput toxicity testing. *Toxicol. Sci.* **142**, 210–224.

Wilkinson, G. R., and Shand, D. G. (1975). Commentary: a physiological approach to hepatic drug clearance. *Clin. Pharmacol. Ther.* **18**, 377–390.

Yoon, M., Efremenko, A., Blaauboer, B. J., and Clewell, H. J. (2014). Evaluation of simple in vitro to in vivo extrapolation approaches for environmental compounds. *Toxicol. in vitro* **28**, 164–170.

Downloaded from http://toxsci.oxfordjournals.org/ at Environmental Protection Agency Library on September 23, 2015

OXFORD

SOT | Society of Toxicology
www.toxsci.oxfordjournals.org

TOXICOLOGICAL SCIENCES, 147(1), 2015, 55–67

doi: 10.1093/toxsci/kfv118
Advance Access Publication Date: June 16, 2015
Research Article

Toxicokinetic Triage for Environmental Chemicals

John F. Wambaugh*,[1], Barbara A. Wetmore†, Robert Pearce*, Cory Strope*,‡, Rocky Goldsmith§, James P. Sluka¶, Alexander Sedykh||, Alex Tropsha||, Sieto Bosgra|||, Imran Shah*, Richard Judson*, Russell S. Thomas*, R. Woodrow Setzer*

*National Center for Computational Toxicology and §National Exposure Research Laboratory, Office of Research and Development, US EPA, Research Triangle Park, North Carolina 27711; †The Hamner Institutes for Health Sciences, Research Triangle Park, North Carolina 27709-2137; ‡Oak Ridge Institute for Science and Education Grantee P.O. Box 117, Oak Ridge, Tennessee 37831-0117, United States; ¶Biocomplexity Institute, Indiana University, Bloomington, Indiana 47405-7105; ||Department of Chemical Biology and Medicinal Chemistry, University of North Carolina, Chapel Hill, North Carolina 27955-7568; and |||The Netherlands Organisation for Applied Scientific Research (TNO), 3700 AJ Zeist, The Netherlands

[1]To whom correspondence should be addressed at National Center for Computational Toxicology, Office of Research and Development, US EPA, 109 T.W Alexander Dr., Research Triangle Park, North Carolina 27711. Fax: (919) 541-1194. E-mail: Wambaugh.john@epa.gov.

Disclaimer: The views expressed in this publication are those of the authors and do not necessarily represent the views for policies of the U.S. Environmental Protection Agency. Reference to commercial products or services does not constitute endorsement.

Downloaded from http://toxsci.oxfordjournals.org/ at Environmental Protection Agency Library on September 23, 2015

ABSTRACT

Toxicokinetic (TK) models link administered doses to plasma, blood, and tissue concentrations. High-throughput TK (HTTK) performs *in vitro* to *in vivo* extrapolation to predict TK from rapid *in vitro* measurements and chemical structure-based properties. A significant toxicological application of HTTK has been "reverse dosimetry," in which bioactive concentrations from *in vitro* screening studies are converted into *in vivo* doses (mg/kg BW/day). These doses are predicted to produce steady-state plasma concentrations that are equivalent to *in vitro* bioactive concentrations. In this study, we evaluate the impact of the approximations and assumptions necessary for reverse dosimetry and develop methods to determine whether HTTK tools are appropriate or may lead to false conclusions for a particular chemical. Based on literature *in vivo* data for 87 chemicals, we identified specific properties (*eg, in vitro* HTTK data, physico-chemical descriptors, and predicted transporter affinities) that correlate with poor HTTK predictive ability. For 271 chemicals we developed a generic HT physiologically based TK (HTPBTK) model that predicts non-steady-state chemical concentration time-courses for a variety of exposure scenarios. We used this HTPBTK model to find that assumptions previously used for reverse dosimetry are usually appropriate, except most notably for highly bioaccumulative compounds. For the thousands of man-made chemicals in the environment that currently have no TK data, we propose a 4-element framework for chemical TK triage that can group chemicals into 7 different categories associated with varying levels of confidence in HTTK predictions. For 349 chemicals with literature HTTK data, we differentiated those chemicals for which HTTK approaches are likely to be sufficient, from those that may require additional data.

Key words: toxicokinetics; high throughput; environmental chemicals; IVIVE

Of the 30 000 chemicals that are estimated to be in wide commercial use, only a small subset has been characterized as to their potential toxicological effects in humans or wildlife (Judson *et al.*, 2008; National Research Council, 1984; USGAO, 2013). High-throughput screening (HTS) using *in vitro* assays, eg, the ToxCast and Tox21 programs, has been proposed as one

Published by Oxford University Press on behalf of Society of Toxicology 2015. This work is written by US Government employees and is in the public domain in the US.

approach to fill these data gaps by analyzing the activity of these chemicals across a broad range of potential biological targets (Bucher, 2008; Judson *et al.*, 2010). One challenge associated with the interpretation of the HTS data has been relating *in vitro* bioactive concentrations with relevant *in vivo* dose values, and doing so on a scale and throughput required to address the large number of chemicals (Judson *et al.*, 2011; Rotroff *et al.*, 2010; Thomas *et al.*, 2013; Tonnelier *et al.*, 2012; Wambaugh *et al.*, 2013, 2014; Wetmore *et al.*, 2012).

For pharmaceutical compounds, *in vitro* to *in vivo* extrapolation (IVIVE) methods have been developed to parameterize toxicokinetic (TK) models that relate blood and tissue concentrations to therapeutic doses for clinical studies. The IVIVE methods typically include limited *in vitro* measurements of hepatic clearance, plasma protein binding, and chemical structure-derived predictions of tissue partitioning (Jamei *et al.*, 2009; Lukacova *et al.*, 2009). The IVIVE methods and resulting TK models are considered effective since the predicted concentrations are often (Wang, 2010) within ~3-fold of the *in vivo* observations (we describe predictions as being "on the order of magnitude" if they are within $\sqrt{10} \approx 3.2$–fold). Ultimately, the human TK of a pharmaceutical compound may be fully characterized in follow-on human clinical trials (Jamei *et al.*, 2009), which is vastly different from the data available for environmental and industrial chemicals where both ethical and cost considerations preclude human testing.

The IVIVE methods developed for pharmaceuticals have been used to parameterize high-throughput TK (HTTK) models for hundreds of environmental and industrial chemicals (Rotroff *et al.*, 2010; Tonnelier *et al.*, 2012; Wetmore *et al.*, 2012, 2013, 2014). The primary example of the application of HTTK models has been to estimate the doses (mg/kg BW/day) needed to produce steady-state plasma concentrations (C_{ss}, in units of μM) equivalent to concentrations that produce bioactivity in *in vitro* assays—this process is often described as "reverse dosimetry" (Rotroff *et al.*, 2010; Tonnelier *et al.*, 2012; Wetmore *et al.*, 2012, 2013, 2014). Reverse dosimetry with HTTK models can provide estimated doses for environmental and industrial chemicals below which significant *in vitro* bioactivity is not expected to occur (Judson *et al.*, 2011; Wetmore *et al.*, 2012). The ratio between the lowest bioactive dose and the maximal expected exposure provides risk-based context to HTS data and is one metric for prioritization of additional chemical testing (Judson *et al.*, 2011; Thomas *et al.*, 2013; Wetmore *et al.*, 2012).

When benchmarked against a limited number of environmental, pesticidal, and industrial chemicals with *in vivo* TK data, HTTK models have demonstrated mixed success, but have generally provided health-protective estimates of bioactive doses (Wetmore *et al.*, 2012; Yoon *et al.*, 2014). The reasons for the discrepancies between steady-state concentrations predicted using HTTK and the concentrations from *in vivo* TK data are not clear. There may be extrapolation issues for environmental chemicals that are not present with pharmaceuticals.

This study evaluated the accuracy of HTTK predictions that were made using the same physiologically motivated, 3-compartment mathematical TK model previously used in reverse dosimetry studies (Rotroff *et al.*, 2010; Tonnelier *et al.*, 2012; Wetmore *et al.*, 2012, 2013, 2014). This assessment was conducted across the 349 chemicals for which the appropriate inputs and data were available. Of these, ~80% of the chemicals (ie, 271), possessed required inputs to parameterize a generic high-throughput physiologically based toxicokinetic (HTPBTK) mathematical model that we employed to test some of the assumptions used in the HTTK-based reverse dosimetry approach for environmental chemicals. HTTK model predictions were further evaluated using available human and rat *in vivo* measurements curated from TK literature.

We found that some properties of pharmaceutical and environmental chemicals correlated with either small or large discrepancies between HTTK predictions and *in vivo*-derived values. Those properties define a "domain of applicability" of chemical property space within which HTTK models may be expected to provide an adequate alternative to more traditional TK methods for reverse dosimetry and other applications. The results of our analyses were integrated into a multi-element TK triage system that organizes chemicals into different categories based on varying degrees of accuracy (eg, on the order, 10× over-estimated, 10× underestimated) of the HTTK predictions with additional categories for situations where more data or alternative approaches are needed to develop suitable TK models. Depending on the accuracy needed for a specific application and the degree of confidence for a particular prediction, this triage system separates those chemicals with which HTTK may be used with confidence from those chemicals that may benefit from specific types of analyses and/or additional experimental data collection.

MATERIALS AND METHODS

In this study, we first replicated the steady-state TK model used in previous studies and developed a new model allowing exploration of the impact of the steady-state assumption. We used these models to analyze the soundness of assumptions used in previous reverse dosimetry HTTK applications as exemplified by the Wetmore *et al.* (2012) study. We then applied statistical methods to determine the chemical-specific properties that correlate with HTTK predictive ability. Among the chemical-specific properties examined, we investigated xenobiotic transporter affinities predicted using quantitative structure–activity relationships (QSAR). The methods and data used for our analysis of HTTK have been made available as a package for the open source R statistical analysis software platform (R Development Core Team, 2013). The package, "httk," can be accessed from the Comprehensive R Archive Network (CRAN) repository (http://cran.r-roject.org/web/packages/httk/, last accessed 22 June 2015). All chemical-specific parameters are listed in Supplementary Table 1 with references.

TK models used. Two general (ie, chemical independent) TK models were used. The first model was intended to replicate the model used in previous reverse dosimetry analyses (Rotroff *et al.*, 2010; Wetmore *et al.*, 2012, 2013). Those analyses were performed using the SimCyp software (Jamei *et al.*, 2009). The first model (illustrated in Supplementary Fig. 1) was a physiologically motivated "3-compartment" model for determining plasma concentrations that assumed no tissue partitioning, elimination due to metabolism of the parent compound in the liver, renal elimination by passive glomerular filtration (GF), and is adjusted for plasma protein binding [ie, GF rate (GFR) × fraction of chemical unbound in plasma]. Metabolism in this model is comparable to the "well-stirred" approximation for hepatic metabolism (Wilkinson and Shand, 1975).

The second general TK model (illustrated in Supplementary Fig. 2) was physiologically based (PBTK) with separate tissue compartments for the gut, liver, lung (unused for dosing in this research, since the inhalation route was not simulated), kidneys, and arterial and venous blood. The rest of the tissues in the body were aggregated. Tissue volumes and blood flows were

Downloaded from http://toxsci.oxfordjournals.org/ at Environmental Protection Agency Library on September 23, 2015

taken from Birnbaum *et al.* (1994). Tissue flows and volumes were scaled to cardiac output and body weights from Davies and Morris (1993), which also provided values for GFR and hematocrit. Absorption from the gut lumen into gut tissue was modeled as a first-order process with an arbitrary, "fast" rate of 1/h. Venous blood from the gut and arterial blood fed separately into the liver, where metabolism was again modeled with the "well-stirred" approximation.

Physico-chemical and partitioning information were collated from various sources. Molecular weight and structure were determined from the DSStox database (http://www.epa.gov/ncct/dsstox, last accessed 22 June 2015) and hydrophobicity was drawn for all compounds from EPI Suite (http://www.epa.gov/opptintr/exposure/pubs/episuite.htm (last accessed 22 June 2015)—measured values used if available, predicted otherwise). Where available, ionization association/dissociation equilibrium constants were curated from the literature; otherwise predictions were based on chemical structure using the SPARC (SPARC Performs Automated Reasoning in Chemistry) model (Hilal *et al.*, 1995). Experimental values for membrane affinities (ie, lipid-bilayer to water concentration ratios) were used where available (Endo *et al.*, 2011) or predicted using a regression of the Endo *et al.* (2011) data based on hydrophobicity and temperature:

$$\log_{10}(K_{npl:water}) = 0.999831 - 0.016578 \times T + 0.881721 \times \log_{10}(K_{octanol:water}),$$

where T is the temperature (°C), $K_{npl:water}$ is the neutral phospholipid-to-water concentration ratio, and $K_{octanol:water}$ is the octanol-to-water concentration ratio.

Chemical-specific tissue to free fraction in plasma partition coefficients were predicted using Schmitt's method (2008a). Tissue-specificity was based upon the cellular fraction of total volume; water, lipid and protein fraction of cellular volume; and distribution of types of lipid (Schmitt, 2008b). Chemical-specificity was based upon plasma protein binding (fup), the hydrophobicity, and any ionization association/dissociation constants. Because we do not have a method for estimating the rate at which chemicals diffuse into tissues, we assumed that all tissues were perfusion-limited; ie, chemical concentrations in tissue, red blood cells, and plasma come to equilibrium instantaneously relative to the flow of blood.

Determination of steady state. We use the term "steady-state" to describe the situation where the chemical concentration in plasma caused by the assumed exposure scenario is unchanging in time. With the assumption of constant infusion dosing, as in Wetmore *et al.* (2012), this is a true steady-state. With constant infusion dosing the flow of chemical into the body is matched perfectly by clearance from the body. For dynamic exposure scenarios (such as exposures separated by time intervals), a quasi-steady-state is determined to occur if the plasma concentration effectively no longer increases across a fixed time interval. For example, if plasma concentration is the same just before the next dose as it was before the current dose, this is quasi-steady-state.

In order to determine if steady-state conditions were achieved, 2 analytic equations were derived from the differential equations of the 3-compartment TK and PBTK models by assuming constant infusion dosing. The analytic solution to the 3-compartment TK model is the equation used for steady-state plasma concentrations (C_{ss}) in previous work (Rotroff *et al.*, 2010; Wetmore *et al.*, 2012, 2013; Wilkinson and Shand, 1975). For the PBTK model, equations were solved numerically to simulate a series of repeated, every 8-h oral doses until the daily averaged venous concentration, just before re-dosing, was within a small tolerance (1%) of the concentration predicted with the analytical solution of the PBTK model. The PBTK simulations assume an initial body burden of no chemical, even though this may not be the case for certain persistent, bioaccumulating, or endogenous chemicals. The equations for the analytic solutions are given in the captions to Supplementary Figures 1 and 2.

In vitro chemical data. *In vitro* data used in this study was extracted from published literature. For environmental, pesticidal, and industrial chemicals, *in vitro* experimental data were obtained primarily from Wetmore *et al.* (2012) and Tonnelier *et al.* (2012). For pharmaceutical compounds these values were compiled from Obach (1999), Jones *et al.* (2002), Shibata *et al.* (2002), Lau *et al.* (2002), Naritomi *et al.* (2003), Ito and Houston (2004), McGinnity *et al.* (2004), Schmitt (2008a), and Obach *et al.* (2008).

Two types of *in vitro* data were extracted in order to parameterize the TK models—intrinsic hepatic clearance and plasma protein binding. The intrinsic metabolic clearance of the parent compound (CL_{int}) by primary hepatocytes (substrate depletion approach) was measured in wells on a multi-compound plate (Shibata *et al.*, 2002). Since only the unbound chemical in the hepatic clearance assay is available for metabolism, CL_{int} was determined from the observed clearance (CL_{uint}) which was divided by the estimated fraction of chemical unbound in the hepatocyte intrinsic clearance assay (f_{uhep}), as estimated using the method of Kilford *et al.* (2008). The Kilford *et al.* (2008) method includes a distribution coefficient estimated from hydrophobicity and ionization. In Wetmore *et al.* (2012), 2 chemical concentrations (1 and 10 μM) were tested, in part to test for saturation of metabolism. We have used only the 1 μM values. Fraction of chemical unbound in the presence of plasma protein (f_{up}) was assessed using rapid equilibrium dialysis (RED) in which 2 wells are separated by a membrane that is permeable to smaller molecules but prevents the plasma protein from migrating from one well to the other (ie, the relative chemical concentration in the 2 linked wells gives the free fraction of chemical) (Waters *et al.*, 2008).

Monte Carlo simulation and parameter distributions. Previous reverse dosimetry analyses (Rotroff *et al.*, 2010; Wetmore *et al.*, 2012) used the SimCYP software (Jamei *et al.*, 2009) to perform a Monte Carlo (MC) simulation of human variability and we have implemented a similar MC simulation ability. To match the assumptions used by SimCYP, normal distributions that were truncated to ensure positive values were used with mean values drawn from the references above and a coefficient of variation of 0.3. Body weight, liver volume, hepatic blood flow, glomerular filtration rate, and CL_{uint} were all varied in this manner. In a change from previous MC simulations, the values for protein binding, f_{up}, were drawn from a censored normal distribution: values were sampled from a uniform distribution between 0% and the limit of detection (LOD) (default of 1% unbound) at a rate proportional to the number of samples from the truncated normal distribution below the LOD. For each chemical, 1000 different combinations of parameters were used to determine C_{ss}, allowing estimation of the 5th, median, and 95th percentiles.

In vivo chemical data. In Wetmore *et al.* (2012), *in vivo* TK and PBTK modeling data for the environmental, pesticidal, and industrial chemicals were collected from the literature and used

Downloaded from http://toxsci.oxfordjournals.org/ at Environmental Protection Agency Library on September 23, 2015

to assess the predictive ability of the human *in vivo* C_{ss} estimation, assuming a 1 mg/kg/day daily oral administration. For pharmaceutical compounds, the measured human clearance (l/day) and volume of distribution (l) in Obach *et al.* (2008) was used to determine C_{ss} for the same dose.

Model compounds for rat IVIVE were chosen based on the availability of HTTK input parameters CL_{uint} and f_{up}. A list was constructed from Ito and Houston (2004), complemented by a group of compounds to which reverse dosimetry was applied in earlier studies (Krug *et al.*, 2013; Piersma *et al.*, 2013). For these compounds, we searched public sources for studies reporting plasma concentration time course data in rat following oral or intravenous administration. Pharmacokinetic data were retrieved from those studies (Supplementary Table 2) by digitizing published figures using TechDig v2.0.

In silico transporter predictions. We used the method of Random Forest (Breiman, 2001) to develop QSAR predictions of transporter affinity (Sedykh *et al.*, 2013). We used the R package "randomForest" by Liaw and Weiner (2002). Experimental data characterizing interaction of chemicals with membrane transporters were compiled from multiple available public sources (Sedykh *et al.*, 2013). The chemicals were represented using Chemistry Development Kit descriptors (Steinbeck *et al.*, 2003) determined from Simplified Molecular-Input Line Entry System strings (Weininger, 1988). Chembench (Walker *et al.*, 2010) was used to standardize chemical structures as well as normalize chemical descriptors to range between 0 and 1. Inhibitors were defined based on a potency threshold of 10 μM except for peptide transporter 1 (PepT1), organic cation transporter 1 (OCT1), and organic anion-transporting polypeptide 2B1 (OATP2B1), for which 100 μM threshold was used due to lower levels of affinity of reported inhibitors. Scores equal to 0 or 1 imply high-confidence predictions that a chemical is a non-substrate or a substrate, respectively, whereas a score of 0.5 indicates an ambiguous prediction (Sedykh *et al.*, 2013). The full list of transporters modeled is identified in Supplementary Table 1, which also contains the QSAR predictions for each compound.

A second model, based upon Bayesian classification, was used to predict interactions of the compounds with organic anion transporter protein (OATP) 1B1 (Van de Steeg *et al.*, 2015). The classification model is based on a database recording the inhibitory potential of 640 FDA-approved drugs from a commercial library (10 μM) on the uptake of [3H]-estradiol-17beta-D-glucuronide (1 μM) in Human Embryonic Kidney 293 cells stably transfected with human OATP1B1. The structural similarity (feature-connectivity bit string 4) to the nearest similar chemical in this training set is used as a measure for potential interaction with OATP1B1. Although this model predicts inhibition of OATP1B1-mediated uptake rather than uptake itself, we assume here that the inhibition is mostly competitive and therefore identifies potential transporter substrates.

HTTK-in vivo discrepancy analysis. The Random Forest algorithm was used to analyze the correlation of chemical descriptors with the discrepancy between HTTK predictions and results based on *in vivo* data. The Random Forest method is cross validated (Breiman, 2001), performing multiple analyses based on different subsets of chemicals and different subsets of chemical descriptors. Fifty thousand regression trees were constructed using random subsets of the data, with a subset of 17 factors considered at each split in the tree, and a minimum terminal node size of 5. Performance of each regression tree was evaluated against the chemicals not used to build that tree. The most important factors in the random forest model were calculated using the method of decrease in node impurities (essentially, a leave 1 factor out method) (Archer and Kimes, 2008). We used the R package "rpart" by Therneau *et al.* (2014) to perform the method of recursive partitioning (Breiman *et al.*, 1984) to develop a regression tree for the full dataset (ie, not cross-validated). Finally, a random forests approach was used to construct a classifier tree for 5 exclusive categories ("on the order," "3.2× under-predicted," "10× under-predicted," "3.2×over-predicted," "10× over-predicted"), with a subset of 17 factors considered at each split, and a minimum terminal node size of 1.

RESULTS

Our HTTK models require chemical-specific data on CL_{int} and f_{up} to predict human C_{ss}. We obtained data from the peer-reviewed literature for a total of 349 chemicals. These chemicals include (non-uniquely) 312 Tox21 chemicals, 248 ToxCast chemicals, 74 pharmaceuticals, and 35 chemicals for which human exposure is monitored by the Centers for Disease Control National Health and Nutrition Examination Survey (CDC, 2012). The distribution of the non-zero values of the CL_{int} and f_{up} data is roughly log-normal and is similar across the curated literature (Supplementary Figs. 3 and 4).

Figure 1 illustrates our ability to reproduce the Wetmore *et al.* (2012) results. As in Wetmore *et al.* (2012), we simulated population variability to determine the median, lower 5th, and upper 95th percentile of plasma concentrations for individuals exposed to the same, fixed dose (1 mg/kg BW/day). Since the upper 95th percentile individuals have higher plasma concentrations for the same exposure, they are considered to be an example of a sensitive population. Any 1 chemical in Figure 1 is indicated by 3 plot points connected by a line. The 3 points correspond to the median, lower 5th, and upper 95th percentiles of

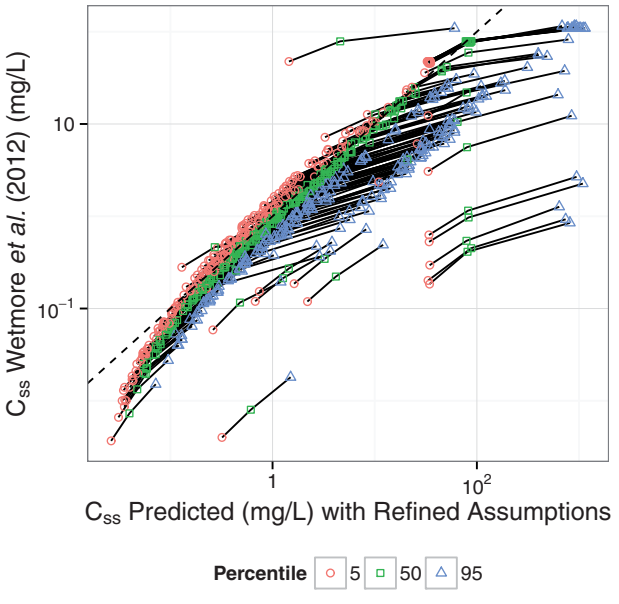

FIG. 1. Comparison of the median, upper, and lower 95th healthy adult human percentiles of steady-state plasma concentration (C_{ss}) predicted on the *y*-axis using SimCyp (Wetmore *et al.*, 2012) and on the *x*-axis using assumptions refined to better reflect screening for environmental chemicals. The C_{ss} values were estimated assuming a steady-state infusion of 1 mg/kg BW/day. Each chemical's median and upper and lower 95th percentiles are connected by a line. The dashed line indicates the identity (perfect predictor) line.

Downloaded from http://toxsci.oxfordjournals.org/ at Environmental Protection Agency Library on September 23, 2015

the C_{ss}. The dashed line indicates the identity (perfect predictor) line—the further a prediction is from the identity line the greater the discrepancy. We describe predictions with large discrepancies as "outliers."

There was good agreement ($R^2 = 0.84$) between our simulations and those in Wetmore *et al.* (2012) for all 3 percentiles. However, this comparison did identify 2 groups of outliers for which the predictions differ due to differing assumptions.

The first group of chemicals in Figure 1 with differing predictions is those that have an upper 95th percentile C_{ss} that was significantly higher than previously estimated, though the median and lower percentile values were unchanged. These chemicals are indicated in Figure 1 by a bent line connecting the 3 quantiles. This predicted difference indicates greater risk for the most sensitive individuals. This difference was due to replacing a default value with a censored distribution for chemicals with a failed RED assay for measuring f_{up} (protein binding). Among other reasons (eg, binding to membrane), the RED assay can fail because the amount of free chemical is below the LOD. In Wetmore *et al.* (2012), the RED assay failed for ~38% of the chemicals. For these chemicals, Wetmore *et al.* (2012) assumed a default value of 0.5% free (roughly half the average LODs). For the analysis shown in Figure 1, we have replaced this default value with a censored distribution in our MC variability simulation (essentially, simulating many different values between 0 and 1%).

There was a second group of chemicals in Figure 1 where the current modeling provided plasma concentration estimates different from Wetmore *et al.* (2012) due to a change in assumptions. This group contained chemicals where differences in the analysis of the hepatic clearance assay results led to different concentrations predicted for all 3 population percentiles in Figure 1 (ie, 3 quantiles connected by a line that are all distant from the identity line). Due to measurement variability and other factors, a linear model may not describe the decrease in parent chemical concentration as a function of time. Previously, a *P*-value threshold of .10 (probability of the null hypothesis of no disappearance of chemical was <10%) was used to determine if the chemical showed significant intrinsic clearance over the time examined. For the results shown in Figure 1, we have required that *P*-values be <.05. For those with a *P*-value >.05, we use a default value of 0 (ie, no hepatic clearance) which acts to increase the estimated plasma concentration for a fixed dose.

Most discrepancies between our predictions and Wetmore *et al.* (2012) disappear ($R^2 \sim 0.90$, Supplementary Fig. 5) if we replace our revised assumptions with the original assumptions of Wetmore *et al.* (2012). However, 8 discrepant chemicals remain due to issues such as the only C_{ss} available in Wetmore *et al.* (2012) was calculated using the 10 μM clearance data. The lone chemical for which we under-predict the value from Wetmore *et al.* (2012) for all 3 population percentiles is Chlorpyrifos-methyl, for which the 10 μM clearance assay was not statistically significant, leading Wetmore *et al.* (2012) to use 0 clearance. Since the clearance assays conducted at 1 μM was statistically significant, we used that value, leading to a larger predicted clearance.

Once we were satisfied that we could reproduce previous results for the majority of chemicals, and understood those cases where we differed, we proceeded to evaluate 3 key assumptions for the calculation of C_{ss}. Previously, chemical partitioning into tissues (eg, volume of distribution) was not determined from HTTK data, necessitating the use of C_{ss} as a dose metric because the concentration at steady-state does not depend on the amount of chemical in tissues. This means that we assume that humans reach steady state with respect to environmental exposures. Using the analytic solution for C_{ss} requires the further assumption of constant infusion dosing. Constant infusion dosing requires that we assume that steady-state plasma concentrations are a reasonable surrogate for peak concentrations which would be caused by other exposure scenarios (eg, exposure at meal times only). Further, constant infusion dosing requires either the assumption that 100% of the chemical is absorbed or the use of additional models to predict absorption. Wetmore *et al.* (2012) selected 100% absorption as being conservative (causing overestimated plasma concentration). By constructing non-steady-state, PBTK models, we can assess the plausibility of these 3 assumptions.

We developed HTPBTK models using Schmitt's method for tissue partitioning (Schmitt, 2008a). We used a generic PBTK model structure that could be parameterized for any chemical using CL_{int} and f_{up} and experimental or QSAR-derived physicochemical properties. Schmitt's method requires a value for protein binding in order to make predictions; therefore, we could only build HTPBTK models for 271 chemicals. Further assumptions about chemical absorption and bioavailability (ie, rapid absorption and 100% bioavailability) were required in order to parameterize the HTPBTK models.

Figure 2 illustrates our evaluation of the HTPBTK model predictions by comparison to literature *in vivo* time course data in rats for 22 chemicals. For a given chemical, the specific TK properties, dose, and route of administration result in different plasma concentration kinetics that we have summarized by the time-integrated plasma concentration (Area Under the Curve, AUC). Neglecting route of administration, we find that HTPBTK is predictive ($R^2 = 0.68$) of *in vivo* data (Fig. 2A). When we estimate a difference between oral exposures (which are subject to absorption and bioavailability) and intravenous and subcutaneous dose routes (which are not), we find slightly greater predictive ability ($R^2 = 0.73$). We systematically over-predict AUC for chemicals administered orally. The average difference between oral and intravenous doses is 6.4 (95% confidence interval 2.3–18), ie, on average AUCs from oral doses are roughly 6 times lower than predicted. This result indicates that the absorption assumptions we used for HTPBPTK are conservative and health protective since they produce higher predicted exposures. In Figure 2B, we show that peak plasma concentration (C_{max}) also appears to be well described by the HTPBTK model ($R^2 \sim 0.68$) and that there is a systematic bias toward over-prediction. The treatments that are over-estimated are predominantly for intravenous doses while predictions for oral doses are more evenly scattered about the identity line. The handful of cases where HTPBTK under-predicts C_{max} are all for oral administration.

Having established that our HTPBTK model predictions are consistent with the *in vivo* data that was available for 22 chemicals (Fig. 2), we conducted a simulation study to evaluate the assumptions used to calculate C_{ss} in previous HTTK reverse dosimetry analyses. In the simulation study, we replaced the infusion dose assumption with a dosing scenario of 3 daily doses totaling 1 mg/kg BW/day (eg, exposure at meal times or from consumer product use), to better reflect the near field sources of exposure that appear to be dominant for environmental chemicals (Wambaugh *et al.*, 2013). As illustrated in Figure 3A, 70% of chemicals (182 of 271) reach steady-state within 28 days, and 90% of chemicals (252 of 271) reach steady-state within 1000 days. However, there were 19 chemicals that required more than 1000 days to reach steady-state (Table 1). TK analyses based upon C_{ss} are inappropriate for these chemicals, suggesting a need for alternative approaches. Approaches based on dynamic TK simulation of the tissue concentrations

Downloaded from http://toxsci.oxfordjournals.org/ at Environmental Protection Agency Library on September 23, 2015

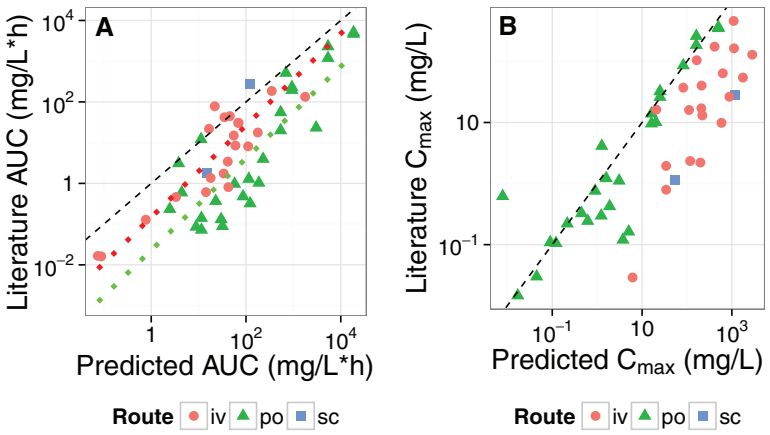

FIG. 2. Evaluation of the predictive ability of HTPBTK models by comparing predictions with *in vivo* measurements in the rat for the AUC (A) and C_{max} (B). Each chemical may have more than one study with potentially different doses and routes. Dose route is indicated by symbols (oral, po—triangle; intravenous, iv—circle; subcutaneous, sc – square). The upper dotted line is the linear regression for intravenous doses, while the lower dotted line is for the oral doses. The dashed line indicates the identity (perfect predictor) line.

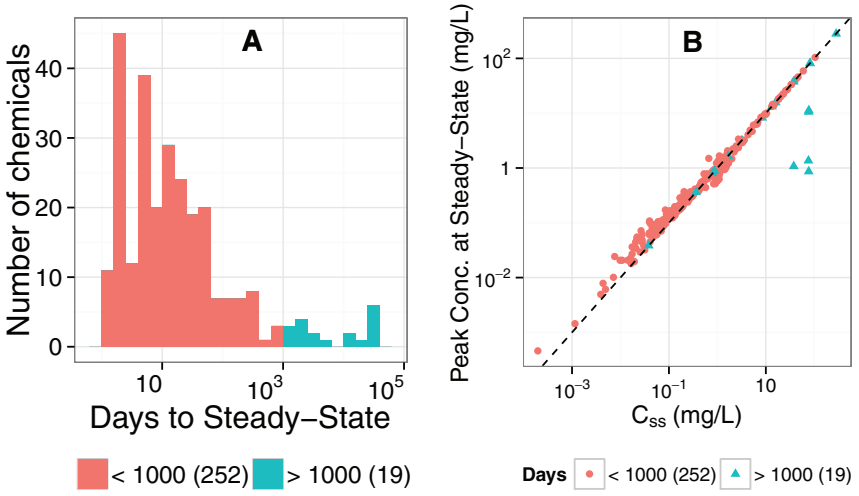

FIG. 3. HTPBTK simulation results evaluating the steady-state infusion assumption to predict C_{ss}. A, Histogram of number of chemicals versus the days needed to effectively reach steady-state assuming 3 daily doses (every 8 h). B, Comparison of peak plasma concentrations due to 3 daily does predicted with the HTPBTK model with the C_{ss} due to a constant infusion exposure as used in Figure 1 and previous reverse dosimetry studies. The dashed line indicates the identity (perfect predictor) line.

likely to be caused over a life-time of exposure may be more appropriate. The 5 chemicals that never reach steady-state (ie, the ratio of the simulated average daily concentration to the analytic C_{ss} never approaches 1) are polychlorinated biphenyls (PCBs), which are known to have long human half-lives (Ritter *et al.*, 2010) and are no longer deliberately in commerce.

With the HTPBTK models and more realistic exposure simulation, we then compared predicted peak concentrations with the C_{ss} derived from the analytical solution to the 3-compartment TK model (Fig. 1). As shown in Figure 3B, the peak concentration for repeated dosing is not different ($R^2 \sim 0.95$) from the C_{ss} predictions under the assumption of constant infusion dosing. Similarly, the average daily concentration at steady-state was nearly identical ($R^2 \sim 0.96$) to the analytical result for C_{ss} used in Wetmore *et al.* (2012) and elsewhere (Supplementary Fig. 6). For rapidly cleared compounds, the peak concentrations from 3 daily doses were within an order of magnitude of C_{ss}.

We then compared HTTK predictions of C_{ss} based on *in vitro* data with C_{ss} values inferred for humans from *in vivo* studies for 11 environmental chemicals (Wetmore *et al.*, 2012) and 74 pharmaceuticals (Obach *et al.*, 2008). Figure 4A illustrates that there is a weak predictive ability ($R^2 \sim 0.34$), but that the errors are mostly conservative (ie, the predicted plasma concentrations based on *in* vitro data are higher than the *in vivo* data indicates). When the perfluorinated chemicals (PFCs) are removed, the R^2 drops to ~0.23. We note that the correlation between the HTTK C_{ss} versus the C_{ss} inferred for humans from *in vivo* studies is lower than observed for AUC and C_{max} predictions in Figure 2. At steady-state, all C_{ss} values are compared for the same fixed dose rate of 1 mg/kg/day. When the HTPBTK predictions are normalized for administered dose, the R^2 for AUC and C_{max} drop to ~0.48 for both, indicating that a portion of the predictive ability of the HTPBTK might be due to the data varying linearly with dose for those chemicals.

Downloaded from http://toxsci.oxfordjournals.org/ at Environmental Protection Agency Library on September 23, 2015

TABLE 1. Chemicals Predicted to Require Long Time Periods to Reach Steady-State

Compound	CAS	Analytic C_{ss} (mg/l)	HTPBTK Average Daily Conc. (mg/l)	Ratio of HTPBTK to Analytic After 100 Years	Years to Steady-State	V_d (l)	K_{el} (h)
Fenpropathrin	39515-41-8	0.36	0.36	0.99	3.0	651.3	0.000162
Perfluorooctanoic acid	335-67-1	81.55	81.39	0.99	3.5	3.4	0.00015
Imazalil	35554-44-0	13.37	13.17	0.99	4.1	24.8	0.000128
Maprotinline	10262-69-8	0.8	0.8	0.99	4.9	480.9	0.000106
Tetraconazole	112281-77-3	15.92	15.67	0.99	5.7	28.9	9.22E−05
Perfluorooctane sulfonic acid	1763-23-1	81.83	81.66	0.99	6.6	6.4	7.92E−05
Isoxaben	82558-50-7	8.4	8.25	0.99	6.8	65.5	7.71E−05
Ddt	50-29-3	0.04	0.04	0.99	7.3	15127.0	3.84E−05
S-bioallethrin	28434-00-6	1.66	1.63	0.99	9.0	434.5	5.85E−05
Fenvalerate	51630-58-1	0.88	0.88	0.99	13.7	1235.3	3.71E−05
Zoxamide	156052-68-5	37.87	37.69	0.99	34.0	71.3	1.55E−05
Oxyfluorfen	42874-03-3	3.21	3.18	0.99	41.7	1033.9	1.26E−05
D-*cis*, *trans*-allethrin	584-79-2	1.35	1.33	0.99	46.7	2763.0	1.13E−05
Emamectin benzoate	155569-91-8	282.45	281.50	0.99	77.7	21.8	6.77E−06
PCB136	38411-22-2	37.68	1.08	0.03	>100	34485.6	3.21E−08
PCB153	35065-27-1	76.7	0.86	0.01	>100	43391.9	1.25E−08
PCB155	33979-03-2	75.67	1.36	0.02	>100	27407.8	2.01E−08
PCB77	32598-13-3	76.21	10.56	0.13	>100	3314.2	1.65E−07
PCB80	33284-52-5	77.06	11.26	0.14	>100	3093.6	1.75E−07

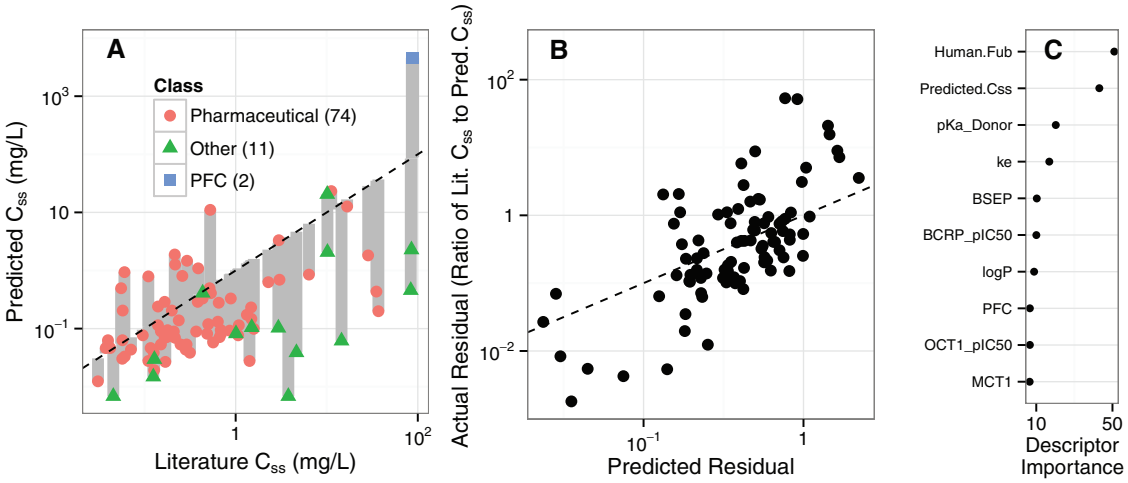

FIG. 4. A, Comparison of HTTK predicted C_{ss} values with measured *in vivo* C_{ss} values from literature studies. Two PFCs are plotted on top of each other. The dashed line indicates the identity (perfect predictor) line. Chemicals plotted below the identity line have predictions greater than literature values, and vice versa. The thick grey lines indicate the discrepancy between measured and predicted values (ie, the residuals). Comparison of the actual residuals calculated from (A) and the residuals predicted using a random forest analysis based on chemical descriptors is shown in (B). The most important factors in the random forest model, as calculated using the method of decrease in node impurities, are shown in (C). These factors are described in detail in Tables 2 and 3.

To identify chemical-specific properties that correlate with reduced HTTK predictive ability, we analyzed the difference between *in vivo* measurements and HTTK predictions (ie, the residuals), shown by thick grey lines in Figure 4A. The method of random forests was used to predict the residual for each chemical with *in vivo* data, as shown in Figure 4B. Chemical properties included chemical-specific physico-chemical properties, *in vitro* intrinsic hepatic clearance, *in vitro* plasma protein binding, and QSAR predictions of transporter affinity. Transporters were included because predictors were available (Sedykh *et al.*, 2013) and they constitute an often important driver of TK (Giacomini *et al.*, 2010; Shugarts and Benet, 2009) that is not included in the steady-state model. A large predicted residual for a specific chemical corresponds to a large expected error. The random forest approach ensures cross-validated predictive ability by averaging the predictions of many models constructed from random subsets of the chemicals and chemical descriptors. The relative importance of the top 10 chemical properties for predicting HTTK residuals (errors) is illustrated in Figure 4C. These factors are described in detail in Tables 2 and 3. Note that all transporters that were included as potential predictors of error were anticipated to be relevant to TK. The relative rankings of specific transporters in Table 2 may reflect the chemical evaluation set that was used.

Downloaded from http://toxsci.oxfordjournals.org/ at Environmental Protection Agency Library on September 23, 2015

TABLE 2. Transporters Associated With Differences Between HTTK Model Predictions and Human *in vivo* C_{ss}

Abbreviation (Gene)	Full Name	Transporter	References	Random Forest Importance[a]	Included in Tree Made From All Data
BSEP (ABCB11)	Bile Salt Export Pump	Hepatocyte bile secretion efflux transporter	Faber *et al.* (2003) and Giacomini *et al.* (2010)	10.3	
BCRP (ABCG2)	Breast cancer resistance protein	Hepatocyte bile and intestinal secretion efflux transporter	Giacomini *et al.* (2010)	9.97	
OCT1 (SLC22A1)	Organic Cation Transporter 1	Hepatocyte influx and intestinal secretion influx transporter	Faber *et al.* (2003) and Giacomini *et al.* (2010)	6.64	
MCT1 (SLC16A1)	Monocarboxylate Transporter 1	Ubiquitous Transporter	Halestrap and Meredith (2004)	6.6	Y
OATP2B1 (SLCO2B1)	Solute carrier organic anion transporter family member 2B1	Hepatocyte and blood-brain barrier influx transporter	Giacomini *et al.* (2010)	5.77	Y
PEPT1 (SLC15A1)	Peptide transporter 1	Intestinal and kidney secretion influx transporter	Giacomini *et al.* (2010)	5.54	Y

[a]Larger value indicates greater relative importance. When multiple predictors for same transporter were available, only the highest reported importance is reported.

TABLE 3. Other Factors Associated With Difference Between HTTK Model Predictions and Human *in vivo* C_{ss}

Factor	Description	Random Forest Importance[a]	Included in Tree Made From All Data
f_{up}	Fraction unbound to plasma protein as measured *in vitro*	51.0	Y
Predicted C_{ss}	Steady-state concentration predicted from *in vitro* measured f_{ub} and C_{lint}	43.1	Y
Ionization (pKa_Donor)	Acid dissociation equilibrium constant	20.2	
Elimination rate (k_e)	Elimination rate as calculated from total clearance (renal + hepatic) predicted from *in vitro* data, divided by V_d	16.9	
Log K_{ow}	Log transformed hydrophobicity (ratio of concentration in octanol to water)	8.86	
Perfluorinated compound (PFC) (yes/no)		6.65	

[a]Larger value indicates greater relative importance.

Although the random forest method produces a cross-validated predictor, the interpretation of how those predictions are achieved can be difficult since the predictions are the average of many different models. A single regression tree for predicting C_{ss} residuals based on all chemicals and all available chemical properties can be created for descriptive purposes (Fig. 5). Error in the HTTK models (ie, large residuals) appears to be driven by predicted C_{ss}, f_{up}, chemical ionization, and 2 of the transporters described in Table 2. We note 2 broad classes of chemicals—those chemicals where HTTK predictions are *on the order* (ie, within ~3.2× or $10^{1/2}$×) of the observed *in vivo* values (~65% of the chemicals), and those chemicals where the errors can be several orders of magnitude (28% of the chemicals were ~6× overestimated, and 8% of chemicals 120× overestimated on average). For this final group of chemicals, the large overestimation by the HTTK models leads to conservative reverse dosimetry predictions (ie, errors that would lead to lower predicted ratios between bioactive doses and the maximal expected exposures, thus leading to a higher predicted risk).

Motivated by the regression tree analysis in Figure 5, which classified all the data but was not suitable for prediction, a second random forest (ie, predictive, rather than descriptive) analysis was conducted. The analysis used the same descriptors as before to classify chemicals into 5 categories based on residual: those chemicals with predictions on the order of the *in vivo* C_{ss} (within ~3.2×), those that were between ~3.2× and 10× over or underestimated, and those that were >10× over or underestimated. The cross-validated classifier had a sensitivity of 79%, a specificity of 54%, and a balanced accuracy of 64% when predicting whether or not a HTTK C_{ss} prediction will be on the order of the *in vivo* measured C_{ss}. Chemicals for which the residuals are predicted to be on the order or overestimated are within the domain of applicability of our HTTK approach; ie, we expect to have either small or conservative errors for reverse dosimetry. Along with identifying those chemicals that never reach steady-state (Table 1) and those chemicals for which the plasma protein binding assay failed, the 5 categories from this random forest classifier allow each chemical to be placed into 1 of 7 categories, as illustrated in Figure 6.

By integrating the various analyses in this study, we developed a TK triage framework that provides guidance on the degree of confidence for a particular prediction and indicates which chemicals may benefit from specific types of analyses or experimental data collection (Table 4). The first step is the collection of basic *in vitro* TK data that allows a prediction to be made for C_{ss}. Second, the parameterization of HTPBTK models using physico-chemical properties and predicted partition coefficients, if possible, allows a determination of the plausibility of reaching steady state. Third, chemical properties that are correlated with large deviations between predicted and observed

Downloaded from http://toxsci.oxfordjournals.org/ at Environmental Protection Agency Library on September 23, 2015

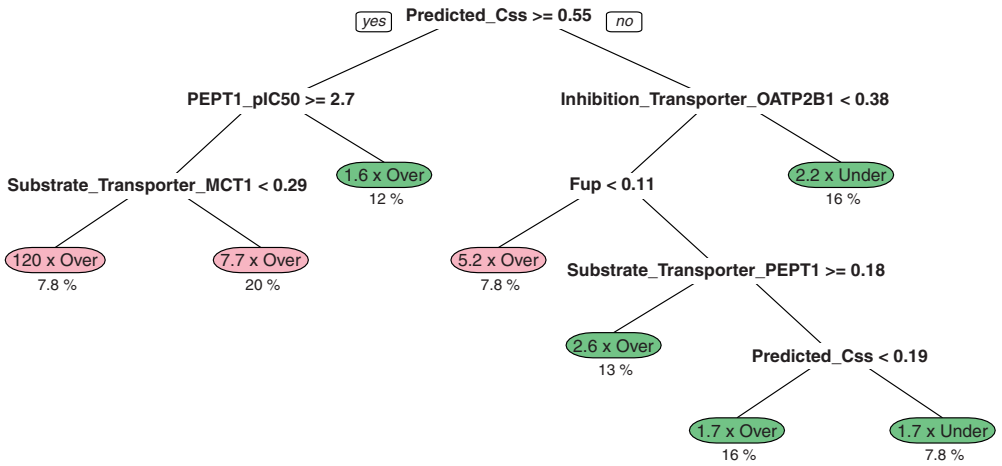

FIG. 5. A recursive partitioning regression tree was used to classify the discrepancy between the C_{ss} predicted from *in vitro* data and the *in vivo* C_{ss} (Obach *et al.*, 2008; Wetmore *et al.*, 2012). Each "leaf" of the tree shows a group of chemicals for which HTTK either overestimates C_{ss} (making conservative predictions) or underestimates C_{ss}. For all but 3 groups, the predictions are on the order of the observed C_{ss} (approximately within a factor of 3.2× greater or lesser). For the other 3 groups, the C_{ss} is 5.2×, 7.7×, and 120× overestimated. The dashed line indicates the identity (perfect predictor) line.

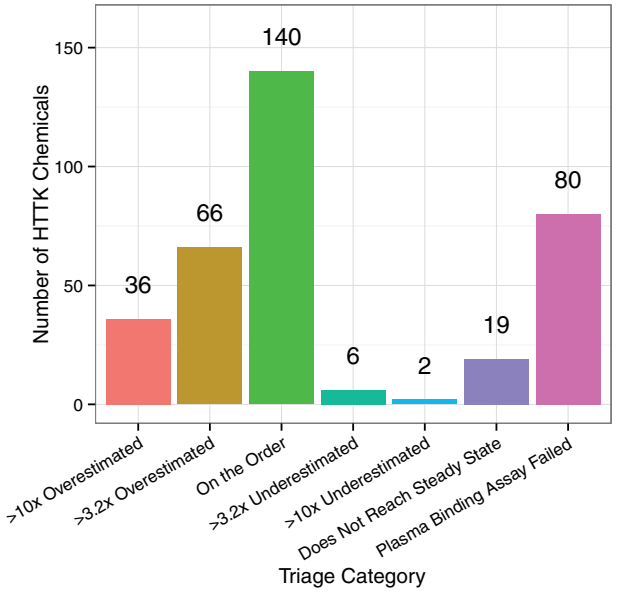

FIG. 6. Distribution of the 349 chemicals with IVIVE data among the triage elements in Table 4. C_{ss} is not meaningful for the chemicals that do not reach steady-state. Chemicals where the protein binding assay failed cannot easily be categorized since f_{up} is an important predictor (Table 3) of discrepancy between HTTK C_{ss} predictions and literature values for C_{ss}. The remaining chemicals are categorized as likely having HTTK predictions for C_{ss} that would be overestimated, underestimated, or on the order (±3.2× the *in vivo* value).

behavior can be used to screen out those chemicals for which HTTK is not expected to perform well. The 4th element of triage addresses those remaining chemicals in greatest need of alternative, perhaps traditional approaches. Different elements of triage may be applied concurrently, depending on the information that is available.

We applied the TK triage (Table 4) to the entire 349 chemical set in Figure 6. We find that a plurality (140) of the chemicals are estimated to be "on the order," ie, the HTTK predicted C_{ss} will be within ~3.2× of the literature value. The third largest category is chemicals for which the protein binding assay failed (80), precluding analysis of time to reach steady-state. However, only 7% of chemicals analyzed for time to reach steady-state did not do so within 1000 days, and we might assume this figure to be similar for these 80 chemicals. Of the remaining 110 chemicals, most (102) are predicted to be overestimated, leading to conservative errors when conducting reverse dosimetry. In total, we predict that the reverse dosimetry assumptions will be appropriate for 89% of the chemicals where the protein binding assay was successful.

DISCUSSION

Efforts to implement the vision outlined in Toxicity Testing in the 21st Century (National Research Council, 2007) include *in vitro* assays to identify potential biological targets of environmental and industrial chemicals (eg, ToxCast, Judson *et al.*, 2010). IVIVE methods are then needed to translate *in vitro* bioactive concentrations into administered doses (Blaauboer *et al.*, 2012; Wetmore *et al.*, 2012). HTS data might then be used in a risk-based context through the comparison of estimated bioactive doses to estimated exposures (Judson *et al.*, 2011; Thomas *et al.*, 2013; Wetmore *et al.*, 2012). Herein, we develop a method for identifying the degree of confidence with which we may apply HTTK in order translate HTS data for chemicals without other TK data. We have formalized this process in a triage system that has categorized 349 chemicals into 7 categories, 5 of which indicate varying degrees of confidence in the HTTK approach and 2 indicate a need for additional data or alternative approaches.

We examined 3 key assumptions in the previous HTTK research: that humans can reach a steady-state with respect to environmental exposures, that steady-state concentration is a reasonable surrogate when exposure is more episodic, and that 100% absorption is reasonable. These assumptions were tested using both simulation studies and direct comparison to *in vivo* data for both pharmaceuticals and environmental chemicals. Based on our analysis we organize HTTK testing into a TK triage framework for environmental chemicals (Table 4). Each element of the framework depends on data collection and/or analysis, and distinguishes those chemicals for which that sort of data is useful from those chemicals for which the approach does not apply. Based on this approach we expect the *in vivo* values to be within ~3.2× of predictions for ~59% the 246 chemicals that both had a successful plasma protein binding estimate and we

Downloaded from http://toxsci.oxfordjournals.org/ at Environmental Protection Agency Library on September 23, 2015

TABLE 4. Elements of HTTK Triage for Environmental Chemicals

	TK Data	Targeted Chemicals	TK Prediction/Consequence	Confidence	Domain of Applicability
1	*In vitro* clearance of parent compound by hepatocytes and binding to plasma protein	HTS compounds	Plasma C_{ss} from constant infusion exposure	If comparison with predicted exposure indicates large AER then infusion C_{ss} should be sufficient	Soluble low volatility (HTS appropriate) compounds
1a	CYP-specific *in vitro* data (Wetmore *et al.*, 2014)	Chemicals with AER near one for general population	Population variability, life-stage variability	Human variations in CYP expression are well characterized	Same as in 1
2	Physico-chemical properties (measured or QSAR)	All chemicals with successful binding *in vitro* assay	Prediction of partition coefficients allows HTPBTK steady-state predictions (including time to steady state) for more realistic exposure modeling	If comparison with predicted exposure indicates large AER then HTPBTK should be sufficient (ie, conservative due to 100% absorption)	QSAR-defined (eg, training set, extrapolation methodology)
3	QSARs for likely transporter substrates	All chemicals with successful binding *in vitro* assay	Assumptions of perfusion-limited tissue partitioning and passive renal excretion by glomerular filtration may be questionable	Can identify those chemicals where the impact is negligible (Fig. 4b)	Chemicals predicted to reach steady state in Tier 2 (Fig. 3a)
3b	Transporter-specific *in vitro* data	Chemicals indicated by QSAR	Tissue-specific accumulation, active secretion/resorption in kidney	Well characterized for non high-throughput applications	Same as in 3
4	*In vivo* oral and iv dose TK study, plasma only	Chemicals with large predicted residuals (Fig. 4b) and those that cannot be tested *in vitro*	Oral bioavailability, absorption rate, volume of distribution, and clearance (refined PBTK model)	If volume of distribution from HTPBTK model and *in vitro* estimate of clearance hold, then refined PBTK model should be excellent	Any compound

AER is the Activity to Exposure Ratio between HTS bioactive reverse dosimetry predictions and exposure.

predict will reach steady-state. We expect conservative errors for an additional ~37% of these 246 chemicals.

The final element of triage incorporates additional *in vitro* or *in vivo* testing for those chemicals that are most in need of additional attention. Admittedly, the domain of applicability for this approach is limited by the domain of chemicals used to conduct this analysis. Since there may be chemical properties that drive HTTK error that may be underrepresented by these chemicals, it will also be important to study at least a few members of diverse and novel classes of environmental and industrial chemicals.

The application of *in vitro* methods to TK is different in the pharmaceutical versus environmental chemical screening domains. For instance, it is expected that some samples of some compounds will be below the LOD of the cost-effective analytical chemistry that is required for the rapid TK screening of thousands of environmental and industrial chemicals (Rousu *et al.*, 2010; Wetmore *et al.*, 2012). When screening environmental and industrial chemicals, resources may not exist for follow-up work and the data must be used as is. This study found that typical assumptions such as half the LOD for protein binding (f_{up}) (Wetmore *et al.*, 2012) may result in an underestimation of C_{ss} values, which may not be health protective. However, this may be offset by other assumptions in the HTTK modeling that tend to produce an overestimate of C_{ss}.

For the metabolic clearance assay, stricter statistical limits are more conservative since they lead to overestimated C_{ss} values (ie, setting metabolic elimination to 0 for P-value $<.05$ instead of P-value $<.1$). However, many of the chemicals that we estimate to have 0 or non-significant clearance in the *in vitro* assays analyzed here may yield significant clearance in more physiological conditions, such as plated hepatocytes over a longer time period. Follow-up measurement of clearance rates using a plated hepatocytes system (Smith *et al.*, 2012) and/or longer times may ensure a more accurate hepatic clearance estimate.

For most environmental and industrial chemicals it is unlikely that there will ever be controlled human TK data. As evaluated by comparison to *in vivo* data, the predictive ability of the HTPBTK methods based on both IVIVE and QSAR-related methods was considerably greater than the HTTK models that assumed steady-state conditions. One possible explanation is that although the evaluation data for the HTPBPTK model predictions (*in vivo* AUCs and C_{max} values) were drawn from diverse literature, the *in vitro* data for this comparison were from a single source (Wetmore *et al.*, 2013). For the steady-state HTTK model evaluation, both the *in vivo* and the *in vitro* data were drawn from diverse literature sources.

Pharmaceuticals are typically small and well-absorbed molecules that are designed for specific biological targets (Lipinski, 2004). In contrast, environmental and industrial chemicals are structurally heterogeneous and may have multiple biological targets (Richard, 2006). Given the diversity of intended applications for environmental and industrial chemicals, their properties can vary greatly from those of pharmaceuticals. Unfortunately, though *in vitro* TK data have been collected for many of the 309 ToxCast Phase I chemicals, only 13 *in vivo* C_{ss} values were available for those chemicals (Wetmore *et al.*, 2012).

Although the HTPBTK models appear promising for predicting AUC and C_{max}, the *in vivo* evaluation data in Figure 2 are drawn from various treatments of only 15 pharmaceutical chemicals and 7 environmental chemicals, thus final

Downloaded from http://toxsci.oxfordjournals.org/ at Environmental Protection Agency Library on September 23, 2015

assessments of the HTPBTK methodology is not yet possible. An effort is needed to collect and organize additional *in vivo* data on environmental and industrial chemicals to confirm the usefulness of HTTK approaches. Generating the data necessary to evaluate HTTK methods does not necessarily require large resources: small, short term, *in vivo* studies—perhaps added to routine toxicological studies—could provide essential information for chemicals and chemical classes that are currently not well modeled. In addition, making existing TK-related data more accessible by creating databases and curating literature or legacy studies could inexpensively expand the available TK information. These *in vivo* TK data can inform important processes that are currently not assayed by HTTK.

The HTTK models analyzed here may omit or inaccurately estimate drivers of TK including: extra-hepatic metabolism; secretion in bile and enterohepatic recirculation; active transport in renal, hepatic, and other tissues; and absorption/bioavailability (Rotroff *et al.*, 2010). Until rapid and cost-effective *in vitro* assays are developed for these processes, QSAR models would seem to provide one-way forward. Unfortunately, QSAR is not yet capable of providing reliable rate constants (eg, transporter velocity); rather, QSAR can estimate how likely or unlikely it is that a process will occur (Sedykh *et al.*, 2013). By integrating the available QSAR predictions into a model to predict when the difference between HTTK predictions and *in vivo* data will be large, we can better identify those compounds in need of follow-up study. However, those chemical properties found to increase predictive error in this current analysis (and therefore indicate that we may be outside the domain of applicability for our methods) apply only to the chemical space we have analyzed thus far. As the approach is applied to new chemicals, additional properties might be identified that play a more significant role in the TK prediction of some of these other chemicals. We must target for further study those chemicals most likely to be subject to transport processes or other drivers of uncertainty as indicated by large errors in HTTK model predictions.

HTTK is intended to complement HTS assays that identify bioactivity of chemicals *in vitro*. As with most HTS assays, we so far have only the means to deal with the parent compound, and do not yet have the tools to deal with any metabolites in a high throughput manner. If these tools were to become available, they would become an important tier in TK triage.

We have shown that HTTK models can be developed from *in vitro* data for many environmental chemicals. The steady-state predictions of these models allow concentrations showing biological activity in HTS assays to be converted into administered dose values. We have evaluated the predictions of these models using comparison to *in vivo* values and HTPBTK simulation studies to identify when HTTK may be used with confidence and when additional, targeted measurements may be necessary.

SUPPLEMENTARY DATA

Supplementary data are available online at http://toxsci.oxfordjournals.org/.

FUNDING

The United States Environmental Protection Agency through its Office of Research and Development funded and managed the research described here. James Sluka was funded by the US EPA (R835001), the NIH (GM077138) and the Biocomplexity Institute at Indiana University. Barbara Wetmore was funded by the American Chemistry Council's Long-Range Research IniInitiative. Sieto Bosgra was funded by the European Commission 7th Framework Program project ChemScreen (GA244236). Alex Tropsha and Alex Sedykh were supported by grants from NIH (GM66940 and R21GM076059), The Johns Hopkins Center for Alternatives to Animal Testing (20011-21) and Boehringer Ingelheim (Canada) Ltd.

ACKNOWLEDGMENTS

We appreciate feedback from Kevin Crofton, Marina Evans, and William Jordan in preparation of this manuscript.

REFERENCES

Archer, K. J., and Kimes, R. V. (2008). Empirical characterization of random forest variable importance measures. *Comput. Stat. Data Anal.* **52**, 2249–2260.

Birnbaum, L., Brown, R., Bischoff, K., Foran, J., Blancato, J., Clewell, H., and Dedrick, R. (1994). *Physiological Parameter Values for PBPK Models*. International Life Sciences Institute, Risk Science Institute, Washington, DC.

Blaauboer, B. J., Boekelheide, K., Clewell, H. J., Daneshian, M., Dingemans, M. M., Goldberg, A. M., Heneweer, M., Jaworska, J., Kramer, N. I., Leist, M., *et al.* (2012). The use of biomarkers of toxicity for integrating in vitro hazard estimates into risk assessment for humans. *Altex* **29**, 411–425.

Breiman, L. (2001). Random forests. *Mach. Learn.* **45**, 5–32.

Breiman, L., Friedman, J., Stone, C. J., and Olshen, R. A. (1984). *Classification and Regression Trees*. CRC Press, Boca Raton.

Bucher, J. R. (2008). Guest editorial: NTP: new initiatives, new alignment. *Environ. Health Perspect.* **116**, A14–A15.

CDC (2012). *National Health and Nutrition Examination Survey*. Available at: http://www.cdc.gov/nchs/nhanes.htm, last accessed 22 June 2015.

Davies, B., and Morris, T. (1993). Physiological parameters in laboratory animals and humans. *Pharm. Res.* **10**, 1093–1095.

Endo, S., Escher, B. I., and Goss, K.-U. (2011). Capacities of membrane lipids to accumulate neutral organic chemicals. *Environ. Sci. Technol.* **45**, 5912–5921.

Faber, K. N., Müller, M., and Jansen, P. L. M. (2003). Drug transport proteins in the liver. *Adv. Drug Deliv. Rev.* **55**, 107–124.

Giacomini, K. M., Huang, S.-M., Tweedie, D. J., Benet, L. Z., Brouwer, K. L., Chu, X., Dahlin, A., Evers, R., Fischer, V., and Hillgren, K. M. (2010). Membrane transporters in drug development. *Nat. Rev. Drug Discov.* **9**, 215–236.

Halestrap, A., and Meredith, D. (2004). The SLC16 gene family—from monocarboxylate transporters (MCTs) to aromatic amino acid transporters and beyond. *Pflugers Arch. Eur. J. Physiol.* **447**, 619–628.

Hilal, S., Karickhoff, S., and Carreira, L. (1995). A rigorous test for SPARC's chemical reactivity models: estimation of more than 4300 ionization pKas. *Quant. Struct. -Act. Relat.* **14**, 348–355.

Ito, K., and Houston, J. B. (2004). Comparison of the use of liver models for predicting drug clearance using in vitro kinetic data from hepatic microsomes and isolated hepatocytes. *Pharm. Res.* **21**, 785–792.

Jamei, M., Marciniak, S., Feng, K., Barnett, A., Tucker, G., and Rostami-Hodjegan, A. (2009). The Simcyp population-based ADME simulator. *Expert Opin. Drug Metab. Toxicol.* **5**, 211–223.

Downloaded from http://toxsci.oxfordjournals.org/ at Environmental Protection Agency Library on September 23, 2015

Jones, O. A., Voulvoulis, N., and Lester, J. N. (2002). Aquatic environmental assessment of the top 25 English prescription pharmaceuticals. *Water Res.* **36**, 5013–5022.

Judson, R. S., Houck, K. A., Kavlock, R. J., Knudsen, T. B., Martin, M. T., Mortensen, H. M., Reif, D. M., Rotroff, D. M., Shah, I., Richard, A. M., *et al.* (2010). In vitro screening of environmental chemicals for targeted testing prioritization: the ToxCast Project. *Environ. Health Perspect.* **118**, 485–492.

Judson, R. S., Kavlock, R. J., Setzer, R. W., Cohen-Hubal, E. A., Martin, M. T., Knudsen, T. B., Houck, K. A., Thomas, R. S., Wetmore, B. A., and Dix, D. J. (2011). Estimating toxicity-related biological pathway altering doses for high-throughput chemical risk assessment. *Chem. Res. Toxicol.* **24**, 451–462.

Judson, R., Richard, A., Dix, D. J., Houck, K., Martin, M., Kavlock, R., Dellarco, V., Henry, T., Holderman, T., Sayre, P., *et al.* (2008). The toxicity data landscape for environmental chemicals. *Environ. Health Perspect.* **117**, 685–695.

Kilford, P. J., Gertz, M., Houston, J. B., and Galetin, A. (2008). Hepatocellular binding of drugs: correction for unbound fraction in hepatocyte incubations using microsomal binding or drug lipophilicity data. *Drug Metab. Dispos.* **36**, 1194–1197.

Krug, A. K., Kolde, R., Gaspar, J. A., Rempel, E., Balmer, N. V., Meganathan, K., Vojnits, K., Baquié, M., Waldmann, T. and Ensenat-Waser, R. (2013). Human embryonic stem cell-derived test systems for developmental neurotoxicity: a transcriptomics approach. *Archives of toxicology* **87**(1), 123–143.

Lau, Y. Y., Sapidou, E., Cui, X., White, R. E., and Cheng, K. C. (2002). Development of a novel in vitro model to predict hepatic clearance using fresh, cryopreserved, and sandwich-cultured hepatocytes. *Drug Metab. Dispos.* **30**, 1446–1454.

Liaw, A., and Wiener, M. (2002). Classification and regression by randomforest. *R News* **2**, 18–22.

Lipinski, C. A., (2004). Lead- and drug-like compounds: the rule-of-five revolution. *Drug Discovery Today: Technologies* **1**(4), 337–341, http://dx.doi.org/10.1016/j.ddtec.2004.11.007.

Lukacova, V., Woltosz, W., and Bolger, M. (2009). Prediction of modified release pharmacokinetics and pharmacodynamics from in vitro, immediate release, and intravenous data. *AAPS J.* **11**, 323–334.

McGinnity, D. F., Soars, M. G., Urbanowicz, R. A., and Riley, R. J. (2004). Evaluation of fresh and cryopreserved hepatocytes as in vitro drug metabolism tools for the prediction of metabolic clearance. *Drug Metab. Dispos.* **32**, 1247–1253.

Naritomi, Y., Terashita, S., Kagayama, A., and Sugiyama, Y. (2003). Utility of hepatocytes in predicting drug metabolism: comparison of hepatic intrinsic clearance in rats and humans in vivo and in vitro. *Drug Metab. Dispos.* **31**, 580–588.

National Research Council (1984). *Toxicity Testing: Strategies to Determine Needs and Priorities*. National Academy Press, Washington, DC.

National Research Council (2007). *Toxicity Testing in the 21st Century: A Vision and a Strategy*. The National Academies Press, Washington, DC.

Obach, R. S. (1999). Prediction of human clearance of twenty-nine drugs from hepatic microsomal intrinsic clearance data: an examination of in vitro half-life approach and nonspecific binding to microsomes. *Drug Metab. Dispos.* **27**, 1350–1359.

Obach, R. S., Lombardo, F., and Waters, N. J. (2008). Trend analysis of a database of intravenous pharmacokinetic parameters in humans for 670 drug compounds. *Drug Metab. Dispos.* **36**, 1385–1405.

Piersma, A., Bosgra, S., Van Duursen, M., Hermsen, S., Jonker, L., Kroese, E., Van der Linden, S., Man, H., Roelofs, M. and Schulpen, S. (2013). Evaluation of an alternative in vitro test battery for detecting reproductive toxicants. *Reproductive Toxicology* **38**, 53–64.

R Development Core Team. (2013). R: A Language and Environment for Statistical Computing, *Version* 3.0.2. R Foundation for Statistical Computing, Vienna, Austria.

Ritter, R., Scheringer, M., MacLeod, M., Moeckel, C., Jones, K. C., and Hungerbühler, K. (2010). Intrinsic human elimination half-lives of polychlorinated biphenyls derived from the temporal evolution of cross-sectional biomonitoring data from the United Kingdom. *Environ. Health Perspect.* **119**, 225–231.

Richard, A. M. (2006). Future of ToxicologyPredictive Toxicology: An Expanded View of "Chemical Toxicity". *Chemical Research in Toxicology* **19**(10), 1257–1262, 10.1021/tx060116u.

Rotroff, D. M., Wetmore, B. A., Dix, D. J., Ferguson, S. S., Clewell, H. J., Houck, K. A., Lecluyse, E. L., Andersen, M. E., Judson, R. S., Smith, C. M., *et al.* (2010). Incorporating human dosimetry and exposure into high-throughput in vitro toxicity screening. *Toxicol. Sci.* **117**, 348–358.

Rousu, T., Hokkanen, J., Pelkonen, O. R., and Tolonen, A. (2010). Applicability of generic assays based on liquid chromatography–electrospray mass spectrometry to study in vitro metabolism of 55 structurally diverse compounds. *Front. Pharmacol.* **1**, 10.

Schmitt, W. (2008a). General approach for the calculation of tissue to plasma partition coefficients. *Toxicol. in vitro* **22**, 457–467.

Schmitt, W. (2008b). Corrigendum to: "General approach for the calculation of tissue to plasma partition coefficients". [Toxicol. in vitro **22** (2008) 457–467]. *Toxicol. in vitro* **22**, 1666.

Sedykh, A., Fourches, D., Duan, J., Hucke, O., Garneau, M., Zhu, H., Bonneau, P., and Tropsha, A. (2013). Human intestinal transporter database: QSAR modeling and virtual profiling of drug uptake, efflux and interactions. *Pharm. Res.* **30**, 996–1007.

Shibata, Y., Takahashi, H., Chiba, M., and Ishii, Y. (2002). Prediction of hepatic clearance and availability by cryopreserved human hepatocytes: an application of serum incubation method. *Drug Metab. Dispos.* **30**, 892–896.

Shugarts, S., and Benet, L. Z. (2009). The role of transporters in the pharmacokinetics of orally administered drugs. *Pharm. Res.* **26**, 2039–2054.

Smith, C. M., Nolan, C. K., Edwards, M. A., Hatfield, J. B., Stewart, T. W., Ferguson, S. S., Lecluyse, E. L., and Sahi, J. (2012). A comprehensive evaluation of metabolic activity and intrinsic clearance in suspensions and monolayer cultures of cryopreserved primary human hepatocytes. *J. Pharm. Sci.* **101**, 3989–4002.

Steinbeck, C., Han, Y., Kuhn, S., Horlacher, O., Luttmann, E., and Willighagen, E. (2003). The Chemistry Development Kit (CDK): an open-source Java library for Chemo- and Bioinformatics. *J. Chem. Inf. Comput. Sci.* **43**, 493–500.

Therneau, T. M., Atkinson, B., and Ripley, B. (2014). *rpart: Recursive partitioning*. R Package Version 4.1(8).

Thomas, R. S., Philbert, M. A., Auerbach, S. S., Wetmore, B. A., Devito, M. J., Cote, I., Rowlands, J. C., Whelan, M. P., Hays, S. M., Andersen, M. E., *et al.* (2013). Incorporating new technologies into toxicity testing and risk assessment: moving from 21st century vision to a data-driven framework. *Toxicol. Sci.* **136**, 4–18.

Tonnelier, A., Coecke, S., and Zaldívar, J.-M. (2012). Screening of chemicals for human bioaccumulative potential with a physiologically based toxicokinetic model. *Arch. Toxicol.* **86**, 393–403.

Downloaded from http://toxsci.oxfordjournals.org/ at Environmental Protection Agency Library on September 23, 2015

USGAO (2013). Toxic substances: EPA has increased efforts to assess and control chemicals but could strengthen its approach. United States Government Accountability Office, Report to Congressional Requesters, GAO-13-249. Published: Mar 22, 2013. Publicly Released: Apr 29, 2013.

van de Steeg, E., Venhorst, J., Jansen, H., Nooijen, I., DeGroot, J., Wortelboer, H., and Vlaming, M. (2015). Generation of Bayesian prediction models for OATP-mediated drug-drug interactions based on inhibition screen of OATP1B1, OATP1B1 15 and OATP1B3. *European Journal of Pharmaceutical Sciences* **70**, 29–36.

Walker, T., Grulke, C. M., Pozefsky, D., and Tropsha, A. (2010). Chembench: a cheminformatics workbench. *Bioinformatics* **26**, 3000–3001.

Wambaugh, J. F., Setzer, R. W., Reif, D. M., Gangwal, S., Mitchell-Blackwood, J., Arnot, J. A., Jolliet, O., Frame, A., Rabinowitz, J., Knudsen, T. B., *et al.* (2013). High throughput models for exposure-based chemical prioritization in the ExpoCast Project. *Environ. Sci. Technol.* **47**, 8479–8488.

Wambaugh, J. F., Wang, A., Dionisio, K. L., Frame, A., Egeghy, P., Judson, R., and Setzer, R. W. (2014). High throughput heuristics for prioritizing human exposure to environmental chemicals. *Environ. Sci. Technol.* **48**, 12760–12767.

Wang, Y.-H. (2010). Confidence assessment of the Simcyp time-based approach and a static mathematical model in predicting clinical drug–drug interactions for mechanism-based CYP3A inhibitors. *Drug Metab. Dispos.* **38**, 1094–1104.

Waters, N. J., Jones, R., Williams, G., and Sohal, B. (2008). Validation of a rapid equilibrium dialysis approach for the measurement of plasma protein binding. *J. Pharm. Sci.* **97**, 4586–4595.

Weininger, D. (1988). SMILES, a chemical language and information system. 1. Introduction to methodology and encoding rules. *J. Chem. Inf. Comput. Sci.* **28**, 31–36.

Wetmore, B. A., Wambaugh, J. F., Ferguson, S. S., Sochaski, M. A., Rotroff, D. M., Freeman, K., Clewell, H. J., III, Dix, D. J., Andersen, M. E., Houck, K. A., *et al.* (2012). Integration of dosimetry, exposure, and high-throughput screening data in chemical toxicity assessment. *Toxicol. Sci.* **125**, 157–174.

Wetmore, B. A., Wambaugh, J. F., Ferguson, S. S., Li, L., Clewell, H. J., Judson, R. S., Freeman, K., Bao, W., Sochaski, M. A., Chu, T.-M., *et al.* (2013). Relative impact of incorporating pharmacokinetics on predicting in vivo hazard and mode of action from high-throughput in vitro toxicity assays. *Toxicol. Sci.* **132**,327–346.

Wetmore, B. A., Allen, B., Clewell, H. J., Parker, T., Wambaugh, J. F., Almond, L. M., Sochaski, M. A., and Thomas, R. S. (2014). Incorporating population variability and susceptible subpopulations into dosimetry for high-throughput toxicity testing. *Toxicol. Sci.* **142**, 210–224.

Wilkinson, G. R., and Shand, D. G. (1975). Commentary: a physiological approach to hepatic drug clearance. *Clin. Pharmacol. Ther.* **18**, 377–390.

Yoon, M., Efremenko, A., Blaauboer, B. J., and Clewell, H. J. (2014). Evaluation of simple in vitro to in vivo extrapolation approaches for environmental compounds. *Toxicol. in vitro* **28**, 164–170.

Downloaded from http://toxsci.oxfordjournals.org/ at Environmental Protection Agency Library on September 23, 2015

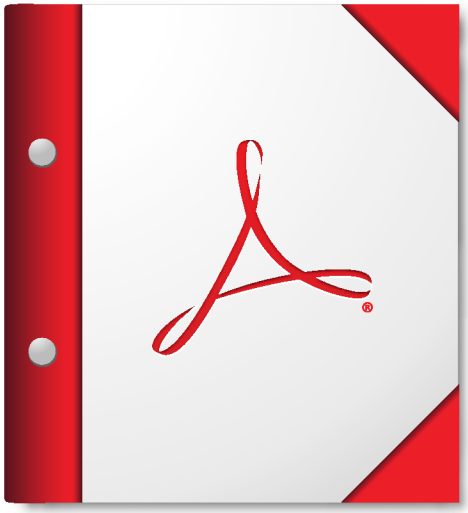

For the best experience, open this PDF portfolio in Acrobat X or Adobe Reader X, or later.

Get Adobe Reader Now!

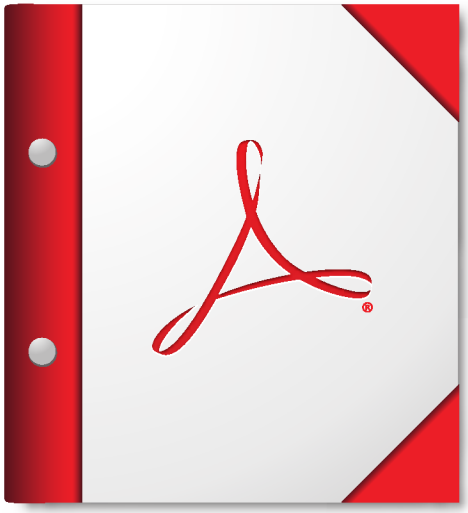

For the best experience, open this PDF portfolio in Acrobat X or Adobe Reader X, or later.

Get Adobe Reader Now!

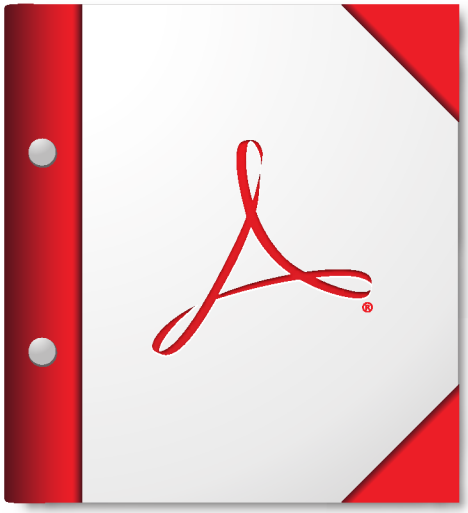

For the best experience, open this PDF portfolio in Acrobat X or Adobe Reader X, or later.

Get Adobe Reader Now!

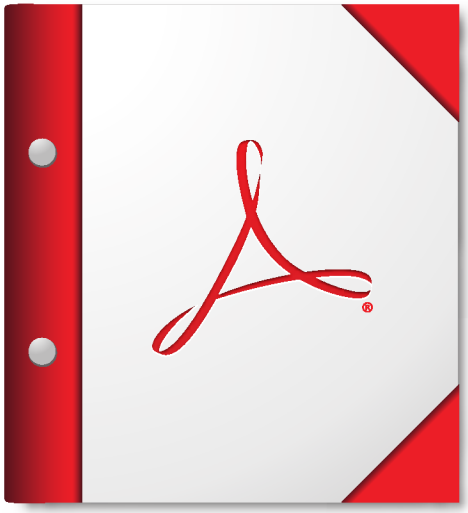

For the best experience, open this PDF portfolio in Acrobat X or Adobe Reader X, or later.

Get Adobe Reader Now!

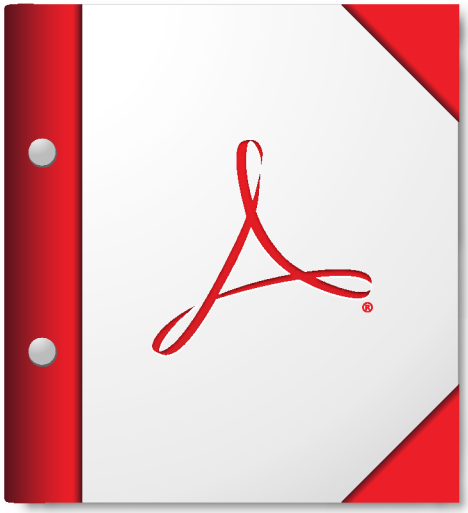

For the best experience, open this PDF portfolio in Acrobat X or Adobe Reader X, or later.

Get Adobe Reader Now!

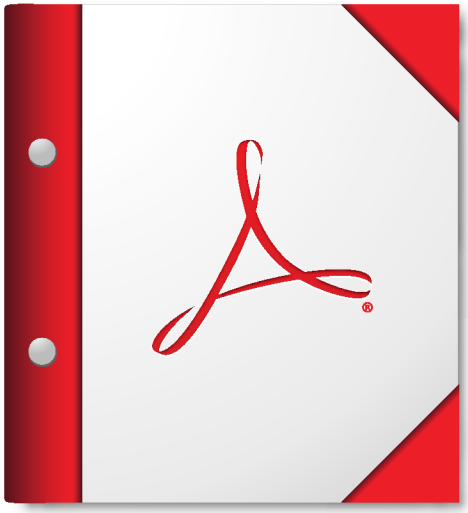

For the best experience, open this PDF portfolio in Acrobat X or Adobe Reader X, or later.

Get Adobe Reader Now!

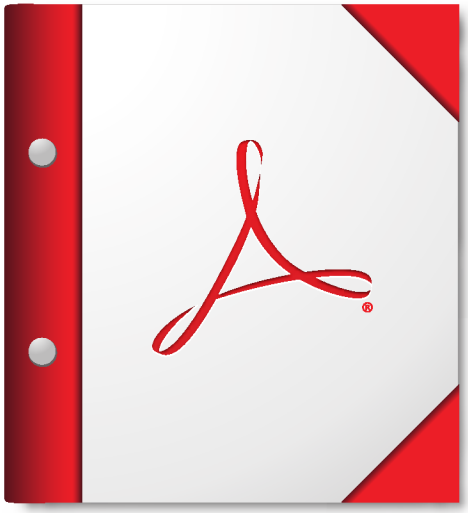

For the best experience, open this PDF portfolio in Acrobat X or Adobe Reader X, or later.

Get Adobe Reader Now!

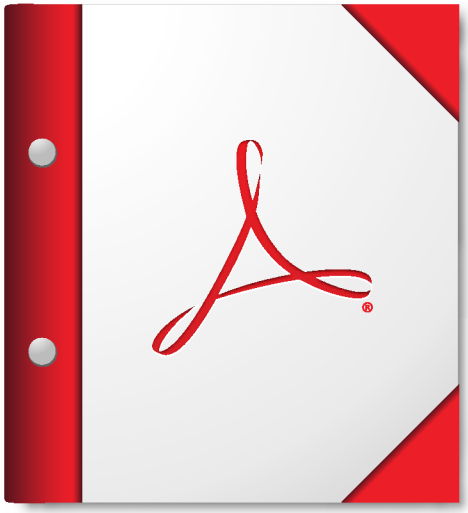

For the best experience, open this PDF portfolio in Acrobat X or Adobe Reader X, or later.

Get Adobe Reader Now!

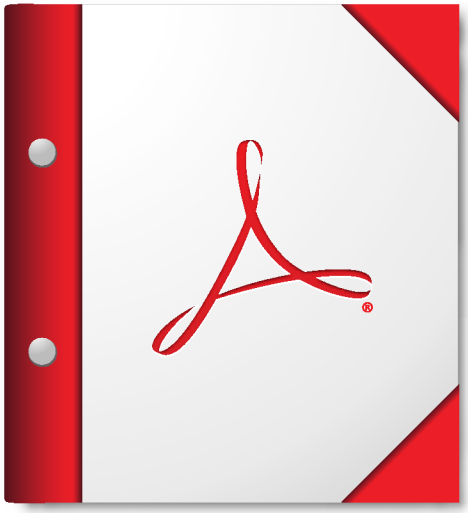

For the best experience, open this PDF portfolio in Acrobat X or Adobe Reader X, or later.

Get Adobe Reader Now!

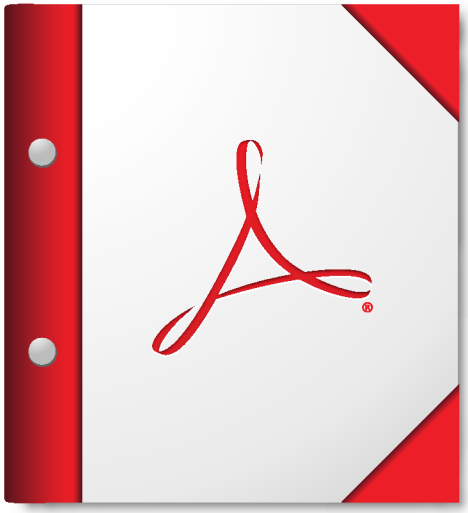

For the best experience, open this PDF portfolio in Acrobat X or Adobe Reader X, or later.

Get Adobe Reader Now!

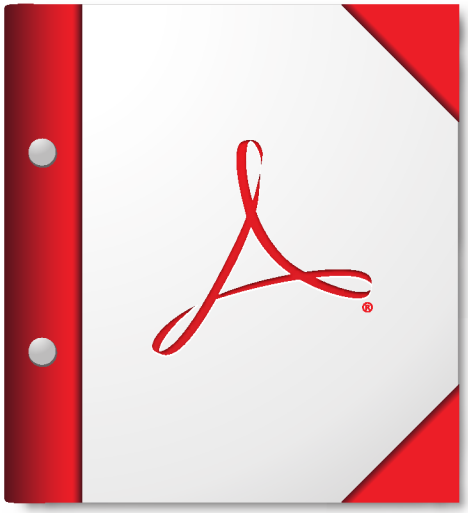

For the best experience, open this PDF portfolio in Acrobat X or Adobe Reader X, or later.

Get Adobe Reader Now!

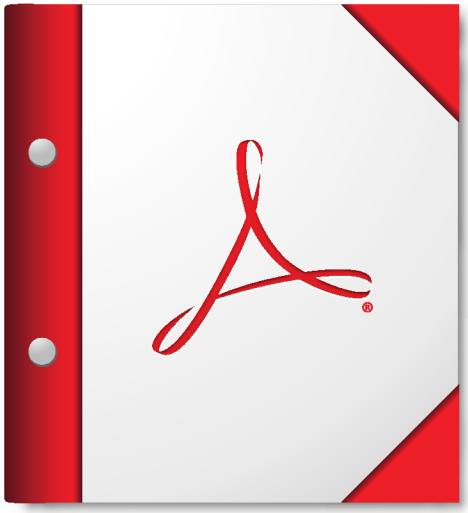

For the best experience, open this PDF portfolio in Acrobat X or Adobe Reader X, or later.

Get Adobe Reader Now!

4/29/20

I agree with the total percentage of effort listed for me.

John Wambaugh

Table of Contents

General_Authors_Publications.....2
LI-266759_Radke_et_al_2018_Phthalates_male_repro_epi_SR.....21
LI-266760_Yost_et_al_2019_DIBP_animal_tox_SR.....51
LI-266761_Blessinger_et_al_2020_Ordinal_dose_response_modeling.....67
Radke_et_al_2019_Development_of_outcome_specific_criteria_for_epi_study_evalua81
Radke_et_al_2019_Phthalates_female_repro_epi_SR.....95
Radke_et_al_2019_Phthalates_metabolic_effects_epi_SR.....114
Radke_et_al_2020_Phthalates_neurodevelopment_epi_SR.....131
Record_of_agreement_Arzuaga.....151
Record_of_agreement_Beverly.....153
Record_of_agreement_Cai.....155
Record_of_agreement_Dishaw.....157
Record_of_agreement_Euling.....159
Record_of_agreement_Hogan.....161
Record_of_agreement_Hotchkiss.....163
Record_of_agreement_Keshava.....165
Record_of_agreement_Klinefelter.....167
Record_of_agreement_Makris.....169
Record_of_agreement_Mudipalli.....171
Record_of_agreement_Radke_Cooper_Meeker_Braun.....173
Record_of_agreement_Saillenfait.....177
Record_of_agreement_Wang.....181
Record_of_agreement_Weaver.....183
Record_of_agreement_Blessinger.....185
Letter_of_support_for_STAA_award_Burke.....187
Letter_of_support_for_STAA_award_Chiu.....189
Letter_of_support_for_STAA_award_Whaley.....191

United States Environmental Protection Agency
Washington, DC 20460

STAA REPORT FOR THE SCIENTIST NOMINATIONS

General Information:

Nomination ID/App ID:	20-094
Research Category Primary:	Health Effects Research and Human Health Risk Assessment (HE)
Research Category Secondary:	Review Articles (RA)
Laboratory/Office Name:	ORD
Nomination Entered By:	Erin Yost

Eligibility Checklist:

[Y] The nominated publication(s) has not been submitted to a previous STAA competition.

[Y] The nominated publication(s) was published on or before January 1, 2017 and on or after January 1,2012

[Y] The principal author was an EPA employee or a PHS employee assigned to EPA when the research was performed

[Y] The EPA authors (includes PHS employees assigned to EPA) contributed collectively a minimum of 50% toward the publication(s)

Nominating Official Name:	Kristina Chialton
Nominating Official Title:	SUPERVISORY BIOLOGIST
Nominating OfficialEmail:	thayer.kris@epa.gov
STAA Coordinator Name:	Kathleen Wiser
STAA Coordinator Email:	wiser.kathi@epa.gov

Justifications:

Justification 1:

The three publications comprising this STAA award nomination represent a collection of work that informs the risk assessment of phthalates using state-of-the-art systematic review methods (Radke et al., 2018, Yost et al., 2019) as well as a dose response assessment method for assessing the phthalate syndrome developed by the EPA's Center for Public Health and Environmental Assessment (Blessinger et al., 2020). These three publications, as well as others listed in the supplemental materials, are part of a special issue in *Environment International* on "Systematic reviews of potential human health outcomes associated with exposure to phthalates" (https://www.sciencedirect.com/journal/environment-international/special-issue/10JT5TGQ846). The special issue is a collection of systematic reviews of epidemiology or animal toxicology data on the health effects of phthalates that were conducted by IRIS program staff, as well as methodological publications that address some of the scientific challenges encountered over the course of conducting the systematic reviews. The scientific contributions of these work primarily relate to improving our understanding of the health effects of phthalate exposure and advancing methods of systematic review for use in complex assessments.

Phthalates, a class of alkyl diesters of phthalic acid, are used in a variety of consumer products including food packaging, cleaning and building materials, cosmetics, personal care, pharmaceuticals, medical devices, and children's toys. Owing to this widespread use, human exposure to phthalates is ubiquitous across all life stages. There is a considerable body of evidence on the potential health effects of exposure to phthalates. In particular, gestational exposure of male rats to phthalates with three to seven (or eight) carbon atoms in the backbone of the alkyl side chain is found to induce a phenotype known as "phthalate syndrome", which is characterized by a collection of male reproductive developmental effects leading to demasculinization of sexual development including permanent malformations of reproductive organs, nipple retention, and decreased anogenital distance.

In December 2019, EPA designated nine phthalates as high priority for risk evaluation under the Toxic Substances Control Act (TSCA) (https://www.epa.gov/assessing-and-managing-chemicals-under-tsca/draft-scope-documents-high-priority-chemicals-undergoing). The majority of the phthalates undergoing risk evaluation by TSCA were found in a 2014 report by the Consumer Product Safety Commission (CPSC) Chronic Hazard Advisory Panel (CHAP) on Phthalates and Phthalate Alternatives to induce phthalate syndrome in rats (https://www.cpsc.gov/chap), and therefore male reproductive toxicity and the potential for cumulative exposure to phthalates with similar modes of action will be key interests in the risk evaluation of these chemicals. These chemicals will move through the process required by TSCA to evaluate any unreasonable risks they may present to human health or the environment. The work in the nominated publications reflects the state of the science on phthalates toxicity and can support development of the TSCA risk evaluations, which are being completed on an aggressive timeline (EPA strategic goal 3.3, Human Health Risk Assessment). Furthermore, the amendments to TSCA under the Frank R. Lautenberg Chemical Safety for the 21st Century Act specifically requires that chemical substances be evaluated for unreasonable risks to "potentially exposed or susceptible subpopulations", which can include infants, children, and pregnant women (https://www.congress.gov/114/plaws/publ182/PLAW-114publ182.pdf). Given the finding that developmental exposures to

certain phthalates are associated with severe male reproductive effects in offspring, our publications support the assessment of risk of phthalate exposure to infants and children in accordance with EPA's Policy on Evaluating Risk to Children (https://www.epa.gov/children/epas-policy-evaluating-risk-children).

The first publication (Radke et al. 2018) is a systematic review of epidemiological data on the male reproductive effects of six phthalates: di(2-ethylhexyl) phthalate (DEHP), diisononyl phthalate (DINP), dibutyl phthalate (DBP), diisobutyl phthalate (DIBP), butyl benzyl phthalate (BBP), and diethyl phthalate (DEP). Five of these phthalates (with the exception of DEP) have been designated as high priority for risk evaluation under TSCA. It is particularly important to consider the epidemiologic studies for this association because there has been some concern that findings in animal studies may not be relevant to humans. While past reviews have examined some of the outcomes included in this review, this is the first systematic review to include all of the key male reproductive effects studied in humans (including semen parameters, testosterone, fecundity/time to pregnancy, pubertal development, anogenital distance, and hypospadias/cryptorchidism). This review shows that there is robust evidence that exposure to DEHP and DBP is associated with male reproductive effects in humans, and moderate evidence for DINP, DIBP, and BBP, with the difference in evidence strength likely due to size of the evidence bases and study sensitivity.

The second publication (Yost et al. 2019) is a systematic review of animal toxicology data on DIBP, focusing on six health outcome categories: male reproductive, female reproductive, developmental, liver, kidney, and cancer. DIBP is one of the phthalates that was designated as high priority for risk evaluation on the 2014 TSCA Workplan under amended TSCA. Because DIBP was introduced as a replacement for DBP, it has been less thoroughly studied; however, the CPSC has recently restricted the use of DIBP in children's toys and childcare items due to evidence of male reproductive toxicity, and biomonitoring trends suggest that DIBP exposures have increased in recent years. To our knowledge, our publication is the only systematic review of DIBP animal toxicology studies and covers a wider range of studies and health outcomes compared to previous reviews of DIBP health outcomes. This review shows that there is robust evidence that DIBP is a male reproductive and developmental toxicant, with gestational exposure leading to permanent effects in offspring, and also identifies suggestive evidence that gestational exposure to DIBP can lead to developmental effects in females.

The third publication (Blessinger et al. 2020) explored how to model a syndrome of endpoints, in this case the phthalate syndrome, where the endpoints are mechanistically related but have a range of severity levels. An ordinal dose-response method was used to model the collection of endpoints that characterize phthalate syndrome in experimental animal studies. The syndrome is most commonly defined as a dichotomous endpoint indicating the presence or absence of one or more male reproductive developmental effects. The dose-response analysis conducted in this publication used an ordinal definition of the endpoint to incorporate severity level, based on impact on fertility. This method provides more reliable benchmark dose estimates than would be obtained by simply modeling the dichotomization of the syndrome at each severity level. Furthermore, it can easily be generalized to include a greater number of endpoint severity levels and thus, the publication demonstrates a more flexible method for modeling syndromes in human health risk assessment, as it can be applied to any syndrome and has broad applicability to the analysis of other classes of chemicals with similar modes of action. Furthermore, the modeling approach would work well when performing a cumulative risk assessment of phthalates, which is a research need outlined in the National Research Council report "Phthalates and Cumulative Risk Assessment: The Tasks Ahead" (https://www.nap.edu/catalog/12528/phthalates-and-cumulative-risk-assessment-the-tasks-ahead).

In addition to their contributions to understanding the health effects of phthalate exposure, the systematic reviews by Radke et al. (2018) and Yost et al. (2019) provide examples of some of the first efforts to use the systematic review methods developed by the EPA's IRIS program for the assessment of environmental chemicals (as described in the IRIS Handbook, summarized in the 2018 NAS report). Systematic reviews are used to summarize the results of multiple primary studies in a transparent and reproducible way, and include several steps including literature search and screening, study evaluation, data extraction, and evidence synthesis and integration. The IRIS program was advised by the National Academy of Sciences (formerly National Research Council) to adopt systematic review methods in the 2011 NAS Formaldehyde report (https://www.nationalacademies.org/our-work/review-of-epas-draft-iris-assessment-of-formaldehyde), as well as in subsequent reviews of the IRIS program during which method development was underway (https://www.nap.edu/catalog/18764/review-of-epas-integrated-risk-information-system-iris-process; https://www.nap.edu/catalog/25086/progress-toward-transforming-the-integrated-risk-information-system-iris-program). The NAS was supportive of the systematic review methods being developed within the IRIS Program (2018). In addition, NAS is currently reviewing the systematic review methods used by EPA's Office of Chemical Safety and Pollution Prevention (OCSPP).

Systematic review methods were originally developed for clinical research projects posing only one or two questions or hypotheses and were instrumental in establishing the efficacy of medical treatments and procedures in the clinical community. Regulatory agencies such as EPA, however, have broader information demands, with questions about multiple exposure scenarios, populations of concerns, and outcomes of interest needing to be addressed to inform the application of the risk assessment paradigm (hazard identification, dose-response, exposure assessment, and risk characterization). There are also discipline-specific considerations that must be incorporated into the review methods (e.g., measuring exposure in epidemiology studies versus administering an intervention in clinical trials). Thus, due to the broader information demands and methodological differences, the systematic review methods used for clinical research must be adapted for use in human health risk assessment (HHRA), which is a considerable challenge that the field has been working towards for several years (EPA strategic goal 3.3, Human Health Risk Assessment). The systematic reviews in this nomination illustrate how to apply systematic review methods to large, complex evidence bases, which is relevant to assessments performed within EPA and by other agencies (see Justification 3A for information on how these systematic reviews have been shared externally beyond their publications).

As supplemental material for this nomination, we have attached four additional publications by Radke et al. (listed below) that were also published as part of the same special issue in *Environment International* and address some of the same questions as the nominated papers. The special issue will also include two additional papers that have not yet been published (and therefore are not included here as supplemental information), which will address issues related to the systematic review of animal toxicology studies for phthalates.

- Radke EG, Glenn BG, Braun JM, Cooper GS. (2019) Phthalate exposure and female reproductive and developmental outcomes: a systematic review of the human epidemiological evidence. Environment International. Published online ahead of Special Issue.
- Radke EG, Galiza A, Thayer KA, Cooper GS. (2019) Phthalate exposure and metabolic outcomes: a systematic review of the human epidemiological evidence. Environment International. Published online ahead of Special Issue.

- Radke EG, Braun JM, Nachman RM, Cooper GS. (2020) Phthalate exposure and neurodevelopment: a systematic review and meta-analysis of the human epidemiological evidence. Environment International. Published online ahead of Special Issue.
- Radke EG, Glenn BG, Galizia A, Persad A, Nachman RM, Bateson T, Wright JM, Navas-Ascien A, Arroyave WD, Puett RC, Harville EW, Pollack AZ, Burns JS, Lynch CD, Sagiv SK, Stein C, Cooper Gs. (2019) Development of outcome-specific criteria for study evaluation in systematic reviews of epidemiology studies. Environment International. Published online ahead of Special Issue.

Justification 2A:

The three nominated publications are a complementary set of work representing different steps of the risk evaluation process for phthalates. The systematic reviews by Radke et al. 2018 and Yost et al. 2019 synthesize the evidence for epidemiology and experimental animal studies, respectively, and can be integrated together to inform hazard identification. Epidemiology and experimental animal studies complement each other in identifying health effects from exposures, as they each bring strengths that address key limitations in the other discipline (i.e., observational epidemiology studies provide evidence in humans, the species of interest, but do not allow for control of exposure; whereas experimental animal studies allow for precise and randomized control of exposure but effects in animals may not be directly relevant to humans). The publication on dose-response by Blessinger et al. 2020 describes a method which can be used to produce reliable benchmark dose estimates for varying levels of severity of the phthalate syndrome; these estimates are used to derive the toxicity values that are ultimately used for risk assessment. Taken together, these three publications showcase cutting edge approaches developed for risk assessment and pave the way for a cumulative phthalate risk assessment.

Justification 2B:

Anuradha Mudipalli (submitted in 2017; no award):

Chapter 6: Airborne carcinogens: Mechanisms of Cancer Pgs151-184.

Book: Air pollution and Health Effects:

Editors: Srikanth S Nadadur, John W Hollingsworth

Molecular and integrative series

Publisher: Springer, 2015

Justification 2C:

The publications we are nominating have no relationship to the book chapter by Anuradha Mudipalli that was nominated in 2017.

Justification 2D:

N/A

Justification 2E:

Xabier Arzuaga, Karen Hogan, Andrew Hotchkiss, Susan Euling, Susan Makris are listed on a concurrent nomination (Makris et al. 2016; citation below). The publication by Makris et al. 2016 represents an example of a systematic review effort by IRIS program staff focused on fetal cardiac effects after trichloroethylene exposure. It is unrelated to the systematic reviews of phthalates.

Makris SL, Scott CS, Fox J, Knudsen TB, Hotchkiss AK, Arzuaga X, Euling SY, Powers CM, Jinot J, Hogan KA, Abbott BD, Hunter ES 3rd, Narotsky MG. A systematic evaluation of the potential effects of trichloroethylene exposure on cardiac development. Reprod Toxicol. 2016 Oct;65:321-358. doi: 10.1016/j.reprotox.2016.08.014. Epub 2016 Aug 27. Review. PubMed PMID: 27575429.

Justification 3A:

The systematic reviews by Radke et al. 2018 and Yost et al. 2019 have been highly cited by other peer-reviewed publications and by the national news media and have been shared by scientific community on Twitter. According to Google Scholar, Radke et al. 2018 has been cited 41 times (with 68 readers and 4 downloads) as and Yost et al. 2019 has been cited 9 times (with 87 readers and 6 downloads). Radke et al. 2018 was cited by the New York Times in the article “The Types of Plastics Families Should Avoid”, which was published on September 19, 2019 (https://www.nytimes.com/article/plastics-to-avoid.html). PlumX Metrics indicate that Radke et al. 2018 has been shared 33 times on Twitter, and Yost et al. 2019 has been shared 8 times on Twitter. The dose-response modeling publication by Blessinger et al. 2020 was published more recently and has not yet been cited (5 readers).

Additionally, the systematic reviews by Radke et al. 2018 and Yost et al. 2019 were presented by the authors to external stakeholders at the National Academy of Sciences “Review of Advances Made to the IRIS Process: A Workshop” (February 1-2, 2018 in Washington, DC) and at the US EPA Board of Scientific Counselors Chemical Safety Subcommittee Meeting (April 10-12, 2019 in Research Triangle Park, NC) as examples of recent improvements to the IRIS systematic review process.

This work contributed to the NAS conclusions that IRIS has made "substantial progress" in implementing recommendations outlined in past reports by the NAS, improving the program's overall scientific and technical performance (https://www.nationalacademies.org/news/2018/04/epas-iris-program-has-made-substantial-progress-says-new-report). These systematic reviews were also used as case studies for multiple meetings and trainings with other government agencies, including staff from the National Toxicology Program, Texas Commission on Environmental Quality, and California Environmental Protection Agency. These presentations illustrate the impact of this work on systematic review practices in the environmental health field.

Three letters of recommendation for this work are attached to the application, from Thomas Burke (Johns Hopkins Bloomberg School of Public Health), Weihsueh Chiu (Texas A&M University), and Paul Whaley (Environment International, Lancaster University).

Justification 3B:

Environment International is one of the top peer-reviewed journals in the environmental health field (cite score: 8.58; impact factor: 7.493), and therefore all articles underwent rigorous review by at least three peer reviewers per journal policy. The journal editors specifically ensured that the systematic review papers by Radke et al. 2018 and Yost et al. 2019 were each reviewed by at least 1-2 reviewers with expertise in phthalates toxicity and 1-2 reviewers with expertise in systematic review methods.

AUTHORS

Contributing Author

Author Name:	Elizabeth Radke		
Professional Title:		Salutation:	
Email:	radke.elizabeth@epa.gov	Organization:	
Mailing Address:			
Street Line 1:			

City:

Zip Code: State:

At time of research was: EPA Employee

Separation Date:

% of Effort: 20

Contributing Author

Author Name: Todd Blessinger

Professional Title: Salutation:

Email: blessinger.todd@epa.gov Organization:

Mailing Address:

Street Line 1:

City:

Zip Code: State:

At time of research was: EPA Employee

Separation Date:

% of Effort: 14

Contributing Author

Author Name: Anne-Marie Saillenfait

Professional Title: Salutation:

Email: anne-marie.saillenfait@inrs.fr Organization:

Mailing Address:

Street Line 1:

City:

Zip Code: State:

At time of research was: Non EPA Personnel

Separation Date:

% of Effort: 2

Contributing Author

Author Name: Susan Euling

Professional Title: Salutation:

Email: euling.susan@epa.gov Organization:

Mailing Address:

Street Line 1:

City:

Zip Code: State:

At time of research was: EPA Employee

Separation Date:

% of Effort: 12

Contributing Author

Author Name: Xabier Arzuaga

Professional Title: Salutation:

Email: arzuaga.xabier@epa.gov Organization:

Mailing Address:

Street Line 1:

City:

Zip Code: State:

At time of research was: EPA Employee

Separation Date:

% of Effort: 3

Contributing Author

Author Name: Glinda Cooper

Professional Title: Salutation:

Email: gscooper1@gmail.com Organization:

Mailing Address:

Street Line 1:

City:

Zip Code: State:

At time of research was: EPA Employee

Separation Date: Fri May 13 00:00:00 GMT 2016

% of Effort: 6

Contributing Author

Author Name: Lily Wang

Professional Title: Salutation:

Email: wang.lily@epa.gov Organization:

Mailing Address:

Street Line 1:

City:

Zip Code: State:

At time of research was: EPA Employee

Separation Date:

% of Effort: 5

Contributing Author

Author Name: Laura Dishaw

Professional Title: Salutation:

Email: dishaw.laura@epa.gov Organization:

Mailing Address:

Street Line 1:

City:

Zip Code: State:

At time of research was: EPA Employee

Separation Date:

% of Effort: 1

Contributing Author

Author Name: Brandiese Beverly

Professional Title: Salutation:

Email: brandy.beverly@nih.gov Organization:

Mailing Address:

Street Line 1:

City:		
Zip Code:		State:
At time of research was:	EPA Employee	
Separation Date:	Sat Jan 07 00:00:00 GMT 2017	
% of Effort:	3	

Contributing Author

Author Name:	Christine Cai	
Professional Title:		Salutation:
Email:	cai.christine@epa.gov	Organization:
Mailing Address:		
Street Line 1:		
City:		
Zip Code:		State:
At time of research was:	EPA Employee	
Separation Date:		
% of Effort:	3	

Contributing Author

Author Name:	Andrew Hotchkiss	
Professional Title:		Salutation:
Email:	hotchkiss.andrew@epa.gov	Organization:
Mailing Address:		
Street Line 1:		

City:

Zip Code: State:

At time of research was: EPA Employee

Separation Date:

% of Effort: 1

Contributing Author

Author Name: Anuradha Mudipalli

Professional Title: Salutation:

Email: mudipalli.anu@epa.gov Organization:

Mailing Address:

Street Line 1:

City:

Zip Code: State:

At time of research was: EPA Employee

Separation Date:

% of Effort: 2

Contributing Author

Author Name: Joseph Braun

Professional Title: Salutation:

Email: joseph_braun_1@brown.edu Organization:

Mailing Address:

Street Line 1:

City:

Zip Code: State:

At time of research was: Non EPA Personnel

Separation Date:

% of Effort: 2

Contributing Author

Author Name: John Meeker

Professional Title: Salutation:

Email: meekerj@umich.edu Organization:

Mailing Address:

Street Line 1:

City:

Zip Code: State:

At time of research was: Non EPA Personnel

Separation Date:

% of Effort: 2

Contributing Author

Author Name: Andre Weaver

Professional Title: Salutation:

Email: weaver.james@epa.gov Organization:

Mailing Address:

Street Line 1:

City:

Zip Code: State:

At time of research was: EPA Employee

Separation Date:

% of Effort: 2

Contributing Author

Author Name: Gary Klinefelter

Professional Title: Salutation:

Email: klinefelter.gary@epa.gov Organization:

Mailing Address:

Street Line 1:

City:

Zip Code: State:

At time of research was: EPA Employee

Separation Date:

% of Effort: 2

Contributing Author

Author Name: Nagalakshmi Keshava

Professional Title: Salutation:

Email: keshava.nagu@epa.gov Organization:

Mailing Address:

Street Line 1:

City:

Zip Code: State:

At time of research was: EPA Employee

Separation Date:

% of Effort: 2

Contributing Author

Author Name: Karen Hogan

Professional Title: Salutation:

Email: hogan.karen@epa.gov Organization:

Mailing Address:

Street Line 1:

City:

Zip Code: State:

At time of research was: EPA Employee

Separation Date:

% of Effort: 2

Contributing Author

Author Name: Susan Makris

Professional Title: Salutation:

Email: makris.susan@epa.gov Organization:

Mailing Address:

Street Line 1:

City:		
Zip Code:		State:
At time of research was:	EPA Employee	
Separation Date:		
% of Effort:	1	

Principal Author

Author Name:	Erin E. Yost	
Professional Title:		Salutation:
Email:	yost.erin@epa.gov	Organization:
Mailing Address:		
Street Line 1:		
City:		
Zip Code:		State:
At time of research was:	EPA Employee	
Separation Date:		
% of Effort:	15	

PUBLICATIONS

Publication 1:

Publication Title:	Phthalate exposure and male reproductive outcomes: A systematic review of the human epidemiological
Publication Date:	Tue Oct 16 00:00:00 GMT 2018
Journal/Publication Method:	Environment International

All Author(s):

Volume:	121	Number:	N/A
Pages:	764-793	Immediately Index:	Immediately Index:
Citation ½ Life:	6.0	Impact Factor:	7.943

Publication 2:

Publication Title:	Hazards of diisobutyl phthalate (DIBP) exposure: A systematic review of animal toxicology studies
Publication Date:	Tue Dec 25 00:00:00 GMT 2018
Journal/Publication Method:	Environment International

All Author(s):

Volume:	125	Number:	N/A
Pages:	579 - 594	Immediately Index:	Immediately Index:
Citation ½ Life:	6.0	Impact Factor:	7.943

Publication 3:

Publication Title:	Ordinal dose-response modeling approach for the phthalate syndrome
Publication Date:	Tue Nov 26 00:00:00 GMT 2019
Journal/Publication Method:	Environment International

All Author(s):

Volume:	134	Number:	N/A
Pages:	105287	Immediately Index:	Immediately Index:

Citation ½ Life:	6.0	Impact Factor:	7.943

Environment International 121 (2018) 764–793

Contents lists available at ScienceDirect

Environment International

journal homepage: www.elsevier.com/locate/envint

Review article

Phthalate exposure and male reproductive outcomes: A systematic review of the human epidemiological evidence

Elizabeth G. Radke[a,*], Joseph M. Braun[b], John D. Meeker[c], Glinda S. Cooper[a,d]

[a] U.S. Environmental Protection Agency, National Center for Environmental Assessment, United States
[b] Brown University, School of Public Health, United States
[c] University of Michigan, School of Public Health, United States
[d] The Innocence Project, United States

ABSTRACT

Objective: We performed a systematic review of the epidemiology literature to identify the male reproductive effects associated with phthalate exposure.

Data sources and study eligibility criteria: Six phthalates were included in the review: di(2-ethylhexyl) phthalate (DEHP), diisononyl phthalate (DINP), dibutyl phthalate (DBP), diisobutyl phthalate (DIBP), butyl benzyl phthalate (BBP), and diethyl phthalate (DEP). The initial literature search (of PubMed, Web of Science, and Toxline) included all studies of male reproductive effects in humans, and outcomes were selected for full systematic review based on data availability.

Study evaluation and synthesis methods: For each outcome, studies were evaluated using criteria defined a priori for risk of bias and sensitivity by two reviewers using a domain-based approach. Evidence was synthesized by outcome and phthalate and strength of evidence was summarized using a structured framework.

Results: The primary outcomes reviewed here are (number of included/excluded studies in parentheses): anogenital distance (6/1), semen parameters (15/9), time to pregnancy (3/5), testosterone (13/8), timing of pubertal development (5/15), and hypospadias/cryptorchidism (4/10). Looking at the overall hazard, there was robust evidence of an association between DEHP and DBP exposure and male reproductive outcomes; this was based primarily on studies of anogenital distance, semen parameters, and testosterone for DEHP and semen parameters and time to pregnancy for DBP. There was moderate evidence of an association between DINP and BBP exposure and male reproductive outcomes based on testosterone and semen parameters for DINP and semen parameters and time to pregnancy for BBP. DIBP and DEP were considered to have slight evidence of an association. For DIBP, the less conclusive evidence was attributed to a more limited literature base (i.e., fewer studies) and lower exposure levels in the population, decreasing the ability to observe an effect. For DEP, the findings were consistent with experimental animal data that suggest DEP does not haves as strong an anti-androgenic effect as other phthalates.

Conclusions and implications of key findings: Overall, despite some inconsistencies across phthalates in the specific outcomes associated with exposure, these results support that phthalate exposure at levels seen in human populations may have male reproductive effects, particularly DEHP and DBP. The relative strength of the evidence reflects differing levels of toxicity as well as differences in the range of exposures studied and the number of available studies.

The views expressed are those of the authors and do not necessarily represent the views or policies of the U.S. EPA.

1. Introduction

Phthalic acid diesters (phthalates) are a class of manmade and multifunction chemicals used in a wide array of consumer and industrial products, including as plasticizers in polyvinyl chloride plastics, excipients in some medications, and scent retainers in some personal care products. Human exposure is ubiquitous across the lifespan, including in utero through maternal exposures. Ingestion, inhalation, and dermal contacts are also routes of exposure for the general population (Johns et al., 2015). After exposure, phthalate diesters are rapidly metabolized to monoester metabolites and excreted in the urine. The group of phthalates encompasses a variety of compounds with different structures, properties, and use. The phthalates, that are the focus of this paper are: di(2-ethylhexyl) phthalate (DEHP), diisononyl phthalate (DINP), dibutyl phthalate (DBP), diisobutyl phthalate (DIBP), butyl benzyl phthalate (BBP), and diethyl phthalate (DEP). Within this group, there are phthalates that are structurally similar and moderately correlated based on human biomonitoring data (e.g., DBP and DiBP). Other are phthalates differ considerably (e.g., long vs short chain; DEP and DEHP); correlations between these phthalates are typically low (Johns et al., 2015).

Phthalates have well documented anti-androgenic activity in rodent studies resulting in reduced circulating testosterone and male reproductive tract abnormalities (Johnson et al., 2012; Howdeshell et al., 2008). Individual studies and reviews in humans and animals, including a recent report from the National Academies of Science (National Academies of Sciences, Engineering, and Medicine, 2017), have investigated male reproductive effects of phthalate exposure, but have

* Corresponding author.
E-mail address: radke-farabaugh.elizabeth@epa.gov (E.G. Radke).

https://doi.org/10.1016/j.envint.2018.07.029
Received 22 February 2018; Received in revised form 22 June 2018; Accepted 20 July 2018
Available online 16 October 2018
0160-4120/ Published by Elsevier Ltd.

Table 1
Primary outcomes included in the systematic review.

Outcome	Background and relevance to male reproductive toxicity
Anogenital distance (AGD)	• Distance from the anus to the genitalia (sexually dimorphic trait with AGD longer in males than females) (Liu et al., 2014). • Externally visible marker shown in animal studies to be a sensitive indicator of prenatal androgen exposure. Decreases in AGD reflect alterations in androgen levels or function during the masculinization programming window (Dent et al., 2015; Dean and Sharpe, 2013). • Susceptible to anti-androgenic environmental exposures.
Semen parameters	• When a couple experiences difficulty getting pregnant, male factor issues (i.e., semen quality) is the sole factor in about 20% of cases and a contributory cause in another 20–30% (Thonneau et al., 1991).
Time to pregnancy	• Fecundity is the biological capacity to reproduce. Time to pregnancy is the primary outcome measure used to study fecundity. • Time to pregnancy displays a reverse j-shaped cumulative distribution with many couples (30–40% conceiving in the first cycle (Buck Louis et al., 2011) and 80–90% of couples being pregnant after up to 12 months of trying (Gnoth et al., 2003). • Time to pregnancy within a couple can be influenced by either male or female exposures, or both (this review focuses on male exposure). • Increases in time to pregnancy are considered indicative of reproductive toxicity (U.S. EPA (U.S. Environmental Protection Agency), 1996, 30,019).
Testosterone	• Plays an important role in the development of the male reproductive system and is necessary for normal male fertility. • Low testosterone levels are associated with adverse conditions (e.g., abnormal sexual differentiation, decreased fertility (U.S. EPA (U.S. Environmental Protection Agency), 1996).
Hypospadias/cryptorchidism	• Hypospadias is the abnormal development of the urethra in males, resulting in the location of the opening of the penis on the underside instead of at the tip. • Cryptorchidism, or undescended testes, can be present at birth (congenital cryptorchidism) or can occur later during infancy and childhood (acquired cryptorchidism).
Pubertal development	• Puberty is a continuous process involving maturation of both the hypothalamic-pituitary-adrenal axis and the hypothalamic-pituitary-gonadal axis. • Hormonal changes during puberty underlie the natural dynamic period of physical and sexual maturation that culminates in the ability to reproduce. • Either early or delayed pubertal onset is considered an adverse effect (U.S. EPA (U.S. Environmental Protection Agency), 1996).

not looked across the full spectrum of male reproductive effects (i.e., from exposures and outcomes during different lifestages, including fetal development, infancy, childhood, puberty, and sexually mature lifestages) in epidemiological studies for DEHP, DINP, DBP, DIBP, BBP, and DEP. Five of the selected phthalates (DEHP, DINP, DBP, DIBP, and BBP) were chosen because they are the most potent with respect to producing the "phthalate syndrome" of male reproductive effects in rats (National Research Council, 2008)and their metabolites have been frequently observed in human populations studies; DEP is not one of the "phthalate syndrome" compounds but was included because it is often the phthalate to which humans have the highest exposure.

We performed a systematic review of the epidemiology literature with the goal of evaluating the strength of evidence of the association between phthalate exposure and male reproductive effects, including the following outcomes: anogenital distance, semen parameters, time to pregnancy (male exposure), testosterone, timing of pubertal development, and hypospadias/cryptorchidism. The human health relevance of these outcomes is summarized briefly in Table 1. These outcomes include a variety of measures relevant to different life-stages: anogenital distance and hypospadias/cryptorchidism may reflect exposure or responsiveness to testosterone during fetal development, pubertal development depends on the functioning of multiple hormonal pathways, and semen parameters and time to pregnancy, measured in adults, are indicators of fertility. Infertility, defined as the inability to conceive after 12 months of unprotected intercourse, has been estimated to affect 15% of couples, and male-related factors are implicated in approximately 20–50% of these cases (Agarwal et al., 2015).

2. Methods

2.1. Literature search and screening

The literature search and screening, study evaluation, data extraction, and evidence synthesis methods are described in detail in the systematic review protocol (Supplemental materials, Section 3). Briefly, epidemiology studies were identified by conducting a single broad literature search on all six phthalates of interest (DEHP, DINP, DBP, DIBP, BBP, DEP) and all outcomes. The Population, Exposure, Comparators, and Outcome (PECO) are available in the protocol (Section 2). The following databases were searched: PubMed, Web of Science, and Toxline, initially in 2013, with updates every 6–12 months through January 2017. Forward and backward searches were also performed. Title/abstract and full text screening was performed by two reviewers.

2.2. Study evaluation

Studies were evaluated by at least two reviewers using uniform approaches for each group of similar studies. Key concerns were risk of bias (factors that affect the magnitude or direction of effect) and insensitivity (factors that limit the ability of a study to detect a true effect) (Cooper et al., 2016). Evaluation was conducted for the following domains: exposure measurement, outcome ascertainment, participant selection, confounding, analysis, sensitivity, and selective reporting. Phthalate and outcome-specific criteria were developed prior to evaluation. For exposure, most of the available studies relied on phthalate metabolite biomarkers (a list of metabolites for each phthalate is provided in the protocol, Section 1.3). Different criteria were developed for short-chain (DEP, DBP, DIBP, BBP) and long-chain (DEHP, DINP) phthalates due to better reliability of single measures for short-chain phthalates. Measurement in urine was considered to be the best proxy of exposure (Johns et al., 2015). Biomarker measures based on samples other than urine (e.g., blood, amniotic fluid, breast milk) were considered to be critically deficient for all short-chain phthalates and for primary metabolites (e.g., MEHP, MINP) of long-chain phthalates (Johns et al., 2015). Rationale for these criteria and additional details for all domains are available in the protocol (Section 4.1.1) and an abbreviated version is available in the key methods supplement. For each study, in each evaluation domain, reviewers reached a consensus rating regarding the utility of the study for hazard identification, with categories of *Good*, *Adequate*, *Deficient*, or *Critically deficient*. These ratings were then combined to reach an overall study confidence classification of *High*, *Medium*, *Low*, or *Uninformative*. Studies were evaluated for their suitability for each outcome investigated, and could receive different ratings for each outcome. Descriptions of each of the categories can be found in the protocol in supplemental materials (Section 4) and the key methods supplement. Study evaluations were documented in Health Assessment Workspace (HAWC), and ratings and rationale are publicly available.

2.3. Evidence synthesis

After study evaluation, the evidence for each outcome was synthesized separately for each phthalate, using the following aspects of an association that may suggest causation: consistency, exposure-response relationship, strength of association, temporal relationship, biological plausibility, and coherence. Based on this synthesis, the evidence was assigned a strength of evidence conclusion of *Robust*, *Moderate*, *Slight*, *Indeterminate*, or *Compelling evidence of no effect*. *Robust* and *Moderate* describe evidence that supports a hazard, differentiated by the quantity and quality of information available to rule out alternative explanations for the results. *Slight* and *Indeterminate* describe evidence that could support a hazard, or could support the absence of a hazard. These categories are generally limited in terms of quantity or confidence level of studies, and serve to encourage additional research across the exposure range experienced by humans. *Compelling evidence of no effect* requires several high confidence studies with consistent null results. The ratings for the individual outcomes were then summarized into an overall conclusion for male reproductive effects by phthalates, using a structured framework available in the key methods supplement and the protocol (Section 6). No statistical quantitative meta-analysis was performed due to substantial differences across studies.

3. Results

An abbreviated version of the literature flow diagram is shown in Fig. 1. Full results of the literature search and screen are described in Supplemental materials. For each outcome, the studies included and excluded based on study evaluation are described in the respective section.

3.1. Anogenital distance

3.1.1. Study selection and evaluation

Based on the exposure evaluation strategy described in the protocol (Section 4.1.1), one study (Huang et al., 2009) was excluded because it was based on the measurement of phthalate metabolites in amniotic fluid. The specific phthalate metabolites examined in the remaining seven papers (describing six studies) and the study evaluations are summarized in Table 2 and full rationale are available at https://hawcprd.epa.gov/summary/visual/100000001/.

All included studies are birth cohorts, varying in size between 73 and 738 mother-child pairs in the analysis sample. All but one were limited to male offspring; (Swan et al., 2015) included both male and female offspring and stratified the analysis by sex. All of the studies were downgraded for exposure assessment as exposure was based on a single spot urine sample. The timing of collection (1st, 2nd, or 3rd trimester) varied among the studies; this variability was not considered to be a basis for downgrading the confidence in the results because the correlation in measures across trimesters is relatively high (Johns et al., 2015). The (Bustamante-Montes et al., 2013) analysis was limited by the fact that MBP, MBzP, and MEP were detected in ≤10% of samples, which is inconsistent with results of biomonitoring studies globally. The corresponding reduction in sensitivity contributed to the overall *low confidence* rating of this study. Limitations of the (Swan, 2008) paper (an extension of the initial study on this topic published by Swan et al., 2015) include a wide age range (1–36 months) and lack of information on the measurement evaluation strategy and standardization and reliability of measures across the different centers. Three studies were classified as *medium confidence* (Bornehag et al., 2015; Swan et al., 2015; Jensen et al., 2016), and the remaining three were classified as *low confidence*.

3.1.2. Results

Fig. 2 provides a comparison of regression coefficients (plotted against the median of exposure for each study) for the three *medium confidence* studies (Bornehag et al., 2015; Swan et al., 2015; Jensen et al., 2016). Because some of the studies used a natural logarithm (ln) transformation of the phthalate metabolite variables and others used a log10 transformation, the regression coefficients in Swan et al., 2015

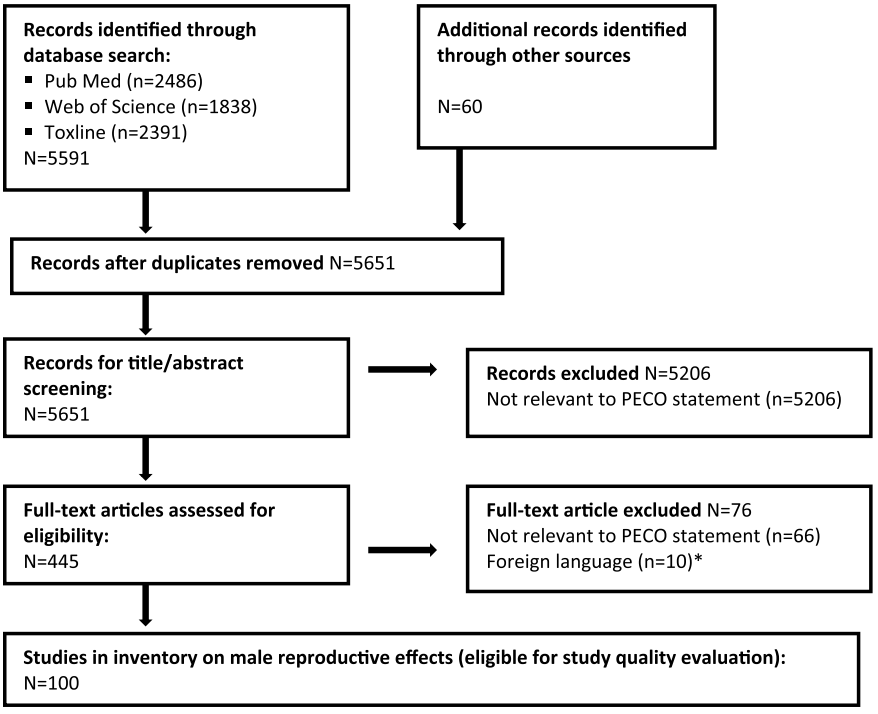

Fig. 1. Literature flow diagram for male reproductive effects of phthalates.
*Did not include studies on male reproductive effects.

Table 2
Epidemiology studies of AGD.

	Reference	Study description			Includes metabolites of:						Study evaluation					
		Population	Exposure	Outcome	DEHP	DINP	DBP	DIBP	BBP	DEP	Exposure	Outcome	Selection	Confounding	Analysis	Overall confidence
Included	(Bornehag et al., 2015)	Birth cohort (N=196 boys) in Sweden	Single urine sample (1st trimester)	AGD at 19-21 mo	✓	✓	✓		✓	✓	A/P	G	G	A	G	Medium
	(Bustamante-Montes et al., 2013)	Birth cohort (N=73 boys) in Mexico	Single urine sample (3rd trimester)	AGD at 1-2 d	✓		✓[a]		✓[a]	✓[a]	P	G	A	A	G	Low
	(Jensen et al., 2016)	Birth cohort (N=273 boys) in Denmark	Single urine sample (26-30 wk gestation)	AGD at 3 mo	✓	✓	✓	✓	✓	✓	A/P	G	G	A	G	Medium
	(Suzuki et al., 2012)	Birth cohort (N=73 boys) in Japan	Single urine sample (3rd trimester)	AGD at 1-3 d	✓		✓		✓	✓	P	A	P	P	A	Low
	(Swan, 2008)	Birth cohort (N=106 boys) in U.S.	Single urine sample (mean 28 wk gestation)	AGD at mean 13 mo (range 1-36)	✓		✓	✓	✓	✓	A/P	P	G	A	P	Low
	(Swan et al., 2015)	Birth cohort (N=365 boys) in U.S.	Single urine sample (1st trimester)	AGD at 1-2 d	✓	✓	✓	✓	✓	✓	A/P	G	A	A	A	Medium
				Total Studies per Phthalate	6	3	5	3	5	5						

	Reference	Reason for Exclusion
Excluded	(Huang et al., 2009)	Critical deficiency in exposure measure (exposure based on amniotic fluid measures)

G = good; A = adequate; D = deficient; A/D = adequate for short chain phthalates, deficient for long chain phthalates.
[a] Study was considered *critically deficient* for this phthalate due to a high percent below the limit of detection (LOD).

and Swan, 2008 with log10 transformations were recalculated (divided by ln10) to make the results directly comparable. Fig. 2 also summarizes in tabular format results (recalculated if applicable) from all studies with the relevant metabolite, including *low confidence* studies.

Evaluation of the evidence for an association between exposure to DEHP and AGD is based on six studies (Fig. 2A). The study with the highest exposure levels for the sum of DEHP metabolites (Bornehag et al., 2015) reported the strongest negative association between DEHP exposure and AGD, and the study with the lowest exposure levels (Jensen et al., 2016) reported the weakest association of the three *medium confidence* studies. (Swan et al., 2015) and (Swan, 2008) also reported statistically significant negative associations with sum DEHP (Swan et al., 2015) and MEHP (Swan, 2008; Swan et al., 2015). Given the consistency across medium confidence studies, evidence of a relationship between AGD and DEHP exposure is considered *moderate*.

Three studies (Bornehag et al., 2015; Swan et al., 2015; Jensen et al., 2016) investigated the association between DINP exposure and AGD (Fig. 2B). (Bornehag et al., 2015), a *medium confidence* study, reported a statistically significant association between shorter AGD with increasing DINP exposure (summed metabolites), while the other two *medium confidence* studies (Swan et al., 2015; Jensen et al., 2016) reported no association between DINP exposure and AGD. The association was observed in the study with the highest exposure levels, which is consistent with a dose response; however, due to the limited number and lack of consistency in the other studies, this evidence is considered *slight*.

The same five studies presented results on the association between DBP (measured by MBP) exposure and AGD (Fig. 2C). (Bornehag et al., 2015) again reported the strongest inverse association between AGD and DBP exposure and the highest exposure levels of MBP in this group of studies. Both (Swan et al., 2015) and (Swan, 2008) also reported inverse associations, with the latter being statistically significant. The remaining two studies reported no association. This evidence is considered *moderate*.

Three studies (Swan et al., 2015; Jensen et al., 2016; Swan, 2008) that examined the association between DIBP (measured by MIBP) and AGD were available (Fig. 2D). (Swan, 2008), a *low confidence* study, and Swan et al., 2015, a *medium confidence* study reported inverse associations, but neither were statistically significant, and the effect size in the latter study was small. The other *medium confidence* study, with higher exposure levels, reported no association. The low exposure levels in all three studies may have decreased sensitivity. This evidence is considered *slight*.

Five studies (Bornehag et al., 2015; Swan et al., 2015; Jensen et al., 2016; Swan, 2008; (Suzuki et al., 2012) presented results on the association between BBP (measured by MBzP) (Fig. 2E) exposure and AGD. Among three *medium confidence* studies, (Bornehag et al., 2015) and (Jensen et al., 2016) reported inverse associations, though neither was statistically significant; the larger effect estimate was seen in the study with higher exposure levels. (Swan et al., 2015) and the two *low confidence* studies (Suzuki et al., 2012; Swan, 2008) reported no association. This evidence is considered *slight*.

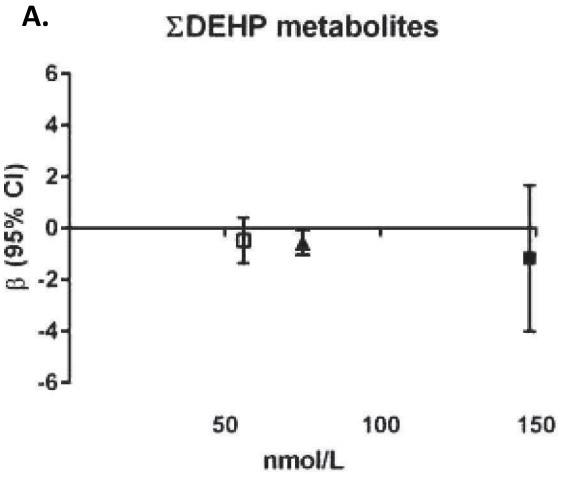

DEHP (measured by sum of DEHP metabolites)			
	Reference, study confidence, N	∑DEHP median, 75th percentile (nmol/L)	Continuous AGD_{as} β (95% CI)
□	**Jensen et al., 2016**, Medium, 245	56, 92	−0.47 (−1.35, 0.41)
▲	**Swan et al., 2015**^, Medium, 365	75, 165	−0.55 (−1.04, −0.06)^
■	**Bornehag et al., 2015**, Medium, 196	148, 221	−1.16 (−4.01, 1.68)
DEHP (measured by MEHP, not on graph)			
	Swan, 2008^, Low, 106	3, 9	−1.52 (p = 0.017)^
	Suzuki et al., 2012, Low, 111	4, 7	−0.23 (−0.41, −0.04)* AGD_{ap}
	Bustamante-Montes et al., 2013, Low, 73	4 (mean)	−0.0049 (p = 0.9) (not log transformed)

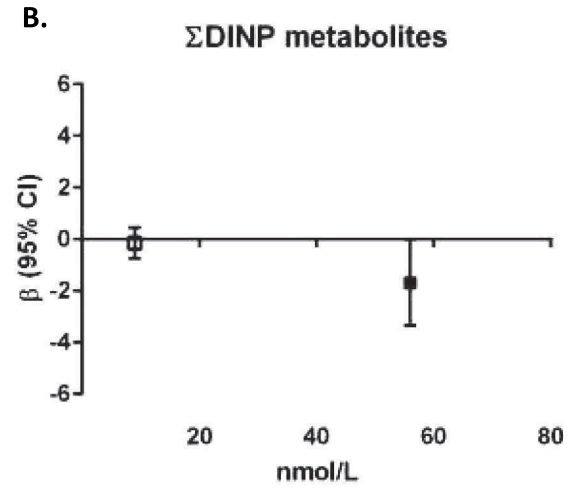

DINP (measured by sum of DINP metabolites)			
	Reference, study confidence, N	∑DINP median, 75th percentile (nmol/L)	Continuous AGD_{as} β (95% CI)
□	**Jensen et al., 2016**, Medium, 245	9, 23	−0.15 (−0.75, 0.44)
■	**Bornehag et al., 2015**, Medium, 196	56, 125	−1.69 (−3.35, −0.02)
DINP (measured by MCiOP, not on graph)			
	Swan et al., 2015^, Medium, 365	13, 45	0.39 (−0.39, 1.16)^

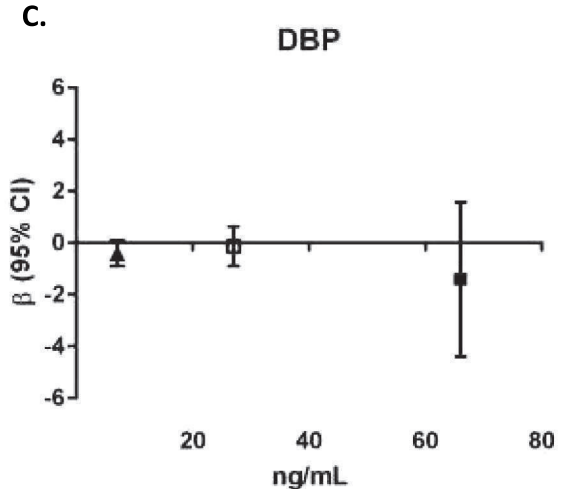

DBP (measured by MBP)			
	Reference, study confidence, N	MBP median, 75th percentile (ng/mL)	Continuous AGD_{as} β (95% CI)
▲	**Swan et al., 2015**^, Medium, 365	7, 17	−0.40 (−0.88, 0.09)^
	Suzuki et al., 2012, Low, 111	7, 17	Not significant (details not reported)
	Swan, 2008^, low, 106	14, 31	−1.41 (p = 0.05)^
□	**Jensen et al., 2016**, Medium, 245	27, 48	−0.13 (−0.89, 0.63)
■	**Bornehag et al., 2015**, Medium, 196	66, 112	−1.41 (−4.39, 1.57)

(caption on next page)

Fig. 2. A–F. Association between phthalate metabolite levels measured in maternal urine samples during pregnancy and AGD in boys.
*$p < 0.05$, results that support an association are shaded. Dark gray represents one or more of the following: $p < 0.05$, large effect size (e.g., OR ≥ 1.5, β ≥ − 0.5), or exposure-response trend across categories of exposure. Light gray represents other supportive results.
^β recalculated to reflect ln transformation of metabolite (from log10).
‡Exposure levels from (Swan et al., 2015).
Exposure level on x-axis is population median for each study, and the axes are scaled the same for all phthalates to facilitate comparison of exposure levels, with the exception of DEHP and DINP, which were reported in nmol/L instead of ng/mL. Each panel depicts results for a metabolite(s) from a different parent phthalate. Studies within each phthalate are sorted by exposure levels. Effect estimates are change in anogenital distance in mm per ln-unit of exposure.

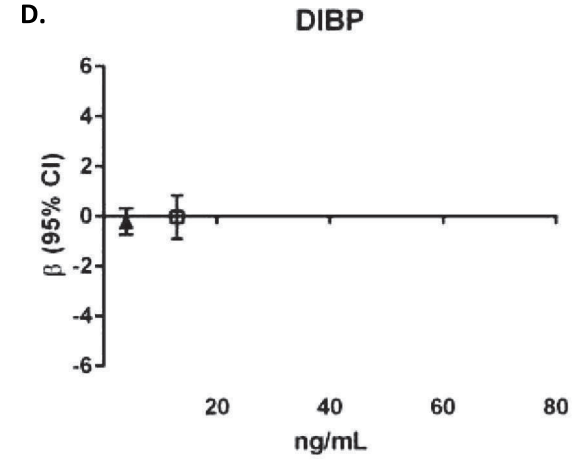

DIBP (measured by MiBP)

Reference, study confidence, N	MiBP median, 75th percentile (ng/mL)	Continuous AGDas β (95% CI)
Swan, 2008^, Low, 106	3, 5[a]	−1.28 (p = 0.1)
▲ **Swan et al., 2015**^, Medium, 365	4, 11	−0.21 (−0.73, 0.31)
□ **Jensen et al., 2016**, Medium, 245	13, 23	−0.03 (−0.90, 0.83)

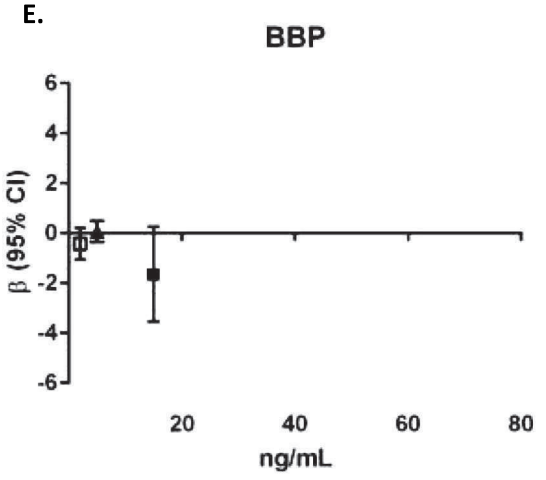

BBP (measured by MBzP)

Reference, study confidence, N	MBzP median, 75th percentile (ng/mL)	Continuous AGD_{as} β (95% CI)
□ **Jensen et al., 2016**, Medium, 245	3, 6	−0.42 (−1.06, 0.21)
▲ **Swan et al., 2015**^, Medium, 365	3, 9	0.07 (−0.35, 0.49)^
Suzuki et al., 2012, Low, 111	4, 9	Not significant (details not reported)
Swan, 2008^, Low, 106	8, 24	−0.14 (p = 0.8)
■ **Bornehag et al., 2015,** Medium, 196	15, 36	−1.66 (−3.56, 0.25)

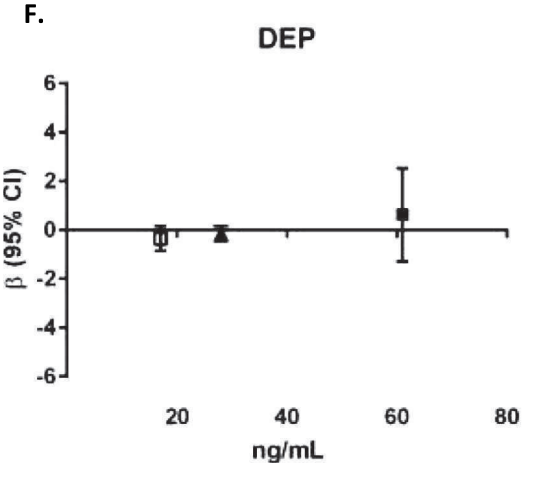

DEP (measured by MEP)

Reference, study confidence, N	MEP median, 75th percentile (ng/mL)	Continuous AGD_{as} β (95% CI)
Suzuki et al., 2012, Low, 111	8, 32	Not significant (details not reported)
□ **Jensen et al., 2016**, Medium, 245	17, 54	−0.34 (−0.84, 0.17)
▲ **Swan et al., 2015**^, Medium, 365	28, 81	−0.14 (−0.45, 0.17)^
■ **Bornehag et al., 2015**, Medium, 196	61, 134	0.63 (−1.29, 2.54)
Swan, 2008^ ‡, Low 106	128, 437[‡]	−1.27 (p = 0.005)^

Fig. 2. (*continued*)

Five studies (Bornehag et al., 2015; Swan et al., 2015: Jensen et al., 2016; Swan, 2008; Suzuki et al., 2012) reported on the association between DEP exposure (measured by MEP) and AGD (Fig. 2E). In the three *medium confidence* studies, there was no evidence of an association. In addition, discordant results (i.e., one positive association and one inverse association) were observed in AGD_{AS} and AGD_{AP} (two different AGD measurements) in both (Jensen et al., 2016) and (Bornehag et al., 2015) (AGD_{AS} result in figure, AGD_{AP} results: Jensen et al., 2016): $\beta = 0.02$ $(-0.54,0.58)$; (Bornehag et al., 2015): $\beta = -1.30$ $(-3.40,0.81)$). Since there is no evidence at this time that one of these AGD measures is a more sensitive measure of response to phthalate exposure, these study findings are considered inconsistent. One *low confidence* study, (Swan, 2008), reported a statistically significant inverse association between MEP and AGD. Overall, evidence is considered *slight*.

In summary, there is *moderate* evidence of an inverse association between AGD and exposure to DEHP and DBP, with mostly consistent results reported among the studies. Evidence for DINP, BBP, DIBP, and DEP is *slight*. The weaker evidence of an association for the DINP, BBP, and DIBP may be due to a combination of low exposure levels (i.e., poor sensitivity) and data availability (i.e., fewer available studies). While evidence for DEP was also rated *slight*, there were high exposure levels, so the relative lack of evidence of an association is consistent with experimental animal data that suggest that this phthalate does not have as strong an anti-androgenic effect as other phthalates. Additional studies, with higher confidence ratings, would be needed to draw a firm conclusion that DEP was not associated with AGD in humans.

3.2. Testosterone in infants

Testosterone plays an important role in the development of the male reproductive system and is therefore an important link between phthalates and other outcomes in this section, such as anogenital distance, hypospadias and cryptorchidism. Three studies (four papers) (Main et al., 2006) (Araki et al., 2016; Araki et al., 2014; Lin et al., 2011) examined the relationship between prenatal phthalate exposure and testosterone levels in newborn boys. Two studies (Main et al., 2006; Araki et al., 2014; Araki et al., 2016) were excluded due to the measurement of exposure in breast milk, blood, and cord blood, respectively, as described in the exposure evaluation strategy (see protocol Section 4.1.1). The remaining *low confidence* study (Lin et al., 2011) was a pregnancy cohort, with phthalate exposure measured in a single spot urine sample during the third trimester, and reproductive hormones measured in cord blood using appropriate methods. Among 81 male newborns, there was no association (Pearson's correlation coefficients for free testosterone: MEP-0.10, MBP-0.11, MBzP 0.05, ΣDEHP 0.06, *p*-values for all > 0.1). This evidence is considered *indeterminate*.

3.3. Semen parameters

3.3.1. Study selection and evaluation

Based on the exposure evaluation, nine of the 28 epidemiology papers (Table 3) identified in the search with data on sperm parameters and exposure in adults were excluded because they used measurements of phthalates in tissues other than urine (i.e., blood or semen) or

Table 3
Epidemiology studies of semen parameters.

	Reference	Study description			Includes metabolites of:						Study evaluation					
		Population	Exposure	Outcome	DEHP	DINP	DBP	DIBP	BBP	DEP	Exposure	Outcome	Selection	Confounding	Analysis	Overall confidence
Included	(Axelsson et al., 2015a) (Axelsson et al., 2015b)	Cross-sectional (N=314) in Sweden; men entering military	Single urine sample; subset with prenatal sample available	Concentration, motility, morphology by WHO guidelines	✓	✓	✓		✓	✓	A/P	A	A	A	A	Medium
	(Bloom et al., 2015)	Cohort (N=375) in U.S.; men from couples trying to conceive	Single urine sample	Concentration, motility, morphology by WHO guidelines in two samples	✓		✓	✓	✓	✓	A/P	A	A	A	A	Medium
	(Den Hond et al., 2015)	Case-control (N=40 cases reduced semen quality/80 controls) in Belgium	Single urine sample	Concentration, motility, morphology by WHO guidelines	✓		✓	✓	✓	✓	A/P	G	P	P	A	Low
	(Han et al., 2014)	Cross-sectional (N=232) in China; general population	Single urine sample	Concentration, motility, morphology by WHO guidelines	✓		✓		✓[a]	✓	A/P	G	P	A	A	Medium
	(Hauser et al., 2006)	Cross-sectional (N=463) in U.S.; men from couples seeking infertility workup	Single urine sample	Concentration, motility, morphology by WHO guidelines	✓		✓		✓	✓	A/P	G	A	A	A	Medium

(*continued on next page*)

Table 3 (*continued*)

	(Herr et al., 2009)	Cross-sectional (N=349) in Germany; men from couples seeking infertility workup	Single urine sample	Concentration, motility, morphology by WHO guidelines	✓						P	A	P	P	P	Low
	(Huang et al., 2013) (Huang et al., 2011)	Cross-sectional (N=62) in Taiwan; factory workers and students	Single urine sample, occupational, air sampling	Concentration, motility, morphology by WHO guidelines	✓						A	A	A	P	A	Medium
	(Jonsson et al., 2005)	Cross-sectional (N=234) in Sweden; men entering military	Single morning urine sample	Concentration, motility, morphology by WHO guidelines	✓[a]		✓		✓	✓	A	A	A	P	A	Medium
	(Jurewicz et al., 2013)	Cross-sectional (N=269) in Poland; men at infertility clinic	Single morning urine sample	Concentration, motility, morphology by WHO guidelines	✓	✓	✓		✓	✓	A/P	A	P	A	A	Medium
	(Liu et al., 2012)	Cross-sectional (N=125) in China; men seeking fertility assessment	Two urine samples several days apart	Concentration, motility, morphology by WHO guidelines	✓		✓		✓[a]	✓	G	G	P	P	A	Medium
	(Pan et al., 2016); Pan et al. (2015)	Cross-sectional (N=1,066) in China; men seeking fertility assessment	Single urine sample	Concentration, motility, morphology by WHO guidelines	✓	✓	✓	✓	✓	✓	A/P	A	A	A	A	Medium
	(Specht et al., 2014) (Lenters et al., 2014)	Cross-sectional (N=589) in Greenland, Poland, Ukraine; men from couples at antenatal visit	Single blood sample (only used for secondary metabolites)	Concentration, motility, morphology by WHO guidelines	✓	✓					P	P	G	A	A	Medium
	Thurston et al. (2016)	Cross-sectional sample (N=420) of male partners from pregnancy cohort in U.S.	Single urine sample	Concentration, motility, morphology by WHO guidelines	✓		✓	✓	✓	✓	A/P	G	A	A	G	Medium
	(Wang et al., 2015b)	Cross-sectional (N=1,040) in China; men seeking semen analysis	Two urine samples collected same day	Concentration, motility, morphology by WHO guidelines	✓		✓		✓	✓	G	G	A	A	G	Medium
	(Wirth et al., 2008)	Cross-sectional (N=45) in U.S.; men seeking fertility assessment	Single morning urine sample	Concentration, motility, morphology by WHO guidelines	✓		✓	✓[a]	✓	✓	A/P	P	P	A	A	Medium
				Total Studies per Phthalate	14	4	12	4	11	12						

Exclu	Reference	Reason for Exclusion
	(Joensen et al., 2012)	Results not presented for individual phthalate metabolites
	(Kranvogl et al., 2014)	Critical deficiencies in multiple evaluation categories
	(Pan et al., 2011)	Critical deficiency in exposure measure (exposure based on measures in semen)
	(Pant et al., 2008)	Critical deficiency in exposure measure (exposure based on measures in semen)
	(Pant et al., 2014)	Critical deficiency in exposure measure (exposure based on measures in semen)
	(Toshima et al., 2012)	Critical deficiency in outcome measure; limited in other categories
	(Wang et al., 2015a)	Critical deficiency in exposure measure (exposure based on measures in semen)
	(Wang et al., 2016b)	Critical deficiency in exposure measure (exposure based on measures in semen); subset of study in Wang et al. (2015b)
	(Zhang et al., 2006)	Critical deficiency in exposure measure (exposure based on measures in semen)

G = good; A = adequate; D = deficient; A/D = adequate for short chain phthalates, deficient for long chain phthalates; WHO = World Health Organization.
[a] Study was considered *critically deficient* for this phthalate due to a high percent below the LOD.

Table 4
Associations between DEHP exposure and semen parameters.

Reference; Study confidence; N	Exposure	Outcome trans-formation	Effect estimate	Metabolite (ng/mL) [median unless otherwise specified]	Sperm concentration (×10^6/ml)	Motility (% normal)	Morphology (% normal)
∑DEHP							
Huang et al. (2011); Medium; 45	No trans-form-ation, air concen-tration	No trans-formation	β (SE; *p*-value)	8/56 (n low/n high exposed) [occupational setting]	−0.19 (0.12; *p* = 0.1)	−0.23 (0.11; *p* = 0.04)	0.014 (0.056, *p* = 0.8) (% abnormal)
(Thurston et al., 2016); Medium; 420	Ln-trans-formed	Log-transformed	β (CI)	MEOHP mean 13 Range 0.5-1320	0.04 (-0.04,0.11)	0.30 (-0.80,1.41)	0.21 (-0.32,0.74)
Wirth et al. (2008); Medium; 45	Tertiles	Dichotomous	OR (CI)	10.1	T2: 1.97 (0.2, 16.1) T3: 6.65 (0.9, 47.3)	T2: 0.7 (0.1–4.4) T3: 0.7 (0.1–4.4)	T2: 1.2 (0.3, 5.4) T3: 1.1 (0.3, 4.7)
Herr et al. (2009); Low; 349	Quartiles	Dichotomous	OR (CI)	4.4	Q2: 0.86 (0.37, 1.97) Q3: 1.11 (0.46, 2.70) Q4: 1.57 (0.60, 4.08)	Q2: 0.61 (0.2, 1.7) Q3: 0.74 (0.3, 2.2) Q4: 0.86 (0.3, 2.9)	Q2: 1.95 (0.7, 5.2) Q3: 0.91 (0.4, 2.1) Q4: 1.26 (0.57, 2.8)
MEOHP							
Bloom et al. (2015); Medium; 375 [related to Wang et al., 2015a]	Ln-trans-formed; 1 IQR difference	Box-Cox transformed	β (CI)	5.7	−1.90 (−3.7, −0.2)*	CD	−3.35 (−11.4, 4.7)
Wang et al. (2015b); Medium; 1,040 [related to Bloom et al., 2015]	Ln-trans-formed	Ln-transformed	β (CI)	5.7	(see row with % change effect estimates)	0.80 (−1.0, 2.6)	−0.10 (−0.8, 0.6)
Huang et al. (2013); Medium; 62	Log trans-formed	No trans-formation	β (CI)	18/92 (low/high exposed)	−0.12 (−0.3, 0.06)	−0.02 (−0.3, −0.07)	−0.001 (−0.07, 0.07)
Den Hond et al. (2015); Low; 120	Ln-trans-formed	No trans-formation	β (SE) for 1 unit increase	7.7 (mean in controls)	0.18 (0.28)	1.73 (4.15)	−0.12 (0.42)
Specht et al. (2014); Medium; 589	Dichotomous	Ln-transformed	Means (CI)	0.2	<LOD: 51.5 ≥LOD: 46.1 (35.3, 60.1)	Not significant (details not reported)	Not significant (details not reported)

(*continued on next page*)

Table 4 (*continued*)

Wang et al. (2015b); Medium; 1,040 [related to Bloom et al., 2015]	Ln-transformed	Ln-transformed	% change (CI)	5.7	4.08% (−9.4, 17.4)	(see results for β effect estimates)	(see row with β effect estimates)
(Pan et al., 2016); Pan et al. (2015); Medium; 1,066	Ln-transformed	Cubic root for concentration	% change (CI)	8.4 IQR 4.8-14.3	−1.3% (-3.6,1.0)	−0.5% (−3.6,2.5)	−2.1% (−5.4,1.2)
Axelsson et al. (2015a); Medium; 314	Quartiles	Cubic root	Mean difference (Q4 vs. Q1)	9.6	−0.06 (−0.48, 0.36)	−6.9 (−13, −1.1)*	−0.42 (−2.4, 1.6)
Wang et al. (2015b); Medium; 1040	Quartiles	Dichotomous	OR (CI)	5.7 7.0	Q2: 0.97 (0.53, 1.79) Q3: 0.82 (0.43, 1.55) Q4: 0.86 (0.47, 1.60)	Q2: 0.86 (0.6, 1.2) Q3: 0.90 (0.6, 1.3) Q4: 0.73 (0.5, 1.1)	
Liu et al. (2012); Medium; 125	Tertiles	Dichotomous	OR (CI)	2.7 (mean)	T2: 1.4 (0.3, 7.7) T3: 0.6 (0.1, 4.2)	T2: 1.0 (0.4, 3.1) T3: 0.6 (0.2, 1.8)	
Hauser et al. (2006); Medium; 463	Quartiles	Dichotomous	OR (CI)	32.1	Q2: 3.1 (0.8, 11.7) Q3: 1.1 (0.3, 4.6) Q4: 1.6 (0.4, 6.3)	Q2: 0.9 (0.4, 2.0) Q3: 0.6 (0.3, 1.3) Q4: 0.8 (0.3, 1.6)	Q2: 1.4 (0.5, 3.7) Q3: 0.5 (0.2, 1.5) Q4: 0.7 (0.3, 2.0)
MEHP							
Jurewicz et al. (2013); Medium; 269	Log transformed	Log transformed	β (p)	8.8	−0.07 (p = 0.3)	−3.85 (p = 0.001)*	1.29 (p = 0.24)
Huang et al. (2013); Medium; 62 (see also means ± SD results)	Log transformed	No transformation	β (CI)	6.3/23[a]	−0.07 (−0.6, 0.5)	−0.55 (−1.0, −0.1)	0.09 (−0.1, 0.3)
Huang et al. (2013); Medium; 62 (see also β results)	Categorical		Means ± SD	6.3/23[a]	Controls: 46.7 ± 32.0 Low: 19.9 ± 14.6 High: 27.8 ± 25.5	Controls: 65.2 ± 10.0 Low: 56.1 ± 18.3 High: 41.4 ± 22.0	Controls: 44.8 ± 7.7 Low: 41.4 ± 9.3 High: 41.4 ± 11.6
Han et al. (2014); Medium; 232	Dichotomous	Dichotomous	OR (CI)	1.1 5th–95th percentile: 0–24	1.15 (0.57, 2.33)	0.48 (0.08, 2.76)	1.18 (0.58, 2.39)

*$p < 0.05$, results that support an association are shaded. Dark gray represents one or more of the following: $p < 0.05$, large effect size (e.g., OR ≥ 1.5, β ≥ −0.5, % difference ≥ 1.0%), or exposure-response trend across categories of exposure. Light gray represents other supportive results.
Q = quartile; T = tertile. Studies are sorted by study confidence level within each metabolite-effect estimate grouping.

Table 5
Associations between DINP exposure and semen parameters.

Reference; Study Confidence Rating; N	Exposure	Outcome transformation	Effect estimate	Metabolite (ng/mL) [median unless otherwise specified]	Sperm concentration (×10^6/ml)	Motility (% normal)	Morphology (% normal)
MCiOP							
Specht et al. (2014) ; Medium; 589	Tertiles	Ln-transformed	Means (CI) by percentile group	0.5 maximum: 42	<25th: 52.8 (43.9, 63.7) 25th–75th: 52.2 (45.1, 60.3) >75th: 51.8 (43.1, 62.2)		
(Pan et al., 2016); Pan et al. (2015); Medium; 1,066	Ln-transformed	Cubic root for concentration	% change (CI)	1.2 IQR: 0.7-2.1	−1.2% (−3.4, 0.9)	−2.4% (−5.2, 0.4%)	−3.4% (−6.4, 0.3)
Axelsson et al. (2015a); Medium; 314	Quartiles	Cubic root	Mean difference (Q4 vs. Q1)	16 range: 1.4–810	−0.08 (−0.49, 0.33)	−1.3 (−7.2, 4.6)	−1.2 (−3.1, 0.81)
MINP							
Jurewicz et al. (2013); Medium; 269	Log transformed	Log transformed	β (p)	1.1 IQR: 0.2–6.4	−0.31 (0.191)	6.21 (0.060)	−9.05 (0.033)*
Specht et al. (2014); Medium; 589	Tertiles	Ln-transformed	Means (CI) by percentile group	0.003 Proxy-MINP (nm) 0.15 (maximum)	<25th: 50.3 (37.8, 67.1) 25th–75th: 48.7 (37.4, 63.4) >75th: 45.5 (34.2, 60.4)		

*$p < 0.05$, results that support an association are shaded. Dark gray represents one or more of the following: $p < 0.05$, large effect size (e.g., OR ≥ 1.5, β ≥ −0.5, % difference ≥ 1.0%), or exposure-response trend across categories of exposure. Light gray represents other supportive results.
Q = quartile; T = tertile. Studies are sorted by study confidence level within each metabolite-effect estimate grouping.

because of other critical deficiencies in methodology or reporting of results. The specific phthalates examined in the remaining 15 studies (19 papers) and their evaluations are summarized in Table 3 (Joensen et al., 2012; Kranvogl et al., 2014; Lenters et al., 2014; Pan et al., 2011, 2016; Pant et al., 2008, 2014; Toshima et al., 2012; Zhang et al., 2006). Full rationale are available at https://hawcprd.epa.gov/summary/visual/100000065/.

Outcome-specific criteria for study evaluation are available in the supplement. Population-based studies were preferred, but clinic or center-based samples were also acceptable as long as they were not limited to volunteers with known male fertility issues. Most of the studies are cross-sectional, varying in size between 45 and 1066 adult males. In most studies, a single urine sample was collected concurrent with outcome assessment (semen analysis). Exceptions are (Liu et al., 2012) and (Wang et al., 2015a, 2015b, 2015c), which had two urine samples several days apart and the same day, respectively. Because the relevant time window of exposure for sperm production was considered to be relatively short (< 90 days), concurrent measurement was not considered a limitation for this outcome. (Specht et al., 2014) used blood samples which were acceptable for secondary metabolites of DEHP and DINP, and (Huang et al., 2011), in which personal air samples were collected during a work shift. All of the studies assessed exposure in adulthood; one study (Axelsson et al., 2015b) additionally examined prenatal exposure, which is considered separately. Thirteen studies were classified as *medium confidence*, and two as *low confidence* (Den Hond et al., 2015, 3,045,496; Herr et al., 2009).

3.3.2. Results

Comparing results across studies is challenging due to the wide variety of analysis methods used. It is important to carefully consider the interpretation of the type of coefficient when comparing across results: for example, results supporting an association between increasing exposure and poorer semen quality will be reflected by a negative coefficient when the outcome is modeled as a continuous variable, and as a positive coefficient when the outcome is modeled as the probability of an unfavorable outcome (e.g., prevalence of sperm concentration $< 15 \times 10^6$ per ml). To facilitate comparisons, the sets of studies reporting each type of metabolite in Table 4 are grouped by type of effect estimate (Beta or OR), and further sorted by overall confidence rating. Studies using dichotomous outcomes (and OR estimates) used World Health Organization guidelines for establishing cutoffs, with all using the 1999 version, with the exception of Wang et al. (2015a, 2015b, 2015c), which used the 2010 version. Both versions are similar in establishing abnormal semen quality (Catanzariti et al., 2013).

Evaluation of the evidence for an association between exposure to DEHP and sperm parameters is based on 14 studies. Results for summed

Table 6
Associations between DBP and semen parameters.

Reference; Study Confidence Rating; N	Exposure	Outcome transformation	Effect estimate	MBP (ng/mL) [median unless otherwise specified]	Sperm concentration (×10^6/ml)	Motility (% normal)	Morphology (% normal)
Wang et al. (2015b); Medium; 1,040	Continuous ln-transformed	No transformation	β (CI)	70	(see row with change effect estimates)	−0.92 (−2.58, 0.75)	−0.40 (−1.07, 0.27)
Bloom et al. (2015); Medium; 375	Continuous ln-transformed; 1 IQR difference	Box-Cox transformed	β (CI)	7	−0.95 (−4.0, 2.1)	−1.22 (−4.0, 1.6)	−7.03 (−21.0, 6.9)
Thurston et al. (2016); Medium; 420	Ln-trans-formed	Log-transformed	β (CI)	15	0.01 (-0.09,0.11)	-0.58 (-2.00, 0.84)	0.22 (-0.46, 0.91)
Jurewicz et al. (2013); Medium; 269	Continuous log transformed	Log transformed (concentration)	β (p)	83	−0.21 (p = 0.11)	−1.55 (p = 0.5)	−2.68 (p = 0.2)
Den Hond et al. (2015); Low; 120	Continuous ln-transformed	No transformation	β (SE)	18.9; 20.7 (mean controls; cases)	0.24 (0.35)	4.21 (5.20)	−0.25 (0.42)
Wang et al. (2015b); Medium; 1,040	Continuous ln-transformed	Ln-transformed (concentration)	% change (CI)	70	−6.18% (1.6, −0.3)	(see row with β effect estimates)	(see row with β effect estimates)
(Pan et al., 2016); Pan et al. (2015); Medium; 1,066	Ln-transformed	Cubic root for concentration	% change (CI)	78	-2.4% (-5.1,0.3)	-1.3% (-4.8,2.3)	-6.5 (-10.3,- 2.7)*
Axelsson et al. (2015a); Medium; 314	Quartiles	Cubic root (concentration)	Mean difference (Q4 vs. Q1)	47	0.04 (−0.38, 0.45)	−7.7 (−14, −1.8)*	0.65 (−1.3, 2.6)
Jonsson et al. (2005); Medium; 234	Quartiles	No transformation	Mean difference (Q4 vs. Q1)	78	−7.9 (−33, 17)	2.1 (−4.0, 8.2)	
Wang et al. (2015b); Medium; 1,040	Quartiles	Dichotomous	OR (CI)	70	Q2: 1.28 (0.7, 2.5) Q3: 0.87 (0.4, 1.8) Q4: 2.01 (1.1, 3.8)*	Q2: 0.74 (0.5, 1.1) Q3: 0.96 (0.7, 1.4) Q4: 1.04 (0.7, 1.5)	
Hauser et al. (2006); Medium; 463	Quartiles	Dichotomous	OR (CI)	18	Q2: 3.1 (1.2, 8.1)* Q3: 2.5 (0.9, 6.7) Q4: 3.3 (1.2, 8.5)*	Q2: 1.5 (0.8, 2.6) Q3: 1.5 (0.8, 2.6) Q4: 1.8 (1.1, 3.2)*	Q2: 0.8 (0.4, 1.6) Q3: 0.9 (0.5, 1.7) Q4: 0.8 (0.4, 1.6)
Han et al. (2014); Medium; 232	Dichotomous	Dichotomous	OR (CI)	19	1.97 (0.97, 4.0)	1.08 (0.7, 1.7)	1.53 (0.8, 3.1)
Reference; Study Confidence Rating; N	**Exposure**	**Outcome transformation**	**Effect estimate**	**MBP (ng/mL) [median unless otherwise specified]**	**Sperm concentration (×10^6/ml)**	**Motility (% normal)**	**Morphology (% normal)**
Wirth et al. (2008); Medium; 45	Dichotomous	Dichotomous	OR (CI)	25	0.5 (0.1, 3.6)	0.8 (0.2, 3.9)	3.3 (0.7, 16.2)
Liu et al. (2012); Medium; 125	Tertiles	Dichotomous	OR (CI)	26 (mean)	Q2: 6.8 (0.6, 75.3) Q3: 12.0 (1.0, 143)*	Q2: 0.5 (0.2, 1.4) Q3: 0.7 (0.3, 2.1)	Q2: 1.0 (0.3, 4.1) Q3: 0.4 (0.1, 2.1)

*$p < 0.05$, results that support an association are shaded. Dark gray represents one or more of the following: $p < 0.05$, large effect size (e.g., OR ≥ 1.5, β ≥ −0.5, % difference ≥ 1.0%), or exposure-response trend across categories of exposure. Light gray represents other supportive results.
Q = quartile; T = tertile. Studies are sorted by study confidence level within each metabolite-effect estimate grouping.

Table 7
Associations between DIBP and semen parameters.

Reference; Study Confidence Rating; N	Exposure	Outcome transformation	Effect estimate	MIBP median (ng/mL)	Sperm concentration (×10⁶/ml)	Motility (% normal)	Morphology (% normal)
Thurston et al. (2016); Medium; 420	Ln-trans-formed	Log-transformed	β (CI)	2.8	0.02 (-0.06,0.11)	0.82 (-0.31,1.96)	0.28 (-0.27,0.83)
Bloom et al. (2015); Medium; 375	Continuous ln-transformed; 1 IQR difference	Box-Cox transformed	β (CI)	4.4	0.46 (-1.90,2.83)	-0.98 (-3.16,1.20)	-4.43 (-15.15,6.29)
Den Hond et al. (2015); Low; 120	Continuous ln-transformed	Continuous, no transformation noted	β (SE)	55 (mean)	0.16 (0.53)	4.81 (3.59)	0.10 (0.33)
(Pan et al., 2016); Pan et al. (2015); Medium; 1,066	Ln-trans-formed	Cubic root for conc	% change (CI)	48	-2.1% (-4.6,0.4)	-2.2% (-5.4,1.1)	-5.3% (-8.9,-1.8)*

*$p < 0.05$, results that support an association are shaded. Dark gray represents one or more of the following: $p < 0.05$, large effect size (e.g., OR ≥ 1.5, β ≥ −0.5, % difference ≥ 1.0%), or exposure-response trend across categories of exposure. Light gray represents other supportive results.
Q = quartile; T = tertile. Studies are sorted by study confidence level within each metabolite-effect estimate grouping.

DEHP metabolites were used when available; if not available, results for MEOHP or MEHP were used (Table 4). An inverse relationship (decreased semen quality with increased DEHP exposure as measured by metabolite levels) was observed for sperm concentration in seven studies, and for motility in four studies. However, of all of the findings, only one for sperm concentration (Bloom et al., 2015) and two for motility (one for MEOHP and one for MEHP) (Axelsson et al., 2015a; Jurewicz et al., 2013) were statistically significant, and there was no indication that studies with higher median exposure levels were more likely to observe an association. The inverse findings were also supported by data (not reviewed systematically) from studies that indicated increased apoptosis (Huang et al., 2014); (Wang et al., 2016b; You et al., 2015), increased reactive oxygen species (ROS) generation (Huang et al., 2014), and increased sperm aneuploidy (Jurewicz et al., 2013)with increasing DEHP exposure, which may help inform potential mechanisms of action. Overall, there is *moderate* evidence of an association between increased DEHP and decreased semen quality, particularly for sperm concentration.

Four *medium confidence* studies examined the association between DINP exposure (measured by MCiOP or MINP) and semen parameters (Table 5). All three studies that looked at morphology (Axelsson et al., 2015a; Pan et al., 2015; Jurewicz et al., 2013) reported an inverse association between exposure and sperm quality, two of the three that looked at motility also reported an association (Axelsson et al., 2015a; Pan et al., 2015), and two of four studies reported an association with concentration (Specht et al., 2014) (Pan et al., 2015), including one with an exposure-response gradient (Specht et al., 2014). However, the only finding that was statistically significant was for morphology in Jurewicz et al. (2013). Given the consistency across studies for morphology, the relationship between DINP exposure and sperm parameters is considered *moderate*.

Twelve studies reported results on the association between DBP exposure (measured by MBP) and semen parameters (Table 6). Eight studies reported decreased concentration with increasing DBP exposure, with statistically significant and monotonic dose-response relationships observed in three (Wang et al., 2015b; Liu et al., 2012; Hauser et al., 2006). These findings were observed across the range of exposures observed in the studies. Seven studies supported an association for motility, including two that were statistically significant (Axelsson et al., 2015a; Hauser et al., 2006), but studies with lower exposure levels were more likely to report an association than studies with higher levels. Of the ten studies that included an evaluation of morphology, six support an association. Evidence for effects on semen were also supported by data (not reviewed systematically) from a study that indicated increased sperm aneuploidy with increased DBP exposure (Jurewicz et al., 2013), which may help inform potential mechanisms of action. No association was observed between DBP exposure and sperm apoptosis in one study (Wang et al., 2016b; You et al., 2015). Overall, due to the consistency across several *medium confidence* studies and the observation of dose-response relationships, evidence of an association between increased DBP exposure and decreased semen quality, specifically sperm concentration, is considered *robust*.

Four studies reported results for DIBP exposure (measured by MIBP) and semen parameters (Table 7). Two *medium confidence* studies (Bloom et al., 2015) reported associations between increasing MIBP concentrations and one or more measures of decreased semen quality. The remaining *medium* confidence (Thurston et al., 2016) and *low* confidence (Den Hond et al., 2015) studies reported no association. Given the limited data and lack of consistency, the relationship between DIBP exposure and semen parameters is considered *slight*.

Ten studies reported results on the association between BBP exposure (measured by MBzP) and semen parameters (Table 8). Four studies that examined sperm concentration and eight studies that examined motility reported an association between increased BBP exposure and decreased sperm quality; for motility, studies with higher exposure levels were more likely to find an association. Statistically significant associations were reported with sperm concentration in two studies (Bloom et al., 2015) (Pan et al., 2015); and with motility in one study (Thurston et al., 2016). Only two studies examining morphology reported an association. Evidence for effects on semen were also supported by data (not reviewed systematically) from a study that reported increased sperm aneuploidy with increased BBP exposure (Jurewicz et al., 2013), which may help inform potential mechanisms of action. No association was observed between BBP exposure and sperm apoptosis in one study (Wang et al., 2016b; You et al., 2015). Overall, due to associations being reported in several *medium confidence* studies, there is *moderate* evidence that BBP exposure is associated with decreased sperm quality, specifically motility.

Twelve studies investigated the association between DEP exposure (measured by MEP) and sperm parameters (Table 9). An inverse relationship (decreased semen quality with increased DEP exposure as measured by metabolite levels) was observed for sperm concentration

Table 8
Associations between BBP and semen parameters.

Reference; Study Confidence Rating; N	Exposure	Outcome transformation	Effect estimate	MBzP median (ng/mL)	Sperm concentration (×10⁶/ml)	Motility (% normal)	Morphology (% normal)
Wang et al. (2015b); Medium; 1,040	Ln-transformed	No transformation	β (CI)	2.9	(see row with % change effect estimates)	0.43 (−0.62, 1.47)	0.20 (−0.22, 0.61)
Bloom et al. (2015); Medium; 375	Ln-transformed; 1 IQR difference	Box-Cox transformed	β (CI)	3.6	−3.09 (−5.52, −0.66)*	−1.67 (−3.92, 0.58)	−5.71 (−16.97, 5.56)
Thurston et al. (2016); Medium; 420	Ln-trans-formed	Log-transformed	β (CI)	11	-0.04 (-0.12,0.04)	-1.47 (-2.61,-0.33)*	-0.19 (-0.75,0.36)
Jurewicz et al. (2013); Medium; 269	Log transformed	Log transformed (concentration)	β (p)	5.2	−0.07 (p = 0.25)	1.86 (0.10)	1.17 (0.28)
Den Hond et al. (2015); Low; 120	Ln-transformed	No transformation	β (SE)	4.5 (mean controls)	−0.03 (0.17)	−1.44 (2.57)	0.30 (0.27)
Wang et al. (2015b); Medium; 1,040	Ln-transformed	Ln-transformed (concentration)	% change (CI)	2.9	1.01% (−3.05, 5.13%)	(see row with β effect estimates)	(see row with β effect estimates)
(Pan et al., 2016); Pan et al. (2015); Medium; 1,066	Ln-transformed	Cubic root for conc	% change (CI)	0.1	-3.4% (-5.9,-0.8)*	-1.8% (-5.1,1.6)	-4.0% (-7.6,-0.4)*
Axelsson et al. (2015a); Medium; 314	Quartiles	Cubic root (concentration)	Mean difference (Q4 vs. Q1)	13	−0.29 (−0.71, 0.13)	−5.4 (−11, 0.56)	−0.79 (−2.8, 1.2)
Reference; Study Confidence Rating; N	**Exposure**	**Outcome transformation**	**Effect estimate**	**MBzP median (ng/mL)**	**Sperm concentration (×10⁶/ml)**	**Motility (% normal)**	**Morphology (% normal)**
Jonsson et al. (2005); Medium; 234	Quartiles	No transformation	Mean difference (Q4 vs. Q1)	16	7.2 (−16, 31)	−4.3 (−10, 1.6)	
Wang et al. (2015b); Medium; 1,040	Quartiles	Dichotomous	OR (CI)	2.9	Q2: 0.88 (0.48, 1.61) Q3: 0.83 (0.44, 1.53) Q4: 0.85 (0.46, 1.58)	Q2: 0.75 (0.51, 1.09) Q3: 1.05 (0.73, 1.52) Q4: 0.93 (0.64, 1.35)	
Hauser et al. (2006); Medium; 463	Quartiles	Dichotomous	OR (CI)	8.0	Q2: 1.1 (0.4, 2.6) Q3: 1.1 (0.4, 2.5) Q4: 1.9 (0.8, 4.3)	Q2: 1.3 (0.7, 2.3) Q3: 1.3 (0.8, 2.3) Q4: 1.3 (0.7, 2.3)	Q2: 0.7 (0.3, 1.4) Q3: 0.9 (0.4, 1.7) Q4: 1.1 (0.6, 1.6)
Wirth et al. (2008); Medium; 45	Dichotomous	No transformation	OR (CI)	17	1.4 (0.3, 6.3)	1.3 (0.3, 5.5)	0.9 (0.2, 3.2)

*$p < 0.05$, results that support an association are shaded. Dark gray represents one or more of the following: $p < 0.05$, large effect size (e.g., OR ≥ 1.5, β ≥ −0.5, % difference ≥ 1.0%), or exposure-response trend across categories of exposure. Light gray represents other supportive results.
Q = quartile. Studies are sorted by study confidence level within each metabolite-effect estimate grouping.

Table 9
Associations between DEP and sperm parameters.

Reference; Study Confidence Rating; N	Exposure	Outcome transformation	Effect estimate	MEP median (ng/mL)	Sperm concentration (×10⁶/ml)	Motility (% normal)	Morphology (% normal)
Wang et al. (2015b); Medium; 1,040	Ln-transformed	No transformation	β (CI)	18	(see row with % change effect estimates)	0.12 (−0.77, 1.02)	−0.25 (−0.60, 0.11)
Bloom et al. (2015); Medium; 375	Ln-transformed; 1 IQR difference	Box-Cox transformed	β (CI)	86	−1.01 (−2.86, 0.85)	−0.83 (−2.54, 0.88)	−1.23 (−9.64, 7.17)
Thurston et al. (2016); Medium; 420	Ln-trans-formed	Log-trans-formed	β (CI)	201	-0.02 (-0.07,0.04)	-0.13 (-0.95,0.69)	0.16 (-0.24,0.55)
Jurewicz et al. (2013); Medium; 269	Log-transformed	Log transformed (concentration)	β (p)	45	−0.07 (0.25)	−3.85 (0.001)*	1.29 (0.24)
Reference; Study Confidence Rating; N	**Exposure**	**Outcome transformation**	**Effect estimate**	**MEP median (ng/mL)**	**Sperm concentration (×10⁶/ml)**	**Motility (% normal)**	**Morphology (% normal)**
Den Hond et al. (2015); Low; 120	Ln-transformed	No transformation noted	β (SE)	50 (mean controls)	0.24 (0.19)	4.62 (2.78)	0.05 (0.24)
Wang et al. (2015b); Medium; 1,040	Ln-transformed	Ln-transformed (concentration)	% change (CI)	18	1.01% (−2.02, 4.08%)	(see row with β effect estimates)	(see row with β effect estimates)
(Pan et al., 2016); Pan et al. (2015); Medium; 1,066	Ln-trans-formed	Cubic root (concentration)	% change (CI)	13	-1.1% (-3.5,1.3)	0.6% (-2.5,3.8)	-1.7% (-5.1,1.8)
Axelsson et al. (2015a); Medium; 314	Quartiles	Cubic root (concentration)	Mean difference (Q4 vs. Q1)	41	0.17 (−0.24, 0.59)	2.6 (−3.3, 8.5)	−0.73 (−2.7, 1.3)
Jonsson et al. (2005); Medium; 234	Quartiles	No transformation	Mean difference (Q4 vs. Q1)	240	5.0 (−15, 25)	−0.4 (−6.4, 5.6)	
Wang et al. (2015b); High; 1,040	Quartiles	Dichotomous	OR (CI)	18	Q2: 1.05 (0.56, 1.98) Q3: 0.94 (0.50, 1.79) Q4: 1.08 (0.58, 2.04)	Q2: 0.88 (0.60, 1.29) Q3: 1.02 (0.71, 1.49) Q4: 0.93 (0.63, 1.36)	
Hauser et al. (2006); Medium; 463	Quartiles	Dichotomous	OR (CI)	158	Q2: 1.5 (0.7, 3.6) Q3: 1.0 (0.4, 2.5) Q4: 1.2 (0.5, 3.0)	Q2: 1.1 (0.6, 1.9) Q3: 0.8 (0.5, 1.5) Q4: 1.0 (0.6, 1.8)	Q2: 0.8 (0.4, 1.6) Q3: 0.7 (0.3, 1.3) Q4: 0.5 (0.3, 1.1)
Han et al. (2014); Medium; 232	Dichotomous	Dichotomous	OR (CI)	3.1	0.78 (0.38, 1.58)	0.96 (0.18, 5.04)	0.88 (0.44, 1.75)
Wirth et al. (2008); Medium; 45	Tertiles	Dichotomous	OR (CI)	108	Q2: 3.6 (0.4, 34.6) Q3: 6.5 (0.6, 73.4)	Q2: 0.7 (0.1, 3.7) Q3: 0.5 (0.1, 2.9)	Q2: 4.2 (0.7, 24.5) Q3: 7.0 (1.0, 48.0)*
Liu et al. (2012); Medium; 125	Tertiles	Dichotomous	OR (CI)	175 (mean)	Q2: 1.4 (0.2, 8.8) Q3: 1.5 (0.2, 9.6)	Q2: 0.7 (0.2, 1.9) Q3: 0.4 (0.1, 1.2)	Q2: 0.2 (0.1, 1.2) Q3: 0.8 (0.2, 3.0)

*$p < 0.05$, results that support an association are shaded. Dark gray represents one or more of the following: $p < 0.05$, large effect size (e.g., OR ≥ 1.5, β ≥ −0.5, % difference ≥ 1.0%), or exposure-response trend across categories of exposure. Light gray represents other supportive results.
Q = quartile. Studies are sorted by study confidence level within each metabolite-effect estimate grouping.

in four studies, for motility in two studies, and for morphology in three studies. No association, or a positive association, was observed in the remaining studies. Given the lack of consistency across studies despite high exposure levels, this evidence is considered *indeterminate*; additional high confidence studies, at high exposure levels, would be needed to conclude there was compelling evidence of no effect.

In summary, there is *moderate* to *robust* evidence of an association between DBP, BBP, DEHP, and DINP exposure and sperm parameters, *slight* evidence for DIBP, and *indeterminate* evidence for DEP. The strongest evidence was observed for sperm concentration, while evidence for motility and morphology was more limited (with the exception of BBP and DINP, respectively). There were notably fewer studies of DIBP, which may explain the lack of an association. DEP had both a reasonable number of studies and high exposure levels without a clear association; these results support differences in DEP's potency or activity relative to other phthalates.

3.4. Time to pregnancy (male exposure)

3.4.1. Study selection

Three studies looked at male exposure to phthalates and its association with time to pregnancy. Two were excluded because the exposure was measured after the outcome (Table 10) (Modigh et al., 2002; Specht et al., 2015). The specific phthalates examined in the

Table 10
Epidemiology studies of time to pregnancy (male exposure).

	Reference	Study description			Includes metabolites of:						Study evaluation					
		Population	Exposure	Outcome	DEHP	DINP	DBP	DIBP	BBP	DEP	Exposure	Outcome	Selection	Confounding	Analysis	Overall confidence
Included	Buck Louis et al. (2014)	Cohort (N=501) in U.S. of couples trying to conceive	Single urine sample at study entry	Cycles to conception (from pregnancy testing, journals, and fertility monitor)	✓	✓[a]	✓	✓	✓	✓	A/P	G	G	A	A	High
Excluded	Reference	Reason for Exclusion														
	Modigh et al. (2002)	Critical deficiency in exposure measure (exposure measured after outcome from occupational records, not validated														
	Specht et al. (2015)	Critical deficiency in exposure measure (exposure measured after outcome, during pregnancy)														

G = good; A = adequate; D = deficient; A/D = adequate for short chain phthalates, deficient for long chain phthalates.
[a] Study was considered *critically deficient* for this phthalate due to a high percent below the LOD.

remaining study are summarized in Table 10. This was a prospective cohort identified through population-based sampling. Based on the criteria described in the outcome-specific criteria (supplement), it was classified as *high confidence*, and the rationale for domain ratings are available at https://hawcprd.epa.gov/rob/study/100000037/.

3.4.2. Results

In Buck Louis et al. (2014), for DBP and BBP (measured by MBP and MBzP, respectively), there were statistically significant associations between increased exposure and increased time to pregnancy, or decreased fecundity (Table 11). Because the study is high confidence and because of the coherence with semen parameters, this evidence is considered *moderate*. For DEHP and DIBP, there was some evidence that increased exposure to these phthalates is associated with increased time to pregnancy, but the results were not statistically significant, and this evidence is considered *slight*. For DEP and DINP, no association was reported; given the limited number of studies and for DINP, the relatively low range of exposures, the evidence is considered *indeterminate*.

Table 11
Association between phthalate metabolites and time to pregnancy in Buck Louis et al. (2014).

Phthalate (metabolite)	Exposure Geometric mean (ng/mL)	Fecundability Ratio (95% CI)
DINP (MINP)	0.07	1.01 (0.90, 1.14)
BBP (MBzP)	2.8	0.77 (0.65, 0.92)*
DIBP (MiBP)	3.4	0.88 (0.74, 1.04)
DBP (MBP)	5.9	0.82 (0.70, 0.97)*
DEHP (MEOHP)	6.1	0.91 (0.79, 1.05)
DEP (MEP)	82.7	1.01 (0.86, 1.18)

*$p < 0.05$, results that support an association are shaded. Dark gray represents one or more of the following: $p < 0.05$, large effect size (e.g., OR ≤ 0.7), or exposure-response trend across categories of exposure. Light gray represents other supportive results.

3.5. Testosterone

3.5.1. Study selection and evaluation

Based on the exposure evaluation criteria, eight of the 21 epidemiology papers (Table 12) identified in the search with data on testosterone were excluded because they used measurements in tissues other than urine (i.e., blood or semen), did not report results for individual metabolites, or did not discuss collection time of outcome sample. The specific phthalates examined in the remaining 13 studies (15 papers) and study evaluations are summarized in Table 12 (Fong et al., 2015; Janjua et al., 2007; Lenters et al., 2014; Li et al., 2011; Pan et al., 2016; Xu et al., 2015). Full rationale for ratings are available at https://hawcprd.epa.gov/summary/visual/100000066/, and outcome-specific criteria are available in the supplement. All of the studies are cross-sectional, varying in sample size between 25 and 1066 adult men in analysis. As with studies of sperm parameters, cross-sectional design with concurrent measurement of exposure and outcome (testosterone concentration) was not considered a limitation. In most studies, a single urine sample was collected concurrent with outcome assessment, with the exception of Wang et al. (2015c), which had two same-day urine samples, and Specht et al. (2014), in which blood samples were used for secondary metabolites of DEHP and DINP. Testosterone was the most studied of the relevant reproductive hormones, and was therefore the focus of this review.

Nine studies (ten papers) were classified as *medium confidence* (Axelsson et al., 2015a; Axelsson et al., 2015b; Pan et al., 2015; Han et al., 2014; Meeker and Ferguson, 2014; Specht et al., 2014; Jurewicz et al., 2013; Mendiola et al., 2011; Meeker et al., 2009);, and four studies were classified as *low confidence* (Chang et al., 2015; Den Hond et al., 2015; Park et al., 2010; Pan et al., 2006).

3.5.2. Results

Evaluation of the association between exposure to DEHP and testosterone is based on 13 studies (Axelsson et al., 2015a; Chang et al., 2015; Den Hond et al., 2015; Pan et al., 2015; Wang et al., 2015c; Han et al., 2014; Meeker and Ferguson, 2014; Specht et al., 2014; Jurewicz et al., 2013; Mendiola et al., 2011; Park et al., 2010; Meeker et al., 2009; Pan et al., 2006). Results for summed DEHP metabolites were used when available; if not available, results for MEOHP (preferred) or MEHP were used. Eight studies (Axelsson et al., 2015a; Wang et al., 2015c; Meeker and Ferguson, 2014; Specht et al., 2014; Jurewicz et al., 2013; Park et al., 2010; Meeker et al., 2009); (Pan et al., 2015); reported decreased testosterone levels with higher DEHP exposure (Table 13), including findings from two studies that were statistically significant (Specht et al., 2014; Jurewicz et al., 2013). The association between DEHP exposure and decreased testosterone did not show a clear response pattern with increasing exposure level or exposure range; however, *medium confidence* studies were more likely to report an association than *low confidence* studies, and *low confidence* studies

Table 12
Epidemiology studies of testosterone.

	Reference	Study description			Includes metabolites of:						Study evaluation					
		Population	Exposure	Outcome	DEHP	DINP	DBP	DIBP	BBP	DEP	Exposure	Outcome	Selection	Confounding	Analysis	Overall confidence
Included	Axelsson et al., 2015(a); Axelsson et al., 2015(b)	Cross-sectional (N=314) in Sweden; men entering military	Single urine sample; subset with prenatal sample available	Total T by immunoassay, morning blood sample	✓	✓	✓		✓	✓	A/P	G	A	A	A	Medium
	Chang et al. (2015)	Case-control based on achieving pregnancy (N=141 cases, 35 controls) in Taiwan	Single urine sample	T by immunoassay; morning blood sample	✓		✓	✓	✓	✓	A/P	G	P	P	P	Low
	Den Hond et al., 2015	Case-control (N=40 cases reduced semen quality/80 controls) in Belgium	Single urine sample	T by immunoassay, adjusted for blood collection time in model	✓		✓	✓	✓	✓	A/P	G	P	P	A	Low
	Han et al., 2014	Cross-sectional (N=232) in China; general population	Single urine sample	T by immunoassay, morning blood sample	✓		✓		✓[a]	✓	A/P	G	P	A	A	Medium
	Jurewicz et al., 2013	Cross-sectional (N=269) in Poland; men at infertility clinic	Single morning urine sample	T by immunoassay, morning blood sample	✓	✓	✓		✓	✓	A/P	A	P	A	A	Medium
	Meeker and Ferguson (2014)	Cross-sectional (N=427) in U.S.; general population	Single urine sample	Total T by mass spectrometry, adjusted for blood collection time in model	✓	✓	✓	✓	✓	✓	A/P	A	G	A	A	Medium
	Meeker et al. (2009)	Cross-sectional (N=425) in U.S.; men from subfertile couples	Single urine sample	Total T by immunoassay, adjusted for blood collection time	✓		✓		✓	✓	A/P	A	G	A	G	Medium
	Mendiola et al. (2011)	Male partners from pregnancy cohort (N=363)	Single urine sample	Total T by immunoassay, adjusted for blood collection time in model	✓						P	A	G	A	A	Medium

(*continued on next page*)

Table 12 (*continued*)

	Pan et al. (2006)	Cross-sectional (N=137) in China; PVC (exposed) and construction (unexposed) workers	Single urine sample	Free T by immunoassay, morning blood sample	✓		✓				A/P	G	P	P	P	Low
	(Pan et al., 2016); Pan et al. (2015)	Cross-sectional (N=1,066) in China; men seeking fertility assessment	Single urine sample	Total T by immunoassay, adjusted for blood collection time in model	✓	✓	✓	✓	✓	✓	A/P	A	A	A	A	Medium
	Park et al. (2010)	Cross-sectional (N=25) in Korea, men working in dental labs	Single pre-shift urine sample	T by immunoassay, morning blood sample	✓						P	P	P	P	P	Low
	Specht et al., 2014; Lenters et al., 2014;	Cross-sectional (N=589) in Greenland, Poland, Ukraine; men from couples at antenatal visit	Single blood sample	T by immunoassay, morning blood sample	✓	✓					P	A	G	A	A	Medium
	Wang et al. (2015c)	Cross-sectional (N=1,040) in China; men seeking semen analysis	Two urine samples collected same day	Total T by direct chemilumin-escence assay, morning blood sample	✓		✓		✓	✓	G	G	A	A	G	Medium
				Total Studies per Phthalate	13	5	10	4	8	9						

Excluded	Reference	Reason for Exclusion
	Fong et al. (2015)	No discussion of or adjustment for collection time of outcome sample.
	Janjua et al. (2007)	Critical deficiency in exposure measure (exposure based on measurement in blood)
	Joensen et al. (2012)	Results not presented for individual phthalate metabolites
	Jonsson et al. (2005)	No discussion of or adjustment for collection time of outcome sample.
	Li et al. (2011)	Critical deficiency in exposure measure (exposure based on measurement in blood, semen; diesters analyzed)
	Pant et al. (2014)	Critical deficiency in exposure measure (exposure based on measurement in semen
	Xu et al. (2015)	Results not presented for individual phthalate metabolites
	Wang et al. (2016b)	Critical deficiency in exposure measure (exposure based on measurement in semen) (note: same study as Wang et al. (2015b))

T = testosterone; G = good; A = adequate; D = deficient; A/E = adequate for short chain phthalates, deficient for long chain phthalates.

[a] Study was considered *critically deficient* for this phthalate due to a high percent below the LOD.

generally had null, rather than conflicting, results. Given the overall consistency among higher confidence studies, this evidence is considered *moderate*.

Five *medium confidence* studies (Axelsson et al., 2015a; Pan et al., 2015; Meeker and Ferguson, 2014; Specht et al., 2014; Jurewicz et al., 2013) investigated the association between DINP exposure (measured by MINP or MCiOP) and testosterone (Table 14). Three studies (Meeker and Ferguson, 2014; Specht et al., 2014)) found decreasing testosterone levels with increasing DINP exposure; the results in two were statistically significant, including an exposure-response gradient in Specht et al., 2014. The evidence for an association between DINP exposure and decreased testosterone is considered *moderate*.

Evaluation of the association between exposure to DBP (measured by MBP) and testosterone is based on ten studies (Axelsson et al., 2015a; Chang et al., 2015; Den Hond et al., 2015; Pan et al., 2015; Wang et al., 2015c; Han et al., 2014; Meeker and Ferguson, 2014; Jurewicz et al., 2013; Meeker et al., 2009; Pan et al., 2006). Five studies (Pan et al., 2015; Meeker and Ferguson, 2014; Meeker et al., 2009; Pan et al., 2006); Wang et al., 2015b) reported results that indicate decreased testosterone levels with increased DBP exposure (Table 15).

Table 13
Associations between DEHP exposure and testosterone.

Reference; Study confidence; N	Transformation	Effect estimate	Metabolite (ng/mL) [median unless otherwise specified]	Exposure IQR (or as specified)	Testosterone effect estimate
∑DEHP					
Mendiola et al. (2011); Medium; 363	Log10 transformed	β (95% CI) for 1 unit increase	0.24 nmol/mL	0.1–0.5	−0.01 (−0.04, 0.03)
Meeker et al. (2009); Medium; 425	Ln-transformed exposure	β (95% CI) for IQR increase	0.31 nmol/mL	0.2–0.7	−6.35 (−17.8, 5.1)
Chang et al. (2015); Low; 176	Ln-transformed exposure and outcome	β (95% CI) for IQR increase	0.15 nmol/mL (mean)		0.98 (0.9, 1.1)Ŧ
Wang et al. (2015c); Medium; 1,040	Ln-transformed exposure and outcome	% difference (95% CI) 1 unit increase	7.9 (MEOHP)	3.9-8.5	−3.7% (−8.0, 0.6)
Meeker and Ferguson (2014); Medium; 160 (12-19 yr)	None reported	% change (95% CI) with IQR increase	4.9 (MEOHP)	3.0-7.4	−8.42% (−24.5, 11.0)
267 (20-40 yr)			4.2 (MEOHP)	2.8-7.1	0.42 (−5.8, 7.1)
Specht et al. (2014); Medium; 589		Means (95% CI) for <25th, 25th–75th, >75th percentile	0.01 nM (Proxy DEHP)	0.01–0.14	Q1: 15.4 (14.3–16.7) Q2: 14.8 (14.0, 15.7) Q3: 14.1 (13.1–15.1) *p* trend <0.05
MEOHP					
Den Hond et al. (2015); Low; 120	Ln-transformed exposure	β ± SE	7.7	3.9–14.0	−0.03 ± 0.04
Pan et al., 2016; Pan et al. (2015); Medium; 1,066	Ln-transformed exposure and outcome	% change (CI)	8.4	4.8-14.3	-1.6% (-2.2,1.0)
Axelsson et al. (2015a); Medium; 314	Ln-transformed exposure and outcome	Mean difference (Q4 vs. Q1)	9.6	0.5–1,100 (range)	−1.0 (−9.7, 8.7)
Park et al. (2010); Low; 25	Ln-transformed exposure	Correlation coefficient	14 (pre-shift)	9.2–19	−0.33 (p = 0.1)
MEHP					
Jurewicz et al. (2013); Medium; 269	Log-transformed exposure	β (p)	8.8	0.6–136 (range)	−0.29 (p = 0.04)
Han et al. (2014); Medium; 232	None reported	Partial correlation coefficient	1.1	0.0–23.8 (5th–95th)	−0.05
Pan et al. (2006); Medium; 137	Log10 transformed outcome	Partial correlation coefficient	562/5 μg/g creatinine (exposed/ unexposed)	210–1,884/ 3.7–10	−0.2 (free testosterone)

*$p < 0.05$, results that support an association are shaded. Dark gray represents one or more of the following: $p < 0.05$, large effect size (e.g., OR ≥ 1.5, β ≥ −0.5, % difference ≥ 1.0%), or exposure-response trend across categories of exposure. Light gray represents other supportive results.
Q = quartile.
Ŧ Coefficient was calculated by study authors with back-transformation of both hormone and phthalate metabolite concentrations. A coefficient < 1.0 indicates a multiplicative decrease in hormone level for an IQR change in exposure.
Units for testosterone differed across studies: ng/mL (Jurewicz et al., 2013, Meeker and Ferguson, 2014, nmol/L (Han et al., 2014, Axelsson et al., 2015a, 2015b, Mendiola et al., 2011, Chang et al., 2015, Pan et al., 2015), nmol/mL (Specht et al., 2014), pg/mL (Pan et al., 2006), ng/dL (Meeker et al., 2009; Den Hond et al., 2015; Wang et al., 2015a, 2015b, 2015c).

Table 14
Associations between DINP exposure and testosterone.

Reference; Study confidence; N	Transformation	Effect estimate	Metabolite (ng/mL) [median unless otherwise specified]	Exposure IQR (or as specified)	Testosterone effect estimate
MINP					
Jurewicz et al. (2013); Medium; 269	Log-transformed exposure	β (p)	1.1	0.2–6.4	0.30 (0.373)
Specht et al. (2014); Medium; 589	Ln-transformed	Means (CI) for <25th, 25th–75th, >75th percentile	0.003 Proxy-MINP (nm)	0.15 (maximum)	Q1: 15.3 (14.2, 16.4) Q2: 14.9 (14.0, 15.8) Q3: 13.9 (12.9, 14.9) *p* trend <0.05
MCiOP					
(Pan et al., 2016); Pan et al. (2015); Medium; 1,066	Ln-transformed	% change (CI)	1.2	0.7-2.1	-2.3% (-4.5,-0.1)*
Meeker and Ferguson (2014); Medium; 160 (12-19 yr)	None reported	% change (95% CI) with IQR increase	14	7.76–43.1	−22.5% (−36.7, −5.18)
267 (20-40 yr)			23	9.28–57.0	−0.33 (−7.09, 6.92)
Axelsson et al. (2015a); Medium; 314	Ln-transformed exposure and outcome	Mean difference (95% CI) Q4 vs. Q1	16	1.4–810 (range)	4.3 (−4.9, 14)

*$p < 0.05$, results that support an association are shaded. Dark gray represents one or more of the following: $p < 0.05$, large effect size (e.g., OR ≥ 1.5, β ≥ −0.5, % difference ≥ 1.0%), or exposure-response trend across categories of exposure. Light gray represents other supportive results.
Q = quartile.
Units for testosterone differed across studies: ng/mL (Jurewicz et al., 2013; Meeker and Ferguson, 2014), nmol/L (Pan et al., 2015), nmol/mL (Specht et al., 2014).

The association in one study (Pan et al., 2015) was statistically significant. There was no clear pattern between observed associations and exposure level or range. This evidence is considered *slight*.

Four studies (Chang et al., 2015; Den Hond et al., 2015; Pan et al., 2015; Meeker and Ferguson, 2014) provided data on the association between DIBP exposure (measured by MIBP) and testosterone (Table 15). Of the four studies, three (Chang et al., 2015; Meeker and Ferguson, 2014) (Pan et al., 2015) found decreased testosterone levels with increasing DIBP exposure; the results in two were statistically significant. The fourth study (Den Hond et al., 2015) reported no association, despite having higher exposure levels for MIBP than other studies in this assessment, but was also rated as *low confidence*. Based on the overall consistency, this evidence is considered *moderate*.

Eight studies (Axelsson et al., 2015a; Chang et al., 2015; Den Hond et al., 2015; Wang et al., 2015c; Meeker and Ferguson, 2014; Jurewicz et al., 2013; Meeker et al., 2009) investigated the association between BBP exposure (measured by MBzP) and testosterone (Table 16). Two studies (Pan et al., 2015; Meeker and Ferguson, 2014) reported an inverse association between BBP exposure and testosterone levels, but they were not statistically significant. Results from some of the remaining studies were in the opposite direction (i.e., a positive association). Given the lack of consistency, this evidence is considered to be *indeterminate*.

Nine studies (Axelsson et al., 2015a; Chang et al., 2015; Den Hond et al., 2015; Wang et al., 2015c; Han et al., 2014; Meeker and Ferguson, 2014; Jurewicz et al., 2013; Meeker et al., 2009) (Pan et al., 2015) investigated the association between DEP (measured by MEP) and testosterone (Table 16). Three studies (Pan et al., 2015; Wang et al., 2015c; Meeker and Ferguson, 2014) reported an inverse association between DEP exposure and testosterone levels, but none were statistically significant. Results from some of the remaining studies were in the opposite direction (i.e., a positive association). Given the lack of consistency despite high exposure levels, this evidence is considered *indeterminate*.

In summary, there is *moderate* evidence of an association between exposure to DEHP, DINP, and DIBP and decreased testosterone levels, *slight* evidence for exposure to DBP, and *indeterminate* evidence for BBP and DEP. In the case of BBP, the reporting of no association in the majority of studies may be explained by the lower exposure levels, and corresponding lower sensitivity to observe an effect. Therefore, the results for BBP are not necessarily inconsistent with the results for the other phthalates. DEP, with both a reasonable number of studies and higher exposure levels, showed no clear association with testosterone levels. This lack of association may reflect an inherent difference in potency or activity towards testosterone relative to other phthalates. This difference is consistent with observations from experimental animal studies.

Table 15
Associations between DBP and DIBP exposure and testosterone.

Reference; Study confidence; N	Transformation	Effect estimate	Metabolite (ng/mL) [median unless otherwise specified]	Exposure IQR (or as specified)	Testosterone effect estimate
DBP (measured by MBP)					
Meeker et al. (2009); Medium; 425	Ln-transformed exposure and outcome (except testosterone)	β (95% CI) for IQR increase	17.7	10.6–32.75	−4.65 (−15.7, 6.33)
Jurewicz et al. (2013); Medium; 269	Log-transformed exposure	β (p)	83	19–1,530 (range)	0.02 (p = 1.0)
Den Hond et al. (2015); Low; 120	Ln-transformed exposure	β ± SE	19	12–42	−0.03 (0.03)
Chang et al. (2015); Low; 176	Ln-transformed exposure and outcome	β (95% CI) for IQR increase₸	11.1 (fertile mean)		0.96 (0.90, 1.02)
Wang et al. (2015c); High; 1,040	Ln-transformed exposure and outcome	% difference (95% CI) 1 unit increase	70	28–84	−1.1% (−4.6, 2.3)
Meeker and Ferguson (2014); Medium; 160 (12-19 yr)	None reported	% change (95% CI) with IQR increase	8.9	5.0–14.3	−19.3% (−37.0, 3.34)
267 (20-40 yr)			7.0	3.9–11.2	−3.85% (−11.0, 3.89)
(Pan et al., 2016); Pan et al. (2015); Medium; 1,066	Ln-transformed exposure and outcome	% change (CI)	78	39-162	-3.9% (-6.6,-1.1)*
Axelsson et al. (2015a); Medium; 314	Ln-transformed exposure and outcome	Mean difference for Q4 vs. Q1 (95% CI)	47	1.0, 690 (range)	2.1 (−11, 7.6)
Han et al. (2014); Medium; 232	None reported	Partial correlation coefficient	18.72	2.10–129.34 (5th–95th)	0.10
Pan et al. (2006); Medium; 137	Log10 transformed outcome	Partial correlation coefficient	548/113 μg/g (exposed/ unexposed)	252–1,493/75–207	−0.253 (free testosterone)
DIBP (measured by MIBP)					
Den Hond et al. (2015); Low; 80/163	Ln-transformed exposure	β ± SE	55	27.0–113.0	0.00 ± 0.03
Chang et al. (2015); Low; 176	Ln-transformed exposure and outcome	β (95% CI) for IQR increase₸	7.6 (fertile mean)		0.92 (0.87, 0.98)*
Meeker and Ferguson (2014); Medium; 160 (12-19 yr)	None reported	% change (95% CI) with IQR increase	7.3	4.3–11.4	−19.9 (−39.4, 5.83)
267 (20-40 yr)			5.1	3.5–9.1	0.39 (−6.26, 7.52)
(Pan et al., 2016); Pan et al. (2015); Medium; 1,066	Ln-transformed exposure and outcome	% change (CI)	48	28-84	-4.1% (-6.7,-1.5)*

*$p < 0.05$, results that support an association are shaded. Dark gray represents one or more of the following: $p < 0.05$, large effect size (e.g., OR ≥ 1.5, β ≥ −0.5, % difference ≥ 1.0%), or exposure-response trend across categories of exposure. Light gray represents other supportive results.

₸ Coefficient was calculated by study authors with back-transformation of both hormone and phthalate metabolite concentrations. A coefficient < 1.0 indicates a multiplicative decrease in hormone level for an IQR change in exposure.

Units for testosterone differed across studies: ng/mL (Jurewicz et al., 2013, Meeker and Ferguson, 2014), nmol/L (Han et al., 2014; Axelsson et al., 2015a, 2015b; Chang et al., 2015; Pan et al., 2015), nmol/mL (Specht et al., 2014), pg/mL (Pan et al., 2006), ng/dL (Meeker et al., 2009, Den Hond et al., 2015, Wang et al., 2015a, 2015b, 2015c).

Table 16
Associations between BBP and DEP exposure and testosterone.

Reference; Study confidence; N	Transformation	Effect estimate	Metabolite (ng/mL) [median unless otherwise specified]	Exposure IQR (or as specified)	Testosterone effect estimate
BBP (measured by MBzP)					
Meeker et al. (2009); Medium; 425	Ln-transformed exposure and outcome (except testosterone)	β (95% CI) for IQR increase	8.2	4.20–15.9	4.58 (−7.91, 17.0)
Jurewicz et al. (2013); Medium; 269	Log-transformed exposure	β (p)	5.2	0.4–205 (range)	−0.09 (p = 0.5)
Den Hond et al. (2015); Low; 120	Ln-transformed exposure	β ± SE	4.5	2.5–9.0	−0.02 ± 0.02
Chang et al. (2015); Low; 176	Ln-transformed exposure and outcome	β (95% CI) for IQR increase₸	0.7 (fertile mean)		0.96 (0.91, 1.02)
Wang et al. (2015c); Medium; 1,040	Ln-transformed exposure and outcome	% difference (95% CI) 1 unit increase	2.9	1.0–3.4	−1.2% (−5.3, 2.9)
Meeker and Ferguson (2014); Medium; 160 (12-19 yr)	None reported	% change (95% CI) with IQR increase	5.8	3.6–11.3	−21.1 (−38.6, 1.30)
267 (20-40 yr)			3.7	2.2–6.7	−4.92 (−12.9, 3.82)
(Pan et al., 2016); Pan et al. (2015); Medium; 1,066	Ln-transformed exposure and outcome	% change (CI)	0.1	<LOD-0.4	-2.6% (-5.3,0.1)
Axelsson et al. (2015a); Medium; 314	Ln-transformed exposure and outcome	Mean difference for Q4 vs. Q1 (95% CI)	13	0.5–260 (range)	2.3 (−2.8, 6.0)
DEP (measured by MEP)					
Meeker et al. (2009); Medium; 425	Ln-transformed exposure and outcome (except testosterone)	β (95% CI) for IQR increase	153	59.9–518	8.87 (−7.18, 24.9)
Jurewicz et al. (2013); Medium; 269	Log-transformed exposure	β (p)	45	3.8–2,483 (range)	0.08 (p = 0.6)
Den Hond et al. (2015); Low; 120	Ln-transformed exposure	β ± SE	50	20.5–110.5	0.01 ± 0.02
Chang et al. (2015); Low; 176	Ln-transformed exposure and outcome	β (95% CI) for IQR increase₸	13 (fertile mean)		1.00 (0.97, 1.04)
Wang et al. (2015c); Medium; 1,040	Ln-transformed exposure and outcome	% difference (95% CI) 1 unit increase	18	7.1–25	−1.7% (−3.8, 0.30)
Meeker and Ferguson (2014); Medium; 160 (12-19 yr)	None reported	% change (95% CI) with IQR increase	26	14.0–46.9	9.46 (−17.1, 44.5)
267 (20-40 yr)			27	12.2–74.7	−3.30 (−9.81, 3.67)
(Pan et al., 2016); Pan et al. (2015); Medium; 1,066	Ln-transformed exposure and outcome	% change (CI)	13	6.6-32	-1.5% (-4.0,1.1)
Axelsson et al. (2015a); Medium; 314	Ln-transformed exposure and outcome	Mean difference for Q4 vs. Q1 (95% CI)	41	2–6,900 (range)	1.0 (−7.9, 11)
Han et al. (2014); Medium; 232	None reported	Partial correlation coefficient	3.1	0.0–59.7 (5th–95th)	−0.01

*$p < 0.05$, results that support an association are shaded. Dark gray represents one or more of the following: $p < 0.05$, large effect size (e.g., OR ≥ 1.5, β ≥ −0.5, % difference ≥ 1.0%), or exposure-response trend across categories of exposure. Light gray represents other supportive results.

₸ Coefficient was calculated by study authors with back-transformation of both hormone and phthalate metabolite concentrations. A coefficient < 1.0 indicates a multiplicative decrease in hormone level for an IQR change in exposure.

Units for testosterone differed across studies: ng/mL (Jurewicz et al., 2013, Meeker and Ferguson, 2014), nmol/L (Han et al., 2014, Axelsson et al., 2015a, 2015b, Chang et al., 2015, Pan et al., 2015), nmol/mL (Specht et al., 2014), pg/mL (Pan et al., 2006), ng/dL (Meeker et al., 2009, Den Hond et al., 2015, Wang et al., 2015a, 2015b, 2015c).

Timing of exposure	Outcome	DEHP	DINP	DBP	DIBP	BBP	DEP
In utero	Anogenital distance	M	S	M	S	S	S
	Hypospadias/cryptorchidism	I	S	S	S	S	I
In utero or childhood	Pubertal development	I	I	I	I	I	I
Adult	Semen parameters	M	M	R	S	M	I
	Time to pregnancy	S	I	M	S	M	I
	Testosterone	M	M	S	M	I	I
	Male repro overall	R	M	R	M	M	S

Robust (R) | Moderate (M) | Slight (S) | Indeterminate (I)

Level of confidence in association

Fig. 3. Summary of epidemiologic evidence of male reproductive effects associated with phthalates.

3.6. Other male reproductive effects

In addition to the health effects already described, systematic reviews were performed for hypospadias/cryptorchidism and timing of pubertal development. These reviews are described in detail in the supplemental materials. In summary, for both outcomes, results were largely inconsistent and the evidence was considered *slight* or *indeterminate* for all phthalates.

3.7. Summary of male reproductive effects

Results for all phthalate-outcome combinations are summarized in Fig. 3. Tables 17–21 present the summary of evidence across outcomes within each phthalate with *moderate* or *robust* evidence of male reproductive toxicity.

Table 17
Evidence profile table for male reproductive effects of DEHP.

Outcome	Studies (design in parentheses)	Factors that increase confidence	Factors that decrease confidence	Summary of findings	Confidence judgement for outcome	Confidence judgement for overall hazard
Anogenital distance	Medium confidence Bornehag et al., 2015 (C) Jensen et al., 2016 (C) Swan et al., 2015 (C) Low confidence Bustamante-Montes et al., 2013 (C) Suzuki et al., 2012 (C) Swan, 2008 (C)	Among medium confidence studies: • Consistency • Exposure-response gradient across studies • Minimal concerns for bias Overall: • finding is consistent with other systematic review/meta-analysis (National Academies of Sciences, Engineering, and Medicine, 2017)	• Low precision in Bornehag et al., 2015	Inverse associations between DEHP exposure and anogenital distance reported in 5/6 studies (Jensen et al., 2016, Swan et al., 2015, Bornehag et al., 2015, Swan, 2008, Suzuki et al., 2012), of which 2 were statistically significant (Swan et al., 2015, Swan, 2008). Among 3 medium confidence studies, effect size increased with increasing exposure levels (Fig. 2).	⊕⊕◯ MODERATE	⊕⊕⊕ ROBUST Supported by coherence across outcomes.
Semen parameters	Medium confidence Axelsson et al., 2015a, 2015b (CS) Bloom et al., 2015 (C) Han et al., 2014 (CS) Hauser et al., 2006 (CS) Huang et al., 2013 (CS) Jurewicz et al., 2013 (CS) Liu et al., 2012 (CS) Pan et al., 2015 (CS) Specht et al., 2014 (CS) Thurston et al., 2016 (CS) Wang et al., 2015a, 2015b, 2015c (CS) Wirth et al., 2008 (CS)	• Minimal concerns for bias • Biological plausibility • Lower study sensitivity could account for most observed inconsistency (i.e., null results in some studies)	• Difficult to assess exposure-response gradient and precision across studies due to differing analyses/presentation of results	Inverse associations between DEHP exposure and sperm concentration in 7/14 studies (Herr et al., 2009, Huang et al., 2011, Wirth et al., 2008, Specht et al., 2014, Bloom et al., 2015, Hauser et al., 2006), of which 1 was statistically	⊕⊕◯ MODERATE for concentration	

(*continued on next page*)

Table 17 (*continued*)

Outcome	Studies (design in parentheses)	Factors that increase confidence	Factors that decrease confidence	Summary of findings	Confidence judgement for outcome	Confidence judgement for overall hazard
	Low confidence Den Hond et al., 2015 (CS) Herr et al., 2009 (CS)			significant (Bloom et al., 2015). Four studies reported an inverse association with motility (Axelsson et al., 2015a; Huang et al., 2013; Huang et al., 2011, and Jurewicz et al., 2013), and 2 were statistically significant (Axelsson et al., 2015a; Jurewicz et al., 2013) (Table 4). Biological plausibility-Studies showed increased apoptosis (Huang et al., 2014); (Wang et al., 2016b; You et al., 2015), increased reactive oxygen species generation (Huang et al., 2014), and increased sperm aneuploidy (Jurewicz et al., 2013) with increased exposure.		
Testosterone	Medium confidence Axelsson et al., 2015a, 2015b (CS) Han et al., 2014 (CS) Jurewicz et al., 2013 (CS) Meeker and Ferguson, 2014 (CS) Meeker et al., 2009 (CS) Mendiola et al., 2011 (C) Pan et al., 2015 (CS) Specht et al., 2014 (CS) Wang et al., 2015c (CS) Low confidence Chang et al. (2015) (CS) Den Hond et al., 2015 (CS) Pan et al., 2006 (CS) Park et al., 2010 (CS)	• Minimal concerns for bias overall • Risk of bias in low confidence studies and lower study sensitivity account for most observed inconsistency • Exposure-response gradient within one study	• Difficult to assess exposure-response gradient and precision across studies due to differing analyses/ presentation of results	Inverse associations between DEHP exposure and testosterone levels in 8/13 studies (Specht et al., 2014, Meeker and Ferguson, 2014, Wang et al., 2015b, Meeker et al., 2009, Axelsson et al., 2015a, Park et al., 2010, Jurewicz et al., 2013, Pan et al., 2015), 2 of which were statistically significant (Specht et al., 2014, Jurewicz et al., 2013), with the former showing an exposure-response trend, other studies did not examine exposure-response gradient (Table 13).	⊕⊕◯ MODERATE	
	Time to Pregnancy Hypospadias/cryptorchidism and pubertal development				⊕◯◯ SLIGHT ◯◯◯ INDETERMINATE	

C: cohort, CC: case-control, CS: cross-sectional.

Table 18
Evidence profile table for male reproductive effects of DINP.

Outcome	Studies (design in parentheses)	Factors that increase confidence	Factors that decrease confidence	Summary of findings	Confidence judgement for outcome	Confidence judgement for overall hazard
Testosterone	Medium confidence Axelsson et al., 2015a, 2015b (CS) Jurewicz et al., 2013 (CS) Meeker and Ferguson, 2014 (CS) Pan et al., 2015 (CS) Specht et al., 2014 (CS)	• Minimal concerns for bias • Large effect size in one study (23% decrease with iqr increase in exposure) • Exposure-response gradient within one study	• Some unexplained inconsistency	Inverse associations between DINP exposure and testosterone levels in 3/5 studies (Specht et al., 2014, Meeker and Ferguson, 2014, Pan et al., 2015), 2 included statistically significant results (Pan et al., 2015, Specht et al., 2014), with the latter being a trend (other studies did not examine exposure-response gradient) (Table 14).	⊕⊕◯ MODERATE	⊕⊕◯ MODERATE Based on testosterone and semen parameters, supported by coherence of slight findings in other outcomes with few available studies
Semen parameters	Medium confidence Axelsson et al., 2015a, 2015b (CS) Jurewicz et al., 2013 (CS) (Pan et al., 2015) (CS) Specht et al., 2014 (CS)	• Minimal concerns for bias • Exposure-response gradient within one study • Consistency for morphology	• Some unexplained inconsistency for concentration	Inverse associations between DINP exposure and sperm morphology in all 4 studies, 1 of which was statistically significant (Jurewicz et al., 2013). 2/3 studies for motility (Pan et al., 2015, Axelsson et al., 2015a) and 2/4 studies for concentration (Specht et al., 2014, Pan et al., 2015) also reported inverse associations (Table 5).	⊕⊕◯ MODERATE	
Anogenital distance, Hypospadias/Cryptorchidism					⊕◯◯ SLIGHT	
Time to pregnancy, pubertal development					◯◯◯ INDETERMINATE	

C: cohort, CC: case-control, CS: cross-sectional.

4. Discussion

With the exception of DEP, all the phthalates included in this systematic review had *moderate* or greater evidence of male reproductive effects; these findings are directly relevant to humans as they generally are based on exposure levels seen in general populations (i.e., not in occupationally exposed settings). The strongest (*robust*) evidence of male reproductive effects comes from studies of DBP and DEHP in adult males. These two phthalates tended to have the largest number of studies, and exposure levels higher than most of the other phthalates (i.e., DINP, DIBP, and BBP).

The differences in data availability and exposure level/range may explain the differing confidence in the associations between these phthalates and male reproductive effects. For DIBP in particular, which might be expected to have similar activity as DBP due to their similarity in structure, there was a considerably smaller number of available studies and lower exposure levels relative to other phthalates. While it is possible there are differences in potency/activity between these phthalates, at this point, inadequate sensitivity of the systematic review (i.e., low exposure levels, fewer studies) for DINP, BBP, and in particular DIBP seems to be a likely explanation. In light of these issues, it would be inappropriate to conclude that substituting DINP for DEHP or DIBP for DBP would be health protective. In contrast, DEP had a similar number of studies as DBP and generally higher exposure levels, but weaker evidence of an association. This is consistent with experimental animal data that suggest that DEP does not have as strong an anti-androgenic effect as other phthalates (Howdeshell et al., 2008).

The results of this review illustrate the difficulty in drawing conclusions across different phthalates (i.e., do phthalates in general cause male reproductive toxicity?). There is *slight* evidence of an association for most of the individual phthalate/outcome combinations, but these are generally marked by inconsistency across available studies and are difficult to draw conclusions from. Looking at the combinations with *moderate* or *robust* evidence, there is little consistency in which outcomes were strongly associated across the six phthalates. Semen parameters were the most consistent, with four phthalates (DBP, DEHP, BBP, and DINP) having *moderate* or *robust* evidence, and as already discussed, there are reasonable explanations for the differences with

Table 19
Evidence profile table for male reproductive effects of DBP.

Outcome	Studies (design in parentheses)	Factors that increase confidence	Factors that decrease confidence	Summary of findings	Confidence judgement for outcome	Confidence judgement for overall hazard
Semen parameters	Medium confidence Axelsson et al., 2015a, 2015b (CS) Bloom et al., 2015 (C) Han et al., 2014 (CS) Hauser et al., 2006 (CS) Jonsson et al., 2005 (CS) Jurewicz et al., 2013 (CS) Liu et al., 2012 (CS) Pan et al., 2015 (CS) Thurston et al., 2016 (CS) Wang et al., 2015c (CS) Wirth et al., 2008 (CS) Low confidence Den Hond et al., 2015 (CS)	• Minimal concerns for bias • Consistency for concentration • Biological plausibility • Exposure-response gradient within three studies	• Difficult to assess exposure-response gradient and precision across studies due to differing analyses/ presentation of results	Inverse associations between DBP exposure and sperm concentration in 8/ 12 studies (Bloom et al., 2015; Jurewicz et al., 2013; Wang et al., 2015a, 2015b, 2015c; Pan et al., 2015; Jonsson et al., 2005; Hauser et al., 2006; Han et al., 2014; Liu et al., 2012), of which 3 were statistically significant and displayed monotonic exposure-response relationships (Wang et al., 2015a; Liu et al., 2012; Hauser et al., 2006). Seven studies reported an inverse association with motility (Wang et al., 2015a, 2015b, 2015c; Bloom et al., 2015; Thurston et al., 2016; Jurewicz et al., 2013; Pan et al., 2015; Axelsson et al., 2015a, 2015b; Hauser et al., 2006), and 2 were statistically significant (Axelsson et al., 2015a; Hauser et al., 2006) (Table 6) Biological plausibility-Studies showed increased sperm aneuploidy (Jurewicz et al., 2013) with increased exposure.	⊕⊕⊕ ROBUST for concentration	⊕⊕⊕ ROBUST Based on semen parameters, supported by coherence across outcomes.
Anogenital distance	Medium confidence Bornehag et al., 2015 (C) Jensen et al., 2016 (C) Swan et al., 2015 (C) Low confidence Suzuki et al., 2012 (C) Swan, 2008 (C)	• Findings largely consistent • Minimal concerns for bias • Finding is consistent with other systematic review/ meta-analysis (National Academies of Sciences, Engineering, and Medicine, 2017)	• Low precision in Bornehag et al., 2015	Inverse associations between DBP exposure and anogenital distance reported in 3/5 studies (Swan et al., 2015, Bornehag et al., 2015, Swan, 2008), of which Swan, 2008 was statistically significant (Fig. 2-C).	⊕⊕◯ MODERATE	
Time to	High confidence Buck Louis et al., 2014 (C)	• Study well conducted	• Single study	Decrease in fecundability with increased DBP	⊕⊕◯ MODERATE	

(continued on next page)

Table 19 (*continued*)

Outcome	Studies (design in parentheses)	Factors that increase confidence	Factors that decrease confidence	Summary of findings	Confidence judgement for outcome	Confidence judgement for overall hazard
pre-gna-ncy		• Large effect size (fecundability OR = 0.82)		exposure in one study (Buck Louis et al., 2014); results were statistically significant (Table 11).		
Hypospadias/cryptorchidism, testosterone					⊕◯◯ SLIGHT	
Pubertal development					◯◯◯ INDETERMINATE	

C: cohort, CC: case-control, CS: cross-sectional, OR = odds ratio.

Table 20
Evidence profile table for male reproductive effects of DIBP.

Outcome	Studies (design in parentheses)	Factors that increase confidence	Factors that decrease confidence	Summary of findings	Confidence judgement for outcome	Confidence judgement for overall hazard
Testoste-rone	Medium confidence Meeker and Ferguson, 2014 (CS) Pan et al., 2015 (CS) Low confidence Chang et al., 2015 (CS) Den Hond et al., 2015 (CS)	• Consistency • Minimal risk of bias in medium confidence studies	• Few studies available • Association in one study only observed in adolescents	Inverse associations between DIBP exposure and testosterone levels in 3/4 studies (Meeker and Ferguson, 2014, Pan et al., 2015, Chang et al., 2015), 2 of which were statistically significant. No studies examined exposure-response gradient (Table 15).	⊕⊕◯ MODERATE	⊕⊕◯ MODERATE Based on testosterone and supported by *slight* evidence in other outcomes, with explanation for weaker observed associations (i.e., sensitivity and few available studies). Results for DBP, a structurally similar phthalate are also supportive.
Anogenital distance, semen parameters, time to pregnancy hypospadias/cryptorchidism					⊕◯◯ SLIGHT	
Pubertal development					◯◯◯ INDETERMINATE	

C: cohort, CC: case-control, CS: cross-sectional.

DIBP and DEP, but the specific parameters with stronger evidence differed across phthalates (concentration for DBP and DEHP, motility for BBP, and morphology for DINP). While DEHP and DBP both had *robust* evidence overall and *moderate* evidence for anogenital distance, DEHP had stronger evidence for testosterone, while DBP had stronger evidence for time to pregnancy. Still, there are mechanistic linkages between all of these outcomes – low testosterone is associated with decreased anogenital distance and semen quality, semen quality is associated with time to pregnancy – and so there is consistency in a broader sense. Still, more consistency within outcomes, across phthalates, would strengthen the confidence in the overall association between phthalates and male reproductive effects. Additional studies with higher sensitivity (i.e., with repeated exposure measures, higher exposure levels/adequate range, and appropriately powered) would be informative. In addition, more evidence on the cumulative effect of phthalates and confounding across phthalates would help reduce uncertainties.

This systematic review benefited from the involvement of experts on phthalates and male reproductive epidemiology throughout the process, from development of the study evaluation criteria through evidence synthesis. However, one important limitation was that we did not perform quantitative meta-analysis to summarize the findings of the studies. This was generally due to differences in the way results were presented across studies. Additionally, further review of mechanistic data for specific outcomes may have clarified the relationship, as would review of animal studies. Discussion of some additional issues that apply to all phthalate studies, such as correlations across phthalates, will be presented in a forthcoming editorial.

Despite these limitations, our results support male reproductive effects as a hazard associated with phthalate exposure in humans, which supports recent regulations by the U.S. Consumer Product Safety Commission to ban certain phthalates in children's toys and other products (CPSC 2017, CPSC 2008). Our findings are consistent with other more limited-scope systematic reviews and meta-analyses that examined some of the outcomes discussed here. NAS also found moderate evidence of an association between DEHP and DBP and anogenital distance, while considering the evidence for infant testosterone and hypospadias to be inadequate (National Academies of Sciences,

Table 21
Evidence profile table for male reproductive effects of BBP.

Outcome	Studies (design in parentheses)	Factors that increase confidence	Factors that decrease confidence	Summary of findings	Confidence judgement for outcome	Confidence judgement for overall hazard
Semen parameters	Medium confidence Axelsson et al., 2015a, 2015b (CS) Bloom et al., 2015 (CS) Hauser et al., 2006 (CS) Jonsson et al., 2005 (CS) Jurewicz et al., 2013 (CS) Pan et al., 2015 (CS) Thurston et al., 2016 (CS) Wang et al., 2015c (CS) Wirth et al., 2008 (CS) Low confidence Den Hond et al., 2015 (CS)	• Minimal concerns for bias • Lower study sensitivity could account for most observed inconsistency for motility • Biological plausibility	• Difficult to assess exposure-response gradient and precision across studies due to differing analyses/ presentation of results	Inverse associations between BBP exposure and sperm concentration in 4/ 10 studies (Bloom et al., 2015; Hauser et al., 2006; Wirth et al., 2008; Pan et al., 2015), of which 2 were statistically significant (Bloom et al., 2015; Pan et al., 2015). Eight studies reported an inverse association with motility (Bloom et al., 2015; Den Hond et al., 2015; Hauser et al., 2006; Axelsson et al., 2015a; Jonsson et al., 2005; Wirth et al., 2008; Pan et al., 2015; Thurston et al., 2016), and 1 was statistically significant (Thurston et al., 2016) (Table 8). Biological plausibility-Studies showed increased sperm aneuploidy (Jurewicz et al., 2013) with increased exposure.	⊕⊕◯ MODERATE for motility	⊕⊕◯ MODERATE Supported by coherence across outcomes.
Time to pregnancy	High confidence Buck Louis et al., 2014 (C)	• Study well conducted • Large effect size (fecundability OR = 0.77)	• Single study	Decrease in fecundability with increased BBP exposure in one study (Buck Louis et al., 2014); results were statistically significant (Table 11).	⊕⊕◯ MODERATE	
Anogenital distance, hypospadias/cryptorchidism					⊕◯◯ SLIGHT	
Testosterone, pubertal development					◯◯◯ INDETERMINATE	

C: cohort, CC: case-control, CS: cross-sectional, OR = odds ratio.

Engineering, and Medicine, 2017). Two meta-analyses on semen parameters and phthalate exposure reported that phthalate exposure was associated with diminished semen quality (Wang et al., 2016a; Cai et al., 2015). This consistency across different review methods provides clear support for our findings.

Acknowledgements

Susan Rieth, Audrey Galizia, Larissa Pardo, Rebecca Nachman, Amanda Persad, Cynthia Yund, Leonid Kopylev, Erin Yost, Xabier Arzuaga, Tom Luben, Susan Euling, Kris Thayer, Courtney Lynch, Jane Burns, Wendy Robinson, Andrew Greenhalgh.

Appendix A. Supplemental materials

Supplementary data to this article can be found online at https://doi.org/10.1016/j.envint.2018.07.029.

References

Agarwal, A., Mulgund, A., Hamada, A., Chyatte, M., 2015. A unique view on male infertility around the globe. Reprod. Biol. Endocrinol. 13.
Araki, A., Mitsui, T., Goudarzi, H., Nakajima, T., Miyashita, C., Itoh, S., Sasaki, S., Cho, K.,

Moriya, K., Shinohara, N., Nonomura, K., Kishi, R., 2016. Prenatal di(2-ethylhexyl) phthalate exposure and disruption of adrenal androgens and glucocorticoids levels in cord blood: the Hokkaido Study. Sci. Total Environ. 581–582, 297–304. https://doi.org/10.1016/j.scitotenv.2016.12.124.

Araki, A., Mitsui, T., Miyashita, C., Nakajima, T., Naito, H., Ito, S., Sasaki, S., Cho, K., Ikeno, T., Nonomura, K., Kishi, R., 2014. Association between maternal exposure to di(2-ethylhexyl) phthalate and reproductive hormone levels in fetal blood: the Hokkaido study on environment and children's health. PLoS One 9, e109039. https://doi.org/10.1371/journal.pone.0109039.

Axelsson, J., Rylander, L., Rignell-Hydbom, A., Jönsson, B.A., Lindh, C.H., Giwercman, A., 2015a. Phthalate exposure and reproductive parameters in young men from the general Swedish population. Environ. Int. 85, 54–60. https://doi.org/10.1016/j.envint.2015.07.005.

Axelsson, J., Rylander, L., Rignell-Hydbom, A., Lindh, C.H., Jönsson, B.A., Giwercman, A., 2015b. Prenatal phthalate exposure and reproductive function in young men. Environ. Res. 138C, 264–270. https://doi.org/10.1016/j.envres.2015.02.024.

Bloom, M.S., Whitcomb, B.W., Chen, Z., Ye, A., Kannan, K., Buck Louis, G.M., 2015. Associations between urinary phthalate concentrations and semen quality parameters in a general population. Hum. Reprod. 30, 2645–2657. https://doi.org/10.1093/humrep/dev219.

Bornehag, C.G., Carlstedt, F., Jönsson, B.A., Lindh, C.H., Jensen, T.K., Bodin, A., Jonsson, C., Janson, S., Swan, S.H., 2015. Prenatal phthalate exposures and anogenital distance in Swedish boys. Environ. Health Perspect. 123, 101–107. https://doi.org/10.1289/ehp.1408163.

Buck Louis, G.M., Schisterman, E.F., Sweeney, A.M., Wilcosky, T.C., Gore-Langton, R.E., Lynch, C.D., Boyd Barr, D., Schrader, S.M., Kim, S., Chen, Z., Sundaram, R., 2011. Designing prospective cohort studies for assessing reproductive and developmental toxicity during sensitive windows of human reproduction and development–the LIFE Study. Paediatr. Perinat. Epidemiol. 25, 413–424. https://doi.org/10.1111/j.1365-3016.2011.01205.x.

Buck Louis, G.M., Sundaram, R., Sweeney, A.M., Schisterman, E.F., Maisog, J., Kannan, K., 2014. Urinary bisphenol A, phthalates, and couple fecundity: the Longitudinal Investigation of Fertility and the Environment (LIFE) study. Fertil. Steril. 101, 1359–1366. https://doi.org/10.1016/j.fertnstert.2014.01.022.

Bustamante-Montes, L.P., Hernández-Valero, M.A., Flores-Pimentel, D., García-Fábila, M., Amaya-Chávez, A., Barr, D.B., Borja-Aburto, V.H., 2013. Prenatal exposure to phthalates is associated with decreased anogenital distance and penile size in male newborns. J. Dev. Orig. Health Dis. 4, 300–306. https://doi.org/10.1017/S2040174413000172.

Cai, H., Zheng, W., Zheng, P., Wang, S., Tan, H., He, G., Qu, W., 2015. Human urinary/seminal phthalates or their metabolite levels and semen quality: a meta-analysis. Environ. Res. 142, 486–494. https://doi.org/10.1016/j.envres.2015.07.008.

Catanzariti, F., Cantoro, U., Lacetera, V., Muzzonigro, G., Polito, M., 2013. Comparison between WHO (World Health Organization) 2010 and WHO 1999 parameters for semen analysis - interpretation of 529 consecutive samples. Arch. Ital. Urol. Androl. 26, 125–129.

Chang, W.H., Li, S.S., Wu, M.H., Pan, H.A., Lee, C.C., 2015. Phthalates might interfere with testicular function by reducing testosterone and insulin-like factor 3 levels. Hum. Reprod. 30, 2658–2670. https://doi.org/10.1093/humrep/dev225.

Cooper, G., Lunn, R., Agerstrand, M., Glenn, B., Kraft, A., Luke, A., Ratcliffe, J., 2016. Study sensitivity: evaluating the ability to detect effects in systematic reviews of chemical exposures. Environ. Int. 92-93, 605–610. https://doi.org/10.1016/j.envint.2016.03.017.

Dean, A., Sharpe, R.M., 2013. Clinical review: anogenital distance or digit length ratio as measures of fetal androgen exposure: relationship to male reproductive development and its disorders [Review]. J. Clin. Endocrinol. Metab. 98, 2230–2238. https://doi.org/10.1210/jc.2012-4057.

Den Hond, E., Tournaye, H., De Sutter, P., Ombelet, W., Baeyens, W., Covaci, A., Cox, B., Nawrot, T.S., Van Larebeke, N., D'Hooghe, T., 2015. Human exposure to endocrine disrupting chemicals and fertility: a case-control study in male subfertility patients [Review]. Environ. Int. 84, 154–160. https://doi.org/10.1016/j.envint.2015.07.017.

Dent, M.P., Carmichael, P.L., Jones, K.C., Martin, F.L., 2015. Towards a non-animal risk assessment for anti-androgenic effects in humans [Review]. Environ. Int. 83, 94–106. https://doi.org/10.1016/j.envint.2015.06.009.

Fong, J.P., Lee, F.J., Lu, I.S., Uang, S.N., Lee, C.C., 2015. Relationship between urinary concentrations of di(2-ethylhexyl) phthalate (DEHP) metabolites and reproductive hormones in polyvinyl chloride production workers. Occup. Environ. Med. 72, 346–353. https://doi.org/10.1136/oemed-2014-102532.

Gnoth, C., Godehardt, D., Godehardt, E., Frank-Herrmann, P., Freundl, G., 2003. Time to pregnancy: results of the German prospective study and impact on the management of infertility. Hum. Reprod. 18, 1959–1966.

Han, X., Cui, Z., Zhou, N., Ma, M., Li, L., Li, Y., Lin, H., Ao, L., Shu, W., Liu, J., Cao, J., 2014. Urinary phthalate metabolites and male reproductive function parameters in Chongqing general population, China. Int. J. Hyg. Environ. Health 217, 271–278. https://doi.org/10.1016/j.ijheh.2013.06.006.

Hauser, R., Meeker, J.D., Duty, S., Silva, M.J., Calafat, A.M., 2006. Altered semen quality in relation to urinary concentrations of phthalate monoester and oxidative metabolites. Epidemiology 17, 682–691. https://doi.org/10.1097/01.ede.0000235996.89953.d7.

Herr, C., zur Nieden, A., Koch, H.M., Schuppe, H.C., Fieber, C., Angerer, J., Eikmann, T., Stilianakis, N., 2009. Urinary di(2-ethylhexyl)phthalate (DEHP)–metabolites and male human markers of reproductive function. Int. J. Hyg. Environ. Health 212, 648–653. https://doi.org/10.1016/j.ijheh.2009.08.001.

Howdeshell, K.L., Rider, C.V., Wilson, V.S., Gray Jr., L.E., 2008. Mechanisms of action of phthalate esters, individually and in combination, to induce abnormal reproductive development in male laboratory rats [Review]. Environ. Res. 108, 168–176. https://doi.org/10.1016/j.envres.2008.08.009.

Huang, L.P., Lee, C.C., Fan, J.P., Kuo, P.H., Shih, T.S., Hsu, P.C., 2013. Urinary metabolites of di(2-ethylhexyl) phthalate relation to sperm motility, reactive oxygen species generation, and apoptosis in polyvinyl chloride workers. Int. Arch. Occup. Environ. Health 87, 635–646. https://doi.org/10.1007/s00420-013-0905-6.

Huang, L.P., Lee, C.C., Hsu, P.C., Shih, T.S., 2011. The association between semen quality in workers and the concentration of di(2-ethylhexyl) phthalate in polyvinyl chloride pellet plant air. Fertil. Steril. 96, 90–94. https://doi.org/10.1016/j.fertnstert.2011.04.093.

Huang, P.C., Kuo, P.L., Chou, Y.Y., Lin, S.J., Lee, C.C., 2009. Association between prenatal exposure to phthalates and the health of newborns. Environ. Int. 35, 14–20. https://doi.org/10.1016/j.envint.2008.05.012.

Huang, T., Saxena, A.R., Isganaitis, E., James-Todd, T., 2014. Gender and racial/ethnic differences in the associations of urinary phthalate metabolites with markers of diabetes risk: national health and nutrition examination survey 2001–2008. Environ. Health 13, 6. https://doi.org/10.1186/1476-069X-13-6.

Janjua, N.R., Mortensen, G.K., Andersson, A.M., Kongshoj, B., Skakkebaek, N.E., Wulf, H.C., 2007. Systemic uptake of diethyl phthalate, dibutyl phthalate, and butyl paraben following whole-body topical application and reproductive and thyroid hormone levels in humans. Environ. Sci. Technol. 41, 5564–5570. https://doi.org/10.1021/es0628755.

Jensen, T.K., Frederiksen, H., Kyhl, H.B., Lassen, T.H., Swan, S.H., Bornehag, C.G., Skakkebaek, N.E., Main, K.M., Lind, D.V., Husby, S., Andersson, A.M., 2016. Prenatal exposure to phthalates and anogenital distance in male infants from a low-exposed Danish cohort (2010–2012). Environ. Health Perspect. 124, 1107–1113. https://doi.org/10.1289/ehp.1509870.

Joensen, U.N., Frederiksen, H., Jensen, M.B., Lauritsen, M.P., Olesen, I.A., Lassen, T.H., Andersson, A.M., Jørgensen, N., 2012. Phthalate excretion pattern and testicular function: a study of 881 healthy Danish men. Environ. Health Perspect. 120, 1397–1403. https://doi.org/10.1289/ehp.1205113.

Johns, L.E., Cooper, G.S., Galizia, A., Meeker, J.D., 2015. Exposure assessment issues in epidemiology studies of phthalates [Review]. Environ. Int. 85, 27–39. https://doi.org/10.1016/j.envint.2015.08.005.

Johnson, K.J., Heger, N.E., Boekelheide, K., 2012. Of mice and men (and rats): phthalate-induced fetal testis endocrine disruption is species-dependent [Review]. Toxicol. Sci. 129, 235–248. https://doi.org/10.1093/toxsci/kfs206.

Jonsson, B.A.G., Richthoff, J., Rylander, L., Giwercman, A., Hagmar, L., 2005. Urinary phthalate metabolites and biomarkers of reproductive function in young men. Epidemiology 16, 487–493. https://doi.org/10.1097/01.ede.0000164555.19041.01.

Jurewicz, J., Radwan, M., Sobala, W., Ligocka, D., Radwan, P., Bochenek, M., Hawuła, W., Jakubowski, L., Hanke, W., 2013. Human urinary phthalate metabolites level and main semen parameters, sperm chromatin structure, sperm aneuploidy and reproductive hormones. Reprod. Toxicol. 42, 232–241. https://doi.org/10.1016/j.reprotox.2013.10.001.

Kranvogl, R., Knez, J., Miuc, A., Vončina, E., Vončina, D.B., Vlaisavljević, V., 2014. Simultaneous determination of phthalates, their metabolites, alkylphenols and bisphenol A using GC-MS in urine of men with fertility problems. Acta Chim. Slov. 61, 110–120.

Lenters, V., Portengen, L., Smit, L.A., Jönsson, B.A., Giwercman, A., Rylander, L., Lindh, C.H., Spanò, M., Pedersen, H.S., Ludwicki, J.K., Chumak, L., Piersma, A.H., Toft, G., Bonde, J.P., Heederik, D., Vermeulen, R., 2014. Phthalates, perfluoroalkyl acids, metals and organochlorines and reproductive function: a multipollutant assessment in Greenlandic, Polish and Ukrainian men. Occup. Environ. Med. 72, 385–393. https://doi.org/10.1136/oemed-2014-102264.

Li, S., Dai, J., Zhang, L., Zhang, J., Zhang, Z., Chen, B., 2011. An association of elevated serum prolactin with phthalate exposure in adult men. Biomed. Environ. Sci. 24, 31–39. https://doi.org/10.3967/0895-3988.2011.01.004.

Lin, L., Wang, S., Chang, Y., Huang, P., Cheng, J., Su, P., Liao, P., 2011. Associations between maternal phthalate exposure and cord sex hormones in human infants. Chemosphere 83, 1192–1199. https://doi.org/10.1016/j.chemosphere.2010.12.079.

Liu, C., Xu, X., Huo, X., 2014. Anogenital distance and its application in environmental health research. Environ. Sci. Pollut. Res. Int. 21, 5457–5464. https://doi.org/10.1007/s11356-014-2570-z.

Liu, L., Bao, H., Liu, F., Zhang, J., Shen, H., 2012. Phthalates exposure of Chinese reproductive age couples and its effect on male semen quality, a primary study. Environ. Int. 42, 78–83. https://doi.org/10.1016/j.envint.2011.04.005.

Main, K.M., Mortensen, G.K., Kaleva, M.M., Boisen, K.A., Damgaard, I.N., Chellakooty, M., Schmidt, I.M., Suomi, A.M., Virtanen, H.E., Petersen, J.H., Andersson, A.M., Toppari, J., Skakkebaek, N.E., 2006. Human breast milk contamination with phthalates and alterations of endogenous reproductive hormones in infants three months of age. Environ. Health Perspect. 114, 270–276. https://doi.org/10.1289/ehp.8075.

Meeker, J.D., Calafat, A.M., Hauser, R., 2009. Urinary metabolites of di(2-ethylhexyl) phthalate are associated with decreased steroid hormone levels in adult men. J. Androl. 30, 287–297. https://doi.org/10.2164/jandrol.108.006403.

Meeker, J.D., Ferguson, K.K., 2014. Urinary phthalate metabolites are associated with decreased serum testosterone in men, women, and children from NHANES 2011–2012. J. Clin. Endocrinol. Metab. 99, 4346–4352. https://doi.org/10.1210/jc.2014-2555.

Mendiola, J., Jørgensen, N., Andersson, A.M., Calafat, A.M., Silva, M.J., Redmon, J.B., Sparks, A., Drobnis, E.Z., Wang, C., Liu, F., Swan, S.H., 2011. Associations between urinary metabolites of di(2-ethylhexyl) phthalate and reproductive hormones in fertile men. Int. J. Androl. 34, 369378. https://doi.org/10.1111/j.1365-2605.2010.01095.x.

Modigh, C.M., Bodin, S.L., Lillienberg, L., Hlman-Hoglund, A., Akesson, B., Axelsson, G., 2002. Time to pregnancy among partners of men exposed to di(2-ethylhexyl)phthalate. Scand. J. Work Environ. Health 28, 418–428.

National Academies of Sciences, Engineering, and Medicine, 2017. Application of Systematic Review Methods in an Overall Strategy for Evaluating Low-Dose Toxicity from Endocrine Active Chemicals. The National Academices Press, Washington, DC. https://doi.org/10.17226/24758.

National Research Council, 2008. Phthalates and Cumulative Risk Assessment: The Tasks Ahead. The National Academies Press, Washington, DC. https://doi.org/10.17226/12528.

Pan, G., Hanaoka, T., Yoshimura, M., Zhang, S., Wang, P., Tsukino, H., Inoue, K., Nakazawa, H., Tsugane, S., Takahashi, K., 2006. Decreased serum free testosterone in workers exposed to high levels of di-n-butyl phthalate (DBP) and di-2-ethylhexyl phthalate (DEHP): a cross-sectional study in China. Environ. Health Perspect. 114, 1643–1648. https://doi.org/10.1289/ehp.9016.

Pan, G., Hanaoka, T., Yu, L., Na, J., Yamano, Y., Hara, K., Ichiba, M., Nakadate, T., Kishi, R., Wang, P., Yin, H., Zhang, S., Feng, Y., 2011. Associations between hazard indices of di-n-butylphthalate and di-2-ethylhexylphthalate exposure and serum reproductive hormone levels among occupationally exposed and unexposed Chinese men. Int. J. Androl. 34, e397–e406. https://doi.org/10.1111/j.1365-2605.2011.01201.x.

Pan, Y., Jing, J., Dong, F., Yao, Q., Zhang, W., Zhang, H., Yao, B., Dai, J., 2015. Association between phthalate metabolites and biomarkers of reproductive function in 1066 Chinese men of reproductive age. J. Hazard. Mater. 300, 729–736. https://doi.org/10.1016/j.jhazmat.2015.08.011.

Pan, Y., Jing, J., Yeung, L.W., Sheng, N., Zhang, H., Yao, B., Dai, J., 2016. Associations of urinary 5-methyl-2′-deoxycytidine and 5-hydroxymethyl-2′-deoxycytidine with phthalate exposure and semen quality in 562 Chinese adult men. Environ. Int. 94, 583–590. https://doi.org/10.1016/j.envint.2016.06.020.

Thonneau, Marchand, S., Tallec, A., Ferial, M.L, Ducot, B., Lansac, J., et al., 1991. Incidence and main causes of infertility in a resident population (1,850,000) of three French regions (1988–1989). Hum. Reprod. 6, 811–816.

Pant, N., Kumar, G., Upadhyay, A.D., Patel, D.K., Gupta, Y.K., Chaturvedi, P.K., 2014. Reproductive toxicity of lead, cadmium, and phthalate exposure in men. Environ. Sci. Pollut. Res. Int. 21, 11066–11074. https://doi.org/10.1007/s11356-014-2986-5.

Pant, N., Shukla, M., Kumar Patel, D., Shukla, Y., Mathur, N., Kumar Gupta, Y., Saxena, D.K., 2008. Correlation of phthalate exposures with semen quality. Toxicol. Appl. Pharmacol. 231, 112–116. https://doi.org/10.1016/j.taap.2008.04.001.

Park, M.S., Yang, Y.J., Hong, Y.P., Kim, S.Y., Lee, Y.P., 2010. Assessment of di (2-ethylhexyl) phthalate exposure by urinary metabolites as a function of sampling time. J. Prev. Med. Public Health 43, 301–308. https://doi.org/10.3961/jpmph.2010.43.4.301.

Specht, I.O., Bonde, J.P., Toft, G., Lindh, C.H., Jönsson, B.A., Jørgensen, K.T., 2015. Serum phthalate levels and time to pregnancy in couples from Greenland, Poland and Ukraine. PLoS One 10, e0120070. https://doi.org/10.1371/journal.pone.0120070.

Specht, I.O., Toft, G., Hougaard, K.S., Lindh, C.H., Lenters, V., Jönsson, B.A., Heederik, D., Giwercman, A., Bonde, J.P., 2014. Associations between serum phthalates and biomarkers of reproductive function in 589 adult men. Environ. Int. 66, 146–156. https://doi.org/10.1016/j.envint.2014.02.002.

Suzuki, Y., Yoshinaga, J., Mizumoto, Y., Serizawa, S., Shiraishi, H., 2012. Foetal exposure to phthalate esters and anogenital distance in male newborns. Int. J. Androl. 35, 236–244. https://doi.org/10.1111/j.1365-2605.2011.01190.x.

Swan, S.H., 2008. Environmental phthalate exposure in relation to reproductive outcomes and other health endpoints in humans [Review]. Environ. Res. 108, 177–184. https://doi.org/10.1016/j.envres.2008.08.007.

Swan, S.H., Sathyanarayana, S., Barrett, E.S., Janssen, S., Liu, F., Nguyen, R.H., Redmon, J.B., TIDES Study Team, 2015. First trimester phthalate exposure and anogenital distance in newborns. Hum. Reprod. 30, 963–972. https://doi.org/10.1093/humrep/deu363.

Thurston, S.W., Mendiola, J., Bellamy, A.R., Levine, H., Wang, C., Sparks, A., Redmon, J.B., Drobnis, E.Z., Swan, S.H., 2016. Phthalate exposure and semen quality in fertile US men. Andrology 4, 632–638. https://doi.org/10.1111/andr.12124.

Toshima, H., Suzuki, Y., Imai, K., Yoshinaga, J., Shiraishi, H., Mizumoto, Y., Hatakeyama, S., Onohara, C., Tokuoka, S., 2012. Endocrine disrupting chemicals in urine of Japanese male partners of subfertile couples: a pilot study on exposure and semen quality. Int. J. Hyg. Environ. Health 215, 502–506. https://doi.org/10.1016/j.ijheh.2011.09.005.

U.S. EPA (U.S. Environmental Protection Agency), 1996. Guidelines for Reproductive Toxicity Risk Assessment. U.S. Environmental Protection Agency, Risk Assessment Forum, Washington, DC, pp. 1–143 (EPA/630/R-96/009).

Wang, C., Yang, L., Wang, S., Zhang, Z., Yu, Y., Wang, M., Cromie, M., Gao, W., Wang, S.L., 2016a. The classic EDCs, phthalate esters and organochlorines, in relation to abnormal sperm quality: a systematic review with meta-analysis [Review]. Sci. Rep. 6, 19982. https://doi.org/10.1038/srep19982.

Wang, S.Y., Wang, Y., Xie, F.Q., Li, Y.X., Wan, X.L., Ma, W.W., Wang, D.C., Wu, Y.H., 2015a. Analysis of PAEs in semen of infertile men. Int. J. Occup. Environ. Health 21, 40–48. https://doi.org/10.1179/2049396714Y.0000000088.

Wang, Y.X., You, L., Zeng, Q., Sun, Y., Huang, Y.H., Wang, C., Wang, P., Cao, W.C., Yang, P., Li, Y.F., Lu, W.Q., 2015b. Phthalate exposure and human semen quality: results from an infertility clinic in China. Environ. Res. 142, 1–9. https://doi.org/10.1016/j.envres.2015.06.010.

Wang, Y.X., Zeng, Q., Sun, Y., Yang, P., Wang, P., Li, J., Huang, Z., You, L., Huang, Y.H., Wang, C., Li, Y.F., Lu, W.Q., 2016b. Semen phthalate metabolites, semen quality parameters and serum reproductive hormones: a cross-sectional study in China. Environ. Pollut. 211, 173–182. https://doi.org/10.1016/j.envpol.2015.12.052.

Wang, Y.X., Zeng, Q., Sun, Y., You, L., Wang, P., Li, M., Yang, P., Li, J., Huang, Z., Wang, C., Li, S., Dan, Y., Li, Y.F., Lu, W.Q., 2015c. Phthalate exposure in association with serum hormone levels, sperm DNA damage and spermatozoa apoptosis: a cross-sectional study in China. Environ. Res. 150, 557–565. https://doi.org/10.1016/j.envres.2015.11.023.

Wirth, J., Rossano, M., Potter, R., Puscheck, E., Daly, D., Paneth, N., Krawetz, S., Protas, B., Diamond, M., 2008. A pilot study associating urinary concentrations of phthalate metabolites and semen quality. Syst Biol Reprod Med 54, 143–154. https://doi.org/10.1080/19396360802055921.

Xu, C., Liu, Q., Liu, H., Heroux, P., Zhang, Q., Jiang, Z.Y., Gu, A., 2015. Low serum testosterone levels are associated with elevated urinary mandelic acid, and strontium levels in adult men according to the us 2011–2012 National Health and Nutrition Examination Survey. PLoS One 10, e0127451. https://doi.org/10.1371/journal.pone.0127451.

You, L., Wang, Y., Zeng, Q., Li, M., Huang, Y., Hu, Yu, Cao, W., Liu, A., Lu, W., 2015. Semen phthalate metabolites, spermatozoa apoptosis, and DNA damage: a cross-sectional study in China. Environ. Sci. Technol. 49, 3805–3812. https://doi.org/10.1021/acs.est.5b00588.

Zhang, Y.H., Zheng, L.X., Chen, B.H., 2006. Phthalate exposure and human semen quality in Shanghai: a cross-sectional study. Biomed. Environ. Sci. 19, 205–209.

Environment International 125 (2019) 579–594

Contents lists available at ScienceDirect

Environment International

journal homepage: www.elsevier.com/locate/envint

Review article

Hazards of diisobutyl phthalate (DIBP) exposure: A systematic review of animal toxicology studies

Erin E. Yost[a,*], Susan Y. Euling[b,1], James A. Weaver[a], Brandiese E.J. Beverly[a,2], Nagalakshmi Keshava[b], Anuradha Mudipalli[a], Xabier Arzuaga[b], Todd Blessinger[b], Laura Dishaw[a], Andrew Hotchkiss[a], Susan L. Makris[b]

[a] U.S. Environmental Protection Agency, National Center for Environmental Assessment, Research Triangle Park, NC, United States of America
[b] U.S. Environmental Protection Agency, National Center for Environmental Assessment, Washington, DC, United States of America

A B S T R A C T

Background: Biomonitoring studies indicate a trend towards increased human exposure to diisobutyl phthalate (DIBP), a replacement for dibutyl phthalate (DBP). Recent reviews have found DIBP to be a male reproductive toxicant, but have not evaluated other hazards of DIBP exposure.

Objective: To inform chemical risk assessment, we performed a systematic review to identify and characterize outcomes within six broad hazard categories (male reproductive, female reproductive, developmental, liver, kidney, and cancer) following exposure of nonhuman mammalian animals to DIBP or the primary metabolite, monoisobutyl phthalate (MIBP).

Methods: A literature search was conducted in four online scientific databases [PubMed, Web of Science, Toxline, and Toxic Substances Control Act Test Submissions 2.0 (TSCATS2)], and augmented by review of regulatory sources as well as forward and backward searches. Studies were identified for inclusion based on defined PECO (Population, Exposure, Comparator, Outcome) criteria. Studies were evaluated using criteria defined a priori for reporting quality, risk of bias, and sensitivity using a domain-based approach. Evidence was synthesized by outcome and life stage of exposure, and strength of evidence was summarized into categories of *robust*, *moderate*, *slight*, *indeterminate*, or *compelling evidence of no effect*, using a structured framework.

Results: Nineteen toxicological studies in rats or mice met the inclusion criteria. There was *robust* evidence that DIBP causes male reproductive toxicity. Male rats and mice exposed to DIBP during gestation had decreased testosterone and adverse effects on sperm or testicular histology, with additional phthalate syndrome effects observed in male rats. There was also evidence of androgen-dependent and -independent male reproductive effects in rats and mice following peripubertal or young adult exposure to DIBP or MIBP, but confidence was reduced because of concerns over risk of bias and sensitivity in the available studies. There was also *robust* evidence that DIBP causes developmental toxicity; specifically, increased post-implantation loss and decreased pre- and postnatal growth. For other hazards, evidence was limited by the small number of studies, experimental designs that were suboptimal for evaluating outcomes, and study evaluation concerns such as incomplete reporting of methods and results. There was *slight* evidence for female reproductive toxicity and effects on liver, and *indeterminate* evidence for effects on kidney and cancer.

Conclusion: Results support DIBP as a children's health concern and indicate that male reproductive and developmental toxicities are hazards of DIBP exposure, with some evidence for female reproductive and liver toxicity. Data gaps include the need for more studies on male reproductive effects following postnatal and adult exposure, and studies to characterize potential hormonal mechanisms in females.

1. Introduction

Diisobutyl phthalate (DIBP) is a member of the phthalate ester class of chemicals and is used as a plasticizer to provide flexibility and durability to a wide variety of industrial and consumer products, including paints, lacquers, printing ink, pulp and paper, carpet, concrete, nail polish, and cosmetics (HSDB, 2017). Because of its use in household products, people are exposed to DIBP via food and indoor environments (Wormuth et al., 2006). DIBP is absorbed via oral ingestion (Koch et al., 2012) and dermal exposure (Elsisi et al., 1989), and is rapidly hydrolyzed to its primary metabolite, monoisobutyl phthalate (MIBP). DIBP and MIBP are distributed systemically in blood (Elsisi et al., 1989; Strucinski et al., 2006), and there is evidence these chemicals can be transferred to human breast milk (Fromme et al., 2011; Latini et al., 2009) and cross the placental barrier (Wittassek et al., 2009).

* Corresponding author.
E-mail address: Yost.Erin@epa.gov (E.E. Yost).
[1] Present affiliation: U.S. Environmental Protection Agency, Office of Children's Health Protection, Washington, DC.
[2] Present affiliation: National Institute of Environmental Health Sciences, National Toxicology Program, Office of Health Assessment and Translation, Research Triangle Park, NC.

https://doi.org/10.1016/j.envint.2018.09.038
Received 22 May 2018; Received in revised form 30 August 2018; Accepted 23 September 2018
Available online 25 December 2018
0160-4120/ Published by Elsevier Ltd. This is an open access article under the CC BY-NC-ND license (http://creativecommons.org/licenses/BY-NC-ND/4.0/).

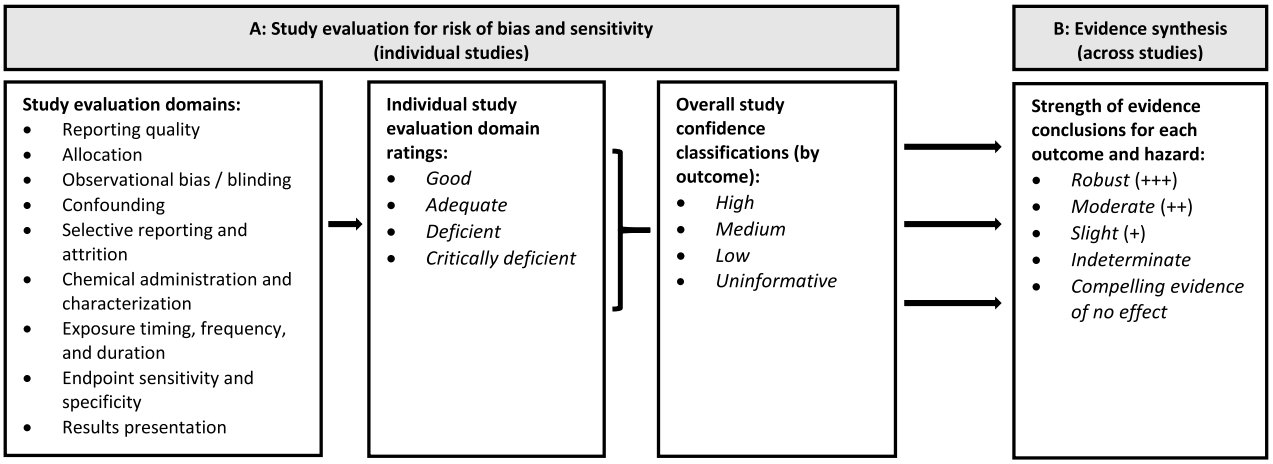

Fig. 1. Summary of (A) study evaluation and (B) strength of evidence characterization for DIBP animal toxicology studies.

Biomonitoring studies indicate that DIBP exposures have increased in recent years, possibly because of DIBP being used as a substitute for other phthalates such as dibutyl phthalate (DBP) (Wittassek et al., 2007; Zota et al., 2014). For instance, data from the National Health and Nutrition Examination Survey (NHANES) indicate that the detection frequency of MIBP in urine increased from 72% of the U.S. general population in 2001–2002 to 96% in 2009–2010. Over this period, urinary concentrations of MIBP increased monotonically, while the metabolites of DBP and several other phthalates decreased (Zota et al., 2014).

Because DIBP was historically used less compared to other phthalates, it has also been relatively less studied. However, recent reviews have characterized DIBP as a male reproductive toxicant (CPSC, 2014; NAS, 2017). Male reproductive toxicity is a common hazard among many phthalates and is generally the greatest concern associated with phthalate exposure. In rats, in utero exposure to phthalates during the critical window of male sexual differentiation produces a phenotype known as “phthalate syndrome”, which is characterized by underdevelopment of male reproductive organs, decreased anogenital distance (AGD), female-like nipple retention, cryptorchidism, and germ cell toxicity (CPSC, 2014; Foster and Gray Jr., 2013; Lioy et al., 2015; National Research Council, 2008). These effects can be causally linked to decreased testicular production of androgens, which are integral to male sexual development; decreased insulin-like-3 (INSL3) hormone, which regulates transabdominal testicular descent; and disruption of seminiferous cord formation, Sertoli cells, and germ cell development via an unknown mode of action (MOA) that is independent of effects on androgen production (Johnson et al., 2012; Martino-Andrade and Chahoud, 2010; National Research Council, 2008).

Based on recommendations following a review by a Chronic Hazard Advisory Panel (CHAP) (CPSC, 2014), which evaluated the effects on children's health of phthalates and phthalate alternatives used in children's toys and child care articles, DIBP is one of eight phthalates that the U.S. Consumer Products Safety Commission (CPSC) has permanently banned from children's toys and care articles at any amount greater than 0.1% [16 CFR § 1307 (2017)]. The CHAP stated that, although DIBP is not widely used in children's toys, it shares a similar anti-androgenic MOA with other banned phthalates, and therefore may contribute to cumulative risks to children. Additionally, the National Academy of Sciences (NAS) recently conducted a systematic review on phthalates and male reproductive tract development with the purpose of evaluating the potential for low-dose toxicity. The NAS concluded that DIBP is a presumed human health hazard based on dose-related effects on testosterone (T) production in animal studies (NAS, 2017).

Systematic review methods have only recently been applied for the purposes of chemical risk assessment, but offer the advantages of being focused, objective, and transparent. The CPSC (2014) and NAS (2017) reviews of phthalates both focused on evaluating epidemiological and toxicological studies with male reproductive outcomes, of which the NAS focused specifically on three phthalate syndrome endpoints (T, anogenital distance, and hypospadias) after gestational exposure. These systematic reviews did not evaluate other hazards caused by phthalate exposure, such as female reproductive effects or effects in other organ systems.

To gain a more comprehensive understanding of the spectrum of effects after DIBP exposure, we performed a systematic review of the animal toxicology literature for DIBP for six broad hazard categories (male reproductive, female reproductive, developmental, liver, kidney, cancer) that have been commonly associated with phthalate exposure.

2. Methods

This systematic review is part of a larger evaluation of health effects after exposure to phthalates, which includes systematic reviews of epidemiological and animal toxicology studies for multiple phthalates that will be published as separate manuscripts. The literature searches and screening, study evaluation, data extraction, and evidence synthesis methods are described in detail in the systematic review protocol (provided as a supplementary file) and summarized here. The systematic review protocol also provides detailed definitions for the terminology used to describe study evaluation and evidence synthesis, which are summarized in Fig. 1. For easier reference, these definitions and key methods from the protocol related to study evaluation and evidence synthesis are also summarized in a separate supplementary file (“key methods supplement”).

2.1. Literature searches and screening

A literature search was conducted in four online scientific databases [PubMed, Web of Science, Toxline, and Toxic Substances Control Act Test Submissions (TSCATS2)], using search terms designed to capture all potentially pertinent studies. Initial database searches were conducted in February 2013, with updates performed every 6–12 months through July 2017 (see protocol Section 3). The results of this literature search were supplemented by forward and backward searches, searching citations from key references, manual search of citations from key regulatory documents, and by addition of references that had been previously identified from an earlier DIBP review effort and added to EPA's Health and Environmental Research Online (HERO) database.

A PECO (Population, Exposure, Comparator, Outcome) was developed to frame the research question and guide the screening of relevant studies. The PECO identifies the following as the inclusion criteria for the systematic review of DIBP animal toxicology studies (see protocol Section 2 for the full PECO):

- Population: Nonhuman mammalian animal species (whole organism) of any life stage.
- Exposure: Any administered dose of DIBP or MIBP as singular compounds, via oral, dermal, or inhalation routes of exposure.
- Comparator: Exposure to vehicle-only or untreated control
- Outcome: Any examination of male reproductive, female reproductive, developmental, liver, kidney, or cancer outcomes.

Title/abstract and full text screening was performed by two reviewers, and all identified animal toxicology studies underwent full-text screening to determine compliance with the PECO. Peer-reviewed studies that contained original data and complied with the PECO were selected for inclusion, and were moved forward for study evaluation. Studies providing supporting health effects data (e.g. mechanistic, genotoxic, or toxicokinetic studies) were also compiled in HERO and annotated during the screening process (https://hero.epa.gov/hero/index.cfm/project/page/project_id/2320).

2.2. Study evaluation

For each study selected for inclusion, the quality and informativeness of the evidence was rated by evaluating domains related to reporting quality, risk of bias, and sensitivity (see protocol Section 4; abbreviated version available in the key methods supplement). Evaluations first considered reporting quality, which refers to whether the study has reported sufficient details to conduct a risk of bias and sensitivity analysis; if a study does not report critical information (e.g. species, test article name) it may be excluded from further consideration. Risk of bias, sometimes referred to as internal validity, is the extent to which the design or conduct of a study may alter the ability to provide accurate (unbiased) evidence to support the relationship between exposures and effects (Higgins, 2011). Sensitivity refers to the extent to which a study is likely to detect a true effect caused by exposure (Cooper et al., 2016).

All study evaluation ratings are documented and publicly available in EPA's version of Health Assessment Workspace Collaborative (HAWC), a free and open source web-based software application (https://hawcprd.epa.gov/assessment/497/). Study evaluation was conducted in the following domains: reporting quality; allocation; observational bias/blinding; confounding; selective reporting and attrition; chemical administration and characterization; exposure timing, frequency and duration; endpoint sensitivity and specificity; and results presentation. For each domain, core questions and basic considerations provided guidance on how a reviewer might evaluate and judge a study for that domain (see Table 9 of the protocol or Table A of the key methods supplement).

At least two reviewers independently assessed each study, and any conflicts were resolved through discussion among reviewers or other technical experts. When information needed for the evaluation was missing from a key study, an attempt was made to contact the study authors for clarification. All communication with study authors was documented and is available in HERO (tagged as Personal Correspondence with Authors), and was annotated in HAWC whenever it was used to inform a study evaluation.

For each study, in each evaluation domain, reviewers reached a consensus on a rating of *Good*, *Adequate*, *Deficient*, or *Critically Deficient*. These individual ratings were then combined to reach an overall study confidence classification of *High*, *Medium*, *Low*, or *Uninformative*. The evaluation process was performed separately for each outcome reported in a study, as the utility of a study may vary for different outcomes.

2.3. Data extraction

Data from included studies were extracted into HAWC (see protocol Section 5). Information was extracted on the study design (species, strain, life stage, exposure characteristics), outcome measurements, and statistical significance as reported by the study authors. Dose levels are presented as mg/kg-day. For dietary exposure studies, dose conversions to mg/kg-day were made using US EPA default food or water consumption rates and body weights for the species/strain and sex of the animal of interest (US EPA, 1988).

2.4. Evidence synthesis

For each outcome, data were synthesized and evaluated across studies according to the age and developmental stage of exposure to account for life stage-specific windows of susceptibility, as recommended by the US EPA (2006). The following considerations were used to articulate the strengths and weaknesses of the available evidence for each outcome [adapted from Hill, 1965; see protocol Section 6.1]: consistency, biological gradient (dose-response), strength (effect magnitude) and precision, biological plausibility, and coherence. Data were synthesized using a narrative approach, with no meta-analysis performed due largely to the heterogeneity of endpoints and study designs considered in this review (see protocol Section 6.2). Syntheses were based primarily on studies of *High* and *Medium* confidence. *Low* confidence studies were generally used to evaluate consistency, or if no or few higher confidence studies are available. When available, informative mechanistic data were used to augment the qualitative syntheses.

Based on this synthesis, each outcome was assigned a strength of evidence conclusion of *Robust*, *Moderate*, *Slight*, *Indeterminate*, *or Compelling evidence of no effect* (see protocol Section 6.3), using the framework outlined in Table 13 of the protocol or Table B of the key methods supplement. *Robust* and *Moderate* describe evidence that supports a hazard, differentiated by the quantity and quality of information available to rule out alternative explanations for the results. *Slight* evidence includes situations in which there is some evidence that supports a hazard but a conclusion of *Moderate* does not apply. *Indeterminate* describes a situation where there are no studies available for that evidence stream or the evidence is inconsistent and cannot provide a basis for making a conclusion in either direction. *Compelling evidence of no effect* represents a situation where extensive evidence across a range of populations and exposures identified no association.

The ratings for individual outcomes were then summarized into an overall strength of evidence conclusion for each of the six hazards (male reproductive, female reproductive, developmental, liver, kidney, cancer). Rationales for strength of evidence conclusions are presented in evidence profile tables using a structured format based on the Grading of Recommendations Assessment, Development and Evaluation (GRADE) approach for evaluating certainty in the evidence (Guyatt et al., 2011; Schunemann et al., 2011).

3. Results

3.1. Study selection

Literature search and screening results are summarized in Fig. 2. The literature search retrieved a total of 1156 unique records for DIBP, of which 31 proceeded to full text screening. Of these, 25 met the defined PECO criteria for inclusion and were moved forward for study evaluation. The studies excluded after full text screening were all animal toxicology studies that did not meet PECO criteria, consisting of three studies that used intraperitoneal injection (Lawrence et al., 1975; Ray et al., 2012; Singh et al., 1972), two studies in nonmammalian species [chickens: Choy, 1975; zebrafish: Sohn et al., 2016], and one behavioral study in mice (Ma et al., 2013). Additionally, the included article by University of Rochester (1954) presented data from multiple experiments, including a rat study that complied with the PECO criteria and was moved forward for study evaluation, and a dog study and several acute studies that were rejected for not meeting the PECO criteria.

At the study evaluation phase, one article was excluded from further consideration because of critical deficiencies in reporting (Eastman

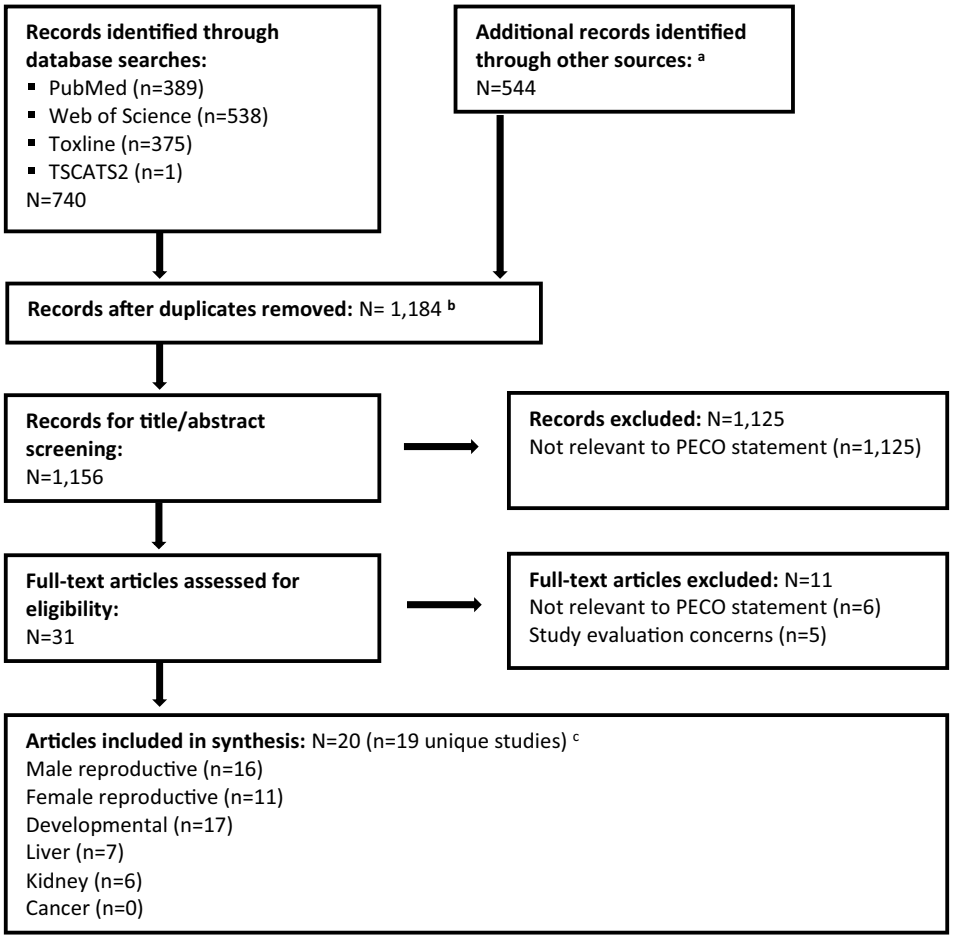

Fig. 2. Literature flow diagram for identifying DIBP animal toxicology studies.
[a] Other sources consisted of forward and backward searches, searching citations from key references, manual search of citations from key regulatory documents, references that had been previously identified from an earlier DIBP review effort, and supplementary materials for articles identified during the literature search.
[b] Includes 28 supplementary materials (not main text articles) that were tagged as records during the literature search. These supplementary materials were not included in the count of records for title/abstract screening.
[c] Most studies reported data on multiple hazards; see Table 1.

Kodak, 1954), and four articles (all of which presented data from the same reproductive toxicity study in rats) were excluded because they tested a single high dose of DIBP (4000 mg/kg-day) that caused a high rate of mortality in the exposed dams (Hardin et al., 1987; Hazleton Laboratories, 1983a, 1983b, 1992). Two of the included articles (Foster et al., 1981; Foster et al., 1982) presented overlapping data from the same animals.[3] Therefore, a total of 20 articles presenting data from 19 unique studies were included in this analysis (Table 1).

3.2. Summary of included studies

Table 1 summarizes the experimental designs and outcomes evaluated in the included studies. All were oral exposures (gavage or diet) of rats or mice. Ten were prenatal developmental toxicity studies that dosed pregnant dams with DIBP; of these, nine exposed rats during gestation only, and one exposed mice either during gestation only or from gestation through weaning (via lactational exposure). The remaining nine studies were postnatal-only exposures of weanling or peripubertal rats or mice to DIBP or MIBP.

Most of the gestational exposure studies were designed with the primary objective of evaluating male reproductive effects in F1 offspring, although two rat studies focused on fetal survival and structural alterations (external, skeletal, and soft tissue/visceral malformations and variations) (BASF, 2007; Saillenfait et al., 2006). Because of the focus on male reproductive effects, four of the rat studies exposed animals only during the critical window of male sexual differentiation (Furr et al., 2014; Hannas et al., 2011; Hannas et al., 2012; Saillenfait et al., 2017), which is approximately between gestation days (GDs) 14–18. Other studies exposed pregnant dams for longer durations, beginning immediately after mating (mice: Wang et al., 2017), within a few days after implantation (rats: BASF, 2007; Howdeshell et al., 2008; Saillenfait et al., 2006), or at mid-gestation (rats: Saillenfait et al., 2008), and continuing through the remainder of gestation. One study in rats (Saillenfait et al., 2008) and one in mice (Wang et al., 2017) allowed dams to give birth and evaluated male reproductive effects in adult F1 offspring, while the remaining rat studies sacrificed dams near the end of gestation and evaluated effects in fetuses. Regardless of the primary objective of the study, all gestational exposure studies provided relevant data on F1 offspring survival, growth, and/or maternal reproductive outcomes.

Six of the postnatal exposure studies exposed sexually immature male rats or mice of varying ages (weanling to peripubertal) for up to 7 days and focused on male reproductive outcomes (Foster et al., 1981; Foster et al., 1982; Oishi and Hiraga, 1980a, 1980b, 1980c, 1980d; Zhu et al., 2010). One study by Sedha et al. (2015) focused on estrogenic outcomes in weanling female rats. Two studies by the University of Rochester (1953, 1954) exposed male or female rats for 1 or 4 months beginning at weaning and focused on general toxicity. All reported information on postnatal growth, and most also reported information on liver and kidney effects.

None of the gestational or postnatal exposure studies provided information on cancer.

3.3. Study evaluation

Overall study confidence classifications by outcome are summarized in Table 1, and heat maps summarizing study evaluation ratings by

[3] Here, we cite Foster et al., 1981 (a peer-reviewed publication) for testis weights and histopathology, and Foster et al., 1982 (an edited book) for liver and kidney weights from the same study.

Table 1
Summary of studies, overall study confidence classifications by outcome[a].

Author (year)	Species (strain)	Exposure life stage and duration	Exposure route	Male reproductive [b]				Female reproductive [c]	
				Testosterone	Morphological development	Reproductive organ weight	Testicular histology and sperm	Morphological development	Maternal body weight
BASF, 2007	Rat (Wistar)	GD 6-20	Diet	-	-	-	-	-	H
Borch et al., 2006	Rat (Wistar)	GD 7-19; GD 7- 20/21	Gavage	H	H	-	M	H	H
Saillenfait et al., 2006	Rat (Sprague-Dawley)	GD 6-20	Gavage	-	H	-	-	H	H
Howdeshell et al., 2008	Rat (Sprague-Dawley)	GD 8-18	Gavage	H	-	-	-	-	M
Saillenfait et al., 2008	Rat (Sprague-Dawley)	GD 12-21	Gavage	-	H	H	H	H	M
Saillenfait et al., 2017	Rat (Sprague-Dawley)	GD 13-19	Gavage	H	H	-	-	-	H
Furr et al., 2014	Rat (Sprague-Dawley)	GD 14-18	Gavage	H	-	-	-	-	L
Hannas et al., 2012	Rat (Sprague-Dawley)	GD 14-18	Gavage	H	-	-	-	-	L
Hannas et al., 2011	Rat (Sprague-Dawley)	GD 14-18	Gavage	H	-	-	-	-	L
Wang et al., 2017	Mouse (ICR)	GD 0-21; GD 0-PND 21	Diet	M	M	M	M	-	L
Sedha et al., 2015	Rat (Wistar)	PND 21-23; PND 21-40	Gavage	-	-	-	-	M	-
Zhu et al., 2010	Rat (Sprague-Dawley); Mouse (C57Bl/6N)	PND 21-28	Gavage	-	-	L	-	-	-
Oishi and Hiraga, 1980a	Mouse (JCL:ICR)	~PND 35-42	Diet	M	-	L	-	-	-
Oishi and Hiraga, 1980b	Rat (JCL:Wistar)	~PND 35-42	Diet	L	-	M	L	-	-
Oishi and Hiraga, 1980c*	Rat (JCL:Wistar)	~PND 35-42	Diet	M	-	M	-	-	-
Oishi and Hiraga, 1980d*	Mouse (JCL:ICR)	~PND 35-42	Diet	M	-	L	-	-	-
Foster et al., 1981, 1982*	Rat (Sprague-Dawley)	"Young"; 6 -day exposure	Gavage	-	-	L	L	-	-
University of Rochester, 1953	Rat (albino; strain not reported)	Weaning to 1 month post-weaning	Diet	-	-	-	-	-	-
University of Rochester, 1954	Rat (albino; strain not reported)	Weaning to 4 months post-weaning	Diet	-	-	M	-	-	-

(continued on next page)

Table 1 (*continued*)

Author (year)	Female reproductive [c]		Developmental [d]			Liver		Kidney	
	Gestation length	Reproductive organ weight	Survival	Growth	Structural alterations	Organ weight	Histopathology	Organ weight	Histopathology
BASF, 2007	-	H	H	H	H	-	-	-	-
Borch et al., 2006	-	-	H	H	-	-	-	-	-
Saillenfait et al., 2006	-	H	H	H	H	-	-	-	-
Howdeshell et al., 2008	-	-	H	-	-	-	-	-	-
Saillenfait et al., 2008	H	-	H	H	-	-	-	-	-
Saillenfait et al., 2017	-	H	H	H	H	-	-	-	-
Furr et al., 2014	-	-	M	-	-	-	-	-	-
Hannas et al., 2012	-	-	M	-	-	-	-	-	-
Hannas et al., 2011	-	-	L	-	-	-	-	-	-
Wang et al., 2017	-	-	H	M	-	M	-	-	-
Sedha et al., 2015	-	M	-	M	-	-	-	-	-
Zhu et al., 2010	-	-	-	-	-	-	-	-	-
Oishi and Hiraga, 1980a	-	-	-	L	-	M	-	M	-
Oishi and Hiraga, 1980b	-	-	-	L	-	M	-	M	-
Oishi and Hiraga, 1980c*	-	-	-	L	-	-	-	-	-
Oishi and Hiraga, 1980d*	-	-	-	L	-	M	-	M	-
Foster et al., 1981, 1982*	-	-	-	-	-	L	-	L	-
University of Rochester, 1953	-	-	-	L	-	M	L	M	L
University of Rochester, 1954	-	-	-	L	-	M	L	M	L

*indicates MIBP study

GD = Gestation day. PND = Postnatal day

[a] High confidence (H), Medium confidence (M), Low confidence (L). Dash (-) indicates outcomes that were not included in a study.

[b] Male reproductive outcomes: Testosterone (testicular production or level measured in testis or serum), morphological development (AGD, nipple retention, hypospadias, cryptorchidism, cleft prepuce, time to puberty), testicular histology and sperm (sperm counts, motility, morphology, histological evaluations of testicular atrophy or azoospermia/oligospermia), reproductive organ weights (testis, epididymides, prostate, seminal vesicles)

[c] Female reproductive outcomes: Maternal body weight (body weight gain during gestation or lactation), gestation length, morphological development (AGD, displaced ovaries, time to puberty), reproductive organ weight (uterus, vagina, ovary)

[d] Developmental outcomes: Survival (fetal viability, fetal mortality, resorptions, pre- or post-implantation loss), growth (pre- or postnatal body weight), malformations/variations (external, skeletal, soft tissue/visceral)

domain are provided in the Supplementary Materials for gestational exposure studies (Fig. S1) and postnatal exposure studies (Fig. S2). Figs. S1 and S2 each provide links to HAWC, where rationale for the study evaluation ratings is documented.

Among the gestational exposure study outcomes, confidence was generally *high*, although some study outcomes were rated *medium* or *low confidence* because of specific concerns. For instance, the rat gestational exposure studies by Furr et al. (2014) and Hannas et al. (2011, 2012) used a relatively small sample size (generally n = 3–4 dams/treatment group) that authors stated did not provide the statistical power to consistently detect anything but rather large alterations in maternal weight gain and fetal viability, or decreases in T production of less than 20–25%; our reviewers determined that the T measurements in these studies had adequate sensitivity, but confidence in the maternal weight gain and fetal survival data was reduced because of sensitivity concerns. For evaluation of maternal toxicity, confidence was reduced in the maternal body weight gain measurements in several studies that did not adjust for gravid uterine weight, the calculation of which is considered preferable because it facilitates the interpretation of maternal toxicity relative to effects on fetal body weight (US EPA, 1991). Additionally, in the only available gestational exposure study in mice (Wang et al., 2017), confidence in male reproductive, body weight, and organ weight data was reduced because data were presented as an average of individual pups, rather than using the litter as the experimental unit. Failure to account for litter effects has the potential to overestimate the statistical significance of experimental findings (Haseman et al., 2001). All rat gestational exposure studies used the litter as the experimental unit for presentation and analysis of F1 offspring data.

All outcomes reported in the postnatal exposure studies were rated as *medium* or *low confidence*. In general, these studies had incomplete reporting of experimental designs and results, which led to concerns for risk of bias and sensitivity. Concerns included lack of information about the age or pubertal status of the animals at the time of exposure, strain of the animals, sample size, or methods used to allocate test animals to experimental groups, and presentation of only qualitative (rather than quantitative) results. For evaluation of male reproductive effects, confidence was reduced in studies that presented only relative testis weight (as a percentage of body weight) without presenting absolute testis weight; it has been shown that testis weights are not modeled well by an organ-to-body weight ratio because testis and body weights are not proportional (Bailey et al., 2004), so this may be a less sensitive measurement compared to absolute testis weight.

3.4. Male reproductive effects

Figures indicating the doses at which statistically significant male reproductive effects occurred are provided in Supplemental Materials (Figs. S3 – S5). Morphological and histopathological effects in F1 postnatal and adult males from the multi-dose study by Saillenfait et al. (2008) are summarized in Figs. S6 and S7, respectively.

3.4.1. Summary of gestational (F1) exposure studies

A dose-related decrease in androgens was observed in male offspring from all rat and mouse gestational exposure studies that evaluated this outcome. This includes six studies that evaluated fetal testicular T production or testicular T or androstenedione (AN) levels in fetal rats (Borch et al., 2006; Furr et al., 2014; Hannas et al., 2011; Hannas et al., 2012; Howdeshell et al., 2008; Saillenfait et al., 2017), and one study that evaluated serum and testicular T levels in adult mice that had been exposed during gestation and/or through weaning (Wang et al., 2017). Across these studies, changes in T were statistically significant at doses as low as 200 mg/kg-day, and the magnitude of effect was often large (decreased up to 96% compared to controls). Several of these studies also reported decreased testicular expression of genes or proteins in the steroidogenesis pathway in rats (Borch et al., 2006; Hannas et al., 2011; Hannas et al., 2012; Saillenfait et al., 2017) and in mice (Wang et al., 2017), providing mechanistic evidence in both species to corroborate the observed decrease in fetal testicular testosterone. The affected genes or proteins included steroid acute regulatory protein (StAR) and scavenger receptor class B type 1 (SR-B1), which are involved in cholesterol uptake and transport; and 3β-hydroxysteroid dehydrogenase (3β-HSD), cytochrome P450 (CYP) side chain cleavage (P450scc or CYP11A1), and CYP17A1, which are steroidogenic enzymes. Hannas et al. (2012) also reported decreased testicular gene expression of INSL3 in rats. Overall, the evidence for decreased fetal testicular T production after gestational exposure was found to be *robust*.

In postnatal and adult male rats that had been exposed during the critical window of male sexual differentiation during gestation, Saillenfait et al. (2008) reported numerous dose-related outcomes that are consistent with decreased testosterone and INSL3: decreased AGD, increased time to puberty (preputial separation), nipple retention, increased rate of external malformations of the reproductive tract (hypospadias, exposed os penis, cryptorchidism,[4] cleft prepuce; Fig. S6), and decreased reproductive organ weights (testis, epididymides, seminal vesicles, prostate). Other gestational exposure studies that evaluated fetal rats also observed decreased male AGD (Borch et al., 2006) and increased incidence of cryptorchidism, with approximately two-thirds of testes in the highest dose group (1000 mg/kg-day) located in the upper half of the abdominal cavity (Saillenfait et al., 2006). Conversely, in weanling and adult mice, male AGD was not affected and effects on testis weight were inconsistent (Wang et al., 2017). It is not clear whether this reflects a species sensitivity difference or a difference in study design. Overall, based on strength of the data in rats, the evidence for effects on male morphological development after gestational exposure was found to be *robust*, and evidence for effects on male reproductive organ weight was found to be *moderate*. In these same animals, histopathological analysis found dose-related increases in lesions in the fetal rat testis (Borch et al., 2006) and adult rat testis (Saillenfait et al., 2008), with oligospermia or total azoospermia[5] in the corresponding epididymides (Saillenfait et al., 2008, Fig. S7). Adult male mice exposed to DIBP during gestation had decreased sperm concentration and motility, which reached statistical significance in mice that were exposed from gestation through weaning (Wang et al., 2017). These outcomes are consistent with effects on sperm development and function that have been observed for other phthalates, which are thought to be mediated via androgen-dependent and -independent pathways (Johnson et al., 2012; National Research Council, 2008). Given the exposure-response gradient and consistency across species, the evidence for effects on testicular histology and sperm parameters was found to be *robust*.

3.4.2. Summary of postnatal (weanling or peripubertal) exposure studies

Effects on androgens (measured as testicular T or serum T or dihydrotestosterone [DHT] levels) were inconsistent across a series of studies by Oishi and Hiraga (1980a, 1980b, 1980c, 1980d), in which immature (~5-week-old) rats or mice were exposed to DIBP or MIBP in the diet for 7 days. In rats, androgen levels were increased compared to controls (Oishi and Hiraga, 1980b, 1980c), whereas testicular T levels in mice were similar (Oishi and Hiraga, 1980a) or significantly decreased (Oishi and Hiraga, 1980d) compared to controls. The life stage of these animals at the time of exposure was inferred to be peripubertal, based on the age of the animals; however, only one of these studies confirmed the pubertal status of the animals [Oishi and Hiraga, 1980c reported that the rats had positive sperm counts and were between puberty and sexual maturity, whereas the pubertal status of animals in

[4] Cryptorchidism is reported as “nonscrotal testis” in in adult males in Saillenfait et al., 2008 and “ectopic testis” in male fetuses in Saillenfait et al., 2006.

[5] Azoospermia refers to a lack of spermatozoa, and oligospermia refers to reduced spermatozoa.

Table 2
Evidence profile table for male reproductive effects of DIBP or MIBP
*indicates MIBP study

Male Reproductive Effects						
Outcome		Available studies	Factors that increase confidence	Factors that decrease confidence	Confidence judgement for outcome	Confidence judgement for overall hazard
Gestational (F1) Exposure	**Testosterone**	**High confidence:** Borch et al., 2006 Furr et al., 2014 Hannas et al., 2011 Hannas et al., 2012 Howdeshell et al., 2008 Saillenfait et al., 2017 **Medium confidence:** Wang et al., 2017	• Consistency • Dose-response gradient • Effect size • Biological plausibility (support from mechanistic evidence) • Minimal concerns for bias and sensitivity		⊕⊕⊕ ROBUST A dose-related decrease in testicular T levels or production (up to -96% compared to control) was observed in all studies in rats and mice that evaluated this outcome. Several of these studies also demonstrated decreased testicular expression of genes and proteins in the steroidogenesis pathway in both rats and mice, which provides support for biological plausibility.	⊕⊕⊕ ROBUST Supported by consistency and coherence across outcomes, with mechanistic evidence (e.g. decreased testicular expression of steroidogenic enzymes and INSL3 in F1 males) providing support for biological plausibility. The greatest weight of evidence came from gestational exposure studies, whereas postnatal exposure studies were limited by risk of bias and sensitivity concerns.
	Male morphological development	**High confidence:** Borch et al., 2006 Saillenfait et al., 2006 Saillenfait et al., 2008 Saillenfait et al., 2017 **Medium confidence:** Wang et al., 2017	• Consistency within rat studies • Dose-response gradient • Effect size • Biological plausibility • Minimal concerns for bias and sensitivity		⊕⊕⊕ ROBUST All rat studies observed a dose-related increase in effects consistent with decreased T and INSL3, including increased time to puberty, decreased AGD, nipple retention, cryptorchidism, non-scrotal testis, hypospadias, and exposed os penis. No effects on AGD were observed in mice (Wang et al., 2017).	
	Reproductive organ weight	**High confidence:** Saillenfait et al., 2008 **Medium confidence:** Wang et al., 2017	• Dose-response gradient and minimal concern for bias and sensitivity in the study by Saillenfait et al., 2008 • Biological plausibility • Coherence with postnatal exposure studies	• Few studies	⊕⊕◯ MODERATE Decreased reproductive organ weights were observed in rats (Saillenfait et al., 2008), whereas a consistent trend in testis weight was not observed in mice (Wang et al., 2017); it is not clear whether this is related to differences in species or study designs. This effect is consistent with decreased T.	
	Testicular histology or sperm evaluation	**High confidence:** Saillenfait et al., 2008 **Medium confidence:** Borch et al., 2006 Wang et al., 2017	• Consistency • Dose-response gradient • Effect size • Biological plausibility		⊕⊕⊕ ROBUST Adverse effects on the testis and/or sperm were observed in rats and mice, including a dose-related increased incidence of pathological lesions of the testis (Borch et al., 2006, Saillenfait et al., 2008), epididymal oligo- or azoopermia	

(*continued on next page*)

Table 2 (*continued*)

Male Reproductive Effects						
Outcome		Available studies	Factors that increase confidence	Factors that decrease confidence	Confidence judgement for outcome	Confidence judgement for overall hazard
					(Saillenfait et al., 2008), and decreased sperm concentration and motility (Wang et al., 2017).	
Postnatal (Weanling or Peripubertal) Exposure	**Testosterone**	**Medium confidence:** Oishi and Hiraga, 1980a Oishi and Hiraga, 1980c* Oishi and Hiraga, 1980d* **Low confidence:** Oishi and Hiraga, 1980b	• Biological plausibility	• Concerns for bias and sensitivity in some studies • Unexplained inconsistency	◯◯◯ INDETERMINATE A dose-related increase in androgen levels was observed in two rat studies (Oishi and Hiraga, 1980b, c), whereas androgen levels were decreased or not changed in two mouse studies (Oishi and Hiraga, 1980a, d).	
	Reproductive organ weight	**Medium confidence:** Oishi and Hiraga, 1980b Oishi and Hiraga, 1980c* U. Rochester, 1954 **Low confidence:** Oishi and Hiraga, 1980a Oishi and Hiraga, 1980d* Foster et al., 1981* Zhu et al., 2010	• Consistency within rat studies • Biological plausibility • Coherence with gestational exposure studies	• Concerns for bias and sensitivity in some studies	⊕⊕⊕ ROBUST In rats, a dose-related decrease in absolute testis weight was consistently observed (Oishi and Hiraga, 1980b, c; Foster et al., 1981; University of Rochester, 1954). In weanling mice, Zhu et al. (2010) observed decreased absolute testis weight in the highest dose group. In peripubertal mice, Oishi and Hiraga (1980a, d) observed increased relative testis weight, which is considered a less reliable metric compared to absolute testis weight.	
	Testicular histology/sperm evaluation	**Low confidence:** Oishi and Hiraga, 1980b Foster et al., 1981*	• Consistency • Biological plausibility • Coherence with gestational exposure studies	• Concerns for bias and sensitivity • Few studies	⊕⊕◯ MODERATE Rats were found to have increased testicular atrophy (Foster et al., 1981) and decreased spermatocytes and spermatogonia (Oishi and Hiraga, 1980a).	

the other three studies was not reported]. Susceptibility to phthalate-induced effects on androgen levels is dependent on the life stage of exposure, with sexually immature animals being more susceptible (Albert and Jégou, 2014; Hotchkiss et al., 2008; National Research Council, 2008). The discord in findings could therefore be based on issues such as timing of exposure and timing of assessment. Given these study concerns and the inconsistency in results across studies, the evidence for effects on T was found to be *indeterminate*.

Despite the inconsistent findings for androgen levels, effects on male reproductive organ weight provide support for an androgen-dependent MOA in animals exposed during weanling and/or peripubertal life stages. A dose-related decrease in absolute and relative testis weight was consistently observed across all rat studies (Foster et al., 1981; Oishi and Hiraga, 1980b, 1980c; University of Rochester, 1954; Zhu et al., 2010), with no significant effects on prostate or seminal vesicle weight (Foster et al., 1981). Decreased absolute testis weights were also observed in 21-day-old mice exposed to DIBP for 7 days (Zhu et al., 2010), although statistically significant effects occurred at higher doses compared to rats in the same study. Conversely, 5-week-old mice exposed to DIBP or MIBP for 7 days had a statistically significant increase in relative testis weight compared to control (Oishi and Hiraga, 1980a, 1980d). Relative testis weight has been found to be an unreliable metric because testis and body weights are not proportional (Bailey et al., 2004), so this result is considered *low confidence* since it could be an artifact of the decreased body weights in the DIBP- and MIBP-treated mice. Nevertheless, results reflect a potential difference in species sensitivity, with rats being more sensitive than mice for effects on testis weight. Overall, reduced testis weight was observed in both species and

was consistent with effects observed in rats exposed to DIBP during gestation, so the evidence for effects on male reproductive organ weight was found to be *robust*.

DIBP- or MIBP-exposed rats had increased testicular atrophy (defined as marked or total loss of germinal epithelium of the seminiferous tubules) (Foster et al., 1981) and decreased spermatocytes and spermatogonia compared to controls (Foster et al., 1981; Oishi and Hiraga, 1980b). These results are considered *low confidence* because authors provided little information on their methods, and neither study provided quantitative results for the observed effects on sperm. However, results are consistent with those observed in rodents exposed to DIBP during gestation (Saillenfait et al., 2008; Wang et al., 2017), and are corroborated by the reported decrease in testis weight in these studies. Evidence for testicular degeneration and effects on sperm was therefore found to be *moderate*.

3.4.3. Synthesis of results for male reproductive effects

Overall, the available studies in rodents provide *robust* evidence that DIBP causes male reproductive toxicity (Table 2). Across the gestational exposure studies, male rats had decreased fetal testicular T and displayed the hallmarks of phthalate syndrome (reduced male reproductive organ weights, hypospadias, cryptorchidism, nipple retention, reduced AGD, germ cell effects), and male mice had decreased T and effects on sperm. These effects are consistent with well-established MOAs for male reproductive effects of phthalates, which act through both androgen-dependent (decreased steroidogenesis leading to decreased androgens) and androgen-independent (decreased INSL3 and germ cell effects) pathways, and are supported by mechanistic data in both rats and mice showing decreased fetal testicular expression of steroidogenic genes/proteins and INSL3. While not all studies reported statistical significance, the direction of effect observed for most outcomes was consistent across the available gestational exposure studies, although some biomarkers observed in rats (decreased AGD and decreased adult male reproductive organ weights) were not observed in the mouse study by Wang et al. (2017).

The database of postnatal exposure studies had more risk of bias and sensitivity concerns compared to the gestational exposure database, but likewise provides evidence of both the androgen-dependent MOA (decreased testis weights) and androgen-independent MOA (increased testicular atrophy and decreased spermatocytes). Although androgens were inconsistently affected across the available postnatal exposure studies for DIBP, this may simply reflect limitations in the study designs, such as uncertainty about the pubertal status of the animals. Pubertal exposure studies for other antiandrogenic phthalates [e.g. DBP and diethylhexyl phthalate (DEHP)] report decreased T as well as androgen-dependent and -independent effects on reproductive development (Noriega et al., 2009; US EPA, 2007).

Strengths of this database include the availability of several *high confidence* gestational exposure studies, with one large multi-dose study that assessed multiple outcomes in postnatal and adult animals that had been exposed to DIBP in utero during the critical window for male reproductive development (Saillenfait et al., 2008). Other strengths are the availability of studies in both rats and mice that assessed similar outcomes, including multi-dose studies in multiple rat strains. Although none of the studies included a direct measurement of male fertility (e.g. mating success), the observed increase in hypospadias, testicular atrophy, and germ cell effects (including azoospermia) suggest that fertility can be affected.

3.5. Female reproductive effects

Figures indicating the doses at which statistically significant female reproductive effects occurred are provided in the Supplementary Materials (Figs. S8 – S9).

3.5.1. Summary of gestational (F1) and postnatal (weanling) exposure studies

Following gestational exposure, Saillenfait et al. (2006) observed a non-significant increase in the incidence of fetuses with displaced ovaries. Borch et al. (2006) reported a significant increase in female AGD/cubic root of body weight, whereas Saillenfait et al. (2008) found a slight but not statistically significant increase in female AGD following gestational exposure with body weight used as a covariate in their statistical analysis. A separate publication of mechanistic data for the Borch et al. (2006) animals (Boberg et al., 2008) reported elevated ovarian aromatase gene expression in DIBP-exposed female fetuses, suggesting a possible endocrine mechanism; ovarian estradiol was also measured but was found to be near the detection limit of the assay with no statistically significant differences between groups (data not shown by authors). In a 20-day pubertal assay in rats, no vaginal opening had occurred in control or DIBP-treated animals when the study was terminated at PND 41, indicating that DIBP did not accelerate the timing of female puberty (Sedha et al., 2015). Although data is limited and the biological implications are unclear, the effects on AGD and ovarian displacement suggest morphological changes in females that are analogous to those observed in male offspring from these studies. Overall, the evidence for effects on female morphological development is considered *slight*.

In female weanling rats exposed to DIBP in a 3-day uterotrophic assay or 20-day pubertal assay, Sedha et al. (2015) found no effects on uterine, paired ovary, or vaginal weight. Because only one study was available, the evidence for effects on reproductive organ weight in developing females is considered *indeterminate*.

3.5.2. Summary of maternal (F0) exposure studies

Only one study (Saillenfait et al., 2008) evaluated gestation length, and reported that there was no effect of DIBP exposure. The evidence for effects on gestation length was considered *indeterminate*.

Maternal body weight parameters were reported in all gestational exposure studies. Of the studies judged to be *high confidence* for this outcome, BASF (2007) reported a significant decrease in maternal body weight gain in Wistar rats after correcting for gravid uterine weight, whereas three other rat studies reported no effect on corrected maternal body weight gain (Borch et al., 2006; Saillenfait et al., 2006; Saillenfait et al., 2017). The remaining studies were judged to have lower confidence because they did not correct for gravid uterine weight. Of these, Howdeshell et al. (2008) observed a decrease in maternal body weight gain, which appears to be a consequence of fetal toxicity (decreased fetal body weights); and the remaining studies reported no effect on maternal weight gain (Furr et al., 2014; Hannas et al., 2011; Hannas et al., 2012; Saillenfait et al., 2008; Wang et al., 2017). Overall, the evidence for effects on maternal body weight gain are considered *slight*.

Saillenfait et al. (2006) reported a significant decrease in gravid uterine weight, which appears to be a secondary effect to reduced fetal body weights in this study, whereas BASF (2007) and Saillenfait et al. (2017) reported no effect on gravid uterine weight. Given this limited amount of information, the evidence for effects on maternal organ weights is considered *indeterminate*.

3.5.3. Synthesis of results for female reproductive effects

Overall, the available studies provide *slight* evidence that DIBP causes female reproductive toxicity following developmental or maternal exposure (Table 3). This database has significant limitations. The exposure durations used in the gestational exposure studies were selected primarily for evaluating male reproductive toxicity and fetal morphological development, and may not be the most sensitive for detecting maternal toxicity. None of the studies included pre-mating, mating, or lactational exposure intervals; therefore, effects on fertility, mating, fecundity (other than litter size effects due to post-implantation loss), and estrous cyclicity were not evaluated. Additionally, limited data were presented on effects in F1 females exposed during gestation, compared to the detailed evaluations of reproductive toxicity in F1 males.

Table 3
Evidence profile table for female reproductive effects of DIBP

Female Reproductive Effects						
Outcome		Available studies	Factors that increase confidence	Factors that decrease confidence	Confidence judgement for outcome	Confidence judgement for overall hazard
Gestational (F1) or Postnatal (Weanling) Exposure	**Female morphological development**	**High confidence:** Saillenfait et al., 2006 Saillenfait et al., 2008 Borch et al., 2006 **Medium confidence:** Sedha et al., 2015	• Biological plausibility (coherence with effects observed in males)	• Concerns for study sensitivity	⊕◯◯ SLIGHT Increased female AGD was observed, but was not always statistically significant (Borch et al., 2006, Saillenfait et al., 2008). A non-significant increase in displaced ovaries was observed by Saillenfait et al., 2006. DIBP did not accelerate female puberty in a 20-day pubertal assay (Sedha et al., 2015).	⊕◯◯ SLIGHT Based on limited evidence for effects on female AGD and ovary displacement in F1 females following gestational exposure, and for effects on maternal weight gain in F0 females following maternal exposure. There were concerns for study sensitivity because most gestational exposure studies were designed to evaluate male reproductive effects, and the exposure windows may not have been the most sensitive for detecting F1 female or maternal toxicity.
	Reproductive organ weight	**Medium confidence:** Sedha et al., 2015		• Single study	◯◯◯ INDETERMINATE No effects on were observed on uterus, ovary, or vagina weight in 3- or 20-day assays in prepubescent females.	
Maternal (F0) Exposure	**Maternal body weight**	**High confidence:** Borch et al., 2006 BASF, 2007 Saillenfait et al., 2006 Saillenfait et al., 2017 **Medium confidence:** Saillenfait et al., 2008 Howdeshell et al., 2008 **Low confidence:** Furr et al., 2014 Hannas et al., 2011 Hannas et al., 2012 Wang et al., 2017	• Dose-response gradient and minimal concern for bias in the study by BASF, 2007	• Concerns for study sensitivity	⊕◯◯ SLIGHT Corrected maternal body weight was significantly decreased in one study (BASF, 2007). Otherwise, any effects on maternal weight gain were concurrent with decreased gravid uterine weight or decreased offspring body weight, and therefore appeared to be secondary effects related to fetal toxicity.	
	Reproductive organ weight	**High confidence:** BASF, 2007 Saillenfait et al., 2006 Saillenfait et al., 2017	• Minimal concerns for bias	• Concerns for study sensitivity	◯◯◯ INDETERMINATE Saillenfait et al., 2006 reported decreased gravid uterine weight, which appeared to be a secondary effect related to fetal toxicity. Otherwise, no effects on female reproductive organ weight were observed.	
	Gestation length	**High confidence:** Saillenfait et al., 2008	• Minimal concern for bias	• Single study • Concerns for study sensitivity	◯◯◯ INDETERMINATE Effects on gestation length were not observed in one study that began exposing dams at mid-gestation, which may not be the most sensitive window of exposure for this endpoint	

3.6. Developmental effects

Figures indicating the doses at which statistically significant developmental effects occurred are provided in the Supplementary Materials (Figs. S10 – S12).

3.6.1. Summary of gestational (F1) exposure studies

Two *high confidence* studies (Howdeshell et al., 2008; Saillenfait et al., 2006) that exposed Sprague-Dawley rats by gavage beginning soon after the time of implantation (GD 8–18 and GD 6–20, respectively) observed a dose-related increase in fetal resorptions per litter, leading to a 52–62% decrease in the number of live fetuses per litter. In contrast, effects on fetal viability were not observed in the other studies that reported this outcome, including two dietary studies that exposed Wistar rats for similar durations (BASF, 2007; Borch et al., 2006), four studies that exposed Sprague-Dawley rats for shorter durations in mid- to late gestation (Furr et al., 2014; Hannas et al., 2011; Hannas et al., 2012; Saillenfait et al., 2008), or in mice exposed throughout gestation (Wang et al., 2017). This variability in results appears to be driven by differences in species, strain, and study design (particularly exposure duration). Reduced fetal survival has also been observed for other phthalates, such as DBP, and evidence suggests that DBP can interfere with pregnancy maintenance by decreasing ovarian progesterone production (Gray Jr et al., 2006). Given this biologically plausible mechanistic hypothesis for other phthalates, and the large effect size and exposure-response gradient observed in Howdeshell et al. (2008) and Saillenfait et al. (2006), the evidence for effects on fetal survival was found to be *robust*.

Postnatal survival following gestational exposure was only evaluated by Saillenfait et al. (2006), who found no effect on the survival of male and female rat pups through weaning. The evidence for effects on postnatal survival was found to be *indeterminate*.

Most studies in rats reported a dose-related decrease in fetal body weights (BASF, 2007; Borch et al., 2006; Saillenfait et al., 2006; Saillenfait et al., 2017) and postnatal and adult body weights (Saillenfait et al., 2008) of animals exposed to DIBP during gestation. No effects on fetal body weight were observed in rats by Saillenfait et al. (2017), and Wang et al. (2017) observed no effects in mice at PND 21 but increased body weight at PND 80, although these two studies tested a single lower dose of DIBP. Given the exposure-response gradient observed in studies that tested a wider range of DIBP doses, the evidence for effects on prenatal growth was found to be *robust*, and evidence for effects on postnatal growth after gestational exposure was found to be *moderate*.

Different results were observed in the two studies that performed detailed analyses of fetal external, skeletal, and soft tissue/visceral malformations and variations following exposure from GD 6–20. In Sprague-Dawley rats, Saillenfait et al. (2006) reported a dose-related increase in the total incidence of external, skeletal, and visceral malformations in fetuses following gestational exposure to DIBP, reaching statistical significance at 750 and 1000 mg/kg-day. In particular, the incidence of fused sternebrae increased statistically significantly with dose, and a variety of other individual malformations of the neural tube, eye, vessels of the heart, vertebral column, and axial skeleton exhibited dose-related increases that were not significant. Dose-related skeletal variations included supernumerary ribs, incomplete ossification of thoracic or lumbar vertebral centra, and assorted variations of the skull and axial skeleton. Dose-related visceral variations included dilation or distention of the ureter and dilated renal pelvis, as well as ectopic testis and displaced ovaries (discussed in the male and female reproductive sections, respectively). Comparatively, in Wistar rats, BASF (2007) did not observe any dose-related trends at doses up to 942 mg/kg-day. In some cases, the frequency of skeletal variations was significantly elevated in treatment groups relative to control; however, the incidences of these variations were consistently within the range of historical control data for that laboratory, suggesting that they were not caused by DIBP treatment. Additionally, no effects on external morphology were observed by Saillenfait et al. (2017) at the single dose tested (250 mg/kg-day). Given that a clear exposure-response gradient was observed in one rat study while no effects were observed in the others, the evidence for effects on fetal structural alterations was found to be *slight*.

3.6.2. Summary of postnatal (weanling or peripubertal) exposure studies

A dose-related decrease in postnatal and adult growth was observed in all available studies that exposed immature rats and mice (Oishi and Hiraga, 1980a, 1980b, 1980c, 1980d; Sedha et al., 2015; University of Rochester, 1953, 1954), which were judged to be *medium* or *low confidence* for this outcome. One limitation is that the studies by Oishi and Hiraga reported decreased food consumption in DIBP and MIBP treated animals, suggesting a palatability issue, so the decreased growth in these animals may have been a secondary effect related to food intake. The studies by University of Rochester did not report food consumption, but also used high doses of DIBP in diet that may have caused palatability issues. Overall, the evidence for effects on growth after postnatal exposure was found to be *moderate*.

3.6.3. Synthesis of results for developmental effects

Overall, the available studies in rodents provide *robust* evidence that DIBP causes developmental toxicity (Table 4). The strongest evidence was available from the gestational exposure studies, which found effects on survival, growth, and fetal structural alterations. One limitation is that many of the studies exposed fetuses only during the major window of male sexual differentiation (e.g. GD 14–18), which may not be the most sensitive for detecting effects on survival or on skeleton or organ system development, and there were no two-generation or continuous breeding studies available. This limits the ability to fully evaluate potential effects on the developing fetus; for instance, none of the rat studies exposed dams prior to implantation, so it was not possible to evaluate effects on preimplantation loss. Nevertheless, the targeted dosing periods are informative of developmental hazards overall, and may provide a starting point for understanding the windows of susceptibility for various outcomes in the developing fetus.

3.7. Liver effects

A figure indicating the doses at which statistically significant effects on liver weight occurred is provided in the Supplementary Materials (Fig. S13).

3.7.1. Summary of available studies

Dose-related increases in relative liver weight were observed in all studies that reported this outcome, consisting of postnatal exposure studies in male rats (Foster et al., 1982; Oishi and Hiraga, 1980b; University of Rochester, 1953, 1954), female rats (University of Rochester, 1954), and male mice (Oishi and Hiraga, 1980a, 1980d); and in weanling and adult male mice that were exposed during gestation (Wang et al., 2017). While the University of Rochester studies did not include a statistical analysis, the average magnitude of effect was large (increased by up to 84% compared to controls); and in all other cases, effects on relative liver weight were statistically significant. Statistically significant increases in absolute liver weight were also observed in some cases (Oishi and Hiraga, 1980b; Wang et al., 2017). The largest increases in liver weight were often seen at doses associated with marked growth retardation, which has the potential to exaggerate the effect of relative weight measurements; however, since the relationship between liver weight and body weight is proportional, changes in relative liver weight are considered informative of toxicity (Bailey et al., 2004). Given the consistent direction of effect across studies and two species, the evidence for effects on liver weight is considered *robust*.

Two of these studies also included a histopathological analysis (University of Rochester, 1953, 1954), and found no difference between treatment and control livers. However, these results are considered *low confidence* because of reporting limitations in these studies. Therefore, the evidence for histopathological effects in the liver is considered *indeterminate*.

Table 4
Evidence profile table for developmental effects of DIBP or MIBP
*indicates MIBP study

Developmental effects

Outcome		Available studies	Factors that increase confidence	Factors that decrease confidence	Confidence judgement for outcome	Confidence judgement for overall hazard
Gestational (F1) Exposure	**Fetal survival**	**High confidence:** BASF, 2007 Borch et al., 2006 Howdeshell et al., 2008 Saillenfait et al., 2006 Saillenfait et al., 2008 Saillenfait et al., 2017 Wang et al., 2017 **Medium confidence:** Hannas et al., 2012 Furr et al., 2014 **Low confidence:** Hannas et al., 2011	• Dose-response gradient, effect size, and minimal concern for bias in studies by Saillenfait et al., 2006 and Howdeshell et al., 2008 • Biological plausibility (support from mechanistic evidence for DBP)		⊕⊕⊕ ROBUST A dose-related increase in post-implantation loss was observed in two Sprague-Dawley rat studies that exposed animals from GD 6-20 and GD 8-18, respectively (Howdeshell et al., 2008, Saillenfait et al., 2006), but not in Wistar rats or mice exposed for a similar duration. Fetal survival was also not affected in studies that exposed Sprague-Dawley rats for shorter durations in mid- to late gestation.	⊕⊕⊕ ROBUST Based on consistent evidence of reduced fetal and postnatal growth across studies, evidence of reduced fetal survival in Sprague-Dawley rats exposed for longer durations in gestation, and slight evidence of structural alterations following gestational exposure.
	Fetal growth	**High confidence:** BASF, 2007 Borch et al., 2006 Saillenfait et al., 2006 Saillenfait et al., 2008 Saillenfait et al., 2017 **Medium confidence:** Wang et al., 2017	• Consistency • Dose-response gradient • Effect size • Minimal concern for bias		⊕⊕⊕ ROBUST A dose-related decrease in fetal body weights or body weights at birth were consistently in rats at higher dose levels, but were not observed in lower dose studies.	
	Fetal structural alterations	**High confidence:** BASF, 2007 Saillenfait et al., 2006 Saillenfait et al., 2017	• Dose-response gradient and minimal concern for bias and sensitivity in the study by Saillenfait et al., 2006	• Few studies	⊕◯◯ SLIGHT A dose-related increase in external, visceral, and skeletal malformations was reported in Sprague-Dawley rats by Saillenfait et al., 2006, but not in a similar study in Wistar rats by BASF, 2007. There were no external malformations in a lower dose study by Saillenfait et al., 2017.	
	Postnatal survival	**High confidence:** Saillenfait et al., 2008	• Minimal concern for bias	• Single study	◯◯◯ INDETERMINATE Effects on postnatal survival following gestational exposure were not observed in the single study that evaluated this outcome.	
	Postnatal growth	**High confidence:** Saillenfait et al., 2008 **Medium confidence:** Wang et al., 2017	• Dose-response gradient and minimal concern for bias in the study by Saillenfait et al., 2008	• Few studies	⊕⊕◯ MODERATE A dose-related decrease in postnatal growth was observed in rats exposed during gestation (Saillenfait et al., 2008), but not in a mouse study that tested a single, lower dose of DIBP (Wang et al., 2017).	
Postnatal (Weanling or Peripubertal) Exposure	**Postnatal growth**	**Medium confidence:** Sedha et al., 2015 **Low confidence:** Oishi and Hiraga, 1980a Oishi and Hiraga, 1980b Oishi and Hiraga, 1980c* Oishi and Hiraga, 1980d* U. Rochester, 1953 U. Rochester, 1954	• Consistency • Dose-response gradient • Effect size	• Concerns for bias and sensitivity in some studies	⊕⊕◯ MODERATE A dose-related decrease in postnatal and adult growth was observed in all available peripubertal exposure studies in rats and mice. However, in the low confidence studies, the reduced growth may have been a secondary effect related to reduced food consumption.	

3.7.2. Synthesis of results for liver effects

Change in organ weight alone has been used as a potentially sensitive indicator for toxicity from chemical exposure (Bailey et al., 2004). In the absence of histopathological changes or supporting biochemical or mechanistic evidence (e.g. changes in hepatic enzyme expression), however, the biological significance of the reported changes in liver weight is inconclusive (Hall et al., 2012). Taken together, the evidence for liver toxicity is considered *slight* (Table S1).

3.8. Kidney effects

A figure indicating the doses at which statistically significant effects on kidney weight occurred is provided in the Supplementary Materials (Fig. S14).

3.8.1. Summary of available studies

Dose-related increases in relatively kidney weight were reported in the 1- and 4-month exposure studies in male and female rats by the University of Rochester (1953, 1954), with more pronounced changes in males compared to females (University of Rochester, 1954), although the authors did not perform a statistical analysis. In contrast, the 7-day exposure studies found that relative kidney weight was statistically significantly decreased in mice exposed to DIBP (Oishi and Hiraga, 1980a), and not significantly changed in mice exposed to MIBP (Oishi and Hiraga, 1980d) or rats exposed to DIBP (Oishi and Hiraga, 1980b). In a 4-day exposure of rats to MIBP, relative kidney weight was increased by 12% compared to controls, although the effect was not significant (Foster et al., 1982). Given these inconsistencies and the limited number of studies, the overall evidence for effects on kidney weight is considered *slight*.

Two of these studies also included a histopathological analysis (University of Rochester, 1953, 1954), and found no difference between treatment and control livers. These histopathology results are considered *low confidence* because of reporting limitations in these studies. The evidence for histopathological effects in the kidney is considered *indeterminate*.

3.8.2. Synthesis of results for kidney effects

Taken together, the available evidence is inadequate to draw conclusions on the effects of DIBP on the kidney. Therefore, the evidence for kidney toxicity is considered *indeterminate* (Table S2).

3.9. Cancer

None of the available studies evaluated cancer in animals exposed to DIBP. The limited number of mutagenicity assays identified in the literature search generally had negative findings (Seed, 1982; Simmon et al., 1977; Zeiger et al., 1982), although genotoxicity assays of DIBP-treated primary human mucosal cells demonstrated DNA damage as measured by the comet assay (Kleinsasser et al., 2000a; Kleinsasser et al., 2000b; Kleinsasser et al., 2001). This was considered inadequate information to evaluate carcinogenicity; thus, the evidence for cancer is considered *indeterminate*.

4. Discussion

The results of this systematic review provide *robust* evidence that DIBP causes male reproductive and developmental toxicity and *slight* evidence for female reproductive toxicity and effects on liver, whereas evidence for effects on kidney and cancer were *indeterminate*. These results corroborate the CPSC (2014) and NAS (2017) conclusions that DIBP is a male reproductive toxic agent, with gestational exposure leading to permanent adverse effects in male offspring, and support DIBP as a children's health concern. The results also provide a reconnaissance of additional effects observed in laboratory animals after DIBP exposure, some of which may share the same mechanisms as the male reproductive effects.

Howdeshell et al. (2008) demonstrated that fetal testosterone production and fetal mortality (post-implantation loss) followed a similar dose-response relationship in rats exposed to a mixture of phthalates during gestation, and suggested that this might be because fetal T production and fetal mortality are both caused by decreased steroidogenesis (decreased testicular testosterone in male fetuses, and decreased ovarian progesterone in dams). While it has been found that DBP decreases maternal ovarian progesterone production in dams exposed at mid-pregnancy (Gray Jr et al., 2006), this has not yet been evaluated for DIBP. Gray Jr et al., 2006 hypothesized that decreased progesterone production could be mediated through decreased ovarian steroidogenesis, similar to the mechanism for decreased testicular steroidogenesis; or may result from disrupted androgen and INSL3 signaling, since those hormones contribute to maintaining the function of the corpora lutea in pregnant rats. There is also some epidemiologic evidence that DIBP is associated with decreased expression of steroidogenic enzymes in the placenta (CYP11A1, CYP19A1, CYP1B1, 17β-hydroxysteroid dehydrogenase) (Adibi et al., 2010) with a significantly stronger association in male placentas compared to female in some cases (Adibi et al., 2017), although results were inconsistent and suggested a possible non-monotonic response.

For male reproductive outcomes, the available studies suggest a sensitivity difference in mice compared to rats; however, there were relatively few mouse studies and all had some concerns for risk of bias and/or sensitivity, so it is difficult to fully delineate species sensitivity differences using the available data. Outcomes associated with the androgen-independent MOA for phthalates (e.g. atrophy of seminiferous cords, germ cell effects) were observed in both species. Conversely, while decreased T was observed in both species, mice did not consistently display the other androgen-dependent outcomes that were observed in rats (e.g. decreased testis weight and AGD). Similar observations on the relative sensitivity of mice and rats have been made for other phthalates, such as DBP. It has also been found that human xenografts (human fetal testis explants into rodents) are less sensitive than rats to the anti-androgenic effects of phthalates, suggesting an interspecies difference in sensitivity; however, the xenograft results have several factors that limit their interpretation, such as concerns about the developmental stage of the human tissues used in the experiments, and high variability in the results (Lioy et al., 2015). In the case of DIBP, results suggest that mice and rats are susceptible to both the androgen-dependent and -independent MOAs, although not all androgen-dependent biomarkers were conserved across species.

The available studies were generally not designed to evaluate female reproductive, liver, or kidney effects, so interpretation of these outcomes is limited. The few studies that evaluated female offspring following gestational exposure provide evidence of morphological effects (displaced ovaries and increased AGD), which could be caused by alterations in hormone signaling analogous to those seen in male offspring. While these observations are compelling, the implications for female fertility are unclear. Literature on the female reproductive effects of phthalates is relatively sparse. A review of phthalate effects in females reported altered steroidogenesis and ovarian function in animal studies, but effects were often inconsistent across studies and the mechanism was unclear (Kay et al., 2013). One study by Hannas et al. (2013) attempted to identify a critical window of exposure for in utero phthalate effects in the female rat, and found a statistically significant increase in vaginal and uterine agenesis in F1 females exposed to a phthalate mixture from GD 8–19; the incidence was lower after exposure from GD 8–13, and there were no female reproductive malformations after exposure from GD 14–19. One female exposed from GD 8–19 had undescended ovaries, located above the kidneys. Although the authors were not able to ascertain the critical window of exposure, they concluded that it appeared to encompass the major period of organogenesis (GD 8–13).

A concurrent systematic review of epidemiological studies of phthalates by our colleagues found *moderate* evidence of an association between DIBP exposure and reduced testosterone in adult cross-

sectional studies, but only *slight* evidence of an association with other male reproductive effects. Comparatively, DBP and several other anti-androgenic phthalates had *robust* evidence of an association with male reproductive toxicity in humans (Radke et al., 2018). Given the effects of DIBP in animal models, the low level of evidence for male reproductive toxicity in humans was likely due to the relatively small number and low sensitivity of the available epidemiological studies that evaluated DIBP exposure. Systematic review of the epidemiological literature also provided *moderate* evidence of an association between DIBP exposure and decreased birth size, and *slight* evidence for an association with preterm birth and spontaneous abortion (Radke et al., under review-a).

Epidemiological evidence also suggests that phthalate exposure may be associated with emerging health outcomes such as neurodevelopmental and metabolic toxicity, with *moderate* evidence of an association between DIBP exposure and diabetes risk, and *slight* evidence of an association with some neurodevelopmental outcomes (Radke et al., in preparation; Radke et al., under review-b). Although emerging health outcomes were not the focus of this systematic review of animal studies, we note that the literature search for DIBP identified one behavioral study (Ma et al., 2013), which reported that mice dosed with 1000 mg/kg-day DIBP via oral gavage for 8 weeks had decreased passive avoidance capability and increased apoptosis of hippocampal cells. We performed a preliminary evaluation of this study and found it to have reporting limitations that reduce confidence in the results (e.g., lack of experimental method detail to determine how memory and learning were measured in the passive avoidance test); however, it does provide suggestive evidence of neurological effects from DIBP exposure.

As a next step towards understanding the quantitative relationship between gestational DIBP exposure and phthalate syndrome in the male rat, an ordinal univariate dose-response analysis of phthalate syndrome was performed by our group using data from Saillenfait et al. (2008), in which endpoints were grouped by severity. This analysis will be available in a forthcoming publication.

This systematic review highlighted several ways in which future studies could provide further insight into the mechanisms and characterization of hazards of DIBP exposure. Most of the available studies were targeted at critical exposure windows for male reproductive toxicity, so it would be useful to design chronic or sub-chronic studies that cover critical windows of exposure for other outcomes. For instance, there are currently no one- or multi-generational reproductive toxicity studies available for DIBP; such a study would assess fertility and fecundity, and would provide a point of reference for comparing reproductive effects in animals exposed as adults versus those exposed in utero. Effects on liver, kidney, and cancer are known hazards for other phthalates, so further research is warranted to characterize these outcomes after exposure to DIBP, in addition to evaluating emerging outcomes such as neurodevelopmental toxicity. Additionally, despite the profound effects of DIBP on testosterone observed in males, data on hormone production in DIBP-exposed females was extremely limited. It would be useful to evaluate steroidogenesis and INSL3 in F1 females to provide a mechanistic understanding of how each sex is affected by gestational DIBP exposure, and to evaluate altered maternal steroidogenesis and INSL3 as a potential contributing factor to reduced fetal survival.

Acknowledgements

This manuscript is dedicated to the memory of Raghu Nath, a biologist at the EPA National Center for Environmental Assessment, who contributed to this systematic review. We would like to acknowledge Anna Chen, Evangela Matthews, Swati Gummadi, Carolyn Gigot, Mefruz Haque (EPA student services contractors), and Carol Starkey (Oak Ridge Institute for Science and Education) for their assistance in data extraction and visualization for this systematic review. We would also like to thank Earl Gray, Justin Conley, and April Luke for their comments on previous drafts of this manuscript.

Disclaimer

The views expressed are those of the authors and do not necessarily represent the views or policies of the U.S. Environmental Protection Agency.

Appendix A. Supplementary data

Supplementary data to this article can be found online at https://doi.org/10.1016/j.envint.2018.09.038.

References

Adibi, J.J., Whyatt, R.M., Hauser, R., Bhat, H.K., Davis, B.J., Calafat, A.M., et al., 2010. Transcriptional biomarkers of steroidogenesis and trophoblast differentiation in the placenta in relation to prenatal phthalate exposure. Environ. Health Perspect. 118, 291–296.

Adibi, J.J., Buckley, J.P., Lee, M.K., Williams, P.L., Just, A.C., Zhao, Y., et al., 2017. Maternal urinary phthalates and sex-specific placental mRNA levels in an urban birth cohort. Environ. Health 16, 35.

Albert, O., Jégou, B., 2014. A critical assessment of the endocrine susceptibility of the human testis to phthalates from fetal life to adulthood. Hum. Reprod. Update 20, 231–249.

Bailey, S.A., Zidell, R.H., Perry, R.W., 2004. Relationships between organ weight and body/brain weight in the rat: what is the best analytical endpoint? Toxicol. Pathol. 32, 448–466.

BASF, 2007. Diisobutylphthalate - Prenatal Developmental Toxicity Study in Wistar Rats Administration in the Diet (2007 update). Document Control Number: 86070000046. Submitted to the U.S. Environmental Protection Agency Under TSCA Section 8d.

Boberg, J., Metzdorff, S., Wortziger, R., Axelstad, M., Brokken, L., Vinggaard, A.M., et al., 2008. Impact of diisobutyl phthalate and other PPAR agonists on steroidogenesis and plasma insulin and leptin levels in fetal rats. Toxicology 250, 75–81.

Borch, J., Axelstad, M., Vinggaard, A.M., Dalgaard, M., 2006. Diisobutyl phthalate has comparable anti-androgenic effects to di-*n*-butyl phthalate in fetal rat testis. Toxicol. Lett. 163, 183–190.

Choy, I., 1975. Effects of sulfathiazole, phthalylsulfathiazole and phthalic acid esters on the development of chick embryos [translated]. Showa Igakkai Zasshi 35, 187–201.

Consumer Product Safety Commission (CPSC), 2014. Chronic Hazard Advisory Panel on Phthalates and Phthalate Alternatives (with Appendices). U.S. Consumer Product Safety Commission, Directorate for Health Sciences, Bethesda, MD.

Cooper, G., Lunn, R., Agerstrand, M., Glenn, B., Kraft, A., Luke, A., et al., 2016. Study sensitivity: evaluating the ability to detect effects in systematic reviews of chemical exposures. Environ. Int. 92-93, 605–610.

Eastman Kodak, 1954. Screening test on the toxicity of diisobutyl phthalate. In: EPA/OTS Doc #878214403. Rochester, NY.

Elsisi, A.E., Carter, D.E., Sipes, I.G., 1989. Dermal absorption of phthalate diesters in rats. Fundam. Appl. Toxicol. 12, 70–77.

Foster, P., Gray Jr.L.E. (Eds.), 2013. Toxic Responses of the Reproductive System. McGraw-Hill Education, New York, NY.

Foster, P.M., Lake, B.G., Thomas, L.V., Cook, M.W., Gangolli, S.D., 1981. Testicular effects and zinc excretion produced by various isomers of monobutyl-*o*-phthalate in the rat. Chem. Biol. Interact. 34, 233–238.

Foster, P.M.D., Lake, B.G., Cook, M.W., Thomas, L.V., Gangolli, S.D. (Eds.), 1982. Structure-Activity Requirements for the Induction of Testicular Atrophy by Butyl Phthalates in Immature Rats: Effect on Testicular Zinc Content. Plenum Press, New York, NY.

Fromme, H., Gruber, L., Seckin, E., Raab, U., Zimmermann, S., Kiranoglu, M., et al., 2011. Phthalates and their metabolites in breast milk–results from the Bavarian Monitoring of Breast Milk (BAMBI). Environ. Int. 37, 715–722.

Furr, J.R., Lambright, C.S., Wilson, V.S., Foster, P.M., Gray Jr., L.E., 2014. A short-term in vivo screen using fetal testosterone production, a key event in the phthalate adverse outcome pathway, to predict disruption of sexual differentiation. Toxicol. Sci. 140, 403–424.

Gray Jr., L.E., Laskey, J., Ostby, J., 2006. Chronic di-*n*-butyl phthalate exposure in rats reduces fertility and alters ovarian function during pregnancy in female Long-Evans hooded rats. Toxicol. Sci. 93, 189–195.

Guyatt, G., Oxman, A.D., Akl, E.A., Kunz, R., Vist, G., Brozek, J., et al., 2011. GRADE guidelines: 1. Introduction-GRADE evidence profiles and summary of findings tables. J. Clin. Epidemiol. 64, 383–394.

Hall, A.P., Elcombe, C.R., Foster, J.R., Harada, T., Kaufmann, W., Knippel, A., et al., 2012. Liver hypertrophy: a review of adaptive (adverse and non-adverse) changes–conclusions from the 3rd International ESTP Expert Workshop. Toxicol. Pathol. 40, 971–994.

Hannas, B.R., Lambright, C.S., Furr, J., Howdeshell, K.L., Wilson, V.S., Gray, L.E., 2011. Dose-response assessment of fetal testosterone production and gene expression levels in rat testes following in utero exposure to diethylhexyl phthalate, diisobutyl phthalate, diisoheptyl phthalate, and diisononyl phthalate. Toxicol. Sci. 123, 206–216.

Hannas, B.R., Lambright, C.S., Furr, J., Evans, N., Foster, P.M.D., Gray, E.L., et al., 2012. Genomic biomarkers of phthalate-induced male reproductive developmental toxicity: a targeted rt-PCR array approach for defining relative potency. Toxicol. Sci. 125, 544–557.

Hannas, B.R., Howdeshell, K.L., Furr, J., Earl Gray Jr., L., 2013. In utero phthalate effects

in the female rat: a model for MRKH syndrome. Toxicol. Lett. 223, 315–321.
Hardin, B.D., Schuler, R.L., Burg, J.R., Booth, G.M., Hazelden, K.P., Mackenzie, K.M., et al., 1987. Evaluation of 60 chemicals in a preliminary developmental toxicity test. Teratog. Carcinog. Mutagen. 7, 29–48.
Haseman, J.K., Bailer, A.J., Kodell, R.L., Morris, R., Portier, K., 2001. Statistical issues in the analysis of low-dose endocrine disruptor data. Toxicol. Sci. 61, 201–210.
Hazleton Laboratories, 1983a. Final Report. Screening of Priority Chemicals for Potential Reproductive Hazard. NIOSH/00133459. OH:NIOSH (The National Institute for Occupational Safety and Health), Cincinnati.
Hazleton Laboratories, 1983b. Screening of Priority Chemicals for Potential Reproductive Hazard (Final Report) With Attachments and Cover Sheet. TSCATS/400290, OTS0516205, Doc I.D. 86-870001624. Shell Oil Company, Houston, TX.
Hazleton Laboratories, 1992. Initial Submission: Screening of Priority Chemicals for Potential Reproductive Hazard (Final Report) With Cover Letter Dated 041492. 88920002015. U.S. Environmental Protection Agency, Washington, DC.
Higgins, J.P.T., 2011. Chapter 8: Assessing Risk of Bias in Included Studies. In: Cochrane Handbook for Systematic Reviews of Interventions Version 5.1.0. The Cochrane Collaboration (updated March 2011).
Hill, A.B., 1965. The environment and disease: association or causation? Proc. R. Soc. Med. 58, 295–300.
Hotchkiss, A.K., Rider, C.V., Blystone, C.R., Wilson, V.S., Hartig, P.C., Ankley, G.T., et al., 2008. Fifteen years after "Wingspread"—environmental endocrine disrupters and human and wildlife health: where we are today and where we need to go. Toxicol. Sci. 105, 235–259.
Howdeshell, K.L., Wilson, V.S., Furr, J., Lambright, C.R., Rider, C.V., Blystone, C.R., et al., 2008. A mixture of five phthalate esters inhibits fetal testicular testosterone production in the Sprague-Dawley rat in a cumulative, dose-additive manner. Toxicol. Sci. 105, 153–165.
HSDB, 2017. Diisobutyl Phthalate. National Library of Medicine, Bethesda, MD.
Johnson, K.J., Heger, N.E., Boekelheide, K., 2012. Of mice and men (and rats): phthalate-induced fetal testis endocrine disruption is species-dependent. Toxicol. Sci. 129, 235–248.
Kay, V.R., Chambers, C., Foster, W.G., 2013. Reproductive and developmental effects of phthalate diesters in females. Crit. Rev. Toxicol. 43, 200–219.
Kleinsasser, N.H., Kastenbauer, E.R., Weissacher, H., Muenzenrieder, R.K., Harreus, U.A., 2000a. Phthalates demonstrate genotoxicity on human mucosa of the upper aerodigestive tract. Environ. Mol. Mutagen. 35, 9–12.
Kleinsasser, N.H., Weissacher, H., Kastenbauer, E.R., Dirschedl, P., Wallner, B.C., Harreus, U.A., 2000b. Altered genotoxicity in mucosal cells of head and neck cancer patients due to environmental pollutants. Eur. Arch. Otorhinolaryngol. 257, 337–342.
Kleinsasser, N.H., Wallner, B.C., Kastenbauer, E.R., Weissacher, H., Harréus, U.A., 2001. Genotoxicity of di-butyl-phthalate and di-iso-butyl-phthalate in human lymphocytes and mucosal cells. Teratog. Carcinog. Mutagen. 21, 189–196.
Koch, H.M., Christensen, K.L.Y., Harth, V., Lorber, M., Brüning, T., 2012. Di-*n*-butyl phthalate (DnBP) and diisobutyl phthalate (DIBP) metabolism in a human volunteer after single oral doses. Arch. Toxicol. 86, 1829–1839.
Latini, G., Wittassek, M., Del Vecchio, A., Presta, G., De Felice, C., Angerer, J., 2009. Lactational exposure to phthalates in southern Italy. Environ. Int. 35, 236–239.
Lawrence, W.H., Malik, M., Turner, J.E., Singh, A.R., Autian, J., 1975. A toxicological investigation of some acute, short-term, and chronic effects of administering di-2-ethylhexyl phthalate (DEHP) and other phthalate esters. Environ. Res. 9, 1–11.
Lioy, P.J., Hauser, R., Gennings, C., Koch, H.M., Mirkes, P.E., Schwetz, B.A., et al., 2015. Assessment of phthalates/phthalate alternatives in children's toys and childcare articles: review of the report including conclusions and recommendation of the chronic Hazard advisory panel of the consumer product safety commission. J. Expo. Sci. Environ. Epidemiol. 25, 343–353.
Ma, N., Liu, S., Gao, P., Cao, P., Xu, H., 2013. Effect of diisobutyl phthalate on learning and memory behavior and apoptosis of hippocampus cells in mice [translated]. Wei Sheng Yan Jiu 42, 57–60.
Martino-Andrade, A.J., Chahoud, I., 2010. Reproductive toxicity of phthalate esters. Mol. Nutr. Food Res. 54, 148–157.
National Academy of Sciences (NAS), 2017. Application of Systematic Review Methods in an Overall Strategy for Evaluating Low-Dose Toxicity from Endocrine Active Chemicals. The National Academies Press, Washington, D.C.
National Research Council, 2008. Phthalates and Cumulative Risk Assessment: The Task Ahead. National Academies Press, Washington, DC.
Noriega, N.C., Howdeshell, K.L., Furr, J., Lambright, C.R., Wilson, V.S., Gray Jr., L.E., 2009. Pubertal administration of DEHP delays puberty, suppresses testosterone production, and inhibits reproductive tract development in male Sprague-Dawley and Long-Evans rats. Toxicol. Sci. 111, 163–178.
Oishi, S., Hiraga, K., 1980a. Effect of phthalic acid esters on mouse testes. Toxicol. Lett. 5, 413–416.
Oishi, S., Hiraga, K., 1980b. Testicular atrophy induced by phthalic acid esters: effect on testosterone and zinc concentrations. Toxicol. Appl. Pharmacol. 53, 35–41.
Oishi, S., Hiraga, K., 1980c. Testicular atrophy induced by phthalic acid monoesters: effects of zinc and testosterone concentrations. Toxicology 15, 197–202.
Oishi, S., Hiraga, K., 1980d. Effects of phthalic acid monoesters on mouse testes. Toxicol. Lett. 6, 239–242.
Radke, E., Nachman, R., Braun, J., Cooper, G., Phthalate exposure and neuropsychological and behavioral effects: a systematic review and meta-analysis of the human epidemiological evidence (in preparation).
Radke, E., Glenn, B., Braun, J., Cooper, G., Phthalate exposure and female reproductive and developmental effects: a systematic review of the human epidemiological evidence (under review-a).
Radke, E., Galizia, A., Thayer, K., Cooper, G. Phthalate exposure and metabolic effects: a systematic review of the human epidemiological evidence (under review-b).
Radke, E.G., Braun, J.M., Meeker, J.D., Cooper, GS., 2018. Phthalate exposure and male reproductive outcomes: A systematic review of the human epidemiological evidence. Environ Int. 121 (Pt 1), 764–793. https://doi.org/10.1016/j.envint.2018.07.029. Epub 2018 Oct 16.
Ray, B., D' Souza, A.S., Kumar, V., Pugazhandhi, B., D'Souza, M.R., Nayak, D., et al., 2012. Ovarian development in Wistar rat treated prenatally with single dose diisobutyl phthalate. Bratisl. Lek. Listy 113, 577–582.
Saillenfait, A.M., Sabate, J.P., Gallissot, F., 2006. Developmental toxic effects of diisobutyl phthalate, the methyl-branched analogue of di-*n*-butyl phthalate, administered by gavage to rats. Toxicol. Lett. 165, 39–46.
Saillenfait, A.M., Sabaté, J.P., Gallissot, F., 2008. Diisobutyl phthalate impairs the androgen-dependent reproductive development of the male rat. Reprod. Toxicol. 26, 107–115.
Saillenfait, A.M., Sabaté, J.P., Denis, F., Antoine, G., Robert, A., Roudot, A.C., et al., 2017. Evaluation of the effects of α-cypermethrin on fetal rat testicular steroidogenesis. Reprod. Toxicol.
Schunemann, H., Hill, S., Guyatt, G., Akl, E.A., Ahmed, F., 2011. The GRADE approach and Bradford Hill's criteria for causation. J. Epidemiol. Community Health 65, 392–395.
Sedha, S., Gautam, A.K., Verma, Y., Ahmad, R., Kumar, S., 2015. Determination of in vivo estrogenic potential of di-isobutyl phthalate (DIBP) and di-isononyl phthalate (DINP) in rats. Environ. Sci. Pollut. Res. Int. 22, 18197–18202.
Seed, J.L., 1982. Mutagenic activity of phthalate esters in bacterial liquid suspension assays. Environ. Health Perspect. 45, 111–114.
Simmon, V.F., Kauhanen, K., Tardiff, R.G. (Eds.), 1977. Mutagenic Activity of Chemicals Identified in Drinking Water. Elsevier/North Holland Press, New York, NY.
Singh, A.R., Lawrence, W.H., Autian, J., 1972. Teratogenicity of phthalate esters in rats. J. Pharm. Sci. 61, 51–55.
Sohn, J., Kim, S., Koschorreck, J., Kho, Y., Choi, K., 2016. Alteration of sex hormone levels and steroidogenic pathway by several low molecular weight phthalates and their metabolites in male zebrafish (*Danio rerio*) and/or human adrenal cell (H295R) line. J. Hazard. Mater. 320, 45–54.
Strucinski, P., Goralczyk, K., Ludwicki, J.K., Czaja, K., Hernik, A., Korcz, W., 2006. Levels of selected organochlorine insecticides, polychlorinated biphenyls, phthalates and perfluorinated aliphatic substances in blood. Rocz. Panstw. Zakl. Hig. 57, 99–112.
University of Rochester, 1953. One month feeding tests of di-isobutyl phthalate with cover letter. In: EPA/OTS Doc #878212229. University of Rochester School of Medicine and Dentistry, Rochester, NY.
University of Rochester, 1954. Preliminary acute toxicity tests and short term feeding tests of rats and dogs given di-isobutyl phthalate and di-butyl phthalate. In: EPA/OTS Doc #878210833. University of Rochester School of Medicine and Dentistry, Rochester, NY.
US EPA, 1988. Recommendations for and documentation of biological values for use in risk assessment. In: EPA/600/6-87/008. U.S. Environmental Protection Agency, Office of Research and Development, Office of Health and Environmental Assessment, Cincinnati, OH.
US EPA, 1991. Guidelines for developmental toxicity risk assessment. In: EPA/600/FR-91/001. U.S. Environmental Protection Agency, Risk Assessment Forum, Washington, DC.
US EPA, 2006. A framework for assessing health risk of environmental exposures to children. In: EPA/600/R-05/093F. U.S. Environmental Protection Agency, Office of Research and Development, National Center for Environmental Assessment, Washington, DC.
US EPA, 2007. Integrated Summary Report for Validation of a Test Method for Assessment of Pubertal Development and Thyroid Function in Juvenile Male Rats as a Potential Screen in the Endocrine Disruptor Screening Program Tier-1 Battery. U.S. Environmental Protection Agency Office of Science Coordination and Policy and Office of Research and Development, Washington, D.C.
Wang, X., Sheng, N., Cui, R., Zhang, H., Wang, J., Dai, J., 2017. Gestational and lactational exposure to di-isobutyl phthalate via diet in maternal mice decreases testosterone levels in male offspring. Chemosphere 172, 260–267.
Wittassek, M., Wiesmuller, G.A., Koch, H.M., Eckard, R., Dobler, L., Muller, J., et al., 2007. Internal phthalate exposure over the last two decades–a retrospective human biomonitoring study. Int. J. Hyg. Environ. Health 210, 319–333.
Wittassek, M., Angerer, J., Kolossa-Gehring, M., Schafer, S.D., Klockenbusch, W., Dobler, L., et al., 2009. Fetal exposure to phthalates-a pilot study. Int. J. Hyg. Environ. Health 212, 492–498.
Wormuth, M., Scheringer, M., Vollenweider, M., Hungerbuhler, K., 2006. What are the sources of exposure to eight frequently used phthalic acid esters in Europeans? Risk Anal. 26, 803–824.
Zeiger, E., Haworth, S., Speck, W., Mortelmans, K., 1982. Phthalate ester testing in the National Toxicology Program's environmental mutagenesis test development program. Environ. Health Perspect. 45, 99–101.
Zhu, X.B., Tay, T.W., Andriana, B.B., Alam, M.S., Choi, E.K., Tsunekawa, N., et al., 2010. Effects of di-iso-butyl phthalate on testes of prepubertal rats and mice. Okajimas Folia Anat. Jpn. 86, 129–136.
Zota, A.R., Calafat, A.M., Woodruff, T.J., 2014. Temporal trends in phthalate exposures: findings from the National Health and Nutrition Examination Survey, 2001–2010. Environ. Health Perspect. 122, 235–241.

Environment International 134 (2020) 105287

Contents lists available at ScienceDirect

Environment International

journal homepage: www.elsevier.com/locate/envint

Ordinal dose-response modeling approach for the phthalate syndrome

Todd D. Blessinger[a,d,*], Susan Y. Euling[b,d], Lily Wang[e], Karen A. Hogan[a,d], Christine Cai[a,d], Gary Klinefelter[c,d], Anne-Marie Saillenfait[f]

[a] Center for Public Health and Environmental Assessment (CPHEA), Mail code 8623R, USA
[b] Office of Children's Health Protection (OCHP), Mail code 1107T, USA
[c] National Health and Environmental Effects Research Lab (NHEERL), USA
[d] United States (US) Environmental Protection Agency, Washington, DC 20460, USA
[e] CPHEA, US Environmental Protection Agency, Mail code B243-01, Research Triangle Park, NC 27711, USA
[f] Institut National de Recherche et de Sécurité, Vandoeuvre, France

ARTICLE INFO

Editor: Adrian Covaci

Keywords:
Phthalate syndrome
Ordinal data analysis
Dose-response modeling
Male reproductive development
Nested model
Diisobutyl phthalate

ABSTRACT

Background: The phthalate syndrome (PS) is a collection of related male reproductive developmental effects, ranging in severity, that have been observed in rats after gestational exposure to developmentally-toxic phthalates. For statistical purposes, the PS is defined as a single endpoint and one dose-response analysis is conducted, rather than conducting multiple analyses on each individual endpoint.
Objective: To improve dose-response modeling approaches for the PS and other syndromes of effects by accounting for differing severity levels among the endpoints.
Methods: Ordinal dose-response modeling was performed on PS data from a published study of diisobutyl phthalate (DIBP) gestational exposure to male Sprague-Dawley rats. To incorporate PS endpoint severity, the endpoints were categorized into ordinal levels based on the expected impact of male developmental endpoint's on fertility. Then, a benchmark dose was estimated for each ordinal level. A bootstrap procedure was used to account for the nested nature of the data, and a sensitivity analysis was performed to assess the bootstrap results. A comparison of the estimates between the ordinal and the dichotomous model was performed.
Results: The ordinal version of the log-logistic model applied to the data categorized by PS endpoint severity level provided benchmark dose estimates that were closer to each other in value and had lower variability than the traditional dichotomous application. The sensitivity analysis confirmed the validity of the bootstrap results.
Conclusion: The ordinal dose-response modeling method accounts for severity differences among dichotomous PS endpoints, can be expanded in the future to include more severity levels, and can be used in both single and cumulative phthalate risk assessments.

1. Introduction

Phthalates esters (referred to as "phthalates") are used as plasticizers and additives for PVC products, nitrocellulose, and concrete (US EPA, 2015). As a result of these uses, phthalate are found in numerous consumer products such as nail polish, makeup, and carpets (US EPA, 2015). Exposure to developmentally toxic phthalates, phthalates with three to seven (or eight) carbon atoms in the backbone of the alkyl side chain, can lead to developmental effects (CPSC, 2014). These phthalates include di-*n*-pentyl (DPENP) (diamyl phthalate), butylbenzyl (BBP), dibutyl (DBP), diisobutyl (DIBP), dihexyl (DHEXP), di(2-ethylhexyl) (DEHP), dicyclohexyl (DCHP), and diisononyl (DINP) (US CPSC, 2014). Further, the human population, including pregnant women, are exposed to multiple phthalates (Koch et al., 2017; Zota et al., 2014; Wittassek et al., 2009; Ye et al., 2008). Therefore, developmentally toxic phthalates are chemicals of concern for children because of the combination of increased cumulative phthalate exposure levels and increased susceptibility during a critical window of development is expected to lead to a greater risk.

Gestational exposure to one or more developmentally toxic phthalates can lead to a set of male reproductive developmental health effects collectively called the phthalate syndrome (PS) in rats (reviewed in Foster, 2006; Fisher et al., 2003; Foster et al., 2001). The phthalate syndrome is characterized by malformations of male reproductive organs (e.g., epididymis, vas deferens, seminal vesicles, prostate, and external genitalia) such as hypospadias and cryptorchidism and

* Corresponding author at: United States (US) Environmental Protection Agency, Washington, DC 20460, USA.
E-mail address: blessinger.todd@epa.gov (T.D. Blessinger).

https://doi.org/10.1016/j.envint.2019.105287
Received 25 May 2019; Received in revised form 17 September 2019; Accepted 23 October 2019
Available online 26 November 2019
0160-4120/ Published by Elsevier Ltd. This is an open access article under the CC BY license (http://creativecommons.org/licenses/BY/4.0/).

developmental effects such as retention of nipples/areolae (sexually dimorphic structures in rodents) and lack of masculinization of the perineum during development, leading to a reduced anogenital distance (AGD) (US CPSC, 2014). The more severe PS endpoints of the male reproductive tract (i.e., malformations) are observed at higher phthalate doses whereas changes in AGD and nipple/areolae retention can be observed at lower phthalate doses as well. Critical windows of exposure for the PS have been defined in rat studies. Gestation is the most sensitive, neonatal and peripubertal exposure is less sensitive, and adulthood is the least sensitive window of exposure (US CPSC, 2014). The modes of action for the PS effects observed in rats after gestational phthalate exposure are due to a decrease in fetal testicular androgens, decreased INSL3 signaling, and fetal germ cell developmental effects (e.g., multinucleated gonocytes) that have not been defined at the molecular level (Makris et al., 2013; van den Driesche et al., 2015; Boekelheide et al., 2009; Howdeshell et al., 2017).

In response to evidence that humans are exposed to multiple phthalates, the National Academy of Sciences convened experts to provide recommendations regarding cumulative risk, resulting in the *Phthalates and Cumulative Risk Assessment* report (NRC, 2008). The committee recommended that a cumulative risk assessment be performed using an approach that evaluates common adverse effects from exposure to phthalates as well as to other chemicals that affect androgen activity. In 2008, Congress banned children's toys and child care articles containing more than 0.1% of DEHP, DBP, and BBP. The U.S. Consumer Product Safety Commission (CPSC)'s Chronic Hazard Advisory Panel (CHAP) on Phthalates and Phthalate Alternatives developed a risk assessment for eight developmentally toxic phthalates (US CPSC, 2014; Review by Lioy et al., 2015), leading to a ban on children's toys and child care articles containing more than 0.1% of five additional phthalates (DINP, DPENP, DHEXP, DCHP, and DIBP). In 2014, EPA added seven phthalates that are still in commerce to their Toxic Substances Control Act (TSCA) Work Plan List for Chemical Assessments list (US EPA, 2014) to determine whether any additional assessment is needed with regard to TSCA-specific uses or exposure scenarios.

There have been efforts to perform dose-response modeling by defining the PS as a single endpoint, as opposed to modeling each individual endpoint separately. In this approach, PS animals are defined as those exhibiting none vs. one or more PS endpoints. In one such evaluation of the PS data after perinatal (part of gestation and part of lactation) di(2-ethylhexyl)phthalate (DEHP) exposure to rats, Gray et al. (2009) designated an animal as having the PS if it had at least one of the PS effects, and found a statistically significant increase in the PS at doses ranging from 11 to 300 mg/kg-day. However, modeling data as dichotomous does not account for differences in severity that exist among PS effects. For example, the consequence of some malformations (e.g., hypospadias, undescended testis) can lead to abnormal reproductive function, impacting fertility. By contrast, other PS endpoints lead to abnormal developmental effects (e.g., retained areolas or nipples) that do not have anticipated impacts on fertility. Therefore, an analysis that incorporates these differences is preferred.

Dose-response modeling of ordinal outcomes has been applied in some recent cases, for example, using U.S. EPA's CatReg software (see, for example, Krewski et al., 2010). In these analyses, CatReg was applied as a meta-analysis in which results from multiple endpoints, often observed across multiple studies, were assigned severity scores based on expert judgement of biological severity and the scores were combined into a single analysis. Chen and Chen (2014) proposed a method to assign ordinal levels based on a latent continuous variable. In addition, the NRC *Phthalates and Cumulative Risk Assessment* report (NRC, 2008; App D) conducted an analysis in which five continuous PS endpoints that are shared between antiandrogen and phthalate chemicals were modeled as part of an antiandrogen chemical cumulative risk assessment case study. The observed responses of five selected endpoints were transformed based on the desirability of response, as determined using consensus expert opinion, and then combined into a unitless score on the interval from 0 to 1, which was analyzed as a continuous, rather than dichotomous, endpoint.

For the analysis presented here, a straightforward extension of the dichotomous log-logistic model to the ordinal case was applied to the individual animal data from a study in which multiple PS endpoints were assessed in male Sprague-Dawley rats exposed to DIBP during gestation (Saillenfait et al., 2008). The ordinal scale was defined by designating two levels of severity for PS endpoints based on knowledge about its relationship to male fertility.

In risk assessment, development of human health risk values, such as reference doses (RfDs) used by EPA, involves the fitting of dose-response models suited to the data type, as well as selection of a low level of response (benchmark response, or BMR) that supports identifying an exposure level (i.e., a benchmark dose, or BMD) that is health protective. Often, the lower confidence bound on the BMD, called the BMDL, is used as a point of departure (POD), which is divided by a series of uncertainty factors to determine a RfD (U.S. EPA, 2002, 2012). When conducting dose-response modeling to develop a risk value for a dichotomous endpoint, a BMD is estimated at only one BMR. However, for the phthalate syndrome, the range of biological significance across the spectrum of different severity PS endpoints supports the development of different BMRs based on the anticipated severity level. Therefore, the BMDs for the two ordinal levels were estimated at different BMRs. The results from the ordinal analysis were then compared with those from dichotomous characterizations of the same data.

2. Materials and methods

2.1. Individual animal PS dataset

The timing of DIBP exposure and endpoint assessment for the Saillenfait et al. (2008) study design are illustrated in Fig. 1. Additional details about the study design, animals, the DIBP and control dose groups, and endpoint assessment methods can be found in Saillenfait et al. (2008). In this study, males were exposed from gestation days (GD) 12–21 by gavage to DIBP and were then sacrificed and necropsied at one of two adult ages, either postnatal day (PND) 76–86 (~postnatal week 11–12, PNW, two males in each litter) or on PND 111–122 (~PNW 16–17, the remaining males in each litter), and were examined for the following endpoints –

- Nipple and areola retention
- Gross abnormalities of external and internal genitalia
- Testes descent
- Histopathological lesions in the testes and epididymis (on either PND 76-86 or on PND 111–122)
- Male reproductive organ weights

Individual animal data from Saillenfait et al. (2008) were provided by the study director, Dr. Saillenfait (co-author). These summary data were reported on a per-litter basis by treatment group in the published article.

2.2. Development of ordinal scale

PS endpoints that were measured as continuous variables, such as anogenital distance (AGD), age of preputial separation (PPS), and male reproductive organ weight decreases, but had no clinical or biological method for assigning ordinal level categories were not included in this analysis. The PS endpoints that were measured as dichotomous variables were therefore included in this analysis. Then, among the dichotomous PS endpoints, they can be characterized as a collection of permanent male reproductive developmental endpoints that are associated with either zero to moderate expected impacts on fertility (level 1), or are associated with severe infertility (level 2). It is important to note that male fertility was not assessed in the Saillenfait et al. (2008) study; sperm quality, sperm quantity, and mating endpoints were not included. Instead, information

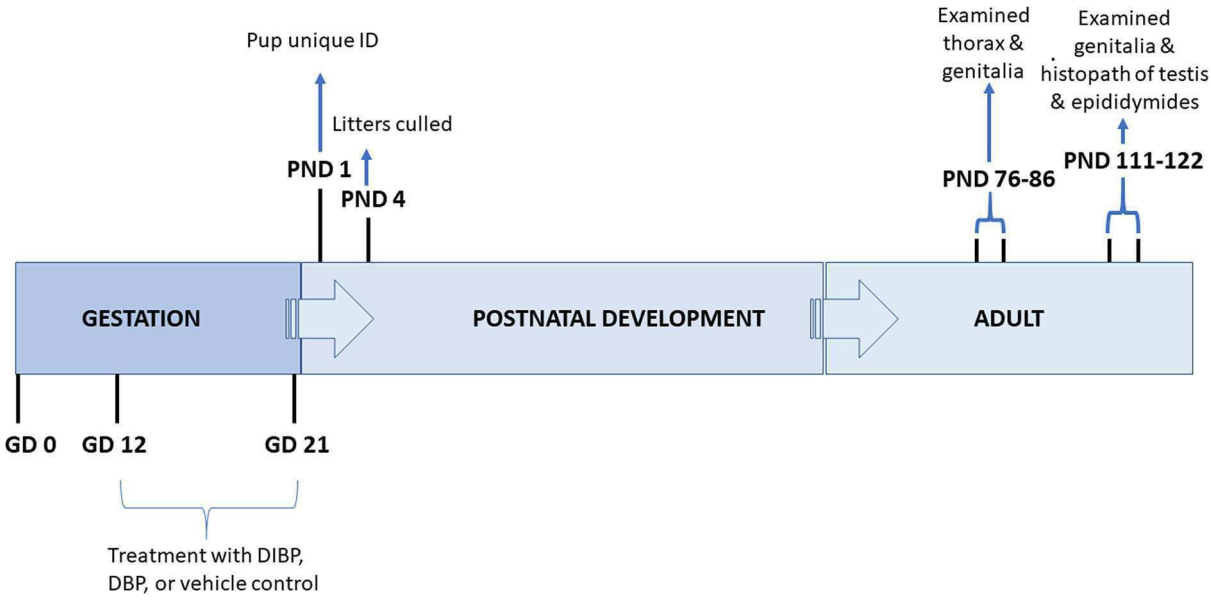

Fig. 1. Illustration of the temporal aspects of the dosing and phthalate syndrome endpoint evaluation in the Saillenfait et al. (2008) study. The figure is limited to the phthalate syndrome endpoints included in this univariate analysis. Sacrificed adult males were shaved and the ventral surface of the thorax was examined for the presence of areolas and/or nipples. The external and internal genitalia were examined for gross abnormalities and for the position of testes. Histopathology was conducted on testes and epididymides. In the Saillenfait et al. (2008) study, Sprague-Dawley female rats were mated to adult male rats of the same strain and from the same supplier. The day that vaginal smears were sperm positive was designated as gestation day 0 (GD 0). Pregnant females were randomly assigned to treatment groups based on body weight at GD 0. Pregnant females were treated once a day with either vehicle alone (olive oil), 500 mg/kg/day DBP, 125 mg/kg/day DIBP, 250 mg/kg/day DIBP, 500 mg/kg/day DIBP, or 625 mg/kg/day DIBP by gavage on GD 12–21. The number of dams per treatment group was 10–14. Postnatal day (PND) 0 was defined as the day of parturition. On PND 4, litters were culled to 10 pups, keeping as many males as possible. Litters with less than 8 pups were not maintained. See Saillenfait et al. (2008) for the numbers of animals and specific endpoints assessed at each life stage. Arrows with vertical bars indicate transitions between three lifestages: gestation, postnatal development, and adulthood. Note that the scale of time is not consistent across the three lifestages.

from experts and the published literature about associations between male organ histopathological endpoints and infertility was utilized. Infertility is a severe effect because a lack of offspring is equivalent to mortality in the next generation. In order to designate an endpoint according to its expected impact on fertility, as delineated above, the expert judgment of toxicologists was used. The ordinal level binning decisions were based on discussions with experts in male development and reproductive toxicology, Gary Klinefelter (co-author), Anne-Marie Saillenfait (co-author), and NCEA's Reproductive and Developmental Toxicity and Neurotoxicity Workgroup, and these decisions are consistent with recommendations of toxicological pathologists (Lanning et al., 2002). The expert evaluation excluded three male reproductive histopathology endpoints, amorphous crystalline material, distorted tubules, and dilated tubule lumen, based on knowledge that sometimes these endpoints may not necessarily be treatment-related (e.g., poor fixation). Therefore, the six animals that exhibited these three endpoints and no other PS endpoints were designated as not having the PS.

For the purposes of this analysis, the PS was defined as an ordinal outcome with one of three separate levels, as follows:

- Level 0: The animal has no PS endpoints (i.e., no male reproductive developmental effects and no male reproductive organ histopathological effects of score 2–5).
- Level 1: The animal has one or more PS endpoints that are associated with zero to moderate expected impacts on fertility, but has no PS endpoints associated with severe impacts on fertility, based on expert judgement.
- Level 2: The animal has one or more PS endpoints that are associated with severe infertility, based on expert judgement.

Animals sacrificed at PNW 11–12 were included in the analysis because all had histopathology examination data (Table 5, Saillenfait et al., 2008) that had gone through peer review of that article. In contrast, animals sacrificed at PNW 16–17 animals were not included because a smaller sample size was assessed for histopathology than the PNW 11–12 group and because the PNW 16–17 histopathology data was not all reported in the Saillenfait et al. (2008) article and therefore did not undergo peer review. To confirm the influence of the histopathological endpoints on the PS levels, the proportion of animals sacrificed at PNW 11–12 whose PS ordinal level classification was increased by the inclusion of histopathology endpoints was calculated, for each dose group.

In order to compare the results of the ordinal method to a dichotomous PS modeling method, the PS was modeled as a single dichotomous endpoint with two different definitions for PS response:

- Any PS: an animal was designated as PS if it had one or more PS endpoints, regardless of severity (analogous to combining levels 1 and 2).
- Severe PS: an animal was designated as PS if it had at least one PS endpoint that is associated with severe infertility (analogous to using only level 2).

2.3. Benchmark response selection to estimate benchmark doses

Among other considerations, BMR selections should generally identify levels of minimal biological significance, with a different BMR corresponding to each ordinal level to address the difference in severity among the PS endpoints. For demonstration purposes, BMRs of 5% and 1% extra risk were selected for ordinal levels 1 (developmental effects associated with zero to moderate anticipated impacts on fertility) and 2 (associated with a severe infertility), respectively, based partly on EPA recommendations regarding biological considerations for determining reference values (US EPA, 2012).

3. Theory and calculation

A log-logistic model was used to model the cumulative probability that the PS level was at least as high as the one observed. That is, for

observed ordinal PS level Y, dose x, and level j for $j = 1, 2$, the cumulative probability was defined as

$$P[Y \geq j|x] = \gamma_j + \frac{1 - \gamma_j}{1 + \exp[-\log(\nu/(1-\nu)) + \beta(\theta_{\nu,j} - \log x)]}, \quad (1)$$

where ν = BMR, $\theta_{\nu,j} = \log(\text{BMD}_j)$ at BMR ν, β = slope, and γ_j = background response rate. This model was chosen because it exhibits greater flexibility in model fitting than some other models such as the logistic. The model form in Eq. (1) does not use the more common intercept-slope parameterization, which is used in EPA's Benchmark Dose Software (BMDS), but instead incorporates the log-BMD as an explicit parameter for ease of estimating the BMD. The relationship between the two model forms is described in more detail in Appendix A. Also observe that the slope was assumed to be constant across levels to maintain monotonicity of the cumulative probability per dose across levels.

The BMDs of interest in this application are the level 1 BMD_{05}, $\theta_{05,1}$, and the level 2 BMD_{01}, $\theta_{01,2}$. Model parameters were estimated using $\nu = 0.01$, so the BMD parameters were estimated initially as $\theta_{01,1}$ and $\theta_{01,2}$. Then $\theta_{05,1}$ was estimated using the relationship

$$\theta_{05,1} = \theta_{01,1} + \frac{c}{\beta}, \quad (2)$$

where $c = \log\left(\frac{0.05/0.95}{0.01/0.99}\right)$. The derivation of this relationship is provided in Appendix A.

As discussed in Section 2.3, the model defined in (1) assumes that the observations are independent, but, in reality, intra-litter correlation exist. Therefore, litter should be included in the model as a random effect because the set of litters that comprises the sample is a random selection from the population of litters. Several mixed model methods exist for modeling ordinal outcomes in the presence of random effects, but they generally require a sufficiently large number of animals per random observation (e.g., EPA's CatReg software, which uses Wald-type estimates). Only two animals per litter (those sacrificed at PNW 11-12) were included in the analysis, so the litters were not large enough to support using these methods. Therefore, a bootstrap resampling method was used instead.

Bootstrap resampling is a method of estimating parameters in which a large number of samples are selected with replacement from the original sample, and a parameter estimate is derived for each resample (see, for example, Efron and Tibshirani, 1994). The PS dataset consists of a two-level nested design, with animal nested within litter and litter treated as a random effect, so it was necessary to use a method of selecting samples that incorporates this design. Van der Leeden et al. (2007) presents three such methods with varying degrees of assumptions. The first two methods require restrictive assumptions on the analysis, such as a linear relationship between the response and model effects, which do not apply to our case. Therefore, the third method, called the "cases bootstrap," was considered most applicable. Under this method, a large number of samples were selected with replacement from the original PS dataset in the following manner. Assuming that there were n_i litters exposed to each dose x_i, for each bootstrap iteration samples were selected by 1) selecting n_i litters with replacement from the set of litters exposed to dose x_i, and 2) for each of the litters selected in the first step, selecting 2 animals with replacement from that litter. Then, the model in (1) was fit to each bootstrap sample and estimates of the parameters computed, including an estimate of log(BMD). These steps were repeated B times (in this case, B = 10,000) to yield B samples and log(BMD) estimates, from which summary statistics such as the mean, standard deviation, and relevant percentiles were computed. The cases bootstrap procedure is described in more detail in Appendix B.

This bootstrap procedure is analogous to fitting the model defined by Eq. (1), where for each level j and dose group i the parameter θ_j is replaced with $\theta_j + u_{k(i)}$, where $u_{k(i)}$ is the random effect of the kth litter nested within the ith dose group, $i = 1, \cdots, n_i$. The selection of the bootstrap samples was done in SAS version 9.4, and the analysis was conducted in SAS Proc NLMIXED. The SAS code and description are provided at Dataset (2019).

Upon fitting the dose-response model to the bootstrap samples, simultaneous confidence intervals for the level 1 BMD_{05} and level 2 BMD_{01} were computed using an adjusted percentile method developed by Mandel and Betensky (2008). Details of this method are provided in Appendix B. The confidence intervals derived from this method have simultaneous coverage of their respective BMDs. Thus, for example, the probability that the 90% confidence intervals for the level 1 BMD_{05} and level 2 BMD_{01} *both* contain their respective parameters is at least 90%. In addition to the Mandel & Betensky intervals, the Bonferroni-adjusted confidence intervals were computed for comparison because the Bonferroni method generally is the most conservative adjustment method, yielding the widest possible simultaneous confidence intervals; thus, it provides a good measure of the most extreme case. Also, the non-simultaneous ("unadjusted") confidence intervals were computed to demonstrate the narrowest possible intervals.

Because the litter sizes were so small, some sensitivity bootstrap analyses were conducted to assess the adequacy of the nested model bootstrap method used and determine if the effect of litter was discernible in the results. In one analysis, the bootstrap method was applied to the original PS dataset disregarding litter. More specifically, a large number of samples (B = 10,000) were selected with replacement from the PS dataset without regard to litter assignment, and the model in (1) was fit to each of these bootstrap samples and parameter estimates computed. In a second analysis, three permutations of the original PS dataset were selected with animals randomly assigned to litters, and the bootstrap analysis with the litter effect included was applied to each permuted sample. The results of these two analyses were compared to the original analysis results. In addition, to demonstrate the application of the model, the model in (1) was applied to the original PS dataset without regard to litter and with no resampling, and the model was fit and parameters estimated using normal-based methods. The equality of slopes across levels was tested in this analysis using an F-test, and the adequacy of the model was tested using a chi-square test.

For comparison to the ordinal dose-response results, a dichotomous dose-response analysis was conducted using the dichotomous PS definitions described in Section 2.2. The modeling was conducted in BMDS version 2.7 using the nested logistic model to incorporate the nested litter design (U.S. EPA, 2016; Allen et al., 1994; Kupper et al., 1986). For each analysis, the model was fit both with and without the dam weight measured immediately prior to dosing included as a covariate, and litter correlations were estimated. The model fit that yielded the lowest AIC value was selected for BMD estimation. In addition, to compare the ordinal PS results to the results from more traditional dose-response methods, selected individual PS endpoints were modeled using this dichotomous analysis.

4. Results

4.1. Groupings of PS endpoints into ordinal levels

The PS endpoints reported by Saillenfait et al. (2008) and included in this analysis (Table 1) were classified according to their developmental effects and their expected associations with fertility, either characterized as zero to moderate anticipated impacts (level 1) or severe impacts (level 2), based on expert input (see Section 2.2). For example, areola/nipple retention is a marker for decreased androgen activity following gestational exposure but is not associated with decreased fertility in adults.

Application of the ordinal PS classifications in Table 1 to the developmental reproductive data for male offspring evaluated at PNW 11–12 is summarized in Table 2. Incidence of the PS (levels 1 and 2 combined) increased in a dose-related manner from 0% in the control to 100% in the highest dose group (625 mg/kg-day), and incidence of PS level 2 increased up to 85% in the highest dose group.

The ordinal level was changed by including histopathology endpoints for 14 out of 114 animals (12%) sacrificed at PNW 11–12. Eleven

Table 1
Proposed severity classifications for PS endpoints reported in Saillenfait et al. (2008), based on the expected impact on fertility (see Materials and Methods for details).

Level 1	Level 2
Male developmental reproductive effects	
• Areola/nipple Retention	• Cleft prepuce • Hypospadias (mild, moderate, or severe) • Exposed os penis • Undescended testes (left, right, or both) • Small penis • Vaginal pouch • Prostate absent • Seminal vesicles abnormal
Epididymis histopathology[a]	
• Interstitial mononuclear cells: grade 2–5 • Oligospermia: grade 2–4 • Grade 5 oligospermia, unilateral (i.e., in only one epid), w/o azoospermia in other epididymis; or azoospermia, unilateral, w/o grade 5 oligospermia in other epididymis • Sloughed cells (caput, cauda, or corpus): grade 2–5 • Granulomatous inflammation: grade 2–4[b] • Tubular necrosis: grade 2–5	• Bilateral grade 5 oligospermia or azoospermia
Testis histopathology[a]	
• Interstitial cell hyperplasia: grade 2-4[b] • Tubular necrosis/mineralization: grade 2–5 • Tubular vacuolation/loss of germ cells: grade 2–4[b] • Seminiferous tubule degeneration-atrophy/hypoplasia: grade 2–4 • Seminiferous tubule degeneration-atrophy/hypoplasia: grade 5 in one testis, grade 1–4 or not present in other testis • Loss of seminiferous tubules: grade 2–4[b]	• Seminiferous tubular degeneration-atrophy/hypoplasia: grade 5 in both testes

[a] Unless otherwise indicated, an animal was designated as having the level 1 endpoint if either side (left or right) had the endpoint.
[b] No animals had grade 5 granulomatous inflammation, grade 2–5 interstitial fibrosis, or grade 5 interstitial cell hyperplasia, tubular vacuolation, or loss of seminiferous tubules.

(11), 2, and 1 animals had levels that increased from 0 to 1, 0 to 2, and 1 to 2, respectively, due to the presence of histopathology endpoints, the most common of these being azoospermia, oligospermia, sloughed cells, and seminiferous tubule degeneration-atrophy/hypoplasia (a list of these animals is provided in Appendix C). The 250 and 500 mg/kg-day groups had more of these animals than the 125 and 625 mg/kg-day groups, probably because the middle dose groups had a more even spread across the ordinal levels than the extreme dose groups. The percent of animals with increased PS levels was considered non-negligible, so it was determined that the histopathology endpoints had a significant influence on the PS level assignments. Thus, the PNW 16–17-sacrificed animals were excluded from the analysis.

4.2. Dose-response analysis of ordinal PS dataset

4.2.1. Litter effect excluded

From the analysis of the ordinal dataset with litter effect excluded, the model exhibited an adequate fit to the data (Table 3; p = 0.213), and the slope was significantly greater than zero (p = 0.009), indicating a significant dose-response relationship. A visual inspection of the fit overlaid on the scatterplot of the dose-response data (Fig. 2ab) also indicates a strong dose-response relationship; the residual plots (Fig. 2cd) also confirm the appropriateness of the log-logistic model for this dataset.

The estimates and SEs of the level 1 BMD_{05} and level 2 BMD_{01} from this analysis and their SEs were similar in magnitude (Table 4, denoted "normal-based"), with the level 2 BMD_{01} being slightly higher than the level 1 BMD_{05}. Although the level 2 BMD_{01} had slightly wider unadjusted and Bonferroni-adjusted confidence intervals (Table 4, denoted "normal-based"), mostly at the high end, the intervals were not especially different in width.

Table 2
Incidence of ordinal PS among male offspring evaluated at PNW 11–12 for each dose group (Saillenfait et al., 2008).

Dose (mg/kg-d[a])	Total Litters Examined	Total Males Examined	Incidence[b]			
			Level 0	Level 1	Level 2	Levels 1 & 2
0	12	24	24 (100%)	0 (0%)	0 (0%)	0 (0%)
125	10	20	18 (90%)	1 (5%)	1 (5%)	2 (10%)
250	14	28	21 (75%)	6 (21%)	1 (4%)	7 (75%)
500	11	22	5 (23%)	9 (41%)	8 (36%)	17 (77%)
625	10	20	0 (0%)	3 (15%)	17 (85%)	20 (100%)

[a] "mg/kg-d" = mg/kg-day.
[b] Ordinal levels 0, 1, and 2 are described in Section 2.2.

4.2.2. Bootstrap analysis

The level 1 BMD_{05} and level 2 BMD_{01} estimates from the 10,000 bootstrap runs (Table 4, labeled "bootstrap") were higher than their

Table 3
Parameter estimates and standard errors (SEs) from fitting model (1) to the ordinal PS dataset, excluding the litter effect.[a]

Parameter	Estimate	Standard Error (SE)
Level 1 background response rate (γ_1)	0.0320	0.0370
Level 2 background response rate (γ_2)	0.0168	0.0180
Slope (β)[b]	4.59	1.11
log(BMD_{05}) for level 1 ($\theta_{05,1}$)	5.17	0.217
log(BMD_{01}) for level 2 ($\theta_{01,2}$)	5.23	0.250

[a] The model fit adequately according to chi-square goodness-of-fit test: $\chi^2_5 = 7.10$, p-value = 0.213 (details in Appendix A). In addition, scatterplots of cumulative incidence rates for levels 1 and 2, with the estimated curve overlayed on each (Fig. 2ab), and residual plots of the estimated curves for the two cumulative incidence rates (Fig. 2cd) indicate adequate model fit.
[b] The slope was statistically significantly greater than zero (t = 4.15; p-value = 0.009). In addition, an F-test on the equality of the slopes yielded a non-significant result ($F_{1,4} = 2.86$; p-value = 0.166).

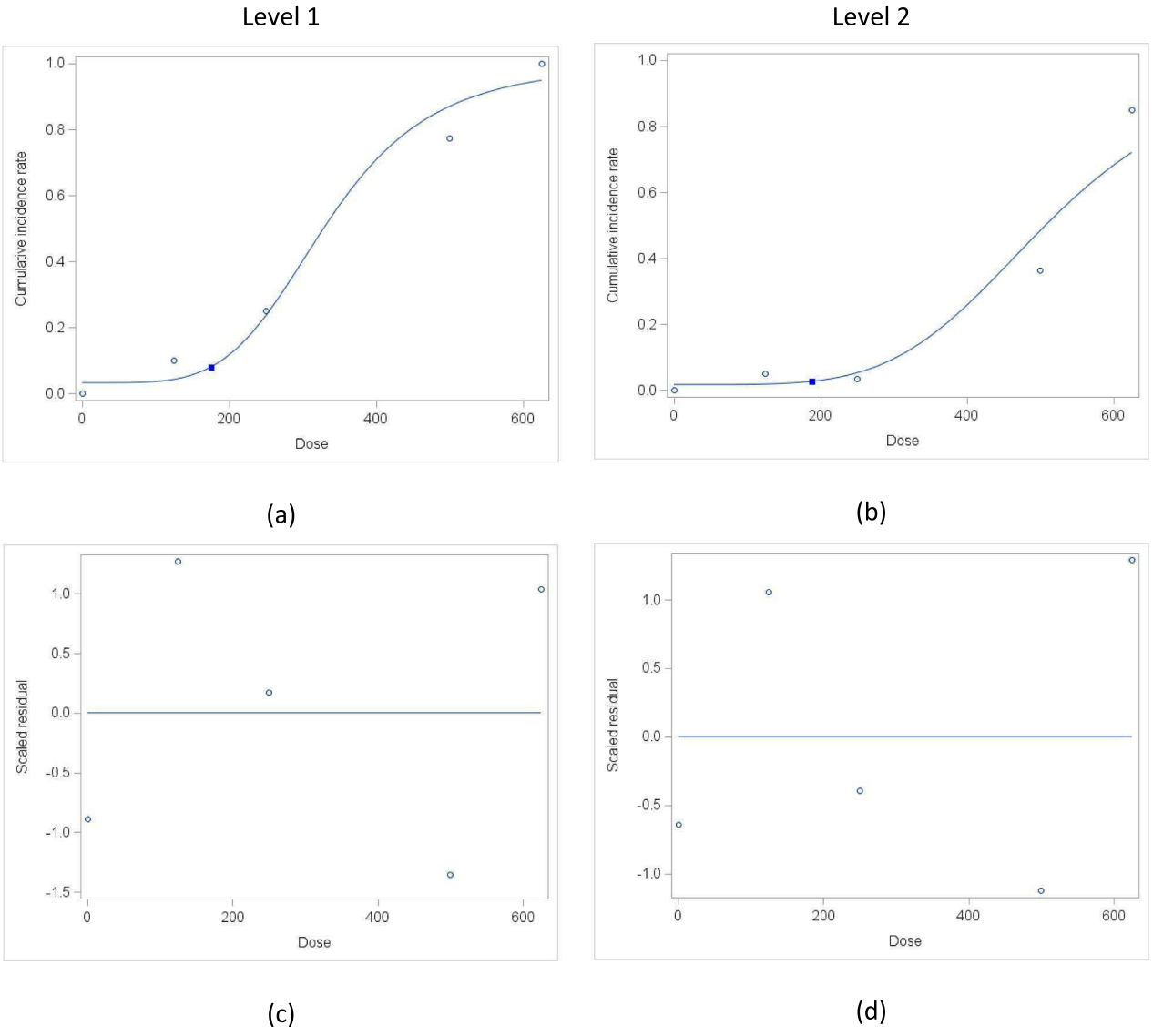

Fig. 2. Plots from ordinal PS analysis with litter effect excluded. The scatter plot of cumulative incidence rate with line plot of fitted cumulative probability curve shown for level 1 (a) and level 2 (b), with the corresponding BMD estimate indicated by a solid square, and residual plots with zero line shown for level 1 (c) and level 2 (d).

Table 4
The estimates, SEs, and 90% and 95% confidence intervals of the BMDs from the normal-based and bootstrap analyses.

Parameter	Analysis	Estimate (mg/kg-d)	SE (mg/kg-d)	CI Type[a]	Two-sided 90% CI (mg/kg-d)	Two-sided 95% CI (mg/kg-d)
Level 1 BMD_{05}	Normal-based	176	38.2[b]	Unadj.	(123, 251)[c]	(115, 269)[c]
				Bonf.	(115, 269)	(108, 286)
	Bootstrap	**215**[d]	**91.8**[d]	Unadj.	(116, 425)	(102, 477)
				M&B	**(111, 428)**	**(98, 478)**
				Bonf.	(102, 477)	(91, 480)
Level 2 BMD_{01}	Normal-based	188	46.9[b]	Unadj.	(125, 283)[c]	(115, 306)[c]
				Bonf.	(115, 306)	(107, 329)
	Bootstrap	**234**[d]	**93.0**[d]	Unadj.	(121, 449)	(105, 478)
				M&B	**(116, 459)**	**(101, 479)**
				Bonf.	(105, 478)	(91, 481)

[a] "Unadj.": CI is not adjusted for multiplicity; "M&B": Mandel & Betensky multiplicity adjustment is applied; "Bonf.": Bonferroni multiplicity adjustment applied; the principal confidence intervals used are in boldface.
[b] The normal-based SEs were computed using the delta method.
[c] The normal-based confidence intervals are t-intervals.
[d] The bootstrap estimates and SEs were the means and standard deviations of the BMD estimates from the 10,000 bootstrap runs.

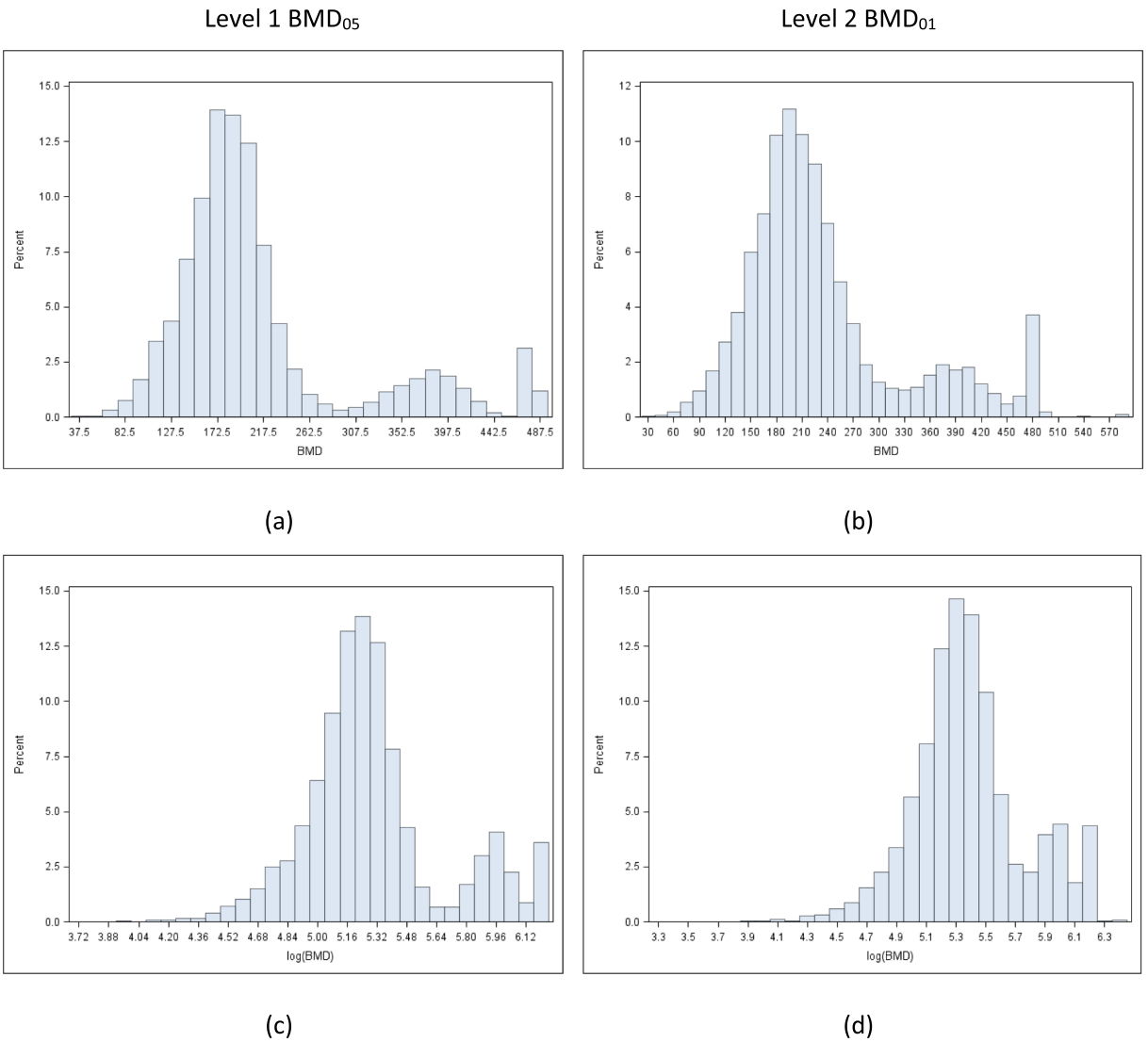

Fig. 3. Histograms from bootstrap analysis of the PS. Shown are the histograms of the untransformed BMD_{05}s for level 1 (a) and the untransformed BMD_{01}s for level 2 (b), and of the log-transformed BMD_{05}s for level 1 (c) and the log-transformed BMD_{01}s for level 2 (d).

corresponding normal-based BMD estimates because of skewness in the distributions of the bootstrap BMD estimates. Also, the bootstrap standard errors of the BMDs (Table 4, labeled "bootstrap") were much higher than their normal-based counterparts because intra-litter correlation resulted in increased variability.

The histograms of the bootstrap distributions of the level 1 BMD_{05} and level 2 BMD_{01} (Fig. 3ab) exhibit significant right skewness, which is common for simulated BMD distributions in our experience. In addition, the distributions are multimodal. Besides the large mode left of center, they each have two additional, smaller modes near the high end. For both distributions, approximately 16% of the BMDs were represented in the two smaller peaks. It is not clear why the distributions exhibit these two extra modes, but it is possible that the extra modes are a result of the limitations of the dataset itself, in the context of the bootstrap sampling, and are not a reflection of the true distribution of the BMDs. The histograms of the bootstrap distributions of the log-transformed level 1 BMD_{05} and level 2 BMD_{01} (Fig. 3cd) are slightly left skewed, but much less skewed than the untransformed BMD distributions. Because the logarithm is an increasing function, the log-transformed BMDs also exhibit two extra modes at the high end. The departures of the untransformed BMD distributions from normality were substantial, making non-normal-based confidence intervals such as the Mandel-Betensky intervals particularly useful.

The Mandel & Betensky bootstrap intervals (Table 4, labeled "M&B") were considerably wider than their respective normal-based intervals, especially at the high end, which reflects the increased variability due to the random litter effect. The Bonferroni intervals were wider than the unadjusted and Mandel & Betensky intervals, but overall the three sets of intervals are similar for each BMD, for both the 90% and 95% cases. A forest plot of the confidence intervals (Fig. 4) demonstrates this similarity and the difference with the normal-based intervals.

For determining RfDs, the lower bounds of these intervals are often used as the PODs; the lower bounds (BMDLs) are used to account for the statistical error in the BMD estimate. The three bootstrap BMDLs in Table 4 are reasonably similar for each BMD, with up to a 13% difference. Ultimately, the Mandel & Betensky intervals are only slightly more conservative than the unadjusted intervals and provide reliable lower bounds to use as PODs.

4.2.3. *Sensitivity bootstrap analysis*

The sensitivity bootstrap analysis with the litter effect disregarded yielded level 1 BMD_{05} and level 2 BMD_{01} estimates of 204 and 220, respectively, which were 5–6% lower than the corresponding estimates in the original bootstrap analysis, and the SEs were 75.6 and 77.0, respectively, which were 17–18% lower than in the original bootstrap analysis. Although these statistics did not differ greatly across the two

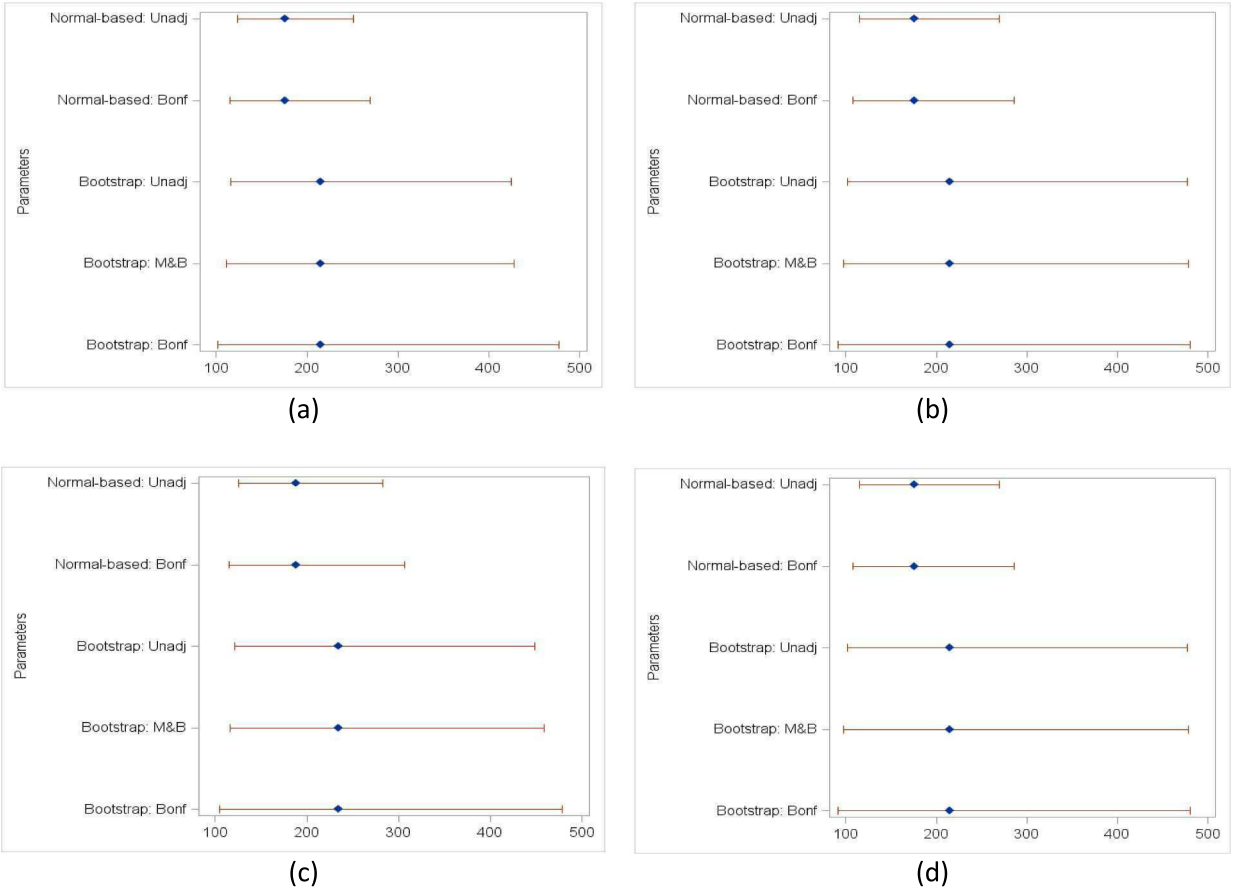

Fig. 4. Forest plots of BMD estimates and confidence intervals for level 1 for the normal-based and bootstrap analyses. Shown are the level 1 BMD_{05} 90% (a) and 95% (b) confidence intervals and the level 2 BMD_{01} with 90% (c) and 95% (d) confidence intervals, with estimates denoted by blue diamonds. (For interpretation of the references to colour in this figure legend, the reader is referred to the web version of this article.)

Table 5
Results from dichotomous dose-response analyses for estimating the "any PS" BMD_{05} and "severe PS" BMD_{01}, with one-sided 95% BMDLs.

Dichotomous Analysis[a]	BMR	BMD (mg/kg-day)	One-sided 95% BMDL[a] (mg/kg-day)
Any PS	5% ER	125	77
Severe PS	1% ER	344	180

[a] The "any PS" and "severe PS" analyses are described in Section 2.2.
[b] The one-sided 95% BMDL corresponds to the lower bound of a two-sided 90% confidence interval; BMDS does not provide the BMDUs for nested dichotomous models, so these are not listed.

analyses, they differed enough to demonstrate that the inclusion of the litter effect was warranted.

The bootstrap analyses on the three permuted samples yielded BMD estimates that were very close (0–1.5% lower) to those from the original analysis and SEs that were somewhat close but slightly more discrepant (3–7% lower). These results demonstrate that the litter assignments in the originally observed dataset have a slight but noticeable influence on the estimated BMD distribution, thus verifying the influence of the litter effect. Furthermore, the differences for the permuted samples were smaller than for the analysis disregarding litter, thus providing additional evidence that the inclusion of the litter effect was warranted. A table of the results of the sensitivity bootstrap analyses and related histograms are provided in Appendix D.

4.3. Comparison to dose-response modeling of dichotomous datasets

The incidence data for the two dichotomous analyses are presented in Table 2 ("levels 1 & 2" for "any PS" and "level 2" for "severe PS"). Unlike the ordinal analysis, for which the BMD estimates were similar between the two severity levels, the BMD estimates from the two dichotomous PS analyses differed considerably. The "severe PS" BMD_{01} estimate was approximately 2.7 times higher than the "any PS" BMD_{05} estimate, and the "severe PS" $BMDL_{01}$ was approximately 2.3 higher than the "any PS" $BMDL_{05}$ (Table 5). In comparison, the bootstrap estimates of the level 1 BMD_{05} and level 2 BMD_{01} (215 and 234 mg/kg-day, respectively) were in the middle of the range from the "any PS" BMD to the "severe PS" BMD. Similarly, the Mandel-Betensky-adjusted 95% level 1 and level 2 BMDLs (98 and 101 mg/kg-day, respectively) were in the middle of the range from the "any PS" BMDL to the "severe PS" BMDL, although slightly closer to the "any PS" BMDL.

In addition, a number of PS endpoints listed in Table 1 were noted by Yost et al. (2019) to exhibit a significant dose-related trend. Several of these endpoints were modeled individually as dichotomous endpoints (Table 6), using the procedure described in Section 3. The BMR used for each endpoint was consistent with the level assignments in Table 1, and the BMDL was calculated with one-sided 95% coverage.

The BMDs of these endpoints ranged from 112 to 480 mg/kg-day, and the BMDLs ranged from 60 to 266 mg/kg-day. These wide ranges reflect the high variability that often arises when modeling multiple endpoints. One of the more biologically relevant endpoints, azoospermia/oligospermia, had one of the lowest BMDs, 117 mg/kg-day, and the lowest BMDL, 60 mg/kg-day, results which are very similar to those from the "any PS" dichotomous approach. In comparison, the bootstrap estimates of the level 1 BMD_{05} and level 2 BMD_{01} (215 and 234 mg/kg-day) and the corresponding Mandel-Betensky-adjusted 95% BMDLs (98 and 101 mg/kg-day) were in the middle of the range outlined by the individual endpoint results.

Table 6
BMD model results from dichotomous analysis of selected PS endpoints.

PS Endpoint	BMR	BMD (mg/kg-day)	BMDL (mg/kg-day)
Hypospadias	1% ER	401	242
Undescended testes	1% ER	342	194
Exposed os penis	1% ER	361	112
Areola or nipple retention	5% ER	317	205
Azoospermia or grade 2–5 oligospermia[a]	5% ER	117	60
Tubular degeneration[b]	5% ER	480	266
Sloughed cells	5% ER	112	67

[a] An animal was designated as having "azoospermia or grade 2–5 oligospermia" if either epididymis had either azoospermia or grade 2–5 oligospermia (or both).

[b] "Tubular degeneration" consisted of tubular degeneration-atrophy/hypoplasia, tubular vacuolation, and loss of seminiferous tubules, all at grades 2–5.

5. Discussion

The ordinal dose-response analysis of PS presented here improves upon the dichotomous analyses because it incorporates severity of effect, and it is a relatively simple extension of the dichotomous analysis. The strengths of the ordinal analysis method are that it provides BMD estimates that are closer to each other in value and have lower variability than the separate dichotomous analyses of the individual PS endpoints. The dichotomous analyses exaggerate variability by not incorporating modeling artifacts due to sparsity of data, especially with regard to the low litter sizes. By contrast, the ordinal PS dataset yielded less variable results because it had higher incidence rates among the middle dose groups and also because the equal slopes in the ordinal analysis draws the level 1 and level 2 curves, and thus the BMD estimates and BMDLs, closer together. This ordinal approach is flexible, as more than two severity levels can be included in other analyses, and it could be applied to dose response assessment of other phthalates and antiandrogens with common effects that may vary in co-occurrence. Therefore, the ordinal approach can be expanded to be broadly applicable to dose-response modeling of any set or syndromes of effects. In addition, the confidence intervals for the BMDs provide simultaneous coverage across the levels, so they can be used in a "post hoc" manner. In other words, either confidence interval, for level 1 BMD_{05} or level 2 BMD_{01}, can be used in subsequent risk assessment even though the data have already been collected and dose-response analysis conducted, and the probabilistic coverage of the interval will not be compromised.

The modeling approach had some limitations, including the lack of consideration of all the continuously measured PS endpoints measured in the Saillenfait et al. (2008) study and the relationships among the PS endpoints. Preliminary investigation of the DIBP data considered here indicated that some endpoints tended to co-occur, for example, for azoospermia, oligospermia, granulomatous inflammation, and interstitial mononuclear cells (data not shown). Only one animal had granulomatous inflammation without also having azoospermia or oligospermia, and no animal had interstitial mononuclear cells without also having the other three. This is not surprising because these four endpoints are mechanistically related. Additionally, the analysis excluded several biologically relevant continuous endpoints such as anogenital distance and reproductive organ weights. In the future, methods for including continuous endpoints in the analysis can be utilized, either by dichotomizing the continuous endpoints using biologically relevant cutoffs, or by doing a multivariate analysis of all PS endpoints that includes the actual observed continuous values. These types of analyses have been explored previously for cerrtain cases (e.g., Catalano et al., 1994; Regan and Catalano, 1999).

The dataset that was analyzed in this study had some strengths and limitations. The Saillenfait et al. (2008) study strengths for modeling included the assessment of numerous male reproductive developmental endpoints, had ~20 dams/dose group, and had available individual animal data, including histopathological examination of the testis and epididymis. The fact that this prenatal exposure toxicity study collected data on a large number of PS endpoints, allowed the model to integrate information on a wide array of male reproductive endpoints. However, the study did not include a direct measure of fertility in the animals, so the categorization had to rely on established associations between male reproductive endpoints, including histopathological endpoints, and male fertility. Also, the small number of animals (two) per litter allowed a very limited estimation of the random variation within litters. The long-established practice of culling of litters to 8–10 offspring on Day 4 resulted in the loss of valuable information. Although this practice was first implemented to reduce the influence of variable litter sizes on related outcomes, statistical methods have advanced sufficiently that re-evaluation of this practice is encouraged. Data on entire litters are essential for investigating complex outcomes such as those addressed here and as shown in other studies (for example, Blystone et al., 2010).

The ordinal analysis of PS conducted here was possible because of the availability of the incidence data for PS endpoints for individual animals, thus allowing the assignment of animals to ordinal levels. In addition, the Saillenfait et al. (2008) study data and methods were well-documented and thoroughly described. Unfortunately, many publications in the peer-reviewed literature do not provide individual animal data or this level of methodological detail. As a result, obtaining individual animal data requires contacting authors and relies on the willingness of authors to collaborate with other scientists, including allowing for additional data analyses. Integrated analysis of multiple endpoints is a growing need in toxicology, and having the data available on an individual animal level is necessary to do many types of these analyses such as multivariate analysis of endpoints. It would be beneficial if journals and scientists publish and share their individual animal data.

Future refinements of the dose-response approach for the PS include (1) further delineation of severity levels; (2) consideration of patterns of responses among the PS endpoints; and (3) inclusion of continuous endpoints using a multivariate analysis approach. As an example of further refinement of severity levels using the Saillenfait et al. (2008) data, level 1 can be split into two levels according to whether a PS endpoint has either (1) no or (2) some more moderate expected association with impacts on fertility. As an example of patterns of responses, analysis of the PS endpoints that co-occur or occur at the lowest doses could be informative for dose response modeling. Understanding the temporal patterns of expression over the course of development and into adulthood could inform precursors to severe effects. In a multivariate approach, both dichotomous and continuous PS outcomes (e.g., anogenital distance, reduced fetal testicular testosterone levels) could be modeled to evaluate the interaction of effects among all of the PS endpoints, as well as the degree of contribution of the individual effects to the PS dose response curve.

The *Phthalates and Cumulative Risk Assessment* report (NRC, 2008) recommended performing a cumulative assessment that included phthalates as well as antiandrogens based on shared male reproductive endpoints. Using data from one phthalate (DIBP), the analysis presented here addresses the required first step in this process – the development of a dose-response approach for the PS endpoints that commonly occur after gestational phthalate or antiandrogen exposure. Once PS modeling is performed within individual phthalate noncancer risk assessments, the next step is to further refine the methodology and develop data to enable performing a cumulative phthalate noncancer risk assessment.

In conclusion, the ordinal dose-response modeling analysis offers an alternative to dichotomous analysis of the PS in which multiple levels of endpoint severity can be incorporated and modeled at different response levels, all in a single analysis. The analysis demonstrated in this investigation included two levels of endpoint severity, but the ordinal analysis is sufficiently flexible so that more levels can be included. Furthermore, the analysis of male reproductive effects as a syndrome leads to more stable BMD estimates.

Declaration of Competing Interest

None.

Acknowledgments

We thank EPA's National Center for Risk Assessment's (NCEA) Reproductive, Developmental, and Neurological Toxicology Workgroup, co-led by Susan Makris and Andrew Kraft, for their expertise and fruitful discussion regarding the severity levels of the male reproductive endpoints. We also thank John Fox and David Farrar for their statistical review of the manuscript.

Disclaimer

The views expressed are those of the authors and do not necessarily represent the views or policies of the U.S. Environmental Protection Agency.

This research did not receive any specific grant from funding agencies in the public, commercial, or not-for-profit sectors.

Appendix A:. Log-logistic model

For the dichotomous case, the most common form of the log-logistic model used in toxicology is

$$\mathrm{P}[Y = 1|x] = \gamma + \frac{1-\gamma}{1+\exp[-(\alpha+\beta\log x)]}$$

where α is the intercept, β is the slope, and γ is the background response rate. For example, this is the model form used in U.S. EPA's Benchmark Dose Software (BMDS). For the ordinal case, this equation would be written

$$\mathrm{P}[Y \geq j|x] = \gamma_j + \frac{1-\gamma_j}{1+\exp[-(\alpha_j+\beta\log x)]}, \tag{A1}$$

where α_j and γ_j are the intercept and background response rate for ordinal level j and β is the slope. Using this model form, estimating the BMD requires expressing the BMD as a function of α_j and β. However, the model can be reparameterized so that the BMD is an explicit parameter in the model using the definition of the BMR, denoted ν:

$$\nu = \frac{\mathrm{P}[Y \geq j|x] - \mathrm{P}[Y \geq j|0]}{1 - \mathrm{P}[Y \geq j|0]}.$$

The BMD associated with this BMR, denoted BMD_ν, is related to the slope and intercept by the equation

$$\log\mathrm{BMD}_\nu = \frac{1}{\beta}[-\alpha_j + \log(\nu/(1-\nu))].$$

Solving this equation for α and substituting it into (A.1) yields Eq. (1), with $\theta_{\nu,j}$ substituted for $\log\mathrm{BMD}_\nu$. The BMD is log-transformed in the equation to improve the normal approximation of its estimate.

The model defined in Eq. (1) was fit to the ordinal PS data using $\nu = 0.01$, and the fit statistics were used to estimate the BMDs of interest, the level 1 BMD_{05}, $\theta_{05,1}$, and the level 2 BMD_{01}, $\theta_{01,2}$. The second of these, $\theta_{01,2}$, was a parameter in the model that was fit, so its estimate and standard error (SE) were automatically output from the model run. $\theta_{05,1}$ was estimated using its relationship to $\theta_{01,1}$, described as follows. For each x, the value in the right-hand side of Eq. (1) must be the same across values of ν, which after simplification implies that the inside of the exponent term in (1) must be the same across ν. Applying this principle to $\nu = 0.01$ and 0.05 yields

$$-\log(0.05/0.95) + \beta(\theta_{05,1} - \log x) = -\log(0.01/0.99) + \beta(\theta_{01,1} - \log x).$$

Solving this equation for $\theta_{05,1}$ yields Eq. (2). The estimate and SE of $\theta_{01,1}$ are listed in the Additional Estimates table of SAS Output A2, under the label "theta_int."

SAS did not automatically compute the goodness-of-fit chi-square test statistic in SAS Proc NLMIXED, so additional code was written to do this computation. The formula used for the test statistic was

$$\chi^2_5 = \sum_{i=1}^{5}\sum_{j=0}^{2}\frac{(O_{ij}-E_{ij})^2}{E_{ij}},$$

where O_{ij} and E_{ij} are the observed and expected incidence frequencies of ordinal level j in the ith dose group. Here, $E_{ij} = n_i \bullet \mathrm{Pr}_i(j)$, where n_i is the number of animals in the ith dose group and $\mathrm{Pr}_i(j)$ is the probability that an animal in the ith dose group has ordinal level j. The degrees of freedom for this test were calculated using the formula $\mathrm{df} = r \times (c-1) - k$, where $r = 5$ is the number of dose groups, $c = 3$ is the number of levels of the ordinal response variable, and $k = 5$ is the number of parameters that are estimated in the model. This procedure is described in Agresti (2010; see Chapter 3).

Appendix B:. Description of bootstrap method and Mandel-Betensky intervals

A large number of bootstrap datasets were randomly selected using the following procedure. For dose x_i, suppose there are J_i litters exposed to that dose, and let Y_{jk} denote the PS incidence of the kth animal in the jth litter for $j = 1, \cdots, J_i$; $k = 1, 2$. That is, for $k = 1, 2$, $Y_{jk} = 1$ if the kth animal in litter has PS, and $Y_{jk} = 0$ otherwise. Select bootstrap samples as follows:

1. Randomly select a sample of size J_i with replacement from the set of litters exposed to dose x_i, and denote this litter j^*_m for $m = 1, \cdots, J_i$. Let $\boldsymbol{Y}^*_{jm} = (Y^*_{1,jm}, Y^*_{2,jm})$ denote the vector of PS incidence in that litter. Note that because the sampling is with replacement, some litters may be selected multiple times, while others may not be selected at all.
2. From each litter j^*_m selected in step 1, randomly select 2 observations from $\boldsymbol{Y}^*_{jm}$, denoted $\boldsymbol{V}^*_{jm} = (V^*_{1,jm}, V^*_{2,jm})$. Note that because the sampling is with replacement, the same observation may be selected twice.

This procedure results in the sample of PS observations $\{\boldsymbol{V}^*_{jm}: m = 1, \cdots, J_i\}$ for dose x_i. When collected across all doses, these samples collectively constitute a dataset of the same nature and size as the original sample of PS observations with litter effect ignored. The dose-response model described in Section 3 was applied to each bootstrap sample and estimates of the level 1 BMD_{05} and level BMD_{01} were obtained. The collection of these estimates across all bootstrap sasmples constituted an estimated distribution of the BMDs.

Simultaneous confidence intervals for the level 1 BMD_{05} and level 2 BMD_{01} using an adjusted percentile bootstrap interval developed by Mandel and Betensky (2008). Here, the lower and upper interval bounds for each BMD were the percentiles of its respective bootstrap-derived BMD distribution, where the rank of each bootstrap sample was redefined based on the coordinate whose rank was most discrepant from its respective median. More explicitly, the sample ranks were redefined as follows:

1. For the bth bootstrap sample and $j = 1, 2$, let $r(b, j) =$ the rank of the jth BMD coordinate taken across all samples, and define the relative rank $r^*(b, j) = |r(b, j) - (B + 1)/2|$ and sign of the relative rank $s^*(b, j) = \text{sign}[r(b, j) - (B + 1)/2]$, where $\text{sign}(x) = 1$ if $x \geq 0$ and -1 if $x < 0$.
2. The final rank of the bth bootstrap sample was based on the redefined ranks across the BMD coordinates associated with that sample's estimate. That is, its rank was defined as $r(b) = (B + 1)/2 + s^*(b, j) \bullet \max_j r^*(b, j)$, where the maximum in this expression is taken across the BMD coordinates in the bth sample.

Appendix C:. Analysis results of assessing influence of histopathology endpoints on ordinal PS levels

Fourteen (14) animals out of a total of 114 (12%) had their PS levels increase because of the presence of histopathology endpoints; 11, 2, and 1 animals had levels that increased from 0 to 1, 0 to 2, and 1 to 2, respectively (see Table C1).

Table C1
Animals sacrificed at PNW 11–12 whose PS level increased due to the presence of histopathology endpoints, including their scores with histopathology excluded and included.

Dose	Litter	Animal	Level w/o histopath	Level w/ histopath
125	26	3	0	2
125	27	1	0	1
250	41	1	0	1
250	44	1	0	1
250	48	4	0	1
250	51	3	0	1
250	52	1	0	1
250	52	3	0	1
500	64	3	0	1
500	73	1	0	1
500	74	1	0	1
500	74	3	0	2
625	82	7	1	2
625	93	1	0	1

Appendix D:. Results of sensitivity bootstrap analysis

See Table D1 and Fig. D1.

Table D1
The estimates, SEs, and 90% and 95% Mandel & Betensky confidence intervals of the BMDs from the original and sensitivity bootstrap analyses.

Parameter	Bootstrap Analysis	Estimate	SE	90% CI	95% CI
Level 1 BMD_{05}	No litter effect	203.6	75.62	(117.5, 393.8)	(104.7, 411.0)
	With litter effect: original sample	214.8	91.81	(111.3, 428.3)	(98.40, 478.2)
	With litter effect: permuted sample 1	213.8	89.47	(108.7, 417.4)	(96.29, 474.8)
	With litter effect: permuted sample 2	211.9	85.69	(111.9, 410.4)	(97.22, 471.3)
	With litter effect: permuted sample 3	214.3	89.30	(112.7, 430.5)	(97.57, 478.0)
Level 2 BMD_{01}	No litter effect	219.8	77.00	(121.0, 402.9)	(105.1, 425.4)
	With litter effect: original sample	233.6	93.01	(116.1, 459.2)	(100.6, 479.2)
	With litter effect: permuted sample 1	232.8	92.8	(111.7, 435.5)	(94.18, 476.1)
	With litter effect: permuted sample 2	230.4	88.52	(113.9, 427.6)	(95.88, 472.8)
	With litter effect: permuted sample 3	234.0	91.24	(115.3, 459.4)	(97.42, 477.7)

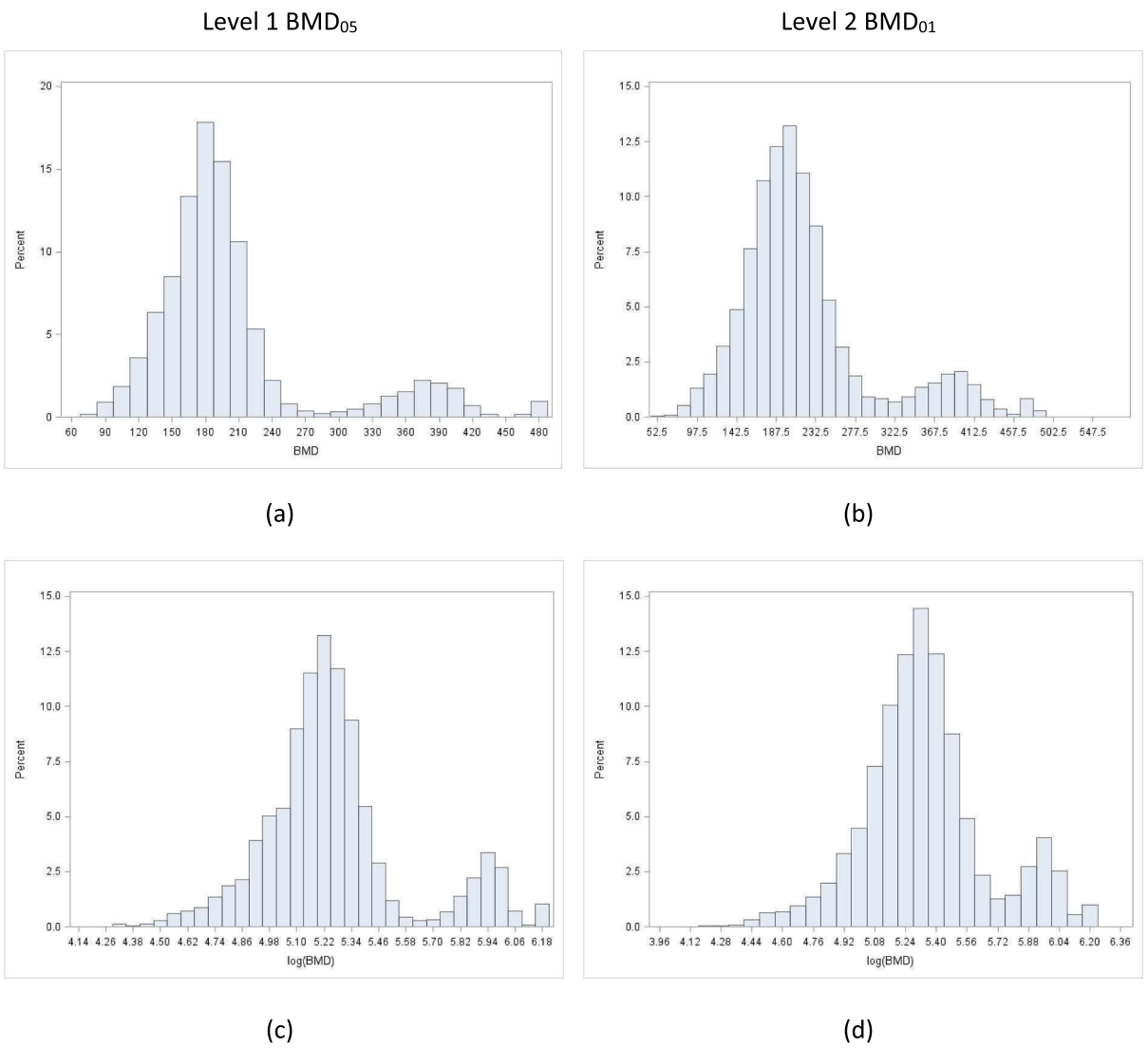

Fig. D1. Histograms from bootstrap analysis of the PS with the litter effect excluded. Shown are the histograms of the untransformed BMD_{05}s for level 1 (a) and the untransformed BMD_{01}s for level 2 (b), and of the log-transformed BMD_{05}s for level 1 (c) and the log-transformed BMD_{01}s for level 2 (d).

Appendix E:. SAS output for ordinal analysis of PS dataset

SAS Output E1: Pertinent sections of the output from the ordinal analysis of the PS dataset in SAS Proc NLMIXED with the slopes allowed to differ across ordinal levels. The results from testing the equality of the slopes are listed in the Contrasts table.

Parameter Estimates

Parameter	Estimate	Standard Error	DF	t Value	Pr > |t|	Alpha	Lower	Upper
gam2	0.02636	0.01973	4	1.34	0.2525	0.05	−0.02843	0.08115
g1	0	.	4	.	.	0.05	.	.
th2	5.6835	0.2525	4	22.51	< 0.0001	0.05	4.9824	6.3845
thd	1.0586	0.3321	4	3.19	0.0333	0.05	0.1365	1.9807
bt1	3.8990	0.7384	4	5.28	0.0062	0.05	1.8488	5.9492
bt2	7.7482	3.0030	4	2.58	0.0613	0.05	−0.5895	16.0859

Contrasts

Label	Num DF	Den DF	F Value	Pr > F
equal slopes	1	4	2.86	0.1662

Additional Estimates

Label	Estimate	Standard Error	DF	t Value	Pr > |t|	Alpha	Lower	Upper
gamma1	0.02636	0.01973	4	1.34	0.2525	0.05	−0.02843	0.08115
gamma2	0.02636	0.01973	4	1.34	0.2525	0.05	−0.02843	0.08115
beta1	3.8990	0.7384	4	5.28	0.0062	0.05	1.8488	5.9492
beta2	7.7482	3.0030	4	2.58	0.0613	0.05	−0.5895	16.0859
theta1	5.0482	0.1694	4	29.79	< 0.0001	0.05	4.5778	5.5187
theta2	5.6835	0.2525	4	22.51	< 0.0001	0.05	4.9824	6.3845
log(beta1)	1.3607	0.1894	4	7.18	0.0020	0.05	0.8349	1.8865
log(beta2)	2.0475	0.3876	4	5.28	0.0062	0.05	0.9714	3.1235

SAS Output E2: Pertinent sections of the output from the ordinal analysis of the PS dataset in SAS Proc NLMIXED with the slopes assumed to be equal across ordinal levels. The estimates and SEs of the BMDs and other parameters of interest are listed in the Additional Estimates table.

Parameter Estimates

Parameter	Estimate	Standard Error	DF	t Value	Pr > |t|	Alpha	Lower	Upper
gam2	0.01675	0.01796	5	0.93	0.3937	0.05	−0.02941	0.06290
g1	0.01526	0.02998	5	0.51	0.6324	0.05	−0.06181	0.09233
th2	5.2359	0.2495	5	20.99	< 0.0001	0.05	4.5946	5.8773
thd	0.4277	0.1016	5	4.21	0.0084	0.05	0.1664	0.6889
bt	4.5913	1.1067	5	4.15	0.0089	0.05	1.7466	7.4361

Additional Estimates

Label	Estimate	Standard Error	DF	t Value	Pr > |t|	Alpha	Lower	Upper
gamma1	0.03201	0.03700	5	0.87	0.4265	0.05	−0.06309	0.1271
gamma2	0.01675	0.01796	5	0.93	0.3937	0.05	−0.02941	0.06290
beta	4.5913	1.1067	5	4.15	0.0089	0.05	1.7466	7.4361
theta1	5.1678	0.2174	5	23.77	< 0.0001	0.05	4.6090	5.7267
theta2	5.2359	0.2495	5	20.99	< 0.0001	0.05	4.5946	5.8773
theta_int	4.8083	0.2993	5	16.07	< 0.0001	0.05	4.0390	5.5776
L1 BMD05	175.53	38.1603	5	4.60	0.0058	0.05	77.4359	273.62
L2 BMD01	187.91	46.8806	5	4.01	0.0102	0.05	67.3950	308.42

References

Agresti, A., 2010. Analysis of Ordinal Categorical Data, second ed. Wiley.

Allen, B.C., Kavlock, R.J., Kimmel, C.A., Faustman, E.M., 1994. Dose-response assessment for developmental toxicity. III. Statistical models. Fundam. Appl. Toxicol. 23 (4), 496–509. https://doi.org/10.1006/faat.1994.1134.

Blystone, C.R., Kissling, G.E., Bishop, J.B., Chapin, R.E., Wolfe, G.W., Foster, P.M., 2010. Determination of the di-(2-ethylhexyl) phthalate NOAEL for reproductive development in the rat: importance of the retention of extra animals to adulthood. Toxicol. Sci. 116 (2), 640–646. https://doi.org/10.1093/toxsci/kfq147.

Boekelheide, K., Kleymenova, E., Liu, K., Swanson, C., Gaido, K.W., 2009. Dose-dependent effects on cell proliferation, seminiferous tubules, and male germ cells in the fetal rat testis following exposure to di(n-butyl) phthalate. Microsc. Res. Tech. 72 (8), 629–638. https://doi.org/10.1002/jemt.20684.

Catalano, P., Ryan, L., Scharfstein, D., 1994. Modeling fetal death and malformation in developmental toxicity studies. Risk Anal. 14 (4), 629–637. https://doi.org/10.1111/j.1539-6924.1994.tb00276.x.

Chen, C.C., Chen, J.J., 2014. Benchmark dose calculation for ordered categorical responses. Risk Anal. 34 (8), 1435–1447. https://doi.org/10.1111/risa.12167.

Dataset, 2019. Data and output for Ordinal Dose-Response Modeling Approach for the Phthalate Syndrome 508. https://doi.org/10.23719/1503702.

Efron, B., Tibshirani, R.J., 1994. An Introduction to the Bootstrap. Chapman & Hall.

Fisher, J.S., Macpherson, S., Marchetti, N., Sharpe, R.M., 2003. Human 'testicular dysgenesis syndrome': a possible model using in-utero exposure of the rat to dibutyl phthalate. Hum. Reprod. 18 (7), 1383–1394. https://doi.org/10.1093/humrep/deg273.

Foster, P.M., 2006. Disruption of reproductive development in male rat offspring following in utero exposure to phthalate esters. Int. J. Androl. 29 (1), 140–147. https://doi.org/10.1111/j.1365-2605.2005.00563.x.

Foster, P.M.D., Mylchreest, E., Gaido, K.W., Sar, M., 2001. Effects of phthalate esters on the developing reproductive tract of male rats. Hum. Reprod. Update 7 (3), 231–235. https://doi.org/10.1111/j.1600-0463.2001.tb05776.x.

Gray Jr, L.E., Barlow, N.J., Howdeshell, K.L., Ostby, J.S., Furr, J.R., Gray, C.L., 2009. Transgenerational effects of Di (2-ethylhexyl) phthalate in the male CRL:CD(SD) rat: added value of assessing multiple offspring per litter. Toxicol. Sci. 110 (2), 411–425. https://doi.org/10.1093/toxsci/kfp109.

Howdeshell, K.L., Hotchkiss, A.K., Gray Jr, L.E., 2017. Cumulative effects of antiandrogenic chemical mixtures and their relevance to human health risk assessment. Int. J. Hyg. Environ. Health. 220 (2 Pt A), 179–188. https://doi.org/10.1016/j.ijheh.2016.11.007.

Koch, H.M., Rüther, M., Schütze, A., Conrad, A., Pälmke, C., Apel, P., Brüning, T., Kolossa-Gehring, M., 2017. Phthalate metabolites in 24-h urine samples of the German Environmental Specimen Bank (ESB) from 1988 to 2015 and a comparison with US NHANES data from 1999 to 2012. Int. J. Hyg. Environ. Health. 220 (2 Pt A), 130–141. https://doi.org/10.1016/j.ijheh.2016.11.003.

Krewski, D., Chambers, A., Birkett, N., 2010. The use of categorical regression in modeling copper exposure-response relationships. J. Toxicol. Environ. Health A 73, 187–207. https://doi.org/10.1080/15287390903340781.

Kupper, L.L., Portier, C., Hogan, M.D., Yamamoto, E., 1986. The impact of litter effects on dose-response modeling in teratology. Biometrics 42 (1), 85–98. https://doi.org/10.2307/2531245.

Lanning, L.L., Creasy, D.M., Chapin, R.E., Mann, P.C., Barlow, N.J., Regan, K.S., Goodman, D.G., 2002. Recommended approaches for the evaluation of testicular and epididymal toxicity. Toxicol. Pathol. 30 (4), 507–520. https://doi.org/10.1080/01926230290105695.

Lioy, P.J., Hauser, R., Gennings, C., Koch, H.M., Mirkes, P.E., Schwetz, B.A., Kortenkamp, A., 2015. Assessment of phthalates/phthalate alternatives in children's toys and childcare articles: Review of the report including conclusions and recommendation of the Chronic Hazard Advisory Panel of the Consumer Product Safety Commission. J. Expo. Sci. Environ. Epidemiol. 25 (4), 343–353.

Makris, S.L., Euling, S.Y., Gray Jr, L.E., Benson, R., Foster, P., 2013. Use of genomic data in risk assessment case study: I. Evaluation of the dibutyl phthalate male reproductive development toxicity data set. Toxicol. Appl. Pharmacol. 271 (3), 336–348. https://doi.org/10.1016/j.taap.2010.09.006.

Mandel, M., Betensky, R.A., 2008. Simultaneous confidence intervals based on the percentile bootstrap approach. Comput. Stat. Data An. 52 (4), 2158–2165. https://doi.org/10.1016/j.csda.2007.07.005.

National Research Council (NRC), 2008. Phthalates and Cumulative Risk Assessment: The Tasks Ahead. Committee on the Health Risks of Phthalates, Board on Environmental Studies and Toxicology, Division on Earth and Life Sciences. The National Academies Press, Washington, DC https://doi.org/10.17226/12528.

Regan, M.M., Catalano, P.J., 1999. Likelihood models for clustered binary and continuous outcomes: application to developmental toxicology. Biometrics 55 (3), 760–768. https://doi.org/10.1111/j.0006-341X.1999.00760.x.

Saillenfait, A.M., Sabaté, J.P., Gallissot, F., 2008. Diisobutyl phthalate impairs the androgen-dependent reproductive development of the male rat. Reprod. Toxicol. 26 (2), 107–115. https://doi.org/10.1016/j.reprotox.2008.07.006.

U.S. Consumer Product Safety Commission (CPSC), 2014. Chronic Hazard Advisory Panel (CHAP) Report on Phthalates and Phthalate Alternatives. 20814. Available online at: https://www.cpsc.gov/s3fs-public/CHAP-REPORT-FINAL%20(1).pdf. Directorate for Health Sciences, Bethesda, MD.

U.S. Environmental Protection Agency (EPA), 2002. A review of the reference dose and reference concentration processes (pp. 1–192). (EPA/630/P-02/002F). Washington, DC: U.S. Environmental Protection Agency, Risk Assessment Forum. Available online at: https://www.epa.gov/sites/production/files/2014-12/documents/rfd-final.pdf.

U.S. EPA, 2012. Benchmark Dose Technical Guidance (EPA/100/R-12/001). Washington, DC: U.S. Environmental Protection Agency, Risk Assessment Forum. Available online at: https://www.epa.gov/sites/production/files/2015-01/documents/benchmark_dose_guidance.pdf.

U.S. EPA, 2014. Toxic Substances Control Act (TSCA) Work Plan for Chemical Assessments: 2014 Update. Office of Pollution Prevention and Toxics, October 2014. Available at: https://www.epa.gov/assessing-and-managing-chemicals-under-tsca/tsca-work-plan-chemical-assessments-2014-update.

U.S. EPA, 2015. Phthalate Action Plan. Available online at: https://www.epa.gov/sites/production/files/2015-09/documents/phthalates_actionplan_revised_2012-03-14.pdf.

U.S. EPA, 2016. BMDS 2.7 User Manual. Available at: https://www.epa.gov/bmds/benchmark-dose-software-bmds-version-27-materials.

van den Driesche, S., McKinnell, C., Calarrão, A., Kennedy, L., Hutchison, G.R., Hrabalkova, L., Jobling, M.S., Macpherson, S., Anderson, R.A., Sharpe, R.M., Mitchell, R.T., 2015. Comparative effects of di(n-butyl) phthalate exposure on fetal germ cell development in the rat and in human fetal testis xenografts. Environ. Health Perspect. 123 (3), 223–230. https://doi.org/10.1289/ehp.1408248.

van der Leeden, R., Meijer, E., 2007. Busing FMTA. Resampling Multilevel Models. Ch. 11 of Handbook of Multilevel Analysis. Springer https://doi.org/10.1007/978-0-387-73186-5_11.

Wittassek, M., Angerer, J., Kolossa-Gehring, M., Schäfer, S.D., Klockenbusch, W., Dobler, L., Günsel, A.K., Müller, A., Wiesmüller, G.A., 2009. Fetal exposure to phthalates–a pilot study. Int. J. Hyg. Environ. Health. 212 (5), 492–498. https://doi.org/10.1016/j.ijheh.2009.04.001.

Ye, X., Pierik, F.H., Hauser, R., Duty, S., Angerer, J., Park, M.M., Burdorf, A., Hofman, A., Jaddoe, V.W., Mackenbach, J.P., Steegers, E.A., Tiemeier, H., Longnecker, M.P., 2008. Urinary metabolite concentrations of organophosphorous pesticides, bisphenol A, and phthalates among pregnant women in Rotterdam, the Netherlands: the Generation R study. Environ. Res. 108 (2), 260–267. https://doi.org/10.1016/j.envres.2008.07.014.

Yost, E.E., Euling, S.Y., Weaver, J.A., Beverly, B.E.J., Keshava, N., Mudipalli, A., Arzuaga, X., Blessinger, T., Dishaw, L., Hotchkiss, A., Makris, S.L., 2019. Hazards of diisobutyl phthalate (DIBP) exposure: a systematic review of animal toxicology studies. Environ. Int. 125, 579–594. https://doi.org/10.1016/j.envint.2018.09.038.

Zota, A.R., Calafat, A.M., Woodruff, T.J., 2014. Temporal trends in phthalate exposures: findings from the National Health and Nutrition Examination Survey, 2001–2010. Environ. Health Perspect. 122 (3), 235–241. https://doi.org/10.1289/ehp.1306681.

Environment International 130 (2019) 104884

Contents lists available at ScienceDirect

Environment International

journal homepage: www.elsevier.com/locate/envint

Development of outcome-specific criteria for study evaluation in systematic reviews of epidemiology studies

Elizabeth G. Radke[a,*], Barbara Glenn[a], Audrey Galizia[a], Amanda Persad[a], Rebecca Nachman[a], Thomas Bateson[a], J. Michael Wright[a], Ana Navas-Acien[b], Whitney D. Arroyave[c], Robin C. Puett[d], Emily W. Harville[e], Anna Z. Pollack[f], Jane S. Burns[g], Courtney D. Lynch[h], Sharon K. Sagiv[i], Cheryl Stein[j], Glinda S. Cooper[a,k]

[a] U.S. Environmental Protection Agency, National Center for Environmental Assessment, United States
[b] Department of Environmental Health Sciences, Columbia University Mailman School of Public Health, United States
[c] Integrated Laboratory Systems, United States
[d] Department of Epidemiology and Biostatistics, University of Maryland School of Public Health, United States
[e] Department of Epidemiology, Tulane University School of Public Health and Tropical Medicine, United States
[f] Department of Global and Community Health, College of Health and Human Services, George Mason University, United States
[g] Department of Environmental Health, Harvard T. H. Chan School of Public Health, United States
[h] Department of Obstetrics and Gynecology, The Ohio State University College of Medicine, United States
[i] Division of Epidemiology, University of California Berkeley, United States
[j] Department of Child and Adolescent Psychiatry, Hassenfeld Children's Hospital at NYU Langone, United States
[k] The Innocence Project, United States

ARTICLE INFO

Handling Editor: Adrian Covaci

ABSTRACT

Introduction and objective: Systematic review tools that provide guidance on evaluating epidemiology studies are receiving increasing attention and support because their application facilitates improved quality of the review, consistency across reviewers, and transparency for readers. The U.S. Environmental Protection Agency's Integrated Risk Information System (IRIS) Program has developed an approach for systematic review of evidence of health effects from chemical exposures that includes structured approaches for literature search and screening, study evaluation, data extraction, and evidence synthesis and integration. This approach recognizes the need for developing outcome-specific criteria for study evaluation. Because studies are assessed at the outcome level, a study could be considered high quality for one investigated outcome, and low quality for another, due to differences in the outcome measures, analytic strategies, how relevant a certain bias is to the outcome, and how the exposure measure relates to the outcome. The objective of this paper is to illustrate the need for outcome-specific criteria in study evaluation or risk of bias evaluation, describe the process we used to develop the criteria, and summarize the resulting criteria.

Methods: We used a process of expert consultation to develop several sets of outcome-specific criteria to guide study reviewers, improve consistency, and ensure consideration of critical issues specific to the outcomes. The criteria were developed using the following domains: outcome assessment, exposure measurement (specifically timing of exposure in relation to outcome; other exposure measurement issues would be addressed in exposure-specific criteria), participant selection, confounding, analysis, and sensitivity (the study's ability to detect a true effect or hazard).

Results: We discuss the application of this process to pregnancy-related outcomes (preterm birth, spontaneous abortion), other reproductive-related outcomes (male reproductive hormones, sperm parameters, time to pregnancy, pubertal development), chronic disease (diabetes, insulin resistance), and acute or episodic conditions (asthma, allergies), and provide examples of the criteria developed. For each outcome the most influential methodological considerations are highlighted including biological sample collection and quality control, sensitivity and specificity of ascertainment tools, optimal timing for recruitment into the study (e.g., preconception, specific trimesters), the etiologically relevant window for exposure assessments, and important potential confounders.

Conclusions: Outcome-specific criteria are an important part of a systematic review and will facilitate study

* Corresponding author.
E-mail addresses: radke-farabaugh.elizabeth@epa.gov, bethradke@gmail.com (E.G. Radke).

https://doi.org/10.1016/j.envint.2019.05.078
Received 13 November 2018; Received in revised form 3 April 2019; Accepted 30 May 2019
Available online 09 July 2019
0160-4120/ Published by Elsevier Ltd. This is an open access article under the CC BY-NC-ND license (http://creativecommons.org/licenses/BY-NC-ND/4.0/).

evaluations by epidemiologists with experience in evaluating studies using systematic review methods who may not have extensive discipline-specific experience in the outcomes being reviewed.

1. Introduction

Application of systematic review methodology to environmental exposures in epidemiologic research is a developing field, with multiple tools (or adaptations of existing tools) addressing some aspect of study quality published in the last several years (Rooney et al., 2016), including Navigation Guide (Woodruff and Sutton, 2014), National Toxicology Program Office of Health Assessment and Translation (NTP, 2015a), European Food Safety Authority (EFSA, 2017), Biomonitoring, Environmental Epidemiology, and Short-Lived Chemicals instrument (Lakind et al., 2015), and the U.S. Environmental Protection Agency's Toxic Substances Control Act evaluations (U.S. EPA, 2018a). Though the specific purpose of these tools differs, they all provide guidance on how to evaluate potential bias in epidemiological studies of environmental and occupational exposures. Use of systematic review tools is intended to improve consistency across reviewers and allow them to interpret and synthesize results in the context of the reliability and validity of each study.

Regardless of the study evaluation tool being used, there is an additional need for evaluations to be exposure- and outcome-specific. A study could be considered high quality for one investigated outcome, and low quality for another, due to, for example, differences in outcome prevalence, measurement error, analytic strategies, study design, and how the timing of exposure assessment relates to the outcome definition. The identification of limitations specific to a particular outcome enhances the ability of the study evaluation tool to transparently document potential selection bias, information bias, and confounding that could distort effect estimates to varying degrees. For example, blinding of outcome assessors may be irrelevant for mortality but critical for assessing a subjective outcome like some motor function tests (Guyatt et al., 2011). Similarly, a study in which exposure is measured concurrent with the presence of a condition may be evaluated as inappropriate for investigating some outcomes, such as diabetes or cancer, when the exposure cannot reflect the relevant etiologic exposure window in earlier years. However, the same study may be acceptable when the exposure is expected to result in short-term effects, such as insulin resistance among non-diabetics. Also, within a single study, reliability of outcome ascertainment may be age-dependent (e.g., asthma in children less than five years may not be reliably ascertained); thus, an outcome could be considered adequate in one age group and critically deficient in another. This type of consideration is not included in tools such as those listed above, because they appropriately are focused on issues that apply regardless of the specific exposure and outcome being reviewed. Thus, there is a need for an additional step in the study evaluation process: the development of specific criteria to supplement the higher-level tool.

In the guidance for the Cochrane Collaboration's Risk of Bias for Non-randomized Studies of Interventions (ROBINS-I) tool, Sterne et al. (2016) emphasize the necessity for both methodological and content expertise. During the planning stages prior to implementing study evaluations, potential issues specific to the methods and content of the studies need to be identified. These go beyond the level of detail that would be included in a well-defined PECO statement that includes explicit descriptions of outcomes to facilitate identification of relevant studies. Rather, the outcome-specific issues could include any methodological or biological factors that would influence confidence in the results of the studies during study evaluation/risk of bias evaluation. For some outcomes, the general considerations or criteria provided in the tools might prove to be adequate for performing an outcome-specific evaluation, but this determination should be made by a reviewer or reviewers with subject matter knowledge to ensure that critical issues are not missed. If subject matter experts identify outcome-specific

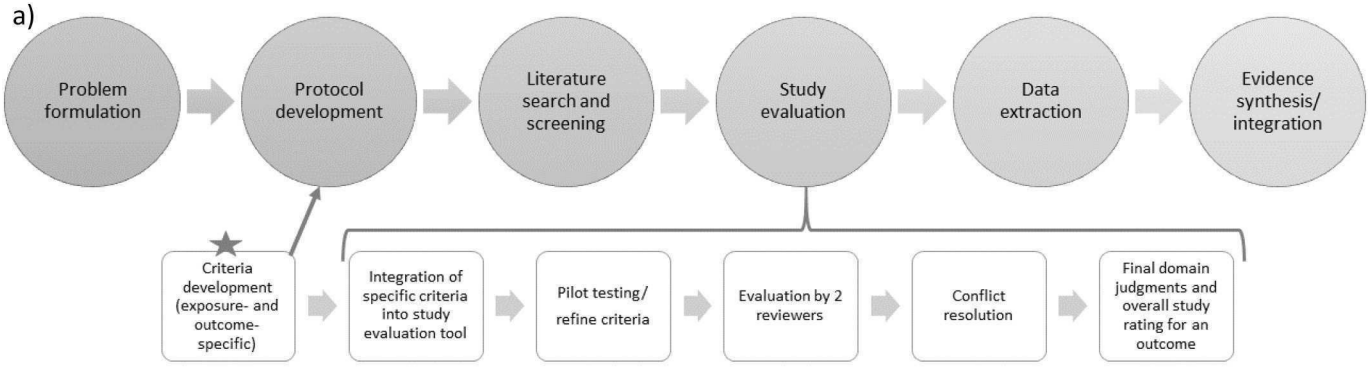

b)

Evaluation domains
Exposure measurement
Outcome ascertainment
Participant selection
Confounding
Analysis
Sensitivity
Selective reporting

Domain judgment	Interpretation
Good	Appropriate study conduct relating to the domain and minor deficiencies not expected to influence results.
Adequate	A study that may have some limitations relating to the domain, but they are not likely to be severe or to have a notable impact on results.
Deficient	Identified biases or deficiencies interpreted as likely to have had a notable impact on the results or prevent reliable interpretation of study findings.
Critically Deficient	A serious flaw identified that makes the observed effect(s) uninterpretable. Studies with a critical deficiency will almost always be considered "uninformative" overall.

Overall Study Rating	Interpretation
High	No notable deficiencies or concerns identified; potential for bias unlikely or minimal; sensitive methodology.
Medium	Possible deficiencies or concerns noted, but resulting bias or lack of sensitivity is unlikely to be of a notable degree.
Low	Deficiencies or concerns were noted, and the potential for substantive bias or inadequate sensitivity could have a significant impact on the study results or their interpretation.
Uninformative	Serious flaw(s) makes study results unusable for hazard identification or dose response.

Fig. 1. a) Illustration of how outcome-specific criteria fits into systematic review process; b) Study evaluation domains and evaluation classifications for determining overall study confidence.

considerations, it is helpful to develop outcome-specific evaluation criteria to guide the evaluations. The criteria can then be used by reviewers without the same level of in-depth specific subject matter knowledge, while further improving consistency and ensuring that critical issues are considered. A similar approach can be used for exposure measurement criteria. However, this step of developing exposure- and outcome-specific criteria is often not done for systematic reviews or the criteria and methods for developing them are not reported. While some higher quality systematic reviews clearly have performed or plan to perform evaluation on an outcome-specific basis and provide some criteria in their papers or protocols (e.g., (NTP, 2017; Lam et al., 2016; NTP, 2015b)), in general published systematic reviews have included criteria to evaluate outcomes inconsistently with variable degrees of specificity. When criteria are incompletely reported, it can be challenging to understand how the study ratings were reached and to compare the results of systematic reviews involving the same outcomes.

The U.S. Environmental Protection Agency's (EPA) Integrated Risk Information System (IRIS) Program has developed an approach for systematic review of evidence of health effects from chemical exposures that includes structured approaches for literature search and screening, study evaluation, data extraction, analysis and synthesis of results (including integration of human, animal, and mechanistic evidence) (Fig. 1). This approach is described in detail in the systematic review protocol for phthalates, available as part of the systematic reviews in this special issue, and in the IRIS Handbook, available at https://hawcprd.epa.gov/assessment/100000039/ (see "attachments"). As described in those documents, the study evaluation approach for observational epidemiology studies uses the principles of the domain-based ROBINS-I tool (Sterne et al., 2016), modified in order to address the specific needs of environmental epidemiology studies (see Morgan et al., 2019 and https://www.bristol.ac.uk/population-health-sciences/centres/cresyda/barr/riskofbias/robins-e/ for information on a concurrent development effort called the ROBINS-E tool). Study evaluation, also called study appraisal or risk of bias evaluation in other tools, as used in the rest of this paper, is designed to assess both risk of bias and study sensitivity (i.e., the ability of a study to observe a true effect or hazard (Cooper et al., 2016)). However, describing the methodology of this larger tool is not the intent of this paper, which focuses more narrowly on development of outcome-specific criteria for study evaluation to improve quality of the reviews by ensuring systematic consideration of critical issues, and improving transparency and consistency across raters. The purpose of this paper is to illustrate the need for outcome-specific criteria in study evaluation or risk of bias evaluation, describe the process we used to develop criteria, and summarize the resulting criteria. While these criteria were developed with the IRIS program context in mind, the considerations and the process for developing them could be easily adapted for use with other study evaluation/risk of bias tools.

2. Methods

We identified outcomes that would benefit from outcome-specific evaluation criteria in planned upcoming systematic reviews and then solicited subject matter experts (consultants) to assist in the development of these criteria. Experts were epidemiologists with several years of training and experience with designing and conducting population-based or occupational studies, with expertise in research evaluating the outcomes they contributed to, largely identified from academic settings, with diverse institutions intentionally selected.

The experts, in collaboration with IRIS scientists, developed outcome-specific evaluation criteria for the following domains (Fig. 1), which were established as part of the study evaluation approach prior to initiation of this effort: outcome ascertainment, relevant time window of exposure (one component of larger exposure measurement domain), participant selection, confounding, analysis, and other attributes, not considered in another domain, that could affect study sensitivity. Selective reporting is another domain considered in the study evaluation tool, but this was not considered to have outcome-specific components and thus is not discussed further in this paper. Under this study evaluation approach, each domain is assigned a rating (Fig. 1) based on outcome-specific criteria as well as criteria that applied to all outcomes. These domain ratings are then combined for an overall study confidence rating for that outcome. The overall rating is reached based on reviewer judgments about the likely impact the noted deficiencies in bias and sensitivity for each domain had on the results and is not a quantitative "score". These decisions, including outcome-specific

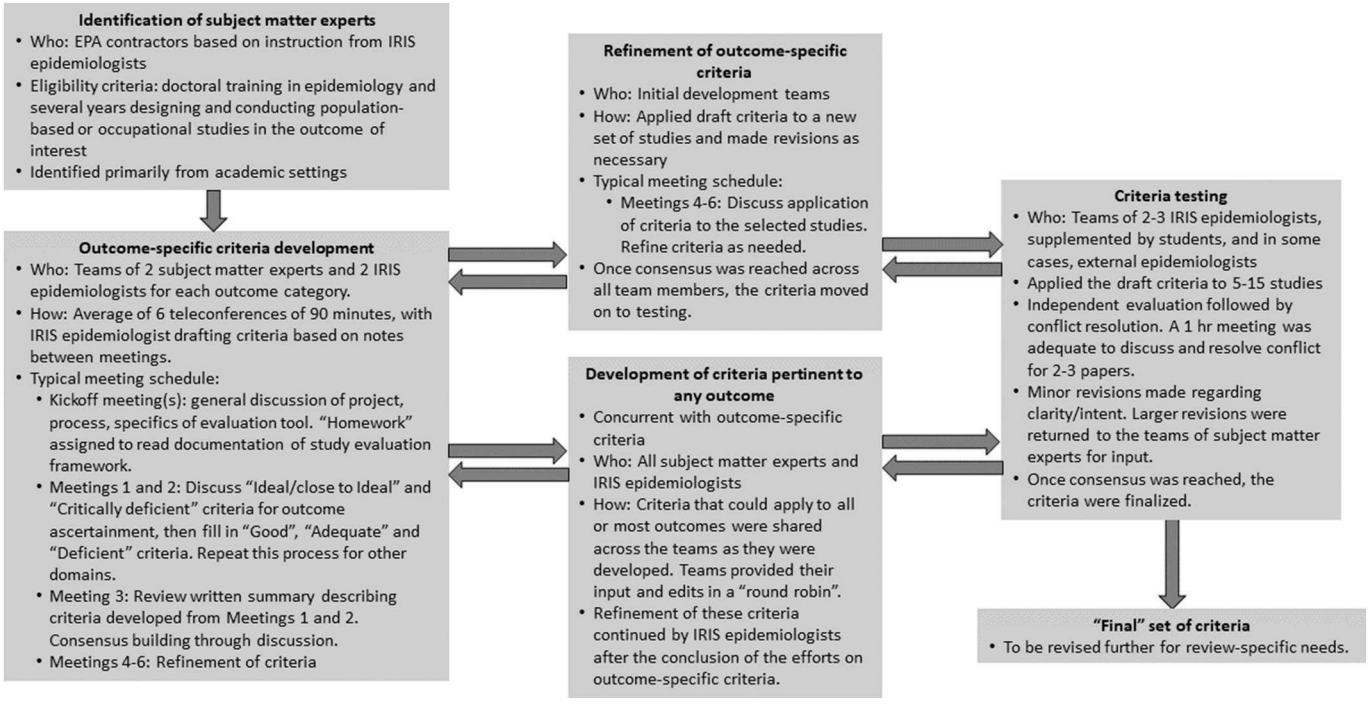

Fig. 2. Process for outcome-specific criteria development.

considerations, inform the synthesis and integration of the evidence looking across studies (Fig. 1). The subject matter experts developed criteria for each classification level (i.e., good, adequate, deficient, critically deficient). Because the criteria are intended to be applicable to any exposure, they were developed with the expectation that they would be a starting place for any systematic review on that outcome but would need to be reviewed and customized for the specific exposure. Most aspects of exposure measurement and other factors that require knowledge of the exposure would be considered separately with exposure-specific criteria. The criteria could be further customized to any other needs specific to the systematic review question. Some study design and conduct issues were relevant to more than one domain (e.g., timing of exposure measures is related to how participants are selected as well as exposure measurement; control of confounding is related to the data analysis). Where there was potential blurring between domains, the criteria were designed to avoid penalizing a study for the same limitation in multiple domains, so issues were assigned to the domain considered most relevant by the experts.

We piloted this process on two related outcomes: asthma and allergies-allergic sensitization. In this phase, we focused on criteria relating to outcome definitions, ascertainment methods and participant selection used in population-based and occupational studies. Two groups of five experts (listed in acknowledgements, coordinated by author WA) discussed a series of directed questions pertaining to these issues for asthma or for allergies; written responses to questions were also provided by the experts. We used this discussion to develop the evaluation criteria for these outcomes, and to refine the expert consultation process for the next set of outcomes.

In this next phase of our evaluation development process (Fig. 2), we focused on three outcome categories, and recruited two subject matter expert consultants for each (author initials in parentheses) –pregnancy outcomes (AP, EH), reproductive effects (JB, CL), and diabetes (AN-A, RP). Two or more IRIS epidemiologists without subject matter expertise (author initials GC, AG, AP) were also included on each development team. The teams had the flexibility to develop separate criteria for related outcomes or multiple outcomes encompassed in the categories. In total, outcome-specific evaluation criteria were developed for ten outcomes: two pregnancy-related (preterm birth, spontaneous abortion), two male reproductive-related (reproductive hormones, semen parameters), two that could be related to either male or female reproductive function (fecundity/time to pregnancy and pubertal development), two diabetes-related (diabetes, insulin resistance among non-diabetics), and two immune-related (asthma, allergy).

During the process of criteria development, core questions were used to define the domains, and a set of corresponding prompting and follow-up questions served to help the teams focus on details relevant to study evaluation for each domain (Table 1). A set of questions pertaining to each domain are central to the IRIS study evaluation approach described in the introduction. Their purpose in the tool is to focus the development of more specific evaluation criteria on sources of bias and study aspects affecting sensitivity for the exposure-outcome combination being reviewed. The teams began by evaluating a set of sample studies drawn primarily from the phthalates literature, as this is a broad, robust database with a large collection of studies examining many different outcomes using a variety of designs, and exposure-specific evaluation criteria had already been developed. The studies were identified in a comprehensive literature search of phthalate epidemiology studies, and approximately six sample studies were selected for each outcome based on representing the different available study designs (and their corresponding strengths and limitations). The discussions began with identification of aspects of an ideal study (i.e., a state-of-the-art observational study design, appropriate to the definition and timeframe for the exposure and endpoints assessed, that would be expected to be free of bias for the domain) and critical deficiencies so severe as to warrant exclusion of the study from future analyses. From there, the criteria for four different rating levels were fleshed out between the two extremes. The development used a consensus building process, with each member offering suggestions regarding content and phrasing of the criteria that were discussed as a group; each team member reviewed the edited versions and offered additional suggestions for discussion if necessary. In general, 2 or 3 rounds of edits were performed for each domain. Any discrepancies of opinion were resolved with further discussion. Once a working set of draft criteria were available, the teams applied them to a second set of sample studies and made revisions as necessary.

As part of this process, it became clear that some considerations/criteria were not outcome-specific, but rather applicable to all or most outcomes. This type of criteria was shared across teams frequently as they were developed to maintain consistency and aid efficiency. Each team could take what had been done already, provide their input and edits, and then share with the other teams. This had the advantage of establishing multi-stakeholder consensus for non-outcome-specific considerations rather than duplicating effort across the teams and producing documents that would require extensive resolution. Outcome-specific criteria were not shared across teams.

Once the criteria were drafted, a team of two to four epidemiologists (author initials GC, ER, BG, AG, AP, TB, MW, acknowledgment initials LP), including at least two IRIS epidemiologists with PhDs in epidemiology, applied the evaluation criteria to a set of 5–15 studies, depending on the number of studies available in the database (i.e., all of the studies in the database were used in testing). For each study, ratings were established for each domain and for overall study confidence (Fig. 1). Members of the team performed evaluations independently, and then discussed discrepancies in evaluation results and difficulties in applying the criteria and came to a consensus rating. When differences occurred, the discussion focused on whether the difference was due to ambiguity in the criterion that needed clarification or a mistake on the part of one of the reviewers (e.g., a reviewer not seeing information that had been provided in the article). Based on this experience of evaluation and reconciliation, the criteria were revised again as needed to address additional issues regarding clarity or intent identified during this process. These edits were generally minor language clarifications, but subject matter experts were available for consultation during the testing phase to answer any questions that arose, and a small number of more substantial changes were returned to them for input. For example, a strict cutoff of participation rate for each rating level was revised to allow for more reviewer judgment in the likely impact of participation rate on the potential for selection bias for each specific study (i.e., considering rationale for why participation is unlikely to be related to exposure). Additional testing, including evaluation of studies from other chemicals, was performed when inconsistency in ratings remained.

3. Results

3.1. Outcome-specific considerations by domain

3.1.1. Outcome ascertainment

This domain is the one that is most unique to each set of outcome-specific criteria. Each outcome uses specific methodologies to determine a “case” and each methodology has inherent specificity, sensitivity and reliability. Criteria for the outcome domain had clearly defined requirements for measurements to be valid (e.g., fasting, sample collection in the morning, exclusion of known diabetics, questionnaires validated in culturally appropriate populations), and other information needed to determine whether the methods were carried out appropriately (e.g., laboratory assays, quality control procedures). Reference to existing guidance or consensus publications on the outcome measurement by expert professional organizations or leading institutions in the field is informative in this section.

Table 1
Questions to guide the development of criteria for each domain in epidemiology studies.

Domain and core question (target bias)	Prompting questions	Follow-up questions
Exposure measurement Does the exposure measure reliably distinguish between levels of exposure in a time window considered most relevant for a causal effect with respect to the development of the outcome? (information bias)	For all: • Does the exposure measure capture the variability in exposure among the participants, considering intensity, frequency, and duration of exposure? • Does the exposure measure reflect a relevant time window? If not, can the relationship between measures in this time and the relevant time window be estimated reliably? • Was the exposure measurement likely to be affected by a knowledge of the outcome? • Was the exposure measurement likely to be affected by the presence of the outcome (i.e., reverse causality)? For case-control studies of occupational exposures: • Is exposure based on a comprehensive job history describing tasks, setting, time period, and use of specific materials? For biomarkers of exposure, general population: • Is a standard assay used? What are the intra- and interassay coefficients of variation? Is the assay likely to be affected by contamination? Are values less than the limit of detection dealt with adequately? • What exposure time-period is reflected by the biomarker? If the half-life is short, what is the correlation between serial measurements of exposure?	Is the degree of exposure misclassification likely to vary by exposure level? If the correlation between exposure measurements is moderate, is there an adequate statistical approach to ameliorate variability in measurements? If there is a concern about the potential for bias, what is the predicted direction or distortion of the bias on the effect estimate (if there is enough information)?
Outcome ascertainment Does the outcome measure reliably distinguish the presence or absence (or degree of severity) of the outcome? (information bias)	For all: • Is outcome ascertainment likely to be affected by knowledge of exposure (e.g., consider access to health care, if based on self-reported history of diagnosis)? For case-control studies: • Is the comparison group without the outcome (e.g., controls in a case-control study) based on objective criteria with little or no likelihood of inclusion of people with the disease? For mortality measures: • How well does cause of death data reflect occurrence of the disease in an individual? How well do mortality data reflect incidence of the disease? For diagnosis of disease measures: • Is diagnosis based on standard clinical criteria? If based on self-report of diagnosis, what is the validity of this measure? For laboratory-based measures (e.g., hormone levels): • Is a standard assay used? Does the assay have an acceptable level of interassay variability? Is the sensitivity of the assay appropriate for the outcome measure in this study population?	Is there a concern that any outcome misclassification is nondifferential, differential, or both? What is the predicted direction or distortion of the bias on the effect estimate (if there is enough information)?
Participant selection Is there evidence that selection into or out of the study (or analysis sample) was jointly related to exposure and to outcome? (selection bias including attrition [primarily], confounding)	For longitudinal cohort: • Did participants volunteer for the cohort based on knowledge of exposure and/or preclinical disease symptoms? Was entry into the cohort or continuation in the cohort related to exposure and outcome? For occupational cohort: • Did entry into the cohort begin with the start of the exposure? • Was follow-up or outcome assessment incomplete, and if so, was follow-up related to both exposure and outcome status? • Could exposure produce symptoms that would result in a change in work assignment/work status (“healthy worker survivor effect”)? For case-control study:	Were differences in participant enrollment and follow-up evaluated to assess bias? If there is a concern about the potential for bias, what is the predicted direction or distortion of the bias on the effect estimate (if there is enough information)? Were appropriate analyses performed to address changing exposures over time in relation to symptoms? Is there a comparison of participants and nonparticipants to address whether differential selection is likely?

(*continued on next page*)

Table 1 (*continued*)

Domain and core question (target bias)	Prompting questions	Follow-up questions
	• Were controls representative of population and time periods from which cases were drawn? • Are hospital controls selected from a group whose reason for admission is independent of exposure? • Could recruitment strategies, eligibility criteria, or participation rates result in differential participation relating to both disease and exposure? For population-based survey: • Was recruitment based on advertisement to people with knowledge of exposure, outcome, and hypothesis?	
Confounding Is confounding of the effect of the exposure likely? (confounding)	Is confounding adequately addressed by considerations in… a. … participant selection (matching or restriction)? b. … accurate information on potential confounders, and statistical adjustment procedures? c. … lack of association between confounder and outcome, or confounder and exposure in the study? d. … information from other sources? Is the assessment of confounders based on a thoughtful review of published literature, potential relationships (e.g., as can be gained through directed acyclic graphing), minimizing potential overcontrol (e.g., inclusion of a variable on the pathway between exposure and outcome)?	If there is a concern about the potential for bias, what is the predicted direction or distortion of the bias on the effect estimate (if there is enough information)?
Analysis Does the analysis strategy and presentation convey the necessary familiarity with the data and assumptions?[a]	• Are missing outcome, exposure, and covariate data recognized, and if necessary, accounted for in the analysis? • Does the analysis appropriately consider variable distributions and modeling assumptions? • Does the analysis appropriately consider subgroups of interest (e.g., based on variability in exposure level or duration, or susceptibility)? • Is an appropriate analysis used for the study design? • Is effect modification considered, based on considerations developed a priori? • Does the study include additional analyses addressing potential biases or limitations (i.e., sensitivity analyses)?	If there is a concern about the potential for bias, what is the predicted direction or distortion of the bias on the effect estimate (if there is enough information)?

[a] The evaluation of the analysis domain is focused on the appropriateness of the analysis rather than any specific form of bias.

3.1.2. Exposure measurement (relevant time window)

Most exposure concerns are addressed in separate exposure-specific criteria, which would be developed for the chemical or other exposure being reviewed. The outcome-specific criteria for the exposure domain focuses on the timing of exposure. For example, this could include: (a) whether exposure could be measured concurrent with the outcome; (b) whether the exposure must be measured prior to development of the outcome, or (c) whether the exposure must be measured during a critical window of exposure (such as gestation, where the critical window of exposure can be a specific trimester). When applying a set of outcome-specific criteria to a specific exposure, all criteria should be reviewed for relevance to a specific chemical; however, it is particularly important to review timing of exposure measures, as differences in half-life or other exposure factors may influence what timing is acceptable. For persistent chemicals, exposure measurement after a diagnosis was made may be acceptable if it is highly likely that behavioral changes after diagnosis did not affect exposure. For chemicals with short half-lives, measuring exposure after a diagnosis may not be acceptable. Outcome-specific factors such as latency and reversibility with the removal of exposure could also influence this domain.

3.1.3. Participant selection

Much of the criteria developed for participant selection applies to all outcomes, such as the reporting of inclusion/exclusion criteria, the participation rate, and comparison of participants and non-participants. There are two main types of outcome-specific considerations for this domain. One is the timing of the participant entry into the study. For example, the evaluation criteria may strongly favor study entry in the first trimester of pregnancy (for preterm birth), or require the population under study to encompass an appropriate age range (e.g., around pubertal onset for pubertal development). Another consideration is whether inclusion/exclusion criteria are appropriate for the population under study. For example, when studying diabetes incidence in a cohort study, diabetics should be excluded at baseline; current asthma symptoms, defined as the occurrence of asthma symptoms or medication use in the last 12 months, should be ascertained among individuals with a previous asthma diagnosis; and for semen parameters, population-based selection (with high participation rates) would be preferred to selection at infertility clinics.

3.1.4. Confounding

Most of the criteria developed for the evaluation of confounding are not outcome-specific, and thus could be applied to all outcomes. The focus for evaluation of confounding is the strategy for identifying confounders. Although a list of known risk factors was developed for each outcome, the lists are not variables that are required for a specific rating (e.g., *Good* or *Adequate*), since association with the exposure is also required for confounding to bias the results, and that cannot be captured in exposure-agnostic evaluation criteria. Rather, variables on the list should be considered as possible confounders, and the strategy for consideration can involve details relating to participant selection and characteristics, study design, and analytic approach.

Table 2
Key outcome-specific considerations for study evaluation[a].

Category	Outcome	Outcome ascertainment	Exposure (relevant time window)	Population selection	Confounding (variables to consider)	Analysis
Pregnancy outcomes	Preterm birth	• Method used to estimate gestational duration (e.g., early pregnancy dating with ultrasound preferred to birth certificate data)	• Must be measured during pregnancy (preferred) or preconception.	• Timing of study entry (1st trimester preferred).	• Age (u-shaped), gender, pre-pregnancy BMI/adiposity, lifestyle factors (physical activity, diet, smoking, alcohol), SES, co-exposures, pregnancy interval, maternal reproductive and clinical factors	• Outcome treated as dichotomous or three-level variable preferred.
	Spontaneous abortion	• Ascertainment of early loss (through daily urine samples) preferred • For clinical loss (> 5 weeks gestation), prospective ascertainment of pregnancy and loss preferred to recall or medical records	• Must be prior to outcome, ideally around conception	• Pregnancy planning couples preferred for identifying early loss. • Population-based or clinic-based with discussion of catchment area preferred to convenience sample • Recruitment prior to end of first trimester preferred	• Age, smoking, alcohol, parity, gravidity, SES, BMI/adiposity, fertility treatment, pregnancy interval, access to healthcare, co-exposures. If paternal exposure is the focus, maternal covariates should also be considered.	• Outcome treated as dichotomous variable preferred, with survival analysis for prospective designs.
Male reproductive	Reproductive hormones	• Time of collection (morning preferred) • Information on laboratory assays, quality control procedures	• Can be measured concurrent with outcome.	• Appropriate comparison group (e.g., similar referral patterns)	• Age, SES, smoking, alcohol use, BMI/adiposity, time of day, co-exposures	• Outcome treated as continuous variable preferred.
	Semen parameters (concentration, motility, morphology)	• Semen analysis on one or more samples. • Manual ascertainment of morphology preferred. • Abstinence time should be collected and considered. • Time between collection and analysis (influences motility) • Information on laboratory methods, quality control procedures	• For adult exposures, exposure measured concurrent with outcome is acceptable. • Must be before identification of infertility problem unless exposure does not change over time	• Selection at setting other than infertility clinic preferred. • Sample not limited to volunteers with known fertility problems unless similar selection in comparison group.	• Age, smoking, BMI, chronic disease status, abstinence time, co-exposures	• Outcome treated as continuous or dichotomous (with justified cut-points) variable.
Male or female reproductive	Pubertal development	• Tanner staging or physical measurements (e.g., testicular volume) by trained physician or investigator preferred	• Must be measured before pubertal onset (prenatal or childhood appropriate)	• Population must span the relevant age range (approximately 11–15 years)	• Age, race/ethnicity, SES, diet, obesity, family history of early or late pubertal onset, co-exposures	• Outcome may be treated as time to event (e.g., puberty onset) or ordinal (e.g., Tanner stage)
	Time to pregnancy	• Prospective measurement of couples discontinuing contraception is preferred. • If recall is used, should be number of cycles or months, and recall time < 10 years is preferred. • Designs where recall is only among pregnant women or where data is collected in categories (< 3 mo., 3–6 mo., etc.) are Poor. • Assessment of time to pregnancy from medical records (e.g., notation about history of infertility) not acceptable.	• Must be prior to conception unless exposure does not vary over time or with pregnancy. • For women: prior to attempt to conceive, including in utero • For men: Period of spermatogenesis for attempted conception	• Couples with no known fecundity impairments strongly preferred. • Sample not limited to couples that achieved pregnancy. • Population-based sampling preferred. Other sampling should be unbiased (e.g., not infertility clinic).	• Age (maternal and paternal), smoking, BMI, SES, co-exposures	• Outcome treated as time to event preferred.

(*continued on next page*)

Table 2 (*continued*)

Category	Outcome	Outcome ascertainment	Exposure (relevant time window)	Population selection	Confounding (variables to consider)	Analysis
Diabetes-related	Diabetes	• Clear definition of diabetes (e.g., ADA); self-report not sole criteria • Fasting requirements • Information on laboratory assays, quality control procedures	• Must be measured before diabetes onset.	• Exclude diabetics at baseline • Cohort followed for sufficient period to allow development of disease	• Age, gender, BMI/adiposity, lifestyle factors (physical activity, diet, smoking, alcohol), SES, co-exposures	• Outcome treated as dichotomous or three-level variable preferred.
	Insulin resistance	• Absence of diabetes • HOMA-IR and HOMA-β, or fasting insulin and fasting glucose • Fasting requirements • Information on laboratory assays, quality control procedures	• Can be measured concurrent with outcome.	• Exclude individuals with known diabetes	• Age, gender, BMI/adiposity, lifestyle factors (physical activity, diet, smoking, alcohol), SES, co-exposures	• Outcome treated as continuous variable preferred.
Asthma and allergies	Asthma	• Self-report using validated questionnaires for physician diagnosed asthma incidence or outcome prevalence (e.g., ATS, ISAAC) or medical record review/ physician confirmation for incidence; • Validation of questionnaires in same population preferred.	• Up to two years prior to ascertainment of incidence or concurrent with prevalence or related outcomes	• Population-based sampling preferred; adults or children > 4 years of age. Consider healthy worker effect in occupational studies.	• Age, sex, race, socioeconomic status, season of outcome measurement (for prevalence and related outcomes), geographic location, co-exposures	• Outcome is dichotomous; effect modification by age (child vs adult) preferred if appropriate
	Allergic sensitization and allergy outcomes	• Ascertainment of sensitization via skin prick test or specific immunoglobulin E levels in blood using validated methods; use of standardized cut-points, distinguishing between food and environmental allergens, and testing a panel of 5–10 allergens preferred. • Ascertainment of site-specific symptoms and outcomes using standardized questionnaires, distinguishing food and other allergy; preferably validated in same population. Ascertainment via self-report of medication use must clarify type of medication.	• Must precede sensitization or symptom onset; or concurrent with prevalence or symptom ascertainment	• Studies among children preferred for sensitization or symptom onset (aged > 4 years). • Self-reported symptoms preferred over restricting to physician diagnosed allergic disease.	• Age, sex, race, socioeconomic status, season of outcome measurement (for prevalence and related outcomes), geographic location, co-exposures	• Stratified analyses of children and adults; age analyzed as effect modifier for studies of sensitization

Abbreviations: ADA (American Diabetes Association), HOMA-IR (Homeostatic model assessment of insulin resistance), HOMA-β (homeostatic model assessment of β-cell function), ATS (American Thoracic Society), ISAAC (International Society of Arthritis and Allergies in Children).

[a] Classification of the considerations in this table into levels (Good, Adequate, Deficient, and Critically deficient) requires additional considerations that apply to all outcomes and outcome-specific considerations. Rationale for the considerations are discussed in the full outcome-specific evaluation criteria (supplementary materials).

Table 3
Criteria for diabetes and insulin resistance.

Level	Exposure measurement	Outcome ascertainment	Participant selection	Confounding	Analysis
Good	Will be developed for the specific exposure Diabetes • Exposure must be measured before diabetes onset (e.g., prospective cohort). Insulin resistance • Can be measured concurrent with outcome. Criteria that apply to all exposures • Valid exposure assessment methods used which represent the etiologically relevant time period of interest. • Exposure misclassification is expected to be minimal.	Diabetes • For undiagnosed cases, American Diabetes Association (ADA) definition with or without repeated measures, and: o Indicates fasting was required. o Includes information on the laboratory test requirements for hemoglobin A1c and for conducting the oral glucose tolerance tests. o Provides some information on assays, quality control procedures, reliability or validity measures. • For diagnosed cases, self-reported physician diagnosis or medical treatment for diabetes can be used. Participants without a diagnosis should be tested to avoid false negatives. Insulin resistance • Homeostatic model assessment (HOMA) of insulin resistance (HOMA-IR) and β-cell function (HOMA-β) in the absence of diabetes from fasting glucose and insulin concentrations measured in plasma. AND/OR • Fasting insulin and fasting glucose measures – indicates fasting was required. Fasting time accounted for in analysis if compliance was an issue. AND • Provides some information on assays, quality control procedures, reliability or validity measures.	Diabetes • Prospective cohort or other design that allows for identification of incident disease. • Must exclude individuals with diabetes at baseline. Prediabetes can be included but should be addressed in analysis via stratification or sensitivity analysis. • Cohort followed for sufficient period to allow for development of disease. Insulin resistance • Cross-sectional studies are appropriate. • Must exclude individuals with known diabetes. Note for both: for studies of children/adolescents, lack of exclusion of diabetes cases may be acceptable due to low prevalence. Criteria that apply to all outcomes • Minimal concern for selection bias based on description of recruitment process. • Exclusion and inclusion criteria specified and would not induce bias. • Participation rate is reported at all steps of study (e.g., initial enrollment, follow-up, selection into analysis sample). If rate is not high, there is appropriate rationale for why it is unlikely to be related to exposure (e.g., comparison between participants and nonparticipants or other available information indicates differential selection is not likely).	Diabetes and Insulin resistance • Risk factors that should be considered as possible confounders include age, gender, BMI/adiposity, lifestyle factors (physical activity, diet, smoking, alcohol), SES, co-exposures Criteria that apply to all outcomes Contains all of the following: • Conveys strategy for identifying key confounders. This may include: a priori biological considerations, published literature, or statistical analyses; with recognition that not all "risk factors" are confounders. • Inclusion of potential confounders in statistical models not based solely on statistical significance criteria (e.g., $p < 0.05$ from stepwise regression). • Does not include variables in the models that have been shown to be influential colliders or intermediates on the causal pathway. • Key confounders are evaluated and considered to be unlikely sources of substantial bias. This will often include: o Presenting the distribution of potential confounders by levels of the exposure and/or the outcomes of interest (with amount of missing data noted); or o Consideration that potential confounders were rare among the study population, or were expected to be poorly correlated with exposure of interest; or o Presenting a progression of model results with adjustment for different potential confounders, including consideration of the function forms of potential confounders, if warranted.	Criteria that apply to all outcomes • Use of an optimal characterization of the outcome variable. • Quantitative results presented (e.g., effect estimates and confidence limits). • Descriptive information about outcome and exposure provided (where applicable): o Amount of missing data noted and addressed appropriately. o For exposure, includes LOD (and percentage less than LOD) and discussion of cut-points and transformations. • Includes analyses that address robustness of findings (e.g., examination of exposure-response, relevant sensitivity analyses). Effect modification examined based only on a priori rationale with sufficient numbers. • No deficiencies in analysis evidence. Discussion of some details may be absent (e.g., examination of outliers).
Adequate	Will be developed for the specific exposure Diabetes • Exposure must be measured before diabetes onset.	Diabetes • ADA definition without repeated measures, and no other information provided. or • The use of medical records with details on criteria used to define	Same as Good, but: Criteria that apply to all outcomes • Enough of a description of the recruitment process to be comfortable that there is no serious risk of bias. • Inclusion and exclusion criteria specified and would not induce bias.	Criteria that apply to all outcomes Similar to Good, but may not have included all key confounders, or less detail may be available on the evaluation of confounders (e.g., sub-bullets in Good). It is possible that residual confounding could explain part of the observed effect, but concern is minimal.	Criteria that apply to all outcomes Same as Good, except: • Descriptive information about exposure provided but may be incomplete; might not have discussed missing data, or cut-points, or shape of distribution.

(*continued on next page*)

Table 3 (*continued*)

Level	Exposure measurement	Outcome ascertainment	Participant selection	Confounding	Analysis
	Insulin resistance • Can be measured concurrent with outcome. Criteria that apply to all exposures • Valid exposure assessment methods used which represent the etiologically relevant time period of interest. • Exposure misclassification may exist but is not expected to greatly change the effect estimate.	diabetes, in the absence of laboratory tests conducted specifically for the study. Insulin resistance • Fasting insulin and fasting glucose measures – no details of fasting or laboratory assays provided.	• Participation rate is incompletely reported but available information indicates participation is unlikely to be related to exposure.		or • Some important analyses that address the robustness of findings are not performed.
Deficient	Will be developed for the specific exposure Diabetes • Exposure must be measured before diabetes onset unless the exposure is persistent in the body. Insulin resistance • Can be measured concurrent with outcome. Criteria that apply to all exposures • Valid exposure assessment methods used which represent the etiologically relevant time period of interest. There may be concerns about reverse causality, but there is no direct evidence that it is influencing the effect estimate. • Exposed groups are expected to contain a notable proportion of unexposed or minimally exposed individuals, the method did not capture important temporal or spatial variation, or there is other evidence of exposure misclassification.	Diabetes • Treatment for diabetes or use of medical records without details on criteria used to define diabetes. or • Self-reported physician diagnosis is the sole criteria for case ascertainment; participants without a diagnosis are not tested and presumed to be non-cases. Insulin resistance – none defined.	Criteria that apply to all outcomes • Little information on recruitment process, selection strategy, sampling framework, and/or participation. OR • Aspects of the recruitment process, selection strategy, sampling framework, or participation raise the potential for bias (e.g., healthy worker effect, survivor bias).	Criteria that apply to all outcomes • Does not include variables in the models that have been shown to be influential colliders or intermediates on the causal pathway. And any of the following: • The potential for bias to explain some of the results is high based on an inability to rule out residual confounding, such as a lack of demonstration that key confounders of the exposure-outcome relationship were considered. • Descriptive information on key confounders (e.g., their relationship relative to the outcomes and exposure levels) are not presented. • Strategy of evaluating confounding is unclear or is not recommended (e.g., based on statistical significance criteria or stepwise regression only).	Criteria that apply to all outcomes • Descriptive information about exposure levels not provided (where applicable). or • Effect estimate presented without standard error or confidence interval. or • Non-optimal analysis methods used (e.g., correlation instead of linear regression)
Critically deficient	Will be developed for the specific exposure Diabetes • Exposure measure does not reflect exposure before onset of diabetes or is known to be affected by disease status.	Diabetes • Studies using self-reported diabetes with no clear information on the questions used to ascertain diabetes status. • Use of glucosuria to identify diabetes cases. • Use of diabetes mortality.	Criteria that apply to all outcomes • Aspects of the processes for recruitment, selection strategy, sampling framework, or participation, or specific available data result in concern that bias resulted in a large impact on effect estimates.	Criteria that apply to all outcomes • Includes variables in the models that have been shown to be influential colliers or intermediates in the causal pathway, indicating that substantial bias is likely from this adjustment. or • Confounding is likely present and not accounted for, indicating that the	Criteria that apply to all outcomes • Results presented as statistically "significant"/"not significant" or just p-values (i.e., without including effect estimates). or • Effect modification examined without clear a priori rationale and without providing main effects.

(*continued on next page*)

Table 3 (*continued*)

Level	Exposure measurement	Outcome ascertainment	Participant selection	Confounding	Analysis
	Criteria that apply to all exposures ● Exposure measurement does not characterize the etiologically relevant period for the outcome or is not valid. ● There is direct evidence that reverse causality could account for the observed association. ● Exposure measurement was not independent of outcome status.	Insulin resistance ● Reporting HOMA-β in the absence of HOMA-IR Criteria that apply to all outcomes ● Invalid/insensitive marker of outcome. ● Outcome ascertainment was not independent from exposure status.		results were most likely due to bias (i.e., confounders associated with the outcome and exposure in the study could explain the majority of the reported results). or	● Analysis methods were not appropriate for the design or data.

3.1.5. Analysis

As with confounding, most of the criteria for evaluation of analysis are not outcome-specific. The criteria include consideration of whether appropriate analysis methods are used, whether quantitative results are presented, and whether there is adequate analysis of the robustness of the findings (e.g., sensitivity analyses). In this group of outcomes, the primary outcome-specific consideration for analysis is the characterization of the outcome variable. For some outcomes, a dichotomous or three-level variable is considered optimal (e.g., preterm birth), while for others, a continuous variable is preferred. The rationale for these preferences is described in the complete sets of criteria.

3.1.6. Sensitivity

Sensitivity issues include a narrow or low exposure range, small sample size, a high percentage below the limit of detection, an inappropriate length of follow-up, and inappropriate choice of referent group (Cooper et al., 2016). Most of these considerations are not outcome-specific, but there are some that are. It is important to note that some issues that reduce sensitivity may be considered in other domains and would not be double counted in the overall study confidence evaluation. Sensitivity is not evaluated on a four-level scale like the other domains, but rather as “adequate” or “deficient”. Since many of the sensitivity considerations are continuous measures, specific criteria were not developed, and classification of this domain relies on review-specific expert judgment on the impact of these limitations.

3.2. Application to study evaluation for specific outcomes

The key considerations identified for each outcome are listed in Table 2, and each outcome has a supplemental file with the full set of criteria. An example of criteria by classification level for diabetes and insulin resistance is in Table 3 and includes criteria that apply to all outcomes identified during the process. A case study of the application of these criteria on a paper by James-Todd et al. (2012) using NHANES data is available at: https://hawcprd.epa.gov/rob/study/100501814/ and additional examples of the application of these criteria across several studies are available in systematic reviews of phthalates (Radke et al., 2018, Radke et al., 2019a,b (forthcoming)). The following discussion highlights some of the important considerations brought out by the expert consultations for each of the major outcome categories.

3.3. Pregnancy outcomes

Pregnancy outcomes present some unique issues due to the short duration and couple dependent nature of a pregnancy. Two pregnancy outcomes were examined during this process: preterm birth (Supplement A) and spontaneous abortion (Supplement B). For both outcomes, timing of entry into the study is important. For preterm birth, participants will ideally be enrolled during the first trimester, since with later study entry some participants who experienced early preterm birth could be excluded. For spontaneous abortion, study entry is ideally preconception (e.g., couples trying to conceive) in order to completely ascertain pregnancy losses, including early (i.e., before clinical detection) loss, but must be in the first trimester. When considering outcome ascertainment, there are different considerations for the two outcomes. For preterm birth, the outcome has a clear definition (i.e., birth prior to 37 weeks gestation), but the sensitivity and specificity of this definition is reliant on the method used to ascertain gestational age. Early pregnancy dating with ultrasound is preferred to less reliable methods, such as retrospective questionnaire or use of administrative records. For spontaneous abortion, ideal measurement of early loss is through the use of daily urine samples, which enable detection of loss prior to clinical ascertainment of pregnancy. Such early detection is not possible in a study that recruits women after clinical recognition of a pregnancy. In those studies, clinical pregnancy loss, which occurs after clinical recognition of pregnancy and prior to 20 weeks of gestation, is

more feasibly ascertained. For both outcomes, exposure measurement should take place prior to the outcome occurring, around conception or during pregnancy. In addition, there are outcome-specific confounding and analysis considerations, and those are available in the supplements.

3.4. Reproductive effects

The criteria for the two male reproductive outcomes (semen parameters [Supplement C] and male reproductive hormones [Supplement D]) focused primarily on the accurate measurement of biological samples (semen and blood, respectively). For semen parameters, concentration, motility, and morphology were the primary measures of interest, and criteria address collection procedures, abstinence time, time from collection to analysis, and laboratory methods. For male reproductive hormones, testosterone, luteinizing hormone, follicle-stimulating hormone, and sex-hormone binding protein were discussed. For all of these hormones, the laboratory methods and quality control were important. In addition, for testosterone, which has diurnal variation, the criteria specify that collection must be in the morning or time of collection addressed in the analysis for a study to be considered acceptable. The criteria for semen parameters also address some specific issues for participant selection, where it is preferred, but not required, that selection occur at a setting other than an infertility clinic. For both of these outcomes, it was considered acceptable to measure the exposure concurrent with the outcome due to the potential for short term response, but it is preferred to more closely alight with the etiologic window (e.g., 90 days prior to sperm collection to account for spermatogenesis).

For the other two reproductive outcomes (time to pregnancy [Supplement E] and pubertal development [Supplement F]), timing of both exposure measurement and study enrollment was more important. For these, the ideal design is a prospective cohort with enrollment and exposure measurement prior to development of the outcome (pregnancy and puberty, respectively). These outcomes also have specific needs for outcome ascertainment. For time to pregnancy, it is preferred to have women from couples discontinuing contraception with close monitoring for pregnancy, but other methods, including retrospective recall by women, are acceptable as well. For pubertal development, Tanner stages can be used for boys and girls, ideally by a trained examiner. Testicular volume and spermarche can also be used for boys, and menarche can be used for girls. For all four reproductive outcomes, there are outcome-specific confounding and analysis considerations, available in the supplements.

3.5. Diabetes and insulin resistance

Studies of diabetes and insulin resistance were also considered (Supplement G), with each outcome presenting unique challenges. For both outcomes, timing of exposure measurement is an important consideration, particularly for exposures with short half-lives. For diabetes, it is important for studies to exclude individuals with diabetes at baseline and include only individuals with incident disease as cases, with exposure measured prior to development of diabetes to establish temporality. Accordingly, prospective designs are generally needed. For insulin resistance, the exposure and outcome can be assessed concurrently as the outcome can be a short-term response. There are also several important criteria for outcome ascertainment. To identify undiagnosed diabetes cases, use of the American Diabetes Association definition is preferred. It includes information about fasting, laboratory test requirements and assays, quality control procedures, and measure reliability/validity. Self-reported physician diagnosis or medical treatment was deemed appropriate to identify diagnosed cases, but additional testing is needed to identify undiagnosed cases. For insulin resistance, individuals with diabetes must be excluded as measures of insulin are not interpretable in the presence of diabetes, especially if diabetes is treated with hypoglycemic medication, as treatment influences insulin production and secretion. Fasting is also required for insulin and glucose measurements. The homeostatic model assessment of insulin resistance (HOMA-IR) is the preferred measure of insulin resistance and is calculated using measurements for insulin and glucose. In addition, there are outcome-specific confounding and analysis considerations, and those are available in the supplements.

3.6. Allergy and asthma

Asthma (Supplement H) and allergy (Supplement I) are related outcomes that that require different approaches depending on whether the outcome is the development of disease (incidence) or symptoms and morbidity among those with prevalent disease. For example, the key exposure window for incident asthma (as well as allergic sensitization) is up to two years prior to diagnosis, while concurrent exposure is most informative for asthma-related symptoms among those with an asthma diagnosis as well as those with allergy-related outcomes. Physician confirmed asthma diagnosis is considered best, but a self-report of physician diagnosed asthma can be used. Self-reported allergy outcomes using a validated questionnaire is preferable to a physician's diagnosis for allergy symptoms as many adults and children self-treat these symptoms at home and do not seek medical treatment. Age should be considered an effect modifier for both asthma and allergy outcomes, with adults and children analyzed separately. This is particularly true with asthma, as adult asthma is often very different from childhood asthma. Asthma cannot accurately be studied in children under 5, and so these children should not be enrolled in studies of asthma symptoms.

4. Discussion

The development and use of outcome-specific criteria that are used to supplement general study evaluation tools for evaluating confidence in individual epidemiology studies is an important step of the systematic review process that has not been well documented, and should be documented in the systematic review protocol. A body of literature on specific health outcomes in relation to chemical exposures may span several decades and comprise a broad spectrum of methodological approaches reflecting an evolving and maturing discipline, as well as differences in reporting detail. The involvement of epidemiologists with subject matter expertise in the outcomes and exposures that are under review is critical to assure that changes in definitions and measurement protocols that have occurred over time are captured, with an understanding of any consequent impacts on the sensitivity and specificity of outcome assessments. This understanding can be translated into criteria for evaluating potential bias and sensitivity for a systematic review. Health assessments of environmental exposure to chemicals and other hazards can involve a broad set of health effects, and ensuring that reviews are conducted by epidemiologists with subject-specific training (e.g., reproductive or respiratory epidemiology) can be challenging. Developing clear criteria also improves transparency of the systematic review.

We have described the methods and results of the approach used by IRIS to develop outcome-specific criteria for a variety of conditions occurring across the lifespan, including pregnancy outcomes, reproductive effects, chronic disease, and acute (episodic) conditions. As mentioned previously, these criteria were developed for use in IRIS assessment products but could be adapted for use with other study evaluation tools. There are several important considerations to note when developing or applying outcome-specific criteria. First, epidemiologists with discipline-specific expertise (e.g., reproductive or respiratory disease) add critical insight into the development of study evaluation tools for bias and sensitivity in environmental and occupational epidemiological studies. Evaluation of studies without input from subject-matter experts would likely miss important nuances. For example, when measuring testosterone, it is important for blood collection to be in the morning, or, if that is not possible, for time of collection

to be addressed in the analysis. Lack of this adjustment is considered a critical deficiency by the subject matter experts, but an epidemiologist without reproductive expertise would likely not have identified this as a source of bias. Even with relevant expertise, however, testing and revision of the criteria are needed to ensure their consistent use and interpretation.

Each set of outcome-specific criteria is not intended to stand-alone, but rather to supplement the existing study evaluation considerations (Table 1 or another tool). The criteria are intended to facilitate reviews by trained, experienced epidemiologists who may not have extensive discipline-specific experience in the outcomes being reviewed. While the availability of these criteria may lessen the requirement of extensive subject-matter expertise, judgments are still required based on understanding of concepts and best practices integral to the field of epidemiology, which is consistent with other programs performing systematic reviews (Rooney et al., 2016; NIEHS, 2015). Conclusions about the impact of potential bias on reported effect measure estimates require gathering information from multiple aspects of a study publication including descriptions of study methods, study groups and data analyses, as well as supporting documentation provided in supplemental documents and earlier publications. This strategy and the evaluation criteria were tested using epidemiologists with doctoral-level training (or masters-level with additional experience), and we caution against generalizing this experience to people with limited knowledge of epidemiology methods and principles.

These outcome-specific criteria are not prescriptive and should not be used as a checklist or as a tool to assign numeric scores for evaluating studies. Rather, they are intended to guide the reviewer to make their own expert judgment by highlighting relevant considerations and their relative importance. Scoring tools or numeric scales frequently mix reporting quality and applicability along with internal validity, and may not accurately account for differences in the impact of a given set of possible biases (Higgins and Green, 2011; Juni et al., 1999; Greenland, 1994). Evaluation should be guided but open-ended and reliant on expert judgment. This includes the ability to consider whether an identified limitation is likely to result in a substantial bias in the effect estimate and the need to account for a limitation in the overall study rating. Limitations identified in some domains may be deemed more important than limitations in other domains, but there is not a set of weights that is applicable to all studies. Judgment is also required on the impact of desired information that is not reported in the paper, which is a frequent occurrence.

In addition, the epidemiologists performing the study evaluations should familiarize themselves with the research on the health effects or outcomes being reviewed and consider the relevance and appropriateness of each criterion to the exposure scenario(s) being assessed. In particular, the timing of exposure measurements in the available studies (e.g., concurrent with outcome assessment or at some point prior) may guide selection of the outcome definitions to be included in the review. For example, among multiple asthma outcomes assessed in a cross-sectional study of indoor air pollution using average concentrations collected concurrent with the assessment of asthma, the definition for current asthma (i.e., asthma symptoms during the past 12 months) would be most relevant to the exposure assessment paradigm rather than an ever/never lifetime diagnosis of asthma.

There are some important limitations of this work. The criteria in the supplemental files is based on the consensus opinions of two subject matter experts and is supported by current literature in the field. However, as with any effort that relies on scientific judgment, there is potential for personal bias to be interjected into the process by individual researchers (Gotzsche and Ionnidis, 2012). Thus, including additional experts would be ideal to decrease the potential for bias, though this may not often be possible due to resource and time limitations facing many federal agencies, regulatory, authorities, and others performing systematic reviews. There are also other sources of curated outcome-specific information developed for clinical research that were not included in this effort, such as core outcome sets (Clarke and Williamson, 2016) and the PhenX Toolkit (Hamilton et al., 2011). These resources are not designed in the context of systematic review and study evaluation and do not include all the outcome measures that are included in epidemiology studies. Nonetheless, have already undergone review and could be useful supplements or resources when developing outcome-specific criteria in the future. Another limitation is that development and testing of these criteria was based on a small selection of studies, and thus the criteria do not represent all the possible scenarios that may be evaluated in the future. Rather, it is expected that the criteria will be “evergreen” and continue to develop and evolve as they are used. It is simply not practical to foresee every outcome-specific eventuality when developing an initial set of criteria, and this combined with the evolving nature of science and the need to include exposure-specific considerations, means that the versions of the criteria in the supplement cannot be used “off the shelf” in a new systematic review, and will need to be modified and tested for the specific review need. There is no expectation that the criteria will ever truly be “final”.

We have described a process for developing outcome-specific criteria for evaluation of individual epidemiology studies. Such criteria development is an important step in the systematic review process and contributes to transparency and consistency. Development of these outcome-specific criteria was a large undertaking that required contributions from many epidemiologists. However, less extensive outcome-specific criteria may be adequate, depending on the health outcome being evaluated. Nevertheless, it is a worthwhile and important step to have someone with research expertise in the outcome under consideration to review the study evaluation criteria to improve transparency and ensure that key issues are addressed. This should be an explicit and documented part of future systematic reviews.

Supplementary data to this article can be found online at https://doi.org/10.1016/j.envint.2019.05.078.

Acknowledgements

We would like to acknowledge the following individuals for their assistance with this project: Asthma and Allergy subject matter experts: Hasan Arshad, Peter Gergen, Elizabeth Matsui, Dan Norbäck, Matthew Perzanowski, Lara Akinbami, Christine Joseph, Felicia Rabito, Carl-Gustaf Bornehag; ICF contractors supporting this project: Michelle Cawley, Ashley Williams; IRIS management: Susan Rieth, Kris Thayer; External epidemiologists providing input during criteria testing: John Meeker, Wendi Robins, Maria Grau Perez; Other IRIS scientific support, including piloting of the criteria: Larissa Pardo, Leonid Kopylev; IRIS student support: Carolyn Gigot, Swati Gummadi, Alex Horansky, Jeff Nathan; EPA technical reviewers: Kristen Rappazzo and Ellen Kirrane.

References

Clarke, M., Williamson, P., 2016. Core outcome sets and systematic reviews. Syst. Rev. 5, 11.

Cooper, G., Lunn, R., Agerstrand, M., Glenn, B., Kraft, A., Luke, A., Ratcliffe, J., 2016. Study sensitivity: evaluating the ability to detect effects in systematic reviews of chemical exposures. Environ. Int. 92–93, 605–610. https://doi.org/10.1016/j.envint.2016.03.017.

EFSA (European Food Safety Authority), 2017. Guidance on the use of the weight of evidence approach in scientific assessments. EFSA J. 15, 4971. https://doi.org/10.2903/j.efsa.2017.4971.

Gotzsche, P., Ionnidis, P., 2012. Content area experts as authors: helpful or harmful for systematic reviews and meta-analyses. BMJ 345.

Greenland, S., 1994. Quality scores are useless and potentially misleading: reply to re: a critical look at some popular analytic methods [editorial]. Am. J. Epidemiol. 140, 300–301. https://doi.org/10.1093/oxfordjournals.aje.a117250.

Guyatt, G.H., Oxman, A.D., Vist, G., Kunz, R., Brozek, J., Alonso-Coello, P., Montori, V., Akl, E.A., Djulbehovic, B., Falck-Ytter, Y., Norris, S.L., Williams, J.W., Atkins, D., Meerpohl, J., Schunemann, H.J., 2011. GRADE guidelines: 4. Rating the quality of evidence-study limitations (risk of bias). J. Clin. Epidemiol. 64, 407–415. https://doi.org/10.1016/j.jclinepi.2010.07.017.

Hamilton, C., Strader, L., Pratt, J., Maiese, D., Hendershot, T., Kwok, R., Hammond, J.,

Huggins, W., Jackman, D., Pan, H., Nettles, D., Beaty, T., Farrer, L., Kraft, P., Marazita, M., Ordovas, J., Pato, C., Spitz, M., Wagener, D., Williams, M., Junkins, H., Harlan, W., Ramos, E., Haines, J., 2011. The PhenX toolkit: get the most from your measures. Am. J. Epidemiol. 174, 253–260.

Higgins, J., Green, S., 2011. Cochrane Handbook for Systematic Reviews of Interventions. Version 5.1.0. The Cochrane Collaboration 2011. http://handbook.cochrane.org.

James-Todd, T., et al., 2012. Urinary phthalate metabolite concentrations and diabetes among women in the National Health and Nutrition Examination Survey (NHANES) 2001-2008. Environ. Health Perspect. 120, 1307–1313.

Juni, P., Witschi, A., Bloch, R., Egger, M., 1999. The hazards of scoring the quality of clinical trials for meta-analysis. JAMA 282, 1054–1060.

Lakind, J.S., Goodman, M., Barr, D.B., Weisel, C.P., Schoeters, G., 2015. Lessons learned from the application of BEES-C: systematic assessment of study quality of epidemiologic research on BPA, neurodevelopment, and respiratory health. Environ. Int. 80, 41–71. https://doi.org/10.1016/j.envint.2015.03.015.

Lam, J., Sutton, P., Kalkbrenner, A., Windham, G., Halladay, A., Koustas, E., Lawler, C., Davidson, L., Daniels, N., Newschaffer, C., Woodruff, T., 2016. A systematic review and meta-analysis of multiple airborne pollutants and autism spectrum disorder. PLoS One 11, e0161851. https://doi.org/10.1371/journal.pone.0161851.

Morgan, R., Thayer, K., Santesso, N., Holloway, A., Blain, R., Eftim, S., Goldstone, A., Ross, P., Ansari, M., Ekl, E., Filippini, T., Hansell, A., Meerpohl, J., Mustafa, R., Verbeek, J., Vinceti, M., Whaley, P., Schunemann, H., GRADE Working Group, 2019. A risk of bias instrument for non-randomized studies of exposures: a users' guide to its application in the context of GRADE. Environ. Int. 122, 168–184.

NIEHS (National Institute for Environmental Health Sciences), 2015. Handbook for Preparing Report on Carcinogens Monographs. U.S. Department of Health and Human Services, Office of the Report on Carcinogens. https://ntp.niehs.nih.gov/ntp/roc/handbook/roc_handbook_508.pdf.

NTP (National Toxicology Program), 2015a. Handbook for conducting a literature-based health assessment using OHAT approach for systematic review and evidence integration. U.S. Dept. of Health and Human Services, National Toxicology Programhttps://ntp.niehs.nih.gov/ntp/ohat/pubs/handbookjan2015_508.pdf.

NTP (National Toxicology Program), 2015b. NTP Monograph: Identifying Research Needs for Assessing Safe Use of High Intakes of Folic Acid [NTP]. National Institute of Environmental Health Sciences, Research Triangle Park, NC. http://ntp.niehs.nih.gov/ntp/ohat/folicacid/final_monograph_508.pdf.

NTP (National Toxicology Program), 2017. Report on carcinogens protocol: Methods for preparing the draft report on carcinogens monograph on antimony trioxide and other antimony compounds. In: Running Title - Antimony: RoC Protocol. National Institute of Environmental Health Sciences, Research Triangle Park, NC.

Radke, E.G., Braun, J.M., Meeker, J.D., Cooper, G.S., 2018. Phthalate exposure and male reproductive outcomes: a systematic review of the human epidemiological evidence. Environ. Int. 121 (Part 1), 764–793. https://doi.org/10.1016/j.envint.2018.07.029.

Radke, E.G., Galizia, A., Thayer, K.A., Cooper, G.S., 2019a. Phthalate exposure and metabolic effects: a systematic review of the human epidemiological evidence. Environ. Int., 104768. https://doi.org/10.1016/j.envint.2019.04.040.

Radke, E.G., Galizia, A., Thayer, K.A., Cooper, G.S., 2019b. Phthalate exposure and metabolic effects: a systematic review of the human epidemiological evidence. Environ. Int., 104768. https://doi.org/10.1016/j.envint.2019.04.040.

Rooney, A.A., Cooper, G.S., Jahnke, G.D., Lam, J., Morgan, R.L., Boyles, A.L., Ratcliffe, J.M., Kraft, A.D., Schünemann, H.J., Schwingl, P., Walker, T.D., Thayer, K.A., Lunn, R.M., 2016. How credible are the study results? Evaluating and applying internal validity tools to literature-based assessments of environmental health hazards. Environ. Int. 92-93, 617–629. https://doi.org/10.1016/j.envint.2016.01.005.

Sterne, J., Higgins, J., Reeves, B., 2016. ROBINS-I: a tool for assessing risk of bias in non-randomized studies of interventions, version 7 march 2016. Br. Med. J. 355, i4919.

U.S. EPA (U.S. Environmental Protection Agency), 2018a. Application of systematic review in TSCA risk evaluations. (740-P1-8001). U.S. Environmental Protection Agency, Office of Chemical Safety and Pollution Prevention, Washington, D.C.https://www.epa.gov/sites/production/files/2018-06/documents/final_application_of_sr_in_tsca_05-31-18.pdf.

Woodruff, T.J., Sutton, P., 2014. The navigation guide systematic review methodology: a rigorous and transparent method for translating environmental health science into better health outcomes [review]. Environ. Health Perspect. 122, 1007–1014. https://doi.org/10.1289/ehp.1307175.

Environment International 130 (2019) 104580

Contents lists available at ScienceDirect

Environment International

journal homepage: www.elsevier.com/locate/envint

Review article

Phthalate exposure and female reproductive and developmental outcomes: a systematic review of the human epidemiological evidence

Elizabeth G. Radke[a,*], Barbara S. Glenn[a], Joseph M. Braun[b], Glinda S. Cooper[a,c]

[a] U.S. Environmental Protection Agency, National Center for Environmental Assessment, United States
[b] Brown University, School of Public Health, United States
[c] The Innocence Project, United States

A B S T R A C T

Objective: We performed a systematic review of the epidemiology literature to identify the female reproductive and developmental effects associated with phthalate exposure.

Data sources and study eligibility criteria: Six phthalates were included in the review: di(2-ethylhexyl) phthalate (DEHP), diisononyl phthalate (DINP), dibutyl phthalate (DBP), diisobutyl phthalate (DIBP), butyl benzyl phthalate (BBP), and diethyl phthalate (DEP). The initial literature search (of PubMed, Web of Science, and Toxline) included all studies of female reproductive and developmental effects in humans, and outcomes were selected for full systematic review based on data availability.

Study evaluation and synthesis methods: For each outcome, studies were evaluated using criteria defined a priori for risk of bias and sensitivity by two reviewers using a domain-based approach. Evidence was synthesized by outcome and phthalate and strength of evidence was summarized using a structured framework.

Results: The primary outcomes reviewed here are (number of included/excluded studies in parentheses): pubertal development (5/13), time to pregnancy (3/4), preterm birth (8/12), and spontaneous abortion (5/0). Among these outcomes, preterm birth had moderate evidence of a positive association with phthalate exposure (specifically DEHP, DBP, and DEP). Exposure levels for BBP, DIBP, and DINP were generally lower than for the phthalates with an observed effect, which may partially explain the difference due to lower sensitivity. Other phthalate/outcome combinations were considered to have slight or indeterminate evidence of an association.

Conclusions and implications of key findings: Overall, these results support that some phthalates may be associated with higher odds of preterm birth in humans, though there is some remaining inconsistency. More evidence is needed on the mechanism and relevant exposure window for this association.

The views expressed are those of the authors and do not necessarily represent the views or policies of the U.S. EPA.

1. Introduction

Phthalates (diesters of phthalic acid) are a class of synthetic chemicals used in many consumer and industrial products, including applications as plasticizers in polyvinyl chloride plastics and as ingredients in some medications and personal care products. Human exposure is ubiquitous across the lifespan, primarily via the oral route, but also through inhalation and dermal contacts (Johns et al., 2015). After exposure, phthalate diesters are rapidly metabolized (estimated half-lives of various phthalate metabolites is approximately 3 to 18 h) to monoester metabolites and excreted in the urine (Johns et al., 2015). The group of phthalates encompasses a variety of compounds with different structures, properties, and use (and relative potency, as shown from animal studies). The most common phthalates, and those focused on here are: di(2-ethylhexyl) phthalate (DEHP), diisononyl phthalate (DINP), dibutyl phthalate (DBP), diisobutyl phthalate (DIBP), butyl benzyl phthalate (BBP), and diethyl phthalate (DEP). The metabolites of each are described in the supplementary materials. Among the group, there are phthalates that are relatively structurally similar and moderately correlated with each other based on human biomonitoring data (e.g., DBP and DIBP). Some phthalates differ considerably in structure and commercial/industrial uses; correlations between these phthalates are typically low.

While male reproductive toxicity is the most commonly discussed hazard of phthalate exposure (NAS, 2017; Johnson et al., 2012; Howdeshell et al., 2008), there has also been substantial study of female reproductive and developmental effects of phthalate exposure. Exposure to some phthalates is higher in women than in men in some studies, which has been hypothesized to be due to higher use of cosmetics (Kay et al., 2013; Fennell et al., 2004; Lovekamp-Swan and Davis, 2003), though this may apply to some phthalates (e.g., DBP, DEP) used in cosmetics more than others. In addition, phthalates can cross the placenta, making developmental effects from in utero exposures a concern (Langonne et al., 1998), particularly given the

* Corresponding author.
E-mail address: radke-farabaugh.elizabeth@epa.gov (E.G. Radke).

https://doi.org/10.1016/j.envint.2019.02.003
Received 24 July 2018; Received in revised form 23 December 2018; Accepted 1 February 2019
Available online 24 July 2019
0160-4120/ Published by Elsevier Ltd. This is an open access article under the CC BY-NC-ND license (http://creativecommons.org/licenses/BY-NC-ND/4.0/).

potential for higher susceptibility in developmental stages. Existing narrative reviews are inconclusive and indicate that there may be an association with some outcomes, most notably preterm birth (Mariana et al., 2016; Hauser and Calafat, 2005; Benjamin et al., 2017), but no systematic review across key female reproductive and developmental effects is available. We performed a systematic review of the epidemiology literature on the female reproductive and developmental effects associated with phthalate exposure. This included review of the following outcomes: pubertal development, time to pregnancy, spontaneous abortion, and preterm birth. In addition, the evidence for some additional outcomes (e.g., ovarian reserve) was reviewed for coherence with the other outcomes and is summarized without systematic review. The human health relevance of these outcomes is summarized briefly in Table 1.

2. Methods

2.1. Literature search and screening

The literature search and screening, study evaluation, data extraction, and evidence synthesis methods are described in detail in the systematic review protocol (Supplement 1, Section 3). Briefly, epidemiology studies were identified by conducting a single broad literature search on all six phthalates of interest (DEHP, DINP, DBP, DIBP, BBP, DEP) and all outcomes. The Population, Exposure, Comparator, and Outcome (PECO) is available in the protocol (Supplement 1, Section 2). The following databases were searched: PubMed, Web of Science, and Toxline, initially in 2013, with updates every 6–12 months through January 2017. Forward and backward searches were also performed. Title/abstract and full text screening was performed by two reviewers to identify studies that met the PECO criteria. In addition, because there was a delay in publication, an updated search and screen was performed in August 2018. The publications from that search that inform each outcome are listed for each outcome and were reviewed to determine if their inclusion would significantly alter the conclusions.

2.2. Study evaluation

Studies were evaluated by at least two reviewers using uniform approaches for each group of similar studies. Key concerns were risk of bias (factors that affect the magnitude or direction of effect) and insensitivity (factors that limit the ability of a study to detect a true effect) (Cooper et al., 2016). Evaluation was conducted for the following domains: exposure measurement, outcome ascertainment, population selection, confounding, analysis, other sensitivity concerns, and selective reporting. These domains were based on the Risk of Bias in Non-randomized Studies of Interventions (ROBINS-I) tool (Sterne et al., 2016), modified for use with environmental exposures by the U.S. Environmental Protection Agency's Integrated Risk Information System. Phthalate and outcome-specific criteria were developed to address issues specific to the evaluation of this chemical and this set of outcomes prior to evaluation. For exposure, most of the available studies relied on phthalate metabolite biomarkers (a list of metabolites for each phthalate is provided in the protocol). Different criteria were developed for short-chain (DEP, DBP, DIBP, BBP) and long-chain (DEHP, DINP) phthalates due to better reliability of single measures for short-chain phthalates. Measurement in urine was considered to be the best proxy of exposure (Johns et al., 2015). Biomarker measures based on samples other than urine (e.g., blood, amniotic fluid, breast milk) were considered to be critically deficient for all short-chain phthalates and for primary metabolites (e.g., MEHP, MINP) of long-chain phthalates. Rationale for these criteria and additional details for all domains are available in the protocol (Supplement 1, Section 4.1.1) and an abbreviated version is available in the key methods supplement (Supplement 2). The outcome-specific criteria are discussed in Radke et al. (forthcoming in special issue).

For each study result, in each evaluation domain, reviewers reached a consensus rating regarding the utility of the study for hazard identification, with categories of *Good*, *Adequate*, *Deficient*, or *Critically deficient*. These ratings were then combined to reach an overall study confidence classification of *High*, *Medium*, *Low*, or *Uninformative*. This overall classification was not based on pre-defined weights for each domain, but rather was based on reviewer judgments, and include the likely impact the noted deficiencies in bias and sensitivity have on the magnitude and direction of effect estimates, which varies depending on the study and/or outcome. Studies were evaluated for their suitability for each outcome investigated, and could receive different ratings for each outcome. Descriptions of each of the evaluation domains and overall confidence categories can be found in the protocol (Supplement 1, Section 4). Study evaluations were documented in Health Assessment Workspace (HAWC), and ratings and rationale are publicly available (links provided in each outcome section).

2.3. Evidence synthesis

After study evaluation, the evidence for each outcome was synthesized separately for each phthalate, using the following aspects of an association that may suggest causation: consistency, exposure-response relationship, strength of association, temporal relationship, biological plausibility, and coherence. In evaluating the evidence for each of these considerations, syntheses also considered the strengths and limitations of each study, with high confidence studies carrying the most weight.

Table 1
Outcomes included in the systematic review.

Outcome	Background and relevance to female reproductive and/or developmental toxicity
Pubertal development	• Puberty is a continuous process involving maturation of both the hypothalamic-pituitary-adrenal axis and the hypothalamic-pituitary-gonadal axis. • Hormonal changes during puberty underlie the natural dynamic period of physical and sexual maturation that culminates in the ability to reproduce. • Changes in the mean age at pubertal onset in either direction would be considered an adverse effect (U.S. EPA, 1996).
Fecundity	• Fecundity is the biological capacity to reproduce. This review includes time to pregnancy as the primary outcome measure used to study fecundity, as well as rate of clinical pregnancy. • Time to pregnancy displays a reverse j-shaped cumulative distribution with many couples (30–40%) conceiving in the first cycle (Buck Louis et al., 2011) and 80–90% of couples being pregnant after up to 12 months of trying (Gnoth et al., 2003). • Fecundity within a couple can be influenced by either male or female exposures, or both (this review focuses on female exposure). Increases in time to pregnancy are considered indicative of reproductive toxicity (U.S. EPA, 1996). • Related outcomes among women seeking infertility treatment are summarized for coherence (without systematic review): oocytes, follicle count, embryo quality, and implantation.
Spontaneous abortion	• Spontaneous abortion or miscarriage is a pregnancy loss occurring before 20 weeks of gestation. • Loss that occurs before the pregnancy is clinically recognized is considered early, or preclinical. • Losses at 5 to roughly 20 weeks gestation are considered clinical loss.
Preterm birth	• Preterm birth, a delivery occurring before 37 weeks gestation, is a relatively common complication of pregnancy, occurring in > 10% of births (Martin et al., 2013). • Changes in gestational duration are considered indicative of reproductive toxicity (U.S. EPA, 1996) and are also reviewed.

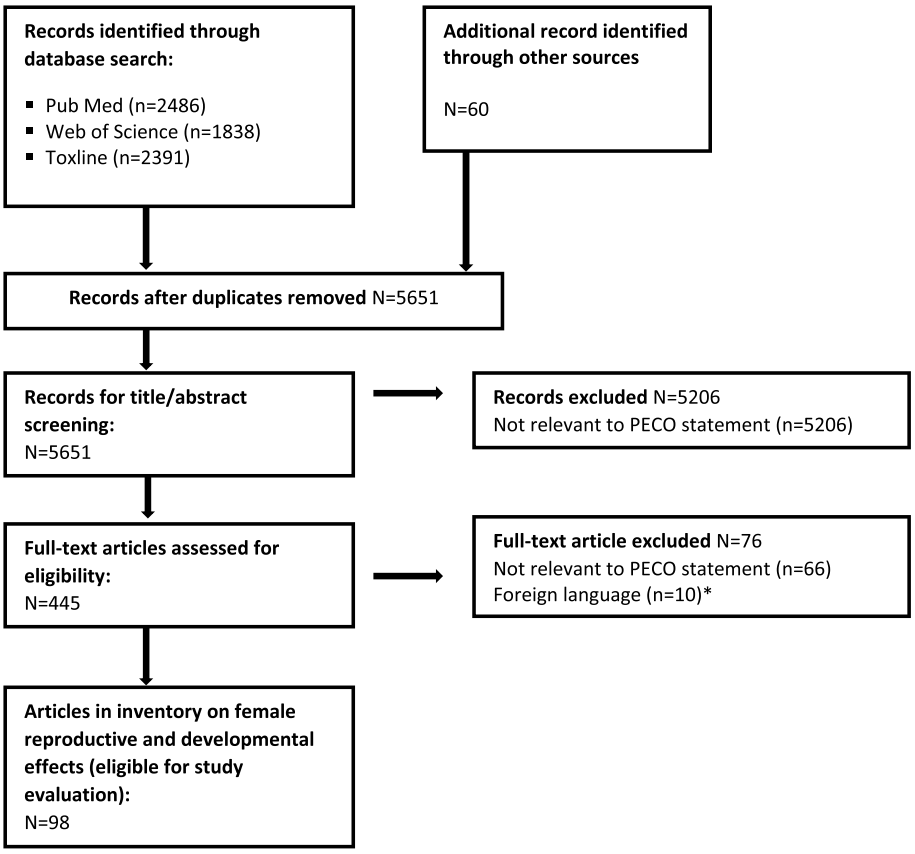

Fig. 1. Literature flow diagram for female reproductive and developmental effects of phthalates.
*Included one study on low birth weight and one on precocious puberty. Based on the abstracts, both would be excluded due to temporality issues.

Based on this synthesis, the evidence was assigned a strength of evidence conclusion of *Robust*, *Moderate*, *Slight*, *Indeterminate*, or *Compelling evidence of no effect*. *Robust* and *Moderate* describe evidence that supports a hazard, differentiated by the quantity and quality of information available to rule out alternative explanations for the results. *Slight* and *Indeterminate* describe evidence for which uncertainties prevents drawing a causal conclusion in either direction. These categories are generally limited in terms of quantity or confidence level of studies, and serve to encourage additional research across the exposure range experienced by humans. *Compelling evidence of no effect* requires several high confidence studies with consistent null results. The ratings for the individual outcomes were then summarized into an overall conclusion for female reproductive and developmental effects by phthalate, using a structured framework available in the key methods supplement (Supplement 2) and the protocol (Supplement 1, Section 6). No statistical quantitative meta-analysis was performed due to substantial differences across studies.

3. Results

The literature flow diagram is shown in Fig. 1 and a list of the included and excluded studies is available at: https://hero.epa.gov/hero/index.cfm/project/page/project_id/2245. For each outcome, there is a summary of the studies included and excluded based on study evaluation, a list of studies identified in the August 2018 update, a presentation of the extracted data (tables and/or figures), and a synthesis of the evidence ending with a judgment of the strength of the evidence in human studies for each phthalate. The studies reviewed from the August 2018 literature update did not influence conclusions, and are not included in Fig. 1.

3.1. Pubertal development

3.1.1. Study selection and evaluation

There were 18 studies (21 papers) that examined female exposure to phthalates and its association with timing of puberty. Thirteen studies were excluded, primarily due to issues with temporality (i.e., exposure was measured post-pubertal onset). Other reasons for exclusion included exposure measurement in tissues other than urine (unless looking at secondary metabolites of DEHP and DINP), exposure measurement by self-report, or critical deficiency in population selection/study design. The specific phthalate metabolites examined in the remaining five studies (seven papers) and the study evaluations are summarized in Table 2. Full rationales are available at https://hawcprd.epa.gov/summary/visual/100000090/.

The included studies varied in sample size, having between 69 and 1170 girls/females included in the analysis. Two studies (Wolff et al., 2014; Mouritsen et al., 2013) examined cohorts of children with phthalate exposure measured prior to pubertal onset. Three studies (Su et al., 2014; Watkins et al., 2014; Hart et al., 2013) were pregnancy cohorts, with exposure measured during gestation and children followed to pubertal onset. The results from the two different time periods (prenatal and childhood) are considered separately in this assessment and both are considered relevant windows of exposure for pubertal onset. For samples collected in utero, the timing in all three studies included the third trimester, with one study (Hart et al., 2013) also collecting samples during the second trimester and one study (Watkins et al., 2017) collecting in all three trimesters. Two studies (Wolff et al., 2014) were classified as medium confidence, and the remaining three (Su et al., 2014; Watkins et al., 2014; Hart et al., 2013; Mouritsen et al., 2013) were classified as low confidence.

Table 2
Epidemiology studies of pubertal development in females.

	Reference	Study description			Includes metabolites of:						Study evaluation					
		Population	Exposure	Outcome	DEHP	DINP	DBP	DIBP	BBP	DEP	Exposure	Outcome	Selection	Confounding	Analysis	Overall confidence
Included	Hart et al. (2013)	Pregnancy cohort (N = 123 girls) in Australia	Blood samples at 18 and 34/36 wks gestation	Prospectively reported age at menarche	✓	✓	✓[a]	✓[a]	✓[a]	✓[a]	D	G	D	D	D	Low
	Mouritsen et al. (2013)	Cohort of children (N = 84 girls) in Denmark enrolled at 6-12 yrs	Urine samples every 6 mo, at least 2 samples averaged	Tanner stages determined by pediatrician	✓	✓	✓[b]	✓[b]	✓	✓	G	G	D	D	D	Low
	Su et al. (2014)	Pregnancy cohort (N = 69 girls) in Taiwan	Single urine sample (3rd trimester)	Tanner stages determined by single examiner	✓		✓		✓	✓	A/D	G	D	D	D	Low
	Watkins et al. (2017); Watkins et al. (2014)	Pregnancy cohort (N = 117 girls) in Mexico	Urine sample in each trimester	Tanner stages determined by pediatrician	✓		✓	✓	✓	✓	G	G	D	A	A	Medium
	Wolff et al. (2017); Wolff et al. (2014); Wolff et al. (2010)	Cohort of girls (N = 1,170) in U.S. enrolled at 6-8 yrs	Single urine sample at baseline	Repeated assessments of Tanner stages by trained examiners	✓		✓	✓	✓	✓	A/D	G	A	G	A	Medium
				Total Studies per Phthalate	7	3	6	5	6	6						

Excluded studies: Exposure measured after development of outcome: Buttke et al. (2012), Chen et al. (2013), Chou et al. (2009), Frederiksen et al. (2012), Hashemipour et al. (2018), Lomenick et al. (2010), Shi et al. (2015), Srilanchakon et al. (2017), Zhang et al. (2015). Exposure measured in blood: Buluş et al. (2016), Lee et al. (2009), Yum et al. (2013). Exposure measured by self-report: Carran and Shaw (2012). No comparison group: Rais-Bahrami et al. (2004). Critical deficiency in population selection: Smerieri et al. (2015).
Additional studies identified in the August 2018 literature update: Binder et al. (2018), Kasper-Sonnenberg et al. (2017). Watkins et al. (2017), an update of Watkins et al. (2014) was also identified in the search and incorporated into the synthesis.
G = good; A = adequate; D = deficient; A/P = adequate for short chain phthalates, deficient for long chain phthalates.
[a]Study was considered *critically deficient* for this phthalate due to measurement in blood.
[b]Study summed DBP and DIBP metabolites.

Table 3
Associations between DEHP exposure and pubertal development.

Reference; Study confidence; N	Outcome	Effect estimate[a]	Mean exposure (IQR) (ng/mL)	Pubertal development timing effect estimate
ΣDEHP				
Childhood Exposure				
Wolff et al. (2017) and Wolff et al. (2014); Medium; 1,141	Age at menarche (n = 1,051)	HR (95% CI)	Median 142 μg/g creatinine	1.00 (0.94, 1.06)
	Age at 1st breast stage 2			1.01 (0.94, 1.09)
	Age at 1st pubic hair stage 2			**0.92 (0.85, 0.99)***
Mouritsen et al. (2013); Low; 84	Age at breast stage 2+ Age at pubic hair stage 2+	Medians in high vs. low exposure	115 (14-4,627)	"no significant difference"
Prenatal Exposure				
Watkins et al. (2014); Medium; 120	Menarche	OR (95% CI)	0.24 μmol/L	1.89 (0.57,6.22)
	Breast stage 2+			**0.66 (0.26,1.69)**
	Pubic hair stage 2+			2.15 (0.62,7.48)
Hart et al. (2013); Low; 121	Age at menarche	Correlation coefficient	4.3 (2.7-7.1)	−0.17, $p = 0.07$
Su et al. (2014); Low; 69	Tanner stage > 1	OR (95% CI)	47 mg/g creatinine	Stage 2: 1.00 (1.00, 1.00) Stage 3: 1.00 (0.99, 1.01)

[a]OR and hazard ratio (HR) < 1 indicate later pubertal development. Bolding of the effect estimate indicates evidence that suggests later onset of puberty, while grey shading indicates evidence that suggests earlier onset of puberty. NR = not reported; Q = quartile, y/n = yes/no *p < 0.05.

3.1.2. Results and synthesis

Evaluation of the association between exposure to DEHP and pubertal development is based on five studies: two with childhood exposure measures (Wolff et al., 2014; Mouritsen et al., 2013) and three with prenatal exposure measures (Su et al., 2014; Watkins et al., 2014; Hart et al., 2013) (Table 3). For childhood exposure, one study reported delayed onset of puberty (Wolff et al., 2014). Results for prenatal exposure were not consistent with that finding, with one study reporting no association (Su et al., 2014; Hart et al., 2013) and two (Watkins et al., 2014; Hart et al., 2013) reporting earlier onset of puberty. Further, the direction of the association was opposite for breast development (delayed with increasing exposure) and pubic hair development (earlier with increasing exposure) in Watkins et al. (2017). Overall, due to lack of consistency and coherence across related measures of puberty, there is *indeterminate* evidence of an effect of DEHP exposure on pubertal development.

Two *low confidence* studies (Mouritsen et al., 2013; Hart et al., 2013) reported on the association between pubertal development and DINP exposure (one with childhood exposure measures, one with prenatal). Neither study reported an association, and this evidence is considered *indeterminate*.

Four studies reported on the association between pubertal development and DBP (two with childhood exposure measures, two with prenatal), although one study reported only a combined estimate for DBP and DIBP (Mouritsen et al., 2013) (Table 4). For childhood exposure, two studies reported later age at pubarche for at least one measure (Wolff et al., 2014; Mouritsen et al., 2013), but results were not consistent across measures. For in utero exposure, one study (Watkins et al., 2017) reported conflicting results for age at menarche (later age with higher MBP exposure) and pubic hair stages (earlier age with higher exposure), the latter of which also conflicted with the results for childhood exposure. In Su et al. (2014), no association was reported. Overall, because of inconsistency and lack of coherence between related measures of puberty, there is *indeterminate* evidence of an effect of DBP exposure on pubertal development.

There are two studies that reported on the potential association of DIBP exposure with pubertal development (one with childhood exposure measures, one with prenatal). For prenatal exposure, Watkins et al. (2014) reported results for menarche and breast and pubic hair development in opposite directions. Other results indicated no association. Overall, there is *indeterminate* evidence of an effect of DIBP exposure on pubertal development.

Evaluation of the evidence of an association between BBP exposure and pubertal development is based on four studies (two with childhood exposure measures, two with prenatal) (Table 5). For childhood exposure, the studies had conflicting results, with one showing earlier onset of puberty (Mouritsen et al., 2013) for breast development and one showing delayed onset of puberty for breast and pubic hair development (Wolff et al., 2014). The effect sizes were small. For prenatal exposure, Watkins et al. (2014) reported earlier onset of breast and pubic hair development, but later onset of menarche with increasing exposure, while Su et al. (2014) reported no association. Overall, there is *indeterminate* evidence of an effect of BBP exposure on pubertal development.

Four studies reported on the association between pubertal development and DEP (two with childhood exposure measures, two with prenatal) (Table 5). For childhood exposure, one study reported earlier onset of puberty for age at menarche (Wolff et al., 2017) and the other study reported no association (Mouritsen et al., 2013). For prenatal exposure, one study (Watkins et al., 2014) showed earlier onset at pubarche with increasing exposure, while the other study (Su et al., 2014) reported no association. Because earlier onset of puberty was observed in both medium confidence studies, overall, there is *slight* evidence of an effect of DEP exposure on pubertal development.

In summary, there is *indeterminate* evidence of an association between pubertal development in females and exposure to phthalates, with the exception of DEP, which has *slight* evidence. Direct comparison of the effect estimates across studies was hindered by the different analysis methods and units, thus the synthesis focused on direction of association, which was inconsistent across endpoints within studies, across studies, and across phthalates, including in medium confidence studies.

3.2. Fecundity

3.2.1. Study selection and evaluation

There were seven studies that examined female exposure to phthalates and its association with time to pregnancy, and three were included in the evaluation. Four studies were excluded (Table 6), primarily due to issues with temporality (i.e., exposure after outcome). The specific phthalate metabolites examined in the remaining three studies and the study evaluations are summarized in Table 6. One additional study examined another outcome related to fecundity, rates of clinical pregnancy (Hauser et al., 2016). Full rationale is available at https://hawcprd.epa.gov/summary/visual/100000091/.

All the included studies of time to pregnancy were prospective cohorts of couples trying to conceive. Time to pregnancy was determined prospectively. All studies employed Cox regression methods to calculate

Table 4
Associations between DBP and DIBP exposure and pubertal development.

Reference; Study Confidence; N	Outcome	Effect estimate	Mean exposure (IQR) (ng/mL)	Pubertal development timing effect estimate
DBP				
Childhood Exposure				
Wolff et al. (2017) and Wolff et al. (2014); Low; 1,141	Age at menarche (n = 1,051)	HR (95% CI)	Median 14 μg/g creatinine	0.98 (0.90, 1.06)
	Age at 1st breast stage 2			0.99 (0.92, 1.08)
	Age at 1st pubic hair stage 2			**0.92 (0.85, 1.00)**
Prenatal Exposure				
Su et al. (2014); Low; 69	Tanner stage > 1	OR (95% CI)	68 mg/g creatinine	Stage 2: 1.00 (0.99, 1.00) Stage 3: 0.99 (0.98, 1.01)
Watkins et al. (2014); Medium; 116	Menarche	OR (95% CI)	57 (26-119) in Watkins et al., 2014	**0.73 (0.22,2.41)**
	Breast stage 2+			1.06 (0.41,2.71)
	Pubic hair stage 2+			2.6 (0.65,10.46)
ΣDBP + DIBP				
Childhood Exposure				
Mouritsen et al. (2013); Low; 84	Age at breast stage 2+	Medians in high vs. low exposure	122 (range 23-904)	Not significant, slightly lower age at pubarche
	Age at pubic hair stage 2+			**Not significant, slightly higher age at pubarche**
DIBP				
Childhood Exposure				
Wolff et al. (2017) and Wolff et al. (2014); Medium; 1,141	Age at menarche (n = 1,051)	HR (95% CI)	Median 48 μg/g creatinine	1.01 (0.94, 1.09)
	Age at 1st breast stage 2			0.97 (0.9, 1.04)
	Age at 1st pubic hair stage 2			0.99 (0.91, 1.07)
Prenatal Exposure				
Watkins et al. (2014); Low; 116	Menarche	OR (95% CI)	2 (1.0-3.6) in Watkins et al., 2014	**0.39 (0.09,1.70)**
	Breast stage 2+			1.21 (0.38,3.90)
	Pubic hair stage 2+			1.65 (0.30,9.03)

[a]OR and hazard ratio (HR) < 1 indicate later pubertal development, [b]Includes MBP and OH-MBP, [c]Includes MIBP and OH-MIBP, Bolding of the effect estimate indicates evidence that suggests later onset of puberty, while grey shading indicates evidence that suggests earlier onset of puberty. NR = not reported; Q = quartile, *p < 0.05

fecundability ORs, in which a lower value (< 1) represents reduced fecundity (increased time to pregnancy). Buck Louis et al. (2014) collected only one urine sample for exposure measurement, while the other two studies analyzed multiple samples when available. Thomsen et al. (2017) included only 242 of the 430 women in the original cohort due to missing urine samples (not collected due to conception in the first cycle or lost during storage). Because time to pregnancy differed in those without urine samples, this was considered a possible selection bias. One study was classified as *high confidence* (Jukic et al., 2016) and two studies were classified as *medium confidence* (Thomsen et al., 2017; Buck Louis et al., 2014). The single study that evaluated rates of pregnancy (Hauser et al., 2016), was a cohort of women undergoing in vitro fertilization and was classified as *high confidence*.

3.2.2. Results and synthesis

Three studies examined the association between DEHP exposure in women and time to pregnancy. Results for metabolites MEHP and MEOHP are provided in Table 7. There is no evidence that higher DEHP exposure is associated with longer time to pregnancy. However, exposure levels were fairly low across the studies, which may have reduced the ability of individual studies to detect associations. The one study examining rates of clinical pregnancy in a population of couples seeking fertility treatment (Hauser et al., 2016) reported lower percentages of participants with a pregnancy with higher exposure to DEHP (Q1: 0.57, 95% CI = 0.45–0.69, Q2: 0.46, 95% CI = 0.36–0.57; Q3: 0.49, 95% CI = 0.38–0.59; Q4: 0.38, 95% CI = 0.28–0.49*, p-trend = 0.04). In addition, three studies (four publications) examined related outcomes in women undergoing in vitro fertilization, and reported decreases in oocytes (Hauser et al., 2016; Machtinger et al., 2018), antral follicle count (Messerlian et al., 2015), embryo quality (Machtinger et al., 2018), and implantation (Hauser et al., 2016), though one study reported no decrease in embryo quality (Wu et al., 2017). Still, because of the lack of supporting evidence from studies on time to pregnancy, which were all of *high* or *medium confidence*, evidence of an association between DEHP exposure in women and fecundity is considered *slight*.

Evaluation of the association between exposure to the other phthalates and time to pregnancy is based on a subset of the studies described for DEHP, with one to three studies for each phthalate (Table 8). With the exception of one study for DEP (Thomsen et al., 2017), no association was reported between higher phthalate exposure and lower fecundity/increased time to pregnancy. This included the single study examining rates of clinical pregnancy (Hauser et al., 2016). There were decreases in related outcomes in women undergoing in vitro fertilization in three studies (four publications) for DBP, DIBP, and DEP in at least one secondary outcome (Hauser et al., 2016; Messerlian et al., 2015; Machtinger et al., 2018; Wu et al., 2017), but based on the lack of association for the primary fecundity outcomes, evidence of an association between fecundity and exposure to DINP, DBP, DIBP, BBP, and DEP is considered *indeterminate*.

3.3. Spontaneous abortion

3.3.1. Study selection and evaluation

There were five studies that examined exposure to phthalates and its association with spontaneous abortion; none were excluded. The specific phthalate metabolites examined in the studies and the study evaluations are summarized in Table 9. Full rationale is available at https://hawcprd.epa.gov/summary/visual/100000092/.

Two studies were preconception general population cohorts (Jukic

Table 5
Associations between BBP and DEP exposure and pubertal development.

Reference; Study Confidence; N	Outcome	Effect estimate	Mean exposure (IQR) (ng/mL)	Pubertal development timing effect estimate
BBP				
Childhood Exposure				
Wolff et al. (2017) and Wolff et al. (2014); Medium; 1,141	Age at menarche (n = 1,051) Age at 1st breast stage 2 Age at 1st pubic hair stage 2	HR (95% CI)	Median 21 μg/g creatinine	0.98 (0.92, 1.05) **0.95 (0.89, 1.01)** **0.92 (0.86, 0.99)***
Mouritsen et al. (2013); Low; 84	Age at breast stage 2+ Age at pubic hair stage 2+	Medians in high vs. low exposure	37 (range 3-433)	Not significant, slightly lower age at pubarche "no significant difference"
Prenatal Exposure				
Su et al. (2014); Low; 69	Tanner stage > 1	OR (95% CI)	17 mg/g	Stage 2: 1.01 (0.99, 1.02) Stage 3: 0.98 (0.91, 1.05)
Watkins et al. (2014); Low; 116	Menarche Breast stage 2+ Pubic hair stage 2+	OR (95% CI)	4 (2.2-7.0) in Watkins et al., 2014	0.92 (0.26,3.25) 1.58 (0.63,3.96) 3.89 (0.96,15.8)
DEP				
Childhood Exposure				
Wolff et al. (2017) and Wolff et al. (2014); Medium; 1,141	Age at menarche (n = 1,051) Age at 1st breast stage 2 Age at 1st pubic hair stage 2	HR (95% CI)	Median 68 μg/g creatinine	1.06 (0.99, 1.14) 1.03 (0.96, 1.09) 0.99 (0.94, 1.06)
Mouritsen et al. (2013); Low; 84	Age at breast stage 2+ Age at pubic hair stage 2+	Medians in high vs. low exposure	36 (range 6-847)	"no significant difference"
Prenatal Exposure				
Su et al. (2014); Low; 69	Tanner stage > 1	OR (95% CI)	65 mg/g creatinine	Stage 2: 1.00 (1.00, 1.01) Stage 3: 0.99 (0.94, 1.03)
Watkins et al. (2014); Low; 116	Menarche Breast stage 2+ Pubic hair stage 2+	OR (95% CI)	114 (41-242) in Watkins et al., 2014	4.33 (1.25,15.0)* 1.49 (0.57,3.88) 2.31 (0.67,7.94)

[a]OR and hazard ratio (HR) < 1 indicate later pubertal development, Bolding of the effect estimate indicates evidence that suggests later onset of puberty, while grey shading indicates evidence that suggests earlier onset of puberty. Studies are sorted by median exposure level, NR = not reported; Q = quartile.
* $p < 0.05$

et al., 2016; Toft et al., 2012), one was a preconception cohort among women receiving assisted reproductive technology (Messerlian et al., 2016) and two were clinic-based, case-control studies (Mu et al., 2015); (Yi et al., 2016). With regards to population selection, the case-control studies only included women who received ultrasound to confirm pregnancy, which represented a potential selection bias as it excludes women who experienced a spontaneous abortion and did not receive an ultrasound. One of the preconception cohorts (Toft et al., 2012) had urine samples for only 56% (242 out of 430) of the cohort participants because urine samples were not collected if conception occurred during the first cycle (n = 111) or because urine samples were lost during the storage period. Time to pregnancy differed between the participants with and without urine samples, which was considered a potential source of selection bias. Two studies were classified as having *high confidence* (Jukic et al., 2016; Messerlian et al., 2016) and the other three (Mu et al., 2015; Toft et al., 2012); (Yi et al., 2016) were classified as having *low confidence*.

3.3.2. Results and synthesis

Evaluation of the evidence of an association between exposure to DEHP and spontaneous abortion (Table 10) is based on five studies, with three studies reporting on early loss, three studies reporting on clinical loss, and one reporting on total loss. Of the two high confidence studies, Messerlian et al. (2016) reported elevated odds of total loss (early and clinical loss combined) with higher exposure while Jukic et al. (2016) reported lower odds of early loss with higher exposure. For early and clinical loss, two low confidence studies reported elevated odds with higher exposure (Toft et al. (2012) for early loss and Yi et al. (2016) for clinical loss), though the effect estimates for one (Mu et al., 2015; Toft et al., 2012) were imprecise. Overall, there is *slight* evidence of an association between DEHP exposure and spontaneous abortion, but there is considerable uncertainty due to inconsistency in the *high* confidence studies.

DINP was measured in two studies (Jukic et al., 2016; Messerlian et al., 2016). No association with early loss or total loss, respectively, was observed. This evidence is considered *indeterminate*.

Evaluation of the evidence of an association between exposure to DBP and spontaneous abortion is based on five studies (Table 11). Jukic et al. (2016), a *high confidence* study, found slightly elevated ORs between early loss and MBP exposure levels. Toft et al. (2012) observed a monotonic increase in OR for early loss with increasing exposure, and an inverse association for clinical loss with increasing exposure. Mu et al. (2015) reported an elevated OR for clinical loss for quartile 4 vs. quartile 1, but an inverse association for quartiles 2 and 3 vs. quartile 1. None of the reported associations were statistically significant. Messerlian et al. (2016), another *high confidence* study, and Yi et al. (2016) reported no association. The results for clinical loss were inconsistent, and the effect estimates for early loss were small and not statistically significant. Overall, there is *slight* evidence of an association between DBP exposure and early spontaneous abortion.

Four studies examined the association between spontaneous abortion and DIBP exposure (Table 11). The two *high confidence* studies, Jukic et al. (2016) and Messerlian et al. (2016) found no relationship between MiBP and early pregnancy loss and total pregnancy loss; however, DIBP exposure levels were lower than those reported for other phthalates and this may have affected study sensitivity. One low confidence study (Yi et al., 2016) also found no increase in clinical loss. Conversely, Mu et al. (2015) reported generally increasing associations

Table 6
Epidemiology studies of fecundity in females

Reference		Study description			Includes metabolites of:						Study evaluation				
		Population	Exposure	Outcome	DEHP	DINP	DBP	DIBP	BBP	DEP	Exposure	Outcome	Selection	Confounding	Analysis	Overall confidence
Included	Buck Louis et al. (2014)	Cohort (N = 501) in U.S. of couples trying to conceive	Single urine sample at study entry	Cycles to conception (measured prospectively)	✓	✓[a]	✓	✓	✓	✓	A/D	G	G	A	A	Medium
	Jukic et al. (2016)	Cohort (N = 221) in U.S. of couples trying to conceive	Three urine samples per cycle, pooled	Cycles to conception (measured prospectively), up to 6 mo	✓	✓	✓	✓	✓	✓	G	G	A	G	A	High
	Thomsen et al. (2017)	Cohort (N = 229) in Denmark of couples trying conceive	1-2 urine samples from final two cycles in study	Cycles to conception (measured prospectively), up to 6 mo	✓		✓		✓	✓	G/A	G	D	A	A	Medium
	Hauser et al. (2016)	Cohort (N = 256) in U.S. of women undergoing IVF	Two urine samples during each IVF (could contribute multiple cycles)	Rate of clinical pregnancy confirmed by ultrasound at ~6 wk	✓	✓	✓	✓	✓	✓	G	A	G	G	G	High
Total Studies per Phthalate					4	2	4	3	4	4						

Excluded studies: Exposure measured after development of outcome: Specht et al. (2015), Vélez et al. (2015), Huang et al. (2016). Exposure categorized as occupational exposure to any phthalate (job exposure matrix): Burdorf et al. (2011). Additional studies identified in the August 2018 literature update: Philips et al. (2018), Buck Louis et al. (2018), G = good; A = adequate; D = poor; A/D = adequate for short chain phthalates, deficient for long chain phthalates; IVF = in vitro fertilization. [a] Study was considered *criticallly deficient* for this phthalate due to a high percent below the LOD.

with increasing exposure, including a statistically significant finding in the 4th vs. 1st quartile. Given the lack of consistency across studies and the reporting of an association in only a single *low confidence* study, the evidence of an association between DIBP exposure and spontaneous abortion is considered *indeterminate*.

Three studies examined the evidence of an association between BBP exposure (measured by MBzP) and spontaneous abortion (Table 11). Toft et al. (2012) found higher ORs with a monotonic trend for early loss, but no association between exposure and clinical loss. Results from Jukic et al. (2016) and Messerlian et al. (2016), *high confidence* studies, did not support this finding despite Jukic et al. (2016) reporting higher BBP exposure levels. Based on this lack of consistency across studies, the evidence of an association between BBP exposure and spontaneous abortion is considered *indeterminate*.

Five studies examined the evidence of an association between DEP exposure and spontaneous abortion. Jukic et al. (2016) and Messerlian et al. (2016), the *high confidence* studies, found no association between MEP levels and early loss or total loss, respectively (Table 11). One *low confidence* study (Yi et al., 2016) also reported no association. Toft et al. (2012) reported slightly elevated ORs for early loss, and moderately elevated ORs for clinical loss. Mu et al. (2015) reported a monotonic increase in ORs with increasing exposure. There was not a clear explanation for the lack of association in the *high confidence* studies, but it is possible that the association is limited to clinical loss. Given this lack of consistency, the evidence for an association between DEP exposure and spontaneous abortion is *slight*.

In summary, there is *slight* evidence of an association between spontaneous abortion and exposure to DEHP, DBP, and DEP. There is generally inconsistency among the high confidence studies.

3.4. Preterm birth

3.4.1. Study selection and evaluation

There were 20 studies (described in 22 publications) that examined exposure to phthalates and its association with preterm birth or gestational duration. Four studies were excluded due to issues with exposure measurement and six studies were excluded due to participant enrollment late in pregnancy (i.e., a majority of participants were enrolled during the third trimester) (Table 12). The specific phthalate metabolites examined in the remaining eight studies (ten publications) and the study evaluations are summarized in Table 12 and full rationale is available at https://hawcprd.epa.gov/summary/visual/100000093/.

Six studies are pregnancy cohorts, and two are case-control studies nested within pregnancy cohorts. These studies vary in size between 60 and 3103 mother-infant pairs included in the analysis. Four studies (Casas et al., 2016; Shoaff et al., 2016; Ferguson et al., 2014b) measured exposure in two or more urine samples, with the levels averaged, while the remaining studies used a single urine sample. Only Ferguson et al. (2014b) additionally analyzed the exposure collections separately. The timing of collection (preconception, 1st, 2nd, or 3rd trimester) varied among the studies; timing variability during pregnancy was not considered to be a basis for downgrading confidence in the results because the critical window is not known. However, preconception exposure resulted in a downgrade in confidence because women may change their diet and overall exposure when they become pregnant, and pregnancy may cause metabolic changes. Five studies (Casas et al., 2016; Gao et al., 2016; Polańska et al., 2016; Watkins et al., 2016; Smarr et al., 2015) analyzed gestational duration as a continuous variable; however, authors of three of these studies (Casas et al., 2016; Gao et al., 2016; Smarr et al., 2015) were contacted and were able to provide analyses with preterm birth as the outcome to improve comparability between studies, and those results are presented here rather than the gestational duration results. Only one study (Ferguson et al., 2014b) stratified by type of preterm birth (i.e., spontaneous preterm birth). Three studies (Casas et al., 2016; Shoaff et al., 2016; Ferguson et al., 2014b) were classified as *high confidence*, and the remaining five

Table 7
Associations between DEHP exposure and time to pregnancy.

Reference; study confidence; N	Mean exposure (IQR) (ng/mL)	Fecundability OR (95% CI)	Fecundability OR unit change
DEHP			
MEHP			
Buck Louis et al. (2014); Medium; 501	4.6	0.99 (0.87, 1.12)	1 SD change (log transformed)
Jukic et al. (2016); High; 221	6.6 (3.8–11)	T2: 1.23 (0.85, 1.79) T3: 1.39 (0.97, 1.97)	T2 and T3 vs. T1
Thomsen et al. (2017); Medium; 229	14.5 (range 0–348)	0.99 (0.72,1.35)	1 unit increase (ln transformed)
MEOHP			
Buck Louis et al. (2014); Medium; 501	Mean 8.7	1.06 (0.91, 1.24)	1 SD change (log transformed)
Jukic et al. (2016); High; 221	33.3 (20–49)	Q2: 1.28 (0.91, 1.81) Q3: 1.11 (0.77, 1.58)	T2 and T3 vs. T1

Fecundability OR < 1 indicates increased time to pregnancy.
Q = quartile; T = tertile. Studies within individual phthalates are sorted by median exposure level.

were classified as *medium confidence*. The bias for all studies was considered likely to be towards the null, if present, due to the possibility of exposure misclassification (see exposure criteria in Supplement 1, Section 4.1.1) and other study-specific limitations.

3.4.2. Results and synthesis

Evaluation of the evidence of an association between exposure to DEHP and preterm birth is based on six studies that analyzed preterm birth as a dichotomous variable (Casas et al., 2016; Gao et al., 2016; Shoaff et al., 2016; Smarr et al., 2015; Ferguson et al., 2014b; Meeker et al., 2009) (Fig. 2, results are sorted by mean exposure level for studies with continuous exposure) and two studies that analyzed gestational duration as a continuous variable (Polańska et al., 2016; Watkins et al., 2016). Of the preterm birth studies, four of the six, including two high confidence studies, reported elevated ORs, with one (Ferguson et al., 2014b) reaching statistical significance, and very similar results among these four studies (OR range for continuous exposure: 1.25–1.33). An exposure-response relationship was observed in Ferguson et al. (2014b) (OR range: 1.23–2.17) and Casas et al. (2016), although the relationship was non-monotonic in the latter study. The largest study (Gao et al., 2016) reported no association, but also had lower levels of exposure than other studies, with only Smarr et al. (2015) reporting lower levels of MEOHP (not shown). This may indicate reduced study sensitivity. The two gestational duration studies reported no association between pregnancy duration and DEHP exposure, but this is not considered inconsistent with the preterm birth results due to the limitations in analyzing gestational duration as a proxy for preterm birth. While there is consistency for preterm birth among multiple medium and high confidence studies in varied settings (e.g., multiple different countries), there is a lack of association in one high confidence study, as well as the largest study, which may be partly explained by lower study sensitivity resulting from low exposure levels. Therefore, there is *moderate* evidence of an association between DEHP exposure and preterm birth.

Two studies of *medium confidence* included results for DINP. Meeker et al. (2009) reported slightly elevated odds (not statistically significant) of preterm birth with higher DINP exposure in a small study (MCiOP OR = 1.3, 95% CI = 0.5–3.9), while Polańska et al., 2016 reported no association with gestational duration (ΣDINP $\beta = -0.03$, SE = 0.08, $p = 0.5$). The evidence for an association between DINP exposure and preterm birth from this one study is considered *slight*.

Evaluation of the evidence of an association between exposure to DBP and preterm birth is based on six studies (Casas et al., 2016; Gao et al., 2016; Shoaff et al., 2016; Smarr et al., 2015; Ferguson et al., 2014b; Meeker et al., 2009) that analyzed preterm birth as a dichotomous variable (Fig. 3; results are sorted by mean exposure level for

Table 8
Associations between DINP, DBP, DIBP, BBP, and DEP exposure and time to pregnancy

Reference; Study confidence; N	Mean exposure (IQR) (ng/mL)	Fecundability OR (95% CI)	Fecundability OR unit change
DINP			
Jukic et al. (2016); High; 221	MCiOP 3.3 (2.3-5.2)	Q2: 0.93 (0.66, 1.32) Q3: 0.96 (0.68, 1.35)	T2 and T3 vs. T1
DBP			
Buck Louis et al. (2014); Medium; 501	10	0.93 (0.77, 1.12)	1 SD change (log transformed)
Jukic et al. (2016); High; 221	80 (49-127)	Q2: 0.90 (0.63, 1.27) Q3: 0.96 (0.68, 1.35)	T2 and T3 vs. T1
Thomsen et al. (2017); Medium; 229	272 (range 10-2,292)	1.03 (0.76,1.39)	1 unit increase (ln transformed)
DIBP			
Jukic et al. (2016); High; 221	3.1 (1.9-5.0)	Q2: 1.16 (0.81, 1.65) Q3: 1.11 (0.77, 1.61)	Tertile vs. T1
Buck Louis et al. (2014); Medium; 501	5.1	0.95 (0.78, 1.14)	1 SD change (log transformed)
BBP			
Buck Louis et al. (2014); Medium; 501	5	0.94 (0.78, 1.13)	1 SD change (log transformed)
Thomsen et al. (2017); Medium; 229	22 (range 1.0-203)	0.88 (0.64,1.19)	1 unit increase (ln transformed)
Jukic et al. (2016); High; 221	40 (25-69)	Q2: 0.76 (0.53, 1.10) Q3: 1.01 (0.73, 1.40)	T2 and T3 vs. T1
DEP			
Thomsen et al. (2017); Medium; 229	379 (range 16-12,357)	0.79 (0.63,0.99)*	1 unit increase (ln transformed)
Buck Louis et al. (2014); Medium; 501	94	0.97 (0.84, 1.12)	1 SD change (log transformed)
Jukic et al. (2016); High; 221	134 (72-296)	Q2: 1.00 (0.71, 1.42) Q3: 0.98 (0.68, 1.40)	T2 and T3 vs. T1

Fecundability OR < 1 indicates increased time to pregnancy. *p < 0.05, results that support an association are shaded. Q = quartile; T = tertile.

Table 9
Epidemiology studies of spontaneous abortion

	Reference	Study description			Includes metabolites of:						Study evaluation					
		Population	Exposure	Outcome	DEHP	DINP	DBP	DIBP	BBP	DEP	Exposure	Outcome	Selection	Confounding	Analysis	Overall confidence
Included	Jukic et al. (2016)	Preconception cohort in U.S. (N = 221 women)	Three urine samples from cycle of conception, pooled	Early pregnancy loss, identified via hCG	✓	✓	✓	✓	✓	✓	G	G	A	G	G	High
	Messerlian et al. (2016)	Cohort of women receiving assisted reproductive technology in U.S. (N = 256)	Two urine samples per conception cycle	Total pregnancy loss and "biochemical" (early) loss identified prospectively	✓	✓	✓	✓	✓	✓	G	G	A	A	A	High
	Mu et al. (2015)	Case-control in China (N = 132 cases, 172 controls) of women receiving ultrasound	Single morning urine sample at 5-13 wks gestation	Clinical pregnancy loss identified by ultrasound	✓		✓	✓	✓[a]	✓	A/P	A	D	D	A	Low
	Toft et al. (2012)	Preconception cohort in Denmark (N = 242 women)	Single urine sample from cycle of conception	Early and clinical pregnancy loss identified through urine samples or medical provider	✓		✓		✓	✓	A/P	G	D	A	A	Low
	Yi et al. (2016)	Case-control in China (N = 150 cases, 172 controls) of women	Single morning urine sample at admission to hospital	Clinical pregnancy low identified by ultrasound	✓		✓	✓		✓	A/P	A	D	A	A	Low
	Total Studies per Phthalate				5	2	5	4	3	5						

Additional studies identified in the August 2018 literature update: Liao et al. (2018), Zhao et al. (2017), Gao et al. (2017). G = good; A = adequate; D = deficient; A/D = adequate for short chain phthalates, deficient for long chain phthalates; hCG = human chorionic gonadotropin. [a] Study was considered *critically deficient* for this phthalate due to a high percent below the LOD.

Table 10
Associations between DEHP metabolite levels and spontaneous abortion

			Early loss		Clinical loss	
Reference; Study Confidence; N	**MEHP median (IQR), (ng/mL)**	**MEOHP median, (ng/mL)**	**MEHP Early loss OR (95% CI)**	**MEOHP Early loss OR (95% CI)**	**MEHP Clinical loss OR (95% CI)**	**MEOHP Clinical loss OR (95% CI)**
Messerlian et al. (2016); High; 256	2.6 (1.5-6.4)	10.2		ΣDEHP Biochemical loss Q2: 2.3 (0.63,8.5) Q3: 2.0 (0.58,7.2) Q4: 3.4 (0.97,11.7) p-trend = 0.04		ΣDEHP Total loss Q2: 1.1 (0.61,2.0) Q3: 1.0 (0.56, 1.8) Q4: 1.6 (0.96, 2.7) p-trend = 0.06
Jukic et al. (2016); High; 221	6.6 (3.8-11)	30.3		ΣDEHP T2: 0.32 (0.13, 0.77)* T3: 0.49 (0.19, 1.24)		
Yi et al. (2016); Low; 300	10.5 (mean)	6.2 (mean)			Continuous 1.78 (1.35,2.34)* Quartiles Q2: 3.3 Q3: 4.0 Q4: 7.2	Continuous 1.28 (0.84,1.95) Quartiles Q2: 1.6 Q3: 1.9 Q4: 4.6
Toft et al. (2012); Low; 242	15.4 (7.5-27)	33.3	T2: 10.83 (1.16, 101) T3: 40.67 (4.48, 370)	T2: 2.16 (0.63, 7.39) T3: 2.73 (0.78, 9.54)	T2: 0.17 (0.03, 0.95)* T3: 0.25 (0.05, 1.28)	T2: 0.55 (0.13, 2.29) T3: 0.55 (0.13, 2.35)
Mu et al. (2015); Low; 304	20.6/4.8 (cases/non-cases) (1.5-103 cases)				Q2: 0.97 (0.47, 1.98) Q3: 0.71 (0.34, 1.51) Q4: 1.30 (0.66, 2.55)	

*$p < 0.05$, results that support an association are shaded. Dark gray represents one or more of the following: $p < 0.05$, large effect size (e.g., OR > = 1.5), or exposure-response trend across categories of exposure. Studies are sorted by median exposure level. Q = quartile; T = tertile.

Table 11
Associations between DBP, DIBP, BBP, and DEP metabolite levels and spontaneous abortion

Reference; Study Confidence; N	Median exposure (IQR), (ng/mL)	Early loss OR (95% CI)	Clinical loss OR (95% CI)
DBP (measured by MBP)			
Messerlian et al. (2016); High; 256	12.6 (6.8-21)	Q2: 0.66 (0.22,1.9) Q3: 0.78 (0.28,2.2) Q4: 0.58 (0.19,1.7)	"No notable association"
Yi et al. (2016); Low; 300	47 (mean)		1.00 (0.67,1.50)
Jukic et al. (2016); High; 221	80 (49-127)	T2: 1.10 (0.47, 2.58) T3: 1.12 (0.46, 2.74)	
Mu et al. (2015); Low; 304	86/44 (cases/noncases) (case IQR 10-240)		Q2: 0.85 (0.44, 1.64) Q3: 0.82 (0.42, 1.59) Q4: 1.33 (0.72, 2.48)
Toft et al. (2012); Low; 242	174 (107-315)	T2: 1.25 (0.38, 4.09) T3: 1.64 (0.52, 5.20)	T2: 0.87 (0.21, 3.57) T3: 0.51 (0.12, 2.21)
DIBP (measured by MIBP)			
Jukic et al. (2016); High; 221	3.1 (1.9-5.0)	T2: 1.08 (0.47, 2.45) T3: 0.73 (0.32, 1.68)	
Messerlian et al. (2016); High; 256	7.2 (3.8-12)	Q2: 0.53 (0.17,1.6) Q3: 1.2 (0.59,2.5) Q4: 0.71 (0.26,1.9)	"No notable association"
Yi et al. (2016); Low; 300	32 (mean)		0.85 (0.60,1.19)
Mu et al. (2015); Low; 304	41/19 (cases/noncases) (case IQR 8.0-125)		Q2: 1.43 (0.71, 2.88) Q3: 1.38 (0.68, 2.79) Q4: 2.48 (1.28, 4.79)*
BBP (measured by MBzP)			
Messerlian et al. (2016); High; 256	3.2 (1.7-6.1)	Q2: 1.2 (0.46,3.3) Q3: 1.2 (0.42,3.2) Q4: 1.1 (0.39,3.1)	"No notable association"
Toft et al. (2012); Low; 242	12 (7.3-23)	T2: 2.39 (0.70, 8.22) T3: 3.11 (0.87, 11.09)	T2: 1.08 (0.25, 4.66) T3: 0.96 (0.20, 4.59)
Jukic et al. (2016); High; 221	40 (25-69)	T2: 1.65 (0.69, 3.98) T3: 0.90 (0.36, 2.27)	
DEP (measured by MEP)			
Yi et al. (2016); Low; 300	12 (mean)		0.75 (0.57,0.98)
Messerlian et al. (2016); High; 256	51 (21-133)	Q2: 0.96 (0.41,2.30) Q3: 0.65 (0.23,1.87) Q4: 0.86 (0.34,2.16)	"No notable association"
Mu et al. (2015); Low; 304	57/16 (cases/noncases) (case IQR 3.8-322)		Q2: 1.04 (0.52, 2.08) Q3: 1.36 (0.70, 2.65) Q4: 1.88 (0.99, 3.58)
Jukic et al. (2016); High; 221	134 (73-296)	T2: 0.73 (0.31, 1.73) T3: 1.06 (0.48, 2.33)	NR
Toft et al. (2012); Low; 242	224 (113-419)	T2: 1.29 (0.43, 3.83) T3: 1.13 (0.36, 3.59)	T2: 2.19 (0.42, 11.45) T3: 4.63 (0.92, 23.26)

*$p < 0.05$, results that support an association are shaded. Dark gray represents one or more of the following: $p < 0.05$, large effect size (e.g., OR > = 1.5), or exposure-response trend across categories of exposure. Light gray represents other supportive results. Studies within individual phthalates are sorted by median exposure level. Q = quartile; T = tertile.

studies with continuous exposure) and two studies that analyzed gestational duration as a continuous variable (Polańska et al., 2016; Watkins et al., 2016). Three studies, including two high confidence, reported elevated odds of preterm birth (OR range: 1.3 to 4.5) with higher exposure (Casas et al., 2016; Ferguson et al., 2014b; Meeker et al., 2009). Statistically significant results were reported in Ferguson et al. (2014b) and Meeker et al. (2009), and the OR in Meeker et al. (2009) was high. The remaining three studies (Gao et al., 2016; Shoaff et al., 2016; Smarr et al., 2015) reported no association or an association with longer gestation; however, the DBP exposure levels in Smarr et al. (2015) were the lowest of the studies, and as such the study may have had lower sensitivity to detect an association. Shoaff et al. (2016) reported statistically significant lower odds of preterm birth with higher exposure. Among the two gestational duration studies, the only association reported between pregnancy duration and DBP exposure was in female infants in Watkins et al., 2016 (for male infants change in days = 0.09, 95% CI = −3.81, 3.99; for female infants change in days = −4.46, 95% CI = −8.25, −0.67*). Overall, while there are some inconsistencies in the results across studies, there is *moderate* evidence of an association between DBP exposure and preterm birth.

Five studies on preterm birth (Casas et al., 2016; Gao et al., 2016; Shoaff et al., 2016; Smarr et al., 2015; Ferguson et al., 2014b; Meeker et al., 2009) and one study on gestational duration (Polańska et al., 2016) investigated the association with exposure to DIBP (Fig. 3). One *high confidence* study (Shoaff et al., 2016) and one *medium confidence* study (Meeker et al., 2009) reported non-statistically significant elevated odds of preterm birth with higher DIBP exposure, while the other three studies reported no association between exposure and preterm birth, and there was no clear pattern between exposure level or range and higher ORs. Polańska et al. (2016) reported no association with gestational duration (β = 0.01, SE = 0.04, $p = 0.8$). DIBP exposure levels were low in all of the studies relative to other phthalates, with the exception of Casas et al. (2016), so the sensitivity to detect an association may have been inadequate. The current evidence is considered *slight*.

Evaluation of the evidence for an association between exposure to BBP and preterm birth is based on six studies (Casas et al., 2016; Gao et al., 2016; Shoaff et al., 2016; Smarr et al., 2015; Ferguson et al., 2014b; Meeker et al., 2009) that analyzed preterm birth as a dichotomous variable (Fig. 3; results are sorted by mean exposure level for studies with continuous exposure variables) and one study that analyzed gestational duration as a continuous variable (Watkins et al., 2016). One *high confidence* study Ferguson et al. (2014b) and one *medium confidence* study (Meeker et al., 2009) reported non-statistically significant elevated odds of preterm birth with increasing BBP exposure, although in Ferguson et al. (2014b) the OR was only slightly elevated. Results from the other four studies (two *high confidence* and two *medium confidence* studies) were either no association or lowered odds. There was no increase in ORs with increasing exposure levels or range. The gestational duration study reported no association between pregnancy duration and BBP exposure (Watkins et al. 2016) male infants change in days (β = 0.27, 95% CI = −4.35, 4.90; female infants change in days (β = −2.60, 95% CI = −7.87, 2.67)). However, BBP exposure in all of the studies was low relative to other phthalates, which may have reduced the sensitivity to detect an association. Therefore, the evidence is considered *slight*.

Of the same six studies that investigated DEP exposure and preterm birth, four studies, including all three high confidence studies (Casas et al., 2016; Shoaff et al., 2016; Ferguson et al., 2014b; Meeker et al., 2009) reported consistent higher odds (OR range: 1.1–1.4) of preterm birth with increasing exposure. These results were not statistically significant, and the effect estimates were smaller than the results for other phthalates, particularly in Meeker et al. (2009). Conversely, Smarr et al. (2015) reported a statistically significant negative association and Gao et al. (2016) reported no association, but these two studies had the lowest exposure levels. Among the two gestational

Table 12
Epidemiology studies of preterm birth/gestational duration

	Reference	Study description			Includes metabolites of:						Study evaluation					
		Population	Exposure	Outcome	DEHP	DINP	DBP	DIBP	BBP	DEP	Exposure	Outcome	Selection	Confounding	Analysis	Overall confidence
Included	Casas et al. (2016)[a]	Pregnancy cohort in Spain (N = 390)	Two urine samples at ~12 and 32 wk gestation	GD calculated from ultrasound and last menstrual period	✓		✓	✓	✓	✓	G	G	G	G	G	High
	Ferguson et al. (2014a); Ferguson et al. (2014b); Chen et al. (2015);	Nested case-control within pregnancy cohort in U.S. (N = 130 cases preterm birth, 352 controls)	Up to four urine samples	GD calculated from ultrasound and last menstrual period	✓		✓	✓	✓	✓	G	G	A	A	G	High
	Gao et al. (2016)[a]	Pregnancy cohort in China (N = 3,103)	Single urine sample in 1st trimester	GD calculated using last menstrual period or ultrasound	✓		✓		✓	✓	A/P	A	A	A	A	Medium
	Meeker et al. (2009)	Nested case-control in pregna cohort in Mexico (N = 30 cases and 30 controls)	Single urine sample in 3rd trimester	GD calculated from last menstrual period (recall)	✓	✓	✓	✓	✓	✓	A/P	A	A	A	A	Medium
	Polańska et al. (2016)	Pregnancy cohort in Poland (N = 165)	Single urine sample in 3rd trimester	GD estimated using last menstrual period or ultrasound	✓	✓	✓	✓	✓[b]	✓	A/P	A	A	G	D	Medium
	Shoaff et al. (2016)	Pregnancy cohort in U.S. (N = 368)	Two urine samples at ~16 and 26 wk gestation	GD calculated from last menstrual period or other method	✓		✓	✓	✓	✓	G	A	A	G	A	High
	Smarr et al. (2015)[a]	Preconception cohort in U.S. (n = 233)	Single urine sample at baseline of trying to conceive	GD calculated from conception identified prospectively	✓	✓[b]	✓	✓	✓	✓	D	G	A	A	A	Medium
	Watkins et al. (2016)	Pregnancy cohort in U.S. (N = 68)	Two urine samples in 1st trimester and at delivery	GD calculated using last menstrual period or ultrasound	✓		✓	✓[c]	✓	✓	G	A	A	A	D	Medium
	Total Studies per Phthalate				6	2	6	5	6	6						

Excluded studies: Exposure based on tissues other than urine: Brucker-Davis et al. (2010), Huang et al. (2009), Huang et al. (2014), Huang et al. (2014), Latini et al. (2003), Li et al. (2016). Exposure based on occupational exposure with unvalidated matrix: Burdorf et al. (2011). Study entry late in pregnancy (most or all enrollment in 3rd trimester): Adibi et al. (2009), Su et al. (2014), Suzuki et al. (2010), Weinberger et al. (2014), Whyatt et al. (2009), Wolff et al. (2008).

G = good; A = adequate; D = deficient; A/D = adequate for short chain phthalates, deficient for long chain phthalates; GD = gestational duration.

[a]Additional analyses pertaining to preterm birth obtained from the study authors.

[b]Considered *critically deficient* for this phthalate due to > 50% less than the LOD.

[c]Results presented for summed DBP (MBP and MIBP), and included in analysis under DBP due to higher exposure levels.

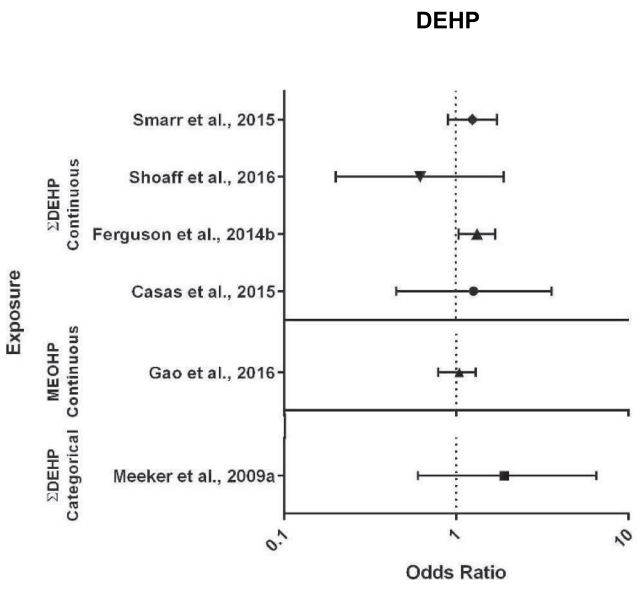

Reference; Study Confidence; N	Mean (IQR) (nm/mL)	OR (95% CI) (continuous ln-transformed exposure with 1 unit change or as specified)
∑DEHP		
Smarr et al. (2015); Medium; 200	0.2 (75th: 0.3)	1.25 (0.90, 1.74) Quartiles Q2: 0.77 (0.26, 2.28) Q3: 1.38 (0.46, 4.13) Q4: 0.93 (0.29, 2.97)
Shoaff et al. (2016); High; 368	0.3 (0.1-0.7)	Continuous, 10-fold change 0.62 (0.20, 1.90)
Ferguson et al. (2014b); High; 482	0.4	1.33 (1.04, 1.70) Quartiles Q2: 1.23 Q3: 1.55 Q4: 2.17 *p* trend = 0.02*
Casas et al. (2016); High; 380	93 ng/mL (range 14-1,429)	1.27 (0.45, 3.62) Quartiles Q2: 1.80 (0.15, 21.33) Q3: 3.32 (0.33, 33.81) Q4: 2.45 (0.23, 25.79)
Meeker et al. (2009b); Medium; 60	0.2 (0.1-0.4)	Dichotomous 1.9 (0.6, 6.5)
MEOHP		
Gao et al. (2016); Medium; 3103	7.5 (4.7-29) ng/mL	1.02 (0.80,1.31)

Fig. 2. Association between DEHP exposure and preterm birth.
*$p < 0.05$, results that support an association are shaded. Dark gray represents one or more of the following: $p < 0.05$, large effect size (e.g., OR ≥ 1.5), or exposure-response trend across categories of exposure. Light gray represents other supportive results.

duration studies, both reported an association between shorter gestational duration and increasing exposure, with statistical significance in one (Polańska et al. (2016) $\beta = -0.2$, SE = 0.1, $p = 0.04$*; Watkins et al. (2016) for male infants change in days = −3.30, 95% CI = −7.94, 1.34; for female infants change in days = −2.86, 95% CI = −9.19, 3.47). Given the reasonable consistency between the studies, the evidence that DEP exposure is associated with higher risk of preterm birth is considered *moderate*.

In addition to the primary effect, one study (Ferguson et al., 2016) showed that oxidative stress may act as a mediator between phthalate exposure and preterm birth, based on a strong association between elevated urinary phthalate metabolites and higher levels of oxidative stress biomarkers in pregnant women. The author noted that oxidative stress can cause apoptosis at the maternal-fetal interface, leading to poor vascularization of the placenta and consequently preeclampsia and/or intrauterine growth restriction during pregnancy. Another study (Adibi et al., 2010) reported that increased urinary phthalate metabolite concentrations were associated with a significant downregulation in the expression of placental genes involved in trophoblast differentiation (PPARγ, AhR, and HCG). There is also evidence from animal studies that phthalates interfere with maternal ovarian function and steroidogenesis, which may have effects on pregnancy maintenance; however, this mechanism in females remains poorly defined (reviewed in Kay et al., 2013). This mechanistic support provides some biological plausibility for the observed associations.

In summary, there is *moderate* evidence of an association between preterm birth and exposure to DEHP, DBP, and DEP. Table 13 presents a summary of the factors that increase and decrease confidence in this evidence. The evidence of an association for the remaining phthalates is considered *slight*. Exposure levels for BBP, DIBP, and DINP were generally lower than for the phthalates with an observed association, which may at least partially explain the differences. On the other hand, in the study where DBP and DIBP levels were similar Casas et al. (2016), there was an association observed for DBP (not statistically significant) but not DIBP.

4. Discussion

Of the outcomes reviewed, preterm birth has the strongest evidence of an association with phthalate exposures (Fig. 4). Three of the six phthalates had *moderate* evidence of a positive association, and the remaining three had *slight* evidence but also fewer studies and/or lower exposure levels that could explain the discrepancy. Looking across, there is evidence that preterm birth is a hazard associated with at least some phthalate exposures in humans. A 1-unit increase in the level of phthalate metabolites was associated with a 20–30% or greater increase in the odds of preterm birth in some studies. This level of increase is of clear public health concern.

Looking across the other outcomes, there is little convincing evidence of an association between phthalate exposure and female reproductive outcomes. Spontaneous abortion had *slight* evidence of an association for some phthalates. More studies on spontaneous abortion with repeated exposure measures, high study sensitivity (e.g., varied exposure levels, large sample size), and prospective outcome ascertainment would help clarify the association. This is particularly true for DEHP since the results of one high confidence study were compelling but the low confidence studies were conflicting. For pubertal development and time to pregnancy, the findings were almost all *indeterminate*, but additional *high* confidence studies may be informative here as well.

For some outcome-phthalate pairs, lower exposure levels than for other phthalates decreased the sensitivity to observe associations with health effects even if they were present in the population and hindered

the interpretability of null findings. This reduced the ability to assess coherence across phthalates. It also is difficult to evaluate the shape of the exposure-response curve in groups exposed at relatively low levels. While there is evidence of non-monotonic dose-response relations between some endocrine disrupting chemicals and health outcomes (Vandenberg et al., 2012), such evidence does not exist for female reproductive outcomes and studies of male reproductive outcomes indicate that such relations are linear (NAS, 2017). It seems unlikely that we would be able to precisely identify any non-monotonic associations given that phthalate biomarker concentrations typically span 2–4 orders of magnitude in most epidemiological studies and human phthalate exposures are several orders of magnitude lower than those used in

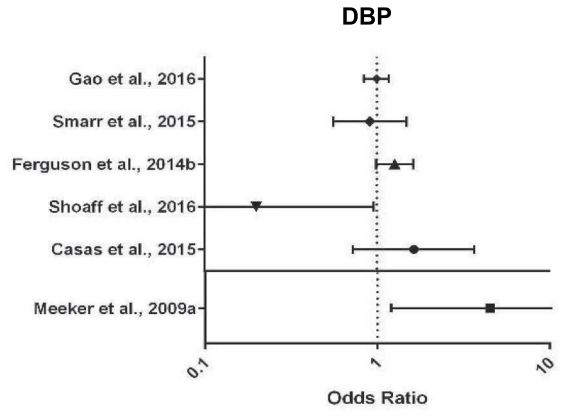

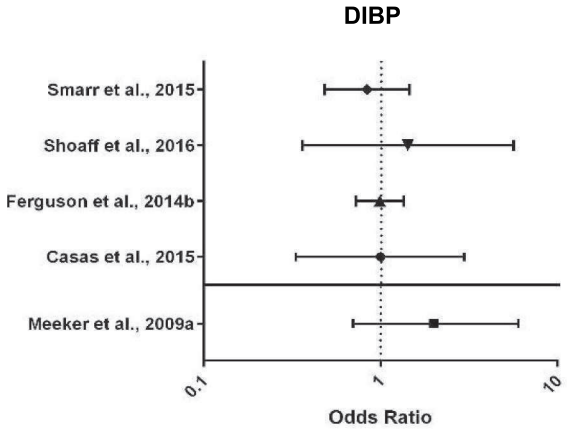

Reference; Study Confidence; N	Exposure mean (IQR) (ng/mL)	OR (95% CI) (continuous ln-transformed exposure with 1 unit change or as specified)
DBP (measured by MBP)		
Smarr et al. (2015); Medium; 2000	6.8 (75th: 15.8)	0.91 (0.56, 1.49) Quartiles Q2: 0.66 (0.23, 1.87) Q3: 0.74 (0.21, 2.57) Q4: 0.68 (0.17, 2.65)
Ferguson et al. (2014b); High; 368	5.7 (2.2-11)	1.27 (0.99, 1.63) Quartiles Q2: 0.82 Q3: 1.57 Q4: 2.25 *p* trend = 0.03
Shoaff et al. (2016); High; 368	27 (23-54)	Continuous, 10-fold change 0.20 (0.04, 0.96)
Casas et al. (2016); High; 380	29 (3.4-403)	1.64 (0.73, 3.67)
Meeker et al. (2009); Medium; 60	33 (21-74)	Dichotomous 4.5 (1.2, 16.6)
Gao et al. (2016); Medium; 3103	42 (24-319)	0.995 (0.84,1.18)
DIBP (measured by MiBP)		
Smarr et al. (2015); Medium; 200	3.7 (75th: 7.7)	0.83 (0.48, 1.44) Quartiles Q2: 1.31 (0.26, 6.65) Q3: 1.21 (0.24, 6.14) Q4: 0.72 (0.06, 9.18)
Shoaff et al. (2016); High; 368	5.7 (2.2-11)	Continuous, 10-fold change 1.41 (0.36, 5.58)
Ferguson et al. (2014b); High; 482	6.8 (4.5-10)	0.98 (0.72, 1.34)
Casas et al. (2016); High; 380	29 (range 4.0-368)	0.99 (0.33, 2.94) Quartiles Q2: 0.94 (0.12, 7.18) Q3: 1.97 (0.33, 11.8) Q4: 0.42 (0.04, 4.99)
Meeker et al. (2009b); Medium; 60	1.9 (0.8-4.1)	Dichotomous 2.0 (0.7, 6.0)

Fig. 3. Association between exposure to DBP, DIBP, BBP, and DEP and preterm birth.
Each panel depicts results for a metabolite(s) from a different parent phthalate; Q = quartile.
*$p < 0.05$, results that support an association are shaded. Dark gray represents one or more of the following: $p < 0.05$, large effect size (e.g., OR ≥ 1.5), or exposure-response trend across categories of exposure. Light gray represents other supportive results.
Tables are sorted within individual phthalates by median exposure level.

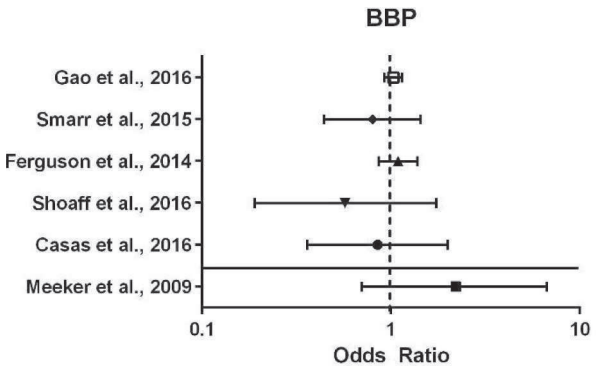

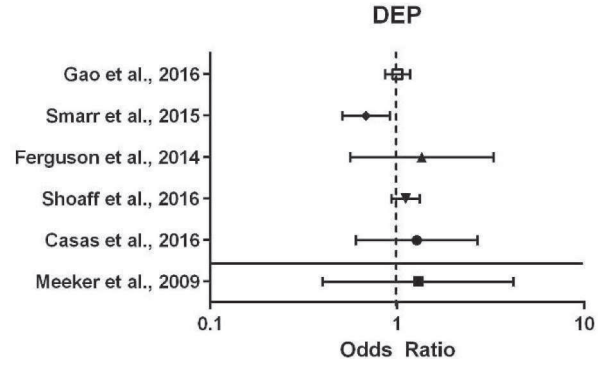

BBP (measured by MBzP)		
Gao et al. (2016); Medium; 3103	0.09 (<LOD-1.1)	1.03 (0.92,1.14)
Smarr et al. (2015); Medium; 200	3.5 (75th: 8.5)	0.80 (0.44, 1.44) Quartiles Q2: 0.43 (0.14, 1.27) Q3: 0.85 (0.27, 2.71) Q4: 0.51 (0.12, 2.17)
Ferguson et al. (2014b); High; 482	6.5 (3.3-12)	1.09 (0.86, 1.38)
Shoaff et al. (2016); High; 268	10 (4.2-24)	Continuous, 10-fold change 0.57 (0.19, 1.74)
Casas et al. (2016); High; 380	11 (range 0.8-336)	0.85 (0.36, 2.00) Quartiles Q2: 0.75 (0.12, 4.87) Q3: 0.70 (0.11, 4.42) Q4: 0.57 (0.09, 3.70)
Meeker et al. (2009b); Medium; 60	2.3 (1.0-5.2)	Dichotomous 2.2 (0.7, 6.7)
DEP (measured by MEP)		
Gao et al. (2016); Medium; 3013	8.8 (4.3-75)	1.002 (0.86,1.17)
Smarr et al. (2015); Medium; 200	101 (75th: 194)	0.68 (0.51, 0.91) Quartiles Q2: 0.44 (0.15, 1.25) Q3: 0.72 (0.25, 2.04) Q4: 0.26 (0.07, 0.89)
Ferguson et al. (2014b); High; 368	131 (54-357)	Continuous, 10-fold change 1.35 (0.56, 3.27)
Shoaff et al. (2016); High; 482	134	1.11 (0.93, 1.32)
Casas et al. (2016); High; 380	336 (range 22-5,115)	1.27 (0.60, 2.68)
Meeker et al. (2009b); Medium; 60	108	Dichotomous 1.3 (0.4, 4.2)

Fig. 3. (*continued*)

animal toxicology studies. However, future studies should employ appropriate methods (e.g., smoothing splines) to identify the presence of any non-monotonic dose-response relations.

Overall, these findings are mostly consistent with past narrative reviews. Mariana et al. (2016) found that the evidence does not support an association between phthalate exposure and precocious puberty and reported weak evidence of an association with birth size. Further, they found that there may be an association between prenatal exposure to phthalates and reduced gestational time. Benjamin et al. (2017) reported associations between phthalates and low gestational duration and spontaneous abortion but did not provide a critical review of the available literature. Both of these reviews included the same compounds examined in this review.

This systematic review benefited from the involvement of experts on phthalates and female reproductive and developmental epidemiology throughout the process, from development of the study evaluation criteria through evidence synthesis. Another strength is that methods for study evaluation and evidence synthesis were predefined in the systematic review protocol, and that studies were evaluated by two reviewers to reduce potential for bias. While study evaluation and evidence synthesis conclusions relied on expert judgment of the reviewers using structured frameworks, this is preferred in the systematic review community due to the limitations of more prescriptive, score-based approaches that tend to focus on reporting quality rather than the impact of identified limitations on the results (Higgins and Green, 2011; Herbison et al., 2006; Juni et al., 1999).

Table 13
Evidence profile table for preterm birth and DEHP, DBP, and DEP.

Phthalate	Studies (design in parentheses)	Factors that increase confidence	Factors that decrease confidence	Summary of findings	Confidence judgment for outcome
DEHP	High confidence Casas et al. (2016) (C) Ferguson et al. (2014a) (CC) Shoaff et al. (2016) (C) Medium confidence Gao et al. (2016) (C) Meeker et al. (2009) (CC) Smarr et al., 2015 (C)	• Minimal concerns for bias • Exposure-response gradient within one study • Biological plausibility	• Some unexplained inconsistency	Increased odds of preterm birth with higher DEHP exposure in 4/6 studies (Casas et al., 2016, Ferguson et al., 2014b, Meeker et al., 2009, Smarr et al., 2015). Statistically significant exposure-response gradient observed in Ferguson et al. (2014b). Similar effect sizes among studies with elevated ORs. Biological plausibility - Ferguson et al. (2016) showed that oxidative stress may act as a mediator between phthalate exposure and preterm birth.	⊕⊕◯ MODERATE
DBP	High confidence Casas et al. (2016) (C) Ferguson et al. (2014a) (CC) Shoaff et al. (2016) (C) Medium confidence Gao et al. (2016) (C) Meeker et al. (2009) (CC) Smarr et al., 2015 (C)	• Minimal concerns for bias • Large effect size in one study (OR = 4.5) • Biological plausibility	• Some unexplained inconsistency	Increased odds of preterm birth with higher DBP exposure in 3/6 studies (Casas et al., 2016; Ferguson et al., 2014b; Meeker et al., 2009), with statistical significant in Ferguson et al. (2014a, b) and Meeker et al. (2009). Biological plausibility - Ferguson et al. (2016) showed that oxidative stress may act as a mediator between phthalate exposure and preterm birth.	⊕⊕◯ MODERATE
DEP	High confidence Casas et al. (2016) (C) Ferguson et al. (2014a) (CC) Shoaff et al. (2016) (C) Medium confidence Gao et al. (2016) (C) Meeker et al. (2009) (CC) Smarr et al., 2015 (C)	• Minimal concerns for bias • Lower study sensitivity (i.e., exposure levels) could account for remaining inconsistency • Biological plausibility		Increased odds of preterm birth with higher DEP exposure in 4/6 studies (Casas et al., 2016; Ferguson et al., 2014b; Meeker et al., 2009; Shoaff et al., 2016). Biological plausibility - Ferguson et al. (2016) showed that oxidative stress may act as a mediator between phthalate exposure and preterm birth.	⊕⊕◯ MODERATE

C: cohort, CC: case-control, CS: cross-sectional, OR = odds ratio.

Outcome	DEHP	DINP	DBP	DIBP	BBP	DEP
Pubertal development	I	I	I	I	I	S
Time to pregnancy	S	I	I	I	I	I
Spontaneous abortion	S	I	S	I	I	S
Preterm birth	M	S	M	S	S	M

Robust (R) Moderate (M) Slight (S) Indeterminate (I)

Level of confidence in association

Fig. 4. Summary of epidemiologic evidence of female reproductive and developmental effects associated with phthalates.

However, while systematic review tools have been in use for some time in studies of clinical interventions, these methods have been introduced in the field of environmental health assessment more recently. Modifications to the existing tools and approaches have been necessary to accommodate challenges inherent to observational studies where exposure is not controlled. However, since the application of these approaches is newer and less tested, we recognize that there may be aspects of the methodology that could benefit from greater transparency for the reader, such as communication of inputs to decisions.

There are other important limitations to note. Due to remaining uncertainty in the database, including inconsistency among some high confidence studies and potential for remaining unidentified confounders, it is not possible to conclusively establish causality from the observational epidemiology studies alone. The integration of this evidence with animal toxicology studies and mechanistic studies could provide additional information to address some of the uncertainty in the epidemiologic evidence and increase the strength of the causal analysis. A complete mechanistic analysis would require additional systematic literature identification and synthesis and was outside the scope of this review. In addition, while a quantitative meta-analysis may have been informative for studies of preterm birth, it was not performed because the necessary analyses were not provided in the same way by all of the studies. A meta-analysis on this topic would ideally be performed using the original datasets, to allow for better exploration of the exposure-response pattern across the studies that contribute data from different exposure ranges, however, this was outside the scope of this review. Discussion of some additional issues that apply to all phthalate studies is presented in a forthcoming editorial. These include the difficulties in assessing health effects of mixtures and separating individual contributions from highly correlated phthalates. Despite these limitations, our systematic review of the epidemiological literature supports an association between some phthalate exposures and preterm birth.

Acknowledgments

We would like to thank Erin Yost, Rebecca Nachman, Susan Rieth, Kris Thayer, Mike Wright, Emily Harville, Anna Pollack, and Andrew Greenhalgh for their contributions to this work.

Appendix A. Supplementary data

Supplementary data to this article can be found online at https://doi.org/10.1016/j.envint.2019.02.003.

References

Adibi, J.J., Hauser, R., Williams, P.L., Whyatt, R.M., Calafat, A.M., Nelson, H., Herrick, R., Swan, S.H., 2009. Maternal urinary metabolites of di-(2-ethylhexyl) phthalate in relation to the timing of labor in a US multicenter pregnancy cohort study. Am. J. Epidemiol. 169, 1015–1024. https://doi.org/10.1093/aje/kwp001.

Adibi, J.J., Whyatt, R.M., Hauser, R., Bhat, H.K., Davis, B.J., Calafat, A.M., Hoepner, L.A., Perera, F.P., Tang, D., Williams, P.L., 2010. Transcriptional biomarkers of steroidogenesis and trophoblast differentiation in the placenta in relation to prenatal phthalate exposure. Environ. Health Perspect. 118, 291–296. https://doi.org/10.1289/ehp.0900788.

Benjamin, S., Masai, E., Kamimura, N., Takahashi, K., Anderson, R.C., Faisal, P.A., 2017. Phthalates impact human health: epidemiological evidences and plausible mechanism of action [review]. J. Hazard. Mater. 340, 360–383. https://doi.org/10.1016/j.jhazmat.2017.06.036.

Binder, A.M., Corvalan, C., Calafat, A.M., Ye, X., Mericq, V., Pereira, A., Michels, K.B., 2018. Childhood and adolescent phenol and phthalate exposure and the age of menarche in Latina girls. Environ. Health 17, 32. https://doi.org/10.1186/s12940-018-0376-z.

Brucker-Davis, F., Wagner-Mahler, K., Bornebusch, L., Delattre, I., Ferrari, P., Gal, J., Boda-Buccino, M., Pacini, P., Tommasi, C., Azuar, P., Bongain, A., Fénichel, P., 2010. Exposure to selected endocrine disruptors and neonatal outcome of 86 healthy boys from Nice area (France). Chemosphere 81, 169–176. https://doi.org/10.1016/j.chemosphere.2010.06.068.

Buck Louis, G.M., Schisterman, E.F., Sweeney, A.M., Wilcosky, T.C., Gore-Langton, R.E., Lynch, C.D., Boyd Barr, D., Schrader, S.M., Kim, S., Chen, Z., Sundaram, R., 2011. Designing prospective cohort studies for assessing reproductive and developmental toxicity during sensitive windows of human reproduction and development—the LIFE study. Paediatr. Perinat. Epidemiol. 25, 413–424. https://doi.org/10.1111/j.1365-3016.2011.01205.x.

Buck Louis, G.M., Sundaram, R., Sweeney, A.M., Schisterman, E.F., Maisog, J., Kannan, K., 2014. Urinary bisphenol A, phthalates, and couple fecundity: the Longitudinal Investigation of Fertility and the Environment (LIFE) study. Fertil. Steril. 101, 1359–1366. https://doi.org/10.1016/j.fertnstert.2014.01.022.

Buck Louis, G.M., Smarr, M.M., Sun, L., Chen, Z., Honda, M., Wang, W., Karthikraj, R., Weck, J., Kannan, K., 2018. Endocrine disrupting chemicals in seminal plasma and couple fecundity. Environ. Res. 163, 64–70. https://doi.org/10.1016/j.envres.2018.01.028.

Buluş, A.D., Aşci, A., Erkekoglu, P., Balci, A., Andiran, N., Koçer-Gümüşel, B., 2016. The evaluation of possible role of endocrine disruptors in central and peripheral precocious puberty. Toxicol. Mech. Methods 26, 493–500. https://doi.org/10.3109/15376516.2016.1158894.

Burdorf, A., Brand, T., Jaddoe, V.W., Hofman, A., Mackenbach, J.P., Steegers, E.A., 2011. The effects of work-related maternal risk factors on time to pregnancy, preterm birth and birth weight: the Generation R Study. Occup. Environ. Med. 68, 197–204. https://doi.org/10.1136/oem.2009.046516.

Buttke, D.E., Sircar, K., Martin, C., 2012. Exposures to endocrine-disrupting chemicals and age of menarche in adolescent girls in NHANES (2003–2008). Environ. Health Perspect. 120, 1613–1618. https://doi.org/10.1289/ehp.1104748.

Carran, M., Shaw, I.C., 2012. New Zealand Malayan war veterans' exposure to dibutylphthalate is associated with an increased incidence of cryptorchidism, hypospadias and breast cancer in their children. N. Z. Med. J. 125, 52–63.

Casas, M., Valvi, D., Ballesteros-Gomez, A., Gascon, M., Fernández, M.F., Garcia-Esteban, R., I iguez, C., Martinez, D., Murcia, M., Monfort, N., Luque, N., Rubio, S., Ventura, R., Sunyer, J., Vrijheid, M., 2016. Exposure to bisphenol A and phthalates during pregnancy and ultrasound measures of fetal growth in the INMA-Sabadell cohort. Environ. Health Perspect. 124, 521–528. https://doi.org/10.1289/ehp.1409190.

Chen, C.Y., Chou, Y.Y., Wu, Y.M., Lin, C.C., Lin, S.J., Lee, C.C., 2013. Phthalates may promote female puberty by increasing kisspeptin activity. Hum. Reprod. 28, 2765–2773. https://doi.org/10.1093/humrep/det325.

Chen, Y.H., Ferguson, K.K., Meeker, J.D., Mcelrath, T.F., Mukherjee, B., 2015. Statistical methods for modeling repeated measures of maternal environmental exposure biomarkers during pregnancy in association with preterm birth. Environ. Health 14, 9. https://doi.org/10.1186/1476-069X-14-9.

Chou, Y.Y., Huang, P.C., Lee, C.C., Wu, M.H., Lin, S.J., 2009. Phthalate exposure in girls during early puberty. J. Pediatr. Endocrinol. Metab. 22, 69–77.

Cooper, G., Lunn, R., Agerstrand, M., Glenn, B., Kraft, A., Luke, A., Ratcliffe, J., 2016. Study sensitivity: evaluating the ability to detect effects in systematic reviews of chemical exposures. Environ. Int. 92-93, 605–610. https://doi.org/10.1016/j.envint.2016.03.017.

Fennell, T.R., Krol, W.L., Sumner, S.C.J., Snyder, R.W., 2004. Pharmacokinetics of dibutylphthalate in pregnant rats. Toxicol. Sci. 82, 407–418. https://doi.org/10.1093/toxsci/kfh294.

Ferguson, K.K., Mcelrath, T.F., Ko, Y.A., Mukherjee, B., Meeker, J.D., 2014a. Variability in

urinary phthalate metabolite levels across pregnancy and sensitive windows of exposure for the risk of preterm birth. Environ. Int. 70C, 118–124. https://doi.org/10.1016/j.envint.2014.05.016.
Ferguson, K.K., Mcelrath, T.F., Meeker, J.D., 2014b. Environmental phthalate exposure and preterm birth. JAMA Pediatr. 168, 61–67. https://doi.org/10.1001/jamapediatrics.2013.3699.
Ferguson, K.K., Chen, Y.H., Vanderweele, T.J., Mcelrath, T.F., Meeker, J.D., Mukherjee, B., 2016. Mediation of the relationship between maternal phthalate exposure and preterm birth by oxidative stress with repeated measurements across pregnancy. Environ. Health Perspect. 125, 488–494. https://doi.org/10.1289/EHP282.
Frederiksen, H., Sørensen, K., Mouritsen, A., Aksglaede, L., Hagen, C.P., Petersen, J.H., Skakkebaek, N.E., Andersson, A.M., Juul, A., 2012. High urinary phthalate concentration associated with delayed pubarche in girls. Int. J. Androl. 35, 216–226. https://doi.org/10.1111/j.1365-2605.2012.01260.x.
Gao, H., Xu, Y.Y., Huang, K., Ge, X., Zhang, Y.W., Yao, H.Y., Xu, Y.Q., Yan, S.Q., Jin, Z.X., Sheng, J., Zhu, P., Hao, J.H., Tao, F.B., 2016. Cumulative risk assessment of phthalates associated with birth outcomes in pregnant Chinese women: a prospective cohort study. Environ. Pollut. 222, 549–556. https://doi.org/10.1016/j.envpol.2016.11.026.
Gao, H., Zhang, Y.W., Huang, K., Yan, S.Q., Mao, L.J., Ge, X., Xu, Y.Q., Xu, Y.Y., Sheng, J., Jin, Z.X., Zhu, P., Tao, X.G., Hao, J.H., Tao, F.B., 2017. Urinary concentrations of phthalate metabolites in early pregnancy associated with clinical pregnancy loss in Chinese women: supplementary materials [supplemental data]. Sci. Rep. 7.
Gnoth, C., Godehardt, D., Godehardt, E., Frank-Herrmann, P., Freundl, G., 2003. Time to pregnancy: results of the German prospective study and impact on the management of infertility. Hum. Reprod. 18, 1959–1966.
Hart, R., Doherty, D.A., Frederiksen, H., Keelan, J.A., Hickey, M., Sloboda, D., Pennell, C.E., Newnham, J.P., Skakkebaek, N.E., Main, K.M., 2013. The influence of antenatal exposure to phthalates on subsequent female reproductive development in adolescence: a pilot study. Reproduction 147, 379–390. https://doi.org/10.1530/REP-13-0331.
Hashemipour, M., Kelishadi, R., Amin, M.M., Ebrahim, K., 2018. Is there any association between phthalate exposure and precocious puberty in girls? Environ. Sci. Pollut. Res. Int. 25, 13589–13596. https://doi.org/10.1007/s11356-018-1567-4.
Hauser, R., Calafat, A.M., 2005. Phthalates and human health [review]. Occup. Environ. Med. 62, 818. https://doi.org/10.1136/oem.2004.017590.
Hauser, R., Gaskins, A.J., Souter, I., Smith, K.W., Dodge, L.E., Ehrlich, S., Meeker, J.D., Calafat, A.M., Williams, P.L., 2016. Urinary phthalate metabolite concentrations and reproductive outcomes among women undergoing in vitro fertilization: results from the EARTH study. Environ. Health Perspect. 124, 831–839. https://doi.org/10.1289/ehp.1509760.
Herbison, P., Hay-Smith, J., Gillespie, W.J., 2006. Adjustment of meta-analyses on the basis of quality scores should be abandoned [review]. J. Clin. Epidemiol. 59, 1249–1256. https://doi.org/10.1016/j.jclinepi.2006.03.008.
Higgins, J.P.T., Green, S., 2011. Cochrane Handbook for Systematic Reviews of Interventions, Version 5.1.0 (Updated March 2011). The Cochrane Collaboration Retrieved from. http://handbook.cochrane.org/.
Howdeshell, K.L., Rider, C.V., Wilson, V.S., Gray Jr., L.E., 2008. Mechanisms of action of phthalate esters, individually and in combination, to induce abnormal reproductive development in male laboratory rats [review]. Environ. Res. 108, 168–176. https://doi.org/10.1016/j.envres.2008.08.009.
Huang, P.C., Kuo, P.L., Chou, Y.Y., Lin, S.J., Lee, C.C., 2009. Association between prenatal exposure to phthalates and the health of newborns. Environ. Int. 35, 14–20. https://doi.org/10.1016/j.envint.2008.05.012.
Huang, Y., Li, J., Garcia, J.M., Lin, H., Wang, Y., Yan, P., Wang, L., Tan, Y., Luo, J., Qiu, Z., Chen, J.A., Shu, W., 2014. Phthalate levels in cord blood are associated with preterm delivery and fetal growth parameters in Chinese women. PLoS ONE 9, e87430. https://doi.org/10.1371/journal.pone.0087430.
Huang, P.C., Tsai, C.H., Liang, W.Y., Li, S.S., Huang, H.B., Kuo, P.L., 2016. Early phthalates exposure in pregnant women is associated with alteration of thyroid hormones. PLoS ONE 11, e0159398. https://doi.org/10.1371/journal.pone.0159398.
Johns, L.E., Cooper, G.S., Galizia, A., Meeker, J.D., 2015. Exposure assessment issues in epidemiology studies of phthalates [review]. Environ. Int. 85, 27–39. https://doi.org/10.1016/j.envint.2015.08.005.
Johnson, K.J., Heger, N.E., Boekelheide, K., 2012. Of mice and men (and rats): phthalate-induced fetal testis endocrine disruption is species-dependent [review]. Toxicol. Sci. 129, 235–248. https://doi.org/10.1093/toxsci/kfs206.
Jukic, A.M., Calafat, A.M., Mcconnaughey, D.R., Longnecker, M.P., Hoppin, J.A., Weinberg, C.R., Wilcox, A.J., Baird, D.D., 2016. Urinary concentrations of phthalate metabolites and bisphenol A and associations with follicular-phase length, luteal-phase length, fecundability, and early pregnancy loss. Environ. Health Perspect. 124, 321–328. https://doi.org/10.1289/ehp.1408164.
Juni, P., Witschi, A., Bloch, R., Egger, M., 1999. The hazards of scoring the quality of clinical trials for meta-analysis. JAMA 282, 1054–1060.
Kasper-Sonnenberg, M., Wittsiepe, J., Wald, K., Koch, H.M., Wilhelm, M., 2017. Pre-pubertal exposure with phthalates and bisphenol A and pubertal development. PLoS ONE 12, e0187922. https://doi.org/10.1371/journal.pone.0187922.
Kay, V.R., Chambers, C., Foster, W.G., 2013. Reproductive and developmental effects of phthalate diesters in females [review]. Crit. Rev. Toxicol. 43, 200–219. https://doi.org/10.3109/10408444.2013.766149.
Langonne, I., Saillenfait, A.M., Payan, J.P., 1998. Comparative embryotoxicity of di-n-butyl phthalate and its main metabolite mono-n-butyl phthalate at midgestation. Teratology 58, 22A.
Latini, G., De Felice, C., Presta, G., Del Vecchio, A., Paris, I., Ruggieri, F., Mazzeo, P., 2003. In utero exposure to di-(2-ethylhexyl)phthalate and duration of human pregnancy. Environ. Health Perspect. 111, 1783–1785. https://doi.org/10.1289/ehp.6202.
Lee, S.W., Lee, W.J., Chae, H.W., Lee, E.B., Kim, J.H., Kim, D.H., Kim, H.S., 2009. Determination of Serum Di-(2-ethylhexyl) Phthalate and Bisphenol A Level in Children With Idiopathic Central Precocious Puberty. 14. pp. 154–162.
Li, B., Xu, X., Zhu, Y., Cao, J., Zhang, Y., Huo, X., 2016. Neonatal phthalate ester exposure induced placental MTs, FATP1 and HFABP mRNA expression in two districts of southeast China. Sci. Rep. 6, 21004. https://doi.org/10.1038/srep21004.
Liao, K.W., Kuo, P.L., Huang, H.B., Chang, J.W., Chiang, H.C., Huang, P.C., 2018. Increased risk of phthalates exposure for recurrent pregnancy loss in reproductive-aged women. Environ. Pollut. 241, 969–977. https://doi.org/10.1016/j.envpol.2018.06.022.
Lomenick, J.P., Calafat, A.M., Melguizo Castro, M.S., Mier, R., Stenger, P., Foster, M.B., Wintergerst, K.A., 2010. Phthalate exposure and precocious puberty in females. J. Pediatr. 156, 221–225. https://doi.org/10.1016/j.jpeds.2009.09.047.
Lovekamp-Swan, T., Davis, B.J., 2003. Mechanisms of phthalate ester toxicity in the female reproductive system [review]. Environ. Health Perspect. 111, 139–145.
Machtinger, R., Gaskins, A.J., Racowsky, C., et al., 2018. Urinary concentrations of biomarkers of phthalates and phthalate alternatives and IVF outcomes. Environ. Int. 111, 23–31 (PMID:29161633).
Mariana, M., Feiteiro, J., Verde, I., Cairrao, E., 2016. The effects of phthalates in the cardiovascular and reproductive systems: a review [review]. Environ. Int. 94, 758–776. https://doi.org/10.1016/j.envint.2016.07.004.
Martin, J.A., Hamilton, B.E., Osterman, M.J., Curtin, S.C., Matthews, T.J., 2013. Births: final data for 2012. Natl. Vital Stat. Rep. 62, 1–68.
Meeker, J.D., Hu, H., Cantonwine, D.E., Lamadrid-Figueroa, H., Calafat, A.M., Ettinger, A.S., Hernandez-Avila, M., Loch-Caruso, R., Tellez-Rojo, M.M., 2009. Urinary phthalate metabolites in relation to preterm birth in Mexico city. Environ. Health Perspect. 117, 1587–1592. https://doi.org/10.1289/ehp.0800522.
Messerlian, C., Souter, I., Gaskins, A.J., Williams, P.L., Ford, J.B., Chiu, Y.H., Calafat, A.M., Hauser, R., Team, E.S., 2015. Urinary phthalate metabolites and ovarian reserve among women seeking infertility care. Hum. Reprod. https://doi.org/10.1093/humrep/.
Messerlian, C., Wylie, B.J., Minguez-Alarcon, L., Williams, P.L., Ford, J.B., Souter, I.C., Calafat, A.M., Hauser, R., Team, E.S., 2016. Urinary concentrations of phthalate metabolites and pregnancy loss among women conceiving with medically assisted reproduction. Epidemiology 27, 879–888. https://doi.org/10.1097/EDE.0000000000000525.
Mouritsen, A., Frederiksen, H., Sørensen, K., Aksglaede, L., Hagen, C., Skakkebaek, N., Main, K., Andersson, A., Juul, A., 2013. Urinary phthalates from 168 girls and boys measured twice a year during a 5 year period: associations with adrenal androgen levels and puberty. J. Clin. Endocrinol. Metab. 98, 3755–3764. https://doi.org/10.1210/jc.2013-1284.
Mu, D., Gao, F., Fan, Z., Shen, H., Peng, H., Hu, J., 2015. Levels of phthalate metabolites in urine of pregnant women and risk of clinical pregnancy loss. Environ. Sci. Technol. 49, 10651–10657. https://doi.org/10.1021/acs.est.5b02617.
NAS, 2017. Application of Systematic Review Methods in an Overall Strategy for Evaluating Low-Dose Toxicity from Endocrine Active Chemicals. https://doi.org/10.17226/24758. https://www.nap.edu/catalog/24758/application-of-systematic-review-methods-in-an-overall-strategy-for-evaluating-low-dose-toxicity-from-endocrine-active-chemicals.
Philips, E.M., Kahn, L.G., Jaddoe, V.W.V., Shao, Y., Asimakopoulos, A.G., Kannan, K., Steegers, E.A.P., Trasande, L., 2018. First trimester urinary bisphenol and phthalate concentrations and time to pregnancy: a population-based cohort analysis. J. Clin. Endocrinol. Metab. 103, 35403547. https://doi.org/10.1210/jc.2018-00855.
Polańska, K., Ligocka, D., Sobala, W., Hanke, W., 2016. Effect of environmental phthalate exposure on pregnancy duration and birth outcomes. Int. J. Occup. Med. Environ. Health 29, 683–697. https://doi.org/10.13075/ijomeh.1896.00691.
Rais-Bahrami, K., Nunez, S., Revenis, M.E., Luban, N.L., Short, B.L., 2004. Follow-up study of adolescents exposed to di(2-ethylhexyl) phthalate (DEHP) as neonates on extracorporeal membrane oxygenation (ECMO) support. Environ. Health Perspect. 112, 1339–1340. https://doi.org/10.1289/ehp.6901.
Shi, H., Cao, Y., Shen, Q., Zhao, Y., Zhang, Z., Zhang, Y., 2015. Association between urinary phthalates and pubertal timing in Chinese adolescents. J. Epidemiol. 25, 574–582. https://doi.org/10.2188/jea.JE20140205.
Shoaff, J.R., Romano, M.E., Yolton, K., Lanphear, B.P., Calafat, A.M., Braun, J.M., 2016. Prenatal phthalate exposure and infant size at birth and gestational duration. Environ. Res. 150, 52–58. https://doi.org/10.1016/j.envres.2016.05.033.
Smarr, M.M., Grantz, K.L., Sundaram, R., Maisog, J.M., Kannan, K., Louis, G.M., 2015. Parental urinary biomarkers of preconception exposure to bisphenol A and phthalates in relation to birth outcomes. Environ. Health 14, 73. https://doi.org/10.1186/s12940-015-0060-5.
Smerieri, A., Testa, C., Lazzeroni, P., Nuti, F., Grossi, E., Cesari, S., Montanini, L., Latini, G., Bernasconi, S., Papini, A.M., Street, M.E., 2015. Di-(2-ethylhexyl) phthalate metabolites in urine show age-related changes and associations with adiposity and parameters of insulin sensitivity in childhood. PLoS ONE 10, e0117831. https://doi.org/10.1371/journal.pone.0117831.
Specht, I.O., Bonde, J.P., Toft, G., Lindh, C.H., Jönsson, B.A., Jørgensen, K.T., 2015. Serum phthalate levels and time to pregnancy in couples from Greenland, Poland and Ukraine. PLoS ONE 10, e0120070. https://doi.org/10.1371/journal.pone.0120070.

Srilanchakon, K., Thadsri, T., Jantarat, C., Thengyai, S., Nosoognoen, W., Supornsilchai, V., 2017. Higher phthalate concentrations are associated with precocious puberty in normal weight Thai girls. J. Pediatr. Endocrinol. Metab. 30, 1293–1298. https://doi.org/10.1515/jpem-2017-0281.

Sterne, J., Higgins, J., Reeves, B., 2016. ROBINS-I: a tool for assessing risk of bias in non-randomized studies of interventions, version 7 March 2016. Br. Med. J. 355, i4919.

Su, P.H., Chen, J.Y., Lin, C.Y., Chen, H.Y., Liao, P.C., Ying, T.H., Wang, S.L., 2014. Sex steroid hormone levels and reproductive development of eight-year-old children following in utero and environmental exposure to phthalates. PLoS ONE 9, e102788. https://doi.org/10.1371/journal.pone.0102788.

Suzuki, Y., Niwa, M., Yoshinaga, J., Mizumoto, Y., Serizawa, S., Shiraishi, H., 2010. Prenatal exposure to phthalate esters and PAHs and birth outcomes. Environ. Int. 36, 699–704. https://doi.org/10.1016/j.envint.2010.05.003.

Thomsen, A.M., Riis, A.H., Olsen, J., Jönsson, B.A., Lindh, C.H., Hjollund, N.H., Jensen, T.K., Bonde, J.P., Toft, G., 2017. Female exposure to phthalates and time to pregnancy: a first pregnancy planner study. Hum. Reprod. 32, 232–238. https://doi.org/10.1093/humrep/dew291.

Toft, G., Jönsson, B.A., Lindh, C.H., Jensen, T.K., Hjollund, N.H., Vested, A., Bonde, J.P., 2012. Association between pregnancy loss and urinary phthalate levels around the time of conception. Environ. Health Perspect. 120, 458–463. https://doi.org/10.1289/ehp.1103552.

U.S. EPA (U.S. Environmental Protection Agency), 1996. Guidelines for Reproductive Toxicity Risk Assessment. Risk Assessment Forum U.S. Environmental Protection Agency, Washington, DC, pp. 1–143(EPA/630/R-96/009). (https://www.epa.gov/sites/production/files/2014-11/documents/guidelines_repro_toxicity.pdf).

Vandenberg, L.N., Colborn, T., Hayes, T.B., Heindel, J.J., Jacobs, D.R., Lee, D.H., Shioda, T., Soto, A.M., vom Saal, F.S., Welshons, W.V., Zoeller, R.T., Myers, J.P., 2012. Hormones and endocrine-disrupting chemicals: low-dose effects and nonmonotonic dose responses [review]. Endocr. Rev. 33, 378–455. https://doi.org/10.1210/er.2011-1050.

Vélez, M.P., Arbuckle, T.E., Fraser, W.D., 2015. Female exposure to phenols and phthalates and time to pregnancy: the Maternal-Infant Research on Environmental Chemicals (MIREC) study. Fertil. Steril. 103, 1011–1020.e1012. https://doi.org/10.1016/j.fertnstert.2015.01.005.

Watkins, D.J., Téllez-Rojo, M.M., Ferguson, K.K., Lee, J.M., Solano-Gonzalez, M., Blank-Goldenberg, C., Peterson, K.E., Meeker, J.D., 2014. In utero and peripubertal exposure to phthalates and BPA in relation to female sexual maturation. Environ. Res. 134, 233–241. https://doi.org/10.1016/j.envres.2014.08.010.

Watkins, D.J., Milewski, S., Domino, S.E., Meeker, J.D., Padmanabhan, V., 2016. Maternal phthalate exposure during early pregnancy and at delivery in relation to gestational age and size at birth: a preliminary analysis. Reprod. Toxicol. 65, 59–66. https://doi.org/10.1016/j.reprotox.2016.06.021.

Watkins, D.J., Sánchez, B.N., Téllez-Rojo, M.M., Lee, J.M., Mercado-García, A., Blank-Goldenberg, C., Peterson, K.E., Meeker, J.D., 2017. Phthalate and bisphenol A exposure during in utero windows of susceptibility in relation to reproductive hormones and pubertal development in girls. Environ. Res. 159, 143–151. https://doi.org/10.1016/j.envres.2017.07.051.

Weinberger, B., Vetrano, A.M., Archer, F.E., Marcella, S.W., Buckley, B., Wartenberg, D., Robson, M.G., Klim, J., Azhar, S., Cavin, S., Wang, L., Rich, D.Q., 2014. Effects of maternal exposure to phthalates and bisphenol A during pregnancy on gestational age. J. Matern. Fetal Neonatal Med. 27, 323–327. https://doi.org/10.3109/14767058.2013.815718.

Whyatt, R.M., Adibi, J.J., Calafat, A.M., Camann, D.E., Rauh, V., Bhat, H.K., Perera, F.P., Andrews, H., Just, A.C., Hoepner, L., Tang, D., Hauser, R., 2009. Prenatal di(2-ethylhexyl)phthalate exposure and length of gestation among an inner-city cohort. Pediatrics 124, e1213–e1220. https://doi.org/10.1542/peds.2009-0325.

Wolff, M.S., Engel, S.M., Berkowitz, G.S., Ye, X., Silva, M.J., Zhu, C., Wetmur, J., Calafat, A.M., 2008. Prenatal phenol and phthalate exposures and birth outcomes. Environ. Health Perspect. 116, 1092–1097. https://doi.org/10.1289/ehp.11007.

Wolff, M.S., Teitelbaum, S.L., Pinney, S.M., Windham, G., Liao, L., Biro, F., Kushi, L.H., Erdmann, C., Hiatt, R.A., Rybak, M.E., Calafat, A.M., 2010. Investigation of relationships between urinary biomarkers of phytoestrogens, phthalates, and phenols and pubertal stages in girls. Environ. Health Perspect. 118, 1039–1046. https://doi.org/10.1289/ehp.0901690.

Wolff, M.S., Teitelbaum, S.L., Mcgovern, K., Windham, G.C., Pinney, S.M., Galvez, M., Calafat, A.M., Kushi, L.H., Biro, F.M., 2014. Phthalate exposure and pubertal development in a longitudinal study of US girls. Hum. Reprod. 29, 1558–1566. https://doi.org/10.1093/humrep/deu081.

Wolff, M.S., Pajak, A., Pinney, S.M., Windham, G.C., Galvez, M., Rybak, M., Silva, M.J., Ye, X., Calafat, A.M., Kushi, L.H., Biro, F.M., Teitelbaum, S.L., Program, BCaER, 2017. Associations of urinary phthalate and phenol biomarkers with menarche in a multiethnic cohort of young girls. Reprod. Toxicol. 67, 56–64. https://doi.org/10.1016/j.reprotox.2016.11.009.

Wu, H., Ashcraft, L., Whitcomb, B.W., Rahil, T., Tougias, E., Sites, C.K., Pilsner, JR., 2017. Parental contributions to early embryo development: influences of urinary phthalate and phthalate alternatives among couples undergoing IVF treatment. Hum. Reprod. 32, 6.

Yi, H., Gu, H., Zhou, T., Chen, Y., Wang, G., Jin, Y., Yuan, W., Zhao, H., Zhang, L., 2016. A pilot study on association between phthalate exposure and missed miscarriage. Eur. Rev. Med. Pharmacol. Sci. 20, 1894–1902.

Yum, T., Lee, S., Kim, Y., 2013. Association between precocious puberty and some endocrine disruptors in human plasma. J. Environ. Sci. Health A Tox. Hazard. Subst. Environ. Eng. 48, 912–917. https://doi.org/10.1080/10934529.2013.762734.

Zhang, Y., Cao, Y., Shi, H., Jiang, X., Zhao, Y., Fang, X., Xie, C., 2015. Could exposure to phthalates speed up or delay pubertal onset and development? A 1.5-year follow-up of a school-based population. Environ. Int. 83, 41–49. https://doi.org/10.1016/j.envint.2015.06.005.

Zhao, R., Wu, Y., Zhao, F., Lv, Y., Huang, D., Wei, J., Ruan, C., Huang, M., Deng, J., Huang, D., Qiu, X., 2017. The risk of missed abortion associated with the levels of tobacco, heavy metals and phthalate in hair of pregnant woman: a case control study in Chinese women. Medicine (Baltimore) 96, e9388. https://doi.org/10.1097/MD.0000000000009388.

Environment International 132 (2019) 104768

Contents lists available at ScienceDirect

Environment International

journal homepage: www.elsevier.com/locate/envint

Review article

Phthalate exposure and metabolic effects: a systematic review of the human epidemiological evidence

Elizabeth G. Radke*, Audrey Galizia, Kristina A. Thayer, Glinda S. Cooper

ABSTRACT

Objective: We performed a systematic review of the epidemiology literature to identify the metabolic effects associated with phthalate exposure.

Data sources and study eligibility criteria: Six phthalates were included in the review: di(2-ethylhexyl) phthalate (DEHP), diisononyl phthalate (DINP), dibutyl phthalate (DBP), diisobutyl phthalate (DIBP), butyl benzyl phthalate (BBP), and diethyl phthalate (DEP). The initial literature search (of PubMed, Web of Science, and Toxline) included all studies of metabolic effects in humans, and outcomes were selected for full systematic review based on data availability.

Study evaluation and synthesis methods: Studies of diabetes and insulin resistance were evaluated using criteria defined a priori for risk of bias and sensitivity by two reviewers using a domain-based approach; studies identified with a pre-defined critical deficiency were excluded. Evidence was synthesized by outcome and phthalate and strength of evidence was summarized using a structured framework. Studies of obesity and renal effects received "screening level" reviews to determine whether full systematic review was warranted.

Results: The primary outcomes reviewed here are (number of included/excluded studies in parentheses): type 2 diabetes (1/3), insulin resistance (13/3), and impaired glucose tolerance and blood glucose in pregnancy (4/2). For DEHP exposure, there was consistency among studies of insulin resistance and coherence with the single included study of diabetes, as well as an observed exposure-response gradient observed in a study of insulin resistance. This evidence is considered moderate. Similarly, for DBP and DIBP exposure, the evidence is considered moderate due to strong positive associations in the diabetes study and coherent results for insulin resistance. For DINP, BBP, and DEP, the evidence is considered slight. No association was reported in the single study of diabetes with BBP and DEP exposure (DINP was not investigated). The available evidence does indicate an association between exposure to these phthalates and insulin resistance, but the small number of studies and the lack of coherence with diabetes decreases confidence. The screening level reviews for obesity and renal effects determined that the currently available evidence is inadequate to assess the associations between these outcomes and phthalate exposure.

Conclusions and implications of key findings: Overall, these results support that phthalate exposure at levels seen in human populations may have metabolic effects. Given the mechanistic support, the large effect sizes for incident diabetes in the single available study, and the coherence with insulin resistance, the association between phthalate exposure and diabetes risk should be considered when assessing the risks and costs of exposure to specific phthalates in humans.

The views expressed are those of the authors and do not necessarily represent the views or policies of the U.S. EPA.

1. Introduction

Human exposure to phthalates (manmade phthalic acid diesters) is ubiquitous because of the widespread use of these chemicals in consumer and industrial products. These compounds have a variety of different structures and properties that determine their uses. Phthalates are used in polyvinyl chloride products and in some medications and personal care products. In general, these diesters are rapidly metabolized to monoester metabolites and are excreted in the urine. Endocrine, and endocrine-disruption, effects on metabolism and on metabolic diseases is a growing area of research with significant public health implications (Heindel et al., 2017). This review focuses on studies of phthalate exposure and metabolic-related outcomes.

The phthalates evaluated in this paper are: di(2-ethylhexyl) phthalate (DEHP), diisononyl phthalate (DINP), dibutyl phthalate (DBP), diisobutyl phthalate (DIBP), butyl benzyl phthalate (BBP), and diethyl phthalate (DEP). Five of the selected phthalates (DEHP, DINP, DBP, DIBP, and BBP) were chosen because they are the most potent with respect to producing the "phthalate syndrome" of male reproductive effects in rats (NAS 2008) and their metabolites have been frequently observed in human populations studies; DEP is not one of the "phthalate syndrome" compounds but was included because it is often the phthalate to which humans have the highest exposure.

Past reviews examined the association between phthalates and diabetes and obesity and found the evidence inadequate to conclude whether an association existed (Kuo et al., 2013; Thayer et al., 2012). However, additional studies have been published in the interim, and no systematic review is available on insulin resistance, an emerging area of research in the phthalate literature. As part of a comprehensive evaluation of the epidemiological literature on phthalates, we performed a systematic review on the association between phthalate exposure and metabolic effects, specifically diabetes, insulin resistance, and obesity. We also examined renal effects because they can be a long-term complication of diabetes and because impaired renal function could affect

* Corresponding author.
E-mail address: bethradke@gmail.com (E.G. Radke).

https://doi.org/10.1016/j.envint.2019.04.040
Received 22 June 2018; Received in revised form 15 April 2019; Accepted 17 April 2019
Available online 10 June 2019
0160-4120/ Published by Elsevier Ltd. This is an open access article under the CC BY-NC-ND license (http://creativecommons.org/licenses/BY-NC-ND/4.0/).

Table 1
Outcomes included in the review.

Outcome	Background and relevance to human health
Diabetes	• Diabetes is a group of metabolic diseases characterized by hyperglycemia due to β-cell dysfunction, insulin resistance, or both. Diabetes can result in long-term complications in different organs, in particular, microvascular and macrovascular complications. • This review focuses on Type 2 (adult onset) diabetes.
Insulin resistance	• Among study subjects without diabetes, fasting blood glucose, insulin, and a related measure based on the homeostatic model assessment of insulin resistance (HOMA-IR) are informative regarding future diabetes risk. • Dysfunctions in insulin production and action in the peripheral tissues are the key pathways in diabetes etiology.
Gestational diabetes	• Gestational diabetes is another form of diabetes that occurs during pregnancy. A history of gestational diabetes is a risk factor for subsequent development of diabetes. • Definitions of gestational diabetes and impaired glucose tolerance are based on measures of blood glucose. All three of these outcomes in pregnant women are reviewed together, separate from the general population.
Obesity	• Excessive body weight, or obesity, is associated with the leading causes of death worldwide, including diabetes, heart disease, stroke, and some types of cancer. • Body mass index (BMI) is a screening tool calculated from a person's weight and height that is moderately correlated with more direct measures of body fat (CDC 2016).
Renal effects	• Kidney function can be assessed by measuring levels of urea, creatinine, and certain dissolved salts in blood and by analyzing protein levels in urine. • Albuminuria is a pathological condition wherein the protein albumin is abnormally present in the urine. Albuminuria is considered a significant risk factor for the development of renal disease. • Renal disease is a long-term complication of diabetes, obesity, and possibly, insulin resistance independent of those two conditions (Whaley-Connell and Sowers, 2017). • Impaired renal function could affect urinary concentration of phthalate metabolites.

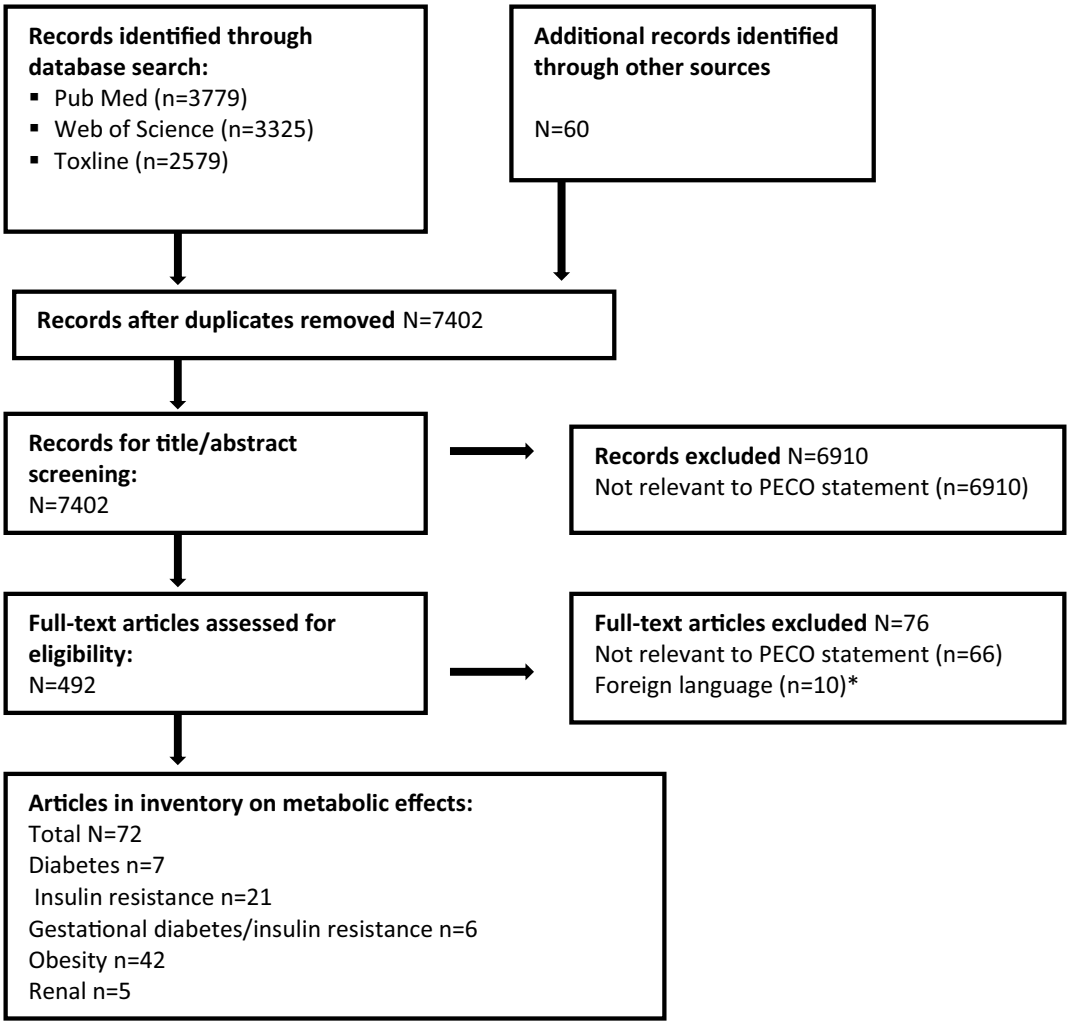

Fig. 1. Literature flow diagram for metabolic effects of phthalates.
*Included one study on insulin resistance and one on obesity. Based on the abstracts, the former would be excluded due to exposure measurement in blood and the latter would be excluded due to temporality issues.
Number of articles in inventory does not account for multiple publications on the same study.

Table 2
Epidemiology studies of diabetes.

Included	Reference	Study description			Includes metabolites of:						Study evaluation					
		Population	Exposure	Outcome	DEHP	DINP	DBP	DIBP	BBP	DEP	Exposure	Outcome	Selection	Confounding	Analysis	Overall confidence
	Sun et al. (2014)	Case-control nested in two cohorts in U.S. (N=971 case-control pairs)	Single urine sample at least one year prior to diagnosis	Self-report of physician diagnosis (validated in cohort)	✓		✓	✓	✓	✓	A/D	G	A	A	G	Medium

Excluded studies (6): exposure measured after development of outcome: James-Todd et al. (2012), Lind et al. (2012), Svensson et al. (2011), Castro-Correia et al. (2018), Dong et al. (2017), Piecha et al. (2016).
G = good; A = adequate; A/D = adequate for short-chain phthalates, deficient for long chain phthalates.

Table 3
Association between phthalate metabolites and type 2 diabetes in Sun et al. (2014).

Phthalate (metabolite)	NHS OR (95% CI)	NHSII OR (95% CI)	Pooled OR (95% CI) for Q4 vs. Q1
DEHP (summed metabolites)	∑DEHP Q2: 0.88 (0.52,1.50) Q3: 1.02 (0.61,1.71) Q4: 1.34 (0.77,2.30) p_{trend}=0.1	∑DEHP Q2: 1.80 (1.07,3.04) Q3: 1.62 (0.95,2.76) Q4: 1.91 (1.04,3.49) p_{trend}=0.2	MEOHP 1.42 (0.95,2.11)
DBP+DIBP (MBP+MIBP)	Q2: 1.26 (0.75,2.12) Q3: 1.01 (0.59,1.73) Q4: 0.91 (0.50,1.68) p_{trend}=0.5	Q2: 1.38 (0.81,2.35) Q3: 1.17 (0.66,2.10) Q4: 3.16 (1.68,5.95) p_{trend}=0.0002	n/a
DBP (MBP)	n/a	Q2: 1.53 (0.90,2.61) Q3: 1.18 (0.67,2.09) Q4: 3.16 (1.69,5.92) p_{trend} =0.0003	n/a
DIBP (MIBP)	n/a	Q2: 1.28 (0.76,2.13) Q3: 1.12 (0.62,2.02) Q4: 2.67 (1.44,4.95) p_{trend} =0.001	n/a
BBP (MBzP)	Q2: 0.91 (0.55,1.51) Q3: 0.85 (0.51,1.40) Q4: 0.82 (0.48,1.43) p_{trend}=0.5	Q2: 0.85 (0.50,1.44) Q3: 1.08 (0.62,1.86) Q4: 1.14 (0.65,2.01) p_{trend}=0.4	0.96 (0.65,1.43)
DEP (MEP)	Q2: 1.13 (0.69,1.84) Q3: 0.98 (0.60,1.61) Q4: 0.72 (0.43,1.20) p_{trend}=0.09	Q2: 1.00 (0.60,1.67) Q3: 0.46 (0.26,0.82) Q4: 0.91 (0.54,1.54) p_{trend}=0.97	0.80 (0.56,1.16)

Exposure levels presented in paper as medians of each quartile.
Results that support an association are shaded. Dark grey represents one or more of the following: $p < 0.05$, large effect size (e.g., OR ≥ 1.5), or exposure-response trend. Light grey represents other supportive results.

interpretation of exposure measures based on urinary concentrations of phthalate metabolites (Table 1). We focus on Type 2 diabetes, which is characterized by insulin resistance and the resulting insulin deficiency due to the inability of the pancreas to produce enough insulin. Obesity is a strong risk factor for Type 2 diabetes, and the highest incidence of Type 2 diabetes is in middle- and older-aged adults. In contrast, Type 1 diabetes involves a different etiology, an autoimmune-mediated destruction of the pancreatic islets of Langerhans cells. Incidence of Type 1 diabetes is highest in children and teenagers.

To make the systematic review more pragmatic, so that limited resources were not utilized to assess bodies of evidence that would likely be inadequate for reaching conclusions about the association, obesity and renal effects received less robust "screening level" reviews to determine the extent and nature of the literature for evidence synthesis. This approach is consistent with recommendations from the National Academies of Science encouraging the U.S. Environmental Protection Agency to explore ways to make systematic review more feasible, including a "rapid review in which components of the systematic review process are simplified or omitted (e.g., the need for two independent reviewers)" (National Academy of Sciences, 2017).

2. Methods

The full methods for this systematic review, including for literature search and screening, study evaluation, data extraction, and evidence synthesis are described in detail in the protocol (Supplemental materials). An abbreviated version is provided below, with references to specific sections of the protocol for ease of reference. In addition, the key tables from the protocol that are necessary to understand how conclusions were reached are included in a separate supplemental file (key methods supplement).

2.1. Literature search and screening

Epidemiology studies were identified by conducting a single broad literature search on all six phthalates of interest (DEHP, DINP, DBP, DIBP, BBP, DEP). The Population, Exposure, Comparators, and Outcome (PECO) criteria are available in the protocol (Section 2.2). The following databases were searched: PubMed, Web of Science, and Toxline, with the initial search in 2013, and updates every 6–12 months through August 2018 (protocol Section 3). Forward and backward searches were also performed. Title/abstract and full text screening was performed by two reviewers.

2.2. Study evaluation

Study evaluation (protocol Section 4.1) was conducted by two reviewers for those outcomes receiving full systematic review (i.e., diabetes, insulin resistance, gestational diabetes). Key concerns were risk of bias (factors that affect the magnitude or direction of effect) and insensitivity (factors that limit the ability of a study to detect a true effect). Evaluation was conducted for the following domains: exposure measurement, outcome ascertainment, participant selection, confounding, analysis, sensitivity, and selective reporting. These domains were based on the Risk of Bias in Non-randomized Studies of Interventions (ROBINS-I) tool (Sterne et al., 2016), modified for use with environmental exposures. Phthalate and outcome-specific criteria

Table 4
Epidemiology studies of insulin resistance (James-Todd et al., 2016a; Lin et al., 2016; Stahlhut et al., 2007).

	Reference	Study description			Includes metabolites of:						Study evaluation					
		Population	Exposure	Outcome	DEHP	DINP	DBP	DIBP	BBP	DEP	Exposure	Outcome	Selection	Confounding	Analysis	Overall confidence
	Studies in Adults															
Included	Chen et al. (2017); Lin et al. (2016)[a]	Cross-sectional analysis of cohort in China of adults and adolescents, follow-up from mass urine screening of children (N=786)	Single urine sample collected in AM	Fasting blood glucose and insulin in serum. HOMA-IR calculated.	✓		✓		✓	✓	A/D	G	D	A	A	Medium
Included	Dales et al. (2018)	Cross-sectional in Canada (Canadian Health Measures Survey 2009-11) (N=2119 adults)	Single urine sample	Fasting blood glucose and insulin. HOMA-IR calculated	✓		✓	✓	✓	✓	A/D	G	G	A	A	Medium
Included	Dirinck et al. (2015)	Cross-sectional in Belgium (N=123) of obese patients at weight clinic	24-hour urine collected day prior to visit	Fasting blood glucose and insulin collected in AM. HOMA-IR calculated.	✓		✓	✓	✓	✓	A/D	A	D	A	A	Low
Included	Attina and Trasande (2015); Huang et al. (2014); James-Todd et al. (2016a); James-Todd et al. (2012); Stahlhut et al. (2007)	Cross-sectional in U.S. (NHANES). Overlapping samples: 2001-08, 12-80 yrs 2001-10, 20-80 yrs 2001-08, Women 20-79 yrs 1999-2002, 18+ yrs (N=3,083 in Huang et al. (2014))	Single urine sample	Fasting blood glucose and insulin collected in AM. HOMA-IR calculated.	✓		✓	✓	✓	✓	A/D	G	G	A	A	Medium
Included	Hong et al. (2009)	Cross-sectional in Korea (N=1131 adults)	Single urine sample collected in AM	Fasting glucose and insulin in serum. HOMA-IR calculated.	✓		✓				A/D	A	D	A	D	Low
Included	Hong et al. (2016)	Cross-sectional in Korea (N=296 women aged 30-49 yrs)	Single first AM urine sample	Fasting blood glucose and insulin collected in AM. HOMA-IR calculated	✓		✓				A/D	G	A	D	A	Medium
Included	Kim and Hong (2014) Kim et al. (2013)	Cohort in Korea (N=560) of older adults (aged 60+) enrolled through community center	Urine samples at up to 5 visits	Fasting glucose and insulin in serum. HOMA-IR calculated.	✓		✓				G	A	A	G	A	Medium

(continued on next page)

Table 4 (*continued*)

Studies in Adolescents																	
Attina and Trasande (2015)	Cross-sectional in U.S. (NHANES). 2009-12, 12-19 yrs (N=356)	Single urine sample	Fasting blood glucose and insulin collected in AM. HOMA-IR calculated.	✓	✓	✓	✓	✓	✓	A/D	G	G	A	A	Medium
Trasande et al. (2013)[a]	Cross-sectional in U.S. (NHANES). 2003-08, 12-19 yrs (N=766)	Single urine sample	Fasting blood glucose and insulin collected in AM. HOMA-IR calculated.	✓		✓	✓	✓	✓	A/D	G	G	A	A	Medium
Studies in Children																	
Carlsson et al. (2018)	Cross-sectional in Thailand (N=107 healthy children)	Single first AM urine sample	Oral glucose tolerance test; insulin sensitivity index calculated	✓	✓	✓		✓	✓	A/D	A	D	D	D	Low
Kataria et al. (2017)	Cross-sectional pilot in U.S. (N=43 healthy children)	Single first AM urine sample	Fasting blood glucose and insulin collected in AM. HOMA-IR calculated	✓	✓					D	G	A	A	D	Low
Saengkaew et al. (2017)	Cross-sectional of overweight/obese children and healthy controls (N=155)	Single AM urine sample	Fasting blood glucose and insulin collected in AM. HOMA-IR calculated			✓				A	G	D	D	D	Low
Watkins et al. (2016)	Birth cohort in Mexico. Subset of offspring (n=250/2,095) had follow-up at 8-14 yrs.	Single maternal sample in 3rd trimester; Single child sample at follow-up	Fasting glucose and insulin in serum. HOMA-IR calculated.	✓		✓[b]	✓[b]	✓	✓	A/D	A	A	D	A	Medium

Excluded studies (3): exposure measurement based on tissue other than urine: Olsén et al. (2012). Approaches for confounding and analysis unclear, incomplete reporting of results: Smerieri et al. (2015), Milošević et al. (2017).
G = good; A = adequate; D = deficient; A/D = adequate for short chain phthalates, deficient for long chain phthalates.
[a]Included estimates in adolescents.
[b]Study summed DBP and DIBP metabolites, and results discussed with DBP because it contributed a larger amount to the total.

were developed prior to evaluation and are described briefly below. Detailed exposure criteria are available in the key methods supplement and the protocol (Section 4.1.1). Detailed outcome-specific evaluation criteria are available in the supplement and summarized briefly below.

For evaluating exposure, most of the available studies relied on phthalate metabolite biomarkers (a list of metabolites for each phthalate is provided in the protocol, Section 1.3). Different criteria were developed for short-chain (DEP, DBP, DIBP, BBP) and long-chain (DEHP, DINP) phthalates due to greater reliability of single biomarker measures for short-chain phthalates. Measurement in urine was considered to be the best proxy of exposure (Johns et al., 2015). Biomarker measures based on samples other than urine (e.g., blood, amniotic fluid, breast milk) were considered to be critically deficient for all short-chain phthalates and for primary metabolites (e.g., MEHP, MINP) of long-chain phthalates (Johns et al., 2015). This critical deficiency was used as a basis for excluding studies from subsequent analyses.

Several outcome-specific criteria were applied across multiple evaluation domains (for more details, see outcome-specific criteria in the supplement). Timing of exposure measurement was an important consideration, particularly given the short half-life of phthalates (3–18 h for phthalate metabolites in a review by Johns et al. (2015)). For diabetes, it is important for studies to exclude individuals with diabetes at baseline and include only individuals with incident disease as cases, with exposure measured prior to development of diabetes in order to establish their temporality. Accordingly, studies of diabetes with exposure measured concurrent with the outcome were excluded, and prospective designs were generally needed for inclusion. For insulin resistance, it is appropriate to measure the exposure and outcome concurrently as the outcome can be a short-term response. Several criteria for outcome ascertainment were also applied. For diabetes, to identify undiagnosed cases, the use of the American Diabetes Association definition with information about required fasting, laboratory test requirements and assays, quality control procedures, and reliability or validity measures were preferred, while self-reported physician diagnosis or medical treatment for diabetes was appropriate for diagnosed cases. For insulin resistance, diabetics must be excluded as measures of

Table 5
Association between DEHP metabolites and insulin resistance in adults and adolescents.

Reference; Study Confidence Rating; N	Median exposure	Exposure IQR	Effect estimate	Fasting glucose	Insulin	HOMA-IR
∑DEHP in Adults						
Huang et al. (2014); medium; 3,083	11.5 μmol/100 g creatinine (women)	6.5-23	Median change (95% CI)	Q2: 1.47 (0.3,2.63) Q3: 1.75 (0.66,2.84) Q4: 2.45 (1.29,3.60) p_{trend}=0.0016*	Q2: 1.74 (1.04,2.45) Q3: 1.99 (1.31,2.66) Q4: 2.60 (1.82,3.38) p_{trend}<0.0001*	Q2: 0.49 (0.31,0.66) Q3: 0.51 (0.34,0.69) Q4: 0.68 (0.47,0.88) p_{trend}<0.0001*
Dales et al. (2016); medium, 2,119	47 ng/mL		β (95% CI) for IQR increase	0.04 (0.00,0.08)*	0.63 (0.21,1.05)*	0.15 (0.04,0.26)*
MEOHP in Adults						
Dirinck et al. (2015); low; 123	6.2 μg/g creatinine	0.8-42 (range)	β (95% CI)	3.88 (-6.19,13.95)	26.62 (0.69,52.5)*	0.31 (-0.72,0.69)
Hong et al. (2016); medium; 296	6.5 μg/g creatinine	3.9-10	β (95% CI)	0.12 (-1.11,1.36)	0.14 (-0.08,0.36)	0.12 (-0.08,0.33)
Chen et al. (2017); medium; 552	17 μg/g creatinine	16	β (95% CI)	-0.001 (-0.01,0.01)	0.003 (-0.07,0.07)	0.001 (-0.07,0.07)
Kim et al. (2013) medium; 560	19 ng/mL	9.5-33	β (95% CI)	0.11 (0.01,0.22)*[Ŧ]	0.70 (0.01,1.40)*[Ŧ]	0.26 (0.01,0.51)*[Ŧ]
MEOHP in Adolescents						
Chen et al. (2017); medium; 234	17 μg/g creatinine	16	β (95% CI)	0.001 (-0.01,0.01)	0.04 (-0.05,0.12)	0.04 (-0.05,0.13)
Attina and Trasande (2015); medium; 356	0.14 μM		β (95% CI)	NR	NR	0.06 (-0.001,0.12)
Trasande et al. (2013); medium; 766	NR		β (95% CI)	NR	NR	0.27 (0.14,0.40)*

Results that support an association are shaded based on effect size and precision. Dark grey represents one or more of the following: $p < 0.05$, large effect size (e.g., OR ≥ 1.5, β ≥ 0.5), or exposure-response trend. Light grey represents other supportive results. Strength of the evidence (i.e., contribution to the synthesis conclusions) from an individual study is influenced by other factors, such as study confidence.
*$p < 0.05$.
[Ŧ]Estimates for total population, including those with history of diabetes. Association for the strata without history of diabetes was not reported.
Hong et al. (2009) reported that no significant association was observed but did not provide quantitative estimates.

insulin are not interpretable in the presence of diabetes, especially if diabetes is treated with hypoglycemic medication, as treatment will influence insulin production and secretion. In addition, fasting insulin and/or glucose measurements were required, and information on testing as described for diabetes was preferred. HOMA-IR was used as the primary measure of insulin resistance when available. In evaluating confounding, the following risk factors were considered possible confounders: age, gender, adiposity/body mass index, lifestyle (physical inactivity, poor diet, smoking, heavy alcohol consumption), and socioeconomic status. It was not required that a study adjusts for all of these variables; rather, the study evaluation considered whether omission of these covariates was likely to have introduced bias into the effect estimates. There is also potential for confounding across the phthalates, particularly when results are similar for two moderately (or higher) correlated phthalates in a study. Study evaluations were not downgraded due to this potential, but it was considered during evidence synthesis as another source of uncertainty in the results.

For each study, in each evaluation domain, reviewers reached a consensus rating regarding the utility of the study for hazard identification, with categories of *Good*, *Adequate*, *Deficient*, or *Critically deficient*. These ratings were then considered together to reach an overall study confidence classification of *High*, *Medium*, *Low*, or *Uninformative*. This overall classification was not based on pre-defined weights of the domains, but rather was based on reviewer judgments, and includes the likely impact the noted deficiencies in bias and sensitivity have on the results, which varies depending on the study and/or outcome. Studies were evaluated for their suitability for each outcome investigated and could receive different ratings for each outcome. Descriptions of each of the categories can be found in the protocol (Section 4) and the key methods supplement. Study evaluations were documented in Health Assessment Workspace (HAWC), and ratings and the rationales are available at links provided in the results.

Table 6
Association between DBP metabolites and insulin resistance in adults and adolescents.

Reference	Median MBP	Exposure IQR	Effect estimate	Fasting glucose	Insulin	HOMA-IR
				Adults		
Huang et al. (2014); medium; 3,083	22 μg/g creatinine	13-36	Median change (95% CI)	Q2: 0.95 (-0.22,2.13) Q3: 1.70 (0.51,2.89) Q4: 1.91 (0.51,3.31) p_{trend}=0.019*	Q2: 1.15 (0.52,1.78) Q3: 1.41 (0.72,2.09) Q4: 1.11 (0.31,1.92) p_{trend}<0.09	Q2: 0.28 (0.11,0.44) Q3: 0.28 (0.11,0.46) Q4: 0.34 (0.15,0.54) p_{trend}<0.006*
Hong et al. (2016); medium; 296	30 μg/g creatinine	21-42	β (95% CI)	-0.37 (-1.38,0.65)	0.06 (-0.13,0.24)	0.04 (-0.13,0.21)
Dales et al. (2016); medium, 2,119	31 ng/mL		β (95% CI) for IQR increase	0.00 (-0.06,0.06)	0.47 (-0.02,0.96)	0.08 (-0.09,0.24)
Chen et al. (2017); medium; 552	38 μg/g creatinine	41	β (95% CI)	0.01 (-0.002,0.01)	0.01 (-0.06,0.08)	0.02 (-0.05,0.09)
Dirinck et al. (2015); low; 123	38 μg/g creatinine	3.9-370 (range)	β (95% CI)	7.27 (-1.29,15.83)	22.52 (3.13,41.90)*	0.29 (-0.05,0.63)
Kim et al. (2013); medium; 560	57 ng/mL	29-158	β (95% CI)	0.06 (-0.04,0.17)[₮]	0.38 (-0.30,1.07)[₮]	0.16 (-0.09,0.40)[₮]
				Adolescents		
Chen et al. (2017); medium; 234	38 μg/g creatinine	41	β (95% CI)	0.01 (-0.001,0.02)	0.002 (-0.08,0.08)	0.01 (-0.07,0.10)
Attina and Trasande (2015); medium; 356	NR		β (95% CI)	NR	NR	0.05 (-0.02,0.12)
Trasande et al. (2013); medium; 766	NR		β (95% CI)	NR	NR	0.13 (0.01,0.26)*

Results that support an association are shaded based on effect size and precision. Dark grey represents one or more of the following: $p < 0.05$, large effect size (e.g., OR ≥ 1.5, β ≥ 0.5), or exposure-response trend. Light grey represents other supportive results. Strength of the evidence (i.e., contribution to the synthesis conclusions) from an individual study is influenced by other factors, such as study confidence. *$p < 0.05$.
[₮]Estimates for total population, including those with history of diabetes. Association for the strata without history of diabetes was not reported.
Hong et al. (2009) reported that no significant association was observed, but did not provide quantitative estimates.

2.3. Evidence synthesis

After study evaluation, the evidence for each outcome was synthesized separately for each phthalate using a structured framework, using the following aspects of an association that may support causation: consistency, exposure-response relationship, strength of association, temporal relationship, biological plausibility, and coherence. In evaluating the evidence for each of these considerations, syntheses also consider study evaluation decisions, with high confidence studies carrying the most weight and consideration of specific strengths and limitations of individual studies described. Based on this synthesis, the evidence was assigned a strength of evidence conclusion of *Robust*, *Moderate*, *Slight*, *Indeterminate*, or *Compelling evidence of no effect*. *Robust* and *Moderate* describe evidence that supports a hazard, differentiated by the quantity and quality of information available to rule out alternative explanations for the results. *Slight* and *Indeterminate* describe evidence for which uncertainties prevent drawing a causal conclusion in either direction. These categories are generally limited in terms of quantity or confidence level of studies, and serve to encourage additional research across the exposure range experienced by humans. *Compelling evidence of no effect* requires several high confidence studies with consistent null results. The ratings for the individual outcomes were then summarized into an overall conclusion for diabetes risk (encompassing incident diabetes and insulin resistance) for each phthalate, using a structured framework available in the key methods supplement and the protocol (Section 6). This structured framework is conceptually similar to and is informed by the well-established Grading of Recommendations, Assessment, Development and Evaluations (GRADE) approach (Schünemann et al., 2013), but is designed to address the challenges specific to the analysis of environmental health data rather than clinical evidence. No statistical quantitative meta-analysis was performed due to substantial differences across studies.

For obesity and renal disease, screening-level reviews were conducted to determine whether new literature suggest full systematic reviews would be warranted and to identify key research gaps. One reviewer identified studies that should be excluded based on exposure

Table 7
Association between DIBP metabolites and insulin resistance in adults and adolescents.

Reference	Median MIBP	Exposure IQR	Effect estimate	Fasting glucose	Insulin	HOMA-IR
			Adults			
Huang et al. (2014); medium; 3,083	4.9 μg/g creatinine (women)	2.6-8.9	Median change (95% CI)	Q2: 1.87 (0.83,2.92) Q3: 2.77 (1.75,3.80) Q4: 3.69 (2.60,4.78) p_{trend}<0.0001	Q2: 1.45 (0.85,2.04) Q3: 1.23 (0.57,1.89) Q4: 1.73 (0.92,2.54) p_{trend}=0.003	Q2: 0.38 (0.23,0.52) Q3: 0.35 (0.19,0.51) Q4: 0.53 (0.33,0.72) p_{trend}=0.0002*
Dales et al. (2016); medium, 2,119	13 ng/mL		β (95% CI) for IQR increase	0.00 (-0.02,0.03)	0.00 (-0.19,0.19)	0.00 (-0.05,0.05)
Dirinck et al. (2015); low; 123	57 μg/g creatinine	7.5-55 (range)	β (95% CI)	5.44 (-3.57,14.5)	7.69 (-15.9,31.3)	0.15 (-0.18,0.47)
			Adolescents			
Attina and Trasande (2015); medium; 356	NR		β (95% CI)	NR	NR	0.03 (-0.05,0.11)
Trasande et al. (2013); medium; 766	NR		β (95% CI)	NR	NR	0.15 (0.04, 0.26)*

Results that support an association are shaded based on effect size and precision. Dark grey represents one or more of the following: $p < 0.05$, large effect size (e.g., OR ≥ 1.5, β ≥ 0.5), or exposure-response trend. Light grey represents other supportive results. Strength of the evidence (i.e., contribution to the synthesis conclusions) from an individual study is influenced by other factors, such as study confidence. *$p < 0.05$.
[Ŧ]Estimates for total population, including those with history of diabetes. Association for the strata without history of diabetes was not reported.

assessment and temporality. The remaining studies were then each evaluated by a single reviewer and were assessed for consistency, while considering whether any observed inconsistency could potentially be attributed to differences in study confidence or exposure level. If this screening level review indicated little consistency among studies, with no clear explanation based on study confidence, then full data extraction and additional evidence analysis and synthesis was not pursued, and the evidence was considered inadequate. The screening level reviews should not be considered as substitutes for systematic review.

Reporting of this systematic review follows the Preferred Reporting Items for Systematic Reviews and Meta-Analyses (PRISMA) guidelines (Moher et al., 2009). The work described herein was federally funded.

3. Results

The literature flow diagram, depicting the identification and disposition of the literature search records, is shown in Fig. 1. A list of all the studies identified in the search that met the PECO criteria is available in the supplement. For each outcome, the included and excluded studies are described in the respective section within the text.

3.1. Type 2 diabetes

3.1.1. Study selection and evaluation

Based on evaluation of temporality, six of the seven epidemiology studies identified in the search with data on type 2 diabetes were excluded because exposure was measured at the same time as ascertainment of diabetes status. One study (Sun et al., 2014), a nested case-control study within two cohorts (Nurses' Health Study (NHS) and NHSII), was identified in the search as having prospective data on diabetes risk. The specific phthalates examined in that study and the evaluation are summarized in Table 2; this study was classified as *medium* confidence and rationales are available in HAWC at https://hawcprd.epa.gov/rob/study/100000200/.

3.1.2. Results

In Sun et al. (2014), there were statistically significant strong positive associations between increased exposure to DBP and DIBP and diabetes risk (Table 3), however pooled results were not available and the positive associations were observed only in participants from NHSII, which is a more homogenous and younger cohort (mean age = 46 vs. 66) with higher exposure levels. In addition, the association was stronger when adjusting for BMI. It is possible that adiposity could lie on the causal pathway between phthalate exposure and diabetes risk, and this should be considered when interpreting the effect estimates. Results were similar for DEHP, but the positive association was smaller and not statistically significant. For BBP and DEP, no association was reported, and no results were available for DINP, so the evidence for these three phthalates is considered indeterminate.

3.2. Insulin resistance

3.2.1. Study selection and evaluation

Three of the 21 publications identified in the search with data on insulin resistance were excluded due to exposure measurement in tissue other than urine or other critical deficiencies. Of the remaining 18 publications, six were based on data from the National Health and Nutrition Examination Survey (NHANES), with different samples but overlapping populations in many. Among the NHANES analyses in adults, one was selected as the primary study (Huang et al., 2014) and the results of the others were reviewed for discrepancies in methods or results. Two NHANES analyses in adolescents did not have overlapping years and were included separately in the review of data in adolescents (Trasande et al., 2013; Attina and Trasande, 2015). Thus, there were a

Table 8
Association between BBP metabolites and insulin resistance in adults and adolescents.

Reference	Median MBzP	Exposure IQR	Effect estimate	Fasting glucose	Insulin	HOMA-IR
Adults						
Chen et al. (2017); medium; 552	1.9 μg/g creatinine	2.4	β (95% CI)	-0.002 (-0.01,0.004)	-0.05 (-0.12,0.01)	-0.06 (-0.12,0.01)
Dales et al. (2016); medium, 2,119	8.4 ng/mL		β (95% CI) for IQR increase	0.00 (-0.02,0.02)	0.03 (-0.20,0.26)	0.00 (-0.06,0.06)
Huang et al. (2014); medium; 3,083	13 μg/g creatinine (women)	7.1-24	Median change (95% CI)	Q2: -0.30 (-1.48,0.87) Q3: -0.06 (-1.25,1.13) Q4: -0.24 (-1.49,1.02) p_{trend}=0.7	Q2: 0.77 (0.16,1.39) Q3: 1.09 (0.39,1.79) Q4: 1.44 (0.50,2.38) p_{trend}=0.007*	Q2: 0.21 (0.06,0.37) Q3: 0.26 (0.09,0.44) Q4: 0.37 (0.15,0.59) p_{trend}<0.003*
Dirinck et al. (2015); low; 123	8.7 μg/g creatinine	0.7-90 (range)	β (95% CI)	8.74 (1.42,16.06)*	14.90 (4.38,34.18)	0.15 (-0.16,0.46)
Adolescents						
Chen et al. (2017); medium; 234	1.9 μg/g creatinine	2.4	β (95% CI)	-0.002 (-0.01,0.01)	0.03 (-0.06,0.13)	0.03 (-0.07,0.13)
Attina and Trasande (2015); medium; 356	NR		β (95% CI)	NR	NR	0.03 (-0.03,0.09)
Trasande et al. (2013); medium; 766	NR		β (95% CI)	NR	NR	0.02 (-0.08,0.13)

Results that support an association are shaded based on effect size and precision. Dark grey represents one or more of the following: $p < 0.05$, large effect size (e.g., OR ≥ 1.5, β ≥ 0.5), or exposure-response trend. Light grey represents other supportive results. Strength of the evidence (i.e., contribution to the synthesis conclusions) from an individual study is influenced by other factors, such as study confidence. *$p < 0.05$.
ŦEstimates for total population, including those with history of diabetes. Association for the strata without history of diabetes was not reported.

total of 13 studies in the review. The specific phthalates examined in these included studies and the evaluations are summarized in Table 4. Rationales for ratings are available at: https://hawcprd.epa.gov/summary/visual/100000076/.

In adults, there were seven studies, including six cross-sectional (Chen et al., 2017; Dales et al., 2018; Dirinck et al., 2015; Huang et al., 2014; Hong et al., 2009; Hong et al., 2016) and one cohort (Kim and Hong, 2014). Three studies reported on adolescents (Chen et al., 2017; Trasande et al., 2013; Attina and Trasande, 2015) and four studies reported on children (Carlsson et al., 2018; Kataria et al., 2017; Saengkaew et al., 2017; Watkins et al., 2016). All used a single urine sample to measure exposure, with the exception of Kim et al. (2013), which collected samples at up to five visits. Eight studies (Chen et al., 2017; Dales et al., 2018; Huang et al., 2014; Hong et al., 2016; Kim and Hong, 2014; Trasande et al., 2013; Attina and Trasande, 2015; Watkins et al., 2016) were classified as medium confidence and the remaining five were classified as low confidence. This set of studies as a whole would be improved with additional studies with repeated exposure measures, and with prospective rather than cross-sectional data collection. However, the strengths of these studies include the wide variety of populations and the availability of data from multiple nationally representative samples, which have large sample sizes and are expected to represent the general population.

3.2.2. Results and synthesis

The majority of available studies examined adult and/or adolescent exposure with concurrent measures of insulin resistance (or repeated measures in the case of Kim et al. (2013)), so these are the focus of this review. Three of the four studies in children were classified as low confidence and the fourth study (Watkins et al., 2016) used an in-utero exposure measure which may not be comparable to the other studies, so results in children are briefly summarized in text only.

Evaluation of the evidence of an association between exposure to DEHP and insulin resistance in adults is based on seven studies (Table 5). Five studies, including four of the five medium confidence studies, reported higher glucose, insulin, and HOMA-IR with higher exposure levels. Results were statistically significant for at least one outcome in four studies and exposure-response gradients were observed for all three outcomes in Huang et al., 2014. However, there is some uncertainty resulting from study limitations. The positive result in Kim et al. (2013) is difficult to interpret because the analysis included subjects with a history of diabetes diagnosis, though this is ameliorated to some extent by an analysis in women adjusting for history of DM and showing consistent results. Additionally, the results in Dirinck et al. (2015) should be interpreted with caution due to the study evaluation concerns. The fact that the latter study had the highest effect estimates could possibly be explained by selection bias, by the specific population (obese patients), or some other factor. In addition, there is potential for residual confounding by diet, but the impact of this is uncertain. While two studies (Huang et al. (2014); Kim et al. (2013)) adjusted for caloric intake, this may not be adequate to adjust for differing exposure levels by food type (e.g., packaged foods). This issue is considered further in the discussion. Despite these limitations, the overall consistency in the direction of the association across studies and the exposure-response gradient observed in a well-conducted and sensitive study increase confidence in the association. In adolescents, only one of the three studies reported higher insulin resistance with higher exposure. The three studies in children found no clear association (Watkins et al.,

Table 9
Association between DEP metabolites and insulin resistance in adults and adolescents.

Reference	Median MEP	Exposure IQR	Effect estimate	Fasting glucose	Insulin	HOMA-IR
Adults						
Dales et al. (2016); medium, 2,119	8.4 ng/mL		β (95% CI) for IQR increase	0.00 (-0.02,0.03)	0.00 (-0.27,0.27)	-0.01 (-0.08,0.06)
Chen et al. (2017); medium; 552	32 μg/g creatinine	63	β (95% CI)	0.00 (-0.01,0.01)	-0.04 (-0.10,0.01)	-0.04 (-0.10,0.01)
Huang et al. (2014); medium; 3,083	182 μg/g creatinine (women)	89-426	Median change (95% CI)	Q2: 1.30 (0.15,2.46) Q3: 0.38 (-0.75,1.51) Q4: 0.49 (-0.80,1.77) p_{trend}=0.8	Q2: 0.25 (-0.50,0.99) Q3: 0.34 (-0.35,1.02) Q4: 0.60 (-0.13,1.34) p_{trend}=0.15	Q2: 0.11 (-0.06,0.27) Q3: 0.10 (-0.07,0.28) Q4: 0.20 (0.03,0.38) p_{trend}<0.006*
Dirinck et al. (2015); low; 123	81 μg/g creatinine	3.4-6865 (range)	β (95% CI)	1.31 (-3.23,5.85)	9.81 (-1.88,21.5)	0.15 (-0.022,0.31)
Adolescents						
Chen et al. (2017); medium; 234	32 μg/g creatinine	63	β (95% CI)	0.001 (-0.01,0.01)	-0.02 (-0.08,0.05)	-0.02 (-0.08,0.05)
Attina and Trasande (2015); medium; 356	NR		β (95% CI)	NR	NR	0.02 (-0.05,0.05)
Trasande et al. (2013); medium; 766	NR		β (95% CI)	NR	NR	-0.07 (-0.16,0.03)

Results that support an association are shaded based on effect size and precision. Dark grey represents one or more of the following: $p < 0.05$, large effect size (e.g., OR ≥ 1.5, β ≥ 0.5), or exposure-response trend. Light grey represents other supportive results. Strength of the evidence (i.e., contribution to the synthesis conclusions) from an individual study is influenced by other factors, such as study confidence. *$p < 0.05$.
[Ŧ]Estimates for total population, including those with history of diabetes. Association for the strata without history of diabetes was not reported.

2016; Carlsson et al., 2018; Kataria et al., 2017).

One medium confidence study included results on the association between DINP and insulin resistance. Attina and Trasande (2015), an NHANES sample of adolescents, reported increased HOMA-IR levels with increasing exposure, with the third tertile being statistically significant (β for tertile 2: 0.07 (−0.09, 0.22), tertile 3: 0.23 (0.08, 0.38)). In addition, one low confidence study in children (Kataria et al., 2017) reported no significant association, but did not report quantitative estimates.

Evaluation of the evidence of an association between exposure to DBP and insulin resistance in adults is based on seven studies (Table 6). Four studies, including three of the five medium confidence studies (Table 6) reported increased glucose, insulin, and/or HOMA-IR. Results in two of these studies were statistically significant, and an exposure-response gradient was observed for glucose and HOMA-IR in Huang et al. (2014). However, in Dales et al. (2018), a weak association was only observed for insulin. Further, as with DEHP, the positive results in Kim et al. (2013) and Dirinck et al. (2015) are difficult to interpret, and there is potential for residual confounding by diet. The other studies reported no association, resulting in some unexplained inconsistency, including between NHANES and CHMS, the nationally representative surveys for fasting glucose and HOMA-IR. This lack of consistency decreases confidence in the association since there is no clear explanation such as study sensitivity (e.g., exposure levels or range) for the differing results. In adolescents, one of the three studies reported higher insulin resistance with higher exposure (Trasande et al., 2013). The three studies in children (Watkins et al., 2016) found no clear association, though there was a statistically significant increase in fasting glucose among pubertal girls based on peripubertal exposure in Watkins et al. (2016) for summed MBP + MIBP.

Three studies reported results on the association between DIBP exposure and insulin resistance in adults (Table 7). One of two medium confidence studies and one low confidence study reported higher glucose, insulin, and HOMA-IR with higher exposure, with Huang et al. (2014) reporting statistical significance for HOMA-IR and exposure-response gradients for glucose and HOMA-IR. However, as with DBP, there was inconsistency between the nationally representative surveys with no clear explanation and the results from Dirinck et al. (2015) have low confidence, and the small number of studies makes evaluating consistency a challenge. As with the other phthalates, there is potential for residual confounding by diet. In adolescents, one of the two studies reported higher insulin resistance with higher exposure (Trasande et al., 2013). Results for BBP (Table 8) and DEP (Table 9) were similar to those of DIBP, though there was no association in adolescents for these phthalates. The studies in children (Watkins et al., 2016) found no clear association for BBP and DEP, though there was a statistically significant increase in fasting glucose among pubertal girls based on peripubertal exposure for DEP.

Overall, across the phthalates, there is generally a stronger association in adults than adolescents and children. Because there was a smaller number of studies of the younger age groups, and there were limitations in the studies that are available, including a lack of exposure information, it is unclear whether this is a true difference and whether it can be explained by changing exposure levels, biological factors, or some other explanation. In addition to the main effects described above, some of the analyses of NHANES data examined differences in the association by sub-population. In Huang et al. (2014), these factors did not generally change the direction of association, but there were

Table 10
Epidemiology studies of gestational diabetes and blood glucose in pregnancy.

	Reference	Study description			Includes metabolites of:						Study evaluation					
		Population	Exposure	Outcome	DEHP	DINP	DBP	DIBP	BBP	DEP	Exposure	Outcome	Selection	Confounding	Analysis	Overall confidence
	Studies in Adults															
Included	James-Todd et al. (2016b)	Sample of women from pregnancy cohort in U.S. (N=352)	Urine samples collected at up to 4 prenatal visits	Impaired glucose tolerance and blood glucose during oral glucose tolerance test	✓		✓		✓	✓	G/A	G	A	A	A	Medium
	James-Todd et al. (2018)	Cohort of women seeking infertility evaluation/ treatment in U.S. (N=245)	Urine samples collected in each trimester	Impaired glucose tolerance and blood glucose during oral glucose tolerance test	✓		✓	✓	✓	✓	G/A	G	G	G	G	High
	Robledo et al. (2015)	Pilot cohort of pregnant women in U.S. (N=72) enrolled at first prenatal visit	Single urine sample	Blood glucose during oral glucose tolerance test.	✓		✓	✓	✓	✓	A/D	D	A	A	A	Low
	Shapiro et al. (2015)	Cohort of pregnant women in U.S. (N=1,885) enrolled in first trimester	Single urine sample	Gestational diabetes and impaired glucose tolerance diagnosed from glucose challenge test	✓		✓		✓	✓	A/D	A	A	A	A	Medium

Excluded studies (2): exposure measurement based on tissue other than urine and high percent non-detects for secondary metabolites of DEHP: Fisher et al. (2018); unable to obtain full text: Zhang et al. (2017).
G = good; A = adequate; D = deficient; A/D = adequate for short chain phthalates, deficient for long chain phthalates.
[a]Included estimates in adolescents.

Table 11
Association between DEHP and blood glucose in pregnant women.

	Reference	Median Exposure	Exposure IQR	Blood glucose 1st trimester Mean (95% CI)	Blood glucose 2nd trimester Mean (95% CI)	Impaired glucose tolerance* OR (95%)
DEHP	**James-Todd et al. (2016b)** medium; 352	0.4 nmol/l (GM)	0.2-0.8	Q1: 110 (100,120) Q2: 115 (105, 127) Q3: 108 (98,118) Q4: 114 (104, 126)	Q1: 117 (106,129) Q2: 110 (100,121) Q3: 109 (99,120) Q4: 110 (100,121) p-trend: 0.16	Q2: 0.46 (0.15,1.40) Q3: 0.74 (0.27,2.04) Q4: 0.25 (0.08,0.85) p-trend: 0.06
	James-Todd et al. (2018) high; 245	0.2 nmol/l	0.1-0.4	Q1: 116 (109,123) Q2: 114 (107,121) Q3: 114 (107,121) Q4: 113 (107,120)	Q1: 111 (105,118) Q2: 111 (105,118) Q3: 115 (109,122) Q4: 116 (109, 123)	no association
	Shapiro et al. (2015) medium; 1,885	7.4 (MEOHP) 11 (MEHHP) 2.6 (MEHP) ng/mL	NR	NR	NR	Q2: 1.0 (0.5,2.0) Q3: 0.6 (0.3,1.5) Q4: 0.9 (0.4,2.3)
	Robledo et al. (2015) low; 72	66 ng/mL	37-101	NR	β (95% CI) T2: 3.82 (-10.22,17.86) T3: -9.97 (-27.11,7.17)	NR

Results that support an association are shaded based on effect size and precision.
*Shapiro includes impaired glucose tolerance and gestational diabetes.
p-Values > 0.20 are not presented. NR = not reported.

Table 12
Association between DBP and DIBP and blood glucose in pregnant women.

	Reference	Median Exposure (ng/mL)	Exposure IQR	Blood glucose 1st trimester Mean (95% CI)	Blood glucose 2nd trimester Mean (95% CI)	Impaired glucose tolerance* OR (95%)
DBP	**James-Todd et al. (2016b)** medium; 352	18 (GM)	11-27	Q1: 115 (104,126) Q2: 113 (103,124) Q3: 114 (103,125) Q4: 109 (99,119) p-trend: 0.13	Q1: 111 (100,123) Q2: 113 (103,125) Q3: 114 (104,125) Q4: 108 (98,119)	Q2: 0.95 (0.31,2.91) Q3: 1.26 (0.43,3.68) Q4: 1.14 (0.37,3.51)
	James-Todd et al. (2018) high; 245	12	6.8-21	Q1: 116 (109,123) Q2: 112 (105,118) Q3: 116 (109, 123) Q4: 113 (107,120)	Q1: 112 (106,119) Q2: 113 (106,120) Q3: 114 (107,121) Q4: 115 (109,122)	no association
	Shapiro et al. (2015) medium; 1,885	13	NR	NR	NR	Q2: 1.8 (0.9,3.6) Q3: 1.3 (0.6,3.0) Q4: 0.8 (0.3,2.2) p-trend: 0.51
	Robledo et al. (2015) low; 72	29	16-57	NR	β (95% CI) T2: 0.11 (-14.71,14.93) T3: -15.61 (-32.99,1.76)	NR
DIBP	**James-Todd et al. (2016b)** medium; 352	7.3 (GM)	4.5-12	Q1: 114 (103,125) Q2: 111 (101,123) Q3: 114 (103,125) Q4: 110 (100,121)	Q1: 111 (100,122) Q2: 109 (99,120) Q3: 110 (100,121) Q4: 114 (104,126) p-trend: 0.17	Q2: 0.47 (0.14,1.58) Q3: 1.16 (0.38,3.54) Q4: 1.79 (0.62,5.16) p-trend: 0.18
	James-Todd et al. (2018) high; 245	6.2	3.3-10	Q1: 118 (111,125) Q2: 114 (107,121) Q3: 114 (107,121) Q4: 111 (104,117) p-trend: 0.15	Q1: 119 (113,126) Q2: 115 (109,122) Q3: 115 (109, 122) Q4: 105 (99,111) p-trend: 0.003	0.37 (0.12,1.16)
	Robledo et al. (2015) low; 72	11	6.7-18	NR	β (95% CI) T2: -2.01 (-16.18,12.17) T3: -18.30 (-35.41,-1.19)	NR

Results that support an association are shaded based on effect size and precision.
*Shapiro includes impaired glucose tolerance and gestational diabetes.
p-Values > 0.20 are not presented. NR = not reported.

differences in strength of association by race/ethnicity and sex. For some phthalates, the association was stronger in black and Hispanic people than in whites. The sex with the stronger association differed by phthalate. Since there were no additional studies that examined these differences, there was limited ability to draw conclusions about the interactions.

3.3. Gestational diabetes

3.3.1. Study selection and evaluation

Two of the six epidemiology studies identified in the search with data on diabetes and/or insulin resistance during pregnancy were excluded due to exposure measurement in tissue other than urine or unavailability in full text. The specific phthalates examined in the remaining four included studies and the evaluations are summarized in Table 10. Rationales for ratings are available at: https://hawcprd.epa.gov/summary/visual/100500026/. All four studies were pregnancy cohorts, with exposure measurement during pregnancy. Two studies collected more than one urine sample (James-Todd et al., 2016b; James-Todd et al., 2018). One study was considered high confidence (James-Todd et al., 2018), two medium confidence (James-Todd et al., 2016b; Shapiro et al., 2015), and one low confidence (Robledo et al., 2015). Looking across the studies, this set of cohorts is generally well-conducted with low risk of bias, but the exposure levels trend slightly lower than in other studies, so sensitivity to observe an effect may be lower.

3.3.2. Results and synthesis

Among the four studies that examined blood glucose and/or impaired glucose tolerance in pregnant women, there was no clear indication of an increase in blood glucose with increased phthalate exposure for DEHP (Table 11), DBP, and DIBP (Table 12). For BBP (Table 13), there were two studies indicating higher blood glucose or impaired glucose tolerance with higher exposure, but neither was statistically significant (James-Todd et al., 2016b; Shapiro et al., 2015). For DEP (Table 13), two studies reported statistically significant associations (James-Todd et al. (2018) for blood glucose and James-Todd et al. (2016b) for impaired glucose tolerance), but the other two studies reported no association. Across the phthalates, with the exception of DEP, the high confidence study (James-Todd et al., 2018) reported no association. This could be due to the lower exposure levels in the study population, which may have reduced study sensitivity.

3.4. Diabetes risk summary

For each phthalate, Table 14 presents a summary of the key factors that increased or decreased confidence in the evidence, a summary of the findings, and an overall judgment of the strength of evidence that considers coherence across the two main outcomes (i.e., type 2 diabetes and insulin resistance), focusing on the studies in adults. For DEHP exposure, there was consistency and an exposure-response gradient in one study for insulin resistance and coherence across diabetes and insulin resistance, though the results for diabetes were not statistically

Table 13
Association between BBP and DEP and blood glucose in pregnant women.

	Reference	Median Exposure (ng/mL or as specified)	Exposure IQR	Blood glucose 1st trimester Mean (95% CI)	Blood glucose 2nd trimester Mean (95% CI)	Impaired glucose tolerance* OR (95%)
BBP	**James-Todd et al. (2016b)** medium; 352	7.4 (GM)	3.3-15	Q1: 108 (98,119) Q2: 118 (108,130) Q3: 112 (102, 122) Q4: 111 (102,122)	Q1: 106 (96,118) Q2: 113 (102,126) Q3: 114 (103,125) Q4: 110 (101,121)	Q2: 1.17 (0.40,3.48) Q3: 1.16 (0.39,3.49) Q4: 1.28 (0.40,4.07)
	James-Todd et al. (2018) high; 245	2.8	1.4-5.4	Q1: 113 (107,120) Q2: 117 (110,124) Q3: 110 (103,116) Q4: 117 (110,124)	Q1: 111 (105,118) Q2: 117 (110,124) Q3: 110 (104,117) Q4: 116 (109,123)	no association
	Shapiro et al. (2015) medium; 1,885	5.8	NR	NR	NR	Q2: 1.3 (0.6,2.8) Q3: 2.0 (0.9, 4.4) Q4: 2.0 (0.9,4.8) p-trend: 0.07
	Robledo et al. (2015) low; 72	16	8.5-37	NR	β (95% CI) T2: -0.82 (-14.37,12.73) T3: -17.26 (-34.12,-0.40)	NR
DEP	**James-Todd et al. (2016b)** medium; 352	133 (GM)	49-325	Q1: 113 (103,125) Q2: 114 (103,125) Q3: 115 (105,126) Q4: 107 (98,118)	Q1: 109 (100,120) Q2: 112 (102,124) Q3: 110 (99,121) Q4: 116 (105,128) p-trend: 0.19	Q2: 2.14 (0.57,8.10) Q3: 2.53 (0.71,8.97) Q4: 7.18 (1.97,26.15) p-trend: <0.01
	James-Todd et al. (2018) high; 245	48	22-144	Q1: 114 (108,121) Q2: 115 (108,122) Q3: 109 (103,116) Q4: 118 (111,125)	Q1: 109 (103,116) Q2: 113 (107,120) Q3: 111 (105,117) Q4: 121 (114,128) p-trend: 0.02	2.48 (0.86,7.20)
	Shapiro et al. (2015) medium; 1,885	39	NR	NR	NR	Q2: 1.0 (0.5,2.0) Q3: 0.8 (0.4,1.7) Q4: 0.7 (0.3,1.5) p-trend: 0.29
	Robledo et al. (2015) low; 72	206	92-525	NR	β (95% CI) T2: 4.45 (-9.30,18.19) T3: 0.18 (-14.57,14.94)	NR

Results that support an association are shaded based on effect size and precision.
*Shapiro includes impaired glucose tolerance and gestational diabetes.
p-Values > 0.20 are not presented. NR = not reported.

significant. Given the overall consistency, but some lingering uncertainty in the evidence, this evidence is considered moderate.

For DBP and DIBP exposure, in contrast, the overall evidence is considered moderate primarily due to the strong positive associations in the single diabetes study. There is substantial unexplained inconsistency in the results for insulin resistance, but some of the results, including exposure-response gradients in one well-conducted study, provide coherence with the incident diabetes results.

For DINP, BBP, and DEP, the evidence is considered slight. No association was reported in the single study of diabetes with BBP and DEP exposure (DINP was not investigated). The available evidence does indicate an association between exposure to these phthalates and insulin resistance, including in pregnant women, but the small number of studies and the lack of coherence with diabetes decreases confidence.

3.5. Obesity

A prior review concluded that the data on obesity and phthalate exposure is inconsistent (Thayer et al., 2012). We conducted a screening level review encompassing these and more recent studies. Twenty-five of the 32 epidemiology studies (described in 35 publications) identified in the search with data on obesity or BMI were excluded (Supplementary Table). The majority were excluded due to issues with temporality (i.e., exposure was measured at the same time as BMI), or due to measurement of exposure in tissues other than urine. Six of the remaining studies focused on obesity in children or infants based on prenatal or childhood exposure. The screening level review of these studies indicated little consistency with no clear explanation based on a preliminary evaluation of study confidence or exposure levels (Supplementary Table). Therefore, a full systematic review was not performed and the evidence is considered inadequate.

Along among the included studies was a single prospective study of adult weight gain (Song et al., 2014), which used the controls from the nested case-control study on type 2 diabetes described previously (Sun et al., 2014) and measured weight gain over ten years. For summed DBP + DIBP and BBP, there were statistically significant associations between increased exposure and weight gain, with exposure-response gradients observed. For DEHP and DEP, no association was observed, and no results were available for DINP. Since the effect sizes for the positive associations were small (approximately 0.3 kg per year) and there is potential for residual confounding by diet (as described for diabetes), the evidence from a single study is considered inadequate to

Table 14
Summary of evidence for diabetes risk in adults.

Phthalate	Outcome	Studies	Factors that increase confidence	Factors that decrease confidence	Summary of findings	Evidence judgment
DEHP	Diabetes	Medium confidence Sun et al. (2014) (nested CC in two C)	• Study well conducted	• Potential for residual confounding by diet • Single study • Imprecision	Positive association between DEHP exposure and type 2 diabetes diagnosis (not statistically significant, Table 3).	⊕⊕◯ MODERATE for diabetes risk
	Insulin resistance in adults	Medium confidence Chen et al. (2017) (CS) Dales et al. (2018) (CS) Hong et al. (2016) (CS) Huang et al. (2014) (CS) Kim et al. (2013) (C) Low confidence Dirinck et al. (2015) (CS) Hong et al. (2009) (CS)	Among medium confidence studies: • Exposure-response gradient observed in one study • Generally consistent results across populations • Minimal concerns for bias	• Potential for residual confounding by diet	Positive association between DEHP exposure and glucose, insulin and/or HOMA-IR in 5 studies (Dales et al., 2018; Dirinck et al., 2015; Huang et al., 2014; Kim et al., 2013; Hong et al., 2016), with statistical significance in four (Table 5). Exposure-response gradients were reported in Huang et al. (2014) for all endpoints (not evaluated in other studies)	Supported by coherence across outcomes and plausible mechanism from animal and in vitro studies
DINP	Insulin resistance in adolescents	Medium confidence Attina and Trasande (2015) (CS)	• Minimal concerns for bias • Exposure-response gradient	• Potential for residual confounding by diet • Single study	Positive association between DINP exposure and HOMA-IR, with statistical significance in the third tertile.	⊕◯◯ SLIGHT
DBP	Diabetes	Medium confidence Sun et al. (2014) (nested CC in two C)	• Strong association • Study well conducted	• Potential for residual confounding by diet • Single study	Strong positive (OR = 3.2 for Q4) statistically significant association between DBP exposure and type 2 diabetes diagnosis (Table 3).	⊕⊕◯ MODERATE
	Insulin resistance in adults	Medium confidence Chen et al. (2017) (CS) Dales et al. (2018) (CS) Hong et al. (2016) (CS) Huang et al. (2014) (CS) Kim et al. (2013) (C) Low confidence Dirinck et al. (2015) (CS) Hong et al. (2009) (CS)	Among medium confidence studies: • Exposure-response gradient observed in one study • Minimal concerns for bias	• Potential for residual confounding by diet	Positive association between DBP exposure and at least one measure of insulin resistance (i.e., glucose, insulin and/or HOMA-IR) in 4 studies (Huang et al., 2014, Dirinck et al., 2015, Dales et al., 2018, Kim et al., 2013), with statistical significance in 2 (Table 6). An exposure-response gradient was reported in Huang et al. (2014) for glucose (not evaluated in other studies).	Supported by coherence across outcomes and plausible mechanism from animal and in vitro studies
DIBP	Diabetes	Medium confidence Sun et al. (2014) (nested CC in two C)	• Strong association • Study well conducted	• Potential for residual confounding by diet • Single study	Strong positive (OR = 2.7 for Q4) statistically significant association between DIBP exposure and type 2 diabetes diagnosis (Table 3).	⊕⊕◯ MODERATE
	Insulin resistance in adults	Medium confidence Dales et al. (2018) (CS) Huang et al. (2014) (CS) Low confidence Dirinck et al. (2015) (CS)	• Exposure-response gradient observed in one study	• Potential for residual confounding by diet • Few studies	Positive association between DIBP exposure and glucose, insulin, and/or HOMA-IR in 2 studies (Huang et al., 2014) (Dirinck et al., 2015) (Table 7). Huang et al. (2014) reported statistical significance for all endpoints and an exposure-response gradient for glucose (not evaluated in other study)	Supported by coherence across outcomes and plausible mechanism from animal and in vitro studies
BBP	Diabetes	Medium confidence Sun et al. (2014) (nested CC in two C)	• Study well conducted	• Potential for residual confounding by diet • Single study	No association reported between type 2 diabetes risk and BBP exposure.	⊕◯◯ SLIGHT
	Insulin resistance in adults	Medium confidence Chen et al. (2017) (CS) Dales et al. (2018) (CS) Huang et al. (2014) (CS) Low confidence Dirinck et al. (2015) (CS)	• Exposure-response gradient observed in one study	• Potential for residual confounding by diet • Few studies • Inconsistency among medium confidence studies	Positive association between BBP exposure and glucose, insulin, and/or HOMA-IR in 2 studies (Dirinck et al., 2015; Huang et al., 2014) (Table 8). Exposure-response gradients were observed for insulin and HOMA-IR in Huang et al. (2014) (not evaluated in other study).	
DEP	Diabetes	Medium confidence Sun et al. (2014) (nested CC in two C)	• Study well conducted	• Potential for residual confounding by diet • Single study	No association reported between type 2 diabetes risk and DEP exposure.	⊕◯◯ SLIGHT

(*continued on next page*)

Table 14 (*continued*)

Phthalate	Outcome	Studies	Factors that increase confidence	Factors that decrease confidence	Summary of findings	Evidence judgment
	Insulin resistance in adults	Medium confidence Chen et al. (2017) (CS) Dales et al. (2018) (CS) Huang et al. (2014) (CS) Low confidence Dirinck et al. (2015) (CS)	● Exposure-response gradient observed in one study ● Consistent results across populations	● Potential for residual confounding by diet ● Few studies	Positive association between DEP exposure and glucose, insulin and/or HOMA-IR in 2 studies (Huang et al., 2014) (Dirinck et al., 2015) (Table 9). Exposure-response gradients were observed for insulin and HOMA-IR in (Huang et al., 2014) (not evaluated in other study).	

C = cohort; CC = case-control; CS = cross-sectional.

draw a conclusion about the association with obesity.

3.6. Renal effects

Five epidemiology studies examined the association between phthalate exposure and renal effects. Three studies were excluded due to critical deficiencies in exposure measurement (Supplementary Table). Both of the remaining studies were considered to be low confidence by a single reviewer due to selection bias (Tsai et al. (2016) or possible reverse causation (Trasande et al. (2014). Because of inconsistency in the results and the availability of only low confidence studies, a full systematic review was not performed, and the evidence is considered inadequate.

4. Discussion

Based on screening-level reviews, the currently available evidence was determined to be inadequate to assess associations between obesity and renal effects and phthalate exposure. It is unlikely that a full systematic review of the existing literature would indicate a clear association, either due to a small number of low confidence studies available or disparate results. The use of screening-level reviews allowed us to avoid using additional resources required for a full systematic review for these outcomes at this time. It is important to note, however, that we do not mean to imply that systematic reviews are not useful in situations where the evidence is inconsistent. To the contrary, systematic review may be particularly beneficial for evidence bases with conflicting results because it provides a process for identifying factors that may explain the discrepancies (e.g., study quality, exposure levels). The benefit gained from the review will depend on the context of the review. In this case, the focus was on identifying key hazards of phthalate exposure with a robust database, and there was a need to be pragmatic in the use of resources to conduct the review.

Evidence for an association between phthalate exposure and diabetes risk is more convincing. The single prospective study that examined incident diabetes as an outcome reported strong associations for multiple phthalates, and several studies reported associations with insulin resistance. When coherence across these outcomes was considered, DEHP, DBP, and DIBP had moderate evidence of an association, and DINP, BBP, and DEP had slight evidence of an association (Table 14).

Diet was considered a possible confounder for the observed association with diabetes and obesity. Only a portion of the studies controlled for diet, and those that did used only caloric intake as a proxy. While this would account for increased exposure simply from eating more in general, there may be other diet-related factors associated with phthalate exposure, such as frequent consumption of packaged/processed foods or fatty foods, which may not be fully accounted for with adjustment for caloric intake, and which may carry an additional risk with respect to diabetes (Micha et al., 2010; Franz et al., 2002; Hu et al., 2001). Phthalates, particularly DEHP and DBP, are present in most food-packaging materials (Balafas et al., 1999) and plastic-packaged food products (Cirillo et al., 2013) and can migrate into food (Serrano et al., 2014a; Castle et al., 1994). This migration is increased with microwave heating (Chen et al., 2008). Phthalate levels in different food types have been reviewed previously and meats (particularly poultry) and fats/oils have been consistently associated with increased phthalate exposure (Serrano et al., 2014a). Since the 2014 review, participants in a pre-defined “fatty, sweet, and ready meal” group had higher exposure to DEHP and DBP in one study (Serrano et al., 2014b). Other foods may vary in phthalate levels, based partly on region (Serrano et al., 2014a). A change in diet to fresh, mostly organic meals prepared without plastics in procurement, cooking, and serving has been shown to reduce DEHP exposure (Rudel et al., 2011). Taken as a whole, it is conceivable that individuals who eat a diet higher in packaged, microwaved, and fatty foods may be at higher risk for

diabetes and obesity, and this diet may also increase phthalate exposure, though the influence of diet may differ by phthalate. The concern would be highest for DEHP, which is commonly used in packaging and is more associated with fatty foods due to its more lipophilic nature (Cao, 2010). DBP, DIBP, BBP are all used in packaging, though perhaps less so than DEHP (Van Holderbeke et al., 2014; Fierens et al., 2012), while DEP is not frequently used in packaging and is less likely to contaminate food (Schettler, 2006). The fact that a similar association with insulin resistance was observed for DEP as the other phthalates reduces the concern about residual confounding overall, but given the small evidence base, it is worth further, more detailed exploration of diet as a potential confounder.

As mentioned in the methods, another important source of potential confounding is across phthalates. When drawing conclusions about associations between individual phthalates and health effects, it can be difficult to conclusively determine that the observed associations are not due to confounding across the phthalates. Correlations between some of the phthalates included in this review are moderately high (e.g., DBP, DIBP, BBP metabolites $r = 0.5$ to 0.7 (Johns et al., 2015)), which increases this concern. While some phthalate studies present multi-pollutant models, this is far from universal, and there are also concerns that bias can be amplified in multipollutant regression models (Weisskopf et al., 2018). Thus, this is an area of uncertainty for reviews of phthalates and other chemical mixtures, and is discussed in more detail in a forthcoming special issue editorial. Our ability to assess this type of confounding is somewhat limited by the different sensitivity of the studies for different phthalates (e.g., due to exposure levels), which reduced the ability to assess coherence across phthalates, and by the fact that we might expect more similar phthalates to be both highly correlated with each other and have similar effects (e.g., DBP and DIBP). However, it is unlikely that this issue would significantly alter the conclusions of this review. None of the associations in this review approached the level of "Robust" evidence, where uncertainty is largely eliminated and alternative explanations for the association such as chance, bias, and confounding are ruled out. Still, this is certainly an important issue for phthalate research moving forward. Methods development to address this concern is a rapidly developing field, and researchers should consider the potential for confounding across phthalates in designing their studies and analyzing data. In addition, given that people are exposed to mixtures of chemicals like phthalates, there may be a benefit in some cases to drawing conclusions for mixtures (such as all phthalates or subclasses of phthalates) rather than for individual chemicals, though this is not without its own complications.

An established mechanism for the association between phthalate exposure and diabetes and insulin resistance would also increase confidence in the association despite the possibility of residual confounding. Plausible mechanisms for the association have been described elsewhere. Phthalates can alter peroxisome proliferator-activated receptors (PPARs), which contribute to adipogenesis, lipid metabolism, and metabolic homeostasis (Benjamin et al., 2017a; Watkins et al., 2016; Attina and Trasande, 2015; Sun et al., 2014; Thayer et al., n.d.). Oxidative stress is another possible mechanism (Watkins et al., 2016).

Given the mechanistic plausibility, the large effect sizes for incident diabetes in the single available study for some phthalates, and the coherence with insulin resistance, the association between phthalate exposure and diabetes risk should be considered when assessing the risks and costs of exposure to specific phthalates in humans. This is consistent with findings by Legler et al. (2015) and Benjamin et al. (2017b) in narrative reviews. Additional prospective research with repeated measures of exposure would further clarify the relationship, as would additional high-quality research on the related metabolic effects (obesity, renal effects) to better understand coherence across outcomes. Discussion of some additional issues that apply to all phthalate studies, is presented in the special issue editorial (forthcoming).

Acknowledgements

We would like to thank Carolyn Gigot, Susan Rieth, Michelle Angrish, Tom Bateson, Erin Yost, Ana Navas-Ascien, Robin Puett, Mike Wright, and Leonid Kopylev for their contributions to this work.

Appendix A. Supplementary data

Supplementary data to this article can be found online at https://doi.org/10.1016/j.envint.2019.04.040.

References

Attina, T.M., Trasande, L., 2015. Association of exposure to di-2-ethylhexylphthalate replacements with increased insulin resistance in adolescents from NHANES 2009–2012. J. Clin. Endocrinol. Metab. 100, 2640–2650. https://doi.org/10.1210/jc.2015-1686.

Balafas, D., Shaw, K.J., Whitfield, F.B., 1999. Phthalate and adipate esters in Australian packaging materials. Food Chem. 65, 279–287.

Benjamin, J.S., Culpepper, C.B., Brown, L.D., Wesolowski, S.R., Jonker, S.S., Davis, M.A., Limesand, S.W., Wilkening, R.B., Hay, W.W., Rozance, P.J., 2017a. Chronic anemic hypoxemia attenuates glucose-stimulated insulin secretion in fetal sheep. Am J Physiol Regul Integr Comp Physiol 312, R492–R500. https://doi.org/10.1152/ajpregu.00484.2016.

Benjamin, S., Masai, E., Kamimura, N., Takahashi, K., Anderson, R.C., Faisal, P.A., 2017b. Phthalates impact human health: epidemiological evidences and plausible mechanism of action [review]. J. Hazard. Mater. 340, 360–383. https://doi.org/10.1016/j.jhazmat.2017.06.036.

Cao, X,. uL, 2010. Phthalate esters in foods: sources, occurrence, and analytical methods. Compr. Rev. Food Sci. Food Saf. 9, 21–43. https://doi.org/10.1111/j.1541-4337.2009.00093.x.

Carlsson, A., Sørensen, K., Andersson, A.M., Frederiksen, H., Juul, A., 2018. Bisphenol a, Phthalate Metabolites and Glucose Homeostasis in Healthy Normal-Weight Children. vol. 7. pp. 232–238. https://doi.org/10.1530/EC-17-0344.

Castle, L., Nichol, J., Gilbert, J., 1994. Migration of mineral hydrocarbons into foods. 4. Waxed paper for packaging dry goods including bread, confectionery and for domestic use including microwave cooking. Food Addit. Contam. 11, 79–89. https://doi.org/10.1080/02652039409374204.

Castro-Correia, C., Correia-Sá, L., Norberto, S., Delerue-Matos, C., Domingues, V., Costa-Santos, C., Fontoura, M., Calhau, C., 2018. Phthalates and type 1 diabetes: is there any link? Environ. Sci. Pollut. Res. Int. 25, 17915–17919. https://doi.org/10.1007/s11356-018-1997-z.

Chen, M.L., Chen, J.S., Tang, C.L., Mao, I.F., 2008. The internal exposure of Taiwanese to phthalate–an evidence of intensive use of plastic materials. Environ. Int. 34, 79–85. https://doi.org/10.1016/j.envint.2007.07.004.

Chen, S.Y., Hwang, J.S., Sung, F.C., Lin, C.Y., Hsieh, C.J., Chen, P.C., Su, T.C., 2017. Mono-2-ethylhexyl phthalate associated with insulin resistance and lower testosterone levels in a young population. Environ. Pollut. 225, 112–117. https://doi.org/10.1016/j.envpol.2017.03.037.

Cirillo, T., Fasano, E., Esposito, F., Prete, E.D., Cocchieri, R.A., 2013. Study on the influence of temperature, storage time and packaging type on di-n-butylphthalate and di(2-ethylhexyl)phthalate release into packed meals. Food Addit Contam Part A Chem Anal Control Expo Risk Assess 30, 403–411. https://doi.org/10.1080/19440049.2012.745198.

Dales, R.E., Kauri, L.M., Cakmak, S., 2018. The associations between phthalate exposure and insulin resistance, β-cell function and blood glucose control in a population-based sample. Sci. Total Environ. 612, 1287–1292. https://doi.org/10.1016/j.scitotenv.2017.09.009.

Dirinck, E., Dirtu, A.C., Geens, T., Covaci, A., Van Gaal, L., Jorens, P.G., 2015. Urinary phthalate metabolites are associated with insulin resistance in obese subjects. Environ. Res. 137, 419–423. https://doi.org/10.1016/j.envres.2015.01.010.

Dong, R., Zhou, T., Chen, J., Zhang, M., Zhang, H., Wu, M., Li, S., Zhang, L., Chen, B., 2017. Gender- and age-specific relationships between phthalate exposures and obesity in Shanghai adults. Arch. Environ. Contam. Toxicol. 73, 431–441. https://doi.org/10.1007/s00244-017-0441-6.

Fierens, T., Servaes, K., Van Holderbeke, M., Geerts, L., De Henauw, S., Sioen, I., Vanermen, G., 2012. Analysis of phthalates in food products and packaging materials sold on the Belgian market. Food Chem. Toxicol. 50, 2575–2583. https://doi.org/10.1016/j.fct.2012.04.029.

Fisher, B.G., Frederiksen, H., Andersson, A.M., Juul, A., Thankamony, A., Ong, K.K., Dunger, D.B., Hughes, I.A., Acerini, C.L., 2018. Serum phthalate and triclosan levels have opposing associations with risk factors for gestational diabetes mellitus. Front Endocrinol (Lausanne) 9, 99. https://doi.org/10.3389/fendo.2018.00099.

Franz, M.J., Bantle, J.P., Beebe, C.A., Brunzell, J.D., Chiasson, J.L., Garg, A., Holzmeister, L.A., Hoogwerf, B., Mayer-Davis, E., Mooradian, A.D., Purnell, J.Q., Wheeler, M., 2002. Evidence-based nutrition principles and recommendations for the treatment and prevention of diabetes and related complications [review]. Diabetes Care 25, 148–198. https://doi.org/10.2337/diacare.25.1.148.

Heindel, J.J., Blumberg, B., Cave, M., Machtinger, R., Mantovani, A., Mendez, M.A., Nadal, A., Palanza, P., Panzica, G., Sargis, R., Vandenberg, L.N., Vom Saal, F., 2017. Metabolism disrupting chemicals and metabolic disorders. Reprod. Toxicol. 68, 3–33. https://doi.org/10.1016/j.reprotox.2016.10.001.

Hong, Y.C., Park, E.Y., Park, M.S., Ko, J.A., Oh, S.Y., Kim, H., Lee, K.H., Leem, J.H., Ha, E.H., 2009. Community level exposure to chemicals and oxidative stress in adult population. Toxicol. Lett. 184, 139–144. https://doi.org/10.1016/j.toxlet.2008.11.001.

Hong, S.H., Sung, Y.A., Hong, Y.S., Ha, E., Jeong, K., Chung, H., Lee, H., 2016. Urinary bisphenol A is associated with insulin resistance and obesity in reproductive-aged women. Clin. Endocrinol. 86, 506–512. https://doi.org/10.1111/cen.13270.

Hu, F.B., van Dam, R.M., Liu, S., 2001. Diet and risk of type II diabetes: the role of types of fat and carbohydrate. Diabetologia 44, 805–817. https://doi.org/10.1007/s001250100.

Huang, T., Saxena, A.R., Isganaitis, E., James-Todd, T., 2014. Gender and racial/ethnic differences in the associations of urinary phthalate metabolites with markers of diabetes risk: national health and nutrition examination survey 2001–2008. Environ. Health 13, 6. https://doi.org/10.1186/1476-069X-13-6.

James-Todd, T., Huang, T., Isganaitis, E., Saxena, A., 2012. Urinary phthalate metabolite concentrations and biomarkers of diabetes risk by race/ethnicity and sex, the National Health and nutrition examination survey 2001–2008 [abstract]. J. Women's Health 21, 992. https://doi.org/10.1089/jwh.2012.ab02.

James-Todd, T.M., Huang, T., Seely, E.W., Saxena, A.R., 2016a. The association between phthalates and metabolic syndrome: the National Health and Nutrition Examination Survey 2001–2010. Environ. Health 15, 52. https://doi.org/10.1186/s12940-016-0136-x.

James-Todd, T.M., Meeker, J.D., Huang, T., Hauser, R., Ferguson, K.K., Rich-Edwards, J.W., Mcelrath, T.F., Seely, E.W., 2016b. Pregnancy urinary phthalate metabolite concentrations and gestational diabetes risk factors. Environ. Int. 96, 118–126. https://doi.org/10.1016/j.envint.2016.09.009.

James-Todd, T.M., Chiu, Y.H., Messerlian, C., Mínguez-Alarcón, L., Ford, J.B., Keller, M., Petrozza, J., Williams, P.L., Ye, X., Calafat, A.M., Hauser, R., Team, E.S., 2018. Trimester-specific phthalate concentrations and glucose levels among women from a fertility clinic. Environ. Health 17, 55. https://doi.org/10.1186/s12940-018-0399-5.

Johns, L.E., Cooper, G.S., Galizia, A., Meeker, J.D., 2015. Exposure assessment issues in epidemiology studies of phthalates [review]. Environ. Int. 85, 27–39. https://doi.org/10.1016/j.envint.2015.08.005.

Kataria, A., Levine, D., Wertenteil, S., Vento, S., Xue, J., Rajendiran, K., Kannan, K., Thurman, J.M., Morrison, D., Brody, R., Urbina, E., Attina, T., Trasande, L., Trachtman, H., 2017. Exposure to bisphenols and phthalates and association with oxidant stress, insulin resistance, and endothelial dysfunction in children. Pediatr. Res. 81, 857–864. https://doi.org/10.1038/pr.2017.16.

Kim, J.H., Hong, Y.C., 2014. HSP70-hom gene polymorphisms modify the association of diethylhexyl phthalates with insulin resistance. Environ. Mol. Mutagen. 55, 727–734. https://doi.org/10.1002/em.21884.

Kim, J.H., Park, H.Y., Bae, S., Lim, Y.H., Hong, Y.C., 2013. Diethylhexyl phthalates is associated with insulin resistance via oxidative stress in the elderly: a panel study. PLoS One 8, e71392. https://doi.org/10.1371/journal.pone.0071392.

Kuo, C.C., Moon, K., Thayer, K.A., Navas-Acien, A., 2013. Environmental chemicals and type 2 diabetes: an updated systematic review of the epidemiologic evidence [review]. Curr Diab Rep 13, 831–849. https://doi.org/10.1007/s11892-013-0432-6.

Legler, J., Fletcher, T., Govarts, E., Porta, M., Blumberg, B., Heindel, J.J., Trasande, L., 2015. Obesity, diabetes, and associated costs of exposure to endocrine-disrupting chemicals in the European Union. J. Clin. Endocrinol. Metab. 100, 1278–1288. https://doi.org/10.1210/jc.2014-4326.

Lin, C.Y., Hsieh, C.J., Lo, S.C., Chen, P.C., Torng, P.L., Hu, A., Sung, F.C., Su, T.C., 2016. Positive association between concentration of phthalate metabolites in urine and microparticles in adolescents and young adults. Environ. Int. 92-93, 157–164. https://doi.org/10.1016/j.envint.2016.04.006.

Lind, P.M., Zethelius, B., Lind, L., 2012. Circulating levels of phthalate metabolites are associated with prevalent diabetes in the elderly. Diabetes Care 35, 1519–1524. https://doi.org/10.2337/dc11-2396.

Micha, R., Wallace, S.K., Mozaffarian, D., 2010. Red and processed meat consumption and risk of incident coronary heart disease, stroke, and diabetes mellitus: a systematic review and meta-analysis [review]. Circulation 121, 2271–2283. https://doi.org/10.1161/CIRCULATIONAHA.109.924977.

Milošević, N., Milić, N., Živanović Bosić, D., Bajkin, I., Perčić, I., Abenavoli, L., Medić Stojanoska, M., 2017. Potential influence of the phthalates on normal liver function and cardiometabolic risk in males. Environ. Monit. Assess. 190, 17. https://doi.org/10.1007/s10661-017-6398-0.

National Academy of Sciences, National Academy of Engineering, Institute of Medicine, 2017. Application of systematic review methods in an overall strategy for evaluating low-dose toxicity from endocrine active chemicals. In: Application of Systematic Review Methods in an Overall Strategy for Evaluating Low-Dose Toxicity from Endocrine Active Chemicals. The National Academies Press, Washington, D.C.. https://doi.org/10.17226/24758.

Olsén, L., Lampa, E., Birkholz, D.A., Lind, L., Lind, P.M., 2012. Circulating levels of bisphenol A (BPA) and phthalates in an elderly population in Sweden, based on the Prospective Investigation of the Vasculature in Uppsala Seniors (PIVUS). Ecotoxicol. Environ. Saf. 75, 242–248. https://doi.org/10.1016/j.ecoenv.2011.09.004.

Piecha, R., Svačina, Š., Malý, M., Vrbík, K., Lacinová, Z., Haluzík, M., Pavloušková, J., Vavrouš, A., Matějková, D., Müllerová, D., Mráz, M., Matoulek, M., 2016. Urine levels of phthalate metabolites and bisphenol A in relation to main metabolic syndrome components: dyslipidemia, hypertension and type 2 diabetes. A pilot study. Cent. Eur. J. Public Health 24, 297–301. https://doi.org/10.21101/cejph.a4704.

Robledo, C.A., Peck, J.D., Stoner, J., Calafat, A.M., Carabin, H., Cowan, L., Goodman, J.R., 2015. Urinary phthalate metabolite concentrations and blood glucose levels during pregnancy. Int. J. Hyg. Environ. Health 218, 324–330. https://doi.org/10.1016/j.ijheh.2015.01.005.

Rudel, R.A., Gray, J.M., Engel, C.L., Rawsthorne, T.W., Dodson, R.E., Ackerman, J.M., Rizzo, J., Nudelman, J.L., Brody, J.G., 2011. Food packaging and bisphenol A and bis (2-ethyhexyl) phthalate exposure: findings from a dietary intervention. Environ. Health Perspect. 119, 914–920. https://doi.org/10.1289/ehp.1003170.

Saengkaew, T., Jantarat, C., Nosoognoen, W., Supornsilchai, V., 2017. Association between Urinary Phthalates and Metabolic Abnormalities in Obese Thai Children and Adolescents. vol. 30. pp. 931–938. https://doi.org/10.1515/jpem-2017-0172.

Schettler, T., 2006. Human exposure to phthalates via consumer products [review]. Int. J. Androl. 29, 134–139. discussion 181-135. https://doi.org/10.1111/j.1365-2605.2005.00567.x.

Updated October 2013 Schünemann, H., Brożek, J., Guyatt, G., Oxman, A. (Eds.), 2013. GRADE handbook for grading quality of evidence and strength of recommendations. The GRADE Working Group. Available from guidelinedevelopment.org/handbook.

Serrano, S.E., Braun, J., Trasande, L., Dills, R., Sathyanarayana, S., 2014a. Phthalates and diet: a review of the food monitoring and epidemiology data [review]. Environ. Health 13, 43. https://doi.org/10.1186/1476-069X-13-43.

Serrano, S.E., Karr, C.J., Seixas, N.S., Nguyen, R.H., Barrett, E.S., Janssen, S., Redmon, B., Swan, S.H., Sathyanarayana, S., 2014b. Dietary phthalate exposure in pregnant women and the impact of consumer practices. Int. J. Environ. Res. Public Health 11, 6193–6215. https://doi.org/10.3390/ijerph110606193.

Shapiro, G.D., Dodds, L., Arbuckle, T.E., Ashley-Martin, J., Fraser, W., Fisher, M., Taback, S., Keely, E., Bouchard, M.F., Monnier, P., Dallaire, R., Morisset, A.S., Ettinger, A.S., 2015. Exposure to phthalates, bisphenol A and metals in pregnancy and the association with impaired glucose tolerance and gestational diabetes mellitus: the MIREC study. Environ. Int. 83, 63–71. https://doi.org/10.1016/j.envint.2015.05.016.

Smerieri, A., Testa, C., Lazzeroni, P., Nuti, F., Grossi, E., Cesari, S., Montanini, L., Latini, G., Bernasconi, S., Papini, A.M., Street, M.E., 2015. Di-(2-ethylhexyl) phthalate metabolites in urine show age-related changes and associations with adiposity and parameters of insulin sensitivity in childhood. PLoS One 10, e0117831. https://doi.org/10.1371/journal.pone.0117831.

Song, Y., Hauser, R., Hu, F.B., Franke, A.A., Liu, S., Sun, Q., 2014. Urinary concentrations of bisphenol A and phthalate metabolites and weight change: a prospective investigation in US women. Int. J. Obes. 38, 1532–1537. https://doi.org/10.1038/ijo.2014.63.

Stahlhut, R.W., van Wijngaarden, E., Dye, T.D., Cook, S., Swan, S.H., 2007. Concentrations of urinary phthalate metabolites are associated with increased waist circumference and insulin resistance in adult U.S. males. Environ. Health Perspect. 115, 876–882. https://doi.org/10.1289/ehp.9882.

Sterne, J., Higgins, J., Reeves, B., 2016. ROBINS-I: a tool for assessing risk of bias in non-randomized studies of interventions, version 7 March 2016. Br. Med. J. 355, i4919.

Sun, Q., Cornelis, M.C., Townsend, M.K., Tobias, D.K., Eliassen, A.H., Franke, A.A., Hauser, R., Hu, F.B., 2014. Association of urinary concentrations of bisphenol A and phthalate metabolites with risk of type 2 diabetes: a prospective investigation in the Nurses' Health Study (NHS) and NHSII cohorts. Environ. Health Perspect. 122, 616–623. https://doi.org/10.1289/ehp.1307201.

Svensson, K., Hernández-Ramírez, R.U., Burguete-García, A., Cebrián, M.E., Calafat, A.M., Needham, L.L., Claudio, L., López-Carrillo, L., 2011. Phthalate exposure associated with self-reported diabetes among Mexican women. Environ. Res. 111, 792–796. https://doi.org/10.1016/j.envres.2011.05.015.

Thayer, K.A., Heindel, J.J., Bucher, J.R., Gallo, M.A., 2012. Role of environmental chemicals in diabetes and obesity: a national toxicology program workshop report [review]. Environ. Health Perspect. 120, 779–789. https://doi.org/10.1289/ehp.1104597.

Thayer, KA; Heindel, JJ; Bucher, JR; Gallo, MA. (In Press) Role of environmental chemicals in diabetes and obesity: a national toxicology program workshop report [review]. Environ. Health Perspect. 120: 779–789. doi:https://doi.org/10.1289/ehp.1104597.

Trasande, L., Attina, T.M., Sathyanarayana, S., Spanier, A.J., Blustein, J., 2013. Race/ethnicity-specific associations of urinary phthalates with childhood body mass in a nationally representative sample. Environ. Health Perspect. 121, 501–506. https://doi.org/10.1289/ehp.1205526.

Trasande, L., Sathyanarayana, S., Trachtman, H., 2014. Dietary phthalates and low-grade albuminuria in US children and adolescents. Clin. J. Am. Soc. Nephrol. 9, 100–109. https://doi.org/10.2215/CJN.04570413.

Tsai, H.J., Chen, B.H., Wu, C.F., Wang, S.L., Huang, P.C., Tsai, Y.C., Chen, M.L., Ho, C.K., Hsiung, C.A., Wu, M.T., 2016. Intake of phthalate-tainted foods and microalbuminuria in children: the 2011 Taiwan food scandal. Environ. Int. 89-90, 129–137. https://doi.org/10.1016/j.envint.2016.01.015.

Van Holderbeke, M., Geerts, L., Vanermen, G., Servaes, K., Sioen, I., De Henauw, S., Fierens, T., 2014. Determination of contamination pathways of phthalates in food products sold on the Belgian market. Environ. Res. 134, 345–352. https://doi.org/10.1016/j.envres.2014.08.012.

Watkins, D.J., Peterson, K.E., Ferguson, K.K., Mercado-García, A., Ortiz, M.T., Cantoral, A., Meeker, J.D., Téllez-Rojo, M.M., 2016. Relating phthalate and BPA exposure to metabolism in peripubescence: the role of exposure timing, sex, and puberty. J. Clin. Endocrinol. Metab. 101, jc20152706. https://doi.org/10.1210/jc.2015-2706.

Weisskopf, M.G., Seals, R.M., Webster, T.F., 2018. Bias amplification in epidemiologic analysis of exposure to mixtures. Environ. Health Perspect. 126 (4), 047003.

Whaley-Connell, A., Sowers, J.R., 2017. Insulin resistance in kidney disease: is there a distinct role separate from that of diabetes or obesity? [review]. Cardiorenal Med 8, 41–49. https://doi.org/10.1159/000479801.

Zhang, Y.W., Gao, H., Huang, K., Xu, Y.Y., Sheng, J., Tao, F.B., 2017. A cohort study on association between the first trimester phthalates exposure and fasting blood glucose level in the third trimester. Zhonghua Liuxingbingxue Zazhi 38, 388–392.

Environment International 137 (2020) 105408

Contents lists available at ScienceDirect

Environment International

journal homepage: www.elsevier.com/locate/envint

Phthalate exposure and neurodevelopment: A systematic review and meta-analysis of human epidemiological evidence

Elizabeth G. Radke[a,*], Joseph M. Braun[b], Rebecca M. Nachman[a], Glinda S. Cooper[a,c]

[a] U.S. Environmental Protection Agency, National Center for Environmental Assessment, United States
[b] Brown University, School of Public Health, United States
[c] The Innocence Project, United States

ARTICLE INFO

Handling Editor: Adrian Covaci

ABSTRACT

Objective: We performed a systematic review of the epidemiology literature to identify the neurodevelopmental effects associated with phthalate exposure.

Data sources and study eligibility criteria: Six phthalates were included in the review: di(2-ethylhexyl) phthalate (DEHP), diisononyl phthalate (DINP), dibutyl phthalate (DBP), diisobutyl phthalate (DIBP), butyl benzyl phthalate (BBP), and diethyl phthalate (DEP). The initial literature search (of PubMed, Web of Science, and Toxline) included all studies of neurodevelopmental effects in humans, and outcomes were selected for full systematic review based on data availability.

Study evaluation and synthesis methods: Studies of neurodevelopmental effects were evaluated using criteria defined *a priori* for risk of bias and sensitivity by two reviewers using a domain-based approach. Evidence was synthesized by outcome and phthalate and strength of evidence was summarized using a structured framework. For studies of cognition and motor effects in children ≤4 years old, a random effects meta-analysis was performed.

Results: The primary outcomes reviewed here are (number of studies in parentheses): cognition (14), motor effects (9), behavior, including attention deficit hyperactivity disorder (20), infant behavior (3), and social behavior, including autism spectrum disorder (7). For each phthalate/outcome combination, there was slight or indeterminate evidence of an association, with the exception of motor effects for BBP, which had moderate evidence.

Conclusions and implications of key findings: Overall, there is not a clear pattern of association between prenatal phthalate exposures and neurodevelopment. There are several possible reasons for the observed null associations related to exposure misclassification, periods of heightened susceptibility, sex-specific effects, and the effects of phthalate mixtures. Until these limitations are adequately addressed in the epidemiology literature, these findings should not be interpreted as evidence that there are no neurodevelopmental effects of phthalate exposure.

The views expressed are those of the authors and do not necessarily represent the views or policies of the U.S. EPA.

1. Introduction

The potential for exposure to endocrine disrupting chemicals (EDCs) to adversely affect neurodevelopment has been widely reported, with plausible mechanisms described (Braun, 2017). Phthalates (phthalic acid diesters) are a class of chemicals within the wider umbrella of EDCs, and past narrative reviews by Braun (2017) and Benjamin et al. (2017) and one systematic review by Ejaredar et al. (2015) suggest that phthalate exposure is associated with a variety of neurodevelopmental outcomes, including autism, ADHD, reduced IQ, and reduced mental and psychomotor development.

Phthalate exposure, primarily via the oral route, but also through inhalation and dermal contact, is ubiquitous in humans due to their widespread use in some consumer and industrial products (Johns et al., 2015). This is true across the lifespan, and the ability of phthalates to cross the placenta as reported by Langonne et al. (1998) increases concern for developmental effects from in utero exposure, particularly when combined with the potential for higher susceptibility in the fetus and child (Braun, 2017). After exposure, phthalate diesters are rapidly metabolized to monoesters (estimated half-lives of various phthalate metabolites is approximately 3–18 h) and excreted in the urine (Johns et al., 2015).

* Corresponding author.
E-mail address: radke-arabaugh.elizabeth@epa.gov (E.G. Radke).

https://doi.org/10.1016/j.envint.2019.105408
Received 28 May 2019; Received in revised form 30 September 2019; Accepted 9 December 2019
Available online 08 February 2020
0160-4120/ © 2019 Published by Elsevier Ltd. This is an open access article under the CC BY-NC-ND license (http://creativecommons.org/licenses/BY-NC-ND/4.0/).

Table 1
Primary outcomes included in the systematic review.

Outcome	Background	Tests or assessments used in this set of studies to assess the outcome
Cognition	• General measure of intelligence. Other categories, including those not reviewed, relate to cognition. • Review focuses on the summary scale of intelligence quotient (IQ) or mental development index (MDI).	• Bayley Scales of Infant Development • Wechsler Intelligence Scale • McCarthy Scales of Children's Abilities
Motor effects	• Capacity to carry out manual motor activities, including coordination. • Review focuses on the summary scale of psychomotor developmental index (PDI) of or motor subscale.	• Bayley Scales of Infant Development • McCarthy Scales of Children's Abilities • Brazelton Neonatal Behavioral Assessment Scale • Bruininks-Oseretsky Test of Motor Proficiency
Behavior	• Broad category that includes dimensions such as anxiety, depression, attention, hyperactivity, aggression, and conduct problems. • Attention-deficit hyperactivity disorder (ADHD) is one of the most common neurobehavioral disorders in children. • Review focuses on the summary scales of internalizing and externalizing behavior.	• Child Behavior Checklist • Behavior Assessment System for Children-Parent Rating Scales • Conners' Parent Rating Scales • Strength and Difficulties Questionnaire • Clinical diagnosis (e.g., ICD codes)
Infant behavior	• Includes components of the other categories, but studies are limited to infants. • Review focuses on the subscales in common across tests – arousal, motor, regulation of state, and nonoptimal reflexes.	• Brazelton Neonatal Behavioral Assessment Scale • NICU Network Neurobehavioral Scale
Social behavior and autism	• Measure of reciprocal social, repetitive, and stereotypic behaviors associated with autism spectrum disorders (ASD). • Review focuses on summary score of autistic behaviors.	• Social Responsiveness Scale • Social Maturity Scale • Autism Diagnostic Observation Schedules

Phthalates encompass compounds with different structures, properties, and use. Some of the most studied phthalates, and those focused on here are: di(2-ethylhexyl) phthalate (DEHP), diisononyl phthalate (DINP), dibutyl phthalate (DBP), diisobutyl phthalate (DIBP), butyl benzyl phthalate (BBP), and diethyl phthalate (DEP). The metabolites of each are described in the supplemental materials. Five of the selected phthalates (DEHP, DINP, DBP, DIBP, BBP) were chosed because they are the most potent with respect to producing the "phthalate syndrome" of male reproductive effects in rats (NAS, 2008) and their metabolites have been frequently observed in human population studies; DEP is not one of the "phthalate syndrome" compounds but was included because it is often the phthalate to which humans have the highest exposure. Among these phthalates, there are some that are relatively structurally similar and moderately correlated with each other based on human biomonitoring data (e.g., DBP and DIBP), while others differ considerably in structure and commercial/industrial uses and correlations between these are typically low (e.g., DEHP and DEP).

A growing number of epidemiological studies have assessed the potential effects of early life phthalate exposure on human health. However, there are important limitations in these studies related to exposure misclassification, periods of heightened susceptibility, persistence of effects past childhood, and confounding. Thus, we performed a systematic review of the epidemiology literature examining the effects of phthalate exposure on infant and child neurodevelopment. This review builds on the past reviews on this topic in several ways. First, it includes in-depth study quality evaluations and study findings are synthesized in the context of those evaluations. In addition, quantitative meta-analysis is used where possible, and the results for individual phthalates are reviewed. Finally, there have been a notable number of new publications on this topic since the last review was published.

2. Methods

The full methods for this systematic review, including for literature search and screening, study evaluation, data extraction, and evidence synthesis are described in detail in the protocol (supplemental materials), which was created for a set of systematic reviews of the human, animal, and mechanistic evidence of all of the phthalates mentioned above. An abbreviated version is provided below, with references to specific sections of the protocol. There are a few minor deviations from the protocol for this review, and those are reflected in this section. In addition, for ease of reference, the key tables from the protocol that are necessary to understand how study evaluation and evidence synthesis conclusions were reached are included in a separate supplemental file (key methods supplement).

2.1. Neurodevelopmental Test Grouping

As neurodevelopment is typically assessed with an array of neurobehavioral or neuropsychological tests that include different domains, clear-cut divisions of these domains is challenging, and psychometric tests often reflect multiple domains. For example, longer mean reaction time (a measure of response time after a stimulus is introduced) on a continuous performance test typically indicates inattention but may also be impacted by slower information processing. Subscales within one test for one neuropsychological category might reflect aspects of another test (i.e., tests are not independent of each other). White et al. (2009) suggested grouping tests into broad categories of cognition, academics, attention, executive function/working memory, language/verbal skills, visuospatial abilities, learning/memory, and motor skills. We roughly follow these recommended groupings for this review, which examines cognition, motor effects, behavior, infant behavior, and social behavior (Table 1). While data on some other neurodevelopmental effects were available, they were not included in this review due to the small number of studies (e.g., language development, anxiety).

2.2. Literature search and screening

Epidemiology studies were identified by conducting a single broad literature search on all six phthalates of interest (DEHP, DINP, DBP, DIBP, BBP, DEP). The Population, Exposure, Comparators, and Outcome (PECO) criteria are available in the protocol (Section 2.2) and is intentionally broad to capture any population with any epidemiologic study design, any exposure to one or more phthalates that were the focus of this review (without restriction by timing of exposure), any comparison population, and any examination of human health effects. The following databases were searched: PubMed, Web of Science, and Toxline, with the initial search in 2013, and updates every 6–12 months through March 2019. Forward and backward searches were also performed. Title/abstract and full text screening were performed by two independent reviewers. The broad inventory of epidemiology studies was then further refined for this analysis, focusing only on the studies that reported any neurodevelopmental outcomes.

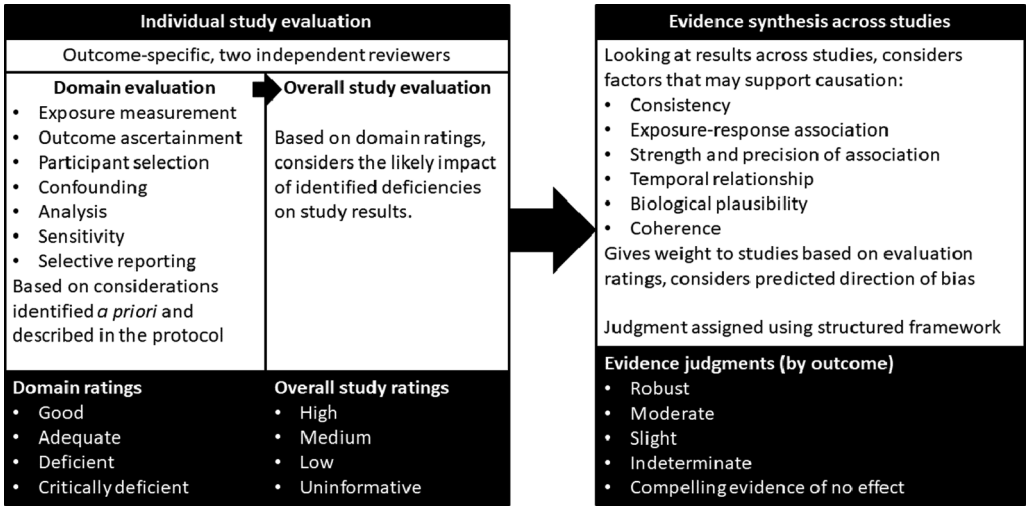

Fig. 1. Summary of study evaluation and evidence synthesis process for the systematic review.

2.3. Study evaluation

Study evaluation (protocol Section 4.1) was conducted by two independent reviewers (authors ER and RN, contributor in acknowledgements CL). Key concerns were risk of bias (factors that affect the magnitude or direction of effect) and insensitivity (factors that limit the ability of a study to detect a true effect). Evaluation was conducted for the following domains: exposure measurement, outcome ascertainment, participant selection, confounding, analysis, sensitivity, and selective reporting (Fig. 1). These domains were based on the Risk of Bias in Non-randomized Studies of Interventions (ROBINS-I) tool (Sterne et al., 2016), modified for use with environmental exposures.

For each study, in each evaluation domain, reviewers reached a consensus rating regarding the utility of the study for hazard identification, with categories of *Good, Adequate, Deficient,* or *Critically deficient*. These ratings were then considered together to reach an overall study confidence classification of *High, Medium, Low,* or *Uninformative* (Fig. 1). This overall classification was not based on pre-defined weights of the domains, but rather on reviewer expert judgments, and include the likely impact the noted deficiencies in bias and sensitivity have on the results, which varies depending on the study and/or outcome. In general, high confidence studies reflect judgments of "good" across all or most domains, and medium confidence studies include adequate or good judgments across most domains, with the impact of any identified limitation not being judged as severe. Studies were evaluated for their suitability for each outcome investigated and could receive different ratings for each outcome. Descriptions of each of the ratings can be found in the protocol (Section 4) and the key methods supplement. Study evaluations were documented in Health Assessment Workspace Collaborative (HAWC).

Criteria and considerations for reaching the study evaluation ratings were developed *a priori* and are described in the protocol and the key methods supplement. This includes: (a) considerations that apply to all exposures and outcomes, (b) evaluation criteria for phthalate exposure measurement, and c) evaluation criteria for studies of neurodevelopment. The exposure- and outcome- specific considerations are summarized briefly here.

For exposure measurement, most of the available studies relied on phthalate metabolite biomarkers (a list of metabolites for each phthalate is provided in the protocol, Section 1.3). Different criteria were developed for short-chain (DEP, DBP, DIBP, BBP) and long-chain (DEHP, DINP) phthalates due to greater reliability of single biomarker measures for short-chain phthalates. Measurement in urine was considered to be the best proxy of exposure (Johns et al., 2015). Biomarker measures based on samples other than urine (e.g., blood, amniotic fluid, breast milk) were considered to be critically deficient for all short-chain phthalates and for primary metabolites (e.g., MEHP, MINP) of long-chain phthalates (Johns et al., 2015) due to the potential for metabolism of phthalate contaminants in other sample types. This critical deficiency was used as a basis for excluding studies from subsequent analyses. In addition, for timing of exposure measures, because of the short half-lives of phthalates, concurrent measurement of exposure was considered not likely to represent exposure at an etiologically relevant period for this set of outcomes, and thus cross-sectional studies were considered uninformative and excluded.

In the other domains, there were several outcome-specific considerations. These are described in detail in the "Evaluation of Studies of Neurodevelopment" criteria in supplemental materials. For outcome ascertainment, tests used in a study should be appropriate for the age range being studied and to the culture language. Any relevant factors such as time of day, computer use, or sleep, should have been considered in the analysis, and some description of the testing environment provided. If there were multiple raters, there should have been some consideration of this (e.g., adjustment for rater, or analysis of interrater reliability). Studies preferably reported results for subscales as well as summary scales. A combination of parent/teacher/self-rating scales with performance-based tests was preferred, but either was acceptable alone. While blinding to exposure is ideal, this information was not commonly reported and it was considered unlikely that participants or the outcome assessors would have knowledge of exposure levels during testing, and thus not blinding or lack of information on blinding was acceptable. Evaluation of confounding was based on the approach used to identify potential confounders; confounders that were considered potentially relevant included child age and sex, maternal age, socioeconomic status, quality of caregiving environment, prenatal tobacco exposure, marital status of parents, and maternal mental health and IQ. It was considered preferable for analyses to use the outcome scales as continuous variables to minimize misclassification and improve statistical power (Sagiv et al., 2015).

2.4. Evidence synthesis

After study evaluation, the evidence across studies for each outcome was synthesized separately for each phthalate using a structured framework (protocol Section 6 and key methods supplement), using the following aspects of an association that may support causation: consistency, exposure-response relationship, strength of association, temporal relationship, biological plausibility, and coherence (Fig. 1), based on the Bradford Hill considerations. In evaluating the evidence for each of these considerations, syntheses also considered study evaluation

decisions, with high confidence studies carrying the most weight and consideration of specific strengths and limitations of individual studies described where relevant. Low confidence studies were primarily used only to evaluate consistency. Based on the synthesis, the evidence for each phthalate-outcome pair was assigned a strength of evidence conclusion of *Robust, Moderate, Slight, Indeterminate,* or *Compelling evidence of no effect. Robust* and *Moderate* describe evidence that supports a hazard, differentiated by the quantity and quality of information available to rule out alternative explanations for the results. *Slight* and *Indeterminate* describe evidence for which uncertainties prevent drawing a causal conclusion in either direction. These categories are generally limited in terms of quantity or confidence level of studies and indicate a need for additional research across the exposure range experienced by humans. *Compelling evidence of no effect* requires several high confidence studies with consistent null results. This structured framework is conceptually similar to and is informed by the Grading of Recommendations, Assessment, Development and Evaluations (GRADE) approach (Schunemann et al., 2013), but is designed to address the challenges specific to the analysis of environmental health data rather than clinical evidence. In the syntheses in this review, only the considerations that contributed to the determination of strength of evidence are explicitly described, but all considerations were applied to each phthalate-outcome combination.

2.5. Meta-analysis

All phthalate-outcome combinations included in this review were considered for meta-analysis, and those with a sufficient proportion of studies that were similar enough with regards to psychometric tests and analysis techniques were selected. These decisions were made using expert judgment rather than *a priori* criteria. For most outcomes, a variety of different psychometric tests were used in the studies (Table 1), which reduced the ability to directly compare the results, and made meta-analyses for most outcomes inappropriate. For very young children ($\leq$4 years old), most studies used a version of Bayley Scales for Infant Development, and this group of studies was considered similar enough for meta-analysis to be used. For each phthalate, a random-effects model was run separately for cognition (Mental Development Index [MDI]) and motor (Psychomotor Development Index [PDI]) effects using the metafor package in R, on medium and high confidence studies with outcomes measured using Bayley Scales of Infant and Toddler Development (BSID). Analyses were repeated with stratification by sex.

3. Results

The literature flow diagram, depicting the identification and disposition of the literature search records, is shown in Fig. 2. The number of publications does not represent the number of studies as in some cases there are multiple publications from the same cohort. In addition, some publications reported on more than one outcome. A list of all the publications identified in the search that met the PECO criteria (i.e., the 52 articles in the final box) is available in the supplement; for each publication this includes the outcomes examined, the status in the review (included, uninformative based on study evaluation, or not reviewed), the rationale for not including, the study name, and the neurodevelopmental tests used. Outcomes with only 1 or 2 available studies were not reviewed further.

3.1. Study selection and evaluation

Due to temporality issues and/or the exposure measurement issues described in the phthalate measurement criteria, we excluded 18 epidemiology studies (2 on cognition, 11 on behavior including ADHD, and 5 on social behavior) identified in the search with data on neurodevelopment and phthalate exposure (Table 2). This included most studies with postnatal exposure measures. The specific phthalate metabolites and outcomes examined in the remaining 26 papers (17 studies) and the study evaluations are summarized in Table 2. Full rationales for the ratings are available in HAWC (https://hawcprd.epa.gov/summary/visual/100500036/).

With one exception, all the included studies are birth cohorts with follow-up in infancy to childhood (newborns to age 11 years), ranging in sample size between 135 and 657 children. The remaining study was a cohort of children admitted to the pediatric intensive care unit (ICU) and followed at 4 years post-admission (Verstraete et al., 2016). Potential for exposure misclassification was a common limitation because exposure was based on a single urine sample in all but three studies (Braun et al., 2014, Gascon et al., 2015, Yolton et al., 2011). The vast majority of the informative studies measured exposure during gestation. Timing of collection varied among studies but was most common in the 3rd trimester; we did not consider this variability to be a basis for downgrading the confidence in the results. One study (Messerlian et al., 2017) measured exposure in the preconception period and two studies measured exposure in neonates in the NICU (Stroustrup et al., 2018; Verstraete et al., 2016). In summary, four studies were classified as *high confidence*, ten studies were classified as *medium confidence*, and three studies were classified as *low confidence*.

3.2. Study results and synthesis by outcome

When discussing study results, we refer to associations with higher and lower exposure to individual phthalates, acknowledging that urinary phthalate metabolite concentrations are used to assess exposure and that exposure is only estimated.

3.3. Cognition

Evaluation of the association between exposure to DEHP and cognition is based on eleven included studies (twelve papers), with a focus on the ten medium and high confidence studies. Four studies (Kim et al., 2011, Téllez-Rojo et al., 2013, Polanska et al., 2014, Li et al., 2019), including one of the two high confidence studies, reported an inverse association, i.e., decreased cognition with increased DEHP exposure in the results unstratified by sex, with effect estimates (β) of −0.5, −0.8, −1.0, and −1.9 per 1 ln-unit increase in DEHP metabolites. In the two studies with the largest effect estimates (Kim et al., 2011; Li et al., 2019), these results were statistically significant (Table 3). Li et al. (2019) reported different associations based on timing of the exposure measure, and the inverse association was present with exposure measurement at 3 years of age but not during gestation (16 or 26 weeks) or at 1, 2, or 4 years. The remaining studies did not support this inverse association, and the other *high confidence* study (Gascon et al., 2015) reported a positive association at age 4. All the studies that reported inverse associations between DEHP and cognition assessed this domain in children $\leq$3 years old, with the exception of Li et al. (2019). There was no apparent trend of greater association in studies with higher exposure levels or wider range. There was some indication of modification by child sex, but the direction was not consistent across studies. Results in girls drove the inverse association in Téllez-Rojo et al. (2013), while the association was stronger in boys in Kim et al. (2011). The results of the meta-analysis of the MDI from the BSID in children 6 months to 3 years were essentially null (Fig. 3A, β = −0.1; 95% CI = −0.8, 0.5). Looking at the sex-specific meta-analyses, there was an inverse association in girls, but the estimate was imprecise (Table 4). Overall, there are indications of an association in some studies, but given the lack of consistency across the available studies, the evidence for cognition and DEHP exposure is considered *slight*.

Three studies provided data on the association between DINP exposure and cognition (Polanska et al., 2014, Nakiwala et al., 2018; Li et al., 2019). An inverse relationship was observed by Polanska et al. (2014) (β = −0.6 (95% CI = −2.0,0.8) and no association was observed in Nakiwala et al. (2018) or Li et al. (2019). This evidence is

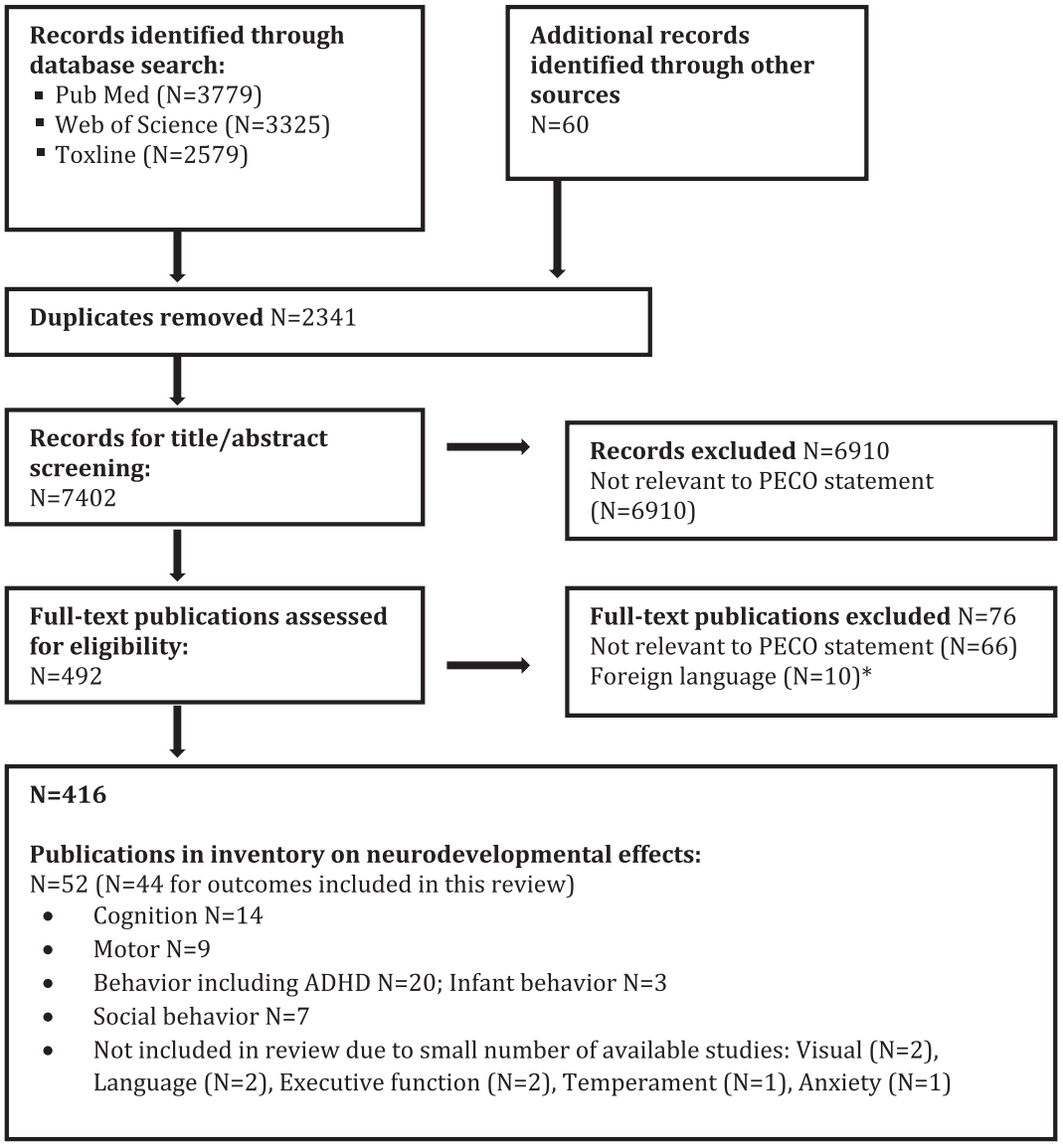

Fig. 2. Literature flow diagram for neurodevelopmental effects of phthalates. *Did not include studies on neuropsychological and behavioral effects.

considered *indeterminate* due to the small amount of available evidence.

Eleven studies reported on the association between DBP exposure and cognition (Table 5). Three studies (Kim et al., 2011, Polanska et al., 2014, Whyatt et al., 2012, Factor-Litvak et al., 2014) reported inverse associations with effect estimates (β) of −0.5, −0.5, −1.1, and −2.7 (statistically significant in Factor-Litvak et al. (2014)). Like DEHP, the association was primarily in children ≤3 years old, but an association was observed in older children in one study (Factor-Litvak et al., 2014). The two high confidence studies (Li et al., 2019; Gascon et al., 2015) reported no association. There is no apparent trend between exposure levels/range and strength of association across studies. There is a suggestion of effect modification by sex, i.e., that girls may be more susceptible to cognitive effects of DBP exposure than boys. Among studies with sex-specific results, girls had stronger associations in most studies (significant associations in girls were observed in two studies, including one (Doherty et al., 2017) in which no association was reported in the non-stratified population. However, there was some inconsistency as a stronger association was observed in boys in one study (Kim et al., 2011) and the association in the high confidence study was in the opposite direction. The results of the meta-analysis of the MDI from the BSID in children 6 months to 3 years were close to null (Fig. 3B, β = −0.2; 95% CI = −0.7, 0.4). Looking at the sex-specific meta-analyses, there was an inverse association in girls, but the estimate was imprecise (Table 4). Overall, given the lack of consistency across studies, the evidence for the association between DBP exposure and cognition is *slight*.

Eight studies reported on the association between DIBP exposure and cognition (Table 6). One medium confidence study (Factor-Litvak et al., 2014) reported an inverse association, which was statistically significant. Some studies had fairly low exposure levels (< 10 ng/mL) compared to other phthalates, which may have reduced sensitivity to observe an effect. However, the studies with the highest exposure levels did not observe an association. As with DBP, there were additional significant results in two of the three studies that examined an interaction with sex, with girls having stronger inverse associations. The results of the meta-analysis of the MDI from the BSID in children 6 months to 3 years were essentially null (Fig. 3C, β = −0.1; 95% CI = −0.6, 0.5). Looking at the sex-specific meta-analyses, there was an imprecise inverse association in girls (Table 4). This evidence is considered *slight*.

Evaluation of the evidence for an association between exposure to BBP and cognition is based on nine studies (Table 7). Four studies (Polanska et al., 2014, Huang et al., 2015, Factor-Litvak et al., 2014, Whyatt et al., 2012, Li et al., 2019) reported inverse associations with

Table 2
Epidemiology studies of neurodevelopmental effects of phthalates.

Study description			Outcomes					Includes metabolites of:						Study evaluation					
Reference(s)	Population	Exposure	Cognition	Motor	Behavior	Infant	Social	DEHP	DINP	DBP	DIBP	BBP	DEP	Exposure	Outcome	Selection	Confound	Analysis	Overall
Braun et al. (2014); Yolton et al. (2011); Li et al. (2019)	Birth cohort (N=389) in U.S.	Two urine samples during gest (16 & 26 wk); additional yearly	C			I		✓		✓	✓	✓	✓	G/A	G	A	G	G	High
Doherty et al. (2017); Mikodovnik et al. (2011); Engel et al. (2010); Engel et al. (2009)	Birth cohort (N=404) in U.S.	Single urine sample (25-40 wk gest)	C	M	B	I	S	✓		✓	✓	✓	✓	A/D	A	A	A	A	Medium
Engel et al. (2018)	Nested case-control (N=802) in birth cohort in Norway	Single urine sample (17 wk gest)			B			✓	✓	✓	✓	✓	✓	A/D	A	A	G	G	Medium
Factor-Litvak et al. (2014); Whyatt et al. (2012); Balalian et al. (2019)	Birth cohort (N=328) in U.S.	Single urine sample (33 wk gest)	C	M	B			✓		✓	✓	✓	✓	A/D	A	A	G	G	Medium
Gascon et al. (2015)	Birth cohort (N=657) in Spain	Two urine samples (12 & 32 wk gest)	C	M	B			✓		✓	✓	✓	✓	G/A	G	G	G	G	High
Huang et al. (2015); Lien et al. (2015)	Birth cohort (N=430) in Taiwan	Single urine sample (28-36 wk gest)	C		B			✓		✓		✓	✓	A/D	A	D	A	G	Medium
Kim et al. (2011)	Birth cohort (N=417) in Korea	Single urine sample (35-41 wk gest)	C	M				✓		✓				A/D	A	A	G	G	Medium
Kim et al. (2017)	Birth cohort (N=175) in Korea	Single urine sample (14-27 wk gest)	C					✓		✓				A/D	A	D	A	A	Medium
Kim et al. (2018)	Birth cohort (N=86) in Korea	Single urine sample (at delivery)	C	M	B		S	✓		✓	✓		✓	D	D	D	A	A	Low
Kobrosly et al. (2014)	Birth cohort (N=153) in U.S.	Single urine sample (10-39 wk gest)			B			✓		✓	✓	✓	✓	A/D	A	A	G	G	Medium
Messerlian et al. (2017)	Preconception cohort (N=166) in U.S.	Multiple urine samples preconception			B			✓		✓	✓	✓	✓	G	A	A	G	G	High
Nakiwala et al. (2018); Philippat et al. (2017)	Birth cohort (N=452 boys) in France	Single urine sample (22-29 wk gest)	C		B			✓	✓	✓	✓	✓	✓	A/D	G	G	G	G	Medium
Polanska et al. (2014)	Birth cohort (N=165) in Poland	Single urine sample (30-34 wk gest)	C	M				✓	✓	✓	✓	✓	✓	A/D	A	A	A	A	Medium
Shin et al. (2018)	Birth cohort (N=201) in U.S.	Multiple samples per trimester					S	✓	✓	✓	✓	✓	✓	G	G	A	G	G	High
Stroustrup et al. (2018)	NICU cohort (N=64) in U.S.	Weekly urine samples in NICU				I		✓						A	G	G	D	A	Low
Téllez-Rojo et al. (2013)	Birth cohort (N=135) in Mexico	Single urine sample (3rd trim)	C	M				✓		✓	✓	✓	✓	A/D	A	A	A	G	Medium
Verstraete et al. (2016)	NICU Cohort (N=549) in Mexico	Multiple plasma samples in NICU		M				✓						D	A	D	D	A	Low
		Total included studies per outcome or phthalate:	11	8	9	3	3	17	4	15	12	12	13						

Excluded
Exposure measured concurrent with outcome - Arbuckle et al. (2016a), Arbuckle et al. (2016b), Cho et al. (2010), Chopra et al. (2014), Hu et al. (2017), Kardas et al. (2015), Kim et al. (2009), Kondolot et al. (2016), Oztop et al. (2018), Park et al. (2014), Park et al. (2015), Testa et al. (2012), Shoaff et al. (2018), Won et al. (2016);
Exposure measurement in blood - Kardas et al. (2015), Minatoya et al. (2016), Minatoya et al. (2018);
Exposure measurement based on type of flooring in home - Larsson et al. (2009);
Exposure measurement based on household dust, which likely does not represent total exposure - Philippat et al. (2015).

C=cognition; M=motor; B=behavior; I=infant behavior; S=social behavior; G=good; A=adequate; D=deficient; G/A=good for short chain phthalates, adequate for long chain phthalates; A/D=adequate for short chain phthalates, deficient for long chain phthalates; wk gest=weeks gestation.
Sample sizes listed may not be accurate for all publications or results reported (the correct sample sizes for individual results are reflected in summary results tables). Studies may have examined additional outcomes not listed in this table (see supplemental file for full list).

C = cognition; M = motor; B = behavior; I = infant behavior; S = social behavior; G = good; A = adequate; D = deficient; G/A = good for short chain phthalates, adequate for long chain phthalates; A/D = adequate for short chain phthalates, deficient for long chain phthalates; wk gest = weeks gestation.
Sample sizes listed may not be accurate for all publications or results reported (the correct sample sizes for individual results are reflected in summary results tables). Studies may have examined additional outcomes not listed in this table (see supplemental file for full list). (See above-mentioned references for further information.)

BBP exposure in the overall populations. The latter study reported statistical significance with exposure measurement at 3 years of age, and a consistent inverse relationship with exposure measurement during gestation (at 16 and 26 weeks) and at 2 years of age; no association was observed with exposure measurement at 1 and 4 years of age. The remaining studies found no association. There was again some indication of modification by child sex, with a stronger indication of an association in girls. The results of the meta-analysis of the MDI from the BSID in children 6 months to 3 years was close to null (Fig. 3D, $\beta = -0.1$; 95% CI $= -0.8, 0.5$). Looking at the sex-specific meta-analyses, there was an inverse association in girls, but the estimate was imprecise (Table 4). Overall, given the lack of consistency, this evidence is considered *slight*.

Nine studies reported on the association between DEP and cognition (Table 8). The two *high confidence* studies (Gascon et al., 2015, Li et al., 2019) reported an inverse association between cognition and DEP exposure. In Li et al. (2019), this association was observed with exposure measurement at 2 and 3 years of age, with the latter being statistically significant, but not with exposure measurement during gestation or at 1 and 4 yrs. The *low confidence* study also reported an inverse association at 1–2 yrs of age. The other studies did not support an association overall. The results of the meta-analysis of the MDI from the BSID in children 6 months to 3 years was null (Fig. 3E, $\beta = 0.3$, 95% CI -0.3, 0.9), as were the sex-specific results (Table 4). There were non-statistically significant associations for girls in one study (Factor-Litvak et al., 2014) and boys in one study (Téllez-Rojo et al., 2013). Because of the lack of association in most studies, even with high exposure levels, this evidence is considered *slight*.

All studies used ln-transformed exposure and βs represent 1 ln-unit increase, except for Gascon, which used log2-transformation and β represent doubling of exposure. Results that support an adverse association are shaded. This represents one or more of the following: $p < 0.05$, $\beta \geq 0.5$, or exposure-response trend across categories of exposure. NR = not reported. GM = geometric mean

*$p < 0.05$

The evidence for cognitive effects is fairly similar across the phthalates in this review. For each phthalate, there are a minority of studies that report inverse associations with cognitive performance, but with considerable inconsistency within each body of evidence that results in low confidence that a causal effect exists. There is no

Table 3
Associations between DEHP metabolites and cognition.

Reference; study confidence; N	Age at outcome measure	Median exposure[a,b]	Exposure IQR (or as specified)	Cognition overall effect estimate β (95% CI)	Cognition in boys β (95% CI)	Cognition in girls β (95% CI)
Included in meta-analysis (age ≤4 yrs, cognition measured using Bayley, medium or high confidence)						
Polanska et al. (2014); medium; 150	2 yr	0.02 nmol/mL	0.3 (95th)	−0.8 (-2.2, 0.6)	NR	NR
Kim et al. (2011); medium; 460	6 mo	8 ng/mL (MEOHP)	3.8–17.1	−1.0 (−1.9, −0.1)*	-1.6 (-2.9,-0.3)*	-0.5 (-1.9,0.9)
Doherty et al. (2017); medium; 258	1-3 yr	0.3 nmol/mL	3.2 (95th)	0.6 (-0.,1.9)	0.1 (-1.5,1.7)	1.8 (-0.1,3.7)
Gascon et al. (2015); high; 367	1 yr	100 μg/g	68–146	0.6 (-1.8,3.1)[c]	0.3 (-3.1,3.7)[c]	0.2 (-3.4,3.7)[c]
	4 yr			2.0 (-0.2,4.2)	2.8 (-0.6,6.2)	1.3 (-1.7,4.3)
Téllez-Rojo et al. (2013); medium; 135	2–3 yr	0.4 nmol/mL (GM)	NR	−0.5 (−2.3, 1.3)	1.5 (-0.8,3.7)	-3.4 (-5.3,-1.6)*
Whyatt et al. (2012); medium; 319	3 yr	19 ng/mL (MEOHP GM)	0.7–1,320 (range)	0.4 (−0.9, 1.6)	1.0 (-1.1,3.1)	-0.2 (-1.9,1.5)
Huang et al. (2015); medium; 251	2-3 yr	59 μg/g (GM)	NR	1.3 (-1.3,3.8)	NR	NR
Not included in meta-analysis						
Kim et al. (2017); medium; 175	6 yr	13 μg/g (MEOHP mean)	NR	3.0 (-2.8,8.7)	NR	NR
Huang et al. (2015); medium; 251	2, 5, 8, and 11 yr	59 μg/g (GM)	NR	−0.1 (−2.2, 2.0)	NR	NR
Nakiwala et al. (2018); medium; 452	5 yr	23 ng/mL (MEOHP)	5.8-87 (5th-95th)	NR	-0.04 (-0.1, 0.06)	NR
Factor-Litvak et al. (2014) (same study as Whyatt et al., 2012)	7 yr	MEHHP		0.2 (−1.2, 1.5)	0.3 (-1.9,2.4)	0.3 (-.14,2.0)
Li et al. (2019); high; 253	5, 8 yr	26 wk gest 87 ng/mL	27-156	0.3 (-1.5,2.1)	NR	NR
		3 yr 94 ng/mL	45-213	-1.9 (-3.7,-0.2)*	NR	NR

[a]Maternal exposure measured during gestation unless otherwise noted.
[b]Results are for summed DEHP metabolites unless specified. All studies used ln-transformed exposure and βs represent 1 ln-unit increase, except for Gascon, which used log2-transformation and β represent doubling of exposure.
[c]Upon request, author provided re-calculated results with ln-transformed exposure and β representing a ln-unit increase, to improve comparability with other studies
One low confidence study (Kim et al., 2018) not shown in table because results were incompletely reported.
Results that support an adverse association are shaded. This represents one or more of the following: $p < 0.05$, $\beta \geq 0.5$, or exposure-response trend across categories of exposure. GM = geometric mean.
*$p < 0.05$.

recognizable pattern of association by study confidence, exposure levels or range, timing of exposure measurement, timing of cognitive assessment, or type of cognitive assessment used. For each phthalate, there is evidence suggestive of stronger associations in girls, but the small number of studies presenting this information hinders interpretation. There are also challenges in assessing coherence across the phthalates and considering whether the phthalates that are most structurally similar and highly correlated in exposure (e.g., DBP and DIBP) have the most similar associations, as exposure levels and thus study sensitivity varies across the phthalates.

3.4. Motor effects

Evaluation of the association between exposure to DEHP and motor effects is based on eight studies (nine publications), with a focus on the six medium and high confidence studies (Table 9). All of these studies examined motor effect in young children (≤4 years), and one study (Balalian et al., 2019, an update of Whyatt et al. (2012)) looked at effects at 11 years. Two medium confidence studies reported an inverse association overall (both sexes combined), with effect estimates (β) of −1.5 and −2.2, the latter of which was statistically significant (Polanska et al. 2014). One low confidence study in children with DEHP exposure in the pediatric intensive care unit (Verstraete et al., 2016) also reported an inverse association. The remaining studies did not support this association. As with cognition, there was some indication of effect modification by child sex, but the direction was not consistent across studies. Results in girls drove the inverse association in Téllez-Rojo et al. (2013), while the association was stronger in boys in Kim et al. (2011). The results of the meta-analysis of the PDI in children 6 months to 3 years indicated a decrease in motor development, but the estimate was imprecise (Fig. 4A, $\beta = -0.4$; 95% CI = −1.4, 0.7). Overall, given the lack of consistency across studies, this evidence is considered *slight*.

Only one study (Polanska et al., 2014) provided results on the association between DINP exposure and motor skills. An inverse

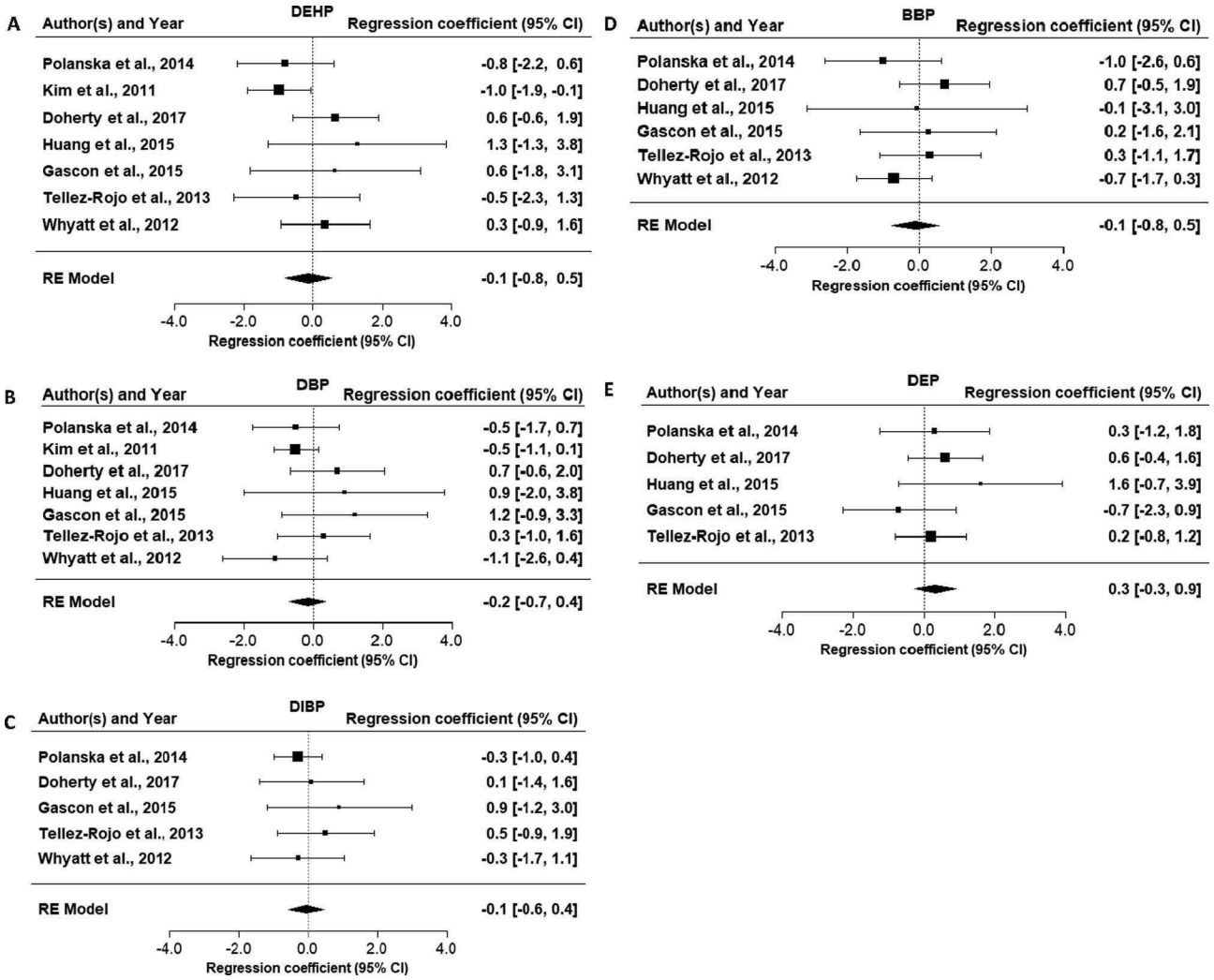

Fig. 3. Forest plots for meta-analysis of phthalate exposure and Bayley Scales of Infant Development Mental Development Index in children ≤ 4 years of age.

Table 4
Sex-specific meta-analysis results for Bayley Scales of Infant Development Mental (MDI) and Psychomotor Development Indices (PDI) in children ≤4 years of age by phthalate.

Phthalate	Girls MDI	Boys MDI	Girls PDI	Boys PDI
DEHP	−0.5 (−2.2, 1.2)	0.1 (−1.2, 1.3)	0.2 (−0.8, 1.3)	0.1 (−1.1, 1.3)
DBP	−0.8 (−2.2, 0.6)	0.4 (−0.8, 1.6)	−0.7 (−1.8, 0.3)	0.0 (−1.7, 1.8)
DIBP	−0.8 (−2.1, 0.6)	0.8 (−0.3, 1.8)	−0.5 (−1.9, 0.9)	−0.1 (−1.4, 1.2)
BBP	−0.7 (−1.6, 0.2)	0.8 (−0.3, 1.9)	−1.6 (−2.6, −0.6)	0.8 (−0.2, 1.9)
DEP	0.3 (−0.8, 1.4)	0.0 (−1.1, 1.2)	0.4 (−0.5, 1.4)	0.4 (−0.5, 1.4)

relationship between cognitive and DINP exposure was observed (β = −1.0 (95% CI = −2.5, 0.5), and without additional studies, this evidence is considered *slight*.

Seven studies (eight publications) reported on the association between DBP exposure and motor skills (Table 10). Three studies (Whyatt et al., 2012, Kim et al., 2011, Polanska et al., 2014) reported decreased in motor skills with higher exposure, with effect estimates (β) of −0.8, −1.2, −2.8 per 1 ln-unit increase in DBP metabolites. Results from one study were statistically significant in 3-year olds (Whyatt et al., 2012) and in an update at 11 years (Balalian et al., 2019). The remaining studies did not support this association. There was again some evidence of effect modification by child sex, but the direction was not consistent across studies. The results of the meta-analysis of the PDI in children 6 months to 3 years were consistent with a decrease in motor development, but the estimate was imprecise (Fig. 4B, β = −0.5; 95% CI = −1.5, 0.5)). Looking at the sex-specific meta-analyses, there was an inverse association in girls, but this estimate was also imprecise (Table 4). Overall, this evidence is considered *slight*.

Evaluation of the association between DIBP exposure and motor effects is based on six studies (seven publications). Three studies (Gascon et al., 2015, Polanska et al., 2014, Whyatt et al., 2012), including the single high confidence study, reported inverse associations with DIBP exposure and motor skills (Table 11). Results from one study were statistically significant in 3 year olds (Whyatt et al., 2012) and 11 year olds (Balalian et al., 2019). Two studies (Doherty et al., 2017, Téllez-Rojo et al., 2013) did not support this association but did have the lowest exposure levels among these studies. Results were generally consistent across the sexes, with the exception of Doherty et al. (2017). The results of the meta-analysis of the PDI in children 6 months to 3 years were consistent with a decrease in motor development, but the

Table 5
Associations between DBP exposure (measured by MBP) and cognition.

Reference; study confidence; N	Age at outcome measure	Median exposure[a]	Exposure IQR (or as specified)	Cognition overall effect estimate β (95% CI)	Cognition in boys β (95% CI)	Cognition in girls β (95% CI)
Included in meta-analysis (age ≤4 yrs, cognition measured using Bayley, medium or high confidence)						
Polanska et al. (2014); medium; 150	2 yr	4 ng/mL	130 (95th)	−0.5 (−1.8, 0.7)	NR	NR
Kim et al. (2011); medium; 460	6 mo	17 ng/mL	5.4–41.1	−0.5 (−1.2, 0.1)	-0.9 (-1.8, -0.05)*	-0.2 (-1.2,0.8)
Gascon et al. (2015); high; 367	1 yr	31 μg/g	20–49	1.2 (-0.9,3.3)[b]	1.5 (-1.6,4.6)[b]	1.4 (-1.5,4.2)[b]
	4 yr			0.8 (-1.1,2.6)[b]	1.7 (-1.4,4.7)[b]	0.4 (-2.0,2.8)[b]
Doherty et al. (2017); medium; 258	1-3 yr	35 ng/mL	202 (95th)	0.7 (-0.7,2.0)	1.7 (0.1,3.3)*	-2.8 (-5.0,-0.5)*
Whyatt et al. (2012); medium, 319		38 ng/mL (GM)	0.2–785 (range)	−1.1 (−2.6, 0.4)	0.3 (-2.0,2.6)	-2.7 (-4.7,-0.7)*
Huang et al. (2015); medium, 251	2-3 yr	78 μg/g (GM)	NR	0.9 (-2.0,3.8)	NR	NR
Téllez-Rojo et al. (2013); medium; 135	2–3 yr	86 ng/mL (GM)	NR	0.3 (−1.0, 1.7)	0.5 (-1.3,2.4)	-0.2 (-2.2,1.8)
Not included in meta-analysis						
Kim et al. (2017); medium; 175	6 yr	30 ng/mL	NR	4.0 (-1.3,9.2)	NR	NR
Factor-Litvak et al. (2014); medium, 328 (same study as Whyatt et al., 2012)	7 yr			−2.7 (−4.3, −1.1)*	-1.9 (-4.3,0.6)	-3.2 (-5.4,-0.9)*
Li et al., 2019; high; 253	5, 8 yr	26 wk gest 23 ng/mL	9-49	0.6 (-0.9,2.2)	NR	NR
		4 yr 22 ng/mL	11-43	2.1 (0.3,3.9)	NR	NR
Nakiwala et al. (2018); medium; 452	5 yr	45 ng/mL	12-444 (5th-95th)	-0.09 (-0.2,0.04)	NR	NR
Huang et al. (2015); medium, 251	2, 5, 8, 11 yr	78 μg/g (GM)		−0.2 (−2.5, 2.1)	NR	NR

[a]Maternal exposure measured during gestation unless otherwise noted.
[b]Upon request, author provided re-calculated results with ln-transformed exposure and β representing a ln-unit increase, to improve comparability with other studies
One low confidence study (Kim et al., 2018) not shown in table because results were incompletely reported.
All studies used ln-transformed exposure and βs represent 1 ln-unit increase, except for Gascon, which used log2-transformation and β represent doubling of exposure.
Results that support an adverse association are shaded. This represents one or more of the following: $p < 0.05$, $\beta \geq 0.5$, or exposure-response trend across categories of exposure. NR = not reported. GM = geometric mean.
*$p < 0.05$.

estimate was imprecise (Fig. 4C, $\beta = -0.4$; 95% CI = −1.1, 0.3)). Looking at the sex-specific meta-analyses, there was an inverse, though imprecise, association in girls (Table 4). Overall, this evidence is considered *slight*.

Evaluation of the evidence for an association between exposure to BBP and motor skills is based on five medium and high confidence studies (Table 12). Four reported inverse associations with BBP exposure in young children, though in one study the inverse association was only in girls (Tellez-Rojo et al., 2013). The inverse effect estimates unstratified by sex were $\beta = -0.4, -0.6, -0.9, -2.2$ and results from the high confidence study were statistically significant (Gascon et al., 2015). The fact that the strongest associations were observed in the high confidence study, which may have had less exposure misclassification due to repeated phthalate measures increases confidence, though this study was also the only one that did not measure motor effects using the BSID instrument, which could also explain differences in results. Since most of the studies performed outcome testing at a similar age (1–4 yrs), it is not clear whether the association persists to older ages, but in one study, the update of Whyatt et al. (2012), there was an inverse association in older children (11 year olds) which was statistically significant in girls (Balaian et al., 2019). Across studies, there was an indication of a stronger association in girls than boys. The results of the meta-analysis of the PDI in children 6 months to 3 years were consistent with a decrease in motor development and approached statistical significance (Fig. 4D, $\beta = -0.7$; 95% CI = −1.4, 0.0). The sex-specific meta-analyses indicated a stronger association among girls (Table 4, $\beta = -1.6$ (95% CI = $-2.6, -0.6$)). Overall, given the consistency in the direction of the association across studies, including in the single high confidence study, and the support of the meta-analysis results, this evidence is considered *moderate* in girls and *slight* in boys.

Five studies reported on the association between DEP and motor skills (Table 13). The one *high confidence* study (Gascon et al., 2015) reported a non-significant inverse association in one-year olds, and a *low confidence* study (Kim et al., 2018) reported a significant association at 6 months. In addition, Balalian et al. (2019) reported an inverse association in 11 year old girls, but not boys. The other studies did not support an association. The results of the meta-analysis of the PDI in children 6 months to 3 years were null (Fig. 4E, $\beta = 0.0$; 95% CI = −0.6, 0.6). Because of the lack of association in most studies, even with high exposure levels, this evidence is considered *indeterminate*.

The evidence of motor effects is stronger than the other outcomes included in this review, though uncertainty still remains. For BBP, the evidence is *moderate* in girls, and a larger proportion of studies for DBP and DIBP indicated an inverse association than in other outcomes, though both of these latter two also had studies that reported positive

Table 6
Associations between DIBP exposure (measured by MIBP) and cognition.

Reference; study confidence; N	Age at outcome measure	Median exposure[a]	Exposure IQR (or as specified)	Cognition overall effect estimate β (95% CI)	Cognition in boys β (95% CI)	Cognition in girls β (95% CI)
Included in meta-analysis (age ≤4 yrs, cognition measured using Bayley, medium or high confidence)						
Téllez-Rojo et al. (2013); medium; 135	2–3 yr	2 ng/mL (GM)		0.5 (−0.9, 1.9)	0.3 (-1.6,2.3)	-0.1 (-1.9,1.7)
Doherty et al. (2017); medium; 258	1-3 yr	6 ng/mL	35 (95th)	0.1 (-1.4,1.6)	1.6 (-0.4,3.5)	-2.3 (-4.3,-0.2)
Whyatt et al. (2012); medium; 319	3 yr	9 ng/mL (GM)	<LOD−374 (range)	−0.3 (−1.6, 1.1)	0.6 (-1.4,2.6)	-1.3 (-3.2,0.5)
Polanska et al. (2014); medium; 150	2 yr	10 ng/mL	359 (95th)	−0.3 (−1.0, 0.4)	NR	NR
Gascon et al. (2015); high; 367	1 yr	32 μg/g	22–48	0.9 (-1.2,3.0)[b]	0.4 (-2.4,3.2)[b]	1.4 (-1.5,4.2)[b]
	4 yr			1.1 (-0.8,3.0)[b]	2.7 (-0.04,5.4)[b]	-0.4 (-3.1,2.4)[b]
Not included in meta-analysis						
Li et al. (2019), high, 253	5, 8 yr	26 wk gest 4 ng/mL	2-11	1.4 (-0.3,3.1)	NR	NR
		4 yr 11 ng/mL	5-23	1.8 (0.0,3.6)	NR	NR
Factor-Litvak et al. (2014); medium; 328 (same study as Whyatt et al., 2012)	7 yr			−2.7 (−4.2, 1.2)*	-2.9 (-5.2,-0.7)*	-2.4 (-4.5,-0.26)*
Nakiwala et al. (2018); medium; 452	5 yr	39 ng/mL	12-168 (5th-95th)	0.05 (-0.05,0.2)	NR	NR

[a]Maternal exposure measured during gestation unless otherwise noted.
[b]Upon request, author provided re-calculated results with ln-transformed exposure and β representing a ln-unit increase, to improve comparability with other studies.
One low confidence study (Kim et al., 2018) not shown in table because results were incompletely reported.
All studies used ln-transformed exposure and βs represent 1 ln-unit increase, except for Gascon, which used log2-transformation and β represent doubling of exposure.
Results that support an adverse association are shaded. This represents one or more of the following: $p < 0.05$, $\beta \geq 0.5$, or exposure-response trend across categories of exposure. NR = not reported. GM = geometric mean
*$p < 0.05$

Table 7
Associations between BBP exposure (measured by MBzP) and cognition.

Reference; Study confidence, N	Age at outcome measure	Median exposure[a]	Exposure IQR (or as specified)	Cognition overall effect estimate β (95% CI)	Cognition in boys β (95% CI)	Cognition in girls β (95% CI)
Included in meta-analysis (age ≤4 yrs, cognition measured using Bayley, medium or high confidence)						
Polanska et al. (2014); medium; 150	2 yr	0.03 ng/mL	0.5 (95th)	−1.0 (−2.6, 0.6)	NR	NR
Téllez-Rojo et al. (2013); medium; 135	2–3 yr	3.5 ng/mL (GM)		0.3 (−1.1, 1.7)	1.3 (-0.4,3.0)	-0.7 (-2.5,1.0)
Gascon et al. (2015); high; 367	1 yr	12 μg/g	7–20	0.3 (-1.7,2.1)[b]	0.4 (-2.1,2.8)[b]	1.0 (-1.9,4.0)[b]
	4 yr			0.5 (-1.3,2.2)[b]	1.1 (-1.3,3.5)[b]	-0.5 (-3.1,2.1)[b]
Doherty et al. (2017); medium; 258	1-3 yr	15 ng/mL	124 (95th)	0.7 (-0.5,2.0)	1.8 (0.1,3.6)	-0.6 (-2.3,1.1)
Huang et al. (2015); medium; 251	2-3 yr	17 μg/g (GM)		0.2 (-3.8,3.6)	NR	NR
Whyatt et al. (2012); medium; 319	3 yr	19 ng/mL (GM)	<LOD−1,110 (range)	−0.7 (−1.8, 0.3)	-0.5 (-2.2,1.3)	-1.1 (-2.5,0.3)
Not included in meta-analysis						
Li et al. (2019); high; 253	5, 8 yr	26 wk gest 8 ng/mL	3-23	-0.5 (-2.2, 1.2)	NR	NR
		3 yr 17 ng/mL	5-42	-2.5 (-4.4, -0.5)*	NR	NR
Huang et al. (2015); medium; 251	2, 5, 8, 11 yr	17 μg/g (GM)		−0.06 (−3.1, 3.0)	NR	NR
Factor-Litvak et al. (2014); medium; 328 (same study as Whyatt et al., 2012)	7 yr			−1.2 (−2.4, 0.1)	-1.5 (-3.4,0.4)	-0.8 (-2.5,0.8)
Nakiwala et al. (2018); medium; 452	5 yr	19 ng/mL	5-114 (5th-95th)	0.02 (-0.1,0.1)	NR	NR

[a]Maternal exposure measured during gestation unless otherwise noted.
[b]Upon request, author provided re-calculated results with ln-transformed exposure and β representing a ln-unit increase, to improve comparability with other studies

Table 8
Associations between DEP exposure (measured by MEP) and cognition.

Reference; Study confidence, N	Age at outcome measure	Median exposure[a]	Exposure IQR (or as specified)	Cognition overall effect estimate β (95% CI)	Cognition in boys β (95% CI)	Cognition in girls β (95% CI)
Included in meta-analysis (age ≤4 yrs, cognition measured using Bayley, medium or high confidence)						
Polanska et al. (2014); medium; 150	2 yr	19 ng/mL	336 (95th)	0.3 (−1.3, 1.8)	NR	NR
Huang et al. (2015); medium; 251	2-3 yr	67 μg/g (GM)		-0.3 (-2.4,1.8)	NR	NR
Téllez-Rojo et al. (2013); medium; 135	2–3 yr	138 ng/mL (GM)		0.2 (−0.8, 1.2)	-0.6 (-2.3,1.0)	1.1 (-0.1,2.2)
Doherty et al. (2017); medium; 258	1-3 yr	172 ng/mL	3372 (95th)	0.6 (-0.5,1.6)	1.0 (-0.5,2.4)	-0.1 (-1.7,1.5)
Gascon et al. (2015); high; 367	1 yr	403 μg/g	199–756	-0.7 (-2.3,0.9)[b]	-0.7 (-2.9,1.4)[b]	-0.8 (-3.0,1.4)[b]
	4 yr			1.0 (-0.4,2.4)[b]	2.1 (-0.01,4.2)[b]	-0.2 (-2.2,1.8)[b]
Not included in meta-analysis						
Huang et al. (2015); medium; 251	2, 5, 8, and 11 yr	67 μg/g (GM)		1.6 (−0.7, 3.9)	NR	NR
Nakiwala et al. (2018); medium; 452	5 yr	100 ng/mL	22-591 (5th-95th)	-0.06 (-0.2,0.04)	NR	NR
Li et al. (2019); high; 253	5, 8 yr	26 wk gest 114 ng/mL	36-319	0.3 (-1.3,1.9)	NR	NR
		3 yr 40 ng/mL	16-83	-2.1 (-3.6,-0.6)*	NR	NR
Factor-Litvak et al. (2014); medium; 328	7 yr	142 ng/mL	70-334	-0.2 (-1.5,1.1)	0.4 (-1.5,2.3)	-0.8 (-2.5,1.0)

[a]Maternal exposure measured during gestation unless otherwise noted.
[b]Upon request, author provided re-calculated results with ln-transformed exposure and β representing a ln-unit increase, to improve comparability with other studies.
One low confidence study (Kim et al., 2018) not shown in table because results were incompletely reported.
All studies used ln-transformed exposure and βs represent 1 ln-unit increase, except for Gascon, which used log2-transformation and β represent doubling of exposure.
Results that support an adverse association are shaded. Thi represents one or more of the following: $p < 0.05$, $\beta \geq 0.5$, or exposure-response trend across categories of exposure. NR = not reported. GM = geometric mean.
*$p < 0.05$.

Table 9
Associations between summed DEHP metabolites and motor effects.

Reference; study confidence; N	Age at outcome measure	Median maternal exposure	Exposure IQR (or as specified)	Motor overall effect estimate β (95% CI)	Motor in boys β (95% CI)	Motor in girls β (95% CI)
Polanska et al. (2014); medium; 150	2 yr	0.02 nmol/mL	0.3 (95th)	−2.2 (−3.6, −0.8)*	NR	NR
Kim et al. (2011); medium; 460	6 mo	8 ng/mL (MEOHP), 10.1 (MEHHP)	3.8–17.1, 4.3–21.4	−1.5 (−3.0, 0.1)	-2.3 (-3.9,-0.6)*	-0.2 (-1.9,1.6)
Doherty et al. (2017); medium; 258		0.3 nmol/mL	3.2 (95th)	0.2 (-1.0,1.4)	0.2 (-1.3,1.8)	0.3 (-1.7,2.2)
Gascon et al. (2015); high; 367	1 yr	100 μg/g	68–146	0.5 (-2.2,3.2)^	0.5 (-3.4,4.4)^	0.5 (-3.4,4.4)^
	4 yr			0.4 (-2.1,2.8)^	0.9 (-3.0,4.8)^	0.02 (-3.1,3.1)^
Téllez-Rojo et al. (2013); medium; 135	2–3 yr	0.4 nmol/mL (GM)	NR	0.01 (−1.5, 1.5)	1.1 (-0.7,2.8)	-1.2 (-3.9,1.5)
Whyatt et al. (2012); medium; 319; **Balalian et al. (2019)**; 209	3 yr	265 ng/mL	137-578	1.3 (−0.3, 2.9)	0.7 (-1.4,2.7)	2.3 (-0.2,4.9)
	11 yr			NR	-0.3 (-1.9,1.3)	-0.2 (-1.3,0.9)

Two low confidence studies (Kim et al., 2018, Verstraete et al., 2016) not shown in table because results were incompletely reported (Kim et al., 2018) or were not summary estimates comparable to the other studies (Verstraete et al., 2016).
All studies used ln-transformed exposure and βs represent 1 ln-unit increase, except for Gascon, which used log2-transformation and β represent doubling of exposure.
Results that support an adverse association are shaded. This represents one or more of the following: $p < 0.05$, $\beta \geq 0.5$, or exposure-response trend across categories of exposure. NR = not reported. GM = geometric mean.
*$p < 0.05$.
^Upon request, author provided re-calculated results with ln-transformed exposure and β representing a ln-unit increase, to improve comparability with other studies.

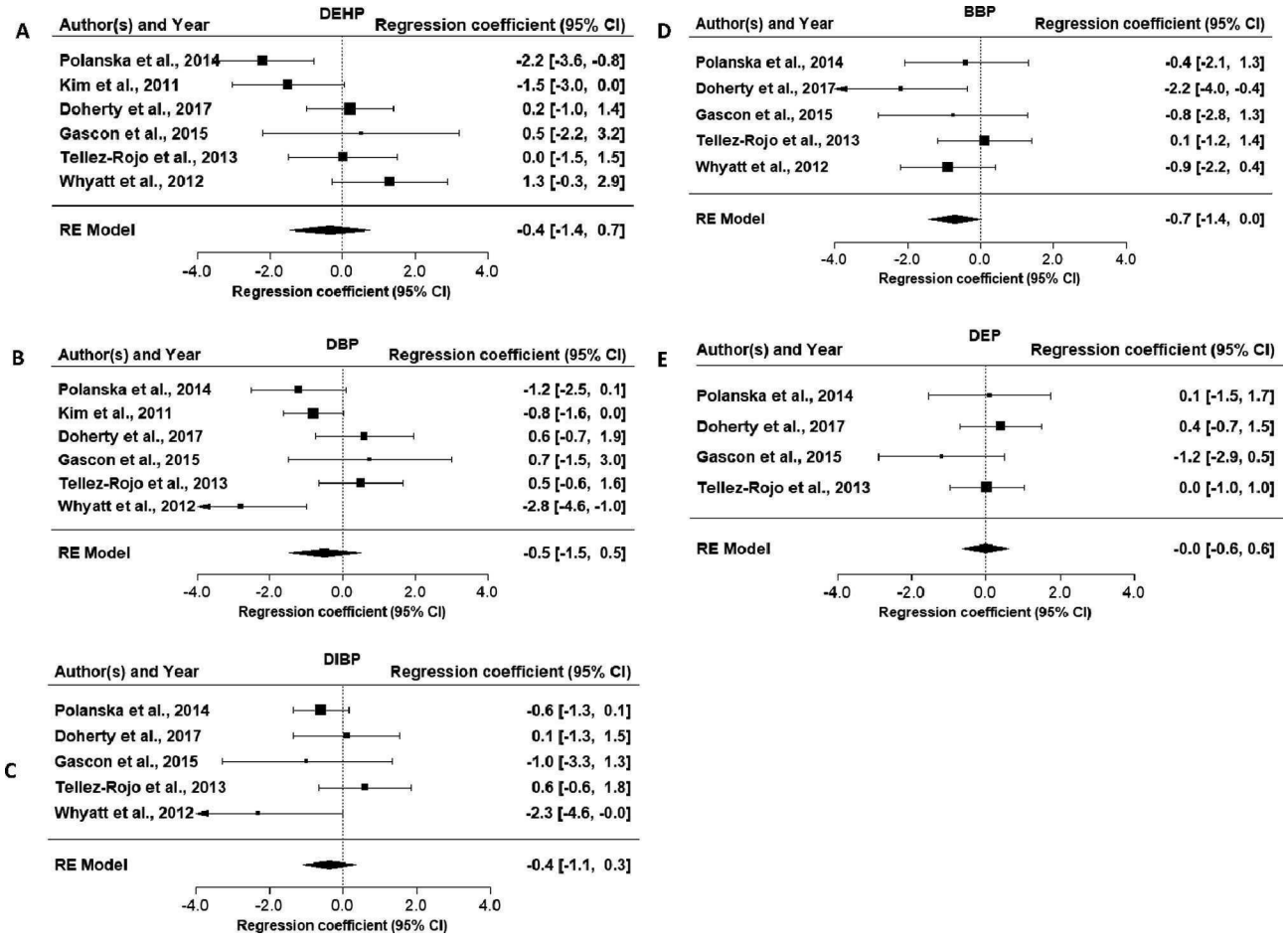

Fig. 4. Forest plots for meta-analyses of phthalate exposure and Bayley Scales of Infant Development Psychomotor Development Index in children ≤ 4 years of age.

Table 10
Associations between DBP exposure (measured by MBP) and motor effects.

Reference; study confidence; N	Age at outcome measure	Median maternal exposure	Exposure IQR (or as specified)	Motor overall effect estimate β (95% CI)	Motor in boys β (95% CI)	Motor in girls β (95% CI)
Polanska et al. (2014); medium; 150	2 yr	4 ng/mL	130 (95th)	−1.2 (−2.5, 0.1)	NR	NR
Kim et al. (2011); medium; 460	6 mo	17 ng/mL	5.4–41.1	−0.8 (−1.6, 0.03)	-1.3 (-2.4,-0.1)	-0.4 (-1.6,0.8)
Gascon et al. (2015); high; 367	1 yr	31 μg/g	20–49	0.7 (-1.5,3.0)^	1.8 (-1.7,5.3)^	0.6 (-2.6,3.7)^
	4 yr			-0.4 (-2.4,1.6)^	0.2 (-3.3,3.6)^	0.2 (-2.3,2.6)^
Doherty et al. (2017); medium; 258	1-3 yr	35 ng/mL	202 (95th)	0.6 (-0.8,1.9)	1.9 (0.3,3.5)	-2.3 (-4.6,0.1)
Whyatt et al. (2012); medium; 319; **Balalian et al. (2019)**; 209	3 yr	37 ng/mL	19-75	−2.8 (−4.6, −1.0)*	-3.1 (-5.8,-0.3)*	-2.4 (-4.9,0.1)
	11 yr			NR	-0.6 (-2.0,0.7)	-2.1 (-3.4,-0.8)*
Téllez-Rojo et al. (2013); medium; 135	2–3 yr	86 ng/mL (GM)	NR	0.5 (−0.7, 1.6)	0.9 (-0.5,2.3)	0.5 (-1.7,2.7)

One low confidence study (Kim et al., 2018) not shown in table because results were incompletely reported.
All studies used ln-transformed exposure and βs represent 1 ln-unit increase, except for Gascon, which used log2-transformation and β represent doubling of exposure.
Results that support an adverse association are shaded. This represents one or more of the following: $p < 0.05$, $\beta \geq 0.5$, or exposure-response trend across categories of exposure. NR = not reported. GM = geometric mean.
*$p < 0.05$.
^Upon request, author provided re-calculated results with ln-transformed exposure and β representing a ln-unit increase, to improve comparability with other studies.

Table 11
Associations between DIBP exposure (measured by MIBP) and motor effects.

Reference; study confidence; N	Age at outcome measure	Median maternal exposure	Exposure IQR (or as specified)	Motor overall effect estimate β (95% CI)	Motor in boys β (95% CI)	Motor in girls β (95% CI)
Téllez-Rojo et al. (2013); medium; 135	2–3 yr	2 ng/mL (GM)	NR	0.6 (-0.7, 1.8)	0.6 (-0.7,2.0)	0.4 (-1.7,2.4)
Doherty et al. (2017); medium; 258	1-3 yr	6 ng/mL	35 (95th)	0.1 (-1.3,1.6)	0.7 (-1.2,2.6)	-0.7 (-2.9,1.6)
Whyatt et al. (2012); medium; 319	3 yr	8 ng/mL	4-16	−2.3 (−3.9, 0.7)*	-2.2 (-4.6,0.2)	-2.3 (-4.6, -0.1)*
Balalian et al. (2019); 209	11 yr			NR	-0.6 (-1.9,0.8)	-1.4 (-2.5,-0.2)*
Polanska et al. (2014); medium; 150	2 yr	10 ng/mL	359 (95th)	−0.6 (−1.3, 0.2)	NR	NR
Gascon et al. (2015); high; 367	1 yr	32 μg/g	22–48	-1.0 (-3.3,1.3)^	-0.8 (-3.9,2.4)^	-0.9 (-4.4,2.7)^
	4 yr			-2.0 (-4.1,0.1)^	-2.0 (-5.1,1.1)^	-1.8 (-4.6,1.0)^

One low confidence study (Kim et al., 2018) not shown in table because results were incompletely reported.
All studies used ln-transformed exposure and βs represent 1 ln-unit increase, except for Gascon, which used log2-transformation and β represent doubling of exposure.
Results that support an adverse association are shaded. This represents one or more of the following: $p < 0.05$, $\beta \geq 0.5$, or exposure-response trend across categories of exposure. Light grey represents other supportive results. NR = not reported.
*$p < 0.05$.
^Upon request, author provided re-calculated results with ln-transformed exposure and β representing a ln-unit increase, to improve comparability with other studies.

(though non-significant) associations. These three phthalates, particularly DBP and DIBP are the most similar structurally and in exposure sources among the phthalates in this review, which increases confidence in the causal association due to coherence across the correlated exposures, though there is remaining potential for confounding across the phthalates that can't be ruled out with the current evidence. Evidence for DEHP, DINP, and DEP is less compelling. For all of the examined phthalates, outside of what was discussed for BBP above, there are no clear patterns of association by study confidence, exposure levels or range, timing of exposure measurement, timing of cognitive assessment, or type of cognitive assessment used. As with cognition, there is evidence suggestive of stronger associations in girls, but additional evidence is needed.

3.5. Behavior

Studies that examined the association between phthalate exposure and behavior generally assessed multiple dimensions of behavior. This included summary scales (i.e., global behavior score, internalizing behaviors, and externalizing behaviors) and clinical scales (e.g., hyperactivity, aggression, anxiety, etc.). This review focused on the summary scales of internalizing and externalizing behavior because they were the most consistently reported across studies. In addition, one prospective study of ADHD was reviewed (Engel et al., 2018).

Nine studies reported on the association between DEHP exposure and behavior, and eight medium to high confidence studies are presented in Table 14. One reported an association between higher

Table 12
Associations between BBP exposure (measured by MBzP) and motor skills.

Reference; Study confidence, N	Age at outcome measure	Median maternal exposure	Exposure IQR (or as specified)	Motor overall effect estimate β (95% CI)	Motor in boys β (95% CI)	Motor in girls β (95% CI)
Polanska et al. (2014); medium; 150	2 yr	0.03 ng/mL	0.5 (95th)	−0.4 (−2.1, 1.3)	NR	NR
Téllez-Rojo et al. (2013); medium; 135	2–3 yr	4 ng/mL (GM)	NR	0.1 (−1.2, 1.4)	1.8 (0.1,3.5)*	-1.2 (-3.3,0.9)
Gascon et al. (2015); high; 367	1 yr	12 μg/g	7–20	-0.8 (-2.8,1.3)^	1.3 (-1.5,4.2)^	-2.8 (-6.0,0.5)^
	4 yr			-2.2 (-4.0,-0.3)^*	-1.4 (-4.2,1.3)^	-2.8 (-5.4,-0.2)^*
Whyatt et al. (2012); medium; 319	3 yr	13 ng/mL	5-27	-0.9 (-2.2,0.4)	-0.6 (-2.7,1.6)	-1.1 (-2.8,0.7)
Balalian et al. (2019); 209	11 yr			NR	-0.9 (-1.8,0.1)	-1.1 (-2.1,-0.1)*
Doherty et al. (2017); medium; 258	1-3 yr	15 ng/mL	124 (95th)	-0.6 (-1.8,0.6)	0.6 (-1.2,2.3)	-2.1 (-3.8,-0.4)

All studies used ln-transformed exposure and βs represent 1 ln-unit increase, except for Gascon, which used log2-transformation and β represent doubling of exposure. Results that support an adverse association are shaded. This represents one or more of the following: $p < 0.05$, $\beta \geq 0.5$, or exposure-response trend across categories of exposure. NR = not reported. GM = geometric mean.
*$p < 0.05$.
^Upon request, author provided re-calculated results with ln-transformed exposure and β representing a ln-unit increase, to improve comparability with other studies.

Table 13
Associations between DEP exposure (measured by MEP) and motor skills.

Reference; Study confidence, N	Age at outcome measure	Median maternal exposure	Exposure IQR (or as specified)	Motor overall effect estimate β (95% CI)	Motor in boys β (95% CI)	Motor in girls β (95% CI)
Polanska et al. (2014); medium; 150	2 yr	19 ng/mL	336 (95th)	0.1 (−1.5, 1.8)	NR	NR
Balalian et al., 2019; medium; 209	11 yr	131 ng/mL	67-302	NR	0.5 (-0.5,1.5)	-1.2 (-2.4,-0.1)*
Téllez-Rojo et al. (2013); medium; 135	2–3 yr	138 ng/mL (GM)	NR	0.02 (−1.0, 1.0)	0.1 (-1.3,1.5)	0.3 (-1.1,1.7)
Doherty et al. (2017); medium; 258	1-3 yr	172 ng/mL	3372 (95th)	0.4 (-0.7,1.5)	0.2 (-1.3,1.6)	0.6 (-1.1,2.3)
Gascon et al. (2015); high; 367	1 yr	403 μg/g	199–756	-1.2 (-2.8,0.6)^	-1.2 (-3.7,1.2)^	-0.2 (-3.6,1.3)^
	4 yr			0.6 (-1.0,2.1)^	2.0 (-0.4,4.4)^	0.5 (-1.8,2.7)^

One low confidence study (Kim et al., 2018) not shown in table because results were incompletely reported.
All studies used ln-transformed exposure and βs represent 1 ln-unit increase, except for Gascon, which used log2-transformation and β represent doubling of exposure.
Results that support an adverse association are shaded. This represents one or more of the following: $p < 0.05$, $\beta \geq 0.5$, or exposure-response trend across categories of exposure. NR = not reported. GM = geometric mean.
*$p < 0.05$.
^Upon request, author provided re-calculated results with ln-transformed exposure and β representing a ln-unit increase, to improve comparability with other studies.

exposure to DEHP and more frequent internalizing and externalizing problems (Lien et al., 2015), but other studies reported no association or, in the study based on preconception exposure, an inverse association (Messerlian et al., 2017). This different exposure window may contribute to the apparent inconsistency. The single medium confidence study of ADHD diagnosis (Engel et al., 2018) reported a significant association between summed DEHP metabolites and ADHD (OR: 1.5, 95% CI 1.1, 1.9), with an exposure-response gradient observed across quintiles of exposure. Based on these latter results, the evidence is considered *slight*; however, there is considerable uncertainty due to inconsistency and lack of association in high confidence studies and lack of additional studies on ADHD diagnosis.

One study examined DINP exposure and behavior in boys (Philippat et al., 2017), and reported no association, and the study of ADHD (Engel et al., 2018) reported no higher odds of ADHD with higher exposure. This evidence is considered *indeterminate*.

Table 14
Associations between DEHP metabolites and behavior.

Reference; study confidence, N	Age at outcome measure	Median maternal exposure	Exposure IQR (or as specified)	Internalizing problems overall β (95% CI)	Externalizing problems overall β (95% CI)	Internalizing problems in boys β (95% CI)	Internalizing problems in girls β (95% CI)	Externalizing problems in boys β (95% CI)	Externalizing problems in girls β (95% CI)
Exposure measured during gestation									
Kobrosly et al. (2014); medium; 153	6–10 yr	12 ng/mL (MEOHP), 13 (MEHHP)(GM)	5–22, 6–24	-0.02 (-0.2,0.1)	-0.04 (-0.2,0.1)	-0.1 (-0.1,0.3)	-0.1 (-0.3,0.1)	0 (-0.2,0.2)	-0.1 (-0.3,0.1)
Gascon et al. (2015); high; 362	7 yr	100 μg/g	68–146	Emotional symptoms RR 1.0 (0.8,1.1)	Conduct problems RR 1.0 (0.8,1.1)	NR	NR	NR	NR
Whyatt et al. (2012); medium; 297	3 yr	19 ng/mL (MEOHP), 40 (MEHHP)(GM)	0.7–1,320, 3–1,840 (ranges)	0.1 (−0.8, 1.0)	"No association"	0.2 (-1.2,1.6)	0.1 (-1.0,1.3)	NR	NR
Lien et al. (2015); medium; 122	8 yr	39 μg/g		1.8 (−0.4, 3.9)	4.38 (2.07, 6.69)*	1.3 (-1.5,4.1)	0.7 (-2.9,4.4)	3.7 (0.1,7.4)*	3.7 (0.4,7.0)*
Philippat et al. (2017); medium; 546	3 yr	0.3 μM/L	0.2-0.4 (33rd-66th)	NR	NR	IRR 1.0 (1.0,1.1)	NR	IRR 1.0 (1.0,1.0)	NR
	5 yr					1.0 (1.0,1.1)		1.0 (1.0,1.1)	
Engel et al. (2010); medium; 188	4–9 yr	0.4 μM/L	0.2–0.9	"No association"	"No association"	NR	NR	NR	NR
Exposure measured preconception									
Messerlian et al. (2017); high; 166	2-9 yr	Preconception Maternal 63 ng/mL	32-99	-2.0 (-3.2,-0.8)*	0.3 (-1.0,1.7)	-5.0 (-9.3,-0.6)*	-2.2 (-3.7,-0.8)*	-0.7 (-2.8,1.3)	0.2 (-1.1,1.5)
		Paternal 93 ng/mL	49-177	-1.8 (-3.1,-0.4)*	-0.4 (-1.7,0.8)	-3.1 (-5.9,-0.4)*	-1.6 (-3.1,-0.03)*	0.2 (-1.5,1.8)	-0.5 (-1.7,0.6)
Attention-deficient hyperactivity disorder (ADHD), exposure measured during gestation									
Engel et al. (2018); medium; 802	n/a	0.2 μM/L	0.2-0.3		OR 1.5 (1.1,1.9)			OR 1.4 (1.0,2.0)	OR 1.6 (1.0,2.6)

One low confidence study (Kim et al., 2018) not shown in table because results were incompletely reported.
All studies used ln-transformed exposure and βs represent 1 ln-unit increase, except for Gascon et al. (2015), which used log2-transformation and β represent doubling of exposure and Philippat et al. (2017) which calculated incidence rate ratios (IRR) for a 1 unit change in test scores for a doubling of exposure. Results that support an adverse association are shaded. This represents one or more of the following: $p < 0.05$, $\beta \geq 0.5$, OR ≥ 0.5, or exposure-response trend across categories of exposure. NR = not reported, GM = geometric mean.
*$p < 0.05$.
^Upon request, author provided re-calculated results with ln-transformed exposure and β representing a ln-unit increase, to improve comparability with other studies.

Table 15
Associations between DBP exposure (measured by MBP) and behavior.

Reference; study confidence, N	Age at outcome measure	Median maternal exposure	Exposure IQR (or as specified)	Internalizing problems overall β (95% CI)	Externalizing problems overall β (95% CI)	Internalizing problems in boys β (95% CI)	Internalizing problems in girls β (95% CI)	Externalizing problems in boys β (95% CI)	Externalizing problems in girls β (95% CI)
Exposure measured during gestation									
Kobrosly et al. (2014); medium; 153	6–10 yr	14 ng/mL (GM)	8–29	-0.1 (-0.3,0.2)	0.1 (-0.2,0.3)	-0.01 (-0.3,0.3)	-0.2 (-0.50.1)	0.2 (-0.1,0.5)	-0.02 (-0.3,0.3)
Gascon et al. (2015); high; 362	7 yr	31 μg/g	20–49	Emotional symptoms RR 0.9 (0.8,1.1)	Conduct problems RR 0.9 (0.8,1.0)	NR	NR	NR	NR
Whyatt et al. (2012); medium; 297	3 yr	38.0 ng/mL (GM)	0.2–785 (range)	1.5 (0.4, 2.5)*	"No association"	2.2 (0.7,3.8)*	1.3 (-0.2,2.7)	NR	NR
Philippat et al. (2017); medium; 546	3 yr	44 ng/mL	33-57 (33rd-66th)	NR	NR	IRR 1.1 (1.0,1.1)*	NR	IRR 1.0 (1.0,1.0)	NR
	5 yr					1.0 (1.0,1.1)		1.0 (1.0,1.1)	
Lien et al. (2015); medium; 122	8 yr	109 μg/g (mean)		2.2 (−1.2, 5.5)	4.3 (0.6, 8)*	0.1 (-5.1,5.3)	3.0 (-1.8,7.8)	-2.5 (-9.5,4.5)	7.6 (3.5,11.8)*
Engel et al. (2010); medium; 188	4–9 yr	0.2 μM/L (from Engel et al., 2009)	0.1–0.3	0.7	1.4*	NR	NR	NR	NR
Exposure measured preconception									
Messerlian et al. (2017); high; 166	2-9 yr	Preconception Maternal 12 ng/mL	7-17	-0.4 (-2.1,1.2)	0.5 (-1.0,2.0)	0.9 (-1.3, 3.1)	-0.8 (-2.4, 0.9)	0.7 (-1.3,2.7)	0.5 (-1.0,2.0)
		Paternal 12 ng/mL	8-19	-0.9 (-2.9,1.1)	-1.2 (-2.5,0.1	2.1 (-1.3,5.4)	-4.5 (-8.0,-1.0)*	-1.4 (-2.8,0.0)*	-1.0 (-2.6,0.6)
Attention-deficient hyperactivity disorder (ADHD), exposure measured during gestation									
Engel et al. (2018); medium; 802	n/a	17 ng/mL	11-31		OR 1.0 (0.8,1.4)			OR 1.0 (0.7,1.3)	OR 1.3 (0.8,2.2)

One low confidence study (Kim et al., 2018) not shown in table because results were incompletely reported.
All studies used ln-transformed exposure and βs represent 1 ln-unit increase, except for Gascon et al. (2015), which used log2-transformation and β represent doubling of exposure and Philippat et al. (2017) which calculated incidence rate ratios (IRR) for a 1 unit change in test scores for a doubling of exposure. Results that support an adverse association are shaded. This represents one or more of the following: $p < 0.05$, $\beta \geq 0.5$, or exposure-response trend across categories of exposure. NR = not reported; GM = geometric mean.
*$p < 0.05$.
ˆUpon request, author provided re-calculated results with ln-transformed exposure and β representing a ln-unit increase, to improve comparability with other studies.

Nine studies examined the association between exposure to DBP and behavior (Table 15). Three studies (Whyatt et al., 2012, Lien et al., 2015, Philippat et al., 2017) reported an association between higher exposure and more frequent internalizing problems, with statistical significance reported in Whyatt et al. (2012) and Philippat et al. (2017). Two studies (Engel et al., 2010, Lien et al., 2015) reported statistically significant results for externalizing problems. The other studies reported no association or, in the study examining preconception exposure, an inverse association (Messerlian et al., 2017). The medium confidence study of ADHD diagnosis also reported no association (Engel et al., 2018). Overall, given the lack of consistency and the lack of positive association in the *high confidence* study (Gascon et al., 2015), the evidence is considered *slight*.

Evaluation of the association between exposure to DIBP and behavior is based on eight studies (Table 16). One study reported an association between higher exposure to DIBP and increased internalizing problems (Whyatt et al., 2012). There were also sex-specific associations for internalizing problems in boys in two studies (Whyatt et al., 2012, Messerlian et al., 2017) and for externalizing problems in boys in one study (Kobrosly et al., 2014). The remaining studies reported no association or, in the study examining preconception exposure, an inverse association (Messerlian et al., 2017), but two of the studies did not report sex-specific associations, so the ability to assess consistency for these effects was limited. The medium confidence study of ADHD diagnosis also reported no association (Engel et al., 2018). This evidence is considered *indeterminate*.

Evaluation of the association between exposure to BBP and behavior is based on seven studies (Table 17). Three studies reported positive associations between higher exposure to BBP and internalizing problems (Whyatt et al., 2012, Gascon et al., 2015, Philippat et al., 2017), and two were statistically significant, though only in 3 year olds for Philippat et al. (2017). One study (Lien et al., 2015) reported a positive association with externalizing problems in girls only, and two studies (Whyatt et al., 2012, Messerlian et al., 2017) reported a positive association with externalizing problems in boys only. One study (Lien et al., 2015) reported a strong inverse association, and the remaining study reported no association (Kobrosly et al., 2014). The single study of ADHD diagnosis (Engel et al., 2018) reported non-significantly higher odds of ADHD with higher exposure (OR: 1.2, 95% CI 0.9, 1.6). Given the lack of consistency within the specific behavior domains and sexes, this evidence is considered *slight*.

Eight studies reported on the association between DEP and behavior (Table 18). One study reported a statistically significant association between higher exposure to DEP and increased externalizing problems (Engel et al., 2010). The remaining studies reported no association or inverse associations (Messerlian et al., 2017, Lien et al., 2015), with Messerlian et al. (2017) examining preconception exposure. The medium confidence study of ADHD diagnosis also reported no association (Engel et al., 2018). This evidence is considered *indeterminate*.

The evidence of behavioral effects of phthalate exposure is largely null. Few studies reported associations between higher exposure and more frequent internalizing or externalizing behaviors. No clear patterns for the observed associations were identified. Across the phthalates, there was some indication that studies using the Child Behavior Checklist (Whyatt et al., 2012, Kobrosly et al., 2014, Lien et al., 2015) were more likely to observe an inverse association, but the data were too sparse to evaluate this thoroughly. There were notable associations with some phthalates observed in the single study of ADHD (Engel et al., 2018), but the lack of additional evidence makes interpretation of these findings difficult.

3.6. Infant neurobehavior

Three studies reported on the association between any phthalate exposure and infant neurobehavior (Table 19). Because of the small number of available studies, the low confidence study is included in the

Table 16
Associations between DIBP exposure (measured by MIBP) and behavior.

Reference; study confidence, N	Age at outcome measure	Median maternal exposure	Exposure IQR (or as specified)	Internalizing problems overall β (95% CI)	Externalizing problems overall β (95% CI)	Internalizing problems in boys β (95% CI)	Internalizing problems in girls β (95% CI)	Externalizing problems in boys β (95% CI)	Externalizing problems in girls β (95% CI)
Exposure measured during gestation									
Kobrosly et al. (2014); medium; 153	6–10 yr	2 ng/mL (GM)	1–5	0.02 (-0.2,0.3)	0.2 (-0.02,0.4)	0.1 (-0.2,0.4)	-0.1 (-0.4,0.2)	0.3 (0.1,0.6)*	0.1 (-0.2,0.3)
Gascon et al. (2015); high; 362	7 yr	32 μg/g	22–48	Emotional symptoms RR 1.0 (0.9,1.2)	Conduct problems RR 1.1 (0.9,1.2)	NR	NR	NR	NR
Whyatt et al. (2012); medium; 297	3 yr	9 ng/mL (GM)	<LOD–374 (range)	1.0 (0, 1.9)	"No association"	1.2 (-0.2,2.6)	1.2 (-0.2,2.6)	NR	NR
Engel et al. (2010); medium; 188	4–9 yr	0.03 μM/L (from Engel et al., 2009)	0.01–0.05	0.5	0.3	NR	NR	NR	NR
Philippat et al. (2017); medium; 546	3 yr	40 ng/mL	29-57 (33rd-66th)	NR	NR	IRR 1.0 (1.0,1.1)	NR	IRR 1.0 (0.9,1.0)	NR
	5 yr					1.0 (0.9,1.1)		1.0 (0.9,1.0)	
Exposure measured preconception									
Messerlian et al. (2017); high; 166	2-9 yr	Preconception Maternal 6 ng/mL	4-10	-0.3 (-1.9,1.4)	1.1 (-0.3,2.5)	0.8 (-1.1,2.6)	-0.7 (-2.4,0.9)	2.1 (0.5,3.8)	0.7 (-0.7,2.0)
		Paternal 6 ng/mL	5-11	-0.9 (-3.1,1.4)	-0.4 (-1.8,1.0)	2.1 (-0.5,4.8)	-2.4 (-5.2,0.4)	-0.4 (-2.4,1.6)	-0.5 (-1.9,1.0)
Attention-deficient hyperactivity disorder (ADHD), exposure measured during gestation									
Engel et al. (2018); medium; 802	n/a	17 ng/mL	10-31		OR 0.9 (0.7,1.2)			OR 1.0 (0.7,1.3)	OR 0.9 (0.5,1.3)

One low confidence study (Kim et al., 2018) not shown in table because results were incompletely reported.
All studies used ln-transformed exposure and βs represent 1 ln-unit increase, except for Gascon et al. (2015), which used log2-transformation and β represent doubling of exposure and Philippat et al. (2017) which calculated incidence rate ratios (IRR) for a 1 unit change in test scores for a doubling of exposure.. Results that support an adverse association are shaded. This represents one or more of the following: $p < 0.05$, $\beta \geq 0.5$, OR ≥ 0.5, or exposure-response trend across categories of exposure. NR = not reported; GM = geometric mean.
*$p < 0.05$.
ˆUpon request, author provided re-calculated results with ln-transformed exposure and β representing a ln-unit increase, to improve comparability with other studies.

table. There was little consistency in the reported associations across studies, and this evidence is considered indeterminate for all phthalates, with the exception of DBP, which is considered *slight* due to statistically significant, though small, associations in multiple domains of neurobehavior in a high confidence study.

3.7. Social behaviors

Four studies, two *high* (Braun et al. 2014, Shin et al. 2018), one *medium* (Miodovnik et al. 2011), and one *low confidence* study (Kim et al., 2018) examined the association between phthalate exposure and

Table 17
Associations between BBP exposure (measured by MBzP) and behavior.

Reference; study confidence, N	Age at outcome measure	Median maternal exposure (ng/mL)	Exposure IQR (or as specified)	Internalizing problems overall β (95% CI)	Externalizing problems overall β (95% CI)	Internalizing problems in boys β (95% CI)	Internalizing problems in girls β (95% CI)	Externalizing problems in boys β (95% CI)	Externalizing problems in girls β (95% CI)
Exposure measured during gestation									
Kobrosly et al. (2014); medium; 153	6–10 yr	7 ng/mL (GM)	3–16.3	0.1 (-0.3,0.1)	0.1 (-0.1,0.2)	-0.04 (-0.3,0.2)	-0.2 (-0.4,0)*	0.2 (-0.03,0.4)	-0.04 (-0.3,0.2)
Gascon et al. (2015); high; 362	7 yr	12 μg/g	7–20	Emotional symptoms RR 1.1 (1.0,1.2)	Conduct problems RR 1.0 (0.9,1.2)	NR	NR	NR	NR
Philippat et al. (2017); medium; 546	3 yr	18 ng/mL	13-27 (33rd-66th)	NR	NR	IRR 1.0 (1.0,1.1)*	NR	IRR 1.0 (1.0,1.0)	NR
	5 yr					1.0 (1.0, 1.1)		1.0 (1.0,1.0)	
Whyatt et al. (2012); medium; 297	3 yr	19 ng/mL	<LOD–1,110 (range)	0.8 (0.1,1.6)*	"No association"	1.8 (0.9,2.7)*	0.3 (-0.8,1.4)	NR	NR
Lien et al. (2015); medium; 122	8 yr	20 μg/g (mean)		-2.9 (-7.4,1.6)	-1.1 (-6.2,3.9)	-2.7 (-8.2,2.9)	-2.8 (-10.3,4.8)	-4.2 (-11.8,3.3)	2.0 (-5.2,9.2)
Exposure measured preconception									
Messerlian et al. (2017); high; 166	2-9 yr	Preconception Maternal 3 ng/mL	2-6	0.2 (-1.3,1.7)	0.4 (-1.1,1.8)	-1.4 (-6.0,3.1)	-0.1 (-1.9,1.7)	0.4 (-1.7,2.4)	0.4 (-1.1,1.8)
		Paternal 4 ng/mL	2-6	0.5 (-1.5,2.5)	-0.4 (-1.7,1.0)	1.8 (-0.8,4.4)	-0.6 (-3.0,1.9)	-0.9 (-2.5,0.7)	-0.2 (-1.6,1.3)
Attention-deficient hyperactivity disorder (ADHD), exposure measured during gestation									
Engel et al. (2018); medium; 802	n/a	4 ng/mL	3-8		OR 1.2 (0.9,1.6)			OR 1.2 (0.9,1.6)	OR 1.2 (0.8,1.8)

All studies used ln-transformed exposure and βs represent 1 ln-unit increase, except for Gascon et al. (2015), which used log2-transformation and β represent doubling of exposure and Philippat et al. (2017) which calculated incidence rate ratios (IRR) for a 1 unit change in test scores for a doubling of exposure. Results that support an adverse association are shaded. This represents one or more of the following: $p < 0.05$, $\beta \geq 0.5$, OR ≥ 0.5, or exposure-response trend across categories of exposure. NR = not reported; GM = geometric mean.
*$p < 0.05$.
ˆUpon request, author provided re-calculated results with ln-transformed exposure and β representing a ln-unit increase, to improve comparability with other studies.

Table 18
Associations between DEP exposure (measured by MEP) and behavior.

Reference; study confidence, N	Age at outcome measure	Median maternal exposure (ng/mL)	Exposure IQR (or as specified)	Internalizing problems overall β (95% CI)	Externalizing problems overall β (95% CI)	Internalizing problems in boys β (95% CI)	Internalizing problems in girls β (95% CI)	Externalizing problems in boys β (95% CI)	Externalizing problems in girls β (95% CI)
Exposure measured during gestation									
Kobrosly et al. (2014); medium; 153	6–10 yr	81 ng/mL (GM)	26–231	-0.1 (-0.2, 0.1)	-0.03 (-0.2,0.1)	-0.02 (-0.2,0.1)	`-0.1 (-0.3,0.1)	-0.02 (-0.2,0.1)	-0.1 (-0.2,0.1)
Philippat et al. (2017); medium; 546	3 yr	97 ng/mL	65-154	NR	NR	IRR 1.0 (1.0,1.0)	NR	IRR 1.0 (1.0,1.0)	NR
	5 yr					1.0 (1.0,1.0)		1.0 (1.0,1.1)	
Lien et al. (2015); medium; 122	8 yr	100 μg/g (mean)		−1.8 (−5.5, 2.0)	−0.5 (−4.6, 3.7)	-0.2 (-5.2,4.8)	-3.0 (-8.6,2.7)	-1.6 (-8.4,5.2)	0.1 (-5.4,5.5)
Gascon et al. (2015); high; 362	7 yr	403 μg/g	199–756	Emotional symptoms RR 1.0 (0.9,1.1)	Conduct problems RR 1.0 (0.9,1.1)	NR	NR	NR	NR
Engel et al. (2010); medium; 188	4–9 yr	2 μM/L (from Engel et al., 2009)	0.8–5	0.8	1.3*	NR	NR	NR	NR
Exposure measured preconception									
Messerlian et al. (2017); high; 166	2-9 yr	Preconception Maternal 46 ng/mL	27-126	-0.6 (-1.9,0.6)	0.3 (-0.8,1.4)	-2.9 (-4.7,-1.2)*	-0.6 (-2.0,0.8)	0.1 (-1.3,1.5)	0.3 (-0.8,1.4)
		Paternal 53 ng/mL	30-125	0.4 (-1.0,1.8)	-0.2 (-1.3,0.9)	0.5 (-5.2,6.2)	0.3 (-1.1,1.7)	-0.7 (-2.3,1.0)	-0.3 (-1.5,0.8)
Attention-deficient hyperactivity disorder (ADHD), exposure measured during gestation									
Engel et al. (2018); medium; 802	n/a	99 ng/mL	32-297		OR 1.0 (0.9,1.2)			OR 1.0 (0.9,1.2)	OR 1.1 (0.9,1.4)

One low confidence study (Kim et al., 2018) not shown in table because results were incompletely reported.
All studies used ln-transformed exposure and βs represent 1 ln-unit increase, except for Gascon et al. (2015), which used log2-transformation and β represent doubling of exposure and Philippat et al. (2017) which calculated incidence rate ratios (IRR) for a 1 unit change in test scores for a doubling of exposure. Results that support an adverse association are shaded. This represents one or more of the following: $p < 0.05$, $\beta \geq 0.5$, or exposure-response trend across categories of exposure. NR = not reported; GM = geometric mean.
*$p < 0.05$.
ˆUpon request, author provided re-calculated results with ln-transformed exposure and β representing a ln-unit increase, to improve comparability with other studies.

autism/social impairment, with most looking at continuous social behaviors and one (Shin et al., 2018) looking at autism spectrum disorder (ASD) as a dichotomous outcome.

For DEHP, both higher confidence studies of social behaviors reported increased autistic behaviors with increasing DEHP exposure (MEHHP β = 1.1 (95% CI −0.8, 3.0) in Braun et al. (2014); ΣDEHP β = 0.8 (95% CI −0.7, 2.4) in Miodovnik et al. (2011), although neither was statistically significant. The high confidence study of ASD

Table 19
Associations between phthalate exposure and infant neurobehavior.

Reference	Age at outcome measure	Exposure	Median maternal exposure	Exposure IQR (or as specified)	Arousal/ Range of state β (SE) or β (95% CI)	Movement/ Motor β (SE) or β (95% CI)	Regulation of state β (SE) or β (95% CI)	Nonoptimal Reflexes β (SE) or β (95% CI)
DEHP								
Yolton et al. (2011); high; 332	5 wk	Log2-trans ∑DEHP	245 ng/mL (GM)		0.03 (0.03)	−0.002 (0.03)	0.03 (0.02)	0.1 (0.1)*
Engel et al. (2009); medium; 274	Newborns	Log-trans high MWP	0.5 μM/L	0.2–0.9	0.1 (−0.04, 0.2)	0.02 (−0.1, 0.1)	−0.1 (−0.2, 0.1)	−0.1
Stroustrup et al. (2018); low; 64	Discharge at 33-37 wk PMA	∑DEHP postnatal	12 ng/mL (MEOHP)	6-25 (MEOHP)		0.03 (-0.1,0.1)	0.1 (0,0.2)	-0.2 (-0.4,0.1)
DBP								
Yolton et al. (2011); high; 332	5 wk	Log2-trans MBP	20 ng/mL (GM)		-0.1 (0.04)*	0.1 (0.03)*	0.1 (0.04)*	-0.1 (0.1)
Low MWP								
Engel et al. (2009); medium; 274	Newborns	Log-trans low MWP	2 μM/L	1.0-5.7	0.01 (-0.1,0.1)	0.1 (-0.01,0.1)	0.04 (-0.1,0.2)	0.04

All studies used ln-transformed exposure and βs represent 1 ln-unit increase, except for Gascon, which used log2-transformation and β represent doubling of exposure. Results that support an adverse association are shaded. This represents one or more of the following: $p < 0.05$, $\beta \geq 0.5$, or exposure-response trend across categories of exposure. NR = not reported. PMA = post menstrual age. MWP = molecular weight phthalates. GM = geometric mean. (See above-mentioned references for further information.)
*$p < 0.05$.
ˆUpon request, author provided re-calculated results with ln-transformed exposure and β representing a ln-unit increase, to improve comparability with other studies.

Outcome	DEHP	DINP	DBP	DIBP	BBP	DEP
Cognition	S	I	S	S	S	S
Motor	S	S	S	S	M*	I
Behavior	S	I	S	I	S	I
Infant behavior	I	I	S	I	I	I
Social behavior	S	I	S	I	I	S

Robust (R) Moderate (M) Slight (S) Indeterminate (I)
Level of confidence in association

Fig. 5. Summary of epidemiologic evidence of neurodevelopmental effects associated with phthalates. *In girls.

(Shin et al., 2018) reported no increased risk of ASD with higher exposure to DEHP (RR = 0.75, 95% CI 0.4, 2.3), though there was an increase in relative risk in a group classified as non-typically developing (RR = 1.4, 95% CI 0.9, 2.1). This group was a heterogenous group, representing children who had either low cognitive ability scores and/or high autism trait scores without reaching the cutoff for the ASD group, and thus the results are difficult to interpret. Overall, this evidence is considered *slight*.

For the remaining phthalates, the results reported by Braun et al. (2014) do not support an association between exposure and autistic behaviors (MIBP β = 0.3 [95% CI −1.5, 2.1]; MBzP β = −0.6 [95% CI −2.7, 1.5]; MBP β = −0.4 [95% CI −2.2, 1.4]; MEP β = −0.5 [95% CI −2.2, 1.3]), while results reported by Miodovnik et al. (2011) do support an association for some phthalates (MBP β = 1.4 [95% CI −0.4, 3.2]; MEP β = 1.4 [95% CI 0.2, 2.5, $p < 0.05$]; individual results for MBzP and MIBP were not reported). In Shin et al. (2018), only DEP had increased risk of ASD with higher exposure (RR = 1.2, 95% CI 0.8, 1.9 for ASD, RR = 1.4, 95% CI 1.0, 1.9 for non-typical development). Given the lack of consistency between the available studies, the evidence is considered *slight* for DBP and DEP and *indeterminate* for DIBP, BBP, and DINP.

4. Discussion

Based on systematic examination of the epidemiological studies of prenatal phthalate exposures and neurodevelopment, there is generally not a clear pattern of associations. Most of the phthalate-outcome pairs have only *slight* or *indeterminate* evidence of an association (Fig. 5), with only motor effects of BBP in girls having *moderate* evidence. This is despite the availability of several medium and high confidence studies examining these associations. There are several possible reasons for the observed null associations, particularly related to reduced sensitivity resulting from exposure misclassification in studies using single phthalate measures and periods of heightened susceptibility, and the effects of phthalate mixtures. These are each discussed further below and until these limitations are adequately addressed in the literature, these findings should not be interpreted as evidence that there are no neurodevelopmental effects of phthalate exposure.

The potential for non-differential exposure misclassification to bias the estimates towards the null is one possible reason for the observed heterogeneity in these study's findings (Perrier et al. 2016). When examining the association between continuous health outcomes and chemicals with substantial temporal within-person variation (e.g., DEHP), effect estimates derived from a study with a single urine sample can be attenuated by 80% and as many as 35 repeated urine samples from a single individual are needed to reduce this attenuation to < 10%. One way to address the issues related to phthalate exposure misclassification is to pool each individual's multiple urine samples, as recommended by Perrier et al. and practiced by others (Perrier et al., 2016), but the majority of available studies rely on a single urine sample.

Studies examining the health effects of prenatal thalidomide and DES show that there are unique periods of susceptibility during development when exposure can cause adverse health effects (Kim and Scialli, 2011, Swan, 2000, Hoover et al. 2011). Thus, there may also be periods of heightened susceptibility to phthalate exposures, as suggested by one study examining the association between neurodevelopmental outcomes and repeated measures of urinary phthalate concentrations during both pregnancy and childhood (Li et al., 2019). If there are discrete periods of susceptibility to phthalate exposures, then the available studies may be unable to adequately assess these associations given that urine samples were collected at various times during development and neurodevelopmental processes during some of these periods of life may not be sensitive to phthalate exposures. One way to address this is to implement new studies with repeated phthalate exposure measures during multiple potentially susceptible periods of life.

Phthalate exposures do not occur in isolation, and individuals are chronically exposed to multiple phthalates on a daily basis across their lifespan. The presented epidemiological studies have examined phthalate exposures using an approach of "one chemical at a time" and one exposure period at a time where they are treated as if they occur in isolation from each other. Thus, these studies have not accurately considered the nature of human exposure to these phthalate "mixtures" or the potential for phthalates to have cumulative effects on human health. Indeed, studies in rodents show that phthalate mixtures can have additive effects on fetal testosterone production (Howdeshell et al., 2008). Future studies will need to employ newly developed statistical tools to quantify the potential neurodevelopmental effects of phthalate mixtures (Braun et al., 2016, Lazarevic et al., 2019).

The studies considered informative in this review were primarily birth cohorts with exposure measurement during gestation (Table 2). Several cross-sectional studies were excluded due to concerns about temporality. Because phthalates do not persist in the body and exposure measures have poor repeatability over time, current exposure was not considered an adequate measure of exposure for an etiologically relevant time period. Including these studies may have influenced the conclusions, particularly for social behaviors, but we felt it was most useful to focus on the highest confidence studies. However, there is potential that recent exposure to phthalates could be associated some neuropsychological outcomes such as cognition, including via a mechanism with thyroid function, and this review was not able to assess this possibility.

We did not undertake this review with an *a priori* expectation of sex-dependent associations. Some studies did report differences in strength and direction of associations for boys and girls. These were generally not consistent across studies, although there was some indication of greater effects for MDI in girls. Many of the studies either did not report or were not adequately powered to assess sex-dependent associations. Future studies should consider this issue and ensure that they are powered to assess a possible interaction with sex.

As mentioned in the introduction, past reviews have presented plausible mechanisms for the association between EDCs and neurodevelopmental effects. In rats, prenatal, pre-adolescent, and adult DEHP exposures cause alterations in learning and hyperactivity that are accompanied by decreased tyrosine hydroxylase neurons, lower brain derived neurotrophic factor levels, and suppression of neuronal excitability and synaptic plasticity in the hippocampus (Holahan et al., 2018) (Li et al., 2018) (Ran et al., 2019). Male rats exposed to DEHP from birth to adulthood had decreased γ-amino butyric acid (GABA) levels in their brain and increased anxiety behaviors that were reversed by the administration of GABA agonists (Carbone et al., 2018). DEHP exposure during puberty caused increased anxiety and reduced social behaviors in female mice (Wang et al., 2016). This was accompanied by decreases in estrogen and dopamine receptors in the striatum. Some phthalates are anti-androgenic and reduce testosterone levels by decreasing steroidogenesis and steroid trafficking gene expression

(Hannas et al., 2011, Howdeshell et al., 2008). Gonadal hormones are critical for sex-specific neurodevelopment and also play an important role in adolescent brain remodeling (Cohen-Bendahan et al., 2005, Dahl et al., 2018). Some phthalates antagonize triiodothyroinine (T3) binding to thyroid receptor-β (Ghisari and Bonefeld-Jorgensen, 2009), reduce cellular T3 uptake (Shimada and Yamauchi, 2004), and affect transcription of the sodium-iodine transporter (Breous et al., 2005). Alterations in prenatal thyroid hormones has been associated with reduced cognition and brain volume (Korevaar et al., 2016).

There are other important limitations to note. There is potential for co-pollutant confounding by other phthalates due to the high correlations across some of the phthalates, and it is difficult to rule this out for estimates of effects of individual phthalates given the available evidence. This issue is related to the "one chemical at a time" issue described above and is discussed in more detail in a forthcoming editorial as an area of uncertainty for reviews of phthalates and other chemical mixtures. However, it is unlikely that it would significantly alter the conclusions of the review due to the amount of uncertainty already present in this evidence. In addition, for most outcomes, we reviewed only the summary measures of the testing instruments because they were the most consistently reported across studies and because of the plethora of data available on clinical subscales. It is possible that stronger conclusions could be reached in looking at a specific subscale or diagnosis, where there may be greater precision around the outcome. There is some support for this in the single study on ADHD diagnosis (Engel et al., 2018), which had a more narrowly defined clinical disorder and found stronger associations than many of the studies of behavior with summary measures of externalizing behavior. This is an important area for future research.

Overall, this detailed systematic review suggests that there is limited evidence that phthalates adversely affect the examined neurodevelopmental domains. However, there are considerable limitations in the existing literature related to exposure misclassification, periods of heightened susceptibility, sex-specific effects, and phthalate mixture effects. Future studies should consider examining additional endpoints, like clinical diagnosis with neurodevelopmental disorders with longitudinal design and repeated exposure measurement. Studies addressing these limitations may provide more compelling evidence of an effect of phthalate exposures on neurodevelopment.

CRediT authorship contribution statement

Elizabeth G. Radke: Conceptualization, Data curation, Methodology, Formal analysis, Visualization, Investigation, Writing - original draft, Writing - review & editing. **Joseph M. Braun:** Conceptualization, Writing - original draft, Writing - review & editing. **Rebecca M. Nachman:** Investigation, Writing - review & editing. **Glinda S. Cooper:** Conceptualization, Methodology, Writing - review & editing.

Acknowledgements

We would like to thank Carolyn Gigot, Cheng-Kuan Lin, Sharon Sagiv, Cheryl Stein, Leonid Kopylev, Laura Dishaw, Amanda Persad, Kris Thayer, Sue Rieth, and Barbara Glenn for their contributions to this work.

Appendix A. Supplementary material

Supplementary data to this article can be found online at https://doi.org/10.1016/j.envint.2019.105408.

References

T.E. Arbuckle, K. Davis, K. Boylan, M. Fisher, J. Fu, Processed data for chms 2007–2009: Bisphenol a, phthalates and lead and learning and behavioral problems in canadian children 6–19 years of age, 8 (2016) 784–802.

Arbuckle, T.E., Davis, K., Boylan, K., Fisher, M., Fu, J., 2016b. Bisphenol a, phthalates and lead and learning and behavioral problems in canadian children 6–11 years of age: Chms 2007–2009. Neurotoxicology 54, 89–98.

Balalian, A.A., Whyatt, R.M., Liu, X., Insel, B.J., Rauh, V.A., Herbstman, J., et al., 2019. Prenatal and childhood exposure to phthalates and motor skills at age 11 years. Environ. Res. 171, 416–427.

Benjamin, S., Masai, E., Kamimura, N., Takahashi, K., Anderson, R.C., Faisal, P.A., 2017. Phthalates impact human health: Epidemiological evidences and plausible mechanism of action. J. Hazard Mater. 340, 360–383. https://doi.org/10.1016/j.jhazmat.2017.06.036. Epub 2017 Jun 19.

Braun, J.M., Kalkbrenner, A.E., Just, A.C., Yolton, K., Calafat, A.M., Sjödin, A., et al., 2014. Gestational exposure to endocrine-disrupting chemicals and reciprocal social, repetitive, and stereotypic behaviors in 4- and 5-year-old children: The home study. Environ. Health. Perspect. 122, 513–520.

Braun, J.M., Gennings, C., Hauser, R., Webster, T.F., 2016. What can epidemiological studies tell us about the impact of chemical mixtures on human health? Environ. Health. Perspect. 124, A6–A9.

Braun, J.M., 2017. Early-life exposure to EDCs: role in childhood obesity and neurodevelopment. Nat. Rev. Endocrinol. 13, 161–173.

Breous, E., Wenzel, A., Loos, U., 2005. The promoter of the human sodium/iodide symporter responds to certain phthalate plasticisers. Mol. Cell. Endocrinol. 244, 75–78.

Carbone, S., Ponzo, O.J., Gobetto, N., Samaniego, Y.A., Reynoso, R., Moguilevsky, J.A., et al., 2018. Effect of di(2-ethylhexyl) phthalate on the neuroendocrine regulation of reproduction in adult male rats and its relationship to anxiogenic behavior: Participation of gabaergic system. Hum. Exp Toxicol:960327118774868.

Cho, S.C., Bhang, S.Y., Hong, Y.C., Shin, M.S., Kim, B.N., Kim, J.W., et al., 2010. Relationship between environmental phthalate exposure and the intelligence of school-age children. Environ. Health. Perspect. 118, 1027–1032.

Chopra, V., Harley, K., Lahiff, M., Eskenazi, B., 2014. Association between phthalates and attention deficit disorder and learning disability in U.S. Children, 6–15 years. Environ. Res. 128, 64–69.

Cohen-Bendahan, C., van de Beek, C., Berenbaum, S., 2005. Prenatal sex hormone effects on child and adult sex-typed behavior: Methods and findings. Neurosci. Biobehav. Rev. 29, 353–384.

Dahl, R.E., Allen, N.B., Wilbrecht, L., Suleiman, A.B., 2018. Importance of investing in adolescence from a developmental science perspective. Nature 554, 441–450.

Doherty, B.T., Engel, S.M., Buckley, J.P., Silva, M.J., Calafat, A.M., Wolff, M.S., 2017. Prenatal phthalate biomarker concentrations and performance on the bayley scales of infant development-ii in a population of young urban children. Environ. Res. 152, 51–58.

Ejaredar, M., Nyanza, E.C., Ten Eycke, K., Dewey, D., 2015. Phthalate exposure and childrens neurodevelopment: A systematic review. Environ. Res. 142, 51–60. https://doi.org/10.1016/j.envres.2015.06.014. Epub 2015 Jun 20.

Engel, S.M., Zhu, C., Berkowitz, G.S., Calafat, A.M., Silva, M.J., Miodovnik, A., et al., 2009. Prenatal phthalate exposure and performance on the neonatal behavioral assessment scale in a multiethnic birth cohort. Neurotoxicology 30, 522–528.

Engel, S.M., Miodovnik, A., Canfield, R.L., Zhu, C., Silva, M.J., Calafat, A.M., et al., 2010. Prenatal phthalate exposure is associated with childhood behavior and executive functioning. Environ. Health. Perspect. 118, 565–571.

Engel, S.M., Villanger, G.D., Nethery, R.C., Thomsen, C., Sakhi, A.K., Drover, S.S.M., et al., 2018. Prenatal phthalates, maternal thyroid function, and risk of attention-deficit hyperactivity disorder in the norwegian mother and child cohort. Environ. Health. Perspect. 126, 057004.

Factor-Litvak, P., Insel, B., Calafat, A.M., Liu, X., Perera, F., Rauh, V.A., et al., 2014. Persistent associations between maternal prenatal exposure to phthalates on child iq at age 7 years. PLoS One 9, e114003.

Gascon, M., Valvi, D., Forns, J., Casas, M., Martínez, D., Júlvez, J., et al., 2015. Prenatal exposure to phthalates and neuropsychological development during childhood. Int. J. Hyg. Environ. Health 218, 550–558.

Ghisari, M., Bonefeld-Jorgensen, E.C., 2009. Effects of plasticizers and their mixtures on estrogen receptor and thyroid hormone functions. Toxicol. Lett. 189, 67–77.

Hannas, B.R., Lambright, C.S., Furr, J., Howdeshell, K.L., Wilson, V.S., Gray, L.E., 2011. Dose-response assessment of fetal testosterone production and gene expression levels in rat testes following in utero exposure to diethylhexyl phthalate, diisobutyl phthalate, diisoheptyl phthalate, and diisononyl phthalate. Toxicol. Sci. 123, 206–216.

Holahan, M.R., Smith, C.A., Luu, B.E., Storey, K.B., 2018. Preadolescent phthalate (dehp) exposure is associated with elevated locomotor activity and reward-related behavior and a reduced number of tyrosine hydroxylase positive neurons in post-adolescent male and female rats. Toxicol. Sci 165, 512–530.

Hoover, R.N., Hyer, M., Pfeiffer, R.M., Adam, E., Bond, B., Cheville, A.L., et al., 2011. Adverse health outcomes in women exposed in utero to diethylstilbestrol. N. Engl. J. Med 365, 1304–1314.

Howdeshell, K.L., Wilson, V.S., Furr, J., Lambright, C.R., Rider, C.V., Blystone, C.R., et al., 2008. A mixture of five phthalate esters inhibits fetal testicular testosterone production in the sprague-dawley rat in a cumulative, dose-additive manner. Toxicol. Sci 105, 153–165.

Hu, D., Wang, Y.X., Chen, W.J., Zhang, Y., Li, H.H., Xiong, L., et al., 2017. Associations of phthalates exposure with attention deficits hyperactivity disorder: A case-control study among chinese children. Environ. Pollut. 229, 375–385.

Huang, H.B., Chen, H.Y., Su, P.H., Huang, P.C., Sun, C.W., Wang, C.J., et al., 2015. Fetal and childhood exposure to phthalate diesters and cognitive function in children up to 12 years of age: Taiwanese maternal and infant cohort study. PLoS One 10, e0131910.

Johns, L.E., Cooper, G.S., Galizia, A., Meeker, J.D., 2015. Exposure assessment issues in

epidemiology studies of phthalates. Environ. Int. 85, 27–39.
Kardas, F., Bayram, A.K., Demirci, E., Akin, L., Ozmen, S., Kendirci, M., et al., 2015. Increased serum phthalates (mehp, dehp) and bisphenol a concentrations in children with autism spectrum disorder: The role of endocrine disruptors in autism etiopathogenesis. J. Child. Neurol. 31, 629–635.
Kim, B.N., Cho, S.C., Kim, Y., Shin, M.S., Yoo, H.J., Kim, J.W., et al., 2009. Phthalates exposure and attention-deficit/hyperactivity disorder in school-age children. Biol. Psychiatry 66, 958–963.
Kim, J.H., Scialli, A.R., 2011. Thalidomide: The tragedy of birth defects and the effective treatment of disease. Toxicol. Sci. 122, 1–6.
Kim, J.I., Hong, Y.C., Shin, C.H., Lee, Y.A., Lim, Y.H., Kim, B.N., 2017. The effects of maternal and children phthalate exposure on the neurocognitive function of 6-year-old children. Environ. Res. 156, 519–525.
Kim, S., Eom, S., Kim, H.J., Lee, J.J., Choi, G., Choi, S., et al., 2018. Association between maternal exposure to major phthalates, heavy metals, and persistent organic pollutants, and the neurodevelopmental performances of their children at 1 to 2years of age- check cohort study. Sci. Total. Environ. 624, 377–384.
Kim, Y., Ha, E.H., Kim, E.J., Park, H., Ha, M., Kim, J.H., et al., 2011. Prenatal exposure to phthalates and infant development at 6 months: prospective mothers and children's environmental health (moceh) study. Environ. Health. Perspect. 119, 1495–1500.
Kobrosly, R.W., Evans, S., Miodovnik, A., Barrett, E.S., Thurston, S.W., Calafat, A.M., et al., 2014. Prenatal phthalate exposures and neurobehavioral development scores in boys and girls at 6–10 years of age. Environ. Health. Perspect. 122, 521–528.
Kondolot, M., Ozmert, E.N., Ascı, A., Erkekoglu, P., Oztop, D.B., Gumus, H., et al., 2016. Plasma phthalate and bisphenol a levels and oxidant-antioxidant status in autistic children. Environ. Toxicol. Pharmacol. 43, 149–158.
Korevaar, T.I.M., Muetzel, R., Medici, M., Chaker, L., Jaddoe, V.W.V., de Rijke, Y.B., et al., 2016. Association of maternal thyroid function during early pregnancy with offspring iq and brain morphology in childhood: A population-based prospective cohort study. Lancet. Diabetes. Endocrinol. 4, 35–43.
Langonne, L., Saillenfait, A.M., Payan, J.P., 1998. Comparative embryotoxicity of di-n-butyl phthalate and its main metabolite mono-n-butyl phthalate at midgestations. Teratology 58, 22A.
Larsson, M., Weiss, B., Janson, S., Sundell, J., Bornehag, C.G., 2009. Associations between indoor environmental factors and parental-reported autistic spectrum disorders in children 6–8 years of age. Neurotoxicology 30, 822–831.
Lazarevic, N., Barnett, A.G., Sly, P.D., Knibbs, L.D., 2019. Statistical methodology in studies of prenatal exposure to mixtures of endocrine-disrupting chemicals: A review of existing approaches and new alternatives. Environ. Health. Perspect. 127, 26001.
Li, L., Li, H., Qu, P., Xiao, M., Zhang, G., Zhang, Q., et al., 2018. An antagonism joint action of lead and di-2-ethylhexyl phthalate explains an improved ability of learning and memory after combined exposure in weaning rats. Biol. Trace. Elem. Res.
Li, N., Papandonatos, G.D., Calafat, A.M., Yolton, K., Lanphear, B.P., Chen, A., et al., 2019. Identifying periods of susceptibility to the impact of phthalates on children's cognitive abilities. Environ. Res. 172, 604–614.
Lien, Y.J., Ku, H.Y., Su, P.H., Chen, S.J., Chen, H.Y., Liao, P.C., et al., 2015. Prenatal exposure to phthalate esters and behavioral syndromes in children at eight years of age: Taiwan maternal and infant cohort study. Environ. Health. Perspect. 123, 95–100.
Messerlian, C., Bellinger, D., Mínguez-Alarcón, L., Romano, M.E., Ford, J.B., Williams, P.L., et al., 2017. Paternal and maternal preconception urinary phthalate metabolite concentrations and child behavior. Environ. Res. 158, 720–728.
Minatoya, M., Naka Jima, S., Sasaki, S., Araki, A., Miyashita, C., Ikeno, T., et al., 2016. Effects of prenatal phthalate exposure on thyroid hormone levels, mental and psychomotor development of infants: the hokkaido study on environment and children's health. Sci. Total. Environ. 565, 1037–1043.
Minatoya, M., Itoh, S., Yamazaki, K., Araki, A., Miyashita, C., Tamura, N., et al., 2018. Prenatal exposure to bisphenol a and phthalates and behavioral problems in children at preschool age: The hokkaido study on environment and children's health. Environ. Health. Prev. Med. 23, 43.
Miodovnik, A., Engel, S.M., Zhu, C., Ye, X., Soorya, L.V., Silva, M.J., et al., 2011. Endocrine disruptors and childhood social impairment. Neurotoxicology 32, 261–267.
Nakiwala, D., Peyre, H., Heude, B., Bernard, J.Y., Béranger, R., Slama, R., et al., 2018. In-utero exposure to phenols and phthalates and the intelligence quotient of boys at 5years. Environ. Health 17, 11.
NAS, 2008. Phthalates and Cumulative Risk Assessment: The Tasks Ahead (2008) Board on Environmental Studies and Toxicology.
Oztop, D.B., Demirci, E., Ozmen, S., Kondolot, M., Kardas, F., Per, H., 2018. Might bpa and phthalates have a role in etiopathogenesis of adhd? Anadolu Psikiyatri Dergisi 19, 300–306.
Park, S., Kim, B.N., Cho, S., Kim, Y., Kim, J., Lee, J.Y., et al., 2014. Association between urine phthalate levels and poor attentional performance in children with attention-deficit hyperactivity disorder with evidence of dopamine gene-phthalate interaction. Int. J. Environ. Res. Public Health 11, 6743–6756.
Park, S., Lee, J.M., Kim, J.W., Cheong, J.H., Yun, H.J., Hong, Y.C., et al., 2015. Association between phthalates and externalizing behaviors and cortical thickness in children with attention deficit hyperactivity disorder. Psychol. Med 45, 1601–1612.
Perrier, F., Giorgis-Allemand, L., Slama, R., Philippat, C., 2016. Within-subject pooling of biological samples to reduce exposure misclassification in biomarker-based studies. Epidemiology 27, 378–388.
Philippat, C., Bennett, D.H., Krakowiak, P., Rose, M., Hwang, H.M., Hertz-Picciotto, I., 2015. Phthalate concentrations in house dust in relation to autism spectrum disorder and developmental delay in the childhood autism risks from genetics and the environment (charge) study. Environ. Health 14, 56.
Philippat, C., Nakiwala, D., Calafat, A.M., Botton, J., De Agostini, M., Heude, B., et al., 2017. Prenatal exposure to nonpersistent endocrine disruptors and behavior in boys at 3 and 5 years. Environ. Health. Perspect 125 097014–097011 097019.
Polanska, K., Ligocka, D., Sobala, W., Hanke, W., 2014. Phthalate exposure and child development: the polish mother and child cohort study. Early. Hum. Dev 90, 477–485.
Ran, D., Luo, Y., Gan, Z., Liu, J., Yang, J., 2019. Neural mechanisms underlying the deficit of learning and memory by exposure to di(2-ethylhexyl) phthalate in rats. Ecotoxicol. Environ. Saf. 174, 58–65.
Sagiv, S.K., Kalkbrenner, A.E., Bellinger, D.C., 2015. Of decrements and disorders: Assessing impairments in neurodevelopment in prospective studies of environmental toxicant exposures. Environ. Health 14, 8.
Shimada, N., Yamauchi, K., 2004. Characteristics of 3,5,3'-triiodothyronine (t3)-uptake system of tadpole red blood cells: Effect of endocrine-disrupting chemicals on cellular t3 response. J. Endocrinol. 183, 627–637.
Shin, H.M., Schmidt, R.J., Tancredi, D., Barkoski, J., Ozonoff, S., Bennett, D.H., et al., 2018. Prenatal exposure to phthalates and autism spectrum disorder in the marbles study. Environ. Health 17, 85.
Shoaff, J.R., Calafat, A.M., Schantz, S.L., Korrick, S.A., 2018. Endocrine disrupting chemical exposure and maladaptive behavior during adolescence. Environ. Res. 172, 231–241.
Sterne, J.A., Hernán, M.A., Reeves, B.C., Savović, J., Berkman, N.D., Viswanathan, M., Henry, D., Altman, D.G., Ansari, M.T., Boutron, I., Carpenter, J.R., Chan, A.W., Churchill, R., Deeks, J.J., Hróbjartsson, A., Kirkham, J., Jüni, P., Loke, Y.K., Pigott, T.D., Ramsay, C.R., Regidor, D., Rothstein, H.R., Sandhu, L., Santaguida, P.L., Schünemann, H.J., Shea, B., Shrier, I., Tugwell, P., Turner, L., Valentine, J.C., Waddington, H., Waters, E., Wells, G.A., Whiting, P.F., Higgins, J.P., 2016. ROBINS-I: a tool for assessing risk of bias in non-randomised studies of interventions. BMJ. 355, i4919. https://doi.org/10.1136/bmj.i4919.
Stroustrup, A., Bragg, J.B., Andra, S.S., Curtin, P.C., Spear, E.A., Sison, D.B., et al., 2018. Neonatal intensive care unit phthalate exposure and preterm infant neurobehavioral performance. PLoS One 13, e0193835.
Swan, S.H., 2000. Intrauterine exposure to diethylstilbestrol: Long-term effects in humans. APMIS 108, 793–804.
Téllez-Rojo, M.M., Cantoral, A., Cantonwine, D.E., Schnaas, L., Peterson, K., Hu, H., et al., 2013. Prenatal urinary phthalate metabolites levels and neurodevelopment in children at two and three years of age. Sci. Total. Environ. 461–462, 386390.
Testa, C., Nuti, F., Hayek, J., De Felice, C., Chelli, M., Rovero, P., et al., 2012. Di-(2-ethylhexyl) phthalate and autism spectrum disorders. ASN Neuro. 4, 223–229.
Verstraete, S., Vanhorebeek, I., Covaci, A., Güiza, F., Malarvannan, G., Jorens, P.G., et al., 2016. Circulating phthalates during critical illness in children are associated with long-term attention deficit: a study of a development and a validation cohort. Intensive. Care. Med 42, 379–392.
Wang, R., Xu, X., Zhu, Q., 2016. Pubertal exposure to di-(2-ethylhexyl) phthalate influences social behavior and dopamine receptor d2 of adult female mice. Chemosphere 144, 1771–1779.
White, R.F., Campbell, R., Echeverria, D., Knox, S.S., Janulewicz, P., 2009. Assessment of neuropsychological trajectories in longitudinal population-based studies of children. J. Epidemiol. Community. Health 63 (Suppl 1), i15–i26.
Whyatt, R.M., Liu, X.H., Rauh, V.A., Calafat, A.M., Just, A.C., Hoepner, L., et al., 2012. Maternal prenatal urinary phthalate metabolite concentrations and child mental, psychomotor, and behavioral development at 3 years of age. Environ. Health. Perspect. 120, 290–295.
Won, E.K., Kim, Y., Ha, M., Burm, E., Kim, Y.S., Lim, H., et al., 2016. Association of current phthalate exposure with neurobehavioral development in a national sample. Int. J. Hyg. Environ. Health 219, 364–371.
Yolton, K., Xu, Y., Strauss, D., Altaye, M., Calafat, A.M., Khoury, J., 2011. Prenatal exposure to bisphenol a and phthalates and infant neurobehavior. Neurotoxicol. Teratol. 33, 558–566.

Yost, Erin

From: Arzuaga, Xabier
Sent: Thursday, April 23, 2020 5:41 PM
To: Yost, Erin
Subject: RE: STAA award submission for phthalates papers- please confirm your % contribution

Hi Erin,
Thank you for putting this together. I agree with the percent contribution you described in your email. Also, I am a co-author in another paper that is being nominated for this award. The citation for the other paper that will be nominated is below. Thanks!
Xabier

Makris SL, Scott CS, Fox J, Knudsen TB, Hotchkiss AK, Arzuaga X, Euling SY, Powers CM, Jinot J, Hogan KA, Abbott BD, Hunter ES 3rd, Narotsky MG. A systematic evaluation of the potential effects of trichloroethylene exposure on cardiac development. Reprod Toxicol. 2016 Oct;65:321-358. doi: 10.1016/j.reprotox.2016.08.014. Epub 2016 Aug 27. Review. PubMed PMID: 27575429.

From: Yost, Erin <Yost.Erin@epa.gov>
Sent: Thursday, April 23, 2020 10:36 AM
To: Blessinger, Todd <blessinger.todd@epa.gov>; Euling, Susan <Euling.Susan@epa.gov>; Arzuaga, Xabier <Arzuaga.Xabier@epa.gov>; brandy.beverly@nih.gov; Weaver, Andre <Weaver.James@epa.gov>; Keshava, Nagalakshmi <Keshava.Nagu@epa.gov>; Mudipalli, Anuradha <Mudipalli.Anu@epa.gov>; Dishaw, Laura <Dishaw.Laura@epa.gov>; Hotchkiss, Andrew <Hotchkiss.Andrew@epa.gov>; Makris, Susan <Makris.Susan@epa.gov>
Subject: RE: STAA award submission for phthalates papers- please confirm your % contribution

I almost forgot- please also let me know if you have been listed as a coauthor on a STAA award application within the last 5 years. If so, we are required to provide a description of this in our application. Thanks so much!

-Erin

From: Yost, Erin
Sent: Thursday, April 23, 2020 10:27 AM
To: Blessinger, Todd <blessinger.todd@epa.gov>; Euling, Susan <Euling.Susan@epa.gov>; Arzuaga, Xabier <Arzuaga.Xabier@epa.gov>; Beverly, Brandy (NIH/NIEHS) [E] <brandy.beverly@nih.gov>; Weaver, Andre <Weaver.James@epa.gov>; Keshava, Nagalakshmi <Keshava.Nagu@epa.gov>; Mudipalli, Anuradha <Mudipalli.Anu@epa.gov>; Dishaw, Laura <Dishaw.Laura@epa.gov>; Hotchkiss, Andrew <Hotchkiss.Andrew@epa.gov>; Makris, Susan <Makris.Susan@epa.gov>
Subject: STAA award submission for phthalates papers- please confirm your % contribution

Dear DIBP paper coauthors,
I hope you all are doing well! I wanted to let you all know that Beth and I are nominating some papers from the phthalates special issue for a STAA award (https://www.epa.gov/research/scientific-and-technological-achievement-award-staa). We are allowed to submit up to 3 published papers as a single package, so we selected the male repro epidemiology paper, the DIBP paper, and the dose-response modeling paper. We need to list the percent contribution of each coauthor to the submission package, so we calculated this by estimating each author's contribution to the individual manuscripts and then dividing that effort across the three papers. **(See the last column in the table below.)**

We are required to submit proof in writing that each author agrees with their estimated percent contribution, so **please reply to this email ASAP and let me know if you agree with your percent contribution.**

FYI, if we win, there are cash prizes that will be divided among EPA authors ($10K, $5K, or $2K), and each EPA author will receive a minimum of $250 regardless of their percent contribution.

Thanks!
-Erin

	DIBP paper	Epi paper	Dose-response paper	Adjusted total % contribution to STAA submission
Beth Radke		60		**20**
Erin Yost	35			**15**
Todd Blessinger	3		40	**14**
Sue Euling	15		20	**12**
Glinda Cooper		20		**6**
Lily Wang			15	**5**
Xabier Arzuaga	10			**3**
Brandy Beverly	10			**3**
Christine Cai			10	**3**
Joe Braun		10		**2**
John Meeker		10		**2**
Andre Weaver	6			**2**
Nagu Keshava	6			**2**
Anu Mudipalli	6			**2**
Gary Klinefelter			5	**2**
Anne-Marie Saillenfait			5	**2**
Karen Hogan			5	**2**
Laura Dishaw	3			**1**
Andrew Hotchkiss	3			**1**
Sue Makris	3			**1**
Total %	100	100	100	**100**

Erin Yost, Ph.D.
Toxicologist
U.S. Environmental Protection Agency
Center for Public Health and Environmental Assessment
Cell phone: 919-841-7926

Yost, Erin

From: Beverly, Brandy (NIH/NIEHS) [E] <brandy.beverly@nih.gov>
Sent: Thursday, April 23, 2020 10:40 AM
To: Yost, Erin
Subject: RE: STAA award submission for phthalates papers- please confirm your % contribution

Hi Erin,

Thanks for reaching out. I'm fine with the breakdown and my percent contribution, and I'm happy to receive an award if I am eligible. Does it matter than I am no longer working there or that the paper was published after I left?

Brandy

_____
Brandiese E.J. Beverly, Ph.D.
Health Scientist
Office of Health Assessment and Translation
National Institute of Environmental Health Sciences/National Toxicology Program
P.O. Box 12233, Mail Drop K2-04
Research Triangle Park, NC 27709

Tel: (984) 287-3112 | Fax: (301) 480-3226
brandy.beverly@nih.gov

From: Yost, Erin <Yost.Erin@epa.gov>
Sent: Thursday, April 23, 2020 10:36 AM
To: Blessinger, Todd <blessinger.todd@epa.gov>; Euling, Susan <Euling.Susan@epa.gov>; Arzuaga, Xabier <Arzuaga.Xabier@epa.gov>; Beverly, Brandy (NIH/NIEHS) [E] <brandy.beverly@nih.gov>; Weaver, Andre <Weaver.James@epa.gov>; Keshava, Nagalakshmi <Keshava.Nagu@epa.gov>; Mudipalli, Anuradha <Mudipalli.Anu@epa.gov>; Dishaw, Laura <Dishaw.Laura@epa.gov>; Hotchkiss, Andrew <Hotchkiss.Andrew@epa.gov>; Makris, Susan <Makris.Susan@epa.gov>
Subject: RE: STAA award submission for phthalates papers- please confirm your % contribution

I almost forgot- please also let me know if you have been listed as a coauthor on a STAA award application within the last 5 years. If so, we are required to provide a description of this in our application. Thanks so much!

-Erin

From: Yost, Erin
Sent: Thursday, April 23, 2020 10:27 AM
To: Blessinger, Todd <blessinger.todd@epa.gov>; Euling, Susan <Euling.Susan@epa.gov>; Arzuaga, Xabier <Arzuaga.Xabier@epa.gov>; Beverly, Brandy (NIH/NIEHS) [E] <brandy.beverly@nih.gov>; Weaver, Andre <Weaver.James@epa.gov>; Keshava, Nagalakshmi <Keshava.Nagu@epa.gov>; Mudipalli, Anuradha <Mudipalli.Anu@epa.gov>; Dishaw, Laura <Dishaw.Laura@epa.gov>; Hotchkiss, Andrew <Hotchkiss.Andrew@epa.gov>; Makris, Susan <Makris.Susan@epa.gov>
Subject: STAA award submission for phthalates papers- please confirm your % contribution

Dear DIBP paper coauthors,

I hope you all are doing well! I wanted to let you all know that Beth and I are nominating some papers from the phthalates special issue for a STAA award (https://www.epa.gov/research/scientific-and-technological-achievement-award-staa). We are allowed to submit up to 3 published papers as a single package, so we selected the male repro epidemiology paper, the DIBP paper, and the dose-response modeling paper. We need to list the percent contribution of each coauthor to the submission package, so we calculated this by estimating each author's contribution to the individual manuscripts and then dividing that effort across the three papers. **(See the last column in the table below.)**

We are required to submit proof in writing that each author agrees with their estimated percent contribution, so **please reply to this email ASAP and let me know if you agree with your percent contribution.**

FYI, if we win, there are cash prizes that will be divided among EPA authors ($10K, $5K, or $2K), and each EPA author will receive a minimum of $250 regardless of their percent contribution.

Thanks!
-Erin

	DIBP paper	Epi paper	Dose-response paper	Adjusted total % contribution to STAA submission
Beth Radke		60		**20**
Erin Yost	35			**15**
Todd Blessinger	3		40	**14**
Sue Euling	15		20	**12**
Glinda Cooper		20		**6**
Lily Wang			15	**5**
Xabier Arzuaga	10			**3**
Brandy Beverly	10			**3**
Christine Cai			10	**3**
Joe Braun		10		**2**
John Meeker		10		**2**
Andre Weaver	6			**2**
Nagu Keshava	6			**2**
Anu Mudipalli	6			**2**
Gary Klinefelter			5	**2**
Anne-Marie Saillenfait			5	**2**
Karen Hogan			5	**2**
Laura Dishaw	3			**1**
Andrew Hotchkiss	3			**1**
Sue Makris	3			**1**
Total %	100	100	100	**100**

Erin Yost, Ph.D.
Toxicologist
U.S. Environmental Protection Agency
Center for Public Health and Environmental Assessment
Cell phone: 919-841-7926

Yost, Erin

From: Cai, Christine
Sent: Monday, April 27, 2020 10:55 AM
To: Blessinger, Todd
Subject: RE: STAA award submission for phthalates papers - please confirm your % contribution

Agree. Best regards, Christine

From: Blessinger, Todd <blessinger.todd@epa.gov>
Sent: Friday, April 24, 2020 2:54 PM
To: Cai, Christine <Cai.Christine@epa.gov>; Euling, Susan <Euling.Susan@epa.gov>; Hogan, Karen <Hogan.Karen@epa.gov>; Klinefelter, Gary <Klinefelter.Gary@epa.gov>; Wang, Lily (Lihong) <wang.lily@epa.gov>; anne-marie.saillenfait@inrs.fr
Subject: STAA award submission for phthalates papers - please confirm your % contribution

Dear phthalates syndrome team,

Erin Yost and Beth Radke of the DIBP team are nominating some articles from the phthalates special issue for a Scientific and Technological Achievement Award (STAA; for more information, see this page: https://www.epa.gov/research/scientific-and-technological-achievement-award-staa). Up to 3 published articles can be submitted as a single package, and one of those being submitted is the ordinal dose-response DIBP article (the other two are the DIBP systematic review article and the male repro epidemiology article). Because you are all co-authors on this article, the percent contribution of each coauthor needs to be listed in the submission package. Beth, Erin, and I calculated percent contributions for each of our respective articles by estimating each author's contribution to the individual manuscripts. Then we divided that effort across the three papers. **(See the last column in the table below for these percents.)**

We would like your input on the contributions we proposed, and we are required to submit proof in writing that each author agrees with their estimated percent contribution. **Please reply to this email ASAP and let me know if you agree with your percent contribution.**

FYI, if we win, there are cash prizes ($10K, $5K, and $2K for levels I, II, and III, respectively) that will be divided among EPA authors according to their contribution to the total effort (in last column of table), and each EPA author will receive a minimum of $250 regardless of their percent contribution.

Thanks!
-Erin

	DIBP paper	Epi paper	Dose-response paper	Adjusted total % contribution to STAA submission
Beth Radke		60		**20**
Erin Yost	35			**15**
Todd Blessinger	3		40	**14**
Sue Euling	15		20	**12**
Glinda Cooper		20		**6**
Lily Wang			15	**5**

Xabier Arzuaga	10			**3**
Brandy Beverly	10			**3**
Christine Cai			10	**3**
Joe Braun		10		**2**
John Meeker		10		**2**
Andre Weaver	6			**2**
Nagu Keshava	6			**2**
Anu Mudipalli	6			**2**
Gary Klinefelter			5	**2**
Anne-Marie Saillenfait			5	**2**
Karen Hogan			5	**2**
Laura Dishaw	3			**1**
Andrew Hotchkiss	3			**1**
Sue Makris	3			**1**
Total %	100	100	100	**100**

Todd Blessinger, Ph.D.
Center for Public Health and Environmental Assessment
U.S. Environmental Protection Agency
Office: 202-564-7641
blessinger.todd@epa.gov

Yost, Erin

From: Dishaw, Laura
Sent: Friday, April 24, 2020 9:00 AM
To: Yost, Erin; Blessinger, Todd; Euling, Susan; Arzuaga, Xabier; brandy.beverly@nih.gov; Weaver, Andre; Keshava, Nagalakshmi; Mudipalli, Anuradha; Hotchkiss, Andrew; Makris, Susan
Subject: RE: STAA award submission for phthalates papers- please confirm your % contribution

I agree with my percent contribution.

I have **not** been a coauthor on a STAA award application in the last 5 years.

From: Yost, Erin <Yost.Erin@epa.gov>
Sent: Thursday, April 23, 2020 10:36 AM
To: Blessinger, Todd <blessinger.todd@epa.gov>; Euling, Susan <Euling.Susan@epa.gov>; Arzuaga, Xabier <Arzuaga.Xabier@epa.gov>; brandy.beverly@nih.gov; Weaver, Andre <Weaver.James@epa.gov>; Keshava, Nagalakshmi <Keshava.Nagu@epa.gov>; Mudipalli, Anuradha <Mudipalli.Anu@epa.gov>; Dishaw, Laura <Dishaw.Laura@epa.gov>; Hotchkiss, Andrew <Hotchkiss.Andrew@epa.gov>; Makris, Susan <Makris.Susan@epa.gov>
Subject: RE: STAA award submission for phthalates papers- please confirm your % contribution

I almost forgot- please also let me know if you have been listed as a coauthor on a STAA award application within the last 5 years. If so, we are required to provide a description of this in our application. Thanks so much!

-Erin

From: Yost, Erin
Sent: Thursday, April 23, 2020 10:27 AM
To: Blessinger, Todd <blessinger.todd@epa.gov>; Euling, Susan <Euling.Susan@epa.gov>; Arzuaga, Xabier <Arzuaga.Xabier@epa.gov>; Beverly, Brandy (NIH/NIEHS) [E] <brandy.beverly@nih.gov>; Weaver, Andre <Weaver.James@epa.gov>; Keshava, Nagalakshmi <Keshava.Nagu@epa.gov>; Mudipalli, Anuradha <Mudipalli.Anu@epa.gov>; Dishaw, Laura <Dishaw.Laura@epa.gov>; Hotchkiss, Andrew <Hotchkiss.Andrew@epa.gov>; Makris, Susan <Makris.Susan@epa.gov>
Subject: STAA award submission for phthalates papers- please confirm your % contribution

Dear DIBP paper coauthors,
I hope you all are doing well! I wanted to let you all know that Beth and I are nominating some papers from the phthalates special issue for a STAA award (https://www.epa.gov/research/scientific-and-technological-achievement-award-staa). We are allowed to submit up to 3 published papers as a single package, so we selected the male repro epidemiology paper, the DIBP paper, and the dose-response modeling paper. We need to list the percent contribution of each coauthor to the submission package, so we calculated this by estimating each author's contribution to the individual manuscripts and then dividing that effort across the three papers. **(See the last column in the table below.)**

We are required to submit proof in writing that each author agrees with their estimated percent contribution, so **please reply to this email ASAP and let me know if you agree with your percent contribution.**

FYI, if we win, there are cash prizes that will be divided among EPA authors ($10K, $5K, or $2K), and each EPA author will receive a minimum of $250 regardless of their percent contribution.

Thanks!

-Erin

	DIBP paper	Epi paper	Dose-response paper	Adjusted total % contribution to STAA submission
Beth Radke		60		**20**
Erin Yost	35			**15**
Todd Blessinger	3		40	**14**
Sue Euling	15		20	**12**
Glinda Cooper		20		**6**
Lily Wang			15	**5**
Xabier Arzuaga	10			**3**
Brandy Beverly	10			**3**
Christine Cai			10	**3**
Joe Braun		10		**2**
John Meeker		10		**2**
Andre Weaver	6			**2**
Nagu Keshava	6			**2**
Anu Mudipalli	6			**2**
Gary Klinefelter			5	**2**
Anne-Marie Saillenfait			5	**2**
Karen Hogan			5	**2**
Laura Dishaw	3			**1**
Andrew Hotchkiss	3			**1**
Sue Makris	3			**1**
Total %	100	100	100	**100**

Erin Yost, Ph.D.
Toxicologist
U.S. Environmental Protection Agency
Center for Public Health and Environmental Assessment
Cell phone: 919-841-7926

Yost, Erin

From: Euling, Susan
Sent: Friday, April 24, 2020 2:55 PM
To: Blessinger, Todd
Subject: RE: STAA award submission for phthalates papers - please confirm your % contribution

Hi Todd,

I confirm my % contribution (listed below in your table) and I do not have STAA applications or awards in the last 5 years.

Sue

From: Blessinger, Todd <blessinger.todd@epa.gov>
Sent: Friday, April 24, 2020 2:54 PM
To: Cai, Christine <Cai.Christine@epa.gov>; Euling, Susan <Euling.Susan@epa.gov>; Hogan, Karen <Hogan.Karen@epa.gov>; Klinefelter, Gary <Klinefelter.Gary@epa.gov>; Wang, Lily (Lihong) <wang.lily@epa.gov>; anne-marie.saillenfait@inrs.fr
Subject: STAA award submission for phthalates papers - please confirm your % contribution

Dear phthalates syndrome team,

Erin Yost and Beth Radke of the DIBP team are nominating some articles from the phthalates special issue for a Scientific and Technological Achievement Award (STAA; for more information, see this page: https://www.epa.gov/research/scientific-and-technological-achievement-award-staa). Up to 3 published articles can be submitted as a single package, and one of those being submitted is the ordinal dose-response DIBP article (the other two are the DIBP systematic review article and the male repro epidemiology article). Because you are all co-authors on this article, the percent contribution of each coauthor needs to be listed in the submission package. Beth, Erin, and I calculated percent contributions for each of our respective articles by estimating each author's contribution to the individual manuscripts. Then we divided that effort across the three papers. **(See the last column in the table below for these percents.)**

We would like your input on the contributions we proposed, and we are required to submit proof in writing that each author agrees with their estimated percent contribution. **Please reply to this email ASAP and let me know if you agree with your percent contribution.**

FYI, if we win, there are cash prizes ($10K, $5K, and $2K for levels I, II, and III, respectively) that will be divided among EPA authors according to their contribution to the total effort (in last column of table), and each EPA author will receive a minimum of $250 regardless of their percent contribution.

Thanks!
-Erin

	DIBP paper	Epi paper	Dose-response paper	Adjusted total % contribution to STAA submission
Beth Radke		60		**20**
Erin Yost	35			**15**

Todd Blessinger	3		40	**14**
Sue Euling	15		20	**12**
Glinda Cooper		20		**6**
Lily Wang			15	**5**
Xabier Arzuaga	10			**3**
Brandy Beverly	10			**3**
Christine Cai			10	**3**
Joe Braun		10		**2**
John Meeker		10		**2**
Andre Weaver	6			**2**
Nagu Keshava	6			**2**
Anu Mudipalli	6			**2**
Gary Klinefelter			5	**2**
Anne-Marie Saillenfait			5	**2**
Karen Hogan			5	**2**
Laura Dishaw	3			**1**
Andrew Hotchkiss	3			**1**
Sue Makris	3			**1**
Total %	100	100	100	**100**

Todd Blessinger, Ph.D.
Center for Public Health and Environmental Assessment
U.S. Environmental Protection Agency
Office: 202-564-7641
blessinger.todd@epa.gov

Yost, Erin

From: Hogan, Karen
Sent: Monday, April 27, 2020 9:26 AM
To: Blessinger, Todd
Subject: RE: STAA award submission for phthalates papers - please confirm your % contribution

Sorry for the delay. The % is fine for me. Plus I don't think I would get any money anyway.
KH

From: Blessinger, Todd <blessinger.todd@epa.gov>
Sent: Friday, April 24, 2020 2:54 PM
To: Cai, Christine <Cai.Christine@epa.gov>; Euling, Susan <Euling.Susan@epa.gov>; Hogan, Karen <Hogan.Karen@epa.gov>; Klinefelter, Gary <Klinefelter.Gary@epa.gov>; Wang, Lily (Lihong) <wang.lily@epa.gov>; anne-marie.saillenfait@inrs.fr
Subject: STAA award submission for phthalates papers - please confirm your % contribution

Dear phthalates syndrome team,

Erin Yost and Beth Radke of the DIBP team are nominating some articles from the phthalates special issue for a Scientific and Technological Achievement Award (STAA; for more information, see this page: https://www.epa.gov/research/scientific-and-technological-achievement-award-staa). Up to 3 published articles can be submitted as a single package, and one of those being submitted is the ordinal dose-response DIBP article (the other two are the DIBP systematic review article and the male repro epidemiology article). Because you are all co-authors on this article, the percent contribution of each coauthor needs to be listed in the submission package. Beth, Erin, and I calculated percent contributions for each of our respective articles by estimating each author's contribution to the individual manuscripts. Then we divided that effort across the three papers. **(See the last column in the table below for these percents.)**

We would like your input on the contributions we proposed, and we are required to submit proof in writing that each author agrees with their estimated percent contribution. **Please reply to this email ASAP and let me know if you agree with your percent contribution.**

FYI, if we win, there are cash prizes ($10K, $5K, and $2K for levels I, II, and III, respectively) that will be divided among EPA authors according to their contribution to the total effort (in last column of table), and each EPA author will receive a minimum of $250 regardless of their percent contribution.

Thanks!
-Erin

	DIBP paper	Epi paper	Dose-response paper	Adjusted total % contribution to STAA submission
Beth Radke		60		**20**
Erin Yost	35			**15**
Todd Blessinger	3		40	**14**
Sue Euling	15		20	**12**
Glinda Cooper		20		**6**

Lily Wang			15	**5**
Xabier Arzuaga	10			**3**
Brandy Beverly	10			**3**
Christine Cai			10	**3**
Joe Braun		10		**2**
John Meeker		10		**2**
Andre Weaver	6			**2**
Nagu Keshava	6			**2**
Anu Mudipalli	6			**2**
Gary Klinefelter			5	**2**
Anne-Marie Saillenfait			5	**2**
Karen Hogan			5	**2**
Laura Dishaw	3			**1**
Andrew Hotchkiss	3			**1**
Sue Makris	3			**1**
Total %	100	100	100	**100**

Todd Blessinger, Ph.D.
Center for Public Health and Environmental Assessment
U.S. Environmental Protection Agency
Office: 202-564-7641
blessinger.todd@epa.gov

Yost, Erin

From: Hotchkiss, Andrew
Sent: Thursday, April 23, 2020 10:34 AM
To: Yost, Erin; Radke-Farabaugh, Elizabeth
Subject: RE: STAA award submission for phthalates papers- please confirm your % contribution

Hi Erin and Beth,

This looks fine for me.

Thanks to you both!

Best regards,
Andrew

From: Yost, Erin <Yost.Erin@epa.gov>
Sent: Thursday, April 23, 2020 10:27 AM
To: Blessinger, Todd <blessinger.todd@epa.gov>; Euling, Susan <Euling.Susan@epa.gov>; Arzuaga, Xabier <Arzuaga.Xabier@epa.gov>; brandy.beverly@nih.gov; Weaver, Andre <Weaver.James@epa.gov>; Keshava, Nagalakshmi <Keshava.Nagu@epa.gov>; Mudipalli, Anuradha <Mudipalli.Anu@epa.gov>; Dishaw, Laura <Dishaw.Laura@epa.gov>; Hotchkiss, Andrew <Hotchkiss.Andrew@epa.gov>; Makris, Susan <Makris.Susan@epa.gov>
Subject: STAA award submission for phthalates papers- please confirm your % contribution

Dear DIBP paper coauthors,
I hope you all are doing well! I wanted to let you all know that Beth and I are nominating some papers from the phthalates special issue for a STAA award (https://www.epa.gov/research/scientific-and-technological-achievement-award-staa). We are allowed to submit up to 3 published papers as a single package, so we selected the male repro epidemiology paper, the DIBP paper, and the dose-response modeling paper. We need to list the percent contribution of each coauthor to the submission package, so we calculated this by estimating each author's contribution to the individual manuscripts and then dividing that effort across the three papers. **(See the last column in the table below.)**

We are required to submit proof in writing that each author agrees with their estimated percent contribution, so **please reply to this email ASAP and let me know if you agree with your percent contribution.**

FYI, if we win, there are cash prizes that will be divided among EPA authors ($10K, $5K, or $2K), and each EPA author will receive a minimum of $250 regardless of their percent contribution.

Thanks!
-Erin

	DIBP paper	Epi paper	Dose-response paper	Adjusted total % contribution to STAA submission
Beth Radke		60		**20**
Erin Yost	35			**15**
Todd Blessinger	3		40	**14**

Sue Euling	15		20	**12**
Glinda Cooper		20		**6**
Lily Wang			15	**5**
Xabier Arzuaga	10			**3**
Brandy Beverly	10			**3**
Christine Cai			10	**3**
Joe Braun		10		**2**
John Meeker		10		**2**
Andre Weaver	6			**2**
Nagu Keshava	6			**2**
Anu Mudipalli	6			**2**
Gary Klinefelter			5	**2**
Anne-Marie Saillenfait			5	**2**
Karen Hogan			5	**2**
Laura Dishaw	3			**1**
Andrew Hotchkiss	3			**1**
Sue Makris	3			**1**
Total %	100	100	100	**100**

Erin Yost, Ph.D.
Toxicologist
U.S. Environmental Protection Agency
Center for Public Health and Environmental Assessment
Cell phone: 919-841-7926

Yost, Erin

From: Keshava, Nagalakshmi
Sent: Thursday, April 23, 2020 10:33 AM
To: Yost, Erin
Subject: RE: STAA award submission for phthalates papers- please confirm your % contribution

Hi Erin,

Thanks for putting this together. I am OK with the calculated percentage contribution.

Hope you and your family are well and staying safe.

Thank you
Nagu

From: Yost, Erin <Yost.Erin@epa.gov>
Sent: Thursday, April 23, 2020 10:27 AM
To: Blessinger, Todd <blessinger.todd@epa.gov>; Euling, Susan <Euling.Susan@epa.gov>; Arzuaga, Xabier <Arzuaga.Xabier@epa.gov>; brandy.beverly@nih.gov; Weaver, Andre <Weaver.James@epa.gov>; Keshava, Nagalakshmi <Keshava.Nagu@epa.gov>; Mudipalli, Anuradha <Mudipalli.Anu@epa.gov>; Dishaw, Laura <Dishaw.Laura@epa.gov>; Hotchkiss, Andrew <Hotchkiss.Andrew@epa.gov>; Makris, Susan <Makris.Susan@epa.gov>
Subject: STAA award submission for phthalates papers- please confirm your % contribution

Dear DIBP paper coauthors,
I hope you all are doing well! I wanted to let you all know that Beth and I are nominating some papers from the phthalates special issue for a STAA award (https://www.epa.gov/research/scientific-and-technological-achievement-award-staa). We are allowed to submit up to 3 published papers as a single package, so we selected the male repro epidemiology paper, the DIBP paper, and the dose-response modeling paper. We need to list the percent contribution of each coauthor to the submission package, so we calculated this by estimating each author's contribution to the individual manuscripts and then dividing that effort across the three papers. **(See the last column in the table below.)**

We are required to submit proof in writing that each author agrees with their estimated percent contribution, so **please reply to this email ASAP and let me know if you agree with your percent contribution.**

FYI, if we win, there are cash prizes that will be divided among EPA authors ($10K, $5K, or $2K), and each EPA author will receive a minimum of $250 regardless of their percent contribution.

Thanks!
-Erin

	DIBP paper	Epi paper	Dose-response paper	Adjusted total % contribution to STAA submission
Beth Radke		60		**20**
Erin Yost	35			**15**
Todd Blessinger	3		40	**14**
Sue Euling	15		20	**12**

Glinda Cooper		20		**6**
Lily Wang			15	**5**
Xabier Arzuaga	10			**3**
Brandy Beverly	10			**3**
Christine Cai			10	**3**
Joe Braun		10		**2**
John Meeker		10		**2**
Andre Weaver	6			**2**
Nagu Keshava	6			**2**
Anu Mudipalli	6			**2**
Gary Klinefelter			5	**2**
Anne-Marie Saillenfait			5	**2**
Karen Hogan			5	**2**
Laura Dishaw	3			**1**
Andrew Hotchkiss	3			**1**
Sue Makris	3			**1**
Total %	100	100	100	**100**

Erin Yost, Ph.D.
Toxicologist
U.S. Environmental Protection Agency
Center for Public Health and Environmental Assessment
Cell phone: 919-841-7926

Yost, Erin

From: Klinefelter, Gary
Sent: Monday, April 27, 2020 3:00 PM
To: Blessinger, Todd
Subject: RE: STAA award submission for phthalates papers - please confirm your % contribution

Todd,

That's fine,
Thanks

Gary

From: Blessinger, Todd <blessinger.todd@epa.gov>
Sent: Friday, April 24, 2020 2:54 PM
To: Cai, Christine <Cai.Christine@epa.gov>; Euling, Susan <Euling.Susan@epa.gov>; Hogan, Karen <Hogan.Karen@epa.gov>; Klinefelter, Gary <Klinefelter.Gary@epa.gov>; Wang, Lily (Lihong) <wang.lily@epa.gov>; anne-marie.saillenfait@inrs.fr
Subject: STAA award submission for phthalates papers - please confirm your % contribution

Dear phthalates syndrome team,

Erin Yost and Beth Radke of the DIBP team are nominating some articles from the phthalates special issue for a Scientific and Technological Achievement Award (STAA; for more information, see this page: https://www.epa.gov/research/scientific-and-technological-achievement-award-staa). Up to 3 published articles can be submitted as a single package, and one of those being submitted is the ordinal dose-response DIBP article (the other two are the DIBP systematic review article and the male repro epidemiology article). Because you are all co-authors on this article, the percent contribution of each coauthor needs to be listed in the submission package. Beth, Erin, and I calculated percent contributions for each of our respective articles by estimating each author's contribution to the individual manuscripts. Then we divided that effort across the three papers. **(See the last column in the table below for these percents.)**

We would like your input on the contributions we proposed, and we are required to submit proof in writing that each author agrees with their estimated percent contribution. **Please reply to this email ASAP and let me know if you agree with your percent contribution.**

FYI, if we win, there are cash prizes ($10K, $5K, and $2K for levels I, II, and III, respectively) that will be divided among EPA authors according to their contribution to the total effort (in last column of table), and each EPA author will receive a minimum of $250 regardless of their percent contribution.

Thanks!
-Erin

	DIBP paper	Epi paper	Dose-response paper	Adjusted total % contribution to STAA submission
Beth Radke		60		**20**

Erin Yost	35			**15**
Todd Blessinger	3		40	**14**
Sue Euling	15		20	**12**
Glinda Cooper		20		**6**
Lily Wang			15	**5**
Xabier Arzuaga	10			**3**
Brandy Beverly	10			**3**
Christine Cai			10	**3**
Joe Braun		10		**2**
John Meeker		10		**2**
Andre Weaver	6			**2**
Nagu Keshava	6			**2**
Anu Mudipalli	6			**2**
Gary Klinefelter			5	**2**
Anne-Marie Saillenfait			5	**2**
Karen Hogan			5	**2**
Laura Dishaw	3			**1**
Andrew Hotchkiss	3			**1**
Sue Makris	3			**1**
Total %	100	100	100	**100**

Todd Blessinger, Ph.D.
Center for Public Health and Environmental Assessment
U.S. Environmental Protection Agency
Office: 202-564-7641
blessinger.todd@epa.gov

Yost, Erin

From: Makris, Susan
Sent: Thursday, April 23, 2020 3:34 PM
To: Yost, Erin
Subject: RE: STAA award submission for phthalates papers- please confirm your % contribution

Erin, I agree with my 1% contribution listed in the table below. I have not been nominated for or received a STAA award in the past 5 years. Sue

Susan Makris
USEPA/ORD/CPHEA, 1200 Pennsylvania Ave. NW, Mailcode 8623R, Washington, DC 20460
202-564-7332 (O), 202-697-2621 (M), 202-564-0296 (F), makris.susan@epa.gov
Courier address: Ronald Reagan Bldg., 1300 Pennsylvania Ave. NW, Rm 71280, Washington, DC 20004

From: Yost, Erin <Yost.Erin@epa.gov>
Sent: Thursday, April 23, 2020 10:36 AM
To: Blessinger, Todd <blessinger.todd@epa.gov>; Euling, Susan <Euling.Susan@epa.gov>; Arzuaga, Xabier <Arzuaga.Xabier@epa.gov>; brandy.beverly@nih.gov; Weaver, Andre <Weaver.James@epa.gov>; Keshava, Nagalakshmi <Keshava.Nagu@epa.gov>; Mudipalli, Anuradha <Mudipalli.Anu@epa.gov>; Dishaw, Laura <Dishaw.Laura@epa.gov>; Hotchkiss, Andrew <Hotchkiss.Andrew@epa.gov>; Makris, Susan <Makris.Susan@epa.gov>
Subject: RE: STAA award submission for phthalates papers- please confirm your % contribution

I almost forgot- please also let me know if you have been listed as a coauthor on a STAA award application within the last 5 years. If so, we are required to provide a description of this in our application. Thanks so much!

-Erin

From: Yost, Erin
Sent: Thursday, April 23, 2020 10:27 AM
To: Blessinger, Todd <blessinger.todd@epa.gov>; Euling, Susan <Euling.Susan@epa.gov>; Arzuaga, Xabier <Arzuaga.Xabier@epa.gov>; Beverly, Brandy (NIH/NIEHS) [E] <brandy.beverly@nih.gov>; Weaver, Andre <Weaver.James@epa.gov>; Keshava, Nagalakshmi <Keshava.Nagu@epa.gov>; Mudipalli, Anuradha <Mudipalli.Anu@epa.gov>; Dishaw, Laura <Dishaw.Laura@epa.gov>; Hotchkiss, Andrew <Hotchkiss.Andrew@epa.gov>; Makris, Susan <Makris.Susan@epa.gov>
Subject: STAA award submission for phthalates papers- please confirm your % contribution

Dear DIBP paper coauthors,
I hope you all are doing well! I wanted to let you all know that Beth and I are nominating some papers from the phthalates special issue for a STAA award (https://www.epa.gov/research/scientific-and-technological-achievement-award-staa). We are allowed to submit up to 3 published papers as a single package, so we selected the male repro epidemiology paper, the DIBP paper, and the dose-response modeling paper. We need to list the percent contribution of each coauthor to the submission package, so we calculated this by estimating each author's contribution to the individual manuscripts and then dividing that effort across the three papers. **(See the last column in the table below.)**

We are required to submit proof in writing that each author agrees with their estimated percent contribution, so **please reply to this email ASAP and let me know if you agree with your percent contribution.**

FYI, if we win, there are cash prizes that will be divided among EPA authors ($10K, $5K, or $2K), and each EPA author will receive a minimum of $250 regardless of their percent contribution.

Thanks!
-Erin

	DIBP paper	Epi paper	Dose-response paper	Adjusted total % contribution to STAA submission
Beth Radke		60		**20**
Erin Yost	35			**15**
Todd Blessinger	3		40	**14**
Sue Euling	15		20	**12**
Glinda Cooper		20		**6**
Lily Wang			15	**5**
Xabier Arzuaga	10			**3**
Brandy Beverly	10			**3**
Christine Cai			10	**3**
Joe Braun		10		**2**
John Meeker		10		**2**
Andre Weaver	6			**2**
Nagu Keshava	6			**2**
Anu Mudipalli	6			**2**
Gary Klinefelter			5	**2**
Anne-Marie Saillenfait			5	**2**
Karen Hogan			5	**2**
Laura Dishaw	3			**1**
Andrew Hotchkiss	3			**1**
Sue Makris	3			**1**
Total %	100	100	100	**100**

Erin Yost, Ph.D.
Toxicologist
U.S. Environmental Protection Agency
Center for Public Health and Environmental Assessment
Cell phone: 919-841-7926

Yost, Erin

From: Mudipalli, Anuradha
Sent: Thursday, April 23, 2020 11:00 AM
To: Yost, Erin
Subject: RE: STAA award submission for phthalates papers- please confirm your % contribution

Again,
I agree with my percent contribution to DIBP paper.

Anuj

From: Yost, Erin <Yost.Erin@epa.gov>
Sent: Thursday, April 23, 2020 10:36 AM
To: Blessinger, Todd <blessinger.todd@epa.gov>; Euling, Susan <Euling.Susan@epa.gov>; Arzuaga, Xabier <Arzuaga.Xabier@epa.gov>; brandy.beverly@nih.gov; Weaver, Andre <Weaver.James@epa.gov>; Keshava, Nagalakshmi <Keshava.Nagu@epa.gov>; Mudipalli, Anuradha <Mudipalli.Anu@epa.gov>; Dishaw, Laura <Dishaw.Laura@epa.gov>; Hotchkiss, Andrew <Hotchkiss.Andrew@epa.gov>; Makris, Susan <Makris.Susan@epa.gov>
Subject: RE: STAA award submission for phthalates papers- please confirm your % contribution

I almost forgot- please also let me know if you have been listed as a coauthor on a STAA award application within the last 5 years. If so, we are required to provide a description of this in our application. Thanks so much!

-Erin

From: Yost, Erin
Sent: Thursday, April 23, 2020 10:27 AM
To: Blessinger, Todd <blessinger.todd@epa.gov>; Euling, Susan <Euling.Susan@epa.gov>; Arzuaga, Xabier <Arzuaga.Xabier@epa.gov>; Beverly, Brandy (NIH/NIEHS) [E] <brandy.beverly@nih.gov>; Weaver, Andre <Weaver.James@epa.gov>; Keshava, Nagalakshmi <Keshava.Nagu@epa.gov>; Mudipalli, Anuradha <Mudipalli.Anu@epa.gov>; Dishaw, Laura <Dishaw.Laura@epa.gov>; Hotchkiss, Andrew <Hotchkiss.Andrew@epa.gov>; Makris, Susan <Makris.Susan@epa.gov>
Subject: STAA award submission for phthalates papers- please confirm your % contribution

Dear DIBP paper coauthors,
I hope you all are doing well! I wanted to let you all know that Beth and I are nominating some papers from the phthalates special issue for a STAA award (https://www.epa.gov/research/scientific-and-technological-achievement-award-staa). We are allowed to submit up to 3 published papers as a single package, so we selected the male repro epidemiology paper, the DIBP paper, and the dose-response modeling paper. We need to list the percent contribution of each coauthor to the submission package, so we calculated this by estimating each author's contribution to the individual manuscripts and then dividing that effort across the three papers. **(See the last column in the table below.)**

We are required to submit proof in writing that each author agrees with their estimated percent contribution, so **please reply to this email ASAP and let me know if you agree with your percent contribution.**

FYI, if we win, there are cash prizes that will be divided among EPA authors ($10K, $5K, or $2K), and each EPA author will receive a minimum of $250 regardless of their percent contribution.

Thanks!
-Erin

	DIBP paper	Epi paper	Dose-response paper	Adjusted total % contribution to STAA submission
Beth Radke		60		**20**
Erin Yost	35			**15**
Todd Blessinger	3		40	**14**
Sue Euling	15		20	**12**
Glinda Cooper		20		**6**
Lily Wang			15	**5**
Xabier Arzuaga	10			**3**
Brandy Beverly	10			**3**
Christine Cai			10	**3**
Joe Braun		10		**2**
John Meeker		10		**2**
Andre Weaver	6			**2**
Nagu Keshava	6			**2**
Anu Mudipalli	6			**2**
Gary Klinefelter			5	**2**
Anne-Marie Saillenfait			5	**2**
Karen Hogan			5	**2**
Laura Dishaw	3			**1**
Andrew Hotchkiss	3			**1**
Sue Makris	3			**1**
Total %	100	100	100	**100**

Erin Yost, Ph.D.
Toxicologist
U.S. Environmental Protection Agency
Center for Public Health and Environmental Assessment
Cell phone: 919-841-7926

Yost, Erin

From: Radke-Farabaugh, Elizabeth
Sent: Thursday, April 23, 2020 12:08 PM
To: Yost, Erin
Subject: FW: STAA award submission for phthalates papers- please confirm your % contribution

Ok, here's all the epi authors on one string.

From: Glinda Cooper <gscooper1@gmail.com>
Sent: Thursday, April 23, 2020 12:06 PM
To: meekerj@umich.edu
Cc: Braun, Joseph <joseph_braun_1@brown.edu>; Radke-Farabaugh, Elizabeth <radke-farabaugh.elizabeth@epa.gov>
Subject: Re: STAA award submission for phthalates papers- please confirm your % contribution

I'm good with what you have done. Good luck!

Glinda

Sent from my iPhone

> On Apr 23, 2020, at 11:07 AM, John Meeker <meekerj@umich.edu> wrote:
>
> Same here, whatever you'd like to do with my % is fine with me.
> Thanks,
> John
>
> On Thu, Apr 23, 2020 at 10:58 AM Braun, Joseph <joseph_braun_1@brown.edu> wrote:
>
> > Looks good to me.
> >
> > Joe
> >
> > **-----**
> > **Joseph M. Braun, RN, MSPH, PhD**
> > Associate Professor of Epidemiology
> > Director, Center for Environmental Health and Technology
> > Brown University School of Public Health
> > Box G-S121-2, Providence, RI 02912, USA
> > Tel: +1 (401) 863-5397
> > **joseph_braun_1@brown.edu**
> > **https://vivo.brown.edu/display/jb93**
> >
> > On Thu, Apr 23, 2020 at 10:55 AM Radke-Farabaugh, Elizabeth <radke-farabaugh.elizabeth@epa.gov> wrote:

Hi Glinda, Joe, and John,

I hope you're all doing well. I checked in with Glinda and Joe already on part of this, but I wanted to share with all of you the proposed % contributions for our submission to an EPA award. We're submitting three papers as a package (attached if you're interested), and have to identify overall contributions to the whole package. I think the contributions for the male repro paper were fairly straightforward, but combining everything to one package was a bit tricky. Because the toxicology paper for DIBP had a lot of coauthors, I felt that the overall contribution to the package for Erin Yost, who with me was the leader of the EI special issue, was too low. So I suggested a few manual adjustments to reflect the overall package contribution vs. individual papers (see table below). Since the percentages are only used to determine the cash award allocation and external authors are not eligible to receive the award, I suggested reducing your percentages for the overall package (not the individual paper). Please let me know if this allocation is acceptable for you.

Thanks,

Beth

From: Yost, Erin <Yost.Erin@epa.gov>
Sent: Thursday, April 23, 2020 10:27 AM
To: Blessinger, Todd <blessinger.todd@epa.gov>; Euling, Susan <Euling.Susan@epa.gov>; Arzuaga, Xabier <Arzuaga.Xabier@epa.gov>; brandy.beverly@nih.gov; Weaver, Andre <Weaver.James@epa.gov>; Keshava, Nagalakshmi <Keshava.Nagu@epa.gov>; Mudipalli, Anuradha <Mudipalli.Anu@epa.gov>; Dishaw, Laura <Dishaw.Laura@epa.gov>; Hotchkiss, Andrew <Hotchkiss.Andrew@epa.gov>; Makris, Susan <Makris.Susan@epa.gov>
Subject: STAA award submission for phthalates papers- please confirm your % contribution

Dear DIBP paper coauthors,

I hope you all are doing well! I wanted to let you all know that Beth and I are nominating some papers from the phthalates special issue for a STAA award (https://www.epa.gov/research/scientific-and-technological-achievement-award-staa). We are allowed to submit up to 3 published papers as a single package, so we selected the male repro epidemiology paper, the DIBP paper, and the dose-response modeling paper. We need to list the percent contribution of each coauthor to the submission package, so we calculated this by estimating each author's contribution to the individual manuscripts and then dividing that effort across the three papers. **(See the last column in the table below.)**

We are required to submit proof in writing that each author agrees with their estimated percent contribution, so **please reply to this email ASAP and let me know if you agree with your percent contribution.**

FYI, if we win, there are cash prizes that will be divided among EPA authors ($10K, $5K, or $2K), and each EPA author will receive a minimum of $250 regardless of their percent contribution.

Thanks!

-Erin

	DIBP paper	Epi paper	Dose-response paper	Adjusted total % contribution to STAA submission
Beth Radke		60		**20**
Erin Yost	35			**15**
Todd Blessinger	3		40	**14**
Sue Euling	15		20	**12**
Glinda Cooper		20		**6**
Lily Wang			15	**5**
Xabier Arzuaga	10			**3**
Brandy Beverly	10			**3**
Christine Cai			10	**3**
Joe Braun		10		**2**
John Meeker		10		**2**
Andre Weaver	6			**2**
Nagu Keshava	6			**2**
Anu Mudipalli	6			**2**
Gary Klinefelter			5	**2**
Anne-Marie Saillenfait			5	**2**
Karen Hogan			5	**2**
Laura Dishaw	3			**1**
Andrew Hotchkiss	3			**1**
Sue Makris	3			**1**
Total %	100	100	100	**100**

Erin Yost, Ph.D.

Toxicologist

U.S. Environmental Protection Agency

Center for Public Health and Environmental Assessment

Cell phone: 919-841-7926

--

John Meeker, ScD, CIH
Professor of Environmental Health Sciences
Professor of Global Public Health
Senior Associate Dean for Research
School of Public Health
University of Michigan

Yost, Erin

From: anne-marie.saillenfait@inrs.fr
Sent: Friday, April 24, 2020 3:12 PM
To: Blessinger, Todd
Subject: Re: FW: STAA award submission for phthalates papers - please confirm your % contribution

Dear Todd,

Thanks à lot for adding me to the list but it would be difficult for me to accept money for my contribution (essentially data of our study), considering the rules of my Institute.
Nevertheless, of course, I would be very honored if you could get this award.

I hope that you do not have too many problems with the virus. Presently I have to work at home but everything is alright till now.
Best regards
Anne Marie Saillenfait

Institut de Recherche et de Sécurité (INRS)
1 Rue du Morvan
CS 60027
54519 Vandoeuvre Cedex
France

tel: 03 83 50 20 39
https://gcc01.safelinks.protection.outlook.com/?url=http%3A%2F%2Fanne-marie.saillenfait%40inrs.fr%2F&data=02%7C01%7Cblessinger.todd%40epa.gov%7C57af57253c6649f5924708d7e8835812%7C88b378b367484867acf976aacbeca6a7%7C0%7C0%7C637233523127429752&sdata=f1sxCv2Wf6gIBsM8LHdvqzfZw2sNpHVkF2ol99ELcoA%3D&reserved=0

-----"Blessinger, Todd" <blessinger.todd@epa.gov> a écrit : -----

==========
A : "anne-marie.saillenfait@inrs.fr" <anne-marie.saillenfait@inrs.fr> De : "Blessinger, Todd" <blessinger.todd@epa.gov> Date : 24/04/2020 20:54 Objet : FW: STAA award submission for phthalates papers - please confirm your % contribution ==========
Dear Anne-Marie,

I hope you are doing well. I want to clarify regarding the email below that I just sent to the phthalate syndrome team. Only EPA employees are eligible for this award (at least the monetary award), but we are required to ask all participants, even those outside EPA, to confirm their contributions. I am going to inquire with the agency as to what recognition is received by non-EPA employees and will let you know.

Thank you,
-Todd

From: Blessinger, Todd
Sent: Friday, April 24, 2020 2:54 PM

To: Cai, Christine <Cai.Christine@epa.gov>; Euling, Susan <Euling.Susan@epa.gov>; Hogan, Karen <Hogan.Karen@epa.gov>; Klinefelter, Gary <Klinefelter.Gary@epa.gov>; Wang, Lily (Lihong) <wang.lily@epa.gov>; anne-marie.saillenfait@inrs.fr
Subject: STAA award submission for phthalates papers - please confirm your % contribution

Dear phthalates syndrome team,

Erin Yost and Beth Radke of the DIBP team are nominating some articles from the phthalates special issue for a Scientific and Technological Achievement Award (STAA; for more information, see this page: https://www.epa.gov/research/scientific-and-technological-achievement-award-staa). Up to 3 published articles can be submitted as a single package, and one of those being submitted is the ordinal dose-response DIBP article (the other two are the DIBP systematic review article and the male repro epidemiology article). Because you are all co-authors on this article, the percent contribution of each coauthor needs to be listed in the submission package. Beth, Erin, and I calculated percent contributions for each of our respective articles by estimating each author's contribution to the individual manuscripts. Then we divided that effort across the three papers. (See the last column in the table below for these percents.)

We would like your input on the contributions we proposed, and we are required to submit proof in writing that each author agrees with their estimated percent contribution. Please reply to this email ASAP and let me know if you agree with your percent contribution.

FYI, if we win, there are cash prizes ($10K, $5K, and $2K for levels I, II, and III, respectively) that will be divided among EPA authors according to their contribution to the total effort (in last column of table), and each EPA author will receive a minimum of $250 regardless of their percent contribution.

Thanks!
-Erin

DIBP paper
Epi paper
Dose-response paper
Adjusted total % contribution to STAA submission Beth Radke
60
20
Erin Yost
35

15
Todd Blessinger
3
40
14
Sue Euling
15
20
12
Glinda Cooper
20
6
Lily Wang

15
5
Xabier Arzuaga
10
3
Brandy Beverly
10
3
Christine Cai

10
3
Joe Braun
10
2
John Meeker
10
2
Andre Weaver
6
2
Nagu Keshava
6
2
Anu Mudipalli
6
2
Gary Klinefelter

5
2
Anne-Marie Saillenfait

5
2
Karen Hogan

5
2
Laura Dishaw
3
1
Andrew Hotchkiss
3
1
Sue Makris
3
1

Total %
100
100
100
100

Todd Blessinger, Ph.D.
Center for Public Health and Environmental Assessment U.S. Environmental Protection Agency
Office: 202-564-7641
blessinger.todd@epa.gov<mailto:blessinger.todd@epa.gov>

Yost, Erin

From: Blessinger, Todd
Sent: Monday, April 27, 2020 3:21 PM
To: Yost, Erin; Radke-Farabaugh, Elizabeth
Subject: FW: STAA award submission for phthalates papers - please confirm your % contribution

Erin and Beth, below is Lily Wang's response the percent contribution. I cut out an intermediate conversation that was unnecessary and distracting.
-Todd

From: Wang, Lily (Lihong) <wang.lily@epa.gov>
Sent: Monday, April 27, 2020 10:45 AM
To: Blessinger, Todd <blessinger.todd@epa.gov>
Subject: RE: STAA award submission for phthalates papers - please confirm your % contribution

Hi Todd,

Thanks for giving the details and context. As I mentioned, I agreed with my %.

Best,
Lily

…
…
…

From: Blessinger, Todd
Sent: Friday, April 24, 2020 2:54 PM
To: Cai, Christine <Cai.Christine@epa.gov>; Euling, Susan <Euling.Susan@epa.gov>; Hogan, Karen <Hogan.Karen@epa.gov>; Klinefelter, Gary <Klinefelter.Gary@epa.gov>; Wang, Lily (Lihong) <wang.lily@epa.gov>; anne-marie.saillenfait@inrs.fr
Subject: STAA award submission for phthalates papers - please confirm your % contribution

Dear phthalates syndrome team,

Erin Yost and Beth Radke of the DIBP team are nominating some articles from the phthalates special issue for a Scientific and Technological Achievement Award (STAA; for more information, see this page: https://www.epa.gov/research/scientific-and-technological-achievement-award-staa). Up to 3 published articles can be submitted as a single package, and one of those being submitted is the ordinal dose-response DIBP article (the other two are the DIBP systematic review article and the male repro epidemiology article). Because you are all co-authors on this article, the percent contribution of each coauthor needs to be listed in the submission package. Beth, Erin, and I calculated percent contributions for each of our respective articles by estimating each author's contribution to the individual manuscripts. Then we divided that effort across the three papers. **(See the last column in the table below for these percents.)**

We would like your input on the contributions we proposed, and we are required to submit proof in writing that each author agrees with their estimated percent contribution. **Please reply to this email ASAP and let me know if you agree with your percent contribution.**

FYI, if we win, there are cash prizes ($10K, $5K, and $2K for levels I, II, and III, respectively) that will be divided among EPA authors according to their contribution to the total effort (in last column of table), and each EPA author will receive a minimum of $250 regardless of their percent contribution.

Thanks!
-Erin

	DIBP paper	Epi paper	Dose-response paper	Adjusted total % contribution to STAA submission
Beth Radke		60		**20**
Erin Yost	35			**15**
Todd Blessinger	3		40	**14**
Sue Euling	15		20	**12**
Glinda Cooper		20		**6**
Lily Wang			15	**5**
Xabier Arzuaga	10			**3**
Brandy Beverly	10			**3**
Christine Cai			10	**3**
Joe Braun		10		**2**
John Meeker		10		**2**
Andre Weaver	6			**2**
Nagu Keshava	6			**2**
Anu Mudipalli	6			**2**
Gary Klinefelter			5	**2**
Anne-Marie Saillenfait			5	**2**
Karen Hogan			5	**2**
Laura Dishaw	3			**1**
Andrew Hotchkiss	3			**1**
Sue Makris	3			**1**
Total %	100	100	100	**100**

Todd Blessinger, Ph.D.
Center for Public Health and Environmental Assessment
U.S. Environmental Protection Agency
Office: 202-564-7641
blessinger.todd@epa.gov

Yost, Erin

From: Weaver, Andre
Sent: Thursday, April 23, 2020 1:07 PM
To: Yost, Erin
Subject: RE: STAA award submission for phthalates papers- please confirm your % contribution

No concerns about the overall % contribution. I have not been nominated for STAA before.

Andre

From: Yost, Erin <Yost.Erin@epa.gov>
Sent: Thursday, April 23, 2020 10:36 AM
To: Blessinger, Todd <blessinger.todd@epa.gov>; Euling, Susan <Euling.Susan@epa.gov>; Arzuaga, Xabier <Arzuaga.Xabier@epa.gov>; brandy.beverly@nih.gov; Weaver, Andre <Weaver.James@epa.gov>; Keshava, Nagalakshmi <Keshava.Nagu@epa.gov>; Mudipalli, Anuradha <Mudipalli.Anu@epa.gov>; Dishaw, Laura <Dishaw.Laura@epa.gov>; Hotchkiss, Andrew <Hotchkiss.Andrew@epa.gov>; Makris, Susan <Makris.Susan@epa.gov>
Subject: RE: STAA award submission for phthalates papers- please confirm your % contribution

I almost forgot- please also let me know if you have been listed as a coauthor on a STAA award application within the last 5 years. If so, we are required to provide a description of this in our application. Thanks so much!

-Erin

From: Yost, Erin
Sent: Thursday, April 23, 2020 10:27 AM
To: Blessinger, Todd <blessinger.todd@epa.gov>; Euling, Susan <Euling.Susan@epa.gov>; Arzuaga, Xabier <Arzuaga.Xabier@epa.gov>; Beverly, Brandy (NIH/NIEHS) [E] <brandy.beverly@nih.gov>; Weaver, Andre <Weaver.James@epa.gov>; Keshava, Nagalakshmi <Keshava.Nagu@epa.gov>; Mudipalli, Anuradha <Mudipalli.Anu@epa.gov>; Dishaw, Laura <Dishaw.Laura@epa.gov>; Hotchkiss, Andrew <Hotchkiss.Andrew@epa.gov>; Makris, Susan <Makris.Susan@epa.gov>
Subject: STAA award submission for phthalates papers- please confirm your % contribution

Dear DIBP paper coauthors,
I hope you all are doing well! I wanted to let you all know that Beth and I are nominating some papers from the phthalates special issue for a STAA award (https://www.epa.gov/research/scientific-and-technological-achievement-award-staa). We are allowed to submit up to 3 published papers as a single package, so we selected the male repro epidemiology paper, the DIBP paper, and the dose-response modeling paper. We need to list the percent contribution of each coauthor to the submission package, so we calculated this by estimating each author's contribution to the individual manuscripts and then dividing that effort across the three papers. **(See the last column in the table below.)**

We are required to submit proof in writing that each author agrees with their estimated percent contribution, so **please reply to this email ASAP and let me know if you agree with your percent contribution.**

FYI, if we win, there are cash prizes that will be divided among EPA authors ($10K, $5K, or $2K), and each EPA author will receive a minimum of $250 regardless of their percent contribution.

Thanks!
-Erin

	DIBP paper	Epi paper	Dose-response paper	Adjusted total % contribution to STAA submission
Beth Radke		60		**20**
Erin Yost	35			**15**
Todd Blessinger	3		40	**14**
Sue Euling	15		20	**12**
Glinda Cooper		20		**6**
Lily Wang			15	**5**
Xabier Arzuaga	10			**3**
Brandy Beverly	10			**3**
Christine Cai			10	**3**
Joe Braun		10		**2**
John Meeker		10		**2**
Andre Weaver	6			**2**
Nagu Keshava	6			**2**
Anu Mudipalli	6			**2**
Gary Klinefelter			5	**2**
Anne-Marie Saillenfait			5	**2**
Karen Hogan			5	**2**
Laura Dishaw	3			**1**
Andrew Hotchkiss	3			**1**
Sue Makris	3			**1**
Total %	100	100	100	**100**

Erin Yost, Ph.D.
Toxicologist
U.S. Environmental Protection Agency
Center for Public Health and Environmental Assessment
Cell phone: 919-841-7926

Yost, Erin

From: Blessinger, Todd
Sent: Thursday, April 30, 2020 8:38 AM
To: Yost, Erin
Subject: RE: STAA award submission for phthalates papers- please confirm your % contribution

I confirm my concurrence with my percent contribution.
-Todd

From: Yost, Erin <Yost.Erin@epa.gov>
Sent: Wednesday, April 29, 2020 10:32 PM
To: Blessinger, Todd <blessinger.todd@epa.gov>
Subject: FW: STAA award submission for phthalates papers- please confirm your % contribution

Hi Todd,
Can you reply to this email chain to confirm that you agree with your percent contribution? The email chain where we originally worked out the % contributions had a lot of distracting side conversations, and it would be good to have a clean record. I'll be submitting the nomination tomorrow (Thursday).

Thanks!
Erin

From: Yost, Erin
Sent: Thursday, April 23, 2020 10:27 AM
To: Blessinger, Todd <blessinger.todd@epa.gov>; Euling, Susan <Euling.Susan@epa.gov>; Arzuaga, Xabier <Arzuaga.Xabier@epa.gov>; Beverly, Brandy (NIH/NIEHS) [E] <brandy.beverly@nih.gov>; Weaver, Andre <Weaver.James@epa.gov>; Keshava, Nagalakshmi <Keshava.Nagu@epa.gov>; Mudipalli, Anuradha <Mudipalli.Anu@epa.gov>; Dishaw, Laura <Dishaw.Laura@epa.gov>; Hotchkiss, Andrew <Hotchkiss.Andrew@epa.gov>; Makris, Susan <Makris.Susan@epa.gov>
Subject: STAA award submission for phthalates papers- please confirm your % contribution

Dear DIBP paper coauthors,
I hope you all are doing well! I wanted to let you all know that Beth and I are nominating some papers from the phthalates special issue for a STAA award (https://www.epa.gov/research/scientific-and-technological-achievement-award-staa). We are allowed to submit up to 3 published papers as a single package, so we selected the male repro epidemiology paper, the DIBP paper, and the dose-response modeling paper. We need to list the percent contribution of each coauthor to the submission package, so we calculated this by estimating each author's contribution to the individual manuscripts and then dividing that effort across the three papers. **(See the last column in the table below.)**

We are required to submit proof in writing that each author agrees with their estimated percent contribution, so **please reply to this email ASAP and let me know if you agree with your percent contribution.**

FYI, if we win, there are cash prizes that will be divided among EPA authors ($10K, $5K, or $2K), and each EPA author will receive a minimum of $250 regardless of their percent contribution.

Thanks!
-Erin

	DIBP paper	Epi paper	Dose-response paper	Adjusted total % contribution to STAA submission
Beth Radke		60		**20**
Erin Yost	35			**15**
Todd Blessinger	3		40	**14**
Sue Euling	15		20	**12**
Glinda Cooper		20		**6**
Lily Wang			15	**5**
Xabier Arzuaga	10			**3**
Brandy Beverly	10			**3**
Christine Cai			10	**3**
Joe Braun		10		**2**
John Meeker		10		**2**
Andre Weaver	6			**2**
Nagu Keshava	6			**2**
Anu Mudipalli	6			**2**
Gary Klinefelter			5	**2**
Anne-Marie Saillenfait			5	**2**
Karen Hogan			5	**2**
Laura Dishaw	3			**1**
Andrew Hotchkiss	3			**1**
Sue Makris	3			**1**
Total %	100	100	100	**100**

Erin Yost, Ph.D.
Toxicologist
U.S. Environmental Protection Agency
Center for Public Health and Environmental Assessment
Cell phone: 919-841-7926

JOHNS HOPKINS
U N I V E R S I T Y

Bloomberg School of Public Health
624 North Broadway/Room 429
Baltimore, MD 21205-2179
410-955-1604
E-mail: tburke1@jhu.edu

Thomas A. Burke, PhD, MPH
Jacob I and Irene B. Fabrikant Professor and Chair in Health, Risk and Society
Director, Risk Sciences and public Policy Institute

April 29, 2020

EPA Science Advisory Board
Science and Technological Achievement Award Selection Committee

I am writing to support the Science and Technological Achievement Award (STAA) nomination of a three paper series on the toxicity and human health effects of phthalate exposure. The papers are: Yost et al., *Hazards of diisobutyl phthalate exposure: A systemativc review of animal toxicology studies* ; Radke et al., *Phthalate exposure and male reproductive outcome: A systematic review of human epidemiological evidence* ; and Blessinger et al., *Ordinal dose-response modeling approach for phthalate syndrome*. These papers represent an outstanding compilation of the state of knowledge of the health effects of these ubiquitous and important compounds. They also advance the methods of systematic review and human health risk assessment. They are outstanding candidates for recognition with the STAA award.

Systematic review is a cornerstone of contemporary health risk assessment. The National Academy of Sciences has advocated the development and use of systematic review to improve the transparency and interpretation of scientific evidence of toxicity and human health effects. The methods are essential to the public health mission of the Agency, perhaps most important to the implementation of the Toxic Substance Control Act. The papers by Yost et al and Radke et al are excellent examples of the conduct of systematic review to evaluate the evidence base for both human epidemiological evidence and animal toxicology. As a Professor and teacher of risk assessment methods, I consider then to be strong examples of very well conducted systematic reviews, objectively compiling the evidence and presenting the key strengths, uncertainties, risk of bias, and findings for each study. I have recommended these papers to my colleagues and students as examples of challenging systematic reviews done well.

Understanding the dose – response relationship for phthalates is essential for assessing potential health risks and informing policy decisions. The Blessinger et al paper builds upon the systematic reviews to examine and present a dose response modeling approach for considering the severity of multiple reproductive endpoints in the risk assessment process. I feel this work advances both the science and methods of risk assessment, and has potential applications in both single compound and cumulative risk assessment.

In summary, I strongly recommend these papers for the STAA award. They address a critical public health issue – reproductive health; provide important contributions to the evidence base for evaluating phthalates; advance the methods of health risk assessment, and address the translation of evidence to inform Agency decision-making. Most importantly they exemplify the excellence and leadership of EPA science.

Sincerely,

Thomas A. Burke, PhD, MPH

cc. Dr. Kristina Thayer

COLLEGE OF VETERINARY MEDICINE
& BIOMEDICAL SCIENCES

Department of Veterinary Integrative Biosciences

TEXAS A&M UNIVERSITY

April 29, 2020

U.S. EPA Center for Public Health and Environmental Assessment
Washington, DC 20460

Dear STAA Review Committee:

I would like to strongly recommend the following package of Phthalates publications for a STAA:

> Radke EG, Braun JM, Meeker JD, Cooper GS. Phthalate exposure and male reproductive outcomes: A systematic review of the human epidemiological evidence. Environ Int. 2018 Dec;121(Pt 1):764-793. doi: 10.1016/j.envint.2018.07.029. Epub 2018 Oct 16. Review. Erratum in: Environ Int. 2019 Apr;125:606-607. PubMed PMID: 30336412.
>
> Yost EE, Euling SY, Weaver JA, Beverly BEJ, Keshava N, Mudipalli A, Arzuaga X, Blessinger T, Dishaw L, Hotchkiss A, Makris SL. Hazards of diisobutyl phthalate (DIBP) exposure: A systematic review of animal toxicology studies. Environ Int. 2019 Apr;125:579-594. doi: 10.1016/j.envint.2018.09.038. Epub 2018 Dec 25. PubMed PMID: 30591249.
>
> Blessinger TD, Euling SY, Wang L, Hogan KA, Cai C, Klinefelter G, Saillenfait AM. Ordinal dose-response modeling approach for the phthalate syndrome. Environ Int. 2020 Jan;134:105287. doi: 10.1016/j.envint.2019.105287. Epub 2019 Nov 26. PubMed PMID: 31783243.

By way of background, I was an environmental health scientist and then branch chief in the U.S. EPA Office of Research and Development from 2002-2015, and worked on numerous human health assessments within the Integrated Risk Information System (IRIS) Program, so I have extensive experience with the review and synthesis of scientific literature to inform policy and decisions. Moreover, I was part of four different EPA teams that received STAA awards from 2007-2014. I have since joined Texas A&M University as a Professor in the Department of Veterinary Integrative Biosciences in the College of Veterinary Medicine and Biomedical Sciences, where I teach, conduct research, and perform service primarily within the Interdisciplinary Faculty of Toxicology. Part of my service has included participating in numerous national and international expert and advisory committees, including membership on the *National Academy of Sciences/National Research Council Committee on Unraveling Low Dose Toxicity: Case Studies of Systematic Review of Evidence*, which used phthalates as a case study. Thus, I am also intimately familiar with systematic review methods both generally as well as specifically applied to phthalates.

In my view, the set of publications above satisfy all five review criteria for STAAs:

(1) The nominated publication(s) have resulted in revised knowledge on the health effects of phthalates, and is expected to represent an important advancement of scientific knowledge relevant to environmental issues and EPA's mission. Phthalates exposure is widespread base on biomonitoring data, and concerns about human health effects have been a major issue for decades. Importantly, these publications together provide not only exemplary examples of application of systematic review to phthalates, but go beyond only hazard identification to advance dose-response methods for complex endpoints such as phthalates syndrome.

Texas Veterinary Medical Center
TAMU 4458
College Station, TX 77843-4458

Tel. 979.845.2828 Fax 979.847.8981
www.vetmed.tamu.edu

(2) All the publications show high degree of originality, creativeness, initiative, and problem-solving ability accompanied by a level of effort required to produce the results. For instance, the systematic reviews of Yost et al. and Radke et al. provide important case studies regarding how concerns about bias can be weighed when upgrading or downgrading confidence in a body of evidence, an area of uncertainty identified in several NRC reports. Additionally, the ordinal dose-response model by Blessinger et al. provides a method for modeling a syndrome of endpoints (in this case, phthalate syndrome) that are mechanistically related but have different levels of severity. Finally, systematic review is an extremely intensive process requiring extensive coordination across a multi-disciplinary team.

(3) These articles will play an important role for risk management of environmental contamination by phthalates, at the local, national and international levels. Although U.S. EPA has decided not to proceed with the IRIS assessment for phthalates, there are numerous phthalates that are currently undergoing high priority risk evaluations under the Toxic Substances Control Action. Not only the results of these analyses, but also the demonstration of appropriate systematic review methods, will be invaluable to EPA's TSCA evaluations. Additionally, many state, local, and international bodies are also concerned about phthalate exposure, and will definitely be drawing upon these articles for their own hazard and risk evaluations. Overall, these articles will likely be highly influential in both the hazard identification and dose-response analyses conducted across the country and the world regarding phthalates.

(4) The extent of the beneficial impact of the accomplishment and the degree to which the accomplishment has been favorably recognized from outside EPA. Almost 10 years ago, U.S. EPA was severely criticized by outside stakeholders as well as the National Research Council for its failure to use consistent and transparent methods in its chemical assessment. This was viewed as a significant detriment to the reliability of IRIS assessments. To address this, NRC recommended that IRIS adopt systematic review methods. The publication of these systematic reviews of phthalates demonstrates that IRIS has been able to rise to the challenge of adapting systematic review methods to meet the needs of the EPA and using this as the foundation of its chemical assessments.

(5) Environment International is widely recognized as one of the top multi-disciplinary environmental health journals in the field, and known to be of high stature and having a high quality of the peer review.

In summary, I have no hesitation in recommending the above publications for the highest level of STAA. These articles exemplify the type of multi-disciplinary, scientifically rigorous, and societally impactful research that scientists at the U.S. EPA are uniquely positioned to conduct. If you have any questions, please do not hesitate to contact me at wchiu@cvm.tamu.edu.

Sincerely yours,

Weihsueh Chiu, PhD
Professor, Veterinary Integrative Biosciences
College of Veterinary Medicine and Biomedical Sciences
Texas A&M University
College Station, TX

28 April 2020

Paul Whaley
Lancaster Environment Centre
Lancaster University
Lancaster
United Kingdom

Letter of Recommendation, US EPA IRIS Program Systematic Reviews on the Health Effects of Exposure to Phthalates

To whom it may concern,

It is my pleasure to write this letter of recommendation in support of consideration of the US EPA IRIS Program Systematic Reviews (SRs) on the health effects of exposure to phthalates for the Scientific and Technological Achievement Award.

I write as Systematic Reviews Editor of *Environment International* (IF 7.94), being the first-ever - and still the sole - specialist editor of environmental health SRs. I was appointed to my position in 2016; under my purview *Environment International* has since become recognised as setting by far the most rigorous and exacting SR publishing standards in our field. In addition to the IRIS Phthalate SRs, I have edited over 200 SR manuscripts. As an editor and researcher, I work with a range of national and international organisations on developing and promoting high-quality SR methods. These include the EU Joint Research Centre, World Health Organization, International Labour Organization, European Food Safety Authority, US National Toxicology Program, US EPA, the GRADE Working Group, and the Evidence-based Toxicology Collaboration, among others.

With that experience, I can confidently attest to the outstanding scientific quality and value of the collection of IRIS Phthalate SRs, as led by Dr Elizabeth Radke and Dr Erin Yost. They are a unique, first-of-their-kind collection of extremely complex SRs of hundreds of studies, subjected to a degree of rigour in external editorial and peer-review process which I believe will have exceeded that applied by a journal to any previous EPA SR. It is an outstanding achievement, serving as an international benchmark in agency-level application of SR methods in chemical assessment.

It is my view is that four main groups have historically been at the forefront of implementing SR methods in the environmental health sciences and its regulatory contexts. These are: the US National Toxicology Program Office of Health Assessment and Translation; the European Food Safety Authority; the World Health Organisation; and (from the academic field) the Navigation Guide at the University of California San Francisco (CA). These organisations have shown real leadership in pioneering SR methods for the environmental health context, using novel methods to conduct high-quality SRs on difficult topics in sometimes highly challenging regulatory environments.

The IRIS Phthalate SRs are a project which, in my opinion, has elevated the US EPA IRIS Program into this top echelon of international scientific leadership in SR methods. It is impossible to capture in a short letter the breadth of progress which the IRIS Phthalate SRs represent in terms of new knowledge, creativeness, and recognition, but I would at least emphasise the following:

- **Progress in development and implementation of SR methods**. Systematic review was revolutionary in the medical sciences. Its widespread adoption in the early 1990s allowed, for the first time, existing evidence of the relative efficacy of medical treatments to be evaluated

according to the same scientific standards as which primary research was being conducted. The consequences for healthcare delivery, in terms of ensuring patients have the most effective treatments and preventing resources being wasted on unnecessary research, have been drastic; the hope is that SR methods will have the same impact in understanding and addressing the impact of environmental challenges have on people's health. The IRIS Phthalate SRs are a quantum shift in delivering on this promise, resolving multiple challenges in application of methods and clarifying research needs in understanding how SR methods need to evolve to handle the specific challenges of analysing environmental health as opposed to clinical research.

- **Delivery of the mission of the US EPA**. It is impossible to develop effective risk management and health policies unless one knows the state of the evidence upon which those policies are based. SR methods, with their approaches to locating all relevant evidence, appraising it for reliability, and making sense of what it means in relation to the information requirements of decision-makers, offer some of the best prospects of that knowledge being attained. It also has to be acknowledged, however, that SRs are extremely resource-intensive projects which take a long time to conduct; finding pragmatic approaches to accelerating the SR process without compromising the integrity of its results is a research priority. Not only have the IRIS Phthalate SRs provided what is arguably the definitive analysis of evidence of potential health harms from phthalate exposure, they identify multiple ways in which the SR process could in future be expedited, including integration of evidence mapping methods into the environmental assessment workflow.
- **Providing a creative response to a scientific challenge**. The US National Resource Council, in its review of the US EPA IRIS Program's methods for conducting health assessments, challenged the IRIS program to implement SR methods in order to deliver its mandate of providing consistent, timely and scientifically robust assessments of health risks posed by exposure to chemical substances. The IRIS Phthalate SRs are, I believe, the first full-blooded response to the NRC's challenge, presenting across multiple independent manuscripts a consistent, systematic approach to assessing health risks posed by exposure to a complex class of compounds. The creativity and discipline required to manage a diverse group of researchers, conducting a huge volume of analysis (almost unprecedented in my experience of SRs), according to a consistent methodology, almost defies description.

Even as the Editor, I find it difficult to account for how such a complex body of work has come together as a coherent whole, and have to satisfy myself with admiring the brilliance and steadfastness of the authors. They and the IRIS Program deserve the highest level of praise and recognition for the delivery of an outstanding body of work.

Yours sincerely,

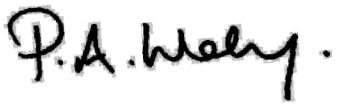

Paul Whaley

Research Fellow, Evidence-based Toxicology Collaboration
Systematic Reviews Editor, *Environment International* (IF 7.9)

Table of Contents

General_Authors_Publications.....2
LI-266684_The_geographic_distribution_and_economic_value_of_climate_change_rel12
LI-266684_uawm_a_996270_sm8196.....24
Amanda_Curry.....31
Chris_Nolte.....33
Neal_Fann.....34
Sharon_Phillips.....35
Susan_Anenberg.....39
Tanya_Spero.....41

United States Environmental Protection Agency
Washington, DC 20460

STAA REPORT FOR THE SCIENTIST NOMINATIONS

General Information:

Nomination ID/App ID:	20-095
Research Category Primary:	Integrated Risk Assessment (IR)
Research Category Secondary:	
Laboratory/Office Name:	OAR
Nomination Entered By:	Patrick Dolwick

Eligibility Checklist:

[Y] The nominated publication(s) has not been submitted to a previous STAA competition.

[Y] The nominated publication(s) was published on or before January 1, 2017 and on or after January 1,2012

[Y] The principal author was an EPA employee or a PHS employee assigned to EPA when the research was performed

[Y] The EPA authors (includes PHS employees assigned to EPA) contributed collectively a minimum of 50% toward the publication(s)

Nominating Official Name:	Erika Sasser
Nominating Official Title:	DIRECTOR
Nominating OfficialEmail:	sasser.erika@epa.gov
STAA Coordinator Name:	Kathleen Wiser
STAA Coordinator Email:	wiser.kathi@epa.gov

Justifications:

Justification 1:

This article demonstrated a framework by which EPA could, for the first time, estimate the geographic scope and magnitude of the potential ground-level ozone increase and associated public health burden under multiple climate scenarios within a relatively near-term time frame (2030). This risk assessment was based on an innovative sequential linkage of a suite of modeling tools designed to quantify: (a) global climate impacts from two greenhouse gas forcing scenarios, (b) the regional climate changes over the United States at a finer spatial resolution, (c) the ground-level ozone impacts driven by the regional climate, and finally (d) the resultant health impacts and economic value of climate-related changes in 2030 ozone air pollution levels in the United States. The paper concluded that even near-term changes to the climate have the potential to substantially affect ground-level ozone. Using a 2030 U.S. emission projection with regional climate fields downscaled from two Representative Concentration Pathways (RCP 6.0 and RCP 8.5), we projected mean temperature increases of 1 to 4°C and climate-driven mean daily 8-hr maximum ozone increases of 1 to 5 ppb across portions of the U.S., though each climate scenario produced ozone levels that varied significantly over space and time. These increased ozone levels were estimated to result in tens to thousands of ozone-related premature deaths and illnesses per year and an economic burden as high as tens of billions of U.S. dollars (2010$).

There were several unique facets to this study beyond the linkage of state-of-the science global and regional climate models with regional air quality and health impact assessment models. Unlike previous studies of the ozone penalty due to a warming climate (e.g., Jacob and Winner, 2009), the estimated ozone effects in the year 2030 utilized an EPA emissions projection that accounted for “on the books” emission control measures that will also influence the level and distribution of ozone precursor emissions. Additionally, this paper characterized the variability in potential ozone-related impacts over both space (by U.S. county) and by climate scenario. Finally, the paper estimated a dollar value associated with the projected ozone-related health impacts, giving insight to the potential economic value of this particular aspect of near-future climate change.

As outlined in “Working Together: FY 2018-2022 U.S. EPA Strategic Plan”, one of EPA’s priority activities is to support attainment of the national ambient air quality standards (NAAQS) by working with our state and tribal partners to develop informed implementation plans to reduce air pollution. The NAAQS attainment deadlines established in the Clean Air Act for ground-level ozone range from 3 to 20 years, which is much shorter than the time frames usually associated with analyses of climate effects on air quality. The work summarized in this paper substantially advanced the scientific knowledge on the subject of near-future ozone levels across the U.S. and provided valuable information to air quality planners. This work was a prime example of EPA’s strategic goal to prioritize robust science by, in part, providing the human exposure and environmental modeling, monitoring, metrics, and information needed to inform air quality decision making at the state, tribal, and local level.

The analytical framework developed in this paper also substantially informed the air quality chapter for the U.S. Global Climate Research Program report: “The Impacts of Climate Change on Human Health in the United States: A Scientific Assessment”. The key finding of this chapter was that climate change will make it harder for any given regulatory approach to reduce ground-level ozone pollution in the future as meteorological conditions become increasingly conducive to forming ozone over most of the United States. This framework also informed additional analyses that were used in the EPA Climate Change Impacts and Risk Analysis (CIRA) project which quantified the physical effects and economic damages under multiple climate change scenarios (U.S. EPA, 2017) and the 4th National Climate Assessment (U.S. Global Change Research Program, 2018).

Justification 2A:

N/A

Justification 2B:

Christopher Nolte: "Does Nudging Squelch the Extremes in Regional Climate Modeling?". Published in Journal of Climate. 2017 Level III award.

Christopher Nolte: "Increasing the credibility of regional climate simulations by introducing subgridscale cloudradiation interactions". Published in JGR-Atmospheres. 2019 Honorable Mention award.

Pat Dolwick: "Dynamic evaluation of CMAQ part I: Separating the effects of changing emissions and changing meteorology on ozone levels between 2002 and 2005 in the eastern US". Published in Atmospheric Environment. 2019. Honorable Mention award.

Tanya Spero (Otte): "WRF-CMAQ two-way coupled system with aerosol feedback: software development and preliminary results". Published in Geosci. Model Dev., 2015. Level III award.

Tanya Spero (Otte): "Does Nudging Squelch the Extremes in Regional Climate Modeling?". Published in Journal of Climate. 2017. Level III award.

Tanya Spero: "Increasing the credibility of regional climate simulations by introducing subgridscale cloudradiation interactions". Published in JGR-Atmospheres. 2019 Honorable Mention award.

Susan Anenberg: "Estimating the National Public Health Burden Associated with Exposure to Ambient PM2.5 and Ozone". Published in Risk Analysis. 2014 Level I award.

Justification 2C:

The publication nominated here focuses on development and demonstration of a framework by which EPA could, for the first time, estimate the geographic scope and magnitude of the potential ground-level ozone increase and associated public health burden under multiple climate scenarios within a relatively near-term time frame (2030). Some of the previous nominated work involves research into individual elements of this framework (i.e., regional climate simulations or AQ/health impact modeling), however the publication nominated here is distinct in that it aggregates the entire framework of tools (global climate modeling, regional climate modeling, regional air quality modeling and regional health impact modeling) to estimate the potential health impacts of a potentially warmer climate.

Justification 2D:

N/A

Justification 2E:

Fann is included as a co-author on an 2020 STAA nomination for a 2018 paper characterizing the health impacts associated with recent wildfire activity. Where that project explored present-day air quality and health relationships in the context of wildfire smoke, the publication nominated here focuses on the relationship between potential future climate change scenarios, ground-level ozone concentrations, and subsequent health impacts.

Justification 3A:

Citation: Fann, N., C.G. Nolte, P. Dolwick, T.L. Spero, A. Curry Brown, S. Phillips, and S. Anenberg, 2015: The geographic distribution and economic value of climate change-related ozone health impacts in the United States in 2030. Journal of the Air & Waste Management Association, 65 (5), 570-580. http://dx.doi.org/10.1080/10962247.2014.996270.

Based on data collected by the RTP Library on April 29, 2020, the Journal of the Air and Waste Management Association has an impact factor of 1.858, an immediacy index of 0.525, and a cited half-life of 12.1. The paper has 4,225 views as of April 29, 2020.

This paper has been cited 66 times in peer reviewed literature since its publication. This paper has informed literature reviews describing the connections between climate and air quality (Fiore et al., 2015; Orru et al., 2017); as well as other modeling estimates future climate impacts on human mortality and morbidity (Garcia-Menendez et al., 2015; Silva et al., 2016; Nassikas et al., 2020).

Further the paper has been cited by a number of major climate assessments, including the Fourth National Climate Assessment (U.S. Global Change Research Program, 2018) and the Impacts of Climate Change on Human Health in the United States: A Scientific Assessment (U.S. Global Climate Change Research Program, 2016). Both of these assessments received major news coverage when they were released with the relationship between between potential climate warming and worsened American health outcomes at the forefront of the media summaries.

Finally, in 2018 the OAQPS authors on this paper (Fann, Curry Brown, Dolwick, and Phillips) won an EPA Silver Medal for this work.

Justification 3B:

The paper went through the standard JAWMA external peer review process.

AUTHORS

Contributing Author

Author Name:	Neal Fann		
Professional Title:		Salutation:	
Email:	fann.neal@epa.gov	Organization:	
Mailing Address:			
Street Line 1:			
City:			
Zip Code:		State:	
At time of research was:	EPA Employee		
Separation Date:			
% of Effort:	30		

Contributing Author

Author Name:	Amanda Curry Brown		
Professional Title:		Salutation:	
Email:	amanda.curry@gmail.com	Organization:	
Mailing Address:			
Street Line 1:			
City:			
Zip Code:		State:	
At time of research was:	EPA Employee		
Separation Date:	Fri Aug 16 00:00:00 GMT 2019		
% of Effort:	5		

Contributing Author

Author Name:	Christopher Nolte		
Professional Title:		Salutation:	Dr.
Email:	nolte.chris@epa.gov	Organization:	
Mailing Address:			
Street Line 1:			
City:			
Zip Code:		State:	
At time of research was:	EPA Employee		
Separation Date:			
% of Effort:	30		

Contributing Author

Author Name:	Tanya Spero		
Professional Title:		Salutation:	
Email:	spero.tanya@epa.gov	Organization:	
Mailing Address:			
Street Line 1:			
City:			
Zip Code:		State:	
At time of research was:	EPA Employee		
Separation Date:			
% of Effort:	13		

Contributing Author

Author Name:	Sharon Phillips	
Professional Title:		Salutation:
Email:	phillips.sharon@epa.gov	Organization:
Mailing Address:		
Street Line 1:		
City:		
Zip Code:		State:
At time of research was:	EPA Employee	
Separation Date:		
% of Effort:	5	

Contributing Author

Author Name:	Susan Anenberg	
Professional Title:		Salutation:
Email:	sanenberg@gwu.edu	Organization:
Mailing Address:		
Street Line 1:		
City:		
Zip Code:		State:
At time of research was:	EPA Employee	
Separation Date:	Fri Jan 29 00:00:00 GMT 2016	
% of Effort:	5	

Principal Author

Author Name:	Patrick D. (Pat) Dolwick		
Professional Title:		Salutation:	
Email:	dolwick.pat@epa.gov	Organization:	
Mailing Address:			
Street Line 1:			
City:			
Zip Code:		State:	
At time of research was:	EPA Employee		
Separation Date:			
% of Effort:	12		

PUBLICATIONS

Publication 1:

Publication Title:	The geographic distribution and economic value of climate change-related ozone health impacts in the		
Publication Date:	Tue Apr 14 00:00:00 GMT 2015		
Journal/Publication Method:	Journal of the Air and Waste Management Association		
All Author(s):			
Volume:	65	Number:	5
Pages:	570-580	Immediately Index:	Immediately Index:
Citation ½ Life:	12.1	Impact Factor:	1.858

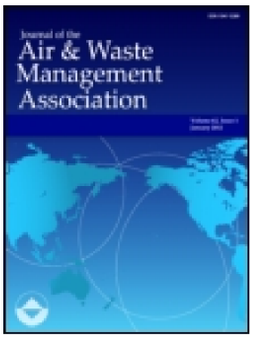

Journal of the Air & Waste Management Association

ISSN: 1096-2247 (Print) 2162-2906 (Online) Journal homepage: https://www.tandfonline.com/loi/uawm20

The geographic distribution and economic value of climate change-related ozone health impacts in the United States in 2030

Neal Fann, Christopher G. Nolte, Patrick Dolwick, Tanya L. Spero, Amanda Curry Brown, Sharon Phillips & Susan Anenberg

To cite this article: Neal Fann, Christopher G. Nolte, Patrick Dolwick, Tanya L. Spero, Amanda Curry Brown, Sharon Phillips & Susan Anenberg (2015) The geographic distribution and economic value of climate change-related ozone health impacts in the United States in 2030, Journal of the Air & Waste Management Association, 65:5, 570-580, DOI: 10.1080/10962247.2014.996270

To link to this article: https://doi.org/10.1080/10962247.2014.996270

View supplementary material

Accepted author version posted online: 22 Dec 2014.
Published online: 14 Apr 2015.

Submit your article to this journal

Article views: 4255

View related articles

View Crossmark data

Citing articles: 55 View citing articles

Full Terms & Conditions of access and use can be found at
https://www.tandfonline.com/action/journalInformation?journalCode=uawm20

TECHNICAL PAPER

The geographic distribution and economic value of climate change-related ozone health impacts in the United States in 2030

Neal Fann,[1,*] Christopher G. Nolte,[2] Patrick Dolwick,[1] Tanya L. Spero,[2] Amanda Curry Brown,[1] Sharon Phillips,[1] and Susan Anenberg[3]

[1]*U.S. Environmental Protection Agency, Office of Air Quality Planning and Standards, Research Triangle Park, NC, USA*
[2]*U.S. Environmental Protection Agency, Office of Research and Development, Research Triangle Park, NC, USA*
[3]*U.S. Chemical Safety and Hazard Investigation Board, Washington, DC, USA*
[*]*Please address correspondence to: Neal Fann, U.S. Environmental Protection Agency, Office of Air Quality Planning and Standards, 109 T. W. Alexander Dr., Research Triangle Park, NC 27711, USA; e-mail: fann.neal@epa.gov*

In this United States-focused analysis we use outputs from two general circulation models (GCMs) driven by different greenhouse gas forcing scenarios as inputs to regional climate and chemical transport models to investigate potential changes in near-term U.S. air quality due to climate change. We conduct multiyear simulations to account for interannual variability and characterize the near-term influence of a changing climate on tropospheric ozone-related health impacts near the year 2030, which is a policy-relevant time frame that is subject to fewer uncertainties than other approaches employed in the literature. We adopt a 2030 emissions inventory that accounts for fully implementing anthropogenic emissions controls required by federal, state, and/or local policies, which is projected to strongly influence future ozone levels. We quantify a comprehensive suite of ozone-related mortality and morbidity impacts including emergency department visits, hospital admissions, acute respiratory symptoms, and lost school days, and estimate the economic value of these impacts. Both GCMs project average daily maximum temperature to increase by 1–4°C and 1–5 ppb increases in daily 8-hr maximum ozone at 2030, though each climate scenario produces ozone levels that vary greatly over space and time. We estimate tens to thousands of additional ozone-related premature deaths and illnesses per year for these two scenarios and calculate an economic burden of these health outcomes of hundreds of millions to tens of billions of U.S. dollars (2010$).

Implications: Near-term changes to the climate have the potential to greatly affect ground-level ozone. Using a 2030 emission inventory with regional climate fields downscaled from two general circulation models, we project mean temperature increases of 1 to 4°C and climate-driven mean daily 8-hr maximum ozone increases of 1–5 ppb, though each climate scenario produces ozone levels that vary significantly over space and time. These increased ozone levels are estimated to result in tens to thousands of ozone-related premature deaths and illnesses per year and an economic burden of hundreds of millions to tens of billions of U.S. dollars (2010$).

Introduction

Climate change can affect air pollutant concentrations in a myriad of ways. Meteorological factors, such as temperatures, cloudiness, precipitation frequency and intensity, wind speeds, and planetary boundary layer heights, are all first-order drivers that influence air quality by determining photochemical reaction rates, vertical mixing, horizontal transport, biogenic emissions, and rates of pollutant removal by wet and dry deposition. Over longer time scales, climate change may also affect land use and population density, modifying emissions and meteorology and thus further affecting air quality. That these factors are related through a number of complex nonlinear pathways makes it challenging to model the individual role of each variable in a comprehensive framework.

For example, many epidemiological studies and risk assessments that examined the influence of climate change on air quality held most factors constant and allowed only a limited number of input parameters to vary (Tagaris et al., 2009; Selin et al., 2009; Bell et al., 2007; Jacobson, 2008; Silva et al., 2013; Post et al., 2012). Bell et al. (2007) project ozone levels to the year 2050 in 50 eastern U.S. cities using the Intergovernmental Panel on Climate Change (IPCC) Fourth Assessment Report A2 emission scenario and describe how climate change increases ozone-related daily mortality by maintaining constant anthropogenic emissions and allowing meteorology to vary over time. That study attempted to isolate the role of climate change on future meteorology and its subsequent effect on human health, holding all other factors constant. Other assessments quantify the effects of historical changes in climate, making it challenging to identify the factor(s) most responsible for climate-related effects. For example, Jacobson (2008) relates historical changes

Journal of the Air & Waste Management Association, 65(5):570–580, 2015. This article not subject to U.S. copyright law. ISSN: 1096-2247 print
DOI: 10.1080/10962247.2014.996270 Submitted October 3, 2014; final version submitted December 3, 2014; accepted December 4, 2014.
Color versions of one or more of the figures in the article can be found online at www.tandfonline.com/uawm.

in CO_2 levels to ambient ozone concentrations and the risk of premature death. Silva et al. (2013) quantifies the human health burden due to total anthropogenic outdoor air pollution and further characterizes the portion of this burden attributable to past climate change.

Climate and air quality modeling are each time and resource intensive, so simulations focus on a limited number of projected years, climate scenarios, and geographic locations (Chang, Zhou, and Fuentes, 2010; Sheffield et al., 2011; Chang, Hao, and Sarnat, 2014; Jackson et al., 2010). Sheffield et al. (2011) relate asthma emergency department visits in the 2020s in the New York City metropolitan area to simulated ozone changes using the IPCC A2 emission scenario. Chang et al. (2014) use a series of general circulation models (GCMs) and regional climate models to estimate the change in ozone-related emergency department visits due to climate change in the Atlanta, GA, metropolitan area.

Taken together, these time, resource and data constraints pose special challenges to disentangling the influence of each factor that might affect climate, air quality, and health. For this reason, analyses of relationships between air quality, climate and health generally alter a subset of input parameters such as the climate model or assumptions regarding future growth in emissions, or limit the geographical extent of the modeled air quality domain. Because calculating health impacts is comparatively computationally efficient, it is relatively easy to test the sensitivity of the results to various input parameters.

We select among the existing suite of climate models, greenhouse gas forcing scenarios, and population projections to examine the scope, magnitude, spatial distribution and economic value of climate-change related air quality and health impacts in the year 2030 relative to meteorology in the year 2000. Specifically, in this analysis we use multiple years within a time slice centered on 2030 from two GCMs and different climate forcing scenarios to account for different assumptions regarding the influence of future greenhouse gas concentrations on climate and to account for year-to-year variability in projected air quality impacts. We characterize the near-term influence of a changing climate on tropospheric ozone-related health impacts near the year 2030, which is a policy-relevant time frame that is subject to fewer uncertainties than previous studies that have focused on 2050 or later (e.g., Post et al., 2012).

In this study, we account for federal air quality policies requiring that areas meet the health-based National Ambient Air Quality Standard (NAAQS) for ozone. Our modeling reflects the emissions controls that have been adopted to reduce anthropogenic emissions of nitrogen oxides (NOx) and volatile organic compounds (VOCs), which will decline significantly between the present day and 2030. Our research aim is not to predict future ozone levels, but rather to quantify and monetize the "climate penalty" (Wu et al., 2008). That is, we seek to estimate the influence of near-term climate change on ozone, and the resulting health impacts and economic burden of those health impacts. We use the same anthropogenic emissions for the historical (ca. 2000) and future (ca. 2030) air quality modeling to isolate the influence of climate change on air quality, employing a 2030 emissions inventory that accounts for fully implementing existing anthropogenic emissions controls, which will strongly influence future tropospheric ozone levels. We quantify a comprehensive suite of ozone-related mortality and morbidity impacts including emergency department visits, hospital admissions, acute respiratory symptoms, and lost school days and estimate the economic value of these impacts. This analytical approach yields estimated climate change-attributable ozone-related premature deaths and illnesses that better account for the baseline atmospheric environment that is expected to prevail in the United States at 2030, as well as differences in climate scenarios and variability in predicted ozone levels across years and locations.

In the following, we first describe the methods we employ to project ozone levels and human health impacts. Next, for each scenario we report the ozone-related health impacts and the economic value of these outcomes; then we discuss the implications of these results.

Methods

Here we apply a suite of modeling tools that are linked sequentially to quantify (a) global climate impacts from specified greenhouse gas forcing scenarios, (b) the resultant regional climate changes over the United States at a higher spatial resolution, (c) the resultant near-surface ozone impacts over the United States driven by the regional climate, and (d) the resultant health impacts and economic value in the United States of climate-related changes in 2030 ozone air pollution levels (Figure 1).

Regional climate modeling

We used fields from two different GCMs that participated in the fifth phase of the Coupled Model Intercomparison Project (CMIP5) (Taylor, Stouffer, and Meehl, 2012). For each GCM, we downscaled two 11-year time slices: the 1995–2005 period from the historical 20th-century experiment, and the period 2025–2035 following one of the Representative Concentration Pathways (RCPs) (van Vuuren et al., 2011):

(1) RCP 8.5 modeled with the National Center for Atmospheric Research/Department of Energy (NCAR/DOE) Community Earth System Model (CESM) (hereafter referred to as "CESM/RCP 8.5").
(2) RCP 6.0 modeled with the NASA Goddard Institute for Space Studies (GISS) Model E2 (hereafter referred to as "GISS/RCP 6.0").

The RCP 8.5 scenario (Riahi et al., 2011) assumes "business as usual," where greenhouse gases will increase substantially over the next century, eventually leading to an 8.5 W m^{-2} radiative forcing level by 2100. The RCP 6.0 scenario (Fujino et al., 2006) assumes a modest degree of mitigation of greenhouse gas emissions such that total radiative forcing will increase over the next century before stabilizing at 6.0 W m^{-2} in 2100.

We downscaled these GCM projections using the Weather Research and Forecasting (WRF) model following techniques described by Bowden et al. (2012) and Otte et al. (2012). We

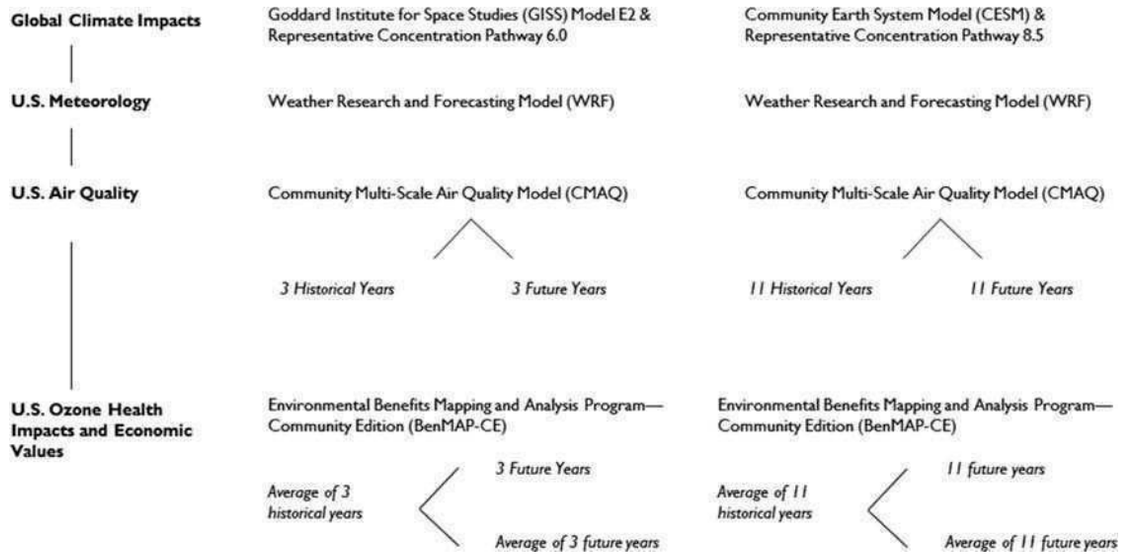

Figure 1. Overview of analytical approach to estimating climate-related ozone changes, health impacts, and economic values.

conducted WRF simulations at 36-km horizontal grid spacing over the United States, incorporating the global climate forcing at the lateral boundaries, through the interior of the domain (following Otte et al., 2012), and in the sea-surface temperatures. It is important to recognize that climate simulated by and downscaled from GCMs for a particular historical (or future) day cannot be compared directly with the actual meteorology that occurred (or will occur) on that day. Rather, the historical period 1995–2005 is intended to be representative of the year 2000, while the future period (2025–2035) is intended to be representative of 2030.

Air quality modeling

The historical and future climate WRF outputs were processed by the Meteorology–Chemistry Interface Processor (MCIP) (Otte and Pleim, 2010) and subsequently input into the Community Multi-scale Air Quality model (CMAQ) version 5.0.1 (Byun and Schere, 2006) to assess how the climate-driven meteorological changes would impact near-surface ozone levels (i.e., concentrations within the lowest model layer, about 38 m deep) over the continental United States. The air quality modeling was also conducted at 36-km grid spacing. While 36-km regional climate and air quality modeling would not be appropriate for projecting future ozone values in individual locations, this resolution is suitable for assessing the sensitivity of future regional-scale ozone levels to climate-driven changes in meteorology. The chemical lateral boundary conditions in the air quality modeling are based on an independent simulation of the year 2011 using the GEOS-Chem global chemical transport model (Bey et al., 2001). The time-varying chemical boundary conditions are used for each year and are unchanged between the base and future climate case. Thus, any changes in ozone transported into the domain are not assessed in this analysis.

For the CESM/RCP 8.5 scenario we used CMAQ to simulate each of the 11 historical years (1995–2005) and 11 future years (2025–2035) to capture the impacts of potential inter-annual variability in the climate response. For the GISS/RCP 6.0 scenario, we identified three historical and three future years that were least conducive, moderately conducive, and most conducive to forming near-surface ozone across the entire continental United States. These years were identified using previous CMAQ simulations of the same 11-year periods that had been forced with present-day emissions, but were otherwise identical to the configuration applied here. The annual number of exceedances of 75 ppb for daily maximum 8-hr ozone were tallied within model grid cells throughout the United States; then the years of each 11-year simulation period were ranked. The most (least) conducive year contained the most (least) exceedances of the threshold, and the moderately conducive year was the median year of each 11-year simulation period. Due to the computational costs associated with air quality modeling, only the regional climate fields from these two 3-year subsets of the GISS/RCP 6.0 were combined with the 2030 emissions in the CMAQ simulations used in the present study.

In this study, only the meteorological conditions (and specific emissions sectors that depend upon meteorology) were changed within the historical and future CMAQ runs to isolate the climate impacts in each scenario—all other input variables were held constant in the air quality modeling scenarios. The emissions were based on U.S. Environmental Protection Agency (EPA) estimates of 2030 levels, which assume the implementation of air quality policies affecting ozone precursor emissions such as the Mercury and Air Toxics Standards and the Tier-2 rule affecting mobile sources (EPA, 2011a,b; EPA, 2012). Biogenic and sea salt emissions were allowed to vary according to climate-driven meteorological changes, but emissions from mobile sources, electrical generating units, and wildfires did not change as a function of climate.

Estimating health impacts

We assess health impacts associated with surface-level ozone in the 5969 36-km grid cells in the continental United

States. In each grid cell, we apply a health impact function relating changes in ambient concentrations with ozone-related adverse outcomes. A log-linear health impact function, which we use to quantify most of the impacts in this analysis, is illustrated by eq 1:

$$\Delta Incidence = Pop \times Y_0 \times \left(exp^{\beta \times \Delta X} - 1\right) \quad (1)$$

where $\Delta Incidence$ is the change in the incidence of a particular health endpoint attributable to the change in ozone concentration (ΔX), Pop and Y_0 are the population and baseline incidence rates for the year 2030, and β is the concentration-response factor drawn from the epidemiology literature. We calculate impacts using the environmental Benefits Mapping and Analysis Program–Community Edition (BenMAP-CE), v1.08 (EPA, 2014), following EPA regulatory analyses and similar studies in the literature (Fann et al., 2011).

We estimated the change in ozone-related adverse human health outcomes of several health endpoints the U.S. Environmental Protection Agency (EPA) quantified in a recent regulatory impact analysis (EPA, 2010) for the Ozone NAAQS. The EPA quantified health outcomes that the EPA Integrated Science Assessment (ISA) determined were causally, or likely to be causally, related to ozone exposure (EPA, 2014). When selecting among epidemiological studies to use as the basis for constructing health impact functions, the agency considered an array of attributes, including statistical design (e.g., time series, case crossover, etc.); time period analyzed; population attributes; population size; and pollutant measures, among other characteristics. In brief, the agency selected studies for which the attributes made them most appropriate for an air pollution health impact analysis. A complete description of the systematic approach to selecting studies can be found in the Regulatory Impact Analysis for the Particulate Matter NAAQS (EPA, 2012). Consistent with the guidance provided by the National Academies of Sciences, and as a means of characterizing uncertainty in the ozone-mortality relationship, we report premature deaths attributable to short-term (i.e., day-to-day) changes in ozone using effect estimates from a suite of multicity studies and meta-analyses (National Research Council, 2008).

For both the GISS/RCP 6.0 and CESM/RCP 8.5 scenarios we estimate air pollution-related health impacts at 2030 using Integrated Climate and Land Use Scenarios (ICLUS) population projections (EPA, 2009; Bierwagen et al., 2010). ICLUS projects the county-level population distribution using assumptions consistent with the IPCC Special Report on Emission Scenarios (SRES) (IPCC, 2000). For this analysis we selected ICLUS projections for SRES A1 and B2, which are roughly consistent with RCP 8.5 and RCP 6.0, respectively. In a sensitivity analysis, we also examine the impact of using ICLUS A1 and B2 population projections to 2050, as well as another population projection developed for 2030 (Woods and Poole, 2012) (Supplemental Figure 1).

We estimate ozone-related effects on premature death, emergency department visits for asthma, hospital visits for respiratory causes, acute respiratory symptoms, and lost school days. We calculate ozone-related premature deaths using cause-specific mortality rates (referenced as Y_0 in the preceding equation) provided by the Centers for Disease Control and Prevention (CDC, 2008) that we projected to the year 2030 using information provided by the U.S. Census Bureau; these projected mortality rates do not account directly for the influence of climate or air quality changes. Morbidity rates are more difficult to project in the future, and we use cause-specific morbidity rates for the year 2007, assuming constant rates over time, though they are likely to change in reality (Tables 1 and 2 of Supplemental Material). We use the seasonal (May–September) average of the 8-hr daily maximum (MDA8) ozone concentration in each 36-km grid cell from CMAQ. Gridded health impact results are aggregated according to six climate regions used by the National Climate Assessment (NCA) in Supplemental Figure 1 (National Climate Assessment, 2014).

Estimating the economic value of health impacts

To estimate the economic value of the health impacts of a changing climate on air quality, we assign a dollar value to the incidence of premature deaths and illnesses occurring in 2030. We derive both cost of illness (COI) and willingness to pay (WTP) measures from the published economic literature, which we then multiply by the counts of adverse health outcomes to express the economic value of these impacts. COI metrics generally account for the value of medical expenditures to treat the adverse outcome and sometimes also the value of the productivity lost due to the illness (e.g., time spent in the hospital). By contrast, WTP measures are generally understood to account for the value that individuals place on both these direct costs as well as the value they place on avoiding pain and suffering (Harrington and Portney, 1987; Berger and Blomquist, 1987). For this reason, economic benefit analyses of air pollution impacts tend to prefer WTP values when they are available.

As in the preceding, we use economic value estimates that are consistent with recent EPA Regulatory Impact Analyses. We estimate the value of statistical life (VSL) to characterize the economic value of ozone-related premature deaths. VSL is a summary measure that expresses the economic value of small changes in the risk of premature death to a large number of people, and is not intended to describe the economic value of any particular life. In this analysis we use a EPA Science Advisory Board-recommended VSL that is derived from a meta-analysis of 26 individual studies (EPA Health Effects Subcommittee, 2010). Because the willingness to pay to reduce mortality and morbidity risk will grow with personal income, and in this analysis we quantify values in a future year, we adjusted each WTP measure; for VSL this value is $9.9 million in 2030 (2010 dollars). We value health outcomes including respiratory hospital admissions, emergency department visits, and lost school days using COI measures and value acute respiratory symptoms using a WTP measure. The source of this literature and the unit values are summarized in Supplemental Table 3.

Results

We first report the ozone-related impacts and dollar values for each of the two climate scenarios that have been calculated using projected ozone levels averaged across the scenario

years. Next we characterize the spatial distribution of these impacts by NCA region and the interannual variability.

Air quality changes

Both the CESM/RCP 8.5 and GISS/RCP 6.0 scenarios are associated with large changes in daily maximum temperatures over the months when ozone levels tend to be highest over the United States. In both scenarios, average daily maximum temperatures are projected to increase by 1–4°C over a broad swath of the continental U.S. (Figure 2). The locations of the largest projected temperature increases vary by scenario, and the average U.S. warming is greater in the CESM/RCP 8.5 scenario, as could be expected. Concurrently, other pollution-relevant weather variables (not shown) are also projected to change. The net effect on near-surface ozone is shown in Figure 2. Seasonal (May–September) mean increases in MDA8 ozone levels of 1–5 ppb are common in the CESM/RCP 8.5 scenario, resulting in more exceedances of the 75-ppb ozone NAAQS than in the historical climate case. The GISS/RCP 6.0 scenario also shows large increases in ozone over some parts of the country (e.g., central United States, California) but projects decreases in ozone over other locations (e.g., Pacific Northwest, Gulf Coast).

Average health impact estimates and economic values in 2030

As a means of describing a central tendency estimate of ozone-related health impacts in the year 2030, we report first the number of premature deaths and illnesses calculated from the average projected ozone values for the 3 individual year GISS/RCP 6.0 and 11 sequential year CESM/RCP 8.5 climate scenarios. We estimate a greater overall number of premature deaths and illnesses for the CESM/RCP 8.5 scenario than the GISS/RCP 6.0 scenario. As shown in Table 1, using GISS/RCP 6.0, we project tens to hundreds of premature deaths, hundreds of respiratory emergency department and hospital visits, tens of thousands of days of missed school, and hundreds of thousands of cases of acute respiratory symptoms. The impact is one order of magnitude greater in each category using CESM/RCP 8.5, as we project hundreds to thousands of premature deaths, thousands of respiratory emergency department and hospital visits, hundreds of thousands of days of missed school, and more than 1 million cases of acute respiratory symptoms.

The estimated economic value of these premature deaths and illnesses is substantial (Table 2). We estimate the value of the hospital admissions, emergency department visits, missed days of school, and acute respiratory symptoms for the

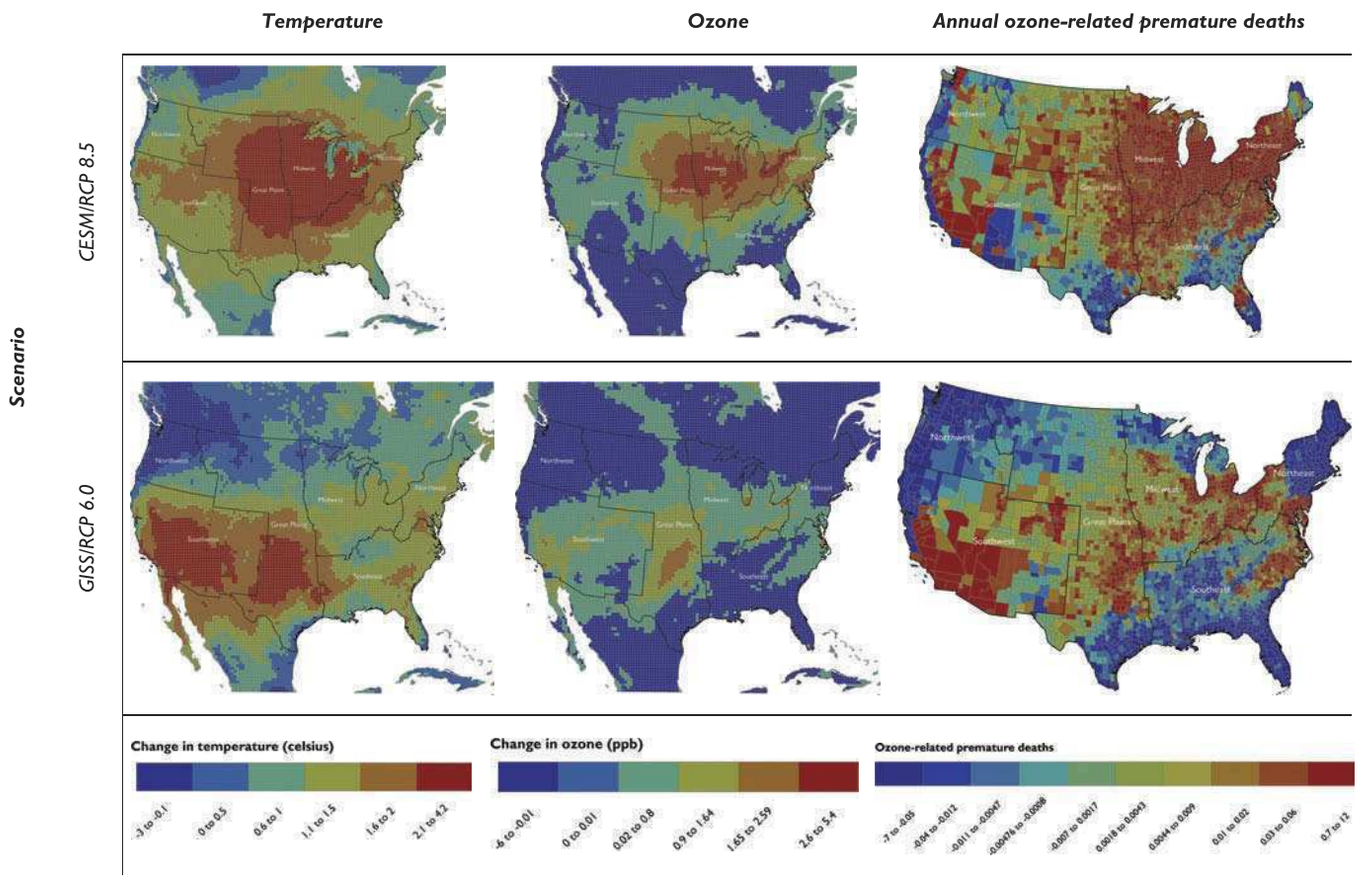

Figure 2. Projected change in average daily maximum temperature, seasonal average maximum daily 8-hr ozone, and ozone-related premature deaths in 2030.

Table 1. Additional ozone-related premature deaths and illnesses attributable to climate change in 2030 in the continental United States (95% confidence intervals)

	Climate scenario[b]	
Health outcome[a]	GISS/RCP 6.0	CESM/RCP 8.5
Alternative estimates of ozone-related premature death (ages 0–99 years)		
Bell et al. (2004)	37	420
	(12–61)	(140–700)
Huang, Dominici, and Bell (2004)	56	640
	(21–92)	(240–1000)
Schwartz (2005)	56	640
	(17–94)	(200–1100)
Bell, Dominici, and Samet (2005)	120	1300
	(56–180)	(630–2000)
Ito, De Leon, and Lippmann (2005)	160	1900
	(98–230)	(1100–2600)
Levy, Chemerynski, and Sarnat (2005)	170	1900
	(110–220)	(1300–2500)
Respiratory hospital admissions (ages 0–1 and 65–99 years)	360	3900
	(65–870)	(1600–8000)
Respiratory emergency department visits (ages 0–99 years)	89	1200
	(82–310)	(1000–4300)
Acute respiratory symptoms (ages 18–64 years)	210,000	1,900,000
	(86,000–330,000)	(780,000–3,000,000)
Missed days of school (ages 5–17 years)	67,000	650,000
	(23,000–150,000)	(230,000–1,500,000)

Notes: [a]Estimates rounded to two significant figures.
[b]The 2030 ozone levels calculated by averaging each modeled year of ozone levels—three selected years for GISS/RCP 6.0 and 2025–2035 for CESM/RCP 8.5.

GISS/RCP 6.0 scenario in the tens of millions of U.S. dollars, and hundreds of millions of dollars for the CESM/RCP 8.5 scenario (2010 dollars). We estimate the value of the additional premature deaths to be in the hundreds of millions of dollars for the GISS/RCP 6.0 scenario, and in the tens of billions of dollars for the CESM/RCP 8.5 scenario. To characterize the total dollar value of the additional premature deaths and illnesses, we report the sum of these impacts, finding that the economic value of these adverse outcomes ranges from $320 million to $1.4 billion for the GISS/RCP 6.0 scenario and from $3.6 to $15 billion for the CESM/RCP 8.5 scenario.

Health impacts by geographic region

In the figures described next, we describe how the ozone-related premature deaths are distributed throughout the United States for each climate scenario. Figure 2 plots the distribution of temperature and ozone (at 36-km grid cells) and climate change-attributable premature deaths (at each county), illustrating the relationship between these three variables. The GISS/RCP 6.0 scenario projects the greatest increases in temperature in the southwestern United States, where CMAQ consequently projects increases in ozone levels. Likewise, we estimate the greatest number of ozone-related deaths to occur in metropolitan areas affected by this temperature change, including Los Angeles, CA, and Dallas, TX. Separately, the CESM/RCP 8.5 scenario projects higher temperatures and ozone levels in the midwestern United States. Under this scenario, we project cities including Chicago, IL, and New York, NY, to see an increase in the number of ozone-related premature deaths.

Interannual variability

The aggregated results already reported do not reflect the substantial year-to-year variability in simulated temperature and ozone changes. Here we examine the influence of meteorological interannual variability on ozone levels and resulting estimated health impacts. We compare several individual future year simulations against the 3-year GISS/RCP 6.0 and 11-year CESM/RCP 8.5 scenario averages of the present-day years to better understand how future inter-annual variability can affect results. We select three future years for each of the two climate models that represent the least conducive, moderately conducive, and most conducive years for forming ozone levels above the current NAAQS for ozone (75 ppb) and predict ozone-related premature deaths in each of those three years using an array of short-term ozone mortality risk coefficients (Table 3). Those years with meteorology projected to be least and moderately conducive to forming ozone in the GISS/RCP 6.0 scenario yield a net reduction in ozone-related deaths and illnesses as compared to a baseline that does not reflect climate change. In the year most conducive to forming ozone in the GISS/RCP 6.0 scenario, we predict a net increase in the number of ozone-related premature deaths. By contrast, the year that is predicted to be least conducive to forming

Table 2. Economic value of ozone-related premature deaths and illnesses attributable to climate change in 2030 (95% confidence intervals, millions of 2010 dollars)

	Climate scenario[b]	
Health outcome[a]	GISS/RCP 6.0	CESM/RCP 8.5
Alternative estimates of ozone-related premature death (ages 0–99 years)		
Bell et al. (2004)	$290 ($24–$870)	$3400 ($280–$10,000)
Huang, Dominici, and Bell (2004)	$450 ($38–$1300)	$5200 ($430–$15,000)
Schwartz (2005)	$450 ($36–$1300)	$5100 ($410–$15,000)
Bell, Dominici, and Samet (2005)	$940 ($82–$2700)	$11,000 ($940–$31,000)
Ito, De Leon, and Lippmann (2005)	$1300 ($120–$3700)	$15,000 ($1400–$42,000)
Levy, Chemerynski, and Sarnat (2005)	$1300 ($120–3600)	$15,000 ($1400–$41,000)
Respiratory hospital admissions (ages 0–1 and 65–99 years)	$11 ($2–$19)	$100 ($10–$130)
Respiratory emergency department visits (ages 0–99 years)	$0.04 ($0.01–$0.1)	$0.5 ($0.3–$1.3)
Acute respiratory symptoms (ages 18–64 years)	$13 ($5–$25)	$120 ($45–$220)
Missed days of school (ages 5–17 years)	$7 ($3–$9.4)	$64 ($28–$91)
Total economic value of ozone-related premature deaths and illnesses		
Sum of Bell et al. 2004 and each morbidity outcome	$320 ($34–$920)	$3600 ($350–$10,000)
Sum of Levy et al. 2005 and each morbidity outcome	$1400 ($130–$3700)	$15,000 ($1500–$41,000)

Notes: [a]Estimates rounded to two significant figures.
[b]The 2030 ozone levels calculated by averaging each modeled year of ozone levels—three selected years for GISS/RCP 6.0 and 2025–2035 for CESM/RCP 8.5.

ozone in the CESM/RCP 8.5 scenario yields a net reduction in ozone-related deaths and illnesses, while the moderately and most conducive years yield substantial increases in ozone health impacts.

All 11 projected years of ozone changes under the CESM/RCP 8.5 scenario were used to examine the annual variability in ozone-related premature deaths within the 6 NCA climate regions (Figure 3). The Northwest, the Great Plains, and the Southwest regions are projected to incur few ozone related health impacts, while the Northeast and Midwest regions are projected to have increases in ozone-related deaths (i.e., reductions in mortality avoided) for most of the years.

Discussion

For the two climate scenarios in which we modeled ozone-related air quality changes in 2030, we estimate hundreds to thousands of premature deaths, hundreds to thousands of respiratory emergency department and hospital visits, tens of thousands to hundreds of thousands of days of missed school, and hundreds of thousands to millions of cases of acute respiratory symptoms. We find that the economic value of these impacts is in the hundreds of millions to billions of dollars. These estimates vary greatly according to the combined climate model and RCP simulated, as we estimate much greater impacts using the CESM/RCP 8.5 scenario than we do with the GISS/RCP 6.0 scenario. Likewise, we find that the scope and magnitude of these impacts vary significantly across the scenarios and between individual years. The CESM/RCP 8.5 scenario generally predicts greater ozone formation in the Midwest, while we estimate higher ozone levels in the Southwest under the GISS/RCP 6.0 scenario. Consistent with previous health impact analyses that account for ozone-related effects, the impacts we report are also greatly influenced by the concentration-response relationship used to quantify the incidence of premature deaths.

This work is similar in some respects to studies published elsewhere in the literature. For example, Post et al. (2012) used an earlier version of the BenMAP tool to quantify climate-

Table 3. Estimated number of additional ozone-related premature deaths and illnesses attributable to projected change in the U.S. climate (95% confidence intervals)

	GISS/RCP 6.0			CESM/RCP 8.5		
	Years least, moderately, and most conducive to forming ozone			Years least, moderately, and most conducive to forming ozone		
Health outcome[a]	Least (2035)	Moderately (2027)	Most (2025)	Least (2028)	Moderately (2030)	Most (2035)
Alternative estimates of ozone–related premature death (ages 0–99 years)						
Bell et al. (2004)	–220 (–75 to –380)	–6 (–2 to –9)	340 (110 to –570)	–32 (–11 to –53)	400 (230–670)	870 (290–1500)
Huang, Dominici, and Bell (2004)	–350 (–130 to –570)	3 (1–4)	520 (190–840)	–48 (–18 to –77)	620 (230–1000)	1,300 (500–2200)
Schwartz (2005)	–340 (–100 to –580)	–8 (–3 to –14)	520 (160–880)	–49 (–15 to –83)	620 (190–1000)	1300 (410–2600)
Bell, Dominici, and Samet (2005)	–720 (–340 to –1,100)	–21 (–10 to –38)	1,100 (520–1,700)	–110 (–53 to –170)	1300 (610–2000)	2800 (1300–4300)
Ito, De Leon, and Lippmann (2005)	–1000 (–600 to –1400)	–25 (–15 to –34)	1500 (920–2100)	–140 (–87 to –200)	1800 (1100–2500)	3900 (2400–5500)
Levy, Chemerynski, and Sarnat (2005)	–1000 (690 to –1300)	–29 (–20 to –38)	1500 (1100–2000)	–160 (–110 to –210)	1800 (1200–2400)	3900 (2700–5200)
Respiratory hospital admissions (ages 0–1 and 65–99 years)	–1900 (–280 to –4100)	–130 (–42 to –260)	3,100 (6800–1100)	–250 (–110 to –560)	3500 (2200–5700)	7500 (5000–12,000)
Respiratory emergency department visits (ages 0–99 years)	–510 (–420 to –1700)	–3 (–14 to –4)	770 (–720 to 2700)	38 (17—86)	1200 (530–2600)	2500 (1100–5600)
Acute respiratory symptoms (ages 18–64 years)	–950,000 (–390,000 to –1,500,000)	–2400 (–380 to –6100)	1,600,000 (650,000–2,500,000)	–180,000 (75,000–280,000)	1,900,000 (780,000–3,000,000)	4,000,000 (1,600,000–6,300,000)
Missed days of school (ages 5–17 years)	–310,000 (–110,00 to –670,000)	–4,000 (–6300 to –1500)	500,000 (180,000–1,100,000)	–81,000 (28,000–110,000)	660,000 (600,000–730,000)	1,400,000 (1,300,000–1,500,000)

Note: [a]Estimates rounded to two significant figures.

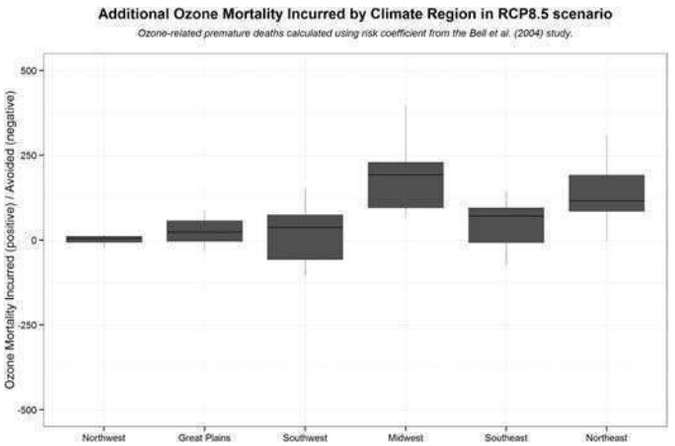

Figure 3. Annual number of climate-attributable ozone-related premature deaths by region and year for the CESM/RCP 8.5 scenario.

change-attributable national-level ozone-related premature death and illnesses and applied similar baseline incidence rates and concentration-response functions. However, that study used year 2050 ozone predictions from seven climate scenarios based on earlier generations of GCMs and did not characterize the economic value of those impacts. That paper reported climate-change-attributable ozone-related premature deaths that varied significantly across scenarios and approaches to projecting future population, and ranged from thousands of additional deaths to hundreds of avoided deaths.

Tagaris et al. (2009) quantified the sensitivity of ozone and fine particle levels in 2050 to marginal changes in precursor emissions including NOx, NH_3, and SO_2 and further quantified the number of premature deaths attributable to changes in these two pollutants. Because that paper reported changes in premature deaths as a function of marginal changes in ozone levels, it is difficult to compare those estimates to the results reported here. Bell et al. (2007), as described earlier, characterized ozone-related impacts in the year 2050 within 50 Eastern cities, holding anthropogenic emissions constant. None of the studies already described assign a dollar value to the avoided/incurred deaths and illnesses.

There are several unique facets to this study. First, we use GCM versions conducted for CMIP5 that include more than 10 years of further model developments beyond those used previously, as well as taking advantage of recent advances in regional climate modeling techniques. Second, we quantify effects in the year 2030 using an EPA emissions inventory that accounts for emission control measures expected to affect the level and distribution of ozone precursor emissions. Third, we characterize the variability in ozone-related impacts over both space (by U.S. county) and time (for each of the projected scenario years). Finally, we assign a dollar value to these projected ozone-related health impacts, giving insight to the potential economic value of this particular aspect of future climate change.

Limitations

As with any analysis of this scope and complexity, there are several notable limitations and uncertainties. First, we considered only two Representative Concentration Pathways (RCP 6.0 and RCP 8.5) that were modeled using two GCMs (GISS and CESM). Modeling each RCP using a different climate scenario means that differences in the predicted ozone levels and health impacts are attributable to both the RCP and the GCM.

Second, several emissions categories that are important to forming ozone, and could potentially be affected by climate (e.g., mobile sources, EGUs, and wildfires), are unchanged between the contemporary-climate and projected-climate air quality modeling. Other studies have shown linkages between a warmer climate and increased evaporative emissions from mobile sources (Rubin et al., 2006), increased electricity usage (Mideksa and Kallbekken, 2010), and increased wildfire activity over parts of the United States (Yue et al., 2013), all of which could lead to even greater health impacts from climate than shown here.

Third, using 36-km grid spacing (as was done here) does not consider potentially important interactions between meteorology, ozone, and health at the local scale, particularly within urban areas. However, adding higher spatial resolution to more finely resolve urban areas would add at least an order of magnitude more computational expense to this analysis. Fourth, we assume concentration-response relationships are constant over time, although changing populations, concentrations, baseline health status, and air pollution mixtures would almost certainly alter the relationship. Likewise, we assume baseline morbidity rates are constant over time, though they are likely to change as a result of changing economic and demographic conditions. Similarly, we did not account for the potential for climate-induced changes in temperature to increase (or decrease) ozone-related risks (Ren, Williams, and Tong, 2006; Ren, Williams, and Mengersen, 2009; Jhun et al., 2014). Fifth, because quantifying climate-induced $PM_{2.5}$ changes is even more strongly related to emissions changes that we did not model (e.g., wildfires), we did not include fine particle levels for this analysis. Many of these assumptions and limitations are consistent with other assessments of future climate-induced air quality changes in the literature (Post et al., 2012).

It is also important to note that this analysis does not account for policies that might mitigate the impacts estimated here, apart from those policies that are already expected to be in place by 2030. For example, while this modeling projects that climate change will create meteorological conditions more conducive to forming ozone, and hence increase the ground-level ozone in many parts of the country, we did not attempt to model air quality management adaptation scenarios that could reduce the level of ozone precursor emissions that would occur in response to these climate-driven impacts. To the extent that climate change increases ambient ozone concentrations (and/or other criteria pollutants) above the health-based air quality standards, the Clean Air Act directs states and municipalities to attain the standard by developing policies to reduce these ambient levels (Bachmann, 2007).

Conclusion

The results of this analysis suggest that for a given level of emissions of ozone precursors, climate change is likely to

increase ambient ozone levels over much of the country by 2030, causing a nontrivial number of premature deaths, respiratory emergency department and hospital visits, missed school, and acute respiratory symptoms. The economic value of these impacts is substantial. In the preceding, we noted that characterizing the influence of a changing climate on air quality and health is computationally intensive, so it is often tailored to specific research questions. In this assessment we describe the number, distribution, and economic value of climate-related ozone health impacts attributable to climate change, as simulated using two global climate models and RCPs. In-depth analysis of the drivers of ozone changes (both meteorological drivers and meteorologically influenced emissions drivers) is underway and will appear in a forthcoming paper focused on the regional climate and air quality simulations. Future analyses should consider applying a single GCM to simulate air quality impacts from multiple RCPs—or use multiple GCMs forced with a single RCP. As air quality science continues to evolve, assessments may also be better able to quantify climate-induced changes in fine particle levels. Future analyses might also attempt to characterize the change in mobile source emissions as a function of changes in temperature. Finally, analyses of the effect of climate change on health could draw upon the small, but growing, body of epidemiological literature finding that temperature modifies air pollution risk.

Disclaimer

The views expressed herein are solely those of the author, and do not necessarily represent the views or positions of the U.S. Government or any of its agencies.

Supplemental Materials

Supplemental data for this article can be accessed at http://dx.doi.org/10.1080/10962247.2014.996270.

References

Bachmann, J. 2007. The A&WMA 2007 critical review—Will the circle be unbroken: A history of the U.S. National Ambient Air Quality Standards. *J. Air Waste Manage. Assoc*. 57(6): 652–97. doi:10.3155/1047-3289.57.6.652.

Bell, M.L., F. Dominici, and J.M. Samet. 2005. A meta-analysis of time-series studies of ozone and mortality with comparison to the national morbidity, mortality, and air pollution study. *Epidemiology* 16(4): 436–45. doi:10.1097/01.ede.0000165817.40152.85.

Bell, M.L., R. Goldberg, C. Hogrefe, P.L. Kinney, K. Knowlton, B. Lynn, J. Rosenthal, C. Rosenzweig, and J.A. Patz. 2007. Climate change, ambient ozone, and health in 50 US cities. *Climatic Change* 82:61–76. doi:10.1007/s10584-006-9166-7

Bell, M.L., A. McDermott, S.L. Zeger, J.M. Samet, and F. Dominici. 2004. Ozone and short-term mortality in 95 US urban communities, 1987–2000. *J. Am. Med. Assoc*. 292(19): 2372–78. doi:10.1001/jama.292.19.2372.

Berger, M.C., and G.C. Blomquist. 1987. Valuing changes in health risks: A comparison of alternative measures. *Southern Economic* 53(4):967–84.

Bey, I., D.J. Jacob, R.M. Yantosca, J.A. Logan, B.D. Field, A.M. Fiore, Q. Li, H.Y. Liu, L.J. Mickley, and M.G. Schultz. 2001. Global modeling of tropospheric chemistry with assimilated meteorology: Model description and evaluation. *J. Geophys. Res*. 106(D19): 23073. doi:10.1029/2001JD000807.

Bierwagen, B.G., D.M. Theobald, C.R. Pyke, A. Choate, P. Groth, J.V. Thomas, and P. Morefield. 2010. National Housing and impervious surface scenarios for integrated climate impact assessments. *Proc. Natl. Acad. Sci. USA* 107(49): 20887–92. doi:10.1073/pnas.1002096107.

Bowden, J.H., T.L. Otte, C.G. Nolte, and M.J. Otte. 2012. Examining interior grid nudging techniques using two-way nesting in the WRF model for regional climate modeling. *J. Climate* 25(8): 2805–23. doi:10.1175/JCLI-D-11-00167.1.

Byun, D., and K.L. Schere. 2006. Review of the governing equations, computational algorithms, and other components of the models—3 Community Multiscale Air Quality (CMAQ) modeling system. *Appl. Mech. Rev.* 59(2): 51. doi:10.1115/1.2128636.

Centers for Disease Control and Prevention. 2008. CDC-Wonder. Wide-Ranging OnLine Data for Epidemiologic Research (CDC Wonder) (data from years 2004–2006). http://wonder.cdc.gov/ (accessed August 15, 2014).

Chang, H.H., H. Hao, and S.E. Sarnat. 2014. A statistical modeling framework for projecting future ambient ozone and its health impact due to climate change. *Atmos. Environ*. 89(June 1): 290–97. doi:10.1016/j.atmosenv.2014.02.037.

Chang, H.H., J. Zhou, and M. Fuentes. 2010. Impact of climate change on ambient ozone level and mortality in southeastern United States. *Int. J. Environ. Res. Public Health* 7(7): 2866–80. doi:10.3390/ijerph7072866.

Fann, N., A.D. Lamson, S.C. Anenberg, K. Wesson, D. Risley, and B.J. Hubbell. 2011. Estimating the national public health burden associated with exposure to ambient PM(2.5) and ozone. *Risk Analysis* 32(1): 81–95. doi:10.1111/j.1539-6924.2011.01630.x.

Fujino, J., R. Nair, M. Kainuma, T. Masui, and Y. Matsuoka. 2006. Multi-gas mitigation analysis on stabilization scenarios using AIM global model. *Energy J* 27:343–53. doi:10.5547/ISSN0195-6574-EJ-VolSI2006-NoSI3-17

Harrington, W., and P.R. Portney. 1987. Valuing the benefits of health and safety regulation. *J. Urban Econ*. 22(1): 101–12. doi:10.1016/0094-1190(87)90052-0.

Huang, Y., F. Dominici, and M. Bell. 2004. Bayesian hierarchical distributed lag models for summer ozone exposure and cardio-respiratory mortality. *Johns Hopkins University Dept. of Biostatistics Working Paper Series* (September 8). http://ideas.repec.org/p/bep/jhubio/1056.html.

International Panel on Climate Change. 2000. Special Report on Emission Scenarios. Cambridge, UK. http://www.ipcc.ch/ipccreports/sres/emission/index.php?idp=0.

Ito, K., S.F. De Leon, and M. Lippmann. 2005. Associations between ozone and daily mortality: Analysis and meta-analysis. *Epidemiology* 16(4): 446–57. doi:10.1097/01.ede.0000165821.90114.7f.

Jackson, J.E., M.G. Yost, C. Karr, C. Fitzpatrick, B.K. Lamb, S.H. Chung, J. Chen, J. Avise, R.A. Rosenblatt, and R.A. Fenske. 2010. Public health impacts of climate change in Washington State: Projected mortality risks due to heat events and air pollution. *Climatic Change* 102(1–2): 159–86. doi:10.1007/s10584-010-9852-3

Jacobson, M.Z. 2008. On the causal link between carbon dioxide and air pollution mortality. *Geophys. Res. Lett*. 35(3): L03809. doi:10.1029/2007GL031101.

Jhun, I., N. Fann, A. Zanobetti, and B. Hubbell. 2014. Effect Modification of ozone-related mortality risks by temperature in 97 US cities. *Environ. Int*. 73C(August 8): 128–34. doi:10.1016/j.envint.2014.07.009.

Levy, J.I., S.M. Chemerynski, and J.A. Sarnat. 2005. Ozone exposure and mortality. *Epidemiology* 16(4): 458–68. doi:10.1097/01.ede.0000165820.08301.b3

Melillo, J., T. Richmond, and G.W. Yohe, ed. 2014. *Climate change impacts in the United States: The third national climate assessment*. Washington, DC. doi:10.7930/J0Z31WJ2.

Mideksa, T.K., and S. Kallbekken. 2010. The impact of climate change on the electricity market: A review. *Energy Policy* 38(7): 3579–85. doi:10.1016/j.enpol.2010.02.035.

National Research Council. 2008. *Estimating Mortality Risk Reduction and Economic Benefits from Controlling Ozone Air Pollution*. Washington, DC: National Academies Press. http://www.nap.edu/catalog.php?record_id=12198.

Otte, T.L., and J.E. Pleim. 2010. The Meteorology-Chemistry Interface Processor (MCIP) for the CMAQ modeling system: Updates through MCIPv3.4.1. *Geosci. Model Dev.* 3(1):243–56. doi:10.5194/gmd-3-243-2010

Otte, T.L., C.G. Nolte, M.J. Otte, and J.H. Bowden. 2012. Does nudging squelch the extremes in regional climate modeling? *J. Climate* 25 (20): 7046–66. doi:10.1175/JCLI-D-12-00048.1.

Post, E.S., A. Grambsch, C. Weaver, P. Morefield, J. Huang, L.-Y. Leung, C.G. Nolte, et al. 2012. Variation in estimated ozone-related health impacts of climate change due to modeling choices and assumptions. *Environ. Health Perspect*. 120(11): 1559–64. doi:10.1289/ehp.1104271.

Ren, C., G.M. Williams, and K. Mengersen. 2009. Temperature enhanced effects of ozone on cardiovascular mortality in assessment using the NMMAPS Data. *Archives* 64(3): 177–84. doi:10.1080/19338240903240749

Ren, C., G.M. Williams, and S. Tong. 2006. Does particulate matter modify the association between temperature and cardiorespiratory diseases? *Environ. Health Perspect*. 1690(11): 1690–96. doi:10.1289/ehp.9266.

Riahi, K., S. Rao, V. Krey, C. Cho, V. Chirkov, G. Fischer, G. Kindermann, N. Nakicenovic, and P. Rafaj. 2011. RCP 8.5—A scenario of comparatively high greenhouse gas emissions. *Climatic Change* 109(1–2): 33–57. doi:10.1007/s10584-011-0149-y

Rubin, J.I., A.J. Kean, R.A. Harley, D.B. Millet, and A.H. Goldstein. 2006. Temperature dependence of volatile organic compound evaporative emissions from motor vehicles. *J. Geophys. Res.* 111(D3): D03305. doi:10.1029/2005JD006458.

Schwartz, J. 2005. How sensitive is the association between ozone and daily deaths to control for temperature? *Am. J. Respir. Crit. Care Med*. 171(6): 627–31. doi:10.1164/rccm.200407-933OC

Selin, N.E., S. Wu, K.M. Nam, J.M. Reilly, S. Paltsev, R.G. Prinn, and M.D. Webster. 2009. Global health and economic impacts of future ozone pollution. *Environ. Res. Lett*. 4(4): 044014. doi:10.1088/1748-9326/4/4/044014.

Sheffield, P.E., K. Knowlton, J.L. Carr, and P.L. Kinney. 2011. Modeling of regional climate change effects on ground-level ozone and childhood asthma. *Am. J. Prevent. Med*. 41(3): 251–57; quiz A3. doi:10.1016/j.amepre.2011.04.017.

Silva, R.A., J.J. West, Y. Zhang, S.C. Anenberg, J.-F. Lamarque, D.T. Shindell, W.J. Collins, et al. 2013. Global premature mortality due to anthropogenic outdoor air pollution and the contribution of past climate change. *Environ. Res. Lett*. 8(3): 034005. doi:10.1088/1748-9326/8/3/034005.

Tagaris, E., K.-J. Liao, A.J. Delucia, L. Deck, P. Amar, and A.G. Russell. 2009. Potential impact of climate change on air pollution-related human health effects. *Environ. Sci. Technol*. 43 (13) (July 1): 4979–88. doi:10.1021/es803650w

Taylor, K.E., R.J. Stouffer, and G.A. Meehl. 2012. An overview of CMIP5 and the experiment design. *Bull. Am. Meteorol. Soc*. 93(4): 485–98. doi:10.1175/BAMS-D-11-00094.1.

U.S. Environmental Protection Agency. 2009. Land-use scenarios: Scenarios consistent with climate change storylines. http://cfpub.epa.gov/ncea/cfm/recordisplay.cfm?deid=203458 (accessed January 13, 2015).

U.S. Environmental Protection Agency. 2010. Regulatory impact assessment for the reconsideration of the National Ambient Air Quality Standard for ozone. Research Triangle Park, NC. http://www.epa.gov/ttn/ecas/regdata/RIAs/s1-supplemental_analysis_full.pdf.

U.S. Environmental Protection Agency. 2011a. Regulatory impact assessment for final transport rule. Research Triangle Park, NC: U.S. EPA.

U.S. Environmental Protection Agency. 2011b. Regulatory impact assessment for the mercury and air toxics standards. http://www.epa.gov/ttn/ecas/regdata/RIAs/matsriafinal.pdf.

U.S. Environmental Protection Agency. 2012. Regulatory impact assessment for the PM NAAQS RIA. Research Triangle Park, NC. http://www.epa.gov/ttn/ecas/regdata/RIAs/finalria.pdf.

U.S. Environmental Protection Agency. 2014. Environmental Benefits Mapping and Analysis Program—Community Edition (BenMAP-CE). Research Triangle Park, NC. www.epa.gov/air/benmap.

U.S. Environmental Protection Agency Health Effects Subcommittee. 2010. Review of EPA's DRAFT Health Benefits of the Second Section 812 Prospective Study of the Clean Air Act. Washington, DC. http://yosemite.epa.gov/sab/sabproduct.nsf/0/72D4EFA39E48CDB28525774500738776/$File/EPA-COUNCIL-10-001-unsigned.pdf.

U.S. Environmental Protection Agency National Center for Environmental Assessment, Research Triangle Park NC, Environmental Media Assessment Group, and J. Brown. 2014. Integrated science assessment of ozone and related photochemical oxidants (Final report). http://cfpub.epa.gov/ncea/isa/recordisplay.cfm?deid=247492 (accessed January 24, 2014).

van Vuuren, D.P., J. Edmonds, M. Kainuma, K. Riahi, A. Thomson, K. Hibbard, G.C. Hurtt, et al. 2011. The representative concentration pathways: An overview. *Climatic Change* 109(1–2): 5–31. doi:10.1007/s10584-011-0148-z. http://link.springer.com/10.1007/s10584-011-0148-z.

Wu, S., L.J. Mickley, E.M. Leibensperger, D.J. Jacob, D. Rind, and D.G. Streets. 2008. Effects of 2000–2050 global change on ozone air quality in the United States. *J. Geophys. Res*. 113(D6): D06302. doi:10.1029/2007JD008917.

Yue, X., L.J. Mickley, J.A. Logan, and J.O. Kaplan. 2013. Ensemble projections of wildfire activity and carbonaceous aerosol concentrations over the western United States in the mid-21st century. *Atmos. Environ*. 77(October 1):767–80. doi:10.1016/j.atmosenv.2013.06.003.

About the Authors

Neal Fann and **Amanda Curry Brown** are policy analysts at the Office of Air Quality Planning and Standards, Office of Air and Radiation in Research Triangle Park, NC

Patrick Dolwick and **Sharon Phillips** are atmospheric scientists at the Office of Air Quality Planning and Standards, Office of Air and Radiation in Research Triangle Park, NC

Christopher G. Nolte and **Tanya L. Spero** are atmospheric scientists at National Exposure Research Laboratory, Office of Research and Development in Research Triangle Park, NC

Susan Anenberg is Deputy Managing Director for Recommendations at the United States Chemical Safety and Hazard Investigation Board in Washington, DC.

Supporting Information for: "The Geographic Distribution and Economic Value of Climate-Related Ozone Health Impacts in the United States in 2030"

Authors:

Part 1: Health Impact Assessment

Estimating air quality concentrations across the population

To quantify the level of ozone among populations in each 36km grid cell, we started with 2010 U.S. Census block-level population data and aggregated population counts to the 36km CMAQ model cells in BenMAP-CE across the continental U.S. This software contains the appropriate age, sex and race stratification that corresponds to the demographic characteristics of the concentration-response relationship specified in the impact function. Using an economic forecasting model, we next projected this national population data to the year 2030, which corresponds to the projected years for the air quality modeling scenarios (Woods and Poole 2012). We estimated the climate-attributable summer-season ozone levels among populations in each grid cell by calculating the difference between each baseline and model projected ozone levels.

Selection of concentration-response relationships and baseline incidence rates

For each sector we assessed the number of ozone-related premature deaths and non-fatal illnesses using concentration-response functions that are drawn from the peer reviewed literature (See Supplemental Material, Table 1) that are generally consistent with recent EPA analyses and other health impact assessments using BenMAP (EPA 2011; Fann et al. 2011).

Finally, we applied baseline incidence rates matched to each health endpoint; these rates are generally consistent with recent EPA analyses (EPA 2011) (See Supplemental Material, Table 2). When quantifying the number of deaths, we apply all-cause baseline mortality rates that have been projected to 2030 using an approach described in US EPA (2012).

Calculating health impacts

To quantify the number of ozone-related deaths and illnesses, for each health endpoint we applied the health impact function summarized in Table 1 below. This procedure generates counts of premature deaths and illnesses for each climate scenario. We also employ a Monte Carlo approach to calculate a distribution around each point estimate, using the standard error reported in each epidemiological study; we report the 95th percentile confidence interval from this distribution. All ozone-related premature deaths are estimated to occur in the year 2030.

Part 2: Supplemental Figures and Tables

Supplemental Material, Table 1. Ozone-Related Health Endpoints and Studies Included

Endpoint	Study	Study Population	Risk Estimate (95th Percentile Confidence Interval)[A]
Premature death			
Daily time series	Bell et al. (2004) (non-accidental)	All ages	β=0.000390 (0.000133)
	Huang et al. (2004) (cardiopulmonary)		β=0.000813 (0.000259)
	Schwartz (2005)(non-accidental)		β=0.000426 (0.000150)
	Bell et al. (2005)(all-cause)		β=0.000794 (0.000212)
	Ito et al. (2005) (non-accidental)		β=0.001173 (0.000239)
	Levy et al. (2005) (all-cause)		β=0.001119 (0.000179)
Hospital Admissions			
Respiratory	*Pooled using random/fixed effects:*	>64 years	
	Schwartz (1995)—ICD 460–519 (all resp)		RR = 1.20 (1.06 – 1.37) per 50 μg/m^3 RR = 1.07 (1.00 – 1.15) per 50 μg/m^3
	Schwartz (1994a, 1994b)—ICD 480–486 (pneumonia)		RR = 1.22 (1.02 – 1.47) per 50 μg/m^3
	Moolgavkar et al. (1997)—ICD 480–487 (pneumonia)		Increase = 5.7% (2.5% – 8.9%) per 15 ppb
	Schwartz (1994b)—ICD 491–492, 494–496 (COPD)		RR=1.57 (2.06—1.020) per 1 ppb
	Moolgavkar et al. (1997)—ICD 490–496 (COPD)		Increase = 4.2% (-1.0% – 9.4%) per 15 ppb
	Burnett (2001)	<2 years	Increase = 33.0 (t-statistic 3.44) per 45.2 ppb
Asthma-related ER visits	*Pooled using random/fixed effects:*	All ages	
	Peel et al. (2005)		RR = 1.022 (0.996 – 1.049) per 25 ppb
	Wilson et al. (2005)		β=0.010 (0.0090) β=0.0060 (0.0110)
Other Health Endpoints			
School absence days	*Pooled estimate:*	5–17 years	
	Gilliland et al. (2001)		Increase = 16.3% (-2.6% - 38.9%) per 20 ppb
	Chen et al. (2000)		β= 0.015763454 (0.0049851)
Minor Restricted Activity Days (MRADs)	Ostro and Rothschild (1989)	18–65 years	β=0.00741 (0.00070)

[A] Values in this column reflect the information reported by each study. When calculating health impacts, relative risk estimates were subsequently converted to beta coefficients.

Supplemental Material, Table 2. Baseline and Prevalence Rates for Included Morbidity and Mortality Endpoints

		Rates	
Endpoint	*Parameter*	*Value*	*Source*[a]
Mortality	Daily or annual mortality rate	Age-, cause-, and county-specific rate	Centers for Disease Control (2008) (rates for 2004–2006)
Hospitalizations	Daily hospitalization rate	Age-, region-, and cause-specific rate	Agency for Healthcare Research and Quality (2007)
Asthma ER Visits	Daily asthma ER visit rate	Age- and region- specific visit rate	Agency for Healthcare Research and Quality (2007)
School Loss Days	Rate per person per year, assuming 180 school days per year	9.9	NCHS (1996) Adams et al. (1999) Table 41
Minor Restricted-Activity Days	Daily MRAD incidence rate per person	0.02137	Ostro and Rothschild (1989)

[a] Healthcare Cost and Utilization Program (HCUP) database contains individual level, state and regional-level hospital and emergency department discharges for a variety of ICD codes.

[b] See ftp://ftp.cdc.gov/pub/Health_Statistics/NCHS/Datasets/NHDS/.

[c] See ftp://ftp.cdc.gov/pub/Health_Statistics/NCHS/Datasets/NHAMCS/.

[d] Lower respiratory symptoms are defined as two or more of the following: cough, chest pain, phlegm, and wheeze.

Supplemental Material, Table 3. Economic unit values

Health Endpoint	Central Estimate of Value Per Statistical Incidence for 2024[A]	Derivation of Distributions of Estimates
Premature death		
Value of a Statistical Life	$9,900,000	The EPA currently recommends a central VSL of $4.8 million (1990$, 1990 income) based on a Weibull distribution fitted to 26 published VSL estimates (5 contingent valuation and 21 labor market studies). The underlying studies, the distribution parameters, and other useful information are available in Appendix B of the EPA's Guidelines for Preparing Economic Analyses (U.S. EPA, 2010).
Hospital visits		
Chronic Lung Disease (18–64)	$22,000	No distributional information available. The COI estimates (lost earnings plus direct medical costs) are based on ICD-9 code-level information (e.g., average hospital care costs, average length of hospital stay, and weighted share of total chronic lung illnesses) reported in Agency for Healthcare Research and Quality (2007) (www.ahrq.gov).
All respiratory (ages 65+)	$36,000	No distributions available. The COI point estimates (lost earnings plus direct medical costs) are based on ICD-9 code level information (e.g., average hospital care costs, average length of hospital stay, and weighted share of total respiratory category illnesses) reported in Agency for Healthcare Research and Quality, 2007 (www.ahrq.gov).
Emergency Department Visits for Asthma	$430	No distributional information available. Simple average of two unit COI values (2000$): (1) $310, from Smith et al. (1997) and (2) $260, from Stanford et al. (1999).
Respiratory Ailments Not Requiring Hospitalization		
School Loss Days	$98	No distribution available. Based on (1) the probability that, if a school child stays home from school, a parent will have to stay home from work to care for the child, and (2) the value of the parent's lost productivity.
Minor Restricted Activity Days (MRADs)	$69	Median WTP estimate to avoid one MRAD from Tolley et al. (1986). Distribution is assumed to be triangular with a minimum of $22 and a maximum of $83, with a most likely value of $52 (2000$). Range is based on assumption that value should exceed WTP for a single mild symptom (the highest estimate for a single symptom—for eye irritation—is $16) and be less than that for a Work Loss Day. The triangular distribution acknowledges that the actual value is likely to be closer to the point estimate than either extreme.

[A] We are unable to project changes in income beyond the year 2024 and so this year is a surrogate for 2030.

	NCA Region	Average of Three Years	Least, Moderately and Most Conducive Years for Forming Ozone		
			Least (2035)	*Moderately (2027)*	*Most (2025)*
ICLUS A1 2030	Northwest	-22	-21	-17	-26
	Great Plains	21	-26	-44	132
	Southwest	35	-53	63	95
	Midwest	41	11	-21	134
	Southeast	-23	-97	7	21
	Northeast	-16	-39	7	-15
ICLUS B2 2030	Northwest	-19	-19	-16	-23
	Great Plains	18	-19	-37	109
	Southwest	31	-49	60	83
	Midwest	43	11	-21	140
	Southeast	-20	-86	2	23
	Northeast	-14	-35	4	-10
Woods & Poole 2030	Northwest	-18	-18	-16	-21
	Great Plains	13	-17	-33	90
	Southwest	28	-49	55	79
	Midwest	37	9	-20	122
	Southeast	-21	-82	0	17
	Northeast	-10	-28	3	-5
ICLUS A1 2050	Northwest	-25	-24	-20	-32
	Great Plains	27	-38	-60	178
	Southwest	51	-69	87	135
	Midwest	46	12	-25	151
	Southeast	-27	-120	14	26
	Northeast	-19	-47	10	-20
ICLUS B2 2050	Northwest	-23	-22	-19	-28
	Great Plains	23	-27	-47	142
	Southwest	44	-64	82	114
	Midwest	50	13	-26	162
	Southeast	-23	-100	5	26
	Northeast	-17	-42	5	-14

Supplemental Figure 1. Additional Ozone-Related Deaths in GISS/RCP 6.0 by Projected Population

References

Adams PF, Hendershot GE, Marano MA. 1999. Current estimates from the National Health Interview Survey, 1996. Vital Health Stat. 10. 1–203.

Agency for Healthcare Research and Quality. 2007. HCUPNet.

Bell ML, Dominici F, Samet JM. 2005. O RIGINAL A RTICLE A Meta-Analysis of Time-Series Studies of Ozone and Mortality With Comparison to the National Morbidity , Mortality , and Air Pollution Study. Epidemiology 16:436–445; doi:10.1097/01.ede.0000165817.40152.85.

Bell ML, McDermott A, Zeger SL, Samet JM, Dominici F. 2004. Ozone and Short-term Mortality in 95 US Urban Communities, 1987-2000. JAMA J. Am. Med. Assoc. 292:2372–2378; doi:10.1001/jama.292.19.2372.

Burnett RT. 2001. Association between Ozone and Hospitalization for Acute Respiratory Diseases in Children Less than 2 Years of Age. Am. J. Epidemiol. 153:444–452; doi:10.1093/aje/153.5.444.

Centers for Disease Control. 2008. CDC-Wonder. Wide-ranging OnLine Data Epidemiol. Res. (CDC Wonder) (data from years 2004–2006).

Chen, Lei Jennison, Brian L. Yang, Wei Omaye ST. 2000. Elementary School Absenteeism and Air Pollution. Inhal. Toxicol. 12:20; doi:http://dx.doi.org/10.1080/08958370050164626.

EPA. 2011. Regulatory Impact Assessment for Final Transport Rule.

Fann N, Lamson AD, Anenberg SC, Wesson K, Risley D, Hubbell BJ. 2011. Estimating the National Public Health Burden Associated with Exposure to Ambient PM(2.5) and Ozone. Risk Anal. 32:81–95; doi:10.1111/j.1539-6924.2011.01630.x.

Gilliland FD, Berhane K, Rappaport EB, Thomas DC, Avol E, Gauderman WJ, et al. 2001. The effects of ambient air pollution on school absenteeism due to respiratory illnesses. Epidemiology 12: 43–54.

Huang Y, Dominici F, Bell M. 2004. Bayesian Hierarchical Distributed Lag Models for Summer Ozone Exposure and Cardio-Respiratory Mortality. Johns Hopkins Univ. Dept. Biostat. Work. Pap. Ser.

Ito K, De Leon SF, Lippmann M. 2005. Associations Between Ozone and Daily Mortality. Epidemiology 16:446–457; doi:10.1097/01.ede.0000165821.90114.7f.

Levy JI, Chemerynski SM, Sarnat J a. 2005. Ozone Exposure and Mortality. Epidemiology 16:458–468; doi:10.1097/01.ede.0000165820.08301.b3.

Moolgavkar SH. 2000. Air pollution and hospital admissions for diseases of the circulatory system in three U.S. metropolitan areas. J. Air Waste Manag. Assoc. 50: 1199–206.

Moolgavkar SH, Luebeck EG, Anderson EL. 1997. Air pollution and hospital admissions for respiratory causes in Minneapolis-St. Paul and Birmingham. Epidemiology 8: 364–70.

NCHS. 1996. The Condition of Education 1996, Indicator 42: Student Absenteeism and Tardiness.

Ostro BD, Rothschild S. 1989. Air pollution and acute respiratory morbidity: An observational study of multiple pollutants. Environ. Res. 50:238–247; doi:10.1016/S0013-9351(89)80004-0.

Peel JL, Tolbert PE, Klein M, Metzger KB, Flanders WD, Todd K, et al. 2005. Ambient Air Pollution and Respiratory Emergency Department Visits. Epidemiology 16:164–174; doi:10.1097/01.ede.0000152905.42113.db.

Schwartz J. 1994a. Air pollution and hospital admissions for the elderly in Detroit, Michigan. Am. J. Respir. Crit. Care Med. 150: 648–55.

Schwartz J. 2005. How sensitive is the association between ozone and daily deaths to control for temperature? Am. J. Respir. Crit. Care Med. 171:627–31; doi:10.1164/rccm.200407-933OC.

Schwartz J. 1994b. PM10, ozone, and hospital admissions for the elderly in Minneapolis-St. Paul, Minnesota. Arch. Environ. Health 49:366–74; doi:10.1080/00039896.1994.9954989.

Schwartz J. 1995. Short term fluctuations in air pollution and hospital admissions of the elderly for respiratory disease. Thorax 50: 531–8.

Smith DH, Malone DC, Lawson KA, Okamoto LJ, Battista C, Saunders WB. 1997. A national estimate of the economic costs of asthma. Am. J. Respir. Crit. Care Med. 156:787–93; doi:10.1164/ajrccm.156.3.9611072.

Stanford R, McLaughlin T, Okamoto LJ. 1999. The cost of asthma in the emergency department and hospital. Am. J. Respir. Crit. Care Med. 160:211–5; doi:10.1164/ajrccm.160.1.9811040.

US EPA. 2012. Regulatory Impact Assessment for the PM NAAQS RIA.

Wilson AM, Wake CP, Kelly T, Salloway JC. 2005. Air pollution, weather, and respiratory emergency room visits in two northern New England cities: an ecological time-series study. Environ. Res. 97:312–21; doi:10.1016/j.envres.2004.07.010.

Woods and Poole. 2012. Woods & Poole.

Wiser, Kathi (Kathleen)

From: Dolwick, Pat
Sent: Thursday, April 30, 2020 10:53 AM
To: Wiser, Kathi (Kathleen)
Subject: EPA-CF-0000000094 (contribution agreeements: 2 of 6)

Here's Amanda Curry Brown's

From: Amanda Curry Brown <amanda.curry@gmail.com>
Sent: Saturday, April 25, 2020 10:08 AM
To: Fann, Neal <Fann.Neal@epa.gov>
Cc: Dolwick, Pat <Dolwick.Pat@epa.gov>
Subject: Re: STAA nomination

Hi guys,

Apologies for not replying to Pat's earlier message. 5% works for me -- in any case, I'm definitely sure I did something equivalent to "much less than everyone else." I think Pat had asked if I'd ever previously contributed to something nominated for an STAA award. I don't think I have... I think I managed to avoid doing science for the most part.

Glad to hear you are both doing ok and surviving the sub-optimality of 2020 as well as can be expected.

Amanda

On Fri, Apr 24, 2020 at 8:05 PM Fann, Neal <Fann.Neal@epa.gov> wrote:

> Hi Amanda—I hope you and your family are well. I'm just following up on that note I sent you earlier from my Gmail account. A super long time ago you co-authored the climate-health paper below looking at climate-attributable ozone impacts. Pat is submitting this for an STAA award. As part of the nomination process, each co-author must confirm his or her contribution to the paper. The team estimated your contribution to be 5%. If this is acceptable to you, can you respond to this e-mail to confirm?
>
> Thanks,
>
> Neal
>
> Neal Fann, Christopher G. Nolte, Patrick Dolwick, Tanya L. Spero, Amanda Curry Brown, Sharon Phillips & Susan Anenberg (2015) The geographic distribution and economic value of climate change-related ozone health impacts in the United States in 2030, Journal of the Air & Waste Management Association, 65:5, 570-580, DOI: 10.1080/10962247.2014.996270

Neal Fann

Health and Environmental Impacts Division

Office of Air Quality Planning and Standards

U.S. Environmental Protection Agency

109 TW Alexander Drive (C539-07)

Research Triangle Park, NC 27711

Phone: (919) 541-0209

Wiser, Kathi (Kathleen)

From: Dolwick, Pat
Sent: Thursday, April 30, 2020 10:59 AM
To: Wiser, Kathi (Kathleen)
Subject: EPA-CF-0000000094 (contribution agreeements: 6 of 6)

Here's Chris Nolte's. Do you need one from me as well?

Thanks for all your help w/ this.

Pat D.

From: Nolte, Chris <Nolte.Chris@epa.gov>
Sent: Wednesday, April 29, 2020 10:05 AM
To: Dolwick, Pat <Dolwick.Pat@epa.gov>; Spero, Tanya <Spero.Tanya@epa.gov>; Fann, Neal <Fann.Neal@epa.gov>; Phillips, Sharon <Phillips.Sharon@epa.gov>
Subject: RE: STAA nomination for Fann et al., JAWMA, 2015???

Has there been any further progress on this nomination? Do you need some kind of statement from each author accepting the proposed author contribution percentages?

If so, then here's mine: I concur with the author contributions proposed by Pat Dolwick below.

Christopher G. Nolte, Ph.D. | Research Physical Scientist
US EPA Office of Research and Development
Center for Environmental Measurement and Modeling
109 T.W. Alexander Drive E243-01 | RTP, NC 27711
nolte.chris@epa.gov | 919-541-2652

From: Dolwick, Pat <Dolwick.Pat@epa.gov>
Sent: Thursday, April 23, 2020 10:20 AM
To: Spero, Tanya <Spero.Tanya@epa.gov>; Fann, Neal <Fann.Neal@epa.gov>; Phillips, Sharon <Phillips.Sharon@epa.gov>; Nolte, Chris <Nolte.Chris@epa.gov>
Subject: RE: STAA nomination for Fann et al., JAWMA, 2015???

Thanks Tanya. I don't recall the original discussions of author order but think your contribution to paper was greater than mine. Regardless … how about: Neal (30), Chris (30), Pat (12), Tanya (13), Amanda (5), Sharon (5), Susan (5)?

Wiser, Kathi (Kathleen)

From: Dolwick, Pat
Sent: Thursday, April 30, 2020 10:55 AM
To: Wiser, Kathi (Kathleen)
Subject: EPA-CF-0000000094 (contribution agreeements: 4 of 6)

Here's Neal Fann's

From: Fann, Neal <Fann.Neal@epa.gov>
Sent: Wednesday, April 22, 2020 12:00 PM
To: Dolwick, Pat <Dolwick.Pat@epa.gov>; Spero, Tanya <Spero.Tanya@epa.gov>; Nolte, Chris <Nolte.Chris@epa.gov>; Phillips, Sharon <Phillips.Sharon@epa.gov>
Subject: RE: STAA nomination for Fann et al., JAWMA, 2015???

Hey Pat.

1. Tanya's proposed percentage contribution looks ok (30% for me), but I'd feel better receiving a share no larger than anyone else.
2. No STAA nominations for the 2015-2020 period.
3. We're submitting a nomination for the wildfire papers this year, in which we reference for this paper. See attached.

I'll take a look at the write-up you sent and provide edits. Thank you again for taking the lead on this!

Wiser, Kathi (Kathleen)

From: Dolwick, Pat
Sent: Thursday, April 30, 2020 10:53 AM
To: Wiser, Kathi (Kathleen)
Subject: EPA-CF-0000000094 (contribution agreeements: 3 of 6)

Here's Sharon Phillips.

From: Phillips, Sharon <Phillips.Sharon@epa.gov>
Sent: Wednesday, April 22, 2020 10:53 PM
To: Dolwick, Pat <Dolwick.Pat@epa.gov>; Nolte, Chris <Nolte.Chris@epa.gov>; Spero, Tanya <Spero.Tanya@epa.gov>; Fann, Neal <Fann.Neal@epa.gov>
Subject: RE: STAA nomination for Fann et al., JAWMA, 2015???

Hi Pat,

Thanks for pushing this nomination forward, as I do believe it is well deserved. I am completely fine with the proposal for allocations you suggest below. I didn't contribute a lot to this paper, however, very appreciative to be included. Great job and best of luck!

Thanks,
Sharon

From: Dolwick, Pat <Dolwick.Pat@epa.gov>
Sent: Wednesday, April 22, 2020 4:36 PM
To: Nolte, Chris <Nolte.Chris@epa.gov>; Spero, Tanya <Spero.Tanya@epa.gov>; Fann, Neal <Fann.Neal@epa.gov>; Phillips, Sharon <Phillips.Sharon@epa.gov>
Subject: RE: STAA nomination for Fann et al., JAWMA, 2015???

Thanks Chris. Will incorporate all the edits and provide more info about USGCRP CHA, CIRA2, and NCA4. Will resend a draft tomorrow (and I agree that the justification writeups probably don't matter much if at all … just avoid saying something non-factual).

Tanya, thanks for sending a proposal for allocations. Based on Neal's comment … what do people think about the following: Neal (30), Chris (30), Tanya (15), Pat (10), Sharon (5), Amanda (5), and Susan (5)? If no one objects, will plan to go w/ that.

Neal … can you be the conduit to Susan? Is anyone in contact w/ Amanda? Planning on checking w/ Kimber.

From: Nolte, Chris <Nolte.Chris@epa.gov>
Sent: Wednesday, April 22, 2020 3:15 PM
To: Dolwick, Pat <Dolwick.Pat@epa.gov>; Spero, Tanya <Spero.Tanya@epa.gov>; Fann, Neal <Fann.Neal@epa.gov>; Phillips, Sharon <Phillips.Sharon@epa.gov>
Subject: RE: STAA nomination for Fann et al., JAWMA, 2015???

All –
A few minor edits here, probably utterly inconsequential.

It's hard to know how much effort to put into this nomination write-up… either the SAB reviewers will like the paper and value the work, or they won't. I won a level II STAA once, but it wasn't because the nomination was amazing. Not that the paper was all that amazing either… I think it was seen as being good and important enough, and at the right time.

From: Dolwick, Pat <Dolwick.Pat@epa.gov>
Sent: Wednesday, April 22, 2020 11:27 AM
To: Spero, Tanya <Spero.Tanya@epa.gov>; Nolte, Chris <Nolte.Chris@epa.gov>; Fann, Neal <Fann.Neal@epa.gov>; Phillips, Sharon <Phillips.Sharon@epa.gov>
Subject: RE: STAA nomination for Fann et al., JAWMA, 2015???

Could you all review/edit the attachment here? It's "Justification #1" and is supposed to explain how the nominated paper "represents research that is innovative and important in advancing the scientific knowledge or technology relevant to EPA's mission … provide a clear and compelling explanation of the relevance, and impact of the research to EPA's mission."

I used a previous justification that Neal provided as a general guide. As you'll see, mostly linked our work to the EPA mission in the context of robust risk assessment science that informs NAAQS attainment. Am open to other directions or perhaps multiple directions. Lightly edited some cut/paste from the paper w/ key results and what made this paper unique. Also cut/paste from EPA strategic goals document where appropriate.

Please edit as needed. This justification only uses around 4K of the allocated 16K, so feel free to add.

Thanks.

From: Dolwick, Pat
Sent: Wednesday, April 22, 2020 10:33 AM
To: Spero, Tanya <Spero.Tanya@epa.gov>; Nolte, Chris <Nolte.Chris@epa.gov>; Fann, Neal <Fann.Neal@epa.gov>; Phillips, Sharon <phillips.sharon@epa.gov>
Subject: RE: STAA nomination for Fann et al., JAWMA, 2015???

Yes. Am in the middle of this now. Hope to have some justifications for the team to review later today.

In the interim, 1) still looking for ideas on percentage contribution; 2) please send me a list of the previous 5 years of STAA nominations and associated publications for each EPA of you … list should be should include publication title, year, and award; and 3) if you have another paper being nominated this year, please send me the information on that.

I'll probably have more requests as we go.

Thanks!

From: Spero, Tanya <Spero.Tanya@epa.gov>
Sent: Wednesday, April 22, 2020 10:26 AM
To: Nolte, Chris <Nolte.Chris@epa.gov>; Dolwick, Pat <Dolwick.Pat@epa.gov>; Fann, Neal <Fann.Neal@epa.gov>
Subject: RE: STAA nomination for Fann et al., JAWMA, 2015???

Pat and Neal –

Do you guys need me to do anything for this?

Tanya

From: Nolte, Chris <Nolte.Chris@epa.gov>
Sent: Friday, April 17, 2020 2:40 PM
To: Dolwick, Pat <Dolwick.Pat@epa.gov>; Fann, Neal <Fann.Neal@epa.gov>; Spero, Tanya <Spero.Tanya@epa.gov>
Subject: RE: STAA nomination for Fann et al., JAWMA, 2015???

#8 Integrated risk assessment sounds good to me. I think #9 connotes research on the efficacy of environmental policies, rather than research that might inform a future policy, in some alternate universe where there were an Administration that cared about science or the environment.

For what it's worth, my 2008 JGR paper was submitted under Transport and Fate. But it didn't have any health component.

From: Dolwick, Pat <Dolwick.Pat@epa.gov>
Sent: Friday, April 17, 2020 2:02 PM
To: Fann, Neal <Fann.Neal@epa.gov>; Spero, Tanya <Spero.Tanya@epa.gov>; Nolte, Chris <Nolte.Chris@epa.gov>
Subject: RE: STAA nomination for Fann et al., JAWMA, 2015???

Thanks Neal. I'll get in touch w/ Kathi. Am good w/ #8.

From: Fann, Neal <Fann.Neal@epa.gov>
Sent: Friday, April 17, 2020 1:56 PM
To: Dolwick, Pat <Dolwick.Pat@epa.gov>; Spero, Tanya <Spero.Tanya@epa.gov>; Nolte, Chris <Nolte.Chris@epa.gov>
Subject: RE: STAA nomination for Fann et al., JAWMA, 2015???

The process is pretty dreadful. I just got added as a BAP user earlier this week, and only after contacting Kathi Wiser, who is the STAA coordinator. Also, pro tip—I discovered that the library will search news articles for any mention of a given paper. This information can come in handy when demonstrating the relevance of the work.

I think that #8 might be a better fit given that this work informed the Climate Health Assessment. #8 also calls out risk assessments in particular. Submitting the manuscript under #9, by contrast, would imply that climate science informs Agency policy.

Thanks for taking the lead on this!

-Neal

From: Dolwick, Pat <Dolwick.Pat@epa.gov>
Sent: Friday, April 17, 2020 1:02 PM
To: Spero, Tanya <Spero.Tanya@epa.gov>; Fann, Neal <Fann.Neal@epa.gov>; Nolte, Chris <Nolte.Chris@epa.gov>
Subject: RE: STAA nomination for Fann et al., JAWMA, 2015???

Hey, so I haven't totally forgotten this. I am on day 3 of superfun times trying to get registered as a BAP provision user. I think this is step 1 of 50, so am probably right on pace. (Seriously, am sure can get this submitted on time.)

Two questions:

1) Any thoughts on the record of percentage agreement? I'm fine w/ 5%. Would guess Sharon, Amanda, and Susan would be ok w/ that allocation as well. (Is that correct that non-EPA'ers still get an allocation?) That would leave you all to divvy up the 80%.
2) Any thoughts on which of the 14 categories to submit this? None are a perfect fit. I'm leaning toward #9 but can see a case for #8. Other suggested categories are welcome as well.

#9 Environmental Policy and Decision-Making Studies (EP): This category covers research pertaining to EPA's policy formulation and regulatory and enforcement responsibilities. It specifically includes environmental policy, environmental justice, anthropology, psychology, sociology, decision making, economics, urban and community planning, transportation, and land-use planning.

#8 Integrated Risk Assessment (IR): This category covers research (observation, experimental, and theoretical) directed towards the goal of integrating human health and ecological risk assessment methods and analysis. It includes processes and modeling research for developing the models to understand, predict, and assess the current and probable future exposure and response of ecosystems to multiple stressors at multiple scales. It also includes risk assessment research for developing and applying assessment methods, indices, and guidelines for quantifying risk to the sustainability and vulnerability of ecosystems from multiple stressors at multiple scales.

From: Spero, Tanya <Spero.Tanya@epa.gov>
Sent: Tuesday, April 07, 2020 10:48 AM
To: Fann, Neal <Fann.Neal@epa.gov>; Dolwick, Pat <Dolwick.Pat@epa.gov>; Nolte, Chris <Nolte.Chris@epa.gov>
Subject: STAA nomination for Fann et al., JAWMA, 2015???

Neal, Pat, and Chris –

What do you all think about putting together a STAA nomination for the Fann et al., JAWMA, 2015, paper? Nominations are due at the end of April.

Tanya

Wiser, Kathi (Kathleen)

From: Dolwick, Pat
Sent: Thursday, April 30, 2020 10:51 AM
To: Wiser, Kathi (Kathleen)
Subject: EPA-CF-0000000094 (contribution agreeements: 1 of 6)

Here's Susan Anenberg's.

From: Anenberg, Susan <sanenberg@email.gwu.edu>
Sent: Thursday, April 23, 2020 10:34 AM
To: Fann, Neal <Fann.Neal@epa.gov>
Cc: Susan Anenberg (sanenberg@gwu.edu) <sanenberg@gwu.edu>; Dolwick, Pat <Dolwick.Pat@epa.gov>
Subject: Re: STAA nomination

That is acceptable to me. Good luck!

On Thu, Apr 23, 2020 at 10:17 AM Fann, Neal <Fann.Neal@epa.gov> wrote:

> Hi Susan—I hope you and your family are well. A super long time ago you co-authored the climate-health paper below looking at climate-attributable ozone impacts. Pat is submitting this for an STAA award. As part of the nomination process, each co-author must confirm his or her contribution to the paper. The team estimated your contribution to be 5%. If this is acceptable to you, can you respond to this e-mail to confirm?
>
> Thanks,
>
> Neal
>
> Neal Fann, Christopher G. Nolte, Patrick Dolwick, Tanya L. Spero, Amanda Curry Brown, Sharon Phillips & Susan Anenberg (2015) The geographic distribution and economic value of climate change-related ozone health impacts in the United States in 2030, Journal of the Air & Waste Management Association, 65:5, 570-580, DOI: 10.1080/10962247.2014.996270
>
> ---
>
> Neal Fann
>
> Health and Environmental Impacts Division
>
> Office of Air Quality Planning and Standards
>
> U.S. Environmental Protection Agency

109 TW Alexander Drive (C539-07)

Research Triangle Park, NC 27711

Phone: (919) 541-0209

--
Susan Anenberg, PhD
Associate Professor
Milken Institute School of Public Health
George Washington University
1-202-994-2392
sanenberg@gwu.edu

Wiser, Kathi (Kathleen)

From: Dolwick, Pat
Sent: Thursday, April 30, 2020 10:57 AM
To: Wiser, Kathi (Kathleen)
Subject: EPA-CF-0000000094 (contribution agreeements: 5 of 6)

Here's Tanya Spero's.

From: Spero, Tanya <Spero.Tanya@epa.gov>
Sent: Wednesday, April 29, 2020 10:18 AM
To: Dolwick, Pat <Dolwick.Pat@epa.gov>
Subject: RE: STAA nomination for Fann et al., JAWMA, 2015???

I agree with the percentage contribution outlined below.

Tanya

From: Dolwick, Pat <Dolwick.Pat@epa.gov>
Sent: Thursday, April 23, 2020 10:20 AM
To: Spero, Tanya <Spero.Tanya@epa.gov>; Fann, Neal <Fann.Neal@epa.gov>; Phillips, Sharon <Phillips.Sharon@epa.gov>; Nolte, Chris <Nolte.Chris@epa.gov>
Subject: RE: STAA nomination for Fann et al., JAWMA, 2015???

Thanks Tanya. I don't recall the original discussions of author order but think your contribution to paper was greater than mine. Regardless … how about: Neal (30), Chris (30), Pat (12), Tanya (13), Amanda (5), Sharon (5), Susan (5)?

Table of Contents

General_Authors_Publications.....2
LI-266504_A_national_statistical_survey_assessment_of_mercury_concentrations_i17
LI-266562_Statistical_Survey_of_Persistent_Organic_Pollutants_Risk_Estimations27
A_national_statistical_survey_assessment_of_mercury_concentrations_in_fillets_38
Statistical_Survey_of_Persistent_Organic_Pollutants_Risk_Estimations_to_human_48
Perfluorinated_compounds_infish_from_US_urban_rivers_and_the_Great_Lakes.....59
Presence_of_pharmaceuticals_in_fish_collected_from_urban_rivers_in_the_US_EPA_70
Percentage_Agreement.....78
STAArecommend-WathenBatt_4-28-20.....80
EPA_STAA_Nomination_review_Muir.....82

United States Environmental Protection Agency
Washington, DC 20460

STAA REPORT FOR THE SCIENTIST NOMINATIONS

General Information:

Nomination ID/App ID:	20-096
Research Category Primary:	Integrated Risk Assessment (IR)
Research Category Secondary:	Environmental Policy and Decision-Making Studies (EP)
Laboratory/Office Name:	ORD
Nomination Entered By:	James Lazorchak

Eligibility Checklist:

[Y] The nominated publication(s) has not been submitted to a previous STAA competition.

[Y] The nominated publication(s) was published on or before January 1, 2017 and on or after January 1,2012

[Y] The principal author was an EPA employee or a PHS employee assigned to EPA when the research was performed

[Y] The EPA authors (includes PHS employees assigned to EPA) contributed collectively a minimum of 50% toward the publication(s)

Nominating Official Name:	Kevin Oshima
Nominating Official Title:	BIOLOGIST
Nominating OfficialEmail:	oshima.kevin@epa.gov
STAA Coordinator Name:	Kathleen Wiser
STAA Coordinator Email:	wiser.kathi@epa.gov

Justifications:

Justification 1:

This nomination package details the comprehensive results of important risk estimates to many high profile organic and inorganic pollutants in a food source for both humans and wildlife. The first nominated paper provides extensive analytical results and risk estimates for a wide range of 50 persistent organic pollutants in fish tissue, including 21 PCB congeners, 8 PBDE congeners, and 21 organochlorine pesticides, "*Statistical Survey of Persistent Organic Pollutants: Risk Estimations to Humans and Wildlife through Consumption of Fish from U.S. Rivers*" (Angela Batt, John B. Wathen, James M. Lazorchak, Anthony R. Olsen, Thomas Kincaid). The second nominated paper, "*A national statistical survey assessment of mercury concentrations in fillets of fish collected in the U.S. EPA national rivers and streams assessment of the continental USA* (John B. Wathen, James M. Lazorchak, Anthony R. Olsen, Angela Batt), is the corresponding assessment of mercury (Hg) contamination in fish fillet tissue.

These risk estimates were conducted as part of the 2008–2009 National Rivers and Streams Assessment (NRSA). The NRSA is a survey of rivers in the 48 conterminous United States used to characterize a broad range of stream water quality, biological, and ecological attributes of U.S. rivers. This powerful, statistically based survey included 540 sites (541 for Hg), with the sites being designated as urban or non-urban based on their inclusion in urban areas. The survey is nationally-representative of the class of waters sampled, with those rivers sampled being 5th order and greater rivers that are boatable. In addition to the risk estimates to so many important contaminant groups, these publications provide one of the largest publicly available data sets for fish tissue concentrations for a very large list of high profile, carcinogenic POPs and organochlorine pesticides. The analytes were described in separate publications because organic and inorganic compounds would be expected to behave quite differently.

The statistical design of this study also produces nationally representative assessment results for three ECO regions each of three National Aquatic Resource Assessment (NARS) ecoregions: West and Mountains (WMTS), Plains and Lowlands (PLNLOW), and Eastern Highlands (EHIGH), in addition to the urban and non-urban subgroups. The statistical framework of the study was designed and published previously by two of the authors, Anthony Olsen and Thomas Kincaid. At each sampling site, multiple fish were collected to form a fish fillet tissue composite. Each sampling site has a weighting factor, and the concentrations of each contaminant determined in the composite fish tissue can be used to provide a national projection of the percent of the types of streams sampled that exceed a given human health criteria value (such as cancer), wildlife criteria value, or aquatic life thresholds, and is expressed as a percentage of stream miles. Results

were used to both estimate contaminant exposures to humans and wildlife that consume fish, and to examine fish tissue contaminant concentration results and patterns between the urban and non-urban sampling locations, and the three ECO regions.

Human Health, Wildlife, and Aquatic Life Risk Estimates

The work conducted in the National Aquatic Resource Surveys, including NRSA, is critical to the mission of the U.S. EPA and supports the Clean Water Act. Supporting populations of fish for human consumption is a primary goal, but the place of fish in the ecological system of waterbodies and in the food webs that exist is also essential to the national environmental health. In many activities at EPA, human and ecosystem health are treated separately, and with good reason. However, there are common threads to the effects of contamination of aquatic life food webs and human exposure. None of the compounds assessed in these studies are beneficial to either humans or wildlife. A large novelty of this body of work is that it explores the exposure of both human and wildlife/aquatic life from the same set of data. Fish fillet composites were analyzed, because human exposure is based on consumption of fish fillets. Documented conversion factors were then used to translate fish fillet concentrations into whole fish estimates for the assessment of wildlife and aquatic life impacts. The variety of compounds involved partition differently into the various parts of fish, and fish vary by species. Accordingly, conversions had to be at least specific to the pollutant group, and involved some informed approximations. Nevertheless, distinctions between human and wildlife exposure were pronounced and informative. The application of appropriate human health and aquatic life criteria to these data resulted in a rare One Health assessment of the contaminant environment of U.S. river habitats and fish.

The survey results were highly informative. Even though PCBs have been banned for decades, they were found in over 93% of samples and exceeded human health cancer screening values in 48% of the national sampled population of river miles, and in 70% of the urban sampled population. PBDEs (92.0%), chlordane (88.5%) and DDT (98.7%) were also detected frequently, although at lower concentrations. Dieldrin was found in 71% of samples, and exceeded human health cancer screening values in 32% of the sampled population. Mercury was detected in every single sample, and found to exceed the fish-tissue based water quality criterion for mercury in over 25% of the sampled population of river miles. In contrast to the human health risk estimates, the PBDEs (minks) and total DDT and chlordane (kingfisher birds) were estimated to be more of a risk to these species of wildlife because of their higher respective sensitivities to these compounds, which shows the importance of the wildlife assessment.

Sample populations were examined in the five additional subpopulations (urban, non-urban, eastern highlands, plains and lowlands, and west and mountains), to determine any patterns of exposure or regional differences. The concentrations of organic contaminants in fish tissue across the country varied markedly by region, and was indicative of the variation in land use and environmental history. Industrial chemicals (PCBs) were found in industrial areas (eastern highlands) and pesticides were detected in fish samples from the plains and lowlands. Among organic chemicals, the elevated concentrations of PCBs in the urban samples are notable. In contrast to the regional differences observed for organics, mercury was found to be ubiquitous. Because much of the distribution of mercury is in large part by atmospheric deposition, distribution across the U.S. as evidenced by fish tissue concentrations was found to vary little by ecoregion.

Co-occurrence of contaminants

Even before statistical analysis of the data, it was evident that many samples contained elevated concentrations of more than one organic contaminant. The combined effects of multiple contaminants and complex chemical mixtures is often poorly defined in the scientific literature. Co-occurrence of the different contaminant groups was investigated, and was described as two or more compounds being present in a given tissue sample at concentrations above their respective medians. Results revealed that the most common mode of co-occurrence (fish from 32% of river sites with concentrations above the median for any compound) was for all four compound groups (PCBs, PBDEs, DDTs, Chlordanes) to co-occur at concentrations above their respective weighted medians. The rarity was for these contaminants to occur singly above the median concentrations as was the case for PCBs in only 4% of the samples. Essentially, application of this analysis demonstrates that there is almost no such thing as exposure to a single contaminant in fish tissue.

Additionally, we are including two papers as supporting evidence of the co-occurrence of contaminants, in this case contaminants of emerging concern (CECs), PFAS and Pharmaceuticals analyzed in a subset of the same composite fish tissue samples as Mercury and the legacy organics. The first paper is:

Stahl, LL, Blaine D. Snyder, Anthony R. Olsen, Thomas M. Kincaid , John B. Wathen, Harry B. McCarty. (2014) Perfluorinated compounds in fish from U.S. urban rivers and the Great Lakes. Science of the Total Environment 499 (2014) 185–195. http://dx.doi.org/10.1016/j.scitotenv.2014.07.126

This paper is offered as a supporting document to the articles nominated as described above. The urban 164 samples from the 2008-2009 NRSA were also analyzed for a suite of 13 perfluorinated compounds. Analyses were limited to these sites for budgetary reasons, but targeting the urban sites seemed appropriate in that it still achieved a national distribution of sites that were considered more likely to be impacted by sources of these then-emerging compounds. With the comprehensive assessment of legacy organic compounds available for the same samples, results of PFAS analyses turned the page from legacy challenges to current and future challenges. Also included in this supporting paper are the results of analyses of samples from 157 nearshore Great Lakes sites collected as part of the National Coastal Condition Assessment. These two sets of data focused Agency attention on the emerging nature of PFAS contamination of fish. The pervasive nature of PFAS in both the NRSA and Great Lakes samples is consistent with other research, and its presence and the presence of substantial concentrations of other long-chain PFAS (PDFA, PFUnA, PFDoA) mark the way to future exposure assessment challenges. This paper is authored by Leanne Stahl, who managed the NRSA and NCCA studies, along with Anthony Olsen, Thomas Kincaid, and John Wathen, who are co-authors on the nominated papers.

The second paper is:

Belinda Huerta, Sara Rodriguez-Mozaz, Jim Lazorchak, Damia Barcelo, Angela Batt, John Wathen, Leanne Stahl. 2018. Presence of pharmaceuticals in fish collected from urban rivers in the U.S. EPA 2008–2009 National Rivers and Streams Assessment. Sci Tot Environ. 634, 542-549.

This paper was a collaboration between Dr. Damia Barcelo's lab, Sara Rodriguez-Moraz, Belinda Huerta, ORD, and OW. Dr Huerta, Sara and Damia previous published a method for measuring pharmaceuticals in fish tissue in 2013. About 6 of the 20 pharmaceuticals included in the fish tissue method were also included in EPA's pharmaceutical assessments of surface water and wastewater. A small subset of 25 fish homogenates the 2008-2009 NRSA survey urban sites were prioritized based on the highest concentrations found in urban

waters, and were analyzed for the presence of those 20 pharmaceuticals. This allowed us to include another high priority emerging contaminant analysis to the suite of fish tissue analytes, and 13 of the 20 pharmaceuticals were detected in at least one fish tissue sample.

Authors for both articles gave their permission for us to use their publications as supporting evidence. In the future as cumulative risk assessment science matures, it will be possible to use the results of all four papers to retrospectively investigate the risk of humans and wildlife consuming fish with multiple contaminants.

The 2008-2009 NRSA survey is the first NRSA, with a second conducted in 2013-2014, and a third sampling conducted in 2018-2019. The results of this first survey provided EPA decision makers with the important information needed to determine which chemical indicators should be included in the future national surveys by providing a baseline on the current state of many important pollutants in the U.S. With so much research effort being invested in emerging contaminant analysis, persistent organic pollutants and mercury are often overlooked. This survey demonstrates that even decades after many of these highly potent, carcinogenic compounds are no longer in use, they are still found at significant levels of concern in food sources. This work also shows that future research for these legacy contaminants is still highly important, especially from the perspective of complex chemical mixtures and investigating multiple routes of exposure. The full data set, including the analytical concentrations of each analyte in each sample, was also published along with the journal articles to encourage future data mining and provide other academic, government, and industry scientists with one of the largest publicly available data sets for these important environmental contaminants.

Justification 2A:

Neither of the papers included in this nomination, or the two supporting papers, have been nominated in previous years. This nomination describes results from the same sample sets collected in the same national survey, however, the two analyte groups were described in separate publications for several reasons. The first reason was the sheer volume of the data generated for over 50 contaminants and in-depth data analysis for so many different contaminant groups. With 540 sampling locations (541 samples for Hg) and 5 subpopulations, whether for one analyte (Hg) or 50 persistent organic pollutants (POPs), presenting, analyzing, and interpreting results of dissimilar compounds, the authors and EPA managers agreed that a single publication would not be feasible. As a second more practical consideration, the Hg samples could be and were analyzed in relatively short timeframe and were available for statistical analysis and interpretation at a much sooner date. Accordingly, the Hg paper was completed and submitted in July of 2014 and was available online in November. The manuscript for the organics paper required a much more complicated, time-consuming analytical and data analysis, and was published in the *Journal of Environmental Science and Technology* in February of 2017. The results of the two publications are complimentary and do build upon each other. The

statistical methodologies used for the analysis of the analytical data were the same, with the exception of the co-occurrence analysis performed in the organics paper. The papers each have a distinct character which reflects the contrasting nature of the contaminants and the different role of the respective authors on the team.

Justification 2B:

Angela Batt

2019 Level II STAA

Nationwide study on the prevalence and potential health effects of contaminants of emerging concern in drinking water

1) Nationwide reconnaissance of contaminants of emerging concern in source and treated drinking waters of the United States, Science of the Total Environment, 2017

2) Comparison of in vitro estrogenic activity and estrogen concentrations in source and treated waters from 25 US drinking water treatment plants, Science of the Total Environment, 2017

3) Per-and polyfluoroalkyl substances in source and treated drinking waters of the United States, Science of the Total Environment, 2017

2016 Level III STAA

1) Evaluating the Extent of Pharmaceuticals in Surface Waters of the United States using a National-Scale Rivers and Streams Assessment Survey, Environmental Toxicology and Chemistry, 2016

2) Concentrations of Prioritized Pharmaceuticals in Effluents from 50 Large Wastewater Treatment Plants in the US and Implications for Risk Estimation, Environmental Pollution, 2014

John Wathen

No previous nominations

Jim Lazorchak

2016 STAA Award Level II

3) Part 1: Laboratory Culture of Centroptilum triangulifer (Ephemeroptera:Baetidae) using a Defined Diet of Three Diatoms. Published in Chemosphere.

4) Part 2: Sensitivity Comparisons of the Mayfly Centroptilum triangulifer to Ceriodaphnia dubia and Daphnia magna using Standard Reference Toxicants: NaCl, KCl and CuSO4. Published in Chemosphere.

5) Elevated Major Ion Concentrations Inhibit Larval Mayfly Growth and Development. Published in Environmental Science & Technology.

2016 Level III STAA

6) Evaluating the Extent of Pharmaceuticals in Surface Waters of the United States using a National-Scale Rivers and Streams Assessment Survey, Environmental Toxicology and Chemistry, 2016

7) Concentrations of Prioritized Pharmaceuticals in Effluents from 50 Large Wastewater Treatment Plants in the US and Implications for Risk Estimation, Environmental Pollution, 2014

Anthony Olsen

2016 Level III STAA

1) Evaluating the Extent of Pharmaceuticals in Surface Waters of the United States using a National-Scale Rivers and Streams Assessment Survey, Environmental Toxicology and Chemistry, 2016

2) Concentrations of Prioritized Pharmaceuticals in Effluents from 50 Large Wastewater Treatment Plants in the US and Implications for Risk Estimation, Environmental Pollution, 2014

Tom Kincaid

2016 Level III STAA

1) Evaluating the Extent of Pharmaceuticals in Surface Waters of the United States using a National-Scale Rivers and Streams Assessment Survey, Environmental Toxicology and Chemistry, 2016

2) Concentrations of Prioritized Pharmaceuticals in Effluents from 50 Large Wastewater Treatment Plants in the US and Implications for Risk Estimation, Environmental Pollution, 2014

Justification 2C:

Four of the authors of this nomination (Angela Batt, Jim Lazorchak, Anthony Olsen, and Tom Kincaid) submitted a nomination for two papers in 2016 that detailed the results of national surveys of effluent and surface water for pharmaceuticals for human prescription use, as identified in 2B. The first paper included in that 2016 nomination, "Evaluating the Extent of Pharmaceuticals in Surface Waters of the United States using a National-Scale Rivers and Streams Assessment Survey" did include samples also collected in the 2008-2009 NRSA survey, however, this paper differs from the current nomination substantially. First, the analyte groups were completely different with very different environmental implications and behaviors. Pharmaceuticals are in the group of emerging contaminants with much to be studied regarding their environmental effects, while persistent organic pollutants are known carcinogens, and many are already withdrawn or regulated. This meant that the resulting information would be used by decision makers in a very different context, and the results would have to be interpreted separately. Second, the pharmaceutical survey was conducted in an entirely different matrix, with the results reported in that 2016 Level III STAA award only being for surface water, and not fish tissue. This also resulted in the analytical analysis for the POPs and pharmaceuticals being conducted using very different analytical methodology. And third, the pharmaceutical analysis in surface water was only performed on a smaller subset of the sampling sites (the 150 urban rivers only), and not the full 540 sites included with the POPs and Hg fish tissue surveys. Therefore, there was no data analysis for urban vs non-urban sub-populations, or the three ECO region groups for the pharmaceuticals. For these reasons, it made much more sense to include the results of the surface water survey with the wastewater survey, as the results of those two studies combined were part of a very important chemical prioritization process for pharmaceuticals in environmental waters. Additionally, John Wathen, was not included as an author on the pharmaceutical paper, but is the first author of the Hg paper, and the second author for the POPs paper. His substantial contribution and expertise in the area of these legacy contaminants applied to this current nomination package is another example of how different these papers really are.

Angela Batt was also included on a 2019 Level II STAA award that presented further research on pharmaceuticals and other emerging contaminants in drinking water. With none of the other four authors of this current nomination being included in that work, and the focus of the work again being pharmaceuticals in drinking water, her 2019 Level II STAA award and this nomination are significantly different.

Jim Lazorchak was included on a 2016 Level II STAA award for the development of a Mayfly method. Again, with none of the other four authors of this current nomination being included in that work, and the focus of that work being in a very different discipline of science altogether (biology vs analytical chemistry), his 2016 Level II STAA award and this nomination are completely unrelated.

Justification 2D:

None of the supplemental information has been included in previous nominations.

Justification 2E:

There are no concurrent nominations by the authors on this nomination.

Justification 3A:

The paper "Statistical Survey of Persistent Organic Pollutants: Risk Estimations to Humans and Wildlife through Consumption of Fish from U.S. Rivers" was published in the *Journal of Environmental Science and Technology (ES&T)*, which has long been considered one of the top journals in the field of Environmental Science, with a current impact factor of 7.149 and cited half-life of 7.8. The journal is published by the American Chemical Society and is highly selective with only a 35% acceptance rate, and seeks to publish papers that are particularly significant and original. *ES&T* is currently the second ranked journal in the Environmental Sciences by Google Scholar, with an H-5 index of 132, second only to *Nature Climate Change* (also with an H-5 index of 132). The Altmetrics provided by the American Chemical Society for this publication track a range of online sources and social media to help researchers monitor and report the attention surrounding their work. This *ES&T* paper has an Altmetric Attention Score of 15, which places it in the top 25% of all research outputs scored by Altmetric. It ranks with a high Attention Score compared to outputs of the same age (being in the 86th percentile), and was shared on Twitter in more than six different countries. The article has been viewed on the *ES&T* website alone over 1080 times, and so far has been sited 20 times, according to Google Scholar. With the time it takes for research of this complexity to be completed (persistent organic pollutants and pesticides in fish tissue), we expect the citations for the relatively newly published paper to increase in time.

The paper "A national statistical survey assessment of mercury concentrations in fillets of fish collected in the U.S. EPA national rivers and streams assessment of the continental USA" was published in the *Chemosphere*, which is another well respected journal in the field of Environmental Science, with a current impact factor of 5.108 and cited half-life of 6.7. The journal is published by Elsevier and is also selective, with a 71% acceptance rate. *Chemosphere* is currently the ninth ranked journal in the Environmental Sciences by Google Scholar, with an H-5 index of 91. This paper has been cited 17 times so far.

Because of the relevance of the NRSA 2008-2009 fish tissue papers, James Lazorchak was asked to participate in an advisory group to design and put content into EPA's "Fish and Shellfish Advisory and Safe Eating Guidelines" website.
https://www.epa.gov/choose-fish-and-shellfish-wisely/fish-and-shellfish-advisories-and-safe-eating-guidelines

In addition to journal metrics, attached to this nomination are two letters of support. The first is from Lisa Larimer and Shari Barash of the Office of Water at the U.S. EPA. They discuss the significance of the contribution of these two journal articles to both the EPA and its decision-making process, and to the

scientific community as well Shari Barash is the Chief of the National Branch in the Standards and Health Protection Division of the Office of Science and Technology in the Office of Water. She is responsible for much of the Water Quality Standards program and assumed responsibility for the EPA Fish Program and Recreational Waters program with the elimination of the Fish Shellfish, Beaches, and Outreach Branch in 2015. Within her branch, Lisa Larimer is the Team Leader of the Fish and Beach Team with responsibility of the Fish Advisory Program, Fish Tissue Contaminant Program (under which these studies were conducted), and EPA's BEACH Program which oversees beach monitoring grants, WQ and advisory data collection, and liaison with EPA regional beach coordinators. The second is from Dr. Derik Muir Dr. Muir who is a Senior Research Scientist and Section Head at Environment Canada - Priority Contaminants Fate and Bioaccumulation at Environment Canada. Dr. Muir is well known internationally as an expert in the distribution, fate and bioaccumulation of priority substances. He has conducted studies on new contaminants in Great Lakes fish, food webs and waters including areas of concern in support of lake area management plans, as well as examined chemical fate and exposures of fish and wildlife in tropical environments as part of global assessments and as a means of supporting training and capacity building in developing countries. Dr. Muir is also Associate Editor, Environmental Chemistry, Environmental Chemistry and Toxicology journal (since 1999).

Justification 3B:

Both papers underwent an intensive internal and external review process prior to publication. Due to the nature of the work and these papers providing risk estimates in a food source for many high profile, cancer causing contaminants, the papers underwent a more extensive internal EPA review, but outside of the Office of Research and Development. For example, the paper "Statistical Survey of Persistent Organic Pollutants: Risk Estimations to Humans and Wildlife through Consumption of Fish from U.S. Rivers" was reviewed by 14 people, including all authors, team members, an internal technical review, extensive QA reviews, and at least four different management reviews, before it was even submitted to *The Journal of Environmental Science and Technology (ES&T)*. As mentioned in the response to Question 3A, *ES&T* is an especially selective journal, with only a 35% acceptance rate. It was the first journal this paper was submitted to and was accepted with the first submission after revisions. There were extensive comments from four reviewers, most of which were very supportive of publishing the work but wanted additional analysis of the extensive amount of data that was unfortunately outside of the scope and length requirements of the article. We were able to successfully respond to comments (a response that required 14 pages of text), and the article was accepted quickly without further review. The mercury paper, "A national statistical survey assessment of mercury concentrations in fillets of fish collected in the U.S. EPA national rivers and streams assessment of the continental USA" was submitted to *Chemosphere* as a first-choice journal after internal EPA review. Chemosphere also included a peer review with two peer reviewers prior to publication, and this manuscript

did require major revisions. In all, 39 comments and authors' responses were tabulated, with 24 comments resulting in changes, additions to, or deletions from the manuscript. We were able to successfully address all reviewers' comments, and the revised manuscript was re-submitted to Chemosphere and was accepted for publication on 11-2-14.

AUTHORS

Contributing Author

Author Name:	Angela Batt		
Professional Title:		Salutation:	Dr.
Email:	batt.angela@epa.gov	Organization:	
Mailing Address:			
Street Line 1:	26 Martin Luther King Drive West		
City:	Cincinnati		
Zip Code:	45268	State:	Ohio
At time of research was:	EPA Employee		
Separation Date:			
% of Effort:	28		

Contributing Author

Author Name:	John Wathen		
Professional Title:		Salutation:	
Email:	wathen.john@epa.gov	Organization:	
Mailing Address:			
	1301 Constitution Ave NW Mail Code:		

Street Line 1:	4305T		
City:	Washington D.C.		
Zip Code:	20460	State:	D.C.
At time of research was:	EPA Employee		
Separation Date:			
% of Effort:	27		

Contributing Author

Author Name:	Athony Olson		
Professional Title:		Salutation:	
Email:	lazorchak.jim@epa.gov	Organization:	
Mailing Address:			
Street Line 1:	200 SW 35th Street		
City:	Corvallis		
Zip Code:	97333	State:	OR
At time of research was:	EPA Employee		
Separation Date:			
% of Effort:	15		

Contributing Author

Author Name:	Thomas Kincaid		
Professional Title:		Salutation:	
Email:	kincaid.tom@epa.gov	Organization:	
Mailing Address:			

Street Line 1:	200 SW 35th Street		
City:	Corvallis		
Zip Code:	97333	State:	OR
At time of research was:	EPA Employee		
Separation Date:			
% of Effort:	10		

Principal Author

Author Name:	James M. (Jim) Lazorchak		
Professional Title:		Salutation:	
Email:	lazorchak.jim@epa.gov	Organization:	
Mailing Address:			
Street Line 1:	26 Martin Luther King Dr W		
City:	Cincinnati		
Zip Code:	45268	State:	Ohio
At time of research was:	EPA Employee		
Separation Date:			
% of Effort:	20		

PUBLICATIONS

Publication 1:

Publication Title:	A national statistical survey assessment of mercury concentrations in fillets of fish collected in t
Publication Date:	Wed Mar 11 00:00:00 GMT 2015

Journal/Publication Method:	Chemosphere		
All Author(s):			
Volume:	122	Number:	N/A
Pages:	52-61	Immediately Index:	Immediately Index:
Citation ½ Life:	6.7	Impact Factor:	5.108

Publication 2:

Publication Title:	Statistical Survey of Persistent Organic Pollutants: Risk Estimations to Humans and Wildlife through		
Publication Date:	Thu Feb 23 00:00:00 GMT 2017		
Journal/Publication Method:	Environmental Science and Technology		
All Author(s):			
Volume:	51	Number:	5
Pages:	3021-3031	Immediately Index:	Immediately Index:
Citation ½ Life:	7.8	Impact Factor:	7.149

Chemosphere 122 (2015) 52–61

Contents lists available at ScienceDirect

Chemosphere

journal homepage: www.elsevier.com/locate/chemosphere

A national statistical survey assessment of mercury concentrations in fillets of fish collected in the U.S. EPA national rivers and streams assessment of the continental USA

John B. Wathen [a,*], James M. Lazorchak [b,1], Anthony R. Olsen [c,2], Angela Batt [b,1]

[a] U.S. Environmental Protection Agency, OW/Office of Science and Technology, 1200 Pennsylvania Avenue, NW (MC4305T), Washington, DC 20460, United States
[b] U.S. Environmental Protection Agency, Office of Research and Development, 26 W. Martin Luther King Drive, Cincinnati, OH 45268, United States
[c] U.S. Environmental Protection Agency, ORD Western Ecology Division, 200 S.W. 35th Street, Corvallis, OR 97333-4902, United States

HIGHLIGHTS

- Hg fish tissue results from 541 U.S. sites on =>5th order streams in 2008–2009.
- Site selection was probabilistic and nationally-representative.
- 25.4% (137 sites, 13071 river miles, (21036 km)) > 300 ug kg^{-1} HH and WV thresholds.
- No difference observed between results from urban vs. non-urban sites or among three eco-regions.
- Most exceedances in top predator species.

ARTICLE INFO

Article history:
Received 8 July 2014
Received in revised form 28 October 2014
Accepted 2 November 2014
Available online 27 November 2014

Handling Editor: Keith Maruya

Keywords:
National rivers
Mercury (Hg)
Human fish consumption
Wildlife fish consumption

ABSTRACT

The U.S. EPA conducted a national statistical survey of fish fillet tissue with a sample size of 541 sites on boatable rivers =>5th order in 2008–2009. This is the first such study of mercury (Hg) in fish tissue from river sites focused on potential impacts to human health from fish consumption to also address wildlife impacts. Sample sites were identified as being urban or non-urban. All sample mercury concentrations were above the 3.33 ug kg^{-1} (ppb) quantitation limit, and an estimated 25.4% (±4.4%) of the 51663 river miles assessed exceeded the U.S. EPA 300 ug kg^{-1} fish-tissue based water quality criterion for mercury, representing 13144 ± 181.8 river miles. Estimates of river miles exceeding comparable aquatic life thresholds (translated from fillet concentrations to whole fish equivalents) in avian species were similar to the number of river miles exceeding the human health threshold, whereas some mammalian species were more at risk than human from lower mercury concentrations. A comparison of means from the non-urban and urban data and among three ecoregions did not indicate a statistically significant difference in fish tissue Hg concentrations at $p < 0.05$.

Published by Elsevier Ltd.

1. Introduction

Mercury (Hg) is a metal that is persistent, bioaccumulative, and toxic in the environment. It is a constituent of minerals in rocks and soil that enters the atmosphere by the natural degassing of the earth's crust and recycling by volatilization of atmospherically deposited mercury, as well as being mobilized to the environment from anthropogenic sources. Human activities have enriched the atmospheric content of mercury by a factor of 7.5 times compared to levels predating emissions from most human activities (Amos et al., 2013). These activities include mining (including gold extraction), manufacturing, Portland cement production, medical waste incineration, and most prominently, the combustion of fossil fuels, especially coal (UNEP, 2008). As of 2005, however, artisan and small scale gold mining were second only to fossil fuel combustion as sources of Hg emissions to the atmosphere (Pacyna et al., 2010). When Hg is deposited in water, a large portion is converted, by chemical and biochemical processes either in sediments or in the water column, from inorganic Hg to toxic methylmercury (MeHg) that bioaccumulates in fish muscle (Sunderland et al., 2009). Despite very effective efforts to reduce emissions of Hg in many countries, including the U.S., Hg emissions from Asia continue to

* Corresponding author. Tel.: +1 (202) 566 0367; fax: +1 (202) 566 0409.
E-mail address: wathen.john@epa.gov (J.B. Wathen).
[1] Tel.: +1 (513) 569 7076; fax: +1 (513) 569 7438.
[2] Tel.: +1 (541) 754 4790.

http://dx.doi.org/10.1016/j.chemosphere.2014.11.005
0045-6535/Published by Elsevier Ltd.

increase (Wilson et al., 2010) with potential implications for increased human exposure in the U.S. and elsewhere (Sunderland et al., 2009; Driscoll et al., 2013). Future levels of Hg emissions will depend on the degree of implementation of measures to remove Hg from fossil fuel combustion emissions in the context of rising demand for electricity (Streets et al., 2009).

Research has shown that exposure to Hg and its compounds through the consumption of fish containing Hg can cause a range of toxic effects in humans, as well as in piscivorous mammalian and avian wildlife (U.S. EPA, 1997). At doses that result from moderate rates of maternal fish consumption, exposure of fetuses to Hg *in utero* can later manifest in children as deficits in subtle neurological end points such as lowered IQ, decrements in motor function, attention, and visuospatial performance (NAS, 2000). Evidence of early childhood effects at low levels of prenatal exposure is clear, and other health effects are likely, including cardiovascular effects and, to a lesser extent, immune system suppression (Karagas et al., 2012). Recent analyses also suggest an association between toenail Hg levels in young adults and the incidence of diabetes in later life (He et al., 2013). The thresholds for neurodevelopmental effects of mercury exposure discussed in this manuscript are based on U.S. EPA reference dose of 0.1 ug kg^{-1} of body weight/day for exposure to Hg (U.S. EPA, 2001b) relative to fish tissue concentrations detected in samples collected by the U.S. EPA. A reference dose (RfD) is an estimate of a daily exposure to the human population (including sensitive subgroups) that is likely to be without an appreciable risk of deleterious effects during a lifetime.

Wildlife are exposed to Hg and MeHg from a variety of environmental sources, mine tailings, industrial effluents, agricultural drain water, impoundments and atmospheric deposition from the electric power generation industry. At the higher levels of the food chain, piscivorous birds and mammals are among the highest risk receptors of MeHg contamination (Wolfe et al., 1998). Toxicity of Hg to piscivorous birds and mammals includes damage to the nervous, excretory, and reproductive systems. (Wolfe et al., 1998). In 1997, EPA identified wet deposition as the primary mechanism by which atmospheric Hg is transported to surface waters and land, although dry deposition may also contribute substantially (U.S. EPA, 1997). More recently, Driscoll et al. (2013) provide a full description of Hg sources, transport and deposition mechanisms, both human health and ecological effects, and cite atmospheric deposition as the primary mechanism of redistribution of mercury.

Large-scale studies of contaminants in fish tissue have found widespread evidence of Hg contamination. In a survey of lakes in the northeastern United States in 1992–1994, the U.S. EPA's Environmental Monitoring and Assessment Program (EMAP) analyzed whole fish composite samples for inorganic and organic contaminants, including Hg. It was found that 26% of northeastern lakes contained fish with Hg levels that exceeded the critical value for humans (200 ug kg^{-1} at that time), 54% of lakes exceeded wildlife critical values for piscivorous mammals (100 ug kg^{-1}), while 98% exceeded wildlife critical values for birds (20 ug kg^{-1}) (Yeardley et al., 1998). During the period 1993–1994, an EMAP survey of fish in the Mid-Atlantic Region found that small fish tissue concentrations exceeded the kingfisher Wildlife Value (30 ug kg^{-1}) over 72% of the stream length. Wildlife Values (WVs,) have been defined as the concentration in fish at which chronic effects to piscivorous wildlife occur (Lazorchak et al., 2003). In 2004 and 2005, the EMAP Great Rivers Assessment measured Hg concentrations in whole fish from the Upper Mississippi, Missouri, and Ohio Rivers to characterize the extent and magnitude of Hg contamination and to identify environmental factors influencing Hg accumulation (Walters et al., 2010). Across all three large river systems, Hg levels exceeded the WV for belted kingfisher in 33–75% of river length and exceeded the human health criteria in 1–7% of river length.

More recently, the U.S. EPA conducted the National Lake Fish Tissue Study (Stahl et al., 2008), which employed a national-scale statistical survey design and targeted human exposure to Hg by focusing on the fillet, the edible portion of collected species. This national lakes study included 486 composite predator fillet samples collected from 500 randomly-selected lakes during 2000–2003. In this nationally representative study, fish tissue from 48.9% of the lake population assessed exceeded the U.S. EPA's 300 ug kg^{-1} human health fish tissue-based water quality criteria (WQC) for Hg (U.S. EPA, 2001a).

The U.S. Geological Survey (USGS) has conducted extensive studies of national and regional fish-tissue contaminant data by combining results of several separate targeted studies conducted over time, analyzing the data and characterizing contaminant levels on the basis of region and watershed type, including propensity for methylation and fish characteristics (Schmitt, 2002; Scudder et al., 2009; Chalmers et al., 2011). These studies have led to identification of patterns and mechanisms of Hg accumulation in fish including the propensity for methylation to occur in watersheds with abundant wetlands (Brigham et al., 2009; Scudder et al., 2009). USGS continues to emphasize locally-focused studies which are national in their distribution (Brigham et al., 2014; Feaster et al., 2014; Chalmers et al., 2014) and explore causative mechanisms for the observed variations in Hg concentrations in a variety of media and settings.

The present work reports the results of a 2008–2009 National Rivers and Streams Assessment (NRSA) survey of rivers in the 48 conterminous United States to investigate Hg concentrations in composited fillet samples (Fig. 1). The survey is nationally-representative of the class of waters (5th order and greater rivers that are boatable) from which the sample of 541 sites was drawn. The fish tissue sampling efforts of this study are focused on providing information for assessments of human health impacts of fish consumption. Results were also used to estimate contaminant exposures to wildlife and aquatic species that consume fish and to compare urban and non-urban sub-groups of sites as well as sites located in each of three National Aquatic Resource Assessment (NARS) ecoregions: West and Mountains (WMTS), Plains and Lowlands (PLNLOW), and Eastern Highlands (EHIGH) (Fig. 1). The design of this study produces assessment results nationally, for three regions, and by urban and non-urban subgroups and relate those results to both human health and wildlife effects. The statistical survey design requires estimates for the assessments to incorporate weights that reflect the stratification and unequal probability of selection. This ensures that the inference (results) apply to all boatable, 5th order and greater rivers in the conterminous states. Results from this study may differ from those employing other non-survey design methods for selection of sites (Peterson et al., 1998).

2. Materials and methods

2.1. NRSA design and site selection

The NRSA included 1924 sites within the conterminous United States that were sampled for a range of environmental indicators, including concentrations of toxic chemicals in fish tissue (U.S. EPA, 2013). Fish tissue samples were collected at a subset of 541 sites that met the three criteria for the river population of interest for the fish tissue contaminant study: (1) boatable U.S. rivers of 5th order and greater (Strahler, 1957); (2) having a permanent fish population; and (3) flowing water during the study period (including the Great Rivers and run-of-the-river ponds, but excluding portions of tidal rivers up to head of salt, and reservoirs). The sample frame was derived from the National Hydrography Dataset (NHD)

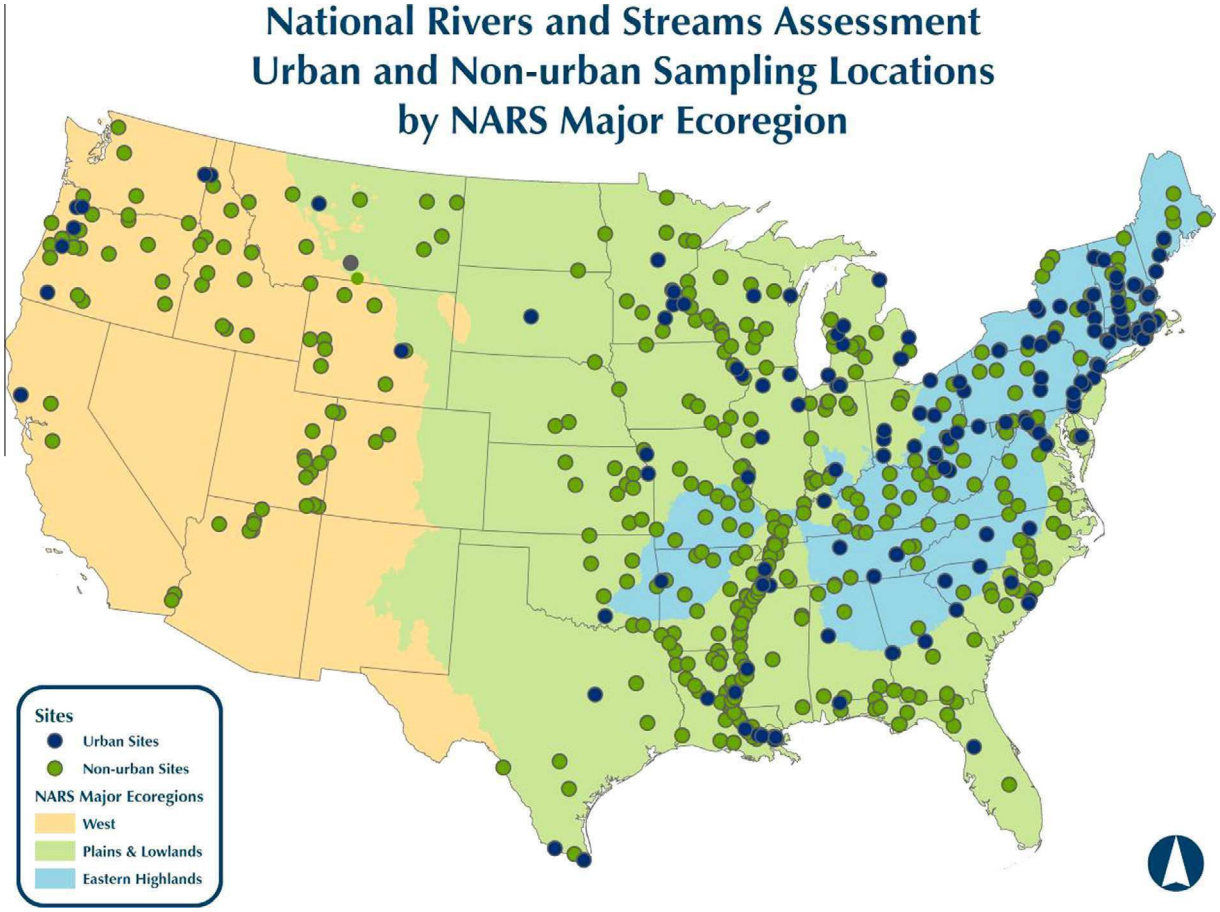

Fig. 1. National map of NRSA 2008–2009 sampling locations (n = 541) within national aquatic resource survey ecoregions.

and included Strahler stream order attributes (http://water.epa.gov/scitech/datait/tools/waters/index.cfm). NHD-Plus and the U.S. Census Bureau national urban boundary GIS coverage layers were used to establish the urban attribute so that both non-urban and urban samples could be identified. Non-urban and urban subpopulations were identified for two purposes. First, analytes other than Hg, including legacy organo-halogen compounds (entire sample set), perfluorinated compounds, and synthetic musks (only the urban subpopulation), were also determined for samples in this study and are being described in other publications. In the case of the perfluorinated compounds and synthetic musks, the smaller urban subpopulation better aligned with the budgetary resources available to perform the analyses. Secondly, the question of variable impacts to non-urban and urban populations and attendant questions of environmental justice are of interest to U.S. EPA. The distinction between urban and non-urban sampling locations was based on the most recent available U.S. Census Bureau data and the following definition: an Urban Area consists of contiguous densely settled census block groups that meet minimum population density requirements, along with adjacent densely settled census blocks that together encompass a population of at least 50 000 people.

Sampling sites were selected using a probability-based approach (Stevens and Olsen, 1999, 2004), generally applying the spatial methodology that had been used for lakes in U.S. EPA's National Lakes Fish Tissue Study (Stahl et al., 2008) to major U.S. rivers (Olsen et al., 2008). Selection probabilities were defined for 5th order or larger rivers in the lower 48 states so that the expected number of urban sites would be at least 150. The numbers of sites where samples were collected were limited by logistical factors, such as failure to obtain a fishing permit, absence of fish of the appropriate species and/or size at a given site, and time constraints for fish sampling. Fish tissue samples were collected from a total of 162 randomly selected urban rivers sites and 379 non-urban river sites. These totals included sampling locations in 46 conterminous states. Sampling included 154 5th order river sites, 162 6th order river sites, 99 7th order river sites and 126 sites from rivers 8th order and above.

2.2. Sample collection

One composite sample containing a single fish species was collected from each site (Fig. 1). Target species and individual specimens for the fish composite samples were selected based on a consistent set of criteria. Species were selected to be ubiquitous, abundant, and easily identified. Individual specimens of the species were selected to be adults of similar size (the length of the smallest individual in a composite could not be less than 75% of the total length of the largest individual) and sufficiently large (i.e., adult specimens) to provide adequate tissue for analysis (U.S. EPA, 2009a).

During required training sessions, all study participants were provided a list of recommended species for fish tissue sampling and were instructed to specifically target those species. A total of 15 species were included in that target list (in the Field Operations Manual and QAPP) and all were predator (typically top carnivore) species. Consistent with the human health context of the study, the focus was on sport/game fish that are commonly consumed by humans and of sufficient size to be of interest to anglers, and species that had a wide geographic distribution. The target species list included members of the sunfish (with largemouth and

smallmouth bass preferred), trout/salmon, pike, temperate bass, perch, and catfish families. Every effort was made to collect the desired species; however, the outcome of the field sampling efforts ultimately depended on the natural diversity and abundance of fish at each sampling site. The fish that were available to be taken dictated the mix of species collected at the sites, similar to conditions that would be encountered by anglers seeking fish for sport or sustenance.

Field teams used active methods (i.e., electrofishing) to collect fish samples from each site during a May through September field sampling period in 2008 and 2009. A routine composite sample consisted of five fish, but composites containing fewer than five fish were accepted in an effort to retain a sample from each target river segment (41% of the composites). The lengths of fish collected were similar in non-urban and urban waters. The mean length of fish taken from non-urban waters was 364.7 mm (min 101 mm, max 790 mm, S.D. 98.3 mm), and the mean length of fish from urban waters was 362.8 mm (min 112.5 mm, max 702 mm, S.D. 93.4 mm) Whole fish were shipped on dry ice to the designated sample preparation laboratories for storage until subsequent preparation (filleting and homogenization).

2.3. Sample preparation

Fish were filleted in the laboratory by trained technicians. In order not to excise fatty tissue likely containing organic contaminants also of interest in this study, scales were removed from fish, then lateral muscle fillets from both sides of each fish were prepared with skin on and the belly flap (ventral muscle and skin) attached. This method maintains consistency in preparing fillet samples for chemical analysis among EPA's national and regional-scale fish tissue studies and follows EPA's Guidance for Assessing Chemical Contaminant Data for Use in Fish Advisories (U.S. EPA, 2000a). By being consistent with this guidance, it enables comparison of fish tissue results among the EPA fish tissue studies and reduces variability for trends analysis when fish tissue studies are repeated periodically.

Fillets were composited using the batch method, where fillets from all of the individual specimens that comprise the sample were homogenized together, regardless of the proportional weight of individual fish. Each composite was homogenized using a tissue grinder, mixed thoroughly to a fine paste of uniform color and texture, and a 1-g aliquot was removed for Hg analysis. Fish collection and handling methods along with details of sample preparation are described in detail in U.S. EPA (2009a).

2.4. Tissue sample analysis

Fillets were analyzed for Hg with a Direct Mercury Analyzer (DMA-80; Milestone, Inc) using EPA method 7473 and Milestone Application note HG-0 (U.S. EPA, 2007). The method detection limit (MDL) was calculated to be 1.49 ug kg^{-1} (ppb or parts per billion) Hg using 40 CFR Part 136, Appendix B (U.S. Government, 2011). The quantitation limit (QL) is 3.33 ug kg^{-1} mercury, based on a low calibration point of 0.001 ug mercury and nominal sample weight of 0.33 g. The certified liquid QC standards for each run were purchased as single elements at 1000 ppm. The primary standard was purchased from Ricca and the secondary QC standard was purchased from Spex Claritas. Two internal standard calibration curves were prepared using standard solutions. The low-range curve included five points ranging from 0 to 0.020 ug and the high range curve included 12 points ranging from 0.030 to 0.400 ug, with each curve yielding R^2 values >0.99. Calibration check standards were run at the beginning and end of each batch for both the low and high curve. A secondary source standard and a sample of certified reference material (CRM DORM-2, dogfish muscle) were also analyzed once per batch. All check standards and reference material measurements were within ±20% of the actual value. Laboratory blanks were run once per batch and were all less than three times the MDL. One laboratory fortified matrix sample (LFM) spiked at a concentration of 25 ug kg^{-1} was run per batch to determine the influence of the matrix, with recoveries being within ±20% of the spiked amount or the result was flagged as estimated. Each batch consisted of 12 samples run in duplicate. Reported values were the mean of two analyses, with the relative percent difference between duplicates being less than 25%. Reported values were not blank-subtracted or recovery-corrected.

2.5. Statistical analysis

The NRSA survey design and survey analysis results in national and regional estimates of contaminant concentrations. The statistical estimates are based on weighted means of the analytical results from sites. The weights are based on the survey design and are the inverse of the probability of selecting a sampling site. The probability of selecting a site depends on the stratification and unequal probability of selection associated with the site. The weights are the total stream length represented by the sample site. Percentiles and mean estimates of fish tissue Hg concentrations were calculated from the data weighted in this manner using routines developed by the U.S. EPA in the statistical calculation package *spsurvey* ***R***. Weighted estimates calculated for the entire sampled population and for each of the sample subregions are listed in Table 1. The minimum and maximum Hg concentrations observed in the 541 samples are also given in Table 1. Additional information on the statistical algorithms employed in site selection and data analysis in the NRSA are available at: http://www.epa.gov/nheerl/arm/analysispages/software.htm (U.S. EPA, 2014). Hg tissue concentration data for the U.S. were depicted graphically as a cumulative distribution frequency (CDF) plot (Fig. 2).

A second statistical task was the assessment of the subgroups relative to each other to determine whether fish tissue Hg concentrations differed significantly between urban and non-urban subgroups and between any two of three geographic sub-regions. A standard normal *z*-test:

$$z = \frac{\text{MeanA} - \text{MeanB}}{\sqrt{(\text{stderrA}^2 + \text{stderrB}^2)}} \quad (1)$$

was used where MeanA is the weighted mean estimate and stderrA is the standard error estimate for MeanA for subgroup A and similarly for subgroup B.

Using regression analyses developed by Peterson and Van Sickle (2007) and Peterson et al. (2004), fish fillet concentrations were translated to equivalent whole body Hg. Using their regression analyses, $[\text{Log}10(\text{whole}) = -0.2712 + 0.9005 * \log 10(\text{fillet})]$, we have estimated exposures and dose to wildlife from Hg concentrations translated from the fillet concentration values obtained in this study to equivalent whole fish Hg concentrations. These whole fish equivalent values were then compared to WVs, as described below, to assess impacts to avian and mammalian wildlife.

3. Results and discussion

The total length of all 5th+ Strahler order U.S. rivers in NHDPlusv2 is 235 945 km (147 465 mi). The total length of all rivers included in the fish tissue study is estimated to be 51 663 mi or 83 144 km (±7027 km). In addition, within the rivers intended to be included in the fish tissue study an estimated 30 407 km (±4488 km) could not be sampled, in many cases due to the inability to obtain fish permits or safety reasons. For some rivers, insufficient information from the survey is available to know whether

Table 1
River length estimates and group percentile and mean estimates for mercury concentration (Hg ww ug kg^{-1}).

Statistic	National n = 541	Non-urban n = 379	Urban n = 162	EHIGH n = 190	PLNLOW n = 280	WMTS n = 71
River miles	51663	40752	10911	14738	29739	7186
River km	83145	65584	17559	23718	47861	11564
5th% ile	37.2	34.6	61.7	45.6	37.2	31.5
25th % ile	96.2	90.9	114.8	100.5	99.7	81.4
50th % ile	175.6	170.5	200.6	176.0	180.1	125.3
75th % ile	302.7	302.6	309.1	274.8	298.8	346.1
95th % ile	583.6	578.8	803.3	535.2	578.8	854.1
Mean	228.9	223.3	250.2	210.0	231.4	257.5
Maximum observed	1419	1419	854	854	1419	1272

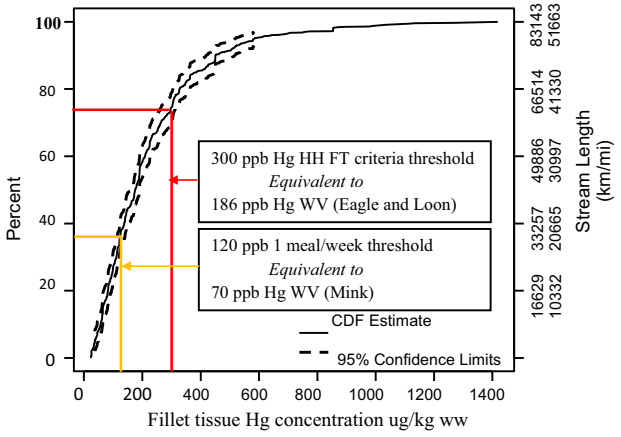

Fig. 2. National estimated Hg fish tissue concentration cumulative distribution (HH FT = human health fish tissue).

the river is boatable. A total of 33993 km (±4803 km) are estimated to be inaccessible due to landowners denying access to the river, and 7257 km (±2208 km) are rivers that were not sampled for other reasons. In addition to the above categories, the total length of 5th+ Strahler order U.S. rivers includes an estimated 57377 km (±7147 km) that are wadeable and 23513 km (±3804 km) that are not rivers or rivers with flowing water and hence do not fall into the population of rivers targeted for the fish tissue study. While the study results apply to the 83144 km, the study was intended to apply to a minimum of 113805 km or a maximum of 155055 km depending on whether the rivers were associated with insufficient information to determine if they were boatable, all not boatable, all boatable, or a combination. The length of 5th+ Strahler order U.S. rivers not included in the study for the reasons cited above was 152801 km (95802 mi).

All (100%) of the 541 fish fillet samples analyzed for Hg content for this national study contained quantifiable levels of Hg above the 3.33 ug kg^{-1} quantitation level for the method. Hg concentrations measured in the fillet samples ranged from 21 ug kg^{-1} to 1419 ug kg^{-1}. The national weighted mean Hg concentration for fillets in fish from U.S. rivers is 228.9 ug kg^{-1} (±18.6 ug kg^{-1}) compared to a weighted mean concentration of 250.2 ug kg^{-1} (±47.8 ug kg^{-1}) for fish fillet samples from only urban rivers and 223.3 ug kg^{-1} (±19.7 ug kg^{-1}) from non-urban rivers. An estimated 25.4% (±4.4%) of the sampled river miles exceeded the U.S. EPA WQC for Hg of 300 ug kg^{-1} (two fish meals/month consumption level) in fish tissue out of 51663 miles (83144 km) of boatable U.S. rivers of 5th order and greater included in the sampled population.

Fig. 2 is a cumulative distribution plot (CDF) of the cumulative percentage of the river length (left y axis) and the corresponding number of river km and miles they represent in the aggregate (right y axis), plotted against the concentrations of Hg in the samples (x axis). Two thresholds are superimposed on the CDF. The red indicator that connects the CDF curve with the x axis marks the point on the distribution at which the 300 ug kg^{-1} criterion value (equivalent to 186 ug kg^{-1} Hg WV (Eagle and Loon) is intersected. The yellow indicator marks the point on the curve intersected by the value of 120 ug kg^{-1} which is the maximum concentration of Hg in fish tissue at which one meal/week can be consumed without exceeding the reference dose for Hg, which is a 170 g portion (6 oz), for a 70 kg individual (Equivalent to 70 ug kg^{-1} Hg WV (Mink)). Table 1 lists the weighted percentile values nationally, as well as for urban and non-urban subgroups and three eco-regional subgroups and the number of sites that each subgroup includes.

3.1. Human health benchmarks

The percentage and number of river miles of fillet sample composites exceeding human health benchmarks provides an index of the extent to which fish from boatable 5th order and higher rivers can be safely consumed by humans. As stated above, this 300 ug kg^{-1} (wet weight) Hg benchmark, contained in the 2001 *Water Quality Criterion for the Protection of Human Health* (U.S. EPA, 2001a) represents a Hg exposure equal to the reference dose for Hg from the consumption of two meals a month.

Based on fish composite samples that exceed the U.S. EPA's 300 ug kg^{-1} human health fish tissue-based WQC (WQC), an estimated 25.4% of the 13071 river miles (21036 km) and a substantial portion of the resource of U.S. rivers 5th order and above as were sampled in this study. This percentage, however, is much lower than the 48.9% (U.S. EPA, 2009b) of U.S. lakes found to exceed this same threshold in the 2000–2003 National Lake Fish Tissue Survey (NLFTS). This difference likely reflects distinctions in a number of areas, among them the contrasting nature of rivers vs. lakes as environments less conducive to methylation, as well as the longer residence time of water in lakes.

Another distinction between the findings of this study vs. NLFTS lies in the species included in the respective sample populations. In this study, all targeted species were top predators, but included catfish. In the NLFTS, bottom dwellers (including catfish) were treated separately. A more appropriate comparison may be made between the 48.9% exceedance of the 300 ug kg^{-1} human health fish tissue-based WQC from the NLFTS and the percentage exceedance of the WQC for smallmouth (25.1%) and largemouth bass (33.4%), which were represented in sufficient numbers to make national inferences. The weighted average exceedance (national values) of the WQC by the smallmouth bass (n = 120) and largemouth bass (n = 114) is 29.2%, which represents the best nationally-representative comparison that can be made between the rivers assessed in this study and the lakes in the NLFTS. As described by Scudder et al. (2009), further characterization of Hg concentrations in fish tissue by land cover and land use is possible, but cannot be resolved at the sample density of this study on a

nationwide basis. Whether compared to the percentage exceedance for all fish (25.4%) of largemouth and smallmouth bass (29.2%), however, exceedance of the WQC in approximately 25–30% of rivers represented by the survey is generally consistent with other current compiled assessments of Hg in fish tissue from U.S. rivers (Scudder et al., 2009; Chalmers et al., 2011) and contrasts markedly with exceedances of the WQC in fish tissue from U.S. lakes of almost 50% (U.S. EPA, 2009b).

The U.S. EPA's 300 ug kg^{-1} human health fish tissue-based WQC for Hg is the regulatory threshold emphasized in this paper, and consumption of two fish meals/month with this Hg concentration is a rate of consumption that is the approximate equivalent of the reference dose (RfD) for Hg. For context, the Hg concentration range for one meal/week consumption is 120–230 ug kg^{-1} and is incorporated in many state fish advisory programs (U.S. EPA, 2011) that the U.S. EPA promotes and for which it provides guidance (U.S. EPA, 2000b). The threshold above which no consumption is recommended (940 ug kg^{-1}, U.S. EPA, 2000b) is exceeded in these data by tissue concentrations from only 1.3% (unweighted percentage) of the sample locations. EPA recommends that pregnant women and nursing mothers should avoid fish with such elevated Hg concentrations (U.S. EPA, 2000b).

3.2. Sub-group differences

It is of interest to the U.S. EPA to understand differences in fish tissue contaminant levels between regions and between urban and non-urban waters. Three means of comparison applied here include the application of the *z*-test as described above, comparisons of the percentages of waters within each of these subgroups that exceed the U.S. EPA's 300 ug kg^{-1} human health fish tissue-based water quality criterion, and comparisons of the means and 95th percentile values for each of the subgroups. The *p*-value for the test of a difference between weighted means of urban and non-urban population subgroups was 0.31 ($z = 1.03$), indicating no statistical difference between the means of 5th order and above urban and non-urban river subgroups. Similarly, when the means of the ecoregion subgroups were compared, the resulting ***p*** values indicate no significant differences among the three ecoregions: EHIGH vs. PLNLOW ($z = 1.25$, $p = 0.21$), EHIGH vs. WMTNS ($z = 1.16$, $p = 0.25$), and WMTNS vs. PLNLOW ($z = 0.63$, $p = 0.53$).

Comparisons of the percentages of weighted river length exceeding the 300 ug kg^{-1} human health fish tissue-based water quality criterion are depicted in Fig. 3. As can be noted, the percent exceeding and not exceeding this criteria value are generally quite uniform, with the WMTS ecoregion being the exception. For all subgroups except the WMTS, the percent of river miles exceeding the criteria value is in the mid 20% range, with the WMTS being the only one that exceeds 30%. Similarly, when means and percentile values across the subgroups are compared (Fig. 4), it can be seen that among the three ecoregions, values for the WMTS exceed those for the EHIGH and PLNLOW regions for the 75th, 90th and 95th percentile groups. Also evident from Fig. 4 is the fact that although there is not a statistically significant difference between the means of the urban and non-urban subgroups, the 90th and 95th percentile data for the urban rivers are elevated relative to the non-urban rivers.

The WMTS is the ecoregion with the smallest number of river locations (***n*** = 71), relative to the PLNLOW (***n*** = 280) and EHIGH (***n*** = 190). As such, statistical analysis of the data for the WMTS is vulnerable to the influence of a few elevated sample values which are inconsistent with the relatively uniform atmospheric deposition otherwise seen across the ecoregions. A sample location in the WMTS with one of the highest fish tissue concentrations observed in the study (854 ug kg^{-1}) was collected in a creek draining a large geothermal area in California with a 100-year history of mercury mining (Kagel et al., 2007). This is the type of local deviation that can mask the pervasive and uniform general character of Hg occurrence and deposition in the U.S. The apparent elevation of Hg in fish tissue in the WMTS suggested by the data in Fig. 4 is not borne out by the *z*-test analysis for significance and is likely attributable to this and potentially another elevated value (1272 ug kg^{-1}) among the data from the Willamette River in OR near areas where historical gold mining occurred.

3.3. Differences in Hg concentration among fish species

As has been observed in other studies (Lazorchak et al., 2003; Peterson and Van Sickle, 2007; U.S. EPA, 2009b), Hg content of fish tissue is dependent upon fish species, size, and trophic level. In this study, weighted Hg concentrations were markedly higher for waters represented by composite samples of predatory species (e.g., largemouth bass, mean Hg = 347 ± 22 ug kg^{-1}) than by bottom dwellers

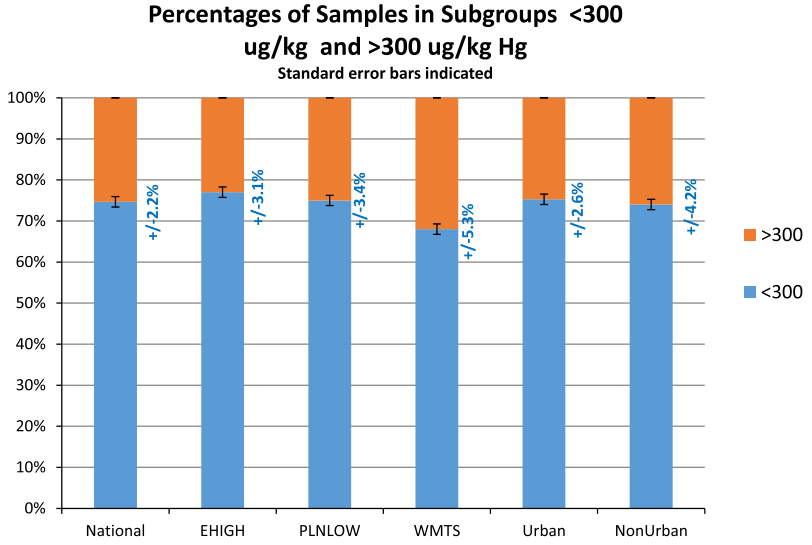

Fig. 3. Percentage of river miles by subgroup exceeding or not exceeding EPA's 300 ug kg^{-1} human health fish tissue-based water quality criterion.

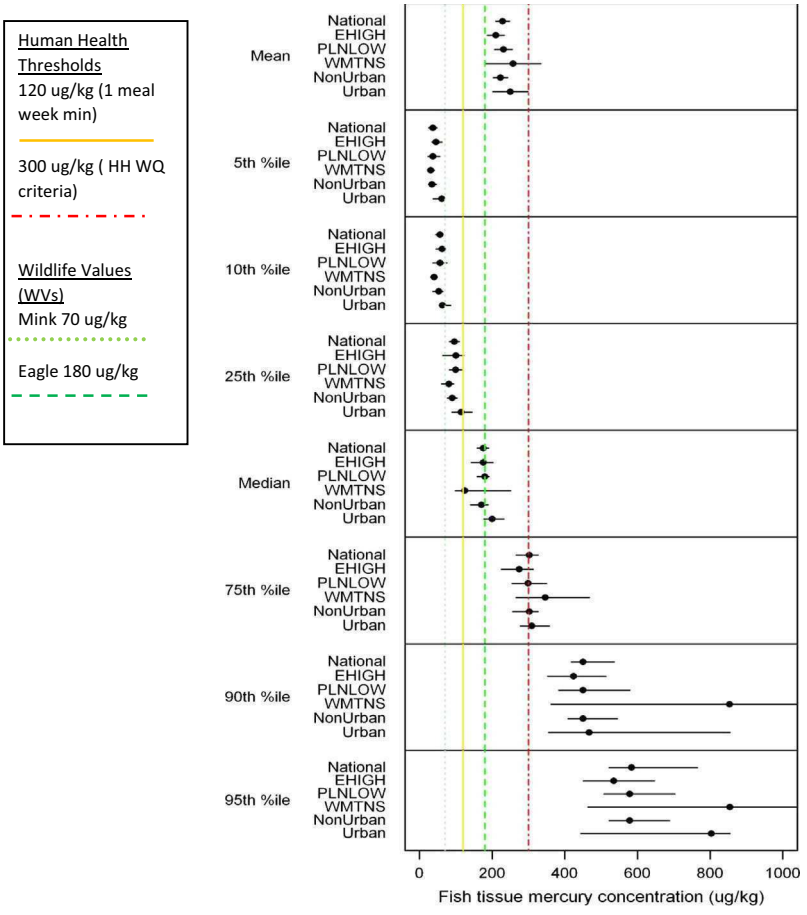

Fig. 4. Estimated percentile values (with 95% confidence limits) for subgroups with human health and wildlife value thresholds.

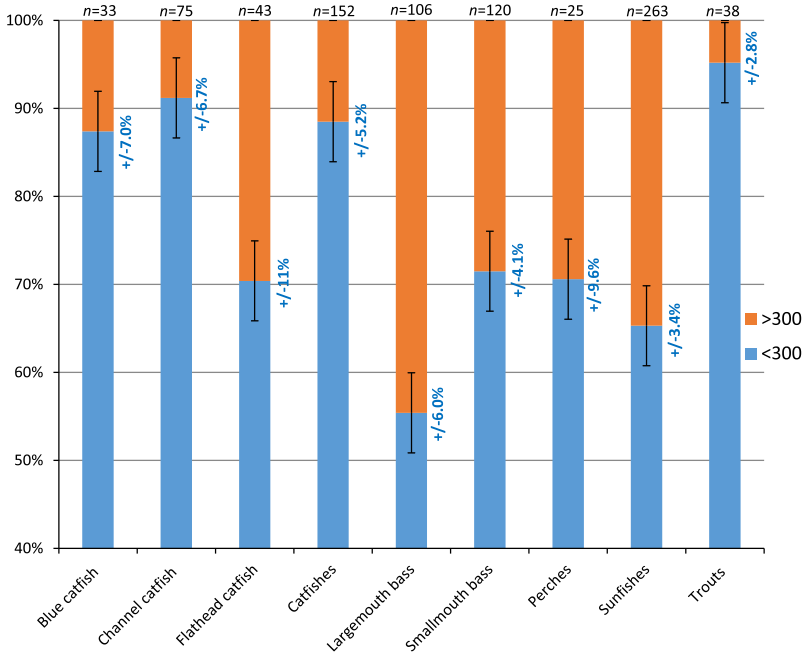

Fig. 5. Percentage of river miles by species/family exceeding EPA's 300 ug kg^{-1} human health fish tissue-based water quality criterion.

(e.g., combined catfish, mean Hg = 143 ± 10 ug kg^{-1}.) Fig. 5 depicts the percent of river miles with species and species groups that exceeded and did not exceed the 300 ug kg^{-1} human health fish tissue-based WQC. Relative to higher (although not significantly so) Hg fish tissue concentrations in the urban river data, the percent of river miles with combined smallmouth and largemouth bass

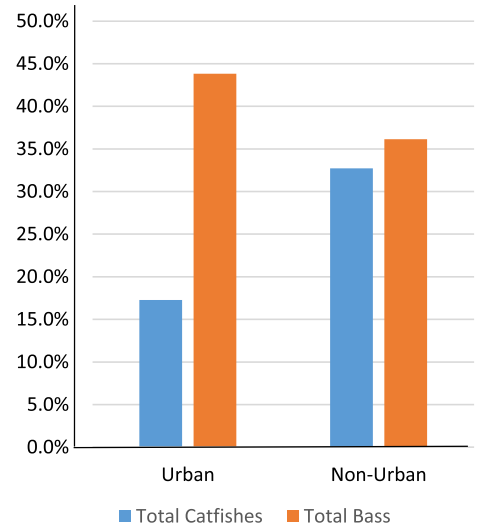

Fig. 6. Relative percentages of catfish and bass species in urban and non-urban waters.

samples were higher in the urban sub-group compared to the non-urban (43.8% vs. 36.1%). Conversely, combined catfish species constituted 32.7% of the river miles analyzed from non-urban sites vs. only 17.3% from urban river sites (Fig. 6).

Scudder et al. (2009) determined that Hg concentrations in fish tissue from largemouth bass from mixed use or undeveloped basins were higher than from urban basins, comparable to non-urban and urban subgroups discussed here. Non-weighted data from this study exhibit a similar distribution, but the smaller ***n*** of the portion of the subgroup that is itself a subgroup is insufficient to draw a national inference. The design of this study is focused on nationally-representative indices of assessment, and this comes at the expense of the ability to resolve distinctions beyond the primary sub-populations described-ecoregions (3), urban vs. non-urban sites, and the species included in Fig. 5. Of further interest relative to the discussion of urban/non-urban Hg fish tissue concentrations, however, may be the predominance of the percentage of bass species over catfish in the urban waters noted above when compared to near parity of the species groups in non-urban waters (Fig. 6). If the tissue of largemouth bass in urban areas is lower in Hg, there are also more of them relative to catfish species than in the non-urban areas, potentially affecting the combined impact of both species and urban/non-urban differential effects. Although not derived from weighted statistics, this factor suggests a possible explanation for the inconsistency between Scudder et al. (2009), Chalmers et al. (2014) among others, and this analysis. As mentioned earlier, because of the weighted probabilistic nature of the sample design, results from this study may differ from those employing other sample design methods (Peterson et al., 1998). Because of the unequal probability of any single sample being in the sample set, methods of comparison other than those employed for these data (*z*-test) are not valid.

3.4. Exceedances of WVs

The data from this study can also be interpreted with respect to the risk posed to piscivorous wildlife. Overall, fillets represent approximately 62% of the whole fish Hg concentration. Therefore, where fillets have Hg concentrations at or about 300 ug kg^{-1}, the dose to birds and mammals will be approximately 186 ug kg^{-1}. Whereas the primary health risk of Hg exposure to humans is neuro-developmental damage to unborn fetuses, Hg has been shown to threaten the survival of piscivorous wildlife (Lazorchak et al., 2003). According to the exposure scenario defined above, bald eagles and loons (WV = 160 and 180 ug kg^{-1}, respectively) will have similar risk levels relative to the applicable thresholds as humans consuming fish containing 300 ug kg^{-1} of Hg. Differences in species sensitivities to Hg consumption are emphasized by comparing mink to otter. Mink will be more at risk using the lower one meal per week (fillet) human threshold of 120 ug kg^{-1} (WV = 70 ug kg^{-1}), and the translated risk to otters will be intermediate between the human risk values in that their WV is 100 ug kg^{-1}. These values can also be compared to the data distribution depicted in Fig. 2.

4. Conclusions

With respect to human health thresholds, we have presented the following findings:

- All (100%) of the 541 fish fillet samples analyzed for Hg content for this national study contained quantifiable levels of Hg above the 3.33 ug kg^{-1} reporting level for the method.
- Nationally, an estimated 25.4% of river miles exceeded the EPA human-health fish tissue-based water quality criterion (WQC) for Hg of 300 ug kg^{-1}. This percentage represents 13 071 river miles (21 154 km) out of a total of 51 663 miles (83 143 km) of U.S. rivers of 5th order and greater included in the sampled population.
- The human health threshold exceedance data from this study also yields an estimate of risk of exposure to aquatic bird and mammal species from consumption of fish by the use of a correction factor for the relative Hg content of fillet tissue, normally consumed by humans, vs. the content of whole fish as are consumed by wildlife. Risk to piscivorous avian species are similar to risks for humans at 300 ug kg^{-1} (two meals per month level of consumption), whereas mink are more at risk than the avian species cited (and humans) when compared to the lower human one meal per week (fillet) threshold of 120 ug kg^{-1}.
- No statistically-significant differences were seen between waters sampled in urban and non-urban rivers, although the mean and 95th percentile values for urban rivers are elevated relative to non-urban rivers and all U.S. rivers.
- Although the percentage of river miles exceeding the 300 ug kg^{-1} criteria value was relatively higher in the WMTS ecoregion than any other of the sub-regional data groupings (>30% vs. ~25%, respectively), and the mean and 90th and 95th percentile values for the WMTS appear elevated relative to other subgroups, the *z*-test for statistical significance did not refute the null hypothesis at greater than the 95% confidence level (69%). The apparent elevation of the WMTS subgroup may be attributable to its smaller sample size in conjunction with one or more locally high fish tissue concentration values associated with local geologic Hg sources, as opposed to fish tissue concentrations related to atmospheric deposition that the findings of this study suggest do not vary significantly across the nation.

This study establishes a national baseline for Hg concentration in fish tissue from U.S. rivers 5th order and greater and compares those concentrations to human health and piscivorous wildlife thresholds. Hg concentrations in fish tissue from all areas of the country represent consumption risks to both humans and piscivorous wildlife in fish collected from approximately a quarter of the river miles. Furthermore, sensitivity to Hg exposure was greater for some aquatic species populations than the risk to humans at a given concentration. The lack of a statistically-significant difference

between fish tissue concentrations from urban vs. non-urban areas and among ecoregions is consistent with the ubiquitous nature of Hg contamination and its primary mechanisms of atmospheric transport and deposition. Differences in the representation of species in urban vs. non-urban rivers in this study may dampen variation seen by others (e.g., Scudder et al., 2009) between Hg concentrations in some species in urban vs. non-urban sites. The observed distinction in these results may also be attributable to the statistical methods of this study which result in national inferences that may not reflect specific local or regional conditions.

Author contributions

All the authors contributed to the initiation of the project, organization of the work, management of the project, analyzed the finished measurement data, and coordinated manuscript preparation. All four authors cooperated in developing the experimental design and writing the manuscript.

Acknowledgements

This study was funded within the U.S. EPA budget with public funds. The results reported here are the products of the combined efforts of many in addition to the authors. Prominent among these efforts is the sample collection supported by federal (USGS) and (many) state agency sampling teams. Within EPA, non-authors who provided significant contributions include Ellen Tarquinio and Sarah Lehmann who managed the overall NRSA project, Leanne Stahl was the overall technical lead for the fish tissue indicator, and the project would not have been possible without the contributions of many other EPA staff. Blaine Snyder of Tetratech and Harry McCarty of CSC played significant roles in project management and data processing and validation. Sample extraction and analysis was performed by Jayme Webb-Turbeville, Tracy Webb-Terbeville, and Ervin Obryan of Dynamac Corp.

References

Amos, H.M., Jacob, D.J., Streets, D.G., Sunderland, E.M., 2013. Legacy Impacts of all-time anthropogenic emissions on the global mercury cycle. Global Biogeochem. Cycles 27, 1–12.

Brigham, M.E., Wentz, D.A., Aiken, G.R., Krabbenhoft, D.P., 2009. Mercury cycling in stream ecosystems. Water column chemistry and transport. Environ. Sci. Technol. 43 (8), 2720–2725.

Brigham, M.E., Sandheinrich, M.B., Gay, D.A., Maki, R.P., Krabbenhoft, D.P., Wiener, J.G., 2014. Environ. Sci. Technol. 2014 (48), 6115–6123.

Chalmers, A.T., Argue, D.M., Gay, D.A., Brigham, M.E., Schmit, C.J., Lorenz, L., 2011. Mercury trends in fish from rivers and lakes in the United States, 1969–2005. Environ. Monit. Assess. 175, 175–191.

Chalmers, A.T., Krabbenhoft, D.P., Van Metre, P.C., Nilles, M.A., 2014. Effects of urbanization on mercury deposition and accumulation in New England. Environ. Pollut. 192, 104–112.

Driscoll, C.T., Mason, R.P., Chan, H.M., Jacob, D.J., Pirrone, N., 2013. Mercury as a global pollutant: sources pathways, and effects. Environ. Sci. Technol. 47, 4967–4983.

Feaster, T.D., Benedict, S.T., Clark, J.M., Bradley, P.M., Conrads, P.A., 2014. Scaling up watershed model parameters—flow and load simulations of the Edisto River Basin, South Carolina, 2007–09: U.S. Geological Survey Scientific Investigations Report 2014-5104, 34 p. <http://dx.doi.org/10.3133/sir20145104>.

He, K., Xun, P., Liu, K., Morris, S., Reis, J., Guallar, E., 2013. Mercury exposure in young adulthood and incidence of diabetes later in life. Diabetes Care 36, 1584–1589. The CARDIA trace element study Diabetes Care published ahead of print February 19, 2013.

Kagel, A., Bates, D., Gawell, K., 2007. A Guide to Geothermal Energy and the Environment. Geothermal Energy Association, Washington, DC. Retrieved February 9 2014. Cite uses deprecated parameters (help); Check date values. In: |access date = (help)Jump up ^ "Calpine Corporation – The Geysers". Retrieved 2008-06-11.

Karagas, M., Choi, A., Oken, E., Horvat, M., Schoeny, R., Kamai, E., Cowell, W., Grandjean, P., Korr, S., 2012. Evidence on the human health effects of low level methylmercury exposure. Environ. Health Perspect. 120 (6), 799–806. http://dx.doi.org/10.1289/ehp.1104494.

Lazorchak, J.M., McCormick, F.H., Henry, T.R., Herlihy, A.T., 2003. Contamination of fish in the mid-atlantic region: an approach to regional indicator selection and wildlife assessment. Environ. Tox. Chem. 22 (3), 545–553.

NAS, 2000. National Academies, Committee on the Toxicological Effects of Methylmercury, Board on Environmental Studies and Toxicology, Commission on Life Sciences. National Research Council. Toxicological Effects of Methylmercury. National Academy Press, Washington, DC.

Olsen, A.R. et al., 2008. Survey design for lakes and reservoirs in the United States to assess contaminants in fish tissue. Environ. Monit. Assess. 150, 91–100.

Pacyna, E.G., Pacyna, J.M., Sundseth, K., Munthe, J., Kindbom, K., Wilson, S., Steenhuisen, F., Maxson, P., 2010. Global emission of mercury to the atmosphere from anthropogenic sources in 2005 and projections to 2020. Atmos. Environ. 44 (20), 2487–2499.

Peterson, S.A., Van Sickle, J., Hughes, R.M., Schacher, J.A., Echols, S.F., 2004. A biopsy procedure for determining fillet and predicting whole-fish mercury concentration. Arch. Environ. Contam. Toxicol. 48, 99–107.

Peterson, S.A., Van Sickle, J., 2007. Mercury concentration in fish from streams and rivers throughout the western United States. Environ. Sci. Technol. 41 (1), 58–65.

Peterson, S.A., Larsen, D.P., Paulsen, S.G., Urquhart, N.S., 1998. Regional lake trophic patterns in the Northeastern United States: three approaches. Environ. Manage. 22 (5), 789–801.

Schmitt, C.J., 2002. Biomonitoring of Environmental Status and Trends (BEST) program: Environmental contaminants and their effects on fish in the Mississippi River basin. U.S. Geological Survey Biological Science Report USGS/BRD/BSR 2002–0004. <http://pubs.er.usgs.gov/usgspubs/bsr/bsr020004>.

Scudder, B.C., Chasar, L.C., Wentz, D.A., Bauch, N.J., Brigham, M.E., Moran, P.W., Krabbenhoft, D.P., 2009, Mercury in fish, bed sediment, and water from streams across the United States, 1998–2005. U.S. Geological Survey Scientific Investigations Report 2009-5109, 74p.

Stahl, L., Snyder, B.D., Olsen, A.R., Pitt, Jennifer L., 2008. Contaminants in fish tissue from US lakes and reservoirs: a national probabilistic study. Environ. Monit. Assess. 150, 3–19. http://dx.doi.org/10.1007/s10661-008-0669-8.

Stevens, D.L., Olsen, A.R., 1999. Spatially restricted surveys over time for aquatic resources. J. Agric. Biol. Environ. Stat. 4 (4), 415–428.

Stevens Jr., D.L., Olsen, A.R., 2004. Spatially balanced sampling of natural resources. J. Am. Stat. Assoc. Theory Methods 99, 465.

Strahler, A.N., 1957. Quantitative analysis of watershed geomorphology. Trans. Am. Geophys. Union 8 (6), 913–920.

Streets, D.G., Zhang, Q., Wu, Y., 2009. Projections of global mercury emissions in 2050. Environ. Sci. Technol. 43 (8), 2983–2988.

Sunderland, E., Krabbenhoft, D.P., Moreau, J.W., Strode, S.A., Landing, W.M., 2009. Mercury sources, distribution, and bioavailability in the North Pacific Ocean: insights from data and models. Global Biogeochem. Cycles 23.

UNEP, 2008. Study on mercury sources and emissions, and analysis of cost and effectiveness of control measures. United Nations Environmental Programme, Division of Technology, Industry and Economics (DTIE) Chemicals Branch, Geneva, Switzerland. <http://www.unep.org/hazardoussubstances/Mercury/tabid/434/Default.aspx> (8/13).

U.S. EPA, 1997. Mercury study report to congress. Office of Air Quality Planning & Standards and Office of Research and Development Volume VI: An Ecological Assessment for Anthropogenic Mercury Emissions in the United States. EPA-452/R-97-008.

U.S. EPA, 2000a. Guidance for assessing chemical contaminant data for use in fish advisories, volume 1: fish sampling and analysis. In: 3rd ed. U.S. EPA, Office of Water, Office of Science and Technology, Washington, DC. EPA 823-B-00-008.

U.S. EPA, 2000b. Guidance for assessing chemical contaminant data for use in fish advisories, volume 2: risk assessment and fish consumption limits. In: 3rd ed. U.S. EPA, Office of Water, Office of Science and Technology, Washington, DC. EPA 823-B-00-008.

U.S. EPA, 2001a. Water Quality Criterion for the Protection of Human Health: Methylmercury. EPA-823-R-01-001. Washington, DC: U.S. Environmental Protection Agency, Office of Water. <http://water.epa.gov/scitech/swguidance/standards/criteria/aqlife/methylmercury/document.cfm> (8/13).

U.S. EPA, 2001. Integrated risk management system. Reference Dose for Chronic Oral Exposure-Methylmercury (MeHg) (CASRN 22967-92-6). Washington, DC. <http://www.epa.gov/iris/subst/0073.htm#reforal>.

U.S. EPA, 2007. EPA Method 7473: mercury in solids and solutions by thermal decomposition amalgamation and atomic absorption spectrophotometry. U.S. Environmental Protection Agency, Office of Research and Development, Environmental Monitoring and Support Laboratory. Cincinnati, OH, 45268.

U.S. EPA, 2009a. National Rivers and Streams Assessment Field Operations Manual. Office of Water, Washington, DC, EPA-841-B-07-009.

U.S. EPA, 2009b. The National Study of Chemical Residues in Lake Fish Tissue. Office of Water, Washington, DC, EPA-823-R-09-006.

U.S. EPA, 2011. 2010 Biennial National Listing of Fish Advisories. U.S. Environmental Protection Agency Report EPA-820-F-11-014.

U.S. EPA, 2013. Rivers and Streams Assessment 2008–2009 A Collaborative Survey DRAFT Office of Wetlands, Oceans and Watersheds Office of Research and Development, Washington, DC 20460 EPA/841/D-13/001.

U.S. EPA, 2014. Aquatic resources monitoring, software downloads for spatial survey design and analysis. Office of Research Development (ORD) National Health Environmental Effects Research Laboratory (NHEERL), Western Ecology Division (WED). <http://www.epa.gov/nheerl/arm/analysispages/software.htm>.

U.S. Government, 2011. Code of Federal Regulations. Title 40 – Protection of Environment Subchapter D – WATER PROGRAMS Part 136 – GUIDELINES

ESTABLISHING TEST PROCEDURES FOR THE ANALYSIS OF POLLUTANTS. Appendix B to Part 136 – Definition and Procedure for the Determination of the Method Detection Limit-Revision 1.11. Government Printing Office, Washington, DC.

Walters, D.M., Bloksom, K.A., Lazorchak, J.M., Jicha, T., Angradi, T.R., Bolgrien, D.W., 2010. Mercury contamination in fish in midcontinent great rivers of the United States: importance of species traits and environmental factors. Environ. Sci. Technol. 44 (8), 2947–2953.

Wilson, S., Munthe, J., Sundseth, K., Kindbom, K., Maxson, P., Pacyna, J., Steenhuisen, F., 2010. Updating historical global inventories of anthropogenic mercury emissions to air. AMAP Technical Report No. 3, Arctic Monitoring and Assess ment Programme (AMAP) Oslo, Norway.

Wolfe, M.F., Schwarzbach, S., Sulaiman, R.A., 1998. Effects of mercury on wildlife: a comprehensive review. Environ. Toxicol. Chem. 17 (2), 140–160.

Yeardley Jr., R.B., Lazorchak, J.M., Paulsen, S., 1998. Elemental fish tissue contamination in northeastern U.S. lakes: evaluation of an approach to regional assessment. Environ. Toxicol. Chem. 17 (9), 1875–1884.

Environmental Science & Technology

Article

pubs.acs.org/est

Statistical Survey of Persistent Organic Pollutants: Risk Estimations to Humans and Wildlife through Consumption of Fish from U.S. Rivers

Angela L. Batt,[†] John B. Wathen,[*,‡] James M. Lazorchak,[†] Anthony R. Olsen,[§] and Thomas M. Kincaid[§]

[†]U.S. Environmental Protection Agency Office of Research and Development National Exposure Research Laboratory, Cincinnati, Ohio 45268, United States

[‡]U.S. Environmental Protection Agency Office of Water Office of Science and Technology, Washington, D.C. 20460, United States

[§]U.S. Environmental Protection Agency Office of Research and Development, National Health and Environmental Effects Research Laboratory, Corvallis, Oregon 97333, United States

Supporting Information

ABSTRACT: U.S. EPA conducted a national statistical survey of fish tissue contamination at 540 river sites (representing 82 954 river km) in 2008−2009, and analyzed samples for 50 persistent organic pollutants (POPs), including 21 PCB congeners, 8 PBDE congeners, and 21 organochlorine pesticides. The survey results were used to provide national estimates of contamination for these POPs. PCBs were the most abundant, being measured in 93.5% of samples. Summed concentrations of the 21 PCB congeners had a national weighted mean of 32.7 μg/kg and a maximum concentration of 857 μg/kg, and exceeded the human health cancer screening value of 12 μg/kg in 48% of the national sampled population of river km, and in 70% of the urban sampled population. PBDEs (92.0%), chlordane (88.5%) and DDT (98.7%) were also detected frequently, although at lower concentrations. Results were examined by subpopulations of rivers, including urban or nonurban and three defined ecoregions. PCBs, PBDEs, and DDT occur at significantly higher concentrations in fish from urban rivers versus nonurban; however, the distribution varied more among the ecoregions. Wildlife screening values previously published for bird and mammalian species were converted from whole fish to fillet screening values, and used to estimate risk for wildlife through fish consumption.

INTRODUCTION

Polychlorinated biphenyls (PCBs), polybrominated diphenyl ethers (PBDEs), and many organochlorine pesticides, such as dichlorodiphenyltrichloroethane (DDT), dieldrin, and chlordane, are well-known persistent organic pollutants (POPs) that have been shown to be ubiquitous in the environment.[1,2] PCBs were widely used in industry and manufacturing as dielectric and coolant fluids, but because of their environmental toxicity and persistence, were banned for use by the U.S. Congress in 1979.[3] PBDEs share a similar chemical structure to PCBs. They are used as flame retardants in numerous consumer products, such as building materials, electronics, furniture, and textiles.[2] The production of octaBDE and pentaBDE commercial mixtures in the United States ended in 2004, leaving decaBDE as the only congener still in production in the U.S., which is also scheduled to be phased out of use.[4] DDT is one of the most recognizable POPs. After concerns were raised that its widespread agricultural use as a pesticide was having serious impacts on the health of the environment,[5] it was banned for use in the United States in 1972.[6] Chlordane and dieldrin were used as pesticides mainly to control termites and other insects in agricultural areas, and both substances having been banned for all agricultural uses in the U.S. by the U.S. EPA since the late 1980s. After its agricultural use was ended, chlordane could continue to be used to control termites around foundations.

The list of possible health effects in humans and wildlife from exposure to these POPs is extensive, and includes cancer, reduced reproduction rates, changes in immune and endocrine end points, and developmental neurotoxic effects.[2,3,7−13] Effects for some POPs, such as PCBs, can also be transgenerational, as the compounds have been found to cross over into the placenta and result in poor attention and behavioral problems in exposed infants and children.[14,15] Most POPs are lipophilic, and have been measured in human serum, blood, breast milk, and other human tissue,[16−21] and in the tissue of a variety of

Received: October 11, 2016
Revised: January 9, 2017
Accepted: February 6, 2017
Published: February 23, 2017

ACS Publications

This article not subject to U.S. Copyright. Published 2017 by the American Chemical Society

DOI: 10.1021/acs.est.6b05162
Environ. Sci. Technol. 2017, 51, 3021−3031

wildlife.[22−29] Not only do they accumulate in tissues, but also they tend to biomagnify in the food chain,[30] and a link between dietary consumption of fish and marine mammals and human blood or serum levels has been observed for several POPs.[31,32] DDT is still detected in food supplies, and food-borne DDT, especially from seafood, remains a significant source of human exposure.[20,33] Although most of these POPs have been banned for use in the U.S. for decades, their persistence and toxicity still make it important to study their potential for exposure today.

This work presents the results of the 2008−2009 National Rivers and Streams Assessment (NRSA) fish tissue indicator, where 50 POPs (Table 1) were measured in 540 composite fish fillet samples collected across the conterminous states (Figure 1). The NRSA is one of several U.S. EPA national probabilistic surveys designed to evaluate the overall condition and health of the nation's waters, and a wide variety of indicators are evaluated. NRSA study results for pharmaceuticals measured in urban surface water, and fish tissue contaminant results for both mercury and perfluorinated compounds have been reported previously.[34−36] Mercury was detected in every one of the 540 samples included in this study, and fillet tissue concentrations in an estimated 25% of the sampled population exceeded the U.S. EPA 300 μg/kg fish-tissue based water quality criteria for mercury.[34] The probabilistic design for this survey provides national estimates of the distribution of these 50 POPs in fifth order and greater U.S. rivers for the assessment of human health impacts of fish consumption. A series of cancer[37] and noncancer[37,38] human health screening values (SVs) were applied to the fillet tissue results. They provide estimates of the percentage of all U.S. river km represented in this study (i.e., the sampled population of rivers) that would be expected to contain POPs that exceed these SVs. Fish fillet tissue contaminant concentrations were also compared to wildlife screening values that were converted from whole fish values to fillet screening values in order to estimate exposure risks to mammals and birds. Geographical distributions of these contaminants were compared, first between urban and nonurban river segments, and then among three aggregated National Aquatic Resource Assessment ecoregions: Eastern Highlands (EHIGH), Plains and Lowlands (PLNLOW), and the West and Mountains (WMTS) (Figure 1).

MATERIALS AND METHODS

2.1. NRSA Design and Site Selection. The NRSA included 1924 sites within the conterminous United States that were sampled for a range of indicators.[39] Fish samples were analyzed from 540 sites on rivers fifth order and greater to determine concentrations of chemicals in fish, including pesticides, PCBs, PBDEs, selenium, and mercury. The 50 POPs listed in Table 1 include 21 out of a possible 209 PCB congeners, 8 PBDE congeners, and 21 organochlorine pesticides and metabolites. The number of congeners of PCBs and PBDEs was limited to allow for the simultaneous analysis of multiple classes of 50 POPs with a single analysis, and the specific congeners were chosen as they have been reported in previous U.S. EPA studies.[22] The mercury findings and fish tissue sample collection design were described previously.[34] Fish tissue samples were collected at sites that had a permanent fish population. Rivers were designated as fifth order or greater based on Strahler stream order.[40] The sampling framework was derived from the National Hydrography Data set (NHD) and included Strahler stream order attributes.[41] The fish sampling sites were classified as two

Table 1. Target analytes with their respective maximum observed method detection limit (MDL) and quantitation limit (QL) (μg/kg wet weight), as described in Method Section 2.3

analyte	CAS number	max MDL	max QL
PCB-8	34883−43−7	0.37	1.99
PCB-18	37680−65−2	0.38	1.23
PCB-28	7012−37−5	0.48	1.53
PCB-44	41464−39−5	1.30	4.13
PCB-52	35693−99−3	0.86	2.73
PCB-66	32598−10−0	1.25	3.97
PCB-77	32598−13−3	0.61	1.93
PCB-101	37680−73−2	0.54	1.72
PCB-105	32598−14−4	0.30	0.95
PCB-118	31508−00−6	0.39	1.24
PCB-126	57465−28−8	0.35	1.11
PCB-128	38380−07−03	0.41	1.30
PCB-138	35065−28−2	2.68	8.52
PCB-153	35065−27−1	0.51	1.63
PCB-169	32774−16−6	0.36	1.14
PCB-170	35065−30−6	0.39	1.24
PCB-180	35065−29−3	0.33	1.05
PCB-187	52663−68−0	0.83	2.62
PCB-195	52663−78−2	0.83	2.63
PCB-206	40186−72−9	0.55	1.74
PCB-209	2051−24−3	0.45	1.43
summed PCBs	a sum of the above 21 congeners		
PBDE-47	5436−43−1	0.37	1.23
PBDE-66	189084−61−5	0.26	0.86
PBDE-99	60348−60−9	0.31	0.99
PBDE-100	189084−64−8	0.52	1.64
PBDE-138	182677−30−1	0.59	1.97
PBDE-153	68631−49−2	0.58	1.93
PBDE-154	207122−16−5	0.55	1.84
PBDE-183	207122−15−4	0.82	2.74
summed PBDE	a sum of the above 8 congeners		
2,4′-DDD	53−19−0	0.37	1.18
4,4′-DDD	72−54−8	0.28	0.89
4,4′-DDE	72−55−9	0.28	0.91
2,4′-DDT	789−02−6	0.30	0.95
4,4′-DDT	55−29−3	0.32	1.02
summed DDT	a sum of the above 5 DDT compounds		
alpha-chlordane (cis-chlordane)	5103−71−9	0.29	0.92
gamma-chlordane (trans-chlordane)	5103−74−2	0.38	1.22
oxychlordane	27304−13−8	0.37	1.18
summed chlordane	a sum of the above 3 chlordane compounds		
dieldrin	60−57−1	0.93	2.95
aldrin	309−00−2	0.30	0.97
alpha-BHC	319−84−6	0.31	1.04
gamma-BHC (lLindane)	58−89−9	0.23	0.73
endosulfan II	33213−65−9	0.46	1.53
endrin	72−20−8	0.37	1.18
endrin ketone	53494−70−5	0.34	1.08
heptachlor	76−44−8	0.28	0.89
heptachlor epoxide	1024−57−3	0.30	0.95
hexachlorobenzene	118−74−1	0.30	0.95
mirex	2385−85−5	0.37	1.18
cis-nonachlor	5103−73−1	0.29	0.99
trans-nonachlor	39765−80−5	0.29	0.92

DOI: 10.1021/acs.est.6b05162
Environ. Sci. Technol. 2017, 51, 3021−3031

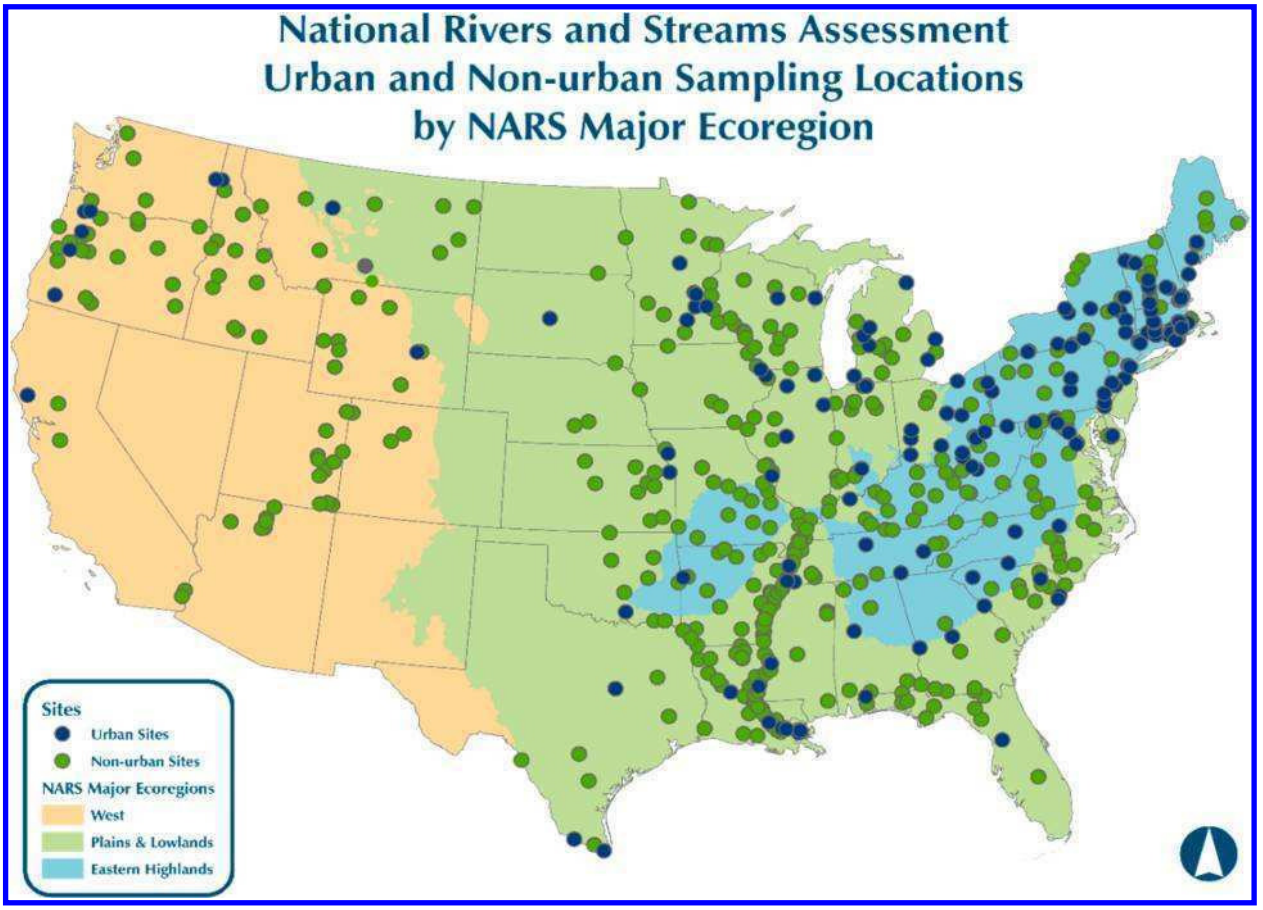

Figure 1. National map of NRSA 2008−2009 sampling locations (n = 540) within national aquatic resource survey ecoregions.

subpopulations: urban and nonurban river segments. NHD-Plus and the U.S. Census Bureau national urban boundary GIS coverage layers were used to identify urban sampling areas, which were defined as densely settled census block groups with a minimum population density of 50 000 people. Sampling sites were selected using a probability-based approach,[42,43] generally applying the spatial methodology used for lakes in U.S. EPA's National Lake Fish Tissue Study[44] to major U.S. rivers. Fish samples were collected from 164 randomly selected urban river sites and 378 nonurban river sites. This included sampling locations in 46 states with the following distribution of river sites: fifth order, 154 sites; sixth order, 161 sites; seventh order, 99 sites; and eighth order and above, 126 sites.

2.2. Sample Collection. One composite sample of a single fish species was collected from each site (Figure 1). A routine composite sample consisted of five fish, but composites containing fewer or greater than five fish were accepted in an effort to retain a sample from each target river segment (51.3% and 1.1% of the composites, respectively). Species were selected to be ubiquitous, abundant, and easily identified. Individual specimens of the species were selected to be adults of similar size (the length of the smallest individual in a composite could not be less than 75% of the total length of the largest individual) and sufficiently large to provide adequate tissue.[45] A total of 15 species were identified in a targeted list, including members of the sunfish (with largemouth and smallmouth bass preferred), trout/salmon, pike, temperate bass, perch, and catfish families. Field teams used active methods, primarily electrofishing, to collect fish samples from each site during the May through September field sampling period in 2008 and 2009. Whole fish were shipped on dry ice to the designated sample preparation laboratory for storage until subsequent fillet tissue sample preparation and analysis. Other aspects of fish collection and handling methods are further described elsewhere.[45]

2.3. Sample Preparation and Analysis. Fish were filleted in the laboratory. Scales were removed, then lateral muscle fillets from both sides of each fish were prepared with skin on and the belly flap (ventral muscle and skin) attached. Fillets from individual specimens that comprised the sample were homogenized together, regardless of the proportional weight of individual fish. Composites were homogenized using a tissue grinder and an 8 g aliquot of homogenate was used for analysis. Wet tissue samples were extracted using pressurized fluid extraction (PFE), followed by sample cleanup with gel permeation chromatography (GPC) and alumina, and clean extracts were analyzed by gas chromatography with electron capture detection (GC-ECD). GC-ECD was chosen as the analysis method since the ECD detection method was found to be more sensitive for the target analytes than some mass spectrometry methods, and provided a very cost-effective analysis for the range of compounds in this study. Full details of the extraction and GC-ECD analysis methods are included in Supporting Information (SI) Document 1. Briefly, 8.0 g of tissue were added to 20 g of anhydrous sodium sulfate and allowed to dry for 1 h. Samples were spiked with a surrogate standard solution and transferred to 33 mL PFE cells fitted with a cellulose filter, and remaining cell volume was filled with drying material. PFE cells were extracted with methylene chloride (50%) and hexane (50%) at 100 °C and 1000 psi for

DOI: 10.1021/acs.est.6b05162
Environ. Sci. Technol. 2017, 51, 3021−3031

three 7 min cycles. Extracts were collected into a 60 mL glass vial, and the volume was reduced to approximately 3 mL using a stream of nitrogen in a 50 °C water bath. Concentrated sample extracts were dried using a 1-in. diameter glass chromatography column packed with 20 g of sodium sulfate and glass wool, and rinsed three times with hexane. Further sample extract cleanup was performed using GPC with a Waters HPLC, followed by solid-phase extraction using columns packed with deactivated alumina-N. Final sample extracts were adjusted to a volume of 1 mL after the addition of 25 μL of an internal standard solution consisting of pentachloronitrobenzene, PCB 96, and PCB 166. These extracts were analyzed using Agilent 6890 gas chromatographs equipped with pressure-pulsed splitless injection, narrow-bore columns and micro ECD detectors. Since ECD detection is not as selective as some mass spectrometry methods available, two separate GC-ECD analyses were performed on instruments equipped with different GC columns, first a primary analysis (Agilent HP-5 capillary column: 30 m length, 0.25 mm diameter and 0.25 μm film thickness), followed by a confirmatory analysis (J&W DB - XLB column, 30 m length, 0.25 mm diameter and 0.25 μm film thickness), with the two different oven programs for both methods being described in SI Document 1. Concentrations of detected analytes were calculated for both the primary and confirmatory analyses. Reported concentrations are a result of the average of the primary and confirmatory analyses, unless the relative percent difference (RPD) in concentrations between the two columns was greater than 30%, in which case, the lesser concentration was reported. If an analyte was not detected in both analyses, it was reported as not-detected.

The method detection limit (MDL, Table 1), which is defined as the minimum concentration of an analyte that can be identified and detected with 99% confidence that the analyte concentration is greater than zero, was determined for each analyte using the procedure described at 40 CFR Part 136 Appendix B.[46] The quantitation limit (QL) was defined as 3 times the MDL, and both the MDL and QL were calculated on the primary and confirmatory columns, and were updated on a yearly basis. Concentrations were reported to the MDL that applied at the time of analysis, however, any concentrations greater than the MDL but less than the QL were flagged as estimated. The maximum MDL and QL observed during the course of the study for each analyte is listed in Table 1. Four quality control samples were analyzed with each extraction batch, including a laboratory reagent blank (LRB), a laboratory fortified blank (LFB), and two laboratory fortified matrix (LFM) samples. The LRB and LFB were prepared from sodium sulfate, and the LFB and LFM were spiked with a mixture of the target analytes to yield a final GC extract concentration of 15 ng/mL. Percent recovery for each analyte was calculated in the LFB and LFM samples. Acceptable target recoveries for all analytes ranged from 70% to 130% for LFB, and from 50% to 150% with a 30% RPD for the duplicate LFM samples. Any analytes or samples which did not meet the predetermined quality criteria of the LFB and LFM samples were reanalyzed, or reported as estimated. Samples were also re-extracted and analyzed if an analyte was present in the LRB above the QL and the analyte was present in the sample above the QL but less than 10 times the detected blank concentration. Standard reference material (SRM) 1947, purchased from National Institute of Standard and Technology (NIST), was used as a certified second source standard to monitor extraction efficiency and instrument quantitation, and was extracted and analyzed with each extraction batch. All data reported in this study were reviewed and validated against the project requirements by a third party not involved in the data generation. Only valid results were used in the statistical analyses. Measured concentrations and qualifiers for each of the 50 contaminants analyzed in the 540 fillet samples are included as SI (Table S1–S3).

2.4. Data Analysis. *National and Subpopulation Estimates.* The NRSA survey design and results provide national and regional estimates of fish tissue contaminant concentrations, and as a result, reported results are expressed as population estimates, and not site or sample summary data. The population estimates are based on weighted analytical results from sampling sites. The weights are based on the survey design and are the inverse of the probability of selecting a sampling site. The probability of selecting a site depends on the stratification and unequal probability of selection associated with the site. The weights are the total river length represented by the sample site. Percentiles and mean population estimates of fish tissue analyte concentrations were calculated from the weighted data, using routines developed by the U.S. EPA in the statistical calculation package *spsurvey* *R*[47] for the R statistical computing environment.[48] In addition to the urban and nonurban subgroups, statistical parameters were generated for three aggregated ecoregions (EHIGH, PLNLOW, and WMTS) used in U.S. EPA National Aquatic Resource Surveys.[49] A standard normal Z-test was used to investigate fish tissue analyte concentration differences between the urban and nonurban subgroups, and between ecoregions:

$$z = \frac{\text{mean}A - \text{mean}B}{\sqrt{(\text{stderr}A^2 + \text{stderr}B^2)}}$$

where mean$A$ is the weighted mean estimate, stderr$A$ is the standard error estimate for mean$A$ for subgroup A, and similarly for subgroup B. Compounds were evaluated by summed groups, including summed PCB and PBDE congeners, total DDT (the five DDT compounds and degradates listed in Table 1), and total chlordane (cis- and trans-chlordane, cis- and trans-nonachlor, and oxychlordane). Prior to summing data into groups, any detections below the MDLs were considered nondetects and the results were treated as zeros during the statistical analysis.

Human Health Risk Estimate. The two categories of human health risk that are reflected in selected SVs are cancer and noncancer (Table 2). The survey design provides national estimates of river kilometers that are expected to contain fish with fillet concentrations that would exceed those screening value thresholds. A cancer SV[37] is based on a level of excess cancer risk from exposure to a carcinogenic substance ranging from 10^{-4} to 10^{-6}. The noncancer SVs are based on a reference dose (RfD) for a toxicant, which is the level of exposure over a lifetime at which no observable adverse effects will occur. Cancer SVs are generally lower than noncancer SVs (Table 2), but the ratio can vary. For this assessment, a cancer SV reflecting 10^{-5} cancer risk has been applied to allow comparison of all the frequently detected compounds across regions, and to be comparable to previous U.S. EPA assessments.[22,26] A noncancer SV was also applied to provide context for the concentrations reported here in terms of thresholds widely used in fish consumption advisories.[37] For the PBDEs, no cancer SV was applied, since the PBDE

DOI: 10.1021/acs.est.6b05162
Environ. Sci. Technol. 2017, 51, 3021−3031

Table 2. Summary of the Human Health Screening Values (SVs) and Wildlife Values (WV), with All Values Being Presented in μg/kg Wet Weight (ppb); and the Applied Fillet to Whole Fish Conversion Factors[a]

compound	cancer SV	noncancer SV	mink WV	kingfisher WV	fillet to whole fish conversion factor
PCBs	12	47	72	242	1.83
PBDEs	N/A	210	21	8.7[b]	1.50
DDT	69	120	216	12.0	1.66
chlordane	67	1200	573	3.1	1.44
dieldrin	1.5	120	20	360	

[a]HH SVs are based on the upper estimates of consuming one 8 oz meal of fish per week. See Methods Section 2.4 for a description of Cancer and Non-Cancer SVs, and WV. [b]Kestril WV instead of Kingfisher, taken from Canadian Environmental Protection Act[38]

congeners represented in this study have not been classified as carcinogenic.[4] Limited RfDs are available for PBDE congeners, however, the California EPA has published fish tissue advisory levels based on noncancer risk.[38]

Wildlife Risk Estimate. The fish tissue study conducted under the 2008−2009 NRSA was designed to assess human health impacts from fish consumption, which is why fillets were targeted for analysis. To estimate the possible risk to wildlife that may be consuming fish collected in this survey, wildlife values (WVs) for mink, kingfisher, and larger birds (if available) that represent thresholds for toxic effects (such as reproductive or development success, organismal viability or growth, effect on population dynamics) were used.[50,51] However, these previously reported WVs represent whole-fish tissue concentrations, so a conversion factor had to be applied to convert whole-fish tissue WVs to fillet WVs. For total PCBs, a conversion factor was averaged from across three references;[28,52,53] one conversion factor was used for DDT and chlordane;[52] and another was identified for PBDEs.[51] All of these conversion factors are listed in Table 2, along with the resulting fillet WVs. Dieldrin WVs were not converted from whole body to fillets, since it has been reported that dieldrin was present in roughly the same average concentrations in game-fish fillets as in whole-body bottom-feeders. No other publications were found that provided information comparing whole fish dieldrin to fillet concentrations from the same fish species.[54] Since a conversion factor for the wildlife values from fillets to whole fish had to be applied, limited inferences can be made for the wildlife results. However, because different species can display very different sensitivities to the same chemicals, the results of the wildlife risk estimate do provide valuable insight into the relative risks of exposure for human, mammalian, and avian species across the different contaminant groups.

Chemical Co-Occurrence. Co-occurrence of the four main chemical groupings was examined using a previously described procedure,[55] Samples that exceeded the weighted median concentrations for any of the four major contaminant groups (PCBs, PBDEs, total chlordane, and total DDT) were identified. Samples that exceeded the respective median concentrations were then compared to calculate the percentage of the samples with concentrations above the median of any one compound group that occurred: (1) singly; (2) with a second contaminant group also above its median; (3) as a combination of any three contaminant groups; or 4) with all four compound groups occurring together above their median concentrations.

3.0. RESULTS AND DISCUSSION

PCBs in Fish Tissue. PCBs were detected in 93.5% of the fish fillet samples, which results in 48% (40 030 river km (±2432 km)) of the national sampled population of rivers having fillet tissue concentrations that exceed the cancer SV of 12 μg/kg, as shown in Table 3. By comparison, nearly 70% of the sampled population of urban rivers had fillet tissue concentrations that exceeded the PCB cancer SV. The maximum summed PCB concentration measured in urban river samples was 857 μg/kg. Among the three ecoregions, PCB detections dominated in the EHIGH, where the mean summed PCB concentration was 47.1 μg/kg. In this ecoregion, fillet tissue concentrations exceeded the PCB cancer SV of 12 μg/kg in 54.3% of the sampled population of EHIGH rivers. The mean summed PCB concentrations in fillet samples from the PLNLOW and WMTS were 30.7 μg/kg and 11.9 μg/kg, respectively. The PCB SV exceedances were lower in these two ecoregions. In the PLNLOW, 50.8% of the sampled population of PLNLOW rivers had fillet concentrations that exceeded the 12 μg/kg SV. By contrast, 23.6% of the WMTS sampled population of rivers exceeded the cancer SV.

The national, ecoregion, urban river, and nonurban river population percentile estimates for the summed PCB concentrations are shown in Figure 2. The national estimate of the median summed PCB concentration is 11.3 μg/kg, which is almost the same as the cancer SV of 12 μg/kg. All of the 75th percentile estimates of fillet concentrations lie between the cancer SV (12 μg/kg, which corresponds to the WMTS estimate) and noncancer SV (47 μg/kg, which corresponds to the urban river estimate). All of the 90th percentile estimates exceed 47 μg/kg except the estimate for the WMTS ecoregion. For the wildlife estimates, fish tissue concentrations in 9.3% of the national sampled population exceed the fillet WV for mink, whereas fish tissue concentrations in only 1.3% of the sampled population exceeded the kingfisher fillet WV. Human SVs for both cancer and noncancer are lower than both PCB WV values, and therefore, in general, the human health SVs are protective of wildlife risks as well.

The relative abundance of the 21 PCB congeners found in fish fillet tissue from nonurban vs urban rivers is shown in SI Figure S-1. All mean PCB congener concentrations are higher in samples from urban rivers than from nonurban rivers, but the magnitude of the difference varies. Congeners 138 and 153 are the most abundant PCBs in both nonurban and urban river fish fillets, which has also been the case in other environmental samples.[16] The coplanar PCBs 77, 126, and 169 (indicated by the arrows in SI Figure S-1) are present only at low concentrations in fillet tissue from both subpopulations. In this study, 21 PCB congeners were quantified out of the full suite of 209 PCB congeners. Since there is additional PCB mass in the samples that was not measured for this study, the summed 21 PCB congeners underestimate the total mass present in the samples. Although this study underestimates the total PCB mass, the congeners analyzed include 10 of the 11 congeners with the highest frequency of environmental occurrence, as well as three dioxin-like congeners.[56] Therefore, the results of this study are still applicable to the human health and wildlife exposure analysis.

PBDEs in Fish Tissue. Similar to PCBs, the eight congeners of PBDEs are commonly detected in fish tissue samples. All of the results presented in Table 3 and SI Figure S-2 indicate higher concentrations in urban river samples than in samples

DOI: 10.1021/acs.est.6b05162
Environ. Sci. Technol. 2017, 51, 3021−3031

Table 3. Weighted POPs Fish Tissue Concentration Results by Site Type and Ecoregion, And Percent River km Exceeding Human Cancer Screening Values (CSV), Noncancer Screening Values, And Wildlife Values (WV)

PCB summed congeners			
statistic	national	nonurban	urban
detects	505/540 sites (93.5%)	343/377 sites (91.0%)	162/163 sites (99.4%)
mean	32.7 ug/kg	26.9 ug/kg	54.2 ug/kg
median	11.3 ug/kg	8.6 ug/kg	23.8 ug/kg
max	857 ug/kg	412 ug/kg	8567 ug/kg
%>CSV (12 ug/kg)	48.0%	42.0%	69.8%
%>non-CSV (47 ug/kg)	16.7%	14.6%	25.7%
%>mink WV (72 ug/kg)	9.3%	8.9%	10.9%
%>KF WV(242 ug/kg)	1.4%	0.7%	3.8%
statistic	EHIGH	PLNLOW	WMTS
sites	189	280	71
mean	47.1 ug/kg	30.7 ug/kg	11.9 ug/kg
median	16.7 ug/kg	12.6 ug/kg	3.8 ug/kg
%>CSV (12 ug/kg)	54.3%	50.8%	23.6%
%>non-CSV (47 ug/kg)	20.2%	18.0%	6.1%
%>mink WV (72 ug/kg)	13.2%	8.5%	4.6%
%>KF WV(242 ug/kg)	3.8%	0.5%	0%

PBDE summed congeners			
statistic	national	nonurban	urban
detects	497/540 sites (92.0%)	340/377 sites (90.2%)	157/163 sites (96.3%)
mean	11.6 ug/kg	8.6 ug/kg	22.5 ug/kg
median	4.7 ug/kg	3.6 ug/kg	8.0 ug/kg
maximum	311 ug/kg	151 ug/kg	310 ug/kg
%>non-CSV (210 ug/kg)	0.3%	0%	1.2%
%>mink WV(21 ug/kg)	14.6%	10.6%	29.1%
%>kestral WV(8.7 ug/kg)	33.4%	29.5%	47.8%
statistic	EHIGH	PLNLOW	WMTS
sites	189	280	71
mean	13.6 ug/kg	10.2 ug/kg	13.2 ug/kg
median	6.8 ug/kg	3.5 ug/kg	4.8 ug/kg
%>non-CSV (210 ug/kg)	0%	0.5%	0%
%>mink WV(21 ug/kg)	17.5%	13.3%	13.9%
%>kestral WV(8.7 ug/kg)	42.0%	31.5%	23.8%

total DDT			
statistic	national	nonurban	urban
detects	533/540 sites (98.7%)	370/377 sites (98.1%)	163/163 sites (100%)
mean	13.8 ug/kg	12.3 ug/kg	19.0 ug/kg
median	6.3 ug/kg	5.7 ug/kg	9.5 ug/kg
maximum	294 ug/kg	170 ug/kg	294 ug/kg
%>CSV (69 ug/kg)	2.3%	1.6%	5.1%
%>mink WV(216 ug/kg)	0.1%	0%	0.3%
%>KF WV(12 ug/kg)	31.6%	28.3%	43.7%
statistic	EHIGH	PLNLOW	WMTS
samples	189	280	71
mean	8.8 ug/kg	16.0 ug/kg	14.6 ug/kg
median	3.6 ug/kg	7.5 ug/kg	4.5 ug/kg
%>CSV (69 ug/kg)	1.0%	2.7%	3.5%
%>mink WV(216 ug/kg)	0.2%	0.03%	0%
%>KF WV(12 ug/kg)	21.0%	36.9%	31.4%

total chlordane			
statistic	national	nonurban	urban
detects	478/540 sites (88.5%)	325/377 sites (86.2%)	153/163 sites (93.9%)
mean	6.3 ug/kg	5.1 ug/kg	10.8 ug/kg
median	2.0 ug/kg	1.6 ug/kg	2.7 ug/kg
maximum	311 ug/kg	87.1 ug/kg	311 ug/kg
%>CSV (67 ug/kg)	0.6%	0.3%	1.6%
%>mink WV(573 ug/kg)	0%	0%	0%
%> KF WV(3.1 ug/kg)	36.9%	34.1 0%	47.2%
statistic	EHIGH	PLNLOW	WMTS
samples	189	280	71
mean	5.7 ug/kg	7.6 ug/kg	2.1 ug/kg
median	2.5 ug/kg	2.2 ug/kg	0.8 ug/kg
%>CSV (67 ug/kg)	1.0%	0.5%	0%
%>mink WV(573 ug/kg)	0%	0%	0%
%> KF WV(3.1 ug/kg)	39.9%	40.9%	14.5%

dieldrin			
statistic	national	nonurban	urban
%>CSV (1.5 ug/kg)	31.2%	28.5	41.2%
statistic	EHIGH	PLNLOW	WMTS
%>CSV (1.5 ug/kg)	24.1%	40.4%	7.8%

from nonurban rivers. In contrast, PBDE results among the three ecoregions show (Table 3) no clear distinctions. SI Figure S-3 shows the relative abundance of individual PBDE congeners in fillet tissue samples from nonurban and urban rivers. PBDE concentrations in fish from U.S. rivers are dominated by BDE 47, followed by BDEs 100 and 99. Only 0.3% of the national sampled population had fillet concentrations that exceeded the 210 μg/kg human health SV for PBDEs (Table 3). The higher noncancer SV for PBDEs relative to PCBs and DDT is a reflection of their lower relative toxicity, but again, limited RfD values are available for PBDEs. The lower toxicity and shorter half-life of PBDEs[57] compared to PCBs[58] could be contributing factors to the lower percentage of the national sampled population having fillet tissue concentrations that exceed the SV for PBDEs. In contrast to PCBs, the applied PBDE WVs are lower than the human health SVs. Summed PBDE results for the wildlife risk estimation showed that fish tissue concentrations in 33.4% of the national sampled population exceed the converted fillet WV for kestrels, and for mink, fish tissue concentrations in 14.5% of the national sampled population exceeded the WV (Table 3).

DOI: 10.1021/acs.est.6b05162
Environ. Sci. Technol. 2017, 51, 3021−3031

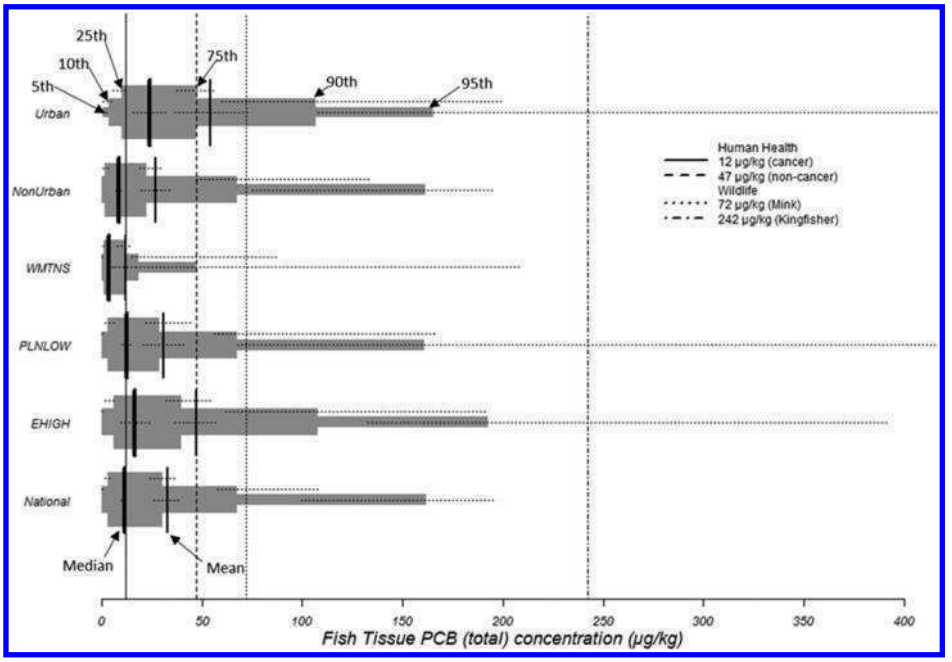

Figure 2. Estimated population percentile distribution for summed PCBs in fish tissue from U.S. river sampling sites, nonurban and urban, and by ecoregion. Confidence intervals for each percentile, mean, and median are represented by the horizontal dashed lines.

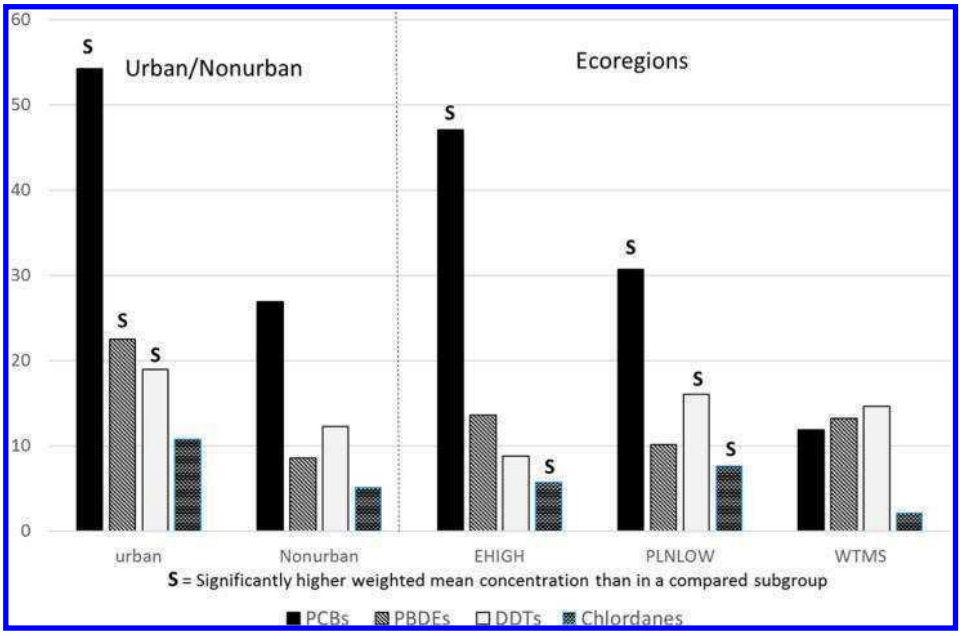

Figure 3. Comparison of weighted mean contaminant concentrations between subgroups in μg/kg (y axis).

OCPs in Fish Tissue. Lower concentrations were observed for the organochlorine pesticides (OCPs) chlordane and total DDT relative to the summed PCBs. Even 28 years after U.S. EPA withdrew approval for its use for underground termite control around the foundations of homes,[59] chlordane was detected in 88.5% of all fish tissue samples and 93.9% of the urban river samples (Table 3). Concentrations exceeded the cancer-based human health SV of 67 μg/kg[44] in fish fillet samples from less than 1% of the sampled population of rivers. When WVs were applied for chlordane, fish tissue concentrations in 36.9% of the national sampled population exceeded the kingfisher fillet WV and fish tissue concentrations in 0% of the national sampled population exceeded the mink fillet WV (Table 3).

Although banned in 1972 (for most uses) in the U.S.,[6] DDT and its metabolites (total DDT) were detected in 100% of the fish samples in this study (Table 3). Concentrations of total DDT were found to be elevated in a few samples. However, the mean concentration (13.8 μg/kg) is well below the human health cancer-based SV of 69 ug/kg for total DDT, and both the percentage of samples and the river length they represent are low (1947 km, ±511 km, Table 3). Only the 95th percentile estimates for total DDT concentrations from urban rivers exceed the cancer-based SV (SI Figure S-4). Additionally, the tissue concentrations for 4,4′-DDT (mean 0.75, median 0.18, maximum 36.3 μg/kg) are much lower than total DDT, which indicates that new sources of DDT are unlikely. The main contributor to total DDT was 4,4′-DDE (mean 10.7, median

DOI: 10.1021/acs.est.6b05162
Environ. Sci. Technol. 2017, 51, 3021−3031

4.7 μg/kg). Fish tissue concentrations in 31.5% of the national sampled population exceeded the WV for total DDT for kingfishers, and fish tissue concentrations in less than 1% of the national sampled population exceeded the WV for mink. Like chlordane, the converted total DDT WV for Kingfishers was lower than that of minks and the human health cancer SVs listed in Table 3, indicating that these organochlorine pesticides may pose more of a risk for avian species.

Analytical results for dieldrin also showed widespread occurrence with a 71% frequency of detection, and dieldrin has a relatively lower cancer SV (1.5 μg/kg). Dieldrin concentrations in fillet samples exceeded this SV in 31.2% of the sampled population of rivers, including 41.2% of urban rivers and 40.4% of PLNLOW rivers (Table 3). Other OCPs detected in this study included aldrin, alpha-BHC, endrin, lindane, endrin ketone, heptachlor epoxide, hexachlorobenzene, and mirex. These other OCPs had detection frequencies of less than 50%, and none of the fillet concentrations exceeded human health SVs for these compounds.

Subpopulation Differences. Concentrations of mercury in fish tissue from these same samples were previously compared across the three ecoregions and between nonurban and urban sites.[34] Those results revealed no significant differences across the subpopulations of rivers, however, different results were observed for the organo-halogen compounds. Figure 3 compares the weighted mean concentrations of the organo-halogens in fish from urban versus nonurban subpopulations and from ecoregions, and the significance of any differences as determined using the Z test are listed in SI Table S4. The means for all chemical groups were higher for samples from urban rivers than those from nonurban rivers. The means for summed PCBs, summed PBDEs, and total DDT were significantly higher for urban river samples, which reflects the greater extent of chemical use and release of a variety of contaminants into rivers in populated areas where they can bioaccumulate in fish. Higher organochlorine concentrations in aquatic environments in urban areas have been documented previously in urban bed sediments.[60] Not only could urban sources from chemical manufacturing, industrial use of chemicals, and domestic application of pesticides contribute to enhanced concentrations in fish tissue from urban waters, but proximity to wastewater treatment plant (WWTP) discharges could also be a factor, since WWTPs have been demonstrated to be an important point source of PCB and PBDE contamination.[61]

Among the ecoregions, summed PCB concentrations in river fish samples from the EHIGH were significantly higher than in samples from both the PLNLOW and WMTS (Figure 3, SI Table S4). Summed PCB concentrations in fish from the PLNLOW were also significantly higher than those from the WMTS. Although summed PBDE concentrations were significantly higher in samples from urban rivers relative to nonurban rivers, there was no significant difference in summed PBDE concentrations among ecoregions. Total chlordane concentrations were found to be significantly higher in fillet tissue samples from rivers in both EHIGH and PLNLOW ecoregions relative to the WMTS ecoregion, but the difference in EHIGH and PLNLOW total chlordane concentrations was not significant ((Figure 3, SI Table S4). Total DDT concentrations in samples from waters in the PLNLOW were significantly higher relative to those from the EHIGH, but unlike total chlordane, the difference in total DDT concentrations among the EHIGH, PLNLOW, and WMTS ecoregions was not significant.

Differences observed in the chemical concentrations relate to various factors, including their historical use and the geographic distribution of these chemical contaminants. Summed PCB concentrations are significantly higher in the EHIGH region relative to both other ecoregions, which reflects the industrial and urban history of this region where PCBs were most predominately used and released into the environment.[60] The ubiquity of PBDEs is consistent with its discharge pathway from dust in homes, through wastewater treatment systems,[21] and then to rivers. Similarly, the predominance of DDT in fish tissue from the PLNLOW ecoregion is consistent with the agricultural character of the middle of the country. The lack of a significant difference between the PLNLOW and WMTS total DDT results is also consistent with the high agricultural use of some states in the WMTS ecoregion. Chlordane, last labeled for use for underground application against termites,[59] persists in the EHIGH and PLNLOW regions but not in the WMTS.

Co-Occurring Contaminants. Co-occurrence of these four chemical groups was examined with the procedure outlined by Thompson and Boekelheide,[55] in which fish tissue concentrations that exceeded their respective median values are used to determine co-occurrence at elevated concentrations. This analysis (Figure 4) revealed that the most common mode of co-occurrence (fish from 32% of river sites with concentrations above the median for any compound) was for all four compound groups to co-occur at concentrations above their respective weighted medians. The next highest category of co-occurrence (16%) was for any three compound groups to co-occur above their median concentrations. PCBs co-occurred with PBDEs in 11% of sampled populations; chlordane with total DDT and PCBs with total DDT each co-occurred in 10% of the sampled population above the medians for these compound groups. The rarity was for these contaminants to occur singly above the median concentrations as was the case for PCBs in 4%, PBDEs and chlordane each in 5%, and total DDT in 7% of samples from the sampled population of rivers.

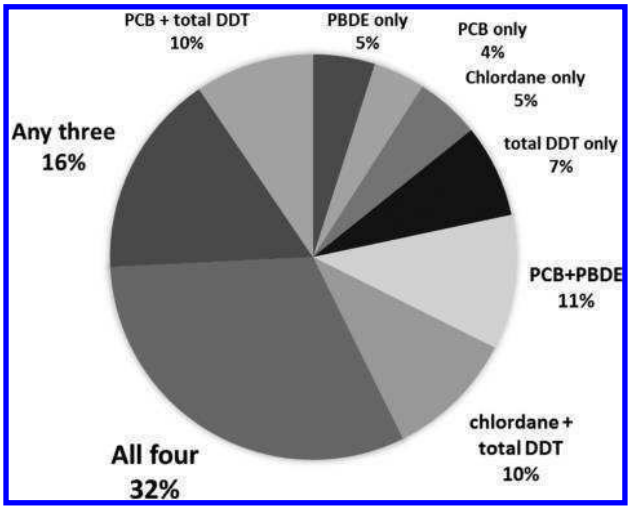

Figure 4. Co-occurrence of PCBs, PBDEs, chlordane, and DDT above respective median values in fish tissue samples from major U.S. Rivers.

The extent of co-occurrence of these compounds at relatively elevated concentrations underscores the exposure risk that is posed by their presence in fish tissue. The U.S. EPA has

DOI: 10.1021/acs.est.6b05162
Environ. Sci. Technol. 2017, 51, 3021−3031

provided approaches to quantify the toxicity of combinations of contaminants based on whether the contaminants are known to have similar or dissimilar modes of toxicity.[62] For compounds with similar modes of toxicity, the doses are considered additive. For dissimilar responses, the risks are considered separately and then combined. Additive risk, however, has been poorly defined and infrequently studied, especially for legacy contaminants, such as PCBs and OCPs no longer in use, that are perceived to be a diminishing threat. Accordingly, the background environmental chemical load and the potential for such additive effects should be taken into consideration when new chemicals, including organo-halogen compounds such as brominated flame retardants or chlorinated antimicrobials, are discharged to surface waters.

Nationally representative data on the occurrence of organic contaminants in fillet tissue of fish from U.S. rivers indicate that PCBs, PBDEs, chlordane, and DDT are still pervasive. PCBs, PBDEs, and total DDT occur at significantly higher concentrations in fish from urban rivers; however, the distribution of chemical groups varies more among the ecoregions. Co-occurrence in fish tissue at concentrations above the medians is typically observed, most frequently (32%) with all four of the chemical classes. This indicates that monitoring of fish tissue for assessment, fish consumption advisories, and the protection of aquatic life continues to be important for both new and legacy organic compounds. Individual organo-halogen compounds seldom occur alone in fish tissue. Therefore, these analytical results should be viewed in the context of co-occurring compounds and assessments of risk to human health and aquatic life that reflect the integrated chemical burden in fish. Any new organo-halogen compounds introduced to the environment will likely add to the existing overall burden of such compounds in fish tissue, since this work has demonstrated that POPs concentrations measured in fish potentially consumed by humans and representative avian and mammalian species still exceed human health SVs and WVs in many U.S. waters today.

■ ASSOCIATED CONTENT

Supporting Information

The Supporting Information is available free of charge on the ACS Publications website at DOI: 10.1021/acs.est.6b05162.

Additional information as noted in the text (PDF)
Tables S1, S2, S3, and S4 (XLSX)

■ AUTHOR INFORMATION

Corresponding Author

*Phone: 202-566-0367; e-mail: wathen.john@epa.gov.

ORCID

Angela L. Batt: 0000-0002-7008-249X

Notes

The authors declare no competing financial interest.

■ ACKNOWLEDGMENTS

This paper has been subjected to review and approved for publication by U.S. EPA's Office of Research and Development and U.S. EPA's Office of Water. The views expressed in this article are those of the authors and do not necessarily reflect the views or policies of the U.S. EPA. Mention of trade names or commercial products does not constitute endorsement or recommendation for use. Additional information for the NRSA program is publically available at https://www.epa.gov/national-aquatic-resource-surveys/nrsa, with additional fish tissue indicator information being available at https://www.epa.gov/fish-tech/fish-tissue-data-collected.epa. The authors would like to acknowledge the many federal and state agencies, and contract crews for their assistance in sample collection; Leanne Stahl, in her role as the U.S. EPA project manager for the 2008-2009 NRSA fish tissue indicator; Ellen Tarquinio and Sarah Lehmann (from the U.S. EPA) for their efforts in executing the larger NRSA study; Blaine Snyder of Tetra Tech and Harry McCarty of CSRA for their technical support; and Lisa Larimer (U.S. EPA) and Leanne Stahl for their reviews of this manuscript. Fish tissue homogenization was performed by GLEC and Dynamac Corporation staff, and sample analysis was performed by staff at Dynamac Corporation, including Gerilyn Ahlers, Michael Eastham, Hayden Miracle, Amy Parks, Ervin O'Bryan, Dan Tettenhorst, Sarah Watson, Jayme Webb-Turbeville, and Tracy Webb-Turbeville.

■ REFERENCES

(1) Muir, D. C. G.; de Wit, C. A. Trends of legacy and new persistent organic pollutants in the circumpolar arctic: Overview, conclusions, and recommendations. *Sci. Total Environ.* **2010**, *408* (15), 3044−3051.

(2) de Wit, C. A. An overview of brominated flame retardants in the environment. *Chemosphere* **2002**, *46* (5), 583−624.

(3) Ming-ch'eng Adams, C. I.; Baker, J. E.; Kjellerup, B. V. Toxicological effects of polychlorinated biphenyls (PCBs) on freshwater turtles in the United States. *Chemosphere* **2016**, *154*, 148−154.

(4) U.S. EPA. *Technical Fact Sheet − Polybrominated Diphenyl Ethers (PBDEs) and Polybrominated Biphenyls (PBBs)*, EPA 505-F-14-006; Office of Solid Waste and Emergency Response 2014.

(5) Carson, R.; Darling, L.; Darling, L. *Silent spring*; Houghton Mifflin; Riverside Press: Boston; Cambridge, MA, 1962.

(6) U.S.EPA Ban of DDT. http://www2.epa.gov/aboutepa/ddt-ban-takes-effect (accessed 12/21/15).

(7) Eriksson, P.; Fischer, C.; Fredriksson, A. Polybrominated diphenyl ethers, A group of brominated flame retardants, can interact with polychlorinated biphenyls in enhancing developmental neurobehavioral defects. *Toxicol. Sci.* **2006**, *94* (2), 302−309.

(8) Leijs, M. M.; Koppe, J. G.; Olie, K.; Van Aalderen, W. M. C.; de Voogt, P.; ten Tusscher, G. W. Effects of dioxins, PCBs, and PBDEs on immunology and hematology in adolescents. *Environ. Sci. Technol.* **2009**, *43* (20), 7946−7951.

(9) Ping, He; Aiguo, Wang; Qiang, Niu; Lijuan, Guo; Tao, Xia; Xuemin, Chen Toxic effect of PBDE-47 on thyroid development, learning, and memory, and the interaction between PBDE-47 and PCB153 that enhances toxicity in rats. *Toxicol. Ind. Health* **2011**, *27* (3), 279−288.

(10) Ross, G. The public health implications of polychlorinated biphenyls (PCBs) in the environment. *Ecotoxicol. Environ. Saf.* **2004**, *59* (3), 275−291.

(11) Vos, J. G.; Dybing, E.; Greim, H. A.; Ladefoged, O.; Lambré, C.; Tarazona, J. V.; Brandt, I.; Vethaak, A. D. Health effects of endocrine-disrupting chemicals on wildlife, with special reference to the European situation. *Crit. Rev. Toxicol.* **2000**, *30* (1), 71−133.

(12) Makey, C. M.; McClean, M. D.; Braverman, L. E.; Pearce, E. N.; He, X. M.; Sjödin, A.; Weinberg, J. M.; Webster, T. F. Polybrominated diphenyl ether exposure and thyroid function tests in North American adults. *Environ. Health Perspect.* **2016**, *124*, 420−425.

(13) Gosavi, R. A.; Knudsen, G. A.; Birnbaum, L. S.; Pedersen, L. C. Mimicking of estradiol binding by flame retardants and their metabolites: a crystallographic analysis. *Environ. Health Perspect.* **2013**, *121*, 1194−1199.

(14) Sagiv, S. K.; Nugent, J. K.; Brazelton, T. B.; Choi, A. L.; Tolbert, P. E.; Altshul, L. M.; Korrick, S. A. Prenatal organochlorine exposure and measures of behavior in infancy using the neonatal behavioral

DOI: 10.1021/acs.est.6b05162
Environ. Sci. Technol. 2017, 51, 3021−3031

assessment scale (NBAS). *Environ. Health Perspect.* **2008**, *116* (5), 666−673.
(15) Sagiv, S. K.; Thurston, S. W.; Bellinger, D. C.; Tolbert, P. E.; Altshul, L. M.; Korrick, S. A. Prenatal organochlorine exposure and behaviors associated with attention deficit hyperactivity disorder in school-aged children. *Am. J. Epidemiol.* **2010**, *171* (5), 593−601.
(16) Abballe, A.; Ingelido, A. M.; De Felip, E., Temporal trends of POPs in human milk from Italy. In *Global Contamination Trends of Persistent Organic Chemicals*, Lam, P. K. S., Ed.; CRC Press: Boca Raton, FL, 2011; pp 381−392.
(17) Adetona, O.; Horton, K.; Sjodin, A.; Jones, R.; Hall, D. B.; Aguillar-Villalobos, M.; Cassidy, B. E.; Vena, J. E.; Needham, L. L.; Naeher, L. P. Concentrations of select persistent organic pollutants across pregnancy trimesters in maternal and in cord serum in Trujillo, Peru. *Chemosphere* **2013**, *91* (10), 1426−1433.
(18) Amodio, E.; Turci, R.; Massenti, M. F.; Di Gaudio, F.; Minoia, C.; Vitale, F.; Firenze, A.; Calamusa, G. Serum concentrations of persistent organic pollutants (POPs) in the inhabitants of a Sicilian city. *Chemosphere* **2012**, *89* (8), 970−974.
(19) Ohta, S.; Ishizuka, D.; Nishimura, H.; Nakao, T.; Aozasa, O.; Shimidzu, Y.; Ochiai, F.; Kida, T.; Nishi, M.; Miyata, H. Comparison of polybrominated diphenyl ethers in fish, vegetables, and meats and levels in human milk of nursing women in Japan. *Chemosphere* **2002**, *46* (5), 689−696.
(20) Zhang, K.; Wei, Y.-L.; Zeng, E. Y. A review of environmental and human exposure to persistent organic pollutants in the Pearl River Delta, South China. *Sci. Total Environ.* **2013**, *463*−*464*, 1093−1110.
(21) Stapleton, H. M.; Eagle, S.; Sjödin, A.; Webster, T. F. Serum PBDEs in a North Carolina toddler cohort: Associations with handwipes, house dust, and socioeconomic variables. *Environ. Health Perspect.* **2012**, *120* (7), 1049−1054.
(22) Blocksom, K. A.; Walters, D. M.; Jicha, T. M.; Lazorchak, J. M.; Angradi, T. R.; Bolgrien, D. W. Persistent organic pollutants in fish tissue in the mid-continental great rivers of the United States. *Sci. Total Environ.* **2010**, *408* (5), 1180−1189.
(23) Byer, J. D.; Lebeuf, M.; Trottier, S.; Raach, M.; Alaee, M.; Stephen Brown, R.; Backus, S.; Casselman, J. M.; Hodson, P. V. Trends of persistent organic pollutants in American eel (*Anguilla rostrata*) from eastern Lake Ontario, Canada, and their potential effects on recruitment. *Sci. Total Environ.* **2015**, *529*, 231−242.
(24) Elliott, J. E.; Brogan, J.; Lee, S. L.; Drouillard, K. G.; Elliott, K. H. PBDEs and other POPs in urban birds of prey partly explained by trophic level and carbon source. *Sci. Total Environ.* **2015**, *524*−*525*, 157−165.
(25) Rigét, F.; Vorkamp, K.; Bossi, R.; Sonne, C.; Letcher, R. J.; Dietz, R. Twenty years of monitoring of persistent organic pollutants in Greenland biota. A review. *Environ. Pollut.* **2016**, *217*, 114−23.
(26) Stahl, L. L.; Snyder, B. D.; Olsen, A. R.; Pitt, J. L. Contaminants in fish tissue from US lakes and reservoirs: a national probabilistic study. *Environ. Monit. Assess.* **2009**, *150* (1), 3−19.
(27) Stahl, L. L.; Snyder, B. D.; Olsen, A. R.; Walters, L. S. A national probabilistic study of polybrominated diphenyl ethers in fish from US lakes and reservoirs. *Environ. Monit. Assess.* **2013**, *185* (12), 10351−10364.
(28) Stone, D. Polybrominated diphenyl ethers and polychlorinated biphenyls in different tissue types from Chinook salmon (*Oncorhynchus tshawytscha*). *Bull. Environ. Contam. Toxicol.* **2006**, *76* (1), 148−154.
(29) Zhou, Y.; Asplund, L.; Yin, G.; Athanassiadis, I.; Wideqvist, U.; Bignert, A.; Qiu, Y.; Zhu, Z.; Zhao, J.; Bergman, Å. Extensive organohalogen contamination in wildlife from a site in the Yangtze River Delta. *Sci. Total Environ.* **2016**, *554*−*555*, 320−328.
(30) Walters, D. M.; Mills, M. A.; Cade, B. S.; Burkard, L. P. Trophic magnification of PCBs and its relationship to the Octanol−water partition coefficient. *Environ. Sci. Technol.* **2011**, *45* (9), 3917−3924.
(31) Gasull, M.; Bosch de Basea, M.; Puigdomènech, E.; Pumarega, J.; Porta, M. Empirical analyses of the influence of diet on human concentrations of persistent organic pollutants: A systematic review of all studies conducted in Spain. *Environ. Int.* **2011**, *37* (7), 1226−1235.
(32) Long, M.; Knudsen, A.-K. S.; Pedersen, H. S.; Bonefeld-Jørgensen, E. C. Food intake and serum persistent organic pollutants in the Greenlandic pregnant women: The ACCEPT sub-study. *Sci. Total Environ.* **2015**, *529*, 198−212.
(33) Schecter, A.; Colacino, J.; Haffner, D.; Patel, K.; Opel, M.; Päpke, O.; Birnbaum, L. Perfluorinated Compounds, Polychlorinated Biphenyls, and Organochlorine Pesticide Contamination in Composite Food Samples from Dallas, Texas, USA. *Environ. Health Perspect* **2010**, *118*, 796−802.
(34) Wathen, J. B.; Lazorchak, J. M.; Olsen, A. R.; Batt, A. A national statistical survey assessment of mercury concentrations in fillets of fish collected in the U.S. EPA national rivers and streams assessment of the continental USA. *Chemosphere* **2015**, *122*, 52−61.
(35) Batt, A. L.; Kincaid, T. M.; Kostich, M. S.; Lazorchak, J. M.; Olsen, A. R. Evaluating the extent of pharmaceuticals in surface waters of the United States using a national-scale rivers and streams assessment survey. *Environ. Toxicol. Chem.* **2016**, *35* (4), 874−881.
(36) Stahl, L. L.; Snyder, B. D.; Olsen, A. R.; Kincaid, T. M.; Wathen, J. B.; McCarty, H. B. Perfluorinated compounds in fish from U.S. urban rivers and the Great Lakes. *Sci. Total Environ.* **2014**, *499*, 185−195.
(37) U.S. EPA. *Guidance for Assessing Chemical Contaminant Data for Use in Fish Advisories; Risk Assessment and Fish Consumption Limits*, EPA 823-B-00-008, 3rd ed. Office of Water: Washington DC, 2000.
(38) California EPA. *Development of Fish Contaminant Goals and Advisory Tissue Levels for Common Contaminants in California Sport Fish: Polybrominated Diphenyl Ethers (PBDEs)*; Pesticide and Environmental Toxicology Branch, Office of Environmental Health Hazard Assessment: Oakland CA, 2011.
(39) U.S. EPA. *Rivers and Streams Assessment 2008−2009 A Collaborative Survey*. Office of Water, Office of Wetlands, Oceans, and Watersheds: Washington, DC, 2013. EPA/841/D-13/001.
(40) Strahler, A. N. Quantitative analysis of watershed geomorphology. *Trans., Am. Geophys. Union* **1957**, *8* (6), 913−920.
(41) U.S.EPA Watershed Assessment, Tracking & Environmental Results System (WATERS). http://water.epa.gov/scitech/datait/tools/waters/index.cfm.
(42) Stevens, D. L.; Olsen, A. R. Spatially Restricted Surveys over Time for Aquatic Resources. *J. Agric. Biol. Environ. Stat.* **1999**, *4* (4), 415−428.
(43) Stevens, D. L.; Olsen, A. R. Spatially Balanced Sampling of Natural Resources. *J. Am. Stat. Assoc.* **2004**, *99* (465), 262−278.
(44) Olsen, A. R.; Snyder, B. D.; Stahl, L. L.; Pitt, J. L. Survey design for lakes and reservoirs in the United States to assess contaminants in fish tissue. *Environ. Monit. Assess.* **2009**, *150* (1−4), 91−100.
(45) U.S. EPA. *National Rivers and Streams Assessment Field Operations Manual*, EPA-841-B-07-009; Office of Environmental Information, Office of Water: Washington, DC, 2009.
(46) U.S. Government. *Code of Federal Regulations. Title 40 − Protection of Environment Subchapter D − Water Programs Part 136 − Guidlines Establishing Test Procedures for the Analysis of Pollutants. Appendix B to Part 136 − Definition and Procedure for the Determination of the Method Detection Limit-Revision 1.11*, Washington, D.C., 2011.
(47) U.S. EPA. *spsurvey: Spatial Survey Design and Analysis. R package version 3.1*, 2015.
(48) RCoreTeam. *R: A Language and Environment for Statistical Computing*; R Foundation for Statistical Computing: Vienna, Austria, https://www.R-project.org/.
(49) U.S. EPA. *Wadeable Streams Assessment*, Office of Water, EPA 841-B-06-002; Office of Environmental Information: Washington, DC, 2006.
(50) Lazorchak, J. M.; McCormick, F. H.; Henry, T. R.; Herlihy, A. T. Contamination of fish in streams of the Mid-Atlantic Region: An approach to regional indicator selection and wildlife assessment. *Environ. Toxicol. Chem.* **2003**, *22* (3), 545−553.
(51) Environment Canada. *Canadian Environmental Protection Act, 1999 Federal Environmental Quality Guidelines Polybrominated Diphenyl Ethers (PBDEs)*, 2013; http://www.ec.gc.ca/ese-ees/05DF7A37-60FF-403F-BB37-0CC697DBD9A3/FEQG_PBDE_EN.pdf.

DOI: 10.1021/acs.est.6b05162
Environ. Sci. Technol. 2017, 51, 3021−3031

(52) U.S. Department of Energy. *Estimation of Whole-Fish Contaminant Concentrations from Fish Fillet Data*. Office of Environmental Management: Oakridge, Tenessee, 1997. U.S. DOE ES/ER/TM-202; https://rais.ornl.gov/documents/tm202.pdf.
(53) USGS. *Concentrations, Loads, and Sources of Polychlorinated Biphenyls, Neponset River and Neponset River Estuary, Eastern Massachusetts*. Scientific Investigations Report 2011−5004 Version 1.1, 2014.
(54) USGS. *Regression Model for Explaining and Predicting Concentrations of Dieldrin in Whole Fish from United States Streams*. Scientific Investigations Report 2006−5020.
(55) Thompson, M. R.; Boekelheide, K. Multiple environmental chemical exposures to lead, mercury and polychlorinated biphenyls among childbearing-aged women (NHANES 1999−2004): Body burden and risk factors. *Environ. Res.* **2013**, *121*, 2351.
(56) McFarland, V. A.; Clarke, J. U. Environmental occurrence, abundance, and potential toxicity of polychlorinated biphenyl congeners: considerations for a congener-specific analysis. *Environ. Health Perspect.* **1989**, *81*, 225−239.
(57) Bhavsar, S. P.; Gandhi, N.; Gewurtz, S. B.; Tomy, G. T. Fate of PBDEs in Juvenile Lake Trout Estimated Using a Dynamic Multichemical Fish Model. *Environ. Sci. Technol.* **2008**, *42* (10), 3724−3731.
(58) Carlson, D. L.; Vault, D. S. D.; Swackhamer, D. L. On the Rate of Decline of Persistent Organic Contaminants in Lake Trout (Salvelinus namaycush) from the Great Lakes, 1970−2003. *Environ. Sci. Technol.* **2010**, *44* (6), 2004−2010.
(59) U.S.EPA. Technology Transfer Network − Clordane; http://www3.epa.gov/ttn/atw/hlthef/chlordan.html (accessed 12/19/15).
(60) Phillips, P. J.; Nowell, L. H.; Gilliom, R. J.; Nakagaki, N.; Murray, K. R.; VanAlstyne, C. Composition, distribution, and potential toxicity of organochlorine mixtures in bed sediments of streams. *Sci. Total Environ.* **2010**, *408*, 594−606.
(61) Samara, F.; Tsai, C. W.; Aga, D. S. Determination of potential sources of PCBs and PBDEs in sediments of the Niagara River. *Environ. Pollut.* **2006**, *139* (3), 489−497.
(62) U.S. EPA. *Guidance for Conducting Health Risk Assessment of Chemical Mixtures*,Risk Assessment Forum Technical Panel, Office of Research and Development, Office of Pesticide Programs, NCEA-C-0148; Office of Pollution Prevention and Toxics and Office of Water: Washington, DC, 1999.

DOI: 10.1021/acs.est.6b05162
Environ. Sci. Technol. 2017, 51, 3021−3031

Chemosphere 122 (2015) 52–61

Contents lists available at ScienceDirect

Chemosphere

journal homepage: www.elsevier.com/locate/chemosphere

A national statistical survey assessment of mercury concentrations in fillets of fish collected in the U.S. EPA national rivers and streams assessment of the continental USA

John B. Wathen [a,*], James M. Lazorchak [b,1], Anthony R. Olsen [c,2], Angela Batt [b,1]

[a] U.S. Environmental Protection Agency, OW/Office of Science and Technology, 1200 Pennsylvania Avenue, NW (MC4305T), Washington, DC 20460, United States
[b] U.S. Environmental Protection Agency, Office of Research and Development, 26 W. Martin Luther King Drive, Cincinnati, OH 45268, United States
[c] U.S. Environmental Protection Agency, ORD Western Ecology Division, 200 S.W. 35th Street, Corvallis, OR 97333-4902, United States

HIGHLIGHTS

- Hg fish tissue results from 541 U.S. sites on =>5th order streams in 2008–2009.
- Site selection was probabilistic and nationally-representative.
- 25.4% (137 sites, 13071 river miles, (21036 km)) > 300 ug kg^{-1} HH and WV thresholds.
- No difference observed between results from urban vs. non-urban sites or among three eco-regions.
- Most exceedances in top predator species.

ARTICLE INFO

Article history:
Received 8 July 2014
Received in revised form 28 October 2014
Accepted 2 November 2014
Available online 27 November 2014

Handling Editor: Keith Maruya

Keywords:
National rivers
Mercury (Hg)
Human fish consumption
Wildlife fish consumption

ABSTRACT

The U.S. EPA conducted a national statistical survey of fish fillet tissue with a sample size of 541 sites on boatable rivers =>5th order in 2008–2009. This is the first such study of mercury (Hg) in fish tissue from river sites focused on potential impacts to human health from fish consumption to also address wildlife impacts. Sample sites were identified as being urban or non-urban. All sample mercury concentrations were above the 3.33 ug kg^{-1} (ppb) quantitation limit, and an estimated 25.4% (±4.4%) of the 51663 river miles assessed exceeded the U.S. EPA 300 ug kg^{-1} fish-tissue based water quality criterion for mercury, representing 13144 ± 181.8 river miles. Estimates of river miles exceeding comparable aquatic life thresholds (translated from fillet concentrations to whole fish equivalents) in avian species were similar to the number of river miles exceeding the human health threshold, whereas some mammalian species were more at risk than human from lower mercury concentrations. A comparison of means from the non-urban and urban data and among three ecoregions did not indicate a statistically significant difference in fish tissue Hg concentrations at $p < 0.05$.

Published by Elsevier Ltd.

1. Introduction

Mercury (Hg) is a metal that is persistent, bioaccumulative, and toxic in the environment. It is a constituent of minerals in rocks and soil that enters the atmosphere by the natural degassing of the earth's crust and recycling by volatilization of atmospherically deposited mercury, as well as being mobilized to the environment from anthropogenic sources. Human activities have enriched the atmospheric content of mercury by a factor of 7.5 times compared to levels predating emissions from most human activities (Amos et al., 2013). These activities include mining (including gold extraction), manufacturing, Portland cement production, medical waste incineration, and most prominently, the combustion of fossil fuels, especially coal (UNEP, 2008). As of 2005, however, artisan and small scale gold mining were second only to fossil fuel combustion as sources of Hg emissions to the atmosphere (Pacyna et al., 2010). When Hg is deposited in water, a large portion is converted, by chemical and biochemical processes either in sediments or in the water column, from inorganic Hg to toxic methylmercury (MeHg) that bioaccumulates in fish muscle (Sunderland et al., 2009). Despite very effective efforts to reduce emissions of Hg in many countries, including the U.S., Hg emissions from Asia continue to

* Corresponding author. Tel.: +1 (202) 566 0367; fax: +1 (202) 566 0409.
E-mail address: wathen.john@epa.gov (J.B. Wathen).
[1] Tel.: +1 (513) 569 7076; fax: +1 (513) 569 7438.
[2] Tel.: +1 (541) 754 4790.

http://dx.doi.org/10.1016/j.chemosphere.2014.11.005
0045-6535/Published by Elsevier Ltd.

increase (Wilson et al., 2010) with potential implications for increased human exposure in the U.S. and elsewhere (Sunderland et al., 2009; Driscoll et al., 2013). Future levels of Hg emissions will depend on the degree of implementation of measures to remove Hg from fossil fuel combustion emissions in the context of rising demand for electricity (Streets et al., 2009).

Research has shown that exposure to Hg and its compounds through the consumption of fish containing Hg can cause a range of toxic effects in humans, as well as in piscivorous mammalian and avian wildlife (U.S. EPA, 1997). At doses that result from moderate rates of maternal fish consumption, exposure of fetuses to Hg *in utero* can later manifest in children as deficits in subtle neurological end points such as lowered IQ, decrements in motor function, attention, and visuospatial performance (NAS, 2000). Evidence of early childhood effects at low levels of prenatal exposure is clear, and other health effects are likely, including cardiovascular effects and, to a lesser extent, immune system suppression (Karagas et al., 2012). Recent analyses also suggest an association between toenail Hg levels in young adults and the incidence of diabetes in later life (He et al., 2013). The thresholds for neurodevelopmental effects of mercury exposure discussed in this manuscript are based on U.S. EPA reference dose of 0.1 ug kg^{-1} of body weight/day for exposure to Hg (U.S. EPA, 2001b) relative to fish tissue concentrations detected in samples collected by the U.S. EPA. A reference dose (RfD) is an estimate of a daily exposure to the human population (including sensitive subgroups) that is likely to be without an appreciable risk of deleterious effects during a lifetime.

Wildlife are exposed to Hg and MeHg from a variety of environmental sources, mine tailings, industrial effluents, agricultural drain water, impoundments and atmospheric deposition from the electric power generation industry. At the higher levels of the food chain, piscivorous birds and mammals are among the highest risk receptors of MeHg contamination (Wolfe et al., 1998). Toxicity of Hg to piscivorous birds and mammals includes damage to the nervous, excretory, and reproductive systems. (Wolfe et al., 1998). In 1997, EPA identified wet deposition as the primary mechanism by which atmospheric Hg is transported to surface waters and land, although dry deposition may also contribute substantially (U.S. EPA, 1997). More recently, Driscoll et al. (2013) provide a full description of Hg sources, transport and deposition mechanisms, both human health and ecological effects, and cite atmospheric deposition as the primary mechanism of redistribution of mercury.

Large-scale studies of contaminants in fish tissue have found widespread evidence of Hg contamination. In a survey of lakes in the northeastern United States in 1992–1994, the U.S. EPA's Environmental Monitoring and Assessment Program (EMAP) analyzed whole fish composite samples for inorganic and organic contaminants, including Hg. It was found that 26% of northeastern lakes contained fish with Hg levels that exceeded the critical value for humans (200 ug kg^{-1} at that time), 54% of lakes exceeded wildlife critical values for piscivorous mammals (100 ug kg^{-1}), while 98% exceeded wildlife critical values for birds (20 ug kg^{-1}) (Yeardley et al., 1998). During the period 1993–1994, an EMAP survey of fish in the Mid-Atlantic Region found that small fish tissue concentrations exceeded the kingfisher Wildlife Value (30 ug kg^{-1}) over 72% of the stream length. Wildlife Values (WVs,) have been defined as the concentration in fish at which chronic effects to piscivorous wildlife occur (Lazorchak et al., 2003). In 2004 and 2005, the EMAP Great Rivers Assessment measured Hg concentrations in whole fish from the Upper Mississippi, Missouri, and Ohio Rivers to characterize the extent and magnitude of Hg contamination and to identify environmental factors influencing Hg accumulation (Walters et al., 2010). Across all three large river systems, Hg levels exceeded the WV for belted kingfisher in 33–75% of river length and exceeded the human health criteria in 1–7% of river length.

More recently, the U.S. EPA conducted the National Lake Fish Tissue Study (Stahl et al., 2008), which employed a national-scale statistical survey design and targeted human exposure to Hg by focusing on the fillet, the edible portion of collected species. This national lakes study included 486 composite predator fillet samples collected from 500 randomly-selected lakes during 2000–2003. In this nationally representative study, fish tissue from 48.9% of the lake population assessed exceeded the U.S. EPA's 300 ug kg^{-1} human health fish tissue-based water quality criteria (WQC) for Hg (U.S. EPA, 2001a).

The U.S. Geological Survey (USGS) has conducted extensive studies of national and regional fish-tissue contaminant data by combining results of several separate targeted studies conducted over time, analyzing the data and characterizing contaminant levels on the basis of region and watershed type, including propensity for methylation and fish characteristics (Schmitt, 2002; Scudder et al., 2009; Chalmers et al., 2011). These studies have led to identification of patterns and mechanisms of Hg accumulation in fish including the propensity for methylation to occur in watersheds with abundant wetlands (Brigham et al., 2009; Scudder et al., 2009). USGS continues to emphasize locally-focused studies which are national in their distribution (Brigham et al., 2014; Feaster et al., 2014; Chalmers et al., 2014) and explore causative mechanisms for the observed variations in Hg concentrations in a variety of media and settings.

The present work reports the results of a 2008–2009 National Rivers and Streams Assessment (NRSA) survey of rivers in the 48 conterminous United States to investigate Hg concentrations in composited fillet samples (Fig. 1). The survey is nationally-representative of the class of waters (5th order and greater rivers that are boatable) from which the sample of 541 sites was drawn. The fish tissue sampling efforts of this study are focused on providing information for assessments of human health impacts of fish consumption. Results were also used to estimate contaminant exposures to wildlife and aquatic species that consume fish and to compare urban and non-urban sub-groups of sites as well as sites located in each of three National Aquatic Resource Assessment (NARS) ecoregions: West and Mountains (WMTS), Plains and Lowlands (PLNLOW), and Eastern Highlands (EHIGH) (Fig. 1). The design of this study produces assessment results nationally, for three regions, and by urban and non-urban subgroups and relate those results to both human health and wildlife effects. The statistical survey design requires estimates for the assessments to incorporate weights that reflect the stratification and unequal probability of selection. This ensures that the inference (results) apply to all boatable, 5th order and greater rivers in the conterminous states. Results from this study may differ from those employing other non-survey design methods for selection of sites (Peterson et al., 1998).

2. Materials and methods

2.1. NRSA design and site selection

The NRSA included 1924 sites within the conterminous United States that were sampled for a range of environmental indicators, including concentrations of toxic chemicals in fish tissue (U.S. EPA, 2013). Fish tissue samples were collected at a subset of 541 sites that met the three criteria for the river population of interest for the fish tissue contaminant study: (1) boatable U.S. rivers of 5th order and greater (Strahler, 1957); (2) having a permanent fish population; and (3) flowing water during the study period (including the Great Rivers and run-of-the-river ponds, but excluding portions of tidal rivers up to head of salt, and reservoirs). The sample frame was derived from the National Hydrography Dataset (NHD)

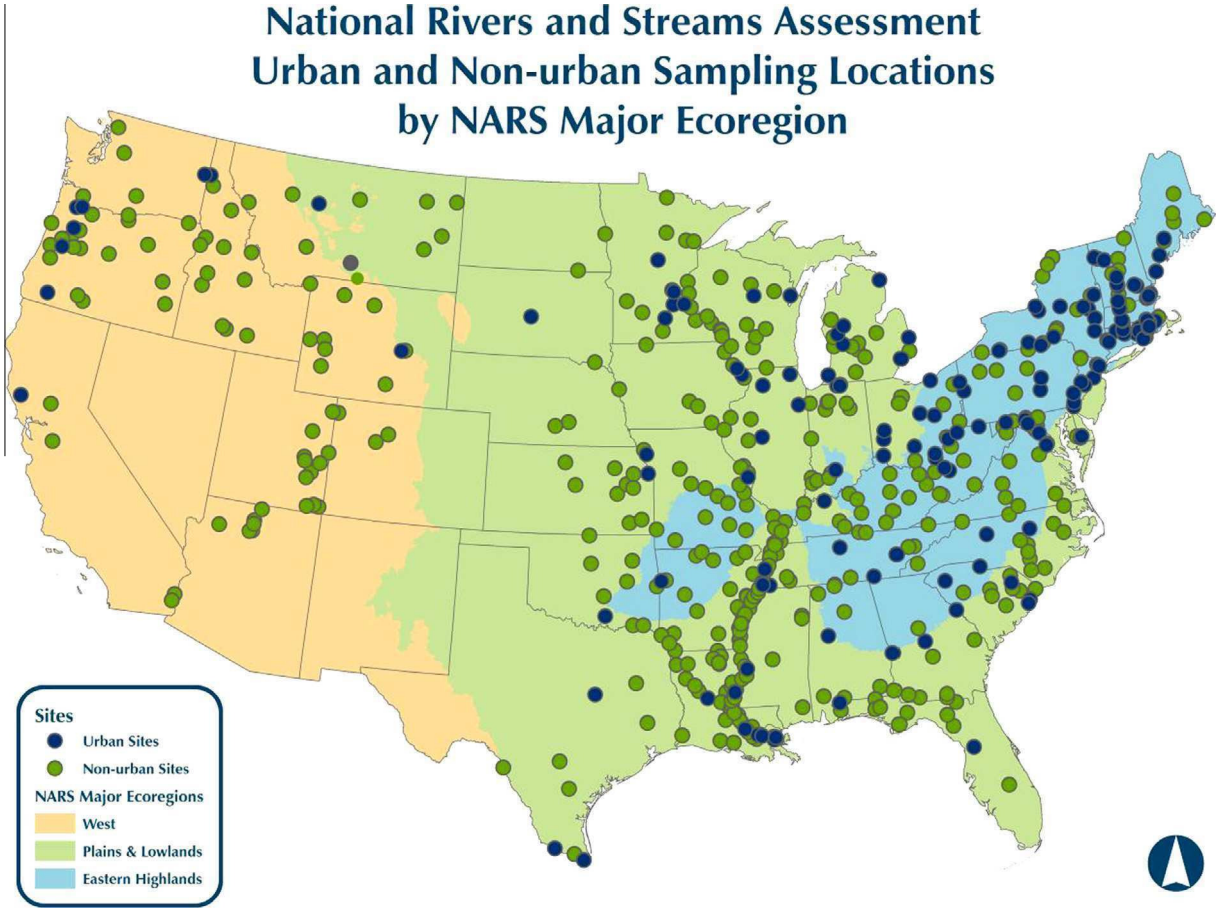

Fig. 1. National map of NRSA 2008–2009 sampling locations (n = 541) within national aquatic resource survey ecoregions.

and included Strahler stream order attributes (http://water.epa.gov/scitech/datait/tools/waters/index.cfm). NHD-Plus and the U.S. Census Bureau national urban boundary GIS coverage layers were used to establish the urban attribute so that both non-urban and urban samples could be identified. Non-urban and urban subpopulations were identified for two purposes. First, analytes other than Hg, including legacy organo-halogen compounds (entire sample set), perfluorinated compounds, and synthetic musks (only the urban subpopulation), were also determined for samples in this study and are being described in other publications. In the case of the perfluorinated compounds and synthetic musks, the smaller urban subpopulation better aligned with the budgetary resources available to perform the analyses. Secondly, the question of variable impacts to non-urban and urban populations and attendant questions of environmental justice are of interest to U.S. EPA. The distinction between urban and non-urban sampling locations was based on the most recent available U.S. Census Bureau data and the following definition: an Urban Area consists of contiguous densely settled census block groups that meet minimum population density requirements, along with adjacent densely settled census blocks that together encompass a population of at least 50 000 people.

Sampling sites were selected using a probability-based approach (Stevens and Olsen, 1999, 2004), generally applying the spatial methodology that had been used for lakes in U.S. EPA's National Lakes Fish Tissue Study (Stahl et al., 2008) to major U.S. rivers (Olsen et al., 2008). Selection probabilities were defined for 5th order or larger rivers in the lower 48 states so that the expected number of urban sites would be at least 150. The numbers of sites where samples were collected were limited by logistical factors, such as failure to obtain a fishing permit, absence of fish of the appropriate species and/or size at a given site, and time constraints for fish sampling. Fish tissue samples were collected from a total of 162 randomly selected urban rivers sites and 379 non-urban river sites. These totals included sampling locations in 46 conterminous states. Sampling included 154 5th order river sites, 162 6th order river sites, 99 7th order river sites and 126 sites from rivers 8th order and above.

2.2. Sample collection

One composite sample containing a single fish species was collected from each site (Fig. 1). Target species and individual specimens for the fish composite samples were selected based on a consistent set of criteria. Species were selected to be ubiquitous, abundant, and easily identified. Individual specimens of the species were selected to be adults of similar size (the length of the smallest individual in a composite could not be less than 75% of the total length of the largest individual) and sufficiently large (i.e., adult specimens) to provide adequate tissue for analysis (U.S. EPA, 2009a).

During required training sessions, all study participants were provided a list of recommended species for fish tissue sampling and were instructed to specifically target those species. A total of 15 species were included in that target list (in the Field Operations Manual and QAPP) and all were predator (typically top carnivore) species. Consistent with the human health context of the study, the focus was on sport/game fish that are commonly consumed by humans and of sufficient size to be of interest to anglers, and species that had a wide geographic distribution. The target species list included members of the sunfish (with largemouth and

smallmouth bass preferred), trout/salmon, pike, temperate bass, perch, and catfish families. Every effort was made to collect the desired species; however, the outcome of the field sampling efforts ultimately depended on the natural diversity and abundance of fish at each sampling site. The fish that were available to be taken dictated the mix of species collected at the sites, similar to conditions that would be encountered by anglers seeking fish for sport or sustenance.

Field teams used active methods (i.e., electrofishing) to collect fish samples from each site during a May through September field sampling period in 2008 and 2009. A routine composite sample consisted of five fish, but composites containing fewer than five fish were accepted in an effort to retain a sample from each target river segment (41% of the composites). The lengths of fish collected were similar in non-urban and urban waters. The mean length of fish taken from non-urban waters was 364.7 mm (min 101 mm, max 790 mm, S.D. 98.3 mm), and the mean length of fish from urban waters was 362.8 mm (min 112.5 mm, max 702 mm, S.D. 93.4 mm) Whole fish were shipped on dry ice to the designated sample preparation laboratories for storage until subsequent preparation (filleting and homogenization).

2.3. Sample preparation

Fish were filleted in the laboratory by trained technicians. In order not to excise fatty tissue likely containing organic contaminants also of interest in this study, scales were removed from fish, then lateral muscle fillets from both sides of each fish were prepared with skin on and the belly flap (ventral muscle and skin) attached. This method maintains consistency in preparing fillet samples for chemical analysis among EPA's national and regional-scale fish tissue studies and follows EPA's Guidance for Assessing Chemical Contaminant Data for Use in Fish Advisories (U.S. EPA, 2000a). By being consistent with this guidance, it enables comparison of fish tissue results among the EPA fish tissue studies and reduces variability for trends analysis when fish tissue studies are repeated periodically.

Fillets were composited using the batch method, where fillets from all of the individual specimens that comprise the sample were homogenized together, regardless of the proportional weight of individual fish. Each composite was homogenized using a tissue grinder, mixed thoroughly to a fine paste of uniform color and texture, and a 1-g aliquot was removed for Hg analysis. Fish collection and handling methods along with details of sample preparation are described in detail in U.S. EPA (2009a).

2.4. Tissue sample analysis

Fillets were analyzed for Hg with a Direct Mercury Analyzer (DMA-80; Milestone, Inc) using EPA method 7473 and Milestone Application note HG-0 (U.S. EPA, 2007). The method detection limit (MDL) was calculated to be 1.49 ug kg^{-1} (ppb or parts per billion) Hg using 40 CFR Part 136, Appendix B (U.S. Government, 2011). The quantitation limit (QL) is 3.33 ug kg^{-1} mercury, based on a low calibration point of 0.001 ug mercury and nominal sample weight of 0.33 g. The certified liquid QC standards for each run were purchased as single elements at 1000 ppm. The primary standard was purchased from Ricca and the secondary QC standard was purchased from Spex Claritas. Two internal standard calibration curves were prepared using standard solutions. The low-range curve included five points ranging from 0 to 0.020 ug and the high range curve included 12 points ranging from 0.030 to 0.400 ug, with each curve yielding R^2 values >0.99. Calibration check standards were run at the beginning and end of each batch for both the low and high curve. A secondary source standard and a sample of certified reference material (CRM DORM-2, dogfish muscle) were also analyzed once per batch. All check standards and reference material measurements were within ±20% of the actual value. Laboratory blanks were run once per batch and were all less than three times the MDL. One laboratory fortified matrix sample (LFM) spiked at a concentration of 25 ug kg^{-1} was run per batch to determine the influence of the matrix, with recoveries being within ±20% of the spiked amount or the result was flagged as estimated. Each batch consisted of 12 samples run in duplicate. Reported values were the mean of two analyses, with the relative percent difference between duplicates being less than 25%. Reported values were not blank-subtracted or recovery-corrected.

2.5. Statistical analysis

The NRSA survey design and survey analysis results in national and regional estimates of contaminant concentrations. The statistical estimates are based on weighted means of the analytical results from sites. The weights are based on the survey design and are the inverse of the probability of selecting a sampling site. The probability of selecting a site depends on the stratification and unequal probability of selection associated with the site. The weights are the total stream length represented by the sample site. Percentiles and mean estimates of fish tissue Hg concentrations were calculated from the data weighted in this manner using routines developed by the U.S. EPA in the statistical calculation package *spsurvey* ***R***. Weighted estimates calculated for the entire sampled population and for each of the sample subregions are listed in Table 1. The minimum and maximum Hg concentrations observed in the 541 samples are also given in Table 1. Additional information on the statistical algorithms employed in site selection and data analysis in the NRSA are available at: http://www.epa.gov/nheerl/arm/analysispages/software.htm (U.S. EPA, 2014). Hg tissue concentration data for the U.S. were depicted graphically as a cumulative distribution frequency (CDF) plot (Fig. 2).

A second statistical task was the assessment of the subgroups relative to each other to determine whether fish tissue Hg concentrations differed significantly between urban and non-urban subgroups and between any two of three geographic sub-regions. A standard normal *z*-test:

$$z = \frac{\text{MeanA} - \text{MeanB}}{\sqrt{(\text{stderrA}^2 + \text{stderrB}^2)}} \quad (1)$$

was used where MeanA is the weighted mean estimate and stderrA is the standard error estimate for MeanA for subgroup A and similarly for subgroup B.

Using regression analyses developed by Peterson and Van Sickle (2007) and Peterson et al. (2004), fish fillet concentrations were translated to equivalent whole body Hg. Using their regression analyses, $[\text{Log}10(\text{whole}) = -0.2712 + 0.9005 * \log 10(\text{fillet})]$, we have estimated exposures and dose to wildlife from Hg concentrations translated from the fillet concentration values obtained in this study to equivalent whole fish Hg concentrations. These whole fish equivalent values were then compared to WVs, as described below, to assess impacts to avian and mammalian wildlife.

3. Results and discussion

The total length of all 5th+ Strahler order U.S. rivers in NHDPlusv2 is 235 945 km (147 465 mi). The total length of all rivers included in the fish tissue study is estimated to be 51 663 mi or 83 144 km (±7027 km). In addition, within the rivers intended to be included in the fish tissue study an estimated 30 407 km (±4488 km) could not be sampled, in many cases due to the inability to obtain fish permits or safety reasons. For some rivers, insufficient information from the survey is available to know whether

Table 1
River length estimates and group percentile and mean estimates for mercury concentration (Hg ww ug kg^{-1}).

Statistic	National n = 541	Non-urban n = 379	Urban n = 162	EHIGH n = 190	PLNLOW n = 280	WMTS n = 71
River miles	51663	40752	10911	14738	29739	7186
River km	83145	65584	17559	23718	47861	11564
5th% ile	37.2	34.6	61.7	45.6	37.2	31.5
25th % ile	96.2	90.9	114.8	100.5	99.7	81.4
50th % ile	175.6	170.5	200.6	176.0	180.1	125.3
75th % ile	302.7	302.6	309.1	274.8	298.8	346.1
95th % ile	583.6	578.8	803.3	535.2	578.8	854.1
Mean	228.9	223.3	250.2	210.0	231.4	257.5
Maximum observed	1419	1419	854	854	1419	1272

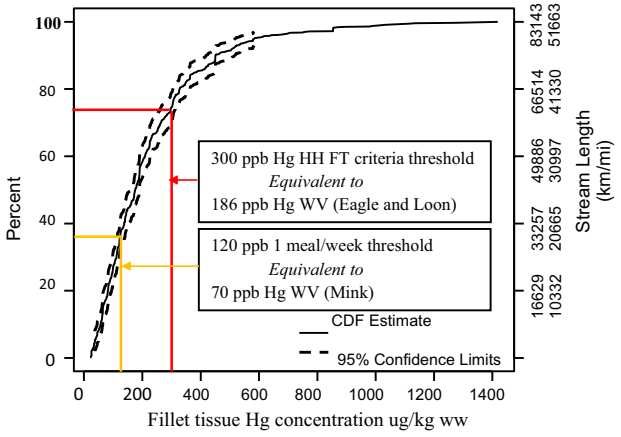

Fig. 2. National estimated Hg fish tissue concentration cumulative distribution (HH FT = human health fish tissue).

the river is boatable. A total of 33993 km (±4803 km) are estimated to be inaccessible due to landowners denying access to the river, and 7257 km (±2208 km) are rivers that were not sampled for other reasons. In addition to the above categories, the total length of 5th+ Strahler order U.S. rivers includes an estimated 57377 km (±7147 km) that are wadeable and 23513 km (±3804 km) that are not rivers or rivers with flowing water and hence do not fall into the population of rivers targeted for the fish tissue study. While the study results apply to the 83144 km, the study was intended to apply to a minimum of 113805 km or a maximum of 155055 km depending on whether the rivers were associated with insufficient information to determine if they were boatable, all not boatable, all boatable, or a combination. The length of 5th+ Strahler order U.S. rivers not included in the study for the reasons cited above was 152801 km (95802 mi).

All (100%) of the 541 fish fillet samples analyzed for Hg content for this national study contained quantifiable levels of Hg above the 3.33 ug kg^{-1} quantitation level for the method. Hg concentrations measured in the fillet samples ranged from 21 ug kg^{-1} to 1419 ug kg^{-1}. The national weighted mean Hg concentration for fillets in fish from U.S. rivers is 228.9 ug kg^{-1} (±18.6 ug kg^{-1}) compared to a weighted mean concentration of 250.2 ug kg^{-1} (±47.8 ug kg^{-1}) for fish fillet samples from only urban rivers and 223.3 ug kg^{-1} (±19.7 ug kg^{-1}) from non-urban rivers. An estimated 25.4% (±4.4%) of the sampled river miles exceeded the U.S. EPA WQC for Hg of 300 ug kg^{-1} (two fish meals/month consumption level) in fish tissue out of 51663 miles (83144 km) of boatable U.S. rivers of 5th order and greater included in the sampled population.

Fig. 2 is a cumulative distribution plot (CDF) of the cumulative percentage of the river length (left y axis) and the corresponding number of river km and miles they represent in the aggregate (right y axis), plotted against the concentrations of Hg in the samples (x axis). Two thresholds are superimposed on the CDF. The red indicator that connects the CDF curve with the x axis marks the point on the distribution at which the 300 ug kg^{-1} criterion value (equivalent to 186 ug kg^{-1} Hg WV (Eagle and Loon) is intersected. The yellow indicator marks the point on the curve intersected by the value of 120 ug kg^{-1} which is the maximum concentration of Hg in fish tissue at which one meal/week can be consumed without exceeding the reference dose for Hg, which is a 170 g portion (6 oz), for a 70 kg individual (Equivalent to 70 ug kg^{-1} Hg WV (Mink)). Table 1 lists the weighted percentile values nationally, as well as for urban and non-urban subgroups and three eco-regional subgroups and the number of sites that each subgroup includes.

3.1. Human health benchmarks

The percentage and number of river miles of fillet sample composites exceeding human health benchmarks provides an index of the extent to which fish from boatable 5th order and higher rivers can be safely consumed by humans. As stated above, this 300 ug kg^{-1} (wet weight) Hg benchmark, contained in the 2001 *Water Quality Criterion for the Protection of Human Health* (U.S. EPA, 2001a) represents a Hg exposure equal to the reference dose for Hg from the consumption of two meals a month.

Based on fish composite samples that exceed the U.S. EPA's 300 ug kg^{-1} human health fish tissue-based WQC (WQC), an estimated 25.4% of the 13071 river miles (21036 km) and a substantial portion of the resource of U.S. rivers 5th order and above as were sampled in this study. This percentage, however, is much lower than the 48.9% (U.S. EPA, 2009b) of U.S. lakes found to exceed this same threshold in the 2000–2003 National Lake Fish Tissue Survey (NLFTS). This difference likely reflects distinctions in a number of areas, among them the contrasting nature of rivers vs. lakes as environments less conducive to methylation, as well as the longer residence time of water in lakes.

Another distinction between the findings of this study vs. NLFTS lies in the species included in the respective sample populations. In this study, all targeted species were top predators, but included catfish. In the NLFTS, bottom dwellers (including catfish) were treated separately. A more appropriate comparison may be made between the 48.9% exceedance of the 300 ug kg^{-1} human health fish tissue-based WQC from the NLFTS and the percentage exceedance of the WQC for smallmouth (25.1%) and largemouth bass (33.4%), which were represented in sufficient numbers to make national inferences. The weighted average exceedance (national values) of the WQC by the smallmouth bass (n = 120) and largemouth bass (n = 114) is 29.2%, which represents the best nationally-representative comparison that can be made between the rivers assessed in this study and the lakes in the NLFTS. As described by Scudder et al. (2009), further characterization of Hg concentrations in fish tissue by land cover and land use is possible, but cannot be resolved at the sample density of this study on a

nationwide basis. Whether compared to the percentage exceedance for all fish (25.4%) of largemouth and smallmouth bass (29.2%), however, exceedance of the WQC in approximately 25–30% of rivers represented by the survey is generally consistent with other current compiled assessments of Hg in fish tissue from U.S. rivers (Scudder et al., 2009; Chalmers et al., 2011) and contrasts markedly with exceedances of the WQC in fish tissue from U.S. lakes of almost 50% (U.S. EPA, 2009b).

The U.S. EPA's 300 ug kg^{-1} human health fish tissue-based WQC for Hg is the regulatory threshold emphasized in this paper, and consumption of two fish meals/month with this Hg concentration is a rate of consumption that is the approximate equivalent of the reference dose (RfD) for Hg. For context, the Hg concentration range for one meal/week consumption is 120–230 ug kg^{-1} and is incorporated in many state fish advisory programs (U.S. EPA, 2011) that the U.S. EPA promotes and for which it provides guidance (U.S. EPA, 2000b). The threshold above which no consumption is recommended (940 ug kg^{-1}, U.S. EPA, 2000b) is exceeded in these data by tissue concentrations from only 1.3% (unweighted percentage) of the sample locations. EPA recommends that pregnant women and nursing mothers should avoid fish with such elevated Hg concentrations (U.S. EPA, 2000b).

3.2. Sub-group differences

It is of interest to the U.S. EPA to understand differences in fish tissue contaminant levels between regions and between urban and non-urban waters. Three means of comparison applied here include the application of the *z*-test as described above, comparisons of the percentages of waters within each of these subgroups that exceed the U.S. EPA's 300 ug kg^{-1} human health fish tissue-based water quality criterion, and comparisons of the means and 95th percentile values for each of the subgroups. The *p*-value for the test of a difference between weighted means of urban and non-urban population subgroups was 0.31 ($z = 1.03$), indicating no statistical difference between the means of 5th order and above urban and non-urban river subgroups. Similarly, when the means of the ecoregion subgroups were compared, the resulting ***p*** values indicate no significant differences among the three ecoregions: EHIGH vs. PLNLOW ($z = 1.25$, $p = 0.21$), EHIGH vs. WMTNS ($z = 1.16$, $p = 0.25$), and WMTNS vs. PLNLOW ($z = 0.63$, $p = 0.53$).

Comparisons of the percentages of weighted river length exceeding the 300 ug kg^{-1} human health fish tissue-based water quality criterion are depicted in Fig. 3. As can be noted, the percent exceeding and not exceeding this criteria value are generally quite uniform, with the WMTS ecoregion being the exception. For all subgroups except the WMTS, the percent of river miles exceeding the criteria value is in the mid 20% range, with the WMTS being the only one that exceeds 30%. Similarly, when means and percentile values across the subgroups are compared (Fig. 4), it can be seen that among the three ecoregions, values for the WMTS exceed those for the EHIGH and PLNLOW regions for the 75th, 90th and 95th percentile groups. Also evident from Fig. 4 is the fact that although there is not a statistically significant difference between the means of the urban and non-urban subgroups, the 90th and 95th percentile data for the urban rivers are elevated relative to the non-urban rivers.

The WMTS is the ecoregion with the smallest number of river locations (***n*** = 71), relative to the PLNLOW (***n*** = 280) and EHIGH (***n*** = 190). As such, statistical analysis of the data for the WMTS is vulnerable to the influence of a few elevated sample values which are inconsistent with the relatively uniform atmospheric deposition otherwise seen across the ecoregions. A sample location in the WMTS with one of the highest fish tissue concentrations observed in the study (854 ug kg^{-1}) was collected in a creek draining a large geothermal area in California with a 100-year history of mercury mining (Kagel et al., 2007). This is the type of local deviation that can mask the pervasive and uniform general character of Hg occurrence and deposition in the U.S. The apparent elevation of Hg in fish tissue in the WMTS suggested by the data in Fig. 4 is not borne out by the *z*-test analysis for significance and is likely attributable to this and potentially another elevated value (1272 ug kg^{-1}) among the data from the Willamette River in OR near areas where historical gold mining occurred.

3.3. Differences in Hg concentration among fish species

As has been observed in other studies (Lazorchak et al., 2003; Peterson and Van Sickle, 2007; U.S. EPA, 2009b), Hg content of fish tissue is dependent upon fish species, size, and trophic level. In this study, weighted Hg concentrations were markedly higher for waters represented by composite samples of predatory species (e.g., largemouth bass, mean Hg = 347 ± 22 ug kg^{-1}) than by bottom dwellers

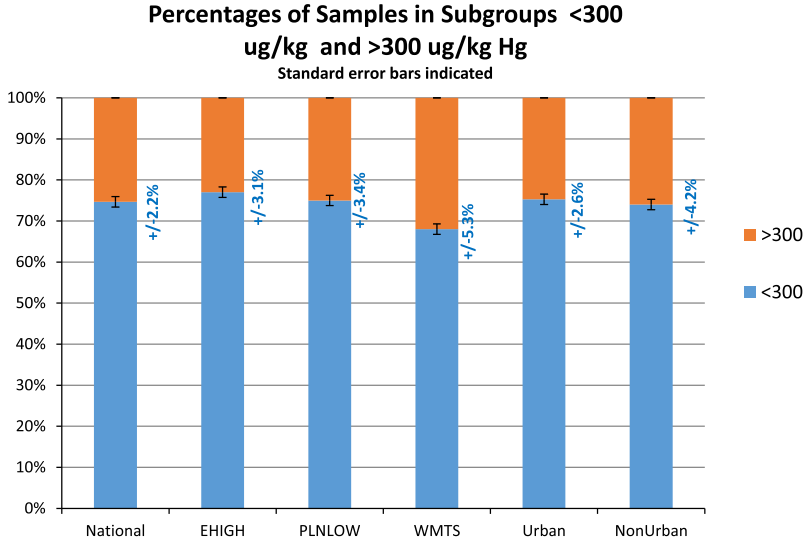

Fig. 3. Percentage of river miles by subgroup exceeding or not exceeding EPA's 300 ug kg^{-1} human health fish tissue-based water quality criterion.

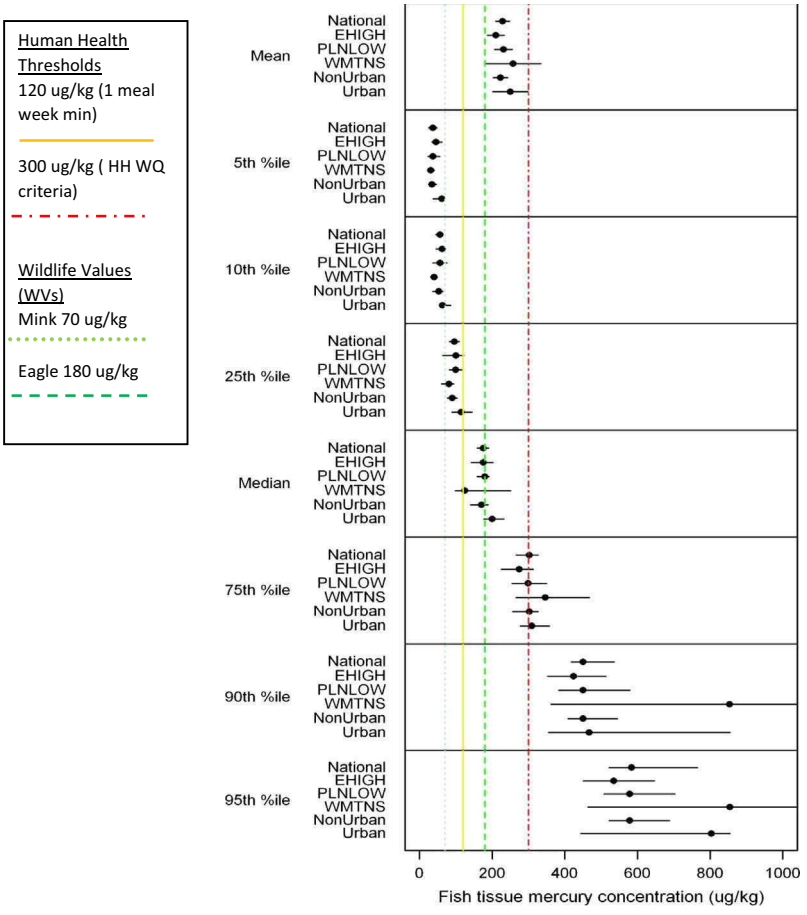

Fig. 4. Estimated percentile values (with 95% confidence limits) for subgroups with human health and wildlife value thresholds.

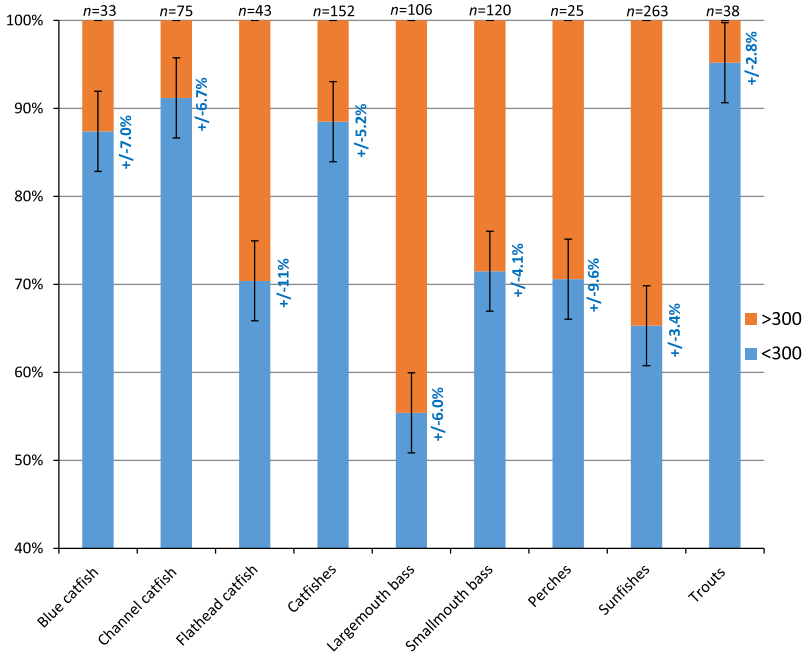

Fig. 5. Percentage of river miles by species/family exceeding EPA's 300 ug kg^{-1} human health fish tissue-based water quality criterion.

(e.g., combined catfish, mean Hg = 143 ± 10 ug kg^{-1}.) Fig. 5 depicts the percent of river miles with species and species groups that exceeded and did not exceed the 300 ug kg^{-1} human health fish tissue-based WQC. Relative to higher (although not significantly so) Hg fish tissue concentrations in the urban river data, the percent of river miles with combined smallmouth and largemouth bass

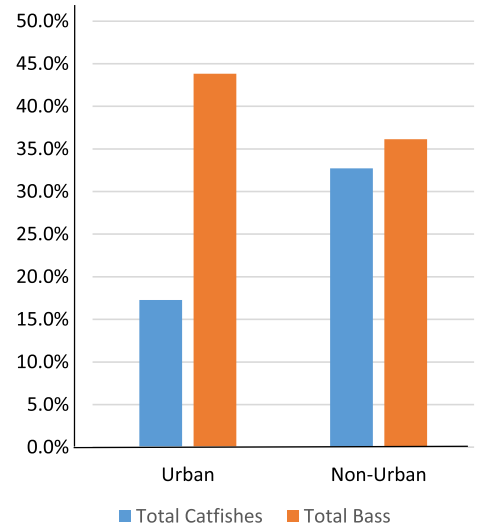

Fig. 6. Relative percentages of catfish and bass species in urban and non-urban waters.

samples were higher in the urban sub-group compared to the non-urban (43.8% vs. 36.1%). Conversely, combined catfish species constituted 32.7% of the river miles analyzed from non-urban sites vs. only 17.3% from urban river sites (Fig. 6).

Scudder et al. (2009) determined that Hg concentrations in fish tissue from largemouth bass from mixed use or undeveloped basins were higher than from urban basins, comparable to non-urban and urban subgroups discussed here. Non-weighted data from this study exhibit a similar distribution, but the smaller ***n*** of the portion of the subgroup that is itself a subgroup is insufficient to draw a national inference. The design of this study is focused on nationally-representative indices of assessment, and this comes at the expense of the ability to resolve distinctions beyond the primary sub-populations described-ecoregions (3), urban vs. non-urban sites, and the species included in Fig. 5. Of further interest relative to the discussion of urban/non-urban Hg fish tissue concentrations, however, may be the predominance of the percentage of bass species over catfish in the urban waters noted above when compared to near parity of the species groups in non-urban waters (Fig. 6). If the tissue of largemouth bass in urban areas is lower in Hg, there are also more of them relative to catfish species than in the non-urban areas, potentially affecting the combined impact of both species and urban/non-urban differential effects. Although not derived from weighted statistics, this factor suggests a possible explanation for the inconsistency between Scudder et al. (2009), Chalmers et al. (2014) among others, and this analysis. As mentioned earlier, because of the weighted probabilistic nature of the sample design, results from this study may differ from those employing other sample design methods (Peterson et al., 1998). Because of the unequal probability of any single sample being in the sample set, methods of comparison other than those employed for these data (*z*-test) are not valid.

3.4. Exceedances of WVs

The data from this study can also be interpreted with respect to the risk posed to piscivorous wildlife. Overall, fillets represent approximately 62% of the whole fish Hg concentration. Therefore, where fillets have Hg concentrations at or about 300 ug kg^{-1}, the dose to birds and mammals will be approximately 186 ug kg^{-1}. Whereas the primary health risk of Hg exposure to humans is neuro-developmental damage to unborn fetuses, Hg has been shown to threaten the survival of piscivorous wildlife (Lazorchak et al., 2003). According to the exposure scenario defined above, bald eagles and loons (WV = 160 and 180 ug kg^{-1}, respectively) will have similar risk levels relative to the applicable thresholds as humans consuming fish containing 300 ug kg^{-1} of Hg. Differences in species sensitivities to Hg consumption are emphasized by comparing mink to otter. Mink will be more at risk using the lower one meal per week (fillet) human threshold of 120 ug kg^{-1} (WV = 70 ug kg^{-1}), and the translated risk to otters will be intermediate between the human risk values in that their WV is 100 ug kg^{-1}. These values can also be compared to the data distribution depicted in Fig. 2.

4. Conclusions

With respect to human health thresholds, we have presented the following findings:

- All (100%) of the 541 fish fillet samples analyzed for Hg content for this national study contained quantifiable levels of Hg above the 3.33 ug kg^{-1} reporting level for the method.
- Nationally, an estimated 25.4% of river miles exceeded the EPA human-health fish tissue-based water quality criterion (WQC) for Hg of 300 ug kg^{-1}. This percentage represents 13 071 river miles (21 154 km) out of a total of 51 663 miles (83 143 km) of U.S. rivers of 5th order and greater included in the sampled population.
- The human health threshold exceedance data from this study also yields an estimate of risk of exposure to aquatic bird and mammal species from consumption of fish by the use of a correction factor for the relative Hg content of fillet tissue, normally consumed by humans, vs. the content of whole fish as are consumed by wildlife. Risk to piscivorous avian species are similar to risks for humans at 300 ug kg^{-1} (two meals per month level of consumption), whereas mink are more at risk than the avian species cited (and humans) when compared to the lower human one meal per week (fillet) threshold of 120 ug kg^{-1}.
- No statistically-significant differences were seen between waters sampled in urban and non-urban rivers, although the mean and 95th percentile values for urban rivers are elevated relative to non-urban rivers and all U.S. rivers.
- Although the percentage of river miles exceeding the 300 ug kg^{-1} criteria value was relatively higher in the WMTS ecoregion than any other of the sub-regional data groupings (>30% vs. ~25%, respectively), and the mean and 90th and 95th percentile values for the WMTS appear elevated relative to other subgroups, the *z*-test for statistical significance did not refute the null hypothesis at greater than the 95% confidence level (69%). The apparent elevation of the WMTS subgroup may be attributable to its smaller sample size in conjunction with one or more locally high fish tissue concentration values associated with local geologic Hg sources, as opposed to fish tissue concentrations related to atmospheric deposition that the findings of this study suggest do not vary significantly across the nation.

This study establishes a national baseline for Hg concentration in fish tissue from U.S. rivers 5th order and greater and compares those concentrations to human health and piscivorous wildlife thresholds. Hg concentrations in fish tissue from all areas of the country represent consumption risks to both humans and piscivorous wildlife in fish collected from approximately a quarter of the river miles. Furthermore, sensitivity to Hg exposure was greater for some aquatic species populations than the risk to humans at a given concentration. The lack of a statistically-significant difference

between fish tissue concentrations from urban vs. non-urban areas and among ecoregions is consistent with the ubiquitous nature of Hg contamination and its primary mechanisms of atmospheric transport and deposition. Differences in the representation of species in urban vs. non-urban rivers in this study may dampen variation seen by others (e.g., Scudder et al., 2009) between Hg concentrations in some species in urban vs. non-urban sites. The observed distinction in these results may also be attributable to the statistical methods of this study which result in national inferences that may not reflect specific local or regional conditions.

Author contributions

All the authors contributed to the initiation of the project, organization of the work, management of the project, analyzed the finished measurement data, and coordinated manuscript preparation. All four authors cooperated in developing the experimental design and writing the manuscript.

Acknowledgements

This study was funded within the U.S. EPA budget with public funds. The results reported here are the products of the combined efforts of many in addition to the authors. Prominent among these efforts is the sample collection supported by federal (USGS) and (many) state agency sampling teams. Within EPA, non-authors who provided significant contributions include Ellen Tarquinio and Sarah Lehmann who managed the overall NRSA project, Leanne Stahl was the overall technical lead for the fish tissue indicator, and the project would not have been possible without the contributions of many other EPA staff. Blaine Snyder of Tetratech and Harry McCarty of CSC played significant roles in project management and data processing and validation. Sample extraction and analysis was performed by Jayme Webb-Turbeville, Tracy Webb-Terbeville, and Ervin Obryan of Dynamac Corp.

References

Amos, H.M., Jacob, D.J., Streets, D.G., Sunderland, E.M., 2013. Legacy Impacts of all-time anthropogenic emissions on the global mercury cycle. Global Biogeochem. Cycles 27, 1–12.

Brigham, M.E., Wentz, D.A., Aiken, G.R., Krabbenhoft, D.P., 2009. Mercury cycling in stream ecosystems. Water column chemistry and transport. Environ. Sci. Technol. 43 (8), 2720–2725.

Brigham, M.E., Sandheinrich, M.B., Gay, D.A., Maki, R.P., Krabbenhoft, D.P., Wiener, J.G., 2014. Environ. Sci. Technol. 2014 (48), 6115–6123.

Chalmers, A.T., Argue, D.M., Gay, D.A., Brigham, M.E., Schmit, C.J., Lorenz, L., 2011. Mercury trends in fish from rivers and lakes in the United States, 1969–2005. Environ. Monit. Assess. 175, 175–191.

Chalmers, A.T., Krabbenhoft, D.P., Van Metre, P.C., Nilles, M.A., 2014. Effects of urbanization on mercury deposition and accumulation in New England. Environ. Pollut. 192, 104–112.

Driscoll, C.T., Mason, R.P., Chan, H.M., Jacob, D.J., Pirrone, N., 2013. Mercury as a global pollutant: sources pathways, and effects. Environ. Sci. Technol. 47, 4967–4983.

Feaster, T.D., Benedict, S.T., Clark, J.M., Bradley, P.M., Conrads, P.A., 2014. Scaling up watershed model parameters—flow and load simulations of the Edisto River Basin, South Carolina, 2007–09: U.S. Geological Survey Scientific Investigations Report 2014-5104, 34 p. <http://dx.doi.org/10.3133/sir20145104>.

He, K., Xun, P., Liu, K., Morris, S., Reis, J., Guallar, E., 2013. Mercury exposure in young adulthood and incidence of diabetes later in life. Diabetes Care 36, 1584–1589. The CARDIA trace element study Diabetes Care published ahead of print February 19, 2013.

Kagel, A., Bates, D., Gawell, K., 2007. A Guide to Geothermal Energy and the Environment. Geothermal Energy Association, Washington, DC. Retrieved February 9 2014. Cite uses deprecated parameters (help); Check date values. In: |access date = (help)Jump up ^ "Calpine Corporation – The Geysers". Retrieved 2008-06-11.

Karagas, M., Choi, A., Oken, E., Horvat, M., Schoeny, R., Kamai, E., Cowell, W., Grandjean, P., Korr, S., 2012. Evidence on the human health effects of low level methylmercury exposure. Environ. Health Perspect. 120 (6), 799–806. http://dx.doi.org/10.1289/ehp.1104494.

Lazorchak, J.M., McCormick, F.H., Henry, T.R., Herlihy, A.T., 2003. Contamination of fish in the mid-atlantic region: an approach to regional indicator selection and wildlife assessment. Environ. Tox. Chem. 22 (3), 545–553.

NAS, 2000. National Academies, Committee on the Toxicological Effects of Methylmercury, Board on Environmental Studies and Toxicology, Commission on Life Sciences. National Research Council. Toxicological Effects of Methylmercury. National Academy Press, Washington, DC.

Olsen, A.R. et al., 2008. Survey design for lakes and reservoirs in the United States to assess contaminants in fish tissue. Environ. Monit. Assess. 150, 91–100.

Pacyna, E.G., Pacyna, J.M., Sundseth, K., Munthe, J., Kindbom, K., Wilson, S., Steenhuisen, F., Maxson, P., 2010. Global emission of mercury to the atmosphere from anthropogenic sources in 2005 and projections to 2020. Atmos. Environ. 44 (20), 2487–2499.

Peterson, S.A., Van Sickle, J., Hughes, R.M., Schacher, J.A., Echols, S.F., 2004. A biopsy procedure for determining fillet and predicting whole-fish mercury concentration. Arch. Environ. Contam. Toxicol. 48, 99–107.

Peterson, S.A., Van Sickle, J., 2007. Mercury concentration in fish from streams and rivers throughout the western United States. Environ. Sci. Technol. 41 (1), 58–65.

Peterson, S.A., Larsen, D.P., Paulsen, S.G., Urquhart, N.S., 1998. Regional lake trophic patterns in the Northeastern United States: three approaches. Environ. Manage. 22 (5), 789–801.

Schmitt, C.J., 2002. Biomonitoring of Environmental Status and Trends (BEST) program: Environmental contaminants and their effects on fish in the Mississippi River basin. U.S. Geological Survey Biological Science Report USGS/BRD/BSR 2002–0004. <http://pubs.er.usgs.gov/usgspubs/bsr/bsr020004>.

Scudder, B.C., Chasar, L.C., Wentz, D.A., Bauch, N.J., Brigham, M.E., Moran, P.W., Krabbenhoft, D.P., 2009, Mercury in fish, bed sediment, and water from streams across the United States, 1998–2005. U.S. Geological Survey Scientific Investigations Report 2009-5109, 74p.

Stahl, L., Snyder, B.D., Olsen, A.R., Pitt, Jennifer L., 2008. Contaminants in fish tissue from US lakes and reservoirs: a national probabilistic study. Environ. Monit. Assess. 150, 3–19. http://dx.doi.org/10.1007/s10661-008-0669-8.

Stevens, D.L., Olsen, A.R., 1999. Spatially restricted surveys over time for aquatic resources. J. Agric. Biol. Environ. Stat. 4 (4), 415–428.

Stevens Jr., D.L., Olsen, A.R., 2004. Spatially balanced sampling of natural resources. J. Am. Stat. Assoc. Theory Methods 99, 465.

Strahler, A.N., 1957. Quantitative analysis of watershed geomorphology. Trans. Am. Geophys. Union 8 (6), 913–920.

Streets, D.G., Zhang, Q., Wu, Y., 2009. Projections of global mercury emissions in 2050. Environ. Sci. Technol. 43 (8), 2983–2988.

Sunderland, E., Krabbenhoft, D.P., Moreau, J.W., Strode, S.A., Landing, W.M., 2009. Mercury sources, distribution, and bioavailability in the North Pacific Ocean: insights from data and models. Global Biogeochem. Cycles 23.

UNEP, 2008. Study on mercury sources and emissions, and analysis of cost and effectiveness of control measures. United Nations Environmental Programme, Division of Technology, Industry and Economics (DTIE) Chemicals Branch, Geneva, Switzerland. <http://www.unep.org/hazardoussubstances/Mercury/tabid/434/Default.aspx> (8/13).

U.S. EPA, 1997. Mercury study report to congress. Office of Air Quality Planning & Standards and Office of Research and Development Volume VI: An Ecological Assessment for Anthropogenic Mercury Emissions in the United States. EPA-452/R-97-008.

U.S. EPA, 2000a. Guidance for assessing chemical contaminant data for use in fish advisories, volume 1: fish sampling and analysis. In: 3rd ed. U.S. EPA, Office of Water, Office of Science and Technology, Washington, DC. EPA 823-B-00-008.

U.S. EPA, 2000b. Guidance for assessing chemical contaminant data for use in fish advisories, volume 2: risk assessment and fish consumption limits. In: 3rd ed. U.S. EPA, Office of Water, Office of Science and Technology, Washington, DC. EPA 823-B-00-008.

U.S. EPA, 2001a. Water Quality Criterion for the Protection of Human Health: Methylmercury. EPA-823-R-01-001. Washington, DC: U.S. Environmental Protection Agency, Office of Water. <http://water.epa.gov/scitech/swguidance/standards/criteria/aqlife/methylmercury/document.cfm> (8/13).

U.S. EPA, 2001. Integrated risk management system. Reference Dose for Chronic Oral Exposure-Methylmercury (MeHg) (CASRN 22967-92-6). Washington, DC. <http://www.epa.gov/iris/subst/0073.htm#reforal>.

U.S. EPA, 2007. EPA Method 7473: mercury in solids and solutions by thermal decomposition amalgamation and atomic absorption spectrophotometry. U.S. Environmental Protection Agency, Office of Research and Development, Environmental Monitoring and Support Laboratory. Cincinnati, OH, 45268.

U.S. EPA, 2009a. National Rivers and Streams Assessment Field Operations Manual. Office of Water, Washington, DC, EPA-841-B-07-009.

U.S. EPA, 2009b. The National Study of Chemical Residues in Lake Fish Tissue. Office of Water, Washington, DC, EPA-823-R-09-006.

U.S. EPA, 2011. 2010 Biennial National Listing of Fish Advisories. U.S. Environmental Protection Agency Report EPA-820-F-11-014.

U.S. EPA, 2013. Rivers and Streams Assessment 2008–2009 A Collaborative Survey DRAFT Office of Wetlands, Oceans and Watersheds Office of Research and Development, Washington, DC 20460 EPA/841/D-13/001.

U.S. EPA, 2014. Aquatic resources monitoring, software downloads for spatial survey design and analysis. Office of Research Development (ORD) National Health Environmental Effects Research Laboratory (NHEERL), Western Ecology Division (WED). <http://www.epa.gov/nheerl/arm/analysispages/software.htm>.

U.S. Government, 2011. Code of Federal Regulations. Title 40 – Protection of Environment Subchapter D – WATER PROGRAMS Part 136 – GUIDELINES

ESTABLISHING TEST PROCEDURES FOR THE ANALYSIS OF POLLUTANTS. Appendix B to Part 136 – Definition and Procedure for the Determination of the Method Detection Limit-Revision 1.11. Government Printing Office, Washington, DC.

Walters, D.M., Bloksom, K.A., Lazorchak, J.M., Jicha, T., Angradi, T.R., Bolgrien, D.W., 2010. Mercury contamination in fish in midcontinent great rivers of the United States: importance of species traits and environmental factors. Environ. Sci. Technol. 44 (8), 2947–2953.

Wilson, S., Munthe, J., Sundseth, K., Kindbom, K., Maxson, P., Pacyna, J., Steenhuisen, F., 2010. Updating historical global inventories of anthropogenic mercury emissions to air. AMAP Technical Report No. 3, Arctic Monitoring and Assess ment Programme (AMAP) Oslo, Norway.

Wolfe, M.F., Schwarzbach, S., Sulaiman, R.A., 1998. Effects of mercury on wildlife: a comprehensive review. Environ. Toxicol. Chem. 17 (2), 140–160.

Yeardley Jr., R.B., Lazorchak, J.M., Paulsen, S., 1998. Elemental fish tissue contamination in northeastern U.S. lakes: evaluation of an approach to regional assessment. Environ. Toxicol. Chem. 17 (9), 1875–1884.

Environmental Science & Technology

Article

pubs.acs.org/est

Statistical Survey of Persistent Organic Pollutants: Risk Estimations to Humans and Wildlife through Consumption of Fish from U.S. Rivers

Angela L. Batt,[†] John B. Wathen,[*,‡] James M. Lazorchak,[†] Anthony R. Olsen,[§] and Thomas M. Kincaid[§]

[†]U.S. Environmental Protection Agency Office of Research and Development National Exposure Research Laboratory, Cincinnati, Ohio 45268, United States

[‡]U.S. Environmental Protection Agency Office of Water Office of Science and Technology, Washington, D.C. 20460, United States

[§]U.S. Environmental Protection Agency Office of Research and Development, National Health and Environmental Effects Research Laboratory, Corvallis, Oregon 97333, United States

Supporting Information

ABSTRACT: U.S. EPA conducted a national statistical survey of fish tissue contamination at 540 river sites (representing 82 954 river km) in 2008−2009, and analyzed samples for 50 persistent organic pollutants (POPs), including 21 PCB congeners, 8 PBDE congeners, and 21 organochlorine pesticides. The survey results were used to provide national estimates of contamination for these POPs. PCBs were the most abundant, being measured in 93.5% of samples. Summed concentrations of the 21 PCB congeners had a national weighted mean of 32.7 μg/kg and a maximum concentration of 857 μg/kg, and exceeded the human health cancer screening value of 12 μg/kg in 48% of the national sampled population of river km, and in 70% of the urban sampled population. PBDEs (92.0%), chlordane (88.5%) and DDT (98.7%) were also detected frequently, although at lower concentrations. Results were examined by subpopulations of rivers, including urban or nonurban and three defined ecoregions. PCBs, PBDEs, and DDT occur at significantly higher concentrations in fish from urban rivers versus nonurban; however, the distribution varied more among the ecoregions. Wildlife screening values previously published for bird and mammalian species were converted from whole fish to fillet screening values, and used to estimate risk for wildlife through fish consumption.

INTRODUCTION

Polychlorinated biphenyls (PCBs), polybrominated diphenyl ethers (PBDEs), and many organochlorine pesticides, such as dichlorodiphenyltrichloroethane (DDT), dieldrin, and chlordane, are well-known persistent organic pollutants (POPs) that have been shown to be ubiquitous in the environment.[1,2] PCBs were widely used in industry and manufacturing as dielectric and coolant fluids, but because of their environmental toxicity and persistence, were banned for use by the U.S. Congress in 1979.[3] PBDEs share a similar chemical structure to PCBs. They are used as flame retardants in numerous consumer products, such as building materials, electronics, furniture, and textiles.[2] The production of octaBDE and pentaBDE commercial mixtures in the United States ended in 2004, leaving decaBDE as the only congener still in production in the U.S., which is also scheduled to be phased out of use.[4] DDT is one of the most recognizable POPs. After concerns were raised that its widespread agricultural use as a pesticide was having serious impacts on the health of the environment,[5] it was banned for use in the United States in 1972.[6] Chlordane and dieldrin were used as pesticides mainly to control termites and other insects in agricultural areas, and both substances having been banned for all agricultural uses in the U.S. by the U.S. EPA since the late 1980s. After its agricultural use was ended, chlordane could continue to be used to control termites around foundations.

The list of possible health effects in humans and wildlife from exposure to these POPs is extensive, and includes cancer, reduced reproduction rates, changes in immune and endocrine end points, and developmental neurotoxic effects.[2,3,7−13] Effects for some POPs, such as PCBs, can also be transgenerational, as the compounds have been found to cross over into the placenta and result in poor attention and behavioral problems in exposed infants and children.[14,15] Most POPs are lipophilic, and have been measured in human serum, blood, breast milk, and other human tissue,[16−21] and in the tissue of a variety of

Received: October 11, 2016
Revised: January 9, 2017
Accepted: February 6, 2017
Published: February 23, 2017

ACS Publications

This article not subject to U.S. Copyright. Published 2017 by the American Chemical Society

DOI: 10.1021/acs.est.6b05162
Environ. Sci. Technol. 2017, 51, 3021−3031

wildlife.[22−29] Not only do they accumulate in tissues, but also they tend to biomagnify in the food chain,[30] and a link between dietary consumption of fish and marine mammals and human blood or serum levels has been observed for several POPs.[31,32] DDT is still detected in food supplies, and food-borne DDT, especially from seafood, remains a significant source of human exposure.[20,33] Although most of these POPs have been banned for use in the U.S. for decades, their persistence and toxicity still make it important to study their potential for exposure today.

This work presents the results of the 2008−2009 National Rivers and Streams Assessment (NRSA) fish tissue indicator, where 50 POPs (Table 1) were measured in 540 composite fish fillet samples collected across the conterminous states (Figure 1). The NRSA is one of several U.S. EPA national probabilistic surveys designed to evaluate the overall condition and health of the nation's waters, and a wide variety of indicators are evaluated. NRSA study results for pharmaceuticals measured in urban surface water, and fish tissue contaminant results for both mercury and perfluorinated compounds have been reported previously.[34−36] Mercury was detected in every one of the 540 samples included in this study, and fillet tissue concentrations in an estimated 25% of the sampled population exceeded the U.S. EPA 300 μg/kg fish-tissue based water quality criteria for mercury.[34] The probabilistic design for this survey provides national estimates of the distribution of these 50 POPs in fifth order and greater U.S. rivers for the assessment of human health impacts of fish consumption. A series of cancer[37] and noncancer[37,38] human health screening values (SVs) were applied to the fillet tissue results. They provide estimates of the percentage of all U.S. river km represented in this study (i.e., the sampled population of rivers) that would be expected to contain POPs that exceed these SVs. Fish fillet tissue contaminant concentrations were also compared to wildlife screening values that were converted from whole fish values to fillet screening values in order to estimate exposure risks to mammals and birds. Geographical distributions of these contaminants were compared, first between urban and nonurban river segments, and then among three aggregated National Aquatic Resource Assessment ecoregions: Eastern Highlands (EHIGH), Plains and Lowlands (PLNLOW), and the West and Mountains (WMTS) (Figure 1).

MATERIALS AND METHODS

2.1. NRSA Design and Site Selection. The NRSA included 1924 sites within the conterminous United States that were sampled for a range of indicators.[39] Fish samples were analyzed from 540 sites on rivers fifth order and greater to determine concentrations of chemicals in fish, including pesticides, PCBs, PBDEs, selenium, and mercury. The 50 POPs listed in Table 1 include 21 out of a possible 209 PCB congeners, 8 PBDE congeners, and 21 organochlorine pesticides and metabolites. The number of congeners of PCBs and PBDEs was limited to allow for the simultaneous analysis of multiple classes of 50 POPs with a single analysis, and the specific congeners were chosen as they have been reported in previous U.S. EPA studies.[22] The mercury findings and fish tissue sample collection design were described previously.[34] Fish tissue samples were collected at sites that had a permanent fish population. Rivers were designated as fifth order or greater based on Strahler stream order.[40] The sampling framework was derived from the National Hydrography Data set (NHD) and included Strahler stream order attributes.[41] The fish sampling sites were classified as two

Table 1. Target analytes with their respective maximum observed method detection limit (MDL) and quantitation limit (QL) (μg/kg wet weight), as described in Method Section 2.3

analyte	CAS number	max MDL	max QL
PCB-8	34883−43−7	0.37	1.99
PCB-18	37680−65−2	0.38	1.23
PCB-28	7012−37−5	0.48	1.53
PCB-44	41464−39−5	1.30	4.13
PCB-52	35693−99−3	0.86	2.73
PCB-66	32598−10−0	1.25	3.97
PCB-77	32598−13−3	0.61	1.93
PCB-101	37680−73−2	0.54	1.72
PCB-105	32598−14−4	0.30	0.95
PCB-118	31508−00−6	0.39	1.24
PCB-126	57465−28−8	0.35	1.11
PCB-128	38380−07−03	0.41	1.30
PCB-138	35065−28−2	2.68	8.52
PCB-153	35065−27−1	0.51	1.63
PCB-169	32774−16−6	0.36	1.14
PCB-170	35065−30−6	0.39	1.24
PCB-180	35065−29−3	0.33	1.05
PCB-187	52663−68−0	0.83	2.62
PCB-195	52663−78−2	0.83	2.63
PCB-206	40186−72−9	0.55	1.74
PCB-209	2051−24−3	0.45	1.43
summed PCBs	a sum of the above 21 congeners		
PBDE-47	5436−43−1	0.37	1.23
PBDE-66	189084−61−5	0.26	0.86
PBDE-99	60348−60−9	0.31	0.99
PBDE-100	189084−64−8	0.52	1.64
PBDE-138	182677−30−1	0.59	1.97
PBDE-153	68631−49−2	0.58	1.93
PBDE-154	207122−16−5	0.55	1.84
PBDE-183	207122−15−4	0.82	2.74
summed PBDE	a sum of the above 8 congeners		
2,4′-DDD	53−19−0	0.37	1.18
4,4′-DDD	72−54−8	0.28	0.89
4,4′-DDE	72−55−9	0.28	0.91
2,4′-DDT	789−02−6	0.30	0.95
4,4′-DDT	55−29−3	0.32	1.02
summed DDT	a sum of the above 5 DDT compounds		
alpha-chlordane (cis-chlordane)	5103−71−9	0.29	0.92
gamma-chlordane (trans-chlordane)	5103−74−2	0.38	1.22
oxychlordane	27304−13−8	0.37	1.18
summed chlordane	a sum of the above 3 chlordane compounds		
dieldrin	60−57−1	0.93	2.95
aldrin	309−00−2	0.30	0.97
alpha-BHC	319−84−6	0.31	1.04
gamma-BHC (lLindane)	58−89−9	0.23	0.73
endosulfan II	33213−65−9	0.46	1.53
endrin	72−20−8	0.37	1.18
endrin ketone	53494−70−5	0.34	1.08
heptachlor	76−44−8	0.28	0.89
heptachlor epoxide	1024−57−3	0.30	0.95
hexachlorobenzene	118−74−1	0.30	0.95
mirex	2385−85−5	0.37	1.18
cis-nonachlor	5103−73−1	0.29	0.99
trans-nonachlor	39765−80−5	0.29	0.92

DOI: 10.1021/acs.est.6b05162
Environ. Sci. Technol. 2017, 51, 3021−3031

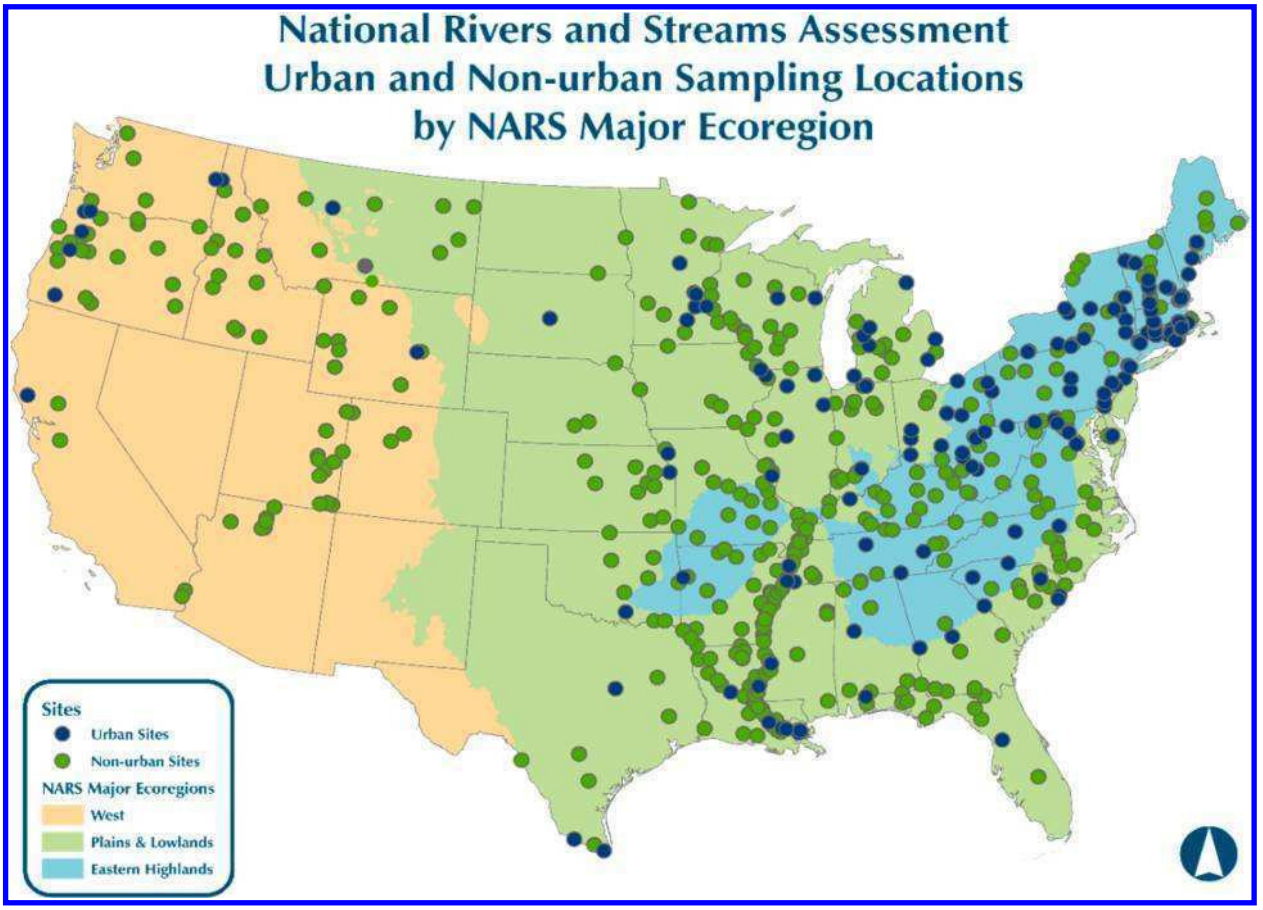

Figure 1. National map of NRSA 2008−2009 sampling locations (n = 540) within national aquatic resource survey ecoregions.

subpopulations: urban and nonurban river segments. NHD-Plus and the U.S. Census Bureau national urban boundary GIS coverage layers were used to identify urban sampling areas, which were defined as densely settled census block groups with a minimum population density of 50 000 people. Sampling sites were selected using a probability-based approach,[42,43] generally applying the spatial methodology used for lakes in U.S. EPA's National Lake Fish Tissue Study[44] to major U.S. rivers. Fish samples were collected from 164 randomly selected urban river sites and 378 nonurban river sites. This included sampling locations in 46 states with the following distribution of river sites: fifth order, 154 sites; sixth order, 161 sites; seventh order, 99 sites; and eighth order and above, 126 sites.

2.2. Sample Collection. One composite sample of a single fish species was collected from each site (Figure 1). A routine composite sample consisted of five fish, but composites containing fewer or greater than five fish were accepted in an effort to retain a sample from each target river segment (51.3% and 1.1% of the composites, respectively). Species were selected to be ubiquitous, abundant, and easily identified. Individual specimens of the species were selected to be adults of similar size (the length of the smallest individual in a composite could not be less than 75% of the total length of the largest individual) and sufficiently large to provide adequate tissue.[45] A total of 15 species were identified in a targeted list, including members of the sunfish (with largemouth and smallmouth bass preferred), trout/salmon, pike, temperate bass, perch, and catfish families. Field teams used active methods, primarily electrofishing, to collect fish samples from each site during the May through September field sampling period in 2008 and 2009. Whole fish were shipped on dry ice to the designated sample preparation laboratory for storage until subsequent fillet tissue sample preparation and analysis. Other aspects of fish collection and handling methods are further described elsewhere.[45]

2.3. Sample Preparation and Analysis. Fish were filleted in the laboratory. Scales were removed, then lateral muscle fillets from both sides of each fish were prepared with skin on and the belly flap (ventral muscle and skin) attached. Fillets from individual specimens that comprised the sample were homogenized together, regardless of the proportional weight of individual fish. Composites were homogenized using a tissue grinder and an 8 g aliquot of homogenate was used for analysis. Wet tissue samples were extracted using pressurized fluid extraction (PFE), followed by sample cleanup with gel permeation chromatography (GPC) and alumina, and clean extracts were analyzed by gas chromatography with electron capture detection (GC-ECD). GC-ECD was chosen as the analysis method since the ECD detection method was found to be more sensitive for the target analytes than some mass spectrometry methods, and provided a very cost-effective analysis for the range of compounds in this study. Full details of the extraction and GC-ECD analysis methods are included in Supporting Information (SI) Document 1. Briefly, 8.0 g of tissue were added to 20 g of anhydrous sodium sulfate and allowed to dry for 1 h. Samples were spiked with a surrogate standard solution and transferred to 33 mL PFE cells fitted with a cellulose filter, and remaining cell volume was filled with drying material. PFE cells were extracted with methylene chloride (50%) and hexane (50%) at 100 °C and 1000 psi for

DOI: 10.1021/acs.est.6b05162
Environ. Sci. Technol. 2017, 51, 3021−3031

three 7 min cycles. Extracts were collected into a 60 mL glass vial, and the volume was reduced to approximately 3 mL using a stream of nitrogen in a 50 °C water bath. Concentrated sample extracts were dried using a 1-in. diameter glass chromatography column packed with 20 g of sodium sulfate and glass wool, and rinsed three times with hexane. Further sample extract cleanup was performed using GPC with a Waters HPLC, followed by solid-phase extraction using columns packed with deactivated alumina-N. Final sample extracts were adjusted to a volume of 1 mL after the addition of 25 μL of an internal standard solution consisting of pentachloronitrobenzene, PCB 96, and PCB 166. These extracts were analyzed using Agilent 6890 gas chromatographs equipped with pressure-pulsed splitless injection, narrow-bore columns and micro ECD detectors. Since ECD detection is not as selective as some mass spectrometry methods available, two separate GC-ECD analyses were performed on instruments equipped with different GC columns, first a primary analysis (Agilent HP-5 capillary column: 30 m length, 0.25 mm diameter and 0.25 μm film thickness), followed by a confirmatory analysis (J&W DB - XLB column, 30 m length, 0.25 mm diameter and 0.25 μm film thickness), with the two different oven programs for both methods being described in SI Document 1. Concentrations of detected analytes were calculated for both the primary and confirmatory analyses. Reported concentrations are a result of the average of the primary and confirmatory analyses, unless the relative percent difference (RPD) in concentrations between the two columns was greater than 30%, in which case, the lesser concentration was reported. If an analyte was not detected in both analyses, it was reported as not-detected.

The method detection limit (MDL, Table 1), which is defined as the minimum concentration of an analyte that can be identified and detected with 99% confidence that the analyte concentration is greater than zero, was determined for each analyte using the procedure described at 40 CFR Part 136 Appendix B.[46] The quantitation limit (QL) was defined as 3 times the MDL, and both the MDL and QL were calculated on the primary and confirmatory columns, and were updated on a yearly basis. Concentrations were reported to the MDL that applied at the time of analysis, however, any concentrations greater than the MDL but less than the QL were flagged as estimated. The maximum MDL and QL observed during the course of the study for each analyte is listed in Table 1. Four quality control samples were analyzed with each extraction batch, including a laboratory reagent blank (LRB), a laboratory fortified blank (LFB), and two laboratory fortified matrix (LFM) samples. The LRB and LFB were prepared from sodium sulfate, and the LFB and LFM were spiked with a mixture of the target analytes to yield a final GC extract concentration of 15 ng/mL. Percent recovery for each analyte was calculated in the LFB and LFM samples. Acceptable target recoveries for all analytes ranged from 70% to 130% for LFB, and from 50% to 150% with a 30% RPD for the duplicate LFM samples. Any analytes or samples which did not meet the predetermined quality criteria of the LFB and LFM samples were reanalyzed, or reported as estimated. Samples were also re-extracted and analyzed if an analyte was present in the LRB above the QL and the analyte was present in the sample above the QL but less than 10 times the detected blank concentration. Standard reference material (SRM) 1947, purchased from National Institute of Standard and Technology (NIST), was used as a certified second source standard to monitor extraction efficiency and instrument quantitation, and was extracted and analyzed with each extraction batch. All data reported in this study were reviewed and validated against the project requirements by a third party not involved in the data generation. Only valid results were used in the statistical analyses. Measured concentrations and qualifiers for each of the 50 contaminants analyzed in the 540 fillet samples are included as SI (Table S1–S3).

2.4. Data Analysis. *National and Subpopulation Estimates.* The NRSA survey design and results provide national and regional estimates of fish tissue contaminant concentrations, and as a result, reported results are expressed as population estimates, and not site or sample summary data. The population estimates are based on weighted analytical results from sampling sites. The weights are based on the survey design and are the inverse of the probability of selecting a sampling site. The probability of selecting a site depends on the stratification and unequal probability of selection associated with the site. The weights are the total river length represented by the sample site. Percentiles and mean population estimates of fish tissue analyte concentrations were calculated from the weighted data, using routines developed by the U.S. EPA in the statistical calculation package *spsurvey* *R*[47] for the R statistical computing environment.[48] In addition to the urban and nonurban subgroups, statistical parameters were generated for three aggregated ecoregions (EHIGH, PLNLOW, and WMTS) used in U.S. EPA National Aquatic Resource Surveys.[49] A standard normal Z-test was used to investigate fish tissue analyte concentration differences between the urban and nonurban subgroups, and between ecoregions:

$$z = \frac{\text{mean}A - \text{mean}B}{\sqrt{(\text{stderr}A^2 + \text{stderr}B^2)}}$$

where mean$A$ is the weighted mean estimate, stderr$A$ is the standard error estimate for mean$A$ for subgroup A, and similarly for subgroup B. Compounds were evaluated by summed groups, including summed PCB and PBDE congeners, total DDT (the five DDT compounds and degradates listed in Table 1), and total chlordane (cis- and trans-chlordane, cis- and trans-nonachlor, and oxychlordane). Prior to summing data into groups, any detections below the MDLs were considered nondetects and the results were treated as zeros during the statistical analysis.

Human Health Risk Estimate. The two categories of human health risk that are reflected in selected SVs are cancer and noncancer (Table 2). The survey design provides national estimates of river kilometers that are expected to contain fish with fillet concentrations that would exceed those screening value thresholds. A cancer SV[37] is based on a level of excess cancer risk from exposure to a carcinogenic substance ranging from 10^{-4} to 10^{-6}. The noncancer SVs are based on a reference dose (RfD) for a toxicant, which is the level of exposure over a lifetime at which no observable adverse effects will occur. Cancer SVs are generally lower than noncancer SVs (Table 2), but the ratio can vary. For this assessment, a cancer SV reflecting 10^{-5} cancer risk has been applied to allow comparison of all the frequently detected compounds across regions, and to be comparable to previous U.S. EPA assessments.[22,26] A noncancer SV was also applied to provide context for the concentrations reported here in terms of thresholds widely used in fish consumption advisories.[37] For the PBDEs, no cancer SV was applied, since the PBDE

DOI: 10.1021/acs.est.6b05162
Environ. Sci. Technol. 2017, 51, 3021−3031

Table 2. Summary of the Human Health Screening Values (SVs) and Wildlife Values (WV), with All Values Being Presented in μg/kg Wet Weight (ppb); and the Applied Fillet to Whole Fish Conversion Factors[a]

compound	cancer SV	noncancer SV	mink WV	kingfisher WV	fillet to whole fish conversion factor
PCBs	12	47	72	242	1.83
PBDEs	N/A	210	21	8.7[b]	1.50
DDT	69	120	216	12.0	1.66
chlordane	67	1200	573	3.1	1.44
dieldrin	1.5	120	20	360	

[a]HH SVs are based on the upper estimates of consuming one 8 oz meal of fish per week. See Methods Section 2.4 for a description of Cancer and Non-Cancer SVs, and WV. [b]Kestril WV instead of Kingfisher, taken from Canadian Environmental Protection Act[38]

congeners represented in this study have not been classified as carcinogenic.[4] Limited RfDs are available for PBDE congeners, however, the California EPA has published fish tissue advisory levels based on noncancer risk.[38]

Wildlife Risk Estimate. The fish tissue study conducted under the 2008−2009 NRSA was designed to assess human health impacts from fish consumption, which is why fillets were targeted for analysis. To estimate the possible risk to wildlife that may be consuming fish collected in this survey, wildlife values (WVs) for mink, kingfisher, and larger birds (if available) that represent thresholds for toxic effects (such as reproductive or development success, organismal viability or growth, effect on population dynamics) were used.[50,51] However, these previously reported WVs represent whole-fish tissue concentrations, so a conversion factor had to be applied to convert whole-fish tissue WVs to fillet WVs. For total PCBs, a conversion factor was averaged from across three references;[28,52,53] one conversion factor was used for DDT and chlordane;[52] and another was identified for PBDEs.[51] All of these conversion factors are listed in Table 2, along with the resulting fillet WVs. Dieldrin WVs were not converted from whole body to fillets, since it has been reported that dieldrin was present in roughly the same average concentrations in game-fish fillets as in whole-body bottom-feeders. No other publications were found that provided information comparing whole fish dieldrin to fillet concentrations from the same fish species.[54] Since a conversion factor for the wildlife values from fillets to whole fish had to be applied, limited inferences can be made for the wildlife results. However, because different species can display very different sensitivities to the same chemicals, the results of the wildlife risk estimate do provide valuable insight into the relative risks of exposure for human, mammalian, and avian species across the different contaminant groups.

Chemical Co-Occurrence. Co-occurrence of the four main chemical groupings was examined using a previously described procedure,[55] Samples that exceeded the weighted median concentrations for any of the four major contaminant groups (PCBs, PBDEs, total chlordane, and total DDT) were identified. Samples that exceeded the respective median concentrations were then compared to calculate the percentage of the samples with concentrations above the median of any one compound group that occurred: (1) singly; (2) with a second contaminant group also above its median; (3) as a combination of any three contaminant groups; or 4) with all four compound groups occurring together above their median concentrations.

3.0. RESULTS AND DISCUSSION

PCBs in Fish Tissue. PCBs were detected in 93.5% of the fish fillet samples, which results in 48% (40 030 river km (±2432 km)) of the national sampled population of rivers having fillet tissue concentrations that exceed the cancer SV of 12 μg/kg, as shown in Table 3. By comparison, nearly 70% of the sampled population of urban rivers had fillet tissue concentrations that exceeded the PCB cancer SV. The maximum summed PCB concentration measured in urban river samples was 857 μg/kg. Among the three ecoregions, PCB detections dominated in the EHIGH, where the mean summed PCB concentration was 47.1 μg/kg. In this ecoregion, fillet tissue concentrations exceeded the PCB cancer SV of 12 μg/kg in 54.3% of the sampled population of EHIGH rivers. The mean summed PCB concentrations in fillet samples from the PLNLOW and WMTS were 30.7 μg/kg and 11.9 μg/kg, respectively. The PCB SV exceedances were lower in these two ecoregions. In the PLNLOW, 50.8% of the sampled population of PLNLOW rivers had fillet concentrations that exceeded the 12 μg/kg SV. By contrast, 23.6% of the WMTS sampled population of rivers exceeded the cancer SV.

The national, ecoregion, urban river, and nonurban river population percentile estimates for the summed PCB concentrations are shown in Figure 2. The national estimate of the median summed PCB concentration is 11.3 μg/kg, which is almost the same as the cancer SV of 12 μg/kg. All of the 75th percentile estimates of fillet concentrations lie between the cancer SV (12 μg/kg, which corresponds to the WMTS estimate) and noncancer SV (47 μg/kg, which corresponds to the urban river estimate). All of the 90th percentile estimates exceed 47 μg/kg except the estimate for the WMTS ecoregion. For the wildlife estimates, fish tissue concentrations in 9.3% of the national sampled population exceed the fillet WV for mink, whereas fish tissue concentrations in only 1.3% of the sampled population exceeded the kingfisher fillet WV. Human SVs for both cancer and noncancer are lower than both PCB WV values, and therefore, in general, the human health SVs are protective of wildlife risks as well.

The relative abundance of the 21 PCB congeners found in fish fillet tissue from nonurban vs urban rivers is shown in SI Figure S-1. All mean PCB congener concentrations are higher in samples from urban rivers than from nonurban rivers, but the magnitude of the difference varies. Congeners 138 and 153 are the most abundant PCBs in both nonurban and urban river fish fillets, which has also been the case in other environmental samples.[16] The coplanar PCBs 77, 126, and 169 (indicated by the arrows in SI Figure S-1) are present only at low concentrations in fillet tissue from both subpopulations. In this study, 21 PCB congeners were quantified out of the full suite of 209 PCB congeners. Since there is additional PCB mass in the samples that was not measured for this study, the summed 21 PCB congeners underestimate the total mass present in the samples. Although this study underestimates the total PCB mass, the congeners analyzed include 10 of the 11 congeners with the highest frequency of environmental occurrence, as well as three dioxin-like congeners.[56] Therefore, the results of this study are still applicable to the human health and wildlife exposure analysis.

PBDEs in Fish Tissue. Similar to PCBs, the eight congeners of PBDEs are commonly detected in fish tissue samples. All of the results presented in Table 3 and SI Figure S-2 indicate higher concentrations in urban river samples than in samples

DOI: 10.1021/acs.est.6b05162
Environ. Sci. Technol. 2017, 51, 3021−3031

Table 3. Weighted POPs Fish Tissue Concentration Results by Site Type and Ecoregion, And Percent River km Exceeding Human Cancer Screening Values (CSV), Noncancer Screening Values, And Wildlife Values (WV)

PCB summed congeners			
statistic	national	nonurban	urban
detects	505/540 sites (93.5%)	343/377 sites (91.0%)	162/163 sites (99.4%)
mean	32.7 ug/kg	26.9 ug/kg	54.2 ug/kg
median	11.3 ug/kg	8.6 ug/kg	23.8 ug/kg
max	857 ug/kg	412 ug/kg	8567 ug/kg
%>CSV (12 ug/kg)	48.0%	42.0%	69.8%
%>non-CSV (47 ug/kg)	16.7%	14.6%	25.7%
%>mink WV (72 ug/kg)	9.3%	8.9%	10.9%
%>KF WV(242 ug/kg)	1.4%	0.7%	3.8%
statistic	EHIGH	PLNLOW	WMTS
sites	189	280	71
mean	47.1 ug/kg	30.7 ug/kg	11.9 ug/kg
median	16.7 ug/kg	12.6 ug/kg	3.8 ug/kg
%>CSV (12 ug/kg)	54.3%	50.8%	23.6%
%>non-CSV (47 ug/kg)	20.2%	18.0%	6.1%
%>mink WV (72 ug/kg)	13.2%	8.5%	4.6%
%>KF WV(242 ug/kg)	3.8%	0.5%	0%

PBDE summed congeners			
statistic	national	nonurban	urban
detects	497/540 sites (92.0%)	340/377 sites (90.2%)	157/163 sites (96.3%)
mean	11.6 ug/kg	8.6 ug/kg	22.5 ug/kg
median	4.7 ug/kg	3.6 ug/kg	8.0 ug/kg
maximum	311 ug/kg	151 ug/kg	310 ug/kg
%>non-CSV (210 ug/kg)	0.3%	0%	1.2%
%>mink WV(21 ug/kg)	14.6%	10.6%	29.1%
%>kestral WV(8.7 ug/kg)	33.4%	29.5%	47.8%
statistic	EHIGH	PLNLOW	WMTS
sites	189	280	71
mean	13.6 ug/kg	10.2 ug/kg	13.2 ug/kg
median	6.8 ug/kg	3.5 ug/kg	4.8 ug/kg
%>non-CSV (210 ug/kg)	0%	0.5%	0%
%>mink WV(21 ug/kg)	17.5%	13.3%	13.9%
%>kestral WV(8.7 ug/kg)	42.0%	31.5%	23.8%

total DDT			
statistic	national	nonurban	urban
detects	533/540 sites (98.7%)	370/377 sites (98.1%)	163/163 sites (100%)
mean	13.8 ug/kg	12.3 ug/kg	19.0 ug/kg
median	6.3 ug/kg	5.7 ug/kg	9.5 ug/kg
maximum	294 ug/kg	170 ug/kg	294 ug/kg
%>CSV (69 ug/kg)	2.3%	1.6%	5.1%
%>mink WV(216 ug/kg)	0.1%	0%	0.3%
%>KF WV(12 ug/kg)	31.6%	28.3%	43.7%
statistic	EHIGH	PLNLOW	WMTS
samples	189	280	71
mean	8.8 ug/kg	16.0 ug/kg	14.6 ug/kg
median	3.6 ug/kg	7.5 ug/kg	4.5 ug/kg
%>CSV (69 ug/kg)	1.0%	2.7%	3.5%
%>mink WV(216 ug/kg)	0.2%	0.03%	0%
%>KF WV(12 ug/kg)	21.0%	36.9%	31.4%

total chlordane			
statistic	national	nonurban	urban
detects	478/540 sites (88.5%)	325/377 sites (86.2%)	153/163 sites (93.9%)
mean	6.3 ug/kg	5.1 ug/kg	10.8 ug/kg
median	2.0 ug/kg	1.6 ug/kg	2.7 ug/kg
maximum	311 ug/kg	87.1 ug/kg	311 ug/kg
%>CSV (67 ug/kg)	0.6%	0.3%	1.6%
%>mink WV(573 ug/kg)	0%	0%	0%
%> KF WV(3.1 ug/kg)	36.9%	34.1 0%	47.2%
statistic	EHIGH	PLNLOW	WMTS
samples	189	280	71
mean	5.7 ug/kg	7.6 ug/kg	2.1 ug/kg
median	2.5 ug/kg	2.2 ug/kg	0.8 ug/kg
%>CSV (67 ug/kg)	1.0%	0.5%	0%
%>mink WV(573 ug/kg)	0%	0%	0%
%> KF WV(3.1 ug/kg)	39.9%	40.9%	14.5%

dieldrin			
statistic	national	nonurban	urban
%>CSV (1.5 ug/kg)	31.2%	28.5	41.2%
statistic	EHIGH	PLNLOW	WMTS
%>CSV (1.5 ug/kg)	24.1%	40.4%	7.8%

from nonurban rivers. In contrast, PBDE results among the three ecoregions show (Table 3) no clear distinctions. SI Figure S-3 shows the relative abundance of individual PBDE congeners in fillet tissue samples from nonurban and urban rivers. PBDE concentrations in fish from U.S. rivers are dominated by BDE 47, followed by BDEs 100 and 99. Only 0.3% of the national sampled population had fillet concentrations that exceeded the 210 μg/kg human health SV for PBDEs (Table 3). The higher noncancer SV for PBDEs relative to PCBs and DDT is a reflection of their lower relative toxicity, but again, limited RfD values are available for PBDEs. The lower toxicity and shorter half-life of PBDEs[57] compared to PCBs[58] could be contributing factors to the lower percentage of the national sampled population having fillet tissue concentrations that exceed the SV for PBDEs. In contrast to PCBs, the applied PBDE WVs are lower than the human health SVs. Summed PBDE results for the wildlife risk estimation showed that fish tissue concentrations in 33.4% of the national sampled population exceed the converted fillet WV for kestrels, and for mink, fish tissue concentrations in 14.5% of the national sampled population exceeded the WV (Table 3).

DOI: 10.1021/acs.est.6b05162
Environ. Sci. Technol. 2017, 51, 3021−3031

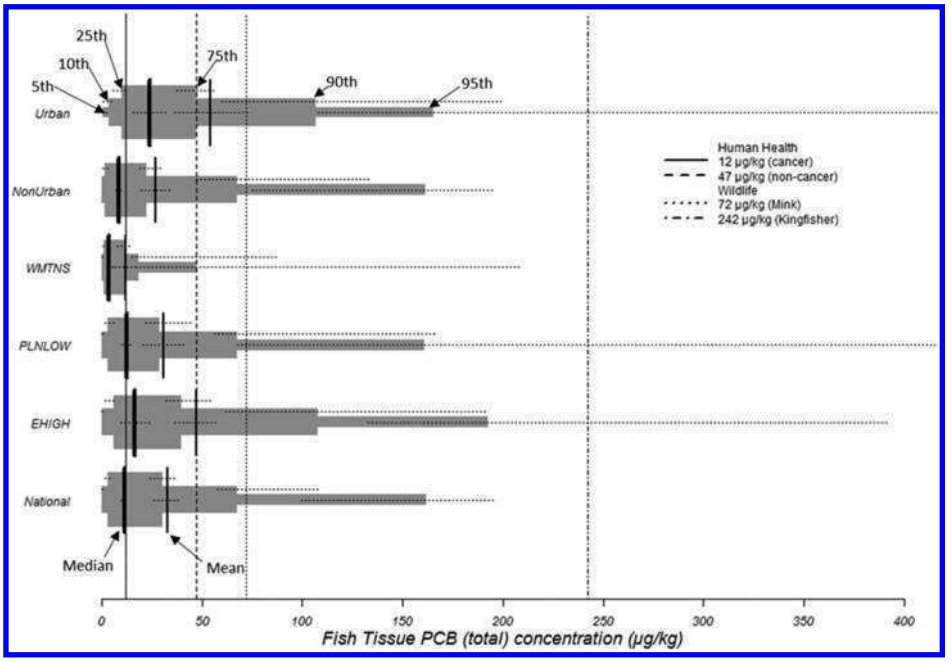

Figure 2. Estimated population percentile distribution for summed PCBs in fish tissue from U.S. river sampling sites, nonurban and urban, and by ecoregion. Confidence intervals for each percentile, mean, and median are represented by the horizontal dashed lines.

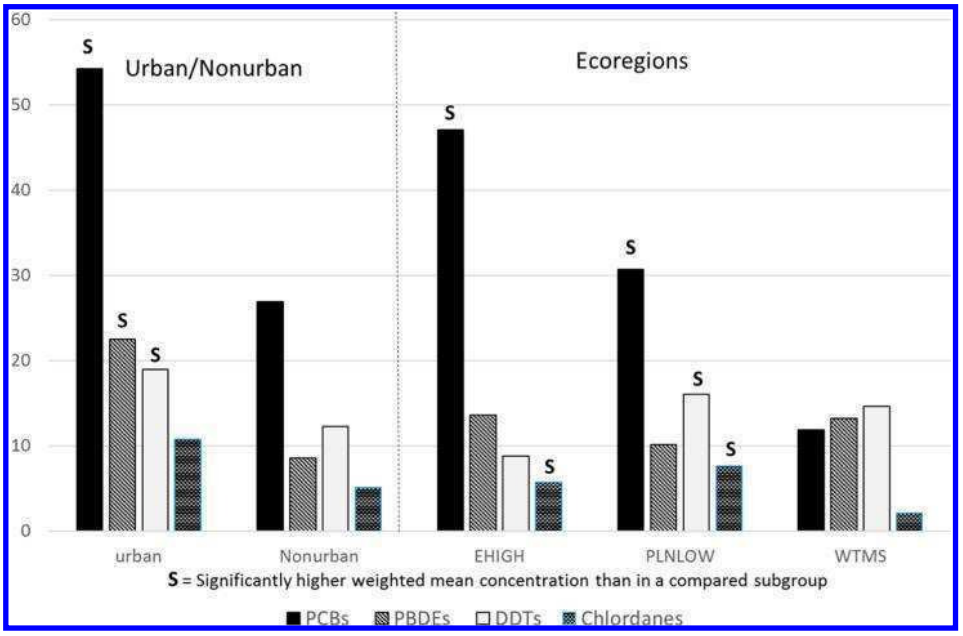

Figure 3. Comparison of weighted mean contaminant concentrations between subgroups in μg/kg (y axis).

OCPs in Fish Tissue. Lower concentrations were observed for the organochlorine pesticides (OCPs) chlordane and total DDT relative to the summed PCBs. Even 28 years after U.S. EPA withdrew approval for its use for underground termite control around the foundations of homes,[59] chlordane was detected in 88.5% of all fish tissue samples and 93.9% of the urban river samples (Table 3). Concentrations exceeded the cancer-based human health SV of 67 μg/kg[44] in fish fillet samples from less than 1% of the sampled population of rivers. When WVs were applied for chlordane, fish tissue concentrations in 36.9% of the national sampled population exceeded the kingfisher fillet WV and fish tissue concentrations in 0% of the national sampled population exceeded the mink fillet WV (Table 3).

Although banned in 1972 (for most uses) in the U.S.,[6] DDT and its metabolites (total DDT) were detected in 100% of the fish samples in this study (Table 3). Concentrations of total DDT were found to be elevated in a few samples. However, the mean concentration (13.8 μg/kg) is well below the human health cancer-based SV of 69 ug/kg for total DDT, and both the percentage of samples and the river length they represent are low (1947 km, ±511 km, Table 3). Only the 95th percentile estimates for total DDT concentrations from urban rivers exceed the cancer-based SV (SI Figure S-4). Additionally, the tissue concentrations for 4,4′-DDT (mean 0.75, median 0.18, maximum 36.3 μg/kg) are much lower than total DDT, which indicates that new sources of DDT are unlikely. The main contributor to total DDT was 4,4′-DDE (mean 10.7, median

DOI: 10.1021/acs.est.6b05162
Environ. Sci. Technol. 2017, 51, 3021−3031

4.7 μg/kg). Fish tissue concentrations in 31.5% of the national sampled population exceeded the WV for total DDT for kingfishers, and fish tissue concentrations in less than 1% of the national sampled population exceeded the WV for mink. Like chlordane, the converted total DDT WV for Kingfishers was lower than that of minks and the human health cancer SVs listed in Table 3, indicating that these organochlorine pesticides may pose more of a risk for avian species.

Analytical results for dieldrin also showed widespread occurrence with a 71% frequency of detection, and dieldrin has a relatively lower cancer SV (1.5 μg/kg). Dieldrin concentrations in fillet samples exceeded this SV in 31.2% of the sampled population of rivers, including 41.2% of urban rivers and 40.4% of PLNLOW rivers (Table 3). Other OCPs detected in this study included aldrin, alpha-BHC, endrin, lindane, endrin ketone, heptachlor epoxide, hexachlorobenzene, and mirex. These other OCPs had detection frequencies of less than 50%, and none of the fillet concentrations exceeded human health SVs for these compounds.

Subpopulation Differences. Concentrations of mercury in fish tissue from these same samples were previously compared across the three ecoregions and between nonurban and urban sites.[34] Those results revealed no significant differences across the subpopulations of rivers, however, different results were observed for the organo-halogen compounds. Figure 3 compares the weighted mean concentrations of the organo-halogens in fish from urban versus nonurban subpopulations and from ecoregions, and the significance of any differences as determined using the Z test are listed in SI Table S4. The means for all chemical groups were higher for samples from urban rivers than those from nonurban rivers. The means for summed PCBs, summed PBDEs, and total DDT were significantly higher for urban river samples, which reflects the greater extent of chemical use and release of a variety of contaminants into rivers in populated areas where they can bioaccumulate in fish. Higher organochlorine concentrations in aquatic environments in urban areas have been documented previously in urban bed sediments.[60] Not only could urban sources from chemical manufacturing, industrial use of chemicals, and domestic application of pesticides contribute to enhanced concentrations in fish tissue from urban waters, but proximity to wastewater treatment plant (WWTP) discharges could also be a factor, since WWTPs have been demonstrated to be an important point source of PCB and PBDE contamination.[61]

Among the ecoregions, summed PCB concentrations in river fish samples from the EHIGH were significantly higher than in samples from both the PLNLOW and WMTS (Figure 3, SI Table S4). Summed PCB concentrations in fish from the PLNLOW were also significantly higher than those from the WMTS. Although summed PBDE concentrations were significantly higher in samples from urban rivers relative to nonurban rivers, there was no significant difference in summed PBDE concentrations among ecoregions. Total chlordane concentrations were found to be significantly higher in fillet tissue samples from rivers in both EHIGH and PLNLOW ecoregions relative to the WMTS ecoregion, but the difference in EHIGH and PLNLOW total chlordane concentrations was not significant ((Figure 3, SI Table S4). Total DDT concentrations in samples from waters in the PLNLOW were significantly higher relative to those from the EHIGH, but unlike total chlordane, the difference in total DDT concentrations among the EHIGH, PLNLOW, and WMTS ecoregions was not significant.

Differences observed in the chemical concentrations relate to various factors, including their historical use and the geographic distribution of these chemical contaminants. Summed PCB concentrations are significantly higher in the EHIGH region relative to both other ecoregions, which reflects the industrial and urban history of this region where PCBs were most predominately used and released into the environment.[60] The ubiquity of PBDEs is consistent with its discharge pathway from dust in homes, through wastewater treatment systems,[21] and then to rivers. Similarly, the predominance of DDT in fish tissue from the PLNLOW ecoregion is consistent with the agricultural character of the middle of the country. The lack of a significant difference between the PLNLOW and WMTS total DDT results is also consistent with the high agricultural use of some states in the WMTS ecoregion. Chlordane, last labeled for use for underground application against termites,[59] persists in the EHIGH and PLNLOW regions but not in the WMTS.

Co-Occurring Contaminants. Co-occurrence of these four chemical groups was examined with the procedure outlined by Thompson and Boekelheide,[55] in which fish tissue concentrations that exceeded their respective median values are used to determine co-occurrence at elevated concentrations. This analysis (Figure 4) revealed that the most common mode of co-occurrence (fish from 32% of river sites with concentrations above the median for any compound) was for all four compound groups to co-occur at concentrations above their respective weighted medians. The next highest category of co-occurrence (16%) was for any three compound groups to co-occur above their median concentrations. PCBs co-occurred with PBDEs in 11% of sampled populations; chlordane with total DDT and PCBs with total DDT each co-occurred in 10% of the sampled population above the medians for these compound groups. The rarity was for these contaminants to occur singly above the median concentrations as was the case for PCBs in 4%, PBDEs and chlordane each in 5%, and total DDT in 7% of samples from the sampled population of rivers.

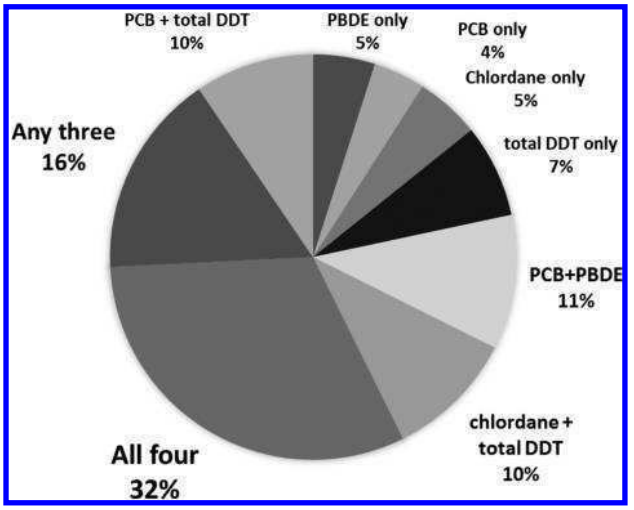

Figure 4. Co-occurrence of PCBs, PBDEs, chlordane, and DDT above respective median values in fish tissue samples from major U.S. Rivers.

The extent of co-occurrence of these compounds at relatively elevated concentrations underscores the exposure risk that is posed by their presence in fish tissue. The U.S. EPA has

DOI: 10.1021/acs.est.6b05162
Environ. Sci. Technol. 2017, 51, 3021−3031

provided approaches to quantify the toxicity of combinations of contaminants based on whether the contaminants are known to have similar or dissimilar modes of toxicity.[62] For compounds with similar modes of toxicity, the doses are considered additive. For dissimilar responses, the risks are considered separately and then combined. Additive risk, however, has been poorly defined and infrequently studied, especially for legacy contaminants, such as PCBs and OCPs no longer in use, that are perceived to be a diminishing threat. Accordingly, the background environmental chemical load and the potential for such additive effects should be taken into consideration when new chemicals, including organo-halogen compounds such as brominated flame retardants or chlorinated antimicrobials, are discharged to surface waters.

Nationally representative data on the occurrence of organic contaminants in fillet tissue of fish from U.S. rivers indicate that PCBs, PBDEs, chlordane, and DDT are still pervasive. PCBs, PBDEs, and total DDT occur at significantly higher concentrations in fish from urban rivers; however, the distribution of chemical groups varies more among the ecoregions. Co-occurrence in fish tissue at concentrations above the medians is typically observed, most frequently (32%) with all four of the chemical classes. This indicates that monitoring of fish tissue for assessment, fish consumption advisories, and the protection of aquatic life continues to be important for both new and legacy organic compounds. Individual organo-halogen compounds seldom occur alone in fish tissue. Therefore, these analytical results should be viewed in the context of co-occurring compounds and assessments of risk to human health and aquatic life that reflect the integrated chemical burden in fish. Any new organo-halogen compounds introduced to the environment will likely add to the existing overall burden of such compounds in fish tissue, since this work has demonstrated that POPs concentrations measured in fish potentially consumed by humans and representative avian and mammalian species still exceed human health SVs and WVs in many U.S. waters today.

■ ASSOCIATED CONTENT

Supporting Information

The Supporting Information is available free of charge on the ACS Publications website at DOI: 10.1021/acs.est.6b05162.

Additional information as noted in the text (PDF)
Tables S1, S2, S3, and S4 (XLSX)

■ AUTHOR INFORMATION

Corresponding Author

*Phone: 202-566-0367; e-mail: wathen.john@epa.gov.

ORCID

Angela L. Batt: 0000-0002-7008-249X

Notes

The authors declare no competing financial interest.

■ ACKNOWLEDGMENTS

This paper has been subjected to review and approved for publication by U.S. EPA's Office of Research and Development and U.S. EPA's Office of Water. The views expressed in this article are those of the authors and do not necessarily reflect the views or policies of the U.S. EPA. Mention of trade names or commercial products does not constitute endorsement or recommendation for use. Additional information for the NRSA program is publically available at https://www.epa.gov/national-aquatic-resource-surveys/nrsa, with additional fish tissue indicator information being available at https://www.epa.gov/fish-tech/fish-tissue-data-collected.epa. The authors would like to acknowledge the many federal and state agencies, and contract crews for their assistance in sample collection; Leanne Stahl, in her role as the U.S. EPA project manager for the 2008-2009 NRSA fish tissue indicator; Ellen Tarquinio and Sarah Lehmann (from the U.S. EPA) for their efforts in executing the larger NRSA study; Blaine Snyder of Tetra Tech and Harry McCarty of CSRA for their technical support; and Lisa Larimer (U.S. EPA) and Leanne Stahl for their reviews of this manuscript. Fish tissue homogenization was performed by GLEC and Dynamac Corporation staff, and sample analysis was performed by staff at Dynamac Corporation, including Gerilyn Ahlers, Michael Eastham, Hayden Miracle, Amy Parks, Ervin O'Bryan, Dan Tettenhorst, Sarah Watson, Jayme Webb-Turbeville, and Tracy Webb-Turbeville.

■ REFERENCES

(1) Muir, D. C. G.; de Wit, C. A. Trends of legacy and new persistent organic pollutants in the circumpolar arctic: Overview, conclusions, and recommendations. *Sci. Total Environ.* **2010**, *408* (15), 3044−3051.

(2) de Wit, C. A. An overview of brominated flame retardants in the environment. *Chemosphere* **2002**, *46* (5), 583−624.

(3) Ming-ch'eng Adams, C. I.; Baker, J. E.; Kjellerup, B. V. Toxicological effects of polychlorinated biphenyls (PCBs) on freshwater turtles in the United States. *Chemosphere* **2016**, *154*, 148−154.

(4) U.S. EPA. *Technical Fact Sheet − Polybrominated Diphenyl Ethers (PBDEs) and Polybrominated Biphenyls (PBBs)*, EPA 505-F-14-006; Office of Solid Waste and Emergency Response 2014.

(5) Carson, R.; Darling, L.; Darling, L. *Silent spring*; Houghton Mifflin; Riverside Press: Boston; Cambridge, MA, 1962.

(6) U.S.EPA Ban of DDT. http://www2.epa.gov/aboutepa/ddt-ban-takes-effect (accessed 12/21/15).

(7) Eriksson, P.; Fischer, C.; Fredriksson, A. Polybrominated diphenyl ethers, A group of brominated flame retardants, can interact with polychlorinated biphenyls in enhancing developmental neurobehavioral defects. *Toxicol. Sci.* **2006**, *94* (2), 302−309.

(8) Leijs, M. M.; Koppe, J. G.; Olie, K.; Van Aalderen, W. M. C.; de Voogt, P.; ten Tusscher, G. W. Effects of dioxins, PCBs, and PBDEs on immunology and hematology in adolescents. *Environ. Sci. Technol.* **2009**, *43* (20), 7946−7951.

(9) Ping, He; Aiguo, Wang; Qiang, Niu; Lijuan, Guo; Tao, Xia; Xuemin, Chen Toxic effect of PBDE-47 on thyroid development, learning, and memory, and the interaction between PBDE-47 and PCB153 that enhances toxicity in rats. *Toxicol. Ind. Health* **2011**, *27* (3), 279−288.

(10) Ross, G. The public health implications of polychlorinated biphenyls (PCBs) in the environment. *Ecotoxicol. Environ. Saf.* **2004**, *59* (3), 275−291.

(11) Vos, J. G.; Dybing, E.; Greim, H. A.; Ladefoged, O.; Lambré, C.; Tarazona, J. V.; Brandt, I.; Vethaak, A. D. Health effects of endocrine-disrupting chemicals on wildlife, with special reference to the European situation. *Crit. Rev. Toxicol.* **2000**, *30* (1), 71−133.

(12) Makey, C. M.; McClean, M. D.; Braverman, L. E.; Pearce, E. N.; He, X. M.; Sjödin, A.; Weinberg, J. M.; Webster, T. F. Polybrominated diphenyl ether exposure and thyroid function tests in North American adults. *Environ. Health Perspect.* **2016**, *124*, 420−425.

(13) Gosavi, R. A.; Knudsen, G. A.; Birnbaum, L. S.; Pedersen, L. C. Mimicking of estradiol binding by flame retardants and their metabolites: a crystallographic analysis. *Environ. Health Perspect.* **2013**, *121*, 1194−1199.

(14) Sagiv, S. K.; Nugent, J. K.; Brazelton, T. B.; Choi, A. L.; Tolbert, P. E.; Altshul, L. M.; Korrick, S. A. Prenatal organochlorine exposure and measures of behavior in infancy using the neonatal behavioral

DOI: 10.1021/acs.est.6b05162
Environ. Sci. Technol. 2017, 51, 3021−3031

assessment scale (NBAS). *Environ. Health Perspect.* **2008**, *116* (5), 666−673.
(15) Sagiv, S. K.; Thurston, S. W.; Bellinger, D. C.; Tolbert, P. E.; Altshul, L. M.; Korrick, S. A. Prenatal organochlorine exposure and behaviors associated with attention deficit hyperactivity disorder in school-aged children. *Am. J. Epidemiol.* **2010**, *171* (5), 593−601.
(16) Abballe, A.; Ingelido, A. M.; De Felip, E., Temporal trends of POPs in human milk from Italy. In *Global Contamination Trends of Persistent Organic Chemicals*, Lam, P. K. S., Ed.; CRC Press: Boca Raton, FL, 2011; pp 381−392.
(17) Adetona, O.; Horton, K.; Sjodin, A.; Jones, R.; Hall, D. B.; Aguillar-Villalobos, M.; Cassidy, B. E.; Vena, J. E.; Needham, L. L.; Naeher, L. P. Concentrations of select persistent organic pollutants across pregnancy trimesters in maternal and in cord serum in Trujillo, Peru. *Chemosphere* **2013**, *91* (10), 1426−1433.
(18) Amodio, E.; Turci, R.; Massenti, M. F.; Di Gaudio, F.; Minoia, C.; Vitale, F.; Firenze, A.; Calamusa, G. Serum concentrations of persistent organic pollutants (POPs) in the inhabitants of a Sicilian city. *Chemosphere* **2012**, *89* (8), 970−974.
(19) Ohta, S.; Ishizuka, D.; Nishimura, H.; Nakao, T.; Aozasa, O.; Shimidzu, Y.; Ochiai, F.; Kida, T.; Nishi, M.; Miyata, H. Comparison of polybrominated diphenyl ethers in fish, vegetables, and meats and levels in human milk of nursing women in Japan. *Chemosphere* **2002**, *46* (5), 689−696.
(20) Zhang, K.; Wei, Y.-L.; Zeng, E. Y. A review of environmental and human exposure to persistent organic pollutants in the Pearl River Delta, South China. *Sci. Total Environ.* **2013**, *463*−*464*, 1093−1110.
(21) Stapleton, H. M.; Eagle, S.; Sjödin, A.; Webster, T. F. Serum PBDEs in a North Carolina toddler cohort: Associations with handwipes, house dust, and socioeconomic variables. *Environ. Health Perspect.* **2012**, *120* (7), 1049−1054.
(22) Blocksom, K. A.; Walters, D. M.; Jicha, T. M.; Lazorchak, J. M.; Angradi, T. R.; Bolgrien, D. W. Persistent organic pollutants in fish tissue in the mid-continental great rivers of the United States. *Sci. Total Environ.* **2010**, *408* (5), 1180−1189.
(23) Byer, J. D.; Lebeuf, M.; Trottier, S.; Raach, M.; Alaee, M.; Stephen Brown, R.; Backus, S.; Casselman, J. M.; Hodson, P. V. Trends of persistent organic pollutants in American eel (*Anguilla rostrata*) from eastern Lake Ontario, Canada, and their potential effects on recruitment. *Sci. Total Environ.* **2015**, *529*, 231−242.
(24) Elliott, J. E.; Brogan, J.; Lee, S. L.; Drouillard, K. G.; Elliott, K. H. PBDEs and other POPs in urban birds of prey partly explained by trophic level and carbon source. *Sci. Total Environ.* **2015**, *524*−*525*, 157−165.
(25) Rigét, F.; Vorkamp, K.; Bossi, R.; Sonne, C.; Letcher, R. J.; Dietz, R. Twenty years of monitoring of persistent organic pollutants in Greenland biota. A review. *Environ. Pollut.* **2016**, *217*, 114−23.
(26) Stahl, L. L.; Snyder, B. D.; Olsen, A. R.; Pitt, J. L. Contaminants in fish tissue from US lakes and reservoirs: a national probabilistic study. *Environ. Monit. Assess.* **2009**, *150* (1), 3−19.
(27) Stahl, L. L.; Snyder, B. D.; Olsen, A. R.; Walters, L. S. A national probabilistic study of polybrominated diphenyl ethers in fish from US lakes and reservoirs. *Environ. Monit. Assess.* **2013**, *185* (12), 10351−10364.
(28) Stone, D. Polybrominated diphenyl ethers and polychlorinated biphenyls in different tissue types from Chinook salmon (*Oncorhynchus tshawytscha*). *Bull. Environ. Contam. Toxicol.* **2006**, *76* (1), 148−154.
(29) Zhou, Y.; Asplund, L.; Yin, G.; Athanassiadis, I.; Wideqvist, U.; Bignert, A.; Qiu, Y.; Zhu, Z.; Zhao, J.; Bergman, Å. Extensive organohalogen contamination in wildlife from a site in the Yangtze River Delta. *Sci. Total Environ.* **2016**, *554*−*555*, 320−328.
(30) Walters, D. M.; Mills, M. A.; Cade, B. S.; Burkard, L. P. Trophic magnification of PCBs and its relationship to the Octanol−water partition coefficient. *Environ. Sci. Technol.* **2011**, *45* (9), 3917−3924.
(31) Gasull, M.; Bosch de Basea, M.; Puigdomènech, E.; Pumarega, J.; Porta, M. Empirical analyses of the influence of diet on human concentrations of persistent organic pollutants: A systematic review of all studies conducted in Spain. *Environ. Int.* **2011**, *37* (7), 1226−1235.
(32) Long, M.; Knudsen, A.-K. S.; Pedersen, H. S.; Bonefeld-Jørgensen, E. C. Food intake and serum persistent organic pollutants in the Greenlandic pregnant women: The ACCEPT sub-study. *Sci. Total Environ.* **2015**, *529*, 198−212.
(33) Schecter, A.; Colacino, J.; Haffner, D.; Patel, K.; Opel, M.; Päpke, O.; Birnbaum, L. Perfluorinated Compounds, Polychlorinated Biphenyls, and Organochlorine Pesticide Contamination in Composite Food Samples from Dallas, Texas, USA. *Environ. Health Perspect* **2010**, *118*, 796−802.
(34) Wathen, J. B.; Lazorchak, J. M.; Olsen, A. R.; Batt, A. A national statistical survey assessment of mercury concentrations in fillets of fish collected in the U.S. EPA national rivers and streams assessment of the continental USA. *Chemosphere* **2015**, *122*, 52−61.
(35) Batt, A. L.; Kincaid, T. M.; Kostich, M. S.; Lazorchak, J. M.; Olsen, A. R. Evaluating the extent of pharmaceuticals in surface waters of the United States using a national-scale rivers and streams assessment survey. *Environ. Toxicol. Chem.* **2016**, *35* (4), 874−881.
(36) Stahl, L. L.; Snyder, B. D.; Olsen, A. R.; Kincaid, T. M.; Wathen, J. B.; McCarty, H. B. Perfluorinated compounds in fish from U.S. urban rivers and the Great Lakes. *Sci. Total Environ.* **2014**, *499*, 185−195.
(37) U.S. EPA. *Guidance for Assessing Chemical Contaminant Data for Use in Fish Advisories; Risk Assessment and Fish Consumption Limits*, EPA 823-B-00-008, 3rd ed. Office of Water: Washington DC, 2000.
(38) California EPA. *Development of Fish Contaminant Goals and Advisory Tissue Levels for Common Contaminants in California Sport Fish: Polybrominated Diphenyl Ethers (PBDEs)*; Pesticide and Environmental Toxicology Branch, Office of Environmental Health Hazard Assessment: Oakland CA, 2011.
(39) U.S. EPA. *Rivers and Streams Assessment 2008−2009 A Collaborative Survey*. Office of Water, Office of Wetlands, Oceans, and Watersheds: Washington, DC, 2013. EPA/841/D-13/001.
(40) Strahler, A. N. Quantitative analysis of watershed geomorphology. *Trans., Am. Geophys. Union* **1957**, *8* (6), 913−920.
(41) U.S.EPA Watershed Assessment, Tracking & Environmental Results System (WATERS). http://water.epa.gov/scitech/datait/tools/waters/index.cfm.
(42) Stevens, D. L.; Olsen, A. R. Spatially Restricted Surveys over Time for Aquatic Resources. *J. Agric. Biol. Environ. Stat.* **1999**, *4* (4), 415−428.
(43) Stevens, D. L.; Olsen, A. R. Spatially Balanced Sampling of Natural Resources. *J. Am. Stat. Assoc.* **2004**, *99* (465), 262−278.
(44) Olsen, A. R.; Snyder, B. D.; Stahl, L. L.; Pitt, J. L. Survey design for lakes and reservoirs in the United States to assess contaminants in fish tissue. *Environ. Monit. Assess.* **2009**, *150* (1−4), 91−100.
(45) U.S. EPA. *National Rivers and Streams Assessment Field Operations Manual*, EPA-841-B-07-009; Office of Environmental Information, Office of Water: Washington, DC, 2009.
(46) U.S. Government. *Code of Federal Regulations. Title 40 − Protection of Environment Subchapter D − Water Programs Part 136 − Guidlines Establishing Test Procedures for the Analysis of Pollutants. Appendix B to Part 136 − Definition and Procedure for the Determination of the Method Detection Limit-Revision 1.11*, Washington, D.C., 2011.
(47) U.S. EPA. *spsurvey: Spatial Survey Design and Analysis. R package version 3.1*, 2015.
(48) RCoreTeam. *R: A Language and Environment for Statistical Computing*; R Foundation for Statistical Computing: Vienna, Austria, https://www.R-project.org/.
(49) U.S. EPA. *Wadeable Streams Assessment*, Office of Water, EPA 841-B-06-002; Office of Environmental Information: Washington, DC, 2006.
(50) Lazorchak, J. M.; McCormick, F. H.; Henry, T. R.; Herlihy, A. T. Contamination of fish in streams of the Mid-Atlantic Region: An approach to regional indicator selection and wildlife assessment. *Environ. Toxicol. Chem.* **2003**, *22* (3), 545−553.
(51) Environment Canada. *Canadian Environmental Protection Act, 1999 Federal Environmental Quality Guidelines Polybrominated Diphenyl Ethers (PBDEs)*, 2013; http://www.ec.gc.ca/ese-ees/05DF7A37-60FF-403F-BB37-0CC697DBD9A3/FEQG_PBDE_EN.pdf.

DOI: 10.1021/acs.est.6b05162
Environ. Sci. Technol. 2017, 51, 3021−3031

(52) U.S. Department of Energy. *Estimation of Whole-Fish Contaminant Concentrations from Fish Fillet Data*. Office of Environmental Management: Oakridge, Tenessee, 1997. U.S. DOE ES/ER/TM-202; https://rais.ornl.gov/documents/tm202.pdf.
(53) USGS. *Concentrations, Loads, and Sources of Polychlorinated Biphenyls, Neponset River and Neponset River Estuary, Eastern Massachusetts*. Scientific Investigations Report 2011−5004 Version 1.1, 2014.
(54) USGS. *Regression Model for Explaining and Predicting Concentrations of Dieldrin in Whole Fish from United States Streams*. Scientific Investigations Report 2006−5020.
(55) Thompson, M. R.; Boekelheide, K. Multiple environmental chemical exposures to lead, mercury and polychlorinated biphenyls among childbearing-aged women (NHANES 1999−2004): Body burden and risk factors. *Environ. Res.* **2013**, *121*, 2351.
(56) McFarland, V. A.; Clarke, J. U. Environmental occurrence, abundance, and potential toxicity of polychlorinated biphenyl congeners: considerations for a congener-specific analysis. *Environ. Health Perspect.* **1989**, *81*, 225−239.
(57) Bhavsar, S. P.; Gandhi, N.; Gewurtz, S. B.; Tomy, G. T. Fate of PBDEs in Juvenile Lake Trout Estimated Using a Dynamic Multichemical Fish Model. *Environ. Sci. Technol.* **2008**, *42* (10), 3724−3731.
(58) Carlson, D. L.; Vault, D. S. D.; Swackhamer, D. L. On the Rate of Decline of Persistent Organic Contaminants in Lake Trout (Salvelinus namaycush) from the Great Lakes, 1970−2003. *Environ. Sci. Technol.* **2010**, *44* (6), 2004−2010.
(59) U.S.EPA. Technology Transfer Network − Clordane; http://www3.epa.gov/ttn/atw/hlthef/chlordan.html (accessed 12/19/15).
(60) Phillips, P. J.; Nowell, L. H.; Gilliom, R. J.; Nakagaki, N.; Murray, K. R.; VanAlstyne, C. Composition, distribution, and potential toxicity of organochlorine mixtures in bed sediments of streams. *Sci. Total Environ.* **2010**, *408*, 594−606.
(61) Samara, F.; Tsai, C. W.; Aga, D. S. Determination of potential sources of PCBs and PBDEs in sediments of the Niagara River. *Environ. Pollut.* **2006**, *139* (3), 489−497.
(62) U.S. EPA. *Guidance for Conducting Health Risk Assessment of Chemical Mixtures*,Risk Assessment Forum Technical Panel, Office of Research and Development, Office of Pesticide Programs, NCEA-C-0148; Office of Pollution Prevention and Toxics and Office of Water: Washington, DC, 1999.

DOI: 10.1021/acs.est.6b05162
Environ. Sci. Technol. 2017, 51, 3021−3031

Science of the Total Environment 499 (2014) 185–195

Contents lists available at ScienceDirect

Science of the Total Environment

journal homepage: www.elsevier.com/locate/scitotenv

Perfluorinated compounds in fish from U.S. urban rivers and the Great Lakes

Leanne L. Stahl [a,1], Blaine D. Snyder [b], Anthony R. Olsen [c], Thomas M. Kincaid [c], John B. Wathen [a], Harry B. McCarty [d]

[a] U.S. Environmental Protection Agency, OW/Office of Science and Technology, 1200 Pennsylvania Avenue, NW (MC 4305), Washington DC 20460, USA
[b] Tetra Tech Inc., Center for Ecological Sciences, 400 Red Brook Boulevard, Suite 200, Owings Mills, MD 21117, USA
[c] ORD/National Health and Environmental Effects Laboratory, Western Ecology Division, 200 S.W. 35th Street, Corvallis, OR 97333, USA
[d] CSC, 6361 Walker Lane, Alexandria, VA 22310, USA

HIGHLIGHTS

- Probability-based surveys allowed the characterization of PFCs in U.S. fish.
- PFOS dominated in frequency of occurrence in fish fillets.
- Cumulative distributions quantified PFOS in fish versus the sampled population.
- PFOS human health screening values (SVs) were applied to fillet results.
- We estimate the proportion of rivers and Great Lakes with fish that exceed SVs.

ARTICLE INFO

Article history:
Received 25 June 2014
Received in revised form 31 July 2014
Accepted 31 July 2014
Available online 2 September 2014

Editor: D. Barcelo

Keywords:
Fish tissue
Perfluorinated compounds
Urban rivers
Great Lakes
Probabilistic survey

ABSTRACT

Perfluorinated compounds (PFCs) have recently received scientific and regulatory attention due to their broad environmental distribution, persistence, bioaccumulative potential, and toxicity. Studies suggest that fish consumption may be a source of human exposure to perfluorooctane sulfonate (PFOS) or long-chain perfluorocarboxylic acids. Most PFC fish tissue literature focuses on marine fish and waters outside of the United States (U.S.). To broaden assessments in U.S. fish, a characterization of PFCs in freshwater fish was initiated on a national scale using an unequal probability design during the U.S. Environmental Protection Agency's (EPA's) 2008–2009 National Rivers and Streams Assessment (NRSA) and the Great Lakes Human Health Fish Tissue Study component of the 2010 EPA National Coastal Condition Assessment (NCCA/GL). Fish were collected from randomly selected locations—164 urban river sites and 157 nearshore Great Lake sites. The probability design allowed extrapolation to the sampled population of 17,059 km in urban rivers and a nearshore area of 11,091 km^2 in the Great Lakes. Fillets were analyzed for 13 PFCs using high-performance liquid chromatography tandem mass spectrometry. Results showed that PFOS dominated in frequency of occurrence, followed by three other longer-chain PFCs (perfluorodecanoic acid, perfluoroundecanoic acid, and perfluorododecanoic acid). Maximum PFOS concentrations were 127 and 80 ng/g in urban river samples and Great Lakes samples, respectively. The range of NRSA PFOS detections was similar to literature accounts from targeted riverine fish sampling. NCCA/GL PFOS levels were lower than those reported by other Great Lakes researchers, but generally higher than values in targeted inland lake studies. The probability design allowed development of cumulative distribution functions (CDFs) to quantify PFOS concentrations versus the sampled population, and the application of fish consumption advisory guidance to the CDFs resulted in an estimation of the proportion of urban rivers and the Great Lakes that exceed human health protection thresholds.

© 2014 Published by Elsevier B.V.

1. Introduction

Perfluorinated compounds (PFCs) are a group of organic chemicals characterized by fluorine atoms bonded to carbon atoms and perfluoroalkyl substances are a subset of PFCs in which all of the hydrogen atoms of an alkane or substituted alkane have been replaced by

E-mail addresses: stahl.leanne@epa.gov (L.L. Stahl), blaine.snyder@tetratech.com (B.D. Snyder), olsen.tony@epa.gov (A.R. Olsen), kincaid.tom@epa.gov (T.M. Kincaid), wathen.john@epa.gov (J.B. Wathen), hmccarty@csc.com (H.B. McCarty).
[1] Tel.: +1 202 566 0404.

http://dx.doi.org/10.1016/j.scitotenv.2014.07.126
0048-9697/© 2014 Published by Elsevier B.V.

fluorine atoms (Buck et al., 2011). Many PFCs have physical properties that make them useful for many consumer and industrial applications, including stain- and water-resistant coatings for carpets and fabric, water- and oil-resistant coatings for paper products, fire-fighting foams, hydraulic fluids, and emulsifiers for photographic film production (Renner, 2001). Naturally occurring fluorinated organic compounds are rare (Lau et al., 2007); however, thousands of different PFCs have been manufactured and used by industry since commercial production began in the 1950s (Lindstrom et al., 2011). Industrial and commercial PFCs include a large number of compounds, such as perfluorocarboxylates, perfluorosulfonates, perfluorosulfonamides, fluorotelomer acids, and fluorotelomer alcohols, among others (Murphy et al., 2012). The global annual production volume of perfluorooctane sulfonate (PFOS) was 3500 metric tons in 2000 and perfluorooctanoic acid (PFOA) production reached 1200 metric tons in 2004 (Lau et al., 2007). PFCs may be released into the environment during manufacture, storage and transport, product use, or disposal (Paul et al., 2008). As a result of their extensive production and use, they have become widely distributed in the environment and detected in water, air, food, wildlife, and humans (Ahrens, 2011).

PFCs can bioaccumulate through food webs and have a long half-life in humans (Houde et al., 2011; Lindstrom et al., 2011). Bioaccumulative potential tends to be higher in longer-chain PFCs than in those with seven or less carbon atoms. Perfluorinated sulfonates have a greater tendency to bioaccumulate than perfluorinated carboxylates, even when their chain lengths are identical (Murphy et al., 2012). Although the highest concentrations of PFCs are typically associated with direct industrial emissions, Giesy and Kannan (2001) observed global distribution of perfluorooctane sulfonate (PFOS) in wildlife, and other researchers have detected PFCs in bird and mammal species taken from remote Arctic regions (Martin et al., 2004a; Butt et al., 2010; Rotander et al., 2012). Houde et al. (2011) reported that recent (2006–2010) monitoring studies focused on PFCs of a variety of chain lengths and configurations; however, PFOS proved to be the predominant PFC detected in species, tissues, and locations around the world.

PFCs are recognized as contaminants of emerging concern (CECs) because they are toxic, ubiquitous, and persistent in the environment (Ahrens, 2011; Houde et al., 2011; Kannan, 2011; Lindstrom et al., 2011). Researchers first noted their broad environmental distribution in the early 2000s (Giesy and Kannan, 2001). Over the past 10 years, high levels of PFCs have been found in surface waters near PFC facilities, wastewater treatment plants, and urban centers, as well as in groundwater in urban areas (Zushi et al., 2012). Investigations of the routes of human exposure to PFCs (e.g., drinking water, dust from upholstered furniture and carpets, food, food packaging, and non-stick cookware) began in the early to mid-2000s and continue today (Taniyasu et al., 2003; Kannan et al., 2004; Lau et al., 2007). The earliest studies of PFCs in humans focused on occupational exposure of workers and manufacturers (Olsen et al., 2003). Studies in industrialized countries worldwide (Kannan et al., 2004; Kuklenyik et al., 2004; Guruge et al., 2005; Lau et al., 2007) indicate that PFCs were present in human blood serum samples from the general population, with highest concentrations reported for PFOS and PFOA. Modeling studies conducted by Fromme et al. (2009) estimated that low level PFC contamination of food may be responsible for most non-occupational exposures in industrialized countries, although there is still uncertainty associated with the role of food as an exposure pathway. Recent studies (Hart et al., 2008; Haug et al., 2010; Holzer et al., 2011) suggest that the consumption of fish from contaminated waters may be a major source of exposure to PFOS or long-chain perfluorocarboxylic acids for some people and that there is still much to learn about PFCs in food sources. Sinclair et al. (2006) found average PFOS concentrations in fish to be 8850-fold greater than levels in surface waters of New York State (i.e., Lake Ontario, Lake Erie, the Finger Lakes, Lake Onondaga, the Erie Canal, the Hudson River, and Lake Champlain), and noted that more information is needed on PFCs in sport fish to assess the risk of potential exposure of humans to these compounds.

Studies of birds, fish, and mammals have shown that PFCs bind to proteins in blood and livers (Jones et al., 2003) and are not lipophilic like many other organic pollutants (Conder et al., 2008). Laboratory animal studies on the toxic effects of PFCs (primarily PFOS and PFOA) show various effects on development, reproduction, and immune function (Murphy et al., 2012). Epidemiological and medical surveillance studies of humans who were occupationally exposed to PFOS or PFOA were summarized in USEPA, 2005, and in general there was no consistent association between PFC blood serum levels and adverse health effects (Steenland et al., 2010; Lindstrom et al., 2011). Recent research by Shankar et al. (2012) found that serum PFOA levels were positively associated with cardiovascular disease and peripheral arterial disease in U.S. adults. Apelberg et al. (2007) found a negative correlation between PFC concentrations in umbilical cord serum and the body weight of newborn babies in the U.S.; however, further study is needed to evaluate the risk of PFCs to infants (Zushi et al., 2012). A study of children (Grandjean et al., 2012) indicated that increased PFOA and PFOS

Fig. 1. National Rivers and Streams Assessment urban river fish tissue sampling locations (164).

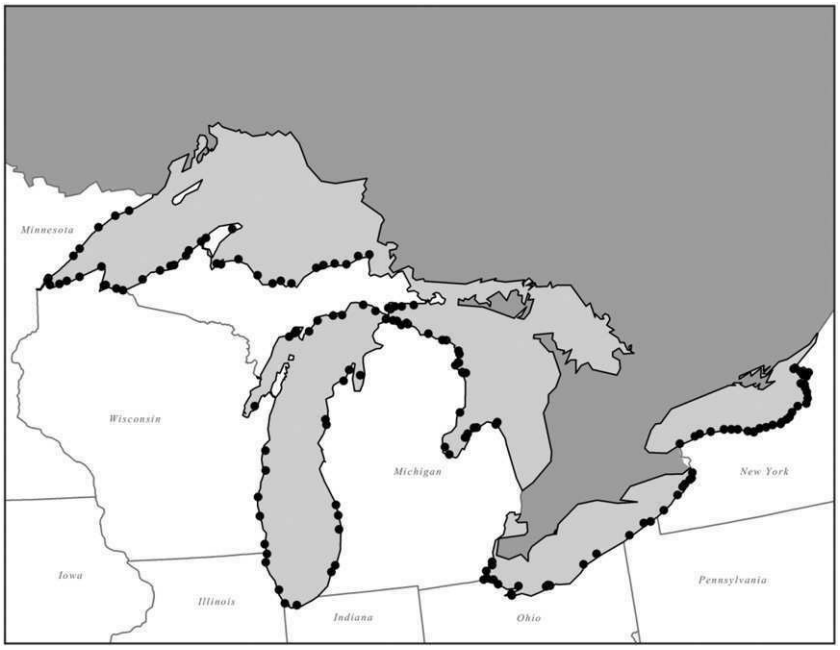

Fig. 2. Great Lakes Human Health Fish Tissue Study sampling locations (157).

exposures were associated with decreased immune response to routine immunizations for children in the five to seven year age group. A 2005–2013 epidemiological study (the C8 Health Project) found probable links between elevated PFOA levels in human blood and ulcerative colitis, thyroid diseases, testicular cancer, kidney cancer, and pre-eclampsia (Frisbee et al., 2009; Steenland et al., 2010; Watkins et al., 2013). Concerns remain about the possible human health effects of PFCs due to the continued use of PFOS, PFOA, and the newer PFCs being introduced as substitutes and to the relatively long half-life of these compounds in humans (e.g., 8.5 year half-life of PFHxS in humans) (Olsen et al., 2007).

Concerns regarding the toxicity of PFCs and their ubiquity in the environment led the U.S. Environmental Protection Agency (EPA) to work with 3M (a leading producer of PFOS) beginning in 2000 to voluntarily phase out production of PFOS and related chemicals in 2002 (Lindstrom et al., 2011; Zushi et al., 2012). Beginning in the same time period, a series of Significant New Use Rules were issued to limit production of PFOS and precursor chemicals in the U.S. (USEPA, 2002). The European Union banned the use of PFOS and its derivatives beginning in 2008 (EU, 2006). In 2009, production and use of PFOS and its precursor perfluorooctyl sulfonyl fluoride were restricted under the Stockholm Convention on Persistent Organic Pollutants. EPA established a PFOA Stewardship Program working with eight major companies toward a 95% reduction in emissions and product contents of PFOA and long-chain PFCs by no later than 2010, and elimination of those emissions by 2015. Despite the restrictions, these compounds are still produced by manufacturers in other parts of the world and enter into the U.S. with imported products. In addition, PFC precursors produced in the U.S. can break down to persistent degradation products that will continue to be contaminants of concern (Murphy et al., 2012; Ahrens, 2011).

To broaden the assessment of CECs in U.S. fish, a comprehensive characterization of PFC contamination in freshwater fish was initiated on a national scale during the U.S. EPA's 2008–09 National Rivers and Streams Assessment (NRSA) (USEPA, 2010a) and during the Great Lakes Human Health Fish Tissue Study component of the 2010 EPA National Coastal Condition Assessment (NCCA/GL) (USEPA, 2010b). For the NRSA, a framework of 1,800 sampling locations contained a statistically representative subset of 164 urban river sites that were 5th order or greater in size based on Strahler stream order classification (Strahler, 1957). Fish were collected at this subset of urban river sites to allow the first nationally representative assessment of PFCs using a

Table 1
Target compounds.

Abbreviation	Name	Formula	Carbon chain length	CAS number[a]	Labeled analog
PFBA	Perfluorobutyric acid	C_3F_7COOH	3	375-22-4	$^{13}C_4$-PFBA [b,c]
PFBS	Perfluorobutane sulfonate	$C_4F_9SO_3$	4	375-73-5[a]	[d]
PFPeA	Perfluoropentanoic acid	C_4F_9COOH	4	2706-90-3	$^{13}C_5$-PFPeA [c]
PFHxA	Perfluorohexanoic acid	$C_5F_{11}COOH$	5	307-24-4	$^{13}C_2$-PFHxA [b,c]
PFHxS	Perfluorhexane sulfonate	$C_6F_{13}SO_3$	6	355-46-4[a]	$^{18}O_2$-PFHxS [c]
PFHpA	Perfluoroheptanoic acid	$C_6F_{13}COOH$	6	375-85-9	$^{13}C_4$-PFHpA [c]
PFOA	Perfluorooctanoic acid	$C_7F_{15}COOH$	7	335-67-1	$^{13}C_4$-PFOA [b,c]
PFOS	Perfluorooctane sulfonate	$C_8F_{17}SO_3$	8	1763-23-1[a]	$^{13}C_4$-PFOS [b,c]
PFOSA	Perfluorooctanesulfonamide	$C_8F_{17}SO_2NH_2$	8	754-91-6	$^{13}C_8$-PFOSA [c]
PFNA	Perfluorononanoic acid	$C_8F_{17}COOH$	8	375-95-1	$^{13}C_5$-PFNA [b,c]
PFDA	Perfluorodecanoic acid	$C_9F_{19}COOH$	9	335-76-2	$^{13}C_2$-PFDA [b,c]
PFUnA	Perfluoroundecanoic acid	$C_{10}F_{21}COOH$	10	2058-94-8	$^{13}C_2$-PFUnA [c]
PFDoA	Perfluorododecanoic acid	$C_{11}F_{23}COOH$	11	307-55-1	$^{13}C_2$-PFDoA [b,c]

[a] CAS number for the parent acid form.
[b] Labeled compound used in the NRSA analysis.
[c] Labeled compound used in the NCCA/GL analysis.
[d] No labeled analog was available for PFBS, so this analyte was quantified using the response for $^{18}O_2$-PFHxS in both studies.

Table 2
Summary of instrumental analysis conditions by study.

	NRSA	NCCA/GL
LC column	C18 reverse phase 10.0 cm × 2.1 mm ID 3.5-μm particle size	C18 reverse phase 10.0 cm × 3.0 mm ID 3.0-μm particle size
Solvent system	Gradient elution with: 90% acetonitrile in water and ammonium acetate in 0.1% acetic acid	Gradient elution with: ammonium acetate in water and methanol
Sample introduction	Negative ion electrospray ionization	Negative ion electrospray ionization
Target compound	Monitored reactions[a]	
PFBA	213 > 169	213 > 169
PFBS	299 > 80, 299 > 99	299 > 80, 299 > 99
PFPeA	263 > 219	263 > 219
PFHxA	313 > 269	313 > 269, 313 > 119
PFHxS	399 > 99, 399 > 80	399 > 99, 399 > 80
PFHpA	363 > 319	363 > 319, 363 > 169
PFOA	413 > 369, 413 > 219	413 > 369, 413 > 169
PFOS	499 > 99, 499 > 80	499 > 99, 499 > 80
PFOSA	498 > 78	498 > 78
PFNA	463 > 419	463 > 419, 463 > 169
PFDA	513 > 469	513 > 469, 513 > 169
PFUnA	563 > 519	563 > 519
PFDoA	613 > 569	613 > 569

[a] Additional ions and reactions were monitored for all of the isotopically labeled standards.

statistically based sampling design. For the NCCA/GL study, fish were collected from 157 randomly selected nearshore sites throughout the five Great Lakes. The objective of the NRSA was to estimate the national distribution of the mean levels (i.e., composite average) of PFCs in fish fillet tissue from urban rivers of the conterminous U.S. Similarly, the objective of the NCCA/GL was to estimate the regional distribution of the mean levels of PFCs in fish fillet tissue from nearshore waters of the Great Lakes within the U.S.

2. Methods

2.1. Sampling site selection

2.1.1. Urban river site selection

The NRSA fish tissue study target population consisted of urban rivers within the conterminous United States that were 5th order or greater in size, had a permanent fish population, and had flowing water during the study period (including the Great Rivers and run-of-the-river ponds, but excluding reservoirs and portions of tidal rivers up to head of salt). The sample frame was derived from the National Hydrography Dataset (NHD) and included attributes of urban land use and Strahler stream order. The urban attribute was based on NHD-Plus (USGS and USEPA, 2007) and the U.S. Census Bureau national urban boundary GIS coverages. The Census Bureau boundaries were buffered 100 m to include a majority of stream features intersecting and coincident with urban areas. Where this buffer did not completely capture all river features within the urban areas (rivers intersecting cities are excluded from the Census Bureau urban areas), the NHD-Plus river area (polygon) features were clipped at a three km buffer around the urban areas and combined with the Census Bureau buffered urban area to create the modified urban database.

Sampling sites were selected using a probability-based approach (Stevens and Olsen, 1999) described as a Generalized Random Tessellation Stratified (GRTS) survey design by Stevens and Olsen (2004). A probability design provides the basis for estimating resource extent and condition, for characterizing trends in extent or condition, and for representing spatial patterns, all with known certainty. To implement the design, the population being sampled had to be explicitly described (in this case, U.S. urban rivers), every element in the population had the opportunity to be sampled with known probability, and the selection process included an explicit random element. Since the specific purpose of the NRSA was to describe the condition of resources on a national basis, a probability-based design was an essential component of the study. Selection probabilities were defined for 5th order or larger rivers in the lower 48 states so that the expected number of urban sites would be at least 150. Fish tissue samples were collected from a total of 164 randomly selected urban rivers during the 2008 and 2009 study period (Fig. 1). That total included sampling locations in 38 states, with 49, 56, 29, and 30 sites in 5th, 6th, 7th, and 8th + order rivers, respectively.

2.1.2. Great Lakes site selection

The NCCA/GL target population included nearshore areas of U.S. waters in the Great Lakes. The GRTS survey design (Stevens and Olsen, 2004) was stratified by Great Lake and country (limited to U.S. waters). The unequal probability of selection was based on the proportion of shoreline length in each of the eight Great Lakes states (Illinois, Indiana, Michigan, Minnesota, New York, Ohio, Pennsylvania, and Wisconsin). The nearshore zone was defined as the region from the shoreline to a depth of 30 m or to a maximum distance of 5 km from the shoreline (i.e., for shallower waters of the Great Lakes). NCCA/GL sites (within the nearshore zone polygons) were randomly selected in the five Great Lakes (Lakes Superior, Michigan, Huron, Erie, and Ontario) bordered by the eight Great Lakes states. The sample frame was derived by EPA/Office of Research and Development's (ORD's) Mid-Continent Ecology Division in Duluth, Minnesota. Fish tissue samples were collected from 157 randomly selected U.S. nearshore locations during the 2010

Table 3
Method detection limits (ng/g) by study.

Chemical	NRSA	NCCA/GL[a]
PFBA	2.70	0.07
PFBS	5.69	0.10
PFPeA	1.42	0.13
PFHxA	2.34	0.07
PFHxS	10.45	0.12
PFHpA	1.25	0.09
PFOA	2.37	0.10
PFOS	5.35	0.13
PFOSA	2.70	0.08
PFNA	2.07	0.08
PFDA	2.63	0.06
PFUnA	2.76	0.11
PFDoA	1.38	0.12

[a] NCCA/GL MDL values are rounded to two decimal places.

study period (Fig. 2). This includes 38, 31, 29, 27, and 32 nearshore areas in Lakes Superior, Michigan, Huron, Erie, and Ontario, respectively.

2.2. Sample collection

Sampling efforts focused on target fish species that were ubiquitous, abundant, easily identified, commonly consumed by humans, and sufficiently large (i.e., adult specimens) to provide adequate tissue for analysis. Field teams used active methods (i.e., electrofishing) to collect fish composite samples from each site primarily during a May through September 2008 and 2009 survey period for the NRSA, and both active (e.g., hook and line) and passive (e.g., gillnetting) methods during a June through mid-November 2010 period for the NCCA/GL. Field procedures stated that each composite should target five adult fish of the same species and similar size (i.e., the smallest individual in a composite was not less than 75% of the total length of the largest individual). Composites containing fewer than five fish were accepted in an effort to retain a sample from each target river (41% of NRSA composites and 77% of NCCA/GL samples had fewer than 5 fish). Whole fish were shipped on dry ice to designated sample preparation laboratories for storage and preparation (filleting and homogenization) prior to analysis. Fish collection and handling methods have been previously described (USEPA, 2009 and USEPA, 2010c).

2.3. Sample preparation

Sample preparation procedures for NRSA and NCCA/GL fish were based on a common approach documented in USEPA, 2010c that included quality control steps to ensure that sample aliquots used for analysis were homogeneous and free from extraneous contamination. Fish were scaled and filleted in the laboratory where lateral muscle fillets from both sides of each fish were prepared with skin on and the belly flap (ventral muscle and skin) attached. Fillets were composited using the batch method, where all of the individual specimens that comprise the sample were homogenized together, regardless of the proportional weight of individual fish. Each composite was homogenized using a tissue grinder and mixed thoroughly to a fine paste of uniform color and texture. A 20-g aliquot was removed for PFC analysis and stored in a glass jar with a polytetrafluoroethylene-free lid liner.

2.4. Tissue analysis

At present, there are no standard analytical methods from EPA or any voluntary consensus standard bodies (VCSBs) for PFC analysis in any matrices. The fish tissue samples in both studies were analyzed using procedures developed and tested by commercial analytical laboratories that are currently considered proprietary, and are therefore only briefly described below.

Approximately 1–5 g of tissue were required for analysis. The sample was spiked with 7 (NRSA) or 12 (NCCA/GL) isotopically labeled standards and extracted by shaking the tissue in a caustic solution of methanol, water, and potassium hydroxide (NRSA) or sodium hydroxide (NCCA/GL). The hydroxide solution was used to break down the tissue and allowed the PFCs to be extracted into the methanol/water. After extraction, the solution was centrifuged to remove the solids and the supernatant liquid was diluted with reagent water (NRSA) or hydrochloric acid to pH <2 (NCCA/GL). The diluted extract was loaded onto a commercially available solid-phase extraction (SPE) cartridge that included a weak anion exchange resin that retained the PFCs. The PFCs were eluted from the SPE cartridge and the eluant was spiked with additional labeled standards and analyzed by high-performance liquid chromatography tandem mass spectrometry (HPLC-MS/MS) for the 13 PFCs in Table 1.

As noted above, there are no standard analytical methods for these contaminants in any matrices, and particularly fish tissue. The two commercial laboratories that analyzed these samples (one laboratory per study) utilized similar, but not identical procedures. The overall instrumental conditions are summarized in Table 2. The analytical procedures yielded results for 13 PFCs in their anion forms (e.g., $C_3F_7COO^-$); however, the results are reported for parent acid forms (e.g., C_3F_7COOH) shown in Table 1. The concentration of each PFC was determined using the responses from one of the isotopically labeled standards added prior to sample extraction, applying the technique known as isotope dilution. As a result, all of the target analyte concentrations were corrected for the recovery of the labeled standards, thereby accounting for extraction efficiencies and losses during cleanup. The recovery of each of those labeled standards was monitored using the additional labeled compounds added after extraction, but prior to analyses. Because commercial suppliers of labeled compounds developed additional

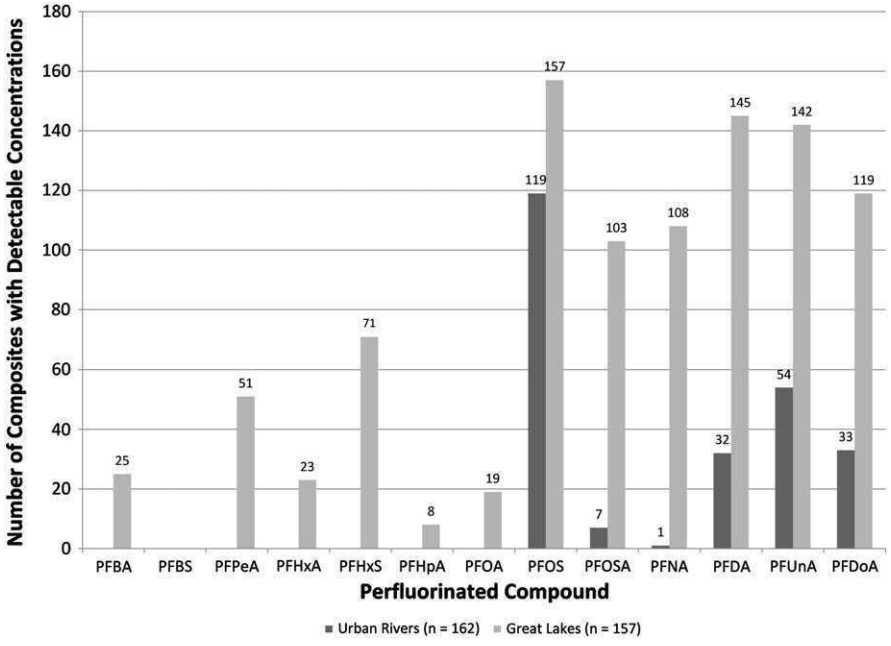

Fig. 3. Number of fish composite samples with detectable concentrations of PFCs from urban rivers (n = 162) and the Great Lakes (n = 157) (Lower chain detection differences may be attributable to lower MDLs in the analytical method applied for the NCCA/GL study).

Table 4
Percentiles for concentrations (ng/g) of PFCs detected in U.S. urban river fish tissue composites.

Chemical	Number of detects	MDL[a]	Percentile[b]				Maximum[b]	Frequency of occurrence[c]
			25th	50th	75th	90th		
PFOS	119	5.35	<MDL	10.7	27.5	41.4	127	73%
PFOSA	7	2.70	<MDL	<MDL	<MDL	<MDL	63.1	4%
PFNA	1	2.07	<MDL	<MDL	<MDL	<MDL	2.48	<1%
PFDA	32	2.63	<MDL	<MDL	<MDL	4.68	28.5	20%
PFUnA	54	2.76	<MDL	<MDL	<MDL	5.74	45.6	33%
PFDoA	33	1.38	<MDL	<MDL	<MDL	3.27	23.8	20%

[a] MDL = Method Detection Limit in ng/g.
[b] Concentrations are statistical estimates for the sampled population of river reaches defined for the study (17,509 river km) with the exception of the maximum concentrations which are maximums observed at 162 sites.
[c] Percent frequency of occurrence values are based on 162 possible PFC detections.

labeled PFCs between the two studies, more labeled compounds were used in the NCCA/GL than in the NRSA (see Table 1). Both of the analytical procedures also involved extensive quality control operations, including method blanks (i.e., aliquots of a clean reference matrix carried through the entire analytical procedure as a check for potential contamination), laboratory control samples, multi-point initial calibrations, and daily calibration verifications, with acceptance criteria for each operation. All analytical results are expressed as wet-weight concentrations in ng/g and reported down to the method detection limit (MDL).

In 1984, the MDL was defined by EPA at 40 CFR Part 136, Appendix B, based on at least seven replicate analyses of a spiked reference matrix (USEPA, 1984). It is calculated as the Student's t-value for the number of replicates multiplied by the standard deviation of the results for the analyte in all of those replicate analyses. The MDLs differed between the NRSA and NCCA/GL, with much lower MDL values for each analyte in the latter study. This difference was driven by two related factors. First, there are no formal analytical methods for determining PFC concentrations in fish tissue published by EPA or any Voluntary Consensus Standards Body. Both of the laboratories that performed the analyses for these studies developed or adapted procedures of their own for measuring PFC levels in a fish tissue matrix. Secondly, without an established method or a large body of fish tissue results, it was difficult to establish the sensitivity (e.g., detection limits) required for the 13 PFCs monitored during the NRSA analyses in 2009. By 2011, the laboratory analyzing NCCA/GL fish tissue samples for PFCs was able to refine its analytical procedures and target lower detection limits after gaining additional experience with PFC analysis in fish tissue and improved insight on expected concentrations (Table 3).

2.5. Data analysis

PFC data were analyzed using R statistical software (R Development Core Team, 2007) and the package "spsurvey" (Kincaid and Olsen, 2012). Data analysis focused on the study objective to develop estimates of the national distribution of mean levels (i.e., river mean or composite average concentrations) of PFCs in urban river fish tissue or regional estimates of mean levels (nearshore mean or composite averages) of PFCs in fish from the nearshore area of the Great Lakes.

The statistical analysis process incorporated elements of the probabilistic survey design and included: site status determination based on reconnaissance; survey design (sample) weights adjustment based on site status; target population estimation (i.e., number of sites that met the study definition of a target river or nearshore Great Lakes location); estimation of the number and proportion of sites in the sampled population (i.e., accessible target rivers or nearshore Great Lakes sites); and estimation of percentiles and cumulative distribution of tissue concentrations by chemical for the sampled population of rivers or Great Lakes locations.

The study design required application of sample weights to the tissue concentrations during data analysis. Sample weights were derived from the various inclusion probabilities assigned to the river size category (i.e., ≥5th order) and urban classification group for the NRSA or shoreline length in each of the eight Great Lakes states for the NCCA/GL. The resulting PFC distributions are described by survey analysis estimates of percentiles and cumulative distribution functions (CDFs) (Zar, 1999) using methods in spsurvey (Kincaid and Olsen, 2012). The CDFs characterize the probability distribution of PFCs in fish tissue as plots of concentrations (x-axis) versus the cumulative number and

Table 5
Percentiles for concentrations (ng/g) of PFCs detected in Great Lakes fish tissue composites.

Chemical	Number of detects	MDL[a]	Percentile[b]				Maximum[b]	Frequency of occurrence[c]
			25th	50th	75th	90th		
PFBA	25	0.07	<MDL	<MDL	<MDL	0.25	1.30	16%
PFPeA	51	0.13	<MDL	<MDL	0.27	0.68	3.00	32%
PFHxA	23	0.07	<MDL	<MDL	<MDL	0.11	0.80	15%
PFHxS	71	0.12	<MDL	<MDL	0.46	1.17	3.50	45%
PFHpA	8	0.09	<MDL	<MDL	<MDL	<MDL	1.00	5%
PFOA	19	0.10	<MDL	<MDL	<MDL	0.16	0.97	12%
PFOS	157	0.13	7.84	15.2	24.9	38.9	80.0	100%
PFOSA	103	0.08	<MDL	0.15	0.43	1.09	4.20	66%
PFNA	108	0.08	<MDL	0.32	0.78	1.60	9.70	69%
PFDA	145	0.06	0.38	0.68	1.60	2.94	13.0	92%
PFUnA	142	0.11	0.67	0.99	2.04	3.69	18.0	90%
PFDoA	119	0.12	<MDL	0.32	0.65	1.05	3.10	76%

[a] MDL = Method Detection Limit in ng/g.
[b] Concentrations are statistical estimates for the nearshore lake area sampled population defined for the study (an area of 11,091 km^2) with the exception of the maximum concentrations which are maximums observed at 157 sites.
[c] Percent frequency of occurrence values are based on 157 possible PFC detections.

Table 6
QC data summary for the NRSA samples (2093 total sample results).

QC operation	Issue	Exceptions	Implications
Multi-point Calibration	None	0	NA
Calibration Verification	None	0	NA
Method Blank Contaminants	None	0	NA
Lab Control Sample	High recovery of PFHxS may indicate high bias	1	PFHxS was not detected in any of the associated samples, so there is no high bias concern (18 field samples).
Labeled Compound Recovery	High recovery of $^{13}C_4$-PFBA may indicate potential bias for native analyte	4	PFBA was not detected in any of the associated samples, so there is no bias concern (4 field samples).
MS/MSD Recovery	None	0	NA
MS/MSD Precision	RPD >40% for PFOS	1	Possible increased uncertainty for PFOS results in the associated samples (20 field samples)

NA = Not applicable.
MS/MSD = Matrix Spike/Matrix Spike Duplicate

percentage (y-axis) of urban river reach length (km) or Great Lake nearshore area (km^2).

3. Results

3.1. Analytical results and statistical estimates

3.1.1. Urban river results

The 164 urban river sampling locations included in the NRSA (Fig. 1) were a statistically representative subset of urban rivers (5th order or greater in size) or a national random sample. Fish collection yielded 162 composite samples (682 total fish) of 25 species for PFC analysis, with three of the recommended target species representing 70% of these composites. Smallmouth bass (*Micropterus dolomieu*), largemouth bass (*Micropterus salmoides*), and channel catfish (*Ictalurus punctatus*) accounted for 34%, 25%, and 11% of the composites, respectively. The set of fillet composites analyzed for PFCs comprised a nationally representative sample whose results can be extrapolated to the sampled population of an estimated urban river length of 17,509 km.

A total of 80% of fish fillet samples contained detectable levels of PFCs; however, seven PFCs were not detected in any fish samples (Fig. 3). No detections were reported for the PFCs with seven or less carbon atoms (PFBA, PFBS, PFPeA, PFHxA, PFHxS, PFHpA, and PFOA). Frequency of occurrence was dominated by PFOS (73%), followed by three other longer-chain PFCs (33% PFUnA, 20% PFDA, and 20% PFDoA) (Table 4). Analytical results and statistical estimates for PFCs detected in urban river samples are presented in Table 4 as maxima and percentiles (ng/g, wet weight), respectively, and reported to three significant figures.

3.1.2. Great Lakes results

The 157 locations sampled for PFCs (Fig. 2) during the NCCA/GL study were a statistically representative subset of the U.S. nearshore area of the five Great Lakes. Fish collection yielded 157 composite samples (423 total fish) of 18 species for PFC analysis. Three of the recommended target species—lake trout (*Salvelinus namaycush*), smallmouth bass, and walleye (*Sander vitreus*)—accounted for 58% of the composites, or 31%, 14%, and 13%, respectively. The fillet composites analyzed for PFCs formed a regionally representative sample, the results of which can be extrapolated to a Great Lakes nearshore surface area of an estimated 11,091 km^2.

All of the NCCA/GL fish fillet samples contained detectable levels of PFCs. No detections were recorded for PFBS; however, other shorter-chain PFCs (i.e., PFBA, PFPeA, PFHxA, PFHxS, PFHpA, and PFOA) that were not detected in NRSA urban river samples were reported for NCCA/GL samples, possibly reflecting the lower NCCA/GL MDLs. Note that MDL values are, by definition, laboratory-specific, procedure- or method-specific, and analyte-specific, and they vary over time. Consistent with the NRSA urban river results, frequency of occurrence was dominated by PFOS (detected in 100% of the NCCA/GL samples) and three other longer-chain PFCs (92% PFDA, 90% PFUnA, and 76% PFDoA). Analytical results and statistical estimates for PFCs detected in

Table 7
QC data summary for the NCCA/GL samples (2041 total sample results).

QC operation	Issue	Exceptions	Implications
Multi-point Calibration	None	0	NA
Calibration Verification	None	0	NA
Method Blank Contaminants	4 PFCs identified in method blanks above the MDL	6	74 PFBA results <5× the associated method blank result were considered non-detects.
		2	34 PFOA results <5× the associated method blank result were considered non-detects.
		1	No effect for PFHxA, all field sample results were >10× the associated method blank result.
		1	2 PFUnA results <5× the associated method blank result were considered non-detects.
Lab Control Sample	High recovery of PFHxA may indicate high bias	1	PFHxA was not detected in any of the associated samples, so there is no high bias concern (14 field samples).
Labeled Compound Recovery	Low recovery	367 of 2041 labeled compound results	Most low recoveries were only marginally below the lower QC limit, and isotope dilution quantitation still functions when the recovery is lower than expected. This affected 112 of 157 PFOSA results. Reducing tissue mass extracted appeared to improve labeled compound recovery.
MS/MSD Recovery	High recovery may indicate high bias	36	15 associated sample results were not affected because the analyte was not detected in the field sample; 21 associated sample results may exhibit a slight high bias.
MS/MSD Precision	RPD >30% for PFOS	0	NA

NA = Not applicable.
MS/MSD = Matrix Spike/Matrix Spike Duplicate.

Great Lakes samples are presented in Table 5 as maxima and percentiles (ng/g, wet weight), respectively, and reported to three significant figures.

3.2. Analytical quality control results

Results from both studies were subjected to extensive review, including all of the QC results. Samples were extracted and analyzed in batches of up to 20 samples, with each batch having its own associated QC samples. All multi-point initial calibrations and daily calibration verifications met the acceptance criteria for both the NRSA and the NCCA/GL. The QC results that did not meet their respective acceptance criteria are summarized in Tables 6 and 7 for the NRSA and NCCA/GL studies, respectively, along with the implications for the data quality of the associated samples. For the NRSA, the mean recovery of the seven labeled compounds added to the samples prior to extraction was 93.3%. For the NCCA/GL, PFBA, PFOA, PFHxA, and PFUnA were detected in a number of the method blanks at concentrations above their respective MDLs. Based on the established data review procedures for both studies, when the results for an analyte in a sample are less than five times the amount reported in the associated method blank, the sample result is considered a non-detect in that sample. However, when the results for an analyte in a sample are greater than 10 times the amount reported in the associated method blank, the sample result is not considered to be affected, since any potential contribution from the method blank is likely less than 10% of the reported amount. The overall implications for the NCCA/GL results are described in Table 7.

The recoveries of the ^{13}C-labeled standards in the NCCA/GL samples were below the acceptance limit of 25% for about 18% of the 2041 labeled compound results (2041 = 13 labeled compounds × 157 samples). Compared to the NRSA, labeled compound recoveries were lower overall and more variable in the NCCA/GL, perhaps in part due to the use of five more labeled compounds. The mean recovery of the twelve labeled compounds added to the samples prior to extraction was 48.9%. Low labeled compound recoveries occurred for the labels associated with all 13 target PFCs, but many of those recoveries were only marginally below the acceptance limits (e.g., 24% versus an acceptance limit of 25%). Isotope dilution quantitation can be utilized even when the recovery of the labeled compound is less than expected. The analyte most affected in the NCCA/GL was PFOSA, where low labeled compound recoveries were noted in 112 of 157 samples; however, the results for the target compounds are still considered usable. Efforts by the laboratory to determine the cause of the low recoveries were inconclusive, but it appeared to be related to the mass of the tissue aliquot that was extracted for some, but not all, species. Ultimately, the laboratory reduced the mass of fish tissue that they extracted from 5 g to 1 g and achieved increased labeled compound recoveries.

4. Discussion

It is difficult to directly compare the results of these two studies to PFC concentrations reported in fish from other studies in the literature due to differences in sample preparation (e.g., skin-on fillets studied here versus skinless fillets or whole bodies in other literature) and analysis (i.e., target PFCs). Most other studies have also been spatially focused on a particular waterbody, or analytically focused on a particular PFC. Despite those differences, most studies, including results presented here for U.S. urban rivers and the Great Lakes, conclude that PFOS is the predominant PFC in fish tissue. In a review of PFCs in aquatic biota, Houde et al. (2011) concluded that PFOS is the predominant PFC in all species, tissues, and locations analyzed around the world. PFOS predominated in freshwater and saltwater fish samples (Houde et al., 2006), was the dominant PFC in fish fillets collected from mountain lakes and rivers at 4000 m elevations in China (Shi et al., 2010), and was reported to levels of 3250 ng/g wet weight in the livers of ornate jobfish (*Pristipomoides argyrogrammicus*), a carnivorous fish species from Japan (Taniyasu et al., 2003). Houde et al. (2011) noted that PFOS appears to have the highest bioaccumulation potential in food webs, and can therefore reach highest concentrations in higher trophic level species. The highest PFOS values from NRSA urban river and NCCA/GL analyses (Tables 4 and 5) were in carnivorous species. NRSA species comparisons (for fishes that dominated in abundance) showed higher PFOS concentrations in largemouth bass than smallmouth bass (Fig. 4), demonstrated by both maximum values and separation of their interquartile ranges. For NCCA/GL species, even though the maximum PFOS value was detected in smallmouth bass, most lake trout concentrations were higher than smallmouth bass or walleye (Fig. 5) shown by the higher interquartile range for lake trout.

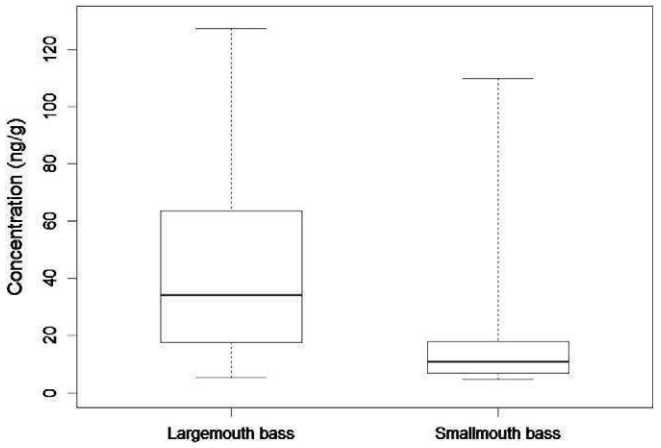

Fig. 4. Minimum, maximum, median and interquartile range (25th and 75th percentiles) of PFOS (ng/g) detected in common fish species from U.S. urban rivers.

Much of the published PFC fish tissue literature focuses on marine fish species and on fish collected outside of the continental U.S. Livers or other organs are often the tissue fraction discussed (Sinclair et al., 2006; Quinete et al., 2009), or fish are processed as whole bodies for analysis rather than as edible fillets (Martin et al., 2004b; Kannan et al., 2005; Furdui et al., 2007; Ye et al., 2008a; De Silva et al., 2011). Direct comparisons of the national NRSA and regional NCCA/GL probabilistic results to other studies are also limited due to differences in waterbody type, sample preparation, analysis, and reporting. Published PFC fish tissue data from freshwater systems of the continental U.S. (including the Great Lakes) are summarized in Table 8, highlighting fillet analysis and wet-weight result reporting that is compatible with the national and regional probabilistic survey designs. A review of the relevant

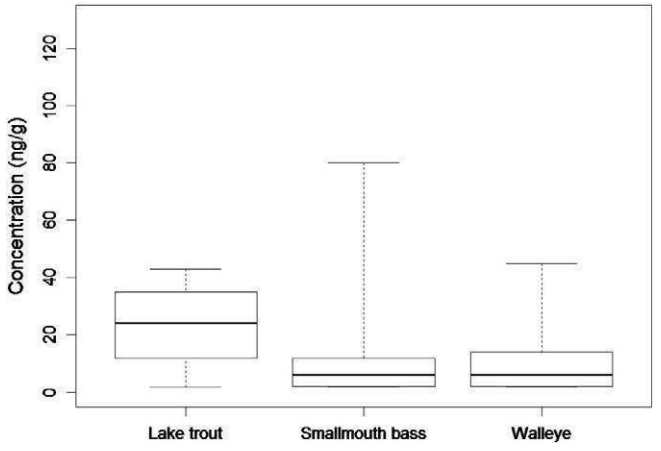

Fig. 5. Minimum, maximum, median, and interquartile range (25th and 75th percentiles) of PFOS (ng/g) detected in common fish species from the Great Lakes.

Table 8
Summary of PFC fish tissue (fillet) results from various U.S. studies (ng/g wet weight).

Author/citation	Location	Waterbody	Species	Number of analyzed PFCs	PFOS (ng/g)		
					min	mean	max
Fillet results, Rivers							
Delinsky et al. (2010)	Minnesota	Mississippi River	Bluegill, black crappie, pumpkinseed [a,b]	10	3.06		2000
Kannan et al. (2005)	Indiana	Calumet River	Smallmouth bass [a,c]	4	2.5	4.5	7.6
Kannan et al. (2005)	Michigan	Raisin River	Smallmouth bass [a,c]	4	2.0	13.2	41.3
Kannan et al. (2005)	Michigan	St. Clair River	Smallmouth bass [a,c]	4	<2.0		2.7
Malinsky et al. (2011)	Mississippi	Mississippi River, pool 2	Black crappie [a,b]	10	n/a	55	n/a
Malinsky et al. (2011)	Mississippi	Mississippi River, pool 2	Bluegill [a,b]	10	105	180	336
Malinsky et al. (2011)	Mississippi	Mississippi River, pool 2	Sauger [a,b]	10	39.8	41.7	43.5
Malinsky et al. (2011)	Mississippi	Mississippi River, pool 2	Smallmouth bass [a,b]	10	54	165	382
Malinsky et al. (2011)	Mississippi	Mississippi River, pool 2	Walleye [a,b]	10	28.5	50.8	83.1
Malinsky et al. (2011)	Mississippi	Mississippi River, pool 3	Bluegill [a,b]	10	74.7	144	221
Malinsky et al. (2011)	Mississippi	Mississippi River, pool 3	Northern Pike [a,b]	10	n/a	50.5	n/a
Malinsky et al. (2011)	Mississippi	Mississippi River, pool 3	Smallmouth bass [a,b]	10	29.7	60.5	105
Malinsky et al. (2011)	Mississippi	Mississippi River, pool 3	Walleye [a,b]	10	50.8	76.4	96.4
Ye et al. (2008b)	Minnesota	Upper Mississippi River (RM1509)	Common carp[a]	10	4.3	9.9	19
Ye et al. (2008b)	Minnesota	Upper Mississippi River (RM 1341)	Common carp[a]	10	11	28	66
Ye et al. (2008b)	Minnesota	Upper Mississippi River (RM 1314)	Common carp[a]	10	15	47	90
Fillet results, Lakes							
Delinsky et al. (2010)	Minnesota	Byllesby Lake	Bluegill, black crappie, pumpkinseed [a,b]	10		1.42	
Delinsky et al. (2010)	Minnesota	Carlos Lake	Bluegill, black crappie, pumpkinseed [a,b]	10		12.3	
Delinsky et al. (2010)	Minnesota	Fall Lake	Bluegill, black crappie, pumpkinseed [a,b]	10		1.08	
Delinsky et al. (2010)	Minnesota	Goose Lake	Bluegill, black crappie, pumpkinseed [a,b]	10		1.25	
Delinsky et al. (2010)	Minnesota	Lac Qui Parle Lake	Bluegill, black crappie, pumpkinseed [a,b]	10		1.31	
Delinsky et al. (2010)	Minnesota	McCarrons Lake	Bluegill, black crappie, pumpkinseed [a,b]	10		47.3	
Delinsky et al. (2010)	Minnesota	Nokomis Lake	Bluegill, black crappie, pumpkinseed [a,b]	10		4.39	
Delinsky et al. (2010)	Minnesota	Pickerel Lake	Bluegill, black crappie, pumpkinseed [a,b]	10		10.0	
Delinsky et al. (2010)	Minnesota	Simley Lake	Bluegill, black crappie, pumpkinseed [a,b]	10		5.13	
Delinsky et al. (2010)	Minnesota	Tamarack Lake	Bluegill, black crappie, pumpkinseed [a,b]	10		1.95	
Delinsky et al. (2010)	Minnesota	Whiteface Reservoir	Bluegill, black crappie, pumpkinseed [a,b]	10		2.29	
Delinsky et al. (2010)	Minnesota	Winona Lake	Bluegill, black crappie, pumpkinseed [a,b]	10		4.7	
Delinsky et al. (2010)	Minnesota	Zumbro Lake	Bluegill, black crappie, pumpkinseed [a,b]	10		52.4	
Giesy and Kannan (2001)	Michigan	Great Lakes (Michigan waters)	Brown trout [a]	4	<6		46
Giesy and Kannan (2001)	Michigan	Great Lakes (Michigan waters)	Chinook salmon [a]	4	7	110	190
Giesy and Kannan (2001)	Michigan	Great Lakes (Michigan waters)	Lake whitefish [a]	4	97	130	170
Giesy and Kannan (2001)	Michigan	Saginaw Bay (Lake Michigan)	Carp [a]	4	60	120	300
Guo et al. (2012)	Ontario	Lake Erie	Lake trout[a,c]	11		27	
Guo et al. (2012)	Ontario	Lake Huron	Lake trout[a,c]	11		8.3	
Guo et al. (2012)	Ontario	Lake Ontario	Lake trout[a,c]	11		46	
Guo et al. (2012)	Ontario	Lake Superior	Lake trout[a,c]	11		0.85	
Kannan et al. (2005)	Michigan	Saginaw Bay (Lake Michigan)	Carp [a,c]	4	59	124	297

[a] Wild caught.
[b] Fillet—skin on.
[c] Fillet—skin off.

literature showed that PFOS was the only PFC analyzed in all studies, with PFOA as the second most reported PFC.

In addition to being commonly reported in relevant studies (Table 8), PFOS was the most commonly detected PFC in both the NRSA and NCCA/GL studies (73% of all urban river samples and 100% of all Great Lakes samples). It was also detected at the highest concentrations among the 13 PFCs included in each of the studies, ranging from 4.8 to 127 ng/g (wet weight) in urban rivers and from 1.9 to 80 ng/g in the Great Lakes (Tables 4 and 5). The range of detections from the NRSA was very similar to the range of PFOS detections in the literature for fillets from riverine fish (Table 8), with the exception of high values reported by Delinsky et al. (2010) and Malinsky et al. (2011). The highest concentration (2000 ng/g) (Table 8) was detected in a composite sample of bluegill fillets collected from Pool 2, an area of the Mississippi River with historically known high PFC concentrations from industrial emissions (Malinsky et al., 2011; Ye et al., 2008b; Delinsky et al., 2010). The second highest concentration was 382 ng/g, detected in a composite sample of smallmouth bass fillets that was also collected from Pool 2 (Malinsky et al., 2011). With the exception of these Mississippi River samples, PFOS tissue levels reported in the literature (Table 8) are comparable to the concentrations observed in the NRSA urban river study. The Mississippi River samples document a specific area of known PFC contamination, whereas the probabilistic results for the NRSA document the national distribution of PFCs in a sampled population of 17,509 U.S. urban river km.

The NCCA/GL PFOS levels were generally higher than values in the literature from studies of other inland lakes (Table 8), but lower than those reported by some other Great Lakes researchers. Maximum PFOS levels of 300 ng/g and 297 ng/g reported by Giesy and Kannan (2001) and Kannan et al. (2005), respectively, were found in common carp (*Cyprinus carpio*) fillets from Saginaw Bay in Lake Michigan. The Saginaw Bay samples may identify an area of elevated PFC contamination; however, the probabilistic results provided by the NCCA/GL study can be extrapolated to a nearshore surface area of 11,091 km^2 in U.S. waters of the Great Lakes. The differences between the Giesy and Kannan (2001) and Kannan et al. (2005) tissue levels and those from the NCCA/GL study may reflect variation between the species analyzed or a change in PFOS levels over time. The latter cannot be determined from these temporally focused studies.

Past temporal trend studies of PFOS have shown increasing concentrations over time. Martin et al. (2004b) documented a four-fold nonlinear increase in whole lake trout homogenates from Lake Ontario between 1980 and 2001. Gewurtz et al. (2012) reported that temporal trend models have not shown a decline in Lake Ontario lake trout PFC concentrations despite the voluntary PFOS (and related chemical) production phase out in 2002. Their power analysis results suggested that

15 years of PFOS data (with a within-year sample size of at least 10) would be required to obtain sufficient power (80%) to detect a 5% decreasing trend in PFOS contamination, which demonstrates the need for continued long-term monitoring.

4.1. Conclusions

Worldwide, studies show that PFOS is the predominant perfluoroalkyl substance in humans and other biota (Kannan, 2011), and it predominated in these national urban river and regional Great Lakes probabilistic fish tissue surveys as well. Fish are noted to be a significant dietary source of PFOS exposure for humans in several locations throughout the world (Houde et al., 2011). For example, Zhang et al. (2010) reported that fish and seafood accounted for a major proportion of the daily intake of PFOS in China. Houde et al. (2011) summarized PFC monitoring studies conducted since 2005 and concluded that fish consumption advisories may need to be considered based on the widespread presence of PFCs and their elevated levels in selected locations. Toxicological reference value information for PFCs is sparse; however, the Minnesota Department of Health developed a PFOS reference dose (RfD) value of 0.000075 mg/kg-day (MDH, 2008a). In February 2014, EPA proposed draft human health reference doses for PFOA and PFOS that are currently under review (Federal Register, 2014). National risk-based consumption limits or human health screening values have not been developed for PFCs in the U.S. The Minnesota Department of Health (MDH) included meal advice categories based on levels of PFOS in fish as part of their statewide Fish Consumption Advisory Program (MDH, 2008b). The MDH sport fish advisory levels recommend consumption of only one meal of fish per week if PFOS concentrations are >40–200 ng/g (wet weight), one meal per month if levels are >200–800, and no consumption at levels greater than 800 ng/g. Michigan Department of Community Health (MDCH) recently used those consumption limits to issue a "do not eat" advisory for all fish in Clarks Marsh, Iosco County, Michigan (south of the former Wurtsmith Air Force Base) due to elevated PFC tissue concentrations (MDCH, 2012). The application of these human health screening values (SV) to the national probabilistic results (Fig. 6) indicates that 10.6% of the sampled population of U.S. urban rivers and 9.0% of the Great Lakes sampled population had PFOS tissue concentrations that exceeded the 40 ng/g SV recommending that fish consumption be restricted to no more than one meal per week. This represents a total of 1856 urban river km and 998 km^2 of the nearshore Great Lakes area, respectively.

Continued development and refinement of tissue advisory levels is warranted as knowledge increases on the toxicity, prevalence, sources, and environmental behavior of PFCs and the overall benefits of fish consumption. Recent research suggests that cooking may reduce PFC concentrations in fish prior to human consumption (and that baking may be the most effective method for reducing PFC levels) (Gobbo et al., 2008). Considering the thermal stability of PFCs, one unresolved aspect of this research is whether cooking truly reduces PFCs or whether it renders them more difficult to extract using the analytical method tested. Continued research in this area should address the issues of PFC extractability and chemical degradation to confirm whether public outreach/education on cooking methods may ultimately help to mitigate human health risks.

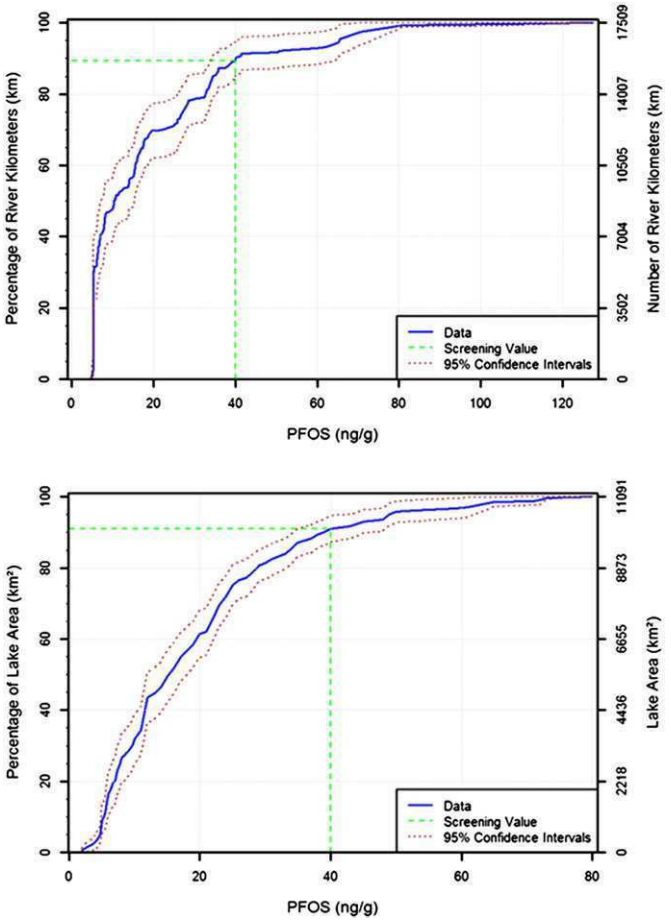

Fig. 6. Cumulative distribution functions (CDFs) of PFOS in fish fillet samples from urban rivers (top graph) and the Great Lakes (bottom graph) with Minnesota Department of Health 1 meal/week human health screening value (dotted line).

Acknowledgments

This study was funded by the U.S. Environmental Protection Agency, and technical support was provided under EPA Contracts EP-C-04-030, EP-C-06-085, EP-C-09-019, and EP-C-10-060. The manuscript has been subjected to review and approved for publication by U.S. EPA's Office of Research and Development and EPA's Office of Water. Approval does not signify that the contents reflect the views of the Agency, nor does mention of trade names or commercial products constitute endorsement or recommendation for use.

This study was made possible by the collaborative efforts of U.S. EPA's Office of Water (OW), EPA's Office of Research and Development (ORD), EPA's Great Lakes National Program Office (GLNPO), and a national network of state, tribal, and federal agency partners. Deep appreciation is expressed to all staff in the participating agencies who conducted site reconnaissance, planned sampling logistics, and collected fish samples. Technical support was provided by study team members from Tetra Tech, Inc. (Tara Cohen, Erik Leppo, Ann Roseberry Lincoln, and John O'Donnell), and CSC (Lynn Walters). Analytical laboratory services were provided by AXYS Analytical Services, Sidney, BC, Canada and TestAmerica, West Sacramento, CA. Appreciation is also expressed to Joyce Donohue (OW), Andrew Lindstrom (ORD), and Elizabeth Murphy (GLNPO) for their technical review and input.

References

Ahrens L. Polyfluoroalkyl compounds in the aquatic environment: a review of their occurrence and fate. J Environ Monit 2011;13:20–31.

Apelberg BJ, Witter FR, Herbstman JB, Calafat AM, Halden RU, Needham LL, et al. Cord serum concentrations of perfluorooctane sulfonate (PFOS) and perfluorooctanoate (PFOA) in relation to weight and size at birth. Environ Health Perspect 2007;115:1670–6.

Buck RC, Franklin J, Berger U, Conder JM, Cousins IT, de Voogt P, et al. Perfluoroalkyl and polyfluoroalkyl substances in the environment: terminology, classification, and origins. Integr Environ Assess Manag 2011;7:513–41.

Butt CM, Berger U, Bossi R, Tomy GT. Levels and trends of poly- and perfluorinated compounds in the arctic environment. Sci Total Environ 2010;408:2936–65.

Conder JM, Hoke RA, De Wolf W, Russell MH, Buck RC. Are PFCAs bioaccumulative? A critical review and comparison with regulatory criteria and persistent lipophilic compounds. Environ Sci Technol 2008;42:995–1003.

De Silva AO, Spencer C, Scott BF, Backus S, Muir DCG. Detection of a cyclic perfluorinated acid, perfluoroethylcyclohexane sulfonate, in the Great Lakes of North America. Environ Sci Technol 2011;45:8060–6.
Del Gobbo L, Tittlemier S, Diamond M, Pepper K, Tague B, Yeudall F, et al. Cooking decreases observed perfluorinated compound concentrations in fish. J Agric Food Chem 2008;56:7551–9.
Delinsky AD, Strynar MJ, McCann PJ, Varns JL, McMillan L, Nakayama SF, et al. Geographical distribution of perfluorinated compounds in fish from Minnesota lakes and rivers. Environ Sci Technol 2010;44:2549–54.
EU. Directive 2006/122/ECOF the European Parliament and of the Council of 12 December; 2006.
Federal Register. Request for nominations for peer reviewers and notice of public comment period for draft health effects documents for perfluorooctanoic acid and perfluorooctane sulfonate. Fed Regist 2014;79(40):11429–30.
Frisbee SJ, Brooks Jr AP, Maher A, Flensborg P, Arnold S, Fletcher T, et al. The C8 health project: design, methods, and participants. Environ Health Perspect 2009;117:1873–82.
Fromme H, Tittlemier SA, Volkel W, Wilhelm M, Twardella D. Perfluorinated compounds–exposure assessment for the general population in Western countries. Int J Hyg Environ Health 2009;212:239–70.
Furdui VI, Stock NL, Ellis DA, Butt CM, Whittle DM, Crozier PW, et al. Spatial distribution of perfluoroalkyl contaminants in lake trout from the Great Lakes. Environ Sci Technol 2007;41:1554–9.
Gewurtz SB, De Silva AO, Backus SM, McGoldrick DJ, Keir MJ, Small J, et al. Perfluoroalkyl contaminants in Lake Ontario lake trout: detailed examination of current status and long-term trends. Environ Sci Technol 2012;46:5842–50.
Giesy JP, Kannan K. Global distribution of perfluorooctane sulfonate in wildlife. Environ Sci Technol 2001;35:1339–42.
Grandjean P, Andersen EW, Budtz-Jorgensen E, Nielsen F, Molbak K, Weihe P, et al. Serum vaccine antibody concentrations in children exposed to perfluorinated compounds. JAMA 2012;307:391–7.
Guo R, Reiner EJ, Bhavsar SP, Helm PA, Mabury SA, Braekevelt E, et al. Determination of polyfluoroalkyl phosphoric acid diesters, perfluoroalkyl phosphonic acids, perfluoroalkyl phosphinic acids, perfluoroalkyl carboxylic acids, and perfluoroalkane sulfonic acids in lake trout from the Great Lakes region. Anal Bioanal Chem 2012;404:2699–709.
Guruge KS, Taniyasu S, Yamashita N, Wijeratna S, Mohotti KM, Seneviratne HR, et al. Perfluorinated organic compounds in human blood serum and seminal plasma: a study of urban and rural tea worker populations in Sri Lanka. J Environ Monit 2005;7:371–7.
Hart K, Kannan K, Tao L, Takahashi S, Tanabe S. Skipjack tuna as a bioindicator of contamination by perfluorinated compounds in the oceans. Sci Total Environ 2008;403:215–21.
Haug LS, Thomsen C, Brantsaeter AL, Kvalem HE, Haugen M, Becher G, et al. Diet and particularly seafood are major sources of perfluorinated compounds in humans. Environ Int 2010;36:772–8.
Hölzer Jr, Göen T, Just P, Reupert R, Rauchfuss K, Kraft M, et al. Perfluorinated compounds in fish and blood of anglers at Lake Möhne, Sauerland area, Germany. Environ Sci Technol 2011;45:8046–52.
Houde M, Martin JW, Letcher RJ, Solomon KR, Muir DCG. Biological monitoring of polyfluoroalkyl substances: a review. Environ Sci Technol 2006;40:3463–73.
Houde M, De Silva AO, Muir DCG, Letcher RJ. Monitoring of perfluorinated compounds in aquatic biota: an updated review. Environ Sci Technol 2011;45:7962–73.
Jones PD, Hu W, De Coen W, Newsted JL, Giesy JP. Binding of perfluorinated fatty acids to serum proteins. Environ Toxicol Chem 2003;22:2639–49.
Kannan K. Perfluoroalkyl and polyfluoroalkyl substances: current and future perspectives. Environ Chem 2011;8:333–8.
Kannan K, Corsolini S, Falandysz J, Fillmann G, Kumar KS, Loganathan BG, et al. Perfluorooctanesulfonate and related fluorochemicals in human blood from several countries. Environ Sci Technol 2004;38:4489–95.
Kannan K, Tao L, Sinclair E, Pastva SD, Jude DJ, Giesy JP. Perfluorinated compounds in aquatic organisms at various trophic levels in a Great Lakes food chain. Arch Environ Contam Toxicol 2005;48:559–66.
Kincaid TM, Olsen AR. Spsurvey: spatial survey design and analysis. R package version 2.5. http://www.epa.gov/nheerl/arm/, 2012.
Kuklenyik Z, Reich JA, Tully JS, Needham LL, Calafat AM. Automated solid-phase extraction and measurement of perfluorinated organic acids and amides in human serum and milk. Environ Sci Technol 2004;38:3698–704.
Lau C, Anitole K, Hodes C, Lai D, Pfahles-Hutchens A, Seed J. Perfluoroalkyl acids: a review of monitoring and toxicological findings. Toxicol Sci 2007;99:366–94.
Lindstrom AB, Strynar MJ, Libelo EL. Polyfluorinated compounds: past, present, and future. Environ Sci Technol 2011;45:7954–61.
Malinsky MD, Jacoby CB, Reagen WK. Determination of perfluorinated compounds in fish fillet homogenates: method validation and application to fillet homogenates from the Mississippi River. Anal Chim Acta 2011;683:248–57.
Martin JW, Smithwick MM, Braune BM, Hoekstra PF, Muir DCG, Mabury SA. Identification of long-chain perfluorinated acids in biota from the Canadian Arctic. Environ Sci Technol 2004a;38:373–80.
Martin JW, Whittle DM, Muir DC, Mabury SA. Perfluoroalkyl contaminants in a food web from Lake Ontario. Environ Sci Technol 2004b;38:5379–85.
MDCH. MDCH issues "do not eat" fish advisory for Clarks Marsh in Losco County. http://www.michigan.gov/mdch/0,4612,7-132-8347-277156-,00.html, 2012.
MDH. Health risk limits for perfluorochemicals: report to the Minnesota Legislature 2008. St. Paul, MN: Environmental Health Division; 2008a [http://www.health.state.mn.us/divs/eh/hazardous/topics/pfcs/finalreport011508.pdf].
MDH. Fish consumption advisory program meal advice categories. http://www.health.state.mn.us/divs/eh/fish/eating/mealadvicetables.pdf, 2008.
Murphy MB, Loi EI, Kwok KY, Lam PK. Ecotoxicology of organofluorous compounds. Top Curr Chem 2012;308:339–63.
Olsen GW, Burris JM, Burlew MM, Mandel JH. Epidemiologic assessment of worker serum perfluorooctanesulfonate (PFOS) and perfluorooctanoate (PFOA) concentrations and medical surveillance examinations. J Occup Environ Med 2003;45:260–70.
Olsen GW, Burris JM, Ehresman DJ, Froehlich JW, Seacat AM, Butenhoff JL, et al. Half-life of serum elimination of perfluorooctanesulfonate, perfluorohexanesulfonate, and perfluorooctanoate in retired fluorochemical production workers. Environ Health Perspect 2007;115:1298–305.
Paul AG, Jones KC, Sweetman AJ. A first global production, emission, and environmental inventory for perfluorooctane sulfonate. Environ Sci Technol 2008;43:386–92.
Quinete N, Wu Q, Zhang T, Yun SH, Moreira I, Kannan K. Specific profiles of perfluorinated compounds in surface and drinking waters and accumulation in mussels, fish, and dolphins from southeastern Brazil. Chemosphere 2009;77:863–9.
R Development Core Team. The R Project for Statistical Computing. Vienna, Austria: R Development Core Team; 2007.
Renner R. Growing concern over perfluorinated chemicals. Environ Sci Technol 2001;35:154A–60A.
Rotander A, Karrman A, van Bavel B, Polder A, Riget F, Auethunsson GA, et al. Increasing levels of long-chain perfluorocarboxylic acids (PFCAs) in Arctic and North Atlantic marine mammals, 1984–2009. Chemosphere 2012;86:278–85.
Shankar A, Xiao J, Ducatman A. Perfluorooctanoic acid and cardiovascular disease in US adults. Arch Intern Med 2012;172:1397–403.
Shi Y, Pan Y, Yang R, Wang Y, Cai Y. Occurrence of perfluorinated compounds in fish from Qinghai-Tibetan Plateau. Environ Int 2010;36:46–50.
Sinclair E, Mayack D, Roblee K, Yamashita N, Kannan K. Occurrence of perfluoroalkyl surfactants in water, fish, and birds from New York State. Arch Environ Contam Toxicol 2006;50:398–410.
Steenland K, Fletcher T, Savitz DA. Epidemiologic evidence on the health effects of perfluorooctanoic acid (PFOA). Environ Health Perspect 2010;118:1100–8.
Stevens Jr DL, Olsen AR. Spatially restricted surveys over time for aquatic resources. J Agric Biol Environ Stat 1999;4:415–28.
Stevens Jr DL, Olsen AR. Spatially balanced sampling of natural resources. J Am Stat Assoc 2004;99:262–78.
Strahler AN. Quantitative analysis of watershed geomorphology. Trans Am Geophys Union 1957;38:913–20.
Taniyasu S, Kannan K, Horii Y, Hanari N, Yamashita N. A survey of perfluorooctane sulfonate and related perfluorinated organic compounds in water, fish, birds, and humans from Japan. Environ Sci Technol 2003;37:2634–9.
US EPA. Guidelines establishing test procedures for the analysis of pollutants under the Clean Water Act; Final Rule and Interim Final Rule, and Proposed Rule, 49 FR 43234. Fed Regist 1984:198. [1984].
US EPA. Perfluoroalkyl sulfonates, significant new use rule, final and supplemental proposed rule. Fed Regist 2002;67:72854–67.
US EPA. Draft risk assessment of the potential human health effects associated with exposure to perfluorooctanic acid and its salts. Washington, DC: Office of Pollution Prevention and Toxics; 2005 [http://www.epa.gov/oppt/pfoa/pubs/pfoarisk.pdf].
US EPA. National rivers and streams assessment field operations manual. Washington, DC: Office of Water; 2009.
US EPA. National rivers and streams assessment quality assurance project plan. Washington, DC: Office of Water, Office of Environmental Information; 2010a.
US EPA. National coastal condition assessment quality assurance project plan. Washington, DC: Office of Water, Office of Environmental Information; 2010b.
US EPA. Quality assurance project plan for laboratory sample preparation and analysis activities: perfluorinated compounds (PFCs) in water and fish tissue from the National Urban River Contaminant of Emerging Concern (CEC) study. Washington, DC: Office of Water, Office of Science and Technology; 2010c.
USGS, US EPA. NHDPlus User Guide. http://www.horizonsystems.com/nhdplus/data/NHDPLUS_UserGuide.pdf, 2007.
Watkins DJ, Josson J, Elston B, Bartell SM, Shin HM, Vieira VM, et al. Exposure to perfluoroalkyl acids and markers of kidney function among children and adolescents living near a chemical plant. Environ Health Perspect 2013;121:625–30.
Ye X, Schoenfuss HL, Jahns ND, Delinsky AD, Strynar MJ, Varns J, et al. Perfluorinated compounds in common carp (*Cyprinus carpio*) fillets from the Upper Mississippi River. Environ Int 2008a;34:932–8.
Ye X, Strynar MJ, Nakayama SF, Varns J, Helfant L, Lazorchak J, et al. Perfluorinated compounds in whole fish homogenates from the Ohio, Missouri, and Upper Mississippi Rivers, USA. Environ Pollut 2008b;156:1227–32.
Zar JH. Biostatistical analysis. Upper Saddle River, NJ: Prentice Hall; 1999.
Zhang T, Sun HW, Wu Q, Zhang XZ, Yun SH, Kannan K. Perfluorochemicals in meat, eggs and indoor dust in China: assessment of sources and pathways of human exposure to perfluorochemicals. Environ Sci Technol 2010;44:3572–9.
Zushi Y, Hogarh J, Masunaga S. Progress and perspective of perfluorinated compound risk assessment and management in various countries and institutes. Clean Techn Environ Policy 2012;14:9–20.

Science of the Total Environment 634 (2018) 542–549

Contents lists available at ScienceDirect

Science of the Total Environment

journal homepage: www.elsevier.com/locate/scitotenv

Presence of pharmaceuticals in fish collected from urban rivers in the U.S. EPA 2008–2009 National Rivers and Streams Assessment

Belinda Huerta [a,*], Sara Rodriguez-Mozaz [a], Jim Lazorchak [b], Damia Barcelo [a,c], Angela Batt [b], John Wathen [d], Leanne Stahl [d]

[a] Catalan Institute for Water Research (ICRA), H_2O Building, Scientific and Technological Park of the University of Girona, Emili Grahit 101, 17003 Girona, Spain
[b] U.S. EPA Office of Research and Development, National Exposure Research Laboratory, 26 W. Martin Luther King Dr, Cincinnati, OH 45268, United States
[c] Water and Soil Quality Research Group, Department of Environmental Chemistry, IDAEA-CSIC, Jordi Girona 18-26, 08034 Barcelona, Spain
[d] U.S. EPA Office of Water, Office of Science and Technology, 1200 Pennsylvania Ave., NW, Washington D.C. 20460, United States

HIGHLIGHTS

- Occurrence of pharmaceuticals in wild fish from 25 polluted river sites in the USA.
- Thirteen pharmaceuticals quantified in fillets at concentrations below 10 ng g^{-1}.
- Venlafaxine, carbamazepine and metabolite were the most prevalent compounds.

GRAPHICAL ABSTRACT

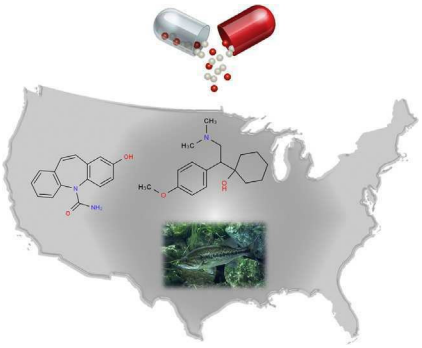

ARTICLE INFO

Article history:
Received 5 February 2018
Received in revised form 29 March 2018
Accepted 31 March 2018
Available online xxxx

Editor: Holden

Keywords:
Pharmaceuticals
Fish
Accumulation
Trophic level

ABSTRACT

Fish are good indicators of aquatic environment pollution because of their capability to uptake pollutants contained in water. Therefore, accumulation of pharmaceutical compounds in freshwater and marine fish and other aquatic organisms has been studied extensively in the last decade. In this context, the present study investigates the occurrence of pharmaceutical compounds in wild fish from 25 polluted river sites in the USA, downstream from wastewater treatment plants (WWTPs). Sample sites constitute a subset of urban rivers investigated in the U.S. EPA's 2008–2009 National Rivers and Streams Assessment. Thirteen pharmaceuticals (out of the twenty compounds analyzed) were quantified in fish fillets at concentrations commonly below 10 ng g^{-1}, in accordance with the findings from previous studies in the USA and Europe. The psychoactive drugs venlafaxine, carbamazepine and its metabolite 2-hydroxy carbamazepine were the most prevalent compounds (58%, 27% and 42%, respectively). This group of drugs is highly prescribed and rather resistant to degradation during conventional treatment in WWTPs as well as in natural aquatic environments. Salbutamol, a drug used to treat asthma, and the diuretic hydrochlorothiazide were also frequently detected (in >20% of the samples). Occurrence of six pharmaceutical families due to chronic exposure at environmental concentrations in water was detected in eight fish species.

© 2018 Elsevier B.V. All rights reserved.

* Corresponding author at: Department of Fisheries and Wildlife, Michigan State University, 480 Wilson Road, East Lansing, MI 48823, United States.
E-mail address: huertabu@msu.edu. (B. Huerta).

https://doi.org/10.1016/j.scitotenv.2018.03.387
0048-9697/© 2018 Elsevier B.V. All rights reserved.

1. Introduction

Many contaminants have been detected in wastewater effluents and surface water in recent years, including pharmaceuticals. Some of these compounds are not completely removed in the wastewater treatment plants (WWTPs) (Kolpin et al., 2002; Kostich et al., 2014) and are released to the environment. Fish and other organisms downstream from WWTP effluent discharges are constantly exposed to mixtures of biologically active pharmaceuticals, which could lead to the alteration of important physiological processes, such as development, reproduction and nervous system function (Liu et al., 2015). This has resulted in an increasing amount of literature exploring environmental occurrence, fate, effects, and risk assessment of these compounds. The impact of the contaminants can be evaluated by assessing selected toxicological effects or by measuring the bioaccumulation of the target compounds in the organisms. Bioaccumulation has indeed been proposed as a hazard criterion itself, since some effects may only be recognized in a later phase of life, are multigenerational effects, or manifest only in higher members of a food web (van der Oost et al., 2003). The accumulation of pharmaceutical compounds in freshwater and marine fish has been studied extensively in the last decade (Huerta et al., 2012; Rodríguez-Mozaz et al., 2017, 2016).

Fish are good indicators of aquatic environment pollution because of their capability to uptake pollutants contained in water through their gills, as well as by ingestion of contaminated forage organisms. First studies were published by Brooks et al. (Brooks et al., 2005) in a single stream, and Ramirez et al. (Ramirez et al., 2009), in a series of streams heavily impacted by effluent discharges in the USA reporting concentrations of psychoactive drugs, antihistamines, and β-blockers in fish tissues. Simultaneously, the presence of psychoactive drugs in fish samples collected in Canada was reported (Chu and Metcalfe, 2007). In these studies, fish tissue concentrations were in the low ng g^{-1} range.

In Europe, initially most of the data on the presence of pharmaceuticals, mainly antibiotics, in aquatic organisms emerged from aquaculture and food control studies closely related to human consumption and regulation demands, where concentrations were found up to 150 ng g^{-1} (Berrada et al., 2008; Cháfer-Pericás et al., 2010). However, in the last few years, the interest in this subject has exponentially increased, and many reports have been published. For instance, anti-inflammatories, psychoactive drugs, and β-blockers were detected in Spain below 10 ng g^{-1} in fish homogenates (Huerta et al., 2013). Other countries, such as Argentina (Valdés et al., 2016), China (Liu et al., 2015; Zhao et al., 2015) or Japan (Tanoue et al., 2014), have also reported the presence of multi-class pharmaceuticals - including antibiotics, anti-inflammatories, β-blockers, synthetic hormones at low concentrations.

There are only limited data available on the effect of pharmaceuticals on aquatic organisms, although some studies have highlighted the link between the bioaccumulation and the possible biological effect of these compounds on aquatic organisms (Margiotta-Casaluci et al., 2014; Mimeault et al., 2005; Valenti et al., 2012). Logically, humans can also be exposed to the pollutants in water and food (Fedorova et al., 2014).

In this context, U.S. EPA conducted the first statistically based survey of persistent and bio-accumulative contaminants in fish designed to assess the condition of streams and rivers. Fish samples commonly consumed by humans were collected at 542 randomly selected river locations in 48 states in 2008–2009 (See website for more details https://www.epa.gov/fish-tech/studies-fish-tissue-contamination). Tissue analyses were conducted on these samples for mercury (Wathen et al., 2015), legacy organics (Batt et al., 2017), and perfluorinated compounds (Stahl et al., 2014). In addition, 182 water samples were collected from 164 targeted urban river sites and analyzed for 46 pharmaceuticals (Batt et al., 2016). The objectives of the present study were to investigate the occurrence of pharmaceutical compounds in 8 wild fish species collected from selected 26 sampling sites downstream from WWTPs (25 polluted and 1 reference site, where none of the target analytes were present).

2. Materials and methods

2.1. Standards and reagents

Chemical standards with a high purity grade (>95%) were purchased from Sigma–Aldrich in the case of atenolol carbamazepine, carazolol, citalopram, clopidogrel, codeine, diazepam, diclofenac, hydrochlorothiazide, levamisole, lorazepam, nadolol, propanolol, salbutamol, and sotalol. Sertraline and velafaxine were purchased from the European Pharmacopeia (EP), while metoprolol was acquired from the US Pharmacopeia (USP). Metabolites 2-hydroxycarbamazepine (2-HydroxyCBZ) and 10, 11-epoxycarbamazepine (10, 11-EpoxyCBZ) were purchased from Toronto Research Chemicals (TRC). Internal standards diazepam-d_5, fluoxetine-d_5, ibuprofen-d_3, and ronidazole-d_3 were purchased from Sigma–Aldrich, while atenolol-d_7, carbamazepine-d_{10}, citalopram-d_4, and hydrochlorothiazide-d_2 were acquired from CDN isotope, as well as antipyrine-d_3 and cimetidine-d_3, used as surrogate standards, and venlafaxine-d_6 was acquired from TRC. All stock standards were prepared in methanol at a concentration of 1000 mg L^{-1} and stored at −20 °C. Fresh working standard solutions (20 and 1 mg L^{-1}) of all compounds were prepared in methanol/water (10:90, *v*/v) before each analytical run.

2.2. Site selection and sample collection

This national fish survey was conducted under the framework of EPA's National Rivers and Streams Assessment (NRSA), a probability-based survey designed to assess the condition of the Nation's streams and rivers (https://www.epa.gov/national-aquatic-resource-surveys/national-rivers-and-streams-assessment-2008-2009-report). Sampling sites were selected using a probability-based approach (Stevens and Olsen, 2004). Field teams applied consistent methods nationwide to collect samples of fish commonly consumed by humans at 542 randomly selected river locations in the lower 48 states during June through October 2008–2009 (see website for more detailed information https://www.epa.gov/fish-tech/studies-fish-tissue-contamination). Rivers were designated as fifth order or greater based on Strahler stream order (Strahler, 1957). The 542 nationwide sites were further stratified into 164 urban river sites where at least one water sample was collected for pharmaceutical analyses. The 164 urban sites were then ranked based on the highest number of target PhACs detected (among the total of 46 pharmaceuticals analyzed in water; Fig. 1).

Among those sites, only 25 sites were selected for analysis of fish tissue samples for 20 pharmaceuticals for this study (see Table S2 & Fig. S1 in Supporting Information). Criteria used for selecting sites for pharmaceutical analyses of fish fillets included:

a) The fish species collected for fish tissue analyses were selected based on a relatively broad continental U.S. distribution, and were also selected by their consumption by humans (see https://www.epa.gov/sites/production/files/2013-/documents/nrsa_field_manual_4_21_09.pdf for target species and size).
b) Forty-six pharmaceuticals, including 6 biologically active metabolites, were measured and reported in the water samples, but only 5 of those (sertraline, atenolol, metoprolol, carbamazepine and hydrochlorothiazide) were in common with the method applied to determine pharmaceutical presence in fish samples. The occurrence of those 5 pharmaceuticals that could be measured not only in water, but also in fish, was used to prioritize the sites for fish tissue analyses. Sites were prioritized based on the highest concentrations found for these 5 pharmaceuticals in water (see Fig. S1). One site (*FW08TX038*) was selected as a reference site, as only one pharmaceutical (the antibiotic sulfamethoxazole) out of 45 was measured sa previous study (Batt et al., 2016).
c) The site had to be proximally 5 miles or less downstream from a WWTP (Wathen et al., 2015), as concentrations of pharmaceuticals are heavily linked to WWTP discharges.

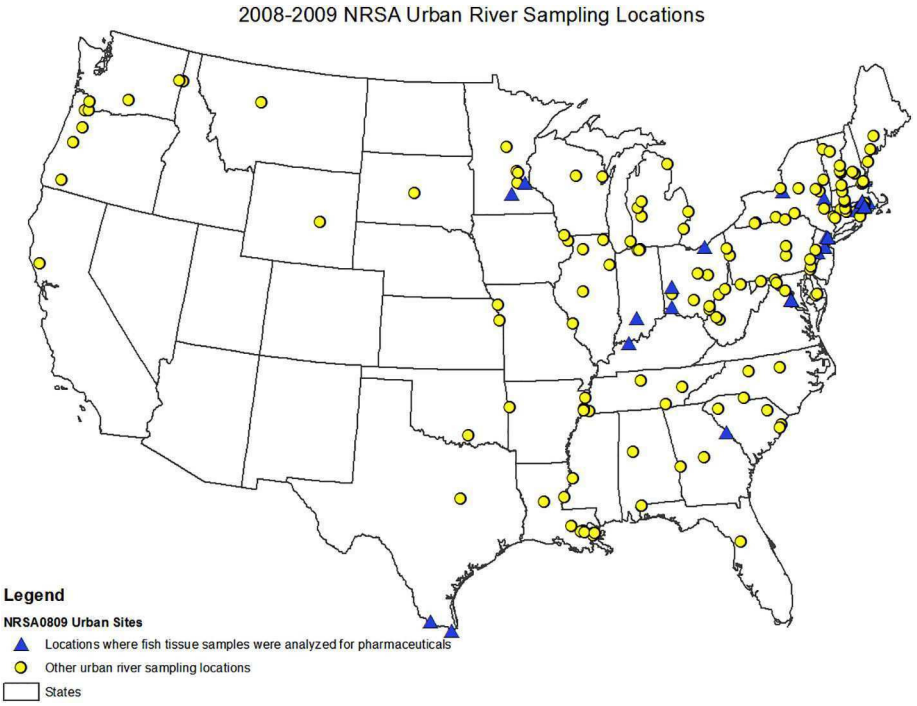

Fig. 1. Map of sample collection locations.

Field teams used active methods, primarily electrofishing, to collect one fish composite sample that consisted of five similarly sized adult fish of the same species from each site. Selected fish species were ubiquitous, abundant, and easily identified. Largemouth and smallmouth bass were the primary species collected for the 2008–2009 National Sand Streams Assessment, accounting for 25% and 34% of all fish composites, respectively. Fish samples were shipped on dry ice to the designated sample preparation laboratory for storage until subsequent fillet tissue sample preparation and analysis. Other aspects of fish collection and handling methods are further described elsewhere (U.S. EPA, 2013).

Fish were filleted in the laboratory. Scales were removed, then lateral muscle fillets from both sides of each fish were prepared with skin on and the belly flap (ventral muscle and skin) attached (US-EPA, 2000). Fillet composites were homogenized using a tissue grinder (Batt et al., 2017; Stahl et al., 2014). Fillet tissue composite samples for this study were freeze-dried and stored at −20° C until analysis. A total of eight fish species were collected for the analysis of pharmaceuticals, including smallmouth bass (*Micropterus dolomieu*), largemouth bass (*Micropterus salmoides*), white sucker (*Catostomus commersonii*), yellow perch (*Perca flavescens*), channel catfish (*Ictalurus punctatus*), common snook (*Centropomus undecimalis*), freshwater drum (*Aplodinotus grunniens*), and spotted bass (*Micropterus punctulatus*).

2.3. Analysis of pharmaceuticals in water

Surface water samples were extracted and analyzed by Batt et al. (Batt et al., 2016) using a previously reported method (Batt et al., 2008). Briefly, 500 mL of each sample was extracted with 150 mg Oasis HLB MCX (Waters) cartridges at an unadjusted pH. Acidic and neutral analytes were eluted by acetonitrile, and basic analytes were eluted by 95% acetonitrile and 5% ammonium hydroxide into separate silanized glass tubes. Immediately before analysis, extracts were concentrated to dryness under a constant flow of nitrogen prior to reconstitution in either 20% acetonitrile (acidic and neutral analytes) or 20% methanol (basic analytes). Reconstituted extracts were analyzed by LC-MS/MS in a Waters Acquity ultra performance liquid chromatograph coupled to a Micromass Quattro Micro triple quadrupole mass spectrometer with an electrospray ionization source operated using multiple reaction monitoring. Analytes were separated on a BEH C18 column (1.0 × 100 mm, 1.7 μm).

2.4. Analysis of pharmaceuticals in fish

Fillet composite samples were treated according to the method developed by Huerta et al. (Huerta et al., 2013). Briefly, 1 g of freeze-dried sample was extracted with methanol in an automated solvent extractor system (ASE® 350, Dionex). Extracts were concentrated to 1 ml and then 250 μl was passed through a preparative column (EnviroPrep, 300 mm × 21.2 mm, 10 μm pore size) in a gel permeation chromatography system (Agilent 1260 Infinity) in tandem with a diode array detector (HPLC-DAD) for lipid removal. Fractions were collected between minutes 13.5 to 26.5 and evaporated to dryness. All fractions from each sample were collected and combined in a final purified extract in methanol/water (10:90) and analyzed by ultra-performance liquid chromatography (UPLC Acquity, Waters, Mildford, USA) coupled to a QTRAP® 5500 (AB SCIEX, Framingham, USA) with electrospray ionization (ESI), according to the method developed by Gros et al. (Gros et al., 2012). An Acquity HSS T_3 with 10 mM formic acid/ammonium formate (pH 3.2) and methanol as the mobile phase at a flow rate of 0.5 mL min^{-1} was applied for the compounds analyzed in the positive mode, whereas an Acquity BEH C_{18} with acetonitrile and 5 mM ammonium acetate/ammonia (pH = 8) as mobile phase at a flow rate of 0.6 mL min^{-1} was used for the compounds analyzed in negative mode. Quantification was performed with a matrix-matched calibration curve together with the internal standard approach (9 labeled compounds) in the concentration range from 0.1 to 50 ng g^{-1}. Methodological blanks were extracted and purified following the same method. One blank was extracted each 10 samples. Analytical blanks were injected together with the samples each 5 injections. Method detection limits (MDL) were in the range of 0.03–0.50 ng g^{-1}.

2.5. Calculation of bioaccumulation factors

Bioaccumulation factors (BAFs, in $L \cdot kg^{-1}$) of pharmaceuticals in fish samples were estimated as the ratio between the concentration of the pharmaceutical in the fish fillet composite ($\mu g\ kg^{-1}$ wet weight) divided by the concentration of the same pharmaceutical in water ($\mu g\ L^{-1}$), assuming stationary state. Predicted BAFs were obtained from the linear regression proposed by Arnot and Gobas (Arnot and Gobas, 2006), using the octanol–water distribution coefficient (D_{ow}) instead of the octanol–water partition coefficient (K_{ow}): log BAF = 0.86 log Dow + 0.12.

3. Results & discussion

3.1. Analysis of pharmaceuticals in fish

A summary of the results are shown in Table 1 (see also Table S3 in Supporting Information). Thirteen pharmaceuticals (out of 20 analyzed) were detected in fish fillets collected from the 25 selected urban sites. In the majority of cases, measured concentrations (all in dry weight in this study) were below 10 ng g^{-1}, as seen in previous studies (Huerta et al., 2013).

Psychoactive drugs (antiepileptics and antidepressants) were the most prevalent therapeutic family in this study, as at least one compound of this group was detected in 15 samples out of 25, and in all fish species (see table S4). Six out of eight psychoactive compounds were detected at least once. This group of drugs is highly prescribed and the consumption of these drugs increased considerably in western countries over the last decade (OECD, 2013). In fact, these compounds have been consistently detected in surface water at relatively high concentrations (Silva et al., 2015). Consequently, they have been frequently measured in tissues (brain, liver, plasma) of fish and mollusks, normally at concentrations in the low ng g^{-1} range (Brooks et al., 2005; Du et al., 2015; Grabicova et al., 2015; Huerta et al., 2013; Silva et al., 2015). This may be cause for concern, as many studies have reported biological alterations (e.g. reproduction, physiology, and behavior alterations in fish) induced by these compounds in aquatic organisms (Silva et al., 2015).

Many of these compounds are relatively hydrophobic (Log $K_{ow} > 3$), therefore they may have the ability to accumulate (Du et al., 2015; Ramírez et al., 2007; Silva et al., 2015). Many of these drugs are weakly alkaline compounds. In waters with a high pH they appear in a neutral form, while in a low pH environment in an ionic form.

Venlafaxine was the most detected compound, in concentrations from below quantification limit to 23 ng g^{-1} (detection frequency: 52%). Venlafaxine is an antidepressant belonging to the class of the serotonin-norepinephrine reuptake inhibitors. This compound has been measured in wastewater effluent and in wastewater-dominated streams at very high concentrations (>1000 ng L^{-1}) in several studies carried out in the USA (Schultz et al., 2010; Schultz and Furlong, 2008). Venlafaxine values found in this study were higher than those found in wild fish from Iberian rivers (Huerta et al., 2013) and from

Table 1
Concentrations (ng g^{-1}, dry weight) of pharmaceuticals in fish fillet composites.

Therapeutic Family	Compound	MQL	Mean Conc. #	Max. Conc.	# Detected*	Fish Species
Anti-inflammatories	Diclofenac	0.2	0.7	0.7	1	White sucker
	Codeine	0.2	–	–	0	–
Antihelmintics	Levamisole	0.1	–	–	0	–
Antiplatelet agent	Clopidogrel	0.1	7.7	8	2	Channel catfish White sucker
β-Blockers	Atenolol	0.2	–	–	0	–
	Carazolol	0.1	–	–	0	–
	Metoprolol	0.7	–	–	0	–
	Nadolol	0.1	2.1	2.3	2	Channel catfish White sucker
	Propanolol	0.3	0.4	0.4	1	Smallmouth bass
	Sotalol	0.9	21.4	37.5	2	Smallmouth bass Yellow perch
Diuretics	Hydrochlorothiazide	0.2	0.8	1.1	5	Channel catfish Common snook Largemouth bass
Psychoactive drug	Carbamazepine	0.1	3	8.2	4	Smallmouth bass Largemouth bass Yellow perch White sucker
	Citalopram	0.4	1.2	2.4	3	Smallmouth bass Yellow perch White sucker
	Diazepam	0.2	1.9	1.9	1	Common snook
	10,11-epoxyCBZ	0.3	–	–	0	–
	2-hydroxyCBZ	0.1	0.7	2.5	5	Smallmouth bass Largemouth bass Channel catfish Freshwater drum
	Lorazepam	1.6	–	–	0	–
	Sertraline	1.1	17.1	17.1	1	White sucker
	Venlafaxine	0.1	4.6	22.9	13	Smallmouth bass Largemouth bass Channel catfish Freshwater drum Common snook Spotted brass
Antiasthmatic	Salbutamol	0.2	3.4	6.5	7	White sucker Channel catfish

* Detected out of 25 samples.
– Not detected.
calculated only with positive samples.

streams in the USA (Schultz et al., 2010) and similar to those detected in caged fishes exposed to effluent from a WWTP (21 ng g^{-1}) (Grabicova et al., 2014). This compound has also been detected previously in marine mollusks at similar (Álvarez-Muñoz et al., 2015) or lower concentrations (up to 3 ng g^{-1}) in samples collected from the Mediterranean (Martínez Bueno et al., 2014, 2013; Moreno-González et al., 2016).

The second most detected psychoactive drug was carbamazepine, which was detected at concentrations up to 8 ng g^{-1}, together with its metabolite 2-hydroxy-carbamazepine, which was detected at lower concentrations (up to 2.5 ng g^{-1}) (detection frequencies were 16% and 20%, respectively). Several studies have previously detected carbamazepine and its metabolites 2-hydroxy-carbamazepine and EPO-Carbamazepine in wild fish (Huerta et al., 2013; Moreno-González et al., 2016; Valdés et al., 2014) at concentrations (in dry weight) similar to this study. Carbamazepine, primarily used for the treatment of epilepsy, is excreted by humans in its unaltered form along with several metabolites, including the metabolite 2-OH-CBZ (Zhang et al., 2008). Both compounds have been found in wastewaters at 219 and 370 ng L^{-1} for carbamazepine and 2-OH-CBZ, respectively (Snip et al., 2016), as well as in surface waters at 32 and 59 ng L^{-1} respectively (Aymerich et al., 2016). Therefore, the presence of 2-OH-CBZ in the fish from the current study could be attributed, on one hand, to the direct uptake of the metabolite from the aquatic environment, and on the other hand, to the metabolization of carbamazepine by the organism itself as other studies suggest. Bioaccumulation and metabolization of carbamazepine in fish were studied in mesocosms experiments by Valdés et al., who detected 2-OH-CBZ and EPO-Carbamazepine in different tissues of *J. multidentata* (Cyprinodontiformes, Anablepidae), although at much lower concentrations than the parent compound (Valdés et al., 2014). The CBZ:2-OH-CBZ ratio obtained ranged between 14:1 and 6:1 for all the organs of *J. multidentata*. However, metabolization of carbamazepine seems to be species dependent, since 2-OH-CBZ was not detected in biota samples from the carbamazepine exposure studies carried out with mussels (*Mytilus galloprovincialis*) (Boillot et al., 2015) or zebra mussel (Daniele et al., 2017) nor in vitro studies using rainbow trout liver fractions (Connors et al., 2013).

Sotalol and nadolol were also detected in fish from a few sampling sites. These compounds belong to the β-blocker therapeutic family, a group of cardiovascular drugs, which are highly prescribed and will be even more in the future due to the great prevalence of hypertension and rapid aging of western populations (Puckowski et al., 2016). Sotalol has been detected at very low concentrations in freshwater fish and mollusks in previous studies (Álvarez-Muñoz et al., 2015; Huerta et al., 2013). Salbutamol and hydrochlorothiazide, both extremely polar and therefore, not likely to be accumulated, were detected also with relatively high prevalence. Salbutamol is widely used in the treatment of asthma, and up to 80% of it is excreted as unchanged compound (Depaolini et al., 2016). Thus, this compound has been detected in wastewater effluents at 48 ng L^{-1} and in surface water below 5 ng L^{-1} (Gros et al., 2012; Santos et al., 2013). Hydrochlorothiazide was detected at levels up to 600 ng L^{-1} in surface waters and 3 μg L^{-1} in effluent waters by Batt et al. (Batt et al., 2016). This is probably due in part to high prescription amounts for hydrochlorothiazide, but also due to its reduced metabolism (for instance, excretion rate as unchanged form is in the range of 80–99%) (Stankiewicz et al., 2015). Both, salbutamol and hydrochlorothiazide, were also previously detected in fish samples at very low concentrations (<20 ng g^{-1}, dry weight) (Huerta et al., 2013; Moreno-González et al., 2016; Valdés et al., 2016).

3.2. Bioaccumulation factors

The calculation of bioaccumulation factors for each particular compound can help to assess its distribution in environmental compartments (biota and water). Bioaccumulation of two pharmaceuticals (hydrochlorothiazide and carbamazepine), among the five compounds analyzed both in water and fish analysis, was assessed. Only these two compounds were present in more than one fish sample, as sertraline was measured in fish only in one sample. Bioaccumulation factors (BAFs) were calculated as the ratio between the concentration of the pharmaceutical in the fish sample divided by the concentration of the same pharmaceutical in water (water concentrations were obtained from the study previously published by Batt et al. (Batt et al., 2016)). Results are presented in Table 2. BAFs were calculated collating data from 4 sampling sites where both water and fish data were available. In both cases, the observed mean BAF was lower (carbamazepine) or higher (hydrochlorothiazide) than the predicted BAF. This is often the case, as changes in pharmaceutical concentrations in river water over time may control effective exposure of fish during their lifespan. Location and time may affect the concentration of a pollutant in water, as well as the mobility of organisms. Thus, a relative disparity between predicted and observed BAFs is expected, and particularly in this case where only a few data points were viable for BAFs calculation due to the limitations of this study (only 5 compounds measured both in water and fish). Other known factors explaining variation in BAFs are, for instance, differences in lipid content among collected fish (higher lipid contents imply a higher capacity to store hydrophobic compounds), size (larger-bodied animals have slower elimination rates) or life stage (age reflects organism effective exposure under pseudo-persistent conditions) (Ruhi et al., 2015). However, lipid normalization has been proved to be ineffective to explain bioaccumulation of pharmaceuticals, in contrast with other organic contaminants (e.g. polychlorinated biphenyls (PCBs), dioxins, furans) (Du et al., 2014; Ramirez et al., 2009).

The bioaccumulation potential is often based on the log K_{ow} (or log P), as it was in the case of the predictive model applied (Arnot and Gobas, 2006). However, when this approach is used with

Table 2
Calculation of BAFs of two selected compounds.

	Carbamazepine	Fish Species	Hydrochlorothiazide	Fish Species
log P	2.8	–	−0.6	–
log Dow (pH 7)	2.8	–	−0.01	–
Max fish conc. (ng g^{-1})	7.4	–	8.4	–
Mean water conc. (ng L^{-1})[a]	97.6	–	55.9	–
Mean fish conc. (ng g^{-1})	3.0	–	0.8	–
Mean BAF (L kg^{-1})	49	–	20	–
Predicted BAF[b]	318	–	0.4	–
Measured BAFs (L kg^{-1})[c]	4.3 ± 0.2	Largemouth bass	4.5 ± 0.5	Largemouth bass
	5.1 ± 0.2	White sucker	9.7 ± 1.2	Channel catfish
	11.3 ± 0.4	Yellow perch	12.5 ± 1.5	Channel catfish
	90.9 ± 3.6	Smallmouth bass	16.7 ± 2.0	Common snook

[a] As published by Batt et al. (Batt et al., 2016).
[b] Log BAF = 0.86 log Dow + 0.12.
[c] Concentration ± analytical standard deviation.

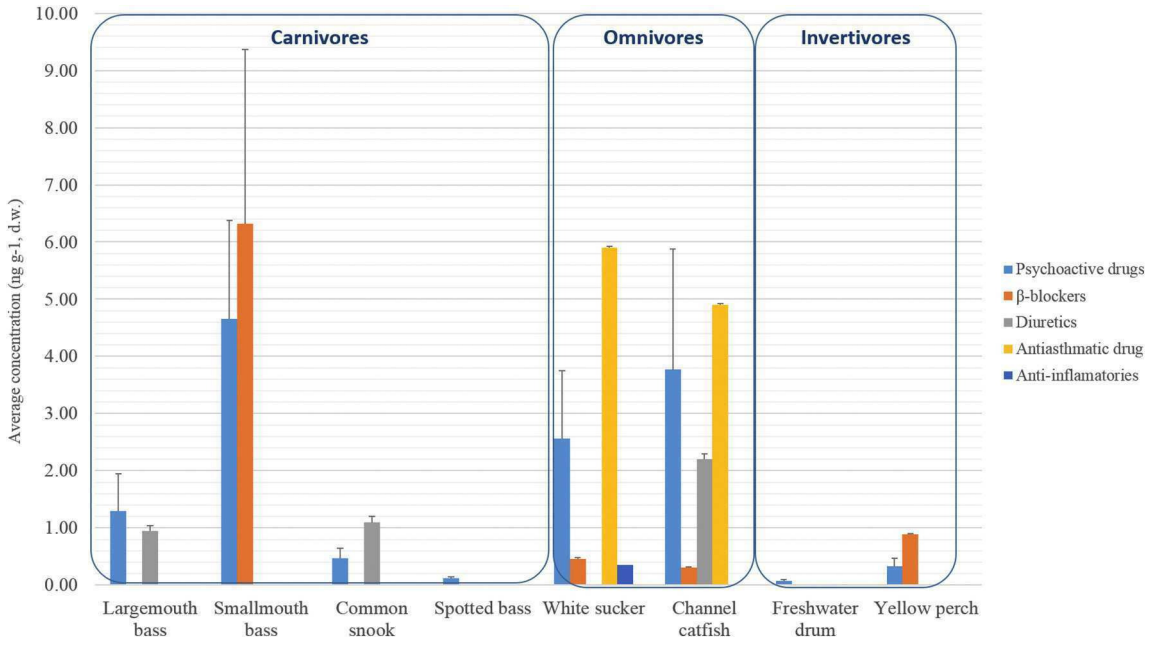

Fig. 2. Pharmaceutical average concentration according to the feeding strategies.

pharmaceuticals, which are ionizable, it forgoes the interactions of charged compounds with the heterogeneous membrane system, which contain polar and charged phospholipids and membrane proteins (Ismail et al., 2014; Puckowski et al., 2016). In this study, however, carbamazepine and hydrochlorothiazide were not ionized, so this approach was considered accurate for this particular case.

In summary, relatively low (when compared with other organic compounds) BAFs values for carbamazepine were calculated in this study, in agreement with previous reports in snails (BAF: 3.2) (Du et al., 2015), crustaceans (BCF: 12.6) (Vernouillet et al., 2010) and fish (BCF: 0.5–9) (Garcia et al., 2012; Tanoue et al., 2015; Valdés et al., 2016) both in field and laboratory studies.

3.3. Trophic niche and accumulation

A total of eight fish species were collected for the analysis of pharmaceuticals, including four carnivores (largemouth bass, smallmouth bass, common snook, spotted bass), two omnivores (white sucker and channel catfish), and two invertivores (yellow perch and freshwater drum). Fig. 2 represents the average accumulation of the measured pharmaceutical groups according to their feeding habits. Among them, channel catfish, white sucker, and smallmouth bass were the ones with a higher number of compounds detected (≥5). Smallmouth bass, channel catfish and white sucker also presented the highest average concentrations among all the species: between 4.9 and 6.3 ng g^{-1} (see Table S4).

There is little information about the degree of influence of the trophic niche and feeding strategy, if any, in the accumulation of pharmaceuticals in fish. In the studies published in the literature, no systematic approach to study species with similar feeding strategies or trophic niche has been found. Although previous studies have assessed concentrations of these contaminants in a variety of species, some of them can be considered comparable to the ones in the present studies. For instance, Brooks et al. (Brooks et al., 2005) detected antidepressants in channel catfish at concentrations ≤10 ng g^{-1} (wet weight). *Silurus glanis,* the European catfish, has also been found to accumulate β-blockers at low concentrations (Huerta et al., 2013). Antibiotics were detected in wild leather catfish (*Clarias fuscus*), with maximum concentrations up to tens of μg kg^{-1} (wet weight) (Zhao et al., 2015). Catfish feeding strategy is considered omnivorous and, in natural conditions, they feed on a large variety of items, including insects, plant seeds, and fish. However, most of the catfishes are carnivorous in the early beginning of their life. Afterwards, their feeding regime switches progressively to an omnivorous one (Bailey and Harrison, 1948).

In contrast, smallmouth bass (*Micropterus dolomieu*) is carnivorous through its lifespan, and its diet consists of crayfish, insects, and smaller fish (Poe et al., 1991). *Catostomus commersonii* is a catastomid (omnivore), which is probably the most broadly studied group in terms of pharmaceutical accumulation (Brooks et al., 2005; Huerta et al., 2013; Ramirez et al., 2009; Tanoue et al., 2015; Zhao et al., 2015). Catastomids feed on organisms located in bottom sediments, most commonly small invertebrates, algae and plant matter. It is still unclear why these three different species, with such diverse feeding strategies, showed more propensity to accumulate pharmaceuticals than others.

4. Conclusions

Evidence of occurrence of pharmaceuticals in fish tissues due to chronic exposure at environmental concentrations in water was established in this study. Thirteen pharmaceuticals were detected in fish fillets from urban systems, although they were measured at concentrations as low as 10 ng g^{-1}, which probably does not represent an immediate risk for the exposed organisms. Psychoactive drugs were the most frequently detected family, with venlafaxine and carbamazepine (and its metabolites) as the most representative compounds.

Acknowledgments

The tissue analyses conducted in the present study were funded by the European Union through the European Regional Development Fund. The present study was partly supported by the Economy and Knowledge Department of the Catalan Government (Consolidated Research Group 2014 SGR 291-ICRA). S. Rodriguez-Mozaz acknowledges Ramon y Cajal research fellowship RYC-2014-16707 from the Spanish Ministry of Economy and Competitiveness. Collection of fish samples for this study was made possible by the collaborative efforts of U.S. EPA's Office of Water and a national network of state, tribal, and federal agency partners. Disclaimer: The views expressed in this perspective are those of the authors and do not necessarily represent the views or policies of the US Environmental Protection Agency. Use of trade names does not imply endorsement of a particular product.

Appendix A. Supplementary data

Supplementary data to this article can be found online at https://doi.org/10.1016/j.scitotenv.2018.03.387.

References

Álvarez-Muñoz, D., Rodríguez-Mozaz, S., Maulvault, A.L., Tediosi, A., Fernández-Tejedor, M., Van den Heuvel, F., Kotterman, M., Marques, A., Barceló, D., 2015. Occurrence of pharmaceuticals and endocrine disrupting compounds in macroalgaes, bivalves, and fish from coastal areas in Europe. Environ. Res. 143, 56–64 Part.

Arnot, J.A., Gobas, F.A., 2006. A review of bioconcentration factor (BCF) and bioaccumulation factor (BAF) assessments for organic chemicals in aquatic organisms. Environ. Rev. 14, 257–297.

Aymerich, I., Acuña, V., Barceló, D., García, M.J., Petrovic, M., Poch, M., Rodriguez-Mozaz, S., Rodríguez-Roda, I., Sabater, S., von Schiller, D., Corominas, L., 2016. Attenuation of pharmaceuticals and their transformation products in a wastewater treatment plant and its receiving river ecosystem. Water Res. 100, 126–136.

Bailey, R.M., Harrison, H.M., 1948. Food habits of the southern channel catfish (*Ictalurus lacustris punctatus*) in the Des Moines River, Iowa. Trans. Am. Fish. Soc. 75, 110–138.

Batt, A.L., Kostich, M.S., Lazorchak, J.M., 2008. Analysis of ecologically relevant pharmaceuticals in wastewater and surface water using selective solid-phase extraction and UPLC−MS/MS. Anal. Chem. 80, 5021–5030.

Batt, A.L., Kincaid, T.M., Kostich, M.S., Lazorchak, J.M., Olsen, A.R., 2016. Evaluating the extent of pharmaceuticals in surface waters of the United States using a national-scale rivers and streams assessment survey. Environ. Toxicol. Chem. 35, 874–881.

Batt, A.L., Wathen, J.B., Lazorchak, J.M., Olsen, A.R., Kincaid, T.M., 2017. Statistical survey of persistent organic pollutants: risk estimations to humans and wildlife though consumption of fish from U.S. rivers. Environ. Sci. Technol. 51 (5), 3021–3031 (acs.est.6b05162).

Berrada, H., Borrull, F., Font, G., Marcé, R.M., 2008. Determination of macrolide antibiotics in meat and fish using pressurized liquid extraction and liquid chromatography-mass spectrometry. J. Chromatogr. A 1208, 83–89.

Boillot, C., Bueno, M.J.M., Munaron, D., Le Dreau, M., Mathieu, O., David, A., Fenet, H., Casellas, C., Gomez, E., 2015. Science of the total environment in vivo exposure of marine mussels to carbamazepine and and metabolization. Sci. Total Environ. 532, 564–570.

Brooks, B.W., Kevin Chambliss, C., Stanley, J.K., Ramirez, A., Banks, K.E., Johnson, R.D., Lewis, R.J., 2005. Determination of select antidepressants in fish from an effluent-dominated stream. Environ. Toxicol. Chem. 24, 464.

Cháfer-Pericás, C., Maquieira, Á., Puchades, R., Company, B., Miralles, J., Moreno, A., 2010. Multiresidue determination of antibiotics in aquaculture fish samples by HPLC-MS/MS. Aquac. Res. 41, 217–225.

Chu, S., Metcalfe, C.D., 2007. Analysis of paroxetine, fluoxetine and norfluoxetine in fish tissues using pressurized liquid extraction, mixed mode solid phase extraction cleanup and liquid chromatography-tandem mass spectrometry. J. Chromatogr. A 1163, 112–118.

Connors, K., Bowen, D., Fitzsimmons, P., Hoffman, A., Chambliss, K., Nichols, J., Brooks, B., 2013. Comparative pharmaceutical metabolism by rainbow trout (*Oncorhynchus mykiss*) liver S9 fractions. Environ. Toxicol. Chem. 32, 1810–1818.

Daniele, G., Fieu, M., Joachim, S., Bado-Nilles, A., Beaudouin, R., Baudoin, P., James-Casas, A., Andres, S., Bonnard, M., Bonnard, I., Geffard, A., Vulliet, E., 2017. Determination of carbamazepine and 12 degradation products in various compartments of an outdoor aquatic mesocosm by reliable analytical methods based on liquid chromatography-tandem mass spectrometry. Environ. Sci. Pollut. Res. 24, 16893–16904.

Depaolini, A.R., Fattore, E., Cappelli, F., Pellegrino, R., Castiglioni, S., Zuccato, E., Fanelli, R., Davoli, E., 2016. Source discrimination of drug residues in wastewater: the case of salbutamol. J. Chromatogr. B 1023–1024, 62–67.

Du, B., Haddad, S.P., Luek, A., Scott, W.C., Saari, G.N., Kristofco, L. a, Connors, K. a, Rash, C., Rasmussen, J.B., Chambliss, C.K., Brooks, B.W., 2014. Bioaccumulation and trophic dilution of human pharmaceuticals across trophic positions of an effluent-dependent wadeable stream. Philos. Trans. R. Soc. Lond. Ser. B Biol. Sci. 369, 1–10.

Du, B., Haddad, S.P., Scott, W.C., Chambliss, C.K., Brooks, B.W., 2015. Pharmaceutical bioaccumulation by periphyton and snails in an effluent-dependent stream during an extreme drought. Chemosphere 119, 927–934.

Fedorova, G., Golovko, O., Randak, T., Grabic, R., 2014. Storage effect on the analysis of pharmaceuticals and personal care products in wastewater. Chemosphere 111, 55–60.

Garcia, S.N., Foster, M., Constantine, L.A., Huggett, D.B., 2012. Field and laboratory fish tissue accumulation of the anti-convulsant drug carbamazepine. Ecotoxicol. Environ. Saf. 84, 207–211.

Grabicova, K., Lindberg, R.H., Östman, M., Grabic, R., Randak, T., Joakim Larsson, D.G., Fick, J., 2014. Tissue-specific bioconcentration of antidepressants in fish exposed to effluent from a municipal sewage treatment plant. Sci. Total Environ. 488–489, 46–50.

Grabicova, K., Grabic, R., Blaha, M., Kumar, V., Cerveny, D., Fedorova, G., Randak, T., 2015. Presence of pharmaceuticals in benthic fauna living in a small stream affected by effluent from a municipal sewage treatment plant. Water Res. 72, 145–153.

Gros, M., Rodríguez-Mozaz, S., Barceló, D., 2012. Fast and comprehensive multi-residue analysis of a broad range of human and veterinary pharmaceuticals and some of their metabolites in surface and treated waters by ultra-high-performance liquid chromatography coupled to quadrupole-linear ion trap tandem. J. Chromatogr. A 1248, 104–121.

Huerta, B., Rodríguez-Mozaz, S., Barceló, D., 2012. Pharmaceuticals in biota in the aquatic environment: analytical methods and environmental implications. Anal. Bioanal. Chem. 404, 2611–2624.

Huerta, B., Jakimska, A., Gros, M., Rodríguez-Mozaz, S., Barceló, D., 2013. Analysis of multiclass pharmaceuticals in fish tissues by ultra-high-performance liquid chromatography tandem mass spectrometry. J. Chromatogr. A 1288, 63–72.

Ismail, N.S., Müller, C.E., Morgan, R.R., Luthy, R.G., 2014. Uptake of contaminants of emerging concern by the bivalves *Anodonta californiensis* and *Corbicula fluminea*. Environ. Sci. Technol. 48, 9211–9219.

Kolpin, D.W., Furlong, E.T., Meyer, M.T., Thurman, E.M., Zaugg, S.D., Barber, L.B., Buxton, H.T., 2002. Pharmaceuticals, hormones, and other organic wastewater contaminants in U.S. streams, 1999−2000: a national reconnaissance. Environ. Sci. Technol. 36, 1202–1211.

Kostich, M.S., Batt, A.L., Lazorchak, J.M., 2014. Concentrations of prioritized pharmaceuticals in effluents from 50 large wastewater treatment plants in the US and implications for risk estimation. Environ. Pollut. 184, 354–359.

Liu, J., Lu, G., Xie, Z., Zhang, Z., Li, S., Yan, Z., 2015. Occurrence, bioaccumulation and risk assessment of lipophilic pharmaceutically active compounds in the downstream rivers of sewage treatment plants. Sci. Total Environ. 511, 54–62.

Margiotta-Casaluci, L., Owen, S.F., Cumming, R.I., De Polo, A., Winter, M.J., Panter, G.H., Rand-Weaver, M., Sumpter, J.P., 2014. Quantitative cross-species extrapolation between humans and fish: the case of the anti-depressant fluoxetine. PLoS One 9.

Martínez Bueno, M.J., Boillot, C., Fenet, H., Chiron, S., Casellas, C., Gómez, E., 2013. Fast and easy extraction combined with high resolution-mass spectrometry for residue analysis of two anticonvulsants and their transformation products in marine mussels. J. Chromatogr. A 1305, 27–34.

Martínez Bueno, M.J., Boillot, C., Munaron, D., Fenet, H., Casellas, C., Gómez, E., 2014. Occurrence of venlafaxine residues and its metabolites in marine mussels at trace levels: development of analytical method and a monitoring program. Anal. Bioanal. Chem. 406, 601–610.

Mimeault, C., Woodhouse, A.J., Miao, X.-S., Metcalfe, C.D., Moon, T.W., Trudeau, V.L., 2005. The human lipid regulator, gemfibrozil bioconcentrates and reduces testosterone in the goldfish, *Carassius auratus*. Aquat. Toxicol. 73, 44–54.

Moreno-González, R., Rodríguez-Mozaz, S., Huerta, B., Barceló, D., León, V.M., 2016. Do pharmaceuticals bioaccumulate in marine molluscs and fish from a coastal lagoon? Environ. Res. 146, 282–298.

OECD, 2013. Health at a Glance 2013: OECD Indicators. https://doi.org/10.1787/health_glance-2013-en.

van der Oost, R., Beyer, J., Vermeulen, N.P., 2003. Fish bioaccumulation and biomarkers in environmental risk assessment: a review. Environ. Toxicol. Pharmacol. 13, 57–149.

Poe, T.P., Hansel, H.C., Vigg, S., Palmer, D.E., Prendergast, L.A., 1991. Feeding of predaceous fishes on out-migrating juvenile salmonids in John Day Reservoir, Columbia River. Trans. Am. Fish. Soc. 120, 405–420.

Puckowski, A., Mioduszewska, K., Łukaszewicz, P., Borecka, M., Caban, M., Maszkowska, J., Stepnowski, P., 2016. Bioaccumulation and analytics of pharmaceutical residues in the environment: a review. J. Pharm. Biomed. Anal. 127, 232–255.

Ramírez, A.J., Mottaleb, M.A., Brooks, B.W., Chambliss, C.K., 2007. Analysis of pharmaceuticals in fish using liquid chromatography-tandem mass spectrometry. Anal. Chem. 79, 3155–3163.

Ramirez, A., Brain, R., Usenko, S., Mottaleb, M., O'Donnell, J., Stahl, L., Wathen, J., Snyder, B., Pitt, J., Perez-Hurtado, P., Dobbins, L., Brooks, B., Chambliss, C., 2009. Occurence of pharmaceuticals and personal care products in fish: results of a national pilot study in the United States. Environ. Toxicol. Chem. 28, 2587–2597.

Rodríguez-Mozaz, S., Huerta, B., Barceló, D., 2016. Bioaccumulation of Emerging Contaminants in Aquatic Biota: Patterns of Pharmaceuticals in Mediterranean River Networks. In: Petrovic, M., Sabater, S., Elosegi, A., Barceló, D. (Eds.), Emerging Contaminants in River Ecosystems: Occurrence and Effects Under Multiple Stress Conditions. Springer International Publishing, Cham, pp. 121–141.

Rodríguez-Mozaz, S., Alvarez-Muñoz, D., Barceló, D., 2017. Pharmaceuticals in the Marine Environment: Analytical Techniques and Applications, in: Environmental Problems in Marine Biology: Methodological Aspects and Applications. Taylor & Francis Publisher. CRC Press, Boca Raton, FL, pp. 268–316.

Ruhi, A., Acuña, V., Barcelò, D., Huerta, B., Mor, J.R., Rodriguez-Mozaz, S., Sabater, S., 2015. Bioaccumulation and trophic magnification of pharmaceuticals and endocrine disruptors in a Mediterranean river food web. Sci. Total Environ. 540, 250–259.

Santos, L.H.M.L.M., Gros, M., Rodriguez-Mozaz, S., Delerue-Matos, C., Pena, A., Barceló, D., Montenegro, M.C.B.S.M., 2013. Contribution of hospital effluents to the load of pharmaceuticals in urban wastewaters: identification of ecologically relevant pharmaceuticals. Sci. Total Environ. 461–462, 302–316.

Schultz, M.M., Furlong, E.T., 2008. Trace analysis of antidepressant pharmaceuticals and their select degradates in aquatic matrixes by LC/ESI/MS/MS. Anal. Chem. 80, 1756–1762.

Schultz, M.M., Furlong, E.T., Kolpin, D.W., Werner, S.L., Schoenfuss, H.L., Barber, L.B., Blazer, V.S., Norris, D.O., Vajda, A.M., 2010. Antidepressant Pharmaceuticals in two U.S. effluent-impacted streams: occurrence and fate in water and sediment, and selective uptake in fish neural tissue. Environ. Sci. Technol. 44, 1918–1925.

Silva, L.J.G., Pereira, A.M.P.T., Meisel, L.M., Lino, C.M., Pena, A., 2015. Reviewing the serotonin reuptake inhibitors (SSRIs) footprint in the aquatic biota: uptake, bioaccumulation and ecotoxicology. Environ. Pollut. 197, 127–143.

Snip, L.J.P., Flores-Alsina, X., Aymerich, I., Rodríguez-Mozaz, S., Barceló, D., Plósz, B.G., Corominas, L., Rodriguez-Roda, I., Jeppsson, U., Gernaey, K.V., 2016. Generation of synthetic influent data to perform (micro)pollutant wastewater treatment modelling studies. Sci. Total Environ. 569–570, 278–290.

Stahl, L.L., Snyder, B.D., Olsen, A.R., Kincaid, T.M., Wathen, J.B., McCarty, H.B., 2014. Perfluorinated compounds in fish from U.S. urban rivers and the Great Lakes. Sci. Total Environ. 499, 185–195.

Stankiewicz, A., Giebułtowicz, J., Stankiewicz, U., Wroczyński, P., Nałęcz-Jawecki, G., 2015. Determination of selected cardiovascular active compounds in environmental aquatic samples – methods and results, a review of global publications from the last 10 years. Chemosphere 138, 642–656.
Stevens, D.L., Olsen, A.R., 2004. Spatially balanced sampling of natural resources. J. Am. Stat. Assoc. 99, 262–278.
Strahler, A.N., 1957. Quantitative analysis of watershed geomorphology. Trans. Am. Geophys. Union 38, 913.
Tanoue, R., Nomiyama, K., Nakamura, H., Hayashi, T., Kim, J.W., Isobe, T., Shinohara, R., Tanabe, S., 2014. Simultaneous determination of polar pharmaceuticals and personal care products in biological organs and tissues. J. Chromatogr. A 1355, 193–205.
Tanoue, R., Nomiyama, K., Nakamura, H., Kim, J.-W., Isobe, T., Shinohara, R., Kunisue, T., Tanabe, S., 2015. Uptake and tissue distribution of pharmaceuticals and personal care products in wild fish from treated-wastewater-impacted streams. Environ. Sci. Technol. 49, 11649–11658.
U.S. EPA, 2013. National Rivers and Streams Assessment Field Operations Manual.
US-EPA, 2000. Fish sampling and analysis. Guid. Assess. Chem. Contam. Data Use Fish Advis. 1, 1–485.
Valdés, M.E., Amé, M.V., Bistoni, M. de los A., Wunderlin, D.A., 2014. Occurrence and bioaccumulation of pharmaceuticals in a fish species inhabiting the Suquia River basin (Cordoba, Argentina). Sci. Total Environ. 472, 389–396.
Valdés, M.E., Huerta, B., Wunderlin, D.A., Bistoni, M.A., Barcelò, D., Rodriguez-Mozaz, S., 2016. Bioaccumulation and bioconcentration of carbamazepine and other pharmaceuticals in fish under field and controlled laboratory experiments. Evidences of carbamazepine metabolization by fish. Sci. Total Environ. 557–558, 58–67.
Valenti, T.W., Gould, G.G., Berninger, J.P., Connors, K.A., Keele, N.B., Prosser, K.N., Brooks, B.W., 2012. Human therapeutic plasma levels of the selective serotonin reuptake inhibitor (SSRI) sertraline decrease serotonin reuptake transporter binding and shelter-seeking behavior in adult male fathead minnows. Environ. Sci. Technol. 46, 2427–2435.
Vernouillet, G., Eullaffroy, P., Lajeunesse, A., Blaise, C., Gagné, F., Juneau, P., 2010. Toxic effects and bioaccumulation of carbamazepine evaluated by biomarkers measured in organisms of different trophic levels. Chemosphere 80, 1062–1068.
Wathen, J.B., Lazorchak, J.M., Olsen, A.R., Batt, A., 2015. A national statistical survey assessment of mercury concentrations in fillets of fish collected in the U.S. EPA national rivers and streams assessment of the continental USA. Chemosphere 122, 52–61.
Zhang, Y., Geißen, S.U., Gal, C., 2008. Carbamazepine and diclofenac: removal in wastewater treatment plants and occurrence in water bodies. Chemosphere 73, 1151–1161.
Zhao, J.L., Liu, Y.S., Liu, W.R., Jiang, Y.X., Su, H.C., Zhang, Q.Q., Chen, X.W., Yang, Y.Y., Chen, J., Liu, S.S., Pan, C.G., Huang, G.Y., Ying, G.G., 2015. Tissue-specific bioaccumulation of human and veterinary antibiotics in bile, plasma, liver and muscle tissues of wild fish from a highly urbanized region. Environ. Pollut. 198, 15–24.

Record of Percentage of Agreement

From: Lazorchak, Jim <Lazorchak.Jim@epa.gov>
Sent: Friday, April 24, 2020 11:51 AM
To: Wathen, John <Wathen.John@epa.gov>
Cc: Olsen, Tony <Olsen.Tony@epa.gov>; Batt, Angela <Batt.Angela@epa.gov>; Kincaid, Tom <Kincaid.Tom@epa.gov>
Subject: Re: STAA Award for NRSA 2008/2009 papers

Proposed percentage of contribution of Co Authors

John – 27%
Angela – 28%
Jim – 20%
Tony – 15%
Tom – 10 %

Jim Lazorchak
Aquatic Biologist U.S. EPA
Aquatic Research Facility Manager

From: Olsen, Tony <Olsen.Tony@epa.gov>
Sent: Friday, April 24, 2020 2:59 PM
To: Lazorchak, Jim <Lazorchak.Jim@epa.gov>; Wathen, John <Wathen.John@epa.gov>
Cc: Batt, Angela <Batt.Angela@epa.gov>; Kincaid, Tom <Kincaid.Tom@epa.gov>
Subject: RE: STAA Award for NRSA 2008/2009 papers

Works for me.

Anthony (Tony) R. Olsen | Pacific Ecological Systems Division | USEPA CPHEA | 200 S.W. 35th Street | Corvallis, OR 97333 | Olsen.Tony@epa.gov | (541) 754-4790

ARM Web Page: http://archive.epa.gov/nheerl/arm/web/html/index.html

NARS Web Page: http://water.epa.gov/type/watersheds/monitoring/aquaticsurvey_index.cfm

From: Kincaid, Tom <Kincaid.Tom@epa.gov>
Sent: Friday, April 24, 2020 1:57 PM
To: Lazorchak, Jim <Lazorchak.Jim@epa.gov>
Cc: Olsen, Tony <Olsen.Tony@epa.gov>; Batt, Angela <Batt.Angela@epa.gov>; Wathen, John <Wathen.John@epa.gov>
Subject: RE: STAA Award for NRSA 2008/2009 papers

Jim,

Hello. I believe that 10% is a reasonable value for my contribution.

Thank you. I hope that everyone seeing this message is healthy and doing well.

Tom

Statistician (Biology)

ORD-CPHEA-PESD-FEB

From: Wathen, John <Wathen.John@epa.gov>
Sent: Tuesday, April 28, 2020 8:38 AM
To: Lazorchak, Jim <Lazorchak.Jim@epa.gov>; Batt, Angela <Batt.Angela@epa.gov>; Olsen, Tony <Olsen.Tony@epa.gov>; Kincaid, Tom <Kincaid.Tom@epa.gov>
Subject: RE: Record of Agreement

I agreed to these percentages.

John – 27%
Angela – 28%
Jim – 20%
Tony – 15%
Tom – 10 %

Jim Lazorchak
Aquatic Biologist U.S. EPA
Aquatic Research Facility Manager

~John Wathen

From: Batt, Angela <Batt.Angela@epa.gov>
Sent: Tuesday, April 28, 2020 7:49 AM
To: Lazorchak, Jim <Lazorchak.Jim@epa.gov>
Subject: RE: STAA Award for NRSA 2008/2009 papers

Yes, I am in agreement with the percentages listed below, and with my percentage being 28%.

Thanks Jim.

Angela L. Batt, Ph.D.
Research Chemist
U.S. Environmental Protection Agency
Office of Research and Development
Center for Environmental Solutions and Emergency Response (CESER)
Cincinnati, OH 45268

April 28, 2020

To whom it may concern:

I am writing to express my strong support for John Wathen in the Office of Water and Angela Batt in the Office of Research and Development (ORD) and the related ORD co-authors for a Scientific and Technical Achievement Award. Their cross-office coordinated research on the accumulation of pollutants such as metals and organics in fish and the risk to both humans and wildlife from eating those fish has advanced the state of knowledge in the area and informs state and tribal fish advisory programs across the nation. Two papers written by John and Angela --"A national statistical survey assessment of mercury concentrations in fillets of fish collected in the U.S. EPA national rivers and streams assessment of the continental USA" (published in Chemosphere) and "Statistical Survey of Persistent Organic Pollutants: Risk Estimations to Humans and Wildlife through Consumption of Fish from U.S. Rivers" (published in Environmental Science & Technology) exemplify their work.

Most papers on pollutant impacts focus on impacts to either wildlife or humans. The papers being nominated for this award innovatively combine the two. Angela and John helped create a "One Health" approach that examined the consumption of fish by both humans and wildlife on a national scope, based on the first national statistical survey of fish tissue in rivers that EPA conducted.

The research described in the articles being nominated directly support EPA's mission and especially the Office of Water's human and aquatic life protection responsibilities. The fish tissue component of the national river and stream assessment that is the origin of data for the two papers is housed in my branch and the funding comes from my budget. The assessment of contaminant concentrations in fish is essential for the formulation of national and state policy regarding these contaminants, including focusing fish consumption advisories and fulfilling CWA requirements under Section 305(b). Since current research tends to focus on emerging contaminants, persistent organic pollutants and mercury are often overlooked. These papers demonstrate that even decades after many of these highly potent, carcinogenic compounds are no longer manufactured or used, they are still found at significant levels of concern in fish. These results are instrumental in helping EPA provide guidance to states and tribes on which pollutants they should monitor and issue fish advisories for.

Communication of the fish tissue concentration results of the national aquatic studies has been a major challenge over the years. For example, previous efforts to document results from similar studies in EPA reports has proven to be resource-intensive. We greatly appreciate the collaboration with ORD on the statistical framework for the national survey, and in the case of these articles, analytical support, aquatic life participation, and paper authorship. The publication of these articles makes the valuable scientific findings broadly available.

The collaboration between the two offices and ensuing innovative peer-reviewed journal articles broadens the use of the data to One Health assessments of the potential for impacts to both the aquatic life and human health communities. This has benefitted both EPA offices, the quality and utility of the assessments, and fulfillment of the Agency mission.

I am pleased to endorse this nomination and thank you for your consideration of these articles for a STAA. Please do not hesitate to contact me by phone (202-566-0996) or email (barash.shari@epa.gov) if you have any questions or if I can be of any additional assistance.

Sincerely,

Shari Z. Barash /s/

Shari Z. Barash
Chief, National Branch
Office of Water, Office of Science and Technology

Environment and Climate Change Canada | Environnement et Changement climatique Canada

Aquatic Contaminants Research Division
867 Lakeshore Rd.,
Burlington, ON L7S 1A1

Phone: 905-319-6921
Fax: 905-336-6430
E-mail: Derek.Muir@Canada.ca

April 30, 2020

Dr. Jim Lazorchak
U.S.EPA ORD
Watershed Management Branch
Watershed & Ecosystem Characterization Division
Cincinnati, OH 45268

Dear Jim,

Thank you for the invitation to comment on the two papers that have been nominated for the STAA Award (Batt et al. "Statistical Survey of Persistent Organic Pollutants: Risk Estimations to Humans and Wildlife through Consumption of Fish from U.S. Rivers", Environ. Sci. Technol. 2017; Whalen et al. "A national statistical survey assessment of mercury concentrations in fillets of fish collected in the U.S. EPA national rivers and streams assessment of the continental USA " Chemosphere 2015. These papers, along with related articles on perfluoroalkyl acids in fish and pharmaceuticals in water and fish, take a highly innovative approach to examining spatial trends of priority toxic contaminants in fish and to assessing the risk to human and wildlife consumers. The innovation begins with the use of a probability-based approach to select sampling sites. This was a key feature of the 2008–09 National Rivers and Streams Assessment (NRSA) river survey upon which the sampling design for collection of fish was based. The NRSA was underpinned by important databases such as the National Hydrography Dataset (NHD) and national urban boundary information from census data. The final sampling framework was a spatially balanced and based on randomly selected sites within defined stream/river reaches distinguishing between urban and non-urban areas. Single pooled samples of fish were then analysed from each location. The spatial balance and representativeness generated by the probabilistic framework allowed the dataset to be interrogated for various questions such as prevailing concentrations of PCBs and mercury in fish at a national levels and within nonurban and urban waters. Also assessments of prevailing concentrations could be done by ecoregion.

The above is highly innovative way to assess spatial trends of contaminants in fish. Other national and international programs that I am familiar with, including the national programs within the European Union's Water Framework Directive (Guidance Document No. 32 on Biota Monitoring) and Canada's national programs (eg Gewurtz et al Environ Int 2013), as well as guidance under the Arctic Monitoring and Assessment Program, stress careful selection of sampling sites, fish size, sample size etc for contaminant trend monitoring. But these programs are rarely able to address questions about prevailing national or regional levels of contaminants because sampling is not statistically spatially balanced. Also interesting questions such as percent of streams/rivers kilometers sampled that exceed guidelines for possible adverse effects cannot be addressed. Why haven't these programs, especially those in Europe, adopted this probabilistic sampling approach, given similar population density and urbanization as many areas of the USA? Possibly the answer to this question is that it requires a high level of commitment over the long term to build upon existing databases such as the NHD, strong basic science (eg Stevens and Olsen 2004), and strong scientific leadership for study design and data interpretation. This strength is evident in the two articles and in

the related reports such as the NRSA technical document (2016). There is simply no other program globally that can bring all of these aspects together in one study.

Another unique aspect of the two studies is that the contaminant concentrations in fish can be compared with aquatic life thresholds as well as human health criteria values. Of course, this is enabled by the strong underlying eco- and mammalian toxicology data for PCBs, DDT, PBDEs and mercury, and the development of wildlife values and reference dose values that has occurred over the past 40+ years, much of it by USEPA labs. But the balanced spatial design allows questions such as what percent of river kilometers exceed these values? It enables watershed or water quality managers to drill down to specific areas of concern. This question is difficult and expensive to answer with conventional non-probabilistic type sampling designs which tend to be very site specific. Indeed an interesting aspect of the study design is how parsimonious it is in terms of samples analysed. Only one pooled sample per site is analysed. But this enables nation wide coverage in a cost effective manner when the sites are statistically representative.

An interesting aspect of the papers by Matt et al and Whalen et al is the convergence of the risks to wildlife and humans. In the case of mercury, the risks to piscivorous avian species were similar to risks for humans consuming 2 fish meals per month, while mink were more at risk than humans. Similarly, from 6.1 to 25% of river km for PCB concentrations in fish exceeded non-cancer screening values, a level which was higher than for mammalian or avian wildlife values. In other words, the human thresholds of concern were protective of fish eating wildlife. Thus both studies contribute very effectively to the “One Health” concept which recognizes ecosystem linkages and shared health problems of humans and wildlife. However, these studies carry more weight than most aquatic environmental risk assessments because of the balanced spatial design and the statistical ability to address broad questions for the entire USA.

It was interesting to look up the articles that have cited the papers by Matt et al and Whalen et al. Major aquatic biota monitoring programs in Germany (Fliedner et al. Environ Pollut 2018), Spain (Eljarrat & Barceló 2018) and China (Sun et al Sci Total Environ 2018) have cited this work. None of the studies have used the probabilistic sampling design, possibly for the reasons mentioned above, but all have taken a similar approach in terms of combining human and wildlife thresholds for assessment of contaminant exposure and possible effects.

In summary, after reading these papers and related studies, I strongly believe that the two articles meet the criteria for Science Quality and Innovation and Scientific Significance for the Scientific and Technical Achievement Award through a combination of novel and innovative design as well as impact within the field of environmental toxicology.

Yours sincerely,

Derek Muir PhD
Fellow Royal Society of Canada, Fellow SETAC, Fellow Chemical Institute of Canada
Senior Research Scientist
Adjunct Professor, University of Toronto, Dept of Chemistry
Adjunct Professor, School of Environmental Sciences, University of Guelph

Table of Contents

General_Authors_Publications.....2
LI-265828_Journal_Article_aws21131.....18
LI-265828_Journal_Article_Supplementary_Information_aws21131-sup-0001-supinfo.30
ScienceMatters+WaterOnlineNewsStory.....57
RecordOfPercentageEmails.....60

STAA REPORT FOR THE SCIENTIST NOMINATIONS

General Information:

Nomination ID/App ID:	20-097
Research Category Primary:	Control Systems and Technology (CS)
Research Category Secondary:	Other Environmental Research (OR)
Laboratory/Office Name:	ORD
Nomination Entered By:	Craig Patterson

Eligibility Checklist:

[Y] The nominated publication(s) has not been submitted to a previous STAA competition.

[Y] The nominated publication(s) was published on or before January 1, 2017 and on or after January 1,2012

[Y] The principal author was an EPA employee or a PHS employee assigned to EPA when the research was performed

[Y] The EPA authors (includes PHS employees assigned to EPA) contributed collectively a minimum of 50% toward the publication(s)

Nominating Official Name:	Regan Murray
Nominating Official Title:	SUPERVISORY INTERDISCIPLINARY SCIENTIST
Nominating OfficialEmail:	murray.regan@epa.gov
STAA Coordinator Name:	Kathleen Wiser
STAA Coordinator Email:	wiser.kathi@epa.gov

Justifications:

Justification 1:

In U.S. EPA's Strategic Plan (FY 2018-2022), EPA's Mission is to work together to protect human health and the environment. Specifically, EPA's Goal 1 prioritizes the delivery of real results to provide Americans with clean air, land, and water, and ensure chemical safety as part of EPA's Core Mission. Tens of thousands of homes, primarily in tribal and disadvantaged communities and the territories, lack access to basic sanitation and drinking water. EPA's Strategic Plan promotes work with states, tribes, territories, and local communities to better safeguard human health; maintain, restore, and improve water quality; and make America's water systems sustainable and secure, supporting new technology and innovation wherever possible. This research aligns with EPA's Strategic Mission and Goal 1 as described below.

Working with EPA Region 8 and Colorado Department of Public Health and Environment (CDPHE), this project focused on improvement of human health in the municipalities of Fountain, Security, and Widefield, Colorado. To deliver real results to Americans, this study provided PFAS water treatment alternatives to rural residents with well water and helped to limit exposure to PFAS in residential drinking water systems. With well water contaminated with Perfluorooctanoic Acid (PFOA) and Perfluorooctane Sulfonate (PFOS) greater than the U.S. EPA health advisory level, reverse osmosis and granular activated carbon water systems were tested with the water quality characteristics and six PFAS contaminants found in Colorado's Widefield Aquifer region groundwater samples. This project also documented the ease of use of these household water systems to assist homeowners with installation, operation and maintenance of their private water treatment systems. According to EPA's Strategic Plan, sustaining the quality of our water resources is essential to safeguarding human health. This research met the Strategic Plan objectives of 1) continuing to protect and restore water resources, including sources of drinking water, from contamination; 2) taking actions to address known and emerging contaminants that endanger human health; and 3) supporting states, tribes, territories, and local communities in implementing water programs by providing guidance, training, and information.

Justification 2A:

n/a

Justification 2B:

EPA Author: Craig Patterson

Publication Title - Nanofiltration Membranes for Removal of Color and Pathogens in Small Public Drinking Water Sources

Year: 2015

Award: n/a

Justification 2C:

The two publications investigate different contaminants, treatment processes, and source waters. This 2020 nomination focuses on removal of PFAS from household well water using reverse osmosis and granular activated carbon adsorption systems. The 2015 nomination focused on removal of color and pathogens from surface water using nanofiltration systems in small utilities.

Justification 2D:

n/a

Justification 2E:

n/a

Justification 3A:

This research study resulted in invited presentations at three national webinars and one international conference in 2018. This research study received an EPA Silver Medal Honor Award in 2019. Since being published, this journal article

has been cited five times and was the most-read paper (36 times) in the Journal of AWWA Water Sciences in 2019. It has also been tweeted three times and is the subject of a Science Matters/Water Online News Story.

1. If research has been invited for presentation at national/international societies

This household water system research on removal of PFAS from well water was the focus of three invited webinars and one international conference that attracted hundreds of national and international attendees as listed below.

1. Patterson, C., Burkhardt, J., Dyment, S., Merritt, S., Zintek, L., Kleinmaier, D., Schupp, D., and Krishnan, E.R., "PFAS Removal Using Household Water Treatment Systems: Point-of-Use (POU)/Point-of-Entry (POE)", Presented at Environmental Council of the States - EPA Bi-Monthly PFAS Call (210 attendees) October 26, 2018.

2. Patterson, C., Burkhardt, J., Dyment, S., Merritt, S., Zintek, L., Kleinmaier, D., Schupp, D., and Krishnan, E.R., "PFAS Removal Using Household Water Treatment Systems: Point-of-Use (POU)/Point-of-Entry (POE)", Presented to EPA Region 8 and the Colorado Department of Public Health and Environment (CDPHE), November 1, 2018.

3. Patterson, C., Burkhardt, J., Dyment, S., Merritt, S., Zintek, L., Kleinmaier, D., Schupp, D. and Krishnan, E.R., "Effectiveness of Point of Entry Systems to Remove Select Per- and Poly- fluoroalkyl Substances from Drinking Water", Presented and published in the Proceedings of American Water Works Association (AWWA) Water Quality Technology Conference (WQTC), Toronto, Ontario, Canada, November 12, 2018.

4. Patterson, C., Burkhardt, J., Dyment, S., Merritt, S., Zintek, L., Kleinmaier, D., Schupp, D., and Krishnan, E.R., "Effectiveness of Point of Entry Systems to Remove Widefield Aquifer Per- and Poly- fluoroalkyl Substances from Water", Region 8 Clu-In Webinar (322 attendees), November 26, 2018.

2. Unique source of funding for research

Project funding was competitively awarded based on a Regional Applied Research Effort (RARE) proposal in 2017 with follow-on EPA PFAS funding in 2020 as described below.

2017 – Region 8 RARE Project funds with Stephen Dyment (OSP) and Steven Merritt (Region 8) "Effectiveness of Point of Entry (POE) Systems to Remove Select Per- and Polyfluoroalkyl Substances from Drinking Water" in Colorado

With per- and polyfluoroalkyl substances (PFAS) contamination at sites in EPA Region 8, a PFAS removal study was designed based on NSF International Standard P473 to determine the capabilities and ease of use of commercially available off-the-shelf reverse osmosis (RO) and granular activated carbon (GAC) point of entry treatment systems. The study was performed using a water matrix that represents Widefield Aquifer groundwater conditions and likely release scenarios from aqueous film forming foam (AFFF) used for firefighting applications.

2020 – Office of Research and Development (ORD), Center for Environmental Solutions and Emergency Response (CESER), Water Infrastructure Division (WID) PFAS funds to continue collaboration with EPA Region 8, CDPHE and residents in Colorado

A PFAS removal study is currently being conducted to determine the capabilities and ease of use of commercially available off-the-shelf household water treatment systems that use anion exchange (AEX) resins. AEX resins have shown excellent PFAS removal capabilities at a public water utility in Widefield, Colorado. This is a follow-on study to the previous RO and GAC studies that will provide guidance on a third household treatment alternative (AEX Resin) for PFAS-contaminated well water to residents of Fountain, Security, and Widefield, Colorado.

3. Any awards Internal/External to EPA that were received for the research

This journal article was the primary reason for the EPA Silver Medal Honor Award for the ORD Water PFAS Team in 2019. The citation on the National Honor Award certificate reads *"For its responsive, high priority, and visible work towards helping homeowners and communities understand and treat PFAS contamination in drinking water".* Excerpts from the write-up for the EPA Silver Medal Honor Award are provided below.

The presence of Per- and Poly-fluoroalkyl Substances (PFAS) in air, land, and water is a major environmental issue, and the heavy use of these chemicals by numerous industries has resulted in hundreds of these chemicals in the environment. Research on the treatment and removal of these compounds is a high priority for EPA due to their harmful human health effects. The Water PFAS Team rapidly formed to address this critical issue. Their efforts included researching the effectiveness of point-of-entry water treatment systems for the removal of PFAS from drinking water and updating the Drinking Water Treatability Database (TDB) to include the latest PFAS treatment and cost information. In a short amount of time, the Team has produced high quality results which have proven to be of interest and use to homeowners and representatives of utilities, consulting firms, states, and EPA regional offices who have attended their webinars and conference presentations.

In 2018, the Water PFAS Team conducted experimental research on the effectiveness of household water treatment systems at removing PFAS from drinking water. The project used Colorado Widefield Aquifer test water, selected because PFAS contamination had been detected in private wells in that area, affecting more than 60,000 residents. The team analyzed PFAS samples, evaluated PFAS removal capabilities, the costs, and the ease of use of several commercially available off-the shelf reverse osmosis (RO) systems and granular activated carbon (GAC) media. The results of this work have been presented at several conferences and webinars, with an overall audience of more than 1,300 individuals.

The Water PFAS Team, with decades of collective experience in drinking water treatment and policy, formed quickly in response to a growing environmental and human health issue. The Team provided timely and useful information on PFAS treatment to several thousand water utilities, decision-makers, and others, as well as providing information to protect more than 60,000 residents of Colorado. Taken together, this research on the PFAS-removing capabilities of RO and GAC systems, and the updates to the TDB are very impactful as water systems and communities seek tools to prevent PFAS exposure from drinking water.

4. Number of times the publication has been downloaded/viewed

Most-Read AWWA Water Science Journal Article of 2019

In 2019, this journal article was the most-read paper in the Journal of AWWA Water Science. The article “Effectiveness of pointofuse/pointofentry systems to remove per and polyfluoroalkyl substances from drinking water” has currently been read 36 times.

5. How many times it has been cited (Google Scholar)

This journal article has been cited five times (Google Scholar lists six citations, but one is a duplicate), read 36 times, tweeted 3 times (in Europe and Australia reaching an upper bound of 31,063 followers) and is the subject of a Science Matters/Water Online news story “EPA Researchers Investigate the Effectiveness of Pointofuse/Pointofentry Systems to Remove Per and Polyfluoroalkyl Substances from Drinking Water” published on January 22, 2020 (see attached supplementary file "ScienceMatters+WaterOnlineNewsStory.docx").

Google Scholar Citations

1. Zeng, C, Atkinson, A, Sharma, N, et al. “Removing per and polyfluoroalkyl substances from groundwaters using activated carbon and ion exchange resin packed columns”, AWWA Wat Sci. 2020;e1172, https://doi.org/10.1002/aws2.1172.

2. Nicholas J. Herkert, John Merrill, Cara Peters, David Bollinger, Sharon Zhang, Kate Hoffman, P. Lee Ferguson, Detlef R. U. Knappe, and Heather M. Stapleton, “Assessing the Effectiveness of Point-of-Use Residential Drinking Water Filters for Perfluoroalkyl Substances (PFASs)”, Environmental Science & Technology Letters 2020 7 (3), 178-184, https://doi.org/10.1021/acs.estlett.0c00004.

3. Ettayapuram Ramaprasad, Azhagiya Singam; Tachachartvanich, Phum; Fourches, Denis; Soshilov, Anatoly; Hsieh, Jennifer C.Y.; La merrill, Michele; et al. (2020): “Structure-Based Virtual Screening of Perfluoroalkyl and Polyfluoroalkyl Substances (PFASs) as Endocrine Disruptors of Androgen Receptor Activity Using Molecular Docking and Machine Learning”, ChemRxiv. Preprint. https://doi.org/10.26434/chemrxiv.11886702.v1.

4. Anthony Saad, Rollie Mills, Hongyi Wan, M. Abdul Mottaleb, Lindell Ormsbee, Dibakar Bhattacharyya, “Thermo-responsive adsorption-desorption of

perfluoroorganics from water using PNIPAm hydrogels and pore functionalized membranes", Journal of Membrane Science, Volume 599, 2020, 117821, ISSN 0376-7388, https://doi.org/10.1016/j.memsci.2020.117821.

5. Minkyu Park, Shimin Wu, Israel J. Lopez, Joseph Y. Chang, Tanju Karanfil, Shane A. Snyder, "Adsorption of perfluoroalkyl substances (PFAS) in groundwater by granular activated carbons: Roles of hydrophobicity of PFAS and carbon characteristics", Water Research, Volume 170, 2020, 115364, ISSN 0043-1354, https://doi.org/10.1016/j.watres.2019.115364.

Tweets

Altmetric reports 3 journal article tweets from 3 users, with an upper bound of 31,063 followers.

Stephanie Dawson (4,798 Followers) @SDawsonBerlin

RT @Science_Open: Strategies to combat a widespread problem for the drinking water industry - #openaccess from @awwa: "Effectiveness of po…

07 Jan 2020

Santiago Campillo (10,822 Followers) @Scruzcampillo

RT @Science_Open: Strategies to combat a widespread problem for the drinking water industry - #openaccess from @awwa: "Effectiveness of po…

07 Jan 2020

ScienceOpen (15,443 Followers) @Science_Open

Strategies to combat a widespread problem for the drinking water industry - #openaccess from @awwa: "Effectiveness of point-of-use/point-of-entry systems to remove per- and polyfluoroalkyl substances from drinking water" #WaterTreatment #WaterScience

6. Letters of Recommendation

Invitation for Conversion of this Journal Article to a Book Chapter

Lt. Col. LeeAnn Raz with the US Air Force provided the following email with a request to convert the journal article into a book chapter as described below. We are in the process of getting ORD Clearance and approval to proceed with publication of the book chapter.

Patterson, C., Burkhardt, J., Schupp, D., Krishnan, E.R., Dyment, S., Merritt, S., Zintek, L., and Kleinmaier, D., “Effectiveness of Point of Entry Systems to Remove Select Per- and Poly- fluoroalkyl Substances from Drinking Water”, Book Chapter in “Forever Chemicals: Environmental, Economic, and Social Equity Concerns with PFAS in the Environment" edited by Racz, L. and Kempisty, D., published by Taylor & Francis (CRC Press) (Invited and Pending) November 2020 (Invited).

From: Racz, LeeAnn Lt Col USAF 1 SOMDG (USA) <leeann.racz.mil@mail.mil>

Sent: Friday, February 7, 2020 5:23 PM

To: Patterson, Craig <Patterson.Craig@epa.gov>

Cc: Kempisty, Dave <david.kempisty@evoqua.com>; LeeAnn Racz <leeann.racz@gmail.com>

Subject: Invitation to Contribute to "Forever Chemicals: Environmental, Economic, and Social Equity Concerns with PFAS in the Environment"

Dear Dr. Patterson,

I read with great interest your recent paper in AWWA Water Science, “Effectiveness of point-of-use/point-of-entry systems to remove per- and polyfluoroalkyl substances from drinking water”. I’d like to invite you to contribute a chapter on this or a related topic to a book I’m publishing with Dr. Dave Kempisty, “Forever Chemicals: Environmental, Economic, and Social Equity Concerns with PFAS in the Environment" with Taylor & Francis (CRC Press). This is a follow-on book to “Perfluoroalkyl Substances in the Environment: Theory, Practice, and Innovation”. Your work would be an outstanding contribution to this project, and I’d be delighted to discuss this opportunity with you.

You may consider reproducing this work as a chapter. If you'd like to use this option, I can help secure the needed permissions from AWWA; we would just need the authors to acknowledge their agreement.

Please let me know when would be a good time to discuss. Looking forward to hearing from you.

LeeAnn Racz

V/r,

LeeAnn Racz, Lt Col, USAF, BSC, PhD, PE, CIH, BCEE

Commander, 1st Special Operations Operational Medical Readiness Squadron

113 Lielmanis Ave, Suite 1D206

Hurlburt Field, FL 32544

Comm: (850) 881-2132

DSN: 641-2132

Justification 3B:

AWWA's Journal of Water Science requires peer review comments and manuscript approval from at least three experts. We successfully responded to 23 comments from three Reviewers. The Editor and Reviewers approved this manuscript for publication after one round of responses to the AWWA Journal of Water Science review comments. No specifics on the journal's impact factor, immediacy index, and citation half-life are available at this time as confirmed by the following email from Taylor Johnson at the U.S. EPA RTP Library.

-----Original Message-----

From: Johnson, Taylor <Johnson.Taylor@epa.gov> On Behalf Of RTP Library

Sent: Wednesday, April 8, 2020 4:32 PM

To: Patterson, Craig <Patterson.Craig@epa.gov>

Subject: RE: STAA Journal Information Request

Good afternoon,

Thank you for contacting EPA-RTP Library. It looks like AWWA Water Science is too new to have generated the journal metrics you have requested. Most of these metrics are updated during the summertime and I think they should be available then.

I'm sorry we couldn't be more helpful, please let us know if you need anything else.

Sincerely,

Taylor

Taylor Abernethy Johnson

Assistant Director

U.S. Environmental Protection Agency Library UNC Contract Staff

109 T.W. Alexander Drive, MD C267-01

Research Triangle Park, NC 27711

Phone: (919) 541-0095

johnson.taylor@epa.gov

AUTHORS

Principal Author

Author Name: Craig Patterson P.E.

Professional Title: Salutation:

Email:	patterson.craig@epa.gov	Organization:	
Mailing Address:			
Street Line 1:	26 W. Martin Luther King Drive		
City:	Cincinnati		
Zip Code:	45268	State:	Ohio
At time of research was:	EPA Employee		
Separation Date:			
% of Effort:	40		

Contributing Author

Author Name:	Jonathan Burkhardt Ph.D.		
Professional Title:		Salutation:	
Email:	burkhardt.jonathan@epa.gov	Organization:	
Mailing Address:			
Street Line 1:			
City:			
Zip Code:		State:	
At time of research was:	EPA Employee		
Separation Date:			
% of Effort:	15		

Contributing Author

Author Name:	Donald Schupp P.E.		
Professional Title:		Salutation:	

Email:	don.schupp@aptim.com	Organization:
Mailing Address:		
Street Line 1:		
City:		
Zip Code:		State:
At time of research was:	Non EPA Personnel	
Separation Date:		
% of Effort:	20	

Contributing Author

Author Name:	E. Radha Krishnan P.E.	
Professional Title:		Salutation:
Email:	radha.krishnan@aptim.com	Organization:
Mailing Address:		
Street Line 1:		
City:		
Zip Code:		State:
At time of research was:	Non EPA Personnel	
Separation Date:		
% of Effort:	5	

Contributing Author

Author Name:	Steven B. Merritt MHP, CIH, REHS	
Professional Title:		Salutation:

Email:	merritt.steven@epa.gov	Organization:
Mailing Address:		
Street Line 1:		
City:		
Zip Code:		State:
At time of research was:	EPA Employee	
Separation Date:		
% of Effort:	5	

Contributing Author

Author Name:	Danielle Kleinmaier	
Professional Title:		Salutation:
Email:	kleinmaier.danielle@epa.gov	Organization:
Mailing Address:		
Street Line 1:		
City:		
Zip Code:		State:
At time of research was:	EPA Employee	
Separation Date:		
% of Effort:	5	

Contributing Author

Author Name:	Stephen Dyment	
Professional Title:		Salutation:

Email:	dyment.stephen@epa.gov	Organization:
Mailing Address:		
Street Line 1:		
City:		
Zip Code:		State:
At time of research was:	EPA Employee	
Separation Date:		
% of Effort:	5	

Contributing Author

Author Name:	Lawrence Zintek Ph.D.	
Professional Title:		Salutation:
Email:	zintek.lawrence@epa.gov	Organization:
Mailing Address:		
Street Line 1:		
City:		
Zip Code:		State:
At time of research was:	EPA Employee	
Separation Date:		
% of Effort:	5	

PUBLICATIONS

Publication 1:

Effectiveness of Point-of-Use/Point-of-Entry Systems to Remove

Publication Title:	Per-and-Poly-fluoroalkyl Substances f		
Publication Date:	Mon Mar 18 00:00:00 GMT 2019		
Journal/Publication Method:	Journal of AWWA Water Science		
All Author(s):			
Volume:	1	Number:	2
Pages:	12	Immediately Index:	Immediately Index:
Citation ½ Life:	NA, See 3B	Impact Factor:	NA, See 3B

Received: 26 October 2018 | Revised: 1 February 2019 | Accepted: 4 February 2019

DOI: 10.1002/aws2.1131

Check for updates

AWWA WATER SCIENCE

ORIGINAL RESEARCH

Effectiveness of point-of-use/point-of-entry systems to remove per- and polyfluoroalkyl substances from drinking water

Craig Patterson[1] | Jonathan Burkhardt[1] | Donald Schupp[2] | E. Radha Krishnan[2] | Stephen Dyment[3] | Steven Merritt[4] | Lawrence Zintek[5] | Danielle Kleinmaier[5]

[1]USEPA, Cincinnati, Ohio

[2]APTIM, Cincinnati, Ohio

[3]USEPA Office of Science Policy, Denver, Colorado

[4]USEPA Region 8, Denver, Colorado

[5]USEPA Region 5, Chicago, Illinois

Correspondence
Craig Patterson, USEPA, 26 W. Martin Luther King Drive, Cincinnati, OH 45268.
Email: patterson.craig@epa.gov

Funding information
USEPA Office of Research and Development

The contamination of groundwater sources with per- and polyfluoroalkyl substances (PFAS) in the United States is a widespread problem for the drinking water industry. Well water supplies in the municipalities of Fountain, Security, and Widefield, Colorado, contain perfluorooctanoic acid and perfluorooctane sulfonate levels greater than the U.S. Environmental Protection Agency (USEPA) health advisory level of 70 ng/L. The source of PFAS has been associated with aqueous film-forming foam at Peterson Air Force Base. To assist property owners and limit the exposure of PFAS to residential drinking water systems, treatability studies were conducted by the USEPA on the PFAS removal effectiveness of commercially available point-of-use/point-of-entry units using reverse osmosis treatment and granular activated carbon adsorbents. Household water systems were tested with a test water containing the water quality characteristics and six PFAS contaminants found in Widefield aquifer region groundwater samples. This study also documents the installation, startup, and continuous/intermittent operation of the treatment systems.

KEYWORDS
drinking water, granular activated carbon, household water treatment, PFAS, point-of-entry, point-of-use, reverse osmosis

1 | INTRODUCTION

The widespread use of per- and polyfluoroalkyl substances (PFAS) over the last half century has resulted in these compounds being detected in environmental media. Although much is unknown, certain PFAS are toxic, resistant to degradation, and bioaccumulate in the food web and, subsequently, in animals and humans. At many sites, it is also likely that PFAS precursors and their degradation products are present; however, limited occurrence data are available due to the lack of comprehensive analytical method capabilities.

Recently, this has been a growing concern for the U.S. Environmental Protection Agency (USEPA)'s Superfund program as these compounds have been identified in groundwater at many high-profile sites across the country, including the Widefield aquifer near Colorado Springs, Colorado. At this site, perfluorooctanoic acid (PFOA), perfluorooctane sulfonate (PFOS), perfluoroheptanoic acid (PFHpA), perfluorobutane sulfonate (PFBS), perfluorohexane sulfonic acid (PFHxS), and perfluorononanoic acid (PFNA) have been detected in the groundwater. Three large water utilities, seven smaller state-regulated utilities, and hundreds of private wells are currently under investigation. At the three large water utilities, nonimpacted surface water from the Pueblo Reservoir is being blended with impacted groundwater sources to meet USEPA's health advisory level (HAL) for combined PFOA and PFOS concentrations. The seven smaller systems and numerous private well owners use the impacted aquifer as

This is an open access article under the terms of the Creative Commons Attribution-NonCommercial-NoDerivs License, which permits use and distribution in any medium, provided the original work is properly cited, the use is non-commercial and no modifications or adaptations are made.
© 2019 The Authors. *AWWA Water Science* published by Wiley Periodicals, Inc. on behalf of American Water Works Association

their sole source of drinking water. On the basis of concentrations found in the Widefield aquifer and USEPA's 2016 HAL of 70 ng/L of combined PFOA and PFOS concentrations (*Federal Register*, 2016), these Widefield aquifer systems are at risk.

Private well owners and small municipalities, where the presence of PFAS is known, are subject to multiyear or even decades-long site-specific investigations, source determinations, risk assessments, and remedial designs and constructions. In addition, many challenges exist at sites managing PFAS contaminants, including the lack of USEPA analytical methods, for the detection of PFAS, their precursors and degradation products, the unknown toxicological impact of many PFAS, and remediation or treatment technologies.

Many private well owners are seeking information on commercially available resources to treat PFAS-contaminated drinking water. Dissemination of the knowledge of the capabilities of commercially available reverse osmosis (RO) and granular activated carbon (GAC) point-of-use (POU) and point-of-entry (POE) treatment systems on PFAS removal would be valuable to those well owners. To match their needs, the PFAS removal systems that were selected for this study were designated to be in accordance with NSF International's Standard P473 (2016).

2 | METHODS AND MATERIALS

To assess the removal effectiveness of the target PFAS present in the Widefield aquifer region, treatability studies were conducted using three commercially available RO treatment systems and two GAC media at the USEPA Test and Evaluation (T&E) facility in Cincinnati, Ohio. RO systems and GAC media were tested using test water simulating the PFAS composition and water quality in the Widefield aquifer region. PFAS samples were analyzed using liquid chromatography/mass spectrometry (LC/MS/MS) at the USEPA Region 5 Chicago Regional Laboratory (CRL) in Chicago, Illinois.

Before RO system and GAC media tests, initial PFAS stability tests were conducted using the same test water to determine the stability of the PFAS compounds in the test water in the 5,000-gal stainless steel RO feed tank and the 55-gal stainless steel GAC media feed drum used in the study. On confirmation of stability, subsequent studies were completed on three RO POU/POE treatment systems, which were tested on the basis of aspects of NSF Standard P473 (NSF International, 2016). In addition, two GAC media were evaluated using rapid small-scale column tests (RSSCTs) per American Society for Testing and Materials D6586-03 (ASTM, 2008).

2.1 | Test water preparation

The feed water was prepared to simulate the PFAS contamination of the Widefield aquifer by adding the PFAS concentrations shown in Table 1. These six PFAS target concentrations are worst-case (maximum) concentrations compiled from historic records (2013–2016) of Widefield aquifer region water samples (Colorado Department of Public Health and Environment [CDPHE], 2016). To align with the NSF P473-specified 2:1 PFOS:PFOA ratio, the PFOA feed concentration was increased from 200 to 800 ng/L.

Cincinnati tap water was added to a 5,000-gal stainless steel tank equipped with a mixer, recirculation pump, and a chiller with a shell-and-tube heat exchanger to control feed water temperature. Sodium thiosulfate (1 mg/L) was added to dechlorinate the test water. The target water quality characteristics specified in Table 2 were maintained throughout the RO and GAC test runs to adhere to the requirements of NSF P473. The test water targets for pH (8.2), total dissolved solids (TDSs) (500 mg/L), and hardness (300 mg/L) were maintained to align with the historic maximum Widefield aquifer well water sampling results (1992–2016) to determine their impact on the longevity and removal capabilities of RO membranes and GAC media.

After the feed water additives dissolved overnight, the target PFAS were measured, mixed, and dissolved in 1 L of deionized water. The PFAS were then added to the 5,000-gal tank and allowed to mix for 3 h for use in the RO treatability study. Before the start of the RO study, approximately 50 gal of the feed water was drained into a 55-gal stainless steel drum equipped with a mixer for use in the GAC RSSCT evaluations. Dehydrated natural organic matter (NOM) of Ohio River water was rehydrated, filtered, and added to the 55-gal drum to increase the total organic carbon (TOC) of the water to above 1 mg/L for the GAC media studies (Pressman et al., 2012).

2.2 | Stability study

A PFAS stability test was run without the RO system and GAC adsorbents over an 8-day period to assess PFAS degradability and sorption in the test apparatus. The

TABLE 1 Test water target per- and polyfluoroalkyl substances (PFAS) composition

CAS number	PFAS compounds	Carbon chain length	Target concentration (ng/L)
375-95-1	PFNA	C9	200
335-67-1	PFOA	C8	800
1763-23-1	PFOS	C8	1,600
375-85-9	PFHpA	C7	200
3871-99-6	PFHxS	C6	1,000
375-73-5	PFBS	C4	300

Note. CAS: Chemical Abstracts Service; PFBS: perfluorobutane sulfonate; PFHpA: perfluoroheptanoic acid; PFHxS: perfluorohexane sulfonic acid; PFNA: perfluorononanoic acid; PFOA: perfluorooctanoic acid; PFOS: perfluorooctane sulfonate.

TABLE 2 Test water target water quality characteristics

General chemistry water parameters	
Temperature (°C)	RO: 25 ± 1°C, GAC: 20 ± 2.5°C
pH (units)	8.2 ± 0.5
Turbidity (ntu)	<1
Free chlorine (mg/L)	<0.2
TOC (mg/L)	RO: Not specified (not adjusted) GAC: >1 mg/L (added as dehydrated NOM)
TDS (mg/L)	RO and GAC: 500 mg/L (added as NaCl)
Hardness (mg/L)	RO: 300 mg/L $CaCO_3$ (added as potassium chloride [KCl], magnesium sulfate [$MgSO_4$], sodium bicarbonate [$NaHCO_3$] and calcium sulfate [$CaSO_4{\cdot}2H_2O$]) GAC: Not specified

Note. $CaCO_3$: calcium carbonate; GAC: granular activated carbon; NaCl: sodium chloride; NOM: natural organic matter; RO: reverse osmosis; TDS: total dissolved solid; TOC: total organic carbon.

concentrations of the six target PFAS remained stable in both the 5,000-gal tank and the 55-gal drum over the 8-day test period. The PFOS concentration was significantly lower than the target concentration due to a lower spike amount inadvertently used when adding the quantity of PFOS to the test water. The PFOS spike amount was corrected in the following test runs. The PFBS concentration was below the detection limit possibly due to the stock solution used during the stability test. A different source of PFBS was secured for the following test runs. These adjustments resolved the concentration discrepancies of PFOS and PFBS during the actual test runs. Although no PFAS degradation or sorption was noted in the stability study, the initial target PFAS concentrations were increased by 25% for the treatability studies as a safety factor to ensure adequate PFAS concentrations for the tests.

2.3 | Analytical methods

PFAS analysis was performed following the USEPA Region 5 standard operating procedure (SOP) for the analysis of polyfluorinated compounds of interest to the Office of Superfund Remediation and Technology Innovation in water, sludge, influent, effluent, and wastewater by multiple reaction monitoring LC/MS/MS (USEPA, 2017). Per the USEPA Region 5 PFAS analytical SOP, 15-mL polypropylene sample containers were weighed before and after sample collection to allow the laboratory to determine the exact sample amount used during analysis. The target volume of a sample per polypropylene container was 5 mL. Because all of the 5-mL sample volumes were analyzed, triplicate samples were collected from both influent and effluent for additional quality assurance/quality control analyses. With a 28-day sample holding time, grab water samples for PFAS analysis were shipped for overnight delivery to the USEPA Region 5 CRL in Chicago, Illinois. All other water quality analyses were performed at the USEPA T&E facility in Cincinnati, Ohio.

2.4 | Analytical sampling plan

Six target PFAS compounds were analyzed in both RO system and GAC media influent and effluent water samples to determine PFAS removal efficiency. The sample plan included analysis of 188 PFAS samples at the CRL in USEPA Region 5 from one stability run and three test runs. Samples were collected from the 5,000-gal stainless steel mix tank and the 55-gal stainless steel drum and analyzed for PFAS, TOC, TDS, hardness, turbidity, pH, temperature, and free available chlorine. Only one free chlorine sample (influent and effluent) was collected at the beginning of each test to ensure that the test water was adequately dechlorinated. Additional information on methods and materials is provided in Appendix S1 (Supplementary Information).

2.5 | RO system design

The installation of each unit was very straightforward. Each of the RO systems was preassembled by the manufacturer before shipment and used quick connects to attach inlet and outlet tubing. The RO systems only required connections to feed water and discharge points for operation. Specifications

TABLE 3 Summary of reverse osmosis (RO) system specifications

RO system	iSpring RCS5T	HydroLogic Evolution RO1000	Flexeon LP-700
Rated capacity[a]	500 gpd (0.35 gpm)	1,000 gpd (0.7 gpm)	700 gpd (0.5 gpm)
Filters included	Sediment filter Carbon prefilter CTO filter RO membrane Carbon postfilter	Carbon prefilter 2 RO membranes	Sediment filter Carbon prefilter 2 RO membranes Carbon postfilter
System recovery[a]	50%	50%, using 1:1 fitting	38%
Booster pump	Yes	No	No
Connections	3/8″ inlet ¼″ outlet (tubing included)	½″ inlet 3/8″ outlet (tubing included)	3/8″ inlet and outlet (tubing not included)
Self-supporting	Yes	Yes	No
Size ($L \times W \times H$)	8.5″ × 15″ × 18.5″	20.5″ × 11″ × 10″	18″ × 10.5″ × 32″
Weight	31 lb	16 lb	38 lb

Note. CTO: carbon block chlorine, taste and odor.
[a]The systems' rated pressure and efficiency are a function of the temperature and pressure of the feed water.

TABLE 4 Reverse osmosis (RO) system replacement filters and membranes

RO system	iSpring RCS5T	HydroLogic Evolution RO1000	Flexeon LP-700
Sediment filter	#FP15 (3–6 months)	Not part of system	#200627 (12 months)
Carbon prefilter	#FG15 (6 months)	#22043 (2,000 gal of purified water)	#200658 (12 months)
Carbon block filter	#FC15 (6 months)	Not part of system	Not part of system
RO membranes	#MS5 (24 months)	#220445 (6–24 months) (requires 2)	#208802 (24 months) (requires 2)
Carbon postfilter	#FT15 (12 months)	Not part of system	#200658 (12 months)

for the three RO systems tested are summarized in Table 3. Table 4 shows the replacement part numbers, replacement frequency, and prices for the replacement filters and membranes in each of the three RO systems.

2.5.1 | iSpring RO system

The five-stage iSpring RO system (iSpring Water Systems, LLC, Alpharetta, GA) was free standing and was preplumbed with a booster pump and color-coded feed and discharge tubing when it was removed from the box. Except for the RO membrane, the filters and cartridges described in Tables 3 and 4 were preinstalled. Wrenches were included to install replacement membranes and filters.

2.5.2 | HydroLogic RO system

The two-stage HydroLogic RO system (HydroLogic Purification Systems, Santa Cruz, CA) was free-standing and included fittings for a 2:1 (green) or 1:1 (orange) waste to pure water ratio. The instructions stated that using the 1:1 fitting (chosen for this study) would provide a higher flow rate but could require more frequent replacement of the RO membranes. Three 90° elbow push fittings, the carbon prefilter, and two RO membranes were installed with wrenches before use. Inlet and outlet tubing was color-coded, and a ball valve at the end of the discharge line was provided for use when water was not needed. A booster pump had to be purchased separately and was installed in front of the HydroLogic RO system.

2.5.3 | Flexeon RO system

The four-stage Flexeon RO System (AXEON Water Technologies, Temecula, CA) was preplumbed with filters when it was removed from the box. The Flexeon RO system was not self-supporting and did not come with a booster pump or inlet and outlet tubing. Except for the RO membrane, the filters and cartridges described in Tables 3 and 4 were preinstalled. A booster pump was purchased separately and was installed in front of the Flexeon RO system.

2.5.4 | Booster pumps

The iSpring unit included an integrated booster pump to create a stable working environment for the RO membrane for situations in which the water feed pressure was not sufficiently high (40–50 psi). A booster pump was purchased separately for the HydroLogic and Flexeon RO systems (HydroLogic Booster Pump Model No. HL29014). The booster pump was installed and included tubing, a pressure gauge, and switches that turned the pumps off when the water supply was stopped or when the discharge line was closed (by a faucet or valve). This would not be needed in a home setup if system pressure is available.

2.5.5 | Modifications for POE use

By themselves, the RO systems tested do not constitute a whole-house POE system; however, with some additional components, each of these RO systems could be part of a POE system. The RO systems tested were designed to produce 500–1,000 gpd (0.35–0.70 gpm), a flow rate that is not suitable for many household activities (bath water, showers, washing machines, dishwashers). In addition, the RO systems do not produce water at a significant pressure. However, it could serve as a POE system with the addition of a 200–500-gal storage tank, a delivery pump, and a 20-gal bladder tank. The storage tank would provide the necessary purified water to the home, and the delivery pump and booster tank would supply the necessary pressure. These RO systems would then be able to refill the storage tank to meet household water demands in real time. However, watering of lawns and gardens and filling swimming pools with treated water would not be a viable option without a much larger GAC or RO system.

TABLE 5 Reverse osmosis (RO) system sampling plan

Day #	Day of week	Time of day	Sample (h)	Time of day	Sample (h)	Time of day	Sample (h)
Day 1	Tuesday	a.m.	Startup[a]	Noon	4	p.m.	8
Day 2	Wednesday	a.m.	24	Noon	30	p.m.	36
Day 3	Thursday	a.m.	48	Noon	54	p.m.	60
Day 4	Friday	a.m.	72	Noon	78	p.m.	84
Day 5	Saturday	2-day stagnation period[a]					
Day 6	Sunday						
Day 7	Monday	a.m.	144	p.m.	148	p.m.	Shutdown[a]

[a]No samples collected.

2.5.6 | RO system sampling plan

The RO systems were originally planned to operate continuously for 4 days, shut down for 2 days, and then operate for another day per NSF P473, as shown in Table 5 (NSF International, 2016). Because of the high use of water from the 5,000-gal tank, the Flexeon and HydroLogic units were operated for 2 days, shut down for 4 days, and then operated for another day. Sampling occurred normally during the period when the units were operating.

The RO systems received test water from a 5,000-gal stainless steel tank. The tank included a mixer and a recirculation pump that recycled the feed water from the bottom to the top of the tank. The feed to the RO system came off the recirculation line. A chiller with a shell and tube heat exchanger was located on the recirculation line to maintain the temperature of the tank at approximately 25°C. A schematic of the RO test system is shown in Figure 1. Figures 2–4 show photographs of the iSpring RCS5T, HydroLogic Evolution RO1000, and the Flexeon LP-700 RO systems, respectively, at the USEPA T&E facility.

Grab samples were collected from each of the RO systems twice or thrice per day during the test period. Grab samples from the influent to the RO system were collected from the recirculation line on the 5,000-gal tank. Grab samples from the effluent of the RO system were collected from the end of the permeate tubing. The flow rate of both the reject (concentrate) and the permeate water was measured throughout the test using a graduated cylinder. This allowed the calculation of the recovery, or efficiency, of the RO system.

2.6 | GAC system design

Two types of GAC media were evaluated using test water: (1) Calgon Filtrasorb 600 AR+ (Calgon Carbon Corporation, Pittsburgh, PA), manufactured from select grades of bituminous coal, and (2) Evoqua 1230CX (Evoqua Water Technologies Pittsburgh, PA), a coconut-based GAC as shown in Table 6. The two GAC media were tested separately using RSSCT methods described in ASTM D6586-03 (2008). Samples were collected every 30 min over an 8-h period.

The representative POE system for GAC filter was an H_2O Filter Warehouse Model FT-1-GAC-20, 4–5 gpm non-backwashing whole house carbon water filter (Omni Filter, Rexford, MT). This filter uses a 35″ (H) × 9″ (D) tank, 30 lb (1 ft^3) GAC, and is rated for 4 gpm with a treatment volume of 150,000 gal. The RSSCT data were scaled up to approximate the use of GAC in this unit.

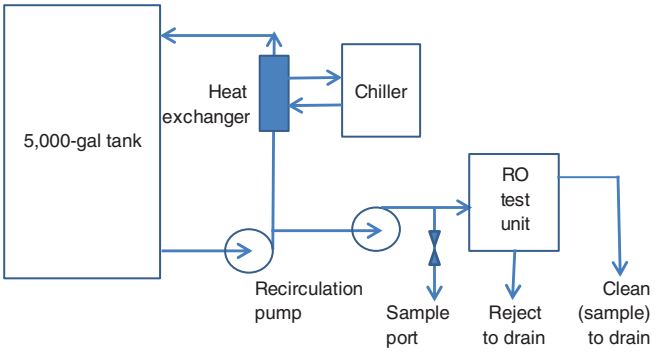

FIGURE 1 Reverse osmosis (RO) test schematic

FIGURE 2 iSpring RCS5T reverse osmosis (RO) system

RSSCTs are based on fixed-bed mass transfer models. The mass transfer models are scaled down from the full-scale adsorber to a small column (SC). Similarity of operation to that of large-scale adsorbers is ensured by properly selecting the particle size, hydraulic loading, and empty bed contact time (EBCT) of the small adsorber. The RSSCT allows the tests to be conducted much more quickly and with less water than full-scale POE tests. Figure 5 shows a schematic of the RSSCT system. Figure 6 shows a photograph of the GAC RSSCT system at the USEPA T&E facility.

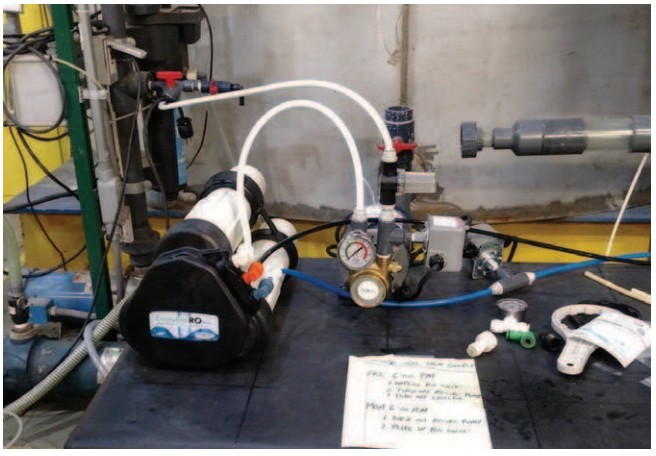

FIGURE 3 HydroLogic evolution RO1000 reverse osmosis (RO) system (with optional booster pump)

FIGURE 4 Flexeon LP-700 reverse osmosis (RO) system

The EBCTs of the large-scale adsorber and the small-scale adsorber are related to the particle sizes of the GAC within the columns according to the following equation (Crittenden et al., 1991):

$$\frac{\mathrm{EBCT_{SC}}}{\mathrm{EBCT_{LC}}} = \left[\frac{d_{\mathrm{p,SC}}}{d_{\mathrm{p,LC}}}\right]^{2-X} = \frac{t_{\mathrm{SC}}}{t_{\mathrm{LC}}},$$

where EBCT is the empty bed contact time; d_{p} is the GAC particle size; and t is the elapsed time to conduct the tests for the RSSCT SCs and the POE large columns (LCs), respectively. X defines the dependence of the intraparticle diffusion coefficient on particle size. In this case, it is assumed that the intraparticle diffusivities do not change with particle size, so $X = 0$. Therefore, the time (minutes) of operation in the LC is proportional to the square of the ratio of the particle sizes in the large and SCs multiplied by the time of operation in the SC.

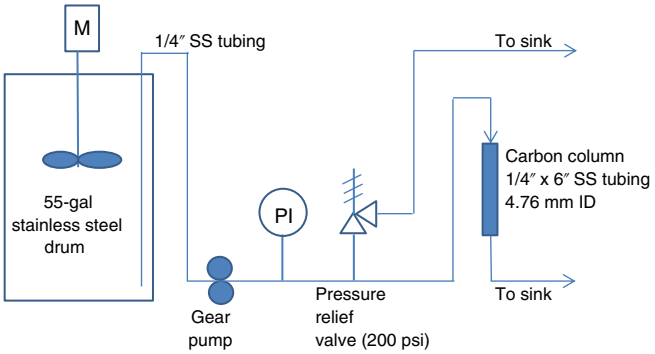

FIGURE 5 Rapid small-scale column test (RSSCT) schematic. ID: inner diameter; M: mixer; PI: pressure indicator; SS: stainless steel

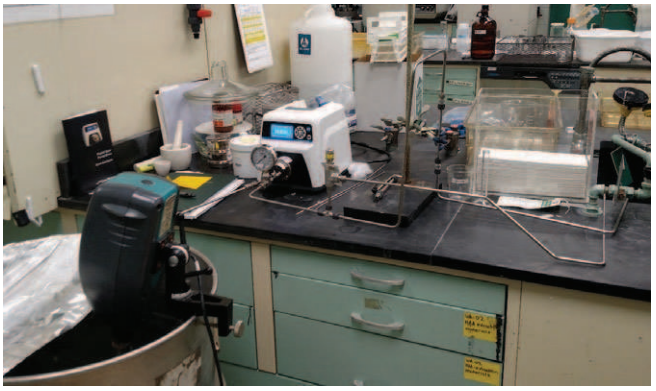

FIGURE 6 Rapid small-scale column test (RSSCT) system

Other equations relating the large and SC operation include the following:

$$\frac{V_{\mathrm{SC}}}{V_{\mathrm{LC}}} = \frac{d_{\mathrm{p,LC}}}{d_{\mathrm{p,SC}}},$$

where V is the velocity in the LC and SC, and

$$M_{\mathrm{SC}} = \mathrm{EBCT_{LC}}\left[\frac{d_{\mathrm{p,SC}}}{d_{\mathrm{p,LC}}}\right]^{2-x} Q_{\mathrm{SC}} \times \rho_{\mathrm{LC}},$$

where M is the mass of GAC in the SC, Q is the flow rate in the SC, and ρ is the GAC density in the LC.

The RSSCT evaluation for this study used a 55-gal stainless steel drum with a mixer as a holding tank for the feed water in a temperature-controlled laboratory. The feed water was pumped through the GAC column using a Masterflex® gear pump (Masterflex, Gelsenkirchen, Germany) at approximately 10 mL/min. The flow rate was measured by collecting water in a graduated cylinder, and it was adjusted to maintain 10 mL/min throughout the study. One-quarter-inch stainless steel tubing was used throughout the system. The inside diameter of the RSSCT column was 4.76 mm. Each type of GAC was ground to a particle size between 170 and 200 mesh with a mortar and pestle. Carbon fines were washed off the crushed GAC with deionized water, and the crushed GAC was dried in a 150°C oven for 4 h. After weighing the crushed GAC for use in the RSSCT, it was added to 40 mL of deionized water and boiled for 10 min to replace the air in the GAC's pores with water. Fiberglass wool was placed in the bottom of the column to keep the GAC inside the column.

On the basis of discussions with GAC vendors offering systems for PFAS removal, an EBCT of 10 min and a GAC RSSCT study duration of 8 h were selected, with a 30-min sample collection frequency. An EBCT of 10 min was selected to provide adequate time for PFAS to absorb GAC and to allow for reasonable GAC replacement frequencies for homeowners. Grab samples from the influent to the RSSCT were collected from the 55-gal drum (Figure 5). Grab samples from the effluent of the RSSCT were collected from the end of the ¼-in. stainless steel tubing every 30 min over an 8-h test period.

TABLE 6 Granular activated carbon (GAC) characteristics and rapid small-scale column test (RSSCT) design parameters

Parameter	Test 1	Test 2
GAC	Evoqua 1230CX	Calgon Filtrasorb 600 AR+
Source	Coconut	Bituminous coal
Density (g/cm^3)	0.45	0.62
Porosity	0.47	0.39
Mesh size	12 × 30	12 × 40
$EBCT_{LC}$ (min)	10	10
$d_{p,LC}$ (mm)	1.150	1.063
$d_{p,SC}$ (mm)	0.0825	0.0825
Scaling factor	194.3	165.9
Q_{SC} (mL/min)	10	10
V_{SC} (mL)	0.515	0.603
M_{SC} (g)	0.2294	0.3742

Note. EBCT: empty bed contact time.

3 | RESULTS AND DISCUSSION

3.1 | RO system studies

Three RO systems were tested: RO#1, iSpring RCS5T 500 gpd (0.35 gpm); RO#2, HydroLogic Evolution 1,000 gpd (0.7 gpm); and RO#3, Flexeon LP-700 gpd (0.5 gpm).

3.1.1 | RO#1 test

The first RO POU/POE system, the iSpring RCS5T (RO#1), was tested over a 7-day period at an average flow rate of 2,285 mL/min. RO#1 was operated on Tuesday through Friday of the first week, shut down over the weekend, and restarted on Monday morning of the following week for the Day 7 samples.

All PFAS in the effluent were reduced below detection for the entire test period. RO#1 also reduced the turbidity, TOC, TDS, and hardness in the effluent. The average permeate flow rate from this unit was approximately 1,020 mL/min, and the average concentrate (reject) flow rate from this unit was approximately 1,265 mL/min. The recovery (flow rate of permeate/flow rate of influent water) of the RO#1 system was approximately 45.

TABLE 7 Removal efficiency of reverse osmosis (RO)#2 per- and polyfluoroalkyl substances (PFAS) results greater than nondetection

PFAS	Time (h)	Influent concentration (ng/L)	Effluent concentration (ng/L)	Removal efficiency (%)
PFOS	0038	1,100	22	98
PFOS[a]	144	1,360	77	94.3
PFOA[a]	144	799	21	97.3
PFHxS	144	844	11	98.7
PFNA	144	210	49	76.7
PFOS	148	1,330	20	98.5

Note. PFHxS: perfluorohexane sulfonic acid; PFNA: perfluorononanoic acid; PFOA: perfluorooctanoic acid; PFOS: perfluorooctane sulfonate; USEPA: U.S. Environmental Protection Agency.
[a]Exceeded the 70 ng/L PFOS + PFOA USEPA health advisory level.

3.1.2 | RO#2 test

The second RO POU/POE system, HydroLogic Evolution RO1000 (RO#2), was tested intermittently over a 7-day period. Because of the increased water volume necessary to test this unit at an average flow rate of 4,895 mL/min, the unit was only operated on Tuesday and Wednesday of the first week before being shut down for the weekend. RO#2 was then restarted on Monday morning of the following week for the Day 7 samples.

Most of the PFAS samples were below the detection limit for the test. However, 6 of 42 RO#2 PFAS sample results were above the detection limit as shown in Table 7 and Figure 7. Five of the PFAS were detected after startup on Day 7.

RO#2 reduced the turbidity, TOC, TDS, and hardness in the effluent as shown in Table 8. Other than a slightly higher effluent turbidity after startup on Day 7, the RO membranes appear to be intact as exhibited by the consistent removal of TOC, TDS, and hardness. Because of the demineralization of the RO-treated water shown in Table 8, a remineralization cartridge may be required to improve taste and to control corrosion in household premise plumbing.

The PFAS compounds found in the effluent may have resulted from the limited number of treatment barriers (activated carbon pre- and postfilters) in the two-stage HydroLogic RO system or a leaking membrane seal because the breakthrough does not correlate to molecular size, as might be expected with a strictly membrane system. However, even the breakthrough of the GAC from the activated carbon pre- and postfilters does not fully match the adsorption properties of the compounds. In addition, it is unclear whether this was a one-time event or whether it is to be expected for the days following Day 7.

The average permeate flow rate from this unit was approximately 2,165 mL/min, and the average concentrate (reject) flow rate from this unit was approximately

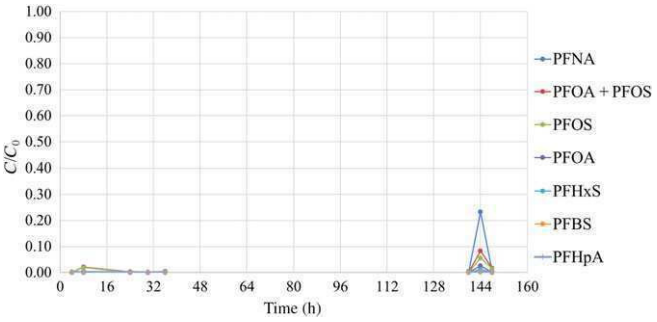

FIGURE 7 Per- and polyfluoroalkyl substances (PFAS) removal versus time for reverse osmosis (RO)#2 test. PFBS: perfluorobutane sulfonate; PFHpA: perfluoroheptanoic acid; PFHxS: perfluorohexane sulfonic acid; PFNA: perfluorononanoic acid; PFOA: perfluorooctanoic acid; PFOS: perfluorooctane sulfonate

TABLE 8 Water quality results from reverse osmosis (RO)#2 test

			Turbidity (ntu)		TOC (mg/L)		TDS (mg/L)		Hardness (mg/L)	
Date	**Day**	**Hours**	**Influent**	**Effluent**	**Influent**	**Effluent**	**Influent**	**Effluent**	**Influent**	**Effluent**
Start-up										
March 13, 2018	1	4	0.38	0.12	1.2	0.48	454	10	298	6
March 13, 2018	1	8	0.40	0.19	1.2	0.18	456	6	247	6
March 14, 2018	2	24	0.31	0.17	1.2	0.21	455	24	247	4
March 14, 2018	2	30	0.33	0.11	1.2	0.16	448	2	247	6
March 14, 2018	2	36	0.28	0.12	1.2	0.16	452	3	260	6
Shutdown and start-up										
March 19, 2018	7	144	0.34	0.54	1.3	0.19	450	16	252	4
March 19, 2018	7	148	0.39	0.12	1.3	0.12	446	6	240	4

Note. TDS: total dissolved solid; TOC: total organic carbon.

2,730 mL/min. The recovery of the RO#2 system was approximately 44%.

3.1.3 | RO#3 test

The third RO POU/POE system, Flexeon LP-700 (RO#3), was tested over a 7-day period. Because of the increased water volume necessary to test this unit at an average flow rate of 4,560 mL/min, the unit was only operated on Tuesday and Wednesday of the first week before being shut down for the weekend. RO#3 was then restarted on Monday morning of the following week for the Day 7 samples.

All PFAS in the effluent were reduced below the detection limit for the entire test. RO#3 also reduced the turbidity, TOC, TDS, and hardness in the effluent. The average permeate flow rate from this unit was approximately 1,260 mL/min, and the average concentrate (reject) flow rate from this unit was approximately 3,300 mL/min. The recovery of the RO#3 system was approximately 28%.

3.2 | RO discussion

The three RO systems were similar in many respects. They were each designed to be installed by a homeowner with basic "handyman" skills or a plumber, if necessary. The RO systems were all equipped with the required filters, membranes, and tools to install and replace these parts. However, the specifics of what was included varied (types of filters, tubing, booster pump, etc.). RO#1 and RO#2 (iSpring and HydroLogic) were self-supporting, while RO#3 (Flexeon) had to be mounted to a wall. Filters and membranes require replacement by the homeowner or plumber on a regular schedule, and all three RO systems generated more reject water than purified water during this study.

Because RO systems tend to increase water corrosivity without additional processes, care should be taken to evaluate potential lead and copper corrosion from the posttreatment premise plumbing for any POE systems. A remineralization cartridge may be required to improve the taste of RO-treated water and for corrosion control in household plumbing. Disposal of reject water via sewer or septic systems may be allowed under a homeowner exemption in many communities; however, special considerations should be made if there is a possibility of recontaminating the aquifer.

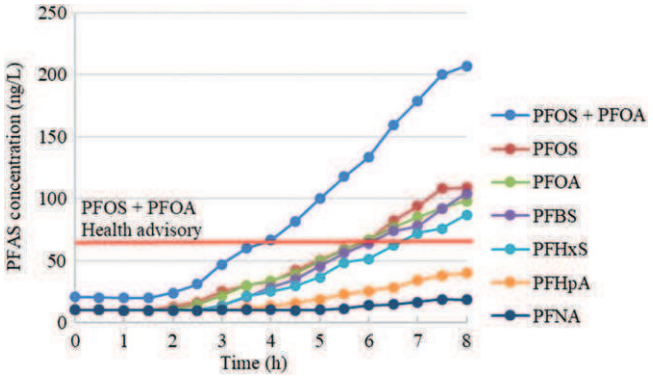

FIGURE 8 Per- and polyfluoroalkyl substances (PFAS) concentrations versus time for granular activated carbon (GAC)#1. PFBS: perfluorobutane sulfonate; PFHpA: perfluoroheptanoic acid; PFHxS: perfluorohexane sulfonic acid; PFNA: perfluorononanoic acid; PFOA: perfluorooctanoic acid; PFOS: perfluorooctane sulfonate

3.3 | GAC media studies

Two GAC media were tested using the test water: GAC#1; Evoqua 1230CX, a coconut-based GAC, and GAC#2; Calgon Filtrasorb 600 AR+, manufactured from select grades of bituminous coal.

3.3.1 | GAC#1 test

The first RSSCT was conducted using Evoqua 1230CX (GAC#1), a coconut-based GAC. The target flow rate was 10 mL/min, and the flow rate was checked every 30 min before samples were collected. Each time, the flow rate was adjusted to maintain 10 mL/min. The flow rate was maintained within 9.6–10.1 mL/min over the course of this test.

No PFAS were detected in the RSSCT effluent for the first 1.5 h of testing. Individual PFAS began to break through the GAC at 2 h and increased with time. The breakthrough time for each PFAS was dependent on the specific compound adsorption properties and its influent concentration. PFOA

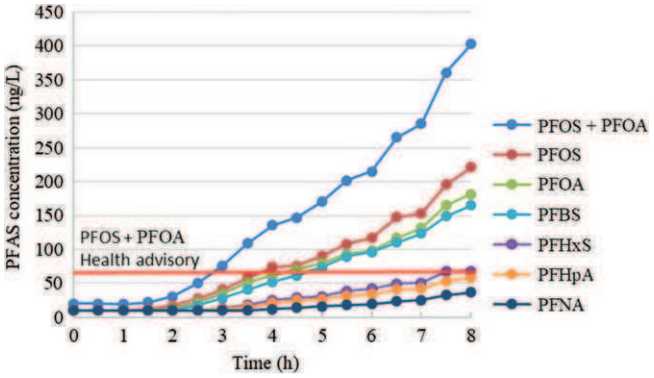

FIGURE 9 Per- and polyfluoroalkyl substances (PFAS) concentrations versus time for granular activated carbon (GAC)#2. PFBS: perfluorobutane sulfonate; PFHpA: perfluoroheptanoic acid; PFHxS: perfluorohexane sulfonic acid; PFNA: perfluorononanoic acid; PFOA: perfluorooctanoic acid; PFOS: perfluorooctane sulfonate

and PFOS were the first compounds detected in the RSSCT effluent, and PFNA was the last compound detected. All PFAS were detected within 5.5 h of testing. By the end of the 8-h testing period, the PFOS and PFBS had the highest concentrations in the effluent, and the PFNA had the lowest concentration in the effluent. Figure 8 shows the PFAS concentrations as a function of time for GAC#1. These results do not match the general results seen by others (Appleman, Dickenson, Bellona, & Higgins, 2013; Dickenson & Higgins, 2016; McCleaf et al., 2017), where the smaller PFAS (e.g., PFBS) generally break through before the longer-chain PFAS (e.g., PFOA and PFOS). However, the PFBS concentration in the test water (260 ng/L) was much lower than the PFOS (1,600 ng/L) and PFOA (800 ng/L) concentrations. The data suggest that, in this case, the combined PFOS + PFOA results may be conservative for controlling the other PFAS. Care must be taken in translating these results to other waters and carbons.

On the basis of the USEPA PFOS and PFOA HAL, GAC#1 lasted for approximately 4 h before the total PFOS and PFOA concentration exceeded 70 ng/L. Using the RSSCT scaling factor for this test (194.3, as shown in Table 6), the simulated life of a GAC filter using GAC#1 with 10 min EBCT would be approximately 800 h (33 days). After this time, the total PFOS and PFOA concentration in the effluent would be expected to exceed the USEPA HAL. GAC#1 treated approximately 4,800 bed volumes of water before exceeding the USEPA PFOS and PFOA HAL. These results suggest that the HAL level of 70 mg/L for combined PFOA and PFOS concentrations is protective when evaluating the breakthrough of the other PFAS studies; however, this is a function of the experimental design chosen in terms of water quality and PFAS studied. Others have shown different results, as mentioned earlier. Aside from a reduction in TOC, no other changes were evident in the water quality parameters for GAC#1.

3.3.2 | GAC#2 test

As a comparison with the coconut-based GAC from Evoqua, a second RSSCT was conducted using Calgon Filtrasorb 600 AR+ (GAC#2), a coal-based GAC. The target flow rate was 10 mL/min, and the flow rate was checked every 30 min before samples were collected. Each time the flow rate was adjusted to maintain 10 mL/min. The flow rate was maintained at 9.5–10.8 mL/min over the course of this test.

No PFAS were detected in the RSSCT effluent for the first hour of testing. Individual PFAS began to break through the GAC at 1.5 h and increased with time. As with GAC#1, PFOA and PFOS were the first compounds detected in the GAC#2 effluent, and PFNA was the last compound detected. All PFAS were detected by 3.5 h of testing. By the end of the 8-h testing period, the PFOA and PFOS had the highest concentrations in the effluent, and the PFNA had the lowest concentration in the effluent. After 8 h of testing, compared with GAC#1, GAC#2 had higher concentrations of each of the PFAS except for PFBS. GAC#2 PFBS reached 70 ng/L 1.5 h later than GAC#1 PFBS. Figure 9 shows the PFAS concentrations as a function of time for GAC#2. These results are similar to those seen for GAC#1 (Evoqua 1230CX). The caveat that the HAL level for PFOA and PFOS may not be protective for PFAS removal made in the GAC#1 discussion also holds true for GAC#2.

On the basis of the USEPA PFOS and PFOA HAL, the GAC#2 lasted for approximately 3 h before the total PFOS and PFOA concentration exceeded 70 ng/L. Using the RSSCT scaling factor for this test (165.9, as shown in Table 6), the simulated life of a GAC filter using GAC#2 with 10 min EBCT would be approximately 480 h (20 days). After this time, the total PFOS and PFOA concentration in the effluent would be expected to exceed the USEPA HAL. GAC#2 treated approximately 2,900 bed volumes of water before exceeding the USEPA PFOS and PFOA HAL. Aside from a reduction in TOC, no other changes were evident in the water quality parameters for GAC#2. The projected life of GAC#1 and GAC#2 is based on the operation of the filters 24 h/day and should be adjusted to account for actual household water usage patterns. Tables of RO and GAC media study results are provided in Appendix S1.

3.4 | GAC media discussion

The representative POE system selected for the GAC filter used a 35″ (*H*) × 9″ (*D*) tank, 30 lb (1 ft^3) GAC, and was rated for 4 gpm with a treatment volume of 150,000 gal. This size unit would only have an EBCT of 2 min, much smaller than a tank with an EBCT of 10 min (as recommended by GAC vendors for PFAS removal).

To meet the EBCT of 10 min, one alternative would be to use two tanks in series that are 65 in. high by 16 in. in diameter, with approximately 240 lb (8 ft^3) GAC. However, scaling up the RSSCT data estimated that the coal-based

Calgon F-600 GAC would have a lifetime of 20 days (2,900 bed volumes) compared with the coconut-based Evoqua GAC lifetime of 33 days (4,800 bed volumes) before requiring replacement based on maximum day PFAS concentrations tested before exceeding the USEPA's HAL of 70 ng/L for PFOS and PFOA. Modeling the results for a lower concentration (average daily concentration) gave bed lives of 545 days (79,000 bed volumes) for the Calgon F-600 GAC and 791 days (115,000 bed volumes) for the Evoqua coconut carbon before requiring replacement as described in Section 4.

Increasing the size of the GAC filter tank or placing two filter tanks in series to lengthen the lifetime of the GAC media for PFAS removal would require additional plumbing and access to drainage lines for backwash wastewater. Replacing wet, contaminated GAC with dry GAC in the home is labor-intensive and requires backwashing to precondition and sort out GAC particle sizes and to remove air. The larger carbon filter tanks will also require additional space that may need to be heated depending on the local environment.

3.5 | RO and GAC residuals management

Residual streams from home residences are exempt from federal regulations as solid/hazardous wastes under the Resource Conservation and Recovery Act. Therefore, homeowners can discharge RO reject water to the publicly owned treatment works. The RO reject wastewater concentrations from RO#1, RO#2, and RO#3 were calculated to range from 7 to 10 μg/L. Therefore, care must be taken when discharging RO wastewaters to private septic or mound systems. Many GAC media manufacturers have carbon reactivation/disposal services. However, household RO and GAC cartridges containing PFAS are not considered hazardous waste and may also be disposed of in household trash.

4 | MODELING OF GAC RESULTS

To investigate the impact of PFAS influent concentrations on GAC (bed volumes to breakthrough at 70 ng/L PFOS + PFOA), a model was used to predict GAC lifetime based on average PFOA (43 ng/L) and PFOS (137 ng/L) concentrations based on historic records (2013–2016) found in Widefield aquifer region water samples (CDPHE, 2016). Adsorption Design Software (AdDesignS™, Houghton, MI) version 1.0, distributed as part of the ETDOT suite, developed by Michigan Technological University (Hokanson, Hand, & Crittenden, 1999; Mertz, Gobin, Hand, Hokanson, & Crittenden, 1994), was used to model the adsorption of PFOA + PFOS compounds.

4.1 | Parameter estimation process

Adsorptive capacity was estimated by calculating the area (integrating) between the influent and effluent concentrations and dividing the resulting value by the mass of carbon in the test apparatus. Any extrapolation of effluent concentration data needed to calculate the total breakthrough point was performed using a line fit for nonzero effluent concentrations and determining the intersection of that line with the average influent concentration. The capacity calculated in this step was used to estimate the Freundlich parameters. The Freundlich isotherm formula is

$$q = K \cdot \bar{C}^{(1/n)},$$

where q is the adsorptive capacity (μg/g), $\bar{C}$ is the average influent concentration (μg/L), and K ((μg/g)(L/μg)$^{(1/n)}$), and n (unitless) are isotherm fitting parameters. The exponential term ($1/n$) was set to 0.45 for all models on the basis of past experience with PFAS modeling. The K estimated in this step was used by the PSDM (pore surface diffusion model) code, as described below.

4.2 | Pore surface diffusion model

The PSDM module from AdDesignS was used to model the adsorption of PFAS onto each carbon (Crittenden, Hutzler, Geyer, Oravitz, & Friedman, 1986; Mertz et al., 1994). AdDesignS uses input information about the adsorption column (diameter, length, flow rate, carbon mass), the adsorptive material/carbon (particle radius, apparent density, porosity), and the adsorbing species (molecular weight, molar volume, and so on). The calculated Freundlich isotherm parameters as described above were used as inputs to AdDesignS. Additional adsorption kinetics parameters were also required by the model. The film diffusion coefficient was calculated by the Gnielinski correlation (Mertz et al., 1994; Sontheimer, Crittenden, & Summers, 1988). The pore diffusion coefficient was calculated from the Hayduk and Laudie correlation (Mertz et al., 1994, Sontheimer et al., 1988). The surface diffusion coefficient was calculated by AdDesignS using the Sontheimer correlation (Mertz et al., 1994, Sontheimer et al., 1988). The surface and pore diffusion and film transfer coefficients were varied to produce a good fit to experimental data. The influent concentrations recorded during GAC RSSCTs 1 and 2 were input into the model. The surface and pore diffusion coefficients were varied to minimize the sum of squared (SSQ) difference between the modeled and experimental effluent concentrations. The minimum SSQ values were recorded with the associated pore and surface diffusion coefficients. PFAS AdDesignS model input parameters are provided in Table 30 of Appendix S1.

4.3 | Application of the model

Adsorption kinetics parameters that resulted in the best match to experimental values were recorded. These were used to model configurations or operating schemes that were not directly tested in the GAC RSSCTs. Specifically, the influent concentrations were reduced from the worst-case (maximum) to average-day concentrations seen in the Widefield aquifer (CDPHE, 2016). Figures 10 and 11 show the model results of effluent concentrations for PFOS and PFOA for both RSSCT experiments using the worst-case (maximum, tested, shown in green) and average-day concentrations (shown in blue) supplied to each carbon. The PFOS + PFOA concentration in the influent was approximately 3,000 ng/L for the worst-case scenario and 180 ng/L for the average day (a 16–17× reduction). For the maximum day, the model predicted an exceedance of the PFOS + PFOA HAL (70 ng/L) after approximately 3,400 bed volumes for Evoqua GAC#1 and approximately 2,700 bed volumes for Calgon GAC#2, which is consistent with the experimental values. Reducing the influent maximum-day concentrations to the average-day concentrations resulted in exceedances of the HAL after approximately 115,000 bed volumes (2.2 years of operation) for GAC#1 and approximately 79,000 bed volumes for GAC#2 (1.5 years of operation). For the 16–17× reduction in influent concentration, the model predicted about 34× (Evoqua) and about 29× (Calgon) improvements in the number of treatable bed volumes before exceedance of the 70 ng/L HAL. This modeling has a number of assumptions (see Table 30 in Appendix S1) on the scale-up approach made in the model fitting, and therefore, it should not be relied on by homeowners. GAC performance should be monitored to determine the bed volumes and time to PFOA + PFOS breakthrough based on the actual well water quality conditions that will vary on the basis of distance from contamination source and source water hydrology.

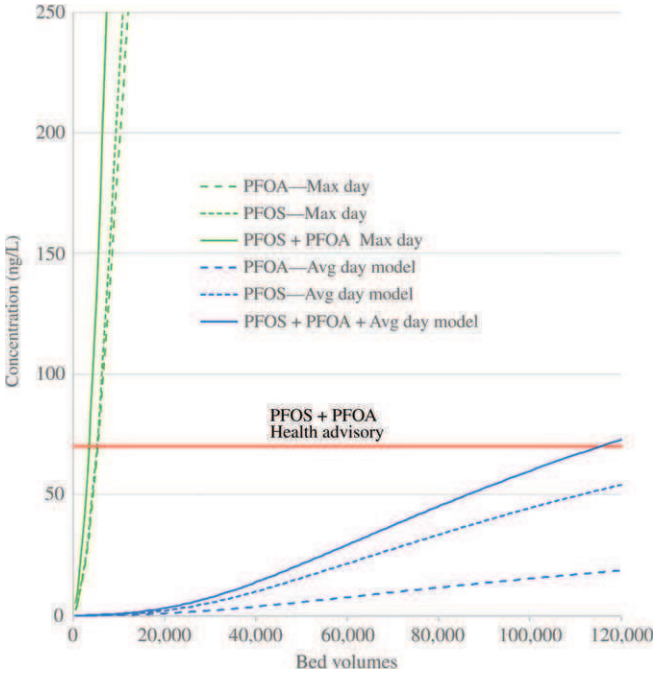

FIGURE 10 Model results of perfluorooctane sulfonate (PFOS) + perfluorooctanoic acid (PFOA) drinking water concentrations versus bed volumes for granular activated carbon (GAC)#1

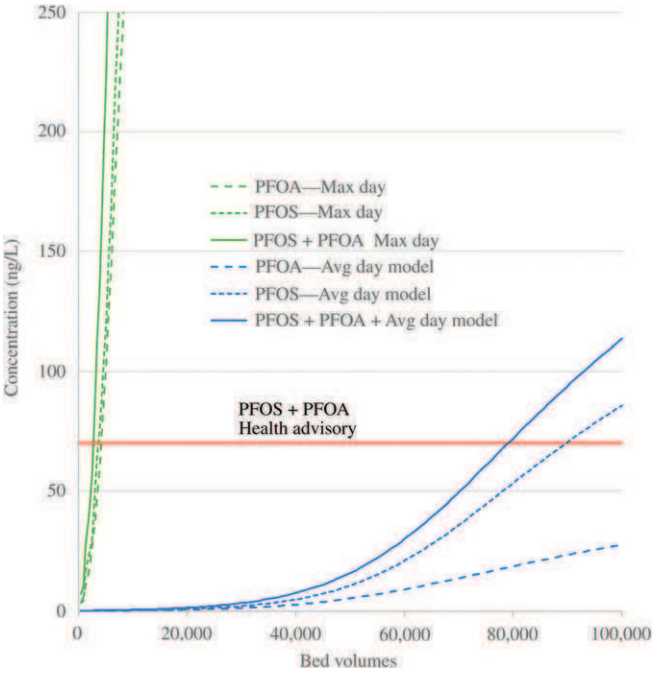

FIGURE 11 Model results of perfluorooctane sulfonate (PFOS) + perfluorooctanoic acid (PFOA) drinking water concentrations versus bed volumes for granular activated carbon (GAC)#2

5 | CONCLUSIONS

In this study, RO and GAC technologies were evaluated to determine their ability as household POU/POE systems to remove PFAS from contaminated groundwater. The RO system and GAC media effluent results were compared for PFOA and PFOS at individual and combined concentrations with the current 70 ng/L USEPA HAL. Both GAC and RO POU/POE systems were shown to have the potential to remove PFAS to below detections under specific water quality conditions, PFAS concentrations, and operational conditions, studied here. However, performance will vary as these conditions vary both spatially and temporally. In addition, long-term performance of these systems, particularly the membrane system, was not tested.

Specifically, each of the three RO systems that was tested successfully removed PFAS from the influent water to below analytical detections for the majority of the sampling events. RO#1 and RO#3 (Flexeon and iSpring) did not show any PFAS in the treated water, while RO#2 (HydroLogic) showed low levels of PFAS in the treated water after shutdown and startup.

The GAC POE systems were evaluated using RSSCT studies to save experimental time. Two different GAC materials were tested in this treatability study: one manufactured from coconut shells and the other manufactured from bituminous coal. While each of the GAC materials tested during this evaluation produced water with little or no PFAS in the effluent, it was found that the coconut-based carbon would treat more water than the coal-based carbon before requiring a replacement. However, the GAC materials may react differently to variations in source water characteristics within the Widefield aquifer region, and additional pilot tests should be performed to ensure the use of the best-performing GAC for each application. In addition, more GAC materials are available that should be considered for testing.

Although this study suggests that using the HAL of 70 ng/L for the combined concentrations of PFOA and PFOS was protective when compared with the breakthrough of the other PFAS, other water qualities may not yield the same results. Differences in water quality, both in terms of PFAS concentrations and background water characteristics, can change this result. Other PFAS are also known to have weaker adsorption characteristics and would break through well before PFOA and PFOS.

If a POU/POE system is correctly designed on the basis of the source water's characteristics and the PFAS found therein, POU/POE water systems can provide relatively inexpensive treatment barriers for PFAS removal in the home. However, analysis of PFAS samples is costly for homeowners and can be a major hurdle in effective removal of PFAS from household water supplies. Proper operation and maintenance and conservative replacement of POU/POE components and media may be one way to circumvent the high cost of monitoring treated household drinking water.

ACKNOWLEDGMENT

The USEPA, through its Office of Research and Development, funded and managed, or partially funded and collaborated in, the research described. This research has been subjected to the Agency's administrative review and has been approved for external publication. Any opinions expressed in this article are those of the author(s) and do not necessarily reflect the views of the Agency; therefore, no official endorsement should be inferred. Any mention of trade names or commercial products does not constitute endorsement or recommendation for use.

ORCID

Craig Patterson https://orcid.org/0000-0002-1435-493X
Jonathan Burkhardt https://orcid.org/0000-0002-2935-4422

REFERENCES

Appleman, T. D., Dickenson, E. R. V., Bellona, C., & Higgins, C. P. (2013). Nanofiltration and granular activated carbon treatment of perfluoroalkyl acids. *Journal of Hazardous Materials*, *260*(9), 740–746.

American Society for Testing and Materials D6586-03. (2008). *Standard practice for the prediction of contaminant adsorption on GAC in aqueous systems using rapid small-scale column tests*. Conshohocken, PA: ASTM International.

Colorado Department of Public Health and Environment. (2016). *PFC levels in drinking water distribution samples collected from the Widefield aquifer region.* Retrieved from https://environmentalrecords.colorado.gov/HPRMWebDrawer/RecordView/1208017

Crittenden, J. C., Reddy, P. S., Arora, H., Trynoski, J., Hand, D. W., Parram, D. L., & Summers, R. S. (1991). Predicting GAC performance with rapid small-scale column tests. *Journal AWWA*, *83*(1), 77–87. https://doi.org/10.1002/j.1551-8833.1991.tb07088.x

Crittenden, J. C., Hutzler, N. J., Geyer, D. G., Oravitz, J. L., & Friedman, G. (1986). Transport of organic compounds with saturated groundwater flow: Model development and parameter sensitivity. *Water Resources Research*, *22*(3), 271–284.

Dickenson, E. R., & Higgins, C. (2016). *Treatment and mitigation strategies for poly- and perfluoroalkyl substances*. (WRF report 4322). Water Research Foundation: Denver, CO.

Federal Register. (2016, May 25). Lifetime health advisories and health effects support documents for perfluorooctanoic acid and perfluorooctane sulfonate. *Federal Register*, *81*(101), 33250. Retrieved from https://www.gpo.gov/fdsys/pkg/FR-2016-05-25/pdf/2016-12361.pdf

Hokanson, D. R., Hand, D. W., & Crittenden, J. W. (1999). *"Adsorption Design Software™ (AdDesignS™)," Copyright 1993–1999*. Houghton, MI: Michigan Technological University. Commercial release: (1999).

McCleaf, P., Englund, S., Östlund, A., Lindegren, K., Wiberg, K., & Ahrens, L. (2017). Removal efficiency of multiple poly- and perfluoroalkyl substances (PFASs) in drinking water using granular activated carbon (GAC) and anion exchange (AE) column tests. *Water Research*, *120*(2017), 77–87.

Mertz, K. A., Gobin, F., Hand, D. W., Hokanson, D. R., & Crittenden, J. C. (1994). *Adsorption design software for windows (AdDesignS)*. Houghton, MI: Michigan Technical University.

National Sanitation Foundation International. (2016). *Draft NSF international protocol, NSF P473-2016, Drinking water treatment units—PFOA & PFOS*. Ann Arbor, MI: Author.

Pressman, J., McCurry, D., Parvez, S., Rice, G., Teuschler, L., Miltner, R., & Speth, T. (2012). Disinfection byproduct formation in reverse-osmosis concentrated and lyophilized natural organic matter from a drinking water source. *Water Research*, *46*(16), 5343–5354.

Sontheimer, H., Crittenden, J. C., & Summers, R. S. (1988). *Activated carbon for water treatment*. Karlsruhe, Germany: DVGW-Forschungsstelle, Engler-Bunte-Institut, University of Karlsruhe, Fed. Rep. of Germany.

U.S. Environmental Protection Agency. (2017). *Standard operating procedure for the analysis of polyfluorinated compounds of interest to OSRTI in water, sludge, influent, effluent, and wastewater by multiple reaction monitoring liquid chromatography/mass spectrometry (LC/MS/MS)*. Chicago, IL: USEPA. CRL Document #OM021, Version #1 (68 pp) (available in Supplementary Information).

SUPPORTING INFORMATION

Additional supporting information may be found online in the Supporting Information section at the end of this article.

How to cite this article: Patterson C, Burkhardt J, Schupp D, et al. Effectiveness of point-of-use/point-of-entry systems to remove per- and polyfluoroalkyl substances from drinking water. *AWWA Wat Sci*. 2019;e1131. https://doi.org/10.1002/aws2.1131

Supplementary Information

for

Effectiveness of Point-of-Use/Point-of-Entry Systems to Remove Per-and-Poly-fluoroalkyl Substances from Drinking Water

Craig Patterson, P.E.[1], Jonathan Burkhardt, Ph.D.[1], Donald Schupp, P.E.[2], E. Radha Krishnan, P.E.[2], Stephen Dyment[3], Steven Merritt[4], Lawrence Zintek, Ph.D.[5] and Danielle Kleinmaier[5]
[1]USEPA, Cincinnati, Ohio
[2]APTIM, Cincinnati, Ohio
[3]USEPA OSP, Denver, Colorado
[4]USEPA Region 8, Denver, Colorado
[5]USEPA Region 5, Chicago, Illinois

Table of Contents

EPA Assessments and Response Actions....3
Table 1. Summary of QA/QC checks for PFAS....4
Table 2. Data qualifiers....5
Table 3. Established MDL and estimated QL for PFAS....5
Table 4. List of analytical methods....6
Table 5. Sample containers, preservation and holding times....7
Table 6. PFAS Concentrations in 5000-gallon tank during stability study....8
Table 7. PFAS Concentrations in 55-gallon drum during stability study....8
Table 8. Water quality parameters in 5000-gallon tank during stability study....9
Table 9. Water quality parameters in 55-gallon drum during stability study....9
Table 10. Influent PFAS concentrations for iSpring RO Test 1....10
Table 11. Effluent PFAS concentrations for iSpring RO Test 1....10
Table 12. Influent water quality parameters for iSpring RO Test 1....11
Table 13. Effluent water quality parameters for iSpring RO Test 1....12
Table 14. Influent PFAS Concentrations for HydroLogic RO Test 2....12
Table 15. Effluent PFAS Concentrations for HydroLogic RO Test 2....13
Table 16. Influent water quality parameters for HydroLogic RO Test 2....13
Table 17. Effluent water quality parameters for HydroLogic RO Test 2....13
Table 18. Influent PFAS Concentrations for Flexeon RO Test 3....14
Table 19. Effluent PFAS Concentrations for Flexeon RO Test 3....14
Table 20. Influent water quality parameters for Flexeon RO Test 3....14
Table 21. Effluent water quality parameters for Flexeon RO Test 3....15
Table 22. Influent PFAS concentrations for Evoqua RSSCT Test 1....15
Table 23. Effluent PFAS concentrations for Evoqua RSSCT Test 1....16
Table 24. Influent water quality parameters for Evoqua RSSCT Test 1....17
Table 25. Effluent water quality parameters for Evoqua RSSCT Test 1....18
Table 26. Influent PFAS concentrations for Calgon RSSCT Test 2....19
Table 27. Effluent PFAS concentrations for Calgon RSSCT Test 2....20
Table 28. Influent water quality parameters for Calgon RSSCT Test 2....21
Table 29. Effluent water quality parameters for Calgon RSSCT Test 2....22
Table 30. PFAS AdDesignS™ Model Input Parameters....23
Figure 1. Model Results of PFAS Concentrations vs. Bed Volumes for GAC RSSCT 1....24
Figure 2. Model Results of PFAS Concentrations vs. Bed Volumes for GAC RSSCT 2....25
Analytical Methods and SOPs....26

EPA Assessments and Response Actions

Readiness reviews and technical system audits were conducted to ensure that all personnel, training, equipment, supplies, and procedures were available and acceptable for environmental data to be collected and to identify and correct of issues that affected data quality. Audits of data quality were conducted on a representative sample of data for the critical target analytes. During data validation, qualifiers were applied to alert the data end user to quality problems that could impact the usability of the data. QA/QC checks for PFAS, definitions of data qualifiers, established MDL and estimated QL for PFAS and RO system and GAC media analytical results with data qualifiers are provided in supplementary information.

The synthetic test water in the stainless steel 55-gallon drum for the GAC media had characteristics based on worst case (maximum) Widefield Aquifer water quality concentrations and/or the requirements of NSF Standard P473: 1) turbidity < 1 NTU, 2) free available chlorine < 0.2 mg/L, 3) pH of 8.2 ± 0.5, 4) temperature of 20 ± 2.5°C, 5) TOC > 1.0 mg/L, and 6) TDS of 500 mg/L.

The synthetic test water in the 5000-gallon stainless steel tank for the RO systems had characteristics based on worst case (maximum) Widefield Aquifer water quality concentrations and/or the requirements of NSF Standard P473: 1) turbidity < 1 Nephelometric Turbidity Unit (NTU), 2) hardness of 300 mg/L (added as potassium chloride [KCl], magnesium sulfate [$MgSO_4$], sodium bicarbonate [$NaHCO_3$] and calcium sulfate [$CaSO_4 \cdot 2H_2O$]), 3) pH of 8.2 ± 0.5, 4) temperature of 25 ± 1 °C (the water temperature was controlled with a chiller and heat exchanger), and 5) TDS of 500 mg/L.

Table 1. Summary of QA/QC checks for PFAS

Parameter	QC Type	Purpose QC	Method	Frequency	Acceptance Criteria
Per-and poly-fluoroalkyl substances (PFAS) (Draft Expanded Region 5 PFC SOP)	Initial calibration	Standardization of instrument	5 to 6 points calibration	Daily	Weighted linear regression curve should have $r^2 \geq 0.98$ and quadratic regression curve should have $r^2 \geq 0.99$ before proceeding with analysis
	Second Source Standard	Assess Calibration curve	An independent standard obtained from different source of calibration standards	Analyzed immediately after the calibration curve	±30% of the true value
	Method Blank (MB)	Assess system/laboratory contamination	Same source reagent water	2 per every 30 samples	≤0.5 of QL
	Continuing calibration checks (CCC) and/or end Calibration check	Assess whether the instrument is within acceptable calibration throughout period in which samples were analyzed	A same source calibration standard	Analysis of mid-level CCC at the end of the analytical sequence	±30% of the true value
	Field duplicate	Assess field sampling precision and homogeneity	Two separate samples collected at the same time	One per every batch of 20 field samples	±30% RPD for samples
	Matrix spike / matrix spike duplicate	Assess the accuracy in a given matrix	A separate aliquot of the sample spiked with known concentrations of analytes	One per every batch of 20 field sample	Recovery ±30 % of the analytes true value
	Field blank	Assess contamination introduced from containers, environment and	Nanopure water with preservatives	One blank per each test matrix	≤0.5 of QL .

Parameter	QC Type	Purpose QC	Method	Frequency	Acceptance Criteria
		reagents			

Table 2. Data qualifiers

Qualifier	Definitions
U	The analyte was analyzed for, but not detected above the reported sample quantitation limit.
J	The analyte was positively identified; the associated numerical value is the approximate concentration of the analyte in the sample. The RL may be increased due to contamination in the blank, or holding times may be exceeded.
K	The result is an estimated quantity, but the result may be biased high.
L	For both detected and non-detected results, the result is estimated but may be biased low.
Q	Used whenever a QC parameter is outside the acceptable limits.
R	The sample results are rejected due to serious deficiencies in the ability to analyze the sample and meet QC criteria. The presence or absence of the analyte cannot be confirmed.

Table 3. Established MDL and estimated QL for PFAS

Contaminants	MDL ng/L	QL ng/L
Per-and poly-fluoroalkyl substances (PFAS)		
Perfluorooctanoic Acid (PFOA)	1.7	10
Perfluorooctane Sulfonate (PFOS)	2.2	10
Perfluoroheptanoic Acid (PFHpA)	1.0	10
Perfluorobutane Sulfonate (PFBS)	0.8	10
Perfluorohexane Sulfonate (PFHxS)	1.2	10
Perfluorononanoic Acid (PFNA)	1.1	10

Note: For each analyte, the lowest calibration standard concentration served as the QL. Actual MDLs and QLs were included with the analytical reports for PFAS analyses. If required, data were reported less than the lowest calibration standard with a “J” qualifier.

Table 4. List of analytical methods

Parameter	Laboratory	Analytical Method / Instrument
Per-and poly-fluoroalkyl substances (PFAS)	EPA Region 5	Region 5 PFC SOP / Waters Acquity H-Class, Waters Xevo TQ-S (LC/MS/MS)
Temperature	T&E Facility	NIST Thermometer
pH	T&E Facility	Standard Method 4500B / Thermo Scientific Orion 5 Star or equivalent, temperature compensated
Turbidity	T&E Facility	HACH® Turbidimeter
Free Chlorine	T&E Facility	HACH® Method 8021 / HACH® Spectrophotometer
Total Organic Carbon (TOC)	T&E Facility	EPA Method 415.3 / Total Organic Carbon (TOC) Analyzer Persulfate-UV Oxidation
Total Dissolved Solids (TDS)	T&E Facility	Wet Chemistry (filtration and evaporation)
Hardness	T&E Facility	EDTA Titrimetric Method / Manual Titration

Table 5. Sample containers, preservation and holding times

Parameter	Sample Containers	Quantity of Influent and Effluent Samples	Preservation	Max. Holding Time
Total Organic Carbon (TOC) (mg/L)	100 mL Amber Glass	1 x 100 mL Influent 1 x 100 mL Effluent	No headspace H_3PO_4, pH<2; Cool ≤6°C	28 days
Total Dissolved Solids (TDS) (mg/L)	1 L HDPE Amber	1 x 1 L Influent 1 x 1 L Effluent	Cool ≤6°C	7 days
Turbidity (NTU)	100 mL HDPE or glass jar or beaker	1 x 100 mL Influent 1 x 100 mL Effluent	Cool ≤6°C	48 hours
Hardness (mg/L)	250 mL HDPE or glass jar	1 x 250 mL Influent 1 x 250 mL Effluent	pH <2, HNO_3	6 months
Free Chlorine* (mg/L)	40-50 mL / Glass beaker	1 x 50 mL Influent 1 x 50 mL Effluent	None	Analyze Immediately
pH (pH Units)	40-50 mL / Glass beaker	1 x 50 mL Influent 1 x 50 mL Effluent	None	Analyze Immediately
Temperature (ºC)	40-50 mL / Glass beaker	1 x 50 mL Influent 1 x 50 mL Effluent	None	Analyze Immediately
Per-and poly-fluoroalkyl substances (PFAS) (ng/L)	15 mL Polypropylene Container	3 x 5 mL Influent 3 x 5 mL Effluent	Cool ≤6°C	28 days
Temperature blank (EPA Region 5)	One 40 mL Vial	1 x 40 mL per cooler	Cool ≤6°C	Measure temperature upon receipt

Table 6. PFAS Concentrations in 5000-gallon tank during stability study

Day	Time (hr)	PFOA (ng/L)	PFOS (ng/L)	PFHpA (ng/L)	PFBS (ng/L)	PFHxS (ng/L)	PFNA (ng/L)
1	0	938 J	130 J	233 J	9.08 JU	938 J	214 J
1	8	919 J	141 J	242 J	9.56 JU	936 J	217 J
2	0	899 J	137 J	247 J	9.85 JU	889 J	211 J
2	8	941 J	139 J	242 J	9.79 JU	952 J	217 J
3	0	940 J	139 J	233 J	9.68 JU	942 J	207 J
3	8	967 J	152 J	244 J	9.38 JU	992 J	227 J
4	0	921 J	147 J	251 J	9.83 JU	958 J	224 J
4	8	963 J	163 J	256 J	9.25 JU	986 J	240 J
5	0	947 J	143 J	253 J	9.41 JU	970 J	221 J
5	8	960 J	155 J	277 J	9.31 JU	1070 J	242 J
8	0	963 J	139 J	252 J	9.82 JU	997 J	220 J
8	8	964 J	141 J	246 J	9.17 JU	964 J	210 J

J – Estimated value; samples received at CRL above 4°C.
U - Below reporting limit.

Table 7. PFAS Concentrations in 55-gallon drum during stability study

Day	Time (hr)	PFOA (ng/L)	PFOS (ng/L)	PFHpA (ng/L)	PFBS (ng/L)	PFHxS (ng/L)	PFNA (ng/L)
1	0	1010 J	172 J	273 J	9.69 JU	1180 J	234 J
1	8	977 J	139 J	240 J	9.42 JU	1020 J	213 J
2	0	1040 J	178 J	256 J	9.64 JU	1050 J	263 J
2	8	1020 J	161 J	261 J	9.56 JU	1030 J	232 J
3	0	1110 J	197 J	259 J	9.98 JU	1030 J	275 J
3	8	1080 J	187 J	277 J	9.28 JU	1060 J	272 J
4	0	1030 J	288 J	257 J	9.45 JU	1060 J	304 J
4	8	870 J	143 J	247 J	9.28 JU	974 J	208 J
5	0	1100 J	173 J	296 J	9.94 JU	1060 J	275 J
5	8	1150 J	191 J	255 J	9.33 JU	1050 J	278 J
8	0	1030 J	247 J	275 J	9.93 JU	1050 J	288 J
8	8	944 J	158 J	280 J	9.52 JU	1040 J	232 J

J – Estimated value; samples received at CRL above 4°C.
U - Below reporting limit.

Table 8. Water quality parameters in 5000-gallon tank during stability study

Day	Time (hr)	Temp (°C)	pH	Turbidity (NTU)	Free Chlorine (mg/L)	TOC (mg/L)	TDS (mg/L)	Hardness (mg $CaCO_3$/L)
1	0	26.6	8.56	0.58	0.01	1.0056	528	266.4
1	8	28.4	8.56	0.34	NA	0.9215	523	262.8
2	0	25.6	8.58	0.38	NA	0.6509	529	262.8
2	8	28.8	8.55	0.31	NA	0.671	528	266.4
3	0	26.6	8.58	0.33	NA	0.6487	549	270.0
3	8	29.1	8.54	0.26	NA	0.6604	544	288.8
4	0	25.0	8.61	0.27	NA	0.7716	538	285.0
4	8	24.9	8.64	0.25	NA	0.6475	541	296.4
5	0	25.3	8.60	0.32	NA	0.649	539	281.2
5	8	25.4	8.64	0.28	NA	0.6462	539	285.0
8	0	27.0	8.61	0.62	NA	0.6977	549	296.4
8	8	26.2	8.63	0.32	NA	0.6619	548	292.6

NA - Not Analyzed

Table 9. Water quality parameters in 55-gallon drum during stability study

Day	Time (hr)	Temp (°C)	pH	Turbidity (NTU)	Free Chlorine (mg/L)	TOC (mg/L)	TDS (mg/L)	Hardness (mg $CaCO_3$/L)
1	0	26.5	8.56	0.57	0.01	1.5149	530	277.2
1	8	24.4	8.58	0.57	NA	1.4847	528	259.2
2	0	22.8	8.58	0.46	NA	1.4713	536	270.0
2	8	22.8	8.58	0.39	NA	1.4599	529	273.6
3	0	22.0	8.58	0.44	NA	1.4347	544	270.0
3	8	22.3	8.56	0.37	NA	1.4516	551	273.6
4	0	21.9	8.60	0.35	NA	1.4696	548	285.0
4	8	21.4	8.59	0.43	NA	1.5247	543	292.6
5	0	21.0	8.58	0.36	NA	1.4095	548	292.6
5	8	21.2	8.60	0.39	NA	1.4134	553	300.2
8	0	21.2	8.61	0.44	NA	1.4402	563	292.6
8	8	20.9	8.63	0.33	NA	1.5439	560	292.6

NA - Not Analyzed

Table 10. Influent PFAS concentrations for iSpring RO Test 1

Day	Time (hr)	PFOA (ng/L)	PFOS (ng/L)	PFHpA (ng/L)	PFBS (ng/L)	PFHxS (ng/L)	PFNA (ng/L)
1	4	878	1570	377	373	1030	280
1	8	1080	2580	375	362	1110	381
2	0	886	2210	343	316	964	326
2	6	907	1690	374	355	1010	314
2	12	1010	2680	384	380 L	1090	365 J
3	0	978	1610	361	353	1140	259
3	6	955	1530	348	348	1030	244
3	12	1080	2230	347	348	1090	352
4	0	881	1370	338	341	977	234
4	6	941	1510	339	338	1060	244
4	12	899	1490	330	324	1030	226
7	0	916	1450	331	332	1020	219
7	4	1040	1690	348	334	1150	258 J

L – Value may be biased low.
J – Value estimated because closing continuing calibration check failed.

Table 11. Effluent PFAS concentrations for iSpring RO Test 1

Day	Time (hr)	PFOA (ng/L)	PFOS (ng/L)	PFHpA (ng/L)	PFBS (ng/L)	PFHxS (ng/L)	PFNA (ng/L)
1	4	9.94 U	9.94 U	9.94 U	9.94 U	9.94 U	9.94 U
1	8	9.65 U	9.65 U	9.65 U	9.65 U	9.65 U	9.65 U
2	0	10.0 U	10.0 U	10.0 U	10.0 U	10.0 U	10.0 U
2	6	9.82 U	9.82 U	9.82 U	9.82 U	9.82 U	9.82 U
2	12	9.69 U	9.69 U	9.69 U	9.69 U	9.69 U	9.69 U
3	0	8.15 U	8.15 U	8.15 U	8.15 U	8.15 U	8.15 U
3	6	9.81 U	9.81 U	9.81 U	9.81 U	9.81 U	9.81 U
3	12	9.47 U	9.47 U	9.47 U	9.47 U	9.47 U	9.47 U
4	0	10.0 U	10.0 U	10.0 U	10.0 U	10.0 U	10.0 U
4	6	9.91 U	9.91 U	9.91 U	9.91 U	9.91 U	9.91 U
4	12	10.1 U	10.1 U	10.1 U	10.1 U	10.1 U	10.1 U
7	0	9.96 U	9.96 U	9.96 U	9.96 U	9.96 U	9.96 U
7	4	9.39 U	9.39 U	9.39 U	9.39 U	9.39 U	9.39 U

U - Below reporting limit.

Table 12. Influent water quality parameters for iSpring RO Test 1

Day	Time (hr)	Temp (°C)	pH	Turbidity (NTU)	Free Chlorine (mg/L)	TOC (mg/L)	TDS (mg/L)	Hardness (mg $CaCO_3$/L)

1	4	22.8	8.47	0.37	0.02	0.7168	573	323.0
1	8	22.0	8.50	0.39	NA	0.7004	564	304.0
2	0	23.0	8.47	0.52	NA	0.6948	566	288.8
2	6	23.0	8.50	0.39	NA	0.7092	544	296.4
2	12	22.8	8.49	0.45	NA	0.6950	571	315.4
3	0	22.5	8.46	0.52	NA	0.8432	576	300.2
3	6	22.5	8.44	0.44	NA	0.7320	568	296.4
3	12	22.4	8.54	0.45	NA	0.7359	554	296.4
4	0	22.3	8.50	0.44	NA	0.7383	564	296.4
4	6	22.2	8.45	0.38	NA	0.6799	514	296.4
4	12	22.1	8.53	0.40	NA	0.6074	555	285.0
7	0	22.4	8.53	0.30	NA	0.4595 LQ	574	285.0
7	4	23.1	8.61	0.34	NA	0.4028 LQ	567	311.6

NA - Not Analyzed

L - For both detected and non-detected results, the result is estimated but may be biased low.

Q - Final check standard recovery was low.

Table 13. Effluent water quality parameters for iSpring RO Test 1

Day	Time (hr)	Temp (°C)	pH	Turbidity (NTU)	Free Chlorine (mg/L)	TOC (mg/L)	TDS (mg/L)	Hardness (mg $CaCO_3$/L)
1	4	23.2	7.20	0.24	0	0.0875 U	7	3.8
1	8	22.2	7.61	0.13	NA	0.1353 U	3	3.8
2	0	22.6	8.10	0.23	NA	0.1463 U	10	1.9
2	6	22.9	7.47	0.13	NA	0.0892 U	8	3.8
2	12	22.6	7.54	0.10	NA	0.1077 U	12	3.8
3	0	22.5	8.45	0.55	NA	0.1005 U	7	1.9
3	6	22.5	7.17	0.34	NA	0.0968 U	4	3.8
3	12	22.5	7.37	0.12	NA	0.2788 U	3	3.8
4	0	22.3	7.69	0.36	NA	0.1012 U	7	3.8
4	6	22.3	7.53	0.17	NA	0.0713 U	6	5.7
4	12	22.5	7.92	0.31	NA	0.1090 LQU	6	3.8
7	0	22.4	7.08	0.16	NA	0.0576 LQU	4	1.9
7	4	22.9	7.38	0.14	NA	0.1671 LQU	3	3.8

NA - Not Analyzed
L - For both detected and non-detected results, the result is estimated but may be biased low.
Q - Final check standard recovery was low.
U - Below detection limit.

Table 14. Influent PFAS Concentrations for HydroLogic RO Test 2

Day	Time (hr)	PFOA (ng/L)	PFOS (ng/L)	PFHpA (ng/L)	PFBS (ng/L)	PFHxS (ng/L)	PFNA (ng/L)
1	4	1190	2810	364	361	1170	413
1	8	806	1100	342	371	881	193
2	0	941	1440	352	382	981	238
2	6	2580	6770	470	377	1930	967
2	12	846	1390	342	372	942	225
7	0	799	1360	325	363	844	210
7	4	805	1330	315	366	910	192

Table 15. Effluent PFAS Concentrations for HydroLogic RO Test 2

Day	Time (hr)	PFOA (ng/L)	PFOS (ng/L)	PFHpA (ng/L)	PFBS (ng/L)	PFHxS (ng/L)	PFNA (ng/L)
1	4	9.49 U	9.49 U	9.49 U	9.49 U	9.49 U	9.49 U
1	8	9.27 U	21.5	9.27 U	9.27 U	9.27 U	9.27 U
2	0	9.72 U	9.72 U	9.72 U	9.72 U	9.72 U	9.72 U
2	6	9.50 U	9.50 U	9.50 U	9.50 U	9.50 U	9.50 U
2	12	9.75 U	9.75 U	9.75 U	9.75 U	9.75 U	9.75 U
7	0	21.4	77.2	10.2 U	10.2 U	10.6	49
7	4	9.88 U	20.2	9.88 U	9.88 U	9.88 U	9.88 U

U - Below reporting limit.

Table 16. Influent water quality parameters for HydroLogic RO Test 2

Day	Time (hr)	Temp (°C)	pH	Turbidity (NTU)	Free Chlorine (mg/L)	TOC (mg/L)	TDS (mg/L)	Hardness (mg $CaCO_3$/L)
1	4	22.1	8.34	0.34	0.02	1.1628	525	292.6
1	8	21.8	8.36	0.30	NA	1.2914	540	296.4
2	0	22.1	8.45	0.33	NA	1.0734	539	292.6
2	6	22.5	8.58	0.38	NA	1.09	531	296.4
2	12	23.1	8.53	0.41	NA	1.1002	524	277.4
7	0	22.2	8.49	0.33	NA	1.1016	514	300.2
7	4	22.8	8.50	0.33	NA	1.1428	507	285.0

NA - Not Analyzed

Table 17. Effluent water quality parameters for HydroLogic RO Test 2

Day	Time (hr)	Temp (°C)	pH	Turbidity (NTU)	Free Chlorine (mg/L)	TOC (mg/L)	TDS (mg/L)	Hardness (mg $CaCO_3$/L)
1	4	22.1	7.77	0.12	0	0.1937 U	18	1.9
1	8	22.3	7.50	0.13	NA	0.1459 U	18	1.9
2	0	22.5	7.16	0.12	NA	0.1245 U	18	1.9
2	6	22.6	7.12	0.16	NA	0.1336 U	12	1.9
2	12	23.4	7.27	0.18	NA	0.1367 U	5	1.9
7	0	22.3	7.55	0.22	NA	0.1510 U	29	1.9
7	4	22.9	7.26	0.24	NA	0.2646 U	7	3.8

NA - Not Analyzed
U - Below detection limit.

Table 18. Influent PFAS Concentrations for Flexeon RO Test 3

Day	Time (hr)	PFOA (ng/L)	PFOS (ng/L)	PFHpA (ng/L)	PFBS (ng/L)	PFHxS (ng/L)	PFNA (ng/L)
1	4	839 J	1400 J	258 J	361 J	976 J	210 J
1	8	1020 J	2920 J	260 J	354 J	1040 J	360 J
2	0	866 J	1620 J	255 J	362 J	983 J	220 J
2	6	1030 J	1810 J	271 J	351 J	1130 J	275 J
2	12	872 J	1660 J	255 J	355 J	927 J	237 J
7	0	800 J	1290 J	240 J	333 J	932 J	192 J
7	4	838 J	1380 J	241 J	336 J	963 J	199 J

J – Estimated value; samples received at CRL above 4°C.

Table 19. Effluent PFAS Concentrations for Flexeon RO Test 3

Day	Time (hr)	PFOA (ng/L)	PFOS (ng/L)	PFHpA (ng/L)	PFBS (ng/L)	PFHxS (ng/L)	PFNA (ng/L)
1	4	9.48 JU	9.48 JU	9.48 JU	9.48 JU	9.48 JU	9.48 JU
1	8	10.3 JU	10.3 JU	10.3 JU	10.3 JU	10.3 JU	10.3 JU
2	0	9.84 JU	9.84 JU	9.84 JU	9.84 JU	9.84 JU	9.84 JU
2	6	9.94 JU	9.94 JU	9.94 JU	9.94 JU	9.94 JU	9.94 JU
2	12	9.56 JU	9.56 JU	9.56 JU	9.56 JU	9.56 JU	9.56 JU
7	0	9.93 JU	9.93 JU	9.93 JU	9.93 JU	9.93 JU	9.93 JU
7	4	10.0 JU	10.0 JU	10.0 JU	10.0 JU	10.0 JU	10.0 JU

J – Estimated value; samples received at CRL above 4°C.
U - Below reporting limit.

Table 20. Influent water quality parameters for Flexeon RO Test 3

Day	Time (hr)	Temp (°C)	pH	Turbidity (NTU)	Free Chlorine (mg/L)	TOC (mg/L)	TDS (mg/L)	Hardness (mg $CaCO_3$/L)
1	4	24.2	8.57	0.38	0.01	1.1895	454	297.7
1	8	22.7	8.53	0.40	NA	1.1729	456	247.0
2	0	22.0	8.58	0.31	NA	1.1834	455	247.0
2	6	22.0	8.61	0.33	NA	1.2248	448	247.0
2	12	22.5	8.58	0.28	NA	1.2074	452	259.7
7	0	24.4	8.48	0.34	NA	1.2755	450	252.0
7	4	23.1	8.48	0.39	NA	1.2984	446	240.0

NA - Not Analyzed

Table 21. Effluent water quality parameters for Flexeon RO Test 3

Day	Time (hr)	Temp (°C)	pH	Turbidity (NTU)	Free Chlorine (mg/L)	TOC (mg/L)	TDS (mg/L)	Hardness (mg $CaCO_3$/L)
1	4	24.2	9.18	0.12	0	0.4828	10	5.7
1	8	23.0	9.01	0.19	NA	0.183	6	5.7
2	0	22.5	8.29	0.17	NA	0.214	24	3.8
2	6	22.4	8.19	0.11	NA	0.1602	2	5.7
2	12	22.6	8.21	0.12	NA	0.1593	3	5.7
7	0	24.7	7.39	0.54	NA	0.1911	16	3.6
7	4	23.5	8.07	0.12	NA	0.1166	6	3.6

NA - Not Analyzed

Table 22. Influent PFAS concentrations for Evoqua RSSCT Test 1

Time (hr)	PFOA (ng/L)	PFOS (ng/L)	PFHpA (ng/L)	PFBS (ng/L)	PFHxS (ng/L)	PFNA (ng/L)
0	989 J	2030 J	296 J	380 J	1140 J	274 J
0.5	1000 J	2740 J	281 J	374 J	1100 J	310 JL
1	989 J	2230 J	279 J	364 J	1100 J	272 J
1.5	984 J	2290 J	278 J	372 J	1090 J	280 J
2	991 J	2490 J	285 J	372 J	1110 J	306 J
2.5	926 J	1740 J	282 J	369 J	1100 J	246 J
3	963 J	1800 J	280 J	372 J	1090 J	249 J
3.5	954 J	2020 J	277 J	375 J	1070 J	266 J
4	982 J	2120 J	287 J	374 J	1070 J	269 J
4.5	971 J	1810 J	281 J	368 J	1080 J	253 J
5	943 J	1940 J	288 J	371 J	1050 J	274 J
5.5	948 J	1750 J	285 J	367 J	999 J	245 J
6	965 J	1670 J	283 J	376 J	1030 J	245 J
6.5	966 J	2370 J	285 J	360 J	1060 J	274 J
7	986 J	1830 J	332 J	405 J	1080 J	264 J
7.5	932 J	1970 J	290 J	369 J	1070 J	264 J
8	1030 J	1870 J	291 J	367 J	1090 J	261 J

J – Estimated value; samples received at CRL above 4°C.
L – Sample result may be biased low.

Table 23. Effluent PFAS concentrations for Evoqua RSSCT Test 1

Time (hr)	PFOA (ng/L)	PFOS (ng/L)	PFHpA (ng/L)	PFBS (ng/L)	PFHxS (ng/L)	PFNA (ng/L)
0	10.3 JU	10.3 JU	10.3 JU	10.3 JU	10.3 JU	10.3 JU
0.5	10.1 JU	10.1 JU	10.1 JU	10.1 JU	10.1 JU	10.1 JU
1	9.98 JU	9.98 JU	9.98 JU	9.98 JU	9.98 JU	9.98 JU
1.5	10.0 JU	10.0 JU	10.0 JU	10.0 JU	10.0 JU	10.0 JU
2	10.9 JK	12.9 J	10.0 JU	10.0 JU	10.0 JU	10.0 JU
2.5	14.7 JK	16.5 J	10.0 JU	10.0 JU	10.0 JU	10.0 JU
3	21.8 J	25.2 J	10.1 JU	13.4 J	13.4 J	10.1 JU
3.5	29.9 J	29.9 J	11.9 JK	20.6 J	21.3 J	10.3 JU
4	33.5 J	33.2 J	13.3 JK	28.5 J	25.1 J	10.1 JU
4.5	39.4 J	42.2 J	15.7 JK	34.7 J	29.7 J	9.87 JU
5	49.5 J	50.5 J	18.9 JK	45.4 J	36.6 J	10.1 JU
5.5	58.7 J	59.2 J	23.0 JK	56.4 J	48.6 J	11.4 J
6	67.0 J	66.5 J	25.6 JK	63.9 J	51.6 J	13.8 J
6.5	77.1 J	82.1 J	28.6 JK	74.0 J	62.3 J	14.7 J
7	85.1 J	93.9 J	34.1 J	77.8 J	72.2 J	16.5 J
7.5	92.1 J	108 J	38.1 J	91.7 J	75.9 J	18.6 J
8	98.1 J	109 J	40.1 J	104 J	87.1 J	18.3 J

J – Estimated value; samples received at CRL above 4°C.
K – Sample result may be biased high.
U – Below reporting limit.

Table 24. Influent water quality parameters for Evoqua RSSCT Test 1

Time (hr)	Temp (°C)	pH	Turbidity (NTU)	Free Chlorine (mg/L)	TOC (mg/L)	TDS (mg/L)	Hardness (mg $CaCO_3$/L)
0	NA	NA	NA	NA	2.5172	NA	NA
0.5	NA	NA	NA	NA	NA	NA	264.0
1	NA	NA	NA	NA	2.4557	NA	NA
1.5	NA	NA	NA	NA	NA	NA	264.0
2	NA	NA	NA	NA	2.4359	NA	NA
2.5	NA	NA	NA	NA	NA	NA	252.0
3	NA	NA	NA	NA	2.4327	NA	NA
3.5	NA	NA	NA	NA	NA	NA	258.0
4	22.3	8.58	0.27	0.02	2.3868	NA	NA
4.5	NA	NA	NA	NA	NA	NA	246.0
5	NA	NA	NA	NA	2.3745	NA	NA
5.5	NA	NA	NA	NA	NA	NA	278.7
6	NA	NA	NA	NA	2.3479	NA	NA
6.5	NA	NA	NA	NA	NA	NA	259.7
7	NA	NA	NA	NA	2.4124	NA	NA
7.5	NA	NA	NA	NA	NA	NA	253.3
8	20.7	8.61	0.38	NA	NA	466	NA

NA - Not Analyzed

Table 25. Effluent water quality parameters for Evoqua RSSCT Test 1

Time (hr)	Temp (°C)	pH	Turbidity (NTU)	Free Chlorine (mg/L)	TOC (mg/L)	TDS (mg/L)	Hardness (mg $CaCO_3$/L)
0	NA	NA	NA	NA	6.0650	NA	NA
0.5	NA	NA	NA	NA	NA	NA	264.0
1	NA	NA	NA	NA	1.4955	NA	NA
1.5	NA	NA	NA	NA	NA	NA	234.0
2	NA	NA	NA	NA	1.521	NA	NA
2.5	NA	NA	NA	NA	NA	NA	240.0
3	NA	NA	NA	NA	1.5571	NA	NA
3.5	NA	NA	NA	NA	NA	NA	258.0
4	22.3	8.60	0.18	0.04	1.6714	NA	NA
4.5	NA	NA	NA	NA	NA	NA	264.0
5	NA	NA	NA	NA	1.7536	NA	NA
5.5	NA	NA	NA	NA	NA	NA	259.7
6	NA	NA	NA	NA	1.8444	NA	NA
6.5	NA	NA	NA	NA	NA	NA	266.0
7	NA	NA	NA	NA	1.8813	NA	NA
7.5	NA	NA	NA	NA	NA	NA	272.3
8	21.8	8.61	0.31	NA	NA	470	NA

NA - Not Analyzed

Table 26. Influent PFAS concentrations for Calgon RSSCT Test 2

Time (hr)	PFOA (ng/L)	PFOS (ng/L)	PFHpA (ng/L)	PFBS (ng/L)	PFHxS (ng/L)	PFNA (ng/L)
0	918 J	1500 J	286 J	377 J	1030 J	246 J
0.5	968 J	2770 J	287 J	370 J	1110 J	324 J
1	941 J	1600 J	287 J	379 J	1060 J	255 J
1.5	1070 J	5210 J	286 J	370 J	1020 J	448 J
2	895 J	1920 J	277 J	361 J	1120 J	253 J
2.5	859 J	1950 J	270 J	359 JL	1080 J	249 J
3	882 J	1680 J	272 J	351 J	1080 J	238 J
3.5	941 J	3630 J	275 J	354 J	1100 J	342 J
4	897 J	1640 J	272 J	347 J	1050 J	232 J
4.5	922 J	1830 J	267 J	348 J	1050 J	248 J
5	904 J	1650 J	272 J	349 J	1110 J	231 J
5.5	891 J	1770 J	270 J	347 J	1080 J	236 J
6	948 J	1700 J	274 J	351 J	1100 J	236 J
6.5	990 J	2050 J	277 J	352 J	1060 J	263 J
7	922 J	1610 J	269 J	348 J	1060 J	235 J
7.5	969 J	2060 J	271 J	348 J	1080 J	272 J
8	959 J	1590 J	267 J	352 J	1090 J	235 J

J – Estimated value; samples received at CRL above 4°C.
L – Sample result may be biased low.

Table 27. Effluent PFAS concentrations for Calgon RSSCT Test 2

Time (hr)	PFOA (ng/L)	PFOS (ng/L)	PFHpA (ng/L)	PFBS (ng/L)	PFHxS (ng/L)	PFNA (ng/L)
0	10.2 JU	10.2 JU	10.2 JU	10.2 JU	10.2 JU	10.2 JU
0.5	10.1 JU	10.1 JU	10.1 JU	10.1 JU	10.1 JU	10.1 JU
1	9.87 JU	9.87 JU	9.87 JU	9.87 JU	9.87 JU	9.87 JU
1.5	10.1 JU	12.0 J	10.1 JU	10.1 JU	10.1 JU	10.1 JU
2	13.3 J	17.8 J	10.3 JU	10.3 JU	10.3 JU	10.3 JU
2.5	22.2 J	27.8 J	10.1 JU	10.1 JU	17.3 J	10.1 JU
3	35.0 J	41.0 J	12.2 J	13.8 J	28.2 J	10.2 JU
3.5	50.7 J	58.5 J	15.8 J	18.2 J	41.2 J	10.0 J
4	61.8 J	74.2 J	21.1 J	25.3 J	52.2 J	12.0 J
4.5	71.0 J	76.3 J	24.8 J	28.6 J	61.7 J	14.1 J
5	79.7 J	90.4 J	26.9 J	30.6 J	73.8 J	16.2 J
5.5	93.8 J	108 J	31.7 J	39.2 J	89.9 J	18.4 J
6	98.2 J	117 J	34.2 J	42.5 J	96.0 J	19.8 J
6.5	117 J	148 J	40.9 J	49.3 J	110 J	23.6 J
7	132 J	153 J	42.3 J	51.1 J	124 J	25.5 J
7.5	165 J	196 J	53.7 J	67.6 J	149 J	32.9 J
8	182 J	221 J	58.0 J	68.1 J	165 J	36.7 J

J – Estimated value; samples received at CRL above 4°C.
U – Below reporting limit.

Table 28. Influent water quality parameters for Calgon RSSCT Test 2

Time (hr)	Temp (°C)	pH	Turbidity (NTU)	Free Chlorine (mg/L)	TOC (mg/L)	TDS (mg/L)	Hardness (mg $CaCO_3$/L)
0	NA	NA	NA	NA	2.3748	NA	NA
0.5	NA	NA	NA	NA	NA	NA	247.0
1	NA	NA	NA	NA	2.5465	NA	NA
1.5	NA	NA	NA	NA	NA	NA	278.7
2	NA	NA	NA	NA	2.5008	NA	NA
2.5	NA	NA	NA	NA	NA	NA	234.0
3	NA	NA	NA	NA	2.4558	NA	NA
3.5	NA	NA	NA	NA	NA	NA	246.0
4	20.3	8.61	0.29	0.01	2.4489	NA	NA
4.5	NA	NA	NA	NA	NA	NA	246.0
5	NA	NA	NA	NA	2.4586	NA	NA
5.5	NA	NA	NA	NA	NA	NA	282.0
6	NA	NA	NA	NA	2.4719	NA	NA
6.5	NA	NA	NA	NA	NA	NA	234.0
7	NA	NA	NA	NA	2.4406	NA	NA
7.5	NA	NA	NA	NA	NA	NA	270.0
8	19.6	8.63	0.32	NA	NA	471	NA

NA - Not Analyzed

Table 29. Effluent water quality parameters for Calgon RSSCT Test 2

Time (hr)	Temp (°C)	pH	Turbidity (NTU)	Free Chlorine (mg/L)	TOC (mg/L)	TDS (mg/L)	Hardness (mg $CaCO_3$/L)
0	NA	NA	NA	NA	0.7078	NA	NA
0.5	NA	NA	NA	NA	NA	NA	266.0
1	NA	NA	NA	NA	0.6413	NA	NA
1.5	NA	NA	NA	NA	NA	NA	285.0
2	NA	NA	NA	NA	0.9649	NA	NA
2.5	NA	NA	NA	NA	NA	NA	246.0
3	NA	NA	NA	NA	1.1623	NA	NA
3.5	NA	NA	NA	NA	NA	NA	234.0
4	21.3	8.71	0.19	-0.03	1.3938	NA	NA
4.5	NA	NA	NA	NA	NA	NA	246.0
5	NA	NA	NA	NA	1.5212	NA	NA
5.5	NA	NA	NA	NA	NA	NA	240.0
6	NA	NA	NA	NA	1.6364	NA	NA
6.5	NA	NA	NA	NA	NA	NA	240.0
7	NA	NA	NA	NA	1.6634	NA	NA
7.5	NA	NA	NA	NA	NA	NA	246.0
8	20.9	8.71	0.20	NA	NA	478	NA

NA - Not Analyzed

Table 30. PFAS AdDesignS™ Model Input Parameters

GAC	PFAS	Kf	K	1/n	dp	ds
Evoqua 1230CX	PFBS	0.00613	19.354317	0.45	8.43E-06	1.31E-10
	PFHpA	0.00808	30.826032	0.45	7.94E-06	1.92E-12
	PFHxS	0.00797	105.445498	0.45	6.26E-06	1.16E-12
	PFNA	0.01077	36.955921	0.45	6.43E-06	1.07E-11
	PFOA	0.00634	91.528488	0.45	6.74E-06	2.34E-12
	PFOS	0.00726	207.547312	0.45	5.6E-06	1.41E-12
Calgon Filtrasorb 600 AR+	PFBS	0.00701	15.680191	0.45	9.25E-06	1.19E-11
	PFHpA	0.0052	12.703420	0.45	7.23E-06	8.68E-11
	PFHxS	0.00513	38.212900	0.45	7.51E-06	2.86E-11
	PFNA	0.00695	15.030018	0.45	6.93E-06	5.89E-11
	PFOA	0.00495	30.815503	0.45	5.28E-06	6.33E-11
	PFOS	0.00567	60.178352	0.45	3.65E-06	7.83E-11

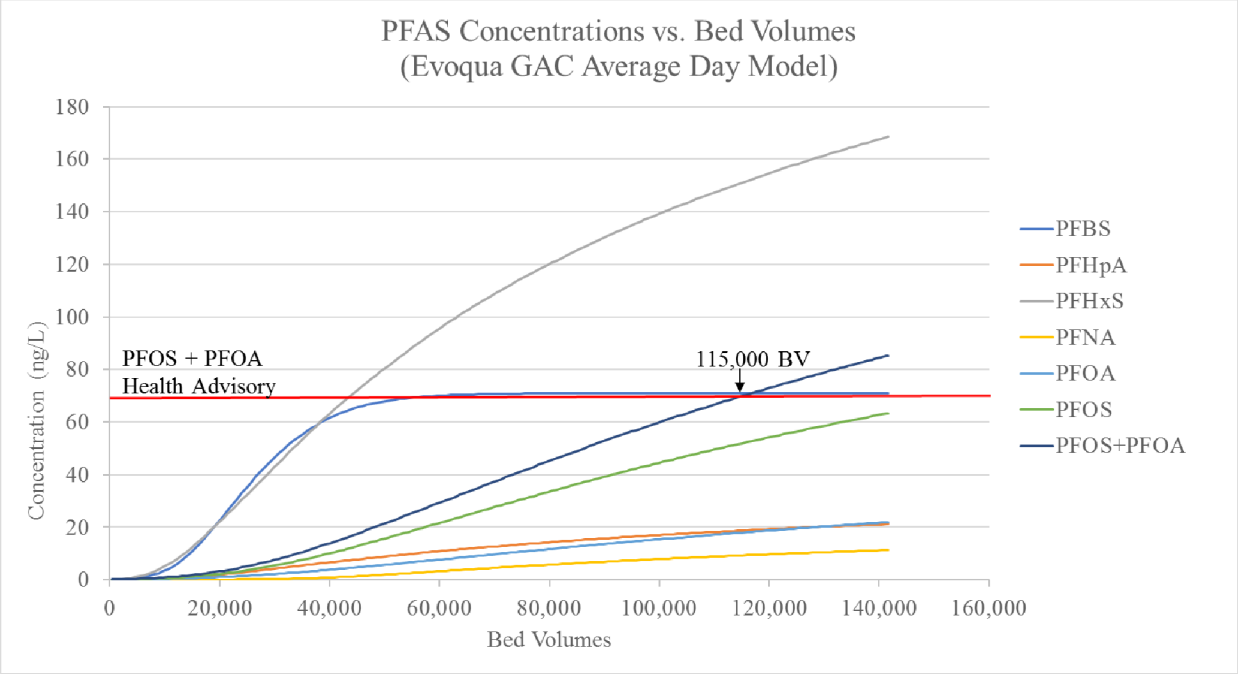

Figure 1. Model Results of PFAS Concentrations vs. Bed Volumes for GAC RSSCT 1

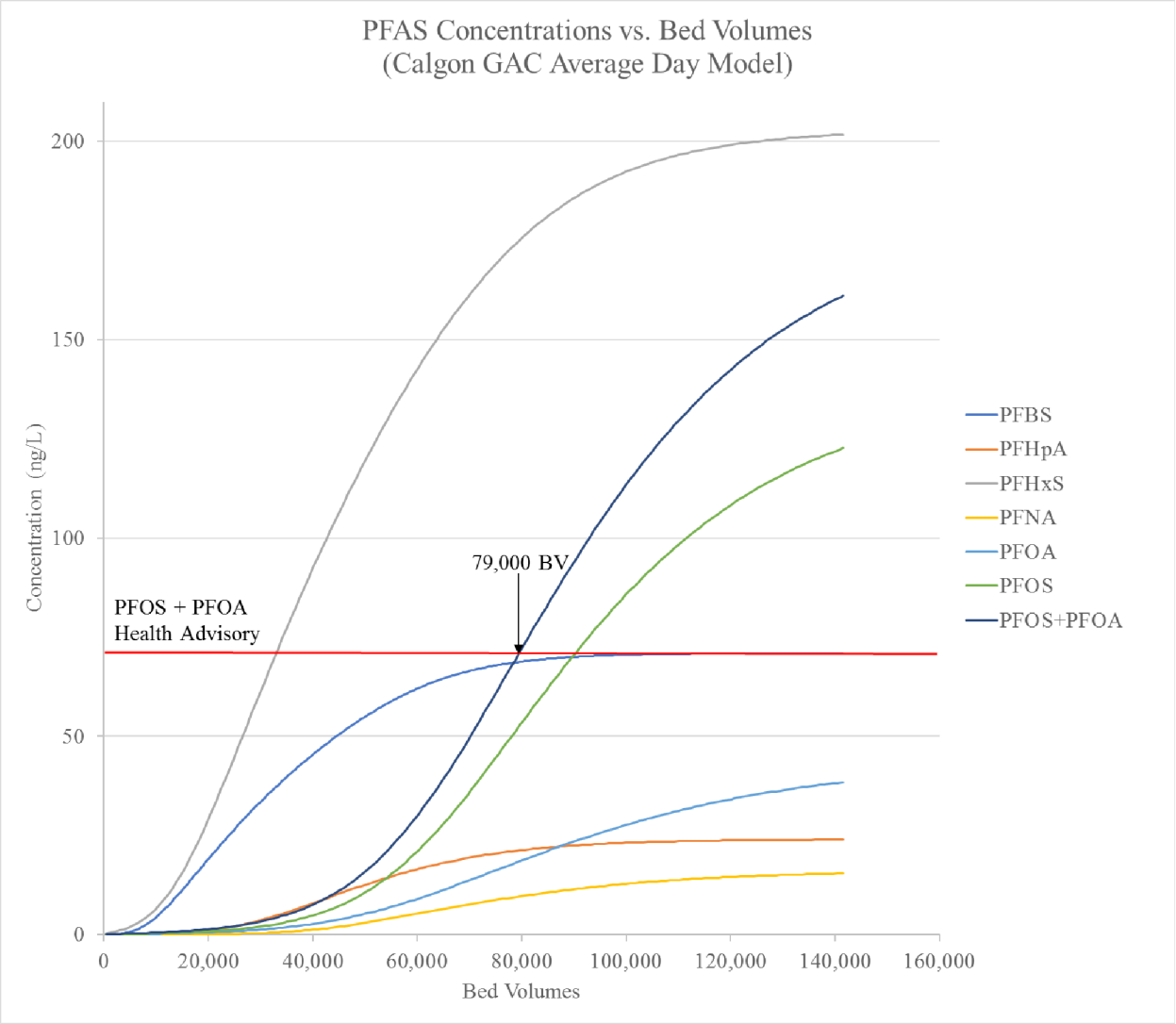

Figure 2. Model Results of PFAS Concentrations vs. Bed Volumes for GAC RSSCT 2

Analytical Methods and SOPs

EPA METHOD 415.3 (TOTAL ORGANIC CARBON)	Appendix B - EPA_415.3.pdf
STANDARD METHOD 4500-H^+ B (pH DETERMINATION USING pH PROBE)	Appendix C - Standard Methods 45
APTIM T&E SOP 510 (TDS DETERMINATION)	TE SOP 510 Total Dissolved Solids 051
APTIM T&E SOP 507 (TURBIDITY DETERMINATION)	507 Turbitidy_gb_RK.pdf
APTIM T&E SOP 503 (HARDNESS DETERMINATION)	503 Total Hardness_20120723.
APTIM T&E SOP 504 (FREE CHLORINE DETERMINATION)	504 Free and Total Chlorine_20110706.p
DRAFT EXPANDED REGION 5 PFC SOP (PFAS DETERMINATION)	Appendix H - Region 5 PFC SOP.pdf

WATER ONLINE

Guest Column | January 22, 2020

EPA Researchers Investigate The Effectiveness Of Point-Of-Use/Point-Of-Entry Systems To Remove Per- And Polyfluoroalkyl Substances From Drinking Water

By U.S. EPA

PFAS are a group of synthetic chemicals that have been in use since the 1940s. PFAS manufacturing and processing facilities, facilities using PFAS in production of other products, airports, and military installations are some of the contributors of PFAS releases into the air, soil, and water. Due to the widespread use of PFAS and their persistence in the environment, most people in the United States have been exposed to PFAS. For homeowners, there is strong interest

in finding a household water treatment system that can be easily installed, if necessary, to reduce the levels of PFAS in their drinking water.

Currently, NSF International has standards PFOA and PFOS, two PFAS compounds. To help homeowners make an informed decision when trying to reduce PFAS in their drinking water, EPA researchers conducted studies on several off-the-shelf, commercially available technologies, including granular activated carbon (GAC), reverse osmosis (RO), and ion exchange treatment systems to determine if they were capable of decreasing PFAS levels in drinking water. Studies for GAC and RO have been completed to date.

In these studies, EPA researchers analyzed water samples for PFAS, pH, temperature, turbidity, total organic carbon, total dissolved solids, hardness, and free available chlorine. The PFAS included in this research were perfluorooctanoic acid (PFOA), perfluorooctane sulfonate (PFOS), perfluoroheptanoic acid (PFHpA), perfluorobutane sulfonate (PFBS), perfluorohexane sulfonic acid (PFHxS), and perfluorononanoic acid (PFNA).

EPA found that both the GAC and RO systems studied were able to reduce PFAS to below laboratory detection limits when used as point-of-entry (where the water enters the whole house) or point-of-use (where water is used in the house, for example a kitchen sink or a bathroom sink) systems. However, water quality conditions, concentrations of PFAS in the water, and operational conditions were shown to affect each of the systems and their effectiveness.

For example, for RO systems, homeowners would be required to replace membranes and filters on a regular schedule to maintain effectiveness. While RO systems were very effective as point-of-use systems, for use as a point-of-entry system to treat water for the entire home, they would require additional components—such as a 200-500-gallon water storage tank, a 20-gallon bladder tank, and a pump with a shutoff switch.

In addition, because RO systems demineralize water, homeowners may have to add mineralization cartridges to point-of-entry RO systems to prevent potential lead and copper corrosion issues within household plumbing.

The RO systems tested included the iSpring RCS5T, the Hydrologic Evolution RO1000 and the Flexeon LP-700. All effluent PFAS results for the iSpring and Flexeon RO systems were non-detect (less than three parts per trillion) during the one-week studies. However, the Hydrologic RO systems were shown to have PFAS concentrations higher than non-detect during intermittent operation. Even in these cases, the membrane removed greater than 75% of the individual PFAS.

GAC systems were also studied on two types of GAC media. Both GAC media (Evoqua 1230CX and Calgon Filtrasorb 600 AR+) were shown to have the potential to remove PFAS to below detection under the specific water quality conditions, PFAS concentrations, and operational conditions used in this study. However, point-of-entry applications, large quantities of GAC would be required to provide enough contact time for removal of PFAS in residents homes.

In conclusion, if a household water system is correctly designed based on the source water's characteristics and the PFAS type and concentrations found within the water, then point-of-use and point-of-entry water systems can provide relatively inexpensive treatment barriers for PFAS removal in the home. It is important to keep in mind that any in-home treatment device should be certified by an independent party, currently available for PFAS (NSF P473), and should be properly maintained to ensure that the treatment system remains effective over time.

For homeowners considering testing to evaluate PFAS in their drinking water, EPA recommends contacting your state to learn if they have state accredited laboratories to test for PFAS. For drinking water, EPA recommends using an EPA testing method.

EPA researchers continue to work with states, tribes, and local communities to develop treatment options to decrease PFAS exposures.

Read the journal article: *Effectiveness of point-of-use/point-of-entry systems to remove per- and polyfluoroalkyl substances from drinking water*.

https://www.epa.gov/sciencematters/epa-researchers-investigate-effectiveness-point-usepoint-entry-systems-remove-and

From: Patterson, Craig <Patterson.Craig@epa.gov>
Sent: Thursday, April 23, 2020 1:13 PM
To: Patterson, Craig <Patterson.Craig@epa.gov>
Subject: Record of Percentage Agreement Craig Patterson

Lead author's name and organization: Craig Patterson, U.S. EPA ORD, Cincinnati, OH

Nominee's name: Craig Patterson

Title of the nominated publication: Effectiveness of Point-of-Use/Point-of-Entry Systems to Remove Per-and-Poly-fluoroalkyl Substances from Drinking Water

I agree with my designated percentage of contribution of 40%

Craig Patterson, P.E.
Environmental Engineer
U.S. EPA M.S. 689
26 W. Martin Luther King Drive
Cincinnati, Ohio 45268
Phone: 513-487-2805
Fax: 513-569-7658
patterson.craig@epa.gov

From: Burkhardt, Jonathan <Burkhardt.Jonathan@epa.gov>
Sent: Thursday, April 9, 2020 9:56 AM
To: Patterson, Craig <Patterson.Craig@epa.gov>
Subject: Record of Percentage Agreement Jonathan Burkhardt

Co-author's name and organization: Jonathan Burkhardt, U.S. EPA ORD, Cincinnati, OH

Nominee's name: Craig Patterson

Title of the nominated publication: Effectiveness of Point-of-Use/Point-of-Entry Systems to Remove Per-and-Poly-fluoroalkyl Substances from Drinking Water

I agree with my designated percentage of contribution of 15%

Jonathan Burkhardt
Center for Environmental Solutions & Emergency Response
Water Infrastructure Division – Drinking Water Management Branch
26 Martin Luther King Drive West
Cincinnati, OH 45268
513-569-7466

From: Schupp, Don <Don.Schupp@aptim.com>
Sent: Tuesday, April 14, 2020 2:04 PM
To: Patterson, Craig <Patterson.Craig@epa.gov>
Subject: Record of Percentage Agreement, Donald Schupp

Co-author's name and organization: Donald Schupp, APTIM Federal Services, LLC, Cincinnati, OH

Nominee's name: Craig Patterson

Title of the nominated publication: Effectiveness of Point-of-Use/Point-of-Entry Systems to Remove Per-and-Poly-fluoroalkyl Substances from Drinking Water

I agree with my designated percentage of contribution of 20%

Don Schupp

DON SCHUPP, P.E.
Engineer 4
APTIM | Government Services
O 513 782 4974
F 513 782 4807
E don.schupp@aptim.com

APTIM

5050 Section Ave.
Cincinnati, OH 45212

APTIM.com

From: Krishnan, Radha <Radha.Krishnan@aptim.com>
Sent: Wednesday, April 15, 2020 11:53 AM
To: Patterson, Craig <Patterson.Craig@epa.gov>
Subject: Record of Percentage Agreement, E. Radha Krishnan

Co-author's name and organization: E. Radha Krishnan, APTIM Federal Services, LLC, Cincinnati, OH

Nominee's name: Craig Patterson

Title of the nominated publication: Effectiveness of Point-of-Use/Point-of-Entry Systems to Remove Per-and-Poly-fluoroalkyl Substances from Drinking Water

I agree with my designated percentage of contribution of 5%

E. Radha Krishnan
APTIM Federal Services, LLC
5050 Section Avenue
Cincinnati, OH 45212

From: Dyment, Stephen <Dyment.Stephen@epa.gov>
Sent: Thursday, April 9, 2020 1:05 PM
To: Patterson, Craig <Patterson.Craig@epa.gov>
Subject: Record of Percentage Agreement- Stephen Dyment

Co-author's name and organization: Stephen Dyment, U.S. EPA ORD, Cincinnati, OH

Nominee's name: Craig Patterson

Title of the nominated publication: Effectiveness of Point-of-Use/Point-of-Entry Systems to Remove Per-and-Poly-fluoroalkyl Substances from Drinking Water

I agree with my designated percentage of contribution of 5%

Stephen Dyment

Stephen Dyment
U.S. EPA Office of Research and Development
Region 8 Superfund and Technology Liaison
1595 Wynkoop Street
Mailcode: 8LAS-TA, Room 5257
Denver, CO 80202-1129

Phone: 303-312-7044
Fax: 303-312-6065
dyment.stephen@epa.gov

Celebrating EPA's 50th Anniversary!
www.epa.gov/50

From: Merritt, Steven <Merritt.Steven@epa.gov>
Sent: Friday, April 10, 2020 11:59 AM
To: Patterson, Craig <Patterson.Craig@epa.gov>
Subject: Record of Percentage Agreement Steve Merritt

Co-author's name and organization: Steven Merritt, U.S. EPA Region 8, Denver, CO

Nominee's name: Craig Patterson

Title of the nominated publication: Effectiveness of Point-of-Use/Point-of-Entry Systems to Remove Per-and-Poly-fluoroalkyl Substances from Drinking Water

I agree with my designated percentage of contribution of 5%

Steven Merritt

Steven B. Merritt, MHP, CIH, REHS
LCDR, USPHS Commissioned Corps
Industrial Hygienist / Radiation Coordinator
U.S. Environmental Protection Agency Region 8
1595 Wynkoop ST (8SEM-EMP)
Denver, CO 80202-1129
303-312-6146 - Work
303-775-7226 - Mobile
Merritt.Steven@epa.gov

From: Zintek, Lawrence <zintek.lawrence@epa.gov>
Sent: Thursday, April 9, 2020 10:02 AM
To: Patterson, Craig <Patterson.Craig@epa.gov>
Subject: Record of Percentage Agreement Lawrence Zintek

Co-author's name and organization: Lawrence Zintek, U.S. EPA Region 5, Chicago, IL

Nominee's name: Craig Patterson

Title of the nominated publication: Effectiveness of Point-of-Use/Point-of-Entry Systems to Remove Per-and-Poly-fluoroalkyl Substances from Drinking Water

I agree with my designated percentage of contribution of 5%

Lawrence Zintek, Ph.D.
US EPA Region 5 Chicago Regional Laboratory
536 South Clark Street
Chicago, IL 60605
312-886-2925

From: Kleinmaier, Danielle <kleinmaier.danielle@epa.gov>
Sent: Friday, April 10, 2020 5:04 PM
To: Patterson, Craig <Patterson.Craig@epa.gov>
Cc: Zintek, Lawrence <zintek.lawrence@epa.gov>
Subject: Record of Percentage Agreement Danielle Kleinmaier

Co-author's name and organization: Danielle Kleinmaier, U.S. EPA Region 5, Chicago, IL

Nominee's name: Craig Patterson

Title of the nominated publication: Effectiveness of Point-of-Use/Point-of-Entry Systems to Remove Per-and-Poly-fluoroalkyl Substances from Drinking Water

I agree with my designated percentage of contribution of 5%

Danielle Kleinmaier, Chemist
US Environmental Protection Agency
Region 5 Analytical Services Branch
[formerly Chicago Regional Laboratory]
536 S. Clark St., 10th Fl. (LAB-10C)
Chicago, IL 60605
(312) 353-9771

Table of Contents

General_Authors_Publications.....2
LI-265947_Price_Heberling_EcolEcon.....12
LI-265947_Price_Heberling_EcolEconSupplemental.....27
LI-265952_Price_et_al-2018-Journal_-_American_Water_Works_Association.....99
Record_of_Percentage_Agreement_James_Price.....105
Record_of_Percentage_Agreement__Christopher_Nietch.....106
Record_of_Percentage_Agreement__Matt_Heberling.....107

United States Environmental Protection Agency
Washington, DC 20460

STAA REPORT FOR THE SCIENTIST NOMINATIONS

General Information:

Nomination ID/App ID:	20-098
Research Category Primary:	Review Articles (RA)
Research Category Secondary:	Environmental Policy and Decision-Making Studies (EP)
Laboratory/Office Name:	ORD
Nomination Entered By:	Matthew Heberling

Eligibility Checklist:

[Y] The nominated publication(s) has not been submitted to a previous STAA competition.

[Y] The nominated publication(s) was published on or before January 1, 2017 and on or after January 1,2012

[Y] The principal author was an EPA employee or a PHS employee assigned to EPA when the research was performed

[Y] The EPA authors (includes PHS employees assigned to EPA) contributed collectively a minimum of 50% toward the publication(s)

Nominating Official Name:	Kevin Oshima
Nominating Official Title:	BIOLOGIST
Nominating OfficialEmail:	oshima.kevin@epa.gov
STAA Coordinator Name:	Kathleen Wiser
STAA Coordinator Email:	wiser.kathi@epa.gov

Justifications:

Justification 1:

There is widespread interest in source water protection (SWP) as a means of maintaining safe drinking water supply and avoiding expenditures at community water systems (CWSs). The nominated research publications: 1) report results from a meta-analysis of studies linking source water quality and water treatment costs, 2) review sources of heterogeneity, and their implications, across studies, 3) identify key knowledge gaps in the literature, and 4) propose approaches for conducting empirical research that can effectively aid CWSs evaluate the efficacy of SWP programs. Findings have implications for national water quality regulations, SWP decisions, and source water quality research.

The submitted publications consolidate available evidence from studies that use cost functions, or related approaches, to quantify the relationship between measures of water quality and treatment costs. Several hundred potentially relevant manuscripts were identified in an initial literature review, of which 24 met established inclusion criteria. From these studies, average elasticities, and their corresponding standard errors, were extracted for key water quality measures, where each elasticity indicates how costs respond to a 1% change in water quality. Forty-six elasticities were obtained for various water quality parameters, such as turbidity, total organic carbon, nitrogen, sediment loading, and phosphorus loading. An additional 29 elasticities were obtained for land use classifications (e.g., forests, agriculture, urban), which are often used as proxies for source water quality. The nominated research also thoroughly reviews key differences between studies, including differences in their motivating factors, data structure, and modeling approach. Key knowledge gaps are highlighted. A threefold approach is proposed for addressing these gaps and for improving the availability, as well as the quality, of data for future research.

These research publications are the first to review and summarize the existing literature estimating statistical relationships between water quality and treatment costs. The calculation of elasticities allows study results to be compared and synthesized across otherwise disparate settings and methods—substantially increasing the usefulness of the review to decision makers. Another innovative component of the research is the inclusion of a table containing detailed information

about the data structure, modeling approach, and statistical model used in each study. The table aids CWSs, regulators, and researchers in identifying studies relevant to their needs. A supplemental Excel file facilitates this process by allowing interested parties to sort studies by key traits and results (attached).

The submitted publications support the Environmental Protection Agency's strategic goal of a cleaner, healthier environment, particularly the objective of providing for clean and safe water. It also supports the Office of Research and Development's research objectives; namely, efforts to develop water quality models and economic analyses to support science-based water quality decisions.

Justification 2A:

Two research publications are being submitted. The first, *The Effects of Source Water Quality on Drinking Water Treatment Costs: A Review and Synthesis of Empirical Literature*, is the more important of the two; it provides a comprehensive review of the literature linking treatment costs to source water quality. It includes the aforementioned meta-analysis of elasticities extracted from the literature and a discussion of key knowledge gaps.

Following a presentation at the 2017 American Water Works Association Water Sustainability Conference (part of a source water protection track) in New Orleans, LA where we discussed some early results of our synthesis, we were invited to prepare another paper on the topic for the Journal American Water Works Association (JAWWA). For this paper, *Economic Support for Decisions on Source Water Protection*, we delved further into the knowledge gaps in the literature and how to address those gaps. Crucially, we provide a threefold research plan for helping CWSs evaluate source water protection programs and identify methods for improving the availability and quality of data for future research.

Justification 2B:

Price

· N/A

Heberling

· 2017 Level III for Comparing Drinking Water Treatment Costs to Source Water Protection Costs Using Time Series Analysis (Heberling, M., C. Nietch, H. Thurston, M. Elovitz, K. Birkenhauer, S. Panguluri, B. Ramakrishnan, E. Heiser, T. Neyer), awarded 2018

Nietch

· 2017 Level III for Comparing Drinking Water Treatment Costs to Source Water Protection Costs Using Time Series Analysis (Heberling, M., C. Nietch, H. Thurston, M. Elovitz, K. Birkenhauer, S. Panguluri, B. Ramakrishnan, E. Heiser, T. Neyer), awarded 2018

· 2017 Level II for an Investigation of the Role of Reservoirs in Removing Excess Reactive Nitrogen from the Environment, awarded 2018:

Beaulieu, J. J., R. L. Smolenski, C. T. Nietch, A. Townsend-Small, M. S. Elovitz, and J. P. Schubauer-Berigan. 2014. Denitrification alternates between a source and sink of nitrous oxide in the hypolimnion of a thermally stratified reservoir. Limnology and Oceanography 59:495-506.

Beaulieu, J. J., C. T. Nietch, and J. L. Young. 2015. Controls on nitrous oxide production and consumption in reservoirs of the Ohio River Basin. Journal of Geophysical Research-Biogeosciences 120:1995-2010.

· 2016 Level II for Development and Application of Test Methods Using a More Relevant and Sensitive Mayfly Species for Assessing Toxicity (Weaver, P., K. Struewing, C. Nietch, J. Lazorchak, B. Johnson, D. Funk, S. DeCelles, D. Buchwalter), awarded 2016

Justification 2C:

Heberling

Comparing Drinking Water Treatment Costs to Source Water Protection Costs Using Time Series Analysis, Level III award, focuses on a single drinking water treatment plant in southwest OH. The current nomination is a synthesis of economic studies that estimate a drinking water treatment cost function. It provides a broader view of the economic literature and synthesizes the approaches used and water quality parameters important in treatment costs.

Nietch

Comparing Drinking Water Treatment Costs to Source Water Protection Costs Using Time Series Analysis, Level III award, focuses on a single drinking water treatment plant in southwest OH. The current nomination is a synthesis of economic studies that estimate a drinking water treatment cost function. It provides a broader view of the economic literature and synthesizes the approaches used and water quality parameters important in treatment costs.

Investigation of the Role of Reservoirs in Removing Excess Reactive Nitrogen from the Environment, Level II award, focuses on excess reactive nitrogen in reservoirs. It does not examine incentives for protecting source water.

Development and Application of Test Methods Using a More Relevant and Sensitive Mayfly Species for Assessing Toxicity, Level II award, has nothing to do with the incentives for protecting source water, rather addressed an ecotoxicology issue.

Justification 2D:

N/A

Justification 2E:

N/A

Justification 3A:

Following publication, the authors received numerous requests of technical assistance related to cited studies or finding additional information. USEPA's Office of Water (Katherine Foreman) requested information on the literature review to support decision making. ICF, a contractor, requested a meeting to discuss how they could use our synthesis to estimate benefits of improvements in water quality as it relates to drinking water treatment costs. Another consultant, George Van Houtven, asked questions about our literature review to support similar work in North Carolina.

Alex Mayer (Professor, Department of Civil & Environmental Engineering, Michigan Technological University) requested information on the studies reviewed in order to look at source water protection in Mexico. Having published the JAWWA paper, Dr. Price was contacted by Ann-Marie Doefhoff and Jordan Parman (Water Quality Scientist, Metro Wastewater Reclamation District, Denver, CO) to discuss economic data that could be used to evaluate the benefits of source water protection or develop a new survey to collect the needed data for analysis.

Our synthesis paper in Ecological Economics has been cited 13 times in Google Scholar. The nominated research citations range from proof that poor water quality has increased the costs of drinking water treatment to the need to look beyond turbidity as a driver of treatment costs (such as pathogens or the effect of forest cover). The JAWWA paper has 3 citations in Google Scholar. In addition, the nominated papers are referenced as evidence to support new rules (e.g., California Water Quality Control Board and Testimony on the Use of Natural Infrastructure for Watershed Restoration and Water Management). Finally, both papers are cited in an US EPA, Office of Water document for estimating the benefits of improved surface water quality. The nominated papers are described as possible support for the development of a tool that estimates avoided drinking water treatment costs with improved water quality.

Justification 3B:

The authors targeted invited presentations and professional meetings for feedback on the ideas, models, and conclusions based on early drafts of the nominated paper. As part of EPA's Small Drinking Water System Webinar Series, the researchers were invited to discuss the potential of source water protection as a cost-effective approach to producing drinking water. Part of this webinar included a draft synthesis of the economic studies. This webinar had over 1100 attendees with all 50 states represented (including 9 Tribes and all 10 EPA Regions), Washington D.C., Puerto Rico, Brazil, Canada, Germany, Japan, the Philippines, and Portugal. In addition, the authors presented at the 2017 American Water Works Association Water Sustainability Conference (part of a source water protection track) in New Orleans, LA and the 2017 American Water Resources Association (AWRA) Annual Conference: in Portland, OR. These all occurred prior to submitting the paper to Ecological Economics.

In addition to the professional meetings, the Office of Research and Development requires two internal reviewers. Because of the importance of this synthesis, we requested an internal review from the Office of Water's Erik Helm who is a respected economist and familiar with these types of studies. We also benefited from the reviews of other economists and policy makers external to the Office of Research and Development. The authors wanted to confirm the interpretations were correct and the paper was consistent with EPA's policy formulation. A draft was sent to economist Dr. William Wheeler (Office of Policy's National Center for Environmental Economics) who requested additional details on the results. We also provided drafts to the Office of Water's Katherine Foreman, Hannah Holsinger, Kara Goodwin, and Bo Williams. Their feedback ranged from improving the clarity to improving the links to decision making. Finally, the paper was externally peer reviewed by 4 reviewers and Editor at Ecological Economics.

AUTHORS

Principal Author

Author Name: Matthew T. Heberling

Professional Title:		Salutation:	Dr.
Email:	heberling.matt@epa.gov	Organization:	
Mailing Address:			
Street Line 1:			
City:			
Zip Code:		State:	
At time of research was:	EPA Employee		
Separation Date:			
% of Effort:	62		

Contributing Author

Author Name:	James Price		
Professional Title:		Salutation:	Dr.
Email:	priceji@uwm.edu	Organization:	
Mailing Address:			
Street Line 1:			
City:			
Zip Code:		State:	
At time of research was:	EPA Employee		
Separation Date:	Fri Jul 19 00:00:00 GMT 2019		
% of Effort:	35		

Contributing Author

Author Name:	Christopher Nietch

Professional Title:		Salutation:	Dr.
Email:	nietch.christopher@epa.gov	Organization:	
Mailing Address:			
Street Line 1:			
City:			
Zip Code:		State:	
At time of research was:	EPA Employee		
Separation Date:			
% of Effort:	3		

PUBLICATIONS

Publication 1:

Publication Title:	The Effects of Source Water Quality on Drinking Water Treatment Costs: A Review and Synthesis of Em		
Publication Date:	Sat Jun 02 00:00:00 GMT 2018		
Journal/Publication Method:	Ecological Economics		
All Author(s):			
Volume:	151	Number:	2018
Pages:	195-209	Immediately Index:	Immediately Index:
Citation ½ Life:	9.4	Impact Factor:	4.281

Publication 2:

Publication Title:	Economic Support for Decisions on Source Water Protection

Publication Date:	Fri Aug 31 00:00:00 GMT 2018		
Journal/Publication Method:	Journal American Water Works Association		
All Author(s):			
Volume:	110	Number:	9
Pages:	56-61	Immediately Index:	Immediately Index:
Citation ½ Life:	18.3	Impact Factor:	0.838

Ecological Economics 151 (2018) 195–209

Contents lists available at ScienceDirect

Ecological Economics

journal homepage: www.elsevier.com/locate/ecolecon

The Effects of Source Water Quality on Drinking Water Treatment Costs: A Review and Synthesis of Empirical Literature

James I. Price*, Matthew T. Heberling

Office of Research and Development, U.S. Environmental Protection Agency, Cincinnati, OH 45268, United States

ARTICLE INFO

Keywords:
Water quality
Source water protection
Community water systems
Drinking water treatment
Avoided treatment costs
Economic analysis

ABSTRACT

Watershed protection, and associated *in situ* water quality improvements, has received considerable attention as a means for mitigating health risks and avoiding expenditures at drinking water treatment plants (DWTPs). This study reviews the literature linking source water quality to DWTP expenditures. For each study, we report information on the modeling approach, data structure, definition of treatment costs and water quality, and statistical methods. We then extract elasticities indicating the percentage change in drinking water treatment costs resulting from a 1% change in water quality. Forty-six elasticities are obtained for various water quality parameters, such as turbidity, total organic carbon (TOC), nitrogen, sediment loading, and phosphorus loading. An additional 29 elasticities are obtained for land use classification (e.g., forest, agricultural, urban), which often proxy source water quality. Findings indicate relatively large ranges in the estimated elasticities of most parameters and land use classifications. However, average elasticities are smaller and ranges typically narrower for studies that incorporated control variables consistent with economic theory in their models. We discuss the implications of these findings for a DWTP's incentive to engage in source water protection and highlight gaps in the literature.

1. Introduction

Drinking water treatment plant (DWTP) design and operation is based on, among other considerations, the physical, chemical, and microbiological characteristics of its source water. Within design limits, DWTPs respond to water quality declines by altering treatment processes (e.g., retention time, chemical dosing, etc.) to meet potable water standards and performance objectives. Dramatic declines in water quality, due to severe algal blooms or the presence of cyanobacteria, may occasionally result in temporary plant shutdowns and drinking water advisories (Henry, 2013; Kansas Department of Health and Environment, 2011; Snider, 2014). When water pollution regularly exceeds design thresholds, DWTPs may purchase new capital assets or develop alternate source water resources (Hanson et al., 2016; Jones et al., 2007), which, in turn, can lead to higher water rates for consumers. The effect of reduced source water quality is thus a potential decrease in consumer welfare and, notwithstanding temporary shutdowns, an unequivocal increase in treatment costs. Estimates of these welfare effects have been included in US Environmental Protection Agency (EPA) assessments of surface water quality regulations (Griffiths et al., 2012).

Source water protection (SWP), defined broadly as actions that safeguard source water conditions from adverse impacts prior to intake, has received growing attention as part of a multi-barrier approach to mitigating water-related health risks and avoiding treatment costs. For instance, the 1996 amendments to the US EPA's Safe Drinking Water Act authorized funding for SWP programs and required states to perform assessments of source waters to determine their susceptibility to contamination (Tiemann, 2014). Recent additions to California's Water Code establish source watersheds as part of a DWTP's infrastructure; financing for repair to source watersheds is also made available (California Water Code §108.5, 2016). Moreover, recent literature indicates that dozens of municipalities are engaged in SWP activities (sometimes referred to as water funds or natural infrastructure), such as land acquisition and management, compensation to landowners for adopting best management practices, and public education campaigns (Abell et al., 2017; Bennett et al., 2014; Carpe Diem West, 2011; Dudley and Stolton, 2003; Gartner et al., 2013; Herbert, 2007). These practices have, in some instances, been linked to reductions in key water quality impairments, including turbidity, pesticides and nutrients, with the latter subsequently linked to lower algae concentrations and a lower probability of algal and cyanobacteria bloom events. Boston has a well-known SWP program. Since the 1980s, the city has undertaken extensive watershed management efforts, at a cost of $135 million for

* Corresponding author.
E-mail addresses: Price.James@epa.gov (J.I. Price), Heberling.Matt@epa.gov (M.T. Heberling).

https://doi.org/10.1016/j.ecolecon.2018.04.014
Received 15 November 2017; Received in revised form 22 March 2018; Accepted 10 April 2018
Available online 02 June 2018
0921-8009/ Published by Elsevier B.V.

land acquisition alone, to avoid the cost of constructing and operating a filtration plant (Alcott et al., 2013). As a result, the city has maintained a waiver from filtration under the US EPA's Surface Water Treatment Rule. Other high-profile examples of municipalities engaged in SWP include New York, Denver, Salt Lake City, San Antonio, Santa Fe, and Seattle (Bennett et al., 2014; Carpe Diem West, 2011). Outside the US, SWP has been adopted by cities as diverse as Munich, Stockholm, Sydney, Tegucigalpa, Tokyo, and Victoria (Capital Regional District, 2017; Dudley and Stolton, 2003).

The notion that SWP is more cost effective than traditional treatment processes is common—but evidence from high-quality benefit-cost analyses (BCAs) is limited (Gartner et al., 2013; Herbert, 2007). The validity of any such analyses partially rests on having an accurate understanding of linkages between ecosystems, hydrologic systems, and DWTPs. This review, motivated to better understand these linkages and to facilitate BCAs, consolidates available evidence from studies that use cost functions, or related approaches, to quantify the relationship between measures of water quality and treatment cost. From these studies, we extract elasticities that indicate how costs respond to marginal changes in water quality. Average elasticities are then calculated for key water quality measures. We discuss the implications of this review for SWP decisions and highlight notable gaps in the literature.

2. Theoretical Framework

Production theory provides an overarching framework for the avoided treatment cost literature (Varian, 1992). Most studies we looked at, regardless of data structure or statistical methods, relate source water quality to treatment costs using either a cost function or price function approach. Some studies use alternate approaches that rely, sometimes implicitly, on the underlying cost minimization assumption inherent in these functions. We address these approaches later. Here we develop cost and price function models for a DWTP using non-purchased source water.

Cost functions define the minimum cost needed to produce a predetermined output. They are well-suited for modeling DWTP behavior, which is usually constrained by some form of revenue control (i.e., caps on revenue, service charges, or rates-of-return) and a requirement to meet customer demand for set water rates (Estache and Rossi, 2002; Renzetti and Dupont, 2009). Cost functions are classified as either short- or long-run. In the short-run, capital inputs are assumed fixed and a DWTP minimizes costs by optimally choosing quantities of the variable inputs. In the long-run, capital is also variable, as new treatment facilities can be constructed or source waters tapped, and optimization occurs in the choice of all inputs. Formally, short- and long-run cost functions for a single-output DWTP are

$$c_{sr} = f(y, P_X, K, Q)$$

$$c_{lr} = f(y, P_X, P_K, Q),$$

where c_{sr} represents short-run total costs, c_{lr} long-run total costs, y the volume of potable water, P_X a vector of variable input prices, P_K a vector of capital input prices, K a vector of quasi-fixed capital inputs, and Q a vector of source water characteristics. For concreteness, Q can be viewed as a set of physical, chemical and microbiological water quality measures. Since these parameters affect a DWTP's choice of treatment technology, capital stock in the short-run function can itself be considered a function of Q (i.e., modeled as $K(Q)$). Statistical estimation of the cost function requires a specified functional form (e.g., linear, Cobb-Douglas, and trans-log).

The price function is a related modeling approach. It is based, as before, on cost minimization, but also hinges on the assumption that water rates are set equal to a DWTP's long-run average costs (Abildtrup et al., 2013). This latter condition is applicable to DWTPs—typically publicly managed systems—that operate under a balanced budget constraint. The price function for such a DWTP is

$$r = f(y, P_X, P_K, Q),$$

where r is the water rate and the remaining elements are defined as before.[1] Similar to the cost function, statistical estimation requires a specified functional form.

3. Literature Search and Selection Criteria

We conducted a thorough search for studies linking treatment costs and source water quality, which considered peer-reviewed and gray literature from multiple disciplines, including economics, environmental science, and civil engineering. Three *ex ante* defined criteria were used to identify studies relevant for this review. Specifically, a study needed to

- establish an original, quantitative functional relationship between costs and source water quality or select proxies for water quality;
- use historic cost information obtained from community water systems (CWSs); and
- clearly describe data sources, methodological procedures, and results.[2]

The criteria are deliberately imprecise in several respects to accommodate the broad spectrum of source water issues facing treatment facilities, and to allow for differences in research aims and data availability. Studies meeting our criteria make use of various physical, chemical, and microbiological water quality parameters. These parameters represent different spatial scales (e.g., source water body, source watershed, etc.) and methods of measurement. Similarly, studies make use of diverse cost measures that vary with respect to expenditure types, timeframes, and units of measurement.

Included in the review are studies that proxy water quality with land use classifications. Broad causal relationships between land use and surface water quality are well established; they indicate that forestland, relative to agriculture and urban land, is associated with lower concentrations of non-point source pollutants (e.g., suspended sediment, nutrients) and more desirable microbiological communities (Baker, 2003; Dudley and Stolton, 2003). Forestland is also associated with better groundwater quality (Lerner and Harris, 2009), which is vulnerable to both point and nonpoint source pollution. Depending on geological and hydrological characteristics of the aquifer, it can take years, decades, or centuries, for surface water to infiltrate to the aquifer wherein it becomes a component of a DWTP's source water (Lerner and Harris, 2009). We consider, but ultimately exclude, studies that employ precipitation and streamflow as proxy measures for water quality. While precipitation often leads to deteriorated water quality via increased runoff, its effects can be ambiguous, being dependent on the importance of the runoff relative to a dilution effect that reduces contaminant concentrations (Holmes, 1988; Vincent et al., 2016). Moreover, both precipitation and streamflow measures confound issues of water availability and water quality, which are known to have distinct effects on treatment costs (Heberling et al., 2015; Renzetti, 2001).

We require that studies use historic cost information from CWSs. Studies employing predicted cost data, pilot programs, or non-community systems are consequently excluded from the review. Predicted costs are expenditures estimated for a certain type of treatment technology, or set of technologies, using engineering or statistical relationships developed elsewhere. These costs, while suitable to many applications, introduce measurement error that can bias estimated

[1] Privately managed systems and public-private partnerships operate under different constraints that give rise to an alternate price function specification equal to the sum of marginal cost and rent paid to the operator. Marginal costs are a function of potable water production, input prices, and source water quality (Abildtrup et al., 2013).

[2] CWSs are defined, in accordance with the US Safe Drinking Water Act, public water systems that supply potable water to at least 15 service connections used by year-round residents or regularly serves at least 25 year-round residents (40 C.F.R. §141.2, 2016).

relationships if they are correlated with model covariates such as output volume or source water quality. This error can be substantial, with predictions differing from actual costs by +50 to −30% (McGivney and Kawamura, 2008). Even when tailored to a specific DWTP, predicted and actual costs will differ since the former are based on historical averages that ignore site-specific differences in some plant design features, operational practices, input prices, and customer characteristics.

Finally, we exclude from the review several studies that are missing vital pieces of information, or are reproduced elsewhere, but that otherwise meet the selection criteria. Most of these studies are not centrally concerned with avoided treatment costs. A complete list of studies not meeting our selection criteria, and a rationale for their exclusion, is available upon request.

4. The Avoided Treatment Cost Literature

An initial literature search identified several hundred potentially relevant manuscripts, from which 24 met the aforementioned criteria. Despite similar frameworks, these studies exhibit considerable heterogeneity due to differences in motivation, data availability, and modeling approaches. Characteristics of the studies are reported in Table A; they pertain, unless otherwise noted, to the preferred specification of the model relating costs to source water quality. Where there is ambiguity about a characteristic, we report the most likely information based on available evidence and note the uncertainty. An augmented version of Table A containing additional information and a database of elasticities that can be sorted or filtered are available in Appendix B - Supplementary material.

4.1. Geography and Motivating Factors

A majority of the 24 selected studies are based in the US (n = 15), with the remainder conducted in Canada, France, India, Japan, Malaysia, and Spain. In the US, roughly 47% (n = 7) use subnational samples (i.e., they evaluate data for a single DWTP or region). The US studies are concentrated in the Midwest (Forster et al., 1987; Forster and Murray, 2007; Heberling et al., 2015), but also include Oregon (Moore and McCarl, 1987), Texas (Dearmont et al., 1998), Oklahoma (Oklahoma Water Resources Board, 2011), and the Great Lakes Region (Murray, 2001). By comparison, 66% of non-US studies use subnational samples. All national level analyses pertain to high-income countries where there is access to DWTP-related databases maintained by government agencies or professional associations.

The selected studies cite a diverse set of objectives and underlying motivations. Nonpoint source pollution from agricultural runoff (e.g., sediment, nutrients, pesticides) is the key concern for many US studies (n = 8), as well as for France-based Abildtrup et al. (2013) and Fiquepron et al. (2013). For these analyses, avoided treatment costs represent a lower-bound estimate of externalities imposed by upstream agriculture. Another more geographically disperse set of studies (n = 7) are principally concerned with how forest landscapes, and associated disturbances (e.g., logging, wildfire), affect source water quality within associated watersheds. In a recent example, Vincent et al. (2016) find a negative correlation between forestland (relative to non-forestland) and short-run treatment cost at Malaysian DWTPs. The correlation is significantly larger for virgin forestland than logged forestland. These analyses, in contrast to those motivated by nonpoint source pollution, view avoided treatment costs to be a lower-bound estimate of ecosystem services benefits provided by forest resources. The remaining studies cite other motivations, including evaluating water quality standards, omitted variable bias in cost efficiency estimates, welfare implications of source water quality changes, and endogeneity between technology choice and ecosystem service values. Avoided treatment costs are a secondary concern for these analyses.

4.2. Data Structure

The specifics of any analysis are largely dictated by the structure and content of available data. Many studies rely on cross-sectional survey data (n = 13) that may not be designed to assess avoided treatment costs. Four studies use data obtained from American Water Works Association member surveys (Holmes, 1988; Mosheim, 2006; Mosheim and Ribaudo, 2017; Piper, 2003). These surveys are primarily intended to provide CWS managers with organizational and operational information about other treatment systems. They are not based on a random sampling framework.

Selected studies also make use of panel (n = 6) and time-series (n = 5) data. While these data may be obtained via surveys, they are more likely to entail direct communication with water providers and more targeted information gathering. An advantage of these data structures is the potential to control for unobserved characteristics (e.g., treatment processes, population traits, input price variation) that when omitted from cross-sectional analyses may bias estimated model coefficients. In practice, however, less than half of the studies using panel or time-series data employ estimation techniques that capitalize on this benefit.

Datasets vary considerably in their number of observations. Among cross-sectional analyses, observations range from fewer than 50 (Ernst et al., 2004; Freeman et al., 2008; Mosheim and Ribaudo, 2017; Oklahoma Water Resources Board, 2011; Renzetti, 2001; Warziniack et al., 2017) to nearly 1000 (Price et al., 2017). The smallest panel datasets contain 5 years of annual observations for fewer than 15 DWTPs (Forster and Murray, 2007; Murray, 2001). In contrast, the largest dataset, exploited by Vincent et al. (2016), contains 15 years of monthly observation for 41 DWTPs. Time-series datasets used by Moore and McCarl (1987), Honey-Rosés et al. (2014), and Heberling et al. (2015) have 247, 963, and 1826 daily observations, respectively. Singh and Mishra (2014) use 144 monthly observations.

Studies can be further classified by their unit of analysis. Most are conducted at the DWTP level (n = 14), and therefore relate expenditures incurred at a treatment facility to measures of that facility's influent water quality. A second group of studies are conducted at the CWS level (n = 8), which often operate multiple DWTPs that draw from source waters with different water quality characteristics. Similarly, Fiquepron et al. (2013) and McDonald and Shemie (2014) use units based on geopolitical boundaries that also contain multiple DWTPs and source waters. Cost data in these studies typically reflect expenditures for all DWTPs within the unit of analysis, while covariates, including source water quality measures, are usually defined as the weighted average across the DWTPs. Most studies evaluate DWTPs that rely on surface water inputs (n = 18), while the remaining studies evaluate both surface water and groundwater facilities. There are no studies that pertain exclusively to groundwater DWTPs. Since surface water systems are on average larger than groundwater systems, the datasets used by selected studies consist of relatively large DWTPs (US EPA, 2009b). In the US, where most facilities are small groundwater systems, the average CWS produces 3700 m^3/day of potable water.[3] By comparison, average production in the US based studies ranges from 3530 to 183,700 m^3/day. Across all studies, the DWTPs evaluated by Abildtrup et al. (2013) and Fiquepron et al. (2013) have the smallest production. In Abildtrup et al. (2013) production ranges from 4 to 7640 m^3/day, with an average of 290 m^3/day. The DWTPs evaluated by Horn (2011) and Warziniack et al. (2017) exhibit the largest range in production; both studies include facilities producing < 600 m^3/day and > 1,000,000 m^3/day.

[3] Authors' calculation based on information provided in US EPA (2009a) and US EPA (2009b).

4.3. Cost, Water Quality, and Control Variables

There are several differences between the cost, water quality, and control variables used in the selected studies. These differences should be considered when comparing results across studies as they will affect estimated relationships between costs and water quality measures irrespective of differences in study sites.

Cost variables are expressed in a variety of different currencies, time periods, and production quantities. For this review, however, the principle difference pertains to the scope of expenditures encompassed by the variable. In their most restricted form, costs are limited to expenditures related to a single type of input. Dearmont et al. (1998), Forster and Murray (2007), and Warziniack et al. (2017) exemplify this approach; they establish a function relationship between expenditures on treatment chemicals and changes in source water quality. Many studies (n = 8) use a broader definition of costs that includes expenditures for multiple inputs into the treatment process (e.g., labor, chemicals, electricity). These costs, henceforth referred to as O&M costs, are themselves heterogeneous, with some studies also including expenditures related to facility maintenance, source water acquisition, and treated water distribution. In their broadest form, costs include expenditures on all variable and capital inputs. Horn (2011), Ernst et al. (2004), and Renzetti (2001) define costs in this manner, where capital expenditures are based on dedicated construction costs, depreciation, and debt payments. Studies utilizing a price function approach (Abildtrup et al., 2013; Fiquepron et al., 2013; Piper, 2003) fall into this category since water rates are assumed to reflect long-run average costs.

Water quality measures can be classified as either water parameters, watershed loading, or land use characteristics. Water parameters describe the physical, chemical, and microbiological traits of source water, and are usually presented in terms of pollutant concentrations. Selected studies employ a variety of parameters, namely: temperature, pH, conductivity, turbidity, total organic carbon (TOC), nitrogen, and calcium carbonate.[4] Turbidity is the most common parameter (n = 12); it is near universally monitored by DWTPs and used by operators to optimize treatment processes, assess performance, and monitor compliance (Crittenden et al., 2012; Pizzi, 2005). Abdul-Rahim and Mohd-Shahwahid (2011) and Dearmont et al. (1998) emphasize the combined effects of particulate matter and acidity/alkalinity on chemical dosage decisions by evaluating the multiplicative interaction of turbidity and pH. A related approach, employed by Freeman et al. (2008) and Renzetti (2001), is to construct a water quality index (WQI) that incorporates multiple water quality parameters. The former index is composed of TOC, turbidity, and alkalinity, and the latter composed of fecal coliform, lead, aluminum, benzene, polychlorinated biphenyl, and trichlorobenzene. In a few studies, rather than source water quality, water quality parameters represent the difference between source water and treatment water quality (Abdul-Rahim and Mohd-Shahwahid, 2011; Dearmont et al., 1998; Forster et al., 1987; Horn, 2011; Mosheim, 2006; Mosheim and Ribaudo, 2017; Piper, 2003). This specification, while likely a more accurate representation of the data generating process, is difficult to implement given that raw and treated water quality data are rarely available in the same database.

In contrast to parameters, watershed loading measures describe the quantity of sediment, nutrients, or pesticides entering surface water due to runoff. We identify these variables with the qualifier *load* (e.g., sediment load, pesticide load). Load measures, broadly speaking, are defined in terms of mass per unit time, and are thus equivalent to the product of a pollutant's concentration and a volumetric flow rate. Fiquepron et al. (2013) include a measure of the proportion of source waters that are in guideline noncompliance, which we also categorize as a loading measure because it concerns contamination at the watershed scale. Finally, land use characteristics describe the proportion of land within an area (e.g., watershed, service area, geopolitical boundary) with a certain land cover or land use designation. The most common categories are forestland, agriculture, and urban—where watersheds with a greater proportion of forestland, or smaller proportions of agriculture and urban land, are expected to have better water quality and lower treatment costs. Classifications such as grassland, rangeland, and barren land are also occasionally employed (Fiquepron et al., 2013; Warziniack et al., 2017). Forster and Murray (2007) and Murray (2001) disaggregate agricultural land by their predominant tillage practices: conventional tillage with < 15% crop residue, conventional tillage with 15–30% crop residue, ridge and mulch tillage, and untilled land. Similarly, Fiquepron et al. (2013) disaggregate agricultural land into low-intensity cereal crop production and higher-intensity vine cultivation, market gardening, and arboriculture. Vincent et al. (2016) decompose forestland by logging practices in their analysis of Malaysian DWTPs.

Control variables (i.e., covariates other than water quality measures) are included in cost and price functions to control for factors that may bias parameters of interest. Economic theory offers some insight in this regard (see Section 2), but fails to provide guidance for a considerable number of possible variables. Moreover, there are circumstances, particularly with panel and time-series analyses, where it would be inappropriate to include variables suggested by theory. Thus, whether a set of control variables captures the key confounding factors depends on the particulars of the data and the modeling procedure. Many studies incorporate control variables, exceptions being Ernst et al. (2004), Freeman et al. (2008), Honey-Rosés et al. (2014), McDonald and Shemie (2014), and Oklahoma Water Resources Board (2011). The most common control variable, consistent with economic theory, is the volume of treated water (i.e., production output). Several studies also explicitly control for some combination of labor, chemical, and energy prices (Holmes, 1988; Horn, 2011; Mosheim, 2006; Mosheim and Ribaudo, 2017; Price et al., 2017; Renzetti, 2001).[5] This price data may be obtained directly from water providers, or are extracted from census data, regional price schedules, and supplier price lists. For short-run cost functions, fixed capital stock, when included, is modeled as treatment capacity (Price et al., 2017) or as the ratio of operating profit and the opportunity cost of capital (Mosheim, 2006; Mosheim and Ribaudo, 2017). For long-run functions, capital prices are defined as the ratio of capital costs to fixed tangible assists (Horn, 2011) or the average interest rate on debt (Renzetti, 2001). Additional control variables pertain to weather conditions, source water type (e.g., surface water, groundwater), systems characteristics (e.g., treatment processes, network density, management regime), and service population characteristics (e.g., population density, residential deliveries, non-residential deliveries). The latter category is relevant when the dependent variable includes distribution costs and it is necessary to control for factors affecting delivery.

4.4. Modeling Approach and Estimation

Most studies, as previously noted, can be classified as using a cost (n = 19) or price (n = 3) function approach. An alternative method, employed by Moore and McCarl (1987) and Honey-Rosés et al. (2014),

[4] Turbidity is a measure of water clarity that is correlated with disease causing microorganisms. TOC is positively associated with chemical usage in water treatment and subsequent increases in the formation of harmful disinfection byproducts (DBPs). Nitrogen, in the form of nitrate, poses a serious health risk for infants. Turbidity, nitrate, and several DBPs are regulated by the US EPA (2009c). Source water temperature, pH, and calcium carbonate (i.e., calcium alkalinity) levels are not typically hazardous but can affect chemical dosing. Conductivity is a measure of dissolved salts and inorganic material, and is a major cost driver in desalination processes. An overview of water treatment stages is available in CDC (2015).

[5] Several other studies implicitly control for input prices, or capital stocks, via the use of spatially concentrated cross-sectional data with little variation across observations, time-series data with time-invariant prices and capital stock, or panel fixed-effects techniques.

is to model factor inputs (e.g., alum usage, energy usage), which are then multiplied *ex post* by input prices to determine cost. Within each of these functional approaches there exist a number of possible model specifications and estimators. Several studies employ univariate models (n = 17), whereby a single equation, or multiple independent equations, relate treatment costs to water quality measures.[6] Remaining studies develop multivariate models that relate costs to water quality measures using a system of equations. For example, treatment costs may be modeled as a function of turbidity (i.e., a cost function) and turbidity modeled as a function of land use characteristics (i.e., a turbidity model). Once model parameters are estimated, the recursive relationship between the two equations can be exploited to estimate the effect of changes in land use on treatment costs. The advantage of this approach is that the cost function contains only those predictors that directly affect the DWTP operations, while still allowing auxiliary land use, or watershed loading measures, to affect costs indirectly. Such models are used with regards to pesticide exceedance (Fiquepron et al., 2013), phosphorus load (Heberling et al., 2015), sediment load (Holmes, 1988), and land use classifications (Forster and Murray, 2007; Murray, 2001; Singh and Mishra, 2014; Warziniack et al., 2017). A smaller set of studies use multivariate models to other ends. Piper (2003) jointly estimates a price function and a water demand function to evaluate how changes in source water quality affect consumer welfare. Both Mosheim (2006) and Renzetti (2001) jointly estimate a cost function and input share equations using seemingly unrelated regression (SUR).

For statistical estimation of a model, it is necessary to specify a functional form. It is possible, although not always practiced, to test multiple specifications to determine the form that best represents the data generating process. We classify studies based on the specified relationship between cost and water quality measures. The log-linear specification is used the most frequently because of its ability to capture nonlinearity and ease of interpretation (n = 14), followed by linear, polynomial, trans-log, and semi-log specifications. The trans-log specification, used only by Mosheim (2006) and Renzetti (2001), is highly flexible; it allows for nonlinearities and complex interactions among covariates.

OLS is the most frequently used estimator among selected studies (n = 11). For many datasets, however, the underlying assumptions of OLS are violated and alternate estimators are more appropriate. Dearmont et al. (1998) and Moore and McCarl (1987) use estimators to address biased variances, and subsequent issues with inference, associated with heteroskedasticity and autocorrelation. Similarly, Abildtrup et al. (2013) and Fiquepron et al. (2013) address endogeneity, as well as heteroskedasticity, concerns in their respective price functions using a three-stage estimator based on instrumental variable and generalized methods of moments. The former study also employs a spatial autocorrelation (SAC) framework, where treatment costs are a function of forestland within a CWS's neighboring service areas, in addition to the immediate area, via a spatial-lag component. Heberling et al. (2015) consider O&M costs using an error correction model (ECM). The model, evaluated with a maximum likelihood estimator (MLE), finds that changes in water quality have both short-term and long-term effects on treatment costs.[7] The MLE is also used by Horn (2011), Mosheim and Ribaudo (2017), and Price et al. (2017) to estimate stochastic cost frontier (SCF) models, which relax the cost minimization assumption by allowing for cost inefficiencies in the production process. Horn (2011) finds that inclusion of source water quality in the cost function significantly affects efficiency estimates for Japanese water providers. Price et al. (2017) find no evidence of this effect for Canadian DWTPs. Vincent et al. (2016) uses panel fixed-effects estimator to account for unobserved heterogeneity between DWTPs. Finally, Piper (2003) employs three stage least squares (3SLS), and Mosheim (2006) and Renzetti (2001) iterative least square (ILS), to jointly estimate their respective systems of equations.

5. Water Quality Elasticities of Cost

From each selected study, we extract water-quality elasticities of cost, which are defined as the percentage change in costs resulting from a 1% change in source water quality. The principal advantage of elasticities is that they are unit-less, and thus allow for the comparison of results across studies using diverse data structures, variable definitions, and statistical methodologies.[8] The elasticities employed here are more precisely defined as point elasticities evaluated at a study's average DWTP. The basic formula is $\eta = (\partial c/\partial q)(\bar{q}/\bar{c})$, where c is the cost measure, q is the source water quality measure, and an overbar denotes the variable mean. Specific formulae depend on several factors, including the specified functional relationship (e.g., linear, log-linear, polynomial, etc.), presence of temporal or spatial lags, whether water quality measures reflect source water conditions or the difference between source and treated water, and whether water quality affects costs directly or indirectly via a linking equation in a multivariate analysis. We make the required calculation for each water quality measure, summing, differencing, and multiplying coefficients as appropriate. Whenever possible we also calculate an elasticity's standard error. These calculations are made using the restrictive assumption of independence between coefficients, which, while clearly erroneous in many cases, is necessary given that covariance matrixes are rarely reported.[9] Descriptions of the calculations used for each study are available in Appendix B.

Elasticities, and corresponding standard errors, from US and non-US studies are presented in Tables 1 and 2, respectively. We test for statistical significance of the elasticities at p-value < 0.1 using one- and two-tailed *t*-test. One-tailed tests are applied to water quality parameters, watershed loading variables, and forestland, since the direction of their effect on treatment costs is unambiguous. Two-tailed tests are applied to other land use classifications. Turbidity elasticities are statistically significant in nearly all instances, ranging from an unexpected −0.11 (Murray, 2001) to 0.30 (Forster and Murray, 2007). The latter estimate suggests that a 1% decrease in turbidity leads to a 0.3% reduction in chemical treatment costs at sample averages. In the Heberling et al. (2015) ECM, a 1% decrease in turbidity has an immediate effect of 0.02%, and a long-term effect of 0.11% on O&M costs. Price et al. (2017) find a similar elasticity of 0.10 on O&M costs, but in a reparameterization of their main model also find that DWTPs using conventional, direct or in-line filtration, and membrane technologies are roughly twice as responsive to changes in turbidity as those using only disinfection technologies. However, these differences are statistically insignificant. Moore and McCarl (1987) relate turbidity to two different cost measures: 1) alum expenditures and 2) alum and lime expenditures. Similarly, Singh and Mishra (2014) relate turbidity to 1) chemical expenditures and 2) O&M expenditures. In both studies, turbidity elasticities are slightly, albeit insignificantly, smaller under the broader definition of costs. Sediment load elasticities, which like

[6] We consider a model to be univariate if it has a single response variable—regardless of the number of independent variables. A multivariate model is a system of equations with multiple response variables.

[7] In the context of an ECM, short-term and long-term delineate immediate single-period relationship from cumulative multiple-period relationships. They are unrelated to the short- and long-run labels used to describe cost functions, which demarcate the variability of capital inputs.

[8] Caution should be taken when making these comparisons as differences in data and statistical methods may produce systematically different elasticities. Economic theory suggests that elasticity will vary with the scope of expenditures included in the cost measure, volume of production, and level of source water quality measures.

[9] If neither standard errors nor t-statistics are reported for a study's estimated coefficients, we calculate, if possible, standard errors corresponding to the reported significance threshold (i.e., a coefficient with a *p*-value < 0.05 is assumed to have a t-statistic of 1.96).

Table 1
Elasticities from U.S. studies.

Reference	Water quality measure	Elasticity	Reference	Water quality measure	Elasticity
Dearmont et al. (1998)	Turbidity	0.27 (0.12)*	McDonald and Shemie (2014)	Sediment load	0.26
	pH	0.27 (0.12)*		Phosphorus load	0.19
Ernst et al. (2004)	L: Non-forest	Ref	Moore and McCarl (1987)	Turbidity (alum)	0.22 (0.02)*
	L: Forest	−0.83		Temperature (alum)	−0.39 (0.12)*
				Turbidity (alum & lime)	0.21
Forster et al. (1987)	Turbidity	0.12 (0.04)*	Mosheim (2006)	Turbidity	0.09 (0.03)*
	Sediment load	0.41 (0.02)*			
Forster and Murray (2007)	Turbidity	0.30 (0.08)*	Mosheim and Ribaudo (2017)	Nitrogen	0.06 (0.02)*
	Pesticide load	0.27 (0.20)*	Murray (2001)	Turbidity	−0.11 (0.12)
	L: Ridge/mulch tilled[a]	Ref		Pesticide load	−0.43 (0.37)
	L: Tilled w/ < 15% residual[a]	0.40 (0.24)*		L: Ridge/mulch tilled[a]	Ref
	L: Tilled w/ 15–30% residual[a]	0.03 (0.03)		L: Tilled w/ < 15% residual[a]	0.10 (0.13)
	L: Untilled[a]	0.02 (0.10)		L: Tilled w/ 15–30% residual[a]	0.11 (0.13)
	L: Non-agriculture[a]	0.60 (0.28)*		L: Untilled[a]	−0.04 (0.12)
				L: Non-agriculture[a]	0.12 (0.15)
Freeman et al. (2008)[b]	TOC	0.77 (0.23)*	Oklahoma Water Resources Board (2011)	TOC	0.55
	WQI	−0.53 (0.23)*	Piper (2003)	Calcium carbonate[c]	0.003 (0.001)*
	L: Forest	−0.38 (0.23)*			
	L: Urban	0.22 (0.10)*			
	L: Non-forest vegetation	−0.15 (0.07)*			
Heberling et al. (2015)	Turbidity (short term)	0.02 (0.01)*	Warziniack et al. (2017)	Turbidity	0.19 (0.11)*
	pH (short term)	−0.04 (0.06)		TOC	0.46 (0.19)*
	TOC (short term)	−0.04 (0.03)		L: Non-forest/non-urban[a]	Ref
	Turbidity (long term)	0.11 (0.04)*		L: Forest (via turbidity)[a]	−0.32 (0.22)*
	pH (long term)	−0.01 (0.06)		L: Urban (via turbidity)[a]	0.08 (0.08)
	TOC (long term)	0.10 (0.29)		L: Forest (via TOC)[a]	−0.06 (0.07)
	Phosphorus load (long term)[a]	0.02 (0.01)*		L: Urban (via TOC)[a]	0.34 (0.56)
Holmes (1988)	Turbidity	0.07 (0.02)*			
	Sediment load[a]	0.05 (0.02)*			

Notes. Water quality measure: L = land use variable; TOC = total organic carbon; WQI = water quality index. Elasticity: Ref = reference land use category.

* Statistically significant at $p < 0.1$. One-tailed test used for water quality parameters, watershed loading variables, and forestland. Two-tailed tests used for all non-forestland classifications.

[a] Elasticity estimated via a multiple-equation recursive relationship.

[b] Study estimates multiple single-predictor regression models; thus, reference land use is all classifications other than the one included in the model.

[c] Variable is defined as the difference between source and treated water quality. Reported elasticity does not adjust for treated water quality and underestimates the effect of source water quality changes on treatment costs.

Table 2
Elasticities from non-U.S. studies.

Reference	Water quality measure	Elasticity	Reference	Water quality measure	Elasticity
Abdul-Rahim and Mohd-Shahwahid (2011)	Turbidity	0.07 (0.03)*	Horn (2011)	TOC	0.06 (0.02)*
	pH	0.07 (0.03)*			
Abildtrup et al. (2013)	L: Agriculture	Ref	Price et al. (2017)	Turbidity	0.10 (0.02)*
	L: Forest (service area)	−0.48 (0.15)*		Turbidity (conventional)	0.12 (0.03)*
	L: Urban (service area)	0.004 (0.03)		Turbidity (filtration)	0.13 (0.05)*
	L: Other (service area)	−0.21 (0.08)*		Turbidity (disinfection)	0.06 (0.04)*
	L: Forest (entire region)	−0.77 (0.26)*		Turbidity (membrane)	0.14 (0.07)*
	L: Urban (entire region)	0.38 (0.22)*		Turbidity (other)	0.08 (0.07)
	L: Other (entire region)	−0.49 (0.36)		Turbidity (untreated)	0.06 (0.08)
Fiquepron et al. (2013)	Nitrate	0.05 (0.01)*	Renzetti (2001)	WQI	0.80 (0.22)*
	Pesticide exceedance[a]	0.02 (0.01)*	Singh and Mishra (2014)	Turbidity (chemical)	0.20 (0.08)*
	L: Urban/agriculture	Ref		Turbidity (O&M)	0.19 (0.07)*
	L: Forest	−0.07 (0.03)*		L: Non-forest[a]	Ref
	L: Grassland	0.02 (0.02)		L: Forest (chemical)[a]	−1.71 (0.87)*
	L: VIARMA	0.02 (0.01)		L: Forest (O&M)[a]	−1.58 (0.80)*
Honey-Rosés et al. (2014)	Conductivity	0.86	Vincent et al. (2016)	L: Non-forest	Ref
				L: Virgin forest	−0.47 (0.19)*
				L: Logged forest	−0.32 (0.14)*

Notes. Water quality measure: L = land use variable; O&M = operation and maintenance; TOC = total organic carbon; VIARMA = vine cultivation, arboriculture, and market gardening; WQI = water quality index. Elasticity: Ref = reference land use category.

* Statistically significant at $p < 0.1$. One-tailed test used for water quality parameters, watershed loading variables, and forestland. Two-tailed tests used for all non-forestland classifications.

[a] Elasticity estimated via a multiple-equation recursive relationship.

turbidity reflect responses to changes in particulate matter, are also significant in all instances, ranging from 0.05 (Holmes, 1988) to 0.41 (Forster et al., 1987).

The TOC elasticities obtained from Freeman et al. (2008), Horn (2011), and Warziniack et al. (2017) are statistically significant, although they range widely from 0.06 to 0.77. In contrast, Heberling et al. (2015) find no significant short- or long-term relationship between TOC and O&M costs. Four elasticities relate to nutrient levels (i.e., nitrogen, nitrate, and phosphorus load), which have been linked to higher algae concentrations, and, when inadequately treated, adverse health outcomes. These elasticities, with the exception of McDonald and Shemie (2014), are statistically significant and fall within the relatively narrow range of 0.02 and 0.06. McDonald and Shemie (2014) find a considerably larger elasticity of 0.19, but insufficient information is provided to test for its significance. Vastly different elasticities, −0.43 and 0.26, are obtained from Forster and Murray (2007) and Murray (2001) for pesticide load. Fiquepron et al. (2013) find an elasticity of 0.02 for pesticide exceedance, indicating that a 1% increase in incidence of pesticide non-compliance is associated with a 0.02% increase in long-run average costs. Finally, Piper (2003) finds an elasticity of 0.003 for calcium carbonate and Honey-Rosés et al. (2014), the only study to evaluate desalinization, find an elasticity of 0.86 for conductivity.

Land use elasticities must be interpreted relative to a reference category, denoted by Ref in Tables 1 and 2. Estimated forest elasticities are universally negative, implying that forestland leads to improved source water quality relative to all other land use classifications. Ernst et al. (2004) model the relationship between treatment costs and forestland using non-forestland as the reference category. They find a forest elasticity of −0.83. This indicates that a 1% increase in forestland within a source watershed—corresponding to an equivalent decrease in non-forestland—will, on average, reduce costs by 0.83%. Freeman et al. (2008), Singh and Mishra (2014), and Vincent et al. (2016) also use non-forestland as a reference category. Singh and Mishra (2014) find considerably larger elasticities, in absolute terms, than those found elsewhere, with a 1% increase in forestland leading to a 1.71% reduction in chemical expenditures and a 1.51% reduction in O&M expenditures. Vincent et al. (2016) distinguish between virgin and logged forestland, finding that a 1% increase in virgin forest reduces O&M costs by 0.47% while an increase in logged forest reduces costs by 0.32%. Results from the Abildtrup et al. (2013) SAC model, where agriculture land serves as the reference category, indicate a forest elasticity of −0.48 for land use changes in the immediate service area and −0.77 when changes in neighboring service areas are incorporated. Lastly, Fiquepron et al. (2013) find a forest elasticity of −0.07 using low-intensity agriculture and urban land as the reference category.

Results for other land use classifications are more ambiguous. Estimated elasticities for urban land are mostly positive, being statistically significant relative to non-urban land in Freeman et al. (2008) and agriculture land in Abildtrup et al. (2013) when changes in neighboring service areas are incorporated. In Warziniack et al. (2017), where land use affects chemical costs indirectly as predictors of turbidity and TOC, the elasticity for urban land is significant with regards to turbidity but insignificant for TOC. Forster and Murray (2007) decompose agricultural land in Ohio watersheds by tillage practices, finding that traditionally tilled land, as well as non-agriculture land, has a positive and significant elasticity relative to conservation tillage. However, a similar analysis of tillage practices in the Great Lakes Region does not support these findings (Murray, 2001). Elasticities for other land use classifications (i.e., grassland, rangeland, vine cultivation) are largely insignificant.

We summarize the findings presented in Tables 1 and 2 by calculating mean elasticities for water quality measures most pertinent to SWP. All elasticities are weighted equally and assumed independent for these calculations, and no attempt is made to group elasticities by DWTP characteristics, modeling approach, or scope of the cost measure. We limit each calculation (i.e., the mean elasticity for each water quality measure) to a single elasticity per study to prevent values from being dominated by analyses with multiple elasticities for the same water quality measure.[10] Three sets of mean elasticities are presented in Table 3. Since these elasticities are calculated from a small, sometimes highly variable, set of observations, values are unlikely representative of all DWTPs. The first set (column 4) is calculated using all relevant elasticities from the selected studies, including those without standard errors. The second set (column 6) is calculated using all relevant elasticities with standard errors, thus allowing standard errors to be calculated for the mean elasticity estimates. Results from this set show a mean turbidity elasticity, based on 12 observations, of 0.14 (CI: 0.10, 0.18).[11] This estimate varies little between US and non-US studies, and has a relatively small standard error compared to other water quality parameters. The mean nitrogen/nitrate elasticity, based on 2 observations, is 0.06 (CI: 0.04, 0.08), and, as with turbidity, varies little between US and non-US studies. In contrast, the mean TOC elasticity is eight times larger among US studies than non-US studies. The mean sediment load, phosphorus load, and pesticide load elasticities, which are based exclusively on US studies, are 0.23 (CI: 0.21, 0.25), 0.02 (CI: 0.00, 0.04), and − 0.08 (CI: -0.49, 0.33), respectively. The negative value for pesticide load counters expectations but is insignificant.

Mean land use elasticities must be interpreted relative to the reference category indicated in parentheses. First, we estimate, based on 5 observations, a mean forest elasticity of −0.67 (CI: −1.10, −0.24) for studies using non-forestland as the reference. This elasticity is slightly smaller among US than non-US studies. Next, we estimate a mean forest elasticity for studies using any combination of non-forestland, agriculture land, or urban land as the reference. The resulting forest elasticity of −0.58 (CI: −0.87, −0.29) is smaller than the previous estimate but remains statistically significant.

The third set of mean elasticities (column 8) is calculated using only studies that mitigate potential omitted variable bias by 1) incorporating control variables consistent with economic theory in their models, or 2) using a panel fixed-effects estimator when panel data is employed. The identification of these studies is necessarily subjective as some control variables, namely input prices, can be implicitly controlled for when there is little variation in these variables across observations (i.e., observations are spatially or temporally concentrated), or through spatial, temporal, or panel fixed effects. We therefore elect to exclude studies that clearly do not account for key confounding factors. Mean elasticities for these studies are generally smaller, and in some instances also have narrower confidence intervals, than previous estimates. The most notable differences are for TOC and sediment load, which now have elasticities of 0.08 (CI: -0.49, 0.65) and 0.05 (CI: 0.01, 0.09), respectively — the former being highly insignificant. The mean turbidity elasticity is slightly smaller at 0.12 (CI: 0.10, 0.14), while the nitrogen/nitrate elasticity, now based on a single observation, is 0.06 (CI: 0.02, 0.10). The forest elasticity for studies using non-forestland as the references category, also based on a single observation, is −0.39 (CI: -0.63, −0.15). There is little change in the forest elasticity from studies using any combination of non-forestland, agriculture land, or urban land as the reference.

[10] Seven studies have multiple elasticities for the same water quality measure. For the mean elasticity calculations, we use the spatial-lag model from Abildtrup et al. (2013), long-term values from Heberling et al. (2015), the alum model from Moore and McCarl (1987), the main model from Price et al. (2017), the O&M model from Singh and Mishra (2014), and turbidity values from Warziniack et al. (2017). We use a land-area weighted average of the virgin and logged forestland elasticities obtained from Vincent et al. (2016).

[11] Values in parentheses refer to 95% confidence intervals (CI).

Table 3
Average elasticities for select water quality measures.

Water quality measure	Classification	All elasticities		Elasticities w/ SE		Elasticities w/ SE from studies using key controls	
		Number of estimates	Mean	Number of estimates	Mean (SE)	Number of estimates	Mean (SE)
Turbidity	US	9	0.14	9	0.14 (0.03)*	4	0.12 (0.01)*
	Non-US	3	0.12	3	0.12 (0.03)*	1	0.10 (0.02)*
	Total	12	0.14	12	0.14 (0.02)*	5	0.12 (0.01)*
TOC	US	4	0.47	3	0.44 (0.14)*	1	0.10 (0.29)
	Non-US	1	0.06	1	0.06 (0.02)*	1	0.06 (0.02)*
	Total	5	0.39	4	0.35 (0.10)*	2	0.08 (0.29)
Nitrogen/Nitrate	US	1	0.06	1	0.06 (0.02)*	1	0.06 (0.02)*
	Non-US	1	0.05	1	0.05 (0.01)*	0	
	Total	2	0.06	2	0.06 (0.01)*	1	0.06 (0.02)*
Sediment load	US	3	0.24	2	0.23 (0.01)*	1	0.05 (0.02)*
	Non-US	0		0		0	
	Total	3	0.24	2	0.23 (0.01)*	1	0.05 (0.02)*
Phosphorus load	US	2	0.10	1	0.02 (0.01)*	1	0.02 (0.01)*
	Non-US	0		0		0	
	Total	2	0.10	1	0.02 (0.01)*	1	0.02 (0.01)*
Pesticide load	US	2	−0.08	2	−0.08 (0.21)	0	
	Non-US	0		0		0	
	Total	2	−0.08	2	−0.08 (0.21)	0	
Forest (non-forest)	US	3	−0.51	2	−0.35 (0.16)*	0	
	Non-US	2	−0.98	2	−0.98 (0.41)*	1	−0.39 (0.12)*
	Total	5	−0.70	4	−0.67 (0.22)*	1	−0.39 (0.12)*
Forest (non-forest, agriculture, urban)	US	3	−0.51	2	−0.35 (0.16)*	0	
	Non-US	4	−0.70	4	−0.70 (0.21)*	2	−0.58 (0.10)*
	Total	7	−0.62	6	−0.58 (0.15)*	2	−0.58 (0.10)*

Note. Reference land use categories are reported in parentheses following the category of interest. Standard errors are reported in parentheses following average elasticities. Mean elasticities are calculated from a small, sometime highly variable, set of observations; thus, caution should be taken when applying these values to other contexts.
Statistically significance for one-tailed test: *$p < 0.1$.

6. Discussion and Conclusion

Water-related ecosystem services are regularly subject to pressure from anthropogenic activities and changing climate conditions. SWP has emerged as a framework for protecting these services; it is widely viewed as an essential and cost-effective component of a multi-barrier approach to providing safe drinking water (Ernst et al., 2004; Gartner et al., 2014; McDonald and Shemie, 2014). Indeed, several regulatory agencies have adopted regulations or guidelines concerning the protection of source watersheds, including in the US EPA's Safe Drinking Water Act. Numerous municipalities are engaged in SWP activities for the expressed purpose of reducing O&M expenditures and averting, or at least delaying, the purchase of costly capital assets at DWTPs (Bennett et al., 2014; Carpe Diem West, 2011; Dudley and Stolton, 2003; Herbert, 2007). For many municipalities, however, SWP policy decisions are made without adequate quantitative information about the impact land management practices have on source water conditions, or the subsequent link between source water conditions and treatment costs (Dudley and Stolton, 2003; Gartner et al., 2013; Ryan, 2000). An improved understanding of these relationships is therefore essential to striking the best possible balance between protecting *in situ* water quality and purifying water via engineered treatment processes, and for improving the design of SWP programs.

We review the literature establishing a functional relationship between treatment costs and source water quality, and, from select studies, extract elasticities reflecting the responsiveness of DWTP expenditures to changes in water quality. Overall, results suggest that marginal changes in water quality measures lead to statistically significant but modest gains in avoided treatment costs. Estimated turbidity elasticities are the most robust; they are markedly consistent given the diversity of data and analytical methods utilized. Elasticities are more varied for other water quality measures, including TOC, phosphorus load, sediment load, and forestland—the latter variation possibly due to heterogeneity in forest types (e.g., temperate, tropical), topography, and management regimes. We also calculate mean elasticities for select water quality measures. These estimates, reported in Table 3, provide a useful summary of existing evidence but should be regarded cautiously given the small number of available observations.

To provide some context to the estimated elasticities, we calculate avoided treatment costs for representative DWTPs from Abildtrup et al. (2013), Forster and Murray (2007), Mosheim (2006), Price et al. (2017), Vincent et al. (2016), and Warziniack et al. (2017). For these DWTPs, the estimated benefit from a 1% reduction in source water turbidity ranges from $121 to $13,060 (2015 USD) annually. The corresponding benefit from a 1% increase in forestland in the source watershed ranges between $201 and $63,293 annually. Whether these benefits justify the cost of SWP activities is highly contextual, depending on site-specific ecologic, hydrologic, and DWTP characteristics. However, some broad insight can be gleaned with regard to forestland impacts on representative DWTPs from Abildtrup et al. (2013), Forster and Murray (2007), Vincent et al. (2016), and Warziniack et al. (2017). In these studies, a 1% increase in forestland corresponds to the conversion of between 955 and 22,680 ha in the average watershed or service area. Costs of forestland conversion and protection vary widely but are usually at least several hundred dollars per hectare (McDonald and Shemie, 2014), implying that SWP costs greatly exceed benefits for these representative DWTPs. Generally speaking, Heberling et al. (2015) and Vincent et al. (2016) reach similar conclusions in their respective analyses. Pyke et al. (2002) find that costs typically exceed benefits for SWP programs using riparian buffers to mitigate agricultural runoff, but that benefits exceed costs for programs using conservation tillage practices. McDonald and Shemie (2014) conclude that SWP is a cost-effective option for 28% of major world cities. Their analysis identifies the least cost approach to SWP using a mix of spatially targeted interventions (e.g., reforestation, riparian restoration, payment to landowner for adopting best management practices), but also relies on a relatively large water quality elasticity of 0.5 to determine benefits. Regardless, evidence suggests that SWP will not be cost effective in most situations where estimated benefits are limited to avoided water treatment expenditures. Accounting for additional

treatment costs (e.g., reservoir dredging and sludge disposal), health impacts, reduced risk of contamination, secondary beneficiaries (e.g., recreationists and homeowners), and potential income streams from managed lands (e.g., logging) may yield different results. In addition, Adhikari et al. (2016) find evidence of household willingness-to-pay for restoration of a source watershed located far from the municipality it supplies. This suggests households may value SWP beyond the benefits from avoided treatments costs and independent of improved recreational experiences, reduced wildfire risk to homes, or aesthetics.

Findings from this review expose several key knowledge gaps. Foremost among these gaps is the relationship between source water quality and long-run treatment costs. The choice of technology at a DWTP is partially determined by source water conditions. McDonald et al. (2016) offer evidence to this effect, finding a negative relationship between source water quality and the probability of using more advanced treatment technologies. Further evidence is found in the numerous accounts of DWTPs augmenting their water treatment infrastructure in response to worsening water conditions. For example, Dunlap et al. (2015) report that Waco, Texas spent $65 million to construct a dissolved air flotation plant in order to mitigate taste and odor problems resulting from frequent algal bloom events. Similarly, Des Moines, Iowa built a nitrate removal facility to address periodic spikes in source water nitrate; and Wichita, Kansas and Celina, Ohio addressed algae-related concerns with the addition of pre-ozonation and granular activated carbon processes to their treatment systems, respectively (Davenport and Drake, 2011; Jones et al., 2007; Oneby and Bollyky, 2006). What is unknown, however, is the extent that source water quality, or uncertainty about future water quality, affects long-run costs after controlling for confounding factors such as the price of capital inputs. While some of these issues are evaluated in Horn (2011), Renzetti (2001), Abildtrup et al. (2013), Fiquepron et al. (2013), and Piper (2003), no definite conclusions can be made regarding the effects of water quality on long-run costs relative to short-run costs. In addition, reservoir dredging, sludge disposal, and *in situ* treatment (e.g., algaecide) are periodic but costly activities that have been ignored in cost function analyses (Babatunde and Zhao, 2007; Buckley et al., 2014). As with capital expenditures, exclusion of these expenditures leads to an underestimation of the effect of source water quality on treatment related costs.

Another knowledge gap concerns the dearth of studies evaluating most water quality measures. Apart from turbidity, where the effect on variable treatment costs appears reasonably well understood, there is an insufficient elasticity of cost estimates from studies that control for confounding factors. Additional research is needed on widespread water quality issues, including TOC, nitrogen and nitrate, phosphorus, algae, and harmful algal and cyanobacteria blooms. Given the heterogeneity of source water conditions, some DWTPs will be affected by less common chemical and biological contaminants (e.g., sodium, perchlorate, trace metals). Evaluation of these parameters is warranted when their effect on treatment costs can be distinguished from that of other water quality measures and when SWP activities can be used to reduce contamination.

Continued research on land use is also needed, particularly with regards to differentiating the effects of various agricultural, forestland, and storm water management practices. For example, similar to Vincent et al. (2016), there is potential to evaluate the relative effects of low-, medium-, and high-intensity forest management approaches on treatment costs. While equilibrium relationships are of primary interest, research on the dynamics between changes in these management practices and treatment costs would also prove beneficial. Related knowledge gaps concern nonlinearities in water quality measures and interactive effects of multiple water quality measures. Results from studies using trans-log and third-order polynomial specifications indicate the presence of complex nonlinearities between treatment costs and water quality measures not captured in most studies. Likewise, results from studies using interaction terms between water quality measures (e.g., Abdul-Rahim and Mohd-Shahwahid, 2011; Dearmont et al., 1998) or WQIs (e.g., Freeman et al., 2008; Renzetti, 2001) suggest there are interactive effects not captured by most studies. Further exploration of these issues would aid BCAs that involve non-marginal changes in source water quality or changes in multiple quality measures.

Water quality elasticities of costs may vary across output levels, treatment technologies, source water types, seasons, and geographic regions. Of selected studies, only Mosheim (2006), Mosheim and Ribaudo (2017), and Price et al. (2017) investigate this type of heterogeneity. A particularly notable gap in the literature concerns small-scale groundwater systems, which comprise the vast majority of treatment systems but have not been evaluated separate from surface water systems.

A final knowledge gap concerns the presence of thresholds in water treatment processes. Cost function analyses usually assume smooth functional relationships between costs and source water quality measures. But these relationships often contain discontinuities related to predefined thresholds in the treatment processes. Beyond a defined threshold, for example, reduced source water quality can trigger utilization of chemical additives (Heberling et al., 2015; Sohn et al., 2008), inactive capital (Honey-Rosés et al., 2013; Jones et al., 2007), and alternate source waters (Towler et al., 2010). In the long-run, as discussed above, it can also trigger the construction of new capital resources. Incorporating thresholds into cost function analyses will be complicated since relevant threshold values will differ by location and are often known only to plant operators; nonetheless, it may ultimately prove a better representation of treatment technology in many situations.

Filling these knowledge gaps will require a multi-pronged approach. Some issues are better suited to cross-sectional or panel data that exhibit considerable variation in treatment technologies, source water, and service population characteristics. Other issues will be better assessed with detailed time-series analysis that can account for certain context-specific aspects of water treatment, such as atypical water quality measures and threshold effects. Likewise, some approaches will be better suited to decision making at national or regional levels and others to a DWTP level. As additional studies become available, meta-regression may help to address some knowledge gaps.

The main obstacle to conducting any analysis is data availability. There exist only a few datasets containing the information required to quantify links between treatment costs and water quality—and many are small non-random samples. Engineering equations offer an alternate approach to assessing these links, but no study to our knowledge has compared behavioral and engineering cost models to determine the validity of this approach. Thus, there is need for both the targeted collection of new data and for the comparison of behavioral and engineering cost models. Doing so will be vital to continued research on avoided treatment costs and benefits of SWP activities.

Declaration of Interest

None.

Acknowledgment/Disclaimer

The views expressed in this article are those of the authors and do not necessarily represent those of the U.S. Environmental Protection Agency. No official agency endorsement should be inferred. We are grateful for helpful comments and feedback from Michael Elovitz, Katherine Foreman, Kara Goodwin, Erik Helm, Hannah Holsinger, Hale Thurston, Will Wheeler, Bo Williams, and four anonymous reviewers.

Appendix A

Table A
Characteristics of selected studies (abbreviations defined in table notes).

Reference	Data characteristics 1. Country 2. Source type 3. Output (Y) in 1000 m^3/day	Data structure 1. Unit of obs. 2. Data type 3. # obs.[a]	Analysis approach 1. Model type 2. Estimator 3. Specification	Dependent variable	Water quality measure	Control variables
Abdul-Rahim and Mohd-Shahwahid (2011)	1. Malaysia 2. SW	1. DWTP 2. PNL 3. $n = 144$ ($i = 6$, $t = 24$)	1. Cost function 2. Panel est.[b] 3. Log-linear	Chemical costs (MYR/m^3/day): Average daily chemical costs per m^3 of output over two-week period.[b]	Turbidity[c] × pH	Treated water Rainy season (dv) FE-DWTP
Abildtrup et al. (2013)	1. France 2. SW & GW 3. Av: 0.29 Mn: 0.004 Mx: 7.64	1. CWS[b] 2. CRS 3. $n = 232$	1. Price function 2. SAC, IV-GMM 3. Linear	Consumer price (EUR/m^3): Average price (publicly managed systems) or marginal price (privately managed systems) per m^3 of residential-use water. Average price is based on consumption of 120 m^3/year. Taxes, abstraction fees, and pollution fees are excluded.	Land use (%): Forest Agriculture (ref) Urban Other	Treated water Population Population density # municipalities # intakes Private system (dv)
Dearmont et al. (1998)	1. USA 2. SW 3. Av: 27.67 Mn: 1.08 Mx: 109.76	1. DWTP 2. PNL 3. $n = 540$ ($i = 12$, $t = 45$)	1. Cost function 2. CHTA 3. Polynomial	Chemical costs (USD/100 MGL/mth): Chemical cost per 100 million gallons of output per month.	Turbidity[c] × pH Chemical contam. (dv)	Treated water Precipitation
Ernst et al. (2004)	1. USA 2. SW	1. DWTP 2. CRS 3. $n = 27$	1. Cost function 2. OLS 3. Polynomial	Total costs (USD/MGL/yr): O&M and amortized capital costs per MGL of output per year.	Land use (%): Forest Non-forest (ref)	
Fiquepron et al. (2013)	1. France 2. SW & GW 3. Av: 0.16 Mn: 0.03 Mx: 0.63	1. Dept. 2. CRS 3. $n = 93$	1. Price function 2. IV-GMM 3. Linear	Consumer price (EUR/m^3): Average price per m^3 of residential-use water based on consumption of 120 m^3/year. Aggregation to the department level is based on survey weights from a stratified sampling procedure.	Nitrate Pesticide exceedance Land use (%): Forest Grassland VIARMA Urban/agriculture (ref)	GW/total intake (%) Population density Private/total systems (%)
Forster et al. (1987)	1. USA 2. SW 3. Av: 3.53 Mn: 1.04 Mx: 23.34	1. DWTP 2. PNL 3. $n = 257$ ($i = 12$, $t = 25$)	1. Cost function 2. OLS 3. Log-linear	Chemical costs (USD/day): Average daily chemical costs over month period.	Turbidity[c] Sediment load	Treated water Retention time

(*continued on next page*)

Table A (*continued*)

Reference	Data characteristics 1. Country 2. Source type 3. Output (Y) in 1000 m^3/day	Data structure 1. Unit of obs. 2. Data type 3. # obs.[a]	Analysis approach 1. Model type 2. Estimator 3. Specification	Dependent variable	Water quality measure	Control variables
Forster and Murray (2007)	1. USA 2. SW 3. Av: 12.71 Mn: 0.23 Mx: 53.40	1. DWTP 2. PNL 3. $n = 55$ ($i = 11$, $t = 5$)	1. Cost function 2. OLS 3. Log-linear	Chemical costs (USD/MGL/yr): Chemical costs per MGL output per year.	Turbidity Pesticide load Land use (%): Tilled w/ < 15% residual Tilled w/ 15–30% residual Ridge/mulch tilled (ref) Untilled Non-agriculture	Treated water
Freeman et al. (2008)	1. USA 2. SW 3. Mn: > 3.79 Mx: < 378.54	1. DWTP 2. CRS 3. $n = 40$	1. Cost function 2. OLS 3. Semi-log	Chemical costs (USD/MGL/yr): Chemical costs per MGL output per year.	TOC WQI Land use (%): Forest Urban Non-forest vegetation	Year (dv)
Heberling et al. (2015)	1. USA 2. SW 3. Av: 18.74 Mn: 2.01 Mx: 38.31	1. DWTP 2. TMS 3. $n = 1826$	1. Cost function 2. ECM, MLE 3. Log-linear	O&M costs (USD/1000 GL/day): Chemical, pumping, and GAC costs per 1000 GL of output per day.	Turbidity pH TOC Phosphorus load Temperature > 23 °C (dv)	Lagged costs Treated water Process shutdown (dv) Pool elevation Years (dv) Spring & summer (dv) Actual TOC measure (dv)
Holmes (1988)	1. USA 2. SW 3. Av: 163.43	1. CWS 2. CRS 3. $n = 132$	1. Cost function 2. OLS 3. Log-linear	O&M costs (1000 USD/yr): Chemical, labor, energy, water acquisition, and distribution costs per year.	Turbidity Sediment load	Treated water Price of labor Price of electricity
Honey-Rosés et al. (2014)	1. Spain 2. SW 3. Av: 82.19	1. DWTP 2. TMS 3. $n = 247$	1. Energy use func. 2. OLS 3. Linear	Energy usage (kWh/m^3/interval): Amount of energy used per m^3 of output per daily/sub-daily interval.	Conductivity	
Horn (2011)	1. Japan 2. SW[b] 3. Av: 38.47 Mn: 0.58 Mx: 1109.48	1. CWS[b] 2. CRS 3. $n = 392$	1. Cost function 2. SCF, MLE 3. Log-linear	Total costs (Million JPY/yr): Source water intake, purification, distribution, dedicated construction, operation, depreciation, and inventory shrinkage costs per year.	TOC[c]	Treated water Price of labor Price of capital
McDonald and Shemie (2014)	1. USA 2. SW	1. Muni. 2. CRS 3. n ≈ 100	1. Cost function 2. OLS 3. Linear	O&M costs (Million USD/yr): O&M costs per year.	Sediment load Phosphorus load	
Moore and McCarl (1987)	1. USA 2. SW	1. DWTP 2. TMS 3. $n = 963$	1. Chemical use func. 2. COAC 3. Eq. (1): Log-linear Eq. (2): Linear	Chemical usage (lbs/day): Amount of alum (Eq. (1)) and lime (Eq. (2)) used per day.	Turbidity (Eq. (1)) Temperature (Eq. (1)) pH (Eq. (2))	Treated water (Eq. (1)) Alum (Eq. (2))

(*continued on next page*)

Table A (*continued*)

Reference	Data characteristics 1. Country 2. Source type 3. Output (Y) in 1000 m^3/day	Data structure 1. Unit of obs. 2. Data type 3. # obs.[a]	Analysis approach 1. Model type 2. Estimator 3. Specification	Dependent variable	Water quality measure	Control variables
Mosheim (2006)	1. USA[d] 2. SW & GW 3. Av: 131.93	1. CWS 2. CRS 3. n = 184	1. Cost function 2. SUR, NL-ILS 3. Translog	O&M costs per year (USD/yr): Chemical, labor, and energy costs per year.	Turbidity[c]	Treated water Price of labor Price of electricity Price of chemicals Capital stock Combined W&WW (dv) Source is SW (dv) Source is GW (dv) Population > 100,000 (dv) Network density Res./total deliveries (%)
Mosheim and Ribaudo (2017)	1. USA[d] 2. SW & GW 3. Av: 146.81	1. CWS 2. CRS 3. n = 48	1. Cost function 2. SCF, MLE 3. Log-linear	O&M costs per year (USD/yr): Chemical, labor, and energy costs per year.	Nitrogen[c]	Treated water Price of labor Price of electricity Price of chemicals Capital stock Agriculture/total N (%)
Murray (2001)[e]	1. USA 2. SW 3. Av: 58.32 Mn: 2.15 Mx: 181.51	1. DWTP 2. PNL 3. n = 65 (i = 13, t = 5)	1. Cost function 2. OLS 3. Log-linear	Chemical costs (USD/MGL/yr): Chemical costs per MGL of output per year.	Turbidity Pesticide load Land use (%): Tilled w/ < 15% residual Tilled w/ 15–30% residual Ridge/mulch tilled (ref) Untilled Non-agriculture	Treated water
Oklahoma Water Resources Board (2011)	1. USA 2. SW	1. DWTP 2. TMS 3. n = 12	1. Cost function 2. OLS[b] 3. Linear	Chemical cost (USD/MGL/mth): Monthly average of chemical costs per MGL of output across eight-year period.	TOC	
Piper (2003)	1. USA[d] 2. SW & GW	1. CWS 2. CRS 3. n = 309	1. Price function 2. 3SLS 3. Log-linear	Consumer price (USD/GL): Average price per GL of residential-use water.	Calcium carbonate[c]	Treated water GW/total intake (%) Source is GW (dv) Population density Debt/assets Regions (dv)

(*continued on next page*)

Table A (*continued*)

Reference	Data characteristics 1. Country 2. Source type 3. Output (Y) in 1000 m^3/day	Data structure 1. Unit of obs. 2. Data type 3. # obs.[a]	Analysis approach 1. Model type 2. Estimator 3. Specification	Dependent variable	Water quality measure	Control variables
Price et al. (2017)	1. Canada 2. SW & GW 3. Av: 12.88	1. DWTP 2. CRS 3. n = 994	1. Cost function 2. SCF, MLE 3. Log-linear	O&M costs (1000 CAD/yr): Chemical, labor, and energy costs for source water acquisition and treatment per year.	Turbidity	Treated water Price of labor Price of electricity Price of chemicals Capacity Conventional treat. (dv) Filtration treat. (dv) Disinfection treat. (dv) Membrane treat. (dv) Other treat. (dv) Source is SW (dv)
Renzetti (2001)	1. Canada 2. SW	1. CWS[b] 2. CRS 3. n = 40	1. Cost function 2. SUR, ILS 3. Translog	Total cost (CAD/yr): Labor, energy, and capital costs per year.	WQI	Treated water Price of labor Price of electricity Price of capital Water availability Var. of water availability Source is lake (dv)
Singh and Mishra (2014)	1. India 2. SW 3. Av: 1310.00[b]	1. DWTP 2. TMS 3. n = 144	1. Cost function 2. OLS[b] 3. Eq. (1): Log-linear Eq. (2): Log-linear	Chemical/O&M costs (INR/ML/mth): Chemical costs per ML of output per month (Eq. (1)). Chemical, energy, repair, maintenance, establishment, and transport costs per ML of output per month (Eq. (2)).	Turbidity Land use (%): Forest Non-forest (ref)	Lagged costs Treated water
Vincent et al. (2016)	1. Malaysia 2. SW 3. Av: 12.61 Mn: 0.06 Mx: 147.70	1. DWTP 2. PNL 3. n = 3894 (i = 41, t = 168)	1. Cost function 2. Panel FE 3. Log-linear	O&M costs (MYR/mth): Chemical, labor, energy, and maintenance cost per month.	Land use (%): Virgin forest Logged forest Non-forest (ref)	Treated water DWTP upgrade (dv) Precipitation Years (dv) Months (dv) FE-DWTP

(*continued on next page*)

Table A (*continued*)

Reference	Data characteristics 1. Country 2. Source type 3. Output (Y) in 1000 m^3/day	Data structure 1. Unit of obs. 2. Data type 3. # obs.[a]	Analysis approach 1. Model type 2. Estimator 3. Specification	Dependent variable	Water quality measure	Control variables
Warziniack et al. (2017)	1. USA 2. SW 3. Av: 183.70 Mn: 0.20 Mx: 4163.90	1. DWTP 2. CRS 3. n = 37	1. Cost function 2. OLS 3. Log-linear	Chemical costs (USD/MGL/yr): Chemical costs per MGL of output per year.	Turbidity TOC Land use (%): Forest Urban Non-forest/non-urban (ref)	Treated water Conventional treat. (dv) Filtration treat. (dv) Disinfection treat. (dv) Advanced treat. (dv)

Notes. Data characteristics: GW = groundwater; SW = surface water. Data structure: DWTP = drinking water treatment plant; CWS = community water system; CRS = cross-sectional data; PNL = panel data; TMS = time series data. Analysis approach: COAC = Cochrane-Orcutt autocorrelation; CHTA = cross-sectional heteroskedastic and time wise autocorrelation; ECM = error correction model; FE = fixed effects; IV-GMM = instrumental variable generalized methods of moments; ILS = iterative least squares; MLE = maximum likelihood estimator; NL-ILS = nonlinear iterative least squares; OLS = ordinary least squares; SUR = seemingly unrelated regression; SAC = spatial autocorrelation; SCF = stochastic cost frontier; 3SLS = three stage least squares. Dependent variable: CAD = Canada dollar; EUR = euro; GL = gallons; GAC = granular activated carbon; INR = India rupee; JPY = Japan yen; O&M = operation and maintenance; MYR = Malaysia ringgit; MGL = million gallons; ML = million liters; USD = USA dollar. Water quality measure: TOC = total organic carbon; VIARMA = vine cultivation, arboriculture, and market gardening; WQI = water quality index. The term load is used to identify water quality measures that pertain to the amount of material entering surface water due to runoff. Reference land use categories, dummy variables, percentage/proportion variables are denoted by (ref), (dv), and (%), respectively.

[a] Total number of observations are denoted by n. For panel data, n is decomposed into the number of panel observations i and time observations t.

[b] Information based on available evidence but uncertainty exists regarding the unit of analysis, estimator, or definition of the dependent variable. Additional information is available in Appendix B.

[c] Variable is defined as the difference between source water and treated water quality.

[d] Study uses data from the 1996 American Water Works Association member survey.

[e] Entry pertains to the Great Lakes Basin analysis; characteristics of the Maumee River Basin analysis are reported in Forster and Murray (2007).

Appendix B. Supplementary Data

Supplementary data to this article can be found online at https://doi.org/10.1016/j.ecolecon.2018.04.014.

References

40 C.F.R. §141.2. 2016.

Abdul-Rahim, A.S., Mohd-Shahwahid, O., 2011. A panel data analysis of timber harvesting operations and its impact on the cost of water treatment. Aust. J. Basic Appl. Sci. 5 (12), 598–601.

Abell, R., Asquith, N., Boccaletti, G., Bremer, L., Chapin, E., Erickson-Quiroz, A., Higgins, J., Johnson, J., Kang, S., Karres, N., Lehner, B., McDonald, R., Raepple, J., Shemie, D., Simmons, E., Sridhar, A., Vigerstøl, K., Vogl, A., Wood, S., 2017. Beyond the Source: The Environmental, Economic and Community Benefits of Source Water Protection. The Nature Conservancy, Arlington, VA.

Abildtrup, J., Garcia, S., Stenger, A., 2013. The effect of forest land use on the cost of drinking water supply: a spatial econometric analysis. Ecol. Econ. 92, 126–136.

Adhikari, D., Thacher, J.A., Chermak, J.M., Berrens, R.P., 2016. Linking forest to faucets in a distant municipal area: public support for forest restoration and water security in Albuquerque, New Mexico. In: Water Economics and Policy. 1650019.

Alcott, E., Ashton, M.S., Gentry, B.S., 2013. Natural and Engineered Solutions for Drinking Water Supplies: Lessons From the Northeastern United States and Directions for Global Watershed Management. CRC Press.

Babatunde, A., Zhao, Y., 2007. Constructive approaches toward water treatment works sludge management: an international review of beneficial reuses. Crit. Rev. Environ. Sci. Technol. 37 (2), 129–164.

Baker, A., 2003. Land use and water quality. Hydrol. Process. 17, 2499–2501.

Bennett, D.E., Gosnell, H., Lurie, S., Duncan, S., 2014. Utility engagement with payments for watershed services in the United States. Ecosyst. Serv. 8, 56–64.

Buckley, M., Beck, N., Bowden, P., Miller, M., Hill, B., Luce, C., Elliot, W., Enstice, N., Podolak, K., Winford, E., 2014. Mokelumne Watershed Avoided Cost Analysis: Why Sierra Fuel Treatments Make Economic Sense. (Auburn, CA).

California Water Code §108.5. 2016.

Capital Regional District, 2017. Greater Victoria Drinking Water Quality: 2016 Annual Report. Capital Regional District Water Quality Program, Victoria, BC.

Carpe Diem West, 2011. Watershed Investment Programs in the American West. Carpe Diem West, Sausalito, CA.

CDC, 2015. Community Water Treatment. Center for Disease Control and Prevention Available from. https://www.cdc.gov/healthywater/drinking/public/water_treatment.html, Accessed date: 15 March 2018.

Crittenden, J.C., Trussell, R.R., Hand, D.W., Howe, K.J., Tchobanoglous, G., 2012. Water quality management strategies. In: MWH's Water Treatment: Principles and Design, 3rd ed. John Wiley and Sons, Hoboken, NJ, pp. 165–224.

Davenport, T., Drake, W., 2011. Grand Lake St. Marys, Ohio—the case for source water protection: nutrients and algae blooms. In: Lakeline, pp. 41–46 (no. Fall).

Dearmont, D., McCarl, B.A., Tolman, D.A., 1998. Costs of water treatment due to diminished water quality: a case study in Texas. Water Resour. Res. 34 (4), 849–853.

Dudley, N., Stolton, S., 2003. Running Pure: The Importance of Forest Protected Areas to Drinking Water. World Bank/WWF Alliance, Gland, Switzerland.

Dunlap, C.R., Sklenar, K.S., Blake, L.J., 2015. A costly endeavor: addressing algae problems in a water supply. J. Am. Water Works Assoc. 107 (5), E255–E262.

Ernst, C., Hopper, K., Summers, D., 2004. Protecting the Source: Land Conservation and the Future of America's Drinking Water (1932807020). Trust for Public Land and American Water Works Association, San Francisco, CA.

Estache, A., Rossi, M.A., 2002. How different is the efficiency of public and private water companies in Asia? World Bank Econ. Rev. 16 (1), 139–148.

Fiquepron, J., Garcia, S., Stenger, A., 2013. Land use impact on water quality: valuing forest services in terms of the water supply sector. J. Environ. Manag. 126, 113–121.

Forster, D.L., Bardos, C.P., Southgate, D.D., 1987. Soil erosion and water treatment costs. J. Soil Water Conserv. 42 (5), 349–352.

Forster, D.L., Murray, C., 2007. Effects of pesticide use and farming practices on water treatment costs in Maumee River basin communities. In: Hitzhusen, Fred J. (Ed.), Economic Valuation of River Systems. Edward Elgar, Chelenham, UK and Northhampton, MA, pp. 115–128.

Freeman, J., Madsen, R., Hart, K., 2008. Statistical Analysis of Drinking Water Treatment Plant Costs, Source Water Quality, and Land Cover Characteristics.

Gartner, T., Mehan III, G.T., Mulligan, J., Roberson, J.A., Stangel, P., Qin, Y., 2014. Protecting forested watersheds is smart economics for water utilities. J. Am. Water Works Assoc. 106 (9), 54–64.

Gartner, T., Mulligan, J., Schmidt, R., Gunn, J., 2013. Natural Infrastructure: Investing in Forested Landscapes for Source Water Protection in the United States. World Resources Institute, Washington, DC.

Griffiths, C., Klemick, H., Massey, M., Moore, C., Newbold, S., Simpson, D., Walsh, P., Wheeler, W., 2012. US Environmental Protection Agency valuation of surface water quality improvements. Rev. Environ. Econ. Policy 6 (1), 130–146.

Hanson, M.J., Keller, A., Boland, M.A., Lazarus, W.F., 2016. The debate about farm nitrates and drinking water. Choices 31 (1), 1–7.

Heberling, M.T., Nietch, C.T., Thurston, H.W., Elovitz, M., Birkenhauer, K.H., Panguluri, S., Ramakrishnan, B., Heiser, E., Neyer, T., 2015. Comparing drinking water treatment costs to source water protection costs using time series analysis. Water Resour. Res. 51 (11), 8741–8756.

Henry, T., 2013. Toxins overwhelm Carroll Township water plant. In: The Blade, (September 7, 2013).

Herbert, E., 2007. Forest management by west coast water utilities: protecting the source? J. Am. Water Works Assoc. 99 (2), 91–106.

Holmes, T.P., 1988. The offsite impact of soil erosion on the water treatment industry. Land Econ. 64 (4), 356–366.

Honey-Rosés, J., Acuña, V., Bardina, M., Brozović, N., Marcé, R., Munné, A., Sabater, S., Termes, M., Valero, F., Vega, À., 2013. Examining the demand for ecosystem services: the value of stream restoration for drinking water treatment managers in the Llobregat River, Spain. Ecol. Econ. 90, 196–205.

Honey-Rosés, J., Schneider, D.W., Brozović, N., 2014. Changing ecosystem service values following technological change. Environ. Manag. 53 (6), 1146–1157.

Horn, T., 2011. Incorporating water purification in efficiency evaluation: evidence from Japanese water utilities. Appl. Econ. Lett. 18, 1789–1794.

Jones, C.S., Hill, D., Brand, G., 2007. Use a multifaceted approach to manage high source-water nitrate. In: Opflow, pp. 20–22 (no. June).

Kansas Department of Health and Environment, 2011. Water Quality Standards White Paper: Chlorophyll-A Criteria for Public Water Supply Lakes and Reservoirs. Kansas Department of Health and Environment Bureau of Water, Topeka, KS.

Lerner, D.N., Harris, B., 2009. The relationship between land use and groundwater resources and quality. Land Use Policy 26, S265–S273.

McDonald, R., Shemie, D., 2014. Urban Water Blueprint: Mapping Conservation Solutions to the Global Water Challenge. The Nature Conservancy, Washington, DC.

McDonald, R.I., Weber, K.F., Padowski, J., Boucher, T., Shemie, D., 2016. Estimating watershed degradation over the last century and its impact on water-treatment costs for the world's large cities. Proc. Natl. Acad. Sci. 113 (32), 9117–9122.

McGivney, W., Kawamura, S., 2008. Cost Estimating Manual for Water Treatment Facilities. Wiley, Hoboken, NJ.

Moore, W.B., McCarl, B.A., 1987. Off-site costs of soil erosion: a case study in the Willamette Valley. West. J. Agric. Econ. 12 (1), 42–49.

Mosheim, R., 2006. A shadow cost function model of the US water industry incorporating water quality and ownership effects. In: Coelli, Tim, Lawrence, Denis (Eds.), Performance Measurement and Regulation of Network Utilities. Edward Elgar, Cheltenham, UK and Northampton, MA, pp. 243–265.

Mosheim, R., Ribaudo, M., 2017. Costs of nitrogen runoff for rural water utilities: a shadow cost approach. Land Econ. 93 (1), 12–39.

Murray, C., 2001. A Study of Pesticide Use, Farming Practices, and Community Drinking Water Treatment Costs in the Maumee and Great Lakes Basins. Department of Agricultural, Environmental, and Development Economics, Ohio State University, Columbus, OH.

Oklahoma Water Resources Board, 2011. Developing In-Lake BMPs to Enhance Raw Water Quality of Oklahoma's Sensitive Water Supply. Oklahoma Water Resources Board, Oklahoma City, OK.

Oneby, M., Bollyky, L.J., 2006. High-pressure Pipeline Pre-ozonation at Wichita, Kansas for Taste and Odor Control. Prepared for the International Conference Ozone and UV. April, 3, 2006, Berlin.

Piper, S., 2003. Impact of water quality on municipal water price and residential water demand and implications for water supply benefits. Water Resour. Res. 39 (5), 1127.

Pizzi, N.G., 2005. Water Treatment Operator Handbook. American Water Works Association, Denver, CO.

Price, J., Renzetti, S., Dupont, D.P., Adamowicz, W., Emelko, M., 2017. Production costs, inefficiency, and source water quality: a stochastic cost frontier analysis of Canadian water utilities. Land Econ. 93 (1), 1–11.

Pyke, G., Becker, W., Head, R., 2002. Efficacy of source water protection for reducing costs of drinking water treatment. Proc. Water Environ. Fed. 2002 (17), 665–677.

Renzetti, S., 2001. Environmental Conditions and the Cost of Water Supply. Prepared for the AWRA/IWLRI-University of Dundee International Specialty Conference. August 6, 2001.

Renzetti, S., Dupont, D.P., 2009. Measuring the technical efficiency of municipal water suppliers: the role of environmental factors. Land Econ. 85 (4), 627–636.

Ryan, D.F., 2000. Synthesis. In: Dissmeyer, George E. (Ed.), Drinking Water From Forests and Grasslands: A Synthesis of the Scientific Literature (General Technical Report No. SRS-39). USDA Forest Service, Asheville, NC.

Singh, S., Mishra, A., 2014. Deforestation-induced costs on the drinking water supplies of the Mumbai metropolitan, India. Glob. Environ. Chang. 27, 73–83.

Snider, A., 2014. Toledo reopens its taps—but algae problems aren't going away. Greenwire (August 4, 2014).

Sohn, B.Y., Park, T.J., Oh, B.S., Kwon, S.B., Kang, J.W., 2008. A case study of the DAF-based drinking water treatment plant in Korea. Sep. Sci. Technol. 43 (15), 3873–3890.

Tiemann, M., 2014. Safe Drinking Water Act (SDWA): A Summary of the Act and Its Major Requirements (CRS Report No. RL31243). Congressional Research Service, Washington, DC.

Towler, E., Rajagopalan, B., Gilleland, E., Summers, R.S., Yates, D., Katz, R.W., 2010. Modeling hydrologic and water quality extremes in a changing climate: a statistical approach based on extreme value theory. Water Resour. Res. 46 (11).

US EPA, 2009a. Factoids: Drinking Water and Ground Water Statistics for 2009. Office of Water, US EPA, Washington, DC.

US EPA, 2009b. 2006 Community Water System Survey (EPA 815-R-09-001). Office of Water, US EPA, Washington, DC.

US EPA, 2009c. National Primary Drinking Water Regulations. US EPA, Washington, DC.

Varian, H.R., 1992. Microeconomic Analysis. Norton & Company.

Vincent, J.R., Ahmad, I., Adnan, N., Burwell III, W.B., Pattanayak, S.K., Tan-Soo, J.-S., Thomas, K., 2016. Valuing water purification by forests: an analysis of Malaysian panel data. Environ. Resour. Econ. 64 (1), 59–80.

Warziniack, T., Sham, C.H., Morgan, R., Feferholtz, Y., 2017. Effect of forest cover on water treatment costs. Water Econ. Policy 3 (4), 175006 1–19.

Notation	
3SLS	three stage least squares.
CAD	Canada dollar
CHTA	cross-sectional heteroskedastic and time wise autocorrelation
COAC	Cochrane-Orcutt autocorrelation
CRS	cross-sectional data
CWS	community water system
DWTP	drinking water treatment plant
ECM	error correction model
EUR	euro
FE	fixed effects
GAC	granular activated carbon
GL	gallons
GW	groundwater
ILS	iterative least squares
INR	India rupee
IV-GMM	instrumental variable generalized methods of moments
JPY	Japan yen
L	Land use variable
MGL	million gallons
ML	million liters
MLE	maximum likelihood estimator
MYR	Malaysia ringgit
NL-ILS	nonlinear iterative least squares
O&M	operation and maintenance
OLS	ordinary least squares
PNL	panel data
SAC	spatial autocorrelation
SCF	stochastic cost frontier
SUR	seemingly unrelated regression
SW	surface water
TMS	time series data
TOC	total organic carbon
USD	USA dollar
VIARMA	vine cultivation, arboriculture, and market gardening
WQI	water quality index

References

Lusardi, P.J. and Consonery, P.J., 1999. Factors affecting filtered water turbidity. *Journal-American Wat*

Bårdsen, G., 1989. Estimation of long run coefficients in error correction models. *Oxford Bulletin of Ec*

er Works Association, *91*(12), pp.28-40.
onomics and Statistics, *51*(3), pp.345-350.

Table B1: Characteristics of Selected Studies (Table A w/ Supplementary Material)

Reference	Data Characteris		
	Country	Source Type	Mean Output (1000 m^3/day)
Abdul-Rahim & Mohd-Shahwahid (2011)	Malaysia	SW	
Abildtrup et al. (2013)	France	SW/GW	0.29
Dearmont et al. (1998)	USA	SW	27.67

Ernst et al. (2004)	USA	SW	
Fiquepron et al. (2013)	France	SW/GW	0.16
Forster et al. (1987)	USA	SW	3.53

Forster & Murray (2007)	USA	SW	12.71
Freeman et al. (2008)	USA	SW	
Heberling et al. (2015)	USA	SW	18.74

Holmes (1988)	USA	SW	163.43
Honey-Rosés et al. (2014)	Spain	SW	82.19
Horn (2011)	Japan	SW†	38.47

McDonald & Shemie (2014)	USA	SW	
Moore & McCarl (1987)	USA	SW	
Mosheim (2006)	USA[§]	SW/GW	131.93

Mosheim & Ribaudo (2017)	USA[§]	SW/GW	146.81
Murray (2001)	USA	SW	58.32
Oklahoma Water Resources Board (2011)	USA	SW	

Piper (2003)	USA[§]	SW/GW	
Price et al. (2017)	Canada	SW/GW	12.88
Renzetti (2001)	Canada	SW	

Singh & Mishra (2014)	India	SW	1310.00†
Vincent et al. (2016)	Malaysia	SW	12.61
Warziniack et al. (2017)	USA	SW	183.70

Notes. The term *load* is used to identify water quality measures that pertain to the amount of material entering s

* Statistically significant at p<0.1. One-tailed test used from water quality parameters, watershed loading variab

« Total number of observations are denoted by *n*. For panel data, *n* is decomposed into the number of panel obse

† Information based on available evidence but uncertainty exists regarding the unit of analysis, estimator, or def

‡ Variable is defined as the difference between source water and treated water quality.

§ Study uses data from the 1996 American Water Works Association member survey.

 Elasticity estimated via a multiple-equation recursive relationship.

stics		Data Structure		
Min. Output (1000 m^3/day)	Max. Output (1000 m^3/day)	Unit of Obs.	Data Type	Num. Obs.[«]
		DWTP	Panel	144 (i=6, t=24)
0.00	7.64	CWS[†]	Cross-section	232
1.08	109.76	DWTP	Panel	540 (i=12, t=45)

		DWTP	Cross-section	27
0.03	0.63	Department	Cross-section	93
1.04	23.34	DWTP	Panel	257 (i=12, t=25)

0.23	53.40	DWTP	Panel	55 (i=11, t=5)
>3.79	<378.54	DWTP	Cross-section	40
2.01	38.31	DWTP	Time series	1826

		CWS	Cross-section	132
		DWTP	Time series	247
0.58	1109.48	CWS†	Cross-section	392

Municipality	Cross-section	≈100
DWTP	Time series	963
CWS	Cross-section	184

		CWS	Cross-section	48
2.15	181.51	DWTP	Panel	65 (i=13, t=5)
		DWTP	Time series	12

CWS	Cross-section	309
DWTP	Cross-section	994
CWS†	Cross-section	40

		DWTP	Time series	144
0.06	147.70	DWTP	Panel	3894 (i=41, t=168)
0.20	4163.90	DWTP	Cross-section	37

urface water due to runoff. Reference land use categories, dummy variables, percentage/proporti
ɔles, and forestland. Two-tailed tests used for all non-forestland classifications.
ervations *i* and time observations *t*.
inition of the dependent variable. Additional information is available in Appendix B (Table B1, (

Analysis Approach		
Model Type	Estimator	Specification
Cost function	Panel estimator[†]	Log-linear
Price function	SAC, IV-GMM	Linear
Cost function	CHTA	Polynomial

Cost function	OLS	Polynomial
Price function	IV-GMM	Linear
Cost function	OLS	Log-linear

Cost function	OLS	Log-linear
Cost function	OLS	Semi-log
Cost function	ECM, MLE	Log-linear

Cost function	OLS	Log-linear
Energy use function	OLS	Linear
Cost function	SCF, MLE	Log-linear

Cost function	OLS	Linear
Chemical use function	COAC	Eq1: Log-linear; Eq2: Linear
Cost function	SUR, NL-ILS	Translog

Cost function	SCF, MLE	Log-linear
Cost function	OLS	Log-linear
Cost function	OLS	Linear

Price function	3SLS	Log-linear
Cost function	SCF, MLE	Log-linear
Cost function	SUR, ILS	Translog

Cost function	OLS[†]	Eq1: Log-linear; Eq2: Log-linear
Cost function	Panel FE	Log-linear
Cost function	OLS	Log-linear

ion variables are denoted by (ref), (d), and (%), respectively.

Column U).

Dependent Variable	Water Parameter
Chemical costs (MYR/m^3/day): Average daily chemical costs per m3 of output over two-week period.[†]	Turbidity[‡] × pH
Consumer price (EUR/m^3): Average price (publicly managed systems) or marginal price (privately managed systems) per m3 of residential-use water. Average price is based on consumption of 120 m3/year. Taxes, abstraction fees, and pollution fees are excluded.	
Chemical costs (USD/100 MGL/mth): Chemical cost per 100 million gallons of output per month.	Turbidity[‡] × pH Chemical contamination (d)

Total costs (USD/MGL/yr): O&M and amortized capital costs per MGL of output per year.	
Consumer price (EUR/m^3): Average price per m3 of residential-use water based on consumption of 120 m3/year. Aggregation to the department level is based on survey weights from a stratified sampling procedure.	Nitrate
Chemical costs (USD/day): Average daily chemical costs over month period.	Turbidity‡

Chemical costs (USD/MGL/yr): Chemical costs per MGL output per year.	Turbidity
Chemical costs (USD/MGL/yr): Chemical costs per MGL output per year.	TOC WQI
O&M costs (USD/1000 GL/day): Chemical, pumping, and GAC costs per 1000 GL of output per day.	Turbidity pH TOC Temperature >23˚C (d)

O&M costs (1000 USD/yr): Chemical, labor, energy, water acquisition, and distribution costs per year.	Turbidity
Energy usage (kWh/m3/interval): Amount of energy used per m3 of output per daily/sub-daily interval.	Conductivity
Total costs (Million JPY/yr): Source water intake, purification, distribution, dedicated construction, operation, depreciation, and inventory shrinkage costs per year.	TOC‡

O&M costs (Million USD/yr): O&M costs per year.	
Chemical usage (lbs/day): Amount of alum (Eq1) and lime (Eq2) used per day.	Turbidity (Eq1) Temperature (Eq1) pH (Eq2)
O&M costs per year (USD/yr): Chemical, labor, and energy costs per year.	Turbidity[‡]

O&M costs per year (USD/yr): Chemical, labor, and energy costs per year.	Nitrate‡
Chemical costs (USD/MGL/yr): Chemical costs per MGL of output per year.	Turbidity
Chemical cost (USD/MGL/mth): Monthly average of chemical costs per MGL of output across eight-year period.	TOC

Consumer price (USD/GL): Average price per GL of residential-use water.	Calcium carbonate‡
O&M costs (1000 CAD/yr): Chemical, labor, and energy costs for source water acquisition and treatment per year.	Turbidity
Total cost (CAD/yr): Labor, energy, and capital costs per year.	WQI

Chemical/O&M costs (INR/ML/mth): Chemical costs per ML of output per month (Eq1). Chemical, energy, repair, maintenance, establishment, and transport costs per ML of output per month (Eq2).	Turbidity
O&M costs (MYR/mth): Chemical, labor, energy, and maintenance cost per month.	
Chemical costs (USD/MGL/yr): Chemical costs per MGL of output per year.	Turbidity TOC

Water Quality Measure		
Watershed Loading	Land Use	Control Variables
		Treated water Rainy season (d) FE-DWTP
	Forest Agriculture (ref) Urban Other	Treated water Population Population density # municipalities # intakes Private system (d)
		Treated water Precipitation

	Forest Non-forest (ref)	
Pesticide exceedance	Forest Grassland VIARMA Urban/agriculture (ref)	GW/total intake (%) Population density Private/total systems (%)
Sediment load		Treated water Retention time

Pesticide load	Tilled w/ <15% residual Tilled w/ 15-30% residual Ridge/mulch tilled (ref) Untilled Non-agriculture	Treated water
	Forest Urban Non-forest vegetation	Year (d)
Phosphorus load		Lagged costs Treated water Process shutdown (d) Pool elevation Years (d) Spring & summer (d) Actual TOC measure (d)

Sediment load

Treated water
Price of labor
Price of electricity

Treated water
Price of labor
Price of capital

Sediment load
Phosphorus load

Treated water (Eq1)
Alum (Eq2)

Treated water
Price of labor
Price of electricity
Price of chemicals
Capital stock
Combined W&WW (d)
Source is SW (d)
Source is GW (d)
Population>100,000 (d)
Network density
Res./total deliveries (%)

		Treated water Price of labor Price of electricity Price of chemicals Capital stock Agriculture/total N (%)
Pesticide load	Tilled w/ <15% residual Tilled w/ 15-30% residual Ridge/mulch tilled (ref) Untilled Non-agriculture	Treated water

Treated water
GW/total intake (%)
Source is GW (d)
Population density
Debt/assets
Regions (d)

Treated water
Price of labor
Price of electricity
Price of chemicals
Capacity
Conventional treat. (d)
Filtration treat. (d)
Disinfection treat. (d)
Membrane treat. (d)
Other treat. (d)
Source is SW (d)

Treated water
Price of labor
Price of electricity
Price of capital
Water availability
Var. of water availability
Source is lake (d)

Forest	Lagged costs
Non-forest (ref)	Treated water

Virgin forest	Treated water
Logged forest	DWTP upgrade (d)
Non-forest (ref)	Precipitation
	Years (d)
	Months (d)
	FE-DWTP

	Treated water
Forest	Conventional treat. (d)
Urban	Filtration treat. (d)
Non-forest/non-urban (ref)	Disinfection treat. (d)
	Advanced treat. (d)

Motivation	Elasticity
Soil erosion from timber harvesting activities	Turbidity‡: 0.07 (0.03)* pH: 0.07 (0.03)*
Nitrate and pesticide levels from agricultural runoff	Forest (service area): -0.48 (0.15)* Forest (entire region): -0.77 (0.26)* Urban (service area): 0.004 (0.03) Urban (entire region): 0.38 (0.22)* Other (service area): -0.21 (0.08)* Other (entire region): -0.49 (0.36)
Sediment loading and chemical contamination from runoff	Turbidity‡: 0.27 (0.12)* pH: 0.27 (0.12)*

Trade-offs between natural and built infrastructure; Ecosystem service benefits of forestland	Forest: -0.83
Ecosystem service benefits of forestland as it pertains to reduced nitrogen and pesticide levels from agricultural runoff	Nitrate: 0.05 (0.01)* Pesticide exceedance□: 0.02 (0.01)* Forest: -0.07 (0.03)* Grassland: 0.02 (0.02) VIARMA: 0.02 (0.01)
Soil erosion from agricultural runoff	Turbidity[‡]: 0.12 (0.04)* Sediment load: 0.41 (0.02)*

Sediment and pesticide runoff resulting from alternative farm management practices	Turbidity: 0.30 (0.08)* Pesticide load: 0.27 (0.20)* Tilled w/ <15% residual: 0.40 (0.24)* Tilled w/ 15-30% residual: 0.03 (0.03) Untilled: 0.02 (0.10) Non-agriculture: 0.60 (0.28)*
Ecosystem service benefits of forestland	TOC: 0.77 (0.23)* WQI: -0.53 (0.23)* Forest: -0.38 (0.23)* Urban: 0.22 (0.10)* Non-forest vegetation: -0.15 (0.07)*
Benefits of source water protection as it pertains to reduced sediment and nutrient loading from agricultural runoff	Turbidity (short term): 0.02 (0.01)* Turbidity (long term): 0.11 (0.04)* pH (short term): -0.04 (0.06) pH (long term): -0.01 (0.06) TOC (short term): -0.04 (0.03) TOC (long term): 0.10 (0.29) Phosphorus load (long term): 0.02 (0.01)*

Soil erosion from agricultural runoff	Turbidity: 0.07 (0.03)* Sediment load□: 0.05 (0.02)*
Endogenous relationship between ecosystem service benefits and water treatment technology	Conductivity: 0.86
Determinants of cost efficiency at water treatment facilities	TOC‡: 0.06 (0.02)*

Sediment and nutrient levels resulting from land use change and agricultural runoff	Sediment load: 0.26 Phosphorus load: 0.19
Soil erosion primarily from agricultural runoff	Turbidity (alum): 0.22 (0.02)* Turbidity (alum & lime): 0.21 Temperature (alum): -0.39 (0.12)*
Determinants of cost and cost efficiency at water treatment facilities; Impact of regulation	Turbidity[‡]: 0.09 (0.03)*

Nitrogen levels primarily from agricultural runoff; Impact of regulation	Nitrate‡: 0.06 (0.02)*
Sediment and pesticide runoff resulting from alternative farm management practices	Turbidity: -0.11 (0.12) Pesticide load: -0.43 (0.37) Tilled w/ <15% residual: 0.10 (0.13) Tilled w/ 15-30% residual: 0.11 (0.13) Untilled: -0.04 (0.12) Non-agriculture: 0.12 (0.15)
Algae levels	TOC: 0.55

Simultaneous modeling of water supply and demand; Welfare effects of improved water quality	Calcium carbonate[‡]: 0.003 (0.001)*
Soil erosion from landscape disturbances (e.g. wildfire, urban development).	Turbidity: 0.10 (0.02)* Turbidity (conventional): 0.12 (0.03)* Turbidity (filtration): 0.13 (0.05)* Turbidity (disinfection): 0.06 (0.04)* Turbidity (membrane): 0.14 (0.07)* Turbidity (other): 0.08 (0.07) Turbidity (untreated): 0.06 (0.08)
Benefits of improved source water characteristics, including water quality, in light of potential climate changes impacts and growing fiscal constraints.	WQI: 0.80 (0.22)*

Degraded urban watersheds resulting from deforestation, high-impact agriculture, and urban development;	Turbidity (chemical): 0.20 (0.08)* Turbidity (O&M): 0.19 (0.07)* Forest (chemical)□: -1.71 (0.87)* Forest (O&M)□: -1.58 (0.80)*
Ecosystem service benefits of forestland	Virgin forest: -0.47 (0.19)* Logged forest: -0.32 (0.14)*
Ecosystem service benefits of forestland	Turbidity: 0.19 (0.11)* TOC: 0.46 (0.19)* Forest (via turbidity)□: -0.32 (0.22)* Forest (via TOC)□: -0.06 (0.07) Urban (via turbidity)□: 0.08 (0.08) Urban (via TOC)□: 0.34 (0.56)

Elasticity Calculation

Turbidity

$\eta = \beta_{WQ} \cdot (WQraw/(WQraw-WQfin))$

$SE(\eta) = SQRT((WQraw/(WQraw-WQfin))^2 \cdot Var(\beta_{WQ}))$

pH

$\eta = \beta_{WQ}$

$SE(\eta) = SE(\beta_{WQ})$

β_{WQ} is the coefficient for the water quality measure of interest; WQraw is mean raw water quality for the measure of interest; W

w/o spatial lag

$\eta = \beta_{WQ} \cdot (WQ/Y)$

$SE(\eta) = SQRT((WQ/Y)^2 \cdot Var(\beta_{WQ}))$

w/ spatial lag

$\eta = (\beta_{WQ}+\beta_{WQlag}) \cdot (WQ/Y)$

$SE(\eta) = SQRT((WQ/Y)^2 \cdot (Var(\beta_{WQ})+Var(\beta_{WQlag})))$

β_{WQ} is the coefficient for the water quality measure of interest; β_{WQlag} is the coefficient for the spatial-lag of the water quality m
Y is the mean of the dependent variable

Turbidity

$\eta = (\beta_{WQ} \cdot WQ_B + 2 \cdot \beta_{WQ2} \cdot WQ_B^2 \cdot (WQ_{Araw} - WQ_{Afin}) + 3 \cdot \beta_{WQ3} \cdot WQ_{Araw} \cdot WQ_B^3 \cdot (WQ_{Araw} - 2 \cdot WQ_{Afin}) + \beta_{WQ3} \cdot WQ_{Afin}^2 \cdot WQ_B) \cdot ((WQ_{Araw})/Y)$

$SE(\eta) = SQRT((WQ_{Araw}/Y)^2 \cdot (WQ_B^2 \cdot Var(\beta_{WQ}) + 4 \cdot WQ_B^4 \cdot (WQ_{Araw} - WQ_{Afin})^2 \cdot Var(\beta_{WQ2}) + 9 \cdot WQ_{Araw}^2 \cdot WQ_B^6 \cdot (WQ_{Araw} - 2 \cdot WQ_{Afin})^2 \cdot Var($

pH

$\eta = (\beta_{WQ} \cdot (WQ_{Araw} - WQ_{Afin}) + 2 \cdot \beta_{WQ2} \cdot (WQ_{Araw} - WQ_{Afin})^2 \cdot WQ_B + 3 \cdot (WQ_{Araw} - WQ_{Afin})^3 \cdot WQ_B^2) \cdot (WQ_B/Y)$

$SE(\eta) = SQRT((WQ_B/Y)^2 \cdot (WQ_{Araw} - WQ_{Afin})^2 \cdot Var(\beta_{WQ}) + 4 \cdot (WQ_{Araw} - WQ_{Afin})^4 \cdot WQ_B^2 \cdot Var(\beta_{WQ2}) + 9 \cdot (WQ_{Araw} - WQ_{Afin})6 \cdot WQ_B^4 \cdot Var(\beta_W$

β_{WQ} is the coefficient for the water quality measure of interest; β_{WQ2} is the coefficient for the square of the water quality measur
measure of interest; WQ_{Araw} is mean raw water turbidity, WQ_{Afin} is mean finished water turbidity; WQ_B is mean pH; Y is the mea

$\eta = (\beta_{WQ} + 2 \cdot \beta_{WQ2} \cdot WQ) \cdot (WQ/Y)$
$SE(\eta) = SQRT((WQ/Y)^2 \cdot (Var(\beta_{WQ}) + 4 \cdot WQ^2 \cdot Var(\beta_{WQ2})))$

β_{WQ} is the coefficient for the water quality measure of interest; β_{WQ2} is the coefficient for the square of the water quality measur
the mean of the dependent variable

Water parameter and land use
$\eta = \beta_{WQ} \cdot (WQ/Y)$
$SE(\eta) = SQRT((WQ/Y)^2 \cdot Var(\beta_{WQ}))$

Watershed loading
$\eta = (\beta_{DEL} \cdot \beta_{WQ}) \cdot (WQ/Y)$
$SE(\eta) = SQRT((WQ/Y)^2 \cdot (Var(\beta_{DEL}) \cdot Var(\beta_{WQ}) + \beta_{DEL}^2 \cdot Var(\beta_{WQ}) + \beta_{WQ}^2 \cdot Var(\beta_{DEL})))$

β_{WQ} is the coefficient for the water quality measure of interest; β_{DEL} is the coefficient for DEL (see Fiquepron et al. (2013) for d
mean of the dependent variable

Water parameter
$\eta = \beta_{WQ} \cdot (WQraw/(WQraw-WQfin))$
$SE(\eta) = SQRT((WQraw/(WQraw-WQfin))^2 \cdot Var(\beta_{WQ}))$

Watershed loading
$\eta = \beta_{WQ}$
$SE(\eta) = SE(\beta_{WQ})$

β_{WQ} is the coefficient for the water quality measure of interest; WQraw is mean raw water quality for the measure of interest; W

Water parameter

$\eta = \beta_{WQ}$

$SE(\eta) = SE(\beta_{WQ})$

Land use

$\eta = \beta_{WQ} \bullet \beta_{LU}$

$SE(\eta) = SQRT(Var(\beta_{WQ}) \bullet Var(\beta_{LU}) + \beta_{WQ}^2 \bullet Var(\beta_{LU}) + \beta_{LU}^2 \bullet Var(\beta_{WQ}))$

β_{WQ} is the coefficient for the water quality parameter of interest; β_{LU} is the coefficient for the land use measure of int

$\eta = \beta_{WQ} \bullet WQ$

$SE(\eta) = SQRT(WQ^2 \bullet Var(\beta_{WQ}))$

β_{WQ} is the coefficient for the water quality measure of interest; WQ is mean water quality for the measure of interest

Water parameter: Short term

$\eta = \beta_{\Delta WQ}$

$SE(\eta) = SE(\beta_{\Delta WQ})$

Water parameter: Long term

$\eta = \beta_{\Delta WQ} + (\beta_{WQ}/-\beta_{ECT})$

$SE(\eta) = SQRT(Var(\beta_{\Delta WQ}) + (1/-\beta_{ECT})^2 \bullet Var(\beta_{WQ}) + (\beta_{WQ}/\beta_{ECT}^2)^2 \bullet Var(\beta_{ECT}))$

Watershed loading

$\eta = (\beta_{\Delta WQ} + (\beta_{WQ}/-\beta_{ECT})) \bullet (\beta_{TPlag0} + \beta_{TPlag1} + \beta_{TPlag2} + \beta_{TPlag3} + \beta_{TPlag4} + \beta_{TPlag5}) \bullet (TP/WQ)$

Define: $C1 = (\beta_{\Delta WQ} + (\beta_{WQ}/-\beta_{ECT}))$; $C2 = (\beta_{TPlag0} + \beta_{TPlag1} + \beta_{TPlag2} + \beta_{TPlag3} + \beta_{TPlag4} + \beta_{TPlag5})$

Define: $Var(C1) = Var(\beta_{\Delta WQ}) + (1/-\beta_{ECT})^2 \bullet Var(\beta_{WQ}) + (\beta_{WQ}/\beta_{ECT}^2)^2 \bullet Var(\beta_{ECT})$; $Var(C2) = Var(\beta_{TPlag0}) + Var(\beta_{TPlag1}) + Var(\beta_{TPlag2})$

$SE(\eta) = SQRT((TP/WQ)^2 \bullet (Var(C1) \bullet Var(C2) + C1^2 \bullet Var(C2) + C2^2 \bullet Var(C1))$

β_{WQ} is the coefficient for the water quality measure of interest (non-dynamic lagged term); $\beta_{\Delta WQ}$ is the coefficient for the error correction term; β_{TPlagi} are coefficients for the lagged TP terms; WQ is mean water quality for the measure

Water parameter

$\eta = \beta_{WQ}$

$SE(\eta) = SE(\beta_{WQ})$

Watershed loading

$\eta = \beta_{WQ} \bullet \beta_{WSL}$

$SE(\eta) = SQRT(Var(\beta_{WQ}) \bullet Var(\beta_{WSL}) + \beta_{WQ}^2 \bullet Var(\beta_{WSL}) + \beta_{WSL}^2 \bullet Var(\beta_{WQ}))$

β_{WQ} is the coefficient for the water quality parameter of interest; β_{WSL} is the coefficient for the watershed loading me

$\eta = \beta_{WQ} \bullet (WQ/Y)$

β_{WQ} is the coefficient for the water quality measure of interest; WQ is mean water quality for the measure of interest; Y is the m

$\eta = \beta_{WQ} \bullet (WQraw/(WQraw-WQfin))$

$SE(\eta) = SQRT((WQraw/(WQraw-WQfin))^2 \bullet Var(\beta_{WQ}))$

β_{WQ} is the coefficient for the water quality measure of interest; WQraw is mean raw water quality for the measure of interest; W

Reported in manuscript

Reported in manuscript

$\eta = \beta_{WQ} \bullet (WQraw/(WQraw-WQfin))$
$SE(\eta) = SQRT((WQraw/(WQraw-WQfin))^2 \bullet Var(\beta_{WQ}))$

β_{WQ} is the coefficient for the water quality measure of interest; WQraw is mean raw water quality for the measure of interest; W

$\eta = \beta_{WQ} \cdot (WQraw/(WQraw-WQfin))$
$SE(\eta) = SQRT((WQraw/(WQraw-WQfin))^2 \cdot Var(\beta_{WQ}))$

β_{WQ} is the coefficient for the water quality measure of interest; WQraw is mean raw water quality for the measure of interest; W

Water parameters
$\eta = \beta_{WQ}$
$SE(\eta) = SE(\beta_{WQ})$

Land use
$\eta = \beta_{WQ} \cdot \beta_{LU}$
$SE(\eta) = SQRT(Var(\beta_{WQ}) \cdot Var(\beta_{LU}) + \beta_{WQ}^2 \cdot Var(\beta_{LU}) + \beta_{LU}^2 \cdot Var(\beta_{WQ}))$

β_{WQ} is the coefficient for the water quality parameter of interest; β_{LU} is the coefficient for the land use measure of int

$\eta = \beta_{WQ} \cdot (WQ/Y)$

β_{WQ} is the coefficient for the water quality measure of interest; WQ is mean water quality for the measure of interest; Y is the m

$\eta = \beta_{WQ} \bullet (WQraw/(WQraw-WQfin))$
$SE(\eta) = SQRT((WQraw/(WQraw-WQfin))^2 \bullet Var(\beta_{WQ}))$

β_{WQ} is the coefficient for the water quality measure of interest; WQraw is mean raw water quality for the measure of interest; W

$\eta = \beta_{WQ}$
$SE(\eta) = SE(\beta_{WQ})$

β_{WQ} is the coefficient for the water quality measure of interest

Reported in manuscript

Water parameters

$\eta = \beta_{WQ}$

$SE(\eta) = SE(\beta_{WQ})$

Land use

$\eta = \beta_{WQ} \cdot \beta_{LU}$

$SE(\eta) = SQRT(Var(\beta_{WQ}) \cdot Var(\beta_{LU}) + \beta_{WQ}^2 \cdot Var(\beta_{LU}) + \beta_{LU}^2 \cdot Var(\beta_{WQ}))$

β_{WQ} is the coefficient for the water quality parameter of interest; β_{LU} is the coefficient for the land use measure of int

$\eta = \beta_{WQ} \cdot (WQ/(1+WQ))$

$SE(\eta) = SQRT((WQ/(1+WQ))^2 \cdot Var(\beta_{WQ}))$

β_{WQ} is the coefficient for the water quality measure of interest; WQ is mean water quality for the measure of interest

Water parameter

$\eta = \beta_{WQ}$

$SE(\eta) = SE(\beta_{WQ})$

Land use

$\eta = \beta_{WQ} \cdot (\beta_{LU} \cdot LU)$

$SE(\eta) = SQRT(LU^2 \cdot Var(\beta_{WQ}) \cdot Var(\beta_{LU}) + (LU \cdot \beta_{WQ})^2 \cdot Var(\beta_{LU}) + (LU \cdot \beta_{LU})^2 \cdot Var(\beta_{WQ}))$

β_{WQ} is the coefficient for the water quality parameter of interest; β_{LU} is the coefficient for the land use measure of int

	Notes
	● The manuscript does not clearly indicate the type of panel-data estimator used for the analysis. ● The manuscript does not clearly indicate which costs are included in the analysis. A description of the data collection process ● Turbidity is defined as the difference between source water and treated water quality. Since no descriptive statistics are repor calculation. Moderate levels of treated-water turbidity have little affect on the elasticity. ● Neither standard errors nor t-statistics are not reported. The maximum standard error consistent with the reported significanc
	● The unit of analysis is reported as water supply services (WSSs). We classify WSSs as CWSs since they can operate multiple analysis operate multiple plants.
	● Turbidity is defined as the difference between source water and treated water quality. Since descriptive statistics for raw wate 0.12 for the elasticity calculation (see Lusardi and Consonery, 1999). Moderate changes in this value have little affect on elastic ● The reported turbidity elasticity differs from the calculated elasticity--likely due to the rounding of reported coefficients. We

● Unit of analysis obtained through personal communication.
● Dependent variable's timeframe obtained through personal communication.
● Dependent variable's definition obtained through personal communication. It is the sum of annual O&M costs and amortized
● Descriptive statistics are not reported. Mean values used for the elasticity calculation are estimated from a scatter plot presen

● Land use elasticities are calculated using results from the reduced form model.

● Statistical estimator obtained through personal communication.
● Turbidity is defined as the difference between source water and treated water quality. Since descriptive statistics for raw wate
0.12 for the elasticity calculation (see Lusardi and Consonery, 1999). Moderate changes in this value have little affect on the el

● The study estimates multiple single-predictor regression models; thus, reference land use is all classifications other than the c

● The standard errors for the ratio of two coefficients is estimated, following Heberling et al. (2015), using the method describe

● Statistical estimator obtained through personal communication.

● Dependent variable's timeframe obtained through personal communication. It is measured at irregular daily and sub-daily int

● The unit of analysis is reported as water utilities. We classify water utilities as CWSs since they can operate multiple DWTPs
operate multiple plants.
● The manuscript does not clearly indicate the type of source water used by the water utilities. We assume, since TOC as the w
water sources.

- Statistical estimator obtained through personal communication.
- Dependent variable's timeframe obtained through personal communication.

- Turbidity is defined as the difference between source water and treated water quality. Mean treated water quality is obtained t

● Nitrate is defined as the difference between source water and treated water quality. Mean treated water quality is obtained thr

● This entry pertains to the Great Lakes Basin analysis; characteristics of the Maumee River Basin analysis are reported in Fors

● Descriptive statistics are not reported. Mean values used for the elasticity calculation are estimated from a scatter plot presen

● Calcium carbonate is defined as the difference between source water and treated water quality. Since descriptive statistics for
calcium carbonate level of 0 for the elasticity calculation. This assumption downwardly biases the estimated elasticity.

● The unit of analysis is reported as water utilities. We classify water utilities as CWSs since they can operate multiple DWTPs
operate multiple plants.

- Descriptive statistics not reported. The manuscript uses an output volume of 1,310,000 m3/day when calculating the affect of
- The manuscript does not clearly indicate the estimator used for the analysis; OLS is the most likely possibility.
- Neither standard errors nor t-statistics are reported. The maximum standard error consistent with the reported significance lev

Table B2: Sortable Database

Item	Reference	Country	Source Type
1	Abdul-Rahim & Mohd-Shahwahid (2011)	Malaysia	SW
2	Abdul-Rahim & Mohd-Shahwahid (2011)	Malaysia	SW
3	Abildtrup et al. (2013)	France	SW & GW
4	Abildtrup et al. (2013)	France	SW & GW
5	Abildtrup et al. (2013)	France	SW & GW
6	Abildtrup et al. (2013)	France	SW & GW
7	Abildtrup et al. (2013)	France	SW & GW
8	Abildtrup et al. (2013)	France	SW & GW
9	Dearmont et al. (1998)	USA	SW
10	Dearmont et al. (1998)	USA	SW
11	Ernst et al. (2004)	USA	SW
12	Fiquepron et al. (2013)	France	SW & GW
13	Fiquepron et al. (2013)	France	SW & GW
14	Fiquepron et al. (2013)	France	SW & GW
15	Fiquepron et al. (2013)	France	SW & GW
16	Fiquepron et al. (2013)	France	SW & GW
17	Forster et al. (1987)	USA	SW
18	Forster et al. (1987)	USA	SW
19	Forster and Murray (2007)	USA	SW
20	Forster and Murray (2007)	USA	SW
21	Forster and Murray (2007)	USA	SW
22	Forster and Murray (2007)	USA	SW
23	Forster and Murray (2007)	USA	SW
24	Forster and Murray (2007)	USA	SW
25	Freeman et al. (2008)	USA	SW
26	Freeman et al. (2008)	USA	SW
27	Freeman et al. (2008)	USA	SW
28	Freeman et al. (2008)	USA	SW
29	Freeman et al. (2008)	USA	SW
30	Heberling et al. (2015)	USA	SW
31	Heberling et al. (2015)	USA	SW
32	Heberling et al. (2015)	USA	SW
33	Heberling et al. (2015)	USA	SW
34	Heberling et al. (2015)	USA	SW
35	Heberling et al. (2015)	USA	SW
36	Heberling et al. (2015)	USA	SW
37	Holmes (1988)	USA	SW
38	Holmes (1988)	USA	SW
39	Honey-Rosés et al. (2014)	Spain	SW
40	Horn (2011)	Japan	SW
41	McDonald and Shemie (2014)	USA	SW

42	McDonald and Shemie (2014)	USA	SW
43	Moore and McCarl (1987)	USA	SW
44	Moore and McCarl (1987)	USA	SW
45	Moore and McCarl (1987)	USA	SW
46	Mosheim (2006)	USA	SW & GW
47	Mosheim and Ribaudo (2017)	USA	SW & GW
48	Murray (2001)	USA	SW
49	Murray (2001)	USA	SW
50	Murray (2001)	USA	SW
51	Murray (2001)	USA	SW
52	Murray (2001)	USA	SW
53	Murray (2001)	USA	SW
54	Oklahoma Water Resources Board (2011)	USA	SW
55	Piper (2003)	USA	SW & GW
56	Price et al. (2017)	Canada	SW & GW
57	Price et al. (2017)	Canada	SW & GW
58	Price et al. (2017)	Canada	SW & GW
59	Price et al. (2017)	Canada	SW & GW
60	Price et al. (2017)	Canada	SW & GW
61	Price et al. (2017)	Canada	SW & GW
62	Price et al. (2017)	Canada	SW & GW
63	Renzetti (2001)	Canada	SW
64	Singh and Mishra (2014)	India	SW
65	Singh and Mishra (2014)	India	SW
66	Singh and Mishra (2014)	India	SW
67	Singh and Mishra (2014)	India	SW
68	Vincent et al. (2016)	Malaysia	SW
69	Vincent et al. (2016)	Malaysia	SW
70	Warziniack et al. (2017)	USA	SW
71	Warziniack et al. (2017)	USA	SW
72	Warziniack et al. (2017)	USA	SW
73	Warziniack et al. (2017)	USA	SW
74	Warziniack et al. (2017)	USA	SW
75	Warziniack et al. (2017)	USA	SW

Notes. The term *load* is used to identify water quality measures that pertain to the am

* Statistically significant at p<0.1. One-tailed test used from water quality parameters

‡ Variable is defined as the difference between source water and treated water quality

Model Type	Water Quality Measure	Footnote	Reference Land Use Category
Cost function	Turbidity	‡	
Cost function	pH		
Price function	L: Forest		Agriculture
Price function	L: Urban		Agriculture
Price function	L: Other		Agriculture
Price function	L: Forest		Agriculture
Price function	L: Urban		Agriculture
Price function	L: Other		Agriculture
Cost function	Turbidity	‡	
Cost function	pH		
Cost function	L: Forest		Non-forest
Price function	Nitrate		
Price function	Pesticide exceedance		
Price function	L: Forest		Urban/agriculture
Price function	L: Grassland		Urban/agriculture
Price function	L: VIARMA		Urban/agriculture
Cost function	Turbidity	‡	
Cost function	Sediment load		
Cost function	Turbidity		
Cost function	Pesticide load		
Cost function	L: Tilled w/ <15% residual		Ridge/mulch tilled
Cost function	L: Tilled w/ 15-30% residual		Ridge/mulch tilled
Cost function	L: Untilled		Ridge/mulch tilled
Cost function	L: Non-agriculture		Ridge/mulch tilled
Cost function	TOC		
Cost function	WQI		
Cost function	L: Forest		Non-forest
Cost function	L: Urban		Non-urban
Cost function	L: Non-forest vegetation		Forest/non-vegetation
Cost function	Turbidity		
Cost function	pH		
Cost function	TOC		
Cost function	Turbidity		
Cost function	pH		
Cost function	TOC		
Cost function	Phosphorus load		
Cost function	Turbidity		
Cost function	Sediment load		
Energy use function	Conductivity		
Cost function	TOC	‡	
Cost function	Sediment load		

Cost function	Phosphorus load		
Chemical use function	Turbidity		
Chemical use function	Temperature		
Chemical use function	pH		
Cost function	Turbidity	‡	
Cost function	Nitrate	‡	
Cost function	Turbidity		
Cost function	Pesticide load		
Cost function	L: Tilled w/ <15% residual		Ridge/mulch tilled
Cost function	L: Tilled w/ 15-30% residual		Ridge/mulch tilled
Cost function	L: Untilled		Ridge/mulch tilled
Cost function	L: Non-agriculture		Ridge/mulch tilled
Cost function	TOC		
Price function	Calcium carbonate	‡	
Cost function	Turbidity		
Cost function	Turbidity		
Cost function	Turbidity		
Cost function	Turbidity		
Cost function	Turbidity		
Cost function	Turbidity		
Cost function	Turbidity		
Cost function	WQI		
Cost function	Turbidity		
Cost function	Turbidity		
Cost function	L: Forest		Non-forest
Cost function	L: Forest		Non-forest
Cost function	L: Forest		Non-forest
Cost function	L: Forest		Non-forest
Cost function	Turbidity		
Cost function	TOC		
Cost function	L: Forest		Non-forest/non-urban
Cost function	L: Urban		Non-forest/non-urban
Cost function	L: Forest		Non-forest/non-urban
Cost function	L: Urban		Non-forest/non-urban

ount of material entering surface water due to runoff.

, watershed loading variables, and forestland. Two-tailed tests used for all non-forestland classifications.

.

Comment	Elasticity	Std. Err.	Statistically Significant*
	0.07	(0.03)	Yes
	0.07	(0.03)	Yes
Service area (w/o spatial autocorrelation)	-0.48	(0.15)	Yes
Service area (w/o spatial autocorrelation)	0.004	(0.03)	No
Service area (w/o spatial autocorrelation)	-0.21	(0.08)	Yes
Entire region (w/ spatial autocorrelation)	-0.77	(0.26)	Yes
Entire region (w/ spatial autocorrelation)	0.38	(0.22)	Yes
Entire region (w/ spatial autocorrelation)	-0.49	(0.36)	No
	0.27	(0.12)	Yes
	0.27	(0.12)	Yes
	-0.83		NA
	0.05	(0.01)	Yes
	0.02	(0.01)	Yes
	-0.07	(0.03)	Yes
	0.02	(0.02)	No
	0.02	(0.01)	No
	0.12	(0.04)	Yes
	0.41	(0.02)	Yes
	0.30	(0.08)	Yes
	0.27	(0.20)	Yes
	0.40	(0.24)	Yes
	0.03	(0.03)	No
	0.02	(0.10)	No
	0.60	(0.28)	Yes
	0.77	(0.23)	Yes
	-0.53	(0.23)	Yes
	-0.38	(0.23)	Yes
	0.22	(0.10)	Yes
	-0.15	(0.07)	Yes
Short term (immediate response)	0.02	(0.01)	Yes
Short term (immediate response)	-0.04	(0.06)	No
Short term (immediate response)	-0.04	(0.03)	No
Long term (total response)	0.11	(0.04)	Yes
Long term (total response)	-0.01	(0.06)	No
Long term (total response)	0.10	(0.29)	No
Long term (total response)	0.02	(0.01)	Yes
	0.07	(0.02)	Yes
	0.05	(0.02)	Yes
	0.86		NA
	0.06	(0.02)	Yes
	0.26		NA

	0.19		NA
Eq1 (alum use eq.)	0.22	(0.02)	Yes
Eq1 (alum use eq.)	-0.39	(0.12)	Yes
Eq2 (lime use eq.)	0.21		NA
	0.09	(0.03)	Yes
	0.06	(0.02)	Yes
	-0.11	(0.12)	No
	-0.43	(0.37)	No
	0.10	(0.13)	No
	0.11	(0.13)	No
	-0.04	(0.12)	No
	0.12	(0.15)	No
	0.55		NA
	0.003	(0.001)	Yes
	0.10	(0.02)	Yes
Conventional (conventional systems)	0.12	(0.03)	Yes
Filtration (direct/in-line filtration systems)	0.13	(0.05)	Yes
Disinfection (disinfection systems)	0.06	(0.04)	Yes
Membrane (membrane systems)	0.14	(0.07)	Yes
Other (other treatment systems)	0.08	(0.07)	No
Untreated (systems w/o treatment)	0.06	(0.08)	No
	0.80	(0.22)	Yes
Chemical (chemical cost eq.)	0.20	(0.08)	Yes
O&M (O&M cost eq.)	0.19	(0.07)	Yes
Chemical (chemical cost eq.)	-1.71	(0.87)	Yes
O&M (O&M cost eq.)	-1.58	(0.80)	Yes
Virgin (virgin forest)	-0.47	(0.19)	Yes
Logged (logged forest)	-0.32	(0.14)	Yes
	0.19	(0.11)	Yes
	0.46	(0.19)	Yes
via turbidity (via turbidity ecol. prod. eq.)	-0.32	(0.22)	Yes
via turbidity (via turbidity ecol. prod. eq.)	0.08	(0.08)	No
via TOC (via TOC ecol. prod. eq.)	-0.06	(0.07)	No
via TOC (via TOC ecol. prod. eq.)	0.34	(0.56)	No

Feature Article

JAMES I. PRICE, MATTHEW T. HEBERLING, AND CHRISTOPHER T. NIETCH

Economic Support for Decisions on Source Water Protection

QUANTIFYING RELATIONSHIPS BETWEEN TREATMENT COSTS AND SOURCE WATER CONDITIONS CAN ESTIMATE AVOIDED-TREATMENT EXPENDITURES AND DETERMINE WHETHER SOURCE WATER PROTECTION WOULD BE COST-EFFECTIVE.

Source water quantity, quality, and reliability are central to the design and operation of public water systems (PWSs). PWSs regularly modify in-plant operations and upgrade capital equipment following changes in source water conditions to optimize performance and maintain compliance with regulatory standards. PWSs may also adopt upstream source water protection (SWP) strategies to safeguard source waters from adverse impacts before treatment, such as agricultural runoff control and watershed restoration to reduce wildfire risks (Carpenter 2017, Gartner et al. 2017).

Around the world, there is growing interest in SWP as a means to reduce certain health risks and avoid treatment expenditures; for example, US federal and state laws recognize the benefits of watershed services and establish funding for SWP activities (California Water Code 2016, CFR 2016). In addition, there are numerous ongoing and emergent watershed management programs whose stated motivations include securing drinking water supplies (Bennett et al. 2014, Carpe Diem West 2011, Herbert 2007).

When considering SWP options, PWSs need evidence-based information on how SWP interventions affect source water conditions and treatment costs (Gartner et al. 2017). By quantifying relationships between treatment costs

Layout imagery by Shutterstock.com/ZwiebackesserI

and various source water conditions, economics can equip PWSs with information needed to estimate avoided-treatment costs and, in conjunction with cost information on SWP activities and in-plant treatment options, show whether SWP is likely to be cost-effective (i.e., the least-cost alternative for meeting the desired objective).

This latter issue is crucial, as evidence suggests that SWP programs are cost-effective only for a fraction of PWSs (Vincent et al. 2016, Heberling et al. 2015, McDonald & Shemie 2014, Hudak et al. 2013, Pyke et al. 2002), except when program costs can be sufficiently distributed across multiple stakeholders (Gartner et al. 2017). Where initial estimates for SWP are projected to be cost-effective, PWSs can pursue more precise economic and hydrologic modeling specific to their treatment system and watershed to better inform the decision-making process. For municipal and state agencies, modeling efforts and cost-effectiveness analyses (CEAs) would most likely consider a broader set of benefits, including those related to recreation, wildfire management, and aesthetics.

The following is a brief review of the state of knowledge regarding the relationship between treatment costs and source water conditions primarily based on experiences in North American PWSs. Key knowledge gaps are also highlighted. In addition, the authors discuss a research agenda that will aid PWSs in evaluating the efficacy of potential SWP programs.

REVIEW OF RESEARCH AND KNOWLEDGE GAPS

Economists rely on statistically estimated cost functions to quantify relationships between treatment costs and source water conditions and subsequently to determine potential avoided-treatment costs. Cost functions are guided by economic theory in which, besides source water conditions, treatment costs depend on a PWS's output volume, price of factor inputs (e.g., electricity rates), and in most instances, fixed capital inputs. The precise form of a cost function depends on several contextual and data-related issues, while input from water treatment engineering is important for refining model specifications and interpreting results. Price and Heberling (2018) provide a review of cost functions, and related approaches, as applied to PWSs and source water quality.

Studies show that marginal improvements in source water quality lead to modest reductions in treatment costs. Evidence of this effect is most robust for turbidity, where recent US- and Canada-based studies showed that a 1% decline in turbidity led to a 0.09–0.11% reduction in variable costs (Price et al. 2017, Heberling et al. 2015, Mosheim 2006). For example, with a $1 million annual-treatment-cost budget, a PWS could save $1,100 per year if a 1% reduction in turbidity led to a 0.11% change in treatment costs. Slightly larger reductions of 0.19 and 0.30% are found when considering the effect of turbidity on just chemical expenditures (Warziniack et al. 2017, Forster & Murray 2007).

Studies have also evaluated how treatment costs are affected by total organic carbon (TOC), nitrate, and calcium carbonate concentrations, as well as the amount of sediment, phosphorus, and pesticides entering source waters from runoff. Findings for these water quality measures are less robust than for turbidity, either being limited to a single study or exhibiting considerable variation across estimates. Among recent US-based studies, a 1% decline in TOC was associated with a 0.46 and 0.77% reduction in chemical costs (Warziniack et al. 2017, Freeman et al. 2008). However, Heberling et al. (2015) found that TOC has no appreciable effect on variable costs. A 1% decline in nitrate concentrations, sediment loading, and phosphorus loading is associated with 0.02, 0.26, and 0.02–0.19% reductions in variable costs, respectively (Mosheim & Ribaudo 2017, Heberling et al. 2015, McDonald & Shemie 2014).

Source water quality also affects expenditures on capital equipment. McDonald et al. (2016) found a positive correlation between the amount of sediment and nutrients entering source watersheds and the probability of adopting more sophisticated treatment technology. There are also numerous instances in which deteriorating source water quality has been anecdotally linked to capital upgrades (Dunlap et al. 2015, Davenport & Drake 2011, Jones et al. 2007, Oneby & Bollyky 2006).

However, because many upgrades are concurrently motivated by a desire to expand treatment capacity or comply with new regulatory standards, it can be difficult to determine what proportion of these costs is attributed to declines in upstream water quality. Evidence from cost functions, which can control for these confounding factors, is limited to a few studies that incorporate capital expenditure into their cost measure (Abildtrup et al. 2013, Fiquepron et al. 2013, Horn 2011, Piper 2003, Renzetti 2001). Taken together, these studies show a negative relationship between total costs and source water quality, but it is unclear whether the inclusion of capital expenditures substantially alters the estimated relationships between treatment costs and source water conditions.

Few cost-function studies have considered how water treatment costs are affected by the availability of source water independent of its impact on water quality via the dilution of contamination or increased runoff. Evidence indicates that water availability, defined as reservoir elevation or streamflow at intake, is negatively correlated with treatment costs (Heberling et al. 2015, Renzetti 2001). Variability in

reservoir elevation and streamflow (i.e., the reliability of water supply) is positively correlated with costs, and under prevailing conditions may have a markedly greater effect on costs than availability (Renzetti 2001).

As is evident from the preceding overview, there are several knowledge gaps in the existing literature. First, there is a need to better understand relationships between treatment costs and key source water quality parameters (e.g., TOC, pH, phosphorus, nitrogen, algae, cyanobacteria), water availability, and variation in water quality parameters and water availability. Second, there is a need to use a cost-function approach to evaluate the relationship between amortized capital expenditures and source water conditions, and to determine whether this relationship differs from those based on variable cost. Third, little is known about how the relationships between treatment costs and source water conditions vary across treatment technologies, production scales, management regimes, and geographic regions. Price et al. (2017) evaluated heterogeneity across treatment technologies, while Mosheim (2006) and Mosheim and Ribaudo (2017) evaluated heterogeneity across production scales—with the latter finding that smaller systems are more adversely affected by marginal changes in water quality than larger systems; however, more research is in order. In particular, the effects that source water conditions have on treatment costs in small-scale groundwater systems have not been adequately studied.

CONSIDERATIONS FOR FUTURE RESEARCH

Building a knowledge base that can effectively aid PWSs in evaluating the efficacy of SWP programs will require a threefold approach. First, case studies should be used to assess avoided-treatment costs at individual PWSs. Cost functions developed for case studies can be tailored to a particular treatment technology, and these are well suited to evaluating the intricacies of source water quality, process modifications, and atypical events such as process shutdown or a spike in pollutants. In some instances, the functions can also account for abrupt changes in treatment that are triggered when source water conditions exceed predefined thresholds (e.g., augmented chemical usage, activation of capital equipment).

Evidence suggests that SWP programs are cost-effective only for a fraction of PWSs, except when program costs can be sufficiently distributed across multiple stakeholders.

Second, multisystem studies should be used to assess average avoided-treatment costs over many PWSs. These studies require a different approach to data acquisition and statistical modeling than case studies. Multisystem studies are suited to evaluating linkages between treatment costs, commonly monitored source water parameters, and land use; they can be used to identify heterogeneity in linkages across treatment technologies, production scales, and geographies.

Third, an updatable database of relevant cost-function studies, including both case studies and multisystem studies, should be developed and maintained to reduce the effort needed by PWSs to find avoided-cost information. Organizing selected studies by characteristics of the treatment system, source water, and modeling approach would further enhance the usefulness of the database. A catalog of cost-function studies related to source water quality, but not source water availability or reliability, is provided through the US Environmental Protection Agency's (USEPA's) Environmental Dataset Gateway (USEPA 2018).

Data constraints are the primary obstacles to both case study and multisystem research approaches. For case studies, data must be obtained directly from PWSs, which, in addition to compiling relevant information, need to partner with researchers and consultants to develop cost functions that reflect their systems' production technology. Since statistical models that analyze data ordered in sequential time intervals are often appropriate for case studies, a common requirement is daily or weekly observations of water treatment costs, production rates, and source water conditions over several years. As a rule of thumb, at least three years of observations are needed to model seasonal patterns in these types of case studies.

For modeling purposes, treatment cost may be defined as all operation-related expenditures or just those pertaining to a subset of treatment processes (e.g., chemical costs); source water variables should include all raw water characteristics that are regularly monitored as part of the treatment process (e.g., turbidity, TOC, pH, temperature, reservoir elevation). Information on discrete changes in treatment processes (e.g., shutdowns, activation of auxiliary equipment) may also be incorporated into the models. Although compiling these data can be burdensome, partner PWSs gain valuable site-specific estimates of avoided-treatment costs to inform SWP decisions. Findings from this kind of analysis, which could be disseminated through the aforementioned database of cost-function studies, would readily benefit nonpartner

PWSs with similar treatment technologies and source water concerns.

Multisystem studies require cross-sectional or panel data obtained from surveys. Cross-sectional data observes many subjects at the same point in time, while panel data observes multiple subjects at several different time periods. The ensuing cost functions, which reflect sample averages, are coarser than those obtained from case studies since they typically employ annual or monthly observations and are unable to control for many site-specific characteristics.

Nonetheless, results from these analyses offer insight into the potential magnitude of avoided-treatment costs that PWSs can use in the initial stages of SWP planning. Findings are also useful for policymakers considering the broader effects of water quality changes.

To the authors' knowledge, a 1996 AWWA questionnaire is the last publicly available survey to simultaneously elicit information on treatment costs and source water conditions for a large number of US PWSs (AWWA 1996). Mosheim (2006), Mosheim and Ribaudo (2017), and Piper (2003) each used the survey to quantify the effects of water quality on costs. More recently, Statistics Canada's Biennial Drinking Water Plants Survey (Statistics Canada 2017) and several small-sample surveys (Warziniack et al. 2017, Freeman et al. 2008, Ernst 2004) collected cost and source water information—but data are not readily available. Surveys like these are necessary for understanding SWP benefits, particularly when there is a desire to evaluate source water conditions over a greater range of values than can be obtained with a case study. Sound design and sampling methods, as well as the ability to verify results, are important to the credibility of survey-based studies. As much as possible, survey administrators should aspire to collect data that are representative of target PWSs, elicit information on all variables relevant to cost-function analyses as dictated by economic theory, and, while balancing privacy concerns, make data available to researchers.

Additional economic analyses, such as benefit–cost analyses (BCAs) or CEAs, are needed to help identify when SWP is cost-effective relative to in-plant treatment. These studies should compare avoided-treatment costs obtained from cost-function studies to SWP program costs (Heberling et al. 2015). BCAs and CEAs should account for the inherent uncertainty in watershed and economic modeling by using the distribution of estimated costs and benefits and estimating the likelihood that SWP options will be cost-effective. Accounting for uncertainty is important because the cost of reducing pollutants via SWP is likely more variable, and that variability is less well understood, than the cost of in-plant treatment. In some instances, BCAs and CEAs will also need to include a probabilistic component accounting for potential landscape disruptions (e.g., wildfire, flooding, chemical spill) that could drastically alter source water conditions. Gartner et al. (2017) found that flooding events are a major motivating factor among PWSs considering SWP.

An interdisciplinary approach is essential to conducting cost-function studies, BCAs, and CEAs. For instance, source water quality is a function of the ecology of the water body (e.g., river, lake, reservoir) or ecosystem (e.g., groundwater) that represents the source, which, in turn, responds in a dynamic manner to physiochemical drivers in watershed loads. These loads are the product of ecological interactions between natural and engineered systems situated on the landscapes draining to the source water. Consequently, understanding the impact of SWP activities on water quality will require interdisciplinary efforts (e.g., by hydrologists, ecologists) in order to develop spatially explicit watershed models linking land use and management practices to water quality parameters (e.g., Elias et al. 2016). Access to geographic information system data on land use and land management data, and the expertise to integrate this information into modeling tools, will be essential to these efforts, as will advances in access to source water information like that being developed for the cloud-based WaterSuite (Benjamin et al. 2018).

The centrality of watershed and water-body ecology in these models underscores the importance of an ecological perspective in linking SWP to changes in treatment costs. Moreover, engineering principles associated with water treatment and watershed management activities are needed to fully appreciate these links and ensuing policy implications. Development of economic analyses thus depends on effective collaboration with ecologists and engineers to adequately account for the changing dynamics resulting from SWP measures.

It is often difficult for PWSs to know whether a proposed SWP program will be cost-effective. Indeed, several PWSs have initiated programs without a formal or complete analysis of the benefits (Gartner et al. 2017). As the types of research outlined here are conducted and made available, possibly through an updatable database, they should help PWSs decide when SWP is likely to be cost-effective and whether to pursue detailed site-specific assessments. While this work is necessarily interdisciplinary, substantial knowledge gaps regarding avoided-treatment costs suggest the need for further economic research. To move forward with these efforts, it will be necessary to consider partnerships between PWSs, or survey developers in the case of multisystem studies, and economists that can help address the general lack of data and studies needed to support SWP decisions.

DISCLAIMER

The views expressed in this article are those of the authors and do not

necessarily represent those of the USEPA. No official agency endorsement should be inferred.

ABOUT THE AUTHORS

James I. Price *(to whom correspondence may be addressed) is a postdoctoral researcher at the USEPA Office of Research and Development, 26 W. Martin Luther King Dr. (MS 483), Cincinnati, OH 45268 USA; Price.James@epa.gov; JamesPrice672@gmail.com. He holds a PhD in economics from the University of New Mexico, Albuquerque, with concentrations in environmental economics and econometrics. Price's recent research centers on estimating the economic benefits of improved water quality.* ***Matthew T. Heberling*** *is a research economist and* ***Christopher T. Nietch*** *is a research ecologist at the USEPA Office of Research and Development in Cincinnati, Ohio.*

https://doi.org/10.1002/awwa.1153

REFERENCES

Abildtrup, J.; Garcia, S.; & Stenger, A., 2013. The Effect of Forest Land Use on the Cost of Drinking Water Supply: A Spatial Econometric Analysis. *Ecological Economics*, 92:126. https://doi.org/10.1016/j.ecolecon.2013.01.004.

AWWA, 1996. WATER:\STATS: The Water Utility Database CD-ROM. AWWA, Denver.

Benjamin, J.; Smith, E.; Kearns, M.; Rosen, J.; & Stevens, K., 2018. Improving Water Utilities' Access to Source Water Protection and Emergency Response Data. *Journal AWWA*, 110:2:E33. https://doi.org/10.5942/jawwa.2018.110.0018.

Bennett, D.E.; Gosnell, H.; Lurie, S.; & Duncan, S., 2014. Utility Engagement With Payments for Watershed Services in the United States. *Ecosystem Services*, 8:56. https://doi.org/10.1016/j.ecoser.2014.02.001.

California Water Code, 2016. California Water Code §108.5, General State Powers Over Water: General State Policy. California Legislative Information, Sacramento, Calif.

Carpe Diem West, 2011. Watershed Investment Programs in the American West. Carpe Diem West, Sausalito, Calif.

Carpenter, A., 2017. Working Together to Solve Source Water Nutrient Issues. *Journal AWWA*, 109:11:58. https://doi.org/10.5942/jawwa.2017.109.0145.

CFR (Code of Federal Regulations), 2016. 40 CFR §141.2, National Primary Drinking Water Regulations: Definitions. United States Government Printing Office, Washington.

Davenport, T. & Drake, W., 2011. Grand Lake St. Marys, Ohio—The Case for Source Water Protection: Nutrients and Algae Blooms. *Lakeline*, Fall 2011:41.

Dunlap, C.R.; Sklenar, K.S.; & Blake, L.J., 2015. A Costly Endeavor: Addressing Algae Problems in a Water Supply. *Journal AWWA*, 107:5:E255. https://doi.org/10.5942/jawwa.2015.107.0055.

Elias, E.; Rodriguez, H.; Srivastava, P.; Dougherty, M.; James, D.; & Smith, R., 2016. Impacts of Forest to Urban Land Conversion and ENSO Phase on Water Quality of a Public Water Supply Reservoir. *Forests*, 7:2:29. https://doi.org/10.3390/f7020029.

Ernst, C., 2004. *Protecting the Source: Land Conservation and the Future of America's Drinking Water.* Trust for Public Land, San Francisco, & AWWA, Denver.

Fiquepron, J.; Garcia, S.; & Stenger, A., 2013. Land Use Impact on Water Quality: Valuing Forest Services in Terms of the Water Supply Sector. *Journal of Environmental Management*, 126:113. https://doi.org/10.1016/j.jenvman.2013.04.002.

Forster, D.L. & Murray, C., 2007. Effects of Pesticide Use and Farming Practices on Water Treatment Costs in Maumee River Basin Communities. In *Economic Valuation of River Systems* (F.J. Hitzhusen, editor), 115–128. Edward Elgar Publishing, Cheltenham, United Kingdom, & Northampton, Mass. https://doi.org/10.4337/9781847208705.

Freeman, J.; Madsen, R.; & Hart, K., 2008. *Statistical Analysis of Drinking Water Treatment Plant Costs, Source Water Quality, and Land Cover Characteristics.* http://cloud.tpl.org/pubs/water-landuse-water-whitepaper.pdf (accessed Nov. 15, 2017).

Gartner, T.; Di Francesco, K.; Ozment, S.; Huber-Stearns, H.; Lichten, N.; & Tognetti, S., 2017. Protecting Drinking Water at the Source: Lessons From US Watershed Investment Programs. *Journal AWWA*, 109:4:30. https://doi.org/10.5942/jawwa.2017.109.0049.

Heberling, M.T.; Nietch, C.T.; Thurston, H.W.; Elovitz, M.; Birkenhauer, K.H.; Panguluri, S.; Ramakrishnan, B.; Heiser, E.; & Neyer, T., 2015. Comparing Drinking Water Treatment Costs to Source Water Protection Costs Using Time Series Analysis. *Water Resources Research*, 51:11:8741. https://doi.org/10.1002/2014WR016422.

Herbert, E., 2007. Forest Management by West Coast Water Utilities: Protecting the Source? *Journal AWWA*, 99:2:91. https://doi.org/10.1002/j.1551-8833.2007.tb07872.x.

Horn, T., 2011. Incorporating Water Purification in Efficiency Evaluation: Evidence From Japanese Water Utilities. *Applied Economics Letters*, 18:18:1789. https://doi.org/10.1080/13504851.2011.564119.

Hudak, J.P.; Dietz, M.E.; Wagner, K.J.; & Ford, R., 2013. Estimating Potential Costs of Watershed Development on Drinking Water Treatment. www.potomacdwspp.org/wp-content/uploads/2015/03EstPotentialCostsWatershedDevelopmentCT.pdf (accessed Sept. 3, 2017).

Jones, C.S.; Hill, D.; & Brand, G., 2007. Use a Multifaceted Approach to Manage High Source-Water Nitrate. *Opflow*, 33:6:20. https://doi.org/10.1002/j.1551-8701.2007.tb02935.x.

McDonald, R.I.; Weber, K.F.; Padowski, J.; Boucher, T.; & Shemie, D., 2016. Estimating Watershed Degradation Over the Last Century and Its Impact on Water-Treatment Costs for the World's Large Cities. *Proceedings of the National Academy of Sciences*, 113:32:9117. https://doi.org/10.1073/pnas.1605354113.

McDonald, R.I. & Shemie, D., 2014. *Urban Water Blueprint: Mapping Conservation Solutions to the Global Water Challenge.* The Nature Conservancy, Washington.

Mosheim, R., 2006. A Shadow Cost Function Model of the US Water Industry Incorporating Water Quality and Ownership Effects. In *Performance Measurement and Regulation of Network Utilities* (T. Coelli & D. Lawrence, editors), 243-265. Edward Elgar Publishing, Cheltenham, United Kingdom, & Northampton, Mass.

Mosheim, R. & Ribaudo, M., 2017. Costs of Nitrogen Runoff for Rural Water Utilities: A Shadow Cost Approach. *Land Economics*, 93:1:12. https://doi.org/10.3368/le.93.1.12.

Oneby, M. & Bollyky, L.J., 2006. High-Pressure Pipeline Pre-Ozonation at Wichita, Kansas, for Taste and Odor Control. Prepared for the International Conference Ozone and UV. Apr. 3, 2006.

Piper, S., 2003. Impact of Water Quality on Municipal Water Price and Residential Water Demand and Implications for Water Supply Benefits. *Water Resources Research*, 39:5:1127. https://doi.org/10.1029/2002WR001592.

Price, J.I. & Heberling, M.T., 2018. The Effects of Source Water Quality on Drinking Water Treatment Costs: A Review and Synthesis of Empirical Literature. *Ecological Economics*, 151:195. https://doi.org/10.1016/j.ecolecon.2018.04.014.

Price, J.I.; Renzetti, S.; Dupont, D.; Adamowicz, W.; & Emelko, M.B., 2017. Production Costs, Inefficiency, and Source Water Quality: A Stochastic Cost Frontier Analysis of Canadian Water Utilities. *Land Economics*, 93:1:1. https://doi.org/10.3368/le.93.1.1.

Pyke, G.W.; Becker, W.C.; & Head, R., 2002. Efficacy of Source Water Protection for Reducing Costs of Drinking Water Treatment. *Proceedings of the Water Environment Federation,* 2002:665. https://doi.org/10.2175/193864702784248629.

Renzetti, S., 2001. Environmental Conditions and the Cost of Water Supply. Proc. AWRA/IWLRI-University of Dundee International Specialty Conf., Dundee, Scotland.

Statistics Canada, 2017. *Biennial Drinking Water Plants Survey*. www23.statcan.gc.ca/imdb/p2SV.pl?Function=getSurvey&Id=423733 (accessed June 27, 2018).

USEPA (US Environmental Protection Agency), 2018. Supplementary Material for "The Effects of Source Water Quality on Drinking Water Treatment Costs: A Review and Synthesis of Empirical Literature." https://doi.org/10.23719/1407619.

Vincent, J.R.; Ahmad, I.; Adnan, N.; Burwell III, W.B.; Pattanayak, S.K.; Tan-Soo, J.-S.; & Thomas, K., 2016. Valuing Water Purification by Forests: An Analysis of Malaysian Panel Data. *Environmental and Resource Economics*, 64:1:59. https://doi.org/10.1007/s10640-015-9934-9.

Warziniack, T.; Sham, C.H.; Morgan, R.; & Feferholtz, Y., 2017. Effect of Forest Cover on Water Treatment Costs. *Water Economics and Policy*, 3:4:1750006. https://doi.org/10.1142/s2382624x17500060.

AWWA RESOURCES

- Pursue Sustainability to Protect Source Water. West, A., 2018. *Opflow*, 44:6:20.
- Improving Water Utilities' Access to Source Water Protection and Emergency Response Data. Benjamin, J.; Smith, E.; Kearns, M.; Rosen, J.; & Stevens, K., 2018. *Journal AWWA*, 110:2:E33.
- Leveraging Source Water Protection Programs Through Effective Partnerships. Walker, L.; Morgan, R.; & Stan gel, P., 2017. *Journal AWWA*, 109:1:58.

These resources have been supplied by *Journal AWWA* staff. For information on these and other AWWA resources, visit www.awwa.org.

From: James I Price
To: Heberling, Matthew
Subject: Record of Percentage Agreement James Price
Date: Wednesday, April 22, 2020 9:54:23 AM

Nominee's name: James I. Price

Title of nominated articles: *The Effects of Source Water Quality on Drinking Water Treatment Costs: A Review and Synthesis of Empirical Literature* and *Economic Support for Decisions on Source Water Protection*

Your name: James I. Price

Professional title:
EPA Postdoc (when relevant research was performed)
Assistant Professor (current)

Percentage on nomination form: 62%

Current affiliation: University of Wisconsin - Milwaukee

Current address:
4050 N Newhall St.
Shorewood, WI 53211

I am in agreement with my designated percentage of contribution as stated on the Scientific and Technological Achievement Awards 2020 Nomination Form.

Sincerely,
James Price

From: Nietch, Christopher
To: Heberling, Matthew
Subject: Record of Percentage Agreement: Christopher Nietch
Date: Wednesday, April 22, 2020 9:35:02 AM

Nominee's name: James I. Price

Title of nominated articles: *The Effects of Source Water Quality on Drinking Water Treatment Costs: A Review and Synthesis of Empirical Literature* and *Economic Support for Decisions on Source Water Protection*

Your name: Christopher T. Nietch

Professional title: Research Ecologist

Percentage on nomination form: 3%

Current affiliation: USEPA/ORD/Center for Environmental Measurement and Modeling/Watershed Management Branch

Current address: 26 W. MLK Dr., Cincinnati, OH. 45268

I am in agreement with my designated percentage of contribution as stated on the Scientific and Technological Achievement Awards 2020 Nomination Form.

Sincerely,
Christopher T. Nietch

==========

Christopher T. Nietch, Ph.D. | Research Ecologist | U.S. EPA | Office of Research and Development
Center for Environmental Measurement and Modelling | Watershed and Ecosystem Characterization Division
Watershed Management Branch | Experimental Stream Facility
26 W. MLK Dr., Cincinnati, OH 45268 | 1003 US HWY 50, Milford, OH 45150
513-569-7460 (Office) | 513-453-5424 (ESF) | 513-317-9394 (Mobile)

From: Heberling, Matthew
To: Heberling, Matthew
Subject: Record of Percentage Agreement: Matt Heberling
Date: Wednesday, April 22, 2020 8:38:07 AM

Nominee's name: James I. Price

Title of nominated articles: *The Effects of Source Water Quality on Drinking Water Treatment Costs: A Review and Synthesis of Empirical Literature* and *Economic Support for Decisions on Source Water Protection*

Your name: Matthew T. Heberling

Professional title: Research Economist

Percentage on nomination form: 35%

Current affiliation: US EPA

Current address:
26 W. M. L. King Dr. (MS 587)
Cincinnati, OH 45268

I am in agreement with my designated percentage of contribution as stated on the Scientific and Technological Achievement Awards 2020 Nomination Form.

Sincerely,
Matt

Matthew T. Heberling, Ph.D.
Research Economist
US EPA/ORD/Center for Environmental Measurement and Modeling/
Watershed & Ecosystem Characterization Division/Watershed Management Branch
26 W. M. L. King Dr. (MS 587)
Cincinnati, OH 45268
Work: (513) 569-7917
Cell: (513) 442-8768

Table of Contents

General_Authors_Publications.....2
LI-266206_Email_approvals_of_the_co-authors_on_their_contributions_to_the_arti9
The_published_PDF_version_of_the_article_on_proteomic_responses_of_BEAS-2b_cel10
Email_approvals_of_the_co-authors_on_their_contributions_to_the_article_for_ST22

United States Environmental Protection Agency
Washington, DC 20460

STAA REPORT FOR THE SCIENTIST NOMINATIONS

General Information:

Nomination ID/App ID:	20-099
Research Category Primary:	Health Effects Research and Human Health Risk Assessment (HE)
Research Category Secondary:	
Laboratory/Office Name:	ORD
Nomination Entered By:	Yue Ge

Eligibility Checklist:

[Y] The nominated publication(s) has not been submitted to a previous STAA competition.

[Y] The nominated publication(s) was published on or before January 1, 2017 and on or after January 1,2012

[Y] The principal author was an EPA employee or a PHS employee assigned to EPA when the research was performed

[Y] The EPA authors (includes PHS employees assigned to EPA) contributed collectively a minimum of 50% toward the publication(s)

Nominating Official Name:	Maureen Gwinn
Nominating Official Title:	BIOLOGIST
Nominating OfficialEmail:	gwinn.maureen@epa.gov
STAA Coordinator Name:	Kathleen Wiser
STAA Coordinator Email:	wiser.kathi@epa.gov

Justifications:

Justification 1:

One of the ORD's long-term research goals is to develop innovative techniques, methodologies, and approaches that can be used to generate scientific data and develop solutions for the rapid screening and identification of environmental hazards/chemicals, and for efficient and accurate assessment of their risks to environmental and human health. Conducting a chemical risk assessment, the major goal of the toxicological study is to define where exposure effects that could be considered potentially toxic to animals and humans occur on the dose-response curve. For this, identification of No-Observed-Adverse-Effect Level (NOAEL) for each environmental hazard/chemical in animals that may be predictive of adverse outcomes in humans is the corner stone of hazard/chemical toxicity testing and risk assessment.

The EPA defines NOAEL as an exposure level at which there are no statistically or biologically significant increases in the frequency or severity of adverse effects between the exposed population and its appropriate control. In an experiment with several NOAELs, the regulatory focus is primarily on the highest one, leading to the common usage of the term NOAEL as the highest exposure without adverse effects. Because of this, the initial opinions or results of NOAELs on where toxic and non-toxic doses and effects occur may change as additional adverse outcomes related to the chemical are generated. Data from longer-term studies may give the toxicologist new or additional perspectives on whether an observation thought to be subtle or minor in a short-term study is an early indicator of a toxicity effect. Another obstacle associated with the applications of NOAEL to chemical toxicity characterization and human health risk assessment is that the NOAEL values generated by traditional toxicity endpoints in the exposed animals are neither accurate nor health protective in many real cases of chemical safety evaluations and risk assessments. In addition, the resulting assessment data obtained from toxicity endpoints-based NOAEL methods and models is very specific to a certain cells, tissues, organs and animal systems and cannot be easily transferred to address other concerns, scenarios, or regulatory decisions. Utilization of toxicity endpoints or adverse

health outcomes-based NOAEL for hazard/chemical identification and risk assessment represents the current and persistent challenges faced by the agency and other risk assessment communities.

Proteins are functional molecules intrinsic to most physiological and pathological processes. Any physiological change and resulting toxicity or adverse health outcome induced by environmental hazard/chemicals is preceded by and reflected in protein changes in the exposed organisms. To some extent, induction of cytotoxicity is a result of interactions among multiple biochemical pathways and proteins involved in the pathways from the perspective of proteomics. Thus, changes at levels of expression and/or phosphorylation of signaling proteins, regulators and biomarkers of toxicity pathways should be sensitive enough to predict adverse outcomes in advance, and even more sensitive than toxicity endpoints-based risk assessment using NOAEL. This work submitted for the application of the 2020 STAA was to demonstrate that critical protein response changes or pathway alterations induced by environmental hazards/chemicals such as Cr (VI) that lead to cytotoxicity conversion could be detected at a non-toxic or NOAEL dose, and be used as protein indicators or biomarkers of toxicity for determination of an adverse effect threshold, a protein based-NOAEL for chemical toxicity characterization with a focus on protein response changes other than toxicity endpoint changes. For this, human BEAS-2B cells were treated with Cr (VI) at the concentrations of 0.3 μM, a nontoxicity dose and 1.8 μM, low toxicity dose respectively. The critical proteomic responses were characterized by measuring protein expression and phosphorylation changes of 15 upstream toxicity pathway regulators using ELISA and identifying downstream differentially expressed proteins using 2-DE in Cr (VI)-treated BEAS-2B cells. This study provided an overall picture of the important protein responses and toxicity pathways that were modulated in the cellular response to Cr (VI) treatments and identified a small set of key proteins and concomitant pathways associated with the toxicity of Cr (VI). Interestingly, this small set of key proteins and pathways involved in glycolysis and gluconeogenesis pathways, protein degradation, and stress responses including inflammation and oxidative stress was already modified to a lower extend in BEAS-2B cells treated with 0.3M of Cr (VI), demonstrating a shift in these pathways from a non-toxic concentration of Cr (VI) to a toxic one.

Thus, this small project supported ORD's long-term research goal of providing scientific knowledge, data, and innovative techniques that can be used to develop solutions to the Agency's highest priority in chemical toxicity characterization and human health risk assessment. The resulting publication has also paved a new avenue for development of protein response-based NOAELs for chemical toxicity characterization and human health risk assessment.

Justification 2A:

n/a

Justification 2B:

n/a

Justification 2C:

n/a

Justification 2D:

n/a

Justification 2E:

n/a

Justification 3A:

This article has been cited multiple times since it was published . We have also been contacted frequently for PDF copies of this article from scientists outside EPA. In addition, the article authors have been invited to present the research results in several prestigious international and national conferences on environmental toxicology such as International Conference on Toxicology (ICT) and SOT, and National Toxicology Program at NIEHS.

Justification 3B:

The research article was first technical reviewed by two research scientists within EPA as a part of the NHEERL review process for submission of this article to publish. The article was then peer-reviewed by three external reviewers who were pointed by the Editor of the journal. The comments on the article from three reviewers were highly positive especially on the innovative ideas and the integrated proteomics approach developed for identification of protein indicators of toxicity conversion. This article could be the first publication ever to address toxicity pathway changes in a biosystem exposed or treated with non-toxic chemical or environmental stressor. Although this was a small research, it was a really innovative and impacted one.

AUTHORS

Principal Author

Author Name:	Yue Ge		
Professional Title:		Salutation:	Dr.
Email:	gesss2019@outlook.com	Organization:	
Mailing Address:			
Street Line 1:	4704 Brook Top Ct		
City:	Raleigh		
Zip Code:	27606	State:	North Carolina
At time of research was:	EPA Employee		

Separation Date:			
% of Effort:	50		

Contributing Author

Author Name:	Jeffrey Ross		
Professional Title:		Salutation:	Dr.
Email:	jeff@piedmontpottery.com	Organization:	
Mailing Address:			
Street Line 1:			
City:			
Zip Code:		State:	
At time of research was:	EPA Employee		
Separation Date:	Mon Oct 15 00:00:00 GMT 2018		
% of Effort:	10		

Contributing Author

Author Name:	Maribel Bruno		
Professional Title:		Salutation:	Ms.
Email:	bruno.maribel@epa.gov	Organization:	
Mailing Address:			
Street Line 1:			
City:			
Zip Code:		State:	
At time of research was:	EPA Employee		

Separation Date:	
% of Effort:	40

PUBLICATIONS

Publication 1:

Publication Title:	Proteomic Responses of BEAS-2B Cells to Nontoxic and Toxic Chromium: Protein Indicators of Cytotoxic		
Publication Date:	Tue Aug 30 00:00:00 GMT 2016		
Journal/Publication Method:	Toxicology Letters		
All Author(s):			
Volume:	264	Number:	1
Pages:	59 -70	Immediately Index:	Immediately Index:
Citation ½ Life:	8.1	Impact Factor:	3.858

From: jeff@piedmontpottery.com <jeff@piedmontpottery.com>
Sent: Monday, April 27, 2020 10:27 AM
To: Ge, Yue <Ge.Yue@epa.gov>
Subject: Re: Good morning. Jeff, a brief update

Hi Yue,
I'm happy that things have been going well for you. I agree to a 10% effort for myself on the paper.

Best wishes,
Jeff

Sent from myMail for iOS

From: Bruno, Maribel <Bruno.Maribel@epa.gov>
Sent: Monday, April 27, 2020 11:13 AM
To: Ge, Yue <Ge.Yue@epa.gov>
Subject: STAA Award

Hello Yue Ge:

Yes I agree with a 40% effort for the STAA award associated with the Chromium publication.

Thank you,
Maribel Bruno

Toxicology Letters 264 (2016) 59–70

Contents lists available at ScienceDirect

Toxicology Letters

journal homepage: www.elsevier.com/locate/toxlet

Proteomic responses of BEAS-2B cells to nontoxic and toxic chromium: Protein indicators of cytotoxicity conversion

Maribel Bruno, Jeffrey Ross, Yue Ge, Ph.D.*

Integrated Systems Toxicology Division, National Health and Environmental Effects Research Laboratory, U.S. Environmental Protection Agency, Research Triangle Park, NC 27711, USA

HIGHLIGHTS

- Integrative proteomics unraveled pathways critical to Cr (VI) toxicity.
- Novel proteins associated with Cr (VI) toxicity were identified.
- Toxic Cr (VI) affected glycolysis, oxidative stress, and proteasome pathways.
- Protein and pathways changes are sensitive indicators of chromium toxicity.

GRAPHICAL ABSTRACT

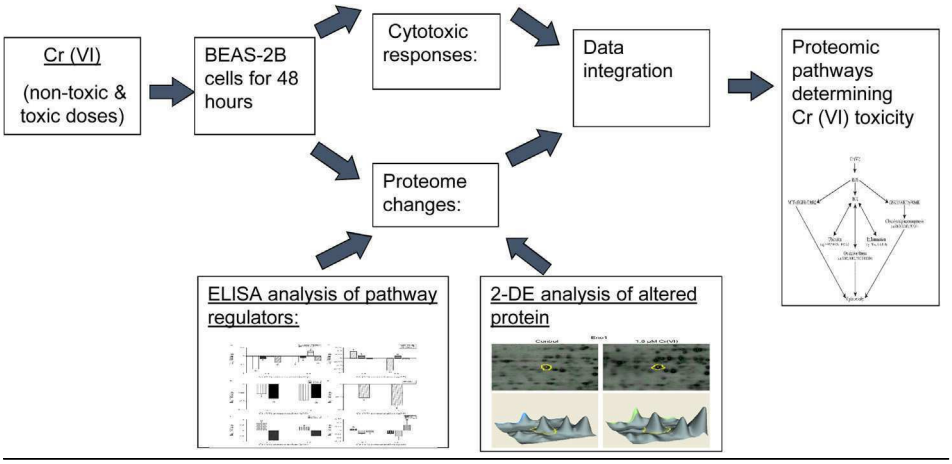

ARTICLE INFO

Article history:
Received 25 March 2016
Received in revised form 25 August 2016
Accepted 30 August 2016
Available online 31 August 2016

Keywords:
Chromium
Protein expression and phosphorylation
Proteomics
Cytotoxicity
Metals
ELISA
Pathways
Mode of action

ABSTRACT

Hexavalent chromium (Cr (VI)) is an environmental human carcinogen which primarily targets lungs. Among a variety of toxic mechanisms, disruption of biological pathways via translational and post-translational modifications represents a key mechanism through which Cr (VI) induces cytotoxicity and carcinogenesis. To identify those disruptions which are altered in response to cytotoxic Cr (VI) exposures, we measured and compared cytotoxicity and changes in expression and phosphorylation status of 15 critical biochemical pathway regulators in human BEAS-2B cells exposed for 48 h to a non-toxic concentration (0.3 μM) and a toxic concentration (1.8 μM) of Cr (VI) by ELISA techniques. In addition, 43 functional proteins which may be altered in response to pathway signaling changes were identified using two dimensional electrophoresis (2-DE) and mass spectrometry. The proteins and fold changes observed in cells exposed to the non-toxic dose of Cr (VI) (0.3 μM) were not necessarily the same as those found in the toxic one (1.8 μM). A subset of signaling proteins that were correlated with the cytotoxic responses of human BEAS-2B cells to Cr (VI) treatments were identified. These proteins include regulators of glycolysis, glycogen synthase kinase 3 beta (GSK3β) and phosphoprotein 70 ribosomal protein s6 kinase

Abbreviations: SOD2, superoxide dismutase 2; ENO1, Enolase 1; UBC, polyubiquitin; GSK3β, glycogen synthase kinase 3β; TNF-α, tissue necrotic factor alpha; MTF-1, metal regulatory transcription factor 1; PSMA2, proteasome α2; PSME1, proteasome activator subunit 1; LDHB, lactate dehydrogenase B; PGAM, phosphoglycerate mutase; TPI1, triosephosphate isomerase; ALDH1A1, aldehyde dehydrogenase 1A1; PRDX3, peroxiredoxin 3; PRDX4, peroxiredoxin 4; MT, metallothionein; p70S6K, phosphoprotein 70 ribosomal protein s6 kinase.

* Corresponding author.
E-mail address: ge.yue@epa.gov (Y. Ge).

http://dx.doi.org/10.1016/j.toxlet.2016.08.025
0378-4274/Published by Elsevier Ireland Ltd.

(p70S6K), a signaling protein associated with oxidative stress and inflammation responses, JNK and metal regulatory transcription factor 1 (MTF-1), and a source of ubiquitin for signaling targeted protein degradation, polyubiquitin C (UBC). In addition, two dimensional gel electrophoresis (2-DE) was applied to identify key alterations in biochemical pathways differentiating between cytotoxic and non-cytotoxic exposures to Cr (VI), including glycolysis and gluconeogenesis, protein degradation, inflammation, and oxidative stress.

Published by Elsevier Ireland Ltd.

1. Introduction

Chromium is an occupational and environmental hazard, and considered to be a human carcinogen (Leonard et al., 2004). It is widely used in industry, especially in painting, steel, and tanning. One of the primary routes of exposure of this metal is inhalation (Leonard et al., 2004). Two of the most common oxidative states of Cr are hexavalent Cr (VI) and trivalent Cr (III), of which Cr (VI) is more toxic (Katz and Salem, 1993). At the DNA level, Cr (VI) induces DNA damage through the formation of Cr-DNA adducts (Zhitkovich, 2011), formation of oxidative DNA damage (Arakawa et al., 2012), and modification of gene methylation status (Nigam et al., 2014). At the RNA level, Cr (VI) induces immune responses, cell growth, and apoptosis through the changes of mRNA expression levels such as the up-regulation of p53 (Quinteros et al., 2008; Permenter et al., 2011; Madejczyk et al., 2015) and Gadd45a (Wu et al., 2012), and down-regulation of glutathione peroxidase in response to oxidative stress (Andrew et al., 2003). At the metabolic levels, Cr (VI) alters cell glycolysis by changing the metabolic rate of carbohydrates (Raghunathan et al., 2010; Sundaram et al., 2012; Pan et al., 2012), which can induce glycolytic enzymes such as M2 pyruvate kinase, phosphoglycerate kinase 1, and enolase α in lung (Lei et al., 2008).

A proteomics study (Pan et al., 2012) associated Cr (VI) exposure with disrupted calcium homeostasis and liver toxicity such as infiltration of mononuclear cells. The induction of p53 and its targets, bax, p21, puma, Gadd45 and apoptosis were also associated with Cr (VI) exposure (Lei et al., 2008). During carcinogenesis, Cr (VI) can stimulate tumor cell growth by inducing signaling proteins including ErbB2 and EGFR (Castorina et al., 2008; Kim et al., 2015), HIF-1α, a subunit of HIF1 transcription factor (Ding and Shi, 2002), and AKT (Beaver et al., 2009). Cr (VI) can also influence post-translational modifications such as phosphorylation of p53 and H2AX (Wang and Shi, 2001; DeLoughery et al., 2015), and biotinylation and acetylation of histone proteins (Xia et al., 2014). Among a variety of toxic mechanisms, disruption of protein function and concomitant biochemical pathways represents a key mechanism through which Cr (VI) induces cytotoxicity and carcinogenesis.

To some extent, induction of cytotoxicity is a result of interactions among multiple biochemical pathways and proteins involved in the pathways from the perspective of proteomics. The present study is to identify key proteomic responses of BEAS-2B cells to Cr (VI) exposures that are critical to the conversion of the cells from nontoxicity to toxicity ones, including the critical toxicity pathways and protein indicators of cytotoxicity conversion. For this, BEAS-2B cells were treated with Cr (VI) at the concentrations of 0.3 μM, a nontoxicity dose and 1.8 μM, low toxicity dose respectively. The critical proteomic responses were characterized by measuring protein expression and phosphorylation changes of 15 upstream toxicity pathway regulators using ELISA and identifying downstream differentially expressed proteins using 2-DE in Cr (VI)-treated BEAS-2B cells. Our hypothesis was that critical protein pathway alterations induced by Cr (VI) that lead to cytotoxicity conversion could be detected as significant changes in protein expression and post-translational modifications. To this end, the alterations in protein expression and phosphorylation identified by both ELISA and 2-DE were correlated with cytotoxicity. Utilization of this integrated proteomic approach, we identified a small subset of signaling proteins and biochemical pathways that are critical to cytotoxic responses and cytotoxicity induction for the first time. This approach also led to the identification of 12 proteins that were not previously associated with Cr (VI) exposure and toxicity as well.

2. Materials and methods

2.1. Materials

BEAS-2B cells were purchased from American Type Culture Collection (Rockville MD, USA). Trypsin Gold (MS-grade) was obtained from Promega (Madison, WI, USA). Dithiothreitol (DTT) was purchased from Bioanalytical (Natick, MA, USA). CyDyes (Cy3, Cy2 and Cy5), Typhoon 9410 scanner, non-linear immobilized pH gradient (IPG) strips (pH 3–11), Ettan IPGPhor™ apparatus, Decyder software, and 2D Image Quant (version 5.1) were manufactured by GE Healthcare (Piscataway, NJ, USA). Methanol (HPLC grade) and glacial acetic acid were purchased from Fisher Scientific (Fair Lawn, NJ, USA). Protean II apparatus was a product from Bio-Rad (Hercules, CA, USA). Protease/phosphatase inhibitors were purchased from Calbiochem (San Diego, CA, USA). IPA Software is a product from Ingenuity Systems (Redwood City, CA, USA). LHC-9 medium, HEPES buffer, saline solution (HBSS) and trypsin neutralizing solution (TNS) were obtained from Lonza (Walkersville, MD, USA). Versene, TrypLE™, Dulbecco's phosphate buffer solution (DPBS) and Sypro Ruby stain were obtained from Life Technologies (Carlsbad, CA, USA). Precast 8–16% gradient polyacrylamide gels were from Jule, Inc (Milford, CT, USA). The Akt, Human Proinflammatory-9 Plex, HIF-1α, Apoptosis, MAPK and EGFR ELISA kits for measurement of protein changes at expression and phosphorylation levels in the treated BEAS-2B cells were from Meso Scale Discovery (Gaithersburg, MD, USA). The human MTF1 kit (Cat. No. MBS928631) was from MyBiosource (San Diego, CA, USA). Trypan blue, neutral red and all other chemicals were obtained from Sigma-Aldrich (St. Louis, MO, USA).

2.2. Treatment of BEAS-2cells with Cr (VI) and cytotoxicity assays

BEAS-2B cells were cultured in LHC-9 medium and treated with 0.3 or 1.8 μM Cr (VI) and incubated for 48 h at 37 °C and 5% CO_2 before harvest from 96-well plate for measurements of cytotoxicity using a neutral red assay and from 150 mm flasks for analysis of protein expression and phosphorylation changes using multiplexed ELISA and 2-DE analysis of protein expression and phosphorylation changes. To determine which time points and doses would be optimal to proteomic and cytotoxicity studies, multiple Cr (VI) doses such as 0, 0.1, 0.3, 1.0, 1.8, 3.0, 4.2, 5.6 and 10 μM were used to treat BEAS-2B cells for 24 and 48 h, respectively. The treatments resulted in 100, 100, 100, 77, 25.5, 6.0, 2.9, 1.4 and 0.4% survival rate, correspondingly. This led us to choose 0.3 and 1.8 μM of Cr (VI) as nontoxic and toxic dose of Cr (VI) for this study. In addition, we also performed 2-DE on BEAS-2B

cells exposed to Cr (VI) for 24 and 48 h to determine the optimal time for proteomic analysis. Our results showed that very few protein changes were observed when the 24 h treatment was performed. Therefore, 48 h exposure was used for this study. Relative cell survival was calculated as the ratio of living cells after exposure to Cr (VI) divided by the number of living cells in untreated controls (Ge et al., 2015). Samples were analyzed in triplicates. A *t*-test was performed to determine statistical significance in cell survival rates or cytotoxicity between control and treated BEA–2 B cells ($P < 0.05$).

2.3. Isolation of total proteins from BEAS-2 cells for 2-DE gel electrophoresis

After the removal of the control and treated BEAS-2B cells from the incubator, 10 ml of ice-cold washing buffer (250 mM sucrose/10 mM Tris solution (pH 7.4)) were added to the cell cultured dishes. Cells were then scraped off from the dishes, transferred to 15 ml conical tubes, and centrifuged at 1300 × *g* for 5 min at 4 °C and washed three times by suspending in ice-cold washing buffer. Cells were then centrifuged at 1300 × *g* for 10 min, and lysed in 0.5 ml of 2-DE sample buffer containing 30 mM Tris (pH 8.8), 2 M urea, 7 M thiourea, 4% CHAPS (w/v), 0.5% Triton X-100, and 10 μl protease/phosphatase inhibitor cocktail. The samples were sonicated for 10 s at a constant duty cycle of 20%, with a 30 s interval (Ultrasonic homogenizer 150 V/T, Biologics, Inc., Manassas, VA). The sonicated cell lysates were then placed on ice for one hour and centrifuged for 5 min at 14,000 × *g*. The supernatants containing total proteins were used for 2-DE analysis. The protein concentration was determined using the 2D Quant kit from GE Healthcare (Ge et al., 2011).

2.4. Protein labeling, 2-DE electrophoresis, and MS analysis

To determine how protein changes may actually lead to the cytotoxic outcome and toxicity pathway alterations, we also analyzed protein expression profiles in the treated BEAS-2B cells using difference in gel electrophoresis as previously described (Ge, Y. el al., 2011). Briefly, each CyDye was mixed with 50 μg of protein sample, and the pooled protein samples were diluted further in the sample buffer (7 M urea, 2 M thiourea, 2%w/v CHAPS, 1% IPG, 13 mM DTT) to the volume of 340 μl for 2-DE analysis. All samples were normalized to the same total protein concentration. Triplicate gels from control and treated protein samples were run. First dimension IEF was carried out in an Ettan IPGphor and precast IPG strips (18 cm, pH 3–11 nonlinear) were employed for the first dimension separation at 20 °C. The proteins in IPG strips were reduced and alkylated by sequential incubation in the equilibration buffer (0.05 M Tris–HCl, pH 8.8, 2% SDS; 30% glycerol, 6 M urea, 0.002% bromophenol blue) plus 0.3 g DTT/10 ml of equilibration buffer for 15 min, and then the equilibration buffer containing 0.9 g/10 ml iodoacetamide for 15 min incubation before the second dimensional electrophoresis. The second dimension SDS-PAGE was performed overnight at 80 V and 4 °C. The resulting 2-DE gels were scanned using a Typhoon 9410 scanner. 520, 580, and 670 nm band pass were used for the scanning of protein samples labeled with Cy2, Cy3, and Cy5 dyes. The scanned 2-DE gel images were imported into Decyder software version 6 for protein quantitation analysis. Protein spots showing greater than 1.2-fold increase or decrease, and with a p value < 0.05 (*t*-test) were selected for protein identification by mass spectrometry (MS). .For the purpose of protein identification using MS, an additional 2-DE gel stained with Sypro-Ruby was run. Briefly, differentially expressed proteins were excised from the gel, digested with trypsin, and analyzed using MS for protein identification. Briefly, gel plugs were de-stained twice using 100 μl of 200 mM ammonium bicarbonate (AMBIC) and 40% (v/v) acetonitrile (ACN), and then 25 mM AMBIC in 50% (v/v) ACN. The de-stained gel plugs were dehydrated using 50 μl of ACN and then dried in vacuum evaporator (Centrivap, Labconco), rehydrated using 10 μl of Proteomics Grade trypsin, and the digested and released protein peptides was desalted using C18 Zip tips (Millipore, Billerica, MA), and spotted onto a stainless steel MALDI plate for MALDI-MS/MS analysis. Proteins were identified using a 4800 MALDI TOF/TOF mass spectrometer (Applied Biosystems, Foster City, CA). MALDI-MS/MS sequencing and the final protein identification was done using Protein Pilot 3.0 software, searching against the human (Homo sapiens) sub-database of the SwissProt protein database (http://expasy.org/sprot/). Mass-selected MALDI-MS/MS spectra acquisition was performed to further increase protein sequence coverage. The reported proteins were identified based on a minimum of two unique MS/MS peptide sequence identifications characterized by the software confidence parameter of 95-99%.

2.5. Pathway and network analysis

After protein identification, the accession numbers and fold changes of the differentially expressed proteins were tabulated in Microsoft Excel and imported into IPA for biological function, molecular function, canonical pathway, and toxlist analyses. The toxlist in IPA reveals biological mechanisms that are related to toxicity on a molecular, cellular, and biochemical level. The statistical significance of each pathway or list was determined by IPA using a Fisher Exact test ($p < 0.05$). In this method, the *p*-value for a given process annotation is calculated by considering the number of identified proteins that participate in that process and the total number of proteins that are known to be associated with that process in the selected reference set. IPA was also used to construct networks of interacting proteins using its database of current knowledge available on genes, proteins, chemicals, normal cellular and disease processes, signaling, and metabolic pathways.

2.6. Multiplex ELISA for measurement of changes at expressions and phosphorylation levels of the 21 pathway regulators

Extraction of total proteins from the control and Cr (VI)-treated BEAS-2B cells, and ELISA assays using MSD Multi-Array kits were performed according to the manufacturer's instructions (Meso Scale Discovery, Gaithersburg, MD). These multiplex ELISA assays allow simultaneous assessment of panels of functionally related proteins. The assays used included the AKT Signaling Assay panel (Cat. No. K1511D-1), which measures phosphorylated AKT (ser473), phosphorylated p70S6K (Thr421/Ser424) and GSK-3β (Ser9), the Human Proinflammatory Cytokine panel (Cat No. K15007B-1), which measures GM-CSF, IFN-ν, IL-1β, IL-2, IL-12p70, IL-6, IL-8, and Tissue necrotic factor alpha (TNF-α), the EGFR Family panel (Cat. No. K15106D-1, which measures EGFR, ErbB2 and IGF-1R), Apoptosis panel (Cat. No. K15106D-1, which measures cleaved PARP (Asp214), cleaved Caspase-3 (Asp175), phospho-p53 (Ser15), and total p53), MAP Kinase Phosphoprotein panel (Cat. No. K15101A-3), which measures Phospho-p38 (Thr180/Tyr182), Phospho-ERK1/2 (Thr202/Tyr204; Thr185/Tyr187), Phospho-JNK (Thr183/Tyr185), and HIF-1α (Cat. No. C11DK-1). The ELISA assays were performed in triplicate. Briefly, 96-well plates were first blocked with the supplied blocking solution, washed either in supplied Tris wash buffer or in phosphate buffered saline containing 0.05% Tween 20 (for cytokine assay only). The plates were blotted dry, and the extracted protein samples were then added. For all the ELISA assays, with the exception of the cytokine assay, protein samples were diluted in appropriate lysis buffer to the concentration of 0.4 or 0.8 μg/μl, depending on the assays. For the cytokine assay, the

protein concentration ranged from 0.74 to 2.16 μg/μl. All samples were normalized to the same total protein concentration. After the incubation with the corresponding primary antibodies that were localized in arrays at the bottom of the 96-wells, the wells were then washed and the corresponding secondary antibody solutions were then added. After the incubation with the secondary antibody, the wells were washed and the Read Buffer was added. The ELISA signals were recorded using the MSD Sector Imager 2400 and analyzed using Discovery Workbench 2006 software (Meso Scale Diagnostics, Gaithersburg, MD) (Ge et al., 2015).

2.7. ELISA for metal regulatory transcription factor 1 (MTF-1)

Media was removed from cells and cells were rinsed with ice-cold PBS (pH 7.4). Cells were scraped and centrifuged for 5 min at 5000 × *g* at 2–8 °C. The supernatant was collected and stored at −80 °C. The 2D quant kit was used to accurately measure protein concentration in samples to be analyzed by 2-DE. Three μg of proteins were used for this assay. Standards were diluted according to manufacturer's specifications. One hundred μl of standard or sample were used per well and incubated for 2 h at 37 °C. The liquid was removed and 100 μl of biotin-avidin (1×) were added to each

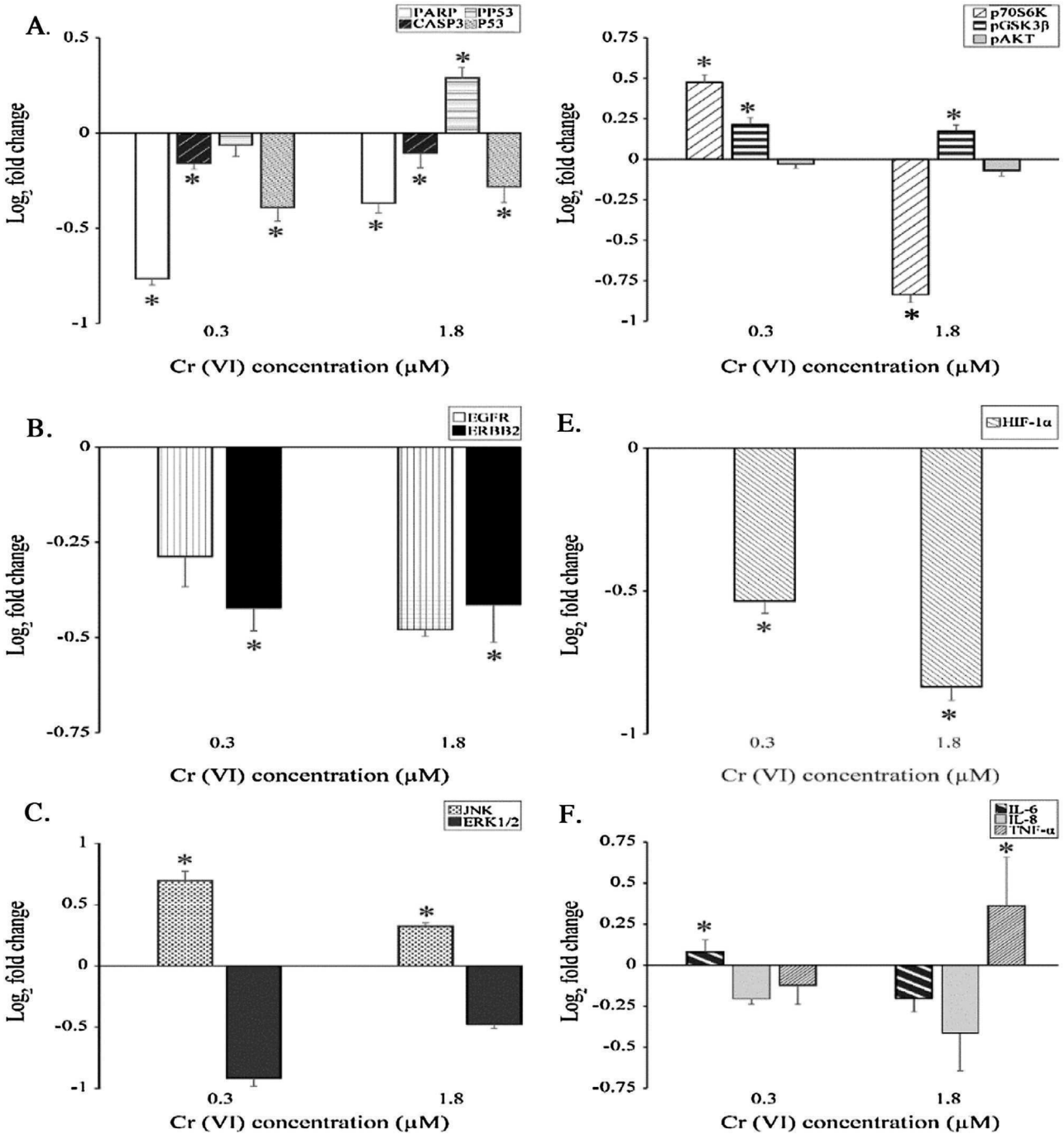

Fig. 1. Changes in protein expression of the 15 pathway regulators induced by Cr (VI). Panel A: Apoptosis panel proteins cleaved PARP, cleaved caspase-3, p53, pp53; Panel B: Two cell growth panel proteins EGFR and ErbB2; Panel C: MAP Kinase panel proteins JNK and ERK1/2; Panel D: phosphorylated p70S6K, GSK3β, and AKT; Panel E: HIF-1α; Panel F: IL-6, IL-8 and TNF-α. X-axis is Cr (VI) concentrations (μM). Y-axis: $\log_2$ relative-fold change of expression and/or phosphorylation levels ± STD compared to untreated controls measured using multiplexed ELISA.

well. Wells were aspirated and washed with buffer 3 times. One hundred μl of HRP-avidin (1x) were added to each well and wells covered and incubated for 1 h at 37 °C. The wash procedure was repeated once more. TMB (3, 3′,5, 5′ tetramethylbenzide) substrate was added to each well and incubated for 15 min at 37 °C in the dark. Fifty μl of stop solution were added and the plate was gently tapped to ensure thorough mixing. The optical density was measured at 450 nm to assess expression of MTF-1 in all samples. Sample MTF-1 concentrations were calculated by comparing to a standard dilution curve of known MTF-1 protein amounts. Samples were run in triplicate.

3. Results

3.1. Overview of responses of cytotoxicity and 21 pathway regulating proteins to Cr (VI) treatment

Exposure of BEAS-2B cells to 0.3 and 1.8 μM Cr (VI) resulted in relative survivals of 100 and 77% survival rate, respectively, when compared to control. They were considered to be nontoxic and toxic exposures, respectively. Fifteen proteins were deregulated, eleven of which were significantly altered at the level of expression or phosphorylation in BEAS-2B cells treated with Cr (VI) at both of the concentrations tested, with $\log_2$ fold-changes ranging from −0.91 to 0.475 (Fig. 1). The down-regulated proteins included EGFR, ErbB2, cleaved-PARP, cleaved caspase-3, pAKT, IL-8, ERK1/2 and HIF-1α. The up-regulated proteins at both concentrations of Cr (VI) were pJNK and pGSK3β. The protein p70S6K was upregulated in cells exposed to 0.3 μM of Cr (VI). In addition, phosphorylated p53 and TNF-α showed similar pattern of expression. They were downregulated in BEAS-2B cells treated with 0.3 μM Cr (VI) and upregulated in cells treated with 1.8 μM Cr (VI). In contrast, IL-6 was slightly upregulated in BEAS-2B cells treated with 0.3 μM of Cr (VI) and downregulated in cells treated with 1.8 μM.

3.2. Identification of differentially expressed proteins in BEAS-2cells treated with Cr (VI) using 2-DE

In addition to the analysis of responses of 15 key signaling proteins regulating metal toxicity pathways, we also investigated novel changes at expression levels of proteins in BEAS-2B cells treated with 0.3 and 1.8 μM Cr (VI) using 2-DE (Fig. 2) and mass

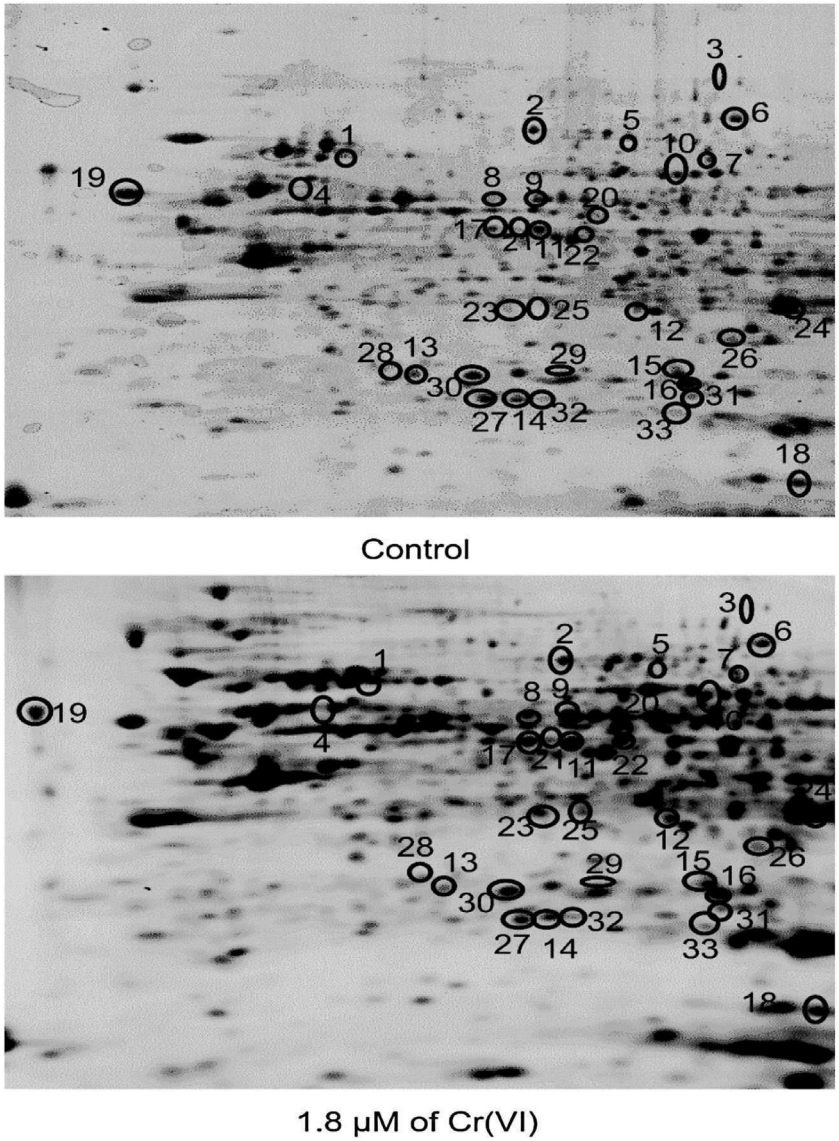

Fig. 2. Representative 2-DE gel images of control and BEAS-2 B cells treated with 1.8 μM of Cr (VI). Fifty micrograms of each protein sample was subjected to 2-DE. Gels were run in triplicate. A *t*-test with a p value < 0.05 was considered statistically significant. Differentially expressed proteins identified were listed in Tables 1a and 1b.

spectrometry. A total of 53 proteins were found to be significantly ($p < 0.05$) altered, at both concentrations of Cr (VI). Forty three proteins were identified by MS from BEAS-2B cells treated with Cr (VI) at two different concentrations (Tables 1a and 1b). Of the identified proteins, 7 proteins were up-regulated in BEAS-2B cells exposed to Cr (VI) and 3 down-regulated in BEAS-2B cells exposed to 0.3 μM of Cr (VI) (Table 1a), whereas 22 were upregulated and 11 downregulated in BEAS-2B cells exposed to 1.8 μM of Cr (VI) (Table 1b). Two proteins, alpha enolase (ENO1) and phosphoglycerate mutase (PGAM1) were increased when compared to controls. As compared to the control, ENO1 expression was increased 1.27 and 1.97 fold in BEAS-2B cells treated with 0.3 and 1.8 μM of Cr (VI), respectively and the fold changes were significant ($p < 0.05$). Since the two dose points were also significant, ENO1 showed a dose response effect with a P value of 0.03. As compared to the control, PGAM1 expression was significantly increased 1.17 and 1.24 fold in BEAS-2B cells exposed to 0.3 and 1.8 μM of Cr (VI), respectively. In addition, 12 differentially expressed proteins identified from this study were found to be associated with Cr (VI) exposure and toxicity for the first time. These proteins were acetylco A acetyl transferase, septin 2, Rab11A, heterogeneous nuclear ribonucleoprotein K, phosphoglycerate mutase 1, isocitrate dehydrogenase, purine nucleoside phosphorylase, 26 s proteasome regulatory subunit 7, proteasome activator complex subunit 1, proteasome subunit alpha 2, tar DNA binding protein 45, and histone H2B.

3.3. Mapping differentially expressed proteins to canonical pathways and toxlists

IPA software was applied to map 43 differentially expressed proteins identified from BEAS-2B cell treated with Cr (VI) at 0.3 and 1.8 μM to predefined molecular functions, diseases, canonical pathways, and toxlists. It was our hypothesis that cellular pathway alterations induced by Cr (VI) that lead to cytotoxicity could be detected as significant changes in protein expression or post-translational modifications. As shown in Table 2, the highest ranked molecular function for 0.3 μM, a nontoxic concentration of Cr (VI), is small molecule biochemistry, but is free radical scavenging for 1.8 μM, a toxic concentration of Cr (VI). This suggests functions associated with small molecules, i.e. metabolism of indole, rather than bigger molecules such as DNA and proteins, are related to a non-toxic dose of Cr (VI). Generation of free radicals and activation of antioxidant systems is a key cytotoxic response of BEAS-2B cells to toxic concentrations of Cr (VI). This result is consistent with the toxlist analysis results in which the top toxlist associated with Cr (VI)-induced toxicity in

Table 1a
List of differentially expressed proteins identified from BEAS-2B cells treated with 0.3 μM of Cr (VI).

Spot #	Abbreviation	Protein ID	Fold change	Accession #	pI	MW (KDa)	Matched peptides	% coverage	P value
1	ACAT2	Acetylco A acetyltransferase cytosol	1.19	B7Z233	8.8	44.61	2	4.5	3.00E − 04
2	ENO1	Alpha-enolase	1.27	P06733	6.99	47.01	5	18.2	1.00E − 16
3	GRP78	78 kDa glucose-regulated protein	−1.24	P11021	5.01	70.44	15	28.9	1.00E − 30
4	Sep-02	Isoform 2 of Septin-2	−1.21	Q15019	6.15	41.46	8	27	2.00E − 10
5	HSD17B10	3-hydroxyacyl-CoA dehydrogenase type-2	1.18	Q99714	7.87	26.78	10	55.6	1.00E − 20
6	H2B1M	Histone H2B	1.2	Q99879	10.32	13.82	5	38.9	6.00E − 10
7	RAB11A	Ras related protein Rab -11A	1.33	P62491	6.14	23.89	3	13.9	2.00E − 06
8	PGAM1	Phosphoglycerate mutase	1.17	P18669	6.8	28.66	2	8.3	1.00E − 04
9	PSMC2	26s protease regulatory subunit 7	1.21	P35998	5.7	48.47	10	26.3	1.00E − 20
10	PNP	purine nucleoside phosphorylase	−1.21	P00491	6.5	32.1	9	37.7	1.00E − 18
1	HSC70	Heat shock 70 kDa protein 1A/1B	1.36	P08107	5.48	69.87	6	11	1.00E − 12
2	LMNA	Prelamin-A/C	−1.22	P02545	6.57	73.76	14	28	2.00E − 28
3	EEF2	Elongation factor 2	−1.22	P13639	6.42	95.14	13	14	1.00E − 26
4	HNRNPK	Heterogeneous nuclear ribonucleoprotein K	−1.25	Q5T6W5	5.39	50.97	5	17	2.00E − 10
5	TF	Serotransferrin	−1.27	P02787	6.7	75.14	5	8	1.00E − 10
6	ACO2	Aconitate hydratase, mitochondrial	−1.17	Q99798	6.85	82.37	15	30	3.00E − 30
7	PCK2	Phosphoenolpyruvate carboxykinase [GTP], mitochondrial	−1.24	Q16822	6.58	67.05	4	7	4.00E − 08
8	HNRNPH1	Heterogeneous nuclear ribonucleoprotein H	1.71	P31943	5.89	49.19	4	13	2.00E − 08
9	ALDHA1	Retinal dehydrogenase 1	1.67	P00352	6.29	54.69	5	17	3.00E − 10
10	HNRNPL	Heterogeneous nuclear ribonucleoprotein L	−1.15	P14866	8.46	64.13	5	9	2.00E − 10
11	ENO1	Alpha-enolase	1.97	P06733	6.99	47.04	5	18	1.00E − 10
12	LASP1	Isoform 2 of LIM and SH3 domain protein	1.36	Q14847	6.61	29.69	4	11	1.00E − 08
13	PRDX4	Peroxiredoxin-4	−1.15	Q13162	5.54	26.55	8	35	1.00E − 16
14	PARK7	Protein DJ-1	1.31	Q99497	6.32	19.88	7	49	1.00E − 14
15	PGAM1	Phosphoglycerate mutase 1	1.24	P18669	6.75	28.65	10	53	1.00E − 20
16	TPI1	Triosephosphate isomerase	1.2	P60174	5.65	30.79	10	52	1.00E − 20
17	ANXA1	Annexin A1	2.04	P04083	6.64	38.56	13	40	1.00E − 26
18	PPIA	Peptidyl-prolyl cis-trans isomerase A	1.16	P62937	7.82	17.87	7	35	1.00E − 14
19	CALR	Calreticulin	−1.17	P27797	4.29	46.43	10	25.9	1.00E − 20
20	LAP3	Cytosol aminopeptidase	1.56	P28838	8.03	56.13	10	23.3	2.00E − 20
21	PCBP1	Poly(rC)binding protein 1	1.28	Q15365	6.66	37.47	2	9	1.00E − 04
22	SEPT11.	Septin 11	1.38	Q9NVA2	6.38	49.24	10	26.1	1.00E − 20
23	IDH3A	Isocitrate dehydrogenase [NAD]subunit α	1.57	P50213	5.71	36.62	5	16.7	1.00E − 10
24	ANXA2	Annexin A2	−1.2	P07355	7.56	38.45	11	36.3	1.00E − 22
25	LDHB	L lactate dehydrogenase B chain	1.77	P07195	5.72	36.48	9	26.9	3.00E − 18
26	ETF1	Electron transfer flavoprotein subunit α	−1.16	P13804	8.62	35.08	4	17.1	1.00E − 08
27	PRDX3	Peroxiredoxin 3	1.27	P30048	7.69	22.69	6	10.1	1.00E − 10
28	PSME1	Proteasome activator complex subunit 1	1.41	Q06323	5.78	28.71	6	26.5	1.00E − 12
29	UQCRFS1	Cytochrome b-c1 complex subunit Rieske	1.43	P47985	8.55	29.68	3	10.6	1.00E − 06
30	HSPB1	HSPB1	1.47	P04792	5.98	22.77	6	17.2	1.00E − 13
31	PSMA2	Proteasome subunit alpha type 2	1.21	P25787	7.12	25.75	4	26.9	2.00E − 08
32	TARDBP	TAR DNA binding protein 43	1.37	Q13148	5.85	44.72	3	9.4	1.00E − 06
33	SOD2	Superoxide dismutase	1.56	P04179	6.86	22.19	7	27	2.40E − 13

Table 1b
List of the differentially expressed proteins identified from BEAS-2B cells treated with 1.8 μM of Cr (VI).

Spot #	Abbreviation	Protein ID	Fold change	Accession #	pI	MW (KDa)	Matched peptides	% coverage	P value
1	HSC70	Heat shock 70 kDa protein 1A/1B	1.36	P08107	5.48	69.87	6	11	1.00E − 12
2	LMNA	Prelamin-A/C	−1.22	P02545	6.57	73.76	14	28	2.00E − 28
3	EEF2	Elongation factor 2	−1.22	P13639	6.42	95.14	13	14	1.00E − 26
4	HNRNPK	Heterogeneous nuclear ribonucleoprotein K	−1.25	Q5T6W5	5.39	50.97	5	17	2.00E − 10
5	TF	Serotransferrin	−1.27	P02787	6.7	75.14	5	8	1.00E − 10
6	ACO2	Aconitate hydratase, mitochondrial	−1.17	Q99798	6.85	82.37	15	30	3.00E − 30
7	PCK2	Phosphoenolpyruvate carboxykinase [GTP], mitochondrial	−1.24	Q16822	6.58	67.05	4	7	4.00E − 08
8	HNRNPH1	Heterogeneous nuclear ribonucleoprotein H	1.71	P31943	5.89	49.19	4	13	2.00E − 08
9	ALDHA1	Retinal dehydrogenase 1	1.67	P00352	6.29	54.69	5	17	3.00E − 10
10	HNRNPL	Heterogeneous nuclear ribonucleoprotein L	−1.15	P14866	8.46	64.13	5	9	2.00E − 10
11	ENO1	Alpha-enolase	1.97	P06733	6.99	47.04	5	18	1.00E − 10
12	LASP1	Isoform 2 of LIM and SH3 domain protein	1.36	Q14847	6.61	29.69	4	11	1.00E − 08
13	PRDX4	Peroxiredoxin-4	−1.15	Q13162	5.54	26.55	8	35	1.00E − 16
14	PARK7	Protein DJ-1	1.31	Q99497	6.32	19.88	7	49	1.00E − 14
15	PGAM1	Phosphoglycerate mutase 1	1.24	P18669	6.75	28.65	10	53	1.00E − 20
16	TPI1	Triosephosphate isomerase	1.2	P60174	5.65	30.79	10	52	1.00E − 20
17	ANXA1	Annexin A1	2.04	P04083	6.64	38.56	13	40	1.00E − 26
18	PPIA	Peptidyl-prolyl cis-trans isomerase A	1.16	P62937	7.82	17.87	7	35	1.00E − 14
19	CALR	Calreticulin	−1.17	P27797	4.29	46.43	10	25.9	1.00E − 20
20	LAP3	Cytosol aminopeptidase	1.56	P28838	8.03	56.13	10	23.3	2.00E − 20
21	PCBP1	Poly(rC)binding protein 1	1.28	Q15365	6.66	37.47	2	9	1.00E − 04
22	SEPT11.	Septin 11	1.38	Q9NVA2	6.38	49.24	10	26.1	1.00E − 20
23	IDH3A	Isocitrate dehydrogenase [NAD]subunit α	1.57	P50213	5.71	36.62	5	16.7	1.00E − 10
24	ANXA2	Annexin A2	−1.2	P07355	7.56	38.45	11	36.3	1.00E − 22
25	LDHB	L lactate dehydrogenase B chain	1.77	P07195	5.72	36.48	9	26.9	3.00E − 18
26	ETF1	Electron transfer flavoprotein subunit α	−1.16	P13804	8.62	35.08	4	17.1	1.00E − 08
27	PRDX3	Peroxiredoxin 3	1.27	P30048	7.69	22.69	6	10.1	1.00E − 10
28	PSME1	Proteasome activator complex subunit 1	1.41	Q06323	5.78	28.71	6	26.5	1.00E − 12
29	UQCRFS1	Cytochrome b-c1 complex subunit Rieske	1.43	P47985	8.55	29.68	3	10.6	1.00E − 06
30	HSPB1	HSPB1	1.47	P04792	5.98	22.77	6	17.2	1.00E − 13
31	PSMA2	Proteasome subunit alpha type 2	1.21	P25787	7.12	25.75	4	26.9	2.00E − 08
32	TARDBP	TAR DNA binding protein 43	1.37	Q13148	5.85	44.72	3	9.4	1.00E − 06
33	SOD2	Superoxide dismutase	1.56	P04179	6.86	22.19	7	27	2.40E − 13

Table 2
Comparisons of the top diseases and disorders, molecular and cell functions, canonical and toxicity pathways identified using IPA analysis of differentially expressed proteins in BEAS-2B cells treated with 0.3 and 1.8 μM of Cr (VI). Only the top ranking one, two, or three identifiers in each category were chosen for this table based on two criteria: IPA's results from a Fisher exact test ($p < 0.05$) and thorough evaluation of previous publications on Cr (VI).

	0.3 μM	1.8 μM
Top Diseases and Disorders	Metabolic disease	Cancer
Top Molecular and Cell functions	Small molecule biochemistry	Free radical scavenging
Top Canonical Pathways	Glycolysis/gluconeogenesis	Glycolysis/gluconeogenesis
	Fatty acid metabolism	Protein ubiquitination pathway
	Lysine degradation	Pyruvate metabolism
Top Toxicity Pathways	Fatty acid metabolism	Oxidative stress
	Cholesterol biosynthesis	Mitochondrial dysfunction

BEAS-2B cells treated with 1.8 μM of Cr (VI) was oxidative stress. Toxlists unravel biological mechanisms that relate to toxicity on a molecular, cellular and biochemical level. Cancer is the highest ranking associated disease identified by IPA. Canonical pathway and toxlist analyses indicated oxidative stress, glycolysis and gluconeogenesis, pyruvate based energy metabolism, and protein ubiquitination/degradation were some of the five highest ranking canonical pathways/toxlist affected by Cr (VI) at the toxic dose.

3.4. Mapping differentially expressed proteins to networks of inter-relationships

The protein network generated by IPA shows the interrelationships between the differentially expressed proteins identified from 2-DE in the present study and other signaling molecules known to interact with them. Fig. 3A is a representative protein network of inter-relationships identified from BEAS-2B cells treated with 0.3 μM of Cr (VI). Fig. 3B is the result of merging two networks showing interrelationships identified from cells treated with 1.8 μM of Cr (VI). As shown in Fig. 3A, UBC is the main hub in the protein network of BEAS-2B cells treated with 0.3 μM of Cr (VI). Clusters of proteins belonging to the RAB11 and the septin families and proteins involved in protein ubiquitination via Proteasome 19S and in glycolysis/gluconeogenesis are circled. The network in Fig. 3B shows clusters of proteins in 26S Proteasome, the RNA binding heteronuclear ribonucleoprotein P (HNRNP) protein family, the Glycolysis/gluconeogenesis pathway, the oxidative stress pathway, and members of the septin family which are circled. The alteration of 26S Proteasome is aligned with one of the top canonical pathways altered by this concentration of Cr (VI) (Table 2) (protein ubiquitination) (Fig. 3B). We found three hubs, the main one being UBC and the minor ones include JNK and NFKB shown in small circles. JNK, which showed to be phosphorylated by ELISA, was associated with oxidative stress proteins and the proteasome pathway, indicated by arrows. Peroxiredoxin 4 (PRDX4) and superoxide dismutase 2 (SOD2) proteins act on JNK

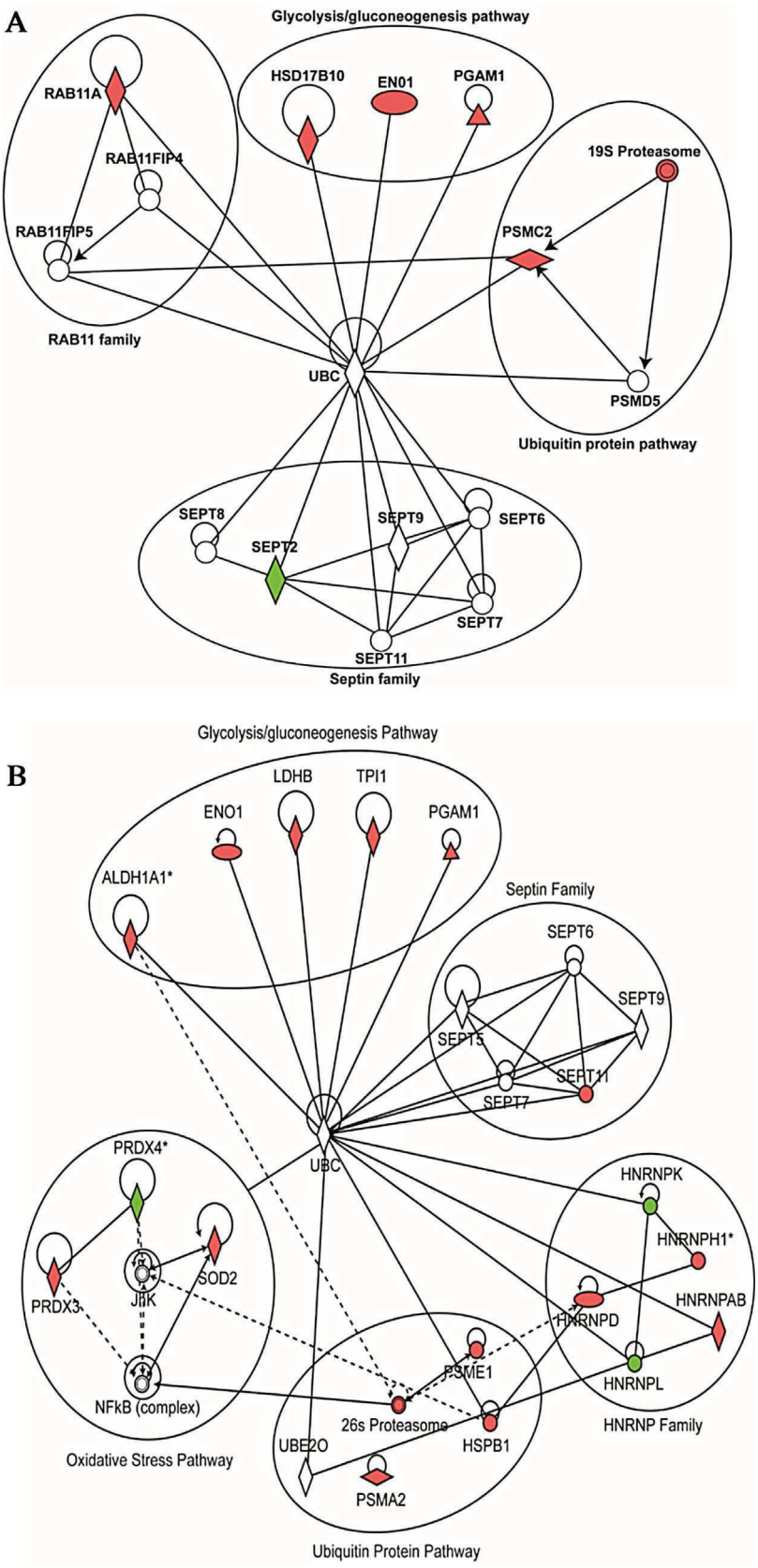

Fig. 3. Networks of proteins showing inter-relationships and pathways which were obtained using IPA. A) The highest ranking network of some differentially expressed proteins identified from BEAS-2B cells treated with 0.3 μM of Cr (VI). B) Merged Networks 1 and 2 of some differentially expressed proteins identified from BEAS-2B cells treated with 1.8 μM of Cr (VI). Solid lines represent direct interactions between molecules; dotted lines represent indirect interactions. Lines connecting the proteins in networks indicate known interrelationships found in the IPA database. Proteins in red were up-regulated and proteins in green were down-regulated in our data set. Molecules labeled in green were downregulated by Cr (VI) exposure; those labeled in red were upregulated. The shapes of nodes in the networks delineate a function: ◇: Enzyme; ⬭: chemical or drug; △: phosphatase; ○: others.

shown by arrows. NFKB, in addition to JNK, linked to oxidative stress proteins, regulates expression of TNFα, induced in our study. Lines connecting the proteins in networks indicate known interrelationships found in the IPA database. Proteins in red were up-regulated and proteins in green were down-regulated in our data set.

3.5. Cr (VI) decreased metal regulatory transcription factor-1 (MTF-1) protein expression

MTF-1 plays important roles in regulating metal-mediated oxidative stress. We, therefore, investigate MTF-1 expression levels in Cr (VI)-treated BEAS-2B cells. As shown in Fig. 4, MTF-1 expression levels were significantly decreased in BEAS-2B cells treated with Cr (VI) at both concentrations of 0.3 and 1.8 μM.

4. Discussion

The overall protein and pathway responses to nontoxic and toxic Cr (VI) treatments were compared to identify key proteome changes that are critical to Cr (VI) toxicity. Proteomic analysis of BEAS-2B cells treated with 1.8 μM of Cr (VI) enabled us to identify the significant effects of Cr (VI) on both protein and cytotoxic responses, and toxic modes of action of Cr (VI). It was our hypothesis that cellular pathway alterations induced by Cr (VI) that lead to cytotoxicity could be detected as significant changes in protein expression or post-translational modification. Furthermore, protein changes and post-translational modifications changes observed in BEAS-2B cells exposed to 0.3 μM of Cr (VI) did not lead to a cytotoxic response whereas changes in cells exposed to 1.8 μM of Cr (VI) did. Based on the protein profiling results, the core protein responses and involved toxicity pathways that lead to deleterious cellular effects of Cr (VI) could be generally classified into four categories. These included glycolysis and glycogenesis, decreased scavenging of ROS and potential cytotoxicity by MTF-1, MAP kinase associated with stress response pathways, and ubiquitin-mediated protein degradation.

The present study extended and expanded the previous Cr (VI) toxicity pathway studies by profiling the expression and phosphorylation changes of both upstream pathway regulating proteins using ELISA and downstream novel proteins involved in multiple biological functions using 2-DE in one experimental system. For this, the overall protein and pathway responses to Cr (VI) treatments were integrated across the individual proteome changes obtained from BEAS-2B cells treated with chromium at both nontoxic and toxic concentrations. The regulating proteins such as MAP kinases, AKT panel proteins, and growth factor panel proteins were chosen for ELISA because they have been reported to be involved in the regulation of toxicity pathways of heavy metals including chromium. In addition, these proteins are expressed at very low abundance in cells and can be detected or measured by more sensitive protein assays such as ELISA, but not by 2-DE.

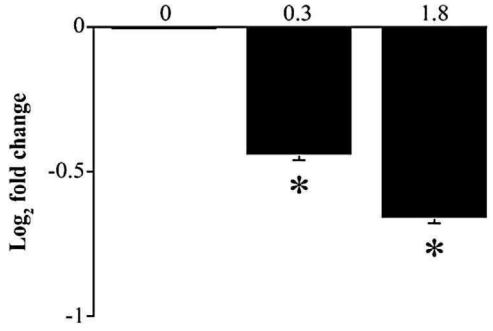

Fig. 4. Cr (VI) decreased MTF-1 expression. The MTF-1 expression levels in BEAS-2B cells treated with 0.3 and 1.8 μM of Cr (VI) were significantly decreased as compared with the control cells. Data represent mean ±STD (N = 3), *, $p < 0.05$.

4.1. Alteration of glycolysis and gluconeogenesis pathways by AKT panel proteins

AKT panel proteins, including phosphorylated AKT, p70S6K, and GSK3β, are the major regulators of glucose metabolism especially glycogenesis pathways (Shimura et al., 2014; Pelicano et al., 2014; Landis and Shaw, 2014). All of these proteins are differentially expressed and/or phosphorylated in BEAS-2B cells treated with 0.3 and 1.8 μM of Cr (VI) (Fig. 5). To assess if the expression levels of AKT, p70S6K, and GSK3β contributed to their phosphorylated states, we also calculated the ratio of phosphorylated over non-phosphorylated proteins (relative phosphorylation level) in BEAS-2B cells treated with Cr (VI). Neither the expressions of AKT panel proteins contributed to their phosphorylated states (Fig. 5). As shown in Fig. 5, phosphorylated AKT was downregulated whereas phosphorylated GSK3β was up-regulated in BEAS-2B cells treated with 0.3 and 1.8 μM of Cr (VI). This is consistent with the previous report that AKT and GSK3β had opposite phosphorylation trends and inhibited each other (Wakatsuki et al., 2011). These results suggested that the activation of glycolysis in Cr (VI)-treated BEAS-2B cells was through the phosphorylation of GSK3β but not AKT.

The protein p70S6K, is a downstream effector of mTOR regulation of glycolysis (Li et al., 2013). Inhibition of mTOR results in decreased phosphorylation of p70S6K, leading to decreased glycolysis in cancer (Frolova et al., 2012). Phosphorylated p70S6K was increased in BEAS-2B cells treated with 0.3 μM of Cr (VI) but decreased in cells treated with 1.8 μM of Cr (VI) (Fig. 5). The dramatic increase and decrease of p70S6K phosphorylation in

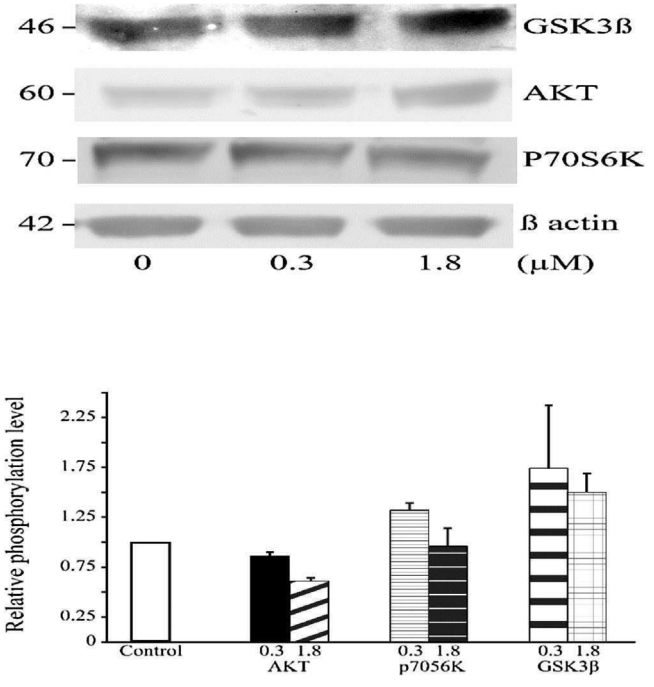

Fig. 5. Western blot analyses of total expression changes and relative phosphorylation levels of AKT panel proteins in Cr (VI)-treated BEAS-2 B cells. Western blot on the top show the total expression changes of AKT panel proteins in BEAS-2B cells treated with Cr (VI). β-actin was used as internal control to normalize protein expression levels. Western blot was developed with AKT, p70S6K, GSK3β, and B-actin primary antibodies (Cell signaling Technology Beverly, MA) and goat anti rabbit HRP-conjugated secondary antibody (Jackson ImmunoResearch, West Grove, PA) according to manufacturer's instructions. The plot below is that of normalized relative phosphorylation levels of AKT panel proteins.

BEAS-2B cells treated with 0.3 and 1.8 μM of Cr (VI) respectively, suggests that glycolysis was significantly increased in the cells treated with 0.3 μM partially via phosphorylated p70S6K. In summary, the alterations of the phosphorylation of the AKT panel proteins especially GSK3β and p70S6K are expected to affect cellular energy metabolism, and consequently influence oxidative phosphorylation rates and ATP levels, and eventually affect cell survival or death.

4.2. Responses of the apoptotic protein biomarkers to Cr (VI) treatments

In order to determine if apoptosis was responsible at least partially for cell death, we performed ELISA assays on a panel of apoptosis markers including p53, pp53 (phosphorylated p53), cleaved caspase 3, and cleaved PARP (Fig. 1). These apoptotic biomarkers were downregulated in BEAS-2B cells treated with 0.3 or 1.8 μM of Cr (VI), except that pp53 was upregulated in BEAS-2B cells treated with 1.8 μM of Cr (VI). In addition, TNFα was found to be upregulated in BEAS-2B cells treated with 1.8 but not 0.3 μM of Cr (VI) (Fig. 1). A previous study unveiled that treating neuroblastoma cells with increasing doses of TNFα for 24 h mediated a dose-dependent decrease in cell survival which was independent of caspase 3 (Alvarez et al., 2011). Therefore, our study was aligned with Alvarez's one that decreased cell survival rate or increased cytotoxicity in BEAS-2B cells treated with 1.8 μM was mediated by TNFα but not by caspases.

4.3. Activation of MAP kinases and stress response pathways

It has been reported that metals invoke a signal cascade that begins with the activation of members of the MAP kinase family which includes JNK and ERK1/2 (Kim et al., 2006). In the present study, JNK is increased and ERK1/2 is decreased at both concentrations of Cr (VI), with a greater magnitude of change observed for both at the lower concentration of Cr (VI). ERK1/2 and JNK regulate a wide variety of key biochemical pathways and cellular processes such as response to oxidative stress, cell proliferation and differentiation, cell cycle and growth, apoptosis, inflammation, and other stress responses (Vlahopoulos and Zoumpourlis, 2004Raman et al., 2007; Rubinfeld and Seger, 2005).

Cytokines including TNFα, IL-6, and IL- 8 are critical for the inflammation process and circulating levels of them were reported to be related to lung toxicity and diseases (Pratheeshkumar et al., 2014; Beaver et al., 2009) Previous studies showed that a direct cytotoxic effect of Cr (VI) on cultured human cells is accompanied by altered expression of pro-inflammatory signaling proteins such as TNFα, IL-6, and IL-8 (Pascal and Tessier, 2004; Pratheeshkumar et al., 2014; Wang et al., 2010; He et al., 2013). Wang et al. (2010) found TNFα mRNA expression increased 2 fold in HACAT cells treated with 30 and 45 μM of Cr (VI) and 3 fold in those treated with 60 and 90 μM of Cr (VI). Our study showed TNFα protein was increased and IL-6 and IL-8 were decreased in BEAS-2B cells treated with 1.8 μM (toxic) of Cr (VI), suggesting that JNK and TNFα play important roles in Cr (VI)-mediated stress responsive pathways and cytotoxicity.

It is known that cells protect themselves against ROS via biological defense systems including antioxidant proteins (Park et al., 2006; Walser et al., 2008). Two of these proteins, peroxiredoxin 3 (PRDX3) and SOD2 were upregulated in BEAS-2B cells treated with 1.8 but not 0.3 μM of Cr (VI). PRDX3 is a peroxidase which is oxidized on its cysteine residues by H_2O_2 (Rhee et al., 2005; Rhee et al., 2001). PRDX3 and SOD2 protect against the damaging effects of ROS by limiting the cellular levels of H_2O_2 (Chen et al., 2008; Myers and Myers, 2009). The fact that SOD2 and PRDX3 were upregulated at the higher concentration of Cr (VI) suggests that excess ROS production is overwhelming baseline antioxidant capacity of cells at our high dose in which may, in part, be mediating Cr (VI)-induced cytotoxicity.

4.4. MTF-1, oxidative stress, and cytotoxicity

Members of the metal regulatory transcription factor (MTF) family activate metallothioneins (MTs), proteins involved in scavenging ROS from cells (Radtke et al., 1995).They can also activate other proteins such as p53 and enolase. O'Shields et al. (2014), microinjected *in vitro* transcribed double negative MTF-1 mRNA into embryos from zebrafish and detected deregulation of p53 and Eno2 in the embryos. The alterations of MTF1, p53 and Eno2 that were detected in our study suggested the possible roles of MTF1 in regulating Cr (VI) toxicity. The down regulation of MTF1 could result in the decreased scavenging of ROS in BEAS-2B cells treated with Cr (VI).

4.5. Protein degradation in BEAS-2cells treated with Cr (VI)

UBC was identified as the protein network hub interacting with proteins that were altered in BEAS-2B cells treated with 0.3 μM of Cr (VI) and strongly linked to many enriched pathways in our analyses (Fig. 3A). Most of the proteins in this network had not been previously linked to Cr (VI)-induced effects. UBC was the main hub in this network and is a source of ubiquitin for signaling targeted protein degradation by the proteasome. PSMC2 was the only protein identified by 2-DE in cells treated with the lower dose of Cr (VI) with a probability to be assigned into the protein ubiquitination/proteasome pathway by IPA. Most likely, other proteins involved in the pathway were statistically deregulated by 0.3 μM of Cr (VI) but perhaps their quantity was insufficient to identify it. Results from BEAS-2B cells suggests UBC may play a role besides protein degradation such as cell cycle and motility in BEAS-2B cells exposed to 0.3 micromolar of Cr (VI).

Conversely, HSP27, proteasome alpha 2 (PSMA2), and proteasome activator subunit 1 (PSME1) induced 1.47, 1.2, and 1.4 fold, respectively in cells treated with 1.8 μM of Cr (VI) were associated with protein ubiquitination. Since protein ubiquitination came up as a main canonical pathway in cells treated with 1.8 μM of Cr (VI), and all the proteins in this pathway were induced, this pathway was activated. UBC played a role in protein degradation in cells exposed to 1.8 μM of Cr (VI). The ubiquitin-proteasome pathways are the major proteolytic systems in the cytosol of eukaryotic cells, catalyzing the selective degradation of short-lived proteins and the rapid elimination of proteins with abnormal conformation (Reinstein, 2004; Wang and Maldonado, 2006). UBC has been shown to be associated with main biological processes such as cell cycle, apoptosis, inflammation via activation of NFκB, and stress response, which are contributors to human cell toxicity and carcinogenicity (Reinstein, 2004; Bochtler et al., 1999; Wang and Maldonado, 2006). In summary, it is clear that the ubiquitin proteins and pathways were also pivotal in 1.8 μM of Cr (VI)-induced cytotoxicity.

4.6. Proteins and pathways correlated with the cytotoxic responses of BEAS-2 cells to Cr (VI)

In the present study, four predominant toxicity pathways in response to toxic concentrations of Cr (VI) were identified such as AKT panel protein-mediated glycolysis and gluconeogenesis pathways, MAP Kinase associated with stress responses, TNFα and pp53 mediated apoptosis independent toxicity pathways and UBC involved in signaling targeted degradation. Importantly, these major toxicity pathways identified by 2-DE profiling studies were consistent with those obtained from ELISA-based assays. For

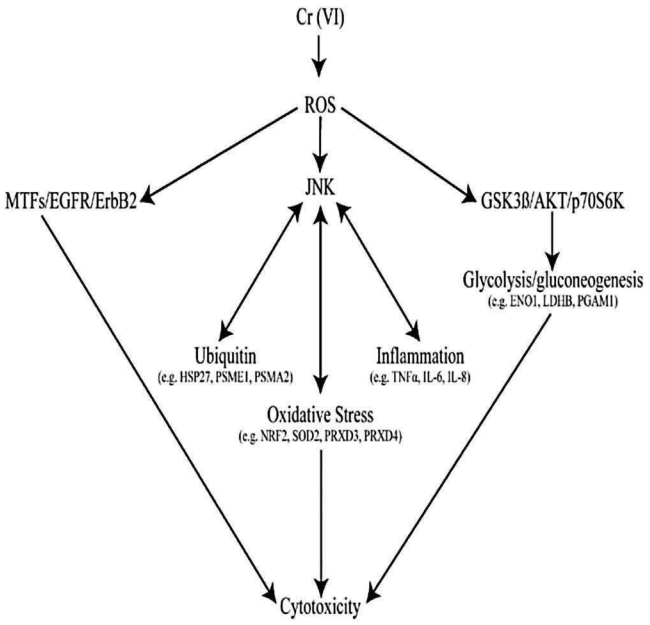

Fig. 6. A proposed core proteins and toxicity pathway map that is critical to Cr toxicity in BEAS-2B cells. The figure is based on interpretation of experimental results identified as statistically significant using IPA and thorough literature searches on proteins altered in our study. Cr (VI) generated ROS which subsequently altered the expression of signaling proteins, JNK and GSK3beta/AKT/p70s6k, associated with oxidative stress/protein ubiquitination/oxidative stress/inflammation and glycolysis/gluconeogenesis, respectively. In BEAS-2B cells exposed to 1.8 of Cr (VI), JNK can act on specific proteins involved in protein ubiquitination/oxidative stress/inflammation and vice versa (shown by arrows pointing in both directions). GSK3β/AKT/p70s6k are mediators of glycolysis/gluconeogenesis (shown with an arrow pointing in only one direction). All of these proteins are correlated with cytotoxicity in BEAS-2B cells exposed to of Cr (VI).

example, the activations of p70S6K and GSK3β identified by ELISA are consistent with the activations of a number of downstream proteins involved in glycolysis, such as Eno 1, Eno 2, and ALDHA1, which were detected by 2-DE. Therefore, these pathways, linked to proteins such as AKT panel proteins and MAP kinases, were likely to be central pathways of Cr (VI) toxicity. Considering all the proteomic results obtained using ELISA and 2-DE, we proposed a core protein and toxicity pathway map (Fig 6) to describe the interplay of these proteins and pathways associated with the cytotoxic responses of BEAS-2B cells to Cr (VI). Protein changes correlated with a cytotoxic outcome where not found in BEAS-2B cells exposed to 0.3 μM of Cr (VI). The diagram was generated based the connectedness of these proteins as hub nodes in the networks of BEAS-2B cells treated with 0.3 and 1.8 μM of Cr (VI) using IPA. In these protein sub-networks, MAP kinases, AKT panel protein, and UBC are the key proteins linked to cytotoxic responses of BEAS-2B cells to Cr (VI).

5. Conclusions

We analyzed proteome changes in BEAS-2B cells treated with Cr (VI) using both ELISA analysis of 15 well-known protein pathway regulators and 2-DE-based proteomic analysis of the protein changes in response to Cr (VI) treatments. This integrated proteomic approach provided an overall picture of the important proteins and toxicity pathways that were modulated in the cellular response to Cr (VI) treatments, and identified a small set of key proteins and concomitant pathways associated with the toxicity of Cr (VI). Interestingly, this small set of key proteins and pathways involved in glycolysis and gluconeogenesis pathways, protein degradation, and stress responses including inflammation and oxidative stress were already modified to a lower extend in BEAS-2B cells treated with 0.3 μM of Cr (VI), demonstrating a shift in these pathways from a non-toxic concentration of Cr (VI) to a toxic one. The present study, therefore, provides an integrated proteomic approach to identify key proteomic responses of BEAS-2B cells to Cr (VI) exposures that are critical to the conversion of the cells from nontoxicity to toxicity ones. Some critical toxicity pathways and protein indicators of cytotoxicity conversion are identified. The identification of key pathways involved in specific toxicity response enables the use of such proteomic signatures as predictive tools to facilitate toxicity screening of chromium and other heavy metals. In addition, our results also demonstrate that proteome alterations in the glycolysis/gluconeogenesis, proteasome, and oxidative stress pathways may be more sensitive indicators of adverse outcomes of toxicant exposures than apical endpoints such as cytotoxicity.

Conflict of interest

None.

Acknowledgement

The authors would like to thank Dr. Brian Chorley and Dr. Medhi Hazari for their very helpful comments on this manuscript. The information in this document has been funded wholly by the US Environmental Protection Agency. It has been subjected to review by the National Health and Environmental Effects Research Laboratory and approved for publication. Approval does not signify that the contents reflect the views of the Agency nor does mention of trade names or commercial products constitute endorsement or recommendation for use.

References

Alvarez, S., Blanco, A., Fresno, M., Munoz-Fernandez, M.A., 2011. TNF-alpha contributes to caspase-3 independent apoptosis in neuroblastoma cells: role of NFAT. PLoS One 6 (1), e16100. doi:http://dx.doi.org/10.1371/journal.pone.0016100.

Andrew, A.S., Warren, A.J., Barchowsky, A., Temple, K.A., Klei, L., Soucy, N.V., Hamilton, J.W., 2003. Genomic and proteomic profiling of responses to toxic metals in human lung cells. Environ. Health Perspect. 111 (6), 825–835.

Arakawa, H., Weng, M.W., Chen, W.C., Tang, M.S., 2012. Chromium(VI) induces both bulky DNA adducts and oxidative DNA damage at adenines and guanines in the p53 gene of human lung cells. Carcinogenesis 33 (10), 1993–2000. doi:http://dx.doi.org/10.1093/carcin/bgs237.

Beaver, L.M., Stemmy, E.J., Constant, S.L., Schwartz, A., Little, L.G., Gigley, J.P., Patierno, S.R., 2009. Lung injury, inflammation and Akt signaling following inhalation of particulate hexavalent chromium. Toxicol. Appl. Pharmacol. 235 (1), 47–56. doi:http://dx.doi.org/10.1016/j.taap.2008.11.018.

Bochtler, M., Ditzel, L., Groll, M., Hartmann, C., Huber, R., 1999. The proteasome. Annu. Rev. Biophys. Biomol. Struct. 28, 295–317. doi:http://dx.doi.org/10.1146/annurev.biophys.28.1.295.

Castorina, A., Tiralongo, A., Cavallo, D., Loreto, C., Carnazza, M.L., Iavicoli, S., D'Agata, V., 2008. Expression profile of ErbB receptor's family in human alveolar type 2-like cell line A549 exposed to hexavalent chromium. Toxicol. In Vitro 22 (2), 541–547. doi:http://dx.doi.org/10.1016/j.tiv.2007.10.003.

Chen, L., Na, R., Gu, M., Salmon, A.B., Liu, Y., Liang, H., Ran, Q., 2008. Reduction of mitochondrial H2O2 by overexpressing peroxiredoxin 3 improves glucose tolerance in mice. Aging Cell 7 (6), 866–878. doi:http://dx.doi.org/10.1111/j.1474-9726.2008.00432.x.

DeLoughery, Z., Luczak, M.W., Ortega-Atienza, S., Zhitkovich, A., 2015. DNA double-strand breaks by Cr (VI) are targeted to euchromatin and cause ATR-dependent phosphorylation of histone H2AX and its ubiquitination. Toxicol. Sci. 143 (1), 54–63. doi:http://dx.doi.org/10.1093/toxsci/kfu207.

Ding, M., Shi, X., 2002. Molecular mechanisms of Cr(VI)-induced carcinogenesis. Mol. Cell. Biochem. 234–235 (1–2), 293–300.

Frolova, O., Samudio, I., Benito, J.M., Jacamo, R., Kornblau, S.M., Markovic, A., Konopleva, M., 2012. Regulation of HIF-1alpha signaling and chemoresistance in acute lymphocytic leukemia under hypoxic conditions of the bone marrow microenvironment. Cancer Biol. Ther. 13 (10), 858–870. doi:http://dx.doi.org/10.4161/cbt.20838.

Ge, Y., Bruno, M., Wallace, K., Winnik, W., Prasad, R.Y., 2011. Proteome profiling reveals potential toxicity and detoxification pathways following exposure of BEAS-2B cells to engineered nanoparticle titanium dioxide. Proteomics 11 (12), 2406–2422. doi:http://dx.doi.org/10.1002/pmic.201000741.

Ge, Y., Bruno, M., Wallace, K., Leavitt, S., Andrews, D., Spassova, M.A., Ross, J.A., 2015. Systematic proteomic approach to characterize the impacts of chemical interactions on protein and cytotoxicity responses to metal mixture exposures. J. Proteom. Res. 14 (1), 183–192. doi:http://dx.doi.org/10.1021/pr500795d.

He, J., Qian, X., Carpenter, R., Xu, Q., Wang, L., Qi, Y., Jiang, B.H., 2013. Repression of miR-143 mediates Cr (VI)-induced tumor angiogenesis via IGF-IR/IRS1/ERK/IL-8 pathway. Toxicol. Sci. 134 (1), 26–38. doi:http://dx.doi.org/10.1093/toxsci/kft101.

Katz, S.A., Salem, H., 1993. The toxicology of chromium with respect to its chemical speciation: a review. J. Appl. Toxicol. 13 (3), 217–224.

Kim, Y.M., Reed, W., Wu, W., Bromberg, P.A., Graves, L.M., Samet, J.M., 2006. Zn2+-induced IL-8 expression involves AP-1, JNK, and ERK activities in human airway epithelial cells. Am. J. Physiol. Lung Cell. Mol. Physiol. 290 (5), L1028–1035. doi:http://dx.doi.org/10.1152/ajplung.00479.2005.

Kim, D., Dai, J., Fai, L.Y., Yao, H., Son, Y.O., Wang, L., Zhang, Z., 2015. Constitutive activation of epidermal growth factor receptor promotes tumorigenesis of Cr (VI)-transformed cells through decreased reactive oxygen species and apoptosis resistance development. J. Biol. Chem. 290 (4), 2213–2224. doi:http://dx.doi.org/10.1074/jbc.M114.619783.

Landis, J., Shaw, L.M., 2014. Insulin receptor substrate 2-mediated phosphatidylinositol 3-kinase signaling selectively inhibits glycogen synthase kinase 3beta to regulate aerobic glycolysis. J. Biol. Chem. 289 (26), 18603–18613. doi:http://dx.doi.org/10.1074/jbc.M114.564070.

Lei, T., He, Q.Y., Cai, Z., Zhou, Y., Wang, Y.L., Si, L.S., Chiu, J.F., 2008. Proteomic analysis of chromium cytotoxicity in cultured rat lung epithelial cells. Proteomics 8 (12), 2420–2429. doi:http://dx.doi.org/10.1002/pmic.200701050.

Leonard, S.S., Roberts, J.R., Antonini, J.M., Castranova, V., Shi, X., 2004. PbCrO4 mediates cellular responses via reactive oxygen species. Mol. Cell. Biochem. 255 (1-2), 171–179.

Li, S., Li, Y., Hu, R., Li, W., Qiu, H., Cai, H., Wang, S., 2013. The mTOR inhibitor AZD8055 inhibits proliferation and glycolysis in cervical cancer cells. Oncol. Lett. 5 (2), 717–721. doi:http://dx.doi.org/10.3892/ol.2012.1058.

Madejczyk, M.S., Baer, C.E., Dennis, W.E., Minarchick, V.C., Leonard, S.S., Jackson, D. A., Lewis, J.A., 2015. Temporal changes in rat liver gene expression after acute cadmium and chromium exposure. PLoS One 10 (5), e0127327. doi:http://dx.doi.org/10.1371/journal.pone.0127327.

Myers, J.M., Myers, C.R., 2009. The effects of hexavalent chromium on thioredoxin reductase and peroxiredoxins in human bronchial epithelial cells. Free Radic. Biol. Med. 47 (10), 1477–1485. doi:http://dx.doi.org/10.1016/j.freeradbiomed.2009.08.015.

Nigam, A., Priya, S., Bajpai, P., Kumar, S., 2014. Cytogenomics of hexavalent chromium (Cr 6+) exposed cells: a comprehensive review. Indian J. Med. Res. 139 (3), 349–370.

O'Shields, B., McArthur, A.G., Holowiecki, A., Kamper, M., Tapley, J., Jenny, M.J., 2014. Inhibition of endogenous MTF-1 signaling in zebrafish embryos identifies novel roles for MTF-1 in development. Biochim. Biophys. Acta 1843 (9), 1818–1833. doi:http://dx.doi.org/10.1016/j.bbamcr.2014.04.015.

Pan, T.L., Wang, P.W., Chen, C.C., Fang, J.Y., Sintupisut, N., 2012. Functional proteomics reveals hepatotoxicity and the molecular mechanisms of different forms of chromium delivered by skin administration. Proteomics 12 (3), 477–489. doi:http://dx.doi.org/10.1002/pmic.201100055.

Park, J.H., Kim, Y.S., Lee, H.L., Shim, J.Y., Lee, K.S., Oh, Y.J., Hwang, S.C., 2006. Expression of peroxiredoxin and thioredoxin in human lung cancer and paired normal lung. Respirology 11 (3), 269–275. doi:http://dx.doi.org/10.1111/j.1440-1843.2006.00849.x.

Pascal, L.E., Tessier, D.M.1, 2004. Cytotoxicity of chromium and manganese to lung epithelial cells in vitro. Toxicol. Lett. 147 (2), 143–151.

Pelicano, H., Zhang, W., Liu, J., Hammoudi, N., Dai, J., Xu, R.H., Huang, P., 2014. Mitochondrial dysfunction in some triple-negative breast cancer cell lines: role of mTOR pathway and therapeutic potential. Breast Cancer Res. 16 (5), 434. doi:http://dx.doi.org/10.1186/s13058-014-0434-6.

Permenter, M.G., Lewis, J.A., Jackson, D.A., 2011. Exposure to nickel, chromium, or cadmium causes distinct changes in the gene expression patterns of a rat liver derived cell line. PLoS One 6 (11), e27730. doi:http://dx.doi.org/10.1371/journal.pone.0027730.

Pratheeshkumar, P., Son, Y.O., Divya, S.P., Roy, R.V., Hitron, J.A., Wang, L., Shi, X., 2014. Luteolin inhibits Cr (VI)-induced malignant cell transformation of human lung epithelial cells by targeting ROS mediated multiple cell signaling pathways. Toxicol. Appl. Pharmacol. 281 (2), 230–241. doi:http://dx.doi.org/10.1016/j.taap.2014.10.008.

Quinteros, F.A., Machiavelli, L.I., Miler, E.A., Cabilla, J.P., Duvilanski, B.H., 2008. Mechanisms of chromium (VI)-induced apoptosis in anterior pituitary cells. Toxicology 249 (2–3), 109–115. doi:http://dx.doi.org/10.1016/j.tox.2008.04.012.

Radtke, F., Georgiev, O., Muller, H.P., Brugnera, E., Schaffner, W., 1995. Functional domains of the heavy metal-responsive transcription regulator MTF-1. Nucl. Acids Res. 23 (12), 2277–2286.

Raghunathan, V.K., Grant, M.H., Ellis, E.M., 2010. Changes in protein expression associated with chronic in vitro exposure of hexavalent chromium to osteoblasts and monocytes: a proteomic approach. J. Biomed. Mater. Res. A 92 (2), 615–625. doi:http://dx.doi.org/10.1002/jbm.a.32396.

Raman, M., Chen, W., Cobb, M.H., 2007. Differential regulation and properties of MAPKs. Oncogene 26 (22), 3100–3112. doi:http://dx.doi.org/10.1038/sj.onc.1210392.

Reinstein, E., 2004. Immunologic aspects of protein degradation by the ubiquitin-proteasome system. Isr. Med. Assoc. J. 6 (7), 420–424.

Rhee, S.G., Kang, S.W., Chang, T.S., Jeong, W., Kim, K., 2001. Peroxiredoxin, a novel family of peroxidases. IUBMB Life 52 (1–2), 35–41. doi:http://dx.doi.org/10.1080/15216540252774748.

Rhee, S.G., Chae, H.Z., Kim, K., 2005. Peroxiredoxins: a historical overview and speculative preview of novel mechanisms and emerging concepts in cell signaling. Free Radic. Biol. Med. 38 (12), 1543–1552. doi:http://dx.doi.org/10.1016/j.freeradbiomed.2005.02.026.

Rubinfeld, H., Seger, R., 2005. The ERK cascade: a prototype of MAPK signaling. Mol. Biotechnol. 31 (2), 151–174. doi:http://dx.doi.org/10.1385/MB:31:2:151.

Shimura, T., Noma, N., Sano, Y., Ochiai, Y., Oikawa, T., Fukumoto, M., Kunugita, N., 2014. AKT-mediated enhanced aerobic glycolysis causes acquired radioresistance by human tumor cells. Radiother. Oncol. 112 (2), 302–307. doi:http://dx.doi.org/10.1016/j.radonc.2014.07.015.

Sundaram, B., Singhal, K., Sandhir, R., 2012. Ameliorating effect of chromium administration on hepatic glucose metabolism in streptozotocin-induced experimental diabetes. Biofactors 38 (1), 59–68. doi:http://dx.doi.org/10.1002/biof.194.

Vlahopoulos, S., Zoumpourlis, V.C., 2004. JNK: a key modulator of intracellular signaling. Biochemistry (Moscow) 69 (8), 844–854.

Wakatsuki, S., Saitoh, F., Araki, T., 2011. ZNRF1 promotes Wallerian degeneration by degrading AKT to induce GSK3B-dependent CRMP2 phosphorylation. Nat. Cell Biol. 13 (12), 1415–1423. doi:http://dx.doi.org/10.1038/ncb2373.

Walser, T., Cui, X., Yanagawa, J., Lee, J.M., Heinrich, E., Lee, G., Dubinett, S.M., 2008. Smoking and lung cancer: the role of inflammation. Proc. Am. Thorac. Soc. 5 (8), 811–815. doi:http://dx.doi.org/10.1513/pats.200809-100TH.

Wang, J., Maldonado, M.A., 2006. The ubiquitin-proteasome system and its role in inflammatory and autoimmune diseases. Cell. Mol. Immunol. 3 (4), 255–261.

Wang, S., Shi, X., 2001. Mechanisms of Cr (VI)-induced p53 activation: the role of phosphorylation, mdm2 and ERK. Carcinogenesis 22 (5), 757–762.

Wang, B.J., Sheu, H.M., Guo, Y.L., Lee, Y.H., Lai, C.S., Pan, M.H., Wang, Y.J., 2010. Hexavalent chromium induced ROS formation, Akt, NF-kappaB, and MAPK activation, and TNF-alpha and IL-1alpha production in keratinocytes. Toxicol. Lett. 198 (2), 216–224. doi:http://dx.doi.org/10.1016/j.toxlet.2010.06.024.

Wu, F., Sun, H., Kluz, T., Clancy, H.A., Kiok, K., Costa, M., 2012. Epigallocatechin-3-gallate (EGCG) protects against chromate-induced toxicity in vitro. Toxicol. Appl. Pharmacol. 258 (2), 166–175. doi:http://dx.doi.org/10.1016/j.taap.2011.10.018.

Xia, B., Ren, X.H., Zhuang, Z.X., Yang, L.Q., Huang, H.Y., Pang, L., Zou, F., 2014. Effect of hexavalent chromium on histone biotinylation in human bronchial epithelial cells. Toxicol. Lett. 228 (3), 241–247. doi:http://dx.doi.org/10.1016/j.toxlet.2014.05.010.

Zhitkovich, A., 2011. Chromium in drinking water: sources, metabolism, and cancer risks. Chem. Res. Toxicol. 24 (10), 1617–1629. doi:http://dx.doi.org/10.1021/tx200251t.

From: jeff@piedmontpottery.com <jeff@piedmontpottery.com>
Sent: Monday, April 27, 2020 10:27 AM
To: Ge, Yue <Ge.Yue@epa.gov>
Subject: Re: Good morning. Jeff, a brief update

Hi Yue,
I'm happy that things have been going well for you. I agree to a 10% effort for myself on the paper.

Best wishes,
Jeff

Sent from myMail for iOS

From: Bruno, Maribel <Bruno.Maribel@epa.gov>
Sent: Monday, April 27, 2020 11:13 AM
To: Ge, Yue <Ge.Yue@epa.gov>
Subject: STAA Award

Hello Yue Ge:

Yes I agree with a 40% effort for the STAA award associated with the Chromium publication.

Thank you,
Maribel Bruno

Table of Contents

General_Authors_Publications.....2
LI-266117_Part_2_Paper_1.....12
LI-266118_Part_2_Paper_2.....40
STAA_Part_2_Sustainable_Hydrogen_Production-Revised.....45
Contribution_to_submitted_papers_for_STAA_award-from_Rajender_Varma.....50
e-mail-Nadagouda.....51
E-mail-Nasir.....52
Part_2_Paper_1.....53
Part_2_Paper_2.....81
Sanny_Verma_Part_01_Confirmation.....86

United States Environmental Protection Agency
Washington, DC 20460

STAA REPORT FOR THE SCIENTIST NOMINATIONS

General Information:

Nomination ID/App ID:	20-100
Research Category Primary:	Sustainability and Innovation (SI)
Research Category Secondary:	Industry and the Environment (IE);Energy and the Environment (EE);Sustainability and Innovation (SI)
Laboratory/Office Name:	ORD
Nomination Entered By:	Mallikarjuna Nadagouda

Eligibility Checklist:

[Y] The nominated publication(s) has not been submitted to a previous STAA competition.

[Y] The nominated publication(s) was published on or before January 1, 2017 and on or after January 1,2012

[Y] The principal author was an EPA employee or a PHS employee assigned to EPA when the research was performed

[Y] The EPA authors (includes PHS employees assigned to EPA) contributed collectively a minimum of 50% toward the publication(s)

Nominating Official Name:	Regan Murray
Nominating Official Title:	SUPERVISORY INTERDISCIPLINARY SCIENTIST
Nominating OfficialEmail:	murray.regan@epa.gov
STAA Coordinator Name:	Kathleen Wiser
STAA Coordinator Email:	wiser.kathi@epa.gov

Justifications:

Justification 1:

The two nominated papers demonstrate the sustainable production of hydrogen from a renewable source (e.g., water and formic acid) and further its utilization in chemical transformation.

Hydrogen production with renewable energies may have an essential role in the future as an energy vector and as a fuel. First nominated paper (Nadagouda, 2019, US Patent) revealed that ruthenium chitosan composite can split water into H_2 and O_2 under microwave irradiation. It performs the dual-task: it produces H_2 under microwave irradiation as well as catalyzing the reduction of a nitro group into an amine. The concept of nitro reduction with a dual-task from the metal catalyst, which involves the production of H_2 through the splitting of water followed by catalytic conversion of a nitro group into amine under microwave conditions, has not been predicted earlier. This patent demonstrates a new dimension to the microwave and catalytic hydrogenation chemistry and opens composite-based materials for H_2 production.

The second nominated paper (Varma, 2016) developed an efficient and sustainable protocol for the generation of hydrogen from formic acid using a bimetallic catalyst, AgPd@g-C_3N_4, under visible light. This bimetallic catalyst was synthesized by reducing silver and palladium salts over graphitic carbon nitride (g-C3N4), enables the concerted reductive formylation of aromatic nitro compounds under photo-chemical conditions using formic acid, which serves the dual role of a hydrogen source and a formylating agent. Formic acid, the simplest carboxylic acid, is found in nature or can be easily synthesized in the laboratory (major by-product of some second-generation biorefinery processes); it is also an important chemical due to its innumerable applications in pharmaceuticals and industry.

Overall, these two papers are influential in fulfilling EPA mission such as “Sustainable Materials Management (SMM)” because these utilize sustainable hydrogen production and also help to combat energy demands that are covered by fossil fuels (https://www.epa.gov/sites/production/files/2015-08/documents/sustainable_materials_management_the_road_ahead.pdf). Over 65% of the world's energy demand is covered by fossil fuels, so hydrogen production developments, offer a more sustainable alternative that limits the production of harmful materials and greenhouse gases. Since these gases are known to be detrimental to the environment and human health, it is apparent that the advantages of this research do not only apply to chemical engineering but also applies to environmental preservation as well as the medical care industry.

Justification 2A:

None of the two nominated papers included in this STAA package have been submitted for the STAA award in the past.

Two articles in this package are necessarily associated with each other as they demonstrate the generation of hydrogen from a renewable source such as form water and formic acid. As mentioned in answer to Question 1, the strength of this study is the breadth of researches that were performed for the utilization of marine waste (chitosan) derived heterogeneous catalyst to produce hydrogen from water (Nadagouda et al., 2019) and generation of hydrogen from formic under visible light irradiation (Varma 2016). All these research studies increase the national scale understanding of sustainable production of hydrogen and its utilization in chemical transformation.

Justification 2B:

Mallikarjuna N. Nadagouda

1. Evaluating Sustainable Pathway to Furanics from Biomass via Heterogeneous Organo-Catalysis Green Chemistry
2. Sustainable Strategy Utilizing Biomass: Visible Light-Mediated Synthesis of g-Valerolactone. Published in ChemCatChem
3. Visible Light Mediated Upgrading of Biomass to Biofuel. Published in Green Chemistry

2017 Honorable Mention STAA

1. The Oxidative C-H activation of amines using protuberant lychee-like goethite. Published in Nature Climate Change
2. Photocatalytic C-H activation and oxidative esterification using Pd@g-C3N4. Published in Catalysis Today
3. Hydroxylation of benzene via C-H activation using bimetallic CuAg@g-C3N4. Published in ACS Sustainable Chemistry and Engineering

2019 Honorable Mention STAA

1. Conversion of spent carbon dioxide into value-added products
2. A sustainable approach to empower the bio-based future: upgrading biomass to value-added products

2019 Level III STTA

Rajender S. Varma

1. Evaluating Sustainable Pathway to Furanics from Biomass via Heterogeneous Organo-Catalysis Green Chemistry
2. Sustainable Strategy Utilizing Biomass: Visible Light-Mediated Synthesis of g-Valerolactone. Published in ChemCatChem
3. Visible Light Mediated Upgrading of Biomass to Biofuel. Published in Green Chemistry

2017 Honorable Mention STAA

1. The Oxidative C-H activation of amines using protuberant lychee-like goethite. Published in Nature Climate Change
2. Photocatalytic C-H activation and oxidative esterification using Pd@g-C3N4. Published in Catalysis Today

3. Hydroxylation of benzene via C-H activation using bimetallic CuAg@g-C3N4. Published in ACS Sustainable Chemistry and Engineering

2019 Honorable Mention STAA

1. Conversion of spent carbon dioxide into value-added products
2. A sustainable approach to empower the bio-based future: upgrading biomass to value-added products

2019 Level III STTA

Justification 2C:

Nadagouda's (2017 Honorable Mention STAA, 2019 Honorable Mention STAA and 2019 Level III STTA) awards are not related to the currently nominated work. The previous works were associated with the upgrading of biomass/waste to value-added products. However, the present work is related to sustainable hydrogen production from a renewable source.

Varma's (2017 Honorable Mention STAA, 2019 Honorable Mention STAA, and 2019 Level III STTA) awards are not related to the currently nominated work. The previous works were related to the upgrading of biomass/waste to value-added products. However, the present work is related to sustainable hydrogen production from a renewable source.

Justification 2D:

None of the supplemental information has been included in previous nominations.

Justification 2E:

There are no concurrent nominations by the authors on this nomination.

Justification 3A:

The first study (Nadagouda 2019) has been accepted as a US patent. Researcher Aminabhavi *et al.* cited and discussed our first research work (Nadagouda 2019) on hydrogen production in his review article (International Journal of Hydrogen Energy, 2019, 44, 10453-10472). The authors have summarized our research findings, indicating, "Recently, Nadagouda et al. revealed that ruthenium chitosan composite could split water into H2 and O2 under microwave irradiation. It performs the dual-task: it produces H2 under microwave irradiation as well as catalyzing the reduction of

a nitro group into an amine. The concept of nitro reduction with a dual-task from the metal catalyst, which involves the production of H2 through the splitting of water followed by catalytic conversion of a nitro group into amine under microwave conditions, has not been predicted earlier. This patent demonstrates a new dimension to the microwave and catalytic hydrogenation chemistry and opens up composite-based materials for H2 production." In this way, our work is particularly well-suited to help other researchers in the United States develop more strategic measures that optimize hydrogen production.

The second nominated paper (Varma, 2016) has been published in the prestigious journal "Green Chemistry" as "Journal Cover Page," which has an Impact Factor of 9.405 and has ranked#3 (h-index: 186) in the "Environmental Science" category. This research work has already been cited in 18 research articles (Google citation search). Prof. Hua et al. from the University of Chinese Medicine, China has highlighted our work, HCOOH/AgPd@g-C3N4, (Varma 2016) in the main body his research article "Wang, Y., Zhan, Z., Zhou, Y., Lei, M. and Hu, L., 2018. A green, efficient, and rapid procedure for the hydrogenation of nitroarenes to formanilides in water. Monatshefte für Chemie-Chemical Monthly, 149(3), pp.527-533." Prof Zhang from china has adopted our work (Varma, 2016) in his research article "Wu, M., Pang, J.H., Song, P.P., Peng, J.J., Xu, F., Li, Q. and Zhang, X.M., 2019. Visible light-driven oxidation of vanillyl alcohol in air with Au–Pd bimetallic nanoparticles on phosphorylated hydrotalcite. New Journal of Chemistry, 43(4), pp.1964-1971."

Justification 3B:

All of the nominated manuscripts underwent anonymous peer review by the journal to which it was submitted for publication.

AUTHORS

Principal Author

Author Name: Mallikarjuna N. Nadagouda

Professional Title: Salutation: Dr.

Email:	nadagouda.mallikarjuna@epa.gov	Organization:	
Mailing Address:			
Street Line 1:	26 West, MLK DR. Cincinnati 45268 OH		
City:	Cincinnati		
Zip Code:	45268	State:	OH
At time of research was:	EPA Employee		
Separation Date:			
% of Effort:	55		

Contributing Author

Author Name:	Nasir Baig		
Professional Title:		Salutation:	Dr.
Email:	nasirchem@gmail.com	Organization:	
Mailing Address:			
Street Line 1:	26 West, MLK Dr		
City:	Cincinnati		
Zip Code:	45268	State:	OH
At time of research was:	Non EPA Personnel		
Separation Date:			
% of Effort:	20		

Contributing Author

Author Name:	Rajender Varma		
Professional Title:		Salutation:	Dr.

Email:	varma.rajender@epa.gov	Organization:	
Mailing Address:			
Street Line 1:	26 West, MLK Dr.		
City:	Cincinnati		
Zip Code:	45268	State:	OH
At time of research was:	EPA Employee		
Separation Date:			
% of Effort:	20		

Contributing Author

Author Name:	Sanny Verma		
Professional Title:		Salutation:	Dr.
Email:	verma.sanny@epa.gov	Organization:	
Mailing Address:			
Street Line 1:	26 West, MLK DR.		
City:	Cincinnati		
Zip Code:	45268	State:	OH
At time of research was:	Non EPA Personnel		
Separation Date:			
% of Effort:	5		

PUBLICATIONS

Publication 1:

A Photoactive bimetallic framework for direct aminoformylation of

Publication Title:	nitroarenes		
Publication Date:	Mon Dec 14 00:00:00 GMT 2020		
Journal/Publication Method:	Green Chemistry		
All Author(s):			
Volume:	18	Number:	1
Pages:	1019-1022	Immediately Index:	Immediately Index:
Citation ½ Life:	4.10	Impact Factor:	9.405

Publication 2:

Publication Title:	Ruthenium on chitosan (ChRu): concerted catalysis for water splitting and reduction. 2019, U.S. Pate		
Publication Date:	Thu Feb 22 00:00:00 GMT 2018		
Journal/Publication Method:	US Patent		
All Author(s):			
Volume:	2019, U.S. Patent 10,189,708	Number:	10,189,708
Pages:	1-20	Immediately Index:	Immediately Index:
Citation ½ Life:	N/A	Impact Factor:	N/A

US 20180050906A1

(19) **United States**

(12) **Patent Application Publication**

(10) **Pub. No.: US 2018/0050906 A1**

(43) **Pub. Date: Feb. 22, 2018**

VARMA et al.

(54) **RUTHENIUM ON CHITOSAN (CHRU): CONCERTED CATALYSIS FOR WATER SPLITTING AND REDUCTION**

(71) Applicant: **Government of the United States as Rep. by the Adm. of the U.S. Environmental Protection Agency**, Washington, DC (US)

(72) Inventors: **Rajender S. VARMA**, Cincinnati, OH (US); **Nasir BAIG**, Cincinnati, OH (US); **Mallikarjuna NADAGOUDA**, Cincinnati, OH (US)

(21) Appl. No.: **15/240,396**

(22) Filed: **Aug. 18, 2016**

Publication Classification

(51) **Int. Cl.**

C01B 3/04	(2006.01)
C07C 209/36	(2006.01)
C01B 13/02	(2006.01)
B01J 23/46	(2006.01)
B01J 31/06	(2006.01)
B01J 35/00	(2006.01)
B01J 37/03	(2006.01)
B01J 37/02	(2006.01)
B01J 37/00	(2006.01)
B01J 19/12	(2006.01)

(52) **U.S. Cl.**

CPC ***C01B 3/042*** (2013.01); ***C07C 209/365*** (2013.01); ***C01B 13/0207*** (2013.01); ***B01J 23/462*** (2013.01); ***B01J 19/126*** (2013.01); ***B01J 35/0006*** (2013.01); ***B01J 37/035*** (2013.01); ***B01J 37/0236*** (2013.01); ***B01J 37/009*** (2013.01); ***B01J 31/061*** (2013.01)

(57) **ABSTRACT**

A process and catalyst for the in situ generation of hydrogen via the microwave irradiation of a ruthenium chitosan composite catalyst has enabled the convenient reduction of nitro compounds in aqueous medium.

Chitosan-Ru (ChRu) composite

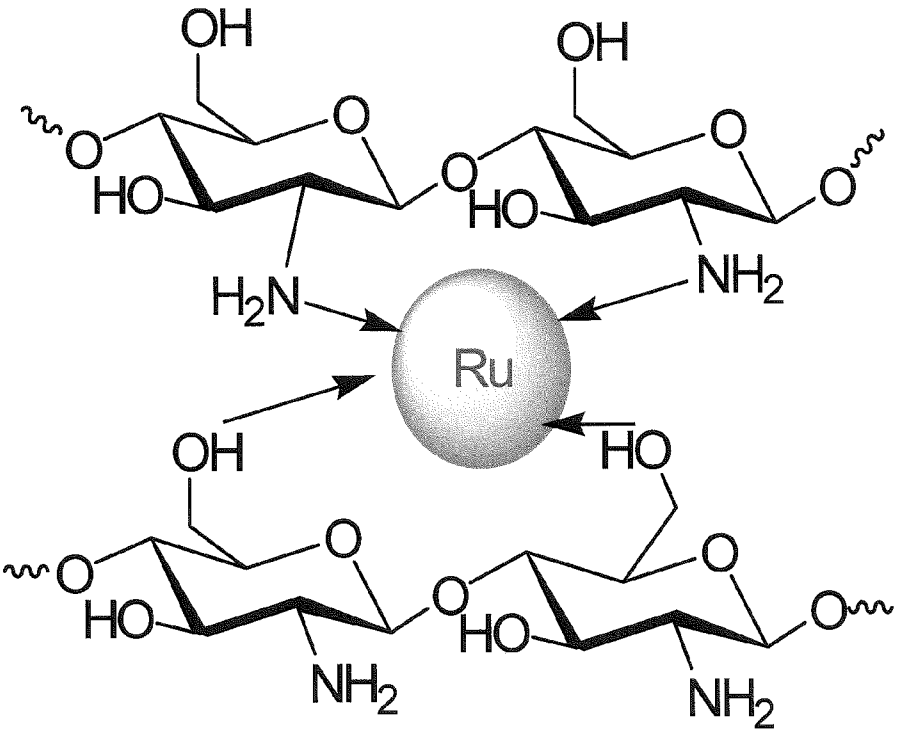

FIG 1.

Chitosan-Ru (ChRu) composite

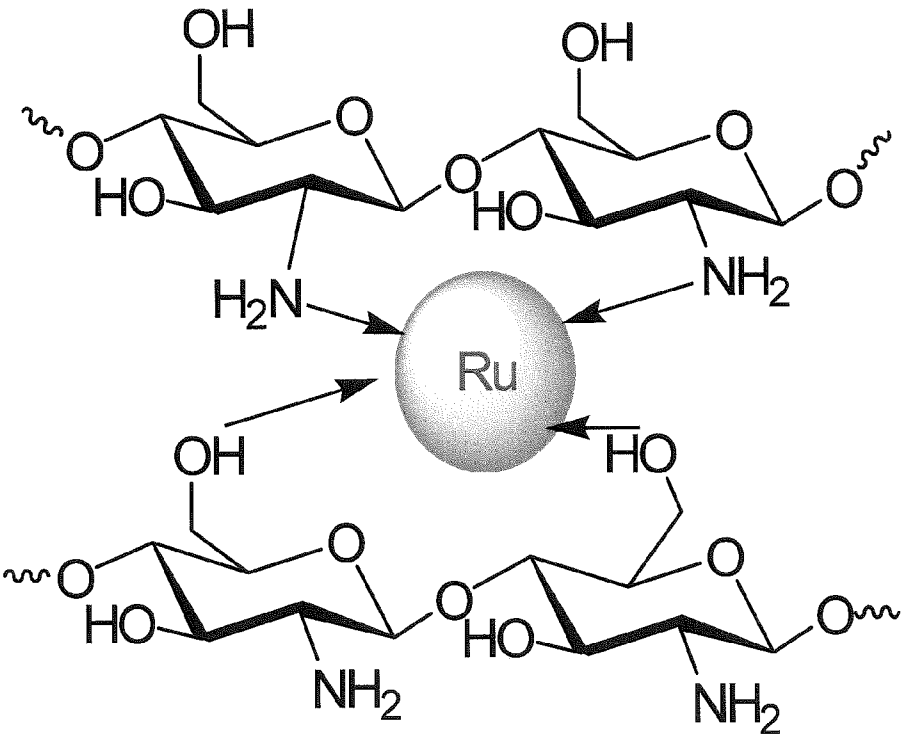

FIG. 2
Sealed microwave tube

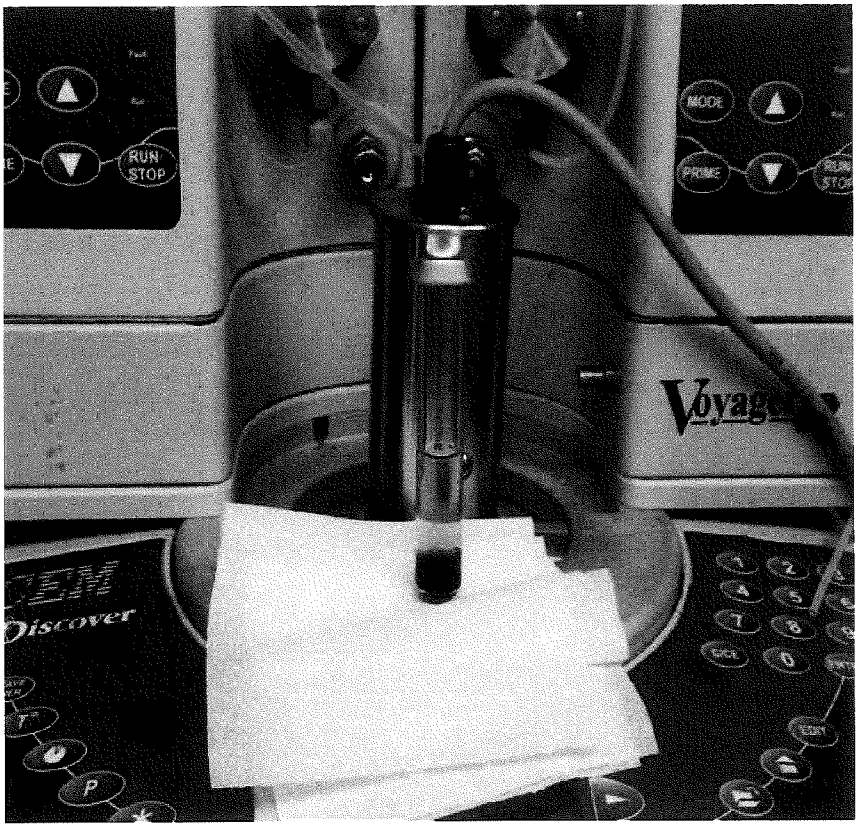

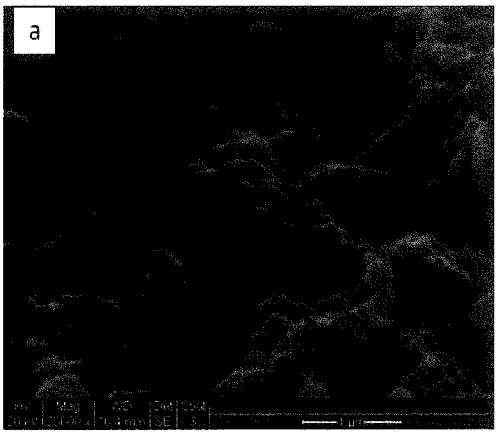

FIG. 3(a)

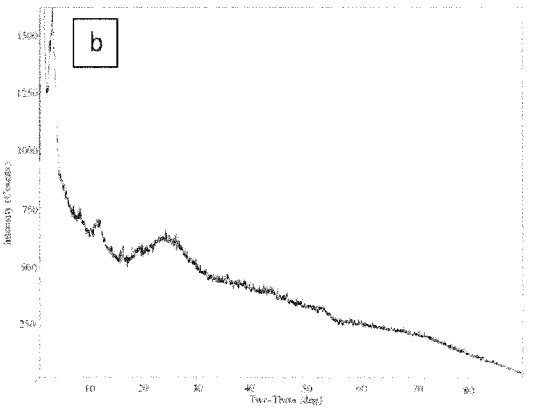

FIG. 3(b)

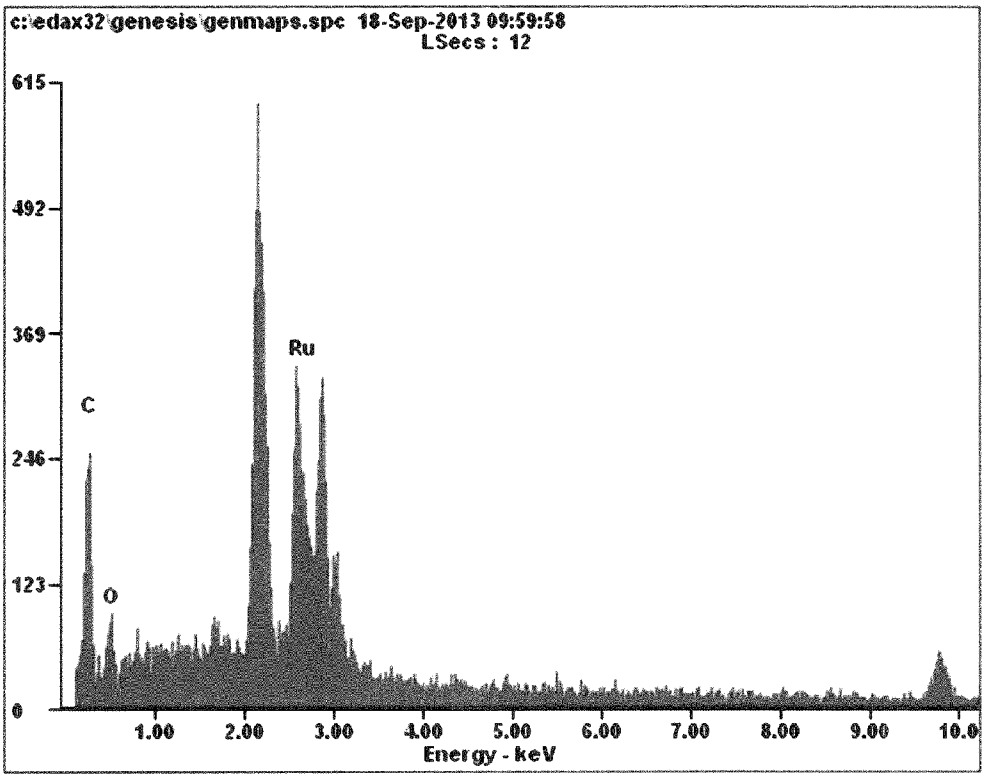

FIG. 3(c)

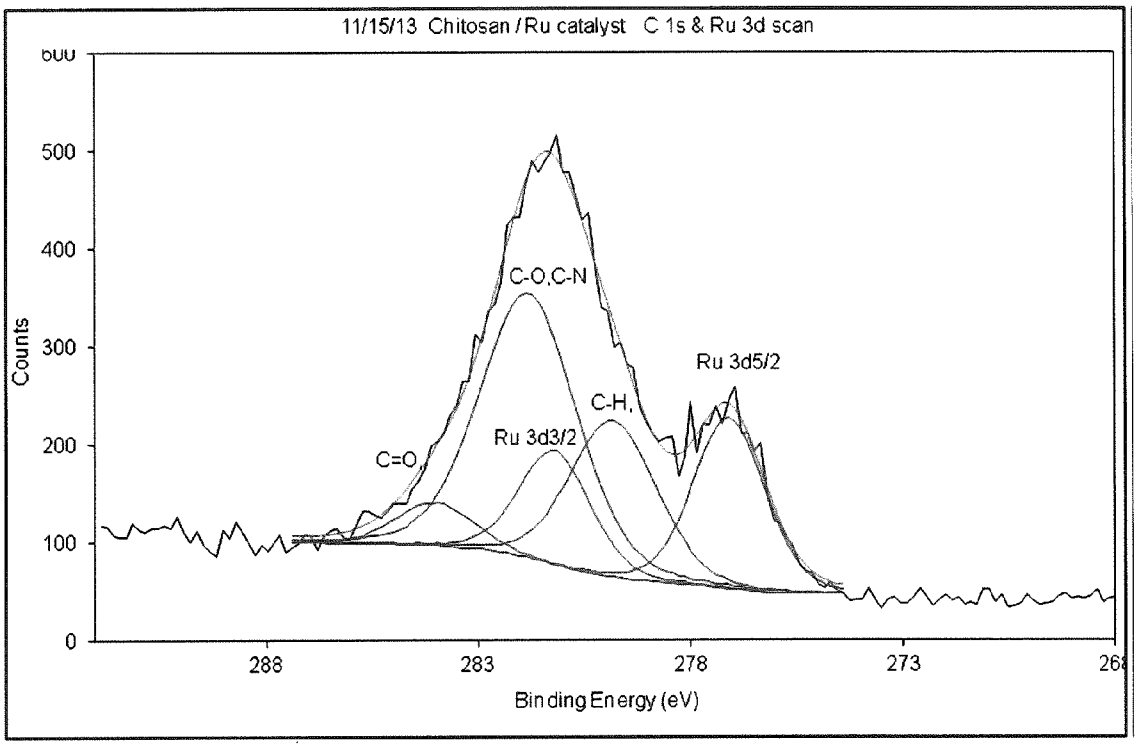
11/15/13 Chitosan / Ru catalyst C 1s & Ru 3d scan
Counts
600
500
400
300
200
100
0
C-O,C-N
Ru 3d5/2
C-H,
Ru 3d3/2
C=O
288
283
278
273
Binding Energy (eV)

FIG. 3(d)

```
File       :C:\Nasir\coupling reaction\Ruthenium reaction\NRB#4139.D
Operator   : Nasir
Acquired   :  6 May 2013   1:21 pm using AcqMethod SAMPLES- 20 MIN_18-NOV-2011.M
Instrument :    Instrument #1
Sample Name: NRB#4139
Misc Info  :
Vial Number: 2
```

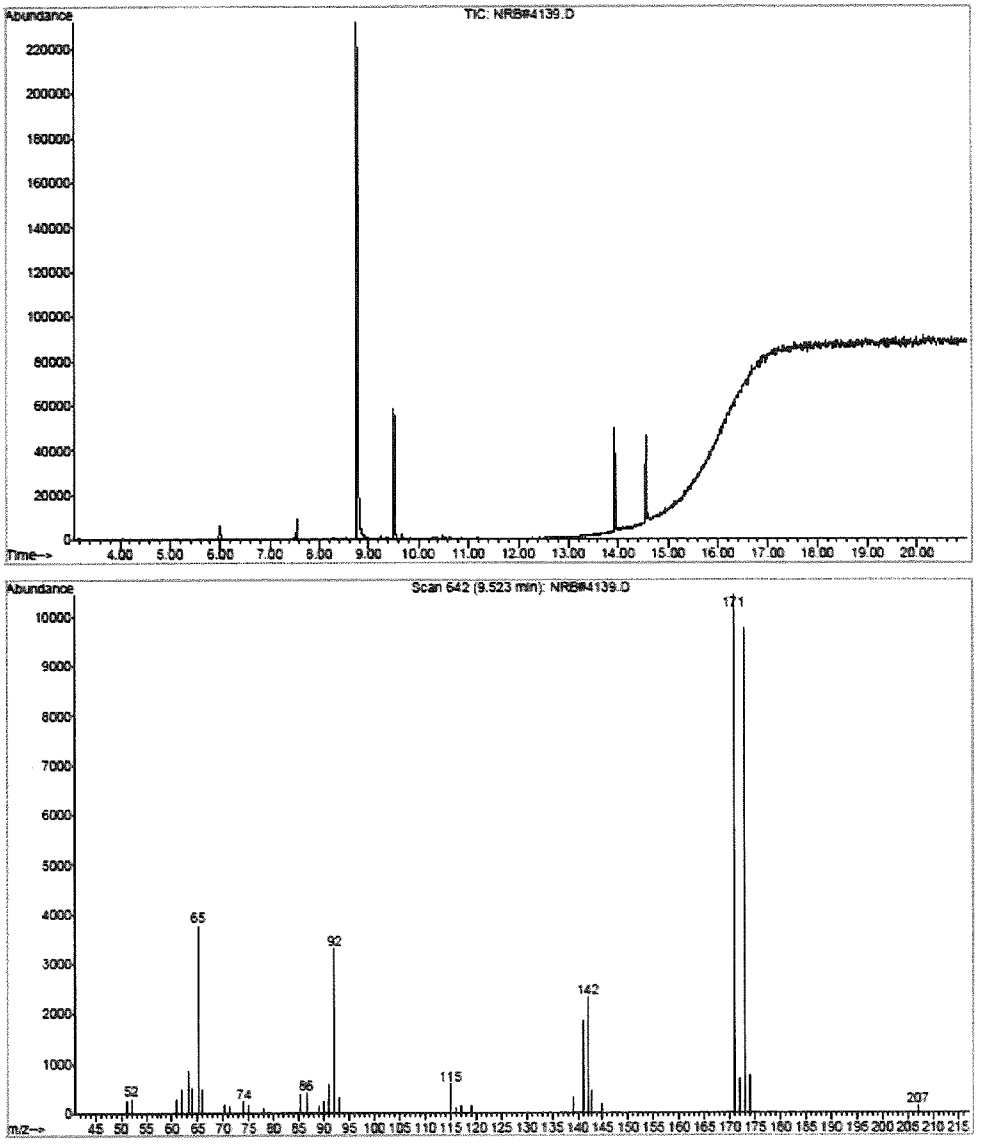

FIG. 4

```
File       :C:\Nasir\coupling reaction\Ruthenium reaction\NRB#4139.D
Operator   : Nasir
Acquired   :  6 May 2013   1:21 pm using AcqMethod SAMPLES- 20 MIN_18-NOV-2011.M
Instrument :    Instrument #1
Sample Name: NRB#4139
Misc Info  :
Vial Number: 2
```

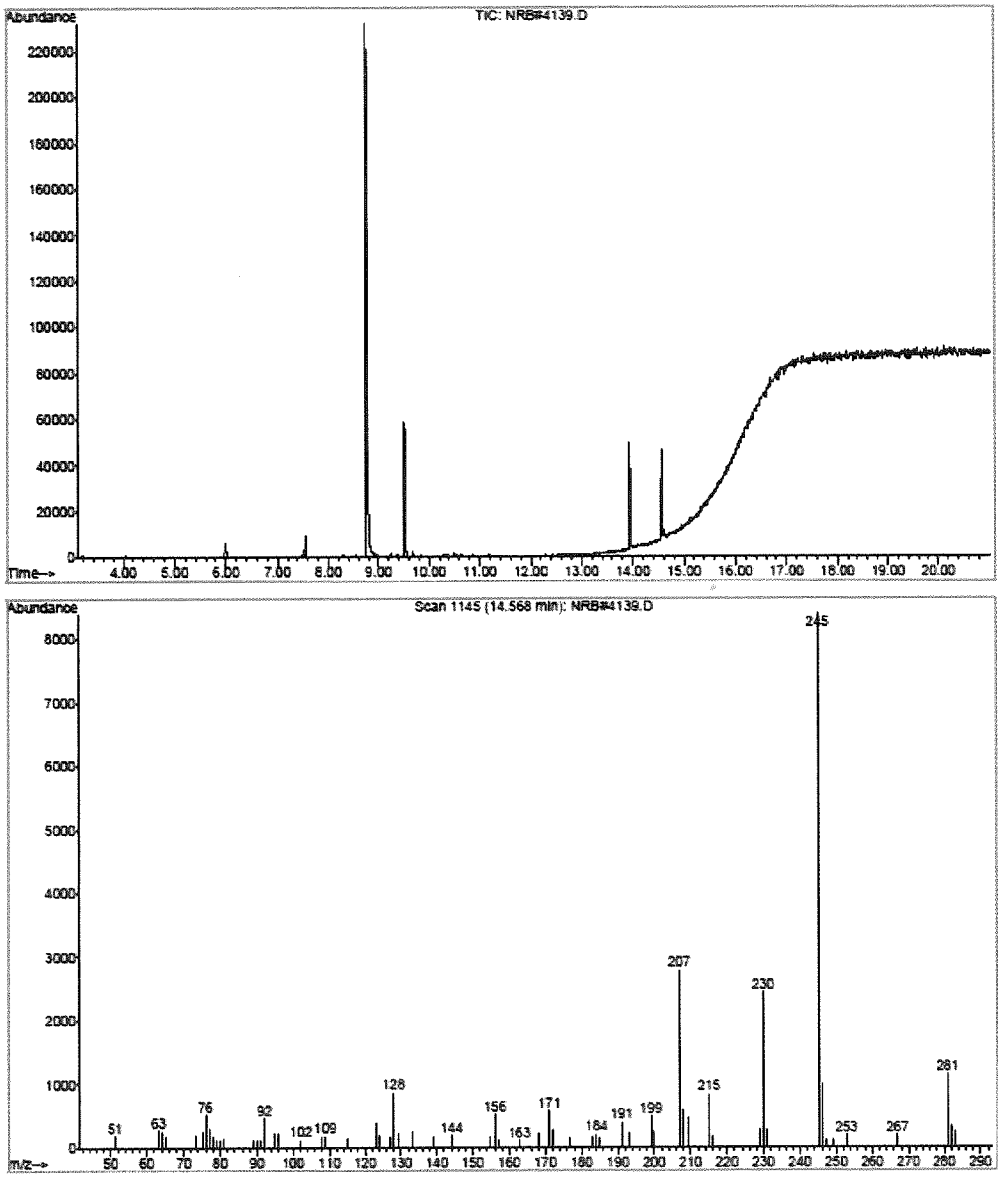

FIG. 5

```
File       :C:\Nasir\coupling reaction\Ruthenium reaction\NRB#4139.D
Operator   : Nasir
Acquired   :  6 May 2013   1:21 pm using AcqMethod SAMPLES- 20 MIN_18-NOV-2011.M
Instrument :    Instrument #1
Sample Name: NRB#4139
Misc Info  :
Vial Number: 2
```

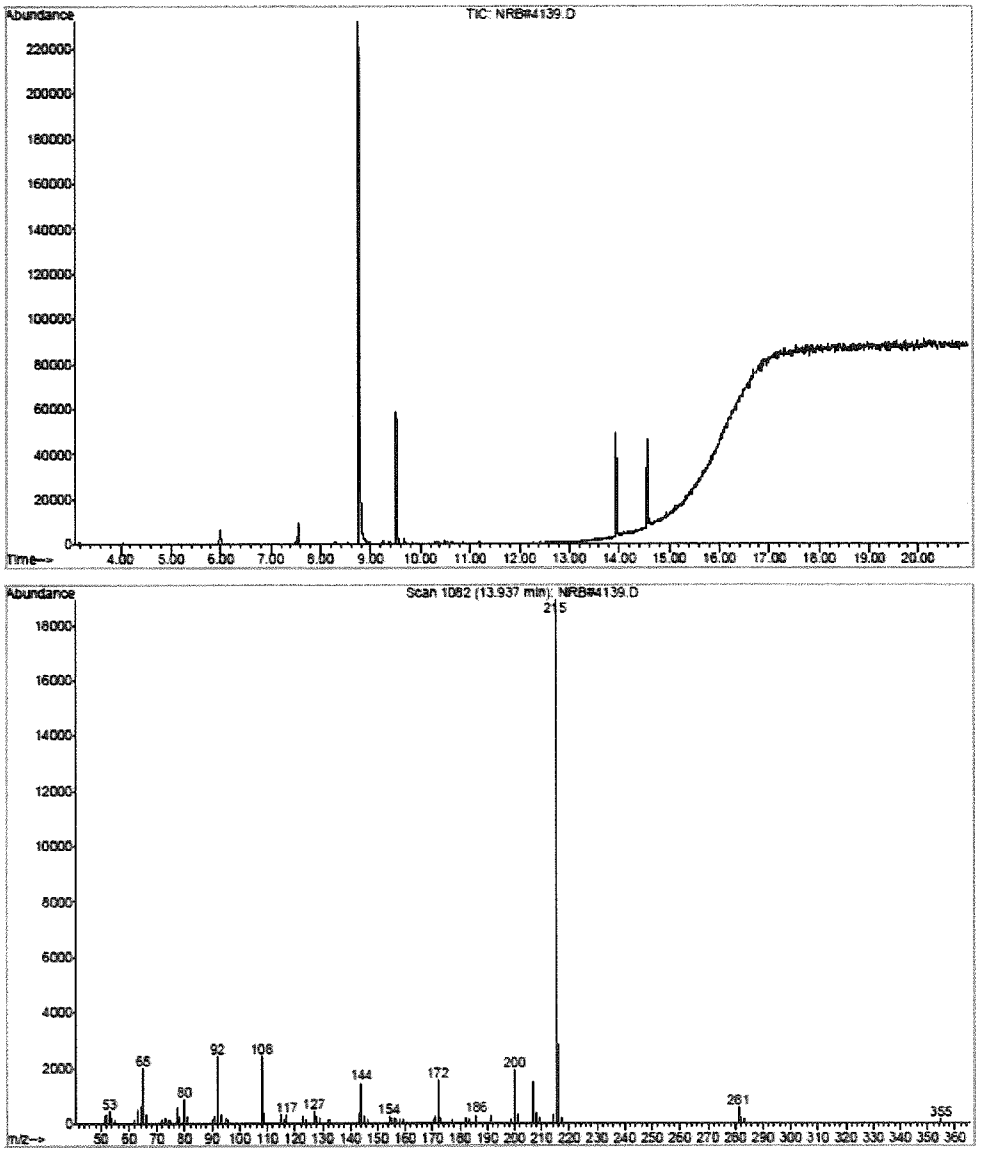

FIG. 6

```
File       :C:\Nasir\coupling reaction\Ruthenium reaction\NRB#4147.D
Operator   : Nasir
Acquired   : 10 May 2013   5:26 pm using AcqMethod SAMPLES- 20 MIN_18-NOV-2011.M
Instrument :    Instrument #1
Sample Name: NRB#4147
Misc Info  :
Vial Number: 1
```

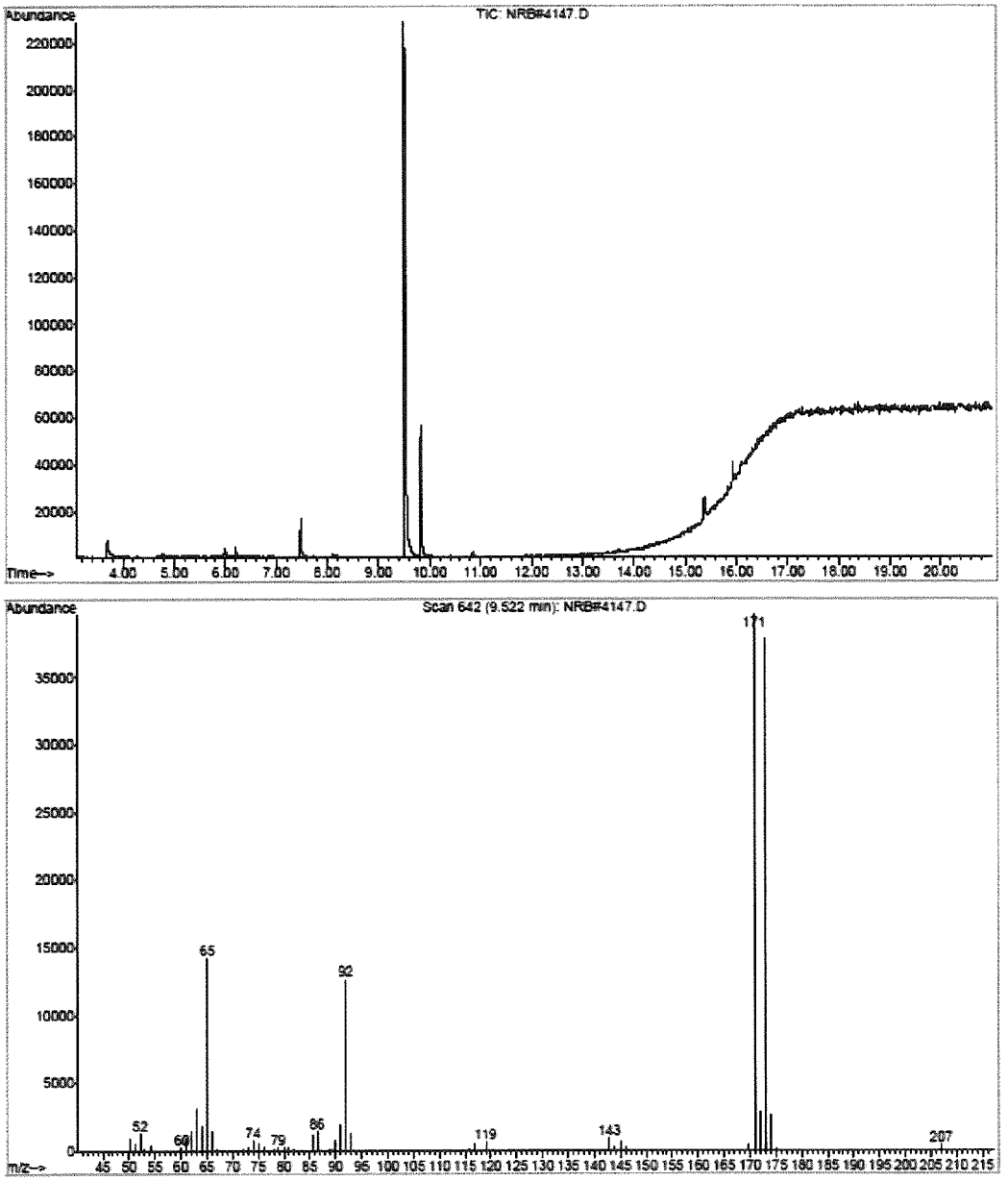

FIG. 7

Data File D:\DATA\NASIR\NASIR000463.D
Sample Name: NRB#4157-3

Acq. Operator : Nasir
Acq. Instrument : Instrument 1 Location : Vial 1
Injection Date : 14-Jun-13, 11:04:16 Inj : 1
Inj Volume : Manually
Acq. Method : C:\CHEM32\1\METHODS\LANDFILL GAS TCD MAR2011.M
Last changed : 6/14/2013 11:03:07 AM by Nasir
Analysis Method : C:\CHEM32\1\METHODS\LANDFILL GAS TCD MAR2011.M
Last changed : 6/14/2013 11:11:16 AM by Nasir
Method Info : Method for Landfill gases - CH4, CO2, CO, H2, N2, O2 Using Porapack N, Mo
Sieve, TCD - Steve Musson

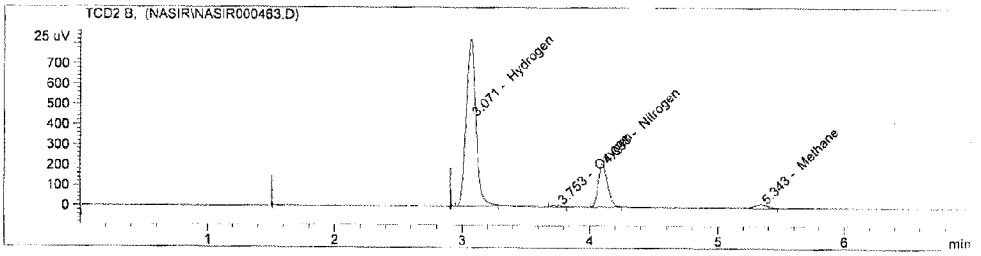

Normalized Percent Report

Sorted By : Signal
Calib. Data Modified : Thursday, January 12, 2012 10:19:23 AM
Multiplier : 1.0000
Dilution : 1.0000
Use Multiplier & Dilution Factor with ISTDs

Signal 1: TCD2 B,

RetTime [min]	Type	Area [25 uV*s]	Amt/Area	Norm %	Grp	Name
2.497		-	-	-		Carbon Dioxide
3.071	BB	4454.34131	4.83147e-3	27.793720		Hydrogen
3.753	BV	43.57506	3.50659e-2	1.973363		Oxygen
4.098	BB	1085.96875	4.84985e-2	68.018808		Nitrogen
5.343	BV	128.70334	1.33206e-2	2.214109		Methane

Totals : 100.000000

2 Warnings or Errors :

Warning : Calibration warnings (see calibration table listing)
Warning : Calibrated compound(s) not found

*** End of Report ***

Instrument 1 6/14/2013 11:11:25 AM Nasir Page 1 of 1

FIG. 8

Data File D:\DATA\NASIR\NASIR000462.D
Sample Name: NRB#4160

```
Acq. Operator   : Nasir
Acq. Instrument : Instrument 1                    Location : Vial 1
Injection Date  : 14-Jun-13, 10:55:56               Inj :   1
                                                  Inj Volume : Manually
Acq. Method     : C:\CHEM32\1\METHODS\LANDFILL GAS TCD MAR2011.M
Last changed    : 6/14/2013 10:53:26 AM by Nasir
Analysis Method : C:\CHEM32\1\METHODS\LANDFILL GAS TCD MAR2011.M
Last changed    : 6/14/2013 11:02:56 AM by Nasir
Method Info     : Method for Landfill gases - CH4, CO2, CO, H2, N2, O2 Using Porapack N, Mol
                  Sieve, TCD - Steve Musson
```

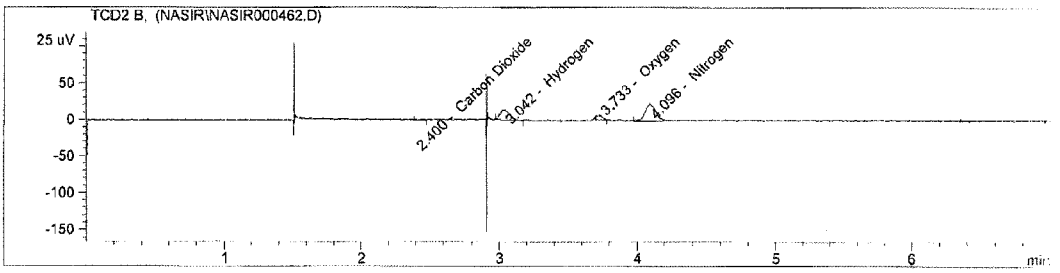


```
                        Normalized Percent Report

Sorted By             :      Signal
Calib. Data Modified  :      Thursday, January 12, 2012 10:19:23 AM
Multiplier            :      1.0000
Dilution              :      1.0000
Use Multiplier & Dilution Factor with ISTDs

Signal 1: TCD2 B,

RetTime  Type     Area      Amt/Area     Norm     Grp   Name
 [min]          [25 uV*s]                 %
-------|------|----------|----------|----------|--|------------------
  2.400 VV        6.80996 4.42418e-2   3.833679     Carbon Dioxide
  3.042 BV       67.58522 4.83147e-3   4.154983     Hydrogen
  3.733 VB       19.34842 3.50659e-2   8.633141     Oxygen
  4.096 VB      135.10970 4.84985e-2  83.378196     Nitrogen
  5.114            -          -          -          Methane

Totals :                              100.000000


2 Warnings or Errors :

Warning : Calibration warnings (see calibration table listing)
Warning : Calibrated compound(s) not found

                            *** End of Report ***
```


FIG. 9

Data File D:\DATA\NASIR\NASIR000472.D
Sample Name: NRB#4163

Acq. Operator : Nasir
Acq. Instrument : Instrument 1 Location : Vial 1
Injection Date : 14-Jun-13, 12:18:54 Inj : 1
Inj Volume : Manually
Acq. Method : C:\CHEM32\1\METHODS\LANDFILL GAS TCD MAR2011.M
Last changed : 6/14/2013 12:18:01 PM by Nasir
Analysis Method : C:\CHEM32\1\METHODS\LANDFILL GAS TCD MAR2011.M
Last changed : 6/14/2013 12:25:54 PM by Nasir
Method Info : Method for Landfill gases - CH4, CO2, CO, H2, N2, O2 Using Porapack N, Mol Sieve, TCD - Steve Musson

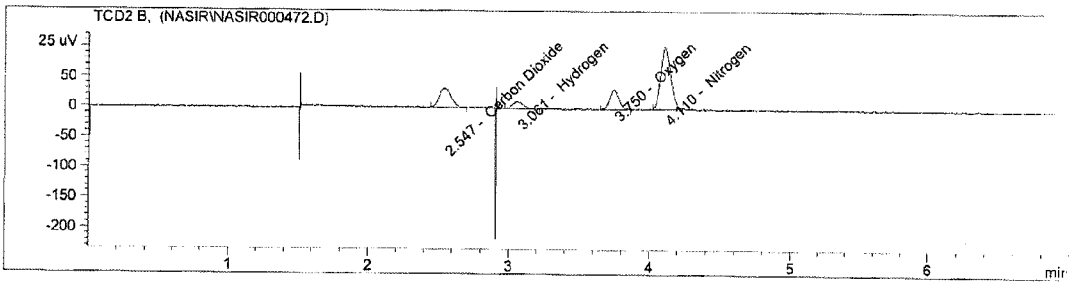

Normalized Percent Report

Sorted By : Signal
Calib. Data Modified : Thursday, January 12, 2012 10:19:23 AM
Multiplier : 1.0000
Dilution : 1.0000
Use Multiplier & Dilution Factor with ISTDs

Signal 1: TCD2 B,

RetTime [min]	Type	Area [25 uV*s]	Amt/Area	Norm %	Grp	Name
2.547	BB	191.11461	4.42418e-2	21.277983		Carbon Dioxide
3.061	BV	65.38754	4.83147e-3	0.795020		Hydrogen
3.750	VB	153.32578	3.50659e-2	13.530192		Oxygen
4.110	BV	527.63409	4.84985e-2	64.396806		Nitrogen
5.114		-	-	-		Methane

Totals : 100.000000

2 Warnings or Errors :

Warning : Calibration warnings (see calibration table listing)
Warning : Calibrated compound(s) not found

*** End of Report ***

Instrument 1 6/14/2013 12:26:03 PM Nasir Page 1 of 1

FIG. 10

Data File D:\DATA\NASIR\NASIR000473.D
Sample Name: NRB#4162

Acq. Operator : Nasir
Acq. Instrument : Instrument 1 Location : Vial 1
Injection Date : 14-Jun-13, 12:27:31 Inj : 1
Inj Volume : Manually
Acq. Method : C:\CHEM32\1\METHODS\LANDFILL GAS TCD MAR2011.M
Last changed : 6/14/2013 12:26:05 PM by Nasir
Analysis Method : C:\CHEM32\1\METHODS\LANDFILL GAS TCD MAR2011.M
Last changed : 6/14/2013 12:34:31 PM by Nasir
Method Info : Method for Landfill gases - CH4, CO2, CO, H2, N2, O2 Using Porapack N, Mol Sieve, TCD - Steve Musson

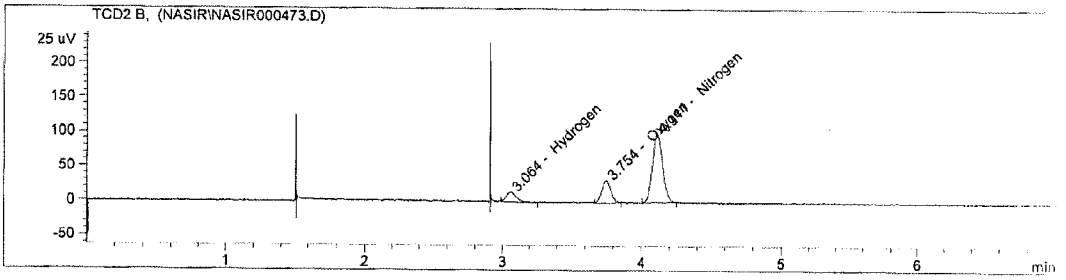

Normalized Percent Report

Sorted By : Signal
Calib. Data Modified : Thursday, January 12, 2012 10:19:23 AM
Multiplier : 1.0000
Dilution : 1.0000
Use Multiplier & Dilution Factor with ISTDs

Signal 1: TCD2 B,

RetTime [min]	Type	Area [25 uV*s]	Amt/Area	Norm %	Grp	Name
2.497		-	-	-		Carbon Dioxide
3.064	VB	75.59394	4.83147e-3	1.225395		Hydrogen
3.754	BV	144.85381	3.50659e-2	17.042162		Oxygen
4.111	BB	502.29285	4.84985e-2	81.732443		Nitrogen
5.114		-	-	-		Methane

Totals : 100.000000

2 Warnings or Errors :

Warning : Calibration warnings (see calibration table listing)
Warning : Calibrated compound(s) not found

*** End of Report ***

Instrument 1 6/14/2013 12:34:40 PM Nasir Page 1 of 1

FIG. 11

Data File D:\DATA\NASIR\NASIR000465.D
Sample Name: NRB#4158-2

Acq. Operator : Nasir
Acq. Instrument : Instrument 1 Location : Vial 1
Injection Date : 14-Jun-13, 11:21:16 Inj : 1
Inj Volume : Manually
Acq. Method : C:\CHEM32\1\METHODS\LANDFILL GAS TCD MAR2011.M
Last changed : 6/14/2013 11:20:22 AM by Nasir
Analysis Method : C:\CHEM32\1\METHODS\LANDFILL GAS TCD MAR2011.M
Last changed : 6/14/2013 11:28:16 AM by Nasir
Method Info : Method for Landfill gases - CH4, CO2, CO, H2, N2, O2 Using Porapack N, Mol Sieve, TCD - Steve Musson

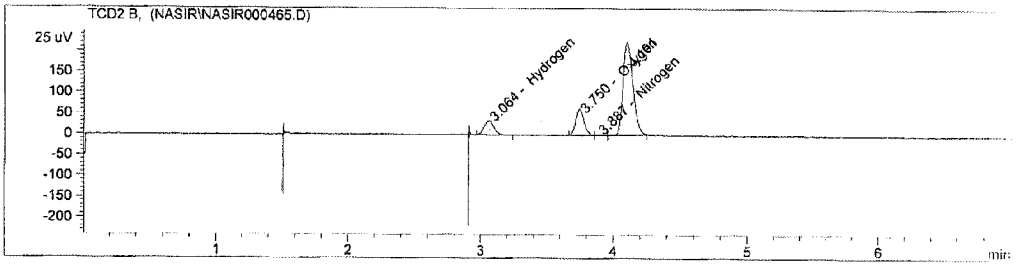

Normalized Percent Report

Sorted By : Signal
Calib. Data Modified : Thursday, January 12, 2012 10:19:23 AM
Multiplier : 1.0000
Dilution : 1.0000
Use Multiplier & Dilution Factor with ISTDs

Signal 1: TCD2 B,

RetTime [min]	Type	Area [25 uV*s]	Amt/Area	Norm %	Grp	Name
2.497		-	-	-		Carbon Dioxide
3.064	BB	170.74980	4.83147e-3	7.396285		Hydrogen
3.750	BV	283.68079	3.50659e-2	89.184455		Oxygen
3.887	VV	7.86376	4.84985e-2	3.419260		Nitrogen
5.114		-	-	-		Methane

Totals : 100.000000

2 Warnings or Errors :

Warning : Calibration warnings (see calibration table listing)
Warning : Calibrated compound(s) not found

*** End of Report ***

FIG. 12

Data File D:\DATA\NASIR\NASIR000461.D
Sample Name: NRB#4159-2

```
Acq. Operator    : Nasir
Acq. Instrument  : Instrument 1                    Location : Vial 1
Injection Date   : 14-Jun-13, 10:46:14                 Inj :  1
                                                  Inj Volume : Manually
Acq. Method      : C:\CHEM32\1\METHODS\LANDFILL GAS TCD MAR2011.M
Last changed     : 6/14/2013 10:40:56 AM by Nasir
Analysis Method  : C:\CHEM32\1\METHODS\LANDFILL GAS TCD MAR2011.M
Last changed     : 6/14/2013 10:53:14 AM by Nasir
Method Info      : Method for Landfill gases - CH4, CO2, CO, H2, N2, O2 Using Porapack N, Mol
                   Sieve, TCD - Steve Musson
```

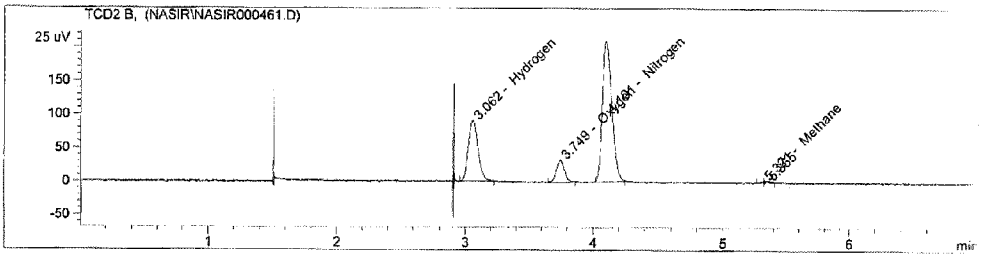

Normalized Percent Report

```
Sorted By             :      Signal
Calib. Data Modified  :      Thursday, January 12, 2012 10:19:23 AM
Multiplier            :      1.0000
Dilution              :      1.0000
Use Multiplier & Dilution Factor with ISTDs

Signal 1: TCD2 B,
```

RetTime [min]	Type	Area [25 uV*s]	Amt/Area	Norm %	Grp	Name
2.497		-	-	-		Carbon Dioxide
3.062	BB	473.96875	4.83147e-3	3.844839		Hydrogen
3.749	VB	147.99077	3.50659e-2	8.713023		Oxygen
4.101	BV	1072.06763	4.84985e-2	87.296958		Nitrogen
5.321	VV	6.49130	1.33206e-2	0.145180		Methane
Totals :				100.000000		

```
2 Warnings or Errors :

Warning : Calibration warnings (see calibration table listing)
Warning : Calibrated compound(s) not found

                        *** End of Report ***
```


FIG. 13

Data File D:\DATA\NASIR\NASIR000470.D
Sample Name: NRB#4164

```
Acq. Operator    : Nasir
Acq. Instrument  : Instrument 1                    Location : Vial 1
Injection Date   : 14-Jun-13, 12:02:28                 Inj :  1
                                                   Inj Volume : Manually
Acq. Method      : C:\CHEM32\1\METHODS\LANDFILL GAS TCD MAR2011.M
Last changed     : 6/14/2013 12:01:29 PM by Nasir
Analysis Method  : C:\CHEM32\1\METHODS\LANDFILL GAS TCD MAR2011.M
Last changed     : 6/14/2013 12:09:28 PM by Nasir
Method Info      : Method for Landfill gases - CH4, CO2, CO, H2, N2, O2 Using Porapack N, Mol
                   Sieve, TCD - Steve Musson
```

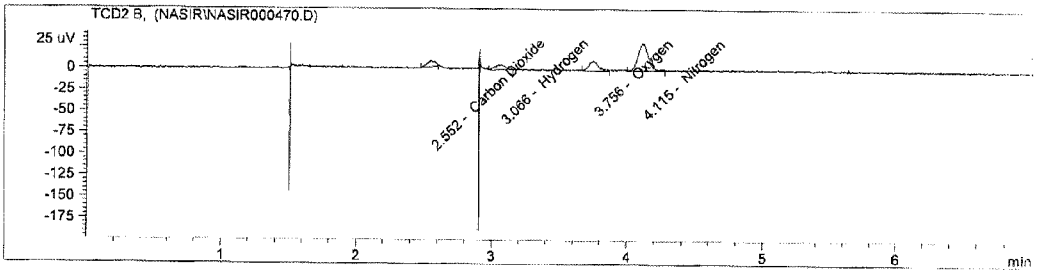

Normalized Percent Report

```
Sorted By             :      Signal
Calib. Data Modified  :      Thursday, January 12, 2012 10:19:23 AM
Multiplier            :      1.0000
Dilution              :      1.0000
Use Multiplier & Dilution Factor with ISTDs

Signal 1: TCD2 B,
```

RetTime [min]	Type	Area [25 uV*s]	Amt/Area	Norm %	Grp	Name
2.552	BB	29.23130	4.42418e-2	11.287271		Carbon Dioxide
3.066	BB	30.54844	4.83147e-3	1.288179		Hydrogen
3.756	BV	57.15428	3.50659e-2	17.492091		Oxygen
4.115	VB	165.21259	4.84985e-2	69.932460		Nitrogen
5.114		-	-	-		Methane

```
Totals :                              100.000000

2 Warnings or Errors :

Warning : Calibration warnings (see calibration table listing)
Warning : Calibrated compound(s) not found

                        *** End of Report ***
```


FIG. 14

Data File D:\DATA\NASIR\NASIR000467.D
Sample Name: NRB#4161

Acq. Operator : Nasir
Acq. Instrument : Instrument 1 Location : Vial 1
Injection Date : 14-Jun-13, 11:37:35 Inj : 1
Inj Volume : Manually
Acq. Method : C:\CHEM32\1\METHODS\LANDFILL GAS TCD MAR2011.M
Last changed : 6/14/2013 11:36:50 AM by Nasir
Analysis Method : C:\CHEM32\1\METHODS\LANDFILL GAS TCD MAR2011.M
Last changed : 6/14/2013 11:44:35 AM by Nasir
Method Info : Method for Landfill gases - CH4, CO2, CO, H2, N2, O2 Using Porapack N, Mol Sieve, TCD - Steve Musson

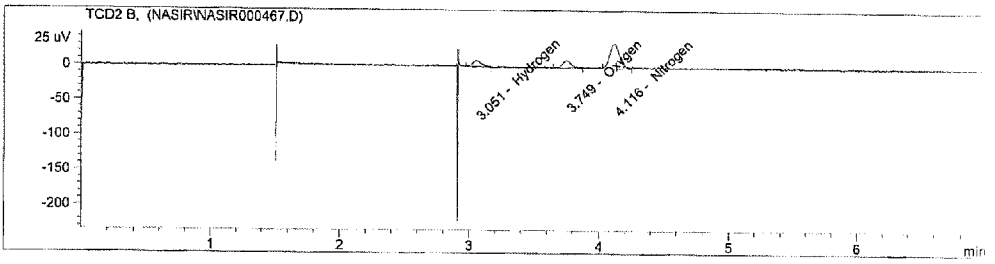

Normalized Percent Report

Sorted By : Signal
Calib. Data Modified : Thursday, January 12, 2012 10:19:23 AM
Multiplier : 1.0000
Dilution : 1.0000
Use Multiplier & Dilution Factor with ISTDs

Signal 1: TCD2 B,

RetTime [min]	Type	Area [25 uV*s]	Amt/Area	Norm %	Grp	Name
2.497		-	-	-		Carbon Dioxide
3.051	BB	42.41637	4.83147e-3	1.902551		Hydrogen
3.749	BB	44.86104	3.50659e-2	14.604207		Oxygen
4.116	BV	185.43852	4.84985e-2	83.493242		Nitrogen
5.114		-	-	-		Methane

Totals : 100.000000

2 Warnings or Errors :

Warning : Calibration warnings (see calibration table listing)
Warning : Calibrated compound(s) not found

*** End of Report ***

Instrument 1 6/14/2013 11:44:44 AM Nasir Page 1 of 1

FIG. 15

Data File D:\DATA\NASIR\NRB000052.D
Sample Name: NRB#4187

Acq. Operator : RFM
Acq. Instrument : Instrument 1 Location : Vial 1
Injection Date : 01-Jul-13, 15:54:21 Inj : 1
Inj Volume : Manually
Acq. Method : C:\CHEM32\1\METHODS\LANDFILL GAS TCD MAR2011.M
Last changed : 7/1/2013 3:53:06 PM by RFM
Analysis Method : C:\CHEM32\1\METHODS\LANDFILL GAS TCD MAR2011.M
Last changed : 7/1/2013 4:01:21 PM by RFM
Method Info : Method for Landfill gases - CH4, CO2, CO, H2, N2, O2 Using Porapack N, Mol Sieve, TCD - Steve Musson

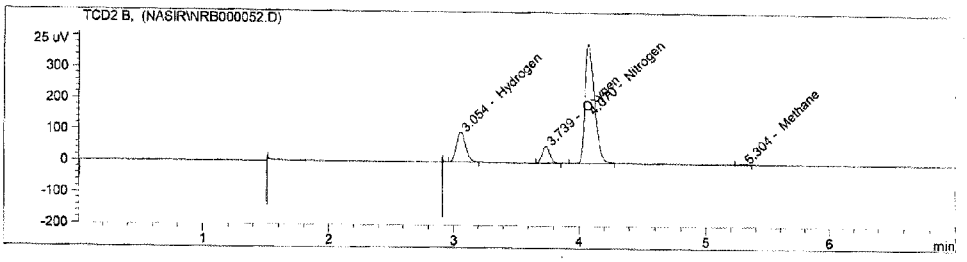

Normalized Percent Report

Sorted By : Signal
Calib. Data Modified : Thursday, January 12, 2012 10:19:23 AM
Multiplier : 1.0000
Dilution : 1.0000
Use Multiplier & Dilution Factor with ISTDs

Signal 1: TCD2 B,

RetTime [min]	Type	Area [25 uV*s]	Amt/Area	Norm %	Grp	Name
2.497		-	-	-		Carbon Dioxide
3.054	BV	497.97028	4.83147e-3	2.262151		Hydrogen
3.739	VB	233.97701	3.50659e-2	7.714312		Oxygen
4.070	BB	1968.34412	4.84985e-2	89.756879		Nitrogen
5.304	BB	21.29068	1.33206e-2	0.266657		Methane

Totals : 100.000000

2 Warnings or Errors :

Warning : Calibration warnings (see calibration table listing)
Warning : Calibrated compound(s) not found

*** End of Report ***

Instrument 1 7/1/2013 4:01:30 PM RFM Page 1 of 1

FIG. 16

Data File D:\DATA\NASIR\NASIR000469.D
Sample Name: NRB#4154-2

```
Acq. Operator   : Nasir
Acq. Instrument : Instrument 1                    Location : Vial 1
Injection Date  : 14-Jun-13, 11:54:17                 Inj :   1
                                                  Inj Volume : Manually
Acq. Method     : C:\CHEM32\1\METHODS\LANDFILL GAS TCD MAR2011.M
Last changed    : 6/14/2013 11:53:02 AM by Nasir
Analysis Method : C:\CHEM32\1\METHODS\LANDFILL GAS TCD MAR2011.M
Last changed    : 6/14/2013 12:01:17 PM by Nasir
Method Info     : Method for Landfill gases - CH4, CO2, CO, H2, N2, O2 Using Porapack N, Mol
                  Sieve, TCD - Steve Musson
```

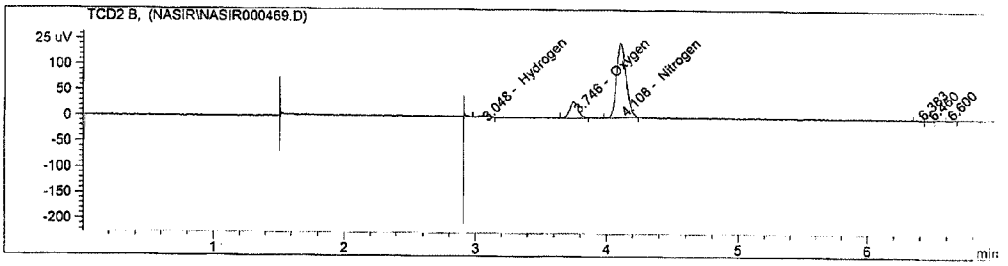

Normalized Percent Report

```
Sorted By             :      Signal
Calib. Data Modified  :      Thursday, January 12, 2012 10:19:23 AM
Multiplier            :      1.0000
Dilution              :      1.0000
Use Multiplier & Dilution Factor with ISTDs

Signal 1: TCD2 B,
```

RetTime [min]	Type	Area [25 uV*s]	Amt/Area	Norm %	Grp	Name
2.497		-	-	-		Carbon Dioxide
3.048	BB	13.26262	4.83147e-3	0.156755		Hydrogen
3.746	BB	144.66556	3.50659e-2	12.409786		Oxygen
4.108	BB	736.94623	4.84985e-2	87.433458		Nitrogen
5.114		-	-	-		Methane
Totals :				100.000000		

```
2 Warnings or Errors :

Warning : Calibration warnings (see calibration table listing)
Warning : Calibrated compound(s) not found

                        *** End of Report ***
```


FIG. 17

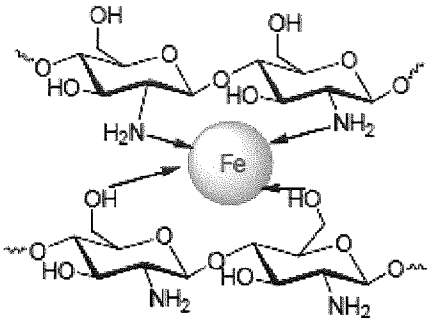

FIG. 18
Chitosan-Fe (ChFe) composite

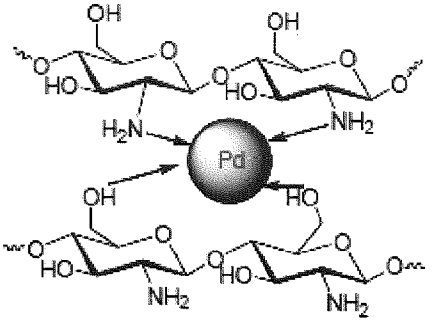

FIG. 19
Chitosan-Pd (ChPd) composite

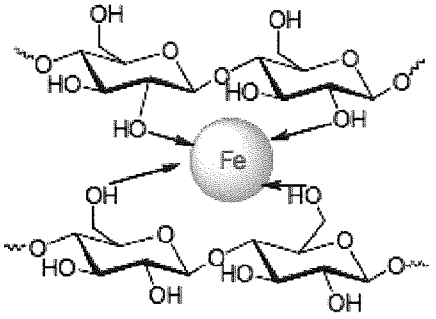

FIG. 20
Cellulose-Fe (CelluFe) composite

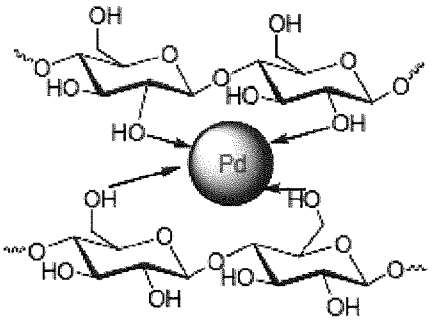

FIG. 21
Cellulose-Pd(CelluPd) composite

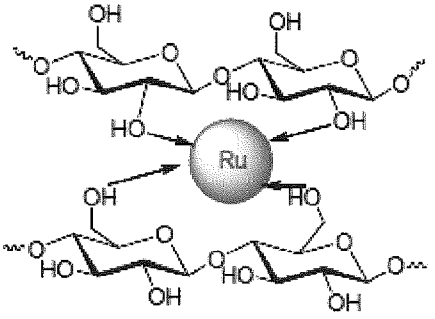

FIG. 22
Cellulose-Ru (CelluRu) composite

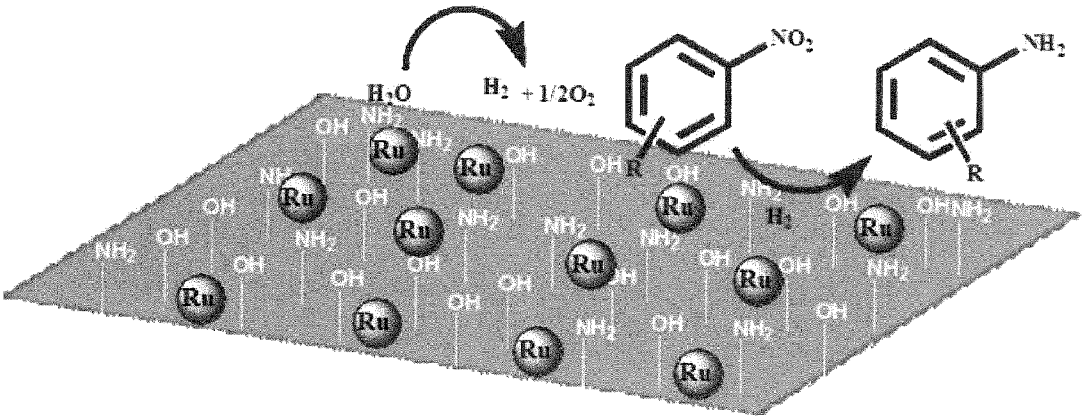

FIG. 23

RUTHENIUM ON CHITOSAN (CHRU): CONCERTED CATALYSIS FOR WATER SPLITTING AND REDUCTION

BACKGROUND

Field of the Invention

[0001] Aspects of the invention relate generally to improved processes and catalysts to split water (i.e., to separate water into hydrogen and oxygen). The invention is particularly useful for the in situ generation of hydrogen via microwave irradiation of a ruthenium chitosan composite catalyst and the convenient reduction of nitro compounds in an aqueous medium.

Description of Related Art

[0002] Increasing energy demands and the impending global warming crisis has forced a paradigm shift in thinking towards the development of carbon-neutral, sustainable and inexpensive energy-consuming strategies. This has inspired scientists to design and develop methods for splitting water, primarily as a means for producing hydrogen (Scheme 1). The total water splitting process consists of two steps: (Step 1) proton reduction and (Step 2) water oxidation. Step 1 requires less energy compared to the key step in water splitting, i.e., water oxidation. Due to the complexity of the Step 2 reaction, the challenges in the water oxidation process involve multiple proton-coupled electron transfer processes and O—O bond formation.

$$2H_2O+h^{\nu}\rightarrow 2H_2+O_2$$

Step 1 $2H^{+}+4e^{-}\rightarrow H_2$

Step 2 $2H_2O\rightarrow O_2+4H^{+}+4e^{-}$

[0003] Scheme 1. Splitting of Water

[0004] There has been great effort over the years to develop a method to split water under a variety of conditions. This includes developing methods such as 1) electrolysis, 2) photoelectrochemical water splitting, 3) photocatalytic water splitting, 4) photobiological water splitting, and 5) thermal decomposition of water.

[0005] Hydrogen production from water using electrical means is not a viable option, as the energy consumed in this process is more than what is produced in the form of hydrogen. Photoelectrochemical, photocatalytic and photobiological methods are no doubt of prime importance in water splitting research. However, to date there has been very limited success due to the high complexity and cost of such methods as well as their low efficiency in producing hydrogen.

[0006] Comprehensive efforts have been made to understand the reaction mechanisms of water splitting using a catalyst. The catalytic concepts center around the use of transition metals or biological systems coupled with sunlight. However, most of the reported literature is confined to the use of conjugated complex ligands or metal oxides, and they are often designed or selected in view of their efficiency in sunlight absorption, thus mimicking nature. There has been little to no progress in the use of low-energy microwaves and non-conjugated ligands in the generation of hydrogen via water splitting.

[0007] In view of the above, there is a need to develop catalysts and reactions capable of splitting water and generating hydrogen. Accordingly, an object of the invention is to provide such a process and catalyst. Other objects will also be apparent from the detailed description of the invention.

SUMMARY OF THE INVENTION

[0008] Broadly stated, the objects of the invention are realized, according to one aspect of the invention, by synthesizing a chitosan-ruthenium catalyst and using this catalyst in a reaction to split water and produce hydrogen. There is no history of using low-energy microwaves and non-conjugated ligands in the generation of hydrogen via water splitting. In continuation of the inventors ongoing efforts to discover the versatility of renewable biopolymers as catalyst supports in organic synthesis, they serendipitously discovered in situ generation of hydrogen via water splitting using a chitosan ruthenium composite under microwave (MW) irradiation conditions. The processes of the invention also relate to the aqueous reduction of nitro compounds.

[0009] In one embodiment, the invention embraces a process for generating hydrogen and oxygen from water. The process includes the following steps: preparing a ruthenium on chitosan catalyst, bringing the catalyst into contact with an aqueous mixture under basic conditions, and applying microwave energy to the aqueous mixture to produce hydrogen and oxygen.

[0010] In one embodiment, the catalyst is prepared by a process including the following steps: suspending chitosan in water; adding $RuCl_3.3H_2O$; adjusting the pH of the mixture to about 8.5 to about 9.5 while continuously stirring the mixture; separating the catalyst from the liquid in the mixture using a centrifuge; and drying the mixture under a vacuum. The pH of the mixture may be adjusted using ammonia, and the catalyst may be dried under a vacuum at about 30° C. to about 60° C.

[0011] In the process of separating water into hydrogen and oxygen, the aqueous mixture may be maintained at about 125° C. during the reaction. In one embodiment, the aqueous mixture is maintained at this temperature for about 30 minutes during the reaction. In another embodiment, K_2CO_3 is used to maintain basic conditions in the aqueous mixture.

[0012] In one embodiment of the invention, the concentration of base in the water is about 0.4 mmol/mL. In another embodiment, the microwave energy is applied at a power of about 100 watts for a time of about 60 to about 70 minutes.

[0013] In one embodiment of the invention, a nitrobenzene compound is added to the aqueous mixture prior to application of microwave energy. The nitrobenzene compound may be 4-bromo-nitrobenzene. In another embodiment of the invention, the reaction also produces a reduced organic compound. The reduced organic compound may comprise a 4-bromo-aniline.

[0014] In one embodiment of the invention, the concentration of hydrogen produced is at least 27.79%.

BRIEF DESCRIPTION OF THE DRAWINGS

[0015] The invention is more fully described by reference to the following detailed description and the accompanying drawings wherein:

[0016] FIG. **1** is a depiction of the Chitosan-Ruthenium (Ch-Ru) composite.

[0017] FIG. **2** shows an experimental set up to perform the MW reaction in a sealed microwave tube.

[0018] FIG. **3**(*a*) provides an SEM image of the ChRu catalyst.

[0019] FIG. **3**(*b*) provides an X-ray diffraction image of the ChRu catalyst.

[0020] FIG. **3**(*c*) provides an energy dispersive spectra (EDS) of ChRu catalyst.

[0021] FIG. **3**(*d*) provides XPS data for the ChRu catalyst.

[0022] FIG. **4** provides GC-MS data confirming the formation of p-amino phenol A.

[0023] FIG. **5** provides GS-MS data confirming the formation of diaryl either B.

[0024] FIG. **6** provides GC-MS data confirming the formation of nitro reduced diaryl either C.

[0025] FIG. **7** provides GC-MS data showing the reduction of nitro group under MW heating conditions exclusively in basic media.

[0026] FIG. **8** provides GC-MS Head Space Analysis data showing the hydrogen concentration produced with the catalyst of the invention, suspended in aqueous K_2CO_3, was exposed to microwave heating for 30 minutes.

[0027] FIG. **9** provides GC-MS Head Space Analysis GC-MS Head Space Analysis data showing the hydrogen concentration produced under the same conditions as in FIG. **8** but using a different base.

[0028] FIG. **10** provides GC-MS Head Space Analysis data showing the hydrogen concentration produced under the same conditions as in FIG. **8** but using a different base.

[0029] FIG. **11** provides GC-MS Head Space Analysis data showing the hydrogen concentration produced under the same conditions as in FIG. **8** but using a different base.

[0030] FIG. **12** provides GC-MS Head Space Analysis data showing the hydrogen concentration produced under the same conditions as in FIG. **8** but using a different base.

[0031] FIG. **13** provides GC-MS Head Space Analysis data showing the hydrogen concentration produced under the same conditions as in FIG. **8** but using a different base.

[0032] FIG. **14** provides GC-MS Head Space Analysis data showing the hydrogen concentration produced under the same conditions as in FIG. **8** but using a different base.

[0033] FIG. **15** provides GC-MS Head Space Analysis data showing the hydrogen concentration produced under the same conditions as in FIG. **8** but using a different base.

[0034] FIG. **16** provides GC-MS Head Space Analysis data showing the hydrogen concentration produced under the same conditions as in FIG. **8** using a lower concentration of K_2CO_3.

[0035] FIG. **17** provides GC-MS Head Space Analysis data showing the hydrogen concentration produced under the same conditions as in FIG. **8** but at a lower temperature (100° C. vs. 125° C.).

[0036] FIG. **18** is a depiction of a Chitosan-Fe (ChFe) composite.

[0037] FIG. **19** is a depiction of a Chitosan-Pd (ChPd) composite.

[0038] FIG. **20** is a depiction of a Cellulose-Fe (CelluFe) composite.

[0039] FIG. **21** is a depiction of a Cellulose-Pd (CelluPd) composite.

[0040] FIG. **22** is a depiction of a Cellulose-Ru (CelluRu) composite.

[0041] FIG. **23** is a depiction of water splitting and nitro compound reduction reactions on a Chitosan-Ruthenium (Ch-Ru) composite catalyst.

DETAILED DESCRIPTION OF THE INVENTION

[0042] Referring more specifically to the drawings, FIG. **1** is a structural representation of the Chitosan-Ru composite catalyst prepared by the inventors. The Chitosan-Ru catalyst has been characterized by SEM (FIG. **3**(*a*)) and X-ray diffraction (XRD)(FIG. **3**(*b*)). The signals pertaining to the Ru metal were not detected in the XRD data, possibly due to complexation with chitosan or its low percentage. However, the presence of the Ru-metal has been confirmed by energy dispersive X-ray spectroscopy (FIG. **3**(*c*)). XPS analysis of ChRu was performed to analyze the oxidation state of the Ru metal; the binding energy peak for Ru $3d_{5/2}$ at 282.5 eV is in accordance with $Ru_{(III)}$ (XPS, FIG. **3**(*d*)). The weight percentage of Ru was found to be 6.41% by inductively coupled plasma-atomic emission spectroscopy (ICP-AES) analysis.

[0043] While demonstrating the application of ruthenium chitosan composite ChRu in C—O aryl bond formation in aqueous media (Scheme 2), the inventors observed the formation of three products: p-amino phenol A (FIG. **4**), expected diaryl ether B (FIG. **5**) and nitro reduced diaryl ether C (FIG. **6**). The detection of reduced nitro group to amine in the product mixture was unexpected, which in turn prompted the inventors to investigate how the reduction of nitro group is feasible under these conditions.

Scheme 2. RuCh catalyzed C—O coupling

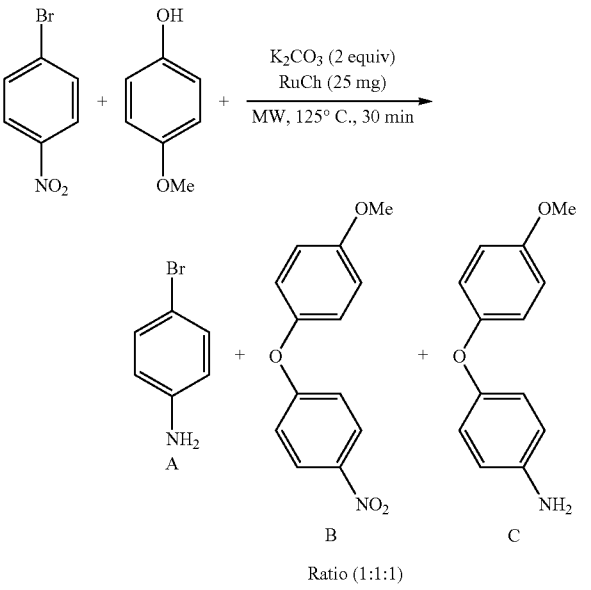

Ratio (1:1:1)

[0044] The study was undertaken with 4-bromo-nitrobenzene as a model substrate in order to find out the best possible conditions for the reduction reaction. The reduction of nitro group occurs under MW heating conditions exclusively in basic media (See Table 1, FIG. **7**).

TABLE 1

Screening for the catalytic reduction of nitro group

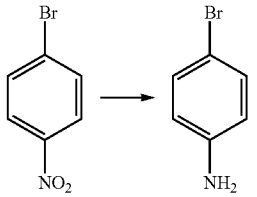

Entry	Catalyst	Base	Temp	Product Yield[a]
1	No catalyst	—	125° C.	0%
2	RuCh (25 mg)	—	125° C.	0%
3	RuCh (25 mg)	K_2CO_3	125° C.	0%
4	RuCh (25 mg)	—	125° C./MW	0%
5	RuChH (25 mg)	K_2CO_3	125° C./MW	89%[b]

[a]Reaction condition: 4-Nitro-bromobenzene (1 mmol), RuCh-catalyst (25 mg), K_2CO_3 (2 mmol), Water 5 mL, MW, 125° C., 30 min; [b]GC Conversion

[0045] After optimizing the reaction conditions that provided an ideal environment for reduction, the inventors searched for the source of the nitro reduction. Their studies led them to hypothesize that hydrogen may be generated in-situ in the reaction mixture, which could be responsible for the reduction of the nitro group. The hydrogen evolution through splitting of water is possible through use of a specially designed, sophisticated and highly conjugated ruthenium metal complex under photochemical conditions. In order to detect the generation of hydrogen in the reaction mixture, the inventors designed an experimental set up to perform the MW reaction in a sealed tube (see FIG. **2**). The design and accompanying conditions prevent the escape of hydrogen gas. The head space analysis of the sealed tube after the reaction would help to identify the gaseous atmosphere over the reaction mixture.

[0046] Accordingly, the inventors carried out experiments and studied the head space atmosphere. The head space analysis after the reaction was encouraging, as the inventors observed that substantial percentages of hydrogen were detected (~27%) (Table 2). Under neutral conditions, no splitting of water was discerned even after prolonged exposure to MW, UV-visible light and conventional heating (Table 2, entries 1-4). However, when the catalyst, suspended in aqueous K_2CO_3, was exposed to MW heating for 30 min, 27.79% of hydrogen (Table 2, entry 8) was detected in head space analysis (FIG. **8**). The experiments were set-up to screen the different bases and their effect on water splitting. Use of Cs_2CO_3 as a base results in 4.15% of hydrogen (Table 2, entry 9, FIG. **9**), whereas $NaHCO_3$, Na_2CO_3 and NaOH provided 0.79% hydrogen (Table 2, entry 10, FIG. **10**), 1.22% hydrogen (Table 2, entry 11, FIG. **11**) and 7.39% hydrogen (Table 2, entry 12, FIG. **12**), respectively, after head space analysis. Other bases, namely KOH, $KHCO_3$ and K_3PO_4, generated 3.84% (Table 2, entry 13, FIG. **13**), 1.28% (Table 2, entry 14, FIG. **14**) and 1.90% (Table 2, entry 15, FIG. **15**) of hydrogen under similar conditions. However, when the concentration of K_2CO_3 was reduced from 2 mmol in 5 mL water to 1 mmol in 5 mL water there was a sharp decline in the hydrogen percentage from 27.79% to 2.26% (Table 2, entry 16, FIG. **16**). The MW exposure at the reduced temperature of 100° C. directly impacts the efficiency of water splitting, thereby reducing the hydrogen percentage to 0.15% (Table entry 17, FIG. **17**). In basic media using K_2CO_3, no hydrogen was detected under conventional heating or UV-Visible light exposure (Table 2, entries 5-7). Having confirmed K_2CO_3 as an ideal base and its appropriate concentration for water splitting under MW, the use of alternative biorenewable support such as cellulose and other metals such as iron and palladium were explored.

TABLE 2

ChRu-catalyzed water splitting under MW

Entry	Catalyst	Base	Time/Temp	Energy source	% Hydrogen[a]
1	ChRu	—	60 min/125° C.	MW	0%
2	ChRu	—	24 h/ambient temp	UV	0%
3	ChRu	—	24 h/ambient temp	Visibile light	0%
4	ChRu	—	24 h/125° C.	oil bath	0%
5	ChRu	K_2CO3	24 h/ambient temp	UV	0%
6	ChRu	K_2CO3	24 h/ambient temp	Visibile light	0%
7	ChRu	K_2CO3	24 h/125° C.	oil bath	0%
8	ChRu	K_2CO_3	30 min/125° C.	MW	27.79%
9	ChRu	Cs_2CO_3	30 min/125° C.	MW	4.15%
10	ChRu	$NaHCO_3$	30 min/125° C.	MW	0.79%
11	ChRu	Na_2CO_3	30 min/125° C.	MW	1.22%
12	ChRu	NaOH	30 min/125° C.	MW	7.39%
13	ChRu	KOH	30 min/125° C.	MW	3.84%
14	ChRu	$KHCO_3$	30 min/125° C.	MW	1.28%
15	ChRu	K_3PO_4	30 min/125° C.	MW	1.90%
16[b]	ChRu	K_2CO_3	30 min/125° C.	MW	2.26%
17[c]	ChRu	K_2CO_3	30 min/100° C.	MW	0.15%

[a]Reaction conditions: Base (2 mmol), water (5 mL);

[b]1 mmol of K_2CO_3, water (5 mL), MW, 125° C.;

[c]Reaction was performed at 100° C., using 2 mmol of K_2CO_3 in 5 mL of water.

[0047] The microwave irradiation of ChFe, ChPd, CelluFe, CelluPd, CelluRu, (see FIGS. **18-22**, respectively) under basic media, using K_2CO_3 as a base was performed without a detectable presence of hydrogen in the head space analysis (Table S1).

TABLE S1

Screeing of water splitting using Fe, Pd and alternative biopolymer

Entry	Catalyst	Base	Time/Temp	Energy source	Hydrogen[a,b]
1	CelluRu	K_2CO_3	30 min/125° C.	Microwave	0.00%
2	CelluPd (II)	K_2CO_3	30 min/125° C.	Microwave	0.00%
3	CelluFe(III)	K_2CO_3	30 min/125° C.	Microwave	0.00%
4	ChFe(III)	K_2CO_3	30 min/125° C.	Microwave	0.00%
5	ChPd (II)	K_2CO_3	30 min/125° C.	Microwave	0.00%

[a]Reaction condition: K_2CO_3 (2 mmol), Water (5 mL), MW, Metal catalyst (25 mg).

[b]Percentage after Head space analysis

TABLE S2

Recycling of ChRu catalyst in nitro reduction

Entry	Substrate	Time	Product	Conversion[a],[b]
Cycle 1	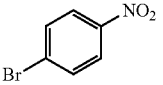	60 min	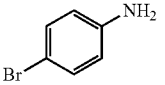	>99%
Cycle 2	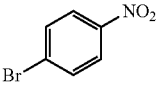	60 min	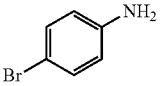	>99%
Cycle 3	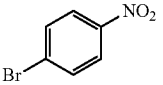	60 min	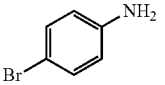	>99%
Cycle 4	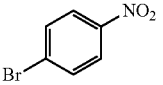	60 min	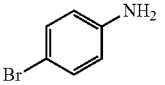	>99%
Cycle 5	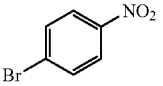	60 min	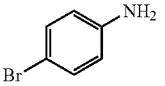	>99%

[a]Reaction condition: 1 mmol of 4-nitro bromobenzene, 2 mmol of K_2CO_3, ChRu (25 mg), 5 mL water, MW, 125° C., 60 min; [b]GC conversion

Scheme 3. Metal-catalyzed reduction of nitro group

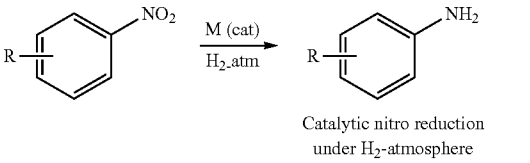

Catalytic nitro reduction under H_2-atmosphere

M = Metal
M = Pd, Pt, Ni, Ru etc

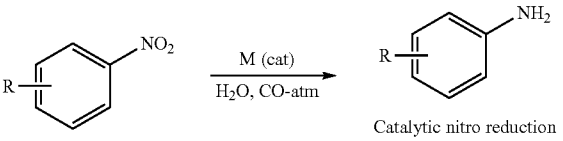

Catalytic nitro reduction using water and CO-mixture as hydrogen source

M = Rh, Ru, Au etc

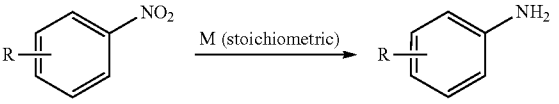

Nitro reduction using stoichiometric amount of metal.

M = Fe, Sn etc

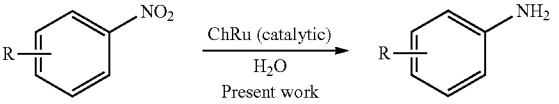

Catalytic reduciton using water as a hydrogen source

M = Fe, Sn etc

[0048] The selective reduction of nitro compounds to amines is one of the very important transformations in organic synthesis, and consequently there are number of procedures for the reduction of nitro compounds (Scheme 3). Due to concern for the environment, the search for simple, chemo-selective, affordable and environmentally benign methods that avoid the use of hazardous and expensive reducing agents in stoichiometric amounts has gained prime importance. The use of a binary mixture of CO and H_2O as a hydrogen source along with specially designed Rh, Au or Ru metal complex catalysts has been considered as one of the most useful methods for nitro reduction. The in-situ generation of hydrogen from water and its utilization in reduction of nitro compounds using simple biodegradable renewable chitosan has never been reported (see bottom, Scheme 3).

TABLE 3

ChRu catalyzed reduction of nitro compund.

Entry	Substrate	Time	Product	Conversion[a],[b]
1	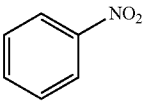	60 min	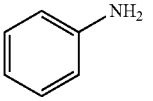	>99%

TABLE 3-continued

ChRu catalyzed reduction of nitro compund.

Entry	Substrate	Time	Product	Conversion[a],[b]
2	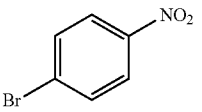	60 min	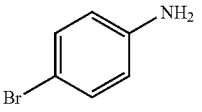	>99%
3	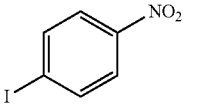	60 min	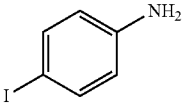	>99%
4	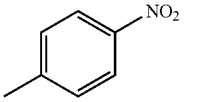	70 min	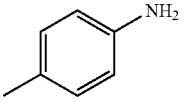	>99%
5	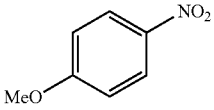	70 min	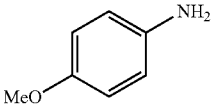	>99%
6	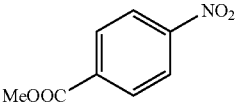	60 min	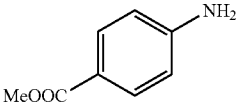	>99%

[a]Reaction condition: 1 mmol of nitro compound, 2 mmol of K_2CO_3, ChRu (25 mg), 5 mL water, MW, 125° C., 60-70 min; [b]GC conversion

[0049] The experimental procedure entailed placing aromatic nitro compound (1 mmol) into a microwave reaction tube, to which K_2CO_3 (2 mmol), ChRu (25 mg) and 5 mL of water were added and exposed to microwave irradiation for 60-70 min at 125° C. The reaction was monitored using GCMS. In almost all the cases, the nitro group is selectively reduced to the corresponding amine (Table 3).

[0050] The recovery of the catalyst is the most important goal in a sustainable organic synthesis. In industrial application of heterogeneous system, the lifetime of the catalyst and its level of reusability are significantly important factors. To demonstrate recyclability of ruthenium chitosan composite, a set of experiments was conducted for the hydrogenation of 4-nitro bromo benzene using the recycled ChRu catalyst. After the completion of the reaction, the catalyst was recovered, washed with acetone, and dried under vacuum. A fresh reaction was then set-up using fresh reactants and recycled catalyst and subjected to MW irradiation. The ChRu catalyst could be used at least five times without any change in its activity. Metal leaching was studied using ICP-AES analysis of the catalyst before and after the completion of the reaction. The Ru concentration was found to be 6.41% before the reaction and 6.35% after the reaction. The very small amount of Ru metal was detected in the aqueous mixture. The negligible amount of Ru leaching may be due to the well-defined structure of chitosan with its abundance of amine and hydroxyl functional groups. While it is only theory, chitosan's advantageous structural characteristics may result in Ru chelating via non-covalent interaction.

Examples

Experimental Procedure for Synthesis of Chitosan Ruthenium Catalyst (ChRu)

[0051] The Ruthenium on Chitosan catalyst was made as follows. Chitosan (3 g, medium molecular weight, Aldrich, CSA #9012-76-4) was suspended in 100 mL of water. To this suspension, 500 mg of $RuCl_3.3H_2O$ was added. The pH was adjusted to 9 using 25% ammonia, and the suspension was continuously stirred overnight. The catalyst was separated using a centrifuge operated at 5000 rpm for 5 minutes. The catalyst was then dried under vacuum at 50° C. for about 2 hours to about 3 hours.

Reduction of Nitro Group

[0052] Nitro compound (e.g., the aromatic nitro compound, 4-bromonitrobenzene, 1.0 mmol), ChRu (25 mg, 0.015, mol %) and K_2CO_3 (2 mmol) were placed in a crimp-sealed thick-walled glass tube equipped with a pressure sensor and a magnetic stirrer. Water (5 mL) was added to the reaction mixture. The reaction tube was placed inside the cavity of a CEM Discover focused microwave synthesis system and operated at 125° C. (temperature monitored by a built-in infrared sensor) and 100 Watts for 60-70 minutes. After completion of the reaction, the catalyst was removed from the reaction mixture using a centrifuge. Reduction of the nitro group has been monitored using GCMS. The clear liquid was cooled slowly, and, in most cases, an analytically pure sample of corresponding amine was obtained. The samples can be isolated from the water medium by simple decantation.

[0053] In brief, the inventors have demonstrated the unprecedented use of pure water as a hydrogen source in the catalytic hydrogenation of nitro compounds wherein ruthenium chitosan composite can split water under microwave irradiation conditions. See FIG. **23**. Ruthenium chitosan composite performs a dual action of producing hydrogen and subsequently catalyzing the reduction of nitro groups to amine under MW irradiation. As a result of this invention, low energy MW has been shown to assist in weakening the O—H bound in water molecules, which results in instigating the splitting of water into hydrogen. These findings may pave the way for the future the expansion of microwave-assisted chemistry in concerted reactions such as hydrogen production from water and hydrogenation.

[0054] As the present invention may be embodied in several forms without departing from the spirit or essential characteristics thereof, it will be understood that the invention is not limited by the details of the foregoing description, unless otherwise specified, but rather should be construed broadly within its spirit and scope as defined in the appended claims, and therefore all changes and modifications that fall within the metes and bounds of the claims. Accordingly, the invention is defined by the appended claims.

REFERENCES

[0055] [1]. R. E. Blankenship, *Molecular Mechanisms of Photosynthesis*, Blackwell Science, Oxford, U.K., 2002.

[0056] [2]. H. J. Lewerenz, L. Peter, *Photoelectrochemical Water Splitting: Materials, Processes and Architectures*, The Royal Society of Chemistry 2013.

[0057] [3]. R. V. D. Krol, M. Gratzel, *Photoelectrochemical Hydrogen Production*, Springer Science, 2012.

[0058] [4]. T. Hisatomi, J. Kubota, K. Domen, *Chem. Soc. Rev.,* 2014, DOI: 10.1039/C3CS60378D

[0059] [5]. A. Kudo, Y. Miseki, *Chem. Soc. Rev.,* 2009, 38, 253-278.

[0060] [6]. J. J. Concepcion, J. W. Jurss, M. K. Brennaman, P. G. Hoertz, A. O. T. Patrocinio, N. Y. Murakami, J. L. Templeton, T. J. Meyer, *Acc. Chem. Res.* 2009, 42, 1954-1965.

[0061] [7]. S. Romain, L. Vigara, A. Llobet, *Acc. Chem. Res.* 2009, 42, 1944-1953.

[0062] [8]. G. S. Parkinson, Z. Novotny, P. Jacobson, M. Schmid, U. Diebold, *J. Am. Chem. Soc.,* 2011, 133, 12650-12655.

[0063] [9]. R. H. Gonçalves, B. H. R. Lima, E. R. Leite, *J. Am. Chem. Soc.,* 2011, 133, 6012-6019.

[0064] [10]. M. Higashi, K. Domen, R. Abe, *J. Am. Chem. Soc.,* 2012, 134, 6968-6971.

[0065] [11]. M. T. Mayer, C. Du, D. Wang, *J. Am. Chem. Soc.,* 2012, 134, 12406-12409.

[0066] [12]. J. Cohen, K. Kim, M. L. Ghirardi, K. Schulten, M. Seibert, P. King, *Biochem. Soc. Trans.* 2005, 33, 80-82.

[0067] [13]. A. S. Fedorov, S. Kosourov, M. Seibert, M. L. Ghirardi, *Appl. Biochem. Biotechnol.* 2005, 403-412.

[0068] [14]. G. Sirasani, L. Tong, and E. P. Balskus, *Angew. Chem. Int. Ed.* 2014, 53, 7785-7788

[0069] [15]. L. Vigh, D. A. Los, I. Horv_th, N. Murata, *Proc. Natl. Acad. Sci*. USA 1993, 90, 9090-9094.

[0070] [16]. X. H. Li, X. Wang, M. Antonietti, *Chem. Sci.,* 2012, 3, 2170

[0071] [17]. K. S. Joya, Y. F. Joya, K. Ocakoglu, R. V. Krol, *Angew. Chem. Int. Ed.* 2013, 52, 10426-10437.

[0072] [18]. R. B. Nasir Baig, R. S. Varma *Chem. Commun.,* 2013, 49, 752-770.

[0073] [19]. R. B. Nasir Baig, B. R. Vaddula, M. A. Gonzalez, R. S. Varma, *RSC Adv.,* 2014, 4, 9103-9106.

[0074] [20]. R. B. Nasir Baig, M. N. Nadagouda, R. S. Varma, *Green Chem.,* 2014, 16, 2122-2127.

[0075] [21]. X. Yang, M. B. Hall, *J. Am. Chem. Soc.,* 2010, 132, 120-130

[0076] [22]. M. J. Krische, Y. Sun, *Acc. Chem. Res.,* 2007, 40, 1237-1237.

[0077] [23]. I. Sorribes, G. Wienhcfer, C. Vicent, K. Junge, Rosa Lusar, M. Beller, *Angew. Chem. Int. Ed.* 2012, 51, 7794-7798.

[0078] [24]. D. Cantillo, M. Baghbanzadeh, C. O. Kappe, *Angew. Chem. Int. Ed.* 2012, 51, 10190-10193.

[0079] [25]. L. He, L. C. Wang, H. Sun, J. Ni, Y. Cao, H. Y. He, K. N. Fan, *Angew. Chem. Int. Ed.* 2009, 48, 9538-9541.

[0080] [26]. C. O. Kappe, *Angew. Chem. Int. Ed.* 2013, 52, 2-7

[0081] [27]. G. B. Dudley, A. E. Stiegman, M. R. Rosana, *Angew. Chem. Int. Ed.* 2013, 52, 2-8.

The invention claimed is:

1. A process for generating hydrogen and oxygen from water, the process comprising preparing a ruthenium on chitosan catalyst, bringing the catalyst into contact with an aqueous mixture under basic conditions, and applying microwave energy to the aqueous mixture to produce hydrogen and oxygen.

2. The process of claim **1** wherein the catalyst is prepared by

(a) suspending chitosan in water;

(b) adding $RuCl_3.3H_2O$;

(c) adjusting the pH of the mixture to about 8.5-9.5 while continuously stirring the mixture;

(d) separating the catalyst from the liquid in the mixture; and

(e) drying the mixture under a vacuum.

3. The process of claim **2** wherein the pH of the mixture is adjusted using ammonia.

4. The process of claim **2** wherein the catalyst is dried under a vacuum at a temperature from about 30-60° C.

5. The process of claim **1** wherein aqueous mixture is maintained at about 125° C. during the reaction.

6. The process of claim **5** wherein the aqueous mixture is maintained at about 125° C. for about 30 minutes during the reaction.

7. The process of claim **1** wherein K_2CO_3 is used to maintain basic conditions in the aqueous mixture.

8. The process of claim **1** wherein the concentration of base in the water is about 0.4 mmol/mL.

9. The process of claim **1** wherein microwave energy is applied at a power of about 100 watts for a time of about 60 to about 70 minutes.

10. The process of claim **1** wherein a nitrobenzene compound is added to the aqueous mixture prior to application of microwave energy.

11. The process of claim **10** wherein the nitrobenzene compound is 4-bromo-nitrobenzene.

12. The process of claim **11** wherein the reaction also produces a reduced organic compound.

13. The process of claim **12** wherein the reduced organic compound comprises a 4-bromo-aniline.

14. The process of claim **1** wherein the concentration of hydrogen produced is at least 4.15%.

15. The process of claim **1** wherein the concentration of hydrogen produced is at least 27.79%.

16. The process of claim **2** wherein the catalyst is separated from the liquid in the mixture using a centrifuge.

* * * * *

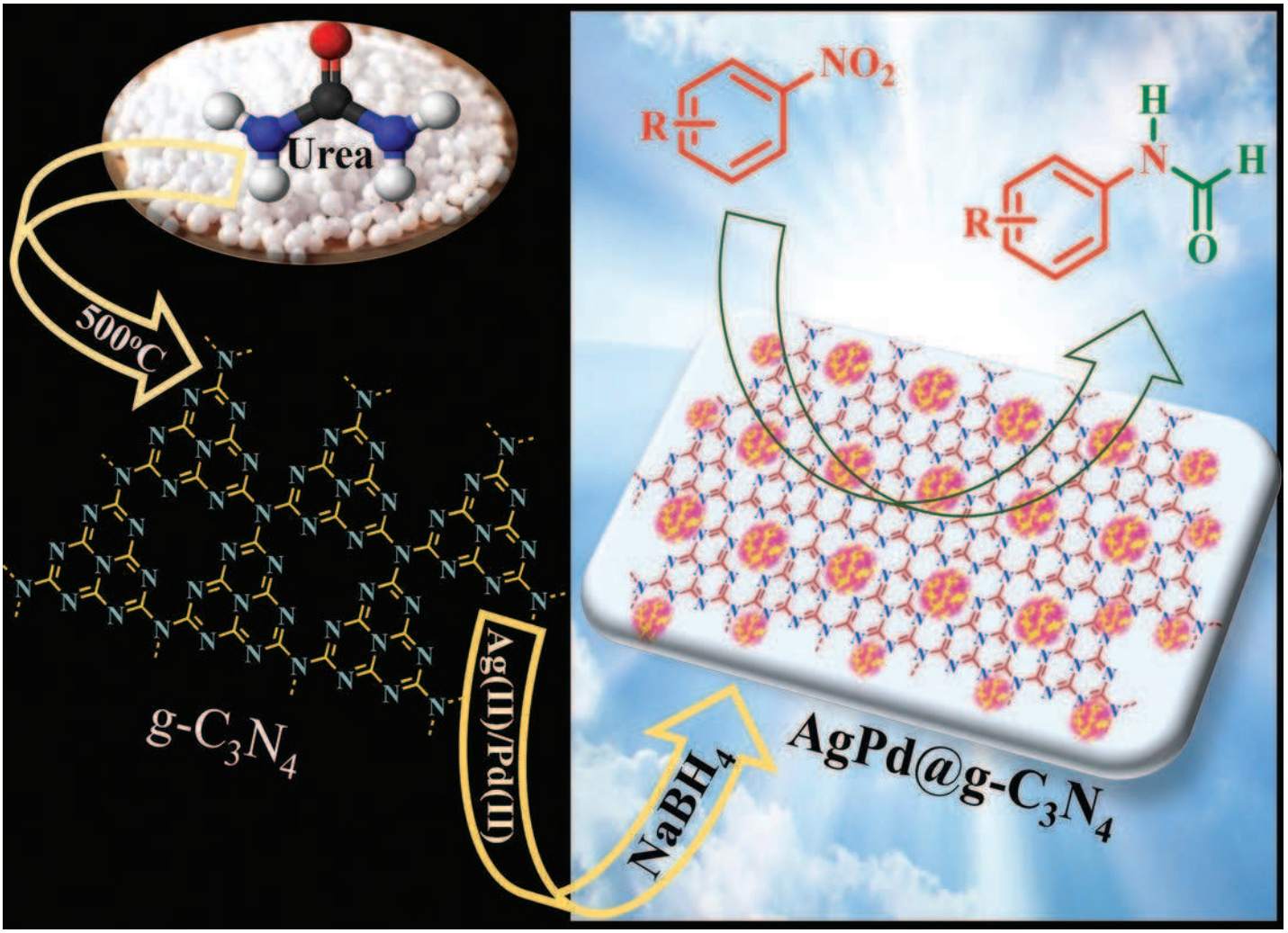

An article presented by Prof. Rajender S. Varma *et al*. of the U.S. Environmental Protection Agency, Cincinnati, USA.

Title: A photoactive bimetallic framework for direct aminoformylation of nitroarenes

A bimetallic catalyst, AgPd@g-C_3N_4, was synthesized by immobilizing silver and palladium nanoparticles over the surface of graphitic carbon nitride (g-C_3N_4) and its utility was demonstrated for the concerted aminoformylation of aromatic nitro compounds under visible light conditions. The entwined AgPd@g-C_3N_4 catalyst was very effective in exploiting formic acid as a source of hydrogen and acting as a formylating agent under photochemical conditions.

As featured in:

See Rajender S. Varma *et al*., *Green Chem*., 2016, **18**, 1019.

ROYAL SOCIETY OF CHEMISTRY

www.rsc.org/greenchem

Registered charity number: 207890

Published on 15 December 2015. Downloaded by US Environmental Protection AG, Cincinnati on 30/03/2016 20:12:36.

Green Chemistry

PAPER

View Article Online
View Journal | View Issue

Cite this: *Green Chem.*, 2016, **18**, 1019

A photoactive bimetallic framework for direct aminoformylation of nitroarenes†

R. B. Nasir Baig,‡[a] Sanny Verma,‡[a] Mallikarjuna N. Nadagouda[b] and Rajender S. Varma*[a]

Received 20th November 2015,
Accepted 14th December 2015

DOI: 10.1039/c5gc02799c

www.rsc.org/greenchem

A bimetallic catalyst, AgPd@g-C_3N_4, synthesized by reducing silver and palladium salts over graphitic carbon nitride (g-C_3N_4), enables the concerted reductive formylation of aromatic nitro compounds under photo-chemical conditions using formic acid, which serves the dual role of a hydrogen source and a formylating agent.

Introduction

The synthesis of amines and their conversion to *N*-formyl derivatives are important reactions in organic synthesis due to their extensive application in natural product synthesis and drug discovery.[1] Conventionally, amino-formyl derivatives have been synthesized from nitro compounds in two separate steps involving nitro reduction followed by *N*-formylation.[2] Most of the earlier developed processes in the reduction of the nitro group use stoichiometric amounts of reagents. The heightened awareness of climate change and the growing importance of pollution prevention have resulted in a dramatic shift to using catalytic reagents instead. In general, the catalytic variant developed for the reduction of nitro compounds often requires high hydrogen pressure and elevated temperature,[3] safety being a worrisome concern for high pressure hydrogenation on the industrial scale. Alternative protocols have been advanced by employing *in situ* generated hydrogen along with a precious metal catalyst. Most of these procedures require vigorous stirring in aqueous media under a carbon monoxide atmosphere,[4] a hazardous and toxic contaminant. Formic acid, available from biomass resources, has been introduced as a safer alternative for the transfer hydrogenation of nitro compounds to generate aryl amines.[5] The formylation of amine has to be carried out subsequently in a separate step. Rutile-supported gold catalyst has achieved such a direct conversion of nitro compounds to *N*-formylamines.[6]

However, this reaction is temperature dependent. At elevated temperatures, it leads to the formation of *N*,*N*-demethylation whereas a slight variation towards the lower side (~60 °C) does not allow the formylation of reduced products.[7] In addition, it requires an inert atmosphere along with the use of organic solvents. Magnetically retrievable palladium catalyst has also been used for the conversion of nitro-arenes to the corresponding *N*-formyl derivatives; the complexity of the catalyst preparation and its higher loading are the main limitations of this method.[8] Iron metal in combination with the corresponding carboxylic acid has been introduced but lower product yields and heating over an extended period of time render this an unproductive and tedious method.[9] This prompted us to develop a simple and sustainable catalyst which can accomplish this transformation in aqueous media under ambient conditions. In continuation of our ongoing efforts to develop sustainable methods[10] that aim for a reduction in chemical waste generation,[11] we have designed a bimetallic AgPd@g-C_3N_4 photoactive heterogeneous catalyst system for the direct transformation of aromatic nitro compounds to *N*-formylamines.

Synthesis and characterization

Graphitic carbon nitride (g-C_3N_4) was synthesized by heating urea in a furnace at 500 °C and the ensuing pale yellow solid was dispersed in water by sonicating over a period of 15 min.[12] Silver and palladium salts ($AgNO_3$ and $Pd(NO_3)_2$) were sequentially added and the reaction mixture was stirred for 12 hours. The reaction temperature was raised to 50 °C and the silver and palladium salts were reduced to Ag(0) and Pd(0) nanoparticles using an excess of sodium borohydride ($NaBH_4$). The reaction mixture was cooled to ambient temperature, centrifuged and the solid was washed with methanol and vacuum

[a]*Sustainable Technology Division, National Risk Management Research Laboratory, U.S. Environmental Protection Agency, MS 443, Cincinnati, Ohio 45268, USA. E-mail: varma.rajender@epa.gov; Fax: +1 513-569-7677; Tel: +1 513-487-2701*
[b]*WQMB, WSWRD, National Risk Management Research Laboratory, U.S. Environmental Protection Agency, MS 443, Cincinnati, Ohio 45268, USA*
†Electronic supplementary information (ESI) available. See DOI: 10.1039/c5gc02799c.
‡These authors contributed equally to this work.

Published on 15 December 2015. Downloaded by US Environmental Protection AG, Cincinnati on 30/03/2016 20:12:36.

dried at 50 °C. The AgPd@g-C_3N_4 catalyst (Fig. 1) was isolated as a fine solid powder.

The catalyst was characterized using transmission electron microscopy, scanning electron microscopy, X-ray photoelectron spectroscopy, X-ray diffraction and inductively coupled plasma atomic emission spectroscopy (ICP-AES).

TEM spectra of the catalyst endorse the formation of single phase silver and palladium nanoparticles with a spherical morphology (Fig. 2). The SEM image of AgPd@g-C_3N_4 and its EDX confirm the immobilization of silver (Ag) and palladium (Pd) nanoparticles over the surface of g-C_3N_4 (Fig. 3). The concentrations of Ag (4.67%) and Pd (4.55%) were determined using ICP-AES analysis. The XPS (Fig. 4) analysis of AgPd@g-C_3N_4 corroborated the formation of palladium and silver nanoparticles on the surface of graphitic carbon nitride, which was further supported by XRD results (Fig. 5).

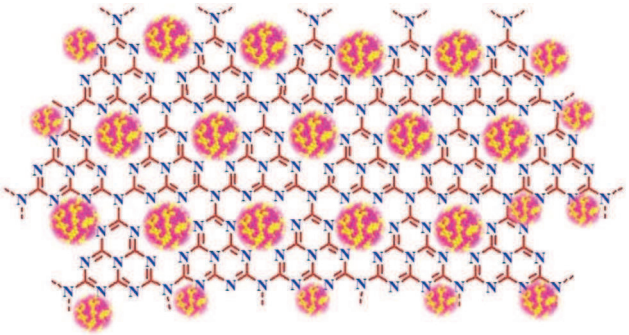

Fig. 1 Structure of AgPd@g-C_3N_4.

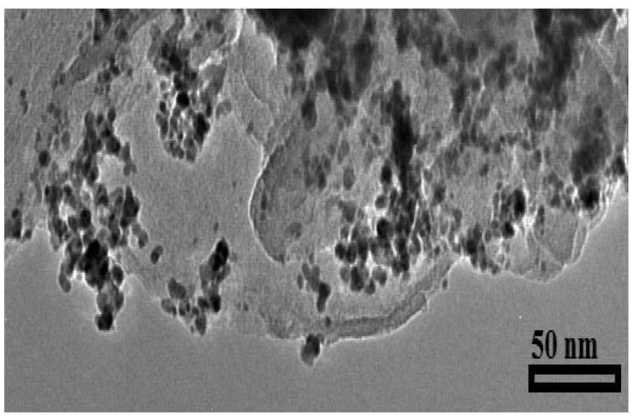

Fig. 2 TEM image of the AgPd@g-C_3N_4 catalyst.

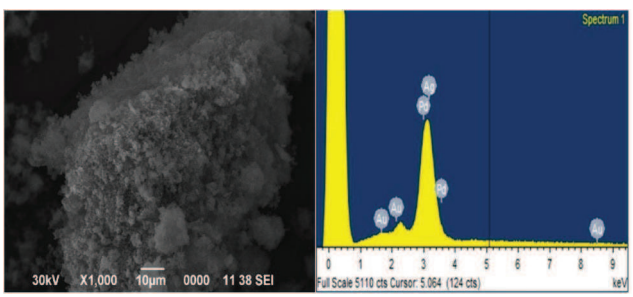

Fig. 3 SEM and EDX data of the AgPd@g-C_3N_4 catalyst.

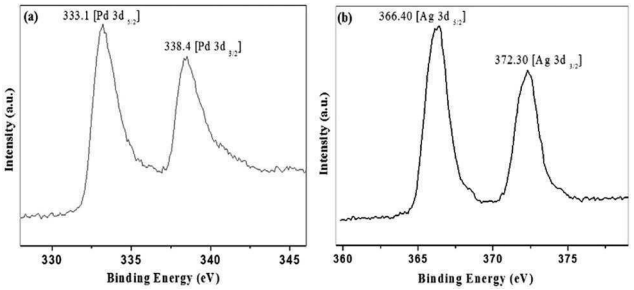

Fig. 4 XPS spectra of AgPd@g-C_3N_4: (a) Pd 3d XPS spectra; (b) Ag 3d XPS spectra.

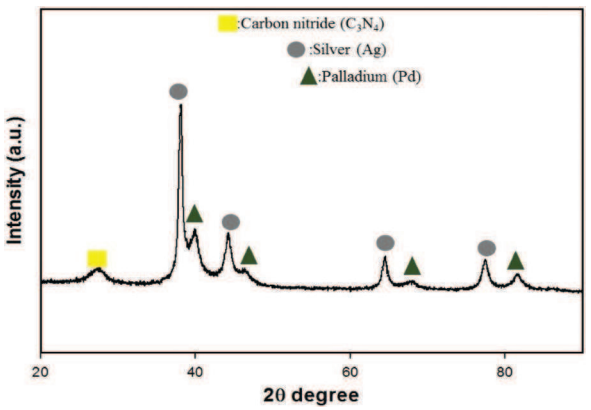

Fig. 5 XRD spectra of the AgPd@g-C_3N_4 catalyst.

Results and discussion

The most important step in the development of the active catalyst was the design and synthesis of a catalytic system for the direct conversion of nitro compounds to *N*-formylamine derivatives, preferably using visible light to drive this reaction. In view of the known prowess of graphitic carbon nitride (g-C_3N_4) as a photo active support,[13] we pursued this approach using formic acid as a reducing as well as a formylating agent in the presence of a bimetallic catalyst.

First, Pd (10 mol%) was immobilized on g-C_3N_4 and tested for the aqueous reductive formylation of the nitro group using formic acid as a hydrogen source; the formation of 47% of the desired product after 12 hours of exposure to visible light (Table 1, entry 1) was encouraging. Increasing the palladium load (Table 1, entry 2) did not improve the catalytic activity whereas low loading decreased the yield to 30% (Table 1,

 This journal is © The Royal Society of Chemistry 2016

Published on 15 December 2015. Downloaded by US Environmental Protection AG, Cincinnati on 30/03/2016 20:12:36.

Table 1 Screening of catalysts for *N*-formylation

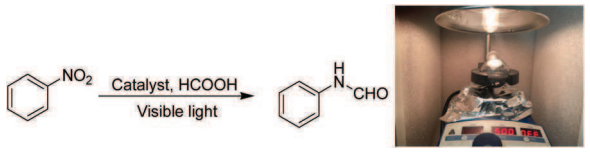

Entry	Catalyst	Time	Yield[a,b]
1	Pd@g-C_3N_4 (10% Pd)	12 h	48%
2	Pd@g-C_3N_4 (20% Pd)	12 h	49%
3	Pd@g-C_3N_4 (5% Pd)	12 h	31%
4	CuPd@g-C_3N_4 (10% Cu : 10% Pd)	12 h	65%
5	CuPd@g-C_3N_4 (10% Cu : 5% Pd)	12 h	55%
6	CuPd@g-C_3N_4 (5% Cu : 10% Pd)	12 h	69%
7	AgPd@g-C_3N_4 (10% Ag : 10% Pd)	2 h	99%
8	AgPd@g-C_3N_4 (10% Ag : 5% Pd)	5 h	88%
9	AgPd@g-C_3N_4 (5% Ag : 10% Pd)	2 h	99%
10	AgPd@g-C_3N_4 (2% Ag : 10% Pd)	5 h	85%
11	Ag@g-C_3N_4 (10% Ag)	24 h	—

[a] Reaction conditions: 1 mmol of nitrobenzene; formic acid (2 mmol); water (1.0 mL); catalyst (25 mg); 40 watt domestic bulb. [b] Isolated yield.

entry 3). These results suggested that Pd@g-C_3N_4 was not sufficiently active to accomplish this transformation. We sought to enhance its activity by adding a catalytic promoter, preferably an abundant material such as copper. Consequently, copper–palladium CuPd@g-C_3N_4 catalysts were synthesized and used, which afforded higher yields (65%) of the desired product (Table 1, entry 4). Various amounts of copper and palladium loadings were next examined (Table 1, entries 5 and 6). The CuPd@g-C_3N_4 catalyst with 10% Cu and 5% Pd (Table 1, entry 5) gave the desired product in 55% yield, whereas the CuPd@g-C_3N_4 catalyst with 5% Cu and 10% Pd gave 69% of the product. A recent report on the use of the Ag–Pd system on an ultrathin support[14] encouraged us to explore the use of silver as a co-catalyst partner, and therefore we synthesized the AgPd@g-C_3N_4 framework. The reaction of nitrobenzene with formic acid in the presence of bimetallic AgPd@g-C_3N_4 gave a quantitative yield of *N*-formyl aniline (Table 1, entry 7, 2 h). The variation in Ag and Pd concentrations in the catalyst played a crucial role in the reductive formylation of the nitro group. The catalyst with 10% Ag and 5% Pd loading required 5 h for the completion of the reaction (Table 1, entry 8). On the other hand, the catalyst system consisting of 5% Ag and 10% Pd gave a quantitative yield of the desired product within 2 h (Table 1, entry 9). Further reduction in the silver concentration led to an increase in the reaction time and a decrease in the product yield (Table 1, entry 10). The reaction with silver alone, Ag@g-C_3N_4, did not show any evidence of reductive formylation products even after 24 hours (Table 1, entry 11).

After establishing the ideal reaction conditions for the catalyst, it was imperative to evaluate the performance of AgPd@g-C_3N_4 with a wide variety of substrates. Accordingly, an array of nitro derivatives were subjected to reductive formylation reactions (Table 2, entries 1–9); all the substrates bearing electron donating (Table 2, entries 2 and 3) and electron withdrawing

Table 2 *N*-Formylation of nitroarenes by AgPd@g-C_3N_4 [a]

Entry	Reactant	Product	Time	Yield[b]
1	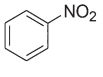	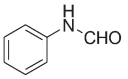	2 h	99%
2	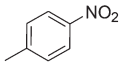	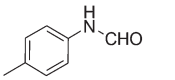	2 h	98%
3	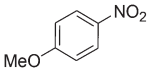	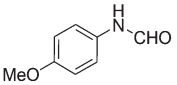	2 h	96%
4	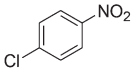	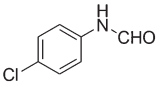	2 h	97%
5	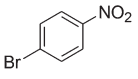	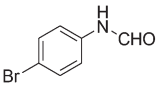	2 h	97%
6	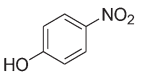	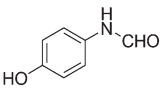	2 h	97%
7	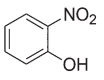	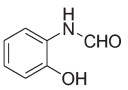	2 h	96%
8	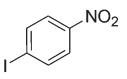	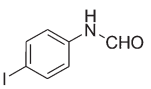	2 h	97%
9	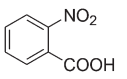	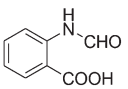	2 h	96%
10	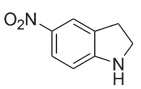	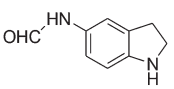	3 h	76%
11	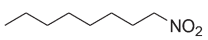	—	12 h	—

[a] Reaction conditions: nitroarenes (1 mmol); formic acid (2 mmol); water (1.0 mL); catalyst (25 mg); 40 watt domestic bulb. [b] Isolated yield.

substituents (Table 2, entries 4–9) were converted to the corresponding amino formyl derivatives. It was difficult to corroborate the reactivity pattern with the nature of the substituents and electronic behavior as most of the reactions were completed within 2 hours.

The recyclability of the catalyst in terms of practical and sustainable use was established using recycling experiments for the reductive formylation of nitrobenzene. After the completion of the first reaction, AgPd@g-C_3N_4 was recovered and reused for the reductive formylation of a fresh batch of nitrobenzene. AgPd@g-C_3N_4 was found to be stable and could be reused several times without losing its activity (ESI, S2†); even

Published on 15 December 2015. Downloaded by US Environmental Protection AG, Cincinnati on 30/03/2016 20:12:36.

after the 6th cycle, nitrobenzene was efficiently converted into *N*-formyl aniline. The reactivity and stability of the catalyst could be attributed to the graphitic carbon nitride (g-C_3N_4) which holds Ag and Pd nanoparticles firmly. The metal leaching in the AgPd@g-C_3N_4 catalyst was studied using ICP-AES analysis of the reaction solvent and the recycled catalyst before and after the reaction. The absence of metals in the mother liquor and the percentage of Ag (4.65%) and Pd (4.54%) in the recycled catalyst confirmed that g-C_3N_4 holds the metals tightly. The negligible metal leaching may be attributed to high porosity and polarity of the g-C_3N_4 support which holds these metals *via* non-covalent interactions.

Conclusions

Silver and palladium were immobilized by reducing their salt forms over a g-C_3N_4 (graphitic carbon nitride) surface. The synthesized AgPd@g-C_3N_4 catalyst was used for the direct amino formylation of an aromatic nitro group under photo-chemical conditions using visible light as a source of energy and formic acid as a reducing as well as a formylating agent. The bimetallic catalyst is highly effective in decomposing formic acid into hydrogen and for use as a formylating agent in a concerted process.

Disclaimer

The views expressed in this article are those of the authors and do not necessarily represent the views or policies of the U.S. Environmental Protection Agency. Any mention of trade names or commercial products does not constitute endorsement or recommendation for use.

Acknowledgements

RBNB and SV were supported by the Postgraduate Research Program of the National Risk Management Research Laboratory administered by the Oak Ridge Institute for Science and Education through an interagency agreement between the U.S. Department of Energy and the U.S. Environmental Protection Agency.

Notes and references

1 (*a*) S. Kotachi, Y. Tsuji, T. Kondo and Y. J. Watanabe, *Chem. Soc., Chem. Commun.*, 1990, 549–550; (*b*) G. W. Kabalka and R. S. Varma, in *Comprehensive Organic Synthesis*, ed. B. M. Trost and I. Fleming, Pergamon, Oxford, 1st edn, 1992, vol. 8, pp. 363–388; (*c*) G. R. Petit, M. V. Kalnins, T. M. H. Liu, E. G. Thomas and K. J. Parent, *Org. Chem.*, 1961, **26**, 2563–2566; (*d*) A. Jackson and O. Meth-Cohn, *J. Chem. Soc., Chem. Commun.*, 1995, 1319–1319.

2 (*a*) A. S. Guram and S. L. Buchwald, *Angew. Chem., Int. Ed. Engl.*, 1995, **34**, 1348–1350; (*b*) M. K. Basu, F. F. Becker and B. K. Banik, *Tetrahedron Lett.*, 2000, **41**, 5603–5722; (*c*) P. Strazzolini, A. G. Giumanini and S. Cauci, *Tetrahedron*, 1990, **46**, 1081–1118.

3 G. S. Vanier, *Synlett*, 2007, 131–135.

4 L. He, L. C. Wang, H. Sun, J. Ni, Y. Cao, H. Y. He and K. N. Fan, *Angew. Chem., Int. Ed.*, 2009, **48**, 9538–9541.

5 X. H. Li, Y. Y. Cai, L. H. Gong, W. Fu, K. X. Wang, H. L. Bao, X. Wei and J. S. Chen, *Chem. – Eur. J.*, 2014, **20**, 16732–16737.

6 X. B. Lou, L. He, Y. Qian, Y. M. Liu, Y. Cao and K. N. Fana, *Adv. Synth. Catal.*, 2011, **353**, 281–286.

7 B. Karimi, F. Mansouri and H. Vali, *ChemPlusChem*, 2015, **80**, 1750–1759.

8 L. Yu, Q. Zhang, S. S. Li, J. Huang, Y. M. Liu, H. Y. He and Y. Cao, *ChemSusChem*, 2015, **8**, 3029–3035.

9 K. Y. Lee, J. M. Kim and J. N. Kim, *Bull. Korean Chem. Soc.*, 2002, **23**, 1355–1498.

10 (*a*) R. S. Varma, *Green Chem.*, 2014, **16**, 2027–2041; (*b*) R. B. Nasir Baig and R. S. Varma, *ACS Sustainable Chem. Eng.*, 2014, **2**, 2155–2158; (*c*) S. Verma, H. P. Mungse, N. Kumar, S. Choudhary, S. L. Jain, B. Sain and O. P. Khatri, *Chem. Commun.*, 2011, **47**, 12673–12675; (*d*) S. Verma, J. L. Bras, S. L. Jain and J. Muzart, *Dalton Trans.*, 2013, **42**, 14454–14459.

11 (*a*) R. B. Nasir Baig, M. N. Nadagouda and R. S. Varma, *Green Chem.*, 2014, **16**, 4333–4338; (*b*) S. Verma, R. Singh, D. Tripathi, P. Gupta, G. M. Bahuguna and S. L. Jain, *RSC Adv.*, 2013, **3**, 4184–4188.

12 (*a*) J. Zhu, P. Xiao, H. Li and S. A. C. Carabineiro, *ACS Appl. Mater. Interfaces*, 2014, **6**, 16449–16465; (*b*) S. Verma, R. B. Nasir Baig, C. Han, M. N. Nadagouda and R. S. Varma, *Green Chem.*, 2016, **18**, 251–254; (*c*) S. Verma, R. B. Nasir Baig, C. Han, M. N. Nadagouda and R. S. Varma, *Chem. Commun.*, 2015, **51**, 15554–15557.

13 Z. Zhao, Y. Sun and F. Dong, *Nanoscale*, 2015, **7**, 15–37.

14 C. Hu, X. Mu, J. Fan, H. Ma, X. Zhao, G. Chen, Z. Zhou and N. Zheng, *ChemNanoMat*, 2015, DOI: 10.1002/cnma.201500162.

 This journal is © The Royal Society of Chemistry 2016

Part 2

Sustainable Hydrogen Production

Research category: 11. Industry and the Environment (IE)
Or
13. Sustainability and Innovation (SI)

[1]. R.S. Varma, B. Nasir, and M. Nadagouda "Ruthenium on chitosan (ChRu): concerted catalysis for water splitting and reduction. 2019, U.S. Patent 10,189,708 **(Citation=1)**

[2]. R. B. Nasir Baig, Sanny Verma, M. N. Nadagouda and R. S. Varma "A Photoactive bimetallic framework for direct aminoformylation of nitroarenes" *Green chem*istry **2016**, *18*, 1019-1022. **(Cover Page; IF= 9.405; immediacy index= 2.24; Citation half-life= 4.10; Citation= 18)**

1. Explain how the nominated paper's represent research that is innovative and important in advancing the scientific knowledge or technology relevant to EPA's mission. It is, important to provide a clear and compelling explanation of the relevance, and impact of the research to EPA's mission (For example, the relevance of the research to one of EPA's strategic goals may be described) (Limit to 16,000 characters including spaces.)

Explanation:

The two nominated papers demonstrate the sustainable production of hydrogen from a renewable source (e.g., water and formic acid) and further its utilization in chemical transformation.

Hydrogen production with renewable energies may have an essential role in the future as an energy vector and as a fuel. First nominated paper (Nadagouda, 2019, US Patent) revealed that ruthenium chitosan composite can split water into H_2 and O_2 under microwave irradiation. It performs the dual-task: it produces H_2 under microwave irradiation as well as catalyzing the reduction of a nitro group into an amine. The concept of nitro reduction with a dual-task from the metal catalyst, which involves the production of H_2 through the splitting of water followed by catalytic conversion of a nitro group into amine under microwave conditions, has not been predicted earlier. This patent demonstrates a new dimension to the microwave and catalytic hydrogenation chemistry and opens composite-based materials for H_2 production.

The second nominated paper (Varma, 2016) developed an efficient and sustainable protocol for the generation of hydrogen from formic acid using a bimetallic catalyst, AgPd@g-C_3N_4, under visible light. This bimetallic catalyst was synthesized by reducing silver and palladium salts over graphitic carbon nitride (g-C3N4), enables the concerted reductive formylation of aromatic nitro

compounds under photo-chemical conditions using formic acid, which serves the dual role of a hydrogen source and a formylating agent. Formic acid, the simplest carboxylic acid, is found in nature or can be easily synthesized in the laboratory (major by-product of some second-generation biorefinery processes); it is also an important chemical due to its innumerable applications in pharmaceuticals and industry.

Overall, these two papers are influential in fulfilling EPA mission such as “Sustainable Materials Management (SMM)” because these utilize sustainable hydrogen production and also help to combat energy demands that are covered by fossil fuels (https://www.epa.gov/sites/production/files/2015-08/documents/sustainable_materials_management_the_road_ahead.pdf). Over 65% of the world's energy demand is covered by fossil fuels, so hydrogen production developments, offer a more sustainable alternative that limits the production of harmful materials and greenhouse gases. Since these gases are known to be detrimental to the environment and human health, it is apparent that the advantages of this research do not only apply to chemical engineering but also applies to environmental preservation as well as the medical care industry.

2A. The EPA Guidelines prohibit resubmission of publications nominated for STAA Awards in previous years. If multiple publications are submitted, provide a comprehensive explanation of the relationship and lengths between subject matter among the different nominated publications. For example, the discussion could describe how one publication builds on the results of a second publication. (Limit to 16,000 characters including spaces.) Enter n/a if blank.

Response:

None of the two nominated papers included in this STAA package have been submitted for the STAA award in the past.

Two articles in this package are necessarily associated with each other as they demonstrate the generation of hydrogen from a renewable source such as form water and formic acid. As mentioned in answer to Question 1, the strength of this study is the breadth of researches that were performed for the utilization of marine waste (chitosan) derived heterogeneous catalyst to produce hydrogen from water (Nadagouda et al., 2019) and generation of hydrogen from formic under visible light irradiation (Varma 2016). All these research studies increase the national scale understanding of sustainable production of hydrogen and its utilization in chemical transformation.

2B. List the previous 5 year's of STAA nominations and associated publications for each EPA author. Categorize the list by author and include publication title, year, and award. (For example, John Smith, publication title(s), year(s), award(s).) (Limit to 16,000 characters including spaces.) Enter n/a if blank.

Response:

Mallikarjuna N. Nadagouda

1. Evaluating Sustainable Pathway to Furanics from Biomass via Heterogeneous Organo-Catalysis Green Chemistry
2. Sustainable Strategy Utilizing Biomass: Visible Light-Mediated Synthesis of g-Valerolactone. Published in ChemCatChem
3. Visible Light Mediated Upgrading of Biomass to Biofuel. Published in Green Chemistry

2017 Honorable Mention STAA

1. The Oxidative C-H activation of amines using protuberant lychee-like goethite. Published in Nature Climate Change
2. Photocatalytic C-H activation and oxidative esterification using Pd@g-C3N4. Published in Catalysis Today
3. Hydroxylation of benzene via C-H activation using bimetallic CuAg@g-C3N4. Published in ACS Sustainable Chemistry and Engineering

2019 Honorable Mention STAA

1. Conversion of spent carbon dioxide into value-added products
2. A sustainable approach to empower the bio-based future: upgrading biomass to value-added products

2019 Level III STTA

Rajender S. Varma

1. Evaluating Sustainable Pathway to Furanics from Biomass via Heterogeneous Organo-Catalysis Green Chemistry
2. Sustainable Strategy Utilizing Biomass: Visible Light-Mediated Synthesis of g-Valerolactone. Published in ChemCatChem
3. Visible Light Mediated Upgrading of Biomass to Biofuel. Published in Green Chemistry

2017 Honorable Mention STAA

1. The Oxidative C-H activation of amines using protuberant lychee-like goethite. Published in Nature Climate Change
2. Photocatalytic C-H activation and oxidative esterification using Pd@g-C3N4. Published in Catalysis Today
3. Hydroxylation of benzene via C-H activation using bimetallic CuAg@g-C3N4. Published in ACS Sustainable Chemistry and Engineering

2019 Honorable Mention STAA

1. Conversion of spent carbon dioxide into value-added products
2. A sustainable approach to empower the bio-based future: upgrading biomass to value-added products

2019 Level III STTA

2C. Provide a description of how this nomination's publication(s) differ from previous (last 5 years) and current nominations by the author(s). (Limit to 16,000 characters including spaces.) Enter n/a if blank.

Response:
Nadagouda's (2017 Honorable Mention STAA, 2019 Honorable Mention STAA and 2019 Level III STTA) awards are not related to the currently nominated work. The previous works were associated with the upgrading of biomass/waste to value-added products. However, the present work is related to sustainable hydrogen production from a renewable source.

Varma's (2017 Honorable Mention STAA, 2019 Honorable Mention STAA, and 2019 Level III STTA) awards are not related to the currently nominated work. The previous works were related to the upgrading of biomass/waste to value-added products. However, the present work is related to sustainable hydrogen production from a renewable source.

2D. Indicate whether previously submitted supplemental information is listed as supplemental information for the current nomination. (Limit to 16,000 characters including spaces.) Enter n/a if blank.

Response:

None of the supplemental information has been included in previous nominations.

2E. If any of the authors have submitted a concurrent nomination to another research category, provide sufficient justification to distinguish the difference between nominations. (Limit to 16,000 characters including spaces.) Enter n/a if blank.

Response:

There are no concurrent nominations by the authors on this nomination.

3A. Please provide substantial evidence for each of the following:
Provide evidence of recognition of the contribution from outside. (Limit to 16,000 characters including spaces.)

Response:

The first study (Nadagouda 2019) has been accepted as a US patent. Researcher Aminabhavi *et al.* cited and discussed our first research work (Nadagouda 2019) on hydrogen production in his review article (International Journal of Hydrogen Energy, 2019, 44, 10453-10472). The authors have summarized our research findings, indicating, "Recently, Nadagouda et al. revealed that ruthenium chitosan composite could split water into H2 and O2 under microwave irradiation. It performs the dual-task: it produces H2 under microwave irradiation as well as catalyzing the reduction of a nitro group into an amine. The concept of nitro reduction with a dual-task from the metal catalyst, which involves the production of H2 through the splitting of water followed by

catalytic conversion of a nitro group into amine under microwave conditions, has not been predicted earlier. This patent demonstrates a new dimension to the microwave and catalytic hydrogenation chemistry and opens up composite-based materials for H2 production." In this way, our work is particularly well-suited to help other researchers in the United States develop more strategic measures that optimize hydrogen production.

The second nominated paper (Varma, 2016) has been published in the prestigious journal "Green Chemistry" as "Journal Cover Page," which has an Impact Factor of 9.405 and has ranked#3 (h-index: 186) in the "Environmental Science" category. This research work has already been cited in 18 research articles (Google citation search). Prof. Hua et al. from the University of Chinese Medicine, China has highlighted our work, HCOOH/AgPd@g-C3N4, (Varma 2016) in the main body his research article "Wang, Y., Zhan, Z., Zhou, Y., Lei, M. and Hu, L., 2018. A green, efficient, and rapid procedure for the hydrogenation of nitroarenes to formanilides in water. Monatshefte für Chemie-Chemical Monthly, 149(3), pp.527-533." Prof Zhang from china has adopted our work (Varma, 2016) in his research article "Wu, M., Pang, J.H., Song, P.P., Peng, J.J., Xu, F., Li, Q. and Zhang, X.M., 2019. Visible light-driven oxidation of vanillyl alcohol in air with Au–Pd bimetallic nanoparticles on phosphorylated hydrotalcite. New Journal of Chemistry, 43(4), pp.1964-1971."

3B Provide an explanation of the external peer review process used to evaluate the scientific merit of the nominated publication(s). (Limit to 16,000 characters including spaces.)

Response

All of the nominated manuscripts underwent anonymous peer review by the journal to which it was submitted for publication.

From: Rajender Varma
To: Nadagouda, Mallikarjuna
Subject: Contribution to submitted papers for STAA award-from Rajender Varma
Date: Monday, April 27, 2020 7:54:38 PM

Dear Dr. Nadagouda,

I wish to confirm that my contribution is 20% for each of the following papers submitted for STAA award.

1. R.S. Varma, B. Nasir, and M. Nadagouda "Ruthenium on chitosan (ChRu): concerted catalysis for water splitting and reduction. 2019, U.S. Patent 10,189,708 **(Citation=1)**

2. R. B. Nasir Baig, Sanny Verma, M. N. Nadagouda and R. S. Varma "A Photoactive bimetallic framework for direct aminoformylation of nitroarenes" *Green chem*istry **2016**, *18*, 1019-1022. **(Cover Page; IF= 9.405; immediacy index= 2.24; Citation half-life= 4.10; Citation= 18)**

Raj

Rajender S. Varma, Ph.D.
U. S. Environmental Protection Agency
ORD, Center for Environmental Solutions and Emergency Response
Water Infrastructure Division/ Chemical Methods and Treatment Branch
26 West Martin Luther King Drive, MS 483
Cincinnati, Ohio 45268, USA

Tel: (513)-487-2701

e-mail: Varma.Rajender@epa.gov

(Highly Cited Researchers 2016, 18, 19; Publons Awardee 2018, 19)

Google Scholar: *https://scholar.google.com/citations?user=kzbCKOQAAAAJ&hl=en*

Research Gate: https://www.researchgate.net/profile/Rajender_Varma/info

From: Nadagouda, Mallikarjuna
To: Nadagouda, Mallikarjuna
Date: Wednesday, April 29, 2020 1:19:36 PM

My contribution to the below publications is 55 % each.

Title of papers:

1. R.S. Varma, B. Nasir, and M. Nadagouda "Ruthenium on chitosan (ChRu): concerted catalysis for water splitting and reduction. 2019, U.S. Patent 10,189,708 **(Citation=1)**

2. R. B. Nasir Baig, Sanny Verma, M. N. Nadagouda and R. S. Varma "A Photoactive bimetallic framework for direct aminoformylation of nitroarenes" *Green chem*istry **2016**, *18*, 1019-1022. **(Cover Page; IF= 9.405; immediacy index= 2.24; Citation half-life= 4.10; Citation= 18)**

Mallikarjuna N. Nadagouda Ph.D.
U. S. Environmental Protection Agency
ORD, Center for Environmental Solutions and Emergency Response
Water Infrastructure Division/ Chemical Methods and Treatment Branch
26 West, Martin Luther King Drive, MS 689, Cincinnati, OH 45268 USA
E-mail: Nadagouda.mallikarjuna@epa.gov
Ph: (513)569-7232

From: Nasir Baig
To: Nadagouda, Mallikarjuna
Subject: Paper contribution
Date: Tuesday, April 28, 2020 12:49:34 PM

Title of papers:

1. R.S. Varma, B. Nasir, and M. Nadagouda "Ruthenium on chitosan (ChRu): concerted catalysis for water splitting and reduction. 2019, U.S. Patent 10,189,708 **(Citation=1)**

2. R. B. Nasir Baig, Sanny Verma, M. N. Nadagouda and R. S. Varma "A Photoactive bimetallic framework for direct aminoformylation of nitroarenes" *Green chem*istry **2016**, *18*, 1019-1022. **(Cover Page; IF= 9.405; immediacy index= 2.24; Citation half-life= 4.10; Citation= 18)**

Acknowledgment/ Confirmation: I, Dr. Nasir Baig was part of the research of the above publications and my contribution for these publications can be valued at 20%.

Best regards

Nasir

--

US 20180050906A1

(19) **United States**

(12) **Patent Application Publication**

(10) **Pub. No.: US 2018/0050906 A1**

(43) **Pub. Date: Feb. 22, 2018**

VARMA et al.

(54) **RUTHENIUM ON CHITOSAN (CHRU): CONCERTED CATALYSIS FOR WATER SPLITTING AND REDUCTION**

(71) Applicant: **Government of the United States as Rep. by the Adm. of the U.S. Environmental Protection Agency**, Washington, DC (US)

(72) Inventors: **Rajender S. VARMA**, Cincinnati, OH (US); **Nasir BAIG**, Cincinnati, OH (US); **Mallikarjuna NADAGOUDA**, Cincinnati, OH (US)

(21) Appl. No.: **15/240,396**

(22) Filed: **Aug. 18, 2016**

Publication Classification

(51) **Int. Cl.**

C01B 3/04	(2006.01)
C07C 209/36	(2006.01)
C01B 13/02	(2006.01)
B01J 23/46	(2006.01)
B01J 31/06	(2006.01)
B01J 35/00	(2006.01)
B01J 37/03	(2006.01)
B01J 37/02	(2006.01)
B01J 37/00	(2006.01)
B01J 19/12	(2006.01)

(52) **U.S. Cl.**

CPC ***C01B 3/042*** (2013.01); ***C07C 209/365*** (2013.01); ***C01B 13/0207*** (2013.01); ***B01J 23/462*** (2013.01); ***B01J 19/126*** (2013.01); ***B01J 35/0006*** (2013.01); ***B01J 37/035*** (2013.01); ***B01J 37/0236*** (2013.01); ***B01J 37/009*** (2013.01); ***B01J 31/061*** (2013.01)

(57) **ABSTRACT**

A process and catalyst for the in situ generation of hydrogen via the microwave irradiation of a ruthenium chitosan composite catalyst has enabled the convenient reduction of nitro compounds in aqueous medium.

Chitosan-Ru (ChRu) composite

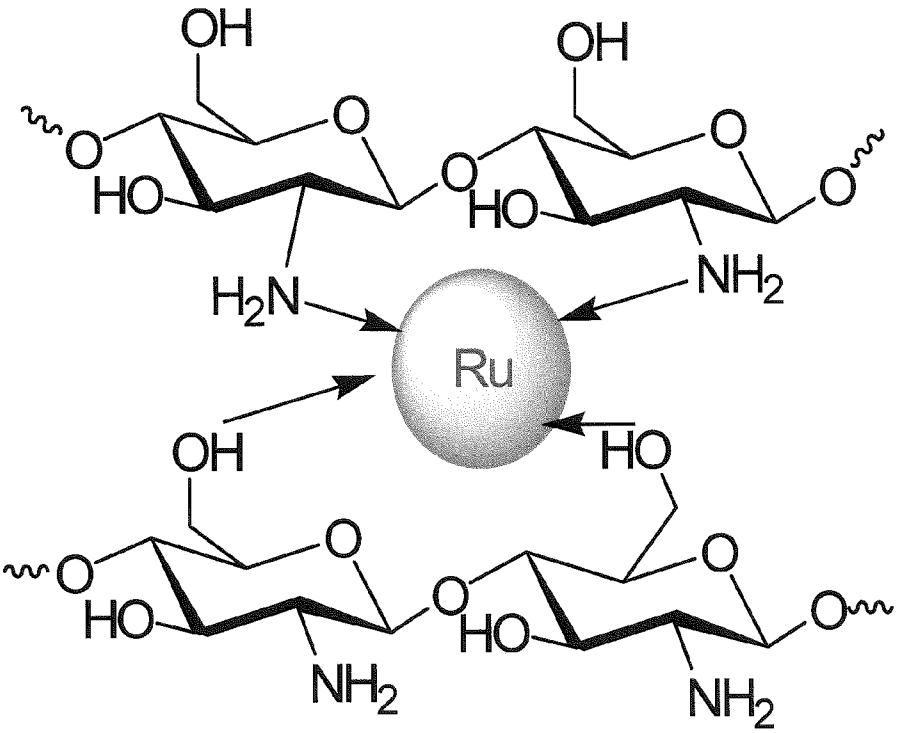

FIG 1.

Chitosan-Ru (ChRu) composite

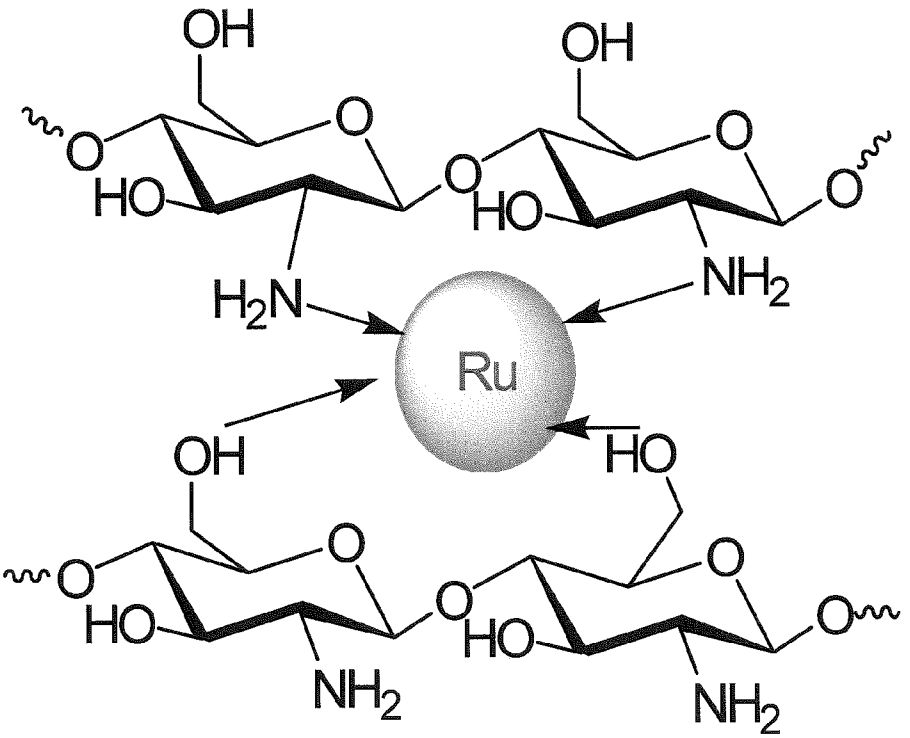

FIG. 2
Sealed microwave tube

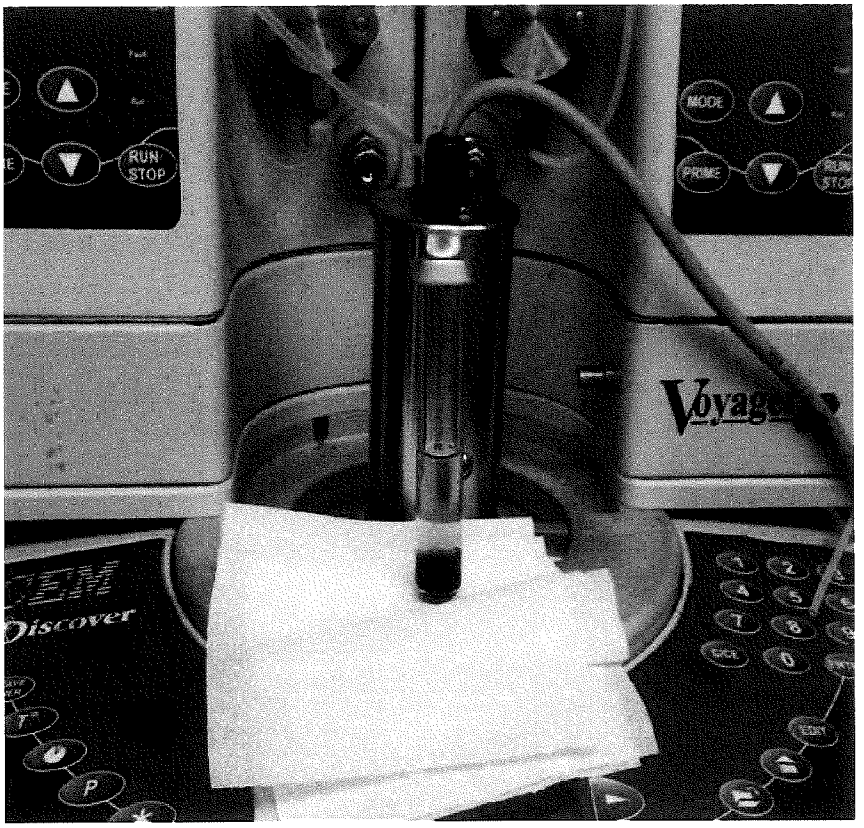

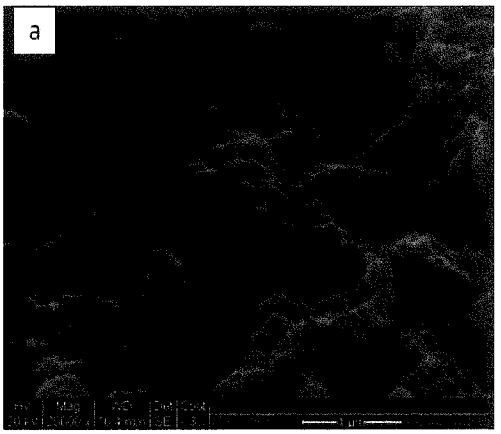

FIG. 3(a)

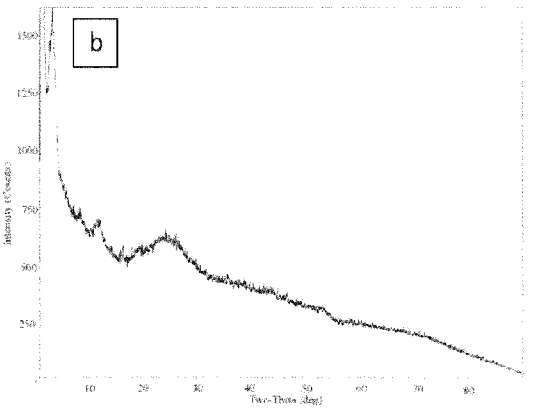

FIG. 3(b)

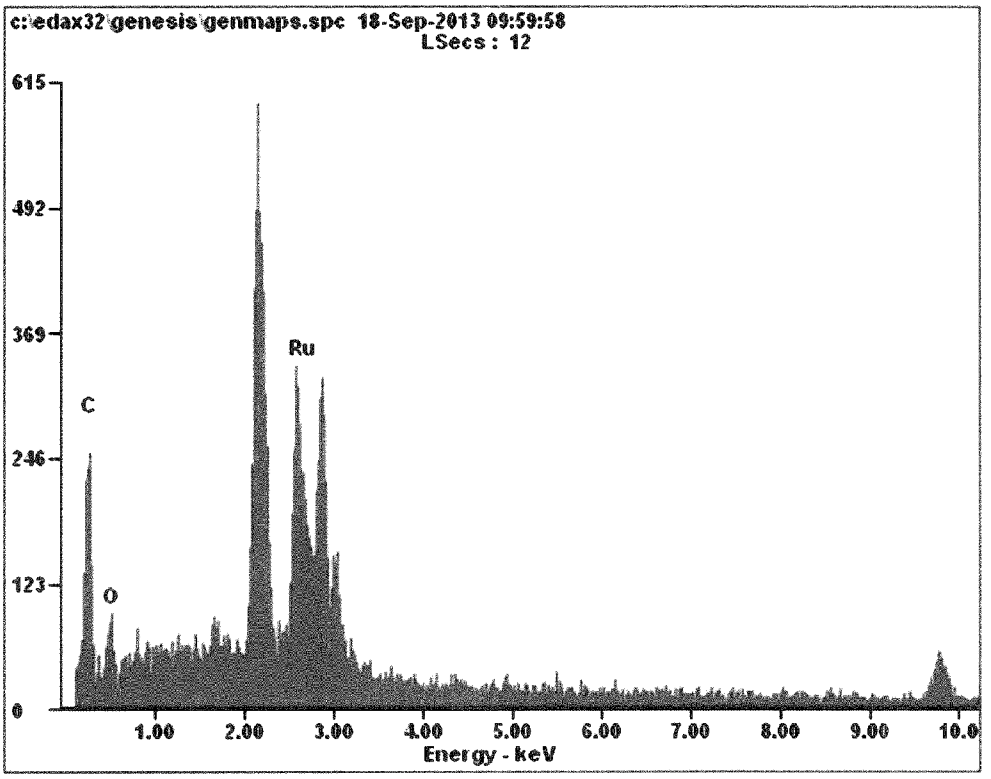

FIG. 3(c)

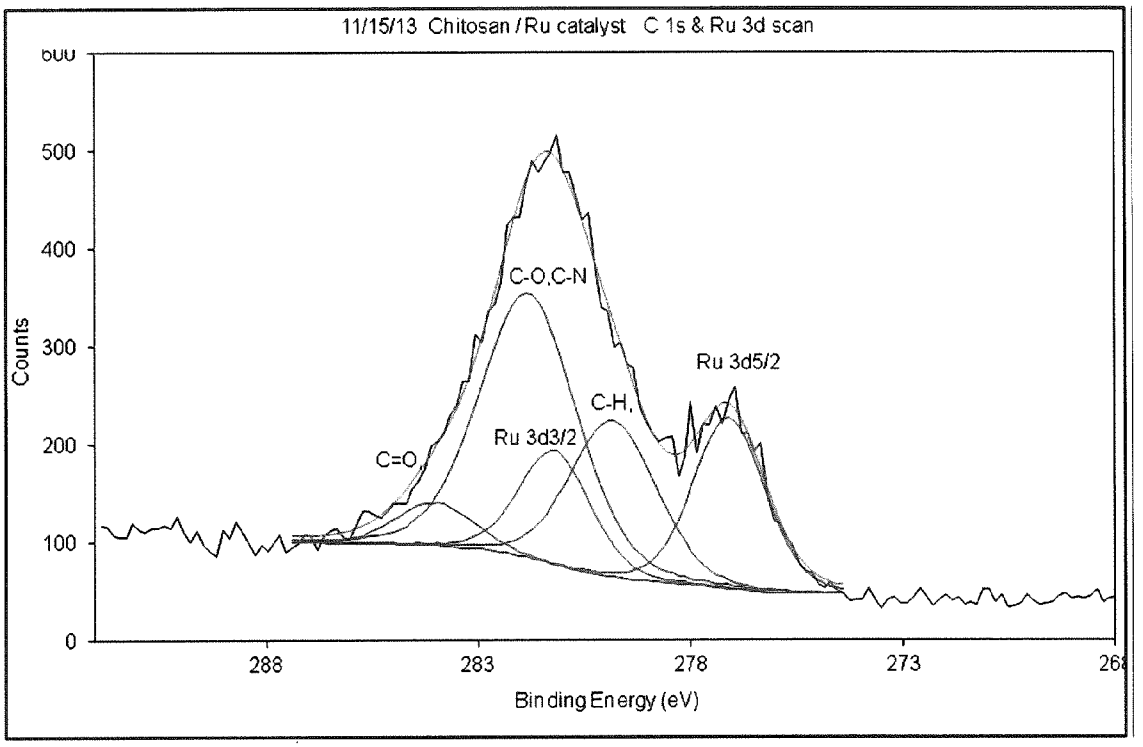
11/15/13 Chitosan / Ru catalyst C 1s & Ru 3d scan
Counts
600
500
400
300
200
100
0
C-O,C-N
Ru 3d5/2
C-H,
Ru 3d3/2
C=O
288
283
278
273
Binding Energy (eV)

FIG. 3(d)

```
File       :C:\Nasir\coupling reaction\Ruthenium reaction\NRB#4139.D
Operator   : Nasir
Acquired   :  6 May 2013   1:21 pm using AcqMethod SAMPLES- 20 MIN_18-NOV-2011.M
Instrument :    Instrument #1
Sample Name: NRB#4139
Misc Info  :
Vial Number: 2
```

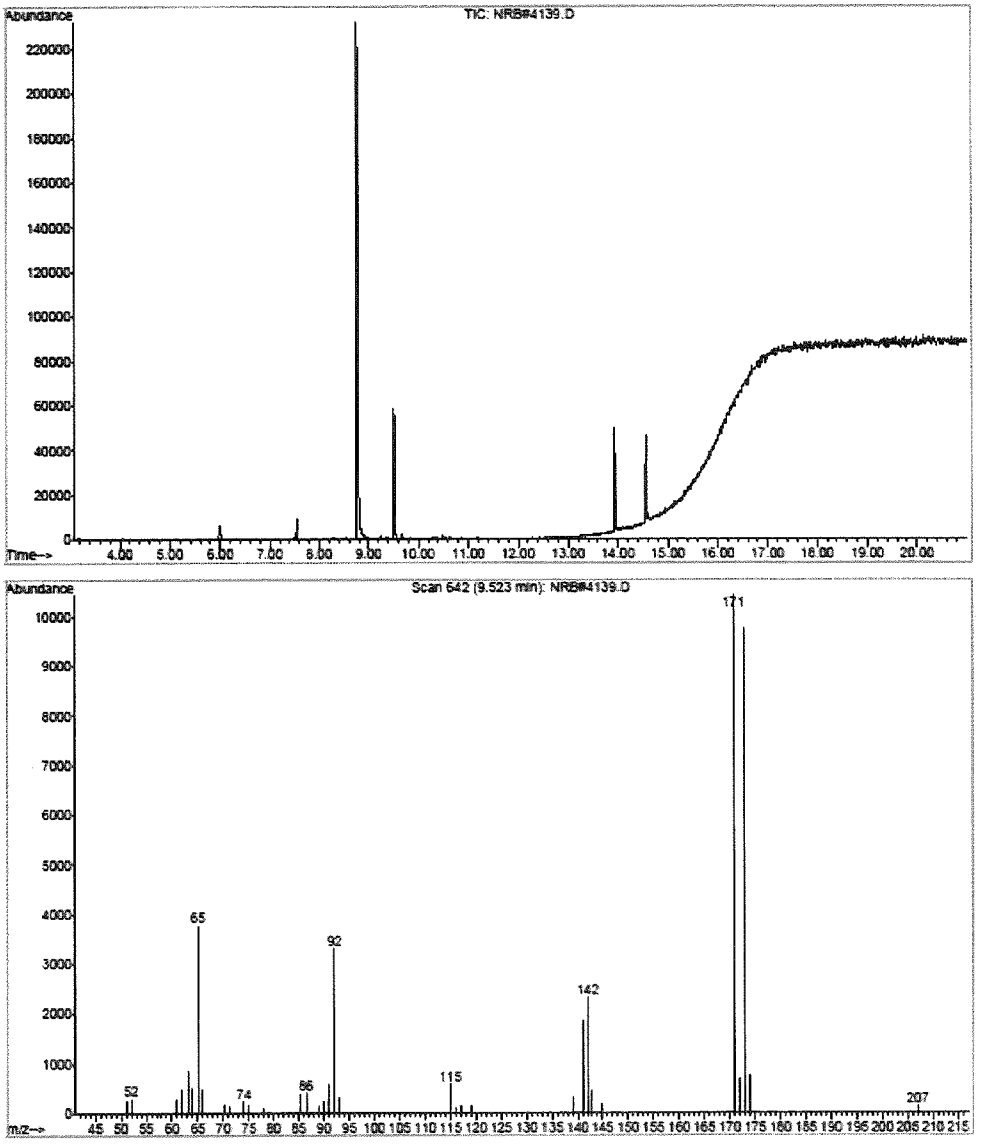

FIG. 4

```
File       :C:\Nasir\coupling reaction\Ruthenium reaction\NRB#4139.D
Operator   : Nasir
Acquired   :  6 May 2013   1:21 pm using AcqMethod SAMPLES- 20 MIN_18-NOV-2011.M
Instrument :    Instrument #1
Sample Name: NRB#4139
Misc Info  :
Vial Number: 2
```

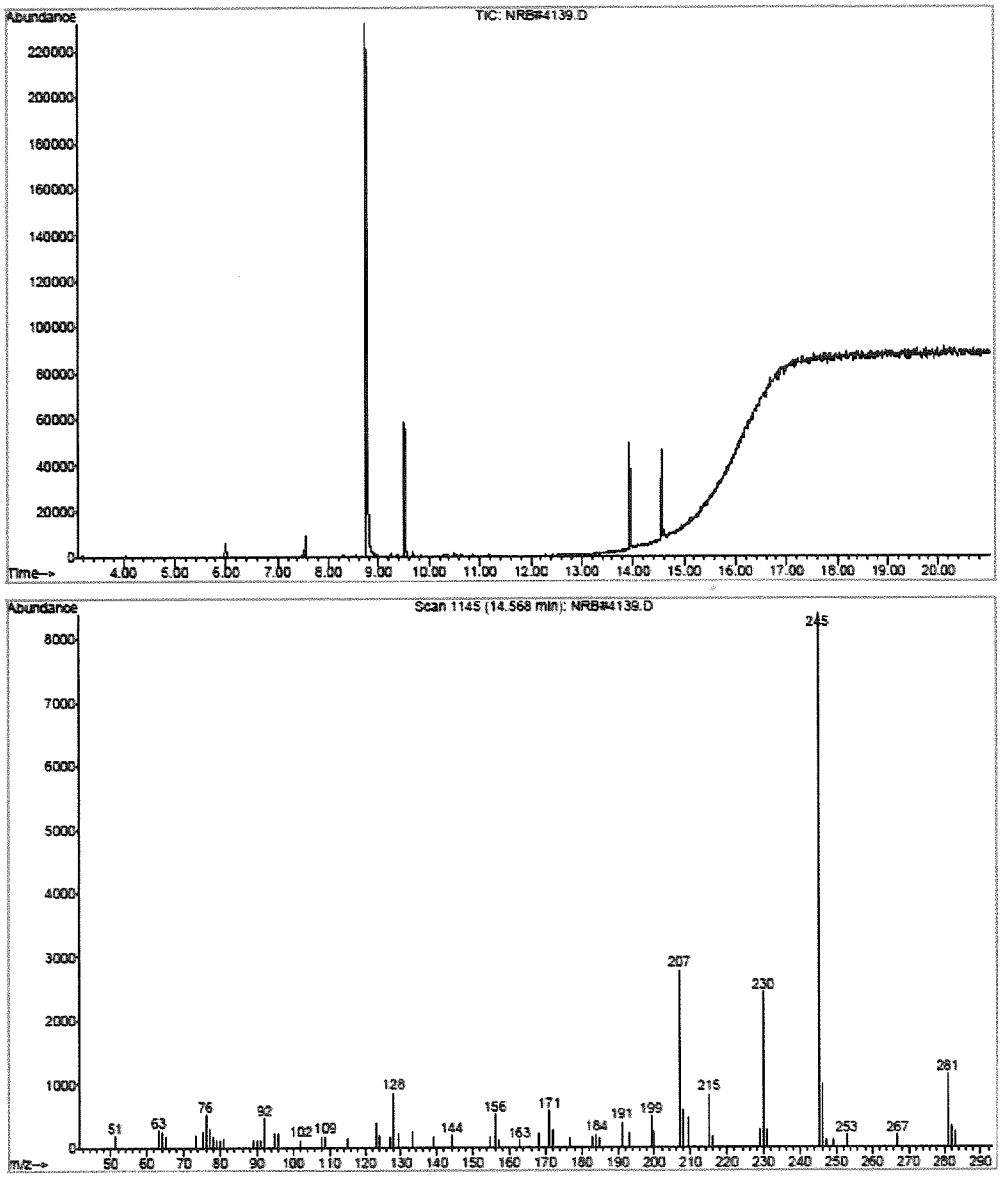

FIG. 5

```
File       :C:\Nasir\coupling reaction\Ruthenium reaction\NRB#4139.D
Operator   : Nasir
Acquired   :  6 May 2013   1:21 pm using AcqMethod SAMPLES- 20 MIN_18-NOV-2011.M
Instrument :    Instrument #1
Sample Name: NRB#4139
Misc Info  :
Vial Number: 2
```

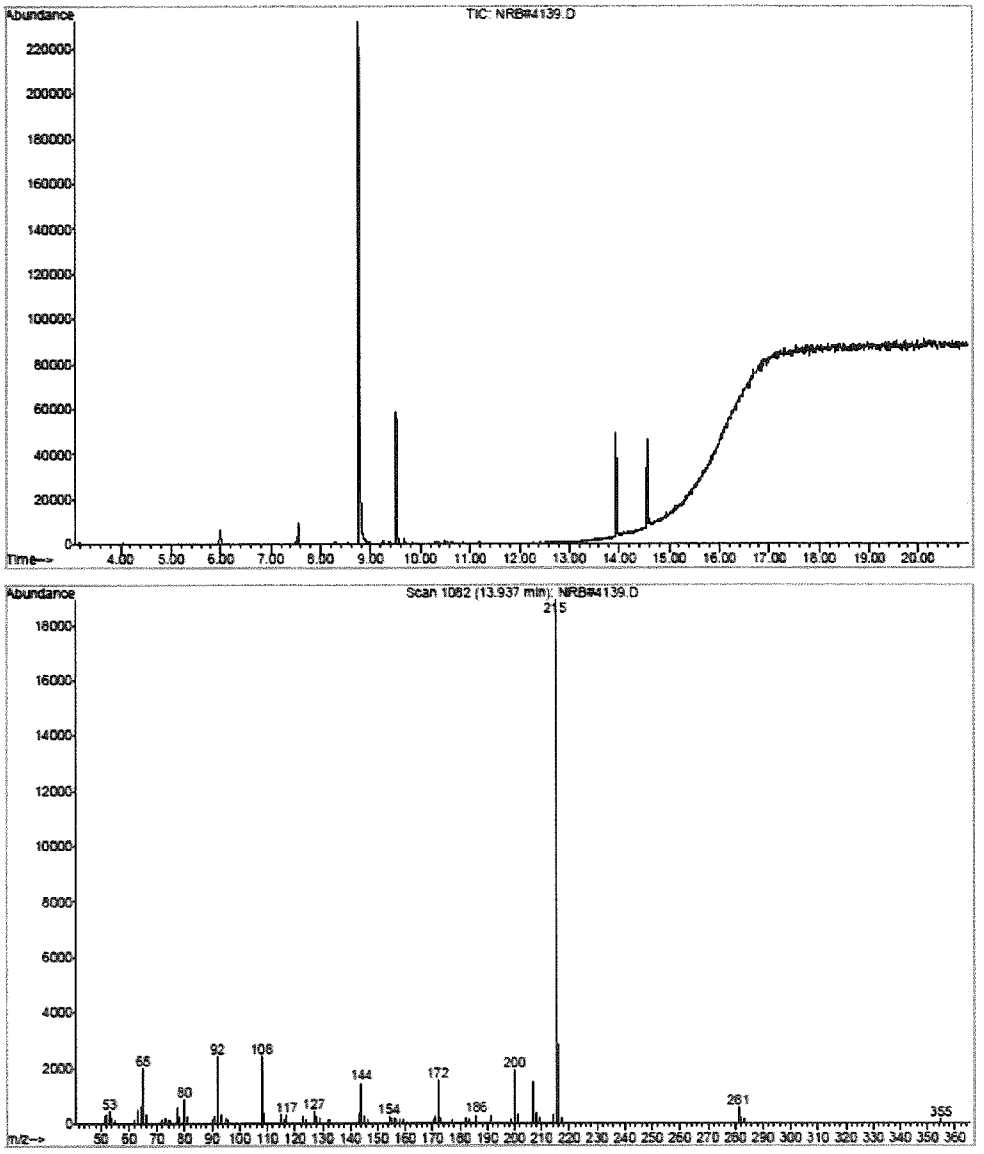

FIG. 6

```
File       :C:\Nasir\coupling reaction\Ruthenium reaction\NRB#4147.D
Operator   : Nasir
Acquired   : 10 May 2013   5:26 pm using AcqMethod SAMPLES- 20 MIN_18-NOV-2011.M
Instrument :    Instrument #1
Sample Name: NRB#4147
Misc Info  :
Vial Number: 1
```

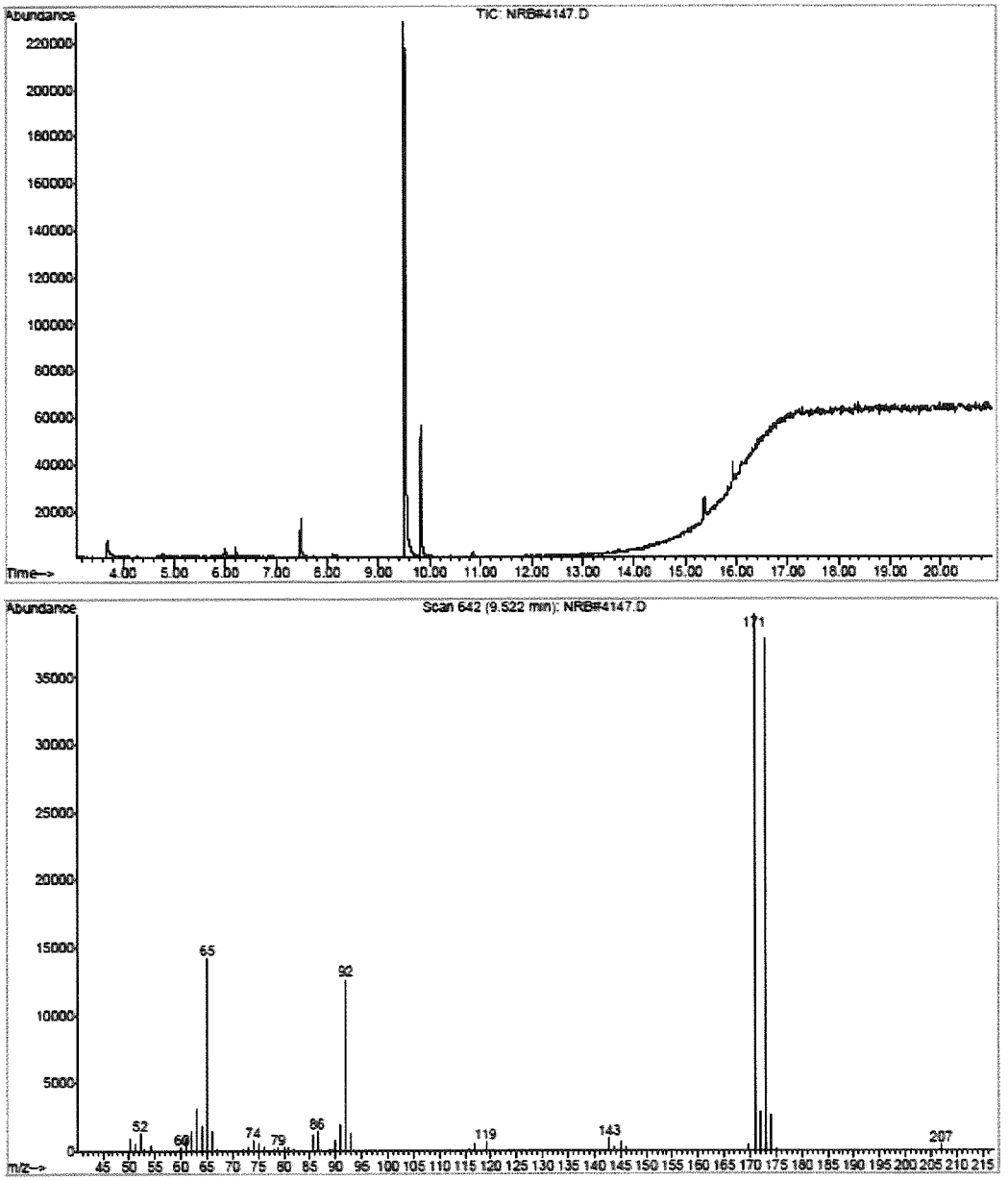

FIG. 7

Data File D:\DATA\NASIR\NASIR000463.D
Sample Name: NRB#4157-3

Acq. Operator : Nasir
Acq. Instrument : Instrument 1 Location : Vial 1
Injection Date : 14-Jun-13, 11:04:16 Inj : 1
Inj Volume : Manually
Acq. Method : C:\CHEM32\1\METHODS\LANDFILL GAS TCD MAR2011.M
Last changed : 6/14/2013 11:03:07 AM by Nasir
Analysis Method : C:\CHEM32\1\METHODS\LANDFILL GAS TCD MAR2011.M
Last changed : 6/14/2013 11:11:16 AM by Nasir
Method Info : Method for Landfill gases - CH4, CO2, CO, H2, N2, O2 Using Porapack N, Mo
Sieve, TCD - Steve Musson

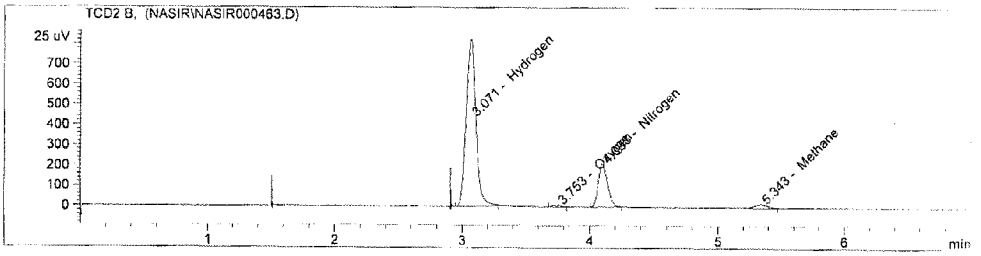

Normalized Percent Report

Sorted By : Signal
Calib. Data Modified : Thursday, January 12, 2012 10:19:23 AM
Multiplier : 1.0000
Dilution : 1.0000
Use Multiplier & Dilution Factor with ISTDs

Signal 1: TCD2 B,

RetTime [min]	Type	Area [25 uV*s]	Amt/Area	Norm %	Grp	Name
2.497		-	-	-		Carbon Dioxide
3.071	BB	4454.34131	4.83147e-3	27.793720		Hydrogen
3.753	BV	43.57506	3.50659e-2	1.973363		Oxygen
4.098	BB	1085.96875	4.84985e-2	68.018808		Nitrogen
5.343	BV	128.70334	1.33206e-2	2.214109		Methane

Totals : 100.000000

2 Warnings or Errors :

Warning : Calibration warnings (see calibration table listing)
Warning : Calibrated compound(s) not found

*** End of Report ***

Instrument 1 6/14/2013 11:11:25 AM Nasir Page 1 of 1

FIG. 8

Data File D:\DATA\NASIR\NASIR000462.D
Sample Name: NRB#4160

```
Acq. Operator   : Nasir
Acq. Instrument : Instrument 1                    Location : Vial 1
Injection Date  : 14-Jun-13, 10:55:56               Inj :   1
                                                  Inj Volume : Manually
Acq. Method     : C:\CHEM32\1\METHODS\LANDFILL GAS TCD MAR2011.M
Last changed    : 6/14/2013 10:53:26 AM by Nasir
Analysis Method : C:\CHEM32\1\METHODS\LANDFILL GAS TCD MAR2011.M
Last changed    : 6/14/2013 11:02:56 AM by Nasir
Method Info     : Method for Landfill gases - CH4, CO2, CO, H2, N2, O2 Using Porapack N, Mol
                  Sieve, TCD - Steve Musson
```

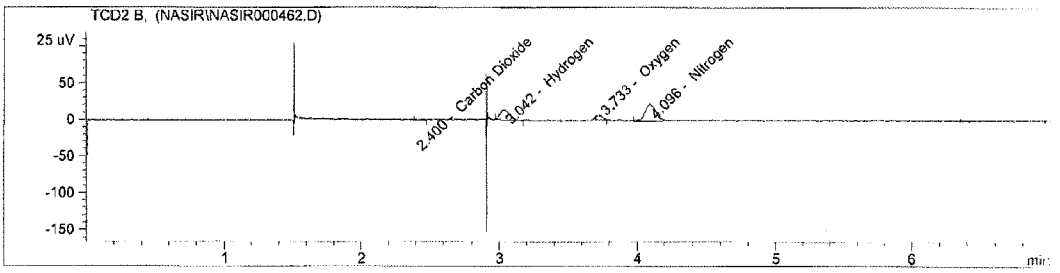


```
                        Normalized Percent Report

Sorted By             :      Signal
Calib. Data Modified  :      Thursday, January 12, 2012 10:19:23 AM
Multiplier            :      1.0000
Dilution              :      1.0000
Use Multiplier & Dilution Factor with ISTDs

Signal 1: TCD2 B,

RetTime  Type     Area      Amt/Area     Norm     Grp   Name
 [min]          [25 uV*s]                 %
-------|------|----------|----------|----------|--|------------------
  2.400 VV        6.80996 4.42418e-2   3.833679     Carbon Dioxide
  3.042 BV       67.58522 4.83147e-3   4.154983     Hydrogen
  3.733 VB       19.34842 3.50659e-2   8.633141     Oxygen
  4.096 VB      135.10970 4.84985e-2  83.378196     Nitrogen
  5.114            -          -          -          Methane

Totals :                              100.000000


2 Warnings or Errors :

Warning : Calibration warnings (see calibration table listing)
Warning : Calibrated compound(s) not found

                            *** End of Report ***
```


FIG. 9

Data File D:\DATA\NASIR\NASIR000472.D
Sample Name: NRB#4163

Acq. Operator : Nasir
Acq. Instrument : Instrument 1 Location : Vial 1
Injection Date : 14-Jun-13, 12:18:54 Inj : 1
Inj Volume : Manually
Acq. Method : C:\CHEM32\1\METHODS\LANDFILL GAS TCD MAR2011.M
Last changed : 6/14/2013 12:18:01 PM by Nasir
Analysis Method : C:\CHEM32\1\METHODS\LANDFILL GAS TCD MAR2011.M
Last changed : 6/14/2013 12:25:54 PM by Nasir
Method Info : Method for Landfill gases - CH4, CO2, CO, H2, N2, O2 Using Porapack N, Mol Sieve, TCD - Steve Musson

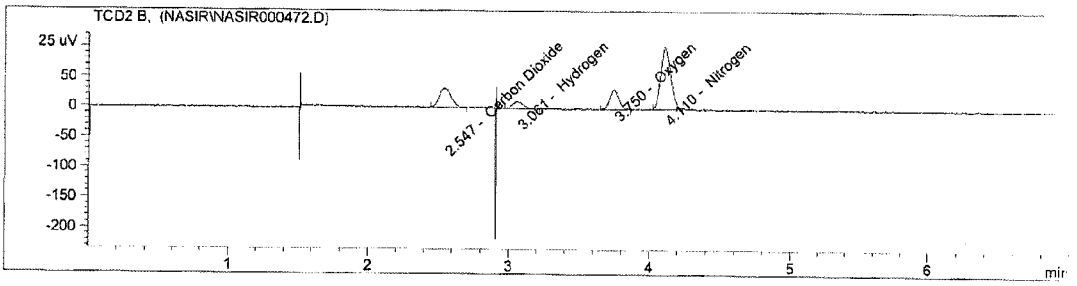

Normalized Percent Report

Sorted By : Signal
Calib. Data Modified : Thursday, January 12, 2012 10:19:23 AM
Multiplier : 1.0000
Dilution : 1.0000
Use Multiplier & Dilution Factor with ISTDs

Signal 1: TCD2 B,

RetTime [min]	Type	Area [25 uV*s]	Amt/Area	Norm %	Grp	Name
2.547	BB	191.11461	4.42418e-2	21.277983		Carbon Dioxide
3.061	BV	65.38754	4.83147e-3	0.795020		Hydrogen
3.750	VB	153.32578	3.50659e-2	13.530192		Oxygen
4.110	BV	527.63409	4.84985e-2	64.396806		Nitrogen
5.114		-	-	-		Methane

Totals : 100.000000

2 Warnings or Errors :

Warning : Calibration warnings (see calibration table listing)
Warning : Calibrated compound(s) not found

*** End of Report ***

Instrument 1 6/14/2013 12:26:03 PM Nasir Page 1 of 1

FIG. 10

Data File D:\DATA\NASIR\NASIR000473.D
Sample Name: NRB#4162

Acq. Operator : Nasir
Acq. Instrument : Instrument 1 Location : Vial 1
Injection Date : 14-Jun-13, 12:27:31 Inj : 1
Inj Volume : Manually
Acq. Method : C:\CHEM32\1\METHODS\LANDFILL GAS TCD MAR2011.M
Last changed : 6/14/2013 12:26:05 PM by Nasir
Analysis Method : C:\CHEM32\1\METHODS\LANDFILL GAS TCD MAR2011.M
Last changed : 6/14/2013 12:34:31 PM by Nasir
Method Info : Method for Landfill gases - CH4, CO2, CO, H2, N2, O2 Using Porapack N, Mol Sieve, TCD - Steve Musson

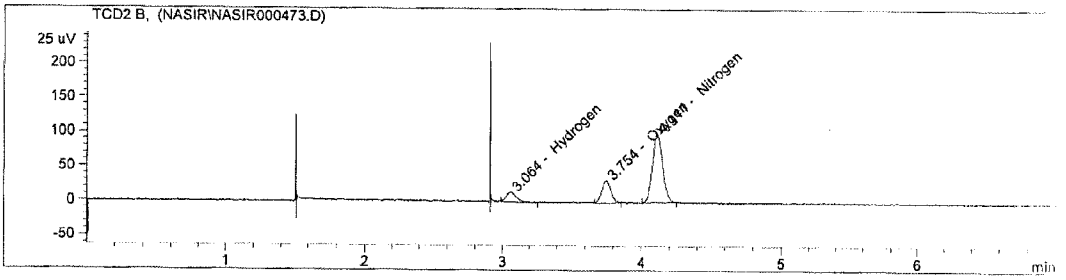

Normalized Percent Report

Sorted By : Signal
Calib. Data Modified : Thursday, January 12, 2012 10:19:23 AM
Multiplier : 1.0000
Dilution : 1.0000
Use Multiplier & Dilution Factor with ISTDs

Signal 1: TCD2 B,

RetTime [min]	Type	Area [25 uV*s]	Amt/Area	Norm %	Grp	Name
2.497		-	-	-		Carbon Dioxide
3.064	VB	75.59394	4.83147e-3	1.225395		Hydrogen
3.754	BV	144.85381	3.50659e-2	17.042162		Oxygen
4.111	BB	502.29285	4.84985e-2	81.732443		Nitrogen
5.114		-	-	-		Methane

Totals : 100.000000

2 Warnings or Errors :

Warning : Calibration warnings (see calibration table listing)
Warning : Calibrated compound(s) not found

*** End of Report ***

Instrument 1 6/14/2013 12:34:40 PM Nasir Page 1 of 1

FIG. 11

Data File D:\DATA\NASIR\NASIR000465.D
Sample Name: NRB#4158-2

Acq. Operator : Nasir
Acq. Instrument : Instrument 1 Location : Vial 1
Injection Date : 14-Jun-13, 11:21:16 Inj : 1
Inj Volume : Manually
Acq. Method : C:\CHEM32\1\METHODS\LANDFILL GAS TCD MAR2011.M
Last changed : 6/14/2013 11:20:22 AM by Nasir
Analysis Method : C:\CHEM32\1\METHODS\LANDFILL GAS TCD MAR2011.M
Last changed : 6/14/2013 11:28:16 AM by Nasir
Method Info : Method for Landfill gases - CH4, CO2, CO, H2, N2, O2 Using Porapack N, Mol Sieve, TCD - Steve Musson

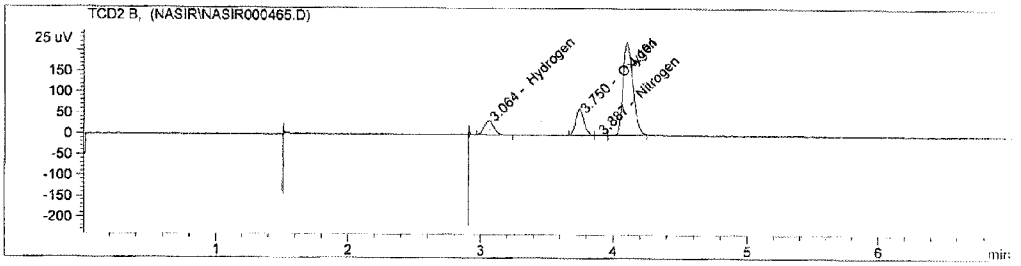

Normalized Percent Report

Sorted By : Signal
Calib. Data Modified : Thursday, January 12, 2012 10:19:23 AM
Multiplier : 1.0000
Dilution : 1.0000
Use Multiplier & Dilution Factor with ISTDs

Signal 1: TCD2 B,

RetTime [min]	Type	Area [25 uV*s]	Amt/Area	Norm %	Grp	Name
2.497		-	-	-		Carbon Dioxide
3.064	BB	170.74980	4.83147e-3	7.396285		Hydrogen
3.750	BV	283.68079	3.50659e-2	89.184455		Oxygen
3.887	VV	7.86376	4.84985e-2	3.419260		Nitrogen
5.114		-	-	-		Methane

Totals : 100.000000

2 Warnings or Errors :

Warning : Calibration warnings (see calibration table listing)
Warning : Calibrated compound(s) not found

*** End of Report ***

FIG. 12

Data File D:\DATA\NASIR\NASIR000461.D
Sample Name: NRB#4159-2

```
Acq. Operator    : Nasir
Acq. Instrument  : Instrument 1                    Location : Vial 1
Injection Date   : 14-Jun-13, 10:46:14                 Inj :  1
                                                  Inj Volume : Manually
Acq. Method      : C:\CHEM32\1\METHODS\LANDFILL GAS TCD MAR2011.M
Last changed     : 6/14/2013 10:40:56 AM by Nasir
Analysis Method  : C:\CHEM32\1\METHODS\LANDFILL GAS TCD MAR2011.M
Last changed     : 6/14/2013 10:53:14 AM by Nasir
Method Info      : Method for Landfill gases - CH4, CO2, CO, H2, N2, O2 Using Porapack N, Mol
                   Sieve, TCD - Steve Musson
```

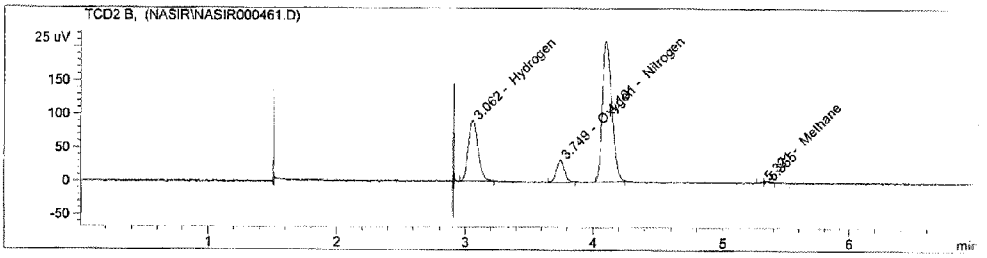

Normalized Percent Report

```
Sorted By             :      Signal
Calib. Data Modified  :      Thursday, January 12, 2012 10:19:23 AM
Multiplier            :      1.0000
Dilution              :      1.0000
Use Multiplier & Dilution Factor with ISTDs

Signal 1: TCD2 B,
```

RetTime [min]	Type	Area [25 uV*s]	Amt/Area	Norm %	Grp	Name
2.497		-	-	-		Carbon Dioxide
3.062	BB	473.96875	4.83147e-3	3.844839		Hydrogen
3.749	VB	147.99077	3.50659e-2	8.713023		Oxygen
4.101	BV	1072.06763	4.84985e-2	87.296958		Nitrogen
5.321	VV	6.49130	1.33206e-2	0.145180		Methane
Totals :				100.000000		

```
2 Warnings or Errors :

Warning : Calibration warnings (see calibration table listing)
Warning : Calibrated compound(s) not found

                        *** End of Report ***
```


FIG. 13

Data File D:\DATA\NASIR\NASIR000470.D
Sample Name: NRB#4164

```
Acq. Operator    : Nasir
Acq. Instrument  : Instrument 1                    Location : Vial 1
Injection Date   : 14-Jun-13, 12:02:28                 Inj :  1
                                                   Inj Volume : Manually
Acq. Method      : C:\CHEM32\1\METHODS\LANDFILL GAS TCD MAR2011.M
Last changed     : 6/14/2013 12:01:29 PM by Nasir
Analysis Method  : C:\CHEM32\1\METHODS\LANDFILL GAS TCD MAR2011.M
Last changed     : 6/14/2013 12:09:28 PM by Nasir
Method Info      : Method for Landfill gases - CH4, CO2, CO, H2, N2, O2 Using Porapack N, Mol
                   Sieve, TCD - Steve Musson
```

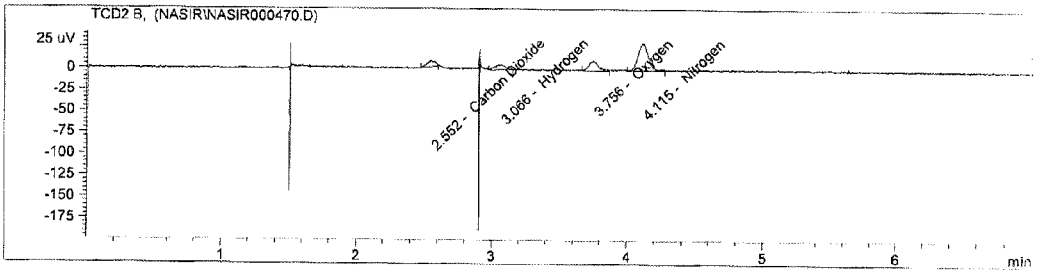

Normalized Percent Report

```
Sorted By             :      Signal
Calib. Data Modified  :      Thursday, January 12, 2012 10:19:23 AM
Multiplier            :      1.0000
Dilution              :      1.0000
Use Multiplier & Dilution Factor with ISTDs

Signal 1: TCD2 B,
```

RetTime [min]	Type	Area [25 uV*s]	Amt/Area	Norm %	Grp	Name
2.552	BB	29.23130	4.42418e-2	11.287271		Carbon Dioxide
3.066	BB	30.54844	4.83147e-3	1.288179		Hydrogen
3.756	BV	57.15428	3.50659e-2	17.492091		Oxygen
4.115	VB	165.21259	4.84985e-2	69.932460		Nitrogen
5.114		-	-	-		Methane

```
Totals :                              100.000000

2 Warnings or Errors :

Warning : Calibration warnings (see calibration table listing)
Warning : Calibrated compound(s) not found

                        *** End of Report ***
```


FIG. 14

Data File D:\DATA\NASIR\NASIR000467.D
Sample Name: NRB#4161

Acq. Operator : Nasir
Acq. Instrument : Instrument 1 Location : Vial 1
Injection Date : 14-Jun-13, 11:37:35 Inj : 1
Inj Volume : Manually
Acq. Method : C:\CHEM32\1\METHODS\LANDFILL GAS TCD MAR2011.M
Last changed : 6/14/2013 11:36:50 AM by Nasir
Analysis Method : C:\CHEM32\1\METHODS\LANDFILL GAS TCD MAR2011.M
Last changed : 6/14/2013 11:44:35 AM by Nasir
Method Info : Method for Landfill gases - CH4, CO2, CO, H2, N2, O2 Using Porapack N, Mol Sieve, TCD - Steve Musson

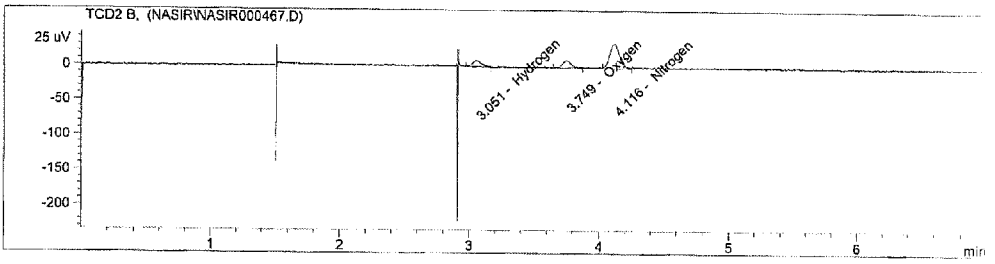

Normalized Percent Report

Sorted By : Signal
Calib. Data Modified : Thursday, January 12, 2012 10:19:23 AM
Multiplier : 1.0000
Dilution : 1.0000
Use Multiplier & Dilution Factor with ISTDs

Signal 1: TCD2 B,

RetTime [min]	Type	Area [25 uV*s]	Amt/Area	Norm %	Grp	Name
2.497		-	-	-		Carbon Dioxide
3.051	BB	42.41637	4.83147e-3	1.902551		Hydrogen
3.749	BB	44.86104	3.50659e-2	14.604207		Oxygen
4.116	BV	185.43852	4.84985e-2	83.493242		Nitrogen
5.114		-	-	-		Methane

Totals : 100.000000

2 Warnings or Errors :

Warning : Calibration warnings (see calibration table listing)
Warning : Calibrated compound(s) not found

*** End of Report ***

Instrument 1 6/14/2013 11:44:44 AM Nasir Page 1 of 1

FIG. 15

Data File D:\DATA\NASIR\NRB000052.D
Sample Name: NRB#4187

Acq. Operator : RFM
Acq. Instrument : Instrument 1 Location : Vial 1
Injection Date : 01-Jul-13, 15:54:21 Inj : 1
Inj Volume : Manually
Acq. Method : C:\CHEM32\1\METHODS\LANDFILL GAS TCD MAR2011.M
Last changed : 7/1/2013 3:53:06 PM by RFM
Analysis Method : C:\CHEM32\1\METHODS\LANDFILL GAS TCD MAR2011.M
Last changed : 7/1/2013 4:01:21 PM by RFM
Method Info : Method for Landfill gases - CH4, CO2, CO, H2, N2, O2 Using Porapack N, Mol Sieve, TCD - Steve Musson

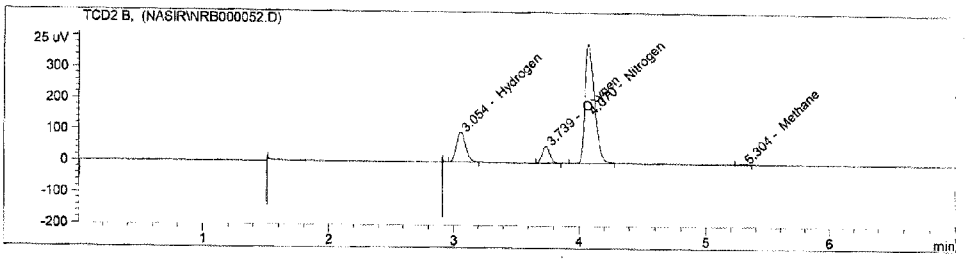

Normalized Percent Report

Sorted By : Signal
Calib. Data Modified : Thursday, January 12, 2012 10:19:23 AM
Multiplier : 1.0000
Dilution : 1.0000
Use Multiplier & Dilution Factor with ISTDs

Signal 1: TCD2 B,

RetTime [min]	Type	Area [25 uV*s]	Amt/Area	Norm %	Grp	Name
2.497		-	-	-		Carbon Dioxide
3.054	BV	497.97028	4.83147e-3	2.262151		Hydrogen
3.739	VB	233.97701	3.50659e-2	7.714312		Oxygen
4.070	BB	1968.34412	4.84985e-2	89.756879		Nitrogen
5.304	BB	21.29068	1.33206e-2	0.266657		Methane

Totals : 100.000000

2 Warnings or Errors :

Warning : Calibration warnings (see calibration table listing)
Warning : Calibrated compound(s) not found

*** End of Report ***

Instrument 1 7/1/2013 4:01:30 PM RFM Page 1 of 1

FIG. 16

Data File D:\DATA\NASIR\NASIR000469.D
Sample Name: NRB#4154-2

```
Acq. Operator   : Nasir
Acq. Instrument : Instrument 1                    Location : Vial 1
Injection Date  : 14-Jun-13, 11:54:17                 Inj :   1
                                                  Inj Volume : Manually
Acq. Method     : C:\CHEM32\1\METHODS\LANDFILL GAS TCD MAR2011.M
Last changed    : 6/14/2013 11:53:02 AM by Nasir
Analysis Method : C:\CHEM32\1\METHODS\LANDFILL GAS TCD MAR2011.M
Last changed    : 6/14/2013 12:01:17 PM by Nasir
Method Info     : Method for Landfill gases - CH4, CO2, CO, H2, N2, O2 Using Porapack N, Mol
                  Sieve, TCD - Steve Musson
```

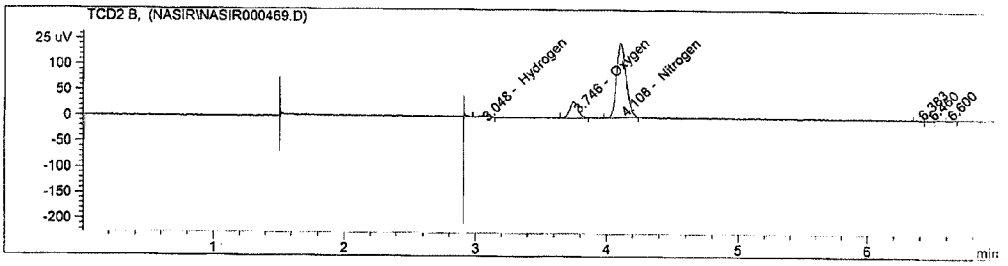

Normalized Percent Report

```
Sorted By             :      Signal
Calib. Data Modified  :      Thursday, January 12, 2012 10:19:23 AM
Multiplier            :      1.0000
Dilution              :      1.0000
Use Multiplier & Dilution Factor with ISTDs

Signal 1: TCD2 B,
```

RetTime [min]	Type	Area [25 uV*s]	Amt/Area	Norm %	Grp	Name
2.497		-	-	-		Carbon Dioxide
3.048	BB	13.26262	4.83147e-3	0.156755		Hydrogen
3.746	BB	144.66556	3.50659e-2	12.409786		Oxygen
4.108	BB	736.94623	4.84985e-2	87.433458		Nitrogen
5.114		-	-	-		Methane
Totals :				100.000000		

```
2 Warnings or Errors :

Warning : Calibration warnings (see calibration table listing)
Warning : Calibrated compound(s) not found

                        *** End of Report ***
```


FIG. 17

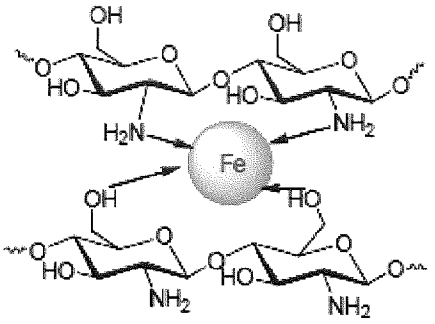

FIG. 18
Chitosan-Fe (ChFe) composite

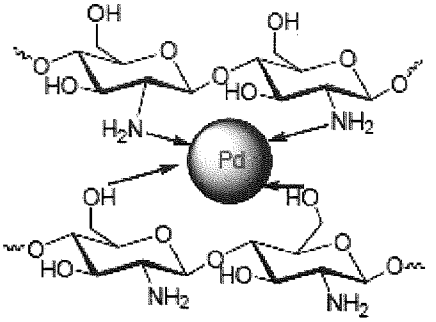

FIG. 19
Chitosan-Pd (ChPd) composite

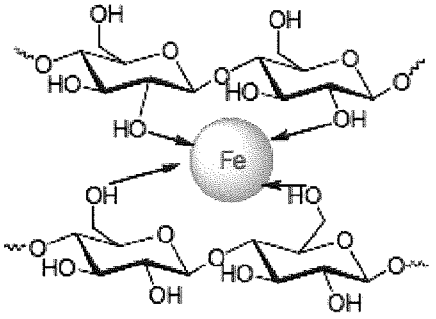

FIG. 20
Cellulose-Fe (CelluFe) composite

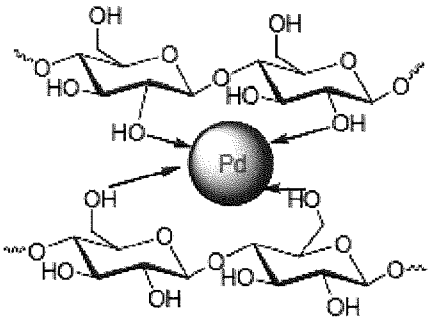

FIG. 21
Cellulose-Pd(CelluPd) composite

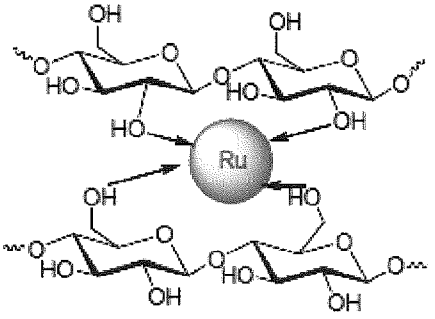

FIG. 22
Cellulose-Ru (CelluRu) composite

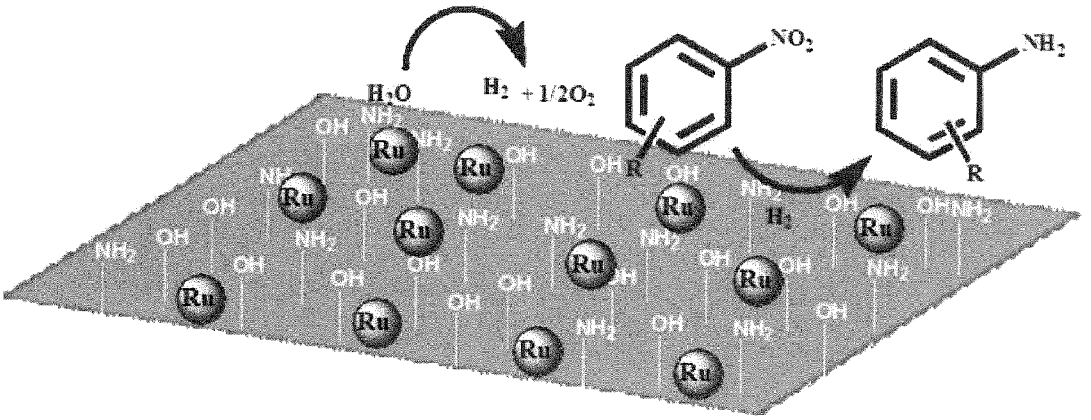

FIG. 23

RUTHENIUM ON CHITOSAN (CHRU): CONCERTED CATALYSIS FOR WATER SPLITTING AND REDUCTION

BACKGROUND

Field of the Invention

[0001] Aspects of the invention relate generally to improved processes and catalysts to split water (i.e., to separate water into hydrogen and oxygen). The invention is particularly useful for the in situ generation of hydrogen via microwave irradiation of a ruthenium chitosan composite catalyst and the convenient reduction of nitro compounds in an aqueous medium.

Description of Related Art

[0002] Increasing energy demands and the impending global warming crisis has forced a paradigm shift in thinking towards the development of carbon-neutral, sustainable and inexpensive energy-consuming strategies. This has inspired scientists to design and develop methods for splitting water, primarily as a means for producing hydrogen (Scheme 1). The total water splitting process consists of two steps: (Step 1) proton reduction and (Step 2) water oxidation. Step 1 requires less energy compared to the key step in water splitting, i.e., water oxidation. Due to the complexity of the Step 2 reaction, the challenges in the water oxidation process involve multiple proton-coupled electron transfer processes and O—O bond formation.

$$2H_2O+h^{\nu}\rightarrow 2H_2+O_2$$

Step 1 $2H^{+}+4e^{-}\rightarrow H_2$

Step 2 $2H_2O\rightarrow O_2+4H^{+}+4e^{-}$

[0003] Scheme 1. Splitting of Water

[0004] There has been great effort over the years to develop a method to split water under a variety of conditions. This includes developing methods such as 1) electrolysis, 2) photoelectrochemical water splitting, 3) photocatalytic water splitting, 4) photobiological water splitting, and 5) thermal decomposition of water.

[0005] Hydrogen production from water using electrical means is not a viable option, as the energy consumed in this process is more than what is produced in the form of hydrogen. Photoelectrochemical, photocatalytic and photobiological methods are no doubt of prime importance in water splitting research. However, to date there has been very limited success due to the high complexity and cost of such methods as well as their low efficiency in producing hydrogen.

[0006] Comprehensive efforts have been made to understand the reaction mechanisms of water splitting using a catalyst. The catalytic concepts center around the use of transition metals or biological systems coupled with sunlight. However, most of the reported literature is confined to the use of conjugated complex ligands or metal oxides, and they are often designed or selected in view of their efficiency in sunlight absorption, thus mimicking nature. There has been little to no progress in the use of low-energy microwaves and non-conjugated ligands in the generation of hydrogen via water splitting.

[0007] In view of the above, there is a need to develop catalysts and reactions capable of splitting water and generating hydrogen. Accordingly, an object of the invention is to provide such a process and catalyst. Other objects will also be apparent from the detailed description of the invention.

SUMMARY OF THE INVENTION

[0008] Broadly stated, the objects of the invention are realized, according to one aspect of the invention, by synthesizing a chitosan-ruthenium catalyst and using this catalyst in a reaction to split water and produce hydrogen. There is no history of using low-energy microwaves and non-conjugated ligands in the generation of hydrogen via water splitting. In continuation of the inventors ongoing efforts to discover the versatility of renewable biopolymers as catalyst supports in organic synthesis, they serendipitously discovered in situ generation of hydrogen via water splitting using a chitosan ruthenium composite under microwave (MW) irradiation conditions. The processes of the invention also relate to the aqueous reduction of nitro compounds.

[0009] In one embodiment, the invention embraces a process for generating hydrogen and oxygen from water. The process includes the following steps: preparing a ruthenium on chitosan catalyst, bringing the catalyst into contact with an aqueous mixture under basic conditions, and applying microwave energy to the aqueous mixture to produce hydrogen and oxygen.

[0010] In one embodiment, the catalyst is prepared by a process including the following steps: suspending chitosan in water; adding $RuCl_3.3H_2O$; adjusting the pH of the mixture to about 8.5 to about 9.5 while continuously stirring the mixture; separating the catalyst from the liquid in the mixture using a centrifuge; and drying the mixture under a vacuum. The pH of the mixture may be adjusted using ammonia, and the catalyst may be dried under a vacuum at about 30° C. to about 60° C.

[0011] In the process of separating water into hydrogen and oxygen, the aqueous mixture may be maintained at about 125° C. during the reaction. In one embodiment, the aqueous mixture is maintained at this temperature for about 30 minutes during the reaction. In another embodiment, K_2CO_3 is used to maintain basic conditions in the aqueous mixture.

[0012] In one embodiment of the invention, the concentration of base in the water is about 0.4 mmol/mL. In another embodiment, the microwave energy is applied at a power of about 100 watts for a time of about 60 to about 70 minutes.

[0013] In one embodiment of the invention, a nitrobenzene compound is added to the aqueous mixture prior to application of microwave energy. The nitrobenzene compound may be 4-bromo-nitrobenzene. In another embodiment of the invention, the reaction also produces a reduced organic compound. The reduced organic compound may comprise a 4-bromo-aniline.

[0014] In one embodiment of the invention, the concentration of hydrogen produced is at least 27.79%.

BRIEF DESCRIPTION OF THE DRAWINGS

[0015] The invention is more fully described by reference to the following detailed description and the accompanying drawings wherein:

[0016] FIG. **1** is a depiction of the Chitosan-Ruthenium (Ch-Ru) composite.

[0017] FIG. **2** shows an experimental set up to perform the MW reaction in a sealed microwave tube.

[0018] FIG. **3**(*a*) provides an SEM image of the ChRu catalyst.

[0019] FIG. **3**(*b*) provides an X-ray diffraction image of the ChRu catalyst.

[0020] FIG. **3**(*c*) provides an energy dispersive spectra (EDS) of ChRu catalyst.

[0021] FIG. **3**(*d*) provides XPS data for the ChRu catalyst.

[0022] FIG. **4** provides GC-MS data confirming the formation of p-amino phenol A.

[0023] FIG. **5** provides GS-MS data confirming the formation of diaryl either B.

[0024] FIG. **6** provides GC-MS data confirming the formation of nitro reduced diaryl either C.

[0025] FIG. **7** provides GC-MS data showing the reduction of nitro group under MW heating conditions exclusively in basic media.

[0026] FIG. **8** provides GC-MS Head Space Analysis data showing the hydrogen concentration produced with the catalyst of the invention, suspended in aqueous K_2CO_3, was exposed to microwave heating for 30 minutes.

[0027] FIG. **9** provides GC-MS Head Space Analysis GC-MS Head Space Analysis data showing the hydrogen concentration produced under the same conditions as in FIG. **8** but using a different base.

[0028] FIG. **10** provides GC-MS Head Space Analysis data showing the hydrogen concentration produced under the same conditions as in FIG. **8** but using a different base.

[0029] FIG. **11** provides GC-MS Head Space Analysis data showing the hydrogen concentration produced under the same conditions as in FIG. **8** but using a different base.

[0030] FIG. **12** provides GC-MS Head Space Analysis data showing the hydrogen concentration produced under the same conditions as in FIG. **8** but using a different base.

[0031] FIG. **13** provides GC-MS Head Space Analysis data showing the hydrogen concentration produced under the same conditions as in FIG. **8** but using a different base.

[0032] FIG. **14** provides GC-MS Head Space Analysis data showing the hydrogen concentration produced under the same conditions as in FIG. **8** but using a different base.

[0033] FIG. **15** provides GC-MS Head Space Analysis data showing the hydrogen concentration produced under the same conditions as in FIG. **8** but using a different base.

[0034] FIG. **16** provides GC-MS Head Space Analysis data showing the hydrogen concentration produced under the same conditions as in FIG. **8** using a lower concentration of K_2CO_3.

[0035] FIG. **17** provides GC-MS Head Space Analysis data showing the hydrogen concentration produced under the same conditions as in FIG. **8** but at a lower temperature (100° C. vs. 125° C.).

[0036] FIG. **18** is a depiction of a Chitosan-Fe (ChFe) composite.

[0037] FIG. **19** is a depiction of a Chitosan-Pd (ChPd) composite.

[0038] FIG. **20** is a depiction of a Cellulose-Fe (CelluFe) composite.

[0039] FIG. **21** is a depiction of a Cellulose-Pd (CelluPd) composite.

[0040] FIG. **22** is a depiction of a Cellulose-Ru (CelluRu) composite.

[0041] FIG. **23** is a depiction of water splitting and nitro compound reduction reactions on a Chitosan-Ruthenium (Ch-Ru) composite catalyst.

DETAILED DESCRIPTION OF THE INVENTION

[0042] Referring more specifically to the drawings, FIG. **1** is a structural representation of the Chitosan-Ru composite catalyst prepared by the inventors. The Chitosan-Ru catalyst has been characterized by SEM (FIG. **3**(*a*)) and X-ray diffraction (XRD)(FIG. **3**(*b*)). The signals pertaining to the Ru metal were not detected in the XRD data, possibly due to complexation with chitosan or its low percentage. However, the presence of the Ru-metal has been confirmed by energy dispersive X-ray spectroscopy (FIG. **3**(*c*)). XPS analysis of ChRu was performed to analyze the oxidation state of the Ru metal; the binding energy peak for Ru $3d_{5/2}$ at 282.5 eV is in accordance with $Ru_{(III)}$ (XPS, FIG. **3**(*d*)). The weight percentage of Ru was found to be 6.41% by inductively coupled plasma-atomic emission spectroscopy (ICP-AES) analysis.

[0043] While demonstrating the application of ruthenium chitosan composite ChRu in C—O aryl bond formation in aqueous media (Scheme 2), the inventors observed the formation of three products: p-amino phenol A (FIG. **4**), expected diaryl ether B (FIG. **5**) and nitro reduced diaryl ether C (FIG. **6**). The detection of reduced nitro group to amine in the product mixture was unexpected, which in turn prompted the inventors to investigate how the reduction of nitro group is feasible under these conditions.

Scheme 2. RuCh catalyzed C—O coupling

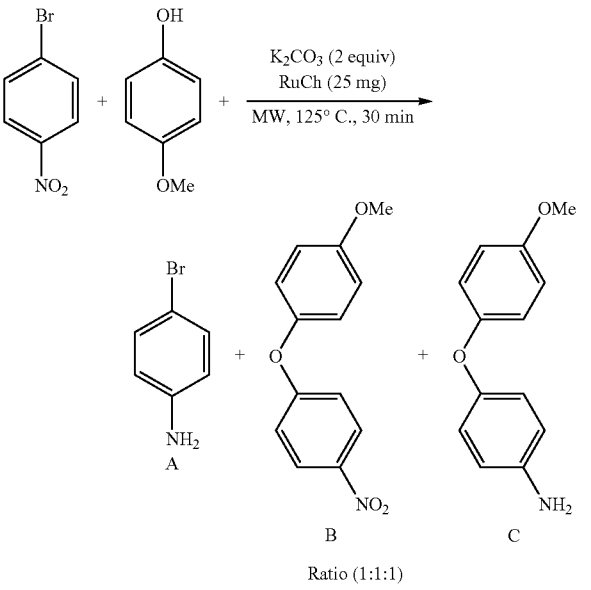

Ratio (1:1:1)

[0044] The study was undertaken with 4-bromo-nitrobenzene as a model substrate in order to find out the best possible conditions for the reduction reaction. The reduction of nitro group occurs under MW heating conditions exclusively in basic media (See Table 1, FIG. **7**).

TABLE 1

Screening for the catalytic reduction of nitro group

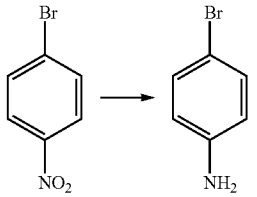

Entry	Catalyst	Base	Temp	Product Yield[a]
1	No catalyst	—	125° C.	0%
2	RuCh (25 mg)	—	125° C.	0%
3	RuCh (25 mg)	K_2CO_3	125° C.	0%
4	RuCh (25 mg)	—	125° C./MW	0%
5	RuChH (25 mg)	K_2CO_3	125° C./MW	89%[b]

[a]Reaction condition: 4-Nitro-bromobenzene (1 mmol), RuCh-catalyst (25 mg), K_2CO_3 (2 mmol), Water 5 mL, MW, 125° C., 30 min; [b]GC Conversion

[0045] After optimizing the reaction conditions that provided an ideal environment for reduction, the inventors searched for the source of the nitro reduction. Their studies led them to hypothesize that hydrogen may be generated in-situ in the reaction mixture, which could be responsible for the reduction of the nitro group. The hydrogen evolution through splitting of water is possible through use of a specially designed, sophisticated and highly conjugated ruthenium metal complex under photochemical conditions. In order to detect the generation of hydrogen in the reaction mixture, the inventors designed an experimental set up to perform the MW reaction in a sealed tube (see FIG. **2**). The design and accompanying conditions prevent the escape of hydrogen gas. The head space analysis of the sealed tube after the reaction would help to identify the gaseous atmosphere over the reaction mixture.

[0046] Accordingly, the inventors carried out experiments and studied the head space atmosphere. The head space analysis after the reaction was encouraging, as the inventors observed that substantial percentages of hydrogen were detected (~27%) (Table 2). Under neutral conditions, no splitting of water was discerned even after prolonged exposure to MW, UV-visible light and conventional heating (Table 2, entries 1-4). However, when the catalyst, suspended in aqueous K_2CO_3, was exposed to MW heating for 30 min, 27.79% of hydrogen (Table 2, entry 8) was detected in head space analysis (FIG. **8**). The experiments were set-up to screen the different bases and their effect on water splitting. Use of Cs_2CO_3 as a base results in 4.15% of hydrogen (Table 2, entry 9, FIG. **9**), whereas $NaHCO_3$, Na_2CO_3 and NaOH provided 0.79% hydrogen (Table 2, entry 10, FIG. **10**), 1.22% hydrogen (Table 2, entry 11, FIG. **11**) and 7.39% hydrogen (Table 2, entry 12, FIG. **12**), respectively, after head space analysis. Other bases, namely KOH, $KHCO_3$ and K_3PO_4, generated 3.84% (Table 2, entry 13, FIG. **13**), 1.28% (Table 2, entry 14, FIG. **14**) and 1.90% (Table 2, entry 15, FIG. **15**) of hydrogen under similar conditions. However, when the concentration of K_2CO_3 was reduced from 2 mmol in 5 mL water to 1 mmol in 5 mL water there was a sharp decline in the hydrogen percentage from 27.79% to 2.26% (Table 2, entry 16, FIG. **16**). The MW exposure at the reduced temperature of 100° C. directly impacts the efficiency of water splitting, thereby reducing the hydrogen percentage to 0.15% (Table entry 17, FIG. **17**). In basic media using K_2CO_3, no hydrogen was detected under conventional heating or UV-Visible light exposure (Table 2, entries 5-7). Having confirmed K_2CO_3 as an ideal base and its appropriate concentration for water splitting under MW, the use of alternative biorenewable support such as cellulose and other metals such as iron and palladium were explored.

TABLE 2

ChRu-catalyzed water splitting under MW

Entry	Catalyst	Base	Time/Temp	Energy source	% Hydrogen[a]
1	ChRu	—	60 min/125° C.	MW	0%
2	ChRu	—	24 h/ambient temp	UV	0%
3	ChRu	—	24 h/ambient temp	Visibile light	0%
4	ChRu	—	24 h/125° C.	oil bath	0%
5	ChRu	K_2CO3	24 h/ambient temp	UV	0%
6	ChRu	K_2CO3	24 h/ambient temp	Visibile light	0%
7	ChRu	K_2CO3	24 h/125° C.	oil bath	0%
8	ChRu	K_2CO_3	30 min/125° C.	MW	27.79%
9	ChRu	Cs_2CO_3	30 min/125° C.	MW	4.15%
10	ChRu	$NaHCO_3$	30 min/125° C.	MW	0.79%
11	ChRu	Na_2CO_3	30 min/125° C.	MW	1.22%
12	ChRu	NaOH	30 min/125° C.	MW	7.39%
13	ChRu	KOH	30 min/125° C.	MW	3.84%
14	ChRu	$KHCO_3$	30 min/125° C.	MW	1.28%
15	ChRu	K_3PO_4	30 min/125° C.	MW	1.90%
16[b]	ChRu	K_2CO_3	30 min/125° C.	MW	2.26%
17[c]	ChRu	K_2CO_3	30 min/100° C.	MW	0.15%

[a]Reaction conditions: Base (2 mmol), water (5 mL);

[b]1 mmol of K_2CO_3, water (5 mL), MW, 125° C.;

[c]Reaction was performed at 100° C., using 2 mmol of K_2CO_3 in 5 mL of water.

[0047] The microwave irradiation of ChFe, ChPd, CelluFe, CelluPd, CelluRu, (see FIGS. **18-22**, respectively) under basic media, using K_2CO_3 as a base was performed without a detectable presence of hydrogen in the head space analysis (Table S1).

TABLE S1

Screeing of water splitting using Fe, Pd and alternative biopolymer

Entry	Catalyst	Base	Time/Temp	Energy source	Hydrogen[a,b]
1	CelluRu	K_2CO_3	30 min/125° C.	Microwave	0.00%
2	CelluPd (II)	K_2CO_3	30 min/125° C.	Microwave	0.00%
3	CelluFe(III)	K_2CO_3	30 min/125° C.	Microwave	0.00%
4	ChFe(III)	K_2CO_3	30 min/125° C.	Microwave	0.00%
5	ChPd (II)	K_2CO_3	30 min/125° C.	Microwave	0.00%

[a]Reaction condition: K_2CO_3 (2 mmol), Water (5 mL), MW, Metal catalyst (25 mg).

[b]Percentage after Head space analysis

TABLE S2

Recycling of ChRu catalyst in nitro reduction

Entry	Substrate	Time	Product	Conversion[a],[b]
Cycle 1	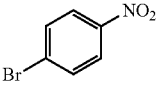	60 min	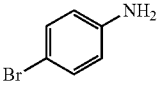	>99%
Cycle 2	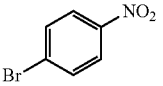	60 min	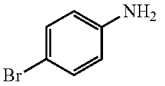	>99%
Cycle 3	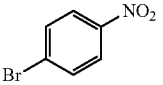	60 min	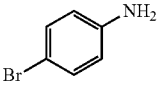	>99%
Cycle 4	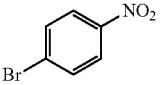	60 min	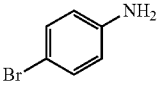	>99%
Cycle 5	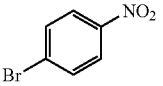	60 min	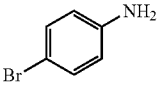	>99%

[a]Reaction condition: 1 mmol of 4-nitro bromobenzene, 2 mmol of K_2CO_3, ChRu (25 mg), 5 mL water, MW, 125° C., 60 min; [b]GC conversion

Scheme 3. Metal-catalyzed reduction of nitro group

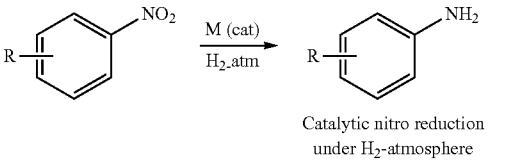

Catalytic nitro reduction under H_2-atmosphere

M = Metal
M = Pd, Pt, Ni, Ru etc

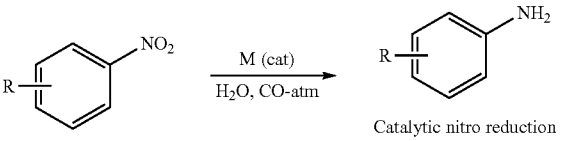

Catalytic nitro reduction using water and CO-mixture as hydrogen source

M = Rh, Ru, Au etc

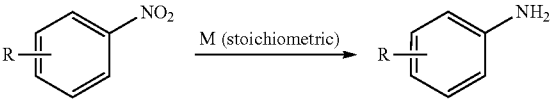

Nitro reduction using stoichiometric amount of metal.

M = Fe, Sn etc

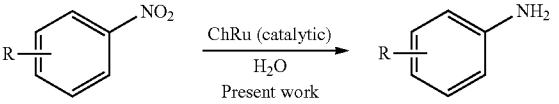

Catalytic reduciton using water as a hydrogen source

M = Fe, Sn etc

[0048] The selective reduction of nitro compounds to amines is one of the very important transformations in organic synthesis, and consequently there are number of procedures for the reduction of nitro compounds (Scheme 3). Due to concern for the environment, the search for simple, chemo-selective, affordable and environmentally benign methods that avoid the use of hazardous and expensive reducing agents in stoichiometric amounts has gained prime importance. The use of a binary mixture of CO and H_2O as a hydrogen source along with specially designed Rh, Au or Ru metal complex catalysts has been considered as one of the most useful methods for nitro reduction. The in-situ generation of hydrogen from water and its utilization in reduction of nitro compounds using simple biodegradable renewable chitosan has never been reported (see bottom, Scheme 3).

TABLE 3

ChRu catalyzed reduction of nitro compund.

Entry	Substrate	Time	Product	Conversion[a],[b]
1	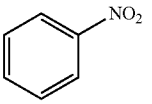	60 min	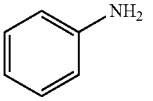	>99%

TABLE 3-continued

ChRu catalyzed reduction of nitro compund.

Entry	Substrate	Time	Product	Conversion[a],[b]
2	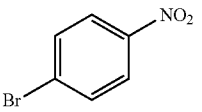	60 min	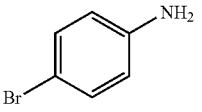	>99%
3	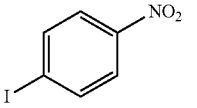	60 min	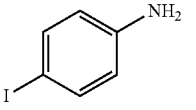	>99%
4	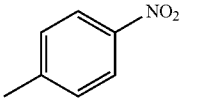	70 min	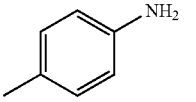	>99%
5	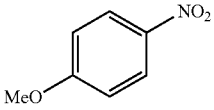	70 min	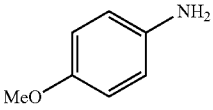	>99%
6	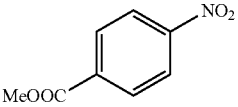	60 min	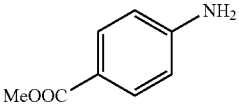	>99%

[a]Reaction condition: 1 mmol of nitro compound, 2 mmol of K_2CO_3, ChRu (25 mg), 5 mL water, MW, 125° C., 60-70 min; [b]GC conversion

[0049] The experimental procedure entailed placing aromatic nitro compound (1 mmol) into a microwave reaction tube, to which K_2CO_3 (2 mmol), ChRu (25 mg) and 5 mL of water were added and exposed to microwave irradiation for 60-70 min at 125° C. The reaction was monitored using GCMS. In almost all the cases, the nitro group is selectively reduced to the corresponding amine (Table 3).

[0050] The recovery of the catalyst is the most important goal in a sustainable organic synthesis. In industrial application of heterogeneous system, the lifetime of the catalyst and its level of reusability are significantly important factors. To demonstrate recyclability of ruthenium chitosan composite, a set of experiments was conducted for the hydrogenation of 4-nitro bromo benzene using the recycled ChRu catalyst. After the completion of the reaction, the catalyst was recovered, washed with acetone, and dried under vacuum. A fresh reaction was then set-up using fresh reactants and recycled catalyst and subjected to MW irradiation. The ChRu catalyst could be used at least five times without any change in its activity. Metal leaching was studied using ICP-AES analysis of the catalyst before and after the completion of the reaction. The Ru concentration was found to be 6.41% before the reaction and 6.35% after the reaction. The very small amount of Ru metal was detected in the aqueous mixture. The negligible amount of Ru leaching may be due to the well-defined structure of chitosan with its abundance of amine and hydroxyl functional groups. While it is only theory, chitosan's advantageous structural characteristics may result in Ru chelating via non-covalent interaction.

Examples

Experimental Procedure for Synthesis of Chitosan Ruthenium Catalyst (ChRu)

[0051] The Ruthenium on Chitosan catalyst was made as follows. Chitosan (3 g, medium molecular weight, Aldrich, CSA #9012-76-4) was suspended in 100 mL of water. To this suspension, 500 mg of $RuCl_3.3H_2O$ was added. The pH was adjusted to 9 using 25% ammonia, and the suspension was continuously stirred overnight. The catalyst was separated using a centrifuge operated at 5000 rpm for 5 minutes. The catalyst was then dried under vacuum at 50° C. for about 2 hours to about 3 hours.

Reduction of Nitro Group

[0052] Nitro compound (e.g., the aromatic nitro compound, 4-bromonitrobenzene, 1.0 mmol), ChRu (25 mg, 0.015, mol %) and K_2CO_3 (2 mmol) were placed in a crimp-sealed thick-walled glass tube equipped with a pressure sensor and a magnetic stirrer. Water (5 mL) was added to the reaction mixture. The reaction tube was placed inside the cavity of a CEM Discover focused microwave synthesis system and operated at 125° C. (temperature monitored by a built-in infrared sensor) and 100 Watts for 60-70 minutes. After completion of the reaction, the catalyst was removed from the reaction mixture using a centrifuge. Reduction of the nitro group has been monitored using GCMS. The clear liquid was cooled slowly, and, in most cases, an analytically pure sample of corresponding amine was obtained. The samples can be isolated from the water medium by simple decantation.

[0053] In brief, the inventors have demonstrated the unprecedented use of pure water as a hydrogen source in the catalytic hydrogenation of nitro compounds wherein ruthenium chitosan composite can split water under microwave irradiation conditions. See FIG. **23**. Ruthenium chitosan composite performs a dual action of producing hydrogen and subsequently catalyzing the reduction of nitro groups to amine under MW irradiation. As a result of this invention, low energy MW has been shown to assist in weakening the O—H bound in water molecules, which results in instigating the splitting of water into hydrogen. These findings may pave the way for the future the expansion of microwave-assisted chemistry in concerted reactions such as hydrogen production from water and hydrogenation.

[0054] As the present invention may be embodied in several forms without departing from the spirit or essential characteristics thereof, it will be understood that the invention is not limited by the details of the foregoing description, unless otherwise specified, but rather should be construed broadly within its spirit and scope as defined in the appended claims, and therefore all changes and modifications that fall within the metes and bounds of the claims. Accordingly, the invention is defined by the appended claims.

REFERENCES

[0055] [1]. R. E. Blankenship, *Molecular Mechanisms of Photosynthesis*, Blackwell Science, Oxford, U.K., 2002.

[0056] [2]. H. J. Lewerenz, L. Peter, *Photoelectrochemical Water Splitting: Materials, Processes and Architectures*, The Royal Society of Chemistry 2013.

[0057] [3]. R. V. D. Krol, M. Gratzel, *Photoelectrochemical Hydrogen Production*, Springer Science, 2012.

[0058] [4]. T. Hisatomi, J. Kubota, K. Domen, *Chem. Soc. Rev.,* 2014, DOI: 10.1039/C3CS60378D

[0059] [5]. A. Kudo, Y. Miseki, *Chem. Soc. Rev.,* 2009, 38, 253-278.

[0060] [6]. J. J. Concepcion, J. W. Jurss, M. K. Brennaman, P. G. Hoertz, A. O. T. Patrocinio, N. Y. Murakami, J. L. Templeton, T. J. Meyer, *Acc. Chem. Res.* 2009, 42, 1954-1965.

[0061] [7]. S. Romain, L. Vigara, A. Llobet, *Acc. Chem. Res.* 2009, 42, 1944-1953.

[0062] [8]. G. S. Parkinson, Z. Novotny, P. Jacobson, M. Schmid, U. Diebold, *J. Am. Chem. Soc.,* 2011, 133, 12650-12655.

[0063] [9]. R. H. Gonçalves, B. H. R. Lima, E. R. Leite, *J. Am. Chem. Soc.,* 2011, 133, 6012-6019.

[0064] [10]. M. Higashi, K. Domen, R. Abe, *J. Am. Chem. Soc.,* 2012, 134, 6968-6971.

[0065] [11]. M. T. Mayer, C. Du, D. Wang, *J. Am. Chem. Soc.,* 2012, 134, 12406-12409.

[0066] [12]. J. Cohen, K. Kim, M. L. Ghirardi, K. Schulten, M. Seibert, P. King, *Biochem. Soc. Trans.* 2005, 33, 80-82.

[0067] [13]. A. S. Fedorov, S. Kosourov, M. Seibert, M. L. Ghirardi, *Appl. Biochem. Biotechnol.* 2005, 403-412.

[0068] [14]. G. Sirasani, L. Tong, and E. P. Balskus, *Angew. Chem. Int. Ed.* 2014, 53, 7785-7788

[0069] [15]. L. Vigh, D. A. Los, I. Horv_th, N. Murata, *Proc. Natl. Acad. Sci*. USA 1993, 90, 9090-9094.

[0070] [16]. X. H. Li, X. Wang, M. Antonietti, *Chem. Sci.,* 2012, 3, 2170

[0071] [17]. K. S. Joya, Y. F. Joya, K. Ocakoglu, R. V. Krol, *Angew. Chem. Int. Ed.* 2013, 52, 10426-10437.

[0072] [18]. R. B. Nasir Baig, R. S. Varma *Chem. Commun.,* 2013, 49, 752-770.

[0073] [19]. R. B. Nasir Baig, B. R. Vaddula, M. A. Gonzalez, R. S. Varma, *RSC Adv.,* 2014, 4, 9103-9106.

[0074] [20]. R. B. Nasir Baig, M. N. Nadagouda, R. S. Varma, *Green Chem.,* 2014, 16, 2122-2127.

[0075] [21]. X. Yang, M. B. Hall, *J. Am. Chem. Soc.,* 2010, 132, 120-130

[0076] [22]. M. J. Krische, Y. Sun, *Acc. Chem. Res.,* 2007, 40, 1237-1237.

[0077] [23]. I. Sorribes, G. Wienhcfer, C. Vicent, K. Junge, Rosa Lusar, M. Beller, *Angew. Chem. Int. Ed.* 2012, 51, 7794-7798.

[0078] [24]. D. Cantillo, M. Baghbanzadeh, C. O. Kappe, *Angew. Chem. Int. Ed.* 2012, 51, 10190-10193.

[0079] [25]. L. He, L. C. Wang, H. Sun, J. Ni, Y. Cao, H. Y. He, K. N. Fan, *Angew. Chem. Int. Ed.* 2009, 48, 9538-9541.

[0080] [26]. C. O. Kappe, *Angew. Chem. Int. Ed.* 2013, 52, 2-7

[0081] [27]. G. B. Dudley, A. E. Stiegman, M. R. Rosana, *Angew. Chem. Int. Ed.* 2013, 52, 2-8.

The invention claimed is:

1. A process for generating hydrogen and oxygen from water, the process comprising preparing a ruthenium on chitosan catalyst, bringing the catalyst into contact with an aqueous mixture under basic conditions, and applying microwave energy to the aqueous mixture to produce hydrogen and oxygen.

2. The process of claim **1** wherein the catalyst is prepared by

(a) suspending chitosan in water;

(b) adding $RuCl_3.3H_2O$;

(c) adjusting the pH of the mixture to about 8.5-9.5 while continuously stirring the mixture;

(d) separating the catalyst from the liquid in the mixture; and

(e) drying the mixture under a vacuum.

3. The process of claim **2** wherein the pH of the mixture is adjusted using ammonia.

4. The process of claim **2** wherein the catalyst is dried under a vacuum at a temperature from about 30-60° C.

5. The process of claim **1** wherein aqueous mixture is maintained at about 125° C. during the reaction.

6. The process of claim **5** wherein the aqueous mixture is maintained at about 125° C. for about 30 minutes during the reaction.

7. The process of claim **1** wherein K_2CO_3 is used to maintain basic conditions in the aqueous mixture.

8. The process of claim **1** wherein the concentration of base in the water is about 0.4 mmol/mL.

9. The process of claim **1** wherein microwave energy is applied at a power of about 100 watts for a time of about 60 to about 70 minutes.

10. The process of claim **1** wherein a nitrobenzene compound is added to the aqueous mixture prior to application of microwave energy.

11. The process of claim **10** wherein the nitrobenzene compound is 4-bromo-nitrobenzene.

12. The process of claim **11** wherein the reaction also produces a reduced organic compound.

13. The process of claim **12** wherein the reduced organic compound comprises a 4-bromo-aniline.

14. The process of claim **1** wherein the concentration of hydrogen produced is at least 4.15%.

15. The process of claim **1** wherein the concentration of hydrogen produced is at least 27.79%.

16. The process of claim **2** wherein the catalyst is separated from the liquid in the mixture using a centrifuge.

* * * * *

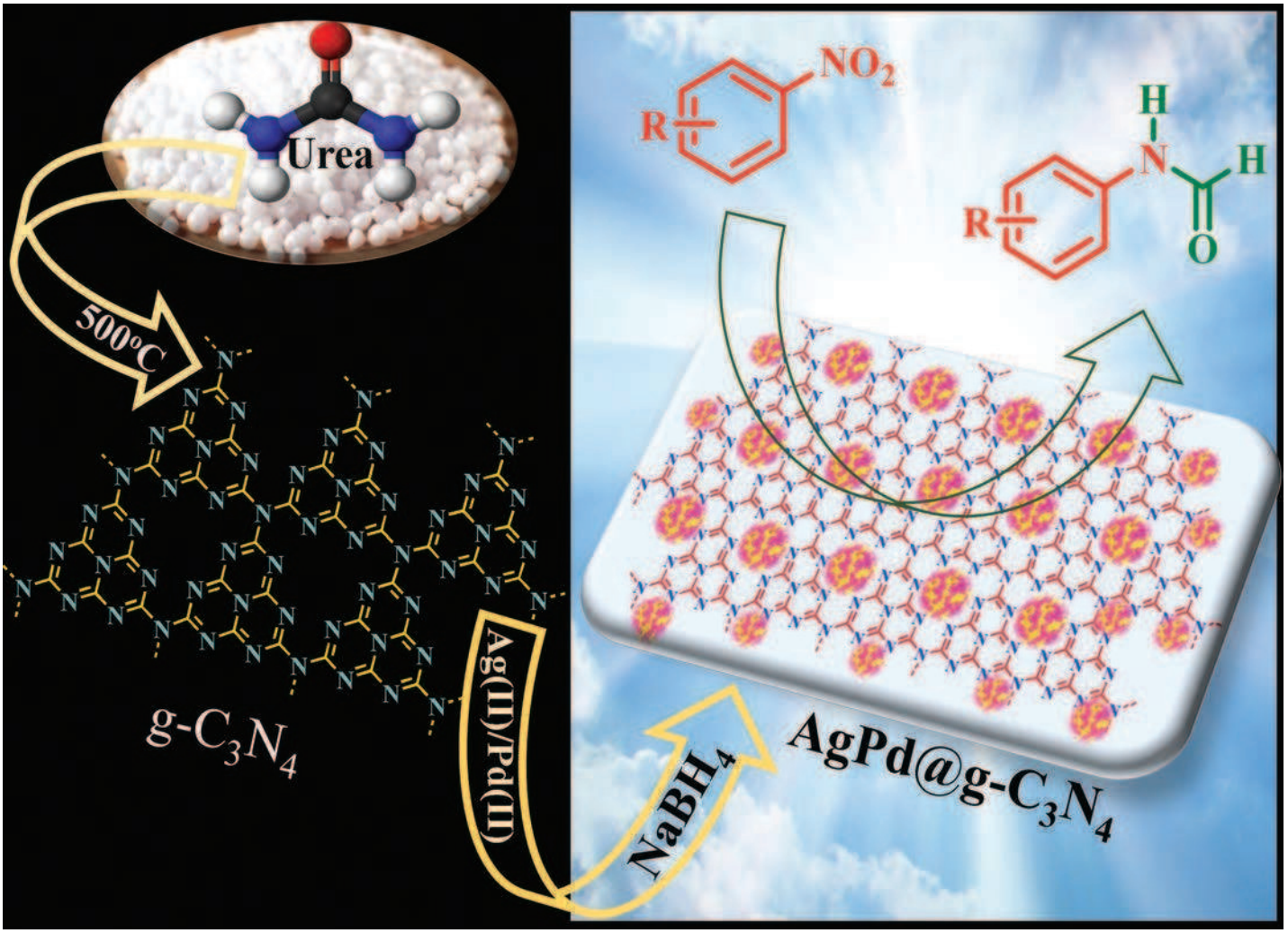

An article presented by Prof. Rajender S. Varma *et al*. of the U.S. Environmental Protection Agency, Cincinnati, USA.

Title: A photoactive bimetallic framework for direct aminoformylation of nitroarenes

A bimetallic catalyst, AgPd@g-C_3N_4, was synthesized by immobilizing silver and palladium nanoparticles over the surface of graphitic carbon nitride (g-C_3N_4) and its utility was demonstrated for the concerted aminoformylation of aromatic nitro compounds under visible light conditions. The entwined AgPd@g-C_3N_4 catalyst was very effective in exploiting formic acid as a source of hydrogen and acting as a formylating agent under photochemical conditions.

As featured in:

See Rajender S. Varma *et al*., *Green Chem*., 2016, **18**, 1019.

ROYAL SOCIETY OF CHEMISTRY

www.rsc.org/greenchem

Registered charity number: 207890

Published on 15 December 2015. Downloaded by US Environmental Protection AG, Cincinnati on 30/03/2016 20:12:36.

Green Chemistry

PAPER

View Article Online
View Journal | View Issue

Cite this: *Green Chem.*, 2016, **18**, 1019

A photoactive bimetallic framework for direct aminoformylation of nitroarenes†

R. B. Nasir Baig,‡[a] Sanny Verma,‡[a] Mallikarjuna N. Nadagouda[b] and Rajender S. Varma*[a]

Received 20th November 2015,
Accepted 14th December 2015

DOI: 10.1039/c5gc02799c

www.rsc.org/greenchem

A bimetallic catalyst, AgPd@g-C_3N_4, synthesized by reducing silver and palladium salts over graphitic carbon nitride (g-C_3N_4), enables the concerted reductive formylation of aromatic nitro compounds under photo-chemical conditions using formic acid, which serves the dual role of a hydrogen source and a formylating agent.

Introduction

The synthesis of amines and their conversion to *N*-formyl derivatives are important reactions in organic synthesis due to their extensive application in natural product synthesis and drug discovery.[1] Conventionally, amino-formyl derivatives have been synthesized from nitro compounds in two separate steps involving nitro reduction followed by *N*-formylation.[2] Most of the earlier developed processes in the reduction of the nitro group use stoichiometric amounts of reagents. The heightened awareness of climate change and the growing importance of pollution prevention have resulted in a dramatic shift to using catalytic reagents instead. In general, the catalytic variant developed for the reduction of nitro compounds often requires high hydrogen pressure and elevated temperature,[3] safety being a worrisome concern for high pressure hydrogenation on the industrial scale. Alternative protocols have been advanced by employing *in situ* generated hydrogen along with a precious metal catalyst. Most of these procedures require vigorous stirring in aqueous media under a carbon monoxide atmosphere,[4] a hazardous and toxic contaminant. Formic acid, available from biomass resources, has been introduced as a safer alternative for the transfer hydrogenation of nitro compounds to generate aryl amines.[5] The formylation of amine has to be carried out subsequently in a separate step. Rutile-supported gold catalyst has achieved such a direct conversion of nitro compounds to *N*-formylamines.[6]

However, this reaction is temperature dependent. At elevated temperatures, it leads to the formation of *N*,*N*-demethylation whereas a slight variation towards the lower side (~60 °C) does not allow the formylation of reduced products.[7] In addition, it requires an inert atmosphere along with the use of organic solvents. Magnetically retrievable palladium catalyst has also been used for the conversion of nitro-arenes to the corresponding *N*-formyl derivatives; the complexity of the catalyst preparation and its higher loading are the main limitations of this method.[8] Iron metal in combination with the corresponding carboxylic acid has been introduced but lower product yields and heating over an extended period of time render this an unproductive and tedious method.[9] This prompted us to develop a simple and sustainable catalyst which can accomplish this transformation in aqueous media under ambient conditions. In continuation of our ongoing efforts to develop sustainable methods[10] that aim for a reduction in chemical waste generation,[11] we have designed a bimetallic AgPd@g-C_3N_4 photoactive heterogeneous catalyst system for the direct transformation of aromatic nitro compounds to *N*-formylamines.

Synthesis and characterization

Graphitic carbon nitride (g-C_3N_4) was synthesized by heating urea in a furnace at 500 °C and the ensuing pale yellow solid was dispersed in water by sonicating over a period of 15 min.[12] Silver and palladium salts ($AgNO_3$ and $Pd(NO_3)_2$) were sequentially added and the reaction mixture was stirred for 12 hours. The reaction temperature was raised to 50 °C and the silver and palladium salts were reduced to Ag(0) and Pd(0) nanoparticles using an excess of sodium borohydride ($NaBH_4$). The reaction mixture was cooled to ambient temperature, centrifuged and the solid was washed with methanol and vacuum

[a]*Sustainable Technology Division, National Risk Management Research Laboratory, U.S. Environmental Protection Agency, MS 443, Cincinnati, Ohio 45268, USA. E-mail: varma.rajender@epa.gov; Fax: +1 513-569-7677; Tel: +1 513-487-2701*
[b]*WQMB, WSWRD, National Risk Management Research Laboratory, U.S. Environmental Protection Agency, MS 443, Cincinnati, Ohio 45268, USA*
†Electronic supplementary information (ESI) available. See DOI: 10.1039/c5gc02799c.
‡These authors contributed equally to this work.

Published on 15 December 2015. Downloaded by US Environmental Protection AG, Cincinnati on 30/03/2016 20:12:36.

dried at 50 °C. The AgPd@g-C_3N_4 catalyst (Fig. 1) was isolated as a fine solid powder.

The catalyst was characterized using transmission electron microscopy, scanning electron microscopy, X-ray photoelectron spectroscopy, X-ray diffraction and inductively coupled plasma atomic emission spectroscopy (ICP-AES).

TEM spectra of the catalyst endorse the formation of single phase silver and palladium nanoparticles with a spherical morphology (Fig. 2). The SEM image of AgPd@g-C_3N_4 and its EDX confirm the immobilization of silver (Ag) and palladium (Pd) nanoparticles over the surface of g-C_3N_4 (Fig. 3). The concentrations of Ag (4.67%) and Pd (4.55%) were determined using ICP-AES analysis. The XPS (Fig. 4) analysis of AgPd@g-C_3N_4 corroborated the formation of palladium and silver nanoparticles on the surface of graphitic carbon nitride, which was further supported by XRD results (Fig. 5).

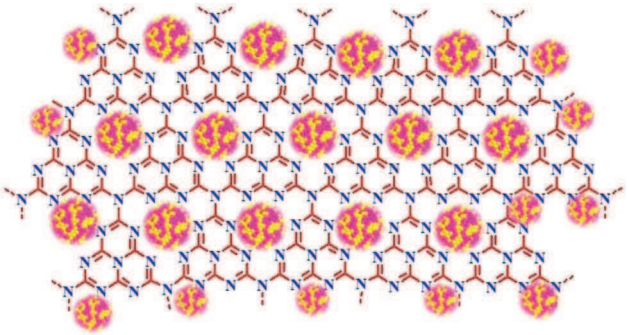

Fig. 1 Structure of AgPd@g-C_3N_4.

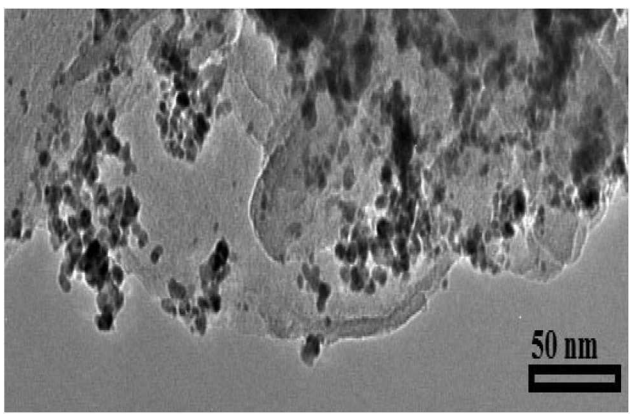

Fig. 2 TEM image of the AgPd@g-C_3N_4 catalyst.

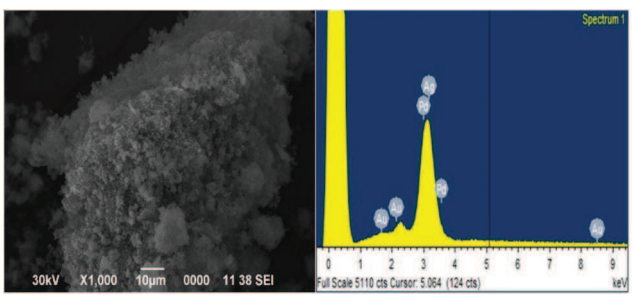

Fig. 3 SEM and EDX data of the AgPd@g-C_3N_4 catalyst.

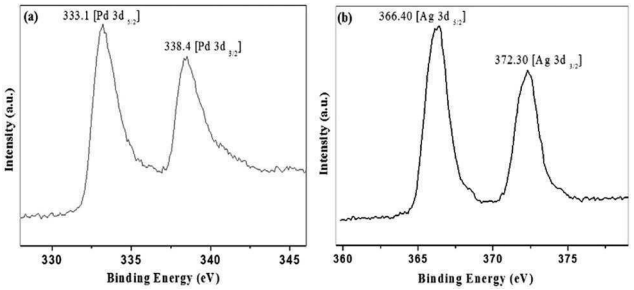

Fig. 4 XPS spectra of AgPd@g-C_3N_4: (a) Pd 3d XPS spectra; (b) Ag 3d XPS spectra.

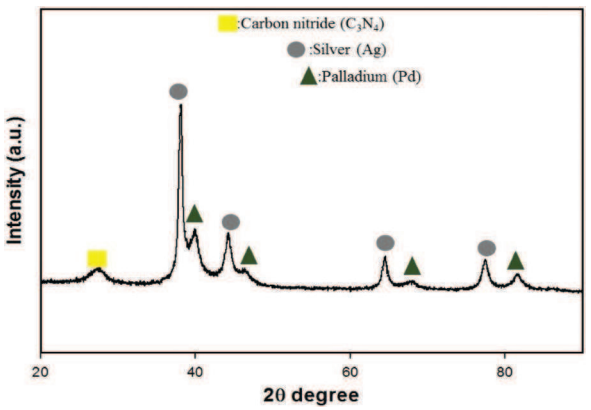

Fig. 5 XRD spectra of the AgPd@g-C_3N_4 catalyst.

Results and discussion

The most important step in the development of the active catalyst was the design and synthesis of a catalytic system for the direct conversion of nitro compounds to *N*-formylamine derivatives, preferably using visible light to drive this reaction. In view of the known prowess of graphitic carbon nitride (g-C_3N_4) as a photo active support,[13] we pursued this approach using formic acid as a reducing as well as a formylating agent in the presence of a bimetallic catalyst.

First, Pd (10 mol%) was immobilized on g-C_3N_4 and tested for the aqueous reductive formylation of the nitro group using formic acid as a hydrogen source; the formation of 47% of the desired product after 12 hours of exposure to visible light (Table 1, entry 1) was encouraging. Increasing the palladium load (Table 1, entry 2) did not improve the catalytic activity whereas low loading decreased the yield to 30% (Table 1,

 This journal is © The Royal Society of Chemistry 2016

Published on 15 December 2015. Downloaded by US Environmental Protection AG, Cincinnati on 30/03/2016 20:12:36.

Table 1 Screening of catalysts for *N*-formylation

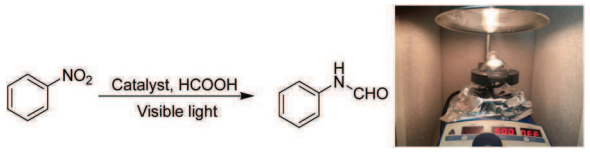

Entry	Catalyst	Time	Yield[a,b]
1	Pd@g-C_3N_4 (10% Pd)	12 h	48%
2	Pd@g-C_3N_4 (20% Pd)	12 h	49%
3	Pd@g-C_3N_4 (5% Pd)	12 h	31%
4	CuPd@g-C_3N_4 (10% Cu : 10% Pd)	12 h	65%
5	CuPd@g-C_3N_4 (10% Cu : 5% Pd)	12 h	55%
6	CuPd@g-C_3N_4 (5% Cu : 10% Pd)	12 h	69%
7	AgPd@g-C_3N_4 (10% Ag : 10% Pd)	2 h	99%
8	AgPd@g-C_3N_4 (10% Ag : 5% Pd)	5 h	88%
9	AgPd@g-C_3N_4 (5% Ag : 10% Pd)	2 h	99%
10	AgPd@g-C_3N_4 (2% Ag : 10% Pd)	5 h	85%
11	Ag@g-C_3N_4 (10% Ag)	24 h	—

[a] Reaction conditions: 1 mmol of nitrobenzene; formic acid (2 mmol); water (1.0 mL); catalyst (25 mg); 40 watt domestic bulb. [b] Isolated yield.

entry 3). These results suggested that Pd@g-C_3N_4 was not sufficiently active to accomplish this transformation. We sought to enhance its activity by adding a catalytic promoter, preferably an abundant material such as copper. Consequently, copper–palladium CuPd@g-C_3N_4 catalysts were synthesized and used, which afforded higher yields (65%) of the desired product (Table 1, entry 4). Various amounts of copper and palladium loadings were next examined (Table 1, entries 5 and 6). The CuPd@g-C_3N_4 catalyst with 10% Cu and 5% Pd (Table 1, entry 5) gave the desired product in 55% yield, whereas the CuPd@g-C_3N_4 catalyst with 5% Cu and 10% Pd gave 69% of the product. A recent report on the use of the Ag–Pd system on an ultrathin support[14] encouraged us to explore the use of silver as a co-catalyst partner, and therefore we synthesized the AgPd@g-C_3N_4 framework. The reaction of nitrobenzene with formic acid in the presence of bimetallic AgPd@g-C_3N_4 gave a quantitative yield of *N*-formyl aniline (Table 1, entry 7, 2 h). The variation in Ag and Pd concentrations in the catalyst played a crucial role in the reductive formylation of the nitro group. The catalyst with 10% Ag and 5% Pd loading required 5 h for the completion of the reaction (Table 1, entry 8). On the other hand, the catalyst system consisting of 5% Ag and 10% Pd gave a quantitative yield of the desired product within 2 h (Table 1, entry 9). Further reduction in the silver concentration led to an increase in the reaction time and a decrease in the product yield (Table 1, entry 10). The reaction with silver alone, Ag@g-C_3N_4, did not show any evidence of reductive formylation products even after 24 hours (Table 1, entry 11).

After establishing the ideal reaction conditions for the catalyst, it was imperative to evaluate the performance of AgPd@g-C_3N_4 with a wide variety of substrates. Accordingly, an array of nitro derivatives were subjected to reductive formylation reactions (Table 2, entries 1–9); all the substrates bearing electron donating (Table 2, entries 2 and 3) and electron withdrawing

Table 2 *N*-Formylation of nitroarenes by AgPd@g-C_3N_4 [a]

Entry	Reactant	Product	Time	Yield[b]
1	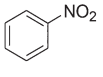	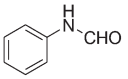	2 h	99%
2	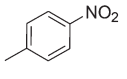	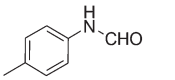	2 h	98%
3	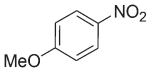	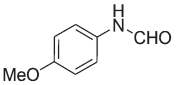	2 h	96%
4	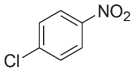	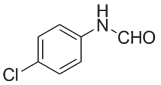	2 h	97%
5	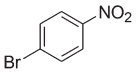	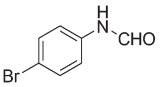	2 h	97%
6	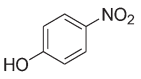	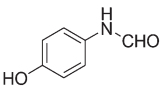	2 h	97%
7	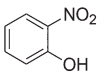	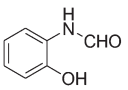	2 h	96%
8	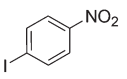	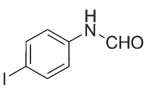	2 h	97%
9	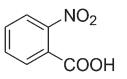	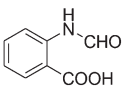	2 h	96%
10	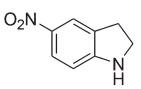	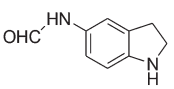	3 h	76%
11	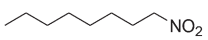	—	12 h	—

[a] Reaction conditions: nitroarenes (1 mmol); formic acid (2 mmol); water (1.0 mL); catalyst (25 mg); 40 watt domestic bulb. [b] Isolated yield.

substituents (Table 2, entries 4–9) were converted to the corresponding amino formyl derivatives. It was difficult to corroborate the reactivity pattern with the nature of the substituents and electronic behavior as most of the reactions were completed within 2 hours.

The recyclability of the catalyst in terms of practical and sustainable use was established using recycling experiments for the reductive formylation of nitrobenzene. After the completion of the first reaction, AgPd@g-C_3N_4 was recovered and reused for the reductive formylation of a fresh batch of nitrobenzene. AgPd@g-C_3N_4 was found to be stable and could be reused several times without losing its activity (ESI, S2†); even

Published on 15 December 2015. Downloaded by US Environmental Protection AG, Cincinnati on 30/03/2016 20:12:36.

after the 6th cycle, nitrobenzene was efficiently converted into *N*-formyl aniline. The reactivity and stability of the catalyst could be attributed to the graphitic carbon nitride (g-C_3N_4) which holds Ag and Pd nanoparticles firmly. The metal leaching in the AgPd@g-C_3N_4 catalyst was studied using ICP-AES analysis of the reaction solvent and the recycled catalyst before and after the reaction. The absence of metals in the mother liquor and the percentage of Ag (4.65%) and Pd (4.54%) in the recycled catalyst confirmed that g-C_3N_4 holds the metals tightly. The negligible metal leaching may be attributed to high porosity and polarity of the g-C_3N_4 support which holds these metals *via* non-covalent interactions.

Conclusions

Silver and palladium were immobilized by reducing their salt forms over a g-C_3N_4 (graphitic carbon nitride) surface. The synthesized AgPd@g-C_3N_4 catalyst was used for the direct amino formylation of an aromatic nitro group under photo-chemical conditions using visible light as a source of energy and formic acid as a reducing as well as a formylating agent. The bimetallic catalyst is highly effective in decomposing formic acid into hydrogen and for use as a formylating agent in a concerted process.

Disclaimer

The views expressed in this article are those of the authors and do not necessarily represent the views or policies of the U.S. Environmental Protection Agency. Any mention of trade names or commercial products does not constitute endorsement or recommendation for use.

Acknowledgements

RBNB and SV were supported by the Postgraduate Research Program of the National Risk Management Research Laboratory administered by the Oak Ridge Institute for Science and Education through an interagency agreement between the U.S. Department of Energy and the U.S. Environmental Protection Agency.

Notes and references

1 (*a*) S. Kotachi, Y. Tsuji, T. Kondo and Y. J. Watanabe, *Chem. Soc., Chem. Commun.*, 1990, 549–550; (*b*) G. W. Kabalka and R. S. Varma, in *Comprehensive Organic Synthesis*, ed. B. M. Trost and I. Fleming, Pergamon, Oxford, 1st edn, 1992, vol. 8, pp. 363–388; (*c*) G. R. Petit, M. V. Kalnins, T. M. H. Liu, E. G. Thomas and K. J. Parent, *Org. Chem.*, 1961, **26**, 2563–2566; (*d*) A. Jackson and O. Meth-Cohn, *J. Chem. Soc., Chem. Commun.*, 1995, 1319–1319.

2 (*a*) A. S. Guram and S. L. Buchwald, *Angew. Chem., Int. Ed. Engl.*, 1995, **34**, 1348–1350; (*b*) M. K. Basu, F. F. Becker and B. K. Banik, *Tetrahedron Lett.*, 2000, **41**, 5603–5722; (*c*) P. Strazzolini, A. G. Giumanini and S. Cauci, *Tetrahedron*, 1990, **46**, 1081–1118.

3 G. S. Vanier, *Synlett*, 2007, 131–135.

4 L. He, L. C. Wang, H. Sun, J. Ni, Y. Cao, H. Y. He and K. N. Fan, *Angew. Chem., Int. Ed.*, 2009, **48**, 9538–9541.

5 X. H. Li, Y. Y. Cai, L. H. Gong, W. Fu, K. X. Wang, H. L. Bao, X. Wei and J. S. Chen, *Chem. – Eur. J.*, 2014, **20**, 16732–16737.

6 X. B. Lou, L. He, Y. Qian, Y. M. Liu, Y. Cao and K. N. Fana, *Adv. Synth. Catal.*, 2011, **353**, 281–286.

7 B. Karimi, F. Mansouri and H. Vali, *ChemPlusChem*, 2015, **80**, 1750–1759.

8 L. Yu, Q. Zhang, S. S. Li, J. Huang, Y. M. Liu, H. Y. He and Y. Cao, *ChemSusChem*, 2015, **8**, 3029–3035.

9 K. Y. Lee, J. M. Kim and J. N. Kim, *Bull. Korean Chem. Soc.*, 2002, **23**, 1355–1498.

10 (*a*) R. S. Varma, *Green Chem.*, 2014, **16**, 2027–2041; (*b*) R. B. Nasir Baig and R. S. Varma, *ACS Sustainable Chem. Eng.*, 2014, **2**, 2155–2158; (*c*) S. Verma, H. P. Mungse, N. Kumar, S. Choudhary, S. L. Jain, B. Sain and O. P. Khatri, *Chem. Commun.*, 2011, **47**, 12673–12675; (*d*) S. Verma, J. L. Bras, S. L. Jain and J. Muzart, *Dalton Trans.*, 2013, **42**, 14454–14459.

11 (*a*) R. B. Nasir Baig, M. N. Nadagouda and R. S. Varma, *Green Chem.*, 2014, **16**, 4333–4338; (*b*) S. Verma, R. Singh, D. Tripathi, P. Gupta, G. M. Bahuguna and S. L. Jain, *RSC Adv.*, 2013, **3**, 4184–4188.

12 (*a*) J. Zhu, P. Xiao, H. Li and S. A. C. Carabineiro, *ACS Appl. Mater. Interfaces*, 2014, **6**, 16449–16465; (*b*) S. Verma, R. B. Nasir Baig, C. Han, M. N. Nadagouda and R. S. Varma, *Green Chem.*, 2016, **18**, 251–254; (*c*) S. Verma, R. B. Nasir Baig, C. Han, M. N. Nadagouda and R. S. Varma, *Chem. Commun.*, 2015, **51**, 15554–15557.

13 Z. Zhao, Y. Sun and F. Dong, *Nanoscale*, 2015, **7**, 15–37.

14 C. Hu, X. Mu, J. Fan, H. Ma, X. Zhao, G. Chen, Z. Zhou and N. Zheng, *ChemNanoMat*, 2015, DOI: 10.1002/cnma.201500162.

 This journal is © The Royal Society of Chemistry 2016

Date: 4/27/2020

R. B. Nasir Baig, Sanny Verma, M. N. Nadagouda and R. S. Varma "A Photoactive bimetallic framework for direct aminoformylation of nitroarenes" Green chemistry 2016, 18, 1019-1022. (Cover Page; IF= 9.405; immediacy index= 2.24; Citation half-life= 4.10; Citation= 18)

I, Dr. Sanny Verma was part of the research of the above publication and my contribution for this publication can be valued at 10%

Best regards

Sanny Verma
US EPA/ORD/CESER/CTMB
26 West Martin Luther King Drive,
Cincinnati, Ohio 45268, USA; Tel: (513)-5697293
E-mail: Verma.Sanny@epa.gov

Table of Contents

General_Authors_Publications.....2
LI-266120_Xue_et_al_2015.....9
Record_of_Percentage_Agreement_Critical_Insight_paper_xx_jg_signed.....24
Record_of_Percentage_Agreement_Critical_Insight_paper_xx_ms_trh_jc_signed.....25
Record_of_Percentage_Agreement_Critical_Insight_paper_xx_ms_na_xm_signed.....26

United States Environmental Protection Agency
Washington, DC 20460

STAA REPORT FOR THE SCIENTIST NOMINATIONS

General Information:

Nomination ID/App ID:	20-101
Research Category Primary:	Integrated Risk Assessment (IR)
Research Category Secondary:	Review Articles (RA);Integrated Risk Assessment (IR);Sustainability and Innovation (SI)
Laboratory/Office Name:	ORD
Nomination Entered By:	Xin Ma

Eligibility Checklist:

[Y] The nominated publication(s) has not been submitted to a previous STAA competition.

[Y] The nominated publication(s) was published on or before January 1, 2017 and on or after January 1,2012

[Y] The principal author was an EPA employee or a PHS employee assigned to EPA when the research was performed

[Y] The EPA authors (includes PHS employees assigned to EPA) contributed collectively a minimum of 50% toward the publication(s)

Nominating Official Name:	Regan Murray
Nominating Official Title:	SUPERVISORY INTERDISCIPLINARY SCIENTIST
Nominating OfficialEmail:	murray.regan@epa.gov
STAA Coordinator Name:	Kathleen Wiser
STAA Coordinator Email:	wiser.kathi@epa.gov

Justifications:

Justification 1:

Although previous siloed community water services are mostly achieved through large centralized infrastructure, sustainable solutions to community water systems require a more comprehensive understanding and assessment of the integrated source-drinking-wastewater systems over their life-cycles. This paper addressed the overarching question: What are the strengths and weaknesses of various sustainability assessment tools, and how do they aid in the design of next-generation community water services? Although many tools (e.g. life cycle assessment, human health risk assessment, footprint and emergy) have been applied to elements of these water services (i.e. water resources, drinking water, storm water or wastewater treatment alone), it is important to develop and combine the system-based tools and metrics in order to holistically evaluate the risks and sustainability of the multi-dimensional urban water systems based on the concept of integrated resource management. The strengths and weaknesses of key system-based tools and metrics are discussed. The thorough review of sustainability tools/metrics provides more insights for future directions to sustainable system designs and the need of how to quantitively measure system adaptability to future changes and infrastructure robustness in community water systems.

Justification 2A:

N/A

Justification 2B:

N/A

Justification 2C:

N/A

Justification 2D:

N/A

Justification 2E:

This research is submitted in Integrated Risk Assessment (IR). The research focuses on the metrics and tools used to quantify risk to the sustainability in urban water systems and vulnerability of ecosystems from multiple stressors at multiple scales.

A concurrent nomination is submitted in the category of Review Articles (RA). It includes not only critical analyses of every major subsystem in existing centralized water systems, providing potential transformative alternatives, but also a conceptual holistic framework of One Water concept and potential tools for such comprehensive analysis. The research provides new insight into sustainable integrated water system design.

Justification 3A:

N/A

Justification 3B:

Water Research is a Journal of the International Water Association (IWA) published by Elservier and one of the leading journals in the field of water science and technology in the world. The external peer review process by Elservier uses the criteria of quality, creativity, originality, accuracy and contribution to the field to evaluate the scientific merit of the publication.

AUTHORS

Principal Author

Author Name: Xin (Cissy) Ma

Professional Title:		Salutation:
Email:	ma.cissy@epa.gov	Organization:
Mailing Address:		
Street Line 1:		
City:		
Zip Code:		State:
At time of research was:	EPA Employee	
Separation Date:		
% of Effort:	56	

Contributing Author

Author Name:	Nicholas Ashbolt	
Professional Title:		Salutation:
Email:	ashbolt@ualberta.ca	Organization:
Mailing Address:		
Street Line 1:		
City:		
Zip Code:		State:
At time of research was:	Non EPA Personnel	
Separation Date:	Tue Apr 01 00:00:00 GMT 2014	
% of Effort:	2	

Contributing Author

Author Name:	Xiaobo Xue

Professional Title:		Salutation:	
Email:	xxue@albany.edu	Organization:	
Mailing Address:			
Street Line 1:			
City:			
Zip Code:		State:	
At time of research was:	Non EPA Personnel		
Separation Date:			
% of Effort:	20		

Contributing Author

Author Name:	Mary Schoen		
Professional Title:		Salutation:	
Email:	mschoen@sollerenvironmental.com	Organization:	
Mailing Address:			
Street Line 1:			
City:			
Zip Code:		State:	
At time of research was:	Non EPA Personnel		
Separation Date:			
% of Effort:	5		

Contributing Author

Author Name:	Troy Hawkins

Professional Title:		Salutation:	
Email:	thawkins@anl.gov	Organization:	
Mailing Address:			
Street Line 1:			
City:			
Zip Code:		State:	
At time of research was:	Non EPA Personnel		
Separation Date:	Wed Apr 30 00:00:00 GMT 2014		
% of Effort:	10		

Contributing Author

Author Name:	Jennifer Cashdollar		
Professional Title:		Salutation:	
Email:	cashdollar.jennifer@epa.gov	Organization:	
Mailing Address:			
Street Line 1:			
City:			
Zip Code:		State:	
At time of research was:	EPA Employee		
Separation Date:			
% of Effort:	5		

Contributing Author

Author Name:	Jay Garland

Professional Title:		Salutation:	
Email:	garland.jay@epa.gov	Organization:	
Mailing Address:			
Street Line 1:			
City:			
Zip Code:		State:	
At time of research was:	EPA Employee		
Separation Date:			
% of Effort:	2		

PUBLICATIONS

Publication 1:

Publication Title:	Critical insights for a sustainability framework to address integrated community water services: Tec		
Publication Date:	Mon Jun 15 00:00:00 GMT 2015		
Journal/Publication Method:	Water Research		
All Author(s):			
Volume:	77	Number:	June 15
Pages:	155-169	Immediately Index:	Immediately Index:
Citation ½ Life:	8.2	Impact Factor:	7.913

Available online at www.sciencedirect.com

ScienceDirect

journal homepage: www.elsevier.com/locate/watres

Review

Critical insights for a sustainability framework to address integrated community water services: Technical metrics and approaches

Xiaobo Xue [a], Mary E. Schoen [b], Xin (Cissy) Ma [c,*], Troy R. Hawkins [c,1], Nicholas J. Ashbolt [d,2], Jennifer Cashdollar [d], Jay Garland [d]

[a] Oak Ridge Institute for Science and Engineering (ORISE), National Risk Management Research Laboratory, U.S. Environmental Protection Agency, 26 West Martin Luther King Drive, Cincinnati, OH 45268, USA
[b] Soller Environmental, 312 NE 82nd St., Seattle, WA 98115, USA
[c] National Risk Management Research Laboratory, U.S. Environmental Protection Agency, 26 West Martin Luther King Drive, Cincinnati, OH 45268, USA
[d] National Exposure Research Laboratory, U.S. Environmental Protection Agency, 26 West Martin Luther King Drive, Cincinnati, OH 45268, USA

ARTICLE INFO

Article history:
Received 7 December 2014
Received in revised form
21 February 2015
Accepted 18 March 2015
Available online 25 March 2015

Keywords:
Water services
Sustainability
System analysis
Integrated water management
Environment

ABSTRACT

Planning for sustainable community water systems requires a comprehensive understanding and assessment of the integrated source-drinking-wastewater systems over their life-cycles. Although traditional life cycle assessment and similar tools (e.g. footprints and emergy) have been applied to elements of these water services (i.e. water resources, drinking water, stormwater or wastewater treatment alone), we argue for the importance of developing and combining the system-based tools and metrics in order to holistically evaluate the complete water service system based on the concept of integrated resource management. We analyzed the strengths and weaknesses of key system-based tools and metrics, and discuss future directions to identify more sustainable municipal water services. Such efforts may include the need for novel metrics that address system adaptability to future changes and infrastructure robustness. Caution is also necessary when coupling fundamentally different tools so to avoid misunderstanding and consequently misleading decision-making.

Published by Elsevier Ltd.

* *Corresponding author*. Tel.: +1 513 569 7828.
E-mail addresses: Xue.Xiaobo@epa.gov (X. Xue), mschoen@sollerenvironmental.com (M.E. Schoen), Ma.Cissy@epa.gov (X.(C. Ma), thawkins@enviance.com (T.R. Hawkins), ashbolt@ualberta.ca (N.J. Ashbolt), Cashdollar.Jennifer@epa.gov (J. Cashdollar), Garland.Jay@epa.gov (J. Garland).
[1] Enviance Corporation, 5780 Fleet Street, Suite 200, Carlsbad, CA 92008, USA.
[2] School of Public Health, University of Alberta, 116 St. and 85 Ave., Edmonton, AB, Canada T6G 2G7.
http://dx.doi.org/10.1016/j.watres.2015.03.017
0043-1354/Published by Elsevier Ltd.

Contents

1. Introduction . . . 2
2. Current status of integrated municipal water management . . . 2
3. Water systems and key considerations . . . 4
4. Metrics and tools for addressing infrastructural system aspects . . . 4
4.1. Human health risk assessment . . . 4
4.2. Economic aspect: cost analysis . . . 5
4.3. Ecosystem outcomes . . . 6
4.3.1. Life cycle assessment of water systems . . . 6
4.3.2. Footprint approaches . . . 7
4.3.3. A thermodynamic approach: emergy analysis . . . 7
5. System resilience and adaptability . . . 8
6. Overlapping and different foci of the tools . . . 8
7. Coupling metrics/tools for integrated water management . . . 9
8. Conclusions . . . 9
Acknowledgments . . . 9
References . . . 10

1. Introduction

In developed regions of the world, community water services are mostly achieved through large engineered centralized systems and through "siloed" water management approaches. Water services defined herein include the provision of safe drinking water, removal and treatment of sewage, and stormwater control. These services have been successful in controlling waterborne disease (OECD, 2011), mitigating flood damage (Jongman et al., 2012) and supporting firefighting (OECD, 2010) at an inexpensive market price (i.e. not full-cost). Increasing water demand, shrinking water resources, more stringent water quality goals, and aging infrastructure have resulted in a major asset management financial gap in countries like the US (US-EPA, 2002), threatening future affordability. Future planning will be more complex with rapidly developing economies and urbanization (WHO, 2012), the necessity to provide adequate ecosystem services (Wenning and Apitz, 2012) and to adapt to more intensified climatic change (IPCC, 2012). Overall, because of increases in population and decreasing water availability, coupled with continuously increasing service costs, and deficiencies in water system resilience, our current water services are not sustainable for future generations (Chang et al., 2012; Strengers and Maller, 2012).

A system level view of integrated water services is necessary to develop more balanced and optimal solutions. Focusing on just one part of the system, such as drinking water or wastewater alone, even when using system analysis tools such as life-cycle assessment (Ghimire et al., 2012; Igos et al., 2014; Lederer and Rechberger, 2010; Lundin et al., 2000; Memon et al., 2007; Mo et al., 2010, 2011; Remy and Jekel, 2008; Tangsubkul et al., 2005a; Tidåker, 2003; Venkatesh and Brattebø, 2012; WHO, 2012) may result in shifting problems to other sectors and miss more effective solutions only possible when the full system is viewed. For example, a full system approach that considers water-fit-for-purpose could lead to the removal of firefighting flow from drinking water provision. Additionally, framing water services around resource recovery (e.g., energy recovered from food and fecal residuals; nutrients returned to food production; and water largely retained within the municipal region) would yield very different system configurations and likely more robust and sustainable water services (Ashbolt, 2011; Otterpohl et al., 2003).

A major shift in resource governance would also be necessary to achieve such coordinated actions (Pahl-Wostl et al., 2012). Complications are evident when jurisdictional issues are raised by the various, and often conflicting stakeholders of source water (Winz et al., 2009) and municipal water services (Malmqvist and Palmquist, 2005). It is therefore no surprise that stakeholder-driven, and systems based approaches (Beall et al., 2011; Chang et al., 2012; Dobbie and Brown, 2014; Lundie et al., 2008; Maheepala et al., 2010; Malmqvist and Palmquist, 2005; Schlüter and Pahl-Wostl, 2007; Winz et al., 2009; Zarghami and Akbariyeh, 2012) are increasingly seen as appropriate ways to address and solve the complexities inherent to community water systems, and their fundamental interactions with regulators and users. Integrated community water management addresses total water cycle management via the engagement of key stakeholders that include city planners, citizens, regulators, utilities and managers of source water for a developed region (Thomas and Durham, 2003).

This paper addressed the overarching question: What are the strengths and weaknesses of various sustainability assessment tools used as a part of integrated community water management, and how do they aid in the design of next-generation community water services? We review a set

Table 1 – Example dimensions, objectives, tools and metrics for integrated municipal water management.

Dimension[a]	Objective	Tool[b]	Metric	Preferred direction	Key references/examples
Human Health	Characterize health effects from exposure to chemical and pathogen hazards	Risk assessment tools	Health-adjusted life years (HALYs), quality adjusted life years (QALYs), disability adjusted life years (DALYs), probability of infection, risk quotient	Minimized	Sometimes combined within the social dimension (Fane et al., 2002) Trade-off between disinfection by-products and pathogens (Havelaar et al., 2000b), Impacts of fecal-contaminated recreational waters (Schoen and Ashbolt, 2010)
	Assess exposure to chemicals and health effects	Life cycle impact assessment	Comparative toxicity units	Minimized	TRACI tool (Bare et al., 2008)
Economic	Capital and operational cost	Life cycle cost analysis	Life cycle cost ($)	Minimized	As used for distribution systems, rainwater use (Ghimire et al., 2012) decentralized wastewater (Wang, 2014) As proposed for green roofs (Carter and Keeler, 2008)
	Evaluate externalities	benefit-cost analysis	net present value ($)	Minimized	
	Characterize capital and operational costs, externalities, employment generation	Trip bottom line reporting	GDP and genuine progress indicator (GPI)	Maximized	Regional scale (Kubiszewski et al., 2013)
Environmental	Assess depletion of water, land and other natural resources	Footprints	Water and ecological footprints	Minimized	Regional, basin, and infrastructure scale (Boulay et al., 2013; Hoekstra and Hung, 2002; Moore et al., 2013; Zeng et al., 2012)
	Calculate energy use	Life cycle assessment (LCA), emergy	Life cycle energy consumption (mj), emergy (sej)	Minimized	Infrastructure scale, water, wastewater, stormwater treatment option (Igos et al., 2014; Lundin et al., 2000; Lyons et al., 2009; Remy and Jekel, 2008; Stokes and Horvath, 2006; Tangsubkul et al., 2005a; Tillman et al., 1998)
	Assess global warming potential	LCA, footprint	Life cycle global warming potential (g CO_2-eq), carbon footprint (g CO_2-eq)	Minimized	
	Assess eutrophication potential	LCA	Life cycle eutrophication potential (g N-eq)	Minimized	
	Assess impact to ecosystem services	Emergy	Emergy (sej)	Minimized, more renewable emergy and most efficient system	Regional, basin, global scale, and treatment options (Campbell and Garmestani, 2012)
Resilience	Evaluate the capacity to deal with change	Literature review and expert opinion, combinations of human health and environmental tools, CREAT	No standard metric- both qualitative and quantitative	Maximized	Limited to date (Cordell and Neset, 2014; Dessai and Hulme, 2007; US-EPA, 2013a), Novel aspects described in current paper

[a] Social and cultural dimensions are beyond the scope of our analysis.
[b] The overlapping areas of the research tools are described in Section 6 and Table 2.

of widely accepted sustainability tools/metrics, their applications to community water services, and potential missing attributes. While this paper focuses on the sustainability assessment tools and not the entire decision-making process, our review emphasizes how these tools can support the creative and adaptive capacities of civil society in a process to identify and assess options that may truly put our community water services on a more sustainable footing.

2. Current status of integrated municipal water management

Integrated Municipal Water Management (IMWM) addresses total water cycle management via the engagement of key stakeholders (Thomas and Durham, 2003). IMWM is a staged and iterative approach used by utilities to plan and manage water supply, wastewater and stormwater systems so as to minimize their impact or restore the natural environment; to maximize their contribution to social and economic vitality; and to engender overall community improvement (Maheepala et al., 2010). In the broader context, this approach is known as integrated resource management (IRM). While IMWM largely focuses on water and its social-environmental context, IRM deliberately spans the various resources (electricity, heat, material, water, nutrients etc.) associated with human systems, and may identify important synergies of other players with the water sector (e.g., co-digestion of food wastes with residuals organics from wastewater (De Gisi et al., 2014; Zeeman et al., 2008)).

While several groups have somewhat independently developed IMWM frameworks (Fuentes et al., 1996; Howe et al., 2011; Kärrman et al., 2011; Lundie et al., 2008; Maheepala et al., 2010; Malmqvist and Palmquist, 2005), all focus on six key components (Kärrman et al., 2011) including participation (why, when, and how stakeholders will participate) (Gabe et al., 2009; Lundie et al., 2008, 2006), vision (goals for the desired future), problem formation (identifying critical problems to be addressed), designing (identifying possible solutions), comparing (assessing among combinations of solutions to meet the vision), and choosing (decision-making and commitment). Often, stakeholder groups are formed to discuss, identify and state the problems to be addressed. As a following stage, three key pillars have been suggested to aid in designing possible solutions. They are composed of the access to a diversity of water sources facilitated by a diversity of centralized and decentralized infrastructure, provision of ecosystem services for the built and natural environment, and socio-political capitals for sustainability and water sensitive behaviors (Wong and Brown, 2009). While various categories of criteria have been suggested to evaluate the solutions, most fall into the following five primary groups including human health, economic, environment, social-cultural dimensions, and an overarching assessment of resilience to future challenges. Example technical metrics and tools to assess/compare community water-related options against stakeholders' objectives are described in Table 1.

Stakeholder participation and socio-behavioral aspects are fundamental in achieving the sustainability of community water services, yet there are various institutional and governance issues that hinder this approach, particularly perceived risks (Dobbie and Brown, 2014) and 'the silos' of water and resource governance (Pahl-Wostl et al., 2012). Numerous examples exist where the public have rejected water treatment approaches due to a lack of engagement or consideration of the socio-cultural aspects of the community (Hurlimann and Dolnicar, 2010; Stenekes et al., 2010). While we recognize the importance of social, cultural and governance aspects when selecting water service systems (Bertera, 2013), this paper primarily focuses on approaches for providing appropriate environmental, engineering, and human health perspectives in the context of informing deliberative stakeholder dialog. A broad range of tools and metrics exist to assess the sustainability of water systems from the technology to the service at watershed, country, and globe levels (Hester and Little, 2013). Here we narrow the list of technical metrics/approaches to those we consider critical to the built water services.

3. Water systems and key considerations

There are various ways to describe the built environment of community water services and associated watersheds. The water service interacts with a range of built and natural infrastructural systems in a complex network. The major flows and stocks of water, materials, energy and residuals are illustrated with conventional (solid boxes) and examples of possible future system elements (dashed boxes) in Fig. 1. This system view illustrates the interconnections within community water systems that tools and metrics need to address.

Starting with the environmental aspects illustrated in Fig. 1, there is a need to account for the many ecological processes and services that support human activities (Brauman et al., 2007; Cochran and Logue, 2011; Dodds et al., 2013). The natural components of the water systems include precipitation, land use, runoff, infiltration, evapotranspiration, surface water, and groundwater sources. These natural components provide source water to the built infrastructure system, process residuals/pollutants, support primary production, shape landscapes, and control local/regional climate. In return, the built infrastructure (i.e., infrastructure that collects, treats, and distributes water/wastewater/stormwater) influences the 'natural' environment through various flows, including leaks from distribution and collection systems, withdrawal from surface and groundwater sources, and discharges to surface and groundwater sources.

The conventional and example future systems (as shown with solid vs. dashed boxes in Fig. 1) differ with regard to the flows and stocks of water, energy, and nutrients. The conventional water infrastructure aims to withdrawal as much water resource to meet the demand and discharge stormwater as much and as fast as possible, resulting in an imbalanced hydrologic cycle and loss of ecosystem services. Alternative infrastructural choices restore the natural hydrology as well as attain other societal goals such as recovery of imbedded energy (via electricity production & heat capture), return of residual nutrients to food production, and maintenance of higher quality water for recreational use. Green and natural infrastructure such as rain gardens, permeable pavements, mature trees and green roofs incorporate natural capitals like vegetation and soil to manage stormwater and restore the

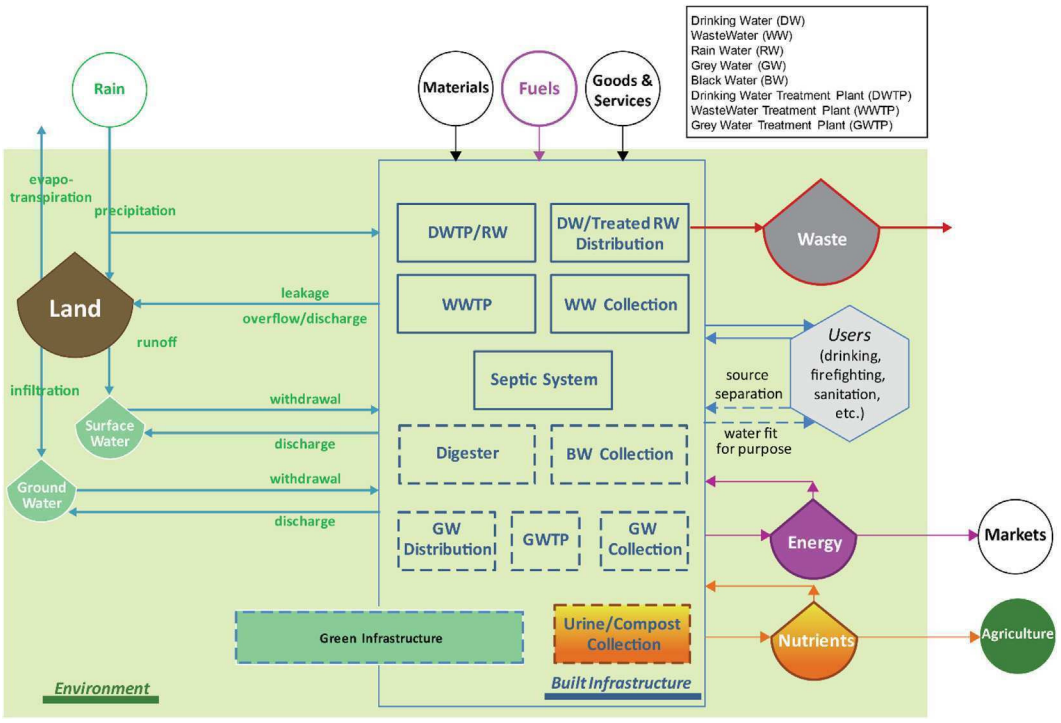

Fig. 1 – System diagram illustrating key elements in community water services. The major flows and stocks of water, materials, energy and residuals of water systems are illustrated. The conventional configurations and example possible future system elements are described with solid and dashed boxes, respectively. DW, RW, GW, BW, DWTP, GWTP, WWTP represent drinking water, rain water, greywater, blackwater, drinking water treatment plant, greywater treatment plant, and wastewater treatment plant, respectively. The arrows represent emergy flows. While the circles mean outside sources of energy, the semicircles describes various storage compartments.

natural hydrological cycle (US-EPA, 2008; Romitelli, 1997; Arden, 2014). Constructed wetlands can be used to simulate natural wetlands and use renewable energy derived from natural systems to replace fossil fuel energy used in conventional treatment technologies to achieve the required purification of water, and restore the hydrological cycle through increasing evapotranspiration and filtration (Odum, 1983).

Current community water services negatively influence nitrogen and phosphorus cycles by releasing large amount of nutrients as waste via combined sewage overflow, wastewater effluent discharge, and sludge application (Tangsubkul et al., 2005b; Tillman et al., 1998), and emitting greenhouse gases during water and wastewater conveyance and treatment (Short et al., 2014). Nitrogen and phosphorus contamination via wastewater is one of the major reasons for nutrient cycle disruption, leading to eutrophication and hypoxia in many coastal and riverine regions (US-EPA, 2013b). Alternative system elements such as urine-diversion toilets and blackwater-only sewers can contain these nutrients for food production and avoid their direct release to the environment, promoting restoration of nutrient cycles.

The example novel system elements capitalize on recent research that identifies decentralized/semi-decentralized systems as more sustainable for the environment (Luthy, 2013). As shown in Fig. 1, the specific decentralized/semi-decentralized processes may include greywater treatment and local reuse (either at the household or community scale); blackwater co-digestion with food waste for energy recovery; diverted urine and feces for fertilizer and soil conditioner (Zeeman et al., 2008); and rainwater harvesting. Greywater accounts for some 70% of residential wastewater in a conventional sewer; separating, treating, and reusing greywater onsite would reduce demand on the outside water resource by up to 70% compared to conventional centralized water systems (and the energy used in its conveyance). Treated greywater has been reliably used for purposes such as irrigation, toilet flushing, and clothes washing in Australia (Barker et al., 2013). Local rainwater harvesting could also provide additional municipal water sources, depending on the level of treatment. Local rainwater harvesting has the extra benefit of enhancing system resilience to storm events, drought and water shortage (Jones and Hunt, 2010).

Essentially, the proposed novel elements change the perspective on water services from the "siloed" and centralized water management thinking into integrated and decentralized/semi-decentralized design following the principles of biomimicy and resource recovery. While the novel elements may present significant potentials in mitigating energy use, resource consumption and nutrient export, the system performances with individual novel elements from environmental, economic, and social perspectives are still not fully understood. The following discussion presents technical tools and metrics that allow us to compare the performances

of conventional and alternative community water systems as presented in Fig. 1 across the dimensions presented in Table 1.

4. Metrics and tools for addressing infrastructural system aspects

We acknowledge that human health, economy, and ecosystem impacts are intertwined. However, we have chosen to classify them separately in order to discuss the metrics and tools explicitly.

4.1. *Human health risk assessment*

The purpose of the human health assessment is to compare the adverse health effects potentially caused by exposures to hazards from water systems. The National Research Council (NRC) risk assessment framework (NRC, 2009) outlines the general steps required to assess risk from microbial and chemical hazards. For the water systems considered, various pathogens (viral, bacterial, parasitic protozoan and helminths) and chemicals (disinfection byproducts, pesticides, metals, etc.) are relevant. When ingested, inhaled, or absorbed through the skin, these pathogens and chemicals may result in a range of health outcomes from acute illness to chronic disease and mortality. Therefore, an ideal human health metric incorporates these various health outcomes. The Health-Adjusted Life Year (HALY) is a class of metrics that transforms any type of morbidity or mortality into an equivalent number of life years (Hofstetter and Hammitt, 2002). The two most common HALYs are Quality Adjusted Life Years (QALY) which measure the actual health quality integrated over time, and the QALY compliment, the Disability Adjusted Life Years (DALYs). DALYs are the sum of years of life lost by premature mortality and years lived with disability (Murray and Acharya, 1997). To calculate DALYs, the time lived with a disability is multiplied by a disability weight to make it comparable with the years of life lost due to premature mortality. In this way, both non-fatal and fatal health outcomes can be considered and compared.

Of the two most commonly reported HALYs, DALYs have been used as a human health metric to compare water system alternatives when health outcomes are seemingly disparate (An et al., 2011; Boulay et al., 2011; Haller et al., 2007; Havelaar and Melse, 2003; Havelaar et al., 2000b; Lundie et al., 2008). Havelaar et al. (2000a) discussed the risks and benefits of drinking water disinfection using the DALY; specifically, the tradeoff between the benefit of reduced microbial infection when implementing ozonation and the potential dis-benefit of an increase in renal cell cancer from the formation of disinfection byproducts was quantified. Since these health outcomes are different in duration, magnitude and impact, overall risk was characterized using the DALY. The analysis supported the use of drinking water disinfection with: "the health benefits of preventing gastroenteritis in the general population and premature death in patients with acquired immunodeficiency syndrome outweighing health losses by premature death from renal cell cancer". However, the magnitude of the overall disinfection benefit varied considerably when key, uncertain parameters were changed, such as the severity weight for gastroenteritis. Furthermore, the DALY was limited by a lack of knowledge and available data for the population exposure assessment. Other potential health metrics, although also dependent upon the same exposure assessment methods, are less data intensive and do not require illness severity and duration data. For example, the probability of infection (Agulló-Barceló et al., 2012; Åström et al., 2007) and the risk quotient (Al Aukidy et al., 2012; Leung et al., 2013), i.e., the observed hazard concentration divided by the acceptable level (NRC, 2012), are useful for a quick comparison of potential risk within a class of hazards.

Risk quotients have been used to evaluate the potential health risks associated with pathogen (adenovirus, *Norovirus*, *Salmonella*, and *Cryptosporidium*) and chemical (DBPs, hormones, pharmaceuticals, pesticides, and other chemicals) for hypothetical wastewater reuse scenarios (NRC, 2012). The probability of infection associated with water and wastewater system use has been assessed separately for conventionally treated drinking water (Petterson, 2010; Teunis et al., 2010; Westrell et al., 2003, 2004), contact with wastewater (Charles, 2009; Schoen and Ashbolt, 2010; Soller et al., 2010), rainwater reuse (Ahmed et al., 2014, 2011), and greywater reuses (Barker et al., 2013).

There is limited analysis that considers the entire community water and wastewater system (Katukiza et al., 2014) and alternative, decentralized system options (Ashbolt et al., 2006). When comparing water system alternatives, the adverse health effects will differ in magnitude for each system option depending on the hazards unique to each water resource, the routes of exposure, and the failure/event impacts of each technology. Computing all the human health metrics for each option is time consuming and unnecessary. Moving forward, the probability of illness and risk quotient can be assessed in a screening-level assessment to identify the most critical human health hazards, for which the DALY is estimated. These metrics may be computed over different time scales to correspond to the functional units and expected system life-times defined by the life cycle assessment and the overall system-level risks as long as the variation in health burden is captured.

4.2. *Economic aspect: cost analysis*

A key, often overriding consideration in any decision related to investment in water infrastructure is the cost. Various methods such as life cycle cost and benefit-cost analyses exist to quantify the costs of water services. While large upfront costs often dominate the discussion of options for providing water services in current centralized systems, the goal of a more complete cost analysis is to weigh initial, direct costs together with costs occurring over the entire life cycle of a system and together with indirect, environmental, societal costs. Examples of direct upfront costs include the costs of planning, materials, and labor. Often, life cycle costs include direct costs associated with materials, constructing, operating, maintaining, and eventually decommissioning or repurposing infrastructure for parts of entire water systems.

Beyond life cycle costs, there are a number of indirect, environmental or societal costs and benefits which should be considered. These include, the cost of health effects caused by

air emissions associated with the electricity used to pump and treat water and wastewater (Fann et al., 2013; Pabi et al., 2013), the cost to heat household hot water (Morales et al., 2013), the cost associated with increased illness from recreational and drinking water pathogen exposures (Collier et al., 2012; Dwight et al., 2005), the cost of imbalanced hydrological cycle and the diversion of water flows from ecological needs versus the electricity savings associated with the increased insulation provided by a green roof (Clark et al., 2008), or the value of green space and natural infrastructure in an urban area provided by rain gardens, vegetation, wetlands or aquifers used for wastewater and stormwater management (Bowman et al., 2012; Page, 2010).

Benefit-cost analysis (BCA), often incorporating a variety of direct and indirect costs and benefits, aims to provide a quantitative assessment in monetary terms for decision making (Arrow et al., 2004; Mishan, 1978). Although BCA has been applied to assess the costs and benefits of various infrastructure projects and policies, the BCA approach has been challenged in the following aspects. First, due to the difficulty to forecast causal relationships, errors such as omitting certain costs and benefits may occur. Second, the ambiguity and uncertainty involved in quantifying and assigning a monetary value to intangible items could lead to an inaccurate analysis. Third, the choice of discount rates can significantly influence the estimated net present values of BCA. Last, BCA assumed the distribution of costs and benefits could theoretically be *corrected* via transfer payments, which may result in double counting.

Moving forward, the coupling of economic impact analyses with sensitivity analysis can identify the influences of key parameters (such as discount rates), incorporate the distributional effects of a decision (US-EPA, 2010), and consdiser a full specturm of costs and benefits connected with risk and life cycle assessment (Hardisty et al., 2013). In addition, there is a need to build a body of knowledge regarding the cost and benefit outcomes associated with less common options for providing water services such as those based on principles of water fit-for-purpose, source-separation of waste streams, material/energy recovery, and the use of natural processes for water treatment. A research agenda to address these issues should include the development of standardized datasets, which can be combined in various configurations to support efficient and fair comparisons of a wide variety of system options. These datasets should support the incorporation and attribution of multiple benefits such as those indirect costs discussed above as well as electricity recovery from biogas, the reuse of nutrient-dense streams and the avoidance of fertilizer production and waste management, capture and reuse of rainwater, and the reuse of greywater for non-potable purposes. It should also include efforts to bound the uncertainty and specify a wide range of human health (Fann et al., 2013) and environmental impacts (Daily and Matson, 2008).

4.3. *Ecosystem outcomes*

Life cycle assessment, footprint analyses and thermodynamic approaches such as emergy analysis are widely utilized tools to assess environmental impacts of products and processes at system levels. The strengths and weaknesses of applying these tools in water resource and infrastructure management are described below.

4.3.1. *Life cycle assessment of water systems*

Life Cycle Assessment (LCA) is a well-established method for quantifying energy consumption and environmental impacts through the entire life-cycle of a product or process. In water systems, a life cycle inventory tracks the energy and material inputs for producing, constructing, operating, and maintaining water and waste services, and associated releases into the air, water and soil environments. Life cycle impact assessment quantifies specific aspects of environmental and human health impacts of services in terms of global warming, eutrophication, acidification, ozone depletion, photochemical oxidation, ecotoxicity, and non-carcinogenic and carcinogenic human health impacts.

LCA approaches have been widely used to analyze the direct and indirect environmental impacts of specific water management elements, i.e., various options for drinking water supply systems, wastewater conveyance and treatment, stormwater management, biosolid systems, or treatment chemicals such as disinfectants and coagulants. A number of comparative LCA studies have provided the comparative energy and environmental evaluation of water system elements at household, community, and city scales in order to assist in selecting preferred options (Lyons et al., 2009; Stokes and Horvath, 2006, 2009; Stokes et al., 2013). The life cycle environmental impacts of water service options are influenced by the choice of system boundaries, functional units, allocation methods, embedded databases, and life cycle impact assessment approaches. The majority of these studies illustrate that the operation phase is the dominating contributor to impacts, compared with the design, construction and demolition phases. The relative contributions of electricity and chemicals are variable, depending on the energy mix, specific treatment technology and local topographic condition. Depending on the choice of life cycle impact assessment approaches, diverse performance indicators are available to evaluate the environmental and human health impacts of water services. However, energy and nutrient related impacts appear to dominate for water services, suggesting a limited number of key LCA measures for water systems, such as global warming potential, energy use and eutrophication potential, as a good starting point for LCA of water systems.

However, there are still shortcomings related to the application of LCA approaches for assessment of water services, such as the lack of consideration of water scarcity, disruption of natural hydrology and impacts of climate and demographic change. Further, several aspects of LCA methodology are still under development, including incorporation of uncertainty and variability assessment, integration of system dynamic processes, inclusion of ecosystem services, reflection of appropriate temporal and spatial scales, and improvement of impact assessment tools.

LCA studies that evaluate the whole anthropogenic water cycle from water extraction to wastewater recycle and reuse are generally lacking (Lundie et al., 2004). Furthermore, LCAs in water systems have yet to explore issues perceived as major concerns of fit-for-purpose water reuse schemes (e.g., pharmaceuticals, personal care products, disinfectant by-

products, pathogens and brine concentrates) (Richardson et al., 2011). There is also little scientific consensus for how to comprehensively assess environmental and human health impacts of water use, although a number of methods and indices have been developed to compile water use inventories, and generate midpoint and endpoint methods for addressing water scarcity (Boulay et al., 2011, 2013; Hanafiah et al., 2011; Pfister et al., 2009).

In order to improve current limitations, the future water LCA efforts should include 1) compiling the life cycle inventory of the whole anthropogenic water cycle including both centralized and decentralized options, 2) development of impact assessment tools to evaluate the environmental and human health impacts of water scarcity and emerging contaminants, and 3) integration with additional pieces such as chemical and microbial associated risk assessment, footprints, emergy, and resilience analysis.

4.3.2. *Footprint approaches*

The "footprint family" of environmental indicators, including carbon footprint (Wiedmann and Minx, 2008), ecological footprint (Wackernagel and Rees, 1996) and water footprint (Zeng et al., 2012), applies life cycle thinking to analyze the environmental releases and resource requirements of products and processes. The Carbon Footprint (CF) for water services accounts for the global warming gas emissions during the design, construction, operation, and decommission stages of community water infrastructure. The Ecological Footprint (EF) (Wackernagel and Rees, 1996) measures the productive land area required to supply the resources consumed and to assimilate the residuals (e.g., CO_2, nitrogen in wastewater) generated for a process or a product or a region. The Water Footprint (WF), initially introduced by Hoekstra and Hung (Hoekstra and Hung, 2002) is analogous to the "ecological footprint" and is used to estimate the volume of water required for the production of goods and services.

Although footprint analysis may provide insight into the design and management of water services, further development and novel indicators are probably necessary in order to form a comprehensive understanding of community water systems and to aid in strategic planning for more sustainable water systems. To date, CF's have been described for production and distribution of drinking water (Mo et al., 2011), collection and treatment of wastewater (Remy and Jekel, 2008), and the handling of sludge (William and Mciwem, 2009). Despite valuable attempts to assess community water systems, the CF arising from the holistic analysis of the drinking, stormwater and wastewater systems requires further development in order to provide an integrated assessment of the built environment water cycle, and more importantly, to provide a systems-level view also suited to assess radically different options. Typical EFs of water services are limited to the measurement of land area, and carbon dioxide emissions during transport and processing of municipal water. The EF does not account for hazardous (chemical and microbial) environmental releases, nor does it measure water (surface and ground) resource availability. The WF is limited to the analysis of embodied virtual water, such as in a nation's economy and to trace water-intensive stages along products' supply chains (Hoekstra et al., 2011). Shortcomings of the WF concept which hinder its use for designing next generation water systems include: 1) an incomplete accounting of the natural and built environment water cycle (Chapagain and Tickner, 2012), 2) limited capability to characterize the temporal and spatial variability of watershed hydrology and related water resource availability (Zeng et al., 2012), 3) no description of ecosystem services, 4) lack of an appropriate description of the environmental and human health risks associated with municipal water (Pfister and Ridoutt, 2013), and 5) an inability to provide solutions towards water resource management and infrastructure design (Chapagain and Tickner, 2012).

In order to overcome the above shortcomings of water footprint for water infrastructure design, the following additional approaches are suggested: 1) incorporation with an integrated bio-physical model to describe natural and the built water cycle with appropriate temporal and spatial resolution; and 2) combination with life cycle impact, risk, emergy analyses to provide a comprehensive understanding of hydrology, environmental and human health risks, and role of ecosystem services.

4.3.3. *A thermodynamic approach: emergy analysis*

Emergy analysis is a system-based method applicable to various scales that incorporates environmental, social, and economic aspects into a common unit of nonmonetary measure (solar energy equivalent joule, sej). Emergy is defined as the available energy of one kind previously used directly and indirectly to make a service or product (Odum, 1996). It is based on the observation of the patterns of energy flows in ecosystems and economic systems during self-organization. It is based on the theory that all systems (ecological, social and economic) are centered on the transformation of available energy. For example, the transformity values (total emergy input required to generate one unit of energy out) for wind energy, and phosphate fertilizer are 1.5E3 sej/J, and 1.0E7 sej/J) (Odum, 1996). This means that the processes generating phosphate fertilizer require considerably more upstream energy investment (geological sedimentary cycle for phosphorus rock to regenerate and the fossil fuels needed in mining and formulating it as fertilizer) than what it takes to regenerate wind energy.

Distinct from the aforementioned approaches, emergy accounting provides a unique platform to combine economic activities (mainly water needs and water disposal) and the hidden ecological costs (via ecosystem services) into a common measuring unit, sej. It represents a fundamental change in perspective from a user-based (i.e., monetary exchange) to donor-based (energy used) value system. This approach allows the behavior of a system as a whole and the interactions between subcomponents to be observed and optimized. This can be applied to water systems with varied components such as water in biological systems, various source waters, drinking water, wastewater, and stormwater. In addition, emergy theory implies that prevailing systems are those where designs maximize available energy by reinforcing resource intake optimally. This statement includes maximizing the resource intake and operating at the optimum efficiency for maximum productivity (Odum, 1996). The same holds for water systems, particularly for community water services. Hence, the current

water management seeking endless sources of new supply, rather than maximizing the productivity and efficiency of the whole system, is not sustainable.

Moving forward, the whole water systems including both natural and built components should be assessed with emergy approach. Although emergy analysis is capable of addressing different scales of systems, it has not been reported for complete community water systems. Rather, emergy studies have largely focused on only one of the subsystems, such as drinking water treatment (Arbault, 2013; Buenfil, 2001), the water distribution system (Buenfil, 2001), wastewater treatment and health effects (Björklund, 2001), wetland treatment (Arias and Brown, 2009; Nelson, 1998), the natural hydrological cycle (Watanabe, 2014), or watersheds (Romitelli, 1997). In addition, the alternative water systems which incorporate hydrological restoration and resource (energy, carbon, nutrients, and water) recovery should be emphasized in the future research agenda for community water services.

5. System resilience and adaptability

While there are many interpretations of resilience, we have adopted a definition suitable for infrastructures, "the ability to prepare for and adapt to changing conditions and withstand and recover rapidly from disruptions" (Stockholm Center, 2007). The concept of resilience was developed for systems where humans and nature co-exist, and describes the capacity of the system to remain within desired states given changing conditions (Folke, 2010). For water services, the desired or operative state provides for critical services such as public health protection, drinking water supply and sanitation needs (Howard et al., 2010).

To enhance the resilience of a community water system to disruptions, improving adaptability of the natural-engineered system is as important as strengthening social preparedness through governance, community outreach and education (Ananda and Proctor, 2013; Bettini et al., 2013; O'Rourke, 2007). The US EPA provides a set of tools (such as CREAT, CBWR, VAST, and WHEAT) to assess the vulnerability of water, wastewater, and combined utilities to loss of service due to natural and human induced risks (US-EPA, 2013a). Most of these tools focus on emergency management planning and stakeholder engagement to identify and improve communication with relevant interconnected stakeholders (i.e., hospitals, agriculture, and power system operators). A few of them include a narrative analysis of adaptive measures to climate change (such as CREAT). While we recognize the importance of the social dimensions, this paper aims to review resilience assessment frameworks that relate to the built infrastructure and interconnected environmental elements with the purpose of ranking alternative engineered water services.

There is no standard resilience assessment approach or metric. Ideally, the assessment should be participatory and identify the system components and interactions, critical requirements for system operation, and potential future changes (Stockholm Resilience Center, 2007). Although both qualitative and quantitative approaches were proposed, qualitative approaches to assess resilience are more common in the literature. Balsells et al. qualitatively compared the resistance, absorption and recovery capacitates of alternative stormwater management options for flooding conditions in Rotterdam and New Orleans (Balsells et al., 2013). The WHO presented a qualitative resilience assessment to identify the vulnerability and adaptive capacity of water services to future climate changes, such as precipitation frequency and intensity (WHO, 2010). On the other hand, Ayyub et al. suggested quantitative resilience metrics incorporating a measure of robustness and rapidity of recovery for various qualities of interests under event disruptions (Ayyub, 2014). Similarly, Hwanga computed a simplified resilience metric as the volume of water not supplied to customers over the duration of a pipe failure event (Hwanga et al., 2013). We are not aware of any applications of a quantitative measure of resilience for a community water system that assesses the multiple dimensions in Table 1 or complex challenge events, such as climate change, hurricane, flooding or drought.

The major limitation of the existing work is the lack of a broad scope of impacts such as energy consumption, ecosystem services, and economic evaluation (Ayyub, 2014). A second limitation is the lack of a comprehensive resilience assessment of both long-term changes and event disruptions. Moving forward, assessing the resilience of alternative water systems should explicitly consider the robustness, adaptive capacity, and rapidity as they relate to the critical requirements identified for the community across the different challenges including population change, climate change, and catastrophic events, either qualitatively or quantitatively. A screening-level qualitative metric based on descriptive summaries of evidence from literature and expert opinions will likely pull from the data collected to estimate the other metrics, such as technical specifications, performance data, or water demand. Following the screening-level assessment, a quantitative metric may be calculated for key challenges —either disruption or system change- and qualities of interest. The quantitative metric will likely require the use of tools previously described to estimate the impact of a challenge on critical services over the duration of the challenge. For example, QMRA may be used to estimate the health impact (in DALYs) resulting from a flooding event over the course of the event and the recovery, given alternative adaptive measures. The resulting health impacts time series can then be used to calculate the robustness and rapidity in combination with other information on time to recovery for the human health dimension of resilience.

6. Overlapping and different foci of the tools

Despite different methodological roots, the discussed tools share overlapping research interests and concerns (Table 2). For example, while the foci of water footprint and water-focused life cycle impact assessment are different, both tools can provide quantitative metrics to support water resource management. The existing water footprint relies on water use indicators in the inventory phase, assuming existing per capita demand will continue. In contrast, the LCA practices emphasize impacts in the areas of human health protection, ecosystem quality, and resources, based on

Table 2 – Considerations included in the discussed tools.

	Considerations	Life cycle assessment[a]	Water footprint[b]	Emergy analysis	Human health risk assessment	Life cycle cost	Benefit-cost analysis[c]	Resilience assessment[d]
Energy Use	Direct energy consumption	X		X		X	X	
	Indirect energy consumption from supply chains	X		X		X	X	
	Energy consumed in the built processes	X		X		X		
	Energy consumed in natural processes			X				
Risks	Direct human health risks	X			X		X	X
	human health risks from supply chain activities	X					X	
	Human health risks from discharge or disposal of products	X			X		X	
	Accidental human health risks				X		X	X
	Occupational human health risks							
	Ecological risks due to the depletion of natural resources	X		X				
Costs	Cost for built processes during design, construction, operation, & decommission stages			X		X	X	X
	Cost for Environmental services			X			X	
Water Use	Direct water consumption	X	X	X		X	X	X
	Indirect water consumption from supply chain/life cycle processes	X	X			X	X	
	Natural water flows	X	X	X				
	Anthropogenic water flows	X	X	X				X

[a] The current practices include neither microbial related risks, nor a complete description of natural and anthropogenic water flows.
[b] The current practices don't contain a complete description of natural and anthropogenic water flows.
[c] The current practices include the environmental and human health consequences which can be monetized.
[d] The most common reported considerations for water systems from literature review are checked in Table 2.

freshwater use inventories and cause-effect chains. Similarly, risk assessment, life cycle impact assessment, and benefit-cost analysis are capable of evaluating the risks of water systems. These three methods differ in the coverage of risks and spatial and temporal resolutions. Life cycle impact assessment systematically evaluates direct, upstream and downstream risk, and risk to built and natural environment. Benefit-cost assessment has a similar coverage but it is generally limited by inclusion of endpoints that can be monetized. Risk assessment may be directed to local microbial and chemical risks due to human exposure of the water flows. Additionally, both emergy analysis and LCA can assess the indirect energy consumption of water systems. The life cycle energy consumption includes the direct and indirect energy consumption from the built processes. In addition to the energy consumption captured by LCA and emergy analysis, the emergy method also accounts for the embedded energy (beyond fossil fuel-based energy) of the supporting natural resources (e.g., groundwater stocks, wetlands, rain and evaportranspiration flows).

Resilience assessment may include any of the considerations relevant to the protection of the human health, a reliable supply of water, ecosystem services, or others depending on the identified critical water services. The most reported considerations for water systems are water supply and human health, marked in Table 2. Ultimately, the considerations of the resilience assessment are specific to the selected future challenges and critical services of the water system. Resilience assessment overlaps in considerations with many of the previously listed tools, but with a view toward performance under future change or challenge rather than nominal conditions.

7. Coupling metrics/tools for integrated water management

Coupling multiple tools appropriately has the potential to better capture the complexities of water systems at different levels and provides a more comprehensive view of sustainable water management. For example, the combination of life cycle assessment, risk assessment and emergy analysis could evaluate the performances of a water system for environmental, built infrastructure and human health dimensions. The human health risk assessment tools provide detailed assessment of chemicals and microbes of water systems, which are currently lacking in other tools like life cycle impact assessments and emergy analysis. Emergy analysis provides a description of ecosystem service landscape where the built infrastructure resides, an important perspective lacking in both life cycle impact and human health risk assessment.

In addition, in order to promote the selection of systems which are robust against hazardous events and resilient in the face of long-term societal or climatic changes, it is important to consider the effect of relevant events and scenarios on the metrics provided by each tool. Too often decisions are focused on nominal and near-term conditions, not including lower probability but high risk failure events and future changes. Resilience assessment could identify the challenges and opportunities for water systems to recover from, and adapt to, long-term and short-term hazards.

The challenge when coupling multiple complex metrics is to convey the objective and scope of each tool and the magnitude as well as uncertainty of each metric, and use them to inform the decision process, together with other social, legal, fiscal considerations and obligations. In practice, time and resource constraints make it difficult to apply all tools and collect all of the information one would ideally synthesize for decision-making. Therefore, a tiered framework for calculating multiple metrics for water systems needs to be developed (Lundie et al., 2008). When presenting results for system options across multiple metrics, it is important to communicate the relative uncertainty for each metric to allow for proper interpretation of qualitative and quantitative results. All of the tools described here involve the use of variable and uncertain inputs for calculation. To represent these sources of uncertainty and variability, metrics are best presented as probabilistic distributions or with error bars. Important information is lost when only considering the best estimate or median results.

Overall, the sustainability tools described above represent distinct research foci, different spatial and temporal resolutions, and various fields of application. Although appropriately coupling these tools can potentially provide a more complete system perspective for various dimensions than a single tool, caution should be taken to clarify the system boundaries and to ensure proper development of the sustainability tools.

8. Conclusions

We conclude that a comprehensive assessment of the whole water cycle (both built and natural water components) and full community water services (including water resources, drinking water, sanitation, firefighting, irrigation, stormwater, wastewater management and ecosystem services) is required to evaluate system sustainability and simply not move issues to other domains and cause unintended consequences. Comprehensive assessment across the entire water cycle that addresses environmental, economic, and human health aspects are lacking. Examples of metrics and tools for such a comprehensive approach are available (Table 1), but their method and dataset limitations for quantifying ecosystem services related to community water systems, novel water system configuration, synergistic water-energy-carbon-fertilizer nexus, and system adaptability to future changes all require further research. Often, they are rarely combined into an integrated sustainability framework to evaluate the built water system without compromising natural water services. Therefore, an imminent research need is the demonstration of this integrated approach with real case studies to support decision making.

Acknowledgments

This project was partially supported by the U.S. Environmental Protection Agency Office of Research and Development through the ORISE Post-Doctoral Fellowship Program

and other project-related supports. The authors would like to acknowledge Michael Gonzalez at U.S. Environmental Protection Agency for his insightful suggestions. The views expressed in this article are those of the authors and do not necessarily reflect the views or policies of the U.S. Environmental Protection Agency. Any mention of specific products or processes does not represent endorsement by the U.S. Environmental Protection Agency.

REFERENCES

Agulló-Barceló, M., Casas-Mangas, R., Lucena, F., 2012. Direct and indirect QMRA of infectious Cryptosporidium oocysts in reclaimed water. J. Water Health 10 (4), 539–548.

Ahmed, W., Gardner, T., Toze, S., 2011. Microbiological quality of roof-harvested rainwater and health risks: a review. J. Environ. Qual. 40 (1), 13–21.

Ahmed, W., Brandes, H., Gyawali, P., Sidhu, J.P., Toze, S., 2014. Opportunistic pathogens in roof-captured rainwater samples, determined using quantitative PCR. Water Res. 53, 361–369.

Al Aukidy, M., Verlicchi, P., Jelic, A., Petrovic, M., Barcelo, D., 2012. Monitoring release of pharmaceutical compounds: occurrence and environmental risk assessment of two WWTP effluents and their receiving bodies in the Po Valley, Italy. Sci. Total Environ. 438, 15–25.

An, W., Zhang, D., Xiao, S., Yu, J., Yang, M., 2011. Quantitative health risk assessment of *Cryptosporidium* in rivers of southern China based on continuous monitoring. Environ. Sci. Technol. 45 (11), 4951–4958.

Ananda, J., Proctor, W., 2013. Collaborative approaches to water management and planning: an institutional perspective. Ecol. Econ. 86, 97–106.

Arbault, D., 2013. Emergy evaluation of water treatment processes. Ecol. Eng. 60 (0), 172–182.

Arden, S., Ma, X., Brown, M., 2014. Ecohydrologic Effects of Urbanization on Evapotranspiration in Shallow Groundwater Table Environments. Water Sci. Technol. 70 (11), 1789–1797 (Special Issue: Modeling the Urban Water Cycle).

Arias, M.E., Brown, M.T., 2009. Feasibility of using constructed treatment wetlands for municipal wastewater treatment in the Bogotá Savannah, Colombia. Ecol. Eng. 35 (7), 1070–1078.

Arrow, K.J., Cropper, M.L., Eads, G.C., Hahn, R.W., Lave, L.B., Noll, R.G., Portney, P.R., Russell, M., Schmalensee, R., Smith, V.K., Stavins, R.N., 2004. Is there a role for benefit-cost analysis in environmental, health, and safety regulation? Science 272, 221–222.

Ashbolt, N.J., 2011. The Short Pipe Path – Safe Water, Energy & Nutrient Recovery. Session 18: Zero Net Energy Facilities and the Future of Wastewater Treatment. Water Environment Foundation, Hyatt Regency McCormick Place, Chicago, Illinois, pp. 1233–1241.

Ashbolt, N.J., Petterson, S.R., Westrell, T., Ottoson, J., Schönning, C., Stenström, T.A., 2006. In: Malmqvist, P.-A., Heinicke, G., Kärrman, E., Stenström, T.A., Svensson, G. (Eds.), Strategic Planning of Sustainable Urban Water Management. IWA Publishing, London, pp. 43–62.

Åström, J., Petterson, S.R., Bergstedt, O., Pettersson, T.J.R., Stenström, T.A., 2007. Evaluation of the microbial risk reduction due to selective closure of the raw water intake before drinking water treatment. J. Water Health 5 (s1), 81–97.

Ayyub, B.M., 2014. Systems resilience for multihazard environments: definition, metrics, and valuation for decision making. Risk Anal. 34 (2), 340–355.

Bare, J.C., Norris, G.A., Pennington, D.W., M, T., 2008. TRACI the tool for the reduction and assessment of chemical and other environmental impacts. J. Ind. Ecol. 6 (3–4), 49–78.

Balsells, M., Barroca, B., Amdal, J.R., Diab, Y., Becue, V., Serre, D., 2013. Analysing urban resilience through alternative stormwater management options: application of the conceptual Spatial Decision Support System model at the neighbourhood scale. Water Sci. Technol. Water Supply 68 (11).

Barker, F.S., O'Toole, J., Sinclair, M.I., Leder, K., Malawaraarachchi, M., Hamilton, A.J., 2013. A probabilistic model of norovirus disease burden associated with greywater irrigation of home-produced lettuce in Melbourne, Australia. Water Res. 47 (3), 1421–1432.

Beall, A., Fiedler, F., Boll, J., Cosens, B., 2011. Sustainable water resource management and participatory system dynamics. Case study: developing the Palouse Basin participatory model. Sustainability 3 (4), 720–742.

Bertera, W.J., 2013. Envision: a sustainability guide for water professionals. J. Am. Water Works Assoc. 105 (7), 50–53.

Bettini, Y., Brown, R., de Haan, F.J., 2013. Water scarcity and institutional change: lessons in adaptive governance from the drought experience of Perth, Western Australia. Water Sci. Technol. 67 (10), 2160–2168.

Björklund, J., 2001. Emergy analysis of municipal wastewater treatment and generation of electricity by digestion of sewage sludge. Resour. Conserv. Recycl. 31, 293–316.

Boulay, A.M., Bulle, C., Bayart, J.B., Deschenes, L., Margni, M., 2011. Regional characterization of freshwater use in LCA: modeling direct impacts on human health. Environ. Sci. Technol. 45, 8948–8957.

Boulay, A.M., Hoekstra, A.Y., Vionnet, S., 2013. Complementarities of water-focused life cycle assessment and water footprint assessment. Environ. Sci. Technol. 47 (21), 11926–11927.

Bowman, T.T., C, J., Thompson, J., Kliebenstein, J., Colletti, J.P., 2012. Multiple approaches to valuation of conservation design and low-impact development features in residential subdivisions. J. Environ. Manag. 2012 (104), 101–103.

Brauman, K.A., Daily, G.C., Duarte, T.K., Mooney, H.A., 2007. The nature and value of ecosystem services: an overview highlighting hydrologic services. Annu. Rev. Environ. Resour. 31 (1), 67–98.

Buenfil, A., 2001. Emergy Evaluation of Water. University of Florida., Gainesville, FL.

Campbell, D.E., Garmestani, A.S., 2012. An energy systems view of sustainability: emergy evaluation of the San Luis Basin, Colorado. J. Environ. Manag. 95 (1), 72–97.

Carter, T., Keeler, A., 2008. Life-cycle cost-benefit analysis of extensive vegetated roof systems. J. Environ. Manag. 87 (4), 350–363.

Chang, N.B., Qi, C., Yang, Y.J., 2012. Optimal expansion of a drinking water infrastructure system with respect to carbon footprint, cost-effectiveness and water demand. J. Environ. Manag. 110C, 194–206.

Chapagain, A.K., Tickner, D., 2012. Water footprint: help or hindrance? Water Altern. 5 (3), 563–581.

Charles, K.J., 2009. Quantitative Microbial Risk Assessment: a Catchment Management Tool to Delineate Buffer Distances for On-Site Sewage Treatment and Disposal Systems in Sydney's Drinking Water Catchments. Doctor of Philosophy. University of New South Wales, Sydney, New South Wales, Australia.

Clark, C., Adriaens, P., Talbot, F., 2008. Green roof valuation: a probabilistic economic analysis of environmental benefits. Environ. Sci. Technol. 42 (6), 2155–2161.

Cochran, B., Logue, C., 2011. A watershed approach to improve water quality: case study of clean water services' Tualatin River program. J. Am. Water Resour. Assoc. 47 (1), 29–38.

Collier, S.A., Stockman, L.J., Hicks, L.A., Garrison, L.E., Zhou, F.J., Beach, M.J., 2012. Direct healthcare costs of selected diseases primarily or partially transmitted by water. Epidemiol. Infect. 140 (11), 2003–2013.
Cordell, D., Neset, T.S.S., 2014. Phosphorus vulnerability: a qualitative framework for assessing the vulnerability of national and regional food systems to the multi-dimensional stressors of phosphorus scarcity. Glob. Environ. Change 24 (1), 108–122.
Daily, G.C., Matson, P.A., 2008. Ecosystem services: from theory to implementation. Proc. Natl. Acad. Sci. 105 (28), 9455–9456.
De Gisi, S., Petta, L., Farina, R., De Feo, G., 2014. Using a new incentive mechanism to improve wastewater sector performance: the case study of Italy. J. Environ. Manag. 132, 94–106.
Dessai, S., Hulme, M., 2007. Assessing the robustness of adaptation decisions to climate change uncertainties: a case study on water resources management in the East of England. Glob. Environ. Change 17 (1), 59–72.
Dobbie, M.F., Brown, R.R., 2014. A framework for understanding risk perception, explored from the perspective of the water practitioner. Risk Anal. 34 (2), 294–308.
Dodds, W.K., Perkin, J.S., Gerken, J.E., 2013. Human impact on freshwater ecosystem services: a global perspective. Environ. Sci. Technol. 47 (16), 9061–9068.
Dwight, R.H.F., M, L., Bakerc, D.B., Semenzad, J.C., Olson, B.H., 2005. Estimating the economic burden from illnesses associated with recreational coastal water pollution—a case study in Orange County, California. J. Environ. Manag. 76, 95–103.
Fane, S.A., Ashbolt, N.J., White, S.B., 2002. Decentralised urban water reuse: the implications of system scale for cost and pathogen risk. Water Sci. Technol. 46 (6–7), 281–288.
Fann, N., Fulcher, C.M., Baker, K., 2013. The recent and future health Burden of air pollution apportioned across U.S. sectors. Environ. Sci. Technol. 47 (8), 3580–3589.
Folke, C., 2010. How Much Disturbance Can a System Withstand? with Roots in Ecology and Complexity Science, Resilience Theory Offers New Ways to Turn Crises into Catalysts for Innovation.
Fuentes, I., Rodriguez, M., Domingo, C.J., del Castinllo, F., Alvar, J., 1996. Urine sample used for congenital toxoplasmosis diagnosis by PCR. J. Clin. Microbiol. 34 (10), 2368–2371.
Gabe, J., Trowsdale, S., Vale, R., 2009. Achieving integrated urban water management: planning top-down or bottom-up? Water Sci. Technol. 59 (10), 1999–2008.
Ghimire, S.R., Watkins Jr., D.W., Li, K., 2012. Life cycle cost assessment of a rain water harvesting system for toilet flushing. Water Sci. Technol. Water Supply 12 (3), 309–320.
Haller, L., Hutton, G., Bartram, J., 2007. Estimating the costs and health benefits of water and sanitation improvements at global level. J. Water Health 5 (4), 467–480.
Hanafiah, M.M., Xenopoulos, M.A., Pfister, S., Leuven, R.S.E.W., Huijbregts, M.A.J., 2011. Charaterization factors for water consumption and greenhouse gas emissions based on freshwater fish species extinction. Environ. Sci. Technol. 45 (12), 5272–5278.
Hardisty, P.E., Sivapalan, M., Humphries, R., 2013. Determing a sustainable and economically optimal wastewater treatment and discharge strategy. J. Environ. Manag. 123, 98–104.
Havelaar, A., Melse, J.M., 2003. Quantifying Public Health Risk in the WHO Guidelines for Drinking-water Quality: a Burden of Disease Approach. RIVM raport 734301022. RIVM, Bilthoven.
Havelaar, A.H., De Hollander, A.E.M., Teunis, P.F.M., Evers, E.G., Van Kranen, H.J., Versteegh, J.F.M., Van Koten, J.E.M., Slob, W., 2000a. Balancing the risks and benefits of drinking water disinfection: disability adjusted life-years on the scale. Environ. Health Perspect. 108 (4), 315–321.
Havelaar, A.H., de Wit, M.A., van Koningsveld, R., van Kempen, E., 2000b. Health burden in the Netherlands due to infection with thermophilic *Campylobacter* spp. Epidemiol. Infect. 125, 505–522.
Hester, E.T., Little, J.C., 2013. Measuring environmental sustainability of water in watersheds. Environ. Sci. Technol. 47 (15), 8083–8090.
Hoekstra, A.Y., Hung, P.Q., 2002. Virtual Water Trade: a Quantification of Virtual Water Flows between Nations in Relation to International Crop Trade. UNESCO-IHE.
Hoekstra, A.Y., Chapagain, A.K., Aldaya, M.M., Mekonnen, M.M., 2011. The Water Footprint Assessment Manual: Setting the Global Standard. Earthscan, London, UK.
Hofstetter, P., Hammitt, J.K., 2002. Selecting human health metrics for environmental decision-support tools. Risk Anal. 22 (5), 965–983.
Howard, G., Charles, K., Pond, K., Brookshaw, A., Hossain, R., Bartram, J., 2010. Securing 2020 vision for 2030: climate change and ensuring resilience in water and sanitation services. J. Water Clim. Change 1 (1), 2–16.
Howe, C.A., Butterworth, J., Smout, I.K., Duffy, A.M., Vairavamoorthy, K., 2011. Sustainable Water Management in Cities of the Future. Final Report of the SWITCH Project 2006–2011.
Hurlimann, A., Dolnicar, S., 2010. When public opposition defeats alternative water projects - the case of Toowoomba Australia. Water Res. 44 (1), 287–297.
Hwanga, H., Forrestera, A., Lanseya, K., 2013. Decentralized Water Reuse: Regional Water Supply System Resilience Benefits.
Igos, E., Benetto, E., Dalle, A., Tiruta-Barna, L., Baudin, I., Méry, Y., 2014. Life cycle assessment of water treatment: the role of infrastructure vs. operation at unit process level. J. Clean. Prod. 65, 424–431.
IPCC, 2012. In: Field, C.B., Barros, V., Stocker, T.F., Qin, D., Dokken, D.J., Ebi, K.L., Mastrandrea, M.D., Mach, K.J., Plattner, G.-K., Allen, S.K., Tignor, M., Midgley, P.M. (Eds.), Managing the Risks of Extreme Events and Disasters to Advance Climate Change Adaptation. Cambridge University Press, Cambridge.
Jones, M.P., Hunt, W.F., 2010. Performance of rainwater harvesting systems in the southeastern United States. Resources. Conserv. Recycl. 54 (10), 623–629.
Jongman, B., Ward, P.J., Aerts, J.C.J.H., 2012. Global exposure to river and coastal flooding: long term trends and changes. Glob. Environ. Change 22 (4), 823–835.
Kärrman, E., Malmqvist, P.A., McConville, J., Pettersson, F., Svensson, G., Wittgren, H.B., 2011. Application of the Urban Water Framework – Systems Analysis in Practice International Water Association. Stockholm, 22–25 May.
Katukiza, A.Y., Ronteltap, M., van der Steen, P., Foppen, J.W., Lens, P.N., 2014. Quantification of microbial risks to human health caused by waterborne viruses and bacteria in an urban slum. J. Appl. Microbiol. 116 (2), 447–463.
Kubiszewski, I., Costanza, R., Franco, C., Lawn, P., Talberth, J., Jackson, T., Aylmer, C., 2013. Beyond GDP: measuring and achieving global genuine progress. Ecol. Econ. 93 (1), 57–68.
Lederer, J., Rechberger, H., 2010. Comparative goal-oriented assessment of conventional and alternative sewage sludge treatment options. Waste Manag. 30 (6), 1043–1056.
Leung, H.W., Jin, L., Wei, S., Tsui, M.M., Zhou, B., Jiao, L., Cheung, P.C., Chun, Y.K., Murphy, M.B., Lam, P.K., 2013. Pharmaceuticals in tap water: human health risk assessment and proposed monitoring framework in china. Environ. Health Perspect. 121 (7), 839–846.

Lundie, S., Peters, G.M., Beavis, P.C., 2004. Life cycle assessment for sustainable metropolitan water systems planning. Environ. Sci. Technol. 38 (13), 3465–3473.
Lundie, S., Peters, G., Ashbolt, N., Lai, E., Livingston, D., 2006. A sustainability framework for the Australian water industry. Water, J. Aust. Water Assoc. 33 (11), 54–59.
Lundie, S., Ashbolt, N., Peters, G., Livingston, D., Lai, E., Kärrman, E., Blaikie, J., Anderson, J., 2008. Sustainability Framework. WSAA Occasional Paper No.17. PART a: Methodology for Evaluating the Overall Sustainability of Urban Water Systems. In: PART B: a Review Comparing the WSAA Sustainability Framework to the Gold Coast Waterfuture Process. Water Services Association of Australia, Melbourne.
Lundin, M., Bengtsson, M., Molander, S., 2000. Life cycle assessment of wastewater systems: Influence of system boundaries and scale on calculated environmental loads. Environ. Sci. Technol. 34 (1), 180–186.
Luthy, R.G., 2013. Design options for a more sustainable urban water environment. Environ. Sci. Technol. 47 (19), 10719–10720.
Lyons, E., Zhang, P., Benn, T., Sharif, F., Li, K., Crittenden, J., Costanza, M., 2009. Life cycle assessment of three water supply systems: importation, reclamation and desalination. Water Sci. Technol. 9 (4), 439–448.
Maheepala, S., Blackmore, J., Diaper, C., Moglia, M., Sharma, A., Kenway, S., 2010. Integrated Urban Water Management Planning Manual. Water Research Foundation, and Commonwealth Scientific Industrial and Research Organisation (CSIRO), Denver.
Malmqvist, P.A., Palmquist, H., 2005. Decision support tools for urban water and wastewater systems—focussing on hazardous flows assessment. Water Sci. Technol. 51 (8), 41–49.
Memon, F.A., Zheng, Z., Butler, D., Shirley-Smith, C., Lui, S., Makropoulos, C., Avery, L., 2007. Life cycle impact assessment of greywater recycling technologies for new developments. Environ. Monit. Assess. 129 (1–3), 27–35.
Mishan, E.J., 1978. Elements of Cost Benefit Analysis. George Allen & Unwin Ltd, London, United Kingdom.
Mo, W., Nasiri, F., Eckelman, M.J., Zhang, Q., Zimmerman, J.B., 2010. Measuring the embodied energy in drinking water supply systems: a case study in the Great Lakes region. Environ. Sci. Technol. 44 (24), 9516–9521.
Mo, W., Zhang, Q., Mihelcic, J.R., Hokanson, D.R., 2011. Embodied energy comparison of surface water and groundwater supply options. Water Res. 45 (17), 5577–5586.
Moore, J., Kissinger, M., Rees, W.E., 2013. An urban metabolism and ecological footprint assessment of Metro Vancouver. J. Environ. Manag. 124, 51–61.
Morales, M.A., Heaney, J.P., Friedman, K.R., Martin, J.M., 2013. Parcel-level model of water and energy end use: effects of indoor water conservation. J. Am. Water Works Assoc. 105 (9), E507–E516.
Murray, C.J., Acharya, A.K., 1997. Understanding DALYs (disability-adjusted life years). J. Health Econ. 16 (6), 703–730.
Nelson, M., 1998. Limestone wetland Mesocosm for Recycling Saline Wastewater in Coastal Yucatan, Mexico. University of Florida, Gainesville, FL.
NRC, 2009. Science and Decisions: Advancing Risk Assessment. National Academies Press, Washington, DC.
NRC, 2012. Water Reuse:Potential for Expanding the Nation's Water Supply through Reuse of Municipal Wastewater. National Academies Press, Washington, DC.
O'Rourke, T.D., 2007. Critical infrastructure, interdependencies, and resilience. Bridge-Washington National Academy of Engineering. Washingt. Acad. Eng. 37 (1), 22.
Odum, E.P., 1983. Basic Ecology. Saunders College Pub, Philadelphia.
Odum, H.T., 1996. Environmental Accounting. John Wiley & Sons, New York.
OECD, 2010. Sustainable Management of Water Resources in Agriculture. OECD Publishing, Paris.
OECD, 2011. An OECD Perspective. OECD. In: Benefits of Investing in Water and Sanitation. OECD Publishing, Paris.
Otterpohl, R., Braun, U., Oldenburg, M., 2003. Innovative technologies for decentralised water-, wastewater and biowaste management in urban and peri-urban areas. Water Sci. Technol. 48 (11–12), 23–32.
Pabi, S., Amarnath, A., Goldstein, R., 2013. Electricity Use and Management in the Municipal Water Supply and Wastewater Industries. Final Report. Electric Power Research Institute, Palo Alto, California.
Page, D., D, P., Toze, S., Bixio, D., Genthe, B., Jimenez Cisneros, B.E., Wintgens, T., 2010. Valuing the subsurface pathogen treatment barrier in water recycling via aquifers for drinking supplies. Water Res. 44 (6), 1841–1852.
Pahl-Wostl, C., Lebel, L., Knieper, C., Nikitina, E., 2012. From applying panaceas to mastering complexity: toward adaptive water governance in river basins. Environ. Sci. Policy 23 (1), 24–34.
Petterson, S., 2010. Development of a Software Tool for Undertaking Comparative Risk Assessment of DBPs and Pathogens in Drinking Water. European Environment Agency, Denmark.
Pfister, S., Ridoutt, B.G., 2013. Water footprint: pitfalls on common ground. Environ. Sci. Technol. 48 (1), 4–4.
Pfister, S., Koehler, A., Hellweg, S., 2009. assessing the environmental impacts of freshwater consumption in LCA. Environ. Sci. Technol. 43 (11), 4098–4104.
Remy, C., Jekel, M., 2008. Sustainable wastewater management: life cycle assessment of conventional and source-separating urban sanitation systems. Water Sci. Technol. 58 (8), 1555–1562.
Richardson, S.D., T, A.T., 2011. Water analysis: emerging contaminants and current issues. Environ. Sci. Technol. 83 (12), 4614–4648.
Romitelli, M.S., 1997. Energy Analysis of Watersheds. University of Florida, Gainsville, FL.
Schlüter, M., Pahl-Wostl, C., 2007. Mechanisms of resilience in common-pool resource management systems: an agent-based model of water use in a river basin. Ecol. Soc. 12 (2), 23.
Schoen, M.E., Ashbolt, N.J., 2010. Assessing pathogen risk to swimmers at non-sewage impacted recreational beaches. Environ. Sci. Technol. 44 (7), 2286–2291.
Short, M.D., Daikeler, A., Peters, G.M., Mann, K., Ashbolt, N.J., Stuetz, R.M., Peirson, W.L., 2014. Municipal gravity sewers: an unrecognised source of nitrous oxide. Sci. Total Environ. 468, 211–218.
Soller, J.A., Schoen, M.E., Bartrand, T., Ravenscroft, J.E., Ashbolt, N.J., 2010. Estimated human health risks from exposure to recreational waters impacted by human and non-human sources of faecal contamination. Water Res. 44 (16), 4674–4691.
Stenekes, N., Colebatch, H.K., Waite, T.D., Ashbolt, N.J., 2010. Risk and governance in water recycling: 'Public acceptance' revisited. Sci. Technol. Hum. Values 31 (2), 107–134.
Stockholm Resilience Center, 2007. Resilience Dictionary.
Stokes, J.R., Horvath, A., 2006. Life cycle energy assessment of alternative water supply systems. Int. J. Life Cycle Assess. 11 (5), 335–343.
Stokes, J.R., Horvath, A., 2009. Energy and air emission effects of water supply. Environ. Sci. Technol. 43 (8), 2680–2687.
Stokes, J.R., Horvath, A., Sturm, R., 2013. Water loss control using pressure management: life-cycle energy and air emission effects. Environ. Sci. Technol. 47 (19), 10771–10780.
Strengers, Y., Maller, C., 2012. Materialising energy and water resources in everyday practices: Insights for securing supply systems. Glob. Environ. Change 22 (3), 754–763.

Tangsubkul, N., Beavis, P., Moore, S.J., Lundie, S., Waite, T.D., 2005a. Life cycle assessment of water recyling technology. Water Resour. Mangement 19 (5), 521–537.
Tangsubkul, N., Moore, S., Waite, T.D., 2005b. Incorporating phosphorus management considerations into wastewater management practice. Environ. Sci. Policy 8 (1), 1–15.
Teunis, P.F.M., Xu, M., Fleming, K.K., Yang, J., Moe, C.L., LeChevallier, M.W., 2010. Enteric virus infection risk from intrusion of sewage into a drinking water distribution network. Environ. Sci. Technol. 44 (22), 8561–8566.
Thomas, J.S., Durham, B., 2003. Integrated Water Resource Management: looking at the whole picture. Desalination 156, 21–28.
Tidåker, P., 2003. Life Cycle Assessment of Grain Production Using Source-separated Human Urine and Mineral Fertiliser. Report 251. Swedish University of Agricultural Sciences, Department of Agricultural Engineering (SLU), Uppsala.
Tillman, A.-M., Svingby, M., Lundström, H., 1998. Life cycle assessment of municipal waste water systems. Int. J. Life Cycle Assess. 3 (3), 145–157.
US-EPA, 2002. The Clean Water and Drinking Water Infrastructure Gap Analysis. Office of Water, United States Environmental Protection Agency, Washington, DC.
US-EPA, 2008. Reducing Urban Heat Islands: Compendium of Strategies.
US-EPA, 2010. Guidelines for Preparing Economic Analyses. U.S. Environmental Protection Agency, National Center for Environmental Economics, Washington, DC (US Forest Service i-Tree ECO, U.S. Forest Service).
US-EPA, 2013a. Community-Based Water Resiliency (CBWR) Tool.
US-EPA, 2013b. Rivers and Streams Assessment 2008–2009, A Collaborative Survey. Office of Wetlands, Oceans and Watersheds. Office of Research and Development, Washington, DC. EPA/841/D-13/001.
Venkatesh, G., Brattebø, H., 2012. Assessment of environmental impacts of an aging and stagnating water supply pipeline network. J. Ind. Ecol. 16 (5), 722–734.
Wackernagel, M., Rees, W.E., 1996. Our Ecological Footprint - Reducing Human Impact on the Earth. New Society Publishers Gabriola Island.
Wang, S., 2014. Values of decentralized systems that avoid investments in idle capacity within the wastewater sector: a theoretical justification. J. Environ. Manag. 136 (c), 68–75.
Watanabe, M., 2014. Dynamic emergy accounting of water and carbon ecosystem services: a model to simulate the impacts of land-use change. Ecol. Model. 27 (1), 113–131.
Wenning, R.J., Apitz, S.E., 2012. Ecosystem services: protecting the commons. Integr. Environ. Assess. Manag. 8 (3), 395–396.
Westrell, T., Bergstedt, O., Stenstrom, T.A., Ashbolt, N.J., 2003. A theoretical approach to assess microbial risks due to failures in drinking water systems. Int. J. Environ. Health Res. 13 (2), 181–197.
Westrell, T., Schonning, C., Stenstrom, T.A., Ashbolt, N.J., 2004. QMRA (quantitative microbial risk assessment) and HACCP (hazard analysis and critical control points) for management of pathogens in wastewater and sewage sludge treatment and reuse. Water Sci. Technol. 50 (2), 23–30.
WHO, 2010. Vision 2030. The Resilience of Water Supply and Sanitation in the Face of Climate Change.
WHO, 2012. Un-water Global Analysis and Assessment of Sanitation and Drinking-water (GLAAS) 2012 Report: the Challenge of Extending and Sustaining Services. World Health Organization, Geneva.
Wiedmann, T., Minx, J., 2008. A definition of 'Carbon footprint'. In: Pertsova, C.C. (Ed.), Ecological Economics Research Trends. Nova Science Publishers, Hauppauge NY, USA.
William, P.F., Mciwem, B., 2009. Influence of anaerobic digestion on the carbon footprint of various sewage sludge treatment options. Water Environ. J. 23 (3), 170–179.
Winz, I., Brierley, G., Trowsdale, S., 2009. The use of system dynamics simulation in water resources management. Water Resour. Manag. 23 (9), 1301–1323.
Wong, T.H., Brown, R.R., 2009. The water sensitive city: principles for practice. Water Sci. Technol. 60 (3), 673–682.
Zarghami, M., Akbariyeh, S., 2012. System dynamics modeling for complex urban water systems: application to the city of Tabriz, Iran. Resour. Conserv. Recycl. 60 (1), 99–106.
Zeeman, G., Kujawa, K., de Mes, T., Hernandez, L., de Graaff, M., Abu-Ghunmi, L., Mels, A., Meulman, B., Temmink, H., Buisman, C., van Lier, J., Lettinga, G., 2008. Anaerobic treatment as a core technology for energy, nutrients and water recovery from source-separated domestic waste(water). Water Sci. Technol. 57 (8), 1207–1212.
Zeng, Z., Liu, J., Koeneman, P.H., Zarate, E., Hoekstra, A.Y., 2012. Assessing water footprint at river basin level: a case study for the Heihe River Basin in northwest China. Hydrol. Earth Syst. Sci. 16 (8), 2985–2994.

Record of Percentage Agreement on the following paper submitted for the 2020 STAA award

Critical insights for a sustainability framework to address integrated community water services: Technical metrics and approaches

Xiaobo Xue, Mary Schoen, Xin (Cissy) Ma, Troy R. Hawkins, and Nicholas Ashbolt. Critical Insights to the Sustainability Framework for Engineering the Next-Generation of US Municipal Water Services: Metrics and Approaches. *Water Research*. 77. 155-169, 2015.

Xiaobo Xue	**20%**	Xiaobo Xue Romero
Mary E. Schoen	**5%**	
Xin (Cissy) Ma	**56%**	
Troy R. Hawkins	**10%**	
Nicholas J. Ashbolt	**2%**	
Jay Garland	**2%**	Jay L Garland
Jennifer Cashdollar	**5%**	

Record of Percentage Agreement on the following paper submitted for the 2020 STAA award

Critical insights for a sustainability framework to address integrated community water services: Technical metrics and approaches

Xiaobo Xue, Mary Schoen, Xin (Cissy) Ma, Troy R. Hawkins, and Nicholas Ashbolt. Critical Insights to the Sustainability Framework for Engineering the Next-Generation of US Municipal Water Services: Metrics and Approaches. *Water Research*. 77. 155-169, 2015.

Xiaobo Xue	**20%**	Xiaobo Xue Roneeko
Mary E. Schoen	**5%**	mary schoen
Xin (Cissy) Ma	**56%**	
Troy R. Hawkins	**10%**	Troy Hawkins
Nicholas J. Ashbolt	**2%**	
Jay Garland	**2%**	
Jennifer Cashdollar	**5%**	JENNIFER CASHDOLLAR Digitally signed by JENNIFER CASHDOLLAR Date: 2020.04.28 08:56:14 -04'00'

Record of Percentage Agreement on the following paper submitted for the 2020 STAA award

Critical insights for a sustainability framework to address integrated community water services: Technical metrics and approaches

Xiaobo Xue, Mary Schoen, Xin (Cissy) Ma, Troy R. Hawkins, and Nicholas Ashbolt. Critical Insights to the Sustainability Framework for Engineering the Next-Generation of US Municipal Water Services: Metrics and Approaches. *Water Research*. 77. 155-169, 2015.

Xiaobo Xue	**20%**	Xiaobo Xue Rone Jo
Mary E. Schoen	**5%**	mary schoen
Xin (Cissy) Ma	**56%**	XIN MA Digitally signed by XIN MA Date: 2020.04.28 16:04:09 -04'00'
Troy R. Hawkins	**10%**	
Nicholas J. Ashbolt	**2%**	
Jay Garland	**2%**	
Jennifer Cashdollar	**5%**	

Table of Contents

General_Authors_Publications.....2
LI-266121_Part_3_Paper_1.....12
LI-266122_Part_3_Paper_2.....17
e-mail_Nasir.....21
e-mail-Nadagouda.....22
My_contribution_to_papers_submitted_for_STAA_award-from_Rajender_Varma.....23
Part_3_Paper_1.....24
Part_3_Paper_2.....29
Sanny_Verma_Part_02_Confirmation.....33
STAA_Part_3_Environmental_upgrading_of_biomass_and_sustainable_development_in_34

United States Environmental Protection Agency
Washington, DC 20460

STAA REPORT FOR THE SCIENTIST NOMINATIONS

General Information:

Nomination ID/App ID:	20-102
Research Category Primary:	Sustainability and Innovation (SI)
Research Category Secondary:	Industry and the Environment (IE);Energy and the Environment (EE);Sustainability and Innovation (SI)
Laboratory/Office Name:	ORD
Nomination Entered By:	Mallikarjuna Nadagouda

Eligibility Checklist:

[Y] The nominated publication(s) has not been submitted to a previous STAA competition.

[Y] The nominated publication(s) was published on or before January 1, 2017 and on or after January 1,2012

[Y] The principal author was an EPA employee or a PHS employee assigned to EPA when the research was performed

[Y] The EPA authors (includes PHS employees assigned to EPA) contributed collectively a minimum of 50% toward the publication(s)

Nominating Official Name:	Regan Murray
Nominating Official Title:	SUPERVISORY INTERDISCIPLINARY SCIENTIST
Nominating OfficialEmail:	murray.regan@epa.gov
STAA Coordinator Name:	Kathleen Wiser
STAA Coordinator Email:	wiser.kathi@epa.gov

Justifications:

Justification 1:

The two nominated papers demonstrate the upgrading of biomass and chemical transformation using environmental-friendly processes.

To preserve resources and maintain environmental and economic sustainability, researchers must develop more efficient technologies for the chemical industry. Currently, they have focused on the lack of available non-renewable organic feedstocks to demonstrate the importance of renewable resources. Upgrading biomass and the development of chemical feedstocks from renewable resources are a sustainable method of reducing dependence on petroleum products. Though upgrading and sustainable development hold many advantages for the environment when applied as a petroleum alternative, they also present a significant challenge, since researchers must chemically modify the bio-derived fuels to make them compatible with existing technology. To solve all these challenges, our first nominated paper (Nadagouda, 2019) developed a technology of magnetically separable heterogeneous bimetallic catalysts for the upgrading of lignin-derived guaiacol to cyclohexanol under visible light. The second nominated paper (Nadagouda, 2017) designed a novel method for supporting photoactive heterogeneous catalysis in organic reactions.

Overall, these two papers significantly justify EPA mission, for example, “Sustainable Materials Management (SMM)” as these research articles demonstrate the utilization of sustainable protocols for the upgrading of biomass and chemical transformation. (https://www.epa.gov/sites/production/files/2015-08/documents/sustainable_materials_management_the_road_ahead.pdf). As we know, chemistry is very crucial for daily life and the extent of its application from the development of organic scaffolds to treat various illnesses in the formation of innovative industrial developments. We develop clean, sustainable methods to synthesize industrially relevant products in the prevention of pollution and the elimination of hazardous waste.

Justification 2A:

None of the two nominated papers consisted of this STAA package have been submit ted for a STAA in the past.

In this package, two papers are essentially related to each other as they demonstrate the environmental upgrading of biomass and sustainable development in organic transformation. As mentioned in answer to Question 1, the strength of this study is the span of researches that was performed for the utilization of sustainable protocols in the upgradation of biomass (Nadagouda, 2019) and organic transformation (Nadagouda, 2017).

All these research studies increase the national scale understanding of environmental upgrading of biomass and sustainable development in organic transformation.

Justification 2B:

Response:

Mallikarjuna N. Nadagouda

1. Evaluating Sustainable Pathway to Furanics from Biomass via Heterogeneous Organo-Catalysis Green Chemistry
2. Sustainable Strategy Utilizing Biomass: Visible Light-Mediated Synthesis of g-Valerolactone. Published in ChemCatChem
3. Visible Light Mediated Upgrading of Biomass to Biofuel. Published in Green Chemistry

2017 Honorable Mention STAA

1. The Oxidative C-H activation of amines using protuberant lychee-like goethite. Published in Nature Climate Change
2. Photocatalytic C-H activation and oxidative esterification using Pd@g-C3N4. Published in Catalysis Today
3. Hydroxylation of benzene via C-H activation using bimetallic CuAg@g-C3N4. Published in ACS Sustainable Chemistry and Engineering

2019 Honorable Mention STAA

1. Conversion of spent carbon dioxide into value-added products
2. A sustainable approach to empower the bio-based future: upgrading biomass to value-added products

2019 Level III STTA

Rajender S. Varma

1. Evaluating Sustainable Pathway to Furanics from Biomass via Heterogeneous Organo-Catalysis Green Chemistry
2. Sustainable Strategy Utilizing Biomass: Visible Light-Mediated Synthesis of g-Valerolactone. Published in ChemCatChem
3. Visible Light Mediated Upgrading of Biomass to Biofuel. Published in Green Chemistry

2017 Honorable Mention STAA

1. The Oxidative C-H activation of amines using protuberant lychee-like goethite. Published in Nature Climate Change
2. Photocatalytic C-H activation and oxidative esterification using Pd@g-C3N4. Published in Catalysis Today
3. Hydroxylation of benzene via C-H activation using bimetallic CuAg@g-C3N4. Published in ACS Sustainable Chemistry and Engineering

2019 Honorable Mention STAA

1. Conversion of spent carbon dioxide into value-added products
2. A sustainable approach to empower the bio-based future: upgrading biomass to value-added products

2019 Level III STTA

Justification 2C:

Nadagouda's (2017 Honorable Mention STAA, 2019 Honorable Mention STAA and 2019 Level III STTA) awards are like the currently nominated work, which are directly connected to sustainable chemistry. However, the sustainable process used in the first paper (Nadagouda 2019) utilizes the chitosan derived carbon nitride as catalyst support, and the second paper demonstrates the oxidation of alcohols under visible light. These are new approaches that have been utilized for the environmental upgrading of biomass and sustainable development in organic transformation, respectively.

Varma's (2017 Honorable Mention STAA, 2019 Honorable Mention STAA, and 2019 Level III STTA) awards are like the currently nominated work, which are directly connected to sustainable chemistry. However, the sustainable process used in the first paper (Nadagouda 2019) utilizes the chitosan derived carbon nitride as catalyst support, and the second

paper demonstrates the oxidation of alcohols under visible light. These are new approaches that have been utilized for the environmental upgrading of biomass and sustainable development in organic transformation, respectively.

Justification 2D:

None of the supplemental information has been included in previous nominations.

Justification 2E:

There are no concurrent nominations by the authors on this nomination.

Justification 3A:

The first nominated paper (Nadagouda et al., 2019) has selected as a part of the themed collection "Green Biorefinery Technologies based on Waste Biomass" by the Royal Society of Chemistry. It has been published in the prestigious journal “Green Chemistry," which has an Impact Factor of 9.405 and has ranked#3 (h-index: 186) in the “Environmental Science” category. This research work has already been cited in 5 research articles (Google citation search). Prof. Reina from Department of Chemical and Process Engineering Department, University of Surrey, United Kingdom has adopted our work on the upgrading of biomass in his research article "Jin, W., Pastor-Pérez, L., Yu, J., Odriozola, J.A., Gu, S. and Reina, T.R., 2020. Cost-effective routes for Catalytic Biomass Upgrading. Current Opinion

in Green and Sustainable Chemistry". Recently, Prof. Bhoi from Department of Mechanical Engineering, Georgia Southern University, GA, USA has adopted and discussed our research work of AgPd/Fe@CNx catalyst for upgrading of lignin-derived guaiacol to cyclohexanol (98%) under visible light irradiation in his article "Ouedraogo, A.S. and Bhoi, P.R., 2020. Recent progress of metals supported catalysts for hydrodeoxygenation of biomass-derived pyrolysis oil. Journal of Cleaner Production 253, 119957"

The second nominated paper (Nadagouda et al., 2017) has been published in the prestigious journal "Tetrahedron," which has an Impact Factor of 2.645 and has ranked#61 (h-index: 209) in the "Pharmacology, Toxicology and Pharmaceutics" category. This research work has already been cited in 19 research articles (Google citation search) since its publication and highlighted in "**Synfacts**" (Polymer-Supported Synthesis) as **Synfacts, 2017, 13(11), p.1222**.

Recently, prof. Hong from South Korea has cited and highlighted our research work (Nadagouda et al., 2017) on his reaserach article "Hong, K., Sajjadi, M., Suh, J.M., Zhang, K., Nasrollahzadeh, M., Jang, H.W., Varma, R.S. and Shokouhimehr, M., 2020. Palladium Nanoparticles on Assorted Nanostructured Supports: Applications for Suzuki, Heck, and Sonogashira Cross-Coupling Reactions. ACS Applied Nano Materials, 3(3), pp.2070-2103."

Justification 3B:

All of the nominated and supporting manuscript underwent anonymous peer review by the journal to which it was submitted for publication.

AUTHORS

Principal Author

Author Name: Mallikarjuna N. Nadagouda

Professional Title: Salutation: Dr.

Email:	nadagouda.mallikarjuna@epa.gov	Organization:	
Mailing Address:			
Street Line 1:	26 West, MLK DR.		
City:	Cincinnati		
Zip Code:	45268	State:	OH
At time of research was:	EPA Employee		
Separation Date:			
% of Effort:	55		

Contributing Author

Author Name:	Rajender Varma		
Professional Title:		Salutation:	Dr.
Email:	varma.rajender@epa.gov	Organization:	
Mailing Address:			
Street Line 1:	26 West, MLK Dr		
City:	Cincinnati		
Zip Code:	45268	State:	OH
At time of research was:	EPA Employee		
Separation Date:			
% of Effort:	20		

Contributing Author

Author Name:	Sanny Verma		
Professional Title:		Salutation:	Dr.

Email:	verma.sanny@epa.gov	Organization:	
Mailing Address:			
Street Line 1:	26 West, MLK Dr		
City:	Cincinnati		
Zip Code:	45268	State:	OH
At time of research was:	Non EPA Personnel		
Separation Date:			
% of Effort:	20		

Contributing Author

Author Name:	Nasir Baig		
Professional Title:		Salutation:	Dr.
Email:	nasirchem@gmail.com	Organization:	
Mailing Address:			
Street Line 1:			
City:			
Zip Code:		State:	
At time of research was:	Non EPA Personnel		
Separation Date:			
% of Effort:	5		

PUBLICATIONS

Publication 1:

Visible light-mediated and water-assisted selective hydrodeoxygenation of

Publication Title:	lignin-derived guaiacol to		
Publication Date:	Tue Jan 29 00:00:00 GMT 2019		
Journal/Publication Method:	Green Chemistry		
All Author(s):			
Volume:	21	Number:	1
Pages:	1253-1257	Immediately Index:	Immediately Index:
Citation ½ Life:	4.10	Impact Factor:	9.405

Publication 2:

Publication Title:	Aerobic oxidation of alcohols in visible light on Pd-grafted Ti cluster		
Publication Date:	Sat Jul 30 00:00:00 GMT 2016		
Journal/Publication Method:	Tetrahedron		
All Author(s):			
Volume:	73	Number:	1
Pages:	5577-5580	Immediately Index:	Immediately Index:
Citation ½ Life:	9.20	Impact Factor:	2.645

Published on 28 January 2019. Downloaded by US Environmental Protection Agency, Cincinnati on 3/18/2019 2:48:24 PM.

Green Chemistry

COMMUNICATION

View Article Online
View Journal | View Issue

Check for updates

Cite this: *Green Chem.*, 2019, **21**, 1253

Received 17th December 2018,
Accepted 28th January 2019

DOI: 10.1039/c8gc03951h

rsc.li/greenchem

Visible light-mediated and water-assisted selective hydrodeoxygenation of lignin-derived guaiacol to cyclohexanol†

Sanny Verma,[a] Mallikarjuna N. Nadagouda[b] and Rajender S. Varma *[c]

A magnetically separable bimetallic AgPd/Fe@CN_x catalyst has been synthesized and utilized for upgrading of lignin-derived guaiacol to cyclohexanol *via* hydrodeoxygenation using formic acid as a source of hydrogen under visible light irradiation. A nitrogen-enriched carbonaceous material, carbon nitride (CN_x), is obtained *via* calcination of chitosan, a marine-derived abundant waste material and subsequently utilized as a support for the immobilization of nanoferrites and silver and palladium nanoparticles. Hydrogen generation from renewable sources such as formic acid and its ideal utilization for the upgrading of biomass-derived guaiacol are the main findings. The synergetic effect of Ag and Pd on the CN_x support enhances the decomposition of formic acid which is aptly utilized for the selective defunctionalization of guaiacol at ambient pressure.

Introduction

The lignocellulosic biomass is abundant and does not affect the food chain.[1] It has mostly been used in the Kraft process to produce pulp and paper[2] wherein energy is produced by the conventional burning of lignin and hemicellulosic residues in black liquor. However, for more efficient and ideal utilization of lignin and hemicellulose fractions of biomass, innovative methods and technologies are sought. Due to the depletion of fossil-based feedstock and striving for carbon-neutral fuels/chemicals, biomass transformations have been investigated intensively.[3–5] Thus, transportation fuel (bio-oil) has been produced *via* flash pyrolysis of biomass in the temperature range of 300–600 °C where lignin fractions have been utilized to produce valued products and fuels.[6]

[a]*Oak Ridge Institute for Science and Education, P. O. Box 117, Oak Ridge, TN, 37831, USA*
[b]*Department of Mechanical and Materials Engineering, Wright State University, Dayton, Ohio 45324, USA*
[c]*Regional Centre of Advanced Technologies and Materials, Department of Physical Chemistry, Faculty of Science, Palacky University, Šlechtitelů 27, 783 71 Olomouc, Czech Republic. E-mail: varma.rajender@epa.gov*
† Electronic supplementary information (ESI) available. See DOI: 10.1039/c8gc03951h

However, bio-oils are highly viscous, corrosive, and acidic (pH = 2.8–3.8) and show low thermal stability due to the presence of oxygen-containing moieties such as phenols, aldehydes, and acids.[7,8] Typically, bio-oils contain 40 wt% oxygen, which necessitates upgrading by transformations of aromatic or naphthenic hydrocarbons *via* the hydrodeoxygenation (HDO) reaction.[9] Catalytic HDO has been proficiently employed for the improvement of product heating value and upgrading of bio-oils as it reduces the oxygen content, especially aromatic $-OCH_3$ and –OH containing scaffolds typified by guaiacol.[10]

Guaiacol (2-methoxyphenol), a lignin-derived model molecule and a typical bio-oil component, can be upgraded to cyclohexanol *via* the hydrodeoxygenation (HDO) process.[11–13] Cyclohexanol has various industrial applications where it can be used as a solvent, or utilized in the synthesis of cyclohexanone and polymers.[14] Due to the presence of stable hydroxyl and methoxyl groups on the aromatic ring in guaiacol, simple hydrogenation is inadequate for the synthesis of cyclohexanol.[15] Hence, the selective removal of the methoxyl group and hydrogenation of the aromatic ring are required for conversion to cyclohexanol. Hitherto, HDO of guaiacol has been investigated using noble catalysts (Pd, Pt, and Ru), conventional hydrotreating sulfide catalysts (CoMoS and NiMoS) and solid acids which lead to hydrogenated oxygen containing compounds namely cyclohexanol and phenol,[16–21] besides fully hydrogenated hydrocarbons such as cyclohexane and benzene.[15]

Wang and Rinaldi developed a protocol for the HDO of bio-oil derived phenolic compounds to cyclohexanols using RANEY®@Ni catalyst at 120 °C with isopropanol as a hydrogen donor.[22] Recently, Jiang *et al.* developed the HDO of guaiacol with cyclohexanol as the primary product in aqueous medium over bimetallic Ni and Co catalysts on γ-Al_2O_3 and ZSM-5 supports.[23] Nakagawa *et al.* reported that the presence of MgO in combination with Ru/C promotes demethoxylation, and hence, increases transformation of guaiacol to cyclohexanol with 80% yield at 160 °C and 1.5 MPa hydrogen pressure.[24] However, basic MgO is not stable in aqueous media although the base helps in demethoxylation and diminishes the unselective

Published on 28 January 2019. Downloaded by US Environmental Protection Agency, Cincinnati on 3/18/2019 2:48:24 PM.

C–O bond dissociation during the HDO process. Tomishige *et al.* developed the Ru–Mn combination for the selective exclusion of the methoxyl group on the substituted phenol to give cyclohexanol with 81% yield at elevated temperature and under hydrogen pressure.[25] Recently, Zhang *et al.* reported the selective conversion of guaiacol to cyclohexanol in water using a metal-solid base bifunctional Ru/ZrO_2-$La(OH)_3$ catalyst at 170 °C and 4 MPa hydrogen pressure in an autoclave.[26] However, the aforementioned reports require high hydrogen pressure, elevated temperature and a prolonged reaction time. Hence, the development of a new efficient catalytic system is still needed to convert guaiacol to cyclohexanol with high stability and selectivity.[27,28]

In continuation of our efforts towards the development of sustainable protocols using heterogeneous catalysts,[29–33] herein, we report a magnetically separable bimetallic AgPd catalyst supported on marine waste chitosan-derived nitrogen-enriched carbon nitride (CN_x), AgPd/Fe@CN_X; the catalyst generates hydrogen from formic acid which can be utilized *in situ* for the selective hydrodeoxygenation of lignin-derived guaiacol under visible light irradiation at ambient pressure.

Synthesis and characterization

Firstly, a nitrogen-enriched carbon nitride support (CN_x) was obtained by the calcination of chitosan at 600 °C for 4 hours under a nitrogen atmosphere. Then, it was dispersed in water for 3 hours using sonication. An aqueous solution of $FeSO_4$ (500 mg in 100 mL) was added dropwise at room temperature to the mixture of CN_x and stirred for 2 hours.[32] A solution of $AgNO_3$ (0.5 mM, in 25 mL water) and $Pd(NO_3)_2$ (0.5 mM, in 25 mL water) was added to the colloidal solution at room temperature and the reaction mixture was further stirred for 4 hours. 1.0 g sodium borohydride ($NaBH_4$) was added, in portions, at 50 °C to reduce the iron sulfate, Ag(I) and Pd(II) to magnetic ferrites, Ag(0) and Pd(0), respectively. This reaction mixture was stirred for the next 12 hours. The ensuing black colored solid was isolated as AgPd/Fe@CN_X using an external magnet, washed with methanol and finally dried at 60 °C under vacuum.[32,34] The obtained AgPd/Fe@CN_X composite powder was further analyzed by various instrumental techniques such as X-ray diffraction (XRD), scanning electron microscopy (SEM), transmission electron microscopy (TEM), X-ray photoelectron spectroscopy (XPS), Brunauer–Emmett–Teller (BET) surface area analysis, FT-IR and inductively coupled plasma atomic emission spectroscopy (ICP-AES). SEM analysis of the CN_X support and AgPd/Fe@CN_X catalyst showed visual differences in images and confirmed the immobilization of silver (Ag), palladium (Pd) nanoparticles and nano-ferrites over the surface of nitrogen-enriched carbon nitride (Fig. 1a and b). TEM analysis validates the formation of single phase Ag nanoparticles, Pd nanoparticles and nano-ferrites with irregular shaped particles in the size range of 10–15 nm (Fig. 1c and d) which is further supported by EDX and SAED analysis of the bimetallic AgPd/Fe@CN_X catalyst (Fig. 2a and b).

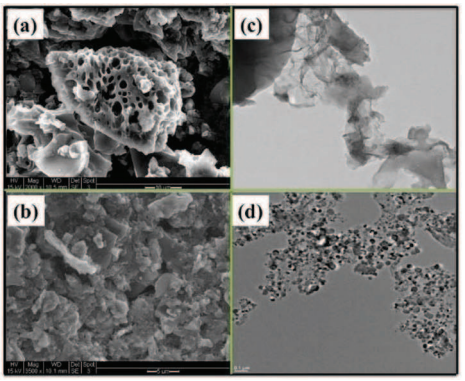

Fig. 1 (a) SEM image of CN_X; (b) SEM image of AgPd/Fe@CN_X; (c) TEM image of CN_X; (d) TEM image of AgPd/Fe@CN_X.

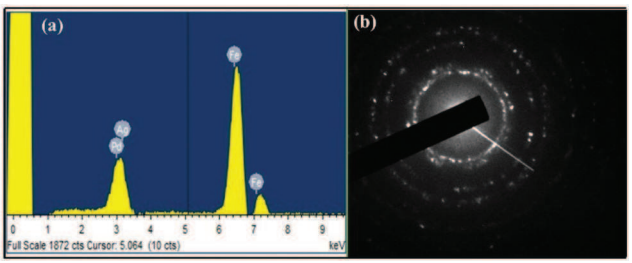

Fig. 2 (a) EDX analysis of AgPd/Fe@CN_X; (b) SAED image of AgPd/Fe@CN_X.

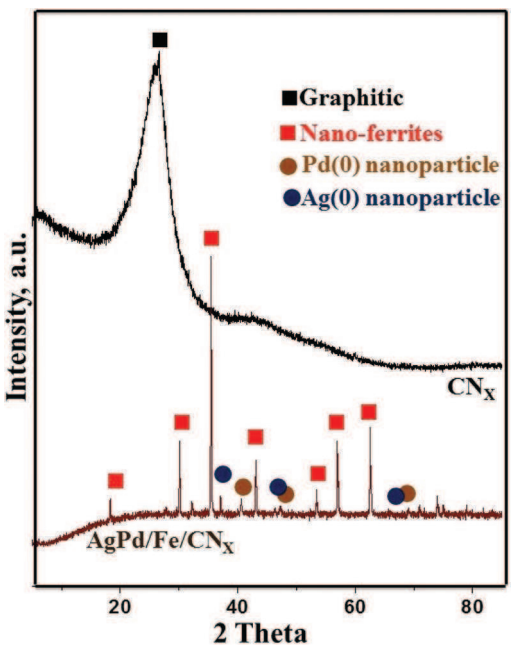

Fig. 3 XRD pattern of CN_X and AgPd/Fe@CN_X.

The XRD and XPS analysis also authenticated the formation of metallic silver and palladium nanoparticles along with nano-ferrites over the CN_X support (Fig. 3 and ESI; Fig. S5†).

 This journal is © The Royal Society of Chemistry 2019

Published on 28 January 2019. Downloaded by US Environmental Protection Agency, Cincinnati on 3/18/2019 2:48:24 PM.

Fig. 3 depicts the XRD patterns of CN_X and the carbon nitride immobilized bimetallic AgPd/Fe@CN_X catalyst. The nitrogen-enriched carbon nitride displayed a diffraction peak at 26.51° which corresponds to the graphitic peak.[46] Loading of metal nanoparticles leads to the disappearance of the diffraction peak at 26.51°. The observed peaks at 5.56°, 27.78°, and 43.01°, respectively, represent the (100), (110), and (210) Bragg reflection as compared with JCPDS standards (00-050-1250) which confirmed the presence of the carbon nitride (CN_X) support. Additionally, the XRD pattern of AgPd/Fe@CN_X corroborated that the bimetallic catalyst was enriched with FeO/Fe_2O_3 [2Θ = 18.21° (111), 30.11° (220), 35.36° (311), 43.16° (400), 53.56° (422), 62.79° (440); JCPDS#00-065-0731], Ag [2Θ = 38.1° (111), 44.27° (200), 64.42° (220); JCPDS#00-004-0783] and Pd [2Θ = 40.11° (111), 46.66° (200), 68.08° (220); JCPDS#00-005-068] nanoparticles (ESI; Fig. S3†). Although the intensity of silver and palladium nanoparticles is not high, their presence has been further confirmed by XPS, EDX and ICP-AES analysis.

A high resolution XPS analysis of CN_X and AgPd/Fe@CN_X was performed (ESI; Fig. S4–S9†). The XPS analysis of the CN_X support resembles the formation of tri-*s*-triazine-based graphitic carbon nitride.[35,36] In the C 1S spectrum, the peak at 284.7 eV (1s–π*C═C) is attributed to a typical transition of graphite and confirms the presence of graphitic carbon in good agreement with the literature.[37,38] The peak at 288.1 eV (1s–π* C–N–C) is ascribed to the characteristic resonance of nitrogen atoms bonded with two carbon atoms in *s*-triazine.[39] In the N 1S spectrum, the signal at 398.5 eV is ascribed to sp^2 nitrogen atoms having two carbon neighboring atoms (–N–C coordination in one tri-*s*-triazine unit) and that at 400.8 eV is attributed to sp^2 nitrogen atoms surrounded by three carbon atoms (N–3C bridging between three tri-*s*-triazine moieties).[40,41] The XPS analysis of AgPd/Fe@CN_X (ESI; Fig. S5†) showed the formation of Pd and Ag nanoparticles on the surface of carbon nitride (CN_X). Two peaks were observed, first one at 338.0 eV with a shoulder at 339.0 eV and the second one at 343.3 eV with a shoulder at 344.8 eV. These peaks were the result of Pd $3d_{5/2}$ and Pd $3d_{3/2}$ (ESI; Fig. S9(e)†). The XPS peaks at 367.9 eV and 373.8 eV could be credited to Ag $3d_{5/2}$ and Ag $3d_{3/2}$ confirming the presence of silver in the zero oxidation state (ESI; Fig. S8(d)†).[31] It is specified in the literature that the binding energy of the metal increases with the increase in the oxidation state; hence, the binding energy at 710.8 eV corresponds to Fe $2p_{3/2}$ in Fe^{2+} in the form of FeO. The satellite peak at 718.1 eV is a characteristic peak of Fe^{3+} in γ-Fe_2O_3, confirming that the catalyst is a combination of FeO/γ-Fe_2O_3 (ESI; Fig. S9(f)†).[42,43] Furthermore, the presence of Pd and Ag was analyzed using ICP-AES and their contents were found to be Pd (2.51%) and Ag (2.48%).

Results and discussion

To upgrade guaiacol, a model component of lignin-derived bio-oil, *via* selective hydrodeoxygenation, a series of catalysts were assessed for *in situ* generation of hydrogen from formic acid under visible light. For this transformation, an array of mono- and bi-metallic catalysts were synthesized on the magnetic nano-ferrite supported nitrogen enriched CN_X support (Table 1). Commercially available homogeneous catalysts such as $Pd(NO_3)_2$, $Cu(NO_3)_2$ and AgCl are ineffective even after 24 hours of exposure (Table 1, entries 1–3). Monometallic TiO_2/Fe@CN_X, Ag/Fe@CN_X, Cu/Fe@CN_X and Pd/Fe@CN_X were synthesized and screened for HDO of 2-methoxyphenol (Table 1, entries 4–7); the first three gave only trace amounts of desired product, while Pd/Fe@CN_X (Table 1, entry 7) delivered only ~5%, not a practically feasible method. We presumed that the lack of *in situ* hydrogen concentration may be responsible for this sluggish reaction due to the slow dissociation of the formic acid. It became apparent that only the monometallic supported catalyst may not be sufficient for HDO under visible light. Hence, in bio-oil upgrading, it is imperative to increase the degree of dissociation of HCOOH by using Pd in the bimetallic form along with nano-ferrites which is known to ease the hydrodeoxygenation of the lignin-derived component.[34] Accordingly, it is crucial to modify the catalyst by adding and utilizing a booster which speeds up the degradation of formic acid without interfering in the reaction.[44] It has also been reported that bimetallic catalysts show enhanced formic acid decomposition rather than single metallic catalysts presumably due to the charge redistribution between metals which leads to strong adsorption of formate ions *via* back donation.[45] Consequently, bimetallics namely Pd/TiO_2/

Table 1 Reaction optimization for upgrading of guaiacol[a]

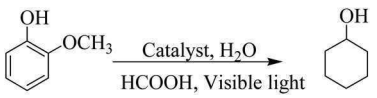

Entry	Catalyst	Time	Yield[b,c]	Conversion[b]
1	$Pd(NO_3)_2$	48 h	—	—
2	$Cu(NO_3)_2$	48 h	—	—
3	AgCl	48 h	—	—
4	TiO_2/Fe@CN_X	48 h	Trace	2%
5	Ag/Fe@CN_X	48 h	Trace	2%
6	Cu/Fe@CN_X	48 h	Trace	2%
7	Pd/Fe@CN_X	48 h	5%	8%
8	Pd/TiO_2/Fe@CN_X	24 h	(90%) 36%	40%
9	Pd–Pt/Fe@CN_X	24 h	(95%) 38%	40%
10	Au–Pd/Fe@CN_X	24 h	(88%) 46%	52%
11	Cu–Pd/Fe@CN_X	24 h	(92%) 55%	60%
12	Co–Pd/Fe@CN_X	24 h	(95%) 62%	65%
13	AgPd/Fe@CN_X	6 h	(>99%) 98%	99%
14[d]	AgPd/Fe@CN_X	24 h	—	—
15[e]	AgPd/Fe@CN_X	24 h	(87%) 35%	40%
16[f]	AgPd/Fe@CN_X	24 h	(93%) 67%	72%

[a] Reaction conditions: Guaiacol (1 mmol), formic acid (5 mmol), catalyst (20 mg), water (1.0 mL), 20 W domestic bulb, room temperature. [b] Conversion and yield are based on GC-MS analysis using *n*-hexadecane (5.0 mmol) as an internal standard. [c] The % in parenthesis indicates the level of selectivity in upgrading of guaiacol. [d] The reaction was performed in the dark at room temperature. [e] The reaction was performed in the dark at 50 °C. [f] The reaction was performed in the dark at 80 °C.

Published on 28 January 2019. Downloaded by US Environmental Protection Agency, Cincinnati on 3/18/2019 2:48:24 PM.

$Fe@CN_X$, Pd–Pt/$Fe@CN_X$, Au–Pd/$Fe@CN_X$, Cu–Pd/$Fe@CN_X$, Co–Pd/$Fe@CN_X$, and AgPd/$Fe@CN_X$ were synthesized and tested for hydrodeoxygenation under visible light (Table 1, entries 8–13). The reaction of guaiacol with Pd/TiO_2/$Fe@CN_X$, Pd–Pt/$Fe@CN_X$, Cu–Pd/$Fe@CN_X$ and Au–Pd/$Fe@CN_X$ gave cyclohexanol in 36%, 38%, 46% and 55% yield, respectively (Table 1, entries 8–10). However, Co–Pd/$Fe@CN_X$ gave a better result as the product yield was 62% after 8 hours of exposure under visible light (Table 1, entry 12). Interestingly, AgPd/$Fe@CN_X$ gave the best result in 98% yield within 6 hours at room temperature (Table 1, entry 13). For better understanding of the photoactivity of the bimetallic AgPd/$Fe@CN_X$ catalyst, the control and thermal experiments were performed in the dark at room temperature (30 °C), 50 °C and 80 °C (Table 1, entries 14–16). The reaction in the dark at room temperature did not give any traces of the product within 24 hours (Table 1, entry 14). Reactions at 50 °C and 80 °C gave cyclohexanol in 35% and 67% yield, respectively, after 24 hours of thermal heating in an oil bath. These experiments show that the bimetallic AgPd/$Fe@CN_X$ catalyst works as a photo-catalyst under visible light irradiation and rather sluggishly under thermal conditions. Moreover, the bimetallic AgPd/Fe/CN_X catalyst has shown higher activity for HDO of guaiacol to cyclohexanol due to the synergistic effect leading to mutual interaction of Ag and Pd nanoparticles with the CN_X support; our claim is corroborated by a report that silver nanoparticles along with palladium atoms significantly enhance the dissociation of formic acid.[45] Undoubtedly, Pd and Ag have proven to be an ideal metallic combination for *in situ* hydrogen generation for upgrading of guaiacol under visible light.

Based on GC-MS analysis outcomes, we have proposed a tentative reaction pathway for the synthesis of cyclohexanol from guaiacol *via* the HDO process. With a careful monitoring of the conversion by GC-MS during 6 hours of the reaction time, the formation of two intermediates namely phenol and cyclohexanone (ESI) was noticed; this has also been recently observed[23] corroborating our proposed mechanism (Fig. 4).

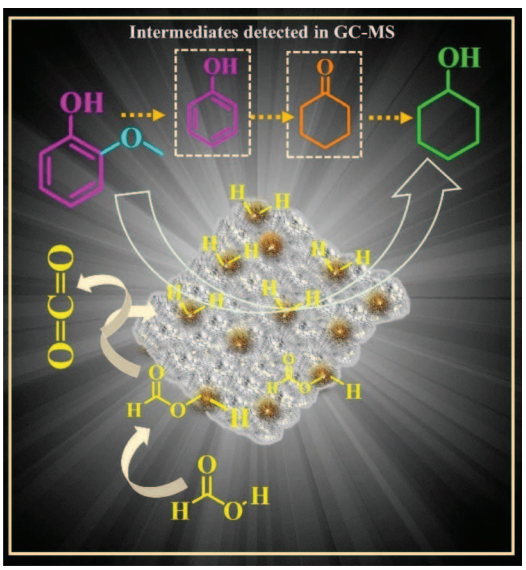

Fig. 4 A tentative reaction pathway for hydrodeoxygenation of guaiacol.

For the industrial application, it is imperative to study the viability, recyclability and stability aspects of the bimetallic AgPd/$Fe@CN_X$ catalyst. Recycling experiments were conducted using guaiacol as the substrate, formic acid as a source of hydrogen and the magnetic AgPd/$Fe@CN_X$ as a catalyst under photochemical conditions. After completion of the reaction, the catalyst was isolated using an external magnet, washed with methanol, dried at 60 °C and recycled for the subsequent HDO reaction of guaiacol. The catalyst was found to be durable and could be reused at least six times without losing its catalytic activity. These recycling experiments confirm that the porous nitrogen enriched CN_X support holds metal nanoparticles firmly *via* non-covalent interactions. This is further supported by the ICP-AES analysis of the mother liquor which does not show any traces of metals; ICP-AES analysis of Fe, Pd and Ag was found to be 4.88%, 2.51% and 2.48% before the reaction and 4.87%, 2.50% and 2.47%, respectively after the six-reaction cycle.

Conclusions

An efficient, sustainable and stable magnetically separable bimetallic AgPd/$Fe@CN_X$ catalyst has been synthesized utilizing an abundant waste material as a support. This heterogeneous catalyst proficiently dehydrogenates formic acid, a renewable chemical hydrogen storage system, to hydrogen and then this *in situ* generated H_2 is utilized for upgrading of lignin-derived bio-oil containing guaiacol, *via* hydrodeoxygenation under visible light irradiation. Furthermore, the bimetallic catalyst shows high reactivity towards dissociation of formic acid to H_2 due to the synergic effect of silver and palladium nanoparticles with nano-ferrites and the nitrogen-enriched carbon nitride support (CN_X), hence, leading to the fast HDO under ambient reaction parameters. The magnetic retrieval quality of AgPd/$Fe@CN_X$ facilitates the catalyst separation during the reaction workup and demonstrates high recyclability with negligible loss of catalytic activity. This highly active catalytic method could be beneficial for the upgrading of renewable lignin to valued components useful in industrial processes.

Conflicts of interest

There are no conflicts of interest to declare.

Notes and references

1 F. H. Isikgor and C. Remzi Becer, *Polym. Chem.*, 2015, **6**, 4497–4559.
2 N.-E. E. Mansouri and J. Salvado, *J. Ind. Crops Prod.*, 2006, **24**, 8–16.
3 M. Besson, P. Gallezot and C. Pinel, *Chem. Rev.*, 2014, **114**, 1827–1870.

 This journal is © The Royal Society of Chemistry 2019

Published on 28 January 2019. Downloaded by US Environmental Protection Agency, Cincinnati on 3/18/2019 2:48:24 PM.

4 W.-J. Liu, W.-W. Li, H. Jiang and H.-Q. Yu, *Chem. Rev.*, 2017, **117**, 6367–6398.
5 G. Fiorentino, M. Ripa and S. Ulgiati, *Biofuels, Bioprod. Biorefin.*, 2017, **11**, 195–214.
6 P. M. Mortensen, J.-D. Grundwaldt, P. A. Jensen, K. G. Knudsen and A. D. Jensen, *Appl. Catal., A*, 2011, **407**, 1–19.
7 P. M. Mortensen, J.-D. Grunwaldt, P. A. Jensen, G. Knudsen and A. D. Jensen, *Catal. Sci. Technol.*, 2014, **4**, 3672–3686.
8 A. Gutierrez, E.-M. Turpeinen, T.-R. Viljava and O. Krause, *Catal. Today*, 2017, **285**, 125–134.
9 Q. Zhang, J. Chang, T. Wang and Y. Xu, *Energy Convers. Manage.*, 2007, **48**, 87–92.
10 P. Mäki-Arvela and D. Yu. Murzin, *Catalysts*, 2017, **7**, 265.
11 E. H. Lee, R. S. Park, H. Kim, S. H. Park, S. C. Jung, J. K. Jeon, S. C. Kim and Y. K. Park, *J. Ind. Eng. Chem.*, 2016, **37**, 18–21.
12 T. Nimmanwudipong, R. C. Runnebaum, D. E. Block and B. C. Gates, *Energy Fuels*, 2011, **25**, 3417–3427.
13 H. Shafaghat, P. S. Sirous Rezaei and W. M. A. W. Daud, *RSC Adv.*, 2015, **5**, 33990–33998.
14 M. T. Musser, Cyclohexanol and Cyclohexanone, in *Ullmann's Encyclopedia of Industrial Chemistry*, Wiley-VCH, Weinheim, 2005.
15 S. Liu, H. Wang, K. J. Smith and C. S. Kim, *Energy Fuels*, 2017, **31**, 6378–6388.
16 S. Boullosa-Eiras, R. Lødeng, H. Bergem, M. Stöcker, L. Hannevold and E. A. Blekkan, *Catal. Today*, 2014, **223**, 44–53.
17 A. H. Zacher, M. V. Olarte, D. M. Santosa, D. C. Elliott and S. B. Jones, *Green Chem.*, 2014, **16**, 491–515.
18 S. K. Kim, D. Yoon, S.-C. Lee and J. Kim, *ACS Catal.*, 2015, **5**, 3292–3303.
19 C. A. Fisk, T. Morgan, Y. Ji, M. Crocker, C. Crofcheck and S. A. Lewis, *Appl. Catal., A*, 2009, **358**, 150–156.
20 P. de Wild, R. Van der Laan, A. Kloekhorst and E. Heeres, *Environ. Prog. Sustainable Energy*, 2009, **28**, 461–469.
21 J. Wildschut, M. Iqbal, F. H. Mahfud, I. M. Cabrera, R. H. Venderbosch and H. J. Heeres, *Energy Environ. Sci.*, 2010, **3**, 962–970.
22 X. Y. Wang and R. Rinaldi, *Energy Environ. Sci.*, 2012, **5**, 8244–8260.
23 M. Zhou, J. Ye, P. Liu, J. Xu and J. Jiang, *ACS Sustainable Chem. Eng.*, 2017, **5**, 8824–8835.
24 Y. Nakagawa, M. Ishikawa, M. Tamura and K. Tomishige, *Green Chem.*, 2014, **16**, 2197–2203.
25 M. Ishikawa, M. Tamura, Y. Nakagawa and K. Tomishige, *Appl. Catal., B*, 2016, **182**, 193–203.
26 G.-Y. Xu, J.-H. Guo, Y.-C. Qu, Y. Zhang, Y. Fu and Q.-X. Guo, *Green Chem.*, 2016, **18**, 5510–5517.
27 M. Kim, J.-M. Ha, K.-Y. Lee and J. Jae, *Catal. Commun.*, 2016, **86**, 113–118.
28 Z. He, M. Hu and X. Wang, *Catal. Today*, 2018, **302**, 136–145.
29 R. S. Varma, *Green Chem.*, 2014, **16**, 2027–2041.
30 S. Verma, R. B. N. Baig, M. N. Nadagouda and R. S. Varma, *ACS Sustainable Chem. Eng.*, 2016, **4**, 1094–1098.
31 S. Verma, R. B. N. Baig, M. N. Nadagouda and R. S. Varma, *Green Chem.*, 2016, **18**, 1327–1331.
32 S. Verma, R. B. Nasir Baig, C. Han, M. N. Nadagouda and R. S. Varma, *Chem. Commun.*, 2015, **51**, 15554–15557.
33 R. S. Varma, *ACS Sustainable Chem. Eng.*, 2016, **4**, 5866–5878.
34 A. K. Singh, S. Jang, J. Y. Kim, S. Sharma, K. C. Basavaraju, M.-G. Kim, K.-R. Kim, J. S. Lee, H. H. Lee and D.-P. Kim, *ACS Catal.*, 2015, **5**, 6964–6972.
35 L. Lin, H. Ou, Y. Zhang and X. Wang, *ACS Catal.*, 2016, **6**, 3921–3931.
36 Y. A. Haleem, Q. He, D. Liu, C. Wang, W. Xu, W. Gan, Y. Zhou, C. Wu, Y. Ding and L. Song, *RSC Adv.*, 2017, **7**, 15390–15396.
37 Q. Guo, Y. Xie, X. Wang, S. Zhang and T. S. Hou, *Chem. Commun.*, 2004, 26–27.
38 C.-B. Cao, Q. Lv and H.-S. Zhu, *Diamond Relat. Mater.*, 2003, **12**, 1070–1074.
39 Y. Zheng, Y. Jiao, Y. Zhu, L. H. Li, Y. Han, Y. Chen, A. Du, M. Jaroniec and S. Z. Qiao, *Nat. Commun.*, 2014, **5**, 1–8.
40 K. Ramesh, M. Prashantha, N. K. Reddy and E. S. R. Gopal, *Integr. Ferroelectr.*, 2010, **117**, 40–48.
41 M. Kim, S. Hwang and J.-S. Yu, *J. Mater. Chem.*, 2007, **17**, 1656–1659.
42 P. Li, E. Y. Jiang and H. L. Bai, *J. Phys. D: Appl. Phys.*, 2011, **44**, 75003.
43 S. Gota, E. Guiot, M. Henriot and M. G. Soyer, *Phys. Rev. B: Condens. Matter Mater. Phys.*, 1999, **60**, 14387.
44 L. Xu, B. Jin, J. Zhang, D.-g. Cheng, F. Chen, Y. An, P. Cui and C. Wan, *RSC Adv.*, 2016, **6**, 46908–46914.
45 K. Tedsree, T. Li, S. Jones, C. W. A. Chan, K. M. K. Yu, P. A. J. Bagot, E. A. Marquis, G. D. W. Smith and S. C. E. Tsang, *Nat. Nanotechnol.*, 2011, **6**, 302–307.
46 S. Verma, M. N. Nadagouda and R. S. Varma, *Sci. Rep.*, 2017, **7**, 13596.

Tetrahedron 73 (2017) 5577–5580

Contents lists available at ScienceDirect

Tetrahedron

journal homepage: www.elsevier.com/locate/tet

Aerobic oxidation of alcohols in visible light on Pd-grafted Ti cluster

Sanny Verma [a,†], R. B. Nasir Baig [a,†], Mallikarjuna N. Nadagouda [b], Rajender S. Varma [a,*]

[a] Sustainable Technology Division, National Risk Management Research Laboratory, U.S. Environmental Protection Agency, MS 443, Cincinnati, OH 45268, USA

[b] WQMB, WSWRD, National Risk Management Research Laboratory, U.S. Environmental Protection Agency, Cincinnati, OH 45268, USA

ARTICLE INFO

Article history:
Received 10 May 2016
Received in revised form 12 July 2016
Accepted 29 July 2016
Available online 30 July 2016

Keywords:
Titanium cluster
Photoactive
Heterogeneous catalysis
Visible light
Aerial oxidation
Palladium nanoparticle

ABSTRACT

The titanium cluster with the reduced band gap has been synthesized having the palladium nanoparticles over the surface, which not only binds to the atmospheric oxygen but also catalyzes the oxidation of alcohols under visible light.

Published by Elsevier Ltd. This is an open access article under the CC BY license (http://creativecommons.org/licenses/by/4.0/).

1. Introduction

The increasing focus on the utilization of visible light energy is due to its abundant nature and its impeccable tolerance towards the environment.[1] Harvesting visible light and performing chemical transformations with it in a concerted process is a high priority chemical research area.[2] Most of the photo-catalysts, especially based on titanium oxide, are active under ultra-violet light (UV);[3] visible light mediated reactions have not received similar attention.[4] There are many photoactive materials available in the literature[4] and a vast majority of them has received casual attention in academic publications due to low activity and/or limited applicability. Titanium-based materials have received maximum consideration as a photoactive material, the major limitation being their wider band gaps, which make it active only under UV irradiation conditions. The activity specific to UV light diminishes its role as a photoactive material, which can utilize solar energy in chemical reactions. Therefore, it becomes imperative to reduce the band gap in titanium materials in order to bring its activity into the visible spectrum of electromagnetic radiation.[5]

Titanium material in combination with metals and other doping elements have been used to reduce the band gap, therefore, sunlight could be utilized for the reaction.[6] Nitrogen doping in titanium oxide has been known to reduce band gap to a great extent.[7] However, the reaction of *N*-doped titanium oxide is uncontrollable in visible light due to its high activity; complete decomposition or mineralization of the organic matter is common occurrence in environmental remediation studies[8] thus rendering this catalyst incongruous in organic synthesis.[9] On the other hand, titanium oxide has been used as a support for the immobilization of transition metals and its application in oxidation chemistry is growing.[10] Hong and co-workers have immobilized palladium and gold combination over the surface of TiO_2 but they lost the ethos of TiO_2 as a photoactive material when the reaction was performed under thermal heating using oxygen atmosphere.[11] In this reaction, gold adsorbs the oxygen in the reaction media and transfers into the reactant via the bimetallic interaction with palladium. The use of titanium oxide becomes irreverent, as its photoactivity has not been utilized. Similarly, Li et al. utilized biosynthesized Au/Pd-TiO_2 supported nanoparticle in the oxidation reaction.[12] We strived to utilize the core property of titanium as photoactive material along with structural modification to create the cluster which can adsorb the atmospheric oxygen and transfer to the reactant in an oxidation process. Accordingly, we prepared nitrogenous titanium cluster, immobilized the palladium to develop photoactive gold-free catalyst, and demonstrated its application in selective oxidation of alcohols; titanium cluster performs the dual task by providing required activation energy and transmitting oxygen in the oxidation step.

* Corresponding author. Fax: +1 513 569 7677; e-mail address: varma.rajender@epa.gov (R.S. Varma).

† Equal contribution.

http://dx.doi.org/10.1016/j.tet.2016.07.070
0040-4020/Published by Elsevier Ltd. This is an open access article under the CC BY license (http://creativecommons.org/licenses/by/4.0/).

2. Result and discussion

In continuation of our desire to develop benign methods for environmental remediation and green synthesis,[13] herein, we report a photoactive palladium-grafted titanium cluster and demonstrated its application in selective oxidation of alcohols to the corresponding carbonyl compounds. Generally, oxidation chemistry is conducted using transition metals along with a supporting co-oxidant.[14] Often, co-oxidants comprise homogenous mix of reagents and catalysts with occasional use of oxygen. However, the utility of oxygen as co-oxidant comes with various detriments that include addition of oxygen absorbing material or metals that can bind oxygen in the reaction such as gold. The main objective here is the adsorption and transmission of the required oxygen for the catalytic process.[15] However, our titanium cluster based catalyst does not require any of these additives and the reaction can be conducted under visible light using oxygen from the atmosphere. The first step in developing the active catalyst was the synthesis of titanium cluster with the significant reduction in the band gap. It has been accomplished by treating titanium (IV) isopropoxide with 4-aminobenzoic acid in isopropanol at 120 °C for 72 h;[16] shiny crystals of titanium clusters ensued which settled down at the bottom of the reaction vessel and were separated by decanting and centrifugation. The Ti-cluster was then suspended in isopropanol and treated with palladium nitrate at 80 °C; palladium salt was reduced and Pd (0) deposited over the cluster. The palladium grafted titanium cluster (Pd@TiC) was separated and its application has been evaluated in the selective oxidation of alcohols (Scheme 1).

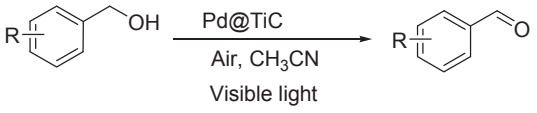

Scheme 1. Pd@TiC catalyzed oxidation of alcohols.

The Pd@TiC catalyst was characterized using scanning electron microscope (SEM) and X-ray diffraction (XRD). The percentage of palladium was determined using inductive coupled plasma atomic emission spectroscopy (ICP-AES) analysis. The SEM images of Ti-cluster and Pd@TiC catalyst illustrate the immobilization of palladium (Pd) nanoparticles (Fig. 1) with the apparent changes in the surface morphology. The immobilization of Pd was further established by XRD (Fig. 2) and the concentration confirmed to be 4.88% by ICP-AES analysis.

The activity of Pd@TiC was evaluated in the aerial oxidation of alcohols under visible light irradiation with benzyl alcohol as a model substrate. The preliminary results obtained during the screening and reaction optimization are summarized in Table 1. The

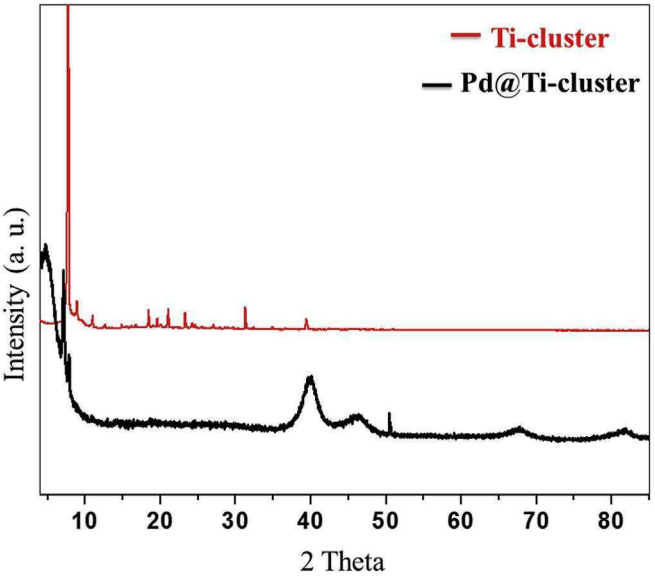

Fig. 2. XRD of Ti-Cluster and Pd@TiC.

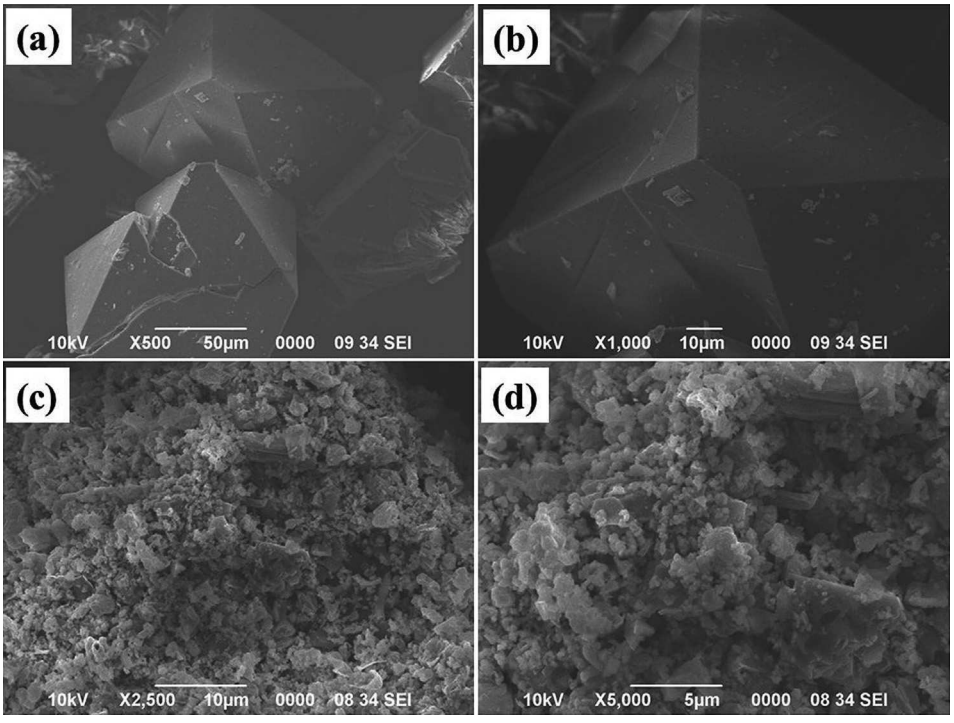

Fig. 1. SEM images of Ti-Cluster (a) Pyramid-like structure and (b) Close view of pyramid; (c) and (d) SEM images of Pd@TiC.

Table 1
Results of screening experiments[a]

Entry	Solvent	Time	Yield[b]
1	H_2O	12 h	45%
2	Toluene	12 h	48%
3	DMF	12 h	16%
4	CH_3CN	8 h	97%

[a] Reaction conditions: Benzyl alcohol (1 mmol), Pd@TiC (25 mg), Solvent (2 mL), 20 W domestic bulb, Air.
[b] Isolated yields.

reaction outcome in different solvents clearly indicate that acetonitrile is the best solvent for this reaction as it gives quantitative yield of the desired product; conventionally used polar solvents (water and DMF) and non-polar solvent (toluene) were in effective in the visible light mediated aerial oxidation of alcohol.

After uncovering the appropriate conditions, the scope of the developed Pd@TiC catalyst was studied in the oxidation of a wide range of alcohols and the results are depicted in Table 2. They clearly demonstrate the excellent activity and selectivity towards the formation of corresponding carbonyl compounds (Table 2; entries 1–8) where electron donating and electron with drawing substituents apparently have trifling effect on the rate of the reaction (Table 2, entries 2–4). The secondary alcohols and heterocyclic alcoholic derivatives were also readily converted to corresponding carbonyl derivatives (Table 2, entries 5–8). The important feature of this reaction was the use of aerial oxygen and solar energy to accomplish the oxidation of alcohol without the formation of any by-product, which is an unprecedented finding.

Table 2
Pd@TiC catalyzed oxidation of alcohols[a]

Entry	Substrate	Product	Yield[b]
1	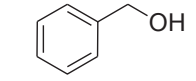	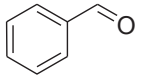	97%
2	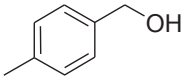	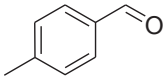	95%
3	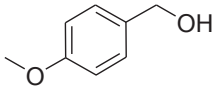	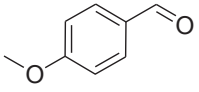	96%
4	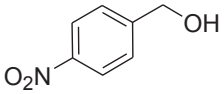	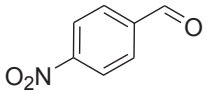	96%
5	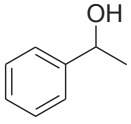	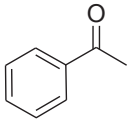	94%
6	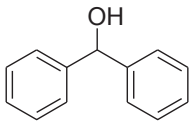	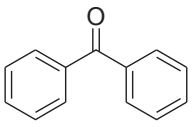	94%
7	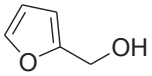	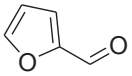	97%
8	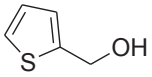	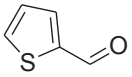	97%

[a] Reaction conditions: Substrate (1 mmol), Pd@TiC (25 mg), CH_3CN (2 mL), 20 W domestic bulb, Air, 8 h.
[b] Isolated yield.

3. Conclusion

We have demonstrated the synthesis of highly dispersed palladium nanoparticles grafted on titanium cluster. The developed Pd@TiC catalyst is found to be a highly effective in the aerial oxidation of alcohols under visible light and its activity is attributed to the reduced band gap, which makes it active under visible light thus harnessing solar energy for the chemical reactions. The Pd@TiC is found to be highly stable and could be recycled several times without any loss in its activity. The most important feature of this catalyst is its ability to bind with the atmospheric oxygen which serves as an oxidant in the reaction cycle.

4. Experimental section

4.1. Synthesis of Pd@TiC catalyst

Titanium (IV) isopropoxide (0.518 mL) was added to a solution of 4-aminobenzoic acid (0.96 g, 7.0 mmol) in 2-propanol (30.0 mL). The reaction mixture was stirred at room temperature for 30 min; an orange-colored slurry was obtained. The slurry was heated at 120 °C for 72 h in a pressure reactor when bright yellow crystals of titanium cluster ensued. The catalyst was isolated by decanting and centrifugation, washed with 2-propanol and dried under vacuum for 2 h. The Ti cluster (100 mg) was then suspended in isopropanol (10 mL) and treated with palladium nitrate (5 mol %) at 80 °C. 2-propanol reduced the Pd metal into Pd-nanoparticle which were deposited over the titanium cluster. The palladium nanoparticle grafted titanium cluster (Pd@TiC) was isolated and characterized using SEM, XRD, and ICP-AES.

4.2. General procedure for the oxidation of alcohols

A 10 mL side-armed round bottomed flask equipped with a magnetic stirring bar and a balloon filled with air was charged with alcohol (1 mmol), catalyst Pd@TiC (25 mg) and acetonitrile (2 mL). The reaction mixture was exposed to visible light irradiation using 20 W domestic bulb (Fig. 3) and the progress of reaction was monitored using TLC. After the completion of the reaction, the Pd@TiC catalyst was separated using a centrifuge and the product was isolated by extracting with ethyl acetate, dried over sodium sulfate, concentrated under reduced pressure and characterized.

Fig. 3. Pictorial representation of the reaction set-up.

4.3. Recycling of Pd@TiC

A set of experiments were performed using benzyl alcohol as a model substrate in acetonitrile solvent. After the completion of each reaction, the Pd@TiC catalyst was recovered using a centrifuge, washed with methanol and reused for the oxidation of fresh batch of benzyl alcohol. The Pd@TiC catalyst could be recycled and reused up to six times without any loss in its activity (Table 3). The metal leaching in reaction with Pd@TiC was examined by ICP-AES analysis before and after the completion of reaction; concentration of palladium was found to be 4.88% before the reaction and 4.87% after the sixth cycle. The ICP-AES of the mother liquor did not show the presence of palladium confirming the fact that titanium cluster holds the Pd nanoparticles tightly.

Table 3
Recycling of Pd@TiC catalyst in the oxidation of benzyl alcohol[a]

Run	1	2	3	4	5	6
Isolated yield	97%	97%	97%	97%	96%	96%

[a] Reaction conditions: Benzyl alcohol (1 mmol), Pd@TiC (25 mg), CH_3CN (2 mL), 20 W domestic bulb, Air.

The SEM image of the Pd@TiC before and after the reaction confirms that there is no significant change in the morphology of the catalyst, which signifies high stability of Pd@TiC during the course of the reaction (Fig. 4).

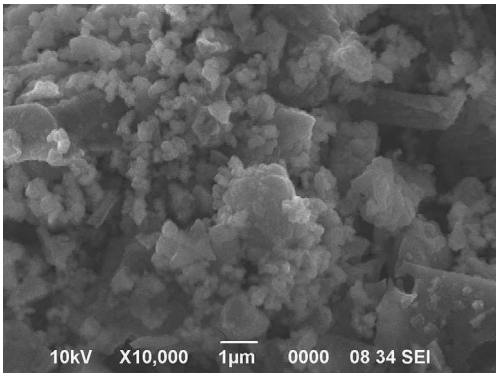

Fig. 4. SEM image of the recycled Pd@TiC.

Disclaimer

The views expressed in this article are those of the authors and do not necessarily represent the views or policies of the U.S. Environmental Protection Agency. Any mention of trade names or commercial products does not constitute endorsement or recommendation for use.

Acknowledgements

SV and RBNB were supported by the Postgraduate Research Program at the National Risk Management Research Laboratory administered by the Oak Ridge Institute for Science and Education through an interagency agreement between the U.S. Department of Energy and the U.S. Environmental Protection Agency.

Supplementary data

Supplementary data associated with this article can be found in the online version, at http://dx.doi.org/10.1016/j.tet.2016.07.070.

References and notes

1. Bita, C. E.; Gerats, T. *Front. Plant Sci.* **2013**, *4*, 273.
2. Li, L.; Zhang, S.; Xu, L.; Wang, J.; Shi, L.-X.; Chen, Z.-N.; Honga, M.; Luo, J. *Chem. Sci.* **2014**, *5*, 3808.
3. Kumar, S. G.; Devi, L. G. *J. Phys. Chem. A* **2011**, *115*, 13211.
4. (a) Prier, C. K.; Rankic, D. A.; MacMillan, D. W. C. *Chem. Rev.* **2013**, *113*, 5322; (b) Kanhere, P.; Chen, Z. *Molecules* **2014**, *19*, 19995.
5. (a) Schneider, J.; Matsuok, M.; Takeuchi, M.; Zhang, J.; Horiuchi, Y.; Anpo, M.; Bahnemann, D. W. *Chem. Rev.* **2014**, *114*, 9919; (b) Colmenares, J. C.; Lisowski, P.; Łomot, D.; Chernyayeva, O.; Lisovytskiy, D. *ChemSusChem* **2015**, *8*, 1676.
6. Zaleska, A. *Recent Pat. Eng.* **2008**, *2*, 157.
7. Cong, Y.; Zhang, J.; Chen, F.; Anpo, M. *J. Phys. Chem. C* **2007**, *111*, 6976.
8. Asahi, R.; Morikawa, T.; Irie, H.; Ohwaki, T. *Chem. Rev.* **2014**, *114*, 9824.
9. Yang, G.; Jiang, Z.; Shi, H.; Xiao, T.; Yan, Z. *J. Mater. Chem.* **2010**, *20*, 5301.
10. Bagheri, S.; Julkapli, N. M.; Bee, S.; Hamid, A. *Sci. World J.* **2014**, *2014*, 727496.
11. Chang, J. B.; Liu, C. H.; Liu, J.; Zhou, Y. Y.; Gao, X.; Wang, S. D. *Nano-Micro Lett.* **2015**, *7*, 307.
12. Hong, Y.; Jing, X.; Huang, J.; Sun, D.; Odoom-Wubah, T.; Yang, F.; Du, M.; Li, Q. *ACS Sustain. Chem. Eng.* **2014**, *2*, 1752.
13. (a) Varma, R. S. *Green Chem.* **2014**, *16*, 2027; (b) Verma, S.; Mungse, H. P.; Kumar, N.; Choudhary, S.; Jain, S. L.; Sain, B.; Khatri, O. P. *Chem. Commun.* **2011**, 12673; (c) Nasir Baig, R. B.; Varma, R. S. *Green Chem.* **2013**, *15*, 1839; (d) Verma, S.; Singh, R.; Tripathi, D.; Gupta, P.; Bahuguna, G. M.; Jain, S. L. *RSC Adv.* **2013**, *3*, 4184; (e) Nasir Baig, R. B.; Varma, R. S. *ACS Sustain. Chem. Eng.* **2014**, *2*, 2155; (f) Nasir Baig, R. B.; Nadagouda, M. N.; Varma, R. S. *Green Chem.* **2014**, *16*, 4333.
14. (a) Verma, S.; Nasir Baig, R. B.; Nadagouda, M. N.; Varma, R. S. *ACS Sustain. Chem. Eng.* **2016**, *4*, 2333; (b) Verma, S.; Baig, R. B. N.; Han, C.; Nadagouda, M. N.; Varma, R. S. *Green Chem.* **2015**, *18*, 251; (c) Verma, S.; Baig, R. B. N.; Nadagouda, M. N.; Varma, R. S. *ACS Sustain. Chem. Eng.* **2016**, *4*, 1094; (d) Verma, S.; Verma, D.; Sinha, A. K.; Jain, S. L. *Appl. Catal. A Gen.* **2015**, *489*, 17; (e) Verma, S.; Aila, M.; Kaul, S.; Jain, S. L. *RSC Adv.* **2014**, *4*, 30598; (f) Verma, S.; Bras, J. Le; Jain, S. L.; Muzart, J. *Appl. Catal. A Gen.* **2013**, *468*, 334; (g) Mungse, H. P.; Verma, S.; Kumar, N.; Sain, B.; Khatri, O. P. *J. Mater. Chem.* **2012**, *22*, 5427.
15. (a) Pina, C. D.; Falletta, E. *Catal. Sci. Technol.* **2011**, *1*, 1564; (b) Biella, S.; Prati, L.; Rossi, M. *J. Mol. Catal. A Chem.* **2003**, *197*, 207.
16. (a) Yuan, S.; Liu, T. F.; Feng, D.; Tian, J.; Wang, K.; Qin, J.; Zhang, Q.; Chen, Y. P.; Bosch, M.; Zou, L.; Teat, S. J.; Dalgarno, S. J.; Zhou, H. C. *Chem. Sci.* **2015**, *6*, 3926; (b) Feng, D.; Wang, K.; Wei, Z.; Chen, Y.-P.; Simon, C. M.; Arvapally, R. K.; Martin, R. L.; Bosch, M.; Liu, T.-F.; Fordham, S.; Yuan, D.; Omary, M. A.; Haranczyk, M.; Smit, B.; Zhou, H.-C. *Nat. Commun.* **2014**, *5*, 5723.

From: Nasir Baig
To: Nadagouda, Mallikarjuna
Subject: Paper contribution
Date: Tuesday, April 28, 2020 12:50:30 PM

Title of paper:

Sanny Verma, R. B. Nasir Baig, M. N. Nadagouda and R. S. Varma "Aerobic oxidation of alcohols in visible light on Pd-grafted Ti cluster" *Tetrahedron* **2017**, *73*, 5577-5580. **(IF= 2.645; immediacy index= 0.65; Citation half-life= 9.20; citations= 19)**

Acknowledgment/ Confirmation: I, Dr. Nasir Baig was part of the research of the above publication and my contribution for this publication can be valued at 10%

best regards

Nasir

--

From: Nadagouda, Mallikarjuna
To: Nadagouda, Mallikarjuna
Date: Wednesday, April 29, 2020 1:32:18 PM

My contribution to the below publications is 55 % each.

1. Sanny Verma, M. N. Nadagouda and R. S. Varma "Visible light-mediated and water-assisted selective hydrodeoxygenation of lignin-derived guaiacol to cyclohexanol" *Green Chem.* **2019**,*21*, 1253-1257. **(IF= 9.405; immediacy index= 2.24; Citation half-life= 4.10; citations= 5)**

From the themed collection: **Green Biorefinery Technologies based on Waste Biomass**

2) Sanny Verma, R. B. Nasir Baig, M. N. Nadagouda and R. S. Varma "Aerobic oxidation of alcohols in visible light on Pd-grafted Ti cluster" *Tetrahedron* **2017**, *73*, 5577-5580. **(IF= 2.645; immediacy index= 0.65; Citation half-life= 9.20; citations= 19)**

Mallikarjuna N. Nadagouda Ph.D.
U. S. Environmental Protection Agency
ORD, Center for Environmental Solutions and Emergency Response
Water Infrastructure Division/ Chemical Methods and Treatment Branch
26 West, Martin Luther King Drive, MS 689, Cincinnati, OH 45268 USA
E-mail: Nadagouda.mallikarjuna@epa.gov
Ph: (513)569-7232

From: Rajender Varma
To: Nadagouda, Mallikarjuna
Subject: My contribution to papers submitted for STAA award-from Rajender Varma
Date: Monday, April 27, 2020 7:57:09 PM

Dear Dr. Nadagouda,

I confirm that my contribution is 20% for each paper listed here and being submitted for the STAA award:

1. Sanny Verma, M. N. Nadagouda and R. S. Varma "Visible light-mediated and water-assisted selective hydrodeoxygenation of lignin-derived guaiacol to cyclohexanol" *Green Chem.* **2019**,*21*, 1253-1257. **(IF= 9.405; immediacy index= 2.24; Citation half-life= 4.10; citations= 5)**

From the themed collection: **Green Biorefinery Technologies based on Waste Biomass**

2. Sanny Verma, R. B. Nasir Baig, M. N. Nadagouda and R. S. Varma "Aerobic oxidation of alcohols in visible light on Pd-grafted Ti cluster" *Tetrahedron* **2017**, *73*, 5577-5580. **(IF= 2.645; immediacy index= 0.65; Citation half-life= 9.20; citations= 19)**

Raj

Rajender S. Varma, Ph.D.
U. S. Environmental Protection Agency
ORD, Center for Environmental Solutions and Emergency Response
Water Infrastructure Division/ Chemical Methods and Treatment Branch
26 West Martin Luther King Drive, MS 483
Cincinnati, Ohio 45268, USA

Tel: (513)-487-2701

e-mail: Varma.Rajender@epa.gov

(Highly Cited Researchers 2016, 18, 19; Publons Awardee 2018, 19)

Google Scholar: *https://scholar.google.com/citations?user=kzbCKOQAAAAJ&hl=en*

Research Gate: https://www.researchgate.net/profile/Rajender_Varma/info

Published on 28 January 2019. Downloaded by US Environmental Protection Agency, Cincinnati on 3/18/2019 2:48:24 PM.

Green Chemistry

COMMUNICATION

View Article Online
View Journal | View Issue

Check for updates

Cite this: *Green Chem.*, 2019, **21**, 1253

Received 17th December 2018,
Accepted 28th January 2019

DOI: 10.1039/c8gc03951h

rsc.li/greenchem

Visible light-mediated and water-assisted selective hydrodeoxygenation of lignin-derived guaiacol to cyclohexanol†

Sanny Verma,[a] Mallikarjuna N. Nadagouda[b] and Rajender S. Varma *[c]

A magnetically separable bimetallic AgPd/Fe@CN_x catalyst has been synthesized and utilized for upgrading of lignin-derived guaiacol to cyclohexanol *via* hydrodeoxygenation using formic acid as a source of hydrogen under visible light irradiation. A nitrogen-enriched carbonaceous material, carbon nitride (CN_x), is obtained *via* calcination of chitosan, a marine-derived abundant waste material and subsequently utilized as a support for the immobilization of nanoferrites and silver and palladium nanoparticles. Hydrogen generation from renewable sources such as formic acid and its ideal utilization for the upgrading of biomass-derived guaiacol are the main findings. The synergetic effect of Ag and Pd on the CN_x support enhances the decomposition of formic acid which is aptly utilized for the selective defunctionalization of guaiacol at ambient pressure.

Introduction

The lignocellulosic biomass is abundant and does not affect the food chain.[1] It has mostly been used in the Kraft process to produce pulp and paper[2] wherein energy is produced by the conventional burning of lignin and hemicellulosic residues in black liquor. However, for more efficient and ideal utilization of lignin and hemicellulose fractions of biomass, innovative methods and technologies are sought. Due to the depletion of fossil-based feedstock and striving for carbon-neutral fuels/chemicals, biomass transformations have been investigated intensively.[3–5] Thus, transportation fuel (bio-oil) has been produced *via* flash pyrolysis of biomass in the temperature range of 300–600 °C where lignin fractions have been utilized to produce valued products and fuels.[6]

[a]*Oak Ridge Institute for Science and Education, P. O. Box 117, Oak Ridge, TN, 37831, USA*
[b]*Department of Mechanical and Materials Engineering, Wright State University, Dayton, Ohio 45324, USA*
[c]*Regional Centre of Advanced Technologies and Materials, Department of Physical Chemistry, Faculty of Science, Palacky University, Šlechtitelů 27, 783 71 Olomouc, Czech Republic. E-mail: varma.rajender@epa.gov*
† Electronic supplementary information (ESI) available. See DOI: 10.1039/c8gc03951h

However, bio-oils are highly viscous, corrosive, and acidic (pH = 2.8–3.8) and show low thermal stability due to the presence of oxygen-containing moieties such as phenols, aldehydes, and acids.[7,8] Typically, bio-oils contain 40 wt% oxygen, which necessitates upgrading by transformations of aromatic or naphthenic hydrocarbons *via* the hydrodeoxygenation (HDO) reaction.[9] Catalytic HDO has been proficiently employed for the improvement of product heating value and upgrading of bio-oils as it reduces the oxygen content, especially aromatic $-OCH_3$ and –OH containing scaffolds typified by guaiacol.[10]

Guaiacol (2-methoxyphenol), a lignin-derived model molecule and a typical bio-oil component, can be upgraded to cyclohexanol *via* the hydrodeoxygenation (HDO) process.[11–13] Cyclohexanol has various industrial applications where it can be used as a solvent, or utilized in the synthesis of cyclohexanone and polymers.[14] Due to the presence of stable hydroxyl and methoxyl groups on the aromatic ring in guaiacol, simple hydrogenation is inadequate for the synthesis of cyclohexanol.[15] Hence, the selective removal of the methoxyl group and hydrogenation of the aromatic ring are required for conversion to cyclohexanol. Hitherto, HDO of guaiacol has been investigated using noble catalysts (Pd, Pt, and Ru), conventional hydrotreating sulfide catalysts (CoMoS and NiMoS) and solid acids which lead to hydrogenated oxygen containing compounds namely cyclohexanol and phenol,[16–21] besides fully hydrogenated hydrocarbons such as cyclohexane and benzene.[15]

Wang and Rinaldi developed a protocol for the HDO of bio-oil derived phenolic compounds to cyclohexanols using RANEY®@Ni catalyst at 120 °C with isopropanol as a hydrogen donor.[22] Recently, Jiang *et al.* developed the HDO of guaiacol with cyclohexanol as the primary product in aqueous medium over bimetallic Ni and Co catalysts on γ-Al_2O_3 and ZSM-5 supports.[23] Nakagawa *et al.* reported that the presence of MgO in combination with Ru/C promotes demethoxylation, and hence, increases transformation of guaiacol to cyclohexanol with 80% yield at 160 °C and 1.5 MPa hydrogen pressure.[24] However, basic MgO is not stable in aqueous media although the base helps in demethoxylation and diminishes the unselective

Published on 28 January 2019. Downloaded by US Environmental Protection Agency, Cincinnati on 3/18/2019 2:48:24 PM.

C–O bond dissociation during the HDO process. Tomishige *et al.* developed the Ru–Mn combination for the selective exclusion of the methoxyl group on the substituted phenol to give cyclohexanol with 81% yield at elevated temperature and under hydrogen pressure.[25] Recently, Zhang *et al.* reported the selective conversion of guaiacol to cyclohexanol in water using a metal-solid base bifunctional Ru/ZrO_2-$La(OH)_3$ catalyst at 170 °C and 4 MPa hydrogen pressure in an autoclave.[26] However, the aforementioned reports require high hydrogen pressure, elevated temperature and a prolonged reaction time. Hence, the development of a new efficient catalytic system is still needed to convert guaiacol to cyclohexanol with high stability and selectivity.[27,28]

In continuation of our efforts towards the development of sustainable protocols using heterogeneous catalysts,[29–33] herein, we report a magnetically separable bimetallic AgPd catalyst supported on marine waste chitosan-derived nitrogen-enriched carbon nitride (CN_x), AgPd/Fe@CN_X; the catalyst generates hydrogen from formic acid which can be utilized *in situ* for the selective hydrodeoxygenation of lignin-derived guaiacol under visible light irradiation at ambient pressure.

Synthesis and characterization

Firstly, a nitrogen-enriched carbon nitride support (CN_x) was obtained by the calcination of chitosan at 600 °C for 4 hours under a nitrogen atmosphere. Then, it was dispersed in water for 3 hours using sonication. An aqueous solution of $FeSO_4$ (500 mg in 100 mL) was added dropwise at room temperature to the mixture of CN_x and stirred for 2 hours.[32] A solution of $AgNO_3$ (0.5 mM, in 25 mL water) and $Pd(NO_3)_2$ (0.5 mM, in 25 mL water) was added to the colloidal solution at room temperature and the reaction mixture was further stirred for 4 hours. 1.0 g sodium borohydride ($NaBH_4$) was added, in portions, at 50 °C to reduce the iron sulfate, Ag(I) and Pd(II) to magnetic ferrites, Ag(0) and Pd(0), respectively. This reaction mixture was stirred for the next 12 hours. The ensuing black colored solid was isolated as AgPd/Fe@CN_X using an external magnet, washed with methanol and finally dried at 60 °C under vacuum.[32,34] The obtained AgPd/Fe@CN_X composite powder was further analyzed by various instrumental techniques such as X-ray diffraction (XRD), scanning electron microscopy (SEM), transmission electron microscopy (TEM), X-ray photoelectron spectroscopy (XPS), Brunauer–Emmett–Teller (BET) surface area analysis, FT-IR and inductively coupled plasma atomic emission spectroscopy (ICP-AES). SEM analysis of the CN_X support and AgPd/Fe@CN_X catalyst showed visual differences in images and confirmed the immobilization of silver (Ag), palladium (Pd) nanoparticles and nano-ferrites over the surface of nitrogen-enriched carbon nitride (Fig. 1a and b). TEM analysis validates the formation of single phase Ag nanoparticles, Pd nanoparticles and nano-ferrites with irregular shaped particles in the size range of 10–15 nm (Fig. 1c and d) which is further supported by EDX and SAED analysis of the bimetallic AgPd/Fe@CN_X catalyst (Fig. 2a and b).

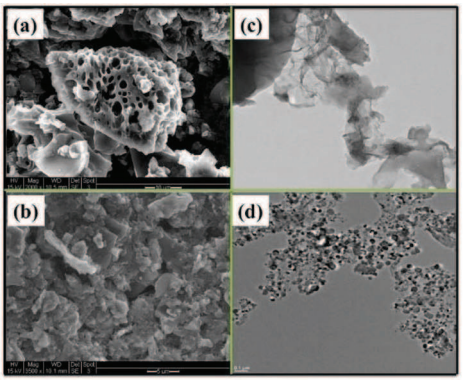

Fig. 1 (a) SEM image of CN_X; (b) SEM image of AgPd/Fe@CN_X; (c) TEM image of CN_X; (d) TEM image of AgPd/Fe@CN_X.

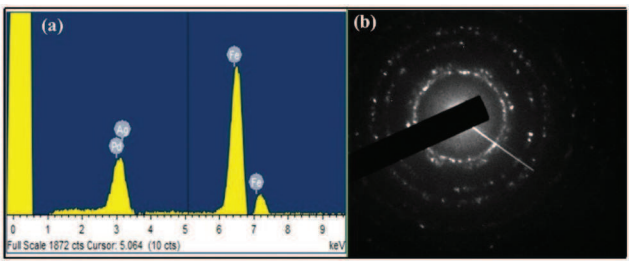

Fig. 2 (a) EDX analysis of AgPd/Fe@CN_X; (b) SAED image of AgPd/Fe@CN_X.

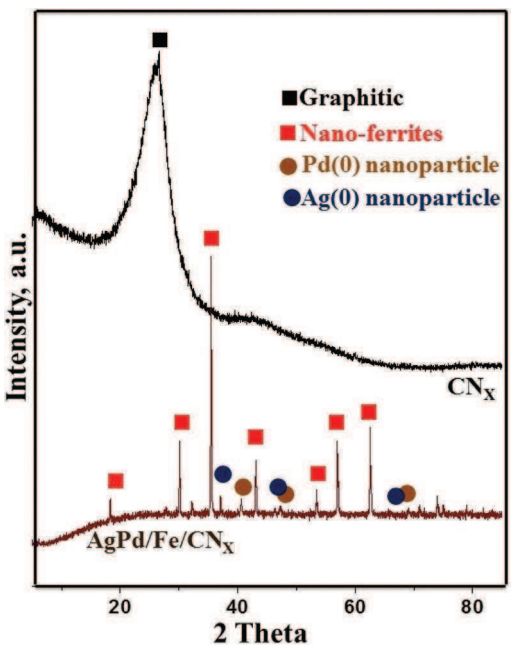

Fig. 3 XRD pattern of CN_X and AgPd/Fe@CN_X.

The XRD and XPS analysis also authenticated the formation of metallic silver and palladium nanoparticles along with nano-ferrites over the CN_X support (Fig. 3 and ESI; Fig. S5†).

 This journal is © The Royal Society of Chemistry 2019

Published on 28 January 2019. Downloaded by US Environmental Protection Agency, Cincinnati on 3/18/2019 2:48:24 PM.

Fig. 3 depicts the XRD patterns of CN_X and the carbon nitride immobilized bimetallic AgPd/Fe@CN_X catalyst. The nitrogen-enriched carbon nitride displayed a diffraction peak at 26.51° which corresponds to the graphitic peak.[46] Loading of metal nanoparticles leads to the disappearance of the diffraction peak at 26.51°. The observed peaks at 5.56°, 27.78°, and 43.01°, respectively, represent the (100), (110), and (210) Bragg reflection as compared with JCPDS standards (00-050-1250) which confirmed the presence of the carbon nitride (CN_X) support. Additionally, the XRD pattern of AgPd/Fe@CN_X corroborated that the bimetallic catalyst was enriched with FeO/Fe_2O_3 [2Θ = 18.21° (111), 30.11° (220), 35.36° (311), 43.16° (400), 53.56° (422), 62.79° (440); JCPDS#00-065-0731], Ag [2Θ = 38.1° (111), 44.27° (200), 64.42° (220); JCPDS#00-004-0783] and Pd [2Θ = 40.11° (111), 46.66° (200), 68.08° (220); JCPDS#00-005-068] nanoparticles (ESI; Fig. S3†). Although the intensity of silver and palladium nanoparticles is not high, their presence has been further confirmed by XPS, EDX and ICP-AES analysis.

A high resolution XPS analysis of CN_X and AgPd/Fe@CN_X was performed (ESI; Fig. S4–S9†). The XPS analysis of the CN_X support resembles the formation of tri-*s*-triazine-based graphitic carbon nitride.[35,36] In the C 1S spectrum, the peak at 284.7 eV (1s–π*C═C) is attributed to a typical transition of graphite and confirms the presence of graphitic carbon in good agreement with the literature.[37,38] The peak at 288.1 eV (1s–π* C–N–C) is ascribed to the characteristic resonance of nitrogen atoms bonded with two carbon atoms in *s*-triazine.[39] In the N 1S spectrum, the signal at 398.5 eV is ascribed to sp^2 nitrogen atoms having two carbon neighboring atoms (–N–C coordination in one tri-*s*-triazine unit) and that at 400.8 eV is attributed to sp^2 nitrogen atoms surrounded by three carbon atoms (N–3C bridging between three tri-*s*-triazine moieties).[40,41] The XPS analysis of AgPd/Fe@CN_X (ESI; Fig. S5†) showed the formation of Pd and Ag nanoparticles on the surface of carbon nitride (CN_X). Two peaks were observed, first one at 338.0 eV with a shoulder at 339.0 eV and the second one at 343.3 eV with a shoulder at 344.8 eV. These peaks were the result of Pd $3d_{5/2}$ and Pd $3d_{3/2}$ (ESI; Fig. S9(e)†). The XPS peaks at 367.9 eV and 373.8 eV could be credited to Ag $3d_{5/2}$ and Ag $3d_{3/2}$ confirming the presence of silver in the zero oxidation state (ESI; Fig. S8(d)†).[31] It is specified in the literature that the binding energy of the metal increases with the increase in the oxidation state; hence, the binding energy at 710.8 eV corresponds to Fe $2p_{3/2}$ in Fe^{2+} in the form of FeO. The satellite peak at 718.1 eV is a characteristic peak of Fe^{3+} in γ-Fe_2O_3, confirming that the catalyst is a combination of FeO/γ-Fe_2O_3 (ESI; Fig. S9(f)†).[42,43] Furthermore, the presence of Pd and Ag was analyzed using ICP-AES and their contents were found to be Pd (2.51%) and Ag (2.48%).

Results and discussion

To upgrade guaiacol, a model component of lignin-derived bio-oil, *via* selective hydrodeoxygenation, a series of catalysts were assessed for *in situ* generation of hydrogen from formic acid under visible light. For this transformation, an array of mono- and bi-metallic catalysts were synthesized on the magnetic nano-ferrite supported nitrogen enriched CN_X support (Table 1). Commercially available homogeneous catalysts such as $Pd(NO_3)_2$, $Cu(NO_3)_2$ and AgCl are ineffective even after 24 hours of exposure (Table 1, entries 1–3). Monometallic TiO_2/Fe@CN_X, Ag/Fe@CN_X, Cu/Fe@CN_X and Pd/Fe@CN_X were synthesized and screened for HDO of 2-methoxyphenol (Table 1, entries 4–7); the first three gave only trace amounts of desired product, while Pd/Fe@CN_X (Table 1, entry 7) delivered only ~5%, not a practically feasible method. We presumed that the lack of *in situ* hydrogen concentration may be responsible for this sluggish reaction due to the slow dissociation of the formic acid. It became apparent that only the monometallic supported catalyst may not be sufficient for HDO under visible light. Hence, in bio-oil upgrading, it is imperative to increase the degree of dissociation of HCOOH by using Pd in the bimetallic form along with nano-ferrites which is known to ease the hydrodeoxygenation of the lignin-derived component.[34] Accordingly, it is crucial to modify the catalyst by adding and utilizing a booster which speeds up the degradation of formic acid without interfering in the reaction.[44] It has also been reported that bimetallic catalysts show enhanced formic acid decomposition rather than single metallic catalysts presumably due to the charge redistribution between metals which leads to strong adsorption of formate ions *via* back donation.[45] Consequently, bimetallics namely Pd/TiO_2/

Table 1 Reaction optimization for upgrading of guaiacol[a]

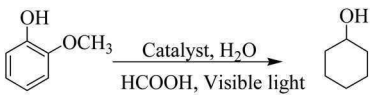

Entry	Catalyst	Time	Yield[b,c]	Conversion[b]
1	$Pd(NO_3)_2$	48 h	—	—
2	$Cu(NO_3)_2$	48 h	—	—
3	AgCl	48 h	—	—
4	TiO_2/Fe@CN_X	48 h	Trace	2%
5	Ag/Fe@CN_X	48 h	Trace	2%
6	Cu/Fe@CN_X	48 h	Trace	2%
7	Pd/Fe@CN_X	48 h	5%	8%
8	Pd/TiO_2/Fe@CN_X	24 h	(90%) 36%	40%
9	Pd–Pt/Fe@CN_X	24 h	(95%) 38%	40%
10	Au–Pd/Fe@CN_X	24 h	(88%) 46%	52%
11	Cu–Pd/Fe@CN_X	24 h	(92%) 55%	60%
12	Co–Pd/Fe@CN_X	24 h	(95%) 62%	65%
13	AgPd/Fe@CN_X	6 h	(>99%) 98%	99%
14[d]	AgPd/Fe@CN_X	24 h	—	—
15[e]	AgPd/Fe@CN_X	24 h	(87%) 35%	40%
16[f]	AgPd/Fe@CN_X	24 h	(93%) 67%	72%

[a] Reaction conditions: Guaiacol (1 mmol), formic acid (5 mmol), catalyst (20 mg), water (1.0 mL), 20 W domestic bulb, room temperature. [b] Conversion and yield are based on GC-MS analysis using *n*-hexadecane (5.0 mmol) as an internal standard. [c] The % in parenthesis indicates the level of selectivity in upgrading of guaiacol. [d] The reaction was performed in the dark at room temperature. [e] The reaction was performed in the dark at 50 °C. [f] The reaction was performed in the dark at 80 °C.

Published on 28 January 2019. Downloaded by US Environmental Protection Agency, Cincinnati on 3/18/2019 2:48:24 PM.

$Fe@CN_X$, Pd–Pt/$Fe@CN_X$, Au–Pd/$Fe@CN_X$, Cu–Pd/$Fe@CN_X$, Co–Pd/$Fe@CN_X$, and AgPd/$Fe@CN_X$ were synthesized and tested for hydrodeoxygenation under visible light (Table 1, entries 8–13). The reaction of guaiacol with Pd/TiO_2/$Fe@CN_X$, Pd–Pt/$Fe@CN_X$, Cu–Pd/$Fe@CN_X$ and Au–Pd/$Fe@CN_X$ gave cyclohexanol in 36%, 38%, 46% and 55% yield, respectively (Table 1, entries 8–10). However, Co–Pd/$Fe@CN_X$ gave a better result as the product yield was 62% after 8 hours of exposure under visible light (Table 1, entry 12). Interestingly, AgPd/$Fe@CN_X$ gave the best result in 98% yield within 6 hours at room temperature (Table 1, entry 13). For better understanding of the photoactivity of the bimetallic AgPd/$Fe@CN_X$ catalyst, the control and thermal experiments were performed in the dark at room temperature (30 °C), 50 °C and 80 °C (Table 1, entries 14–16). The reaction in the dark at room temperature did not give any traces of the product within 24 hours (Table 1, entry 14). Reactions at 50 °C and 80 °C gave cyclohexanol in 35% and 67% yield, respectively, after 24 hours of thermal heating in an oil bath. These experiments show that the bimetallic AgPd/$Fe@CN_X$ catalyst works as a photo-catalyst under visible light irradiation and rather sluggishly under thermal conditions. Moreover, the bimetallic AgPd/Fe/CN_X catalyst has shown higher activity for HDO of guaiacol to cyclohexanol due to the synergistic effect leading to mutual interaction of Ag and Pd nanoparticles with the CN_X support; our claim is corroborated by a report that silver nanoparticles along with palladium atoms significantly enhance the dissociation of formic acid.[45] Undoubtedly, Pd and Ag have proven to be an ideal metallic combination for *in situ* hydrogen generation for upgrading of guaiacol under visible light.

Based on GC-MS analysis outcomes, we have proposed a tentative reaction pathway for the synthesis of cyclohexanol from guaiacol *via* the HDO process. With a careful monitoring of the conversion by GC-MS during 6 hours of the reaction time, the formation of two intermediates namely phenol and cyclohexanone (ESI) was noticed; this has also been recently observed[23] corroborating our proposed mechanism (Fig. 4).

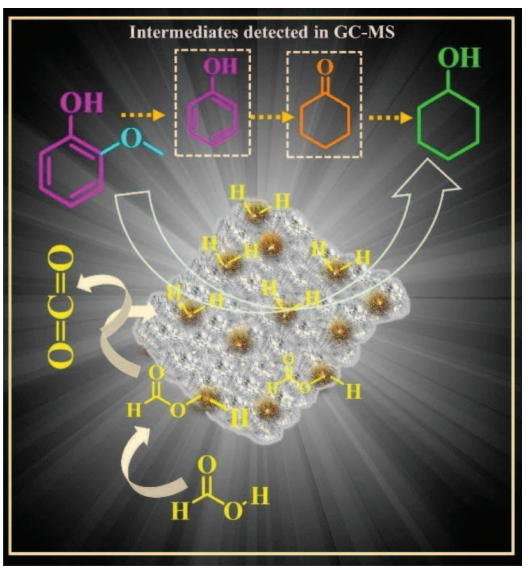

Fig. 4 A tentative reaction pathway for hydrodeoxygenation of guaiacol.

For the industrial application, it is imperative to study the viability, recyclability and stability aspects of the bimetallic AgPd/$Fe@CN_X$ catalyst. Recycling experiments were conducted using guaiacol as the substrate, formic acid as a source of hydrogen and the magnetic AgPd/$Fe@CN_X$ as a catalyst under photochemical conditions. After completion of the reaction, the catalyst was isolated using an external magnet, washed with methanol, dried at 60 °C and recycled for the subsequent HDO reaction of guaiacol. The catalyst was found to be durable and could be reused at least six times without losing its catalytic activity. These recycling experiments confirm that the porous nitrogen enriched CN_X support holds metal nanoparticles firmly *via* non-covalent interactions. This is further supported by the ICP-AES analysis of the mother liquor which does not show any traces of metals; ICP-AES analysis of Fe, Pd and Ag was found to be 4.88%, 2.51% and 2.48% before the reaction and 4.87%, 2.50% and 2.47%, respectively after the six-reaction cycle.

Conclusions

An efficient, sustainable and stable magnetically separable bimetallic AgPd/$Fe@CN_X$ catalyst has been synthesized utilizing an abundant waste material as a support. This heterogeneous catalyst proficiently dehydrogenates formic acid, a renewable chemical hydrogen storage system, to hydrogen and then this *in situ* generated H_2 is utilized for upgrading of lignin-derived bio-oil containing guaiacol, *via* hydrodeoxygenation under visible light irradiation. Furthermore, the bimetallic catalyst shows high reactivity towards dissociation of formic acid to H_2 due to the synergic effect of silver and palladium nanoparticles with nano-ferrites and the nitrogen-enriched carbon nitride support (CN_X), hence, leading to the fast HDO under ambient reaction parameters. The magnetic retrieval quality of AgPd/$Fe@CN_X$ facilitates the catalyst separation during the reaction workup and demonstrates high recyclability with negligible loss of catalytic activity. This highly active catalytic method could be beneficial for the upgrading of renewable lignin to valued components useful in industrial processes.

Conflicts of interest

There are no conflicts of interest to declare.

Notes and references

1 F. H. Isikgor and C. Remzi Becer, *Polym. Chem.*, 2015, **6**, 4497–4559.
2 N.-E. E. Mansouri and J. Salvado, *J. Ind. Crops Prod.*, 2006, **24**, 8–16.
3 M. Besson, P. Gallezot and C. Pinel, *Chem. Rev.*, 2014, **114**, 1827–1870.

 This journal is © The Royal Society of Chemistry 2019

Published on 28 January 2019. Downloaded by US Environmental Protection Agency, Cincinnati on 3/18/2019 2:48:24 PM.

4 W.-J. Liu, W.-W. Li, H. Jiang and H.-Q. Yu, *Chem. Rev.*, 2017, **117**, 6367–6398.
5 G. Fiorentino, M. Ripa and S. Ulgiati, *Biofuels, Bioprod. Biorefin.*, 2017, **11**, 195–214.
6 P. M. Mortensen, J.-D. Grundwaldt, P. A. Jensen, K. G. Knudsen and A. D. Jensen, *Appl. Catal., A*, 2011, **407**, 1–19.
7 P. M. Mortensen, J.-D. Grunwaldt, P. A. Jensen, G. Knudsen and A. D. Jensen, *Catal. Sci. Technol.*, 2014, **4**, 3672–3686.
8 A. Gutierrez, E.-M. Turpeinen, T.-R. Viljava and O. Krause, *Catal. Today*, 2017, **285**, 125–134.
9 Q. Zhang, J. Chang, T. Wang and Y. Xu, *Energy Convers. Manage.*, 2007, **48**, 87–92.
10 P. Mäki-Arvela and D. Yu. Murzin, *Catalysts*, 2017, **7**, 265.
11 E. H. Lee, R. S. Park, H. Kim, S. H. Park, S. C. Jung, J. K. Jeon, S. C. Kim and Y. K. Park, *J. Ind. Eng. Chem.*, 2016, **37**, 18–21.
12 T. Nimmanwudipong, R. C. Runnebaum, D. E. Block and B. C. Gates, *Energy Fuels*, 2011, **25**, 3417–3427.
13 H. Shafaghat, P. S. Sirous Rezaei and W. M. A. W. Daud, *RSC Adv.*, 2015, **5**, 33990–33998.
14 M. T. Musser, Cyclohexanol and Cyclohexanone, in *Ullmann's Encyclopedia of Industrial Chemistry*, Wiley-VCH, Weinheim, 2005.
15 S. Liu, H. Wang, K. J. Smith and C. S. Kim, *Energy Fuels*, 2017, **31**, 6378–6388.
16 S. Boullosa-Eiras, R. Lødeng, H. Bergem, M. Stöcker, L. Hannevold and E. A. Blekkan, *Catal. Today*, 2014, **223**, 44–53.
17 A. H. Zacher, M. V. Olarte, D. M. Santosa, D. C. Elliott and S. B. Jones, *Green Chem.*, 2014, **16**, 491–515.
18 S. K. Kim, D. Yoon, S.-C. Lee and J. Kim, *ACS Catal.*, 2015, **5**, 3292–3303.
19 C. A. Fisk, T. Morgan, Y. Ji, M. Crocker, C. Crofcheck and S. A. Lewis, *Appl. Catal., A*, 2009, **358**, 150–156.
20 P. de Wild, R. Van der Laan, A. Kloekhorst and E. Heeres, *Environ. Prog. Sustainable Energy*, 2009, **28**, 461–469.
21 J. Wildschut, M. Iqbal, F. H. Mahfud, I. M. Cabrera, R. H. Venderbosch and H. J. Heeres, *Energy Environ. Sci.*, 2010, **3**, 962–970.
22 X. Y. Wang and R. Rinaldi, *Energy Environ. Sci.*, 2012, **5**, 8244–8260.
23 M. Zhou, J. Ye, P. Liu, J. Xu and J. Jiang, *ACS Sustainable Chem. Eng.*, 2017, **5**, 8824–8835.
24 Y. Nakagawa, M. Ishikawa, M. Tamura and K. Tomishige, *Green Chem.*, 2014, **16**, 2197–2203.
25 M. Ishikawa, M. Tamura, Y. Nakagawa and K. Tomishige, *Appl. Catal., B*, 2016, **182**, 193–203.
26 G.-Y. Xu, J.-H. Guo, Y.-C. Qu, Y. Zhang, Y. Fu and Q.-X. Guo, *Green Chem.*, 2016, **18**, 5510–5517.
27 M. Kim, J.-M. Ha, K.-Y. Lee and J. Jae, *Catal. Commun.*, 2016, **86**, 113–118.
28 Z. He, M. Hu and X. Wang, *Catal. Today*, 2018, **302**, 136–145.
29 R. S. Varma, *Green Chem.*, 2014, **16**, 2027–2041.
30 S. Verma, R. B. N. Baig, M. N. Nadagouda and R. S. Varma, *ACS Sustainable Chem. Eng.*, 2016, **4**, 1094–1098.
31 S. Verma, R. B. N. Baig, M. N. Nadagouda and R. S. Varma, *Green Chem.*, 2016, **18**, 1327–1331.
32 S. Verma, R. B. Nasir Baig, C. Han, M. N. Nadagouda and R. S. Varma, *Chem. Commun.*, 2015, **51**, 15554–15557.
33 R. S. Varma, *ACS Sustainable Chem. Eng.*, 2016, **4**, 5866–5878.
34 A. K. Singh, S. Jang, J. Y. Kim, S. Sharma, K. C. Basavaraju, M.-G. Kim, K.-R. Kim, J. S. Lee, H. H. Lee and D.-P. Kim, *ACS Catal.*, 2015, **5**, 6964–6972.
35 L. Lin, H. Ou, Y. Zhang and X. Wang, *ACS Catal.*, 2016, **6**, 3921–3931.
36 Y. A. Haleem, Q. He, D. Liu, C. Wang, W. Xu, W. Gan, Y. Zhou, C. Wu, Y. Ding and L. Song, *RSC Adv.*, 2017, **7**, 15390–15396.
37 Q. Guo, Y. Xie, X. Wang, S. Zhang and T. S. Hou, *Chem. Commun.*, 2004, 26–27.
38 C.-B. Cao, Q. Lv and H.-S. Zhu, *Diamond Relat. Mater.*, 2003, **12**, 1070–1074.
39 Y. Zheng, Y. Jiao, Y. Zhu, L. H. Li, Y. Han, Y. Chen, A. Du, M. Jaroniec and S. Z. Qiao, *Nat. Commun.*, 2014, **5**, 1–8.
40 K. Ramesh, M. Prashantha, N. K. Reddy and E. S. R. Gopal, *Integr. Ferroelectr.*, 2010, **117**, 40–48.
41 M. Kim, S. Hwang and J.-S. Yu, *J. Mater. Chem.*, 2007, **17**, 1656–1659.
42 P. Li, E. Y. Jiang and H. L. Bai, *J. Phys. D: Appl. Phys.*, 2011, **44**, 75003.
43 S. Gota, E. Guiot, M. Henriot and M. G. Soyer, *Phys. Rev. B: Condens. Matter Mater. Phys.*, 1999, **60**, 14387.
44 L. Xu, B. Jin, J. Zhang, D.-g. Cheng, F. Chen, Y. An, P. Cui and C. Wan, *RSC Adv.*, 2016, **6**, 46908–46914.
45 K. Tedsree, T. Li, S. Jones, C. W. A. Chan, K. M. K. Yu, P. A. J. Bagot, E. A. Marquis, G. D. W. Smith and S. C. E. Tsang, *Nat. Nanotechnol.*, 2011, **6**, 302–307.
46 S. Verma, M. N. Nadagouda and R. S. Varma, *Sci. Rep.*, 2017, **7**, 13596.

Tetrahedron 73 (2017) 5577–5580

Contents lists available at ScienceDirect

Tetrahedron

journal homepage: www.elsevier.com/locate/tet

Aerobic oxidation of alcohols in visible light on Pd-grafted Ti cluster

Sanny Verma [a,†], R. B. Nasir Baig [a,†], Mallikarjuna N. Nadagouda [b], Rajender S. Varma [a,*]

[a] Sustainable Technology Division, National Risk Management Research Laboratory, U.S. Environmental Protection Agency, MS 443, Cincinnati, OH 45268, USA

[b] WQMB, WSWRD, National Risk Management Research Laboratory, U.S. Environmental Protection Agency, Cincinnati, OH 45268, USA

ARTICLE INFO

Article history:
Received 10 May 2016
Received in revised form 12 July 2016
Accepted 29 July 2016
Available online 30 July 2016

Keywords:
Titanium cluster
Photoactive
Heterogeneous catalysis
Visible light
Aerial oxidation
Palladium nanoparticle

ABSTRACT

The titanium cluster with the reduced band gap has been synthesized having the palladium nanoparticles over the surface, which not only binds to the atmospheric oxygen but also catalyzes the oxidation of alcohols under visible light.

Published by Elsevier Ltd. This is an open access article under the CC BY license (http://creativecommons.org/licenses/by/4.0/).

1. Introduction

The increasing focus on the utilization of visible light energy is due to its abundant nature and its impeccable tolerance towards the environment.[1] Harvesting visible light and performing chemical transformations with it in a concerted process is a high priority chemical research area.[2] Most of the photo-catalysts, especially based on titanium oxide, are active under ultra-violet light (UV);[3] visible light mediated reactions have not received similar attention.[4] There are many photoactive materials available in the literature[4] and a vast majority of them has received casual attention in academic publications due to low activity and/or limited applicability. Titanium-based materials have received maximum consideration as a photoactive material, the major limitation being their wider band gaps, which make it active only under UV irradiation conditions. The activity specific to UV light diminishes its role as a photoactive material, which can utilize solar energy in chemical reactions. Therefore, it becomes imperative to reduce the band gap in titanium materials in order to bring its activity into the visible spectrum of electromagnetic radiation.[5]

Titanium material in combination with metals and other doping elements have been used to reduce the band gap, therefore, sunlight could be utilized for the reaction.[6] Nitrogen doping in titanium oxide has been known to reduce band gap to a great extent.[7] However, the reaction of *N*-doped titanium oxide is uncontrollable in visible light due to its high activity; complete decomposition or mineralization of the organic matter is common occurrence in environmental remediation studies[8] thus rendering this catalyst incongruous in organic synthesis.[9] On the other hand, titanium oxide has been used as a support for the immobilization of transition metals and its application in oxidation chemistry is growing.[10] Hong and co-workers have immobilized palladium and gold combination over the surface of TiO_2 but they lost the ethos of TiO_2 as a photoactive material when the reaction was performed under thermal heating using oxygen atmosphere.[11] In this reaction, gold adsorbs the oxygen in the reaction media and transfers into the reactant via the bimetallic interaction with palladium. The use of titanium oxide becomes irreverent, as its photoactivity has not been utilized. Similarly, Li et al. utilized biosynthesized Au/Pd-TiO_2 supported nanoparticle in the oxidation reaction.[12] We strived to utilize the core property of titanium as photoactive material along with structural modification to create the cluster which can adsorb the atmospheric oxygen and transfer to the reactant in an oxidation process. Accordingly, we prepared nitrogenous titanium cluster, immobilized the palladium to develop photoactive gold-free catalyst, and demonstrated its application in selective oxidation of alcohols; titanium cluster performs the dual task by providing required activation energy and transmitting oxygen in the oxidation step.

* Corresponding author. Fax: +1 513 569 7677; e-mail address: varma.rajender@epa.gov (R.S. Varma).

† Equal contribution.

http://dx.doi.org/10.1016/j.tet.2016.07.070
0040-4020/Published by Elsevier Ltd. This is an open access article under the CC BY license (http://creativecommons.org/licenses/by/4.0/).

2. Result and discussion

In continuation of our desire to develop benign methods for environmental remediation and green synthesis,[13] herein, we report a photoactive palladium-grafted titanium cluster and demonstrated its application in selective oxidation of alcohols to the corresponding carbonyl compounds. Generally, oxidation chemistry is conducted using transition metals along with a supporting co-oxidant.[14] Often, co-oxidants comprise homogenous mix of reagents and catalysts with occasional use of oxygen. However, the utility of oxygen as co-oxidant comes with various detriments that include addition of oxygen absorbing material or metals that can bind oxygen in the reaction such as gold. The main objective here is the adsorption and transmission of the required oxygen for the catalytic process.[15] However, our titanium cluster based catalyst does not require any of these additives and the reaction can be conducted under visible light using oxygen from the atmosphere. The first step in developing the active catalyst was the synthesis of titanium cluster with the significant reduction in the band gap. It has been accomplished by treating titanium (IV) isopropoxide with 4-aminobenzoic acid in isopropanol at 120 °C for 72 h;[16] shiny crystals of titanium clusters ensued which settled down at the bottom of the reaction vessel and were separated by decanting and centrifugation. The Ti-cluster was then suspended in isopropanol and treated with palladium nitrate at 80 °C; palladium salt was reduced and Pd (0) deposited over the cluster. The palladium grafted titanium cluster (Pd@TiC) was separated and its application has been evaluated in the selective oxidation of alcohols (Scheme 1).

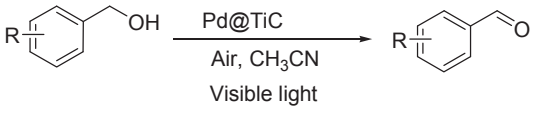

Scheme 1. Pd@TiC catalyzed oxidation of alcohols.

The Pd@TiC catalyst was characterized using scanning electron microscope (SEM) and X-ray diffraction (XRD). The percentage of palladium was determined using inductive coupled plasma atomic emission spectroscopy (ICP-AES) analysis. The SEM images of Ti-cluster and Pd@TiC catalyst illustrate the immobilization of palladium (Pd) nanoparticles (Fig. 1) with the apparent changes in the surface morphology. The immobilization of Pd was further established by XRD (Fig. 2) and the concentration confirmed to be 4.88% by ICP-AES analysis.

The activity of Pd@TiC was evaluated in the aerial oxidation of alcohols under visible light irradiation with benzyl alcohol as a model substrate. The preliminary results obtained during the screening and reaction optimization are summarized in Table 1. The

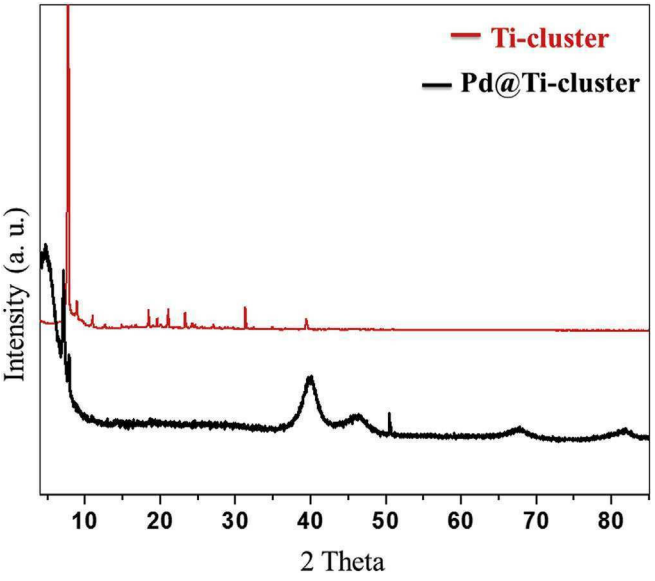

Fig. 2. XRD of Ti-Cluster and Pd@TiC.

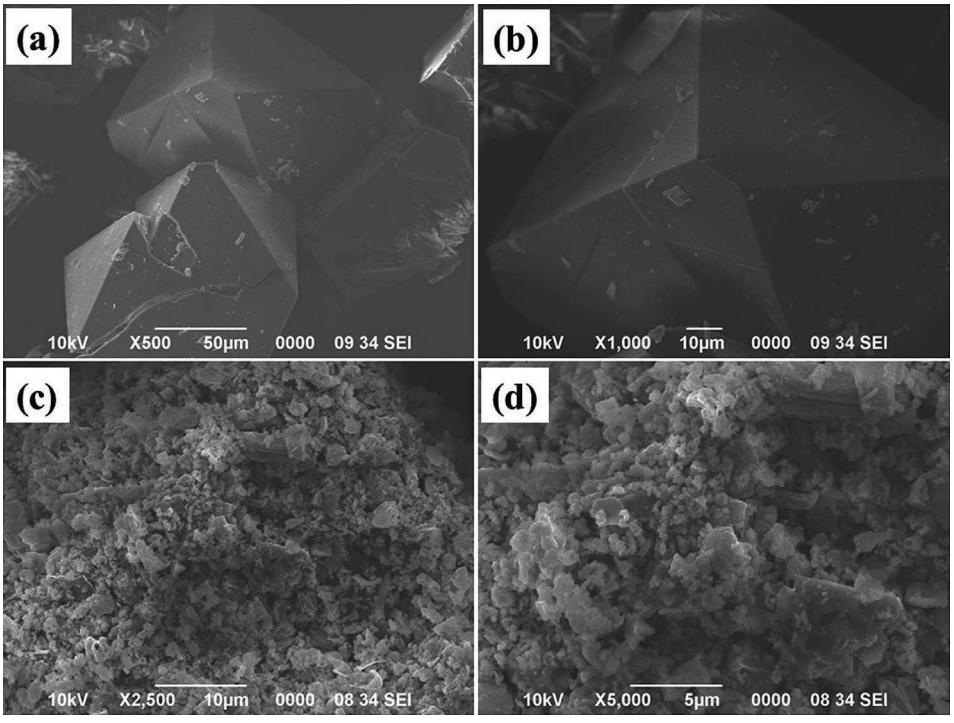

Fig. 1. SEM images of Ti-Cluster (a) Pyramid-like structure and (b) Close view of pyramid; (c) and (d) SEM images of Pd@TiC.

Table 1
Results of screening experiments[a]

Entry	Solvent	Time	Yield[b]
1	H_2O	12 h	45%
2	Toluene	12 h	48%
3	DMF	12 h	16%
4	CH_3CN	8 h	97%

[a] Reaction conditions: Benzyl alcohol (1 mmol), Pd@TiC (25 mg), Solvent (2 mL), 20 W domestic bulb, Air.
[b] Isolated yields.

reaction outcome in different solvents clearly indicate that acetonitrile is the best solvent for this reaction as it gives quantitative yield of the desired product; conventionally used polar solvents (water and DMF) and non-polar solvent (toluene) were in effective in the visible light mediated aerial oxidation of alcohol.

After uncovering the appropriate conditions, the scope of the developed Pd@TiC catalyst was studied in the oxidation of a wide range of alcohols and the results are depicted in Table 2. They clearly demonstrate the excellent activity and selectivity towards the formation of corresponding carbonyl compounds (Table 2; entries 1–8) where electron donating and electron with drawing substituents apparently have trifling effect on the rate of the reaction (Table 2, entries 2–4). The secondary alcohols and heterocyclic alcoholic derivatives were also readily converted to corresponding carbonyl derivatives (Table 2, entries 5–8). The important feature of this reaction was the use of aerial oxygen and solar energy to accomplish the oxidation of alcohol without the formation of any by-product, which is an unprecedented finding.

Table 2
Pd@TiC catalyzed oxidation of alcohols[a]

Entry	Substrate	Product	Yield[b]
1	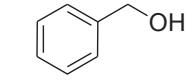	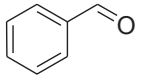	97%
2	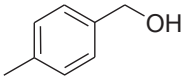	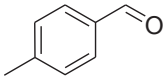	95%
3	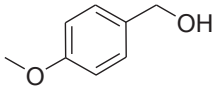	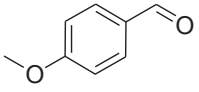	96%
4	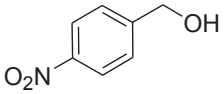	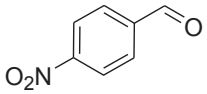	96%
5	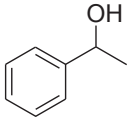	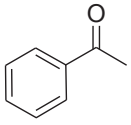	94%
6	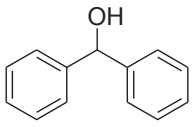	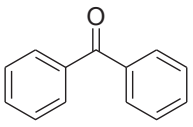	94%
7	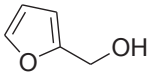	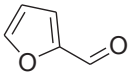	97%
8	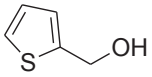	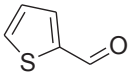	97%

[a] Reaction conditions: Substrate (1 mmol), Pd@TiC (25 mg), CH_3CN (2 mL), 20 W domestic bulb, Air, 8 h.
[b] Isolated yield.

3. Conclusion

We have demonstrated the synthesis of highly dispersed palladium nanoparticles grafted on titanium cluster. The developed Pd@TiC catalyst is found to be a highly effective in the aerial oxidation of alcohols under visible light and its activity is attributed to the reduced band gap, which makes it active under visible light thus harnessing solar energy for the chemical reactions. The Pd@TiC is found to be highly stable and could be recycled several times without any loss in its activity. The most important feature of this catalyst is its ability to bind with the atmospheric oxygen which serves as an oxidant in the reaction cycle.

4. Experimental section

4.1. Synthesis of Pd@TiC catalyst

Titanium (IV) isopropoxide (0.518 mL) was added to a solution of 4-aminobenzoic acid (0.96 g, 7.0 mmol) in 2-propanol (30.0 mL). The reaction mixture was stirred at room temperature for 30 min; an orange-colored slurry was obtained. The slurry was heated at 120 °C for 72 h in a pressure reactor when bright yellow crystals of titanium cluster ensued. The catalyst was isolated by decanting and centrifugation, washed with 2-propanol and dried under vacuum for 2 h. The Ti cluster (100 mg) was then suspended in isopropanol (10 mL) and treated with palladium nitrate (5 mol %) at 80 °C. 2-propanol reduced the Pd metal into Pd-nanoparticle which were deposited over the titanium cluster. The palladium nanoparticle grafted titanium cluster (Pd@TiC) was isolated and characterized using SEM, XRD, and ICP-AES.

4.2. General procedure for the oxidation of alcohols

A 10 mL side-armed round bottomed flask equipped with a magnetic stirring bar and a balloon filled with air was charged with alcohol (1 mmol), catalyst Pd@TiC (25 mg) and acetonitrile (2 mL). The reaction mixture was exposed to visible light irradiation using 20 W domestic bulb (Fig. 3) and the progress of reaction was monitored using TLC. After the completion of the reaction, the Pd@TiC catalyst was separated using a centrifuge and the product was isolated by extracting with ethyl acetate, dried over sodium sulfate, concentrated under reduced pressure and characterized.

Fig. 3. Pictorial representation of the reaction set-up.

4.3. Recycling of Pd@TiC

A set of experiments were performed using benzyl alcohol as a model substrate in acetonitrile solvent. After the completion of each reaction, the Pd@TiC catalyst was recovered using a centrifuge, washed with methanol and reused for the oxidation of fresh batch of benzyl alcohol. The Pd@TiC catalyst could be recycled and reused up to six times without any loss in its activity (Table 3). The metal leaching in reaction with Pd@TiC was examined by ICP-AES analysis before and after the completion of reaction; concentration of palladium was found to be 4.88% before the reaction and 4.87% after the sixth cycle. The ICP-AES of the mother liquor did not show the presence of palladium confirming the fact that titanium cluster holds the Pd nanoparticles tightly.

Table 3
Recycling of Pd@TiC catalyst in the oxidation of benzyl alcohol[a]

Run	1	2	3	4	5	6
Isolated yield	97%	97%	97%	97%	96%	96%

[a] Reaction conditions: Benzyl alcohol (1 mmol), Pd@TiC (25 mg), CH_3CN (2 mL), 20 W domestic bulb, Air.

The SEM image of the Pd@TiC before and after the reaction confirms that there is no significant change in the morphology of the catalyst, which signifies high stability of Pd@TiC during the course of the reaction (Fig. 4).

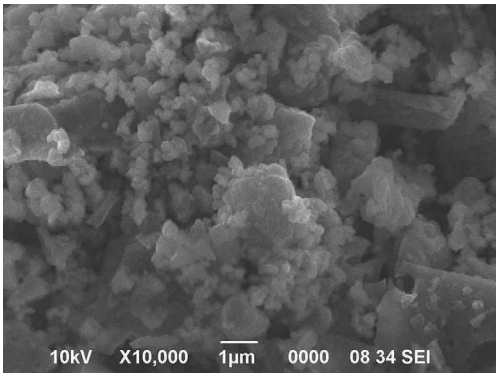

Fig. 4. SEM image of the recycled Pd@TiC.

Disclaimer

The views expressed in this article are those of the authors and do not necessarily represent the views or policies of the U.S. Environmental Protection Agency. Any mention of trade names or commercial products does not constitute endorsement or recommendation for use.

Acknowledgements

SV and RBNB were supported by the Postgraduate Research Program at the National Risk Management Research Laboratory administered by the Oak Ridge Institute for Science and Education through an interagency agreement between the U.S. Department of Energy and the U.S. Environmental Protection Agency.

Supplementary data

Supplementary data associated with this article can be found in the online version, at http://dx.doi.org/10.1016/j.tet.2016.07.070.

References and notes

1. Bita, C. E.; Gerats, T. *Front. Plant Sci.* **2013**, *4*, 273.
2. Li, L.; Zhang, S.; Xu, L.; Wang, J.; Shi, L.-X.; Chen, Z.-N.; Honga, M.; Luo, J. *Chem. Sci.* **2014**, *5*, 3808.
3. Kumar, S. G.; Devi, L. G. *J. Phys. Chem. A* **2011**, *115*, 13211.
4. (a) Prier, C. K.; Rankic, D. A.; MacMillan, D. W. C. *Chem. Rev.* **2013**, *113*, 5322; (b) Kanhere, P.; Chen, Z. *Molecules* **2014**, *19*, 19995.
5. (a) Schneider, J.; Matsuok, M.; Takeuchi, M.; Zhang, J.; Horiuchi, Y.; Anpo, M.; Bahnemann, D. W. *Chem. Rev.* **2014**, *114*, 9919; (b) Colmenares, J. C.; Lisowski, P.; Łomot, D.; Chernyayeva, O.; Lisovytskiy, D. *ChemSusChem* **2015**, *8*, 1676.
6. Zaleska, A. *Recent Pat. Eng.* **2008**, *2*, 157.
7. Cong, Y.; Zhang, J.; Chen, F.; Anpo, M. *J. Phys. Chem. C* **2007**, *111*, 6976.
8. Asahi, R.; Morikawa, T.; Irie, H.; Ohwaki, T. *Chem. Rev.* **2014**, *114*, 9824.
9. Yang, G.; Jiang, Z.; Shi, H.; Xiao, T.; Yan, Z. *J. Mater. Chem.* **2010**, *20*, 5301.
10. Bagheri, S.; Julkapli, N. M.; Bee, S.; Hamid, A. *Sci. World J.* **2014**, *2014*, 727496.
11. Chang, J. B.; Liu, C. H.; Liu, J.; Zhou, Y. Y.; Gao, X.; Wang, S. D. *Nano-Micro Lett.* **2015**, *7*, 307.
12. Hong, Y.; Jing, X.; Huang, J.; Sun, D.; Odoom-Wubah, T.; Yang, F.; Du, M.; Li, Q. *ACS Sustain. Chem. Eng.* **2014**, *2*, 1752.
13. (a) Varma, R. S. *Green Chem.* **2014**, *16*, 2027; (b) Verma, S.; Mungse, H. P.; Kumar, N.; Choudhary, S.; Jain, S. L.; Sain, B.; Khatri, O. P. *Chem. Commun.* **2011**, 12673; (c) Nasir Baig, R. B.; Varma, R. S. *Green Chem.* **2013**, *15*, 1839; (d) Verma, S.; Singh, R.; Tripathi, D.; Gupta, P.; Bahuguna, G. M.; Jain, S. L. *RSC Adv.* **2013**, *3*, 4184; (e) Nasir Baig, R. B.; Varma, R. S. *ACS Sustain. Chem. Eng.* **2014**, *2*, 2155; (f) Nasir Baig, R. B.; Nadagouda, M. N.; Varma, R. S. *Green Chem.* **2014**, *16*, 4333.
14. (a) Verma, S.; Nasir Baig, R. B.; Nadagouda, M. N.; Varma, R. S. *ACS Sustain. Chem. Eng.* **2016**, *4*, 2333; (b) Verma, S.; Baig, R. B. N.; Han, C.; Nadagouda, M. N.; Varma, R. S. *Green Chem.* **2015**, *18*, 251; (c) Verma, S.; Baig, R. B. N.; Nadagouda, M. N.; Varma, R. S. *ACS Sustain. Chem. Eng.* **2016**, *4*, 1094; (d) Verma, S.; Verma, D.; Sinha, A. K.; Jain, S. L. *Appl. Catal. A Gen.* **2015**, *489*, 17; (e) Verma, S.; Aila, M.; Kaul, S.; Jain, S. L. *RSC Adv.* **2014**, *4*, 30598; (f) Verma, S.; Bras, J. Le; Jain, S. L.; Muzart, J. *Appl. Catal. A Gen.* **2013**, *468*, 334; (g) Mungse, H. P.; Verma, S.; Kumar, N.; Sain, B.; Khatri, O. P. *J. Mater. Chem.* **2012**, *22*, 5427.
15. (a) Pina, C. D.; Falletta, E. *Catal. Sci. Technol.* **2011**, *1*, 1564; (b) Biella, S.; Prati, L.; Rossi, M. *J. Mol. Catal. A Chem.* **2003**, *197*, 207.
16. (a) Yuan, S.; Liu, T. F.; Feng, D.; Tian, J.; Wang, K.; Qin, J.; Zhang, Q.; Chen, Y. P.; Bosch, M.; Zou, L.; Teat, S. J.; Dalgarno, S. J.; Zhou, H. C. *Chem. Sci.* **2015**, *6*, 3926; (b) Feng, D.; Wang, K.; Wei, Z.; Chen, Y.-P.; Simon, C. M.; Arvapally, R. K.; Martin, R. L.; Bosch, M.; Liu, T.-F.; Fordham, S.; Yuan, D.; Omary, M. A.; Haranczyk, M.; Smit, B.; Zhou, H.-C. *Nat. Commun.* **2014**, *5*, 5723.

Date: 4/27/2020

[1]. Sanny Verma, M. N. Nadagouda and R. S. Varma "Visible light-mediated and water-assisted selective hydrodeoxygenation of lignin-derived guaiacol to cyclohexanol" *Green Chem.* **2019**,*21*, 1253-1257. **(IF= 9.405; immediacy index= 2.24; Citation half-life= 4.10; citations= 5)**

From the themed collection: **Green Biorefinery Technologies based on Waste Biomass**

[2]. Sanny Verma, R. B. Nasir Baig, M. N. Nadagouda and R. S. Varma "Aerobic oxidation of alcohols in visible light on Pd-grafted Ti cluster" *Tetrahedron* **2017**, *73*, 5577-5580. **(IF= 2.645; immediacy index= 0.65; Citation half-life= 9.20; citations= 19)**

I, Dr. Sanny Verma was part of the research of the above publication and my contribution for this publication can be valued at 20%

Best regards

Sanny Verma
US EPA/ORD/CESER/CTMB
26 West Martin Luther King Drive,
Cincinnati, Ohio 45268, USA; Tel: (513)-5697293
E-mail: Verma.Sanny@epa.gov

Part 3

Environmental upgrading of biomass and sustainable development in organic transformation

Research category: 11. Industry and the Environment (IE)
Or
13. Sustainability and Innovation (SI)

[1]. Sanny Verma, M. N. Nadagouda and R. S. Varma "Visible light-mediated and water-assisted selective hydrodeoxygenation of lignin-derived guaiacol to cyclohexanol" *Green Chem.* **2019**,*21*, 1253-1257. **(IF= 9.405; immediacy index= 2.24; Citation half-life= 4.10; citations= 5)**

From the themed collection: **Green Biorefinery Technologies based on Waste Biomass**

[2]. Sanny Verma, R. B. Nasir Baig, M. N. Nadagouda and R. S. Varma "Aerobic oxidation of alcohols in visible light on Pd-grafted Ti cluster" *Tetrahedron* **2017**, *73*, 5577-5580. **(IF= 2.645; immediacy index= 0.65; Citation half-life= 9.20; citations= 19)**

1. Explain how the nominated paper's represent research that is innovative and important in advancing the scientific knowledge or technology relevant to EPA's mission. It is, important to provide a clear and compelling explanation of the relevance, and impact of the research to EPA's mission (For example, the relevance of the research to one of EPA's strategic goals may be described) (Limit to 16,000 characters including spaces.)

Explanation:

The two nominated papers demonstrate the upgrading of biomass and chemical transformation using environmental-friendly processes.

To preserve resources and maintain environmental and economic sustainability, researchers must develop more efficient technologies for the chemical industry. Currently, they have focused on the lack of available non-renewable organic feedstocks to demonstrate the importance of renewable resources. Upgrading biomass and the development of chemical feedstocks from renewable resources are a sustainable method of reducing dependence on petroleum products. Though upgrading and sustainable development hold many advantages for the environment when applied as a petroleum alternative, they also present a significant challenge, since researchers must chemically modify the bio-derived fuels to make them compatible with existing technology. To solve all these challenges, our first nominated paper (Nadagouda, 2019) developed a technology of magnetically separable heterogeneous bimetallic catalysts for the upgrading of lignin-derived guaiacol to cyclohexanol under visible light. The second nominated paper (Nadagouda, 2017) designed a novel method for supporting photoactive heterogeneous catalysis in organic reactions.

Overall, these two papers significantly justify EPA mission, for example, “Sustainable Materials Management (SMM)” as these research articles demonstrate the utilization of sustainable protocols for the upgrading of biomass and chemical transformation. (https://www.epa.gov/sites/production/files/2015-08/documents/sustainable_materials_management_the_road_ahead.pdf). As we know, chemistry is very crucial for daily life and the extent of its application from the development of organic scaffolds to treat various illnesses in the formation of innovative industrial developments. We develop clean, sustainable methods to synthesize industrially relevant products in the prevention of pollution and the elimination of hazardous waste.

2A. The EPA Guidelines prohibit resubmission of publications nominated for STAA Awards in previous years. If multiple papers are submitted, provide a comprehensive explanation of the relationship and lengths between subject matter among the different nominated publications. For example, the discussion could describe how one publication builds on the results of a second publication. (Limit to 16,000 characters including spaces.) Enter n/a if blank.

Response:

None of the two nominated papers consisted of this STAA package have been submit ted for a STAA in the past.

In this package, two papers are essentially related to each other as they demonstrate the environmental upgrading of biomass and sustainable development in organic transformation. As mentioned in answer to Question 1, the strength of this study is the span of researches that was performed for the utilization of sustainable protocols in the upgradation of biomass (Nadagouda, 2019) and organic transformation (Nadagouda, 2017).

All these research studies increase the national scale understanding of environmental upgrading of biomass and sustainable development in organic transformation.

2B. List the previous 5 year's of STAA nominations and associated publications for each EPA author. Categorize the list by author and include publication title, year, and award. (For example, John Smith, publication title(s), year(s), award(s).) (Limit to 16,000 characters including spaces.) Enter n/a if blank.

Response:

Mallikarjuna N. Nadagouda

1. Evaluating Sustainable Pathway to Furanics from Biomass via Heterogeneous Organo-Catalysis Green Chemistry
2. Sustainable Strategy Utilizing Biomass: Visible Light-Mediated Synthesis of g-Valerolactone. Published in ChemCatChem
3. Visible Light Mediated Upgrading of Biomass to Biofuel. Published in Green Chemistry

2017 Honorable Mention STAA

1. The Oxidative C-H activation of amines using protuberant lychee-like goethite. Published in Nature Climate Change
2. Photocatalytic C-H activation and oxidative esterification using Pd@g-C3N4. Published in Catalysis Today
3. Hydroxylation of benzene via C-H activation using bimetallic CuAg@g-C3N4. Published in ACS Sustainable Chemistry and Engineering

2019 Honorable Mention STAA

1. Conversion of spent carbon dioxide into value-added products
2. A sustainable approach to empower the bio-based future: upgrading biomass to value-added products

2019 Level III STTA

Rajender S. Varma

1. Evaluating Sustainable Pathway to Furanics from Biomass via Heterogeneous Organo-Catalysis Green Chemistry
2. Sustainable Strategy Utilizing Biomass: Visible Light-Mediated Synthesis of g-Valerolactone. Published in ChemCatChem
3. Visible Light Mediated Upgrading of Biomass to Biofuel. Published in Green Chemistry

2017 Honorable Mention STAA

1. The Oxidative C-H activation of amines using protuberant lychee-like goethite. Published in Nature Climate Change
2. Photocatalytic C-H activation and oxidative esterification using Pd@g-C3N4. Published in Catalysis Today
3. Hydroxylation of benzene via C-H activation using bimetallic CuAg@g-C3N4. Published in ACS Sustainable Chemistry and Engineering

2019 Honorable Mention STAA

1. Conversion of spent carbon dioxide into value-added products
2. A sustainable approach to empower the bio-based future: upgrading biomass to value-added products

2019 Level III STTA

2C. Provide a description of how this nomination's publication(s) differ from previous (last 5 years) and current nominations by the author(s). (Limit to 16,000 characters including spaces.) Enter n/a if blank.

Response:

Nadagouda's (2017 Honorable Mention STAA, 2019 Honorable Mention STAA and 2019 Level III STTA) awards are like the currently nominated work, which are directly connected to sustainable chemistry. However, the sustainable process used in the first paper (Nadagouda 2019) utilizes the chitosan derived carbon nitride as catalyst support, and the second paper demonstrates the oxidation of alcohols under visible light. These are new approaches that have been utilized for the environmental upgrading of biomass and sustainable development in organic transformation, respectively.

Varma's (2017 Honorable Mention STAA, 2019 Honorable Mention STAA, and 2019 Level III STTA) awards are like the currently nominated work, which are directly connected to sustainable chemistry. However, the sustainable process used in the first paper (Nadagouda 2019) utilizes the chitosan derived carbon nitride as catalyst support, and the second paper demonstrates the oxidation of alcohols under visible light. These are new approaches that have been utilized for the environmental upgrading of biomass and sustainable development in organic transformation, respectively.

2D. Indicate whether previously submitted supplemental information is listed as supplemental information for the current nomination. (Limit to 16,000 characters including spaces.) Enter n/a if blank.

Response:

None of the supplemental information has been included in previous nominations.

2E. If any of the authors have submitted a concurrent nomination to another research category, provide sufficient justification to distinguish the difference between nominations. (Limit to 16,000 characters including spaces.) Enter n/a if blank.

Response:

There are no concurrent nominations by the authors on this nomination.

3A. Please provide substantial evidence for each of the following:
Provide evidence of recognition of the contribution from outside. (Limit to 16,000 characters including spaces.)

Response:

The first nominated paper (Nadagouda et al., 2019) has selected as a part of the themed collection "Green Biorefinery Technologies based on Waste Biomass" by the Royal Society of Chemistry. It has been published in the prestigious journal “Green Chemistry," which has an Impact Factor of 9.405 and has ranked#3 (h-index: 186) in the “Environmental Science” category. This research work has already been cited in 5 research articles (Google citation search). Prof. Reina from Department of Chemical and Process Engineering Department, University of Surrey, United Kingdom has adopted our work on the upgrading of biomass in his research article "Jin, W., Pastor-Pérez, L., Yu, J., Odriozola, J.A., Gu, S. and Reina, T.R., 2020. Cost-effective routes for Catalytic Biomass Upgrading. Current Opinion in Green and Sustainable Chemistry”. Recently, Prof. Bhoi from Department of Mechanical Engineering, Georgia Southern University, GA, USA has adopted and discussed our research work of AgPd/Fe@CNx catalyst for upgrading of lignin-derived guaiacol to cyclohexanol (98%) under visible light irradiation in his article “Ouedraogo, A.S. and Bhoi, P.R., 2020. Recent progress of metals supported catalysts for hydrodeoxygenation of biomass-derived pyrolysis oil. Journal of Cleaner Production 253, 119957”

The second nominated paper (Nadagouda et al., 2017) has been published in the prestigious journal “Tetrahedron," which has an Impact Factor of 2.645 and has ranked#61 (h-index: 209) in the “Pharmacology, Toxicology and Pharmaceutics” category. This research work has already been cited in 19 research articles (Google citation search) since its publication and highlighted in “**Synfacts**” (Polymer-Supported Synthesis) as **Synfacts, 2017, 13(11), p.1222**.

Recently, prof. Hong from South Korea has cited and highlighted our research work (Nadagouda et al., 2017) on his reaserach article “Hong, K., Sajjadi, M., Suh, J.M., Zhang, K., Nasrollahzadeh, M., Jang, H.W., Varma, R.S. and Shokouhimehr, M., 2020. Palladium Nanoparticles on Assorted Nanostructured Supports: Applications for Suzuki, Heck, and Sonogashira Cross-Coupling Reactions. ACS Applied Nano Materials, 3(3), pp.2070-2103.”

3B Provide an explanation of the external peer review process used to evaluate the scientific merit of the nominated publication(s). (Limit to 16,000 characters including spaces.)

Response

All of the nominated and supporting manuscript underwent anonymous peer review by the journal to which it was submitted for publication.

Table of Contents

General_Authors_Publications.....2
LI-266150_Maxwell_2018_Environ_Res_Lett_13_083002-2.....13
Maxwell_2018_Environ_Res_Lett_13_083002-2.....30
RPA_Maxwell.....47
RPA_Kiessling.....48
RPA_Buckley.....49
EPA_Award_Letter_-_Kiessling_and_Maxwell_2020.....50

United States Environmental Protection Agency
Washington, DC 20460

STAA REPORT FOR THE SCIENTIST NOMINATIONS

General Information:

Nomination ID/App ID:	20-103
Research Category Primary:	Review Articles (RA)
Research Category Secondary:	Environmental Policy and Decision-Making Studies (EP)
Laboratory/Office Name:	ORD
Nomination Entered By:	Keely Maxwell

Eligibility Checklist:

[Y] The nominated publication(s) has not been submitted to a previous STAA competition.

[Y] The nominated publication(s) was published on or before January 1, 2017 and on or after January 1,2012

[Y] The principal author was an EPA employee or a PHS employee assigned to EPA when the research was performed

[Y] The EPA authors (includes PHS employees assigned to EPA) contributed collectively a minimum of 50% toward the publication(s)

Nominating Official Name:	Shawn Ryan
Nominating Official Title:	GENERAL ENGINEER
Nominating OfficialEmail:	ryan.shawn@epa.gov
STAA Coordinator Name:	Kathleen Wiser
STAA Coordinator Email:	wiser.kathi@epa.gov

Justifications:

Justification 1:

EPA's Strategic Plan for FY2018-2022 has three goals, the first of which is to "Deliver a cleaner, safer, and healthier environment for all Americans and future generations by carrying out the Agency's core mission." Within this goal, Objective 1.3 focuses on the revitalization of land and the prevention of contamination. Specifically, EPA aims to "provide better leadership and management to properly clean up contaminated sites to revitalize and return the land back to communities." Many researchers have addressed this objective through technical studies, including exposure assessments, development of sampling and analysis methods, and studying chemical fate and transport. While these studies are important for expediting EPA's core mission, they miss a critical piece of the puzzle, which is how social contexts may affect environmental cleanup processes and outcomes.

With this fact in mind, a team of researchers in the EPA Office of Research and Development's (ORD) Center for Environmental Solutions and Emergency Response (CESER), Homeland Security Materials Management Division (HSMMD) has taken the initiative to apply social science theories and methods to the topic of environmental cleanups. This research uses the term 'cleanup' broadly, to include both remediation or removal at contaminated sites that may be managed through different EPA offices (e.g. Superfund, brownfields, emergency management). This research begins to answer the following questions: How do social factors (e.g. demographics, regional cultures, community values) affect cleanup processes? What are the social impacts during cleanup activities? And what are the social outcomes of completed cleanups?

HSMMD (formerly, National Homeland Security Research Center) scientists are experts in engineering, chemistry, toxicology, and microbiology, among other specialties. This team of researchers in HSMMD, in contrast, is comprised of social scientists. Following a 2016 "social science boot camp" for non-social scientists in ORD, the team met with boot camp participants from HSMMD to discuss potential social science research on self-help decontamination. 'Self-help decontamination' describes actions that households and businesses can take to clean interior surfaces after a radiological release. When reviewing the materials, the team realized that addressing this specific topic necessitated a more comprehensive analysis of what

the social sciences had to say about decontamination writ large. Thus, they decided to carry out a literature review. This research effort is wholly original and was carried out entirely by this small team, which established the review's scope,

research questions, and methodology. For example, the team quickly realized that the review had to include a wide variety of environmental cleanups in order to achieve effective coverage of the literature.

The nominated article lays the foundation for this research by systematically reviewing existing social scientific literature to assess the state of knowledge on this topic. The nominated article is novel in several respects. It engages a new area of research for EPA on social variables affecting cleanups. It targets literature in the social sciences, including anthropology, economics, geography, and sociology. The review uses qualitative analysis, which contrasts to the largely quantitative approaches used in other reviews conducted by EPA scientists. Finally, it provides an intellectual framework for advancing a relatively new area of research on contaminated site cleanups within the authors' discipline of environmental anthropology.

The review's synthesis of existing literature finds that studies fall primarily into three themes: effects on cleanup worker health, public engagement and decision-making, and societal benefits of cleaned-up sites. Studies of cleanup worker health were mostly epidemiological analyses done after large-scale incidents (e.g. Chernobyl). They point to social contexts of cleanup worker health including protective measures, vulnerable populations, and stigma. Studies of cleanup decision-making revealed the social and political dimensions of technical decisions and established the importance of public engagement. Studies of societal benefits of cleaned-up sites most commonly stemmed from economics literature, which used hedonic pricing models to evaluate changes in property values in areas near Superfund sites before and after cleanup.

This review's critical analysis of the literature identifies research trends as well as important gaps. Specifically, the review found three main areas of research need: 1) more mixed methods and interdisciplinary engagement within the literature, 2) more comparative studies between different types of environmental cleanup situations, and 3) further investigation in social science topics such as labor practices, race, gender, and power relations. It's important to note that, while many case studies of cleanup incidents exist, no other article has reviewed this area of social science research in such a rigorous way. In so doing, this article aids researchers' ability to

learn from these case studies. It also serves guidepost for future research in an emerging area of study within the social sciences.

Another important contribution that this article makes to the advancement of scientific knowledge is that it analyzes literature from multiple disciplines, to see how this topic is being addressed from different perspectives. For example, while economists evaluate the benefits of Superfund remediation in terms of housing value, sociologists are more concerned about potential neighborhood gentrification. The approach this article took serves to break down research silos that so often limit or constrain creative environmental problem solving. It also underscores the point that this area of research transcends disciplinary boundaries, meaning that it involves cross-cutting themes that are important to all types of environmental researchers.

In addition to laying the foundation for future research, this article also has strong applications to environmental policy and practice. It highlights ways, as synthesized from the literature, in which environmental cleanups can achieve better social and environmental outcomes. For example, the article outlines suggestions from the literature for improving support for the health of cleanup practitioners through increased worker benefits and services. These suggestions could address issues of worker burnout or increase worker efficiency. The article also points to examples of effective public engagement strategies, which can be used to reinforce EPA's community involvement program– an integral component of Superfund cleanups. Finally, it can help EPA better communicate the importance of the remediation and removal work it does, whether at National Priority List sites, brownfields, or removal sites, including the difference it makes in communities. The authors gave a training session on 'Brownfields Feud: Challenging Community Engagement Assumptions' at the 2019 National Brownfields Training Conference based upon the review and subsequent research on this topic.

Overall, this review article deepens understanding of the body of social science literature on environmental cleanups. It not only opens the door to a new area of research but leads the way into the future. It brings together research that had yet to be put into conversation which each other and makes connections that may inspire the next generation of interdisciplinary science on environmental cleanups.

Justification 2A:

n/a

Justification 2B:

n/a

Justification 2C:

n/a

Justification 2D:

n/a

Justification 2E:

n/a

Justification 3A:

The nominated article has had significant recognition outside of the Agency for its advancement in scientific knowledge and relevance to environmental issues. After publication, this work was recognized for its significance and impact. *Environmental Research Letters*, the journal in which it was published, selected it as an Editor's Featured Article; an honor given only to articles that are deemed the very best based on originality, significance, scientific impact, and broad appeal. Within the first week of publication it was downloaded 325 times, and to date (4/27/2020) it has been downloaded 3,450 times and cited 4 times. It was even added to the syllabus of an environmental anthropology class by a professor at the University of North Carolinal Chapel Hill. These statistics demonstrate a burgeoning interest in this topic within the research community and recognition of the significance of this article to this topic.

The authors of the paper have also been selected to present the findings from the research at several important professional scientific venues. For example, the authors chaired and organized a panel focused on social science and environmental cleanup at the 2018 Society for Applied Anthropology (SfAA) Annual Meeting. The panel not only featured the findings from the literature review, but also provided a platform to gather researchers around this topic area. There was such a tremendous interest in this emerging area, that the SfAA panel led to further academic collaborations around this topic – namely a forthcoming special issue in the *Journal of Environmental Management*. The authors were also invited to present a paper or poster at: the 2018 International Decontamination Research and Development Conference, the 2018 Association for Environmental Studies and Sciences Annual Meeting, the 2019 Natural Hazards Workshop Researcher Meeting, and the 2019 Association for American Geographers Annual Meeting.

The positive reception that this publication has received shows that it speaks to multidisciplinary audiences, thereby increasing its impact. The authors have presented to anthropologists, environmental scientists, decontamination researchers, hazards and disasters researchers, and geographers. The article was published in an environmental science journal and has also received positive reception in the authors' home discipline of environmental anthropology. Moreover, the meeting venues at which the authors presented the article's findings demonstrate the review's relevance and appeal to both researchers and practitioners doing cleanup work.

Additionally, the research team was awarded funding to do additional work on this topic by EPA's Office of Research and Development to carry out an EPA Pathfinder to Innovation Project (PIP) in 2019. Pathfinder to Innovation Projects are intended to transform sustainability and environmental protection by integrating innovative ideas into the major EPA research programs. The PIP project builds upon the findings from the paper, using them as a springboard for future research and tool development.

Justification 3B:

The nominated article was submitted to the journal *Environmental Research Letters* and successfully went through the journal's standard peer review process to evaluate its scientific merit. *Environmental Research Letters* requires researchers seeking to publish a review article to first submit an abstract and outline of the review article for approval by the journal's Editorial Board. This initial approval is necessary to even be allowed to submit a manuscript for consideration. The authors received this initial approval, including some suggestions from the Editorial Board, and prepared the manuscript. Then, the submitted manuscript was reviewed by three peer reviewers through a single-blind peer review process.

Overall the authors received very positive reviews and only had to make minor revisions before the article was accepted for publication. Reviewers commented especially on the potential impact of the paper and its importance to the area of study as well as for environmental policy. For example, one reviewer stated,

"In my view, this is an excellent review, and a much-needed contribution to the interdisciplinary literature on the intersections between environmental cleanup and the broad spectrum of relevant social sciences knowledge and areas of inquiry. An improved understanding of these intersections has the potential to significantly and beneficially inform environmental policy, as well as advance theories of people and the environment. The review's identification of dominant themes in the extant literature, as well as key research gaps, are particularly valuable."

Another positive comment that the authors received from a reviewer was the applications our paper has for practitioners working in the field. It was explained that the review "will be very useful both for people working in technical and also social stuff related to site remediation."

These reviewer comments provide further evidence that this article is influential in several key ways – advancing a theoretical framework, supporting future research, informing environmental policy, and guiding applied work. Rarely do review articles have such a broad impact.

AUTHORS

Principal Author

Author Name:	Keely B. Maxwell	
Professional Title:		Salutation:
Email:	maxwell.keely@epa.gov	Organization:
Mailing Address:		
Street Line 1:		
City:		
Zip Code:		State:
At time of research was:	EPA Employee	
Separation Date:		
% of Effort:	50	

Contributing Author

Author Name:	Brittany Kiessling	
Professional Title:		Salutation:
Email:	kiessling.brittany@epa.gov	Organization:
Mailing Address:		
Street Line 1:		
City:		
Zip Code:		State:
At time of research was:	Non EPA Personnel	

Separation Date:			
% of Effort:	35		

Contributing Author

Author Name:	Jenifer Buckley		
Professional Title:		Salutation:	
Email:	jenifer.a.buckley@gmail.com	Organization:	
Mailing Address:			
Street Line 1:			
City:			
Zip Code:		State:	
At time of research was:	Non EPA Personnel		
Separation Date:			
% of Effort:	15		

PUBLICATIONS

Publication 1:

Publication Title:	How clean is clean: a review of the social science of environmental cleanups		
Publication Date:	Thu Aug 16 00:00:00 GMT 2018		
Journal/Publication Method:	Environmental Research Letters		
All Author(s):			
Volume:	13	Number:	8
		Immediately	Immediately

Pages:	083002	Index:	Index:
Citation ½ Life:	89.8	Impact Factor:	6.192

Environmental Research Letters

TOPICAL REVIEW • **OPEN ACCESS**

How clean is clean: a review of the social science of environmental cleanups

To cite this article: Keely Maxwell *et al* 2018 *Environ. Res. Lett.* **13** 083002

View the article online for updates and enhancements.

This content was downloaded from IP address 161.80.170.183 on 16/08/2018 at 12:25

Environmental Research Letters

TOPICAL REVIEW

How clean is clean: a review of the social science of environmental cleanups

Keely Maxwell[1], **Brittany Kiessling**[2] and **Jenifer Buckley**[3]

[1] US Environmental Protection Agency (EPA), United States of America
[2] Oak Ridge Institute for Science & Education Research Participant at EPA, United States of America
[3] American Association for the Advancement of Science, Science & Technology Policy Fellowship, Program Participant at EPA, United States of America

E-mail: maxwell.keely@epa.gov

Keywords: decontamination, remediation, social science, Superfund, brownfields, megasites, public engagement

OPEN ACCESS

RECEIVED
31 August 2017

REVISED
30 July 2018

ACCEPTED FOR PUBLICATION
1 August 2018

PUBLISHED
16 August 2018

Original content from this work may be used under the terms of the Creative Commons Attribution 3.0 licence.

Any further distribution of this work must maintain attribution to the author(s) and the title of the work, journal citation and DOI.

Abstract

Environmental cleanup may involve decontaminating an area affected by a radiological release, containing an oil spill, or remediating a Superfund site or brownfield. It is a key component of how environmental agencies work to protect public health and the environment. There are many publications on technical protocols for cleanup and waste disposal. Additionally, there has been much social science work on the social problems of environmental contamination. However, social science research on cleanup itself has been much more scattered across disciplines and incidents. To date, there has not been a comprehensive review of the social factors that affect cleanup processes and outcomes. Such social factors may include cultural worldviews that shape stakeholder perspectives on 'how clean is clean' and social relationships among stakeholders. This article fills this gap by providing an interdisciplinary literature review of the social science of environmental cleanup. Three principal themes emerged from the 97 articles that met selection criteria: effects on cleanup worker health, public engagement and decision-making, and societal benefits of cleaned-up sites. The review points to areas where further research is needed. For example, there is a lack of mixed methods and interdisciplinary engagement within the literature. Additionally, few articles compare cleanup situations. There is also a need for further investigation into specific social science topics such as labor practices, gender, race, and power relationships. To address these gaps, we argue for the development of a comprehensive framework or model as well as the exploration of broader questions complicating cleanups. Overall, this area of research has significant potential to benefit environmental cleanup policy and practice worldwide, while advancing social theory about people and the environment.

1. Introduction and background

Cleaning up toxic contaminants and hazardous waste is a cornerstone of environmental protection in the United States (US) and abroad. In the US, there are 1345 sites on the Superfund National Priority List (NPL) and an estimated 450 000 contaminated brownfields properties. Approximately 53 million people (17% of the US population) live within 3 miles of a Superfund site (EPA 2015), making cleanups vital to public health. Environmental cleanup is also part of emergency response to oil spills, industrial and transportation accidents, and homeland security threats. In this paper, 'cleanup' refers to any part of the assessment, characterization, containment, removal, remediation, and waste disposal of chemical, biological, and radiological materials. Some hazardous waste sites, such as Love Canal and Warren County, North Carolina, play important roles in the history of US environmental policy and environmental justice. Others, such as historic industrial buildings contaminated with mercury or residential yards with high levels of lead in the soil, may not be nationally renowned yet still pose a risk to human health and require an extensive and costly cleanup.

Table 1 shows the range of situations included as environmental cleanup for the purposes of this analysis. It follows US Environmental Protection Agency

© 2018 The Author(s). Published by IOP Publishing Ltd

(EPA) categorizations and US policy approaches to provide consistency. Other countries may use slightly different categorizations (e.g. megasites, polluted sites), policy approaches (e.g. soil protection policies), and funding sources. The overarching goal of environmental cleanup is to protect human health and the environment, but there are differences among statutory requirements for achieving this goal. Each situation involves specific terminologies, activities, and phases. The term *remediation* refers to long-term actions at Superfund and brownfield sites to remove contaminants from different environmental media. Techniques include capping hazardous waste sites, dredging sediments in water bodies, and bioremediating using microbes to treat contaminated soil or groundwater on site. The term *decontamination*, in contrast, is more commonly used in emergency response when a substance is released that poses an 'imminent and substantial threat' to public health or the environment (40 CFR 300 1994). Decontamination refers to the inactivation, immobilization, or reduction of contaminants from a surface. For example, rooms containing *Bacillus anthracis* (the bacterium that causes anthrax) can be fumigated with chemicals to inactivate the spores. Surfaces contaminated with radiological materials can undergo physical or chemical decontamination. Responses to smaller release incidents are called *removal actions*. After an oil spill from an overturned truck, for example, contaminated soils are removed to be treated and disposed of elsewhere.

The cleanup situations in table 1 differ in several respects: the cause of contamination, materials handled, statutory authority, institutions involved, steps followed, funding stream, and future reuse. This diversity of cleanup situations is one indication of the complex social and political dynamics involved. Environmental and public health agencies, tribes, industry, private contractors, and community groups all play roles. Actions and timelines vary, as do the threat to human health, public engagement, and cost. Different cleanup situations use different criteria for cleanup standards. Superfund sites are cleaned to national standards, for example, whereas brownfields rely on state standards.

Cleanups take place everywhere from tribal lands to private residences on time scales of days to decades. During cleanups, stakeholders with existing social and power relationships engage in new ways. Stakeholders may not all use the same technical terms or even speak the same language. They may have competing ideas about health risks at a site, when is it clean enough, what does 'clean' even mean, and what constitutes appropriate post-cleanup land use (Fowlkes and Miller 1982, Interstate Technology and Regulatory Council ITRC 2002, van Horn and Chilik 1988, National Research Council 2005, McCaffrey and Baver 2006, Layzer 2012, Cram 2015).

Research from several social science disciplines has addressed social conflicts during cleanup (Fowlkes and Miller 1982), institutional decision-making (Interstate Technology and Regulatory Council ITRC 2002, Franco and Bouri 2010), and cost-benefit analysis (Hamilton and Viscusi 1999). Many studies are specific to a particular site such as Chernobyl in the Ukraine (Petryna 1995, Smith 2005) or Hanford in the United States (Gray and Becker 1993, Gephart 2003). To date, however, there has not been a comprehensive review of the social, economic, institutional, political, and cultural factors that affect cleanup processes and outcomes. Such a review is necessary to begin to develop an overarching framework to explain the social dynamics of environmental cleanup.

To fill this knowledge gap, we conducted a systematic, interdisciplinary literature review of the social science of environmental cleanups. The purpose of the review was to understand the current state of this literature and to identify key social variables that affect cleanup activities and outcomes. The review covered publications from anthropology, archeology, economics, environmental justice, environmental management, epidemiology, human geography, policy, public health, psychology, science and technology studies (STS), and sociology. Three common areas of investigation emerged from the review: physical and mental health of cleanup workers, public engagement in decision-making, and evaluation of societal benefits of cleanups.

The review should be of interest to social scientists, environmental scientists, and technical experts involved in cleanup decisions. It provides a baseline synthesis of scientific knowledge about the social dynamics of environmental cleanups. It also identifies research gaps, including a lack of cross-disciplinary fertilization and uneven coverage and comparison of cleanup situations. Overall, the review supports the development of an interdisciplinary systems framework for analyzing environmental cleanups and evaluating societal benefits.

2. Methods

2.1. Overview

This article uses a systematic literature review method, which involves article search and selection protocol, a defined research question or hypothesis, and a quantitative summary of results (Grant and Booth 2009, Singh 2017). It differs from systematic review methods from the clinical health literature in two respects. It provides a numerical analysis of article metadata but does not do a statistical analysis of article results (e.g. effect size) (Singh 2017). Instead, it uses a qualitative thematic synthesis or critical review to analyze the literature (Hart 1998, Thomas and Harden 2008, Grant and Booth 2009). Qualitative analysis is appropriate because this is exploratory research to identify social variables, not test a specific hypothesis. Figure 1 shows a preferred reporting items for systematic review and meta-analysis (PRISMA) diagram of the systematic search and selection process used (Moher *et al* 2009).

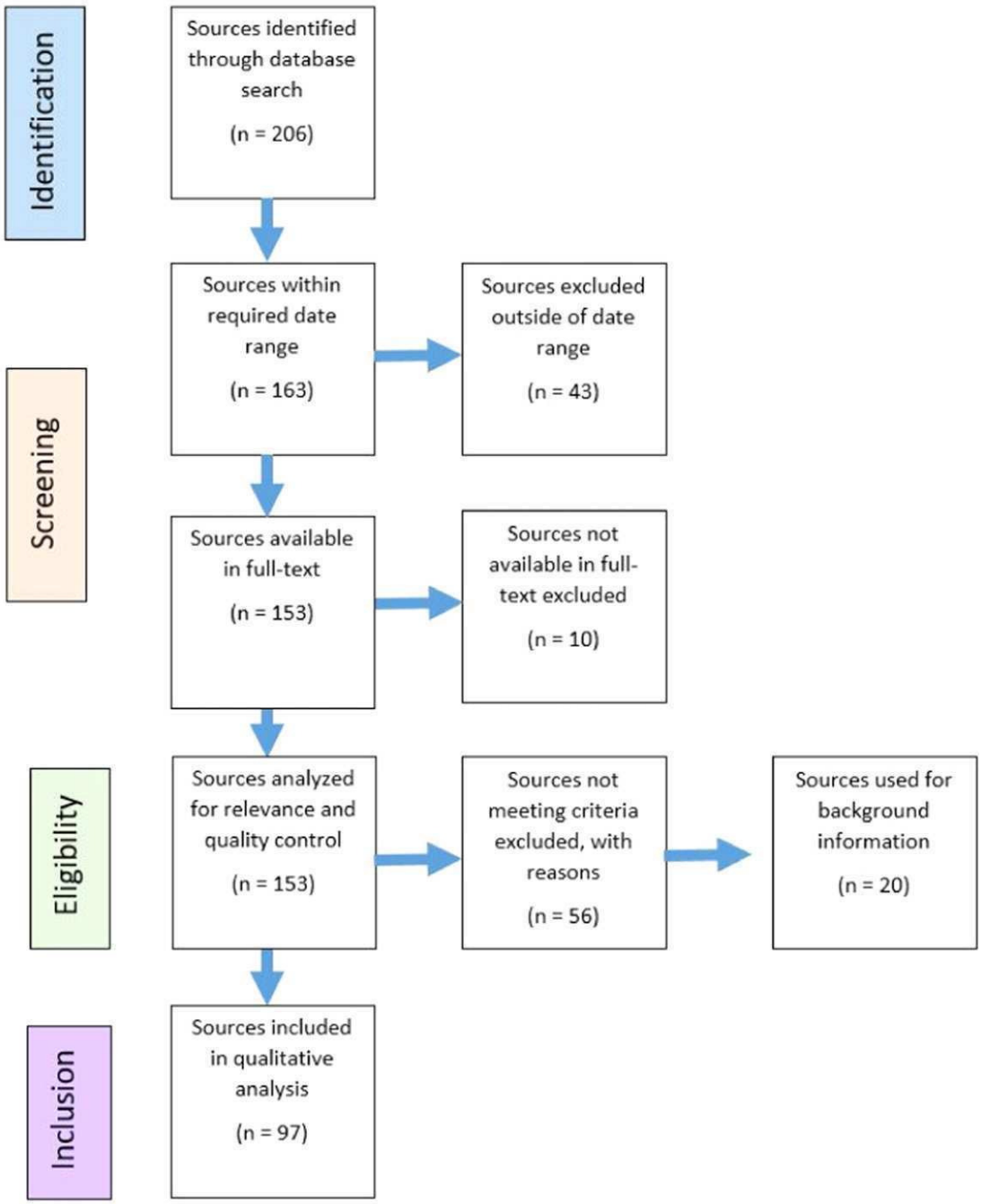

Figure 1. A PRISMA flow diagram illustrating the literature search process.

Literature sources included peer-reviewed journal articles, books, book chapters, e-books, and gray literature such as government agency reports. We included articles for review if the following criteria applied: (1) they use theories and/or methods from a social science discipline; (2) they address one or more social dimensions of environmental cleanups; (3) they were published in the last 25 years (1992–2017); (4) they meet quality control criteria (see below); and (5) they are written in English.

The five selection criteria allowed for inclusion of a diversity of publication types covering multiple disciplines, institutions, and countries. We excluded articles that provide a descriptive account of social conflict during a cleanup but do not use social theory or methods to analyze it. For example, our search returned technical assessments and reports about specific sites, but many of them did not have clear connections to social theory or employ social science research methods (e.g. interviews, surveys), so they were excluded from the analysis. We also excluded articles that address the social impacts of contamination but not decontamination. We limited the search to publications within the last 25 years to capture work published on cleanup actions under US environmental laws (e.g. Comprehensive Environmental Response,

Table 1. Types of environmental cleanups considered in this article (categorizations follow EPA 2017, 2018).

Cleanup category	Definition	Examples	Cleanup steps	Statutory authority	Funding
Emergency response	Response to oil spills, chemical, biological, radiological releases, and large-scale national emergencies.	• Natural disaster (medical waste, household hazardous waste, orphan containers, flood debris) • Oil spill • Train derailment • Chemical spill	• Removal assessment • Removal action	• CERCLA • SARA • Clean Water Act • National Contingency Plan • Oil Pollution Act • Stafford Act • Presidential Directives	• Stafford Act • Oil Spill Liability Trust Fund
Superfund sites/NPL sites	Uncontrolled or abandoned sites or properties where hazardous waste or other contamination is located. A contaminated site is generally considered a 'Superfund site' if the federal government is or plans to be involved in cleanup efforts. Note: NPL sites are those on the NPL; Superfund sites can be proposed or deleted from the list.	• Lead • Asbestos • Dioxin • Radiation • Agriculture runoff • Heavy metals • Industrial spill • Excludes coal mines	• Preliminary assessment/site investigation • NPL site listing • Remedial investigation/feasibility study • Records of decision • Remedial design/remedial action • Construction completion • Post-construction completion • NPL deletion • Site reuse/redevelopment	• CERCLA • SARA	• EPA grants • Technical Assistance Grants Program • Superfund Job Training Initiative • Superfund • Cost recovery
Brownfield sites	Real properties, the expansion, development, or reuse of which may be complicated by the presence of a hazardous substance, pollutant, or contaminant.	• Asbestos • Lead • Mine-scarred land • Former industrial site	• Assessment • Cleanup	• State environmental laws • Small Business Liability Relief and Brownfields Revitalization Act	• EPA Brownfields program grants • State response programs • State voluntary cleanup programs

Table 1. (Continued.)

Cleanup category	Definition	Examples	Cleanup steps	Statutory authority	Funding
					• Tax credits
State sites	Sites addressed by state, not EPA	All types of contaminants	• Depends on state	• State environmental laws	• State funding
Resource Conservation and Recovery Act (RCRA) corrective action	Treatment, storage and disposal facilities regulated under RCRA may have releases into the environment that require cleanup.	• Hazardous waste • Solid waste • Injection wells • Landfills	• Flexible may include: • Initial site assessment • Site characterization • Interim actions • Evaluate remedial alternatives • Implement remedy • Track process • Long-term care	• RCRA • Hazardous and Solid Waste Amendments (HSWA)	• Responsible parties
Underground storage tank sites (USTs)	Sites that contain contamination from petroleum products or Superfund hazardous substances released from underground storage tanks.	• Petroleum containers • Underground pipelines • Hazardous chemicals • Not septic tank, fuel container $<$1100 gal.	• Site characterization/assessment • Corrective action • Site closure	• RCRA • Solid Waste Disposal Act • Energy Policy Act of 2005	• Leaking Underground Storage Tank Trust Fund
Federal facilities	Properties owned or operated by the US government that may contain environmental contamination from unexploded ordnance, radioactive waste, or other hazardous substances.	• Military munitions • Unexploded ordnance • Hazardous chemicals • Federally owned wastewater treatment facilities	• Depends on site • Some federal facilities may be Superfund sites and follow Superfund steps.	• RCRA • HSWA • Safe Drinking Water Act • Clean Air Act • Clean Water Act • Oil Pollution Act	• Superfund • Department of Defense (DOD) • Department of Energy (DOE)

Compensation and Liability Act (CERCLA), Superfund Amendments and Reauthorization Act (SARA)), as well as homeland security incidents and technological disasters. We limited articles to English publications to avoid misinterpretations that could affect data quality. The articles had to be research articles, not book reviews, commentaries, or policy documents.

2.2. Quality control

We evaluated the articles according to a checklist of nine quality standards: focus, verity, integrity, rigor, soundness, applicability and utility, clarity and completeness, uncertainty and variability, and evaluation and review (EPA 2003, 2013). We evaluated gray literature sources according to these standards. If sources did not meet at least six of the nine quality standards, we did not include them. Because peer-reviewed sources such as books and journal articles are already evaluated by a similar system, we presumed that they met quality standards. We did assess the applicability of each source and the appropriate use of social science theory and methods for all articles, which served as another layer of quality assessment.

2.3. Literature search and analysis

We conducted keyword searches in the following databases: ScienceDirect, Springer, ProQuest, Anthrosource, Web of Science, our institutional library catalog, and Google Scholar. This search strategy covered a wide range of publications in social science, environmental science, homeland security, risk analysis, and other related areas. We also found sources via snowballing, i.e., using citations in articles already retrieved. Keywords used to search include place names, contaminants, social science concepts, and cleanup actions (see table 2). Searches included alterative spellings, e.g. cleanup, clean-up, clean up. Keyword strings varied depending on the database's topical focus and search capability.

Since many of the searches turned up technical and engineering articles outside the scope of this review, a quick reading of the source's title and abstract ascertained its possible relevance. We recorded the number of relevant hits in an Access® database. For sources that made it through this first round of selection, we entered bibliographic information into an Access® database and EndNote® library. We searched bibliographic databases until article saturation was achieved, that is, additional keyword searches failed to turn up new relevant articles.

The second step of the review was to acquire and read a full-text version of each source. We eliminated some articles at this step because of access limitations. We evaluated full-text articles for compliance with the five selection criteria described above. To reach agreement on source selection, we each ranked the articles on a one-to-three compliance scale: (1) did not meet the criteria; (2) met some but not all; (3) met all criteria. We totaled the rankings for each source and then discussed sources that ranked below a seven out of nine to reach consensus on whether they should be included. At this stage, we evaluated gray literature sources using the quality control standards described above.

The third and final stage of the review process involved a close textual reading of the selected articles and thematic evaluation of article contents. We recorded research notes in EndNote® for each article's topic, research methods, cleanup situation, and main argument. We then created mind maps to identify major themes and conducted a thematic synthesis of article content (Hart 1998, Thomas and Harden 2008). We also conducted a quantitative analysis of article metadata using NVivo®. We coded metadata for each source by geographic location in which the research took place, phase of cleanup addressed, type of

Table 2. A list of keywords and search strings used in the literature search.

Search keywords and search strings	
Actor network theory decontamination	Hazardous waste cleanup
Anthrax/Amerithrax	How clean is clean
Anthrax/Amerithrax and decontamination	Libby, Montana
Bikini atoll/Marshall Islands	Livestock carcass disposal
Biosafety	Love Canal
Biosecurity	Love Canal and remediation
BP/Deepwater Horizon	Milwaukee (Cryptosporidium outbreak)
Brownfield	Minot, North Dakota
BSE	Mitigation
Chemical spill	Nuclear
Chemical spill and clean-up	Nuclear waste disposal
Chernobyl	Oil spill
Chernobyl and social impacts	Oil spill and clean-up
Clean-up	Oil spill and cleanup and social impacts
Cleanup and radiation	Oil train derailment/Lac-Mégantic
Clean-up and social effects	Pensacola, Florida—Mt. Dioxin
Clean-up and toxic spill	Plague
Clearance	Radiological
Community	Remediation
Construction	Rocky flats
Cost	Social impacts and cleanup
Decontamination	Social impacts and decontamination
Disaster and clean-up	Social stigma
Ebola and social stigma	Superfund and clean-up
Endicott, NY—IBM	Superfund, CERCLA
Foreign animal disease threat	TB sanatorium
Fukushima and remediation	Three Mile Island
Fukushima, Japan	Three Mile Island and cleanup
Gold King Mine	Toxic spill
Hanford	Vieques, Puerto Rico
Hanford and cleanup	World trade center and clean-up
Hansen's disease/leper colony	

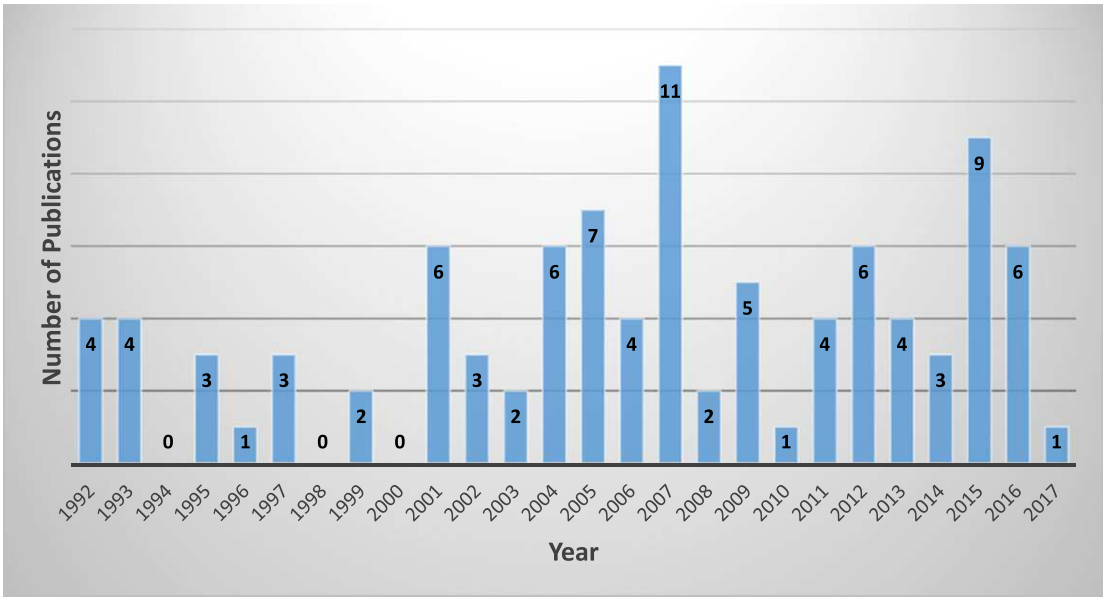

Figure 2. The distribution of sources by publication year ($n = 97$).

contaminant, discipline, and methodology. We then tabulated these metadata categories.

There were limitations to this systematic literature review. The review addresses the social dimensions of cleanup, which is only a subset of the social impacts of contamination. The bibliographic databases searched might not contain all relevant publications. While the review did include non-US materials, the search and selection protocol used did not require international representation and may not have captured all international publications. For example, the databases used to find gray literature may not contain reports published in other countries. Alternatively, a source may have been in a database but not discoverable using the keywords selected. The term Superfund originates from US policy and may not be applicable elsewhere. An article framed around social theory might not use the technical language of decontamination. The review only included sources available via institutional library holdings and interlibrary loan agreements, which were limited. The English language criterion may have excluded relevant materials written in Russian, Japanese, and other languages. Because this research does not conduct a statistical analysis of article data, results are not skewed by not including every article published on a topic, as with quantitative reviews (Thomas and Harden 2008, Singh 2017). Our search did reach conceptual saturation, that is, it captured the range of concepts found in the literature (Thomas and Harden 2008).

3. Results and synthesis

3.1. The landscape of the literature

A total of 97 relevant articles was analyzed. Figure 2 shows the distribution of sources by publication year. The year 2007 has the greatest number of publications ($n = 11$), while 1994, 1988, and 2000 have none. There is a slight increase in coverage since 2000, but no apparent trend in peaks and valleys. For example, only two of the articles from the early 2000s analyze cleanup after the 9/11 attack on the World Trade Center, even though that incident involved a huge cleanup effort from the US. Given the wealth of remediation, removal, and decontamination activity in the US and elsewhere, finding only 97 relevant sources suggests that environmental cleanup may not be a popular topic in the social sciences.

Of the 97 sources found, 75 refer to specific case studies. The most common case studies are Chernobyl ($n = 10$), the Exxon Valdez oil spill ($n = 7$), and the Deepwater Horizon oil spill ($n = 5$). These case studies illustrate the predominance of social science analysis of emergency response to disasters. Figure 3 also highlights this trend. Most of the cleanup situations found in the literature are emergency response ($n = 48$) or Superfund sites ($n = 35$). Cleanups of brownfields and federal facilities are less well represented, as are smaller scale emergency response situations.

Figure 4 shows the distribution of cleanup situations that the articles analyze. The literature includes sites in United States, Belgium, Ukraine, China, England, Japan, South Korea, Liberia, Spain, Sweden, Finland, Canada, and Italy. There is none to limited coverage of cleanups in Africa, Latin America, Australia, and Asia.

The case studies analyze 18 Superfund sites in the US: Amchitka Island, Alaska; City of Bloomington, Indiana; RSR Corporation Site, Dallas, Texas; Emmell's Septic Landfill, New Jersey; Endicott, New York; Fresno Municipal Sanitary Landfill, California; Central

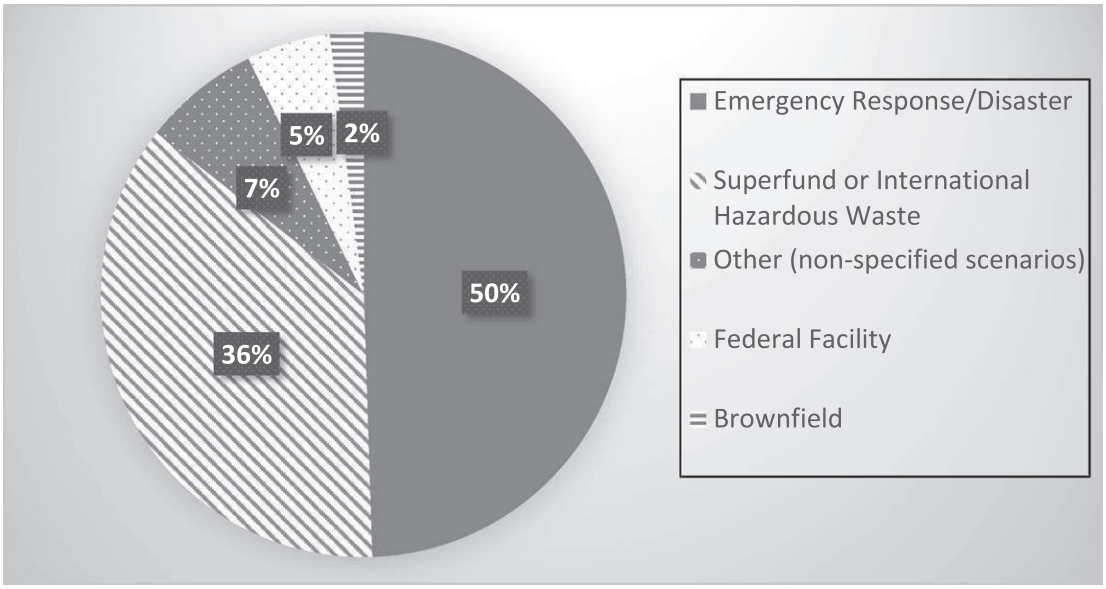

Figure 3. The percentage of literature sources ($n = 97$) covering each cleanup situation.

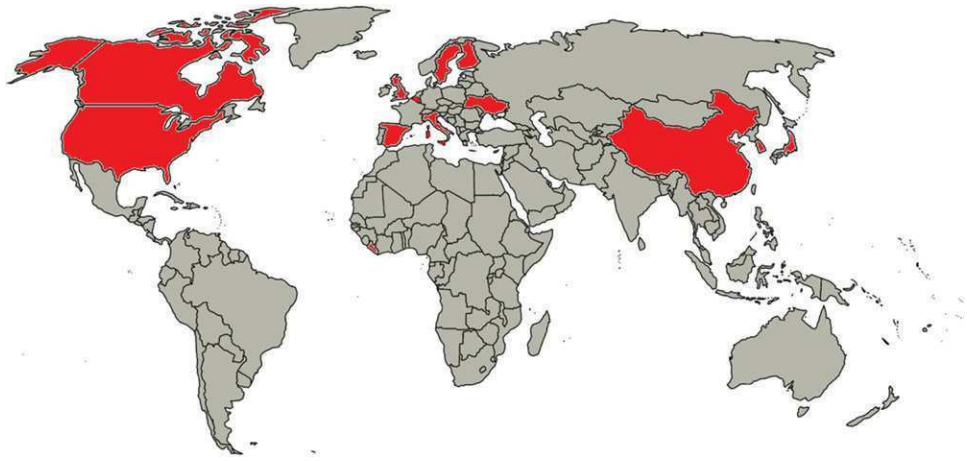

Figure 4. The countries highlighted in red were represented in case studies.

Chemical in Hagerstown, Maryland; Gowanus Canal, New York; Hanford, Washington; Los Alamos National Laboratory, New Mexico; Love Canal, New York; Middlefield-Ellis-Whisman, California; Tar Creek, Oklahoma; Rentokil Inc., Virginia; Rocky Flats, Colorado; Shell Oil Co dumpsite on the Swinomish Reservation, Washington; Three Mile Island, Pennsylvania; and Waukegan Harbor, Illinois.

The literature covers different phases of cleanups: pre-cleanup, during cleanup, and post-cleanup. Fifteen sources address the pre-cleanup phase, ten sources address the cleanup itself, and 30 sources address post-cleanup. Forty-two sources address multiple phases. The articles do not all delineate phases in the same way, nor does their terminology correspond exactly to the steps listed in table 1, which impeded comparison of the case studies.

The articles come from seven academic disciplines: anthropology, economics, human geography, policy and management, public health and medicine, sociology, and STS. They use a wide range of research methods, e.g. interviews, surveys, focus groups, and economic modeling. The most common methods are secondary analysis of existing data ($n = 24$) and interviews ($n = 21$). Figure 5 shows the distribution of academic disciplines and method type. To analyze methodological differences, we used four main method categorizations: qualitative, quantitative, mixed methods, secondary analysis. By mixed methods, we mean any study that combines quantitative and qualitative methods (Merriam and Tisdell 2015). By secondary analysis, we mean any study that reviewed the data or findings of other studies. The academic areas with the most representation in the literature are policy and

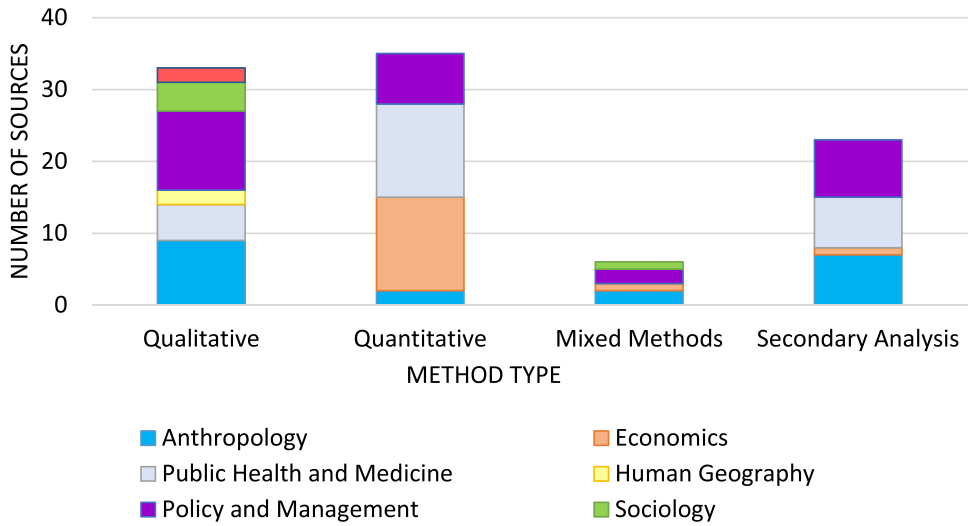

Figure 5. Methods used within the sources ($n = 97$) divided by discipline.

management ($n = 28$), public health and medicine ($n = 25$), and anthropology ($n = 20$). There is a near-even split between studies using qualitative ($n = 33$) and quantitative methods ($n = 35$). Far fewer studies use mixed methods ($n = 6$) such as integrating quantitative survey data with qualitative interviews or combining economic modeling with participant observation. As we will discuss later in this paper, the lack of mixed methods may be a result of limited cross-disciplinary engagement on this topic.

3.2. Worker health

One of the prominent themes in the literature is the analysis of short- and long-term impacts on the physical and mental health of cleanup workers. The articles document health problems among workers involved in the containment, removal, and remediation of toxic contaminants. They focus on notable case studies such as the 9/11 attacks on the World Trade Center, Deepwater Horizon oil spill, and Chernobyl and Fukushima nuclear disasters. The number of cleanup workers exposed to health risks is significant, particularly in large disasters. Over 800 000 'liquidators' worked with radiologically contaminated materials at Chernobyl between 1986 and 1989 alone (Bay and Oughton 2005). Formal measures of the number of cleanup workers may not even include residents, business owners, and others who initiate work on their own (Allen 2007).

The most common and longest studied aspect of worker health is cancer, followed by mental health and other aspects of physical health. The articles document that cleanup workers suffer from high rates of cancer (Bebeshko and Bobyliova 2002, Bay and Oughton 2005), prevalence of post-traumatic stress disorder and depression (Allen and D'Elia 2015, Bromet 2014, Laidra *et al* 2015, Horn *et al* 2016, Maeda and Oe 2015, Viel *et al* 1997, Zvolensky *et al* 2015), substance abuse (Bromet 2014, Laidra *et al* 2015), and respiratory diseases (Herbstman *et al* 2005). Many of these studies are retrospective, reviewing health data collected years before the analysis; or longitudinal, analyzing worker cohorts many years after a disaster (Bebeshko and Bobyliova 2002, Chernobyl Forum 2005, Eglite *et al* 2009).

While the studies use primarily epidemiological methods, this body of work also illuminates the broader social context of cleanup work. We highlight three aspects of this social context here. First, the articles raise concerns about workplace safety, i.e. protective gear, training, and information (Suárez *et al* 2005, Allen 2007, Wheeler *et al* 2007). Second, they touch on issues of environmental justice and ethics. They note that vulnerable populations, including prison inmates and immigrants, are unequally burdened with cleanup tasks and consequently exposed to greater health risks (Koo *et al* 1995, D'Andrea and Reddy 2013, Laidra *et al* 2015). Finally, the literature highlights the problem of stigma against people involved in cleanup activities (Bay and Oughton 2005, Chernobyl Forum 2005, Schneider 2012, Magill *et al* 2013, Bromet 2014, Pellecchia *et al* 2015). For example, Chernobyl liquidators were ostracized from their communities because people feared that radiation exposure was somehow contagious (Bay and Oughton 2005, Chernobyl Forum 2005, Bromet 2014).

3.3. Decision-making and public engagement

A second common theme found in the articles is decision-making and public engagement. These studies establish the necessity of public engagement by illuminating the social and political dimensions of technical cleanup decisions (e.g. Frickel 2012). Technical decisions made throughout cleanups include:

- where to sample for contaminants,
- how to analyze samples,
- how to set and meet quality control standards for data collection and analysis,
- what is the extent of contamination,
- which removal and remediation techniques to use,
- what cleanup levels to set,
- whether cleanup has achieved the desired reduction in contamination and health risks,
- where and how to dispose of the waste,
- what ongoing monitoring is necessary, and
- what types of post-cleanup land use are appropriate.

In addition, specific cleanup situations may require their own decisions. In the US, for example, CERCLA law requires determinations about whether to list a site on the NPL and when a site is clean enough to warrant deletion from the list.

The studies indicate that public views shape cleanup decisions as much as experts' technical determinations do. Moreover, lay and technical perceptions of risk often differ. Jorgensen (2016) observes that decisions about radiological cleanup depend on how affected people understand and tolerate risk. In a review of Superfund cleanup activities at the US Department of Energy's (DOE) Hanford Site, Gray and Becker (1993) argue that decisions have been driven more by public anxiety and politics than by scientific data. Affected communities may not accept agencies' technical determinations about health risks, remediation techniques, and cleanup levels. Instead, they apply socially contextual determinations of their own.

The articles further suggest that agencies' setting of technical standards itself has socio-political dimensions. Standards are set amid scientific debates tied to institutional power dynamics. Auer (2010), for example, describes negotiations between Finland and Sweden concerning tests to measure organochlorines in water. He argues that advances in testing technology in fact increased confusion in these negotiations, and warns that science and technology do not guarantee consensual decision-making.

The articles highlight trust as a critical social dimension of decision-making (Raimond 2001, Gephart 2003, Allen 2007, Cheong and Hazelwood 2015). Lack of trust in environmental officials undermined public trust in the information agencies provided following Hurricane Katrina, particularly when agencies appeared to undervalue local knowledge (Allen 2007). A long history of secrecy and concealment at former nuclear weapons production sites impedes public trust in cleanup activity at these sites (Raimond 2001, Gephart 2003). A lack of trust also exacerbated emergency responders' problems communicating with residents of Grand Isle, Louisiana, an insular community, during the Deepwater Horizon oil spill (Cheong and Hazelwood 2015).

The articles examine how decisions about future reuse of a site shape risk determinations and cleanup actions. They argue that present and future risks from existing contamination, remediation actions, and residual contamination following remediation must be balanced and considered in decision-making (Gochfeld *et al* 2007). They point out that when goals and options are not well defined, cleanup is hampered by uncertainty (Gray and Becker 1993). Recognizing these limitations, Beling *et al* (2007) suggest that Superfund processes allow for contingency planning.

Finally, the articles underscore the importance of public engagement to decision-making, even for technical decisions (Raimond 2001, Pellecchia *et al* 2015). The need to build consensus, share power, and establish trust is a recurring theme (e.g., Raimond 2001, Allen 2007, Jorgensen 2016). Ferris (1993) argues that cleanup solutions are more enduring at sites with higher community participation. Dukes (2007) posits that contaminated sites are an opportunity to build cumulative knowledge by including the public in deliberative, adaptive decision-making. Authors also point to challenges encountered during public engagement. For example, communities are not homogenous and may have internal socioeconomic and power inequalities. Participatory outreach may not reach all affected stakeholders (Miller 2016). Additionally, contamination incidents can exacerbate community divisions (Raimond 2001).

3.4. Evaluating societal benefits of cleanup

A third theme in the social science literature is evaluation of the broader societal benefits of cleanup. The articles found by this review primarily evaluated economic benefits in the form of housing value. The majority use hedonic pricing models to analyze local property values. Hedonic pricing is a revealed preference method that associates an increase in housing value after cleanup with the amenity value of living in an uncontaminated place. The articles apply hedonic pricing to housing around Superfund sites in the US (Kiel 1995, McClusky and Rausser 2003, Chattopadhyay *et al* 2005, Messer *et al* 2006, Noonan *et al* 2007, Greenstone and Gallagher 2008, Gamper-Rabindran and Timmins 2011, 2013). A few studies apply it to other cleanup situations, e.g. along nuclear waste transport routes (Gawande and Jenkins-Smith 2001), and near hazardous waste sites not on the NPL (Ketkar 1992, Ihlanfeldt and Taylor 2004). This method also provides a way of measuring stigma associated with site discovery, listing, and other cleanup actions (Kiel 1995, McClusky and Rausser 2003, Messer *et al* 2006). Post-cleanup housing values can be compared to pre-cleanup values to

determine whether stigma is overcome (Gamper-Rabindran and Timmins 2011, 2013).

We note methodological differences among the articles in their selection of regression models and datasets, radial distance of properties from a site (e.g. one mile, three miles), spatial unit of analysis (e.g. census tract, census block), type of property (e.g. owner-occupied housing, commercial), and timeline (e.g. after construction complete, after deletion). The authors also came to differing conclusions about the societal benefits of cleanups. The majority agrees that property values do increase after cleanup (Ketkar 1992, Ihlanfeldt and Taylor 2004, Chattopadhyay *et al* 2005, Gamper-Rabindran and Timmins 2011, Gamper-Rabindran and Timmins 2013). However, the amount of the estimated increase varies greatly, as do authors' interpretations of these numbers. Noonan *et al* (2007) posit that while direct impacts on housing are minimal, there may be positive indirect effects such as increased neighborhood investment. Kiel (1995) finds that housing prices do not recover enough to overcome initial stigma of site discovery and listing. Delaying cleanup worsens property value losses (Messer *et al* 2006). Greenstone and Gallagher (2008) argue that local property value increases are small relative to the high costs of Superfund cleanup. In contrast, Ihlanfeldt and Taylor (2004) argue that even high cleanup costs can be offset by increases in property values and, in turn, property taxes.

A few of the articles also discuss how cleanups may spur neighborhood gentrification (Noonan *et al* 2007, Gamper-Rabindran and Timmins 2011, 2013). With gentrification, housing prices increase but residents are priced out of the housing market. Neighborhood demographics can shift along the lines of race, class, and ethnicity. Gentrification is an environmental justice concern and can be an unintended social outcome of environmental cleanup.

4. Discussion

4.1. Trends in the literature

This literature review provides extensive evidence that social variables affect cleanup processes and outcomes in several ways. Cleanup activities affect worker health. Technical decisions are shaped by social and political dimensions. Completed cleanups have local socio-economic consequences.

The review uncovers several trends in the literature. First, there is limited geographic coverage in social science analysis of environmental cleanups. The dearth of articles about many parts of the world shown in figure 4 may be due in part to the limitations highlighted in the methods section 2.3. It may also reflect national differences in environmental policies, remediation activities, and terminology. A third possible explanation is the reliance that the social science literature has on case studies, particularly of highly visible incidents such as the Deepwater Horizon oil spill and Fukushima nuclear accident. These incidents mobilize extensive cleanup efforts, media attention, research interest, and funding. They involve complex social dynamics that can be studied over time. One repercussion of the reliance on high-profile incidents is that analysis of other types of contaminants and cleanup situations is limited. For example, site reports indicate that stakeholder engagement and public participation positively influence brownfields redevelopment in Europe (Payá Pérez and Peláez Sánchez 2017). Brownfields sites, however, comprised the smallest portion of articles (2%) found by this search. Moreover, there is limited comparison of case studies in the literature, which would be generative of social science theory of decontamination.

A second trend is that the articles operate largely in disciplinary silos. Anthropological studies of decontamination discourse are not in conversation with economic works on hedonic pricing. Epidemiological articles on cleanup worker health do not engage with the broader social science literature on labor practices, worker identity, and embodied stigma. Thus, the social context of cleanup work is missing: how do people come to be in this work, what are their work experiences, and how does it affect households and communities as well as individual health? The silo-ization of the literature is also apparent in that while the case studies uncover diverse social aspects of cleanups, they often lack a theoretical grounding. Observed trends in methodologies provide further evidence of silo-ization. The limited use of mixed methods, such as combining health surveys with ethnography, indicates a lack of interdisciplinary engagement. Another methodological gap is the relatively low number of ethnographic accounts of cleanup experiences. One exception is Little's (2012) study of people living with vapor mitigation systems installed in their houses as part of remediation of the IBM Endicott Superfund site in New York state. Ethnographic studies of cleanup workers, community activists, and agency staff would shed light on social relationships, cultural worldviews, decision-making, and health.

4.2. Future research needs

The review identifies research gaps in the four thematic areas. Na *et al* (2012) and D'Andrea and Reddy (2013) mention differences between male and female cleanup workers' risk exposure and health impacts. A deeper discussion of the gendered nature of cleanup work is absent. Zvolensky *et al* (2015) report how adverse mental health impacts to cleanup workers correlate with financial problems. It points to the need to investigate how cleanup work affects families and households as well as worker populations. The Chernobyl case studies primarily analyze possible health effects of low-dose radiation exposure over a long period of time (Barnes 2001, Bay and Oughton 2005,

Eglite *et al* 2009, Krasnov *et al* 2015, Laidra *et al* 2015). There is a need for longitudinal studies of other types of cleanup work.

In terms of public engagement, the articles do address how trust is lost and how mistrust affects cleanups (e.g., Eisenman *et al* 2004, Allen 2007, Ritchie *et al* 2013). However, there is limited coverage of research on how to build trust and maintain it over time. Future research could examine best practices in building consensus, sharing power, and establishing trust among stakeholders. It could field test strategies for effective public engagement in different cleanup situations.

The reliance found in this literature on hedonic pricing affords a relatively limited basis for measuring societal benefits of environmental cleanups. The studies primarily use this technique at Superfund sites, so its application to other cleanup situations and non-US sites remains untested. Hedonic pricing does not capture social consequences such as neighborhood gentrification. Cleanups may well benefit society in ways other than property values. New methods for evaluating societal benefits—and costs—should be developed and tested for their applicability to different cleanup situations. Methodological challenges remain for how to measure benefits that are not easily quantifiable, such as changes to risk perception and improved stakeholder relationships.

Greater comparison among sites within a given country and internationally is needed. It would help answer research questions about: how does stigma differ when radiological, chemical, or biological contaminants are involved? Are public engagement strategies transferable among Superfund, brownfields, and emergency response? Does post-cleanup gentrification play out differently in cities, suburbs, and rural areas? What are similarities and differences in public engagement strategies, worker health protection, and post-remediation property values when comparing sites internationally? Site comparison can help identify technical, policy, and public engagement approaches that foster achievement of positive social and environmental outcomes (Coulon *et al* 2016, Payá Pérez and Peláez Sánchez 2017). It can also assess how multi-criteria decision support tools (e.g., human health risk assessment (Wcislo *et al* 2016), integrated assessment modeling (Schädler *et al* 2012)) support cleanup decision-making (see Norrman *et al* 2016 for an example).

The review found that there is no overarching model or framework to explain how social dynamics affect cleanup activities, the origins of these dynamics, and what the social impacts of cleanup activities and outcomes of cleanup completion are. We suggest that a comprehensive framework should be developed. One possible theoretical foundation is a socio-environmental systems (SES) approach that addresses interactions between social and biophysical systems (Machlis *et al* 1997, Musters *et al* 1998). SES has largely focused on ecosystems, land use, and urban ecology, and does not always directly address human health, though, so a framework might also benefit from incorporating elements from health risk assessment (Wcislo *et al* 2016). Social science theory that situates people's relationships with chemicals, toxics, and post-industrial sites in a broader culture and political economic context (Fortun 2012, Shapiro and Kirksey 2017) may be informative, but challenging to incorporate into a model. Participatory socio-environmental modeling techniques may allow site-specific details to emerge (Gray *et al* 2018). This analysis identifies several important factors to address in a framework: multiple phases of cleanup actions; positive and negative social impacts (e.g. stigma); the social as well as toxicological context of worker health; governance approaches to public engagement, trust, and stigma; scientific decision-making; institutional roles and constraints; and measures of societal outcomes of cleanup.

4.3. Application to policy and practice

The case studies present strategies to help cleanups achieve positive social and environmental outcomes. For example, steps can be taken to support the health of workers and community members. In the US, removal and remediation is often done by contractors and sub-contractors. The US Government Accountability Office (2006) reports that DOE provided incentives for contractors to meet health and safety standards at the Rocky Flats Superfund site. Moreover, it encouraged contractors to share the incentives with workers. Providing additional worker benefits such as counseling, financial management, and transition aid can aid worker health and reduce local economic shock after cleanups are complete (US Government Accountability Office 2006, Zvolensky *et al* 2015). Counseling services could be provided for affected communities through coordination with health organizations. Overall, this body of literature prompts us to reevaluate cost-benefit analysis of remediation by considering the toll it takes on workers (Leigh and Hoskin 1999, Lowe *et al* 2015). It also underscores the importance of providing mental health services for cleanup workers and affected communities, in addition to physical health monitoring.

The articles detail techniques that have been used for effective public engagement. Halfacre (2009) suggests using focus groups to elicit concerns of underrepresented stakeholder groups as a complement to community-wide meetings. Burger *et al* (2005) describe a process of consensus building that engages citizens and scientists in development of a science plan. The National Research Council (2005) outlines steps to help achieve socially acceptable cleanup standards. Zaferatos (2006) stresses the importance doing truly meaningful consultation when working with Tribal Nations. Unfortunately, it may be difficult for agencies to adopt these best practices and adapt them

to different cleanup situations given limited authority, budgets, and staffing.

It may be more challenging to put into practice hedonic pricing methods to evaluate cleanup outcomes. They may be of limited applicability to emergency response and the other non-Superfund cleanup situations listed in table 1. It takes expertise, time, and funding to obtain and analyze local housing data. These economic articles do suggest changes to policy and practice. The observation that delaying cleanup worsens property value losses provides a strong impetus for getting cleanups done in a timely manner (Ketkar 1992, Sigman 2001, Ihlanfeldt and Taylor 2004, Messer *et al* 2006). The observation that stigma can increase as additional cleanup actions are announced (Messer *et al* 2006) is a reason to carefully craft communications and public engagement so as not to inadvertently increase stigma.

4.4. Complicating cleanups

Agency definitions, case study descriptions, and statutory language often characterize environmental cleanups as involving discrete sites or incidents, established cleanup goals, a prescribed set of steps and actions, and measurable transition from a contaminated site to a cleaned-up one. This literature review instead reveals a fuzziness to the boundaries of what a site is, timeline for when cleanup begins and ends, and the social meaning of contamination, decontamination, and clean. For example, many hazardous waste sites have more than one contaminant. Site assessment, remediation, and community engagement may need to address uncertainties about cumulative health risks from multiple contaminants.

The spatial unboundedness of sites is made apparent by the extent of cleanup activities, workers, and community impacts in large-scale disasters such as the Deepwater Horizon and Exxon Valdez oil spills (Shaw 1992, Russell *et al* 1993, Bond 2013). It is underscored by the complexities of managing cleanup goals and actions at Superfund sites that are dozens of square miles or more with varying levels of contaminants across the site (Gray and Becker 1993, Burger *et al* 2004). Even smaller sites may be physically cordoned off but still retain community ties and be of local cultural or historical significance (Bluestone 2007, Kirkwood 2007). The final disposal location for waste that is removed also complicates the idea of what a site is. Waste disposal sites may be enmeshed in environmental justice struggles of their own (Wright 2011).

Articles delineate cleanup phases differently than the official steps detailed in table 1, bringing cleanup timelines into question (e.g. Ketkar 1992, Bittner 1993, Anspaugh 1996, Page 1997, Allen 2007). The predominance of multi-phase analysis in the literature suggests it is important to analyze cleanups holistically, rather than in discrete parts. It also suggests that remediation and incident response steps are experienced as loosely bounded temporal phenomena. Site discovery, listing, and assessment may be iterative processes rather than a single act (Zaferatos 2006). Moreover, there is a temporal collapse of pre- and post-cleanup during decision-making. Cleanup levels are set based on health risk assessments, as well as on expected post-cleanup land use (Gephart 2003, Masco 2004, Gochfeld *et al* 2007). How clean is clean thus differs for sites intended for residential, industrial, or conservation use. Being able to assess redevelopment options early on is important (Wcislo *et al* 2016).

Stakeholders who bring different needs, values, and goals to the table contest the meaning of how clean is clean (Hoffman 1995, Gephart 2003, Cheong 2012). Approaches that use only technical criteria to determine when a site is cleaned-up and do not take social contexts into account are not likely to resolve these conflicts (Elcock *et al* 2004, Auer 2010, Frickel 2012). At Love Canal, for example, only a single guideline about dioxin was used as a standard for reoccupation habitability despite the multitude of contaminants at the site (Hoffman 1995). The nuclear era itself has led to modifications of what is considered background levels of radiation against which the health effects of contamination are measured (Masco 2004).

Cleanup complexities require further research to advance social theory about contaminated and post-contaminated lands and bodies, i.e. theories of the Anthropocene, disasters, late-industrialism, chemo-ethnography, and infrastructure-society relations (Fortun 2012, Moore 2016, Anand 2017, Barrios 2017, Malhi 2017, Shapiro and Kirksey 2017). Understanding these complexities is of more than theoretical importance, since debates over how clean is clean can contribute to cleanup delays (Page 1997). Being able to understand and navigate these complexities can resolve social conflicts that arise, allow cleanups to proceed despite scientific uncertainty, and support informed decision-making that considers potential social and economic outcomes.

5. Conclusions

This literature review highlights the complex ways that social factors affect environmental cleanup processes and outcomes. It establishes what we term the 'social science of decontamination' as an area of study. There are an emerging number of articles, books, and gray literature from a variety of academic disciplines that address this topic.

Several important themes emerge from the review. Public health and epidemiological studies document the impact of environmental cleanups on worker physical and mental health. Many of these focus on the case study of Chernobyl. This research lays the foundation for discussions of worker rights and the connection between social vulnerabilities and environmental cleanup work. Another theme in the literature is the focus on

improving decision-making and risk analysis processes. Many of these studies assert the importance of public engagement and the need for more public involvement in cleanup decisions to improve outcomes and avoid conflicts. They also highlight how decisions about future reuse of sites shape risk determinations and cleanup actions, demonstrating the importance of using a systems approach and analyzing cleanups as a multi-phase process. The third major theme in the literature is evaluation of societal outcomes of cleanup, primarily through hedonic price models of property values near Superfund sites in the US.

Despite the variety of literature relating to the social science of decontamination, there is still a need for further studies due to specific gaps. The studies utilize a wide array of qualitative and quantitative research methods, but there is a lack of mixed methods and interdisciplinary engagement within the social sciences. Many articles rely on case studies of large-scale disasters or Superfund sites, leaving room for comparisons of how social dynamics differ among cleanup situations. In particular, more international comparisons would aid understanding of how these dynamics play out in places with different forms of governance and social histories. Development of a comprehensive framework or model is necessary to advance the social science of decontamination. Broader questions complicating cleanups need to be explored. Further investigation into specific topics such as labor practices, gender, race, and power relationships is also necessary. Overall, this area of research has significant potential to benefit environmental cleanup policy and practice, as well as advance social theory about people and the environment.

Acknowledgments

This project was supported in part by an appointment to the Internship/Research Participation Program at the EPA's Office of Research and Development, administered by the Oak Ridge Institute for Science and Education through an interagency agreement between DOE and EPA. It was also supported by an American Association for the Advancement of Science, Science & Technology Policy Fellowship participant at the EPA Office of Research & Development, National Homeland Security Research Center, Threat & Consequence Assessment Division. Many thanks to Bruce Duncan, Katie Williams, Emily Snyder, Shawn Ryan, and the anonymous journal referees. Their thoughtful reviews helped improve the article.

Disclaimer

The authors declare no conflicts of interest with the publication of this research. EPA funded & managed the research described. It has been subjected to the Agency's review & has been approved for publication & distribution. Note that approval does not signify that the contents necessarily reflect the views of the Agency. Mention of trade names, products, or services does not convey official EPA approval, endorsement, or recommendation.

ORCID iDs

Keely Maxwell https://orcid.org/0000-0002-0802-4723
Brittany Kiessling https://orcid.org/0000-0003-3124-7375
Jenifer Buckley https://orcid.org/0000-0002-8294-1482

References

40 CFR 300 1994 National Oil and Hazardous Substances Pollution Contingency Plan, Final rule
Allen B 2007 Environmental justice, local knowledge, and after-disaster planning in New Orleans *Technol. Soc.* **29** 153–9
Allen P and D'Elia C 2015 What lies beneath: the BP oil spill and the need for new response models *Curr. Psychol.* **34** 587–96
Anand N 2017 *Hydraulic City: Water and the Infrastructures of Citizenship in Mumbai* (Durham: Duke University Press)
Anspaugh L 1996 A risk-based approach to cleanup—problems and pitfalls *Assessing the Risks of Nuclear and Chemical Contamination in the Former Soviet Union* ed E J Kirk (Dordrecht: Springer Netherlands) pp 29–32
Auer M 2010 Better science and worse diplomacy: negotiating the cleanup of the Swedish and Finnish pulp and paper industry *Int. Environ. Agreements: Politics, Law Econ.* **10** 65–84
Barnes J 2001 Sensitivity syndromes' related to radiation exposures *Med. Hypotheses* **57** 453–8
Barrios R 2017 What does catastrophe reveal for whom? The anthropology of crises and disasters at the onset of the anthropocene *Annu. Rev. Anthropol.* **46** 151–66
Bay I and Oughton D 2005 Social and economic effects *Chernobyl—Catastrophe and Consequences* (Berlin: Springer) pp 239–66
Bebeshko V and Bobyliova O 2002 Medical consequences of the Chernobyl nuclear power plant accident: experience of 15-year studies *Int. Congr. Ser.* **1234** 267–79
Beling P A, Lambert J H, Rahman F A, Overstreet G O and Slutzky D 2007 Systems analysis and adaptive learning for portfolio management of Superfund sites *Reclaiming the Land: Rethinking Superfund Institutions, Methods and Practices* ed G P Macey and J Z Cannon (New York: Springer) pp 129–68
Bittner J 1993 Cultural resources and the Exxon Valdez oil spill: an overview *Paper presented at the Exxon Valdez Oil Spill Symp. (Anchorage, Alaska)*
Bluestone D 2007 Toxic sites as places of culture and memory: adaptive management for citizenship *Reclaiming the Land: Rethinking Superfund Institutions, Methods and Practices* ed G P Macey and J Z Cannon (New York: Springer) pp 245–66
Bond D 2013 Governing disaster: the political life of the environment during the BP oil spill *Cultural Anthropol.* **28** 694–715
Bromet E J 2014 Emotional consequences of nuclear power plant disasters *J. Health Phys.* **106** 206–10
Burger J *et al* 2005 Science, policy, and stakeholders: developing a consensus science plan for Amchitka Island, Aleutians, Alaska *Environ. Manage.* **35** 557–68
Burger J, Greenberg M, Powers C and Gochfeld M 2004 Reducing the footprint of contaminated lands: US Department of Energy sites as a case study *Risk Manage.* **6** 41–63
Chattopadhyay S, Braden J and Patunru A 2005 Benefits of hazardous waste cleanup: new evidence from survey- and market-based property value approaches *Contemp. Econ. Policy* **23** 357–75
Cheong S-M 2012 Fishing and tourism impacts in the aftermath of the Hebei-Spirit Oil Spill *J. Coast. Res.* **28** 1648–53

Cheong S-M and Hazelwood E 2015 Insularity and oil spill response in Grand Isle *GeoJournal* **80** 679–87
Chernobyl Forum 2005 *Chernobyl's Legacy: Health, Environmental and Socio-Economic impacts and Recommendations to the Governments of Belarus* IAEA/PI/A.87 Rev.2 / 06-09181 International Atomic Energy Agency (IAEA)
Coulon F 2016 *Land Contamination and Brownfield management Policy Development in China: Learning from the UK Experience* China UK Partnership for Contaminated Land Management
Cram S 2015 Becoming Jane: the making and unmaking of Hanford's nuclear body *Environ. Plan. D-Soc. Space* **33** 796–812
D'Andrea M and Reddy G 2013 Health consequences among subjects involved in Gulf oil spill clean-up activities *Am. J. Med.* **126** 966–74
Dukes E F 2007 Rethinking community involvement for Superfund site reuse: the case for consensus-building in adaptive management *Reclaiming the Land: Rethinking Superfund Institutions, Methods and Practices* ed G P Macey and J Z Cannon (New York: Springer) pp 211–44
Eglite M, Zvagule T, Rainsford K, Reste J, Curbakova E and Kurjane N 2009 Clinical aspects of the health disturbances in Chernobyl Nuclear Power Plant accident clean-up workers (liquidators) from Latvia *Inflammopharmacology* **17** 163–9
Eisenman D, Wold C, Setodji C, Hickey S, Lee B, Stein B and Long A 2004 Will public health's response to terrorism be fair? Racial/ethnic variations in perceived fairness during a bioterrorist event *Biosecur. Bioterrorism: Biodef. Strategy, Pract. Sci.* **2** 146–56
Elcock D, Klemic G and Taboas A 2004 Establishing remediation levels in response to a radiological dispersal event (or 'dirty bomb') *Environ. Sci. Technol.* **38** 2505–12
EPA 2002 *Challenges Faced during the Environmental Protection Agency's Response to Anthrax and Recommendations for Enhancing Responses Capabilities: a Lessons Learned Report* (Washington, DC: EPA)
EPA 2003 *A Summary of General Assessment Factors for Evaluating the Quality of Scientific and Technical Information* EPA 100/B-03/001 EPA
EPA 2013 *National Center for Environmental Assessment (NCEA) Office of Research and Development Quality Management Plan for Scientific Research* ORDQMP-01-01 EPA
EPA 2015 *Population Surrounding 1388 Superfund Remedial Sites* EPA
EPA 2017 Types of contaminated sites https://epa.gov/enforcement/types-contaminated-sites (Accessed: 20 March 2018)
EPA 2018 Emergency response https://epa.gov/emergency-response (Accessed: 20 March 2018)
Ferris D 1994 Communities of color and hazardous waste cleanup: expanding public participation in the federal Superfund program *Fordham Urban Law J.* **21** 671–88
Fortun K 2012 Ethnography in late industrialism *Cultural Anthropol.* **27** 446–64
Fowlkes M R and Miller P Y 1983 *Love Canal: The Social Construction of Disaster* 83 03 07 039 FEMA
Franco C and Bouri N 2010 Environmental decontamination following a large-scale bioterrorism attack: Federal progress and remaining gaps *Biosecur. Bioterrorism: Biodef. Strategy, Pract. Sci.* **8** 107–17
Frickel S 2012 Missing New Orleans: tracking knowledge and ignorance through an urban hazardscape *Histories of the Dustheap: Waste, Material Cultures, Social Justice* ed S Foote and E Mazzolini (Cambridge, Massachusetts: MIT Press) pp 97–117
Gamper-Rabindran S and Timmins C 2011 Hazardous waste cleanup, neighborhood gentrification, and environmental justice: evidence from restricted access census block data *Am. Econ. Rev.* **101** 5
Gamper-Rabindran S and Timmins C 2013 Does cleanup of hazardous waste sites raise housing values? Evidence of spatially localized benefits *J. Environ. Econ. Manage.* **65** 345–60
Gawande K and Jenkins-Smith H 2001 Nuclear waste transport and residential property values: estimating the effects of perceived risks *J. Environ. Econ. Manage.* **42** 207–33
Gephart R 2003 *Hanford: A Conversation About Nuclear Waste and Cleanup* (Columbus, Ohio: Battelle Press)
Gochfeld M, Burger J, Friedlander B and Powers C 2007 Approaches for assessing hazards and risks to workers and the public from contaminated land *Remediation* **18** 29–57
Grant M J and Booth A 2009 A typology of reviews: an analysis of 14 review types and associated methodologies *Health Inf. Libr. J.* **26** 91–108
Gray R and Becker C 1993 Environmental cleanup: the challenge at the Hanford site, Washington, USA *Environ. Manage.* **17** 461
Gray S *et al* 2018 Purpose, processes, partnerships, and products: four Ps to advance participatory socio-environmental modeling *Ecol. Appl.* **28** 46–61
Greenstone M and Gallagher J 2008 Does hazardous waste matter? Evidence from the housing market and the Superfund program *Q. J. Econ.* **123** 951–1003
Halfacre A 2009 The use of focus groups in assessing ethnic and racial group concerns about nuclear waste cleanup *Public Participation and Better Environmental Decisions: The Promise and Limits of Participatory Processes for the Quality of Environmentally Related Decision-Making* ed F H J M Coenen (Dordrecht: Springer) pp 35–55
Hamilton J and Viscusi W 1999 How costly is 'clean'? An analysis of the benefits and costs of Superfund site remediations *J. Policy Anal. Manage.* **18** 2–27
Hart C 1998 *Doing a Literature Review: Releasing the Social Science Research Imagination* (London: SAGE)
Herbstman J, Frank R, Schwab M, Williams D, Samet J, Breysse P and Geyh A 2005 Respiratory effects of inhalation exposure among workers during the clean-up effort at the World Trade Center disaster site *Environ. Res.* **99** 85–92
Hoffman A 1995 An uneasy rebirth at Love Canal *Environment* **37** 4
Horn S *et al* 2016 Latent typologies of posttraumatic stress disorder in World Trade Center responders *J. Psychiatric Res.* **83** 151–9
Ihlanfeldt K and Taylor L 2004 Externality effects of small-scale hazardous waste sites: evidence from urban commercial property markets *J. Environ. Econ. Manage.* **47** 117–39
Interstate Technology and Regulatory Council (ITRC) 2002 *Determining Cleanup Goals at Radioactively Contaminated Sites: Case Studies* ITRC
Jorgensen T 2016 The new 'normal': stakeholders and radiation protection limits in a post-9/11 world *J. Health Phys.* **111** 227–31
Ketkar K 1992 Hazardous waste sites and property values in the state of New Jersey *Appl. Econ.* **24** 647–59
Kiel K 1995 Measuring the impact of the discovery and cleaning of identified hazardous waste sites on house values *Land Econ.* **71** 428–35
Kirkwood N 2007 CHAT: approaches to long-term planning for the Tar Creek Superfund Site, Ottawa County, Oklahoma *Reclaiming the Land: Rethinking Superfund Institutions, Methods and Practices* ed G P Macey and J Z Cannon (New York: Springer) pp 267–92
Koo D, Goldman L and Baron R 1995 Irritant dermatitis among workers cleaning up a pesticide spill: California 1991 *Am. J. Ind. Med.* **27** 545–53
Krasnov V, Kryukov V, Samedova E, Emelianova I and Ryzhova I 2015 Early aging in Chernobyl clean-up workers: long-term study *BioMed Research International* **2015** 1–5
Laidra K, Rahu K, Tekkel M, Aluoja A and Leinsalu M 2015 Mental health and alcohol problems among Estonian cleanup workers 24 years after the Chernobyl accident *Soc. Psychiatry Psychiatric Epidemiol.* **50** 1753–60
Layzer J 2012 *The Environmental Case: Translating Values into Policy* (Washington, DC: CQ Press)
Leigh J P and Hoskin A 1999 Hazards for nearby residents and cleanup workers of waste sites *J. Occup. Environ. Med.* **41** 331–48

Little P C 2012 Another angle on pollution experience: toward an anthropology of the emotional ecology of risk mitigation *ETHOS* **40** 431–52
Lowe S, Kwok R, Payne J, Engel L, Galea S and Sandler D 2015 Mental health service use by cleanup workers in the aftermath of the Deepwater Horizon oil spill *Soc. Sci. Med.* **130** 125–34
Machlis G E, Force J E and Burch W R 1997 The human ecosystem: I. The human ecosystem as an organizing concept in ecosystem management *Soc. Nat. Res.* **10** 347–67
Maeda M and Oe M 2015 The Great East Japan Earthquake: Tsunami and nuclear disaster *Traumatic Stress and Long-Term Recovery: Coping with Disasters and Other Negative Life Events* ed K Cherry (Cham: Springer) pp 71–90
Magill C, Wilson T and Okada T 2013 Observations of tephra fall impacts from the 2011 shinmoedake eruption, Japan *Earth, Planets Space* **65** 18
Malhi Y 2017 The concept of the anthropocene *Annu. Rev. Environ. Res.* **42** 77–104
Masco J 2004 Mutant ecologies: radioactive life in post—Cold War New Mexico *Cultural Anthropol.* **19** 517–50
McCaffrey K and Baver S 2006 'Ni una bomba mas': reframing the Vieques struggle *Beyond Sun and Sand: Caribbean Environmentalisms. Rutgers* ed S Baver and B Lynch (Rutgers: Rutgers University Press)
McCluskey J and Rausser G 2003 Hazardous waste sites and housing appreciation rates *J. Environ. Econ. Manage.* **45** 166–76
Merriam S B and Tisdell E J 2015 . *Qualitative Research: A Guide to Design and Implementation* 4th edn (San Francisco, CA: Jossey-Bass)
Messer K, Schulze W, Hackett K, Cameron T and McClelland G 2006 Can stigma explain large property value losses? The psychology and economics of Superfund *Environ. Res. Econ.* **33** 299–324
Miller J 2016 Is urban greening for everyone? Social inclusion and exclusion along the Gowanus Canal *Urban Forestry Urban Greening* **19** 285–94
Moher D, Liberati A, Tetzlaff J, Altman D G and The P G 2009 Preferred reporting items for systematic reviews and meta-analyses: the PRISMA statement *Ann. Intern. Med.* **151** 264–9
Moore A 2016 Anthropocene anthropology: reconceptualizing contemporary global change *J. R. Anthropol. Inst.* **22** 27–46
Musters C J M, de Graaf H J and ter Keurs W J 1998 Defining socio-environmental systems for sustainable development *Ecol. Econ.* **26** 243–58
Na J U, Sim M, Jo I and Song H 2012 The duration of acute health problems in people involved with the cleanup operation of the Hebei Spirit oil spill *Mar. Pollut. Bull.* **64** 1246–51
National Research Council 2005 *Reopening Public Facilities After a Biological Attack: A Decision Making Framework* National Academies Press (https://doi.org/10.17226/11324)
Noonan D, Krupka D and Baden B 2007 Neighborhood dynamics and price effects of Superfund site clean-up *J. Reg. Sci.* **47** 665–92
Norrman J *et al* 2016 Integration of the subsurface and the surface sectors for a more holistic approach for sustainable redevelopment of urban brownfields *Sci. Total Environ.* **563–564** 879–89
Page G 1997 The social, economic, business, and policy dimensions of bioremediation techniques *Biotechnology for Waste Management and Site Restoration: Technological, Educational, Business, Political Aspects* ed C Ronneau and O Bitchaeva (Dordrecht: Springer) pp 9–18
Payá Pérez A and Peláez Sánchez S 2017 *European Achievements in Soil Remediation and Brownfield Redevelopment* (European Union)
Pellecchia U, Crestani R, Decroo T, Bergh R and Al-Kourdi Y 2015 Social consequences of ebola containment measures in Liberia *PLoS One* **10** 1–12
Petryna A 1995 Sarcophagus: Chernobyl in historical light *Cultural Anthropol.* **10** 196–220
Raimond R R 2001 *Trust and Conflict in Public Participation*. Colorado Department of Public Health and Environment
Ritchie L, Gill D and Farnham C 2013 Recreancy revisited: beliefs about institutional failure following the Exxon Valdez oil spill *Soc. Nat. Res.* **26** 655–71
Russell J, Downs M, Petterson J and Palinkas L 1993 Psychological and social impacts of the Exxon Valdez oil spill and cleanup *Paper presented at the Exxon Valdez Oil Spill Symp. (Anchorage, Alaska)*
Schneider D 2012 Purification or profit: Milwaukee and the contradictions of sludge *Histories of the Dustheap* ed S Foote and E Mazzolini (Cambridge, MA: MIT Press)
Schädler S, Morio M, Bartke S and Finkel M 2012 Integrated planning and spatial evaluation of megasite remediation and reuse options *J. Contaminant Hydrol.* **127** 88–100
Shapiro N and Kirksey E 2017 Chemo-ethnography: an introduction *Cultural Anthropol.* **32** 481–93
Shaw D 1992 The Exxon Valdez oil spill: ecological and social consequences *Environ. Conservation* **19** 253–8
Sigman H 2001 The pace of progress at Superfund sites: policy goals and interest group influence *J. Law Econ.* **44** 315–44
Singh S 2017 How to conduct and interpret systematic reviews and meta-analyses *Clin. Transl. Gastroenterol.* **8** e93
Smith J T 2005 *Chernobyl—Catastrophe and consequences* (Berlin: Springer)
Suárez B *et al* 2005 Acute health problems among subjects involved in the cleanup operation following the Prestige oil spill in Asturias and Cantabria (Spain) *Environ. Res.* **99** 413–24
Thomas J and Harden A 2008 Methods for the thematic synthesis of qualitative research in systematic reviews *BMC Med. Res. Methodol.* **8** 45
US Government Accountability Office 2006 *Nuclear Cleanup of Rocky Flats: DOE can use Lessons Learned to Improve Oversight of other Sites' Cleanup Activities (GAO-06-352)* GAO-06-352 US Government Accountability Office
Van Horn C and Chilik Y 1988 How clean is clean? A case study of the nation's no. 1 Superfund toxic dump *Environ. Impact Assess. Rev.* **8** 133–48
Viel J F, Curbakova E, Dzerve B, Eglite M, Zvagule T and Vincent C 1997 Risk factors for long-term mental and psychosomatic distress in Latvian Chernobyl liquidators *Environ. Health Perspect.* **105** 1539–44
Wcislo E, Bronder J, Bubak A, Rodriguez-Valdes E and Gallebo J L R 2016 Human health risk assessment in restoring safe and productive use of abandoned contaminated sites *Environ. Int.* **94** 436–48
Wheeler K *et al* 2007 Asthma diagnosed after 11 september 2001 among rescue and recovery workers: findings from the world trade center health registry *Environ. Health Perspect.* **115** 1584–90
Wright B 2011 Race, place, and the environment in the aftermath of Katrina *Anthropol. Work Rev.* **32** 4–8
Zaferatos N C 2006 Environmental justice in Indian Country: dumpsite remediation on the Swinomish Indian Reservation *Environ. Manage.* **38** 896–909
Zvolensky M *et al* 2015 Post-disaster stressful life events and WTC-related posttraumatic stress, depressive symptoms, and overall functioning among responders to the world trade center disaster *J. Psychiatric Res.* **61** 97–105

Environmental Research Letters

TOPICAL REVIEW • **OPEN ACCESS**

How clean is clean: a review of the social science of environmental cleanups

To cite this article: Keely Maxwell *et al* 2018 *Environ. Res. Lett.* **13** 083002

View the article online for updates and enhancements.

This content was downloaded from IP address 161.80.170.183 on 16/08/2018 at 12:25

Environmental Research Letters

TOPICAL REVIEW

How clean is clean: a review of the social science of environmental cleanups

Keely Maxwell[1], **Brittany Kiessling**[2] and **Jenifer Buckley**[3]

[1] US Environmental Protection Agency (EPA), United States of America
[2] Oak Ridge Institute for Science & Education Research Participant at EPA, United States of America
[3] American Association for the Advancement of Science, Science & Technology Policy Fellowship, Program Participant at EPA, United States of America

E-mail: maxwell.keely@epa.gov

Keywords: decontamination, remediation, social science, Superfund, brownfields, megasites, public engagement

OPEN ACCESS

RECEIVED
31 August 2017

REVISED
30 July 2018

ACCEPTED FOR PUBLICATION
1 August 2018

PUBLISHED
16 August 2018

Original content from this work may be used under the terms of the Creative Commons Attribution 3.0 licence.

Any further distribution of this work must maintain attribution to the author(s) and the title of the work, journal citation and DOI.

Abstract

Environmental cleanup may involve decontaminating an area affected by a radiological release, containing an oil spill, or remediating a Superfund site or brownfield. It is a key component of how environmental agencies work to protect public health and the environment. There are many publications on technical protocols for cleanup and waste disposal. Additionally, there has been much social science work on the social problems of environmental contamination. However, social science research on cleanup itself has been much more scattered across disciplines and incidents. To date, there has not been a comprehensive review of the social factors that affect cleanup processes and outcomes. Such social factors may include cultural worldviews that shape stakeholder perspectives on 'how clean is clean' and social relationships among stakeholders. This article fills this gap by providing an interdisciplinary literature review of the social science of environmental cleanup. Three principal themes emerged from the 97 articles that met selection criteria: effects on cleanup worker health, public engagement and decision-making, and societal benefits of cleaned-up sites. The review points to areas where further research is needed. For example, there is a lack of mixed methods and interdisciplinary engagement within the literature. Additionally, few articles compare cleanup situations. There is also a need for further investigation into specific social science topics such as labor practices, gender, race, and power relationships. To address these gaps, we argue for the development of a comprehensive framework or model as well as the exploration of broader questions complicating cleanups. Overall, this area of research has significant potential to benefit environmental cleanup policy and practice worldwide, while advancing social theory about people and the environment.

1. Introduction and background

Cleaning up toxic contaminants and hazardous waste is a cornerstone of environmental protection in the United States (US) and abroad. In the US, there are 1345 sites on the Superfund National Priority List (NPL) and an estimated 450 000 contaminated brownfields properties. Approximately 53 million people (17% of the US population) live within 3 miles of a Superfund site (EPA 2015), making cleanups vital to public health. Environmental cleanup is also part of emergency response to oil spills, industrial and transportation accidents, and homeland security threats. In this paper, 'cleanup' refers to any part of the assessment, characterization, containment, removal, remediation, and waste disposal of chemical, biological, and radiological materials. Some hazardous waste sites, such as Love Canal and Warren County, North Carolina, play important roles in the history of US environmental policy and environmental justice. Others, such as historic industrial buildings contaminated with mercury or residential yards with high levels of lead in the soil, may not be nationally renowned yet still pose a risk to human health and require an extensive and costly cleanup.

Table 1 shows the range of situations included as environmental cleanup for the purposes of this analysis. It follows US Environmental Protection Agency

© 2018 The Author(s). Published by IOP Publishing Ltd

(EPA) categorizations and US policy approaches to provide consistency. Other countries may use slightly different categorizations (e.g. megasites, polluted sites), policy approaches (e.g. soil protection policies), and funding sources. The overarching goal of environmental cleanup is to protect human health and the environment, but there are differences among statutory requirements for achieving this goal. Each situation involves specific terminologies, activities, and phases. The term *remediation* refers to long-term actions at Superfund and brownfield sites to remove contaminants from different environmental media. Techniques include capping hazardous waste sites, dredging sediments in water bodies, and bioremediating using microbes to treat contaminated soil or groundwater on site. The term *decontamination*, in contrast, is more commonly used in emergency response when a substance is released that poses an 'imminent and substantial threat' to public health or the environment (40 CFR 300 1994). Decontamination refers to the inactivation, immobilization, or reduction of contaminants from a surface. For example, rooms containing *Bacillus anthracis* (the bacterium that causes anthrax) can be fumigated with chemicals to inactivate the spores. Surfaces contaminated with radiological materials can undergo physical or chemical decontamination. Responses to smaller release incidents are called *removal actions*. After an oil spill from an overturned truck, for example, contaminated soils are removed to be treated and disposed of elsewhere.

The cleanup situations in table 1 differ in several respects: the cause of contamination, materials handled, statutory authority, institutions involved, steps followed, funding stream, and future reuse. This diversity of cleanup situations is one indication of the complex social and political dynamics involved. Environmental and public health agencies, tribes, industry, private contractors, and community groups all play roles. Actions and timelines vary, as do the threat to human health, public engagement, and cost. Different cleanup situations use different criteria for cleanup standards. Superfund sites are cleaned to national standards, for example, whereas brownfields rely on state standards.

Cleanups take place everywhere from tribal lands to private residences on time scales of days to decades. During cleanups, stakeholders with existing social and power relationships engage in new ways. Stakeholders may not all use the same technical terms or even speak the same language. They may have competing ideas about health risks at a site, when is it clean enough, what does 'clean' even mean, and what constitutes appropriate post-cleanup land use (Fowlkes and Miller 1982, Interstate Technology and Regulatory Council ITRC 2002, van Horn and Chilik 1988, National Research Council 2005, McCaffrey and Baver 2006, Layzer 2012, Cram 2015).

Research from several social science disciplines has addressed social conflicts during cleanup (Fowlkes and Miller 1982), institutional decision-making (Interstate Technology and Regulatory Council ITRC 2002, Franco and Bouri 2010), and cost-benefit analysis (Hamilton and Viscusi 1999). Many studies are specific to a particular site such as Chernobyl in the Ukraine (Petryna 1995, Smith 2005) or Hanford in the United States (Gray and Becker 1993, Gephart 2003). To date, however, there has not been a comprehensive review of the social, economic, institutional, political, and cultural factors that affect cleanup processes and outcomes. Such a review is necessary to begin to develop an overarching framework to explain the social dynamics of environmental cleanup.

To fill this knowledge gap, we conducted a systematic, interdisciplinary literature review of the social science of environmental cleanups. The purpose of the review was to understand the current state of this literature and to identify key social variables that affect cleanup activities and outcomes. The review covered publications from anthropology, archeology, economics, environmental justice, environmental management, epidemiology, human geography, policy, public health, psychology, science and technology studies (STS), and sociology. Three common areas of investigation emerged from the review: physical and mental health of cleanup workers, public engagement in decision-making, and evaluation of societal benefits of cleanups.

The review should be of interest to social scientists, environmental scientists, and technical experts involved in cleanup decisions. It provides a baseline synthesis of scientific knowledge about the social dynamics of environmental cleanups. It also identifies research gaps, including a lack of cross-disciplinary fertilization and uneven coverage and comparison of cleanup situations. Overall, the review supports the development of an interdisciplinary systems framework for analyzing environmental cleanups and evaluating societal benefits.

2. Methods

2.1. Overview

This article uses a systematic literature review method, which involves article search and selection protocol, a defined research question or hypothesis, and a quantitative summary of results (Grant and Booth 2009, Singh 2017). It differs from systematic review methods from the clinical health literature in two respects. It provides a numerical analysis of article metadata but does not do a statistical analysis of article results (e.g. effect size) (Singh 2017). Instead, it uses a qualitative thematic synthesis or critical review to analyze the literature (Hart 1998, Thomas and Harden 2008, Grant and Booth 2009). Qualitative analysis is appropriate because this is exploratory research to identify social variables, not test a specific hypothesis. Figure 1 shows a preferred reporting items for systematic review and meta-analysis (PRISMA) diagram of the systematic search and selection process used (Moher *et al* 2009).

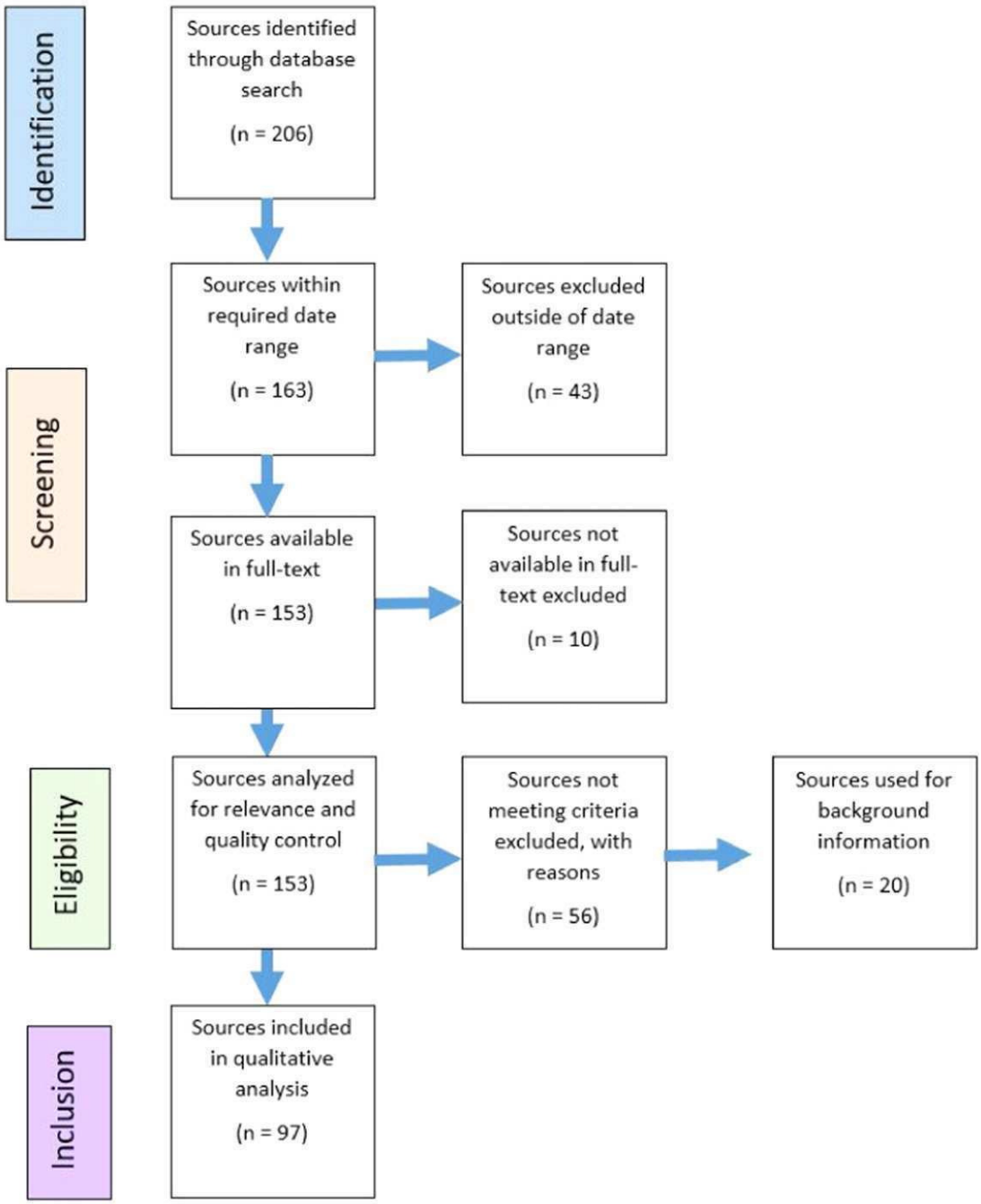

Figure 1. A PRISMA flow diagram illustrating the literature search process.

Literature sources included peer-reviewed journal articles, books, book chapters, e-books, and gray literature such as government agency reports. We included articles for review if the following criteria applied: (1) they use theories and/or methods from a social science discipline; (2) they address one or more social dimensions of environmental cleanups; (3) they were published in the last 25 years (1992–2017); (4) they meet quality control criteria (see below); and (5) they are written in English.

The five selection criteria allowed for inclusion of a diversity of publication types covering multiple disciplines, institutions, and countries. We excluded articles that provide a descriptive account of social conflict during a cleanup but do not use social theory or methods to analyze it. For example, our search returned technical assessments and reports about specific sites, but many of them did not have clear connections to social theory or employ social science research methods (e.g. interviews, surveys), so they were excluded from the analysis. We also excluded articles that address the social impacts of contamination but not decontamination. We limited the search to publications within the last 25 years to capture work published on cleanup actions under US environmental laws (e.g. Comprehensive Environmental Response,

Table 1. Types of environmental cleanups considered in this article (categorizations follow EPA 2017, 2018).

Cleanup category	Definition	Examples	Cleanup steps	Statutory authority	Funding
Emergency response	Response to oil spills, chemical, biological, radiological releases, and large-scale national emergencies.	• Natural disaster (medical waste, household hazardous waste, orphan containers, flood debris) • Oil spill • Train derailment • Chemical spill	• Removal assessment • Removal action	• CERCLA • SARA • Clean Water Act • National Contingency Plan • Oil Pollution Act • Stafford Act • Presidential Directives	• Stafford Act • Oil Spill Liability Trust Fund
Superfund sites/NPL sites	Uncontrolled or abandoned sites or properties where hazardous waste or other contamination is located. A contaminated site is generally considered a 'Superfund site' if the federal government is or plans to be involved in cleanup efforts. Note: NPL sites are those on the NPL; Superfund sites can be proposed or deleted from the list.	• Lead • Asbestos • Dioxin • Radiation • Agriculture runoff • Heavy metals • Industrial spill • Excludes coal mines	• Preliminary assessment/site investigation • NPL site listing • Remedial investigation/feasibility study • Records of decision • Remedial design/remedial action • Construction completion • Post-construction completion • NPL deletion • Site reuse/redevelopment	• CERCLA • SARA	• EPA grants • Technical Assistance Grants Program • Superfund Job Training Initiative • Superfund • Cost recovery
Brownfield sites	Real properties, the expansion, development, or reuse of which may be complicated by the presence of a hazardous substance, pollutant, or contaminant.	• Asbestos • Lead • Mine-scarred land • Former industrial site	• Assessment • Cleanup	• State environmental laws • Small Business Liability Relief and Brownfields Revitalization Act	• EPA Brownfields program grants • State response programs • State voluntary cleanup programs

Table 1. (Continued.)

Cleanup category	Definition	Examples	Cleanup steps	Statutory authority	Funding
					• Tax credits
State sites	Sites addressed by state, not EPA	All types of contaminants	• Depends on state	• State environmental laws	• State funding
Resource Conservation and Recovery Act (RCRA) corrective action	Treatment, storage and disposal facilities regulated under RCRA may have releases into the environment that require cleanup.	• Hazardous waste • Solid waste • Injection wells • Landfills	• Flexible may include: • Initial site assessment • Site characterization • Interim actions • Evaluate remedial alternatives • Implement remedy • Track process • Long-term care	• RCRA • Hazardous and Solid Waste Amendments (HSWA)	• Responsible parties
Underground storage tank sites (USTs)	Sites that contain contamination from petroleum products or Superfund hazardous substances released from underground storage tanks.	• Petroleum containers • Underground pipelines • Hazardous chemicals • Not septic tank, fuel container $<$1100 gal.	• Site characterization/assessment • Corrective action • Site closure	• RCRA • Solid Waste Disposal Act • Energy Policy Act of 2005	• Leaking Underground Storage Tank Trust Fund
Federal facilities	Properties owned or operated by the US government that may contain environmental contamination from unexploded ordnance, radioactive waste, or other hazardous substances.	• Military munitions • Unexploded ordnance • Hazardous chemicals • Federally owned wastewater treatment facilities	• Depends on site • Some federal facilities may be Superfund sites and follow Superfund steps.	• RCRA • HSWA • Safe Drinking Water Act • Clean Air Act • Clean Water Act • Oil Pollution Act	• Superfund • Department of Defense (DOD) • Department of Energy (DOE)

Compensation and Liability Act (CERCLA), Superfund Amendments and Reauthorization Act (SARA)), as well as homeland security incidents and technological disasters. We limited articles to English publications to avoid misinterpretations that could affect data quality. The articles had to be research articles, not book reviews, commentaries, or policy documents.

2.2. Quality control

We evaluated the articles according to a checklist of nine quality standards: focus, verity, integrity, rigor, soundness, applicability and utility, clarity and completeness, uncertainty and variability, and evaluation and review (EPA 2003, 2013). We evaluated gray literature sources according to these standards. If sources did not meet at least six of the nine quality standards, we did not include them. Because peer-reviewed sources such as books and journal articles are already evaluated by a similar system, we presumed that they met quality standards. We did assess the applicability of each source and the appropriate use of social science theory and methods for all articles, which served as another layer of quality assessment.

2.3. Literature search and analysis

We conducted keyword searches in the following databases: ScienceDirect, Springer, ProQuest, Anthrosource, Web of Science, our institutional library catalog, and Google Scholar. This search strategy covered a wide range of publications in social science, environmental science, homeland security, risk analysis, and other related areas. We also found sources via snowballing, i.e., using citations in articles already retrieved. Keywords used to search include place names, contaminants, social science concepts, and cleanup actions (see table 2). Searches included alterative spellings, e.g. cleanup, clean-up, clean up. Keyword strings varied depending on the database's topical focus and search capability.

Since many of the searches turned up technical and engineering articles outside the scope of this review, a quick reading of the source's title and abstract ascertained its possible relevance. We recorded the number of relevant hits in an Access® database. For sources that made it through this first round of selection, we entered bibliographic information into an Access® database and EndNote® library. We searched bibliographic databases until article saturation was achieved, that is, additional keyword searches failed to turn up new relevant articles.

The second step of the review was to acquire and read a full-text version of each source. We eliminated some articles at this step because of access limitations. We evaluated full-text articles for compliance with the five selection criteria described above. To reach agreement on source selection, we each ranked the articles on a one-to-three compliance scale: (1) did not meet the criteria; (2) met some but not all; (3) met all criteria. We totaled the rankings for each source and then discussed sources that ranked below a seven out of nine to reach consensus on whether they should be included. At this stage, we evaluated gray literature sources using the quality control standards described above.

The third and final stage of the review process involved a close textual reading of the selected articles and thematic evaluation of article contents. We recorded research notes in EndNote® for each article's topic, research methods, cleanup situation, and main argument. We then created mind maps to identify major themes and conducted a thematic synthesis of article content (Hart 1998, Thomas and Harden 2008). We also conducted a quantitative analysis of article metadata using NVivo®. We coded metadata for each source by geographic location in which the research took place, phase of cleanup addressed, type of

Table 2. A list of keywords and search strings used in the literature search.

Search keywords and search strings	
Actor network theory decontamination	Hazardous waste cleanup
Anthrax/Amerithrax	How clean is clean
Anthrax/Amerithrax and decontamination	Libby, Montana
Bikini atoll/Marshall Islands	Livestock carcass disposal
Biosafety	Love Canal
Biosecurity	Love Canal and remediation
BP/Deepwater Horizon	Milwaukee (Cryptosporidium outbreak)
Brownfield	Minot, North Dakota
BSE	Mitigation
Chemical spill	Nuclear
Chemical spill and clean-up	Nuclear waste disposal
Chernobyl	Oil spill
Chernobyl and social impacts	Oil spill and clean-up
Clean-up	Oil spill and cleanup and social impacts
Cleanup and radiation	Oil train derailment/Lac-Mégantic
Clean-up and social effects	Pensacola, Florida—Mt. Dioxin
Clean-up and toxic spill	Plague
Clearance	Radiological
Community	Remediation
Construction	Rocky flats
Cost	Social impacts and cleanup
Decontamination	Social impacts and decontamination
Disaster and clean-up	Social stigma
Ebola and social stigma	Superfund and clean-up
Endicott, NY—IBM	Superfund, CERCLA
Foreign animal disease threat	TB sanatorium
Fukushima and remediation	Three Mile Island
Fukushima, Japan	Three Mile Island and cleanup
Gold King Mine	Toxic spill
Hanford	Vieques, Puerto Rico
Hanford and cleanup	World trade center and clean-up
Hansen's disease/leper colony	

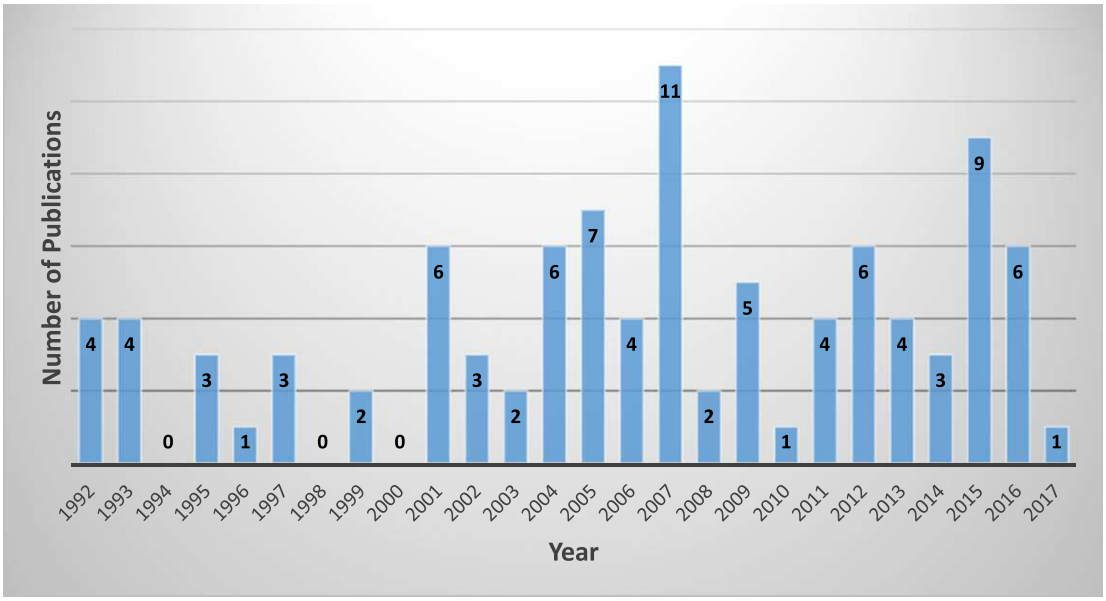

Figure 2. The distribution of sources by publication year ($n = 97$).

contaminant, discipline, and methodology. We then tabulated these metadata categories.

There were limitations to this systematic literature review. The review addresses the social dimensions of cleanup, which is only a subset of the social impacts of contamination. The bibliographic databases searched might not contain all relevant publications. While the review did include non-US materials, the search and selection protocol used did not require international representation and may not have captured all international publications. For example, the databases used to find gray literature may not contain reports published in other countries. Alternatively, a source may have been in a database but not discoverable using the keywords selected. The term Superfund originates from US policy and may not be applicable elsewhere. An article framed around social theory might not use the technical language of decontamination. The review only included sources available via institutional library holdings and interlibrary loan agreements, which were limited. The English language criterion may have excluded relevant materials written in Russian, Japanese, and other languages. Because this research does not conduct a statistical analysis of article data, results are not skewed by not including every article published on a topic, as with quantitative reviews (Thomas and Harden 2008, Singh 2017). Our search did reach conceptual saturation, that is, it captured the range of concepts found in the literature (Thomas and Harden 2008).

3. Results and synthesis

3.1. The landscape of the literature

A total of 97 relevant articles was analyzed. Figure 2 shows the distribution of sources by publication year. The year 2007 has the greatest number of publications ($n = 11$), while 1994, 1988, and 2000 have none. There is a slight increase in coverage since 2000, but no apparent trend in peaks and valleys. For example, only two of the articles from the early 2000s analyze cleanup after the 9/11 attack on the World Trade Center, even though that incident involved a huge cleanup effort from the US. Given the wealth of remediation, removal, and decontamination activity in the US and elsewhere, finding only 97 relevant sources suggests that environmental cleanup may not be a popular topic in the social sciences.

Of the 97 sources found, 75 refer to specific case studies. The most common case studies are Chernobyl ($n = 10$), the Exxon Valdez oil spill ($n = 7$), and the Deepwater Horizon oil spill ($n = 5$). These case studies illustrate the predominance of social science analysis of emergency response to disasters. Figure 3 also highlights this trend. Most of the cleanup situations found in the literature are emergency response ($n = 48$) or Superfund sites ($n = 35$). Cleanups of brownfields and federal facilities are less well represented, as are smaller scale emergency response situations.

Figure 4 shows the distribution of cleanup situations that the articles analyze. The literature includes sites in United States, Belgium, Ukraine, China, England, Japan, South Korea, Liberia, Spain, Sweden, Finland, Canada, and Italy. There is none to limited coverage of cleanups in Africa, Latin America, Australia, and Asia.

The case studies analyze 18 Superfund sites in the US: Amchitka Island, Alaska; City of Bloomington, Indiana; RSR Corporation Site, Dallas, Texas; Emmell's Septic Landfill, New Jersey; Endicott, New York; Fresno Municipal Sanitary Landfill, California; Central

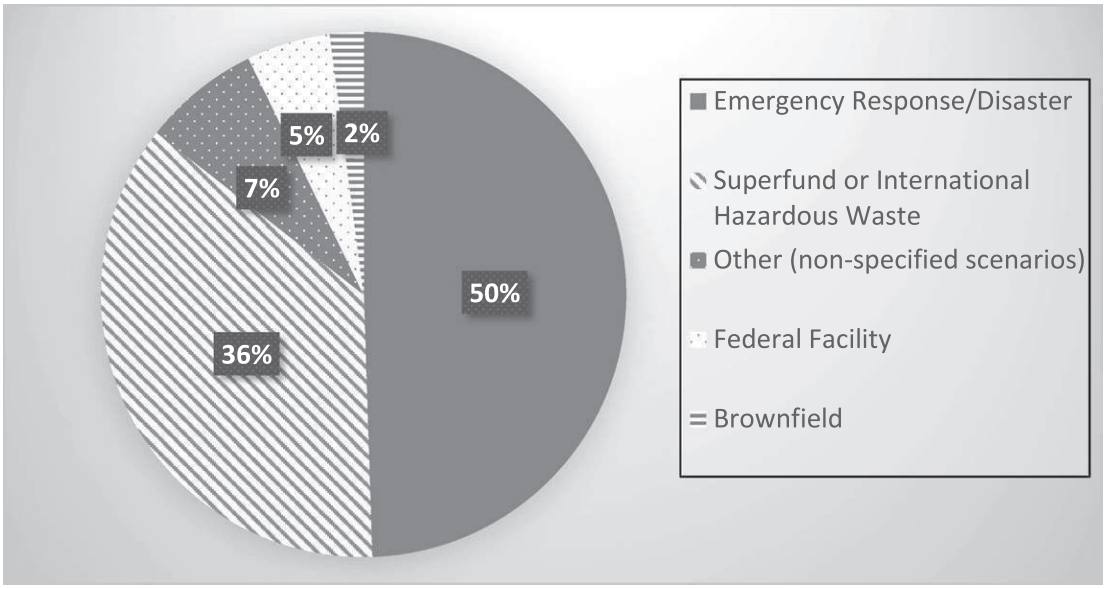

Figure 3. The percentage of literature sources ($n = 97$) covering each cleanup situation.

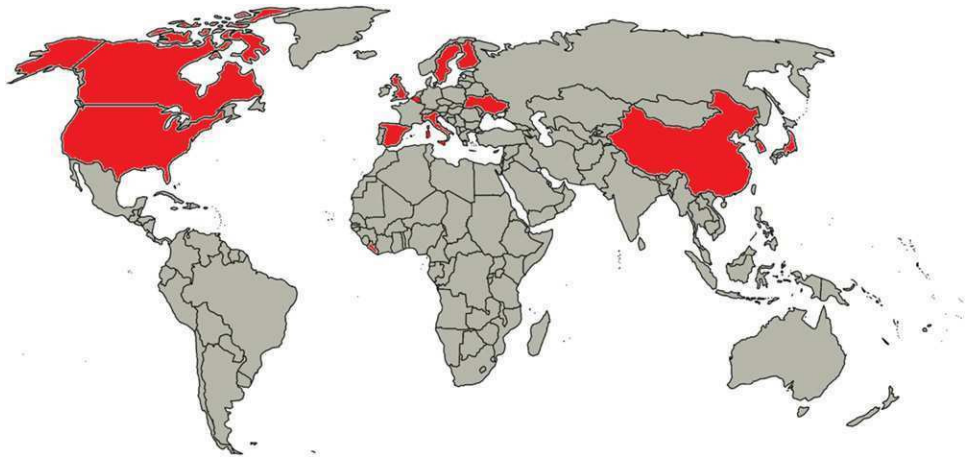

Figure 4. The countries highlighted in red were represented in case studies.

Chemical in Hagerstown, Maryland; Gowanus Canal, New York; Hanford, Washington; Los Alamos National Laboratory, New Mexico; Love Canal, New York; Middlefield-Ellis-Whisman, California; Tar Creek, Oklahoma; Rentokil Inc., Virginia; Rocky Flats, Colorado; Shell Oil Co dumpsite on the Swinomish Reservation, Washington; Three Mile Island, Pennsylvania; and Waukegan Harbor, Illinois.

The literature covers different phases of cleanups: pre-cleanup, during cleanup, and post-cleanup. Fifteen sources address the pre-cleanup phase, ten sources address the cleanup itself, and 30 sources address post-cleanup. Forty-two sources address multiple phases. The articles do not all delineate phases in the same way, nor does their terminology correspond exactly to the steps listed in table 1, which impeded comparison of the case studies.

The articles come from seven academic disciplines: anthropology, economics, human geography, policy and management, public health and medicine, sociology, and STS. They use a wide range of research methods, e.g. interviews, surveys, focus groups, and economic modeling. The most common methods are secondary analysis of existing data ($n = 24$) and interviews ($n = 21$). Figure 5 shows the distribution of academic disciplines and method type. To analyze methodological differences, we used four main method categorizations: qualitative, quantitative, mixed methods, secondary analysis. By mixed methods, we mean any study that combines quantitative and qualitative methods (Merriam and Tisdell 2015). By secondary analysis, we mean any study that reviewed the data or findings of other studies. The academic areas with the most representation in the literature are policy and

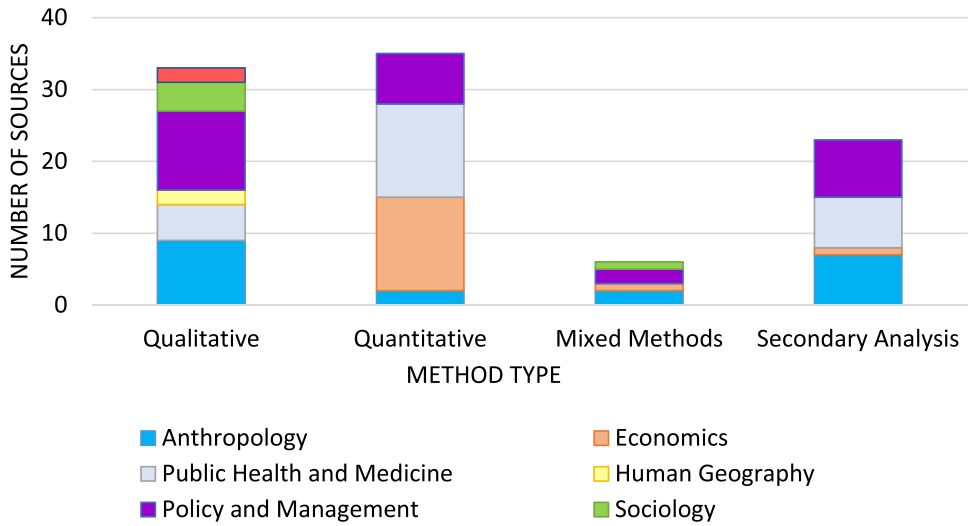

Figure 5. Methods used within the sources ($n = 97$) divided by discipline.

management ($n = 28$), public health and medicine ($n = 25$), and anthropology ($n = 20$). There is a near-even split between studies using qualitative ($n = 33$) and quantitative methods ($n = 35$). Far fewer studies use mixed methods ($n = 6$) such as integrating quantitative survey data with qualitative interviews or combining economic modeling with participant observation. As we will discuss later in this paper, the lack of mixed methods may be a result of limited cross-disciplinary engagement on this topic.

3.2. Worker health

One of the prominent themes in the literature is the analysis of short- and long-term impacts on the physical and mental health of cleanup workers. The articles document health problems among workers involved in the containment, removal, and remediation of toxic contaminants. They focus on notable case studies such as the 9/11 attacks on the World Trade Center, Deepwater Horizon oil spill, and Chernobyl and Fukushima nuclear disasters. The number of cleanup workers exposed to health risks is significant, particularly in large disasters. Over 800 000 'liquidators' worked with radiologically contaminated materials at Chernobyl between 1986 and 1989 alone (Bay and Oughton 2005). Formal measures of the number of cleanup workers may not even include residents, business owners, and others who initiate work on their own (Allen 2007).

The most common and longest studied aspect of worker health is cancer, followed by mental health and other aspects of physical health. The articles document that cleanup workers suffer from high rates of cancer (Bebeshko and Bobyliova 2002, Bay and Oughton 2005), prevalence of post-traumatic stress disorder and depression (Allen and D'Elia 2015, Bromet 2014, Laidra *et al* 2015, Horn *et al* 2016, Maeda and Oe 2015, Viel *et al* 1997, Zvolensky *et al* 2015), substance abuse (Bromet 2014, Laidra *et al* 2015), and respiratory diseases (Herbstman *et al* 2005). Many of these studies are retrospective, reviewing health data collected years before the analysis; or longitudinal, analyzing worker cohorts many years after a disaster (Bebeshko and Bobyliova 2002, Chernobyl Forum 2005, Eglite *et al* 2009).

While the studies use primarily epidemiological methods, this body of work also illuminates the broader social context of cleanup work. We highlight three aspects of this social context here. First, the articles raise concerns about workplace safety, i.e. protective gear, training, and information (Suárez *et al* 2005, Allen 2007, Wheeler *et al* 2007). Second, they touch on issues of environmental justice and ethics. They note that vulnerable populations, including prison inmates and immigrants, are unequally burdened with cleanup tasks and consequently exposed to greater health risks (Koo *et al* 1995, D'Andrea and Reddy 2013, Laidra *et al* 2015). Finally, the literature highlights the problem of stigma against people involved in cleanup activities (Bay and Oughton 2005, Chernobyl Forum 2005, Schneider 2012, Magill *et al* 2013, Bromet 2014, Pellecchia *et al* 2015). For example, Chernobyl liquidators were ostracized from their communities because people feared that radiation exposure was somehow contagious (Bay and Oughton 2005, Chernobyl Forum 2005, Bromet 2014).

3.3. Decision-making and public engagement

A second common theme found in the articles is decision-making and public engagement. These studies establish the necessity of public engagement by illuminating the social and political dimensions of technical cleanup decisions (e.g. Frickel 2012). Technical decisions made throughout cleanups include:

- where to sample for contaminants,
- how to analyze samples,
- how to set and meet quality control standards for data collection and analysis,
- what is the extent of contamination,
- which removal and remediation techniques to use,
- what cleanup levels to set,
- whether cleanup has achieved the desired reduction in contamination and health risks,
- where and how to dispose of the waste,
- what ongoing monitoring is necessary, and
- what types of post-cleanup land use are appropriate.

In addition, specific cleanup situations may require their own decisions. In the US, for example, CERCLA law requires determinations about whether to list a site on the NPL and when a site is clean enough to warrant deletion from the list.

The studies indicate that public views shape cleanup decisions as much as experts' technical determinations do. Moreover, lay and technical perceptions of risk often differ. Jorgensen (2016) observes that decisions about radiological cleanup depend on how affected people understand and tolerate risk. In a review of Superfund cleanup activities at the US Department of Energy's (DOE) Hanford Site, Gray and Becker (1993) argue that decisions have been driven more by public anxiety and politics than by scientific data. Affected communities may not accept agencies' technical determinations about health risks, remediation techniques, and cleanup levels. Instead, they apply socially contextual determinations of their own.

The articles further suggest that agencies' setting of technical standards itself has socio-political dimensions. Standards are set amid scientific debates tied to institutional power dynamics. Auer (2010), for example, describes negotiations between Finland and Sweden concerning tests to measure organochlorines in water. He argues that advances in testing technology in fact increased confusion in these negotiations, and warns that science and technology do not guarantee consensual decision-making.

The articles highlight trust as a critical social dimension of decision-making (Raimond 2001, Gephart 2003, Allen 2007, Cheong and Hazelwood 2015). Lack of trust in environmental officials undermined public trust in the information agencies provided following Hurricane Katrina, particularly when agencies appeared to undervalue local knowledge (Allen 2007). A long history of secrecy and concealment at former nuclear weapons production sites impedes public trust in cleanup activity at these sites (Raimond 2001, Gephart 2003). A lack of trust also exacerbated emergency responders' problems communicating with residents of Grand Isle, Louisiana, an insular community, during the Deepwater Horizon oil spill (Cheong and Hazelwood 2015).

The articles examine how decisions about future reuse of a site shape risk determinations and cleanup actions. They argue that present and future risks from existing contamination, remediation actions, and residual contamination following remediation must be balanced and considered in decision-making (Gochfeld *et al* 2007). They point out that when goals and options are not well defined, cleanup is hampered by uncertainty (Gray and Becker 1993). Recognizing these limitations, Beling *et al* (2007) suggest that Superfund processes allow for contingency planning.

Finally, the articles underscore the importance of public engagement to decision-making, even for technical decisions (Raimond 2001, Pellecchia *et al* 2015). The need to build consensus, share power, and establish trust is a recurring theme (e.g., Raimond 2001, Allen 2007, Jorgensen 2016). Ferris (1993) argues that cleanup solutions are more enduring at sites with higher community participation. Dukes (2007) posits that contaminated sites are an opportunity to build cumulative knowledge by including the public in deliberative, adaptive decision-making. Authors also point to challenges encountered during public engagement. For example, communities are not homogenous and may have internal socioeconomic and power inequalities. Participatory outreach may not reach all affected stakeholders (Miller 2016). Additionally, contamination incidents can exacerbate community divisions (Raimond 2001).

3.4. Evaluating societal benefits of cleanup

A third theme in the social science literature is evaluation of the broader societal benefits of cleanup. The articles found by this review primarily evaluated economic benefits in the form of housing value. The majority use hedonic pricing models to analyze local property values. Hedonic pricing is a revealed preference method that associates an increase in housing value after cleanup with the amenity value of living in an uncontaminated place. The articles apply hedonic pricing to housing around Superfund sites in the US (Kiel 1995, McClusky and Rausser 2003, Chattopadhyay *et al* 2005, Messer *et al* 2006, Noonan *et al* 2007, Greenstone and Gallagher 2008, Gamper-Rabindran and Timmins 2011, 2013). A few studies apply it to other cleanup situations, e.g. along nuclear waste transport routes (Gawande and Jenkins-Smith 2001), and near hazardous waste sites not on the NPL (Ketkar 1992, Ihlanfeldt and Taylor 2004). This method also provides a way of measuring stigma associated with site discovery, listing, and other cleanup actions (Kiel 1995, McClusky and Rausser 2003, Messer *et al* 2006). Post-cleanup housing values can be compared to pre-cleanup values to

determine whether stigma is overcome (Gamper-Rabindran and Timmins 2011, 2013).

We note methodological differences among the articles in their selection of regression models and datasets, radial distance of properties from a site (e.g. one mile, three miles), spatial unit of analysis (e.g. census tract, census block), type of property (e.g. owner-occupied housing, commercial), and timeline (e.g. after construction complete, after deletion). The authors also came to differing conclusions about the societal benefits of cleanups. The majority agrees that property values do increase after cleanup (Ketkar 1992, Ihlanfeldt and Taylor 2004, Chattopadhyay *et al* 2005, Gamper-Rabindran and Timmins 2011, Gamper-Rabindran and Timmins 2013). However, the amount of the estimated increase varies greatly, as do authors' interpretations of these numbers. Noonan *et al* (2007) posit that while direct impacts on housing are minimal, there may be positive indirect effects such as increased neighborhood investment. Kiel (1995) finds that housing prices do not recover enough to overcome initial stigma of site discovery and listing. Delaying cleanup worsens property value losses (Messer *et al* 2006). Greenstone and Gallagher (2008) argue that local property value increases are small relative to the high costs of Superfund cleanup. In contrast, Ihlanfeldt and Taylor (2004) argue that even high cleanup costs can be offset by increases in property values and, in turn, property taxes.

A few of the articles also discuss how cleanups may spur neighborhood gentrification (Noonan *et al* 2007, Gamper-Rabindran and Timmins 2011, 2013). With gentrification, housing prices increase but residents are priced out of the housing market. Neighborhood demographics can shift along the lines of race, class, and ethnicity. Gentrification is an environmental justice concern and can be an unintended social outcome of environmental cleanup.

4. Discussion

4.1. Trends in the literature

This literature review provides extensive evidence that social variables affect cleanup processes and outcomes in several ways. Cleanup activities affect worker health. Technical decisions are shaped by social and political dimensions. Completed cleanups have local socio-economic consequences.

The review uncovers several trends in the literature. First, there is limited geographic coverage in social science analysis of environmental cleanups. The dearth of articles about many parts of the world shown in figure 4 may be due in part to the limitations highlighted in the methods section 2.3. It may also reflect national differences in environmental policies, remediation activities, and terminology. A third possible explanation is the reliance that the social science literature has on case studies, particularly of highly visible incidents such as the Deepwater Horizon oil spill and Fukushima nuclear accident. These incidents mobilize extensive cleanup efforts, media attention, research interest, and funding. They involve complex social dynamics that can be studied over time. One repercussion of the reliance on high-profile incidents is that analysis of other types of contaminants and cleanup situations is limited. For example, site reports indicate that stakeholder engagement and public participation positively influence brownfields redevelopment in Europe (Payá Pérez and Peláez Sánchez 2017). Brownfields sites, however, comprised the smallest portion of articles (2%) found by this search. Moreover, there is limited comparison of case studies in the literature, which would be generative of social science theory of decontamination.

A second trend is that the articles operate largely in disciplinary silos. Anthropological studies of decontamination discourse are not in conversation with economic works on hedonic pricing. Epidemiological articles on cleanup worker health do not engage with the broader social science literature on labor practices, worker identity, and embodied stigma. Thus, the social context of cleanup work is missing: how do people come to be in this work, what are their work experiences, and how does it affect households and communities as well as individual health? The silo-ization of the literature is also apparent in that while the case studies uncover diverse social aspects of cleanups, they often lack a theoretical grounding. Observed trends in methodologies provide further evidence of silo-ization. The limited use of mixed methods, such as combining health surveys with ethnography, indicates a lack of interdisciplinary engagement. Another methodological gap is the relatively low number of ethnographic accounts of cleanup experiences. One exception is Little's (2012) study of people living with vapor mitigation systems installed in their houses as part of remediation of the IBM Endicott Superfund site in New York state. Ethnographic studies of cleanup workers, community activists, and agency staff would shed light on social relationships, cultural worldviews, decision-making, and health.

4.2. Future research needs

The review identifies research gaps in the four thematic areas. Na *et al* (2012) and D'Andrea and Reddy (2013) mention differences between male and female cleanup workers' risk exposure and health impacts. A deeper discussion of the gendered nature of cleanup work is absent. Zvolensky *et al* (2015) report how adverse mental health impacts to cleanup workers correlate with financial problems. It points to the need to investigate how cleanup work affects families and households as well as worker populations. The Chernobyl case studies primarily analyze possible health effects of low-dose radiation exposure over a long period of time (Barnes 2001, Bay and Oughton 2005,

Eglite *et al* 2009, Krasnov *et al* 2015, Laidra *et al* 2015). There is a need for longitudinal studies of other types of cleanup work.

In terms of public engagement, the articles do address how trust is lost and how mistrust affects cleanups (e.g., Eisenman *et al* 2004, Allen 2007, Ritchie *et al* 2013). However, there is limited coverage of research on how to build trust and maintain it over time. Future research could examine best practices in building consensus, sharing power, and establishing trust among stakeholders. It could field test strategies for effective public engagement in different cleanup situations.

The reliance found in this literature on hedonic pricing affords a relatively limited basis for measuring societal benefits of environmental cleanups. The studies primarily use this technique at Superfund sites, so its application to other cleanup situations and non-US sites remains untested. Hedonic pricing does not capture social consequences such as neighborhood gentrification. Cleanups may well benefit society in ways other than property values. New methods for evaluating societal benefits—and costs—should be developed and tested for their applicability to different cleanup situations. Methodological challenges remain for how to measure benefits that are not easily quantifiable, such as changes to risk perception and improved stakeholder relationships.

Greater comparison among sites within a given country and internationally is needed. It would help answer research questions about: how does stigma differ when radiological, chemical, or biological contaminants are involved? Are public engagement strategies transferable among Superfund, brownfields, and emergency response? Does post-cleanup gentrification play out differently in cities, suburbs, and rural areas? What are similarities and differences in public engagement strategies, worker health protection, and post-remediation property values when comparing sites internationally? Site comparison can help identify technical, policy, and public engagement approaches that foster achievement of positive social and environmental outcomes (Coulon *et al* 2016, Payá Pérez and Peláez Sánchez 2017). It can also assess how multi-criteria decision support tools (e.g., human health risk assessment (Wcislo *et al* 2016), integrated assessment modeling (Schädler *et al* 2012)) support cleanup decision-making (see Norrman *et al* 2016 for an example).

The review found that there is no overarching model or framework to explain how social dynamics affect cleanup activities, the origins of these dynamics, and what the social impacts of cleanup activities and outcomes of cleanup completion are. We suggest that a comprehensive framework should be developed. One possible theoretical foundation is a socio-environmental systems (SES) approach that addresses interactions between social and biophysical systems (Machlis *et al* 1997, Musters *et al* 1998). SES has largely focused on ecosystems, land use, and urban ecology, and does not always directly address human health, though, so a framework might also benefit from incorporating elements from health risk assessment (Wcislo *et al* 2016). Social science theory that situates people's relationships with chemicals, toxics, and post-industrial sites in a broader culture and political economic context (Fortun 2012, Shapiro and Kirksey 2017) may be informative, but challenging to incorporate into a model. Participatory socio-environmental modeling techniques may allow site-specific details to emerge (Gray *et al* 2018). This analysis identifies several important factors to address in a framework: multiple phases of cleanup actions; positive and negative social impacts (e.g. stigma); the social as well as toxicological context of worker health; governance approaches to public engagement, trust, and stigma; scientific decision-making; institutional roles and constraints; and measures of societal outcomes of cleanup.

4.3. Application to policy and practice

The case studies present strategies to help cleanups achieve positive social and environmental outcomes. For example, steps can be taken to support the health of workers and community members. In the US, removal and remediation is often done by contractors and sub-contractors. The US Government Accountability Office (2006) reports that DOE provided incentives for contractors to meet health and safety standards at the Rocky Flats Superfund site. Moreover, it encouraged contractors to share the incentives with workers. Providing additional worker benefits such as counseling, financial management, and transition aid can aid worker health and reduce local economic shock after cleanups are complete (US Government Accountability Office 2006, Zvolensky *et al* 2015). Counseling services could be provided for affected communities through coordination with health organizations. Overall, this body of literature prompts us to reevaluate cost-benefit analysis of remediation by considering the toll it takes on workers (Leigh and Hoskin 1999, Lowe *et al* 2015). It also underscores the importance of providing mental health services for cleanup workers and affected communities, in addition to physical health monitoring.

The articles detail techniques that have been used for effective public engagement. Halfacre (2009) suggests using focus groups to elicit concerns of underrepresented stakeholder groups as a complement to community-wide meetings. Burger *et al* (2005) describe a process of consensus building that engages citizens and scientists in development of a science plan. The National Research Council (2005) outlines steps to help achieve socially acceptable cleanup standards. Zaferatos (2006) stresses the importance doing truly meaningful consultation when working with Tribal Nations. Unfortunately, it may be difficult for agencies to adopt these best practices and adapt them

to different cleanup situations given limited authority, budgets, and staffing.

It may be more challenging to put into practice hedonic pricing methods to evaluate cleanup outcomes. They may be of limited applicability to emergency response and the other non-Superfund cleanup situations listed in table 1. It takes expertise, time, and funding to obtain and analyze local housing data. These economic articles do suggest changes to policy and practice. The observation that delaying cleanup worsens property value losses provides a strong impetus for getting cleanups done in a timely manner (Ketkar 1992, Sigman 2001, Ihlanfeldt and Taylor 2004, Messer *et al* 2006). The observation that stigma can increase as additional cleanup actions are announced (Messer *et al* 2006) is a reason to carefully craft communications and public engagement so as not to inadvertently increase stigma.

4.4. Complicating cleanups

Agency definitions, case study descriptions, and statutory language often characterize environmental cleanups as involving discrete sites or incidents, established cleanup goals, a prescribed set of steps and actions, and measurable transition from a contaminated site to a cleaned-up one. This literature review instead reveals a fuzziness to the boundaries of what a site is, timeline for when cleanup begins and ends, and the social meaning of contamination, decontamination, and clean. For example, many hazardous waste sites have more than one contaminant. Site assessment, remediation, and community engagement may need to address uncertainties about cumulative health risks from multiple contaminants.

The spatial unboundedness of sites is made apparent by the extent of cleanup activities, workers, and community impacts in large-scale disasters such as the Deepwater Horizon and Exxon Valdez oil spills (Shaw 1992, Russell *et al* 1993, Bond 2013). It is underscored by the complexities of managing cleanup goals and actions at Superfund sites that are dozens of square miles or more with varying levels of contaminants across the site (Gray and Becker 1993, Burger *et al* 2004). Even smaller sites may be physically cordoned off but still retain community ties and be of local cultural or historical significance (Bluestone 2007, Kirkwood 2007). The final disposal location for waste that is removed also complicates the idea of what a site is. Waste disposal sites may be enmeshed in environmental justice struggles of their own (Wright 2011).

Articles delineate cleanup phases differently than the official steps detailed in table 1, bringing cleanup timelines into question (e.g. Ketkar 1992, Bittner 1993, Anspaugh 1996, Page 1997, Allen 2007). The predominance of multi-phase analysis in the literature suggests it is important to analyze cleanups holistically, rather than in discrete parts. It also suggests that remediation and incident response steps are experienced as loosely bounded temporal phenomena. Site discovery, listing, and assessment may be iterative processes rather than a single act (Zaferatos 2006). Moreover, there is a temporal collapse of pre- and post-cleanup during decision-making. Cleanup levels are set based on health risk assessments, as well as on expected post-cleanup land use (Gephart 2003, Masco 2004, Gochfeld *et al* 2007). How clean is clean thus differs for sites intended for residential, industrial, or conservation use. Being able to assess redevelopment options early on is important (Wcislo *et al* 2016).

Stakeholders who bring different needs, values, and goals to the table contest the meaning of how clean is clean (Hoffman 1995, Gephart 2003, Cheong 2012). Approaches that use only technical criteria to determine when a site is cleaned-up and do not take social contexts into account are not likely to resolve these conflicts (Elcock *et al* 2004, Auer 2010, Frickel 2012). At Love Canal, for example, only a single guideline about dioxin was used as a standard for reoccupation habitability despite the multitude of contaminants at the site (Hoffman 1995). The nuclear era itself has led to modifications of what is considered background levels of radiation against which the health effects of contamination are measured (Masco 2004).

Cleanup complexities require further research to advance social theory about contaminated and post-contaminated lands and bodies, i.e. theories of the Anthropocene, disasters, late-industrialism, chemo-ethnography, and infrastructure-society relations (Fortun 2012, Moore 2016, Anand 2017, Barrios 2017, Malhi 2017, Shapiro and Kirksey 2017). Understanding these complexities is of more than theoretical importance, since debates over how clean is clean can contribute to cleanup delays (Page 1997). Being able to understand and navigate these complexities can resolve social conflicts that arise, allow cleanups to proceed despite scientific uncertainty, and support informed decision-making that considers potential social and economic outcomes.

5. Conclusions

This literature review highlights the complex ways that social factors affect environmental cleanup processes and outcomes. It establishes what we term the 'social science of decontamination' as an area of study. There are an emerging number of articles, books, and gray literature from a variety of academic disciplines that address this topic.

Several important themes emerge from the review. Public health and epidemiological studies document the impact of environmental cleanups on worker physical and mental health. Many of these focus on the case study of Chernobyl. This research lays the foundation for discussions of worker rights and the connection between social vulnerabilities and environmental cleanup work. Another theme in the literature is the focus on

improving decision-making and risk analysis processes. Many of these studies assert the importance of public engagement and the need for more public involvement in cleanup decisions to improve outcomes and avoid conflicts. They also highlight how decisions about future reuse of sites shape risk determinations and cleanup actions, demonstrating the importance of using a systems approach and analyzing cleanups as a multi-phase process. The third major theme in the literature is evaluation of societal outcomes of cleanup, primarily through hedonic price models of property values near Superfund sites in the US.

Despite the variety of literature relating to the social science of decontamination, there is still a need for further studies due to specific gaps. The studies utilize a wide array of qualitative and quantitative research methods, but there is a lack of mixed methods and interdisciplinary engagement within the social sciences. Many articles rely on case studies of large-scale disasters or Superfund sites, leaving room for comparisons of how social dynamics differ among cleanup situations. In particular, more international comparisons would aid understanding of how these dynamics play out in places with different forms of governance and social histories. Development of a comprehensive framework or model is necessary to advance the social science of decontamination. Broader questions complicating cleanups need to be explored. Further investigation into specific topics such as labor practices, gender, race, and power relationships is also necessary. Overall, this area of research has significant potential to benefit environmental cleanup policy and practice, as well as advance social theory about people and the environment.

Acknowledgments

This project was supported in part by an appointment to the Internship/Research Participation Program at the EPA's Office of Research and Development, administered by the Oak Ridge Institute for Science and Education through an interagency agreement between DOE and EPA. It was also supported by an American Association for the Advancement of Science, Science & Technology Policy Fellowship participant at the EPA Office of Research & Development, National Homeland Security Research Center, Threat & Consequence Assessment Division. Many thanks to Bruce Duncan, Katie Williams, Emily Snyder, Shawn Ryan, and the anonymous journal referees. Their thoughtful reviews helped improve the article.

Disclaimer

The authors declare no conflicts of interest with the publication of this research. EPA funded & managed the research described. It has been subjected to the Agency's review & has been approved for publication & distribution. Note that approval does not signify that the contents necessarily reflect the views of the Agency. Mention of trade names, products, or services does not convey official EPA approval, endorsement, or recommendation.

ORCID iDs

Keely Maxwell https://orcid.org/0000-0002-0802-4723
Brittany Kiessling https://orcid.org/0000-0003-3124-7375
Jenifer Buckley https://orcid.org/0000-0002-8294-1482

References

40 CFR 300 1994 National Oil and Hazardous Substances Pollution Contingency Plan, Final rule
Allen B 2007 Environmental justice, local knowledge, and after-disaster planning in New Orleans *Technol. Soc.* **29** 153–9
Allen P and D'Elia C 2015 What lies beneath: the BP oil spill and the need for new response models *Curr. Psychol.* **34** 587–96
Anand N 2017 *Hydraulic City: Water and the Infrastructures of Citizenship in Mumbai* (Durham: Duke University Press)
Anspaugh L 1996 A risk-based approach to cleanup—problems and pitfalls *Assessing the Risks of Nuclear and Chemical Contamination in the Former Soviet Union* ed E J Kirk (Dordrecht: Springer Netherlands) pp 29–32
Auer M 2010 Better science and worse diplomacy: negotiating the cleanup of the Swedish and Finnish pulp and paper industry *Int. Environ. Agreements: Politics, Law Econ.* **10** 65–84
Barnes J 2001 Sensitivity syndromes' related to radiation exposures *Med. Hypotheses* **57** 453–8
Barrios R 2017 What does catastrophe reveal for whom? The anthropology of crises and disasters at the onset of the anthropocene *Annu. Rev. Anthropol.* **46** 151–66
Bay I and Oughton D 2005 Social and economic effects *Chernobyl—Catastrophe and Consequences* (Berlin: Springer) pp 239–66
Bebeshko V and Bobyliova O 2002 Medical consequences of the Chernobyl nuclear power plant accident: experience of 15-year studies *Int. Congr. Ser.* **1234** 267–79
Beling P A, Lambert J H, Rahman F A, Overstreet G O and Slutzky D 2007 Systems analysis and adaptive learning for portfolio management of Superfund sites *Reclaiming the Land: Rethinking Superfund Institutions, Methods and Practices* ed G P Macey and J Z Cannon (New York: Springer) pp 129–68
Bittner J 1993 Cultural resources and the Exxon Valdez oil spill: an overview *Paper presented at the Exxon Valdez Oil Spill Symp. (Anchorage, Alaska)*
Bluestone D 2007 Toxic sites as places of culture and memory: adaptive management for citizenship *Reclaiming the Land: Rethinking Superfund Institutions, Methods and Practices* ed G P Macey and J Z Cannon (New York: Springer) pp 245–66
Bond D 2013 Governing disaster: the political life of the environment during the BP oil spill *Cultural Anthropol.* **28** 694–715
Bromet E J 2014 Emotional consequences of nuclear power plant disasters *J. Health Phys.* **106** 206–10
Burger J *et al* 2005 Science, policy, and stakeholders: developing a consensus science plan for Amchitka Island, Aleutians, Alaska *Environ. Manage.* **35** 557–68
Burger J, Greenberg M, Powers C and Gochfeld M 2004 Reducing the footprint of contaminated lands: US Department of Energy sites as a case study *Risk Manage.* **6** 41–63
Chattopadhyay S, Braden J and Patunru A 2005 Benefits of hazardous waste cleanup: new evidence from survey- and market-based property value approaches *Contemp. Econ. Policy* **23** 357–75
Cheong S-M 2012 Fishing and tourism impacts in the aftermath of the Hebei-Spirit Oil Spill *J. Coast. Res.* **28** 1648–53

Cheong S-M and Hazelwood E 2015 Insularity and oil spill response in Grand Isle *GeoJournal* **80** 679–87
Chernobyl Forum 2005 *Chernobyl's Legacy: Health, Environmental and Socio-Economic impacts and Recommendations to the Governments of Belarus* IAEA/PI/A.87 Rev.2 / 06-09181 International Atomic Energy Agency (IAEA)
Coulon F 2016 *Land Contamination and Brownfield management Policy Development in China: Learning from the UK Experience* China UK Partnership for Contaminated Land Management
Cram S 2015 Becoming Jane: the making and unmaking of Hanford's nuclear body *Environ. Plan. D-Soc. Space* **33** 796–812
D'Andrea M and Reddy G 2013 Health consequences among subjects involved in Gulf oil spill clean-up activities *Am. J. Med.* **126** 966–74
Dukes E F 2007 Rethinking community involvement for Superfund site reuse: the case for consensus-building in adaptive management *Reclaiming the Land: Rethinking Superfund Institutions, Methods and Practices* ed G P Macey and J Z Cannon (New York: Springer) pp 211–44
Eglite M, Zvagule T, Rainsford K, Reste J, Curbakova E and Kurjane N 2009 Clinical aspects of the health disturbances in Chernobyl Nuclear Power Plant accident clean-up workers (liquidators) from Latvia *Inflammopharmacology* **17** 163–9
Eisenman D, Wold C, Setodji C, Hickey S, Lee B, Stein B and Long A 2004 Will public health's response to terrorism be fair? Racial/ethnic variations in perceived fairness during a bioterrorist event *Biosecur. Bioterrorism: Biodef. Strategy, Pract. Sci.* **2** 146–56
Elcock D, Klemic G and Taboas A 2004 Establishing remediation levels in response to a radiological dispersal event (or 'dirty bomb') *Environ. Sci. Technol.* **38** 2505–12
EPA 2002 *Challenges Faced during the Environmental Protection Agency's Response to Anthrax and Recommendations for Enhancing Responses Capabilities: a Lessons Learned Report* (Washington, DC: EPA)
EPA 2003 *A Summary of General Assessment Factors for Evaluating the Quality of Scientific and Technical Information* EPA 100/B-03/001 EPA
EPA 2013 *National Center for Environmental Assessment (NCEA) Office of Research and Development Quality Management Plan for Scientific Research* ORDQMP-01-01 EPA
EPA 2015 *Population Surrounding 1388 Superfund Remedial Sites* EPA
EPA 2017 Types of contaminated sites https://epa.gov/enforcement/types-contaminated-sites (Accessed: 20 March 2018)
EPA 2018 Emergency response https://epa.gov/emergency-response (Accessed: 20 March 2018)
Ferris D 1994 Communities of color and hazardous waste cleanup: expanding public participation in the federal Superfund program *Fordham Urban Law J.* **21** 671–88
Fortun K 2012 Ethnography in late industrialism *Cultural Anthropol.* **27** 446–64
Fowlkes M R and Miller P Y 1983 *Love Canal: The Social Construction of Disaster* 83 03 07 039 FEMA
Franco C and Bouri N 2010 Environmental decontamination following a large-scale bioterrorism attack: Federal progress and remaining gaps *Biosecur. Bioterrorism: Biodef. Strategy, Pract. Sci.* **8** 107–17
Frickel S 2012 Missing New Orleans: tracking knowledge and ignorance through an urban hazardscape *Histories of the Dustheap: Waste, Material Cultures, Social Justice* ed S Foote and E Mazzolini (Cambridge, Massachusetts: MIT Press) pp 97–117
Gamper-Rabindran S and Timmins C 2011 Hazardous waste cleanup, neighborhood gentrification, and environmental justice: evidence from restricted access census block data *Am. Econ. Rev.* **101** 5
Gamper-Rabindran S and Timmins C 2013 Does cleanup of hazardous waste sites raise housing values? Evidence of spatially localized benefits *J. Environ. Econ. Manage.* **65** 345–60
Gawande K and Jenkins-Smith H 2001 Nuclear waste transport and residential property values: estimating the effects of perceived risks *J. Environ. Econ. Manage.* **42** 207–33
Gephart R 2003 *Hanford: A Conversation About Nuclear Waste and Cleanup* (Columbus, Ohio: Battelle Press)
Gochfeld M, Burger J, Friedlander B and Powers C 2007 Approaches for assessing hazards and risks to workers and the public from contaminated land *Remediation* **18** 29–57
Grant M J and Booth A 2009 A typology of reviews: an analysis of 14 review types and associated methodologies *Health Inf. Libr. J.* **26** 91–108
Gray R and Becker C 1993 Environmental cleanup: the challenge at the Hanford site, Washington, USA *Environ. Manage.* **17** 461
Gray S *et al* 2018 Purpose, processes, partnerships, and products: four Ps to advance participatory socio-environmental modeling *Ecol. Appl.* **28** 46–61
Greenstone M and Gallagher J 2008 Does hazardous waste matter? Evidence from the housing market and the Superfund program *Q. J. Econ.* **123** 951–1003
Halfacre A 2009 The use of focus groups in assessing ethnic and racial group concerns about nuclear waste cleanup *Public Participation and Better Environmental Decisions: The Promise and Limits of Participatory Processes for the Quality of Environmentally Related Decision-Making* ed F H J M Coenen (Dordrecht: Springer) pp 35–55
Hamilton J and Viscusi W 1999 How costly is 'clean'? An analysis of the benefits and costs of Superfund site remediations *J. Policy Anal. Manage.* **18** 2–27
Hart C 1998 *Doing a Literature Review: Releasing the Social Science Research Imagination* (London: SAGE)
Herbstman J, Frank R, Schwab M, Williams D, Samet J, Breysse P and Geyh A 2005 Respiratory effects of inhalation exposure among workers during the clean-up effort at the World Trade Center disaster site *Environ. Res.* **99** 85–92
Hoffman A 1995 An uneasy rebirth at Love Canal *Environment* **37** 4
Horn S *et al* 2016 Latent typologies of posttraumatic stress disorder in World Trade Center responders *J. Psychiatric Res.* **83** 151–9
Ihlanfeldt K and Taylor L 2004 Externality effects of small-scale hazardous waste sites: evidence from urban commercial property markets *J. Environ. Econ. Manage.* **47** 117–39
Interstate Technology and Regulatory Council (ITRC) 2002 *Determining Cleanup Goals at Radioactively Contaminated Sites: Case Studies* ITRC
Jorgensen T 2016 The new 'normal': stakeholders and radiation protection limits in a post-9/11 world *J. Health Phys.* **111** 227–31
Ketkar K 1992 Hazardous waste sites and property values in the state of New Jersey *Appl. Econ.* **24** 647–59
Kiel K 1995 Measuring the impact of the discovery and cleaning of identified hazardous waste sites on house values *Land Econ.* **71** 428–35
Kirkwood N 2007 CHAT: approaches to long-term planning for the Tar Creek Superfund Site, Ottawa County, Oklahoma *Reclaiming the Land: Rethinking Superfund Institutions, Methods and Practices* ed G P Macey and J Z Cannon (New York: Springer) pp 267–92
Koo D, Goldman L and Baron R 1995 Irritant dermatitis among workers cleaning up a pesticide spill: California 1991 *Am. J. Ind. Med.* **27** 545–53
Krasnov V, Kryukov V, Samedova E, Emelianova I and Ryzhova I 2015 Early aging in Chernobyl clean-up workers: long-term study *BioMed Research International* **2015** 1–5
Laidra K, Rahu K, Tekkel M, Aluoja A and Leinsalu M 2015 Mental health and alcohol problems among Estonian cleanup workers 24 years after the Chernobyl accident *Soc. Psychiatry Psychiatric Epidemiol.* **50** 1753–60
Layzer J 2012 *The Environmental Case: Translating Values into Policy* (Washington, DC: CQ Press)
Leigh J P and Hoskin A 1999 Hazards for nearby residents and cleanup workers of waste sites *J. Occup. Environ. Med.* **41** 331–48

Little P C 2012 Another angle on pollution experience: toward an anthropology of the emotional ecology of risk mitigation *ETHOS* **40** 431–52
Lowe S, Kwok R, Payne J, Engel L, Galea S and Sandler D 2015 Mental health service use by cleanup workers in the aftermath of the Deepwater Horizon oil spill *Soc. Sci. Med.* **130** 125–34
Machlis G E, Force J E and Burch W R 1997 The human ecosystem: I. The human ecosystem as an organizing concept in ecosystem management *Soc. Nat. Res.* **10** 347–67
Maeda M and Oe M 2015 The Great East Japan Earthquake: Tsunami and nuclear disaster *Traumatic Stress and Long-Term Recovery: Coping with Disasters and Other Negative Life Events* ed K Cherry (Cham: Springer) pp 71–90
Magill C, Wilson T and Okada T 2013 Observations of tephra fall impacts from the 2011 shinmoedake eruption, Japan *Earth, Planets Space* **65** 18
Malhi Y 2017 The concept of the anthropocene *Annu. Rev. Environ. Res.* **42** 77–104
Masco J 2004 Mutant ecologies: radioactive life in post—Cold War New Mexico *Cultural Anthropol.* **19** 517–50
McCaffrey K and Baver S 2006 'Ni una bomba mas': reframing the Vieques struggle *Beyond Sun and Sand: Caribbean Environmentalisms. Rutgers* ed S Baver and B Lynch (Rutgers: Rutgers University Press)
McCluskey J and Rausser G 2003 Hazardous waste sites and housing appreciation rates *J. Environ. Econ. Manage.* **45** 166–76
Merriam S B and Tisdell E J 2015 . *Qualitative Research: A Guide to Design and Implementation* 4th edn (San Francisco, CA: Jossey-Bass)
Messer K, Schulze W, Hackett K, Cameron T and McClelland G 2006 Can stigma explain large property value losses? The psychology and economics of Superfund *Environ. Res. Econ.* **33** 299–324
Miller J 2016 Is urban greening for everyone? Social inclusion and exclusion along the Gowanus Canal *Urban Forestry Urban Greening* **19** 285–94
Moher D, Liberati A, Tetzlaff J, Altman D G and The P G 2009 Preferred reporting items for systematic reviews and meta-analyses: the PRISMA statement *Ann. Intern. Med.* **151** 264–9
Moore A 2016 Anthropocene anthropology: reconceptualizing contemporary global change *J. R. Anthropol. Inst.* **22** 27–46
Musters C J M, de Graaf H J and ter Keurs W J 1998 Defining socio-environmental systems for sustainable development *Ecol. Econ.* **26** 243–58
Na J U, Sim M, Jo I and Song H 2012 The duration of acute health problems in people involved with the cleanup operation of the Hebei Spirit oil spill *Mar. Pollut. Bull.* **64** 1246–51
National Research Council 2005 *Reopening Public Facilities After a Biological Attack: A Decision Making Framework* National Academies Press (https://doi.org/10.17226/11324)
Noonan D, Krupka D and Baden B 2007 Neighborhood dynamics and price effects of Superfund site clean-up *J. Reg. Sci.* **47** 665–92
Norrman J *et al* 2016 Integration of the subsurface and the surface sectors for a more holistic approach for sustainable redevelopment of urban brownfields *Sci. Total Environ.* **563–564** 879–89
Page G 1997 The social, economic, business, and policy dimensions of bioremediation techniques *Biotechnology for Waste Management and Site Restoration: Technological, Educational, Business, Political Aspects* ed C Ronneau and O Bitchaeva (Dordrecht: Springer) pp 9–18
Payá Pérez A and Peláez Sánchez S 2017 *European Achievements in Soil Remediation and Brownfield Redevelopment* (European Union)
Pellecchia U, Crestani R, Decroo T, Bergh R and Al-Kourdi Y 2015 Social consequences of ebola containment measures in Liberia *PLoS One* **10** 1–12
Petryna A 1995 Sarcophagus: Chernobyl in historical light *Cultural Anthropol.* **10** 196–220
Raimond R R 2001 *Trust and Conflict in Public Participation*. Colorado Department of Public Health and Environment
Ritchie L, Gill D and Farnham C 2013 Recreancy revisited: beliefs about institutional failure following the Exxon Valdez oil spill *Soc. Nat. Res.* **26** 655–71
Russell J, Downs M, Petterson J and Palinkas L 1993 Psychological and social impacts of the Exxon Valdez oil spill and cleanup *Paper presented at the Exxon Valdez Oil Spill Symp. (Anchorage, Alaska)*
Schneider D 2012 Purification or profit: Milwaukee and the contradictions of sludge *Histories of the Dustheap* ed S Foote and E Mazzolini (Cambridge, MA: MIT Press)
Schädler S, Morio M, Bartke S and Finkel M 2012 Integrated planning and spatial evaluation of megasite remediation and reuse options *J. Contaminant Hydrol.* **127** 88–100
Shapiro N and Kirksey E 2017 Chemo-ethnography: an introduction *Cultural Anthropol.* **32** 481–93
Shaw D 1992 The Exxon Valdez oil spill: ecological and social consequences *Environ. Conservation* **19** 253–8
Sigman H 2001 The pace of progress at Superfund sites: policy goals and interest group influence *J. Law Econ.* **44** 315–44
Singh S 2017 How to conduct and interpret systematic reviews and meta-analyses *Clin. Transl. Gastroenterol.* **8** e93
Smith J T 2005 *Chernobyl—Catastrophe and consequences* (Berlin: Springer)
Suárez B *et al* 2005 Acute health problems among subjects involved in the cleanup operation following the Prestige oil spill in Asturias and Cantabria (Spain) *Environ. Res.* **99** 413–24
Thomas J and Harden A 2008 Methods for the thematic synthesis of qualitative research in systematic reviews *BMC Med. Res. Methodol.* **8** 45
US Government Accountability Office 2006 *Nuclear Cleanup of Rocky Flats: DOE can use Lessons Learned to Improve Oversight of other Sites' Cleanup Activities (GAO-06-352)* GAO-06-352 US Government Accountability Office
Van Horn C and Chilik Y 1988 How clean is clean? A case study of the nation's no. 1 Superfund toxic dump *Environ. Impact Assess. Rev.* **8** 133–48
Viel J F, Curbakova E, Dzerve B, Eglite M, Zvagule T and Vincent C 1997 Risk factors for long-term mental and psychosomatic distress in Latvian Chernobyl liquidators *Environ. Health Perspect.* **105** 1539–44
Wcislo E, Bronder J, Bubak A, Rodriguez-Valdes E and Gallebo J L R 2016 Human health risk assessment in restoring safe and productive use of abandoned contaminated sites *Environ. Int.* **94** 436–48
Wheeler K *et al* 2007 Asthma diagnosed after 11 september 2001 among rescue and recovery workers: findings from the world trade center health registry *Environ. Health Perspect.* **115** 1584–90
Wright B 2011 Race, place, and the environment in the aftermath of Katrina *Anthropol. Work Rev.* **32** 4–8
Zaferatos N C 2006 Environmental justice in Indian Country: dumpsite remediation on the Swinomish Indian Reservation *Environ. Manage.* **38** 896–909
Zvolensky M *et al* 2015 Post-disaster stressful life events and WTC-related posttraumatic stress, depressive symptoms, and overall functioning among responders to the world trade center disaster *J. Psychiatric Res.* **61** 97–105

Maxwell, Keely

From: Maxwell, Keely
Sent: Monday, April 20, 2020 10:08 AM
To: Kiessling, Brittany; Jenifer Buckley
Cc: Maxwell, Keely
Subject: Record of Percentage Agreement- Keely Maxwell

To whom it may concern:

I agree with my designated percentage of contribution of effort to this article, as listed in the nomination form and below.

Name and organization: Keely Maxwell, US Environmental Protection Agency
Nominee's name: Keely Maxwell
Title of nominated publication: How clean is clean: a review of the social science of environmental cleanups

Percentage contributions of effort:

Keely Maxwell	50%
Brittany Kiessling	35%
Jenifer Buckley	15%

Sincerely,

Keely Maxwell

General Anthropologist, US EPA Office of Research & Development
(202) 564-5266

Maxwell, Keely

From: Kiessling, Brittany
Sent: Monday, April 20, 2020 10:28 AM
To: Maxwell, Keely; Jenifer Buckley
Subject: RE: Record of Percentage Agreement- Brittany Kiessling

To whom it may concern:

I agree with my designated percentage of contribution of effort to this article, as listed in the nomination form and below.

Name and organization: Brittany Kiessling, US Environmental Protection Agency (current)/ ORISE Participant at US Environmental Protection Agency (at time of publication)
Nominee's name: Keely Maxwell
Title of nominated publication: How clean is clean: a review of the social science of environmental cleanups

Percentage contributions of effort:

Keely Maxwell	50%
Brittany Kiessling	35%
Jenifer Buckley	15%

Sincerely,

Brittany Kiessling, PhD
Social Scientist
Center for Environmental Solutions and Emergency Response
Office of Research and Development
US Environmental Protection Agency
1200 Pennsylvania Ave., NW
Washington, DC 20460
Office: 202-564-2603
Mobile: 305-504-6896

Maxwell, Keely

From: Jenifer Buckley <jenifer.a.buckley@gmail.com>
Sent: Tuesday, April 21, 2020 10:43 PM
To: Maxwell, Keely
Cc: Kiessling, Brittany
Subject: Record of Percentage Agreement- Jenifer Buckley

I agree with my designated percentage of contribution of effort to this article, as listed in the nomination form and below.

Name and organization: Jenifer Buckley, AAAS Science & Technology Policy Fellow hosted by US EPA at time of research. No current research affiliation
Nominee's name: Keely Maxwell
Title of nominated publication: How clean is clean: a review of the social science of environmental cleanups

Percentage contributions of effort:

Keely Maxwell	50%
Brittany Kiessling	35%
Jenifer Buckley	15%

_____

Jenifer Buckley
jenifer.a.buckley@gmail.com, jeniferbuckley.com
608-421-2386, skype jenifer.buckley

Michigan Technological University

Department of Social Sciences

April 24, 2020

Dr. Shawn Ryan
Division Director
Environmental Protection Agency
Washington DC

Dear Dr. Ryan,

I am writing this letter of reference in regard to your Scientific and Technological Achievement Awards for 2020. In the category of Review Awards, I'd like to enthusiastically support the nomination of Brittany Kiessling and Keely Maxwell (Office of Research and Development) for their outstanding paper titled "How Clean is Clean? A review of the social science of environmental cleanups." Published in 2018 in *Environmental Research Letters* it is a significant piece of research that is much needed in the social scientific study of Superfund and other toxic sites and environmental cleanup in general. It breaks new ground and steers social scientists in a direction that is needed for public policy of contaminated communities and strategies for decontamination.

As an anthropologist who has studied two major Superfund copper mining sites, and supervised graduate research of other sites, I have followed the research of Kiessling and Maxwell for several years. They have systematically tackled the major piece of research and analysis that has been lacking in social analysis of contaminated sites – namely an overview that rises above the site-specific case studies that are presented at conferences and in published articles. As they note in their article, of the 97 articles reviewed 75 are case studies. What has been lacking in the social science of contaminated sites and their cleanup is a comparative perspective. This is the forte of anthropologists (both Kiessling and Maxwell have their PhDs in anthropology) who seek to find the common themes among diverse cultures and geographies that reflect the scope of human society. In this article, their findings reveal that the disciplines who study the social dynamics of contaminated sites rarely speak to one another, do not build upon the research of others, and thus have created a landscape of scattered findings that make it difficult to assess a number of vital factors that contribute to the success, failure, or gaps in environmental cleanup programs. Kiessling and Maxwell focus on prominent areas of overlap in the literature: worker health, public engagement, and societal benefits of cleanup. Yet, as they note, several important factors limit the findings of this comparison: geographical inclusion of diverse sites and types of contamination, the vigorous application of a more mixed methodological approach, and an interdisciplinary discussion of social aspects of contamination. Thus, their call for a social science of decontamination is a breakthrough after decades (since the 1980s) of fragmented economic, sociological, political science, and anthropological studies of contaminated communities and effects of cleanup policies.

209 Academic Office Building | 1400 Townsend Drive, Houghton, MI 49931-1295
906-487-2113 | socialsciences@mtu.edu | **mtu.edu/social-sciences**

Michigan Tech is an EOE which includes protected veterans and individuals with disabilities.

I am especially impressed by the Kiessling and Maxwell contribution to because I have also witnessed the framing, execution, and discussion of their research effort while they have worked at EPA. Because of my own interest in Superfund sites, public engagement, and policy reform, I have followed their research for several years, attended their conference presentations, and steered my own graduate students toward their work. They carefully and systematically identified the major gaps in our knowledge in their 2018 publication and have subsequently organized panels and a special journal issue in *Journal of Environmental Management* to move their work to the next phase.

Their continued work, as framed by their 2018 article, points to specific directions that need attention if we are to effectively tackle policy implementation, evaluation, and reform in the successful decontamination of communities. Social science research needs to advance to match the work of the physical and biological sciences that have begun to identify new methods and strategies for reducing the public risk to exposure of toxic sites and long-term contamination that plagues many communities. The absence of a coordinated voice from the social sciences with their mixed qualitative and quantitative approaches impedes our understanding of how best to tackle the expensive, long-term process of ridding communities from harmful legacy contaminants. In my estimation, Kiessling and Maxwell's work has begun this much needed effort and deserves recognition by EPA for paving the path forward. It is a most impressive contribution!

Sincerely,

Carol

Carol A MacLennan

Professor Emerita and Research Scholar
Social Sciences and Great Lakes Research Center
Michigan Technological University
Senior Scholar
School for Advanced Research
Co-President, Association for Anthropology of Policy
Contact Information:
10 Recado Rd
Santa Fe, NM 87508
906-370-9632
camac@mtu.edu
https://sarweb.org/sar-researchers/carol-maclennan/

Table of Contents

General_Authors_Publications.....2
LI-266167_STAA_combined_%_memos.....14
STAA_combined_%_memos.....23
Regli_et_al_2015.....32
Regli_SI.....41

United States Environmental Protection Agency
Washington, DC 20460

STAA REPORT FOR THE SCIENTIST NOMINATIONS

General Information:

Nomination ID/App ID:	20-104
Research Category Primary:	Environmental Policy and Decision-Making Studies (EP)
Research Category Secondary:	Health Effects Research and Human Health Risk Assessment (HE)
Laboratory/Office Name:	ORD
Nomination Entered By:	Michael Elovitz

Eligibility Checklist:

[Y] The nominated publication(s) has not been submitted to a previous STAA competition.

[Y] The nominated publication(s) was published on or before January 1, 2017 and on or after January 1,2012

[Y] The principal author was an EPA employee or a PHS employee assigned to EPA when the research was performed

[Y] The EPA authors (includes PHS employees assigned to EPA) contributed collectively a minimum of 50% toward the publication(s)

Nominating Official Name:	Kevin Oshima
Nominating Official Title:	BIOLOGIST
Nominating OfficialEmail:	oshima.kevin@epa.gov
STAA Coordinator Name:	Kathleen Wiser
STAA Coordinator Email:	wiser.kathi@epa.gov

Justifications:

Justification 1:

Beginning around 2010, numerous drinking water utilities, surface water plants predominantly in EPA's Regions 3 and 4, were reporting unusually high formation of trihalomethane (THM) disinfection byproducts (DBPs) in their finished drinking water. The high THM formation was seemingly the result of atypically high percentages of brominated THM species. In subsequent years, further investigations (by the collective research community) at some utilities revealed elevated bromide concentration in the source waters. This led to considerable attention by the research community to identify the various possible sources of the bromide, most notably industrial activities such as unconventional energy extraction, coal-fired power plants, and textile and electronics manufacturing.

These bromide-related issues occurred during a period when staff in Office of Water's (OW) Standards and Risk Management Branch (SRMD/OGWDW/OW) were beginning their work on the *Six Year Review* (SYR3) of the *Microbial* and *Disinfectant/Disinfectant By-Product Rules*. The impact of the elevated bromide in source waters was recognized by both OW and the drinking water treatment community. In a very general sense, the elevated bromide concentrations could have direct implications for increased risk from DBP-associated bladder cancer. Previous ORD findings support a role for brominated THMs in the etiology of DBP-associated bladder cancer. SRMD/OGWDW/OW began developing a strategy for addressing the impacts due to the anthropogenic bromide inputs with the intent of leveraging the *Clean Water Act* through development of an ambient water quality criteria for bromide. Towards this end, OW began a risk assessment and understood the importance of writing a peer-review journal article that characterized the potential impact of bromide inputs on DBP formation and the associated bladder cancer. OW also saw this as an opportunity for risk assessment aspects of the paper to inform its *Six Year Review*.

When asked by SRMD/OGWDW/OW in various phases of the development of the paper, ORD provided rapid analysis and interpretive language of the scientific literature on toxicology, DBP formation chemistry and equations, and epidemiology to support the fundamental basis for the paper. In 2015, OW needed to accelerate the completion of the paper for submission to peer review. This was largely prompted by a spring 2015 presentation that the *American Water Works Association* (AWWA) gave to OGWDW that indicated that many drinking water utilities could experience significant costs in complying with the *Stage 2 DBPR* because of elevated bromide concentrations projected to occur in drinking water sources. ORD scientists were pivotal in helping to see the manuscript to completion and submission to the journal *Environmental Science & Technology* (*ES&T*, current Impact factor: 7.149). Following initial acceptance by the journal (accepted with revisions), the authors agreed that due to the potential for policy implications, the paper warranted a much more thorough *Supplemental Information* section to provide a clear explanation of the data analysis and modeling underlying the paper. The timely and critical input of ORD co-authors in responding to peer review comments received in

August 2015, and developing the extended *Supplemental Information* section, allowed for the paper to be published in *ES&T* in October 2015 (Regli et al. 2015). Completion of the paper by 2015 was an important deadline for OW to allow for the paper's inclusion in the SYR3 support documents that only include references published by 2015.

The paper is relevant to EPA's mission of protecting America's waters. The paper was used as an important reference to support the OGWDW's current *Six Year Review* of the *Microbial and Disinfectant/Disinfectant By-Product Rules*, which was completed in 2016. The paper informs increased weight-of-evidence for bladder cancer being associated with exposure from DBPs, particularly brominated THM species, that occur as a result of drinking water chlorination practices. The paper also provides a basis for estimating potential public health implications of bromide discharges from industrial sources in the nation's source drinking waters, thereby supporting the potential for leveraging remediation under the *Clean Water Act*. The success of this manuscript and the leadership of this multi-disciplinary team is a model of cross-cutting research to tackle a very challenging problem and demonstrated need and is a rare cross OW and ORD collaboration that led to a publication.

Justification 2A:

n/a

Justification 2B:

1. Michael Elovitz: *Denitrification alternates between a source and sink of nitrous oxide in the hypolimnion of a thermally stratified reservoir* (published 2014); 2017 STAA nomination (*Investigating the Role of Reservoirs in Removing Excess Reactive Nitrogen*); 2017 Level II STAA award.
2. Michael Elovitz: *Comparing drinking water treatment costs to source water protection costs using time series analysis* (published 2015); 2017 STAA nomination (same title as publication); 2017 Level III STAA award.
3. Michael Messner: *Total coliform and E. coli in public water systems using undisinfected ground water in the United States* (published 2017); 2018 STAA nomination; no award

Justification 2C:

The past and concurrent (see justification 2E) STAA nominations do not have any direct relationship to this nomination. This nomination neither built upon, nor relied upon this e other nominations in any way.

1. Michael Elovitz: *Denitrification alternates between a source and sink of nitrous oxide in the hypolimnion of a thermally stratified reservoir* (published 2014); 2017 STAA nomination (*Investigating the Role of Reservoirs in Removing Excess Reactive Nitrogen*); 2017 Level II STAA award. This paper has no relation to the topic of the current nomination

2. Michael Elovitz: *Comparing drinking water treatment costs to source water protection costs using time series analysis* (published 2015); 2017 STAA nomination (same title as publication); 2017 Level III STAA award. This paper has no relation to the topic of the current nomination. Neither paper built upon, nor relied upon the other in any way.

3. Michael Messner: *Total coliform and E. coli in public water systems using undisinfected ground water in the United States* (published 2017); 2018 STAA nomination; no award. This paper has no relation to the topic of the current nomination. Neither paper built upon, nor relied upon the other in any way.

4. John Michael Wright: concurrent 2020 STAA (category #3 [Health Effects Research and Human Health Risk Assessment]); *Disinfection By-Product Exposures and the Risk of Specific Cardiac Birth Defects*. Environmental Health Perspectives 2017;125:269–277. This paper is an epidemiological study of cardiac birth defects that was conducted based on primary data in Massachusetts and has no relation to the topic of the current nomination. The paper does not relate to this nomination as they are very different health end-points.

Justification 2D:

n/a

Justification 2E:

John Michael Wright is (concurrently) submitting a manuscript under STAA category #3 [Health Effects Research and Human Health Risk Assessment] entitled:

"Disinfection By-Product Exposures and the Risk of Specific Cardiac Birth Defects." *Environmental Health Perspectives* 2017;125:269–277.

This Wright-paper is an epidemiological study of cardiac birth defects that was conducted based on primary data in Massachusetts and has no relation to the topic of the current nomination. The Wright-paper does not relate to this nomination as they are very different health end-points. Dr. Wright is the only author on his submission with nexus with this nomination.

Justification 3A:

Citations:

To date, according to Google Scholar, the paper has been cited 62 times.

Downloads/Views:

According to the Journal, there have been 1738 Views/downloads.

Altmetric Score:

3

Invited presentations:

The core of the nominated publication was the topic of an invited talk by lead-author Stig Regli at one of the prestigious Gordon Research Conferences (GRC) – *2015 Drinking Water Disinfection By-Products: Charting the Horizons of Interdisciplinary Research and Application in Water Disinfection, By-Products, Water Reuse and Public Health*. The talk entitled "DBP Research: Roadmap for the Future" was part of a session entitled "The Way Foreword, Future DBP Research and Regulation". Dr. Regli also gave an invited follow-up talk focusing on some of the core aspects of the paper at the following GRC conference – *2017 Drinking Water Disinfection By-Products: Disinfection 2100: Linking Engineering, Chemistry, Toxicology and Epidemiology to Reduce Exposure to Toxicity Drivers While Curtailing Pathogens*. The talk entitled "New Regulatory Approaches to Minimizing DBP Toxicity Drivers" was part of the session entitled "Disinfection Systems of the Future: How Can We Minimize Toxicity Drivers?".

The GRC conferences are known across the globe for their slogan “Frontiers of Science”. The conferences are a small, highly selective group of scientists and the subject matter of each talk is selected to fill a specific niche. The invitations afforded the two authors to present the research that is a fundamental core of the paper, as well as supporting information, is high recognition of the impact of the work.

The toxicological underpinnings of the research comprising this nominated publication was the topic of an invited talk by co-author Dr. Rex Pegram at the same 2015 GRC conference. The talk entitled "What are the Forcing Agents Involved with Disinfection By-Product Toxicity?" was part of the aforementioned “The Way Forward, Future Disinfection By-Product Research and Regulation” session. The mechanistic information linking brominated trihalomethane exposure to human bladder cancer was also presented by Dr. Pegram at the *48th Annual Meeting of the Environmental Mutagenesis and Genomics Society* as an invited symposium lecture entitled, “Molecular Mechanisms by which Chlorinated Water Causes Bladder Cancer”, in September, 2017.

Internal (EPA) Awards:

The EPA authors on this paper received a 2016 ORD Award for “*Exceptional/Outstanding Technical Assistance to the Regions or Program Offices. Anthropogenic Bromide Impact Assessment Group”.* This 2016 award recognized the *exception collaborative interaction* between ORD scientists, and Program Office scientists, working across multiple disciplines to achieve the goal of the assessment of the impact of anthropogenic sources of bromide on drinking water treatment. The paper currently being nominated is the outcome of that collaborative effort. The ORD award emphasized the collaborative effort which was evident in 2016. This STAA nomination aims to recognize the scientific and policy impacts that the paper has led to in the years since publication.

Justification 3B:

The journal *Environmental Science and Technology* (ES&T) is largely considered the preeminent peer-reviewed research journal on environmental science and engineering topics (current impact factor 7.149). The journal is known to have a very rigorous peer-review process both for novelty of the research and editorial quality. All manuscripts that are deemed acceptable scholarship by an initial screening of an associate editor are sent for thorough external peer-review to experts in the field. Manuscripts are typically evaluated by three or more experts. This paper was published under the journal topic of “Policy Analysis”, which is a specific category of research that focuses on nexus of science, engineering and policy.

The paper went through the ES&T peer-review process comprising three anonymous peer-reviews and correspondence with an associate editor. While the anonymous peer-reviewers and editor judged the initial submission with unanimous positive ratings ("accept with minor revisions"), the authors and some of the reviewers felt that due to the potential for policy implications, the paper warranted a much more thorough *Supplemental Information* section to provide a clear explanation of the data analysis and modeling underlying the paper (associated SI section is part of this nomination).

Upon the minor revisions to the main paper, and the new extended SI section, the paper received a second review by the three anonymous reviewers, and the associated editor, and was published in 2015.

AUTHORS

Principal Author

Author Name:	Michael S. Elovitz		
Professional Title:		Salutation:	Dr.
Email:	elovitz.michael@epa.gov	Organization:	
Mailing Address:			
Street Line 1:	26 W MARTIN LUTHER KING DR		
City:	CINCINNATI		
Zip Code:	45268	State:	Ohio
At time of research was:	EPA Employee		
Separation Date:			
% of Effort:	10		

Contributing Author

Author Name:	Michael Messner

Professional Title:		Salutation:	Dr.
Email:	messner.michael@epa.gov	Organization:	
Mailing Address:			
Street Line 1:	USEPA Headquarters William Jefferson Clinton Building 1200 Pennsylvania Avenue, N. W.		
City:	Washington		
Zip Code:	20460	State:	DC
At time of research was:	EPA Employee		
Separation Date:			
% of Effort:	15		

Contributing Author

Author Name:	John Michael Wright		
Professional Title:		Salutation:	Dr.
Email:	wright.michael@epa.gov	Organization:	
Mailing Address:			
Street Line 1:	26 W MARTIN LUTHER KING DR		
City:	CINCINNATI		
Zip Code:	45268	State:	Ohio
At time of research was:	EPA Employee		
Separation Date:			
% of Effort:	5		

Contributing Author

Author Name:	Jimmy Chen		
Professional Title:		Salutation:	Dr.
Email:	chen.jimmy@epa.gov	Organization:	
Mailing Address:			
Street Line 1:	U.S. Environmental Protection Agency Office of Ground Water and Drinking Water 1200 Pennsylvania Ave., NW (Mail Stop 4607)		
City:	Washington		
Zip Code:	20460	State:	DC
At time of research was:	EPA Employee		
Separation Date:			
% of Effort:	20		

Contributing Author

Author Name:	Rex Pegram		
Professional Title:		Salutation:	Dr.
Email:	pegram.rex@epa.gov	Organization:	
Mailing Address:			
Street Line 1:	09 T.W. Alexander Drive Mail Code: B105-03		
City:	Research Triangle Park		
Zip Code:	27709	State:	NC
At time of research was:	EPA Employee		
Separation Date:			
% of Effort:	5		

Contributing Author

Author Name:	Stig Regli		
Professional Title:		Salutation:	Mr.
Email:	regli.stig@epa.gov	Organization:	
Mailing Address:			
Street Line 1:	USEPA Headquarters William Jefferson Clinton Building 1200 Pennsylvania Avenue, N. W. Mail Code: 4607M		
City:	Washington		
Zip Code:	20460	State:	DC
At time of research was:	EPA Employee		
Separation Date:			
% of Effort:	30		

Contributing Author

Author Name:	Susan Ricahrdson		
Professional Title:		Salutation:	Dr.
Email:	richardson.susan@sc.edu	Organization:	
Mailing Address:			
Street Line 1:	Department of Chemistry and Biochemistry University of South Carolina 631 Sumter Street		
City:	Columbia		
Zip Code:	29208	State:	SC
At time of research was:	Non EPA Personnel		

Separation Date:			
% of Effort:	5		

Contributing Author

Author Name:	T.J. Pepping		
Professional Title:		Salutation:	Mr.
Email:	tj_pepping@abtassoc.com	Organization:	
Mailing Address:			
Street Line 1:	6130 Executive Boulevard		
City:	Rockville		
Zip Code:	20852	State:	MD
At time of research was:	Non EPA Personnel		
Separation Date:			
% of Effort:	5		

Contributing Author

Author Name:	Frank Letkiewicz		
Professional Title:		Salutation:	Dr.
Email:	frank.letkiewicz@cadmusgroup.com	Organization:	
Mailing Address:			
Street Line 1:	7700 Old Georgetown Road,		
City:	Bethesda		
Zip Code:	20814	State:	MD
At time of research was:	Non EPA Personnel		

Separation Date:	
% of Effort:	5

PUBLICATIONS

Publication 1:

Publication Title:	Estimating Potential Increased Bladder Cancer Risk Due to Increased Bromide Concentrations in Source		
Publication Date:	Wed Oct 21 00:00:00 GMT 2015		
Journal/Publication Method:	Environmental Science & Technology		
All Author(s):			
Volume:	49	Number:	22
Pages:	13094-1310	Immediately Index:	Immediately Index:
Citation ½ Life:	7.10	Impact Factor:	7.149

MEMO

Subject: Record of Percentage Agreement

Nominee's name: Stig Regli

Title of nominated articles: *Estimating potential increased bladder cancer risk due to increased bromide concentrations in sources of disinfected drinking waters*

Your name: Stig Regli
Professional title: Senior Leader – Policy Analyst
Percentage on nomination form: 30%
Current affiliation: USEPA
Current address: OGWDW (4607), USEPA; 1200 Pennsylvania Avenue NW; Washington DC 20260

I am in agreement with my designated percentage of contribution as stated on the Scientific and Technological Achievement Awards 2020 Nomination Form.

Sincerely,

Stig Regli

MEMO

Subject: Record of Percentage Agreement

Nominee's name: Stig Regli

Title of nominated articles: *Estimating potential increased bladder cancer risk due to increased bromide concentrations in sources of disinfected drinking waters*

Your name: Jimmy Chen
Professional title:
Percentage on nomination form: 20%
Current affiliation:
Current address:

I am in agreement with my designated percentage of contribution as stated on the Scientific and Technological Achievement Awards 2020 Nomination Form.

Sincerely,

04/27/2020

Jimmy Chen

MEMO

Subject: Record of Percentage Agreement

Nominee's name: Stig Regli

Title of nominated articles: *Estimating potential increased bladder cancer risk due to increased bromide concentrations in sources of disinfected drinking waters*

Your name: Michael Messner
Professional title: Mathematical Statistician
Percentage on nomination form: 15%
Current affiliation: USEPA/OW
Current address:

I am in agreement with my designated percentage of contribution as stated on the Scientific and Technological Achievement Awards 2020 Nomination Form.

Sincerely,
Your name

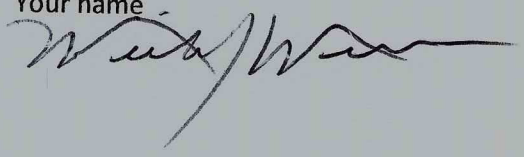

MEMO

Subject: Record of Percentage Agreement

Nominee's name: Stig Regli

Title of nominated articles: *Estimating potential increased bladder cancer risk due to increased bromide concentrations in sources of disinfected drinking waters*

Your name: Michael S. Elovitz
Professional title:
Percentage on nomination form: 10%
Current affiliation: US EPA/ ORD/CEMM/WECD
Current address: 26 West MLK Dr. Cincinnati, OH 45268

I am in agreement with my designated percentage of contribution as stated on the Scientific and Technological Achievement Awards 2020 Nomination Form.

Sincerely,

4/27/2020

X

Michael Elovitz
Branch Chief; WMB/WECD/CEMM/ORD
Signed by: MICHAEL ELOVITZ

MEMO

Subject: Record of Percentage Agreement

Nominee's name: Stig Regli

Title of nominated articles: *Estimating potential increased bladder cancer risk due to increased bromide concentrations in sources of disinfected drinking waters*

Your name: Frank J. Letkiewicz
Professional title: Principal
Percentage on nomination form: 5%
Current affiliation: The Cadmus Group, LLC
Current address: 7700 Old Georgetown Road, Bethesda, MD 20814

I am in agreement with my designated percentage of contribution as stated on the Scientific and Technological Achievement Awards 2020 Nomination Form.

Sincerely,

Frank Letkiewicz

MEMO

Date: April 27, 2020

Subject: Record of Percentage Agreement

Nominee's name: Stig Regli

Title of nominated articles: *Estimating potential increased bladder cancer risk due to increased bromide concentrations in sources of disinfected drinking waters*

Your name: Rex A. Pegram
Professional title: Research Biologist
Percentage on nomination form: 5%
Current affiliation: U.S EPA/ORD/CCTE/CCED/ETTB
Current address: 3004 Jehon Court, Apex, NC 27502

I am in agreement with my designated percentage of contribution as stated on the Scientific and Technological Achievement Awards 2020 Nomination Form.

Sincerely,

Rex A. Pegram

MEMO

Subject: Record of Percentage Agreement

Nominee's name: Stig Regli

Title of nominated articles: *Estimating potential increased bladder cancer risk due to increased bromide concentrations in sources of disinfected drinking waters*

Your name: T. J. Pepping
Professional title: Senior Analyst
Percentage on nomination form: 5%
Current affiliation: Abt Associates, Inc.
Current address: 6130 Executive Blvd, Rockville, MD 20852

I am in agreement with my designated percentage of contribution as stated on the Scientific and Technological Achievement Awards 2020 Nomination Form.

Sincerely,

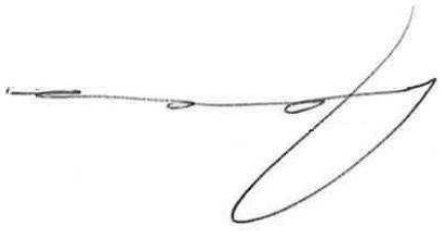

T.J. Pepping

MEMO

Subject: Record of Percentage Agreement

Nominee's name: Stig Regli

Title of nominated articles: *Estimating potential increased bladder cancer risk due to increased bromide concentrations in sources of disinfected drinking waters*

Your name: Susan D. Richardson
Professional title: Arthur Sease Williams Professor of Chemistry
Percentage on nomination form: 5%
Current affiliation: Department of Chemistry & Biochemistry, University of South Carolina
Current address: Department of Chemistry & Biochemistry, University of South Carolina, 631 Sumter St., Columbia, SC 29208

I am in agreement with my designated percentage of contribution as stated on the Scientific and Technological Achievement Awards 2020 Nomination Form.

Sincerely,
Susan Richardson

4-27-20

MEMO

Subject: Record of Percentage Agreement

Nominee's name: Stig Regli

Title of nominated articles: *Estimating potential increased bladder cancer risk due to increased bromide concentrations in sources of disinfected drinking waters*

Your name: Dr. John Michael Wright
Professional title: Epidemiologist
Percentage on nomination form: 5%
Current affiliation: ORD/CPHEA/CPAD
Current address: USEPA (MS-A110) 26 West Martin Luther King Drive Cincinnati, OH 45268

I am in agreement with my designated percentage of contribution as stated on the Scientific and Technological Achievement Awards 2020 Nomination Form.

Sincerely,

J. Michael Wright

MEMO

Subject: Record of Percentage Agreement

Nominee's name: Stig Regli

Title of nominated articles: *Estimating potential increased bladder cancer risk due to increased bromide concentrations in sources of disinfected drinking waters*

Your name: Stig Regli
Professional title: Senior Leader – Policy Analyst
Percentage on nomination form: 30%
Current affiliation: USEPA
Current address: OGWDW (4607), USEPA; 1200 Pennsylvania Avenue NW; Washington DC 20260

I am in agreement with my designated percentage of contribution as stated on the Scientific and Technological Achievement Awards 2020 Nomination Form.

Sincerely,

Stig Regli

MEMO

Subject: Record of Percentage Agreement

Nominee's name: Stig Regli

Title of nominated articles: *Estimating potential increased bladder cancer risk due to increased bromide concentrations in sources of disinfected drinking waters*

Your name: Jimmy Chen
Professional title:
Percentage on nomination form: 20%
Current affiliation:
Current address:

I am in agreement with my designated percentage of contribution as stated on the Scientific and Technological Achievement Awards 2020 Nomination Form.

Sincerely,

04/27/2020

Jimmy Chen

MEMO

Subject: Record of Percentage Agreement

Nominee's name: Stig Regli

Title of nominated articles: *Estimating potential increased bladder cancer risk due to increased bromide concentrations in sources of disinfected drinking waters*

Your name: Michael Messner
Professional title: Mathematical Statistician
Percentage on nomination form: 15%
Current affiliation: USEPA/OW
Current address:

I am in agreement with my designated percentage of contribution as stated on the Scientific and Technological Achievement Awards 2020 Nomination Form.

Sincerely,
Your name

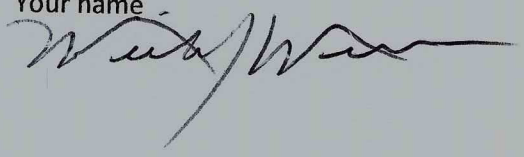

MEMO

Subject: Record of Percentage Agreement

Nominee's name: Stig Regli

Title of nominated articles: *Estimating potential increased bladder cancer risk due to increased bromide concentrations in sources of disinfected drinking waters*

Your name: Michael S. Elovitz
Professional title:
Percentage on nomination form: 10%
Current affiliation: US EPA/ ORD/CEMM/WECD
Current address: 26 West MLK Dr. Cincinnati, OH 45268

I am in agreement with my designated percentage of contribution as stated on the Scientific and Technological Achievement Awards 2020 Nomination Form.

Sincerely,

4/27/2020

X

Michael Elovitz
Branch Chief; WMB/WECD/CEMM/ORD
Signed by: MICHAEL ELOVITZ

MEMO

Subject: Record of Percentage Agreement

Nominee's name: Stig Regli

Title of nominated articles: *Estimating potential increased bladder cancer risk due to increased bromide concentrations in sources of disinfected drinking waters*

Your name: Frank J. Letkiewicz
Professional title: Principal
Percentage on nomination form: 5%
Current affiliation: The Cadmus Group, LLC
Current address: 7700 Old Georgetown Road, Bethesda, MD 20814

I am in agreement with my designated percentage of contribution as stated on the Scientific and Technological Achievement Awards 2020 Nomination Form.

Sincerely,

Frank Letkiewicz

MEMO

Date: April 27, 2020

Subject: Record of Percentage Agreement

Nominee's name: Stig Regli

Title of nominated articles: *Estimating potential increased bladder cancer risk due to increased bromide concentrations in sources of disinfected drinking waters*

Your name: Rex A. Pegram
Professional title: Research Biologist
Percentage on nomination form: 5%
Current affiliation: U.S EPA/ORD/CCTE/CCED/ETTB
Current address: 3004 Jehon Court, Apex, NC 27502

I am in agreement with my designated percentage of contribution as stated on the Scientific and Technological Achievement Awards 2020 Nomination Form.

Sincerely,

Rex A. Pegram

MEMO

Subject: Record of Percentage Agreement

Nominee's name: Stig Regli

Title of nominated articles: *Estimating potential increased bladder cancer risk due to increased bromide concentrations in sources of disinfected drinking waters*

Your name: T. J. Pepping
Professional title: Senior Analyst
Percentage on nomination form: 5%
Current affiliation: Abt Associates, Inc.
Current address: 6130 Executive Blvd, Rockville, MD 20852

I am in agreement with my designated percentage of contribution as stated on the Scientific and Technological Achievement Awards 2020 Nomination Form.

Sincerely,

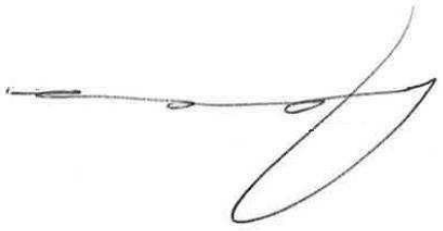

T.J. Pepping

MEMO

Subject: Record of Percentage Agreement

Nominee's name: Stig Regli

Title of nominated articles: *Estimating potential increased bladder cancer risk due to increased bromide concentrations in sources of disinfected drinking waters*

Your name: Susan D. Richardson
Professional title: Arthur Sease Williams Professor of Chemistry
Percentage on nomination form: 5%
Current affiliation: Department of Chemistry & Biochemistry, University of South Carolina
Current address: Department of Chemistry & Biochemistry, University of South Carolina, 631 Sumter St., Columbia, SC 29208

I am in agreement with my designated percentage of contribution as stated on the Scientific and Technological Achievement Awards 2020 Nomination Form.

Sincerely,
Susan Richardson

4-27-20

MEMO

Subject: Record of Percentage Agreement

Nominee's name: Stig Regli

Title of nominated articles: *Estimating potential increased bladder cancer risk due to increased bromide concentrations in sources of disinfected drinking waters*

Your name: Dr. John Michael Wright
Professional title: Epidemiologist
Percentage on nomination form: 5%
Current affiliation: ORD/CPHEA/CPAD
Current address: USEPA (MS-A110) 26 West Martin Luther King Drive Cincinnati, OH 45268

I am in agreement with my designated percentage of contribution as stated on the Scientific and Technological Achievement Awards 2020 Nomination Form.

Sincerely,

J. Michael Wright

Environmental Science & Technology

Policy Analysis

pubs.acs.org/est

Estimating Potential Increased Bladder Cancer Risk Due to Increased Bromide Concentrations in Sources of Disinfected Drinking Waters

Stig Regli,*[,†] Jimmy Chen,[†] Michael Messner,[†] Michael S. Elovitz,[‡] Frank J. Letkiewicz,[§] Rex A. Pegram,[∥] T.J. Pepping,[†,⊥] Susan D. Richardson,[#] and J. Michael Wright[▽]

[†]Office of Ground Water and Drinking Water, U.S. Environmental Protection Agency, Washington, D.C. 20460, United States

[‡]Office of Research and Development, National Risk Management Laboratory, U.S. Environmental Protection Agency, Cincinnati, Ohio 45268, United States

[§]The Cadmus Group, Bethesda, Maryland 20814, United States

[∥]Office of Research and Development, National Health and Environmental Effects Research Laboratory, U.S. Environmental Protection Agency, Research Triangle Park, North Carolina 27711, United States

[⊥]Oak Ridge Institute for Science and Education Internship/Research Participation Program, U.S. Department of Energy, Oak Ridge, Tennessee 37830, United States

[#]Department of Chemistry and Biochemistry, University of South Carolina, Columbia, South Carolina 29208, United States

[▽]Office of Research and Development, National Center for Environmental Assessment, U.S. Environmental Protection Agency, Cincinnati, Ohio 45268, United States

Supporting Information

ABSTRACT: Public water systems are increasingly facing higher bromide levels in their source waters from anthropogenic contamination through coal-fired power plants, conventional oil and gas extraction, textile mills, and hydraulic fracturing. Climate change is likely to exacerbate this in coming years. We estimate bladder cancer risk from potential increased bromide levels in source waters of disinfecting public drinking water systems in the United States. Bladder cancer is the health end point used by the United States Environmental Protection Agency (EPA) in its benefits analysis for regulating disinfection byproducts in drinking water. We use estimated increases in the mass of the four regulated trihalomethanes (THM4) concentrations (due to increased bromide incorporation) as the surrogate disinfection byproduct (DBP) occurrence metric for informing potential bladder cancer risk. We estimate potential increased excess lifetime bladder cancer risk as a function of increased source water bromide levels. Results based on data from 201 drinking water treatment plants indicate that a bromide increase of 50 μg/L could result in a potential increase of between 10^{-3} and 10^{-4} excess lifetime bladder cancer risk in populations served by roughly 90% of these plants.

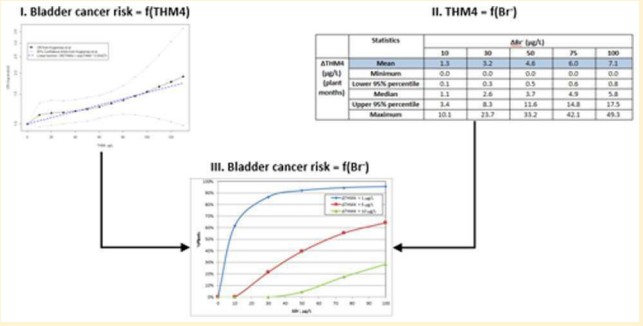

INTRODUCTION

In recent years, drinking water utilities in various regions of the U.S. have expressed concerns over increased bromide levels in their source waters.[1−4] In addition to natural sources of bromide from salt water intrusion or geologic formations, there are new anthropogenic bromide releases from coal-fired power plants, conventional oil and gas extraction, textile mills, and hydraulic fracturing activities. Bromide reacts with aqueous chlorine in the form of hypochlorous acid (HOCl) to form hypobromous acid (HOBr) which reacts with organic material to form brominated disinfection byproducts (DBPs) such as brominated trihalomethanes (THMs) and haloacetic acids (HAAs). Increased bromide concentration in the source water may induce changes in concentrations and speciation of DBPs in the finished water. These changes in DBP formation may also result in increased risk of adverse health effects, such as bladder cancer, due to long-term drinking water usage.

BACKGROUND

Regulatory Context. DBPs are an unintended consequence from disinfection used to minimize risk from pathogens in drinking water. DBPs are complex mixtures in drinking water supplies, most obviously in the formation of chlorination DBPs, and are influenced by source water quality and physicochemical treatment processes. The United States EPA

Received: July 21, 2015
Revised: October 16, 2015
Accepted: October 21, 2015
Published: October 21, 2015

Downloaded via US EPA RESEARCH TRIANGLE PARK on April 27, 2020 at 13:38:36 (UTC).
See https://pubs.acs.org/sharingguidelines for options on how to legitimately share published articles.

© 2015 American Chemical Society

DOI: 10.1021/acs.est.5b03547
Environ. Sci. Technol. 2015, 49, 13094−13102

has regulated DBPs in public drinking water systems since 1979[5−7] mainly due to concern for their carcinogenicity in humans. Epidemiological studies indicate an association between exposure to chlorinated drinking water and bladder cancer.[8−13] Increased incidence of bladder cancer has also been associated with exposure to higher THM4 levels in drinking water.[10,11,14−17] In its economic analysis to support the Stage 2 DBP regulation,[7] EPA used estimated bladder cancer cases avoided as the health effects metric for quantifying the benefits under the new regulation. Since they are the predominant DBPs, THMs and HAAs are considered surrogate measures for the co-occurrence of other DBPs in systems using chlorination.

Why Brominated DBPs are a Concern. Given the multitude of DBPs present in drinking water, a key remaining challenge is to determine which mixtures of DBPs are of most toxicological concern. Among DBPs formed in chlorinated drinking water, bromine-containing species may pose greater health risks than those containing only chlorine.[17−19] DNA damage and induction of gene mutations are important basic mechanisms (genotoxicity) by which chemicals can cause cancer. In many cases, chemical carcinogens are transformed by metabolizing enzymes to "activated" metabolites that react with DNA to produce mutations. A hypothesis has been developed linking bladder cancer risk to population variation in the ability to metabolize brominated trihalomethanes (BrTHMs) to genotoxic metabolites. BrTHMs, but not chloroform, were found to be mutagenic in Salmonella via metabolic activation by the enzyme, glutathione *S*-transferase theta-1 (GSTT1).[20,21] Ross and Pegram[22,23] subsequently demonstrated that GSTT1 is active in the urinary tract and that GSTT1-mediated metabolism of bromodichloromethane (BDCM) produces reactive intermediates that covalently bind DNA and deoxyguanosine, which is consistent with the possibility it is a mutagenic carcinogen. GSTT1 is polymorphically expressed in humans, which has enabled epidemiologists to compare bladder cancer risks in people that have (i.e., GSTT1(+)) and do not have (i.e., GSTT1-null) this enzyme. Cantor et al.[16] found that people with the GSTT1(+) genotype were at significantly greater risk (odds ratio (OR) = 2.2; 95% confidence interval (CI): 1.1−4.3) for developing bladder cancer when exposed to the upper THM4 exposure quartile (>49 μg/L) compared to GSTT1-null participants who had no increased risk at the same exposure level. Cantor et al.[16] also examined the role of genetic variation in another enzyme, GST zeta 1 (GSTZ1), which is involved in HAA metabolism and elimination.[24,25] Study participants in the highest THM4 exposure quartile (>49 μg/L) had a 1.8 (95%CI: 0.9−3.5) increased risk of bladder cancer compared to those in the lowest quartile (<8 μg/L THM4). Those with both the GSTT1(+) genotype and a genotype (CT/TT) that causes lower activity of GSTZ1 had a 5.9-fold (95%CI: 1.8−19.0) increased risk for bladder cancer. The Cantor et al. study[16] therefore suggests that the BrTHMs and the HAAs may both play a role in the etiology of DBP-induced human bladder cancer. Approximately 80% of the U.S population has the GSTT1(+) genotype, and 30% has the GSTZ1 (CT/TT) genotype;[26−28] thus, people with the combination of both high-risk genotypes comprise approximately 24% (0.8 × 0.3) of the U.S. population. Noteworthy is that much of the Cantor et al.[16] study population was exposed to drinking water with THM4 concentrations having a higher proportion of BrTHMs than in most U.S. drinking water supplies (see Supporting Information (SI)). Thus, the exposure-response relationship observed between exposure from THM4 concentrations and bladder cancer risk in the Cantor et al. 2010 study may be more pronounced than what might be found for the general US population and for which we later model (based on a meta-analysis which does not include the Cantor et al.[16] data).

Consistent with the findings for the BrTHMs, brominated DBPs, in general, are more genotoxic, cytotoxic, and carcinogenic than chlorinated DBPs based on toxicological data.[18,19] A comprehensive genotoxicity database containing more than 80 DBPs was created that examined DNA damage in Chinese hamster ovary cells.[18,19] This database allowed genotoxicity comparisons of several different DBP classes, along with the effect of bromide vs chloride substituents and monohalo vs dihalo vs trihalo substituents. Brominated species were found generally to be more genotoxic than chlorinated species. For example, bromoacetic acid is more than an order of magnitude more genotoxic than chloroacetic acid. This same pattern is also observed in *Salmonella*, as well as in new human cell data.[29,30] However, there is not a consistent relationship between toxicity and the degree of bromine substitution in dihalo and trihalocompounds.[21,31] The significantly higher genotoxicity of brominated versus chlorinated DBP species is also apparent when the bromo- and chloro-DBPs of different classes (beyond only THMs and HAAs) are summed together.[18,19]

Bromide DBP Chemistry and Exposure Implications. Additional occurrence of bromide in source waters increases the formation of brominated DBPs with disinfection using chlorine,[32−40] chloramines,[41−46] ozone,[39−41,47] and chlorine dioxide.[41,48] The resultant speciation shift from primarily chlorinated compounds to more heavily brominated compounds occurs across every compound class, including the THMs, HAAs, haloacetonitriles, halonitromethanes, haloaldehydes, haloketones, haloamides, and halofuranones, as well as new DBP classes recently discovered, including halobenzoquinones[49,50] and other new brominated aromatic DBPs.[51] As such, source waters having higher levels of bromide cause a shift from species like chloroform, dichloroacetic acid, trichloronitromethane, and MX (3-chloro-4-(dichloromethyl)-5-hydroxy-2(5*H*)-furanone) to bromoform, dibromoacetic acid, tribromonitromethane, and brominated MX analogues resulting in higher mass of DBPs. Increased bromine substitution on a carbon atom generally renders these DBPs less stable due to steric hindrance and electronic effects.

It is also important to note that increased bromide levels not only increases the overall mass of DBPs due to the higher mass of bromine (80 Da) relative to chlorine (35.5 Da), but research has also shown that the molar mass of the DBPs formed increases especially for THMs, HAAs, and haloacetonitriles.[52−54] This can be explained by the increased reactivity, as reaction rates of HOBr with natural organic matter are at least 10 times faster than with HOCl.[52,53,55] In addition, HOBr is more efficient at substitution reactions than chlorine, such that aqueous bromine is substituted more into organic structures, whereas chlorine tends to cleave carbon bonds and produce relatively less halogen substitution.[53]

DBP formation and degradation is complex and exposure assessment remains a key challenge in epidemiological studies. The impact of certain water-use activities and specific exposure routes are important considerations when evaluating the relationship between DBPs and bladder cancer. The physicochemical properties of DBPs can determine exposure route and impact absorption, metabolism, excretion, and distribution in the body (i.e., bioavailability). HAAs, for example, are neither volatile nor very permeable to skin; therefore, ingestion is

DOI: 10.1021/acs.est.5b03547
Environ. Sci. Technol. 2015, 49, 13094−13102

considered the most important HAA exposure route. THMs, in contrast, result in multiroute exposures largely due to their volatility and skin permeability.[56] Backer et al.[57] reported that 10 min post-exposure blood levels of brominated THMs in participants that took showers were 3.7- to 5.1-fold greater than in participants that drank 1 L of tap water. Similarly, maximum blood concentrations of BDCM, area under the blood concentration vs time curve (integrated exposure over time), and half-lives in human participants attained after dermal exposures to water containing BDCM averaged 35-, 79-, and 7-fold greater than in subjects exposed to the same BDCM dose via the oral route.[58] These significant route-dependent differences in BDCM exposure metrics are important, because they demonstrate that much more BDCM will likely reach the bladder from dermal and inhalation exposures than by ingestion and that this relationship should pertain to other BrTHMs.[57,58] Higher blood concentrations, and thus, higher extra-hepatic target tissue doses associated with the dermal and inhalation exposures are due to the bypass of first-pass liver metabolism.[57,58] Due to limitations in water-use activity data over one's lifetime, only one epidemiological study of bladder cancer has been able to characterize route-specific effect estimates. Villanueva et al.[59] reported an OR for bladder cancer in participants with upper quartile ingestion levels of >35 μg/day of THM4 versus those with no reported consumption of chlorinated water (odds ratios (OR) = 1.35; 95%CI: 0.92—1.99). These effect estimates were smaller than the metric based on duration of shower or bath (OR = 1.83; 95%CI: 1.17—2.87) for the highest showering/bathing exposure quartile (duration × THM4 water concentration) as compared to the lowest quartile. This suggests that for this study population, which was essentially the same as that of Cantor et al.,[16] the bladder cancer risk associated with exposure to DBPs may be more attributed to the dermal/inhalation route than ingestion.

■ ANALYSIS

Overview. Given the association between bladder cancer and THM4 noted in epidemiological studies, and the impact of bromide on BrTHMs and other DBPs, we postulate that a population served by a utility producing drinking water with increased THM4 due to increased bromide levels in its source water may be subject to increased bladder cancer risk. Increased bromide levels in source waters from anthropogenic activities are a concern, since bromide is difficult to remove by treatment.[1] We estimate potential increased bladder cancer risk for U.S. populations using disinfected public drinking water systems with increased bromide in their source waters by

I. estimating potential increase in bladder cancer risk as a function of increased THM4 levels in finished water,
II. estimating increased THM4 levels in finished waters attributed to increased bromide levels in source waters, and
III. consolidating "I" and "II" to estimate potential increase in bladder cancer risk as a function of increased bromide levels in source water on a national level.

In sum, we are estimating the potential increase in bladder cancer risk that might result from an increase in THM4 concentration (and associated DBPs) due specifically to increased bromide in the source water.

Data Analysis I—Bladder Cancer Risk Estimates. In the Economic Analysis (EA) for the Stage 2 Disinfectants and Disinfection Byproduct Rule (DBPR), the EPA estimated the annual baseline bladder cancer cases attributable to DBP exposure prior to the Stage 1 DBPR and estimated reductions in the THM4 concentrations that would result from the new regulation, and from these estimated associated reductions in annual incidence of bladder cancer.[60] EPA derived three estimates of bladder cancer incidence attributable to chlorination DBPs in drinking water using data from five case-control epidemiological studies,[8−12,61] a meta-analysis,[13] and a pooled data analysis.[14] The respective attributable risk estimates were 2−17% (for the range of the five case control studies), 16% for the central estimate of the meta-analysis, and 17% for the central estimate of the pooled analysis. In its EA, EPA assumed there is a linear relationship between average THM4 concentration and bladder cancer risk and that the estimated percent reduction in national average THM4 concentration resulting from regulation would correspond to the same percent reduction in bladder cancer cases attributable to exposure from drinking water. EPA based this assumption largely on the pooled data analysis[14] which showed a dose−response relationship of increasing ORs as a function of cumulative THM4 exposure for which the best estimate appeared largely linear.[14,60] For low probability outcomes, odds and outcome probability are nearly equal, so OR (the ratio of odds with exposure to odds without exposure) is nearly equal to the ratio of risk with exposure to risk without exposure.

Development of Risk Function. The National Cancer Institute estimates that for 2014, 74 690 new cases of bladder cancer will be diagnosed in the United States and approximately 2.4% of men and women will be diagnosed with bladder cancer in their lifetimes.[62] This proportion represents the lifetime risk of bladder cancer in the U.S. due to all causes, including DBPs. Lifetime odds of bladder cancer is the lifetime probability (2.4%) divided by its complement: 0.024/(1−0.024) = 0.02459. Note that the denominator (1−0.024 = 0.976) is nearly 1, so the odds is not much different from the lifetime probability (0.024). This lifetime odds value will be used in later calculations of the change in risk with changes in THM4 concentrations.

Estimates noted in previous epidemiological studies suggest that bladder cancer risk generally increases with THM4 levels and with duration of exposure. As such, EPA used estimates from the pooled analysis[14] and more detailed data provided by the authors of that analysis[63] in the Stage 2 EA,[60] which reported ORs as a continuous function of average THM4 concentration. The estimates, shown in Table 1, were based on a pooled analysis of data obtained from six case-control studies. The confidence intervals shown in Table 1 reflect uncertainty about the central estimates (OR).

The ORs of Table 1 were found by fitting a spline function to pooled data from the six epidemiological studies included in the pooled analysis. The curve in Figure 1 is complex; concave near the origin, convex in the middle and nearly linear at higher exposure levels. Given the wide confidence bands about the curve, there is considerable uncertainty about the actual relationship between exposure and risk. In the Stage 2 EA, EPA used a simpler linear relationship between exposure and the bladder cancer OR and used unweighted least-squares regression to characterize the linear relationship. A line was fit to the ORs of Table 1 and additional lines were fit to the upper and lower confidence limit estimates. The central estimate is

$$\mathrm{OR} = 1 + 0.00581 \times C$$

where C is the average (lifetime) concentration of THM4 (μg/L).

DOI: 10.1021/acs.est.5b03547
Environ. Sci. Technol. 2015, 49, 13094−13102

Table 1. Odds Ratio Estimates and Weights Used for Bladder Cancer Associated with THM4 Exposure

average THM4 (μg/L)	OR (95% CI)[a]	ln(OR) (95% CI)	SE[b]	weight[c]	adjusted weight[d]
0	1.00	0	0	0	
10	1.13 (0.96, 1.33)	0.122 (−0.041, 2.85)	0.083	14.5	0.0035
20	1.16 (0.98, 1.38)	0.148 (−0.020, 0.322)	0.087	52.5	0.0125
30	1.17 (1.00, 1.37)	0.157 (0.000, 0.315)	0.080	139.5	0.0333
40	1.19 (1.02, 1.39)	0.174 (0.020, 0.329)	0.079	256.7	0.0613
50	1.22 (1.04, 1.43)	0.199 (0.039, 0.358)	0.081	378.8	0.0905
60	1.26 (1.08, 1.47)	0.231 (0.077, 0.385)	0.079	582.0	0.1390
70	1.32 (1.12, 1.55)	0.278 (0.113, 0.438)	0.083	713.2	0.1704
80	1.38 (1.14, 1.68)	0.322 (0.131, 0.519)	0.099	654.0	0.1562
90	1.46 (1.13, 1.89)	0.378 (0.122, 0.637)	0.131	470.4	0.1124
100	1.55 (1.11, 2.17)	0.438 (0.104, 0.775)	0.171	341.9	0.0817
110	1.66 (1.07, 2.55)	0.507 (0.068, 0.936)	0.222	246.5	0.0589
120	1.77 (1.03, 3.06)	0.571 (0.030, 1.118)	0.278	186.6	0.0446
130	1.90 (0.98, 3.66)	0.641 (−0.20, 1.297)	0.336	149.6	0.0357

[a]Odds Ratios and confidence intervals were provided by Kogevinas and Villanueva.[63] [b]Standard Error (SE) = Interval width divided by 3.92. [c]Weight = $((\text{TTHM4}/\text{SE})^2)/1000$. [d]Adjusted weight is the weight divided by the sum of the weights.

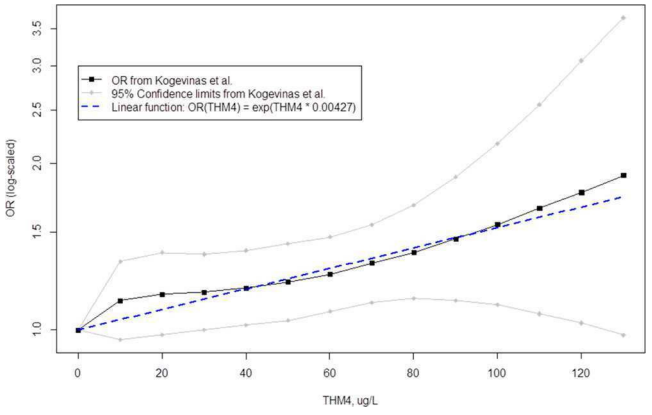

Figure 1. Bladder cancer risk from six epidemiological studies as a function of THM exposure from residential concentration data (derived from personal communication with Kogevinas and Villanueva[63]).

The values in Table 1 were weighted equally, although the confidence limits show that uncertainty varies across the range of THM4 exposure. To more properly account for this, we derived a weighted mean slope as follows:

- The response variable was changed to ln(OR). As shown in Figure 1, this normalized the errors so that the upper and lower confidence limits are symmetric about ln(OR).
- The weight used for each record (row) of Table 1 is based on its uncertainty, expressed as standard error. The standard error (s) is derived from the confidence interval width:
  - s = (ln(upper 95% confidence limit) − ln(lower 95% confidence limit))/($z_{0.975} - z_{0.025}$)
  - z = quantile of the standard normal distribution and $z_{0.975} - z_{0.025} = 3.92$
- The variance of the slope (ln(OR)/THM4) estimated from a single record of Table 1 is then $s^2/\text{THM4}^2$
- The unadjusted weight for each row of the table is the inverse of the variance of the slope (weight = $\text{THM4}^2/s^2$) and these are multiplied by a constant (the sum of unadjusted weights) so that the sum of adjusted weights is 1.
- Finally, the estimated overall slope is the sum, across rows, of adjusted weight times ln(OR)/THM4. The result is 0.00427 and the resulting function is shown as a dashed line in Figure 1.

The weighted slope (0.00427) is smaller than EPA's unweighted estimate (0.00581),[60] because it gives less weight to the three lowest nonzero exposure levels (THM4 = 10, 20, and 30) and also to the highest (THM4 = 130). The following equation relates ORs to average THM4 exposure:

$$\text{OR}(\text{THM4}) = e^{\text{THM4}\times 0.00427}$$

Based on this function and assuming average pre-Stage 1 exposure at 38.05 μg/L which EPA estimated in its EA for the Stage 2 DBPR,[60] baseline risk (r_0 = lifetime bladder cancer risk with zero THM4 exposure) can be derived as follows:

$$\text{OR}_{38.05\mu\text{g/L}} = e^{38.05\times 0.00427}$$

$$\text{pre-Stage 1 odds/baseline odds} = 1.176$$

$$0.02459/(r_0/(1 - r_0)) = 1.176$$

Solving for r_o:

$$r_0 = 0.02047$$

where baseline odds are associated with exposure to 0 μg/L.

Baseline odds is therefore 0.02047/(1−0.02047) = 0.02090. From the function relating ORs to THM4, the additional risk posed by a 1 μg/L increase in THM4 (r_1) will depend on the initial conditions (THM4 exposure level and lifetime bladder cancer risk). The additional risk will be smallest for the case with zero THM4 exposure (r_0 = 0.02047):

$$r_1/(1 - r_1) = 0.02090 \times e^{1\times 0.00427} = 0.02099$$

$$r_1 = 0.02099/(1 + 0.02099)$$

$$r_1 = 0.02056$$

$$r_1 - r_0 = 0.02056 - 0.02047 = 0.00009$$

If lifetime risk is greater than r_0, then the risk associated with a 1 μg/L increase is slightly increased. Consider the case where the average THM4 level changes from the pre-Stage 1 mean of 38.05 μg/L to 39.05 μg/L and pre-Stage 1 lifetime risk is $r_{38.05}$ = 0.024. From above, the pre-Stage 1 odds is 0.0246 and the additional risk is calculated as shown below:

$$r_{39.05}/(1 - r_{39.05}) = 0.0246 \times e^{1\times\backslash\, 0.00427} = 0.0247$$

$$r_{39.05} = 0.0241$$

The additional risk due to the 1 μg/L increase is 0.0241−0.024 = 0.0001 or 10^{-4}. The simple relationship of approximately 10^{-4} added lifetime risk per 1 μg/L increase in THM4 holds over the THM4 range expected for systems in

DOI: 10.1021/acs.est.5b03547
Environ. Sci. Technol. 2015, 49, 13094−13102

compliance with Stage 2 (see Table S1). We believe this is the smallest increase that one would reasonably consider, given that the magnitude of uncertainty is difficult to estimate.

Data Analysis II—THM4 Increases from Increased Bromide Levels. We used the Surface Water Analytical Tool (SWAT), version 1.1 (see SI for further information) that the EPA used in its Stage 2 EA[60,64] to assess the impacts of an increase of bromide levels in source waters on THM4 levels in public drinking water distribution systems. This version of SWAT was used by the EPA to estimate treatment and associated water quality changes for different regulatory options. SWAT uses source water and treatment data collected under the Information Collection Rule (ICR)[65] from July 1997 through December 1998 from 273 large plants using surface water sources representing a total population of over 100 million people contained in the AUX8 ICR data set. An overarching consideration for our analysis was to estimate the potential impact of increasing source water bromide on a subset of these plants that were assumed to be in compliance with the Stage 2 DBPR. Post-Stage 2 DBPR national level data sets are not available. Therefore, we attempted to utilize the AUX8 ICR data set in such a way as to include plants that, based on their ICR data and SWAT modeling, would likely have met the Stage 2 DBPR MCL of 80/60 μg/L (THM4/HAA5) at maximum residence time sample sites in the distribution system. In other words, if a plant was predicted (SWAT model predictions of THM4 and HAA5, based on ICR data inputs) to be within the annual average 80/60 compliance metric, then that plant would not likely make treatment changes (e.g., switch to chloramines) and would be operating today as it did during the ICR. Based on these criteria, 201 plants, comprising 2089 plant months, were identified and included in the analysis (see SI).

For the purpose of our modeling, we assumed that any ICR data entry for bromide concentration that was below the minimum reporting level (MRL) was equivalent to the reporting limit (i.e., 20 μg/L). This is consistent with the EPA's approach when conducting SWAT modeling to support the Stage 2 EA. The modeling with an assumption of half of the reporting limit is included in the SI to illustrate a sensitivity analysis of different values assigned to those below MRL. We also used the THM4 values predicted by SWAT at the average residence time in the distribution system (vs the maximum residence time, which would likely overestimate mean exposure for the entire residential population served by the plant) to estimate increases in THM4 concentration in treated drinking water (i.e., concentrations that would occur in households) as a function of increased bromide concentration in the source water. This assumption should better represent most of the exposed population for a given system.

To predict the impact of increased bromide on THM4 formation, for each of the plant months, we increased the source water bromide concentration by different increments (see Table 2) while keeping the other THM4 formation equation input parameters unchanged from their original ICR values. Changes in THM4 concentrations from increases in influent bromide (denoted as "ΔBr^-") are denoted as "ΔTHM4."

Table 2 shows the summary statistics of ΔTHM4 as a function of ΔBr^- predicted by the SWAT, indicating the predicted ΔTHM4 concentrations consistently increased, on average, by roughly an order of magnitude less than the increase in bromide. Such predicted results are consistent with a theoretical analysis that a simple replacement of chloride atom by bromide atom leads to a higher mass-based concentration of DBPs due to a higher molecular weight of bromide. However, there is a diminishing rate of increased ΔTHM4 as the ΔBr^- increases, indicating that organic precursors could be a limiting factor for formation of THMs with higher bromide concentration. For instance, the mean ΔTHM4 is 1.3 μg/L at the $\Delta Br^-$of 10 μg/L (i.e., 0.13 μg/L ΔTHM4 per μg/L ΔBr^-), compared to the mean ΔTHM4 7.1 μg/L at the ΔBr^- of 100 μg/L (i.e., 0.07 μg/L ΔTHM4 per μg/L ΔBr^-). Table 2 also indicates that ΔTHM4 at a given ΔBr^- varies across the 2089 plant-months. This variability is due not just to the variability in baseline bromide, but due to variations of other factors affecting THM4 formation, including source water quality (total organic carbon (TOC), ultraviolet absorbance at wavelength of 254 nanonmeters (UV254), temperature), operational conditions (disinfectant type, disinfectant dose, pH adjustments, changes in TOC and UV254), and residence time in the distribution system, characteristics essentially inherent in the SWAT model. These variations can occur from plant to plant, or within a specific plant due to temporal fluctuations.

Table 2. THM4 increases (ΔTHM4) as a Function of Increased Bromide Levels in Source Water (ΔBr^-)

		ΔBr^- (μg/L)				
	statistics	10	30	50	75	100
ΔTHM4 (μg/L) (plant months)	mean	1.3	3.2	4.6	6.0	7.1
	minimum	0.0	0.0	0.0	0.0	0.0
	lower 95% percentile	0.1	0.3	0.5	0.6	0.8
	median	1.1	2.6	3.7	4.9	5.8
	upper 95% percentile	3.4	8.3	11.6	14.8	17.5
	maximum	10.1	23.7	33.2	42.1	49.3

Given the wide range of initial baseline bromide or THM4 concentrations among the 201 plants examined, ranging from <20 μg/L to 400 μg/L as plant means (see SI), we assessed the impact of source water bromide increases (i.e., ΔBr^-) as a function of these baseline conditions. For this purpose, we predicted the resulting ΔTHM4 based on a single ΔBr^- of 50 μg/L (which was in the middle of the range of concentrations we considered and appeared to be a plausible increase in bromide concentration from anthropogenic effects).[1,4,66] As the mean baseline source water bromide level was lower, the ΔTHM4 per μg/L ΔBr^- tended to be higher, and as the baseline THM4 level increased, the ΔTHM4 tended to increase. Plants using only chlorine as a disinfectant had the highest mean ΔTHM4 across all treatment configuration categories. However, some plants within the categories that used chlorine, ozone, or chlorine dioxide as a primary disinfectant and chloramine as secondary disinfectant frequently also had high ΔTHM4 values. More detailed analyses are included in the SI.

Data Analysis III—Potential Risk Increases from Increased Bromide Levels in Source Water. The results predicted by the SWAT model from Data Analysis II were linked with the risk function from Data Analysis I. Since bladder cancer is associated with long-term exposure, annual plant mean increases in THM4 concentration are more relevant than plant month estimates to inform potential risk. Figure 2 characterizes the estimated annual plant mean ΔTHM4 as a function of ΔBr^- across 201 plants.

Figure 2 illustrates the percent of the 201 plants that were estimated to exceed a mean ΔTHM4 concentration of 1, 5, or

DOI: 10.1021/acs.est.5b03547
Environ. Sci. Technol. 2015, 49, 13094−13102

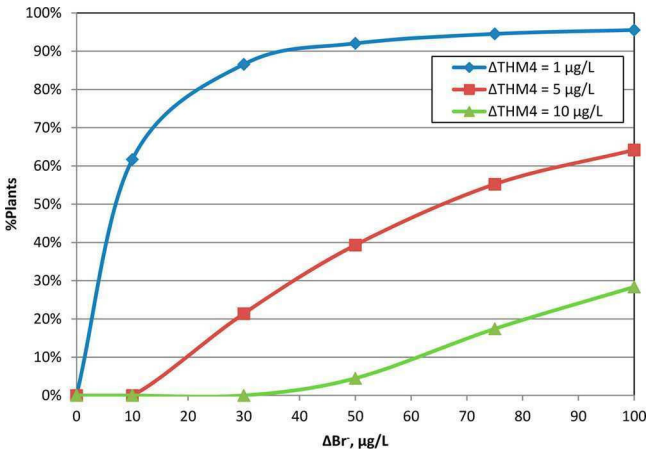

Figure 2. Percentage of plants with plant mean ΔTHM4 exceeding 1, 5, or 10 μg/L as function of ΔBr^-.

10 μg/L as a function of different mean ΔBr^-concentrations. For example, the ΔTHM4 line of 1 μg/L indicates that a mean increase of 50 μg/L bromide above the baseline would result in greater than 90% of plants incurring at least 1 μg/L THM4 increase at the average residence time location in the distribution system. From Data Analysis I, this suggests that such increases over a lifetime could correspond to a potential increase of greater than 10^{-4} excess lifetime bladder cancer risk. Similarly, the Δ10 μg/L THM4 line indicates that about 5% and 30% of all the plants are predicted to incur at least an increase of 10 μg/L THM4 if their source water bromide concentration increased by 50 μg/L, or 100 μg/L, respectively, which could correspond to a potential increase of greater than 10^{-3} excess lifetime bladder cancer risk.

DISCUSSION

We estimated potential increases in bladder cancer risk from increased bromide levels in source waters of disinfected public drinking water systems in the United States. As shown in Figure 2, our analysis indicates that roughly 90% of the plants could incur increases of between 1 and 10 μg/L THM4 if their mean source water bromide concentration were to increase by 50 μg/L above the baseline, and that such increases could correspond to excess lifetime bladder cancer risk of between 10^{-4} and 10^{-3}. Given an increase of 50 μg/L of mean bromide concentration in source water, 40% of the plants would incur a plant mean ΔTHM4 of greater than 5 μg/L. Furthermore, the greatest increases would be expected to occur when baseline mean source water bromide concentrations are lowest and the baseline mean THM4 concentrations are highest (see SI). Depending on the baseline THM4 concentration, these projected increases in source water bromide concentrations could also pose challenges for utilities to comply with the Stage 2 DBPR MCL (see SI).

While we recognize there is yearly variation of source water quality, our predictions are incremental relative to the baseline, and therefore we believe that differences in our prediction due to source water baseline variation will be relatively small (see SI). Since naturally occurring source water bromide levels can be quite high and variable (e.g., due to drought and precipitation events), relying on additional bromide (and THM) monitoring data to inform their contributions and potential risk implications from anthropogenic activity could be quite burdensome and challenging. Our approach has the advantage of characterizing the potential risk implications of increased bromide levels in source waters without relying on these additional measurements. Given our analysis and a designated increased source water bromide concentration level of concern (e.g., a level corresponding to a potential increased excess lifetime bladder cancer risk of between 10^{-4} and 10^{-3} or greater), we suggest that hydrodynamic modeling of in-stream dilution (not the subject of this paper) could be used to estimate point source bromide discharge levels that could lead to a bromide source water level of concern being exceeded for drinking water systems downstream of the discharge. One limitation in our analysis is not having sufficient data to develop confidence bounds around our ΔTHM4 estimates (see SI). Nevertheless, we think the methodology we have used to derive our estimates is sound, and we think that most plants (especially those having some free chlorine contact time) having a mean increase of 50 μg/L of bromide in their source water will likely incur at least a mean THM4 increase of 1 μg/L, and often more, in their delivered water (see SI).

While our analysis builds on that used in EPA's Stage 2 EA, it includes several enhancements and new information that strengthens the basis for the modeling approach considered here. We have improved the function for estimating bladder cancer risk that expresses the OR as a function of mean THM4 by using the log transformed variance to weight the observations thereby better accounting of the uncertainty of the exposure data from the epidemiological studies. Also, we only include the estimated increase in mass of the THM4 concentration (from elevated bromide levels in the source water) as the reference DBP occurrence metric for informing potential increased bladder cancer risk. The Stage 2 EA relied on decreased mass of THM4 as the surrogate measure (for risk reduction). This introduced more uncertainty than in our analysis for this paper since such reductions could result from a variety of remedial measures that might have more impact on reducing chloroform than the potentially more toxic brominated species (e.g., aeration) or contributing other types of DBP risk (e.g., chloramination). Given the more recent scientific data adding to the evidence base (e.g., pharmacokinetics, the importance of multiple routes of exposure, more epidemiological studies indicating a relationship between elevated THM4 and elevated bladder cancer risk, and relative toxicity of brominated versus chlorinated species), we believe there is less uncertainty in the risk analysis in this paper than in the Stage 2 DBPR EA. We also recognize that the analysis may underestimate bladder cancer risk, since we do not attribute any increase in risk that might result from increased toxicity due to higher concentrations and relative proportions of brominated DBP species.

In our analysis, we assumed, as the EPA did in its EA, that a linear relationship exists between the average THM4 concentration and the OR, whereas this relationship may actually be supra or super linear across different concentration ranges. Since we assumed that there is no risk above the baseline risk at 0 μg/L THM4 (the OR = 1.0), the slope for the linear relationship in Figure 1 was derived with the intercept forced to 1.0 and 0 μg/L. The implication of the linearity assumption is that the associated increased lifetime bladder cancer risk of 10^{-4} associated with a ΔTHM4 increase of 1 μg/L is nearly constant across the full range of mean baseline THM4 concentrations that could occur. We believe the assumption of linearity from increased THM4 concentration due to bromide increase across the full range of THM4 baseline concentrations is reasonable.

DOI: 10.1021/acs.est.5b03547
Environ. Sci. Technol. 2015, 49, 13094−13102

This is supported by empirical evidence of genotoxic mechanisms implicated in the carcinogenicity of the brominated THMs[20−23,67] and approximate linearity in bladder cancer risk was observed in epidemiological studies of THM4 exposures within the range of most plant baseline THM4 concentrations (presented in Figure 1).

Although recent studies have added to the weight of evidence between exposure to chlorinated drinking water and elevated bladder cancer risk, we recognize that substantial uncertainty remains in our risk estimates and in some of the underlying epidemiological estimates that propagate throughout our analysis. For example, one major source of uncertainty stems from exposure assessment efforts that rely on HAA5 and THM4 as surrogates for the relevant DBP mixtures in chlorinated drinking water, especially since different populations encounter various DBP speciation proportions and exposure mixtures.[36] For example, the THM4 exposure metric potentially acts as a surrogate for many of the chlorinated DBP species, but it should also be recognized that the same THM4 concentration in one water may have a very different mix of THM species and associated co-occurring DBPs, when compared to another water with the same THM4 concentration. Consequently, the respective risks from these waters might be substantially different even though they have the same THM4 concentration. In addition, if the nonchlorinated species (e.g., brominated DBPs) are the most important from a toxicological perspective, then using THM4 and HAA5 to estimate risk might not fully capture the most relevant DBP mixtures of interest. Thus, exposure measurement error from using an imperfectly correlated surrogate like THM4 in epidemiological studies could result in an underestimate of the bladder cancer risk from long-term exposure if a causal relationship exists. Despite these uncertainties, there is more evidence today than at the time of EPA's EA to suggest a basis for causality. Indeed, in 2014 the International Agency for Research on Cancer (IARC) advisory panel nominated, as a high priority, that disinfected water used for showering, bathing, swimming, or drinking be evaluated for its carcinogenicity based on ubiquitous exposure and extensive new mechanistic evidence of specific DBP toxicity, including molecular epidemiological studies.[68]

As in EPA's Stage 2 EA, the scope of our analysis is a national perspective, and it should be recognized that, for a given drinking water system, estimates could vary widely especially across different disinfection treatment types. Also, since causality has not yet been established, and our risk estimates are associated with relatively small changes in THM4 concentrations, we do not consider these estimates as definitive. However, this analysis does provide a potential model for assessment of additional risk due to increased bromide in source water, thus addressing a problem of increasing importance for U.S. drinking water systems.

■ ASSOCIATED CONTENT

Supporting Information

The Supporting Information is available free of charge on the ACS Publications website at DOI: 10.1021/acs.est.5b03547.

Additional details on SWAT and it is associated model components, supplemental analyses, QA/QC, and other discussions about the analyses (PDF)

■ AUTHOR INFORMATION

Corresponding Author

*Phone: (202)-564-5270; fax: (202)-564-3758; e-mail: regli.stig@epa.gov.

Notes

The authors declare no competing financial interest.

■ ACKNOWLEDGMENTS

This project was supported in part by an appointment to the Research Participation Program at the Office of Water administered by the Oak Ridge Institute for Science and Education through an interagency agreement between the Department of Energy and EPA. Although the work was reviewed by EPA and approved for publication, it may not necessarily reflect official Agency policy or opinions expressed. We are grateful for the rigorous review by Patricia Murphy, Jeff Swartout, and the *ES&T* peer reviewers that strengthened the paper.

■ REFERENCES

(1) States, S.; Cyprych, G.; Stoner, M.; Wydra, F.; Kuchta, J.; Monnell, J.; Casson, L. Marcellus Shale drilling and brominated THMs in Pittsburgh, Pa., drinking water. *Journal American Water Works Association.* **2013**, *105*, E432−E448.

(2) Hladik, M. L.; Focazio, M. J.; Engle, M. Discharges of produced waters from oil and gas extraction via wastewater treatment plants are sources of disinfection by-products to receiving streams. *Sci. Total Environ.* **2014**, *466−467*, 1085−1093.

(3) Wilson, J. M.; VanBriesen, J. M. Oil and gas produced water management and surface drinking water sources in Pennsylvania. *Environ. Pract.* **2012**, *14*, 288−300.

(4) McTigue, N. E.; Cornwell, D. A.; Graf, K.; Brown, R. Occurrence and consequences of increased bromide in drinking water sources. *J. Am. Water Works Ass.* **2014**, *106* (11), E492−E508.

(5) U.S. Environmental Protection Agency. National Interim Primary Drinking Water Regulations: Control of Trihalomethanes in Drinking Water. *Fed Regist.* **1979**, *44* (231), 68624−68707.

(6) U.S. Environmental Protection Agency. National Primary Drinking Water Regulations: Disinfectants and Disinfection By-products. *Fed Regist.* **1998**, *63* (241), 69389−69476.

(7) U.S. Environmental Protection Agency. National Primary Drinking Water Regulations: Stage 2 Disinfectants and Disinfection Byproducts Rule. *Fed Regist.* **2006**, *71*, 388−493.

(8) Cantor, K. P.; Hoover, R.; Hartge, P.; Drinking Water Source and Bladder Cancer: A Case-Control Study. In *Water Chlorination: Chemistry, Environmental Impact and Health Effects*; Jolley, R. L., Bull, R. J., Davis, W. P., Eds.; Lewis Publishers, Inc.: Chelsea, MI, 1985; Vol. *5*, pp 145−152.

(9) McGeehin, M. A.; Reif, J. S.; Becher, J. C.; Mangione, E. J. Case Control Study of Bladder Cancer and Water Disinfections Methods in Colorado. *Am. J. Epidemiol.* **1993**, *18*, 138.

(10) King, W. D.; Marrett, L. D. Case-control study of bladder cancer and chlorination by-products in treated water (Ontario, Canada). *Cancer Cause Control.* **1996**, *7*, 596−604.

(11) Cantor, K. P.; Lunch, C. F.; Hildesheim, M.; Dosemeci, M.; Lubin, J.; Alavanja, M.; Craun, G. F. Drinking Water Source and Chlorination Byproducts I. Risk of Bladder Cancer. *Epidemiology* **1998**, *9* (1), 21−28.

(12) Freedman, M.; Cantor, K. P.; Lee, N. L.; Chen, L. S.; Lei, H. H.; Ruhl, C. E.; Wang, S. S. Bladder Cancer and Drinking Water: A Population-Based Case Control Study in Washington County, Maryland. *Cancer Cause Control.* **1997**, *8* (5), 738−744.

(13) Villanueva, C. M.; Fernandez, F.; Malats, M.; Grimalt, J. O.; Kogevinas, M. A. A meta-analysis of studies on individual consumption of chlorinated drinking water and bladder cancer. *J. Epidemiol Community Health.* **2003**, *57*, 166−173.

DOI: 10.1021/acs.est.5b03547
Environ. Sci. Technol. 2015, 49, 13094−13102

(14) Villanueva, C. M.; Cantor, K. P.; Cordier, S.; Jaakkola, J. J.; King, W. D.; Lynch, C. F.; Porru, S.; Kogevinas, M. Disinfection byproducts and bladder cancer: a pooled analysis. *Epidemiology* **2004**, *15*, 357−367.
(15) Bove, G. E.; Rogerson, P. A.; Vena, J. E. Case Control Study of the Effects of Trihalomethanes on Urinary Bladder Cancer Risk. *Arch. Environ. Occup. Health* **2007**, *62* (1), 39−47.
(16) Cantor, K. P.; Villanueva, C. M.; Silverman, D. T.; Figueroa, J. D.; Real, F. X.; Garcia-Closas, M.; Malats, N.; Chanock, S.; Yeager, M.; Tardon, A.; Garcia-Closas, R.; Serra, C.; Carrato, A.; Castaño-Vinyals, G.; Samanic, C.; Rothman, N.; Kogevinas, M. Polymorphisms in *GSTT1, GSTZ1,* and *CYP2E1,* disinfection by-products, and risk of bladder cancer in Spain. *Environ. Health Perspect.* **2010**, *118*, 1545−1550.
(17) Costet, N.; Villanueva, C. M.; Jaakkola, J. J. K.; Kogevinas, M.; Cantor, K. P.; King, W. D.; Lynch, C. F.; Nieuwenhuijsen, M. J.; Cordier, S. Water disinfection by-products and bladder cancer: is there a European specificity? A pooled and meta-analysis of European case-control studies. *Occup. Environ. Med.* **2011**, *68* (5), 379−385.
(18) Richardson, S. D.; Plewa, M. J.; Wagner, E. D.; Schoeny, R.; DeMarini, D. M. Occurrence, genotoxicity, and carcinogenicity of regulated and emerging disinfection by-products in drinking water: a review and roadmap for research. *Mutat. Res., Rev. Mutat. Res.* **2007**, *636*, 178−242.
(19) Plewa, M. J.; Wagner, E. D.; Muellner, M. G.; Hsu, K. M.; Richardson, S. D. Comparative mammalian cell toxicity of N-DBPs and C-DBPs. In *Occurrence, Formation, Health Effects and Control of Disinfection By-Products in Drinking Water*; Karanfil, T., Krasner, S. W., Westerhoff, P., Xie, Y., Eds.; American Chemical Society: Washington, DC, 2008; Vol. *995*, pp 36−50.
(20) Pegram, R. A.; Andersen, M. E.; Warren, S. H.; Ross, T. M.; Claxton, L. D. Glutathione *S*-transferase-mediated mutagenicity of trihalomethanes in *Salmonella typhimurium* TA1535: contrasting results with bromodichloromethane and chloroform. *Toxicol. Appl. Pharmacol.* **1997**, *144*, 183−188.
(21) DeMarini, D. M.; Shelton, M. L.; Warren, S. H.; Ross, T. M.; Shim, J.-Y.; Richard, A. M.; Pegram, R. A. Glutathione S-transferase-mediated induction of GC to At transitions by halomethanes in Salmonella. *Environ. Mol. Mutagen.* **1997**, *30*, 440−447.
(22) Ross, M. K.; Pegram, R. A. Glutathione Transferase Theta 1−1-dependent Metabolism of the Water Disinfection Byproduct Bromodichloromethane. *Chem. Res. Toxicol.* **2003**, *16*, 216−226.
(23) Ross, M. K.; Pegram, R. A. In vitro biotransformation and genotoxicity of the drinking water disinfection byproduct bromodichloromethane: DNA binding mediated by glutathione transferase theta 1−1. *Toxicol. Appl. Pharmacol.* **2004**, *195*, 166−181.
(24) Board, P. G.; Anders, M. W. Human glutathione transferase zeta. *Methods Enzymol.* **2005**, *401*, 61−77.
(25) Saghir, S. A.; Schultz, I. R. Toxicokinetics and oral bioavailability of halogenated acetic acids mixtures in naïve and GSTzeta-depleted rats. *Toxicol. Sci.* **2005**, *84*, 214−224.
(26) National Center for Biotechnology Information; National Institutes of Health. Database of Single Nucleotide Polymorphisms. http://www.ncbi.nlm.nih.gov/snp/ (accessed July 2, 2014).
(27) United States Census Bureau. Population Estimates Vintage 2008: National Tables. http://www.census.gov/poptest/data/historical/2000s/vintage_2008 (accessed August 26, 2014).
(28) Ginsberg, G. S.; Smolenski, S.; Hattis, D.; Guyton, K. Z.; Johns, D. O.; Sonawane, B. Genetic polymorphisms in glutathione transferases (GST): Population distribution of GSTM1, T1, and P1 conjugating activity. *J. Toxicol. Environ. Health, Part B* **2009**, *12*, 389−439.
(29) Attene-Ramos, M. S.; Wagner, E. D.; Plewa, M. J. Comparative human cell toxicogenomic analysis of monohaloacetic acid drinking water disinfection byproducts. *Environ. Sci. Technol.* **2010**, *19*, 7206−7212.
(30) Escobar-Hoyos, L. F.; Hoyos-Giraldo, L. S.; Londono-Velasco, E.; Reyes-Carvajal, I.; Saavedra-Trujillo, D.; Carvajal-Varona, S.; Sanchez-Gomez, A.; Wagner, E. D.; Plewa, M. J. Genotoxic and clastogenic effects of monohaloacetic acid drinking water disinfection by-products in primary human lymphocytes. *Water Res.* **2013**, *47*, 3282−3290.
(31) Plewa, M. J.; Simmons, J. E.; Richardson, S. D.; Wagner, E. D. Mammalian cell cytotoxicity and genotoxicity of the haloacetic acids, a major class of drinking water disinfection by-products. *Environ. Mol. Mutagen.* **2010**, *51*, 871−878.
(32) Krasner, S. W.; McGuire, M. J.; Jacangelo, J. G.; Patania, N. L.; Reagan, K. M.; Aieta, E. M. The occurrence of disinfection by-products in US drinking water. *J. Am. Water Works Assoc.* **1989**, *81*, 41−53.
(33) Heller-Grossman, L.; Manka, J.; Limoni-Relis, B.; Rebhun, M. Formation and distribution of haloacetic acids, THM and TOX in chlorination of bromide-rich lake water. *Water Res.* **1993**, *27*, 1323−1331.
(34) Rathbun, R. E. Bromine incorporation factors for trihalomethane formation for the Mississippi, Missouri, and Ohio Rivers. *Sci. Total Environ.* **1996**, *192*, 111−118.
(35) Petri, M.; Wilker, M.; Stabel, H. H.; Gilbert, E. Formation of brominated disinfection by-products after chlorination of water from Lake Constance depending on treatment steps and bromide concentration. *Acta Hydrochim. Hydrobiol.* **1997**, *25*, 319−328.
(36) McLain, J. L.; Obolensky, A.; Shukairy, H. M. Disinfection by-product speciation. In *Information Collection Rule Data Analysis*; McGuire, M. J., McLain, J. L., Obolensky, A., Eds.; Awwa Research Foundation and American Water Works Association: Denver, CO, 2002; pp 141−168.
(37) Obolensky, A.; Singer, P. C. Halogen substitution patterns among disinfection byproducts in the Information Collection Rule database. *Environ. Sci. Technol.* **2005**, *39*, 2719−2730.
(38) Lekkas, T. D.; Nikolaou, A. D. Development of predictive models for the formation of trihalomethanes and haloacetic acids during chlorination of bromide-rich water. *Water Qual. Res. J. Can.* **2004**, *39*, 149−159.
(39) Krasner, S. W.; Weinberg, H. S.; Richardson, S. D.; Pastor, S. J.; Chinn, R.; Sclimenti, M. J.; Onstad, G. D.; Thruston, A. D., Jr. Occurrence of a new generation of disinfection byproducts. *Environ. Sci. Technol.* **2006**, *40*, 7175−7185.
(40) Sohn, J.; Amy, G.; Yoon, Y. Bromide ion incorporation into brominated disinfection by-products. *Water, Air, Soil Pollut.* **2006**, *174*, 265−277.
(41) Zhang, X.; Echigo, S.; Minear, R. A.; Plewa, M. J. Characterization and comparison of disinfection by-products of four major disinfectants. In *Natural Organic Matter and Disinfection By-Products: Characterization and Control*; Barrett, S. E., Krasner, S. W., Amy, G. L., Eds.; American Chemical Society: Washington D.C., 2000; Vol. *761*, pp 299−314.
(42) Diehl, A. C.; Speitel, G. E.; Symons, J. M.; Krasner, S. W.; Hwang, S. J. DBP formation during chloramination. *J. Am. Water Works Assoc.* **2000**, *92*, 76−90.
(43) Yang, X.; Shang, C. Chlorination byproduct formation in the presence of humic acid, model nitrogenous organic compounds, ammonia, and bromide. *Environ. Sci. Technol.* **2004**, *38*, 4995−5001.
(44) Richardson, S. D.; Fasano, F.; Ellington, J. J.; Crumley, F. G.; Buettner, K. M.; Evans, J. J.; Blount, B. C.; Silva, L. K.; Waite, T. J.; Luther, G. W.; McKague, A. B.; Miltner, R. J.; Wagner, E. D.; Plewa, M. J. Occurrence and Mammalian Cell Toxicity of Iodinated Disinfection Byproducts in Drinking Water. *Environ. Sci. Technol.* **2008**, *42*, 8330−8338.
(45) Hua, G.; Reckhow, D. A. Evaluation of bromine substitution factors of DBPs during chlorination and chloramination. *Water Res.* **2012**, *46*, 4208−4216.
(46) Chu, W.; Gao, N.; Yin, D.; Krasner, S. W. Formation and speciation of nine haloacetamides, an emerging class of nitrogenous DBPs, during chlorination or chloramination. *J. Hazard. Mater.* **2013**, *260*, 806−812.
(47) Richardson, S. D.; Thruston, A. D., Jr.; Caughran, T. V.; Chen, P. H.; Collette, T. W.; Floyd, T. L.; Schenck, K. M.; Lykins, B. W., Jr.; Sun, G.-R.; Majetich, G. Identification of new drinking water

DOI: 10.1021/acs.est.5b03547
Environ. Sci. Technol. 2015, 49, 13094−13102

disinfection byproducts formed in the presence of bromide. *Environ. Sci. Technol.* **1999**, *33*, 3378−3383.
(48) Richardson, S. D.; Thruston, A. D., Jr.; Rav-Acha, C.; Groisman, L.; Popilevsky, I.; Juraev, O.; Glezer, V.; McKague, A. B.; Plewa, M. J.; Wagner, E. D. Tribromopyrrole, brominated acids, and other disinfection byproducts produced by disinfection of drinking water rich in bromide. *Environ. Sci. Technol.* **2003**, *37*, 3782−3793.
(49) Zhao, Y. L.; Qin, F.; Boyd, J. M.; Anichina, J.; Li, X.-F. Characterization and determination of chloro- and bromo-benzoquinones as new chlorination disinfection byproducts in drinking water. *Anal. Chem.* **2010**, *82*, 4599−4605.
(50) Zhao, Y. L.; Anichina, J.; Lu, X. F.; Bull, R. J.; Krasner, S. W.; Hrudey, S. E.; Li, X.-F. Occurrence and formation of chloro- and bromo-benzoquinones during drinking water disinfection. *Water Res.* **2012**, *46*, 4351−4360.
(51) Pan, Y.; Zhang, X. R. Four groups of new aromatic halogenated disinfection byproducts: effect of bromide concentration on their formation and speciation in chlorinated drinking water. *Environ. Sci. Technol.* **2013**, *47*, 1265−1273.
(52) Hua, G.; Reckhow, D. A.; Kim, J. Effect of bromide and iodide ions on the formation and speciation of disinfection byproducts during chloramination. *Environ. Sci. Technol.* **2006**, *40*, 3050−3056.
(53) Westerhoff, P.; Chao, P.; Mash, H. Reactivity of natural organic matter with aqueous chlorine and bromine. *Water Res.* **2004**, *38*, 1502−1513.
(54) Wu, W. W.; Chadik, P. A. Effect of bromide ion on haloacetic acid formation during chlorination of a Biscayne aquifer water. *J. Environ. Eng.* **1998**, *124*, 932−938.
(55) Uyak, V.; Toroz, I. Investigation of bromide ion effects on disinfection by-products formation and speciation in an Istanbul water supply. *J. Hazard. Mater.* **2007**, *149*, 445−451.
(56) Xu, X.; Mariano, T. M.; Laskin, J. D.; Weisel, C. P. Percutaneous absorption of trihalomethanes, haloacetic acids, and haloketones. *Toxicol. Appl. Pharmacol.* **2002**, *184*, 19−26.
(57) Backer, L. C.; Ashley, D. A.; Bonin, M. A.; Cardinali, F. L.; Kieszak, S. M.; Wooten, J. V. Household exposures to drinking water DBPs: whole blood THM levels. *J. Exposure Anal. Environ. Epidemiol.* **2000**, *10*, 321−326.
(58) Leavens, T. L.; Blount, B. C.; DeMarini, D. M.; Madden, M. C.; Valentine, J. L.; Case, M. W.; Silva, L. K.; Warren, S. H.; Hanley, N. M.; Pegram, R. A. Disposition of bromodichloromethane in humans following oral and dermal exposure. *Toxicol. Sci.* **2007**, *99*, 432−445.
(59) Villanueva, C. M.; Cantor, K. P.; Grimalt, J. O.; Malats, N.; Silverman, D.; Tardon, A.; Garcia-Closas, R.; Serra, C.; Carrato, A.; Castaño-Vinyals, G.; Marcos, R.; Rothman, N.; Real, F. X.; Dosemeci, M.; Kogevinas, M. Bladder cancer and exposure to water disinfection by-products through ingestion, bathing, showering, and swimming in pools. *Am. J. Epidemiol.* **2007**, *165*, 148−156.
(60) U.S. Environmental Protection Agency. *Economic Analysis for the Final Stage 2 Disinfectants and Disinfection Byproducts Rule*, EPA 815-R-05-010; Office of Water; Office of Ground Water and Drinking Water: Washington, DC, 2005.
(61) Cantor, K. P.; Hoover, R.; Hartge, P.; Mason, T. J.; Silverman, D. T.; Altman, R.; Austin, D. F.; Child, M. A.; Key, C. R.; Marrett, L. D.; Myers, M. H.; Narayana, A. S.; Levin, L. I.; Sullivan, J. W.; Swanson, G. M.; Thomas, D. B.; West, D. W. Bladder Cancer, Drinking Water Source, and Tap Water Consumption: A Case-Control Study. *J. Natl. Cancer Inst.* **1987**, *79* (6), 1269−1279.
(62) National Cancer Institute; Surveillance, Epidemiology, and End Results Program Stat Fact Sheets: Bladder Cancer. http://seer.cancer.gov/statfacts/html/urinb.html (accessed July 2, 2014).
(63) Kogevinas, M.; Villanueva, C. Personal communication regarding THM exposure levels presented in Villanueva et al (2004); July 15, 2005.
(64) U.S. Environmental Protection Agency. *Appendices to the Economic Analysis for the Final Stage 2 Disinfectants and Disinfection Byproducts Rule*, EPA 815-R-05-010; Office of Water; Office of Ground Water and Drinking Water: Washington, DC, 2005; Vol. *I*, A-E2.
(65) U.S. Environmental Protection Agency. National Primary Drinking Water Regulations: Monitoring Requirements for Public Drinking Water Supplies; Final Rule. *Fed Regist. 61*(94) 24354 − May 14, **1996**.
(66) Parker, K. M.; Zeng, T.; Harkness, J.; Vengosh, A.; Mitch, W. A. Enhanced Formation of Disinfection By-Products in Shale Gas Wastewater-Impacted Drinking Water Supplies. *Environ. Sci. Technol.* **2014**, *48*, 11161.
(67) Kogevinas, M.; Villanueva, C. M.; Font-Ribera, L.; Liviac, D.; Bustamante, M.; Espinoza, F.; Nieuwenhuijsen, M. J.; Espinsoza, A.; Fernandez, P.; DeMarini, D. M.; Grimalt, J. O.; Grummt, T.; Marcos, R. Genotoxic effects in swimmers exposed to disinfection by-products in indoor swimming pools. *Environ. Health Perspect.* **2010**, *118*, 1531−1537.
(68) Straift, K.; Loomis, D.; Guyton, K.; Grosse, Y.; Lauby-Secretan, B.; El Ghissassi, F.; Bouvard, V.; Benbrahim-Tallaa, L.; Guha, N.; Mattock, H. Future priorities for the IARC Monographs. *Lancet Oncol.* **2014**, *15* (7), 683−684.

DOI: 10.1021/acs.est.5b03547
Environ. Sci. Technol. 2015, 49, 13094−13102

Estimating Potential Increased Bladder Cancer Risk Due to Increased Bromide Concentrations in Sources of Disinfected Drinking Waters

Supporting Information

STIG REGLI,[†] JIMMY CHEN,[†] MICHAEL MESSNER,[†] MICHAEL S. ELOVITZ,[‡] FRANK J. LETKIEWICZ,[§] REX A. PEGRAM, [¶] T.J. PEPPING,[†,∥] SUSAN D. RICHARDSON, [††] J. MICHAEL WRIGHT[‡‡]

[†]*Office of Ground Water and Drinking Water, U.S. Environmental Protection Agency, Washington, DC,* [‡]*Office of Research and Development, National Risk Management Laboratory, U.S. Environmental Protection Agency, Cincinnati, OH,* [§]*The Cadmus Group, Bethesda, MD,* [¶]*Office of Research and Development, National Health and Environmental Effects Research Laboratory, U.S. Environmental Protection Agency, Research Triangle Park, NC,* [∥]*Oak Ridge Institute for Science and Education Internship/Research Participation Program, U.S. Department of Energy, Oak Ridge, TN,* [††]*Department of Chemistry and Biochemistry, University of South Carolina, Columbia, SC,* [‡‡]*Office of Research and Development, National Center for Environmental Assessment, U.S. Environmental Protection Agency, Cincinnati, OH*

Table of Contents

A. Comparative THM speciation in drinking water supplies of the Cantor et al. 2010 study population, versus in the United States. 3

B. Estimated impacts of additional 1 μg/L THM4 over a range of baseline THM4 concentrations 4

C. Overview of SWAT components 4

D. SWAT analysis plant month screening process and results 5

E. Sensitivity analysis of ΔTHM4 based on ½ MRL substitution 8

F. More detailed analyses of the distribution of ΔTHM4 across plants for ΔBr^- of 50 μg/L 9

G. The impact of ΔBr^- 50 μg/L as a function of treatment type and disinfection type 11

H. Compliance with the MCL for THM4 13

I. Description of WTP Model and applicability 14

J. Quality checks for predicting ΔTHM4 as a function of increased bromide 20

K. Supporting Information References 30

Table of Tables

Table S1. Estimated impacts of Additional 1 µg/L THM4 over a range of baseline THM4 concentrations .. 4
Table S2. Source Water Quality Parameters and Average Residence Time in Distribution System (DS) (Based on 2089 Plant Months for 201 Plants) 6
Table S3. ΔTHM4 Based on ½ MRL Bromide Concentration Substitution (Based on 2089 Plant Months for 201 Plants) 8
Table S4. ΔTHM4 at ΔBr^- of 50 µg/L for Different Treatment Types and Disinfectant Types 12
Table S5. Sensitivity Analysis of ΔTHM4 at ΔBr^- of 50 µg/L for Different Treatment Types and Disinfectant Types Based on ½ MRL Substitution 13
Table S6. ΔTHM4 and Experimental Conditions in Bromide Spiking Studies 29

Table of Figures

Figure S1. Accumulative Distribution of 1998 Baseline Bromide Levels in Source Water among 201 ICR Plants 7
Figure S2. Percentages of Plants in Each Interval of Plant Mean ΔTHM4 9
Figure S3. ΔTHM4 for ΔBr^- of 50 µg/L, as Function of Baseline (Initial) Br^- Levels 10
Figure S4. ΔTHM4 for ΔBr^- of 50 µg/L, as a Function of Baseline (Initial) Predicted THM4 Levels 11
Figure S5. Number of Plants with LRAA THM4 Levels at the DS_MAX Location > 80 µg/L as a Function of ΔBr^- 14
Figure S6. Comparison of Observed versus Predicted THM4 Levels among 661 Common Plant Months . 22
Figure 7. Comparison of Observed versus Predicted THM4 Levels among 375 Common Plant Months with CL2/CL2 only 23
Figure S8. ΔTHM4 at ΔBr^- of 50 µg/L with Plant Months shown in Figure S6: All Plant Months, Non-outlier Months, and 10% Outlier Months 25
Figure S9. Annual Plant Mean ΔTHM4 at ΔBr^- of 50 µg/L: among All 201 Plants, Non-outlier Plants, and Outlier Plants 26
Figure S10. Annual Plant Mean ΔTHM4 at ΔBr^- of 50 µg/L: among All Plants with CL2/CL2 only, Non-outlier Plants, and Outlier Plants 26
Figure S11. ΔTHM4 as a Function of Varying Increases in Bromide among All 2089 Plant Months 27

A. Comparative THM speciation in drinking water supplies of the Cantor et al. 2010 study population, versus in the United States.

Salas et al. 2013[1] (Table 2) includes THM speciation concentration estimates for the study populations considered in the Cantor et al. study.[2] Four of the six county populations (Alicante, Barcelona, Sababdal, and Tenerife) had sum THM3 (bromodichloromethane, dibromochloromethane, and bromoform) concentrations greater than the chloroform concentration and represented more than 50% of the total study population (768/1436). This represents a much greater proportion of brominated THM species than generally found in drinking water of the US population. Figure 6.1 from McLain et al.[3] indicates that 84% (6788/7982 samples) of the US population receiving disinfected waters from more than 200 utilities serving greater than 100,000 people had chloroform concentrations greater than the sum THM3 concentrations. Thus, the exposure-response relationship observed between THM4 concentrations and bladder cancer risk in the Cantor et al. study may be more pronounced than what might be found for the overall U.S. population.

B. Estimated impacts of additional 1 μg/L THM4 over a range of baseline THM4 concentrations

Table S1. Estimated impacts of Additional 1 μg/L THM4 over a range of baseline THM4 concentrations

Change of THM4 Concentration (μg/L)	Additional Lifetime Bladder Cancer Risk
0 → 1	0.000085
10 → 11	0.000089
20 → 21	0.000093
30 → 31	0.000097
40 → 41	0.000101
50 → 51	0.000105
60 → 61	0.000110
70 → 71	0.000114
80 → 81	0.000119

C. Overview of SWAT components

EPA used the *Surface Water Analytical Tool* (SWAT) model to estimate changes in technology and THM4 concentrations in drinking water predicted to occur when utilities complied with the Stage 1 and Stage 2 DBP Rules.[4] The SWAT program (Version 1.1)[5] consists of four components – User Interface, Auxiliary Database 8 (Aux8), Water Treatment Plant Model, and Decision Tree Program. The SWAT user manual[5] provides a detailed program description and assumptions, but since only the first three components are relevant to this paper only these are briefly described below:

- **User Interface -** A Microsoft Windows™ interface enables the user to specify the disinfection and DBP regulatory criteria, as well as numerous other conditions for a SWAT run. As described later, the "validation" mode in the interface (without any assumptions) was selected for modeling. By doing so, the decision tree program in the SWAT was bypassed (i.e., without making any changes on the existing treatment operations) whenever a SWAT run was executed.
- **Aux8 -** Aux8 is a Microsoft Access™ database that holds inputs and outputs for SWAT analyses. Aux8 initially contains a specific subset of data extracted from Auxiliary Database 1 of the primary ICR database[6] that was needed as inputs to run the SWAT. The initial data in Aux8 (as part of the inputs) includes source water quality, treatment plant characteristics, unit processes, chemical additions, and distribution system characteristics for ICR plants and systems. Cumulated THM4 and HAA5 levels at two distribution system sample sites (i.e., at the average and maximum residence time sample sites in distribution systems) are computed as part of the outputs for each plant month that have the necessary input values. The prediction at the

theoretical average residence time (designated as DS_AVG) was based on a mean residence time for each plant (the mean residence time comprising the average of the so-called "distribution system equivalent sampling point" (DSE), two average distribution system times, and one maximum residence time, as reported in the DBP ICR).

- **Water Treatment Plant Model (WTP Model) -** The WTP Model predicts treated drinking water quality given source water quality conditions, water treatment plant configuration and operation. It consists of a series of algorithms that predict levels of DBP precursors (i.e., bromide, TOC and UVA_{254}), pH values, disinfectant decay, and cumulated concentrations of DBPs (i.e., THM4 and HAA5) formed from reactions of chlorine and chloramine with the aforementioned precursors. Section SI.I describes the WTP model and discusses its applicability.

SWAT allows a user to run the program in the "validation" mode to generate the water quality parameter values at various stages of treatment, and model DBP formation as a function of the water quality values for the existing treatment conditions as reported in the ICR (i.e. without any changes to the treatment train). The modeling results presented in this paper are based on the outputs generated in this mode. Specifically, to evaluate the impacts of an increase of bromide levels in source waters on THM4 levels in distribution systems, the records of bromide in source water in the Aux8 database were increased by specific intervals (i.e., by 0, 10, 30, 50, 75, and 100 µg/L of Br^-) for every plant month in Aux8. For each of these intervals, SWAT was run under the "validation" mode, thus predicting the impact of bromide on THM4 levels at DS_AVG with no change in treatment and other source water quality parameters.

D. SWAT analysis plant month screening process and results

As was done for the Economic Analysis of Stage 2 DBPR, the first step in this screening was to include Aux8 data for only the last 12 months (January to December, 1998) of the 18-month ICR collection period to focus on a one-year cycle. Initially, in our ICR data set there were 273 plants (comprising 2,784 plant months) in Aux8. Seven plants were excluded because they only had three or fewer plant months of data and did not have representative monitoring results in each of four quarters for a one-year cycle.

The SWAT model was run to make predictions of THM4 and HAA5 at the maximum residence time (designated as DS_MAX) for each month of data that a plant had water quality data available (4 to 12 months of data depending on the utility), and the annual average THM4 and HAA5 concentration for each of the plants was determined from the mean of those predicted values. This screening step

suggested that 64 (of the remaining 266 plants) would not meet the 80/60 µg/L of THM4/HAA5 (MCLs under Stage 2 DBPR) as an annual average at the maximum residence time. The SWAT always predicts higher THM4/HAA5 levels at DS_MAX than at DS_AVG due to longer residence times for DS_MAX and the MCLs under Stage 2 DBPR were based on a locational running average at the highest site. Thus, using the maximum residence time for the screening step is consistent with the requirements under Stage 2 DBPR. By excluding the 64 plants 202 plants remained for the analysis. Furthermore, it was found that one plant had a "zero" value of THM4/HAA5 for all of its plant months. This plant was also excluded for the analysis. In addition, one plant month was excluded because an implausibly high pH value of 14 was reported. As a result of the screening process, 201 plants (with 2089 plant months) were used for the analysis presented in this paper.

Table S2 indicates the range of parameters from the ICR data set that was used for predicting the baseline THM4 occurrence among 201 ICR plants. The table includes the summary statistics for each parameter, showing the variation among plant months. The minimum reporting limit (MRL) for bromide during the ICR was 20 µg/L. Those bromide records under the MRL were replaced with 20 µg/L of MRL for the analysis (which is consistent with the approach for national estimates with the SWAT presented in the Economic Analysis of Stage 2 DBPR[4]). See next section for a sensitivity analysis with this assumption.

Table S2. Source Water Quality Parameters and Average Residence Time in Distribution System (DS) (Based on 2089 Plant Months for 201 Plants)

	pH	Temperature (ºC)	TOC (mg/L)	UV254 (cm^{-1})	Bromide (µg/L)	Average Residence Time in DS (Hour) DS_AVG
Mean	7.6	15.5	2.9	0.09	53.2	35.3
5%ile	6.5	4.0	1	0.02	20.0	3.1
Median	7.7	15.3	2.5	0.06	23.0	28.9
95%ile	8.4	27.5	6.0	0.22	190.6	90.8

Figure S1 shows a cumulative distribution of bromide levels as annual plant means among 201 plants, along with the minimum and maximum levels during the 12 months of the 1998 ICR monitoring period (indicated by whiskers), which define the baseline of bromide occurrence in source water. The embedded figure is to provide better resolution at the lower range of source water bromide levels.

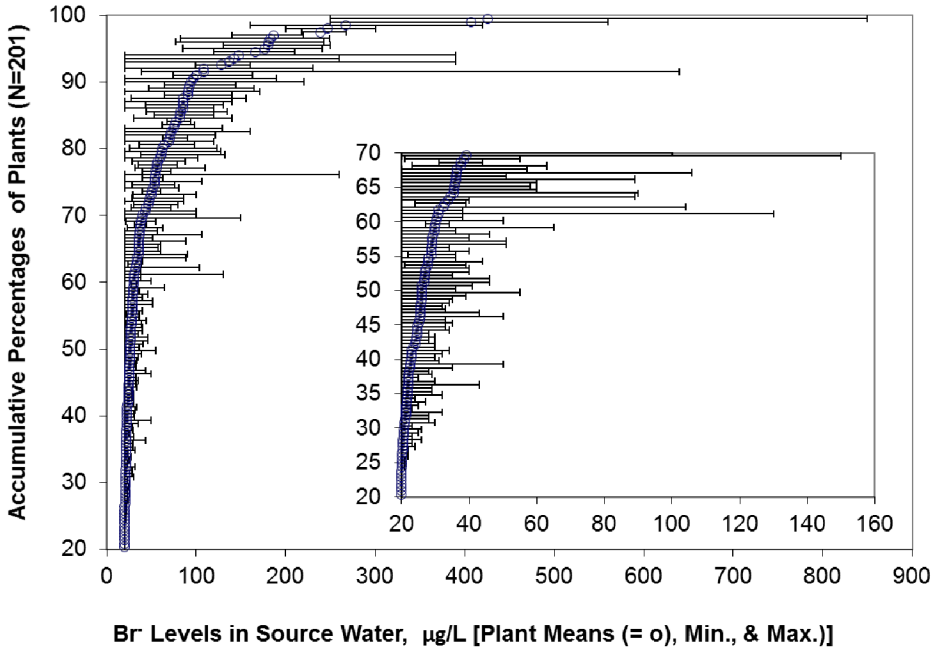

Figure S1. Accumulative Distribution of 1998 Baseline Bromide Levels in Source Water among 201 ICR Plants

During the analysis of the ICR data used to support the Stage 2 DBPR rule development the question arose how representative 1998 was versus other years. While this year was recognized as unusual since it was the warmest and fifth wettest year on record since 1895, because of large regional variations in temperature and rainfall and their unknown effect on source water quality, it was deemed too difficult, without additional year to year regional water quality data, to generalize the representativeness of the ICR data[7]. For similar reasons we have not tried to generalize the representativeness of the 1998 ICR source water quality data as it might pertain to today's source water quality (other than noting the likely increase of bromide due to anthropogenic sources). We recognize this introduces some uncertainty in our model predictions. However, regarding baseline source water bromide occurrence, we do not think this introduces a major uncertainty in our model predictions because, as described in subsequent SI.E, the proportional predicted change in THM4 concentration as a function of increased bromide source water concentration does not differ substantially for different assumed incremental increases of bromide in the source water.

E. Sensitivity analysis of ΔTHM4 based on ½ MRL substitution

In our model we include all records with bromide concentrations less than the MRL of 20 µg/L by assuming their value is 20 µg/L, recognizing that this probably leads to an underestimate of the increased THM4 level resulting from increased bromide in the source water. To better characterize the potential effects of our assumption we conducted a sensitivity analysis as follows.

Table S3 shows the resulting ΔTHM4 when a bromide concentration of 10 µg/L (i.e. ½ the MRL) is used as the baseline for samples that were below detection limit (bromide concentration increases from 10 to 60 µg/L at ΔBr^- of 50 µg/L) rather than the MRL of 20 µg /L (increase from 20 to 70 µg/L as indicated in Table 2). A comparison of summary statistics between Table 2 and Table S3 (e.g., mean ΔTHM4 at 50 µg/L of ΔBr^-, 4.6 versus 5.5 µg/L) indicates the THM4 level is greater (by about 38% to 14% as ΔBr^- varied from 10 to 100 µg/L) when ½ MRL is used, thus suggesting that our analysis using the MRL value is likely underestimating the increase in THM4 as a result of increased Br^- in source waters. See Section SI.J for more discussion on bias of predicted ΔTHM4.

Table S3. ΔTHM4 Based on ½ MRL Bromide Concentration Substitution (Based on 2089 Plant Months for 201 Plants)

	Statistics	ΔBr^- (µg/L)				
		10	**30**	**50**	**75**	**100**
ΔTHM4 (µg/L) when bromide MRL = 10 µg /L	**Mean**	1.8	4.0	5.5	7.0	8.1
	Minimum	0.0	0.0	0.0	0.0	0.0
	5% percentile	0.1	0.4	0.5	0.7	0.8
	Median	1.3	3.1	4.4	5.5	6.5
	95% percentile	5.2	11.0	14.8	18.2	20.8
	Maximum	16.1	33.7	44.8	54.9	62.7

F. More detailed analyses of the distribution of ΔTHM4 across plants for ΔBr⁻ of 50 µg/L

For a further evaluation of the effect of a 50 µg/L increase in bromide on ΔTHM4, the annual mean ΔTHM4 for each plant (denoted "plant mean ΔTHM4") was calculated by first averaging all plant month values over a 12-month period for each plant. The 201 plant mean ΔTHM4 values ranged from < 1 µg/L to ≥ 10 (up to 12) µg/L and were grouped into eleven ranges with 1 µg/L as an incremental interval. Figure S2 shows a distribution of 201 plants among these eleven ΔTHM4 intervals. The percentage in each of the intervals ranges from 4.5% to 15.4% of the 201 plants, indicating a relatively even distribution. For the specific plants within each of the eleven bins in Figure S2, annual means for baseline bromide and baseline THM4 were then calculated for each plant. Then for each of the eleven bins, a mean value of the plant means was calculated, thus determining eleven values of average plant mean baseline bromide concentrations, and eleven values of average of plant mean baseline THM4 concentrations.

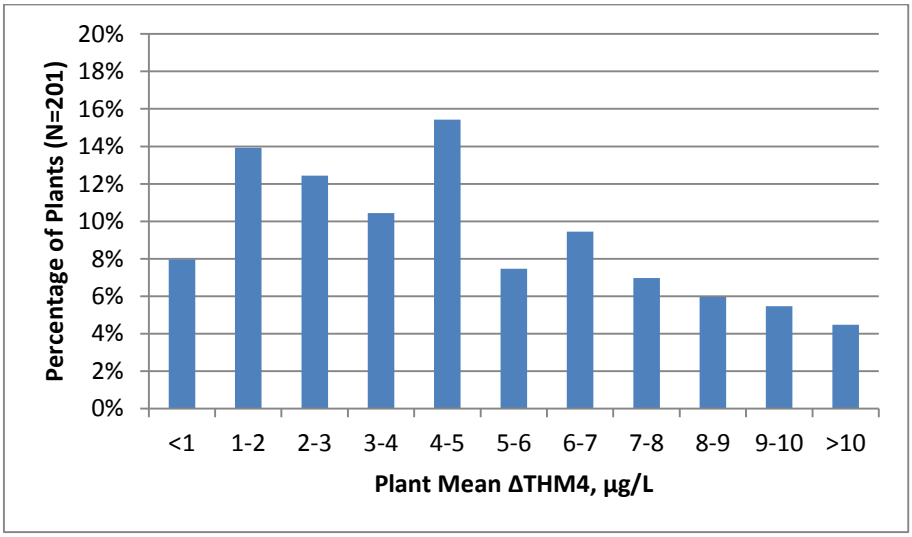

Figure S2. Percentages of Plants in Each Interval of Plant Mean ΔTHM4

Figure S3 indicates that as the average of the plant mean baseline bromide concentration decreases, ΔTHM4 increases. This observation could be explained by the hypothesis that when the baseline bromide concentrations are low, the THM4 speciation will likely be dominated by low-molecular weight chlorinated species, and increases in bromide concentration will lead to higher incorporation of Br (for Cl) in the THM4. In contrast, Figure S4 illustrates that as the average of the plant mean baseline THM4 concentration increases, ΔTHM4 increases. Since one potential surrogate for identifying the general THM4 formation potential of given water is the actual baseline THM4 concentration, this observation could be explained by the hypothesis that when baseline THM4 levels are higher, there are higher

intrinsic THM4 formation potentials, and hence a greater potential to incorporate more of the Br into brominated THM4 at a given ΔBr^-. These figures, however, should not be viewed as foundations for quantitative models. They explore two relationships independently and suggest that both relationships are important. As independent relationships, they do not reflect combined effects of baseline bromide and baseline THM4 concentrations, such as the impacts of increased bromide on plants that may have low baseline bromide, but low THM4 concentrations, or high baseline bromide and high THM4 concentrations. However, these trends do help us understand the types of plants that may be impacted the most from increases in source water bromide, and thus may help focus future efforts at monitoring and assessment.

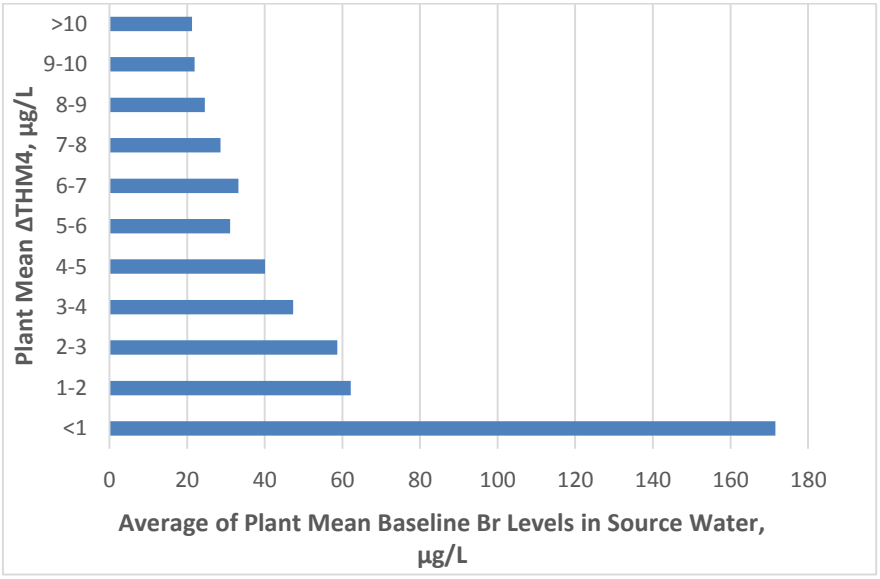

Figure S3. ΔTHM4 for ΔBr^- of 50 µg/L, as Function of Baseline (Initial) Br^- Levels

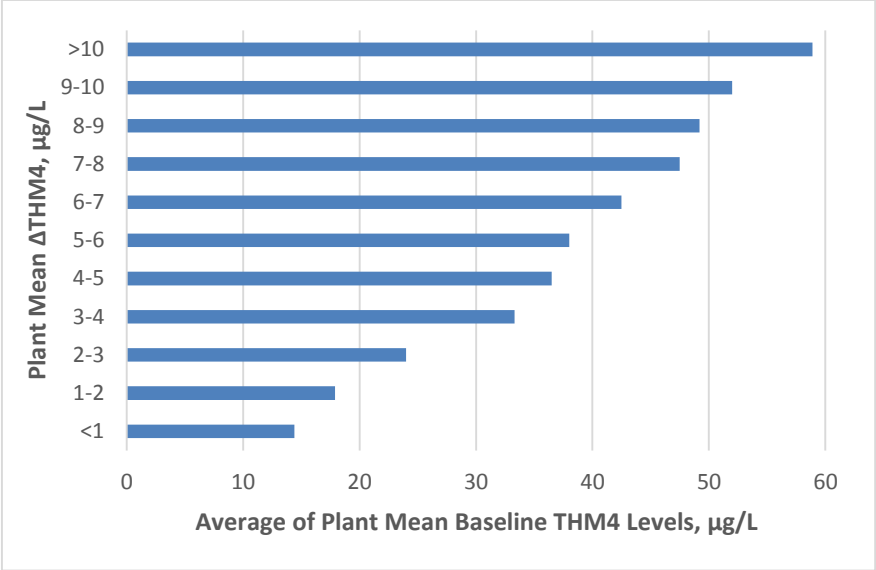

Figure S4. ΔTHM4 for ΔBr⁻ of 50 µg/L, as a Function of Baseline (Initial) Predicted THM4 Levels

G. The impact of ΔBr⁻ 50 µg/L as a function of treatment type and disinfection type

To further illustrate factors influencing the ΔTHM4 from the ΔBr⁻, we examined the impact of ΔBr⁻ of 50 µg/L as a function of treatment type and disinfection type. Pooling all plant months within a category of treatment type and disinfectant type, Table S4 indicates that systems using only free chlorine as their primary and secondary disinfectant type (CL2/CL2), versus those that used combinations of disinfectants [e.g., CL2, ozone or chlorine dioxide (CLX) as their primary disinfectant, and chloramine (CLM) as a secondary disinfectant], had higher mean ΔTHM4 values. For example, for conventional plants the mean ΔTHM4 is 6.0 µg/L for plants using chlorine as both primary disinfectant and as a residual, compared to 3.7 µg/L and 3.3 µg/L for other primary disinfectants and chloramines as a disinfectant residual, respectively. While there is not much difference on mean baseline THM4 levels (in range of 32.3 – 38.3 µg/L), the mean baseline Br levels in source water for the plant months with CL2/CL2 (28 µg/L) are more than 2 times lower than the ones for plant months with other disinfectant types. This observation suggests that, in general, the formation of THM4s in water treatment plants using chlorine only are more sensitive to an increase in source water Br⁻ levels (whose baseline levels are relatively low) than the treatment plants using other disinfectants. Table S4 also indicates that the ΔTHM4 in the softening plants is significantly lower than that of other treatment plants' baseline source water Br⁻ levels. This can be explained by softening plants having significantly higher bromide levels in their source waters, as well as low mean baseline THM4 levels. An additional sensitivity analysis was performed under the assumption that any measured bromide concentrations below the MRL would be

replaced by ½ the MRL rather than the MRL, as shown in Table S5. Overall, mean ΔTHM4 was higher in this sensitivity analysis. This was largely due to the plants using chlorine as a secondary disinfectant. The difference in the mean ΔTHM4 when comparing the original analysis in Table S4 and the sensitivity analysis in Table S5 was higher among the CL2/CL2 plants for both Conventional and Other treatment type categories.

Table S4. ΔTHM4 at ΔBr^- of 50 µg/L for Different Treatment Types and Disinfectant Types

Treatment Type	Disinfectant Types[1] (Primary/ Secondary)	Number of Plant Months	Mean ΔTHM4 (µg/L)	90% Probability Interval of ΔTHM4 (µg/L) (5th to 95th %ile)	Mean Baseline Br^- Levels in Source Water (µg/L)	Mean Baseline THM4 Levels (µg/L)
All Plants	**Any**	2,089	4.6	0.5 – 11.6	53	33.9
Conventional	**CL2/CL2**	947	6.0	1.2 - 12.7	28	37.0
	CL2/CLM CL2_CLM/CLM CLM/CLM	468	3.3	0.5 – 9.3	70	32.3
	Ozone/CL2 Ozone/CLM CLX/CL2 CLX/CLM	95	3.7	0.84 – 10.0	135	38.3
Softening[2]	**Any**	291	1.8	0.2 – 5.2	106	21.8
Others[3]	**CL2/CL2**	162	6.1	1.1 - 12.4	24	36.8
	CL2/CLM CL2_CLM/CLM	38	4.5	2.0 – 9.1	55	39.5
	Ozone/CL2 Ozone/CLM	41	4.5	0.3 - 10.1	34	42.4

1. Abbreviations: CL2 – free chlorine; CLM – Chloramines; CLX – Chlorine Dioxide; primary means first disinfectant applied whereas as secondary means applied sometime after primary disinfectant and/or the disinfectant residual in the distribution system
2. Softening plants include: SOFT - Softening, CS/SOFT – Coagulation/Sedimentation/Softening, & TS/SOFT - Two Stage Softening
3. Others include: DF – Direct Filtration, ILF – In-Line Filtration, SSF – Slow Sand filtration, UNFILT/SW – Unfiltered Surface Water, MEMBRANES – Membrane Filtration, & OTHER

Table S5. Sensitivity Analysis of ΔTHM4 at ΔBr^- of 50 µg/L for Different Treatment Types and Disinfectant Types Based on ½ MRL Substitution

Treatment Type	Disinfectant Types[1] (Primary/ Secondary)	Number of Plant Months	Mean ΔTHM4 (µg/L)	90% Probability Interval of ΔTHM4 (5th to 95th Percentile)	Mean Baseline Br^- Levels in Source Water (µg/L)	Mean Baseline THM4 Levels (µg/L)	Difference in Mean ΔTHM4 Compared to MRL of 20 µg Br/L
All Plants	**Any**	2,089	5.5	0.5 - 14.8	48.6	32.6	0.9
Conventional	**CL2/CL2**	947	7.3	1.3 - 16.5	22.8	35.2	1.3
	CL2/CLM CL2_CLM/CLM CLM/CLM	468	3.7	0.5 - 11.1	66.3	31.8	0.4
	Ozone/CL2 Ozone/CLM CLX/CL2 CLX/CLM	95	4.6	0.9 - 13.5	130.1	37.0	0.9
Softening[2]	**Any**	291	2.0	0.2 - 5.9	103.7	21.6	0.2
Others[3]	**CL2/CL2**	162	7.8	1.5 - 16.6	16.3	34.4	1.7
	CL2/CLM CL2_CLM/CLM	38	4.8	1.9 - 9.1	53.9	39.1	0.3
	Ozone/CL2 Ozone/CLM	41	5.0	0.4 - 13.7	29.5	41.5	0.5

1. Abbreviations: CL2 – free chlorine; CLM – Chloramines; CLX – Chlorine Dioxide; primary means first disinfectant applied whereas as secondary means applied sometime after primary disinfectant and/or the disinfectant residual in the distribution system
2. Softening plants include: SOFT - Softening, CS/SOFT – Coagulation/Sedimentation/Softening, & TS/SOFT - Two Stage Softening
3. Others include: DF – Direct Filtration, ILF – In-Line Filtration, SSF – Slow Sand filtration, UNFILT/SW – Unfiltered Surface Water, MEMBRANES – Membrane Filtration, & OTHER

H. Compliance with the MCL for THM4

An increase of THM4 levels resulting from an elevation of bromide levels in source water could not only lead to increased potential long-term health risks due to incrementally higher THM4 concentrations, but could also affect the compliance status of water systems, especially those having baseline THM4 concentrations already near the MCL. As described earlier, all of 201 plants included in this analysis have baseline LRAA THM4 levels at the DS_MAX location < 80 µg/L (i.e., the MCL under Stage 2 DBPR).

Figure S5 indicates that as ΔBr^- increases, an increasing number of plants could have LRAA THM4 levels that exceed 80 µg/L at the DS_MAX location, implying that these plants could have become non-

compliant at the given ΔBr^- or made new treatment changes to comply. Eight of the 13 and ten of the 18 plants at the respective ΔBr^- of 50 and 100 µg/L used only chlorine as the disinfectant, while the other plants predicted to exceed the MCL used chloramine as a residual disinfectant. It should be noted that although the THM4 MCL of the Stage 2 DBPR is calculated as a LRAA, a seasonal increase of bromide levels in source water (which could be compounded by a drought condition) could make it difficult for water utilities to continue meeting the existing THM4 MCL without making changes in their existing treatment conditions if their baseline LRAA THM4 levels were close to the MCLs.

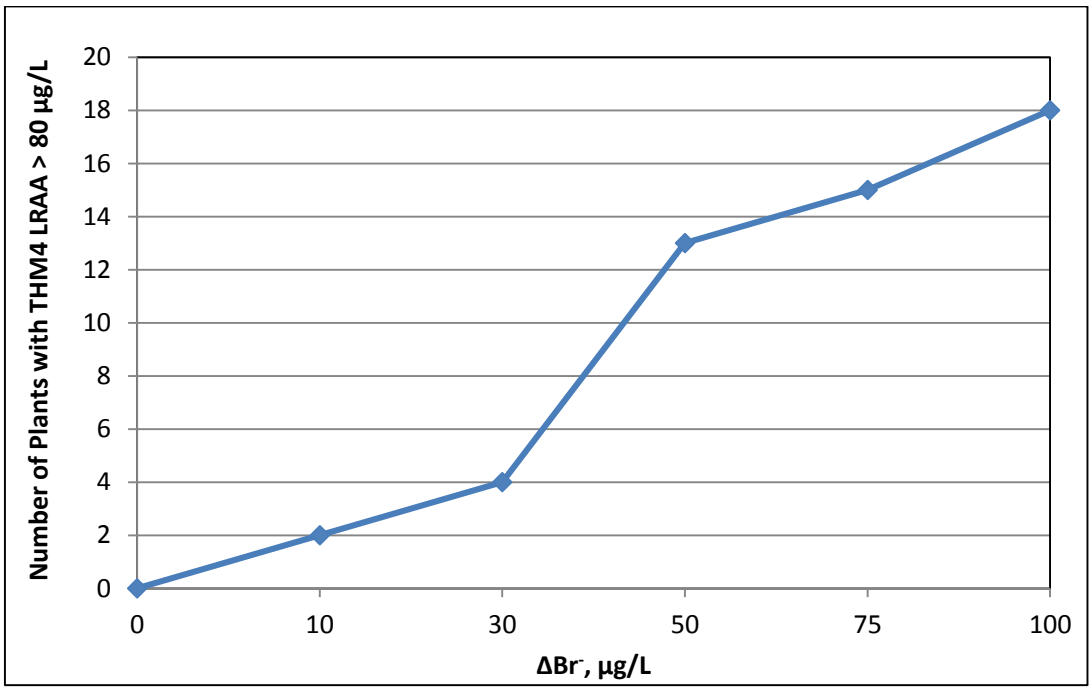

Figure S5. Number of Plants with LRAA THM4 Levels at the DS_MAX Location > 80 µg/L as a Function of ΔBr^-

I. Description of WTP Model and applicability

The formation of disinfection byproducts resulting from hypochlorite-based treatment processes has been a research focus since the recognition of THM formation in the 1970s. The vast amount of research has afforded numerous models for estimating their formation under a wide variety of conditions. A compendium of many of the THM formation modes can be found in a review article by Chowdhury, et al.[8] In almost all cases, the models comprise an empirical mathematical relationship between the concentration of THMs formed and specific measurable parameters thought to influence their formation. Chief among these parameters are descriptors for the concentrations of the chemical

reactants: free-chlorine, chloramine, Br^-, H^+ and/or OH^- (i.e. pH), and the organic matter (providing the carbon atom reaction center for the THM molecule). Along with temperature and reaction time, these parameters are known, based on principles of physical chemistry, to influence chemical reactions. Hence, despite the empirical nature of most of the formation models, there are some theoretical underpinnings for many of the model parameters.

Of particular importance to the risk estimate presented in this paper is the impact of bromide concentration, and more specifically increased bromide concentration, on THM4 formation. In a very general sense, it is well known that an increase in bromide concentration leads to an increased incorporation of Br in THM4. Due to the higher molecular weight of Br (79.9 g/mol) versus Cl (35.45 g/mol), greater incorporation of Br leads to a higher formation of THM4 on a mass-basis. There is less data, and less consistency, on whether increased bromide leads to an overall increase in THM4s on a molar-basis under conditions typically found in the real world. Various studies have examined the effect of bromide on THM formation; however oftentimes the reaction conditions are not particularly relevant to a typical drinking water treatment plant. Bromide levels in some of the studies may start at above 100 µg/L and increase to mg/L levels.

For example, Hua, et al.[9] found that increasing bromide from sub-ppb levels to ca. 2400 ppb increased the molar concentration of THM4s by as much as 58%. However, increases of 159 ppb, still a very large increase relative to average national ambient levels, caused only an 18% increase in the molar concentration. Hu, et al.[10] performed similar lab-based experiments on both a raw and a treated water at two pHs. At pH 8, raw water, containing 64 ppb Br^- and 4.1 mg/L DOC, formed 925 nM THM4, whereas, spikes of 205 and 410 µg/L Br^- increased the THM4 to 988 and 1084 nM, respectively. For the treated water containing half the DOC (2.2 mg/L), 72 µg/L Br^- formed 270 nM THM4, while spikes of 110 and 220 µg/L Br^- increased THM4 to 286 and 324 nM, respectively. THM4 increases at pH 6 were less than those at pH 8. These are relatively small increases in molar THM4 considering the rather large increases in Br^-. Ged and Boyer[11] examined simulated saltwater intrusion of a groundwater source and found that from an ambient Br^- level of 38 µg/L and 330 nM TM4 (pH 8, DOC = 1.4 mg/), increases in bromide of 21 and 68 µg/L resulted in 320 and 380 nM THM4, respectively. The fact that molar concentrations of THM4 may be far less affected by bromide increases than mass-based concentrations might suggest that a mole-based regulate-by-group approach for THM4 may be less sensitive to THM species changes.

Aside from the direct impact of increasing Br^- on THM formation, there are important confounding effects of HOCl:DOC ratio, HOCl:Br^- ratio, Br^-:DOC ratio, pH, and reaction time that can affect both the incorporation of bromide into THMs, as well as the overall concentration of THMs. When the concentration of precursor is limiting relative to the oxidant, as it might be with a well-run treatment process, the potentially greater halogenation efficiency of HOBr over HOCl may not be as important as either oxidant might be able to fully react with the limited THM precursors. These effects may not always be accounted for in lab-based experiments where concentrations of reactants are sometimes elevated. These effects have been explored in a variety of ways, yet with the exception of pH and time, they are not often integrated into THM formation models. Moreover, there does not appear to be a single THM4 formation model that is adequate for covering a multitude of scenarios such as conventional treatment under the impact of increasing bromide, enhanced treatment (GAC/membranes, ozonation) under consistent bromide, or enhanced treatment under increasing bromide. These scenarios would seemingly require a more explicit treatment of the relative concentrations of HOCl, Br^- and precursor.

In developing the Economic Analysis for Stage 2 DBPR,[4] EPA relied on empirical models to estimate THM4 formation. The models themselves relied on both lab-based and field-based data sets. Initial development of the THM formation model resulted from an EPA-contracted study.[12] This study employed a lab-based approach and examined THM formation in both untreated as well as coagulated waters. For the raw water studies, 12 different source waters of varying DOC content (concentration and character) and ambient bromide were examined. Temperature, pH, initial chlorine concentration (dose), and reaction time were varied systematically. In addition, bromide was spiked at three additional concentrations (+100, +200, +300 µg/L) above the ambient concentrations, providing a total bromide range of 7 - 600 µg/L. For the coagulated water study, a subset of eight waters was coagulated with alum and ferric salts. The temperature and pH were set at pH 7.5 and 20 °C, respectively, but initial chlorine concentration (dose), and reaction time were varied. The bromide concentration was not altered from the ambient concentration, thus providing a more limited, but very relevant for this paper's analysis, bromide range of 23 - 308 µg/L. As described in the Economic Analysis of Stage 2 DBPR[4] and the User Manual for WTP model (version 2.0[5]), separate empirical equations for THM4 formation as a function of various parameters were developed for the raw and coagulated waters to reflect different DBP formation chemistry at different treatment stages.

$THM4_{raw} = 0.0412(TOC_{raw})^{1.098}(Cl_2)^{0.152}(Br^-_{raw})^{0.068}(T)^{0.609}(pH_{raw})^{1.601}(t)^{0.263}$

where:

$THM4_{raw}$ = raw water THM4 (μg/L)
TOC_{raw} = raw water TOC (mg-C/L): $1.2 \le TOC_{raw} \le 10.6$
Cl_2 = applied chlorine dose (mg/L): $1.51 \le Cl_2 \le 33.55$
Br^-_{raw} = raw water bromide concentration (μg/L): $7 \le Br^-_{raw} \le 600$
T = temperature (°C): $15 \le T \le 25$
pH_{raw} = raw water pH: $6.5 \le pH \le 8.5$
t = reaction time (hour): $2 \le t \le 168$

$THM4_{treated} = 23.9(TOC \times UVA)^{0.403}(Cl_2)^{0.225}(Br^-)^{0.141}(1.027)^{(T-20)}(1.156)^{(pH-7.5)}(t)^{0.264}$

where:

$THM4_{treated}$ = treated water THM4 (μg/L): $13 \le THM4 \le 690$
TOC = treated water TOC (mg/L): $1.00 \le TOC \le 7.77$
UVA = treated water UVA (cm^{-1}): $0.016 \le UVA \le 0.215$
Cl_2 = applied chlorine dose (mg/L): $1.11 \le Cl_2 \le 24.75$
Br^- = treated water bromide concentration (μg/L): $23 \le Br^- \le 308$
T = temperature (°C): $15 \le T \le 25$
pH = treated water pH: $6.5 \le pH \le 8.5$
t = reaction time (hour): $2 \le t \le 168$

It should be noted that the origin of the equation for treated water was provided by Sohn and Sohn, et al.[13,14] Sohn reanalyzed treated water data from the EPA-contracted study,[12] and developed a model that included UV absorbance at 254nm (UVA) for organic matter quality/character.

Because the study examining THM formation in coagulated waters was conducted at a single pH and temperature, Sohn used pH and temperature adjustment equations based on the pH and temperature effects demonstrated in the raw water dataset. Both THM formation models show positive correlation with chlorine dose, temperature, pH, bromide concentration, TOC concentration, and reaction time. The coagulated-water model also shows positive correlation with UVA.

With these equations along with a series of predictive equations for water quality parameters, given a set of initial source water conditions and treatment conditions, the WTP model first predicts the changes of water quality parameters after treatment and then predicts the formation of DBPs. Subsequently, the model computes the cumulated DBP levels in treated water. The SWAT Version 1.1 (released in 2001) was used for this paper. SWAT contains WTP Model Version 2.0, which predicts THM4 formation under different chlorination and chloramination scenarios based on input data for a specific plant month. With respect to the THM formation equations discussed above, the WTP model

predicts changes in TOC, UVA, pH, chlorine and chloramine (i.e. chlorine and chloramine decay) of the water as it flows through different treatment steps in a given plant. Of the 201 plants examined in this paper, various treatment processes and disinfection practices (with various disinfectant types) that affect the THM4 prediction are indicated in Table S4 or S5. The WTP User Manual, as discussed in the Stage 2 EA Appendices,[5] and Solarik, et al.[15] describe how each of these scenarios was considered within the WTP model. Overall, THM4 formation is predicted using the raw water equation (above) for chlorination practices prior to sedimentation. The treated water equation is used for chlorination practices post-sedimentation. THM4 formation due to chloramination is calculated using the treated water equation, but with a scaler multiplier to reduce the formation (see below). Chlorine dioxide and ozone do not contribute the predicted THM4 value, however, ozone can affect some of the inputs to the THM4 equation, such as DOC, UV and Br^-.

As part of the SWAT development, the WTP model (including THM4 formation equations) was assessed for the ability to predict THM4 formation. This assessment utilized the national field dataset from the database of Information Collection Rule.[16] As described by Swanson et al.[7], the calibration examined the predictions for THM4 at finished water and DS_AVG location, and compared them to the measured values at these two locations. There was an understanding that distribution system values at maximum residence time also were of regulatory interest. However, there was also likely greater uncertainty in model inputs, such as residence time for these distribution system sample points. As such, the model calibration was performed on higher quality data.

Overall, the WTP model was calibrated and validated with the ICR DBP monitoring data from water treatment plants from water utilities serving 100,000 or more people in the U.S. The calibration was focused on optimizing the prediction of the central tendency of the entirety of (pooled) monthly Aux8 data in order for SWAT to be used as a tool for national-level analyses. Those plant months with chlorine and chloramine conditions were calibrated separately. Subsequent validation of the ICR-calibrated WTP model confirmed the ability of the WTP model to predict DBP formation on a national level, with some adjustment factors applied within the SWAT. The calibration suggested a simple adjustment factor (called a *calibration adjustment* in the EA) of 0.77 could considerably improve the THM predictions of the ICR utilities using the WTP model. This exercise was denoted as a “calibration” of the THM formation equations:

$THM4_{cal} = THM4_{orig} \times (1/0.77)$

Where:

$THM4_{cal}$ = is the estimated concentration of THM4 after calibration

$THM4_{orig}$ = is the estimated concentration of THM4 calculated by the WTP model.

Further analyses of plants employing chloramination for distribution system residual found that THM4 formation in these plants could be better predicted using a calibration multiplier of 0.3:

$THM4_{CLM} = 0.3 \times THM4_{treated}$

Where:

$THM4_{CLM}$ = is the estimated concentration of THM4 from chloramination

$THM4_{treated}$ = is the estimated concentration of THM4 calculated using the treated water equation and for the equivalent amount of chlorine.

Finally, the calibrated WTP model was also evaluated on its ability to predict THM4 formation for a specific utility. Input data for a specific utility were entered into the WTP model and the predicted THM4 was compared to the ICR measured THM4 for different points in the distribution system (average and maximum hydraulic times as per the ICR definitions). Unlike the evaluation for national trends, the system-specific comparison indicated considerable (ca. 45%) relative error in the predictions.[7] Section J below further discusses the applicability and uncertainties of the SWAT along with the WTP model used in this paper.

There are two additional points regarding the WTP model and its applicability to modeling the ICR plants. First, the THM4 equations were applied to ICR water quality inputs outside the boundary conditions of the original 1998 Amy et al. study[12] (see equations above). This is especially relevant for the inclusion of ICR temperature and pH data outside the somewhat narrow ranges shown above. In particular, the ICR data included a considerable number of plant months with temperatures below the Amy study boundary conditions. Nonetheless, for the 201 plants in this study there was no distinct trend in the THM4 residuals as a function of temperature, suggesting that WTP model was not biased with respect to temperature despite the extrapolation outside the boundary conditions (results not

shown). Overall, the SWAT analysis showed that the WTP model was reasonably capable of predicting distributions of THM4 on a national level. This is despite the empirical nature of both the THM models as and other WTP model components, as well as simplifications of ICR data inputs (see Section J below for more discussion).

Second, the various empirical equations within the WTP model affecting THM4 predictions, including changes in water quality (e.g. UVA, pH, TOC) and the two THM4 equations themselves, were developed from external datasets (i.e. various reports in the literature). The calibration for the ICR Aux8 dataset involved simple scaler and intercept adjustments of the model predictions (see Table 8.2 in Amy et al.[12]), and not recalibration of specific model coefficients (with the exception of equations that have coefficients as overall multipliers). The fact that the WTP model performs as well as it does at predicting THM4 formation on a central tendency national level from an independent data set (the exception of the simple calibration factors) speaks to some extent of the model's strength. Whether this strength is due to, or in spite of, the model's relative complexity, there is a certain level of confidence that the predictions are capturing the effects of realistic THM4 formation drivers, such as bromide.

J. Quality checks for predicting ∆THM4 as a function of increased bromide

The ideal method for estimating model uncertainty (and potential bias) for ΔTHM4 predictions as a function of ΔBr^- would be to compare model predictions with the measured response in THM4 from an increase in bromide. Full-scale experiments would need to be done to measure THM4 at baseline bromide conditions, as well as after a bromide addition in the source water (i.e. a bromide spiking study at the full-scale). The other source water characteristics, and treatment conditions, would need to be held constant during such tests to isolate the effect of the bromide. Furthermore, one would need such data for a nationally representative set of source water and treatment conditions to allow for the analysis of model bias across the changing nature of the water chemistry and treatment conditions in a given year. Due to the temporal variability of source water and treatment conditions within and across plants, the prospect for obtaining such a data set would likely be cost prohibitive. However, absent such data, we can still inform potential systematic model bias and provide perspective on uncertainty for our estimation of $\Delta THM4/\Delta Br^-$.

A strength of the ICR data used for generating our estimates is the extent of source water quality, treatment information, THM measurements in the distribution system, and the (intended) linkage of this data, when it was collected, within and across the plants to support national regulatory impact analysis.

Much of the data collected under the ICR was designed to inform the use of and further development of DBP formation predictive equations.[4] A weakness of the ICR data is the uncertainty associated with the measured and reported information, and model error associated with the use of this information. The large scatter of differences between predicted THMs versus measured values has historically been recognized by those involved with the evaluation and calibration of the WTP model[5,7] and in the use of this data in conducting national regulatory impact analysis.[4]

A fundamental premise in our modeling approach is that much of the error associated with differences between predicted versus observed THM4 would be factored out by the modeling approach we use to estimate ΔTHM4 as a function of increased bromide; i.e., subtracting the THM4 estimate with no bromide addition from the THM4 estimate with bromide addition. We will illustrate the effects of this subtraction process in subsequent analysis described later in this section. Also, while we will not be able to quantify the uncertainty of our estimates, we will also later provide a basis for why we think our estimates are reasonable.

To evaluate potential systemic model bias that may be associated with our estimates, we first compared the measured THM4 values reported in the ICR database for each plant quarter (since only quarterly THM4 data was available) with the predicted THM4 value based on water quality and treatment data for the same month associated with the quarterly THM4 measurement. Comparisons of predicted versus observed THM4 were only made for months which contained both the measured THM4 value and the model input parameters that allowed the model prediction for that month (N = 661). Figure S6 indicates no correlation between observed versus predicted values (R^2 = -0.093) with a trend for predicted values being less than the observed values (Slope = 0.76). Figure S6 also identifies 10% of the values having the greatest difference between observed versus predictive. The regression values which excludes this 10% subset is substantially improved, showing some correlation and much less underestimation of predicted versus observed values (R^2 = 0.32, Slope = 0.92).

We used the 10% exclusion criteria of ICR data, as Swanson et al.[7] did to allow for use of more reliable data when evaluating the accuracy of the WTP for predicting THM4. Our own examination of these "outlier" data revealed obvious discrepancies, especially among plants designated as using multiple disinfectants (suggesting either a data entry error or incorrect reporting of treatment type for a given month). Factors contributing to the scatter in Figure S6 include uncertainty with measurement and reporting of input values for the parameters used either directly in the THM4 predictive equations (e.g.

residence time, chlorine dose), or used indirectly but having an impact on terms in the equations (e.g., reported treatment conditions such as coagulant dose, or initial source water quality); errors in measurement and reporting of THMs (e.g. non-Lagrangian sampling affecting the linkage between source water measurements and THM4 measurements); and WTP model error.

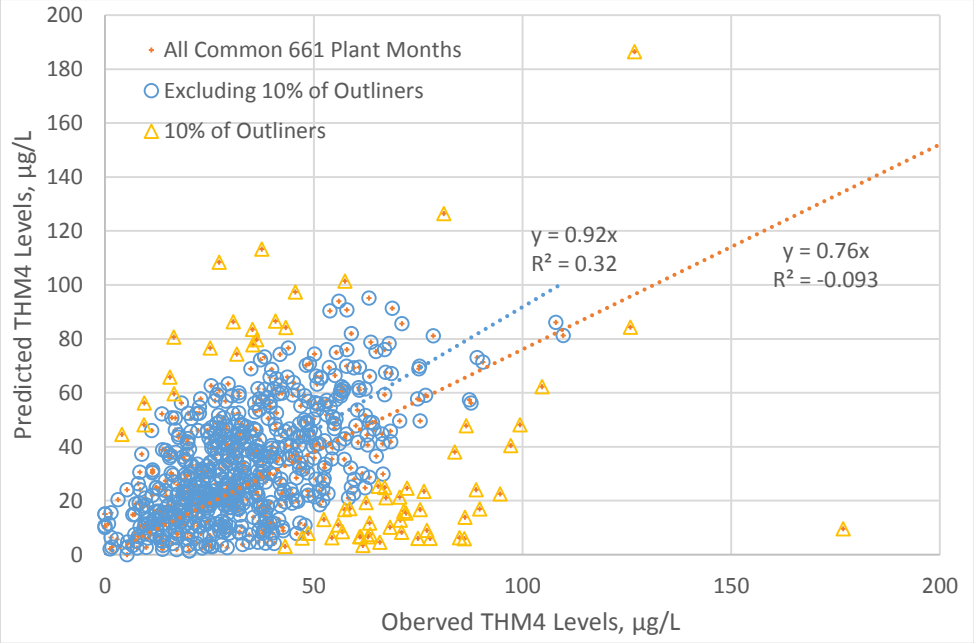

Figure S6. Comparison of Observed versus Predicted THM4 Levels among 661 Common Plant Months

Figure S7 illustrates the same comparison of observed versus predicted data as was done in Figure S6, but for plants using chlorine as their only disinfectant (both as primary and secondary distribution system residual). Given that both slopes for chlorine only plants (with and without exclusion of outliers) in Figures S6 and S7 are close to 1.0, little systematic bias for prediction of THM4 is apparent among systems using only chlorine as their disinfectant. It is expected that the WTP model is better at estimating THM4 for chlorine-only plants than for plants using multiple disinfectants because of the calibration process focused primarily on chlorine-only plants. The WTP model is expected to be challenged in making accurate predictions of THM4 by plants that use chloramines as a primary disinfectant (denoted as CLM or CL2_CLM for the primary disinfectant). These plants have variable, and often difficult to characterize, free chlorine contact periods prior to ammonia addition. The WTP model's ability to accurately predict THM4 formation for these specific plant types will thus be dependent on accurate characterization of these processes.

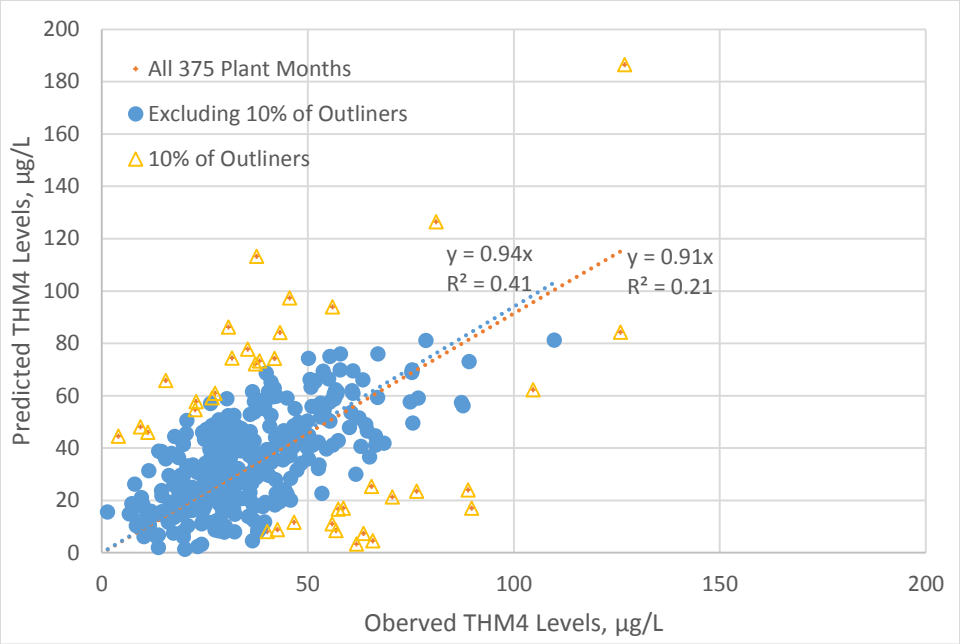

Figure 7. Comparison of Observed versus Predicted THM4 Levels among 375 Common Plant Months with CL2/CL2 only

The scatter of data illustrated in Figures S6 and S7 clearly indicates the potential for error in using the WTP to predict estimate individual THM4. However, the lack of model fit may have as much to do with inaccurate input data and matching THM4 data as the inability of the model to predict THM4 formation. We are not that concerned with the scatter of the data in Figures S6 and S7 (i.e., high variability in over or underestimation of THM4) since we are really only interested in the ability of the WTP model to predict the impact of increased bromide. Our assumption is that most of the error associated with the causative factors of under- or over-estimation will be factored out with the modeling approach we have taken for estimating THM4 as a function of increased bromide.

Our modeling approach is based on the premise that the WTP has an inherent ability of predicting realistic levels of THM4, and estimating the influence the key factors affecting increases of THM4, including the effects of bromide. In particular, increases in bromide are expected to always lead to increases in THM4, both theoretically (i.e. in the real world) and based on the THM4 equations. In addition, while the ICR database of water quality and treatment operation may not describe a specific plant completely accurately, with the tendency to over-predict formation as often as it under-predicts formation (e.g. slopes approaching 1.0 in Figures S6 and S7) , it does provide a reasonable national

representation of combinations of water qualities and treatment. As such, we think that the WTP model with inputs from the Aux8 database is providing realistic predictions of national level THM4 formation.

To test our assumption that our modeling approach for estimating ΔTHM4 (as a function of increased bromide) largely factors out errors associated with the ICR data and model prediction for THM4, we compared estimates of ΔTHM4 at an increase of 50 μg/l in the source water, among the "outlier" plants versus "non-outlier" plants described in Figure S6. Figure S8 indicates a comparable 90th percentile of ΔTHM4 (first whisker above the box) for the "outlier" and "non-outlier" plant months, which we think supports our assumption that the ΔTHM4 predictions at baseline and at elevated bromide levels are realistic in magnitude and in the effect of bromide, even if the prediction is for an "outlier." We expect a lower median and interquartile (25th to 75th percentile range) for the "outlier" versus the "non-outlier" plants because the outlier plants comprise a higher proportion of plants using chloramines, and use of chloramines greatly reduces THM4 formation regardless of bromide content. Since the WTP model captures this sensitivity, we would expect in general, lower ΔTHM4 estimates for plants using chloramines with little or no preceding free chlorine contact time.

Since the estimation of potential increases in bladder cancer incidence is based on long-term exposure, we also wanted to examine ΔTHM4 level for each plant on an annual mean basis (annual plant mean ΔTHM4). Plant mean values were calculated as the mean of all plant-month predictions for a given plant (ranging from 4 to 12 plant months per plant). A plant was denoted an "outlier" plant if one of its possible four plant-month predictions was denoted an outlier in the previous analysis. The 66 outlier plant months of Figure S6 were associated with 46 of the 201 plants. Comparing annual plant mean ΔTHM4 for outlier versus non-outlier plants shows very comparable distributions of ΔTHM4 even for the plants that had been identified as having at least one outlier quarterly prediction (Figure S9). This further supports our assumption that our models prediction of the effect of increased bromide is insensitive to whatever contributed to the large differences between the measured and predicted THM4 levels illustrated in Figures S6 and S7. A similar analysis examining chlorine-only plants showed fairly even distributions of the annual plant means for both the non-outlier and outlier plants (Figure S10).

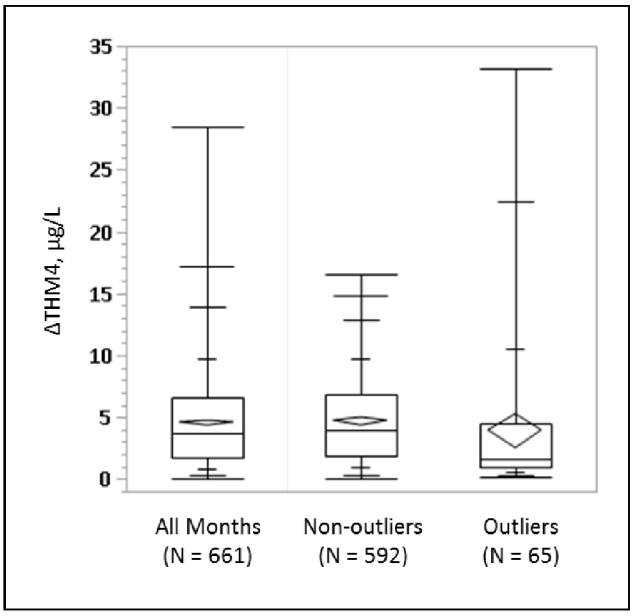

Figure S8. ΔTHM4 at ΔBr^- of 50 µg/L with Plant Months shown in Figure S6: All Plant Months, Non-outlier Months, and 10% Outlier Months

(Note: The quantile box plots display the box representing the 25th and 75th quantiles. The horizontal line within the box depicts the median sample value, while the diamond contains the mean and the upper/lower 95% of the mean. The whiskers (from the center outward) depict: 10th/90th, 2.5th/97.5th; 0.5th/99.5th, and min/max quantiles. Note that the 0.5th/99.5th whiskers are typically overlapping with the min/max outmost whiskers. This key pertains to subsequent box and whisker plots.)

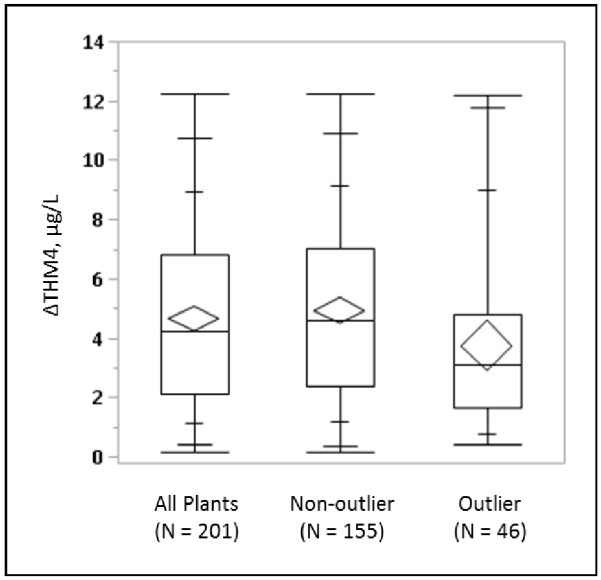

Figure S9. Annual Plant Mean ΔTHM4 at ΔBr⁻ of 50 µg/L: among All 201 Plants, Non-outlier Plants, and Outlier Plants

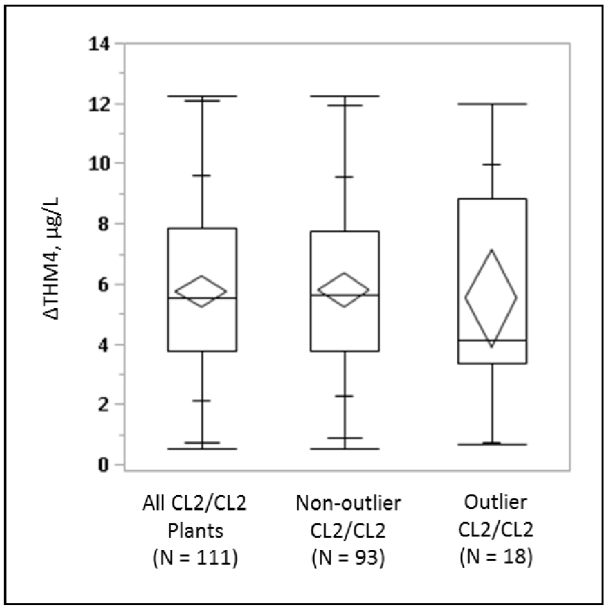

Figure S10. Annual Plant Mean ΔTHM4 at ΔBr⁻ of 50 µg/L: among All Plants with CL2/CL2 only, Non-outlier Plants, and Outlier Plants

We next examined the distributions of ΔTHM4 plant means among all plant types to illustrate the full range of the modeled effects of incremental bromide increase (+ 10, 30, 50, 75, 100 µg/L) in source water (Figure S11). The relative distribution of ΔTHM4 as function of increased bromide appears to be about the same across all bromide concentration increases. Note that Figure S11 represents another depiction of the data shown in Table 2 (main text).

While we think the analysis presented above supports a reasonable approach for making national estimates of ΔTHM4 as a function of increased bromide, we still have not informed overall model uncertainty for our estimates. We recognize that if different experiments and data had been used to develop the WTP model, the resulting predictive equations would be different and generated different ΔTHM4 estimates. While the range for this uncertainty cannot be quantified (i.e., the standard error of our ΔTHM4 estimates) from our available data, to ground truth the reasonableness of our model estimates, we reviewed the available research for additional perspective.

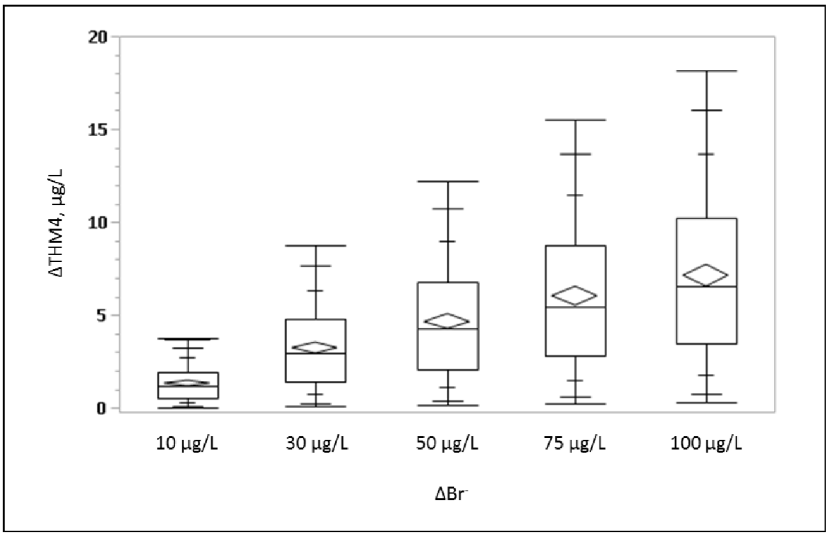

Figure S11. ΔTHM4 as a Function of Varying Increases in Bromide among All 2089 Plant Months

As we discussed above, the best evidence that our ΔTHM4 estimates are reasonable would come from full-scale spiking studies at multiple plants wherein all water quality and treatment was held constant, but bromide was increased (or decreased) to examine the effect on THM4. Data of this nature does not exist. However, in recent years there have been some reports of increased bromide in source waters, and concomitant increased THM4 and bromine incorporation in the THM4.[17,18] Though impossible to control for other changing water quality and treatment impacts, the anecdotal reports suggest that bromide increases are leading to THM4 increases. Moreover, the fact that the THM4 increases for most

plants are measurable, and oftentimes putting the utility near an MCL violation, this further suggests that the THM4 increases are considerably greater than the lower bound of 1 µg/L considered in our estimates in Figure 2.

In the absence of controlled field data, we can look to lab-scale spiking studies to help assess the magnitude of THM4 increases from increases in bromide. Although the effect of bromide on THMs has been known for some time, and bromide spiking studies have been performed for as long, there are few studies that examined relatively low initial bromide levels (e.g. baseline bromide < 150 µg/L) and also had relatively modest bromide increases, such as in the range of 50 to 100 µg/L.[19] Table S6 summarizes the results from a selection of lab studies with bromide concentrations most relevant to this paper.

Table S6. ΔTHM4 and Experimental Conditions in Bromide Spiking Studies

Water Source	DOC (TOC) [mg/L]	Cl_2 dose [mg/L]	Reaction time [hr]	pH	Br^- [µg/L] (increase from baseline)	THM4 [µg/L] (increase from baseline)	Reference
raw	4.1	UFC conditions		6	64 (baseline)	84 (baseline)	10
					205 (+141)	97 (+13)	
		UFC conditions		8	64 (baseline)	117.3 (baseline)	
					205 (+141)	137 (+20)	
treated	2.2	UFC conditions		6	72 (baseline)	24 (baseline)	
					110 (+38)	26 (+2)	
					220 (+148)	35 (+10.8)	
		UFC conditions		8	72 (baseline)	39 (baseline)	
					110 (+38)	44 (+6)	
					220 (+148)	58 (+19)	
humic acid isolate	3	4	48	6	0 (baseline)	76 (baseline)	20
					40 (+40)	84 (+9)	
					80 (+80)	91 (+16)	
					120 (+120)	97 (+21)	
raw ground water	1.4	2.8	24	8	38 (baseline)	43 (baseline)	11
					59 (+21)	44 (+1)	
					106 (+68)	60 (+17)	
					197 (+159)	87 (+44)	
raw	8.5	6.2	48	7	9 (baseline)	138 (baseline)	21†
					169 (+160)	185 (+47)	
raw	5.3	5	48	7	63 (baseline)	158 (baseline)	
					223 (+160)	212 (+54)	
raw	7.5	6	48	7.5	100 (baseline)	145 (baseline)	22†
					350 (+250)	186 (+41)	
raw‡	unk	1.5	336	unk	39 (baseline)	102 (baseline)	18
					99 (+60)	121 (+19)	
					139 (+100)	113 (+11)	
raw	4.6	5	24	7	210 (baseline)	180 (baseline)	23†
					360 (+150)	224 (+44)	
raw	5.6	16.9	48	6.5	51 (baseline)	212 (baseline)	24
					301 (+250)	265 (+53)	

† data extracted from figures within cited reference, and therefore estimated; ‡ experiments performed at 30 °C; unk = unknown; UFC = Uniform Formation Conditions

Consistent with the Amy lab study[12], which was the training set for the THM4 formation equations in the WTP model, these lab studies generally showed an increase of 1 to 20 µg/L THM4 for increases in Br^- of 20 to 100 µg/L. While these reports still do not help assess the uncertainty in our model estimates, we feel they add to the weight of evidence that the envelope of change in THM4 levels from the range of Br^- increases explored in this paper is reasonable. Note that even among the studies that had data at what we feel are more relevant bromide concentrations, one must also use caution in that the chlorine doses, or chlorine:DOC ratios may not be realistic, and differing reaction times may play a role as brominated THMs generally form faster than chloroform.

The data in Table S6, however, only summarizes the effect of bromide on chlorination. Data of this type for chloramination is lacking. Of the 201 plants modeled in this paper, only 111 were chlorine-only plants for all plant months. A large number of the plants (40) practiced a combination of chlorine and chloramine for the primary disinfectant, followed by chloramine in the distribution system (CL2_CLM/CLM plants). As mentioned above, this disinfection scenario is potentially challenging to characterize by the WTP model both in terms of data input and model simulation. Moreover, these plants had considerable THM4 levels measured during the ICR period (interquartile range of 23 - 46 µg/L, and 90th%ile of 61 µg/L). Whereas we have reasonable confidence that our estimates of ΔTHM4 for chlorine-only plants (based on treatment plant reports and lab studies), we recognize more uncertainty in the predictions for chloramine plants.

In summary, despite these reality checks, the weakest aspect of our analysis is not having sufficient data to develop confidence bounds around our ΔTHM4 estimates. Nevertheless, we think the THM4 predictive equations used in the WTP model are among the best available, and we have confidence that most plants having an increase in 50 µg/L of Br^- in their source water will incur at least an increase of 1 µg/L THM4, and often much greater than 1 µg/L.

K. Supporting Information References

[1] Salas, L.A.; Cantor, K.P.; Tardon, A.; Serra, C.; Carrato, A.; Garcia-Closas, R.; Rothman, N.; Malats, N.; Silverman, D.; Kogevinas, M.; Villanueva, C.M. Biological and statistical approaches for modeling exposures to specific trihalomethanes and bladder cancer risk. *Am J Epidemiol.* **2013***, 178* (4), 652–660.

[2] Cantor, K.P.; Villanueva, C.M.; Silverman, D.T.; Figueroa, J.D.; Real, F.X.; Garcia-Closas, M.; Malats, N.; Chanock, S.; Yeager, M.; Tardon, A; Garcia-Closas, R.; Serra, C.; Carrato, A; Castaño-Vinyals, G.; Samanic,

C.; Rothman, N.; Kogevinas, M. Polymorphisms in *GSTT1, GSTZ1,* and *CYP2E1,* disinfection by-products, and risk of bladder cancer in Spain. *Environ. Health Perspect*. **2010**, *118*, 1545-1550.

[3] McLain, J. L.; Obolensky, A.; Shukairy, H. M. Disinfection by-product speciation. In *Information Collection Rule Data Analysis*, McGuire, M. J., McLain, J. L., Obolensky, A., Eds.; Awwa Research Foundation and American Water Works Association: Denver, CO; 2002; pp 141-168.

[4] U.S. Environmental Protection Agency. *Economic Analysis for the Final Stage 2 Disinfectants and Disinfection Byproducts Rule*; EPA 815-R-05-010; Office of Water; Office of Ground Water and Drinking Water: Washington, DC, 2005.

[5] U.S. Environmental Protection Agency. *Appendices to the Economic Analysis for the Final Stage 2 Disinfectants and Disinfection Byproducts Rule. Volume I (A-E2).*; EPA 815-R-05-010; Office of Water; Office of Ground Water and Drinking Water: Washington, DC, 2005

[6] U.S. Environmental Protection Agency. *ICR Auxiliary 1 Database, Version 5.0*; EPA 815-C-00-002; Office Water: Washington, DC, 2000.

[7] Swanson, W.J.; Chowdhury, Z.K.; Aburto, L.; Summers, R.S. Predicting ICR surface water plant behavior with the Water Treatment Plant Model. In *Information Collection Rule Data Analysis*, McGuire, M.J., McLain, J.L., Obolensky, A., Eds.; Awwa Research Foundation and American Water Works Association: Denver, CO; 2002; pp 199-223.

[8] Chowdhury, S.; Champagne, P.; McLellan, P. J., Models for predicting disinfection byproduct (DBP) formation in drinking waters: A chronological review. *Science of The Total Environment.* **2009,** *407*, (14), 4189-4206.

[9] Hua, G.; Reckhow, D. A.; Kim, J., Effect of Bromide and Iodide Ions on the Formation and Speciation of Disinfection Byproducts during Chlorination. *Environmental Science & Technology.* **2006,** *40*, (9), 3050-3056.

[10] Hu, J.; Song, H.; Karanfil, T., Comparative Analysis of Halonitromethane and Trihalomethane Formation and Speciation in Drinking Water: The Effects of Disinfectants, pH, Bromide, and Nitrite. *Environmental Science & Technology* **2009,** *44*, (2), 794-799.

[11] Ged, E.C.; Boyer, T.H.; Effect of seawater intrusion on formation of bromine-containing trihalomethanes and haloacetic acids during chlorination. *Desalination.* **2014**, *345*, 85-93.

[12] Amy G.; Siddiqui, M.S.; Ozekin, K.; Zhu, H.W.; Wang, C. Empirically based models for predicting chlorination and ozonation by-products: Trihalomethanes, haloacetic acids, chloral hydrate, and bromate; EPA 815-R-98-005; U.S. Environmental Protection Agency; Office of Water; Office of Ground Water and Drinking Water: Cincinnati, OH, 1998.

[13] Sohn, J.; Amy, G.; Cho, J.; Lee, Y.; Yoon, Y., Disinfectant decay and disinfection by-products formation model development: chlorination and ozonation by-products. *Water Research* **2004,** *38*, (10), 2461-2478.

[14] Sohn, J. Comprehensive Assessment and Modeling of Disinfection By-products (DBPs), DBP Precursors, and Disinfectants. University of Colorado, Boulder, 2000.

[15] Solarik, G.; Summers, R. S.; Sohn, J.; Swanson Warren, J.; Chowdhury Zaid, K.; Amy Gary, L., Extensions and Verification of the Water Treatment Plant Model for Disinfection By-Product Formation. In *Natural Organic Matter and Disinfection By-Products*, American Chemical Society: 2000; Vol. 761, pp 47-66.

[167] U.S. Environmental Protection Agency. National Primary Drinking Water Regulations: Monitoring Requirements for Public Drinking Water Supplies: Cryptosporidium, Giardia, Viruses, Disinfection By-products, Water Treatment Plant Data and Other Information Requirements. *Fed. Regis.* **2006**, *61* (94), 24353-24388.

[17] McTigue, N.E.; Cornwell, D.A.; Graf, K.; Brown, R. Occurrence and consequences of increased bromide in drinking water sources. *J. Am. Water Works Ass.* **2014**, *106* (11), E492-E508.

[18] States, S.; Cyprych, G.; Stoner, M.; Wydra, F.; Kuchta, J.; Monnell, J.; Casson, L. Marcellus Shale drilling and brominated THMs in Pittsburgh, Pa., drinking water. *Journal American Water Works Association.* **2013**, *105*, E432-E448.

[19] Ged, E.C.; Chadik, P.A.; Boyer, T.H. Predictive capability of chlorination disinfection byproducts models. *Journal of Environmental Management*. **2015**, *149*, 253-262.

[20] Chowdhury, S.; Champagne, P.; McLellan, J.P. Investigating effects of bromide ions on trihalomethanes and developing model for predicting bromodichloromethane in drinking water. *Water Research.* **2010**. *44(7)*, 2349-2359.

[21] Reckhow, D. A.; Hua, G.; Kim, J.; Hatcher, P.; Caccamise, S. A. L.; Sachdeva, R. *Characterization of Total Organic Halogen Produced During Disinfection Processes - 2755* AWWA Research Foundation: 2007.

[22] Liu, S.; Zhu, Z.; Qiu, Y.; Zhao, J., Effect of ferric and bromide ions on the formation and speciation of disinfection byproducts during chlorination. *Journal of Environmental Sciences* **2011,** *23*, (5), 765-772.

[23] Uyak, V.; Toroz, I., Investigation of bromide ion effects on disinfection by-products formation and speciation in an Istanbul water supply. *Journal of Hazardous Materials* **2007,** *149*, (2), 445-451.

[24] Zaid Chowdhury. **2015**. Personal communication.

Table of Contents

General_Authors_Publications.....2
LI-266168_DonohueBMCinfetDis.....9
LI-266168_DonohueannalATS.....18
LI-266169_DonohueBMCinfetDis.....26
Wymer_%_Agreement.....35
Donohue_%_Agreement.....36

United States Environmental Protection Agency
Washington, DC 20460

STAA REPORT FOR THE SCIENTIST NOMINATIONS

General Information:

Nomination ID/App ID:	20-105
Research Category Primary:	Health Effects Research and Human Health Risk Assessment (HE)
Research Category Secondary:	Health Effects Research and Human Health Risk Assessment (HE)
Laboratory/Office Name:	ORD
Nomination Entered By:	Maura Donohue

Eligibility Checklist:

[Y] The nominated publication(s) has not been submitted to a previous STAA competition.

[Y] The nominated publication(s) was published on or before January 1, 2017 and on or after January 1,2012

[Y] The principal author was an EPA employee or a PHS employee assigned to EPA when the research was performed

[Y] The EPA authors (includes PHS employees assigned to EPA) contributed collectively a minimum of 50% toward the publication(s)

Nominating Official Name:	Regan Murray
Nominating Official Title:	SUPERVISORY INTERDISCIPLINARY SCIENTIST
Nominating OfficialEmail:	murray.regan@epa.gov
STAA Coordinator Name:	Kathleen Wiser
STAA Coordinator Email:	wiser.kathi@epa.gov

Justifications:

Justification 1:

Data on the national prevalence of Nontuberculous Mycobacteria (NTM) in the Unites States was non-existent. This is because NTMs and their diseases are not monitored by the Centers for Disease Control and Prevention (CDC). However, NTM (*Mycobacterium avium*) is a priority for the EPA because it is on the Safe Drinking Water Act, Candidate Contaminant List (CCL), and hence we need a national benchmark to track prevalence. NTMs cause both infections and respiratory diseases in humans, with Pulmonary NTM diseases being the severest form. Transmission of the disease is through the inhalation of aerosols containing the bacteria. The United States (US) spends a billion dollars per year on treating NTM related diseases. NTMs are water-borne bacteria routinely isolated from drinking water. NTMs are highly resistant to water treatment chemical disinfectants (chlorine and chloramine). Therefore, exposure though drinking water is highly probable.

I took a creative and unconventional approach to address this programmatic /research need, by reaching out to state health departments. I found that health departments in some states like Ohio tracked NTM prevalence. These state health departments provided me with anonymized data on NTM cases. Using this data, I calculated the yearly NTM prevalence rate in each of these states, going back 6 years (2008-2013). I found that NTM prevalence rates had increased in all 5 states (Ohio, Wisconsin, Missouri, Maryland and Mississippi) that had provided me data (Donohue et al, 2016).

· This publication was downloaded 2,737 times on the journal website (as of 4/24/20).

· This publication was cited 37 times according to Google Scholar.

· This article was published in the Annals of the American Thoracic Society which has an impact factor of 4.026.

I expanded my investigation to understand if the NTM species-specific infection rates had changed over time. This is important information because it can help us

prioritize which NTM species we should monitor (among the more than 100 known NTM species). Health departments form 4 states (Ohio, Wisconsin, Missouri, and Mississippi) provided me anonymized case data by NTM species. Using this data and historical public health records, I found that between 1994 and 2014, *M. abscessus-chelonae* group and *M. avium* complex linked NTM cases increased by 322% and 149%, respectively. I estimated that approximately 50,000 NTM cases per year could be projected for the nation; serving as a baseline indicator for the potential NTM disease burden per year in the US (Donohue MJ, 2018).

· This publication was downloaded 1,673 times on the journal website (as of 4/24/20).

· This publication was cited 31 times according to Google Scholar.

· This article was published in the BMC infectious diseases which has an impact factor of 2.951.

Impact on EPA mission:

As a result of these two publications, the EPA can update its health advisory document, cost burden analysis, and help evaluate EPA policies and to help reduce NTM-disease prevalence in the US.

Justification 2A:

These two publications are closely related to each other. The first publication established the prevalence of NTM patients in 5 states. The second publication builds on this research by focusing on the specifies specific NTM prevalence rates. It also looked at the seasonality of NTM prevalence.

Justification 2B:

The nominated publications address an epidemiological knowledge gap regarding NTM prevalence rate in the US. This work was not nominated in past STAA nomination years. Dr. Donohue's research primarily focuses on analytical method development for pathogens detection and quantification in drinking water.

Justification 2C:

The author Maura Donohue has received the following STAA awards for her research efforts.

1) Donohue, Maura plus 39 other authors, Nationwide study on the prevalence and potential health effects of contaminants of emerging concern in drinking water. **2019-Level II, STAA award**

2) Donohue, Maura plus 12 other authors of the Detection and quantification of Legionella and Nontuberculous Mycobacterium in drinking water. **2016 Level III STAA Award**

Justification 2D:

n/a-not applicable

Justification 2E:

Maura Donohue has a concurrent STAA nomination. Dr. Lisa Melynk is submitting a STAA nomination for research effort centered on Strontium absorption into food. Dr. Donohue also participated in Dr. Melynk Strontium study. Dr. Donohue specific activities within the Strontium study were gathering food sources, purchasing equipment, identifying and setting-up collaborations, writing a section within the manuscript, editing manuscript and creating study design figure.

There is no research overlap between Dr. Donohue's NTM epidemiological papers and Strontium absorption paper. Even the timeline of the two research efforts did not over lap. The epidemiological papers were drafted in 2015-2017. The Strontium work was preformed 2018-2019.

Justification 3A:

Due to this research I have been asked by Dr. Rebecca Prevots (National Health Institute, Gaithersburg, MD) and Dr. Ettie Lipner (National Jewish Hospital, Bolder CO) to collaborate on a NTM research effort in Florida.

These NTM papers filled a data gap in this research field as demonstrated by being cited 17 times per year. (37 +31 cites/4 years).

Donohue MJ, Wymer L. Increasing Prevalence Rate of NTM Infections in Five States. Ann Am Thorac Soc. 2016**.**

· This publication was downloaded 2,737 times on the journal website (as of 4/24/20).

· In 4 years, this publication was cited 37 times according to Google Scholar.

· This article was published in the Annals of the American Thoracic Society which has an impact factor of 4.026 and a low acceptance rate (19%) .

Donohue MJ., Increasing NTM reporting rates and species diversity in clinical laboratory reports. BMC Infect Dis. 2018.

· This publication was downloaded 1,673 times on the journal website (as of 4/24/20).

· In 2 years, this publication was cited 31 times according to Google Scholar.

· This article was published in the BMC infectious diseases which has an impact factor of 2.951.

Justification 3B:

Both papers underwent extensive internal and external (Journal) review. Each paper required two internal technical reviews by EPA experts. In addition, these papers had to clear branch- and division- level review. Both papers were also subjected to Office of Water policy review, prior to journal submission. The Annals of Thoracic Society has a 19% acceptance rate for original research. At the Annals of Thoracic Society Journal the submitted article underwent editorial judgment and received comments from three experts. The article was accepted for publication. The article submitted to BMC Infectious Diseases underwent editorial review and review from five experts. The article was accepted for publication.

AUTHORS

Principal Author

Author Name:	Maura J. Donohue		
Professional Title:		Salutation:	Dr.
Email:	donohue.maura@epa.gov	Organization:	
Mailing Address:			
Street Line 1:	26 W. Martin Luther King Dr.		
City:	Cincinnati		
Zip Code:	45268	State:	OH
At time of research was:	EPA Employee		
Separation Date:			
% of Effort:	90		

Contributing Author

Author Name:	Larry Wymer		
Professional Title:		Salutation:	Mr.
Email:	wymer.larry@epa.gov	Organization:	
Mailing Address:			
Street Line 1:	26 W Martin Luther King Dr.		
City:	Cincinnati		
Zip Code:	45268	State:	OH
At time of research was:	EPA Employee		
Separation Date:			
% of Effort:	10		

PUBLICATIONS

Publication 1:

Publication Title:	Increasing Prevalence Rate of Nontuberculous Mycobacteria Infections in Five States, 2008-2013		
Publication Date:	Thu Dec 01 00:00:00 GMT 2016		
Journal/Publication Method:	Ann Am Thorac Soc.		
All Author(s):			
Volume:	13	Number:	12
Pages:	2143-2150	Immediately Index:	Immediately Index:
Citation ½ Life:	3.1	Impact Factor:	4.026

Publication 2:

Publication Title:	Increasing nontuberculous mycobacteria reporting rates and species diversity identified in clinical		
Publication Date:	Tue Apr 10 00:00:00 GMT 2018		
Journal/Publication Method:	BMC Infectious Diseases		
All Author(s):			
Volume:	18	Number:	1
Pages:	163-	Immediately Index:	Immediately Index:
Citation ½ Life:	4.6	Impact Factor:	2.565

Donohue *BMC Infectious Diseases* (2018) 18:163
https://doi.org/10.1186/s12879-018-3043-7

BMC Infectious Diseases

RESEARCH ARTICLE Open Access

Increasing nontuberculous mycobacteria reporting rates and species diversity identified in clinical laboratory reports

Maura J. Donohue

Abstract

Background: Nontuberculous Mycobacteria (NTM) are environmental microorganisms that can affect human health. A 2009–2010 occurrence survey of NTM in potable tap water samples indicated an increased recovery rate for many clinically significant species such as *M. avium* (30%) and *M. abscessus* (12%). To determine if these trends by species were mirrored in human infections, isolation rates of NTM species identified in clinical laboratory reports from four states were evaluated.

Method: Clinical laboratory reports from the Mississippi, Missouri, Ohio, and Wisconsin Health Departments were used to investigate the species of NTM isolated from human specimens in 2014. The NTM positive specimen reports were tabulated for each species and complex/group. The number of reports by month were used to investigate seasonal trends. The 2014 isolation rates were compared to historic values to examine longitudinal trends.

Results: The positive rate of NTM specimens increased from 8.2 per 100,000 persons in 1994 to 16 per 100,000 persons in 2014 (or 13.3 per 100,000 after excluding *Mycobacterium gordonae*). Changes in NTM diversity were observed in complex/groups known to be clinically significant. Between 1994 and 2014 the rate implicating *M. abscesses-chelonae* group and *M. avium* complex increased by 322 and 149%, respectively.

Conclusions: Based on public health data supplied by the four State's Health Departments and the 2014 U.S. population, 50,976 positive NTM specimen reports per year were projected for the nation; serving as an indicator for the national potential disease burden that year.

Keywords: Nontuberculous mycobacteria (NTM), Clinical laboratory reports, Species, Epidemiology, Isolation rates, Report rates, Seasonal, United States

Background

Data from recent studies demonstrate an increasing prevalence of Nontuberculous Mycobacteria (NTM) infections in the United States [1–3]. NTM are of environmental origin and can impact a wide variety of tissues and body fluids causing both respiratory (chronic bronchopulmonary disease) illnesses and dermal infections [4]. NTM infections may also compound the respiratory ailments of individuals with Cystic Fibrosis [5], Chronic Obstructive Pulmonary Disease (COPD) [6, 7] and Acquired Immunodeficiency Syndrome (AIDS) [8, 9].

NTM's natural habitats are aquatic and soil environments [10]. Since the majority (77.4% [11] to 91.5% [12]) of NTMs are isolates from pulmonary specimens, exposure likely occurs through the aerosolization or aspiration of water and or soil particulates. NTM infections or illnesses are not generally communicable, although there are a few documented cases of person-to-person transmission [13, 14]. Additionally, highly populated areas have a higher NTM infection rate and positive specimen counts than other regions of the U.S. [15, 16].

NTM is a broad classification term that is applied to a group of approximately 186 currently recognized unique mycobacterium species [17]. The majority do not have an impact on human health. Thus, it is important to identify the species causing an infection in cases where

Correspondence: Donohue.maura@epa.gov
United States Environmental Protection Agency, 26 W. Martin Luther King Dr. Mail Stop 587, Cincinnati, Ohio 45268, USA

BioMed Central

© The Author(s). 2018 **Open Access** This article is distributed under the terms of the Creative Commons Attribution 4.0 International License (http://creativecommons.org/licenses/by/4.0/), which permits unrestricted use, distribution, and reproduction in any medium, provided you give appropriate credit to the original author(s) and the source, provide a link to the Creative Commons license, and indicate if changes were made. The Creative Commons Public Domain Dedication waiver (http://creativecommons.org/publicdomain/zero/1.0/) applies to the data made available in this article, unless otherwise stated.

symptoms are sufficient to support specimen collection. Knowledge of the NTM species identity will guide the therapeutic treatment prescribed by the physician and provide clues relative to exposure source and route.

This study catalogued the NTM species in human-specimen clinical reports from four States (Mississippi, Missouri, Ohio, and Wisconsin) during the 2014 calendar year with the goal of identifying the species with the most frequent impact on human health. The dates for the case report submissions were examined to determine if there was any indication of seasonality. In addition, the 2014 findings were compared to those from an earlier 1994 Centers for Disease Control and Prevention (CDC) report of NTM infections (19) to evaluate if prevalence had increased over the last 20 years.

Methods

Study design

Four states (Mississippi, Missouri, Ohio, and Wisconsin) that required NTM positive specimen results to be submitted to their respective state health departments were asked if they would provide the following data from their disease surveillance network: the number of positive NTM reports by species and the number of positive NTM reports by month for the 2014 calendar year. The respective health departments agreed to participate and provided the requested information to the U.S. EPA. Table 1 summarizes the information received from the four states. No personal identifiers were shared with U.S. EPA, therefore maintaining the privacy for the individuals associated with all report records. This study was determined to be exempt from Institution Review Board review by U.S. EPA.

Data

Four health departments provided U.S. EPA with the number of NTM reports by species for the 2014 calendar year. The methods used to isolate NTMs were either through culture [18] or the Becton Dixon BACTEC™ Mycobacteria Growth Indicator Tube (MGIT™) [19]. All four states largely used mycolic acid analysis and DNA probes (Hologic, Marlborough, MA) for species identification. Some laboratories sequenced an isolate's *hsp65* or *rpoB* gene for NTM identification (Table 1).

Cases implicating all non-NTM isolates, as well as, isolates of *M. bovis* and *M. marinum* were removed from the data set for this analysis. Cattle and fish, not water, are the sources of infection for *M. bovis* and *M. marinum* species; thus, they were not considered in this evaluation.

Analysis

Report rates for NTMs were calculated for each state by dividing the number of positive NTM case reports by the July 1, 2014 state population. Calculation of these rates used 2014 U.S. population estimates for each state as follows (Table 1): Mississippi: 2,993,443; Missouri: 6,063,827; Ohio: 11,597,998; Wisconsin: 5,759,432 and U.S.: 318,563,456. The percentage of the total was calculated for each species or group identified by each state using Microsoft Excel.

CDC does not routinely collect NTM specimen reports. Periodically, over the past 40 years, CDC has published a few papers and reports that examined the epidemiology of NTMs in the U.S. These papers examined NTM prevalence by the number of laboratory reports generated by each state [20–22]. The 1994 historical data for each of the four states was extracted from the Butler and Crawford, 1999 document. This document contains the number of reports and report rate by species for each state in the U.S for the years 1993–1996. In the 1990's, laboratories were using either culture bases methods [18] or BD MGIT™ systems [19] for bacterial enrichment and DNA/RNA

Table 1 Health departments data sources and NTM identification method for the year 2014

State	Data source	Year	NTM identification method	NTM laboratory report	Report rate[a]
Mississippi	Mississippi's public health laboratories + accredited laboratories (hospitals and/01 commercial laboratories)	2014	HPLC and DNA probes	529	17.6
Missouri	Missouri's public health laboratories + few hospitals + commercial laboratories	2014	HPLC and DNA probes	879	14.5
Ohio	Ohio's public health laboratories + hospitals + commercial laboratories	2014	HPLC, DNA probes, sequencing of the *hsp65* and *rpoB* gene and biochemical test	1379	11.8
Wisconsin		2014	HPLC and DNA probes and inconclusive isolates are sequenced.	1413	24.5
Total				4200	16.0

[a] Rate per 100,000 persons

probes (Hologic, Marlborough, MA) and or mycolic acid analysis for identification [23]. In 2014, the majority of laboratories were still using these culture and identification methods. Thus, supporting a comparison between the two-time periods 1994 and 2014. Chi-square and Fisher Exact tests for significant differences between the two data sets were determined using SigmaPlot 13.0.

Species grouping

Many of the NTM species have similar characteristics and have been placed into groups of two to seven species (Table 2) with some species being ungrouped. The species identified by the states were summed by their group for this analysis to facilitate a comparison between the historical 1994 data and the 2014 data. For example, 1541 samples identified as M. *avium* complex (MAC) positive specimens were combined with 705 reports identified as *M. avium* species and 6 reports identified as *M. intracellulare* species to give a total of 2252 reports for the MAC group. Table 2 lists the NTM species reports that were combined to represent each NTM group/complex/clad unit for the comparison.

Monthly reports

The Mississippi, Missouri, and Ohio Health Departments provided the U.S. EPA with the number of NTM specimen reports by month for the year 2014. Mississippi data are publicly available at the Monthly Reportable Disease Statistics website: http://msdh.ms.gov/msdhsite/_static/14,0,261.html. The Wisconsin Health Department was unable to supply their data in this format; thus, there is no evaluation of cases per month for the state of Wisconsin. The monthly report data were used to determine if report frequency exhibited any seasonal trends.

Results

NTM species in laboratory reports

The Mississippi, Missouri, Ohio, and Wisconsin disease network had 4200 NTM positive specimen reports submitted in 2014. The overall NTM prevalence rate was 16.0 reports per 100,000 persons (or 13.3 per 100,000 excluding *Mycobacterium gordonae*). This rate is much higher than that reported by the CDC in 1994. Based on the 2014 data, a national estimate of 50,976 positive NTM specimen reports are projected during that year.

The distributions by state for the total NTM positive specimens are as follows: Wisconsin (33.6%), Ohio (32.8%), Missouri (20.9%) and Mississippi (12.6%) (Additional file 1: Table S1-S4). The complex/group assignment to which an isolate was speciated varied across the states. Three percent of the reports identified the isolates only to the genus-level. Forty-three percent of the reports assigned the isolates only to a specific complex/group, and 54% of reports provided the species name (Table 2). In all, 52 species were identified by name in the state reports. Isolates classified only by their complex/group designation primarily belonged to the *M. avium* complex (MAC), *M. chelonae-abscessus* or *M. fortuitum* groups. Table 2 provides the data for all the species identified and ascribes each species to its designated complex or group. The five most common species isolated from human specimens were *M. avium* 705/4200 (17%), *M. gordonae* 688/4200 (16%), *M. chelonae* 135/4200 (3.2%), *M. fortuitum* 110/4200 (2.6%), and *M. mucogenicum* 104/4200 (2.5%) (Table 2). These species accounted for 41.4% of the total demonstrating the broad range of species identified among the samples collected for analysis.

NTM increased reporting frequency

NTM positive specimen reports have increased between 1994 and 2014 from 1950 to 2400, equivalent to an increase of 8.2 per 100,000 persons per year to 16.0 per 100,000 persons per year. The three complexes/groups that had statistically significant increases in the frequency of detections were the: *M. chelonae-abscessus* group, *M. fortuitum* group and *M. avium* complex. The percentage increase of these clinically important species, as established by American Thoracic Society and Infectious Disease Society of America, (ATS/IDSA) [4] between 1994 and 2014 is significant: 322% (94 to 440 reports), 194% (105 to 343 reports), and 149% (816 to 2252 reports), respectively (Fig. 1). On the other hand, Fig. 1 illustrates a decline in the number of positive specimen reports for other species: *M. xenopi (− 15%), M. kansasii (− 30%), M. terrae (− 40%), M. scrofulaceum (− 55%)* and *M. flavescens* (none detected).

Longitudinal analysis for the MAC species

Figure 2 illustrates the report rate of *M. avium per* 100,000 persons over time for the four states. In 2014, the combined report rate of *M. avium* for Mississippi, Missouri, Ohio, and Wisconsin was 8.5 per 100,000 persons (Fig. 2). This is 2.5 times more reports than the numbers reported in 1994 [20]. The species detections for Ohio and Wisconsin increased more than five-fold suggesting a comparable increase in the respiratory infections disease burden.

NTMs reports by month

When the 2014 positive specimens per month for each state were plotted (Fig. 3) there was no evidence for a seasonal pattern to the potential disease burden. The peak month for each state differed: February for Mississippi, April for Ohio, and July for Missouri. Data from Wisconsin were not segregated by month.

Table 2 NTMs identified from human specimens in Mississippi, Missouri, Ohio, and Wisconsin, 2014

Identified to Genus	Complex/Group Totals	Identified to NTM Complex/Group	Identified to NTM Species	Count	Percentage	Rate[a]
NTM				132	3.14	0.50
	MAC complex (Total)			2252	53.62	8.53
		MAC complex		1541	36.69	5.83
			M. avium	705	16.79	2.67
			M. intracellulare	6	0.14	0.02
	MAIS Complex (Total)			20	0.48	0.08
		MAIS Complex		17	0.40	0.06
			M. scrofulaceum	3	0.07	0.01
	M. *chelonae-abscessus* Group (Total)			440	10.48	1.67
		M. chelonae-abscessus Group		122	2.90	0.46
			M. abscessus	62	1.48	0.23
			M. bolletii	5	0.12	0.51
			M. chelonae	135	3.21	0.00
			M. franklinii	1	0.02	0.02
			M. immunogenum	4	0.10	
			M. massiliense	2	0.05	
			M. mucogenicum	104	248	0.39
			M. phocaicum	5	0.12	0.02
	M. fortuitum Group (Total)			343	8.17	1.30
		M. fortuitum Group		143	3.40	0.54
			M. conceptionense	2	0.05	0.01
			M. fortuitum	110	2.62	0.42
			M. houstonense	1	0.02	0.00
			M. neworleansense	2	0.05	0.01
			N. peregrinum	76	1.81	0.29
			M. porcinum	5	0.12	0.02
			M. septicum	4	0.10	0.02
	M. gordonae (Total)		*M. gordonae*	689	16.40	2.61
	M. xenopi (Total)		*M. xenopi*	54	1.29	0.20
	M. kansasii Clade (Total)			100	2.38	0.38
			M. gastri	1	0.02	0.00
			M. kansasii	99	2.36	0.37
	M. haemophilum (Total)			7	0.17	0.03
			M. haemophilum	2	0.05	0.01
			M. malmoense	5	0.12	0.02
	M. terrae Complex (Total)			60	1.43	0.23
			M. arupense	21	0.50	0.08
			M. kumamotonense	1	0.02	0.00
			M. nonchromogenicum	10	0.24	0.04
			M. terrae	28	0.67	0.11
	M. smegmatis (Total)			17	0.40	0.06
			M. goodii	7	0.17	0.03
			M. mageritense	4	0.10	0.02
			M. smegmatis	4	0.10	0.02
			M. wolinskyi	2	0.05	0.01

Table 2 NTMs identified from human specimens in Mississippi, Missouri, Ohio, and Wisconsin, 2014 *(Continued)*

Identified to Genus	Complex/Group Totals	Identified to NTM Complex/Group	Identified to NTM Species	Count	Percentage	Rate[a]
	M. simiae Complex (Total)			45	1.07	0.17
			M. interjectum	2	0.05	0.01
			M. kubicae	2	0.07	0.01
			M. lentiflavum	15	0.36	0.06
			M. parascrofulaceum	2	0.05	0.01
			M. simiae	22	0.52	0.08
			M. triplex	1	0.02	0.00
	Ungrouped NTM (Total)			41	0.98	0.16
			M. algericum	1	0.02	0.00
			M. aurum	1	0.02	0.00
			M. bacteremicum	1	0.02	0.00
			M. branderi	1	0.02	0.00
			M. celatum	1	0.02	0.00
			M. cosmeticum	4	0.10	0.02
			M. frederiksbergense	1	0.02	0.00
			M. iranicum	1	0.02	0.00
			M. nebraskense	2	0.05	0.01
			M. neoaurum	6	0.14	0.02
			M. paraffinicum	9	0.21	0.03
			M. pulveris	1	0.02	0.00
			M. sphagni	1	0.02	0.00
			M. szulgai	10	0.24	0.04
			M. vaccae	1	0.02	0.00

[a]Rate per 100,000 persons

Discussion

Case reports are the bedrock for disease surveillance in the U.S. Unfortunately, CDC's National Notifiable Disease Surveillance System (NNDSS) does not routinely collect data on NTM positive laboratory reports or disease cases on a national basis. In recent years, state health departments are allowing other public and private laboratories to submit reports into their disease surveillance systems due to the increase capability of private and public labs to identify NTMs in human specimens and improvements in electronic reporting. The state NTM data reports capture information that reflects potential respiratory infections among both the young and elderly, as well as, the poor and the uninsured population groups often underrepresented in studies of disease burden based on Medicare part B and/or health care insurance records. However, there are limitations to these state data. The NTM reports are not generally scrutinized for accuracy or completeness during data entry. The procedures for isolating the NTM species from the specimen could yield false positives due to laboratory contamination. In addition, more than one report could belong to the same individual if more than one specimen was collected during the course of a single disease episode in order to evaluate treatment efficacy. Thus, the NTM specimen reports can overestimate the burden of disease. Yet, the report rate of 13.3 per 100,000 is similar to 13.7 per 100,000 persons (North Carolina) [12] and 17.2 reports per 100,000 persons (Oregon) [11] other estimates of NTM prevalence in the U.S. Additionally, the estimate of 50,976 NTM reports in the U.S. per annum derived by using the state NTM reports is of the same order of magnitude as the estimated 86,244 cases identified using Medicare part B records [24]. Multiple lines of evidence demonstrate an increase in NTM prevalence [1–3] and report rates [12], strengthening the conclusion that NTM infections in the U.S. have increased. These lines of evidence also elevate the concern for NTM-related diseases in the U.S., identifying a need to search for controllable sources of exposure that will guide risk mitigation measures [25].

In this study, fifty-two NTM species were identified from human specimens. Twenty eight percent (52/186) of recognized NTM species are represented in the specimen reports. The four most frequently identified NTM groups or species that were common across the four states were: MAC, *M. fortuitum*, *M. gordonae*, and *M. chelonae-abscessus* groups. This observation was supported by data from other regions and states within the U.S. [11, 12, 26].

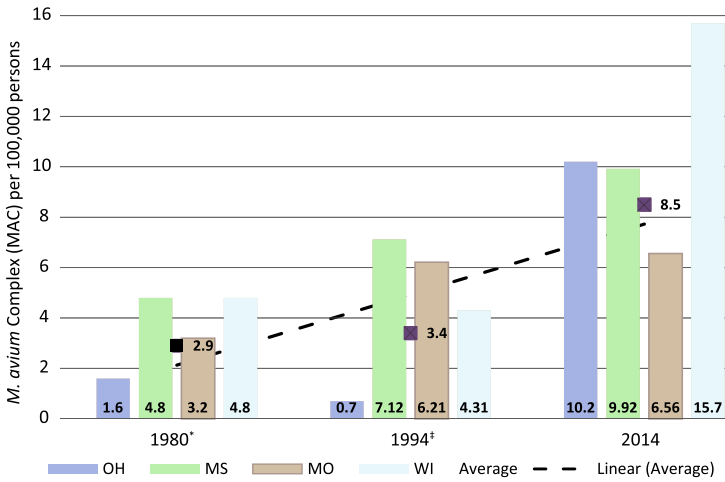

Fig. 1 Numbers, rates, and percent change of NTM reports by species, 1994 and 2014 comparison. See Table 2 for clarity on which NTM species were considered in each complex or group. *2014: *M. chelonae-abscessus* Group plus. *M. mucogenicum-phocaicum* report numbers were combined, ‡ NS = Not significant, § per 100,000 persons: 1994 population 23,795,000 (as reported by Butler and Crawford, 1999); 2014 population 26,414,700

The increase in the number of NTM positive reports is not solely due to population growth. From 1994 to 2014, the population in these four states increased by 2.1 million people. Using the CDC 1994 report rate of 8.2 per 100,000 persons [20], this population increase should have only added 172 reports. Instead the number of reports for the four states is 4200 positive reports. This number was greater than 2000 more reports than predicted. The reason for this increase is probably multifactorial. One important factor that likely led to the larger case count is the increase in electronic reporting by laboratories who perform sample analyses to state databases. Established common portals for data entry can be used by state laboratories, large research hospitals, as well as, commercial laboratories to facilitate improved record keeping. However, despite the impact of technology on better reporting, the increase in the number of reports is substantial enough to support the conclusion that more individuals are experiencing NTM related episodes impacting their health now than they did two decades ago.

NTM Species	1994 Number	1994 Rate§	2014 Number	2014 Rate§	P Value	Percent Change (rate)
M. chelonae-abscessus Group*	94	0.40	440	1.67	P = <0.001	321.6
M. smegmatis	1	0.00	4	0.02	NS‡	260.3
M. fortuitum Group	105	0.44	343	1.30	P = <0.001	194.2
M. avium Complex	816	3.43	2252	8.53	P = <0.001	148.6
M. malmoense	2	0.01	5	0.02	NS	125.2
M. szulgai	4	0.02	10	0.04	NS	125.2
M. simiae	14	0.06	22	0.08	NS	41.5
M. gordonae	573	2.41	689	2.61	P = <0.001	8.3
M. vaccae	1	0.00	1	0.00	NS	-9.9
M. xenopi	57	0.24	54	0.20	P = <0.001	-14.6
M. kansasii Clade	128	0.54	100	0.38	P = <0.001	-29.6
M. terrae	42	0.18	28	0.11	P = <0.001	-39.9
M. scrofulaceum	6	0.03	3	0.01	NS	-54.9
M. flavescens	6	0.03	0	0.00	P = 0.002	-100

* 2014: *M. chelaonae-absessus* Group plus. *M. mucogenicum-phocaicum* report numbers were combined.
‡ NS=Non-significant
§ per 100,000 persons: 1994 population 23,795,000 (as reported by Butler and Crawford), 1999; 2014 population 26,414,700

Fig. 2 Longitudinal analysis (1980–2014) of *M. avium* complex report rate per 100,000 persons for Mississippi, Missouri, Ohio, Wisconsin, and combined. * Butler and Crawford, 1999: 1994 rates

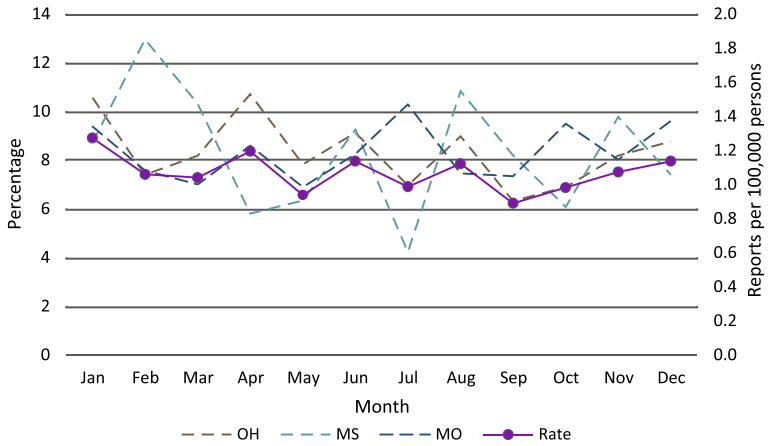

Fig. 3 NTM reports by state by month

There was an increase in the MAC positive reports from 3.4 per 100,000 in 1994 to 8.5 per 100,000 in 2014 (Fig. 2). Numerous factors could have contributed to the increase in prevalence including: increased medical awareness of NTM related infections/diseases, improvement of laboratory identification techniques, increases in exposure modalities and human activities associated with water and/or soils. The increased MAC detection rates for the four states suggest a need for improved risk communication efforts between the public health sector and populations at risk for NTM infections. The NTM family of microorganisms and their contribution to respiratory illnesses are seldom topics for the popular press and media. There is a need for a better communications strategy targeting the general population on both the signs and symptoms of NTM infections and measures that will help minimize risk.

The shifts in detection frequency for either an NTM group or species should be considered in any assessment of population risk. Not all NTM species have the same symptoms nor impact on human health. Species within the *M. chelonae-abscessus* and *M. fortuitum* groups are those commonly identified in "outbreak" investigations [27–29]. These outbreaks can include dermal infections of either the skin or soft tissue and pulmonary problems. Dermal signs and symptoms reported were immediate post contact rash onset, septic arthritis, or cutaneous infections of the skin [27–29]. The source of the infection is typically found to be a non-potable or potable water source that has been contaminated with NTMs. Species in the MAC grouping have been the most clinically significant because they cause the majority of NTM related illnesses and diseases [3, 30].

The increases in a state's population alone do not account for the increased number of cases reported by the state health departments. However, changes within the population can contribute to the increase. For example, a state population could contain more elderly individuals with co-morbidity factors such as COPD or people suffering from suppression of their immune response than in the past. Changes in routes of exposure are also important. MAC infections are usually respiratory, but not communicable [4]. Therefore, changes in bathroom construction that promote showering over bathing (especially for the elderly) increases the likelihood for inhalation exposure and infection when potable water is the source of transmission. A recent survey of NTM presence in tap water found 78% (202/258) of the samples collected were positive for NTM [31]. Since inhalation is believed to be the main route of exposure [4], the increased use of shower water aerators could also be an important feature associated with an increase in population exposure [32]. Recently, several publications [33] have outlined measures, such as, cleaning showerheads and removing aerators as protective measures for avoiding exposure to NTMs [34, 35].

There is no seasonal pattern to NTM reports. The lack of seasonality suggests exposure routes for illness and or disease occur year-round and may not be influenced by seasonal changes in activities of the at-risk population. This is probably due to the fact that pulmonary NTM lung infections and/or diseases are not acute illnesses. Common signs and symptoms of the respiratory problems are shortness of breath and fatigue [4]. These vague symptoms may not be addressed in a timely manner, lengthening the time between illness onset and consultation with a physician because of symptom persistence. This delay could potentially dampen the opportunity to link a positive specimen as a result of physician consultation to the time the symptoms were first noted. As a result, a potential NTM report is filed with the state long past the time of infection acquisition.

Conclusion

Knowledge of the NTM species most frequently associated with adverse human health consequences will assist epidemiological investigators to identify likely sources and modes of exposure associated with these types of infections. By identifying the sources of the NTM infections, strategies can be implemented to control for the occurrence of NTMs and/or procedures can be adopted to mitigate exposure routes associated with the risks. NTMs and their related disease manifestations result in a significant, medical, human health burden, especially among the elderly [2, 15]. As the U.S. population ages, the public health burden from NTM associated disorders is expected to increase. Thus, it is important to conduct research to identify the major exposure routes and environmental sources of dissemination to identify and implement practices that will limit human exposures to NTM infections.

Disclaimer

The United States Environmental Protection Agency through its Office of Research and Development funded and managed the research described here. It has been subjected to Agency's administrative review and approved for publication. The views expressed in this paper are those of the authors and do not necessarily reflect the views or policies of the United States Environmental Protection Agency.

Additional file

Additional file 1: Table S1. Nontuberculous mycobacteria reported by Missouri, 2014. **Table S2.** Nontuberculous mycobacteria reported by Mississippi, 2014; **Table S3.** Nontuberculous mycobacteria reported by Ohio, 2014. **Table S4.** Nontuberculous mycobacteria reported by Wisconsin, 2014. Provisional counts of NTM reports by State and NTM Species. (DOCX 26 kb)

Abbreviations

AIDS: Acquired immunodeficiency syndrome; ATS/IDSA: American thoracic society and infectious disease society of America; CDC: Center for disease control and prevention; COPD: Chronic obstructive pulmonary disease; MAC: *M. avium* complex; NNDSS: National notifiable disease surveillance system; NTM: Nontuberculous mycobacteria; U.S. EPA: United States environmental protection agency; U.S.: United States

Acknowledgements

The author sincerely thanks the state health departments of the states of, Mississippi, Missouri, Ohio and Wisconsin for their assistance with providing data and to Dr. Cynthia Yund for her mentorship.

Funding

The author received no funding for this research.

Availability of data and materials

All data analyzed during this study are included in this published article, and its Additional files.

Author's contributions

The author met all four criteria for authorship suggested by the international committee of journal editors. Study concept and design, acquisition of data, analysis and interpretation of data, drafting of the manuscript, critical revision of the manuscript for important intellectual content, and statistical analysis: MJD. The author read and approved the final manuscript.

Ethics approval and consent to participate

This study was determined to be exempt from Institution review board review by United States environmental protection agency.

Consent for publication

Not applicable.

Competing interests

The author declare that they have no competing interests.

Publisher's Note

Springer Nature remains neutral with regard to jurisdictional claims in published maps and institutional affiliations.

Received: 13 November 2017 Accepted: 12 March 2018
Published online: 10 April 2018

References

1. Adjemian J, Olivier KN, Seitz AE, Holland SM, Prevots DR. Prevalence of nontuberculous mycobacterial lung disease in U.S. Medicare beneficiaries. Am J Respir Crit Care Med. 2012;185(8):881–6.
2. Donohue MJ, Wymer L. Increasing prevalence rate of nontuberculous mycobacteria infections in five states, 2008-2013. Ann Am Thorac Soc. 2016; 13(12):2143–50.
3. Prevots DR, Shaw PA, Strickland D, Jackson LA, Raebel MA, Blosky MA, Montes de Oca R, Shea YR, Seitz AE, Holland SM, et al. Nontuberculous mycobacterial lung disease prevalence at four integrated health care delivery systems. Am J Respir Crit Care Med. 2010;182(7):970–6.
4. Griffith DE, Aksamit T, Brown-Elliott BA, Catanzaro A, Daley C, Gordin F, Holland SM, Horsburgh R, Huitt G, Iademarco MF, et al. An official ATS/IDSA statement: diagnosis, treatment, and prevention of nontuberculous mycobacterial diseases. Am J Respir Crit Care Med. 2007;175(4):367–416.
5. Olivier KN, Weber DJ, Lee JH, Handler A, Tudor G, Molina PL, Tomashefski J, Knowles MR, Nontuberculous Mycobacteria in Cystic Fibrosis Study G. Nontuberculous mycobacteria. II: nested-cohort study of impact on cystic fibrosis lung disease. Am J Respir Crit Care Med. 2003;167(6):835–40.
6. Huang CT, Tsai YJ, Wu HD, Wang JY, Yu CJ, Lee LN, Yang PC. Impact of non-tuberculous mycobacteria on pulmonary function decline in chronic obstructive pulmonary disease. Int J Tuberc Lung Dis. 2012;16(4):539–45.
7. Lewis AG Jr, Dunbar FP, Lasche EM, Bond JO, Lerner EN, Wharton DJ, Hardy AV, Davies R. Chronic pulmonary disease due to atypical mycobacterial infections. Am Rev Respir Dis. 1959;80:188–99.
8. Horsburgh CR Jr, Selik RM. The epidemiology of disseminated nontuberculous mycobacterial infection in the acquired immunodeficiency syndrome (AIDS). Am Rev Respir Dis. 1989;139(1):4–7.
9. Petrini B, Svahn A, Julander I, Kallenius G, Ostlund L. Prevalence of mycobacterium avium complex infection in AIDS patients. Scand J Infect Dis. 1991;23(4):511–2.
10. Gruft H, Loder A, Osterhout M, Parker BD, Falkinham JO 3rd. Postulated sources of Mycobacterium intracellulare and Mycobacterium scrofulaceum infection: isolation of mycobacteria from estuaries and ocean waters. Am Rev Respir Dis. 1979;120(6):1385–8.
11. Cassidy PM, Hedberg K, Saulson A, McNelly E, Winthrop KL. Nontuberculous mycobacterial disease prevalence and risk factors: a changing epidemiology. Clin Infect Dis. 2009;49(12):e124–9.
12. Smith GS, Ghio AJ, Stout JE, Messier KP, Hudgens EE, Murphy MS, Pfaller SL, Maillard JM, Hilborn ED. Epidemiology of nontuberculous mycobacteria isolations among Central North Carolina residents, 2006-2010. J Infect. 2016; 72(6):678–86.
13. Bryant JM, Grogono DM, Parkhill J, Floto RA. Transmission of M abscessus in patients with cystic fibrosis – Authors' reply. Lancet. 2013;382(9891):504.
14. Bryant JM, Grogono DM, Rodriguez-Rincon D, Everall I, Brown KP, Moreno P, Verma D, Hill E, Drijkoningen J, Gilligan P, et al. Emergence and spread of a

human-transmissible multidrug-resistant nontuberculous mycobacterium. Science. 2016;354(6313):751–7.
15. Winthrop KL, Varley CD, Ory J, Cassidy PM, Hedberg K. Pulmonary disease associated with nontuberculous mycobacteria, Oregon, USA. Emerg Infect Dis. 2011;17(9):1760–1.
16. du Moulin GC, Sherman IH, Hoaglin DC, Stottmeier KD. Mycobacterium avium complex, an emerging pathogen in Massachusetts. J Clin Microbiol. 1985;22(1):9–12.
17. Parte AC. LPSN—list of prokaryotic names with standing in nomenclature. Nucleic Acids Res. 2014;42(D1):D613–D616. https://doi.org/10.1093/nar/gkt1111. http://www.bacterio.net. Accessed 19 Mar 2018.
18. Manual of clinical microbiology, Eleventh edn. In: Jorgensen JH, Pfaller MA, Carroll KC, Funke G, Landry ML, Richter SS, Warnock DW, editors. Washington: ASM Press; 2015.
19. Pfyffer GE, Welscher HM, Kissling P, Cieslak C, Casal MJ, Gutierrez J, Rusch-Gerdes S. Comparison of the mycobacteria growth Indicator tube (MGIT) with radiometric and solid culture for recovery of acid-fast bacilli. J Clin Microbiol. 1997;35(2):364–8.
20. Butler WR, Crawford JT. Nontuberculous mycobacteria reported to the public health laboratory information system by state public health laboratories United States, 1993-1996: Georgia: Centers for Disease Control and Prevention, National Center for Infectious Diseases; 1999. p. 1–51.
21. Good RC. From the Center for Disease Control. Isolation of nontuberculous mycobacteria in the United States, 1979. J Infect Dis. 1980;142(5):779–83.
22. Good RC, Snider DE Jr. Isolation of nontuberculous mycobacteria in the United States, 1980. J Infect Dis. 1982;146(6):829–33.
23. Butler WR, Guthertz LS. Mycolic acid analysis by high-performance liquid chromatography for identification of Mycobacterium species. Clin Microbiol Rev. 2001;14(4):704–26. table of contents
24. Strollo SE, Adjemian J, Adjemian MK, Prevots DR. The burden of pulmonary nontuberculous mycobacterial disease in the United States. Ann Am Thorac Soc. 2015;12(10):1458–64.
25. Bergey's manual of systematic bacteriology, 5, 2nd. New York: Springer-Verlag; 2012.
26. Henkle E, Hedberg K, Schafer S, Novosad S, Winthrop KL. Population-based incidence of pulmonary nontuberculous mycobacterial disease in Oregon 2007 to 2012. Ann Am Thorac Soc. 2015;12(5):642–7.
27. D'Antonio S, Rogliani P, Paone G, Altieri A, Alma MG, Cazzola M, Puxeddu E. An unusual outbreak of nontuberculous mycobacteria in hospital respiratory wards: association with nontuberculous mycobacterial colonization of hospital water supply network. Int J Mycobacteriol. 2016;5(2):244–7.
28. Jung SY, Kim BG, Kwon D, Park JH, Youn SK, Jeon S, Um HY, Kwon KE, Kim HJ, Jung HJ, et al. An outbreak of joint and cutaneous infections caused by non-tuberculous mycobacteria after corticosteroid injection. Int J Infect Dis. 2015;36:62–9.
29. Kennedy BS, Bedard B, Younge M, Tuttle D, Ammerman E, Ricci J, Doniger AS, Escuyer VE, Mitchell K, Noble-Wang JA, et al. Outbreak of Mycobacterium chelonae infection associated with tattoo ink. N Engl J Med. 2012;367(11):1020–4.
30. Bodle EE, Cunningham JA, Della-Latta P, Schluger NW, Saiman L. Epidemiology of nontuberculous mycobacteria in patients without HIV infection, new York City. Emerg Infect Dis. 2008;14(3):390–6.
31. Donohue MJ, Mistry JH, Donohue JM, O'Connell K, King D, Byran J, Covert T, Pfaller S. Increased frequency of nontuberculous mycobacteria detection at potable water taps within the United States. Environ Sci Technol. 2015; 49(10):6127–33.
32. Hines SA, Chappie DJ, Lordo RA, Miller BD, Janke RJ, Lindquist HA, Fox KR, Ernst HS, Taft SC. Assessment of relative potential for legionella species or surrogates inhalation exposure from common water uses. Water Res. 2014; 56:203–13.
33. Nishiuchi Y, Iwamoto T, Maruyama F. Infection sources of a common non-tuberculous mycobacterial pathogen, Mycobacterium avium complex. Front Med. 2017;4:27.
34. Falkinham JO 3rd. Current epidemiologic trends of the nontuberculous mycobacteria (NTM). Curr Environ Health Rep. 2016;3(2):161–7.
35. Thomson R, Tolson C, Carter R, Coulter C, Huygens F, Hargreaves M. Isolation of nontuberculous mycobacteria (NTM) from household water and shower aerosols in patients with pulmonary disease caused by NTM. J Clin Microbiol. 2013;51(9):3006–11.

Submit your next manuscript to BioMed Central and we will help you at every step:

- We accept pre-submission inquiries
- Our selector tool helps you to find the most relevant journal
- We provide round the clock customer support
- Convenient online submission
- Thorough peer review
- Inclusion in PubMed and all major indexing services
- Maximum visibility for your research

Submit your manuscript at
www.biomedcentral.com/submit

BioMed Central

Increasing Prevalence Rate of Nontuberculous Mycobacteria Infections in Five States, 2008–2013

Maura J. Donohue and Larry Wymer

U.S. Environmental Protection Agency, Office of Research and Development, National Exposure Research Laboratory, Cincinnati, Ohio

ORCID ID: 0000-0001-5584-8680 (M.J.D.).

Abstract

Rationale: Many nontuberculous mycobacteria (NTM) are clinically significant pathogens that cause disease in a variety of different human organs and tissues.

Objectives: A population-based study was undertaken to investigate the prevalence of patients with a positive specimen for NTM within five states of the United States.

Methods: We determined the case and age distribution of patients with at least one specimen positive for NTM, using data submitted to the disease surveillance systems of five states (Maryland, Mississippi, Missouri, Ohio, and Wisconsin) between 2008 and 2013. Crude, age-specific, and age-adjusted prevalence rates per 100,000 persons were calculated for each state.

Measurements and Main Results: From 2008 to 2013, a total of 24,226 NTM cases were reported to the disease surveillance systems of the five states. The overall average annual age-adjusted prevalence rate rose from 8.7 to 13.9 per 100,000 persons between the beginning and end of the surveillance period. The number of cases and case rate in the 50–80+-year age group was higher than in the 0–49-year age group. Prevalence by age category differed among the five states. The highest number of NTM cases was observed in Mississippi for the 80+-year age group, whereas Wisconsin observed the highest number of NTM cases in the 60- to 69-year age group.

Conclusions: From 2008 to 2013, the number of patients with positive specimens for NTM rose. This trend is likely to continue in the coming decade as the U.S. population ages. To reduce the prevalence of NTM infections, medical guidance for susceptible populations is needed regarding actions that can be taken to avoid sources and routes of exposure to NTMs if the disease burden is to be reduced.

Keywords: nontuberculous mycobacteria; epidemiology; prevalence; United States

(Received in original form May 10, 2015; accepted in final form September 2, 2016)

The U.S. Environmental Protection Agency, through its Office of Research and Development, funded and managed the research described here. It has been subjected to agency's administrative review and approved for publication. The views expressed in this paper are those of the authors and do not necessarily reflect the views or policies of the U.S. Environmental Protection Agency.

Author Contributions: Study concept and design, M.J.D.; acquisition of data, M.J.D. and L.W.; analysis and interpretation of data, M.J.D. and L.W.; drafting of the manuscript, M.J.D.; critical revision of the manuscript for important intellectual content: M.J.D. and L.W.; and statistical analysis, M.J.D and L.W.

Correspondence and requests for reprints should be addressed to Maura J. Donohue, Ph.D., U.S. Environmental Protection Agency, 26 W. Martin Luther King Drive, Mail Stop 587, Cincinnati, OH 45268. E-mail: Donohue.maura@epa.gov

Ann Am Thorac Soc Vol 13, No 12, pp 2143–2150, Dec 2016
Copyright © 2016 by the American Thoracic Society
DOI: 10.1513/AnnalsATS.201605-353OC
Internet address: www.atsjournals.org

Nontuberculous mycobacteria (NTM) infections and/or diseases include chronic bronchopulmonary disease (NTM lung disease), cervical or other lymphadenitis, skin and soft tissue diseases, skeletal infections, disseminated infections, and catheter-related infections (1). In the 1950s, NTM became a clinically significant bacterium because of its repeated isolation from patients experiencing respiratory symptoms similar to those caused by *Mycobacterium tuberculosis* (TB). Among all the NTM-associated infections and diseases, respiratory-related infections are the most common. In the general population, women aged 50 years or older carry the greatest burden for NTM infections and/or diseases (2). Patients with HIV^+/AIDS (3, 4) and those with cystic fibrosis (5) are susceptible.

Unlike tuberculosis, NTM infections and/or diseases are not thought to be passed directly from person to person. Instead, these environmental microorganisms seem to be transmitted to humans from nonbiological sources by inhalation or contact with contaminated water or soil particles. NTMs have thick, waxy cell walls that cause them to partition out of water and adhere to surfaces (biofilms). This protects

them from inactivation by common microbial disinfectants and high temperatures (6). Thus, they can colonize potable water distributions systems, including household and facility plumbing.

In a recent paper, Donohue and colleagues reported that nearly all the samples they collected at water faucets from homes and facilities were positive for NTM. *Mycobacterium avium*, *Mycobacterium abscessus*, and *Mycobacterium mucogenicum* persisted at many of the locations, based on their detection in two or more samples collected from the same location and tap at intervals separated by months (7).

Both *M. avium* and *M. abscessus* are clinically relevant species. These two species are the etiological agents most often responsible for causing NTM lung disease in the United States (8–10). The study by Donohue and coauthors indicated that exposure can potentially occur daily and repeatedly as a result of the persistence of the microorganisms in potable water at points of use, such as kitchen and bathroom faucets and drinking water fountains (7).

Prevalence is a measure of the amount of an infection and/or disease within a given population. In the United States, few institutions (e.g., health departments, state and/or federal agencies) track NTM cases. In 1981–1983, a U.S. national estimate of NTM prevalence, as defined by an individual with an NTM culture-positive specimen, was 2.4 cases per 100,000 (5,469 cases/228.5 million people) (11). In recent years, only a few studies tried to estimate a population-based prevalence of NTM. At this time, the reported rates range from 12.6 to 17.3 cases per 100,000 persons (12, 13). However, these estimates are limited in scope and reflect the prevalence of NTMs only in one particular state (10, 13–15), region (9, 16, 17), or hospital (12, 18). Because prevalence of NTM infections and diseases varies greatly across the United States, it is important to evaluate NTM prevalence on a state-by-state basis (12, 13, 17, 18).

This study was conducted to estimate the population-based prevalence of NTM cases from five states (Missouri, Mississippi, Maryland, Ohio, and Wisconsin) during a period of 6 years. For each state, age-specific rates were calculated and assessed for differences and general trends associated with age.

Methods

Study Design

An internet and literature search was conducted to identify states that included NTM cases on their reportable disease list. Six states were identified (Figure 1). On all states' Reportable Disease Lists, NTM infections are classified as Mycobacteria Disease Other than Tuberculosis (MOTT). Five of the six states confirmed that they collected case reports on NTM. Although NTM is listed on Virginia's Reportable Disease List, the NTM reports were not electronically accessible at the time of the

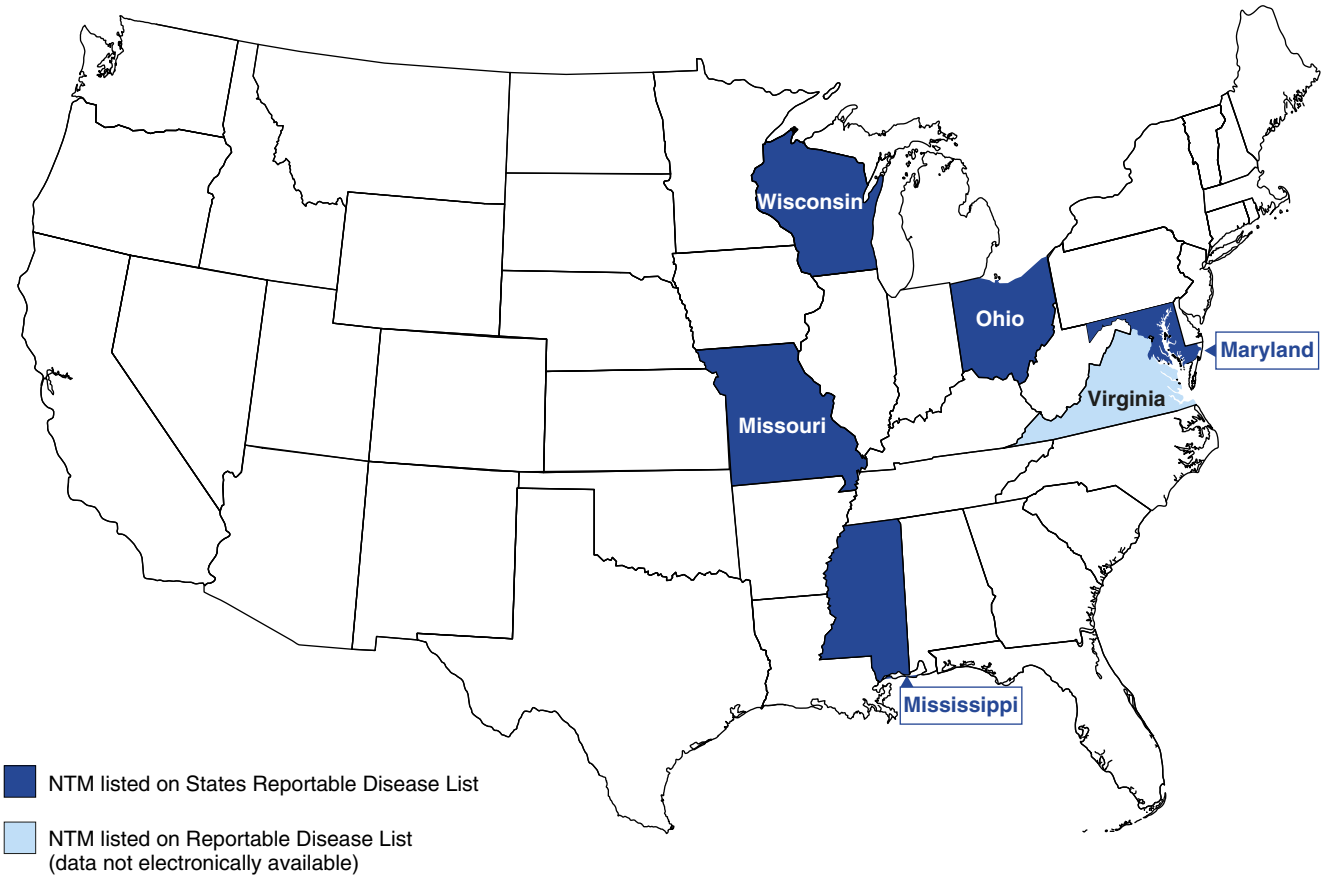

Figure 1. States that collect data on nontuberculous mycobacteria cases.

data request. Each state's disease surveillance network is populated with reports from state and commercial laboratories and hospitals.

In each of the five states from which data were available for our analysis, the health department compiled the number of cases by the following age groups: 0–39, 40–49, 50–59, 60–69, 70–79, and ⩾80 years, and unknown. From each state, the U.S. Environmental Protection Agency received only a spreadsheet containing the number of NTM cases by age group; no personal identifiers were given. In this report, the terms "case" and "infection" refer to a unique individual who gave a specimen that was determined to be culture-positive for NTM.

Laboratory procedures for NTM identification were similar across the five states. A portion of the specimen was used to inoculate growth media (Lowestein-Jensen, Middlebrook 7H9, or Mycobacteria Growth Incubation Tubes broth) (BD & Company, Franklin Lakes, NJ). After 3–10 days of growth, an acid-fast smear was performed. Simultaneously, the culture was prepped for high-performance liquid chromatography analysis to determine the identity of the NTM. If the isolate was not identified by that technique, Accuprobes (Hologic Inc., Marlborough, MA), PCR, DNA sequencing, or biochemical analysis was performed to support classification. This study was exempted from institutional review board review by the U.S. Environmental Protection Agency.

U.S. 2010 Census demographic data (total population, age, and sex) were collected from the U.S. Census Bureau for each state: Maryland, Mississippi, Missouri, Ohio, and Wisconsin. Populations for each age group were supplied by U.S. Census Bureaus' American fact finder (8). The 2010 Census data were used for the prevalence analysis because this census year falls in the timeframe of collected state data.

Statistical Analyses

A crude prevalence rate of number of cases per 100,000 residents was calculated for each state, using July 1, 2010, population estimates. The annual age-specific rates were calculated using the following equation: ([total number of cases in each age group/state's 2010 population within the age group]/6 years). The age-adjusted prevalence rates were standardized against the U.S. 2000 population weighted age distribution. Resulting rates were summed (19). The changes in annual prevalence numbers across the period were calculated in Microsoft Excel. Standard regression and ordinal logistics were used to model the prevalence rate as a function of year (time) and by state. In addition, one-way ANOVA and 95% confidence intervals (95% CIs) were determined using SAS 9.3/SAS STAT 12.1.

Results

Overall Age-Adjusted Prevalence

In total, 24,226 NTM cases were reported by the five states between 2008 and 2013. The combined population from these states represented 10.3% of the U.S. population in 2010. Overall, the 6-year prevalence was 75.8 cases per 100,000 persons or 12.6 cases per 100,000 persons per year. In Table 1, crude, age-adjusted prevalence rates and the number of cases reported by each state are provided.

The age-adjusted prevalence rate when averaged for the five states ranged from 8.7 cases per 100,000 persons (95% CI, 5.7–12.8 cases per 100,000 persons) in 2008 to 13.9 cases per 100,000 persons (95% CI, 9.2–19.6 cases per 100,000 persons) in 2013 (Table 1). The annual percentage change across these five states was a positive 9.9% increase per year. The increase in the annual number of cases per year across the 5 years was significant ($P < 0.001$) for all age groups and for the 50–80+ age groups. The slight positive increase for the 0–49 age group was not significant (Figure 2).

NTM infections are more common in the elderly than in the young. Age-related changes in prevalence were examined, using the data for different age groups provided to the U.S. Environmental Protection Agency by the states (Figure 2). In 2008, the prevalence rate for the 50–80+ age

Table 1. Annual patient prevalence of nontuberculous mycobacteria, 2008–2013

State*	State population (thousands)†	Data type	Prevalence (total number of patients (cases/100,000 population) reported each year					
			2008	2009	2010	2011	2012	2013
Maryland	5,773.6	Crude‡	9.9 (574)	7.8 (449)	6.2 (359)	6.6 (383)	8.7 (504)	9.6 (556)
		Adjusted§	9.5	7.4	5.9	6.2	8.4	9.2
Mississippi	2,967.3	Crude	10.5 (313)	11.4 (339)	13.9 (413)	12.0 (355)	13.4 (397)	14.1 (419)
		Adjusted	10.2	11.1	13.6	11.7	12.9	13.6
Missouri	5,988.9	Crude	6.0 (358)	16.8 (1,005)	5.5 (327)	15.5 (931)	11.8 (709)	14.6 (876)
		Adjusted	5.5	15.5	4.9	14.4	10.8	13.3
Ohio	11,536.5	Crude	6.5 (749)	8.2 (947)	11.4 (1,319)	11.2 (1,197)	11.9 (1,365)	12.7 (1,469)
		Adjusted	5.8	7.4	10.0	9.1	10.5	11.3
Wisconsin	5,687.0	Crude	16.7 (951)	20.9 (1,187)	23.0 (1,309)	23.7 (1,350)	27. 8 (1,582)	27.0 (1,534)
		Adjusted	15.4	18.9	21.2	21.5	25.4	24.6
Total	31,953.3	Crude	9.2 (2,945)	12.3 (3,927)	11.7 (3,727)	13.2 (4,216)	14.3 (4,557)	15.2 (4,854)
		Adjusted	8.7	11.3	10.6	12.1	13.1	13.9

*State Health Department Provided Disclaimers: Maryland, case counts are provisional; Mississippi, case counts are provisional; Missouri, case counts are provisional; Ohio, some cases reports may contain more than one organism and some people may have two or more laboratory results in a cases that should have been reported as separate; and Wisconsin, case counts are provisional.
†U.S. Census 2010.
‡Crude prevalence rate as reported by the state (number of cases).
§Age-adjusted value is the sum age-adjusted numbers provided by each state.

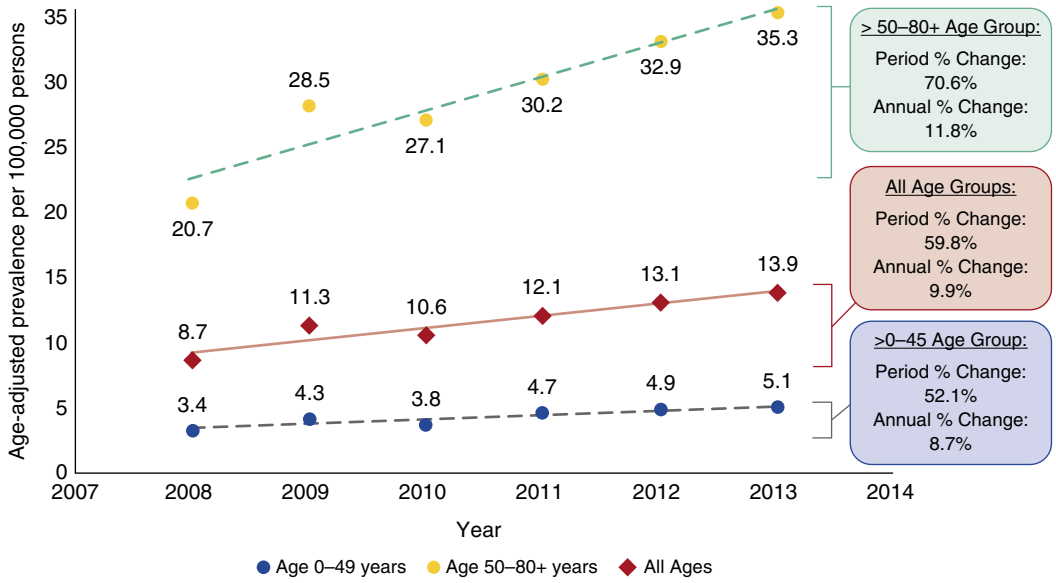

Figure 2. The average age-adjusted annual prevalence of nontuberculous mycobacteria case rate per 100,000 persons. Brackets show the range of change from 2008 to 2013.

group started at 20.7 cases per 100,000 persons (95% CI, 14.4–31.6 cases per 100,000 persons) and climbed to 35.3 cases per 100,000 persons (95% CI, 23.8–49.7 cases per 100,000 persons) by 2013. This was a 70.6% increase over the course of 6 years, for an 11.8% increase per year.

The younger age group of 0–49 years had an 8.7% increase in cases per year. In 2008, the 0–49-year age group started at 3.4 cases per 100,000 persons (95% CI, 1.7–5.3 cases per 100,000 persons) and rose to 5.1 cases per 100,000 persons (95% CI, 2.9–7.4 cases per 100,000 persons) by 2013 (Figure 2). These two age groups showed the annual increased rate for the 50–80+ age group and the 0–49-year age group to be 2.6 and 0.3 cases per 100,000 persons, respectively. Both standard regression ($P > 0.0017$) and ordinal logistics ($P > 0.0002$) modeling of the data showed year (time) variable to be highly significant. The state variable and year/state interaction ($P > 0.3$ and $P > 0.998$) were not significant predictors of prevalence.

Age-Adjusted Prevalence by State

Each state had its own unique trend during the 6-year period. The yearly prevalence rate was most variable for Missouri. Both Ohio and Wisconsin saw a steady increase in prevalence across the 6-year period. Population-adjusted prevalence values were relatively stable for Maryland and Mississippi. Regression and ordinal logistics analysis of the data indicated that there were no statistical differences in slope across the five states. Therefore, on average, each state independently observed an increase of one case per 100,000 persons per year (95% CI, 0.38–1.45).

Age-Specific Rates by State

Between 2008 and 2013, age-specific rates of NTM cases were as expected. In general, the number of cases increased with age (Figure 3). The age group that had the lowest average case rate was the 0–39-year age group, at 3 cases per 100,000 persons. The age group that had the highest average case rate was the >80+ age group, with 64 NTM cases per 100,000. Maryland, Missouri, and Ohio had very similar age-specific rates, yet there were some unique trends seen in Mississippi and Wisconsin. An 84% change in rate was observed between the 70–79 and the 80+ age groups in Mississippi. Although most other states saw a modest rise of 11–24% between these two age groups, Wisconsin had a very different age-specific profile than the other states. The 70–79 age group had the highest rate of 90 cases per 100,000 persons.

Discussion

National and state reportable disease lists track diseases that affect the population. These lists name specific microorganisms and diseases of known clinical importance. NTM is not a nationally recognized reportable disease. However, in Maryland, Mississippi, Missouri, Ohio, and Wisconsin, NTM infections are reportable at a state level. In most of these states, cases are from laboratory surveillance, where a patient has submitted a specimen that tested positive for NTM. The states use the NTM information for a variety of purposes other than tracking NTM infections among their respective populations.

Although many entities (state and commercial laboratories and large hospitals) submit reports into the state's disease surveillance network, the likelihood of NTM being underreported is still high because of state budget restrictions and lack of resources. States' epidemiologists primarily use NTM reports to find TB cases and to clarify the AIDS/HIV status of their patient population. Mississippi's health department observed that 3% of all TB cases have, at one time, an NTM-positive specimen. According to the independent reports from the states, the yearly increases in cases is strong enough ($P < 0.001$ by regression analysis) to support the conclusion that NTM infections are becoming more common in the United States.

Early epidemiological studies of NTM used both isolate reports and patient

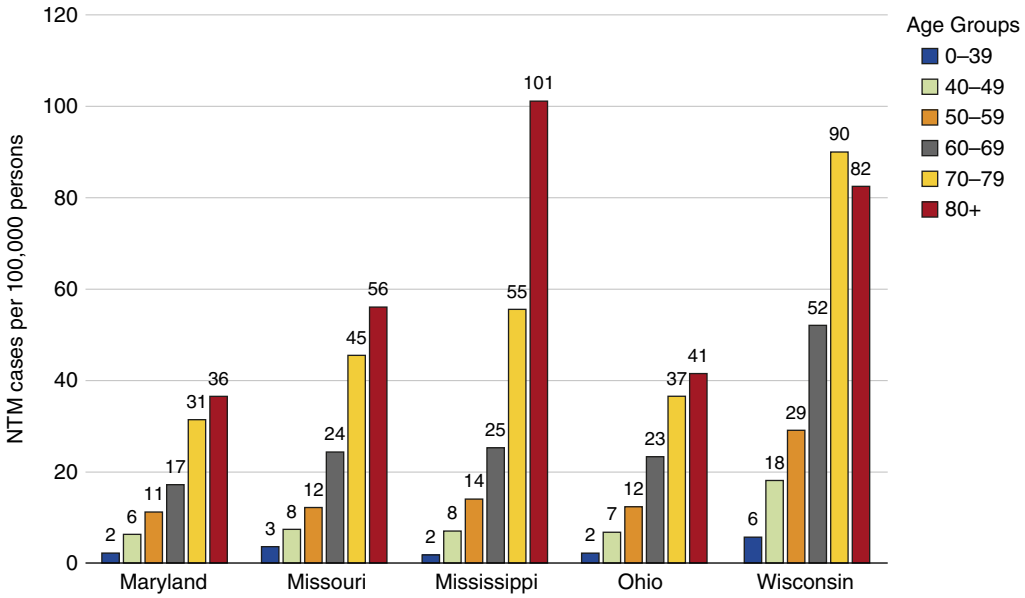

Figure 3. Nontuberculous mycobacteria case age-specific rates by state for the years 2008–2013.

numbers as a way to examine the prevalence of NTM disease in a population. In the case of NTM, isolation-based numbers can overestimate the prevalence of NTM disease in a population because more than one species of NTM can be isolated from a single specimen, and not all individuals who produce a specimen that grows an NTM have an NTM disease requiring medical treatment. An approach that has been taken to distinguish between an individual in the "infection state" (which may or may not require treatment) vs the "disease state" is to apply the 2007 American Thoracic Society's (ATS)/Infectious Disease Society of America (IDSA)'s microbiological criteria to the isolation base numbers (9, 13). Unfortunately, applying ATS/IDSA's microbiological criteria was not done to this data set because each state provided only the number of cases per age group, and not the number of isolates per case.

The other approach used to estimate NTM prevalence is patient-level data. This approach reduces the overestimation in isolation rates, but can lead to overestimating NTM lung disease prevalence. This is a result of inclusion of patient-level data for NTM infection of tissues other than the lungs. Patient-level data provide information about the number of people within a population who had symptoms and a positive specimen result for NTM. Although this study did not investigate the anatomic site of infection, other population-based studies have shown that pulmonary specimens (sputum, lavage, etc.) account for roughly 77–93% of the reported cases (13, 20).

A study by O'Brien and colleagues of NTM disease in the United States in 1981–1983 (11) was used to discern whether the state-provided case numbers by age were reasonable. The O'Brien study used state reports on the number of patients with an NTM-positive specimen from 46 centers in 33 states, using a methodology that is similar to that used in the current study. Interestingly, the study demonstrated the same bimodal case by age distribution (Figure 4) observed in this study. The similarity in the distribution of cases between this study and O'Brien and coauthors demonstrates that the patient-level data are a viable tool for examining NTM's effect on a population. A more detailed analysis of the two data sets is not possible because in 2007, ATS/IDSA changed the NTM lung disease criteria (1).

In this study, the total NTM prevalence increased between 2008 and 2013 from 8.7 to 13.9 cases per 100,000 persons. These values are consistent with those reported by other studies. Cassidy and colleagues (13) reported an average of 12.5 cases per 100,000 persons in 2005–2006, and Smith and colleagues (15) reported an average of 15.9 cases per 100,000 persons in 2006–2010. Marras and colleagues and Al Houquani and colleagues studied NTM patient prevalence in Ontario, Canada, in 1997–2003, 2007, and 1998–2010. They observed a 6.3% annual increase in number of patients with a positive NTM specimen, from 12.4 persons per 100,000 in 1997 to 22.2 persons per 100,000 persons by 2010 (20–22). These values are higher than those in this study and in other U.S.-focused studies, but still support the outcome reported here.

The five states in the current study all had different patient prevalence rates. Wisconsin had the highest prevalence of the five states. It is similar to those from the three Ontario studies. This is not surprising because Wisconsin and Ontario are geographically in the same region, both bordering the North American Great Lakes. Adjemian and colleagues identified Milwaukee, Wisconsin, and other regions as high-risk areas for NTM lung disease (16). This result is corroborated by the 2013 Wisconsin data: 57% of the patients reporting an NTM-positive specimen in the state came from Milwaukee County (23). The Adjemian study identified environmental risk factors such as evapotranspiration, population density, and higher levels of copper and sodium in the soil as predictive for a high risk for pulmonary NTM disease (16). The states of Mississippi, Missouri, and Ohio had

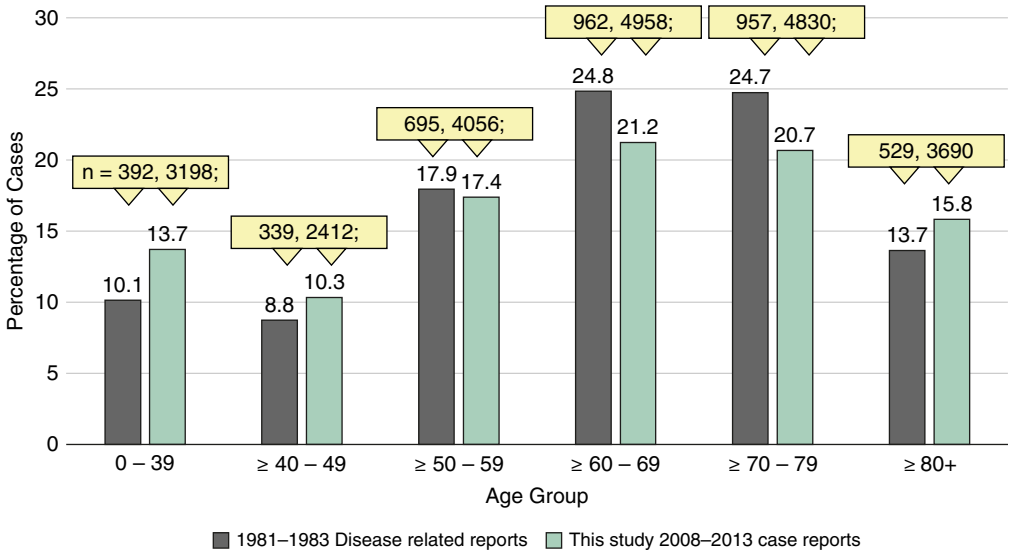

Figure 4. Comparison of the distribution of nontuberculous mycobacteria cases (total) by age group. The box contains the raw "n" values for each bar.

similar patient prevalence rates (14.4, 13.8, and 11.9 cases per 100,000 persons, respectively) in 2013.

The distributions of the NTM age-specific rates are similar, but slight differences do exist across the five states (Figure 3). These differences suggest there are factors other than age that could influence the rate in a particular age group. NTMs are environmental bacteria. Their natural habitat is soil and water. The hydrology of these 5 states differs; this can influence environmental distributions of NTM and patterns of exposure.

In addition, although these states have no significant population difference by age groups, they do have differences by race and industry. Maryland and Mississippi have a higher black population, at 29% and 37%, respectively, compared with Ohio and Wisconsin, at 12% and 6%, respectively (8). These states also have different industries that make up their economic base and that could influence the prevalence of NTM infections. Metalworkers are prone to NTM respiratory infections (24, 25). Differences in demographics and occupations can affect the potential for NTM infections and/or disease within a state. The information from the state Reportable Disease Registries do not provide the data necessary to quantitatively or qualitatively determine the potential effect of these variables on the similarities and differences in the prevalence outcomes between states.

Examining population trends can help identify the effect an infection or disease rate can have on risk for the population as a whole. NTM infections and/or diseases predominantly affect the elderly. In 2011, the front edge of the baby boomer (1946–1964) generation became 65 years old. This generation is now entering the age range with an increased risk for NTM infections and/or diseases (Figure 5). The baby boomers have a higher percentage of females than males, and approximately 60% suffer from at least one chronic disease (cancer, chronic lower respiratory disease, diabetes, hypocholesteremia, hypertension, and obesity) (26). These chronic diseases are often cause of death in the elderly and those 55–64 years old, and potentially contribute to their susceptibility to NTM exposures.

There is a known relationship between chronic obstructive pulmonary disease, which is included in the chronic lower respiratory disease category, and lung disease resulting from NTM (5, 9, 27–31). In a recent report published by the U.S. Health and Human Services, chronic lower respiratory disease-related deaths have risen from 56,050 (rank 5 as a leading cause of death) in 1980 to 149,205 (rank 3) in 2013 (26). By 2025, 25% of the U.S. population will be older than 60 years. This future demographic trend will likely increase the prevalence of NTM infections and/or diseases in the United States in the years to follow (Figure 5), adding to the cost of medical care for the elderly.

Whether the observed increase in the number of patients with a positive NTM specimen is the result of new exposure routes is largely unknown. Activities that may increase a person's exposure to NTM can include hobbies (e.g., gardening), water use patterns (e.g., humidifiers, showering, and water aerobics), and facilities visited (e.g., medical facilities, thermal spas, large retirement facilities). The 2015 study by Donohue and coauthors found NTM in 78% of the "at the tap" potable water samples tested, providing evidence that potable water is a major potential source of NTM exposure. Both the frequency of NTM detection and colony counts were higher than observed in earlier studies (7, 32).

As the number of patients with NTM increases, the amount of money spent on diagnosis and treatment will climb. With approximately 47,510–52,739 persons currently affected (with 47,510 persons in 2014, the persons [age-adjusted] = [estimated prevalence rate for 0–49 years of age, 2014] × [2014 estimated 0–49 age population] + [estimated prevalence rate for ⩾50–80+ years of age, 2014] × [2014 estimated ⩾50–80+ years age population] or 52,739 persons = [(0.054 × 209,565.5 thousand persons) + (0.379 × 109,291.6 thousand persons] and 2014, persons (general population) = [estimated prevalence rate in 2014] × [estimated U.S. population in 2014] or 47,510 persons = [0.149] × [318,857.1 thousand persons]) and average doctor's visits having a level

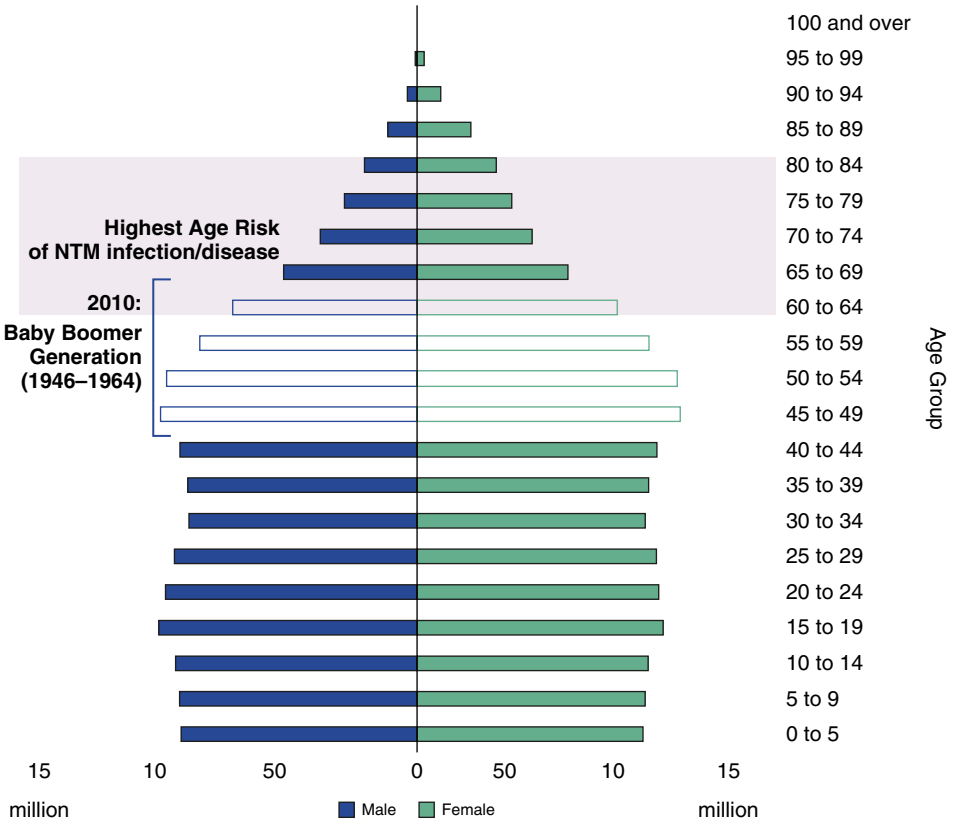

Figure 5. U.S. 2010 population by age and sex. NTM = nontuberculous mycobacteria.

3 visit cost of $139/visit (2015) (33), an estimated $6.6 to $7.3 million per year will be spent on the care of patients who are culture-positive for NTM. Once hospitalization is required, the financial cost increases significantly. Strollo and colleagues estimated that in 2014, 1.4 billion dollars was spent on the treatment of NTM pulmonary disease in the United States (34).

To help reduce the costly healthcare effect of NTM infections and improve the population quality of life, the need to expand surveillance on a national basis is increasingly important. Identifying areas affected by NTM, understanding which NTM species are causing the most disease, and determining whether there are seasonal factors that contribute to the NTM infection/disease rate will provide valuable information for healthcare providers. This information will help improve surveillance and inform the development of measures to protect public health. Surveillance tools are especially important and necessary to identify exposure pathways and understand the effect of disease on a population. Because of NTM's environmental link and its effect on human health, having public health officers and environmental researchers working together to improve surveillance of exposure routes will be beneficial. ■

Author disclosures are available with the text of this article at www.atsjournals.org.

Acknowledgment: The authors sincerely thank the health departments of Maryland, Mississippi, Missouri, Ohio, and Wisconsin for their assistance with providing the data.

References

1 Griffith DE, Aksamit T, Brown-Elliott BA, Catanzaro A, Daley C, Gordin F, Holland SM, Horsburgh R, Huitt G, Iademarco MF, *et al.*; ATS Mycobacterial Diseases Subcommittee; American Thoracic Society; Infectious Disease Society of America. An official ATS/IDSA statement: diagnosis, treatment, and prevention of nontuberculous mycobacterial diseases. *Am J Respir Crit Care Med* 2007;175:367–416.

2 Billinger ME, Olivier KN, Viboud C, de Oca RM, Steiner C, Holland SM, Prevots DR. Nontuberculous mycobacteria-associated lung disease in hospitalized persons, United States, 1998-2005. *Emerg Infect Dis* 2009;15:1562–1569.

3 Horsburgh CR Jr, Selik RM. The epidemiology of disseminated nontuberculous mycobacterial infection in the acquired immunodeficiency syndrome (AIDS). *Am Rev Respir Dis* 1989;139:4–7.

4 Prince DS, Peterson DD, Steiner RM, Gottlieb JE, Scott R, Israel HL, Figueroa WG, Fish JE. Infection with *Mycobacterium avium* complex in patients without predisposing conditions. *N Engl J Med* 1989;321: 863–868.

5 Olivier KN, Weber DJ, Lee JH, Handler A, Tudor G, Molina PL, Tomashefski J, Knowles MR; Nontuberculous Mycobacteria in Cystic Fibrosis Study Group. Nontuberculous mycobacteria. II: nested-cohort study of impact on cystic fibrosis lung disease. *Am J Respir Crit Care Med* 2003;167: 835–840.

6 Norton CD, LeChevallier MW, Falkinham JO III. Survival of *Mycobacterium avium* in a model distribution system. *Water Res* 2004;38:1457–1466.
7 Donohue MJ, Mistry JH, Donohue JM, O'Connell K, King D, Byran J, Covert T, Pfaller S. Increased frequency of nontuberculous mycobacteria detection at potable water taps within the United States. *Environ Sci Technol* 2015;49:6127–6133.
8 U.S. Census Bureau (U.S. Census Bureau). P12, American FactFinder: Sex by Age. 2010 Census. Washington, DC: U.S. Census Bureau; 2010 [accessed 2015 Feb 23]. Available from: http://factfinder2.census.gov
9 Prevots DR, Shaw PA, Strickland D, Jackson LA, Raebel MA, Blosky MA, Montes de Oca R, Shea YR, Seitz AE, Holland SM, *et al*. Nontuberculous mycobacterial lung disease prevalence at four integrated health care delivery systems. *Am J Respir Crit Care Med* 2010;182:970–976.
10 Winthrop KL, McNelley E, Kendall B, Marshall-Olson A, Morris C, Cassidy M, Saulson A, Hedberg K. Pulmonary nontuberculous mycobacterial disease prevalence and clinical features: an emerging public health disease. *Am J Respir Crit Care Med* 2010;182:977–982.
11 O'Brien RJ, Geiter LJ, Snider DE Jr. The epidemiology of nontuberculous mycobacterial diseases in the United States: results from a national survey. *Am Rev Respir Dis* 1987;135:1007–1014.
12 Bodle EE, Cunningham JA, Della-Latta P, Schluger NW, Saiman L. Epidemiology of nontuberculous mycobacteria in patients without HIV infection, New York City. *Emerg Infect Dis* 2008;14:390–396.
13 Cassidy PM, Hedberg K, Saulson A, McNelly E, Winthrop KL. Nontuberculous mycobacterial disease prevalence and risk factors: a changing epidemiology. *Clin Infect Dis* 2009;49:e124–e129.
14 Henkle E, Hedberg K, Schafer S, Novosad S, Winthrop KL. Population-based incidence of pulmonary nontuberculous mycobacterial disease in Oregon 2007 to 2012. *Ann Am Thorac Soc* 2015;12:642–647.
15 Smith GS, Ghio AJ, Stout JE, Messier KP, Hudgens EE, Murphy MS, Pfaller SL, Maillard JM, Hilborn ED. Epidemiology of nontuberculous mycobacteria isolations among central North Carolina residents, 2006-2010. *J Infect* 2016;72:678–686.
16 Adjemian J, Olivier KN, Seitz AE, Falkinham JO III, Holland SM, Prevots DR. Spatial clusters of nontuberculous mycobacterial lung disease in the United States. *Am J Respir Crit Care Med* 2012;186:553–558.
17 Adjemian J, Olivier KN, Seitz AE, Holland SM, Prevots DR. Prevalence of nontuberculous mycobacterial lung disease in U.S. Medicare beneficiaries. *Am J Respir Crit Care Med* 2012;185:881–886.
18 Satyanarayana G, Heysell SK, Scully KW, Houpt ER. Mycobacterial infections in a large Virginia hospital, 2001-2009. *BMC Infect Dis* 2011;11:113.
19 National Cancer Institute Surveillance Epidemiology and End Results System. SEER*Stat Tutorials: Calculating Age-adjusted Rates. Bethesda, MD; National Cancer Institute; 2016 [accessed 2016 Jul 26]. Available from: http://seer.cancer.gov/seerstat/tutorials/aarates/definition.html
20 Marras TK, Daley CL. Epidemiology of human pulmonary infection with nontuberculous mycobacteria. *Clin Chest Med* 2002;23:553–567.
21 Al Houqani M, Jamieson F, Chedore P, Mehta M, May K, Marras TK. Isolation prevalence of pulmonary nontuberculous mycobacteria in Ontario in 2007. *Can Respir J.* 2011;18(1):19–24.
22 Marras TK, Mendelson D, Marchand-Austin A, May K, Jamieson FB. Pulmonary nontuberculous mycobacterial disease, Ontario, Canada, 1998-2010. *Emerg Infect Dis* 2013;19:1889–1891.
23 Hygiene WSLo. Wisconsin Mycobacteriology Laboratory Network Data Report: 2014. In: Services WDoH, editor. Madison, WI: Wisconsin State Laboratory of Hygiene; 2014 [accessed 2015 May 23]. p. 4. Available from: http://www.slh.wisc.edu/wp-content/uploads/2015/04/WMLN-Isolation-Data-table-Cumulative-2014.pdf
24 Centers for Disease Control and Prevention (CDC). Respiratory illness in workers exposed to metalworking fluid contaminated with nontuberculous mycobacteria: Ohio, 2001. *MMWR Morb Mortal Wkly Rep* 2002;51:349–352.
25 Kapoor R, Yadav JS. Expanding the mycobacterial diversity of metalworking fluids (MWFs): evidence showing MWF colonization by *Mycobacterium abscessus*. *FEMS Microbiol Ecol* 2012;79:392–399.
26 U.S. Department of Health and Human Services. Health, United States, 2014: With Special Feature on Adults Aged 55–64. Hyattsville, MD: U.S. Department of Health and Human Services; 2015 [accessed 2016 May 10]. Available from: http://www.cdc.gov/nchs/data/hus/hus14.pdf
27 Daley CL, Griffith DE. Pulmonary non-tuberculous mycobacterial infections. *Int J Tuberc Lung Dis.* 2010;14:665–671.
28 Griffith DE, Girard WM, Wallace RJ Jr. Clinical features of pulmonary disease caused by rapidly growing mycobacteria: an analysis of 154 patients. *Am Rev Respir Dis* 1993;147:1271–1278.
29 Hadjiliadis D, Adlakha A, Prakash UB. Rapidly growing mycobacterial lung infection in association with esophageal disorders. *Mayo Clin Proc* 1999;74:45–51.
30 Huang CT, Tsai YJ, Wu HD, Wang JY, Yu CJ, Lee LN, Yang PC. Impact of non-tuberculous mycobacteria on pulmonary function decline in chronic obstructive pulmonary disease. *Int J Tuberc Lung Dis.* 2012;16(4):539–545.
31 Witty LA, Tapson VF, Piantadosi CA. Isolation of mycobacteria in patients with pulmonary alveolar proteinosis. *Medicine (Baltimore)* 1994;73:103–109.
32 Covert TC, Rodgers MR, Reyes AL, Stelma GN Jr. Occurrence of nontuberculous mycobacteria in environmental samples. *Appl Environ Microbiol* 1999;65:2492–2496.
33 Healthcare BlueBook. Office Visit, Established Patient, Level 3. 2015 [accessed 2015 Jul 9]. Available from: https://healthcarebluebook.com/page_ProcedureDetails.aspx?id=225&dataset=MD
34 Strollo SE, Adjemian J, Adjemian MK, Prevots DR. The burden of pulmonary nontuberculous mycobacterial disease in the United States. *Ann Am Thorac Soc* 2015;12:1458–1464.

Donohue *BMC Infectious Diseases* (2018) 18:163
https://doi.org/10.1186/s12879-018-3043-7

BMC Infectious Diseases

RESEARCH ARTICLE Open Access

Increasing nontuberculous mycobacteria reporting rates and species diversity identified in clinical laboratory reports

Maura J. Donohue

Abstract

Background: Nontuberculous Mycobacteria (NTM) are environmental microorganisms that can affect human health. A 2009–2010 occurrence survey of NTM in potable tap water samples indicated an increased recovery rate for many clinically significant species such as *M. avium* (30%) and *M. abscessus* (12%). To determine if these trends by species were mirrored in human infections, isolation rates of NTM species identified in clinical laboratory reports from four states were evaluated.

Method: Clinical laboratory reports from the Mississippi, Missouri, Ohio, and Wisconsin Health Departments were used to investigate the species of NTM isolated from human specimens in 2014. The NTM positive specimen reports were tabulated for each species and complex/group. The number of reports by month were used to investigate seasonal trends. The 2014 isolation rates were compared to historic values to examine longitudinal trends.

Results: The positive rate of NTM specimens increased from 8.2 per 100,000 persons in 1994 to 16 per 100,000 persons in 2014 (or 13.3 per 100,000 after excluding *Mycobacterium gordonae*). Changes in NTM diversity were observed in complex/groups known to be clinically significant. Between 1994 and 2014 the rate implicating *M. abscesses-chelonae* group and *M. avium* complex increased by 322 and 149%, respectively.

Conclusions: Based on public health data supplied by the four State's Health Departments and the 2014 U.S. population, 50,976 positive NTM specimen reports per year were projected for the nation; serving as an indicator for the national potential disease burden that year.

Keywords: Nontuberculous mycobacteria (NTM), Clinical laboratory reports, Species, Epidemiology, Isolation rates, Report rates, Seasonal, United States

Background

Data from recent studies demonstrate an increasing prevalence of Nontuberculous Mycobacteria (NTM) infections in the United States [1–3]. NTM are of environmental origin and can impact a wide variety of tissues and body fluids causing both respiratory (chronic bronchopulmonary disease) illnesses and dermal infections [4]. NTM infections may also compound the respiratory ailments of individuals with Cystic Fibrosis [5], Chronic Obstructive Pulmonary Disease (COPD) [6, 7] and Acquired Immunodeficiency Syndrome (AIDS) [8, 9].

NTM's natural habitats are aquatic and soil environments [10]. Since the majority (77.4% [11] to 91.5% [12]) of NTMs are isolates from pulmonary specimens, exposure likely occurs through the aerosolization or aspiration of water and or soil particulates. NTM infections or illnesses are not generally communicable, although there are a few documented cases of person-to-person transmission [13, 14]. Additionally, highly populated areas have a higher NTM infection rate and positive specimen counts than other regions of the U.S. [15, 16].

NTM is a broad classification term that is applied to a group of approximately 186 currently recognized unique mycobacterium species [17]. The majority do not have an impact on human health. Thus, it is important to identify the species causing an infection in cases where

Correspondence: Donohue.maura@epa.gov
United States Environmental Protection Agency, 26 W. Martin Luther King Dr. Mail Stop 587, Cincinnati, Ohio 45268, USA

BioMed Central

© The Author(s). 2018 **Open Access** This article is distributed under the terms of the Creative Commons Attribution 4.0 International License (http://creativecommons.org/licenses/by/4.0/), which permits unrestricted use, distribution, and reproduction in any medium, provided you give appropriate credit to the original author(s) and the source, provide a link to the Creative Commons license, and indicate if changes were made. The Creative Commons Public Domain Dedication waiver (http://creativecommons.org/publicdomain/zero/1.0/) applies to the data made available in this article, unless otherwise stated.

symptoms are sufficient to support specimen collection. Knowledge of the NTM species identity will guide the therapeutic treatment prescribed by the physician and provide clues relative to exposure source and route.

This study catalogued the NTM species in human-specimen clinical reports from four States (Mississippi, Missouri, Ohio, and Wisconsin) during the 2014 calendar year with the goal of identifying the species with the most frequent impact on human health. The dates for the case report submissions were examined to determine if there was any indication of seasonality. In addition, the 2014 findings were compared to those from an earlier 1994 Centers for Disease Control and Prevention (CDC) report of NTM infections (19) to evaluate if prevalence had increased over the last 20 years.

Methods

Study design

Four states (Mississippi, Missouri, Ohio, and Wisconsin) that required NTM positive specimen results to be submitted to their respective state health departments were asked if they would provide the following data from their disease surveillance network: the number of positive NTM reports by species and the number of positive NTM reports by month for the 2014 calendar year. The respective health departments agreed to participate and provided the requested information to the U.S. EPA. Table 1 summarizes the information received from the four states. No personal identifiers were shared with U.S. EPA, therefore maintaining the privacy for the individuals associated with all report records. This study was determined to be exempt from Institution Review Board review by U.S. EPA.

Data

Four health departments provided U.S. EPA with the number of NTM reports by species for the 2014 calendar year. The methods used to isolate NTMs were either through culture [18] or the Becton Dixon BACTEC™ Mycobacteria Growth Indicator Tube (MGIT™) [19]. All four states largely used mycolic acid analysis and DNA probes (Hologic, Marlborough, MA) for species identification. Some laboratories sequenced an isolate's *hsp65* or *rpoB* gene for NTM identification (Table 1).

Cases implicating all non-NTM isolates, as well as, isolates of *M. bovis* and *M. marinum* were removed from the data set for this analysis. Cattle and fish, not water, are the sources of infection for *M. bovis* and *M. marinum* species; thus, they were not considered in this evaluation.

Analysis

Report rates for NTMs were calculated for each state by dividing the number of positive NTM case reports by the July 1, 2014 state population. Calculation of these rates used 2014 U.S. population estimates for each state as follows (Table 1): Mississippi: 2,993,443; Missouri: 6,063,827; Ohio: 11,597,998; Wisconsin: 5,759,432 and U.S.: 318,563,456. The percentage of the total was calculated for each species or group identified by each state using Microsoft Excel.

CDC does not routinely collect NTM specimen reports. Periodically, over the past 40 years, CDC has published a few papers and reports that examined the epidemiology of NTMs in the U.S. These papers examined NTM prevalence by the number of laboratory reports generated by each state [20–22]. The 1994 historical data for each of the four states was extracted from the Butler and Crawford, 1999 document. This document contains the number of reports and report rate by species for each state in the U.S for the years 1993–1996. In the 1990's, laboratories were using either culture bases methods [18] or BD MGIT™ systems [19] for bacterial enrichment and DNA/RNA

Table 1 Health departments data sources and NTM identification method for the year 2014

State	Data source	Year	NTM identification method	NTM laboratory report	Report rate[a]
Mississippi	Mississippi's public health laboratories + accredited laboratories (hospitals and/01 commercial laboratories)	2014	HPLC and DNA probes	529	17.6
Missouri	Missouri's public health laboratories + few hospitals + commercial laboratories	2014	HPLC and DNA probes	879	14.5
Ohio	Ohio's public health laboratories + hospitals + commercial laboratories	2014	HPLC, DNA probes, sequencing of the *hsp65* and *rpoB* gene and biochemical test	1379	11.8
Wisconsin		2014	HPLC and DNA probes and inconclusive isolates are sequenced.	1413	24.5
Total				4200	16.0

[a] Rate per 100,000 persons

probes (Hologic, Marlborough, MA) and or mycolic acid analysis for identification [23]. In 2014, the majority of laboratories were still using these culture and identification methods. Thus, supporting a comparison between the two-time periods 1994 and 2014. Chi-square and Fisher Exact tests for significant differences between the two data sets were determined using SigmaPlot 13.0.

Species grouping

Many of the NTM species have similar characteristics and have been placed into groups of two to seven species (Table 2) with some species being ungrouped. The species identified by the states were summed by their group for this analysis to facilitate a comparison between the historical 1994 data and the 2014 data. For example, 1541 samples identified as M. *avium* complex (MAC) positive specimens were combined with 705 reports identified as *M. avium* species and 6 reports identified as *M. intracellulare* species to give a total of 2252 reports for the MAC group. Table 2 lists the NTM species reports that were combined to represent each NTM group/complex/clad unit for the comparison.

Monthly reports

The Mississippi, Missouri, and Ohio Health Departments provided the U.S. EPA with the number of NTM specimen reports by month for the year 2014. Mississippi data are publicly available at the Monthly Reportable Disease Statistics website: http://msdh.ms.gov/msdhsite/_static/14,0,261.html. The Wisconsin Health Department was unable to supply their data in this format; thus, there is no evaluation of cases per month for the state of Wisconsin. The monthly report data were used to determine if report frequency exhibited any seasonal trends.

Results

NTM species in laboratory reports

The Mississippi, Missouri, Ohio, and Wisconsin disease network had 4200 NTM positive specimen reports submitted in 2014. The overall NTM prevalence rate was 16.0 reports per 100,000 persons (or 13.3 per 100,000 excluding *Mycobacterium gordonae*). This rate is much higher than that reported by the CDC in 1994. Based on the 2014 data, a national estimate of 50,976 positive NTM specimen reports are projected during that year.

The distributions by state for the total NTM positive specimens are as follows: Wisconsin (33.6%), Ohio (32.8%), Missouri (20.9%) and Mississippi (12.6%) (Additional file 1: Table S1-S4). The complex/group assignment to which an isolate was speciated varied across the states. Three percent of the reports identified the isolates only to the genus-level. Forty-three percent of the reports assigned the isolates only to a specific complex/group, and 54% of reports provided the species name (Table 2). In all, 52 species were identified by name in the state reports. Isolates classified only by their complex/group designation primarily belonged to the *M. avium* complex (MAC), *M. chelonae-abscessus* or *M. fortuitum* groups. Table 2 provides the data for all the species identified and ascribes each species to its designated complex or group. The five most common species isolated from human specimens were *M. avium* 705/4200 (17%), *M. gordonae* 688/4200 (16%), *M. chelonae* 135/4200 (3.2%), *M. fortuitum* 110/4200 (2.6%), and *M. mucogenicum* 104/4200 (2.5%) (Table 2). These species accounted for 41.4% of the total demonstrating the broad range of species identified among the samples collected for analysis.

NTM increased reporting frequency

NTM positive specimen reports have increased between 1994 and 2014 from 1950 to 2400, equivalent to an increase of 8.2 per 100,000 persons per year to 16.0 per 100,000 persons per year. The three complexes/groups that had statistically significant increases in the frequency of detections were the: *M. chelonae-abscessus* group, *M. fortuitum* group and *M. avium* complex. The percentage increase of these clinically important species, as established by American Thoracic Society and Infectious Disease Society of America, (ATS/IDSA) [4] between 1994 and 2014 is significant: 322% (94 to 440 reports), 194% (105 to 343 reports), and 149% (816 to 2252 reports), respectively (Fig. 1). On the other hand, Fig. 1 illustrates a decline in the number of positive specimen reports for other species: *M. xenopi (− 15%), M. kansasii (− 30%), M. terrae (− 40%), M. scrofulaceum (− 55%)* and *M. flavescens* (none detected).

Longitudinal analysis for the MAC species

Figure 2 illustrates the report rate of *M. avium per* 100,000 persons over time for the four states. In 2014, the combined report rate of *M. avium* for Mississippi, Missouri, Ohio, and Wisconsin was 8.5 per 100,000 persons (Fig. 2). This is 2.5 times more reports than the numbers reported in 1994 [20]. The species detections for Ohio and Wisconsin increased more than five-fold suggesting a comparable increase in the respiratory infections disease burden.

NTMs reports by month

When the 2014 positive specimens per month for each state were plotted (Fig. 3) there was no evidence for a seasonal pattern to the potential disease burden. The peak month for each state differed: February for Mississippi, April for Ohio, and July for Missouri. Data from Wisconsin were not segregated by month.

Table 2 NTMs identified from human specimens in Mississippi, Missouri, Ohio, and Wisconsin, 2014

Identified to Genus	Complex/Group Totals	Identified to NTM Complex/Group	Identified to NTM Species	Count	Percentage	Rate[a]
NTM				132	3.14	0.50
	MAC complex (Total)			2252	53.62	8.53
		MAC complex		1541	36.69	5.83
			M. avium	705	16.79	2.67
			M. intracellulare	6	0.14	0.02
	MAIS Complex (Total)			20	0.48	0.08
		MAIS Complex		17	0.40	0.06
			M. scrofulaceum	3	0.07	0.01
	M. *chelonae-abscessus* Group (Total)			440	10.48	1.67
		M. chelonae-abscessus Group		122	2.90	0.46
			M. abscessus	62	1.48	0.23
			M. bolletii	5	0.12	0.51
			M. chelonae	135	3.21	0.00
			M. franklinii	1	0.02	0.02
			M. immunogenum	4	0.10	
			M. massiliense	2	0.05	
			M. mucogenicum	104	248	0.39
			M. phocaicum	5	0.12	0.02
	M. fortuitum Group (Total)			343	8.17	1.30
		M. fortuitum Group		143	3.40	0.54
			M. conceptionense	2	0.05	0.01
			M. fortuitum	110	2.62	0.42
			M. houstonense	1	0.02	0.00
			M. neworleansense	2	0.05	0.01
			N. peregrinum	76	1.81	0.29
			M. porcinum	5	0.12	0.02
			M. septicum	4	0.10	0.02
	M. gordonae (Total)		*M. gordonae*	689	16.40	2.61
	M. xenopi (Total)		*M. xenopi*	54	1.29	0.20
	M. kansasii Clade (Total)			100	2.38	0.38
			M. gastri	1	0.02	0.00
			M. kansasii	99	2.36	0.37
	M. haemophilum (Total)			7	0.17	0.03
			M. haemophilum	2	0.05	0.01
			M. malmoense	5	0.12	0.02
	M. terrae Complex (Total)			60	1.43	0.23
			M. arupense	21	0.50	0.08
			M. kumamotonense	1	0.02	0.00
			M. nonchromogenicum	10	0.24	0.04
			M. terrae	28	0.67	0.11
	M. smegmatis (Total)			17	0.40	0.06
			M. goodii	7	0.17	0.03
			M. mageritense	4	0.10	0.02
			M. smegmatis	4	0.10	0.02
			M. wolinskyi	2	0.05	0.01

Table 2 NTMs identified from human specimens in Mississippi, Missouri, Ohio, and Wisconsin, 2014 *(Continued)*

Identified to Genus	Complex/Group Totals	Identified to NTM Complex/Group	Identified to NTM Species	Count	Percentage	Rate[a]
	M. simiae Complex (Total)			45	1.07	0.17
			M. interjectum	2	0.05	0.01
			M. kubicae	2	0.07	0.01
			M. lentiflavum	15	0.36	0.06
			M. parascrofulaceum	2	0.05	0.01
			M. simiae	22	0.52	0.08
			M. triplex	1	0.02	0.00
	Ungrouped NTM (Total)			41	0.98	0.16
			M. algericum	1	0.02	0.00
			M. aurum	1	0.02	0.00
			M. bacteremicum	1	0.02	0.00
			M. branderi	1	0.02	0.00
			M. celatum	1	0.02	0.00
			M. cosmeticum	4	0.10	0.02
			M. frederiksbergense	1	0.02	0.00
			M. iranicum	1	0.02	0.00
			M. nebraskense	2	0.05	0.01
			M. neoaurum	6	0.14	0.02
			M. paraffinicum	9	0.21	0.03
			M. pulveris	1	0.02	0.00
			M. sphagni	1	0.02	0.00
			M. szulgai	10	0.24	0.04
			M. vaccae	1	0.02	0.00

[a]Rate per 100,000 persons

Discussion

Case reports are the bedrock for disease surveillance in the U.S. Unfortunately, CDC's National Notifiable Disease Surveillance System (NNDSS) does not routinely collect data on NTM positive laboratory reports or disease cases on a national basis. In recent years, state health departments are allowing other public and private laboratories to submit reports into their disease surveillance systems due to the increase capability of private and public labs to identify NTMs in human specimens and improvements in electronic reporting. The state NTM data reports capture information that reflects potential respiratory infections among both the young and elderly, as well as, the poor and the uninsured population groups often underrepresented in studies of disease burden based on Medicare part B and/or health care insurance records. However, there are limitations to these state data. The NTM reports are not generally scrutinized for accuracy or completeness during data entry. The procedures for isolating the NTM species from the specimen could yield false positives due to laboratory contamination. In addition, more than one report could belong to the same individual if more than one specimen was collected during the course of a single disease episode in order to evaluate treatment efficacy. Thus, the NTM specimen reports can overestimate the burden of disease. Yet, the report rate of 13.3 per 100,000 is similar to 13.7 per 100,000 persons (North Carolina) [12] and 17.2 reports per 100,000 persons (Oregon) [11] other estimates of NTM prevalence in the U.S. Additionally, the estimate of 50,976 NTM reports in the U.S. per annum derived by using the state NTM reports is of the same order of magnitude as the estimated 86,244 cases identified using Medicare part B records [24]. Multiple lines of evidence demonstrate an increase in NTM prevalence [1–3] and report rates [12], strengthening the conclusion that NTM infections in the U.S. have increased. These lines of evidence also elevate the concern for NTM-related diseases in the U.S., identifying a need to search for controllable sources of exposure that will guide risk mitigation measures [25].

In this study, fifty-two NTM species were identified from human specimens. Twenty eight percent (52/186) of recognized NTM species are represented in the specimen reports. The four most frequently identified NTM groups or species that were common across the four states were: MAC, *M. fortuitum*, *M. gordonae*, and *M. chelonae-abscessus* groups. This observation was supported by data from other regions and states within the U.S. [11, 12, 26].

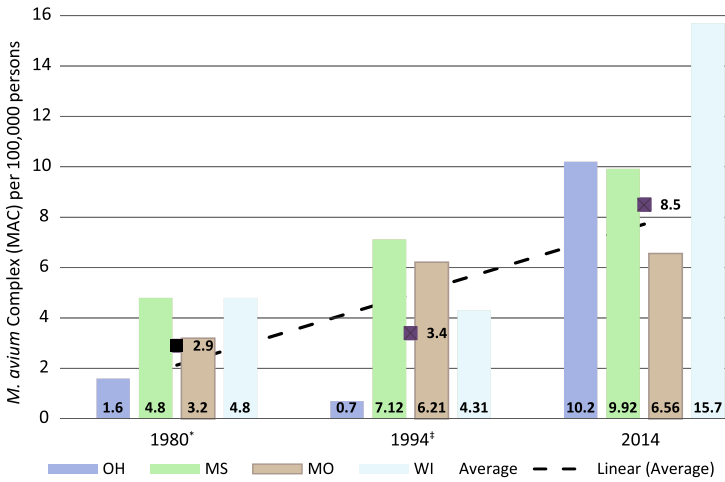

Fig. 1 Numbers, rates, and percent change of NTM reports by species, 1994 and 2014 comparison. See Table 2 for clarity on which NTM species were considered in each complex or group. *2014: *M. chelonae-abscessus* Group plus. *M. mucogenicum-phocaicum* report numbers were combined, ‡ NS = Not significant, § per 100,000 persons: 1994 population 23,795,000 (as reported by Butler and Crawford, 1999); 2014 population 26,414,700

The increase in the number of NTM positive reports is not solely due to population growth. From 1994 to 2014, the population in these four states increased by 2.1 million people. Using the CDC 1994 report rate of 8.2 per 100,000 persons [20], this population increase should have only added 172 reports. Instead the number of reports for the four states is 4200 positive reports. This number was greater than 2000 more reports than predicted. The reason for this increase is probably multifactorial. One important factor that likely led to the larger case count is the increase in electronic reporting by laboratories who perform sample analyses to state databases. Established common portals for data entry can be used by state laboratories, large research hospitals, as well as, commercial laboratories to facilitate improved record keeping. However, despite the impact of technology on better reporting, the increase in the number of reports is substantial enough to support the conclusion that more individuals are experiencing NTM related episodes impacting their health now than they did two decades ago.

NTM Species	1994 Number	1994 Rate§	2014 Number	2014 Rate§	P Value	Percent Change (rate)
M. chelonae-abscessus Group*	94	0.40	440	1.67	P = <0.001	321.6
M. smegmatis	1	0.00	4	0.02	NS‡	260.3
M. fortuitum Group	105	0.44	343	1.30	P = <0.001	194.2
M. avium Complex	816	3.43	2252	8.53	P = <0.001	148.6
M. malmoense	2	0.01	5	0.02	NS	125.2
M. szulgai	4	0.02	10	0.04	NS	125.2
M. simiae	14	0.06	22	0.08	NS	41.5
M. gordonae	573	2.41	689	2.61	P = <0.001	8.3
M. vaccae	1	0.00	1	0.00	NS	-9.9
M. xenopi	57	0.24	54	0.20	P = <0.001	-14.6
M. kansasii Clade	128	0.54	100	0.38	P = <0.001	-29.6
M. terrae	42	0.18	28	0.11	P = <0.001	-39.9
M. scrofulaceum	6	0.03	3	0.01	NS	-54.9
M. flavescens	6	0.03	0	0.00	P = 0.002	-100

* 2014: *M. chelaonae-absessus* Group plus. *M. mucogenicum-phocaicum* report numbers were combined.
‡ NS=Non-significant
§ per 100,000 persons: 1994 population 23,795,000 (as reported by Butler and Crawford), 1999; 2014 population 26,414,700

Fig. 2 Longitudinal analysis (1980–2014) of *M. avium* complex report rate per 100,000 persons for Mississippi, Missouri, Ohio, Wisconsin, and combined. * Butler and Crawford, 1999: 1994 rates

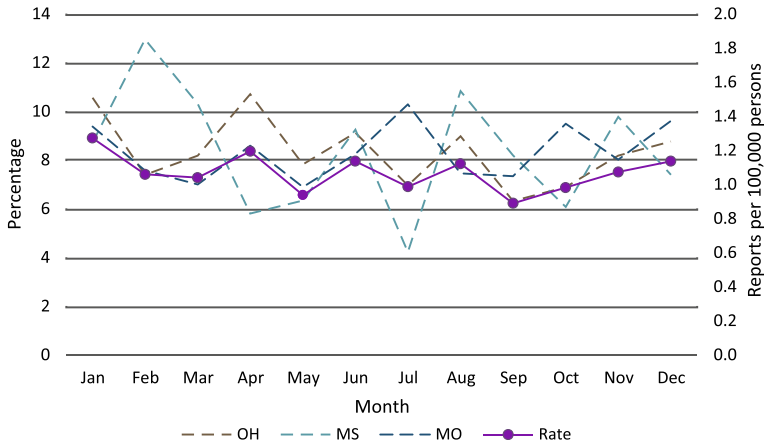

Fig. 3 NTM reports by state by month

There was an increase in the MAC positive reports from 3.4 per 100,000 in 1994 to 8.5 per 100,000 in 2014 (Fig. 2). Numerous factors could have contributed to the increase in prevalence including: increased medical awareness of NTM related infections/diseases, improvement of laboratory identification techniques, increases in exposure modalities and human activities associated with water and/or soils. The increased MAC detection rates for the four states suggest a need for improved risk communication efforts between the public health sector and populations at risk for NTM infections. The NTM family of microorganisms and their contribution to respiratory illnesses are seldom topics for the popular press and media. There is a need for a better communications strategy targeting the general population on both the signs and symptoms of NTM infections and measures that will help minimize risk.

The shifts in detection frequency for either an NTM group or species should be considered in any assessment of population risk. Not all NTM species have the same symptoms nor impact on human health. Species within the *M. chelonae-abscessus* and *M. fortuitum* groups are those commonly identified in "outbreak" investigations [27–29]. These outbreaks can include dermal infections of either the skin or soft tissue and pulmonary problems. Dermal signs and symptoms reported were immediate post contact rash onset, septic arthritis, or cutaneous infections of the skin [27–29]. The source of the infection is typically found to be a non-potable or potable water source that has been contaminated with NTMs. Species in the MAC grouping have been the most clinically significant because they cause the majority of NTM related illnesses and diseases [3, 30].

The increases in a state's population alone do not account for the increased number of cases reported by the state health departments. However, changes within the population can contribute to the increase. For example, a state population could contain more elderly individuals with co-morbidity factors such as COPD or people suffering from suppression of their immune response than in the past. Changes in routes of exposure are also important. MAC infections are usually respiratory, but not communicable [4]. Therefore, changes in bathroom construction that promote showering over bathing (especially for the elderly) increases the likelihood for inhalation exposure and infection when potable water is the source of transmission. A recent survey of NTM presence in tap water found 78% (202/258) of the samples collected were positive for NTM [31]. Since inhalation is believed to be the main route of exposure [4], the increased use of shower water aerators could also be an important feature associated with an increase in population exposure [32]. Recently, several publications [33] have outlined measures, such as, cleaning showerheads and removing aerators as protective measures for avoiding exposure to NTMs [34, 35].

There is no seasonal pattern to NTM reports. The lack of seasonality suggests exposure routes for illness and or disease occur year-round and may not be influenced by seasonal changes in activities of the at-risk population. This is probably due to the fact that pulmonary NTM lung infections and/or diseases are not acute illnesses. Common signs and symptoms of the respiratory problems are shortness of breath and fatigue [4]. These vague symptoms may not be addressed in a timely manner, lengthening the time between illness onset and consultation with a physician because of symptom persistence. This delay could potentially dampen the opportunity to link a positive specimen as a result of physician consultation to the time the symptoms were first noted. As a result, a potential NTM report is filed with the state long past the time of infection acquisition.

Conclusion

Knowledge of the NTM species most frequently associated with adverse human health consequences will assist epidemiological investigators to identify likely sources and modes of exposure associated with these types of infections. By identifying the sources of the NTM infections, strategies can be implemented to control for the occurrence of NTMs and/or procedures can be adopted to mitigate exposure routes associated with the risks. NTMs and their related disease manifestations result in a significant, medical, human health burden, especially among the elderly [2, 15]. As the U.S. population ages, the public health burden from NTM associated disorders is expected to increase. Thus, it is important to conduct research to identify the major exposure routes and environmental sources of dissemination to identify and implement practices that will limit human exposures to NTM infections.

Disclaimer

The United States Environmental Protection Agency through its Office of Research and Development funded and managed the research described here. It has been subjected to Agency's administrative review and approved for publication. The views expressed in this paper are those of the authors and do not necessarily reflect the views or policies of the United States Environmental Protection Agency.

Additional file

Additional file 1: Table S1. Nontuberculous mycobacteria reported by Missouri, 2014. **Table S2.** Nontuberculous mycobacteria reported by Mississippi, 2014; **Table S3.** Nontuberculous mycobacteria reported by Ohio, 2014. **Table S4.** Nontuberculous mycobacteria reported by Wisconsin, 2014. Provisional counts of NTM reports by State and NTM Species. (DOCX 26 kb)

Abbreviations

AIDS: Acquired immunodeficiency syndrome; ATS/IDSA: American thoracic society and infectious disease society of America; CDC: Center for disease control and prevention; COPD: Chronic obstructive pulmonary disease; MAC: *M. avium* complex; NNDSS: National notifiable disease surveillance system; NTM: Nontuberculous mycobacteria; U.S. EPA: United States environmental protection agency; U.S.: United States

Acknowledgements

The author sincerely thanks the state health departments of the states of, Mississippi, Missouri, Ohio and Wisconsin for their assistance with providing data and to Dr. Cynthia Yund for her mentorship.

Funding

The author received no funding for this research.

Availability of data and materials

All data analyzed during this study are included in this published article, and its Additional files.

Author's contributions

The author met all four criteria for authorship suggested by the international committee of journal editors. Study concept and design, acquisition of data, analysis and interpretation of data, drafting of the manuscript, critical revision of the manuscript for important intellectual content, and statistical analysis: MJD. The author read and approved the final manuscript.

Ethics approval and consent to participate

This study was determined to be exempt from Institution review board review by United States environmental protection agency.

Consent for publication

Not applicable.

Competing interests

The author declare that they have no competing interests.

Publisher's Note

Springer Nature remains neutral with regard to jurisdictional claims in published maps and institutional affiliations.

Received: 13 November 2017 Accepted: 12 March 2018
Published online: 10 April 2018

References

1. Adjemian J, Olivier KN, Seitz AE, Holland SM, Prevots DR. Prevalence of nontuberculous mycobacterial lung disease in U.S. Medicare beneficiaries. Am J Respir Crit Care Med. 2012;185(8):881–6.
2. Donohue MJ, Wymer L. Increasing prevalence rate of nontuberculous mycobacteria infections in five states, 2008-2013. Ann Am Thorac Soc. 2016; 13(12):2143–50.
3. Prevots DR, Shaw PA, Strickland D, Jackson LA, Raebel MA, Blosky MA, Montes de Oca R, Shea YR, Seitz AE, Holland SM, et al. Nontuberculous mycobacterial lung disease prevalence at four integrated health care delivery systems. Am J Respir Crit Care Med. 2010;182(7):970–6.
4. Griffith DE, Aksamit T, Brown-Elliott BA, Catanzaro A, Daley C, Gordin F, Holland SM, Horsburgh R, Huitt G, Iademarco MF, et al. An official ATS/IDSA statement: diagnosis, treatment, and prevention of nontuberculous mycobacterial diseases. Am J Respir Crit Care Med. 2007;175(4):367–416.
5. Olivier KN, Weber DJ, Lee JH, Handler A, Tudor G, Molina PL, Tomashefski J, Knowles MR, Nontuberculous Mycobacteria in Cystic Fibrosis Study G. Nontuberculous mycobacteria. II: nested-cohort study of impact on cystic fibrosis lung disease. Am J Respir Crit Care Med. 2003;167(6):835–40.
6. Huang CT, Tsai YJ, Wu HD, Wang JY, Yu CJ, Lee LN, Yang PC. Impact of non-tuberculous mycobacteria on pulmonary function decline in chronic obstructive pulmonary disease. Int J Tuberc Lung Dis. 2012;16(4):539–45.
7. Lewis AG Jr, Dunbar FP, Lasche EM, Bond JO, Lerner EN, Wharton DJ, Hardy AV, Davies R. Chronic pulmonary disease due to atypical mycobacterial infections. Am Rev Respir Dis. 1959;80:188–99.
8. Horsburgh CR Jr, Selik RM. The epidemiology of disseminated nontuberculous mycobacterial infection in the acquired immunodeficiency syndrome (AIDS). Am Rev Respir Dis. 1989;139(1):4–7.
9. Petrini B, Svahn A, Julander I, Kallenius G, Ostlund L. Prevalence of mycobacterium avium complex infection in AIDS patients. Scand J Infect Dis. 1991;23(4):511–2.
10. Gruft H, Loder A, Osterhout M, Parker BD, Falkinham JO 3rd. Postulated sources of Mycobacterium intracellulare and Mycobacterium scrofulaceum infection: isolation of mycobacteria from estuaries and ocean waters. Am Rev Respir Dis. 1979;120(6):1385–8.
11. Cassidy PM, Hedberg K, Saulson A, McNelly E, Winthrop KL. Nontuberculous mycobacterial disease prevalence and risk factors: a changing epidemiology. Clin Infect Dis. 2009;49(12):e124–9.
12. Smith GS, Ghio AJ, Stout JE, Messier KP, Hudgens EE, Murphy MS, Pfaller SL, Maillard JM, Hilborn ED. Epidemiology of nontuberculous mycobacteria isolations among Central North Carolina residents, 2006-2010. J Infect. 2016; 72(6):678–86.
13. Bryant JM, Grogono DM, Parkhill J, Floto RA. Transmission of M abscessus in patients with cystic fibrosis – Authors' reply. Lancet. 2013;382(9891):504.
14. Bryant JM, Grogono DM, Rodriguez-Rincon D, Everall I, Brown KP, Moreno P, Verma D, Hill E, Drijkoningen J, Gilligan P, et al. Emergence and spread of a

human-transmissible multidrug-resistant nontuberculous mycobacterium. Science. 2016;354(6313):751–7.
15. Winthrop KL, Varley CD, Ory J, Cassidy PM, Hedberg K. Pulmonary disease associated with nontuberculous mycobacteria, Oregon, USA. Emerg Infect Dis. 2011;17(9):1760–1.
16. du Moulin GC, Sherman IH, Hoaglin DC, Stottmeier KD. Mycobacterium avium complex, an emerging pathogen in Massachusetts. J Clin Microbiol. 1985;22(1):9–12.
17. Parte AC. LPSN—list of prokaryotic names with standing in nomenclature. Nucleic Acids Res. 2014;42(D1):D613–D616. https://doi.org/10.1093/nar/gkt1111. http://www.bacterio.net. Accessed 19 Mar 2018.
18. Manual of clinical microbiology, Eleventh edn. In: Jorgensen JH, Pfaller MA, Carroll KC, Funke G, Landry ML, Richter SS, Warnock DW, editors. Washington: ASM Press; 2015.
19. Pfyffer GE, Welscher HM, Kissling P, Cieslak C, Casal MJ, Gutierrez J, Rusch-Gerdes S. Comparison of the mycobacteria growth Indicator tube (MGIT) with radiometric and solid culture for recovery of acid-fast bacilli. J Clin Microbiol. 1997;35(2):364–8.
20. Butler WR, Crawford JT. Nontuberculous mycobacteria reported to the public health laboratory information system by state public health laboratories United States, 1993-1996: Georgia: Centers for Disease Control and Prevention, National Center for Infectious Diseases; 1999. p. 1–51.
21. Good RC. From the Center for Disease Control. Isolation of nontuberculous mycobacteria in the United States, 1979. J Infect Dis. 1980;142(5):779–83.
22. Good RC, Snider DE Jr. Isolation of nontuberculous mycobacteria in the United States, 1980. J Infect Dis. 1982;146(6):829–33.
23. Butler WR, Guthertz LS. Mycolic acid analysis by high-performance liquid chromatography for identification of Mycobacterium species. Clin Microbiol Rev. 2001;14(4):704–26. table of contents
24. Strollo SE, Adjemian J, Adjemian MK, Prevots DR. The burden of pulmonary nontuberculous mycobacterial disease in the United States. Ann Am Thorac Soc. 2015;12(10):1458–64.
25. Bergey's manual of systematic bacteriology, 5, 2nd. New York: Springer-Verlag; 2012.
26. Henkle E, Hedberg K, Schafer S, Novosad S, Winthrop KL. Population-based incidence of pulmonary nontuberculous mycobacterial disease in Oregon 2007 to 2012. Ann Am Thorac Soc. 2015;12(5):642–7.
27. D'Antonio S, Rogliani P, Paone G, Altieri A, Alma MG, Cazzola M, Puxeddu E. An unusual outbreak of nontuberculous mycobacteria in hospital respiratory wards: association with nontuberculous mycobacterial colonization of hospital water supply network. Int J Mycobacteriol. 2016;5(2):244–7.
28. Jung SY, Kim BG, Kwon D, Park JH, Youn SK, Jeon S, Um HY, Kwon KE, Kim HJ, Jung HJ, et al. An outbreak of joint and cutaneous infections caused by non-tuberculous mycobacteria after corticosteroid injection. Int J Infect Dis. 2015;36:62–9.
29. Kennedy BS, Bedard B, Younge M, Tuttle D, Ammerman E, Ricci J, Doniger AS, Escuyer VE, Mitchell K, Noble-Wang JA, et al. Outbreak of Mycobacterium chelonae infection associated with tattoo ink. N Engl J Med. 2012;367(11):1020–4.
30. Bodle EE, Cunningham JA, Della-Latta P, Schluger NW, Saiman L. Epidemiology of nontuberculous mycobacteria in patients without HIV infection, new York City. Emerg Infect Dis. 2008;14(3):390–6.
31. Donohue MJ, Mistry JH, Donohue JM, O'Connell K, King D, Byran J, Covert T, Pfaller S. Increased frequency of nontuberculous mycobacteria detection at potable water taps within the United States. Environ Sci Technol. 2015; 49(10):6127–33.
32. Hines SA, Chappie DJ, Lordo RA, Miller BD, Janke RJ, Lindquist HA, Fox KR, Ernst HS, Taft SC. Assessment of relative potential for legionella species or surrogates inhalation exposure from common water uses. Water Res. 2014; 56:203–13.
33. Nishiuchi Y, Iwamoto T, Maruyama F. Infection sources of a common non-tuberculous mycobacterial pathogen, Mycobacterium avium complex. Front Med. 2017;4:27.
34. Falkinham JO 3rd. Current epidemiologic trends of the nontuberculous mycobacteria (NTM). Curr Environ Health Rep. 2016;3(2):161–7.
35. Thomson R, Tolson C, Carter R, Coulter C, Huygens F, Hargreaves M. Isolation of nontuberculous mycobacteria (NTM) from household water and shower aerosols in patients with pulmonary disease caused by NTM. J Clin Microbiol. 2013;51(9):3006–11.

Submit your next manuscript to BioMed Central and we will help you at every step:

- We accept pre-submission inquiries
- Our selector tool helps you to find the most relevant journal
- We provide round the clock customer support
- Convenient online submission
- Thorough peer review
- Inclusion in PubMed and all major indexing services
- Maximum visibility for your research

Submit your manuscript at
www.biomedcentral.com/submit

BioMed Central

WL

Wymer, Larry

Donohue, Maura

2:10 PM

Record of Percentage Agreement-Larry Wymer

Retention Policy 10 years (Capstone approach) (10 years) Expires 4/22/2030

Dear STAA Committee Members

In Maura Donohue's 2020 STAA nomination for the following paper;

- **Donohue MJ**, Wymer L. Increasing Prevalence Rate of Nontuberculous Mycobacteria Infections in Five States, 2008-2013. Ann Am Thorac Soc. 2016 Dec;13(12):2143-2150.
- **Donohue MJ.**, Increasing nontuberculous mycobacteria reporting rates and species diversity identified in clinical laboratory reports. BMC Infect Dis. 2018 Apr 10;18(1):163.

I, Larry Wymer, am in agreement with the listed total percentage of effort of 10%.

Sincerely,

Larry J. Wymer
Mathematical Statistician
U.S. Environmental Protection Agency
CEMM/MEB
26 West Martin Luther King Dr
Cincinnati OH 45268
513.569.7252

Mon 4/27/2020 11:02 AM

Donohue, Maura

Donohue Percentage of Effort

To Donohue, Maura

Retention Policy 10 years (Capstone approach) (10 years) Expires 4/25/2030

Dear STAA Committee Members

In Maura Donohue's 2020 STAA nomination for the following paper;

- **Donohue MJ**, Wymer L. Increasing Prevalence Rate of Nontuberculous Mycobacteria Infections in Five States, 2008-2013. Ann Am Thorac Soc. 2016 Dec;13(12):2143-2150.
- **Donohue MJ.**, Increasing nontuberculous mycobacteria reporting rates and species diversity identified in clinical laboratory reports. BMC Infect Dis. 2018 Apr 10;18(1):163.

I, Maura Donohue, am in agreement with the listed total percentage of effort of 90%.

Sincerely,

Maura J. Donohue, Ph.D
US Environmental Protection Agency
Center of Environmental Solutions and Emergency Response (CESER)
Water Infrastructure Division
26 W. Martin Luther King Drive
Cincinnati, OH 45268
513-569-7634
Donohue.maura@epa.gov

Table of Contents

General_Authors_Publications.....2
LI-266296_Sarwar_et_al_2015_article.....24
LI-266297_Gantt_et_al_2017.....33
LI-266299_Sarwar_et_al_2019.....42
SI_Gantt_et_al_2017.....62
SI_Sarwar_et_al_2019.....69
SI_Sarwar_et_al_2015.....76
Muniz-Unamunzaga_et_al_2018.....83
Li_et_al__2019.....93
Record_of_percent_agreement_contribution.....110

STAA REPORT FOR THE SCIENTIST NOMINATIONS

General Information:

Nomination ID/App ID:	20-106
Research Category Primary:	Transport and Fate (TF)
Research Category Secondary:	Other Environmental Research (OR)
Laboratory/Office Name:	ORD
Nomination Entered By:	Golam Sarwar

Eligibility Checklist:

[Y] The nominated publication(s) has not been submitted to a previous STAA competition.

[Y] The nominated publication(s) was published on or before January 1, 2017 and on or after January 1,2012

[Y] The principal author was an EPA employee or a PHS employee assigned to EPA when the research was performed

[Y] The EPA authors (includes PHS employees assigned to EPA) contributed collectively a minimum of 50% toward the publication(s)

Nominating Official Name:	Alan Vette
Nominating Official Title:	SUPERVISORY PHYSICAL SCIENTIST (DEPUTY DIRECTOR)
Nominating OfficialEmail:	vette.alan@epa.gov
STAA Coordinator Name:	Kathleen Wiser
STAA Coordinator Email:	wiser.kathi@epa.gov

Justifications:

Justification 1:

Many current ozone non-attainment areas are located near coastal areas in the U.S. The improvement to the chemical mechanism in the Community Multiscale Air Quality (CMAQ) model introduced in these three papers are particularly targeted to address the National Ambient Air Quality Standard (NAAQS) related issues in these areas. CMAQ is an EPA-developed three-dimensional comprehensive air quality model that is widely used in the U.S. and globally for developing air pollution control strategies and conducting air quality research. Policymakers and researchers have utilized CMAQ on a variety of spatial scales ranging from fine-scale single-source studies to hemispheric-scale international transport studies. During some of these larger-scale applications, CMAQ persistently over-predicted ozone near coastal areas. As the NAAQS for ozone has been lowered, correcting for these over-predictions became a priority as state and local environmental agencies began the process of determining future compliance with the lowered NAAQS for ozone.

To address this shortcoming, we performed a comprehensive literature search in which we reviewed several studies suggesting that seawater can emit halogen compounds such as bromine and iodine which can participate in atmospheric chemical reactions to destroy ozone. The chemical mechanisms in CMAQ did not employ such reactions and were not adequate in predicting ozone over seawater and coastal areas. We also evaluated studies describing oceanic halogen emissions and atmospheric reactions of halogens and identified the most suitable method for estimating these emissions and relevant atmospheric chemical reactions for CMAQ. During the process, we also consulted investigators who have previously developed such emissions and reactions. These nominated papers focus on halogen-related advances to the heart of CMAQ: its chemical mechanism that solves for the hundreds of chemical reactions in the atmosphere involving ozone (O_3), oxides of nitrogen (NO_x), volatile organic compounds (VOC), carbon monoxide (CO), sulfur dioxide (SO_2), and many other compounds. In these papers, we 1) implemented oceanic halogen emissions and related chemical reactions into CMAQ, 2) linked them with the chemical reactions in the commonly used Carbon Bond chemical mechanism, 3) included the impact of these halogens on enhanced ozone depositional loss over seawater, and 4) performed model simulations on a variety of domains and configurations and analyzed the resulting change in predictions.

The main findings from these papers are that halogen chemistry enhances ozone deposition, reduces ozone concentrations, and improves model performance compared to observed ozone over coastal areas as well as some inland regions. These articles also quantify the impact of halogen chemistry on the intercontinental transport of ozone and estimates of background ozone. In Sarwar et al. (2019), for example, we show that background ozone estimates in the Western U.S. are reduced by halogen chemistry along the coast and well inland. Because few air quality models include this halogen chemistry, it is likely that background ozone has been overestimated in previous model-based studies.

As both developers and users of CMAQ, we are always concerned with how any change to the model affects its performance. The detailed halogen chemistry contains more than 90 chemical reactions involving 33 additional chemical species and takes a substantially more computational resource for completing model simulations. Therefore, we developed a condensed halogen chemistry to account for halogen-mediated ozone loss and implemented it in each of CMAQ's three chemical mechanisms. Model simulations with the condensed halogen chemistry are computationally efficient and can be applied to a modeling domain containing the U.S. and surrounding areas with limited oceanic area. This effort required us to develop creative methods for balancing scientific detail with computational limits and innovative ways to evaluate both the accuracy of the implementation and the predictions.

Because there are no existing guidelines for this type of work and the chemical mechanism is of high importance to EPA modeling efforts, we have also had to implement procedures for ensuring careful and open analysis and documentation of the halogen emissions, chemistry, and deposition and how these processes affect other pollutants like ozone. This effort has resulted in a significant advancement in the description of the chemical mechanisms and depositional processes that are supported by CMAQ. We have publicly released the detailed halogen chemistry with the Carbon Bond chemical mechanism, the condensed halogen chemistry combined with each of the three chemical mechanisms, and the enhanced ozone deposition over seawater. The most significant outcome of this work is that policy- and decision-makers can have confidence that by using the CMAQ model, they are

taking advantage of the most state-of-the-art chemical information and deposition scheme available and the model with the current science can now be used for developing policy decisions.

The CMAQ with the Carbon Bond chemical mechanism containing the condensed halogen chemistry and enhanced ozone deposition has become the default base model that EPA/OAQPS has used in several regulatory actions such as the 2018 Risk and Exposure Assessment Planning Document for the Secondary NOx/SOx/PM NAAQS, 2018 National Air Toxics Assessment (NATA) assessment, the 2019 Draft Policy Assessment for the Ozone NAAQS (background O_3 section) and the 2020 Policy Assessment for the PM NAAQS. The hemispheric CMAQ model with detailed halogen chemistry has been used for creating boundary conditions in some of these actions.

One of EPA's strategic goals is to deliver a cleaner, safer, and healthier environment for all Americans and the EPA has developed several long-term performance goals to achieve this strategic goal. For example, EPA's long-term performance goals include improving air quality and reducing number of non-attainment areas for NAAQS, prioritizing robust science to improve air quality, and delivering state-of-the-art tools for state and local environmental agencies to use in identifying effective emission reduction strategies to meet the NAAQS. Thus, the research described in these papers has the dual benefit of advancing the science in CMAQ and helping the EPA support its long-term performance goals of improving air quality and reducing the number areas currently in non-attainment with the NAAQS.

Justification 2A:

The three articles focus on various aspects halogen (bromine and iodine) chemistry and can be characterized as 1) initial implementation, 2) application to local air quality, and 3) comprehensive evaluation. Sarwar et al. (2015) focuses on the implementation of the enhanced ozone deposition scheme and atmospheric halogen chemistry in CMAQ. Specifically, it describes the details of the enhanced ozone deposition scheme that accounts for the interaction of atmospheric ozone with iodide present in seawater, oceanic halogen emissions, and atmospheric halogen reactions in the hemispheric CMAQ model. In this article, we performed a series of

simulations over the entire Northern Hemisphere (using 108-km horizontal grids) for a summer period to estimate the impact of enhanced ozone deposition and the impact of halogen chemistry on atmospheric ozone concentrations. We compared model predictions with observed data from remote sites in the Northern Hemisphere and documented that the predictions with enhanced ozone deposition and halogen chemistry improves the model performance. Because this halogen chemistry

substantially increased computational time in CMAQ, we also developed a computationally efficient halogen mediated ozone loss for model applications in areas with limited seawater.

For air quality impact analysis involving regulatory applications, the USEPA/OAQPS and many other users apply CMAQ over the continental U.S. using 12-km horizontal grids. Thus, Gantt et al. (2017) focus on the application of the model over the continental U.S. employing 12-km horizontal grids and employed boundary conditions generated from the hemispheric CMAQ model. In this article, we performed a series of model simulations for a summer period and estimated the impact of enhanced ozone deposition as well as the impact of halogen chemistry on atmospheric ozone over the continental U.S. We compared model predictions with observed data in the U.S. and showed that the predictions with enhanced ozone deposition and halogen chemistry lowers ozone concentrations and improved model performance especially near the coastal areas. In addition, we also used the condensed halogen chemistry, developed in the Sarwar et al. (2015) article, and demonstrated that the use of such condensed reaction produces reasonable ozone predictions compared to those with the detailed halogen chemistry. This ensures that the users of the condensed halogen chemistry can expect reasonable predictions for their model applications.

In Sarwar et al. (2019), we further refined the halogen emissions and chemistry developed in the first article. We added aqueous-phase bromine reactions as well as heterogeneous reactions for halogen species. We used hemispheric CMAQ and performed simulations without and with the halogen chemistry for an entire year and determined the seasonal and diurnal impacts of halogen chemistry on ozone. We documented that the halogen chemistry is active throughout the year and decreases ozone concentration without changing the diurnal profile of ozone. The halogen chemistry, however, does not have a strong seasonal influence on ozone. It improves model performance when compared to observations especially at coastal sites and over seawater. To isolate the impacts of bromine chemistry and iodine chemistry, we performed simulations separately and determined that iodine chemistry is four times more effective in reducing atmospheric ozone than the bromine chemistry. By performing additional simulations, we also determined that the halogen chemistry modulates intercontinental transport and lowers the background ozone imported to the U.S.

Justification 2B:

Golam Sarwar

2015 Level 3 STAA

1. Examining the impact of heterogeneous nitryl chloride production on air quality across the United States, (2012)

2. Importance of tropospheric $CINO_2$ chemistry across the Northern Hemisphere, (2014)

Brett Gantt

2015 Level 3 STAA

1. Near Road Modeling and Measurement of Cerium Containing Particles Generated by Nanoparticle Diesel Fuel Additive Use, (2014)

2. Inhaled Diesel Emissions Generated with Cerium Oxide Nanoparticle Fuel Additive Induce Adverse Pulmonary and Systemic Effects, (2014)

3. Predicting the Effects of Nanoscale Cerium Additives in Diesel Fuel on Regional Scale Air Quality, (2014)

Heather Simon

2015 Level 3 STAA

1. Near Road Modeling and Measurement of Cerium Containing Particles Generated by Nanoparticle Diesel Fuel Additive Use, (2014)

2. Inhaled Diesel Emissions Generated with Cerium Oxide Nanoparticle Fuel Additive Induce Adverse Pulmonary and Systemic Effects, (2014)

3. Predicting the Effects of Nanoscale Cerium Additives in Diesel Fuel on Regional Scale Air Quality, (2014)

2015 Level 3 STAA

1. Examining the impact of heterogeneous nitryl chloride production on air quality across the United States, (2012)

2. Importance of tropospheric $CINO_2$ chemistry across the Northern Hemisphere, (2014)

2015 Level 3 STAA

1. A Direct Sensitivity Approach to Predict Hourly Ozone Resulting from Compliance with the National Ambient Air Quality Standard, (2013)

2015 STAA nomination without any award

1. Compilation and Interpretation of Photochemical Model Statistics Published between 2006 and 2012, (2012)

2019 Honorable Mention STAA

1. Dynamic evaluation of CMAQ part I: Separating the effects of changing emissions and changing meteorology on ozone levels between 2002 and 2005 in the eastern US, (2015)

2. Dynamic Evaluation of CMAQ part II: Evaluation of Relative Response Factor Metrics for Ozone Non-Attainment demonstration (2015)

2019 Honorable Mention STAA

1. Ozone Trends Across the United States over a Period of Decreasing NOx and VOC Emissions, (2015)

2. Assessing Temporal and Spatial Patterns of Observed and Predicted Ozone in Multiple Urban Area, (2016)

Rohit Mathur

2015 Level 3 STAA

1. Near Road Modeling and Measurement of Cerium Containing Particles Generated by Nanoparticle Diesel Fuel Additive Use, (2014)

2. Inhaled Diesel Emissions Generated with Cerium Oxide Nanoparticle Fuel Additive Induce Adverse Pulmonary and Systemic Effects, (2014)

3. Predicting the Effects of Nanoscale Cerium Additives in Diesel Fuel on Regional Scale Air Quality, (2014)

2015 Level 3 STAA

1. Examining the impact of heterogeneous nitryl chloride production on air quality across the United States, (2012)

2. Importance of tropospheric $ClNO_2$ chemistry across the Northern Hemisphere, (2014)

2015 Level 3 STAA

1. WRF-CMAQ Two-way Coupled System with Aerosol Feedback: Software Development and Preliminary Results, (2012)

Donna Schwede

2015 Level 3 STAA

1. Processes of Ammonia Air-Surface Exchange in a Fertilized Zea mays Canopy, (2013)

2. Linking Agricultural Management and Air-Quality models for Regional to National-Scale Nitrogen Deposition Assessments, (2012)

3. Evaluation of a Regional Air-Quality Model with Bidirectional NH3 Exchange Coupled to an Agro-ecosystem Model, (2013)

2019 Honorable Mention STAA

1. Modeling the current and future roles of particulate organic nitrates in the southeastern United States, (2015)

2. On the implications of aerosol liquid water and phase separation for organic aerosol mass, (2017)

3. Simulating aqueous phase isoprene-epoxydiol (IEPOX) secondary organic aerosol production during the 2013 southern oxidant and aerosol study (SOAS), (2017)

Kristen Foley

2019 Honorable Mention STAA

1. Dynamic evaluation of CMAQ part I: Separating the effects of changing emissions and changing meteorology on ozone levels between 2002 and 2005 in the eastern US, (2015)

2. Dynamic Evaluation of CMAQ part II: Evaluation of Relative Response Factor Metrics for Ozone Attainment demonstrations, (2015)

Kathleen Fahey

2015 Level 3 STAA

1. Near Road Modeling and Measurement of Cerium Containing Particles Generated by Nanoparticle Diesel Fuel Additive Use, (2014)

2. Inhaled Diesel Emissions Generated with Cerium Oxide Nanoparticle Fuel Additive Induce Adverse Pulmonary and Systemic Effects, (2014)

3. Predicting the Effects of Nanoscale Cerium Additives in Diesel Fuel on Regional Scale Air Quality, (2014)

Tanya Spero

2015 Level 3 STAA

1. WRF-CMAQ Two-way Coupled System with Aerosol Feedback: Software Development and Preliminary Results, (2012)

2017 Level 3 STAA

1. Does Nudging Squelch the Extremes in Regional Climate Modeling? (2012)

2019 Honorable Mention STAA

1. Increasing the credibility of regional climate simulations by introducing subgrid-scale cloud – radiation interactions, (2014)

William Hutzell

2019 Honorable Mention STAA

1. Modeling the current and future roles of particulate organic nitrates in the southeastern United States, (2015)

2. On the implications of aerosol liquid water and phase separation for organic aerosol mass, (2017)

3. Simulating aqueous phase isoprene-epoxydiol (IEPOX) secondary organic aerosol production during the 2013 southern oxidant and aerosol study (SOAS), (2017)

Justification 2C:

This nomination deals with bromine and iodine chemistry and its impacts on ozone. None of the previous nominations focused on this topic.

Justification 2D:

Supplemental information listed in this nomination was not submitted in any previous STAA applications.

Justification 2E:

Tanya Spero has submitted a concurrent nomination for the 2015 Fann et al. article (The geographic distribution and economic value of climate change-related ozone health impacts in the United States in 2030) which addresses projected changes to air quality and health in the United States in 2030 due to climate change. The nomination submitted in this package addresses halogen chemistry and its impact on ozone. Thus, the focus of the current nomination is entirely different from the concurrent Tanya Spero nomination.

Justification 3A:

Both the detailed and the condensed halogen chemistry and enhanced ozone deposition scheme in CMAQ are being regularly used by researchers and regulators in the U.S. and in many other countries. The model with such options has been released and is publicly available from an archive at the USEPA. The Carbon Bond chemical mechanism with the condensed halogen chemistry and enhanced ozone deposition scheme has been adopted by the EPA/OAQPS as its base model for regulatory applications. Many state and local agencies are also using the model with such options. Current users of the Carbon Bond chemical mechanism with the condensed halogen chemistry and enhanced ozone deposition include the consortium of states represented by the Lake Michigan Air Directors Consortium (Illinois, Indiana, Michigan, Wisconsin and Ohio), New York, Maryland, and several other air agencies. In addition, the condensed halogen chemistry has been combined with all three chemical mechanisms. Currently CMAQ has more than 2000 users world-wide; all users of the current CMAQ model are using the condensed halogen chemistry and enhanced ozone deposition scheme.

Several users are currently using the CMAQ model with the detailed halogen chemistry. For example, the Technical University of Madrid (Spain), the University of Maryland, the University of Houston, the Hong Kong University of Science & Technology, and the Air Quality Forecasting team at the National Oceanic and Atmospheric Administration are currently using the halogen chemistry in the Carbon Bond chemical mechanism.

The primary authors of the nominated papers have been invited to speak at numerous national and international conferences on the halogen chemistry, enhanced ozone deposition and their implementation in CMAQ. These have included multiple presentations at the *33rd International* Technical Meeting on *Air Pollution Modelling* and *its Application (*Miami, Florida, USA, August 26-30, 2013*), the 13th Annual* Community Modeling and Analysis System Conference (Chapel Hill, NC, USA , October 27-29, 2014), *the 14th Annual* Community Modeling and Analysis System Conference (Chapel Hill, NC, USA, October 5-7, 2015), *the 15th Annual*

Community Modeling and Analysis System Conference (Chapel Hill, NC, USA, October 24-26, 2016), *the 16th Annual* Community Modeling and Analysis System Conference (Chapel Hill, NC, USA , October 23-25, 2017), and the 2018 joint international conference on ABaCAS and CMAS-Asia-Pacific Conference (Beijing, China, May 21-23, 2018).

Justification 3B:

Each manuscript followed a rigorous peer review process established by ORD and OAQPS before submitting for journal peer review. Within ORD, each paper was reviewed by two EPA scientists, Quality Assurance Manager, Branch Chief, the Associate Division Director for Science. The principal authors were responsible for addressing all comments. A parallel set of reviews were also performed within the Air Quality Assessment Division of EPA/OAR/OAQPS, with additional reconciliation of comments.

The Sarwar et al. (2015) and the Gantt et al. (2017) articles were submitted to *Environmental Science & Technology*, because it is an authoritative source of information in a wide range of environmental disciplines. It is published by the American Chemical Society, which is a leader in providing access to chemistry-related information and research. The focus of these articles fit in well with wide range target audience. The Sarwar et al. (2019) paper was submitted to *Atmospheric Environment*, because of its international coverage of air pollution research/applications and focus on atmospheric chemistry. Sarwar et al. (2019) fits well with *Atmospheric Environment*'s target audience of air quality researchers and policymakers. *Environmental Science & Technology* and *Atmospheric Environment* both require that submissions successfully pass a series of extensive anonymous peer review, to the satisfaction of the editor, prior to acceptance. These international journals maintain a large list of potential reviewers. Two to three anonymous external peer reviewers, chosen by the journals, provided comments for each of the articles. In general, the external review comments were minor and constructive, and all comments were satisfactorily addressed by the authors before the papers were accepted for publication. In addition, the panel of the sixth external peer review of the CMAQ model reviewed the halogen chemistry and provided positive feedback for including it in the model.

AUTHORS

Principal Author

Author Name:	Golam Sarwar		
Professional Title:		Salutation:	
Email:	sarwar.golam@epa.gov	Organization:	

Mailing Address:		
Street Line 1:		
City:		
Zip Code:		State:
At time of research was:	EPA Employee	
Separation Date:		
% of Effort:	30	

Contributing Author

Author Name:	Kristen Foley	
Professional Title:		Salutation:
Email:	foley.kristen@epa.gov	Organization:
Mailing Address:		
Street Line 1:		
City:		
Zip Code:		State:
At time of research was:	EPA Employee	
Separation Date:		
% of Effort:	10	

Contributing Author

Author Name:	Rohit Mathur	
Professional Title:		Salutation:
Email:	mathur.rohit@epa.gov	Organization:

Mailing Address:		
Street Line 1:		
City:		
Zip Code:		State:
At time of research was:	EPA Employee	
Separation Date:		
% of Effort:	9	

Contributing Author

Author Name:	Brett Gantt	
Professional Title:		Salutation:
Email:	gantt.brett@epa.gov	Organization:
Mailing Address:		
Street Line 1:		
City:		
Zip Code:		State:
At time of research was:	EPA Employee	
Separation Date:		
% of Effort:	20	

Contributing Author

Author Name:	Donna Schwede	
Professional Title:		Salutation:
Email:	schwede.donna@epa.gov	Organization:

Mailing Address:			
Street Line 1:			
City:			
Zip Code:		State:	
At time of research was:	EPA Employee		
Separation Date:			
% of Effort:	6		

Contributing Author

Author Name:	Alfonso Saiz-Lopez		
Professional Title:		Salutation:	
Email:	a.saiz@csic.es	Organization:	
Mailing Address:			
Street Line 1:			
City:			
Zip Code:		State:	
At time of research was:	Non EPA Personnel		
Separation Date:			
% of Effort:	6		

Contributing Author

Author Name:	Jia Xing		
Professional Title:		Salutation:	
Email:	xingjia@mail.tsinghua.edu.cn	Organization:	

Mailing Address:		
Street Line 1:		
City:		
Zip Code:		State:
At time of research was:	Non EPA Personnel	
Separation Date:		
% of Effort:	4	

Contributing Author

Author Name:	William T Hutzell	
Professional Title:		Salutation:
Email:	hutzell.bill@epa.gov	Organization:
Mailing Address:		
Street Line 1:		
City:		
Zip Code:		State:
At time of research was:	EPA Employee	
Separation Date:		
% of Effort:	2	

Contributing Author

Author Name:	Tomás Sherwen	
Professional Title:		Salutation:
Email:	tomas.sherwen@york.ac.uk	Organization:

Mailing Address:		
Street Line 1:		
City:		
Zip Code:		State:
At time of research was:	Non EPA Personnel	
Separation Date:		
% of Effort:	2	

Contributing Author

Author Name:	Kathleen Fahey	
Professional Title:		Salutation:
Email:	fahey.kathleen@epa.gov	Organization:
Mailing Address:		
Street Line 1:		
City:		
Zip Code:		State:
At time of research was:	EPA Employee	
Separation Date:		
% of Effort:	3	

Contributing Author

Author Name:	Daiwen Kang	
Professional Title:		Salutation:
Email:	kang.daiwen@epa.gov	Organization:

Mailing Address:		
Street Line 1:		
City:		
Zip Code:		State:
At time of research was:	EPA Employee	
Separation Date:		
% of Effort:	2	

Contributing Author

Author Name:	Heather Simon	
Professional Title:		Salutation:
Email:	simon.heather@epa.gov	Organization:
Mailing Address:		
Street Line 1:		
City:		
Zip Code:		State:
At time of research was:	EPA Employee	
Separation Date:		
% of Effort:	2	

Contributing Author

Author Name:	Tanya L Spero	
Professional Title:		Salutation:
Email:	spero.tanya@epa.gov	Organization:

Mailing Address:			
Street Line 1:			
City:			
Zip Code:		State:	
At time of research was:	EPA Employee		
Separation Date:			
% of Effort:	2		

Contributing Author

Author Name:	Hosein Foroutan		
Professional Title:		Salutation:	
Email:	hosein@vt.edu	Organization:	
Mailing Address:			
Street Line 1:			
City:			
Zip Code:		State:	
At time of research was:	Non EPA Personnel		
Separation Date:			
% of Effort:	2		

PUBLICATIONS

Publication 1:

Publication Title:	Impact of enhanced ozone deposition and halogen chemistry on tropospheric ozone over the Northern He

Publication Date:	Tue Jul 07 00:00:00 GMT 2015		
Journal/Publication Method:	Environmental Science & Technology		
All Author(s):			
Volume:	49	Number:	15
Pages:	9203-9211	Immediately Index:	Immediately Index:
Citation ½ Life:	7.8	Impact Factor:	7.149

Publication 2:

Publication Title:	The impact of iodide-mediated ozone deposition and halogen chemistry on surface ozone concentrations		
Publication Date:	Wed Jan 04 00:00:00 GMT 2017		
Journal/Publication Method:	Environmental Science & Technology		
All Author(s):			
Volume:	51	Number:	3
Pages:	1458-1466	Immediately Index:	Immediately Index:
Citation ½ Life:	7.8	Impact Factor:	7.149

Publication 3:

Publication Title:	Influence of bromine and iodine chemistry on annual, seasonal, diurnal, and background ozone: CMAQ		
Publication Date:	Tue Jun 11 00:00:00 GMT 2019		
Journal/Publication Method:	Atmospheric Environment		

All Author(s):			
Volume:	213	Number:	15
Pages:	395-404	Immediately Index:	Immediately Index:
Citation ½ Life:	9.3	Impact Factor:	4.012

Environmental Science & Technology

Article

pubs.acs.org/est

Impact of Enhanced Ozone Deposition and Halogen Chemistry on Tropospheric Ozone over the Northern Hemisphere

Golam Sarwar,*[,†] Brett Gantt,[†] Donna Schwede,[†] Kristen Foley,[†] Rohit Mathur,[†] and Alfonso Saiz-Lopez[‡]

[†]National Exposure Research Laboratory, Environmental Protection Agency, Research Triangle Park, North Carolina 27711, United States

[‡]Atmospheric Chemistry and Climate Group, Institute of Physical Chemistry Rocasolano, CSIC, Madrid 28006, Spain

Supporting Information

ABSTRACT: Fate of ozone in marine environments has been receiving increased attention due to the tightening of ambient air quality standards. The role of deposition and halogen chemistry is examined through incorporation of an enhanced ozone deposition algorithm and inclusion of halogen chemistry in a comprehensive atmospheric modeling system. The enhanced ozone deposition treatment accounts for the interaction of iodide in seawater with ozone and increases deposition velocities by 1 order of magnitude. Halogen chemistry includes detailed chemical reactions of organic and inorganic bromine and iodine species. Two different simulations are completed with the halogen chemistry: without and with photochemical reactions of higher iodine oxides. Enhanced deposition reduces mean summer-time surface ozone by ∼3% over marine regions in the Northern Hemisphere. Halogen chemistry without the photochemical reactions of higher iodine oxides reduces surface ozone by ∼15% whereas simulations with the photochemical reactions of higher iodine oxides indicate ozone reductions of ∼48%. The model without these processes overpredicts ozone compared to observations whereas the inclusion of these processes improves predictions. The inclusion of photochemical reactions for higher iodine oxides leads to ozone predictions that are lower than observations, underscoring the need for further refinement of the halogen emissions and chemistry scheme in the model.

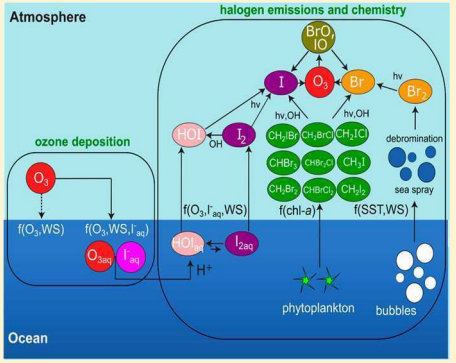

1.0. INTRODUCTION

Ozone (O_3) has been linked to adverse effects on human health[1] and ecosystems.[2] To mitigate these effects, air quality standards have been periodically revised, which has led to the tightening of ambient air quality standards for O_3. The tightened ambient air quality standards make the determination of background O_3 levels more important. Background levels of O_3 are affected by mixing ratios over the ocean, which are influenced greatly by the chemicals present in the sea surface microlayer. These chemical compounds can be emitted to the atmosphere and affect atmospheric chemistry and can also serve as a chemical sink to enhance deposition to the seawater surface. Studies have suggested that O_3 deposition over seawater is highly variable due to variations in atmospheric O_3 mixing ratio and deposition velocity (flux/mixing ratio), with reported deposition velocities ranging from 0.009 to ∼0.27 cm s^{-1}.[3,4] The deposition velocity over seawater is dependent on a number of factors including the atmospheric turbulence and the chemical composition of the seawater. Although several compounds in seawater can interact with O_3[5−7] and the presence of other compounds can affect such interactions,[8] there is still much uncertainty in modeling these interactions. Considerably more consensus has been reached on the interaction between O_3 and iodide in the seawater. Developing reliable spatial distributions of iodide concentrations in seawater is key and concentrations have been estimated using various proxies, including chlorophyll-*a* (chl-*a*),[9] nitrate,[10] and sea surface temperature (SST).[10,11] Several models of the enhanced deposition of O_3 over seawater have been proposed ranging from complex approaches such as that of Fairall et al.[12] to more simple approaches such as that of Chang et al.[5] Oh et al.[9] employed the simple approach of Chang et al.[5] and linked O_3 dry deposition velocities to satellite-derived chl-*a* concentrations and reported a maximum surface O_3 decrease of 2.5 ppbv offshore of Galveston, Texas. Although the Oh et al.[9] study suggests enhanced deposition of O_3 over seawater can affect atmospheric O_3 in areas of the Gulf of Mexico, little is known about its importance in other coastal areas.

Although several studies have postulated that bromine and iodine emitted from the ocean impact atmospheric chemistry,[13−15] recent measurements of speciated halogen species with advanced instrumentation have confirmed the presence of an oceanic halogen emission source.[16−20] The sea−air flux and associated chemistry of bromine- and iodine-containing compounds affects new particle formation, mercury cycling, oxidative capacity, and O_3 mixing ratio of the marine atmosphere.[17,21−23] These halogen species undergo photolysis

Received: April 1, 2015
Revised: June 24, 2015
Accepted: July 6, 2015
Published: July 7, 2015

Downloaded via US EPA RESEARCH TRIANGLE PARK on April 2, 2020 at 14:44:50 (UTC).
See https://pubs.acs.org/sharingguidelines for options on how to legitimately share published articles.

© 2015 American Chemical Society

DOI: 10.1021/acs.est.5b01657
Environ. Sci. Technol. 2015, 49, 9203−9211

and react with oxidants to release iodine or bromine, which can then catalytically react with O_3 to reduce its levels in the marine atmosphere. With the increasing focus on background O_3 levels, marine halogen sources/chemistry have been the subject of several recent laboratory, field, and modeling studies.[24−38] Laboratory studies report that the reactions of O_3 and marine aerosols can release halogens[24,27] and water surface properties can also affect these reactions.[26,28] Although the reaction of O_3 with bromide is generally low,[39] some studies reveal the possibility of a surface-mediated reaction that can enhance the reaction rate leading to the loss of O_3 and release of gaseous bromine.[24,25,28]

In recent years, several modeling studies have attempted to represent marine halogen emission sources and atmospheric chemistry with increasing levels of complexity. Beginning with the one-dimensional modeling work of halogen chemistry in the atmosphere,[29,30] various marine emission sources such as halocarbons,[31,32] sea spray aerosol (SSA) bromine,[33] and iodine/hypoiodous acid[11] and chemical reactions such as photolysis of higher iodine oxides[34] have been implemented into global chemical transport models. Saiz-Lopez et al.[35] found that tropospheric O_3 loss due to marine halogen emissions can have a climatically relevant radiative impact whereas Parrella et al.[36] postulate that the inclusion of bromine chemistry improves model prediction of preindustrial O_3 observations and leads to differential mercury lifetimes in preindustrial and present-day conditions. Long et al.[37] report that bromine activated from SSA reduces marine boundary layer O_3 by >20% over most of the tropics and >75% over the Southern Ocean. Despite the demonstrated impact of enhanced deposition of O_3 over seawater and marine halogen emissions/chemistry on O_3 mixing ratios, these processes are currently not accounted for in most regional air quality models. The reaction between O_3 and dissolved iodide in seawater not only decreases atmospheric O_3 but also generates halogen emissions that activate the atmospheric chemistry of reactive halogens. The loss of atmospheric O_3 due to the reaction of O_3 and dissolved iodide in seawater is modeled using enhanced deposition velocity. In this study, we quantify the impact of enhanced O_3 deposition and marine halogen emissions and chemistry on tropospheric O_3 mixing ratios over the Northern Hemisphere.

2.0. METHODOLOGY

2.1. Model Description. The Community Multiscale Air Quality (CMAQ) modeling system is a comprehensive regional air quality model accounting for interactions among major atmospheric processes.[40] Many studies have employed the regional CMAQ model and demonstrated its skill in simulating ambient pollutants.[41−44] Mathur et al.[45,46] recently extended the model capabilities for applications to the Northern Hemisphere. Sarwar et al.[47] applied the hemispheric CMAQ model for examining the impacts of heterogeneous nitryl chloride chemistry in the Northern Hemisphere whereas Xing et al.[48] used the model for evaluating air quality trends. Here, we employ the online hemispheric CMAQ model using a horizontal resolution of 108-km and 44 vertical layers.[48] The CB05TUCl chemical mechanism[42] that integrates chlorine chemistry with the Carbon Bond mechanism was used. Emissions inputs are described in Sarwar et al.[47] and meteorological fields are detailed in Xing et al.[48] In the following sections, we describe the model implementation of enhanced O_3 deposition (section 2.2), halogen chemistry (section 2.3), and halogen emissions (section 2.4).

2.2. Deposition of Species. CMAQ accounts for both the dry and wet deposition of model species, and these treatments have been described in Byun et al.[40] These deposition approaches have been updated to include the necessary parameters for modeling the loss of bromine and iodine species (section 2.3). Here we focus on updates to the deposition of O_3.

The deposition velocity (v_d) for gas species is parametrized in CMAQ using the familiar resistance analogy:[49]

$$v_d = (R_a + R_b + R_s)^{-1} \quad (1)$$

where the aerodynamic resistance (R_a) accounts for atmospheric turbulence, the boundary layer resistance (R_b) represents diffusion across the quasi-laminar near-surface layer, and the surface resistance (R_s) accounts for the uptake by the surface. In CMAQ, the R_s for water surfaces is calculated as[12,50]

$$R_s = \left(\frac{Sc}{Pr}\right)^{2/3} ((H_{eff})(k)(\rho_a/\rho_w)^{0.5}(u_*))^{-1} \quad (2)$$

where Sc = Schmidt number (unitless), Pr = Prandtl number (unitless), H_{eff} = dimensionless effective Henry's Law constant (ratio of aqueous to gas phase), k = von Karman constant (0.4), ρ_a = density of air (g cm^{-3}), ρ_w = density of water (g cm^{-3}) and u_* = friction velocity (m s^{-1}).

The v_d value obtained using eqs 1 and 2 is referred to here as the standard deposition velocity and is used for most chemical species.

We revised the standard deposition velocity calculation to account for the enhanced deposition of O_3 due to the reaction with iodide in seawater. Similar to the work by Oh et al.,[9] we implemented the approach of Chang et al.[5] In this parametrization, R_s over seawater is calculated as

$$R_s = \frac{1}{H_{eff}(ak_w + (\lambda D)^{1/2})} = \frac{1}{pk_w + q} \quad (3)$$

where k_w = gas transfer velocity (m s^{-1}), a = chemical enhancement factor, $(\lambda D)^{1/2}$ = chemical loss of O_3, p = $(a)(H_{eff})$ = 1.75, and q = $(\lambda D)^{1/2}$ (H_{eff}). The values for k_w and q are calculated as

$$k_w = \frac{k(\rho_a/\rho_w)^{0.5}(u_*)}{\left(\frac{Sc}{Pr}\right)^{2/3}} \quad (4)$$

$$q = [(k_i)(C_i)(d_w)]^{0.5}(H_{eff}) \quad (5)$$

where k_i is the second-order kinetic rate constant, C_i = concentrations of iodide in seawater (calculated using eq 9), and d_w = diffusion coefficient of O_3 in water (m^2 s^{-1}). Magi et al.[51] reported a temperature dependent k_i ranging from 3.2 × 10^8 to 2.4 × 10^9 for a temperature range of 276−293 K that increases with increasing water temperature. We have used a constant value of 2.0 × 10^9 in our study.[52] Thus, our simulated impacts of enhanced O_3 deposition at lower water temperature will be somewhat greater than the real impacts. Similarly, simulated impacts of enhanced O_3 deposition at higher water temperature will be lower than the real impacts. The v_d value obtained using eqs 1 and 3 is referred here as the enhanced deposition velocity. Values of R_a and R_b are determined using the same procedures in the standard and enhanced deposition velocity calculations.

CMAQ-derived standard O_3 deposition velocities over seawater are less than 0.01 cm s^{-1} whereas the enhanced O_3

DOI: 10.1021/acs.est.5b01657
Environ. Sci. Technol. 2015, 49, 9203−9211

deposition velocities generally range between 0.01 and 0.04 cm s^{-1} (Figure S.1 of the Supporting Information). The median CMAQ-estimated standard and enhanced deposition velocities for O_3 over seawater are ~0.001 and 0.025 cm s^{-1}, respectively. Helmig et al.[4] reported median O_3 deposition velocities over different seawater ranging from 0.009 to 0.27 cm s^{-1}; therefore, the enhanced deposition velocities agree better with observations than the standard deposition velocities. However, further increases are needed for improving the agreement with observed deposition velocities.

2.3. Halogen Chemistry. Several investigators have examined the role of bromine chemistry on O_3.[32,33,36,53] We use the Yang et al.[33] bromine chemistry with 5 additional reactions to account for the interactions of BrO with ClO and with DMS and BrO.[32,54] A complete list of the bromine gas phase chemical reactions implemented in CMAQ can be found in Table S.1 of the Supporting Information.

Numerous investigators have studied iodine chemistry,[32,34,55] with Saiz-Lopez et al.[34] reporting a comprehensive mechanism of iodine gas phase chemical reactions, including photolysis of higher iodine oxides (I_2O_2, I_2O_3, and I_2O_4), listed in Table S.2 of the Supporting Information. Although previous studies[56,57] suggested that higher iodine oxides impact aerosol formation, Saiz-Lopez et al.[34] found that they also play a role in atmospheric chemistry and included their photochemical reactions in a global model. The Saiz-Lopez et al. study included two sets of iodine chemistry: one set without the photolysis of I_2O_2, I_2O_3, and I_2O_4 (lower limit) and the other set with the photolysis of I_2O_2, I_2O_3, and I_2O_4 (upper limit). We completed two different model simulations with the halogen chemistry similar to that of Saiz-Lopez et al.[34] without and with the photochemical reactions of higher iodine oxides.

Yang et al.[33] considered heterogeneous hydrolysis of bromine nitrate ($BrONO_2$) on aerosols, which we also use R1. We calculate the heterogeneous reaction rate of $BrONO_2$ using $k_{BrONO_2} = \gamma cA/4$, where γ = reactive uptake coefficient, c = mean molecular speed (m s^{-1}) (a function of temperature), and A = aerosol surface area (m^2 m^{-3}). Consistent with Yang et al.,[33] we used $\gamma = 0.3$ following the recommendation of the International Union of Pure and Applied Chemistry (IUPAC). The recent IUPAC[58] evaluation provides values of 0.15−1.0 for the uptake coefficient of $BrONO_2$ on liquid substrates.

$$BrONO_2(g) + H_2O(aq) \rightarrow HOBr(g) + HNO_3(g) \quad (R1)$$

2.4. Halogen Emissions. Marine emissions of bromine- and iodine-containing compounds fall into three categories with distinct formation mechanisms: (1) halocarbons, (2) inorganic bromine, and (3) inorganic iodine. Halocarbons are produced in the ocean by phytoplankton and macroalgae and typically have elevated oceanic concentrations in regions of high biological activity.[59] Halocarbon emissions are adapted from the Community Atmosphere Model with Chemistry (CAM-Chem)[35] and the Comprehensive Air quality Model with extensions (CAMx).[60] The halocarbons include five bromocarbons ($CHBr_3$, CH_2Br_2, CH_2BrCl, $CHBrCl_2$, $CHBr_2Cl$) and four iodocarbons (CH_3I, CH_2ICl, CH_2IBr, CH_2I_2) and their emissions are estimated using monthly average climatological chl-*a* concentrations derived from the Moderate Resolution Imaging Spectroradiometer (MODIS) aboard the Aqua satellite (oceancolor.gsfc.nasa.gov/cgi/l3) and projected to the polar stereographic coordinate system used in the hemispheric CMAQ model. For each halocarbon, the emission rate is calculated as

$$E_{HC} = (O_F + S_F) \times A_{GC} \times 1.2 \times 10^{-11} \times f_{HC} \times f_{DP} \times [\text{chl}-a] \quad (6)$$

where E_{HC} = halocarbon emission rate (moles s^{-1}), O_F = open ocean zone fraction of the grid cell, S_F = surf zone fraction of the grid cell, A_{GC} = grid cell area (m^2), 1.2×10^{-11} represents a base emission rate, f_{HC} = a species-dependent emission factor, and f_{DP} = a diurnal profile factor based on the grid cell local hour peaking at noon. Values of f_{HC} and f_{DP} from CAMx[60] are used.

Unlike halocarbons, which are directly emitted from the ocean surface, SSA are the source of the one inorganic bromine compound (Br_2).[33] Bromine depletion in SSA is acidity dependent and thought to be due to the uptake of gaseous HOBr[61] or HOCl[62] from the heterogeneous reaction of N_2O_5 on aerosol surfaces. We use the simplified treatment of bromine release from SSA[33] as

$$P_{SSA} = (O_F + S_F) \times A_{GC} \times 0.965 \times 10^{-16} \times U_{10}^{3.41} \times (0.38 + 0.054 \times \text{SSTC}) \times \rho_{SSA} \quad (7)$$

$$E_{Br_2} = 0.8624 \times P_{SSA} \times R_a \times \text{DF}/\text{MW}_{Br_2} \quad (8)$$

where P_{SSA} = mass production of SSA with dry radius <10 μm (g s^{-1}), 0.965×10^{-16} represents total volume flux of SSA at a wind speed of 1 m s^{-1} and relative humidity of 0%, U_{10} = 10 m wind speed (m s^{-1}), SSTC is the sea surface temperature in °C, ρ_{SSA} = dry SSA density (2.165×10^3 g m^{-3}), E_{Br_2} = Br_2 emission rate (moles s^{-1}), R_a = sea-salt Br/NaCl mass ratio (0.00223 g g^{-1}), DF = bromine depletion factor (0.5), and MW_{Br_2} = molecular weight of Br_2. In CMAQ, NaCl represents 86.24% of the SSA emissions; thus, we use a factor of 0.8624 to calculate NaCl emissions. Spatially, Br_2 emissions are consistent with the distribution of SSA emissions, which are positively related to U_{10} and SST in CMAQ as recently implemented by Gant et al.[63]

Mahajan et al.[64] compared model predictions to observed halogen species over the Atlantic Ocean and reported that current iodine fluxes are inadequate to explain the observed IO levels and additional iodine sources are needed. McDonald et al.[11] developed a parametrization for estimating emissions of two inorganic iodine species (HOI and I_2) based on the surface mixing ratios of O_3 in the atmosphere, iodide concentration at the sea surface, and wind speed. This parametrization is based on the production of HOI and I_2 from the reaction of iodide and O_3 in the interfacial layer of the ocean surface.[18] Following the global analysis from Chance et al.,[10] we follow the MacDonald et al.[11] approach to estimate I_2 and HOI emissions that are driven by sea surface iodide concentrations ($[I_{(aq)}^-]$) based on SST:

$$[I_{(aq)}^-] = 1.46 \times 10^6 \times \exp\left(\frac{-9134}{\text{SST}}\right) \quad (9)$$

DOI: 10.1021/acs.est.5b01657
Environ. Sci. Technol. 2015, 49, 9203−9211

$$E_{HOI} = (O_F + S_F) \times A_{GC} \times 1.16 \times 10^{-14} \times [O_3] \times \left(4.15 \times 10^5 \times \left(\frac{\sqrt{[I_{(aq)}^-]}}{ws}\right) - \left(\frac{20.6}{ws}\right) - 23600 \times \sqrt{[I_{(aq)}^-]}\right) \quad (10)$$

$$E_{I_2} = (O_F + S_F) \times A_{GC} \times 1.16 \times 10^{-14} \times [O_3] \times [I_{(aq)}^-]^{1.3} \times (1.74 \times 10^9 - (6.54 \times 10^8 \times \ln ws)) \quad (11)$$

where E_{HOI} = HOI emission rates (mole s^{-1}), E_{I_2} = I_2 emission rates (mol s^{-1}), [O_3] = surface O_3 mixing ratios (ppbv), and ws = wind speed (m s^{-1}). We also set a lower limit of 3 m s^{-1} for wind speed following McDonald et al.[11]

Hemispheric halocarbons and inorganic halogen emissions estimates are shown in Table 1. Global halocarbon emissions

Table 1. Halogen Emissions Estimates[a]

species	hemispheric summer estimates in this study (Gg)	global annual estimates in this study (Gg)	global annual estimates from published studies (Gg)
$CHBr_3$	100.1	525	533
CH_2Br_2	17.2	90	67.3
CH_2BrCl	2.0	11	10.0
$CHBr_2Cl$	4.9	26	19.7
$CHBrCl_2$	4.8	17	22.6
CH_3I	44.9	236	303
CH_2ICl	49.2	258	234
CH_2IBr	18.3	96	87.3
CH_2I_2	24.4	128	116
Br_2	274 (Br)		1150–2090 (Br)
			1420 (Br)
HOI + 2xI_2	736 (I)		1900 (I)

[a]Global annual estimates of halocarbon emissions are taken from Ordóñez et al.,[32] global annual estimates of Br_2 are taken from Yang et al.[33] and Parrella et al.,[36] and global annual estimates of HOI + 2xI_2 are taken from Saiz-Lopez et al.[34]

can be calculated using publicly available global chl-*a* data. Using such data, we calculated global halocarbon emissions and compared to the values reported by others. Our global halocarbon emissions estimates compare well with values reported by Ordóñez et al.[32] Calculation of global inorganic halogen emissions requires global wind speed, SST, and O_3 fields. Because our modeling domain only covers the Northern Hemisphere, we could not accurately estimate global emissions of Br_2, HOI, and I_2. Our extrapolated global Br_2 emissions estimate is likely to be greater than the estimate of Parrella et al.[36] but is similar to the higher estimate of Yang et al.[33] Our estimate accounts for the temperature effect on SSA; hence our Br_2 estimates extrapolated from the Northern Hemisphere during summer-time conditions will be higher than those estimated without considering the temperature effect. Our Br_2 estimates are within the uncertainty factor of 4.0 for SSA sources.[65]

Prados-Roman et al.[66] implemented the McDonald et al.[11] parametrization into the CAM-Chem model and reported an annual global inorganic iodine emissions estimate of ~1900 Gg(I). Our extrapolated global inorganic iodine emissions are likely to be greater than this value due to different O_3, SST, wind-speed fields. CMAQ predicted surface O_3 mixing ratios are higher than those predicted by CAM-Chem. The surface layer height in CMAQ is ~20 m and we use wind-speeds at 10 m for calculating inorganic iodine emissions. In contrast, the surface layer height in CAM-Chem is ~150 m and Prados-Roman et al.[66] used CAM-Chem model first layer wind-speeds for calculating these emissions. Differences in O_3 and wind-speed lead to greater iodine emissions in CMAQ. Additionally, we focus on summer-time when halogen emissions are likely to be greater than those in the winter-time. Similar to the Prados-Roman et al.[66] estimates, our calculation also suggests that 95% of the inorganic iodine emissions are in the form of HOI and 5% are in the form of I_2.

2.5. Simulation Details. Four different model simulations were conducted. The first simulation (Case A) was completed using the standard O_3 deposition velocity over seawater and the CB05TUCl mechanism. The second simulation (Case B) was completed using the enhanced O_3 deposition over seawater and the CB05TUCl mechanism. The third simulation (Case C) was completed using the enhanced O_3 deposition over seawater, the CB05TUCl mechanism, and halogen chemistry without the photolysis of higher iodine oxides. The fourth simulation (Case D) was completed using the enhanced O_3 deposition over seawater, the CB05TUCl mechanism, and halogen chemistry with the photolysis of higher iodine oxides. Differences between Cases A and B are attributable to the enhanced deposition over seawater. Differences between Cases B and C simulation results are attributable to halogen chemistry without the photolysis of higher iodine oxides whereas the differences between Cases B and D are attributable to halogen chemistry with the photolysis of higher iodine oxides. Each simulation was completed for four months (May–August) in 2006. May was used as model spin-up period and results of the three summer months (June–August) are analyzed.

3.0. RESULTS AND DISCUSSSION

3.1. Distribution of Halogen Species. The predicted mean surface mixing ratios for all halogen species over marine regions for Case C are presented in Table 2. HBr, produced via reactions of Br with HO_2 and aldehydes, contributes the highest percentage of total bromine. $CHBr_3$ is the second most abundant bromine species due to large emissions and a relatively long atmospheric lifetime. Br_2 is an emitted species but can also be formed in the atmosphere and is the third most abundant bromine species. CH_2Br_2 is an emitted species that only reacts with OH and is the fourth most abundant species. The fifth most abundant species is HOBr, which is produced only by chemical reactions.

The most abundant iodine species, I_2O_3, is a reaction product that does not participate in any other chemical reactions. The I_2O_3 mixing ratio decreases only via dry and wet deposition; enabling it to accumulate in the atmosphere. HOI is the second most abundant iodine species and is formed through primary emissions and secondary formation. CH_3I is the third most abundant iodine species due to its large emission rates and long atmospheric lifetime. $IONO_2$ is the fourth highest abundant iodine species.

Predicted surface BrO and IO mixing ratios (daytime mean over marine regions) are 0.3 and 1.2 pptv, respectively. Because the rate constants for the reactions of Br + O_3 and I + O_3 are

DOI: 10.1021/acs.est.5b01657
Environ. Sci. Technol. 2015, 49, 9203–9211

Table 2. Predicted Mean Surface Mixing Ratios of Halogen Species (Case C)[a]

species	mean mixing ratio (pptv)	percent distribution (%)	species	mean mixing ratio (pptv)	percent distribution (%)
HBr	6.8	33.6	I_2O_3	5.0	58.6
$CHBr_3$	2.2	32.6	HOI	2.5	14.6
Br_2	1.3	13.1	CH_3I	2.1	12.2
CH_2Br_2	0.9	8.7	$IONO_2$	0.8	5.0
HOBr	1.3	6.4	IO	0.6	3.7
$CHBr_2Cl$	0.2	1.8	CH_2ICl	0.3	1.9
$BrONO_2$	0.2	1.1	I	0.2	0.9
BrO	0.2	0.8	I_2	0.1	0.7
$CHBrCl_2$	0.1	0.7	INO_2	0.1	0.6
CH_2BrCl	0.1	0.7	HI	0.1	0.6
CH_2IBr	0.1	0.3	CH_2I_2	<0.1	0.5
$BrNO_2$	<0.1	0.2	CH_2IBr	0.1	0.4
Br	<0.1	<0.1	OIO	<0.1	0.3
BrCl	<0.1	<0.1	I_2O_2	<0.1	<0.1
total Br	20.2		INO	<0.1	<0.1
			I_2O_4	<0.1	<0.1
			ICl	<0.1	<0.1
			total I	17.1	

[a]Total Br and Total I are calculated as follows. Total Br = $3xCHBr_3$ + HBr + $2xBr_2$ + $2xCH_2Br_2$ + HOBr + $BrONO_2$ + $2xCHBr_2Cl$ + BrO + CH_2BrCl + $CHBrCl_2$ + CH_2IBr + $BrNO_2$ + Br + BrCl. Total I = $2xI_2O_2$ + $2xI_2O_3$ + $2x\ I_2O_4$ + HOI+ CH_3I + $IONO_2$ + IO + CH_2ICl + I + $2xI_2$ + INO_2 + HI+ $2xCH_2I_2$ + CH_2IBr+ OIO + INO + ICl.

similar; the higher IO value relative to BrO suggests that the iodine chemistry is more effective in reducing O_3 than bromine chemistry. Saiz-Lopez et al.[35] compiled BrO and IO data from ground and ship-based measurements. Ground-based measured BrO ranged 0.5−2.0 pptv and ship-based BrO ranged 3.0−3.6 pptv whereas ground-based IO ranged 0.2−2.4 pptv and ship-based IO level was ∼3.5 pptv. Prados-Roman et al.[19] reported IO measurements of 0.4−1.0 pptv in the global marine boundary layer. Mahajan et al.[64] reported a daytime average measurement of 2.8 pptv for BrO and 1.5 pptv for IO at Cape Verde in Atlantic Ocean. Thus, the halogen chemistry without the photolysis of higher iodine oxides successfully reproduces these observed halogen oxides. Higher levels (∼100 pptv) of BrO have been measured in the boundary layer of the Dead Sea.[67,68] Our model results are lower than these high observed values over the Dead Sea, which contains 86 times more bromide than typical ocean water.[69] Tas et al.[69] studied the atmospheric bromine chemistry over the Dead Sea using a one-dimensional model and reported that high levels of bromide in the Dead Sea water and release of halogen species from airborne aerosols are not adequate to capture the observed BrO values. In their study, the addition of two heterogeneous reactions significantly improved the BrO predictions: the $BrONO_2$ heterogeneous reaction and the bromine explosion reaction. Our model uses typical ocean water bromide levels and does not use the bromine explosion reaction. Although our model uses the $BrONO_2$ heterogeneous reaction, the uptake coefficient is 2.5 times lower than the value used in their study. These differences likely caused our model predictions of BrO to be lower than high observed data over the Dead Sea.

3.2. Impact of Enhanced O_3 Deposition and Halogen Chemistry on O_3. Predicted mean O_3 averaged over all marine regions obtained with the standard deposition velocity is ∼27 ppbv at surface and increases with altitude reaching ∼330 ppbv at the highest model layer. The percent reductions due to the enhanced deposition and halogen chemistry are shown in Figure 1. The impact of the enhanced deposition is the highest

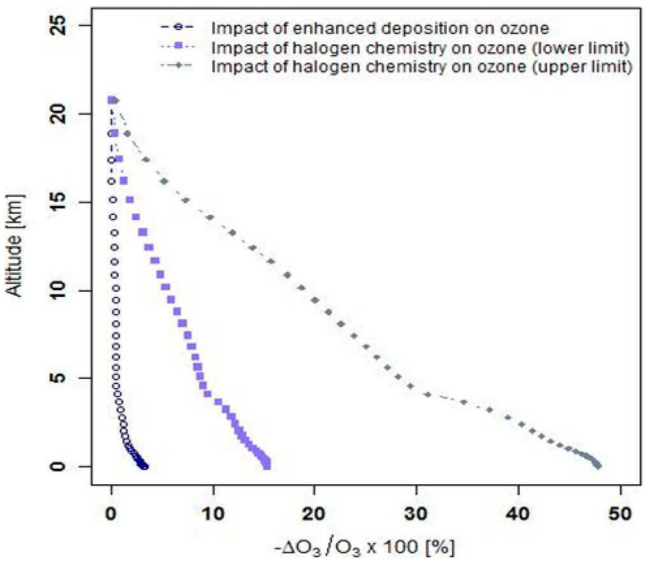

Figure 1. Percent reduction of O_3 due the enhanced deposition and halogen chemistry.

at the surface (∼3%), sharply decreases with height, and is expectedly negligible at higher altitudes. Though the impact of the halogen chemistry is also the highest at the surface, decreasing with height, it can effectively reduce O_3 concentrations throughout the lower troposphere. Although halogen chemistry without photolysis of higher iodine oxides reduces surface O_3 mixing ratios over marine regions by 15%, including the photolysis of these oxides results in a more substantial decrease in surface O_3 mixing ratios averaging nearly 48%. As noted in section 3.1, I_2O_3 is the most abundant iodine species and the inclusion of its photolytic reaction reduces I_2O_3 mixing ratios and generates iodine, which participates in O_3 destruction.

The spatial distributions of summer-time mean surface O_3 mixing ratios predicted by Case A and reduction due to enhanced deposition velocity and halogen chemistry are presented in Figure 2. Higher O_3 mixing ratios are predicted over terrestrial and coastal areas than over remote marine regions. Enhanced deposition reduces O_3 mixing ratios by 1.0−2.0 ppbv over most marine regions and by 2.0−3.0 ppbv over some coastal regions. The impact of the enhanced deposition in remote marine areas is relatively small due to lower absolute mixing ratios. Halogen chemistry without photolysis of higher iodine oxides reduces O_3 mixing ratios in the majority of the modeling domain. However, the reduction is greater over the marine environment than over land. O_3 mixing ratios are reduced by 4.0−6.0 ppbv over most remote marine regions and over 6.0 ppbv occurs in several coastal areas. Over most terrestrial regions near the coast, O_3 mixing ratios are reduced by 2.0−4.0 ppbv due to halogen chemistry. The inclusion of the photochemical reactions of higher iodine oxides has a large impact on predicted O_3 mixing ratios, with reductions of 12−24 ppbv over large swaths of the marine domain.

Yang et al.[33] reported that bromine chemistry reduces 4−6% of monthly mean summer-time tropospheric O_3 in Northern

DOI: 10.1021/acs.est.5b01657
Environ. Sci. Technol. 2015, 49, 9203−9211

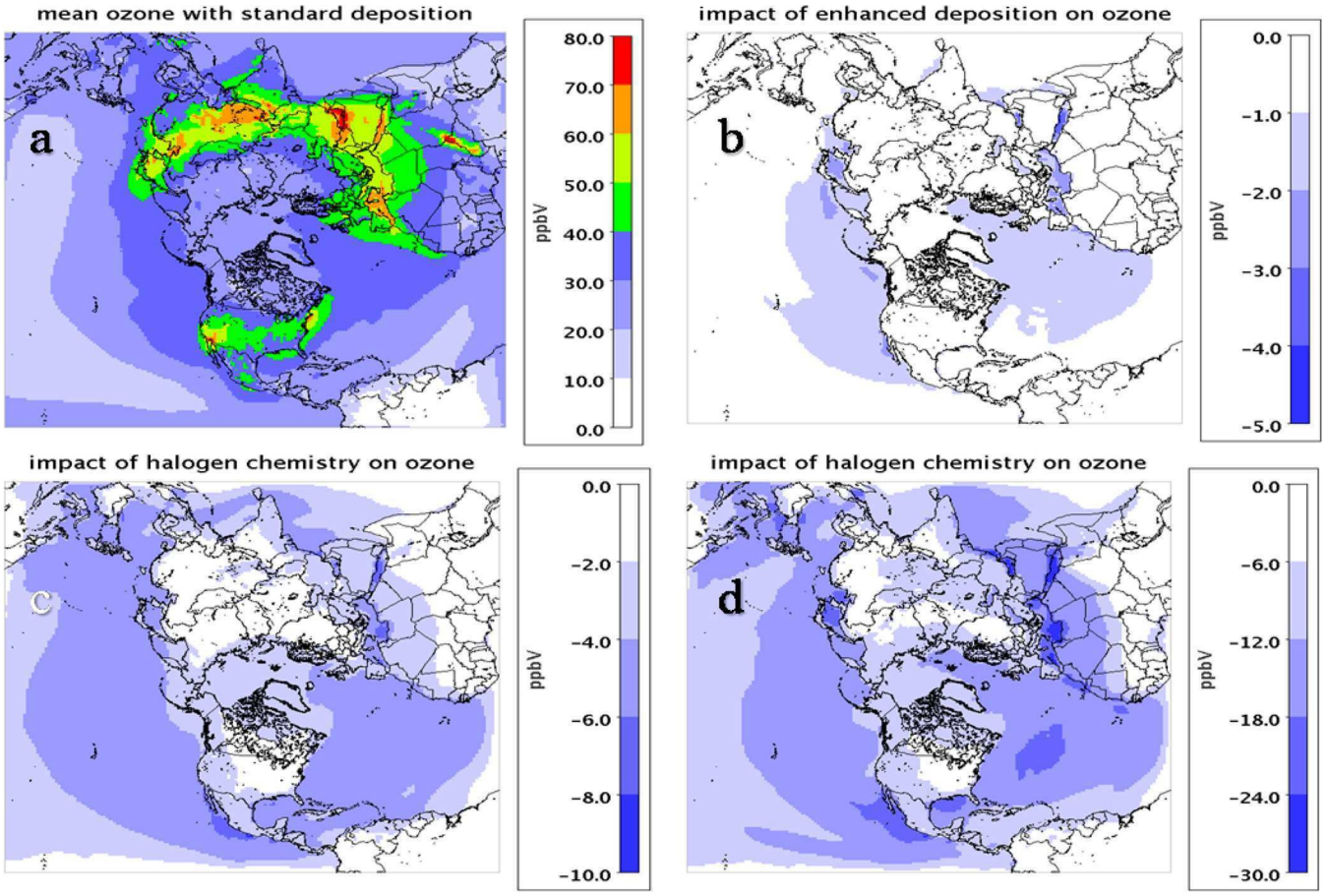

Figure 2. (a) Spatial distribution of predicted mean summer-time O_3 with the standard deposition (b) reduction of O_3 due to enhanced deposition (c) reduction of O_3 due to the halogen chemistry without photolysis of higher iodine oxides (d) reduction of O_3 due to the halogen chemistry with photolysis of higher iodine oxides.

Hemisphere whereas Parrella et al.[36] reported a global tropospheric O_3 reduction of 6.5% due to the bromine chemistry. Saiz-Lopez et al.[34] reported that iodine chemistry reduces annual mean tropical tropospheric O_3 by 9% and 16% for the simulations without and with photolysis of higher iodine oxides, respectively. Saiz-Lopez et al.[35] reported tropical tropospheric O_3 loss of 6−20% due to combined bromine and iodine chemistry. The halogen chemistry mediated O_3 reductions in this study are greater than those reported by others due to bromine chemistry or iodine chemistry alone but similar to values reported by others studying the combined effects of bromine and iodine chemistry. The reduction of O_3 mixing ratios due to halogen chemistry with photolysis of higher iodine species in this study is greater than values reported by other investigators.

3.3. Impact of Halogen Chemistry on Selected Chemical Species. Mahajan et al.[64] compared model predictions to observed data from Cape Verde and reported a typical observed peak noon value of 0.25 pptv for OH, 18 pptv for HO_2, and 72 for HO_2:OH ratio. They found that their baseline model simulation under-predicts OH by ∼13%, overpredicts HO_2 by ∼14%, and overpredicts HO_2:OH compared to observations, but improves with the inclusion of halogen chemistry. The inclusion of the halogen chemistry in our simulations decreased mean OH by 1% and HO_2 by 11%, and lowered the HO_2:OH from 104 to 93 over marine regions. Though we cannot directly compare our predictions to observations, our results qualitatively agree with those reported by Mahajan et al.[64] Several halogen compounds react with HO_2, reducing both its mixing ratio and the mixing ratio of H_2O_2 (by 17%) over marine regions. Because H_2O_2 and O_3 are important oxidizing agents for aqueous-phase conversion of SO_2 into sulfate, the production of sulfate via the aqueous-phase oxidation by H_2O_2 and O_3 decreases with the inclusion of halogen chemistry.

3.4. Comparison with Observed Data. Model predictions are compared to the observed data at selected monitoring sites from the World Data Centre for Greenhouse Gases (http://ds.data.jma.go.jp/gmd/wdcgg). Because a relatively coarse horizontal grid-size is used in this study, we limit our comparisons to 13 background sites (Table S.3 of the Supporting Information) where enhanced deposition and halogen chemistry are effective in reducing O_3. The median observed O_3 for these sites is 27 ppbv (Figure 3), which is overpredicted by ∼6 ppbv in Case A. The simulation with enhanced deposition (Case B) improves model performance by lowering the median prediction by ∼1 ppbv. The simulation including halogen chemistry without photolysis of higher iodine oxides (Case C) further reduces the surface O_3 mixing ratios by 5 ppbv. Case D, which uses halogen chemistry with photolysis of higher iodine oxides, has a more substantial reduction of surface O_3 mixing ratios averaging 12 ppbv compared to that of Case B. The inclusion of enhanced deposition and halogen chemistry without photolysis of higher iodine oxides improves

DOI: 10.1021/acs.est.5b01657
Environ. Sci. Technol. 2015, 49, 9203−9211

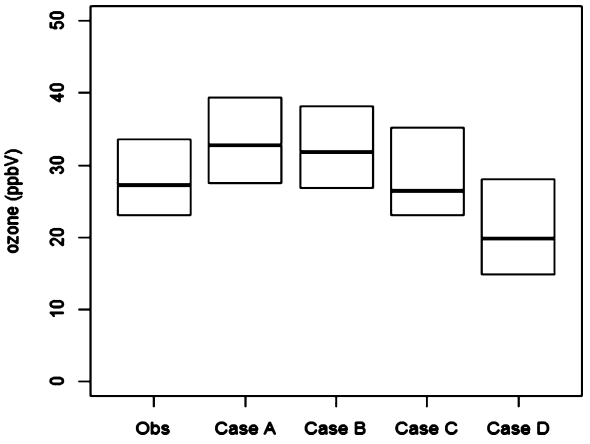

Figure 3. Comparison of model predictions with observed data. Lower bar in the box represents 25th percentile, middle bar represents the median and the upper bar represents 75 percentile values.

model performance. When the photolysis reactions are included in Case D, the surface O_3 mixing ratios are underpredicted by the model. This evaluation suggests that additional research is needed to further refine the halogen emissions and chemistry.

3.5. Effective First-Order Rate Constant for Halogen Mediated O_3 Loss. The application of regional air quality models demands computational efficiency. Because the inclusion of detailed halogen chemistry increases computational time (in our case by more than 25%), simplifications such as the first-order rate constant can be used for calculating halogen mediated O_3 loss in these computationally intensive model applications. The following relationship between the first-order rate constant values, k_{O_3} (s^{-1}), and the atmospheric pressures, P (Pa) is obtained using nonlinear least-squares estimation (R^2 = 0.97) (Figure S.2 of the Supporting Information).

$$k_{O_3}(P) = 1.0000 \times 10^{-40} e^{7.7400\times10^{-4}\times P} + 4.0582 \times 10^{-09} e^{5.7451\times10^{-5}\times P} \quad (12)$$

3.6. Future Work. We examined the impacts of enhanced O_3 deposition and halogen chemistry on summer-time O_3. Future work is needed to quantify the impact of these processes during other seasons. Our enhanced deposition scheme neglects several factors such as the possible reaction of dimethyl sulfide[5] and dissolved organic carbon[7] with O_3 as well as the effects of water salinity[70] and surface properties.[8] Our study uses a simplified Br_2 emission scheme that may contain large uncertainties. Studies suggest that heterogeneous reactions involving marine aerosols and O_3 can release bromine and iodine.[24,25,27] Our study does not include the bromine explosion reaction[69] that may occur in some marine boundary layers. Although we have attempted to include the most important atmospheric bromine and iodine reactions, it is possible that other reactions not included in this study may also affect model results. Photochemical reactions of higher iodine oxides in the halogen chemistry treatment contain large uncertainties. Thus, future effort should focus on reducing these uncertainties and re-examining the impacts with improved enhanced deposition scheme and halogen chemistry. Previous studies employing regional air quality models have shown overpredictions of O_3 in coastal areas[71−73] and may need to be re-examined with a more realistic representation of enhanced O_3 deposition and halogen chemistry as presented in this study. Some of these studies also have revealed that lateral boundary conditions used in regional models play an important role in O_3 predictions; this suggests that future studies focusing on O_3 predictions in coastal areas should use boundary conditions generated from hemispheric or global models that include enhanced O_3 deposition and halogen chemistry.

■ ASSOCIATED CONTENT

Supporting Information

Daily averaged standard and enhanced ozone deposition velocity for a typical day, plot of first-order halogen mediated O_3 loss rate and atmospheric pressure, gas-phase bromine chemistry used in the study, gas-phase iodine chemistry used in the study, and list of monitoring sites used in model comparison. The Supporting Information is available free of charge on the ACS Publications website at DOI: 10.1021/acs.est.5b01657.

■ AUTHOR INFORMATION

Corresponding Author

*Golam Sarwar. Address: U.S. EPA, 109 T.W. Alexander Drive, Research Triangle Park, NC 27711, USA. Tel.: 919-541-2669. Fax: 919-541-1379. E-mail: sarwar.golam@epa.gov.

Notes

Although this paper has been reviewed by EPA and approved for publication, it does not necessarily reflect EPA's policies or views.

The authors declare no competing financial interest.

■ REFERENCES

(1) Devlin, R.; Folinsbee, L.; Biscardi, F.; Hatch, G.; Becker, S.; Madden, M.; Robbins, M.; Koren, H. Inflammation and cell damage induced by repeated exposure of humans to ozone. *Inhalation Toxicol.* **1997**, *9*, 211−235.

(2) Felzer, B. S.; Cronin, T.; Reilly, J. M.; Melillo, J. M.; Wang, X. Impacts of ozone on trees and crops. *C. R. Geosci.* **2007**, *339*, 784−798.

(3) Gallagher, M. W.; Beswick, K. M.; McFiggans, G.; Coe, H.; Choularton, T. W. Ozone dry deposition velocities for coastal waters. *Water, Air, Soil Pollut.: Focus* **2001**, *1*, 233−242.

(4) Helmig, D.; Lang, E. K.; Bariteau, L.; Boylan, P.; Fairwall, C. W.; Ganzeveld, L.; Hara, J. E.; Hueber, J.; Pallandt, M. Atmosphere-ocean ozone fluxes during the TexAQS 2006, STRATUS 2006, GOMECC 2007, GasEx 2008, and AMMA 2008 cruises. *J. Geophys. Res.* **2012**, *117*, D04305.

(5) Chang, W.; Heikes, B. G.; Lee, M. Ozone deposition to the sea surface: chemical enhancement and wind speed dependence. *Atmos. Environ.* **2004**, *38*, 1053−1059.

(6) Ganzeveld, L.; Helmig, D.; Fairall, C. W.; Hare, J.; Pozzer, A. Atmosphere-ocean ozone exchange - a global modeling study of biogeochemical, atmospheric and water-side turbulence dependencies. *Global Biogeochemical Cycle* **2009**, *23*, GB4021.

(7) Shaw, M. D.; Carpenter, L. J. Modification of ozone deposition and I_2 emissions at the air-aqueous interface by dissolved organic carbon of marine origin. *Environ. Sci. Technol.* **2013**, *47*, 10947−10954.

(8) Resser, D. I.; Donaldson, D. J. Influence of water surface properties on the heterogeneous reaction between $O_{3(g)}$ and $I_{(aq)}^-$. *Atmos. Environ.* **2011**, *45*, 6116−6120.

(9) Oh, I.-B.; Byun, D. W.; Kim, H.-C.; Kim, S.; Cameron, B. Modeling the effect of iodide distribution on ozone deposition to seawater surface. *Atmos. Environ.* **2008**, *42*, 4453−4466.

(10) Chance, R.; Baker, A. R.; Carpenter, L.; Jickells, T. D. The distribution of iodide at the sea surface. *Environmental Science: Processes and Impacts* **2014**, *16*, 1841−1859.

DOI: 10.1021/acs.est.5b01657
Environ. Sci. Technol. 2015, 49, 9203−9211

(11) MacDonald, S. M.; Martin, J. C. G.; Chance, R.; Warriner, S.; Saiz-Lopez, A.; Carpenter, L. J.; Plane, J. M. C. A laboratory characterisation of inorganic iodine emissions from the sea surface: dependence on oceanic variables and parameterisation for global modelling. *Atmos. Chem. Phys.* **2014**, *14*, 5841−5852.
(12) Fairall, C. W.; Helmig, D.; Ganzeveld, L.; Hare, J. Water-side turbulence enhancement of ozone deposition to the ocean. *Atmos. Chem. Phys.* **2007**, *7*, 443−451.
(13) Peters, C.; Pechtl, S.; Stutz, J.; Hebestreit, K.; Hönninger, G.; Heumann, K. G.; Schwarz, A.; Winterlik, J.; Platt, U. Reactive and organic halogen species in three different European coastal environments. *Atmos. Chem. Phys.* **2005**, *5*, 3357−3375.
(14) Mahajan, A. S.; Oetjen, H.; Saiz-Lopez, A.; Lee, J. D.; McFiggans, G. B.; Plan, J. M. C. Reactive iodine species in a semi-polluted environment. *Geophys. Res. Lett.* **2009**, *36*, L16803.
(15) Simpson, W. R.; Brown, S. S.; Saiz-Lopez, A.; Thornton, J. A.; Von Glasow, R. Tropospheric Halogen Chemistry: Sources, Cycling, and Impacts. *Chem. Rev.* **2015**, *115*, 4035−4062.
(16) Alicke, B.; Hebestreit, K.; Stutz, J.; Platt, U. Iodine oxide in the marine boundary layer. *Nature* **1999**, *397*, 572−573.
(17) Read, K. A.; Mahajan, A. S.; Carpenter, L. J.; Evans, M. J.; Faria, B. V. E.; Heard, D. E.; Hopkins, J. R.; Lee, J. D.; Moller, S. J.; Lewis, A. C.; Mendes, L.; McQuaid, J. B.; Oetjen, H.; SaizLopez, A.; Pilling, M. J.; Plane, J. M. C. Extensive halogen mediated ozone destruction over the tropical Atlantic Ocean. *Nature* **2008**, *453*, 1232−1235.
(18) Carpenter, L. J.; MacDonald, S. M.; Shaw, M. D.; Kumar, R.; Saunders, R. W.; Parthipan, R.; Wilson, J.; Plane, J. M. C. Atmospheric iodine levels influenced by sea surface emissions of inorganic iodine. *Nat. Geosci.* **2013**, *6*, 108−111.
(19) Prados-Roman, C.; Cuevas, C. A.; Hay, T.; Fernandez, R. P.; Mahajan, A. S.; Royer, S.-J.; Gali, M.; Simo, R.; Dachs, J.; Großmann, K.; Kinnison, D. E.; Lamarque, J.-F.; Saiz-Lopez, A. Iodine oxide in the global marine boundary layer. *Atmos. Chem. Phys.* **2015**, *15*, 583−593.
(20) Mahajan, A. S.; Gómez Martín, J. C.; Hay, T. D.; Royer, S.-J.; Yvon-Lewis, S.; Liu, Y.; Hu, L.; Prados-Roman, C.; Ordóñez, C.; Plane, J. M. C.; Saiz-Lopez, A. Latitudinal distribution of reactive iodine in the Eastern Pacific and its link to open ocean sources. *Atmos. Chem. Phys.* **2012**, *12*, 11609−11617.
(21) O'Dowd, C.; Jimenez, J.; Bahreini, R.; Flagan, R.; Seinfeld, J.; Hameri, K.; Pirjola, L.; Kulmala, M.; Jennigns, S.; Hoffmann, T. Marine aerosol formation from biogenic iodine emissions. *Nature* **2002**, *417*, 632−636.
(22) Holmes, C. D.; Jacob, D. J.; Corbitt, E. S.; Mao, J.; Yang, X.; Talbot, R.; Slemr, F. Global atmospheric model for mercury including oxidation by bromine atoms. *Atmos. Chem. Phys.* **2010**, *10*, 12037−12057.
(23) Saiz-Lopez, A.; von Glasow, R. Reactive halogen chemistry in the troposphere. *Chem. Soc. Rev.* **2012**, *41*, 6448−6472.
(24) Hunt, S. W.; Roeselová, M.; Wang, W.; Wingen, L. M.; Knipping, E. M.; Tobias, D. J.; Dabdub, D.; Finlayson-Pitts, B. J. Formation of molecular bromine from the reaction of ozone with deliquesced NaBr aerosol: evidence for interface chemistry. *J. Phys. Chem. A* **2004**, *108*, 11559−11572.
(25) Clifford, C.; Donaldson, D. J. Direct experimental evidence for a heterogeneous reaction of ozone with bromide at the air-aqueous interface. *J. Phys. Chem. A* **2007**, *111*, 9809−9814.
(26) Rouvière, A.; Ammann, M. The effect of fatty acid surfactants on the uptake of ozone to aqueous halogenide particles. *Atmos. Chem. Phys.* **2010**, *10*, 11489−11500.
(27) Pillar, E. A.; Guzman, M. I.; Rodruguez, J. M. Conversion of iodide to hypoiodous acid and iodine in aqueous microdroplets exposed to ozone. *Environ. Sci. Technol.* **2013**, *47*, 10971−10979.
(28) Lee, M.-T.; Brown, M. A.; Kato, S.; Kleibert, A.; Türler, A.; Ammann, M. Competition between organics and bromide at the aqueous solution−air interface as seen from ozone uptake kinetics and x-ray photoelectron spectroscopy. *J. Phys. Chem. A* **2015**, *119*, 4600−4608.
(29) vonGlasow, R.; Sander, R.; Bott, A.; Crutzen, P. J. Modeling halogen chemistry in the marine boundary layer. 1. Cloud-free MBL. *J. Geophys. Res.* **2002**, *107*, 4341.
(30) Von Glasow, R.; Sander, R.; Bott, A.; Crutzen, P. J. Modeling halogen chemistry in the marine boundary layer. 2. Interactions with sulfur and cloud-covered MBL. *J. Geophys. Res.* **2002**, *107*, 4323.
(31) Warwick, N. J.; Pyle, J. A.; Carver, G. D.; Yang, X.; Savage, N. H.; O'Connor, F. M.; Cox, R. A. Global modeling of biogenic bromocarbons. *J. Geophys. Res.* **2006**, *111*, D24305.
(32) Ordóñez, C.; Lamarque, J.-F.; Tilmes, S.; Kinnison, D. E.; Atlas, E. L.; Blake, D. R.; Sousa Santos, G.; Brasseur, G.; Saiz-Lopez, A. Bromine and iodine chemistry in a global chemistry-climate model: description and evaluation of very short-lived oceanic sources. *Atmos. Chem. Phys.* **2012**, *12*, 1423−1447.
(33) Yang, X.; Cox, R. A.; Warwick, N. J.; Pyle, J. A.; Carver, G. D.; O'Connor, F. M.; Savage, N. H. Tropospheric bromine chemistry and its impacts on ozone: A model study. *J. Geophys. Res.* **2005**, *110*, D23311.
(34) Saiz-Lopez, A.; Fernandez, R. P.; Ordóñez, C.; Kinnison, D. E.; Gómez Martín, J. C.; Lamarque, J.-F.; Tilmes, S. Iodine chemistry in the troposphere and its effect on ozone. *Atmos. Chem. Phys.* **2014**, *14*, 13119−13143.
(35) Saiz-Lopez, A.; Lamarque, J.-F.; Kinnison, D. E.; Tilmes, S.; Ordóñez, C.; Orlando, J. J.; Conley, A. J.; Plane, J. M. C.; Mahajan, A. S.; Sousa Santos, G.; Atlas, E. L.; Blake, D. R.; Sander, S. P.; Schauffler, S.; Thompson, A. M.; Brasseur, G. Estimating the climate significance of halogen-driven ozone loss in the tropical marine troposphere. *Atmos. Chem. Phys.* **2012**, *12*, 3939−3949.
(36) Parrella, J. P.; Jacob, D. J.; Liang, Q.; Zhang, Y.; Mickley, L. J.; Miller, B.; Evans, M. J.; Yang, X.; Pyle, J. A.; Theys, N.; Van Roozendael, M. Tropospheric bromine chemistry: implications for present and pre-industrial ozone and mercury. *Atmos. Chem. Phys.* **2012**, *12*, 6723−6740.
(37) Long, M. S.; Keene, W. C.; Easter, R. C.; Sander, R.; Liu, X.; Kerkweg, A.; Erickson, D. Sensitivity of tropospheric chemical composition to halogen-radical chemistry using a fully coupled size-resolved multiphase chemistry−global climate system: halogen distributions, aerosol composition, and sensitivity of climate-relevant gases. *Atmos. Chem. Phys.* **2014**, *14*, 3397−3425.
(38) Rouvière, A.; Sosedova, Y.; Markus Ammann, M. Uptake of ozone to deliquesced KI and mixed KI/NaCl aerosol particles. *J. Phys. Chem. A* **2010**, *114*, 7085−7093.
(39) Liu, Q.; Schurter, L. M.; Muller, C. E.; Aloisio, S.; Francisco, J. S.; Margerum, D. W. Kinetics and mechanisms of aqueous ozone reactions with bromide, sulfite, hydrogen sulfite, iodide, and nitrite ions. *Inorg. Chem.* **2001**, *40*, 4436−4442.
(40) Byun, D.; Schere, K. L. Review of the governing equations, computational algorithms, and other components of the Models-3 Community Multiscale Air Quality (CMAQ) Modeling System. *Appl. Mech. Rev.* **2006**, *59*, 51−77.
(41) Foley, K. M.; Roselle, S. J.; Appel, K. W.; Bhave, P. V.; Pleim, J. E.; Otte, T. L.; Mathur, R.; Sarwar, G.; Young, J. O.; Gilliam, R. C.; Nolte, C. G.; Kelly, J.; Gilliland, A. B.; Bash, J. O. Incremental Testing of the Community Multiscale Air Quality (CMAQ) Modeling System Version 4.7. *Geosci. Model Dev.* **2010**, *3*, 205−226.
(42) Sarwar, G.; Simon, H.; Bhave, P.; Yarwood, G. Examining the impact of heterogeneous nitryl chloride production on air quality across the United States. *Atmospheric Chemistry & Physics* **2012**, *12*, 1−19.
(43) Appel, K. W.; Pouliot, G.; Simon, H.; Sarwar, G.; Pye, H. O. T.; Napelenok, S.; Akhtar, F.; Roselle, S. J. Evaluation of dust and trace metal estimates from the Community Multiscale Air Quality (CMAQ) model version 5.0. *Geosci. Model Dev.* **2013**, *6*, 883−899.
(44) Sarwar, G.; Godowitch, J.; Henderson, B. H.; Fahey, K.; Pouliot, G.; Hutzell, W. T.; Mathur, R.; Kang, D.; Goliff, W. S.; Stockwell, W. R. A comparison of atmospheric composition using the Carbon Bond and Regional Atmospheric Chemistry Mechanisms. *Atmos. Chem. Phys.* **2013**, *13*, 9695−9712.

DOI: 10.1021/acs.est.5b01657
Environ. Sci. Technol. 2015, 49, 9203−9211

(45) Mathur, R.; Gilliam, R.; Bullock, O. R.; Roselle, S.; Pleim, J.; Wong, D.; Binkowski, F.; Streets, D. Extending the applicability of the community multiscale air quality model to hemispheric scales: motivation, challenges, and progress. In *Air Pollution Modeling and its Applications XXI, The NATO Science for Peace and Security Programme*; Steyn, D. G., Trini, S., Eds.; Springer: Dordrecht, The Netherlands, 2012; Chapter 30, pp 175−179.
(46) Mathur, R.; Roselle, S.; Young, J.; Kang, D. Representing the effects of long-range transport and lateral boundary conditions in regional air pollution models. In *Air Pollution Modeling and its Application XXII, The NATO Science for Peace and Security Programme*; Steyn, D. G., Builtjes, P. J. H., Timmermans, R. M. A., Eds.; Springer: Heidelberg, Germany, 2014; Chapter 51, pp 303−308.
(47) Sarwar, G.; Simon, H.; Xing, J.; Mathur, R. Importance of tropospheric $ClNO_2$ chemistry across the Northern Hemisphere. *Geophys. Res. Lett.* **2014**, *41*, 4050−4058.
(48) Xing, J.; Mathur, R.; Pleim, J.; Hogrefe, C.; Gan, C.-M.; Wong, D. C.; Wei, C.; Gilliam, R.; Pouliot, G. Observations and modeling of air quality trends over 1990−2010 across the Northern Hemisphere: China, the United States and Europe. *Atmos. Chem. Phys.* **2015**, *15*, 2723−2747.
(49) Wesley, M. L. Parameterization of surface resistances to gaseous dry deposition in regional scale numerical models. *Atmos. Environ.* **1989**, *23*, 1293−1304.
(50) Slinn, W. G. N.; Hasse, L.; Hicks, B. B.; Hogan, A. W.; Lal, D.; Liss, P. S.; Munnich, K. O.; Sehmel, G. A.; Vittori, O. Some aspects of the transfer of atmospheric trace constituents past the air-sea interface. *Atmos. Environ.* **1978**, *12*, 2055−2087.
(51) Magi, L.; Schweitzer, F.; Pallares, C.; Cherif, S.; Mirabel, P.; George, C. Investigation of the uptake rate of ozone and methylhydroperoxide by water surfaces. *J. Phys. Chem. A* **1997**, *101* (27), 4943−4949.
(52) Garland, J. A.; Elzerman, A. W.; Penkett, S. A. The mechanism for dry deposition of ozone to seawater surfaces. *J. Geophys. Res.* **1980**, *85* (12), 7488−7492.
(53) Fernandez, R. P.; Salawitch, R. J.; Kinnison, D. E.; Lamarque, J.-F.; Saiz-Lopez, A. Bromine partitioning in the tropical tropopause layer: implications for stratospheric injection. *Atmos. Chem. Phys.* **2014**, *14*, 13391−13410.
(54) Sommariva, R.; Glasow, R. Multiphase Halogen Chemistry in the Tropical Atlantic Ocean. *Environ. Sci. Technol.* **2012**, *46* (19), 10429−10437.
(55) Solomon, S.; Garcia, R. R.; Ravishankara, A. R. On the role of iodine in ozone depletion. *J. Geophys. Res.* **1994**, *99* (D10), 20491−20499.
(56) Hoffmann, T.; O'Dowd, C. D.; Seinfeld, J. H. Iodine oxide homogeneous nucleation: an explanation for coastal new particle production. *Geophys. Res. Lett.* **2001**, *28* (No. 10), 1949−1952.
(57) Burkholder, J. B.; Curtius, J.; Ravishankara, A. R.; Lovejoy, E. R. Laboratory studies of the homogeneous nucleation of iodine oxides. *Atmos. Chem. Phys.* **2004**, *4*, 19−34.
(58) Ammann, M.; Cox, R. A.; Crowley, J. N.; Jenkin, M. E.; Mellouki, A.; Rossi, M. J.; Troe, J.; Wallington, T. J. Evaluated kinetic and photochemical data for atmospheric chemistry: Volume VI − heterogeneous reactions with liquid substrates. *Atmos. Chem. Phys.* **2013**, *13*, 8045−8228. IUPAC Task Group on Atmospheric Chemical Kinetic Data Evaluation, http://iupac.pole-ether.fr/index.html.
(59) Liss, P. S.; Marandino, C.; Dahl, E. E.; Helmig, D.; Hintsa, E. J.; Hughes, C.; Johnson, M. T.; Moore, R. M.; Plane, J. M. C.; Quack, B.; Singh, H. B.; Stefels, J.; Glasow, R.; Williams, J. Short-Lived Trace Gases in the Surface Ocean and the Atmosphere Ocean-Atmosphere Interactions of Gases and Particles; Springer: Berlin, Germany, 2014; pp 1−54, DOI: 10.1007/978-3-642-25643-1_1.
(60) Yarwood, G.; Jung, J.; Ou, N.; Emery, C. *Improving CAMx performance in simulating ozone transport from the Gulf of Mexico, Final Report for the Texas Commission on Environmental Quality*; Project No. 0626408I, 2012.
(61) Fan, S.-M.; Jacob, D. J. Surface ozone depletion in Arctic spring sustained by bromine reactions on aerosols. *Nature* **1992**, *359*, 522−524.
(62) Vogt, R.; Crutzen, P. J.; Sander, R. A mechanism for halogen release from sea-salt aerosol in the remote marine boundary layer. *Nature* **1996**, *383*, 327−330.
(63) Gantt, B.; Kelly, J. T.; Bash, J. O. Updating sea spray aerosol emissions in the Community Multiscale Air Quality (CMAQ) model version 5.0.2. *Geoscientific Model Development Discussions* **2015**, *8*, 3905−3939.
(64) Mahajan, A. S.; Plane, J. M. C.; Oetjen, H.; Mendes, L.; Saunders, R. W.; Saiz-Lopez, A.; Jones, C. E.; Carpenter, L. J.; McFiggans, G. B. Measurement and modelling of tropospheric reactive halogen species over the tropical Atlantic Ocean. *Atmos. Chem. Phys.* **2010**, *10*, 4611−4624.
(65) Lewis, E. R.; Schwartz, S. E. *Sea Salt Aerosol Production: Mechanisms, Methods, Measurements, And Models − A Critical Review*; Geophysical Monograph Series, Vol. 152; AGU: Washington, DC, 2004.
(66) Prados-Roman, C.; Cuevas, C. A.; Fernandez, R. P.; Kinnison, D. E.; Lamarque, J.-F.; Saiz-Lopez, A. A negative feedback between anthropogenic ozone pollution and enhanced ocean emissions of iodine. *Atmos. Chem. Phys.* **2015**, *15*, 2215−2224.
(67) Matveev, V.; Peleg, M.; Rosen, D.; Tov-Alper, D. S.; Hebestreit, K.; Stutz, J.; Platt, U.; Blake, D.; Luria, M. Bromine-oxide-ozone interaction over the Dead Sea. *J. Geophys. Res.* **2001**, *16* (No., D10), 10375−10387.
(68) Holla, R., Schmitt, S., Frieß, U., Pöhler, D., Zingler, J., Corsmeier, U., Platt, U., Vertical distribution of BrO in the boundary layer at the Dead Sea. *Environ. Chem.*, EN14224, Accepted 27 March **2015**, DOI: 10.1071/EN14224.
(69) Tas, E.; Peleg, M.; Pedersen, D. U.; Matveev, V.; Pour Biazar, A.; Luria, M. Measurement-based modeling of bromine chemistry in the boundary layer: 1. Bromine chemistry at the Dead Sea. *Atmos. Chem. Phys.* **2006**, *6*, 5589−5604.
(70) Colman, L.; Varghese, S.; Tripathi, O. P.; Jennings, S. G.; O'Dowd, C. D. Regional-scale ozone deposition to North-East Atlantic waters. *Adv. Meteorol.* **2010**, *2010*, No. 243701.
(71) Eder, B. K.; Yu, S. A Performance evaluation of the 2004 release of Models-3 CMAQ. *Atmos. Environ.* **2006**, *40* (26), 4811−4824.
(72) Han, Z.; Sakurai, T.; Ueda, H.; Carmichael, G. R.; Streets, D.; Hayami, H.; Wang, Z.; Holloway, T.; Engardt, M.; Hozumi, Y.; Park, S. U.; Kajino, M.; Sarttelet, K.; Fung, C.; Bennet, C.; Thongboonchoo, N.; Tang, Y.; Chang, A.; Matsuda, K.; Amman, M. MICS-Asia II: Model intercomparison and evaluation of ozone and relevant species. *Atmos. Environ.* **2008**, *42* (15), 3491−3509.
(73) Appel, W.; Chemel, C.; Roselle, S. J.; Francis, X. V.; Rong-Ming, H.; Sokhi, R. S.; Rao, S. T.; Galmarini, S. Examination of the Community Multiscale Air Quality (CMAQ) Model Performance over the North American and European Domains. *Atmos. Environ.* **2012**, *53*, 142−155.

DOI: 10.1021/acs.est.5b01657
Environ. Sci. Technol. 2015, 49, 9203−9211

Environmental Science & Technology

Article

pubs.acs.org/est

The Impact of Iodide-Mediated Ozone Deposition and Halogen Chemistry on Surface Ozone Concentrations Across the Continental United States

Brett Gantt,[†] Golam Sarwar,*[,‡] Jia Xing,[‡] Heather Simon,[†] Donna Schwede,[‡] William T. Hutzell,[‡] Rohit Mathur,[‡] and Alfonso Saiz-Lopez[§]

[†]Office of Air Quality Planning and Standards, US Environmental Protection Agency, Research Triangle Park, North Carolina 27711, United States

[‡]National Exposure Research Laboratory, Office of Research and Development, US Environmental Protection Agency, Research Triangle Park, North Carolina 27711, United States

[§]Department of Atmospheric Chemistry and Climate, Institute of Physical Chemistry Rocasolano, CSIC, Madrid 28006, Spain

Supporting Information

ABSTRACT: The air quality of many large coastal areas in the United States is affected by the confluence of polluted urban and relatively clean marine airmasses, each with distinct atmospheric chemistry. In this context, the role of iodide-mediated ozone (O_3) deposition over seawater and marine halogen chemistry accounted for in both the lateral boundary conditions and coastal waters surrounding the continental U.S. is examined using the Community Multiscale Air Quality (CMAQ) model. Several nested simulations are conducted in which these halogen processes are implemented separately in the continental U.S. and hemispheric CMAQ domains, the latter providing lateral boundary conditions for the former. Overall, it is the combination of these processes within both the continental U.S. domain and from lateral boundary conditions that lead to the largest reductions in modeled surface O_3 concentrations. Predicted reductions in surface O_3 concentrations occur mainly along the coast where CMAQ typically has large overpredictions. These results suggest that a realistic representation of halogen processes in marine regions can improve model prediction of O_3 concentrations near the coast.

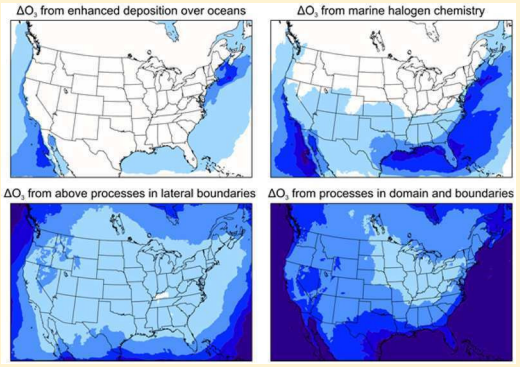

INTRODUCTION

A large portion of the U.S. population lives in coastal areas where surface ozone (O_3) concentrations can vary in part due to the relative mixture of urban and marine airmasses. Ozone can be formed locally in urban plumes[1] and can be transported to coastal areas from regional, national and international sources.[2−6] Additionally, onshore/offshore flow patterns can result in local or regional O_3 precursors being advected into marine environments before reacting to form O_3 and recirculating back into populated areas.[1,7−11] Models and observations show that O_3 can build up over water bodies near large urban areas due, in part, to lower deposition velocities over water than land, shallower boundary layers, and ship emissions.[9,12−15] It is in this context that we examine the role of iodide-mediated O_3 deposition over seawater and marine halogen chemistry in both the coastal waters surrounding the continental U.S. and lateral boundary conditions using the Community Multiscale Air Quality (CMAQ) model.

Previous studies in urban environments have shown that gas-phase chlorine emissions (Cl_2 and HOCl)[16−18] and chloride from sea-salt[19,20] can lead to increases in O_3 concentrations as a result of NO_2 release via photolysis of $ClNO_2$ and through the rapid oxidation of methane and other hydrocarbons by chlorine radicals. Conversely, halogens can deplete O_3 in remote and marine environments.[21] This has been shown to occur from reactions of O_3 with bromine and iodine[22−25] originating from the ocean surface[25−30] and through iodide-mediated enhanced deposition onto the ocean surface.[31]

Despite the demonstrated impact of marine halogen chemistry and iodide-mediated O_3 deposition over the ocean on surface concentrations, these processes are currently not accounted for in most chemical transport models. A multi-model comparison of global and hemispheric chemical transport models found systematic overpredictions of surface O_3 at regionally representative coastal sites in the Pacific Northwest and Florida/Gulf Coast.[32] Overprediction of surface O_3 concentrations in marine air masses by multimodel ensembles is also reported for Japanese islands in the East

Received: July 15, 2016
Revised: December 13, 2016
Accepted: January 4, 2017
Published: January 4, 2017

ACS Publications © 2017 American Chemical Society

DOI: 10.1021/acs.est.6b03556
Environ. Sci. Technol. 2017, 51, 1458−1466

China Sea.[33] In recent years, several modeling studies have attempted to implement marine halogen emission sources and chemistry to better represent marine boundary layer chemistry.[34−37]

In this study, we apply the recently described implementation of iodide-mediated O_3 deposition over seawater and marine halogen chemistry in the hemispheric version of the CMAQ model[38] to the continental U.S. (CONUS) domain. Compared to the coarse resolution of the hemispheric domain, the finer spatial resolution CONUS domain is expected to better to simulate the complex ocean-land-atmosphere interactions in the coastal zone while providing an opportunity to quantify the impact of these processes on the boundary conditions. Sarwar et al.[38] demonstrated that the inclusion of iodide-mediated O_3 deposition and marine halogen chemistry in the hemispheric version of CMAQ reduces the large model overpredictions of surface O_3 in remote marine and coastal regions throughout the Northern Hemisphere. However, extensive evaluation of CMAQ O_3 predictions using the national monitoring networks is more appropriate with finer horizontal resolution than the coarse model grids of the hemispheric domain. Additionally, the CONUS model domain can more closely capture the mesoscale meteorology that impacts the formation and transport of O_3 in coastal areas. Employing a widely used CMAQ model domain covering the continental U.S., we used the same iodide-mediated O_3 deposition and marine halogen chemistry implemented by Sarwar et al.[38] to isolate their impacts over coastal waters where the boundaries of typical regional model applications are specified. Additionally, we examined impacts of a parametrized version of the marine halogen chemistry on surface O_3 predictions within the continental U.S. domain.

MATERIALS AND METHODS

Model Description. The CMAQ model[39] employed in this study has been used to simulate ambient pollutant concentrations in many research and regulatory applications.[20,40−43] Here, we employ CMAQ version 5.0 to simulate air quality over the continental U.S. using a horizontal grid resolution of 12-km. The vertical extent of the model, spanning from surface to 100 mb, is discretized with 35 layers of variable thickness with the first layer having a depth of 20 m. The model uses the CB05TUCl chemical mechanism[20] that integrates chlorine chemistry with the Carbon Bond mechanism. Anthropogenic emissions were derived from the 2005 National Emissions Inventory while biogenic emissions were derived from the Biogenic Emissions Inventory System version 3.14.[44] Emissions used in this study have been described elsewhere.[41] Meteorological fields were developed using the Weather Research and Forecasting (WRF3.4) model.[45] The configuration and evaluation of WRF have previously described by Hogrefe et al.[46] Boundary conditions were generated from the hemispheric CMAQ simulations described in Sarwar et al.[38] covering the Northern Hemisphere with a horizontal grid resolution of 108-km and 44 vertical layers from the surface to 50 mb.

Iodide-Mediated O_3 Deposition over Seawater. Ozone deposition velocities over seawater predicted by CMAQ version 5.0 (median value ∼0.001 cm s^{-1}) are well below the recently documented observed O_3 deposition velocities that range from 0.009 to 0.06 cm s^{-1} over the open ocean and up to 0.27 cm s^{-1} in coastal waters.[47,48] Following the work of Chang et al.[49] and Oh et al.,[31] Sarwar et al.[38] revised the deposition of O_3 to ocean surfaces in CMAQ to account for the reaction of dissolved O_3 and iodide in seawater. This study uses the procedure described by Sarwar et al.[38] for O_3 deposition over seawater, which calculates the O_3 deposition velocity as a function of both wind speed and dissolved iodide in surface seawater (which itself is a function of sea surface temperature[50]). The value of dissolved iodide in surface seawater used for calculating O_3 deposition velocities is consistent with the values previously used to calculate marine emissions of inorganic iodine.[51] Accounting for these seawater reactions in CMAQ enhances the deposition of O_3 by increasing the deposition velocity from ≪0.01 cm s^{-1} to values in the range of 0.01−0.04 cm s^{-1} which are within the range of observed open ocean values, as noted above.

Marine Halogen Chemistry. The implementation of chlorine, bromine, and iodine chemistry in CMAQ has been previously described in detail[20,38] and consists of 25 chlorine reactions adapted from Tanaka et al.,[17] 39 bromine reactions adapted from Yang et al.[34] and 53 iodine reactions adapted from Saiz-Lopez et al.[37] Marine emissions of halogen species in CMAQ fall into three categories: (1) halocarbons, (2) inorganic bromine, and (3) inorganic iodine. Halocarbon emissions include five bromocarbons and four iodocarbons, inorganic bromine is represented with one bromine species, and inorganic iodine emissions include two iodine species. The three halogen emission categories have different formation mechanisms, with halocarbons driven by chlorophyll-*a* concentrations, inorganic bromine driven by sea spray aerosol emissions, and inorganic iodine species driven by a combination of atmospheric O_3, iodide concentration at the sea surface, and wind speed. Model inputs of chlorophyll-*a* concentrations[52] are derived from the Moderate Resolution Imaging Spectroradiometer (MODIS) aboard the Aqua satellite and projected to the Lambert conformal coordinate system used in the CMAQ domain.

Parameterized Marine Halogen Chemistry. Because the inclusion of detailed marine halogen chemistry increases computational time by >25%, Sarwar et al.[38] derived a first-order rate constant parametrizing the impacts of detailed marine halogen chemistry on predicted O_3 concentrations. This O_3 loss rate constant was developed using a nonlinear least-squares regression of the vertically resolved difference between the O_3 production and loss rates for all marine regions in the Northern Hemisphere in simulations with and without detailed marine halogen chemistry (see the Supporting Information from Sarwar et al.[38] for more information). In CMAQ, the rate constant is applied to all oceanic grid cells as a function of atmospheric pressure as follows:

$$k_{O3}(P) = 1.0000 \times 10^{-40} e^{7.7400\times10^{-4}\times P} + 4.0582 \times 10^{-09} e^{5.7451\times10^{-5}\times P} \quad (1)$$

where k_{O3} is the halogen mediated first order O_3 loss rate (s^{-1}) and P is the pressure (Pa).

Simulation Details. Six different simulations were completed for assessing the impacts of iodide-mediated deposition, halogen chemistry, and boundary conditions on O_3 concentrations (see Table 1). The first simulation (Case A) was completed using CB05TUCl with chlorine chemistry but without marine halogen chemistry or iodide-mediated O_3 deposition over seawater. Time-varying boundary conditions for Case A were generated from the hemispheric CMAQ results without any iodide-mediated O_3 deposition and halogen chemistry.[38] The second simulation (Case B) was completed

DOI: 10.1021/acs.est.6b03556
Environ. Sci. Technol. 2017, 51, 1458−1466

Table 1. Configuration of CMAQ Model Sensitivity Simulations in the Continental U.S. Domain and Lateral Boundary Conditions

	continental U.S. configuration		hemispheric configuration	
cases	iodide-mediated O_3 deposition	halogen chemistry	iodide-mediated O_3 deposition	halogen chemistry
Baseline[a]	no	no	no	no
Case B	yes	no	no	no
Case C	no	detailed	no	no
Case D	no	no	yes	detailed
Case E	yes	detailed	yes	detailed
Revised[b]	yes	parametrized	yes	detailed

[a]This simulation is also referred to as the Case A simulation. [b]This simulation is also referred to as the Case F simulation.

using CB05TUCl chemistry and iodide-mediated O_3 deposition. The third simulation (Case C) was completed using CB05TUCl and detailed marine halogen chemistry.[38] The boundary conditions for Cases B and C were identical to those of Case A. The fourth simulation (Case D) was completed using CB05TUCl but the boundary conditions for the model were generated from the hemispheric CMAQ results with iodide-mediated deposition and detailed halogen chemistry.[38] The fifth simulation (Case E) was completed using the CB05TUCl, iodide-mediated O_3 deposition, detailed halogen chemistry, and boundary conditions with iodide-mediated deposition and detailed halogen chemistry used in Case D. Finally, the sixth simulation (Case F) was completed using the CB05TUCl, iodide-mediated O_3 deposition, parametrized halogen chemistry, and boundary conditions with iodide-mediated deposition and detailed halogen chemistry used in Case D. Each simulation was completed for August 2006 with a 10-day spin-up period ending July 31st The spin-up period for the hemispheric CMAQ simulations used for boundary conditions was three-month. Hereafter, Case A will be referred to as the "Baseline" simulation and Case F the "Revised" simulation.

Differences between the Baseline and Case B simulations are attributed to iodide-mediated O_3 deposition and differences between the Baseline and Case C are attributed to the impact of detailed marine halogen chemistry active within the continental model domain alone. Differences between the Baseline and Case D simulations isolate the impact of iodide-mediated O_3 deposition and detailed marine halogen chemistry in the lateral boundary conditions. Differences between the Baseline and Case E represent the combined effects of iodide-mediated O_3 deposition, detailed marine halogen chemistry, and lateral boundary conditions. Similar to the Baseline/Case E comparison, the Baseline/Revised simulation differences show the combined effects of these processes but with parametrized halogen chemistry. We determine model errors introduced by parametrizing marine halogen chemistry by comparing the differences between the Case E and Revised simulations.

RESULTS

Impact of Marine Halogen Chemistry and Iodide-Mediated O_3 Deposition on Surface O_3 Concentrations in the Continental U.S. Domain. Figure 1 shows that the inclusion of iodide-mediated O_3 deposition over seawater and halogen chemistry in lateral boundary conditions and/or within the continental U.S. domain have distinct impacts on the spatial distribution and magnitude of monthly mean surface maximum daily 8-h average (MDA8) O_3 concentrations relative to the Baseline simulation. Iodide-mediated O_3 deposition, when applied only within the continental U.S. domain, has impacts of <1−2 ppb on inland and marine surface O_3 concentrations with the exception of areas just along the southern Pacific and northern Atlantic coasts which have predicted O_3 reductions up to 2 ppb inland and 3 ppb offshore (see Figure 1a). These hotspots of O_3 reduction also have high O_3 deposition rates in the Baseline simulation (due to moderate/high surface O_3 concentrations and wind speeds) that are further enhanced by the inclusion of the O_3-iodide reaction in seawater.

Relative to iodide-mediated O_3 deposition, detailed marine halogen chemistry in the continental U.S. domain (see Figure 1b) results in monthly mean MDA8 O_3 reductions that are greater in magnitude and occur further inland. Unlike deposition changes which only affect the surface layer, marine halogen chemistry reduces O_3 in all model layers and can therefore impact regional O_3 concentrations. Widespread areas over the Pacific, Atlantic, and Gulf of Mexico have reductions in surface O_3 concentrations around 3 ppb, whereas areas along the Baja California and Gulf of Mexico coasts have O_3 reductions in excess of 4 ppb. The short oceanic fetch near the boundaries of the regional domain results in little O_3 impact from either iodide-mediated O_3 deposition or detailed marine halogen chemistry.

When iodide-mediated O_3 deposition and detailed halogen chemistry are included solely in the hemispheric CMAQ simulations used to generate lateral boundary conditions for the continental U.S. domain (see Figure 1c), reductions of 4−5 ppb in surface MDA8 O_3 concentrations are predicted at the boundaries with lesser (1−2 ppb) reductions over much of the continental U.S. In the western U.S., high elevation areas in vicinity of the Great Basin have relatively greater reductions of surface O_3 than the surrounding lower elevations areas because they are more likely to be influenced by free tropospheric air masses that are affected by the larger O_3 reductions in the lateral boundary conditions.[53] Along the western edge of the CONUS domain, the lateral boundary conditions have monthly mean MDA8 O_3 reductions of ∼5 ppb from the surface up to 1 km (and by >2 ppb for all vertical layers up to 50 mb) when iodide-mediated O_3 deposition and detailed halogen chemistry are included in the hemispheric CMAQ simulations. Supporting Information Figure S1 shows that the Revised simulation had a similar reduction in O_3 concentrations above the surface at coastal and near-coastal sites when compared to the Baseline simulation. Including iodide-mediated O_3 deposition and marine halogen chemistry in both the lateral boundary conditions and within the continental U.S. domain results in widespread surface O_3 concentration reductions in excess of 5 ppb over the ocean and 1−4 ppb over land as shown in Figure 1d. The largest inland surface O_3 reductions occur near the coasts, with the western U.S. and Gulf Coast typically having greater reductions than the northeastern U.S. due to the differences in the wind directions between these regions. The magnitude of these reductions is similar to that of the Sarwar et al.[38] hemispheric CMAQ results.

Detailed vs Parametrized Marine Halogen Chemistry. Although the first order rate constant used in the parametrized marine halogen chemistry simulations was derived from simulations with detailed marine halogen chemistry, spatial differences in the halogen emissions and long atmospheric lifetimes of several halogen species result in subtle differences in

DOI: 10.1021/acs.est.6b03556
Environ. Sci. Technol. 2017, 51, 1458−1466

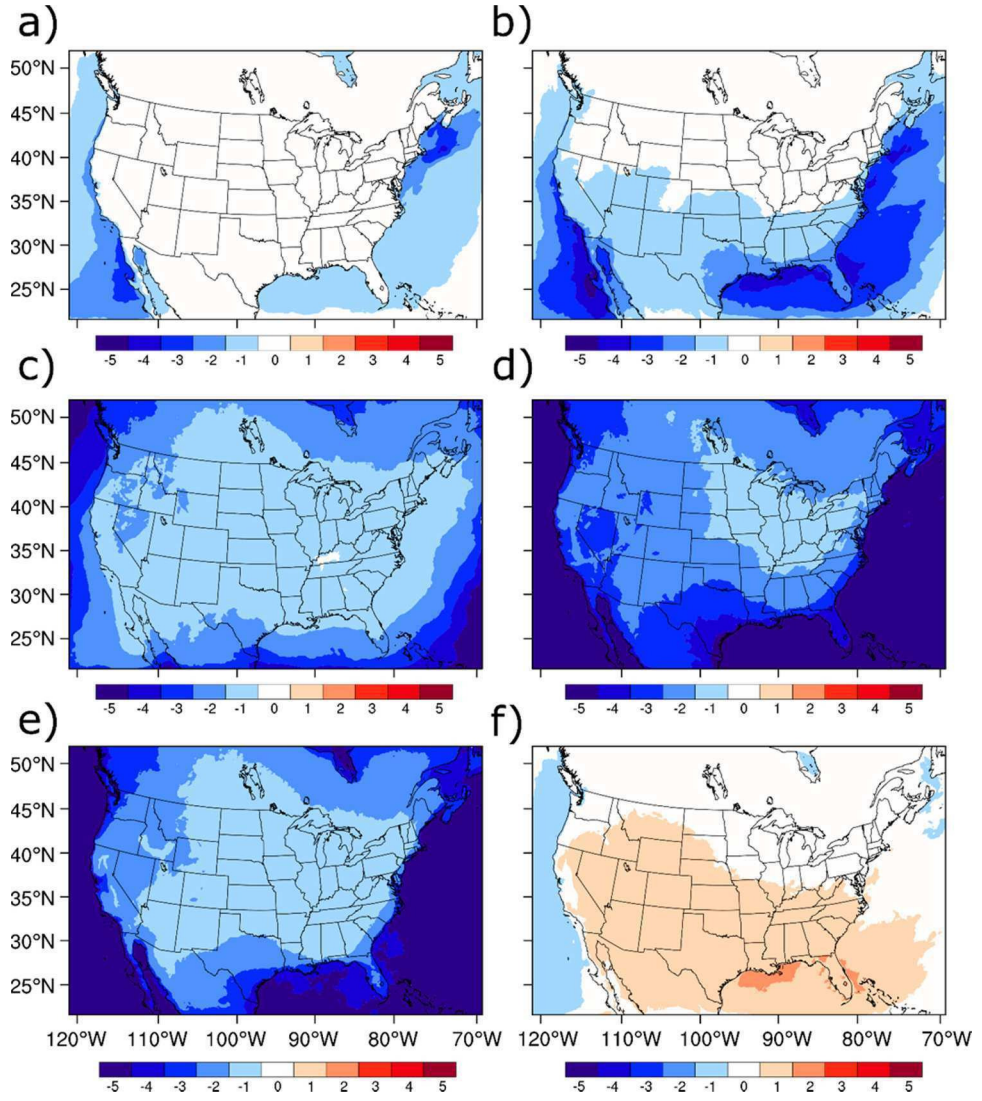

Figure 1. Average monthly mean changes in predicted surface MDA8 O_3 concentrations (in units of ppb) for August 2006 due to (a) iodide-mediated deposition solely in the CONUS domain (Case B minus Baseline), (b) detailed halogen chemistry solely in the CONUS domain (Case C minus Baseline), (c) iodide-mediated deposition and detailed halogen chemistry solely in hemispheric domain (i.e., represented in the lateral boundary conditions for the CONUS domain) (Case D minus Baseline), (d) the combination of iodide-mediated deposition and detailed halogen chemistry in both the CONUS and hemispheric domains (Case E minus Baseline), (e) combination of iodide-mediated deposition and parametrized marine halogen chemistry in the CONUS domain and iodide-mediated deposition and detailed halogen chemistry in the lateral boundary conditions (Revised minus Baseline), and (f) parametrized marine halogen chemistry in the CONUS domain relative to that of detailed marine halogen chemistry (Revised minus Case E). Note that when the scale labels of this and subsequent figures are situated in the middle of the color block, they represent the middle of the range indicated by the color.

the surface O_3 impacts. A comparison of Figure 1e and d shows that O_3 reductions in the simulation with parametrized marine halogen chemistry are similar to that of detailed marine halogen chemistry, with inland and marine regions having a 1−4 and ≥5 ppb reduction, respectively. A difference plot of the two simulations in Figure 1f, however, shows that the simulation with parametrized marine halogen chemistry has lower O_3 concentrations over most of the Pacific Ocean and higher O_3 concentrations over much of the Gulf of Mexico, Atlantic Ocean, and most inland regions due to the impact of sea surface temperature and halogen lifetime on modeled O_3. Unlike the parametrized marine halogen chemistry simulations, the detailed chemistry simulation includes sea surface temperature-dependent inorganic iodine emissions and chemical reactions between halogens and O_3 occurring well inland. Because predicted surface O_3 concentrations in the detailed and parametrized halogen chemistry simulations are typically within 1 ppb over most inland regions of the continental U.S. and the parametrized marine halogen chemistry requires significantly less computational time, this Revised simulation was used for comparison to ambient measurements as described below.

Comparison with TexAQS Ship-Based O_3 Measurements. The 2006 Texas Air Quality Study - Gulf of Mexico Atmospheric Composition and Climate Study (TexAQS/GoMACCS[54]) campaign provides a valuable data set for evaluating CMAQ surface O_3 predictions over the Gulf of Mexico during this time period. Throughout August 2006, the NOAA research vessel Ronald H. Brown (R/V Brown) measured surface O_3 concentrations (see Figure 2a) in the north-central Gulf of Mexico near Houston, TX. Figure 2b shows that the Baseline CMAQ predictions overpredict O_3 in the north-central Gulf of Mexico by 10−12 ppb with the

DOI: 10.1021/acs.est.6b03556
Environ. Sci. Technol. 2017, 51, 1458−1466

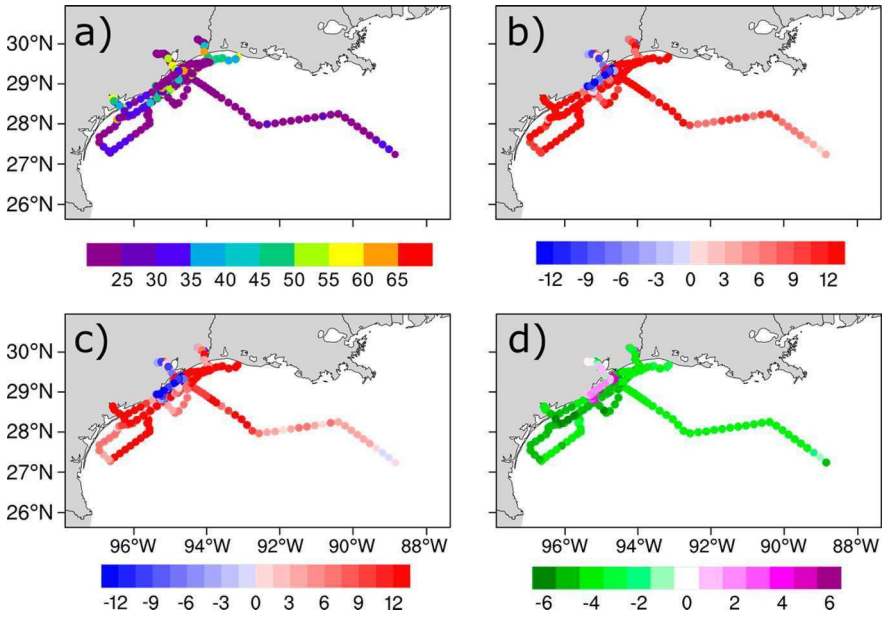

Figure 2. (a) Observed surface O_3 concentrations from R/V Ronald H. Brown during the August 2006 period of the TexAQS campaign (b) mean bias for Baseline simulation (c) mean bias for Revised simulation, and d) changes in mean bias between the Baseline and Revised simulations. The green colors in (d) represent locations where the Revised simulation had a lower model bias (improved prediction) and purple colors represent locations where the Revised simulation had a higher model bias (worse prediction). All units are in ppb.

exception of isolated underpredictions near Houston-Galveston and Port Arthur, TX where high NOx levels suggest O_3 titration. The largest overpredictions occur near the coast, but overpredictions of 5−10 ppb extend well offshore into the Gulf of Mexico. The change in mean bias between the Baseline and Revised simulations in Figure 2d shows a widespread 3−4 ppb bias reduction in the Revised simulation offshore in the Gulf of Mexico and slightly higher bias reductions (up to 6 ppb) near the coast. Coastal urban areas like Houston where the Baseline simulation underpredicts O_3 concentrations experience a slight degradation in the O_3 model bias (1−2 ppb larger underprediction) with the implementation of iodide-mediated O_3 deposition and marine halogen chemistry in the Revised CMAQ simulation. The modeled O_3 underprediction in Houston likely occurs due to several factors including uncertainties in emissions, grid resolution, or the complex chemistry of the area.

For all hourly averaged O_3 measurements in August 2006 from the R/V Brown matched in space to the hourly model concentration, the Revised simulation has a reduced normalized mean bias (49.2 to 34.2%) and normalized mean error (65.9 to 53.2%) and has a slightly improved Pearson's correlation efficient (0.66 to 0.69) relative to the Baseline simulation.

Comparison with MDA8 Surface O_3 Measurements Across the Continental U.S. Figure 3 shows that CMAQ generally overpredicts O_3 during periods with the lowest observed concentrations (likely dominated by marine air-masses) and underpredicts O_3 during the highest concentrations (likely dominated by urban airmasses), with the greatest improvement in model performance occurring during these low concentrations. This pattern of overpredicting low concentrations and underpredicting high concentrations is present in previous versions of CMAQ, and is still an active area of research.[40] When only sites immediately along the coastline are considered in the analysis, the Revised simulation had an even greater improvement of the predicted MDA8 O_3 mean bias (see Supporting Information Figure S2).

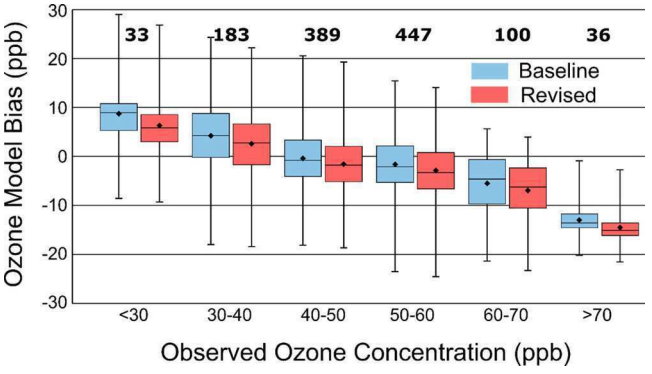

Figure 3. Monthly mean MDA8 bias in August 2006 for the Baseline and Revised simulations, binned by observed MDA8 O_3 concentrations retrieved from the EPA Air Quality System (AQS) database. The lower bar in the box represents 25th percentile, middle bar represents the median, and upper bar represents 75th percentile values. The mean values are given by the diamonds, maximum and minimum values are shown by the error bars, and the numbers in bold indicate the total number of monitors in each O_3 concentration bin.

Similar to previous modeling studies having systematic overprediction of surface O_3 concentrations at nonurban coastal sites in the continental U.S.,[32,55] comparison of observed MDA8 surface O_3 measurements (see Figure 4a, Supporting Information Figure S3) with the Baseline CMAQ simulation reveals overpredictions in the monthly mean MDA8 O_3 concentrations by 5−10 ppb at several coastal sites in California, Gulf of Mexico, and southeast U.S. for August 2006 (see Figure 4b, Supporting Information Figure S4). The insets within Supporting Information Figure S4 reveal divergent model biases for O_3 in the Baseline simulation at urban and nonurban sites along the coast, with underpredictions at some urban sites near Los Angeles, CA, Houston, TX, and New Orleans, LA and overpredictions outside urban regions. The Baseline simulation shows a previously reported[40] systematic

DOI: 10.1021/acs.est.6b03556
Environ. Sci. Technol. 2017, 51, 1458−1466

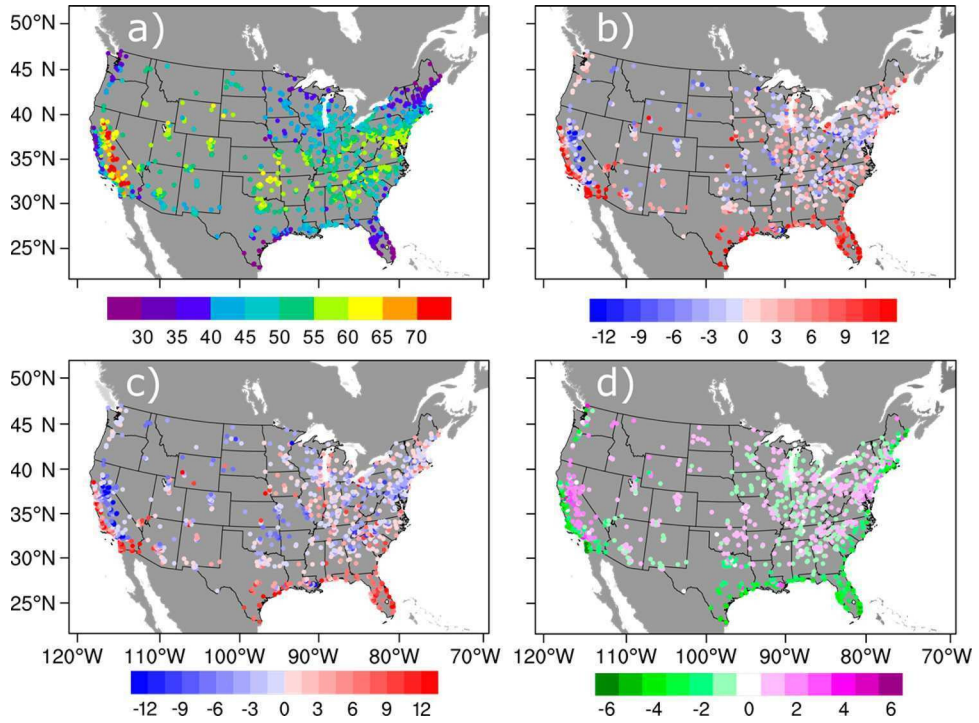

Figure 4. (a) Observed monthly mean surface O_3 concentrations from the EPA Air Quality System (AQS) sites in August 2006, (b) mean bias for the Baseline simulation at AQS sites (c) mean bias for the Revised simulation at AQS sites and (d) change in mean bias between the Baseline and Revised simulations at AQS sites. The green colors in (d) represent sites where the Revised simulation had a lower mean bias (improved prediction) and purple colors represent sites where the Revised simulation had a higher mean bias (worse prediction). All units are in ppb.

overprediction of surface O_3 concentrations over the entire continental U.S. at the lowest observed values and underprediction at the highest observed values (see Figure 3).

Comparison of the monthly mean bias in the Baseline (Figure 4b) and Revised (Figure 4c) simulations shows that the Revised simulation has lower bias at many sites in the continental U.S. relative to the Baseline. Generally, the consistent O_3 concentration reduction in the Revised simulation results in lower bias when the Baseline simulation is biased high and higher bias when the Baseline simulation is biased low (see Figure 4c, Supporting Information Figure S5). The largest reductions in monthly mean bias were along the California coast, where the bias are reduced by >5 ppb (see Figure 4d, Supporting Information Figure S6). In high O_3 concentration areas near the coast such as the Central Valley of California and the metropolitan region from Washington DC to New York City, O_3 underpredictions in the Baseline simulation are exacerbated in the Revised simulation. The higher bias in some coastal urban and inland areas in California may be due to emissions uncertainties and complex meteorology which is poorly predicted in fine scale (4 km) simulations,[56] let alone the 12 km model resolution of the CONUS domain. Along the Gulf and Atlantic coasts, the Revised simulation has reductions in the bias of 2−3 ppb for the majority of sites, similar to the bias reductions in the offshore and near-coastal nonurban TexAQS predictions. Because the Revised simulation has consistent reductions in O_3 concentrations across the continental U.S. relative to the Baseline simulation, the pattern of overpredictions/underpredictions at low/high observed concentrations is retained in the Revised simulation (see Figure 3). The preponderance of very low observed O_3 concentrations at coastal sites (see Supporting Information Figure S3) that are affected by iodide-mediated O_3 deposition and marine halogen chemistry results in greater reduction of the bias at the lowest observed concentrations than increases in the bias at the highest observed concentrations (see Figure 3).

DISCUSSION

As health science continues to support the lowering of standards for ozone and many criteria pollutants, realistic simulation of the processes affecting background O_3 concentrations has become increasingly important to the development of air quality management plans for attaining these lower standards.[57] This work shows the importance of properly representing marine halogen processes including emissions, chemistry, and deposition in chemical transport models such as CMAQ to the prediction of surface O_3 concentrations at coastal (and some inland) sites during low O_3 periods. The spatially variable impact of lateral boundary conditions on model predictions of O_3 in the CONUS domain was also demonstrated, highlighting the importance of including these marine halogen processes in global/hemispheric models that feed the lateral boundary conditions.[58−60] Including these marine halogen processes in the model does not completely alleviate overpredictions of low surface O_3 concentrations along the coast and over the open ocean, and exacerbates underpredictions of high surface O_3 concentrations in some near-coast areas like the Central Valley of California and the metropolitan region from Washington DC to New York City. Many factors are likely responsible for these persistent over- and underpredictions, including model representation of boundary layer mixing or ventilation processes and uncertain emissions. For a comprehensive evaluation of O_3 model performance at sites across the U.S. using the latest public release of CMAQ, see Appel et al.[61]

DOI: 10.1021/acs.est.6b03556
Environ. Sci. Technol. 2017, 51, 1458−1466

While previous studies have examined the factors affecting O_3 deposition on a local or regional scale,[31,49] marine halogen emissions and their impact on atmospheric chemistry have been studied mainly using global models.[27,29,35,36] These different domains may have distinct factors affecting marine halogen emissions due to the preponderance of coastal vs open ocean waters within the domain. The uncertainty in the marine halogen emissions used in this study is also particularly high because of the scarcity of marine halogen observations to evaluate the model performance.

Not yet included in these simulations is the impact of seawater dimethyl sulfide, dissolved organic carbon, bromine, or dissolved salts on the O_3 deposition over seawater which has recently been studied using the hemispheric CMAQ model.[62] Further improvement in the predicted O_3 concentrations over marine regions could be achieved through the use of planetary boundary layer parametrizations based on eddy-diffusivity–mass-flux concepts[63] or the inclusion of photochemical reactions of higher iodine oxides.[37] Additional future work may also include extending both the hemispheric and CONUS CMAQ simulations with these marine halogen processes over an entire year to better understand their impact on the seasonal variability of surface concentrations and vertical profiles of O_3 and other oxidants and to enable long-lived halocarbons to release their reactive halogen atoms. As both long-range transport patterns and design value calculations have a seasonal component, this annual simulation would better quantify the impact of marine halogen processes to regulatory-based model predictions of O_3.

■ ASSOCIATED CONTENT

Supporting Information

The Supporting Information is available free of charge on the ACS Publications website at DOI: 10.1021/acs.est.6b03556.

Additional information as noted in the text (PDF)

■ AUTHOR INFORMATION

Corresponding Author

*Phone: 919-541-2669; fax: 919-541-1379; e-mail: sarwar.golam@epa.gov.

ORCID

Brett Gantt: 0000-0001-7217-2715

Author Contributions

The manuscript was written through contributions of all authors. All authors have given approval to the final version of the manuscript.

Notes

This article represents the authors' views and not necessarily those officially of the EPA.

The authors declare no competing financial interest.

■ ACKNOWLEDGMENTS

The Community Multiscale Air Quality (CMAQ) model (CMAQv5.0) was used for generating the model results. The CMAQ model can be downloaded from www.cmascenter.org. We also acknowledge James Johnson with NOAA-PMEL for the use of the R/V Ronald H. Brown ozone data measured during TexAQS-GoMACCS 2006 and Gary Morris formerly of Valparaiso University for the ozonesonde data measured during the INTEX-B Ozonesonde Network Study. All plots and analyses were performed using the NCAR Command Language (Version 6.3.0), UCAR/NCAR/CISL/TDD: http://dx.doi.org/10.5065/D6WD3XH5. Lastly, we greatly appreciate the comments of the three anonymous reviewers.

■ REFERENCES

(1) Parrish, D. D.; Hanwant, S. B.; Molina, L.; Madronich, S. Air quality progress in North American megacities: A review. *Atmos. Environ.* **2011**, *45*, 7015–7025.

(2) Mao, H.; Talbot, R. Role of meteorological processes in two New England ozone episodes during summer 2001. *J. Geophys. Res.* **2004**, *109*, D20305.

(3) Chen, M.; Talbot, R.; Mao, H.; Sive, B.; Chen, J.; Griffin, R. J. Air mass classification in coastal New England and its relationship to meteorological conditions. *J. Geophys. Res.* **2007**, *112*, D10S05.

(4) Parrish, D. D.; Millet, D. B.; Goldstein, A. H. Increasing ozone in marine boundary layer inflow at the west coasts of North America and Europe. *Atmos. Chem. Phys.* **2009**, *9*, 1303–1323.

(5) Huang, M.; Carmichael, G. R.; Adhikary, B.; Spak, S. N.; Kulkarni, S.; Cheng, Y. F.; Wei, C.; Tang, Y.; Parrish, D. D.; Oltmans, S. J.; et al. Impacts of transported background ozone on California air quality during the ARCTAS-CARB period – a multi-scale modeling study. *Atmos. Chem. Phys.* **2010**, *10*, 6947–6968.

(6) Zhang, H.; Ying, Q. Contributions of local and regional sources of NOx to ozone concentrations in Southeast Texas. *Atmos. Environ.* **2011**, *45*, 2877–2887.

(7) Yimin, M.; Lyons, T. J. Recirculation of coastal urban air pollution under a synoptic scale thermal trough in Perth, Western Australia. *Atmos. Environ.* **2003**, *37*, 443–454.

(8) Boucouvala, D.; Bornstein, R. Analysis of transport patterns during an SCOS97-NARSTO episode. *Atmos. Environ.* **2003**, *37* (Suppl. 2), 73–94.

(9) Banta, R. M.; Seniff, C. J.; Nielsen-Gammon, J.; Darby, L. S.; Ryerson, T. B.; Alvarez, R. J.; Sandberg, S. R.; Williams, E. J.; Trainer, M. A bad air day in Houston. *Bull. Am. Meteorol. Soc.* **2005**, *86* (5), 657–669.

(10) Darby, L. S. Cluster analysis of surface winds in Houston, Texas, and the impact of wind patterns on ozone. *J. Appl. Meteorol.* **2005**, *44*, 1788–1806.

(11) Loughner, C. P.; Tzortziou, M.; Follette-Cook, M.; Pickering, K. E.; Goldberg, D.; Satam, C.; Weinheimer, A.; Crawford, J. H.; Knapp, D. J.; Montzka, D. D.; et al. Impact of bay-breeze circulations on surface air quality and boundary layer export. *J. Appl. Meteorol. Clim.* **2014**, *53*, 1697–1713.

(12) Angevine, W. M.; Senff, C. J.; White, A. B.; Williams, E. J.; Koermer, J.; Miller, S. T. K.; Talbot, R.; Johnston, P. E.; McKeen, S. A.; Downs, T. Coastal boundary layer influence on pollutant transport in New England. *J. Appl. Meteorol.* **2004**, *43*, 1425–1437.

(13) Goldberg, D. L.; Loughner, C. P.; Tzortziou, M.; Stehr, J. W.; Pickering, K. E.; Marufu, L. T.; Dickerson, R. R. Higher surface ozone concentrations over the Chesapeake Bay than over the adjacent land: Observations and models from the DISCOVER-AQ and CBODAQ campaigns. *Atmos. Environ.* **2014**, *84*, 9–19.

(14) Cleary, P. A.; Fuhrman, N.; Schulz, L.; Schafer, J.; Fillingham, J.; Bootsma, H.; McQueen, J.; Tang, Y.; Langel, T.; McKeen, S.; et al. Ozone distributions over southern Lake Michigan: comparisons between ferry-based observations, shoreline-based DOAS observations and model forecasts. *Atmos. Chem. Phys.* **2015**, *15*, 5109–5122.

(15) Burley, J. D.; Theiss, S.; Bytnerowicz, A.; Gertler, A.; Schilling, S.; Zielinska, B. Surface ozone in the Lake Tahoe basin. *Atmos. Environ.* **2015**, *109*, 351–369.

(16) Chang, S. Y.; McDonald-Buller, E.; Kimura, Y.; Yarwood, G.; Neece, J.; Russell, M.; Tanaka, P.; Allen, D. Sensitivity of urban ozone formation to chlorine emission estimates. *Atmos. Environ.* **2002**, *36*, 4991–5003.

(17) Tanaka, P. L.; Riemer, D. D.; Change, S. H.; Yarwood, G.; McDonald-Buller, E. C.; Apel, E. C.; Orlando, J. J.; Silva, P. J.; Jimenez, J. L.; Canagaratna, M. R.; et al. Direct evidence for chlorine-enhanced

urban ozone formation in Houston, Texas. *Atmos. Environ.* **2003**, *37*, 1393−1400.
(18) Sarwar, G.; Bhave, P. V. Modeling the effect of chlorine emissions on ozone levels over the eastern United States. *J. Appl. Meteorol. Clim.* **2007**, *46*, 1009−1019.
(19) Simon, H.; Kimura, Y.; McGaughey, G.; Allen, D. T.; Brown, S. S.; Osthoff, H. D.; Roberts, J. M.; Byun, D.; Lee, D. Modeling the impact of $ClNO_2$ on ozone formation in the Houston area. *J. Geophys. Res.* **2009**, *114*, D00F03.
(20) Sarwar, G.; Simon, H.; Bhave, P.; Yarwood, G. Examining the impact of heterogeneous nitryl chloride production on air quality across the United States. *Atmos. Chem. Phys.* **2012**, *12*, 6455−6473.
(21) Saiz-Lopez, A.; von Glasow, R. Reactive halogen chemistry in the troposphere. *Chem. Soc. Rev.* **2012**, *41*, 6448−6472.
(22) Chameides, W. L.; Davis, D. D. Iodine: Its possible role in tropospheric photochemistry. *J. Geophys. Res.* **1980**, *85* (C12), 7383−7398.
(23) Solomon, S.; Garcia, R. R.; Ravishankara, A. R. On the role of iodine in ozone depletion. *J. Geophys. Res.* **1994**, *99*, 20491−20499.
(24) Saiz-Lopez, A.; Mahajan, A. S.; Salmon, R. A.; Bauguitte, S. J.-B.; Jones, A. E.; Roscoe, H. K.; Plane, J. M. C. Boundary layer halogens in coastal Antarctica. *Science* **2007**, *317*, 348−351.
(25) Read, K. A.; Mahajan, A. S.; Carpenter, L. J.; Evans, M. J.; Faria, B. V. E.; Heard, D. E.; Hopkins, J. R.; Lee, J. D.; M?ller, S. J.; Lewis, A. C.; et al. Extensive halogen mediated ozone destruction over the tropical Atlantic Ocean. *Nature* **2008**, *453*, 1232−1235.
(26) Alicke, B.; Hebestreit, K.; Stutz, J.; Platt, U. Iodine oxide in the marine boundary layer. *Nature* **1999**, *397*, 572−573.
(27) Mahajan, A. S.; Gómez Martín, J. C.; Hay, T. D.; Royer, S.-J.; Yvon-Lewis, S.; Liu, Y.; Hu, L.; Prados-Roman, C.; Ordóñez, C.; Plane, J. M. C.; et al. Latitudinal distribution of reactive iodine in the Eastern Pacific and its link to open ocean sources. *Atmos. Chem. Phys.* **2012**, *12*, 11609−11617.
(28) Carpenter, L. J.; MacDonald, S. M.; Shaw, M. D.; Kumar, R.; Saunders, R. W.; Parthipan, R.; Wilson, J.; Plane, J. M. C. Atmospheric iodine levels influenced by sea surface emissions of inorganic iodine. *Nat. Geosci.* **2013**, *6*, 108−111.
(29) Prados-Roman, C.; Cuevas, C. A.; Hay, T.; Fernandez, R. P.; Mahajan, A. S.; Royer, S.-J.; Gali, M.; Simo, R.; Dachs, J.; Großmann, K.; et al. Iodine oxide in the global marine boundary layer. *Atmos. Chem. Phys.* **2015**, *15*, 583−593.
(30) Simpson, W. R.; Brown, S. S.; Saiz-Lopez, A.; Thornton, J. A.; Von Glasow, R. Tropospheric Halogen Chemistry: Sources, Cycling, and Impacts. *Chem. Rev.* **2015**, *115*, 4035−4062.
(31) Oh, I.-B.; Byun, D. W.; Kim, H.-C.; Kim, S.; Cameron, B. Modeling the effect of iodide distribution on ozone deposition to seawater surface. *Atmos. Environ.* **2008**, *42*, 4453−4466.
(32) Reidmiller, D. R.; Fiore, A. M.; Jaffe, D. A.; Bergmann, D.; Cuvelier, C.; Dentener, F. J.; Duncan, B. N.; Folberth, G.; Gauss, M.; Gong, S.; et al. The influence of foreign vs. North American emissions on surface ozone in the US. *Atmos. Chem. Phys.* **2009**, *9*, 5027−5042.
(33) Han, Z.; Sakurai, T.; Ueda, H.; Carmichael, G. R.; Streets, D.; Hayami, H.; Wang, Z.; Holloway, T.; Engardt, M.; Hozumi, Y.; et al. MICS-Asia II: Model intercomparison and evaluation of ozone and relevant species. *Atmos. Environ.* **2008**, *42* (15), 3491−3509.
(34) von Glasow, R.; von Kuhlmann, R.; Lawrence, M. G.; Platt, U.; Crutzen, P. J. Impact of reactive bromine chemistry in the troposphere. *Atmos. Chem. Phys.* **2004**, *4*, 2481−2497.
(35) Yang, X.; Cox, R. A.; Warwick, N. J.; Pyle, J. A.; Carver, G. D.; O'Connor, F. M.; Savage, N. H. Tropospheric bromine chemistry and its impacts on ozone: A model study. *J. Geophys. Res.* **2005**, *110*, D23311.
(36) Ordóñez, C.; Lamarque, J.-F.; Tilmes, S.; Kinnison, D. E.; Atlas, E. L.; Blake, D. R.; Sousa Santos, G.; Brasseur, G.; Saiz-Lopez, A. Bromine and iodine chemistry in a global chemistry-climate model: description and evaluation of very short-lived oceanic sources. *Atmos. Chem. Phys.* **2012**, *12*, 1423−1447.
(37) Saiz-Lopez, A.; Fernandez, R. P.; Ordóñez, C.; Kinnison, D. E.; Gómez Martín, J. C.; Lamarque, J.-F.; Tilmes, S. Iodine chemistry in the troposphere and its effect on ozone. *Atmos. Chem. Phys.* **2014**, *14*, 13119−13143.
(38) Sarwar, G.; Gantt, B.; Schwede, D.; Foley, K.; Mathur, R.; Saiz-Lopez, A. Impact of enhanced ozone deposition and halogen chemistry on tropospheric ozone over the Northern Hemisphere. *Environ. Sci. Technol.* **2015**, *49* (15), 9203−9211.
(39) Byun, D.; Schere, K. L. Review of the governing equations, computational algorithms, and other components of the Models-3 Community Multiscale Air Quality (CMAQ) Modeling System. *Appl. Mech. Rev.* **2006**, *59*, 51−77.
(40) Foley, K. M.; Roselle, S. J.; Appel, K. W.; Bhave, P. V.; Pleim, J. E.; Otte, T. L.; Mathur, R.; Sarwar, G.; Young, J. O.; Gilliam, R. C.; et al. Incremental Testing of the Community Multiscale Air Quality (CMAQ) Modeling System Version 4.7. *Geosci. Model Dev.* **2010**, *3*, 205−226.
(41) Appel, K. W.; Pouliot, G.; Simon, H.; Sarwar, G.; Pye, H. O. T.; Napelenok, S.; Akhtar, F.; Roselle, S. J. Evaluation of dust and trace metal estimates from the Community Multiscale Air Quality (CMAQ) model version 5.0. *Geosci. Model Dev.* **2013**, *6*, 883−899.
(42) Sarwar, G.; Simon, H.; Xing, J.; Mathur, R. Importance of tropospheric $ClNO_2$ chemistry across the Northern Hemisphere. *Geophys. Res. Lett.* **2014**, *41*, 4050−4058.
(43) Xing, J.; Mathur, R.; Pleim, J.; Hogrefe, C.; Gan, C.-M.; Wong, D. C.; Wei, C.; Gilliam, R.; Pouliot, G. Observations and modeling of air quality trends over 1990−2010 across the Northern Hemisphere: China, the United States and Europe. *Atmos. Chem. Phys.* **2015**, *15*, 2723−2747.
(44) Schwede, D.; Pouliot, G.; Pierce, T. Changes to the biogenic emissions inventory system version 3 (BEIS3), 4th Annual CMAS Models-3 Users' Conference, September 26−28 2005, UNC-Chapel Hill, NC, available at: https://www.cmascenter.org/conference/2005/abstracts/2_7.pdf.
(45) Skamarock, W. C.; Klemp, J. B.; Dudhia, J.; Gill, D. O.; Barker, D. M.; Duda, M. G.; Huang, X.-Y.; Wang, W.; Powers, J. G. *ADescription of the Advanced Research WRF Version 3, NCAR/TN-475+STR*; Mesoscale and Microscale Meteorology Division, National Center for Atmospheric Research: Cambridge, MA, 2008
(46) Hogrefe, C.; Pouliot, G.; Wong, D.; Torian, A.; Roselle, S.; Pleim, J.; Mathur, R. Annual application and evaluation of the online coupled WRF−CMAQ system over North America under AQMEII phase 2. *Atmos. Environ.* **2015**, *115*, 683−694.
(47) Ganzeveld, L.; Helmig, D.; Fairall, C. W.; Hare, J.; Pozzer, A. Atmosphere-ocean ozone exchange: A global modeling study of biogeochemical, atmospheric, and waterside turbulence dependencies. Global. *Biogeochem. Cycles* **2009**, *23*, GB4021.
(48) Helmig, D.; Lang, E. K.; Bariteau, L.; Boylan, P.; Fairall, C. W.; Ganzeveld, L.; Hara, J. E.; Hueber, J.; Pallandt, M. Atmosphere-ocean ozone fluxes during the TexAQS 2006, STRATUS 2006, GOMECC 2007, GasEx 2008, and AMMA 2008 cruises. *J. Geophys. Res.* **2012**, *117*, D04305.
(49) Chang, W.; Heikes, B. G.; Lee, M. Ozone deposition to the sea surface: chemical enhancement and wind speed dependence. *Atmos. Environ.* **2004**, *38*, 1053−1059.
(50) Chance, R.; Baker, A. R.; Carpenter, L.; Jickells, T. D. The distribution of iodide at the sea surface. *Environ. Sci.: Processes Impacts* **2014**, *16*, 1841−1859.
(51) MacDonald, S. M.; Gómez Martín, J. C.; Chance, R.; Warriner, S.; Saiz-Lopez, A.; Carpenter, L. J.; Plane, J. M. C. A laboratory characterisation of inorganic iodine emissions from the sea surface: dependence on oceanic variables and parameterisation for global modelling. *Atmos. Chem. Phys.* **2014**, *14*, 5841−5852.
(52) Hu, C.; Lee, Z.; Franz, B. Chlorophyll *a* algorithms for oligotrophic oceans: A novel approach based on three-band reflectance difference. *J. Geophys. Res.* **2012**, *117* (C1), C01011.
(53) Cooper, O. R.; Gao, R. S.; Tarasick, D.; Leblanc, T.; Sweeney, C. Long-term ozone trends at rural ozone monitoring sites across the United States, 1990−2010. *J. Geophys. Res.-Atmos.* **2012**, *117*, D22307.
(54) Parrish, D. D.; Allen, D. T.; Bates, T. S.; Estes, M.; Fehsenfeld, F. C.; Feingold, G.; Ferrare, R.; Hardesty, R. M.; Meagher, J. F.;

DOI: 10.1021/acs.est.6b03556
Environ. Sci. Technol. 2017, 51, 1458−1466

Nielsen-Gammon, J. W.; et al. Overview of the Second Texas Air Quality Study (TexAQS II) and the Gulf of Mexico Atmospheric Composition and Climate Study (GoMACCS). *J. Geophys. Res.* **2009**, *114*, D00F13.
(55) Dolwick, P.; Akhtar, F.; Baker, K. R.; Possiel, N.; Simon, H.; Tonnesen, G. Comparison of background ozone estimates over the western United States based on two separate model methodologies. *Atmos. Environ.* **2015**, *109*, 282−296.
(56) Kelly, J. T.; Baker, K. R.; Nowak, J. B.; Murphy, J. G.; Markovic, M. Z.; VandenBoer, T. C.; Ellis, R. A.; Neuman, J. A.; Weber, R. J.; Roberts, J. M. Fine-scale simulation of ammonium and nitrate over the South Coast Air Basin and San Joaquin Valley of California during CalNex-2010. *J. Geophys. Res.-Atmos.* **2014**, *119*, 3600−3614.
(57) Environmental Protection Agency (EPA). Implementation of the 2015 Primary Ozone NAAQS: Issues Associated with Background Ozone White Paper for Discussion. 2015, https://www.epa.gov/sites/production/files/2016-03/documents/whitepaper-bgo3-final.pdf.
(58) Tang, Y.; Lee, P.; Tsidulko, M.; Huang, H. C.; McQueen, J. T.; DiMego, G. J.; Emmons, L. K.; Pierce, R. B.; Lin, H. M.; Kang, D.; et al. The impact of chemical lateral boundary conditions on CMAQ predictions of tropospheric ozone over the continental United States. *Environ. Fluid Mech.* **2009**, *9* (1), 43−58.
(59) Schere, K.; Flemming, J.; Vautard, R.; Chemel, C.; Colette, A.; Hogrefe, C.; Bessagnet, B.; Meleux, F.; Mathur, R.; Roselle, S.; et al. Trace gas/aerosol boundary concentrations and their impacts on continental-scale AQMEII modeling domains. *Atmos. Environ.* **2012**, *53*, 38−50.
(60) Henderson, B. H.; Akhtar, F.; Pye, H. O. T.; Napelenok, S. L.; Hutzell, W. T. A database and tool for boundary conditions for regional air quality modeling: description and evaluation. *Geosci. Model Dev.* **2014**, *7*, 339−360.
(61) Appel, K. W.; Napelenok, S. L.; Foley, K. M.; Pye, H. O. T.; Hogrefe, C.; Luecken, D. J.; Bash, J. O.; Roselle, S. J.; Pleim, J. E.; Foroutan, H.; et al. Overview and evaluation of the Community Multiscale Air Quality (CMAQ) model version 5.1. *Geosci. Model Dev. Discuss.* **2016**, 1.
(62) Sarwar, G.; Kang, D.; Foley, K.; Schwede, D.; Gantt, B.; Mathur, R. Technical note: Examining ozone deposition over seawater. *Atmos. Environ.* **2016**, *141*, 255−262.
(63) Huang, H.-Y.; Hall, A.; Teixeira, J. Evaluation of the WRF PBL parameterizations for marine boundary layer clouds: Cumulus and stratocumulus. *Mon. Weather Rev.* **2013**, *141*, 2265−2271.

DOI: 10.1021/acs.est.6b03556
Environ. Sci. Technol. 2017, 51, 1458−1466

Atmospheric Environment 213 (2019) 395–404

Contents lists available at ScienceDirect

Atmospheric Environment

journal homepage: www.elsevier.com/locate/atmosenv

Influence of bromine and iodine chemistry on annual, seasonal, diurnal, and background ozone: CMAQ simulations over the Northern Hemisphere

Golam Sarwar[a,*], Brett Gantt[b], Kristen Foley[a], Kathleen Fahey[a], Tanya L. Spero[a], Daiwen Kang[a], Rohit Mathur[a], Hosein Foroutan[c], Jia Xing[d], Tomás Sherwen[e,f], Alfonso Saiz-Lopez[g]

[a] National Exposure Research Laboratory, US Environmental Protection Agency, RTP, North Carolina, 27711, USA
[b] Office of Air Quality Planning and Standards, US Environmental Protection Agency, RTP, NC, 27711, USA
[c] The Charles E. Via, Jr. Department of Civil & Environmental Engineering, Virginia Tech, Blacksburg, 24061, USA
[d] State Key Joint Laboratory of Environmental Simulation and Pollution Control, School of Environment, Tsinghua University, Beijing, 100084, China
[e] Wolfson Atmospheric Chemistry Laboratories, Department of Chemistry, University of York, UK
[f] National Centre for Atmospheric Science, Department of Chemistry, University of York, UK
[g] Department of Atmospheric Chemistry and Climate, Institute of Physical Chemistry Rocasolano, CSIC, Madrid, 28006, Spain

ARTICLE INFO

Keywords:
Bromine
Iodine
Ozone
Background ozone
CMAQ

ABSTRACT

Bromine and iodine chemistry has been updated in the Community Multiscale Air Quality (CMAQ) model to better capture the influence of natural emissions from the oceans on ozone concentrations. Annual simulations were performed using the hemispheric CMAQ model without and with bromine and iodine chemistry. Model results over the Northern Hemisphere show that including bromine and iodine chemistry in CMAQ not only reduces ozone concentrations within the marine boundary layer but also aloft and inland. Bromine and iodine chemistry reduces annual mean surface ozone over seawater by 25%, with lesser ozone reductions over land. The bromine and iodine chemistry decreases ozone concentration without changing the diurnal profile and is active throughout the year. However, it does not have a strong seasonal influence on ozone over the Northern Hemisphere. Model performance of CMAQ is improved by the bromine and iodine chemistry when compared to observations, especially at coastal sites and over seawater. Relative to bromine, iodine chemistry is approximately four times more effective in reducing ozone over seawater over the Northern Hemisphere (on an annual basis). Model results suggest that the chemistry modulates intercontinental transport and lowers the background ozone imported to the United States.

1. Introduction

Although anthropogenic emissions of nitrogen oxides (NO_x) and volatile organic compounds (VOC) within the United States (U.S.) have a large influence on ambient surface ozone (O_3) concentrations, other processes such as natural emissions, stratospheric intrusions, and long-range transport can affect surface O_3 concentrations at some locations within the U.S. Among these natural emissions are chemical compounds from the ocean surface that can reduce atmospheric O_3 concentrations through catalytic reactions. Bromine reactions deplete O_3 in the tropical marine boundary layer (Dickerson et al., 1999) and when combined with iodine reactions, they can deplete O_3 much faster than would have been expected if they acted individually (Saiz-Lopez et al., 2007; Mahajan et al., 2010). Bromine and iodine are produced in the ocean through both biotic and abiotic pathways resulting in measurable concentrations of both organic and inorganic species within the marine boundary layer. Several modeling studies have implemented marine bromine and iodine emission sources and chemistry with increasing levels of scope, ranging from one-dimensional models (e.g. von Glasow et al., 2002a; von Glasow et al., 2002b) to global chemical transport models (e.g. Ordó ez et al., 2012; Saiz-Lopez et al., 2012; Saiz-Lopez et al., 2014; Fernandez et al., 2014; Sherwen et al., 2016a; Sherwen et al., 2016b).

A disconnect between anthropogenic precursor emissions and surface O_3 concentrations at some U.S. sites has led to an increased focus on background O_3 (Fiore et al., 2002, 2003, 2014). The U.S. Environmental Protection Agency (EPA) considers background O_3 to be any O_3 formed from sources or processes other than U.S. manmade emissions of NO_x, VOC, methane, and carbon monoxide (EPA, 2016). Previous photochemical modeling studies (Parrish et al., 2009a; Cooper et al.,

* Corresponding author. US EPA, 109 T.W. Alexander Drive, Research Triangle Park, NC, 27711, USA.
E-mail address: sarwar.golam@epa.gov (G. Sarwar).

https://doi.org/10.1016/j.atmosenv.2019.06.020
Received 19 October 2018; Received in revised form 7 June 2019; Accepted 8 June 2019
Available online 11 June 2019
1352-2310/ Published by Elsevier Ltd.

2010; Zhang et al., 2011; McDonald-Buller et al., 2011) which estimated the contribution of background sources on U.S. O_3 concentrations have found that (1) seasonal mean background concentrations are highest in the Intermountain West, (2) seasonal mean background concentrations are generally highest in the Spring and early Summer, (3) background impacts can occur on episodic and non-episodic scales, and (4) air quality models are not capable of estimating background values accurately on a daily basis.

Background O_3 levels in coastal areas are affected by marine boundary layer chemistry, which is influenced by atmosphere-ocean interactions. Several previous studies examined the impacts on O_3 by bromine (e.g. Ordó ez et al., 2012; Fernandez et al., 2014; Yang et al., 2005; Parrella et al., 2012; Schmidt et al., 2016; Breton et al., 2017) and iodine chemistry (e.g. Saiz-Lopez et al., 2014; Sherwen et al., 2016a; Sherwen et al., 2016b; McFiggans et al., 2000; Long et al., 2014; Badia et al., 2019). Sarwar et al. (2015), Gantt et al. (2017), and Mu iz-Unamunzaga et al. (2018) showed that including marine bromine and iodine chemistry in the Community Multiscale Air Quality (CMAQ) model not only reduces summertime marine boundary layer O_3 concentrations by more than 5 ppbv, but also reduces O_3 in the free troposphere and inland areas far from the coast. In this study, we refine the marine bromine and iodine chemistry in the CMAQ model and extend the simulations to examine its influence on annual, seasonal, diurnal, and background O_3.

2. Methodology

CMAQ is a 3-D chemical transport model containing comprehensive treatments of many important atmospheric processes and is widely used for both regulatory and research purposes (e.g. Appel et al., 2013; Appel et al., 2017; Ring et al., 2018; Qiao et al., 2018). We use the hemispheric version (Mathur et al., 2017) of CMAQ version 5.2 (www.epa.gov/cmaq) to simulate the year 2006 with meteorological fields generated from the Weather Research and Forecasting (WRFv3.8.1) model employing the Thompson microphysics option (Skamarock et al., 2008). WRF results were further processed using the Meteorology Chemistry Interface Processor (Otte and Pleim, 2010) (MCIPv4.3) to prepare CMAQ-ready meteorological files. The model vertical extent reaches to 50 hPa containing 44 layers of varying thickness and uses 108-km horizontal grid spacings. The surface layer has a thickness of 20 m.

The 2005 Carbon Bond chemical mechanism (CB05e51) containing updated toluene, oxidized nitrogen, and isoprene reactions (Appel et al., 2017) is combined with the chlorine (Sarwar et al., 2012), bromine, and iodine chemistry for this study. Sarwar et al. (2015) incorporated an initial version of bromine and iodine chemistry into CMAQ and examined its lower and upper limits of the impacts on O_3. The upper limit included photolysis of higher iodine oxides while the lower limit did not. The model without the photolysis of iodine oxides yielded lesser reduction of O_3 over seawater (15%) compared to the model with the photolysis of iodine oxides which reduced O_3 by 48%. Since this 48% reduction resulted in unrealistically low O_3 concentrations in Sarwar et al. (2015), photolysis rates of higher iodine oxides have not been included in any publicly available version of the CMAQ model. Sarwar et al. (2015) also included one heterogeneous reaction of bromine nitrate.

In this study, the CMAQ bromine and iodine chemistry described in Sarwar et al. (2015) is further improved to include photolysis of higher iodine oxides (Tables S1–S2), several heterogeneous reactions of bromine and iodine species (Table S3) with aerosol chloride (Cl^-) and bromide (Br^-), and refined bromine and halocarbon emissions. In the previous CMAQ model, photolysis rates of higher iodine oxides were calculated using absorption cross-section and quantum yield from Saiz-Lopez et al. (2014). Sherwen et al. (2016a) used absorption cross-section and quantum yield of iodine nitrate for calculating photolysis rates of higher iodine oxides which is now used in the CMAQ model.

We also incorporate several aqueous-phase reactions of bromine species following Long et al. (2013) (Table S4). Cloud chemistry of bromine species was added to the CMAQ cloud module "AQCHEM-KMT" (Fahey et al., 2017) using the Kinetic PreProcessor (KPP) v.2.2.3 (Damian et al., 2002). AQCHEM-KMT simulates the evolution of species in and around cloud water by calculating kinetic mass transfer between gas and aqueous phases, interstitial aerosol scavenging, dissociation of ionic species, aqueous phase chemical reactions, and wet deposition.

Sarwar et al. (2015) used halocarbon, inorganic bromine, and inorganic iodine emissions in the CMAQ model, the rates of which are refined in this study. For halocarbon species, the emission rates are calculated following the procedures of Ordó ez et al. (2012) and Yarwood et al. (2010):

$$E_{HC} = E_{base} \times (O_F + S_F) \times A_{GC} \times f_{HC} \times f_{DP} \times \text{chl-}a \quad (1)$$

Where, E_{HC} is the halocarbon emission rates (moles s^{-1}), E_{base} represents the halocarbon base emission rate (moles s^{-1}), O_F is the open ocean fraction of a grid cell, S_F is the surf zone fraction of a grid cell, A_{GC} is the grid cell area (m^2), f_{HC} is a species-dependent emission factor, f_{DP} is a diurnal profile factor, and chl-*a* is the monthly climatological chlorophyll value (mg m^{-3}) from the Moderate Resolution Imaging Spectroradiometer (MODIS).

In Sarwar et al. (2015), chl-*a* values were capped at 1.0 following Yarwood et al. (2010); in this study, we used the actual chl-*a* values from MODIS which can be greater than 1.0 in coastal areas. This change in chl-*a* values necessitated a revision in the base emission rate from 1.2×10^{-11} in Sarwar et al. (2015) to 6.9×10^{-12} to replicate the global estimates of halocarbon emissions reported by Ordó ez et al. (2012). This revision was done outside the CMAQ framework by using the native MODIS derived global land/ocean grid areas and chl-*a* values. We iterated the base emission rate until suitable agreement with the Ordó ez et al. (2012) estimates was reached. The use of the revised base emission rate and the actual chl-*a* values reduces the total hemispheric halocarbon emissions estimates by ~20% compared to the estimates of Sarwar et al. (2015). It also changes the allocation of halocarbon emissions to different grid-cells. More halocarbon emissions are now allocated to coastal areas and less are allocated to open oceans compared to the estimates of Sarwar et al. (2015).

Refinement of the inorganic emissions included the replacement of the simplified treatment of directly emitting inorganic bromine emissions (Yang et al., 2005 and Sarwar et al., 2015) with the physically-based heterogeneous chemistry of bromine and iodine species (Table S3) following Fernandez et al. (2014) and Sherwen et al. (2016b). This required a revision to the sea spray emissions in CMAQ (Gantt et al., 2015) to include Br^- in the chemical speciation. Specifically, the sea spray emissions are speciated by mass (gm/gm) following Millero (1996): $Cl^- = 0.5528$, $Na^+ = 0.3080$, $SO_4^{2-} = 0.0775$, $Ca^{2+} = 0.0118$, $Mg^{2+} = 0.0367$, $K^+ = 0.0113$, and $Br^- = 0.0019$. We also updated the minimum wind speed in the inorganic iodine emissions parameterization (McDonald et al., 2014) from 3 m s^{-1} in Sarwar et al. (2015) to 5 m s^{-1} following the value used for the GEOS-Chem model (Sherwen et al., 2016a) which reduces the emissions estimates by ~15%. Hemispheric halocarbon and inorganic iodine emission rates, along with global estimates reported in previous studies, are shown in Table 1. Generally, our halocarbon emissions estimates for the Northern Hemisphere are lower than the reported global estimates while inorganic iodine emissions estimates fall between the reported ranges of global estimates.

We performed six annual simulations for this study that can be grouped in three pairs. In the first pair, one simulation used CB05e51 along with the chlorine chemistry (hereto referred as "No_Br/I"), while the other added bromine and iodine chemistry ("Added_Br/I"). A second set of simulations was completed to investigate the influence of the bromine and iodine chemistry independently. In this second pair,

Table 1
Halocarbon and inorganic iodine emissions estimates.

Species	Hemispheric annual estimates in this study (Gg)	Global annual estimates from published studies (Gg)
$CHBr_3$	301	533
CH_2Br_2	51.5	67.3
CH_2BrCl	6.1	10.0
$CHBr_2Cl$	14.8	19.7
$CHBrCl_2$	14.5	22.6
CH_3I	135	303
CH_2ICl	148	234
CH_2IBr	54.4	87.3
CH_2I_2	73	116
HOI + $2xI_2$	2052	1900–3230

Note: Global annual estimates of halocarbon emissions are taken from Ordó ez et al. (2012), global annual estimates of HOI + 2 × I_2 are taken from Saiz-Lopez et al. (2014) and Sherwen et al. (2016a).

one simulation added only bromine chemistry updates ("Added_Br") while the other added only iodine chemistry updates ("Added_I"). The final set of simulations was completed to investigate the impact of bromine and iodine chemistry on background O_3 over the U.S. For the third pair, the model chemistry was identical to the first pair but with anthropogenic emission sources over North America were zeroed out ("No_Br/I_NoAnth" and "Added_Br/I_NoAnth", respectively). All the annual simulations were completed with a three-month spin-up period (October–December of 2005) and initialized from previous model results (Xing et al., 2016).

3. Results and discusssion

3.1. Predicted BrO (bromine monoxide) and IO (iodine monoxide)

BrO and IO are reaction products of the bromine and iodine chemistry. Annual mean daytime BrO and IO concentrations are shown in Fig. 1. BrO concentrations of 0–0.8 pptv are predicted over large oceanic areas. However, higher values (> 0.8 pptv) are also predicted over limited areas of mid-latitude oceans. In contrast, IO concentrations of 0–3.0 pptv are predicted over large oceanic areas and higher values (> 3.0 pptv) are predicted only over limited oceanic areas.

The current bromine/iodine chemistry enhances BrO and IO levels compared to the previous version of the chemistry without the photolysis of higher iodine oxides in CMAQ (Sarwar et al., 2015). For example, predicted summertime BrO levels with the previous version rarely exceed 0.5 pptv over the mid-latitude oceanic areas. In contrast, predicted BrO levels with the current version exceed 1.0 pptv over large portions of the mid-latitude oceanic areas. Overall, the current chemistry increases surface BrO levels by a factor of ~2.0 averaged over the entire seawater. Predicted summertime IO levels over most areas of seawater range from 0.5 to 1.5 pptv and 0.5–3.0 pptv for the previous and current versions of the chemistry, respectively. Overall, the current chemistry increases surface IO levels by a factor of ~1.5 averaged over the entire seawater. The BrO enhancement occurs primarily due to the inclusion of aqueous-phase and heterogeneous reactions while the IO enhancement occurs due to the inclusion of photolysis of higher iodine oxides and the heterogeneous reactions.

Table 2
A comparison of observed daytime BrO and IO concentrations with CMAQ predictions.

Location	Species	Observed value (pptv)	Predicted value (pptv)
Cape Verde Islands[a]	BrO	2.8	0.7
Dagebüll, Germany[b]	BrO	0.4	0.1
Brittany, France[b]	BrO	1.5	0.03
Mace Head, Ireland[c]	BrO	2.3	0.05
Cape Verde Islands[a]	IO	1.5	1.2
Dagebüll, Germany[b]	IO	0.7	0.8
Brittany, France[b]	IO	1.5	0.2
Mace Head, Ireland[d]	IO	1.2	0.14
Tenrife, Spain[d]	IO	1.2	1.1

Note: a - Mahajan et al. (2010); b – Peters et al. (2005); c – Saiz-Lopez et al. (2006); d – Allan et al. (2000). Cape Verde values represent daytime average of long-term measurements; CMAQ predicted annual daytime mean values are compared. Values at other locations represent daytime average over campaign; CMAQ predicted monthly daytime mean values are compared. Peters et al. (2005) reported average values for the entire campaign which we multiplied by 2.0 to estimate daytime average values.

We compare model predictions with published values from different years for an approximate evaluation of the bromine and iodine chemistry in CMAQ. Predicted BrO levels are lower than observed values at all locations (Table 2). CMAQ predicted values are also lower than ground-based daytime BrO measurements of < 0.5–2.0 pptv and ship-based daytime BrO measurements of < ~3.0–3.6 pptv (Saiz-Lopez et al., 2012). Thus, CMAQ generally under-predicts BrO levels. In contrast, CMAQ predicted values are similar to observed IO levels at Cape Verde Islands; Tenrife, Spain; Dagebüll, Germany but are lower than observed values at Brittany, France and Mace Head, Ireland (Table 2). Dix et al. (2013) measured IO concentrations over the Pacific

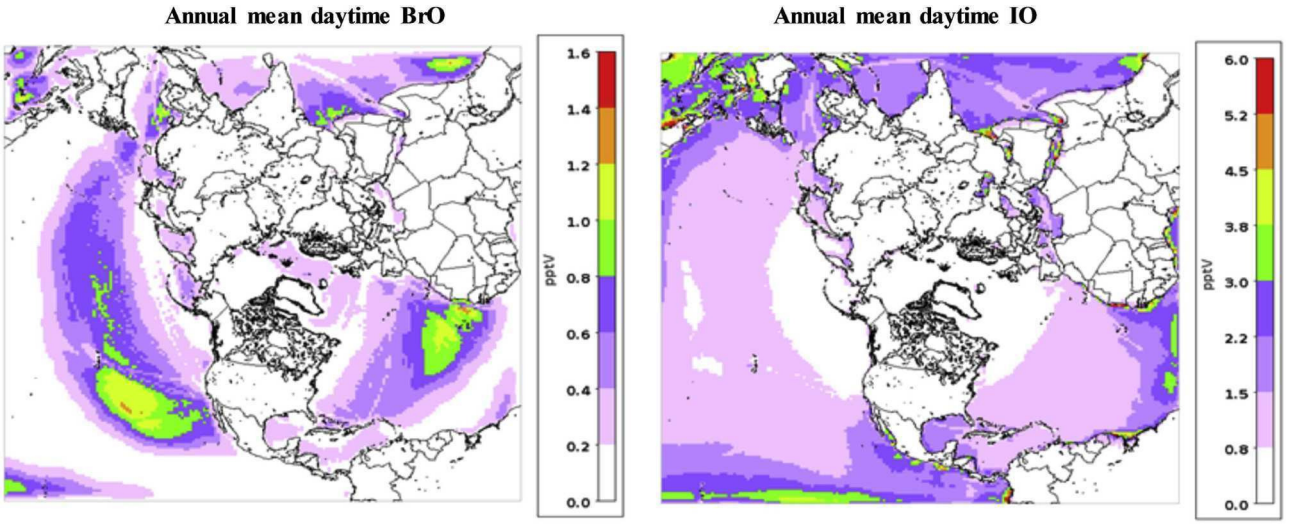

Fig. 1. Simulated annual mean daytime surface BrO and IO concentrations with the bromine and iodine chemistry (Added_Br/I). Annual mean concentrations were multiplied by 2.0 to estimate approximate annual mean daytime BrO and IO concentrations.

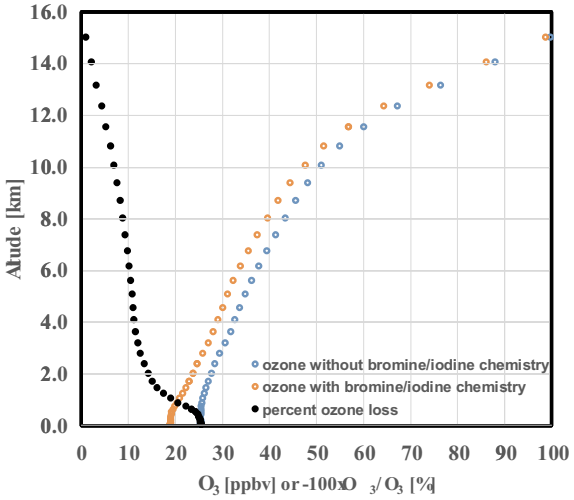

Fig. 2. Simulated annual mean O_3 over seawater in the Northern Hemisphere without (No_Br/I) and with the bromine and iodine chemistry (Added_Br/I) and annual mean percent reduction of O_3 by the bromine and iodine chemistry [100 x (Added_Br/I − No_Br/I)/No_Br/I].

Ocean in January of 2010 and reported an average value of 0.5 pptv inside the marine boundary layer. CMAQ predicted surface layer values range from 0.4 to 1.0 pptv over the region. Saiz-Lopez et al. (2012) reported that ground-based daytime IO measurements range from < 0.2 to 2.4 pptv while ship-based daytime IO measurements range ~3.5 pptv. CMAQ predicted IO levels are similar to these reported observed values. Thus, CMAQ generally captures observed IO values.

3.2. Influence on annual mean O_3

Annual mean surface O_3 concentration over seawater without bromine and iodine chemistry is ~25 ppbv and increases with altitude (Fig. 2). Consistent with the results of Sherwen et al. (2016b), the bromine and iodine chemistry reduces mean surface O_3 over seawater by 25% and reduces O_3 throughout the lower troposphere. Such reduction occurs due primarily to the reactions of O_3 with bromine and iodine radicals generated from photolysis and reactions of halocarbons and inorganic bromine and iodine species with hydroxyl radical. The influence of bromine and iodine chemistry on O_3 decreases with altitude and is negligible at ~15 km. Saiz-Lopez et al. (2014) and Sarwar et al. (2015) reported lower and upper limits (17–27% and 15–48%) of the impacts on O_3; and the O_3 changes reported in this study fall within their published ranges.

The spatial distribution of the annual mean O_3 without bromine and iodine chemistry is shown in Fig. 3a with the highest values over portions of Asia, Africa, and the western U.S. and lower values predicted over seawater (especially over remote oceanic areas). The inclusion of bromine and iodine chemistry reduces surface O_3 by 3–12 ppbv over large areas of seawater (Fig. 3b) and by 3–6 ppbv in many coastal areas including the Pacific, Gulf of Mexico, and Atlantic coasts. Its impact on O_3 over land is smaller than that over seawater, although all areas of the U.S. have a predicted ~2 ppbv or greater reduction in O_3 from the bromine and iodine chemistry.

The bromine and iodine chemistry in this study is more efficient in reducing O_3 over seawater compared to the previous version of the chemistry without the photolysis of higher iodine oxides in CMAQ (Sarwar et al., 2015). For example, the previous chemistry reduces summer-time O_3 over seawater generally by 2–8 ppbv while the current chemistry reduces O_3 over seawater by 3–12 ppbv. Both versions of the bromine and iodine chemistry have similar impacts over land areas.

3.3. Influence on diurnal variation of O_3

To examine the influence of the bromine and iodine chemistry on the diurnal variation of O_3, we calculated a mean diurnal profile for an area over the Atlantic Ocean (see Fig. 3a) by averaging across all days in the annual simulation for each hour of the day, as shown in Fig. 4a. The area is selected to minimize the influence of anthropogenic emissions on O_3. Predicted O_3 levels with the bromine and iodine chemistry are lower (by 7–8 ppbv) than those in simulations without the bromine and iodine chemistry. There is a pronounced diurnal cycle in both simulations, as O_3 concentrations increase from midnight and peak in the morning, then decrease to a minimum value in the afternoon before increasing again. This diurnal variation results from low concentrations of O_3 precursors over remote areas of seawater that limit O_3 production as has been previously reported by Read et al. (2008). In contrast, the O_3 levels over land typically peak in the afternoon due to the higher concentrations of O_3 precursors (David and Nair, 2011). When bromine and iodine chemistry are excluded, O_3 is reduced primarily by the photolysis of O_3 and its reaction with hydroperoxy radical (HO_2). Adding bromine and iodine chemistry creates more pathways to O_3 reduction. Thus, the bromine and iodine chemistry reduces O_3; however, it does not alter the diurnal profile of O_3. While the diurnal cycle

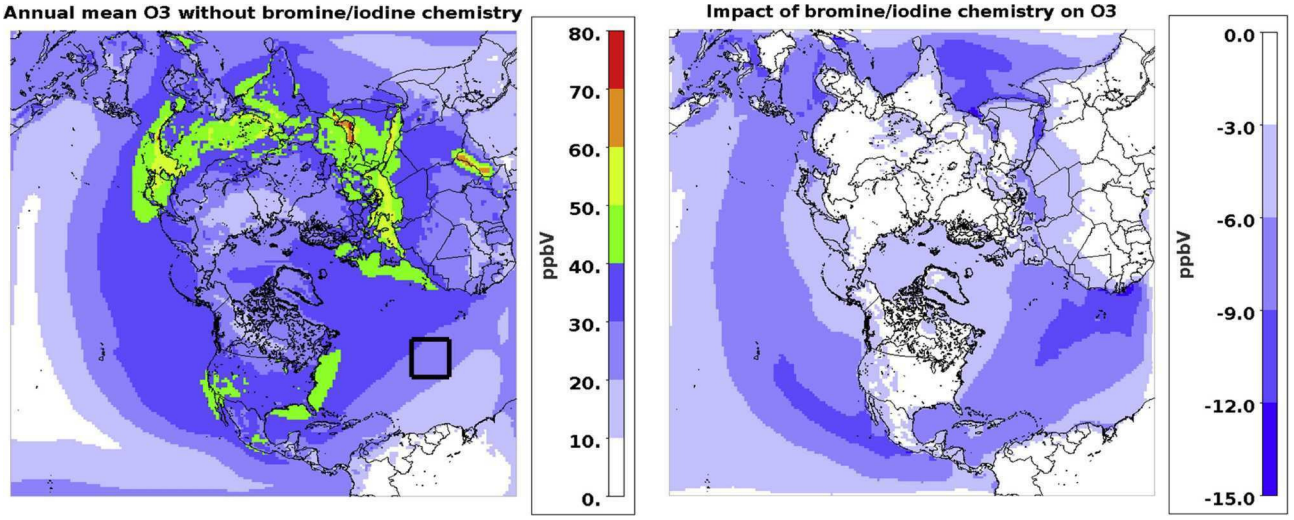

Fig. 3. (a) Annual mean surface O_3 without the bromine and iodine chemistry (No_Br/I) (b) influence of the bromine and iodine chemistry on annual mean O_3 (Added_Br/I − No_Br/I). Black square box is the area over which diurnal, day-to-day, and monthly variations are calculated as shown in Figs. 4 and 5.

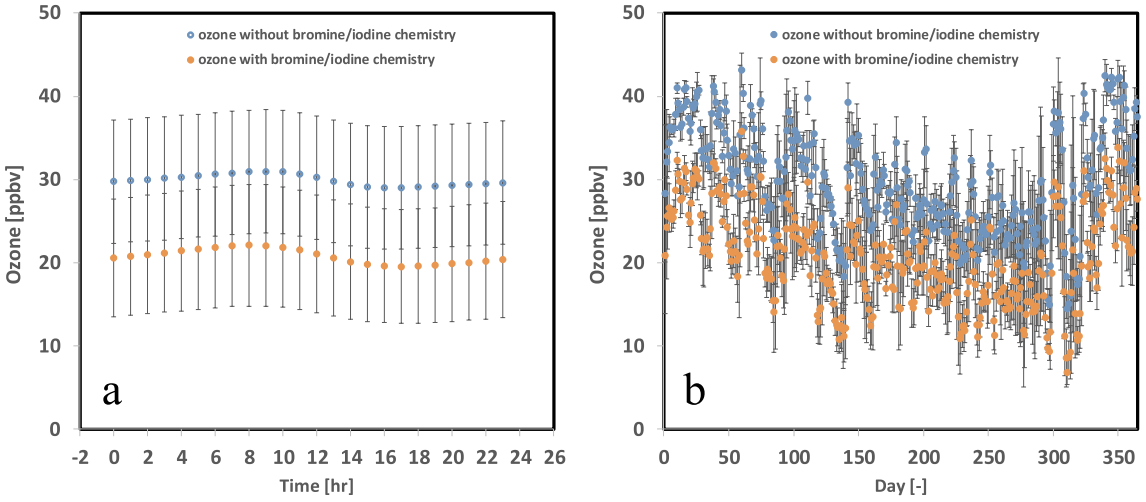

Fig. 4. (a) Influence of the bromine and iodine chemistry on diurnal variation of surface O_3 (b) influence of the bromine and iodine chemistry on the day-to-day variation of surface O_3. Blue circle – No_Br/I and orange circle – Added_Br/I. (For interpretation of the references to color in this figure legend, the reader is referred to the Web version of this article.)

of O_3 without the bromine and iodine chemistry varies slightly with locations due to precursors, meteorology and other factors, the bromine and iodine chemistry does not alter the diurnal cycle at any location but rather simply reduces O_3 concentrations.

3.4. Influence on the day-to-day variation of O_3

To examine the day-to-day variation of the bromine and iodine chemistry impacts on O_3, we first calculated daily-mean O_3 values for each grid cell over seawater. We then calculated a mean daily value from the same area over the Atlantic Ocean (see Fig. 3a). Bromine and iodine chemistry reduces O_3 on each day of the year (Fig. 4b), but the magnitude of the reduction varies from day to day. Such variation depends on multiple factors including existing atmospheric O_3 levels and wind speed. The O_3 levels can influence the daily variation in two ways: 1) higher O_3 concentrations increase inorganic iodine emissions which react with and reduce O_3 and 2) higher O_3 increases the reaction rates with bromine and iodine which reduces O_3. Wind speed can influence the daily variation in two ways: 1) lower wind speed enhances inorganic iodine emissions (McDonald et al., 2014) which further reduce O_3 and 2) lower wind speed increases available reaction time between O_3 and bromine/iodine species which can also reduce additional O_3. Bromine and iodine chemistry most efficiently reduces O_3 at low wind speeds and high existing O_3 concentrations.

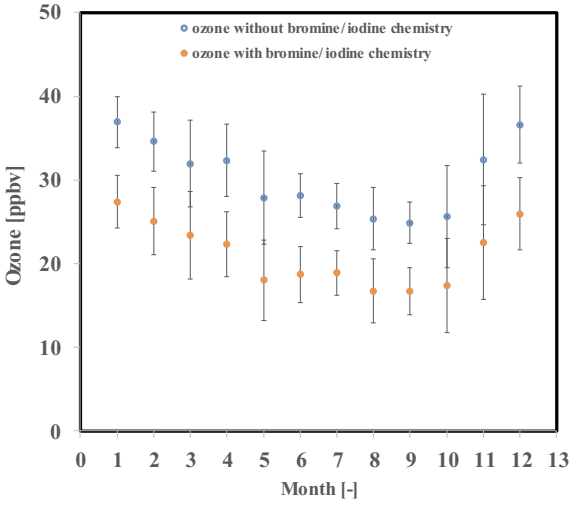

Fig. 5. Influence of the bromine and iodine chemistry on month-to-month variation of surface O_3. Error bars are represented with two standard deviation. Blue circle – No_Br/I and orange circle – Added_Br/I. (For interpretation of the references to color in this figure legend, the reader is referred to the Web version of this article.)

3.5. Seasonal variation of the influence on O_3

To examine the seasonal variation of the bromine and iodine chemistry impacts on O_3, we first calculated monthly mean O_3 from daily-mean values for each grid cell over seawater. We then calculated a mean value from the same area over the Atlantic Ocean (see Fig. 3a). Mean O_3 levels are highest in cooler months and lowest in warmer months (Fig. 5) due to the low O_3 precursor levels over seawater that limit O_3 production and cause loss processes to control O_3 concentrations. Photolysis of O_3 and its reaction with HO_2 are two dominant loss processes over seawater (Breton et al., 2017). The loss via photolysis is highest in warmer months due to high actinic flux. Atmospheric HO_2 levels are high in warmer months due to higher photochemical activity; thus, the loss of O_3 via its reaction with HO_2 is also high in warmer months. Bromine and iodine chemistry reduces monthly mean O_3 by ~8–10 ppbv. The reduction of O_3 from bromine and iodine chemistry is largest in December and lowest in July. Bromine and iodine chemistry reduces seasonal mean surface O_3 in Winter (December–February) by 9.9 ppbv, Spring (March–May) by 9.5 ppbv, Summer (June–August) by 8.7 ppbv, and Fall (September–November) by 8.8 ppbv. If the entire seawater is considered, bromine and iodine chemistry reduces mean surface O_3 over seawater by 6.9 ppbv, 6.8 ppbv, 5.9 ppbv, and 6.2 ppbv in Winter, Spring, Summer, and Fall, respectively. Slightly greater O_3 losses occur in the Winter and Spring seasons due primarily to the bromine chemistry and the fact that lower temperatures in cooler months promote efficient partitioning of hydrobromic acid into Br^- which enhances heterogeneous production of ozone-reacting bromine species.

3.6. Influence on background O_3

By comparing the pair of simulations with anthropogenic emission sources over North America zeroed out, we are able estimate the impact of iodine and bromine chemistry on background O_3 over North America. The bromine and iodine chemistry reduces seasonal mean background O_3 over the U.S. in all seasons (Fig. 6) with the greatest reduction occurring in the Winter and Spring (2–6 ppbv) followed by

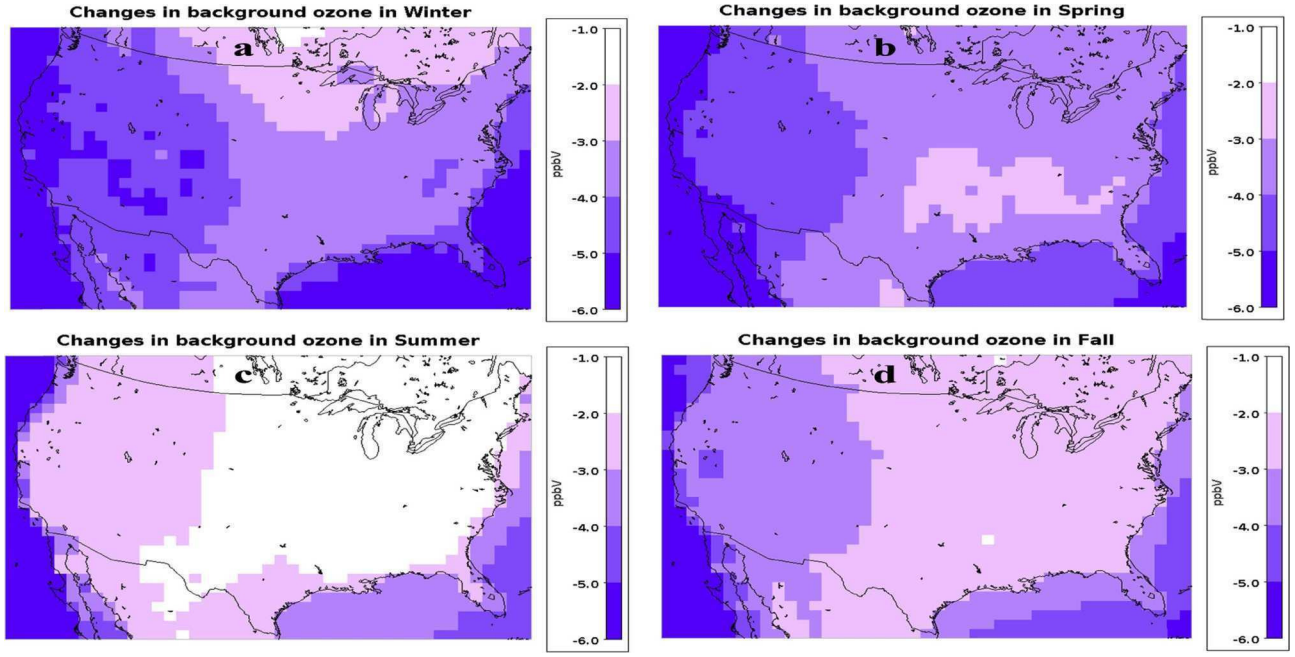

Fig. 6. Influence of the bromine and iodine chemistry (Added_Br/I_NoAnth – No_Br/I_NoAnth) on seasonal mean background O_3 over the U.S. (a) Winter (b) Spring (c) Summer (d) Fall. Winter: December–February; Spring: March–May; Summer: June–August; Fall: September–November.

the Fall (2–4 ppbv) and Summer (1–3 ppbv). For all seasons, bromine and iodine chemistry reduces more O_3 over the western U.S. and coastal areas than over other inland areas, which is consistent with the results shown in Fig. 3b. The springtime reductions in the western U.S. are in areas that have some of the highest background O_3 concentrations in the U.S. (Dolwick et al., 2015). These substantial reductions in background O_3 from the bromine and iodine chemistry suggest that atmospheric models without this chemistry potentially overpredict background O_3. Our results corroborate the findings of Wang et al. (2015) who reported that halogen chemistry affects the intercontinental transport of O_3.

3.7. Isolating the impacts of bromine and iodine chemistry on O_3

Fig. 7 shows that bromine and iodine chemistry have different impacts on O_3 concentrations; bromine chemistry reduces annual mean surface O_3 over limited areas of seawater by 2–4 ppbv (Fig. 7a) while the iodine chemistry reduces O_3 by 2–10 ppbv over most oceanic areas (Fig. 7b). Iodine chemistry affects model prediction over the entire U.S. and reduces annual mean O_3 by 1–2 ppbv over the eastern U.S., 2–3 ppbv over the western U.S., and 3–4 ppbv over some coastal areas. In contrast, bromine chemistry reduces annual mean O_3 by < 1 ppbv over U.S. On average, bromine chemistry reduces annual mean O_3 over seawater by 1.2 ppbv while iodine chemistry reduces O_3 by 5.2 ppbv. Iodine chemistry is more efficient in reducing O_3 than the bromine chemistry due to several factors. The rate constant for the I + O_3 reaction is ~10% greater than that of the Br + O_3 reaction (Ordó ez et al., 2012). Iodine recycles at a faster rate than bromine due to higher photolysis rates of I_2/HOI compared to Br_2/HOBr as well as the presence of higher iodine oxides in the model. Additionally, the inorganic iodine emissions rates are a function of dissolved O_3 and iodide present in seawater (Carpenter et al., 2013) and are higher when atmospheric O_3 concentrations are higher. Such factors in iodine chemistry reduce O_3 over seawater more efficiently than that of bromine chemistry. Lower O_3 concentrations over the marine environment due to iodine chemistry are transported inland resulting in lower O_3 over land.

3.8. Influence of iodine and bromine chemistry on O_3 model performance

In addition to the direct comparison between model simulations, we

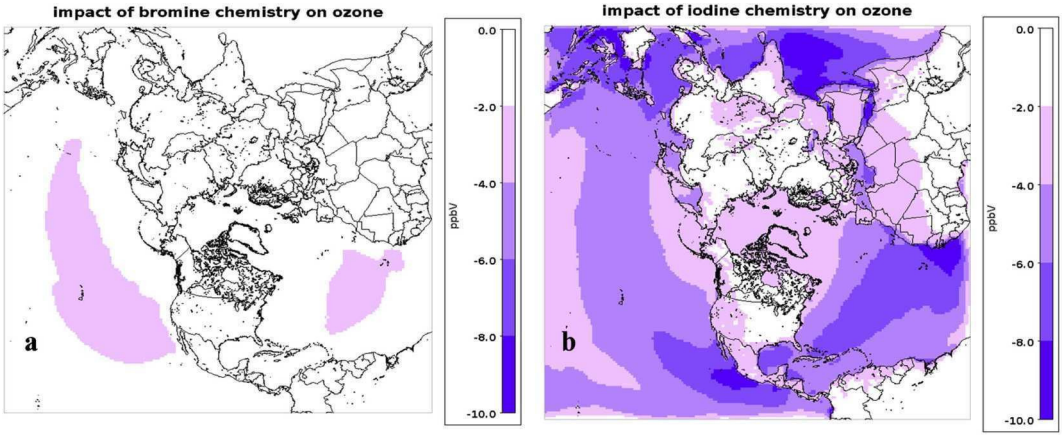

Fig. 7. Changes in annual mean surface O_3 with (a) bromine chemistry (Added_Br − No_Br/I) and (b) iodine chemistry (Added_I − No_Br/I).

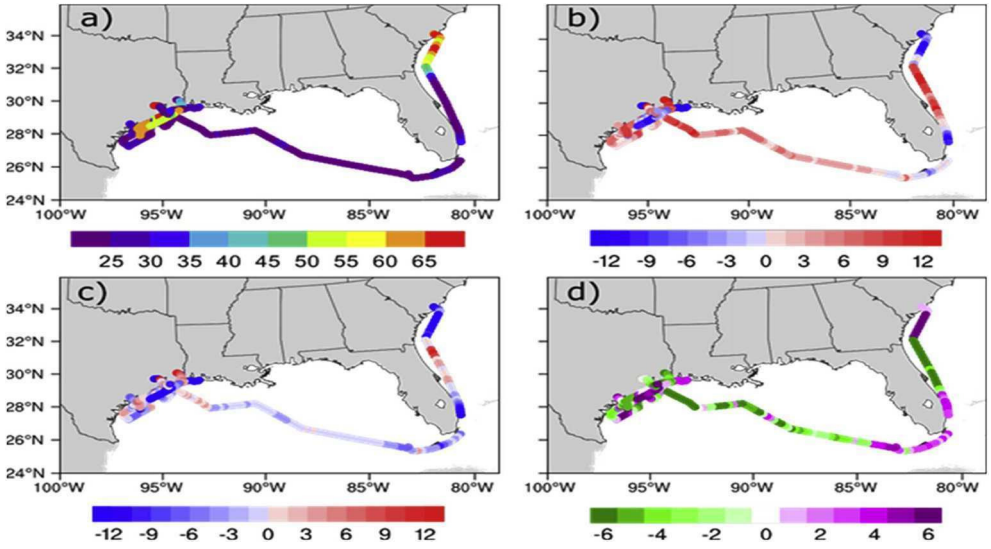

Fig. 8. (a) Observed surface O_3 concentrations from R/V Ronald H. Brown during August 2006 of the TexAQS campaign (Parrish et al., 2009b) (b) model mean bias for the model without any bromine and iodine chemistry (No_Br/I – Observations) (c) model mean bias for the model with the bromine and iodine chemistry (Added_Br/I – Observations), and (d) differences in the model absolute mean bias between simulations without and with bromine and iodine chemistry (|Added_Br/I – Observations| – |No_Br/I – Observations|). The green colors in (d) represent locations where the simulation with the bromine and iodine chemistry had a lower model bias (improved prediction), and purple colors represent locations where the simulation with the bromine and iodine chemistry had a higher model bias (worse prediction). All units are in ppbv. (For interpretation of the references to color in this figure legend, the reader is referred to the Web version of this article.)

have also evaluated the simulations without and with bromine and iodine chemistry against both ship-based and land-based O_3 observations. The ship-based surface measurements used for this evaluation are over the Gulf of Mexico from the 2006 Texas Air Quality Study (Parrish et al., 2009b) (TexAQS). Observed O_3 concentrations during the August 2006 period of the TexAQS campaign are generally less than 30 ppbv, though higher values were measured over some coastal waters off Texas, South Carolina and Georgia (Fig. 8a). Model mean bias values (Fig. 8b–c) show that neither model simulation captures the high observed values near some coastal waters which results in a negative bias. The model without the bromine and iodine chemistry, however, has a positive bias (median bias +4.7 ppbv) over most areas in the remote ocean while the model with the bromine and iodine chemistry typically has a slight negative bias (median bias −1.0 ppbv, 95% of the observations have a bias within ± 30 ppbv) for these areas. We also compared the performance of the simulations without and with bromine and iodine chemistry by calculating the difference in the absolute mean bias between the two simulations. In this calculation, positive values mean that the simulation with bromine and iodine chemistry has a higher absolute bias (further from observations) while negative values indicate that it has a lower absolute bias (closer to observations). The difference in absolute mean bias shown in Fig. 8d reveals that the

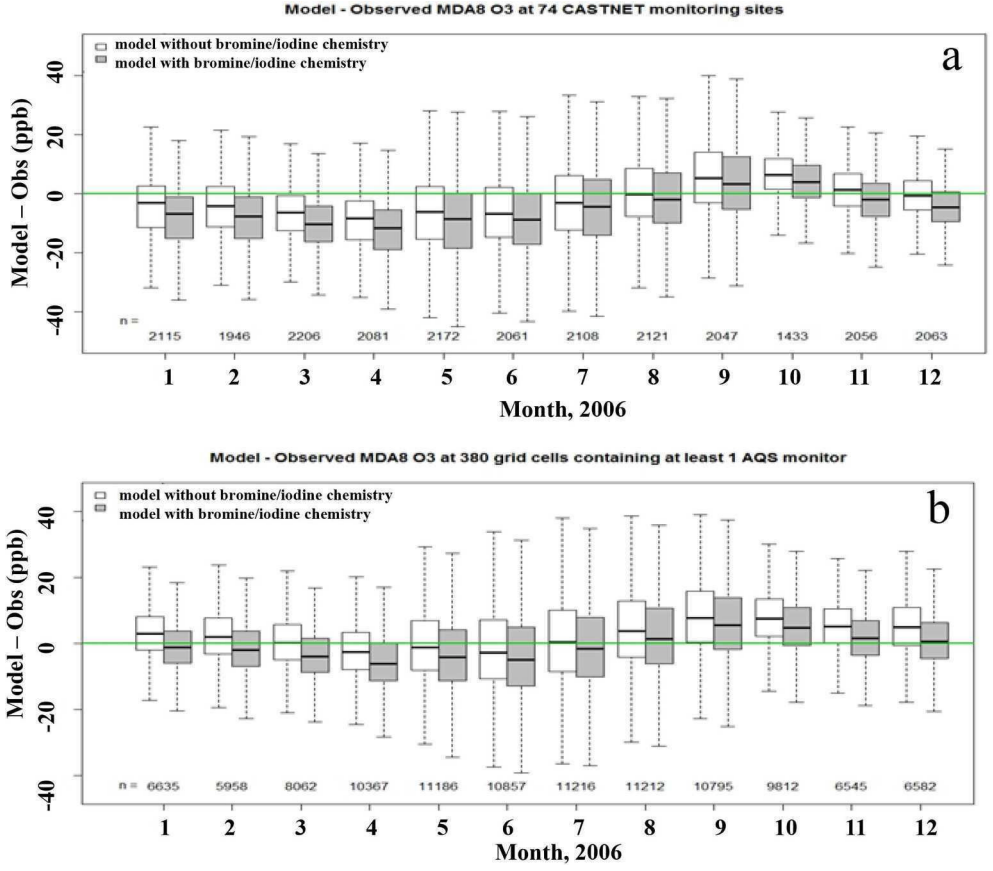

Fig. 9. Monthly mean bias without (No_Br/I – Observations) and with (Added_Br/I – Observations) the bromine and iodine chemistry at all (a) CASTNET and (b) AQS sites. AQS observations falling within the same grid cell are first averaged prior to comparing to the model value. Lower bar in the box represents the 25th percentile, middle bar represents the median and the upper bar represents the 75 percentile values. The lowest horizontal bar represents the minimum value while the highest horizontal bar represents the maximum value.

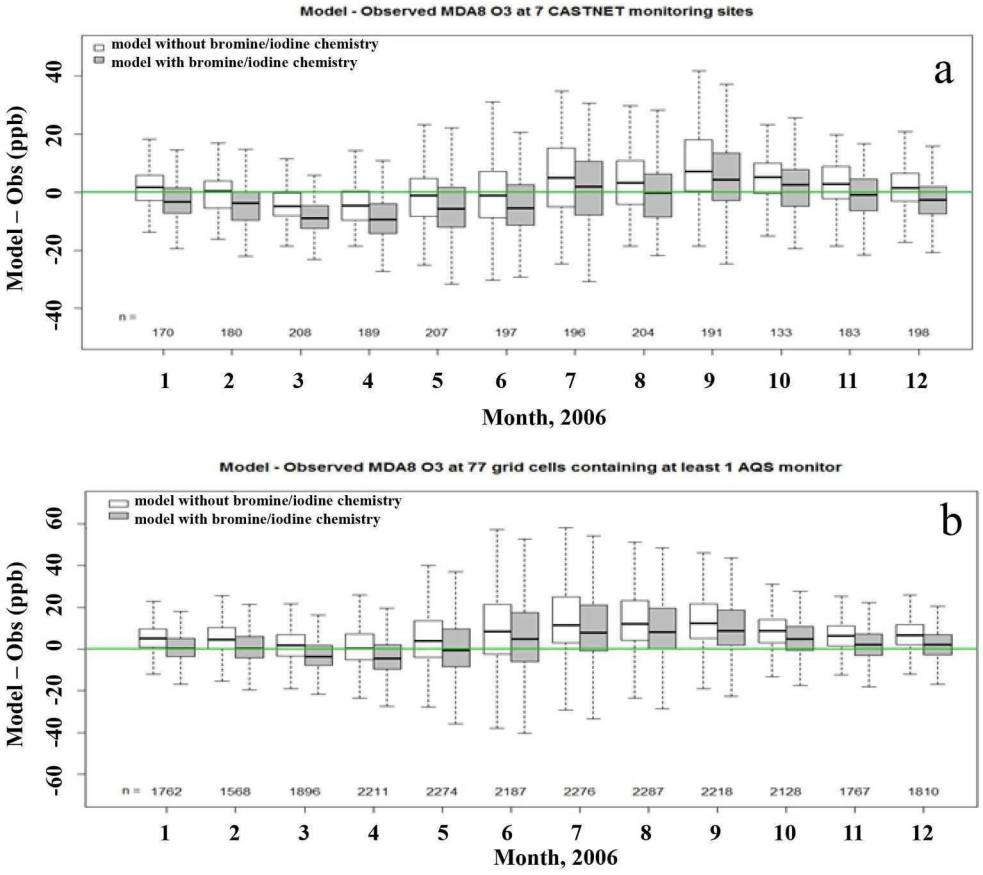

Fig. 10. Monthly mean bias without (No_Br/I – Observations) and with (Added_Br/I – Observations) the bromine and iodine chemistry at coastal (a) CASTNET and (b) AQS sites. AQS observations falling within the same grid cell are first averaged prior to comparing to the model value. Lower bar in the box represents the 25th percentile, middle bar represents the median and the upper bar represents the 75 percentile values. The lowest horizontal bar represents the minimum value while the highest horizontal bar represents the maximum value.

inclusion of bromine and iodine chemistry generally reduces the bias by 2–6 ppbv over the ocean without much degradation in other regions.

The simulations without and with bromine and iodine chemistry were also evaluated against observations in the U.S. from the Clean Air Status and Trends Network (CASTNET) and the USEPA's Air Quality System (AQS). CASTNET and AQS include sites at mainly remote and mainly urban locations, respectively. Monthly mean bias for the simulation without the bromine and iodine chemistry varies (−8 to +4 ppbv for CASTNET sites and −3 to +7 ppbv for AQS sites), with negative biases (underprediction) for several months (January–August and December at CASTNET sites and April–June for AQS sites) and positive biases (overprediction) for other months (Fig. 9). The inclusion of bromine and iodine chemistry generally improves O_3 predictions in the Fall at both the CASTNET and AQS sites and deteriorates the model predictions in the Spring. In the Winter and Summer, the simulation with bromine and iodine chemistry generally has degraded predictions at the CASTNET sites and improved predictions at the AQS sites.

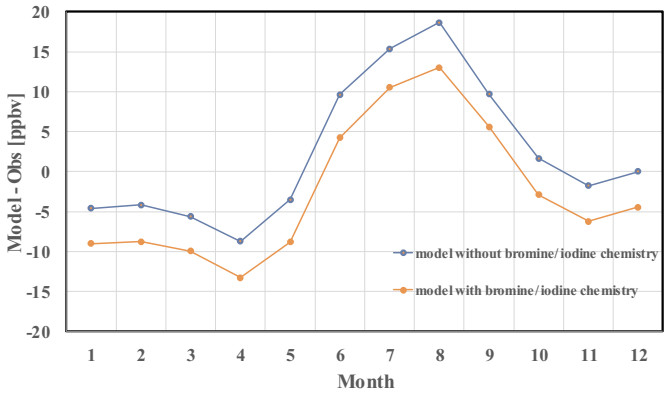

Fig. 11. Monthly mean bias without (No_Br/I – Observations) and with (Added_Br/I – Observations) the bromine and iodine chemistry at monitoring sites in Japan.

When only the coastal sites are considered, the monthly mean biases for the simulation without bromine and iodine chemistry are positive for January–February and July–December at CASTNET sites (Fig. 10a) and for all months at AQS sites (Fig. 10b). Differences between the simulations without and with bromine and iodine chemistry are more noticeable for the coastal sites, with a larger number of months having improved predictions when bromine and iodine chemistry is included. This is especially true at coastal AQS sites where the bromine and iodine chemistry improves model performance for all months except March and April. Gantt et al. (2017) compared model (using a 12-km horizontal grid resolution) predictions for August 2006 with observations from the 2006 ship-based TexAQS and coastal AQS sites and reported that the model without bromine and iodine chemistry generally over-predicts O_3 while the bromine and iodine chemistry improves the model performance. Model performance shown in Figs. 8 and 10 for August is consistent with results of Gantt et al. (2017).

The hemispheric domain also allows for model evaluation against O_3 observations from monitors in Japan as part of the Acid Deposition Monitoring Network in East Asia (www.eanet.asia/eanet) (Fig. 11). The simulation without bromine and iodine chemistry underpredicts O_3 (by 2–9 ppbv) during the cooler months (January–May and November) and overpredicts (by 2–19 ppbv) in the warmer months (June–September). Including bromine and iodine chemistry further deteriorates O_3 model performance in the cooler months but improves model performance in warmer months. This seasonality is consistent with Kyo et al. (2019) which reported CMAQ overpredictions of O_3 during the summertime over Japan.

4. Summary

Regional chemical transport models like CMAQ are routinely applied to specific geographic areas for developing air pollutant control strategies. Often the boundary conditions for the regional models are adapted from hemispheric and global models to capture the broader influence of global pollution on the focal region. The results of this study reveal that bromine and iodine chemistry not only affects O_3 over seawater but also over land, improves model performance for coastal sites, and reduces the predicted background ozone. These combined impacts provide strong evidence that bromine and iodine chemistry should be considered for inclusion in air quality models used for O_3 applications.

Appendix A. Supplementary data

Supplementary data to this article can be found online at https://doi.org/10.1016/j.atmosenv.2019.06.020.

Disclaimer

The views expressed in this paper are those of the authors and do not necessarily represent the views or policies of the U.S. EPA.

Declaration of interests

- The authors declare that they have no known competing financial interests or personal relationships that could have appeared to influence the work reported in this paper.
- The authors declare the following financial interests/personal relationships which may be considered as potential competing interests:

References

Allan, B.J., McFiggans, G., Plane, J.M.C., 2000. Observations of iodine monoxide in the remote marine boundary layer. J. Geophys. Res. 105 (D11), 14363–14369 2000.

Appel, K.W., Pouliot, G., Simon, H., Sarwar, G., Pye, H.O.T., Napelenok, S., Akhtar, F., Roselle, S.J., 2013. Evaluation of dust and trace metal estimates from the Community Multiscale Air Quality (CMAQ) model version 5.0. Geosci. Model Dev. (GMD) 6, 883–899 2013.

Appel, K.W., Napelenok, S., Foley, K.M., Pye, H.O.T., Hogrefe, C., Luecken, D.J., Bash, J.O., Roselle, S.J., Pleim, J.E., Foroutan, H., Hutzell, W., Pouliot, G., Sarwar, G., Sarwar, G., Fahey, K., Gantt, B., Gilliam, R.C., Kang, D., Mathur, R., Schwede, D., Spero, T., Wong, D.C., Young, J., 2017. Overview and evaluation of the Community Multiscale Air Quality (CMAQ) model version 5.1. Geosci. Model Dev. (GMD) 10, 1703–1732 2017.

Badia, A., Reeves, C.E., Baker, A.R., Saiz-Lopez, A., Volkamer, R., Koenig, T.K., Apel, E.C., Hornbrook, R.S., Carpenter, L.J., Andrews, S.J., Sherwen, T., von Glasow, R., 2019. Importance of reactive halogens in the tropical marine atmosphere: a regional modelling study using WRF-Chem. Atmos. Chem. Phys. 19, 3161–3189. https://doi.org/10.5194/acp-19-3161-2019.

Breton, M.L., Bannan, T.J., Shallcross, D.E., Khan, M.A., Evans, M.J., Lee, J., Lidster, R., Andrews, S., Carpenter, L.J., Schmidt, J., Jacob, D., Harris, N.R.P., Bauguitte, S., Gallagher, M., Bacak, A., Leather, K.E., Percival, C.J., 2017. Enhanced Ozone Loss by Active Inorganic Bromine Chemistry in the Tropical Troposphere, vol. 155. pp. 21–28 2017.

Carpenter, L.J., MacDonald, S.M., Shaw, M.D., Kumar, R., Saunders, R.W., Parthipan, R., Wilson, J., Plane, J.M.C., 2013. Atmospheric iodine levels influenced by sea surface emissions of inorganic iodine. Nat. Geosci. 6, 108–111 2013.

Cooper, O.R., Parrish, D.D., Stohl, A., Trainer, M., Nédélec, P., Thouret, V., Cammas, J.P., Oltmans, S.J., Johnson, B.J., Tarasick, D., Leblanc, T., McDermid, I.S., Jaffe, D., Gao, R., Stith, J., Ryerson, T., Aikin, K., Campos, T., Weinheimer, A., Avery, M.A., 2010. Increasing springtime ozone mixing ratios in the free troposphere over western North America. Nature 463, 344–348 2010.

Damian, V., Sandu, A., Damian, M., Potra, F., Carmichael, G.R., 2002. The Kinetic PreProcessor KPP – a software environment for solving chemical kinetics. Comput. Chem. Eng. 26 (11), 1567–1579 2002.

David, L.M., Nair, P.R., 2011. Diurnal and seasonal variability of surface ozone and NOx at a tropical coastal site: association with mesoscale and synoptic meteorological conditions. J. Geophys. Research 116, D10303.

Dickerson, R.R., Rhoads, K.P., Carsey, T.P., Oltmans, S.J., Burrows, J.P., Crutzen, P.J., 1999. Ozone in the remote marine boundary layer: a possible role for halogens. Geophys. Res. 104, 21385–21395.

Dix, B., Baider, S., Bresch, J.F., Hall, S.R., Schmidt, K.,S., Wang, S., Volkamer, R., 2013. Detection of iodine monoxide in the tropical free troposphere. Proc. Natl. Acad. Sci. Unit. States Am. 110 (6), 2035–2040 2013.

Dolwick, P., Akhtar, F., Baker, K.R., Possiel, N., Simon, H., Tonnesen, G., 2015. Comparison of background ozone estimates over the western United States based on two separate model methodologies. Atmos. Environ. 109, 282–296 2015.

Environmental Protection Agency, 2016. Implementation of the 2015 Primary Ozone NAAQS: Issues Associated with Background Ozone White Paper for Discussion. accessed at. https://www.epa.gov/sites/production/files/2016-03/documents/whitepaper-bgo3-final.pdf.

Fahey, K.M., Carlton, A.G., Pye, H.O.T., Baek, J., Hutzell, W.T., Stanier, C.O., Baker, K.R., Appel, K.W., Jaoui, M., Offenberg, J.H., 2017. A framework for expanding aqueous chemistry in the Community Multiscale Air Quality (CMAQ) model version 5.1. Geosci. Model Dev. (GMD) 10, 1587–1605 2017.

Fernandez, R.P., Salawitch, R.J., Kinnison, D.E., Lamarque, J.-F., Saiz-Lopez, A., 2014. Bromine partitioning in the tropical tropopause layer: implications for stratospheric injection. Atmos. Chem. Phys. 14, 13391–13410 2014.

Fiore, A.M., Jacob, D.L., Bey, I., Yantosca, R.M., Field, B.D., Fusco, A.C., Wilkinson, J.G., 2002. Background ozone over the United States in summer: origin, trend, and contribution to pollution episodes. J. Geophys. Res. 107 (D15), 4275.

Fiore, A.M., Jacob, D.J., Liu, H., Yantosca, R.M., Fairlie, T.D., Li, Q., 2003. Variability in surface ozone background over the United States: implications for air quality policy. J. Geophys. Res. 108 (D24), 4787.

Fiore, A.M., Oberman, J.T., Lin, M., Zhang, L., Clifton, O.E., Jacob, D.J., Naik, V., Horowitz, L.W., Pinto, J.P., Milly, G.P., 2014. Estimating North American background ozone in U.S. surface air with two independent global models: variability, uncertainties, and recommendations. Atmos. Environ. 96, 284–300.

Gantt, B., Kelly, J.T., Bash, J.O., 2015. Updating sea spray aerosol emissions in the Community Multiscale Air Quality (CMAQ) model version 5.0.2. Geosci. Model Dev. (GMD) 8, 3733–3746. https://doi.org/10.5194/gmd-8-3733-2015. 2015.

Gantt, B., Sarwar, G., Xing, J., Simon, H., Schwede, D., Hutzell, W.T., Mathur, R., Saiz-Lopez, A., 2017. The impact of iodide-mediated ozone deposition and halogen chemistry on surface ozone concentrations across the continental United States. Environ. Sci. Technol. 51 (3), 1458–1466 2017.

Kyo, K., Morino, Y., Yamaji, K., Chatani, S., 2019. Uncertainties in O_3 concentrations simulated by CMAQ over Japan using four chemical mechanisms. Atmos. Environ. 198, 448–462 2019.

Long, M.S., Keene, W.C., Easter, R., Sander, R., Kerkweg, A., Erickson, D., Liu, X., Ghan, S., 2013. Implementation of the chemistry module MECCA (v2.5) in the modal aerosol version of the Community Atmosphere Model component (v3.6.33) of the Community Earth System Model. Geosci. Model Dev. (GMD) 6, 255–262. 2013. https://doi.org/10.5194/gmd-6-255-2013.

Long, M.S., Keene, W.C., Easter, R.C., Sander, R., Liu, X., Kerkweg, A., Erickson, D., 2014. Sensitivity of tropospheric chemical composition to halogen-radical chemistry using a fully coupled size-resolved multiphase chemistry–global climate system: halogen distributions, aerosol composition, and sensitivity of climate-relevant gases. Atmos. Chem. Phys. 14, 3397–3425 2014.

Mahajan, A.S., Plane, J.M.C., Oetjen, H., Mendes, L., Saunders, R.W., Saiz-Lopez, A., Jones, C.E., Carpenter, L.J., McFiggans, G.B., 2010. Measurement and modelling of tropospheric reactive halogen species over the tropical Atlantic Ocean. Atmos. Chem. Phys. 10, 4611–4624 2010.

Mathur, R., Xing, J., Gilliam, R., Sarwar, G., Hogrefe, C., Pleim, J., Pouliot, G., Roselle, S., Spero, T., Wong, D.C., Young, J., 2017. Extending the community Multiscale Air quality (CMAQ) modeling system to hemispheric scales: process considerations and initial applications. Atmos. Chem. Phys. 17, 1–25 2017.

McDonald, S.M., Martin, J.C.G., Chance, R., Warriner, S., Saiz-Lopez, A., Carpenter, L.J., Plane, J.M.C., 2014. A laboratory characterisation of inorganic iodine emissions from the sea surface: dependence on oceanic variables and parameterisation for global modelling. Atmos. Chem. Phys. 14, 5841–5852 2014.

McDonald-Buller, E.C., Allen, D.T., Brown, N., Jacob, D.J., Jaffe, D.A., Kolb, C.E., Lefohn, A.S., Oltmans, S., Parrish, D.D., Yarwood, G., Zhang, L., 2011. Establishing policy relevant background (PRB) ozone concentrations in the United States. Environ. Sci. Technol. 45 (22), 9484–9497 2011.

McFiggans, G., Plane, J.M.C., Allan, B.J., Carpenter, L.J., Coe, H., O'Dowd, C., 2000. A modeling study of iodine chemistry in the marine boundary layer. J. Geophys. Res. 105 (D11), 14371–14385 2000.

Millero, F.J., 1996. Chemical Oceanography, second ed. CRC Press, Boca Raton, FL.

Mu iz-Unamunzaga, M., Borge, B., Sarwar, G., Gantt, B., Paz, D.P., Cuevas, C.A., Saiz-Lopez, A., 2018. Ocean halogen and sulfur emissions influence air quality in the coastal megacity of Los Angeles. Sci. Total Environ. 610–611, 1536–1545 2018.

Ordó ez, C., Lamarque, J.-F., Tilmes, S., Kinnison, D.E., Atlas, E.L., Blake, D.R., Sousa Santos, G., Brasseur, G., Saiz-Lopez, A., 2012. Bromine and iodine chemistry in a global chemistry-climate model: description and evaluation of very short-lived oceanic sources. Atmos. Chem. Phys. 12, 1423–1447 2012.

Otte, T.L., Pleim, J.E., 2010. The Meteorology-Chemistry Interface Processor (MCIP) for the CMAQ modeling system: updates through MCIPv3.4.1. Geosci. Model Dev. (GMD) 3, 243–256 2010.

Parrella, J.P., Jacob, D.J., Liang, Q., Zhang, Y., Mickley, L.J., Miller, B., Evans, M.J., Yang, X., Pyle, J.A., Theys, N., Van Roozendael, M., 2012. Tropospheric bromine chemistry: implications for present and pre-industrial ozone and mercury. Atmos. Chem. Phys. 12, 6723–6740 2012.

Parrish, D.D., Millet, D.B., Goldstein, A.H., 2009a. Increasing ozone in marine boundary layer air inflow at the west coasts of North America and Europe. Atmos. Chem. Phys. 9, 1303–1323 2009a.

Parrish, D.D., Allen, D.T., Bates, T.S., Estes, M., Fehsenfeld, F.C., Feingold, G., Ferrare, R., Hardesty, R.M., Meagher, J.F., Nielsen-Gammon, J.W., Pierce, R.B., Ryerson, T.B., Seinfeld, J.H., Williams, E.J., 2009b. Overview of the second Texas air quality study

(TexAQS II) and the Gulf of Mexico atmospheric composition and climate study (GoMACCS). J. Geophys. Res. 114 2009b.
Peters, C., Pechtl, S., Stutz, J., Hebestreit, K., Hönninger, G., Heumann, K.G., Schwarz, A., Winterlik, J., Platt, U., 2005. Reactive and organic halogen species in three different European coastal environments. Atmos. Chem. Phys. 5, 3357–3375 2005.
Qiao, X., Ying, Q., Li, X., Zhang, H., Hu, J., Tang, Y., Chen, X., 2018. Source apportionment of $PM_{2.5}$ for 25 Chinese provincial capitals and municipalities using a source-oriented Community Multiscale Air Quality model. Atmos. Environ. 612, 462–471 2018.
Read, K.A., Mahajan, A.S., Carpenter, L.J., Evans, M.J., Faria, B.V.E., Heard, D.E., Hopkins, J.R., Lee, J.D., Moller, S.J., Lewis, A.C., Mendes, L., McQuaid, J.B., Oetjen, H., Saiz-Lopez, A., Pilling, M.J., Plane, J.M.C., 2008. Extensive halogen mediated ozone destruction over the tropical Atlantic Ocean. Nature 453, 1232–1235 2008.
Ring, A.M., Canty, T.P., Anderson, D.C., Vinciguerra, T.P., e, H., Goldberg, D.L., Ehrman, S.H., Dickerson, R.R., Salawitch, R.J., 2018. Evaluating commercial marine emissions and their role in air quality policy using observations and the CMAQ model. Atmos. Environ. 173, 96–107 2018.
Sarwar, G., Simon, H., Bhave, P., G Yarwood, G., 2012. Examining the impact of heterogeneous nitryl chloride production on air quality across the United States. Atmos. Chem. Phys. 12, 1–19 2012.
Sarwar, G., Gantt, B., Schwede, D., Foley, K., Mathur, R., Saiz-Lopez, A., 2015. Impact of enhanced ozone deposition and halogen chemistry on tropospheric ozone over the Northern Hemisphere. Environ. Sci. Technol. 49 (15), 9203–9211 2015.
Saiz-Lopez, A., Shillito, J.A., Coe, H., Plane, J.M.C., 2006. Measurements and modelling of I_2, IO, OIO, BrO, and NO_3 in the mid-latitude marine boundary layer. Atmos. Chem. Phys. 6, 1513–1528 2006.
Saiz-Lopez, A., Mahajan, A.S., Salmon, R.A., Bauguitte, S.J.-B., Jones, A.E., Roscoe, H.K., Plane, J.M.C., 2007. Boundary layer halogens in coastal Antarctica. Science 317 (5836), 348–351. https://doi.org/10.1126/science.1141408. 2007.
Saiz-Lopez, A., Lamarque, J.-F., Kinnison, D.E., Tilmes, S., Ordó ez, C., Orlando, J.J., Conley, A.J., Plane, J.M.C., Mahajan, A.S., Sousa Santos, G., Atlas, E.L., Blake, D.R., Sander, S.P., Schauffler, S., Thompson, A.M., Brasseur, G., 2012. Estimating the climate significance of halogen-driven ozone loss in the tropical marine troposphere. Atmos. Chem. Phys. 12 (9), 3939–3949. https://doi.org/10.5194/acp-12-3939-2012. 2012.
Saiz-Lopez, A., Fernandez, R.P., Ordó ez, C., Kinnison, D.E., Gómez Martín, J.C., Lamarque, J.-F., Tilmes, S., 2014. Iodine chemistry in the troposphere and its effect on ozone. Atmos. Chem. Phys. 14, 13119–13143 2014.
Schmidt, J.A., Jacob, D.J., Horowitz, H.M., Hu, L., Sherwen, T., Evans, M.J., Liang, Q., Suleiman, R.M., Oram, D.E., Breton, M.L., Percival, C.J., Wang, S., Dix, B., Volkamer, R., 2016. Modeling the observed tropospheric BrO background: importance of multiphase chemistry and implications for ozone, OH, and mercury. J. Geophys. Res.-Atmos. 121, 11819–11835 2016.
Sherwen, T., Evans, M.J., Carpenter, L.J., Andrews, S.J., Lidster, R.T., Dix, B., Koenig, T.K., Sinreich, R., Ortega, I., Volkamer, R., Saiz-Lopez, A., Prados-Roman, C., Mahajan, A.S., Ordó ez, C., 2016a. Iodine's impact on tropospheric oxidants: a global model study in. GEOS-Chem. Atmos. Chem. Phys. 16, 1161–1186 2016a.
Sherwen, T., Schmidt, J.A., Evans, M.J., Carpenter, L.J., Großmann, K., Eastham, S.D., Jacob, D.J., Dix, B., Koenig, T.K., Sinreich, R., Ortega, I., Volkamer, R., Saiz-Lopez, A., Prados-Roman, C., Mahajan, A.S., Ordó ez, C., 2016b. Global impacts of tropospheric halogens (Cl, Br, I) on oxidants and composition in GEOS-Chem. Atmos. Chem. Phys. 16, 12239–12271 2016b.
Skamarock, W.C., Klemp, J.B., Dudhia, J., Grill, D.O., Barker, D.M., Duda, M.G., Huang, X.-Y., Wang, W., Powers, J.G., 2008. A Description of the Advanced Research WRF Version 3. NCAR Tech Note NCAR/TN 475 STR. pp. 125 [Available from: UCAR Communications, P.O. Box 3000, Boulder, CO 80307].
von Glasow, R., Sander, R., Bott, A., Crutzen, P.J., 2002a. Modeling of halogen chemistry in the marine boundary layer. 1. Cloud-free MBL. J. Geophys. Res. B 107, 4341 2002.
von Glasow, R., Sander, R., Bott, A., Crutzen, P.J., 2002b. Modeling halogen chemistry in the marine boundary layer. 2. Interactions with sulfur and cloud-covered MBL. J. Geophys. Res. 107, 4323 2002.
Wang, S., Schmidt, J.A., Baidar, S., Coburn, S., Dix, B., Koenig, T.K., Apel, E., Bowdalo, D., Campos, T.L., Eloranta, E., Evans, M.J., DiGangi, J.P., Zondlo, M.A., Gao, R., Haggerty, J.A., Hall, S.R., Hornbrook, R.S., Jacob, D., Morley, B., Pierce, B., Reeves, M., Romashkin, P., Schure, A., Volkamer, R., 2015. Active and widespread halogen chemistry in the tropical and subtropical free troposphere. Proc. Natl. Acad. Sci. Unit. States Am. 112 (30), 9281–9286 2015.
Xing, J., Mathur, R., Pleim, J., Hogrefe, C., Wang, J., Gan, C.-M., Sarwar, G., Wong, D., McKeen, S., 2016. Representing the effects of stratosphere-troposphere exchange on 3D O_3 distributions in chemistry transport models using a potential vorticity based parameterization. Atmos. Chem. Phys. 16, 10865–10877. https://doi.org/10.5194/acp-16-10865-2016. 2016.
Yang, X., Cox, R.A., Warwick, N.J., Pyle, J.A., Carver, G.D., O'Connor, F.M., Savage, N.H., 2005. Tropospheric bromine chemistry and its impacts on ozone: a model study. J. Geophys. Res. 110, D23311 2005.
Yarwood, G., Jung, J., Whitten, G.Z., Heo, G., Mellberg, J., Estes, M., 2010. Updates to the carbon bond mechanism for version 6 (CB6). In: Presented at the 9th Annual CMAS Conference, Chapel Hill, NC, October 11-13, 2010, . Available at: https://www.cmascenter.org/conference/2010/abstracts/emery_updates_carbon_2010.pdf.
Zhang, L., Jacob, D.J., Downey, N.V., Wood, D.A., Blewitt, D., Carouge, C.C., van Donkelaar, A., Jones, D.B.A., Murray, L.T., Wang, Y., 2011. Improved estimate of the policy-relevant background ozone in the United States using the GEOS-Chem global model with 1/2° x 2/3° horizontal resolution over North America. Atmos. Environ. 45 (37), 6769–6776 2011.

Supporting Information for:

The Impact of Iodide-Mediated Ozone Deposition and Halogen Chemistry on Surface Ozone Concentrations Across the Continental United States

Brett Gantt,[†] Golam Sarwar,[*,‡] Jia Xing,[‡] Heather Simon,[†] Donna Schwede,[‡] William T. Hutzell,[‡] Rohit Mathur,[‡] Alfonso Saiz-Lopez[§]

[†]Office of Air Quality Planning and Standards, US Environmental Protection Agency, Research Triangle Park, North Carolina 27711, United States

[‡]National Exposure Research Laboratory, Office of Research and Development, US Environmental Protection Agency, Research Triangle Park, North Carolina 27711, United States

[§]Department of Atmospheric Chemistry and Climate, Institute of Physical Chemistry Rocasolano, CSIC, Madrid 28006, Spain

Corresponding Author
[*]Phone: 919-541-2669, fax: 919-541-1379, email: sarwar.golam@epa.gov

This supporting information contains 7 pages, 6 figures.

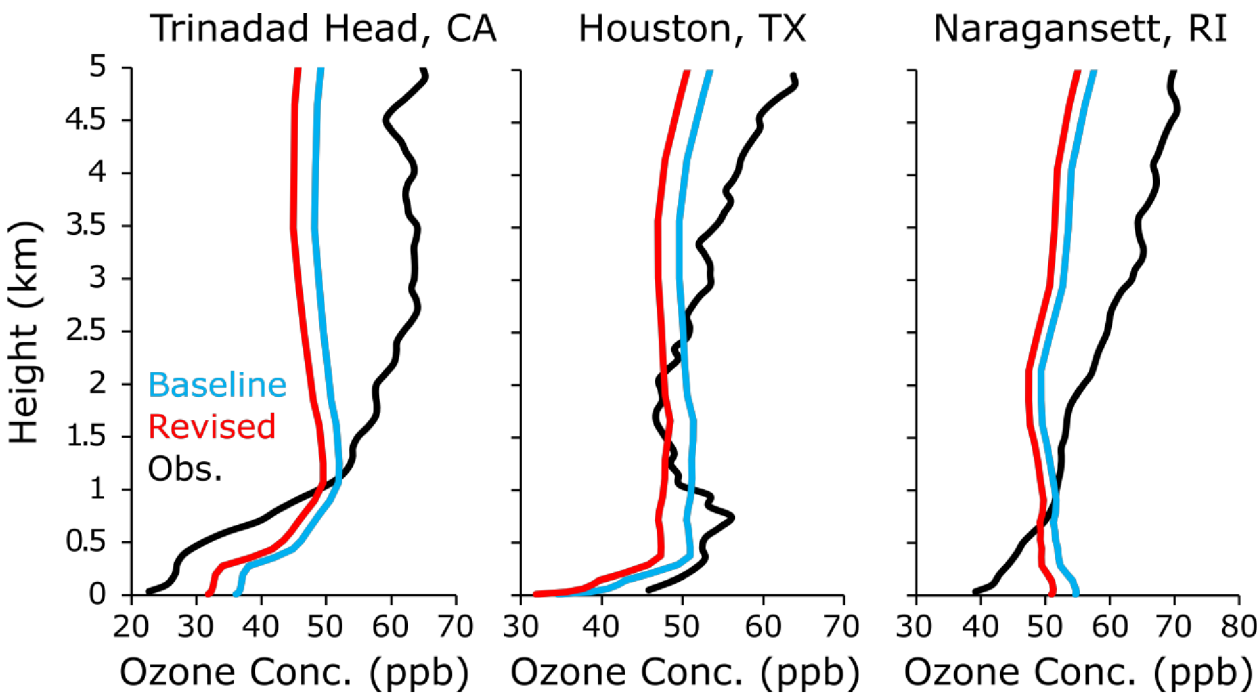

Figure S1. Monthly mean vertically-resolved ozone concentrations (in units of ppb) for August 2006 as observed by ozonesondes at coastal or near-coastal sites from the Global Monitoring Division of NOAA's Earth System Research Laboratory (Trinadad Head, CA: 41.06°N, 124.15°W; Naragansett, RI: 41.49°N, 71.42°W) and as part of the INTEX-B Ozonesonde Network Study (Houston, TX: 29.72°N, 95.30°W).

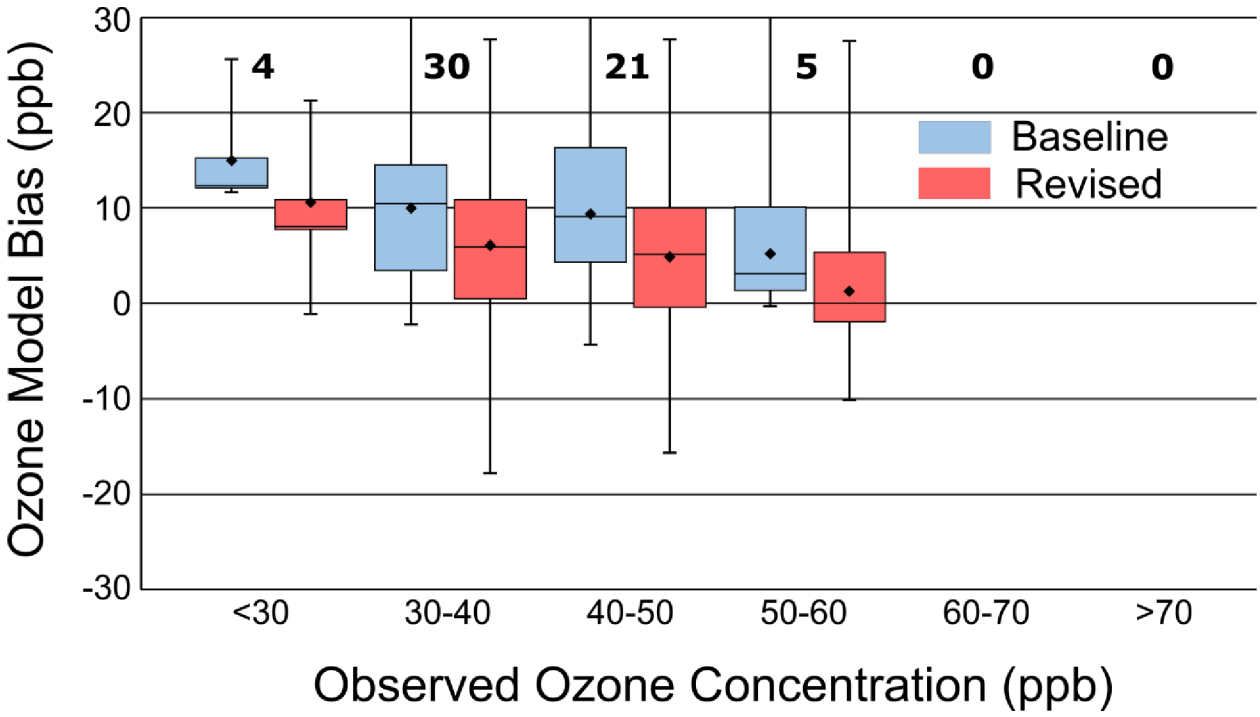

Figure S2. Monthly mean MDA8 bias in August 2006 for the Baseline and Revised simulations, binned by observed MDA8 O_3 concentrations at coastal sites (in CMAQ grids with nonzero surf zone) retrieved from the EPA Air Quality System (AQS) database. The lower bar in the box represents 25th percentile, middle bar represents the median, and upper bar represents 75th percentile values. The mean values are given by the diamonds, maximum and minimum values are shown by the error bars, and the numbers in bold indicate the total number of monitors in each O_3 concentration bin.

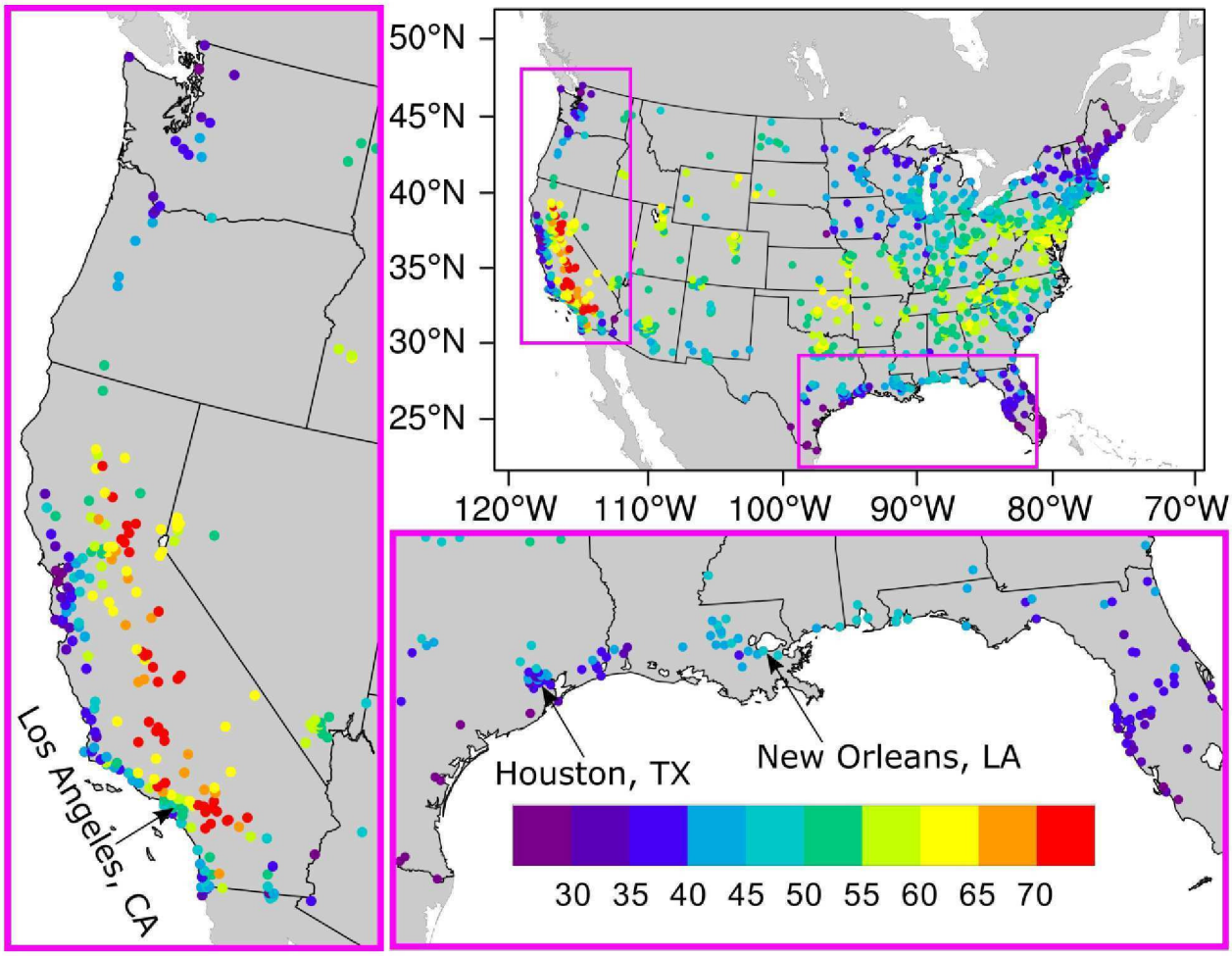

Figure S3. Monthly mean observed surface MDA8 ozone concentrations (in units of ppb) for August 2006 retrieved from EPA's Air Quality System database.

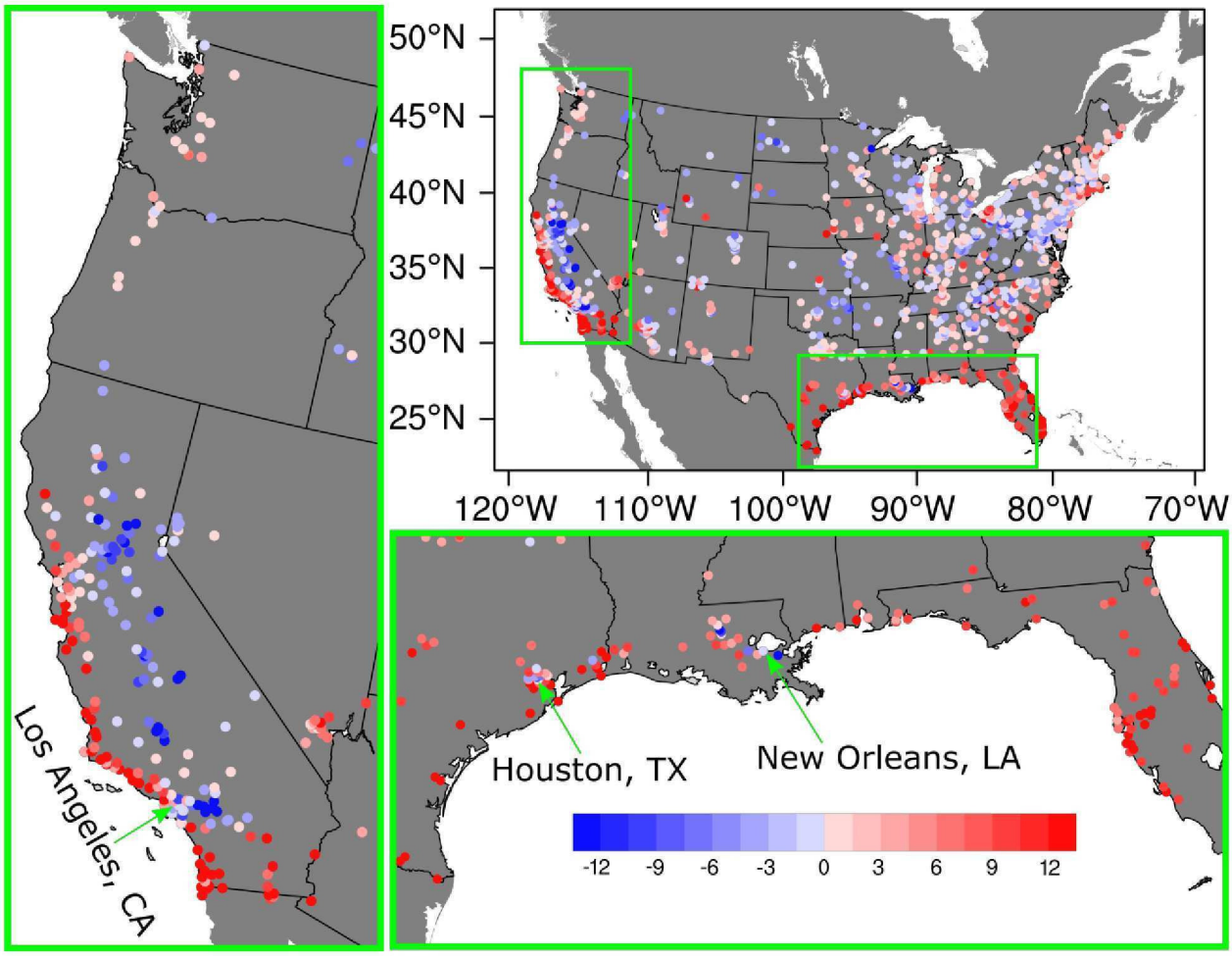

Figure S4. Monthly mean bias of MDA8 ozone concentrations (in units of ppb) for the Baseline simulation at EPA's Air Quality System sites during August 2006. Cooler/warmer colors represent sites where Baseline predictions were lower/higher than observed data.

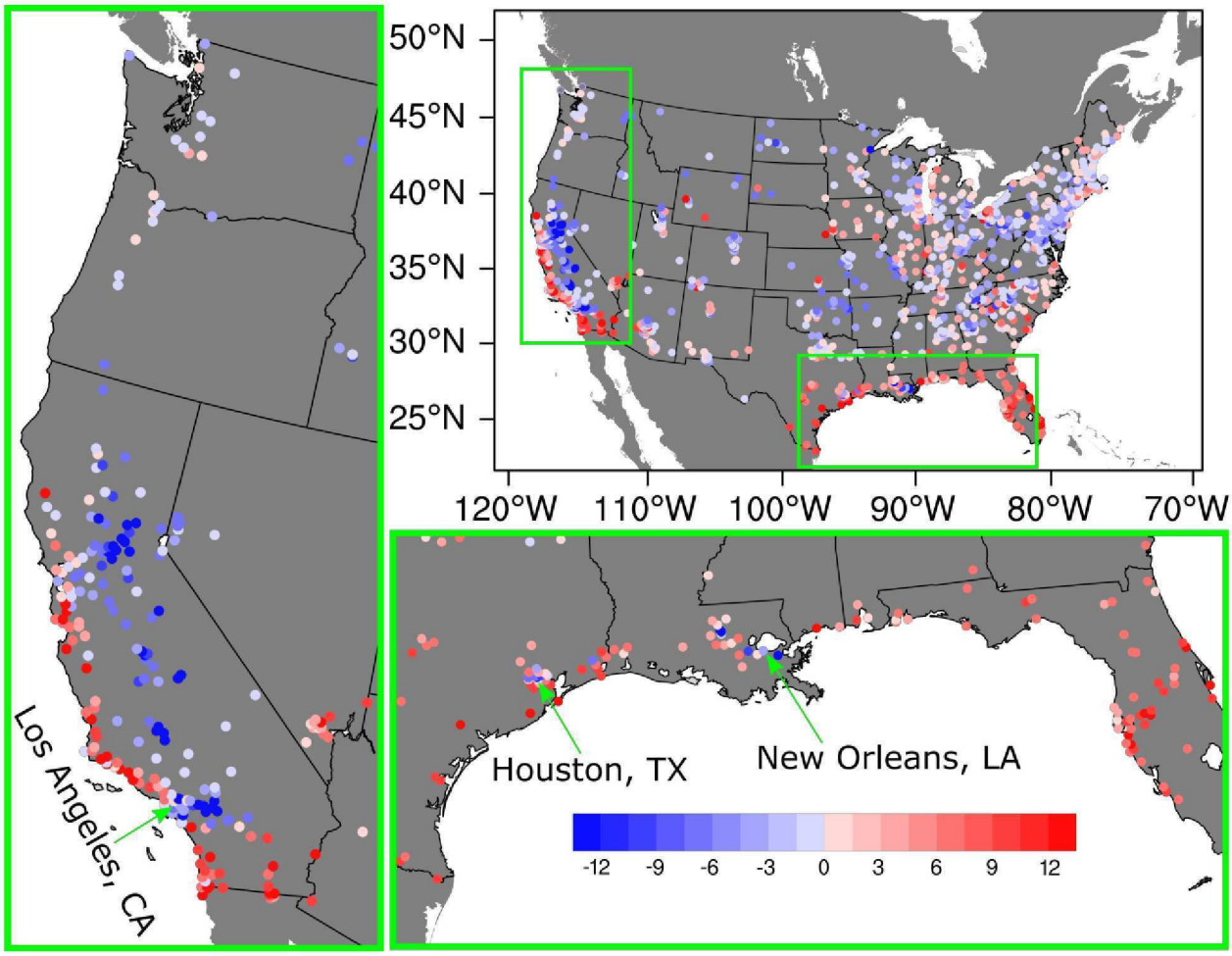

Figure S5. Monthly mean bias of MDA8 ozone concentrations (in units of ppb) for the Revised simulation at EPA's Air Quality System sites during August 2006. Cooler/warmer colors represent sites where Baseline predictions were lower/higher than observed data.

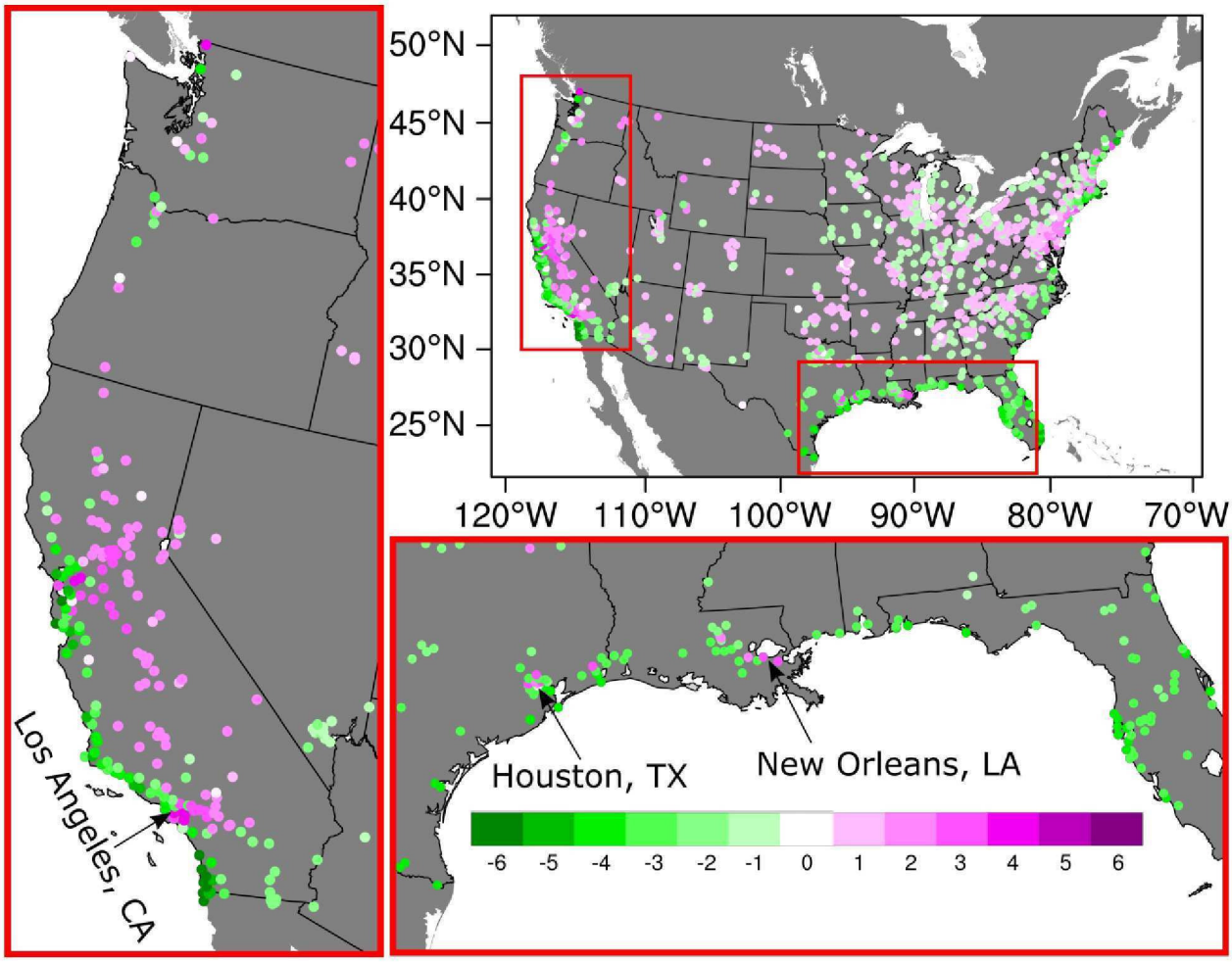

Figure S6. Change in mean bias (in units of ppb) for MDA8 O_3 concentrations between the Baseline and Revised simulations at the EPA Air Quality System sites during August 2006. Green colors represent sites where the Revised simulation had a lower mean bias (improved prediction) and purple colors represent sites where the Revised simulation had a higher mean bias (worse prediction).

Supplemental Information for:

Influence of bromine and iodine chemistry on annual, seasonal, diurnal, and background ozone

Golam Sarwar[1], Brett Gantt[2], Kristen Foley[1], Kathleen Fahey[1], Tanya L. Spero[1], Daiwen Kang[1], Rohit Mathur[1], Hosein Foroutan[3], Jia Xing[4], Tomás Sherwen[5,6], Alfonso Saiz-Lopez[7]

[1] National Exposure Research Laboratory, US Environmental Protection Agency, RTP, North Carolina 27711, USA

[2] Office of Air Quality Planning and Standards, US Environmental Protection Agency, RTP, NC 27711, USA

[3] Department of Biomedical Engineering and Mechanics, Virginia Tech, Blacksburg, VA 24061, USA

[4] State Key Joint Laboratory of Environmental Simulation and Pollution Control, School of Environment, Tsinghua University, Beijing 100084, China

[5]Wolfson Atmospheric Chemistry Laboratories, Department of Chemistry, University of York, UK

[6]National Centre for Atmospheric Science, Department of Chemistry, University of York, UK

[7]Department of Atmospheric Chemistry and Climate, Institute of Physical Chemistry Rocasolano, CSIC, Madrid 28006, Spain

E-mail: sarwar.golam@epa.gov

Number of Pages: 7
Number of Tables: 4
Number of Figures: 1

Tables:
S1 – Gas-phase bromine chemistry
S2 – Gas-phase iodine chemistry
S3 – Heterogeneous reactions of bromine and iodine reactions
S4 – Aqueous-phase bromine chemistry

Figures:
S1. Location of coastal sites at (a) Clean Air Status and Trends Network (CASTNet) and (b) the USEPA's Air Quality System (AQS)

Table S1: Gas-phase bromine chemistry

Rx level	Reaction	Rate Expression [a]	Ref
BR01	$Br + O_3 = BrO + O_2$	$1.6\times 10^{-11}e^{-780/T}$	4,5
BR02	$BrO + HO_2 = HOBr + O_2$	$4.5\times 10^{-12}e^{460/T}$	4,5
BR03	$Br + HO_2 = HBr + O_2$	$4.8\times 10^{-12}\ e^{-310/T}$	4,5
BR04	$HBr + OH = Br + H_2O$	$6.7\times 10^{-12}e^{155/T}$	4,5
BR05	$BrO + BrO = 2.0\ Br + O_2$	$1.4\times 10^{-12}e^{210/T}$	4,5
BR06	$BrO + BrO = BR_2 + O_2$	$2.9\times 10^{-14}e^{840/T}$	4,5
BR07	$BrO + NO = Br + NO_2$	$8.8\times 10^{-12}e^{260/T}$	4,5
BR08	$Br + BrNO_3 = BR_2 + NO_3$	4.9×10^{-11}	4,5
BR09	$BR_2 + OH = HOBr + Br$	$2.1\times 10^{-11}e^{240/T}$	4,5
BR10	$BrO + OH = Br + HO_2$	$1.7\times 10^{-11}e^{250/T}$	4,5
BR11	$Br + NO_3 = BrO + NO_2$	1.6×10^{-11}	4,5
BR12	$BrO + NO_2 = BrNO_3$	$k_o = 5.2\ x\ 10^{-31}(T/300)^{-3.2}$; $k_\infty = 6.9\ x\ 10^{-12}(T/300)^{-2.9}$; F = 0.6 and N = 1.0	4,5
BR13	$Br + NO_2 = BrNO_2$	$k_o = 4.2\ x\ 10^{-31}(T/300)^{-2.4}$; $k_\infty = 2.7\ x\ 10^{-11}(T/300)^{0.0}$; F = 0.6 and N = 1.0	4,5
BR14	$BrO + ClO = Br + Cl$	$4.7\times 10^{-12}e^{320/T}$	4,5
BR15	$Br + FORM = HBr + HO_2 + CO$	$1.7\times 10^{-11}e^{-800/T}$	4,5
BR16	$Br + ALD2 = HBr + C_2O_3$	$1.3\times 10^{-11}e^{-360/T}$	4,5
BR17	BrO + MEO2 = 0.8 HOBr + 0.2 BR + FORM	$2.7\times 10^{-14}\ e^{1600/T}$	4,5
BR18	$CH_3Br + OH = Br + FORM$	$2.9\times 10^{-12}e^{-1230/T}$	4,5
BR19	MB3 + OH = 3 Br + CO	$1.0\times 10^{-12}e^{-388/T}$	4,5
BR20	MB2 + OH = 2 Br + HO2 + CO	$2.0\times 10^{-12}e^{-840/T}$	4,5
BR21	MB2C + OH = 2 Br + Cl + CO	$9.0\times 10^{-13}e^{-420/T}$	4,5
BR22	MBC2 + OH = Br + 2 Cl + CO	$9.4\times 10^{-13}e^{-510/T}$	4,5
BR23	MBC + OH = Br + Cl + CO + HO2	$2.1\times 10^{-12}e^{-880/T}$	4,5
BR24	DMS + BrO = MEO2 + Br	$1.5\times 10^{-14}e^{1000/T}$	5
BR25	$BrCl = Br + Cl$	Photolysis	5
BR26	$BrO = Br + O$	Photolysis	5
BR27	$HOBr = OH + Br$	Photolysis	5
BR28	$BrNO_3 = BrO + NO_2$	Photolysis	5
BR29	$BrNO_3 = Br + NO_3$	Photolysis	5
BR30	$BrNO_2 = Br + NO_2$	Photolysis	5
BR31	$Br_2 = 2\ Br$	Photolysis	5
BR32	MB3 = 3 Br + HO2 + CO	Photolysis	5
BR33	MB2C = 2 Br + Cl + HO2 + CO	Photolysis	5
BR34	MBC2 = Br + 2 Cl + HO2 + CO	Photolysis	5

Note:
Br = bromine atom, O_3 = ozone, O_2 = oxygen, BrO =bromine oxide, HO_2 = hydroperoxy radical, HOBr = hypobromous acid, HBr = hydrobromic acid, OH = hydroxyl radical, Br_2 = molecular bromine, NO = nitric oxide, NO_2 = nitrogen dioxide, $BrNO_3$ = bromine nitrate, NO_3 = nitrate, FORM = formaldehyde, ALD2 = acetaldehyde, CO = carbon monoxide, C_2O_3 = acetylperoxy radical, CH_3Br=methyl bromide, MB3 = bromoform, MB2 = methylene bromide, MB2C = dibromochloromethane, MBC2 = bromodichloromethane, MBC = methylene bromochloride, $BrNO_2$=nitryl bromide, BrCl= bromine chloride, H_2O = water vapor, DMS=dimethylsulfide, SO2 = sulfur dioxide, MSA = methanesulfonic acid.

[a] First order rate constants are in units of sec^{-1}, second order rate constants are in units of $cm^3\ molecule^{-1}\ sec^{-1}$. Temperatures (T) are in K. Rate constants for reaction BR12 and BR13 are described by the falloff expression of the form $k=\{k_o[M]/(1+k_o[M]/k_\infty)\}\ F^z$, where $Z=\{(1/N)+\log_{10}[k_o[M]/k_\infty]^2\}^{-1}$, where [M] is the total pressure in molecules/cm^3, and k_o, k_∞, F, and N are indicated in the table.

Table S2: Gas-phase iodine chemistry

Rx level	Reaction	Rate Expression [a]	Ref
IO01	$I + O_3 = IO + O_2$	$2.1 \times 10^{-11} e^{-830/T}$	4-7
IO02	$I + HO_2 = HI + O_2$	$1.5 \times 10^{-11} e^{-1090/T}$	4-7
IO03	$I_2 + OH = HOI + I$	2.1×10^{-10}	4-7
IO04	$HI + OH = I + H_2O$	$1.6 \times 10^{-11} e^{440/T}$	4-7
IO05	$HOI + OH = IO + H_2O$	5.0×10^{-12}	4-7
IO06	$IO + HO_2 = HOI + O_2$	$1.4 \times 10^{-11} e^{540/T}$	4-7
IO07	$IO + NO = I + NO_2$	$7.15 \times 10^{-12} e^{300/T}$	4-7
IO08	$INO + INO = I_2 + 2\ NO$	$8.4 \times 10^{-11} e^{-2620/T}$	4-7
IO09	$INO_2 + INO_2 = I2 + 2\ NO_2$	$4.7 \times 10^{-13} e^{-1670/T}$	4-7
IO10	$I_2 + NO_3 = I + INO_3$	1.5×10^{-12}	4-7
IO11	$INO_3 + I = I_2 + NO_3$	$9.1 \times 10^{-11} e^{-146/T}$	4-7
IO12	$I + BrO = IO + Br$	1.2×10^{-11}	4-7
IO13	$IO + Br = I + BrO$	2.70×10^{-11}	4-7
IO14	$IO + BrO = Br + I + O_2$	$1.5 \times 10^{-11} e^{510/T}$	4-7
IO15	$IO + ClO = I + Cl$	$4.7 \times 10^{-12} e^{280/T}$	4-7
IO16	$OIO + OIO = I_2O_4$	$1.5 \times 10^{-10} e^{0/T}$	4-7
IO17	$OIO + NO = IO + NO_2$	$1.1 \times 10^{-12} e^{542/T}$	4-7
IO18	$IO + IO = 0.4OIO + 0.4I + 0.6I_2O_2$	$5.4 \times 10^{-11} e^{180/T}$	4-7
IO19	$IO + OIO = I_2O_3$	1.5×10^{-10}	4-7
IO20	$I_2O_2 = OIO + I$	$2.5 \times 10^{14}\ e^{-9770/T}$	4-7
IO21	$I_2O_4 = 2OIO$	$3.8 \times 10^{-2} e^{0/T}$	4-7
IO22	$INO_2 = I + NO_2$	$9.94 \times 10^{17}\ e^{-11859/T}$	4-7
IO23	$INO_3 = IO + NO_2$	$2.1 \times 10^{15}\ e^{-13670/T}$	4-7
IO24	$I + NO = INO$	$k_o = 1.8 \times 10^{-32}(T/300)^{-1.0}$; $k_\infty = 1.7 \times 10^{-11}(T/300)^{-0.0}$; F = 0.6 and N = 1.0	4-7
IO25	$I + NO_2 = INO_2$	$k_o = 3.0 \times 10^{-31}(T/300)^{-1.0}$; $k_\infty = 6.6 \times 10^{-11}(T/300)^{-0.0}$; F = 0.6 and N = 1.0	4-7
IO26	$IO + NO_2 = INO_3$	$k_o = 7.7 \times 10^{-31}(T/300)^{-5.0}$; $k_\infty = 1.6 \times 10^{-11}(T/300)^{-0.4}$; F = 0.4 and N = 1.0	4-7
IO27	$CH_3I + OH = I + HO_2 + H_2O$	$4.3 \times 10^{-12} e^{-1120//T}$	4-7
IO28	$IO + DMS = I + MEO2$	$3.2 \times 10^{-13} e^{-925/T}$	4-7
IO29	$CH_3I = I + MEO2$	Photolysis	5
IO30	$CH_2I_2 = 2.0\ I$	Photolysis	5
IO31	$CH_2IBr = I + Br$	Photolysis	5
IO32	$CH_2ICl = I + Cl$	Photolysis	5
IO33	$I_2 = 2.0\ I$	Photolysis	5
IO34	$IO = I + O$	Photolysis	5
IO35	$OIO = I + O_2$	Photolysis	5
IO36	$INO = I + NO$	Photolysis	5
IO37	$INO_2 = I + NO_2$	Photolysis	5
IO38	$INO_3 = I + NO_3$	Photolysis	5
IO39	$HOI = I + OH$	Photolysis	5
IO40	$ICl = I + Cl$	Photolysis	5
IO41	$I_2O_2 = I + OIO$	Photolysis	6
IO42	$I_2O_3 = IO + OIO$	Photolysis	6
IO43	$I_2O_4 = OIO + OIO$	Photolysis	6
IO44	$IBr = I + Br$	Photolysis	5

Note:
I = iodine atom, O_3 = ozone, O_2 = oxygen, IO = iodine oxide, OIO =iodine dioxide, HO_2 = hydroperoxy radical, HI = hydroiodic acid, NO = nitric oxide, NO_2 = nitrogen dioxide, HOI = hypoiodous acid, I_2O_2 =di-iodine dioxide, I_2O_3=di-iodine trioxide, I_2O_4= diiodine tetroxide, I_2 = molecular iodine, OH = hydroxyl radical, NO_3 = nitrate, $IONO_2$ = iodine nitrate, INO_2=nitryl iodide, INO=nitrosyl iodide, HNO_3=nitric acid,

ICl= iodine monochloride, CH_3I=methyl iodide, CH_2I_2=methylene iodide, CH_2IBr=bromoiodomethane, CH_2ICl=chloroiodomethane, Br = bromine atom, BrO =bromine oxide, Cl = atomic chlorine, ClO = chlorine oxide.

[a] First order rate constants are in units of sec^{-1}, second order rate constants are in units of cm^3 $molecule^{-1}$ sec^{-1}. Temperatures (T) are in K. Rate constants for reaction IO24-26 are described by the falloff expression of the form $k=\{k_o[M]/(1+k_o[M]/k_\infty)\}$ F^z, where $Z=\{(1/N)+\log_{10}[k_o[M]/k_\infty]^2\}^{-1}$, where [M] is the total pressure in molecules/cm^3, and k_o, k_∞, F, and N are indicated in the table.

Table S3: Heterogeneous reactions of bromine and iodine species

Reactions on aerosols			
Rx level	Reaction	Uptake coefficient	Reference
HET_HBR_BR	HBr →Br^-	$1.3\times 10^{-8}e^{4290/T}$	Ammann et al. (2013)
HET_BRNO3_WA	$BrNO_3$(+ H_2O)→HOBr + HNO_3	0.03	Deiber et al. (2004)
HET_HOBR_CL	HOBr + Cl^-→BrCl	0.08	Fernandez et al. (2014)
HET_HOBR_BR	HOBr + Br^-→Br_2	0.02	Fernandez et al. (2014)
HET_I2O2	I_2O_2→	0.02	Sherwen et al. (2016)
HET_I2O3	I_2O_3→	0.02	Sherwen et al. (2016)
HET_I2O4	I_2O_4 →	0.02	Sherwen et al. (2016)
HET_INO3_CL	INO_3 + Cl^-→ICl + HNO_3	0.005	Saiz-Lopez et al. (2014)
HET_INO3_BR	INO_3 + Br^-→IBr + HNO_3	0.005	Saiz-Lopez et al. (2014)
HET_INO2_CL	INO_2 + Cl^-→ICl + HONO	0.01	Saiz-Lopez et al. (2014)
HET_INO2_BR	INO_2 + Br^-→IBr + HONO	0.01	Saiz-Lopez et al. (2014)
HET_HOI_CL	HOI + Cl^-→ICl	0.005	Sherwen et al. (2016)
HET_HOI_BR	HOI + Br^-→IBr	0.005	Sherwen et al. (2016)
Reactions on ice crystals			
Rx level	Reaction	Uptake coefficient	
HET_HOBR_HBR	HOBr + HBr →Br_2 + H_2O	0.12	Fernandez et al. (2014)
HET_HOBR_HCL	HOBr + HCl →BrCl + H_2O	0.30	Fernandez et al. (2014)
HET_HOCL_HBR	HOCl + HBr →BrCl + H_2O	0.20	Fernandez et al. (2014)

Note:
First order rate constant for heterogeneous reaction is calculated using the following expression:

$$k_{het} = \left(\frac{\tilde{d}}{2D} + \frac{4}{\bar{c}\gamma}\right)^{-1} A$$

Where $\tilde{d}$represents the effective diameter, D represents the diffusivity in air, $\bar{c}$ is the mean molecular velocity, A is the aerosol surface area concentration, and γ is the reactive uptake coefficient. Second order rate constants for reactions involving Cl^-or Br^- are calculated by dividing the first order rate constant by [Cl^-] or [Br^-] concentrations. Second order rate constants on ice-crystals are calculated by dividing the first order rate constant by the [HBr] or [HCl] concentrations.

For the HOBr heterogeneous reaction, Fernandez et al. (2014) used an uptake coefficient of 0.1 and a yield of 0.65 and 0.35 reaction products Br_2 and BrCl, respectively. We assume that 80% of the reaction proceeds with the chloride pathway and 20% proceeds with the bromide pathway and use an uptake coefficient of 0.08 (0.1 x 0.8) forHET_HOBR_CL and 0.02 (0.1 x 0.2) forHET_HOBR_BR.

For the INO3 heterogeneous reaction, Saiz-Lopez et al. (2014) used an uptake coefficient of 0.01 and a yield of 0.5 and 0.5 for reaction products IBr and ICl, respectively. We use an uptake coefficient of 0.005 (0.01 x 0.5) forHET_INO3_CL and 0.005 (0.01 x 0.5) forHET_INO3_BR.

For the INO2 heterogeneous reaction, Saiz-Lopez et al. (2014) used an uptake coefficient of 0.02 and a yield of 0.5 and 0.5 for reaction products IBr and ICl, respectively. We use an uptake coefficient of 0.01 (0.02 x 0.5) forHET_INO2_CL and 0.01 (0.02 x 0.5) forHET_INO2_BR.

For the HOI heterogeneous reaction, Sherwen et al. (2016) used an uptake coefficient of 0.01 while Saiz-Lopez et al. (2014) used a yield of 0.5 and 0.5 for reaction products IBr and ICl, respectively. We use an uptake coefficient of 0.005 (0.01 x 0.5) forHET_HOI_CL and 0.005 (0.01 x 0.5) for HET_HOI_BR.

Table S4: Aqueous-phase bromine reactions. Reactions and coefficients come from Long et al. (2013) and the references therein unless otherwise noted. Wet deposition was calculated for all new aqueous species in the model (Fahey et al., 2017)

Chemical kinetic reactions	Rate constant (k_r) in appropriate units of M,s (298K)	$-E_a/R$ (K)	Notes[#]
Br_2 (+ H_2O) → Br^- + HOBr + H^+	9.7E1	-7457	$k(T)(M^{-n+1}s^{-1}) = k_r exp\left[\frac{-E_a}{R}\left(\frac{1}{T}-\frac{1}{298}\right)\right]$
HOBr + Br^- + H^+ → Br_2	1.6E10		
Br^- + HOCl + H^+ → BrCl	1.32E6		
HOBr + Cl^- + H^+ → BrCl	2.3E10		
BrCl (+H_2O) → Cl^- + HOBr + H^+	3.0E6		
Mass transfer between phases	D_g (m^2/s) x 10^5	α^*	Notes[#]
HBr (g) ↔ HBr (aq)	1.216	0.032	$k_{mt,i}(s^{-1}) = \left(\frac{r^2}{3D_{g,i}} + \frac{4r}{3\bar{v}_i\alpha_i}\right)^{-1}$
HOBr (g) ↔ HOBr (aq)	1.101	0.5	
HOCl (g) ↔ HOCl (aq)	1.267	0.5	$\bar{v}_i = \sqrt{\frac{8RT}{MW_i\pi}}$
BrCl (g) ↔ BrCl (aq)	1.19	0.38	
Br_2 (g) ↔ Br_2 (aq)	1.0	0.038	
Ionic dissociation	Equilibrium constant, K_{eq} (M)		
HBr (aq) ↔ H^+ (aq) + Br^- (aq)	1.0E9		

[*]Treated as T independent here.

[#]E_a is the activation energy, MW is the molecular weight, $D_{g,i}$ is the gas phase diffusion coefficient (m^2/s), α_i is the accommodation coefficient, R is the gas constant, T is temperature, and, r is the droplet radius (m)

Rate constants are calculated using the following expression:

$$k(T)(M^{-n+1}s^{-1}) = k_r exp\left[\frac{-E_a}{R}\left(\frac{1}{T}-\frac{1}{298}\right)\right]$$

Where, T is temperature, E_a is the activation energy, and R is the gas constant.

Mass transfer between gas and aqueous phases is calculated using the following expression:

$$k_{mt,i}(s^{-1}) = \left(\frac{r^2}{3D_{g,i}} + \frac{4r}{3\bar{v}_i\alpha_i}\right)^{-1}$$

Where, r is the droplet radius (m), $D_{g,i}$ is the gas phase diffusion coefficient (m^2/s), $\bar{v}_i$is the mean molecular speed (m/s), and α_i is the accommodation coefficient, R is the gas constant, T is temperature, and MW is the molecular weight.

Figure S1: Location of coastal sites at (a) Clean Air Status and Trends Network (CASTNet) and (b) the USEPA's Air Quality System (AQS)

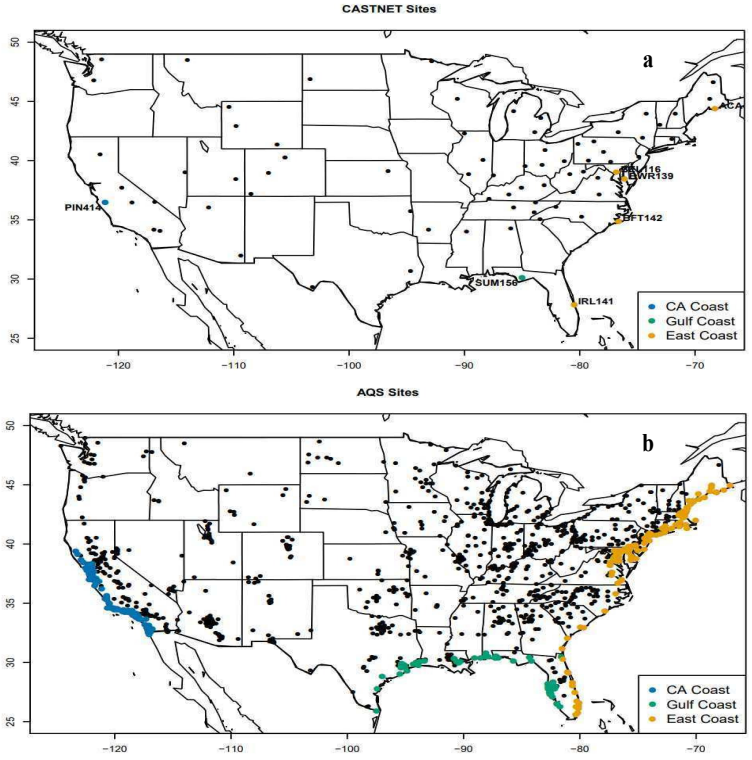

Supplemental Information for:

Impact of enhanced ozone deposition and halogen chemistry on tropospheric ozone over the Northern Hemisphere

Golam Sarwar[1,*], Brett Gantt[1], Donna Schwede[1], Kristen Foley[1], Rohit Mathur[1], Alfonso Saiz-Lopez[2]

[1] National Exposure Research Laboratory, Environmental Protection Agency, Research Triangle Park, North Carolina, USA

[2] Atmospheric Chemistry and Climate Group, Institute of Physical Chemistry Rocasolano, CSIC, Spain

*Corresponding author contact information: e-mail: sarwar.golam@epa.gov

Number of Pages: 7

Number of Figures: 2

Number of Tables: 3

Figures:

S.1 – Daily averaged (a) standard and (b) enhanced ozone deposition velocity for a typical day
S.2 – A plot of first order halogen mediated O_3 loss rate and atmospheric pressure

Tables:

S.1 – Gas-phase bromine chemistry used in the study
S.2 – Gas-phase iodine chemistry used in the study
S.3 – List of monitoring sites used in model comparison

Calculation of an effective first order rate constant for halogen mediated O_3 loss

An effective first order rate constant (k_{O3}) for halogen mediated O_3 loss is calculated by subtracting the first order O_3 loss rate obtained without halogen chemistry from that obtained with halogen chemistry (without photolysis of higher iodine oxides). The first order O_3 loss rate for each simulation is calculated by subtracting the total O_3 production rate from the total O_3 loss rate and dividing the result by O_3:

$$\text{First order } O_3 \text{ loss rate} = \left(\sum k_i[O_3][R_i] - \sum k_j[X_j][Y_j] \right)/O_3 \quad (1)$$

where R_i is the species involved in reactions with O_3, and X_i and Y_i are the species involved in reactions producing O_3. The first order O_3 loss rate with the halogen chemistry over marine regions is greater than that obtained without the halogen chemistry. A daytime average k_{O3} value for each grid-cell is then calculated by using all daytime values in summer. Finally, a layer average k_{O3} is calculated by using all daytime averaged k_{O3} values over all marine regions for each model layer. The relationship between the layer averaged k_{O3} (s^{-1}) values and the corresponding atmospheric pressures, P (Pa) is then obtained using nonlinear least squares estimation (Figure S.2).

Our calculated surface k_{O3} is 2.4×10^{-6} s^{-1}. Using data from Read et al.[1], we also derive a similar value for surface k_{O3} (~80% of our value). Our calculated value is slightly greater than the value derived from Read et al.[1], likely due to the fact that we averaged values over all marine regions in the Northern Hemisphere during summer while Read et al.[1] only analyzed annual O_3 measurements from the Cape Verde archipelago.

Figures

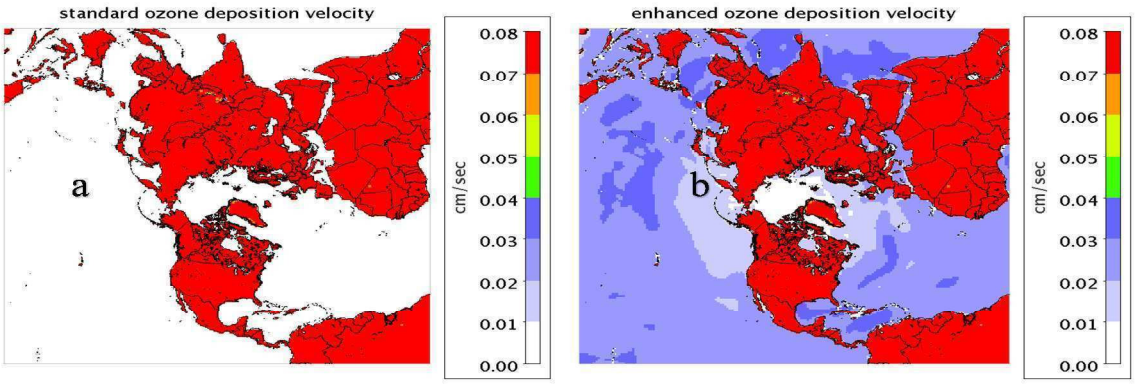

Figure S.1: Daily averaged (a) standard and (b) enhanced ozone deposition velocity for a typical day

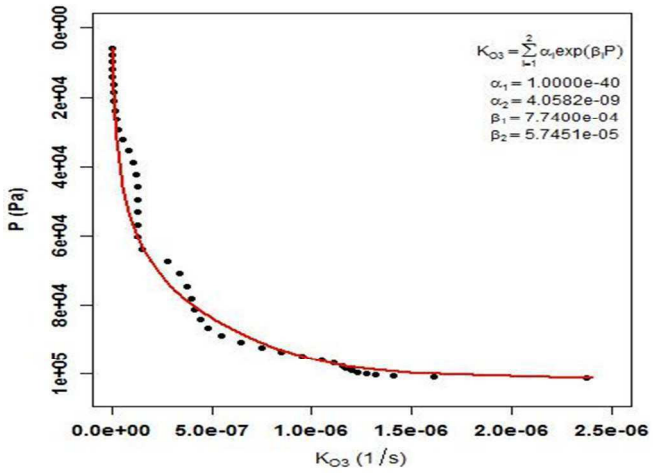

Figure S.2: A plot of first order halogen mediated O_3 loss rate and atmospheric pressure

Table S.1: Gas-phase bromine chemistry used in the study[2-4]

Rx level	Reaction	Rate constant (k)
BR01	$Br + O_3 = BrO + O_2$	$1.7 \times 10^{-11}\ e^{-800/T}$
BR02	$BrO + HO_2 = HOBr + O_2$	$3.7 \times 10^{-12}\ e^{545/T}$
BR03	$Br + HO_2 = HBr + O_2$	$1.4 \times 10^{-11}\ e^{-590/T}$
BR04	$HBr + OH = Br + H_2O$	1.1×10^{-11}
BR05	$BrO + BrO = 2.0\ Br + O_2$	2.7×10^{-12}
BR06	$BrO + BrO = BR_2 + O_2$	$2.9 \times 10^{-14}\ e^{840/T}$
BR07	$BrO + NO = Br + NO_2$	$8.7 \times 10^{-12}\ e^{260/T}$
BR08	$Br + BrONO_2 = BR_2 + NO_3$	$1.78 \times 10^{-11}\ e^{365/T}$
BR09	$BR_2 + OH = HOBr + Br$	$1.9 \times 10^{-11}\ e^{240/T}$
BR10	$BrO + OH = Br + HO_2$	7.5×10^{-11}
BR11	$Br + NO_3 = BrO + NO_2$	1.6×10^{-11}
BR12	$Br + FORM = HBr + HO_2 + CO$	$1.7 \times 10^{-11}\ e^{-800/T}$
BR13	$Br + ALD2 = HBr + C_2O_3$	$1.3 \times 10^{-11}\ e^{-360/T}$
BR14	$Br + ALDX = HBr + C_XO_3$	9.7×10^{-12}
BR15	$BrO + MEO2 = HOBr + FORM$	4.1×10^{-12}
BR16	$BrO + MEO2 = Br + FORM + HO_2$	1.6×10^{-12}
BR17	$BrO + C_2O_3 = Br + MEO2$	1.7×10^{-12}
BR18	$CHBr_3 + OH = 3\ Br$	$1.6 \times 10^{-12}\ e^{-710/T}$
BR19	$CH_3Br + OH = Br$	$4.0 \times 10^{-12}\ e^{-1470/T}$
BR20	$CH_2Br_2 + OH = 2\ Br$	$2.4 \times 10^{-12}\ e^{-900/T}$
BR21	$CHBr_2Cl + OH = 2\ Br + Cl$	$2.4 \times 10^{-12}\ e^{-900/T}$
BR22	$CHBrCl_2 + OH = Br + 2\ Cl$	$2.4 \times 10^{-12}\ e^{-900/T}$
BR23	$CH_2BrCl + OH = Br + Cl$	$2.4 \times 10^{-12}\ e^{-930/T}$
BR24	$BrO + NO_2 = BrONO_2$	$k_o = 5.2 \times 10^{-31}\ (T/300)^{-3.2}$; $k_\infty = 6.9 \times 10^{-12}\ (T/300)^{-2.9}$; F = 0.6 and N = 1.0
BR25	$Br + NO_2 = BrNO_2$	$k_o = 4.2 \times 10^{-31}\ (T/300)^{-2.4}$; $k_\infty = 2.7 \times 10^{-11}\ (T/300)^{0.0}$; F = 0.6 and N = 1.0
BR26	$BrO + ClO = Br + Cl$	$9.5 \times 10^{-13}\ e^{550/T}$
BR27	$BrO + ClO = Br + Cl + O_2$	$2.3 \times 10^{-12}\ e^{260/T}$
BR28	$BrO + ClO = BrCl + O_2$	$4.1 \times 10^{-13}\ e^{290/T}$
BR29	$DMS + BrO = Br + MEO2$	$1.54 \times 10^{-14}\ e^{1000/T}$
BR30	$BrCl = Br + Cl$	Photolysis
BR31	$BrO = Br + O$	Photolysis
BR32	$HOBr = OH + Br$	Photolysis
BR33	$BrONO_2 = BrO + NO_2$	Photolysis
BR34	$BrONO_2 = Br + NO_3$	Photolysis
BR35	$BrNO_2 = Br + NO_2$	Photolysis
BR36	$Br_2 = 2\ Br$	Photolysis
BR37	$CHBr_3 = 3\ Br$	Photolysis
BR38	$CHBr_2Cl = 2\ Br + Cl$	Photolysis
BR39	$CHBrCl_2 = Br + 2\ Cl$	Photolysis

Note: First order rate constants are in units of sec^{-1}, second order rate constants are in units of $cm^3\ molecule^{-1}\ sec^{-1}$. Temperatures (T) are in Kelvin. Rate constants for BR24 and BR25 is described by the falloff expression of the form $k=\{k_o[M]/(1+k_o[M]/k_\infty)\}\ F^z$, where $Z=[1+\{(1/N)\log_{10}(k_o\ [M]/k_\infty)\}^2]^{-1}$, where [M] is the total pressure in molecules/cm^3, and k_o, k_∞, F, and N are indicated in table. The original reaction in BR26 contains OClO which is represented by Cl since it is not accounted for in the current CMAQ chlorine chemistry. Br = bromine atom, O_3 = ozone, O_2 = oxygen, BrO =bromine oxide, HO_2 = hydroperoxy radical, HOBr = hypobromous acid, HBr = hydrobromic acid, OH = hydroxyl radical, Br_2 = molecular bromine, NO = nitric oxide, NO_2 = nitrogen dioxide, $BrONO_2$ = bromine nitrate, NO_3 = nitrate, FORM = formaldehyde, ALD2 = acetaldehyde, ALDX = propionaldehyde and higher aldehydes, CO = carbon monoxide, C_2O_3 = acetylperoxy radical, C_XO_3 = higher acylperoxy radicals, $CHBr_3$=bromoform, CH_3Br=methyl bromide, CH_2Br_2= methylene bromide, $CHBr_2Cl$= dibromochloromethane, $CHBrCl_2$= bromodichloromethane, CH_2BrCl= methylene bromochloride, $BrNO_2$=nitryl bromide, BrCl= bromine chloride, H_2O = water vapor, DMS=dimethylsulfide.

Table S.2: Gas-phase iodine chemistry used in the study[5]

Rx level	Reaction	Rate constant (k)
IO01	$I + O_3 = IO + O_2$	$2.1 \times 10^{-11}\, e^{-830/T}$
IO02	$IO + O_3 = OIO + O_2$	3.0×10^{-16}
IO03	$I + HO_2 = HI + O_2$	$1.5 \times 10^{-11}\, e^{-1090/T}$
IO04	$IO + NO = I + NO_2$	$7.15 \times 10^{-12}\, e^{300/T}$
IO05	$IO + HO_2 = HOI + O_2$	$1.4 \times 10^{-11}\, e^{540/T}$
IO06	$IO + IO = OIO + I$	$2.13 \times 10^{-11}\, e^{180/T} \times [\, 1 + e^{-P/191.42}\,]$
IO07	$IO + IO = I_2O_2$	$3.27 \times 10^{-11}\, e^{180/T} \times [\, 1 - 0.65\, e^{-P/191.42}\,]$
IO08	$IO + OIO = I_2O_3$	$w_1\, e^{w_2 T}$ $w_1 = 4.68 \times 10^{-10} - 1.38 \times 10^{-5}\, e^{-0.75\,P/1.62} + 5.51 \times 10^{-10}\, e^{-0.75\,P/199.32}$ $w_2 = -3.31 \times 10^{-3} - 5.14 \times 10^{-3}\, e^{-0.75\,P/325.68} - 4.44 \times 10^{-3}\, e^{-0.75\,P/40.81}$
IO09	$OIO + OIO = I_2O_4$	$w_1\, e^{w_2 T}$ $w_1 = 1.16 \times 10^{-9} - 7.79 \times 10^{-10}\, e^{-0.75\,P/22.09} + 1.03 \times 10^{-9}\, e^{-0.75\,P/568.15}$ $w_2 = -8.13 \times 10^{-3} - 3.82 \times 10^{-3}\, e^{-0.75\,P/45.57} - 6.43 \times 10^{-3}\, e^{-0.75\,P/417.95}$
IO10	$I_2 + O = IO + I$	1.25×10^{-10}
IO11	$IO + O = I + O_2$	1.4×10^{-10}
IO12	$IO + OH = HO_2 + I$	1.0×10^{-10}
IO13	$I_2O_2 = OIO + I$	$w_1\, e^{w_2 T}$ $w_1 = 3.54 \times 10^{10} + 1.85 \times 10^{11}\, 0.75\,P - 1.45 \times 10^{8}\, (0.75\,P)^2 + 6.07 \times 10^{4}\, (0.75\,P)^3$ $w_2 = -9681.65 - 346.95\, e^{-0.75\,P/343.25} + 251.78\, e^{-0.75\,P/44.14}$
IO14	$I_2O_2 = 2{*}IO$	$w_1\, e^{w_2 T}$ $w_1 = 2.55 \times 10^{11} - 4.41 \times 10^{9}\, 0.75\,P + 8.56 \times 10^{7}\, (0.75\,P)^2 + 1.42 \times 10^{4}\, (0.75\,P)^3$ $w_2 = -11466.82 + 597.01\, e^{-0.75\,P/1382.62} - 167.33\, e^{-0.75\,P/43.75}$
IO15	$I_2O_4 = 2{*}OIO$	$w_1\, e^{w_2 T}$ $w_1 = -1.92 \times 10^{14} + 4.67 \times 10^{13}\, 0.75\,P - 3.68 \times 10^{8}\, (0.75\,P)^2 - 3.09 \times 10^{6}\, (0.75\,P)^3$ $w_2 = -12302.15 + 252.78\, e^{-0.75\,P/46.12} + 437.62\, e^{-0.75\,P/428.44}$
IO16	$I_2 + OH = HOI + I$	1.8×10^{-10}
IO17	$I_2 + NO_3 = I + IONO_2$	1.5×10^{-12}
IO18	$I + NO_3 = IO + NO_2$	1.0×10^{-10}
IO19	$OH + HI = I + H_2O$	$1.6 \times 10^{-11}\, e^{440/T}$
IO20	$I + IONO_2 = I_2 + NO_3$	$9.1 \times 10^{-11}\, e^{-146/T}$
IO21	$HOI + OH = IO + H_2O$	2.0×10^{-13}
IO22	$IO + DMS = I + MEO2$	$3.2 \times 10^{-13}\, e^{-925/T}$
IO23	$INO_2 = I + NO_2$	$1.0 \times 10^{18}\, e^{-13670/T}$
IO24	$IONO_2 = IO + NO_2$	$w_1\, e^{w_2 T}$ $w_1 = -2.63 \times 10^{13} + 4.32 \times 10^{12}\, 0.75\,P + 3.73 \times 10^{8}\, (0.75\,P)^2 - 6.28 \times 10^{5}\, (0.75\,P)^3$ $w_2 = -13847.85 + 240.34\, e^{-0.75\,P/49.27} + 451.34\, e^{-0.75\,P/436.87}$
IO25	$INO + INO = I_2 + 2\,NO$	$8.4 \times 10^{-11}\, e^{-2620/T}$
IO26	$INO_2 + INO_2 = I2 + 2\,NO_2$	$4.7 \times 10^{-13}\, e^{-1670/T}$
IO27	$OIO + NO = IO + NO_2$	$1.1 \times 10^{-12}\, e^{542/T}$
IO28	$HI + NO_3 = I + HNO_3$	$1.3 \times 10^{-12}\, e^{-1830/T}$
IO29	$IO + BrO = Br + I + O_2$	$0.3 \times 10^{-11}\, e^{510/T}$
IO30	$IO + BrO = Br + OIO$	$1.2 \times 10^{-11}\, e^{510/T}$
IO31	$I + BrO = IO + Br$	1.44×10^{-11}
IO32	$IO + ClO = I + Cl$	$2.585 \times 10^{-12}\, e^{280/T}$
IO33	$IO + ClO = I + Cl + O_2$	$1.175 \times 10^{-12}\, e^{280/T}$
IO34	$IO + ClO = ICl + O_2$	$9.4 \times 10^{-13}\, e^{280/T}$
IO35	$IO + Br = I + BrO$	2.49×10^{-11}
IO36	$IO + NO_3 = OIO + NO_2$	9.0×10^{-12}
IO37	$IO + MEO2 = FORM + I + HO_2$	2.0×10^{-12}
IO38	$CH_3I + OH = I + HO_2 + H_2O$	$2.9 \times 10^{-12}\, e^{-1100/T}$
IO39	$I + NO_2 = INO_2$	$k_o = 3.0 \times 10^{-31}\, (T/300)^{-1.0}$; $k_\infty = 6.6 \times 10^{-11}\, (T/300)^{-0.0}$; F = 0.6 and N = 1.0
IO40	$IO + NO_2 = IONO_2$	$k_o = 6.5 \times 10^{-31}\, (T/300)^{-3.5}$; $k_\infty = 7.6 \times 10^{-12}\, (T/300)^{-1.5}$; F = 0.6 and N = 1.0
IO41	$I + NO = INO$	$k_o = 1.8 \times 10^{-32}\, (T/300)^{-1.0}$; $k_\infty = 1.7 \times 10^{-11}\, (T/300)^{-0.0}$; F = 0.6 and N = 1.0
IO42	$CH_3I = I + MEO2$	Photolysis
IO43	$CH_2I_2 = 2.0\,I$	Photolysis
IO44	$CH_2IBr = I + Br$	Photolysis
IO45	$CH_2ICl = I + Cl$	Photolysis
IO46	$I_2 = 2.0\,I$	Photolysis
IO47	$IO = I + O$	Photolysis
IO48	$OIO = I + O_2$	Photolysis
IO49	$INO = I + NO$	Photolysis
IO50	$INO_2 = I + NO_2$	Photolysis
IO51	$IONO_2 = I + NO_3$	Photolysis
IO52	$HOI = I + OH$	Photolysis
IO53	$ICl = I + Cl$	Photolysis

IO54	I_2O_2 = I + OIO	Photolysis*
IO55	I_2O_3 = IO + OIO	Photolysis*
IO56	I_2O_4 = OIO + OIO	Photolysis*

Note: First order rate constants are in units of sec^{-1}, second order rate constants are in units of cm^3 $molecule^{-1}$ sec^{-1}. Temperatures (T) are in Kelvin. Rate constants for IO39-IO41 are described by the falloff expression of the form $k=\{k_o[M]/(1+k_o[M]/k_\infty)\}$ F^Z, where $Z=[1+\{(1/N)\log_{10}(k_o[M]/k_\infty)\}^2]^{-1}$, where [M] is the total pressure in molecules/cm^3, and k_o, k_∞, F, and N are indicated in table. Values have been rounded-off for IO08, IO09, IO13, IO14, IO15, and IO23. The original reaction in IO32 contains OClO which is represented by Cl since it is not accounted for in the current CMAQ chlorine chemistry. I = iodine atom, O_3 = ozone, O_2 = oxygen, IO = iodine oxide, OIO =iodine dioxide, HO_2 = hydroperoxy radical, HI = hydroiodic acid, NO = nitric oxide, NO_2 = nitrogen dioxide, HOI = hypoiodous acid, I_2O_2 =di-iodine dioxide, I_2O_3=di-iodine trioxide, I_2O_4=diiodine tetroxide, I_2 = molecular iodine, OH = hydroxyl radical, NO_3 = nitrate, $IONO_2$ = iodine nitrate, INO_2=nitryl iodide, INO=nitrosyl iodide, HNO_3=nitric acid, ICl= iodine monochloride, CH_3I=methyl iodide, CH_2I_2=methylene iodide, CH_2IBr=bromoiodomethane, CH_2ICl=chloroiodomethane, Br = bromine atom, BrO =bromine oxide, Cl = atomic chlorine, ClO = chlorine oxide. *Only used for Case D.

Table S.3: List of monitoring sites used in model comparison (http://ds.data.jma.go.jp/gmd/wdcgg)

Location	Latitude (degree)	Longitude (degree)
Trinidad Head, California, USA	41.05	-124.15
Ragged Pt., Barbados	13.17	-59.43
Tudor Hill, Bermuda	32.27	-64.87
Mauna Loa, Hawaii, USA	19.54	-155.58
Barrow, Alaska, USA	71.32	-156.60
Minamitorishima, Japan	24.28	153.98
Tsukuba, Japan	36.05	140.13
Ryori, Japan	39.03	141.82
Yonagunijima, Japan	24.47	123.02
Heimaey, Iceland	63.40	-20.28
Mace Head, Ireland	53.33	-9.90
Westerland, Germany	54.93	8.32
Kollumerwaard, Netherland	53.33	6.28

SI REFERENCE

1. Read, K. A.; Mahajan, A. S.; Carpenter, L. J.; Evans, M. J.; Faria, B. V. E.; Heard, D. E.; Hopkins, J. R.; Lee, J. D.; Moller, S. J.; Lewis, A. C.; Mendes, L.; McQuaid, J. B.; Oetjen, H.; SaizLopez, A.; Pilling, M. J.; Plane, J. M. C. Extensive halogen mediated ozone destruction over the tropical Atlantic Ocean. Nature, 2008, 453, 1232–1235.
2. Yang, X.; Cox, R. A.; Warwick, N. J.; Pyle, J. A.; Carver, G. D.; O'Connor, F. M.; Savage, N. H. Tropospheric bromine chemistry and its impacts on ozone: a model study. Journal of Geophysical Research, 2005, 110, D23311.
3. Ordóñez, C.; Lamarque, J.-F.; Tilmes, S.; Kinnison, D. E.; Atlas, E. L.; Blake, D. R.; Sousa Santos, G.; Brasseur, G.; Saiz-Lopez, A. Bromine and iodine chemistry in a global chemistry-climate model: description and evaluation of very short-lived oceanic sources. Atmospheric Chemistry & Physics, 2012, 12, 1423-1447.
4. Sommariva, R.; Glasow, R. Multiphase Halogen Chemistry in the Tropical Atlantic Ocean. Environmental Science & Technology, 2012, 46 (19), 10429–10437.
5. Saiz-Lopez, A.; Fernandez, R. P.; Ordóñez, C.; Kinnison, D. E.; Gómez Martín, J. C.; Lamarque, J.-F.; Tilmes, S. Iodine chemistry in the troposphere and its effect on ozone. Atmospheric Chemistry & Physics, 2014, 14, 13119-13143.

Science of the Total Environment 610–611 (2018) 1536–1545

Contents lists available at ScienceDirect

Science of the Total Environment

journal homepage: www.elsevier.com/locate/scitotenv

The influence of ocean halogen and sulfur emissions in the air quality of a coastal megacity: The case of Los Angeles

Maria Muñiz-Unamunzaga [a], Rafael Borge [b], Golam Sarwar [c], Brett Gantt [c], David de la Paz [b], Carlos A. Cuevas [a,*], Alfonso Saiz-Lopez [a,*]

[a] Department of Atmospheric Chemistry and Climate, Institute of Physical Chemistry Rocasolano, CSIC, Madrid 28006, Spain
[b] Environmental Modelling Laboratory, Department of Chemical & Environmental Engineering, Technical University of Madrid (UPM), Madrid, Spain
[c] National Exposure Research Laboratory, Environmental Protection Agency, Research Triangle Park, NC 27711, United States

HIGHLIGHTS

- Natural marine emissions (Cl, Br, I and DMS) included in CMAQ simulations over LA.
- Oceanic halogens and DMS may play an important role on coastal urban areas.
- Substantial changes in the levels of key urban atmospheric oxidants (OH, HO_2 and NO_3).
- O_3 and NO_2 ambient levels decreased by 5 ppbv and 2.5 ppbv in Los Angeles city.
- 10% increase in secondary organic aerosol (SOA) due to dimethyl sulphide (DMS).

GRAPHICAL ABSTRACT

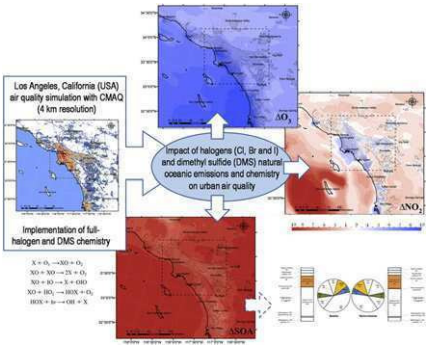

ARTICLE INFO

Article history:
Received 1 March 2017
Received in revised form 23 May 2017
Accepted 12 June 2017
Available online 28 June 2017

Editor: D. Barcelo

Keywords:
Marine natural emissions
Halogens
DMS
CMAQ
Los Angeles
Urban air quality

ABSTRACT

The oceans are the main source of natural halogen and sulfur compounds, which have a significant influence on the oxidizing capacity of the marine atmosphere; however, their impact on the air quality of coastal cities is currently unknown. We explore the effect of marine halogens (Cl, Br and I) and dimethyl sulfide (DMS) on the air quality of a large coastal city through a set of high-resolution (4-km) air quality simulations for the urban area of Los Angeles, US, using the Community Multiscale Air Quality (CMAQ model). The results indicate that marine halogen emissions decrease ozone and nitrogen dioxide levels up to 5 ppbv and 2.5 ppbv, respectively, in the city of Los Angeles. Previous studies suggested that the inclusion of chlorine in air quality models leads to the generation of ozone in urban areas through photolysis of nitryl chloride ($ClNO_2$). However, we find that when considering the chemistry of Cl, Br and I together the net effect is a reduction of surface ozone concentrations. Furthermore, combined ocean emissions of halogens and DMS cause substantial changes in the levels of key urban atmospheric oxidants such as OH, HO_2 and NO_3, and in the composition and mass of fine particles. Although the levels of ozone, NO_3 and HO_x are reduced, we find a 10% increase in secondary organic aerosol (SOA) mean concentration, attributed to the increase in aerosol acidity and sulfate aerosol formation when combining DMS and bromine. Therefore, this new pathway for enhanced SOA formation may potentially help with current model under predictions of urban SOA. Although further observations and research are needed to establish these preliminary conclusions, this first city-scale investigation suggests that the inclusion of oceanic halogens and DMS in air quality models may improve regional air quality predictions over coastal cities around the world.

© 2017 Elsevier B.V. All rights reserved.

* Corresponding authors.
E-mail addresses: ccuevas@iqfr.csic.es (C.A. Cuevas), a.saiz@csic.es (A. Saiz-Lopez).

http://dx.doi.org/10.1016/j.scitotenv.2017.06.098
0048-9697/© 2017 Elsevier B.V. All rights reserved.

1. Introduction

The world's population and urbanization rates are increasing, and with it the number of megacities – cities with over 10 million inhabitants. Many megacities such as Los Angeles, California in the United States are located in coastal regions (Fig. 1). Due to its large urban population and meteorological and geographic conditions, California has historically suffered from severe air quality problems, especially in regard to high ozone concentrations (Neuman et al., 2012). The urban area of Los Angeles is part of the South Coast Air Basin (SoCAB), which is surrounded by mountainous terrain and the Pacific Ocean (Fig. 1). These geographical features cause pollution to be trapped in the basin, leading to increased pollution levels that can negatively affect human health and ecosystems (Kim et al., 2016). Since the early 1960s, a tightening of ambient quality standards has led to strong air pollution controls in SoCAB in order to reduce anthropogenic emissions of nitrogen oxides ($NO_x = NO_2 + NO$) and volatile organic compounds (VOCs) that are the main precursors of tropospheric ozone (Pollack et al., 2013). Despite significant anthropogenic emission reduction during the last decades (Fujita et al., 2013), the concentrations of ozone and particulate matter (PM) in Los Angeles in 2015 still exceeded the corresponding air quality standards.

Nonetheless, urban air quality can also be influenced by natural emissions as marine air masses confluence with polluted urban air. Halogenated species produced in the oceans by biological and photochemical processes are emitted to the marine atmosphere where they undergo photolysis and reaction with atmospheric oxidants to release reactive iodine, bromine and chlorine radicals, which can then catalytically destroy tropospheric O_3 in the troposphere (Simpson et al., 2015) and in the stratosphere (Fernandez et al., 2017; Hossaini et al., 2015; Oman et al., 2016). Halogenated compounds can also alter the oxidative capacity of the marine troposphere by changing the budget and balance of

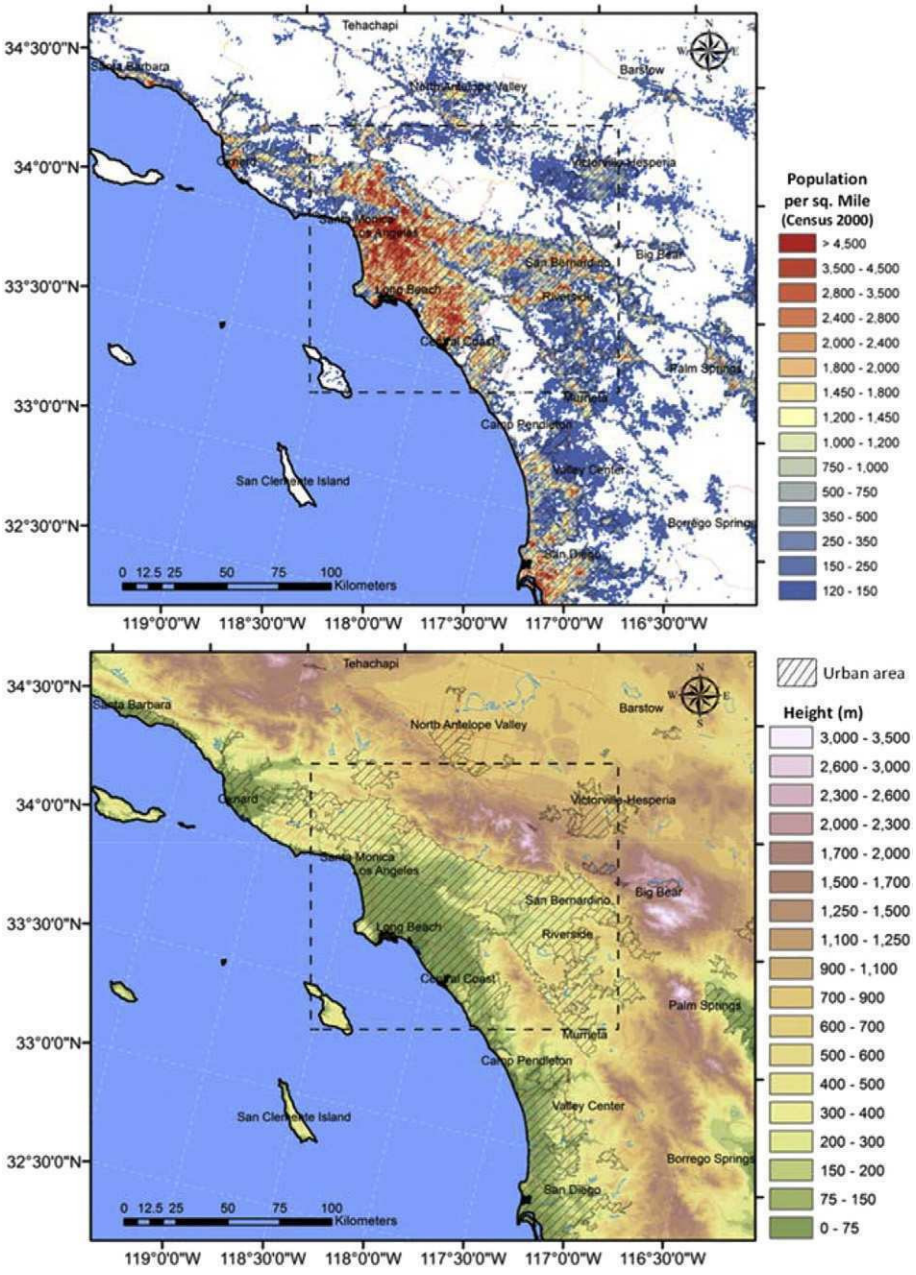

Fig. 1. Representation of population in California per square mile according to Census 2000 in the domain (upper panel), and geographical features of Los Angeles area along with the location of selected monitoring sites (bottom panel).

important atmospheric oxidants such as NO_x and HO_x ($HO_x = HO_2 + OH$) (Saiz-Lopez and von Glasow, 2012). Previous global modelling studies have shown that combined chlorine-bromine-iodine chemistries can deplete up to 20% of ozone in remote and clean marine environments (Saiz-Lopez et al., 2012a; Sherwen et al., 2016). Conversely, chlorine compounds released via heterogeneous reaction on marine aerosols can increase ground-level O_3 concentration in coastal polluted regions (Hossaini et al., 2016; Osthoff et al., 2008; Tham et al., 2016), that in turn, affect PM concentration (Chan et al., 2017). An increase of 1.0–6.0 ppbv in 8-h daily maximum O_3 concentration due to chlorine activation on marine aerosols was estimated for the North Hemisphere (Sarwar et al., 2014) and across the United States (Sarwar et al., 2012). However, multi-model assessments using global and regional chemical transport models have still found systematic overpredictions of surface ozone concentrations at representative coastal sites over North America and South East Asia (Han et al., 2008; Reidmiller et al., 2009). Remarkably, observations made at the Californian coast (La Jolla) have reported significant and highly variable levels of dihalogens (Cl_2, Br_2 and I_2) in polluted coastal air, suggesting a possible role of this chemistry in coastal urban air quality (Finley and Saltzman, 2008). However, despite their detection in polluted coastal air and their demonstrated ability to alter the oxidative capacity of the marine atmosphere (Simpson et al., 2015), the omission of natural halogen sources altogether (Cl, Br and I) and their combined chemistry in air quality models has so far prevented a comprehensive evaluation of their effect on air quality within and around coastal megacities through high-resolution simulations.

Dimethyl sulfide (DMS) is produced by many species of phytoplankton in the oceans and emitted to the atmosphere (Stefels et al., 2007) where, following reactions with oxidants (OH, NO_3 and BrO) (Boucher et al., 2003; Breider et al., 2010), represents the primary source of sulfate aerosol over remote ocean regions. Sulfate aerosols can impact climate via direct and indirect effects on radiation and clouds (Haywood and Boucher, 2000). Hence, DMS plays an important role in the Earth's global climate system, although its influence on urban aerosol formation on coastal cities remains poorly assessed. Here, we investigate the potential of marine halogens (Cl, Br and I) and DMS to influence the levels of key pollutants with relevant health impacts (Delamater et al., 2012) in the megacity of Los Angeles, and surrounding areas, through a set of city-scale air quality simulations. We explore the resulting implications for air quality policies relevant to coastal urban areas.

2. Methods

2.1. Model

High-resolution simulations were performed using the Community Multiscale Air Quality (CMAQ v5.1) regional model (Appel et al., 2017), with the Carbon Bond chemical mechanism (Whitten et al., 2010) and the chlorine chemistry scheme (Sarwar et al., 2015; Sarwar et al., 2014). The model is used to assess the impact of ocean emissions and combined chemical processes of halogens (iodine, bromine and chlorine) and DMS on air quality levels of Los Angeles and SoCAB using a horizontal grid resolution of 4 km and 35 vertical levels. Simulations were completed for August (used as a spin up period) and September of 2006. The Community Multiscale Air Quality (CMAQ) model (https://github.com/USEPA/CMAQ) is a chemical transport model containing comprehensive treatment of all important atmospheric processes related to air pollution. It has been widely used throughout the world in a variety of applications. The skill of the model has been demonstrated by evaluating the model predictions against numerous observational datasets (Appel et al., 2007; Appel et al., 2017; Appel et al., 2013; Foley et al., 2010; Appel et al., 2008). The chlorine implementation in CMAQ was previously evaluated using, among others, the $ClNO_2$ observations made during the CALNEX campaign that took place in California in 2010 (Mielke et al., 2013; Riedel et al., 2012). However, the chemistry was modified to include iodine and bromine (further details can be found in (Gantt et al., 2017; Sarwar et al., 2015)) and DMS reactions.

2.2. Emissions and meteorological data

Marine emissions of halogen species are divided into halocarbons, inorganic bromine and inorganic iodine, according to (Gantt et al., 2017) and references therein. (Sarwar et al., 2015) and (Xing et al., 2015) described the emissions and meteorological datasets for the outermost domain while (Appel et al., 2017) and (Hogrefe et al., 2015) described the emissions and meteorological datasets for the intermediate domain. The Sparse Matrix Operator Kernel Emissions (SMOKE) system (Houyoux et al., 2000) was used to prepare model-ready emissions for the innermost domain. Anthropogenic emission datasets were taken from the 2005 Version 4.2 US EPA emission modelling platform, based on the National Emission Inventory (NEI) version 3 and harmonized with emissions submitted by California Air Resources Board (CARB) inventory. Biogenic emissions were calculated in-line using the Biogenic Emissions Inventory System version 3.14 (Schwede et al. 2005). Halogen (Sarwar et al., 2015) and DMS (Lana et al., 2011) emissions were calculated in-line.

Meteorology and non-oceanic biogenic emissions are identical for all the simulations presented. The Meteorology from the Weather Research and Forecasting (WRFv3.7.1) model (Skamarock, 2008) was used to drive the chemical transport model in all three nested domains. WRF was initialized from global NCEP FNL Operational Model Global Tropospheric Analyses with a spatial resolution of 1° × 1° and a temporal resolution of 6 h (http://dx.doi.org/10.5065/D6M043C6) while sea surface temperature is updated daily from NCEP SST global analyses with 0.5° resolution (http://polar.ncep.noaa.gov/sst/rtg_low_res).

2.3. Observation data

Observed data was retrieved from the Environmental Protection Agency (EPA) Air Quality System (AQS) database for September 2006 (http://aqsdr1.epa.gov/aqsweb/aqstmp/airdata/download_files.html). Eight monitoring sites located in the area of Los Angeles were selected in order to compare modeled ozone concentration to observed data (Table 1).

Table 1
Situation and information of selected monitoring sites from the Environmental Protection Agency (EPA) Air Quality System (AQS) database.

Air quality monitoring station	Site number	Lat (°)	Lon (°)	Elevation (m.a.s.l.)
West Los Angeles	060370113	34.05	−118.46	91
Burbank	060371002	34.18	−118.32	168
Los Angeles-1(LA-1)	060371103	34.07	−118.23	87
Lynwood	060371301	33.93	−118.21	27
Pico Rivera	060371602	34.01	−118.07	75
Pasadena	060372005	34.13	−118.13	250
Long Beach	060374002	33.82	−118.19	6
Los Angeles-2(LA-2)	060375005	33.95	−118.43	21

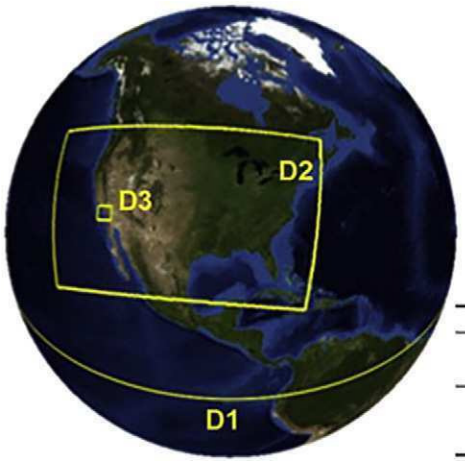

CMAQ				
Domain	Horizontal resolution (km)	Geographic scope	X-Y dimensions (km)	Vertical levels
D1	108	Northern Hemisphere		44
D2	12	US CONUS	459 x 299	35
D3	4	Los Angeles	324 x 288	35

Fig. 2. CMAQ modelling domains.

2.4. Simulation cases

Simulations were performed for three nested model domains (Fig. 2). The outermost domain covers the Northern Hemisphere using 108-km horizontal grid-resolution, the intermediate domain covers the continental United States using 12-km horizontal grid-resolution, and the innermost domain covers the South Coast Air Basin using 4-km horizontal grid-resolution. Results from the outermost domain provided boundary conditions for the intermediate domain while the results from the intermediate domain provided boundary conditions for the innermost domain. The analysis focuses on the innermost domain. Three simulations were completed for each domain. The first simulation used the Carbon Bond chemical mechanism without any halogen or DMS chemistry (Baseline simulation). The second simulation (Case B or full-halogen simulation) used the Carbon Bond chemical mechanism with chlorine, bromine, iodine, and DMS chemistry (Tables S1–S3). This setup allows assessing the sensitivity of ambient air concentration levels of criteria pollutants such as O_3, NO_2 or $PM_{2.5}$ to marine emissions (halogens and DMS simultaneously) at city-scale for the first time. One sensitivity simulation is run to assess the individual role of chlorine chemistry for which we used the Carbon Bond chemical mechanism and the chlorine chemistry alone.

3. Results and discussion

3.1. Effect on O_3, NO_2, secondary organic aerosols and HO_2/OH and NO_2/NO ratios

Model results are compared with surface ozone observations (at the sites listed in Table 1) to understand whether observed changes contribute to improve model predictions (Fig. 3) and thus, support the validity of the additions being tested. In the whole domain, normalized mean bias is reduced from 13.5% to 4.9% when marine halogen and DMS emissions are considered in the simulation.

A noticeable impact on monthly mean surface ozone concentrations relative to the Baseline is found when marine halogen emissions are included in the simulation (Fig. 4). Surface ozone levels are reduced all over the modelling domain. This impact is higher closer to the Californian coast and decreases into the interior of continental US. The combined chemistry of the three halogen species destroys surface ozone by 2 ppbv (3%) on average over most inland regions, while 2.5–5 ppbv (5–10%) are reduced in coastal areas (Fig. 5). The effect on NO_2 ambient concentration levels (panel B) is strongly conditioned by the distribution of emission sources. While concentrations increase over non-urbanized areas (up to 15% over the ocean), the effect of halogens over the urban

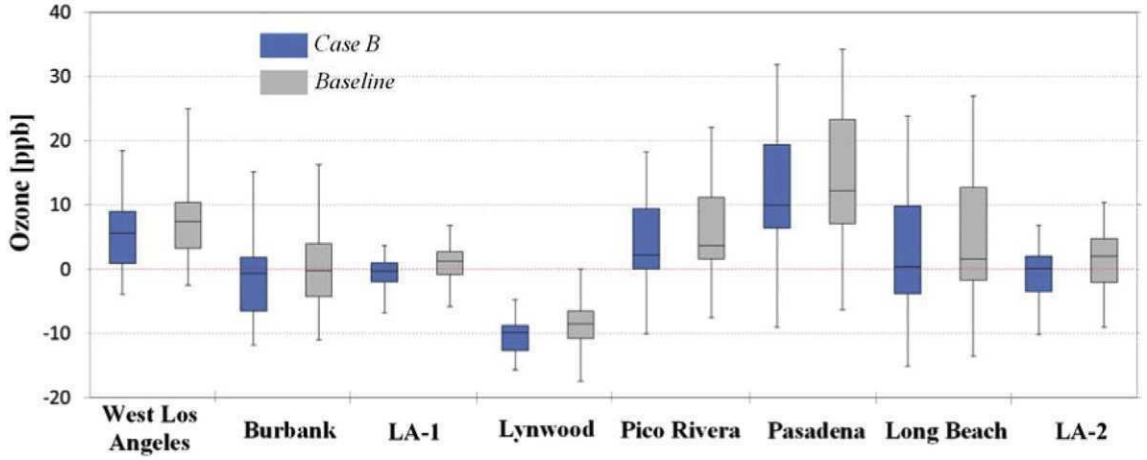

Fig. 3. Distribution of hourly O_3 bias (predicted – observed) for September 2006 for Case B (full halogen and DMS chemistry) and Baseline simulations. Lower bar in the box represents 25th percentile, middle bar represents the median and the upper one 75 percentile values. Maximum and minimum values are shown by error bars.

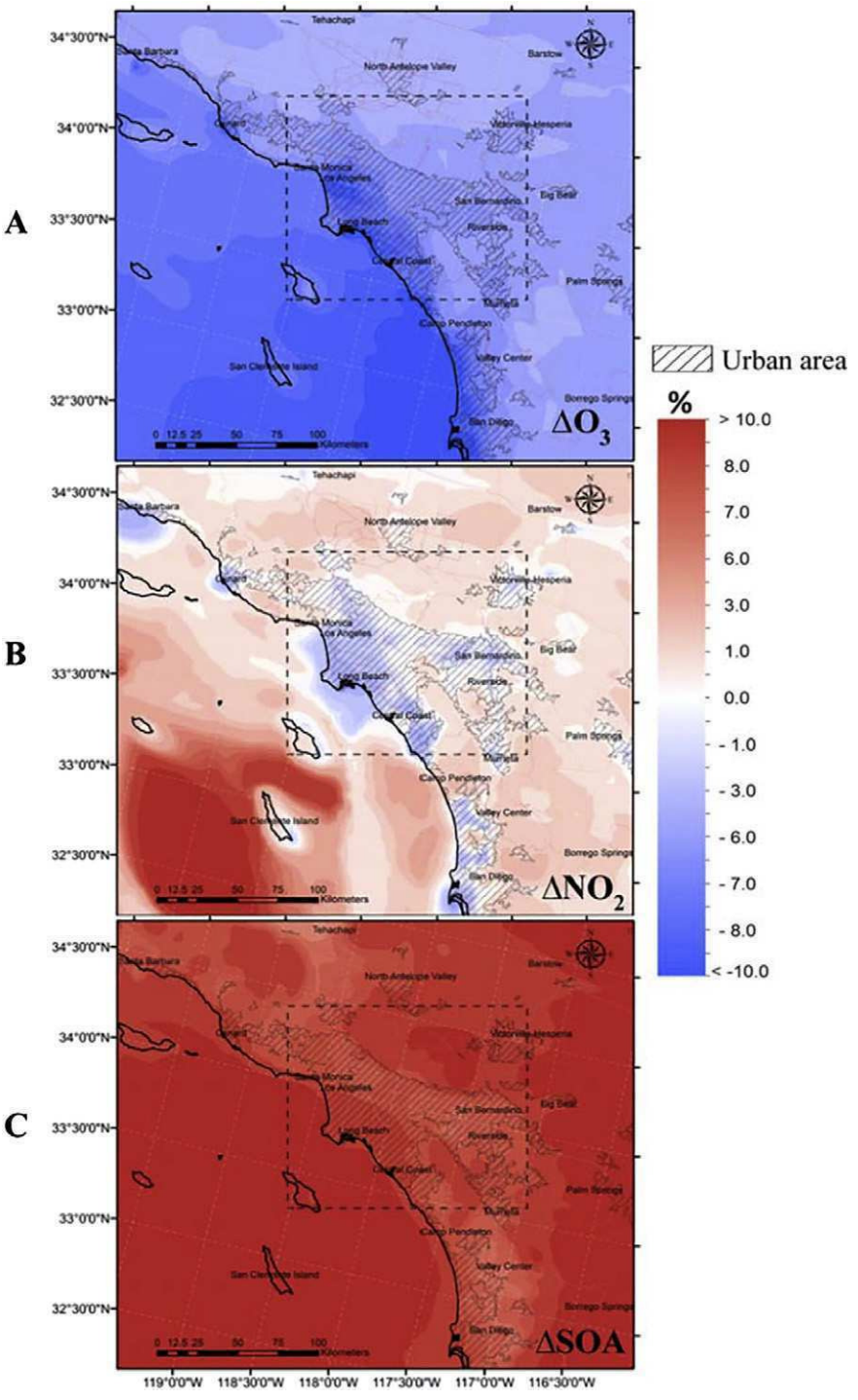

Fig. 4. Impact of the implementation of marine halogens and DMS on the Los Angeles region. The maps show the relative variation of ground level ozone (A), nitrogen dioxide (B) and secondary organic aerosols (C) relative to the baseline scenario (no halogen/DMS).

areas is the opposite, with a maximum reduction of nearly 5% in NO_2 concentrations for downtown Los Angeles (around 3 ppb). In polluted areas halogen chemistry shifts the NO_x partitioning to NO, while in non-polluted areas with high concentrations of halogens the reaction between XO and NO shifts the balance to NO_2 (Fig. 7) (Mahajan et al., 2009; Saiz-Lopez et al., 2012b). Finally, panel C shows how the inclusion of DMS and halogens brings about a clear increase of regional levels of secondary organic aerosol (SOA). Although maximum relative increments are found over the sea and non-urbanized inland areas, the increase over Los Angeles is as high as 10%, which leads to a net SOA fraction increase of 0.2 $\mu g \cdot m^{-3}$ (Fig. 5).

The coastal side of Los Angeles has reductions in monthly mean surface ozone concentration around 3–4 ppbv, and up to 5 ppbv in downtown Los Angeles, which represents a decrease of 10% relative to the Baseline simulation without halogens (Fig. 6). The impact of halogen chemistry gradually decreases inland, where surface ozone concentrations are depleted by 2–2.5 ppbv or less, such as in San Bernardino where ozone is reduced by 1 ppbv (around 4%). Although the net effect clearly diminishes inland, the distribution of ozone variations throughout the day at both locations is similar. Maximum reductions (3–5 ppbv) occur during the afternoon (from 13 to 17 h local time) when maximum concentrations are typically observed (this is why reductions

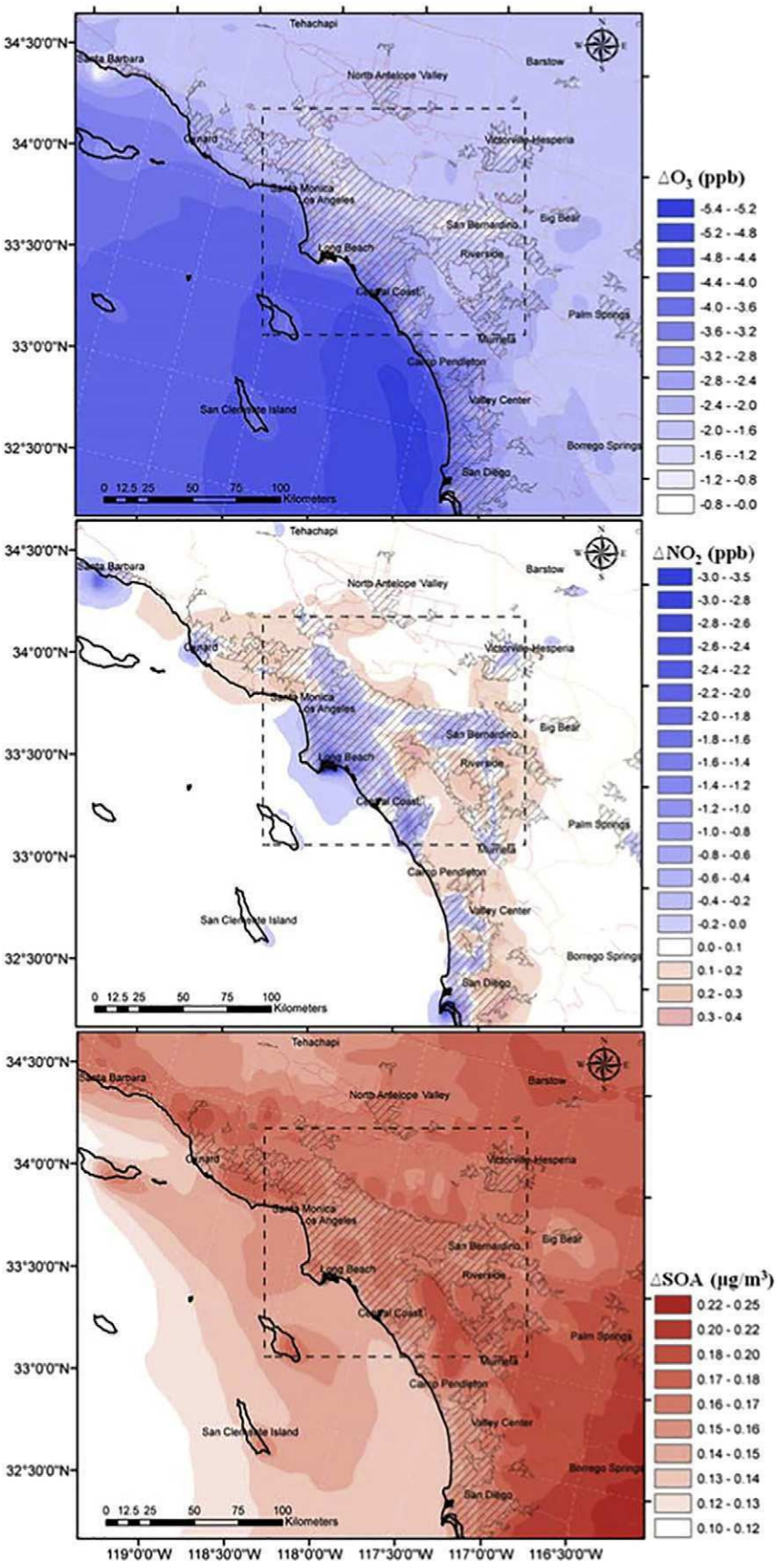

Fig. 5. Average monthly variations (absolute values) in predicted surface O_3, NO_2 and SOA concentrations for September 2006 due to natural marine emissions (halogen/DMS model run – Baseline scenario).

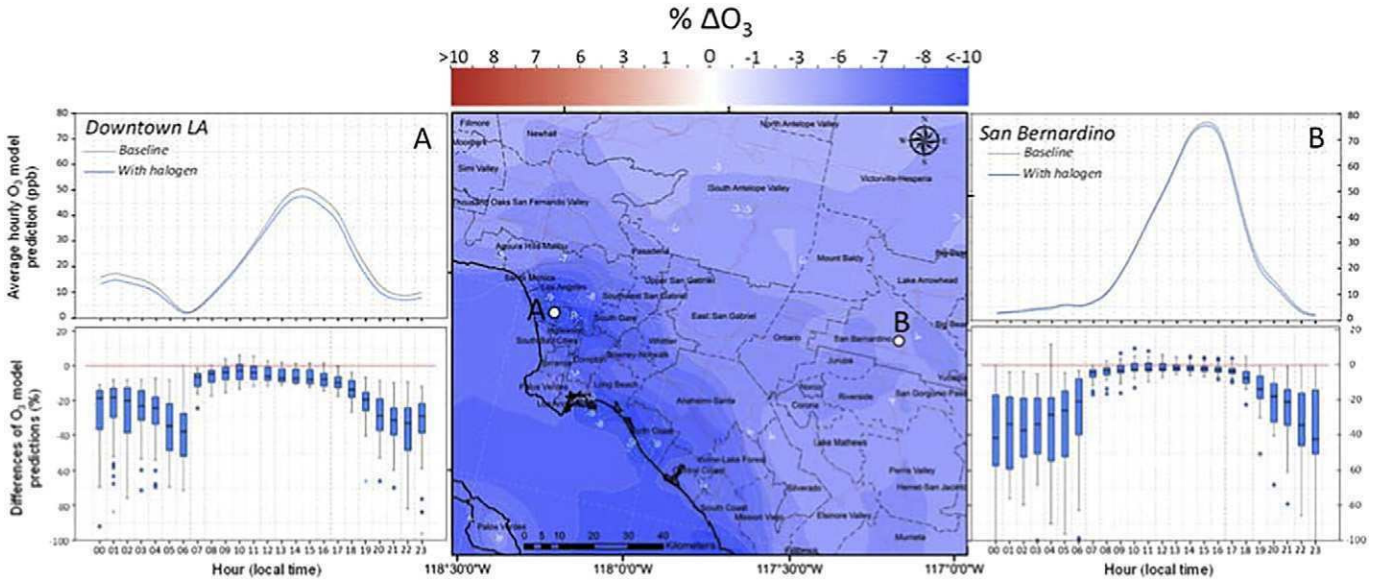

Fig. 6. Detail of surface ozone variations (Case B – Baseline) in Los Angeles urban area (contained by dotted square in Fig. 1). Left and right panels show the average daily concentration pattern during the period simulated (Sept. 2006) in downtown Los Angeles (A) and San Bernardino (B).

relative to the baseline scenario are small, less than 5% as an average). Conversely, small variations during the low ozone concentration period (nighttime and early morning) result in large relative reductions, 30% and 40% as an average over downtown Los Angeles and San Bernardino, respectively. These variations however show a considerable spread pointing out that ozone destruction is affected by local factors such as meteorological conditions and variations on emission patterns.

It is well known that the inclusion of chlorine in air quality models leads to the generation of ozone in urban areas through the heterogeneous production and subsequent photolysis of nitryl chloride (Sarwar et al., 2012). We therefore ran a sensitivity simulation with the heterogeneous production of nitryl chloride and gas phase chlorine only. In agreement with previous studies (Sarwar et al., 2014), our simulation indicates that chlorine chemistry alone increases monthly mean ozone concentrations by approximately 1–2 ppbv in the city of Los Angeles. However, the results from the Case B simulation, where full halogen chemistry is considered, shows that the net effect is the destruction of ozone dominated by iodine and bromine chemistry, which prevails over the ozone production by chlorine. Ozone is depleted directly with catalytic cycles involving the self-reactions of XO radicals (where X = Br, I) as rate determining (reactions 1–5). Indirect reduction in ozone also occurs as halogens decrease the HO_2/OH ratio (reactions 4–5) (Saiz-Lopez and von Glasow, 2012) (Fig. 7, Tables S1–S3):

$$X + O_3 \rightarrow XO + O_2 \quad (1)$$

$$XO + XO \rightarrow 2X + O_2 \quad (2)$$

$$XO + IO \rightarrow X + OIO \quad (3)$$

$$XO + HO_2 \rightarrow HOX + O_2 \quad (4)$$

$$HOX + h\nu \rightarrow OH + X \quad (5)$$

Baseline and Case B model predictions are compared to observed data retrieved from the Environmental Protection Agency (EPA) Air Quality System (AQS) database. For this, we use measurements from 8 representative sites located in Los Angeles (Table 1). This comparison indicates

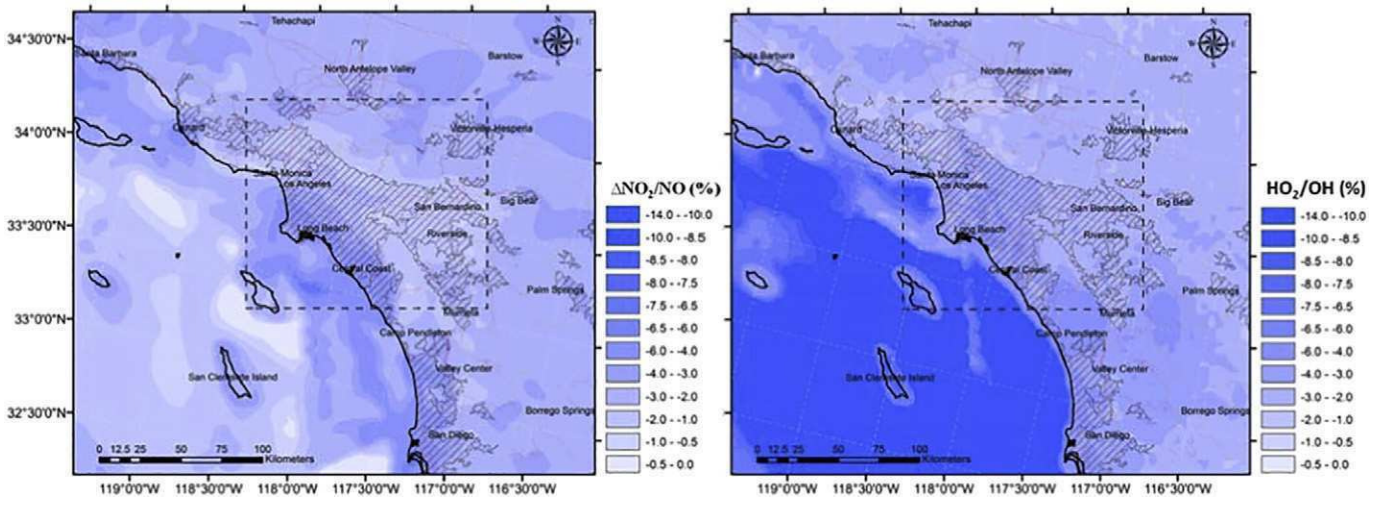

Fig. 7. NO_2/NO and HO_2/OH modeled daytime ratio changes between Case B (full halogen and DMS chemistry) and Baseline simulations.

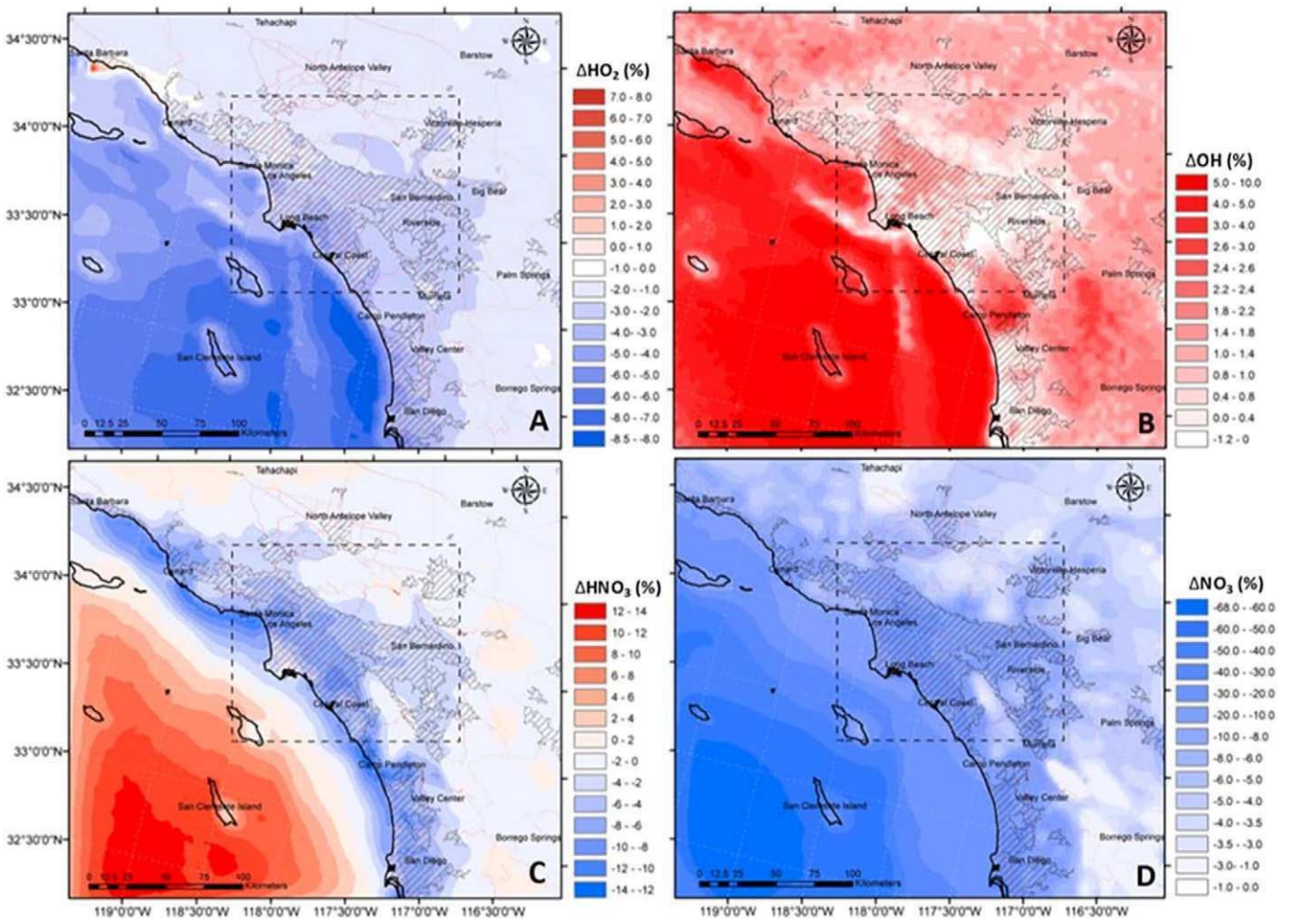

Fig. 8. Daytime concentration change between full-halogen and baseline simulation (%) in HO_2 (A), OH (B), monthly variation of HNO_3 (C) and nighttime concentration change for NO_3 (D).

that in general our Baseline CMAQ simulation overpredicted the monthly average ozone concentrations by 3–10 ppbv across the city of Los Angeles during September 2006 (Fig. 3). The monthly mean ozone concentration predictions from the Baseline simulation have a normalized mean bias of 13.5%, a normalized mean error of 15.8% and a correlation coefficient of 0.79. Case B simulation (full halogen) improves model performance by reducing ozone concentrations around 2–5 ppbv at most sites. The simulation with halogens clearly improves statistics relative to the Baseline simulation, producing a normalized mean bias of 4.9%, normalized mean error of 11.7% and correlation coefficient of 0.81.

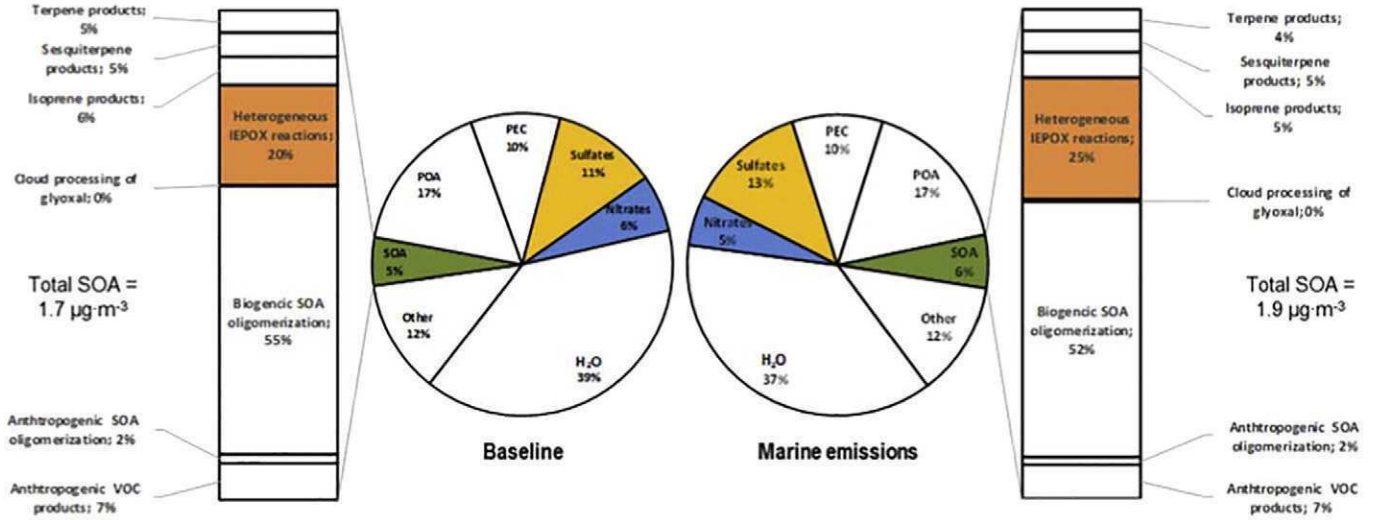

Fig. 9. Composition of $PM_{2.5}$ in downtown Los Angeles according to the baseline scenario and the incorporation of DMS and halogen chemistry (Marine emissions): PEC – Primary elemental carbon, POA – Primary organic aerosol, SOA – Secondary organic aerosol. Average monthly concentrations are 33.7 $\mu g \cdot m^{-3}$ and 33.1 $\mu g \cdot m^{-3}$ respectively.

In coastal urban areas, halogen chemistry reactions involving criteria pollutants such as NO_2 can also be important for air quality. Fig. 5 shows a reduction of up to 2.5 ppbv (5%) in the monthly mean NO_2 concentrations over the city of Los Angeles when halogen chemistry is implemented. By contrast, the monthly mean NO concentration is increased around 1–2 ppbv (5–10%). This decrease in the NO_2/NO ratio (Fig. 7) is driven by the halogen-catalyzed reduction in ozone levels which in turn reduces the efficiency of the reaction $O_3 + NO$ to yield NO_2.

3.2. Effect on NO_3 and HNO_3

Our results show that the combined inclusion of marine halogens and DMS can also exert an impact on the modeled levels of the main urban atmospheric oxidants, HO_x and nitrate (NO_3) radicals. We find that the main nocturnal oxidant, NO_3, formed by the reaction of $O_3 + NO_2$, decreases by 20–50% (2–4 pptv) in Los Angeles (Fig. 8). The reduction of NO_3 in Case B is driven by *i*) direct reaction with DMS, which represents a major sink for marine and coastal NO_3 (Andreae et al., 1985) and *ii*) indirectly due to the reduction of O_3 and NO_2 in the presence of halogens. This decreased oxidation capacity in the nocturnal atmosphere of Los Angeles has important air quality implications since NO_3-mediated oxidation of VOCs proceeds to form organic aerosol. The diurnal OH mean concentration is minimally altered (increase of 1–2%) by halogen chemistry; however, the levels of HO_2 are reduced by about 4% (Fig. 8) through reactions 4–5, leading to an overall decrease in the levels of HO_x radicals over Los Angeles. The other important pollutant affected by the inclusion of halogens is nitric acid (HNO_3), which forms through daytime reaction of $OH + NO_2$, and nighttime heterogeneous hydrolysis of N_2O_5. Monthly mean HNO_3 concentration (Fig. 8) over the city decreases 6–10%, due to the halogen-driven reduction in NO_2 and subsequently N_2O_5. However, HNO_3 concentration is increased over the ocean due to the increase in OH and NO_2 levels in that region. All this highlights that marine natural halogens have the potential to significantly impact the oxidative capacity of the urban atmosphere of coastal megacities.

3.3. Effect on aerosol composition

Fig. 9 shows that the implementation of ocean emissions of halogen and DMS in the model has a non-negligible impact on aerosol total mass and composition over the Los Angeles area. For instance, in downtown Los Angeles, the composition of secondary inorganic aerosols is modified, showing an increment of aerosol sulfate mass around 10%, mainly due to a oxidation of DMS, and a decrease of aerosol nitrates of 14%. While the increase of the sulfates is quite consistent throughout the area modeled, the influence of marine emissions on nitrate levels, associated with the reduction in the concentrations of HNO_3, decreases inland to a modeled aerosol nitrate reduction of 7% at San Bernardino. The increase in the sulfate fraction is driven by the oxidation of DMS, the most important oceanic gaseous precursor for sulfate aerosol over the ocean. The combined chemistry of NO_3, OH and BrO oxidants increases the oxidation of DMS and consequently the total sulfate fraction in the Case B simulation. The resulting effect is an increase in the aerosol acidity which has important atmospheric implications for secondary aerosol formation. According to our simulations, the concentration of hydronium ion (H_3O^+), used for the computation of acid-catalyzed uptake of isoprene epoxydiols (IEPOX) onto aqueous aerosol, is increased by 15–30% in the Los Angeles area.

We now turn to the effect of marine emissions of DMS and halogens in the formation of additional aerosol mass from secondary organic aerosol (SOA). SOA forms when VOCs, mainly isoprene, react with oxidants such as ozone, NO_3 and HO_x radicals, to form low-volatility compounds that can partition to the aerosol phase (Ortega et al., 2016). Surprisingly, even though the concentration of ozone, NO_3 and HO_x is lower (Fig. 8), Fig. 4 shows an increment over the modelling domain between 0.12 and 0.22 $\mu g/m^3$ (10%) of monthly mean SOA concentration when DMS and halogens are considered. Over Los Angeles, the increase ranges from 10% (Downtown) to 8% in the surrounding areas such as San Bernardino. According to our simulation, aged isoprene-derived compounds constitute the predominant fraction of SOA which is consistent with previous studies in this area (Hayes et al., 2015; Hayes et al., 2013). We estimate an increase of oligomerization reactions of biogenic species although the largest difference in modeled SOA in Case B is due to a larger production of IEPOX from isoprene peroxy radicals (RO_2) related to aerosol-phase aqueous processes. We find that the inclusion of DMS and halogen chemistry results in an increase in aerosol acidity due to DMS oxidation by NO_3, OH and BrO leading to more sulfate formation. The BrO impact on DMS oxidation is comparable to that of NO_3, but less than OH, and is particularly large over the ocean and much less inland. Aerosol acidity has been shown to increase substantially the SOA mass yields from isoprene (Pye et al., 2013; Surratt et al., 2010; Surratt et al., 2007). Therefore, DMS-mediated increase in aerosol sulfate represents a pathway for enhanced SOA formation that may help to some extent with the discrepancy, at least over coastal megacities, between observed and predicted SOA that indicates there is still a significant amount of "missing urban SOA" currently not included in atmospheric models (Pye et al., 2013; de Gouw et al., 2005; Heald et al., 2005; Volkamer et al., 2006; Woody et al., 2016).

4. Summary and conclusions

We have conducted model simulations to explore for the first time at city-scale resolution the effect of halogens and DMS on the air quality of a coastal megacity. The results indicate that natural halogenated and sulfur species emitted from the ocean have a non-negligible impact on the air quality of the megacity of Los Angeles. This includes changes in the concentration of some of the main criteria pollutants and in the composition and mass of fine particles. We therefore suggest that air quality in coastal cities is sensitive to this marine atmospheric chemistry, therefore this chemistry should be included in regional air quality models to accurately reproduce the O_3, NO_x and particulate matter levels measured by air quality monitoring networks. In-depth diagnostic evaluation of model performance involving observation of relevant species is needed to establish more precisely the role of marine trace gases on urban atmospheres and to review the corresponding gas-phase chemistry as well as formation pathways of secondary aerosols. Additional observations and modelling studies are also needed to understand the overall influence of marine halogen/DMS emissions on air pollution in other coastal megacities around the world.

Disclaimer

The views expressed in this article are those of the author[*s*] and do not necessarily represent the views or policies of the U.S. Environmental Protection Agency.

Acknowledgments

This work was supported by the Consejo Superior de Investigaciones Científicas (CSIC).

Appendix A. Supplementary data

Supplementary data to this article can be found online at http://dx.doi.org/10.1016/j.scitotenv.2017.06.098.

References

Andreae, M.O., Ferek, R.J., Bermond, F., Byrd, K.P., Engstrom, R.T., Hardin, S., et al., 1985. Dimethyl sulfide in the marine atmosphere. J. Geophys. Res. Atmos. 90, 12891–12900.
Appel, K.W., Gilliland, A.B., Sarwar, G., Gilliam, R.C., 2007. Evaluation of the community multiscale air quality (CMAQ) model version 4.5: sensitivities impacting model performance: part I—ozone. Atmos. Environ. 41, 9603–9615.

Appel, K.W., Bhave, P.V., Gilliland, A.B., Sarwar, G., Roselle, S.J., 2008. Evaluation of the community multiscale air quality (CMAQ) model version 4.5: sensitivities impacting model performance; part II—particulate matter. Atmos. Environ. 42, 6057–6066.

Appel, K.W., Pouliot, G.A., Simon, H., Sarwar, G., Pye, H.O.T., Napelenok, S.L., et al., 2013. Evaluation of dust and trace metal estimates from the community multiscale air quality (CMAQ) model version 5.0. Geosci. Model Dev. 6, 883–899.

Appel, K.W., Napelenok, S.L., Foley, K.M., Pye, H.O.T., Hogrefe, C., Luecken, D.J., et al., 2017. Description and evaluation of the community multiscale air quality (CMAQ) modeling system version 5.1. Geosci. Model Dev. 10, 1703–1732.

Boucher, O., Moulin, C., Belviso, S., Aumont, O., Bopp, L., Cosme, E., et al., 2003. DMS atmospheric concentrations and sulphate aerosol indirect radiative forcing: a sensitivity study to the DMS source representation and oxidation. Atmos. Chem. Phys. 3, 49–65.

Breider, T.J., Chipperfield, M.P., Richards, N.A.D., Carslaw, K.S., Mann, G.W., Spracklen, D.V., 2010. Impact of BrO on dimethylsulfide in the remote marine boundary layer. Geophys. Res. Lett. 37 (n/a-n/a).

Chan, K.L., Wang, S., Liu, C., Zhou, B., Wenig, M.O., Saiz-Lopez, A., 2017. On the summertime air quality and related photochemical processes in the megacity Shanghai, China. Sci. Total Environ. 580, 974–983.

Delamater, P.L., Finley, A.O., Banerjee, S., 2012. An analysis of asthma hospitalizations, air pollution, and weather conditions in Los Angeles County, California. Sci. Total Environ. 425, 110–118.

Fernandez, R.P., Kinnison, D.E., Lamarque, J.F., Tilmes, S., Saiz-Lopez, A., 2017. Impact of biogenic very short-lived bromine on the Antarctic ozone hole during the 21st century. Atmos. Chem. Phys. 17, 1673–1688.

Finley, B.D., Saltzman, E.S., 2008. Observations of Cl_2, Br_2, and I_2 in coastal marine air. J. Geophys. Res. Atmos. 113 (n/a-n/a).

Foley, K.M., Roselle, S.J., Appel, K.W., Bhave, P.V., Pleim, J.E., Otte, T.L., et al., 2010. Incremental testing of the community multiscale air quality (CMAQ) modeling system version 4.7. Geosci. Model Dev. 3, 205–226.

Fujita, E.M., Campbell, D.E., Stockwell, W.R., Lawson, D.R., 2013. Past and future ozone trends in California's South Coast Air Basin: reconciliation of ambient measurements with past and projected emission inventories. J. Air Waste Manage. Assoc. 63, 54–69.

Gantt, B., Sarwar, G., Xing, J., Simon, H., Schwede, D., Hutzell, W.T., et al., 2017. The impact of iodide-mediated ozone deposition and halogen chemistry on surface ozone concentrations across the continental United States. Environ. Sci. Technol. 51, 1458–1466.

de Gouw, J.A., Middlebrook, A.M., Warneke, C., Goldan, P.D., Kuster, W.C., Roberts, J.M., et al., 2005. Budget of organic carbon in a polluted atmosphere: results from the New England air quality study in 2002. J. Geophys. Res. Atmos. 110 (n/a-n/a).

Han, Z., Sakurai, T., Ueda, H., Carmichael, G.R., Streets, D., Hayami, H., et al., 2008. MICS-Asia II: model intercomparison and evaluation of ozone and relevant species. Atmos. Environ. 42, 3491–3509.

Hayes, P.L., Ortega, A.M., Cubison, M.J., Froyd, K.D., Zhao, Y., Cliff, S.S., et al., 2013. Organic aerosol composition and sources in Pasadena, California, during the 2010 CalNex campaign. J. Geophys. Res. Atmos. 118, 9233–9257.

Hayes, P.L., Carlton, A.G., Baker, K.R., Ahmadov, R., Washenfelder, R.A., Alvarez, S., et al., 2015. Modeling the formation and aging of secondary organic aerosols in Los Angeles during CalNex 2010. Atmos. Chem. Phys. 15, 5773–5801.

Haywood, J., Boucher, O., 2000. Estimates of the direct and indirect radiative forcing due to tropospheric aerosols: a review. Rev. Geophys. 38, 513–543.

Heald, C.L., Jacob, D.J., Park, R.J., Russell, L.M., Huebert, B.J., Seinfeld, J.H., et al., 2005. A large organic aerosol source in the free troposphere missing from current models. Geophys. Res. Lett. 32 (n/a-n/a).

Hogrefe, C., Pouliot, G., Wong, D., Torian, A., Roselle, S., Pleim, J., et al., 2015. Annual application and evaluation of the online coupled WRF–CMAQ system over North America under AQMEII phase 2. Atmos. Environ. 115, 683–694.

Hossaini, R., Chipperfield, M.P., Montzka, S.A., Rap, A., Dhomse, S., Feng, W., 2015. Efficiency of short-lived halogens at influencing climate through depletion of stratospheric ozone. Nat. Geosci. 8, 186–190.

Hossaini, R., Chipperfield, M.P., Saiz-Lopez, A., Fernandez, R., Monks, S., Feng, W., et al., 2016. A global model of tropospheric chlorine chemistry: organic versus inorganic sources and impact on methane oxidation. J. Geophys. Res. Atmos. 121, 14,271–14,297.

Houyoux, M.R., Vukovich, J.M., Coats, C.J., Wheeler, N.J.M., Kasibhatla, P.S., 2000. Emission inventory development and processing for the seasonal model for regional air quality (SMRAQ) project. J. Geophys. Res. Atmos. 105, 9079–9090.

Kim, S.W., McDonald, B.C., Baidar, S., Brown, S.S., Dube, B., Ferrare, R.A., et al., 2016. Modeling the weekly cycle of NO_x and CO emissions and their impacts on O_3 in the Los Angeles-South Coast Air Basin during the CalNex 2010 field campaign. J. Geophys. Res. Atmos. 121, 1340–1360.

Lana, A., Bell, T.G., Simó, R., Vallina, S.M., Ballabrera-Poy, J., Kettle, A.J., et al., 2011. An updated climatology of surface dimethlysulfide concentrations and emission fluxes in the global ocean. Glob. Biogeochem. Cycles 25 (n/a-n/a).

Mahajan, A.S., Oetjen, H., Saiz-Lopez, A., Lee, J.D., McFiggans, G.B., Plane, J.M.C., 2009. Reactive iodine species in a semi-polluted environment. Geophys. Res. Lett. 36 (n/a-n/a).

Mielke, L.H., Stutz, J., Tsai, C., Hurlock, S.C., Roberts, J.M., Veres, P.R., et al., 2013. Heterogeneous formation of nitryl chloride and its role as a nocturnal NOx reservoir species during CalNex-LA 2010. J. Geophys. Res. Atmos. 118, 10,638–10,652.

Neuman, J.A., Trainer, M., Aikin, K.C., Angevine, W.M., Brioude, J., Brown, S.S., et al., 2012. Observations of ozone transport from the free troposphere to the Los Angeles basin. J. Geophys. Res. Atmos. 117 (n/a-n/a).

Oman, L.D., Douglass, A.R., Salawitch, R.J., Canty, T.P., Ziemke, J.R., Manyin, M., 2016. The effect of representing bromine from VSLS on the simulation and evolution of Antarctic ozone. Geophys. Res. Lett. 43, 9869–9876.

Ortega, A.M., Hayes, P.L., Peng, Z., Palm, B.B., Hu, W., Day, D.A., et al., 2016. Real-time measurements of secondary organic aerosol formation and aging from ambient air in an oxidation flow reactor in the Los Angeles area. Atmos. Chem. Phys. 16, 7411–7433.

Osthoff, H.D., Roberts, J.M., Ravishankara, A.R., Williams, E.J., Lerner, B.M., Sommariva, R., et al., 2008. High levels of nitryl chloride in the polluted subtropical marine boundary layer. Nat. Geosci. 1, 324–328.

Pollack, I.B., Ryerson, T.B., Trainer, M., Neuman, J.A., Roberts, J.M., Parrish, D.D., 2013. Trends in ozone, its precursors, and related secondary oxidation products in Los Angeles, California: a synthesis of measurements from 1960 to 2010. J. Geophys. Res. Atmos. 118, 5893–5911.

Pye, H.O.T., Pinder, R.W., Piletic, I.R., Xie, Y., Capps, S.L., Lin, Y.-H., et al., 2013. Epoxide pathways improve model predictions of isoprene markers and reveal key role of acidity in aerosol formation. Environ. Sci. Technol. 47, 11056–11064.

Reidmiller, D.R., Fiore, A.M., Jaffe, D.A., Bergmann, D., Cuvelier, C., Dentener, F.J., et al., 2009. The influence of foreign vs. North American emissions on surface ozone in the US. Atmos. Chem. Phys. 9, 5027–5042.

Riedel, T.P., Bertram, T.H., Crisp, T.A., Williams, E.J., Lerner, B.M., Vlasenko, A., et al., 2012. Nitryl chloride and molecular chlorine in the coastal marine boundary layer. Environ. Sci. Technol. 46, 10463–10470.

Saiz-Lopez, A., von Glasow, R., 2012. Reactive halogen chemistry in the troposphere. Chem. Soc. Rev. 41, 6448–6472.

Saiz-Lopez, A., Lamarque, J.F., Kinnison, D.E., Tilmes, S., Ordóñez, C., Orlando, J.J., et al., 2012a. Estimating the climate significance of halogen-driven ozone loss in the tropical marine troposphere. Atmos. Chem. Phys. 12, 3939–3949.

Saiz-Lopez, A., Plane, J.M.C., Baker, A.R., Carpenter, L.J., von Glasow, R., Gómez Martín, J.C., et al., 2012b. Atmospheric chemistry of iodine. Chem. Rev. 112, 1773–1804.

Sarwar, G., Simon, H., Bhave, P., Yarwood, G., 2012. Examining the impact of heterogeneous nitryl chloride production on air quality across the United States. Atmos. Chem. Phys. 12, 6455–6473.

Sarwar, G., Simon, H., Xing, J., Mathur, R., 2014. Importance of tropospheric ClNO2 chemistry across the Northern Hemisphere. Geophys. Res. Lett. 41, 4050–4058.

Sarwar, G., Gantt, B., Schwede, D., Foley, K., Mathur, R., Saiz-Lopez, A., 2015. Impact of enhanced ozone deposition and halogen chemistry on tropospheric ozone over the northern Hemisphere. Environ. Sci. Technol. 49, 9203–9211.

Schwede, D., Pouliot, G., Pierce, T., 26–28 September 2005. Paper presented at 4th Annual CMAS Models-3 Users' Conference "Changes to the biogenic emissions inventory system version 3 (BEIS3)", 4th Annual CMAS Models-3 Users' Conference, 464 UNC-Chapel Hill, NC. available at: https://www.cmascenter.org/conference/2005/abstracts/2_7.pdf.

Sherwen, T., Schmidt, J.A., Evans, M.J., Carpenter, L.J., Großmann, K., Eastham, S.D., et al., 2016. Global impacts of tropospheric halogens (cl, Br, I) on oxidants and composition in GEOS-Chem. Atmos. Chem. Phys. 16, 12239–12271.

Simpson, W.R., Brown, S.S., Saiz-Lopez, A., Thornton, J.A., RV, Glasow, 2015. Tropospheric halogen chemistry: sources, cycling, and impacts. Chem. Rev. 115, 4035–4062.

Skamarock, W.C., 2008. A Description of the Advanced Research WRF Version 3. Tech. Rep. NCAR/TN-475 + STRNational Center for Atmospheric Research, Cambridge, MA.

Stefels, J., Steinke, M., Turner, S., Malin, G., Belviso, S., 2007. Environmental constraints on the production and removal of the climatically active gas dimethylsulphide (DMS) and implications for ecosystem modelling. Biogeochemistry 83, 245–275.

Surratt, J.D., Kroll, J.H., Kleindienst, T.E., Edney, E.O., Claeys, M., Sorooshian, A., et al., 2007. Evidence for Organosulfates in secondary organic aerosol. Environ. Sci. Technol. 41, 517–527.

Surratt, J.D., Chan, A.W.H., Eddingsaas, N.C., Chan, M., Loza, C.L., Kwan, A.J., et al., 2010. Reactive intermediates revealed in secondary organic aerosol formation from isoprene. Proc. Natl. Acad. Sci. 107, 6640–6645.

Tham, Y.J., Wang, Z., Li, Q., Yun, H., Wang, W., Wang, X., et al., 2016. Significant concentrations of nitryl chloride sustained in the morning: investigations of the causes and impacts on ozone production in a polluted region of northern China. Atmos. Chem. Phys. 16, 14959–14977.

Volkamer, R., Jimenez, J.L., San Martini, F., Dzepina, K., Zhang, Q., Salcedo, D., et al., 2006. Secondary organic aerosol formation from anthropogenic air pollution: Rapid and higher than expected. Geophys. Res. Lett. 33 (n/a-n/a).

Whitten, G.Z., Heo, G., Kimura, Y., McDonald-Buller, E., Allen, D.T., Carter, W.P.L., et al., 2010. A new condensed toluene mechanism for carbon bond: CB05-TU. Atmos. Environ. 44, 5346–5355.

Woody, M.C., Baker, K.R., Hayes, P.L., Jimenez, J.L., Koo, B., Pye, H.O.T., 2016. Understanding sources of organic aerosol during CalNex-2010 using the CMAQ-VBS. Atmos. Chem. Phys. 16, 4081–4100.

Xing, J., Mathur, R., Pleim, J., Hogrefe, C., Gan, C.M., Wong, D.C., et al., 2015. Observations and modeling of air quality trends over 1990–2010 across the northern Hemisphere: China, the United States and Europe. Atmos. Chem. Phys. 15, 2723–2747.

Atmos. Chem. Phys., 19, 15321–15337, 2019
https://doi.org/10.5194/acp-19-15321-2019
© Author(s) 2019. This work is distributed under
the Creative Commons Attribution 4.0 License.

Atmospheric Chemistry and Physics
Open Access
EGU

Impact of halogen chemistry on summertime air quality in coastal and continental Europe: application of the CMAQ model and implications for regulation

Qinyi Li[1], Rafael Borge[2], Golam Sarwar[3], David de la Paz[2], Brett Gantt[4], Jessica Domingo[2], Carlos A. Cuevas[1], and Alfonso Saiz-Lopez[1]

[1]Department of Atmospheric Chemistry and Climate, Institute of Physical Chemistry Rocasolano, CSIC, Madrid 28006, Spain
[2]Environmental Modelling Laboratory, Department of Chemical & Environmental Engineering, Universidad Politécnica de Madrid (UPM), Madrid, Spain
[3]National Exposure Research Laboratory, Environmental Protection Agency, Research Triangle Park, NC 27711, USA
[4]Office of Air Quality Planning and Standards, Environmental Protection Agency, Research Triangle Park, NC 27711, USA

Correspondence: Alfonso Saiz-Lopez (a.saiz@csic.es)

Received: 19 February 2019 – Discussion started: 23 April 2019
Revised: 21 October 2019 – Accepted: 28 October 2019 – Published: 16 December 2019

Abstract. Halogen (Cl, Br, and I) chemistry has been reported to influence the formation of secondary air pollutants. Previous studies mostly focused on the impact of chlorine species on air quality over large spatial scales. Very little attention has been paid to the effect of the combined halogen chemistry on air quality over Europe and its implications for control policy. In the present study, we apply a widely used regional model, the Community Multiscale Air Quality Modeling System (CMAQ), incorporated with the latest halogen sources and chemistry, to simulate the abundance of halogen species over Europe and to examine the role of halogens in the formation of secondary air pollution. The results suggest that the CMAQ model is able to reproduce the level of O_3, NO_2, and halogen species over Europe. Chlorine chemistry slightly increases the levels of OH, HO_2, NO_3, O_3, and NO_2 and substantially enhances the level of the Cl radical. Combined halogen chemistry induces complex effects on OH (ranging from -0.023 to 0.030 pptv) and HO_2 (in the range of -3.7 to 0.73 pptv), significantly reduces the concentrations of NO_3 (as much as 20 pptv) and O_3 (as much as 10 ppbv), and decreases NO_2 in highly polluted regions (as much as 1.7 ppbv); it increases NO_2 (up to 0.20 ppbv) in other areas. The maximum effects of halogen chemistry occur over oceanic and coastal regions, but some noticeable impacts also occur over continental Europe. Halogen chemistry affects the number of days exceeding the European Union target threshold for the protection of human beings and vegetation from ambient O_3. In light of the significant impact of halogen chemistry on air quality, we recommend that halogen chemistry be considered for inclusion in air quality policy assessments, particularly in coastal cities.

1 Introduction

Halogen (Cl, Br, and I) species and related processes have been known to deplete stratospheric ozone (O_3) for several decades (Molina and Rowland, 1974; Farman et al., 1985). In the troposphere, the chemistry of halogens has been described in detail in recent reviews and references therein (Saiz-Lopez and von Glasow, 2012; Simpson et al., 2015), so it is just briefly outlined here. Halogen species affect the concentration of air pollutants by, e.g., directly destroying O_3 (Reaction R1), indirectly decreasing O_3 production by reducing NO_2 (Reactions R2 and R3), and influencing the NO/NO_2 ratio (Reactions R2 and R4) and the HO_2/OH ratio (Reactions R5 and R6). The budgets of NO_x ($NO + NO_2$) and HO_x ($OH + HO_2$) also affect the formation of O_3 (e.g., Sillman, 1999; Li et al., 2018).

$$X\,(Cl, Br, I) + O_3 \rightarrow XO + O_2 \qquad (R1)$$

$$XO + NO_2 \rightarrow XONO_2 \quad \text{(R2)}$$

$$XONO_2 + H_2O(l) \rightarrow HOX + HNO_3(l) \quad \text{(R3)}$$

$$XO + NO \rightarrow X + NO_2 \quad \text{(R4)}$$

$$XO + HO_2 \rightarrow HOX + O_2 \quad \text{(R5)}$$

$$HOX + h\nu \rightarrow OH + X \quad \text{(R6)}$$

The chlorine radical (Cl) initiates the oxidation of hydrocarbons (Reaction R7), including methane (CH_4) and non-methane volatile organic compounds (NMVOCs), in a similar way to the OH radical, reducing the lifetime of CH_4 and NMVOCs and leading to the formation of O_3 in the presence of NO_x (Thornton et al., 2010).

$$RH + Cl \rightarrow HCl + RO_2 \quad \text{(R7)}$$

The combined effect of halogen chemistry on air quality is therefore complicated and depends heavily on local conditions, e.g., atmospheric compositions and oxidative capacity (Sherwen et al., 2017; Muñiz-Unamunzaga et al., 2018). Evaluation of the complex role of halogen chemistry in air quality requires the employment of advanced, high-resolution chemical transport models.

A number of modeling studies have been conducted to investigate the impact of individual halogen species on air quality. The chemistry of chlorine, mainly that of nitryl chloride ($ClNO_2$), has been reported to increase the oxidation capacity and the formation of O_3 in recent studies (Sarwar et al., 2012, 2014; Li et al., 2016; Sherwen et al., 2017; Sommariva et al., 2018). Bromine (Fernandez et al., 2014) and iodine (Saiz-Lopez et al., 2014) chemistry are reported to decrease the concentration of O_3 over oceanic and terrestrial regions.

Only a few regional modeling studies have explored the combined influence of halogen chemistry on air quality. The first modeling study with combined halogen (Cl, Br, and I) chemistry was conducted by Sarwar et al. (2015), who used a hemispheric version of the Community Multiscale Air Quality (CMAQ) model (Byun and Ching, 1999; Byun and Schere, 2006; Mathur et al., 2017) and reported a decrease in surface O_3 by $\sim 15\,\%$ to $\sim 48\,\%$ over the Northern Hemisphere by Br and I. Gantt et al. (2017) then utilized the CMAQ model to explore the role of halogen chemistry at a regional scale over the continental United States (US). While these studies focused on the Northern Hemisphere and the continental US, Muñiz-Unamunzaga et al. (2018) applied the full halogen chemistry version of CMAQ with a resolution of 4 km and reported an up to 5 ppbv decrease in O_3 in the city of Los Angeles, California, US. Sherwen et al. (2017) used a global model, GEOS-Chem, in a regional configuration (with a grid size of $0.25^\circ \times 0.315^\circ$, $\sim 25\,\text{km} \times \sim 25\,\text{km}$) and predicted a large decrease in O_3, on average 13.5 pptv (25 %) and as much as 28.9 pptv (45 %), in Europe. Sarwar et al. (2019) further updated the halogen chemistry in the CMAQ model and reported a reduction of 3 to 12 ppbv in annual average O_3 over seawater, 3 to 6 ppbv over coastal areas, and 3 ppbv over inland areas by Br and I. These previous regional studies using various models (or versions of models) in different areas reported a large range of the halogen impact on O_3, highlighting the uncertainty in this research field.

The regulation of air quality and the control of air pollutants emission in Europe started in the early 1970s and over 40 years of effort has successfully improved air quality throughout Europe (EEA, 2018a). Nonetheless, poor air quality persists in major cities like Madrid, Paris, and London (EEA, 2018a); this shows the need for continued air quality management and effective policy. Because the influence of halogens on air quality is uncertain and potentially has an impact on air quality management decisions, we have conducted regional simulations using the latest version of the CMAQ model implemented with comprehensive halogen sources and chemistry (Sarwar et al., 2019) to examine the overall effect of halogen species on air pollution over Europe. Considering that the grid size has a noticeable impact on air quality model predictions (Sommariva et al., 2018), we used a CMAQ model domain with 12 km horizontal resolution (higher than the previous studies on the halogen impact covering Europe) to simulate the levels of halogen species over Europe, examine the effect on the oxidation capacity and the concentration of air pollutants, and explore the potential implications for air quality policy related to NO_2 and O_3.

2 Method and materials

2.1 Data

The meteorological inputs for the CMAQ model were obtained from the Weather Research and Forecasting model (WRF 3.7.1) (Skamarock and Klemp, 2008; Borge et al., 2008a) as an offline input. The WRF model was initialized from global reanalyses from the National Centers for Environmental Prediction (NCEP) Global Forecast System (GFS) with a spatial resolution of $1^\circ \times 1^\circ$ and a temporal resolution of 6 h (available online at http://rda.ucar.edu/datasets/ds083.2/, last access: 22 November 2019), which was updated daily from NCEP global analyses with 0.5° resolution (available online at http://www.nco.ncep.noaa.gov/pmb/products/sst/, last access: 22 November 2019). NCEP's ADP global upper-air (NCAR archive ds351.0) and global surface observations (NCAR archive ds461.0) were used to drive the simulation with a Newtonian relaxation technique in the WRF model.

Anthropogenic emissions for the year 2016 were taken from the $0.1^\circ \times 0.1^\circ$ gridded EMEP inventory (EMEP/CEIP, 2014). It should be noted that no anthropogenic chlorine sources are included in our emission inventory. The temporal profiles and vertical distribution needed to resolve the

emissions were those used in the EuroDelta experiment (van Loon et al., 2007). Biogenic emissions were estimated using the Model of Emissions of Gases and Aerosols from Nature (MEGANv2.10) (Guenther et al., 2012). All emissions were gridded to our model domain, temporally allocated, and chemically speciated using the Sparse Matrix Operator Kernel Emissions (SMOKE) model version 3.6.5 (UNC, 2015; Borge et al., 2008b).

In addition, we used measurement data on NO_2 and O_3 from over 400 background stations (traffic and industrial stations are not included) across Europe from the database AirBase (public air quality database system of the EEA, 2018a) to compare the results of our simulation with observations (Fig. 1). Among these stations, 315 are located in inland areas (208 for NO_2 and 266 for O_3), and 125 are located in coastal areas (83 for NO_2 and 93 for O_3).

2.2 Modeling system

The CMAQ model is widely used and includes comprehensive representations of many essential atmospheric processes. The skill of the model in reproducing observed air quality has been demonstrated in many previous studies (Foley et al., 2010; Appel et al., 2013, 2017; Mathur et al., 2017), including applications over Europe (Borge et al., 2008a; Appel et al., 2012; Solazzo et al., 2017). CMAQ version 5.2 (https://www.epa.gov/cmaq, last access: 22 November 2019; https://doi.org/10.5281/zenodo.1167892, US EPA ORD, 2017) containing the Carbon Bond chemical mechanism (Appel et al., 2017) with halogen chemistry was used in this study. We updated the chlorine chemistry of Sarwar et al. (2012) and implemented it in CMAQ version 5.2 (Table S1 in the Supplement). The heterogeneous hydrolysis of dinitrogen pentoxide (N_2O_5) can produce $ClNO_2$ and nitric acid (HNO_3) in the presence of particulate chloride. In the absence of particulate chloride, the heterogeneous hydrolysis of N_2O_5 produces only HNO_3. Sarwar et al. (2015) implemented the initial bromine and iodine chemistry in CMAQ, which has recently been updated by Sarwar et al. (2019). The updates include revising the gas-phase bromine and iodine reactions, incorporating several heterogeneous reactions of bromine and iodine species, incorporating several aqueous-phase bromine reactions, and revising the iodine and bromine emissions. We combine the updated chlorine, bromine, and iodine chemistry with the Carbon Bond chemical mechanism and use it in this study.

2.3 Simulation setup

A detailed description of physics and other model options (Table S2) can be found in de la Paz et al. (2016). The CMAQ model is applied over a domain covering the entirety of Europe (Fig. 1) with 12 km horizontal resolution. The vertical extent of the model extended from the surface to 100 mbar and contained 35 layers with an average surface layer thickness of approximately 20 m. The CMAQ chemical transport model is configured to use the piecewise parabolic method to describe advection processes, the Asymmetric Convective Model (version 2) to describe vertical diffusion processes, and the multiscale method to describe horizontal diffusion processes. Gas-phase chemistry, aqueous chemistry, aerosol processes, and dry and wet deposition were also included. The Rosenbrock solver was used for gas-phase chemistry.

The study was completed for the month of July 2016 with a spin-up period of 30 d. We performed three simulations to isolate the effect of halogen chemistry on air quality (in brackets is the name of the scenario used hereafter):

1. base model without halogen chemistry (BASE),
2. BASE with chlorine chemistry (CL), and
3. CL with Br and I chemistry (HAL).

The BASE model simulation includes the Carbon Bond 2015 chemical mechanism but does not contain any halogen chemistry, and only HNO_3 is produced from the heterogeneous hydrolysis of N_2O_5. The CL simulation contains the Carbon Bond chemical mechanism with chlorine chemistry and considers $ClNO_2$ and HNO_3 production from the heterogeneous uptake of N_2O_5 on the aerosol surface. The HAL simulation contains the Carbon Bond chemical mechanism with full halogen chemistry and produces $ClNO_2$ and HNO_3 from the heterogeneous uptake of N_2O_5 on the aerosol surface.

Boundary conditions for the model were derived from the hemispheric CMAQ simulations (Mathur et al., 2017). Three different annual simulations were conducted using the hemispheric CMAQ model for 2016: the first simulation used the Carbon Bond chemical mechanism without any halogen chemistry, the second simulation used the Carbon Bond chemical mechanism and the chlorine chemistry, and the third simulation used the Carbon Bond chemical mechanism and the full halogen chemistry. Results from the corresponding hemispheric CMAQ simulation were used to generate boundary conditions for the BASE, CL, and HAL simulations. Therefore, the difference between CL and BASE simulations represents the impact of the chlorine chemistry on air quality, and the difference between HAL and BASE simulations represents the effect of halogen chemistry on air quality.

3 Results and discussion

3.1 Evaluation of model performance

The performance of the CMAQ model in simulating air quality over Europe is evaluated using observation data collected from > 400 measurement stations. We separate the stations into coastal (within 24 km of the coast) and continental stations (Fig. 1). Table 1 presents the statistics of the model performance for O_3 and NO_2 for BASE and HAL simulations.

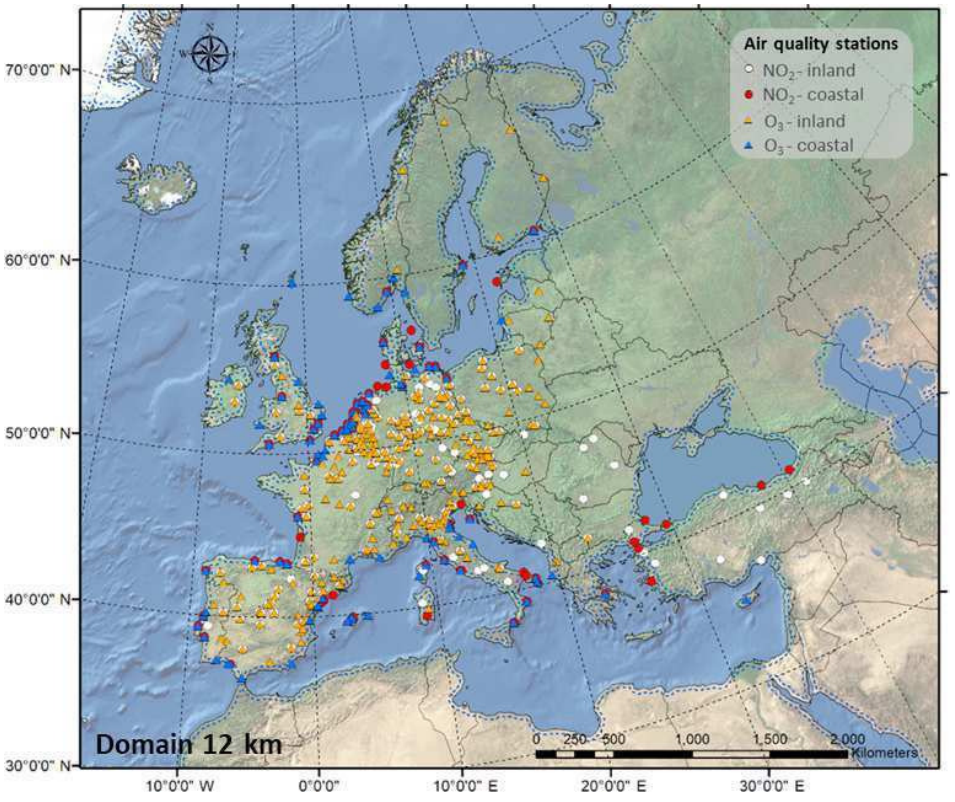

Figure 1. Geographic representation of the modeling domain and the air quality stations used for model evaluation.

The BASE and HAL simulations generally reproduce the concentration levels and the temporal variations of O_3 and NO_2 both at coastal and continental stations. The correlation coefficients between simulations and observations (Fig. S1 in the Supplement) show that CMAQ satisfactorily reproduces the variation of O_3 and NO_2 over most of Europe, especially the coastal regions (> 0.6 for O_3 and > 0.4 for NO_2). The BASE simulation underpredicts O_3 compared to observations at both coastal and continental stations (Table 1), possibly due to the uncertainty of the NMVOC emission inventory (Sherwen et al., 2017) and the underestimated NO_x (Table 1). The HAL simulation slightly improves the correlation coefficient of O_3 but decreases the average level of O_3 compared to the BASE case. Diurnal variation plots (Fig. S2) suggest that both BASE and HAL simulations can reproduce the temporal patterns of O_3.

The BASE simulation underpredicts NO_2 compared to observations at both coastal and continental stations (Table 1). Such an underestimation of NO_2 can occur for many reasons, including (1) positive artifacts of NO_2 monitors (Jung et al., 2017), (2) underestimation of NO_x in the emission inventory, and (3) rapid transformation of NO_2 into HNO_3 in the model compared to the real atmosphere. Model performance is reasonable as the NO_2 underestimation is relatively small. The HAL case predicted very similar NO_2 concentrations (Table 1).

Overall, the evaluation of CMAQ results over Europe demonstrates that the model is capable of reproducing the levels of atmospheric chemical species and can be used to investigate the impact of halogen chemistry on air quality over Europe. It also suggests that the incorporation of halogen chemistry changes the model performance for O_3 concentrations by a small margin without a noticeable impact on the model performance for NO_2.

3.2 Simulated halogen species

Average surface concentrations of the inorganic halogen species predicted in the HAL simulation over the ocean are summarized in Table 2. HCl is the dominant chlorine species, with an average level of 247.9 pptv representing over 96 % of the total inorganic chlorine (Cl_y), while the average $ClNO_2$ and HOCl is 4.9 pptv (1.9 %) and 3.8 pptv (1.5 %), respectively, with the remaining species contributing less than 1 %. The Br_y species are relatively evenly partitioned, with HOBr (1.06 pptv, 27.0 %), BrCl (0.71 pptv, 18.2 %), $BrNO_3$ (0.67 pptv, 16.9 %), HBr (0.66 pptv, 16.8 %), and Br_2 (0.33 pptv, 8.4 %) being the abundant species, while the remaining species contribute < 5 %. HOI (5.1 pptv, 52.0 %), INO_3 (2.8 pptv, 28.7 %), and IO (1.0 pptv, 10.3 %) contribute over 90 % of I_y over the ocean, while the remaining species contribute ~ 10 %. The predicted average concentrations of

Table 1. Statistical summary of model performance.

Statistics	O_3 ($\mu g\,m^{-3}$)				NO_2 ($\mu g\,m^{-3}$)			
	Coastal		Inland		Coastal		Inland	
	Base	HAL	Base	HAL	Base	HAL	Base	HAL
MB	−0.9	−6.8	−2.3	−6.6	−3.7	−3.7	−3.1	−3.1
ME	16.9	17.5	19.7	20.2	5.8	5.8	5.7	5.6
RMSE	22.6	23.1	25.8	26.4	7.7	7.7	7.2	7.2
r	0.65	0.67	0.60	0.61	0.44	0.44	0.42	0.42
IOA	0.64	0.62	0.62	0.61	0.31	0.31	0.18	0.19

MB: mean bias, RMSE: root mean square error, r: correlation coefficient, IOA: index of agreement.

the critical halogen radicals, Cl, BrO, and IO, are 2.0×10^{-4}, 0.03, and 0.4 pptv, respectively, over the ocean in Europe.

The spatial distributions of key halogen species are shown in Fig. 2. The HAL simulation with full halogen chemistry simulates generally higher $ClNO_2$ levels (with the highest monthly average value of 113.0 pptv) along the coast of the Mediterranean Sea and the North Sea with some influence into continental Europe, especially in Germany. The simulated HCl shows a similar pattern to that of $ClNO_2$ but with a much higher concentration ($>$ 10 times higher). The predicted BrO levels over Europe are low (average value $\sim$ 0.17 pptv), with the largest predicted value occurring within the Arctic Circle, while GEOS-Chem predicted $>$ 1.0 pptv of BrO in the Mediterranean Sea (Sherwen et al., 2017). The predicted IO peaks over the Mediterranean region with a maximum value of 6.9 pptv.

Direct measurements of halogen species are very scarce and not available for the period covered in the present study (July 2016). Since a direct comparison is not possible, here we present a comparison of the simulated concentrations with observations from previous studies (Table 3) to provide an approximate assessment of the representation of halogen species in the HAL simulation of the CMAQ model over Europe.

Numerous $ClNO_2$ measurements have been reported around the globe, which show that $ClNO_2$ is ubiquitous in the boundary layer, with maximum values ranging from hundreds to thousands of parts per trillion by volume in polluted coastal (Osthoff et al., 2008; Wang et al., 2016) and continental regions (Tham et al., 2016; Thornton et al., 2010). A few campaigns have been conducted in Europe. Phillips et al. (2012) reported a maximum value of 800 pptv for $ClNO_2$ in Hessen, Germany, where CMAQ predicts a concentration of 273 pptv. Bannan et al. (2015) observed a peak value of 724 pptv in London where CMAQ predicts a concentration of 802 pptv. Simulations with the GEOS-Chem model (Sherwen et al., 2017) reported maximum values of 110 and 140 pptv in Hessen and London, respectively. Several field campaigns have been conducted in Weybourne in the past few years to measure $ClNO_2$. Sherwen et al. (2017) reported a peak concentration of 946 pptv. Bannan et al. (2017) reported a peak value of 65 pptv, and Sommariva et al. (2018) reported a peak value of 1100 pptv in summer, 75.6 pptv in autumn, and 733 pptv in winter. CMAQ simulated a maximum of 373 pptv at that location, while GEOS-Chem predicted 458 pptv. Sommariva et al. (2018) also reported measurements of $ClNO_2$ in Leicester with a maximum value of 274 pptv in spring, 74.2 pptv in summer, and 248 pptv in winter, with a peak value at Penlee Point of 922 pptv. CMAQ predicted a maximum of 274 pptv in Leicester and 319 pptv at Penlee Point. Eger et al. (2019) conducted shipborne observations of $ClNO_2$ in the Mediterranean Sea and reported up to 600 pptv $ClNO_2$ during their campaign, which is similar to the prediction of the present study.

The observed levels of HCl in Europe range from $<$ 100 to 5000 pptv (Hossaini et al., 2016, and the references therein). The CMAQ model predicted monthly average concentrations of HCl of 6.3 to 1249 pptv, which is similar to the observation ranges. GEOS-Chem (Sherwen et al., 2017) predicted a maximum of 12 pptv for HCl, which is significantly lower than the measurements in Europe.

BrO measurements have been reported at ground-based sites and during the ship cruises, which generally demonstrate a range of 0.5 to 2.0 pptv maximum values for land measurements and 3.0 to 3.6 pptv for ship measurements (Saiz-Lopez and von Glasow, 2012). BrO observations have been reported at several coastal sites in Europe. BrO levels of up to 6.5 pptv (Saiz-Lopez et al., 2004) and 7.5 pptv (Mahajan et al., 2009) were reported in Mace Head and Brittany, respectively. CMAQ predicts 10.1 and 0.4 pptv at those locations, which are lower than the measurements. Sherwen et al. (2017) also predicted small values, with a maximum of 0.8 pptv in Mace Head and 0.5 pptv in Brittany. An extremely high level of BrO, $\sim$ 100 pptv, was observed over the Dead Sea (Matveev et al., 2001; Holla et al., 2015). CMAQ is not able to reproduce such a high level of BrO due to the lower bromide content in typical ocean water (which was used in the present study for the Dead Sea) compared to the exceptionally high bromide content in the Dead Sea (Tas et al., 2006; Sarwar et al., 2015).

Table 2. Simulated average concentrations of inorganic halogen species over the ocean.

Species	Concentration (ppt)	Percentage (%)	Species	Concentration (ppt)	Percentage (%)	Species	Concentration (ppt)	Percentage (%)
HCl	247.9	96.1	HOBr	1.06	27.0	HOI	5.1	52.0
$ClNO_2$	4.9	1.9	BrCl	0.71	18.2	INO_3	2.8	28.7
HOCl	3.8	1.5	$BrNO_3$	0.67	16.9	IO	1.0	10.3
$ClNO_3$	1.2	0.5	HBr	0.66	16.8	I	0.4	4.0
ClO	0.25	0.1	BrO	0.38	9.7	I_2O_3	0.3	3.1
Cl_2	0.02	0.008	Br_2	0.33	8.4	HI	0.1	1.0
Cl	0.0002	0.0001	$BrNO_2$	0.09	2.4	I_2	0.05	0.5
–			Br	0.03	0.7	INO	0.03	0.3
–			–			I_2O_2	0.01	0.1
–			–			INO_2	0.01	0.1
–			–			I_2O_4	0.004	< 0.1
Total Cl	258.1	100	Total Br	3.9	100	Total I	9.8	100

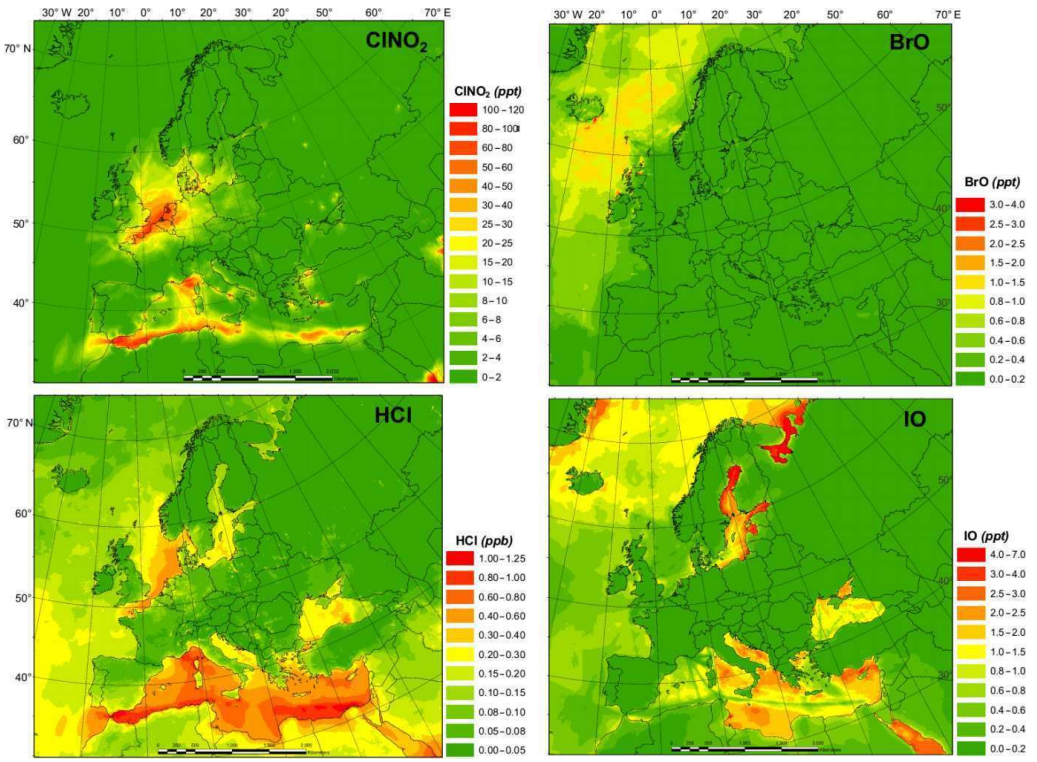

Figure 2. Monthly average $ClNO_2$, HCl, BrO, and IO concentration in the HAL simulation.

Global measurements show that the IO levels observed by ground-based campaigns were generally between 0.2 and 2.4 pptv, while those by ship measurement were ∼ 3.5 pptv (Saiz-Lopez and von Glasow, 2012). Observations of IO have also been conducted in Europe. Maximum IO levels of 4.0–50.0 pptv were measured at Mace Head (Allan et al., 2000; Commane et al., 2011). CMAQ predicts a value of 3.9 pptv at Mace Head, while GEOS-Chem predicted a value of 0.6 pptv (Sherwen et al., 2017). In Brittany, up to 7.7–30.0 pptv of IO were observed by Bitter et al. (2005) and Furneaux et al. (2010). CMAQ predicts 1.1 pptv of IO at Brittany and Sherwen et al. (2017) predicted 0.07 pptv. A maximum IO concentration of 2.0 pptv was reported in Dagebüll (Peters et al., 2005), and CMAQ predicts 9.0 pptv at that site, while GEOS-Chem predicted 1.8 pptv (Sherwen et al., 2017). Prados-Roman et al. (2015) reported the level of IO during a ship-based campaign in the range of < 0.4 to > 1.4 pptv (daytime average) around the globe and 0.4 to 0.5 pptv (daytime average) in the south of Spain and the west of Africa

Table 3. Comparison of observed and simulated halogen species.

Location	Species	Observation[a]	Simulation[b]
Hessen, Germany[c]	$ClNO_2$	800.0	273.4
London, United Kingdom[d]	$ClNO_2$	724.0	801.5
Weybourne, United Kingdom[e]	$ClNO_2$	65	373
Weybourne, United Kingdom[f]	$ClNO_2$	946	373
Weybourne, United Kingdom[g]	$ClNO_2$	1100 (summer), 75.6 (autumn), 733 (winter)	373
Leicester, United Kingdom[g]	$ClNO_2$	274 (spring), 74.2 (summer), 248 (winter)	274
Penlee Point, United Kingdom[g]	$ClNO_2$	922	319
Mace Head, Ireland[h]	BrO	6.5	10.1
Brittany, France[i]	BrO	7.5	0.4
Dead Sea[j]	BrO	100.0	0.2
Mace Head, Ireland[k]	IO	4.0–50.0	3.9
Brittany, France[l]	IO	7.7–30.0	1.1
Dagebüll, Germany[m]	IO	2.0	9.0
Atlantic Ocean[n]	IO	0.4 to 0.5 (daytime average)	0.4 to 2.0 (daytime average)

[a] Maximum value (pptv). [b] Maximum value (pptv) from the HAL simulation. [c] Phillips et al. (2012). [d] Bannan et al. (2015). [e] Bannan et al. (2017). [f] Sherwen et al. (2017). [g] Sommariva et al. (2018). [h] Saiz-Lopez et al. (2004). [i] Mahajan et al. (2009). [j] Matveev et al. (2001), Holla et al. (2015). [k] Allan et al. (2000), Commane et al. (2011). [l] Britter et al. (2005), Furneaux et al. (2010). [m] Peters et al. (2005). [n] Prados-Roman et al. (2015)

(over the Atlantic); the present study predicted 0.4 to 2.0 pptv (daytime average) of IO over those areas.

3.3 Influence of halogen chemistry on the atmospheric oxidation capacity

Figure 3 shows the monthly average concentrations of the OH and HO_2 radicals predicted by the BASE simulation as well as the impact of chlorine chemistry (CL-BASE) and the full halogen chemistry (HAL-BASE) on the simulated OH and HO_2 levels. In the BASE simulation, the highest OH concentration levels are predicted over the oceans, especially along ship tracks, with a maximum value of 0.38 pptv ($\sim 9.5 \times 10^6$ molecule cm^{-3}). The chlorine chemistry slightly increased the OH level over most of the domain by up to 0.0041 pptv (1.0×10^5 molecule cm^{-3}). The impact of the halogen chemistry has competing effects on OH concentrations, with a maximum increase of 0.030 pptv (7.5×10^5 molecule cm^{-3}) and a reduction of as much as 0.023 pptv (5.8×10^5 molecule cm^{-3}). The BASE simulation predicts the highest values of HO_2 over the Mediterranean Sea, with a maximum value of 21 pptv. The chlorine chemistry increases the HO_2 level in the areas of elevated $ClNO_2$ predictions (Figs. 2 and 3). The further addition of halogen chemistry lowers the HO_2 as much as 3.7 pptv and increases HO_2 up to 0.73 pptv compared to the BASE simulation. The overall difference of HO_2 because of halogens was -0.59 pptv in the European domain. The effect of halogen chemistry on OH and HO_2 is the combined effect of the following four pathways: (1) conversion of HO_2 to OH via XO (Reactions R5 and R6), in which HO_2 decreases and OH increases; (2) reduction of O_3 (Reaction R1 and Fig. 7) and the reduced production of OH by O_3 photolysis, in which both OH and HO_2 decrease; (3) increase in NO_2 (Reaction R4 and Fig. 7) and the enhanced consumption of OH by the reaction with NO_2, in which both OH and HO_2 decrease; and (4) increased oxidation of VOCs due to halogens in which both OH and HO_2 increase. Pathway (1) leads to the increase in OH and decrease in HO_2 over coastal areas, the Mediterranean Sea, and the Baltic Sea (except the ship tracks). Pathway (2) results in a decrease in OH and HO_2 over the remote ocean. Pathways (2), (3), and (4) result in a decrease in OH and an increase or decrease in HO_2 along the ship tracks in the Mediterranean Sea.

Sarwar et al. (2015) reported a small overall decrease in OH (1 %) and a significant decrease in HO_2 (11 %) in the Northern Hemisphere due to bromine and iodine chemistry. Their results suggest a considerable reduction of the HO_2/OH ratio, which is consistent with the present study. Muñiz-Unamunzaga et al. (2018) found a slight increase in diurnal OH (1 %–2 %) and a noticeable decrease in HO_2 (4 %), leading to a decrease in HO_2/OH in Los Angeles, California. Sherwen et al. (2017) suggested that OH was reduced across their European domain due to halogen chemistry and concluded that the shift of HO_2 to OH by XO could not compensate for the decrease in OH due to the loss of O_3. Another GEOS-Chem study, however, predicted an increase in OH over the Mediterranean Sea (Stone et al., 2018). The discrepancy among previous studies and between those works and the present one is difficult to deduce and requires further investigation. Several possible causes could lead to different simulated levels of halogens and their impact on oxidants, including the different mechanisms of producing and recycling halogen species (Sarwar et al., 2019), spatial resolution (Sommariva et al., 2018), emission inventory (Wang

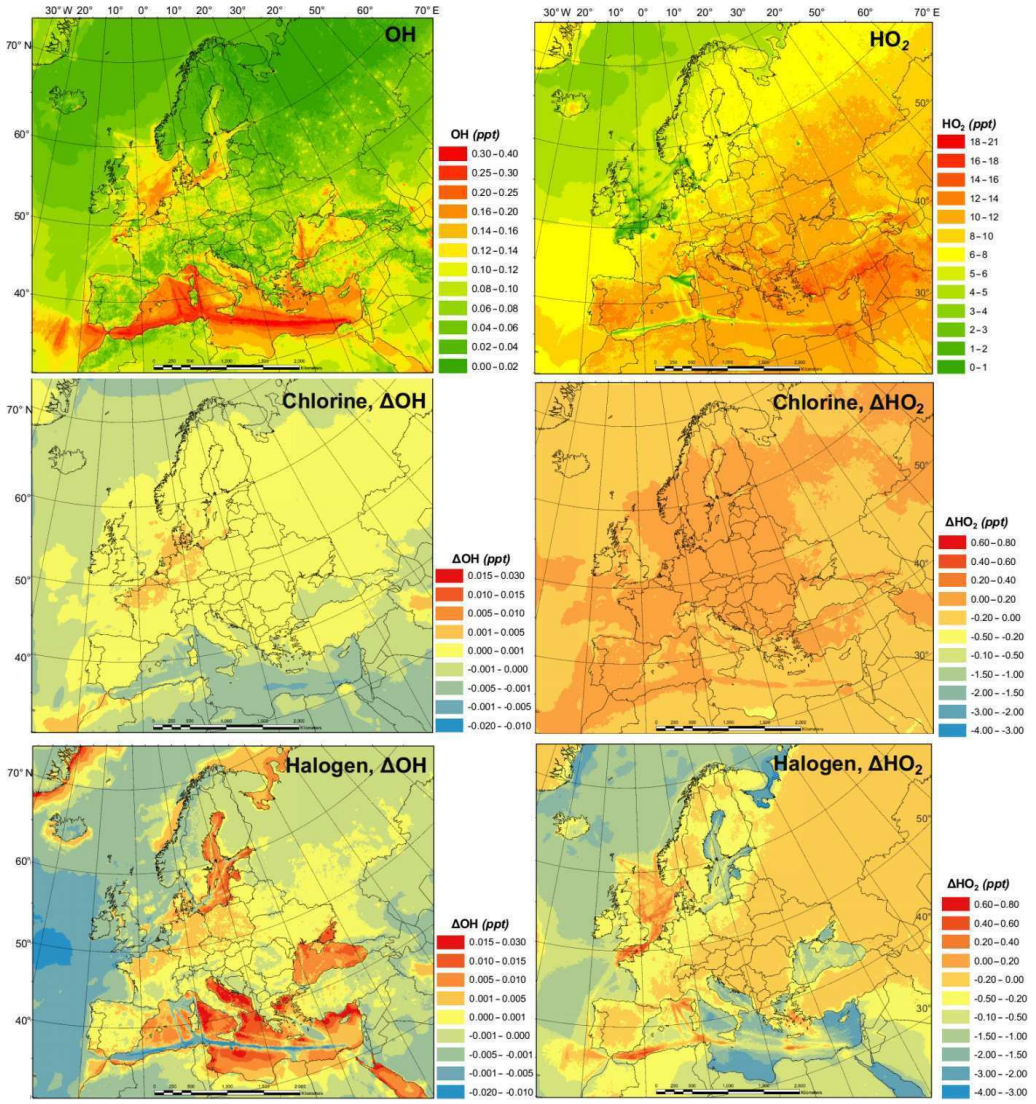

Figure 3. Monthly average OH and HO_2 concentration in the BASE simulation and changes due to chlorine (CL) and full halogen chemistry (HAL).

et al., 2019), and different spatiotemporal scale of interest (Stone et al., 2018).

Figure 4 presents the monthly average prediction of NO_3 and Cl radicals in the BASE scenario and the influence of chlorine (CL-BASE) and halogen chemistry (HAL-BASE) on the levels of NO_3 and Cl. The BASE simulation predicted relatively high NO_3 concentrations over the Mediterranean Sea along the busy shipping tracks. Although concentrations as high as 71 pptv are found, the majority of oceanic regions have concentrations in the range of 10 to 40 pptv and between 0 and 4 pptv over land. The chlorine chemistry slightly increases the NO_3 radical due to the increase in O_3 (see Sect. 3.4). In contrast, the halogen chemistry considerably reduces NO_3 concentrations by as much as 20 pptv in the nighttime over the Mediterranean Sea. Muñiz-Unamunzaga et al. (2018) reported a 20 %–50 % (2 to 4 pptv) decrease in the NO_3 radical in Los Angeles, California, when considering the halogen chemistry.

In the BASE simulation, the Cl concentration was negligible because there was no relevant chlorine source incorporated in the CMAQ model. The CL simulation contains the production of $ClNO_2$ and its subsequent photolysis, which increases the Cl concentration to as high as 7.0×10^{-4} pptv ($\sim 1.75 \times 10^4$ atom cm^{-3}). The HAL simulation predicted a very similar magnitude and spatial distribution of chlorine concentration. Sherwen et al. (2017) reported Cl concentrations less than 1.4×10^4 atom cm^{-3} ($\sim 5.6 \times 10^{-4}$ pptv) over Europe, comparable to our prediction. Hossaini et al. (2016) reported more than 1.0×10^4 atom cm^{-3} ($\sim 4.0 \times 10^{-4}$ pptv) of chlorine over Asia, Europe, and North America, with a maximum of 8.5×10^4 atom cm^{-3} ($\sim 3.4 \times 10^{-3}$ pptv), using a global chemical transport model (TOMCAT) that in-

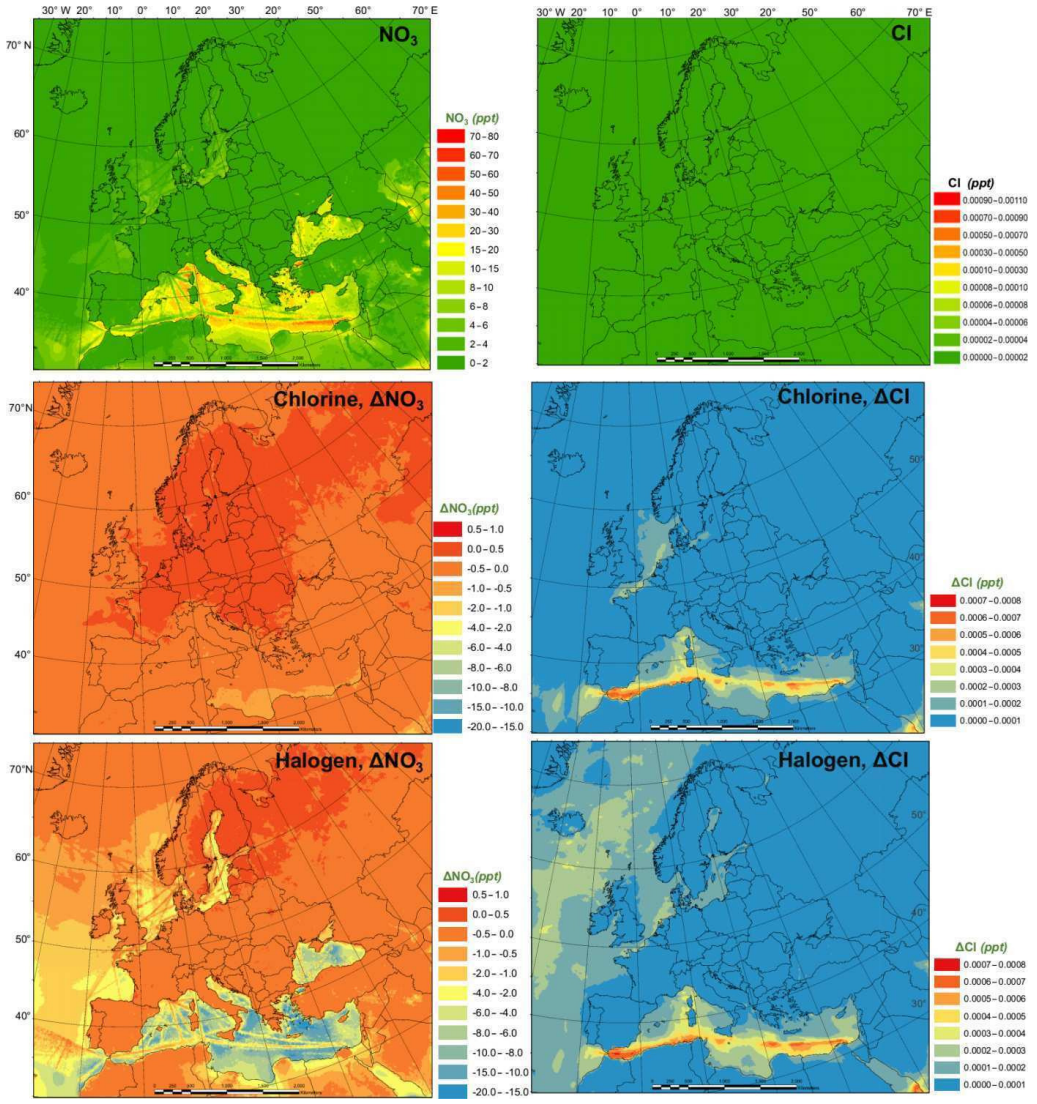

Figure 4. Monthly average NO_3 and Cl radical concentrations in the BASE simulation and changes induced by chlorine (CL) and full halogen chemistry (HAL).

corporated chlorine sources from sea salt dechlorination, coal and biomass burning, oxidation of natural and anthropogenic chlorocarbon, and heterogeneous reactions on sea salt and sulfate aerosol. In their study, Hossaini et al. (2016) used the Reactive Emission Inventory of Chlorine (Keene et al., 1999), which Wang et al. (2019) reported to be unrealistic for present-day applications.

The current study and previous studies simulated a broad range of surface Cl concentrations, although they were all within the scope of the reported observed (observation-based calculation) values of 10^3 to 10^5 atom cm^{-3} ($\sim 4.0 \times 10^{-5}$ to 4.0×10^{-3} pptv) according to the review of Saiz-Lopez and von Glasow (2012). In light of the considerable variation of observed and model-predicted Cl levels, further study may be needed to comprehensively evaluate the significant role of Cl in the troposphere.

Figures 5 and 6 demonstrate the monthly average of the daily maximum concentrations of OH, HO_2, NO_3, and Cl in the BASE simulation and also the impact of chlorine (CL-BASE) and the halogen chemistry (HAL-BASE). The maximum values of OH, HO_2, and Cl were predicted during the daytime, but they peak at different hours with Cl in the early morning and OH and HO_2 later in the day, while the highest levels of the NO_3 radical were simulated during nighttime.

The monthly averages of the daily maxima of OH, HO_2, NO_3, and Cl (Figs. 5 and 6) have similar spatial patterns and higher concentrations (or changes in concentration) compared to those of the monthly averages (Figs. 3 and 4). The monthly average of the daily maximum OH (HO_2 and NO_3) radical is 3.7 (2.5 and 3.4) times the monthly average OH (HO_2 and NO_3) concentration in the BASE simulations, while both the monthly average of the daily maximum and

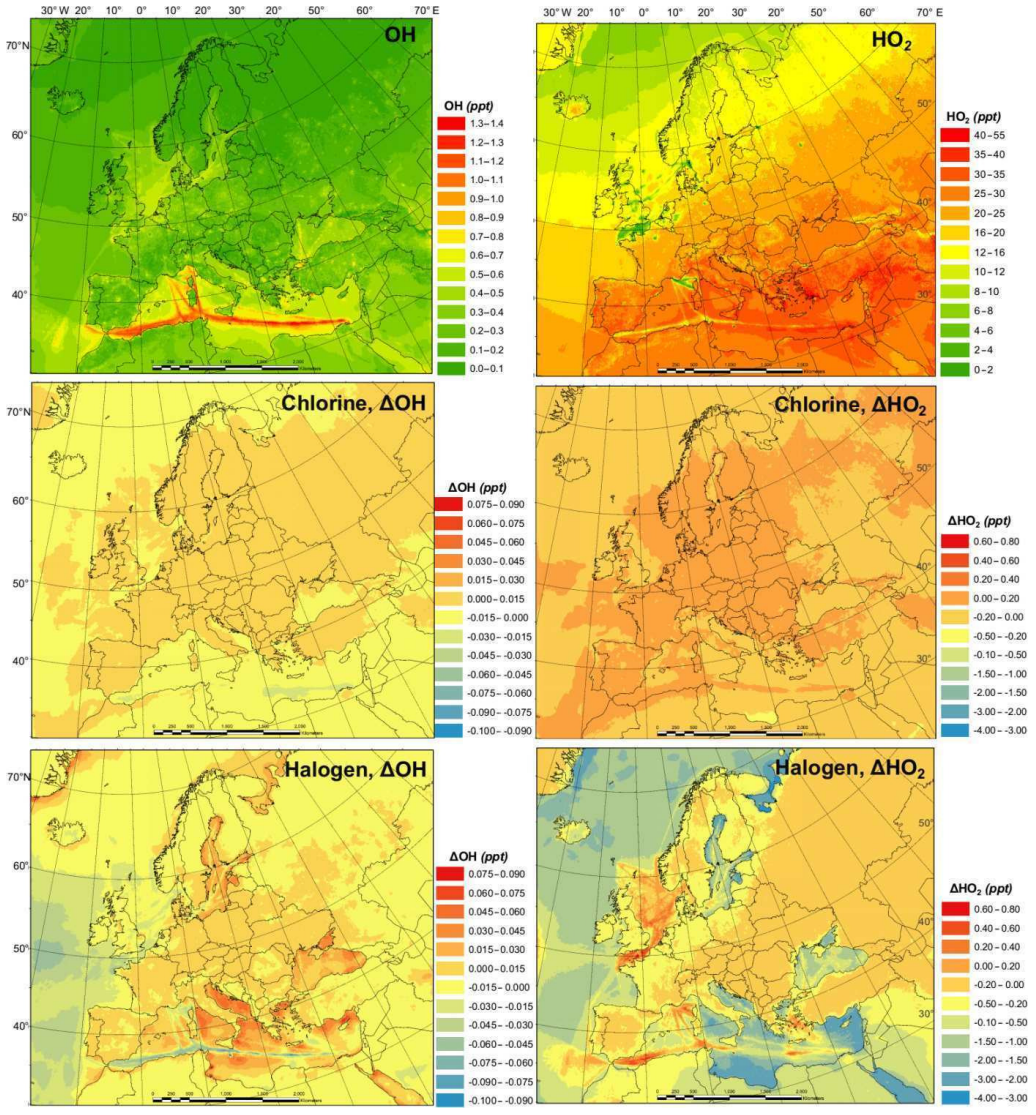

Figure 5. Monthly average of daily maximum concentrations of OH and HO_2 in the BASE simulation and changes due to chlorine (CL) and full halogen chemistry (HAL).

monthly average Cl show negligible values. The monthly average of daily maximum changes in the OH (HO_2) concentration due to the chlorine and halogen chemistry has a magnitude of −0.10 to 0.09 pptv (−4.0 to 0.8 pptv), which is wider than (the same as) that of the monthly averages, i.e., −0.020 to 0.03 pptv (−4.0 to 0.8 pptv). For the NO_3 (Cl) radicals, the magnitude of changes in the monthly average is −20 to 1.0 pptv (0.0 to 0.0008 pptv), while that in the monthly average of daily maximums is −55 to 1.0 pptv (0.0 to 0.0055 pptv).

We also examine the diurnal variations of the four radicals in the BASE and HAL scenarios (Figs. S3 and S4). Halogens have a small effect on the diurnal pattern of OH. HO_2 is reduced by halogens, especially in the midday. The NO_3 radical is strongly decreased throughout the night after the addition of halogens. The Cl atom is released by the halogen chemistry in the early morning. The significant effects of halogen chemistry on the diurnal variation of OH, HO_2, NO_3, and Cl radicals highlight the role of halogen chemistry in regulating the atmospheric oxidation capacity throughout the day, with the highest effect on Cl in the early morning, maximum effects on OH and HO_2 in daytime, and the largest effect on NO_3 at night.

3.4 Impact of halogen chemistry on regulated gaseous air pollutants

The monthly average modeled NO_2 and O_3, two major gaseous air pollutants in Europe, and the effect of chlorine and halogen chemistry on the two regulated gaseous species are shown in Fig. 7. The BASE simulation produced

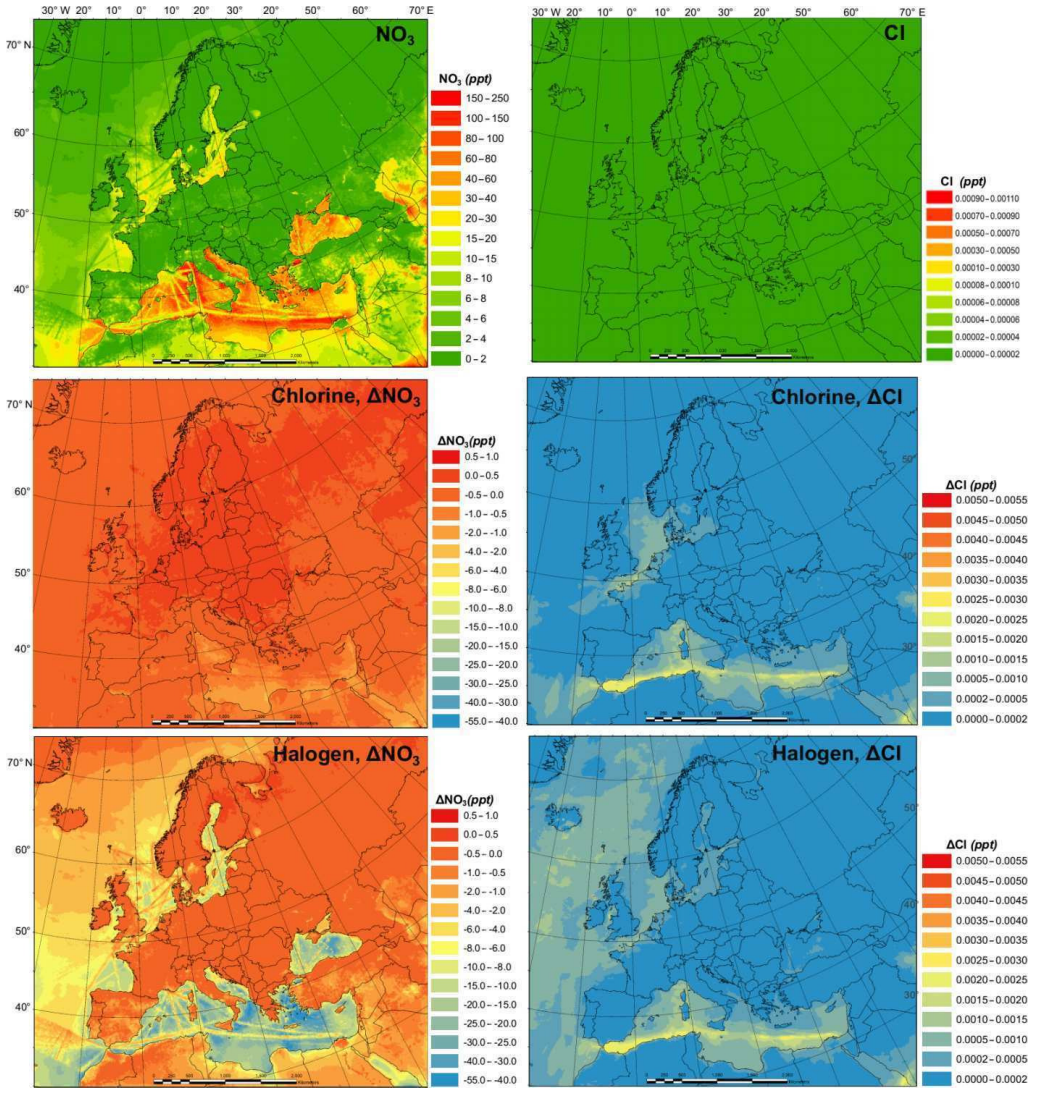

Figure 6. Monthly average of daily maximum concentrations of NO_3 and the Cl radical in the BASE simulation and changes induced by chlorine (CL) and full halogen chemistry (HAL).

many hot spots of NO_2 over Europe in the vicinity of major cities and ship trajectories. The chlorine chemistry slightly increases the level of NO_2 (by up to 0.038 ppbv) in the majority of the domain since (1) the production and the subsequent photolysis of $ClNO_2$ recycles the NO_x and extends its lifetime, which increases both NO_2 and NO (Figs. 7 and S5), and (2) the increased O_3 level (Fig. 7) enhances the transformation of NO to NO_2, which increases NO_2 and decreases NO (Figs. 7 and S2). Some grid cells show a decrease in NO_2 (as much as 0.09 ppbv) because the enhanced oxidative capacity (Sect. 3.3) promotes the cleansing of NO_2 via OH, forming HNO_3. The full halogen chemistry enhances NO_2 (up to 0.20 ppbv) over the North Sea and the Mediterranean Sea and decreases NO_2 (by as much as 1.7 ppbv) in the most polluted hot spots. The increase in NO_2 occurs through the reactions of XO with NO. Meanwhile, in the most polluted regions, the NO–NO_2 balance is predominantly controlled by the reactions of NO with HO_2 and O_3. With the decrease in HO_2 and O_3 due to the halogen chemistry, the transformation of NO to NO_2 is reduced, which leads to decreasing NO_2 and increasing NO.

The monthly average O_3 concentration over Europe from the BASE simulation was relatively high (up to 57 ppbv), especially over southern Europe where higher temperatures and more intensive radiation promote the formation of this secondary pollutant. Chlorine chemistry increases O_3 levels over the land of Europe with a maximum increment of 0.22 ppbv and decreases O_3 over the oceanic area by as much as 0.76 ppbv. The full halogen chemistry decreases O_3 throughout the domain, with a maximum reduction of 10 ppbv. On average, the halogen chemistry reduces the O_3 concentration by more than 3.0 ppbv in coastal Europe and

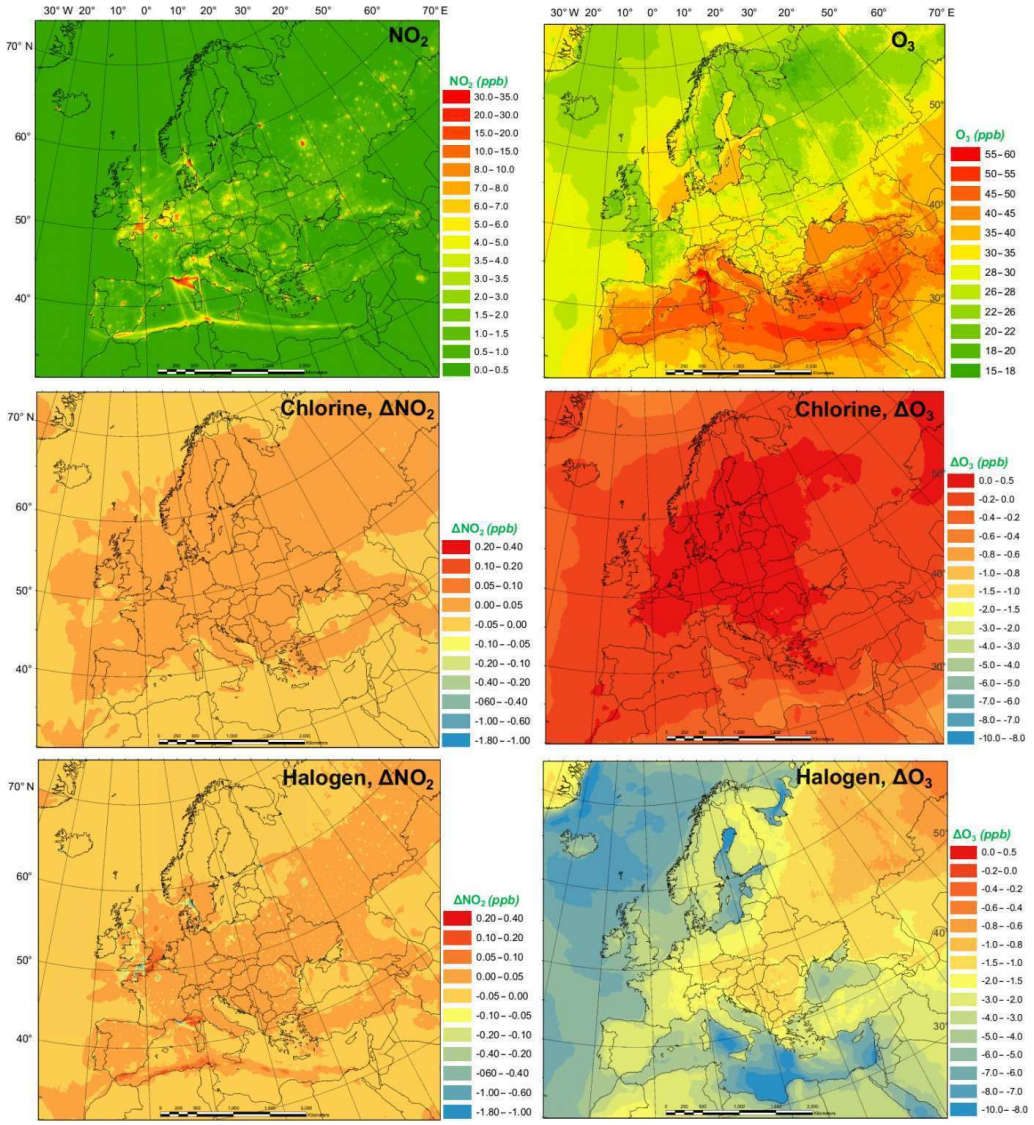

Figure 7. Monthly average NO_2 and O_3 concentration in the BASE simulation and changes induced by chlorine (CL) and full halogen chemistry (HAL).

by over 2.0 ppbv over western and central Europe (nearly 1000 km from the ocean). Our model simulation highlights the fact that halogen chemistry has a large impact on O_3 concentrations over oceanic areas and a moderate impact on O_3 over coastal and continental regions of Europe.

Muñiz-Unamunzaga et al. (2018) reported a decrease of −2.0 ppbv O_3 in the inland areas of the western US (several hundred kilometers from the ocean) and a reduction of 2.5 to 5.0 ppbv O_3 in the coastal regions due to the full halogen chemistry. Sarwar et al. (2015) suggested that the inclusion of halogen processes reduced O_3 concentrations by 2.0 to 4.0 ppbv over most of the terrestrial regions in the Northern Hemisphere and over 6.0 ppbv in some coastal areas. Sherwen et al. (2017) used a revised version of GEOS-Chem (Sherwen et al., 2016) with halogen chemistry to show substantial reductions in O_3 over Europe, with an average reduction of 13.5 ppbv in the domain and a maximum of 28.9 ppbv in some locations.

3.5 Implications for policy assessment

The current air quality management in Europe has two main objectives: (1) to protect human health and (2) to protect the environment. While many plans and measures have prioritized particulate matter (PM) or NO_2, policies to reduce O_3 concentrations are still needed (EEA, 2018a). The World Health Organization (WHO) Air Quality Guidelines value for O_3 (maximum daily 8 h mean of 100 $\mu g\,m^{-3}$) was exceeded in 96 % of all the reporting stations in Europe, although this is especially true for areas near the Mediterranean

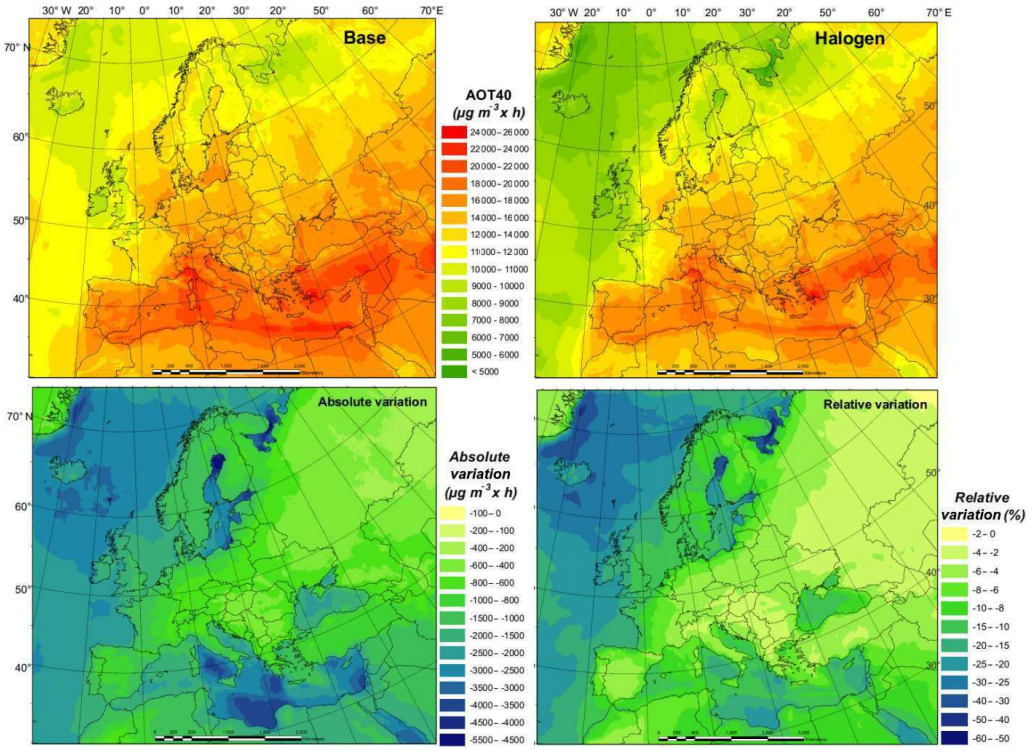

Figure 8. AOT40 for July in the BASE and HAL simulations and absolute and relative changes between the two simulations.

Sea. According to the European Environment Agency's latest report, 12 % of the EU-28 urban population is exposed to O_3 concentrations above the European Union target value threshold (a maximum daily 8 h mean of 120 µg m^{-3} is not to be exceeded on more than 25 d yr^{-1}, as set out by the Directive 2008/50/EC) in 2016. Apart from significant potential health effects (Jerrett et al., 2009; Malley et al., 2017), O_3 is also known to have a negative impact on vegetation (Mills et al., 2011). The target value for the protection of vegetation (18 000 µg m^{-3} h^{-1} accumulated over May to July), based on the AOT40 index (Accumulated Ozone exposure over a Threshold of 40 ppbv), was exceeded for about 31 % of all agricultural land in all European countries. The critical level for this pollutant (10 000 µg m^{-3} h^{-1} accumulated over April to September) was exceeded in 60 % of the total forest area of the continent in 2016 (EEA, 2018a).

Since our experiment covers only 1 month, it is not possible to assess the impact of halogen chemistry on these two indexes. Nonetheless, we have compared the results of both maximum daily 8 h mean and 1-month AOT40 (over July; Fig. 8) for the BASE and HAL simulations. The relative variation provides a good indication of the potential impact of considering halogens in our modeling system in the estimation of legally relevant indexes.

We find that halogen chemistry strongly affects the ambient O_3 concentration and may need to be considered in the formulation of plans and strategies for O_3 non-attainment areas. We see differences between BASE and HAL simulations (over land in July 2016) as high as 12 % and 36 % for the number of days with daily maximum 8 h O_3 over 120 µg m^{-3} and the monthly average daily maximum 8 h O_3 level, respectively (Figs. S6 and S7). Furthermore, we notice strong regional differences, mainly between coastal and inland areas. The considerable effect of halogen chemistry on air quality implies the need to improve the robustness and accuracy of modeling tools to design customized policies to control O_3.

In Sect. 3.3 and 3.4, we have also discussed the effect of halogen chemistry on the partitioning of OH/HO_2 and NO/NO_2. The budgets of HO_x and NO_x are key parameters to accurately simulate the formation of O_3 and its response to the reduction of precursors, namely NO_x and VOCs (e.g., Li et al., 2018). Air quality models are predominantly used to formulate air pollution control policy by examining the responses of O_3 levels to various reduction rates of NO_x and/or VOCs. The models that do not include the comprehensive halogen chemistry can potentially lead to different O_3 concentration responses to NO_x and/or VOC emission changes in Europe.

This study also demonstrates that chlorine chemistry affects the formation of O_3. The current policy is only designed to control the long-lived chlorinated species (Hossaini et al., 2015) but not reactive chlorine species, e.g., HCl, chloride, and short-lived chlorocarbons, from coal burn-

ing, biomass burning, and industrial activities. The coal-fired power plants in the EU (EEA, 2018b; Kuklinska et al., 2015) can potentially provide chlorine sources, making the implications of halogen chemistry even more relevant.

4 Conclusion

We applied the CMAQ model with comprehensive halogen chemistry (Cl, Br, and I) to conduct high-resolution simulations for examining the impact of halogen chemistry on air quality over Europe.

The comparison of model results with observations from over 400 monitoring sites indicates that the CMAQ model is capable of reproducing the concentrations and temporal variations of air pollutants over Europe and can be employed to study the impact of halogen chemistry in Europe. The comparison of predicted halogen species concentrations with measurements suggests that the CMAQ model is able to predict observed levels of chlorine and iodine species, although it underestimates bromine species.

Chlorine chemistry enhances the atmospheric oxidation capacity by significantly increasing the level of the Cl radical and affects the levels of OH, HO_2, NO_3, O_3, and NO_2. The combined halogen chemistry marginally increases the level of OH and reduces HO_2, NO_3, and O_3. The impact of halogen chemistry on the ambient concentration of NO_2 is smaller but non-negligible.

Halogen chemistry significantly influences the atmospheric oxidation capacity throughout the day by imposing the highest effect on Cl in the early morning, maximum effects on OH and HO_2 in daytime, and the largest effect on NO_3 at night. Halogen chemistry can have a strong influence on atmospheric composition over oceanic and coastal regions but also some noticeable impacts over continental Europe. This study highlights the potential benefit of incorporating halogen chemistry into air quality models for policy development.

Although the incorporation of the halogen chemistry may improve the capabilities of 3-D Eulerian chemical transport models, we acknowledge that large uncertainties still exist in the assessment of the halogen chemistry impact due to emission inventories (e.g., chlorine emission inventory; Wang et al., 2019), model configurations (e.g., grid size; Sommariva et al., 2018), and chemical mechanisms (e.g., photolysis rate of iodine oxides, recycling rate of halogen species on aerosol; Simpson et al., 2015). Further field, laboratory, and theoretical studies are needed to constrain modeling studies for evaluating the impacts of halogen chemistry on air quality and for assessing air quality policy implications.

Data availability. The data used and demonstrated in this study are available upon the request to the corresponding author.

Supplement. The supplement related to this article is available online at: https://doi.org/10.5194/acp-19-15321-2019-supplement.

Author contributions. ASL designed the research. GS and BG conducted the CMAQ modeling. RB, DP, JD, GS, BG, QL, and ASL analyzed the results. QL, RB, GS, and ASL wrote the paper with contributions from all authors.

Competing interests. The authors declare that they have no conflict of interest.

Disclaimer. The views expressed in this paper are those of the authors and do not necessarily represent the views or policies of the U.S. EPA.

Financial support. This research has been supported by the European Commission, H2020 Research Infrastructures (CLIMAHAL (grant no. 726349)).

Review statement. This paper was edited by Michel Van Roozendael and reviewed by three anonymous referees.

References

Allan, B. J., McFiggans, G., Plane, J. M. C., and Coe, H.: Observations of iodine monoxide in the remote marine boundary layer, J. Geophys. Res., 105, 14363–14369, https://doi.org/10.1029/1999JD901188, 2000.

Appel, K. W., Chemel, C., Roselle, S. J., Francis, X. V, Hu, R.-M., Sokhi, R. S., Rao, S. T., and Galmarini, S.: Examination of the Community Multiscale Air Quality (CMAQ) model performance over the North American and European domains, Atmos. Environ., 53, 142–155, https://doi.org/10.1016/j.atmosenv.2011.11.016, 2012.

Appel, K. W., Pouliot, G. A., Simon, H., Sarwar, G., Pye, H. O. T., Napelenok, S. L., Akhtar, F., and Roselle, S. J.: Evaluation of dust and trace metal estimates from the Community Multiscale Air Quality (CMAQ) model version 5.0, Geosci. Model Dev., 6, 883–899, https://doi.org/10.5194/gmd-6-883-2013, 2013.

Appel, K. W., Napelenok, S. L., Foley, K. M., Pye, H. O. T., Hogrefe, C., Luecken, D. J., Bash, J. O., Roselle, S. J., Pleim, J. E., Foroutan, H., Hutzell, W. T., Pouliot, G. A., Sarwar, G., Fahey, K. M., Gantt, B., Gilliam, R. C., Heath, N. K., Kang, D., Mathur, R., Schwede, D. B., Spero, T. L., Wong, D. C., and Young, J. O.: Description and evaluation of the Community Multiscale Air Quality (CMAQ) modeling system version 5.1, Geosci. Model Dev., 10, 1703–1732, https://doi.org/10.5194/gmd-10-1703-2017, 2017.

Bannan, T. J., Murray Booth, A., Bacak, A., Muller, J. B. A., Leather, K. E., Le Breton, M., Jones, B., Young, D., Coe, H., Allan, J., Visser, S., Slowik, J. G., Furger, M., Prévôt, A. S. H., Lee, J., Dunmore, R. E., Hopkins, J. R., Hamilton, J. F., Lewis, A. C.,

Whalley, L. K., Sharp, T., Stone, D., Heard, D. E., Fleming, Z. L., Leigh, R., Shallcross, D. E., and Percival, C. J.: The first UK measurements of nitryl chloride using a chemical ionization mass spectrometer in central London in the summer of 2012, and an investigation of the role of Cl atom oxidation, J. Geophys. Res., 120, 5638–5657, https://doi.org/10.1002/2014JD022629, 2015.

Bannan, T. J., Bacak, A., Le Breton, M., Flynn, M., Ouyang, B., McLeod, M., Jones, R., Malkin, T. L., Whalley, L. K., Heard, D. E., Bandy, B., Khan, M. A. H., Shallcross, D. E., and Percival, C. J.: Ground and airborne UK measurements of nitryl chloride: An investigation of the role of Cl atom oxidation at Weybourne Atmospheric Observatory, J. Geophys. Res.-Atmos., 122, 11154–11165, https://doi.org/10.1002/2017JD026624, 2017

Bitter, M., Ball, S. M., Povey, I. M., and Jones, R. L.: A broadband cavity ringdown spectrometer for in-situ measurements of atmospheric trace gases, Atmos. Chem. Phys., 5, 2547–2560, https://doi.org/10.5194/acp-5-2547-2005, 2005.

Borge, R., Alexandrov, V., José del Vas, J., Lumbreras, J., and Rodríguez, E.: A comprehensive sensitivity analysis of the WRF model for air quality applications over the Iberian Peninsula, Atmos. Environ., 42, 8560–8574, https://doi.org/10.1016/j.atmosenv.2008.08.032, 2008a.

Borge, R., Lumbreras, J., and Rodríguez, E.: Development of a high-resolution emission inventory for Spain using the SMOKE modelling system: A case study for the years 2000 and 2010, Environ. Model. Softw., 23, 1026–1044, https://doi.org/10.1016/j.envsoft.2007.11.002, 2008b.

Byun, D. and Schere, K. L.: Review of the Governing Equations, Computational Algorithms, and Other Components of the Models-3 Community Multiscale Air Quality (CMAQ) Modeling System, Appl. Mech. Rev., 59, 51–77, https://doi.org/10.1115/1.2128636, 2006.

Byun, D. W. and Ching, J. K. S.: Science Algorithms of the EPA MODELS-3 Community Multiscale Air Quality (CMAQ) Modelling System. U.S. Environmental Protection Agency, Washington, D.C., EPA/600/R-99/030 (NTIS PB2000-100561), 1999.

Commane, R., Seitz, K., Bale, C. S. E., Bloss, W. J., Buxmann, J., Ingham, T., Platt, U., Pöhler, D., and Heard, D. E.: Iodine monoxide at a clean marine coastal site: observations of high frequency variations and inhomogeneous distributions, Atmos. Chem. Phys., 11, 6721–6733, https://doi.org/10.5194/acp-11-6721-2011, 2011.

de la Paz, D., Borge, R., and Martilli, A.: Assessment of a high resolution annual WRF-BEP/CMAQ simulation for the urban area of Madrid (Spain), Atmos. Environ., 144, 282–296, https://doi.org/10.1016/j.atmosenv.2016.08.082, 2016.

EEA (European Environmental Agency): Air Quality in Europe – 2018 report, EEA, Luxembourg, 12/2018, 83 pp., https://doi.org/10.2800/777411, 2018a.

EEA (European Environmental Agency): European Union emission inventory report 1990–2016 under the UNECE Convention on Long-range Transboundary Air Pollution (LRTAP), EEA, Luxembourg, 6/2018, 150 pp., https://doi.org/10.2800/571876, 2018b.

Eger, P. G., Friedrich, N., Schuladen, J., Shenolikar, J., Fischer, H., Tadic, I., Harder, H., Martinez, M., Rohloff, R., Tauer, S., Drewnick, F., Fachinger, F., Brooks, J., Darbyshire, E., Sciare, J., Pikridas, M., Lelieveld, J., and Crowley, J. N.: Shipborne measurements of $ClNO_2$ in the Mediterranean Sea and around the Arabian Peninsula during summer, Atmos. Chem. Phys., 19, 12121–12140, https://doi.org/10.5194/acp-19-12121-2019, 2019.

EMEP/CEIP: Present state of emissions as used in EMEP models, available at: http://www.ceip.at/webdab_emepdatabase/emissions_emepmodels (last access: 22 November 2019), 2014.

Farman, J. C., Gardiner, B. G., and Shanklin, J. D.: Large losses of total ozone in Antarctica reveal seasonal ClO_x/NO_x interaction, Nature, 315, 207–210, https://doi.org/10.1038/315207a0, 1985.

Fernandez, R. P., Salawitch, R. J., Kinnison, D. E., Lamarque, J.-F., and Saiz-Lopez, A.: Bromine partitioning in the tropical tropopause layer: implications for stratospheric injection, Atmos. Chem. Phys., 14, 13391–13410, https://doi.org/10.5194/acp-14-13391-2014, 2014.

Foley, K. M., Roselle, S. J., Appel, K. W., Bhave, P. V., Pleim, J. E., Otte, T. L., Mathur, R., Sarwar, G., Young, J. O., Gilliam, R. C., Nolte, C. G., Kelly, J. T., Gilliland, A. B., and Bash, J. O.: Incremental testing of the Community Multiscale Air Quality (CMAQ) modeling system version 4.7, Geosci. Model Dev., 3, 205–226, https://doi.org/10.5194/gmd-3-205-2010, 2010.

Furneaux, K. L., Whalley, L. K., Heard, D. E., Atkinson, H. M., Bloss, W. J., Flynn, M. J., Gallagher, M. W., Ingham, T., Kramer, L., Lee, J. D., Leigh, R., McFiggans, G. B., Mahajan, A. S., Monks, P. S., Oetjen, H., Plane, J. M. C., and Whitehead, J. D.: Measurements of iodine monoxide at a semi polluted coastal location, Atmos. Chem. Phys., 10, 3645–3663, https://doi.org/10.5194/acp-10-3645-2010, 2010.

Gantt, B., Sarwar, G., Xing, J., Simon, H., Schwede, D., Hutzell, W. T., Mathur, R., and Saiz-Lopez, A.: The Impact of Iodide-Mediated Ozone Deposition and Halogen Chemistry on Surface Ozone Concentrations Across the Continental United States, Environ. Sci. Technol., 51, 1458–1466, https://doi.org/10.1021/acs.est.6b03556, 2017.

Guenther, A. B., Jiang, X., Heald, C. L., Sakulyanontvittaya, T., Duhl, T., Emmons, L. K., and Wang, X.: The Model of Emissions of Gases and Aerosols from Nature version 2.1 (MEGAN2.1): an extended and updated framework for modeling biogenic emissions, Geosci. Model Dev., 5, 1471–1492, https://doi.org/10.5194/gmd-5-1471-2012, 2012.

Holla, R., Schmitt, S., Frieß, U., Pöhler, D., Zingler, J., Corsmeier, U., and Platt, U.: Vertical distribution of BrO in the boundary layer at the Dead Sea, Environ. Chem., 12, 438–460, https://doi.org/10.1071/EN14224, 2015.

Hossaini, R., Chipperfield, M. P., Saiz-Lopez, A., Harrison, J. J., Von Glasow, R., Sommariva, R., Atlas, E., Navarro, M., Montzka, S. A., Feng, W., Dhomse, S., Harth, C., Mühle, J., Lunder, C., O'Doherty, S., Young, D., Reimann, S., Vollmer, M. K., Krummel, P. B., and Bernath, P. F.: Growth in stratospheric chlorine from short-lived chemicals not controlled by the Montreal Protocol, Geophys. Res. Lett., 42, 4573–4580, https://doi.org/10.1002/2015GL063783, 2015.

Hossaini, R., Chipperfield, M. P., Saiz-Lopez, A., Fernandez, R., Monks, S., Feng, W., Brauer, P., and Von Glasow, R.: A global model of tropospheric chlorine chemistry: Organic versus inorganic sources and impact on methane oxidation, J. Geophys. Res., 121, 14271–14297, https://doi.org/10.1002/2016JD025756, 2016.

Jerrett, M., Burnett, R. T., Pope, C. A., Ito, K., Thurston, G., Krewski, D., Shi, Y., Calle, E., and Thun, M.: Long-Term Ozone

Exposure and Mortality, New Engl. J. Med., 360, 1085–1095, https://doi.org/10.1056/NEJMoa0803894, 2009.

Jung, J., Lee, J., Kim, B., and Oh, S.: Seasonal variations in the NO_2 artifact from chemiluminescence measurements with a molybdenum converter at a suburban site in Korea (downwind of the Asian continental outflow) during 2015–2016, Atmos. Environ., 165, 290–300, 2017.

Keene, W., Khalil, M. A. K., Erickson, D., McCulloch, A., Graedel, T. E., Lobert, J. M., Aucott, M. L., Gong, S. L., Harper, D. B., Kleiman, G., Midgley, P., Moore, R. M., Seuzaret, C., Sturges, W. T., Benkovitz, C. M., Koropalov, V., Barrie, L. A., and Li, Y. F.: Composite global emissions of reactive chlorine from anthropogenic and natural sources: Reactive Chlorine Emissions Inventory, J. Geophys. Res., 104, 8429–8440, 1999.

Kuklinska, K., Wolska, L., and Namiesnik, J.: Air quality policy in the U.S. and the EU – a review, Atmos. Pollut. Res., 6, 129–137, https://doi.org/10.5094/APR.2015.015, 2015.

Li, Q., Zhang, L., Wang, T., Tham, Y. J., Ahmadov, R., Xue, L., Zhang, Q., and Zheng, J.: Impacts of heterogeneous uptake of dinitrogen pentoxide and chlorine activation on ozone and reactive nitrogen partitioning: improvement and application of the WRF-Chem model in southern China, Atmos. Chem. Phys., 16, 14875–14890, https://doi.org/10.5194/acp-16-14875-2016, 2016.

Li, Q., Zhang, L., Wang, T., Wang, Z., Fu, X., and Zhang, Q.: "New" Reactive Nitrogen Chemistry Reshapes the Relationship of Ozone to Its Precursors, Environ. Sci. Technol., 52, 2810–2818, https://doi.org/10.1021/acs.est.7b05771, 2018.

Mahajan, A. S., Oetjen, H., Lee, J. D., Saiz-Lopez, A., McFiggans, G. B., and Plane, J. M. C.: High bromine oxide concentrations in the semi-polluted boundary layer, Atmos. Environ., 43, 3811–3818, https://doi.org/10.1016/j.atmosenv.2009.05.033, 2009.

Malley, C. S., Henze, D. K., Kuylenstierna, J. C. I., Vallack, H. W., Davila, Y., Anenberg, S. C., Turner, M. C., and Ashmore, M. R.: Updated Global Estimates of Respiratory Mortality in Adults ≥ 30 Years of Age Attributable to Long-Term Ozone Exposure, Environ. Health Persp., 125, 87021, https://doi.org/10.1289/EHP1390, 2017.

Mathur, R., Xing, J., Gilliam, R., Sarwar, G., Hogrefe, C., Pleim, J., Pouliot, G., Roselle, S., Spero, T. L., Wong, D. C., and Young, J.: Extending the Community Multiscale Air Quality (CMAQ) modeling system to hemispheric scales: overview of process considerations and initial applications, Atmos. Chem. Phys., 17, 12449–12474, https://doi.org/10.5194/acp-17-12449-2017, 2017.

Matveev, V., Peleg, M., Rosen, D., Tov-Alper, D. S., Hebestreit, K., Stutz, J., Platt, U., Blake, D., and Luria, M.: Bromine oxide–ozone interaction over the Dead Sea, J. Geophys. Res., 106, 10375–10387, https://doi.org/10.1029/2000JD900611, 2001.

Mills, G., Pleijel, H., Braun, S., Büker, P., Bermejo, V., Calvo, E., Danielsson, H., Emberson, L., Fernández, I. G., Grünhage, L., Harmens, H., Hayes, F., Karlsson, P.-E., and Simpson, D.: New stomatal flux-based critical levels for ozone effects on vegetation, Atmos. Environ., 45, 5064–5068, https://doi.org/10.1016/j.atmosenv.2011.06.009, 2011.

Molina, M. J. and Rowland, F. S.: Stratospheric sink for chlorofluoromethanes: chlorine atom-catalysed destruction of ozone, Nature, 249, 810–812, https://doi.org/10.1038/249810a0, 1974.

Muñiz-Unamunzaga, M., Borge, R., Sarwar, G., Gantt, B., de la Paz, D., Cuevas, C. A., and Saiz-Lopez, A.: The influence of ocean halogen and sulfur emissions in the air quality of a coastal megacity: The case of Los Angeles, Sci. Total Environ., 610–611, 1536–1545, https://doi.org/10.1016/j.scitotenv.2017.06.098, 2018.

Osthoff, H. D., Roberts, J. M., Ravishankara, A. R., Williams, E. J., Lerner, B. M., Sommariva, R., Bates, T. S., Coffman, D., Quinn, P. K., Dibb, J. E., Stark, H., Burkholder, J. B., Talukdar, R. K., Meagher, J., Fehsenfeld, F. C., and Brown, S. S.: High levels of nitryl chloride in the polluted subtropical marine boundary layer, Nat. Geosci., 1, 324–328, https://doi.org/10.1038/ngeo177, 2008.

Peters, C., Pechtl, S., Stutz, J., Hebestreit, K., Hönninger, G., Heumann, K. G., Schwarz, A., Winterlik, J., and Platt, U.: Reactive and organic halogen species in three different European coastal environments, Atmos. Chem. Phys., 5, 3357–3375, https://doi.org/10.5194/acp-5-3357-2005, 2005.

Phillips, G. J., Tang, M. J., Thieser, J., Brickwedde, B., Schuster, G., Bohn, B., Lelieveld, J., and Crowley, J. N.: Significant concentrations of nitryl chloride observed in rural continental Europe associated with the influence of sea salt chloride and anthropogenic emissions, Geophys. Res. Lett., 39, L10811, https://doi.org/10.1029/2012GL051912, 2012.

Prados-Roman, C., Cuevas, C. A., Hay, T., Fernandez, R. P., Mahajan, A. S., Royer, S.-J., Galí, M., Simó, R., Dachs, J., Großmann, K., Kinnison, D. E., Lamarque, J.-F., and Saiz-Lopez, A.: Iodine oxide in the global marine boundary layer, Atmos. Chem. Phys., 15, 583–593, https://doi.org/10.5194/acp-15-583-2015, 2015.

Saiz-Lopez, A. and von Glasow, R.: Reactive halogen chemistry in the troposphere, Chem. Soc. Rev., 41, 6448–6472, https://doi.org/10.1039/c2cs35208g, 2012.

Saiz-Lopez, A., Plane, J. M. C., and Shillito, J. A.: Bromine oxide in the mid-latitude marine boundary layer, Geophys. Res. Lett., 31, L03111, https://doi.org/10.1029/2003GL018956, 2004.

Saiz-Lopez, A., Fernandez, R. P., Ordóñez, C., Kinnison, D. E., Gómez Martín, J. C., Lamarque, J.-F., and Tilmes, S.: Iodine chemistry in the troposphere and its effect on ozone, Atmos. Chem. Phys., 14, 13119–13143, https://doi.org/10.5194/acp-14-13119-2014, 2014.

Sarwar, G., Simon, H., Bhave, P., and Yarwood, G.: Examining the impact of heterogeneous nitryl chloride production on air quality across the United States, Atmos. Chem. Phys., 12, 6455–6473, https://doi.org/10.5194/acp-12-6455-2012, 2012.

Sarwar, G., Simon, H., Xing, J., and Mathur, R.: Importance of tropospheric $ClNO_2$ chemistry across the Northern Hemisphere, Geophys. Res. Lett., 41, 4050–4058, https://doi.org/10.1002/2014GL059962, 2014.

Sarwar, G., Gantt, B., Schwede, D., Foley, K., Mathur, R., and Saiz-Lopez, A.: Impact of Enhanced Ozone Deposition and Halogen Chemistry on Tropospheric Ozone over the Northern Hemisphere, Environ. Sci. Technol., 49, 9203–9211, https://doi.org/10.1021/acs.est.5b01657, 2015.

Sarwar, G., Gantt, B., Foley, K., Fahey, K., Spero T. L., Kang, D., Mathur, R., Hosein F., Xing, J., Sherwen, T., and Saiz-Lopez, A.: Influence of bromine and iodine chemistry on annual, seasonal, diurnal, and background ozone: CMAQ simulations over the Northern Hemisphere, Atmos. Environ., 213, 395–404, 2019.

Sherwen, T., Schmidt, J. A., Evans, M. J., Carpenter, L. J., Großmann, K., Eastham, S. D., Jacob, D. J., Dix, B., Koenig, T. K., Sinreich, R., Ortega, I., Volkamer, R., Saiz-Lopez, A., Prados-Roman, C., Mahajan, A. S., and Ordóñez, C.: Global impacts of tropospheric halogens (Cl, Br, I) on oxidants and composition in GEOS-Chem, Atmos. Chem. Phys., 16, 12239–12271, https://doi.org/10.5194/acp-16-12239-2016, 2016.

Sherwen, T., Evans, M. J., Sommariva, R., Hollis, L. D. J., Ball, S. M., Monks, P. S., Reed, C., Carpenter, L. J., Lee, J. D., Forster, G., Bandy, B., Reeves, C. E., and Bloss, W. J.: Effects of halogens on European air-quality, Faraday Discuss., 200, 75–100, https://doi.org/10.1039/c7fd00026j, 2017.

Sillman, S.: The relation between ozone, NO_x and hydrocarbons in urban and polluted rural environments, Atmos. Environ., 33, 1821–1845, https://doi.org/10.1016/S1352-2310(98)00345-8, 1999.

Simpson, W. R., Brown, S. S., Saiz-Lopez, A., Thornton, J. A., and Von Glasow, R.: Tropospheric Halogen Chemistry: Sources, Cycling, and Impacts, Chem. Rev., 115, 4035–4062, https://doi.org/10.1021/cr5006638, 2015.

Skamarock, W. C. and Klemp, J. B.: A time-split nonhydrostatic atmospheric model for weather research and forecasting applications, J. Comput. Phys., 227, 3465–3485, https://doi.org/10.1016/j.jcp.2007.01.037, 2008.

Solazzo, E., Hogrefe, C., Colette, A., Garcia-Vivanco, M., and Galmarini, S.: Advanced error diagnostics of the CMAQ and Chimere modelling systems within the AQMEII3 model evaluation framework, Atmos. Chem. Phys., 17, 10435–10465, https://doi.org/10.5194/acp-17-10435-2017, 2017.

Sommariva, R., Hollis, L. D. J., Sherwen, T., Baker, A. R., Ball, S. M., Bandy, B. J., Bell, T. G., Chowdhury, M. N., Cordell, R. L., Evans, M. J., Lee, J. D., Reed, C., Reeves, C. E., Roberts, J. M., Yang, M., and Monks, P. S.: Seasonal and geographical variability of nitryl chloride and its precursors in Northern Europe, Atmos. Sci. Lett., 19, e844, https://doi.org/10.1002/asl.844, 2018.

Stone, D., Sherwen, T., Evans, M. J., Vaughan, S., Ingham, T., Whalley, L. K., Edwards, P. M., Read, K. A., Lee, J. D., Moller, S. J., Carpenter, L. J., Lewis, A. C., and Heard, D. E.: Impacts of bromine and iodine chemistry on tropospheric OH and HO_2: comparing observations with box and global model perspectives, Atmos. Chem. Phys., 18, 3541–3561, https://doi.org/10.5194/acp-18-3541-2018, 2018.

Tas, E., Peleg, M., Pedersen, D. U., Matveev, V., Pour Biazar, A., and Luria, M.: Measurement-based modeling of bromine chemistry in the boundary layer: 1. Bromine chemistry at the Dead Sea, Atmos. Chem. Phys., 6, 5589–5604, https://doi.org/10.5194/acp-6-5589-2006, 2006.

Tham, Y. J., Wang, Z., Li, Q., Yun, H., Wang, W., Wang, X., Xue, L., Lu, K., Ma, N., Bohn, B., Li, X., Kecorius, S., Größ, J., Shao, M., Wiedensohler, A., Zhang, Y., and Wang, T.: Significant concentrations of nitryl chloride sustained in the morning: investigations of the causes and impacts on ozone production in a polluted region of northern China, Atmos. Chem. Phys., 16, 14959–14977, https://doi.org/10.5194/acp-16-14959-2016, 2016.

Thornton, J. A., Kercher, J. P., Riedel, T. P., Wagner, N. L., Cozic, J., Holloway, J. S., Dubé, W. P., Wolfe, G. M., Quinn, P. K., Middlebrook, A. M., Alexander, B., and Brown, S. S.: A large atomic chlorine source inferred from mid-continental reactive nitrogen chemistry, Nature, 464, 271–274, https://doi.org/10.1038/nature08905, 2010.

UNC (University of North Carolina at Chapel Hill): SMOKE v3.6.5 User's Manual, Institute for the Environment, available at: https://www.cmascenter.org/smoke/documentation/3.6.5/html (last access: 22 November 2019), 2015.

US EPA Office of Research and Development (ORD): CMAQ (Version 5.2), Zenodo, https://doi.org/10.5281/zenodo.1167892, 30 June 2017.

van Loon, M., Vautard, R., Schaap, M., Bergström, R., Bessagnet, B., Brandt, J., Builtjes, P. J. H., Christensen, J. H., Cuvelier, C., Graff, A., Jonson, J. E., Krol, M., Langner, J., Roberts, P., Rouil, L., Stern, R., Tarrasón, L., Thunis, P., Vignati, E., White, L., and Wind, P.: Evaluation of long-term ozone simulations from seven regional air quality models and their ensemble, Atmos. Environ., 41, 2083–2097, https://doi.org/10.1016/j.atmosenv.2006.10.073, 2007.

Wang, T., Tham, Y. J., Xue, L., Li, Q., Zha, Q., Wang, Z., Poon, S. C. N., Dubé, W. P., Blake, D. R., Louie, P. K. K., Luk, C. W. Y., Tsui, W., and Brown, S. S.: Observations of nitryl chloride and modeling its source and effect on ozone in the planetary boundary layer of southern China, J. Geophys. Res.-Atmos., 121, 2476–2489, https://doi.org/10.1002/2015JD024556, 2016.

Wang, X., Jacob, D. J., Eastham, S. D., Sulprizio, M. P., Zhu, L., Chen, Q., Alexander, B., Sherwen, T., Evans, M. J., Lee, B. H., Haskins, J. D., Lopez-Hilfiker, F. D., Thornton, J. A., Huey, G. L., and Liao, H.: The role of chlorine in global tropospheric chemistry, Atmos. Chem. Phys., 19, 3981–4003, https://doi.org/10.5194/acp-19-3981-2019, 2019.

From: Kang, Daiwen <Kang.Daiwen@epa.gov>
Sent: Tuesday, April 21, 2020 11:09 AM
To: Sarwar, Golam <Sarwar.Golam@epa.gov>
Subject: RE: Record of Percent Agreement for the 2020 STAA award

Hi Sarwar,

Yes, I agree. Thanks for putting this together.

Best regards,

Daiwen

From: Sarwar, Golam <Sarwar.Golam@epa.gov>
Sent: Tuesday, April 21, 2020 11:07 AM
To: Kang, Daiwen <Kang.Daiwen@epa.gov>
Subject: Record of Percent Agreement for the 2020 STAA award

Hi Daiwen:

Please let me know if you agree by replying the mail.

Please also let me know if you are applying to the 2020 STAA since the application requires identifying all concurrent nominations.

Thanks,
Sarwar

From: Sarwar, Golam
Sent: Friday, April 17, 2020 10:21 AM
To: Gantt, Brett <Gantt.Brett@epa.gov>; Schwede, Donna <Schwede.Donna@epa.gov>; Foley, Kristen <Foley.Kristen@epa.gov>; Mathur, Rohit <Mathur.Rohit@epa.gov>; Simon, Heather <Simon.Heather@epa.gov>; Hutzell, Bill <Hutzell.Bill@epa.gov>; Fahey, Kathleen <Fahey.Kathleen@epa.gov>; Spero, Tanya <Spero.Tanya@epa.gov>; Kang, Daiwen <Kang.Daiwen@epa.gov>
Subject: Record of Percent Agreement for the 2020 STAA award

Date: 4/17/2020
Subject: Record of Percent Agreement for the 2020 STAA award

Dear co-authors,

I plan to nominate the following publications for the 2020 Science and Technological Achievement Awards. The Award requires a record of percentage agreement which is shown below. Please reply to indicate agreement or disagreement to the proposed agreement.

Contributing authors	Organization	Percent agreement
Golam Sarwar	EPA/ORD/CEMM	30
Brett Gantt	EPA/OAR/OAQPS/AQAD	20
Kristen Foley	EPA/ORD/CEMM	10
R. Mathur	EPA/ORD/CEMM	9
Donna Schwede	EPA/ORD/CEMM	6
Alfonso Saiz-Lopez	Institute of Physical Chemistry, Spain	6
Jia Xing	Tsinghua University, China	4
K. Fahey	EPA/ORD/CEMM	3
D. Kang	EPA/ORD/CEMM	2

Heather Simon	EPA/OAR/OAQPS/AQAD	2
Tanya L. Spero	EPA/ORD/CEMM	2
W.T. Hutzell	EPA/ORD/CEMM	2
Hosein Foroutan	Virginia Tech, Blacksburg 24061, USA	2
Tomás Sherwen	University of York, UK	2

Article:

Sarwar, G., Gantt, B., Schwede, D., Foley, K., Mathur, R., Saiz-Lopez, A.: Impact of enhanced ozone deposition and halogen chemistry on tropospheric ozone over the Northern Hemisphere, Environmental Science & Technology, 49 (15), 9203-9211, 2015.

Gantt, B., Sarwar, G., Xing, J., Simon, H., Schwede, D., Hutzell, W. T., Mathur, R, Saiz-Lopez, A.: The impact of iodide-mediated ozone deposition and halogen chemistry on surface ozone concentrations across the continental United States, Environmental Science & Technology, 51 (3), 1458-1466, 2017.

Sarwar, G., Gantt, B., Foley, K., Fahey, K., Spero, T.L., Kang, D., Mathur, R., Foroutan, H., Xing, J., Sherwen, T., Saiz-Lopez, A.: Influence of bromine and iodine chemistry on annual, seasonal, diurnal, and background ozone: CMAQ simulations over the Northern Hemisphere, Atmospheric Environment, 213, 395-404, 2019.

Thanks,
Golam Sarwar
Research Physical Scientist
Center for Environmental Measurement & Modeling
Office of Research and Development
US Environmental Protection Agency

From: Hutzell, Bill <Hutzell.Bill@epa.gov>
Sent: Monday, April 20, 2020 5:13 PM
To: Sarwar, Golam <Sarwar.Golam@epa.gov>
Subject: RE: Record of Percent Agreement for the 2020 STAA award

Sarwar, I endorse the percentages. Thanks for considering me. -Bill

From: Sarwar, Golam <Sarwar.Golam@epa.gov>
Sent: Monday, April 20, 2020 3:47 PM
To: Hutzell, Bill <Hutzell.Bill@epa.gov>
Subject: FW: Record of Percent Agreement for the 2020 STAA award

Hi Bill:

Please let me know if you agree by replying the mail.

Thanks,
Sarwar

From: Sarwar, Golam
Sent: Friday, April 17, 2020 10:21 AM
To: Gantt, Brett <Gantt.Brett@epa.gov>; Schwede, Donna <Schwede.Donna@epa.gov>; Foley, Kristen <Foley.Kristen@epa.gov>; Mathur, Rohit <Mathur.Rohit@epa.gov>; Simon, Heather <Simon.Heather@epa.gov>; Hutzell, Bill <Hutzell.Bill@epa.gov>; Fahey, Kathleen <Fahey.Kathleen@epa.gov>; Spero, Tanya <Spero.Tanya@epa.gov>; Kang, Daiwen <Kang.Daiwen@epa.gov>
Subject: Record of Percent Agreement for the 2020 STAA award

Date: 4/17/2020
Subject: Record of Percent Agreement for the 2020 STAA award

Dear co-authors,

I plan to nominate the following publications for the 2020 Science and Technological Achievement Awards. The Award requires a record of percentage agreement which is shown below. Please reply to indicate agreement or disagreement to the proposed agreement.

Contributing authors	Organization	Percent agreement
Golam Sarwar	EPA/ORD/CEMM	30
Brett Gantt	EPA/OAR/OAQPS/AQAD	20
Kristen Foley	EPA/ORD/CEMM	10
R. Mathur	EPA/ORD/CEMM	9
Donna Schwede	EPA/ORD/CEMM	6
Alfonso Saiz-Lopez	Institute of Physical Chemistry, Spain	6
Jia Xing	Tsinghua University, China	4
K. Fahey	EPA/ORD/CEMM	3
D. Kang	EPA/ORD/CEMM	2
Heather Simon	EPA/OAR/OAQPS/AQAD	2
Tanya L. Spero	EPA/ORD/CEMM	2
W.T. Hutzell	EPA/ORD/CEMM	2
Hosein Foroutan	Virginia Tech, Blacksburg 24061, USA	2
Tomás Sherwen	University of York, UK	2

Article:

Sarwar, G., Gantt, B., Schwede, D., Foley, K., Mathur, R., Saiz-Lopez, A.: Impact of enhanced ozone deposition and halogen chemistry on tropospheric ozone over the Northern Hemisphere, Environmental Science & Technology, 49 (15), 9203-9211, 2015.

Gantt, B., Sarwar, G., Xing, J., Simon, H., Schwede, D., Hutzell, W. T., Mathur, R, Saiz-Lopez, A.: The impact of iodide-mediated ozone deposition and halogen chemistry on surface ozone concentrations across the continental United States, Environmental Science & Technology, 51 (3), 1458-1466, 2017.

Sarwar, G., Gantt, B., Foley, K., Fahey, K., Spero, T.L., Kang, D., Mathur, R., Foroutan, H., Xing, J., Sherwen, T., Saiz-Lopez, A.: Influence of bromine and iodine chemistry on annual, seasonal, diurnal, and background ozone: CMAQ simulations over the Northern Hemisphere, Atmospheric Environment, 213, 395-404, 2019.

Thanks,
Golam Sarwar
Research Physical Scientist
Center for Environmental Measurement & Modeling
Office of Research and Development
US Environmental Protection Agency

From: Jia Xing <xingjia@tsinghua.edu.cn>
Sent: Monday, April 20, 2020 1:53 PM
To: Sarwar, Golam <Sarwar.Golam@epa.gov>
Subject: Re: FW: Record of Percent Agreement for the 2020 STAA award

Hi Sarwar,

I'm so sorry for the late responding...Thank you so much for including me in the application! Actually, I'm honored to be included, and I have no problem with that.

Hope we can continue to work together on this area in the future.

Best,
Jia

Sarwar, Golam <Sarwar.Golam@epa.gov> 于2020年4月21日周二 上午12:19写道：

Hi Jia:

I am forwarding the email that I sent you last week; please reply.

Thanks,
Sarwar

From: Sarwar, Golam
Sent: Friday, April 17, 2020 10:28 AM
To: Jia Xing <xingj02@gmail.com>; Jia Xing <xingjia@mail.tsinghua.edu.cn>
Subject: Record of Percent Agreement for the 2020 STAA award

Date: 4/17/2020
Subject: Record of Percent Agreement for the 2020 STAA award

Dear co-authors,

I plan to nominate the following publications for the 2020 Science and Technological Achievement Awards. The Award requires a record of percentage agreement which is shown below. Please reply to indicate agreement or disagreement to the proposed agreement.

Contributing authors	Organization	Percent agreement
Golam Sarwar	EPA/ORD/CEMM	30
Brett Gantt	EPA/OAR/OAQPS/AQAD	20
Kristen Foley	EPA/ORD/CEMM	10
R. Mathur	EPA/ORD/CEMM	9
Donna Schwede	EPA/ORD/CEMM	6
Alfonso Saiz-Lopez	Institute of Physical Chemistry, Spain	6
Jia Xing	Tsinghua University, China	4
K. Fahey	EPA/ORD/CEMM	3
D. Kang	EPA/ORD/CEMM	2
Heather Simon	EPA/OAR/OAQPS/AQAD	2
Tanya L. Spero	EPA/ORD/CEMM	2
W.T. Hutzell	EPA/ORD/CEMM	2
Hosein Foroutan	Virginia Tech, Blacksburg 24061, USA	2
Tomás Sherwen	University of York, UK	2

Article:
Sarwar, G., Gantt, B., Schwede, D., Foley, K., Mathur, R., Saiz-Lopez, A.: Impact of enhanced ozone deposition and halogen chemistry on tropospheric ozone over the Northern Hemisphere, Environmental Science & Technology, 49 (15), 9203-9211, 2015.
Gantt, B., Sarwar, G., Xing, J., Simon, H., Schwede, D., Hutzell, W. T., Mathur, R, Saiz-Lopez, A.: The impact of iodide-mediated ozone deposition and halogen chemistry on surface ozone concentrations across the continental United States, Environmental Science & Technology, 51 (3), 1458-1466, 2017.
Sarwar, G., Gantt, B., Foley, K., Fahey, K., Spero, T.L., Kang, D., Mathur, R., Foroutan, H., Xing, J., Sherwen, T., Saiz-Lopez, A.: Influence of bromine and iodine chemistry on annual, seasonal, diurnal, and background ozone: CMAQ simulations over the Northern Hemisphere, Atmospheric Environment, 213, 395-404, 2019.

Thanks,
Golam Sarwar

Research Physical Scientist
Center for Environmental Measurement & Modeling
Office of Research and Development
US Environmental Protection Agency

From: Gantt, Brett <Gantt.Brett@epa.gov>
Sent: Monday, April 20, 2020 10:59 AM
To: Sarwar, Golam <Sarwar.Golam@epa.gov>
Subject: RE: Record of Percent Agreement for the 2020 STAA award

Hi Sarwar,
Confirming the proposed agreement.
Brett

From: Sarwar, Golam <Sarwar.Golam@epa.gov>
Sent: Friday, April 17, 2020 10:21 AM
To: Gantt, Brett <Gantt.Brett@epa.gov>; Schwede, Donna <Schwede.Donna@epa.gov>; Foley, Kristen <Foley.Kristen@epa.gov>; Mathur, Rohit <Mathur.Rohit@epa.gov>; Simon, Heather <Simon.Heather@epa.gov>; Hutzell, Bill <Hutzell.Bill@epa.gov>; Fahey, Kathleen <Fahey.Kathleen@epa.gov>; Spero, Tanya <Spero.Tanya@epa.gov>; Kang, Daiwen <Kang.Daiwen@epa.gov>
Subject: Record of Percent Agreement for the 2020 STAA award

Date: 4/17/2020
Subject: Record of Percent Agreement for the 2020 STAA award

Dear co-authors,

I plan to nominate the following publications for the 2020 Science and Technological Achievement Awards. The Award requires a record of percentage agreement which is shown below. Please reply to indicate agreement or disagreement to the proposed agreement.

Contributing authors	Organization	Percent agreement
Golam Sarwar	EPA/ORD/CEMM	30
Brett Gantt	EPA/OAR/OAQPS/AQAD	20
Kristen Foley	EPA/ORD/CEMM	10
R. Mathur	EPA/ORD/CEMM	9
Donna Schwede	EPA/ORD/CEMM	6
Alfonso Saiz-Lopez	Institute of Physical Chemistry, Spain	6
Jia Xing	Tsinghua University, China	4
K. Fahey	EPA/ORD/CEMM	3
D. Kang	EPA/ORD/CEMM	2
Heather Simon	EPA/OAR/OAQPS/AQAD	2
Tanya L. Spero	EPA/ORD/CEMM	2
W.T. Hutzell	EPA/ORD/CEMM	2
Hosein Foroutan	Virginia Tech, Blacksburg 24061, USA	2
Tomás Sherwen	University of York, UK	2

Article:
Sarwar, G., Gantt, B., Schwede, D., Foley, K., Mathur, R., Saiz-Lopez, A.: Impact of enhanced ozone deposition and halogen chemistry on tropospheric ozone over the Northern Hemisphere, Environmental Science & Technology, 49 (15), 9203-9211, 2015.

Gantt, B., Sarwar, G., Xing, J., Simon, H., Schwede, D., Hutzell, W. T., Mathur, R, Saiz-Lopez, A.: The impact of iodide-mediated ozone deposition and halogen chemistry on surface ozone concentrations across the continental United States, Environmental Science & Technology, 51 (3), 1458-1466, 2017.
Sarwar, G., Gantt, B., Foley, K., Fahey, K., Spero, T.L., Kang, D., Mathur, R., Foroutan, H., Xing, J., Sherwen, T., Saiz-Lopez, A.: Influence of bromine and iodine chemistry on annual, seasonal, diurnal, and background ozone: CMAQ simulations over the Northern Hemisphere, Atmospheric Environment, 213, 395-404, 2019.

Thanks,
Golam Sarwar
Research Physical Scientist
Center for Environmental Measurement & Modeling
Office of Research and Development
US Environmental Protection Agency

From: Alfonso Saiz López <a.saiz@csic.es>
Sent: Monday, April 20, 2020 5:28 AM
To: Sarwar, Golam <Sarwar.Golam@epa.gov>
Subject: Re: Record of Percent Agreement for the 2020 STAA award

Dear Golam,
Thanks for checking and please go ahead with the nomination! fingers crossed!
Hope you and your family are staying safe and healthy in these difficult times!

Best,
Alfonso

Alfonso Saiz-Lopez
Department of Atmospheric Chemistry and Climate
Instituto de Química Física Rocasolano, CSIC
Serrano 119, 28006 Madrid
Tf: (+34) 91-7459526
Fax: (+34) 91-5642431
Web: http://ac2.iqfr.csic.es
--
Affiliate Scientist at Atmospheric Chemistry Division/NCAR, Boulder, USA

El 17/04/2020 a las 16:25, Sarwar, Golam escribió:
Date: 4/17/2020
Subject: Record of Percent Agreement for the 2020 STAA award

Dear Alfonso,

I plan to nominate the following publications for the 2020 Science and Technological Achievement Awards. The Award requires a record of percentage agreement which is shown below. Please reply to indicate agreement or disagreement to the proposed agreement.

Contributing authors	Organization	Percent agreement
Golam Sarwar	EPA/ORD/CEMM	30
Brett Gantt	EPA/OAR/OAQPS/AQAD	20
Kristen Foley	EPA/ORD/CEMM	10
R. Mathur	EPA/ORD/CEMM	9
Donna Schwede	EPA/ORD/CEMM	6
Alfonso Saiz-Lopez	Institute of Physical Chemistry, Spain	6

Jia Xing	Tsinghua University, China	4
K. Fahey	EPA/ORD/CEMM	3
D. Kang	EPA/ORD/CEMM	2
Heather Simon	EPA/OAR/OAQPS/AQAD	2
Tanya L. Spero	EPA/ORD/CEMM	2
W.T. Hutzell	EPA/ORD/CEMM	2
Hosein Foroutan	Virginia Tech, Blacksburg 24061, USA	2
Tomás Sherwen	University of York, UK	2

Article:

Sarwar, G., Gantt, B., Schwede, D., Foley, K., Mathur, R., Saiz-Lopez, A.: Impact of enhanced ozone deposition and halogen chemistry on tropospheric ozone over the Northern Hemisphere, Environmental Science & Technology, 49 (15), 9203-9211, 2015.

Gantt, B., Sarwar, G., Xing, J., Simon, H., Schwede, D., Hutzell, W. T., Mathur, R, Saiz-Lopez, A.: The impact of iodide-mediated ozone deposition and halogen chemistry on surface ozone concentrations across the continental United States, Environmental Science & Technology, 51 (3), 1458-1466, 2017.

Sarwar, G., Gantt, B., Foley, K., Fahey, K., Spero, T.L., Kang, D., Mathur, R., Foroutan, H., Xing, J., Sherwen, T., Saiz-Lopez, A.: Influence of bromine and iodine chemistry on annual, seasonal, diurnal, and background ozone: CMAQ simulations over the Northern Hemisphere, Atmospheric Environment, 213, 395-404, 2019.

Thanks,
Golam Sarwar
Research Physical Scientist
Center for Environmental Measurement & Modeling
Office of Research and Development
US Environmental Protection Agency

From: Tomás Sherwen <tomas.sherwen@york.ac.uk>
Sent: Monday, April 20, 2020 4:49 AM
To: Sarwar, Golam <Sarwar.Golam@epa.gov>
Subject: Re: Record of Percent Agreement for the 2020 STAA award

Dear Sarwar,

I hope you are managing OK at this difficult time.

I am happy with whatever you decide for percentages.

My best wishes,

Tomas
--
Dr Tomás Sherwen
Research Scientist
National Centre for Atmospheric Science (NCAS)
Wolfson Atmospheric Chemistry Laboratories (WACL)
Department of Chemistry, University of York, York, YO10 5DD

On Fri, 17 Apr 2020 at 15:24, Sarwar, Golam <Sarwar.Golam@epa.gov> wrote:

> Date: 4/17/2020
> Subject: Record of Percent Agreement for the 2020 STAA award

Dear Tomas,

I plan to nominate the following publications for the 2020 Science and Technological Achievement Awards. The Award requires a record of percentage agreement which is shown below. Please reply to indicate agreement or disagreement to the proposed agreement.

Contributing authors	Organization	Percent agreement
Golam Sarwar	EPA/ORD/CEMM	30
Brett Gantt	EPA/OAR/OAQPS/AQAD	20
Kristen Foley	EPA/ORD/CEMM	10
R. Mathur	EPA/ORD/CEMM	9
Donna Schwede	EPA/ORD/CEMM	6
Alfonso Saiz-Lopez	Institute of Physical Chemistry, Spain	6
Jia Xing	Tsinghua University, China	4
K. Fahey	EPA/ORD/CEMM	3
D. Kang	EPA/ORD/CEMM	2
Heather Simon	EPA/OAR/OAQPS/AQAD	2
Tanya L. Spero	EPA/ORD/CEMM	2
W.T. Hutzell	EPA/ORD/CEMM	2
Hosein Foroutan	Virginia Tech, Blacksburg 24061, USA	2
Tomás Sherwen	University of York, UK	2

Article:
Sarwar, G., Gantt, B., Schwede, D., Foley, K., Mathur, R., Saiz-Lopez, A.: Impact of enhanced ozone deposition and halogen chemistry on tropospheric ozone over the Northern Hemisphere, Environmental Science & Technology, 49 (15), 9203-9211, 2015.
Gantt, B., Sarwar, G., Xing, J., Simon, H., Schwede, D., Hutzell, W. T., Mathur, R, Saiz-Lopez, A.: The impact of iodide-mediated ozone deposition and halogen chemistry on surface ozone concentrations across the continental United States, Environmental Science & Technology, 51 (3), 1458-1466, 2017.
Sarwar, G., Gantt, B., Foley, K., Fahey, K., Spero, T.L., Kang, D., Mathur, R., Foroutan, H., Xing, J., Sherwen, T., Saiz-Lopez, A.: Influence of bromine and iodine chemistry on annual, seasonal, diurnal, and background ozone: CMAQ simulations over the Northern Hemisphere, Atmospheric Environment, 213, 395-404, 2019.

Thanks,
Golam Sarwar
Research Physical Scientist
Center for Environmental Measurement & Modeling
Office of Research and Development
US Environmental Protection Agency

From: Hosein Foroutan <hosein@vt.edu>
Sent: Friday, April 17, 2020 2:03 PM
To: Sarwar, Golam <Sarwar.Golam@epa.gov>
Subject: Re: Record of Percent Agreement for the 2020 STAA award

Hi Sarwar,
Thanks for letting me know. Sure - I agree with the proposed percentage.
Best of luck with the nomination!
Hosein
--
Hosein Foroutan, Ph.D.
Assistant Professor
Environmental and Water Resources
The Charles E. Via, Jr. Department of Civil & Environmental Engineering
Virginia Tech

417 Durham Hall (0246), 1145 Perry St., Blacksburg, VA 24061
Phone: (540) 232-8400
AIRFlowS Lab

On Fri, Apr 17, 2020 at 10:22 AM Sarwar, Golam <Sarwar.Golam@epa.gov> wrote:

Date: 4/17/2020
Subject: Record of Percent Agreement for the 2020 STAA award

Dear co-authors,
I plan to nominate the following publications for the 2020 Science and Technological Achievement Awards. The Award requires a record of percentage agreement which is shown below. Please reply to indicate agreement or disagreement to the proposed agreement.

Contributing authors	Organization	Percent agreement
Golam Sarwar	EPA/ORD/CEMM	30
Brett Gantt	EPA/OAR/OAQPS/AQAD	20
Kristen Foley	EPA/ORD/CEMM	10
R. Mathur	EPA/ORD/CEMM	9
Donna Schwede	EPA/ORD/CEMM	6
Alfonso Saiz-Lopez	Institute of Physical Chemistry, Spain	6
Jia Xing	Tsinghua University, China	4
K. Fahey	EPA/ORD/CEMM	3
D. Kang	EPA/ORD/CEMM	2
Heather Simon	EPA/OAR/OAQPS/AQAD	2
Tanya L. Spero	EPA/ORD/CEMM	2
W.T. Hutzell	EPA/ORD/CEMM	2
Hosein Foroutan	Virginia Tech, Blacksburg 24061, USA	2
Tomás Sherwen	University of York, UK	2

Article:
Sarwar, G., Gantt, B., Schwede, D., Foley, K., Mathur, R., Saiz-Lopez, A.: Impact of enhanced ozone deposition and halogen chemistry on tropospheric ozone over the Northern Hemisphere, Environmental Science & Technology, 49 (15), 9203-9211, 2015.
Gantt, B., Sarwar, G., Xing, J., Simon, H., Schwede, D., Hutzell, W. T., Mathur, R, Saiz-Lopez, A.: The impact of iodide-mediated ozone deposition and halogen chemistry on surface ozone concentrations across the continental United States, Environmental Science & Technology, 51 (3), 1458-1466, 2017.
Sarwar, G., Gantt, B., Foley, K., Fahey, K., Spero, T.L., Kang, D., Mathur, R., Foroutan, H., Xing, J., Sherwen, T., Saiz-Lopez, A.: Influence of bromine and iodine chemistry on annual, seasonal, diurnal, and background ozone: CMAQ simulations over the Northern Hemisphere, Atmospheric Environment, 213, 395-404, 2019.

Thanks,
Golam Sarwar
Research Physical Scientist
Center for Environmental Measurement & Modeling
Office of Research and Development
US Environmental Protection Agency

From: Spero, Tanya <Spero.Tanya@epa.gov>
Sent: Friday, April 17, 2020 11:45 AM
To: Sarwar, Golam <Sarwar.Golam@epa.gov>
Subject: RE: Record of Percent Agreement for the 2020 STAA award

Sarwar –

I agree with the proposed Record of Percent Agreement.

Tanya

From: Sarwar, Golam <Sarwar.Golam@epa.gov>
Sent: Friday, April 17, 2020 10:21 AM
To: Gantt, Brett <Gantt.Brett@epa.gov>; Schwede, Donna <Schwede.Donna@epa.gov>; Foley, Kristen <Foley.Kristen@epa.gov>; Mathur, Rohit <Mathur.Rohit@epa.gov>; Simon, Heather <Simon.Heather@epa.gov>; Hutzell, Bill <Hutzell.Bill@epa.gov>; Fahey, Kathleen <Fahey.Kathleen@epa.gov>; Spero, Tanya <Spero.Tanya@epa.gov>; Kang, Daiwen <Kang.Daiwen@epa.gov>
Subject: Record of Percent Agreement for the 2020 STAA award

Date: 4/17/2020
Subject: Record of Percent Agreement for the 2020 STAA award

Dear co-authors,

I plan to nominate the following publications for the 2020 Science and Technological Achievement Awards. The Award requires a record of percentage agreement which is shown below. Please reply to indicate agreement or disagreement to the proposed agreement.

Contributing authors	Organization	Percent agreement
Golam Sarwar	EPA/ORD/CEMM	30
Brett Gantt	EPA/OAR/OAQPS/AQAD	20
Kristen Foley	EPA/ORD/CEMM	10
R. Mathur	EPA/ORD/CEMM	9
Donna Schwede	EPA/ORD/CEMM	6
Alfonso Saiz-Lopez	Institute of Physical Chemistry, Spain	6
Jia Xing	Tsinghua University, China	4
K. Fahey	EPA/ORD/CEMM	3
D. Kang	EPA/ORD/CEMM	2
Heather Simon	EPA/OAR/OAQPS/AQAD	2
Tanya L. Spero	EPA/ORD/CEMM	2
W.T. Hutzell	EPA/ORD/CEMM	2
Hosein Foroutan	Virginia Tech, Blacksburg 24061, USA	2
Tomás Sherwen	University of York, UK	2

Article:

Sarwar, G., Gantt, B., Schwede, D., Foley, K., Mathur, R., Saiz-Lopez, A.: Impact of enhanced ozone deposition and halogen chemistry on tropospheric ozone over the Northern Hemisphere, Environmental Science & Technology, 49 (15), 9203-9211, 2015.

Gantt, B., Sarwar, G., Xing, J., Simon, H., Schwede, D., Hutzell, W. T., Mathur, R, Saiz-Lopez, A.: The impact of iodide-mediated ozone deposition and halogen chemistry on surface ozone concentrations across the continental United States, Environmental Science & Technology, 51 (3), 1458-1466, 2017.

Sarwar, G., Gantt, B., Foley, K., Fahey, K., Spero, T.L., Kang, D., Mathur, R., Foroutan, H., Xing, J., Sherwen, T., Saiz-Lopez, A.: Influence of bromine and iodine chemistry on annual, seasonal, diurnal, and background ozone: CMAQ simulations over the Northern Hemisphere, Atmospheric Environment, 213, 395-404, 2019.

Thanks,
Golam Sarwar
Research Physical Scientist
Center for Environmental Measurement & Modeling
Office of Research and Development
US Environmental Protection Agency

From: Foley, Kristen <Foley.Kristen@epa.gov>
Sent: Friday, April 17, 2020 11:04 AM
To: Sarwar, Golam <Sarwar.Golam@epa.gov>
Subject: RE: Record of Percent Agreement for the 2020 STAA award

Dear Sarwar,

I agree with percentages.

Best regards,
Kristen

Kristen M. Foley, Ph.D.
Research Statistician
Atmospheric & Environmental Systems Modeling Division
U.S. Environmental Protection Agency
109 T.W. Alexander Dr., MD E243-04
Research Triangle Park, NC 27711
foley.kristen@epa.gov | 919 541 5367

From: Sarwar, Golam <Sarwar.Golam@epa.gov>
Sent: Friday, April 17, 2020 10:21 AM
To: Gantt, Brett <Gantt.Brett@epa.gov>; Schwede, Donna <Schwede.Donna@epa.gov>; Foley, Kristen <Foley.Kristen@epa.gov>; Mathur, Rohit <Mathur.Rohit@epa.gov>; Simon, Heather <Simon.Heather@epa.gov>; Hutzell, Bill <Hutzell.Bill@epa.gov>; Fahey, Kathleen <Fahey.Kathleen@epa.gov>; Spero, Tanya <Spero.Tanya@epa.gov>; Kang, Daiwen <Kang.Daiwen@epa.gov>
Subject: Record of Percent Agreement for the 2020 STAA award

Date: 4/17/2020
Subject: Record of Percent Agreement for the 2020 STAA award

Dear co-authors,

I plan to nominate the following publications for the 2020 Science and Technological Achievement Awards. The Award requires a record of percentage agreement which is shown below. Please reply to indicate agreement or disagreement to the proposed agreement.

Contributing authors	Organization	Percent agreement
Golam Sarwar	EPA/ORD/CEMM	30
Brett Gantt	EPA/OAR/OAQPS/AQAD	20
Kristen Foley	EPA/ORD/CEMM	10
R. Mathur	EPA/ORD/CEMM	9
Donna Schwede	EPA/ORD/CEMM	6
Alfonso Saiz-Lopez	Institute of Physical Chemistry, Spain	6
Jia Xing	Tsinghua University, China	4
K. Fahey	EPA/ORD/CEMM	3
D. Kang	EPA/ORD/CEMM	2
Heather Simon	EPA/OAR/OAQPS/AQAD	2
Tanya L. Spero	EPA/ORD/CEMM	2
W.T. Hutzell	EPA/ORD/CEMM	2
Hosein Foroutan	Virginia Tech, Blacksburg 24061, USA	2
Tomás Sherwen	University of York, UK	2

Article:

Sarwar, G., Gantt, B., Schwede, D., Foley, K., Mathur, R., Saiz-Lopez, A.: Impact of enhanced ozone deposition and halogen chemistry on tropospheric ozone over the Northern Hemisphere, Environmental Science & Technology, 49 (15), 9203-9211, 2015.

Gantt, B., Sarwar, G., Xing, J., Simon, H., Schwede, D., Hutzell, W. T., Mathur, R, Saiz-Lopez, A.: The impact of iodide-mediated ozone deposition and halogen chemistry on surface ozone concentrations across the continental United States, Environmental Science & Technology, 51 (3), 1458-1466, 2017.

Sarwar, G., Gantt, B., Foley, K., Fahey, K., Spero, T.L., Kang, D., Mathur, R., Foroutan, H., Xing, J., Sherwen, T., Saiz-Lopez, A.: Influence of bromine and iodine chemistry on annual, seasonal, diurnal, and background ozone: CMAQ simulations over the Northern Hemisphere, Atmospheric Environment, 213, 395-404, 2019.

Thanks,
Golam Sarwar
Research Physical Scientist
Center for Environmental Measurement & Modeling
Office of Research and Development
US Environmental Protection Agency

From: Schwede, Donna <Schwede.Donna@epa.gov>
Sent: Friday, April 17, 2020 10:51 AM
To: Sarwar, Golam <Sarwar.Golam@epa.gov>
Subject: RE: Record of Percent Agreement for the 2020 STAA award

Thank you for including me Sarwar. I really have done much since the early implementation, so 6% may be generous. If anyone else feels they deserve a higher percent, please feel free to decrease mine.

From: Sarwar, Golam <Sarwar.Golam@epa.gov>
Sent: Friday, April 17, 2020 10:21 AM
To: Gantt, Brett <Gantt.Brett@epa.gov>; Schwede, Donna <Schwede.Donna@epa.gov>; Foley, Kristen <Foley.Kristen@epa.gov>; Mathur, Rohit <Mathur.Rohit@epa.gov>; Simon, Heather <Simon.Heather@epa.gov>; Hutzell, Bill <Hutzell.Bill@epa.gov>; Fahey, Kathleen <Fahey.Kathleen@epa.gov>; Spero, Tanya <Spero.Tanya@epa.gov>; Kang, Daiwen <Kang.Daiwen@epa.gov>
Subject: Record of Percent Agreement for the 2020 STAA award

Date: 4/17/2020
Subject: Record of Percent Agreement for the 2020 STAA award

Dear co-authors,

I plan to nominate the following publications for the 2020 Science and Technological Achievement Awards. The Award requires a record of percentage agreement which is shown below. Please reply to indicate agreement or disagreement to the proposed agreement.

Contributing authors	Organization	Percent agreement
Golam Sarwar	EPA/ORD/CEMM	30
Brett Gantt	EPA/OAR/OAQPS/AQAD	20
Kristen Foley	EPA/ORD/CEMM	10
R. Mathur	EPA/ORD/CEMM	9
Donna Schwede	EPA/ORD/CEMM	6
Alfonso Saiz-Lopez	Institute of Physical Chemistry, Spain	6
Jia Xing	Tsinghua University, China	4
K. Fahey	EPA/ORD/CEMM	3
D. Kang	EPA/ORD/CEMM	2
Heather Simon	EPA/OAR/OAQPS/AQAD	2

Tanya L. Spero	EPA/ORD/CEMM	2
W.T. Hutzell	EPA/ORD/CEMM	2
Hosein Foroutan	Virginia Tech, Blacksburg 24061, USA	2
Tomás Sherwen	University of York, UK	2

Article:

Sarwar, G., Gantt, B., Schwede, D., Foley, K., Mathur, R., Saiz-Lopez, A.: Impact of enhanced ozone deposition and halogen chemistry on tropospheric ozone over the Northern Hemisphere, Environmental Science & Technology, 49 (15), 9203-9211, 2015.

Gantt, B., Sarwar, G., Xing, J., Simon, H., Schwede, D., Hutzell, W. T., Mathur, R, Saiz-Lopez, A.: The impact of iodide-mediated ozone deposition and halogen chemistry on surface ozone concentrations across the continental United States, Environmental Science & Technology, 51 (3), 1458-1466, 2017.

Sarwar, G., Gantt, B., Foley, K., Fahey, K., Spero, T.L., Kang, D., Mathur, R., Foroutan, H., Xing, J., Sherwen, T., Saiz-Lopez, A.: Influence of bromine and iodine chemistry on annual, seasonal, diurnal, and background ozone: CMAQ simulations over the Northern Hemisphere, Atmospheric Environment, 213, 395-404, 2019.

Thanks,
Golam Sarwar
Research Physical Scientist
Center for Environmental Measurement & Modeling
Office of Research and Development
US Environmental Protection Agency

From: Fahey, Kathleen <Fahey.Kathleen@epa.gov>
Sent: Friday, April 17, 2020 10:46 AM
To: Sarwar, Golam <Sarwar.Golam@epa.gov>
Subject: RE: Record of Percent Agreement for the 2020 STAA award

Hi, Sarwar-

Looks fine to me.

Good luck!
Kathleen

From: Sarwar, Golam <Sarwar.Golam@epa.gov>
Sent: Friday, April 17, 2020 10:21 AM
To: Gantt, Brett <Gantt.Brett@epa.gov>; Schwede, Donna <Schwede.Donna@epa.gov>; Foley, Kristen <Foley.Kristen@epa.gov>; Mathur, Rohit <Mathur.Rohit@epa.gov>; Simon, Heather <Simon.Heather@epa.gov>; Hutzell, Bill <Hutzell.Bill@epa.gov>; Fahey, Kathleen <Fahey.Kathleen@epa.gov>; Spero, Tanya <Spero.Tanya@epa.gov>; Kang, Daiwen <Kang.Daiwen@epa.gov>
Subject: Record of Percent Agreement for the 2020 STAA award

Date: 4/17/2020
Subject: Record of Percent Agreement for the 2020 STAA award

Dear co-authors,

I plan to nominate the following publications for the 2020 Science and Technological Achievement Awards. The Award requires a record of percentage agreement which is shown below. Please reply to indicate agreement or disagreement to the proposed agreement.

Contributing authors	Organization	Percent agreement
Golam Sarwar	EPA/ORD/CEMM	30

Brett Gantt	EPA/OAR/OAQPS/AQAD	20
Kristen Foley	EPA/ORD/CEMM	10
R. Mathur	EPA/ORD/CEMM	9
Donna Schwede	EPA/ORD/CEMM	6
Alfonso Saiz-Lopez	Institute of Physical Chemistry, Spain	6
Jia Xing	Tsinghua University, China	4
K. Fahey	EPA/ORD/CEMM	3
D. Kang	EPA/ORD/CEMM	2
Heather Simon	EPA/OAR/OAQPS/AQAD	2
Tanya L. Spero	EPA/ORD/CEMM	2
W.T. Hutzell	EPA/ORD/CEMM	2
Hosein Foroutan	Virginia Tech, Blacksburg 24061, USA	2
Tomás Sherwen	University of York, UK	2

Article:

Sarwar, G., Gantt, B., Schwede, D., Foley, K., Mathur, R., Saiz-Lopez, A.: Impact of enhanced ozone deposition and halogen chemistry on tropospheric ozone over the Northern Hemisphere, Environmental Science & Technology, 49 (15), 9203-9211, 2015.

Gantt, B., Sarwar, G., Xing, J., Simon, H., Schwede, D., Hutzell, W. T., Mathur, R, Saiz-Lopez, A.: The impact of iodide-mediated ozone deposition and halogen chemistry on surface ozone concentrations across the continental United States, Environmental Science & Technology, 51 (3), 1458-1466, 2017.

Sarwar, G., Gantt, B., Foley, K., Fahey, K., Spero, T.L., Kang, D., Mathur, R., Foroutan, H., Xing, J., Sherwen, T., Saiz-Lopez, A.: Influence of bromine and iodine chemistry on annual, seasonal, diurnal, and background ozone: CMAQ simulations over the Northern Hemisphere, Atmospheric Environment, 213, 395-404, 2019.

Thanks,
Golam Sarwar
Research Physical Scientist
Center for Environmental Measurement & Modeling
Office of Research and Development
US Environmental Protection Agency

From: Mathur, Rohit <Mathur.Rohit@epa.gov>
Sent: Friday, April 17, 2020 10:32 AM
To: Sarwar, Golam <Sarwar.Golam@epa.gov>
Subject: RE: Record of Percent Agreement for the 2020 STAA award

Hi Sarwar:
I agree with the percentage agreement as shown in the table in your email.
Thanks, Rohit

Rohit Mathur, Ph.D. | Center for Environmental Measurement & Modeling | Office of Research & Development | U.S. Environmental Protection Agency | (919) 541-1483 | mathur.rohit@epa.gov

From: Sarwar, Golam <Sarwar.Golam@epa.gov>
Sent: Friday, April 17, 2020 10:21 AM
To: Gantt, Brett <Gantt.Brett@epa.gov>; Schwede, Donna <Schwede.Donna@epa.gov>; Foley, Kristen <Foley.Kristen@epa.gov>; Mathur, Rohit <Mathur.Rohit@epa.gov>; Simon, Heather <Simon.Heather@epa.gov>; Hutzell, Bill <Hutzell.Bill@epa.gov>; Fahey, Kathleen <Fahey.Kathleen@epa.gov>; Spero, Tanya <Spero.Tanya@epa.gov>; Kang, Daiwen <Kang.Daiwen@epa.gov>
Subject: Record of Percent Agreement for the 2020 STAA award

Date: 4/17/2020

Subject: Record of Percent Agreement for the 2020 STAA award

Dear co-authors,

I plan to nominate the following publications for the 2020 Science and Technological Achievement Awards. The Award requires a record of percentage agreement which is shown below. Please reply to indicate agreement or disagreement to the proposed agreement.

Contributing authors	Organization	Percent agreement
Golam Sarwar	EPA/ORD/CEMM	30
Brett Gantt	EPA/OAR/OAQPS/AQAD	20
Kristen Foley	EPA/ORD/CEMM	10
R. Mathur	EPA/ORD/CEMM	9
Donna Schwede	EPA/ORD/CEMM	6
Alfonso Saiz-Lopez	Institute of Physical Chemistry, Spain	6
Jia Xing	Tsinghua University, China	4
K. Fahey	EPA/ORD/CEMM	3
D. Kang	EPA/ORD/CEMM	2
Heather Simon	EPA/OAR/OAQPS/AQAD	2
Tanya L. Spero	EPA/ORD/CEMM	2
W.T. Hutzell	EPA/ORD/CEMM	2
Hosein Foroutan	Virginia Tech, Blacksburg 24061, USA	2
Tomás Sherwen	University of York, UK	2

Article:

Sarwar, G., Gantt, B., Schwede, D., Foley, K., Mathur, R., Saiz-Lopez, A.: Impact of enhanced ozone deposition and halogen chemistry on tropospheric ozone over the Northern Hemisphere, Environmental Science & Technology, 49 (15), 9203-9211, 2015.

Gantt, B., Sarwar, G., Xing, J., Simon, H., Schwede, D., Hutzell, W. T., Mathur, R, Saiz-Lopez, A.: The impact of iodide-mediated ozone deposition and halogen chemistry on surface ozone concentrations across the continental United States, Environmental Science & Technology, 51 (3), 1458-1466, 2017.

Sarwar, G., Gantt, B., Foley, K., Fahey, K., Spero, T.L., Kang, D., Mathur, R., Foroutan, H., Xing, J., Sherwen, T., Saiz-Lopez, A.: Influence of bromine and iodine chemistry on annual, seasonal, diurnal, and background ozone: CMAQ simulations over the Northern Hemisphere, Atmospheric Environment, 213, 395-404, 2019.

Thanks,
Golam Sarwar
Research Physical Scientist
Center for Environmental Measurement & Modeling
Office of Research and Development
US Environmental Protection Agency

From: Simon, Heather <Simon.Heather@epa.gov>
Sent: Friday, April 17, 2020 10:23 AM
To: Sarwar, Golam <Sarwar.Golam@epa.gov>
Subject: RE: Record of Percent Agreement for the 2020 STAA award

Hi Sarwar,

I concur with my percent contribution (2%) listed below.

-Heather

Heather Simon, PhD
Air Quality Modeling Group
Office of Air Quality Planning and Standards
U.S. Environmental Protection Agency

Tel: (919) 541-1803

From: Sarwar, Golam <Sarwar.Golam@epa.gov>
Sent: Friday, April 17, 2020 10:21 AM
To: Gantt, Brett <Gantt.Brett@epa.gov>; Schwede, Donna <Schwede.Donna@epa.gov>; Foley, Kristen <Foley.Kristen@epa.gov>; Mathur, Rohit <Mathur.Rohit@epa.gov>; Simon, Heather <Simon.Heather@epa.gov>; Hutzell, Bill <Hutzell.Bill@epa.gov>; Fahey, Kathleen <Fahey.Kathleen@epa.gov>; Spero, Tanya <Spero.Tanya@epa.gov>; Kang, Daiwen <Kang.Daiwen@epa.gov>
Subject: Record of Percent Agreement for the 2020 STAA award

Date: 4/17/2020
Subject: Record of Percent Agreement for the 2020 STAA award

Dear co-authors,

I plan to nominate the following publications for the 2020 Science and Technological Achievement Awards. The Award requires a record of percentage agreement which is shown below. Please reply to indicate agreement or disagreement to the proposed agreement.

Contributing authors	Organization	Percent agreement
Golam Sarwar	EPA/ORD/CEMM	30
Brett Gantt	EPA/OAR/OAQPS/AQAD	20
Kristen Foley	EPA/ORD/CEMM	10
R. Mathur	EPA/ORD/CEMM	9
Donna Schwede	EPA/ORD/CEMM	6
Alfonso Saiz-Lopez	Institute of Physical Chemistry, Spain	6
Jia Xing	Tsinghua University, China	4
K. Fahey	EPA/ORD/CEMM	3
D. Kang	EPA/ORD/CEMM	2
Heather Simon	EPA/OAR/OAQPS/AQAD	2
Tanya L. Spero	EPA/ORD/CEMM	2
W.T. Hutzell	EPA/ORD/CEMM	2
Hosein Foroutan	Virginia Tech, Blacksburg 24061, USA	2
Tomás Sherwen	University of York, UK	2

Article:

Sarwar, G., Gantt, B., Schwede, D., Foley, K., Mathur, R., Saiz-Lopez, A.: Impact of enhanced ozone deposition and halogen chemistry on tropospheric ozone over the Northern Hemisphere, Environmental Science & Technology, 49 (15), 9203-9211, 2015.

Gantt, B., Sarwar, G., Xing, J., Simon, H., Schwede, D., Hutzell, W. T., Mathur, R, Saiz-Lopez, A.: The impact of iodide-mediated ozone deposition and halogen chemistry on surface ozone concentrations across the continental United States, Environmental Science & Technology, 51 (3), 1458-1466, 2017.

Sarwar, G., Gantt, B., Foley, K., Fahey, K., Spero, T.L., Kang, D., Mathur, R., Foroutan, H., Xing, J., Sherwen, T., Saiz-Lopez, A.: Influence of bromine and iodine chemistry on annual, seasonal, diurnal, and background ozone: CMAQ simulations over the Northern Hemisphere, Atmospheric Environment, 213, 395-404, 2019.

Thanks,
Golam Sarwar

Research Physical Scientist
Center for Environmental Measurement & Modeling
Office of Research and Development
US Environmental Protection Agency

Table of Contents

General_Authors_Publications.....2
LI-266212_Barron_et_al_2015_-_Barron-MOA-STAA-2020.....12
LI-266213_Carriger_et_al_2016_-_Barron-MOA-STAA-2020.....18
LI-266214_Martin_et_al_2015_-_Barron-MOA-STAA-2020.....32
Barron-MOA-STAA-2020-percent_contribution_agreements.....52
Barron_et_al_2015_-_Barron-MOA-STAA-2020.....55
Carriger_et_al_2016_-_Barron-MOA-STAA-2020.....61
Martin_et_al_2015_-_Barron-MOA-STAA-2020.....75

United States Environmental Protection Agency
Washington, DC 20460

STAA REPORT FOR THE SCIENTIST NOMINATIONS

General Information:

Nomination ID/App ID:	20-107
Research Category Primary:	Other Environmental Research (OR)
Research Category Secondary:	
Laboratory/Office Name:	ORD/CEMM/GEMMD
Nomination Entered By:	Matthew Harwell

Eligibility Checklist:

[Y] The nominated publication(s) has not been submitted to a previous STAA competition.

[Y] The nominated publication(s) was published on or before January 1, 2017 and on or after January 1,2012

[Y] The principal author was an EPA employee or a PHS employee assigned to EPA when the research was performed

[Y] The EPA authors (includes PHS employees assigned to EPA) contributed collectively a minimum of 50% toward the publication(s)

Nominating Official Name:	Susan George
Nominating Official Title:	DIRECTOR, GULF ECOLOGY DIVISION
Nominating OfficialEmail:	george.elizabeth@epa.gov
STAA Coordinator Name:	Kathleen Wiser
STAA Coordinator Email:	wiser.kathi@epa.gov

Justifications:

Justification 1:

Mode of toxic action (MOA) has been recognized as a key determinant of chemical toxicity and as an alternative to chemical class-based predictive toxicity modeling. However, global development of quantitative structure activity relationship (QSAR) and other predictive models has been limited by the availability of a comprehensive high quality MOA database. Together, the three papers advance the development and application of mode of action classification in aquatic toxicology by incorporating state of the science mechanism-based toxic-action classification. MOAtox supports EPA's strategic goal to provide cleaner, safer and healthier environments by providing a system of MOA classification that will facilitate knowledge-based chemical screening and assessments based on mode of toxic action.

The research was invited and presented at the *"Establishment of the Eco-TTC Approach for Environmental Risk Assessment of Chemicals: An International Workshop"* held in Ottawa, ON, Canada on September 18 and 19, 2017.

Overall, these publications have been cited (Google Scholar) **88 times** and "viewed" **375 times**

Barron MG (70), Lilavois CR (20), Martin TM. 2015 (10). MOAtox: a comprehensive mode of action and acute aquatic toxicity database for predictive model development. *Aquat Tox* 16:102-107.

58 cites; 118 views

Carriger JF (45), Martin TM (20), Barron MG (35). 2016.

A Bayesian network model for predicting aquatic toxicity mode of action using two dimensional theoretical molecular descriptors. *Aquat Tox* 180:11-24.

11 cites, 66 views

Martin TM (45), Young DM (10), Lilavois CR (10), Barron MG (35). 2015. Comparison of global and mode of action-based models for aquatic toxicity. *SAR QSAR Environ Res* 26:245-262.

19 cites, 191 views

Justification 2A:

The three publications are linked by the development and application of the MOAtox database of mode of action (MOA) classifications. Barron et al. (2015) developed the MOAtox database and MOA classification system. Martin et al. (2015) used the MOAtox classification system of Barron et al. (2015) to build and validate models to predict MOA in aquatic organisms using molecular descriptors of chemical structure. Carriger et al. (2016) then used MOAtox and the molecular descriptor models of Martin et al. to develop and apply a Bayesian network that was able to select the most important descriptors and classify MOA was 80% accuracy.

Justification 2B:

Mace Barron:

2017-2018 Scientific and Technological Achievement Award (STAA) – Level 3 Award:

Awkerman, J.A., S. Raimondo, C. R. Jackson, and M. G. Barron. 2014. Augmenting species sensitivity distributions with interspecies toxicity estimation models. Environmental Toxicology and Chemistry. 33: 688-695

Willming, M. M., C. R. Lilavois, M.G. Barron, and S. Raimondo. 2016. Acute toxicity prediction to threatened and endangered species using Interspecies Correlation Estimation (ICE) models. Environ Sci Technol. 50: 10700-10707

2017-18 Scientific and Technological Achievement Award (STAA) – Level 3:

Awkerman, J.A., B. Hemmer, A. Almario, C.R. Jackson, M.G. Barron, S. Raimondo. 2016. Spatially explicit risk assessment of estuarine fish after Deepwater Horizon Oil spill: trade-off in complexity and parsimony. Ecological Applications. 26:1708-1720.

Raimondo, S., C.R. Jackson, J. Krzykwa, B.L. Hemmer, M.G. Barron. 2014. Developmental toxicity of Louisiana crude oiled-spiked sediment to zebrafish. Ecotoxicology and Environmental Safety. 108: 265-272.

Raimondo, S., B.L. Hemmer, C.R. Jackson, J. Krzykwa, A. Almario, J.A. Awkerman, M.G. Barron. 2016. Effects of Louisiana crude oil on the sheepshead minnow (Cyrpinodon variegatus) during a life-cycle exposure to laboratory oiled sediment. Environmental Toxicology. 31: 1627-1639.

2015-2016 Scientific and Technological Achievement Award (STAA) - Honorable Mention, Assessing Impacts of Oil and Oil Products on Marine and Estuarine Ecosystems. Barron, M., M. Hemmer, and C. Jackson. Development of aquatic toxicity benchmarks for oil products using species sensitivity distributions. Integrated Environmental Assessment and Management. Allen Press, Inc., Lawrence, KS, USA, 9(4): 610-615, (2013).

John Carriger: No 2016-2020 STAA awards

Crystal Lilavois:

2015-2016 Scientific and Technological Achievement Award (STAA) - Honorable Mention, Assessing Impacts of Oil and Oil Products on Marine and Estuarine Ecosystems. Barron, M., M. Hemmer, and C. Jackson. Development of aquatic toxicity benchmarks for oil products using species sensitivity distributions. Integrated Environmental Assessment and Management. Allen Press, Inc., Lawrence, KS, USA, 9(4): 610-615, (2013).

2017-2018 Scientific and Technological Achievement Award (STAA) – Level 3 Award:

Awkerman, J.A., S. Raimondo, C. R. Jackson, and M. G. Barron. 2014. Augmenting species sensitivity distributions with interspecies toxicity estimation models. Environmental Toxicology and Chemistry. 33: 688-695

Willming, M. M., C. R. Lilavois, M.G. Barron, and S. Raimondo. 2016. Acute toxicity prediction to threatened and endangered species using Interspecies Correlation Estimation (ICE) models. Environ Sci Technol. 50: 10700-10707

2017-18 Scientific and Technological Achievement Award (STAA) – Level 3:

Awkerman, J.A., B. Hemmer, A. Almario, C.R. Jackson, M.G. Barron, S. Raimondo. 2016. Spatially explicit risk assessment of estuarine fish after Deepwater Horizon Oil spill: trade-off in complexity and parsimony. Ecological Applications. 26:1708-1720.

Raimondo, S., C.R. Jackson, J. Krzykwa, B.L. Hemmer, M.G. Barron. 2014. Developmental toxicity of Louisiana crude oiled-spiked sediment to zebrafish. Ecotoxicology and Environmental Safety. 108: 265-272.

Raimondo, S., B.L. Hemmer, C.R. Jackson, J. Krzykwa, A. Almario, J.A. Awkerman, M.G. Barron. 2016. Effects of Louisiana crude oil on the sheepshead minnow (Cyrpinodon variegatus) during a life-cycle exposure to laboratory oiled sediment. Environmental Toxicology. 31: 1627-1639.

Todd Martin: No 2016-2020 STAA awards

Doug Young: No 2016-2020 STAA awards

Justification 2C:

This is the first STAA submission for MOAtox related publications. There is no overlap with previous STAA awards or submissions.

Justification 2D:

There is no overlap of SI with any previous STAA awards or submissions.

Justification 2E:

There are no concurrent nominations relating to this STAA award submission.

Justification 3A:

The MOAtox database and classification system has been incorporated into the international computational tool EnviroTox (https://envirotoxdatabase.org/) as one a mode of action assignment scheme. The MOAtox system is also the basis of aquatic toxicity mode of action classification in EPA's T.E.S.T structure activity modeling tool (www.epa.gov/chemical-research/toxicity-estimation-software-tool-test). Additionally, the paper has been utilized and cited by authors in over 20 countries.

Justification 3B:

Each of the three articles had the following external peer review: (1) each article was reviewed by one reviewer outside of EPA as part of the initial EPA clearance; and (2) each article was then reviewed by two anonymous peer reviewers as part of each journal's publication requirement.

AUTHORS

Contributing Author

Author Name: Todd Martin

Professional Title:		Salutation:	
Email:	martin.todd@epa.gov	Organization:	
Mailing Address:			
Street Line 1:	USEPA 26 West Martin Luther King Drive Mail Code: 483		
City:	Cincinnati		
Zip Code:	45268	State:	OH
At time of research was:	EPA Employee		
Separation Date:			
% of Effort:	25		

Contributing Author

Author Name:	Crystal Lilavois		
Professional Title:		Salutation:	
Email:	lilavois.crystal@epa.gov	Organization:	
Mailing Address:			
Street Line 1:	Office of Research and Development, U.S. EPA 1 Sabine Island Drive		
City:	Gulf Breeze		
Zip Code:	32561	State:	FL
At time of research was:	EPA Employee		
Separation Date:			
% of Effort:	10		

Contributing Author

Author Name:	Mace Barron		
Professional Title:		Salutation:	
Email:	barron.mace@epa.gov	Organization:	
Mailing Address:			
Street Line 1:	Office of Research and Development, U.S. EPA 1 Sabine Island Drive		
City:	Gulf Breeze		
Zip Code:	32561	State:	FL
At time of research was:	EPA Employee		
Separation Date:			
% of Effort:	45		

Contributing Author

Author Name:	Douglas Young		
Professional Title:		Salutation:	
Email:	young.douglas@epa.gov	Organization:	
Mailing Address:			
Street Line 1:	USEPA 26 West Martin Luther King Drive Mail Code: 236		
City:	Cincinnati		
Zip Code:		State:	OH
At time of research was:	EPA Employee		
Separation Date:			
% of Effort:	3		

Contributing Author

Author Name:	John Carriger		
Professional Title:		Salutation:	
Email:	carriger.john@epa.gov	Organization:	
Mailing Address:			
Street Line 1:	USEPA 26 West Martin Luther King Drive Mail Code: 190		
City:	Cincinnati		
Zip Code:		State:	OH
At time of research was:	EPA Employee		
Separation Date:			
% of Effort:	17		

PUBLICATIONS

Publication 1:

Publication Title:	MOAtox: a comprehensive mode of action and acute aquatic toxicity database for predictive model deve		
Publication Date:	Wed Apr 01 00:00:00 GMT 2015		
Journal/Publication Method:	Aquatic Toxicology		
All Author(s):			
Volume:	16	Number:	1
Pages:	102-107	Immediately Index:	Immediately Index:
Citation ½ Life:	7.0	Impact Factor:	3.557

Publication 2:

Publication Title:	A Bayesian network model for predicting aquatic toxicity mode of action using two dimensional theore		
Publication Date:	Tue Nov 01 00:00:00 GMT 2016		
Journal/Publication Method:	Aquatic Toxicology		
All Author(s):			
Volume:	180	Number:	1
Pages:	11-24	Immediately Index:	Immediately Index:
Citation ½ Life:	7.0	Impact Factor:	4.129

Publication 3:

Publication Title:	Comparison of global and mode of action-based models for aquatic toxicity		
Publication Date:	Wed Mar 18 00:00:00 GMT 2015		
Journal/Publication Method:	SAR and QSAR in Environmental Research		
All Author(s):			
Volume:	26	Number:	3
Pages:	245-262	Immediately Index:	Immediately Index:
Citation ½ Life:	6.5	Impact Factor:	2.287

Aquatic Toxicology 161 (2015) 102–107

Contents lists available at ScienceDirect

Aquatic Toxicology

journal homepage: www.elsevier.com/locate/aquatox

MOAtox: A comprehensive mode of action and acute aquatic toxicity database for predictive model development

M.G. Barron[a,*], C.R. Lilavois[a], T.M. Martin[b]

[a] U.S. Environmental Protection Agency, Office of Research Development, Gulf Ecology Division, Gulf Breeze, FL, USA
[b] U.S. Environmental Protection Agency, Office of Research Development, Sustainable Technology Division, Cincinnati, OH, USA

ARTICLE INFO

Article history:
Received 19 November 2014
Received in revised form 31 January 2015
Accepted 2 February 2015
Available online 7 February 2015

Keywords:
QSAR
Toxicity
Model
Mode of action
Fish
Invertebrate

ABSTRACT

The mode of toxic action (MOA) has been recognized as a key determinant of chemical toxicity and as an alternative to chemical class-based predictive toxicity modeling. However, the development of quantitative structure activity relationship (QSAR) and other models has been limited by the availability of comprehensive high quality MOA and toxicity databases. The current study developed a dataset of MOA assignments for 1213 chemicals that included a diversity of metals, pesticides, and other organic compounds that encompassed six broad and 31 specific MOAs. MOA assignments were made using a combination of high confidence approaches that included international consensus classifications, QSAR predictions, and weight of evidence professional judgment based on an assessment of structure and literature information. A toxicity database of 674 acute values linked to chemical MOA was developed for fish and invertebrates. Additionally, species-specific measured or high confidence estimated acute values were developed for the four aquatic species with the most reported toxicity values: rainbow trout (*Oncorhynchus mykiss*), fathead minnow (*Pimephales promelas*), bluegill (*Lepomis macrochirus*), and the cladoceran (*Daphnia magna*). Measured acute toxicity values met strict standardization and quality assurance requirements. Toxicity values for chemicals with missing species-specific data were estimated using established interspecies correlation models and procedures (Web-ICE; http://epa.gov/ceampubl/fchain/webice/), with the highest confidence values selected. The resulting dataset of MOA assignments and paired toxicity values are provided in spreadsheet format as a comprehensive standardized dataset available for predictive aquatic toxicology model development.

Published by Elsevier B.V.

1. Introduction

In aquatic toxicology, mode of action (MOA) has been defined phenomenologically based on whole organism responses, identified from effects at the cellular or organ level, or based on the primary mechanism of toxicity initiated at the receptor level (Barron et al., 2002; Suter, 2007). MOA has been recognized as a key determinant of chemical toxicity and as an alternative to chemical class-based predictive toxicity modeling. Early work on determining chemical mode of action in aquatic organisms focused on industrial compounds that were largely of moderate polarity, low toxicity and acted through narcosis, a non-specific reversible baseline mode of whole organism toxicity (Konemann, 1981; Call et al., 1985). Based on a suite of behavioral/morphological responses in rainbow trout (*Onchorhynchus mykiss*), McKim et al. (1987) established several modes of action including narcosis, oxidative phosphorylation uncoupler, acetylcholinesterase (AChE) inhibitor, or stimulant-like. Verhaar et al. (1992) categorized chemicals into one of four MOA classes based on structural rules: (1) inert compounds causing narcosis, (2) less inert more toxic compounds causing polar narcosis, (3) reactive compounds with enhanced toxicity, and (4) compounds with specific or receptor mediated toxicity. Russom et al. (1997) utilized an extensive fathead minnow (*Pimephales promelas*) acute toxicity and behavioral database to extend MOA categorization to three narcosis MOAs and five specific MOAs (AChE inhibition, uncoupling, reactivity, seizure mechanisms, and respiratory inhibition). Other approaches to MOA assignment and categorization have included assessments of *in vitro* activity and cross species receptor homology for pharmaceutical compounds (Escher et al., 2005; Christen et al., 2010).

In contrast to empirical and rule-based categorization approaches, Martin et al. (2013) utilized two dimensional descriptor assignments and machine-based learning algorithms to develop a computational chemistry approach to MOA assignment

* Corresponding author at: U.S. Environmental Protection Agency, Office of Research and Development, Gulf Ecology Division, 1 Sabine Island Drive, Gulf Breeze, FL 32561, USA. Tel.: +1 850 934 9223; fax: +1 850 934 2402.
E-mail address: Barron.mace@epa.gov (M.G. Barron).

http://dx.doi.org/10.1016/j.aquatox.2015.02.001
0166-445X/Published by Elsevier B.V.

for six broad and seven specific MOAs. This computational chemistry-based approach calculated up to 700 structural and property descriptors for each chemical and developed prediction models based on multi-linear regression models and decision tree algorithms. As part of that work, a dataset of 924 acute aquatic toxicity MOA assignments were developed using a combination of high confidence approaches that included international consensus classifications, quantitative structure activity relationship (QSAR) predictions, and weight of evidence professional judgment based on an assessment of structure and literature information.

The objective of the current study was to develop a comprehensive standardized dataset of aquatic toxicity values and MOA assignments. The current research expands the Martin et al. (2013) dataset to over 1200 chemicals including metals and organometallics, increases the number of specific MOA categories, and refines some of the pesticide neurotoxicity MOA categories to be less general and more mechanism-based. The categorization scheme was comprised of six broad and 31 specific MOA categories that encompassed the major acute toxicity MOAs reported in aquatic invertebrates and fish. Chemicals in the MOA dataset were then linked to a dataset of high confidence acute aquatic toxicity values developed for this study to create a database of 674 chemicals with species-specific acute toxicity values. The MOA-aquatic toxicity database (MOAtox) development focused on the four most commonly reported aquatic test species with toxicity endpoint data in the ECOTOX database (USEPA, 2014): rainbow trout, the cladoceran (*Daphnia magna*), fathead minnow, and bluegill (*Lepomis macrochirus*). These species represented 22% of the 300,000 ECOTOX records with toxicity endpoint data (Fairbrother et al., 2014). Additionally, generic fish and aquatic invertebrate acute toxicity values were developed from the geometric mean of all measured toxicity values that met strict quality assurance and standardization requirements. Toxicity values for chemicals with missing species-specific data were estimated using established interspecies correlation models and procedures (Web-ICE; http://epa.gov/ceampubl/fchain/webice/), with the highest confidence values selected (Raimondo et al., 2010, 2013). The development of this comprehensive standardized dataset is intended to facilitate the development of predictive aquatic toxicity and MOA models. The larger MOA dataset could support MOA-based assessments of chemical mixtures, such as applying a toxic units approach to chemicals with the same specific MOA.

2. Methods

2.1. MOA category and dataset development

An aquatic toxicity MOA categorization scheme was developed for a diversity of metals, organometallics, pesticides, and other organics that appear in the ECOTOX database (USEPA, 2014), based on earlier work determining chemical modes of acute toxic action in fish (Konemann 1981; Call et al., 1985; McKim et al., 1987; Russom et al., 1997; USEPA, 2012; Martin et al., 2013). The categorization scheme was comprised of six broad and 31 specific MOA categories that encompassed the major MOAs reported in aquatic invertebrates and fish. Broad MOA categories included narcosis, AChE inhibition, neurotoxicity, iono/osmoregulatory/circulatory impairment, reactivity, and electron transport inhibition (Supplementary information; Table S1). Specific MOAs were developed as subcategories of the broad MOAs based on either chemical structure or known mechanism of action. A total of 1213 chemicals were assigned to a broad and specific MOA category following the general procedures of Martin et al. (2013). This involved using a combination of high confidence assignments including, international consensus classifications (*e.g.*, IRAC, 2014), QSAR predictions (USEPA, 2012), and weight of evidence professional judgment by considering a combination of assessment of structure (*e.g.*, analogous structure; moiety/functional group presence) and literature information on MOA, mechanism of action and toxicity pathways (*e.g.*, Russom et al., 1997; Nendza and Müller 2000; Schüürmann et al., 2003; Spycher et al., 2004). Chemicals with an uncertain MOA assignment were excluded from the database.

2.2. Toxicity dataset development

Toxicity dataset development focused on determining acute toxicity values for three fish species (rainbow trout, fathead minnow, and bluegill) and *Daphnia* for chemicals in the MOA dataset. These four taxa were selected, because they have been the most commonly reported aquatic test species with acute toxicity endpoint data in the ECOTOX database (USEPA, 2014). First, measured aquatic toxicity values were obtained from the US EPA's ICE Aquatic Toxicity Database (Raimondo et al., 2013a). This database is comprised of 5500 acute EC/LC50 values for 180 species and 1260 chemicals that have been obtained from a diversity of sources (primarily ECOTOX) then subjected to a rigorous quality assurance review and standardization procedure (Raimondo et al., 2010). Each toxicity record included in the dataset met specific requirements for: (1) test chemical identity and purity, (2) test procedures, conditions, reporting, and quality control, and (3) test organism life stage. Additionally, toxicity values for selected compounds were normalized based on water quality parameters, and outliers and central tendency were determined in cases of multiple reported values as documented in Raimondo et al. (2013a). Mean fish and mean aquatic invertebrate toxicity values were also computed from the geometric mean of all standardized values available for each chemical. Similarly, a mean *Daphnia* genus value was computed from all standardized values for each chemical with available data.

Missing species-specific toxicity data were then estimated using established interspecies correlation estimation (ICE) models available in the USEPA Web-ICE tool (http://epa.gov/ceampubl/fchain/webice/; Raimondo et al., 2010, 2013b). ICE models are log-linear least square regressions of chemical sensitivity relationships between a surrogate and predicted taxon. Toxicity values in the Aquatic Toxicity Database for all available surrogate species were used to estimate acute toxicity for those chemicals with missing measured data for rainbow trout, *D. magna*, fathead minnow, or bluegill. This procedure resulted in multiple estimated values for many chemicals because ICE models were available for multiple surrogate species.

2.3. Determination of best estimated value

A systematic process was used to determine a best toxicity estimate for any of the four species with multiple predicted values based on model uncertainty and performance criteria. First, each surrogate species ICE model was evaluated to determine if it met the following statistical criteria: mean square error of less than or equal to 0.94, coefficient of determination greater than 0.6, and the upper 95th percentile confidence limit was within five fold of the predicted toxicity value. If multiple models met all three statistical criteria, these models were evaluated to determine if they met the following additional criteria: taxonomic distance between the surrogate and predicted species was less than or equal to four (same Class), model cross validation success was greater than 85%, and degrees of freedom were greater than 8. If multiple models met all criteria, the best estimated value was computed from the geometric mean of the model predicted values.

2.4. Ranking and assessment of estimated values

Each estimated value in the MOAtox database received a qualitative ranking based on the number of statistical criteria met (Supplementary information; Table S2): level P1 (highest confidence estimate; all three model criteria met), P2 (two met), P3 (one met), and P4 (lowest confidence; no statistical criteria met). Estimated values were not included in the MOAtox database for those chemicals with species-specific measured values. However, toxicity values were also estimated and ranked for those chemicals with measured values to allow an assessment of accuracy. Accuracy was determined from the proportion of species-specific estimated values within two, five, and ten fold of measured values. Correlations between species-specific estimated and measured values were determined from simple log–log linear regressions.

3. Results

3.1. MOA assignments

The MOA dataset was comprised of 1213 chemicals assigned to one of six broad acute toxicity MOA categories and one of 31 specific MOA subcategories (Tables 1, S1, and S2). The predominant MOAs and chemical classes in the database (>40 chemicals) were AChE inhibition (carbamates and organophosphates), narcosis (nonpolar, polar, and ester compounds), neurotoxicity (pyrethroids and alicyclics), and uncouplers of oxidative phosphorylation (*e.g.*, polychlorinated and nitrophenols and amines) (Tables 1 and S1).

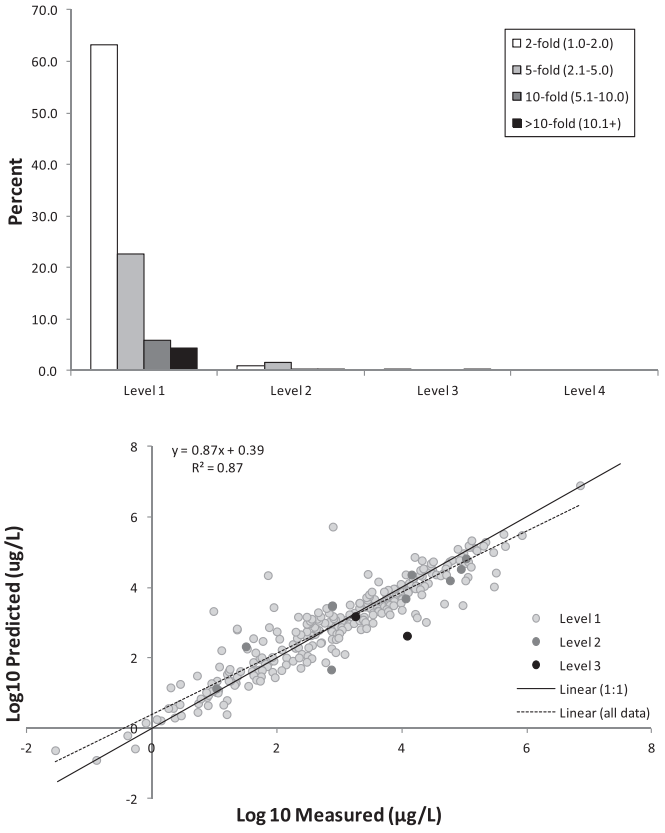

Fig. 1. Prediction accuracy of estimated toxicity values by uncertainty level (upper panel), and correlation between measured and predicted toxicity values (lower panel) in bluegill.

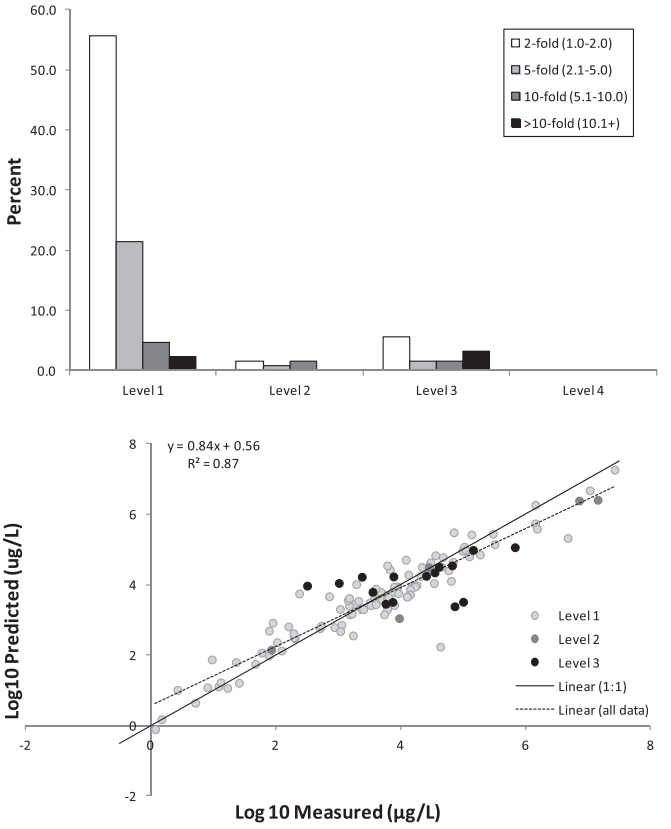

Fig. 2. Prediction accuracy of estimated toxicity values by uncertainty level (upper panel), and correlation between measured and predicted toxicity values (lower panel) in fathead minnows.

3.2. Toxicity values

Of the 1213 chemicals in the MOA dataset, 614 had measured values in fish and 424 had measured values in invertebrates determined as the geomeans of standardized acute toxicity data (Table 2). There were 671 chemicals in the MOA dataset that had either a measured or estimated taxa-specific acute toxicity value for *Daphnia*, bluegill, fathead minnow, or rainbow trout (Table 2). Estimated values for the three fish species were primarily comprised of level 1 (highest confidence; >85%) values, whereas, in *D. magna* the majority of estimated values were level 3 (62%) (Table 2 and Figs. 1–4). Over 60% of the estimated values in the three fish species were within two fold of standardized measured values, and 87% were within five fold (Table 2 and Figs. 1–4). Prediction accuracy was lower for *D. magna*, with only 61% of estimated values within five fold of measured values (Table 2 and Fig. 4). In the three fish species, estimated values were highly correlated with measured values ($R^2 > 0.87$; Figs. 1–4), whereas, there was greater variance in the relationship for *D. magna* ($R^2 = 0.69$; Fig. 4).

4. Discussion

In aquatic toxicology, MOA-based toxicity prediction has primarily focused on organic chemicals acting through polar and nonpolar narcosis. Although compounds causing narcosis are structurally diverse and represent the largest class of organic chemicals produced globally, the narcosis MOA does not encompass more toxic compounds, such as pesticides, metals, and other chemicals acting through specific mechanisms and toxicity pathways. The current study builds upon the earlier work of Konemann (1981), Russom et al. (1997), Verhaar et al. (2000), and others to expand the chemical coverage and MOA categories to include

Table 1
Description of mode of action (MOA) categories used in the MOAtox database and number of chemicals within each MOA.[a]

Broad MOA (*n*)[b]	Specific MOA	Chemical class	Structural features	Example chemicals	#Chemicals in Database[a]	
					MOA	MOAtox
AChE inhibition (285)	Carbamate	Carbamate insecticides	Oxime and methyl carbamate	Aldicarb, carbaryl, methiocarb	74	19
	Organophosphate	Organophosphorus insecticides	Organophosphates, organothiophosphates	Chlorpyrifos, malathion, terbufos	211	58
Iono/osmoregulatory/ circulatory impairment (55)	Metallic iono/osmoregulatory impairment	Heavy metals, transition metals	Divalent metals	Copper, zinc	18	15
	Other	Inorganics	Chemical specific	Ammonia	6	4
	Methemoglobinemia	Chemical specific, nitrites	Chemical specific	Aminopropiophenone, sodium nitrite	6	1
	Anticoagulation	Coumarin rodenticides	Coumarin moiety	Dicoumarol, bromadiolone	25	7
Narcosis (465)[c]	Ester	Mono or diesters,	Diverse structures, non-reactive	Bromoxynil butyrate, methyl acetate, phenyl salicylate	48	41
	Non-polar	Neutral organics	Moderate polarity	Benzene, ethanol, metolachlor	347	283
	Polar	Polar organics	Single nitro or <3 halogens	4-Nonylphenol, pyridine, triclosan	61	55
Neurotoxicity (200)	Alicyclic GABA antagonism	Acyclic organochlorines	Cyclodiene, hexachlorocyclohexane	Aldrin, lindane	42	17
	Diphenyl sodium channel modulation	Diphenyl organochlorines	Halogenated bridged diphenyls	DDT, methoxychlor	11	7
	GABA agonism	Lactone insecticides	Macrocyclic lactones	Abamectin	16	2
	Other	Various	Chemical specific	Phenobarbital	8	3
	Pyrazole GABA antagonism	Pyrazole insecticides	Phenyl pyrazoles,	Fipronil,	6	1
	Pyrethroid sodium channel modulation	Pyrethroid insecticide	Pyrethroid ether, oxime, ester moieties	Cypermethrin,	102	24
	Sodium channel blocking	Oxidiazine insecticides	Oxidiazine moiety	Indoxacarb	3	1
	Nicotinic acetylcholine receptor agonism	Neonicotinoid insecticides	Nicotine analogs	Acetamiprid, dinotefuran	8	6
	Strychnine	Strychnines	Strychnine moiety	Strychnine	4	1
Reactivity (111)	Acrylate	Acrylates	Acrylate moiety	Acrylonitrile	8	7
	Alkylation	Various	Reactive leaving group (*e.g.*, alkene)	2-Propenamide	38	30
	Carbonyl	Various	Reactive carbonyl	Formalin	13	11
	Chromate	Chromates	Chromate moiety	Sodium dichromate	3	0
	Cyanate/nitrile	Cyanates, nitriles	Cyanate or nitrile moiety	Allyl isothiocyanate	9	8
	Di/trinitroaromatic	Nitrobenzenes	Poly nitrobenzene moiety	2,3,5-Trinitrobenzene	14	14
	Hydrazine	Hydrazines	Hydrazine moiety	Monomethylhydrazine	4	3
	Other	Various	Chemical specific	Quinoline	19	14
	Phosphide	Phosphides	Phosphide moiety	Calcium phosphide	3	0
Electron transport inhibition (97)	Oxidative phosphorylation inhibition	Inorganics, antimycins trialkyltins	Chemical specific	Cyanide, antimycin a, tributyl tin	20	13
	Uncoupling oxidative phosphorylation	Nitro or halo-phenols, pyridines, anilines	Chemical specific	2,4-Dinitrophenol, pentachlorophenol	55	21
	Arsenical respiratory inhibition	Arsenicals	Arsenites, arsenates	Sodium arsenite	22	1

[a] See Supplemental Tables S1 and S2 for complete databases.
[b] Total number of chemicals within the broad MOA category.
[c] Includes 9 chemicals with a specific MOA of NA (not assigned).

metallic compounds, new MOAs (*e.g.*, methemaglobinemia), and subcategories of neurotoxicity and electron transport inhibition consistent with the IRAC international insecticide classification system (IRAC, 2014). The categorization scheme was comprised of six broad and 31 specific MOA categories that encompassed the major MOAs reported in aquatic invertebrates and fish. The reactivity MOA included nine structure-based subcategories determined largely from Russom et al. (1997) and U.S. EPA QSAR models

Table 2
Number of chemicals with measured and predicted toxicity values for each taxa group within the MOAtox database (Table S2).

Taxa	Measured toxicity values	Species-specific estimated toxicity values[a]				Total number
		Level 1	Level 2	Level 3	Level 4	
Bluegill	306	323	36	3	0	668
Fathead	298	314	6	48	1	667
Rainbow trout	336	294	2	35	0	667
Daphnia[b]	328	54	12	263	12	669
Fish	614	NA	NA	NA	NA	615
Invertebrates	424	NA	NA	NA	NA	425

[a] Model uncertainty level of estimated taxa-specific values (1 highest confidence). NA: not applicable.
[b] Measured values include *D. magna* (319), *D. pulex* (15), *D. galeata* (2), and *D. carinata* (2). Estimated values are for *D. magna*.

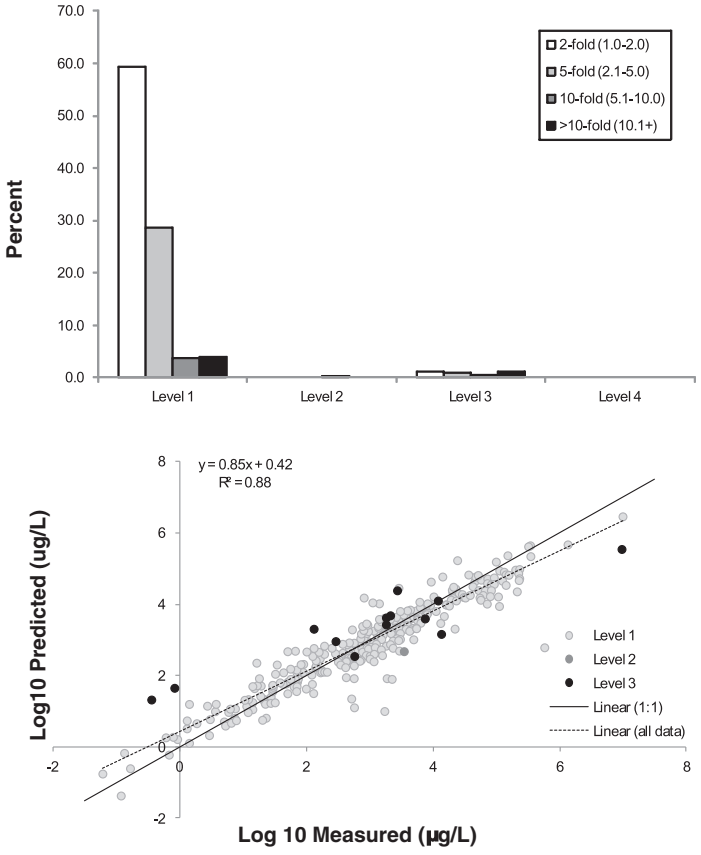

Fig. 3. Prediction accuracy of estimated toxicity values by uncertainty level (upper panel), and correlation between measured and predicted toxicity values (lower panel) in rainbow trout.

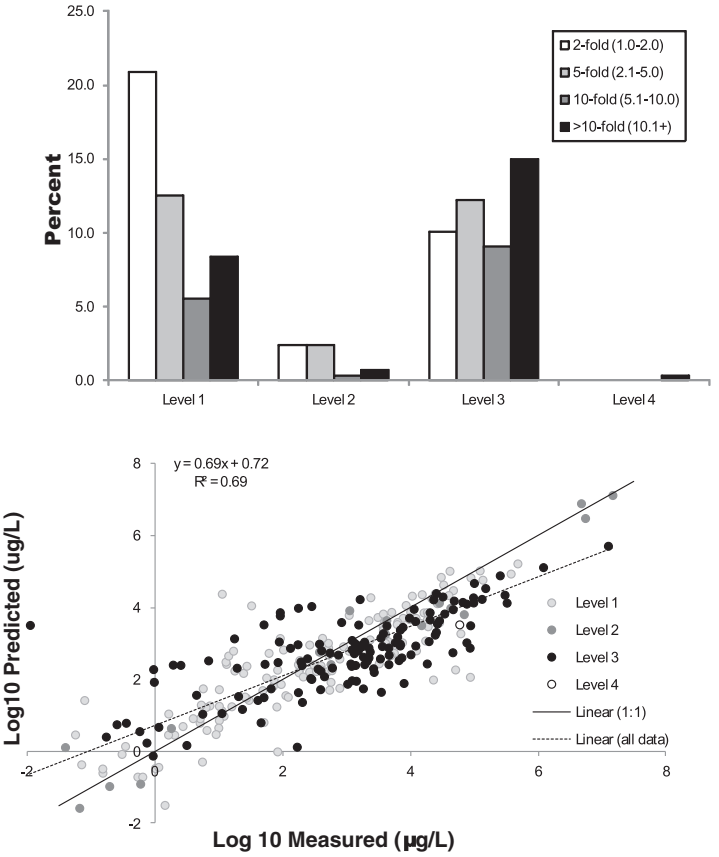

Fig. 4. Prediction accuracy of estimated toxicity values by uncertainty level (upper panel), and correlation between measured and predicted toxicity values (lower panel) in *D. magna*.

that used a fragment-based MOA assignment approach (USEPA, 2012). The specific MOA of alkylation encompassed a structurally diverse group of nucleophiles, electrophiles, and proelectrophiles of varying potency. Additional research is needed to refine the reactivity MOA in general, and the alkylation specific MOA in particular because of the diversity of structures and reactivity mechanisms.

An inherent uncertainty in the MOA assignments is whether the same MOA is applicable to both fish and the large diversity of aquatic invertebrates. Multiple studies of chemicals with a narcosis MOA have shown similar critical body residues in several aquatic taxa, suggesting similar intrinsic species sensitivity, and mechanism of action (Barron et al., 2002). Species sensitivity distributions for AChE inhibitors show distinct differences in fish and invertebrates, but these appear to relate to species-specific sensitivity rather than differing MOA (Awkerman et al., 2014; Russom et al., 2014). MOAs may be similar across taxa, because the basic biochemical systems and molecular targets affected may be generally conserved across many animal species (LaLone et al., 2013). However, applicability of the MOA assignments to the large diversity in aquatic species is a significant uncertainty and an area of future research. Compounds that had very specific acting insecticidal mechanisms (*e.g.*, insect growth or molt inhibitors) were excluded from the database because of uncertain or unlikely applicability to toxic action in fish.

In many applications, MOA-based model development can be considered a better alternative to chemical class-based profiling and predictive toxicity modeling. Chemical MOA is a key determinant of hazard, provides information on underlying toxicity pathways, and allows for grouping across multiple chemical classes. However, the development of QSAR and other predictive models have been generally limited by the availability of large high quality MOA and toxicity databases. For example, previously available toxicity datasets have been dominated by non-polar and polar narcotics. The MOAtox database was developed as a comprehensive standardized dataset intended to facilitate predictive aquatic toxicology model development for a diversity of chemical classes and MOAs. The taxa-specific component of the database focused on the four most commonly reported aquatic test species in order to maximize chemical and MOA diversity, and minimize the number of estimated values. Additionally, generic toxicity values for fish and aquatic invertebrates were determined from only measured values to increase the chemical domain and applicability of the MOAtox dataset for QSAR and other predictive model development. However, only 24 additional chemicals were gained from using all available fish compared to measured values in the three focus fish species, illustrating the predominance of existing test data for these species in aquatic toxicology. In contrast, the taxa group of all aquatic invertebrates comprised an additional 96 chemicals relative to the *Daphnia* only category.

The toxicity data used in the current study were standardized to limit extrinsic variation caused by differences in toxicity test conditions and variability in reported values. This approach removed a large amount of measured toxicity values. Additional research would be needed to determine the optimum level of standardization needed. In addition to predictive model development, the MOA dataset presented here should also support MOA-based assessments of chemical mixtures, such as applying a toxic units approach (additivity) to chemicals with the same specific MOA. Future work will include periodic expansion and refinement of the database and MOA categories, as well as developing an internet accessible and searchable platform.

Acknowledgements

We thank Larisa Lee and Julie Krzykwa for dataset development and quality assurance support. This paper has been reviewed according to EPA guidelines, but the opinions expressed in this work are those of the authors and do not represent the policies or opinions of the U.S. EPA.

Appendix A. Supplementary data

Supplementary data associated with this article can be found, in the online version, at http://dx.doi.org/10.1016/j.aquatox.2015.02.001.

References

Awkerman, J.S., Raimondo, S., Jackson, C.R., Barron, M.G., 2014. Augmenting aquatic species sensitivity distributions with interspecies toxicity estimation models. Environ. Toxicol. Chem. 33, 688–695.

Barron, M.G., Hansen, J., Lipton, J., 2002. Association between contaminant tissue residues and adverse effects in aquatic organisms. Rev. Environ. Contamin. Toxicol. 173, 1–37.

Call, D.J., Brooke, L.T., Knuth, M.L., Poirier, S.H., Hoglund, M.D., 1985. Fish subchronic toxicity prediction model for industrial organic chemicals that produce narcosis. Environ. Toxicol. Chem. 4, 335–341.

Christen, V., Hickmann, S., Rechenberg, B., Fent, K., 2010. Highly active human pharmaceuticals in aquatic systems: a concept for their identification based on their mode of action. Aquat. Toxicol. 96 (February (3)), 167–181.

Escher, B.I., Bramaz, N., Eggen, R.I.L., Richter, M., 2005. *In vitro* assessment of modes of toxic action of pharmaceuticals in aquatic life. Environ. Sci. Technol. 39, 3090–3100.

Fairbrother, A., Barron, M.G., Johnson, M.S., 2014. Chapter 42: methods in ecotoxicology. In: Hayes, A.W., Kruger, C.L. (Eds.), Hayes' Principles and Methods of Toxicology. , Sixth ed. Taylor & Frances, Boca Raton, FL, pp. 2024–2065.

IRAC, 2014. IRAC MoA classification scheme, Insecticide Resistance Action Committee, February 2014, Version 7.3. 24 p, www.irac-online.org/documents/moa-classification/?ext=pdf

Konemann, W.H., 1981. Quantitative structure-activity relationship in fish toxicity studies, Part 1. Relationship for 50 industrial pollutants. Toxicology 19, 209–282.

LaLone, C.A., Villeneuve, D.L., Burgoon, L.D., Russom, C.L., Helgen, H.W., Berninger, J.P., Tietge, J.E., Severson, M.N., Cavallin, J.E., Ankley, G.T., 2013. Molecular target sequence similarity as a basis for species extrapolation to assess the ecological risk of chemicals with known modes of action. Aquat. Tox. 144–145, 141–154.

Martin, T.M., Grulke, C.M., Young, D.M., Russom, C.L., Wang, N., Jackson, C.R., Barron, M.G., 2013. Prediction of aquatic toxicity mode of action using linear discriminant and random forest models. J. Chem. Info. Model. 53, 2229–2239.

McKim, J.M., Bradbury, S.P., Niemi, G.J., 1987. Fish acute toxicity syndromes and their use in the QSAR approach to hazard assessment. Environ. Health Perspect. 71, 171–186.

Nendza, M., Müller, M., 2000. Discriminating toxicant classes by mode of action: 2. Physico-chemical descriptors. Quant. Struct. -Act. Relat. 19, 581–598.

Raimondo, S., Jackson, C.R., Barron, M.G., 2010. Influence of taxonomic relatedness and chemical mode of action in acute interspecies estimation models for aquatic species. Environ. Sci. Technol. 44, 7711–7716.

Raimondo, S., Jackson, C.R., Barron, M.G., 2013a. ICE aquatic toxicity database documentation. In: Office of Research and Development. U.S. Environmental Protection Agency, Gulf Breeze, FL http://epa.gov/ceampubl/fchain/webice/iceDownloads.html

Raimondo, S., Jackson, C.R., Barron, M.G., 2013b. Web-based interspecies correlation estimation (Web-ICE) for acute toxicity: user manual. In: Office of Research and Development. U.S. Environmental Protection Agency, Gulf Breeze, FL (Version 3.1. EPA/600/R-12/603).

Russom, C.L., Bradbury, S.P., Broderius, S.J., Hammermeister, D.E., Drummond, R.A., 1997. Predicting modes of toxic action from chemical structure: acute toxicity in the fathead minnow (*Pimephales promelas*). Environ. Toxicol. Chem. 16, 948–967.

Russom, C.L., LaLone, C.A., Villeneuve, D.L., Ankley, G.T., 2014. Development of an adverse outcome pathway for acetylcholinesterase inhibition leading to acute mortality. Environ. Toxicol. Chem. 33, 2157–2169.

Schüürmann, G., Aptula, A.O., Kühne, R., Ebert, R.-U., 2003. Stepwise discrimination between four modes of toxic action of phenols in the tetrahymena pyriformis assay. Chem. Res. Toxicol. 16, 974–987.

Spycher, S., Nendza, M., Gasteiger, J., 2004. Comparison of different classification methods applied to a mode of toxic action dataset. QSAR Comb. Sci. 23, 779–791.

Suter II, G.W., 2007. Modes and mechanisms of action. Chapter 7. In: Suter, G.W. (Ed.), Ecological Risk Assessment. , second edition. CRC Press, Boca Raton, FL, USA, pp. 105–109.

USEPA, 2012. ASTER User Guide: ASTER System, Version 2.0. U.S. Environmental Protection Agency (2012) http://cfpub.epa.gov/ecotox/blackbox/help/ASTER.pdf

USEPA, 2014. ECOTOX User Guide: ECOTOXicology Database System, Version 4.0. U.S. Environmental Protection Agency (2014) http://www.epa.gov/ecotox/

Verhaar, H.J.M., van Leeuwen, C.J., Hermens, J.L.M., 1992. Classifying environmental pollutants part 1, Structure activity relationships for prediction of aquatic toxicity. Chemosphere 25, 471–491.

Verhaar, H.J.M., Solbe, J., Speksnijder, J., van Leeuwen, C.J., Hermens, J.L.M., 2000. Classifying environmental pollutants: part 3. External validation of the classification system. Chemosphere 40, 875–883.

Aquatic Toxicology 180 (2016) 11–24

Contents lists available at ScienceDirect

Aquatic Toxicology

journal homepage: www.elsevier.com/locate/aquatox

A Bayesian network model for predicting aquatic toxicity mode of action using two dimensional theoretical molecular descriptors

John F. Carriger[a], Todd M. Martin[b], Mace G. Barron[a,*]

[a] U.S. Environmental Protection Agency, Office of Research and Development, Gulf Ecology Division, Gulf Breeze, FL, 32561, United States
[b] U.S. Environmental Protection Agency, Office of Research and Development, Sustainable Technology Division, Cincinnati, OH, 45220, United States

ARTICLE INFO

Article history:
Received 18 July 2016
Received in revised form 6 September 2016
Accepted 7 September 2016
Available online 13 September 2016

Keywords:
Mode of action
Aquatic toxicity
Bayesian network
Markov blanket
Chemical descriptors

ABSTRACT

The mode of toxic action (MoA) has been recognized as a key determinant of chemical toxicity, but development of predictive MoA classification models in aquatic toxicology has been limited. We developed a Bayesian network model to classify aquatic toxicity MoA using a recently published dataset containing over one thousand chemicals with MoA assignments for aquatic animal toxicity. Two dimensional theoretical chemical descriptors were generated for each chemical using the Toxicity Estimation Software Tool. The model was developed through augmented Markov blanket discovery from the dataset of 1098 chemicals with the MoA broad classifications as a target node. From cross validation, the overall precision for the model was 80.2%. The best precision was for the AChEI MoA (93.5%) where 257 chemicals out of 275 were correctly classified. Model precision was poorest for the reactivity MoA (48.5%) where 48 out of 99 reactive chemicals were correctly classified. Narcosis represented the largest class within the MoA dataset and had a precision and reliability of 80.0%, reflecting the global precision across all of the MoAs. False negatives for narcosis most often fell into electron transport inhibition, neurotoxicity or reactivity MoAs. False negatives for all other MoAs were most often narcosis. A probabilistic sensitivity analysis was undertaken for each MoA to examine the sensitivity to individual and multiple descriptor findings. The results show that the Markov blanket of a structurally complex dataset can simplify analysis and interpretation by identifying a subset of the key chemical descriptors associated with broad aquatic toxicity MoAs, and by providing a computational chemistry-based network classification model with reasonable prediction accuracy.

Published by Elsevier B.V.

1. Introduction

The mode of toxic action (MoA) has been recognized as a key determinant of chemical toxicity but MoA classification in aquatic toxicology has been generally limited to either narrow domains of applicability, highly complex or simplistic assignment schemes, or poor prediction accuracy (Russom et al., 1997; Nendza and Muller 2007; Enoch et al., 2008; Barron et al., 2015). Generally two approaches have been used to develop structure-based models to predict aquatic toxicity MoA: identification of substructural indicators based on the presence of specific molecular features (e.g., Verhaar et al., 1992; Russom et al., 1997; Nendza and Muller 2007; Enoch et al., 2008), and use of neural networks, hierarchical clustering or other machine learning methods with theoretical descriptors that describe a broad array of electronic, topological, and other features of a chemical (e.g., Yao et al., 2005; He and Jurs, 2005). Recently, Martin et al. (2013) used two dimensional chemical descriptors and machine based learning algorithms to predict aquatic toxicity MoA using a database of 924 chemicals. Linear discriminant analysis (LDA) and random forest MoA assignment models had high internal concordance and specificity and produced overall MoA prediction accuracies of 85–88% (Martin et al., 2013). Barron et al. (2015) developed an integrated dataset of MoA assignments for over 1200 chemicals that included a diversity of metals, pesticides and other organic compounds that encompassed six broad and 31 specific MoAs for fish and aquatic invertebrates. Martin et al. (2015) then utilized this expanded MoA database to predict global or specific aquatic toxicity MoA with methods such as LDA and multiple linear regression. Mode of action prediction accuracy was greatest for acetylcholinesterase inhibitors and lowest for other neurotoxicants, the structurally diverse group of reactive chemicals, and MoAs with low representation in the database (Martin et al., 2015).

* Corresponding author.
E-mail address: barron.mace@epa.gov (M.G. Barron).

http://dx.doi.org/10.1016/j.aquatox.2016.09.006
0166-445X/Published by Elsevier B.V.

Bayesian networks have seen increasing use in hazard and risk assessment (Burden and Winkler, 2000; Billoir et al., 2008; Iorio et al., 2009), but only limited application in aquatic toxicity and MoA prediction. A Bayesian network is a graphical representation of a joint probability distribution. The structure of a Bayesian network consists of individual nodes (i.e., random variables) connected by arcs (arrows) reflecting a dependence structure between the variables. Bayesian networks are built in a directed manner often reflecting causality between the variables though this is not a requirement. The absence of an arc between nodes signifies that the variables are conditionally independent. Algorithms are available for learning a Bayesian network structure from data. These algorithms can often be useful in high dimensional data where the structure and conditional dependence are not readily apparent. The automated learning process of a Bayesian network structure can either be unsupervised or supervised. In contrast to a more generalized representation of a joint probability distribution in unsupervised learning of a Bayesian network's structure, supervised learning focuses on representing the relationship of predictor nodes to a target variable. Bayesian networks have not been previously used to predict MoA, but have been applied in machine learning applications for diverse fields from cancer prediction to marketing and finance.

The objective of the current study was to elucidate the connection between molecular descriptors and MoA, and develop a Bayesian network prediction model for classifying chemicals by aquatic toxicity MoA. The model was developed following the steps of discretization, structure learning, network selection and validation, and sensitivity analysis. The study utilized a recently published dataset containing over one thousand chemicals with MoA assignments (Barron et al., 2015), and two dimensional chemical descriptors generated for each chemical. Machine-learned Bayesian networks were chosen for their capabilities in analyzing uncertainties, and accounting for covariation among multiple variables (Barber, 2012). For the current study, we focus on learning the Markov blanket of the data set with the MoA broad classifications as a target node. The Markov blanket of a target node consists of the node's parents, children, and the nodes that share children with the target node (Korb and Nicholson, 2004). The target node or node in question, is screened from the rest of the nodes in the network from its Markov blanket if the value of each of the nodes in the blanket is known. Fig. 1 shows an illustration of the concept. If the A_i predictor nodes in Fig. 1 are known for certain, then no other node (i.e., the B_i nodes) will provide any additional information on the target variable. Identifying the Markov blanket of a complex dataset with numerous variables can simplify analytical and computational requirements by providing a subset of the key predictors in a dataset that are highly informative for making probabilistic inferences on a target variable.

2. Methods

2.1. General approach

The approach to database and network model development is described in detail in the subsections below. The database used in developing and validating the Bayesian classification network was comprised of a dataset of known MoA assignments and a dataset of two dimensional theoretical chemical descriptors for over 1000 chemicals. Six preliminary models were initially constructed with two different discretization levels and three Markov blanket algorithms. An optimal structural coefficient was selected for each model from trade-offs between internal precision and structural complexity. A 10-fold cross validation was implemented for each candidate model and a final network was selected with the highest empirical performance from overall precision. Sensitivity analyses on the selected model examined the strengths of the relationships between the variables, and the capabilities of maximizing MoA probabilities using individual and multiple descriptors.

2.2. MoA and descriptor database development

The MoA dataset was based on the MOAtox database of Barron et al. (2015) that encompassed the six broad acute aquatic toxicity categories of acetylcholinesterase inhibition (AChEI), narcosis, electron transport inhibition (ETI), ionoregulatory/osmoregulatory/circulatory impairment (IOCI), other neurotoxicity, and reactivity. Those MoA assignments had been determined for aquatic invertebrates and fish toxicity from over 1200 chemicals using a combination of international consensus classifications, QSAR predictions, and weight of evidence professional judgment based on an assessment of structural features and literature information (Barron et al., 2015). Up to 790 two dimensional theoretical molecular descriptors were then calculated for each chemical following the method of Martin et al. (2015) using the computational chemistry application TEST (USEPA, 2016). The descriptor classes included E-state values and E-state counts, constitutional descriptors, topological descriptors, walk and path counts, connectivity, information content, two-dimensional autocorrelation, Burden eigenvalue, molecular properties, Kappa, hydrogen bond acceptor/donor counts, molecular distance edge and molecular fragment counts (USEPA, 2008; Zhu et al., 2009; Martin et al., 2013, 2015). Definitions of key descriptors are in Supplemental Table S1 and available for download from the TEST internet site (USEPA, 2008). Chemicals were removed from the database that included metals, other inorganic compounds, and organic salts because of the inability to compute descriptors for these ionic compounds leaving a total of 1098 chemicals used in the Bayesian network.

2.3. Bayesian network development

2.3.1. -Discretization

All Bayesian network analysis was conducted with Bayesialab 5.4.3 (Bayesia S.A.S., 2015). Each chemical entry in the MoA and descriptor dataset was used except several descriptors only containing zeroes were removed prior to analysis. Continuous variables were discretized using the decision tree algorithm with the broad MoA variable as the target node for choosing levels. The decision tree algorithm maximizes the information content between a target node (i.e., MoA) and predictor (i.e., a descriptor) from the discretization levels. In case of failure of the decision tree discretization algorithm to identify intervals, we used density approximation, k-means discretization, and normalized equal distance in that order of priority for selecting a discretization algorithm. Discretization was run twice using both three and four discretization intervals as initial specifications in the algorithms. The number of intervals for the descriptors was chosen as a compromise between representation of the distribution and data availability for estimating probabilities (Conrady and Jouffe, 2015).

2.3.2. -Structure learning

After discretizing the continuous variables, three supervised structure learning methods were applied. The first was a Markov blanket (MB) analysis and the second was an augmented Markov blanket (AMB) analysis and the third was a minimal augmented Markov blanket (MAMB) analysis. The MB analysis searches for the parents, children, and spouses of the target node. The AMB first identifies the MB and then the relationships among the parent, son, and spouse nodes (Fig. 1). The MAMB prunes the MB by

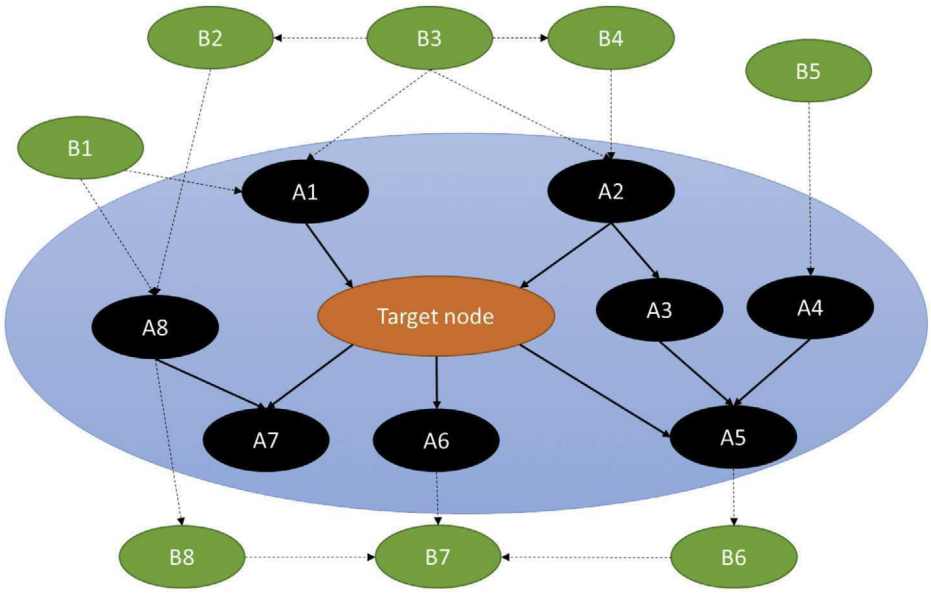

Fig. 1. Representation of a Markov blanket in a Bayesian network. The orange (center) oval is a target node or the variable of ultimate inferential interest in the analysis. The black ovals labelled A_i are variables that are used for predictions and are in the Markov blanket of the target node (i.e., either children, parents, or spouses of the target node). The green (bottom) ovals labelled B_i are variables in the problem domain but not in the Markov blanket. (For interpretation of the references to colour in this figure legend, the reader is referred to the web version of this article.)

eliminating nodes from the blanket through an additional equivalence class unsupervised learning step.

Bayesialab uses the minimum description length of candidate networks in its score-based algorithms for comparing Bayesian network structures (Conrady and Jouffe, 2015). The structural coefficient (SC) modifies the complexity of the network through weighting the structure encoding (in bits) of the Bayesian network. In a Markov blanket analysis, the SC can influence the number of descriptors selected in the blanket as well as their connectivity. We adjusted the SC by finding the optimal value between complexity and data representation/precision similar to Harris et al. (2016) and Conrady and Jouffe (2015). The SC analysis generated networks with each of the supervised learning algorithms (i.e., MB, AMB, MAMB) and discretization levels with SCs ranging from 0.5 to 6.0 at 0.1 intervals. Bayesian networks with lower (< 0.5) SC values were found to be difficult to computationally manage because of higher model complexity. Plotting the SC values against the structure:target precision ratio for each of the generated networks helped to visually identify candidate SCs. The inflection of the structure:target precision ratio plot was located to identify a SC that optimally did not underfit or overfit the model (Bayesia, 2010; Harris et al., 2016). The target precision was also examined as a function of the SC before final selection where the height of the curve was used to prioritize the SC. In case of constant values for the precision across the range of SCs, the structure/data ratio was plotted against the SC to further enhance descriptor representation or prevent overfitting. A single SC value was identified for all candidate models except for the MAMB model with three discretization levels where two different SCs were tested.

2.3.3. -Network selection and validation

Targeted cross validation (k fold) was used to estimate the performance of the networks in out of sample predictions (Stone, 1974; Conrady and Jouffe, 2015). Prior to cross-validation work, a virtual data point was added to every conditional and unconditional probability table cell to prevent impossible assignments in the cross-validation and to improve later inferential analysis. The k-folds cross validation method splits the data set into k equal sized sets and uses k-1 sets for learning the model and one for validation. This is repeated for k rounds and synthesized results are reported (Conrady and Jouffe, 2011). The data were randomly split into 10 sets for a 10 fold cross validation. The k-folds cross validation method was used to compare the precision of these candidate models and the final selected model was built with the AMB algorithm with three discretization levels and a SC of 1. Cross validation results are discussed for this model including reliability and precision statistics from an occurrence matrix. The reliability statistic related the number of predictions that should have been a MoA to the occurrences that were predicted to be that or another MoA. The precision statistic related the number of occurrences that were predicted for a MoA to the total occurrences that should have been predicted as that or another MoA. Total precision sums the correct predictions for each MoA and relates this value to the total number of predictions that were made. All precision and reliability statistics were expressed as percentages.

For the AMB network with three discretization levels, a final check on the connections identified among the descriptors was made for overfitting based on the Kullback-Leibler divergence for the arcs between descriptors (Bayesia, 2010). This check for lack of dependence was done for each parent-child relationship in the AMB network that was previously identified with the minimum description length score-based algorithm. The validity of the connections among the descriptors that was identified by the learning algorithm was examined using a statistical independence test (G_{KL}-test; p-values greater than 0.05 provide evidence of independence) (Bayesia, 2010). From the tests, the p-values or independence probabilities, were used to check the significance of each identified relationship between the descriptors or between the descriptors and the target node (Thai et al., 2012; Harris et al., 2016).

2.3.4. -Sensitivity analysis

A comprehensive sensitivity analysis examined the relationship among the descriptors in the selected network and helped hone in on the influence of individual descriptors on MoA prediction. The sensitivity analysis was conducted using higher, moderate or lower values of the descriptors with each MoA. For a broad understanding of the relationships between variables, the highest and lowest values of mutual information, Pearson's correlation, Kullback-Leibler

divergence, and node force between variables were examined globally on the network. Mutual information was used to examine the probabilistic dependence between the nodes in the network. Pearson's correlation gave a measure of the linear strength of the relationship between the variables. The Kullback-Leibler divergence can be used as a measure of the information gain from assuming a joint relationship between two variables in a network compared to an assumption of independence. Node force sums the Kullback Leibler divergence input to a node and output by the node. The nodes that have more direct relationships and greater dependence with other nodes have the highest node force. Sensitivity of each MoA to each descriptor was examined in tornado plots that displayed the influence of knowledge of the descriptor values on the probability of each MoA and provided information on the maximum strength of the individual relationships between each MoA and descriptor. The tornado plots display the range between the lowest and highest probability that can be achieved for each MoA from hard evidence placed on the corresponding descriptor states.

A target dynamic profile analysis (TDP) (Bayesia, 2010) identified a pathway of states of the descriptors most likely to reduce uncertainty on the MoAs. The TDP checked the sensitivity of each MoA to multiple descriptors by maximizing their probability as the search criteria optimization specification. This analysis uses a search that can take into account the joint probability of the evidence to diminish the impact of low probability scenarios. Only hard evidence was used to establish the TDP under the assumption that there would be minimal uncertainty on the descriptors' states for a given chemical.

A target optimization tree (Bayesia, 2010) was also used to identify additional pathways for reducing uncertainty on the MoAs from knowledge of descriptors in the Markov blanket. This allowed a fuller consideration of different evidence from multiple variables (descriptors). The tree presented a visualization of the hard evidence set for predicting a MoA through an exhaustive search that can also take into account the joint probability of the evidence to diminish the impact of low probability states. We limited the target optimization tree to three descriptors for depth of evidence and a maximum of two alternate trees corresponding to the breadth of evidence and utilized hard evidence for its derivation. Both the TDP and target optimization tree analyses were run twice, once using the joint probability of the evidence to weight the search methods and once not considering it but only considering the maximization of the probability of the MoA. The probability changes from initial marginal probability to final probability for the MoAs were used to score the pathways in the target optimization trees. When the joint probability of the evidence was considered in the tree construction, the probability change to the MoA was weighted by the joint probability of the evidence to calculate the optimization score.

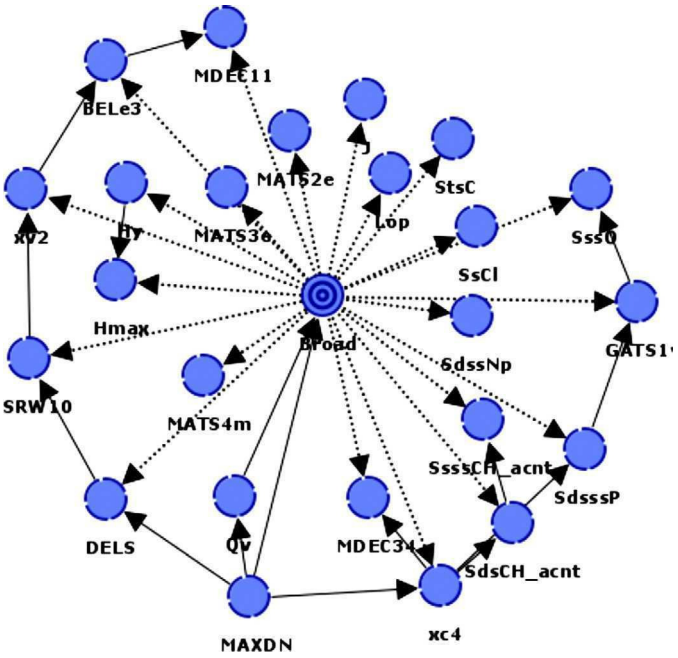

Fig. 2. Structural components of the augmented Markov blanket model used for classifying modes of toxic action using chemical descriptors. The target (predicted) node (*Broad*) contains the broad mode of toxic action categories in its variable states. Dashed arcs delineate relationships where *Broad* is a parent node of a descriptor. Inferences made within the model are omnidirectional so that observing a descriptor changes the probability of the other descriptors as well as the target node depending on all other observations in the model and the conditional independence relationships contained in the structure.

3. Results

3.1. Network precision and reliability

The total precision for the selected AMB model (Fig. 2) with three discretizations was 80.2% (Table 1). The best precision was for the AChEI MoA (93.5%) where 257 chemicals out of 275 were correctly classified. Model precision was poorest for the reactivity MoA (48.5%) where only 48 out of 99 reactive chemicals were correctly classified. Narcosis represented the largest class within the MoA dataset and had a precision of 80.0%, reflecting the total precision across all of the MoAs. False negatives for chemicals with the narcosis MoA most often fell into the ETI, neurotoxicity or reactivity MoAs. False negatives for all other MoAs were most often narcosis.

Table 1
Global cross validation results for mode of toxic action (MoA) predicted from chemical descriptors (n = number of chemicals in dataset). Data are: % reliability (R%) and% precision (P%). Row titles and numerical values in parentheses pertain to predicted cases and column titles and numerical values are for actual cases.

MoA	AChEI[a] (275)		ETI[b] (61)		IOCI[c] (18)		Narcosis (460)		Neurotoxicity (185)		Reactivity (99)	
	R %	P %	R %	P %	R %	P %	R %	P %	R %	P %	R %	P %
AChEI[1] (276)	93	93	0	0	0	0	5.1	3.0	1.5	2.2	0.4	1.0
ETI[2] (76)	0	0	55	69	0	0	33	5.4	0	0	12	9.1
IOCI[3] (14)	0	0	0	0	86	67	7.1	0.2	7.1	0.5	0	0
Narcosis (471)	3.8	6.6	3.4	26	1.1	28	78	80	5.5	14	8.1	38
Neurotoxicity (184)	0	0	1.1	3.3	0.54	5.6	13	5.2	84	83	1.6	3.0
Reactivity (77)	0	0	1.3	1.6	0	0	36	6.1	0	0	62	48

[a] Acetylcholinesterase inhibition.
[b] Electron transport inhibition.
[c] Iono/osmoregulatory/circulatory impairment.

3.2. Global model results

The structure of the selected AMB model contained over a dozen connections between the descriptors in the Markov blanket of the MoA variable (Fig. 2). The p-values for each of the variable relationships were all 0.0000% from the G_{KL}-test indicating that the evidence is not strong enough to disprove the links identified by the AMB algorithm. The highest Kullback-Leibler divergence was between the MAXDN and Broad MoA nodes (0.5256) and the lowest was between SdsCH_acnt and SsssCH_acnt (0.0523). The highest mutual information was found between the broad MoA and SRW10 nodes (0.4913). The lowest was between xc4 and SdsCH_acnt (0.0495). The highest positive Pearson's correlation was between Broad and SdsssP (0.6839). The lowest positive correlation was between Broad and SdssNp (0.0055). The highest negative Pearson's correlation was between SdsssP and GATS1v (-0.6065) and the lowest negative Pearson's correlation was between Broad and DELS (−0.0044). Aside from the node force of the Broad MoA variable (5.2611), the highest node force was for MAXDN (1.2074). The lowest was for StsC (0.0553). The highest outgoing force for a descriptor was MAXDN (1.2074) followed by xc4 (0.3767). Thirteen descriptors had zero values for outgoing force indicating that these are leaf variables in the network. The lowest non-leaf descriptor outgoing force was for SdsCH_acnt (0.0523). The highest incoming force for a descriptor was for xc4 (0.5539) followed by DELS (0.5405) and SRW10 (0.5069). The lowest incoming force was for StsC (0.0553). MAXDN had a zero for incoming force indicating that it is a root variable with no parents.

3.3. Mode of toxic action sensitivity to individual descriptors

The sensitivity of each MoA to the individual descriptors is based on changes to the probability of each broad MoA from changes to each descriptor individually while allowing the other descriptors to co-vary with the state changes for a descriptor of concern (Fig. 3). The Supporting information contains separate tornado plots of the sensitivity of each MoA to each individual descriptor (Figs. S1–S6).

AChEI had the greatest sensitivity to changes in SdsssP with ranges from 0.081 to 0.95 probability depending on the state, indicating the importance of a phosphate group. GATS1 v was the second most influential individual descriptor but J was also influential and is capable of raising the probability of AChEI to the second highest level below SdsssP. ETI was most sensitive to SdssNp, suggesting that the number of nitro groups is critical in defining the MoA. Based on the range of probabilities for ETI, Hmax was the second most influential descriptor and Qv also has the potential to raise the probability of ETI to greater than 0.30. Weak positive relationships were found between ETI and most of the descriptors. Electron transport inhibitors were poorly represented in the database.

The number of data points available for IOCI was the lowest in comparison with other MoAs. Iono/osmoregulatory/circulatory impairment had Hmax as the most influential descriptor followed by BELe3, SRW10, and Qv. None of the states of the individual descriptors could raise the probability of IOCI above 0.20 on their own. The low overall probabilities for IOCI in the tornado plot indicates weak positive relationships with individual descriptors and the IOCI MoA.

In contrast, narcosis was the best represented MoA in the database. The descriptor with the greatest influence on the narcosis MoA was MAXDN with a probability range of 0.12 to 0.76. DELS and MATS3e could raise the probability of narcosis to greater values than MAXDN but MAXDN can lower the probability more giving it an overall greater range of potential probability changes than DELS and MATS3e. Numerous descriptors could lower the narcosis MoA to lower probabilities such as SRW10, which was the second most sensitive descriptor, xv2, xc4, SdsssP, SsCL, and SdssNP.

The neurotoxicity MoA was most sensitive to SsCl which has the potential to raise the probability of neurotoxicity from 0.11 to 0.99 alone. Although individual findings at multiple descriptors can lower the probability of neurotoxicity to less than 0.1, five descriptor states can raise the probability of its occurrence to greater than 0.5 (SsCl, MDEC34, SRW10, SsssCH_acnt, and BELe3).

The probability of reactivity was most sensitive to SdssNp. The range of probabilities of reactivity from this one descriptor extended from slightly lower than reactivity's initial probability (0.090) to 0.34. Several other descriptors could raise the initial probability of reactivity from 0.090 to a posterior probability of greater than 0.20. Like IOCI, reactivity had relatively weak positive relationships with the individual descriptors and several descriptor states that could lower the posterior probability of reactivity to close to zero from individual findings at their states.

3.4. Mode of toxic action optimization by multiple descriptors

The results from the TDP analyses are displayed in the Supporting information. Findings on multiple descriptors could lead to equal or greater than 0.99 probability of a MoA both when the joint probability of the evidence was considered in developing the pathway and when it was not. For the models that did not consider the joint probability of the evidence when selecting descriptors, fewer descriptors were necessary to reach the final probabilities of a MoA. The first nodes in the tornado plots that have the potential to affect the greatest range of probabilities were always the first nodes chosen in the TDP with the exception of ETI, IOCI, neurotoxicity, and reactivity when the joint probability was taken into account, and narcosis without taking into account the joint probability of the evidence. These initial descriptors chosen for the TDP were within the top six descriptors that individually created greater range variation with the target state or MoA's probability.

From the existing database alone, multiple descriptors are able to identify MoAs with high certainty even when constrained to follow paths that reflect the available data. For AChEI, only two descriptors were needed to reach or exceed 0.99 probability when considering the joint probability of the evidence and when not considering it. This was largely due to the influence of SdsssP which was the first descriptor for each and which achieved a greater than 0.94 probability of AChEI from one of its states alone. After SdsssP, different descriptors were identified in each of AChEI's target dynamic profiles for achieving a probability of 0.99. For ETI, only two descriptors were needed to reach or exceed a 0.99 probability of its occurrence without the joint probability considered but six descriptors were needed with the joint probability considered. For IOCI, five descriptors were needed to reach or exceed 0.99 probability without the joint probability considered and seven with the joint probability considered. For narcosis, eleven were needed with the joint probability considered and two without the joint probability considered. For neurotoxicity, an outcome on one descriptor was the minimum needed without the joint probability considered and three descriptor outcomes with the joint probability considered. For reactivity, nine descriptors were needed with the joint probability considered and four were needed without the joint probability considered.

Several descriptors that were used in the TDP to reach or exceed 0.99 probability for a single MoA were found to be unique to certain MoAs or were found multiple times across MoAs. For unique descriptors prioritized to reach 0.99 probability, Lop was only found in AChE joint, MAXDN was unique to narcosis joint, MATS3e and SssO were unique to narcosis and MDEC34 and xv2 were only in neurotoxicity joint. Hmax was in both ETI and ETI joint as well as IOCI and IOCI joint. SdssNp was in ETI, ETI joint, narcosis joint, and reactivity. Qv was in ETI joint, IOCI, narcosis joint, and reactivity joint. Bele3, GATS1v, Hy, J, SdsCH_acnt, SdsssP, SRW10, SsCl,

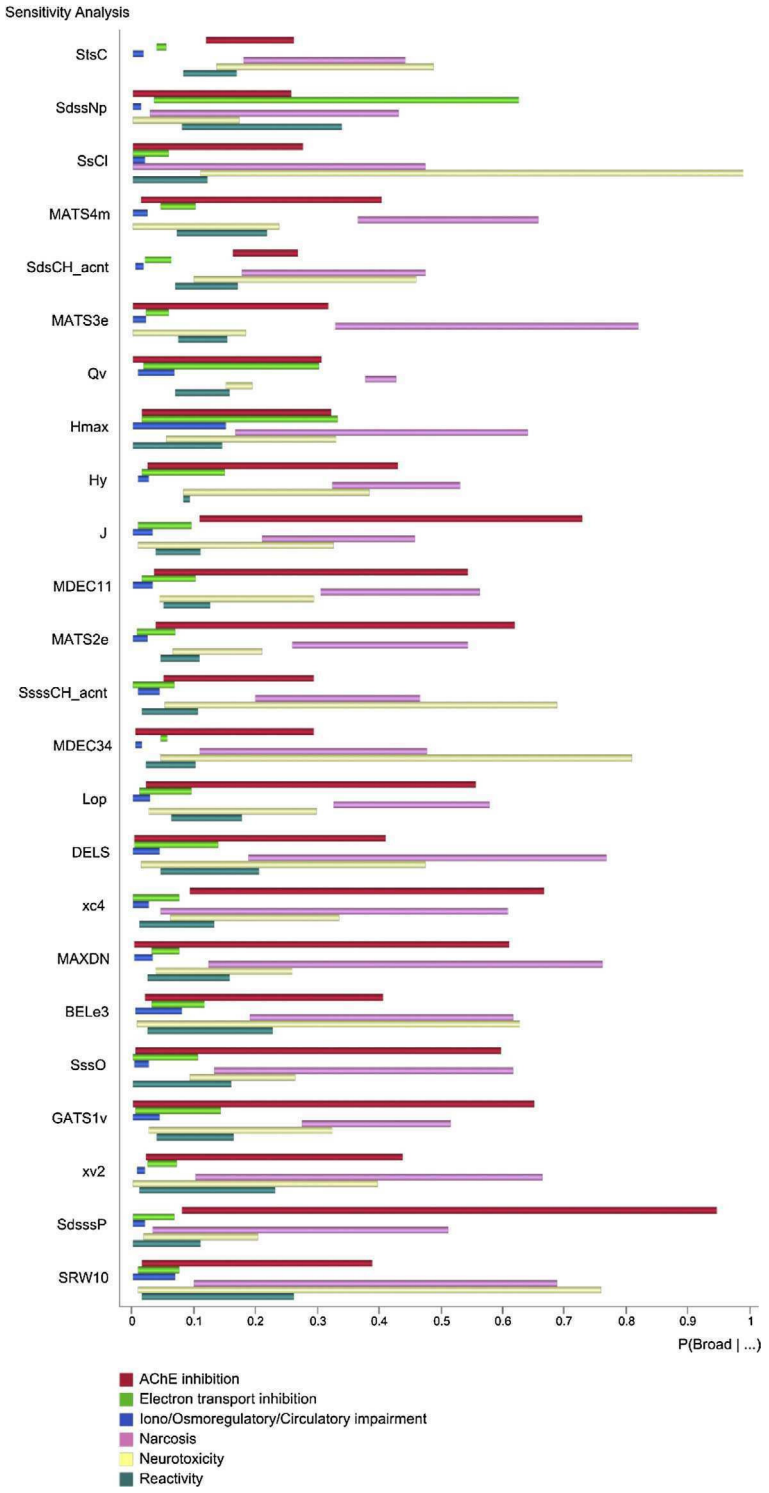

Fig. 3. Sensitivity of the chemical modes of toxic action to each of the descriptors. Horizontal bars represent the range of probabilities for each mode of toxic action (i.e., the conditional probability of the broad mode of toxic action (P(Broad| . . .)) (x-axis)) from findings at the individual descriptors listed on the y-axis.

SsssCH_acnt, and xc4 were found in at least three MoA's TDPs and used prior to or at the point of reaching 0.99. The rest of the descriptors that were prioritized for optimally reaching 0.99 (i.e., DELS, MDEC11, StsC) were found twice across the MoA's TDPs.

To examine multiple pathways for identifying the MoAs, target optimization trees were developed. Fig. 4 contains the target optimization tree for AChEI while taking into account the joint probability of the evidence and Fig. 5 contains the target optimization tree for AChEI without the joint probability of the evidence taken into account in the development of the pathways. All pathways in Figs. 4 and 5 led to a probability of AChEI that is greater than 0.98. The red highlighted box at the leaf of the tree contains the final scenario with the highest overall score based on the joint probability (if considered in the evidence determination) and the change in probability from the initial probability of the MoA displayed in the root of the tree. Both of the primary (first) pathways

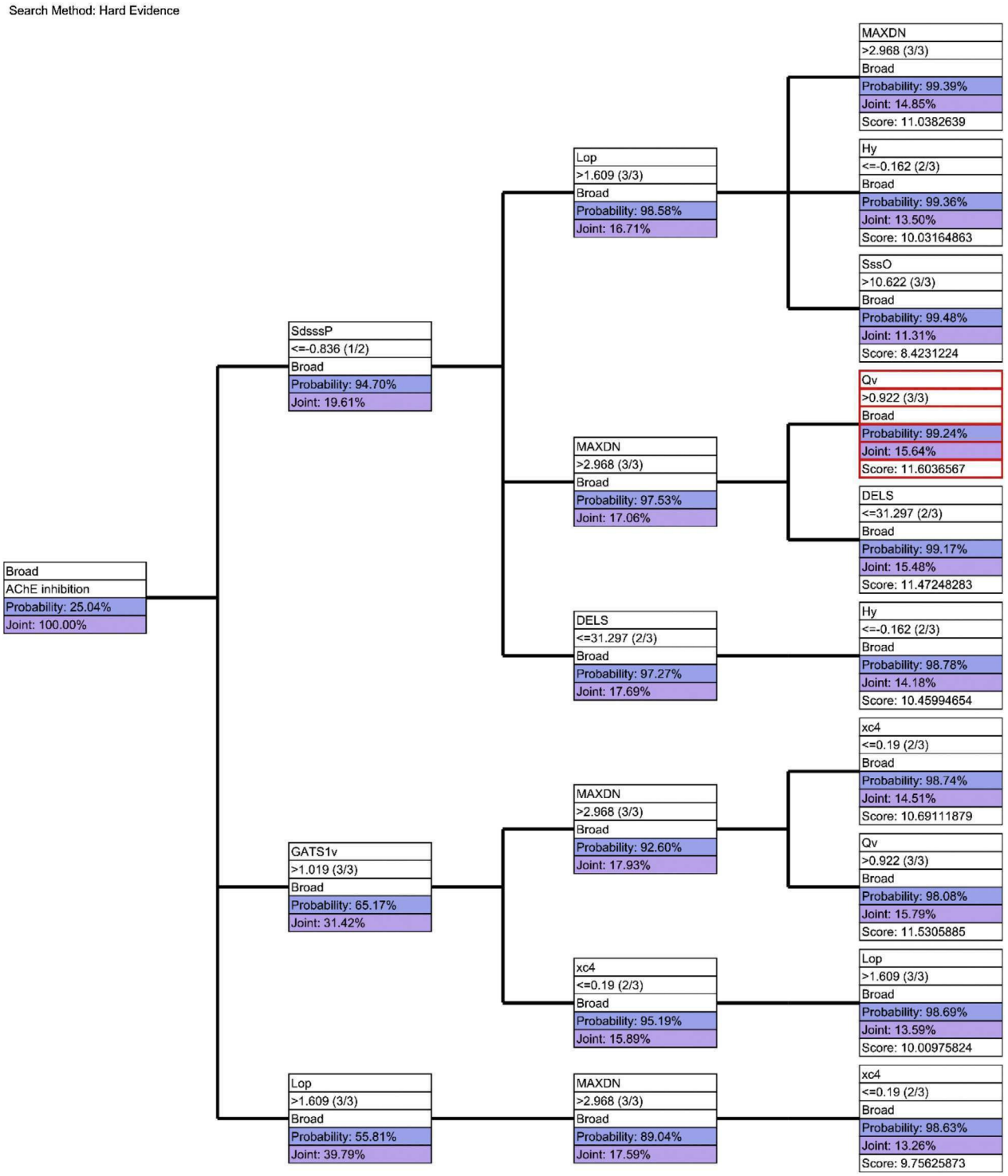

Fig. 4. Target optimization tree for acetylcholinesterase inhibition (AChEI) with the joint probability of the evidence taken into consideration. The rows on the leaves contain the score for the pathway built on the probability change from the prior probability of the mode of toxic action weighted by the final joint probability. The red highlighted descriptor (Qv) is the terminal node of the pathway with the highest score. (For interpretation of the references to colour in this figure legend, the reader is referred to the web version of this article.)

in the target optimization trees for AChEI duplicate the steps in the corresponding TDPs. The two nodes in the TDP that optimally led to a probability of AChEI that was greater than 0.99 probability were SdsssP and J when the joint probability was not considered. In the same target optimization tree, SdsssP only appeared in one pathway as the initial variable and J appeared in two pathways, as an initial and secondarily selected variable. When the joint probability was considered (Fig. 4), J was no longer in the target optimization tree but SdsssP was still selected early and raised the probability of AChEI the most in the first branching. The highest scoring pathway with the joint probability contained SdsssP, MAXDN, and Qv leading to a 0.99 probability of AChEI. The highest scoring pathway

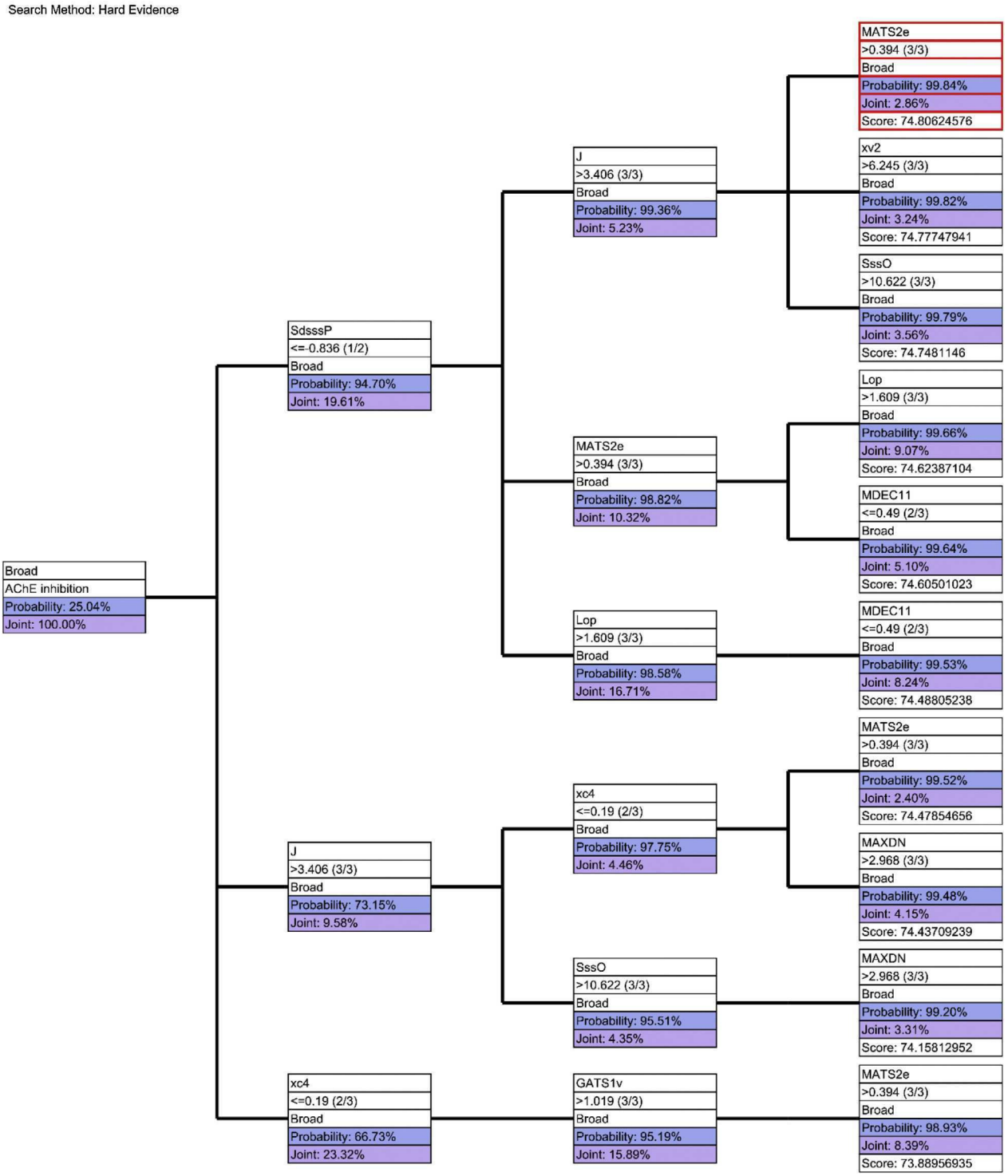

Fig. 5. Target optimization tree for acetylcholinesterase inhibition (AChEI) without taking into account the joint probability of the evidence. The rows on the leaves contain the score for the pathway built on the probability change from prior probabilities before findings on descriptors are entered. The red highlighted descriptor (MATS2e) is the terminal node state of the pathway with the highest score. (For interpretation of the references to colour in this figure legend, the reader is referred to the web version of this article.)

without consideration of the joint probability contained SdsssP, J, and MATS2e leading to a probability of 0.998 (near certainty) of AChEI.

Neurotoxicity had the second highest precision from cross validation and its target optimization trees are displayed in Figs. 6 and 7, with and without the joint probability of the evidence weighted in the pathways, respectively. Like AChEI, multiple scenarios with at most three predictors can lead to a probability equal to or greater than 0.99 for the neurotoxicity MoA. The lowest final probability was 0.98 in a few lineages with the joint probability of the evidence considered. An outcome on only one descriptor was necessary to reach a 0.99 probability of neutotoxicity (SsCl) in the target optimization tree that did not consider the joint probability. For the target optimization tree that did consider the joint

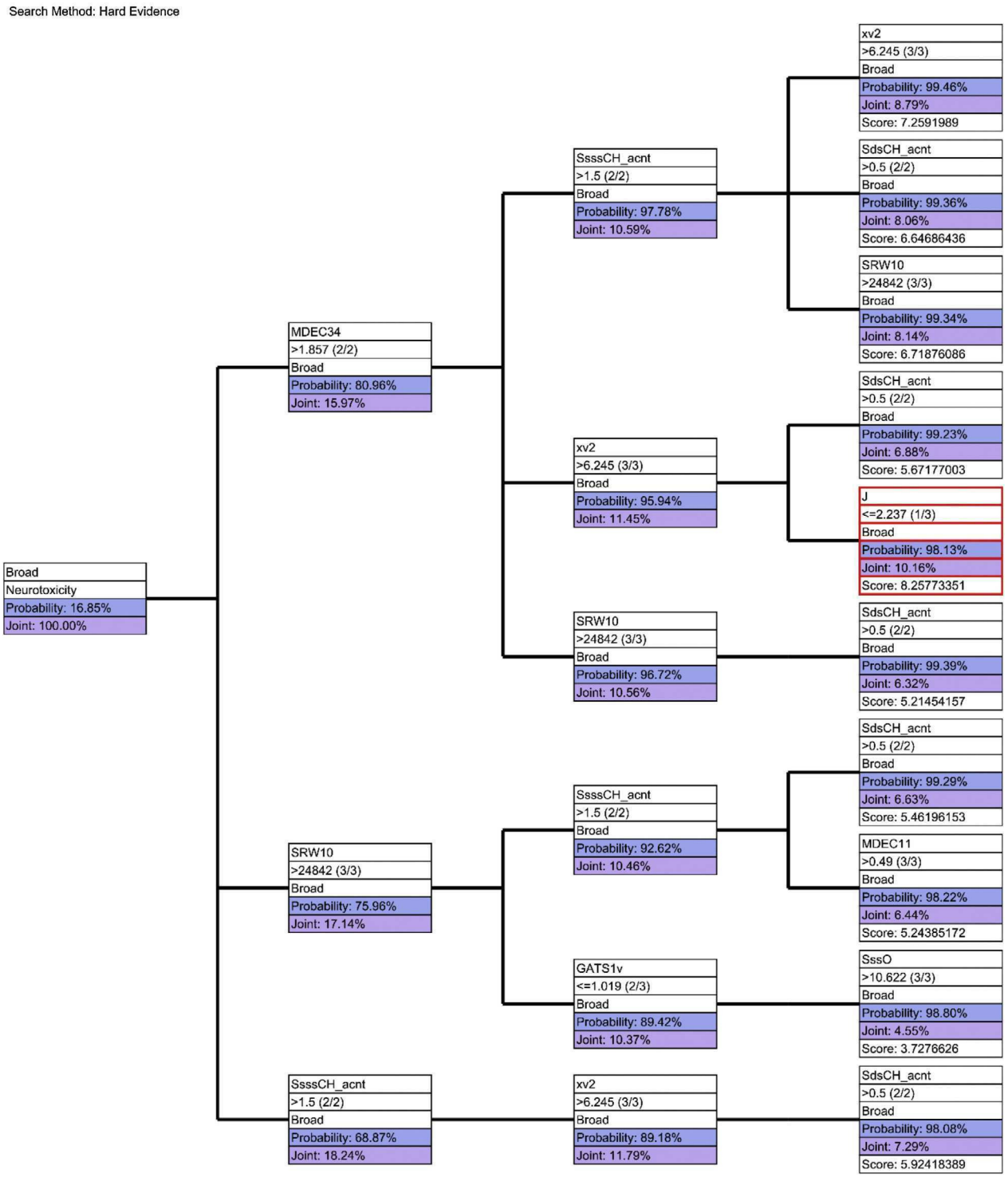

Fig. 6. Target optimization tree for neurotoxicity with the joint probability of the evidence taken into consideration. The rows on the leaves contain the score for the pathway built on the probability change weighted by the final joint probability. The red highlighted descriptor (J) is the terminal node state of the pathway with the highest score. (For interpretation of the references to colour in this figure legend, the reader is referred to the web version of this article.)

probability, SsCl was not selected at all. When the joint probability was considered, the 0.99 probability was still commonly reached but required several additional descriptors. The highest scoring pathway in the tree that considered the joint probability contained MDEC34, xv2, and J in the same order of priority. The highest scoring pathway in the tree that did not consider the joint probability contained SsCl, MDEC34, and SssO, duplicating the TDP. Both led to a probability of neurotoxicity greater than 0.98.

As can be seen, for AChEI and neurotoxicity several possible descriptor groupings can lead to a high probability of the MoA being true based on a few descriptors alone including the number of phosphate groups and chlorine atoms, respectively. Figs. 8 and 9 contain the target optimization trees for narcosis. By contrast, some scenarios contained final probabilities that were lower than AChEI and neurotoxicity target optimization tree pathways, especially when the joint probability of the evidence was considered in the tree

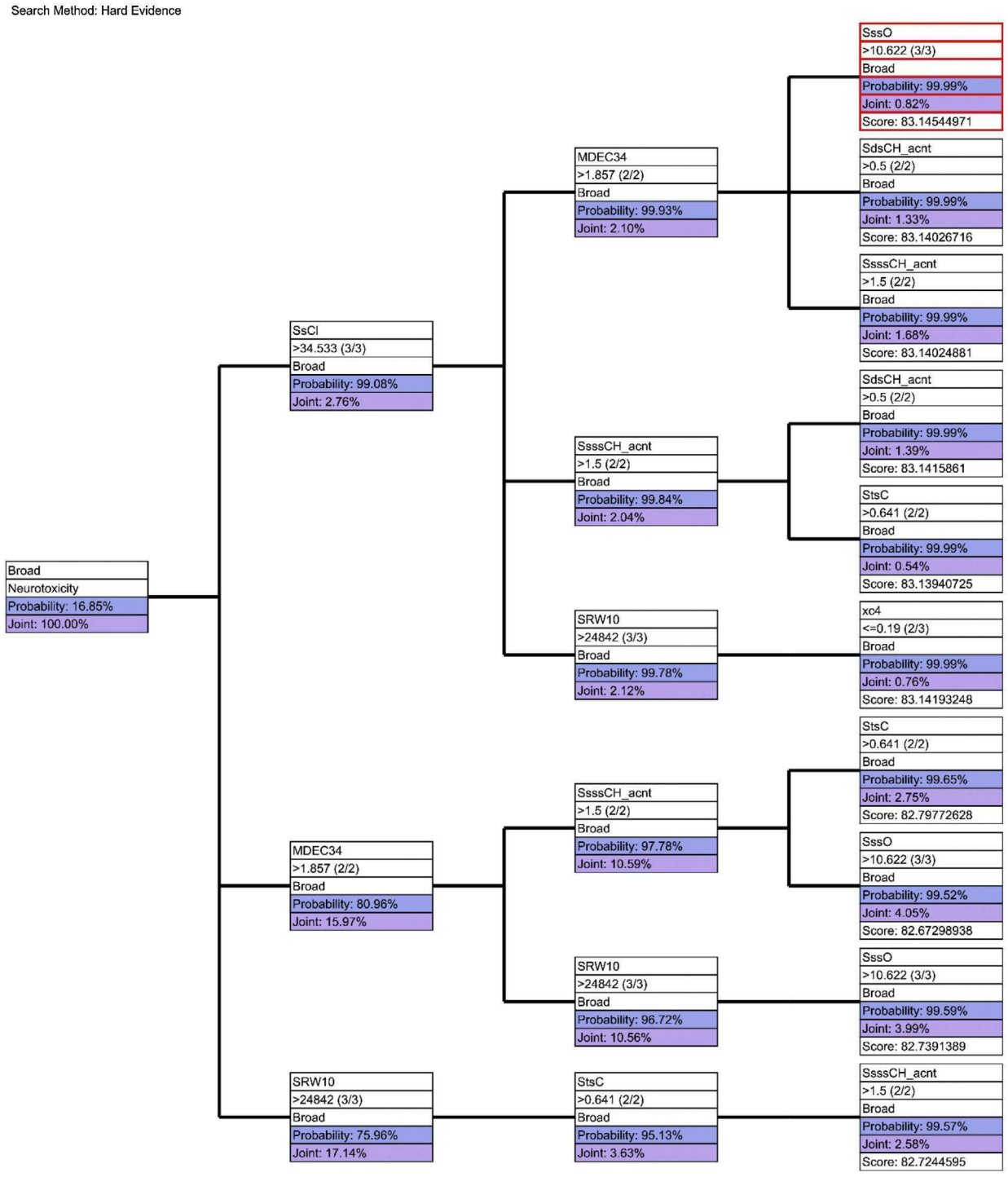

Fig. 7. Target optimization tree for neurotoxicity without taking into account the joint probability of the evidence. The rows on the leaves contain the score for the pathway built on the probability change. The red highlighted descriptor (SssssO) is the terminal node state of the pathway with the highest score. (For interpretation of the references to colour in this figure legend, the reader is referred to the web version of this article.)

development. From the TDP analysis above, it was also observed that narcosis took as many or more descriptors when compared to the corresponding TDPs of neurotoxicity and AChEI to raise the probability to near certainty (0.99 or above). The final probabilities range from 0.76 to 0.91 at the terminal evidence set for scenarios with consideration of the joint probability. Additional descriptors could raise these probabilities further but the trees were constrained for examining the capabilities of only a handful of descriptors in predicting the MoAs. Without consideration of the joint probability, probabilities of narcosis being true ranged from 0.93 to near certainty. The highest scoring pathway with the joint probability considered contained MAXDN, SdsCH_acnt, and Qv, duplicating the TDP. The highest scoring pathway without consideration of the joint probability contained MATS3e, SssO, and DELS, also duplicating the initial evidence set of the TDP. Narcosis and neurotoxicity both contained SssO in their highest scoring pathways without considering the joint probability. Narcosis and AChEI both contained MAXDN and Qv in their highest

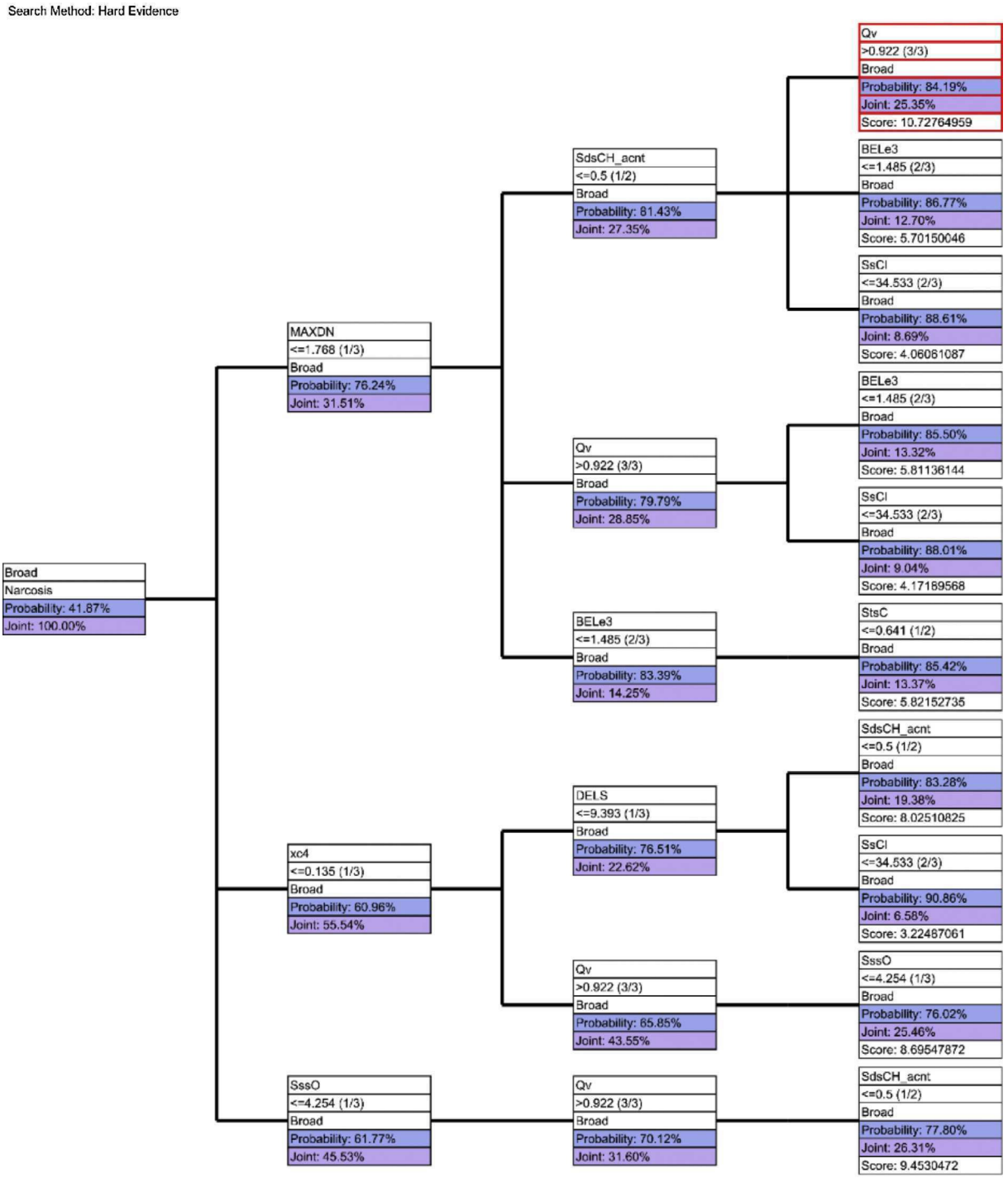

Fig. 8. Target optimization tree for narcosis with the joint probability of the evidence taken into consideration. The rows on the leaves contain the score for the pathway built on the probability change weighted by the final joint probability. The red highlighted box (Qv) is the terminal node state of the pathway with the highest score. (For interpretation of the references to colour in this figure legend, the reader is referred to the web version of this article.)

scoring pathways with the joint probability considered. Neurotoxicity and AChEI both contained J in highest scoring pathways. For neurotoxicity, J was in the pathway that considered the joint probability and for AchEI it was in the pathway without consideration of the joint probability. Additional target optimization trees for the other modes of action are found in the Supporting information.

4. Discussion

Compound classification methods offer the ability to associate structural features and chemical properties with specific types of biological activities and to screen for and predict biologically active compounds (Bajorath, 2001). Molecular similarity is the basis of these approaches, which typically requires the use of chemical descriptors that capture a broad range of molecular

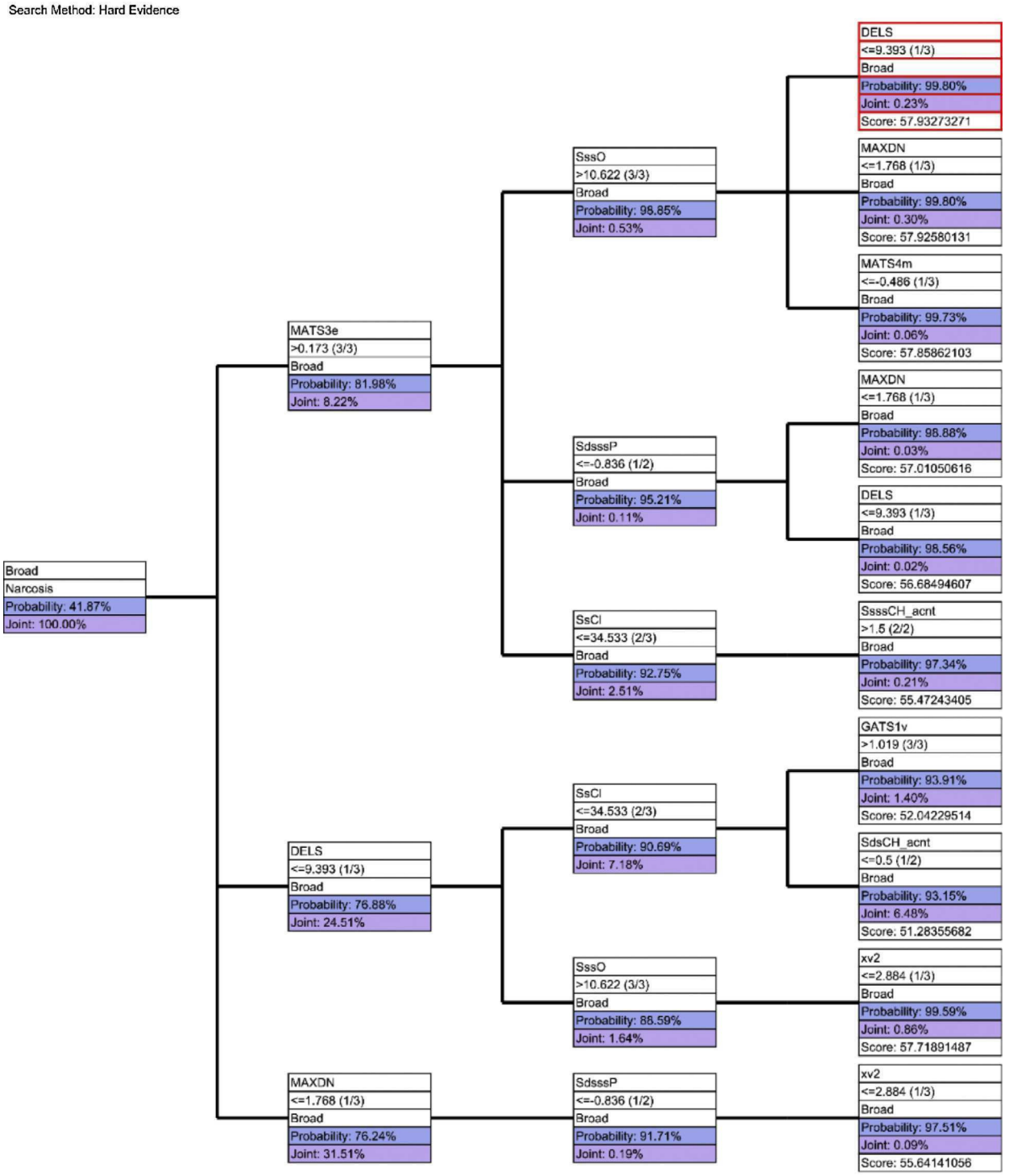

Fig. 9. Target optimization tree for narcosis without taking into account the joint probability of the evidence. The rows on the leaves contain the score for the pathway built on the probability change. The red highlighted box (DELS) is the terminal node state of the pathway with the highest score. (For interpretation of the references to colour in this figure legend, the reader is referred to the web version of this article.)

characteristics and definition of the theoretical chemical space of the model (Martin et al., 2002; Bajorath 2001). Hundreds of molecular descriptors are available in the literature that can be calculated using computational chemistry software such as Dragon which provides more than 1600 theoretical descriptors (e.g., Mauri et al., 2006). In the current study, a diversity of two dimensional chemical descriptors were calculated and assigned using the computational chemistry application TEST (USEPA, 2008, 2016), including E-state values and E-state counts, constitutional descriptors, topological descriptors, walk and path counts, connectivity, information content, two-dimensional autocorrelation, Burden eigenvalue, molecular property, Kappa, hydrogen bond acceptor/donor counts, molecular distance edge and molecular fragment counts (Martin et al., 2013, 2015). Previous studies have demonstrated high performance of two dimensional descriptors in both molecular similarity analysis and compound classification

(Bajorath, 2001), although they have seen only limited application in aquatic toxicology (e.g., Papa et al., 2005; Martin et al., 2013, 2015).

Interpretation of computational chemistry descriptors is typically challenging because they are based on hundreds of calculated attributes of a molecule that may have positive or negative values. For example, the electrotopological state index represents the electronic state of an atom as perturbed from electronic influence of other atoms in the molecule (Hall and Kier, 1995). The index reflects the contribution of a specific group of atoms (e.g., –CH3, =CH2-) and depends on the environment of that group of atoms within a specific molecule (Hall and Kier, 1995). As another example, Qv is a whole molecule polarity index that decreases in value as polarity increases (Votano et al., 2004). Of the over 700 descriptors assigned by the TEST computational chemistry application, only 24 were used to establish a Markov blanket around the MoA variable and 22 of these 24 were in a pathway prior to reaching or at the point of exceeding 0.99 probability of a MoA in the TDP analysis. The Markov blanket analysis used in the current network provided a method that reduced the inherent complexity of numerous chemical descriptor assignments by determining the most important predictors in terms of probabilistic dependence with the MoAs.

The Bayesian network had an overall prediction accuracy (model precision) of 80%, which is similar to the 86% accuracy (correct fraction) of the LDA model of Martin et al. (2015) using two dimensional theoretical chemical descriptors and the same MoA dataset of Barron et al. (2015). AChEI MoA had the highest prediction accuracy in both the network (93.5%) and LDA (98%), and reactivity the lowest (network: 48%; LDA: 33%). Prediction accuracy of chemicals with an MoA of neurotoxicity was highest in the network model (83%; LDA: 65%), whereas narcosis prediction accuracy was highest in LDA (98%) compared to the network (80%) (Martin et al., 2015). These results suggest that MoA prediction accuracy may be a function of the intrinsic uncertainty in the theoretical descriptors and MoA classification, rather than fundamental differences in the statistical modeling approach. As knowledge of MoA assignments and theoretical relationships between descriptors and MoAs advances, model performance and predictive capabilities should likewise improve.

For machine learned Bayesian networks, the minimum description length scores are useful for establishing the relationships among variables from the available data. With deterministic models, rules can be difficult to establish and interpret and complexity can overwhelm understanding of the model and the processes being represented. However, the nonparametric quantitative methods used in the current approach require larger amounts of data than might be found in some datasets. For the current model, MoAs with low numbers of data generally had relatively diminished predictive accuracy and data coverage for establishing conditional probabilities. In contrast, Martin et al. (2013, 2015) attributed poor predication accuracy of the reactivity MoA to a large range in reactivity mechanisms and general structural diversity. Within the current model, pathways constrained to a relatively small number of descriptors still led to high probabilities for each MoA despite varying data coverage.

Bayesian approaches can decompose complex multivariate problems into graphical networks that can be visualized and that support bidirectional inferences under various levels of uncertainty. The probabilistic focus inherent in a Bayesian network is also conducive to improvements in structuring and quantification as the knowledge and evidence improves over time. Coupling a Bayesian network with subjective interpretations of probability maintains focus on missing information and the imprecision from insufficient knowledge of true relationships. In the current study, the MOATox database of Barron et al. (2015) was taken as the best compendium of knowledge currently available regarding the acute aquatic toxicity MoA for a diversity of chemicals. The ability to predict unknown MoAs from existing data will become more precise as the knowledge base of MoA increases. Bayesian frameworks can provide useful pathways to improved predictive and diagnostic tools for aquatic toxicology and other problems with high dimensional data and multiple uncertain outcomes.

Acknowledgments

This research was supported in part by an appointment to the ORISE participant research program supported by an interagency agreement between the U.S. EPA and the U.S. Department of Energy. We thank Tom Stockton and Chris Grulke for review of a draft of the manuscript. The conclusions may not necessarily reflect the views of EPA and no official endorsement should be inferred.

Appendix A. Supplementary data

Supplementary data associated with this article can be found, in the online version, at http://dx.doi.org/10.1016/j.aquatox.2016.09.006.

References

Bajorath, J., 2001. Selected concepts and investigations in compound classification, molecular descriptor analysis, and virtual screening. J. Chem. Inf. Comput. Sci. 41, 233–245.
Barber, D., 2012. Bayesian Reasoning and Machine Learning. Cambridge University Press, Cambridge, UK.
Barron, M.G., Lilavois, C.R., Martin, T.M., 2015. A comprehensive mode of action and acute aquatic toxicity database for predictive model development. Aquat. Toxicol. 16, 102–107.
Bayesia S.A.S, 2015. Bayesialab Software Version 5.4.3 (Accessed 05/16/2016) http://www.bayesia.com/.
Bayesia, 2010. Bayesialab User Guide. Bayesia S.A.S., Laval Cedex, France.
Billoir, E., Delignette-Muller, M.L., Péry, A.R.R., Charles, S., 2008. A Bayesian approach to analyzing ecotoxicological data. Environ. Sci. Technol 42, 8978–8984.
Burden, F.R., Winkler, D.A., 2000. A quantitative structure-activity relationships model for the acute toxicity of substituted benzenes to *Tetrahymena pyriformis* using Bayesian-regularized neural networks. Chem. Res. Toxicol 13, 436–440.
Conrady, S., Jouffe, L., 2011. Microarray Analysis with Bayesian Networks: Using Bayesialab for Cancer Type Classification. Bayesia USA, Franklin, TN.
Conrady, S., Jouffe, L., 2015. Bayesian Networks and Bayesialab: A Practical Introduction for Researchers. Bayesia USA, Franklin, TN.
Enoch, S.J., Hewitt, M., Cronin, M.T.D., Azam, S., Madden, J.C., 2008. Classification of chemicals according to mechanism of aquatic toxicity: an evaluation of the implementation of the Verhaar scheme in Toxtree. Chemosphere 73, 243–248.
Hall, L.H., Kier, L.B., 1995. Electrotopological state indices for atom types: a novel combination of electronic, topological, and valence state information. J. Chem. Inf. Comput. Sci. 35, 1039–1045.
Harris, M., Bhuvaneshwar, K., Natarajan, T., Sheahan, L., Wang, D., Tadesse, M.G., Shoulson, I., Filice, R., Steadman, K., Pishvaian, M.J., Madhavan, S., Deeken, J., Pharmacogenomic characterization of gemcitabine response –a framework for data integration to enable personalized medicine. Pharmacogenetics and Genomics 24 (2): 81–93.
He, L., Jurs, P.C., 2005. Assessing the reliability of QSAR model's predictions. J. Mol. Graph. Model. 23, 503–523.
Iorio, F., Tagliaferri, R., di Bernardo, D., 2009. Identifying network of drug mode of action by gene expression profiling. J. Comput. Biol. 16, 241–251.
Korb, K.K., Nicholson, A.E., 2004. Bayesian Artificial Intelligence. Chapman & Hall/CRC, Boca Raton, FL.
Martin, Y.C., Kofron, J.L., Traphagen, L.M., 2002. Do structurally similar molecules have similar biological activitiy? J. Med. Chem. 45, 4350–4358.
Martin, T.M., Grulke, C.M., Young, D.M., Russom, C.L., Wang, N., Jackson, C.R., Barron, M.G., 2013. Prediction of aquatic toxicity mode of action using linear discriminant and random forest models. J. Chem. Info. Model. 53, 2229–2239.
Martin, T.M., Young, D.M., Lilavois, C.R., Barron, M.G., 2015. Comparison of global and mode of action-based models for aquatic toxicity. SAR QSAR Environ. Res. 26, 245–262.
Mauri, A., Consonni, V., Pavan, M., Todeschini, R., 2006. MATCH. Commun. Math. Comput. Chem. 56, 237–248.
Nendza, M., Muller, M., 2007. Discriminating toxicant classes by mode of action: 3: Substructure indicators. SAR QSAR Environ. Res. 18, 155–168.
Papa, E., Villa, F., Gramatica, P., 2005. Statistically validated QSARs, based on theoretical descriptors, for modeling aquatic toxicity of organic chemicals in *Pimephales promelas* (fathead minnow). J. Chem. Inf. Model. 45, 1256–1266.
Russom, C.L., Bradbury, S.P., Broderius, S.J., Hammermeister, D.E., Drummond, R.A., 1997. Predicting modes of toxic action from chemical structure: acute toxicity

in the fathead minnow (Pimephales promelas). Environ. Toxicol. Chem. 16, 948–967.
Stone, M., 1974. Cross-validatory choice and assessment of statistical predictions (with discussion). J. R. Stat. Soc. Ser. B (Methodol.) 36 (2), 111–147.
Thai, H., Campo, D.S., Lara, J., Dimitrova, Z., Ramachandran, S., Xia, G., Ganova-Raeva, L., Teo, C.-G., Lok, A., Khudyakov, Y., 2012. Convergence and coevoluation of Hepatitis B virus drug resistance. Nat. Commun. 3, 789.
USEPA, 2008. Molecular Descriptors Guide. Description of the Molecular Descriptors Appearing in the Toxicity Estimation Software Tool. V. 1.0.2. U.S. Environmental Protection Agency www.epa.gov/chemical-research/molecular-descriptors-guide.
USEPA, 2016. User's Guide for T.E.S.T. (version 4.2) (Toxicity Estimation Software Tool). A Program to Estimate Toxicity from Molecular Structure. EPA/600/R-16/058. U.S. Environmental Protection Agency, Cincinnati, OH (63 pp.) www.epa.gov/chemical-research/toxicity-estimation-software-tool-test.
Verhaar, H.J.M., van Leeuwen, C.J., Hermens, J.L.M., 1992. Classifying environmental pollutants part 1, Structure activity relationships for prediction of aquatic toxicity. Chemosphere 25, 471–491.
Votano, J.R., Parham, M., Hall, L.H., Kier, L.B., Oloff, S., Tropsha, A., Xie, Q., Tong, W., 2004. Three new consensus QSAR models for the prediction of Ames genotoxicity. Mutagenesis 19, 365–377.
Yao, X.J., Panaye, A., Doucet, J.P., Chen, H.F., Zhang, R.S., Fan, B.T., Liu, M.C., Hu, Z.D., 2005. Comparative classification study of toxicity mechanisms using support vector machines and radial basis function neural networks. Anal. Chim. Acta 535, 259–273.
Zhu, H., Martin, T.M., Ye, L., Sedykh, A., Young, D.M., Tropsha, A., 2009. Quantitative structure-activity relationship modeling of rat acute toxicity by oral exposure. Chem. Res. Toxicol. 22, 1913–1921.

This article was downloaded by: [US EPA Library]
On: 01 July 2015, At: 08:06
Publisher: Taylor & Francis
Informa Ltd Registered in England and Wales Registered Number: 1072954 Registered office: Mortimer House, 37-41 Mortimer Street, London W1T 3JH, UK

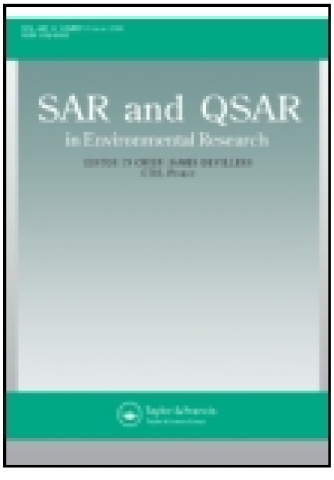

CrossMark
Click for updates

SAR and QSAR in Environmental Research

Publication details, including instructions for authors and subscription information:
http://www.tandfonline.com/loi/gsar20

Comparison of global and mode of action-based models for aquatic toxicity

T.M. Martin[a], D.M. Young[a], C.R. Lilavois[b] & M.G. Barron[b]

[a] National Risk Management Research Laboratory, US Environmental Protection Agency, Cincinnati, OH, USA

[b] National Health and Environmental Effects Research Laboratory, US Environmental Protection Agency, Gulf Breeze, Florida, USA

Published online: 18 Mar 2015.

To cite this article: T.M. Martin, D.M. Young, C.R. Lilavois & M.G. Barron (2015) Comparison of global and mode of action-based models for aquatic toxicity, SAR and QSAR in Environmental Research, 26:3, 245-262, DOI: 10.1080/1062936X.2015.1018939

To link to this article: http://dx.doi.org/10.1080/1062936X.2015.1018939

PLEASE SCROLL DOWN FOR ARTICLE

Taylor & Francis makes every effort to ensure the accuracy of all the information (the "Content") contained in the publications on our platform. However, Taylor & Francis, our agents, and our licensors make no representations or warranties whatsoever as to the accuracy, completeness, or suitability for any purpose of the Content. Any opinions and views expressed in this publication are the opinions and views of the authors, and are not the views of or endorsed by Taylor & Francis. The accuracy of the Content should not be relied upon and should be independently verified with primary sources of information. Taylor and Francis shall not be liable for any losses, actions, claims, proceedings, demands, costs, expenses, damages, and other liabilities whatsoever or howsoever caused arising directly or indirectly in connection with, in relation to or arising out of the use of the Content.

This article may be used for research, teaching, and private study purposes. Any substantial or systematic reproduction, redistribution, reselling, loan, sub-licensing, systematic supply, or distribution in any form to anyone is expressly forbidden. Terms &

Conditions of access and use can be found at http://www.tandfonline.com/page/terms-and-conditions

Downloaded by [US EPA Library] at 08:06 01 July 2015

SAR and QSAR in Environmental Research, 2015
Vol. 26, No. 3, 245–262, http://dx.doi.org/10.1080/1062936X.2015.1018939

Taylor & Francis
Taylor & Francis Group

Comparison of global and mode of action-based models for aquatic toxicity

T.M. Martin[a]*, D.M. Young[a], C.R. Lilavois[b] and M.G. Barron[b]

[a]*National Risk Management Research Laboratory, US Environmental Protection Agency, Cincinnati, OH, USA;* [b]*National Health and Environmental Effects Research Laboratory, US Environmental Protection Agency, Gulf Breeze, Florida, USA*

(*Received 21 November 2014; in final form 10 February 2015*)

Downloaded by [US EPA Library] at 08:06 01 July 2015

The ability to estimate aquatic toxicity is a critical need for ecological risk assessment and chemical regulation. The consensus in the literature is that mode of action (MOA) based toxicity models yield the most toxicologically meaningful and, theoretically, the most accurate results. In this study, a two-step prediction methodology was developed to estimate acute aquatic toxicity from molecular structure. In the first step, one-against-the-rest linear discriminant analysis (LDA) models were used to predict the MOA. The LDA models were able to predict the MOA with 85.8–88.8% accuracy for broad and specific MOAs, respectively. In the second step, a multiple linear regression (MLR) model corresponding to the predicted MOA was used to predict the acute aquatic toxicity value. The MOA-based approach was found to yield similar external prediction accuracy (r^2 = 0.529–0.632) to a single global MLR model (r^2 = 0.551–0.562) fit to the entire training set. Overall, the global hierarchical clustering approach yielded a higher combination of accuracy and prediction coverage (r^2 = 0.572, coverage = 99.3%) than the other approaches. Utilizing multiple two-dimensional chemical descriptors in MLR models yielded comparable results to using only the octanol–water partition coefficient (log K_{ow}).

Keywords: mode of action; quantitative structure–activity relationship (QSAR); linear discriminant analysis (LDA); multiple linear regression; aquatic toxicity; octanol–water partition coefficient

1. Introduction

There are three general approaches for developing quantitative structure–activity relationship (QSAR) models for diverse datasets that apply (1) global models using flexible machine learning techniques, (2) local models based on sets of clearly defined congeners (class based approach) and (3) local models based on a common mode of toxic action (MOA) [1]. Several previous studies have indicated the most toxicologically meaningful results can be obtained using a mode of action (MOA) based approach [2–6]. For example, Yuan et al. [7] reported that MOA-based local models yielded superior results to a global model for predicted acute toxicity to a standard fish test species, the fathead minnow (*Pimephales promelas*).

Global approaches to modelling aquatic toxicity include k nearest neighbours (kNN) [8,9] or nearest neighbours [10], support vector machines (SVM) [11], multilinear regression (MLR) [10,12–14], MLR using only structurally similar chemicals from the training set [15],

*Corresponding author. Email: martin.todd@epa.gov

This work was authored as part of the Contributors' official duties as Employees of the United States Government and is therefore a work of the United States Government. In accordance with 17 USC. 105, no copyright protection is available for such works under US Law.

group contribution methods [16,17], partial least squares [18,19], artificial neural networks (ANNs) [12,20], associative neural networks (ASNN) [21] and hierarchical clustering (HC) [10,22]. The advantage of global methods is that machine learning allows the development of model(s), which do not require the determination of chemical class or MOA. This makes it easier to develop models for diverse datasets. The disadvantage of global methods is that it is possible to overfit a dataset with too many non-biologically relevant chemical descriptors.

Previous QSAR research in aquatic toxicology has largely been focused on developing models for specific chemical classes (reviewed by Netzeva et al. [1]). Early QSAR studies used a single chemical property of hydrophobicity, usually modelled as the log of the octanol–water partition coefficient (log K_{ow}) to estimate toxicity for large classes of industrial chemicals of moderate polarity [23]. The Ecological Structure Activity Relationships (ECOSAR) program within the Estimation Program Interface (EPI) Suite [24] uses class-based models to calculate aquatic toxicity based on log K_{ow} for a variety of chemical groups including pesticides, dyes and reactive compounds, as well as traditional solvent-like chemicals.

An advantage of class based models is that structurally similar chemicals should be toxicologically similar. However, Russom et al. [25] illustrated that chemicals within the same chemical class can act through different MOAs. For example, hydroquinones emerge as an outlier from models for phenols [26], and chlorinated phenols exhibit polar narcosis and uncoupling of oxidative phosphorylation depending on the number of chlorines [25]. Disadvantages of class-based methods include: the uncertainty in precisely defining a chemical class; chemicals can possess functional groups for more than one chemical class; and sometimes insufficient data are available to develop a model for specific chemical classes.

Several researchers have developed MOA-based models to predict aquatic toxicity LC_{50} values [1,7,13,27]. Claeys et al. developed models for chronic aquatic toxicity for the nonpolar narcosis and polar narcosis MOAs using the octanol–water partition coefficient [27]. Many models are available, but the predictive power can be confounded by the need for 'a priori' selection of the appropriate MOA model [28]. Several researchers have developed methods to assign chemicals to particular aquatic toxicity modes of action [28–38]. A variety of techniques have been utilized including linear discriminant analysis (LDA) [28,29,37], binary logistic regression [30], Adaboost [31], decision tree models [33], counter propagation neural networks and multinomial logistic regression [39], and support vector machines [34,36].

In a previous paper [38], we developed a 'one-against-the-rest' LDA approach to predict aquatic toxicity MOA. Separate discriminant models were developed for each results category and the predicted category yielded the highest score from all the different models. In the current study, fathead minnow acute toxicity is predicted using a two-step process. In the first step, LDA models are used to predict MOA and then acute toxicity is predicted using the multilinear regression model corresponding to each chemical's predicted MOA. This approach is similar to that utilized by ASTER (ASessment Tools for the Evaluation of Risk) to estimate aquatic toxicity, except that ASTER utilizes a fragment-based MOA assignment approach and log K_{ow} based linear regression toxicity models [25,40]. Here we compare the MOA-based model results with global methods including hierarchical clustering and a single MLR model fit to the entire training set. Additionally we investigate whether MOA-based MLR models fit to multiple two-dimensional (2D) descriptors yield better results than models fitted only to log K_{ow}.

In this study there are two datasets (one with 1015 chemicals, one with 793 chemicals). The first is used to develop models to predict the toxicity MOA. The training set is ~80% and the prediction set is ~20% of this dataset. The second dataset is used to develop models to predict quantitative fathead minnow toxicity. A total of 372 chemicals in the second dataset

Downloaded by [US EPA Library] at 08:06 01 July 2015

have LC_{50} values as well as MOA values (thus they are also present in the first dataset). These chemicals are used for the training set. The chemicals in the second dataset with unknown MOA are used as the prediction set for predicting the LC_{50} value. The chemicals in this set represent a true external set in that none of the chemicals are present in the training set for the MOA or LC_{50} models.

2. Materials and methods

2.1 *MOA dataset*

A dataset of 1015 chemicals was developed for 11 MOAs based on their mode of acute toxic action in fish (Table 1). This dataset represents a slight expansion of the database used in a previous study to include additional specific MOAs [38]. Neurotoxicity categories were expanded from two specific MOAs (organochlorine and pyrethroid) to seven [pyrethroid sodium channel modulation, alicyclic γ-aminobutyric acid (GABA) antagonism, diphenyl sodium channel modulation, GABA agonism, pyrazole GABA antagonism, sodium channel

Downloaded by [US EPA Library] at 08:06 01 July 2015

Table 1. Summary of the mode of action (MOA) dataset used in developing MOA-based QSAR models.

MOA	*MOA subcategory*	*Characteristics*	*Count*
AChE inhibition	Carbamate	Carbamate moiety	69
	Organo-phosphate	Pphosphate or thiophosphate moiety	199
Narcosis	Ester	Diverse structures, mono or diesters	44
	Nonpolar	Diverse structures, not ionizable	299
	Polar	Phenols, anilines, pyridines; single nitro or <4 halogens	59
Neurotoxicity	Pyrethroid sodium channel modulation	Pyrethroid analogs	65
	Alicyclic GABA antagonism	Aliphatic and cyclic	26
	Diphenyl sodium channel modulation	Diphenyl	11
	GABA agonism	Macrocyclic lactones	13
	Other	Diverse structures	6
	Pyrazole GABA antagonism	Pyrazole	6
	Sodium channel blocking	Urea with trifluoro group	2
Reactivity	*NA*	Electrophiles, proelectrophiles	91
Uncoupling Oxidative Phosphorylation	*NA*	>1 nitro or >3 halogenated phenols, anilines, pyridines	48
Not AChE Inhibition	Carbamate	Carbamate moiety	40
	Organophosphate	Phosphate or thiophosphate moeity	9
Anticoagulation	Vitamin K antagonism	Coumarins	17
nAChR agonism	*NA*	Nicotine or neconicotinoids	8
nAChR antagonism	*NA*	Piperidine with alkyl chain	1
Methaeglobinaemia	*NA*	Benzene ring with amino and ketone substituents	1
Oxidative phosphorylation inhibition	*NA*	Pyridine with urea and nitrobenzene	1
Total			1015

NA: not applicable.

blocking, and other]. However, the number of chemicals with the broad neurotoxicity MOA only increased from 124 to 129 chemicals. This refinement provided greater structural similarity within each specific MOA as well as consistency with international pesticide MOA classification [41]. The number of chemicals with the acetylcholinesterase (AChE) inhibition broad MOA was increased from 199 to 268.

The dataset was developed using a combination of high confidence assignments, including biological responses in fish acute toxicity assays [25], international consensus classifications such as the Insecticide Resistance Action Committee's (IRAC) MOA classification tool [41], ASTER [40] predictions, and weight of evidence professional judgment based on assessment of structure and literature information (see Table S1 in the supplemental material which is available via the multimedia link on the online article webpage). The molecular structures for the chemicals in the overall dataset were obtained using the procedure detailed by Young and colleagues [10].

One of 11 broad MOAs was assigned to each chemical: AChE inhibition; narcosis; neurotoxicity; reactivity; uncoupling oxidative phosphorylation; anticoagulation; nicotinic acetylcholine receptor (nACHR) agonism; nACHR antagonism; methemoglobinemia; and oxidative phosphorylation inhibition (see Table 1). The first column in Table 1 indicates 'broad' MOAs, while the first and second columns taken together indicate 'specific' MOAs. Models were developed for both broad and specific MOAs. The MOA dataset were randomly subdivided into training (~80% of chemicals, 802 chemicals) and validation set (~20%, 213 chemicals) within each MOA and MOA subcategory (see Table S1 in the supplemental material which is available via the multimedia link on the online article webpage). This 802 chemical training set was used to build LDA models to predict MOA.

Downloaded by [US EPA Library] at 08:06 01 July 2015

2.2 *Fathead minnow LC_{50} data set*

The fathead minnow LC_{50} endpoint represents the concentration in freshwater which kills half of the test fish in 96 hours. The dataset for this endpoint was obtained from the ECOTOX aquatic toxicity database (http://cfpub.epa.gov/ecotox/). Compounds were restricted to the following elements: C, H, O, N, F, Cl, Br, I, S, P, Si and As. In addition, compounds must represent a single pure component (salts, undefined isomeric mixtures, polymers or mixtures were removed). For chemicals with multiple LC_{50} values in ECOTOX, the geometric median value was used. Chemicals with known MOA (372 chemicals) were placed in the training set and chemicals with unknown MOA (421 chemicals) were placed in the prediction set. This was done so that chemicals in the prediction set will have an external prediction of the MOA and then the toxicity value. The 372 chemical training set was used to build multiple models (one for each MOA) to predict the quantitative LC_{50} value. The chemicals in the LC_{50} training set are also present in the 1015 MOA dataset.

2.3 *Prediction methodology*

Fathead minnow acute toxicity values were predicted using a two-step process. In the first step, one-against-the-rest LDA models were used to predict each chemical's broad or specific MOA. In the second step, the LC_{50} value was predicted using the multilinear regression model corresponding to the predicted MOA. Several MOAs had an insufficient number of chemicals with an available LC_{50} values to include in QSAR toxicity estimation. These included anticoagulation, nAChR agonism and antagonism, diphenyl sodium channel modulation, and GABA agonism.

The methodology for estimating MOA using LDA is described in a previous publication [38] and is described briefly below. An LDA model is essentially a multilinear regression model [30]:

$$Score = \sum_{i=1}^{n} a_i x_i + a_0 \quad (1)$$

where a_i is the fitted constant for parameter i, x_i is the ith molecular descriptor, and a_0 is the model intercept. Chemicals with a given MOA are assigned a score of 1. Chemicals that do not have the given MOA are assigned a score of 0. For example, when building a model for the AChE inhibition-organophosphate MOA, famphur (*O*-(4-((dimethylamino)sulphonyl)phenyl) *O*,*O*-dimethyl thiophosphate) would be assigned a score of 1 while ethanol would be assigned a score of 0 (since it has the narcosis-nonpolar MOA).

Descriptors are selected (and regression constants fitted) using a genetic algorithm based approach so the model can match the experimental values for the training set. A pool of 790 descriptors was obtained from the US Environmental Protection Agency (US EPA) chemical descriptor and toxicity estimation tool, T.E.S.T. [40]. The descriptor classes included E-state values and E-state counts, constitutional descriptors, topological descriptors, walk and path counts, connectivity, information content, two-dimensional autocorrelation, Burden eigenvalue, molecular property (such as the octanol–water partition coefficient), Kappa, hydrogen bond acceptor/donor counts, molecular distance edge and molecular fragment counts [40].

LDA models were built for each MOA that contained at least five chemicals, consistent with a minimum recommended ratio of 5:1 [42]. However, using a minimum ratio of 67 chemicals per descriptor (about 11 descriptors per model) yielded the best results based on re-substitution sensitivity, which was the fraction of positive chemicals correlated accurately to the number of positive chemicals in the training set. The MOA for new chemicals was determined by first calculating the score for all the LDA models, then selecting the predicted MOA with the highest score. MOA assignments were only included where the maximum predicted score was ≥0.5.

The training set included several carbamate and organophosphate chemicals that were structurally similar to AChE inhibitors, but were known not to have an AChE inhibition MOA. These chemicals were assigned a score of zero when building LDA models for AChE inhibition to facilitate the development of models that could distinguish between potent and non-potent AChE inhibitors. Chemicals with a non-AChE inhibition MOA were not used when building LDA models for other MOAs. These chemicals were added so that no all carbamates and organophosphates would be predicted to be AChE inhibitors.

Before any QSAR model can be used to make a prediction for a test chemical, it must be determined whether the test chemical falls within the domain of applicability (or AD) for the model. The first constraint, the model ellipsoid constraint, checks if the test chemical is within the multidimensional ellipsoid defined by the ranges of descriptor values for the chemicals in the training set (for the descriptors appearing in the model). The model ellipsoid constraint is satisfied if the leverage of the test compound (h_{00}) is less than the maximum leverage value for all the compounds used in the model [43]. The second constraint, the R_{max} constraint, checks if the distance from the test chemical to the centroid of the training set is less than the maximum distance for any chemical in the training set to the its centroid. The fragment constraint [10] was not applied in this study since it was not found to improve prediction concordance [38]. Finally, the maximum score from all the LDA models must exceed 0.5 as mentioned above.

Downloaded by [US EPA Library] at 08:06 01 July 2015

LC_{50} values were predicted using a multilinear regression model for toxicity:

$$Tox = \sum b_i x_i + b_0 \quad (2)$$

where b_i is the fitted constant for parameter i, x_i is the ith molecular descriptor, and b_0 is the model intercept. The descriptors were selected using a genetic algorithm approach as outlined previously [10]. The minimum ratio of chemicals to descriptors was set at 5:1 for QSAR modelling. An LC_{50} model was developed for all the MOAs that had at least five chemicals in the LC_{50} training set. The model ellipsoid and R_{max} constraints described above were used to define the applicability domain of the LC_{50} models. In addition to the 2D descriptors from T.E.S.T. described above, single descriptor models were developed using log K_{ow}. The log K_{ow} was taken from EPISUITE [24], denoted from here on as ELOGP. If an experimental value is available, that value was used. If an experimental value was not available, the calculated value from EPISUITE was used.

Downloaded by [US EPA Library] at 08:06 01 July 2015

3. Results and discussion

3.1 *Results*

3.1.1 *Internal model statistics for LDA models*

All the LDA models had high correlations in terms of concordance (fraction of chemicals predicted correctly) and specificity (fraction of negative chemicals predicted correctly) (see Table 2). However, for several of the specific MOAs (narcosis-ester, narcosis-polar, neurotoxicity-diphenyl sodium channel modulation, and reactivity), we were unable to achieve high sensitivity (fraction of positive chemicals predicted correctly) values. Greatly increasing the number of descriptors did not yield models with good sensitivity (i.e. ≥0.5). The reactivity MOA contained a variety of structural classes and thus different reactive mechanisms, which may explain why it was difficult to consistently identify the MOA of reactive compounds. In future research, we may divide the reactivity MOA into several specific MOAs such as acylation, isocyanate reactivity, nucleophilic substitution, alkylation/arylation and sulfhydryl reactivity. The correlation for narcosis-polar may have achieved low sensitivity due to ambiguity about the structural differences between chemicals in the narcosis-polar and narcosis-nonpolar categories. For example, it has been demonstrated that *ortho* substitutions on a pyridine can shift the MOA from narcosis-polar (e.g. pyridine) to narcosis-nonpolar narcosis (e.g. 2-ethylpyridine), presumably due to steric hindrance [25].

3.1.2 *Results for MOA prediction set*

The overall prediction accuracy for the different QSAR techniques was excellent, with concordance of 88.8 and 85.8% for the specific and broad MOAs, respectively (Table 3). These results were comparable with those obtained in our previous publication using a slightly different MOA dataset [38]. The specific MOAs achieved a higher accuracy, but at the sacrifice of a lower prediction coverage (fraction of chemicals which can be predicted): 73.3% of chemicals for specific MOAs compared with 94.5% for broad MOAs.

The prediction accuracies for each MOA were highly correlated with the training set sensitivities. For example the AChE inhibition–carbamate chemicals were predicted with perfect accuracy (the training set sensitivity was 100%), while the reactive chemicals were predicted with 46.2% accuracy (the training set sensitivity was 47.2%). This similarity is not unexpected since the overall dataset was divided into training and prediction sets randomly

Table 2. Modelling statistics for the training dataset used in developing MOA-based models using LDA.

Broad MOA	*Concordance**	*Sensitivity†*	*Specificity‡*
AChE inhibition	0.970	0.995	0.961
Anticoagulation	0.999	0.923	1.000
nAChR agonism	0.997	0.833	0.999
Narcosis	0.890	0.938	0.855
Neurotoxicity	0.969	0.768	0.998
Reactivity	0.942	0.472	0.991
Uncoupler	0.982	0.658	0.999
Specific MOA			
AChE inhibition-carbamate	0.986	1.000	0.985
AChE inhibition-organophosphate	0.991	0.994	0.991
Anticoagulation-vitamin K antagonism	0.999	0.923	1.000
nAChR agonism	0.997	0.833	0.999
Narcosis-ester	0.969	0.371	0.997
Narcosis-nonpolar	0.815	0.636	0.897
Narcosis-polar	0.961	0.383	0.999
Neurotoxicity-alicyclic GABA antagonism	0.995	0.800	1.000
Neurotoxicity-diphenyl sodium channel modulation	0.990	0.000	1.000
Neurotoxicity-GABA agonism	1.000	1.000	1.000
Neurotoxicity-pyrethroid sodium channel modulation	0.982	0.827	0.993
Reactivity	0.942	0.472	0.991
Uncoupling oxidative phosphorylation	0.982	0.658	0.999

*Concordance is the fraction of chemicals predicted correctly.
†Sensitivity is the fraction of positive chemicals predicted correctly.
‡Specificity is the fraction of negative chemicals predicted correctly.

Downloaded by [US EPA Library] at 08:06 01 July 2015

with equal distributions of each mode of action. Several of the specific MOAs had 0% accuracy (neurotoxicity-other, neurotoxicity-pyrazole GABA antagonism, neurotoxicity-sodium channel blocking, and oxidative phosphorylation inhibition) due to the fact there was insufficient chemicals in the MOA training set to build an LDA model. Chemicals falling under these MOAs were not used to calculate the overall accuracy (Table 3). About 60% of the non-AChE inhibitors were still predicted to be AChE inhibitors, indicating the LDA models still predominately predict chemicals with carbamate or organophosphate substructures to be AChE inhibitors.

3.1.3 *LDA model descriptors*

The LDA models for each MOA are given in the supplemental material (Tables S2 and S3) which is available via the multimedia link on the online article webpage. The most common descriptors selected include molecular fragment counts [40], autocorrelation [44], E-state [45] and constitutional [46]. The definitions for the descriptors appearing in the LDA models are given in the T.E.S.T. user's guide [40]. The molecular fragment count descriptors are given by Martin et al. [10]. Some of the fragments were initially developed so they captured specific modes of action as detailed by Russom et al. [25].

Table 3. Summary results for the MOA prediction set for specific and broad MOA categories.

	Exp. count	*Correct fraction*	*Predict fraction*	*Training set sensitivity*
Specific MOA				
AChE inhibition-carbamate	14	1.000	0.929	1.000
AChE inhibition-organophosphate	40	1.000	1.000	0.994
Anticoagulation-vitamin K antagonism	4	1.000	1.000	0.923
Narcosis-ester	9	0.333	0.333	0.371
Narcosis-nonpolar	60	0.919	0.617	0.636
Narcosis-polar	12	0.667	0.500	0.383
Neurotoxicity-alicyclic GABA antagonism	6	0.800	0.833	0.800
Neurotoxicity-diphenyl sodium channel modulation	3	N/A	0.000	0.000
Neurotoxicity-GABA agonism	3	1.000	0.667	1.000
Neurotoxicity-pyrethroid sodium channel modulation	13	1.000	0.846	0.827
Reactivity	19	0.462	0.684	0.472
Uncoupler	10	0.875	0.800	0.658
nAChR agonism	2	1.000	0.500	0.833
Neurotoxicity-other	2	0.000	1.000	N/A*
Neurotoxicity-pyrazole GABA antagonism	2	0.000	0.500	N/A
Neurotoxicity-sodium channel blocking	1	0.000	1.000	N/A
Oxidative phosphorylation inhibition	1	0.000	1.000	N/A
Non-AChE inhibition-carbamate	8	0.500	0.500	N/A
Non-AChE inhibition-organophosphate	2	0.000	1.000	N/A
Overall**	195	0.888	0.733	N/A
Broad MOA				
AChE inhibition	54	0.981	1.000	0.995
Anticoagulation	4	0.750	1.000	0.923
Narcosis	81	0.975	0.975	0.938
Neurotoxicity	30	0.654	0.867	0.768
Reactivity	19	0.333	0.789	0.472
Uncoupler	11	0.700	0.909	0.658
nAChR agonism	2	0.500	1.000	0.833
Non-AChE inhibition	10	0.4	1	N/A
Overall*	201	0.858	0.945	N/A

*LDA model is not available for this MOA.
**Omitting MOAs without an explicit LDA model.

One benefit of LDA models is they are inherently interpretable. It was found the fragment counts selected in the LDA models are similar to those in the scheme proposed by Verhaar et al. [47] or the US EPA's ASTER [40]. For example, the model for AChE inhibition–organophosphate included the count of oxygens attached to two phosphorus atoms and the count of OH fragments attached to phosphorus.

3.1.4 *Internal model statistics for LC_{50} models*

In general, the LC_{50} MLR models based on 2D descriptors had acceptable statistics (r^2 and $q^2 > 0.5$) (Table 4). q^2 is the one leave-one-out cross-validated r^2. AChE inhibition–carbamate

Downloaded by [US EPA Library] at 08:06 01 July 2015

Table 4. LC_{50} Statistics for the fathead minnow acute toxicity training set.

	2D descriptors*				Only ELOGP		
	Number of descriptors	q^2	r^2	MAE	q^2	r^2	MAE
Broad MOA							
AChE inhibition	7	0.780	0.853	0.263	0.417	0.476	0.573
Narcosis	32	0.917	0.946	0.249	0.845	0.849	0.411
Neurotoxicity	4	0.829	0.902	0.380	0.642	0.701	0.668
Reactivity	8	0.636	0.713	0.460	0.350	0.391	0.737
Uncoupler	4	0.891	0.930	0.178	0.687	0.742	0.387
Specific MOA							
AChE inhibition–carbamate	1	−1.599	0.237	0.338	−0.920	0.002	0.390
AChE inhibition–organophosphate	5	0.662	0.767	0.363	0.439	0.515	0.559
Narcosis–ester	3	0.897	0.941	0.172	0.816	0.868	0.288
Narcosis–nonpolar	30	0.971	0.982	0.150	0.872	0.877	0.372
Narcosis–polar	9	0.914	0.944	0.221	0.874	0.889	0.299
Neurotoxicity–alicyclic GABA antagonism	1	0.635	0.717	0.566	−0.768	0.157	1.091
Neurotoxicity–pyrethroid sodium channel modulation	1	0.930	0.955	0.122	−3.720	0.360	0.482
Reactivity	8	0.636	0.713	0.460	0.350	0.391	0.737
Uncoupler	4	0.891	0.930	0.178	0.687	0.742	0.387

*q^2 is the leave one out correlation coefficient, r^2 is the coefficient of determination, and MAE is the mean absolute error.

Downloaded by [US EPA Library] at 08:06 01 July 2015

was the only MOA with poor internal statistics ($q^2 = -1.599$ and $r^2 = 0.237$). A likely explanation for this is there were few chemicals that had both this MOA and an experimental toxicity value, allowing for only one descriptor to be utilized maintaining a minimum ratio of five chemicals per descriptor. In all cases, the utilization of multiple 2D descriptors yielded better internal statistics than using only ELOGP. This result is not surprising since using additional descriptors can allow a model to fit idiosyncrasies in a dataset. However, in several cases (AChE inhibition–carbamate, neurotoxicity–alicyclic GABA antagonism and neurotoxicity–pyrethroid sodium channel modulation), a single two dimensional T.E.S.T. descriptor was able to correlate the training set data better than ELOGP. For these MOAs, IC (information content), XLOGP2 (square of the XLOGP octanol–water partition coefficient) and IE-ADJMM (mean information content on the edge adjacency magnitude) were selected, respectively. Two out of the three MOAs are described by information content descriptors (which are a measure of molecular symmetry). Neurotoxicity–alicyclic GABA antagonism is still a function of the octanol–water partition coefficient.

3.1.5 *Results for LC_{50} prediction set*

Analysis of the external LC_{50} prediction set results showed MOA-based models had similar or lower prediction accuracy compared with global models (Table 5). The specific MOA LDA models were able to achieve a higher prediction accuracy (in terms of r^2) than the broad MOA LDA models, but at the sacrifice of a lower prediction coverage. The global hierarchical clustering method (runs #5 and 6) yielded superior results to the MOA-based methods (runs #1–4) based on both prediction accuracy and coverage (Table 5). The hierarchical

Table 5. Summary statistics for the acute toxicity prediction set.

#	*MOA type*	*Method*	*Descriptor set*	r^2	*Coverage*
1	broad	LDA	all 2D	0.529	84.8
2	specific	LDA	all 2D	0.632	49.3
3	broad	LDA	ELOGP	0.579	87.3
4	specific	LDA	ELOGP	0.630	57.3
5	global	hierarchical clustering	all 2D	0.572	99.3
6	global	hierarchical clustering	ALOGP	0.568	90.2
7	global	Single model	all 2D	0.551	91.4
8	global	Single model	ALOGP	0.562	90.2

clustering method yielded 99.3% coverage, which can be explained by the fact that it makes predictions using several different models. If one compares the hierarchical clustering method (run #5) with the broad LDA method (run #1) for the predictions in common, the results do not change (r^2 = 0.579 for run#5 vs. r^2 = 0.528 for run #1). A single global MLR model achieved slightly higher prediction accuracy and coverage than the MOA-based approach (comparing runs #1 and #7). If one compares the predictions in common, the prediction accuracy is identical (r^2 = 0.528).

Analysis of the external LC_{50} prediction set results showed that QSAR models based on multiple 2D descriptors had similar results to those based solely on ELOGP (Table 5). The predictions in common for these runs are compared in Table 6.

For specific MOAs, the overall mean absolute error (MAE) was lower using 2D descriptors in the LC_{50} models. For broad MOAs, the overall error is lower using only ELOGP in

Table 6. Comparison of LC_{50} predictions using 2D descriptors and only ELOGP for the LC_{50} models (run #1 vs. #3 and run #2 vs. #4 in Table 5).

	Count	*MAE 2D**	*MAE ELOGP**
Specific MOA			
Narcosis-nonpolar	135	0.537	0.567
Narcosis-polar	17	0.47	0.456
Narcosis-ester	7	0.575	0.634
AChE inhibition-organophosphate	5	1.46	1.248
Reactivity	42	0.65	0.634
Uncoupling oxidative phosphorylation	7	0.833	1.05
All MOAs	213	0.587	0.605
All but narcosis	54	0.749	0.745
Broad MOA			
Narcosis	326	0.623	0.589
AChE inhibition	9	1.583	1.232
Neurotoxicity	1	1.76	0.436
Reactivity	21	0.66	0.74
Uncoupler	7	0.833	1.05
All MOAs	364	0.656	0.622
All but narcosis	38	0.939	0.906

*MAE 2D and MAE ELOGP are the mean absolute errors for models based on multiple 2d descriptors and solely on ELOGP, respectively.

Downloaded by [US EPA Library] at 08:06 01 July 2015

the LC_{50} models. One would expect the prediction accuracy using 2D descriptors would be higher for chemicals which did not have the narcosis MOA because the toxicity of chemicals with more specific MOAs are not only controlled by partitioning. However, the results indicate there was no advantage in using descriptors in addition to ELOGP in the MLR LC_{50} models (see 'All but narcosis' rows in Table 6). One explanation may be the intercept of the models may be more important in predicting the LC_{50} for some MOAs. For example, for the AChE inhibition–carbamate specific MOA, the LC_{50} model using 2D descriptors was

$$Tox = -0.09 \times ic + 4.95$$

where ic = information content descriptor.

The model using ELOGP was

$$Tox = -0.02 \times ELOGP + 4.77$$

It is interesting to note that if one only uses only ALOGP (Ghose–Crippen octanol–water coefficient [48] as calculated by T.E.S.T. [40]) for the hierarchical calculations, the prediction accuracy is similar (r^2 = 0.568), but the prediction coverage is lower (coverage = 90.2%). Using a single MLR model with 2D descriptors (run #7) yielded slightly worse results (r^2 = 0.551, coverage = 91.4%) than the hierarchical clustering method. Using a single MLR model with just ALOGP yielded similar results to those for the MLR with 2D descriptors (r^2 was slightly higher, but the coverage was slightly lower). This indicates the additional descriptors do not improve the external prediction accuracy for the global model.

3.1.6 *LC_{50} model descriptors*

The LC_{50} models for each MOA are given in the supplemental material (Tables S4 and S5) which is available via the multimedia link on the online article webpage. The most common 2D descriptors selected include autocorrelation, molecular fragment and E-state descriptors. It is interesting to note that 10 out of the 14 LC_{50} models using T.E.S.T. descriptors (see Table S4 and S5 in the supplementary material which is available via the multimedia link on the online article webpage) contained some form of log K_{ow} descriptor (ALOGP, ALOGP2, XLOGP and XLOGP2). The specific MOAs, which did not contain a log K_{ow} descriptor, were AChE inhibition–carbamate, narcosis–ester and neurotoxicity–pyrethroid sodium channel modulation.

3.2 *Discussion*

3.2.1 *Analysis of poorly predicted chemicals using MOA-based QSAR models*

One of the disadvantages of MOA-based methods is that an incorrectly predicted MOA can lead to a large error in the estimated toxicity value. Table 7 lists predictions for the broad LDA method (run #1 in Table 5) for poorly predicted chemicals (MAE ≥ 2 log units) that have a second highest LDA score ≥0.25. MOA1 and MOA2 are the predicted MOAs, which have the first and second highest score from the LDA models, respectively. Pred1 and Pred2 are the toxicity scores using the LC_{50} model for MOA1 and MOA2, respectively. Of the chemicals in Table 7, 9/10 were underpredicted which makes sense in that most of them were predicted to have the narcosis MOA. For chemicals where the second highest LDA score indicates the reactivity MOA, the predicted toxicities are much more accurately predicted using the reactivity LC_{50} model (MAE is reduced from 2.3 log units

Downloaded by [US EPA Library] at 08:06 01 July 2015

Table 7. Poorly predicted chemicals with large second highest LDA scores (≥0.25).

Chemical	*MOA1*	*MOA2*	*Exp.*	*Pred1*	*Pred2*
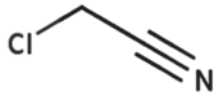 Chloroacetonitrile	Narcosis	Reactivity	4.75	1.54	3.65
Ethylene oxide	Narcosis	Reactivity	2.72	0.55	3.51
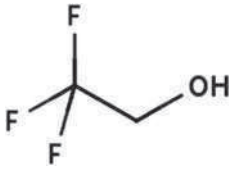 Trifluoroethanol	Narcosis	Reactivity	2.93	0.89	3.67
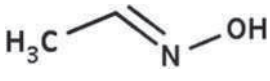 Acetaldehyde oxime	Narcosis	Reactivity	2.89	0.88	4.07
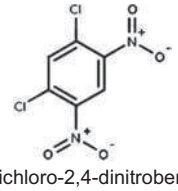 1,5-Dichloro-2,4-dinitrobenzene	Uncoupler	Reactivity	6.78	4.78	5.51
Salicylanilide	Narcosis	Uncoupler	7.43	4.36	4.65
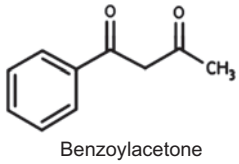 Benzoylacetone	Narcosis	Anticoagulant	5.17	3.08	N/A
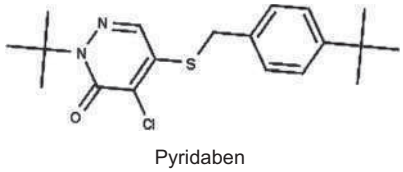 Pyridaben	Narcosis	Neurotoxicity	8.20	5.81	7.65

(*Continued*)

Downloaded by [US EPA Library] at 08:06 01 July 2015

Table 7. (*Continued*).

Chemical	*MOA1*	*MOA2*	*Exp.*	*Pred1*	*Pred2*
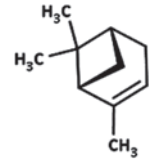 (+)-alpha-Pinene	Narcosis	Neurotoxicity	5.69	3.47	N/A
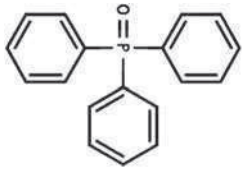 Triphenylphosphine oxide	AChE inhibition	Neurotoxicity	3.72	6.34	8.24

LDA models are based on broad MOAs and the LC50 models are fit to 2D descriptors.
Pred 1 and Pred 2 are the predictions using MOA1 and MOA2, respectively.
Exp. is the experimental value in -log(mol/L).

Downloaded by [US EPA Library] at 08:06 01 July 2015

to 1.0). All of these compounds are reactive according to the expert scheme outlined by Russom et al. [25]; (chloroacetonitrile is a halogenated nitrile, ethylene oxide is an epoxide, trifluoroethanol is a halogenated alcohol, acetaldehyde oxime is an oxime and 1,5-dichloro-2,4-dinitrobenzene has two nitro groups on one ring without an aniline or phenol substructure. The LDA methodology did not select reactivity for these compounds, but it suggests that one should examine the structure by hand when the second highest score is somewhat large (i.e. ≥0.25).

A prediction could not be made for benzoylacetone using MOA2 (since there is no LC_{50} model for the anticoagulant MOA) or for (+)alpha-pinene (since the applicability domain for neurotoxicity could not be met). In these cases, making no prediction is better than a poor prediction using MOA1. In the case of triphenylphosphine oxide, predictions are even worse for the second MOA. Visual inspection of this compound would indicate that this compound is probably a narcotic (due to a lack of single-bonded oxygens attached to the phosphorus) which would explain the overpredicted toxicity. Pyridaben is much better predicted using the neurotoxicity LC_{50} model. Salicylanilide is underpredicted using either the narcosis or uncoupler models, despite an expected uncoupler MOA.

3.2.2 *Analysis of poorly predicted chemicals using MLR model fit to entire training set*

One of the disadvantages of fitting a single model to the entire training set is that it may not correctly capture the trends in the toxicity for all modes of action. Table 8 lists the poor predictions (MAE ≥ 2 log units) for a single MLR model (run #7 in Table 5). These predictions are compared with those for broad MOA-based models (run #1 in Table 5). With the exception of fenoprop-isoctyl and 1,4-bis(chloromethyl)benzene, the MOA-based models had a lower prediction error. Despite the fact that 11 out of the 12 chemicals were predicted to have the narcosis MOA, the majority were overpredicted by both methods.

Table 8. Comparison of poorly predicted chemicals using a single model (run #7 in Table 5) with those from MOA-based models selected by the broad LDA approach (run #1 in Table 5).

	Exp –log (LC_{50} mol/L)			
Chemical	*Experimental*	*MLR 2D*	*Broad LDA*	*Predicted MOA*
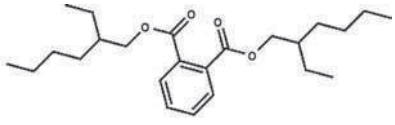 Bis(2-ethylhexyl) phthalate	2.55	8.13	7.83	Narcosis
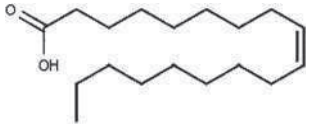 9-Octadecenoic acid	3.14	8.18	7.31	Narcosis
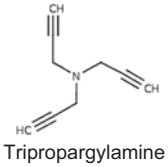 Tripropargylamine	2.65	7.15	5.28	Reactivity
Salicylanilide	7.43	4.16	4.36	Narcosis
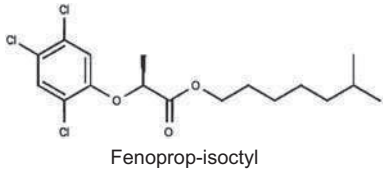 Fenoprop-isoctyl	4.24	7.36	8.14	Narcosis
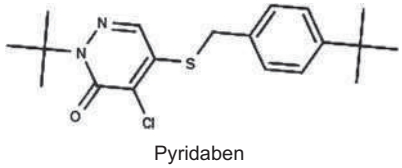 Pyridaben	8.20	5.34	5.81	Narcosis
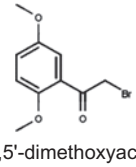 2-Bromo-2',5'-dimethoxyacetophenone	6.65	3.86	4.00	Narcosis
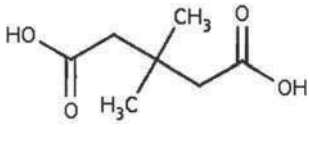 3,3-Dimethylglutaric acid	1.06	3.70	1.49	Narcosis

(*Continued*)

Downloaded by [US EPA Library] at 08:06 01 July 2015

Table 8. (*Continued*).

Chemical	Exp –log (LC_{50} mol/L)			Predicted MOA
	Experimental	*MLR 2D*	*Broad LDA*	
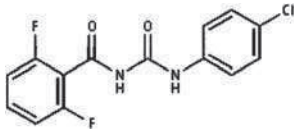 Diflubenzuron	2.86	5.44	5.18	Narcosis
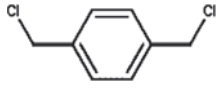 1,4-Bis(chloromethyl)benzene	6.65	4.27	3.68	Narcosis
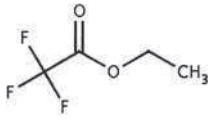 Ethyl trifluoroacetate	1.15	3.48	2.92	Narcosis
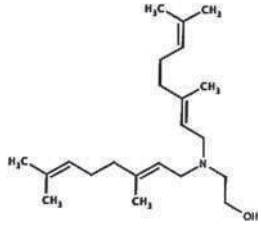 (E,E)-2-(Bis(3,7-dimethyl-2,6-octadienyl)amino)ethanol	6.41	8.62	7.41	Narcosis

Downloaded by [US EPA Library] at 08:06 01 July 2015

4. Conclusions

In this study, a two-step MOA-based approach was developed to estimate aquatic toxicity. The MOA-based approach was found to yield similar external prediction accuracy (r^2 = 0.529–0.632) to a single global MLR model (r^2 = 0.551–0.562). Overall, the global hierarchical clustering approach yielded higher combination of accuracy and prediction coverage (r^2 = 0.572, coverage = 99.3%) than the MOA-based approach (r^2 = 0.529–0.632, coverage = 49.3–87.3%). In addition, it was determined that multiple 2D descriptors achieved the same prediction accuracy as MLR models based only on the octanol–water partition coefficient. Finally, it was determined that in some cases that an incorrect mode of action can lead to large prediction errors when there is a competing MOA (LDA score ≥0.25). The results of this study indicate that, while MOA-based approaches may appear biologically relevant, they may not impart superior external prediction accuracy. However, the MOA-based approach can give toxicologists greater confidence in the predicted values since the models are based less on a 'black box' approach. The use of both MOA-based and global approaches in a consensus approach [49] can provide even greater confidence.

Supporting information

The mode of action datasets and the LDA and LC_{50} models are available in the supplementary material which is available via the multimedia link on the online article webpage.

Acknowledgement

The opinions expressed in this work are those of the authors and do not represent the policies or opinions of the US EPA.

References

[1] T.I. Netzeva, M. Pavan, and A.P. Worth, *Review of (quantitative) structure-activity relationships for acute aquatic toxicity*, QSAR Comb. Sci. 27 (2008), pp. 77–90.

[2] R. Benigni and A.M. Richard, *QSARS of mutagens and carcinogens: Two case studies illustrating problems in the construction of models for noncongeneric chemicals*, Mutat. Res.-Genet. Tox. 371 (1996), pp. 29–46.

[3] T.W. Schultz, G.D. Sinks, and A.P. Bearden, *QSAR in aquatic toxicology: A mechanism of action approach comparing toxic potency to* Pimephales promelas, Tetrahymena pyriformis, *and* Vibrio fischeri, in *Comparative QSAR*, J. Devillers, ed., Taylor & Francis, New York, 1998, pp. 51–109.

[4] S.G. Abernethy, D. MacKay, and L.S. McCarty, *'Volume fraction' correlation for narcosis in aquatic organisms: The key role of partitioning*, Environ. Toxicol. Chem. 7 (1988), pp. 469–481.

[5] M.T.D. Cronin and T.W. Schultz, *Structure-toxicity relationships for phenols to* Tetrahymena pyriformis, Chemosphere 32 (1996), pp. 1453–1468.

[6] O.G. Mekenyan and G.D. Veith, *Relationships between descriptors for hydrophobicity and soft electrophilicity in predicting toxicity*, SAR QSAR Environ. Res. 1 (1993), pp. 335–344.

[7] H. Yuan, Y.-Y. Wang, and Y.-Y. Cheng, *Mode of action-based local QSAR modeling for the prediction of acute toxicity in the fathead minnow*, J. Molec. Graph. Model. 26 (2007), pp. 327–335.

[8] W.F. Zheng and A. Tropsha, *Novel variable selection quantitative structure-property relationship approach based on the k-nearest-neighbor principle*, J. Chem. Inf. Comp. Sci. 40 (2000), pp. 185–194.

[9] M. Cassotti, D. Ballabio, V. Consonni, A. Mauri, I.V. Tetko, and R. Todeschini, *Prediction of acute aquatic toxicity toward* Daphnia magna *by using the GA-kNN method*, Altern. Lab. Anim. 42 (2014), pp. 31–41.

[10] T.M. Martin, P. Harten, R. Venkatapathy, S. Das, and D.M. Young, *A hierarchical clustering methodology for the estimation of toxicity*, Toxicol. Mech. Method. 18 (2008), pp. 251–266.

[11] C.X. Xue, R.S. Zhang, H.X. Liu, X.J. Yao, M.C. Liu, Z.D. Hu, and B.T. Fan, *An Accurate QSPR study of O–H bond dissociation energy in substituted phenols based on support vector machines*, J. Chem. Inf. Comp. Sci. 44 (2004), pp. 669–677.

[12] D.V. Eldred, C.L. Weikel, P.C. Jurs, and K.L.E. Kaiser, *Prediction of fathead minnow acute toxicity of organic compounds from molecular structure*, Chem Res. Toxicol. 12 (1999), pp. 670–678.

[13] E. Papa, F. Villa, and P. Gramatica, *Statistically validated QSARs, based on theoretical descriptors, for modeling aquatic toxicity of organic chemicals in* Pimephales promelas *(fathead minnow)*, J. Chem. Inf. Model. 45 (2005), pp. 1256–1266.

[14] J.A. Castillo-Garit, Y. Marrero-Ponce, J. Escobar, F. Torrens, and R. Rotondo, *A novel approach to predict aquatic toxicity from molecular structure*, Chemosphere 73 (2008), pp. 415–427.

[15] J.F. Contrera, E.J. Matthews, and R.D. Benz, *Predicting the carcinogenic potential of pharmaceuticals in rodents using molecular structural similarity and E-state indices*, Regul. Toxicol. Pharm. 38 (2003), pp. 243–259.

[16] K.L.E. Kaiser and S.P. Niculescu, *Using probabilistic neural networks to model the toxicity of chemicals to the fathead minnow* (Pimephales promelas)*: A study based on 865 chemicals*, Chemosphere 38 (1999), pp. 3237–3245.

Downloaded by [US EPA Library] at 08:06 01 July 2015

[17] T.M. Martin and D.M. Young, *Prediction of the acute toxicity (96-h LC_{50}) of organic compounds to the fathead minnow* (Pimephales promelas) using a group contribution method, Chem Res. Toxicol. 14 (2001), pp. 1378–1385.
[18] T. Öberg, *A general structure-property relationship to predict the enthalpy of vaporisation at ambient temperatures*, SAR QSAR Environ. Res. 18 (2007), pp. 127–139.
[19] T. Öberg, *A QSAR for baseline toxicity: Validation, domain of application, and prediction*, Chem Res. Toxicol. 17 (2004), pp. 1630–1637.
[20] A. Cherkasov, *Inductive QSAR descriptors. Distinguishing compounds with antibacterial activity by artificial neural networks*, Int. J. Mol. Sci. 6 (2005), pp. 63–86.
[21] Virtual Computational Chemistry Laboratory (VCCLAB), *Associative Neural Network,* VCCLAB, Munich, 2007; software available at http://www.vcclab.org/lab/asnn/.
[22] L. He and P.C. Jurs, *Assessing the reliability of QSAR model's predictions*, J. Mol. Graph. Model. 23 (2005), pp. 503–523.
[23] H. Könemann, *Quantitative structure-activity relationships in fish toxicity studies Part 1: Relationship for 50 industrial pollutants*, Toxicology 19 (1981), pp. 209–221.
[24] US Enviromental Protection Agency (US EPA), *Estimation Programs Interface Suite™ for Microsoft® Windows, v 4.11*. (2014), US EPA, Washington DC; software available at http://www.epa.gov/opptintr/exposure/pubs/episuitedl.htm.
[25] C.L. Russom, S.P. Bradbury, S.J. Broderius, D.E. Hammermeister, and R.A. Drummond, *Predicting modes of toxic action from chemical structure: Acute toxicity in the fathead minnow (*Pimephales Promelas*)*, Environ. Toxicol. Chem. 16 (1997), pp. 948–967.
[26] M.T.D. Cronin, A.O. Aptula, J.C. Duffy, T.I. Netzeva, P.H. Rowe, I.V. Valkova, and T. Wayne Schultz, *Comparative assessment of methods to develop QSARs for the prediction of the toxicity of phenols to* Tetrahymena pyriformis, Chemosphere 49 (2002), pp. 1201–1221.
[27] L. Claeys, F. Iaccino, C.R. Janssen, P. Van Sprang, and F. Verdonck, *Development and validation of a quantitative structure–activity relationship for chronic narcosis to fish*, Environ. Toxicol. Chem. 32 (2013), pp. 2217–2225.
[28] M. Nendza and M. Müller, *Discriminating toxicant classes by mode of action: 2. Physico-chemical descriptors*, Quant. Struct.-Act. Rel, 19 (2000), pp. 581–598.
[29] A.O. Aptula, T.I. Netzeva, I.V. Valkova, M.T.D. Cronin, T.W. Schultz, R. Kühne, and G. Schüürmann, *Multivariate discrimination between modes of toxic action of phenols*, Quant. Struct.-Act. Rel, 21 (2002), pp. 12–22.
[30] G. Schüürmann, A.O. Aptula, R. Kühne, and R.-U. Ebert, *Stepwise discrimination between four modes of toxic action of phenols in the* Tetrahymena pyriformis *assay*, Chem Res. Toxicol. 16 (2003), pp. 974–987.
[31] B. Niu, Y. Jin, W. Lu, and G. Li, *Predicting toxic action mechanisms of phenols using AdaBoost Learner*, Chemom. Intell. Lab. Syst. 96 (2009), pp. 43–48.
[32] S. Spycher, M. Nendza, and J. Gasteiger, *Comparison of different classification methods applied to a mode of toxic action data set*, QSAR Comb. Sci. 23 (2004), pp. 77–791.
[33] U. Norinder, P. Lidén, and H. Boström, *Discrimination between modes of toxic action of phenols using rule based methods*, Mol. Divers. 10 (2006), pp. 207–212.
[34] X.J. Yao, A. Panaye, J.P. Doucet, H.F. Chen, R.S. Zhang, B.T. Fan, M.C. Liu, and Z.D. Hu, *Comparative classification study of toxicity mechanisms using support vector machines and radial basis function neural networks*, Anal. Chim. Acta 535 (2005), pp. 259–273.
[35] S. Ren, *Predicting three narcosis mechanisms of aquatic toxicity*, Toxicol. Lett. 133 (2002), pp. 127–139.
[36] L. Michielan, L. Pireddu, M. Floris, and S. Moro, *Support vector machine (SVM) as alternative tool to assign acute aquatic toxicity warning labels to chemicals*, Mol. Inform. 29 (2010), pp. 51–64.
[37] S.C. Basak, G.D. Grunwald, G.E. Host, G.J. Niemi, and S.P. Bradbury, *A comparative study of molecular similarity, statistical, and neural methods for predicting toxic modes of action*, Environ. Toxicol. Chem. 17 (1998), pp. 1056–1064.

Downloaded by [US EPA Library] at 08:06 01 July 2015

[38] T.M. Martin, C.M. Grulke, D.M. Young, C.L. Russom, N.Y. Wang, C.R. Jackson, and M.G. Barron, *Prediction of aquatic toxicity mode of action using linear discriminant and random forest models*, J. Chem. Inf. Model. 53 (2013), pp. 2229–2239.
[39] S. Spycher, E. Pellegrini, and J. Gasteiger, *Use of structure descriptors to discriminate between modes of toxic action of phenols*, J. Chem. Inf. Model. 45 (2005), pp. 200–208.
[40] Un Environmental Protection Agency (US EPA), *ASTER (Assessment Tools for the Evaluation of Risk)*, US EPA, Washington DC, 2012; software available at http://www.epa.gov/med/Prods_Pubs/aster.htm.
[41] Insecticide Resistance Action Committee (IRAC), *IRAC MoA Classification Scheme,* IRAC International MoA Working Group, 2012; software available at http://www.irac-online.org/eClassification/.
[42] L. Eriksson, J.S. Jaworska, A.P. Worth, M.T.D. Cronin, R.M. McDowell, and P. Gramatica, *Methods for reliability and uncertainty assessment and for applicability evaluations of classification- and regression-based QSARs*, Environ. Health Persp. 111 (2003), pp. 1361–1375.
[43] D.C. Montgomery, *Introduction to Linear Regression Analysis*, John Wiley & Sons, New York, 1982.
[44] R. Todeschini and V. Consonni, *Handbook of Molecular Descriptors*, Wiley-VCH, Weinheim, Germany, 2000.
[45] L.B. Kier and L.H. Hall, *Molecule Structure Description: The Electrotopological State*, Academic Press, New York, 1999.
[46] Talete, *Dragon Version 6*, Talete SRL, Milan, Italy, 2006; software available at http://www.talete.mi.it/products/dragon_description.htm.
[47] H.J.M. Verhaar, C.J. van Leeuwen, and J.L.M. Hermens, *Classifying environmental pollutants. 1: Structure-activity relationships for prediction of aquatic toxicity*, Chemosphere 25 (1992), pp. 471–491.
[48] A.K. Ghose, V.N. Viswanadhan, and J.J. Wendoloski, *Prediction of hydrophilic (lipophilic) properties of small organic molecules using fragmental methods: An analysis of ALOGP and CLOGP methods*, J. Phys. Chem. 102 (1998), pp. 3762–3772.
[49] H. Zhu, T.M. Martin, L. Ye, A. Sedykh, D.M. Young, and A. Tropsha, *Quantitative structure−activity relationship modeling of rat acute toxicity by oral exposure*, Chem Res. Toxicol. 22 (2009), pp. 1913–1921.

Downloaded by [US EPA Library] at 08:06 01 July 2015

From: Carriger, John <Carriger.John@epa.gov>
Sent: Friday, April 17, 2020 9:47 AM
To: Barron, Mace <Barron.Mace@epa.gov>
Subject: RE: ACTION NEEDED: Record of Percentage Agreement for MOAtox STAA award nomination.....

Coauthor: John Carriger, US EPA/ORD/CESER/LRTD
Nominee: Mace Barron
Publications:
Barron MG (70%), Lilavois CR (20%), Martin TM. 2015 (10%). MOAtox: a comprehensive mode of action and acute aquatic toxicity database for predictive model development. Aquat Tox 16:102-107.

Carriger JF (50%), Martin TM (20%), Barron MG (30%). 2016.
A Bayesian network model for predicting aquatic toxicity mode of action using two dimensional theoretical molecular descriptors. Aquat Tox 180:11-24.

Martin TM (45%), Young DM (10%), Lilavois CR (10%), Barron MG (35%). 2015. Comparison of global and mode of action-based models for aquatic toxicity. SAR QSAR Environ Res 26:245-262.

I, John Carriger, agree with the designated percentages.

John Carriger
U.S. Environmental Protection Agency
CESER, AWBERC
e: carriger.john@epa.gov

From: Lilavois, Crystal <Lilavois.Crystal@epa.gov>
Sent: Thursday, April 16, 2020 2:33 PM
To: Barron, Mace <Barron.Mace@epa.gov>
Subject: RE: ACTION NEEDED: Record of Percentage Agreement for MOAtox STAA award nomination.....

Coauthor: Crystal Lilavois, US EPA/ORD/CEMM/GEMMD
Nominee: Mace Barron
Publications:
I, Crystal Lilavois, agree with the designated percentages.

Barron MG (70%), Lilavois CR (20%), Martin TM. 2015 (10%). MOAtox: a comprehensive mode of action and acute aquatic toxicity database for predictive model development. Aquat Tox 16:102-107.

Carriger JF (50%), Martin TM (20%), Barron MG (30%). 2016.
A Bayesian network model for predicting aquatic toxicity mode of action using two dimensional theoretical molecular descriptors. Aquat Tox 180:11-24.

Martin TM (45%), Young DM (10%), Lilavois CR (10%), Barron MG (35%). 2015. Comparison of global and mode of action-based models for aquatic toxicity. SAR QSAR Environ Res 26:245-262.

Crystal R. Lilavois
U.S. Environmental Protection Agency
Gulf Ecosystem Measurement and Modeling Division
1 Sabine Island Drive
Gulf Breeze, FL 32561
t: (850)934-9389
e: lilavois.crystal@epa.gov

From: Martin, Todd <Martin.Todd@epa.gov>
Sent: Friday, April 17, 2020 9:44 AM
To: Barron, Mace <Barron.Mace@epa.gov>
Subject: RE: ACTION NEEDED: Record of Percentage Agreement for MOAtox STAA award nomination.....

Coauthor: Todd Martin, US EPA/ORD/CCTE/CCED
Nominee: Mace Barron
Publications:

- Barron MG (70), Lilavois CR (20), Martin TM. 2015 (10). MOAtox: a comprehensive mode of action and acute aquatic toxicity database for predictive model development. Aquat Tox 16:102-107. 58 cites; 118
- Carriger JF (45), Martin TM (20), Barron MG (35). 2016. A Bayesian network model for predicting aquatic toxicity mode of action using two dimensional theoretical molecular descriptors. Aquat Tox 180:11-24. 11 cites, 66 views
- Martin TM (45), Young DM (10), Lilavois CR (10), Barron MG (35). 2015. Comparison of global and mode of action-based models for aquatic toxicity. SAR QSAR Environ Res 26:245-262. 19 cites, 191 views

I, Todd Martin, agree with the designated percentages.

Todd Martin
CCTE, AWBERC
Martin.todd@epa.gov

From: Young, Douglas <Young.Douglas@epa.gov>
Sent: Friday, April 17, 2020 9:04 AM
To: Barron, Mace <Barron.Mace@epa.gov>
Subject: RE: ACTION NEEDED: Record of Percentage Agreement for MOAtox STAA award nomination.....

I, Douglas Young, agree with Mace Barron's assignment of percent contributions.

Barron MG (70%), Lilavois CR (20%), Martin TM. 2015 (10%). MOAtox: a comprehensive mode of action and acute aquatic toxicity database for predictive model development. Aquat Tox 16:102-107.

Carriger JF (50%), Martin TM (20%), Barron MG (30%). 2016.
A Bayesian network model for predicting aquatic toxicity mode of action using two dimensional theoretical molecular descriptors. Aquat Tox 180:11-24.

Martin TM (45%), Young DM (10%), Lilavois CR (10%), Barron MG (35%). 2015. Comparison of global and mode of action-based models for aquatic toxicity. SAR QSAR Environ Res 26:245-262.

Douglas Young
Assistant Center Director
Center for Computational Toxicology and Exposure
U.S. Environmental Protection Agency
26 W. MLK Dr.
Cincinnati, OH 45268
o: (513) 569-7624; f: (513) 569-7677; m: (513) 633-1330

From: Barron, Mace <Barron.Mace@epa.gov>
Sent: Monday, April 20, 2020 12:55 PM
To: Barron, Mace <Barron.Mace@epa.gov>
Subject: Record of Percentage Agreement for MOAtox STAA award nomination.....

Coauthor: Mace Barron
Nominee: Mace Barron
Publications:
Barron MG (70%), Lilavois CR (20%), Martin TM. 2015 (10%). MOAtox: a comprehensive mode of action and acute aquatic toxicity database for predictive model development. Aquat Tox 16:102-107.

Carriger JF (50%), Martin TM (20%), Barron MG (30%). 2016.
A Bayesian network model for predicting aquatic toxicity mode of action using two dimensional theoretical molecular descriptors. Aquat Tox 180:11-24.

Martin TM (45%), Young DM (10%), Lilavois CR (10%), Barron MG (35%). 2015. Comparison of global and mode of action-based models for aquatic toxicity. SAR QSAR Environ Res 26:245-262.

I, Mace Barron, agree with the designated percentages.

Mace G Barron, PhD
Office of Research and Development, U.S. EPA
1 Sabine Island Drive, Gulf Breeze, FL 32561
(D) 850 934 9223; (C) 850 449 6339
barron.mace@epa.gov

Aquatic Toxicology 161 (2015) 102–107

Contents lists available at ScienceDirect

Aquatic Toxicology

journal homepage: www.elsevier.com/locate/aquatox

MOAtox: A comprehensive mode of action and acute aquatic toxicity database for predictive model development

M.G. Barron[a,*], C.R. Lilavois[a], T.M. Martin[b]

[a] U.S. Environmental Protection Agency, Office of Research Development, Gulf Ecology Division, Gulf Breeze, FL, USA
[b] U.S. Environmental Protection Agency, Office of Research Development, Sustainable Technology Division, Cincinnati, OH, USA

ARTICLE INFO

Article history:
Received 19 November 2014
Received in revised form 31 January 2015
Accepted 2 February 2015
Available online 7 February 2015

Keywords:
QSAR
Toxicity
Model
Mode of action
Fish
Invertebrate

ABSTRACT

The mode of toxic action (MOA) has been recognized as a key determinant of chemical toxicity and as an alternative to chemical class-based predictive toxicity modeling. However, the development of quantitative structure activity relationship (QSAR) and other models has been limited by the availability of comprehensive high quality MOA and toxicity databases. The current study developed a dataset of MOA assignments for 1213 chemicals that included a diversity of metals, pesticides, and other organic compounds that encompassed six broad and 31 specific MOAs. MOA assignments were made using a combination of high confidence approaches that included international consensus classifications, QSAR predictions, and weight of evidence professional judgment based on an assessment of structure and literature information. A toxicity database of 674 acute values linked to chemical MOA was developed for fish and invertebrates. Additionally, species-specific measured or high confidence estimated acute values were developed for the four aquatic species with the most reported toxicity values: rainbow trout (*Oncorhynchus mykiss*), fathead minnow (*Pimephales promelas*), bluegill (*Lepomis macrochirus*), and the cladoceran (*Daphnia magna*). Measured acute toxicity values met strict standardization and quality assurance requirements. Toxicity values for chemicals with missing species-specific data were estimated using established interspecies correlation models and procedures (Web-ICE; http://epa.gov/ceampubl/fchain/webice/), with the highest confidence values selected. The resulting dataset of MOA assignments and paired toxicity values are provided in spreadsheet format as a comprehensive standardized dataset available for predictive aquatic toxicology model development.

Published by Elsevier B.V.

1. Introduction

In aquatic toxicology, mode of action (MOA) has been defined phenomenologically based on whole organism responses, identified from effects at the cellular or organ level, or based on the primary mechanism of toxicity initiated at the receptor level (Barron et al., 2002; Suter, 2007). MOA has been recognized as a key determinant of chemical toxicity and as an alternative to chemical class-based predictive toxicity modeling. Early work on determining chemical mode of action in aquatic organisms focused on industrial compounds that were largely of moderate polarity, low toxicity and acted through narcosis, a non-specific reversible baseline mode of whole organism toxicity (Konemann, 1981; Call et al., 1985). Based on a suite of behavioral/morphological responses in rainbow trout (*Onchorhynchus mykiss*), McKim et al. (1987) established several modes of action including narcosis, oxidative phosphorylation uncoupler, acetylcholinesterase (AChE) inhibitor, or stimulant-like. Verhaar et al. (1992) categorized chemicals into one of four MOA classes based on structural rules: (1) inert compounds causing narcosis, (2) less inert more toxic compounds causing polar narcosis, (3) reactive compounds with enhanced toxicity, and (4) compounds with specific or receptor mediated toxicity. Russom et al. (1997) utilized an extensive fathead minnow (*Pimephales promelas*) acute toxicity and behavioral database to extend MOA categorization to three narcosis MOAs and five specific MOAs (AChE inhibition, uncoupling, reactivity, seizure mechanisms, and respiratory inhibition). Other approaches to MOA assignment and categorization have included assessments of *in vitro* activity and cross species receptor homology for pharmaceutical compounds (Escher et al., 2005; Christen et al., 2010).

In contrast to empirical and rule-based categorization approaches, Martin et al. (2013) utilized two dimensional descriptor assignments and machine-based learning algorithms to develop a computational chemistry approach to MOA assignment

* Corresponding author at: U.S. Environmental Protection Agency, Office of Research and Development, Gulf Ecology Division, 1 Sabine Island Drive, Gulf Breeze, FL 32561, USA. Tel.: +1 850 934 9223; fax: +1 850 934 2402.
E-mail address: Barron.mace@epa.gov (M.G. Barron).

http://dx.doi.org/10.1016/j.aquatox.2015.02.001
0166-445X/Published by Elsevier B.V.

for six broad and seven specific MOAs. This computational chemistry-based approach calculated up to 700 structural and property descriptors for each chemical and developed prediction models based on multi-linear regression models and decision tree algorithms. As part of that work, a dataset of 924 acute aquatic toxicity MOA assignments were developed using a combination of high confidence approaches that included international consensus classifications, quantitative structure activity relationship (QSAR) predictions, and weight of evidence professional judgment based on an assessment of structure and literature information.

The objective of the current study was to develop a comprehensive standardized dataset of aquatic toxicity values and MOA assignments. The current research expands the Martin et al. (2013) dataset to over 1200 chemicals including metals and organometallics, increases the number of specific MOA categories, and refines some of the pesticide neurotoxicity MOA categories to be less general and more mechanism-based. The categorization scheme was comprised of six broad and 31 specific MOA categories that encompassed the major acute toxicity MOAs reported in aquatic invertebrates and fish. Chemicals in the MOA dataset were then linked to a dataset of high confidence acute aquatic toxicity values developed for this study to create a database of 674 chemicals with species-specific acute toxicity values. The MOA-aquatic toxicity database (MOAtox) development focused on the four most commonly reported aquatic test species with toxicity endpoint data in the ECOTOX database (USEPA, 2014): rainbow trout, the cladoceran (*Daphnia magna*), fathead minnow, and bluegill (*Lepomis macrochirus*). These species represented 22% of the 300,000 ECOTOX records with toxicity endpoint data (Fairbrother et al., 2014). Additionally, generic fish and aquatic invertebrate acute toxicity values were developed from the geometric mean of all measured toxicity values that met strict quality assurance and standardization requirements. Toxicity values for chemicals with missing species-specific data were estimated using established interspecies correlation models and procedures (Web-ICE; http://epa.gov/ceampubl/fchain/webice/), with the highest confidence values selected (Raimondo et al., 2010, 2013). The development of this comprehensive standardized dataset is intended to facilitate the development of predictive aquatic toxicity and MOA models. The larger MOA dataset could support MOA-based assessments of chemical mixtures, such as applying a toxic units approach to chemicals with the same specific MOA.

2. Methods

2.1. MOA category and dataset development

An aquatic toxicity MOA categorization scheme was developed for a diversity of metals, organometallics, pesticides, and other organics that appear in the ECOTOX database (USEPA, 2014), based on earlier work determining chemical modes of acute toxic action in fish (Konemann 1981; Call et al., 1985; McKim et al., 1987; Russom et al., 1997; USEPA, 2012; Martin et al., 2013). The categorization scheme was comprised of six broad and 31 specific MOA categories that encompassed the major MOAs reported in aquatic invertebrates and fish. Broad MOA categories included narcosis, AChE inhibition, neurotoxicity, iono/osmoregulatory/circulatory impairment, reactivity, and electron transport inhibition (Supplementary information; Table S1). Specific MOAs were developed as subcategories of the broad MOAs based on either chemical structure or known mechanism of action. A total of 1213 chemicals were assigned to a broad and specific MOA category following the general procedures of Martin et al. (2013). This involved using a combination of high confidence assignments including, international consensus classifications (*e.g.*, IRAC, 2014), QSAR predictions (USEPA, 2012), and weight of evidence professional judgment by considering a combination of assessment of structure (*e.g.*, analogous structure; moiety/functional group presence) and literature information on MOA, mechanism of action and toxicity pathways (*e.g.*, Russom et al., 1997; Nendza and Müller 2000; Schüürmann et al., 2003; Spycher et al., 2004). Chemicals with an uncertain MOA assignment were excluded from the database.

2.2. Toxicity dataset development

Toxicity dataset development focused on determining acute toxicity values for three fish species (rainbow trout, fathead minnow, and bluegill) and *Daphnia* for chemicals in the MOA dataset. These four taxa were selected, because they have been the most commonly reported aquatic test species with acute toxicity endpoint data in the ECOTOX database (USEPA, 2014). First, measured aquatic toxicity values were obtained from the US EPA's ICE Aquatic Toxicity Database (Raimondo et al., 2013a). This database is comprised of 5500 acute EC/LC50 values for 180 species and 1260 chemicals that have been obtained from a diversity of sources (primarily ECOTOX) then subjected to a rigorous quality assurance review and standardization procedure (Raimondo et al., 2010). Each toxicity record included in the dataset met specific requirements for: (1) test chemical identity and purity, (2) test procedures, conditions, reporting, and quality control, and (3) test organism life stage. Additionally, toxicity values for selected compounds were normalized based on water quality parameters, and outliers and central tendency were determined in cases of multiple reported values as documented in Raimondo et al. (2013a). Mean fish and mean aquatic invertebrate toxicity values were also computed from the geometric mean of all standardized values available for each chemical. Similarly, a mean *Daphnia* genus value was computed from all standardized values for each chemical with available data.

Missing species-specific toxicity data were then estimated using established interspecies correlation estimation (ICE) models available in the USEPA Web-ICE tool (http://epa.gov/ceampubl/fchain/webice/; Raimondo et al., 2010, 2013b). ICE models are log-linear least square regressions of chemical sensitivity relationships between a surrogate and predicted taxon. Toxicity values in the Aquatic Toxicity Database for all available surrogate species were used to estimate acute toxicity for those chemicals with missing measured data for rainbow trout, *D. magna*, fathead minnow, or bluegill. This procedure resulted in multiple estimated values for many chemicals because ICE models were available for multiple surrogate species.

2.3. Determination of best estimated value

A systematic process was used to determine a best toxicity estimate for any of the four species with multiple predicted values based on model uncertainty and performance criteria. First, each surrogate species ICE model was evaluated to determine if it met the following statistical criteria: mean square error of less than or equal to 0.94, coefficient of determination greater than 0.6, and the upper 95th percentile confidence limit was within five fold of the predicted toxicity value. If multiple models met all three statistical criteria, these models were evaluated to determine if they met the following additional criteria: taxonomic distance between the surrogate and predicted species was less than or equal to four (same Class), model cross validation success was greater than 85%, and degrees of freedom were greater than 8. If multiple models met all criteria, the best estimated value was computed from the geometric mean of the model predicted values.

2.4. Ranking and assessment of estimated values

Each estimated value in the MOAtox database received a qualitative ranking based on the number of statistical criteria met (Supplementary information; Table S2): level P1 (highest confidence estimate; all three model criteria met), P2 (two met), P3 (one met), and P4 (lowest confidence; no statistical criteria met). Estimated values were not included in the MOAtox database for those chemicals with species-specific measured values. However, toxicity values were also estimated and ranked for those chemicals with measured values to allow an assessment of accuracy. Accuracy was determined from the proportion of species-specific estimated values within two, five, and ten fold of measured values. Correlations between species-specific estimated and measured values were determined from simple log–log linear regressions.

3. Results

3.1. MOA assignments

The MOA dataset was comprised of 1213 chemicals assigned to one of six broad acute toxicity MOA categories and one of 31 specific MOA subcategories (Tables 1, S1, and S2). The predominant MOAs and chemical classes in the database (>40 chemicals) were AChE inhibition (carbamates and organophosphates), narcosis (nonpolar, polar, and ester compounds), neurotoxicity (pyrethroids and alicyclics), and uncouplers of oxidative phosphorylation (*e.g.*, polychlorinated and nitrophenols and amines) (Tables 1 and S1).

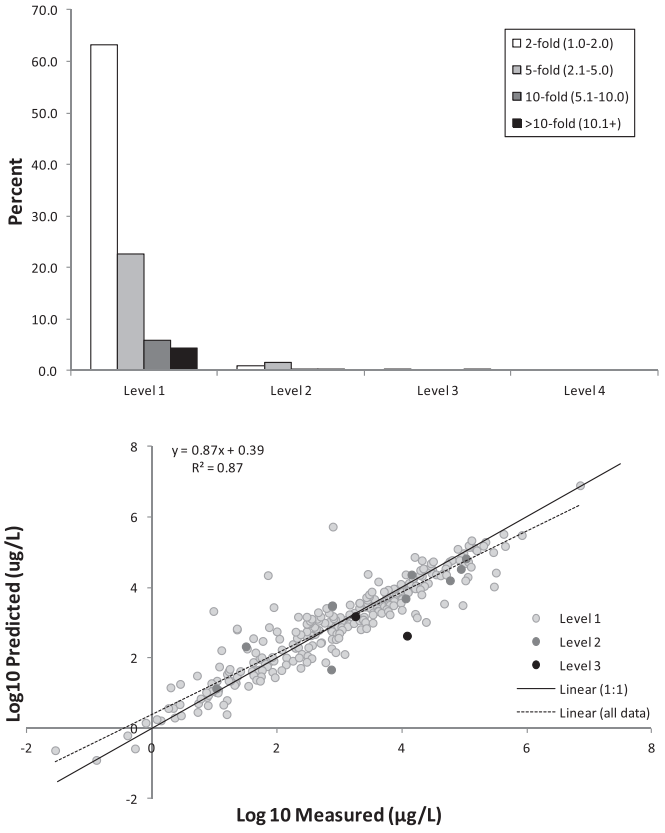

Fig. 1. Prediction accuracy of estimated toxicity values by uncertainty level (upper panel), and correlation between measured and predicted toxicity values (lower panel) in bluegill.

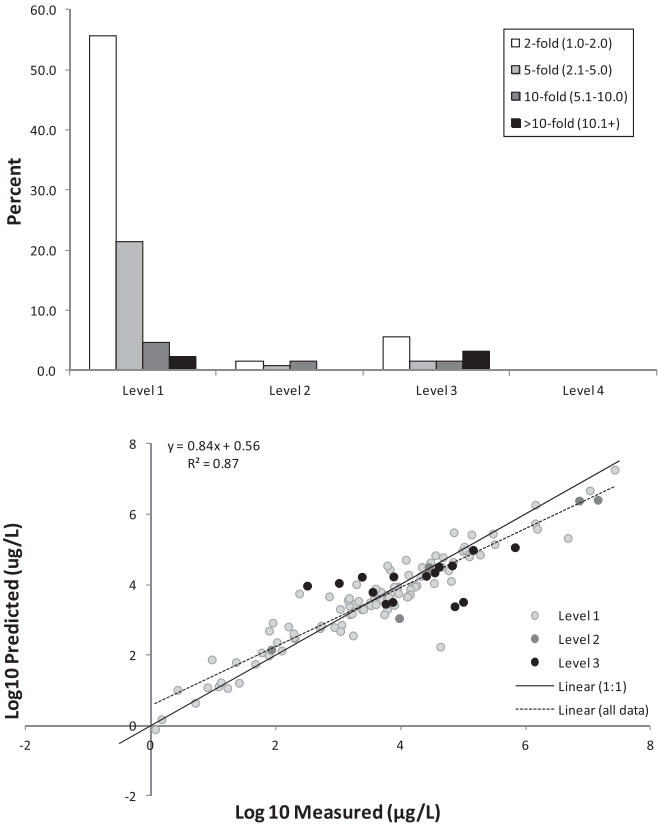

Fig. 2. Prediction accuracy of estimated toxicity values by uncertainty level (upper panel), and correlation between measured and predicted toxicity values (lower panel) in fathead minnows.

3.2. Toxicity values

Of the 1213 chemicals in the MOA dataset, 614 had measured values in fish and 424 had measured values in invertebrates determined as the geomeans of standardized acute toxicity data (Table 2). There were 671 chemicals in the MOA dataset that had either a measured or estimated taxa-specific acute toxicity value for *Daphnia*, bluegill, fathead minnow, or rainbow trout (Table 2). Estimated values for the three fish species were primarily comprised of level 1 (highest confidence; >85%) values, whereas, in *D. magna* the majority of estimated values were level 3 (62%) (Table 2 and Figs. 1–4). Over 60% of the estimated values in the three fish species were within two fold of standardized measured values, and 87% were within five fold (Table 2 and Figs. 1–4). Prediction accuracy was lower for *D. magna*, with only 61% of estimated values within five fold of measured values (Table 2 and Fig. 4). In the three fish species, estimated values were highly correlated with measured values ($R^2 > 0.87$; Figs. 1–4), whereas, there was greater variance in the relationship for *D. magna* ($R^2 = 0.69$; Fig. 4).

4. Discussion

In aquatic toxicology, MOA-based toxicity prediction has primarily focused on organic chemicals acting through polar and nonpolar narcosis. Although compounds causing narcosis are structurally diverse and represent the largest class of organic chemicals produced globally, the narcosis MOA does not encompass more toxic compounds, such as pesticides, metals, and other chemicals acting through specific mechanisms and toxicity pathways. The current study builds upon the earlier work of Konemann (1981), Russom et al. (1997), Verhaar et al. (2000), and others to expand the chemical coverage and MOA categories to include

Table 1
Description of mode of action (MOA) categories used in the MOAtox database and number of chemicals within each MOA.[a]

Broad MOA (*n*)[b]	Specific MOA	Chemical class	Structural features	Example chemicals	#Chemicals in Database[a]	
					MOA	MOAtox
AChE inhibition (285)	Carbamate	Carbamate insecticides	Oxime and methyl carbamate	Aldicarb, carbaryl, methiocarb	74	19
	Organophosphate	Organophosphorus insecticides	Organophosphates, organothiophosphates	Chlorpyrifos, malathion, terbufos	211	58
Iono/osmoregulatory/ circulatory impairment (55)	Metallic iono/osmoregulatory impairment	Heavy metals, transition metals	Divalent metals	Copper, zinc	18	15
	Other	Inorganics	Chemical specific	Ammonia	6	4
	Methemoglobinemia	Chemical specific, nitrites	Chemical specific	Aminopropiophenone, sodium nitrite	6	1
	Anticoagulation	Coumarin rodenticides	Coumarin moiety	Dicoumarol, bromadiolone	25	7
Narcosis (465)[c]	Ester	Mono or diesters,	Diverse structures, non-reactive	Bromoxynil butyrate, methyl acetate, phenyl salicylate	48	41
	Non-polar	Neutral organics	Moderate polarity	Benzene, ethanol, metolachlor	347	283
	Polar	Polar organics	Single nitro or <3 halogens	4-Nonylphenol, pyridine, triclosan	61	55
Neurotoxicity (200)	Alicyclic GABA antagonism	Acyclic organochlorines	Cyclodiene, hexachlorocyclohexane	Aldrin, lindane	42	17
	Diphenyl sodium channel modulation	Diphenyl organochlorines	Halogenated bridged diphenyls	DDT, methoxychlor	11	7
	GABA agonism	Lactone insecticides	Macrocyclic lactones	Abamectin	16	2
	Other	Various	Chemical specific	Phenobarbital	8	3
	Pyrazole GABA antagonism	Pyrazole insecticides	Phenyl pyrazoles,	Fipronil,	6	1
	Pyrethroid sodium channel modulation	Pyrethroid insecticide	Pyrethroid ether, oxime, ester moieties	Cypermethrin,	102	24
	Sodium channel blocking	Oxidiazine insecticides	Oxidiazine moiety	Indoxacarb	3	1
	Nicotinic acetylcholine receptor agonism	Neonicotinoid insecticides	Nicotine analogs	Acetamiprid, dinotefuran	8	6
	Strychnine	Strychnines	Strychnine moiety	Strychnine	4	1
Reactivity (111)	Acrylate	Acrylates	Acrylate moiety	Acrylonitrile	8	7
	Alkylation	Various	Reactive leaving group (*e.g.*, alkene)	2-Propenamide	38	30
	Carbonyl	Various	Reactive carbonyl	Formalin	13	11
	Chromate	Chromates	Chromate moiety	Sodium dichromate	3	0
	Cyanate/nitrile	Cyanates, nitriles	Cyanate or nitrile moiety	Allyl isothiocyanate	9	8
	Di/trinitroaromatic	Nitrobenzenes	Poly nitrobenzene moiety	2,3,5-Trinitrobenzene	14	14
	Hydrazine	Hydrazines	Hydrazine moiety	Monomethylhydrazine	4	3
	Other	Various	Chemical specific	Quinoline	19	14
	Phosphide	Phosphides	Phosphide moiety	Calcium phosphide	3	0
Electron transport inhibition (97)	Oxidative phosphorylation inhibition	Inorganics, antimycins trialkyltins	Chemical specific	Cyanide, antimycin a, tributyl tin	20	13
	Uncoupling oxidative phosphorylation	Nitro or halo-phenols, pyridines, anilines	Chemical specific	2,4-Dinitrophenol, pentachlorophenol	55	21
	Arsenical respiratory inhibition	Arsenicals	Arsenites, arsenates	Sodium arsenite	22	1

[a] See Supplemental Tables S1 and S2 for complete databases.
[b] Total number of chemicals within the broad MOA category.
[c] Includes 9 chemicals with a specific MOA of NA (not assigned).

metallic compounds, new MOAs (*e.g.*, methemaglobinemia), and subcategories of neurotoxicity and electron transport inhibition consistent with the IRAC international insecticide classification system (IRAC, 2014). The categorization scheme was comprised of six broad and 31 specific MOA categories that encompassed the major MOAs reported in aquatic invertebrates and fish. The reactivity MOA included nine structure-based subcategories determined largely from Russom et al. (1997) and U.S. EPA QSAR models

Table 2
Number of chemicals with measured and predicted toxicity values for each taxa group within the MOAtox database (Table S2).

Taxa	Measured toxicity values	Species-specific estimated toxicity values[a]				Total number
		Level 1	Level 2	Level 3	Level 4	
Bluegill	306	323	36	3	0	668
Fathead	298	314	6	48	1	667
Rainbow trout	336	294	2	35	0	667
Daphnia[b]	328	54	12	263	12	669
Fish	614	NA	NA	NA	NA	615
Invertebrates	424	NA	NA	NA	NA	425

[a] Model uncertainty level of estimated taxa-specific values (1 highest confidence). NA: not applicable.
[b] Measured values include *D. magna* (319), *D. pulex* (15), *D. galeata* (2), and *D. carinata* (2). Estimated values are for *D. magna*.

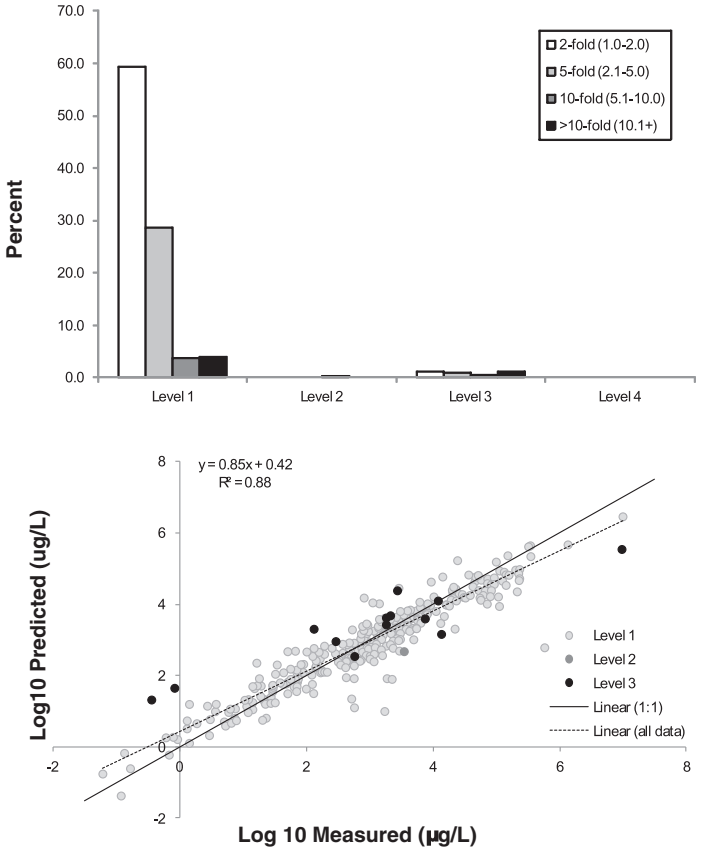

Fig. 3. Prediction accuracy of estimated toxicity values by uncertainty level (upper panel), and correlation between measured and predicted toxicity values (lower panel) in rainbow trout.

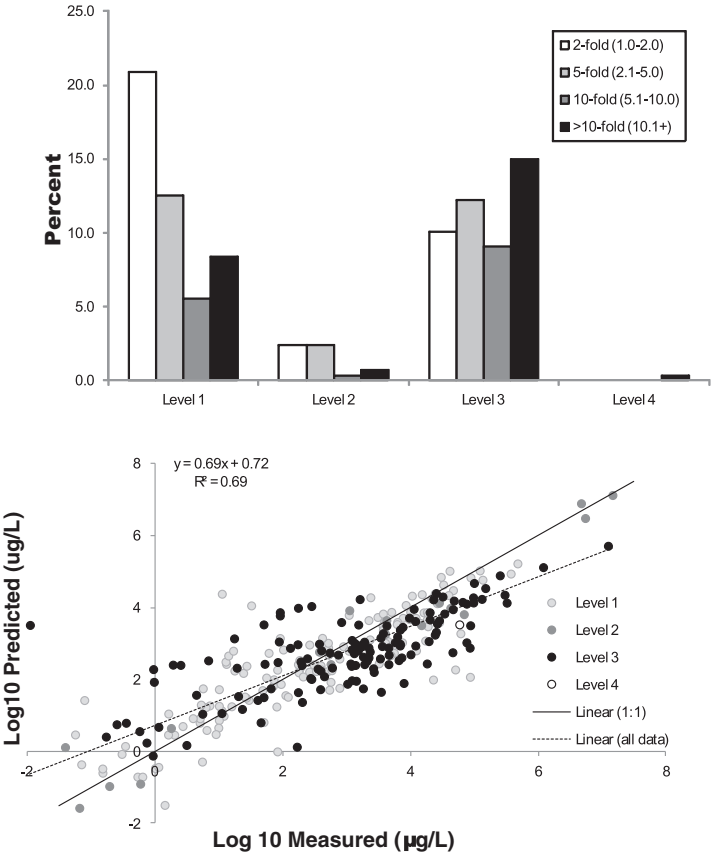

Fig. 4. Prediction accuracy of estimated toxicity values by uncertainty level (upper panel), and correlation between measured and predicted toxicity values (lower panel) in *D. magna*.

that used a fragment-based MOA assignment approach (USEPA, 2012). The specific MOA of alkylation encompassed a structurally diverse group of nucleophiles, electrophiles, and proelectrophiles of varying potency. Additional research is needed to refine the reactivity MOA in general, and the alkylation specific MOA in particular because of the diversity of structures and reactivity mechanisms.

An inherent uncertainty in the MOA assignments is whether the same MOA is applicable to both fish and the large diversity of aquatic invertebrates. Multiple studies of chemicals with a narcosis MOA have shown similar critical body residues in several aquatic taxa, suggesting similar intrinsic species sensitivity, and mechanism of action (Barron et al., 2002). Species sensitivity distributions for AChE inhibitors show distinct differences in fish and invertebrates, but these appear to relate to species-specific sensitivity rather than differing MOA (Awkerman et al., 2014; Russom et al., 2014). MOAs may be similar across taxa, because the basic biochemical systems and molecular targets affected may be generally conserved across many animal species (LaLone et al., 2013). However, applicability of the MOA assignments to the large diversity in aquatic species is a significant uncertainty and an area of future research. Compounds that had very specific acting insecticidal mechanisms (*e.g.*, insect growth or molt inhibitors) were excluded from the database because of uncertain or unlikely applicability to toxic action in fish.

In many applications, MOA-based model development can be considered a better alternative to chemical class-based profiling and predictive toxicity modeling. Chemical MOA is a key determinant of hazard, provides information on underlying toxicity pathways, and allows for grouping across multiple chemical classes. However, the development of QSAR and other predictive models have been generally limited by the availability of large high quality MOA and toxicity databases. For example, previously available toxicity datasets have been dominated by non-polar and polar narcotics. The MOAtox database was developed as a comprehensive standardized dataset intended to facilitate predictive aquatic toxicology model development for a diversity of chemical classes and MOAs. The taxa-specific component of the database focused on the four most commonly reported aquatic test species in order to maximize chemical and MOA diversity, and minimize the number of estimated values. Additionally, generic toxicity values for fish and aquatic invertebrates were determined from only measured values to increase the chemical domain and applicability of the MOAtox dataset for QSAR and other predictive model development. However, only 24 additional chemicals were gained from using all available fish compared to measured values in the three focus fish species, illustrating the predominance of existing test data for these species in aquatic toxicology. In contrast, the taxa group of all aquatic invertebrates comprised an additional 96 chemicals relative to the *Daphnia* only category.

The toxicity data used in the current study were standardized to limit extrinsic variation caused by differences in toxicity test conditions and variability in reported values. This approach removed a large amount of measured toxicity values. Additional research would be needed to determine the optimum level of standardization needed. In addition to predictive model development, the MOA dataset presented here should also support MOA-based assessments of chemical mixtures, such as applying a toxic units approach (additivity) to chemicals with the same specific MOA. Future work will include periodic expansion and refinement of the database and MOA categories, as well as developing an internet accessible and searchable platform.

Acknowledgements

We thank Larisa Lee and Julie Krzykwa for dataset development and quality assurance support. This paper has been reviewed according to EPA guidelines, but the opinions expressed in this work are those of the authors and do not represent the policies or opinions of the U.S. EPA.

Appendix A. Supplementary data

Supplementary data associated with this article can be found, in the online version, at http://dx.doi.org/10.1016/j.aquatox.2015.02.001.

References

Awkerman, J.S., Raimondo, S., Jackson, C.R., Barron, M.G., 2014. Augmenting aquatic species sensitivity distributions with interspecies toxicity estimation models. Environ. Toxicol. Chem. 33, 688–695.

Barron, M.G., Hansen, J., Lipton, J., 2002. Association between contaminant tissue residues and adverse effects in aquatic organisms. Rev. Environ. Contamin. Toxicol. 173, 1–37.

Call, D.J., Brooke, L.T., Knuth, M.L., Poirier, S.H., Hoglund, M.D., 1985. Fish subchronic toxicity prediction model for industrial organic chemicals that produce narcosis. Environ. Toxicol. Chem. 4, 335–341.

Christen, V., Hickmann, S., Rechenberg, B., Fent, K., 2010. Highly active human pharmaceuticals in aquatic systems: a concept for their identification based on their mode of action. Aquat. Toxicol. 96 (February (3)), 167–181.

Escher, B.I., Bramaz, N., Eggen, R.I.L., Richter, M., 2005. *In vitro* assessment of modes of toxic action of pharmaceuticals in aquatic life. Environ. Sci. Technol. 39, 3090–3100.

Fairbrother, A., Barron, M.G., Johnson, M.S., 2014. Chapter 42: methods in ecotoxicology. In: Hayes, A.W., Kruger, C.L. (Eds.), Hayes' Principles and Methods of Toxicology. , Sixth ed. Taylor & Frances, Boca Raton, FL, pp. 2024–2065.

IRAC, 2014. IRAC MoA classification scheme, Insecticide Resistance Action Committee, February 2014, Version 7.3. 24 p, www.irac-online.org/documents/moa-classification/?ext=pdf

Konemann, W.H., 1981. Quantitative structure-activity relationship in fish toxicity studies, Part 1. Relationship for 50 industrial pollutants. Toxicology 19, 209–282.

LaLone, C.A., Villeneuve, D.L., Burgoon, L.D., Russom, C.L., Helgen, H.W., Berninger, J.P., Tietge, J.E., Severson, M.N., Cavallin, J.E., Ankley, G.T., 2013. Molecular target sequence similarity as a basis for species extrapolation to assess the ecological risk of chemicals with known modes of action. Aquat. Tox. 144–145, 141–154.

Martin, T.M., Grulke, C.M., Young, D.M., Russom, C.L., Wang, N., Jackson, C.R., Barron, M.G., 2013. Prediction of aquatic toxicity mode of action using linear discriminant and random forest models. J. Chem. Info. Model. 53, 2229–2239.

McKim, J.M., Bradbury, S.P., Niemi, G.J., 1987. Fish acute toxicity syndromes and their use in the QSAR approach to hazard assessment. Environ. Health Perspect. 71, 171–186.

Nendza, M., Müller, M., 2000. Discriminating toxicant classes by mode of action: 2. Physico-chemical descriptors. Quant. Struct. -Act. Relat. 19, 581–598.

Raimondo, S., Jackson, C.R., Barron, M.G., 2010. Influence of taxonomic relatedness and chemical mode of action in acute interspecies estimation models for aquatic species. Environ. Sci. Technol. 44, 7711–7716.

Raimondo, S., Jackson, C.R., Barron, M.G., 2013a. ICE aquatic toxicity database documentation. In: Office of Research and Development. U.S. Environmental Protection Agency, Gulf Breeze, FL http://epa.gov/ceampubl/fchain/webice/iceDownloads.html

Raimondo, S., Jackson, C.R., Barron, M.G., 2013b. Web-based interspecies correlation estimation (Web-ICE) for acute toxicity: user manual. In: Office of Research and Development. U.S. Environmental Protection Agency, Gulf Breeze, FL (Version 3.1. EPA/600/R-12/603).

Russom, C.L., Bradbury, S.P., Broderius, S.J., Hammermeister, D.E., Drummond, R.A., 1997. Predicting modes of toxic action from chemical structure: acute toxicity in the fathead minnow (*Pimephales promelas*). Environ. Toxicol. Chem. 16, 948–967.

Russom, C.L., LaLone, C.A., Villeneuve, D.L., Ankley, G.T., 2014. Development of an adverse outcome pathway for acetylcholinesterase inhibition leading to acute mortality. Environ. Toxicol. Chem. 33, 2157–2169.

Schüürmann, G., Aptula, A.O., Kühne, R., Ebert, R.-U., 2003. Stepwise discrimination between four modes of toxic action of phenols in the tetrahymena pyriformis assay. Chem. Res. Toxicol. 16, 974–987.

Spycher, S., Nendza, M., Gasteiger, J., 2004. Comparison of different classification methods applied to a mode of toxic action dataset. QSAR Comb. Sci. 23, 779–791.

Suter II, G.W., 2007. Modes and mechanisms of action. Chapter 7. In: Suter, G.W. (Ed.), Ecological Risk Assessment. , second edition. CRC Press, Boca Raton, FL, USA, pp. 105–109.

USEPA, 2012. ASTER User Guide: ASTER System, Version 2.0. U.S. Environmental Protection Agency (2012) http://cfpub.epa.gov/ecotox/blackbox/help/ASTER.pdf

USEPA, 2014. ECOTOX User Guide: ECOTOXicology Database System, Version 4.0. U.S. Environmental Protection Agency (2014) http://www.epa.gov/ecotox/

Verhaar, H.J.M., van Leeuwen, C.J., Hermens, J.L.M., 1992. Classifying environmental pollutants part 1, Structure activity relationships for prediction of aquatic toxicity. Chemosphere 25, 471–491.

Verhaar, H.J.M., Solbe, J., Speksnijder, J., van Leeuwen, C.J., Hermens, J.L.M., 2000. Classifying environmental pollutants: part 3. External validation of the classification system. Chemosphere 40, 875–883.

Aquatic Toxicology 180 (2016) 11–24

Contents lists available at ScienceDirect

Aquatic Toxicology

journal homepage: www.elsevier.com/locate/aquatox

A Bayesian network model for predicting aquatic toxicity mode of action using two dimensional theoretical molecular descriptors

John F. Carriger[a], Todd M. Martin[b], Mace G. Barron[a,*]

[a] U.S. Environmental Protection Agency, Office of Research and Development, Gulf Ecology Division, Gulf Breeze, FL, 32561, United States
[b] U.S. Environmental Protection Agency, Office of Research and Development, Sustainable Technology Division, Cincinnati, OH, 45220, United States

ARTICLE INFO

Article history:
Received 18 July 2016
Received in revised form 6 September 2016
Accepted 7 September 2016
Available online 13 September 2016

Keywords:
Mode of action
Aquatic toxicity
Bayesian network
Markov blanket
Chemical descriptors

ABSTRACT

The mode of toxic action (MoA) has been recognized as a key determinant of chemical toxicity, but development of predictive MoA classification models in aquatic toxicology has been limited. We developed a Bayesian network model to classify aquatic toxicity MoA using a recently published dataset containing over one thousand chemicals with MoA assignments for aquatic animal toxicity. Two dimensional theoretical chemical descriptors were generated for each chemical using the Toxicity Estimation Software Tool. The model was developed through augmented Markov blanket discovery from the dataset of 1098 chemicals with the MoA broad classifications as a target node. From cross validation, the overall precision for the model was 80.2%. The best precision was for the AChEI MoA (93.5%) where 257 chemicals out of 275 were correctly classified. Model precision was poorest for the reactivity MoA (48.5%) where 48 out of 99 reactive chemicals were correctly classified. Narcosis represented the largest class within the MoA dataset and had a precision and reliability of 80.0%, reflecting the global precision across all of the MoAs. False negatives for narcosis most often fell into electron transport inhibition, neurotoxicity or reactivity MoAs. False negatives for all other MoAs were most often narcosis. A probabilistic sensitivity analysis was undertaken for each MoA to examine the sensitivity to individual and multiple descriptor findings. The results show that the Markov blanket of a structurally complex dataset can simplify analysis and interpretation by identifying a subset of the key chemical descriptors associated with broad aquatic toxicity MoAs, and by providing a computational chemistry-based network classification model with reasonable prediction accuracy.

Published by Elsevier B.V.

1. Introduction

The mode of toxic action (MoA) has been recognized as a key determinant of chemical toxicity but MoA classification in aquatic toxicology has been generally limited to either narrow domains of applicability, highly complex or simplistic assignment schemes, or poor prediction accuracy (Russom et al., 1997; Nendza and Muller 2007; Enoch et al., 2008; Barron et al., 2015). Generally two approaches have been used to develop structure-based models to predict aquatic toxicity MoA: identification of substructural indicators based on the presence of specific molecular features (e.g., Verhaar et al., 1992; Russom et al., 1997; Nendza and Muller 2007; Enoch et al., 2008), and use of neural networks, hierarchical clustering or other machine learning methods with theoretical descriptors that describe a broad array of electronic, topological, and other features of a chemical (e.g., Yao et al., 2005; He and Jurs, 2005). Recently, Martin et al. (2013) used two dimensional chemical descriptors and machine based learning algorithms to predict aquatic toxicity MoA using a database of 924 chemicals. Linear discriminant analysis (LDA) and random forest MoA assignment models had high internal concordance and specificity and produced overall MoA prediction accuracies of 85–88% (Martin et al., 2013). Barron et al. (2015) developed an integrated dataset of MoA assignments for over 1200 chemicals that included a diversity of metals, pesticides and other organic compounds that encompassed six broad and 31 specific MoAs for fish and aquatic invertebrates. Martin et al. (2015) then utilized this expanded MoA database to predict global or specific aquatic toxicity MoA with methods such as LDA and multiple linear regression. Mode of action prediction accuracy was greatest for acetylcholinesterase inhibitors and lowest for other neurotoxicants, the structurally diverse group of reactive chemicals, and MoAs with low representation in the database (Martin et al., 2015).

* Corresponding author.
E-mail address: barron.mace@epa.gov (M.G. Barron).

http://dx.doi.org/10.1016/j.aquatox.2016.09.006
0166-445X/Published by Elsevier B.V.

Bayesian networks have seen increasing use in hazard and risk assessment (Burden and Winkler, 2000; Billoir et al., 2008; Iorio et al., 2009), but only limited application in aquatic toxicity and MoA prediction. A Bayesian network is a graphical representation of a joint probability distribution. The structure of a Bayesian network consists of individual nodes (i.e., random variables) connected by arcs (arrows) reflecting a dependence structure between the variables. Bayesian networks are built in a directed manner often reflecting causality between the variables though this is not a requirement. The absence of an arc between nodes signifies that the variables are conditionally independent. Algorithms are available for learning a Bayesian network structure from data. These algorithms can often be useful in high dimensional data where the structure and conditional dependence are not readily apparent. The automated learning process of a Bayesian network structure can either be unsupervised or supervised. In contrast to a more generalized representation of a joint probability distribution in unsupervised learning of a Bayesian network's structure, supervised learning focuses on representing the relationship of predictor nodes to a target variable. Bayesian networks have not been previously used to predict MoA, but have been applied in machine learning applications for diverse fields from cancer prediction to marketing and finance.

The objective of the current study was to elucidate the connection between molecular descriptors and MoA, and develop a Bayesian network prediction model for classifying chemicals by aquatic toxicity MoA. The model was developed following the steps of discretization, structure learning, network selection and validation, and sensitivity analysis. The study utilized a recently published dataset containing over one thousand chemicals with MoA assignments (Barron et al., 2015), and two dimensional chemical descriptors generated for each chemical. Machine-learned Bayesian networks were chosen for their capabilities in analyzing uncertainties, and accounting for covariation among multiple variables (Barber, 2012). For the current study, we focus on learning the Markov blanket of the data set with the MoA broad classifications as a target node. The Markov blanket of a target node consists of the node's parents, children, and the nodes that share children with the target node (Korb and Nicholson, 2004). The target node or node in question, is screened from the rest of the nodes in the network from its Markov blanket if the value of each of the nodes in the blanket is known. Fig. 1 shows an illustration of the concept. If the A_i predictor nodes in Fig. 1 are known for certain, then no other node (i.e., the B_i nodes) will provide any additional information on the target variable. Identifying the Markov blanket of a complex dataset with numerous variables can simplify analytical and computational requirements by providing a subset of the key predictors in a dataset that are highly informative for making probabilistic inferences on a target variable.

2. Methods

2.1. General approach

The approach to database and network model development is described in detail in the subsections below. The database used in developing and validating the Bayesian classification network was comprised of a dataset of known MoA assignments and a dataset of two dimensional theoretical chemical descriptors for over 1000 chemicals. Six preliminary models were initially constructed with two different discretization levels and three Markov blanket algorithms. An optimal structural coefficient was selected for each model from trade-offs between internal precision and structural complexity. A 10-fold cross validation was implemented for each candidate model and a final network was selected with the highest empirical performance from overall precision. Sensitivity analyses on the selected model examined the strengths of the relationships between the variables, and the capabilities of maximizing MoA probabilities using individual and multiple descriptors.

2.2. MoA and descriptor database development

The MoA dataset was based on the MOAtox database of Barron et al. (2015) that encompassed the six broad acute aquatic toxicity categories of acetylcholinesterase inhibition (AChEI), narcosis, electron transport inhibition (ETI), ionoregulatory/osmoregulatory/circulatory impairment (IOCI), other neurotoxicity, and reactivity. Those MoA assignments had been determined for aquatic invertebrates and fish toxicity from over 1200 chemicals using a combination of international consensus classifications, QSAR predictions, and weight of evidence professional judgment based on an assessment of structural features and literature information (Barron et al., 2015). Up to 790 two dimensional theoretical molecular descriptors were then calculated for each chemical following the method of Martin et al. (2015) using the computational chemistry application TEST (USEPA, 2016). The descriptor classes included E-state values and E-state counts, constitutional descriptors, topological descriptors, walk and path counts, connectivity, information content, two-dimensional autocorrelation, Burden eigenvalue, molecular properties, Kappa, hydrogen bond acceptor/donor counts, molecular distance edge and molecular fragment counts (USEPA, 2008; Zhu et al., 2009; Martin et al., 2013, 2015). Definitions of key descriptors are in Supplemental Table S1 and available for download from the TEST internet site (USEPA, 2008). Chemicals were removed from the database that included metals, other inorganic compounds, and organic salts because of the inability to compute descriptors for these ionic compounds leaving a total of 1098 chemicals used in the Bayesian network.

2.3. Bayesian network development

2.3.1. -Discretization

All Bayesian network analysis was conducted with Bayesialab 5.4.3 (Bayesia S.A.S., 2015). Each chemical entry in the MoA and descriptor dataset was used except several descriptors only containing zeroes were removed prior to analysis. Continuous variables were discretized using the decision tree algorithm with the broad MoA variable as the target node for choosing levels. The decision tree algorithm maximizes the information content between a target node (i.e., MoA) and predictor (i.e., a descriptor) from the discretization levels. In case of failure of the decision tree discretization algorithm to identify intervals, we used density approximation, k-means discretization, and normalized equal distance in that order of priority for selecting a discretization algorithm. Discretization was run twice using both three and four discretization intervals as initial specifications in the algorithms. The number of intervals for the descriptors was chosen as a compromise between representation of the distribution and data availability for estimating probabilities (Conrady and Jouffe, 2015).

2.3.2. -Structure learning

After discretizing the continuous variables, three supervised structure learning methods were applied. The first was a Markov blanket (MB) analysis and the second was an augmented Markov blanket (AMB) analysis and the third was a minimal augmented Markov blanket (MAMB) analysis. The MB analysis searches for the parents, children, and spouses of the target node. The AMB first identifies the MB and then the relationships among the parent, son, and spouse nodes (Fig. 1). The MAMB prunes the MB by

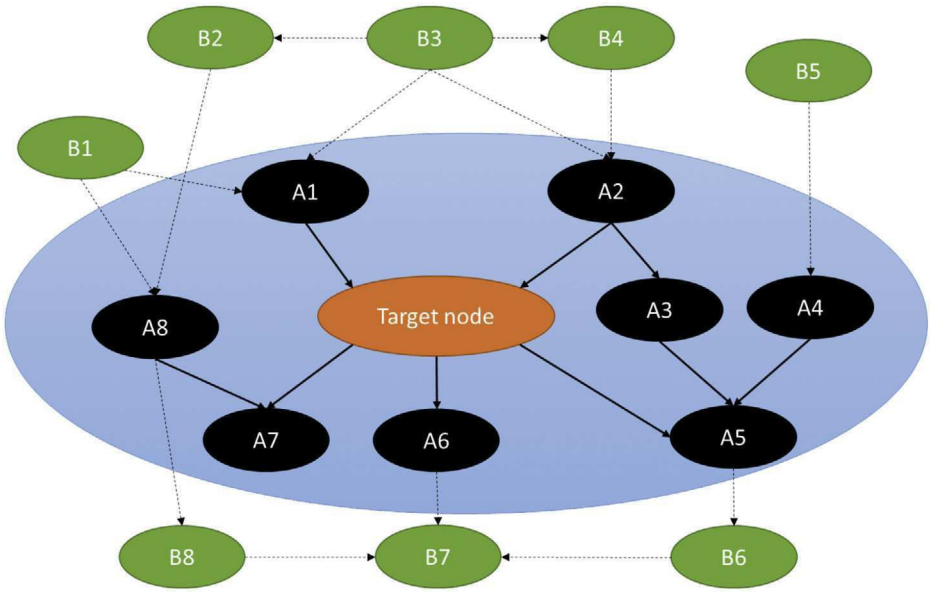

Fig. 1. Representation of a Markov blanket in a Bayesian network. The orange (center) oval is a target node or the variable of ultimate inferential interest in the analysis. The black ovals labelled A_i are variables that are used for predictions and are in the Markov blanket of the target node (i.e., either children, parents, or spouses of the target node). The green (bottom) ovals labelled B_i are variables in the problem domain but not in the Markov blanket. (For interpretation of the references to colour in this figure legend, the reader is referred to the web version of this article.)

eliminating nodes from the blanket through an additional equivalence class unsupervised learning step.

Bayesialab uses the minimum description length of candidate networks in its score-based algorithms for comparing Bayesian network structures (Conrady and Jouffe, 2015). The structural coefficient (SC) modifies the complexity of the network through weighting the structure encoding (in bits) of the Bayesian network. In a Markov blanket analysis, the SC can influence the number of descriptors selected in the blanket as well as their connectivity. We adjusted the SC by finding the optimal value between complexity and data representation/precision similar to Harris et al. (2016) and Conrady and Jouffe (2015). The SC analysis generated networks with each of the supervised learning algorithms (i.e., MB, AMB, MAMB) and discretization levels with SCs ranging from 0.5 to 6.0 at 0.1 intervals. Bayesian networks with lower (< 0.5) SC values were found to be difficult to computationally manage because of higher model complexity. Plotting the SC values against the structure:target precision ratio for each of the generated networks helped to visually identify candidate SCs. The inflection of the structure:target precision ratio plot was located to identify a SC that optimally did not underfit or overfit the model (Bayesia, 2010; Harris et al., 2016). The target precision was also examined as a function of the SC before final selection where the height of the curve was used to prioritize the SC. In case of constant values for the precision across the range of SCs, the structure/data ratio was plotted against the SC to further enhance descriptor representation or prevent overfitting. A single SC value was identified for all candidate models except for the MAMB model with three discretization levels where two different SCs were tested.

2.3.3. -Network selection and validation

Targeted cross validation (k fold) was used to estimate the performance of the networks in out of sample predictions (Stone, 1974; Conrady and Jouffe, 2015). Prior to cross-validation work, a virtual data point was added to every conditional and unconditional probability table cell to prevent impossible assignments in the cross-validation and to improve later inferential analysis. The k-folds cross validation method splits the data set into k equal sized sets and uses k-1 sets for learning the model and one for validation. This is repeated for k rounds and synthesized results are reported (Conrady and Jouffe, 2011). The data were randomly split into 10 sets for a 10 fold cross validation. The k-folds cross validation method was used to compare the precision of these candidate models and the final selected model was built with the AMB algorithm with three discretization levels and a SC of 1. Cross validation results are discussed for this model including reliability and precision statistics from an occurrence matrix. The reliability statistic related the number of predictions that should have been a MoA to the occurrences that were predicted to be that or another MoA. The precision statistic related the number of occurrences that were predicted for a MoA to the total occurrences that should have been predicted as that or another MoA. Total precision sums the correct predictions for each MoA and relates this value to the total number of predictions that were made. All precision and reliability statistics were expressed as percentages.

For the AMB network with three discretization levels, a final check on the connections identified among the descriptors was made for overfitting based on the Kullback-Leibler divergence for the arcs between descriptors (Bayesia, 2010). This check for lack of dependence was done for each parent-child relationship in the AMB network that was previously identified with the minimum description length score-based algorithm. The validity of the connections among the descriptors that was identified by the learning algorithm was examined using a statistical independence test (G_{KL}-test; p-values greater than 0.05 provide evidence of independence) (Bayesia, 2010). From the tests, the p-values or independence probabilities, were used to check the significance of each identified relationship between the descriptors or between the descriptors and the target node (Thai et al., 2012; Harris et al., 2016).

2.3.4. -Sensitivity analysis

A comprehensive sensitivity analysis examined the relationship among the descriptors in the selected network and helped hone in on the influence of individual descriptors on MoA prediction. The sensitivity analysis was conducted using higher, moderate or lower values of the descriptors with each MoA. For a broad understanding of the relationships between variables, the highest and lowest values of mutual information, Pearson's correlation, Kullback-Leibler

divergence, and node force between variables were examined globally on the network. Mutual information was used to examine the probabilistic dependence between the nodes in the network. Pearson's correlation gave a measure of the linear strength of the relationship between the variables. The Kullback-Leibler divergence can be used as a measure of the information gain from assuming a joint relationship between two variables in a network compared to an assumption of independence. Node force sums the Kullback Leibler divergence input to a node and output by the node. The nodes that have more direct relationships and greater dependence with other nodes have the highest node force. Sensitivity of each MoA to each descriptor was examined in tornado plots that displayed the influence of knowledge of the descriptor values on the probability of each MoA and provided information on the maximum strength of the individual relationships between each MoA and descriptor. The tornado plots display the range between the lowest and highest probability that can be achieved for each MoA from hard evidence placed on the corresponding descriptor states.

A target dynamic profile analysis (TDP) (Bayesia, 2010) identified a pathway of states of the descriptors most likely to reduce uncertainty on the MoAs. The TDP checked the sensitivity of each MoA to multiple descriptors by maximizing their probability as the search criteria optimization specification. This analysis uses a search that can take into account the joint probability of the evidence to diminish the impact of low probability scenarios. Only hard evidence was used to establish the TDP under the assumption that there would be minimal uncertainty on the descriptors' states for a given chemical.

A target optimization tree (Bayesia, 2010) was also used to identify additional pathways for reducing uncertainty on the MoAs from knowledge of descriptors in the Markov blanket. This allowed a fuller consideration of different evidence from multiple variables (descriptors). The tree presented a visualization of the hard evidence set for predicting a MoA through an exhaustive search that can also take into account the joint probability of the evidence to diminish the impact of low probability states. We limited the target optimization tree to three descriptors for depth of evidence and a maximum of two alternate trees corresponding to the breadth of evidence and utilized hard evidence for its derivation. Both the TDP and target optimization tree analyses were run twice, once using the joint probability of the evidence to weight the search methods and once not considering it but only considering the maximization of the probability of the MoA. The probability changes from initial marginal probability to final probability for the MoAs were used to score the pathways in the target optimization trees. When the joint probability of the evidence was considered in the tree construction, the probability change to the MoA was weighted by the joint probability of the evidence to calculate the optimization score.

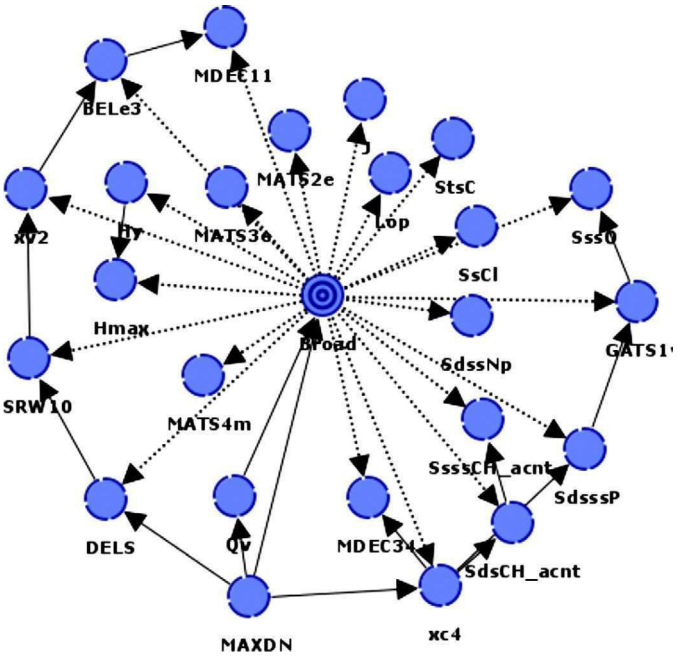

Fig. 2. Structural components of the augmented Markov blanket model used for classifying modes of toxic action using chemical descriptors. The target (predicted) node (*Broad*) contains the broad mode of toxic action categories in its variable states. Dashed arcs delineate relationships where *Broad* is a parent node of a descriptor. Inferences made within the model are omnidirectional so that observing a descriptor changes the probability of the other descriptors as well as the target node depending on all other observations in the model and the conditional independence relationships contained in the structure.

3. Results

3.1. Network precision and reliability

The total precision for the selected AMB model (Fig. 2) with three discretizations was 80.2% (Table 1). The best precision was for the AChEI MoA (93.5%) where 257 chemicals out of 275 were correctly classified. Model precision was poorest for the reactivity MoA (48.5%) where only 48 out of 99 reactive chemicals were correctly classified. Narcosis represented the largest class within the MoA dataset and had a precision of 80.0%, reflecting the total precision across all of the MoAs. False negatives for chemicals with the narcosis MoA most often fell into the ETI, neurotoxicity or reactivity MoAs. False negatives for all other MoAs were most often narcosis.

Table 1
Global cross validation results for mode of toxic action (MoA) predicted from chemical descriptors (n = number of chemicals in dataset). Data are: % reliability (R%) and% precision (P%). Row titles and numerical values in parentheses pertain to predicted cases and column titles and numerical values are for actual cases.

MoA	AChEI[a] (275)		ETI[b] (61)		IOCI[c] (18)		Narcosis (460)		Neurotoxicity (185)		Reactivity (99)	
	R %	P %	R %	P %	R %	P %	R %	P %	R %	P %	R %	P %
AChEI[1] (276)	93	93	0	0	0	0	5.1	3.0	1.5	2.2	0.4	1.0
ETI[2] (76)	0	0	55	69	0	0	33	5.4	0	0	12	9.1
IOCI[3] (14)	0	0	0	0	86	67	7.1	0.2	7.1	0.5	0	0
Narcosis (471)	3.8	6.6	3.4	26	1.1	28	78	80	5.5	14	8.1	38
Neurotoxicity (184)	0	0	1.1	3.3	0.54	5.6	13	5.2	84	83	1.6	3.0
Reactivity (77)	0	0	1.3	1.6	0	0	36	6.1	0	0	62	48

[a] Acetylcholinesterase inhibition.
[b] Electron transport inhibition.
[c] Iono/osmoregulatory/circulatory impairment.

3.2. Global model results

The structure of the selected AMB model contained over a dozen connections between the descriptors in the Markov blanket of the MoA variable (Fig. 2). The p-values for each of the variable relationships were all 0.0000% from the G_{KL}-test indicating that the evidence is not strong enough to disprove the links identified by the AMB algorithm. The highest Kullback-Leibler divergence was between the MAXDN and Broad MoA nodes (0.5256) and the lowest was between SdsCH_acnt and SsssCH_acnt (0.0523). The highest mutual information was found between the broad MoA and SRW10 nodes (0.4913). The lowest was between xc4 and SdsCH_acnt (0.0495). The highest positive Pearson's correlation was between Broad and SdsssP (0.6839). The lowest positive correlation was between Broad and SdssNp (0.0055). The highest negative Pearson's correlation was between SdsssP and GATS1v (-0.6065) and the lowest negative Pearson's correlation was between Broad and DELS (−0.0044). Aside from the node force of the Broad MoA variable (5.2611), the highest node force was for MAXDN (1.2074). The lowest was for StsC (0.0553). The highest outgoing force for a descriptor was MAXDN (1.2074) followed by xc4 (0.3767). Thirteen descriptors had zero values for outgoing force indicating that these are leaf variables in the network. The lowest non-leaf descriptor outgoing force was for SdsCH_acnt (0.0523). The highest incoming force for a descriptor was for xc4 (0.5539) followed by DELS (0.5405) and SRW10 (0.5069). The lowest incoming force was for StsC (0.0553). MAXDN had a zero for incoming force indicating that it is a root variable with no parents.

3.3. Mode of toxic action sensitivity to individual descriptors

The sensitivity of each MoA to the individual descriptors is based on changes to the probability of each broad MoA from changes to each descriptor individually while allowing the other descriptors to co-vary with the state changes for a descriptor of concern (Fig. 3). The Supporting information contains separate tornado plots of the sensitivity of each MoA to each individual descriptor (Figs. S1–S6).

AChEI had the greatest sensitivity to changes in SdsssP with ranges from 0.081 to 0.95 probability depending on the state, indicating the importance of a phosphate group. GATS1 v was the second most influential individual descriptor but J was also influential and is capable of raising the probability of AChEI to the second highest level below SdsssP. ETI was most sensitive to SdssNp, suggesting that the number of nitro groups is critical in defining the MoA. Based on the range of probabilities for ETI, Hmax was the second most influential descriptor and Qv also has the potential to raise the probability of ETI to greater than 0.30. Weak positive relationships were found between ETI and most of the descriptors. Electron transport inhibitors were poorly represented in the database.

The number of data points available for IOCI was the lowest in comparison with other MoAs. Iono/osmoregulatory/circulatory impairment had Hmax as the most influential descriptor followed by BELe3, SRW10, and Qv. None of the states of the individual descriptors could raise the probability of IOCI above 0.20 on their own. The low overall probabilities for IOCI in the tornado plot indicates weak positive relationships with individual descriptors and the IOCI MoA.

In contrast, narcosis was the best represented MoA in the database. The descriptor with the greatest influence on the narcosis MoA was MAXDN with a probability range of 0.12 to 0.76. DELS and MATS3e could raise the probability of narcosis to greater values than MAXDN but MAXDN can lower the probability more giving it an overall greater range of potential probability changes than DELS and MATS3e. Numerous descriptors could lower the narcosis MoA to lower probabilities such as SRW10, which was the second most sensitive descriptor, xv2, xc4, SdsssP, SsCL, and SdssNP.

The neurotoxicity MoA was most sensitive to SsCl which has the potential to raise the probability of neurotoxicity from 0.11 to 0.99 alone. Although individual findings at multiple descriptors can lower the probability of neurotoxicity to less than 0.1, five descriptor states can raise the probability of its occurrence to greater than 0.5 (SsCl, MDEC34, SRW10, SsssCH_acnt, and BELe3).

The probability of reactivity was most sensitive to SdssNp. The range of probabilities of reactivity from this one descriptor extended from slightly lower than reactivity's initial probability (0.090) to 0.34. Several other descriptors could raise the initial probability of reactivity from 0.090 to a posterior probability of greater than 0.20. Like IOCI, reactivity had relatively weak positive relationships with the individual descriptors and several descriptor states that could lower the posterior probability of reactivity to close to zero from individual findings at their states.

3.4. Mode of toxic action optimization by multiple descriptors

The results from the TDP analyses are displayed in the Supporting information. Findings on multiple descriptors could lead to equal or greater than 0.99 probability of a MoA both when the joint probability of the evidence was considered in developing the pathway and when it was not. For the models that did not consider the joint probability of the evidence when selecting descriptors, fewer descriptors were necessary to reach the final probabilities of a MoA. The first nodes in the tornado plots that have the potential to affect the greatest range of probabilities were always the first nodes chosen in the TDP with the exception of ETI, IOCI, neurotoxicity, and reactivity when the joint probability was taken into account, and narcosis without taking into account the joint probability of the evidence. These initial descriptors chosen for the TDP were within the top six descriptors that individually created greater range variation with the target state or MoA's probability.

From the existing database alone, multiple descriptors are able to identify MoAs with high certainty even when constrained to follow paths that reflect the available data. For AChEI, only two descriptors were needed to reach or exceed 0.99 probability when considering the joint probability of the evidence and when not considering it. This was largely due to the influence of SdsssP which was the first descriptor for each and which achieved a greater than 0.94 probability of AChEI from one of its states alone. After SdsssP, different descriptors were identified in each of AChEI's target dynamic profiles for achieving a probability of 0.99. For ETI, only two descriptors were needed to reach or exceed a 0.99 probability of its occurrence without the joint probability considered but six descriptors were needed with the joint probability considered. For IOCI, five descriptors were needed to reach or exceed 0.99 probability without the joint probability considered and seven with the joint probability considered. For narcosis, eleven were needed with the joint probability considered and two without the joint probability considered. For neurotoxicity, an outcome on one descriptor was the minimum needed without the joint probability considered and three descriptor outcomes with the joint probability considered. For reactivity, nine descriptors were needed with the joint probability considered and four were needed without the joint probability considered.

Several descriptors that were used in the TDP to reach or exceed 0.99 probability for a single MoA were found to be unique to certain MoAs or were found multiple times across MoAs. For unique descriptors prioritized to reach 0.99 probability, Lop was only found in AChE joint, MAXDN was unique to narcosis joint, MATS3e and SssO were unique to narcosis and MDEC34 and xv2 were only in neurotoxicity joint. Hmax was in both ETI and ETI joint as well as IOCI and IOCI joint. SdssNp was in ETI, ETI joint, narcosis joint, and reactivity. Qv was in ETI joint, IOCI, narcosis joint, and reactivity joint. Bele3, GATS1v, Hy, J, SdsCH_acnt, SdsssP, SRW10, SsCl,

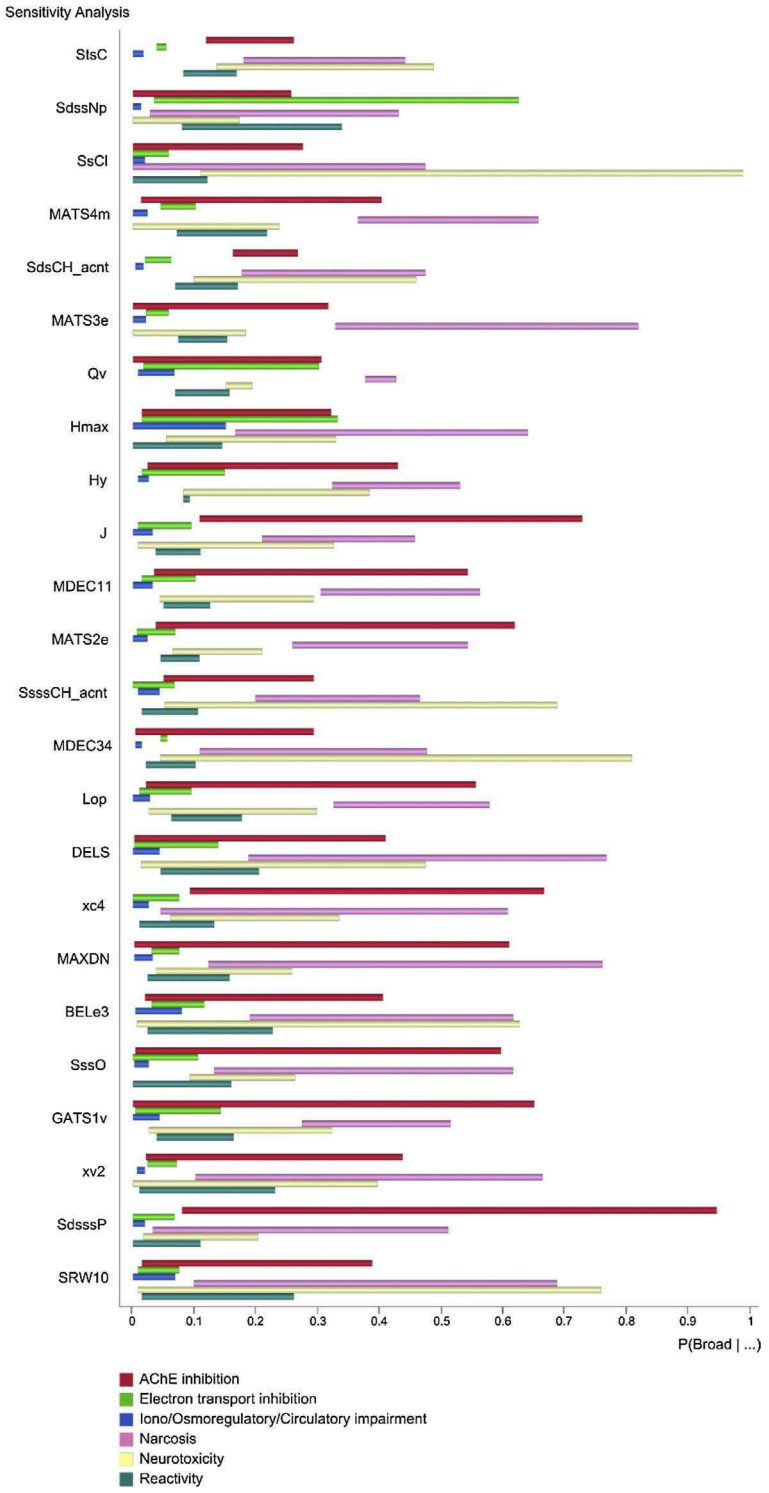

Fig. 3. Sensitivity of the chemical modes of toxic action to each of the descriptors. Horizontal bars represent the range of probabilities for each mode of toxic action (i.e., the conditional probability of the broad mode of toxic action (P(Broad| . . .)) (x-axis)) from findings at the individual descriptors listed on the y-axis.

SsssCH_acnt, and xc4 were found in at least three MoA's TDPs and used prior to or at the point of reaching 0.99. The rest of the descriptors that were prioritized for optimally reaching 0.99 (i.e., DELS, MDEC11, StsC) were found twice across the MoA's TDPs.

To examine multiple pathways for identifying the MoAs, target optimization trees were developed. Fig. 4 contains the target optimization tree for AChEI while taking into account the joint probability of the evidence and Fig. 5 contains the target optimization tree for AChEI without the joint probability of the evidence taken into account in the development of the pathways. All pathways in Figs. 4 and 5 led to a probability of AChEI that is greater than 0.98. The red highlighted box at the leaf of the tree contains the final scenario with the highest overall score based on the joint probability (if considered in the evidence determination) and the change in probability from the initial probability of the MoA displayed in the root of the tree. Both of the primary (first) pathways

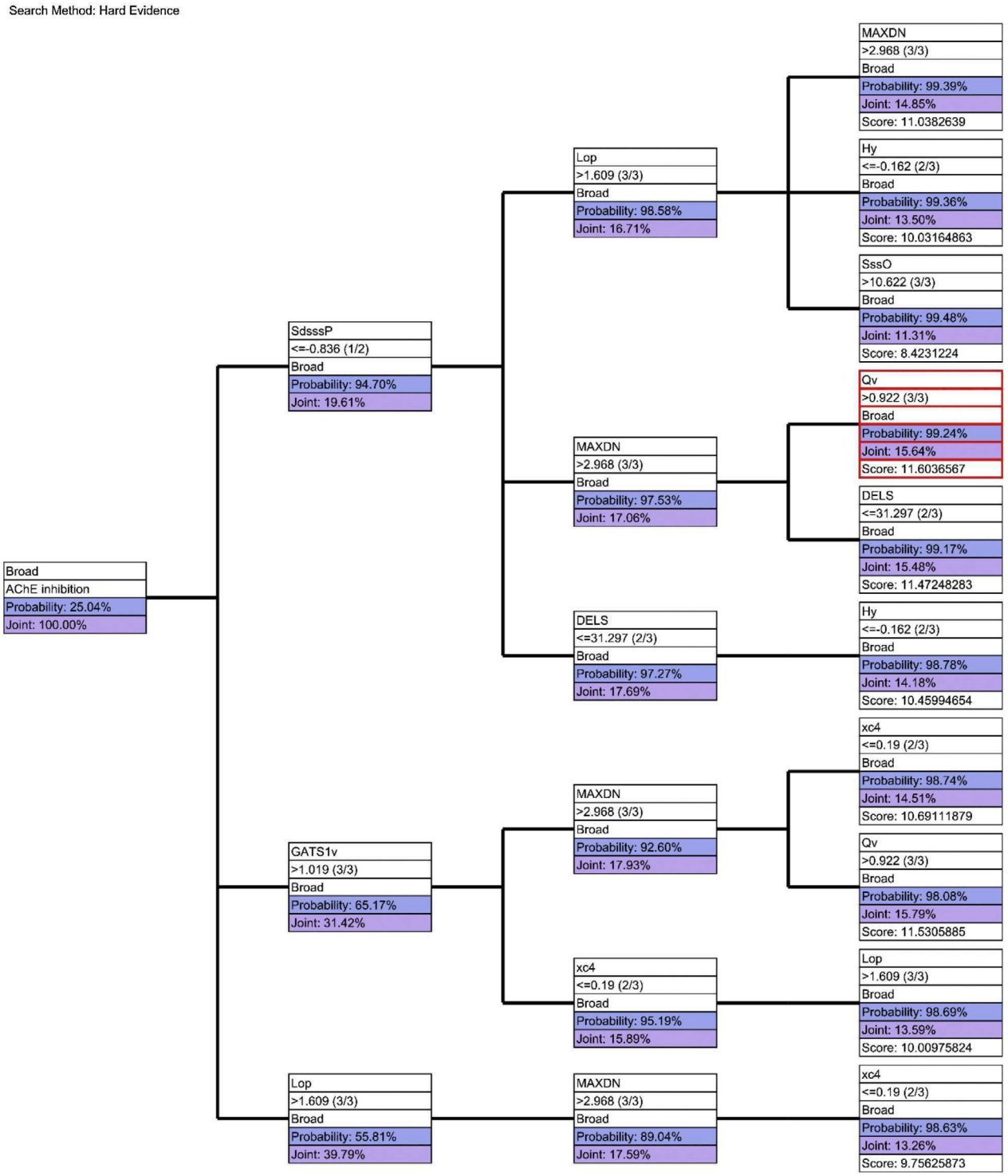

Fig. 4. Target optimization tree for acetylcholinesterase inhibition (AChEI) with the joint probability of the evidence taken into consideration. The rows on the leaves contain the score for the pathway built on the probability change from the prior probability of the mode of toxic action weighted by the final joint probability. The red highlighted descriptor (Qv) is the terminal node of the pathway with the highest score. (For interpretation of the references to colour in this figure legend, the reader is referred to the web version of this article.)

in the target optimization trees for AChEI duplicate the steps in the corresponding TDPs. The two nodes in the TDP that optimally led to a probability of AChEI that was greater than 0.99 probability were SdsssP and J when the joint probability was not considered. In the same target optimization tree, SdsssP only appeared in one pathway as the initial variable and J appeared in two pathways, as an initial and secondarily selected variable. When the joint probability was considered (Fig. 4), J was no longer in the target optimization tree but SdsssP was still selected early and raised the probability of AChEI the most in the first branching. The highest scoring pathway with the joint probability contained SdsssP, MAXDN, and Qv leading to a 0.99 probability of AChEI. The highest scoring pathway

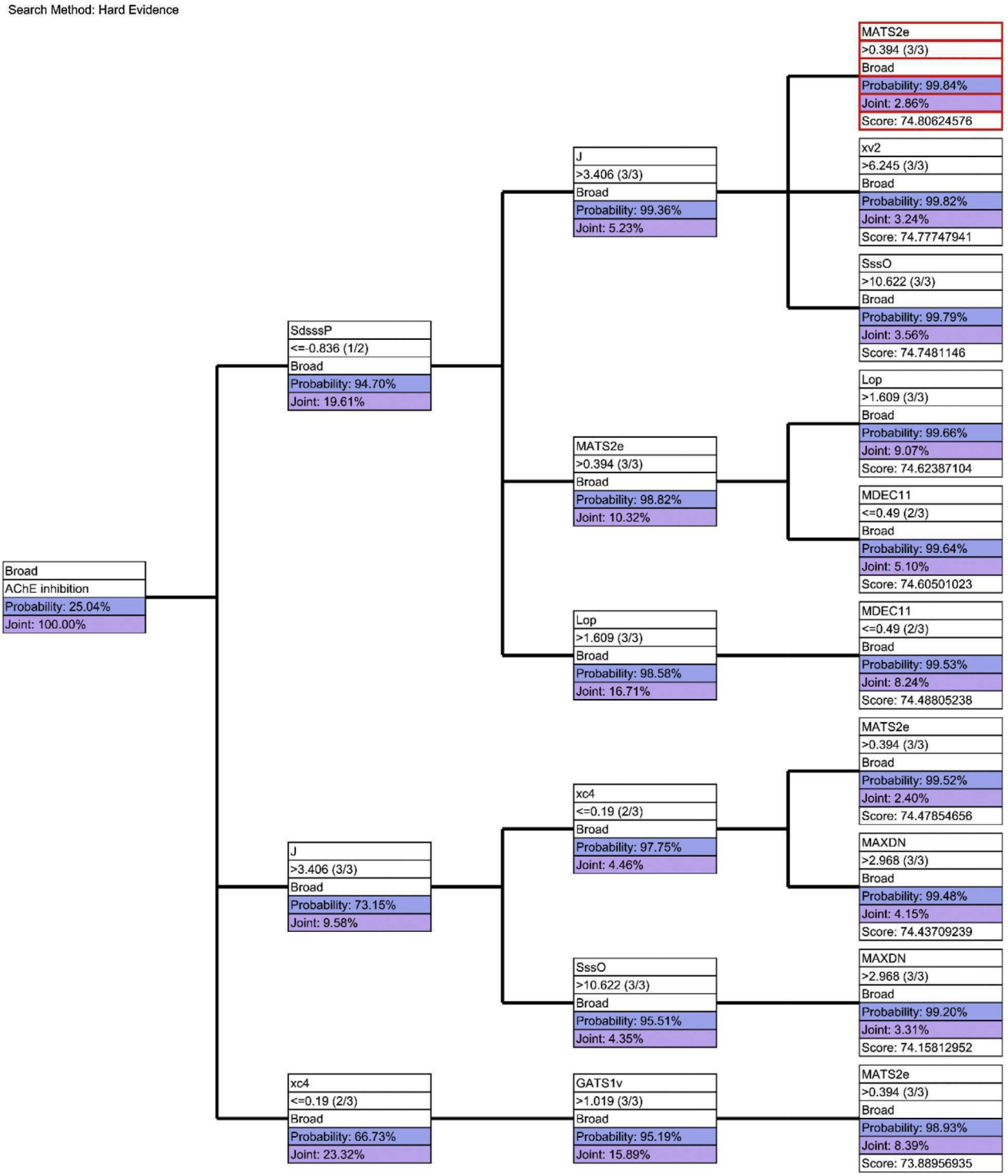

Fig. 5. Target optimization tree for acetylcholinesterase inhibition (AChEI) without taking into account the joint probability of the evidence. The rows on the leaves contain the score for the pathway built on the probability change from prior probabilities before findings on descriptors are entered. The red highlighted descriptor (MATS2e) is the terminal node state of the pathway with the highest score. (For interpretation of the references to colour in this figure legend, the reader is referred to the web version of this article.)

without consideration of the joint probability contained SdsssP, J, and MATS2e leading to a probability of 0.998 (near certainty) of AChEI.

Neurotoxicity had the second highest precision from cross validation and its target optimization trees are displayed in Figs. 6 and 7, with and without the joint probability of the evidence weighted in the pathways, respectively. Like AChEI, multiple scenarios with at most three predictors can lead to a probability equal to or greater than 0.99 for the neurotoxicity MoA. The lowest final probability was 0.98 in a few lineages with the joint probability of the evidence considered. An outcome on only one descriptor was necessary to reach a 0.99 probability of neutotoxicity (SsCl) in the target optimization tree that did not consider the joint probability. For the target optimization tree that did consider the joint

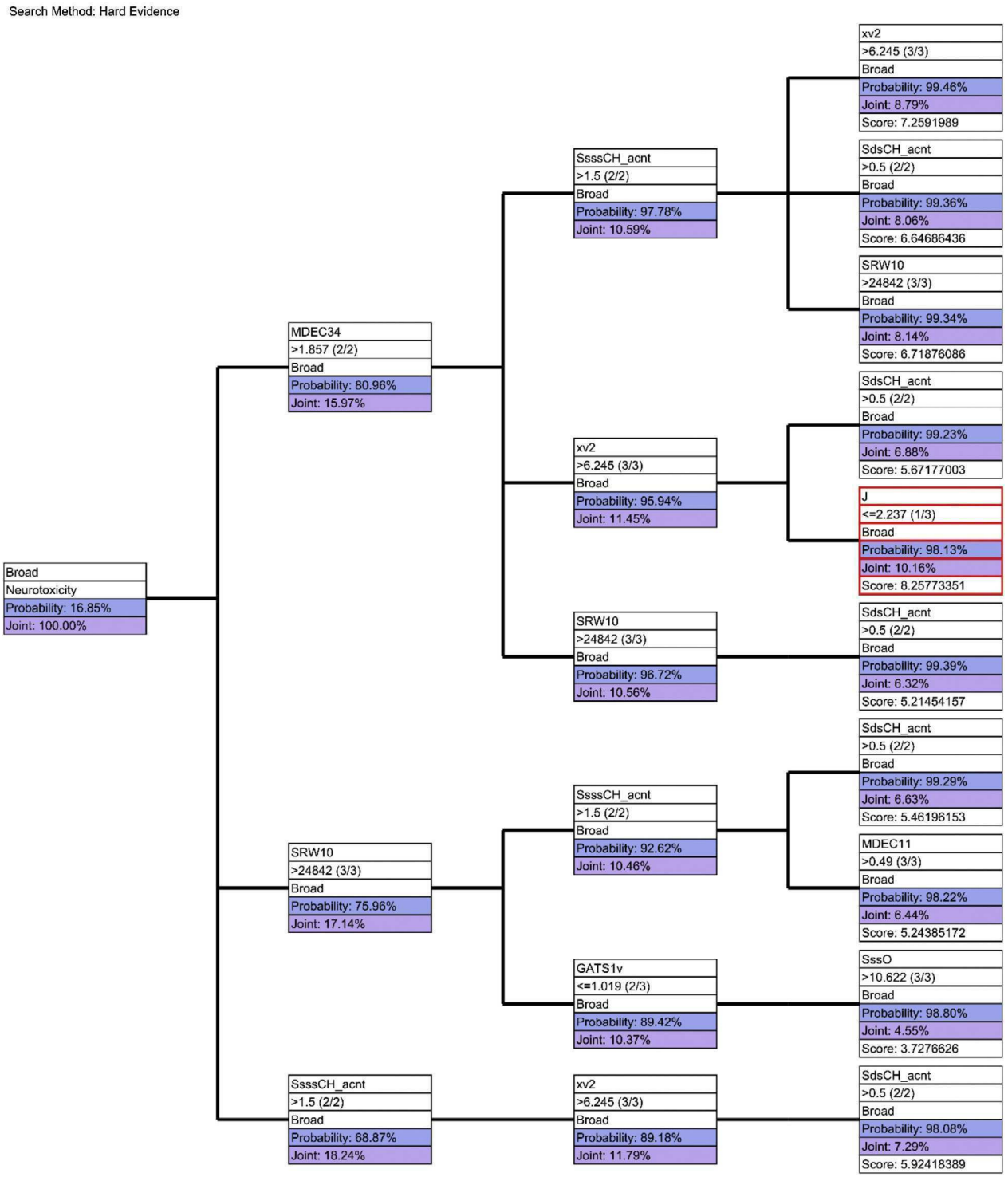

Fig. 6. Target optimization tree for neurotoxicity with the joint probability of the evidence taken into consideration. The rows on the leaves contain the score for the pathway built on the probability change weighted by the final joint probability. The red highlighted descriptor (J) is the terminal node state of the pathway with the highest score. (For interpretation of the references to colour in this figure legend, the reader is referred to the web version of this article.)

probability, SsCl was not selected at all. When the joint probability was considered, the 0.99 probability was still commonly reached but required several additional descriptors. The highest scoring pathway in the tree that considered the joint probability contained MDEC34, xv2, and J in the same order of priority. The highest scoring pathway in the tree that did not consider the joint probability contained SsCl, MDEC34, and SssO, duplicating the TDP. Both led to a probability of neurotoxicity greater than 0.98.

As can be seen, for AChEI and neurotoxicity several possible descriptor groupings can lead to a high probability of the MoA being true based on a few descriptors alone including the number of phosphate groups and chlorine atoms, respectively. Figs. 8 and 9 contain the target optimization trees for narcosis. By contrast, some scenarios contained final probabilities that were lower than AChEI and neurotoxicity target optimization tree pathways, especially when the joint probability of the evidence was considered in the tree

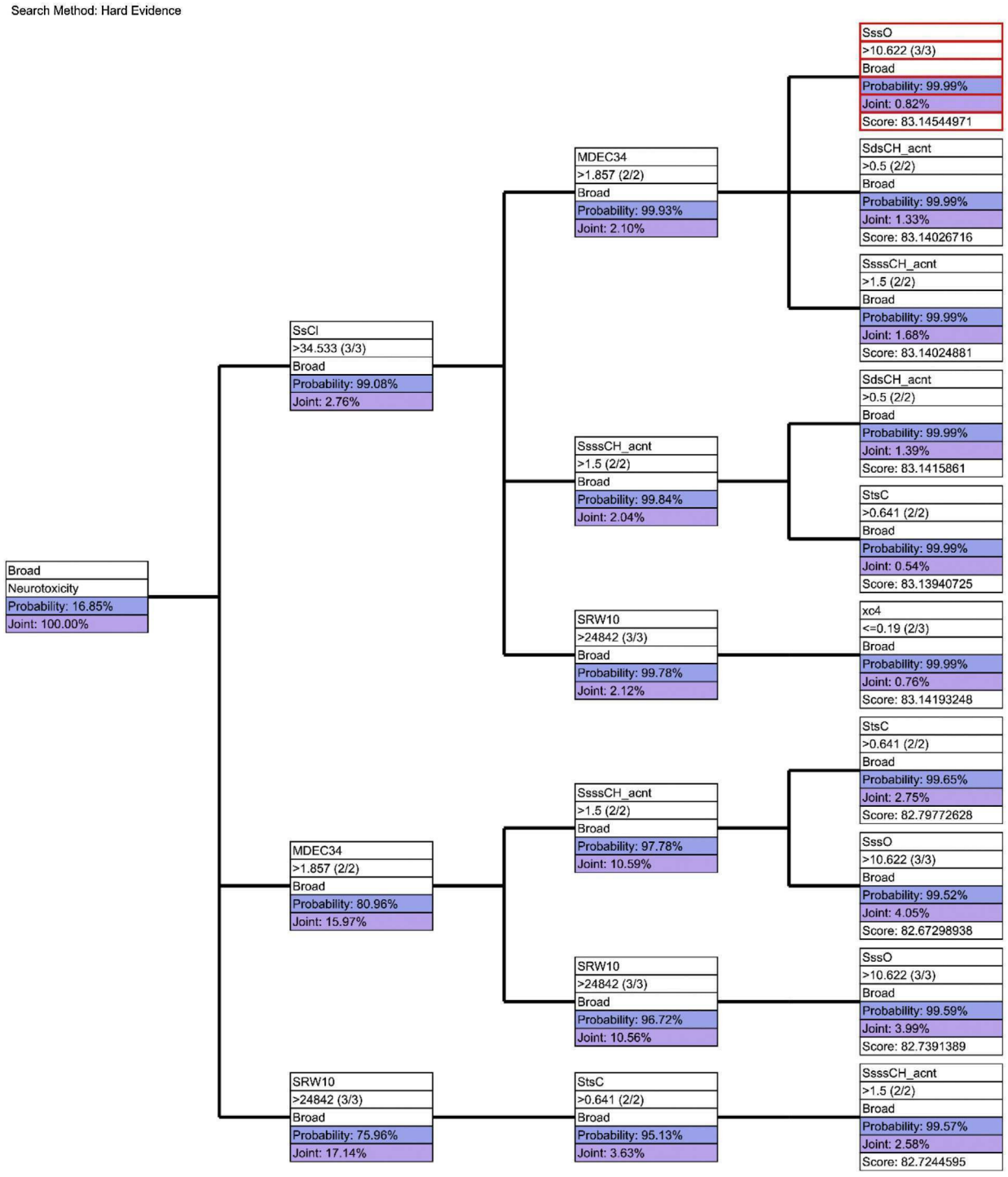

Fig. 7. Target optimization tree for neurotoxicity without taking into account the joint probability of the evidence. The rows on the leaves contain the score for the pathway built on the probability change. The red highlighted descriptor (SssssO) is the terminal node state of the pathway with the highest score. (For interpretation of the references to colour in this figure legend, the reader is referred to the web version of this article.)

development. From the TDP analysis above, it was also observed that narcosis took as many or more descriptors when compared to the corresponding TDPs of neurotoxicity and AChEI to raise the probability to near certainty (0.99 or above). The final probabilities range from 0.76 to 0.91 at the terminal evidence set for scenarios with consideration of the joint probability. Additional descriptors could raise these probabilities further but the trees were constrained for examining the capabilities of only a handful of descriptors in predicting the MoAs. Without consideration of the joint probability, probabilities of narcosis being true ranged from 0.93 to near certainty. The highest scoring pathway with the joint probability considered contained MAXDN, SdsCH_acnt, and Qv, duplicating the TDP. The highest scoring pathway without consideration of the joint probability contained MATS3e, SssO, and DELS, also duplicating the initial evidence set of the TDP. Narcosis and neurotoxicity both contained SssO in their highest scoring pathways without considering the joint probability. Narcosis and AChEI both contained MAXDN and Qv in their highest

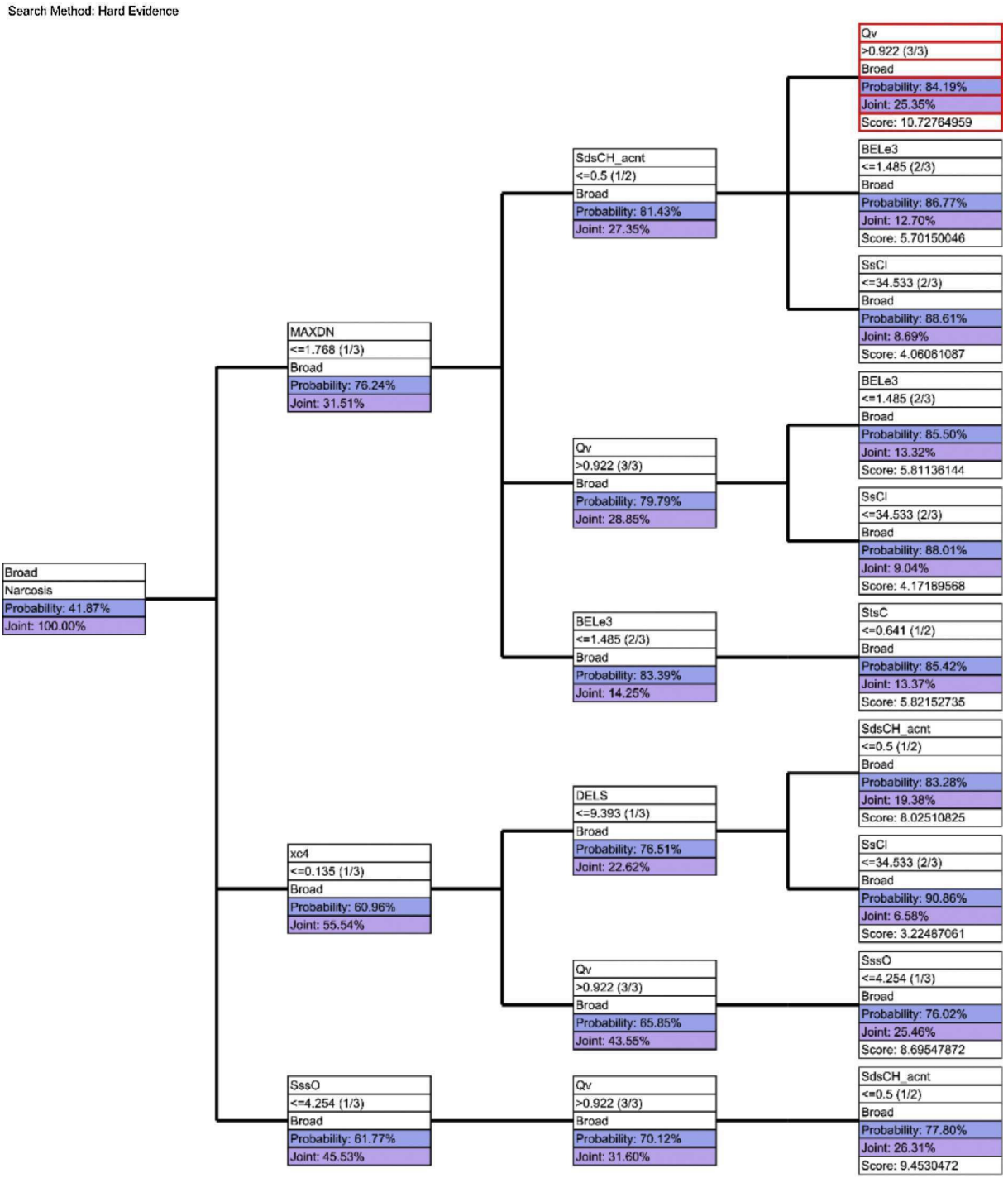

Fig. 8. Target optimization tree for narcosis with the joint probability of the evidence taken into consideration. The rows on the leaves contain the score for the pathway built on the probability change weighted by the final joint probability. The red highlighted box (Qv) is the terminal node state of the pathway with the highest score. (For interpretation of the references to colour in this figure legend, the reader is referred to the web version of this article.)

scoring pathways with the joint probability considered. Neurotoxicity and AChEI both contained J in highest scoring pathways. For neurotoxicity, J was in the pathway that considered the joint probability and for AchEI it was in the pathway without consideration of the joint probability. Additional target optimization trees for the other modes of action are found in the Supporting information.

4. Discussion

Compound classification methods offer the ability to associate structural features and chemical properties with specific types of biological activities and to screen for and predict biologically active compounds (Bajorath, 2001). Molecular similarity is the basis of these approaches, which typically requires the use of chemical descriptors that capture a broad range of molecular

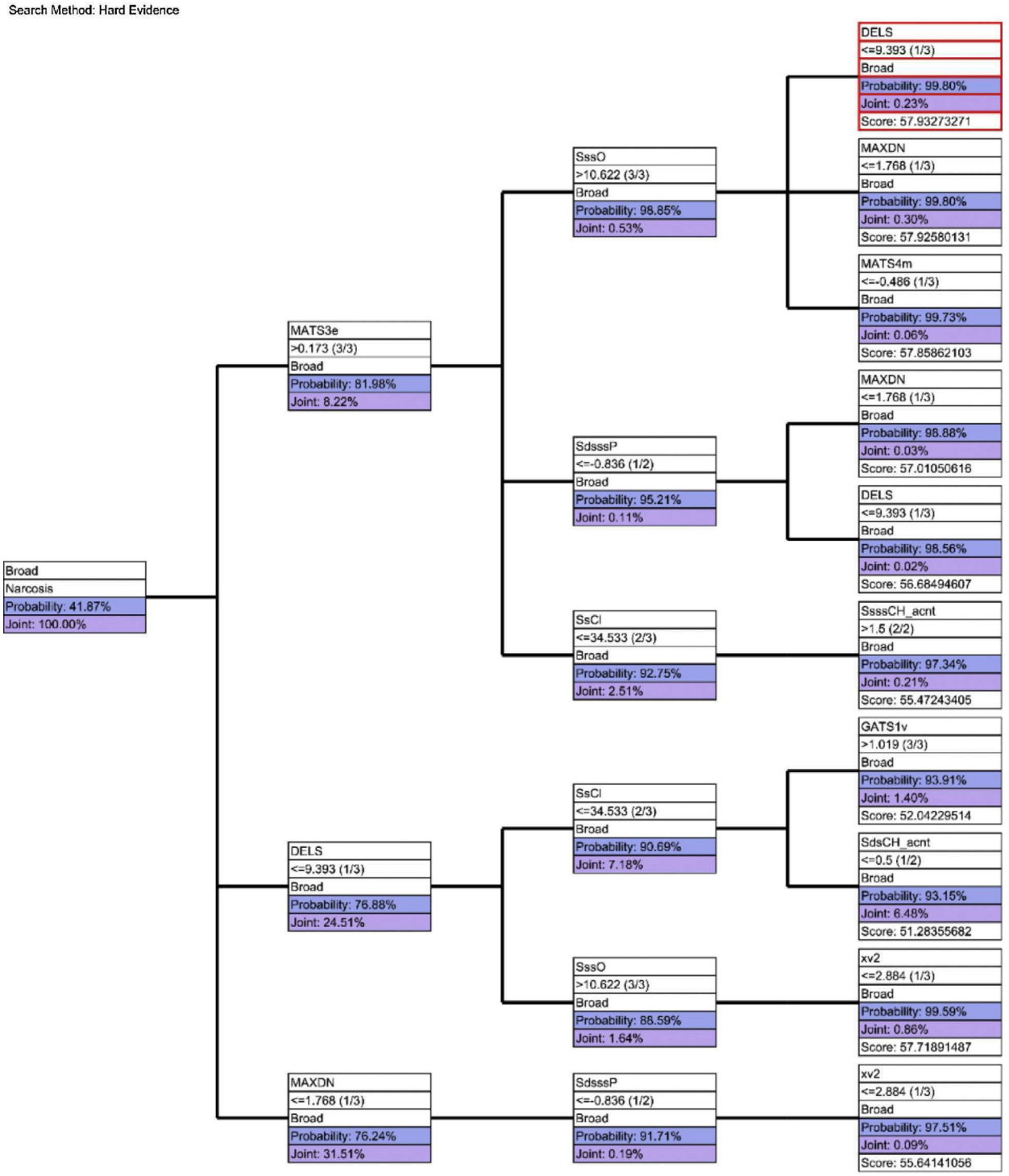

Fig. 9. Target optimization tree for narcosis without taking into account the joint probability of the evidence. The rows on the leaves contain the score for the pathway built on the probability change. The red highlighted box (DELS) is the terminal node state of the pathway with the highest score. (For interpretation of the references to colour in this figure legend, the reader is referred to the web version of this article.)

characteristics and definition of the theoretical chemical space of the model (Martin et al., 2002; Bajorath 2001). Hundreds of molecular descriptors are available in the literature that can be calculated using computational chemistry software such as Dragon which provides more than 1600 theoretical descriptors (e.g., Mauri et al., 2006). In the current study, a diversity of two dimensional chemical descriptors were calculated and assigned using the computational chemistry application TEST (USEPA, 2008, 2016), including E-state values and E-state counts, constitutional descriptors, topological descriptors, walk and path counts, connectivity, information content, two-dimensional autocorrelation, Burden eigenvalue, molecular property, Kappa, hydrogen bond acceptor/donor counts, molecular distance edge and molecular fragment counts (Martin et al., 2013, 2015). Previous studies have demonstrated high performance of two dimensional descriptors in both molecular similarity analysis and compound classification

(Bajorath, 2001), although they have seen only limited application in aquatic toxicology (e.g., Papa et al., 2005; Martin et al., 2013, 2015).

Interpretation of computational chemistry descriptors is typically challenging because they are based on hundreds of calculated attributes of a molecule that may have positive or negative values. For example, the electrotopological state index represents the electronic state of an atom as perturbed from electronic influence of other atoms in the molecule (Hall and Kier, 1995). The index reflects the contribution of a specific group of atoms (e.g., –CH3, =CH2-) and depends on the environment of that group of atoms within a specific molecule (Hall and Kier, 1995). As another example, Qv is a whole molecule polarity index that decreases in value as polarity increases (Votano et al., 2004). Of the over 700 descriptors assigned by the TEST computational chemistry application, only 24 were used to establish a Markov blanket around the MoA variable and 22 of these 24 were in a pathway prior to reaching or at the point of exceeding 0.99 probability of a MoA in the TDP analysis. The Markov blanket analysis used in the current network provided a method that reduced the inherent complexity of numerous chemical descriptor assignments by determining the most important predictors in terms of probabilistic dependence with the MoAs.

The Bayesian network had an overall prediction accuracy (model precision) of 80%, which is similar to the 86% accuracy (correct fraction) of the LDA model of Martin et al. (2015) using two dimensional theoretical chemical descriptors and the same MoA dataset of Barron et al. (2015). AChEI MoA had the highest prediction accuracy in both the network (93.5%) and LDA (98%), and reactivity the lowest (network: 48%; LDA: 33%). Prediction accuracy of chemicals with an MoA of neurotoxicity was highest in the network model (83%; LDA: 65%), whereas narcosis prediction accuracy was highest in LDA (98%) compared to the network (80%) (Martin et al., 2015). These results suggest that MoA prediction accuracy may be a function of the intrinsic uncertainty in the theoretical descriptors and MoA classification, rather than fundamental differences in the statistical modeling approach. As knowledge of MoA assignments and theoretical relationships between descriptors and MoAs advances, model performance and predictive capabilities should likewise improve.

For machine learned Bayesian networks, the minimum description length scores are useful for establishing the relationships among variables from the available data. With deterministic models, rules can be difficult to establish and interpret and complexity can overwhelm understanding of the model and the processes being represented. However, the nonparametric quantitative methods used in the current approach require larger amounts of data than might be found in some datasets. For the current model, MoAs with low numbers of data generally had relatively diminished predictive accuracy and data coverage for establishing conditional probabilities. In contrast, Martin et al. (2013, 2015) attributed poor predication accuracy of the reactivity MoA to a large range in reactivity mechanisms and general structural diversity. Within the current model, pathways constrained to a relatively small number of descriptors still led to high probabilities for each MoA despite varying data coverage.

Bayesian approaches can decompose complex multivariate problems into graphical networks that can be visualized and that support bidirectional inferences under various levels of uncertainty. The probabilistic focus inherent in a Bayesian network is also conducive to improvements in structuring and quantification as the knowledge and evidence improves over time. Coupling a Bayesian network with subjective interpretations of probability maintains focus on missing information and the imprecision from insufficient knowledge of true relationships. In the current study, the MOATox database of Barron et al. (2015) was taken as the best compendium of knowledge currently available regarding the acute aquatic toxicity MoA for a diversity of chemicals. The ability to predict unknown MoAs from existing data will become more precise as the knowledge base of MoA increases. Bayesian frameworks can provide useful pathways to improved predictive and diagnostic tools for aquatic toxicology and other problems with high dimensional data and multiple uncertain outcomes.

Acknowledgments

This research was supported in part by an appointment to the ORISE participant research program supported by an interagency agreement between the U.S. EPA and the U.S. Department of Energy. We thank Tom Stockton and Chris Grulke for review of a draft of the manuscript. The conclusions may not necessarily reflect the views of EPA and no official endorsement should be inferred.

Appendix A. Supplementary data

Supplementary data associated with this article can be found, in the online version, at http://dx.doi.org/10.1016/j.aquatox.2016.09.006.

References

Bajorath, J., 2001. Selected concepts and investigations in compound classification, molecular descriptor analysis, and virtual screening. J. Chem. Inf. Comput. Sci. 41, 233–245.
Barber, D., 2012. Bayesian Reasoning and Machine Learning. Cambridge University Press, Cambridge, UK.
Barron, M.G., Lilavois, C.R., Martin, T.M., 2015. A comprehensive mode of action and acute aquatic toxicity database for predictive model development. Aquat. Toxicol. 16, 102–107.
Bayesia S.A.S, 2015. Bayesialab Software Version 5.4.3 (Accessed 05/16/2016) http://www.bayesia.com/.
Bayesia, 2010. Bayesialab User Guide. Bayesia S.A.S., Laval Cedex, France.
Billoir, E., Delignette-Muller, M.L., Péry, A.R.R., Charles, S., 2008. A Bayesian approach to analyzing ecotoxicological data. Environ. Sci. Technol 42, 8978–8984.
Burden, F.R., Winkler, D.A., 2000. A quantitative structure-activity relationships model for the acute toxicity of substituted benzenes to *Tetrahymena pyriformis* using Bayesian-regularized neural networks. Chem. Res. Toxicol 13, 436–440.
Conrady, S., Jouffe, L., 2011. Microarray Analysis with Bayesian Networks: Using Bayesialab for Cancer Type Classification. Bayesia USA, Franklin, TN.
Conrady, S., Jouffe, L., 2015. Bayesian Networks and Bayesialab: A Practical Introduction for Researchers. Bayesia USA, Franklin, TN.
Enoch, S.J., Hewitt, M., Cronin, M.T.D., Azam, S., Madden, J.C., 2008. Classification of chemicals according to mechanism of aquatic toxicity: an evaluation of the implementation of the Verhaar scheme in Toxtree. Chemosphere 73, 243–248.
Hall, L.H., Kier, L.B., 1995. Electrotopological state indices for atom types: a novel combination of electronic, topological, and valence state information. J. Chem. Inf. Comput. Sci. 35, 1039–1045.
Harris, M., Bhuvaneshwar, K., Natarajan, T., Sheahan, L., Wang, D., Tadesse, M.G., Shoulson, I., Filice, R., Steadman, K., Pishvaian, M.J., Madhavan, S., Deeken, J., Pharmacogenomic characterization of gemcitabine response –a framework for data integration to enable personalized medicine. Pharmacogenetics and Genomics 24 (2): 81–93.
He, L., Jurs, P.C., 2005. Assessing the reliability of QSAR model's predictions. J. Mol. Graph. Model. 23, 503–523.
Iorio, F., Tagliaferri, R., di Bernardo, D., 2009. Identifying network of drug mode of action by gene expression profiling. J. Comput. Biol. 16, 241–251.
Korb, K.K., Nicholson, A.E., 2004. Bayesian Artificial Intelligence. Chapman & Hall/CRC, Boca Raton, FL.
Martin, Y.C., Kofron, J.L., Traphagen, L.M., 2002. Do structurally similar molecules have similar biological activitiy? J. Med. Chem. 45, 4350–4358.
Martin, T.M., Grulke, C.M., Young, D.M., Russom, C.L., Wang, N., Jackson, C.R., Barron, M.G., 2013. Prediction of aquatic toxicity mode of action using linear discriminant and random forest models. J. Chem. Info. Model. 53, 2229–2239.
Martin, T.M., Young, D.M., Lilavois, C.R., Barron, M.G., 2015. Comparison of global and mode of action-based models for aquatic toxicity. SAR QSAR Environ. Res. 26, 245–262.
Mauri, A., Consonni, V., Pavan, M., Todeschini, R., 2006. MATCH. Commun. Math. Comput. Chem. 56, 237–248.
Nendza, M., Muller, M., 2007. Discriminating toxicant classes by mode of action: 3: Substructure indicators. SAR QSAR Environ. Res. 18, 155–168.
Papa, E., Villa, F., Gramatica, P., 2005. Statistically validated QSARs, based on theoretical descriptors, for modeling aquatic toxicity of organic chemicals in *Pimephales promelas* (fathead minnow). J. Chem. Inf. Model. 45, 1256–1266.
Russom, C.L., Bradbury, S.P., Broderius, S.J., Hammermeister, D.E., Drummond, R.A., 1997. Predicting modes of toxic action from chemical structure: acute toxicity

in the fathead minnow (Pimephales promelas). Environ. Toxicol. Chem. 16, 948–967.
Stone, M., 1974. Cross-validatory choice and assessment of statistical predictions (with discussion). J. R. Stat. Soc. Ser. B (Methodol.) 36 (2), 111–147.
Thai, H., Campo, D.S., Lara, J., Dimitrova, Z., Ramachandran, S., Xia, G., Ganova-Raeva, L., Teo, C.-G., Lok, A., Khudyakov, Y., 2012. Convergence and coevoluation of Hepatitis B virus drug resistance. Nat. Commun. 3, 789.
USEPA, 2008. Molecular Descriptors Guide. Description of the Molecular Descriptors Appearing in the Toxicity Estimation Software Tool. V. 1.0.2. U.S. Environmental Protection Agency www.epa.gov/chemical-research/molecular-descriptors-guide.
USEPA, 2016. User's Guide for T.E.S.T. (version 4.2) (Toxicity Estimation Software Tool). A Program to Estimate Toxicity from Molecular Structure. EPA/600/R-16/058. U.S. Environmental Protection Agency, Cincinnati, OH (63 pp.) www.epa.gov/chemical-research/toxicity-estimation-software-tool-test.
Verhaar, H.J.M., van Leeuwen, C.J., Hermens, J.L.M., 1992. Classifying environmental pollutants part 1, Structure activity relationships for prediction of aquatic toxicity. Chemosphere 25, 471–491.
Votano, J.R., Parham, M., Hall, L.H., Kier, L.B., Oloff, S., Tropsha, A., Xie, Q., Tong, W., 2004. Three new consensus QSAR models for the prediction of Ames genotoxicity. Mutagenesis 19, 365–377.
Yao, X.J., Panaye, A., Doucet, J.P., Chen, H.F., Zhang, R.S., Fan, B.T., Liu, M.C., Hu, Z.D., 2005. Comparative classification study of toxicity mechanisms using support vector machines and radial basis function neural networks. Anal. Chim. Acta 535, 259–273.
Zhu, H., Martin, T.M., Ye, L., Sedykh, A., Young, D.M., Tropsha, A., 2009. Quantitative structure-activity relationship modeling of rat acute toxicity by oral exposure. Chem. Res. Toxicol. 22, 1913–1921.

This article was downloaded by: [US EPA Library]
On: 01 July 2015, At: 08:06
Publisher: Taylor & Francis
Informa Ltd Registered in England and Wales Registered Number: 1072954 Registered office: Mortimer House, 37-41 Mortimer Street, London W1T 3JH, UK

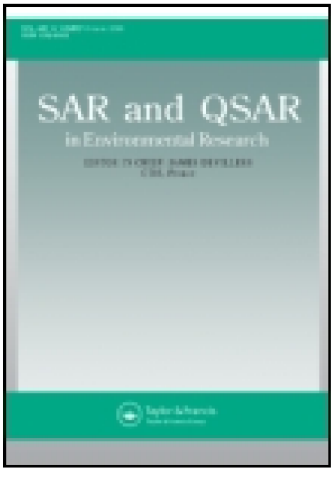

CrossMark
Click for updates

SAR and QSAR in Environmental Research

Publication details, including instructions for authors and subscription information:
http://www.tandfonline.com/loi/gsar20

Comparison of global and mode of action-based models for aquatic toxicity

T.M. Martin[a], D.M. Young[a], C.R. Lilavois[b] & M.G. Barron[b]

[a] National Risk Management Research Laboratory, US Environmental Protection Agency, Cincinnati, OH, USA

[b] National Health and Environmental Effects Research Laboratory, US Environmental Protection Agency, Gulf Breeze, Florida, USA

Published online: 18 Mar 2015.

To cite this article: T.M. Martin, D.M. Young, C.R. Lilavois & M.G. Barron (2015) Comparison of global and mode of action-based models for aquatic toxicity, SAR and QSAR in Environmental Research, 26:3, 245-262, DOI: 10.1080/1062936X.2015.1018939

To link to this article: http://dx.doi.org/10.1080/1062936X.2015.1018939

PLEASE SCROLL DOWN FOR ARTICLE

Taylor & Francis makes every effort to ensure the accuracy of all the information (the "Content") contained in the publications on our platform. However, Taylor & Francis, our agents, and our licensors make no representations or warranties whatsoever as to the accuracy, completeness, or suitability for any purpose of the Content. Any opinions and views expressed in this publication are the opinions and views of the authors, and are not the views of or endorsed by Taylor & Francis. The accuracy of the Content should not be relied upon and should be independently verified with primary sources of information. Taylor and Francis shall not be liable for any losses, actions, claims, proceedings, demands, costs, expenses, damages, and other liabilities whatsoever or howsoever caused arising directly or indirectly in connection with, in relation to or arising out of the use of the Content.

This article may be used for research, teaching, and private study purposes. Any substantial or systematic reproduction, redistribution, reselling, loan, sub-licensing, systematic supply, or distribution in any form to anyone is expressly forbidden. Terms &

Conditions of access and use can be found at http://www.tandfonline.com/page/terms-and-conditions

Downloaded by [US EPA Library] at 08:06 01 July 2015

SAR and QSAR in Environmental Research, 2015
Vol. 26, No. 3, 245–262, http://dx.doi.org/10.1080/1062936X.2015.1018939

Taylor & Francis
Taylor & Francis Group

Comparison of global and mode of action-based models for aquatic toxicity

T.M. Martin[a]*, D.M. Young[a], C.R. Lilavois[b] and M.G. Barron[b]

[a]*National Risk Management Research Laboratory, US Environmental Protection Agency, Cincinnati, OH, USA;* [b]*National Health and Environmental Effects Research Laboratory, US Environmental Protection Agency, Gulf Breeze, Florida, USA*

(*Received 21 November 2014; in final form 10 February 2015*)

Downloaded by [US EPA Library] at 08:06 01 July 2015

The ability to estimate aquatic toxicity is a critical need for ecological risk assessment and chemical regulation. The consensus in the literature is that mode of action (MOA) based toxicity models yield the most toxicologically meaningful and, theoretically, the most accurate results. In this study, a two-step prediction methodology was developed to estimate acute aquatic toxicity from molecular structure. In the first step, one-against-the-rest linear discriminant analysis (LDA) models were used to predict the MOA. The LDA models were able to predict the MOA with 85.8–88.8% accuracy for broad and specific MOAs, respectively. In the second step, a multiple linear regression (MLR) model corresponding to the predicted MOA was used to predict the acute aquatic toxicity value. The MOA-based approach was found to yield similar external prediction accuracy (r^2 = 0.529–0.632) to a single global MLR model (r^2 = 0.551–0.562) fit to the entire training set. Overall, the global hierarchical clustering approach yielded a higher combination of accuracy and prediction coverage (r^2 = 0.572, coverage = 99.3%) than the other approaches. Utilizing multiple two-dimensional chemical descriptors in MLR models yielded comparable results to using only the octanol–water partition coefficient (log K_{ow}).

Keywords: mode of action; quantitative structure–activity relationship (QSAR); linear discriminant analysis (LDA); multiple linear regression; aquatic toxicity; octanol–water partition coefficient

1. Introduction

There are three general approaches for developing quantitative structure–activity relationship (QSAR) models for diverse datasets that apply (1) global models using flexible machine learning techniques, (2) local models based on sets of clearly defined congeners (class based approach) and (3) local models based on a common mode of toxic action (MOA) [1]. Several previous studies have indicated the most toxicologically meaningful results can be obtained using a mode of action (MOA) based approach [2–6]. For example, Yuan et al. [7] reported that MOA-based local models yielded superior results to a global model for predicted acute toxicity to a standard fish test species, the fathead minnow (*Pimephales promelas*).

Global approaches to modelling aquatic toxicity include k nearest neighbours (kNN) [8,9] or nearest neighbours [10], support vector machines (SVM) [11], multilinear regression (MLR) [10,12–14], MLR using only structurally similar chemicals from the training set [15],

*Corresponding author. Email: martin.todd@epa.gov

This work was authored as part of the Contributors' official duties as Employees of the United States Government and is therefore a work of the United States Government. In accordance with 17 USC. 105, no copyright protection is available for such works under US Law.

group contribution methods [16,17], partial least squares [18,19], artificial neural networks (ANNs) [12,20], associative neural networks (ASNN) [21] and hierarchical clustering (HC) [10,22]. The advantage of global methods is that machine learning allows the development of model(s), which do not require the determination of chemical class or MOA. This makes it easier to develop models for diverse datasets. The disadvantage of global methods is that it is possible to overfit a dataset with too many non-biologically relevant chemical descriptors.

Previous QSAR research in aquatic toxicology has largely been focused on developing models for specific chemical classes (reviewed by Netzeva et al. [1]). Early QSAR studies used a single chemical property of hydrophobicity, usually modelled as the log of the octanol–water partition coefficient (log K_{ow}) to estimate toxicity for large classes of industrial chemicals of moderate polarity [23]. The Ecological Structure Activity Relationships (ECOSAR) program within the Estimation Program Interface (EPI) Suite [24] uses class-based models to calculate aquatic toxicity based on log K_{ow} for a variety of chemical groups including pesticides, dyes and reactive compounds, as well as traditional solvent-like chemicals.

An advantage of class based models is that structurally similar chemicals should be toxicologically similar. However, Russom et al. [25] illustrated that chemicals within the same chemical class can act through different MOAs. For example, hydroquinones emerge as an outlier from models for phenols [26], and chlorinated phenols exhibit polar narcosis and uncoupling of oxidative phosphorylation depending on the number of chlorines [25]. Disadvantages of class-based methods include: the uncertainty in precisely defining a chemical class; chemicals can possess functional groups for more than one chemical class; and sometimes insufficient data are available to develop a model for specific chemical classes.

Several researchers have developed MOA-based models to predict aquatic toxicity LC_{50} values [1,7,13,27]. Claeys et al. developed models for chronic aquatic toxicity for the nonpolar narcosis and polar narcosis MOAs using the octanol–water partition coefficient [27]. Many models are available, but the predictive power can be confounded by the need for 'a priori' selection of the appropriate MOA model [28]. Several researchers have developed methods to assign chemicals to particular aquatic toxicity modes of action [28–38]. A variety of techniques have been utilized including linear discriminant analysis (LDA) [28,29,37], binary logistic regression [30], Adaboost [31], decision tree models [33], counter propagation neural networks and multinomial logistic regression [39], and support vector machines [34,36].

In a previous paper [38], we developed a 'one-against-the-rest' LDA approach to predict aquatic toxicity MOA. Separate discriminant models were developed for each results category and the predicted category yielded the highest score from all the different models. In the current study, fathead minnow acute toxicity is predicted using a two-step process. In the first step, LDA models are used to predict MOA and then acute toxicity is predicted using the multilinear regression model corresponding to each chemical's predicted MOA. This approach is similar to that utilized by ASTER (ASessment Tools for the Evaluation of Risk) to estimate aquatic toxicity, except that ASTER utilizes a fragment-based MOA assignment approach and log K_{ow} based linear regression toxicity models [25,40]. Here we compare the MOA-based model results with global methods including hierarchical clustering and a single MLR model fit to the entire training set. Additionally we investigate whether MOA-based MLR models fit to multiple two-dimensional (2D) descriptors yield better results than models fitted only to log K_{ow}.

In this study there are two datasets (one with 1015 chemicals, one with 793 chemicals). The first is used to develop models to predict the toxicity MOA. The training set is ~80% and the prediction set is ~20% of this dataset. The second dataset is used to develop models to predict quantitative fathead minnow toxicity. A total of 372 chemicals in the second dataset

Downloaded by [US EPA Library] at 08:06 01 July 2015

have LC_{50} values as well as MOA values (thus they are also present in the first dataset). These chemicals are used for the training set. The chemicals in the second dataset with unknown MOA are used as the prediction set for predicting the LC_{50} value. The chemicals in this set represent a true external set in that none of the chemicals are present in the training set for the MOA or LC_{50} models.

2. Materials and methods

2.1 *MOA dataset*

A dataset of 1015 chemicals was developed for 11 MOAs based on their mode of acute toxic action in fish (Table 1). This dataset represents a slight expansion of the database used in a previous study to include additional specific MOAs [38]. Neurotoxicity categories were expanded from two specific MOAs (organochlorine and pyrethroid) to seven [pyrethroid sodium channel modulation, alicyclic γ-aminobutyric acid (GABA) antagonism, diphenyl sodium channel modulation, GABA agonism, pyrazole GABA antagonism, sodium channel

Downloaded by [US EPA Library] at 08:06 01 July 2015

Table 1. Summary of the mode of action (MOA) dataset used in developing MOA-based QSAR models.

MOA	*MOA subcategory*	*Characteristics*	*Count*
AChE inhibition	Carbamate	Carbamate moiety	69
	Organo-phosphate	Pphosphate or thiophosphate moiety	199
Narcosis	Ester	Diverse structures, mono or diesters	44
	Nonpolar	Diverse structures, not ionizable	299
	Polar	Phenols, anilines, pyridines; single nitro or <4 halogens	59
Neurotoxicity	Pyrethroid sodium channel modulation	Pyrethroid analogs	65
	Alicyclic GABA antagonism	Aliphatic and cyclic	26
	Diphenyl sodium channel modulation	Diphenyl	11
	GABA agonism	Macrocyclic lactones	13
	Other	Diverse structures	6
	Pyrazole GABA antagonism	Pyrazole	6
	Sodium channel blocking	Urea with trifluoro group	2
Reactivity	*NA*	Electrophiles, proelectrophiles	91
Uncoupling Oxidative Phosphorylation	*NA*	>1 nitro or >3 halogenated phenols, anilines, pyridines	48
Not AChE Inhibition	Carbamate	Carbamate moiety	40
	Organophosphate	Phosphate or thiophosphate moeity	9
Anticoagulation	Vitamin K antagonism	Coumarins	17
nAChR agonism	*NA*	Nicotine or neconicotinoids	8
nAChR antagonism	*NA*	Piperidine with alkyl chain	1
Methaeglobinaemia	*NA*	Benzene ring with amino and ketone substituents	1
Oxidative phosphorylation inhibition	*NA*	Pyridine with urea and nitrobenzene	1
Total			1015

NA: not applicable.

blocking, and other]. However, the number of chemicals with the broad neurotoxicity MOA only increased from 124 to 129 chemicals. This refinement provided greater structural similarity within each specific MOA as well as consistency with international pesticide MOA classification [41]. The number of chemicals with the acetylcholinesterase (AChE) inhibition broad MOA was increased from 199 to 268.

The dataset was developed using a combination of high confidence assignments, including biological responses in fish acute toxicity assays [25], international consensus classifications such as the Insecticide Resistance Action Committee's (IRAC) MOA classification tool [41], ASTER [40] predictions, and weight of evidence professional judgment based on assessment of structure and literature information (see Table S1 in the supplemental material which is available via the multimedia link on the online article webpage). The molecular structures for the chemicals in the overall dataset were obtained using the procedure detailed by Young and colleagues [10].

One of 11 broad MOAs was assigned to each chemical: AChE inhibition; narcosis; neurotoxicity; reactivity; uncoupling oxidative phosphorylation; anticoagulation; nicotinic acetylcholine receptor (nACHR) agonism; nACHR antagonism; methemoglobinemia; and oxidative phosphorylation inhibition (see Table 1). The first column in Table 1 indicates 'broad' MOAs, while the first and second columns taken together indicate 'specific' MOAs. Models were developed for both broad and specific MOAs. The MOA dataset were randomly subdivided into training (~80% of chemicals, 802 chemicals) and validation set (~20%, 213 chemicals) within each MOA and MOA subcategory (see Table S1 in the supplemental material which is available via the multimedia link on the online article webpage). This 802 chemical training set was used to build LDA models to predict MOA.

Downloaded by [US EPA Library] at 08:06 01 July 2015

2.2 *Fathead minnow LC_{50} data set*

The fathead minnow LC_{50} endpoint represents the concentration in freshwater which kills half of the test fish in 96 hours. The dataset for this endpoint was obtained from the ECOTOX aquatic toxicity database (http://cfpub.epa.gov/ecotox/). Compounds were restricted to the following elements: C, H, O, N, F, Cl, Br, I, S, P, Si and As. In addition, compounds must represent a single pure component (salts, undefined isomeric mixtures, polymers or mixtures were removed). For chemicals with multiple LC_{50} values in ECOTOX, the geometric median value was used. Chemicals with known MOA (372 chemicals) were placed in the training set and chemicals with unknown MOA (421 chemicals) were placed in the prediction set. This was done so that chemicals in the prediction set will have an external prediction of the MOA and then the toxicity value. The 372 chemical training set was used to build multiple models (one for each MOA) to predict the quantitative LC_{50} value. The chemicals in the LC_{50} training set are also present in the 1015 MOA dataset.

2.3 *Prediction methodology*

Fathead minnow acute toxicity values were predicted using a two-step process. In the first step, one-against-the-rest LDA models were used to predict each chemical's broad or specific MOA. In the second step, the LC_{50} value was predicted using the multilinear regression model corresponding to the predicted MOA. Several MOAs had an insufficient number of chemicals with an available LC_{50} values to include in QSAR toxicity estimation. These included anticoagulation, nAChR agonism and antagonism, diphenyl sodium channel modulation, and GABA agonism.

The methodology for estimating MOA using LDA is described in a previous publication [38] and is described briefly below. An LDA model is essentially a multilinear regression model [30]:

$$Score = \sum_{i=1}^{n} a_i x_i + a_0 \quad (1)$$

where a_i is the fitted constant for parameter i, x_i is the ith molecular descriptor, and a_0 is the model intercept. Chemicals with a given MOA are assigned a score of 1. Chemicals that do not have the given MOA are assigned a score of 0. For example, when building a model for the AChE inhibition-organophosphate MOA, famphur (*O*-(4-((dimethylamino)sulphonyl)phenyl) *O*,*O*-dimethyl thiophosphate) would be assigned a score of 1 while ethanol would be assigned a score of 0 (since it has the narcosis-nonpolar MOA).

Descriptors are selected (and regression constants fitted) using a genetic algorithm based approach so the model can match the experimental values for the training set. A pool of 790 descriptors was obtained from the US Environmental Protection Agency (US EPA) chemical descriptor and toxicity estimation tool, T.E.S.T. [40]. The descriptor classes included E-state values and E-state counts, constitutional descriptors, topological descriptors, walk and path counts, connectivity, information content, two-dimensional autocorrelation, Burden eigenvalue, molecular property (such as the octanol–water partition coefficient), Kappa, hydrogen bond acceptor/donor counts, molecular distance edge and molecular fragment counts [40].

LDA models were built for each MOA that contained at least five chemicals, consistent with a minimum recommended ratio of 5:1 [42]. However, using a minimum ratio of 67 chemicals per descriptor (about 11 descriptors per model) yielded the best results based on re-substitution sensitivity, which was the fraction of positive chemicals correlated accurately to the number of positive chemicals in the training set. The MOA for new chemicals was determined by first calculating the score for all the LDA models, then selecting the predicted MOA with the highest score. MOA assignments were only included where the maximum predicted score was ≥0.5.

The training set included several carbamate and organophosphate chemicals that were structurally similar to AChE inhibitors, but were known not to have an AChE inhibition MOA. These chemicals were assigned a score of zero when building LDA models for AChE inhibition to facilitate the development of models that could distinguish between potent and non-potent AChE inhibitors. Chemicals with a non-AChE inhibition MOA were not used when building LDA models for other MOAs. These chemicals were added so that no all carbamates and organophosphates would be predicted to be AChE inhibitors.

Before any QSAR model can be used to make a prediction for a test chemical, it must be determined whether the test chemical falls within the domain of applicability (or AD) for the model. The first constraint, the model ellipsoid constraint, checks if the test chemical is within the multidimensional ellipsoid defined by the ranges of descriptor values for the chemicals in the training set (for the descriptors appearing in the model). The model ellipsoid constraint is satisfied if the leverage of the test compound (h_{00}) is less than the maximum leverage value for all the compounds used in the model [43]. The second constraint, the R_{max} constraint, checks if the distance from the test chemical to the centroid of the training set is less than the maximum distance for any chemical in the training set to the its centroid. The fragment constraint [10] was not applied in this study since it was not found to improve prediction concordance [38]. Finally, the maximum score from all the LDA models must exceed 0.5 as mentioned above.

Downloaded by [US EPA Library] at 08:06 01 July 2015

LC_{50} values were predicted using a multilinear regression model for toxicity:

$$Tox = \sum b_i x_i + b_0 \quad (2)$$

where b_i is the fitted constant for parameter i, x_i is the ith molecular descriptor, and b_0 is the model intercept. The descriptors were selected using a genetic algorithm approach as outlined previously [10]. The minimum ratio of chemicals to descriptors was set at 5:1 for QSAR modelling. An LC_{50} model was developed for all the MOAs that had at least five chemicals in the LC_{50} training set. The model ellipsoid and R_{max} constraints described above were used to define the applicability domain of the LC_{50} models. In addition to the 2D descriptors from T.E.S.T. described above, single descriptor models were developed using log K_{ow}. The log K_{ow} was taken from EPISUITE [24], denoted from here on as ELOGP. If an experimental value is available, that value was used. If an experimental value was not available, the calculated value from EPISUITE was used.

Downloaded by [US EPA Library] at 08:06 01 July 2015

3. Results and discussion

3.1 *Results*

3.1.1 *Internal model statistics for LDA models*

All the LDA models had high correlations in terms of concordance (fraction of chemicals predicted correctly) and specificity (fraction of negative chemicals predicted correctly) (see Table 2). However, for several of the specific MOAs (narcosis-ester, narcosis-polar, neurotoxicity-diphenyl sodium channel modulation, and reactivity), we were unable to achieve high sensitivity (fraction of positive chemicals predicted correctly) values. Greatly increasing the number of descriptors did not yield models with good sensitivity (i.e. ≥0.5). The reactivity MOA contained a variety of structural classes and thus different reactive mechanisms, which may explain why it was difficult to consistently identify the MOA of reactive compounds. In future research, we may divide the reactivity MOA into several specific MOAs such as acylation, isocyanate reactivity, nucleophilic substitution, alkylation/arylation and sulfhydryl reactivity. The correlation for narcosis-polar may have achieved low sensitivity due to ambiguity about the structural differences between chemicals in the narcosis-polar and narcosis-nonpolar categories. For example, it has been demonstrated that *ortho* substitutions on a pyridine can shift the MOA from narcosis-polar (e.g. pyridine) to narcosis-nonpolar narcosis (e.g. 2-ethylpyridine), presumably due to steric hindrance [25].

3.1.2 *Results for MOA prediction set*

The overall prediction accuracy for the different QSAR techniques was excellent, with concordance of 88.8 and 85.8% for the specific and broad MOAs, respectively (Table 3). These results were comparable with those obtained in our previous publication using a slightly different MOA dataset [38]. The specific MOAs achieved a higher accuracy, but at the sacrifice of a lower prediction coverage (fraction of chemicals which can be predicted): 73.3% of chemicals for specific MOAs compared with 94.5% for broad MOAs.

The prediction accuracies for each MOA were highly correlated with the training set sensitivities. For example the AChE inhibition–carbamate chemicals were predicted with perfect accuracy (the training set sensitivity was 100%), while the reactive chemicals were predicted with 46.2% accuracy (the training set sensitivity was 47.2%). This similarity is not unexpected since the overall dataset was divided into training and prediction sets randomly

Table 2. Modelling statistics for the training dataset used in developing MOA-based models using LDA.

Broad MOA	*Concordance**	*Sensitivity†*	*Specificity‡*
AChE inhibition	0.970	0.995	0.961
Anticoagulation	0.999	0.923	1.000
nAChR agonism	0.997	0.833	0.999
Narcosis	0.890	0.938	0.855
Neurotoxicity	0.969	0.768	0.998
Reactivity	0.942	0.472	0.991
Uncoupler	0.982	0.658	0.999
Specific MOA			
AChE inhibition-carbamate	0.986	1.000	0.985
AChE inhibition-organophosphate	0.991	0.994	0.991
Anticoagulation-vitamin K antagonism	0.999	0.923	1.000
nAChR agonism	0.997	0.833	0.999
Narcosis-ester	0.969	0.371	0.997
Narcosis-nonpolar	0.815	0.636	0.897
Narcosis-polar	0.961	0.383	0.999
Neurotoxicity-alicyclic GABA antagonism	0.995	0.800	1.000
Neurotoxicity-diphenyl sodium channel modulation	0.990	0.000	1.000
Neurotoxicity-GABA agonism	1.000	1.000	1.000
Neurotoxicity-pyrethroid sodium channel modulation	0.982	0.827	0.993
Reactivity	0.942	0.472	0.991
Uncoupling oxidative phosphorylation	0.982	0.658	0.999

*Concordance is the fraction of chemicals predicted correctly.
†Sensitivity is the fraction of positive chemicals predicted correctly.
‡Specificity is the fraction of negative chemicals predicted correctly.

Downloaded by [US EPA Library] at 08:06 01 July 2015

with equal distributions of each mode of action. Several of the specific MOAs had 0% accuracy (neurotoxicity-other, neurotoxicity-pyrazole GABA antagonism, neurotoxicity-sodium channel blocking, and oxidative phosphorylation inhibition) due to the fact there was insufficient chemicals in the MOA training set to build an LDA model. Chemicals falling under these MOAs were not used to calculate the overall accuracy (Table 3). About 60% of the non-AChE inhibitors were still predicted to be AChE inhibitors, indicating the LDA models still predominately predict chemicals with carbamate or organophosphate substructures to be AChE inhibitors.

3.1.3 *LDA model descriptors*

The LDA models for each MOA are given in the supplemental material (Tables S2 and S3) which is available via the multimedia link on the online article webpage. The most common descriptors selected include molecular fragment counts [40], autocorrelation [44], E-state [45] and constitutional [46]. The definitions for the descriptors appearing in the LDA models are given in the T.E.S.T. user's guide [40]. The molecular fragment count descriptors are given by Martin et al. [10]. Some of the fragments were initially developed so they captured specific modes of action as detailed by Russom et al. [25].

Table 3. Summary results for the MOA prediction set for specific and broad MOA categories.

	Exp. count	*Correct fraction*	*Predict fraction*	*Training set sensitivity*
Specific MOA				
AChE inhibition-carbamate	14	1.000	0.929	1.000
AChE inhibition-organophosphate	40	1.000	1.000	0.994
Anticoagulation-vitamin K antagonism	4	1.000	1.000	0.923
Narcosis-ester	9	0.333	0.333	0.371
Narcosis-nonpolar	60	0.919	0.617	0.636
Narcosis-polar	12	0.667	0.500	0.383
Neurotoxicity-alicyclic GABA antagonism	6	0.800	0.833	0.800
Neurotoxicity-diphenyl sodium channel modulation	3	N/A	0.000	0.000
Neurotoxicity-GABA agonism	3	1.000	0.667	1.000
Neurotoxicity-pyrethroid sodium channel modulation	13	1.000	0.846	0.827
Reactivity	19	0.462	0.684	0.472
Uncoupler	10	0.875	0.800	0.658
nAChR agonism	2	1.000	0.500	0.833
Neurotoxicity-other	2	0.000	1.000	N/A*
Neurotoxicity-pyrazole GABA antagonism	2	0.000	0.500	N/A
Neurotoxicity-sodium channel blocking	1	0.000	1.000	N/A
Oxidative phosphorylation inhibition	1	0.000	1.000	N/A
Non-AChE inhibition-carbamate	8	0.500	0.500	N/A
Non-AChE inhibition-organophosphate	2	0.000	1.000	N/A
Overall**	195	0.888	0.733	N/A
Broad MOA				
AChE inhibition	54	0.981	1.000	0.995
Anticoagulation	4	0.750	1.000	0.923
Narcosis	81	0.975	0.975	0.938
Neurotoxicity	30	0.654	0.867	0.768
Reactivity	19	0.333	0.789	0.472
Uncoupler	11	0.700	0.909	0.658
nAChR agonism	2	0.500	1.000	0.833
Non-AChE inhibition	10	0.4	1	N/A
Overall*	201	0.858	0.945	N/A

*LDA model is not available for this MOA.
**Omitting MOAs without an explicit LDA model.

One benefit of LDA models is they are inherently interpretable. It was found the fragment counts selected in the LDA models are similar to those in the scheme proposed by Verhaar et al. [47] or the US EPA's ASTER [40]. For example, the model for AChE inhibition–organophosphate included the count of oxygens attached to two phosphorus atoms and the count of OH fragments attached to phosphorus.

3.1.4 *Internal model statistics for LC_{50} models*

In general, the LC_{50} MLR models based on 2D descriptors had acceptable statistics (r^2 and $q^2 > 0.5$) (Table 4). q^2 is the one leave-one-out cross-validated r^2. AChE inhibition–carbamate

Downloaded by [US EPA Library] at 08:06 01 July 2015

Table 4. LC_{50} Statistics for the fathead minnow acute toxicity training set.

	2D descriptors*				Only ELOGP		
	Number of descriptors	q^2	r^2	MAE	q^2	r^2	MAE
Broad MOA							
AChE inhibition	7	0.780	0.853	0.263	0.417	0.476	0.573
Narcosis	32	0.917	0.946	0.249	0.845	0.849	0.411
Neurotoxicity	4	0.829	0.902	0.380	0.642	0.701	0.668
Reactivity	8	0.636	0.713	0.460	0.350	0.391	0.737
Uncoupler	4	0.891	0.930	0.178	0.687	0.742	0.387
Specific MOA							
AChE inhibition–carbamate	1	−1.599	0.237	0.338	−0.920	0.002	0.390
AChE inhibition–organophosphate	5	0.662	0.767	0.363	0.439	0.515	0.559
Narcosis–ester	3	0.897	0.941	0.172	0.816	0.868	0.288
Narcosis–nonpolar	30	0.971	0.982	0.150	0.872	0.877	0.372
Narcosis–polar	9	0.914	0.944	0.221	0.874	0.889	0.299
Neurotoxicity–alicyclic GABA antagonism	1	0.635	0.717	0.566	−0.768	0.157	1.091
Neurotoxicity–pyrethroid sodium channel modulation	1	0.930	0.955	0.122	−3.720	0.360	0.482
Reactivity	8	0.636	0.713	0.460	0.350	0.391	0.737
Uncoupler	4	0.891	0.930	0.178	0.687	0.742	0.387

*q^2 is the leave one out correlation coefficient, r^2 is the coefficient of determination, and MAE is the mean absolute error.

Downloaded by [US EPA Library] at 08:06 01 July 2015

was the only MOA with poor internal statistics ($q^2 = -1.599$ and $r^2 = 0.237$). A likely explanation for this is there were few chemicals that had both this MOA and an experimental toxicity value, allowing for only one descriptor to be utilized maintaining a minimum ratio of five chemicals per descriptor. In all cases, the utilization of multiple 2D descriptors yielded better internal statistics than using only ELOGP. This result is not surprising since using additional descriptors can allow a model to fit idiosyncrasies in a dataset. However, in several cases (AChE inhibition–carbamate, neurotoxicity–alicyclic GABA antagonism and neurotoxicity–pyrethroid sodium channel modulation), a single two dimensional T.E.S.T. descriptor was able to correlate the training set data better than ELOGP. For these MOAs, IC (information content), XLOGP2 (square of the XLOGP octanol–water partition coefficient) and IE-ADJMM (mean information content on the edge adjacency magnitude) were selected, respectively. Two out of the three MOAs are described by information content descriptors (which are a measure of molecular symmetry). Neurotoxicity–alicyclic GABA antagonism is still a function of the octanol–water partition coefficient.

3.1.5 *Results for LC_{50} prediction set*

Analysis of the external LC_{50} prediction set results showed MOA-based models had similar or lower prediction accuracy compared with global models (Table 5). The specific MOA LDA models were able to achieve a higher prediction accuracy (in terms of r^2) than the broad MOA LDA models, but at the sacrifice of a lower prediction coverage. The global hierarchical clustering method (runs #5 and 6) yielded superior results to the MOA-based methods (runs #1–4) based on both prediction accuracy and coverage (Table 5). The hierarchical

Table 5. Summary statistics for the acute toxicity prediction set.

#	*MOA type*	*Method*	*Descriptor set*	r^2	*Coverage*
1	broad	LDA	all 2D	0.529	84.8
2	specific	LDA	all 2D	0.632	49.3
3	broad	LDA	ELOGP	0.579	87.3
4	specific	LDA	ELOGP	0.630	57.3
5	global	hierarchical clustering	all 2D	0.572	99.3
6	global	hierarchical clustering	ALOGP	0.568	90.2
7	global	Single model	all 2D	0.551	91.4
8	global	Single model	ALOGP	0.562	90.2

clustering method yielded 99.3% coverage, which can be explained by the fact that it makes predictions using several different models. If one compares the hierarchical clustering method (run #5) with the broad LDA method (run #1) for the predictions in common, the results do not change (r^2 = 0.579 for run#5 vs. r^2 = 0.528 for run #1). A single global MLR model achieved slightly higher prediction accuracy and coverage than the MOA-based approach (comparing runs #1 and #7). If one compares the predictions in common, the prediction accuracy is identical (r^2 = 0.528).

Analysis of the external LC_{50} prediction set results showed that QSAR models based on multiple 2D descriptors had similar results to those based solely on ELOGP (Table 5). The predictions in common for these runs are compared in Table 6.

For specific MOAs, the overall mean absolute error (MAE) was lower using 2D descriptors in the LC_{50} models. For broad MOAs, the overall error is lower using only ELOGP in

Table 6. Comparison of LC_{50} predictions using 2D descriptors and only ELOGP for the LC_{50} models (run #1 vs. #3 and run #2 vs. #4 in Table 5).

	Count	*MAE 2D**	*MAE ELOGP**
Specific MOA			
Narcosis-nonpolar	135	0.537	0.567
Narcosis-polar	17	0.47	0.456
Narcosis-ester	7	0.575	0.634
AChE inhibition-organophosphate	5	1.46	1.248
Reactivity	42	0.65	0.634
Uncoupling oxidative phosphorylation	7	0.833	1.05
All MOAs	213	0.587	0.605
All but narcosis	54	0.749	0.745
Broad MOA			
Narcosis	326	0.623	0.589
AChE inhibition	9	1.583	1.232
Neurotoxicity	1	1.76	0.436
Reactivity	21	0.66	0.74
Uncoupler	7	0.833	1.05
All MOAs	364	0.656	0.622
All but narcosis	38	0.939	0.906

*MAE 2D and MAE ELOGP are the mean absolute errors for models based on multiple 2d descriptors and solely on ELOGP, respectively.

Downloaded by [US EPA Library] at 08:06 01 July 2015

the LC_{50} models. One would expect the prediction accuracy using 2D descriptors would be higher for chemicals which did not have the narcosis MOA because the toxicity of chemicals with more specific MOAs are not only controlled by partitioning. However, the results indicate there was no advantage in using descriptors in addition to ELOGP in the MLR LC_{50} models (see 'All but narcosis' rows in Table 6). One explanation may be the intercept of the models may be more important in predicting the LC_{50} for some MOAs. For example, for the AChE inhibition–carbamate specific MOA, the LC_{50} model using 2D descriptors was

$$Tox = -0.09 \times ic + 4.95$$

where ic = information content descriptor.

The model using ELOGP was

$$Tox = -0.02 \times ELOGP + 4.77$$

It is interesting to note that if one only uses only ALOGP (Ghose–Crippen octanol–water coefficient [48] as calculated by T.E.S.T. [40]) for the hierarchical calculations, the prediction accuracy is similar (r^2 = 0.568), but the prediction coverage is lower (coverage = 90.2%). Using a single MLR model with 2D descriptors (run #7) yielded slightly worse results (r^2 = 0.551, coverage = 91.4%) than the hierarchical clustering method. Using a single MLR model with just ALOGP yielded similar results to those for the MLR with 2D descriptors (r^2 was slightly higher, but the coverage was slightly lower). This indicates the additional descriptors do not improve the external prediction accuracy for the global model.

3.1.6 *LC_{50} model descriptors*

The LC_{50} models for each MOA are given in the supplemental material (Tables S4 and S5) which is available via the multimedia link on the online article webpage. The most common 2D descriptors selected include autocorrelation, molecular fragment and E-state descriptors. It is interesting to note that 10 out of the 14 LC_{50} models using T.E.S.T. descriptors (see Table S4 and S5 in the supplementary material which is available via the multimedia link on the online article webpage) contained some form of log K_{ow} descriptor (ALOGP, ALOGP2, XLOGP and XLOGP2). The specific MOAs, which did not contain a log K_{ow} descriptor, were AChE inhibition–carbamate, narcosis–ester and neurotoxicity–pyrethroid sodium channel modulation.

3.2 *Discussion*

3.2.1 *Analysis of poorly predicted chemicals using MOA-based QSAR models*

One of the disadvantages of MOA-based methods is that an incorrectly predicted MOA can lead to a large error in the estimated toxicity value. Table 7 lists predictions for the broad LDA method (run #1 in Table 5) for poorly predicted chemicals (MAE ≥ 2 log units) that have a second highest LDA score ≥0.25. MOA1 and MOA2 are the predicted MOAs, which have the first and second highest score from the LDA models, respectively. Pred1 and Pred2 are the toxicity scores using the LC_{50} model for MOA1 and MOA2, respectively. Of the chemicals in Table 7, 9/10 were underpredicted which makes sense in that most of them were predicted to have the narcosis MOA. For chemicals where the second highest LDA score indicates the reactivity MOA, the predicted toxicities are much more accurately predicted using the reactivity LC_{50} model (MAE is reduced from 2.3 log units

Downloaded by [US EPA Library] at 08:06 01 July 2015

Table 7. Poorly predicted chemicals with large second highest LDA scores (≥0.25).

Chemical	*MOA1*	*MOA2*	*Exp.*	*Pred1*	*Pred2*
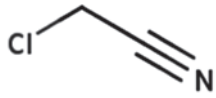 Chloroacetonitrile	Narcosis	Reactivity	4.75	1.54	3.65
Ethylene oxide	Narcosis	Reactivity	2.72	0.55	3.51
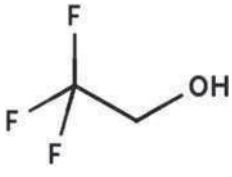 Trifluoroethanol	Narcosis	Reactivity	2.93	0.89	3.67
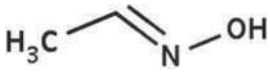 Acetaldehyde oxime	Narcosis	Reactivity	2.89	0.88	4.07
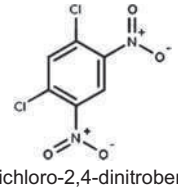 1,5-Dichloro-2,4-dinitrobenzene	Uncoupler	Reactivity	6.78	4.78	5.51
Salicylanilide	Narcosis	Uncoupler	7.43	4.36	4.65
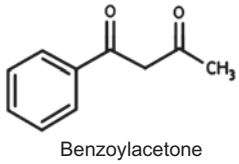 Benzoylacetone	Narcosis	Anticoagulant	5.17	3.08	N/A
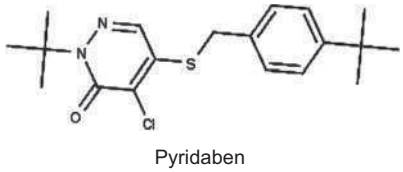 Pyridaben	Narcosis	Neurotoxicity	8.20	5.81	7.65

(*Continued*)

Downloaded by [US EPA Library] at 08:06 01 July 2015

Table 7. (*Continued*).

Chemical	*MOA1*	*MOA2*	*Exp.*	*Pred1*	*Pred2*
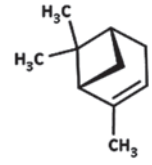 (+)-alpha-Pinene	Narcosis	Neurotoxicity	5.69	3.47	N/A
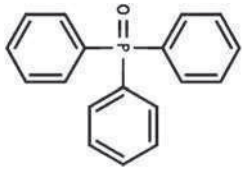 Triphenylphosphine oxide	AChE inhibition	Neurotoxicity	3.72	6.34	8.24

LDA models are based on broad MOAs and the LC50 models are fit to 2D descriptors.
Pred 1 and Pred 2 are the predictions using MOA1 and MOA2, respectively.
Exp. is the experimental value in -log(mol/L).

Downloaded by [US EPA Library] at 08:06 01 July 2015

to 1.0). All of these compounds are reactive according to the expert scheme outlined by Russom et al. [25]; (chloroacetonitrile is a halogenated nitrile, ethylene oxide is an epoxide, trifluoroethanol is a halogenated alcohol, acetaldehyde oxime is an oxime and 1,5-dichloro-2,4-dinitrobenzene has two nitro groups on one ring without an aniline or phenol substructure. The LDA methodology did not select reactivity for these compounds, but it suggests that one should examine the structure by hand when the second highest score is somewhat large (i.e. ≥0.25).

A prediction could not be made for benzoylacetone using MOA2 (since there is no LC_{50} model for the anticoagulant MOA) or for (+)alpha-pinene (since the applicability domain for neurotoxicity could not be met). In these cases, making no prediction is better than a poor prediction using MOA1. In the case of triphenylphosphine oxide, predictions are even worse for the second MOA. Visual inspection of this compound would indicate that this compound is probably a narcotic (due to a lack of single-bonded oxygens attached to the phosphorus) which would explain the overpredicted toxicity. Pyridaben is much better predicted using the neurotoxicity LC_{50} model. Salicylanilide is underpredicted using either the narcosis or uncoupler models, despite an expected uncoupler MOA.

3.2.2 *Analysis of poorly predicted chemicals using MLR model fit to entire training set*

One of the disadvantages of fitting a single model to the entire training set is that it may not correctly capture the trends in the toxicity for all modes of action. Table 8 lists the poor predictions (MAE ≥ 2 log units) for a single MLR model (run #7 in Table 5). These predictions are compared with those for broad MOA-based models (run #1 in Table 5). With the exception of fenoprop-isoctyl and 1,4-bis(chloromethyl)benzene, the MOA-based models had a lower prediction error. Despite the fact that 11 out of the 12 chemicals were predicted to have the narcosis MOA, the majority were overpredicted by both methods.

Table 8. Comparison of poorly predicted chemicals using a single model (run #7 in Table 5) with those from MOA-based models selected by the broad LDA approach (run #1 in Table 5).

	Exp –log (LC_{50} mol/L)			
Chemical	*Experimental*	*MLR 2D*	*Broad LDA*	*Predicted MOA*
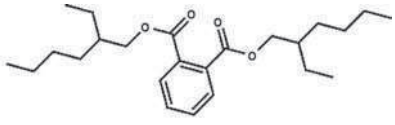 Bis(2-ethylhexyl) phthalate	2.55	8.13	7.83	Narcosis
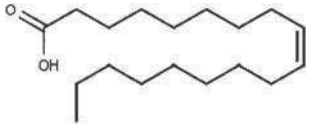 9-Octadecenoic acid	3.14	8.18	7.31	Narcosis
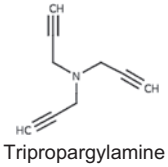 Tripropargylamine	2.65	7.15	5.28	Reactivity
Salicylanilide	7.43	4.16	4.36	Narcosis
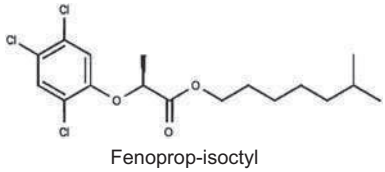 Fenoprop-isoctyl	4.24	7.36	8.14	Narcosis
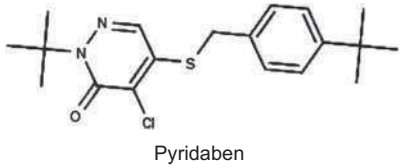 Pyridaben	8.20	5.34	5.81	Narcosis
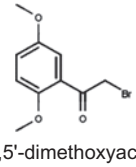 2-Bromo-2',5'-dimethoxyacetophenone	6.65	3.86	4.00	Narcosis
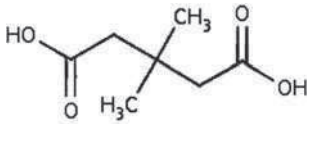 3,3-Dimethylglutaric acid	1.06	3.70	1.49	Narcosis

(*Continued*)

Downloaded by [US EPA Library] at 08:06 01 July 2015

Table 8. (*Continued*).

Chemical	Exp –log (LC_{50} mol/L)			Predicted MOA
	Experimental	*MLR 2D*	*Broad LDA*	
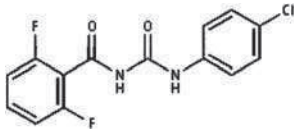 Diflubenzuron	2.86	5.44	5.18	Narcosis
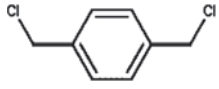 1,4-Bis(chloromethyl)benzene	6.65	4.27	3.68	Narcosis
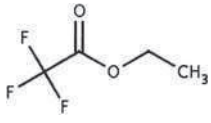 Ethyl trifluoroacetate	1.15	3.48	2.92	Narcosis
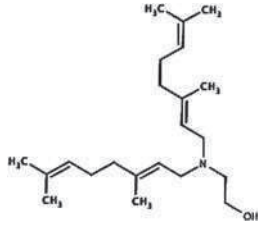 (E,E)-2-(Bis(3,7-dimethyl-2,6-octadienyl)amino)ethanol	6.41	8.62	7.41	Narcosis

Downloaded by [US EPA Library] at 08:06 01 July 2015

4. Conclusions

In this study, a two-step MOA-based approach was developed to estimate aquatic toxicity. The MOA-based approach was found to yield similar external prediction accuracy (r^2 = 0.529–0.632) to a single global MLR model (r^2 = 0.551–0.562). Overall, the global hierarchical clustering approach yielded higher combination of accuracy and prediction coverage (r^2 = 0.572, coverage = 99.3%) than the MOA-based approach (r^2 = 0.529–0.632, coverage = 49.3–87.3%). In addition, it was determined that multiple 2D descriptors achieved the same prediction accuracy as MLR models based only on the octanol–water partition coefficient. Finally, it was determined that in some cases that an incorrect mode of action can lead to large prediction errors when there is a competing MOA (LDA score ≥0.25). The results of this study indicate that, while MOA-based approaches may appear biologically relevant, they may not impart superior external prediction accuracy. However, the MOA-based approach can give toxicologists greater confidence in the predicted values since the models are based less on a 'black box' approach. The use of both MOA-based and global approaches in a consensus approach [49] can provide even greater confidence.

Supporting information

The mode of action datasets and the LDA and LC_{50} models are available in the supplementary material which is available via the multimedia link on the online article webpage.

Acknowledgement

The opinions expressed in this work are those of the authors and do not represent the policies or opinions of the US EPA.

References

[1] T.I. Netzeva, M. Pavan, and A.P. Worth, *Review of (quantitative) structure-activity relationships for acute aquatic toxicity*, QSAR Comb. Sci. 27 (2008), pp. 77–90.

[2] R. Benigni and A.M. Richard, *QSARS of mutagens and carcinogens: Two case studies illustrating problems in the construction of models for noncongeneric chemicals*, Mutat. Res.-Genet. Tox. 371 (1996), pp. 29–46.

[3] T.W. Schultz, G.D. Sinks, and A.P. Bearden, *QSAR in aquatic toxicology: A mechanism of action approach comparing toxic potency to* Pimephales promelas, Tetrahymena pyriformis, *and* Vibrio fischeri, in *Comparative QSAR*, J. Devillers, ed., Taylor & Francis, New York, 1998, pp. 51–109.

[4] S.G. Abernethy, D. MacKay, and L.S. McCarty, *'Volume fraction' correlation for narcosis in aquatic organisms: The key role of partitioning*, Environ. Toxicol. Chem. 7 (1988), pp. 469–481.

[5] M.T.D. Cronin and T.W. Schultz, *Structure-toxicity relationships for phenols to* Tetrahymena pyriformis, Chemosphere 32 (1996), pp. 1453–1468.

[6] O.G. Mekenyan and G.D. Veith, *Relationships between descriptors for hydrophobicity and soft electrophilicity in predicting toxicity*, SAR QSAR Environ. Res. 1 (1993), pp. 335–344.

[7] H. Yuan, Y.-Y. Wang, and Y.-Y. Cheng, *Mode of action-based local QSAR modeling for the prediction of acute toxicity in the fathead minnow*, J. Molec. Graph. Model. 26 (2007), pp. 327–335.

[8] W.F. Zheng and A. Tropsha, *Novel variable selection quantitative structure-property relationship approach based on the k-nearest-neighbor principle*, J. Chem. Inf. Comp. Sci. 40 (2000), pp. 185–194.

[9] M. Cassotti, D. Ballabio, V. Consonni, A. Mauri, I.V. Tetko, and R. Todeschini, *Prediction of acute aquatic toxicity toward* Daphnia magna *by using the GA-kNN method*, Altern. Lab. Anim. 42 (2014), pp. 31–41.

[10] T.M. Martin, P. Harten, R. Venkatapathy, S. Das, and D.M. Young, *A hierarchical clustering methodology for the estimation of toxicity*, Toxicol. Mech. Method. 18 (2008), pp. 251–266.

[11] C.X. Xue, R.S. Zhang, H.X. Liu, X.J. Yao, M.C. Liu, Z.D. Hu, and B.T. Fan, *An Accurate QSPR study of O–H bond dissociation energy in substituted phenols based on support vector machines*, J. Chem. Inf. Comp. Sci. 44 (2004), pp. 669–677.

[12] D.V. Eldred, C.L. Weikel, P.C. Jurs, and K.L.E. Kaiser, *Prediction of fathead minnow acute toxicity of organic compounds from molecular structure*, Chem Res. Toxicol. 12 (1999), pp. 670–678.

[13] E. Papa, F. Villa, and P. Gramatica, *Statistically validated QSARs, based on theoretical descriptors, for modeling aquatic toxicity of organic chemicals in* Pimephales promelas *(fathead minnow)*, J. Chem. Inf. Model. 45 (2005), pp. 1256–1266.

[14] J.A. Castillo-Garit, Y. Marrero-Ponce, J. Escobar, F. Torrens, and R. Rotondo, *A novel approach to predict aquatic toxicity from molecular structure*, Chemosphere 73 (2008), pp. 415–427.

[15] J.F. Contrera, E.J. Matthews, and R.D. Benz, *Predicting the carcinogenic potential of pharmaceuticals in rodents using molecular structural similarity and E-state indices*, Regul. Toxicol. Pharm. 38 (2003), pp. 243–259.

[16] K.L.E. Kaiser and S.P. Niculescu, *Using probabilistic neural networks to model the toxicity of chemicals to the fathead minnow* (Pimephales promelas)*: A study based on 865 chemicals*, Chemosphere 38 (1999), pp. 3237–3245.

Downloaded by [US EPA Library] at 08:06 01 July 2015

[17] T.M. Martin and D.M. Young, *Prediction of the acute toxicity (96-h LC_{50}) of organic compounds to the fathead minnow* (Pimephales promelas) using a group contribution method, Chem Res. Toxicol. 14 (2001), pp. 1378–1385.
[18] T. Öberg, *A general structure-property relationship to predict the enthalpy of vaporisation at ambient temperatures*, SAR QSAR Environ. Res. 18 (2007), pp. 127–139.
[19] T. Öberg, *A QSAR for baseline toxicity: Validation, domain of application, and prediction*, Chem Res. Toxicol. 17 (2004), pp. 1630–1637.
[20] A. Cherkasov, *Inductive QSAR descriptors. Distinguishing compounds with antibacterial activity by artificial neural networks*, Int. J. Mol. Sci. 6 (2005), pp. 63–86.
[21] Virtual Computational Chemistry Laboratory (VCCLAB), *Associative Neural Network,* VCCLAB, Munich, 2007; software available at http://www.vcclab.org/lab/asnn/.
[22] L. He and P.C. Jurs, *Assessing the reliability of QSAR model's predictions*, J. Mol. Graph. Model. 23 (2005), pp. 503–523.
[23] H. Könemann, *Quantitative structure-activity relationships in fish toxicity studies Part 1: Relationship for 50 industrial pollutants*, Toxicology 19 (1981), pp. 209–221.
[24] US Enviromental Protection Agency (US EPA), *Estimation Programs Interface Suite™ for Microsoft® Windows, v 4.11*. (2014), US EPA, Washington DC; software available at http://www.epa.gov/opptintr/exposure/pubs/episuitedl.htm.
[25] C.L. Russom, S.P. Bradbury, S.J. Broderius, D.E. Hammermeister, and R.A. Drummond, *Predicting modes of toxic action from chemical structure: Acute toxicity in the fathead minnow (*Pimephales Promelas*)*, Environ. Toxicol. Chem. 16 (1997), pp. 948–967.
[26] M.T.D. Cronin, A.O. Aptula, J.C. Duffy, T.I. Netzeva, P.H. Rowe, I.V. Valkova, and T. Wayne Schultz, *Comparative assessment of methods to develop QSARs for the prediction of the toxicity of phenols to* Tetrahymena pyriformis, Chemosphere 49 (2002), pp. 1201–1221.
[27] L. Claeys, F. Iaccino, C.R. Janssen, P. Van Sprang, and F. Verdonck, *Development and validation of a quantitative structure–activity relationship for chronic narcosis to fish*, Environ. Toxicol. Chem. 32 (2013), pp. 2217–2225.
[28] M. Nendza and M. Müller, *Discriminating toxicant classes by mode of action: 2. Physico-chemical descriptors*, Quant. Struct.-Act. Rel, 19 (2000), pp. 581–598.
[29] A.O. Aptula, T.I. Netzeva, I.V. Valkova, M.T.D. Cronin, T.W. Schultz, R. Kühne, and G. Schüürmann, *Multivariate discrimination between modes of toxic action of phenols*, Quant. Struct.-Act. Rel, 21 (2002), pp. 12–22.
[30] G. Schüürmann, A.O. Aptula, R. Kühne, and R.-U. Ebert, *Stepwise discrimination between four modes of toxic action of phenols in the* Tetrahymena pyriformis *assay*, Chem Res. Toxicol. 16 (2003), pp. 974–987.
[31] B. Niu, Y. Jin, W. Lu, and G. Li, *Predicting toxic action mechanisms of phenols using AdaBoost Learner*, Chemom. Intell. Lab. Syst. 96 (2009), pp. 43–48.
[32] S. Spycher, M. Nendza, and J. Gasteiger, *Comparison of different classification methods applied to a mode of toxic action data set*, QSAR Comb. Sci. 23 (2004), pp. 77–791.
[33] U. Norinder, P. Lidén, and H. Boström, *Discrimination between modes of toxic action of phenols using rule based methods*, Mol. Divers. 10 (2006), pp. 207–212.
[34] X.J. Yao, A. Panaye, J.P. Doucet, H.F. Chen, R.S. Zhang, B.T. Fan, M.C. Liu, and Z.D. Hu, *Comparative classification study of toxicity mechanisms using support vector machines and radial basis function neural networks*, Anal. Chim. Acta 535 (2005), pp. 259–273.
[35] S. Ren, *Predicting three narcosis mechanisms of aquatic toxicity*, Toxicol. Lett. 133 (2002), pp. 127–139.
[36] L. Michielan, L. Pireddu, M. Floris, and S. Moro, *Support vector machine (SVM) as alternative tool to assign acute aquatic toxicity warning labels to chemicals*, Mol. Inform. 29 (2010), pp. 51–64.
[37] S.C. Basak, G.D. Grunwald, G.E. Host, G.J. Niemi, and S.P. Bradbury, *A comparative study of molecular similarity, statistical, and neural methods for predicting toxic modes of action*, Environ. Toxicol. Chem. 17 (1998), pp. 1056–1064.

Downloaded by [US EPA Library] at 08:06 01 July 2015

[38] T.M. Martin, C.M. Grulke, D.M. Young, C.L. Russom, N.Y. Wang, C.R. Jackson, and M.G. Barron, *Prediction of aquatic toxicity mode of action using linear discriminant and random forest models*, J. Chem. Inf. Model. 53 (2013), pp. 2229–2239.
[39] S. Spycher, E. Pellegrini, and J. Gasteiger, *Use of structure descriptors to discriminate between modes of toxic action of phenols*, J. Chem. Inf. Model. 45 (2005), pp. 200–208.
[40] Un Environmental Protection Agency (US EPA), *ASTER (Assessment Tools for the Evaluation of Risk)*, US EPA, Washington DC, 2012; software available at http://www.epa.gov/med/Prods_Pubs/aster.htm.
[41] Insecticide Resistance Action Committee (IRAC), *IRAC MoA Classification Scheme,* IRAC International MoA Working Group, 2012; software available at http://www.irac-online.org/eClassification/.
[42] L. Eriksson, J.S. Jaworska, A.P. Worth, M.T.D. Cronin, R.M. McDowell, and P. Gramatica, *Methods for reliability and uncertainty assessment and for applicability evaluations of classification- and regression-based QSARs*, Environ. Health Persp. 111 (2003), pp. 1361–1375.
[43] D.C. Montgomery, *Introduction to Linear Regression Analysis*, John Wiley & Sons, New York, 1982.
[44] R. Todeschini and V. Consonni, *Handbook of Molecular Descriptors*, Wiley-VCH, Weinheim, Germany, 2000.
[45] L.B. Kier and L.H. Hall, *Molecule Structure Description: The Electrotopological State*, Academic Press, New York, 1999.
[46] Talete, *Dragon Version 6*, Talete SRL, Milan, Italy, 2006; software available at http://www.talete.mi.it/products/dragon_description.htm.
[47] H.J.M. Verhaar, C.J. van Leeuwen, and J.L.M. Hermens, *Classifying environmental pollutants. 1: Structure-activity relationships for prediction of aquatic toxicity*, Chemosphere 25 (1992), pp. 471–491.
[48] A.K. Ghose, V.N. Viswanadhan, and J.J. Wendoloski, *Prediction of hydrophilic (lipophilic) properties of small organic molecules using fragmental methods: An analysis of ALOGP and CLOGP methods*, J. Phys. Chem. 102 (1998), pp. 3762–3772.
[49] H. Zhu, T.M. Martin, L. Ye, A. Sedykh, D.M. Young, and A. Tropsha, *Quantitative structure−activity relationship modeling of rat acute toxicity by oral exposure*, Chem Res. Toxicol. 22 (2009), pp. 1913–1921.

Downloaded by [US EPA Library] at 08:06 01 July 2015

Table of Contents

General_Authors_Publications.....2
LI-266232_Published_Manuscript_for_LI-266232_(ES&T_2019).....18
LI-266233_Published_Manuscript_for_LI-266233_(J_Chrom_A).....29
LI-266234_Published_Manuscript_for_LI-266234_(ES&T_2015).....36
Published_Manuscript_for_LI-266234_(ES&T_2015).....45
Supplemental_materials_provided_to_Journal_for_LI-266234_(ES&T_2015).....54
Supplemental_materials_provided_to_Journal_for_LI-266233_(J_Chrom_A).....68
Published_Manuscript_for_LI-266233_(J_Chrom_A).....73
Published_Manuscript_for_LI-266232_(ES&T_2019).....80

STAA REPORT FOR THE SCIENTIST NOMINATIONS

General Information:

Nomination ID/App ID:	20-108
Research Category Primary:	Monitoring and Measurement Methods (MM)
Research Category Secondary:	
Laboratory/Office Name:	ORD
Nomination Entered By:	James McCord

Eligibility Checklist:

[Y] The nominated publication(s) has not been submitted to a previous STAA competition.

[Y] The nominated publication(s) was published on or before January 1, 2017 and on or after January 1,2012

[Y] The principal author was an EPA employee or a PHS employee assigned to EPA when the research was performed

[Y] The EPA authors (includes PHS employees assigned to EPA) contributed collectively a minimum of 50% toward the publication(s)

Nominating Official Name:	Kevin Oshima
Nominating Official Title:	BIOLOGIST
Nominating OfficialEmail:	oshima.kevin@epa.gov
STAA Coordinator Name:	Kevin Oshima
STAA Coordinator Email:	oshima.kevin@epa.gov

Justifications:

Justification 1:

The work presented in this package represents a growing effort to create, validate, and apply a new approach to monitoring environ to protect human health and the environment. This research supports both the scientific community, through its innovative techniqu the application of cutting edge science to solve issues presented by emerging contaminants in cooperation with our state partners. E package represent a stage in the development and application of non-targeted analysis (NTA) using high-resolution mass spectrome contaminants known as per- and polyfluorinated alkyl substances (PFAS). PFAS have been a significant agency priority for many y focus following the May 2018 National Leadership Summit on PFAS, and a 2019/2020 PFAS specific action plan laying out the ag class. The research in this STAA package have been critical in laying the groundwork for the current agency vision on PFAS monit subsection of the 2019 action plan "Development of Field and Laboratory Methods to Measure PFAS in the Environment" (https://www.epa.gov/pfas/epas-pfas-action-plan) specifically citing two of the papers in this package (McCord 2018, and Strynar 2 continued development.

Non-targeted analysis represents a departure from traditional environmental pollutant measuring methods because sampling and an pre-conceptions for the targeted chemical(s) of interest. Rather than a defined panel of analytes to quantify, samples are either scree chemicals, such as found on the EPA Comptox Chemicals Dashboard, or chemicals can be identified strictly by their behavior in th combination of computer software and expert analysis. The Strynar et al. 2015 manuscript in this package demonstrates the power o has historically been monitored for PFAS using targeted methods (EPA method 537) but we sought to apply NTA techniques to ide The study detected novel PFAS with limited toxicity information, and the response from the public for more information and the st ORD / NC response was significant (cf Justification 3). The initial Strynar et al. 2015 study was significant for its ability to detect u and statistically demonstrate their introduction by a specific waste stream, but was unable to provide chemical structures of all the u limitations, and was unable to provide concentrations of analytes for making risk assessment decisions, due to limitations of NTA g addressed in follow-up studies also included in this package. Non-targeted analysis is predominantly used for discovery and screeni its ability to describe concentrations or integrate with risk assessment decision making processes. McCord et al. 2018 was able to d chemical, known as HFPO-DA or GenX, and used a series of surrogate chemicals to estimate concentrations of other species. Whil utilized approach in many biology fields, providing quantitative estimates of NTA compounds without standards is still an unsolve applications. We were able to provide semi-quantitative estimates to support decision making and the surrogate similarities were us concentration estimates of unknowns. McCord and Strynar 2019 used an improved mass spectrometer to fragment molecules and p of chemicals in the Cape Fear river and developed a statistical clustering approach to show relationships between detected chemica predict the association of chemicals which were mapped to internal industrial processing lines (CBI not disclosed beyond NC inves contamination was originating from more than just the GenX process; ultimately NC required controls for all effluents leaving the f

This research has both supported and influenced agency priorities over the last several years; during the last ORD planning cycle th the safe and sustainable water resources task to provide novel monitoring technologies for occurrence, exposure, and effect for indi the current strategic research action plan PFAS are a major component of almost every research program. Four out of the six have s

applying non-targeted analysis for PFAS work, at least in part due to the utility of the approach demonstrated here. In fact, during t
Community of Science meeting, 8/10 Regions listed emerging PFAS topics as one of their two primary areas of concern for the reg
demonstrated by the integration of the ORD research on emerging contaminants, the Region 4 management of state concerns, and s
consistent with ORD's goal of cooperative federalism as a response to environmental challenges. Following the success of this worl
studies have been undertaken with NJ, NY, WV, MI, and KY with more anticipated in the future. This STAA nomination thus repr
demonstrably valuable to EPA and our partners at both the discovery of emerging contaminants and in providing a framework for t
focusing on a topic of significant national priority.

Justification 2A:

The package contains three manuscripts (submitted as LI-266232, LI-266233, and LI-266234) which describe continuous research
Fear River of North Carolina. LI-266234 described the initial discovery of novel pollutants in the Cape Fear River, a major watersh
drinking water to between 3-5 million inhabitants of the state. The manuscript used a high resolution mass spectrometer and provid
compounds based on comparison to patent literature and industry documents of a local manufacturer of fluorinated chemicals, inclu
substances (PFAS). A few years later, the authors attempted to expand on the initial discovery by applying more modern mass spec
technology and data analysis to confirm structures, abundances, and origins of these species, which would form the basis of LI-266

Before the data analysis for LI-266232 could be completed, a news article was published in the Star News (
https://www.starnewsonline.com/news/20170607/toxin-taints-cfpua-drinking-water/1) detailing the detection of the chemicals iden
up study with NC State (Sun et al, Legacy and Emerging Perfluoroalkyl Substances Are Important Drinking Water Contaminants i
Carolina. ES & T Letters, 2016, 3(12), 415-419, DOI: 10.1021/acs.estlett.6b00398). The Chemours company had been identified as
described, and the public outcry from residents of eastern North Carolina, as well as the state legislature and environmental protecti
significant and the state formally reached out to ORD through Region 4 contacts to gain immediate access to the ongoing research.
interest was a compound known as HFPO-DA (or GenX) and LI-266233 was released as a formalized, single-lab validated quantita
samples collected by EPA and by NC Department of Environmental Quality (NCDEQ). Data generated on the additional samples i
released directly to NCDEQ and the public over the course of 2017-2018 prior to finalization of the manuscripts submitted in this p
identify additional compounds not found in the initial study, and was able to demonstrate that actions by Chemours were insufficie
chemicals, even after taking initial steps required by NCDEQ. Eventually, Chemours and NCDEQ entered into a consent order whe
compounds detected in all three manuscripts and provide for cleanup.

The ongoing story of the monitored region and the role that data from each of the three manuscripts played requires the submission
address underlying research without including all of the interrelated papers would paint an incomplete picture of the significance of
communities and the state/regional EPA partners who were heavily engaged in the work.

Justification

2B:

n/a

Justification 2C:

n/a

Justification 2D:

n/a

Justification 2E:

Mark Strynar and Seth Newton are listed each as 5% contributors for an STAA nomination this cycle containing the following publ

Rager JE, Strynar MJ, Liang S, McMahen RL, Richard AM, Grulke CM, Wambaugh JF, Isaacs KK, Judson R, Williams AJ, Sobus J spectrometry data with exposure and toxicity forecasts to advance high-throughput environmental monitoring. Environ Int. 2016 M 7.943; Immediacy Index = 1.108; Cited Half-Life = 6.0; Times Cited = 75.

Sobus JR, Wambaugh JF, Isaacs KK, Williams AJ, McEachran AD, Richard AM, Grulke CM, Ulrich EM, Rager JE, Strynar MJ, N non-targeted analysis research and chemical safety evaluations at the US EPA. J Expo Sci Environ Epidemiol. 2018 Sep;28(5):411 Immediacy Index = 1.277; Cited Half-Life = 8.1; Times Cited = 24.

The similarity between the two packages exists only in the fact that mass spectrometry, non-targeted methods were employed in bo listed above, however, are focused on the application of risk-assessment approaches to high-throughput data collection and the inte available information as part of EPA DSSTox. In contrast, this STAA package focuses on the detection of novel compounds with n environmental detection, quantitation, and response/monitoring of affected regions rather than high-throughput risk assessment or t

Justification 3A:

This STAA package is comprised of three manuscripts with the full citations listed below:

LI-266234:

Mark Strynar, Sonia Dagnino, Rebecca McMahen, Shuang Liang, Andrew Lindstrom, Erik Andersen, Larry McMillan, Michael Th
Ball. Identification of Novel Perfluoroalkyl Ether Carboxylic Acids (PFECAs) and Sulfonic Acids (PFESAs) in Natural Waters Us
Mass Spectrometry (TOFMS). Environmental Science & Technology, 2015, 49(19), 11622-11630, DOI: 10.1021/acs.est.5b01215

LI-266233:

James McCord, Seth Newton, Mark Strynar. Validation of quantitative measurements and semi-quantitative estimates of emerging
(PFECAs) and hexafluoroprolyene oxide acids (HFPOAs). Journal of Chromatography A, 2018, 1551, 52-58, DOI: 10.1016/j.chro

LI-266232:

James McCord and Mark Strynar. Identification of Per- and Polyfluoroalkyl Substances in the Cape Fear River by High Resolution
Screening Environmental Science & Technology, 2019, 53(9), 4717-4727, DOI: 10.1021/acs.est.8b06017

The three manuscripts form a cohesive, in-depth, and long-term examination of a closely related series of compounds in a widely ir
Carolina. Each builds chronologically both in terms of scientific advances, and also in terms of the importance to the affected comr
EPA response to the work and its implications.

LI-266234 (ES&T 2015, Impact Factor = 7.149; Immediacy Index = 1.141; Cited Half-Life = 7.8):

Initial work on the discovery and monitoring of emerging per- and polyfluorinated alkyl substances in NC was described, where a r
tentatively identified using cutting edge non-targeted analysis techniques and high resolution mass spectrometry. By current metric
Scholar) and 3636 Views (ACS). All told, the approach was the main topic of five invited talks at national/international conference
of the work and as a direct result of the outgrowth of interest in its results. The talks are as follows:

Investigations of per- and polyfluorinated compounds in environmental samples and contemporary products. MJ Strynar, JP McCo
Hopkins, M Sun, A Lindstrom. 256th ACS National Meeting in Boston, MA, Aug. 19-23, 2018.

Investigations of per- and polyfluorinated compounds in environmental samples and contemporary products. MJ Strynar, JP McCo
Hopkins, M Sun, A Lindstrom. 2018 Toxicology and Risk Assessment Conference (TRAC), Cincinnati, OH, April 23 - 26, 2018.

Discovery of Emerging Per-and Polyfluoroalkyl Substances. M Strynar, JP McCord, JR Lang, A Lindstrom, Z Hopkins, D Knappe
(WRRI) Conference, Raleigh, NC, March 14 - 15, 2018.

Mark Strynar, Seth Newton, Rebecca McMahen, Larry McMillan, and Andrew Lindstrom. Emerging per- and polyfluorinated com
Emerging Environmental Contaminants Southeast Regional ACS Conference (SERMACS), Columbia, SC, Oct. 23-27, 2016

Determination of perfluoroalkyl ether carboxylic acids (PFECAs) and sulfonic acids (PFESAs) in North Carolina surface water usi
Dagnino, Rebecca McMahen, Shuang Liang, Andrew Lindstrom, Erik Andersen, Larry McMillan, Michael Thurman, Imma Ferrer
Vancouver, BC, Canada November 9-13th, 2014

Interest and impact of this work has extended beyond the scientific community, with six science and health news articles directly ci
the following years. The articles are:

"The Hunt is on for GenX Chemicals in People", C&E News. April 7, 2019; "EPA Continues to Approve Toxic PFAS Chemicals I
The Intercept, Oct 25, 2018; "GenX chemicals taint sediments", C&E News. April 6, 2018; "GenX Pollution. What Happened? and
Aug 18, 2017; "Cooper Takes Aim at Chemours, GenX, Other Chemicals" North Carolina Health News. Jul 17, 2017; "Another Ur
Fear River" North Carolina Health News. Jun 20, 2017.

The Star News (Wilmington, NC) and The Intercept(online) published a series of articles related to PFAS along with the cited refer
Wilmington, NC resulted directly in the work accomplished in manuscript 2. Major public interest focused around one of the chem
intense national and local interest. In fact, the general assembly of North Carolina specifically asked to be briefed on the techniques
and availability of high resolution mass spectrometers for detection and analysis of GenX and other emerging contaminants" Mark
Carolina, House Select Committee on North Carolina River Quality, State Legislative Building, Raleigh, North Carolina February
2018, https://www.ncleg.net/documentsites/committees/house2017-185/Meetings/5%20-%20Feb%2021%202018/HSC%20River%

LI-266233 (J. Chrom. A, Impact Factor = 3.858; Immediacy Index = 0.832; Cited Half-Life = 9.3):

The discovery of a novel class of emerging PFAS contaminants in the major watershed in NC was troublesome due to the large am
assessment of these compounds. There were no methods, especially not validated methods, for the direct quantitation of chemicals
approach for the quantification of chemicals in some of the classes described in manuscript 1. The methods paper currently has 14 c
discussion of the approaches were a major talk, "A Deeper Dive into PFAS Analysis," at a the 2019 joint conference of American C
(ACEC) and the Groundwater Professionals of North Carolina. The work detailed in the manuscript was of such significant interest
and the general public that the NC Department of Environmental Quality hosted and distributed data from the work as it was being
website for public consumption (https://deq.nc.gov/news/key-issues/genx-investigation) and continues to update the website with re
decisions related to manuscripts in this package. The work was incorporated into a state level risk assessment for GenX
(https://deq.nc.gov/state-releases-first-water-quality-data-updated-health-information-genx-cape-fear-river-0) and both James McC
briefings to the North Carolina general assembly and departments of environmental and water quality.

Following the initial validation and testing conducted by the STAA authors, quantitative methods were transferred to EPA Region 4
of GenX related testing for the cooperative EPA/state investigation and response. Methods based on those generated in ORD were u
responding to NC's ongoing PFAS investigations. Eurofins and TestAmerica both offered GenX as part of their PFAS suite using a
to EPA numbered method 537, to 537.1, was undertaken to include GenX and a select few other PFAS, which are now widely teste
PFAS is under development to use the alternative solid phase extraction media for many PFAS, including GenX. EPA 533 is simila
manuscript 2, where it was referred to as a "modified method 537" approach.

LI-266234 (ES&T 2019, Impact Factor = 7.149; Immediacy Index = 1.141; Cited Half-Life = 7.8):

While manuscript 2 detailed the approach to quantifying the major analyte of public interest, GenX, manuscript 3 detailed the conc
unanticipated analytes. Manuscript 3 followed up the approach used in manuscript 1 using modern instrumentation and approaches
Cape Fear river to a degree that was not possible during the intial sampling, validating tentative IDs provided in the initial manuscr
determin the likely sources, and connecting temporal trends observed with ongoing actions by NC regulators as the result of the mo
and 2. Current metrics indicate the manuscript has 13 citations (Google Scholar) and 1694 Views (ACS). Thus far, the manuscript l
international level talks:

Non-Targeted Analysis Approaches in Environmental Chemistry. JP McCord. Meeting of the International Society for Indoor Air C
Sources, Monitoring and Evaluation of Chemical Pollutants, Feb 13, 2020

Multimedia, Non-Targeted Examination of Emerging PFAS Sources. JP McCord, MJ Strynar. Annual Meeting of the North Ameri
Environmental Toxicology and Chemistry (SETAC). Toronto, Canada, Nov 3 - 7, 2019

The fully resolved list of identified compounds from manuscript 3 and manuscript 1 was directly used in a consent order entered in
company (https://files.nc.gov/ncdeq/GenX/2019-02-20-Final-Revised-Proposed-Consent-Order-with-attachments-and-signatures.p
emissions of PFAS. The identifications were used to require Chemours to provide both standards for quantitation, and toxicity info
risk assessment to affected communities.

For the body of work described here, the EPA authors have been formally recognized for their service.

Mark Strynar, Andy Lindstrom, and Seth Newton received the 2017 EPA National Honor Award Gold Medal for Exceptional Serv

“Cape Fear River (PFAS Public Health Action Team)” For discovering and partnering to remedy the public health threat of PFAS
and drinking water of ~300,000 NC residents

Mark, James, and Andy were awarded the 2018 EPA Bronze Medal for Commendable Service: NERL-NRMRL Regional PFAS Su

James McCord received the 2019 NERL Early Career in Research award, in part for the work described here.

Justification 3B:

The external review process for the manuscripts in this STAA nomination was that required by the peer-reviewed journals they we
consisted of a primary editorial review by an associate editor with a specialty in the content area, followed by a three-member peer
unaffiliated subject matter experts (typically environmental science and engineering). The authors are blind to the contents of their
of their comments and rulings on the scientific merit and editorial quality of the manuscripts. All the manuscripts in this STAA no
suggestion of minor editorial revisions, which were performed by the primary author(s) of each manuscript before publication.

Both ES&T and J. Chrom. A ask reviewers to assess publications on the basis of originality, scientific accuracy, and widespread ut
communities. ES&T defines its scope as "...major advances, trends, and challenges in environmental science, technology, and polic

understanding in the environmental field." while J. Chrom. A focuses on "...fundamental research on all aspects of separation scien
scrutiny will be placed on the degree of novelty and significance of the research and the extent to which it adds to existing knowled

AUTHORS

Contributing Author

Author Name:	Seth Newton	
Professional Title:		Salutation:
Email:	newton.seth@epa.gov	Organization:
Mailing Address:		
Street Line 1:		
City:		
Zip Code:		State:
At time of research was:	EPA Employee	
Separation Date:		
% of Effort:	7	

Contributing Author

Author Name:	Andrew Lindstrom	
Professional Title:		Salutation:
Email:	lindstrom.andrew@epa.gov	Organization:
Mailing Address:		
Street Line 1:		
City:		

Zip Code:		State:
At time of research was:	EPA Employee	
Separation Date:		
% of Effort:	7	

Contributing Author

Author Name:	Mark J Strynar	
Professional Title:		Salutation:
Email:	strynar.mark@epa.gov	Organization:
Mailing Address:		
Street Line 1:		
City:		
Zip Code:		State:
At time of research was:	EPA Employee	
Separation Date:		
% of Effort:	40	

Contributing Author

Author Name:	James P McCord	
Professional Title:		Salutation:
Email:	mccord.james@epa.gov	Organization:
Mailing Address:		
Street Line 1:		
City:		

Zip Code:		State:
At time of research was:	EPA Employee	
Separation Date:		
% of Effort:	30	

Contributing Author

Author Name:	Larry McMillain	
Professional Title:		Salutation:
Email:	mcmillan.larry-rtp@epa.gov	Organization:
Mailing Address:		
Street Line 1:		
City:		
Zip Code:		State:
At time of research was:	Non EPA Personnel	
Separation Date:		
% of Effort:	2	

Contributing Author

Author Name:	Sonia Dagnino	
Professional Title:		Salutation:
Email:	sonia.dagnino@imperial.ac.uk	Organization:
Mailing Address:		
Street Line 1:		
City:		

Zip Code:		State:
At time of research was:	Non EPA Personnel	
Separation Date:		
% of Effort:	2	

Contributing Author

Author Name:	Shuang Liang	
Professional Title:		Salutation:
Email:	sliang2@ncsu.edu	Organization:
Mailing Address:		
Street Line 1:		
City:		
Zip Code:		State:
At time of research was:	Non EPA Personnel	
Separation Date:		
% of Effort:	2	

Contributing Author

Author Name:	Carol Ball	
Professional Title:		Salutation:
Email:	carol_ball@agilent.com	Organization:
Mailing Address:		
Street Line 1:		
City:		

Zip Code:		State:
At time of research was:	Non EPA Personnel	
Separation Date:		
% of Effort:	2	

Contributing Author

Author Name:	Michael Thurman	
Professional Title:		Salutation:
Email:	mthurman@ono.com	Organization:
Mailing Address:		
Street Line 1:		
City:		
Zip Code:		State:
At time of research was:	Non EPA Personnel	
Separation Date:		
% of Effort:	2	

Contributing Author

Author Name:	Rebecca McMahen	
Professional Title:		Salutation:
Email:	mcmahen.rebecca@epa.gov	Organization:
Mailing Address:		
Street Line 1:		
City:		

Zip Code:		State:
At time of research was:	Non EPA Personnel	
Separation Date:		
% of Effort:	2	

Contributing Author

Author Name:	Imma Ferrer	
Professional Title:		Salutation:
Email:	imma.ferrer@colorado.edu	Organization:
Mailing Address:		
Street Line 1:		
City:		
Zip Code:		State:
At time of research was:	Non EPA Personnel	
Separation Date:		
% of Effort:	2	

Contributing Author

Author Name:	Erik Andersen	
Professional Title:		Salutation:
Email:	eanderse4@gmail.com	Organization:
Mailing Address:		
Street Line 1:		
City:		

Zip Code:		State:
At time of research was:	EPA Employee	
Separation Date:	Sat Dec 31 00:00:00 GMT 2016	
% of Effort:	2	

PUBLICATIONS

Publication 1:

Publication Title:	Identification of Per- and Polyfluoroalkyl Substances in the Cape Fear River by High Resolution Mass	
Publication Date:	Wed Apr 17 00:00:00 GMT 2019	
Journal/Publication Method:	Environmental Science & Technology	
All Author(s):		
Volume:	53	Num
Pages:	4717-4727	Imm
Citation ½ Life:	7.8	Impa

Publication 2:

Publication Title:	Validation of quantitative measurements and semi-quantitative estimates of emerging perfluoroetherca	
Publication Date:	Fri May 25 00:00:00 GMT 2018	
Journal/Publication Method:	Journal of Chromatography A	
All Author(s):		
Volume:	1551	Num
Pages:	52-58	Imm
Citation ½ Life:	9.3	Impa

Publication 3:

Publication Title:	Identification of Novel Perfluoroalkyl Ether Carboxylic Acids (PFECAs) and Sulfonic Acids (PFESAs) i	
Publication Date:	Tue Oct 06 00:00:00 GMT 2015	
Journal/Publication Method:	Environmental Science and Technology	
All Author(s):		
Volume:	49	Nur
Pages:	11622-1163	Imn
Citation ½ Life:	7.8	Imp

Environmental Science & Technology

Article

Cite This: Environ. Sci. Technol. 2019, 53, 4717−4727

pubs.acs.org/est

Identification of Per- and Polyfluoroalkyl Substances in the Cape Fear River by High Resolution Mass Spectrometry and Nontargeted Screening

James McCord[†] and Mark Strynar*[,‡]

[†]National Exposure Research Laboratory, U.S. Environmental Protection Agency, Oak Ridge Institute for Science and Education, Research Triangle Park, Durham, North Carolina 27711, United States

[‡]National Exposure Research Laboratory, U.S. Environmental Protection Agency, Research Triangle Park, Durham, North Carolina 27711, United States

Supporting Information

ABSTRACT: Ongoing chemical development in response to regulation of historical perfluorinated compounds, (i.e., perfluorooctanoic acid (PFOA) and perfluorooctanesulfonic acid (PFOS)) has resulted in a proliferation of novel per- and polyfluorinated species. Screening and monitoring for these emerging chemicals benefit from a nontargeted approach due to a lack of necessary standards and a paucity of information about the replacement chemistries. In this paper, we apply nontargeted screening to the Cape Fear River of North Carolina, a fluorochemically impacted watershed. The continued presence of perfluorinated ether acids was confirmed, with a total of 37 unique chemical formulas comprising 58 isomers detected. Structural determination was carried out by LC-MS/MS to determine isomeric structures where possible. Novel structures determined included perfluorinated ether acid species containing two acidic sites, polyfluorinated ether acids containing a single hydrogenation, and previously unreported perfluorinated ether acids. Compounds identified by an initial nontargeted screen were monitored over repeated sampling to track long-term reductions in PFAS content during emission source control. Hierarchical clustering of the time course data was used to associate groups of chemicals based on their trends over time. Six clusters were identified and showed some similarity in chemical class; they are believed to represent the byproducts of different fluorochemical production lines.

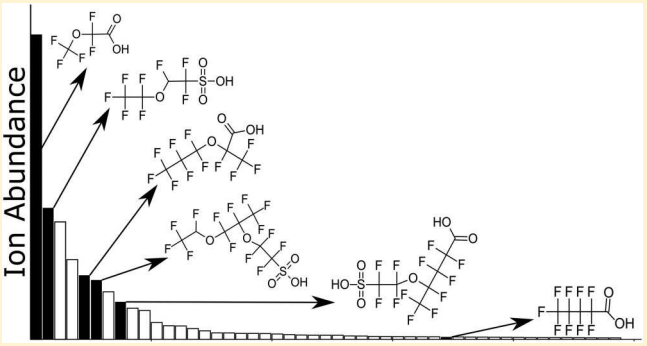

INTRODUCTION

Fluorinated polymers and fluorosurfactants are constantly evolving due to in-demand consumer and industrial products with a long and complicated history of environmental impacts.[1] A consequence of the ubiquity of per- and polyfluoroalkyl substances (PFASs) in industry is their extensive environmental infiltration due to their use as manufacturing aids, production as waste, and release as degradations and side-products of manufactured products. PFASs possess exemplary thermochemical inertness, and fluorinated carbons are resistant to biological breakdown,[2] which is the cause of their persistent nature in the environment[3] and was the driving rationale for the erroneous assumption of biological inertness for over 25 years.[4]

The most historically dominant PFAS species, perfluorooctanesulfonate (PFOS) and perfluorooctanoic acid (PFOA), were used extensively before triggering domestic and international action due to concerns about their negative toxicological effects and bioaccumulation potential.[5−7] Long-term toxicological studies demonstrated that these species have broad spectrum influence and require exposure controls.[8,9] Coinciding with the environmental studies in the previous decade, domestic manufacturing began phasing out PFOA and PFOS,[10,11] but the chemical qualities of fluorochemicals are difficult, or impossible, to replicate using nonfluorinated species.[12,13] Consequently, industries developed fluorinated alternatives, including short-chain PFASs and perfluoroalkyl ether acids, to replace legacy long-chain PFASs.[14,15]

A chief difficulty with chemical phase-out is the assurance that replacement chemicals from the same class demonstrate improved environmental and human health profiles. Historically, reliance on chemicals within a single chemical class has not markedly overcome fundamental issues presented by the original compounds (e.g., the replacement of polychlorinated biphenyls with short-chain chlorinated paraffins or the

Received: October 25, 2018
Revised: February 25, 2019
Accepted: March 14, 2019
Published: April 17, 2019

Downloaded via US EPA OFFICE OF ENVIRONMENTAL INFO on April 29, 2020 at 12:41:52 (UTC).
See https://pubs.acs.org/sharingguidelines for options on how to legitimately share published articles.

ACS Publications © 2019 American Chemical Society

DOI: 10.1021/acs.est.8b06017
Environ. Sci. Technol. 2019, 53, 4717−4727

emerging replacements for brominated flame retardants).[16,17] Due to the aforementioned uniqueness of fluorinated compounds, there may be challenges to the prospect of alleviating the toxicological effects associated with PFOA/PFOS or legacy PFASs by using related chemistries.[13,18] One company has introduced a new line of "short-chain" PFOS replacements which exhibit nearly identical structures but potentially better biological clearance rates.[19] Others have introduced branched polymeric surfactants with "low-bioaccumulation potential".[20] Still, more manufacturers have created species with interspersed ether-oxygen linkages[21] or partial hydrogenation.[22] The net result is a proliferation of product chemicals, precursors, and degradation products with limited publicly available toxicological and physical data due to the proprietary nature of these compounds. Monitoring this vast new chemical landscape requires the development of new analytical methodologies.

High-resolution mass spectrometry (HRMS) has a proven track record in compound elucidation and environmental screening that is well suited to the task of identifying and monitoring emerging pollutants through accurate chemical prediction and structural elucidation.[23−28] HRMS approaches have been applied to numerous environmental samples collected around fluorochemical point sources to identify new unregulated compounds. For example, new structures were resolved in water located around Chinese manufacturing facilities[28] and in river water from domestic sites.[29] Potential structures were assigned to numerous PFASs in Alabama[26] and previously in the Cape Fear River of North Carolina.[29,30] In each case, spatial and/or temporal sampling was used to compare impacted and baseline water samples, while identifying molecular features associated with the fluorochemical waste stream.

In North Carolina, discovery of the chemical hexafluoropropylene oxide dimer acid (HFPO-DA) sparked intense scrutiny of its long-term effects, resulting in the establishment of a preliminary NC state drinking water health goal.[31] Since initial reporting by media outlets,[32] the "chemical" GenX has been used as a public synonym for HFPO-DA. While GenX has occupied the center of the debate regarding fluorochemical contamination in the Cape Fear River, the presence of other fluorinated chemicals of related classes is also of interest. We combine the previously demonstrated nontargeted approach with techniques for structural assignment by tandem mass spectrometry (MS/MS) to identify the additional fluorochemical species affecting the Cape Fear watershed.

METHODS

Sample Collection. Surface water grab samples were collected in May 2017 from the main flow of the Cape Fear River and its tributaries at the William O. Huske Lock and Dam. An "upstream" sample was collected approximately 2 miles upstream of the dam, representative of the background contents of the river. A "downstream" sample was collected immediately above the dam, representative of the impacts of nearby (<1 mile) manufacturing outfall (Supporting Information Figure 91). Longitudinal grab samples of the manufacturing outfall were collected weekly by the North Carolina Department of Environmental Quality (NCDEQ) throughout the summer of 2017,[33] and follow-up samples were collected at the original sampling locations in February 2018. At each site, water was collected in a precleaned one liter high-density polyethyelene (HDPE) Nalgene bottle according to an established procedure.[34]

The collected water was processed as previously described, after stabilization with the addition of 5 mL 35% nitric acid.[26] In brief, one liter of water was measured in an HDPE graduated cylinder, and the sample bottle was washed with 10 mL of methanol to desorb analytes adhered to the interior of the bottle. The water and methanol were pooled in the bottle and filtered using a Whatman GF/A glass fiber filter. From this filtered sample, 500 mL of liquid was concentrated using a SPC10-P Sep-Pak concentrator onto an Oasis WAX Plus SPE cartridge (225 mg sorbent, 60 μm particle size) that had been preconditioned with methanol (MeOH) and water per manufacturer instructions. SPE cartridges were washed with 4 mL of pH 4 acetate buffer, followed by 4 mL of neutral methanol, and then compounds were eluted in 4 mL of 0.1% NH_4OH in MeOH. The methanol wash fraction could have contained nonacidic PFAS, but preliminary experiments did not detect these in samples from the Cape Fear, so they were discarded in the work for this manuscript. The eluent was evaporated under a nitrogen stream at 40 °C to a final volume of 1 mL and diluted 4-fold with 2.5 mM ammonium formate. A method blank was prepared in parallel using laboratory deionized water.

Sample Analysis and Data Processing. Initial mass spectrometry (MS) analysis on the collected water samples was carried out by liquid chromatography coupled to time-of-flight (TOF) in a fashion previously described;[29] instrument details are located in the Supporting Information. MS sample data was postprocessed using a software workflow of Agilent ProFinder, MassHunter, and Mass Profiler. Samples were subjected to batch recursive molecular feature extraction (MFE) in ProFinder using previously determined thresholds for this instrument and separation gradient (Supporting Information Table 3). A molecular feature, as defined by the software, consists of a specific isotopic distribution with a distinct extracted ion chromatogram peak abundance and is assigned a monoisotopic mass and retention time. Molecular features identified in the method blank were removed from the sample data, and the remaining values were exported for comparison in Mass Profiler. Samples collected downstream of the known fluorochemical point source were compared to upstream samples, which should be free of species introduced by the intervening facility. Pairwise comparison was used to identify features unique to the downstream samples as well as species which were significantly increased (>3-fold increase in integrated peak area). The list of the top 100 most abundant unique and statistically significant species was exported and prepared as an inclusion list for further MS/MS investigation.

Structural investigation of the molecular features was performed using an Agilent 1260 Infinity UPLC coupled to an Agilent 6530 quadrupole time-of-flight (QTOF). Parameters for LC separation were the same as the initial TOF analysis, but MS settings were adjusted to allow collection of MS/MS fragmentation spectra of the targeted inclusion list from the TOF analysis. Modifications to the MS collection are detailed in the Supporting Information.

The raw data collected from QTOF MS/MS experiments was processed using ProFinder, followed by filtering to isolate features for closer inspection. Comparison of precursor and fragment masses allowed a maximum 5 ppm precursor and 20 ppm fragment mass error; average mass error was ∼1 ppm, consistent with the performance specifications of the instru-

DOI: 10.1021/acs.est.8b06017
Environ. Sci. Technol. 2019, 53, 4717−4727

ment. Features were individually examined to determine structures where possible. For each mass-to-charge (m/z) identified at the formula level or better (Confidence 4+), an ±10 ppm extracted ion chromatogram of the theoretical precursor mass was generated to determine retention times (Supporting Information Figures 1−83). Composite MS/MS spectra consisting of multiple averaged MS/MS scans at collision induced dissociation (CID) energies of 10 and 25 V; spectrawere generated for individual isomers of each precursor, where possible.

The list of molecular features was sorted by integrated peak area and the isotopic distributions for each of the molecular features; a putative empirical formula was assigned using MassHunter's formula generator tool. This assignment is a score obtained by matching the feature's accurate mass and isotopic distribution with theoretical values calculated using known isotopic distributions of a potential formula's constituent elements (i.e., 1.1% ^{13}C, 0.4% ^{15}N, etc.). Allowed atoms included C, H, N, O, S, F, Cl, Br, and P. For compounds with only poorly scoring isotopic matches (e.g., <70%), background subtraction of the precursor spectrum was carried out against a background of the 0.2 min regions immediately preceding and following the chromatographic peak, and a second attempt at formula assignment was made.

The MS/MS spectra collected for each molecular feature were manually examined to ascertain the accuracy of the precursor formula and attempt to resolve molecular structures. Emphasis was placed on chemicals demonstrating a negative mass defect—the difference between the exact and nominal mass of the compound, a common signature of halogenation.[22] It is worth noting that this is only a rough proxy for the inclusion of critical atoms of interest (i.e F, Cl, Br) in small molecules and significant supporting data is necessary to classify an unknown as a PFAS.[35] Fragment ions were assigned partial empirical formulas based on exact monoisotopic mass using a similar process to the precursor mass but using the precursor formula as the list of allowed atoms. Potential formulas were compared against the existing EPA's Comptox Chemicals Dashboard,[36] an internally maintained PFAS database, and extant literature, including publications, patents, and the CAS registry, to obtain known potential structures. Potential structures were also generated *de novo* based on observed fragments and related chemicals. A degree-of-confidence assessment for each chemical feature was assigned based on the Schymanski classification.[37] Briefly, where verified standards existed for a proposed structure, comparison with the retention time and MS/MS structure of the standard was carried out; matches were assigned a confidence level of 1. In the absence of a confirmed standard, fragment ions were compared to available standards with similar substructures and empirical or *in silico* library spectra; probable structures were assigned a confidence level of 2. Where structures could not be completely resolved by MS/MS, partial elucidation of chemical class/structure was based on diagnostic fragments and relationship to identified compounds; tentative candidates were assigned a confidence level of 3. In absence of quality MS/MS spectra or where incompatible tentative candidates could not be resolved, only a molecular formula was determined; molecular formula level assignments were given a confidence level of 4. Features with lower confidence were not reported here.

Clustering of Non-Targeted Chemical Features by Time Trend. The samples collected in May 2017 and February 2018 bracketed significant changes to the Cape Fear River as the result of regulatory actions by NCDEQ against the Chemours company.[33] As part of their ongoing monitoring, the state collected water samples proximate to the waste outfall into the Cape Fear River over several months during the summer of 2017. These samples were acquired from NCDEQ, analyzed by TOF-MS as described, and the ion abundances for the species were monitored over the sampling time points. Abundance measurements for each chemical were normalized to the highest abundance for the feature across all sampling points for that chemical. Time trends of chemical features were hierarchical clustered for similarity with *hclust* in R (3.4.4) using Euclidean distance and the "Ward.D2" clustering criterion;[38] cluster p-values were calculated using *pvclust*[39] with 10000 bootstrap iterations and filtered to $p < 0.05$.

RESULTS AND DISCUSSION

Feature extraction from surface water collected upstream of a fluorochemical manufacturing site yielded ∼120 distinct molecular features. Features with PFAS-like MS signatures were all from the legacy perfluorinated acids (PFBA, PFPeA, PFHxA, PFHpA, PFHxS, PFOA, and PFOS). No additional PFAS species were detected in the samples. The existence of these fluorinated compounds in the surface water is expected, because of their persistent nature and ubiquitous use in preceding years, and has been previously reported.[40−44]

Feature extraction from the sample immediately downstream from the fluorochemical manufacturer yielded a significantly larger amount of ∼260 distinct molecular features of which nearly 200 possess the negative mass defect marker indicative of potential halogenation (Supporting Information Table 1). A comparison of the total signal intensity of species with a negative mass defect in the upstream and downstream samples indicates that while ∼15% of the total ion current for the upstream sample is resultant from perfluorinated acids above, the downstream sample is, by total ion intensity, >90% composed of species with a negative mass defect. Further, the ambient PFASs detected upstream make up <1% of the total ion intensity in the downstream sample. Clearly, wastewater discharge from the fluorochemical manufacture introduces a significant number of compounds to the river besides the legacy perfluorinated acids detailed in EPA 537[45] (Supporting Information Table 1).

Manual curation of detected chemical features yielded 58 distinct chromatographically resolved PFAS peaks, corresponding to 38 unique molecular formulas. Recent efforts have been made to identify novel contaminant species in fluorochemically impacted water supplies by the US EPA and other groups.[26,46−49] Cross-referencing literature lists of expected monoisotopic masses and their hypothetical structures against the molecular features observed in this study accounts for roughly half of the unique features, with the remainder being unidentified based on literature comparison.

The features were individually examined to determine novel structures as described in the Methods section (Supporting Information Table 2). For each mass-to-charge (m/z) identified at the formula level or better, an extracted ion chromatogram of the precursor mass was generated to determine retention times (Supporting Information Figures 1−83). Composite MS/MS spectra consisting of multiple averaged MS/MS scans at 10 and 25 CID settings were

DOI: 10.1021/acs.est.8b06017
Environ. Sci. Technol. 2019, 53, 4717−4727

Table 1. Identified Perfluorinated Ether Acids

ID	Conf	Formula	Theoretical [M]	ppm error	Isomers	CAS	Ref
1	1	$C_3HF_5O_3$	179.9846	1.68	1	674-13-5	29
2	1	$C_4HF_7O_3$	229.9814	2.18	2	13140-29-9, 377-73-1	29
3	1/2b	$C_4HF_7O_4$	245.9763	0.41	1	39492-88-1	29
4	2b	$C_5HF_9O_3$	279.9782	1.43	1	267239-61-2	29
5	3	$C_5HF_9O_4$	295.9731	2.71	1		
6	1	$C_5HF_9O_5$	311.968	0.96	1	39492-89-2	29
7	1	$C_6HF_{11}O_3$	329.975	1.22	1	13252-13-6	29
8	3	$C_6HF_{11}O_4$	345.9699	0.58	1		
9	3	$C_6HF_{11}O_5$	361.9648	0.83	1		
10	1	$C_6HF_{11}O_6$	377.9597	1.59	1		29
11	4	$C_8HF_{13}O_4$	407.9667	0.25	1		
12	3	$C_7HF_{13}O_5$	411.9616	1.46	1		
13	1	$C_7HF_{13}O_7$	443.9515	0.90	1		29
14	2b	$C_4HF_9O_4S$	315.94518	1.97	1	113507-82-7	29
15	3	$C_5HF_{11}O_4S$	365.94199	0.85	1		
16	1	$C_7HF_{13}O_5S$	443.93371	0.20	1	29311-67-9	29
17	3	$C_8HF_{15}O_5S$	493.93052	0.04	1		

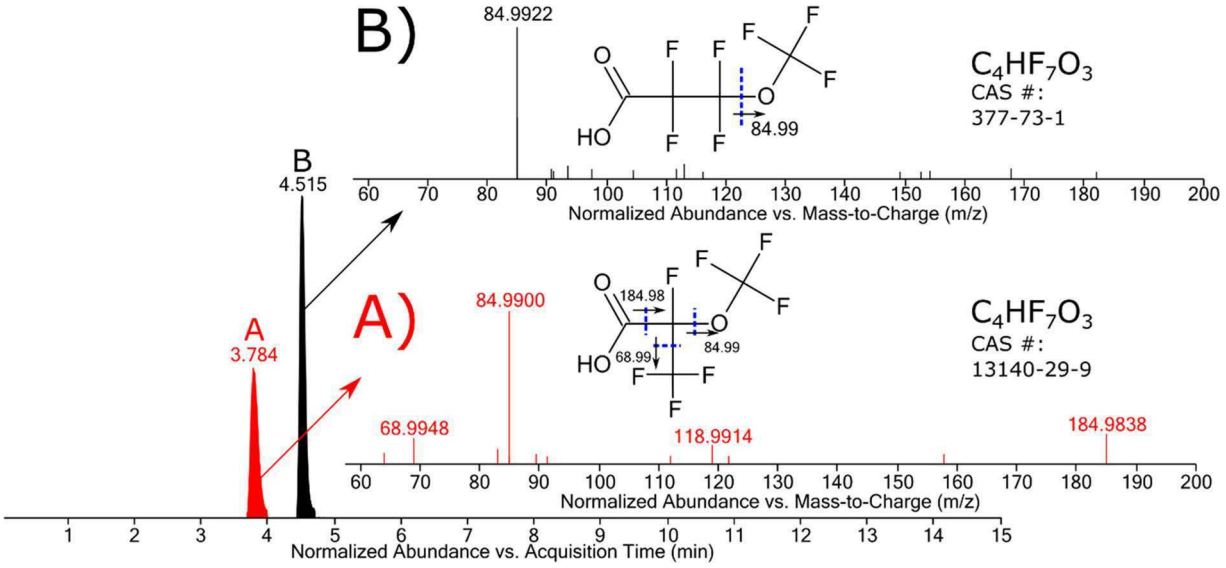

Figure 1. Determination of isomeric branching of perfluorinated ether compounds based on MS/MS fragmentation patterns. Compound 2A elutes at 3.8 min and has multiple major mass fragments. Compound 2B elutes later at 4.5 min and fragments only at the terminal ether linkage.

generated for individual isomers of each precursor, where possible (Supporting Information Figures 1−83).

Group A: Perfluorinated Ether Acids. A frequently observed PFAS class is that of fluoroether acids (here Group A), which exist with a general formula $CF_3(CF_2)_n(CF_2O)_m(R_1)$, where the headgroup, R_1, is an acidic moiety such as −COOH or $-SO_3H$.[29,30] These were expected to be the primary contaminants identified in the survey, given that nearby production includes perfluorinated polyvinyl ethers, empirical formula $(CF_2)_n(CF_2O)_m$. The production of the ammonium salt of 2,3,3,3-tetrafluoro-2-(heptafluoropropoxy) propanoic acid,[21] where $n = 3$, $m = 1$, R1 = COOH is shown in the above scheme, and "Nafion", a copolymer of tetrafluoroethylene and perfluoro(4-methyl-3,6-dioxaoct-7-ene)sulfonic acid, a monomer where $n = 3$, $m = 2$, $R_1 = SO_3H$ is shown as above.[50] Numerous molecules in this series were found during this sampling event (Table 1).

Compound 2 was identified previously in historical sampling in the river basin;[29] however, the UPLC separation resolved two isomeric structures with different MS/MS fragmentation patterns (Figure 1), which was not observed for other Group A species. The more abundant isomer of compound 2 (2B) is available as a standard, and its MS/MS fragmentation pattern and retention were confirmed to match the tentative assignment. The additional isomer is currently not commercially available and was assigned on the basis of MS/MS fragmentation and the shift in reverse phase retention time, indicative of increased branching (Schymanski Level 2b).[51]

The primary fragments for perfluorinated ether carboxylic acids are typically decarboxylation (neutral loss of 43.9898 Da) and production of the terminal ether fragment (here CF_3O^-, 84.99067 Da). Sulfonated acids produce a sulfonate (SO_3^-, 79.9568 Da) fragment instead of a decarboxylation, but the primary structural fragment remains the terminal ether. These patterns were observed across all Group A compounds, but the lack of significant internal fragmentation makes it difficult to assign complete linkage isomerization of longer perfluorinated

DOI: 10.1021/acs.est.8b06017
Environ. Sci. Technol. 2019, 53, 4717−4727

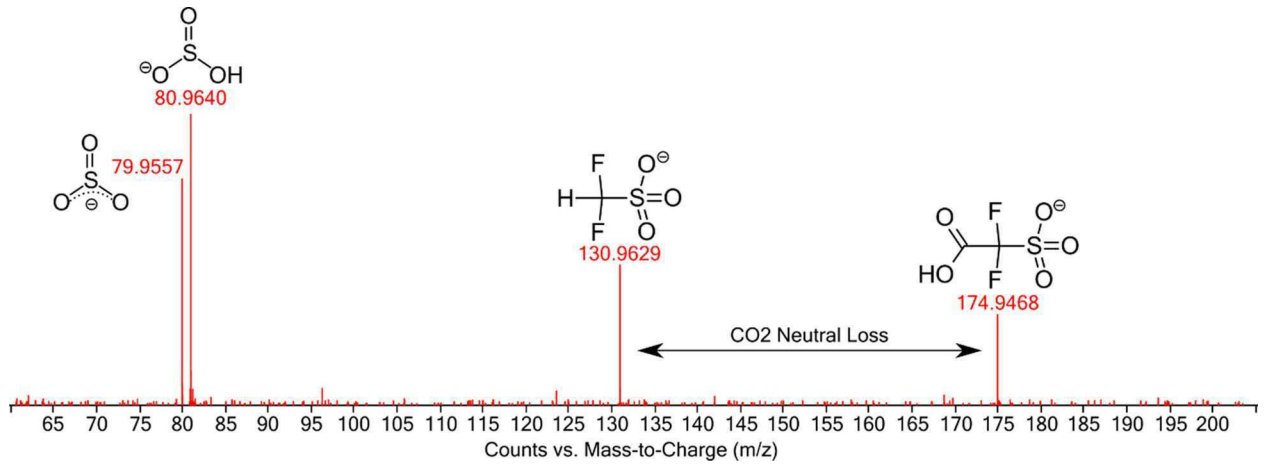

Figure 2. Annotated MS/MS spectrum of precursor m/z 174.9496 (compound 18), assigned the molecular formula $C_2H_2F_2O_5S$.

Table 2. Identified Perfluorinated Ether Acids with Multiple Acidic Sites

ID	Conf	Formula	Theoretical [M]	ppm error	Isomers	CAS	Ref
18	2b	$C_2H_2F_2O_5S$	175.9591	0.57	1	422-67-3	55
19	2b/3	$C_5H_2F_8O_6S$	341.9444	2.35	2	790642-73-8	55
20	3	$C_6H_2F_{10}O_5$	343.9743	2.33	1	919005-07-5	56
21	4	$C_7H_3F_{11}O_7S$	439.9424	0.68	2		
22	2b/3	$C_7H_2F_{12}O_6S$	441.938	0.23	2	852157-01-8	57
23	2b/3	$C_8H_2F_{14}O_7S$	507.9298	1.18	2	1235024-21-1	57
24	2b/3	$C_7H_3F_{13}O_8S_2$	525.9062	0.19	2	916340-65-3	58

ethers based on MS/MS alone, and many compounds remain level 3 identifications.

The initial patent description of the polyvinyl ether process refers to the creation of multiple competing side reactions and low molecular weight polyfluoro-ether byproducts,[52,53] which have been used as reactants and starting materials in more complicated copolymer production schemes.[54] Without further information about manufacturing processes, it is not immediately clear which reactions and waste streams yield the perfluoroether compounds detected and whether they are primary or secondary waste products. Further, broader nontargeted efforts would be necessary to determine whether they are contained in finished products directly impacting consumers or only in the nearby environment; however, the spatial and temporal correlation of detected species is highly suggestive of the point source (i.e., manufacturing outfall).

Group B: Multi-Headed Perfluoroether Species. Perfluoroether species previously described can be thought of in a more general sense as compounds with the form R_1-$(CF_2)_n(CF_2O)_m$-R_2, where R_1 and R_2 are both variable head groups. While R_1 is CF_3 for the Group A perfluorinated acids previously discussed, some compounds were observed with multiple acidic groups (R_1, R_2 = −COOH or $-SO_3H$). This group of compounds was identified in both −1 and −2 charge states and had initial predicted formulas suggesting an overabundance of oxygens which could only be structurally supported by multiple acidic sites on the perfluorinated backbone. Further, diagnostic ions for CO_2 and/or SO_3 were observed (Figure 2). We grouped these species as Group B, multiply sulfonated and/or carboxylated perfluorinated ether acids (Table 2).

While these species have not been previously reported in environmental media, to the best of our knowledge, the literature of fluorochemical manufacturers proposes a few possible structures in this group, primarily as side products in fluoropolymer production and degradation.[55−57] The formation of short chain fluorosulfonyl ($-SO_2F$) and acyl fluoride (−COF) fluoroethers formed as byproducts or intermediate steps in fluoropolymer synthesis is the likely source of precursor compounds that degrade into the observed compounds.[52] Aqueous hydrolysis of the acid fluoride intermediates during production or water treatment yields the familiar carboxylic acid (−COOH) and sulfonic acid moieties ($-SO_3H$), while more basic conditions (e.g., KOH, Na_2CO_3, etc.) yield further hydrolysis products (Scheme 1). These full and partial hydrolysis reactions are well-known steps in fluoropolymer production and in the abatement of fluoroether salts.[59−61]

Scheme 1. Transformation of a Fluorosulfonyl/Acyl Fluoride Fluoroether to Sulfonate End Products by Hydroloysis

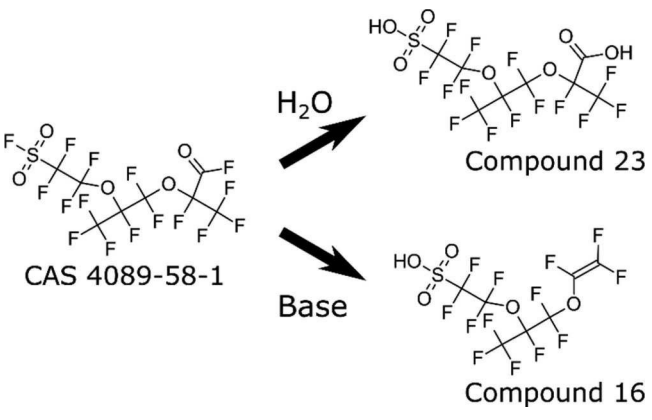

DOI: 10.1021/acs.est.8b06017
Environ. Sci. Technol. 2019, 53, 4717−4727

Table 3. Identified Polyfluorinated Ether Acids with a Single Hydrogen Substitution

ID	Conf	Formula	Theoretical [M]	ppm error	Isomers	CAS	Ref
25	2b/3	$C_3H_2F_6O_4S$	247.9578	1.62	3	905363-45-3	58
26	1	$C_4H_2F_8O_4S$	297.9546	1.35	1	905363-44-2	58
27	2b/3	$C_5H_2F_{10}O_4S$	347.9514	1.15	3	935443-55-3	58
28	3	$C_6H_2F_{12}O_4S$	397.9482	1.51	2		
29	3	$C_8H_2F_{14}O_4S$	459.9450	0.00	3		
30	2b/3	$C_5H_2F_8O_3$	261.9876	1.15	3	919005-00-8, 919005-13-3	56
31	2b/3	$C_6H_2F_{10}O_3$	311.9844	1.61	3	919005-19-9	56
32	3	$C_7H_2F_{12}O_3$	361.9812	3.05	1	919005-26-8	56
33	3	$C_6H_2F_{12}O_5S$	413.9431	0.00	2		
34	1	$C_7H_2F_{14}O_5S$	463.9399	1.30	2	749836-20-2	29
35	4	$C_9H_2F_{16}O_6S$	541.9317	0.00	1		
36	1	$C_8H_2F_{14}O_4$	427.9730	2.11	1	773804-62-9	
37	4	$C_8H_2F_{14}O_7$	475.9577	4.42	2		

Group C: Single-H Containing Polyfluorinated Acids. Another subset of fluorinated compounds, Group C, was identified with molecular formulas containing a single F → H substitution compared to that in the Group A perfluorinated ether compounds (Table 3). For example, compound 14 ($C_4HO_4SF_9$) and compound 26 ($C_4H_2O_4SF_8$) differ by the substitution of a hydrogen for a fluorine. These compounds are highly isomerized, and MS/MS fragmentation is frequently insufficient to unequivocally assign the structure; the structures presented in the Supporting Information (Table S-2) are representative of a single observed isomer.

The production of polyfluorosulfonic acid ethers of the form R-OCF**H**−CF_2−SO_3 was described in early patent filings,[58] and their use as fluoropolymer surfactants was mentioned in a follow up.[62] The use and production of these chemicals as part of Nafion manufacturing is assumed to be responsible for at least some of the observed species. In contrast to the previously mentioned literature structures, MS/MS fragmentation of some polyether sulfonate isomers indicates that the single hydrogen substitution occurs on the tail ether rather than adjacent to the head; for example, the fragment C_2HF_4O− (116.9969 Da) from one isomer of compound 30 (Supporting Information Figure 64) is derived from a two carbon polyfluorinated ether unit (Supporting Information Table S-4). These species are assumed to be products of the fluorosulfonyl and/or acyl fluoride species which produced Group B but further decomposed. The complete loss of a headgroup (e.g., decarboxylation) during production, waste treatment, or naturally in surface water would yield a compound with a single hydrogen in that site (Scheme 2). Thermally decarboxylated perfluoroether species are noted as potentially undesirable byproducts of fluoropolymer production in the patent literature of fluoropolymer production,[60] and partially decarboxylated species are noted as possible products from multiply acidic species such as Group B chemicals.[63]

Scheme 2. Transformation by Decarboxylation of Sulfonated Carboxylic Acid Perfluoroether to Yield the Polyfluorosulfonic Acid

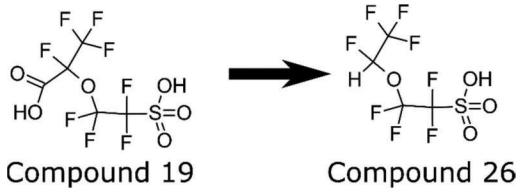

Presence and Prevalence of Novel Species. The lack of authentic standards limits the potential for quantitative measurements of novel compounds; relative abundance and semiquantitative estimates of emerging compounds are all that are available. However, this information remains useful for targeting individual chemicals for follow-up study and for monitoring environmental changes in response to systemic actions. Our examination of the May 2017 downstream sample could assign 35 of the top 50 most abundant features, corresponding to ∼90% of the total ion current in the sample (Figure 3). While ion abundances are sensitive to many aspects of the sample matrix and molecules, the structural similarity of the fluoroethers would suggest some similarity in instrument response, and that species can be roughly compared. At least one species of each of the three major chemical groups outlined (groups A, B, and C) exhibited a higher ion abundance than the HFPO-DA species with a targeted health goal. Further, of the targeted compounds detailed in EPA 537,[45] only perfluoropentanoic acid (PFPeA) is present in the top 50; thus, the fluorochemical load in the system would be greatly underestimated by traditional targeted approaches. Additionally, including the compounds previously detailed in studies of the Cape Fear River[29,30] accounts for only ∼50% of the total ion intensity in the initial sample, suggesting that even single-time-point nontargeted survey can fail to sufficiently capture the chemical complexity of a location.

An advantage of nontargeted analysis is the historical data banking of samples and the ability to perform relative quantification across disparate sample sets. The comparison of chemical species abundance over the time period from May 2017 to February 2018 revealed several distinct abundance patterns from simple visual inspection (Figure 4). Many fluoroether species exhibited exponential decline in concentration (Figure 4, left) while others showed lagging or even temporarily increased abundances (Figure 4, center and right).

Matrices of the weekly relative ion abundance of each of the identified chemical features over the eight sampling points were clustered for similarity using Ward's clustering criterion implemented in R *hclust*;[38] *p*-value calculations for clusters were performed using multiscale bootstrap resampling implemented in the *pvclust* package. Clustering of the time-trend data yielded six distinct chemical clusters (Figure 5, Supporting Information Figures 84−89).

DOI: 10.1021/acs.est.8b06017
Environ. Sci. Technol. 2019, 53, 4717−4727

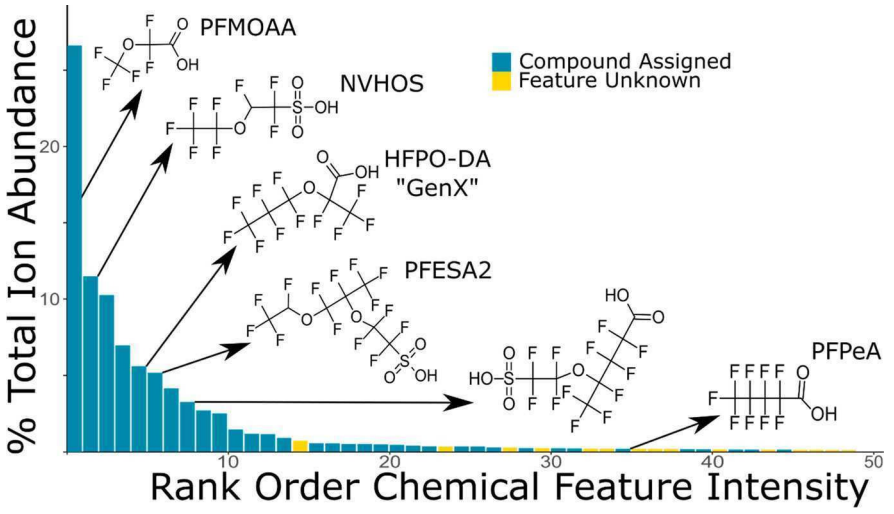

Figure 3. Total ion abundance as a percentage of the sum of all chemical features for compounds identified in a May 2017 sample of the Cape Fear River downstream of a fluorochemical manufacturer. Selected highly abundant compounds confirmed by standards obtained from and labeled by Chemours include: compounds 1 (PFMOAA), 26 (NVHOS), 7 (HFPO-DA), 34 (PFESA2), 22 (PFESA4), and perfluoropentanoic acid (PFPeA).

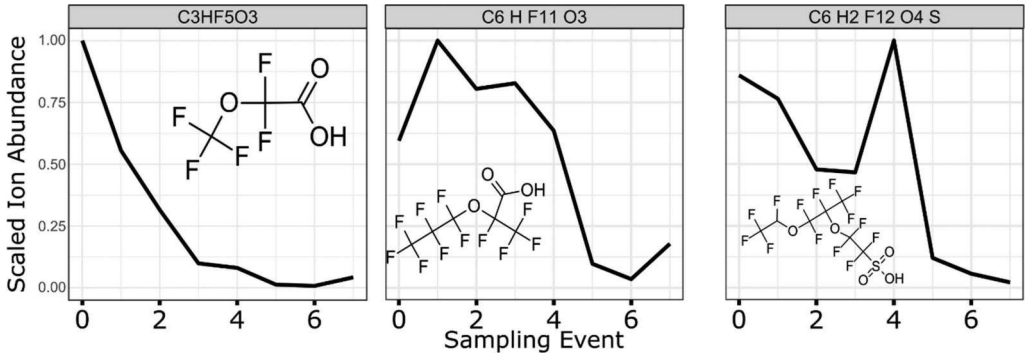

Figure 4. Scaled ion abundance of three chemical features confirmed by standard and detected in the Cape Fear River over a time course sample. Time points one to six were taken weekly beginning June 19, 2017 with time points zero and seven being collected in May 2017 and February 2018, respectively.

These clusters support the hypothesis that multiple production processes generate distinct groups of the chemicals observed in the Cape Fear River, as the compound abundances are correlated over time and are chemically similar based on naive classification. For example, the cluster at branch 16 (Figure 5) contains the H-substituted sulfonic acid ethers from Group C. These compounds abruptly and almost uniformly vanish following the initial sampling event (Supporting Information Figure 86), while the clusters at branches 13 and 18 contain the perfluoroether carboxylic acids and their associated H substituted versions; both classes exponentially and smoothly decrease from the early sampling events (Supporting Information Figures 84,87). Other clusters contain more chemical variation, as well as more complex time-trend patterns, that may be reflective of species with multiple sources or processes involving multiple PFAS classes.

It is worth noting that the chemical assignment provided to each feature is not required for clustering. Application of the clustering approach reveals chemical feature relationships that could be used to target unidentified species for follow-up analysis based on their close association with compounds of interest (e.g., HFPO-DA), and occurs before the assignment of formulas or structures.

Environmental Impact. The phase-out of PFOA/PFOS and longer-chain PFAS materials has led to an increased prevalence of replacement chemicals. The chemical groups detailed here are derived from processes and procedures that are over 20 years old within the fluorochemical production industry but are only now becoming apparent due to increased scrutiny of environmental media and the proliferation of nontargeted methodologies. Fluorinated ethers such as those described here have been reported in the Cape Fear River previously.[29,30] Similar structures have been reported in numerous locations worldwide, indicating that emerging PFAS are every bit as ubiquitous as their PFOA/PFOS antecedents.[64,65] Physiochemical characteristics of similar perfluorinated ether compounds suggest that the fluoroether substances are of reduced health impact compared to similarly sized perfluorinated acids, but retain some degree of health risk.[66] Further, longer-chain perfluorinated ethers are not currently regulated similarly to long chain perfluorinated acids and exhibit similar bioaccumulation potential, as evidenced by the preliminary reporting in human blood in spite of their relative low abundance in surface water.[67] Efforts to determine reasonable health levels for these emerging compounds are ongoing. During the preparation of this manuscript, the state of North Carolina set a drinking water health goal for a single perfluorinated ether acid (PFECA) compound, HFPO-DA, at 140 ng/L, based on their assessment of human health risk from available data submitted in the European Union.[31,68,69]

DOI: 10.1021/acs.est.8b06017
Environ. Sci. Technol. 2019, 53, 4717−4727

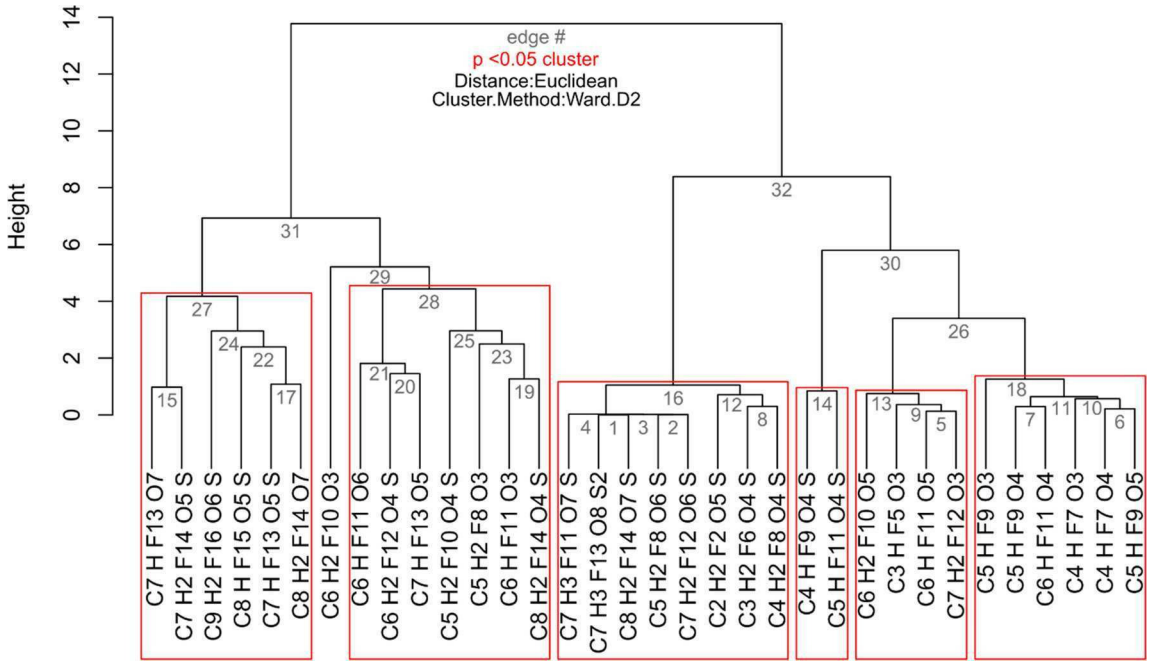

Figure 5. Clustering of identified chemical features from scaled ion-abundance of features detected in the Cape Fear River in eight sampling events between May 2017 and February 2018.

Sulfonated ether substances in this measurement series are primarily associated with sulfonated fluoropolymer production, specifically the Nafion polymer, and are of lesser widespread concern due to the limited manufacture of such polymers and their primary application being energy-related technologies, such as fuel cells.[50] Nevertheless, for locations that are exposed to such manufacturing waste streams, sulfonated fluorinated acids have shown higher accumulation potential and toxicological effects than equivalent carboxylic acids.[19] Further, other sulfonated ether acids, such as F-53B, have shown equivalent bioaccumulation potential as the regulated perfluorinated sulfonic acid PFOS.[70,71] Other sulfonated fluoroether species have begun to be detected by other groups, but they exhibit different structural elements and likely have different origins that need to be examined independently.[64,72] The continued appearance of new PFAS species necessitates an increase in the generation of toxicological profiling and monitoring efforts to assess human risk from exposure to these novel chemicals.

With regards to human exposure, it has been demonstrated that perfluoroether compounds are poorly cleared by water treatment processes, including activated carbon, and the most effective method of removal is through source control.[30,73] Long-term monitoring of impacted watersheds remains an important tool for both detecting new chemical species over multiyear time scales and for determining shorter-term changes in local chemical load. An application of this approach to other watersheds has been effective for other chemical classes, such as surfactants.[23,47] During the course of this study, our monitoring activities resulted in the cessation of discharge from the vinyl ether production at the source manufacturing location, which resulted in a concomitant decrease in PFECAs hypothesized to derive from that process, but not in the immediate reduction of the perfluorinated ether sulfonic acid (PFESAs) species since they derive from a different source than the PFECAs.[33] Targeted methods and single time-point nontargeted surveys can easily miss transient chemicals or underestimate chemical loads for exposure assessment; some species spiked as much as 5-fold during the sampling period (cluster branch 27, Supporting Information Figure 88), even as other compounds were declining. The proactive application of a nontargeted screening approach is capable of identifying and monitoring chemicals present in the water, even prior to complete structural elucidation or toxicological analysis and provides a useful tool toward those ends.

■ ASSOCIATED CONTENT

Supporting Information

The Supporting Information is available free of charge on the ACS Publications website at DOI: 10.1021/acs.est.8b06017.

All detected chemical features, assigned chemical species, software settings for molecular feature extraction, common MS/MS fragments of PFAS compounds, chromatographic traces for molecular ions of chemical features, composite MS/MS fragmentation spectra of chemical features, scaled abundance time trends for chemical features, statistical validation of chemical feature clustering, sampling map (PDF)

Cape Fear upstream and downstream data (XLSX)

■ AUTHOR INFORMATION

Corresponding Author

*Phone: 919-541-3706. E-mail: strynar.mark@epa.gov.

ORCID

James McCord: 0000-0002-1780-4916

Mark Strynar: 0000-0003-3472-7921

Author Contributions

The manuscript was written through contributions of all authors. All authors have given approval to the final version of the manuscript.

Notes

The authors declare no competing financial interest.

DOI: 10.1021/acs.est.8b06017
Environ. Sci. Technol. 2019, 53, 4717−4727

■ ACKNOWLEDGMENTS

The U.S. Environmental Protection Agency, through its Office of Research and Development, funded and managed the research described here. This document has been reviewed by the U.S. Environmental Protection Agency, Office of Research and Development, and approved for publication. The views expressed in this article are those of the authors and do not necessarily represent the views or policies of the U.S. Environmental Protection Agency. This research was supported in part by an appointment to the Postdoctoral Research Program at the National Exposure Research Laboratory administered by the Oak Ridge Institute for Science and Education through Interagency Agreement DW89992431601 between the U.S. Department of Energy and the U.S. Environmental Protection Agency.

■ REFERENCES

(1) Lindstrom, A. B.; Strynar, M. J.; Libelo, E. L. Polyfluorinated Compounds: Past, Present, and Future. *Environ. Sci. Technol.* **2011**, *45* (19), 7954.

(2) Sargent, J. W.; Seffl, R. In *Properties of perfluorinated liquids, Federation proceedings*, 1970; pp 1699−1703.

(3) Rahman, M. F.; Peldszus, S.; Anderson, W. B. Behaviour and fate of perfluoroalkyl and polyfluoroalkyl substances (PFASs) in drinking water treatment: A review. *Water Res.* **2014**, *50*, 318−340.

(4) Grandjean, P.; Clapp, R. Changing Interpretation of Human Health Risks from Perfluorinated Compounds. *Public Health Rep.* **2014**, *129* (6), 482−485.

(5) *Provisional Health Advisories for Perfluorooctanoic Acid (PFOA) and Perfluorooctane Sulfonate (PFOS)*. In United States Environmental Protection Agency: Washington DC, 2009.

(6) Report of the Conference of the Parties of the Stockholm Convention on Persistent Organic Pollutants on the work of its fourth meeting 2009.

(7) Proposal for a COUNCIL DECISION on the submission, on behalf of the European Union, of a proposal for the listing of additional chemicals in Annex A to the Stockholm Convention on Persistent Organic Pollutants. In Council of the European Union: 2016.

(8) MacNeil, J.; Steenland, N. K.; Shankar, A.; Ducatman, A. A cross-sectional analysis of type II diabetes in a community with exposure to perfluorooctanoic acid (PFOA). *Environ. Res.* **2009**, *109* (8), 997−1003.

(9) Steenland, K.; Fletcher, T.; Savitz, D. A. Epidemiologic Evidence on the Health Effects of Perfluorooctanoic Acid (PFOA). *Environ. Health Perspect.* **2010**, *118* (8), 1100−1108.

(10) Fact Sheet: 2010/2015 PFOA Stewardship Program. https://www.epa.gov/assessing-and-managing-chemicals-under-tsca/fact-sheet-20102015-pfoa-stewardship-program.

(11) EPA and 3M Announce phase out of PFOS. https://yosemite.epa.gov/opa/admpress.nsf/0/33aa946e6cb11f35852568e1005246b4.

(12) Kissa, E. *Fluorinated surfactants and repellents*. CRC Press: 2001; Vol. 97.

(13) Bowman, J. S. Fluorotechnology is critical to modern life: the FluoroCouncil counterpoint to the Madrid Statement. *Environ. Health Perspect.* **2015**, *123* (5), A112.

(14) Scheringer, M.; Trier, X.; Cousins, I. T.; de Voogt, P.; Fletcher, T.; Wang, Z.; Webster, T. F. Helsingør Statement on poly- and perfluorinated alkyl substances (PFASs). *Chemosphere* **2014**, *114*, 337−339.

(15) Wang, Z.; Cousins, I. T.; Scheringer, M.; Hungerbühler, K. Fluorinated alternatives to long-chain perfluoroalkyl carboxylic acids (PFCAs), perfluoroalkane sulfonic acids (PFSAs) and their potential precursors. *Environ. Int.* **2013**, *60*, 242.

(16) Strempel, S.; Scheringer, M.; Ng, C. A.; Hungerbühler, K. Screening for PBT Chemicals among the "Existing" and "New" Chemicals of the EU. *Environ. Sci. Technol.* **2012**, *46* (11), 5680−5687.

(17) Fantke, P.; Weber, R.; Scheringer, M. From incremental to fundamental substitution in chemical alternatives assessment. *Sustainable Chemistry and Pharmacy* **2015**, *1*, 1−8.

(18) Blum, A.; Balan, S. A.; Scheringer, M.; Trier, X.; Goldenman, G.; Cousins, I. T.; Diamond, M.; Fletcher, T.; Higgins, C.; Lindeman, A. E. The Madrid statement on poly-and perfluoroalkyl substances (PFASs). *Environ. Health Perspect.* **2015**, *123* (5), A107.

(19) DeWitt, J. C. *Toxicological Effects of Perfluoroalkyl and Polyfluoroalkyl Substances*. 2015.

(20) Marchionni, G.; Tortelli, V.; Wlassics, I.; Kapeliouchko, V. Method for manufacturing fluoropolymers. US8703889B2, 2014.

(21) DuPont GenX Processing Aid for Making Fluoropolymer Resins. In *Chemours*: 2010.

(22) Trier, X.; Granby, K.; Christensen, J. H. Polyfluorinated surfactants (PFS) in paper and board coatings for food packaging. *Environ. Sci. Pollut. Res.* **2011**, *18* (7), 1108−1120.

(23) Schymanski, E. L.; Singer, H. P.; Slobodnik, J.; Ipolyi, I. M.; Oswald, P.; Krauss, M.; Schulze, T.; Haglund, P.; Letzel, T.; Grosse, S.; Thomaidis, N. S.; Bletsou, A.; Zwiener, C.; Ibáñez, M.; Portolés, T.; de Boer, R.; Reid, M. J.; Onghena, M.; Kunkel, U.; Schulz, W.; Guillon, A.; Noyon, N.; Leroy, G.; Bados, P.; Bogialli, S.; Stipaničev, D.; Rostkowski, P.; Hollender, J. Non-target screening with high-resolution mass spectrometry: critical review using a collaborative trial on water analysis. *Anal. Bioanal. Chem.* **2015**, *407* (21), 6237−6255.

(24) Chibwe, L.; Titaley, I. A.; Hoh, E.; Simonich, S. L. M. Integrated framework for identifying toxic transformation products in complex environmental mixtures. *Environ. Sci. Technol. Lett.* **2017**, *4* (2), 32−43.

(25) Knolhoff, A. M.; Croley, T. R. Non-targeted screening approaches for contaminants and adulterants in food using liquid chromatography hyphenated to high resolution mass spectrometry. *Journal of Chromatography A* **2016**, *1428*, 86−96.

(26) Newton, S.; McMahen, R.; Stoeckel, J. A.; Chislock, M.; Lindstrom, A.; Strynar, M. Novel Polyfluorinated Compounds Identified Using High Resolution Mass Spectrometry Downstream of Manufacturing Facilities near Decatur, Alabama. *Environ. Sci. Technol.* **2017**, *51* (3), 1544−1552.

(27) Ferrer, I.; Thurman, E. M. Liquid chromatography/time-of-flight/mass spectrometry (LC/TOF/MS) for the analysis of emerging contaminants. *TrAC, Trends Anal. Chem.* **2003**, *22* (10), 750.

(28) Liu, Y.; Pereira, A. D. S.; Martin, J. W. Discovery of C5−C17 Poly-and Perfluoroalkyl Substances in Water by In-Line SPE-HPLC-Orbitrap with In-Source Fragmentation Flagging. *Anal. Chem.* **2015**, *87* (8), 4260.

(29) Strynar, M.; Dagnino, S.; McMahen, R.; Liang, S.; Lindstrom, A.; Andersen, E.; McMillan, L.; Thurman, M.; Ferrer, I.; Ball, C. Identification of novel perfluoroalkyl ether carboxylic acids (PFECAs) and sulfonic acids (PFESAs) in natural waters using accurate mass time-of-flight mass spectrometry (TOFMS). *Environ. Sci. Technol.* **2015**, *49* (19), 11622.

(30) Sun, M.; Arevalo, E.; Strynar, M.; Lindstrom, A.; Richardson, M.; Kearns, B.; Pickett, A.; Smith, C.; Knappe, D. R. U. Legacy and Emerging Perfluoroalkyl Substances Are Important Drinking Water Contaminants in the Cape Fear River Watershed of North Carolina. *Environ. Sci. Technol. Lett.* **2016**, *3* (12), 415−419.

(31) *NC DHHS Preliminary Risk Assessment FAQ for GenX (Perfluoro2-propoxypropanoic acid)*. In North Carolina Department of Health and Human Services: 2017.

(32) Hagerty, V., Toxin taints CFPUA drinking water. *StarNews* 2017.

(33) NC Department of Environmental Quality GenX Investigation. https://deq.nc.gov/news/hot-topics/genx-investigation/.

(34) Nakayama, S. F.; Strynar, M. J.; Reiner, J. L.; Delinsky, A. D.; Lindstrom, A. B. Determination of perfluorinated compounds in the Upper Mississippi River Basin. *Environ. Sci. Technol.* **2010**, *44* (11), 4103.

DOI: 10.1021/acs.est.8b06017
Environ. Sci. Technol. 2019, 53, 4717−4727

(35) Sleno, L. The use of mass defect in modern mass spectrometry. *J. Mass Spectrom.* **2012**, *47* (2), 226−36.
(36) McEachran, A. D.; Sobus, J. R.; Williams, A. J. Identifying known unknowns using the US EPA's CompTox Chemistry Dashboard. *Anal. Bioanal. Chem.* **2017**, *409* (7), 1729−1735.
(37) Schymanski, E. L.; Jeon, J.; Gulde, R.; Fenner, K.; Ruff, M.; Singer, H. P.; Hollender, J. Identifying small molecules via high resolution mass spectrometry: communicating confidence. *Environ. Sci. Technol.* **2014**, *48* (4), 2097.
(38) Murtagh, F.; Legendre, P. Ward's Hierarchical Agglomerative Clustering Method: Which Algorithms Implement Ward's Criterion? *Journal of Classification* **2014**, *31* (3), 274−295.
(39) Suzuki, R.; Shimodaira, H. Pvclust: an R package for assessing the uncertainty in hierarchical clustering. *Bioinformatics* **2006**, *22* (12), 1540−1542.
(40) Hu, X. C.; Andrews, D. Q.; Lindstrom, A. B.; Bruton, T. A.; Schaider, L. A.; Grandjean, P.; Lohmann, R.; Carignan, C. C.; Blum, A.; Balan, S. A.; Higgins, C. P.; Sunderland, E. M. Detection of Poly- and Perfluoroalkyl Substances (PFASs) in U.S. Drinking Water Linked to Industrial Sites, Military Fire Training Areas, and Wastewater Treatment Plants. *Environ. Sci. Technol. Lett.* **2016**, *3* (10), 344−350.
(41) Arsenault, G.; Chittim, B.; McAlees, A.; McCrindle, R.; Riddell, N.; Yeo, B. Some issues relating to the use of perfluorooctanesulfonate (PFOS) samples as reference standards. *Chemosphere* **2008**, *70* (4), 616−25.
(42) Hansen, K. J.; Clemen, L. A.; Ellefson, M. E.; Johnson, H. O. Compound-specific, quantitative characterization of organic fluorochemicals in biological matrices. *Environ. Sci. Technol.* **2001**, *35* (4), 766−70.
(43) Giesy, J. P.; Kannan, K. Global distribution of perfluorooctane sulfonate in wildlife. *Environ. Sci. Technol.* **2001**, *35* (7), 1339−42.
(44) Buck, R. C.; Franklin, J.; Berger, U.; Conder, J. M.; Cousins, I. T.; de Voogt, P.; Jensen, A. A.; Kannan, K.; Mabury, S. A.; van Leeuwen, S. P. J. Perfluoroalkyl and Polyfluoroalkyl Substances in the Environment: Terminology, Classification, and Origins. *Integr. Environ. Assess. Manage.* **2011**, *7* (4), 513−541.
(45) Shoemaker, J.; Grimmett, P.; Boutin, B. *Method 537. Determination of selected perfluorinated alkyl acids in drinking water by solid phase extraction and liquid chromatography/tandem mass spectrometry (LC/MS/MS)*. U.S. Environmental Protection Agency: Washington, DC, 2009.
(46) J Place, B.; Field, J. *Identification of Novel Fluorochemicals in Aqueous Film-Forming Foams Used by the US Military*. 2012; Vol. *46*, p 7120−7.
(47) Hollender, J.; Schymanski, E. L.; Singer, H. P.; Ferguson, P. L. Nontarget Screening with High Resolution Mass Spectrometry in the Environment: Ready to Go? *Environ. Sci. Technol.* **2017**, *51* (20), 11505−11512.
(48) Gebbink, W. A.; van Asseldonk, L.; van Leeuwen, S. P. J. Presence of Emerging Per- and Polyfluoroalkyl Substances (PFASs) in River and Drinking Water near a Fluorochemical Production Plant in the Netherlands. *Environ. Sci. Technol.* **2017**, *51* (19), 11057−11065.
(49) Xiao, F.; Golovko, S. A.; Golovko, M. Y. Identification of novel non-ionic, cationic, zwitterionic, and anionic polyfluoroalkyl substances using UPLC−TOF−MSE high-resolution parent ion search. *Anal. Chim. Acta* **2017**, *988*, 41−49.
(50) Mauritz, K. A.; Moore, R. B. State of understanding of Nafion. *Chem. Rev.* **2004**, *104* (10), 4535−4586.
(51) Burda, J.; Kuraš, M.; Kříž, J.; Vodička, L. Relationship between retention behaviour and molecular structure of alkanes in reversed phase high performance liquid chromatography. *Fresenius' Z. Anal. Chem.* **1985**, *321* (6), 549−552.
(52) Franklin, G. W.; James, C. D. Fluorocarbon vinyl ether polymers. 3,282,875, 1966.
(53) Milian, J. A. S.; Moore, J. E. P.; Sousa, E. H. Fluorocarbon ethers derived from hexafluoropropylene epoxide. 3,250,808, 1966.
(54) Liang, B.; Hung, M. H.; Resnick, P. R. Co-production of perfluoromethyl perfluorovinyl ether and perfluoroethyl perfluorovinyl ether. US5777179A, 1998.
(55) Takasaki, M.; Nakagawa, Y.; Sakiyama, Y.; Tanabe, K.; Ookubo, K.; Sato, N.; Minamide, T.; Nakayama, H.; Hori, M. Degradation Study of Perfluorosulfonic Acid Polymer Electrolytes: Approach from Decomposition Product Analysis. *J. Electrochem. Soc.* **2013**, *160* (4), F413−F416.
(56) Hintzer, K.; Jürgens, M.; Kaspar, H.; Koenigsmann, H.; Lochhaas, K. H.; Maurer, A. R.; Schwertfeger, W.; Zipplies, T.; Mayer, L.; Dadalas, M. C. Method of making fluoropolymer dispersion. 7,671,112 B2, 2010.
(57) Zhou, C.; Guerra, M. A.; Qiu, Z.-M.; Zawodzinski, T. A.; Schiraldi, D. A. Chemical Durability Studies of Perfluorinated Sulfonic Acid Polymers and Model Compounds under Mimic Fuel Cell Conditions. *Macromolecules* **2007**, *40* (24), 8695−8707.
(58) Junk, C.; Harmer, M.; Feiring, A.; Schadt, F.; Schnepp, Z. Hydrofluoroalkanesulfonic acids from fluorovinyl ethers. 7,834,209, 2005−06−07, 2006.
(59) Brothers, P. D.; Leung, L. H.; Gangal, S. V. Abatement of Fluoroether Carboxylic Acids or Salts Employed in Fluoropolymer Resin Manufacture. 2015/0203427 A1 2009−11−12, 2009.
(60) Nappa Mario, J. Improved Process For Preparing Fluorocarbon Polyethers. EP 0337743 B1, 1989/04/12, 1994.
(61) Ezzell Bobby, R.; Carl William, P.; Mod William, A. Preparation, Decarboxylation And Polymerization Of Novel Acid Fluorides And Resulting Monomers. US 4687821 A, 1983/07/05, 1987.
(62) Peng, S.; Hung, M. H.; Junk, C. P.; Tang, P. L. Fluoroalkyl ether sulfonate surfactants. US 7,977,426 B2, 2010.
(63) Marchionni, G.; Petricci, S.; Spataro, G.; Pezzin, G. A study of the thermal decarboxylation of three perfluoropolyether salts. *J. Fluorine Chem.* **2003**, *124* (2), 123−130.
(64) Pan, Y.; Zhang, H.; Cui, Q.; Sheng, N.; Yeung, L. W. Y.; Sun, Y.; Guo, Y.; Dai, J. Worldwide Distribution of Novel Perfluoroether Carboxylic and Sulfonic Acids in Surface Water. *Environ. Sci. Technol.* **2018**, *52* (14), 7621−7629.
(65) Wang, Z.; DeWitt, J. C.; Higgins, C. P.; Cousins, I. T. A Never-Ending Story of Per- and Polyfluoroalkyl Substances (PFASs)? *Environ. Sci. Technol.* **2017**, *51* (5), 2508−2518.
(66) Wang, Z.; Cousins, I. T.; Scheringer, M.; Hungerbuehler, K. Hazard assessment of fluorinated alternatives to long-chain perfluoroalkyl acids (PFAAs) and their precursors: status quo, ongoing challenges and possible solutions. *Environ. Int.* **2015**, *75*, 172−9.
(67) Hoppin, J.; Knappe, D.; Smart, R.; May, K.; Collier, D.; DeWitt, J. The GenX Exposure Study: Center for Human Health and the Environment. https://chhe.research.ncsu.edu/the-genx-exposure-study/.
(68) *NC DHHS Risk Assessment FAQ, July 2017*. In North Carolina Department of Health and Human Services: 2017.
(69) Agency, E. C. Ammonium 2,3,3,3-tetrafluoro-2-(heptafluoropropoxy)propanoate Acute Toxicity Endpoint Summary. https://echa.europa.eu/registration-dossier/-/registered-dossier/2679/7/3/1.
(70) Shi, Y.; Vestergren, R.; Zhou, Z.; Song, X.; Xu, L.; Liang, Y.; Cai, Y. Tissue Distribution and Whole Body Burden of the Chlorinated Polyfluoroalkyl Ether Sulfonic Acid F-53B in Crucian Carp (Carassius carassius): Evidence for a Highly Bioaccumulative Contaminant of Emerging Concern. *Environ. Sci. Technol.* **2015**, *49* (24), 14156−14165.
(71) Briels, N.; Ciesielski, T. M.; Herzke, D.; Jaspers, V. L. B. Developmental Toxicity of Perfluorooctanesulfonate (PFOS) and Its Chlorinated Polyfluoroalkyl Ether Sulfonate Alternative F-53B in the Domestic Chicken. *Environ. Sci. Technol.* **2018**, *52* (21), 12859−12867.
(72) Rotander, A.; Kärrman, A.; Toms, L.-M. L.; Kay, M.; Mueller, J. F.; Gómez Ramos, M. J. Novel Fluorinated Surfactants Tentatively Identified in Firefighters Using Liquid Chromatography Quadrupole

DOI: 10.1021/acs.est.8b06017
Environ. Sci. Technol. 2019, 53, 4717−4727

Time-of-Flight Tandem Mass Spectrometry and a Case-Control Approach. *Environ. Sci. Technol.* **2015**, *49* (4), 2434−2442.
(73) Hopkins, Z. R.; Sun, M.; DeWitt, J. C.; Knappe, D. R. U. Recently Detected Drinking Water Contaminants: GenX and Other Per- and Polyfluoroalkyl Ether Acids. *J. - Am. Water Works Assoc.* **2018**, *110* (7), 13−28.

DOI: 10.1021/acs.est.8b06017
Environ. Sci. Technol. 2019, 53, 4717−4727

Journal of Chromatography A, 1551 (2018) 52–58

Contents lists available at ScienceDirect

Journal of Chromatography A

journal homepage: www.elsevier.com/locate/chroma

Validation of quantitative measurements and semi-quantitative estimates of emerging perfluoroethercarboxylic acids (PFECAs) and hexfluoroprolyene oxide acids (HFPOAs)

James McCord[a], Seth Newton[b], Mark Strynar[b,*]

[a] Oak Ridge Institute for Science and Education, National Exposure Research Laboratory, U.S. Environmental Protection Agency, Research Triangle Park, NC, United States

[b] National Exposure Research Laboratory, U.S. Environmental Protection Agency, Research Triangle Park, NC, 27711, United States

ARTICLE INFO

Article history:
Received 11 January 2018
Received in revised form 20 March 2018
Accepted 22 March 2018
Available online 23 March 2018

Keywords:
Perfluoroalkyl substances
HFPO-DA
GenX
Cape fear river
LC–MS

ABSTRACT

Legacy perfluorinated compounds exhibit significant environmental persistence and bioaccumulation potential, which has spawned an ongoing effort to introduce replacement compounds with reduced toxicological risk profiles. Many of these emerging chemical species lack validated quantitative methods, and, frequently, appropriate analytical standards for accurate monitoring and identification. To fill this knowledge gap, a general method for the quantitative determination of perfluoroether carboxylic acids (PFECAs) by LC–MS/MS was single-lab validated on spike-recovery samples in surface, drinking, and wastewater for a variety of perfluorinated ether standards. Relative error measurements for spike-recovery samples in each matrix ranged from 0.36% to 25.9%, with an average error of 10% overall. Coefficient of variation (CV) for each compound ranged from 10 to 28% with an average of 17%. The quantitative methodology was applied during repeated weekly monitoring of the Cape Fear River during remediation of PFECA hexafluoropropyloxide dimer-acid (HFPO-DA), known by the brand name "GenX." Semi-quantitative concentration estimates for emerging PFECA compounds lacking analytical standards was also carried out using surrogate calibration curves and mass labeled HFPO-DA as an internal standard. Estimates of the emerging compounds were possible using matched standards, but application of the estimation methodology to compounds with known concentration revealed that such estimates may possess up to an order of magnitude, or more, in uncertainty due to the difficulty of matching with an appropriate standard. Nevertheless, the estimation biases are primarily systematic (extraction efficiency and instrument response) rather than stochastic, enabling the collection of time-course data; both HFPO-DA and the emerging compounds were reduced in surface water and drinking water concentration of several orders of magnitude after removal of the source waste stream.

Published by Elsevier B.V.

1. Introduction

Per- and polyfluoroalkyl substances (PFASs) are recalcitrant environmental pollutants which have become a focus of significant public health interest in recent years [1]. In particular, the widely used compounds perfluorooctanoic acid (PFOA) and perfluorooctanesulfonate (PFOS) were found to have a negative toxicological profile and bioaccumulation potential [2,3], resulting in publication of a drinking water health advisory by the EPA [3,4], international restrictions [5], and pressure for banning under the Stockholm Convention on Persistent Organic Pollutants [6]. The primary manufacturers of these molecules phased out US production of PFOS/PFOA and related chemical species in the 2000s [7,8]. However, fluorinated surfactants, such as PFOA and PFOS, as well as the fluorinated polymer products whose production they support, exhibit unique chemical properties that are of substantial value in the textiles and consumer products industries [9]. As a consequence, numerous alternative chemistries have emerged to replace the discontinued species [10–12], with estimates as high as several thousand species [13].

One broad class of the replacement chemicals are fluorinated ether compounds [11], which consist of a series of short chain perfluorinated carbons linked by ether oxygens and capped with an acidic head group (Table 1). Many species demonstrating this general fluorinated ether structure have been detected in locations where fluorochemical manufacturing

* Corresponding author.
E-mail address: strynar.mark@epa.gov (M. Strynar).

https://doi.org/10.1016/j.chroma.2018.03.047
0021-9673/Published by Elsevier B.V.

Table 1
A) Reference perfluoro-ether carboxylic acids included in the PFECA standard mixture and B) emerging perfluorinated ether species lacking analytical standards.

A) Perfluorinated Ether Standards			
Compound Name	CAS	Formula	Structure
Perfluoro(4-oxapentanoic acid) ("Surrogate 1")	863090–89-5	$C_5HF_9O_3$	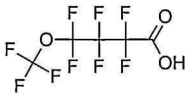
Perfluoro(3,6-dioxaheptanoic acid) ("Surrogate 2")	151772–58-6	$C_5HF_9O_4$	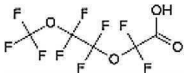
Perfluoro(3-oxabutanoic acid) ("Surrogate 3")	377–73-1	$C_4HF_7O_3$	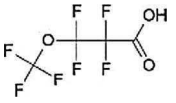
Perfluro(5-oxa-6-dimethylhexanoic) acid ("Surrogate 4")	801212–59-9	$C_7HF_{13}O_3$	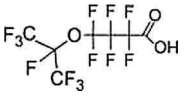
Perfluoro(2-methyl-3-oxahexanoic) acid ("HFPO-DA")	13252–13-6	$C_6HF_{11}O_3$	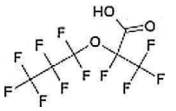
B) Emerging Compounds			
Compound Name	CAS	Formula	Structure
Perfluoro-methoxyacetic acid (PFMOAA)	674–13-5	$C_3HF_5O_3$	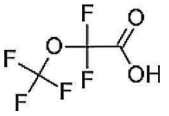
Perfluoro-3,5-dioxahexanoic acid (PFO2HxA)	39492–88-1	$C_4HF_7O_4$	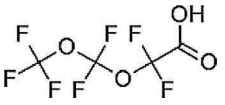
Perfluoro-3,5,7-trioxaoctanoic acid (PFO3OA)	39492–89-2	$C_5HF_9O_5$	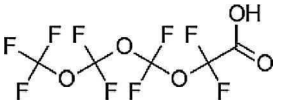

impacts the water supply [14,17], but toxicological data of these emerging compounds are limited. One particular chemical, 2,3,3,3-Tetrafluoro-2-(heptafluoropropoxy) propanoic acid, also known as hexafluoropropylene oxide dimer acid (HFPO-DA), or the trade name of its ammonium salt, GenX, [18] was designed as a fluorochemical processing surfactant that meets the requirements of the EPA PFASs management program [18,19]. HFPO-DA, and other HFPO related products have been found in significant concentrations in the discharge from certain fluorochemical manufacturing sites [14,16,20]. The limited toxicological studies of the HFPO-DA compound indicate that *acute* toxicity and metabolism are of limited concern for the replacement chemical, [21–24] but long-term exposure effects require additional study. [23–27] The detection of the compound in the Cape Fear River in North Carolina sparked an intensive investigation and establishment of a statewide health goal [28] amid concerns over its potential long-term effects.

HFPO-DA is but one of an amalgamation of related fluorochemical compounds emerging as pollutants of interest in surface, ground, and drinking water, and, while existing non-targeted methodologies have allowed for the detection of novel structures, [12–16] quantitative methods will be necessary for long term environmental monitoring and health effects studies regarding new fluorochemicals like HFPO-DA/GenX. Existing methodologies, such as EPA method 537, were developed for the analysis of legacy compounds, straight chain perfluorinated carboxylic acids and sulfonates, in drinking water, but there is substantial need for general methods sufficient to analyze known and emerging compounds in environmental matrices. Further, as emerging contaminants frequently lack authenticated standards, methods for tracking and estimating fluorochemical concentrations are needed for monitoring environmental levels of unknown contaminants. Here we demonstrate a quantitative sample preparation and LC–MS/MS method suitable for emerging perfluoroether compounds, validate it in multiple water source matrices, and apply it to the ongoing monitoring of an impacted watershed. Further, we estimate concentrations and conduct time course monitoring of perfluoroether compounds with no existing standards by using closely related surrogate species to model instrument responses and construct non-matched calibration curves.

2. Materials and methods

2.1. Preparation of PFECA standards

Reference standards of perfluoroether carboxylic acids were obtained from Synquest Laboratories (Table 1) along with $13C_3$ labeled 2,3,3,3-Tetrafluoro-2-(heptafluoropropoxy) propanoic acid (HFPO-DA) for use as an internal standard (Wellington Labs).

A stock solution of each standard was prepared in 95:5 methanol:2.5 M NaOH to prevent the formation of the methyl ester. From these stocks, a mixed PFECA standard was prepared containing equal mass of each native species and diluted to the desired final concentrations in methanol.

Standard PFECA solution mixtures were prepared using water sourced from three locations as the background matrices. Background matrix water was sourced as followed: surface water collected from Discovery Lake, Research Triangle Park, NC, waste water collected from Jacksonville Wastewater Treatment facility effluent, Jacksonville, NC, and drinking water collected from a laboratory faucet in the Environmental Protection Agency office in Research Triangle Park, NC. Each source sample was collected into one liter pre-cleaned high-density polyethyelene (HDPE) Nalgene bottles and spiked with a standard mixture of PFECAs (Table 1) at either 0, 50, or 200 ng/L. Five replicates of these matrix spiked samples were prepared for each combination of background matrix (Surface Water, Waste Water, Drinking Water) and PFECA level (Blank, Low Spike, High Spike) resulting in 45 samples. The prepared spiked samples were stabilized by pH adjustment to pH ~ 2 with the addition of 5 mL of 35% nitric acid. A set of samples of the PFECA mixture at 0, 10, 25, 50, 100, 150, 200, and 250 ng/L was also prepared in deionized water (DI) and processed immediately in tandem to construct calibration curves.

2.2. Environmental sampling

Fluorochemical contaminated water samples were acquired from North Carolina Department of Environmental Quality (NCDEQ) at a location near the industrial waste outfall for a local fluorochemical manufacturer, as well as from downstream drinking water treatment plants. Location 1 was the source water drawn from the Cape Fear River for a downstream water treatment facility and Location 2 was finished drinking water delivered to Wilmington, NC. Each sample was collected in a one liter HDPE bottle and stabilized by pH adjustment with nitric acid as previously described [29]. Samples were stored at room temperature, extracted and analyzed within five days of the sampling date.

2.3. Solid phase extraction of PFECAs from aqueous matrix

The previously prepared, stabilized samples were decanted into a 1000 mL HDPE graduated cylinder and their total volume recorded; water in excess of 1000 mL was discarded. The maximum oversampling possible in a one liter HDPE bottle is ~10%, allowing a worst case 10% bias if 100% of in-solution PFASs bind to the bottle surface and the maximum amount of excess water is discarded. This scenario can be avoided by not filling bottles completely; the maximum sample collection overfill was <10 mL in this sample set. The sample bottle was then rinsed with 10 mL of methanol to remove any compounds that partially adhere during sample processing and storage; the retained water was returned to the bottle alongside the methanol. An internal standard of $^{13}C_3$ labeled HFPO-DA was added to each water sample at a concentration of 100 ng/L of sample, and shaken vigorously before being vacuum filtered through a Whatman GF/A glass filter.

Oasis weak anion exchange (WAX) Plus (225 mg) solid phase extraction (SPE) cartridges (Waters Corporation) were conditioned according to the manufacturer instructions, as follows: the SPE cartridges were equilibrated under 10 mL/min methanol flow for 2.5 min, followed by 2.5 min of deionized water (DI) at 10 mL/min; flow was maintained through a SPC10-P Sep-Pak concentrator binary piston pump (Waters Corporation). Samples were concentrated at a flow rate of 10 mL/min for 50 min (500 mL total volume) and SPE cartridges were removed for later elution. The Sep-Pak system was flushed with 25 mL of methanol (2.5 min at 10 mL/min) between sample cartridges to prevent sample carryover.

After sample concentration, the SPE cartridges were washed with 4 mL of 25 mM pH 4.0 acetate/acetic acid buffer, followed by a wash of 4 mL of neutral methanol. Compounds of interest were then eluted with 4 mL of freshly prepared 0.1% ammonium hydroxide in methanol and evaporated in a polypropylene tube at 40°C under a dry nitrogen stream to a final volume of ~ 1 mL. The evaporated samples were diluted 4-fold in 2.5 mM ammonium acetate to match the starting conditions for liquid chromatography.

2.4. LC–MS/MS data acquisition and quantification

LC–MS/MS quantification took place on a Waters Acquity ultra performance liquid chromatograph which had been modified to replace OEM PTFE filters and solvent plumbing with stainless steel or PEEK tubing and incorporate a PFC isolation column (Waters P/N 176001744). The chromatographic separation was carried out using a Waters ACQUITY UPLC BEH C18 column (2.1 mm × 50 mm, 1.7 μm), a flow rate of 500 μL/min, 50 μL injection volume, and a binary mobile phase gradient with mobile phases A (95:5, 2.5 mM ammonium acetate: Methanol) and B (95:5, Methanol: 2.5 mM ammonium acetate). The gradient program was a follows: 10–85% B (5 min), 85–100% (0.1 min), 100% (hold for 1.9 min), 100–10% (0.1 min), 10% (hold for 1.9 min). Detection and quantitation was performed with an interfaced Waters Quattro Premier XE triple quadrupole mass spectrometer in negative mode (Supplemental Table 1) with individual transition parameters for each PFECA species analyzed (Table 2). Stable isotope labeled (SIL) HFPO-DA was used as an internal standard for all measured compounds.

MRM transitions were previously optimized for the four surrogate perfluoroether compounds and HFPO-DA using available standards. Additional transitions for three emerging PFECAs previously described (Table 1, Supplemental Fig. 1–3), [16] but currently lacking analytical standards, were selected using direct infusion of extracts prepared from the Cape Fear River. For method validation, the MRM method contained only the surrogate and HFPO-DA transitions, while environmental samples included the three MRM transitions for the emerging PFECAs as well.

The PFECA mixture was used to prepare an eight-point calibration curve for each constituent PFECA standard for quantitation. Ion abundances were normalized to the HFPO-DA internal standard intensity and curves were fitted as a concentration weighted (1/x) quadratic curve with two injections per concentration. For spike recovery experiments, quantitation was derived from the matching standard curve. For quantitative measurements of HFPO-DA and semi-quantitative estimates for the emerging PFECAs in environmental samples, systematic application of each surrogate standard curve was used to calculate estimated concentrations.

3. Results and discussion

3.1. Spike-recovery validation

Representative figures of merit were calculated for the quantitative spike recovery assessment based on the five sample preparations for each combination of background matrix and concentration (Fig. 1). For each replicate, the relative percentage error (RE) ranges from 0.36% to 25.9%, with an average of ~10% when aggregated across compounds and background matrices (Table 3). Sample precision was calculated with average coefficient of variation of 17% across matrices and spike levels (Table 3). A method limit of detection (LOD) for PFECAs was estimated at 16 ng/L using a 3X signal-to-noise cutoff. The method noise was estimated as the standard deviation of repeated injections of the 10 ng/L calibration

Table 2
Multiple reaction monitoring (MRM) transition table for surrogate and emerging PFECAs analyzed in this study.

Species	Molecular Formula	Precursor Mass (Da)	Product Mass (Da)	Cone Voltage (V)	Collision Energy (eV)
Surrogate 1	$C_5HF_9O_3$	279.0	84.9	14	22
			134.8	22	24
Surrogate 2	$C_5HF_9O_4$	295.0	84.9	10	26
			200.9	10	10
Surrogate 3	$C_4HF_7O_3$	229.0	84.9	10	10
			184.9	22	18
Surrogate 4	$C_7HF_{13}O_3$	379.0	184.8	16	12
			134.9	16	34
HFPO-DA	$C_6HF_{11}O_3$	329.2	168.9	10	12
			286.9	10	6
HFPO-DA IS	$[13C]_3C_3HF_{11}O_3$	332.2	168.9	10	12
			286.9	10	6
PFMOAA	$C_3HF_9O_5$	178.9	84.9	10	12
PFO2HxA	$C_4HF_7O_4$	245.0	84.9	22	18
			178.8	22	4
PFO3OA	$C_5HF_9O_5$	311.1	84.9	22	20
			150.8	22	4

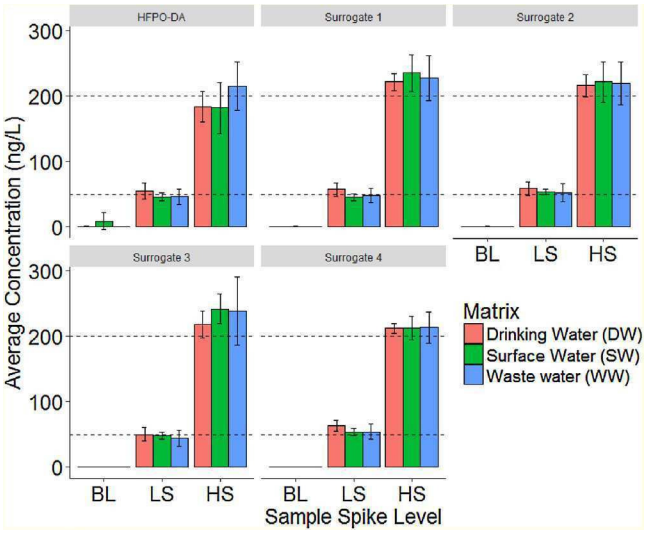

Fig. 1. Measured PFECA concentrations for a synthetic PFECA mixture in varying matrices at 200 ng/L (HS), 50 ng/L (LS), and 0 ng/L (BL) spike levels, with 95% confidence intervals.

Table 3
Calculated relative percentage error (RE) and coefficient of variation (CV) for measurements (n = 5) in waste water (WW), surface water (SW) and drinking water (DW) matrices for a series of PFECA compounds.

Compound	Matrix	RE (%)	CV (%)
HFPO-DA	DW	9.2	20%
	SW	8.6	20%
	WW	7.4	25%
Surrogate 1	DW	12.9	14%
	SW	13.4	14%
	WW	9.1	22%
Surrogate 2	DW	13.0	14%
	SW	9.2	12%
	WW	7.5	23%
Surrogate 3	DW	4.7	17%
	SW	12.2	12%
	WW	15.6	28%
Surrogate 4	DW	15.9	10%
	SW	7.0	10%
	WW	7.5	19%

curve point. This reported LOD value is not a physical limitation, and can be reduced through modifications to the SPE concentration step, sample blowdown, or injection volume to increase the on-column analyte load and improve sensitivity, or use of an MS platform with better intrinsic sensitivity.

For the HFPO-DA compound, the measurement retains accuracy regardless of matrix or sample concentration within the range of the calibration curve; all measurements correspond to their theoretical values within the 95% confidence interval and demonstrate acceptable RE (<10%) and CV (<30%) values. However, the other PFECA compounds demonstrate a small, systemic overestimation of their concentration in some background matrices. This effect is attributable to a non-matched internal standard, and can be corrected in the future as appropriate stable isotope labeled species become available. The reproducibility of the assay is still high; CVs of the surrogate compounds are equivalent or better than HFPO-DA with one exception, and the RE remains under 20% in all cases, with results from each matrix being statistically indistinguishable from each other. Thus, the methodology can be generally applied even in absence of matched internal standards. Of note, a single replicate of waste water – high spike was excluded from the collection sample set due to a significant contaminant in the preparation. Investigation of the sample revealed significant (>5-fold) signal suppression of HFPO-DA and the SIL HFPO-DA standard in only that prep. HFPO-DA quantification was unaffected due to the matched internal standard, but surrogate concentration estimates were >3.5 standard deviation outliers due to the suppressed SIL used for normalization. This event demonstrates that caution remains necessary when using non-matched internal standards, especially in heterogeneous matrices such as waste water.

3.2. Application in longitudinal monitoring of HFPO-DA

Initial environmental samples obtained in June 2017 from fluorochemical manufacturing outfall, surface, and drinking water far exceeded the designated calibration range and required significant dilution to enter the calibration curve range for accurate quantitation. Following this sampling, the manufacturer ceased waste stream emissions from one of their manufacturing lines and the measured concentrations of all monitored species dramatically declined in both the direct outfall and downstream locations (Figs. 2 and 3). Of note, local contamination from pumps and piping at the manufacturing site are hypothesized to be the cause of the persistently high concentrations in the waste outfall through the third sampling week in spite of the immediate decline observed at downstream locations. Continuous monitoring of both outfall and impacted drinking water sites demonstrated minor daily variation but consistent reduction below North Carolina's targeted health goal of 140 ng/L [28].

Blank, low spike, and high spiked standard mixtures were carried to the sampling site as field blanks each week and returned for QC analysis. Throughout the sampling course, QC samples mea-

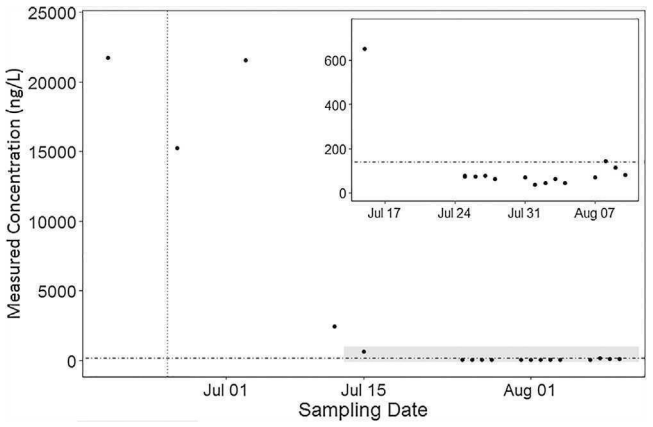

Fig. 2. Measured HFPO-DA concentrations in manufacturing outfall over time. The vertical line indicates diversion of PFECA generating waste stream, the horizontal line indicates targeted HFPO-DA health goal (140 ng/L), inset shows shaded region.

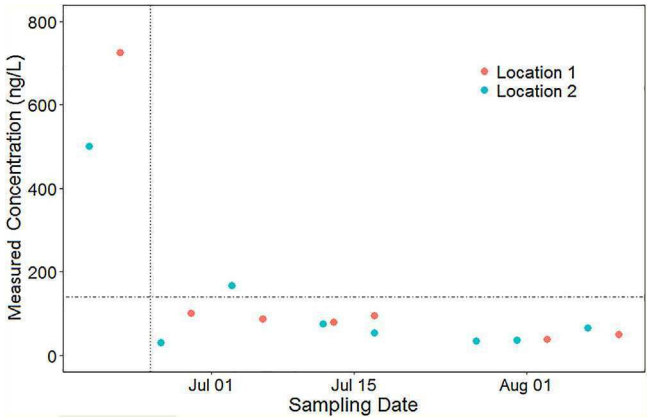

Fig. 3. Measured HFPO-DA concentrations at drinking water treatment plants located in the Cape Fear River basin. Vertical line indicates diversion of PFECA generating waste stream, horizontal line indicates targeted health goal (140 ng/L).

sured were quantified with an average RE of 22%. Each week, a randomly selected 10% subset of the environmental samples were replicated and inter-replicate CVs were <10%, demonstrating long term method stability and precision.

3.3. Semi-quantitative estimates of emerging PFECAs

For compounds tentatively identified as PFMOAA, PFO2HxA, and PFO3OA [16], the lack of a matched standard and reliance on a surrogate internal standard limits the potential accuracy of quantitative efforts. Nevertheless, semi-quantitative estimates can inform public health decisions and provide focus for further development of analytical methods [30]. The PFECA mixture was used to prepare an eight-point calibration curve for each constituent PFECA standard. Ion abundances were normalized to the HFPO-DA internal standard intensity and calibration curves were fitted as a concentration weighted (1/x) quadratic curve. Estimated concentrations for the three emerging compounds, which lack standards, and HFPO-DA were obtained using each of the five calibration curves each sampling week, as well as a global estimate curve built from the response of all five individual surrogates.

To establish an estimate of the level of error when using surrogate compounds for concentration estimates, the HFPO-DA value from its matched calibration curve was compared to values obtained using the calibration curves from the four surrogate compounds. The surrogate estimated concentrations yielded average errors of 1.3%, 0.6%, 48%, and 0.3% for Surrogates 1–4 respectively. The three closely matching surrogates, 1, 2 and 4, elute within a 1-min window, very near the HFPO-DA peak (Supplemental Fig. 4–7). As a consequence, they demonstrate remarkably little bias in estimated concentrations for HFPO-DA, unlike Surrogate 3, which elutes much earlier in the chromatographic run, and has significant peak distortions resulting from its more hydrophilic character than the other species. Surrogate 3 however, does have a more similar chromatographic profile to PFMOAA and PFO2HXA. For the HFPO-DA, a best case scenario of a closely matched chemical structure for the calibration curve and internal standard yields accurate results within the error margins of the matched curve and standard, while a poorly matched species yields a several-fold, but still manageable, level of bias in estimation. Matching of surrogates can be performed empirically, by selecting similar chemical structures and confirming similar chromatographic and MS performance, but a general solution to determining “good” surrogate matches is beyond the scope of this paper.

The emerging species exhibit significantly more variability in estimated concentrations compared to the surrogate standards (Fig. 4). Structurally, the emerging compounds appear similar to the surrogate PFECA compounds, however, their elution time indicates substantially higher hydrophilicity consistent with their low molecular weight and increased oxygen content; PFMOAA elutes nearly in the void volume, and PFO2HxA falls somewhere between the PFMOAA and surrogate standards (Supplemental Fig. 5). Further, the extraction efficiency of non-targeted species in SPE is currently unknown, and can contribute to significant variability, but we assume the binding to be consistently high when using anion exchange phases with easily ionized species such as perfluoroacids [31].

The systematic dissimilarity between the lower molecular weight emerging compounds and the surrogate standards impacts the concentration estimates. The predicted concentrations are

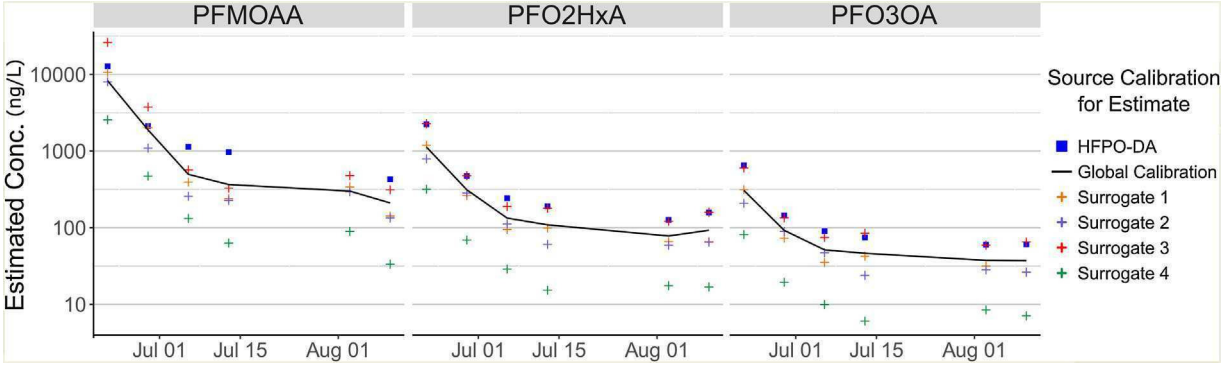

Fig. 4. Estimated concentrations of three emerging PFECA compounds at Location 2, using five surrogate calibration curves and a global calibration of all species.

consistent in their ordering, with HFPO-DA estimate being the highest value and Surrogate 4 underestimating that value by ~10-fold.

The systematic bias of estimated concentration is consistent across sampling location and date, implying it is intrinsic to the process, likely the result of hydrophobic bias in the chromatography and/or electrospray that cannot be corrected for without more closely matched calibration curve and/or internal standard. A conservative application of the variation between the five closely related PFECA standards suggests the error of the global average is on the order of ten-fold and can be considered semi-quantitative at best. Regardless, using the global average calibration curve of the PFECA standards provides a rough estimate of concentration that can be useful for directing further work. The most recent PFMOAA estimate range still falls partially above the health goal for HFPO-DA and it is worthy of further scrutiny, while the other compounds have been reduced below that target level, even when using the highest estimate of the concentration.

Nevertheless, all three of the non-standard PFECA compounds demonstrated substantial reduction over time as the result of halted upstream emission, similarly to the behavior of the HFPO-DA compound. This signifies that all the related PFECA compounds likely derive from the single fluoropolymer manufacturing process whose waste was diverted. Further, time trends indicate that the overall concentration has dropped ~2 orders of magnitude, similar to the HFPO-DA, regardless of the calibration source used. This methodology is therefore suitable for tracking temporal changes in compounds lacking standards even though the specific estimation of concentrations remains highly uncertain, presuming that such species can be detected by LC–MS.

4. Conclusion

The ongoing proliferation of new perfluorinated species to serve industrial chemical need in absence of the legacy compounds PFOA and PFOS is a burgeoning topic in environmental and public health with substantial interest. Monitoring efforts for these new species require a robust, generalized method for quantitative determinations of exposure. The availability of a SIL internal standard for HFPO-DA allows for robust analysis of this species, and allows its use as a surrogate internal standard for other compounds barring the production of matching SIL perfluoroethers. The methodology presented here is robust to variations in the environmental matrix (tap, surface, and waste water) and offers an extended range of sensitivity through the use of multiple concentration steps. Nevertheless, the calibration range utilized, with a method limit of detection ~10 ng/L, is sufficient for exposure monitoring, as the existing health advisory/goal levels for both the legacy and emerging perfluorinated compounds are around an order of magnitude higher. Lower health targets for legacy species exist in some states [32], and increased concentration factors or improved instrument sensitivity would be necessary to achieve the necessary lower method detection limits.

The same sample preparation technique can be applied to the analysis of only partially characterized species assuming chemically similar standards are available for purchase. Using one or more related species to construct calibration curves, even with surrogate internal standards, allows for an estimation of concentrations that can inform future research and policy efforts in environmental exposure. This can act as supplemental and supporting information to other mass spectrometry related monitoring efforts in non-targeted analysis. For species with some available structural information and a closely related standard, the error is on the same order as the method variation and theoretically suitable for quantitative work. However, this should be consisted a stop-gap technique prior to the acquisition of standards or validation of the assumption of similar extraction efficiency and instrument response. suitable for quantitative work. The estimates from less closely matched calibrations curves vary by >10-fold depending on the selected calibration species, but nevertheless can reveal accurate time-trend data for determining the impact of systemic changes and determining whether multiple species have correlated behaviors in response to an intervention.

Acknowledgements

The United States Environmental Protection Agency, through its Office of Research and Development, funded and managed the research described here. It has been subjected to Agency administrative review and approved for publication. James McCord was supported by an appointment to the Internship/Research Participation Program at the Office of Research and Development, U.S. Environmental Protection Agency, administered by the Oak Ridge Institute for Science and Education through an interagency agreement between the U.S. Department of Energy and EPA. Thanks are extended to the North Carolina Department of Environmental Quality for collecting the water samples used for the longitudinal monitoring application.

Appendix A. Supplementary data

Supplementary data associated with this article can be found, in the online version, at https://doi.org/10.1016/j.chroma.2018.03.047.

References

[1] A.B. Lindstrom, M.J. Strynar, E.L. Libelo, Polyfluorinated Compounds: past, present, and future, Environ. Sci. Technol. 45 (19) (2011) 7954.
[2] T. Stahl, D. Mattern, H. Brunn, Toxicology of perfluorinated compounds, Environ. Sci. Eur. 23 (1) (2011) 38.
[3] Lifetime Health Advisories and Health Effects Support Documents for Perfluorooctanoic Acid and Perfluorooctane Sulfonate, E. P. A., Ed. Federal Register, United States, 2016, pp 33250–33251.
[4] Provisional Health Advisories for Perfluorooctanoic Acid (PFOA) and Perfluorooctane Sulfonate (PFOS), United States Environmental Protection Agency, Washington DC, 2009.
[5] Report of the Conference of the Parties of the Stockholm Convention on Persistent Organic Pollutants on the Work of Its Fourth Meeting, 2009.
[6] Proposal for a COUNCIL DECISION on the Submission, on Behalf of the European Union, of a Proposal for the Listing of Additional Chemicals in Annex A to the Stockholm Convention on Persistent Organic Pollutants, Council of the European Union, 2016.
[7] Fact Sheet: 2010/ PFOA Stewardship Program, 2015 https://www.epa.gov/assessing-and-managing-chemicals-under-tsca/fact-sheet-20102015-pfoa-stewardship-program.
[8] EPA and 3 M Announce Phase Out of PFOS, 2018 https://yosemite.epa.gov/opa/admpress.nsf/0/33aa946e6cb11f35852568e1005246b4.
[9] E. Kissa, Fluorinated Surfactants and Repellents, vol. 97, CRC Press, 2001.
[10] M. Scheringer, X. Trier, I. Cousins, P. T.; de Voogt, T. Fletcher, Z. Wang, T.F. Webster, Helsingør Statement on poly- and perfluorinated alkyl substances (PFASs), Chemosphere 114 (2014) 337–339.
[11] Z. Wang, I.T. Cousins, M. Scheringer, K. Hungerbühler, Fluorinated alternatives to long-chain perfluoroalkyl carboxylic acids (PFCAs), perfluoroalkane sulfonic acids (PFSAs) and their potential precursors, Environ. Int. 60 (2013) 242.
[12] F. Xiao, Emerging poly- and perfluoroalkyl substances in the aquatic environment: a review of current literature, Water Res. 124 (2017) 482–495.
[13] Z. Wang, J.C. DeWitt, C.P. Higgins, I.T. Cousins, A never-Ending story of per- and polyfluoroalkyl substances (PFASs), Environ. Sci. Technol. 51 (5) (2017) 2508–2518.
[14] M. Sun, E. Arevalo, M. Strynar, A. Lindstrom, M. Richardson, B. Kearns, A. Pickett, C. Smith, D.R.U. Knappe, Legacy and emerging perfluoroalkyl substances are important drinking water contaminants in the cape fear river watershed of north carolina, Environ. Sci. Technol. Lett. 3 (12) (2016) 415–419.
[15] S. Newton, R. McMahen, J.A. Stoeckel, M. Chislock, A. Lindstrom, M. Strynar, Novel polyfluorinated compounds identified using high resolution mass spectrometry downstream of manufacturing facilities near Decatur, alabama, Environ. Sci. Technol. 51 (3) (2017) 1544–1552.
[16] M. Strynar, S. Dagnino, R. McMahen, S. Liang, A. Lindstrom, E. Andersen, L. McMillan, M. Thurman, I. Ferrer, C. Ball, Identification of novel perfluoroalkyl ether carboxylic acids (PFECAs) and sulfonic acids (PFESAs) in natural waters

using accurate mass time-of-flight mass spectrometry (TOFMS), Environ. Sci. Technol. 49 (19) (2015) 11622.
[17] F. Heydebreck, J. Tang, Z. Xie, R. Ebinghaus, Alternative and legacy perfluoroalkyl substances: differences between european and chinese River/Estuary systems, Environ. Sci. Technol. 49 (14) (2015) 8386–8395.
[18] DuPont™ GenX Processing Aid for Making Fluoropolymer Resins, Chemours, 2010.
[19] Risk Management for Per- and Polyfluoroalkyl Substances (PFASs) Under TSCA, United States Environmental Protection Agency, Washington DC, 2015.
[20] Y. Pan, H. Zhang, Q. Cui, N. Sheng, L.W. Yeung, Y. Guo, Y. Sun, J. Dai, First report on the occurrence and bioaccumulation of hexafluoropropylene oxide trimer acid: an emerging concern, Environ. Sci. Technol. 51 (17) (2017) 9553–9560.
[21] S.A. Gannon, W.J. Fasano, M.P. Mawn, D.L. Nabb, R.C. Buck, L.W. Buxton, G.W. Jepson, S. Frame, R. Absorption, distribution, metabolism, excretion, and kinetics of 2,3,3,3-tetrafluoro-2-(heptafluoropropoxy)propanoic acid ammonium salt following a single dose in rat, mouse, and cynomolgus monkey, Toxicology 340 (2016) 1–9.
[22] J.M. Caverly Rae, L. Craig, T.W. Slone, S.R. Frame, L.W. Buxton, G.L. Kennedy, Evaluation of chronic toxicity and carcinogenicity of ammonium 2,3,3,3-tetrafluoro-2-(heptafluoropropoxy)-propanoate in Sprague–Dawley rats, Toxicol. Rep. 2 (2015) 939–949.
[23] R.A. Hoke, B.D. Ferrell, T.L. Sloman, R.C. Buck, L. Buxton, W. Aquatic hazard, bioaccumulation and screening risk assessment for ammonium 2,3,3, 3-tetrafluoro-2-(heptafluoropropoxy)-propanoate, Chemosphere 149 (2016) 336–342.
[24] B.R. Rushing, Q. Hu, J.N. Franklin, R.L. McMahen, S. Dagnino, C.P. Higgins, M.J. Strynar, J.C. DeWitt, Evaluation of the immunomodulatory effects of 2,3,3,3-Tetrafluoro-2-(Heptafluoropropoxy)-Propanoate in C57BL/6 mice, Toxicol. Sci. 156 (1) (2017) 179–189.
[25] E.C. Agency, Ammonium 2,3,3,3-tetrafluoro-2-(heptafluoropropoxy)propanoate Acute Toxicity Endpoint Summary, 2018 https://echa.europa.eu/registration-dossier/-/registered-dossier/2679/7/3/1.
[26] M.Z.P. Beekman, A. Muler, W. de Vriew, P. Janssen, M. Zeilmaker, Evaluation of Substances Used in the GenX Technology by Chemours, The Dutch National Institute for Public Health and the Environment (RIVM), Dordrecht, 2016.
[27] C. Smit, Research into Indicative Water Quality Standards for Substances Used in the GenX Technology, The Dutch National Institute for Public Health and the Environment (RIVM), 2017.
[28] NC DHHS Preliminary Risk Assessment FAQ for GenX (Perfluoro2-propoxypropanoic Acid), North Carolina Department of Health and Human Services, 2017.
[29] S.F. Nakayama, M.J. Strynar, J.L. Reiner, A.D. Delinsky, A.B. Lindstrom, Determination of perfluorinated compounds in the upper mississippi river basin, Environ. Sci. Technol. 44 (11) (2010) 4103.
[30] Environmental Decisions in the Face of Uncertainty, National Research Council, 2013.
[31] K.-U. Goss, The pKa values of PFOA and other highly fluorinated carboxylic acids, Environ. Sci. Technol. 42 (2) (2008) 456–458.
[32] Maximum Contamination Level Recommendation for Perfluorooctanoic Acid in Drinking Water, Drinking Water Quality Institute, New Jersey, 2017.

Environmental Science & Technology

Article

pubs.acs.org/est

Identification of Novel Perfluoroalkyl Ether Carboxylic Acids (PFECAs) and Sulfonic Acids (PFESAs) in Natural Waters Using Accurate Mass Time-of-Flight Mass Spectrometry (TOFMS)

Mark Strynar,*[,†] Sonia Dagnino,[†,‡] Rebecca McMahen,[†,‡] Shuang Liang,[†,‡] Andrew Lindstrom,[†] Erik Andersen,[†] Larry McMillan,[§] Michael Thurman,[∥] Imma Ferrer,[∥] and Carol Ball[⊥]

[†]National Exposure Research Laboratory, U.S. Environmental Protection Agency, Research Triangle Park, North Carolina 27711, United States

[‡]Oak Ridge Institute for Science and Education, Oak Ridge, Tennessee 37831 United States

[§]National Caucus and Center on Black Aged, Inc., Durham, North Carolina 27713, United States

[∥]Center for Environmental Mass Spectrometry, University of Colorado Boulder, Boulder, Colorado 80309, United States

[⊥]Agilent Technologies Inc., Wilmington, Delaware 19808, United States

Supporting Information

ABSTRACT: Recent scientific scrutiny and concerns over exposure, toxicity, and risk have led to international regulatory efforts resulting in the reduction or elimination of certain perfluorinated compounds from various products and waste streams. Some manufacturers have started producing shorter chain per- and polyfluorinated compounds to try to reduce the potential for bioaccumulation in humans and wildlife. Some of these new compounds contain central ether oxygens or other minor modifications of traditional perfluorinated structures. At present, there has been very limited information published on these "replacement chemistries" in the peer-reviewed literature. In this study we used a time-of-flight mass spectrometry detector (LC-ESI-TOFMS) to identify fluorinated compounds in natural waters collected from locations with historical perfluorinated compound contamination. Our workflow for discovery of chemicals included sequential sampling of surface water for identification of potential sources, nontargeted TOFMS analysis, molecular feature extraction (MFE) of samples, and evaluation of features unique to the sample with source inputs. Specifically, compounds were tentatively identified by (1) accurate mass determination of parent and/or related adducts and fragments from in-source collision-induced dissociation (CID), (2) in-depth evaluation of in-source adducts formed during analysis, and (3) confirmation with authentic standards when available. We observed groups of compounds in homologous series that differed by multiples of CF_2 (m/z 49.9968) or CF_2O (m/z 65.9917). Compounds in each series were chromatographically separated and had comparable fragments and adducts produced during analysis. We detected 12 novel perfluoroalkyl ether carboxylic and sulfonic acids in surface water in North Carolina, USA using this approach. A key piece of evidence was the discovery of accurate mass in-source n-mer formation (H^+ and Na^+) differing by m/z 21.9819, corresponding to the mass difference between the protonated and sodiated dimers.

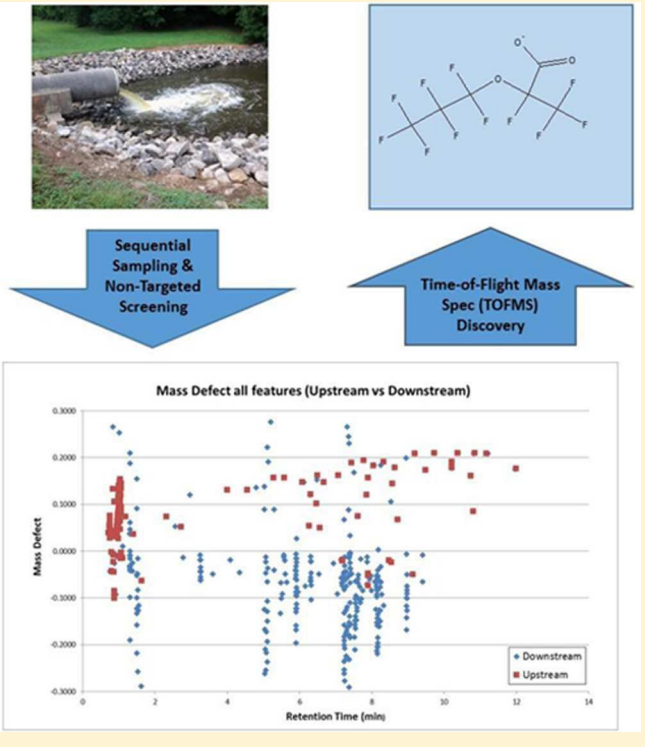

INTRODUCTION

Perfluoroalkyl and polyfluoroalkyl substances (PFASs) have unique physical and structural properties that make them extremely resistant to chemical and thermal degradation. As a result, PFASs have been used in a wide range of consumer

Received: March 10, 2015
Revised: August 7, 2015
Accepted: August 30, 2015
Published: September 22, 2015

Downloaded via US EPA OFFICE OF ENVIRONMENTAL INFO on April 29, 2020 at 12:45:11 (UTC).
See https://pubs.acs.org/sharingguidelines for options on how to legitimately share published articles.

ACS Publications © 2015 American Chemical Society

DOI: 10.1021/acs.est.5b01215
Environ. Sci. Technol. 2015, 49, 11622−11630

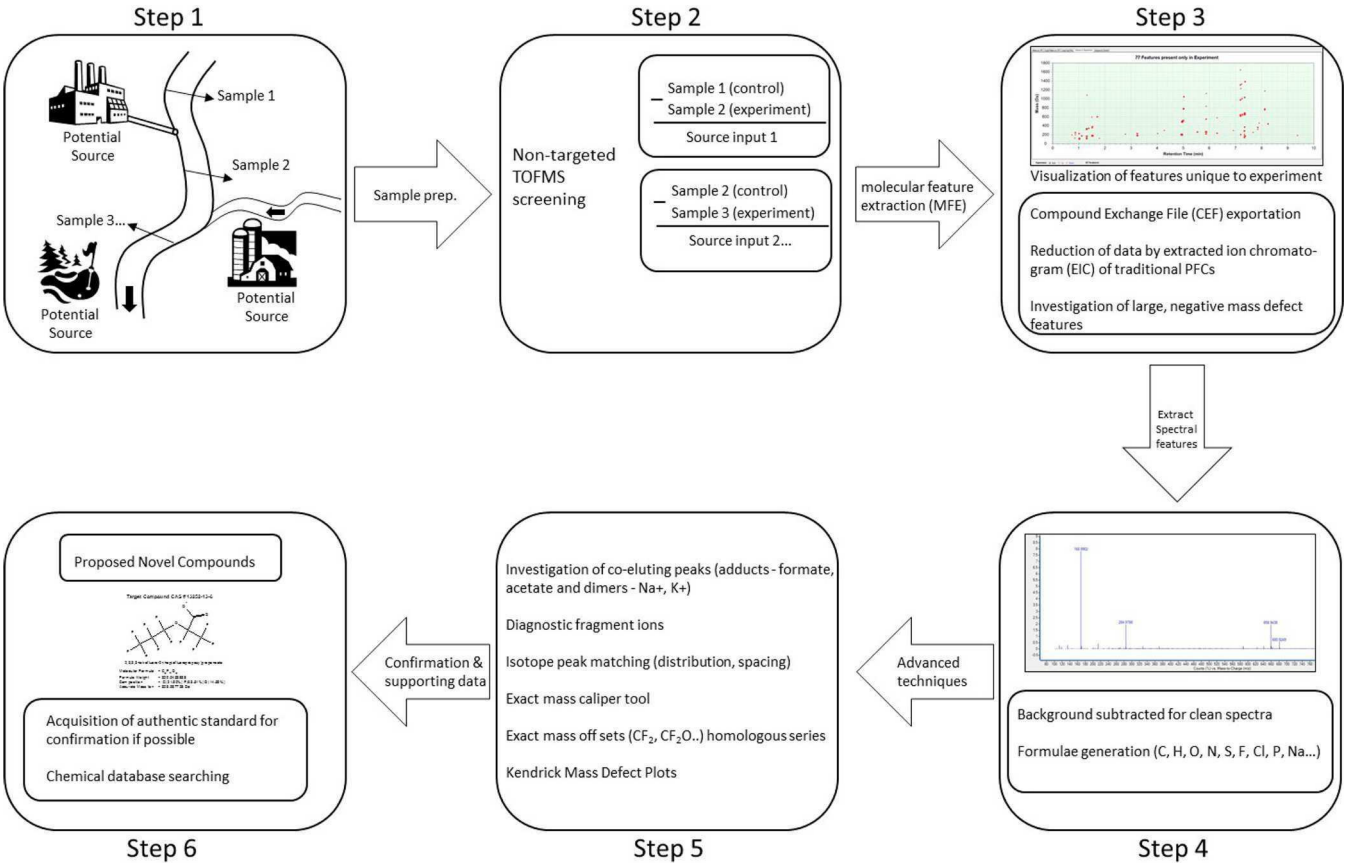

Figure 1. Sample workflow for TOFMS discovery.

products and industrial applications.[1] Between 1950 and 2000, the eight-carbon PFASs, including perfluorooctanoic acid (PFOA) and perfluorooctanesulfonate (PFOS), were among the most commonly produced and used perfluorinated compounds. PFASs have been detected in many environmental and biological matrices across the globe for a number of years,[2] and this ubiquity has led to mounting concerns about exposure and potential toxicity. As a result, many international regulatory efforts have been enacted to reduce, substitute, or eliminate long-chain (8 consecutive perfluorinated carbons or longer) PFASs from products and waste streams. In the United States, eight major fluorochemical manufacturers entered into a voluntary stewardship agreement with the U.S. Environmental Protection Agency (EPA) to phase out the use and production of long-chain perfluorinated chemistries by 2015.[3] To take their place, manufacturers have started using alternative chemistries that may include both shorter-chain perfluorinated (<C8) and/or polyfluorinated materials. For example, some of these replacement compounds still have the traditional perfluorinated carbon regions, but they are broken into shorter units by insertion of ether oxygens at regular intervals. These ether linked compounds are still technically classified as perfluorinated if all carbons are substituted with fluorine and polyfluorinated if any carbon is occupied by a hydrogen rather than a fluorine.[4] The rationale is that the addition of oxygens would likely make the replacement chemistry more labile to degradation, and thus more favorable for usage. However, to date the chemical manufacturers have disclosed little information publicly concerning the chemical structures and potential toxicities of the replacement PFASs now being produced. This makes it extremely difficult for independent research groups to evaluate their environmental distributions and potential toxicities.

A rare exception is a peer-reviewed publication on 4,8-dioxa-3H-perfluorononanoate (ADONA) (Supporting Information Figure S1), a polyfluorinated alternative to PFOA which is said to have a "more favorable toxicological profile".[5] This single journal article was published by its manufacturer, but standards for this new material have not been made available (to our knowledge) for comprehensive ecological or toxicological evaluation. Manufacturers typically submit more detailed information concerning compound structure, potential toxicity, environmental fate, and projected production volumes to regulatory authorities prior to large-scale production (e.g., the U.S. EPA's premanufacture notice process), but this information is held as confidential business information and cannot be disclosed to the general research community.

One example of industrial producers manufacturing replacement compounds is outlined in an executed draft consent order from the state of West Virginia to DuPont Corporation allowing the discharge of a new fluorinated compound into the Ohio river, at the Washington Works facility (West Virginia).[6] This is the same facility that has been the source of historical PFOA contamination of local surface and groundwater due to industrial manufacture and discharge and is the center of a court-ordered investigation by the C8 science panel to determine if PFOA exposure in the local human population has led to adverse health effects.[7] A number of recent epidemiological studies have indicated that exposure to PFOA at this location has been associated with adverse human health outcomes.[8,9]

DOI: 10.1021/acs.est.5b01215
Environ. Sci. Technol. 2015, 49, 11622−11630

Typical environmental occurrence investigations have for years focused on targeted analysis for specific analytes of interest. Highly precise and sensitive LC and GC MS/MS methods have been developed to quantify contaminants of concern. A more recent approach for environmental sample analysis has been the use of high-resolution mass spectrometry (HRMS) for these efforts. Some researchers have used nontargeted or suspect screening effectively in demonstrating many chemical classes in wastewater effluent without the use of reference standards.[11−13] These approaches have begun to rely more heavily on the use of databases, accurate mass searches, and HRMS molecular formula prediction capabilities for discovery. Confirmation with authentic standards still remains the "gold standard". Schymanski et al.[14] reported on five levels of confidence in identifying small molecules using HRMS ranging from exact mass matches, through molecular formula prediction, tentative candidate structures, library match searches, and finally confirmation with a reference standard. This is the type of approach that we use in this work to identify previously undescribed PFASs in surface water.

As it is mostly unknown what is being produced to replace traditional perfluorinated compounds, a series of sampling events was conducted to collect water samples with determination of new per- and polyfluorinated substances as a goal. In Nakayama et al.,[10] a sampling of surface water in the Cape Fear River Basin in North Carolina indicated sources of perfluorinated compounds intermittently spread throughout the drainage basin. A follow-up investigation with more focused sampling to determine sources was not conducted. However, based on this early work, there was some indication that there were PFASs sources in the Fayetteville, NC area. More recent surface water sampling trips in this region indicated continued elevated concentrations of traditional perfluorinated compounds, supporting the Nakayama et al.[10] findings. One such source was known to be downstream of the industrial effluent discharge of a fluorochemical production facility. Further investigation of these samples for identification and occurrence of potential replacement chemistries was undertaken.

MATERIALS AND METHODS

Sample Workflow for Discovery. A diagram of the workflow we used for novel compound discovery in surface water samples is shown in Figure 1. It is a six-step process that starts with sequential sampling of water, followed by nontargeted screening, visualization of detected peaks, further investigation of suspect features, advanced TOFMS techniques, and, last, compound confirmation with authentic standards when available. Using this approach, it becomes possible to detect chemicals that enter a waterway from a source (point or nonpoint) between sampling locations. This can then be used for such purposes as source elucidation, compound discovery, or both. In the following sections we will be referring to Figure 1 and the specific step in the process to which we are referring.

Sample Collection. In the summer of 2012, water samples were collected at locations on the Cape Fear River and its tributaries, with some locations having previously been found to contain measurable PFASs.[15] Grab samples were taken from the bank and bridge crossings with a lab-made dip sampler or a stainless steel Kemmerer sampler, and stored in a 1-L HDPE bottle following the procedures described in Nakayama et al.[16] Samples (n = 9) were acquired from the main flow of the Cape Fear River including from just south of the city of Fayetteville, NC to the bridge crossing in the town of Tar Heel, NC. Duplicate samples, trip spikes, and trip blanks were included in this sampling. This sampling also included tributaries to the Cape Fear River along the same stretch of river where reclaimed wastewater treatment plant (WWTP) and industrial effluent streams occurred (Figure 1, step 1).

Sample Analysis for Traditional PFASs. Samples were prepared and analyzed according to the methods of Nakayama et al.[16] In brief, water samples were stabilized with addition of nitric acid and stored at ambient temperature prior to analysis (<7 days). Each water sample was measured in a graduated cylinder, and the sampling bottle was washed with 10 mL of methanol to solubilize analytes that may have become sorbed to the container wall during shipping and storage. The water was then placed back in the methanol-washed bottle with the methanol rinsate, spiked with a mixture of internal standards, and filtered through a glass fiber filter. A volume, typically 500 mL, of water was concentrated on a Waters WAX SPE cartridge using a positive displacement pump. The cartridge was eluted with basic methanol (0.3% NH_4OH) and the eluent was concentrated via evaporation under N_2 gas to 1 mL and prepared for analysis. A procedural blank was prepared as described above using 500 mL of in-house DI water. Traditional PFASs (C_4−C_{10} perfluorocarboxylic acids (PFCAs); perfluorobutanesulfonate (PFBS), perfluorohexanesulfonate (PFHxS), and PFOS) analysis was performed using a Waters Acquity ultra performance liquid chromatograph interfaced with a Waters Quattro Premier XE triple quadrupole mass spectrometer (UPLC-MS/MS) (Waters, Milford, MA, USA).

TOFMS Investigation of Novel Fluorinated Compounds. The extraction method used for traditional PFASs analysis was also used for elucidation of novel compounds. Elevated concentrations of traditional PFASs in samples were used as an indication of samples that were likely closer to sources (Figure S2). Sample analysis was performed using an Agilent 1100 series HPLC interfaced with a 6210 series Accurate-Mass LC-TOF system (Agilent Technologies, Palo Alto, CA). The mass spectrometer was operated in electrospray ionization (ESI) negative mode and any drift in the mass accuracy of the TOF was continuously corrected by infusion of two reference compounds (purine (m/z 119.03632) and the acetate adduct of hexakis (1H,1H,3H-tetrafluoropropoxy) phosphazine (m/z 980.016375)) via dual-ESI sprayer. Chromatographic separation was accomplished using an Eclipse Plus C8 column (2.1 × 50 mm, 3.5 μm; Agilent). The method consisted of the following conditions: 0.2 mL/min flow rate; column at 30 °C; mobile phases: A: ammonium formate buffer (0.4 mM) and DI water/methanol (95:5 v/v), and B: ammonium formate (0.4 mM) and methanol/DI water (95:5 v/v); gradient: 0−15 min a linear gradient from 75:25 A/B to 15:85 A/B; with a 4 min post time for equilibration.

Identification of Suspect Features. The total ion chromatogram (TIC) of each water sample was subjected to the software molecular feature extraction algorithm (MFE) and was restricted to the 100 most intense features m/z 50−1700 based on peak height. A molecular feature is defined as a single accurate mass with a specific retention time and an integrated area count. Compounds identified in the solvent and procedural blank samples were used to develop a mass exclusion list to subtract from subsequent unknown samples. After molecular features were identified, they were exported as a Compound Exchange File (.CEF) and imported into Mass Profiler to compare upstream with downstream samples.

DOI: 10.1021/acs.est.5b01215
Environ. Sci. Technol. 2015, 49, 11622−11630

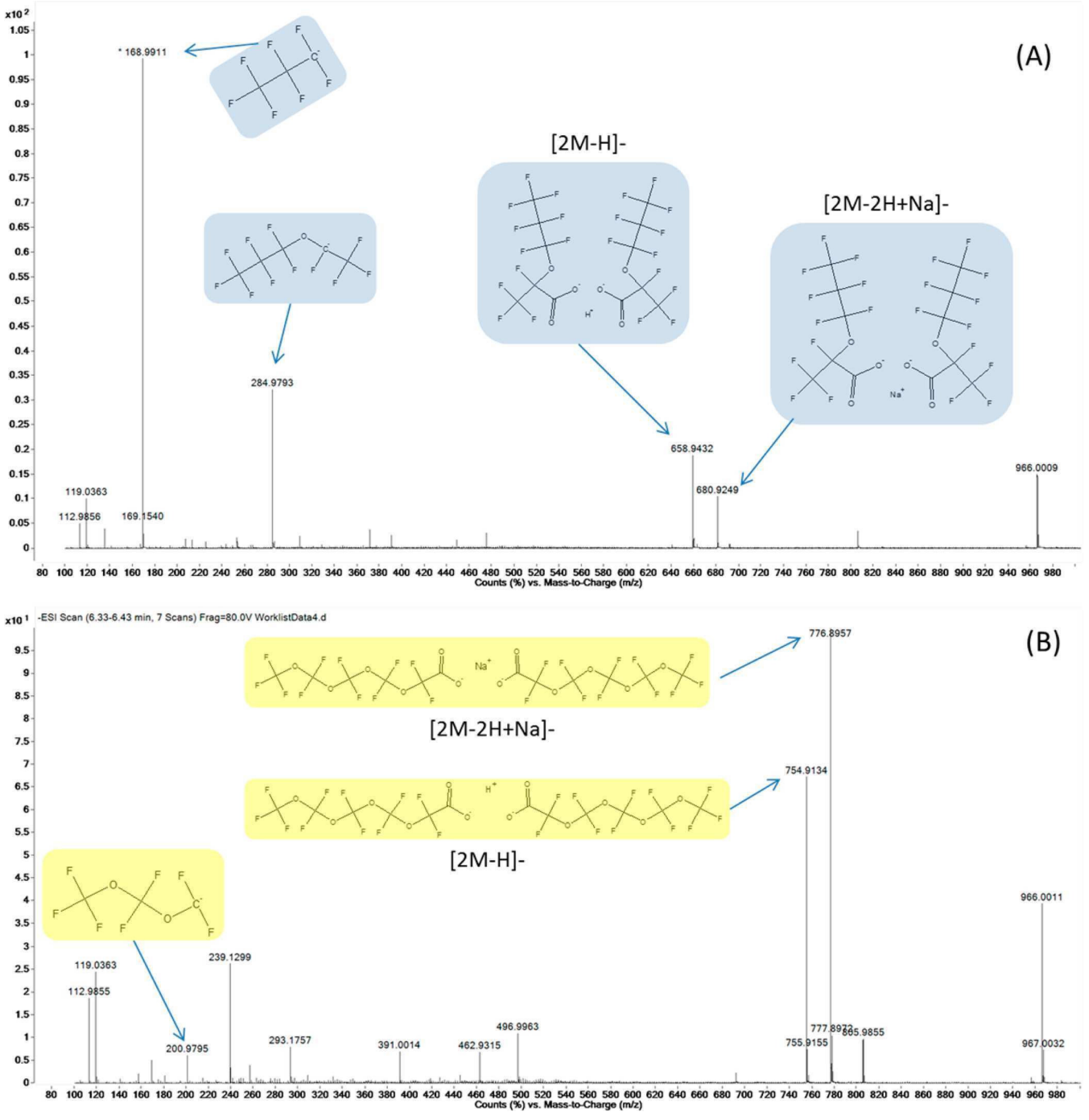

Figure 2. ESI negative spectra for two example perfluorinated ether carboxylic acids found in water: (A) $C_6HF_{11}O_3$ (retention time 5.9−6.0 min) and (B) $C_6HF_{11}O_6$ (retention time 6.5−6.6 min). Note: in spectrum (A and B) *m/z* 112.9856, 119.0363, and 966.0007 are reference masses for continuous mass calibration. Peaks not pointed out are not associated with the compound of interest.

Pairwise comparisons of sequential samples in river flow (Figure 1 step 2) were used to identify those requiring further investigation. For instance, features found in the downstream sample that were not found in the upstream sample indicate a source (point or nonpoint) exists between the two sampling locations (Figure 1 step 3). Further investigation of peaks with larger area counts using the "identify compounds" feature in the software and additional analyses of samples were used for confirmation. Perfluorinated compounds already identified with traditional UPLC-MS/MS analysis were eliminated from this remaining list further narrowing the unknown compounds requiring follow-up scrutiny.

Poly- and perfluorinated compounds tend to have a negative mass defect due to the presence of multiple fluorine and oxygen atoms. Negative mass defect means that the exact mass of a compound is less than the nominal mass.[17] For instance, the exact mass of perfluorooctanoate ($C_8F_{15}O_2$) is 412.9664, whereas the nominal mass is 413 Da. In this instance negative mass defect compounds only found in the downstream sample were further explored. An additional characteristic of samples that are contaminated with per- and polyfluorinated com-

DOI: 10.1021/acs.est.5b01215
Environ. Sci. Technol. 2015, 49, 11622−11630

Table 1. Accurate Mass of Polyfluorinated Compounds and In-Source Artifacts Found in Extracted Water Samples

number	formula	CAS no.	name	[M][a]	$[M-H]^-$ m/z	$[2M-2H+Na]^-$ m/z	$[2M-H]^-$ m/z
Monoether PFECAs							
1	$C_3HF_5O_3$			179.9846	178.9773	380.9438	358.9619
2	$C_4HF_7O_3$			229.9813	228.9740	480.9372	458.9553
3	$C_5HF_9O_3$	863090-89-5		279.9782	278.9709	580.9310	558.9491
4	$C_6HF_{11}O_3$	13252-13-6	undecafluoro-2-methyl-3-oxahexanoic acid	329.9750	328.9677	680.9247	658.9427
5	$C_7HF_{13}O_3$			379.9718	378.9645	780.9182	758.9363
6	$C_8HF_{15}O_3$			429.9686	428.9613	880.9118	858.9299
Polyether PFECAs							
7	$C_7HF_{13}O_7$	39492-91-6	perfluoro-3,5,7,9,11-pentaoxadodecanoic acid	443.9515	442.9442	908.8776	886.8957
8	$C_6HF_{11}O_6$	39492-90-5	perfluoro-3,5,7,9-butaoxadecanoic acid	377.9598	376.9525	776.8942	754.9123
9	$C_5HF_9O_5$	39492-89-2	perfluoro-3,5,7-propaoxaoctanoic acid	311.9681	310.9608	644.9108	622.9289
10	$C_4HF_7O_4$	39492-88-1	perfluoro-3,5-dioxahexanoic acid	245.9764	244.9691	512.9274	490.9455
PFESAs							
11	$C_7HF_{13}O_5S$	66796-30-3[b]		443.9337	442.9264		
12	$C_7H_2F_{14}O_5S$			463.9399	462.9326		
Other							
	Na^+			22.9892			
	H^+			1.0073			
	CF_2O			65.9917			
	CF_2			49.9968			

[a]Indicates the monoisotopic mass of the neutral species. [b]CAS number for Nafion copolymer.

pounds is the presence of multiple peaks that differ by exactly ± m/z 49.9968 and/or 65.9917, corresponding to a difference of CF_2 and CF_2O, respectively. This happens because PFAS synthesis is an industrial process that yields a distribution of products that differ primarily in chain length and/or degree of isomerization. Compounds identified as having a negative mass defect and differing from another peak by ± m/z 49.9968 and 65.9917 are highly likely to be polyfluorinated compounds. Selected samples were also analyzed by QTOF to aid with confirmation of proposed structures (generously provided by colleagues mentioned in the Acknowledgments).

TOFMS Experimental Workflow. Once an unknown compound with negative mass defect was noted, it was isolated from other mass spectral data in the following way: An extracted ion chromatogram (EIC) was generated from the total ion chromatogram (TIC) using the m/z identified. The EIC was then used to do a background subtraction of the spectral region both immediately before and after the detected peak (typically ±0.1 min) (Figure 1 step 4). The center of the detected peak was extracted for the mass spectral information, and the background spectrum was subtracted for a clean spectrum. This was necessary to eliminate, to the best of our ability, competing spectral peaks that were coeluting and not associated with the spectrum being investigated. This would include, but is not limited to, spectral signals originating from the reference compounds (constantly infused to maintain a lock on mass assignments) and their fragments. Once suspect spectral signals were isolated, a series of experiments were conducted to induce in-source fragmentation ions to aid with compound identification based on the work of Ferrer and Thurman.[18] Specifically, a series of methods with differing fragmentor voltages (80−190 V) were run in sequence to look for diagnostic ions that emerged as fragmentor voltage increased. In addition, common adducts such as Na^+, NH_4^+, acetate, etc. were used to aid with compound identification. Detected spectral features were subjected to molecular formula generation using the elements (C, H, O, N, S, P, Cl and F).[19] Formulas generated were scored based on accurate mass, isotope abundance (compound mass distributions attributable to elemental mass distributions e.g., 1.1% ^{13}C, 0.2% ^{18}O, etc.) and isotope distribution (for example, slight differences in isotope mass such as when an m+2 peak is from two ^{13}C or a single ^{18}O) . Only scores >75% were considered for further exploration. Figure 1 steps 4 and 5 outline the advanced TOFMS techniques used to discover novel chemical species.

RESULTS

With the approach described above, sites were identified for further investigation when a large increase in number and magnitude (area counts) of unknown compounds was found in downstream samples. In addition, a very large increase (greater than 2 orders of magnitude) in concentration of historically measured PFAAs also persisted for many river miles downstream of a certain point (Figure S2) consistent with observations in Nakayama et al.[10] Interestingly, the profile of the historically measured PFASs contributing to the total PFASs found at each location was seen to dramatically change near this location (Figure S3). The major compounds contributing to this increase were perfluoropentanoic acid (PFPeA), followed by perfluoroheptanoic acid (PFHpA) and perfluorobutanoic acid (PFBA). It was evident that there was a significant source (total historically measured PFASs concentration increased by >100 times) of per- and polyfluorinated compounds near this location. Plotting the samples (CFR004 upstream vs CFR002 downstream) in MassProfiler for visualization indicated that there were 77 features that were unique to the downstream sample (Figure S4) with many (n = 69) having negative mass defects. In this figure (S4) the size of the symbol is proportional to the area counts of the molecular feature. Traditional PFASs with known concentrations (in Figure S2) are included for comparison purposes. Peaks with larger areas were investigated first under the assumption that these concentrations would be among the highest. Additional

DOI: 10.1021/acs.est.5b01215
Environ. Sci. Technol. 2015, 49, 11622−11630

pairwise comparisons were done on all sequential samples, however results indicated that samples downstream of CFR003 were simply dilutions of a source input. Samples were chosen for additional scrutiny where there was sufficient analytical signal without saturation of the detector which compromises mass accuracy.

Dimers and Fragments. It became evident that in multiple instances several of the larger peaks had a number of common characteristics: (1) negative mass defect, (2) multiple related chromatographic peaks differing by ± m/z 49.9968 and/or 65.9917 (± a CF_2 group and/or a CF_2O group), and (3) apparent noncovalent homodimers linked by either a proton or sodium ion. For example, at a retention time of 5.9−6.0 min, two large peaks emerged from the spectra with m/z of 658.9462 and 680.9256 (Figure 2A). After careful evaluation, it became apparent that these were the proton-bound and sodium-bound in-source homodimers of undecafluoro-2-methyl-3-oxahexanoic acid ($C_6HF_{11}O_3$) (Table 1). These differed by m/z 21.9819, the difference between the Na^+ and H^+ versions of the dimer. It is important to note that the $[M - H]^-$ peak (m/z 328.9677), which one might expect to be the most prominent, was barely distinguishable from the background signal at this point because the in-source ionization conditions so heavily favored the formation of these dimers. Given the prominence of the $C_6HF_{11}O_3$ compound in this sample, we postulated that a homologous series of related perfluorinated ether carboxylic acids (PFECAs), differing from the first compound by either the addition or deletion of CF_2 units (m/z 49.9968) might also be present. An EIC for each of the hypothetical masses, based on sequential addition or deletion of CF_2 units (m/z 49.9968) was extracted from the TIC, with the resulting series of related PFECAs presented in Figure S5. Although not specifically shown in this Figure, we also observed the presence of the analogous sodium and proton bound dimers for each compound identified in this homologous series of PFECAs ($C_{(n=3-8)}HF_{(n=5-15)}O_3$ (Table 1). To obtain additional evidence supporting the proposed structure of the compounds eluting at 5.9 min, additional experiments were conducted by altering the fragmentor voltage in order to try to form diagnostic ions from the m/z of 658.9427 and 680.9247 dimers eluting at this time. Figure S6 shows diagnostic dimer and fragment ions resulting from in-source CID that are consistent with the structure proposed for the $C_6HF_{11}O_3$ compound. The major ions found are also shown in Figure S10. Extracted spectra comparable to those shown in Figure S6, differing only by the loss of CF_2 groups, were investigated as well (Figure S7) lending credence to the postulated structure(s) and discussed in more detail in the following section.

Confirmation of Structure. An online search of the formula and proposed structure of the $C_6HF_{11}O_3$ compound eluting at 5.9 min led to a tentative match in a "grey-literature" citation that mentions a new-generation processing aid for the production of high-performance fluoropolymers identified only as C3 dimer acid/salt (CAS 13252-13-6) (Figure S6).[6] With a CAS number, it was possible to purchase an authentic standard (Synquest Laboratories, Alachua, FL) to compare for retention times and mass spectral ionization patterns. The authentic standard compared very well with the tentatively identified compound found in water samples (±0.051 min RT; ± m/z 0.0002 (0.51 ppm) (Figure 1 step 6). Additional authentic standards for other compounds in this homologous series were not commercially available. However, common spectral patterns and adducts were observed differing only by repeating CF_2 units, as supporting information for compound identification of a homologous series of PFECAs (Figure S7).

Additional Perfluorinated Ether Acids. Figure S4 shows that there are a number of features that are present in the water sample downstream of a potential input location that are not in the upstream sample. Evident in Figure S4 are a pronounced series of peaks that appear as vertical lines, likely from coeluting and related chemicals (see later discussion on in-source n-mer formation). A number of these peaks exhibited negative mass defects. Further investigation of the TOFMS spectra indicated two peaks coeluting at 6.5 min (m/z 776.8942 and 754.9123) with a mass difference of m/z 21.9819, again suggesting the presence of in-source proton- and sodium-bound homodimers (Figure 2B). Knowing this information, we postulated an exact mass of m/z 376.9525 for the $[M - H]^-$ ion (Table 1). We further postulated a homologous series based on addition and deletion of CF_2 units, but exact masses corresponding to ± m/z 49.9968 were not detected. Given reports of industrial producers making greater use of ether oxygens to limit the size of perfluorinated regions within a given molecule, we postulated that a homologous series could also be based on the repeating units of CF_2O, with an exact mass offset of ± (m/z 65.9917).[17,20] Searching the sample for m/z 376.9525 ± this hypothetical CF_2O offset did yield another homologous series (Figure S8). In addition, as was previously the case, each of these new compounds was also found to form sodium-bound and proton-bound homodimers, providing further support for the proposed structures (Table 1). Confirmation of these compounds with authentic standards was not possible. It should be noted that in the homologous series shown, the chemical $C_3HF_5O_3$ (m/z 178.9773) is a common feature (Table 1) to the previously identified homologous series. Taken together, the exact mass of the proposed structures, the offset by a CF_2O, and the exact mass of the in-source dimers formed, all support the occurrence of this additional homologous series. One compound in this homologous series ($C_4HF_7O_4$ [M − H] 244.9691 Table 1) was subjected to QTOF analysis leading to a series of accurate mass fragments consistent with the proposed structure (Figure S9). The accurate mass fragments show the sequential breakage of the ether oxygen bonds and the resulting fragment ions.

In-Source *n*-mer Formation. Multiple peaks originally thought to be of polymeric origin (m/z 1176.8353 and 1576.7769) were determined to be sodium-bound n-mers of m/z 376.9525 already identified (Figure S12). The retention time of these peaks (6.5 min) indicates this is an in-source phenomenon, as they coelute (Figure S4). In-source artifacts occur in the ESI source and can include such things as the formation of adducts (formate, Na^+, H^+, NH_4^+), fragments, dimers, trimers, and combinations of the above. Peaks that do not coelute, or are chromatographically separated, are generally considered not to be in-source artifacts. The observed spectra (Figure S12) include the formation of n-mers[17] including 2 and 3 bound sodium cations in addition to the compounds shown in Figure S11. The formation of other n-mers with >1 bound sodium was seen as well for additional PFECAs found in this work (data not shown). Recent work by Trier et al.[17] indicates that the formation of these polyfluorinated surfactant clusters occurs in the MS source in the gas phase and are pH and concentration dependent.[17] However, this phenomenon may also be instrument-specific as sample dilution in this study did not lead to loss of these in-source dimers being formed. Similar

DOI: 10.1021/acs.est.5b01215
Environ. Sci. Technol. 2015, 49, 11622−11630

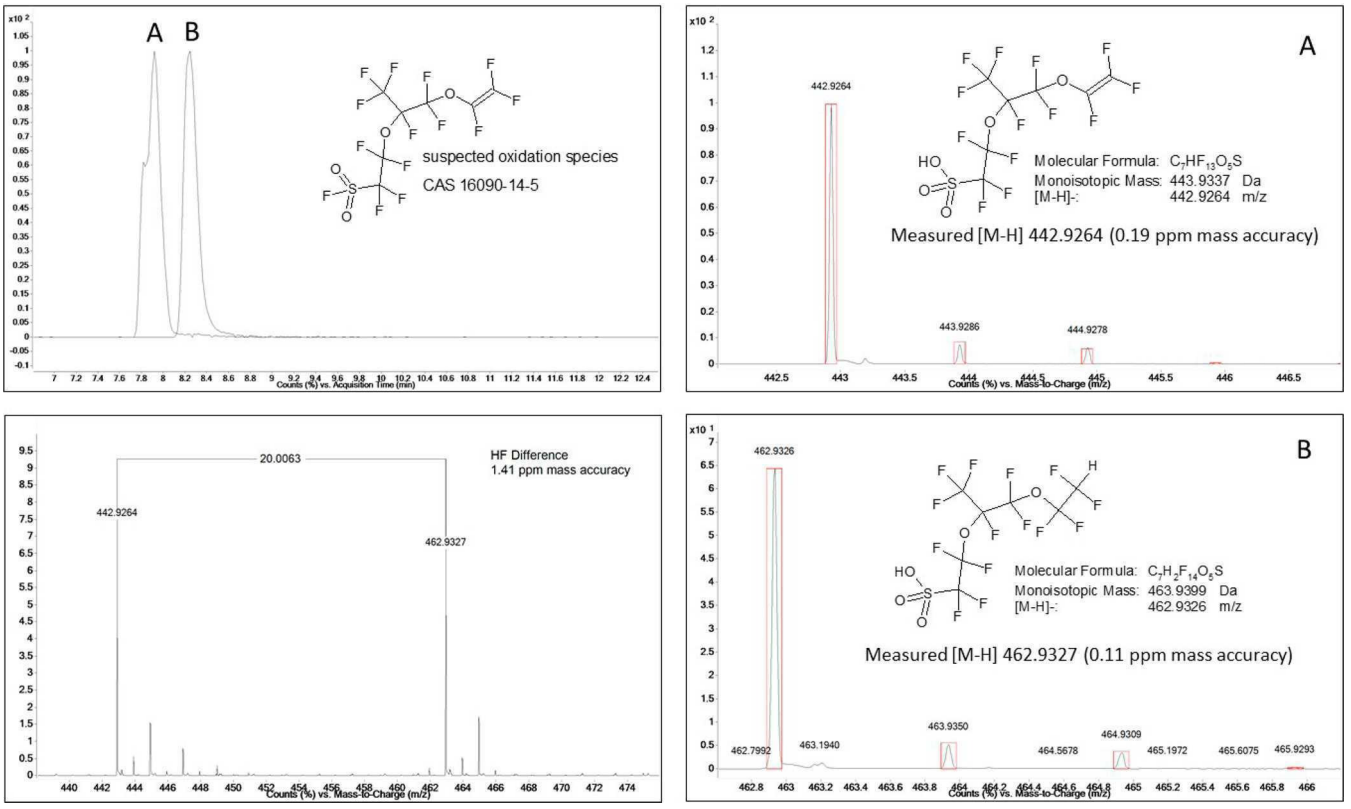

Figure 3. Suspected perfluoro ether sulfonic acids identified in water. Oxidation species are likely products of CAS 16090-14-5, a perfluorinated ether sulfonyl fluoride. Chromatogram shown of two resolved peaks (A,B) and isotope cluster matching of measured versus exact mass. Red boxes indicate the exact mass for the suspected formulas, compared to the accurate mass profile spectrum. Mass difference between two species is an HF (m/z 20.0063−1.41 ppm mass accuracy).

sodium- and proton-bound, as well as mobile phase, modifier (i.e., formate) adducts have been shown by Trier et al.[17] for perfluorocarboxylic acids and mono-PAPs (perfluorinated alkyl phosphates).

Perfluoroalkyl Ether Sulfonic Acid (PFESA) Identification. Records of groundwater monitoring at a fluorochemical manufacturing plant with wells in close proximity to our sampling site indicate PFOA in μg/L concentrations.[21] This document also indicated a sulfonated tetrafluoroethylene based fluoropolymer-copolymer with the trade name Nafion was also produced at this facility. Our data provide evidence that materials related to this compound are also emitted into the river at this point. Figure 3 shows the chemical structures of the suspected oxidation species and resulting transformation products tentatively identified in our samples. An EIC of m/z 442.9264, which is the exact mass of the $[M - H]^-$ moiety of the copolymer containing the sulfonate group (IUPAC name 1,1,2,2-tetrafluoro-2-({1,1,1,2,3,3-hexafluoro-3-[(trifluorovinyl)-oxy]-2-propanyl}oxy)ethanesulfonic acid), suggests this compound is present in the water. In addition, spectral evidence supports the detection of a related compound which is consistent with the addition of an HF ($[M - H]^-$ m/z 462.9327) (IUPAC name 1,1,2,2-tetrafluoro-2-{[1,1,1,2,3,3-hexafluoro-3-(1,1,2,2-tetrafluoroethoxy) propan-2-yl]oxy}-ethanesulfonic acid). The two suspected compounds differ by the mass of HF (m/z 20.0062−1.41 ppm mass accuracy) (Figure 3). These compounds elute as two discrete chromatographic peaks, likely explained by the position occupied by the H and F additions. It is possible that these chemicals originate from the oxidation of ethanesulfonyl fluoride, 2-[1-[difluoro-[(t(fluoroethenyl)oxy]methyl]-1,2,2,2-tetrafluoroethoxy]-1,1,2,2-tetrafluoro- (CAS 16090-14-5) which may have been in use at this industrial location.[22] These compounds would thus be classified as perfluoroalkyl ether sulfonic acids (PFESA).[4] However, unlike previous perfluorinated ether carboxylic acid compounds found in this study, in-source proton- and sodium-bound dimers were not found for these perfluorinated ether sulfonates. In addition, a homologous series based on CF_2 or CF_2O additions was not found. We have not been able to obtain an authentic standard for confirmation of this proposed structure.

DISCUSSION

It has been well-known for a number of years that, due to the toxicity and persistence of perfluorinated compounds, industrial producers are moving toward shorter chain per- and polyfluorinated compound homologues. However, it is not well-known which compounds are being produced as replacements for historic perfluorinated compounds (e.g., PFOS and PFOA). Peer-reviewed literature showing the chemical structure of manufactured per- and polyfluorinated replacement compounds is sparse. An example of one such publication from 3M Corporation indicated that the compound ADONA (4,8-dioxa-3H-perfluorononanoate) is being made to replace ammonium perfluorooctanoate (APFO) as an emulsifier in the manufacture of fluoropolymers.[5] The data presented in this study and Figure S1 indicate that the manufacture and release of per- and polyfluorinated compounds with CF_2 units interspersed with ether oxygen linkages likely is ongoing. A more recent study suggests that polyfluoroalkyl ether

DOI: 10.1021/acs.est.5b01215
Environ. Sci. Technol. 2015, 49, 11622−11630

compounds are being produced and that the number and spacing of ether oxygen linkages and size of the resulting per- and polyfluorinated compound may be manufacturer-specific including other major fluorochemical producers (DuPont, 3M, Solvay, and Asahi).[20] However, there are little to no data in the peer-reviewed literature on most of these compounds. The use of HRMS appears to be an ideal technique to use for discovery and occurrence of new PFASs being released into the environment.

As illustrated in this research, identification of previously undescribed compounds in environmental matrices can be made difficult by the formation of a multitude of in-source artifacts such as in-source gas phase adducts, *n*-mers, and the presence of a homologous series of per- and polyfluorinated compounds. D'Agostino and Mabury identified novel fluorinated surfactants in aqueous film-forming foams (AFFF) and commercial surfactant concentrates using high-resolution mass spectrometry.[23] Their results imply that there are a number of additional fluorinated compounds being produced and emitted into the environment that are unknown to most analysts. The use of TOFMS or other high-resolution mass spectrometers and the workflow we demonstrated (Figure 1) appears to be a useful way to determine occurrence and emissions of new and emerging fluorinated compounds for environmental occurrence efforts.

Schymanski et al. report on identifying small molecules via HRMS, with five levels of confidence.[14] As has been noted earlier, one of the pitfalls of discovery work is the lack of authentic standards at times. As such the highest level of confidence for confirmed structure (Level 1) can be made to one compound in this effort, with the remaining compounds falling in the categories of tentative candidate(s) (Level 3) or probable structure (Level 2).[14] An additional line of evidence we present that Schymanski et al. appear not to is the presence of a homologous series (CF_2, CF_2O) as evidence for compound identification.

The manufacture of shorter-chain perfluorinated and polyfluorinated compounds may have an advantageous effect on biological persistence and bioaccumulation. Two recent publications deemed "The Helsingor Statement"[24] and the "Madrid Statement"[25] explore the state of the science related to poly- and perfluorinated alkyl substances. Shorter straight-chain homologues of perfluorocarboxylic acids (<C_6) and sulfonic acids (<PFBS) have been shown to be cleared quickly from mammalian species tested and thus are not expected to bioaccumulate as readily as PFOS and PFOA.[26] However, the environmental persistence of these shorter chain perfluorinated compounds is likely to be no different from that of the related longer-chain acids. The conventional wisdom is the perfluorinated ether compounds will be more labile than the *n*-alkyl perfluorinated homologues with ether oxygen linkages being more susceptible to chemical or microbial attack. However, as the CF_2 bond in perfluorinated compounds is not at all open to microbial attack due to its bond strength, even the slightest degree of degradation of a per- or and polyfluorinated ether compound would be considered "more" labile. Environmental degradation or toxicology studies associated with the compounds identified in this study were not found by the authors in the peer-reviewed literature at the time of writing this Article. Although data are scarce, the few perfluoropolyethers (PFPEs) to have undergone any kind of degradation studies show little to no biodegradation or hydrolysis.[20] These data mainly come from the European Chemical Agency (ECHA) database of registered substances and associated information.[27] Past studies have demonstrated poor removal efficiency for historical PFASs from source water to drinking water in conventional systems (i.e., treatments that do not include granular activated charcoal (GAC)). It is unknown if these PFECAs and PFESAs are removed by conventional WWTP processes.

Environmental Implications. We demonstrate the presence of a series of novel perfluorinated ether carboxylic and sulfonic acid(s) found to be in natural waters using a nontargeted workflow (Figure 1). The compounds consist of a homologous series of per- and polyfluorinated compounds with repeating units of CF_2 or CF_2O subunits. LC-TOFMS investigations of accurate mass dimers and *n*-mers (proton- or sodium-bound) in addition to diagnostic fragment ions support these findings. Further unidentified compounds with negative mass defects are likely also of per- and polyfluorinated origin, but have not yet been identified and are undergoing further analytical scrutiny. Nontargeted screening and discovery of novel species in samples such as reported here is an ongoing process. Additional environmental samples from other locations may be needed to identify additional chemistries.

Once a xenobiotic compound is identified in the environment, it falls upon the scientific community to begin monitoring efforts to find the extent of contamination of newly discovered species. In addition, toxicological and degradation investigations of identified compounds can commence once a compound has been identified. The procurement of authentic compounds for use in these types of investigations may be a major limiting factor in conducting such investigations, as most of these compounds appear not to be commercially available. More research will need to be conducted on these perfluorinated ether carboxylic and sulfonic acids concerning environmental occurrence, toxicology, and degradation potential.

■ ASSOCIATED CONTENT

Supporting Information

The Supporting Information is available free of charge on the ACS Publications website at DOI: 10.1021/acs.est.5b01215.

Additional information including tables, figures, chemicals structures, and spectra (PDF)

■ AUTHOR INFORMATION

Corresponding Author

*Phone: 919-541-3706; e-mail: strynar.mark@epa.gov.

Notes

The authors declare no competing financial interest.

■ ACKNOWLEDGMENTS

We thank Agilent Technologies for their support of this effort through a TOFMS and travel/training CRADA with the U.S. EPA (CRADA 437-A-12) and in particular Joe Weitzel for his support of this work. In addition, we thank Mike Hays (USEPA), and Chris Higgins and Simon Roberts (Colorado School of Mines) for the use of their QTOFs in confirmation of select compounds identified. We also thank John Offenberg, Michelle Angrish, and Mike Hays for their review of this manuscript. The United States Environmental Protection Agency through its Office of Research and Development funded and managed the research described here. It has been subjected to Agency review and approved for publication.

DOI: 10.1021/acs.est.5b01215
Environ. Sci. Technol. 2015, 49, 11622−11630

Mention of trade names or commercial products does not constitute endorsement or recommendation for use.

REFERENCES

(1) Lindstrom, A. B.; Strynar, M. J.; Libelo, E. L. Polyfluorinated Compounds: Past, Present, and Future. *Environ. Sci. Technol.* **2011**, *45* (19), 7954−7961.

(2) Houde, M.; De Silva, A. O.; Muir, D. C. G.; Letcher, R. J. Monitoring of Perfluorinated Compounds in Aquatic Biota: An Updated Review. *Environ. Sci. Technol.* **2011**, *45* (19), 7962−7973.

(3) U.S. EPA. *2010/15 PFOA Stewardship Program*. http://www.epa.gov/oppt/pfoa/pubs/stewardship/index.html.

(4) Buck, R. C.; Franklin, J.; Berger, U.; Conder, J. M.; Cousins, I. T.; de Voogt, P.; Jensen, A. A.; Kannan, K.; Mabury, S. A.; van Leeuwen, S. P. Perfluoroalkyl and polyfluoroalkyl substances in the environment: terminology, classification, and origins. *Integr. Environ. Assess. Manage.* **2011**, *7* (4), 513−41.

(5) Gordon, S. C. Toxicological evaluation of ammonium 4,8-dioxa-3H-perfluorononanoate, a new emulsifier to replace ammonium perfluorooctanoate in fluoropolymer manufacturing. *Regul. Toxicol. Pharmacol.* **2011**, *59* (1), 64−80.

(6) West Virginia Department of Environmental Protection. *Executed Draft Consent Order No. 7418*. http://www.dep.wv.gov/pio/Documents/DuPont%20Final%20Version.pdf.

(7) Steenland, K.; Fletcher, T.; Savitz, D. A. Epidemiologic Evidence on the Health Effects of Perfluorooctanoic Acid (PFOA). *Environ. Health Perspect.* **2010**, *118* (8), 1100−1108.

(8) MacNeil, J.; Steenland, N. K.; Shankar, A.; Ducatman, A. A cross-sectional analysis of type II diabetes in a community with exposure to perfluorooctanoic acid (PFOA). *Environ. Res.* **2009**, *109* (8), 997−1003.

(9) Steenland, K.; Tinker, S.; Frisbee, S.; Ducatman, A.; Vaccarino, V. Association of Perfluorooctanoic Acid and Perfluorooctane Sulfonate With Serum Lipids Among Adults Living Near a Chemical Plant. *Am. J. Epidemiol.* **2009**, *170* (10), 1268−1278.

(10) Nakayama, S.; Strynar, M.; Helfant, L.; Egeghy, P.; Ye, X.; Lindstrom, A. B. Perfluorinated Compounds in the Cape Fear Drainage Basin in North Carolina. *Environ. Sci. Technol.* **2007**, *41*, 5271−5276.

(11) Hollender, J.; Bourgin, M.; Fenner, K. B.; Longrée, P.; Mcardell, C. S.; Moschet, C.; Ruff, M.; Schymanski, E. L.; Singer, H. P. Exploring the Behaviour of Emerging Contaminants in the Water Cycle using the Capabilities of High Resolution Mass Spectrometry. *Chimia* **2014**, *68* (11), 793−798.

(12) Schymanski, E. L.; Singer, H. P.; Longrée, P.; Loos, M.; Ruff, M.; Stravs, M. A.; Ripollés Vidal, C.; Hollender, J. Strategies to Characterize Polar Organic Contamination in Wastewater: Exploring the Capability of High Resolution Mass Spectrometry. *Environ. Sci. Technol.* **2014**, *48* (3), 1811−1818.

(13) Schymanski, E. L.; Singer, H. P.; Slobodnik, J.; Ipolyi, I. M.; Oswald, P.; Krauss, M.; Schulze, T.; Haglund, P.; Letzel, T.; Grosse, S.; Thomaidis, N. S.; Bletsou, A.; Zwiener, C.; Ibanez, M.; Portoles, T.; de Boer, R.; Reid, M. J.; Onghena, M.; Kunkel, U.; Schulz, W.; Guillon, A.; Noyon, N.; Leroy, G.; Bados, P.; Bogialli, S.; Stipanicev, D.; Rostkowski, P.; Hollender, J. Non-target screening with high-resolution mass spectrometry: critical review using a collaborative trial on water analysis. *Anal. Bioanal. Chem.* **2015**, *407*, 6237.

(14) Schymanski, E. L.; Jeon, J.; Gulde, R.; Fenner, K.; Ruff, M.; Singer, H. P.; Hollender, J. Identifying Small Molecules via High Resolution Mass Spectrometry: Communicating Confidence. *Environ. Sci. Technol.* **2014**, *48* (4), 2097−2098.

(15) Nakayama, S.; Strynar, M. J.; Helfant, L.; Egeghy, P.; Ye, X.; Lindstrom, A. B. Perfluorinated compounds in the Cape Fear Drainage Basin in North Carolina. *Environ. Sci. Technol.* **2007**, *41* (15), 5271−6.

(16) Nakayama, S. F.; Strynar, M. J.; Reiner, J. L.; Delinsky, A. D.; Lindstrom, A. B. Determination of Perfluorinated Compounds in the Upper Mississippi River Basin. *Environ. Sci. Technol.* **2010**, *44* (11), 4103−4109.

(17) Trier, X.; Granby, K.; Christensen, J. H. Tools to discover anionic and nonionic polyfluorinated alkyl surfactants by liquid chromatography electrospray ionisation mass spectrometry. *J. Chromatogr. A* **2011**, *1218* (40), 7094−104.

(18) Ferrer, I.; Thurman, E. M. *Liquid Chromatography Time-of-Flight Mass Spectrometry*; Wiley: Hoboken, NJ, 2009.

(19) Kind, T.; Fiehn, O. Seven Golden Rules for heuristic filtering of molecular formulas obtained by accurate mass spectrometry. *BMC Bioinf.* **2007**, *8* (1), 105.

(20) Wang, Z.; Cousins, I. T.; Scheringer, M.; Hungerbühler, K. Fluorinated alternatives to long-chain perfluoroalkyl carboxylic acids (PFCAs), perfluoroalkane sulfonic acids (PFSAs) and their potential precursors. *Environ. Int.* **2013**, *60* (0), 242−248.

(21) NCDENR. *Onsite PFOA Groundwater Monitoring Report 12-9-13*; p 6. https://edm.nc.gov/DENR-Portal/; full text search HW_F_NCD047368642_12-09-2013_GW_GMR.

(22) USEPA. Envirofacts. http://iaspub.epa.gov/enviro/tsca.get_chem_info?v_registry_id=110000559609. 2015.

(23) D'Agostino, L. A.; Mabury, S. A. Identification of novel fluorinated surfactants in aqueous film forming foams and commercial surfactant concentrates. *Environ. Sci. Technol.* **2014**, *48* (1), 121−9.

(24) Scheringer, M.; Trier, X.; Cousins, I. T.; de Voogt, P.; Fletcher, T.; Wang, Z.; Webster, T. F. Helsingør Statement on poly- and perfluorinated alkyl substances (PFASs). *Chemosphere* **2014**, *114* (0), 337−339.

(25) Blum, A.; Balan, S.A.; Scheringer, M.; Goldenman, G.; Trier, X.; Cousins, I.; Diamond, M.; Fletcher, T.; Higgins, C.; Lindeman, A. A.; Peaslee, G.; de Voogt, P.; Wang, Z.; Weber, R. Madrid Statement. *Environ. Health Perspect.* **2015**, *123*, A107.

(26) Lau, C.; Anitole, K.; Hodes, C.; Lai, D.; Pfahles-Hutchens, A.; Seed, J. Perfluoroalkyl acids: a review of monitoring and toxicological findings. *Toxicol. Sci.* **2007**, *99* (2), 366−94.

(27) European Chemical Agency (ECHA). Registered Substances. http://echa.europa.eu/information-on-chemicals/registered-substances. 2015.

DOI: 10.1021/acs.est.5b01215
Environ. Sci. Technol. 2015, 49, 11622−11630

Cpd	Mass	Avg Mass	m/z	RT	Vol	Vol %	Z Count	Saturated	Group	Cpds/Group
1	195.9336	196.1177	194.9264	0.31	882172	7.04	1		1	1
2	298.0494	298.2903	297.0421	0.31	18290	0.15	1		2	3
3	286.0545	287.1295	285.0473	0.32	30933	0.25	1		2	3
4	312.0565	313.0574	311.0492	0.32	37632	0.3	1		2	3
5	300.0609	300.9733	299.0536	0.32	40901	0.33	1		3	4
6	328.0679	329.0040	327.0606	0.32	36673	0.29	1		3	4
7	280.0325	282.1246	279.0252	0.33	80466	0.64	1		3	4
8	266.0404	268.3195	265.0331	0.33	100281	0.8	1		3	4
9	254.0402	254.2842	253.0329	0.34	29950	0.24	1		4	1
10	294.0432	295.0913	293.0360	0.34	66872	0.53	1		5	1
11	953.2294	953.2924	316.7359	0.37	145527	1.16	1		6	1
12	340.0782	341.9594	339.0709	0.39	89696	0.72	1		7	1
13	324.0757	325.1782	323.0685	0.4	36284	0.29	1		8	2
14	300.0790	300.2774	299.0717	0.4	24402	0.19	1		8	2
15	981.0235	981.2056	980.0162	0.46	78087	0.62	1		9	1
16	352.1010	352.8799	351.0935	0.48	29836	0.24	1		10	3
17	312.0902	312.2557	311.0830	0.48	18195	0.15	1		10	3
18	368.1078	368.3103	367.1006	0.48	15870	0.13	1		10	3
19	348.0928	349.1671	347.0855	0.49	28972	0.23	1		11	1
20	324.0956	324.2579	323.0882	0.5	43242	0.35	1		12	3
21	314.0990	314.2874	313.0917	0.5	30869	0.25	1		12	3
22	380.1130	380.3399	379.1057	0.5	36689	0.29	1		12	3
23	408.1196	408.4002	407.1124	0.51	25573	0.2	1		13	2
24	272.0890	272.2808	271.0817	0.51	35723	0.29	1		13	2
25	296.0905	296.2620	295.0834	0.51	85235	0.68	1		14	2
26	440.1353	440.3672	439.1281	0.52	23672	0.19	1		14	2
27	364.1086	366.5730	363.1013	0.54	214683	1.71	1		15	1
28	406.1212	406.3506	405.1136	0.54	51366	0.41	1		16	5
29	340.1112	340.9763	339.1039	0.54	162195	1.29	1		16	5
30	310.1021	310.3302	309.0949	0.54	94463	0.75	1		16	5
31	254.0758	254.2456	253.0683	0.54	110240	0.88	1		16	5
32	318.0876	319.2258	317.0803	0.54	70745	0.56	1		16	5
33	242.0791	242.2322	241.0718	0.55	72805	0.58	1		17	3
34	354.1158	355.1973	353.1085	0.55	155805	1.24	1		17	3
35	280.0884	280.3220	279.0811	0.55	59696	0.48	1		17	3
36	215.0228	215.1451	214.0155	0.58	40045	0.32	1		18	1
37	286.1039	286.2385	285.0966	0.59	150092	1.2	1		19	1
38	448.1503	449.3769	447.1428	0.6	56337	0.45	1		20	1
39	390.1257	390.3900	389.1184	0.62	19901	0.16	1		21	1
40	450.1567	451.4408	449.1494	0.65	51376	0.41	1		22	1
41	191.0689	191.2460	190.0617	0.69	18621	0.15	1		23	2
42	214.9709	215.2066	213.9636	0.7	99324	0.79	1		23	2
43	304.1005	305.3301	303.0932	0.73	93258	0.74	1		24	1
44	400.1539	400.4113	399.1466	0.8	36295	0.29	1		25	1
45	376.1413	376.2215	375.1339	0.86	49703	0.4	1		26	1
46	439.9417	440.6217	438.9344	0.88	556781	4.44	1		27	1
47	362.1389	362.3609	361.1316	0.92	33601	0.27	1		28	2

48	376.1398	376.4300	375.1325	0.92	31514	0.25	1	28	2
49	256.0413	256.1857	255.0340	0.99	34703	0.28	1	29	1
50	272.0705	272.6509	271.0633	1.01	47149	0.38	1	30	1
51	385.2567	385.4603	384.2494	1.1	22846	0.18	1	31	1
52	272.0715	272.1977	271.0643	1.11	57013	0.46	1	32	1
53	119.0484	119.1576	118.0411	1.16	70937	0.57	1	33	1
54	136.0524	136.1384	135.0451	1.26	41724	0.33	1	34	1
55	272.0744	272.4550	271.0671	1.34	31840	0.25	1	35	1
56	312.1104	312.3088	311.1031	1.35	29818	0.24	1	36	2
57	286.0868	286.2517	285.0795	1.35	100005	0.8	1	36	2
58	246.0604	246.5037	245.0531	1.37	21876	0.17	1	37	1
59	184.1097	184.2162	183.1024	1.42	76200	0.61	1	38	1
60	297.9546	298.0997	296.9474	1.46	195345	1.56	1	39	1
61	286.0890	286.2163	285.0818	1.53	75786	0.6	1	40	1
62	312.1075	312.2859	311.1002	1.57	59160	0.47	1	41	1
63	310.1130	310.2517	309.1057	1.58	103908	0.83	1	42	1
64	292.0984	292.2783	291.0911	1.69	36804	0.29	1	43	1
65	222.0899	222.2170	221.0827	1.77	31217	0.25	1	44	1
66	133.0640	133.1415	132.0568	1.89	140046	1.12	1	45	1
67	263.9828	264.0480	262.9755	2.12	116628	0.93	1	46	1
68	210.1023	210.2098	209.0950	2.29	426110	3.4	1	47	1
69	411.0499	411.2090	410.0427	2.36	27649	0.22	1	48	1
70	320.1624	320.3453	319.1551	2.47	103948	0.83	1	49	1
71	348.1897	348.6814	347.1824	2.51	52384	0.42	1	50	1
72	256.1674	256.3363	255.1601	2.53	36397	0.29	1	51	1
73	320.1629	320.3712	319.1557	2.6	45596	0.36	1	52	1
74	256.1673	256.3302	255.1601	2.69	189366	1.51	1	53	1
75	295.0726	295.3023	294.0653	2.87	69943	0.56	1	54	1
76	254.1518	254.3135	253.1445	2.88	89957	0.72	1	55	1
77	304.1661	304.3669	303.1588	2.9	23753	0.19	1	56	1
78	346.1771	346.7616	345.1698	3	26078	0.21	1	57	1
79	274.1246	274.2890	273.1173	3.03	33811	0.27	1	58	1
80	371.0615	371.3030	370.0542	3.03	64002	0.51	1	59	1
81	269.9899	270.0368	268.9826	3.13	57706	0.46	1	60	2
82	313.9799	314.0357	312.9727	3.13	139278	1.11	1	60	2
83	400.1213	401.2695	399.1140	3.53	204442	1.63	1	61	1
84	288.1397	288.2941	287.1324	3.56	39297	0.31	1	62	1
85	400.1222	401.3180	399.1150	3.63	63382	0.51	1	63	1
86	252.1724	252.3218	251.1651	3.71	51873	0.41	1	64	1
87	294.1824	294.3609	293.1751	3.77	40767	0.33	1	65	1
88	363.9769	364.0510	362.9697	3.85	121026	0.97	1	66	1
89	399.9437	400.1155	398.9364	3.92	98873	0.79	1	67	1
90	240.1369	240.2720	239.1296	3.95	38708	0.31	1	68	1
91	304.1676	304.3119	303.1603	3.96	47120	0.38	1	69	1
92	332.1983	332.6390	331.1911	4.08	30855	0.25	1	70	1
93	432.1795	432.3781	431.1722	4.22	31950	0.26	1	71	1
94	498.1762	498.5351	248.0801	4.23	91389	0.73	2	72	1
95	266.1647	266.3293	265.1574	4.33	28689	0.23	1	73	2

96	448.1425	448.3194	447.1352	4.34	50843	0.41	1	73	2
97	438.2471	438.4420	437.2398	4.38	34749	0.28	1	74	3
98	421.2563	421.4991	420.2491	4.38	40797	0.33	1	74	3
99	413.9731	414.0628	412.9658	4.38	156068	1.25	1	74	3
100	312.1936	312.3841	311.1863	4.44	29137	0.23	1	75	1
101	278.1879	278.3582	277.1806	4.5	22512	0.18	1	76	1
102	366.1723	366.3626	365.1650	4.54	20941	0.17	1	77	1
103	499.9367	500.1106	498.9294	4.72	73427	0.59	1	78	1
104	499.9367	500.1131	498.9294	4.82	144408	1.15	1	79	1
105	250.1569	250.2745	249.1496	4.83	27855	0.22	1	80	1
106	460.2099	460.5383	459.2026	4.84	87728	0.7	1	81	1
107	318.1461	318.3339	317.1388	4.85	24031	0.19	1	82	1
108	266.1554	266.3911	265.1482	5.07	109543	0.87	1	83	1
109	278.1886	278.4158	277.1814	5.09	23684	0.19	1	84	1
110	298.1601	298.3942	297.1528	5.22	388408	3.1	1	85	1
111	312.1761	312.4356	311.1688	5.52	875516	6.99	1	86	1
112	294.1870	294.3018	293.1797	5.69	32205	0.26	1	87	1
113	326.1913	326.3991	325.1840	5.71	69040	0.55	1	88	1
114	326.1918	326.4731	325.1846	5.8	707237	5.64	1	89	1
115	422.2341	422.5330	421.2269	5.83	752026	6	1	90	1
116	322.2271	322.3979	321.2199	5.87	26813	0.21	1	91	1
117	340.2069	340.4663	339.1997	6.16	126285	1.01	1	92	1
118	256.2398	256.3946	255.2325	8.1	56505	0.45	1	93	1
119	682.3027	682.7184	681.2955	9.93	154999	1.24	1	94	1
120	284.2707	284.4659	283.2634	11.14	64329	0.51	1	95	1
121	404.3134	404.5241	403.3061	11.48	94645	0.76	1	96	1
122	382.3801	382.6025	381.3728	13.11	65265	0.52	1	97	1
123	396.3955	396.6206	395.3882	13.31	26600	0.21	1	98	1
124	410.4115	410.6165	409.4042	13.42	101466	0.81	1	99	1
125	438.4431	438.6833	437.4358	13.87	147103	1.17	1	100	1
126	466.4747	466.7288	465.4674	14.49	126941	1.01	1	101	1

Quality Score	Mass Defect
100	-0.0736
87	0.0421
86.6	0.0473
100	0.0492
87	0.0536
87	0.0606
89.7	0.0252
100	0.0331
92.4	0.0329
98.5	0.036
100	-0.2641
80	0.0709
91.2	0.0685
87	0.0717
87	0.0162
92.6	0.0935
95.2	0.083
82	0.1006
83.2	0.0855
87	0.0882
82.3	0.0917
86.9	0.1057
100	0.1124
84.6	0.0817
87	0.0834
99.7	0.1281
85.1	0.1013
80.5	0.1136
84.9	0.1039
85.6	0.0949
99.9	0.0683
87	0.0803
100	0.0718
82.7	0.1085
87	0.0811
96.6	0.0155
100	0.0966
89.1	0.1428
89.7	0.1184
91.4	0.1494
100	0.0617
100	-0.0364
93.6	0.0932
90.5	0.1466
91.1	0.1339
100	-0.0656
88.9	0.1316

84.3	0.1325
100	0.034
87	0.0633
100	0.2494
100	0.0643
100	0.0411
100	0.0451
99.4	0.0671
89	0.1031
99	0.0795
100	0.0531
100	0.1024
100	-0.0526
100	0.0818
100	0.1002
100	0.1057
100	0.0911
100	0.0827
100	0.0568
100	-0.0245
100	0.095
100	0.0427
100	0.1551
92.6	0.1824
100	0.1601
80	0.1557
100	0.1601
100	0.0653
100	0.1445
98.9	0.1588
80	0.1698
100	0.1173
100	0.0542
100	-0.0174
100	-0.0273
100	0.114
100	0.1324
100	0.115
100	0.1651
87.2	0.1751
100	-0.0303
100	-0.0636
100	0.1296
100	0.1603
100	0.1911
100	0.1722
100	0.0801
100	0.1574

100	0.1352
100	0.2398
100	0.2491
100	-0.0342
100	0.1863
100	0.1806
89.1	0.165
100	-0.0706
100	-0.0706
100	0.1496
100	0.2026
100	0.1388
100	0.1482
100	0.1814
100	0.1528
100	0.1688
100	0.1797
82.9	0.184
100	0.1846
100	0.2269
100	0.2199
100	0.1997
93.1	0.2325
100	0.2955
100	0.2634
100	0.3061
94.9	0.3728
100	0.3882
94.2	0.4042
100	0.4358
100	0.4674

Cpd	Mass	Avg Mass	m/z	RT	Vol	Vol %	Z Count	Saturated	Group	Cpds/Group
1	195.9335	196.1274	194.9263	0.31	1277673	0.52	1		1	1
2	175.9575	176.1428	174.9502	0.32	128095	0.05	1		2	1
3	273.9560	274.0983	272.9487	0.35	893478	0.36	1		3	1
4	291.9469	292.0991	290.9396	0.37	82068	0.03	1		4	1
5	120.0417	120.1139	119.0345	0.37	56430	0.02	1		5	1
6	180.0631	180.1518	179.0558	0.38	51910	0.02	1		6	1
7	341.9445	342.1018	340.9372	0.4	1961449	0.8	1		7	1
8	325.9500	326.1259	324.9428	0.41	75414	0.03	1		8	1
9	249.9683	250.0318	248.9610	0.42	235520	0.1	1		9	1
10	113.9929	114.0209	112.9856	0.42	9963533	4.06	1	S	10	1
11	1034.9946	1035.2465	1033.9873	0.43	185007	0.08	1		11	1
12	341.9449	342.0794	340.9376	0.49	847790	0.35	1		12	1
13	120.0000	120.0197	118.9927	0.5	242003	0.1	1		13	2
14	163.9894	164.0294	162.9821	0.5	1382091	0.56	1		13	2
15	1084.9913	1085.1971	1083.9840	0.51	14125	0.01	1		14	1
16	343.9741	344.0549	342.9668	0.51	941276	0.38	1		15	1
17	391.9405	392.1413	390.9332	0.52	135679	0.06	1		16	1
18	389.9448	390.0319	388.9375	0.53	94677	0.04	1		17	1
19	403.9478	404.0326	402.9406	0.54	99435	0.04	1		18	1
20	593.8720	594.0694	592.8647	0.55	176206	0.07	1		19	2
21	601.8671	602.6480	600.8598	0.55	57152	0.02	1		19	2
22	179.9842	180.0286	178.9770	0.57	64392236	26.23	1	S	20	1
23	135.9944	136.0178	134.9871	0.58	1435367	0.58	1		21	1
24	247.9581	248.0940	246.9509	0.59	320342	0.13	1		22	2
25	381.9509	382.0488	380.9437	0.59	823557	0.34	1		22	2
26	439.9413	440.0185	438.9340	0.66	4367951	1.78	1		23	1
27	896.9111	897.7850	895.9038	0.67	36294	0.01	1		24	1
28	343.9439	344.0097	342.9366	0.68	62812	0.03	1		25	1
29	213.1001	213.2155	212.0928	0.7	484668	0.2	1		26	1
30	441.9384	442.1024	440.9311	0.74	6177922	2.52	2		27	1
31	377.9422	378.1287	376.9349	0.74	228122	0.09	1		28	1
32	896.9113	897.7153	895.9040	0.77	144123	0.06	1		29	2
33	901.8670	902.7145	900.8597	0.77	116823	0.05	1		29	2
34	343.9407	344.0987	342.9334	0.78	441267	0.18	1		30	2
35	461.9240	462.0246	460.9168	0.78	95062	0.04	1		30	2
36	439.9417	440.0238	438.9340	0.8	18298698	7.45	2	S	31	1
37	298.1356	299.0322	297.1283	0.86	54991	0.02	1		32	1
38	308.1255	308.3285	307.1181	0.89	105808	0.04	1		33	1
39	210.0921	210.2352	209.0848	0.89	30879	0.01	1		34	1
40	296.1262	296.3080	295.1189	0.9	171982	0.07	1		35	1
41	410.1627	411.1035	409.1554	0.9	188627	0.08	1		36	2
42	425.9424	426.1312	424.9352	0.9	128145	0.05	1		36	2
43	314.1326	314.9716	313.1253	0.9	122383	0.05	1		37	3
44	366.1550	367.3087	365.1478	0.9	274591	0.11	1		37	3

45	423.9472	424.0251	422.9399	0.9	75624	0.03	1		37	3
46	272.0709	272.2477	271.0636	0.91	60042	0.02	1		38	1
47	247.9575	248.1406	246.9503	0.92	93776	0.04	1		39	3
48	179.9845	180.0148	178.9772	0.92	336619	0.14	1		39	3
49	268.1301	268.3154	267.1228	0.93	82847	0.03	1		39	3
50	280.1284	280.3292	279.1212	0.93	102663	0.04	1		40	1
51	208.0767	208.1968	207.0694	0.94	47077	0.02	1		41	1
52	213.9866	214.0363	212.9794	0.95	112049	0.05	1		42	1
53	384.9859	385.0801	383.9786	0.95	33536	0.01	1		43	1
54	457.9322	458.0076	456.9249	0.96	129890	0.05	1		44	2
55	282.1395	282.3470	281.1322	0.96	44726	0.02	1		44	2
56	362.1415	362.3863	361.1342	0.96	29258	0.01	1		45	3
57	510.9785	511.1078	509.9712	0.96	19285	0.01	1		45	3
58	361.9507	362.1132	360.9434	0.96	165523	0.07	1		45	3
59	155.0945	155.2166	154.0872	0.97	28550	0.01	1		46	2
60	185.9917	186.0251	184.9845	0.97	214068	0.09	1		46	2
61	229.9816	230.0218	228.9744	0.97	210939	0.09	1		47	2
62	489.9388	490.0195	488.9315	0.97	25980	0.01	1		47	2
63	507.9293	508.1352	506.9220	0.99	144709	0.06	1		48	1
64	525.9069	526.1979	261.9465	1	883521	0.36	2		49	1
65	1172.8942	1173.3774	1171.8869	1.03	31033	0.01	1		50	1
66	297.9534	298.1009	296.9461	1.04	27115808	11.05	1	S	51	2
67	612.9348	613.2301	611.9275	1.04	8013074	3.26	1	S	51	2
68	927.9170	928.3647	926.9098	1.04	443884	0.18	1		52	3
69	1557.8778	1558.6109	1556.8705	1.04	199029	0.08	1		52	3
70	1242.8983	1243.4660	1241.8910	1.04	901874	0.37	1		52	3
71	1562.8346	1563.4165	1561.8273	1.05	46300	0.02	1		53	2
72	979.9484	980.3679	978.9412	1.05	82015	0.03	1		53	2
73	1247.8531	1248.3032	1246.8458	1.05	140304	0.06	1		54	1
74	1452.8731	1453.4081	1451.8658	1.06	29160	0.01	1		55	1
75	822.9095	823.2213	821.9022	1.07	72416	0.03	1		56	1
76	932.8720	933.2657	931.8647	1.08	34024	0.01	1		57	3
77	507.9291	508.1283	506.9218	1.08	342530	0.14	1		57	3
78	681.9933	682.3307	680.9860	1.08	97215	0.04	1		57	3
79	827.8632	828.1747	826.8559	1.1	38442	0.02	1		58	1
80	617.8904	618.1621	616.8831	1.11	525656	0.21	1		59	2
81	565.9118	566.1057	564.9045	1.11	319969	0.13	1		59	2
82	791.8483	792.0819	790.8410	1.17	364323	0.15	1		60	1
83	310.1113	310.2404	309.1040	1.43	26749	0.01	1		61	1
84	507.9304	508.1643	506.9231	1.67	108766	0.04	1		62	1
85	499.9590	500.0961	498.9517	1.83	17495	0.01	1		63	1
86	133.0641	133.1659	132.0568	1.9	52322	0.02	1		64	2
87	344.1487	344.3048	343.1414	1.9	40091	0.02	1		64	2
88	499.9594	500.0803	498.9521	1.92	40594	0.02	1		65	1
89	519.9491	520.0711	518.9418	1.92	26562	0.01	1		66	1

90	535.9268	536.2027	534.9195	1.95	893618	0.36	1	67	1
91	565.9368	566.2326	564.9295	1.96	114282	0.05	2	68	1
92	344.1474	344.3160	343.1401	1.98	66481	0.03	1	69	1
93	563.9211	564.0408	562.9138	2	36034	0.01	1	70	1
94	535.9266	536.2080	534.9193	2.04	1837073	0.75	1	71	1
95	565.9365	566.1931	564.9292	2.06	242928	0.1	2	72	1
96	344.1479	344.2942	343.1406	2.07	79233	0.03	1	73	1
97	509.9597	510.0667	508.9524	2.09	63894	0.03	1	74	1
98	219.9937	220.0347	218.9864	2.09	214273	0.09	1	75	2
99	263.9836	264.0330	262.9763	2.09	527194	0.21	1	75	2
100	595.9482	596.2827	594.9409	2.1	52984	0.02	1	76	1
101	563.9176	564.0170	562.9103	2.12	252500	0.1	1	77	1
102	541.9315	542.1199	540.9242	2.13	997841	0.41	2	78	1
103	539.9352	540.0239	538.9279	2.15	59979	0.02	1	79	1
104	298.1429	298.4293	297.1356	2.18	57531	0.02	1	80	2
105	344.1477	344.3029	343.1404	2.18	81925	0.03	1	80	2
106	409.9682	410.0532	408.9609	2.21	28246	0.01	1	81	1
107	526.9563	527.2576	525.9490	2.22	70694	0.03	1	82	1
108	255.0637	255.2656	254.0565	2.26	21861	0.01	1	83	2
109	311.9836	312.1751	310.9763	2.26	44125	0.02	1	83	2
110	210.1019	210.2102	209.0947	2.27	272606	0.11	1	84	1
111	411.0505	411.2562	410.0432	2.3	21137	0.01	1	85	1
112	295.9896	296.0599	294.9823	2.31	152775	0.06	1	86	1
113	311.9846	312.0466	310.9773	2.32	87772	0.04	1	87	1
114	591.9620	592.0581	590.9547	2.33	25790	0.01	1	88	1
115	279.9784	280.0299	278.9711	2.33	243940	0.1	1	89	1
116	559.9565	560.0930	558.9493	2.34	328680	0.13	1	90	3
117	525.9538	526.0581	524.9466	2.34	59623	0.02	1	90	3
118	235.9886	236.0289	234.9814	2.34	490114	0.2	1	90	3
119	344.1483	344.3374	343.1410	2.4	31586	0.01	1	91	1
120	320.1622	320.3082	319.1549	2.41	47571	0.02	1	92	1
121	347.9508	348.0964	346.9436	2.5	2045288	0.83	1	93	2
122	482.9841	483.0930	481.9768	2.5	60359	0.02	1	93	2
123	284.1272	284.2839	283.1199	2.55	43489	0.02	1	94	1
124	311.9507	312.0813	310.9434	2.57	126640	0.05	1	95	2
125	438.2815	438.4829	437.2742	2.57	58217	0.02	1	95	2
126	359.9515	360.1152	358.9442	2.58	119459	0.05	1	96	1
127	256.1674	256.3481	255.1601	2.6	178136	0.07	1	97	1
128	347.9511	348.1148	346.9438	2.66	131858	0.05	1	98	1
129	300.1926	300.3639	299.1853	2.67	29564	0.01	1	99	1
130	482.9842	483.1745	481.9770	2.7	71813	0.03	1	100	2
131	315.9452	316.0985	314.9379	2.71	144327	0.06	1	100	2
132	254.1520	254.2893	253.1447	2.75	34401	0.01	1	101	3
133	541.9489	542.0520	540.9417	2.75	20330	0.01	1	101	3
134	295.9732	296.0229	294.9660	2.75	926958	0.38	1	101	3

135	607.9410	608.0809	606.9337	2.78	258227	0.11	1		102	2
136	629.9229	630.0481	628.9156	2.78	35406	0.01	1		102	2
137	347.9510	348.1033	346.9437	2.79	132651	0.05	1		103	1
138	641.9419	642.0531	640.9346	2.79	71652	0.03	1		104	1
139	973.8511	974.0914	972.8438	2.9	348552	0.14	1		105	1
140	809.9097	810.0638	808.9025	3.22	19666	0.01	1		106	1
141	475.9594	476.1508	474.9521	3.22	1627634	0.66	1		107	1
142	397.9482	398.0949	396.9410	3.25	374016	0.15	1		108	1
143	663.9246	664.0133	662.9173	3.25	34615	0.01	1		109	2
144	641.9429	642.0752	640.9356	3.25	289585	0.12	1		109	2
145	1027.8722	1028.0658	1026.8649	3.31	30443	0.01	1		110	1
146	1033.8884	1034.0884	1032.8811	3.31	231423	0.09	1		111	3
147	659.9485	660.1063	658.9412	3.31	10244704	4.17	1	S	111	3
148	329.9747	330.0605	328.9674	3.31	790546	0.32	1		111	3
149	285.9851	286.0395	284.9778	3.31	1204695	0.49	1		112	4
150	371.9627	372.0282	370.9554	3.31	175596	0.07	1		112	4
151	637.9418	638.0610	636.9345	3.31	78372	0.03	1		112	4
152	681.9320	682.0733	680.9248	3.31	1625367	0.66	1		112	4
153	1250.9761	1251.2573	1249.9688	3.32	151002	0.06	1		113	2
154	673.9146	674.1512	672.9073	3.32	227931	0.09	1		113	2
155	169.9964	170.0241	168.9891	3.32	1401750	0.57	1		114	1
156	827.9166	828.0485	826.9093	3.39	18969	0.01	1		115	1
157	475.9592	476.1449	474.9519	3.4	1986550	0.81	1		116	1
158	439.9922	440.0714	438.9850	3.41	46653	0.02	1		117	1
159	673.9147	674.1330	672.9075	3.42	148861	0.06	1		118	1
160	365.9420	366.1010	364.9347	3.46	1240180	0.51	1		119	1
161	413.9431	414.1026	412.9358	3.49	329563	0.13	1		120	1
162	527.9357	528.1218	526.9284	3.52	429474	0.17	1		121	1
163	400.1210	401.3107	399.1137	3.53	128391	0.05	1		122	1
164	310.1775	310.3530	309.1702	3.56	21119	0.01	1		123	1
165	459.9642	460.1494	458.9569	3.58	51465	0.02	1		124	1
166	381.9124	382.4956	380.9051	3.59	144740	0.06	1		125	1
167	400.1220	401.0840	399.1147	3.61	36731	0.01	1		126	1
168	713.9213	714.0488	712.9140	3.66	17515	0.01	1		127	1
169	345.9695	346.0389	690.9319	3.66	453304	0.18	1		128	3
170	251.9832	252.0340	250.9760	3.66	1208021	0.49	1		128	3
171	451.9943	452.3388	450.9870	3.67	29698	0.01	1		128	3
172	413.9430	414.1146	412.9358	3.68	78950	0.03	1		129	2
173	361.9809	362.0513	360.9736	3.68	305833	0.12	1		129	2
174	719.9507	720.0851	718.9434	3.72	87804	0.04	1		130	1
175	459.9647	460.1604	458.9575	3.73	66465	0.03	1		131	1
176	294.1831	294.3737	293.1758	3.76	38489	0.02	1		132	1
177	719.9503	720.0817	718.9431	3.81	47645	0.02	1		133	1
178	363.9769	364.0530	362.9697	3.84	95495	0.04	1		134	1
179	397.9471	398.1076	396.9398	3.85	2307328	0.94	1		135	1

180	575.9529	576.1532	574.9456	3.86	83077	0.03	1		136	1
181	427.9725	428.0768	426.9652	3.88	275079	0.11	1		137	2
182	361.9648	362.0209	360.9574	3.88	230054	0.09	1		137	2
183	944.9069	945.2536	943.8996	3.92	574349	0.23	1		138	3
184	949.8616	950.1600	948.8543	3.92	149454	0.06	1		138	3
185	463.9391	464.1220	462.9318	3.92	8228612	3.35	1	S	138	3
186	427.9727	428.0518	426.9654	3.94	154496	0.06	1		139	1
187	575.9527	576.0534	574.9454	3.96	35276	0.01	1		140	1
188	415.9377	416.0231	414.9304	3.97	28029	0.01	1		141	1
189	773.9258	774.0620	772.9185	3.98	41823	0.02	1		142	1
190	777.9021	778.0823	776.8948	3.99	955864	0.39	1		143	2
191	1177.8418	1178.0907	1176.8345	3.99	124702	0.05	1		143	2
192	1571.7635	1571.9673	1570.7563	3.99	25471	0.01	1		144	1
193	755.9186	756.1116	754.9113	4.01	13702602	5.58	1	S	145	1
194	377.9598	378.0471	376.9525	4.02	948121	0.39	1		146	1
195	1298.9606	1299.2697	1297.9533	4.02	251812	0.1	1		147	1
196	949.8625	950.1881	948.8552	4.03	212881	0.09	1		148	4
197	944.9076	945.2366	943.9003	4.03	387150	0.16	1		148	4
198	1263.8221	1264.1926	1262.8148	4.03	53805	0.02	1		148	4
199	863.8822	864.1472	862.8750	4.03	387704	0.16	1		148	4
200	463.9389	464.1142	462.9316	4.03	5308408	2.16	1	S	149	2
201	465.1208	465.4624	464.1135	4.03	34052	0.01	1		149	2
202	1177.8423	1178.1187	1176.8350	4.08	154028	0.06	1		150	1
203	777.9022	778.0656	776.8949	4.08	1274250	0.52	1		151	1
204	483.9845	484.3418	482.9772	4.14	64168	0.03	1		152	1
205	773.9260	774.0419	772.9188	4.15	81697	0.03	1		153	1
206	427.9390	428.1335	426.9317	4.17	66119	0.03	1		154	1
207	432.1791	432.3924	431.1718	4.22	20662	0.01	1		155	1
208	463.9395	464.1294	462.9323	4.23	122169	0.05	1		156	1
209	443.9332	444.1223	442.9259	4.25	163690	0.07	1		157	1
210	329.9745	330.0469	328.9672	4.25	69710	0.03	1		158	1
211	448.1413	448.2944	447.1341	4.34	53819	0.02	1		159	1
212	459.9447	460.1365	458.9375	4.36	184841	0.08	1		160	1
213	438.2483	438.4682	437.2410	4.38	17948	0.01	1		161	1
214	421.2574	421.4655	420.2501	4.38	39508	0.02	1		162	1
215	413.9737	414.0487	412.9664	4.39	92629	0.04	1		163	2
216	463.9395	464.1064	462.9323	4.39	97598	0.04	1		163	2
217	251.9834	252.0213	250.9761	4.4	267217	0.11	1		164	2
218	346.1450	346.4469	345.1378	4.4	54121	0.02	1		164	2
219	411.9613	412.1006	410.9542	4.41	116821	0.05	1		165	1
220	317.9749	318.0252	316.9676	4.42	283213	0.12	1		166	1
221	351.9771	352.0335	350.9698	4.51	259021	0.11	1		167	3
222	427.9727	428.0545	426.9654	4.51	388365	0.16	1		167	3
223	533.9969	534.2859	532.9896	4.51	49696	0.02	1		167	3
224	493.9303	494.1142	492.9231	4.51	450644	0.18	1		168	1

225	286.2144	286.3535	285.2071	4.53	120376	0.05	1	169	1
226	477.9357	478.0903	476.9284	4.54	554833	0.23	1	170	1
227	429.9682	430.0509	428.9610	4.56	60340	0.02	1	171	1
228	427.9567	428.0311	426.9494	4.59	104636	0.04	1	172	1
229	477.9354	478.1107	476.9281	4.66	280997	0.11	1	173	1
230	909.8851	910.0666	908.8778	4.73	425296	0.17	1	174	2
231	887.9021	888.1108	886.8949	4.73	2491605	1.02	1	174	2
232	1364.9536	1365.1625	1363.9463	4.73	43543	0.02	1	175	2
233	443.9510	444.0265	442.9437	4.74	222771	0.09	1	175	2
234	549.9759	550.3783	548.9686	4.76	85719	0.03	1	176	1
235	499.9363	500.1110	498.9290	4.82	112711	0.05	1	177	1
236	460.2087	460.4738	459.2014	4.85	54902	0.02	1	178	1
237	1013.9020	1014.0587	1012.8948	5.02	19051	0.01	1	179	4
238	991.9207	992.0884	990.9138	5.02	314826	0.13	2	179	4
239	601.9837	602.5497	600.9764	5.03	42295	0.02	1	179	4
240	185.9917	186.0189	184.9844	5.03	1417652	0.58	1	179	4
241	266.1551	266.4021	265.1478	5.08	75892	0.03	1	180	1
242	278.1880	278.3638	277.1807	5.1	23325	0.01	1	181	1
243	460.2094	460.4358	459.2022	5.11	43018	0.02	1	182	1
244	509.9426	510.0233	1018.8795	5.22	132056	0.05	1	183	2
245	615.9667	616.3624	614.9594	5.22	36677	0.01	1	183	2
246	298.1601	298.3901	297.1529	5.22	285398	0.12	1	184	1
247	529.9616	530.0582	528.9543	5.24	79722	0.03	1	185	1
248	312.1761	312.4422	311.1688	5.52	719651	0.29	1	186	1
249	294.1858	294.3198	293.1785	5.69	17488	0.01	1	187	1
250	326.1916	326.3684	325.1843	5.71	50584	0.02	1	188	1
251	326.1916	326.4680	325.1843	5.8	621132	0.25	1	189	1
252	422.2339	422.5501	421.2266	5.83	559991	0.23	1	190	1
253	322.2280	322.3557	321.2207	5.87	21440	0.01	1	191	1
254	340.2070	340.4827	339.1997	6.16	107329	0.04	1	192	1
256	682.3027	682.6191	681.2954	9.92	75900	0.03	1	194	1
257	284.2715	284.4843	283.2642	11.13	63936	0.03	1	195	1
258	404.3135	404.5240	403.3062	11.48	76189	0.03	1	196	1

Quality Score	Mass Defect
100	-0.0737
100	-0.0498
100	-0.0513
100	-0.0604
100	0.0345
100	0.0558
97.6	-0.0628
87	-0.0572
100	-0.039
100	-0.0144
100	-0.0127
100	-0.0624
100	-0.0073
100	-0.0179
91.6	-0.016
100	-0.0332
100	-0.0668
100	-0.0625
87	-0.0594
100	-0.1353
100	-0.1402
100	-0.023
100	-0.0129
100	-0.0491
80	-0.0563
86.2	-0.066
100	-0.0962
86.6	-0.0634
100	0.0928
100	-0.0689
100	-0.0651
100	-0.096
100	-0.1403
100	-0.0666
100	-0.0832
80	-0.066
82.5	0.1283
88.6	0.1181
100	0.0848
95.1	0.1189
91.7	0.1554
100	-0.0648
87.7	0.1253
94.3	0.1478

100	-0.0601
80	0.0636
100	-0.0497
87	-0.0228
93.9	0.1228
90.2	0.1212
100	0.0694
100	-0.0206
92.4	-0.0214
99.6	-0.0751
80.7	0.1322
87	0.1342
98.4	-0.0288
96.9	-0.0566
100	0.0872
100	-0.0155
100	-0.0256
90.6	-0.0685
98.9	-0.078
92	-0.0535
100	-0.1131
100	-0.0539
100	-0.0725
100	-0.0902
100	-0.1295
100	-0.109
100	-0.1727
100	-0.0588
100	-0.1542
92.8	-0.1342
100	-0.0978
100	-0.1353
100	-0.0782
87	-0.014
100	-0.1441
100	-0.1169
100	-0.0955
100	-0.159
100	0.104
96	-0.0769
100	-0.0483
100	0.0568
100	0.1414
100	-0.0479
100	-0.0582

100	-0.0805
80	-0.0705
100	0.1401
100	-0.0862
100	-0.0807
100	-0.0708
100	0.1406
100	-0.0476
100	-0.0136
100	-0.0237
100	-0.0591
100	-0.0897
100	-0.0758
100	-0.0721
80	0.1356
100	0.1404
100	-0.0391
100	-0.051
100	0.0565
100	-0.0237
100	0.0947
100	0.0432
100	-0.0177
100	-0.0227
100	-0.0453
100	-0.0289
100	-0.0507
100	-0.0534
100	-0.0186
100	0.141
100	0.1549
100	-0.0564
100	-0.0232
100	0.1199
100	-0.0566
100	0.2742
100	-0.0558
100	0.1601
100	-0.0562
100	0.1853
100	-0.023
100	-0.0621
100	0.1447
81.9	-0.0583
100	-0.034

100	-0.0663
94.7	-0.0844
100	-0.0563
100	-0.0654
84.7	-0.1562
98.6	-0.0975
100	-0.0479
97.5	-0.059
100	-0.0827
100	-0.0644
97.3	-0.1351
100	-0.1189
100	-0.0588
100	-0.0326
100	-0.0222
100	-0.0446
100	-0.0655
100	-0.0752
100	-0.0312
100	-0.0927
80	-0.0109
100	-0.0907
100	-0.0481
100	-0.015
100	-0.0925
100	-0.0653
100	-0.0642
100	-0.0716
100	0.1137
100	0.1702
100	-0.0431
100	-0.0949
100	0.1147
100	-0.086
100	-0.0681
100	-0.024
100	-0.013
100	-0.0642
100	-0.0264
97.7	-0.0566
100	-0.0425
100	0.1758
100	-0.0569
100	-0.0303
100	-0.0602

100	-0.0544
92.1	-0.0348
100	-0.0426
100	-0.1004
100	-0.1457
100	-0.0682
100	-0.0346
100	-0.0546
100	-0.0696
100	-0.0815
100	-0.1052
100	-0.1655
80	-0.2437
93.3	-0.0887
90.2	-0.0475
100	-0.0467
100	-0.1448
100	-0.0997
100	-0.1852
100	-0.125
100	-0.0684
81	0.1135
80	-0.165
83.9	-0.1051
100	-0.0228
100	-0.0812
100	-0.0683
100	0.1718
100	-0.0677
100	-0.0741
100	-0.0328
100	0.1341
100	-0.0625
100	0.241
100	0.2501
100	-0.0336
100	-0.0677
81.6	-0.0239
100	0.1378
100	-0.0458
100	-0.0324
100	-0.0302
100	-0.0346
100	-0.0104
100	-0.0769

100	0.2071
100	-0.0716
100	-0.039
100	-0.0506
100	-0.0719
100	-0.1222
100	-0.1051
80	-0.0537
100	-0.0563
80	-0.0314
100	-0.071
100	0.2014
98.7	-0.1052
100	-0.0862
100	-0.0236
100	-0.0156
100	0.1478
100	0.1807
100	0.2022
100	-0.1205
100	-0.0406
100	0.1529
100	-0.0457
100	0.1688
100	0.1785
87	0.1843
100	0.1843
100	0.2266
100	0.2207
100	0.1997
100	0.2954
100	0.2642
100	0.3062

SUPPORTING INFORMATION

Non-targeted screening based identification of per- and polyfluoroalkyl substances in the Cape Fear River by high resolution mass spectrometry

James McCord[1], Mark Strynar[2]*

1 Oak Ridge Institute for Science and Education, National Exposure Research Laboratory, U.S. Environmental Protection Agency, Research Triangle Park, NC

2 National Exposure Research Laboratory, U.S. Environmental Protection Agency, Research Triangle Park, North Carolina 27711, United States

91 Figures, 3 Tables, 32 Pages

TOF Analysis and Molecular Feature Screening

Initial mass spectrometry (MS) analysis was carried out with an Agilent 1100 series HPLC interfaced with an Agilent 6210 TOF system. Chromatographic separation was carried out an InfinityLab Poroshell 120 EC-C8 column (2.1 × 50 mm, 2.7 µm; Agilent) with method conditions as follows: 0.3 mL/min flow rate; column at 30 °C; mobile phases A: ammonium formate buffer (0.4 mM) in water/methanol (95:5 v/v), and mobile phase B: ammonium formate (0.4 mM) in methanol/water (95:5 v/v); gradient: 0−15 min a linear gradient from 75:25 A/B to 15:85 A/B; with a 4 min post time for equilibration. TOF data collection was accomplished in negative mode electrospray ionization with a dual-electrospray source providing purine and hexakis phosphazine as internal reference masses from the secondary spray. The instrument was operated in 4GHz high resolution mode with a mass window of 100-1700 m/z.

QTOF-MS/MS Instrument Parameters

Structural investigation of the molecular features was performed using an Agilent 1260 Infinity UPLC coupled to a 6530 QTOF. Chromatographic separation was carried out similarly to the TOF analysis, but with MS parameters altered to allow for data-dependent MS/MS acquisition. The MS was operated in 2GHz extended dynamic range mode with an MS mass range of 100-1700 m/z and an MS/MS mass range of 60-1000 m/z. Scan rates were set to vary based on precursor abundance with a target of 10,000 counts/spectrum and cap of 250 ms of ion collection. A minimum precursor threshold of 5,000 counts was set, along with an active exclusion window of twelve seconds after five spectral collections. A preferential inclusion list of the 50 most abundant species from the TOF analysis was set, along with an exclusion list of the reference mass ions and molecular features assigned to the blank. The collection of MS/MS spectra took place at fixed collision energies of 10 and 25 with a narrow (~1.3 m/z) precursor isolation window.

Extracted Ion Chromatograms and MS/MS spectra for Identified Per/Polyfluorinated Ether Compounds

Extracted ion chromatograms were prepared by extracting the theoretical [M-H] ion mass with a mass accuracy of +/- 10ppm. Chromatographically resolved isomers of the same molecular formula are assigned letters A, B, C etc. Features in black have MS/MS spectra, features in grey were not able to be isolated for MS/MS fragmentation. Cleavage locations for major fragments are shown with red dashed lines for chemical structures that could be accurately assigned on the basis of MS/MS. Some common fragments are listed in Table S-4.

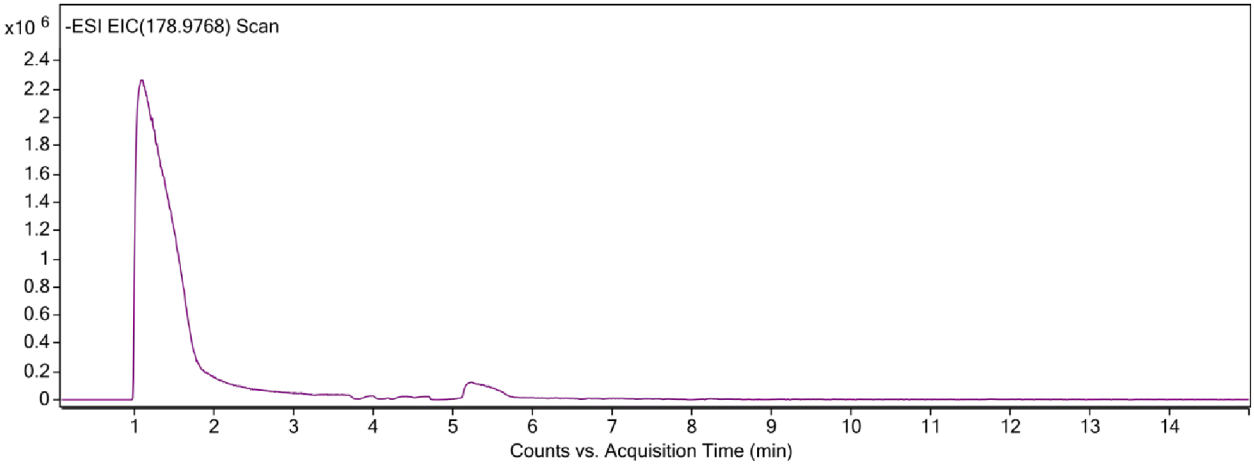

Figure 1. Extracted Ion Chromatogram for Cmp01

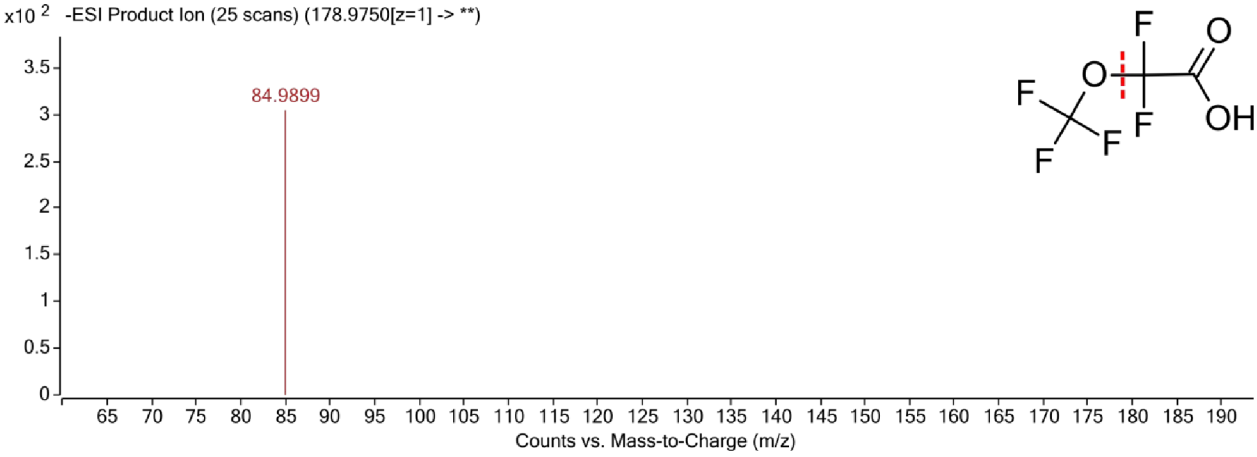

Figure 2. Average MS/MS Spectrum for Cmp01 @ 10/25 CID

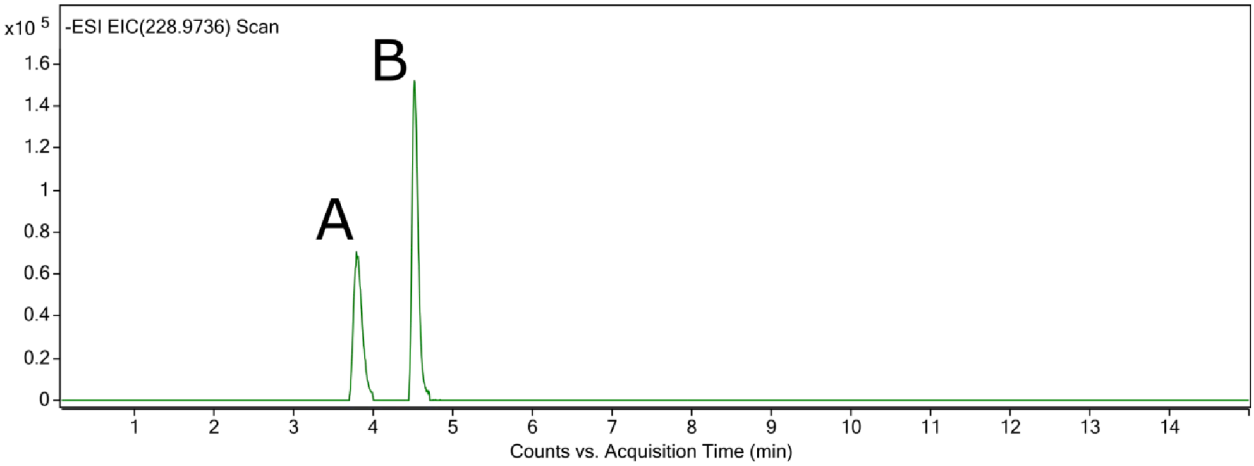

Figure 3. Extracted Ion Chromatogram for Cmp02

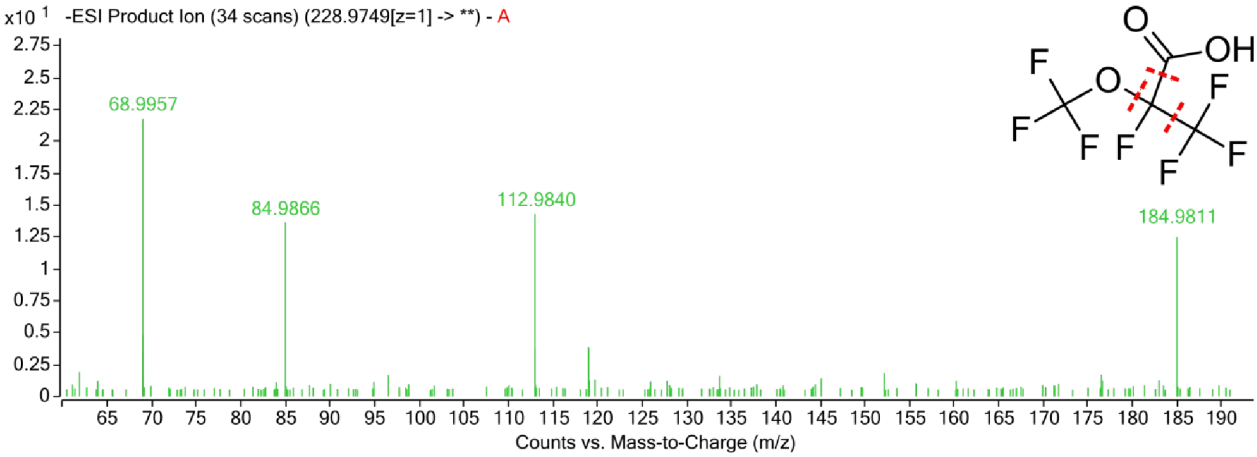

Figure 4. Average MS/MS Spectrum for Cmp02a @ 10/25 CID

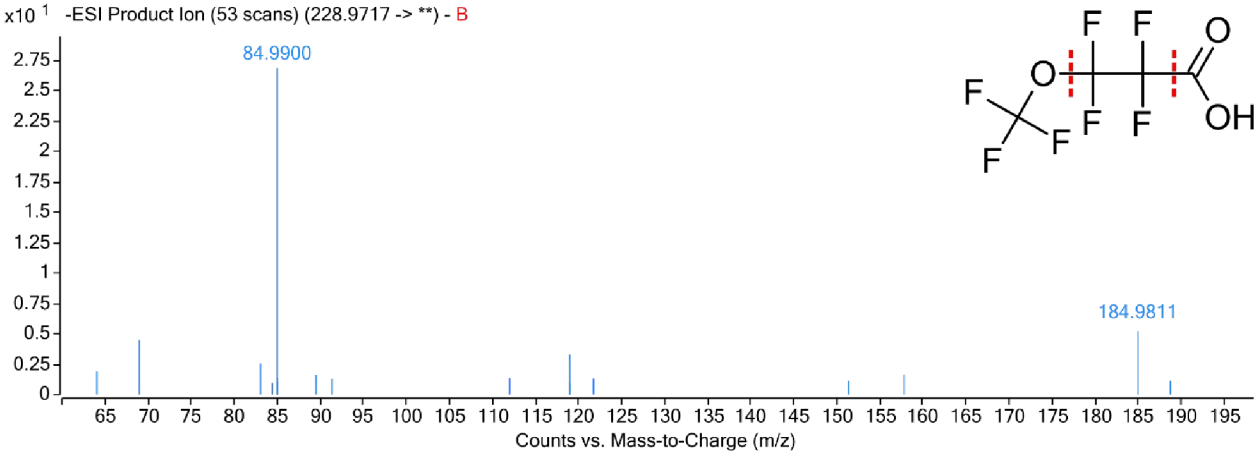

Figure 5. Average MS/MS Spectrum for Cmp02b @ 10/25 CID

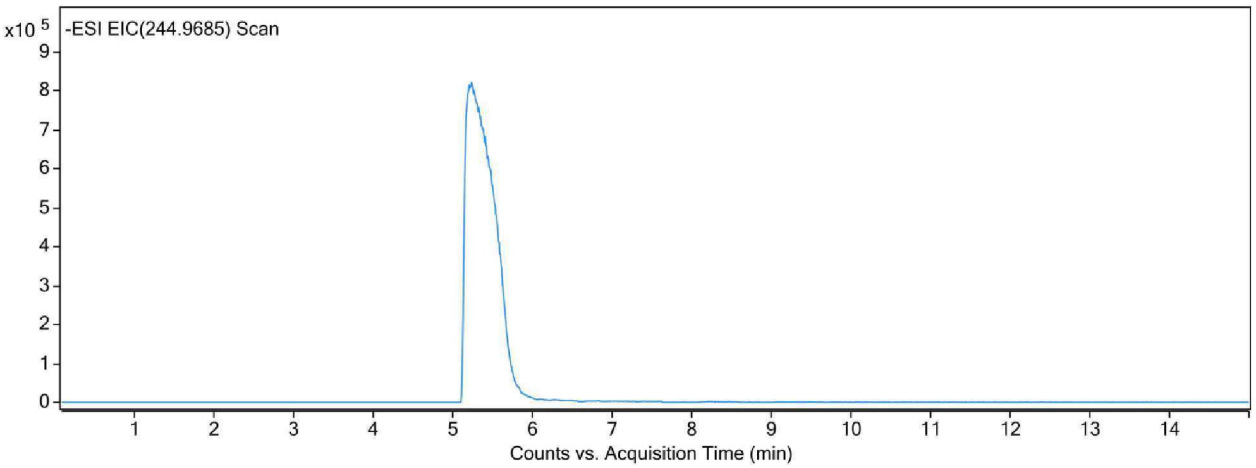

Figure 6. Extracted Ion Chromatogram for Cmp03

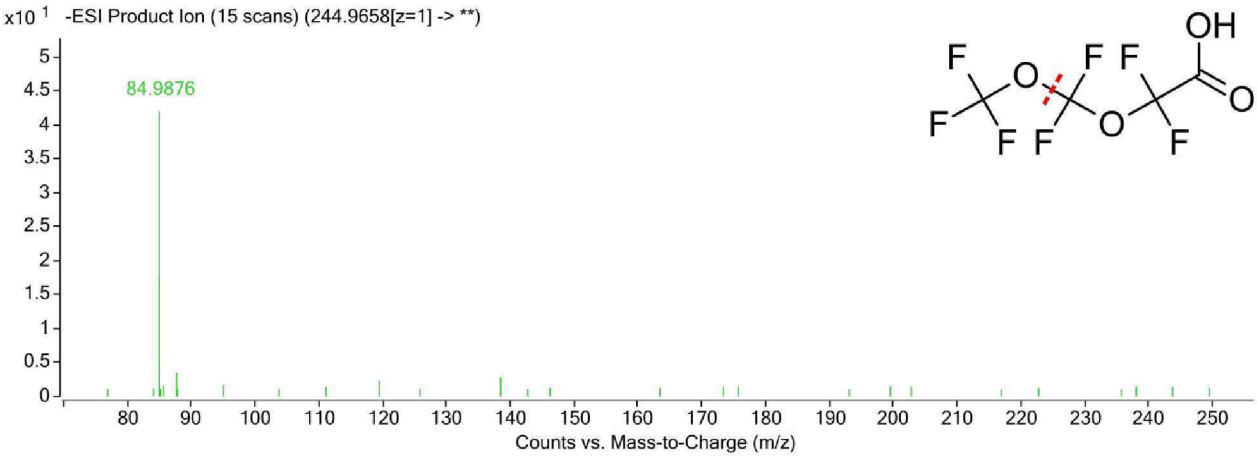

Figure 7. Average MS/MS Spectrum for Cmp03 @ 10/25 CID

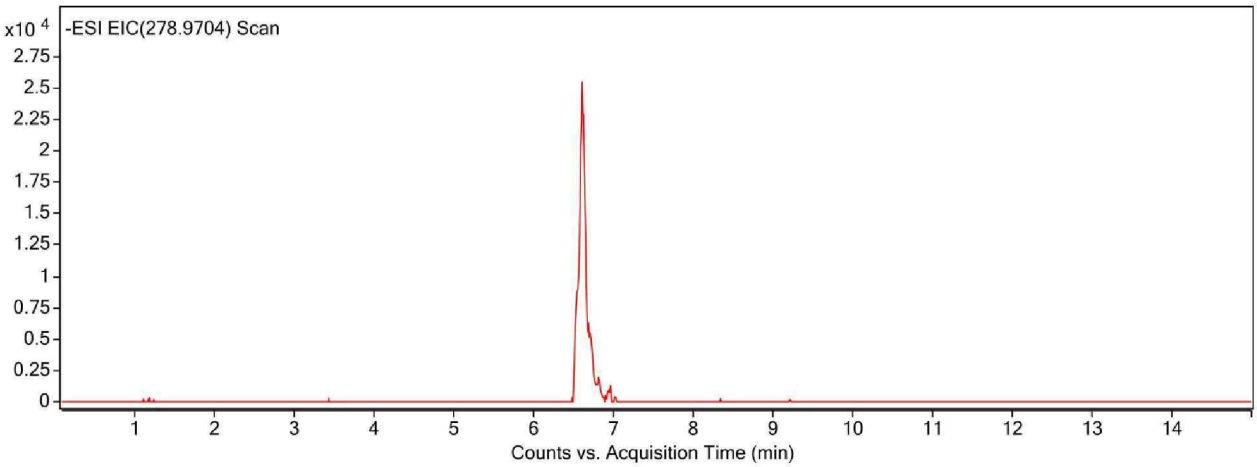

Figure 8. Extracted Ion Chromatogram for Cmp04

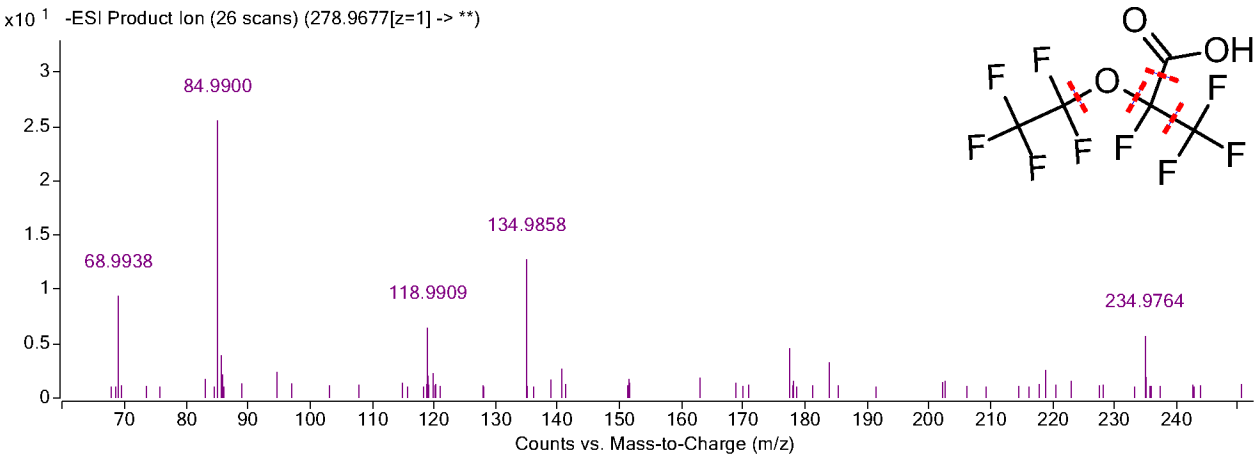

Figure 9. Average MS/MS Spectrum for Cmp04 @ 10/25 CID

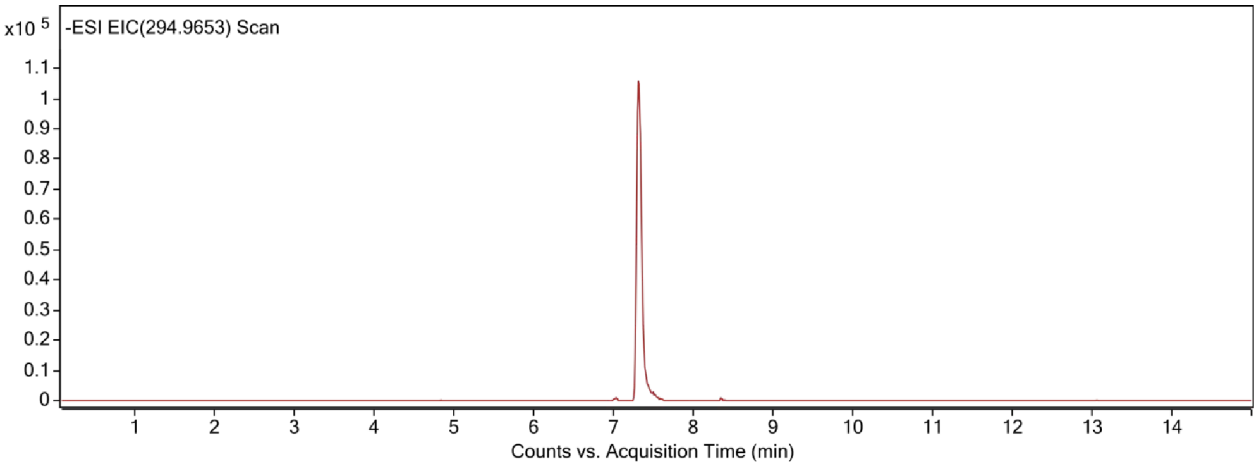

Figure 10. Extracted Ion Chromatogram for Cmp05

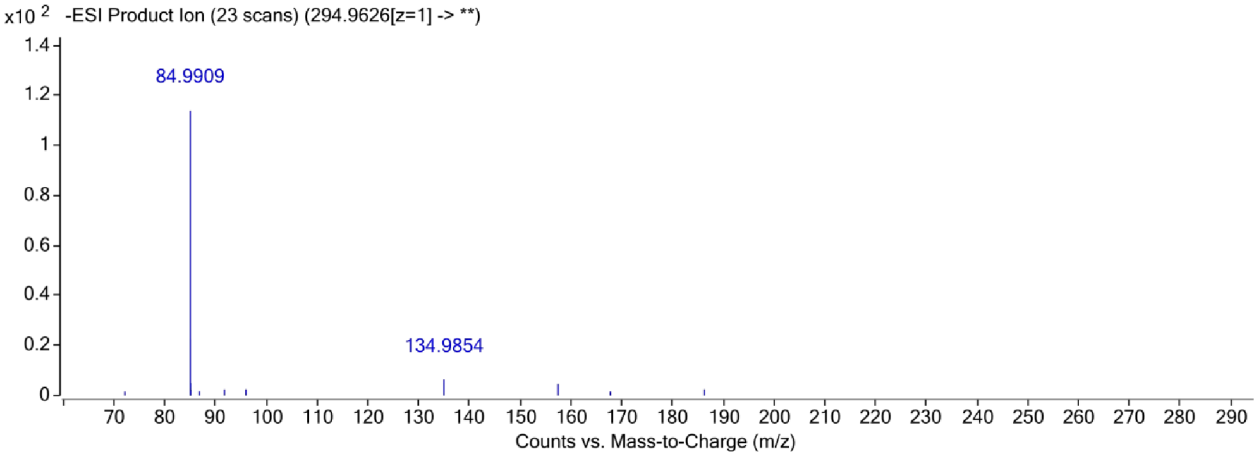

Figure 11. Average MS/MS Spectrum for Cmp05 @ 10/25 CID

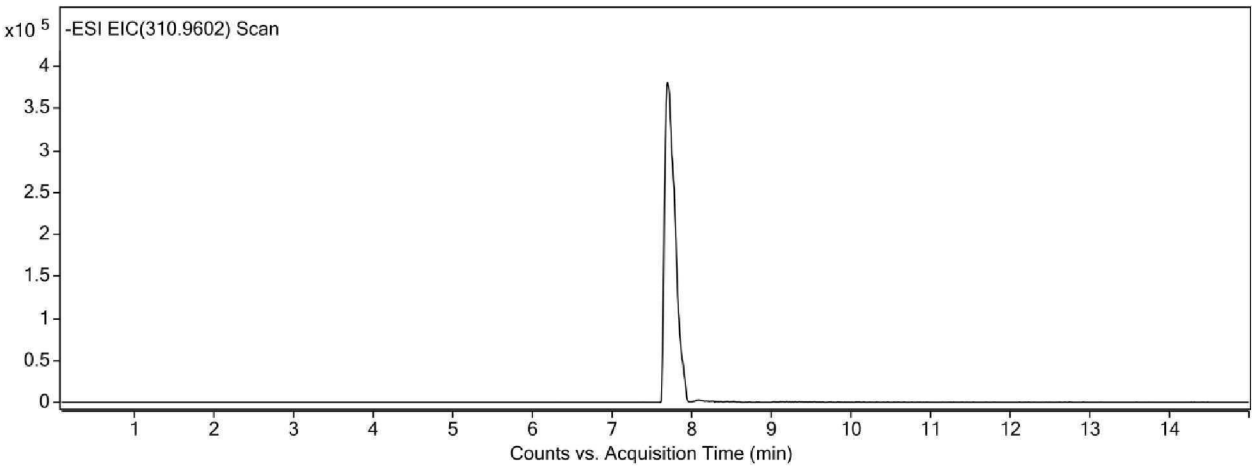

Figure 12. Extracted Ion Chromatogram for Cmp06

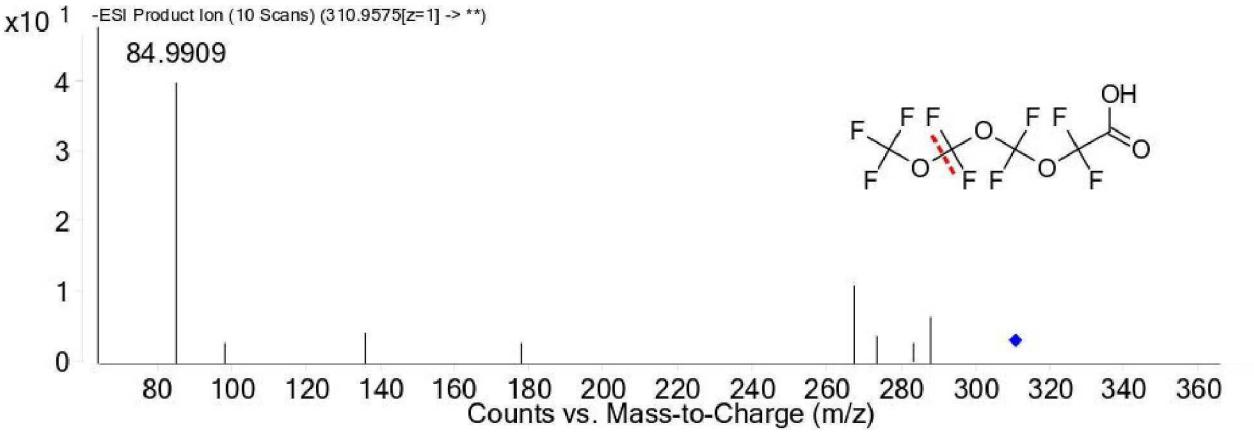

Figure 13. Average MS/MS Spectrum for Cmp06 @ 10/25 CID

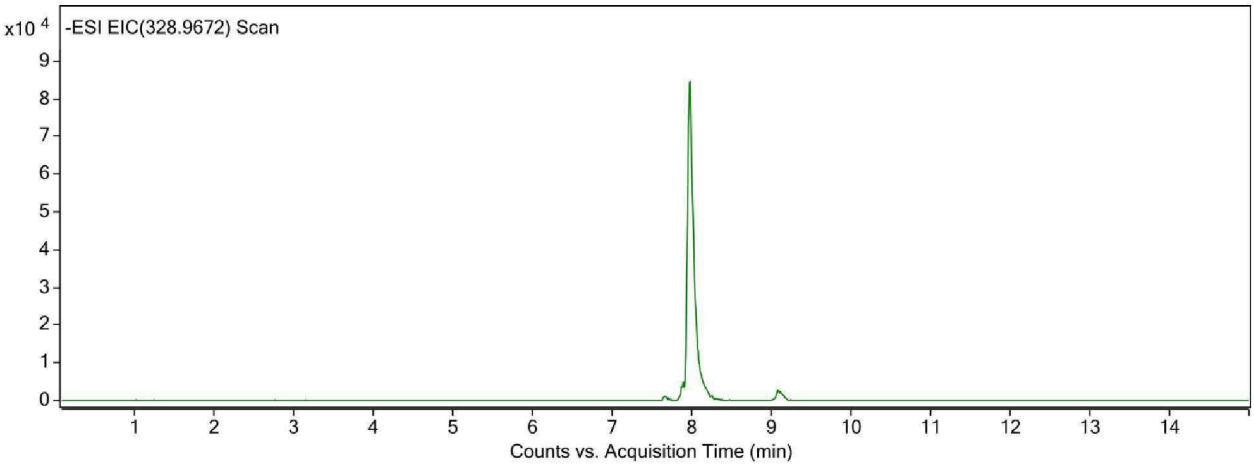

Figure 14. Extracted Ion Chromatogram for Cmp07

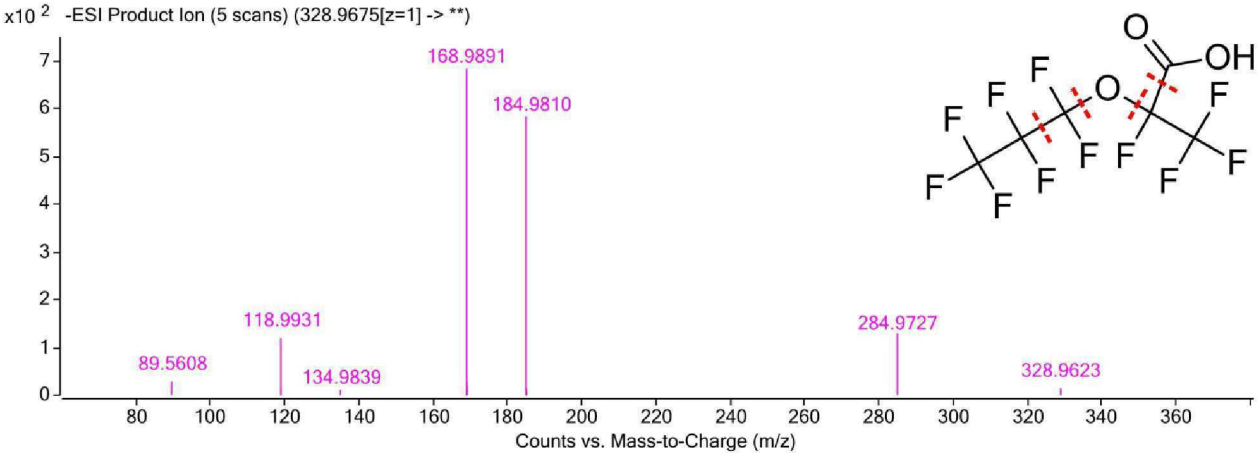

Figure 15. Average MS/MS Spectrum for Cmp07 @ 10/25 CID

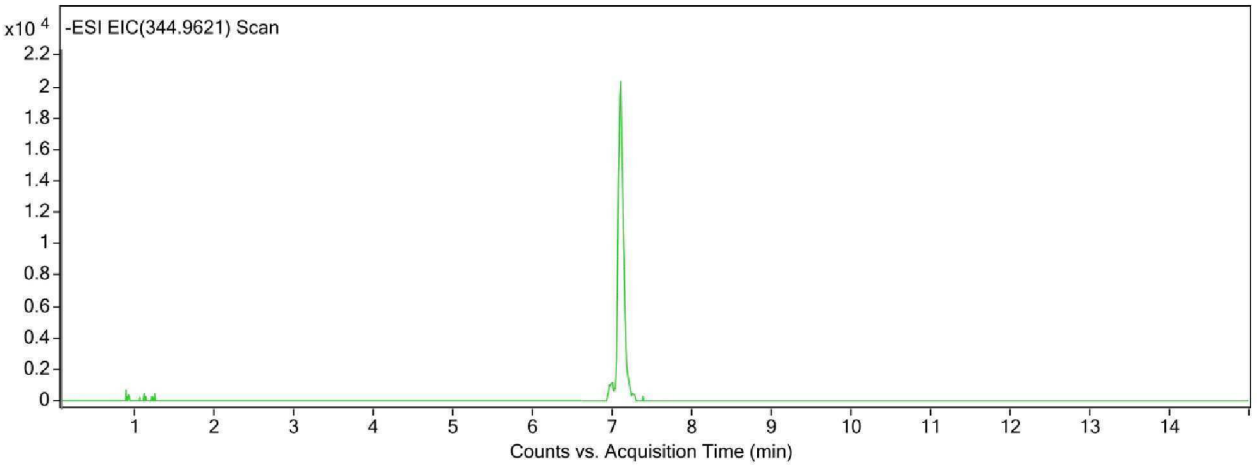

Figure 16. Extracted Ion Chromatogram for Cmp08

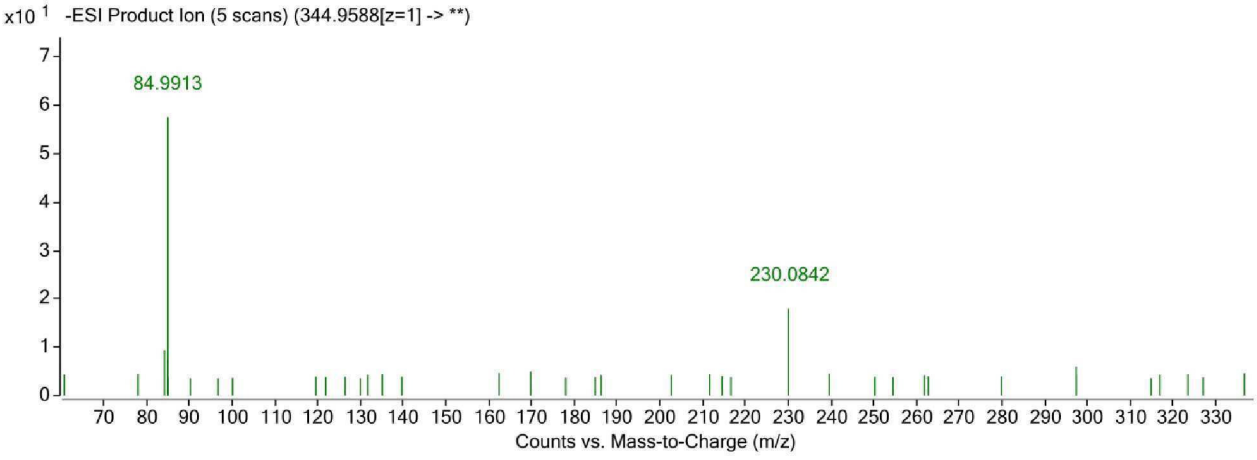

Figure 17. Average MS/MS Spectrum for Cmp08 @ 10/25 CID

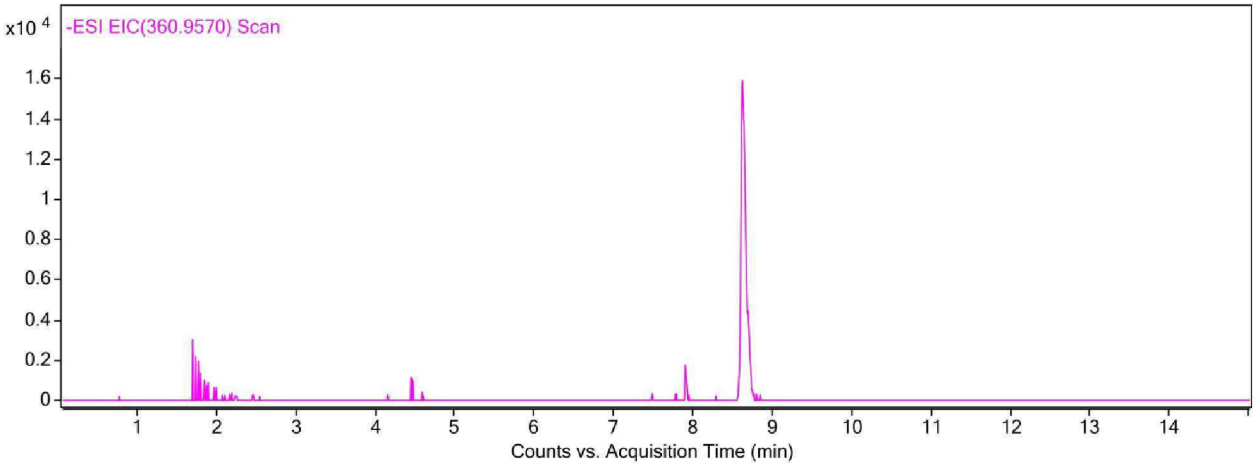

Figure 18. Extracted Ion Chromatogram for Cmp09

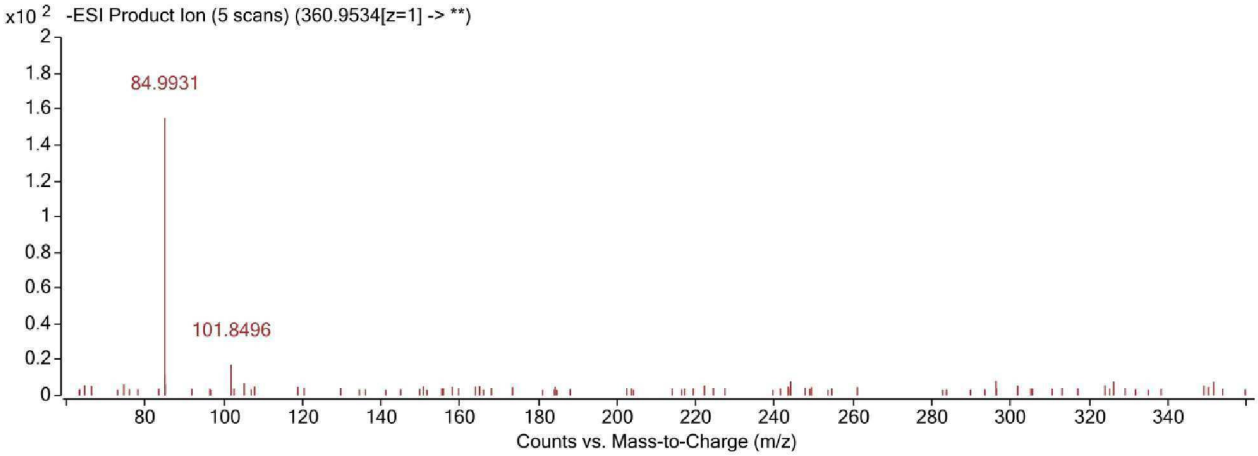

Figure 19. Average MS/MS Spectrum for Cmp09 @ 10/25 CID

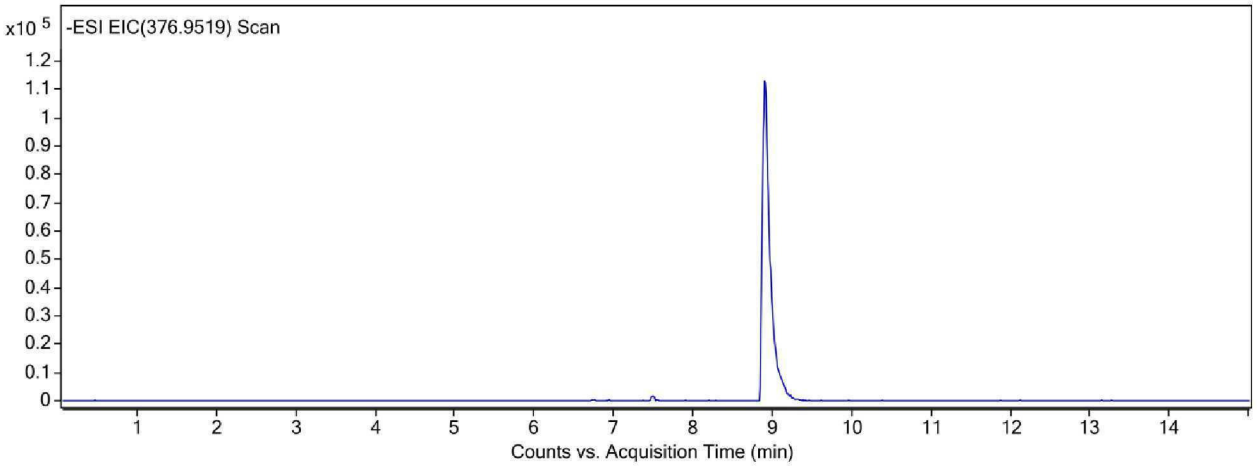

Figure 20. Extracted Ion Chromatogram for Cmp10

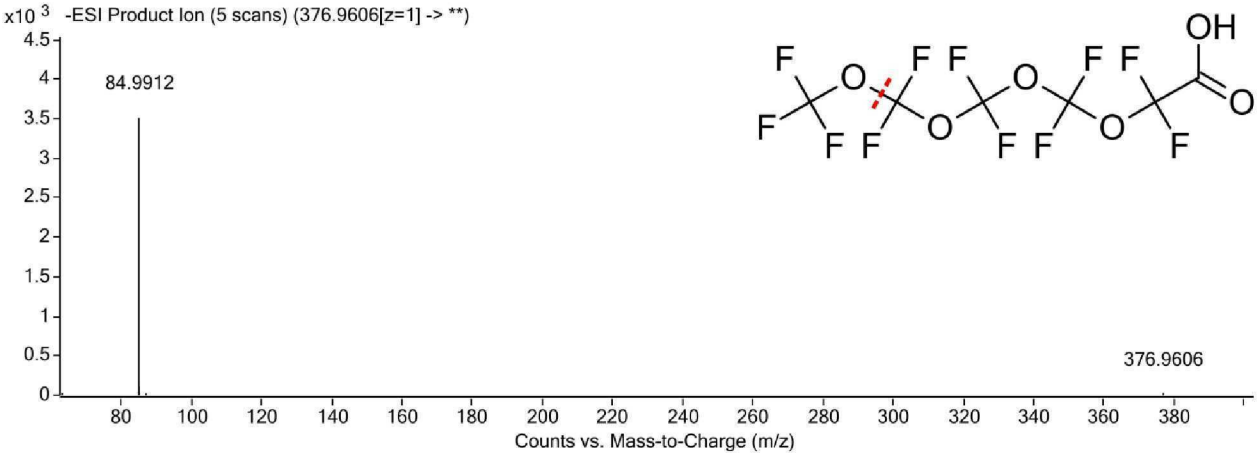

Figure 21. Average MS/MS Spectrum for Cmp10 @ 10/25 CID

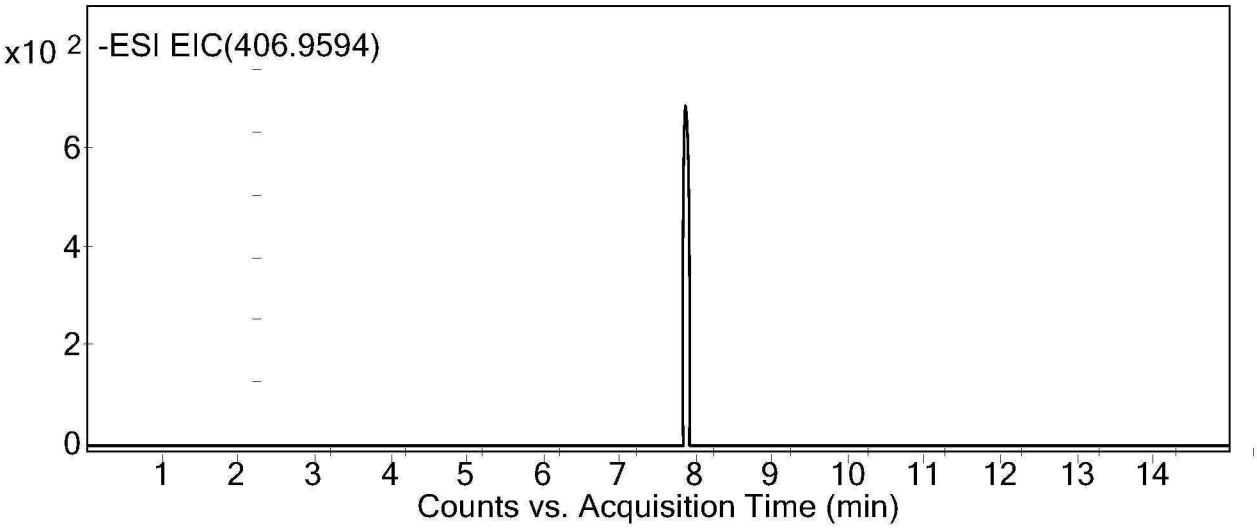

Figure 22. Extracted Ion Chromatogram for Cmp 11

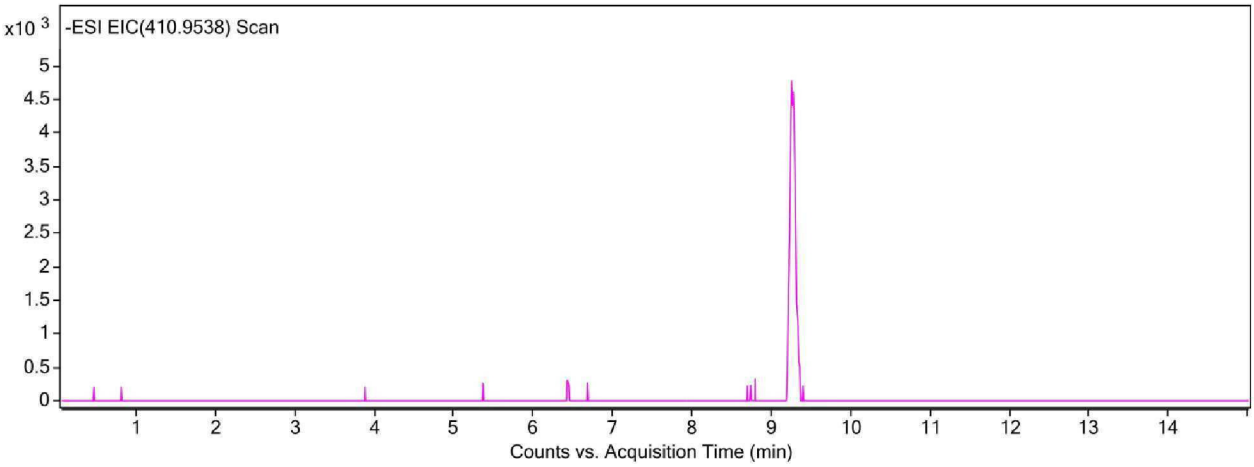

Figure 23. Extracted Ion Chromatogram for Cmp12

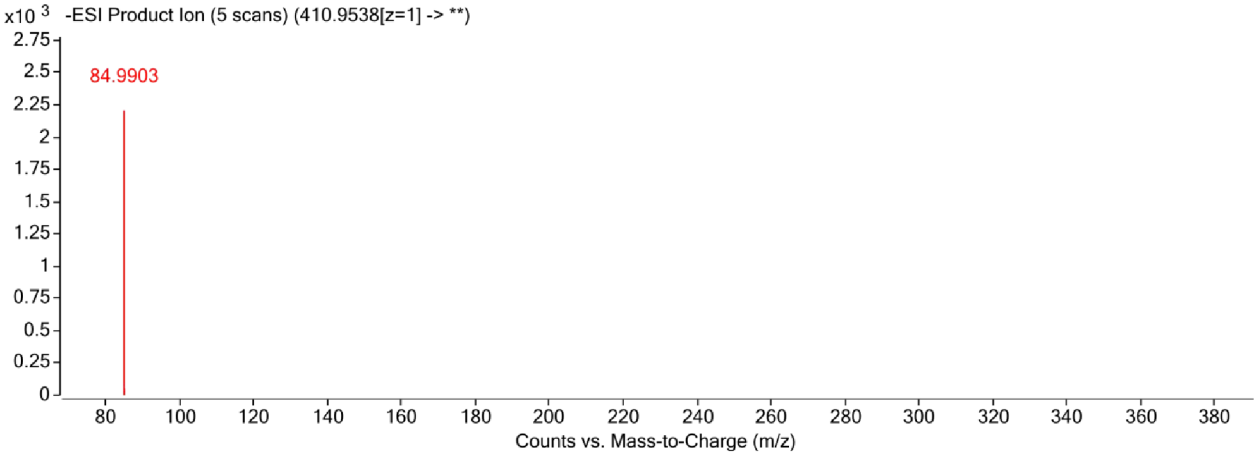

Figure 24. Average MS/MS Spectrum for Cmp12 @ 10/25 CID

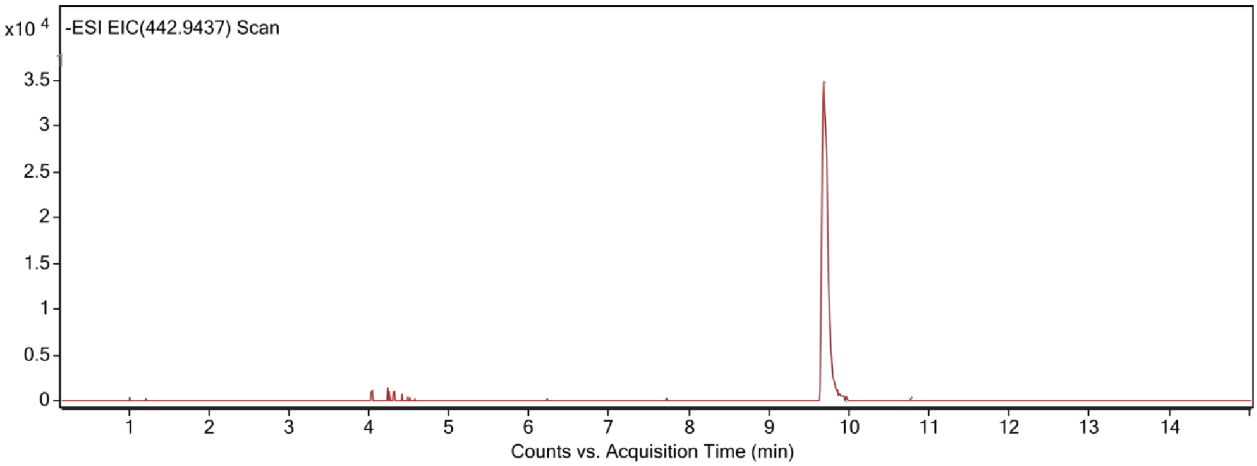

Figure 25. Extracted Ion Chromatogram for Cmp13

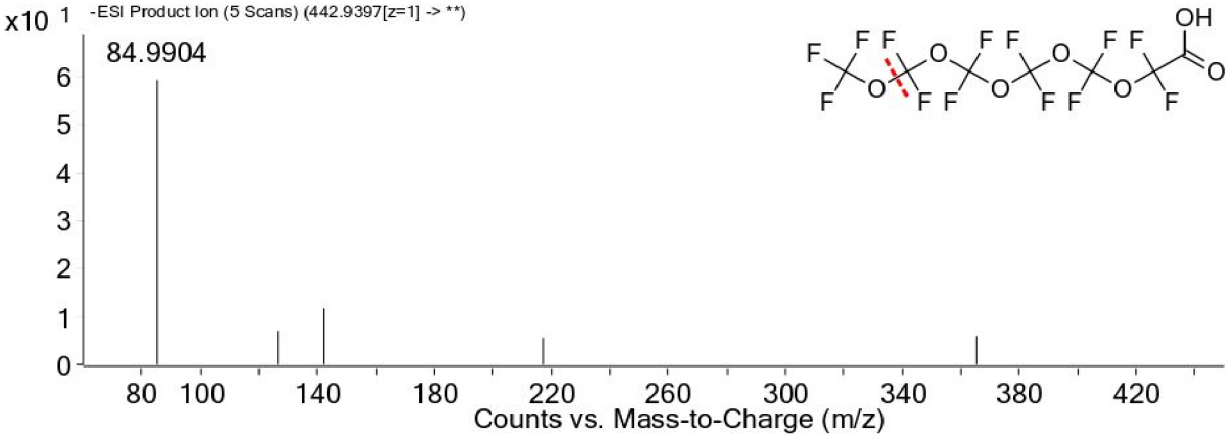

Figure 26. Average MS/MS Spectrum for Cmp13 @ 10/25 CID

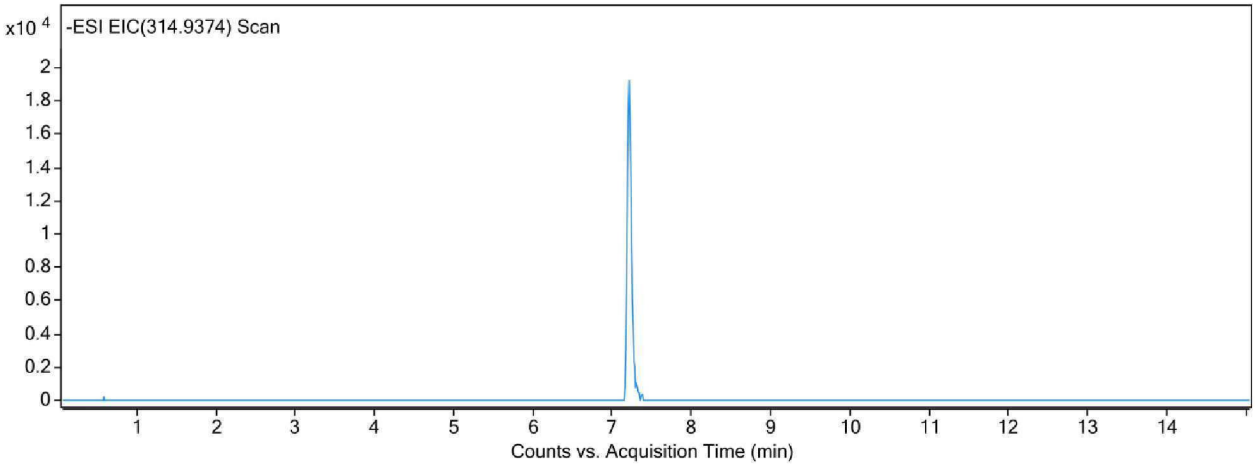

Figure 27. Extracted Ion Chromatogram for Cmp14

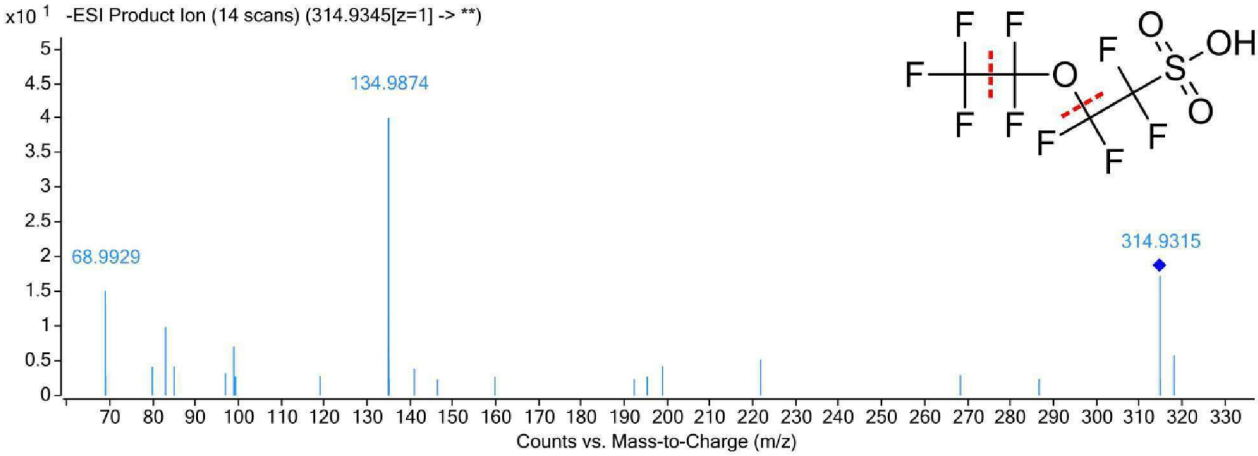

Figure 28. Average MS/MS Spectrum for Cmp14 @ 10/25 CID

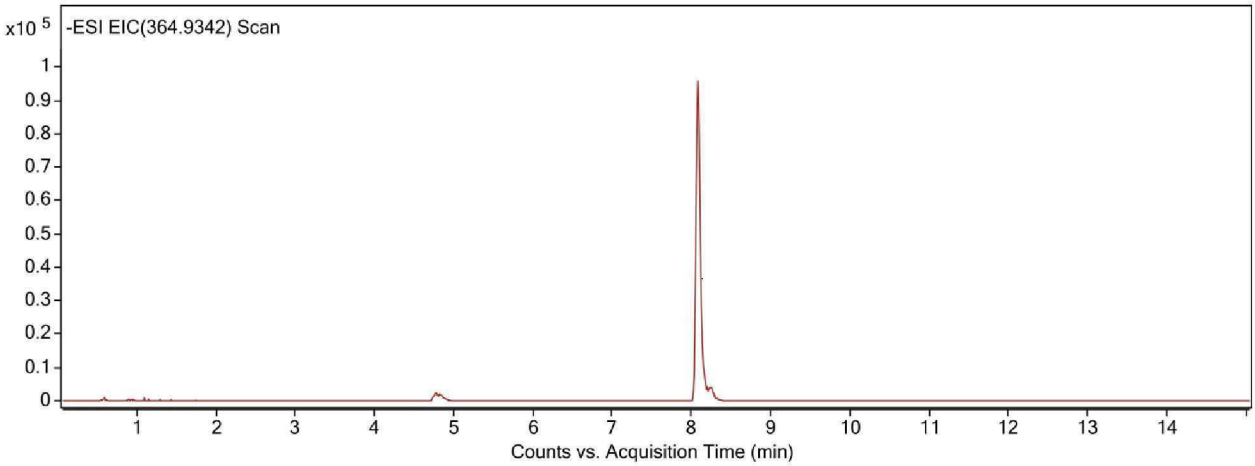

Figure 29. Extracted Ion Chromatogram for Cmp15

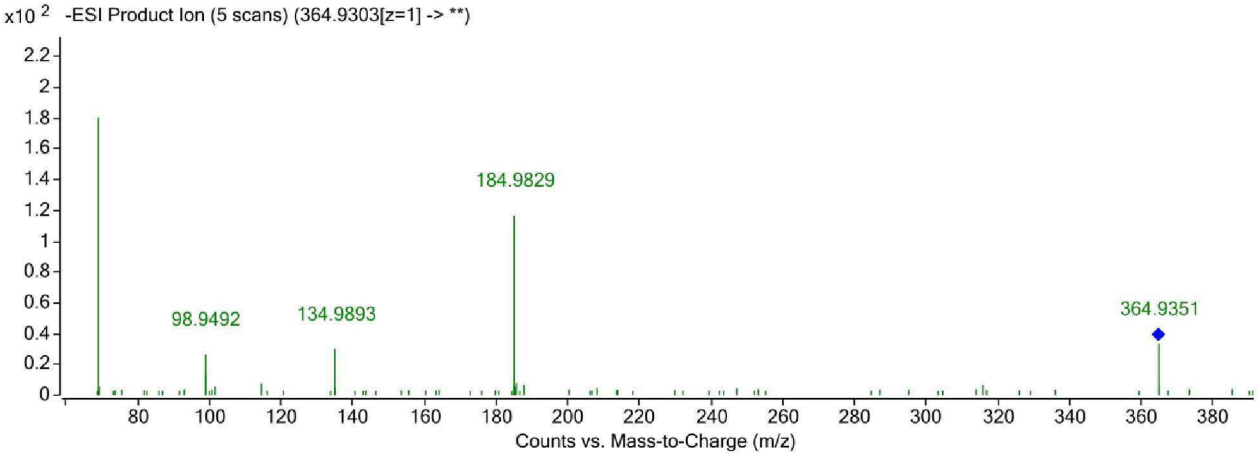

Figure 30. Average MS/MS Spectrum for Cmp15 @ 10/25 CID

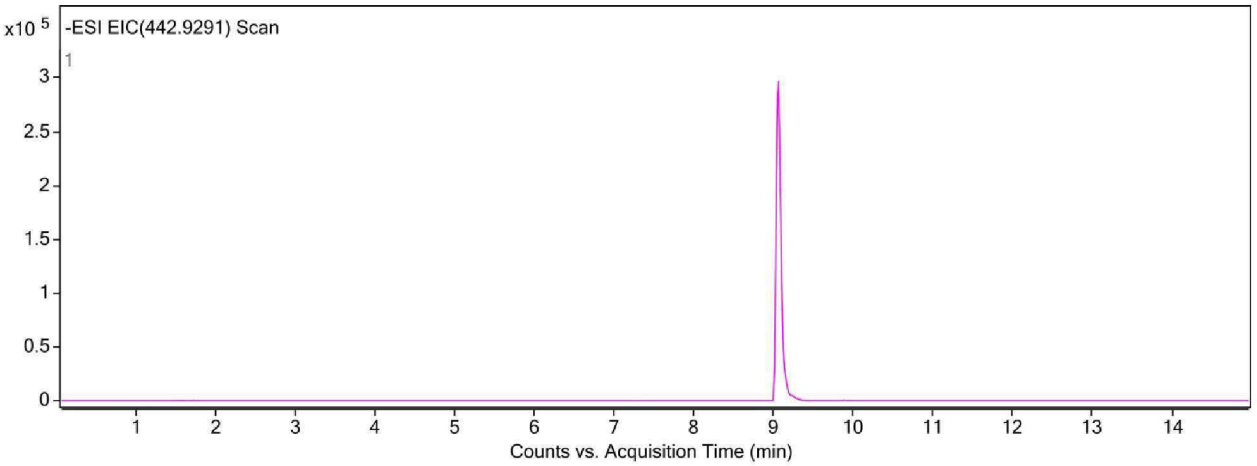

Figure 31. Extracted Ion Chromatogram for Cmp16

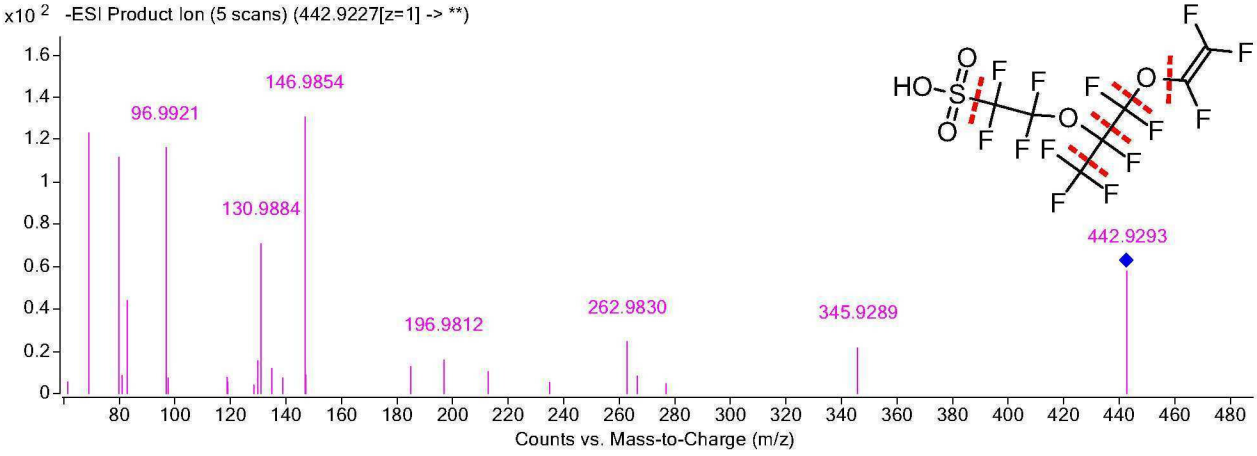

Figure 32. Average MS/MS Spectrum for Cmp16 @ 10/25 CID

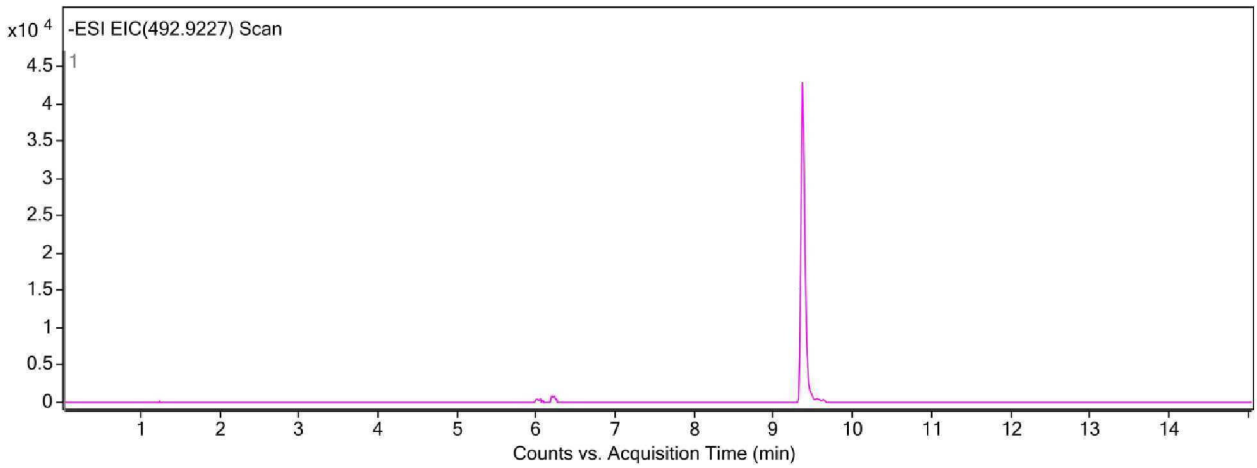

Figure 33. Extracted Ion Chromatogram for Cmp17

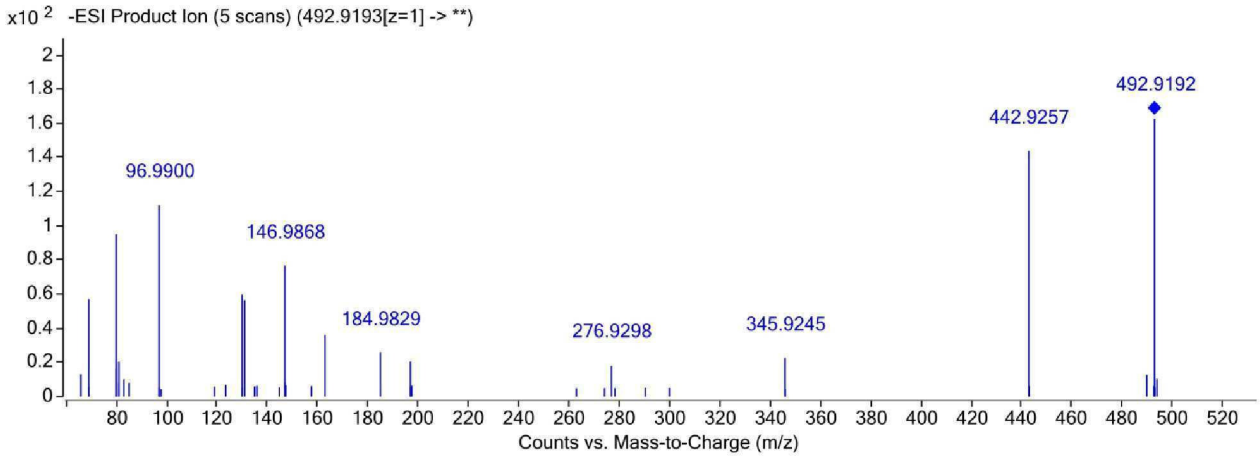

Figure 34. Average MS/MS Spectrum for Cmp17 @ 10/25 CID

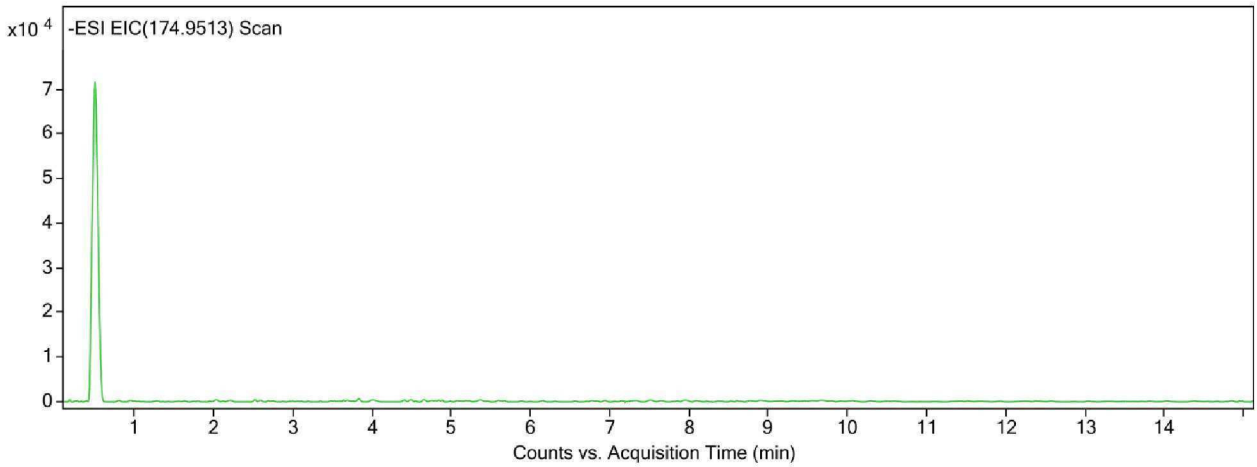

Figure 35. Extracted Ion Chromatogram for Cmp18

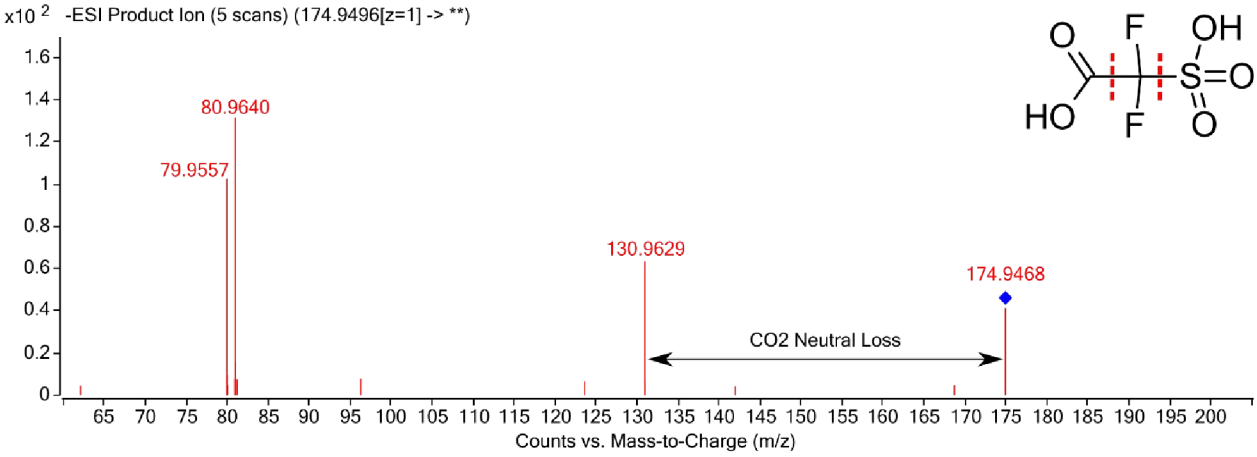

Figure 36. Average MS/MS Spectrum for Cmp18 @ 10/25 CID

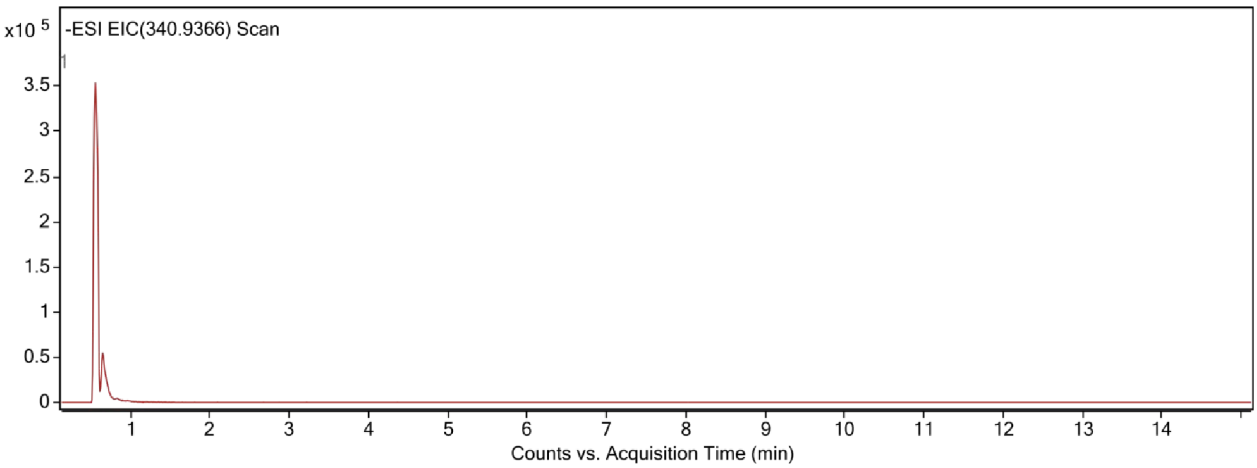

Figure 37. Extracted Ion Chromatogram for Cmp19

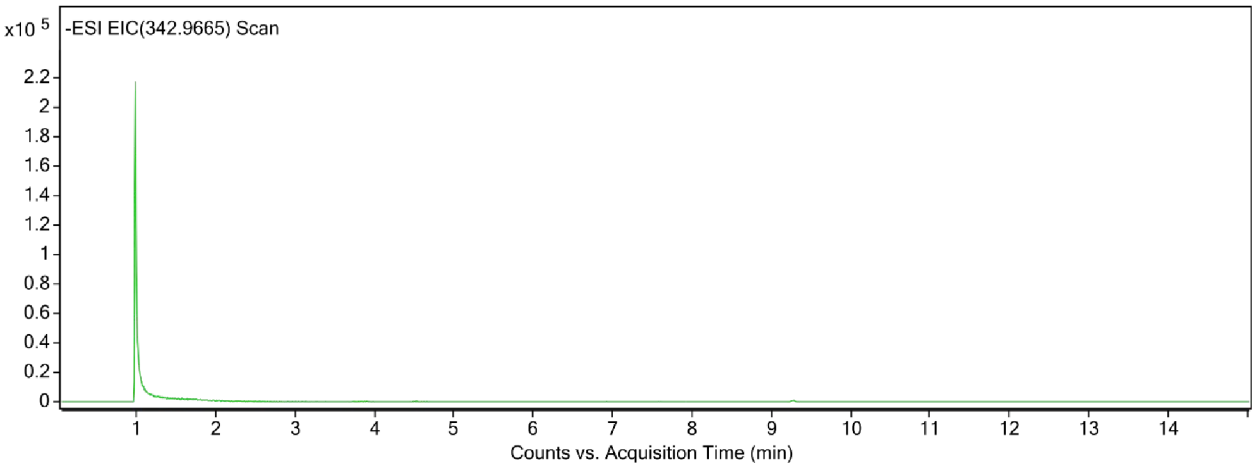

Figure 38. Extracted Ion Chromatogram for Cmp20

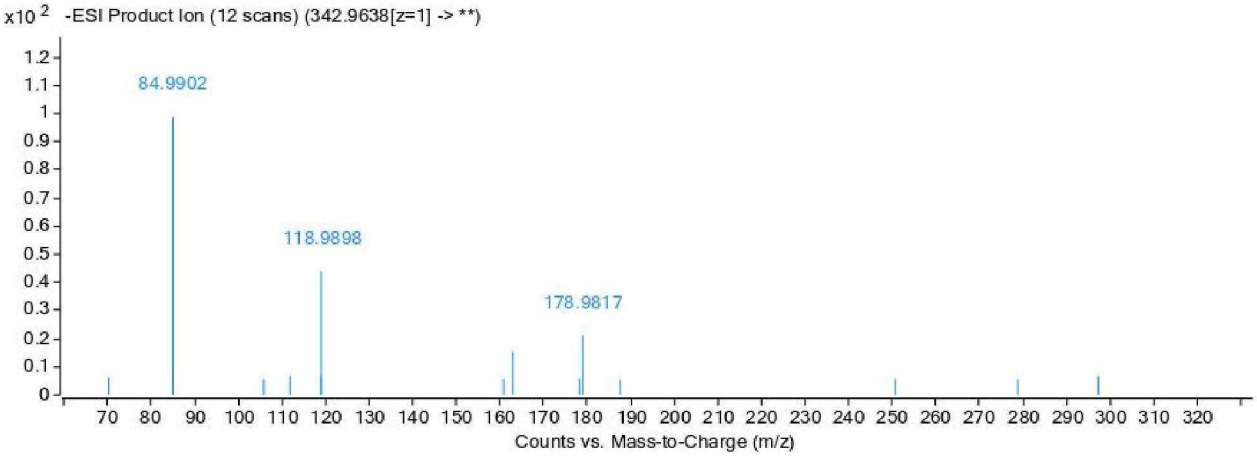

Figure 39. Average MS/MS Spectrum for Cmp20 @ 10/25 CID

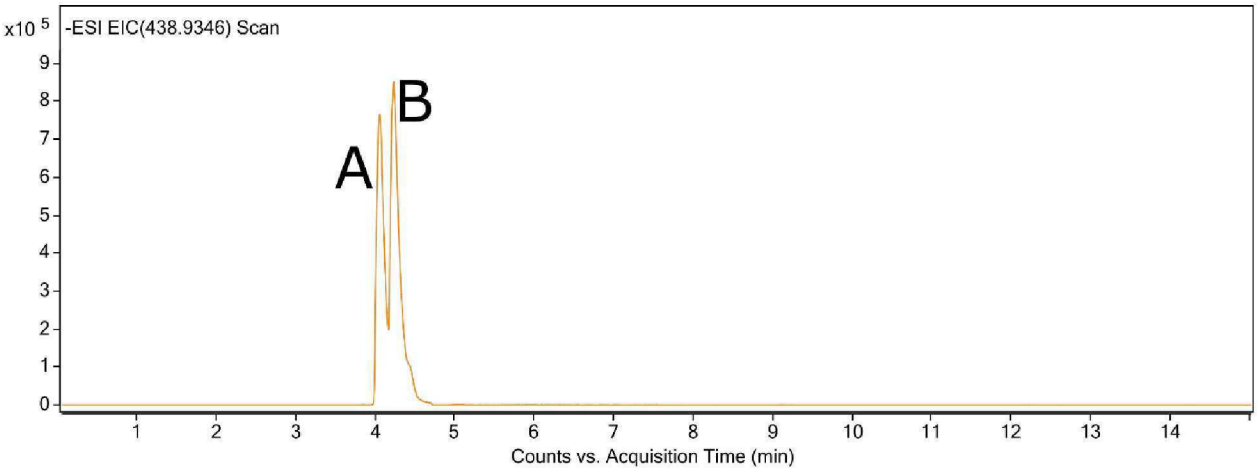

Figure 40. Extracted Ion Chromatogram for Cmp21

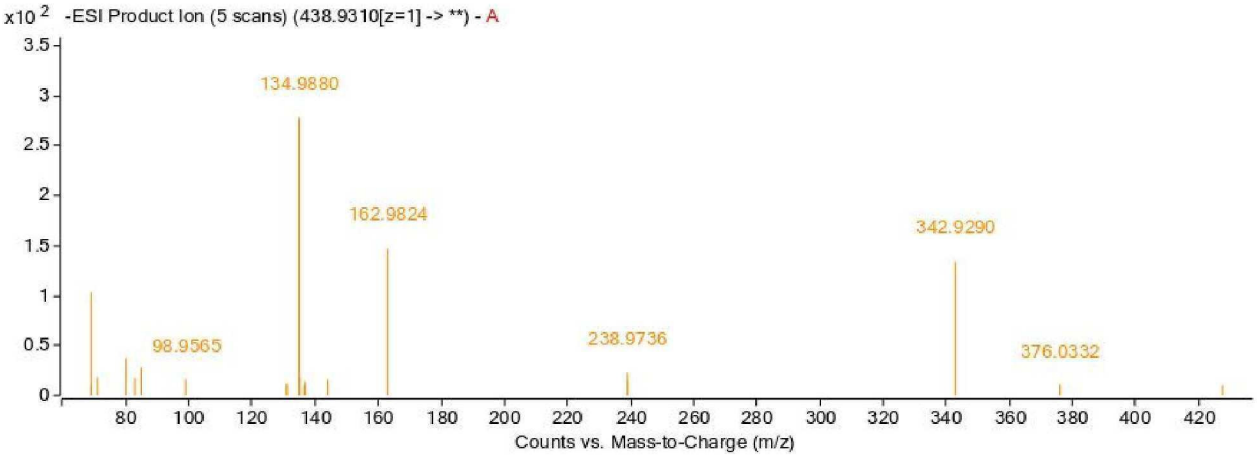

Figure 41. Average MS/MS for Cmp21a @ 10/25 CID

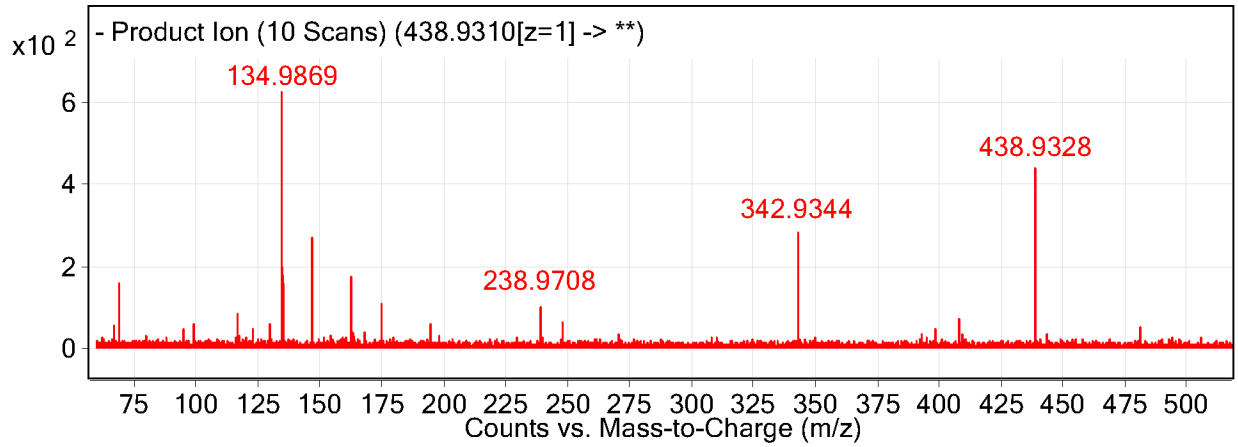

Figure 42. Average MS/MS for Cmp21b @ 10/25 CID

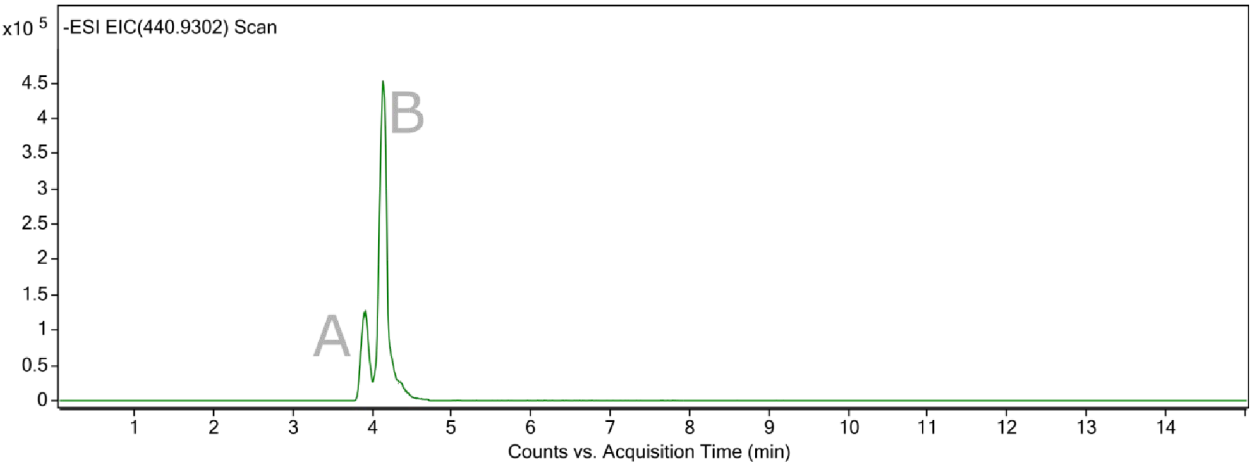

Figure 43. Extracted Ion Chromatogram for Cmp22

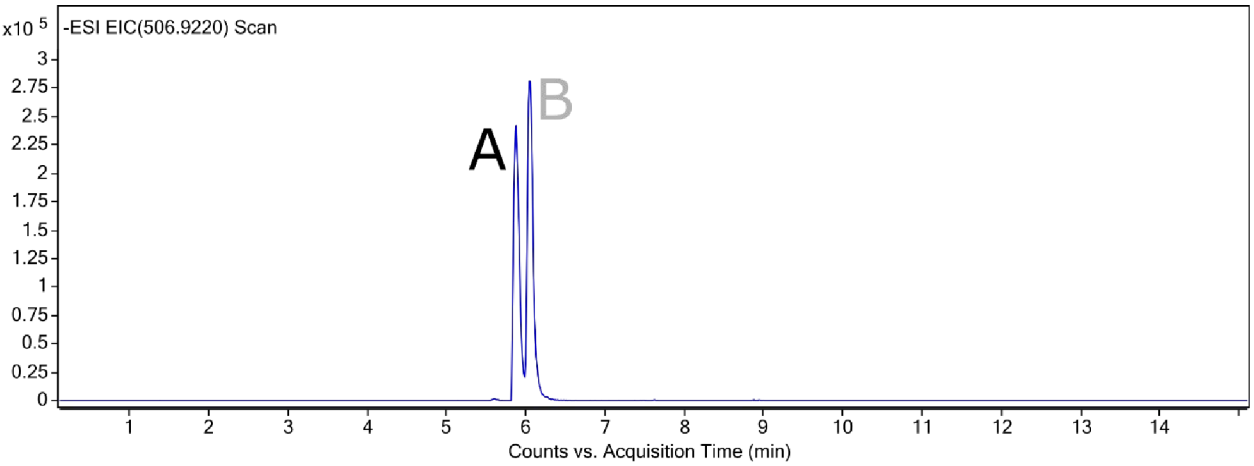

Figure 44. Extracted Ion Chromatogram for Cmp23

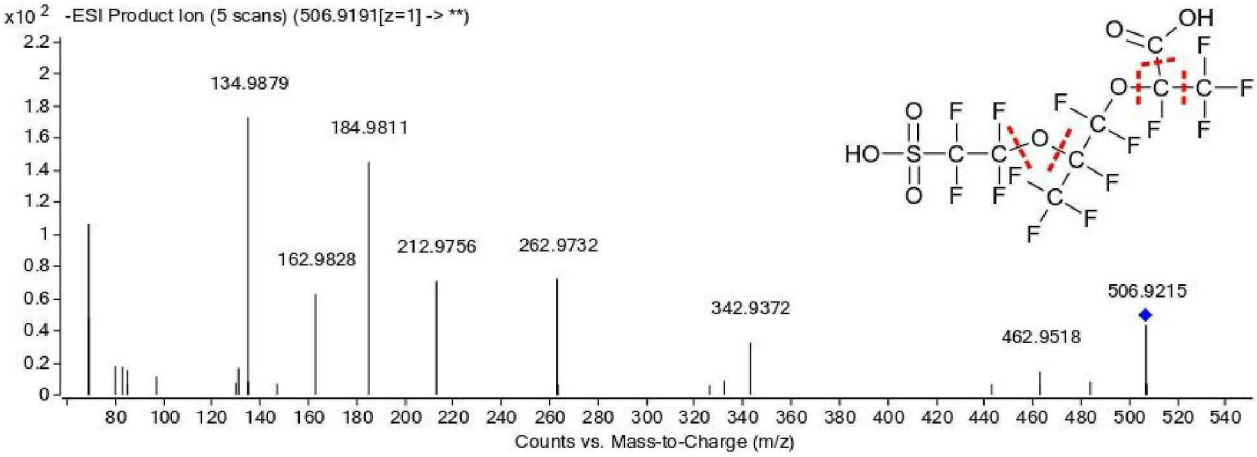

Figure 45. Average MS/MS spectrum for Cmp 23a @ CID 10/25

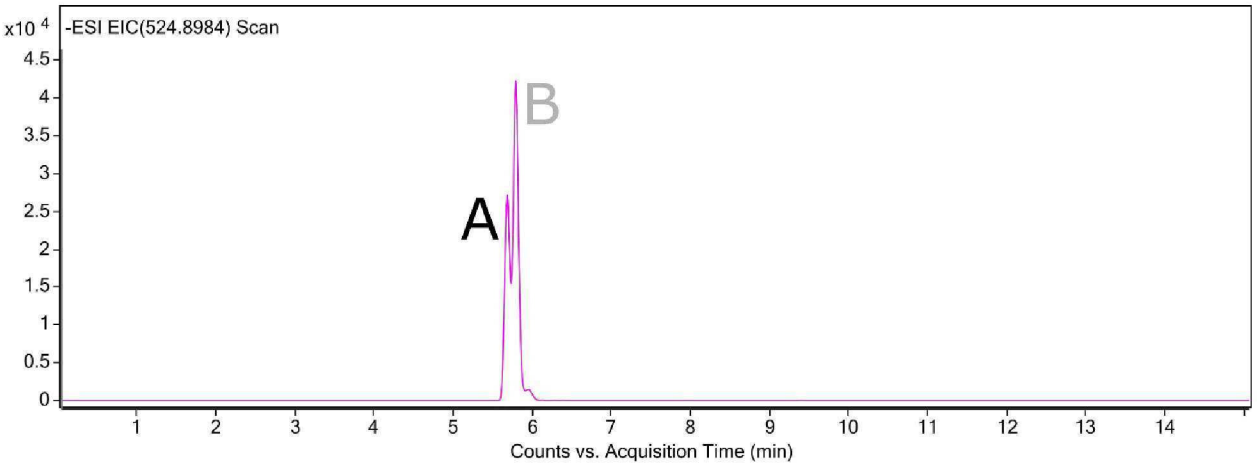

Figure 46. Extracted Ion Chromatogram for Cmp24

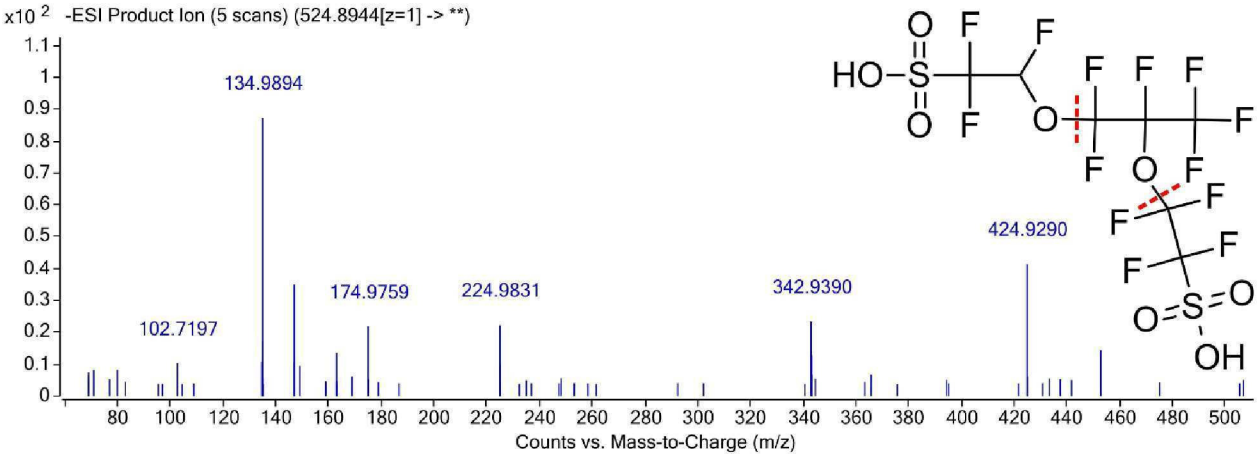

Figure 47. Average MS/MS Spectrum for Cmp24a @ 10/25 CID

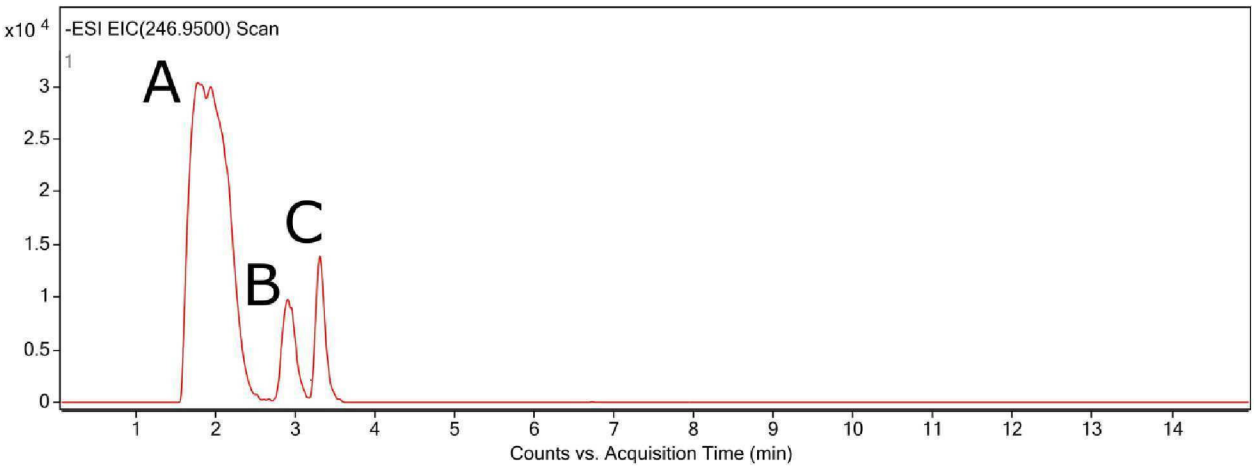

Figure 48. Extracted Ion Chromatogram for Cmp25

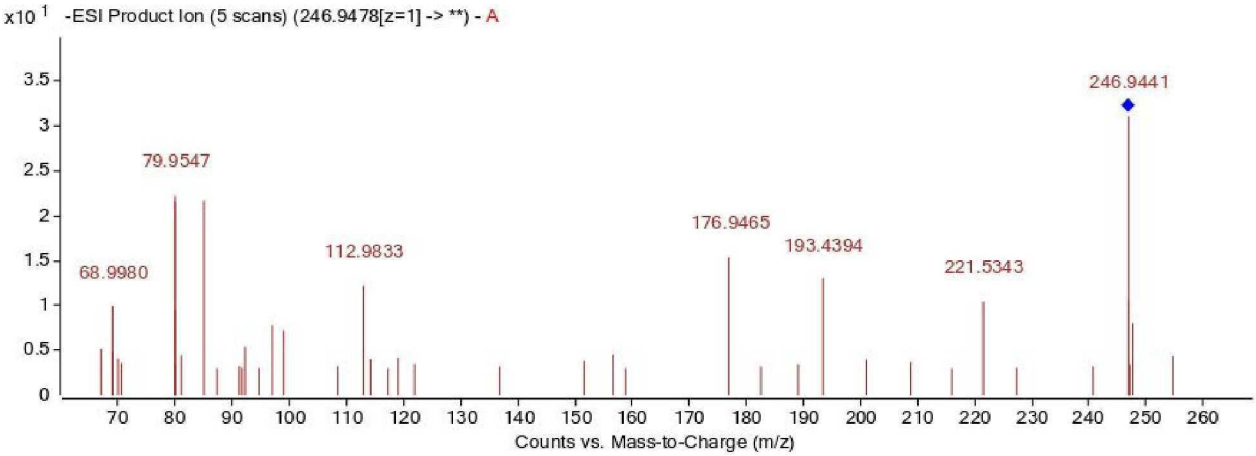

Figure 49. Average MS/MS for Cmp 25a @ 10/25 CID

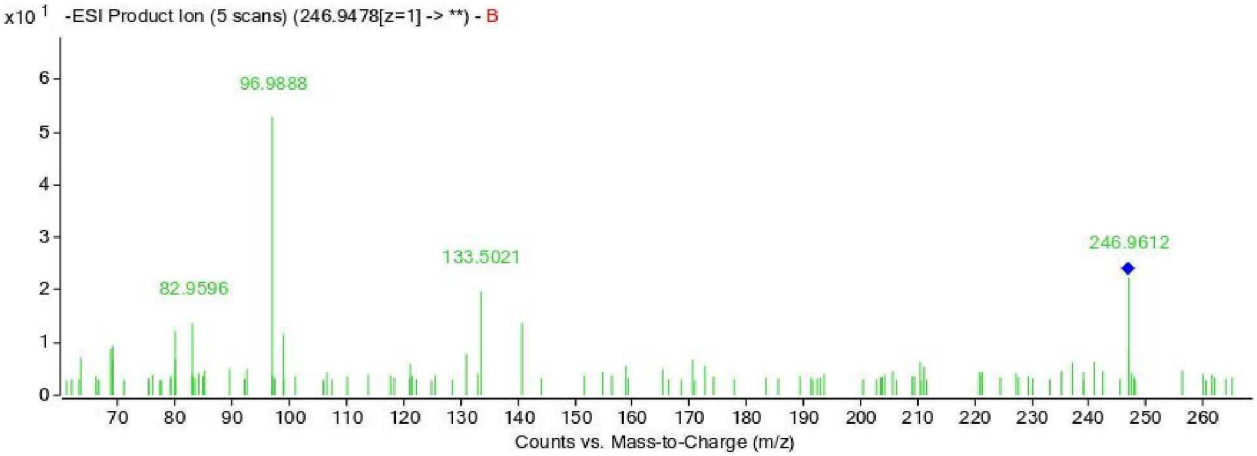

Figure 50. Average MS/MS for Cmp 25b @ 10/25 CID

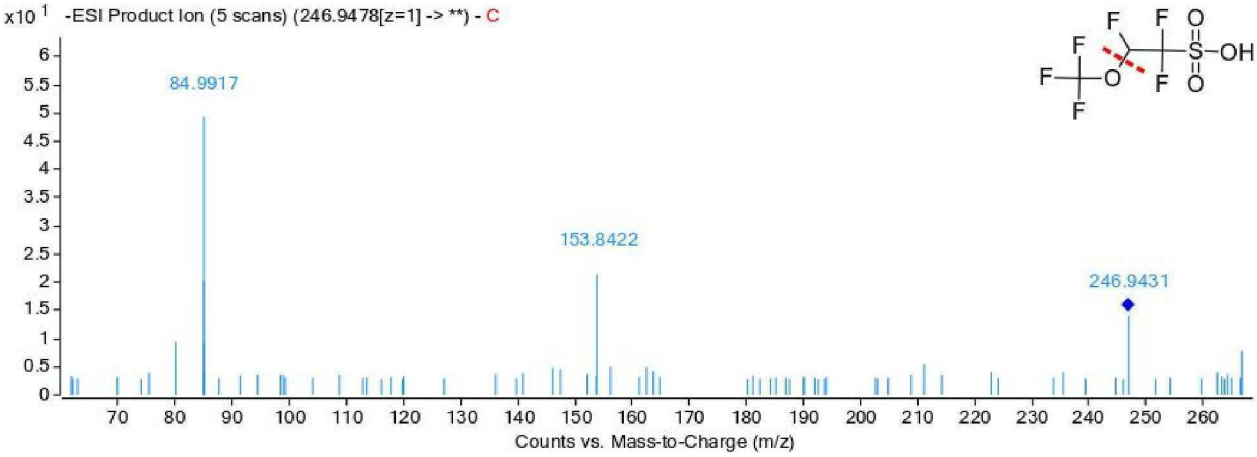

Figure 51. Average MS/MS for Cmp 25c @ 10/25 CID

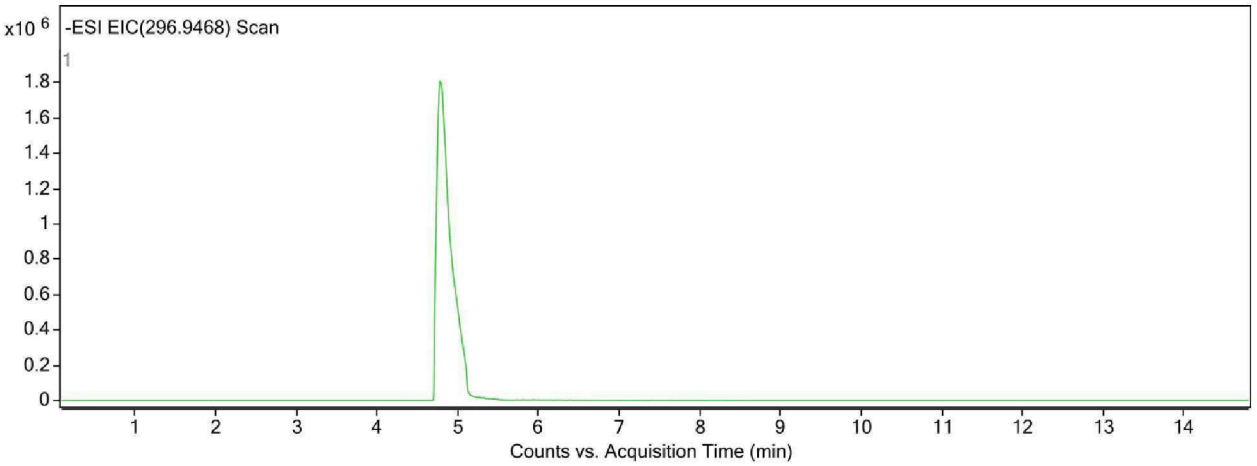

Figure 52. Extracted Ion Chromatogram for Cmp26

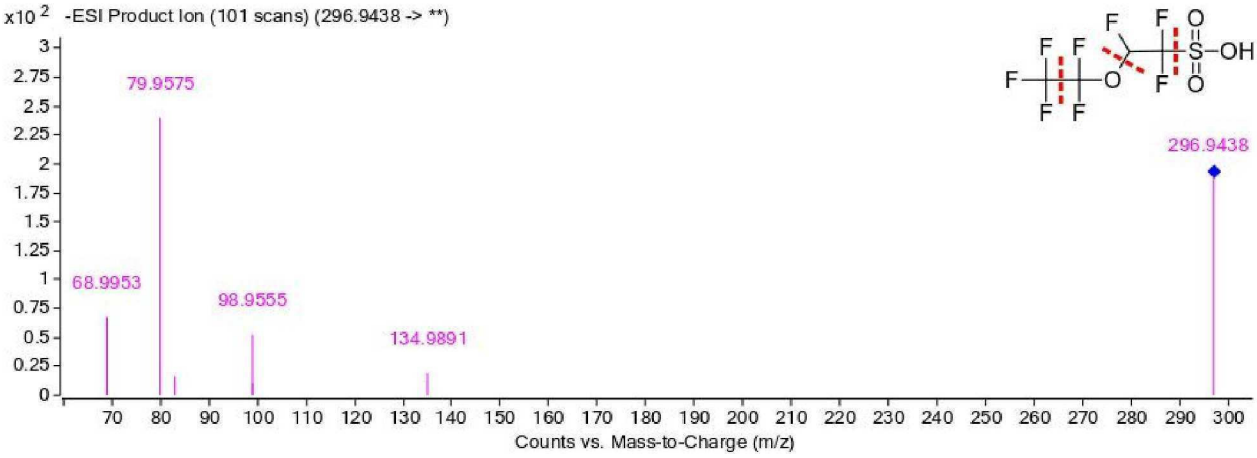

Figure 53. Average MS/MS for Cmp 26 @ 10/25 CID

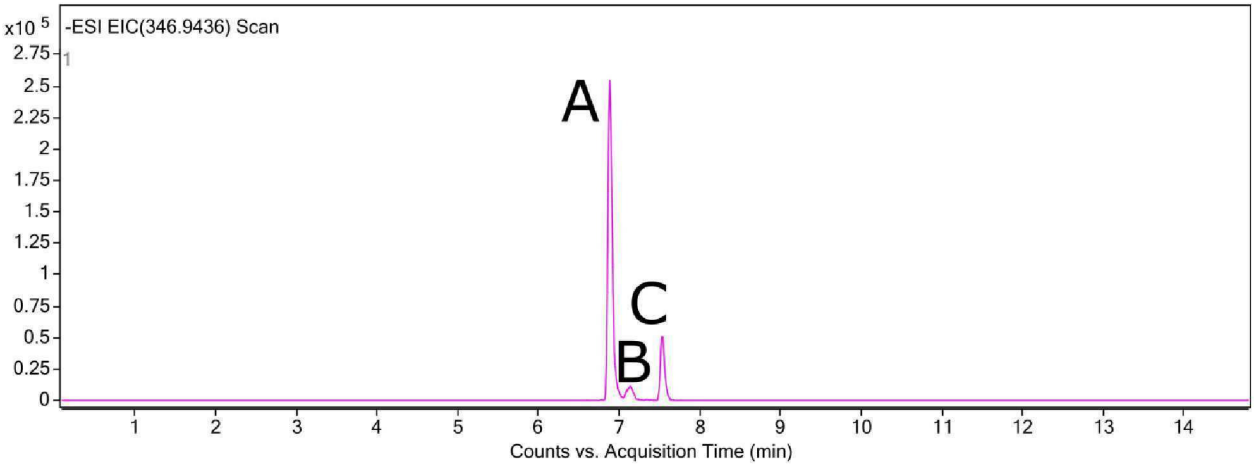

Figure 54. Extracted Ion Chromatogram for Cmp27

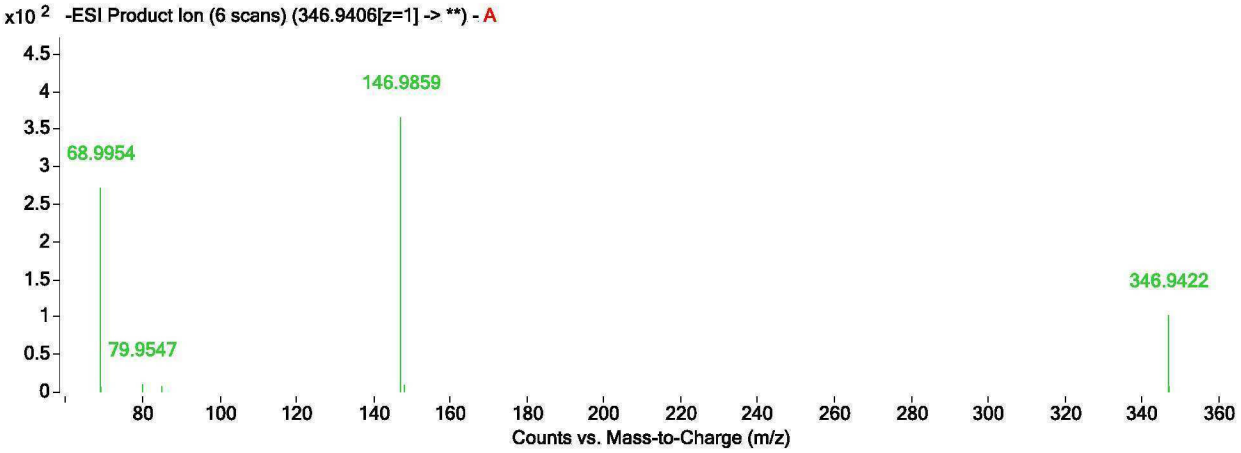

Figure 55. Average MS/MS Spectrum for Cmp 27a @ 10/25 CID

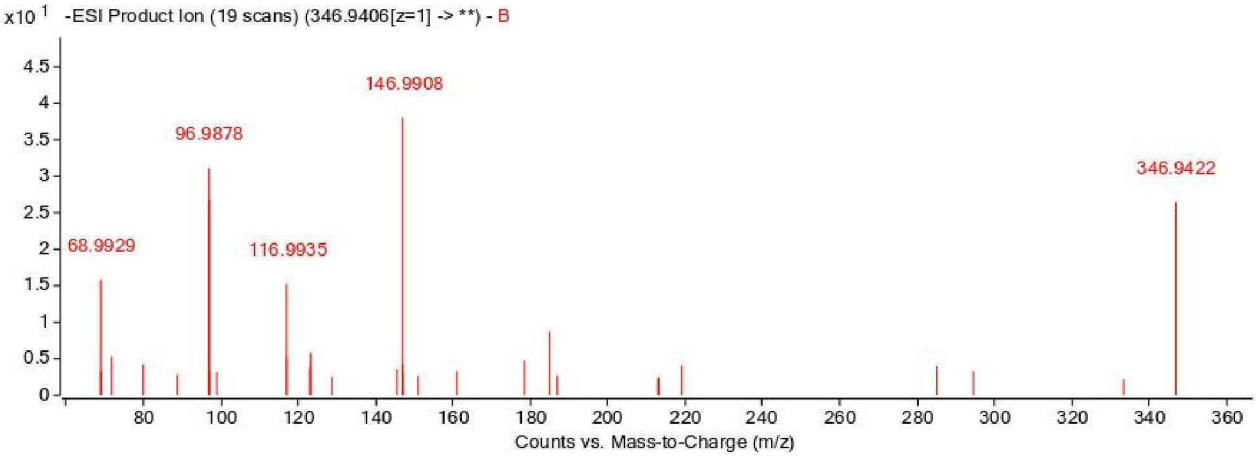

Figure 56. Average MS/MS Spectrum for Cmp 27b @ 10/25 CID

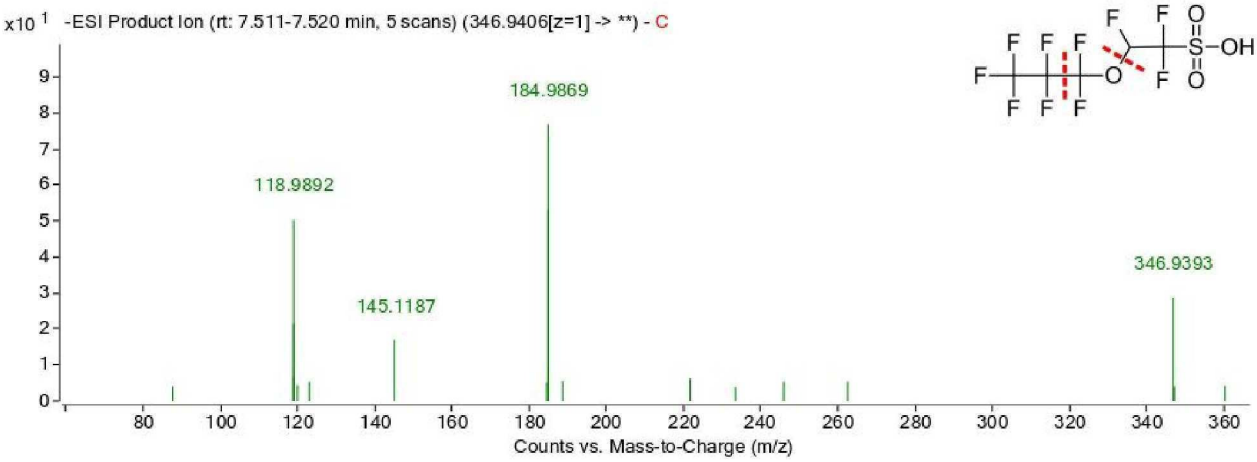

Figure 57. Average MS/MS Spectrum for Cmp 27c @ 10/25 CID

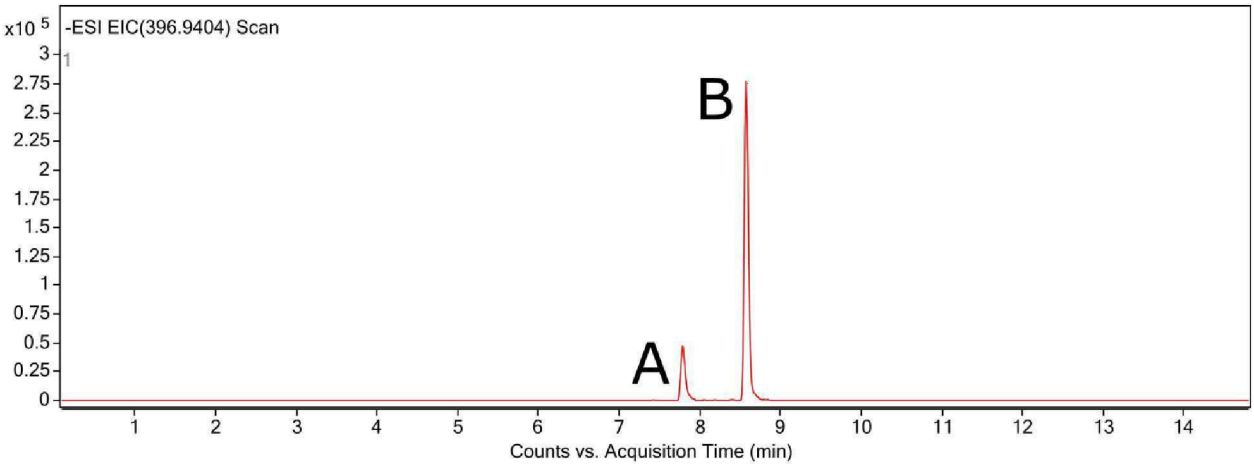

Figure 58. Extracted Ion Chromatogram for Cmp28

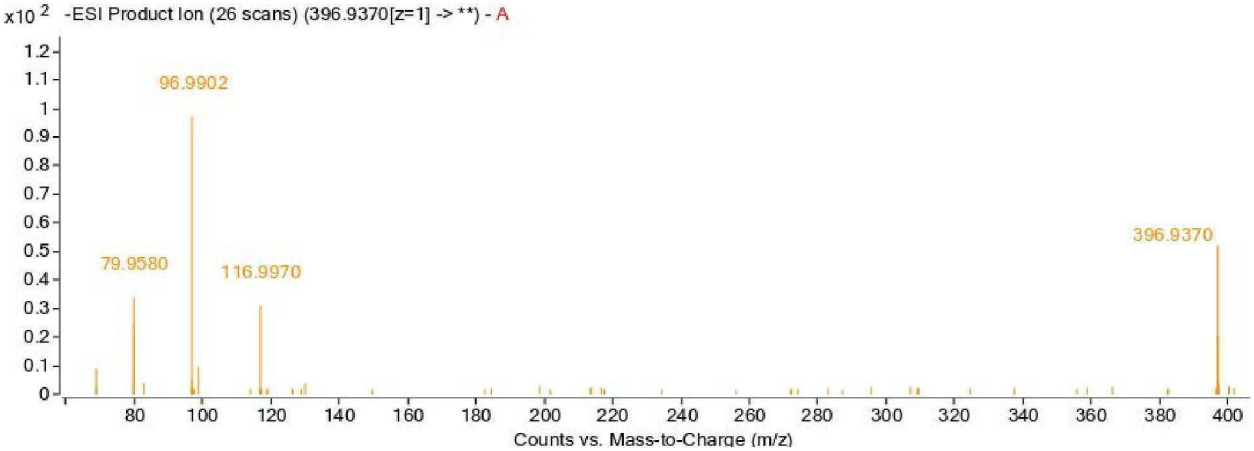

Figure 59. Average MS/MS Spectrum for Cmp 28a @ 10/25 CID

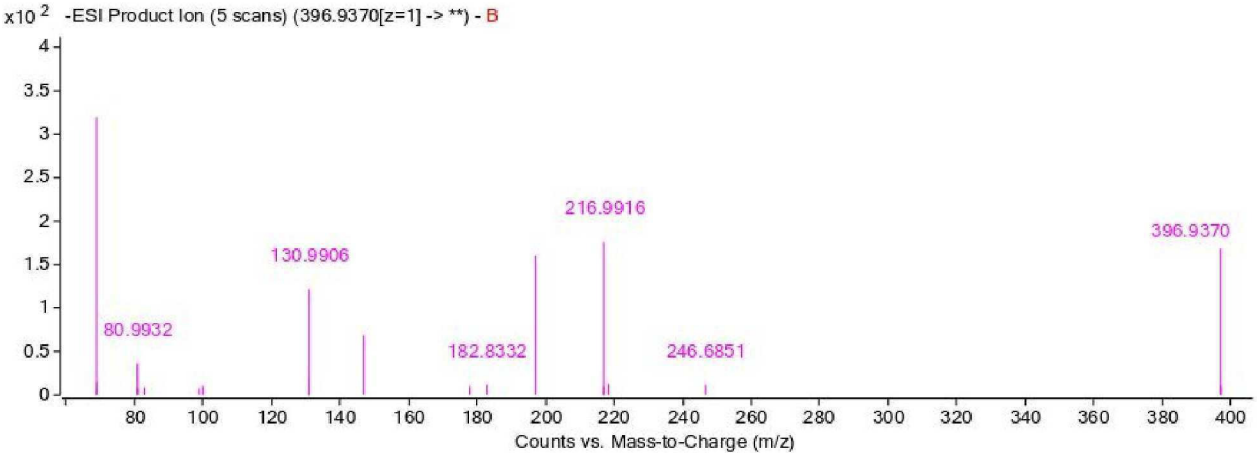

Figure 60. Average MS/MS Spectrum for Cmp 28b @ 10/25 CID

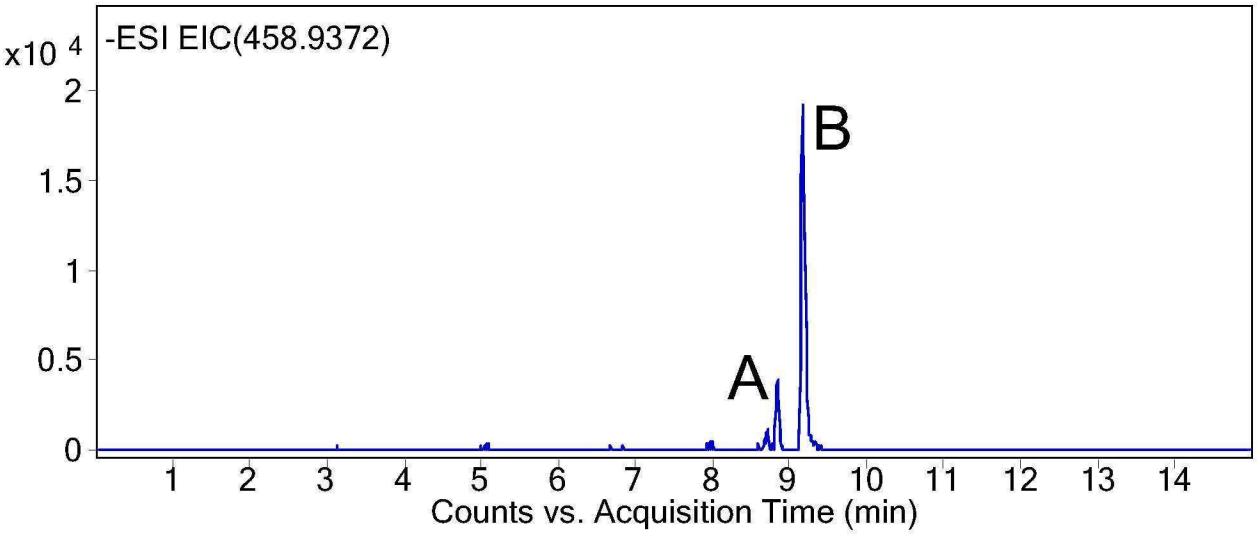

Figure 61. Extracted Ion Chromatogram for Cmp 29

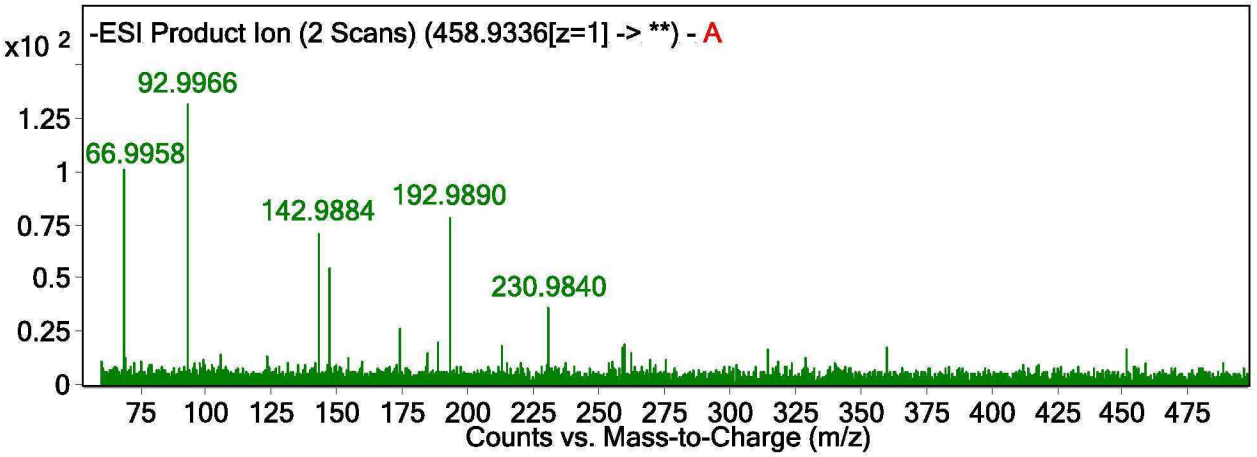

Figure 62. MS/MS Spectrum for Cmp 29a @ 10/25 CID

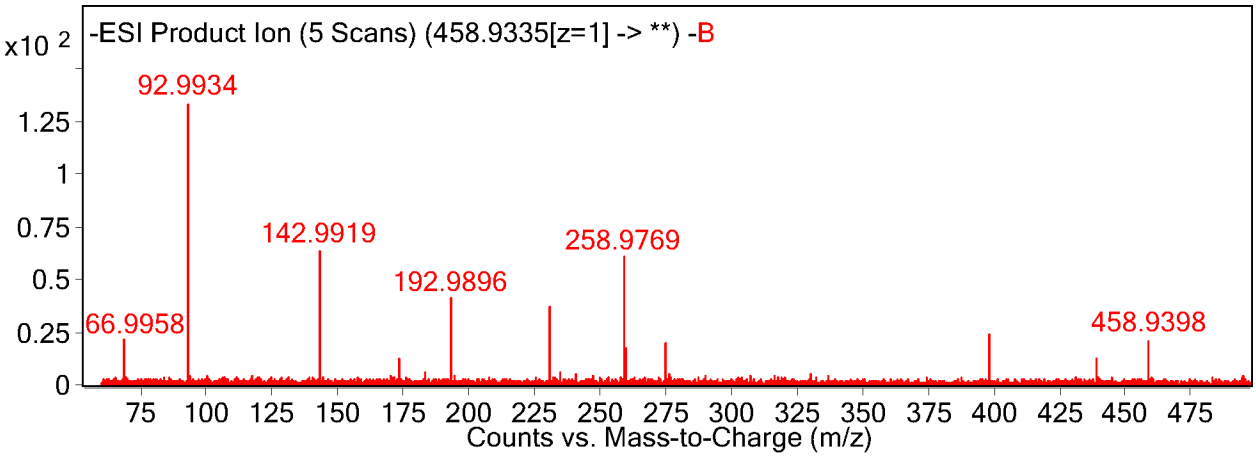

Figure 63. MS/MS Spectrum for Cmp 29b @ 10/25 CID

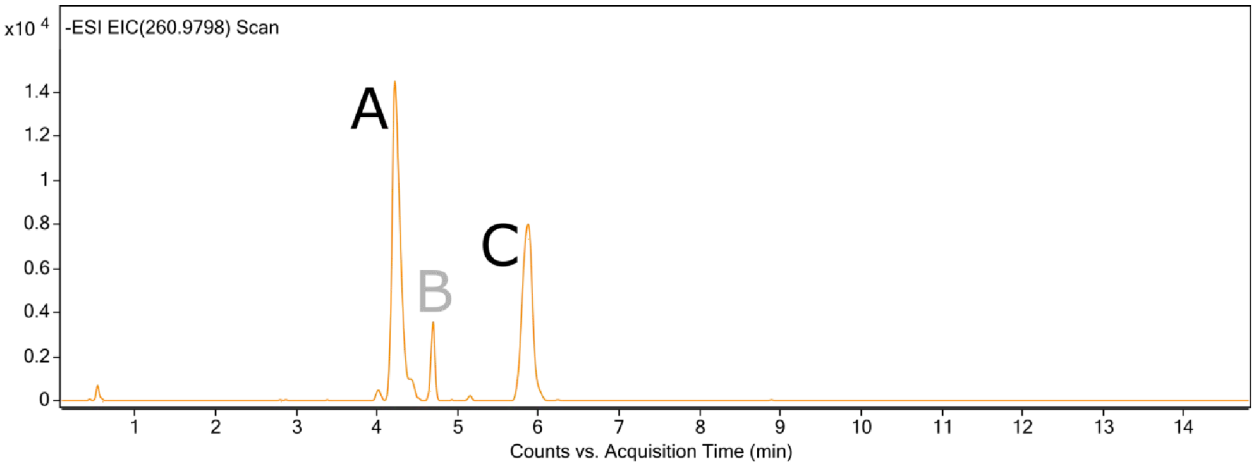

Figure 64. Extracted Ion Chromatogram for Cmp30

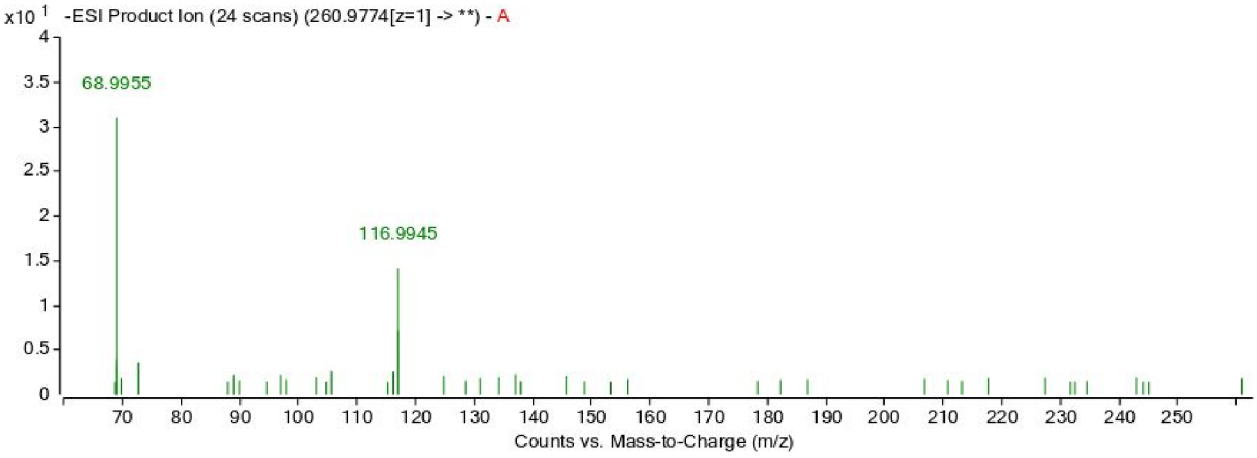

Figure 65. Average MS/MS for Cmp30a @ 10/25 CID

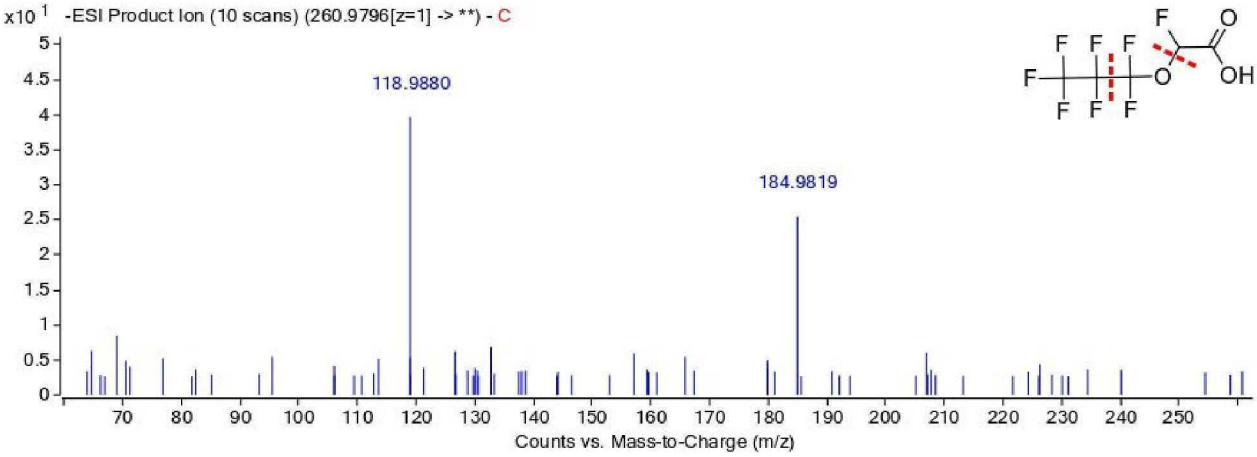

Figure 66. Average MS/MS Spectrum for Cmp30c @ 10/25 CID

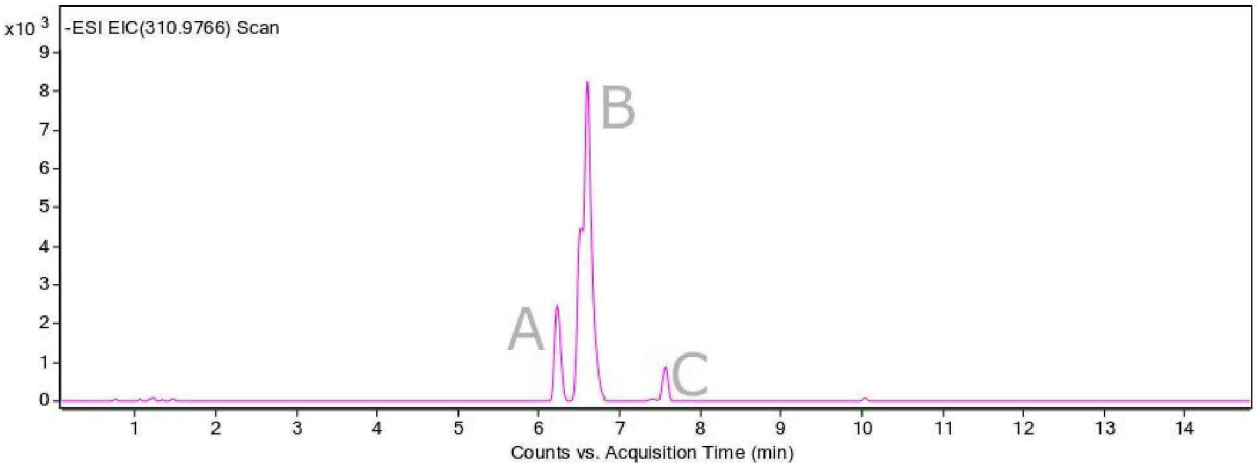

Figure 67. Extracted Ion Chromatogram for Cmp31

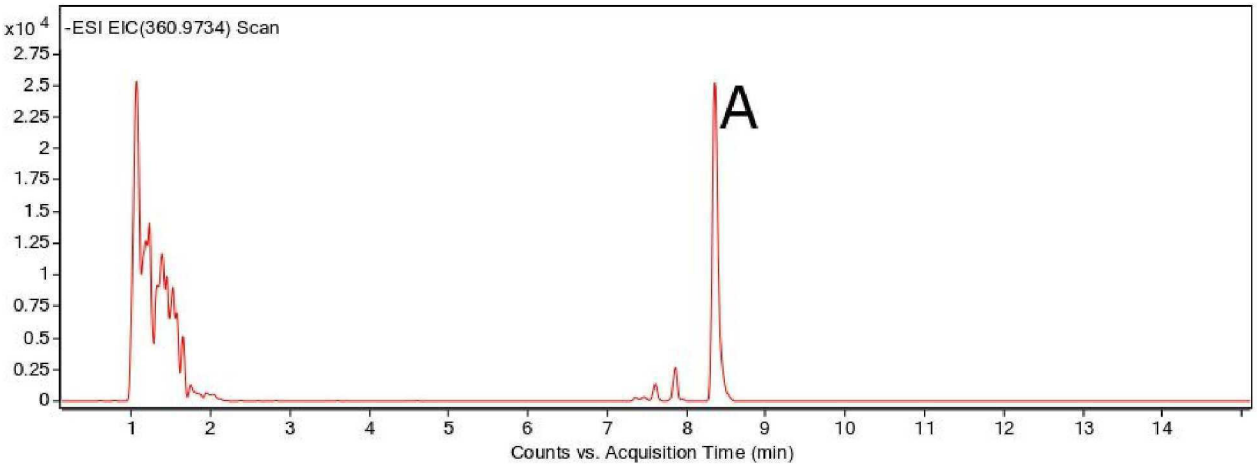

Figure 68. Extracted Ion Chromatogram for Cmp32. Peak at retention time ~1 minute is not a unique chemical feature.

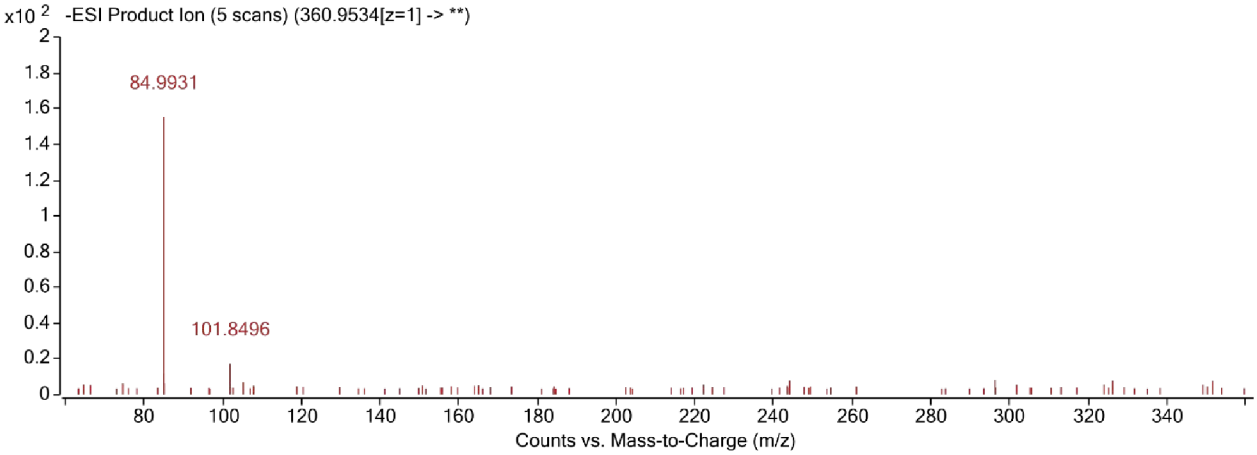

Figure 69. Average MS/MS Spectrum for Cmp32 @10/25 CID

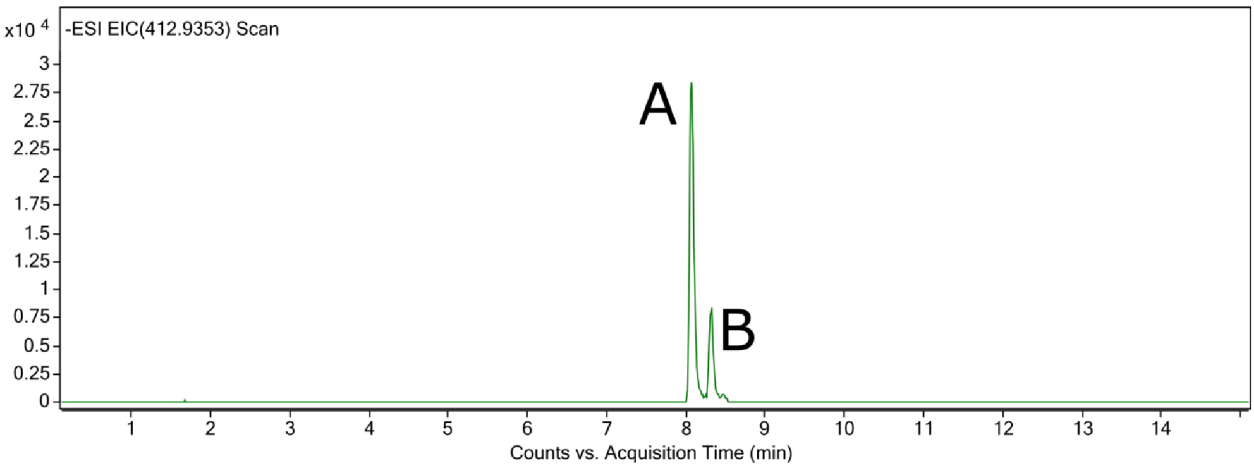

Figure 70. Extracted Ion Chromatogram for Cmp33

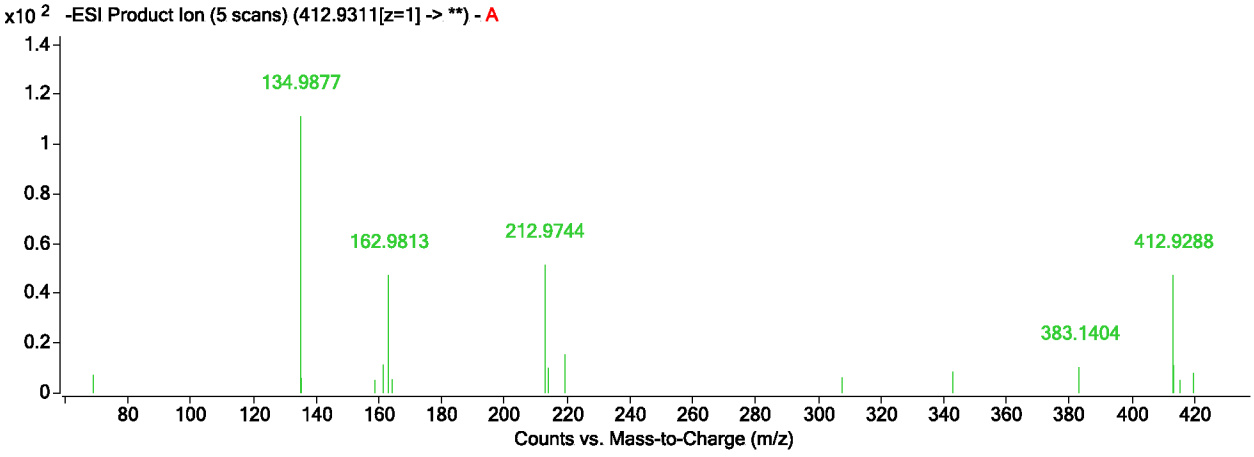

Figure 71. Average MS/MS Spectrum for Cmp33a @ 10/25 CID

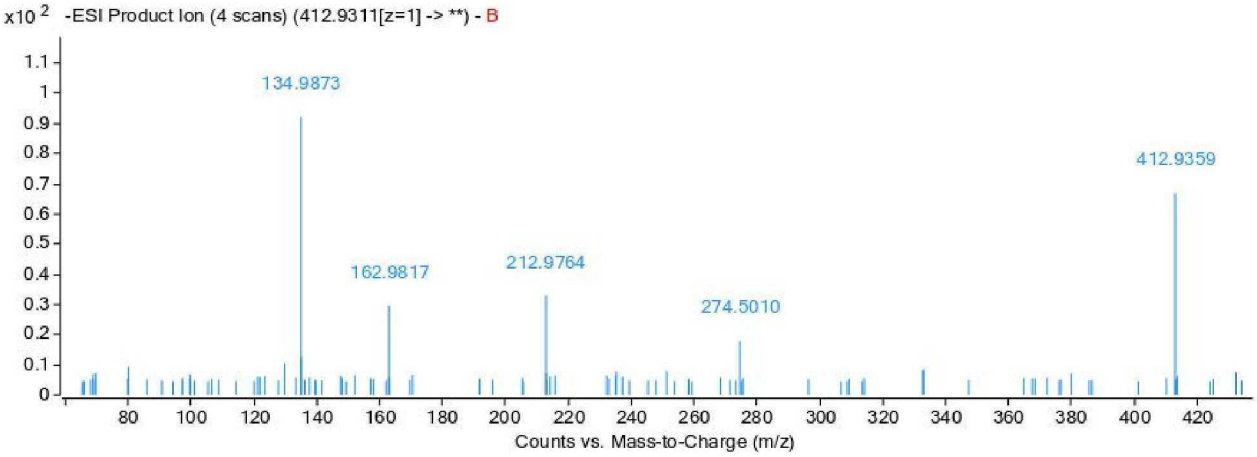

Figure 72. Average MS/MS Spectrum for Cmp33b @ 10/25 CID

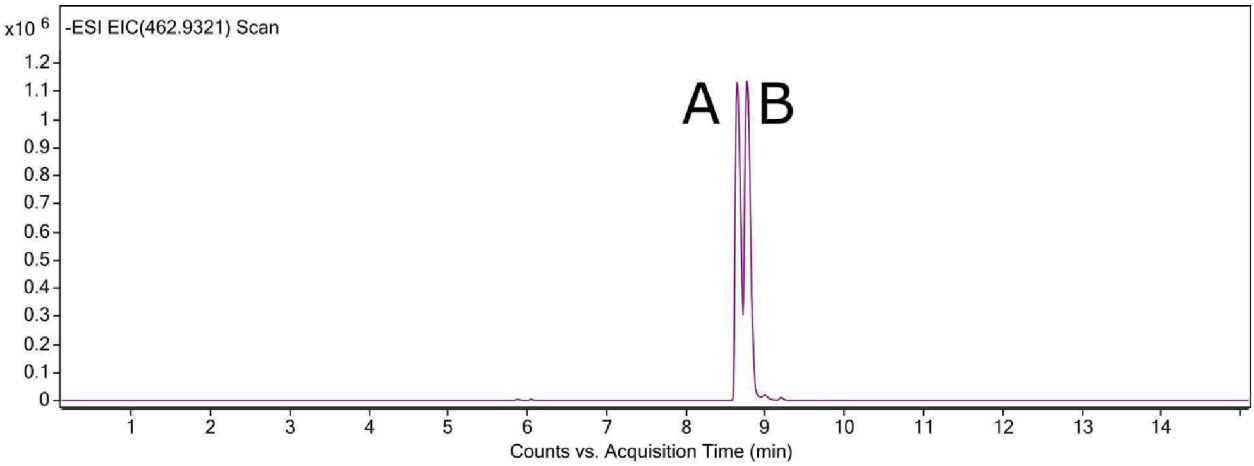

Figure 73. Extracted Ion Chromatogram for Cmp34

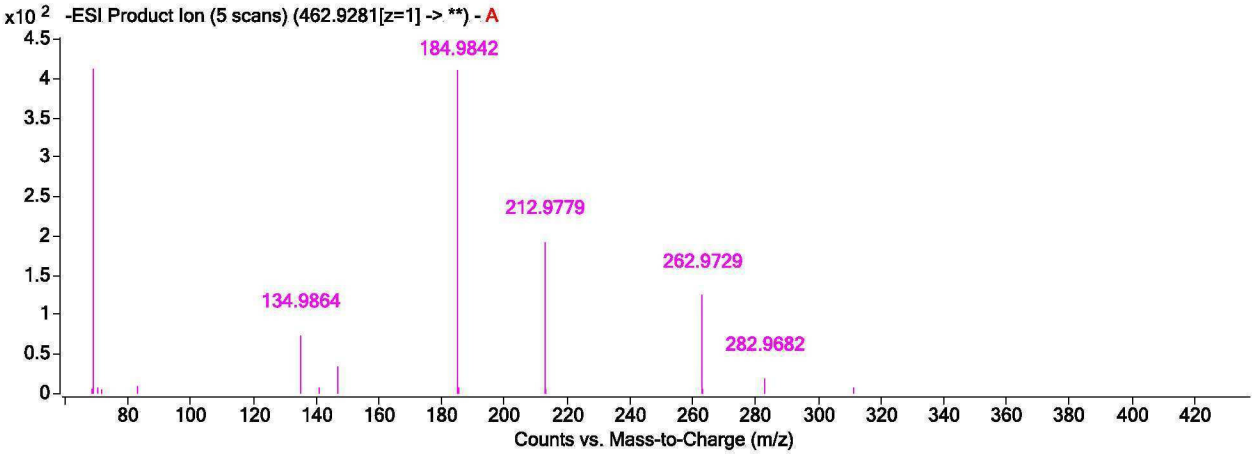

Figure 74. Average MS/MS Spectrum for Cmp34a @ 10/25 CID

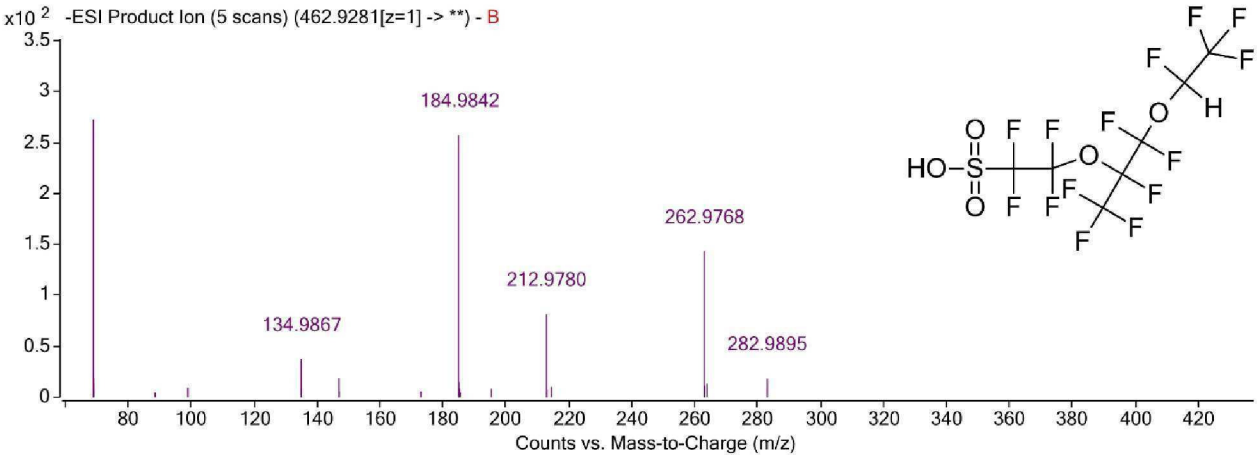

Figure 75. Average MS/MS Spectrum for Cmp34b @ 10/25 CID

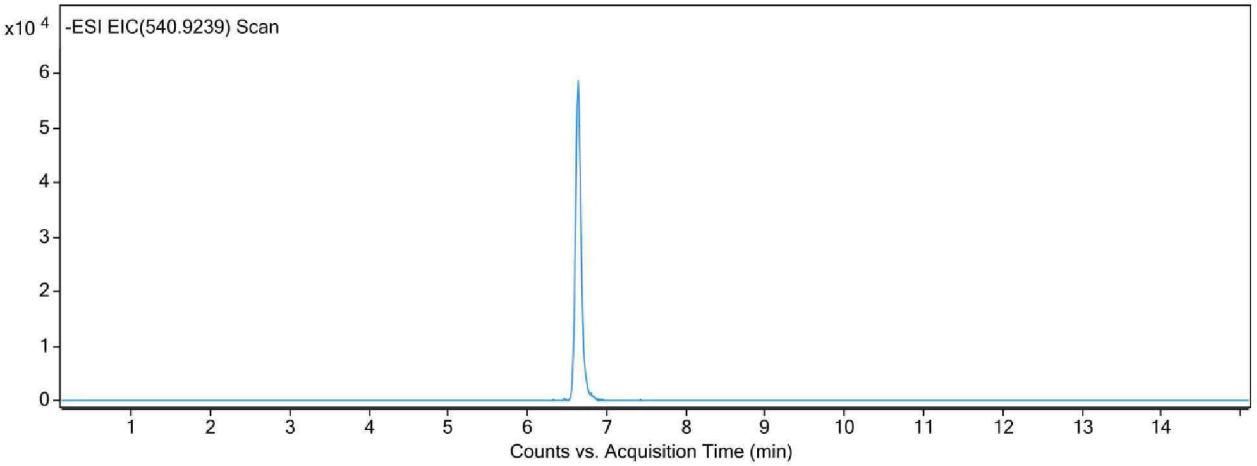

Figure 76. Extracted Ion Chromatogram for Cmp35

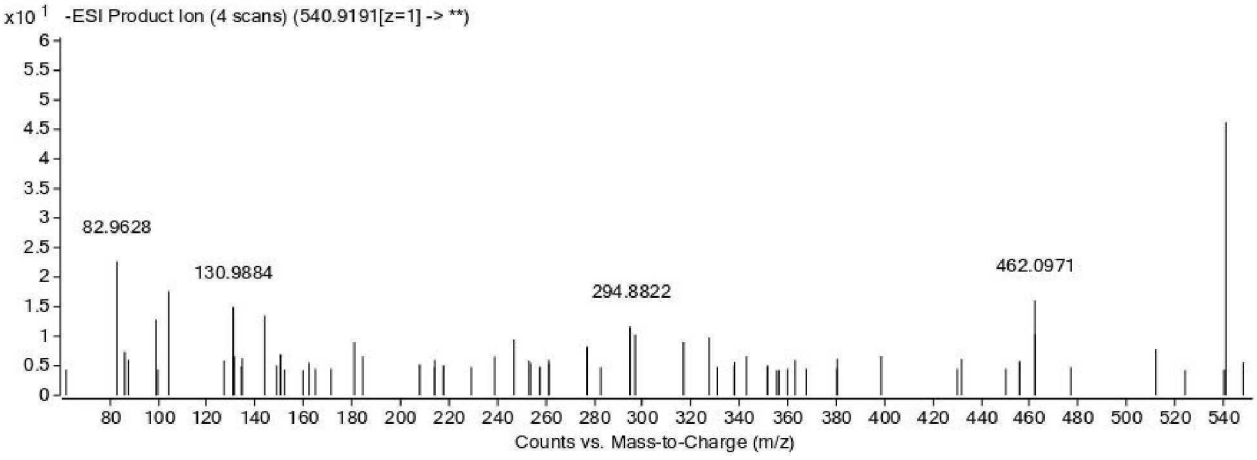

Figure 77. Average MS/MS Spectrum for Cmp35 @ 10/25 CID

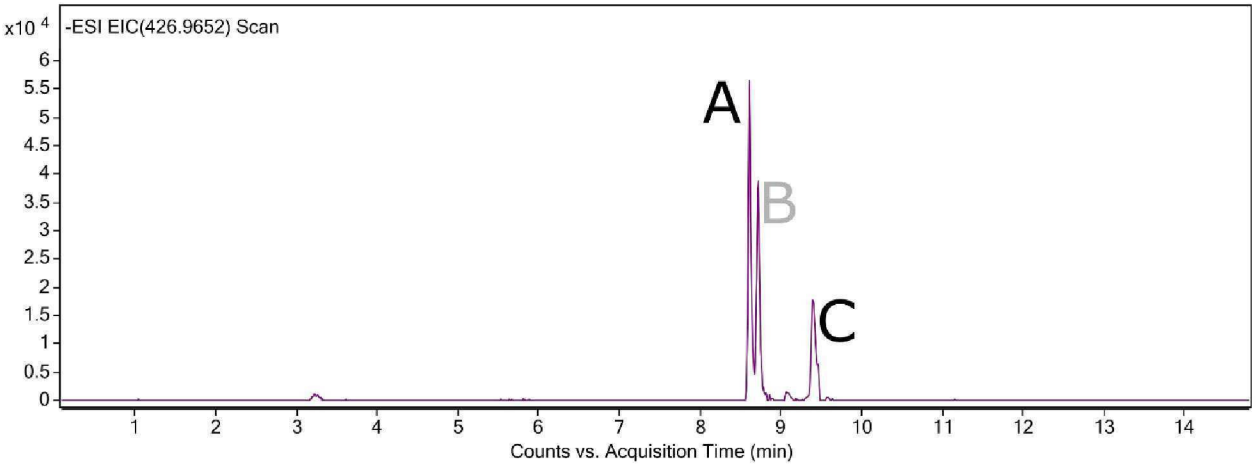

Figure 78. Extracted Ion Chromatogram for Cmp36

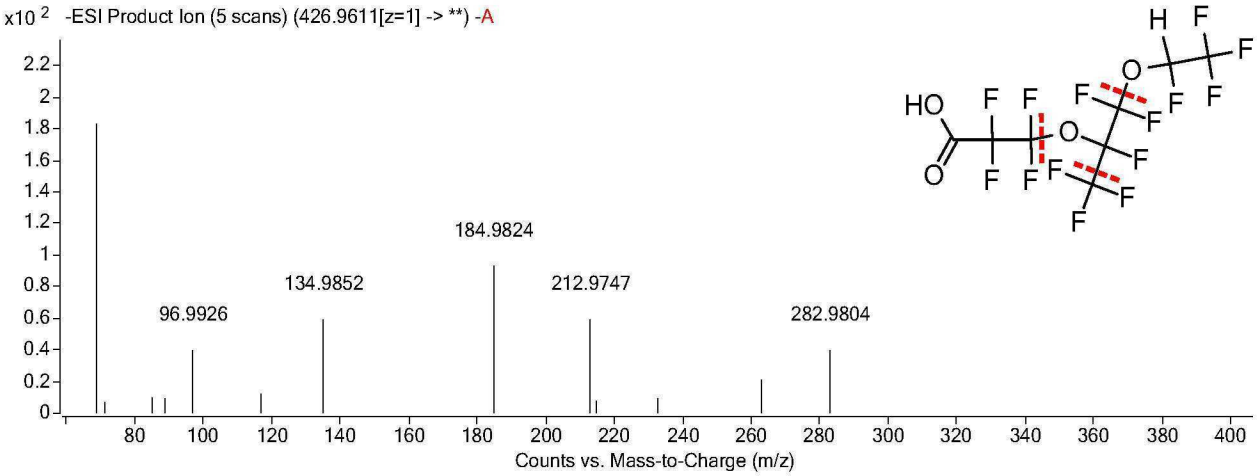

Figure 79. Average MS/MS Spectrum for Cmp 36a @ 10/25 CID

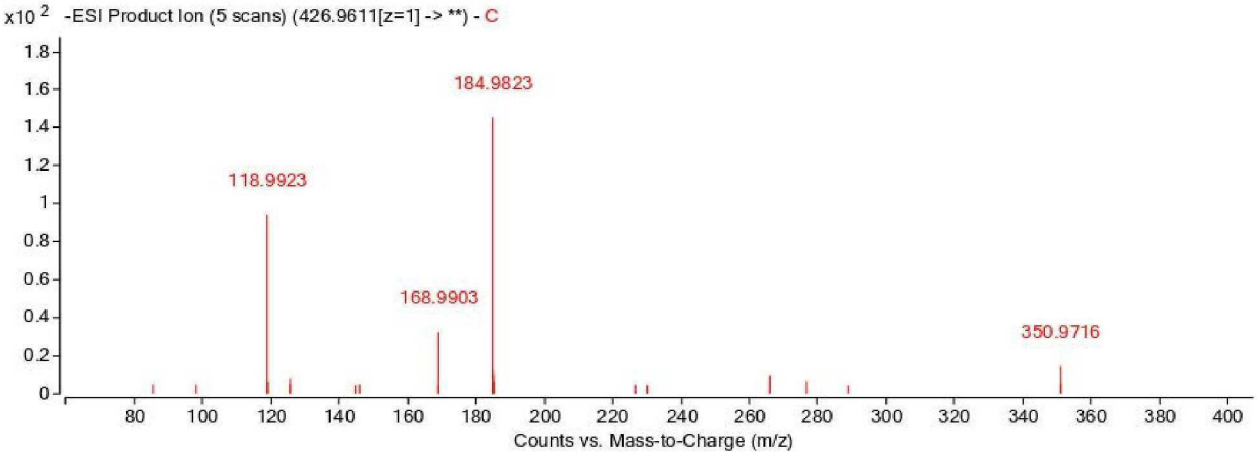

Figure 80. Average MS/MS Spectrum for Cmp 36b @ 10/25 CID

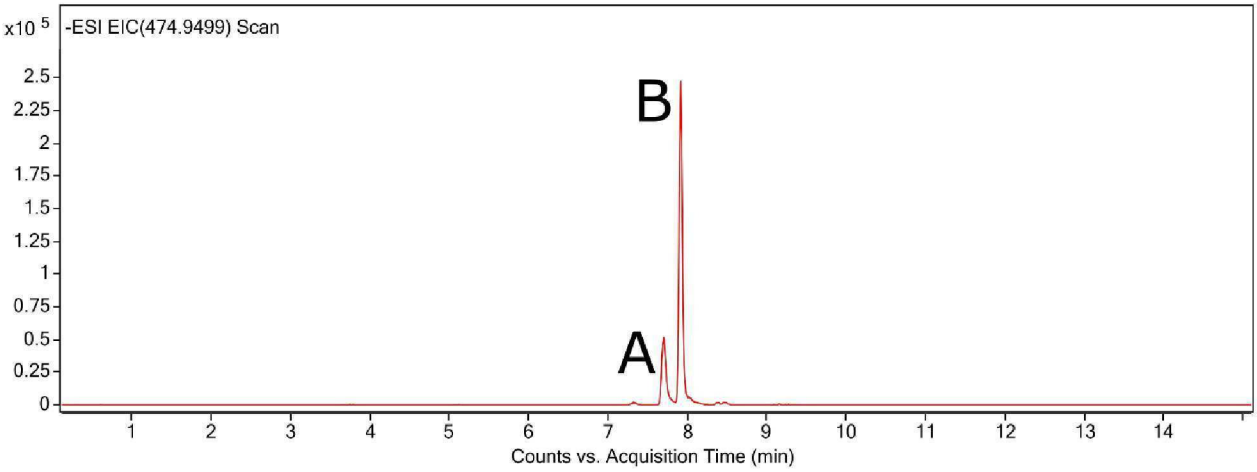

Figure 81. Extracted Ion Chromatogram for Cmp37

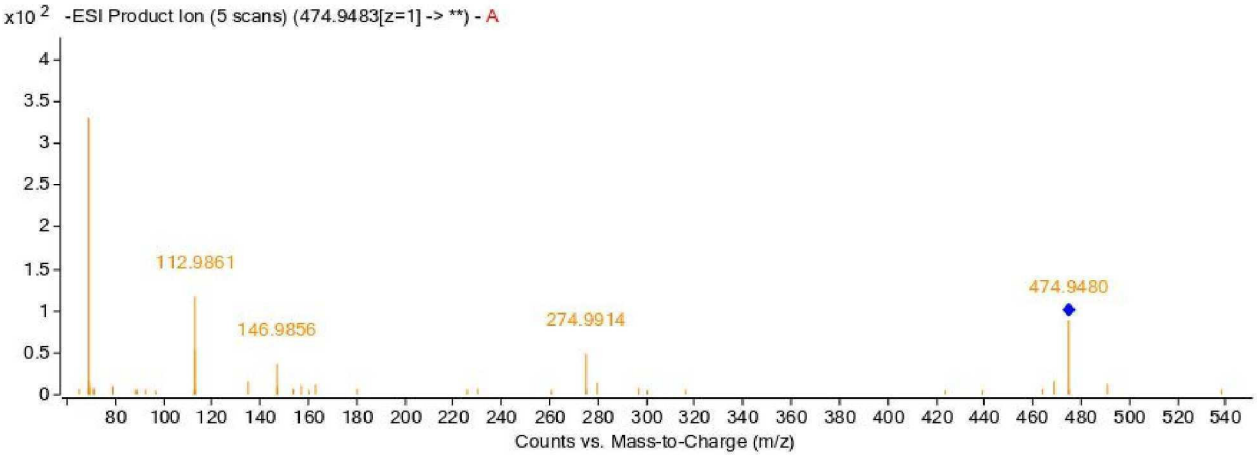

Figure 82. Average MS/MS Spectrum for Cmp37a @ 10/25 CID

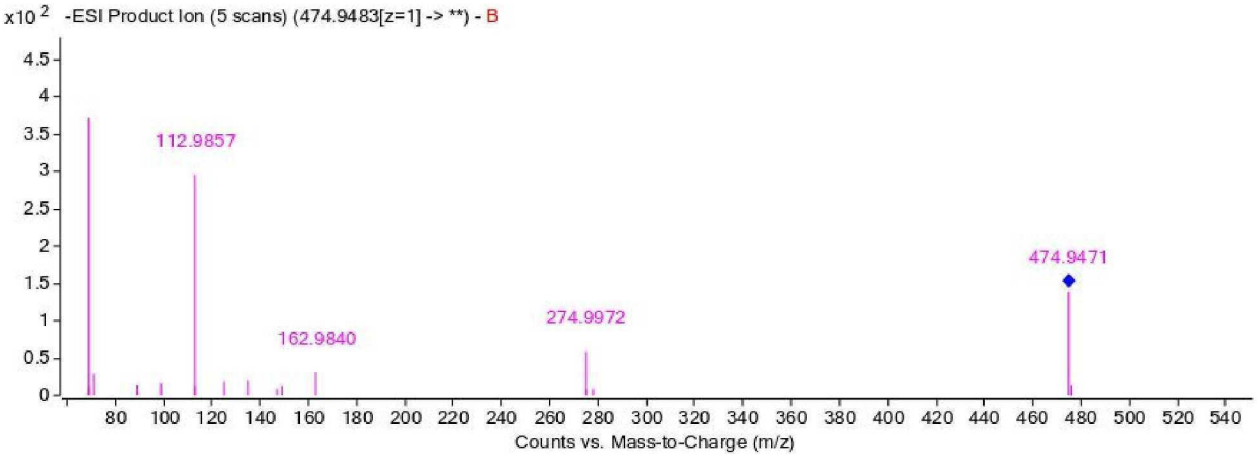

Figure 83. Average MS/MS Spectrum for Cmp37b @ 10/25 CID

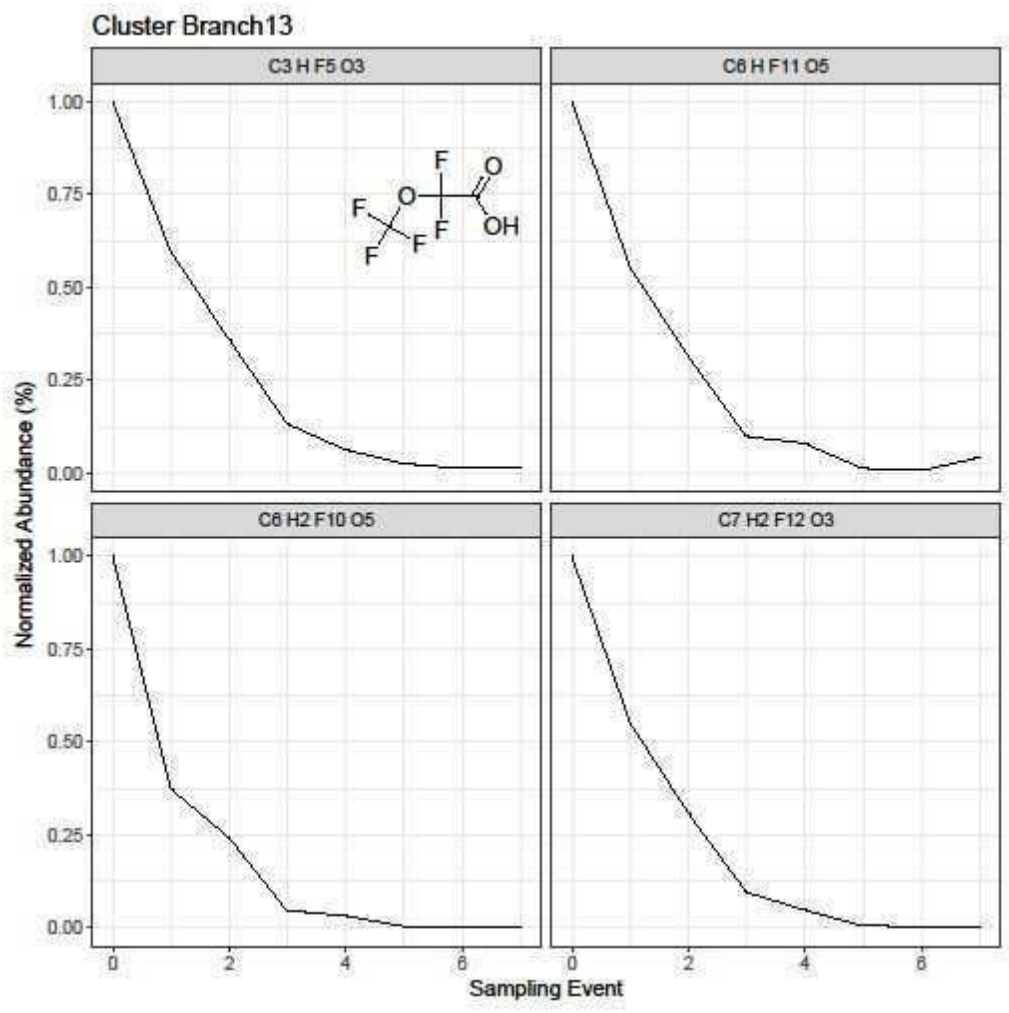

Figure 84. Cluster Branch 13

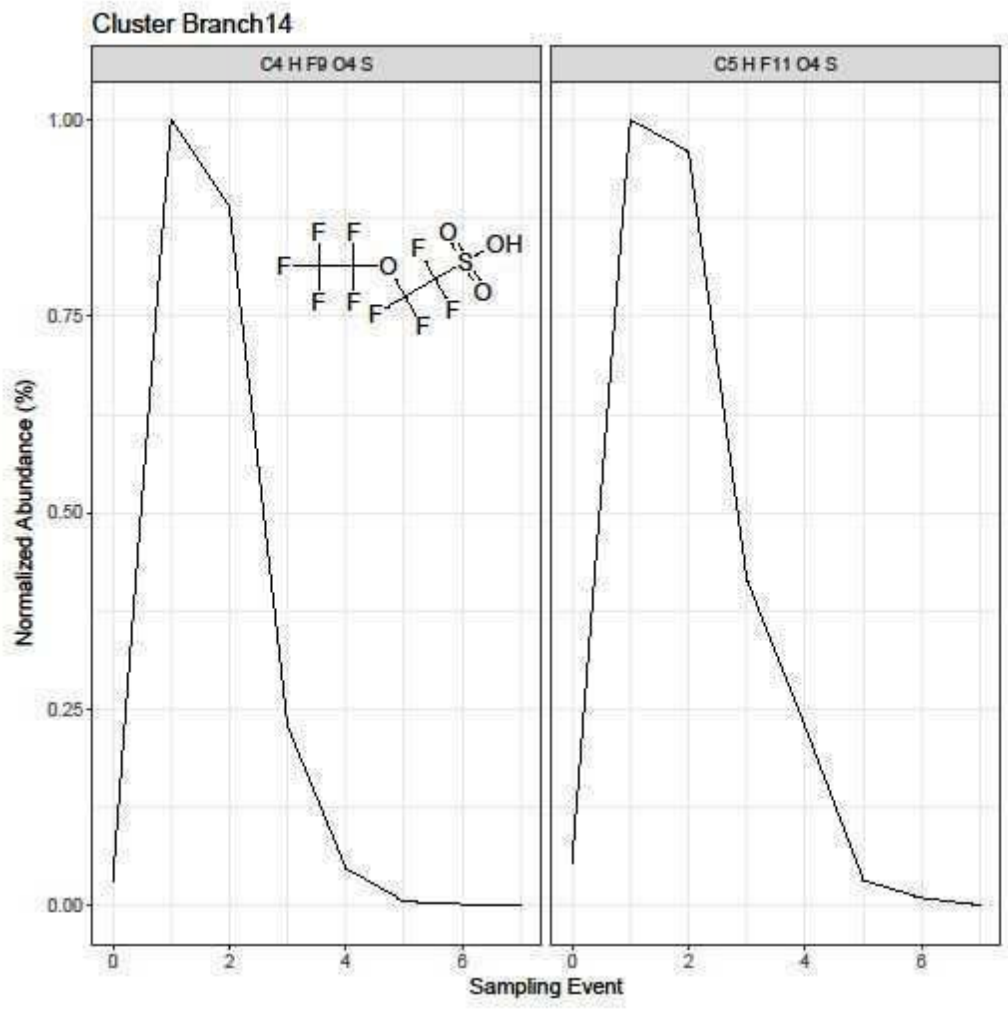

Figure 85. Cluster Branch 14

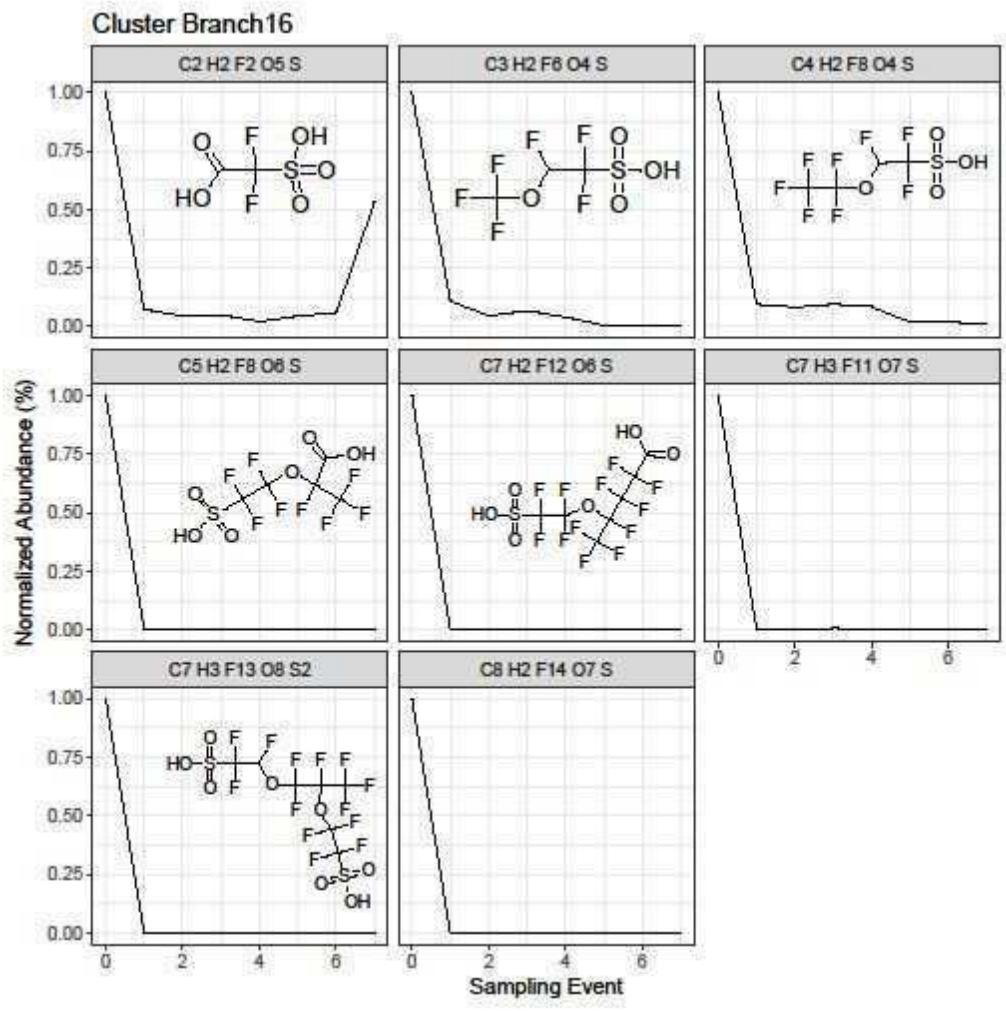

Figure 86. Cluster Branch 16

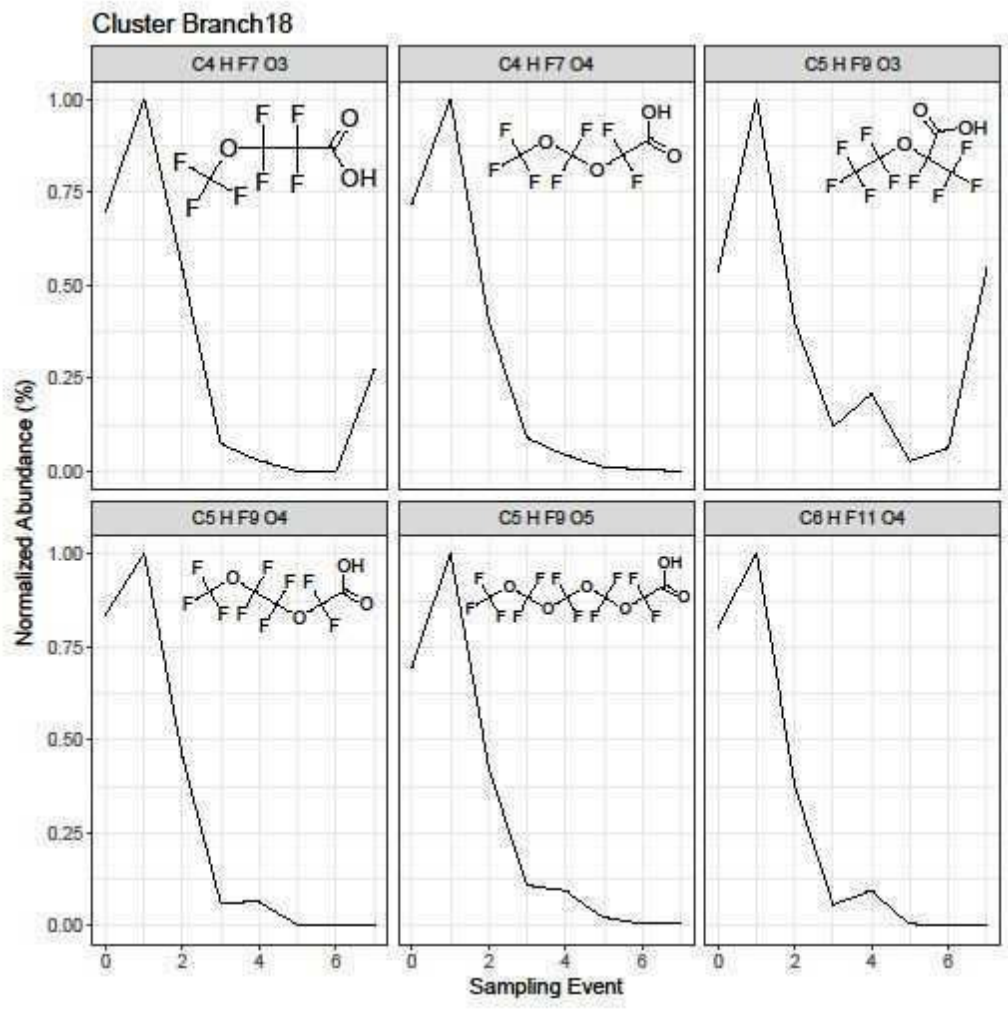

Figure 87. Cluster Branch 18

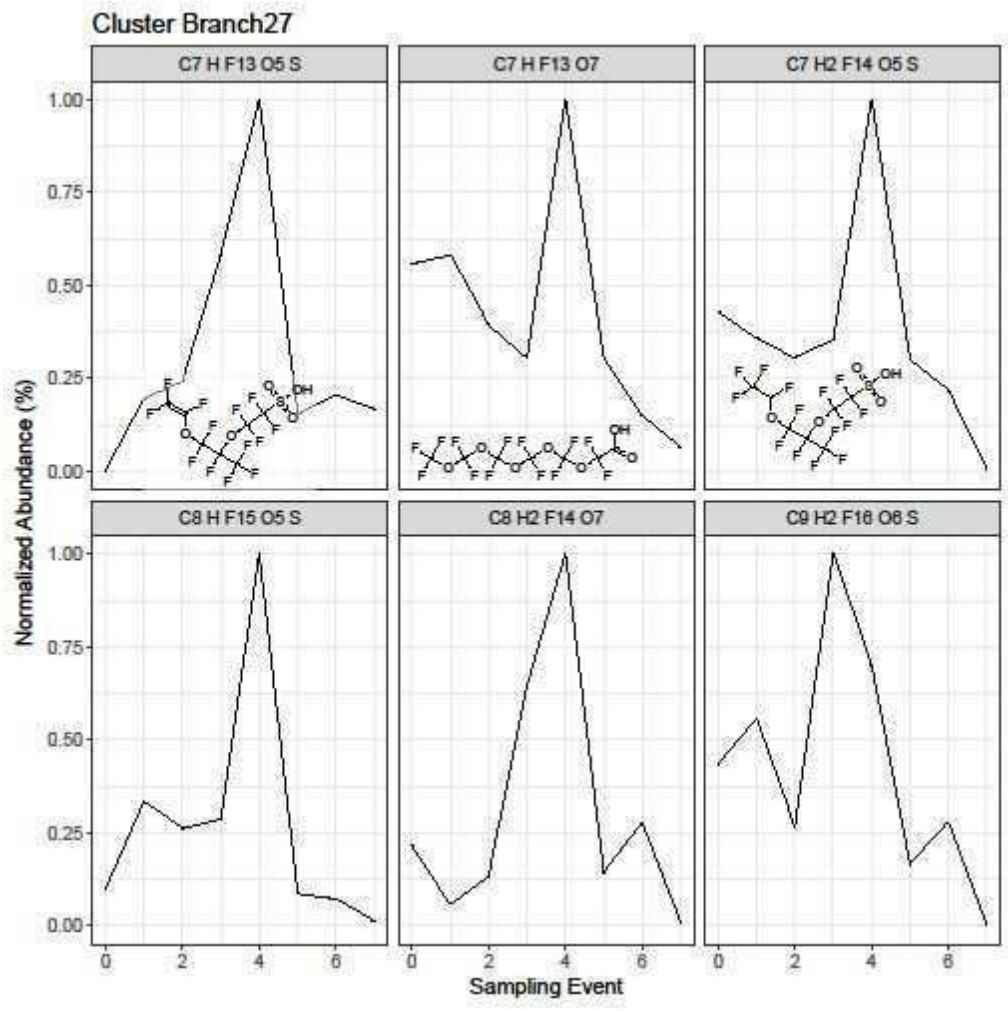

Figure 88. Cluster Branch 27

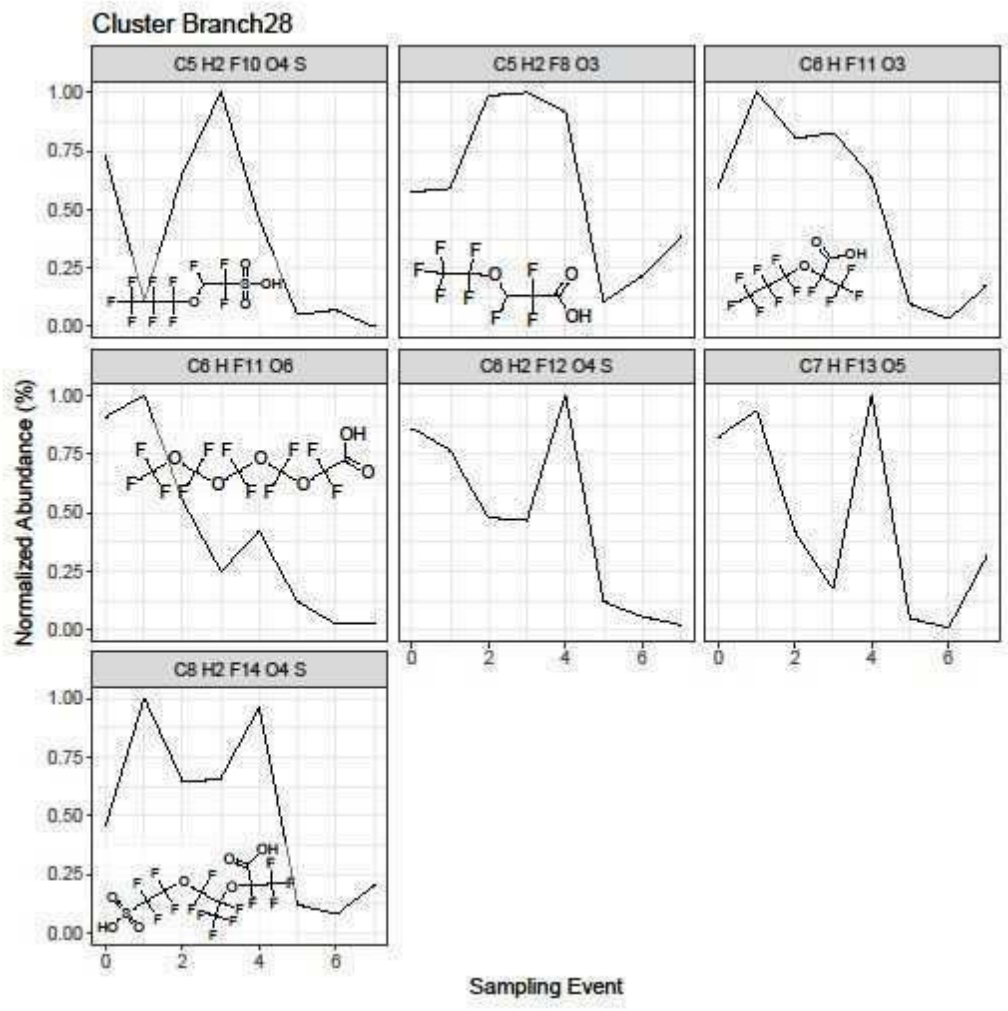

Figure 89. Cluster Branch 28

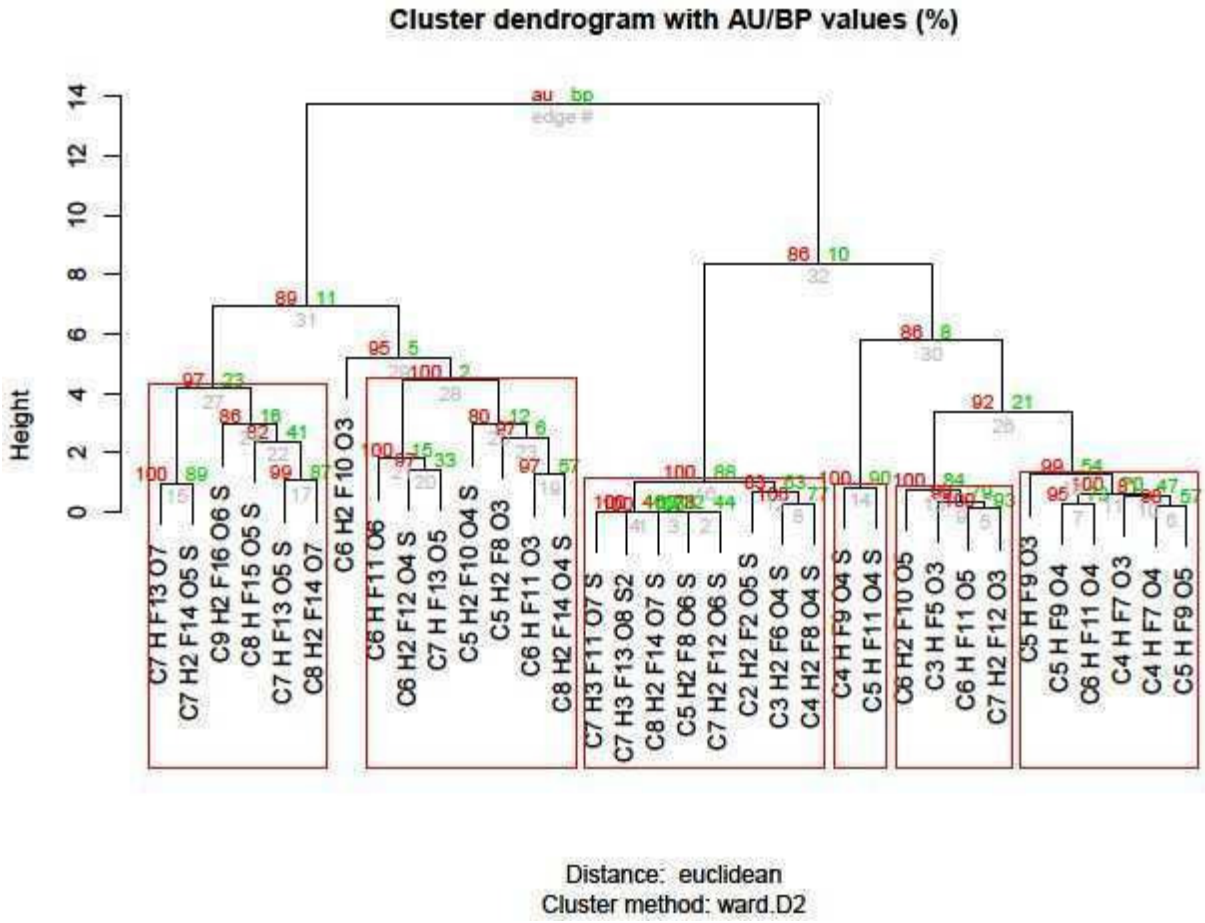

Figure 90. pvclust Ward.D2 clustering of time trend abundance of fluorinated chemical features detected in the Cape Fear River over a longitudinal sampling period.

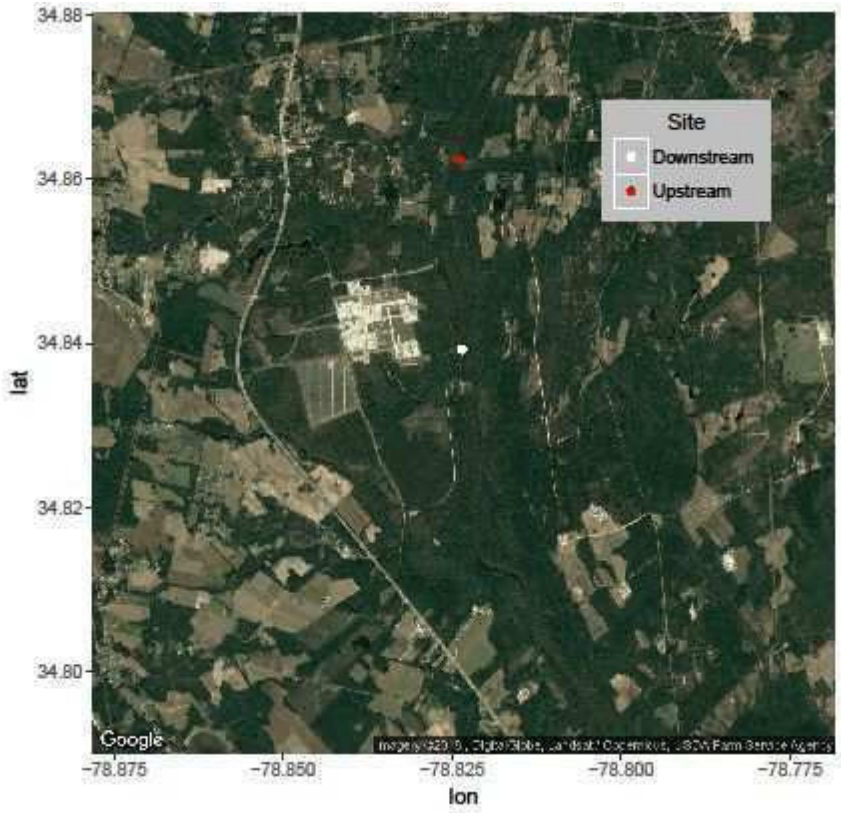

Figure 91. Sampling Map

Table S-2: List of all identified PFAS compounds and structures

ID	Confidence	Formula	Class	Theoretical Neutral Mass (Da)	Observed ion mass (m/z)	Observed Mass Error (ppm)	# Isomers	CAS	Ref	Structure
0	1	$C_2HO_2F_3$		113.9929	112.9855	3.54	1	76-05-1		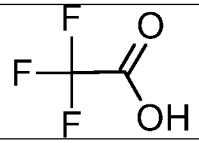
1	1	$C_3HO_3F_5$	A	179.9846	178.9765	1.68	1	674-13-5	[1]	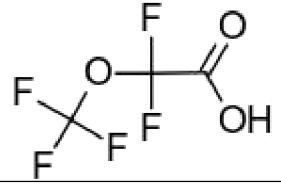
2	1	$C_4HO_3F_7$	A	229.9814	228.9741	2.18	2	13140-29-9, 377-73-1	[1]	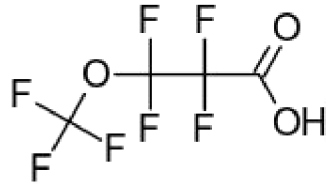 AND 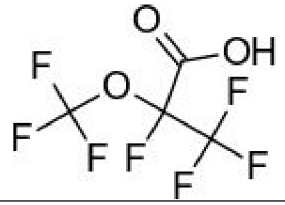
3	1/2b	$C_4HO_4F_7$	A	245.9763	244.9686	0.41	1	39492-88-1	[1]	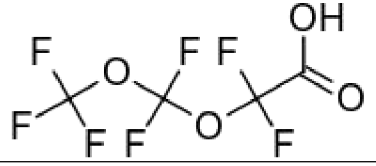

4	2b	$C_5HO_3F_9$	A	279.9782	278.9708	1.43	1	267239-61-2	[1]	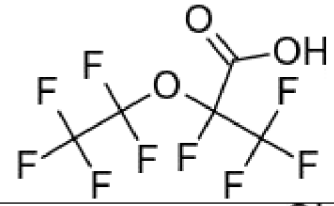
5	3	$C_5HO_4F_9$	A	295.9731	294.9661	2.71	1			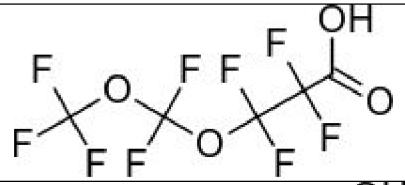
6	1	$C_5HO_5F_9$	A	311.968	310.9605	0.96	1	39492-89-2	[1]	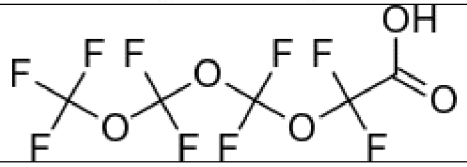
7	1	$C_6HO_3F_{11}$	A	329.975	328.9676	1.22	1	13252-13-6	[1]	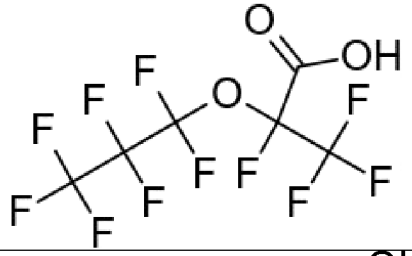
8	3	$C_6HO_4F_{11}$	A	345.9699	344.9623	0.58	1			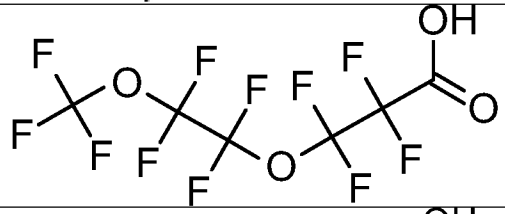
9	3	$C_6HO_5F_{11}$	A	361.9648	360.9573	0.83	1			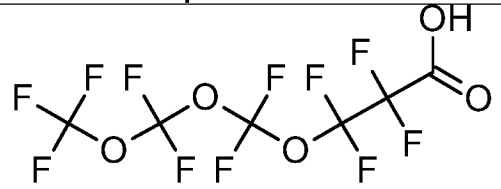

10	1	$C_6HO_6F_{11}$	A	377.9597	376.9525	1.59	1		[1]	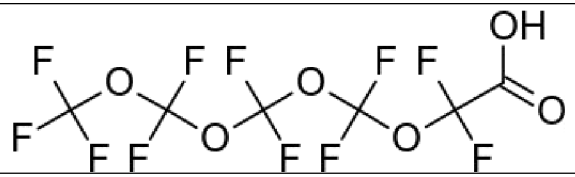
11	4	$C_8HO_4F_{13}$	A	407.9667	406.9588	0.25	1			
12	3	$C_7HO_5F_{13}$	A	411.9616	410.9544	1.46	1			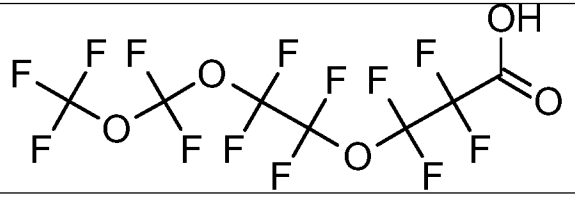
13	1	$C_7HO_7F_{13}$	A	443.9515	442.9433	0.90	1		[1]	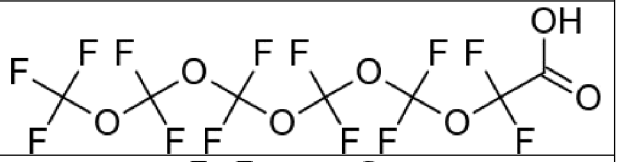
14	2b	$C_4HO_4SF_9$	A	315.94518	314.938	1.97	1	113507-82-7	[1]	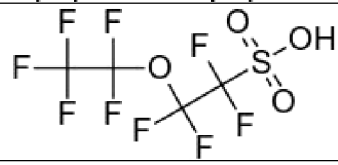
15	3	$C_5HO_4SF_{11}$	A	365.94199	364.9345	0.85	1			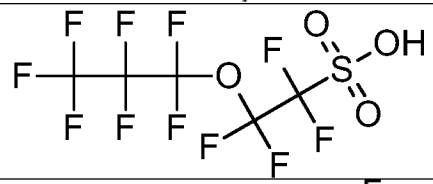
16	1	$C_7HO_5SF_{13}$	A	443.93371	442.926	0.20	1	29311-67-9	[1]	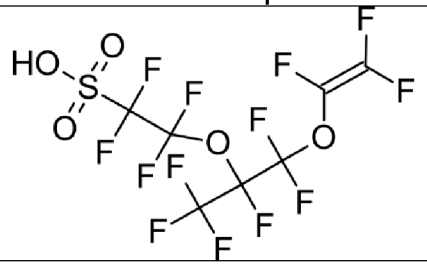

17	3	$C_8HO_5SF_{15}$	A	493.93052	492.9227	0.04	1			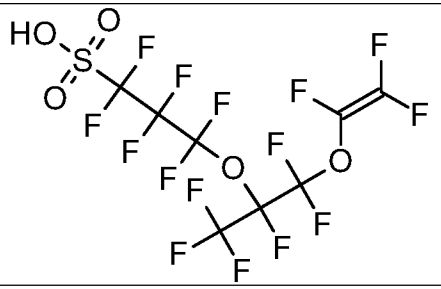
18	2b	$C_2H_2O_5SF_2$	B	175.9591	174.9514	0.57	1	422-67-3	[2]	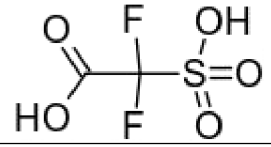
19	2b/3	$C_5H_2O_6SF_8$	B	341.9444	340.9374	2.35	2	790642-73-8	[2]	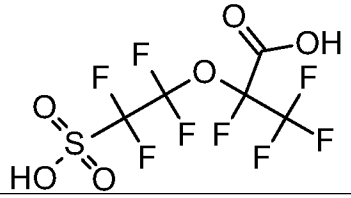
20	3	$C_6H_2O_5F_{10}$	B	343.9743	342.9673	2.33	1	919005-07-5	[3]	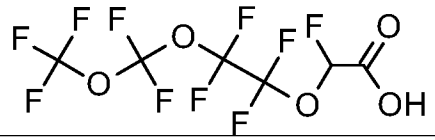
21	4	$C_7H_3O_7SF_{11}$	B	439.9424	438.9343	0.68	2			
22	2b/3	$C_7H_2O_6SF_{12}$	B	441.938	440.9303	0.23	2	852157-01-8	[4]	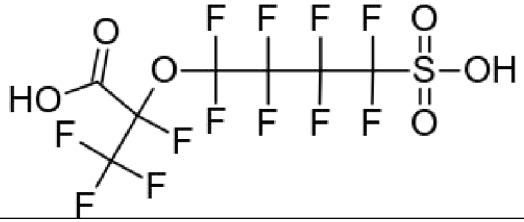

23	2b/3	$C_8H_2O_7SF_{14}$	B	507.9298	506.9226	1.18	2	1235024-21-1	[4]	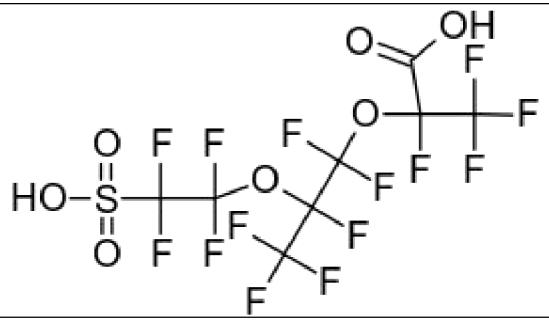
24	2b/3	$C_7H_3F_{13}O_8S_2$	B	525.9062	524.8983	0.19	2	916340-65-3	[5]	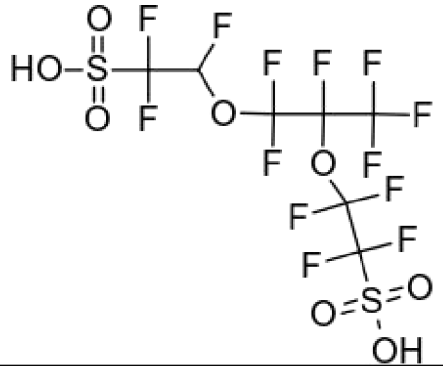
25	2b/3	$C_3H_2O_4SF_6$	C	247.9578	246.9504	1.62	3	905363-45-3	[5]	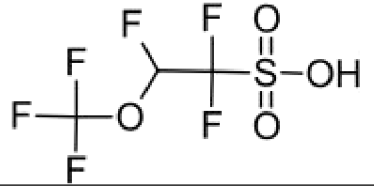
26	1	$C_4H_2O_4SF_8$	C	297.9546	296.9472	1.35	1	905363-44-2	[5]	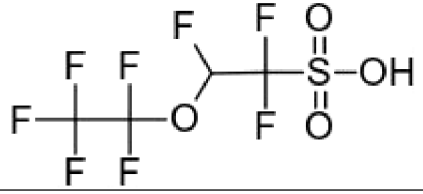

27	2b/3	$C_5H_2O_4SF_{10}$	C	347.9514	346.944	1.15	3	935443-55-3	5	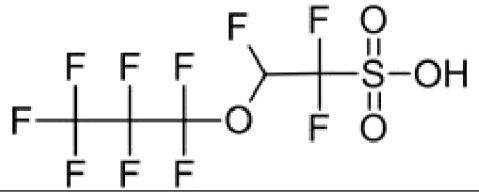
28	3	$C_6H_2O_4SF_{12}$	C	397.9482	396.941	1.51	2			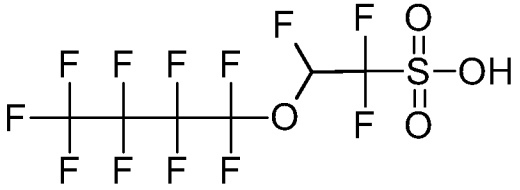
29	3	$C_8H_2O_4SF_{14}$	C	459.945	458.9372	0.00	3			
30	2b/3	$C_5H_2O_3F_8$	C	261.9876	260.9801	1.15	3	919005-00-8, 919005-13-3	3	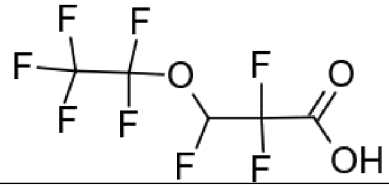
31	2b/3	$C_6H_2O_3F_{10}$	C	311.9844	310.9771	1.61	3	919005-19-9	3	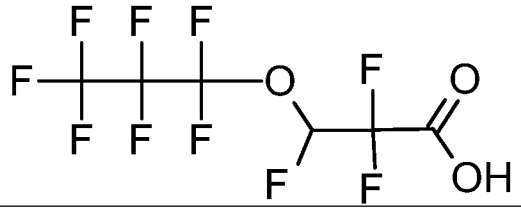
32	3	$C_7H_2O_3F_{12}$	C	361.9812	360.9723	3.05	1	919005-26-8	3	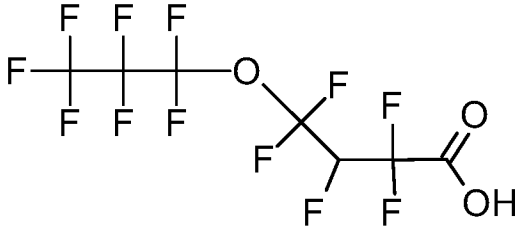

33	3	$C_6H_2O_5SF_{12}$	C	413.9431	412.9353	0.00	2			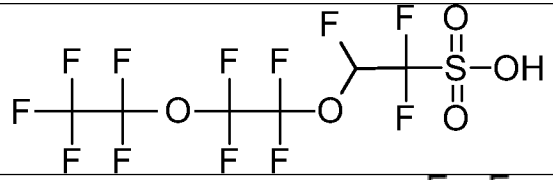
34	1	$C_7H_2O_5SF_{14}$	C	463.9399	462.9315	1.30	2	749836-20-2	[1]	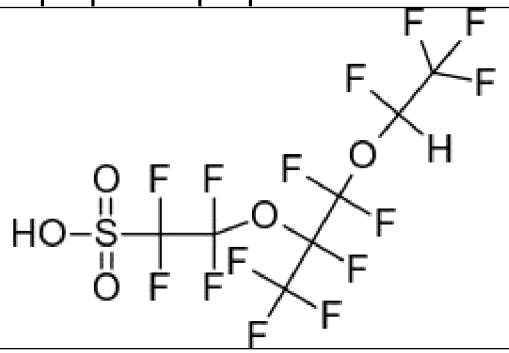
35	4	$C_9H_2O_6SF_{16}$	C	541.9317	540.9239	0.00	1			
36	1	$C_8H_2O_4F_{14}$	C	427.973	426.9643	2.11	1	773804-62-9		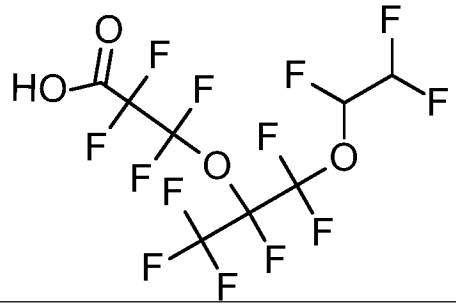
37	4	$C_8H_2O_7F_{14}$	C	475.9577	474.952	4.42	2			

Table S-3: Profinder settings for peak extraction and integration

Profinder Parameter	Setting Value
Extraction Peak Height Filter	800 counts
Permitted Ion(s)	+H/-H
Feature Extraction Isotope Model	Common organic molecules
Allowed Charge States	1-2
Compound Ion Count Threshold	Two or more ions
RT Tolerance	0.40min + 0.0%
Mass Tolerance	20.00ppm + 2.0mDa
Post-Processing Absolute Height Filter	>= 10000 counts in one sample
Post-Processing MFE Score Filter	>= 75 in one sample
Peak Integration Algorithm	Agile 2
Peak Integration Height Filter	>= 5000 counts
Find By Ion Absolute Height Filter	>= 7500 counts in one sample
Find By Ion Score Filter	>= 50.00 in one sample

Table S-4: Common MS/MS Fragments of per and poly-fluorinated ethers

Formula	*m/z*	Structure
CF3-	68.99575	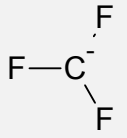
HSO3-	80.96519	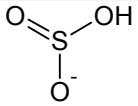
CF3O-	84.99067	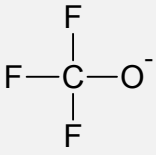
C2F3O-	96.99067	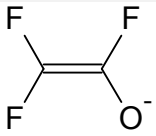
C2HF4O-	116.99690	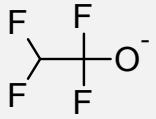

C2F5-	118.99257	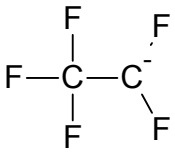
C2F5O-	134.98748	
C3F5O-	146.98748	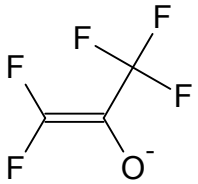
C3F7-	168.98937	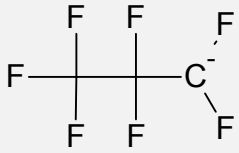

References included in Supplemental Information

1. Strynar, M.; Dagnino, S.; McMahen, R.; Liang, S.; Lindstrom, A.; Andersen, E.; McMillan, L.; Thurman, M.; Ferrer, I.; Ball, C., Identification of novel perfluoroalkyl ether carboxylic acids (PFECAs) and sulfonic acids (PFESAs) in natural waters using accurate mass time-of-flight mass spectrometry (TOFMS). *Environ. Sci. Technol.* **2015,** *49*, (19), 11622.
2. Takasaki, M.; Nakagawa, Y.; Sakiyama, Y.; Tanabe, K.; Ookubo, K.; Sato, N.; Minamide, T.; Nakayama, H.; Hori, M., Degradation Study of Perfluorosulfonic Acid Polymer Electrolytes: Approach from Decomposition Product Analysis. *Journal of The Electrochemical Society* **2013,** *160*, (4), F413-F416.
3. Hintzer, K.; Jürgens, M.; Kaspar, H.; Koenigsmann, H.; Lochhaas, K. H.; Maurer, A. R.; Schwertfeger, W.; Zipplies, T.; Mayer, L.; Dadalas, M. C. Method of making fluoropolymer dispersion. 7,671,112 B2, 2010.
4. Zhou, C.; Guerra, M. A.; Qiu, Z.-M.; Zawodzinski, T. A.; Schiraldi, D. A., Chemical Durability Studies of Perfluorinated Sulfonic Acid Polymers and Model Compounds under Mimic Fuel Cell Conditions. *Macromolecules* **2007,** *40,* (24), 8695-8707.
5. Junk, C.; Harmer, M.; Feiring, A.; Schadt, F.; Schnepp, Z. Hydrofluoroalkanesulfonic acids from fluorovinyl ethers. 7,834,209, 2005-06-07, 2006.

Environmental Science & Technology

Article

pubs.acs.org/est

Identification of Novel Perfluoroalkyl Ether Carboxylic Acids (PFECAs) and Sulfonic Acids (PFESAs) in Natural Waters Using Accurate Mass Time-of-Flight Mass Spectrometry (TOFMS)

Mark Strynar,*[,†] Sonia Dagnino,[†,‡] Rebecca McMahen,[†,‡] Shuang Liang,[†,‡] Andrew Lindstrom,[†] Erik Andersen,[†] Larry McMillan,[§] Michael Thurman,[∥] Imma Ferrer,[∥] and Carol Ball[⊥]

[†]National Exposure Research Laboratory, U.S. Environmental Protection Agency, Research Triangle Park, North Carolina 27711, United States

[‡]Oak Ridge Institute for Science and Education, Oak Ridge, Tennessee 37831 United States

[§]National Caucus and Center on Black Aged, Inc., Durham, North Carolina 27713, United States

[∥]Center for Environmental Mass Spectrometry, University of Colorado Boulder, Boulder, Colorado 80309, United States

[⊥]Agilent Technologies Inc., Wilmington, Delaware 19808, United States

Supporting Information

ABSTRACT: Recent scientific scrutiny and concerns over exposure, toxicity, and risk have led to international regulatory efforts resulting in the reduction or elimination of certain perfluorinated compounds from various products and waste streams. Some manufacturers have started producing shorter chain per- and polyfluorinated compounds to try to reduce the potential for bioaccumulation in humans and wildlife. Some of these new compounds contain central ether oxygens or other minor modifications of traditional perfluorinated structures. At present, there has been very limited information published on these "replacement chemistries" in the peer-reviewed literature. In this study we used a time-of-flight mass spectrometry detector (LC-ESI-TOFMS) to identify fluorinated compounds in natural waters collected from locations with historical perfluorinated compound contamination. Our workflow for discovery of chemicals included sequential sampling of surface water for identification of potential sources, nontargeted TOFMS analysis, molecular feature extraction (MFE) of samples, and evaluation of features unique to the sample with source inputs. Specifically, compounds were tentatively identified by (1) accurate mass determination of parent and/or related adducts and fragments from in-source collision-induced dissociation (CID), (2) in-depth evaluation of in-source adducts formed during analysis, and (3) confirmation with authentic standards when available. We observed groups of compounds in homologous series that differed by multiples of CF_2 (m/z 49.9968) or CF_2O (m/z 65.9917). Compounds in each series were chromatographically separated and had comparable fragments and adducts produced during analysis. We detected 12 novel perfluoroalkyl ether carboxylic and sulfonic acids in surface water in North Carolina, USA using this approach. A key piece of evidence was the discovery of accurate mass in-source n-mer formation (H^+ and Na^+) differing by m/z 21.9819, corresponding to the mass difference between the protonated and sodiated dimers.

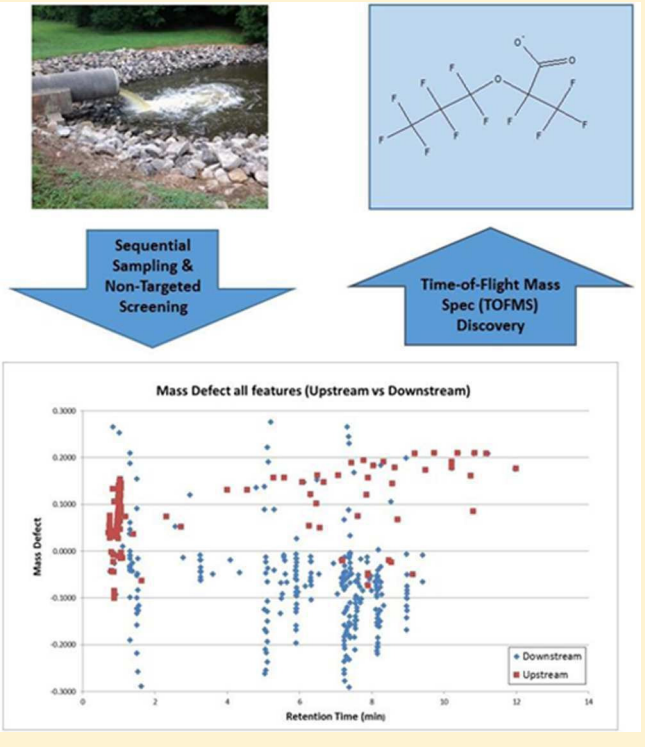

INTRODUCTION

Perfluoroalkyl and polyfluoroalkyl substances (PFASs) have unique physical and structural properties that make them extremely resistant to chemical and thermal degradation. As a result, PFASs have been used in a wide range of consumer

Received: March 10, 2015
Revised: August 7, 2015
Accepted: August 30, 2015
Published: September 22, 2015

Downloaded via US EPA OFFICE OF ENVIRONMENTAL INFO on April 29, 2020 at 12:45:11 (UTC).
See https://pubs.acs.org/sharingguidelines for options on how to legitimately share published articles.

ACS Publications © 2015 American Chemical Society

DOI: 10.1021/acs.est.5b01215
Environ. Sci. Technol. 2015, 49, 11622−11630

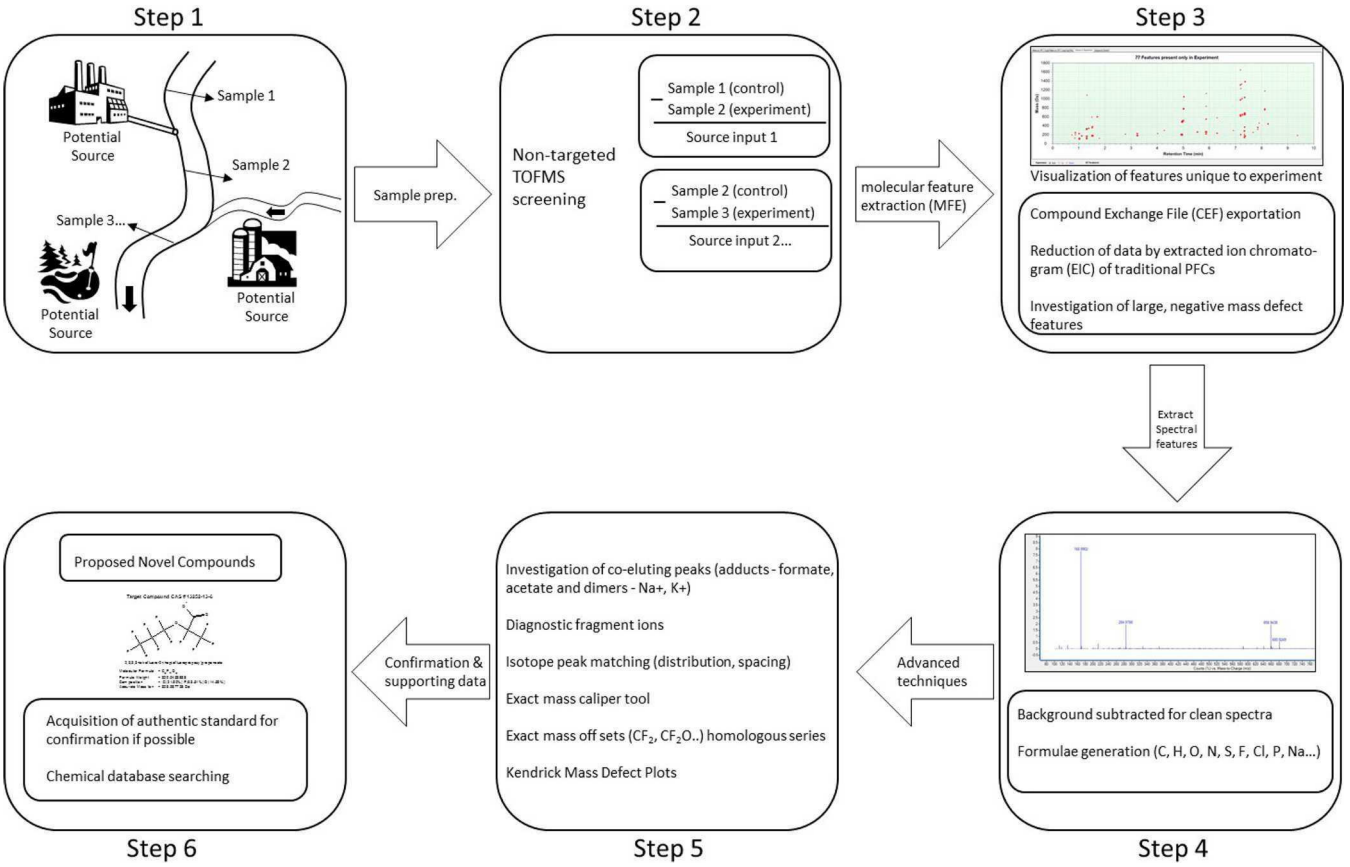

Figure 1. Sample workflow for TOFMS discovery.

products and industrial applications.[1] Between 1950 and 2000, the eight-carbon PFASs, including perfluorooctanoic acid (PFOA) and perfluorooctanesulfonate (PFOS), were among the most commonly produced and used perfluorinated compounds. PFASs have been detected in many environmental and biological matrices across the globe for a number of years,[2] and this ubiquity has led to mounting concerns about exposure and potential toxicity. As a result, many international regulatory efforts have been enacted to reduce, substitute, or eliminate long-chain (8 consecutive perfluorinated carbons or longer) PFASs from products and waste streams. In the United States, eight major fluorochemical manufacturers entered into a voluntary stewardship agreement with the U.S. Environmental Protection Agency (EPA) to phase out the use and production of long-chain perfluorinated chemistries by 2015.[3] To take their place, manufacturers have started using alternative chemistries that may include both shorter-chain perfluorinated (<C8) and/or polyfluorinated materials. For example, some of these replacement compounds still have the traditional perfluorinated carbon regions, but they are broken into shorter units by insertion of ether oxygens at regular intervals. These ether linked compounds are still technically classified as perfluorinated if all carbons are substituted with fluorine and polyfluorinated if any carbon is occupied by a hydrogen rather than a fluorine.[4] The rationale is that the addition of oxygens would likely make the replacement chemistry more labile to degradation, and thus more favorable for usage. However, to date the chemical manufacturers have disclosed little information publicly concerning the chemical structures and potential toxicities of the replacement PFASs now being produced. This makes it extremely difficult for independent research groups to evaluate their environmental distributions and potential toxicities.

A rare exception is a peer-reviewed publication on 4,8-dioxa-3H-perfluorononanoate (ADONA) (Supporting Information Figure S1), a polyfluorinated alternative to PFOA which is said to have a "more favorable toxicological profile".[5] This single journal article was published by its manufacturer, but standards for this new material have not been made available (to our knowledge) for comprehensive ecological or toxicological evaluation. Manufacturers typically submit more detailed information concerning compound structure, potential toxicity, environmental fate, and projected production volumes to regulatory authorities prior to large-scale production (e.g., the U.S. EPA's premanufacture notice process), but this information is held as confidential business information and cannot be disclosed to the general research community.

One example of industrial producers manufacturing replacement compounds is outlined in an executed draft consent order from the state of West Virginia to DuPont Corporation allowing the discharge of a new fluorinated compound into the Ohio river, at the Washington Works facility (West Virginia).[6] This is the same facility that has been the source of historical PFOA contamination of local surface and groundwater due to industrial manufacture and discharge and is the center of a court-ordered investigation by the C8 science panel to determine if PFOA exposure in the local human population has led to adverse health effects.[7] A number of recent epidemiological studies have indicated that exposure to PFOA at this location has been associated with adverse human health outcomes.[8,9]

DOI: 10.1021/acs.est.5b01215
Environ. Sci. Technol. 2015, 49, 11622−11630

Typical environmental occurrence investigations have for years focused on targeted analysis for specific analytes of interest. Highly precise and sensitive LC and GC MS/MS methods have been developed to quantify contaminants of concern. A more recent approach for environmental sample analysis has been the use of high-resolution mass spectrometry (HRMS) for these efforts. Some researchers have used nontargeted or suspect screening effectively in demonstrating many chemical classes in wastewater effluent without the use of reference standards.[11−13] These approaches have begun to rely more heavily on the use of databases, accurate mass searches, and HRMS molecular formula prediction capabilities for discovery. Confirmation with authentic standards still remains the "gold standard". Schymanski et al.[14] reported on five levels of confidence in identifying small molecules using HRMS ranging from exact mass matches, through molecular formula prediction, tentative candidate structures, library match searches, and finally confirmation with a reference standard. This is the type of approach that we use in this work to identify previously undescribed PFASs in surface water.

As it is mostly unknown what is being produced to replace traditional perfluorinated compounds, a series of sampling events was conducted to collect water samples with determination of new per- and polyfluorinated substances as a goal. In Nakayama et al.,[10] a sampling of surface water in the Cape Fear River Basin in North Carolina indicated sources of perfluorinated compounds intermittently spread throughout the drainage basin. A follow-up investigation with more focused sampling to determine sources was not conducted. However, based on this early work, there was some indication that there were PFASs sources in the Fayetteville, NC area. More recent surface water sampling trips in this region indicated continued elevated concentrations of traditional perfluorinated compounds, supporting the Nakayama et al.[10] findings. One such source was known to be downstream of the industrial effluent discharge of a fluorochemical production facility. Further investigation of these samples for identification and occurrence of potential replacement chemistries was undertaken.

MATERIALS AND METHODS

Sample Workflow for Discovery. A diagram of the workflow we used for novel compound discovery in surface water samples is shown in Figure 1. It is a six-step process that starts with sequential sampling of water, followed by nontargeted screening, visualization of detected peaks, further investigation of suspect features, advanced TOFMS techniques, and, last, compound confirmation with authentic standards when available. Using this approach, it becomes possible to detect chemicals that enter a waterway from a source (point or nonpoint) between sampling locations. This can then be used for such purposes as source elucidation, compound discovery, or both. In the following sections we will be referring to Figure 1 and the specific step in the process to which we are referring.

Sample Collection. In the summer of 2012, water samples were collected at locations on the Cape Fear River and its tributaries, with some locations having previously been found to contain measurable PFASs.[15] Grab samples were taken from the bank and bridge crossings with a lab-made dip sampler or a stainless steel Kemmerer sampler, and stored in a 1-L HDPE bottle following the procedures described in Nakayama et al.[16] Samples (n = 9) were acquired from the main flow of the Cape Fear River including from just south of the city of Fayetteville, NC to the bridge crossing in the town of Tar Heel, NC. Duplicate samples, trip spikes, and trip blanks were included in this sampling. This sampling also included tributaries to the Cape Fear River along the same stretch of river where reclaimed wastewater treatment plant (WWTP) and industrial effluent streams occurred (Figure 1, step 1).

Sample Analysis for Traditional PFASs. Samples were prepared and analyzed according to the methods of Nakayama et al.[16] In brief, water samples were stabilized with addition of nitric acid and stored at ambient temperature prior to analysis (<7 days). Each water sample was measured in a graduated cylinder, and the sampling bottle was washed with 10 mL of methanol to solubilize analytes that may have become sorbed to the container wall during shipping and storage. The water was then placed back in the methanol-washed bottle with the methanol rinsate, spiked with a mixture of internal standards, and filtered through a glass fiber filter. A volume, typically 500 mL, of water was concentrated on a Waters WAX SPE cartridge using a positive displacement pump. The cartridge was eluted with basic methanol (0.3% NH_4OH) and the eluent was concentrated via evaporation under N_2 gas to 1 mL and prepared for analysis. A procedural blank was prepared as described above using 500 mL of in-house DI water. Traditional PFASs (C_4−C_{10} perfluorocarboxylic acids (PFCAs); perfluorobutanesulfonate (PFBS), perfluorohexanesulfonate (PFHxS), and PFOS) analysis was performed using a Waters Acquity ultra performance liquid chromatograph interfaced with a Waters Quattro Premier XE triple quadrupole mass spectrometer (UPLC-MS/MS) (Waters, Milford, MA, USA).

TOFMS Investigation of Novel Fluorinated Compounds. The extraction method used for traditional PFASs analysis was also used for elucidation of novel compounds. Elevated concentrations of traditional PFASs in samples were used as an indication of samples that were likely closer to sources (Figure S2). Sample analysis was performed using an Agilent 1100 series HPLC interfaced with a 6210 series Accurate-Mass LC-TOF system (Agilent Technologies, Palo Alto, CA). The mass spectrometer was operated in electrospray ionization (ESI) negative mode and any drift in the mass accuracy of the TOF was continuously corrected by infusion of two reference compounds (purine (m/z 119.03632) and the acetate adduct of hexakis (1H,1H,3H-tetrafluoropropoxy) phosphazine (m/z 980.016375)) via dual-ESI sprayer. Chromatographic separation was accomplished using an Eclipse Plus C8 column (2.1 × 50 mm, 3.5 μm; Agilent). The method consisted of the following conditions: 0.2 mL/min flow rate; column at 30 °C; mobile phases: A: ammonium formate buffer (0.4 mM) and DI water/methanol (95:5 v/v), and B: ammonium formate (0.4 mM) and methanol/DI water (95:5 v/v); gradient: 0−15 min a linear gradient from 75:25 A/B to 15:85 A/B; with a 4 min post time for equilibration.

Identification of Suspect Features. The total ion chromatogram (TIC) of each water sample was subjected to the software molecular feature extraction algorithm (MFE) and was restricted to the 100 most intense features m/z 50−1700 based on peak height. A molecular feature is defined as a single accurate mass with a specific retention time and an integrated area count. Compounds identified in the solvent and procedural blank samples were used to develop a mass exclusion list to subtract from subsequent unknown samples. After molecular features were identified, they were exported as a Compound Exchange File (.CEF) and imported into Mass Profiler to compare upstream with downstream samples.

DOI: 10.1021/acs.est.5b01215
Environ. Sci. Technol. 2015, 49, 11622−11630

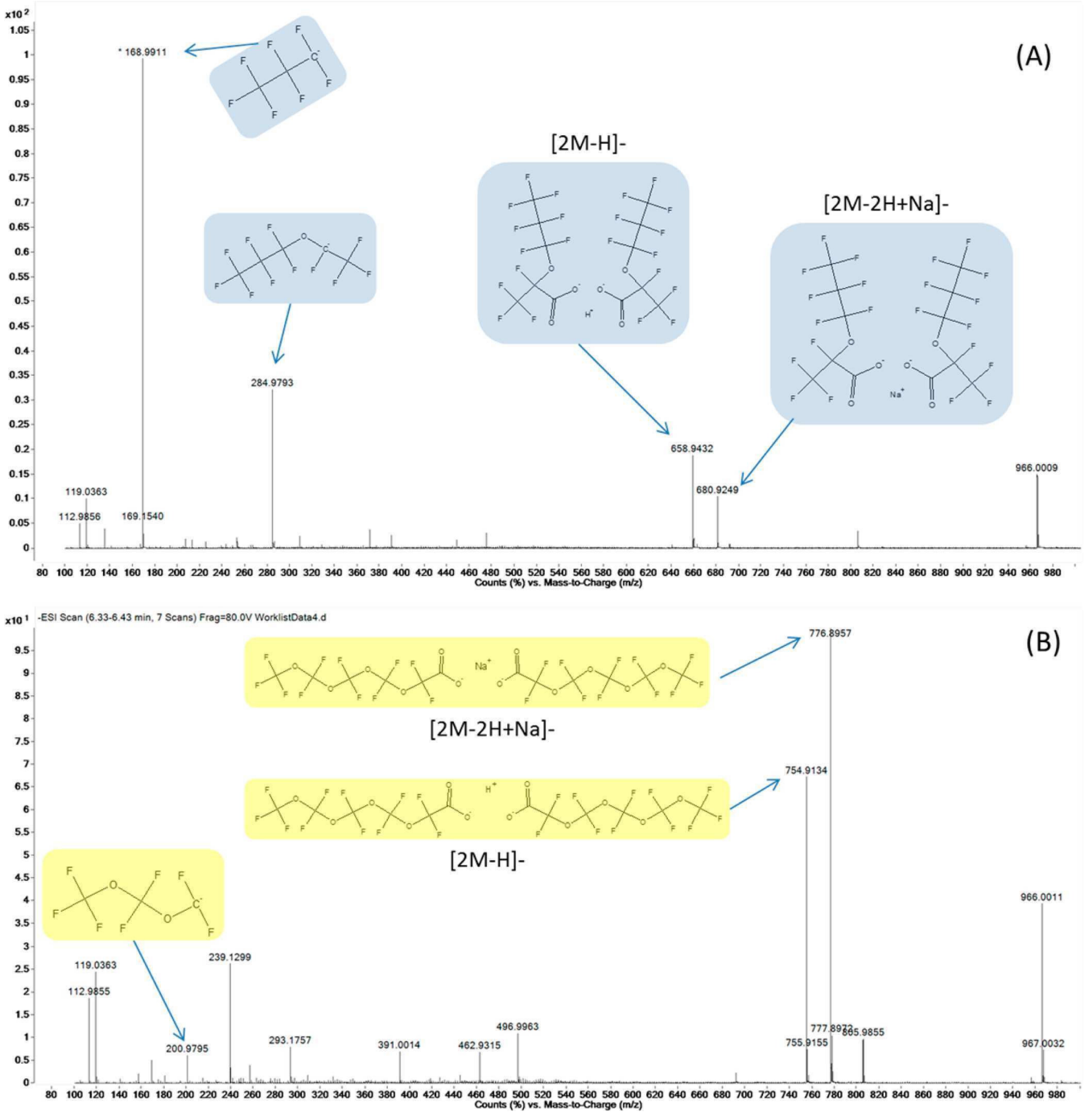

Figure 2. ESI negative spectra for two example perfluorinated ether carboxylic acids found in water: (A) $C_6HF_{11}O_3$ (retention time 5.9−6.0 min) and (B) $C_6HF_{11}O_6$ (retention time 6.5−6.6 min). Note: in spectrum (A and B) *m/z* 112.9856, 119.0363, and 966.0007 are reference masses for continuous mass calibration. Peaks not pointed out are not associated with the compound of interest.

Pairwise comparisons of sequential samples in river flow (Figure 1 step 2) were used to identify those requiring further investigation. For instance, features found in the downstream sample that were not found in the upstream sample indicate a source (point or nonpoint) exists between the two sampling locations (Figure 1 step 3). Further investigation of peaks with larger area counts using the "identify compounds" feature in the software and additional analyses of samples were used for confirmation. Perfluorinated compounds already identified with traditional UPLC-MS/MS analysis were eliminated from this remaining list further narrowing the unknown compounds requiring follow-up scrutiny.

Poly- and perfluorinated compounds tend to have a negative mass defect due to the presence of multiple fluorine and oxygen atoms. Negative mass defect means that the exact mass of a compound is less than the nominal mass.[17] For instance, the exact mass of perfluorooctanoate ($C_8F_{15}O_2$) is 412.9664, whereas the nominal mass is 413 Da. In this instance negative mass defect compounds only found in the downstream sample were further explored. An additional characteristic of samples that are contaminated with per- and polyfluorinated com-

DOI: 10.1021/acs.est.5b01215
Environ. Sci. Technol. 2015, 49, 11622−11630

Table 1. Accurate Mass of Polyfluorinated Compounds and In-Source Artifacts Found in Extracted Water Samples

number	formula	CAS no.	name	[M][a]	$[M-H]^-$ m/z	$[2M-2H+Na]^-$ m/z	$[2M-H]^-$ m/z
Monoether PFECAs							
1	$C_3HF_5O_3$			179.9846	178.9773	380.9438	358.9619
2	$C_4HF_7O_3$			229.9813	228.9740	480.9372	458.9553
3	$C_5HF_9O_3$	863090-89-5		279.9782	278.9709	580.9310	558.9491
4	$C_6HF_{11}O_3$	13252-13-6	undecafluoro-2-methyl-3-oxahexanoic acid	329.9750	328.9677	680.9247	658.9427
5	$C_7HF_{13}O_3$			379.9718	378.9645	780.9182	758.9363
6	$C_8HF_{15}O_3$			429.9686	428.9613	880.9118	858.9299
Polyether PFECAs							
7	$C_7HF_{13}O_7$	39492-91-6	perfluoro-3,5,7,9,11-pentaoxadodecanoic acid	443.9515	442.9442	908.8776	886.8957
8	$C_6HF_{11}O_6$	39492-90-5	perfluoro-3,5,7,9-butaoxadecanoic acid	377.9598	376.9525	776.8942	754.9123
9	$C_5HF_9O_5$	39492-89-2	perfluoro-3,5,7-propaoxaoctanoic acid	311.9681	310.9608	644.9108	622.9289
10	$C_4HF_7O_4$	39492-88-1	perfluoro-3,5-dioxahexanoic acid	245.9764	244.9691	512.9274	490.9455
PFESAs							
11	$C_7HF_{13}O_5S$	66796-30-3[b]		443.9337	442.9264		
12	$C_7H_2F_{14}O_5S$			463.9399	462.9326		
Other							
	Na^+			22.9892			
	H^+			1.0073			
	CF_2O			65.9917			
	CF_2			49.9968			

[a]Indicates the monoisotopic mass of the neutral species. [b]CAS number for Nafion copolymer.

pounds is the presence of multiple peaks that differ by exactly ± m/z 49.9968 and/or 65.9917, corresponding to a difference of CF_2 and CF_2O, respectively. This happens because PFAS synthesis is an industrial process that yields a distribution of products that differ primarily in chain length and/or degree of isomerization. Compounds identified as having a negative mass defect and differing from another peak by ± m/z 49.9968 and 65.9917 are highly likely to be polyfluorinated compounds. Selected samples were also analyzed by QTOF to aid with confirmation of proposed structures (generously provided by colleagues mentioned in the Acknowledgments).

TOFMS Experimental Workflow. Once an unknown compound with negative mass defect was noted, it was isolated from other mass spectral data in the following way: An extracted ion chromatogram (EIC) was generated from the total ion chromatogram (TIC) using the m/z identified. The EIC was then used to do a background subtraction of the spectral region both immediately before and after the detected peak (typically ±0.1 min) (Figure 1 step 4). The center of the detected peak was extracted for the mass spectral information, and the background spectrum was subtracted for a clean spectrum. This was necessary to eliminate, to the best of our ability, competing spectral peaks that were coeluting and not associated with the spectrum being investigated. This would include, but is not limited to, spectral signals originating from the reference compounds (constantly infused to maintain a lock on mass assignments) and their fragments. Once suspect spectral signals were isolated, a series of experiments were conducted to induce in-source fragmentation ions to aid with compound identification based on the work of Ferrer and Thurman.[18] Specifically, a series of methods with differing fragmentor voltages (80−190 V) were run in sequence to look for diagnostic ions that emerged as fragmentor voltage increased. In addition, common adducts such as Na^+, NH_4^+, acetate, etc. were used to aid with compound identification. Detected spectral features were subjected to molecular formula generation using the elements (C, H, O, N, S, P, Cl and F).[19] Formulas generated were scored based on accurate mass, isotope abundance (compound mass distributions attributable to elemental mass distributions e.g., 1.1% ^{13}C, 0.2% ^{18}O, etc.) and isotope distribution (for example, slight differences in isotope mass such as when an m+2 peak is from two ^{13}C or a single ^{18}O) . Only scores >75% were considered for further exploration. Figure 1 steps 4 and 5 outline the advanced TOFMS techniques used to discover novel chemical species.

RESULTS

With the approach described above, sites were identified for further investigation when a large increase in number and magnitude (area counts) of unknown compounds was found in downstream samples. In addition, a very large increase (greater than 2 orders of magnitude) in concentration of historically measured PFAAs also persisted for many river miles downstream of a certain point (Figure S2) consistent with observations in Nakayama et al.[10] Interestingly, the profile of the historically measured PFASs contributing to the total PFASs found at each location was seen to dramatically change near this location (Figure S3). The major compounds contributing to this increase were perfluoropentanoic acid (PFPeA), followed by perfluoroheptanoic acid (PFHpA) and perfluorobutanoic acid (PFBA). It was evident that there was a significant source (total historically measured PFASs concentration increased by >100 times) of per- and polyfluorinated compounds near this location. Plotting the samples (CFR004 upstream vs CFR002 downstream) in MassProfiler for visualization indicated that there were 77 features that were unique to the downstream sample (Figure S4) with many (n = 69) having negative mass defects. In this figure (S4) the size of the symbol is proportional to the area counts of the molecular feature. Traditional PFASs with known concentrations (in Figure S2) are included for comparison purposes. Peaks with larger areas were investigated first under the assumption that these concentrations would be among the highest. Additional

DOI: 10.1021/acs.est.5b01215
Environ. Sci. Technol. 2015, 49, 11622−11630

pairwise comparisons were done on all sequential samples, however results indicated that samples downstream of CFR003 were simply dilutions of a source input. Samples were chosen for additional scrutiny where there was sufficient analytical signal without saturation of the detector which compromises mass accuracy.

Dimers and Fragments. It became evident that in multiple instances several of the larger peaks had a number of common characteristics: (1) negative mass defect, (2) multiple related chromatographic peaks differing by ± m/z 49.9968 and/or 65.9917 (± a CF_2 group and/or a CF_2O group), and (3) apparent noncovalent homodimers linked by either a proton or sodium ion. For example, at a retention time of 5.9−6.0 min, two large peaks emerged from the spectra with m/z of 658.9462 and 680.9256 (Figure 2A). After careful evaluation, it became apparent that these were the proton-bound and sodium-bound in-source homodimers of undecafluoro-2-methyl-3-oxahexanoic acid ($C_6HF_{11}O_3$) (Table 1). These differed by m/z 21.9819, the difference between the Na^+ and H^+ versions of the dimer. It is important to note that the $[M - H]^-$ peak (m/z 328.9677), which one might expect to be the most prominent, was barely distinguishable from the background signal at this point because the in-source ionization conditions so heavily favored the formation of these dimers. Given the prominence of the $C_6HF_{11}O_3$ compound in this sample, we postulated that a homologous series of related perfluorinated ether carboxylic acids (PFECAs), differing from the first compound by either the addition or deletion of CF_2 units (m/z 49.9968) might also be present. An EIC for each of the hypothetical masses, based on sequential addition or deletion of CF_2 units (m/z 49.9968) was extracted from the TIC, with the resulting series of related PFECAs presented in Figure S5. Although not specifically shown in this Figure, we also observed the presence of the analogous sodium and proton bound dimers for each compound identified in this homologous series of PFECAs ($C_{(n=3-8)}HF_{(n=5-15)}O_3$ (Table 1). To obtain additional evidence supporting the proposed structure of the compounds eluting at 5.9 min, additional experiments were conducted by altering the fragmentor voltage in order to try to form diagnostic ions from the m/z of 658.9427 and 680.9247 dimers eluting at this time. Figure S6 shows diagnostic dimer and fragment ions resulting from in-source CID that are consistent with the structure proposed for the $C_6HF_{11}O_3$ compound. The major ions found are also shown in Figure S10. Extracted spectra comparable to those shown in Figure S6, differing only by the loss of CF_2 groups, were investigated as well (Figure S7) lending credence to the postulated structure(s) and discussed in more detail in the following section.

Confirmation of Structure. An online search of the formula and proposed structure of the $C_6HF_{11}O_3$ compound eluting at 5.9 min led to a tentative match in a "grey-literature" citation that mentions a new-generation processing aid for the production of high-performance fluoropolymers identified only as C3 dimer acid/salt (CAS 13252-13-6) (Figure S6).[6] With a CAS number, it was possible to purchase an authentic standard (Synquest Laboratories, Alachua, FL) to compare for retention times and mass spectral ionization patterns. The authentic standard compared very well with the tentatively identified compound found in water samples (±0.051 min RT; ± m/z 0.0002 (0.51 ppm) (Figure 1 step 6). Additional authentic standards for other compounds in this homologous series were not commercially available. However, common spectral patterns and adducts were observed differing only by repeating CF_2 units, as supporting information for compound identification of a homologous series of PFECAs (Figure S7).

Additional Perfluorinated Ether Acids. Figure S4 shows that there are a number of features that are present in the water sample downstream of a potential input location that are not in the upstream sample. Evident in Figure S4 are a pronounced series of peaks that appear as vertical lines, likely from coeluting and related chemicals (see later discussion on in-source n-mer formation). A number of these peaks exhibited negative mass defects. Further investigation of the TOFMS spectra indicated two peaks coeluting at 6.5 min (m/z 776.8942 and 754.9123) with a mass difference of m/z 21.9819, again suggesting the presence of in-source proton- and sodium-bound homodimers (Figure 2B). Knowing this information, we postulated an exact mass of m/z 376.9525 for the $[M - H]^-$ ion (Table 1). We further postulated a homologous series based on addition and deletion of CF_2 units, but exact masses corresponding to ± m/z 49.9968 were not detected. Given reports of industrial producers making greater use of ether oxygens to limit the size of perfluorinated regions within a given molecule, we postulated that a homologous series could also be based on the repeating units of CF_2O, with an exact mass offset of ± (m/z 65.9917).[17,20] Searching the sample for m/z 376.9525 ± this hypothetical CF_2O offset did yield another homologous series (Figure S8). In addition, as was previously the case, each of these new compounds was also found to form sodium-bound and proton-bound homodimers, providing further support for the proposed structures (Table 1). Confirmation of these compounds with authentic standards was not possible. It should be noted that in the homologous series shown, the chemical $C_3HF_5O_3$ (m/z 178.9773) is a common feature (Table 1) to the previously identified homologous series. Taken together, the exact mass of the proposed structures, the offset by a CF_2O, and the exact mass of the in-source dimers formed, all support the occurrence of this additional homologous series. One compound in this homologous series ($C_4HF_7O_4$ [M − H] 244.9691 Table 1) was subjected to QTOF analysis leading to a series of accurate mass fragments consistent with the proposed structure (Figure S9). The accurate mass fragments show the sequential breakage of the ether oxygen bonds and the resulting fragment ions.

In-Source *n*-mer Formation. Multiple peaks originally thought to be of polymeric origin (m/z 1176.8353 and 1576.7769) were determined to be sodium-bound n-mers of m/z 376.9525 already identified (Figure S12). The retention time of these peaks (6.5 min) indicates this is an in-source phenomenon, as they coelute (Figure S4). In-source artifacts occur in the ESI source and can include such things as the formation of adducts (formate, Na^+, H^+, NH_4^+), fragments, dimers, trimers, and combinations of the above. Peaks that do not coelute, or are chromatographically separated, are generally considered not to be in-source artifacts. The observed spectra (Figure S12) include the formation of n-mers[17] including 2 and 3 bound sodium cations in addition to the compounds shown in Figure S11. The formation of other n-mers with >1 bound sodium was seen as well for additional PFECAs found in this work (data not shown). Recent work by Trier et al.[17] indicates that the formation of these polyfluorinated surfactant clusters occurs in the MS source in the gas phase and are pH and concentration dependent.[17] However, this phenomenon may also be instrument-specific as sample dilution in this study did not lead to loss of these in-source dimers being formed. Similar

DOI: 10.1021/acs.est.5b01215
Environ. Sci. Technol. 2015, 49, 11622−11630

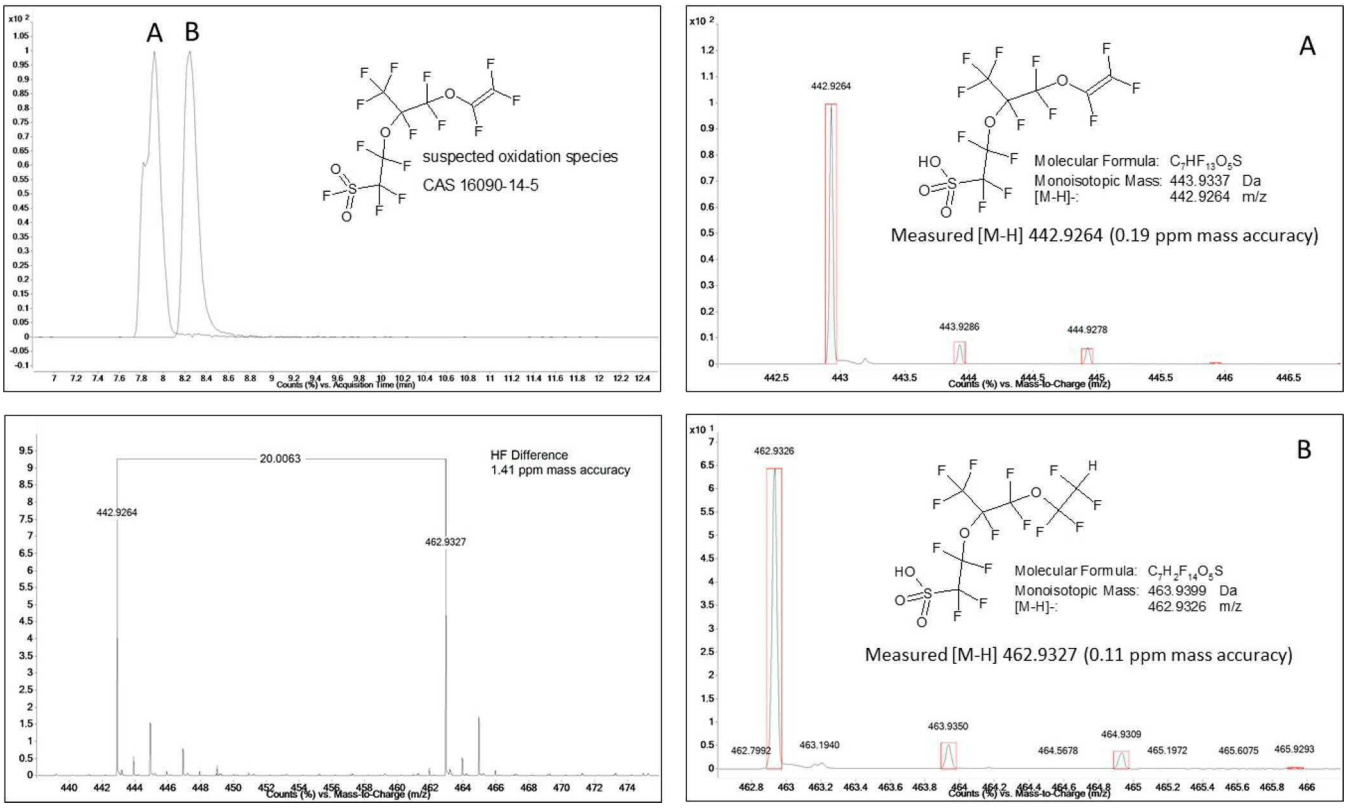

Figure 3. Suspected perfluoro ether sulfonic acids identified in water. Oxidation species are likely products of CAS 16090-14-5, a perfluorinated ether sulfonyl fluoride. Chromatogram shown of two resolved peaks (A,B) and isotope cluster matching of measured versus exact mass. Red boxes indicate the exact mass for the suspected formulas, compared to the accurate mass profile spectrum. Mass difference between two species is an HF (m/z 20.0063−1.41 ppm mass accuracy).

sodium- and proton-bound, as well as mobile phase, modifier (i.e., formate) adducts have been shown by Trier et al.[17] for perfluorocarboxylic acids and mono-PAPs (perfluorinated alkyl phosphates).

Perfluoroalkyl Ether Sulfonic Acid (PFESA) Identification. Records of groundwater monitoring at a fluorochemical manufacturing plant with wells in close proximity to our sampling site indicate PFOA in μg/L concentrations.[21] This document also indicated a sulfonated tetrafluoroethylene based fluoropolymer-copolymer with the trade name Nafion was also produced at this facility. Our data provide evidence that materials related to this compound are also emitted into the river at this point. Figure 3 shows the chemical structures of the suspected oxidation species and resulting transformation products tentatively identified in our samples. An EIC of m/z 442.9264, which is the exact mass of the $[M - H]^-$ moiety of the copolymer containing the sulfonate group (IUPAC name 1,1,2,2-tetrafluoro-2-({1,1,1,2,3,3-hexafluoro-3-[(trifluorovinyl)-oxy]-2-propanyl}oxy)ethanesulfonic acid), suggests this compound is present in the water. In addition, spectral evidence supports the detection of a related compound which is consistent with the addition of an HF ($[M - H]^-$ m/z 462.9327) (IUPAC name 1,1,2,2-tetrafluoro-2-{[1,1,1,2,3,3-hexafluoro-3-(1,1,2,2-tetrafluoroethoxy) propan-2-yl]oxy}-ethanesulfonic acid). The two suspected compounds differ by the mass of HF (m/z 20.0062−1.41 ppm mass accuracy) (Figure 3). These compounds elute as two discrete chromatographic peaks, likely explained by the position occupied by the H and F additions. It is possible that these chemicals originate from the oxidation of ethanesulfonyl fluoride, 2-[1-[difluoro-[(t(fluoroethenyl)oxy]methyl]-1,2,2,2-tetrafluoroethoxy]-1,1,2,2-tetrafluoro- (CAS 16090-14-5) which may have been in use at this industrial location.[22] These compounds would thus be classified as perfluoroalkyl ether sulfonic acids (PFESA).[4] However, unlike previous perfluorinated ether carboxylic acid compounds found in this study, in-source proton- and sodium-bound dimers were not found for these perfluorinated ether sulfonates. In addition, a homologous series based on CF_2 or CF_2O additions was not found. We have not been able to obtain an authentic standard for confirmation of this proposed structure.

DISCUSSION

It has been well-known for a number of years that, due to the toxicity and persistence of perfluorinated compounds, industrial producers are moving toward shorter chain per- and polyfluorinated compound homologues. However, it is not well-known which compounds are being produced as replacements for historic perfluorinated compounds (e.g., PFOS and PFOA). Peer-reviewed literature showing the chemical structure of manufactured per- and polyfluorinated replacement compounds is sparse. An example of one such publication from 3M Corporation indicated that the compound ADONA (4,8-dioxa-3H-perfluorononanoate) is being made to replace ammonium perfluorooctanoate (APFO) as an emulsifier in the manufacture of fluoropolymers.[5] The data presented in this study and Figure S1 indicate that the manufacture and release of per- and polyfluorinated compounds with CF_2 units interspersed with ether oxygen linkages likely is ongoing. A more recent study suggests that polyfluoroalkyl ether

DOI: 10.1021/acs.est.5b01215
Environ. Sci. Technol. 2015, 49, 11622−11630

compounds are being produced and that the number and spacing of ether oxygen linkages and size of the resulting per- and polyfluorinated compound may be manufacturer-specific including other major fluorochemical producers (DuPont, 3M, Solvay, and Asahi).[20] However, there are little to no data in the peer-reviewed literature on most of these compounds. The use of HRMS appears to be an ideal technique to use for discovery and occurrence of new PFASs being released into the environment.

As illustrated in this research, identification of previously undescribed compounds in environmental matrices can be made difficult by the formation of a multitude of in-source artifacts such as in-source gas phase adducts, *n*-mers, and the presence of a homologous series of per- and polyfluorinated compounds. D'Agostino and Mabury identified novel fluorinated surfactants in aqueous film-forming foams (AFFF) and commercial surfactant concentrates using high-resolution mass spectrometry.[23] Their results imply that there are a number of additional fluorinated compounds being produced and emitted into the environment that are unknown to most analysts. The use of TOFMS or other high-resolution mass spectrometers and the workflow we demonstrated (Figure 1) appears to be a useful way to determine occurrence and emissions of new and emerging fluorinated compounds for environmental occurrence efforts.

Schymanski et al. report on identifying small molecules via HRMS, with five levels of confidence.[14] As has been noted earlier, one of the pitfalls of discovery work is the lack of authentic standards at times. As such the highest level of confidence for confirmed structure (Level 1) can be made to one compound in this effort, with the remaining compounds falling in the categories of tentative candidate(s) (Level 3) or probable structure (Level 2).[14] An additional line of evidence we present that Schymanski et al. appear not to is the presence of a homologous series (CF_2, CF_2O) as evidence for compound identification.

The manufacture of shorter-chain perfluorinated and polyfluorinated compounds may have an advantageous effect on biological persistence and bioaccumulation. Two recent publications deemed "The Helsingor Statement"[24] and the "Madrid Statement"[25] explore the state of the science related to poly- and perfluorinated alkyl substances. Shorter straight-chain homologues of perfluorocarboxylic acids (<C_6) and sulfonic acids (<PFBS) have been shown to be cleared quickly from mammalian species tested and thus are not expected to bioaccumulate as readily as PFOS and PFOA.[26] However, the environmental persistence of these shorter chain perfluorinated compounds is likely to be no different from that of the related longer-chain acids. The conventional wisdom is the perfluorinated ether compounds will be more labile than the *n*-alkyl perfluorinated homologues with ether oxygen linkages being more susceptible to chemical or microbial attack. However, as the CF_2 bond in perfluorinated compounds is not at all open to microbial attack due to its bond strength, even the slightest degree of degradation of a per- or and polyfluorinated ether compound would be considered "more" labile. Environmental degradation or toxicology studies associated with the compounds identified in this study were not found by the authors in the peer-reviewed literature at the time of writing this Article. Although data are scarce, the few perfluoropolyethers (PFPEs) to have undergone any kind of degradation studies show little to no biodegradation or hydrolysis.[20] These data mainly come from the European Chemical Agency (ECHA) database of registered substances and associated information.[27] Past studies have demonstrated poor removal efficiency for historical PFASs from source water to drinking water in conventional systems (i.e., treatments that do not include granular activated charcoal (GAC)). It is unknown if these PFECAs and PFESAs are removed by conventional WWTP processes.

Environmental Implications. We demonstrate the presence of a series of novel perfluorinated ether carboxylic and sulfonic acid(s) found to be in natural waters using a nontargeted workflow (Figure 1). The compounds consist of a homologous series of per- and polyfluorinated compounds with repeating units of CF_2 or CF_2O subunits. LC-TOFMS investigations of accurate mass dimers and *n*-mers (proton- or sodium-bound) in addition to diagnostic fragment ions support these findings. Further unidentified compounds with negative mass defects are likely also of per- and polyfluorinated origin, but have not yet been identified and are undergoing further analytical scrutiny. Nontargeted screening and discovery of novel species in samples such as reported here is an ongoing process. Additional environmental samples from other locations may be needed to identify additional chemistries.

Once a xenobiotic compound is identified in the environment, it falls upon the scientific community to begin monitoring efforts to find the extent of contamination of newly discovered species. In addition, toxicological and degradation investigations of identified compounds can commence once a compound has been identified. The procurement of authentic compounds for use in these types of investigations may be a major limiting factor in conducting such investigations, as most of these compounds appear not to be commercially available. More research will need to be conducted on these perfluorinated ether carboxylic and sulfonic acids concerning environmental occurrence, toxicology, and degradation potential.

■ ASSOCIATED CONTENT

Supporting Information

The Supporting Information is available free of charge on the ACS Publications website at DOI: 10.1021/acs.est.5b01215.

Additional information including tables, figures, chemicals structures, and spectra (PDF)

■ AUTHOR INFORMATION

Corresponding Author

*Phone: 919-541-3706; e-mail: strynar.mark@epa.gov.

Notes

The authors declare no competing financial interest.

■ ACKNOWLEDGMENTS

We thank Agilent Technologies for their support of this effort through a TOFMS and travel/training CRADA with the U.S. EPA (CRADA 437-A-12) and in particular Joe Weitzel for his support of this work. In addition, we thank Mike Hays (USEPA), and Chris Higgins and Simon Roberts (Colorado School of Mines) for the use of their QTOFs in confirmation of select compounds identified. We also thank John Offenberg, Michelle Angrish, and Mike Hays for their review of this manuscript. The United States Environmental Protection Agency through its Office of Research and Development funded and managed the research described here. It has been subjected to Agency review and approved for publication.

DOI: 10.1021/acs.est.5b01215
Environ. Sci. Technol. 2015, 49, 11622−11630

Mention of trade names or commercial products does not constitute endorsement or recommendation for use.

REFERENCES

(1) Lindstrom, A. B.; Strynar, M. J.; Libelo, E. L. Polyfluorinated Compounds: Past, Present, and Future. *Environ. Sci. Technol.* **2011**, *45* (19), 7954−7961.

(2) Houde, M.; De Silva, A. O.; Muir, D. C. G.; Letcher, R. J. Monitoring of Perfluorinated Compounds in Aquatic Biota: An Updated Review. *Environ. Sci. Technol.* **2011**, *45* (19), 7962−7973.

(3) U.S. EPA. *2010/15 PFOA Stewardship Program*. http://www.epa.gov/oppt/pfoa/pubs/stewardship/index.html.

(4) Buck, R. C.; Franklin, J.; Berger, U.; Conder, J. M.; Cousins, I. T.; de Voogt, P.; Jensen, A. A.; Kannan, K.; Mabury, S. A.; van Leeuwen, S. P. Perfluoroalkyl and polyfluoroalkyl substances in the environment: terminology, classification, and origins. *Integr. Environ. Assess. Manage.* **2011**, *7* (4), 513−41.

(5) Gordon, S. C. Toxicological evaluation of ammonium 4,8-dioxa-3H-perfluorononanoate, a new emulsifier to replace ammonium perfluorooctanoate in fluoropolymer manufacturing. *Regul. Toxicol. Pharmacol.* **2011**, *59* (1), 64−80.

(6) West Virginia Department of Environmental Protection. *Executed Draft Consent Order No. 7418*. http://www.dep.wv.gov/pio/Documents/DuPont%20Final%20Version.pdf.

(7) Steenland, K.; Fletcher, T.; Savitz, D. A. Epidemiologic Evidence on the Health Effects of Perfluorooctanoic Acid (PFOA). *Environ. Health Perspect.* **2010**, *118* (8), 1100−1108.

(8) MacNeil, J.; Steenland, N. K.; Shankar, A.; Ducatman, A. A cross-sectional analysis of type II diabetes in a community with exposure to perfluorooctanoic acid (PFOA). *Environ. Res.* **2009**, *109* (8), 997−1003.

(9) Steenland, K.; Tinker, S.; Frisbee, S.; Ducatman, A.; Vaccarino, V. Association of Perfluorooctanoic Acid and Perfluorooctane Sulfonate With Serum Lipids Among Adults Living Near a Chemical Plant. *Am. J. Epidemiol.* **2009**, *170* (10), 1268−1278.

(10) Nakayama, S.; Strynar, M.; Helfant, L.; Egeghy, P.; Ye, X.; Lindstrom, A. B. Perfluorinated Compounds in the Cape Fear Drainage Basin in North Carolina. *Environ. Sci. Technol.* **2007**, *41*, 5271−5276.

(11) Hollender, J.; Bourgin, M.; Fenner, K. B.; Longrée, P.; Mcardell, C. S.; Moschet, C.; Ruff, M.; Schymanski, E. L.; Singer, H. P. Exploring the Behaviour of Emerging Contaminants in the Water Cycle using the Capabilities of High Resolution Mass Spectrometry. *Chimia* **2014**, *68* (11), 793−798.

(12) Schymanski, E. L.; Singer, H. P.; Longrée, P.; Loos, M.; Ruff, M.; Stravs, M. A.; Ripollés Vidal, C.; Hollender, J. Strategies to Characterize Polar Organic Contamination in Wastewater: Exploring the Capability of High Resolution Mass Spectrometry. *Environ. Sci. Technol.* **2014**, *48* (3), 1811−1818.

(13) Schymanski, E. L.; Singer, H. P.; Slobodnik, J.; Ipolyi, I. M.; Oswald, P.; Krauss, M.; Schulze, T.; Haglund, P.; Letzel, T.; Grosse, S.; Thomaidis, N. S.; Bletsou, A.; Zwiener, C.; Ibanez, M.; Portoles, T.; de Boer, R.; Reid, M. J.; Onghena, M.; Kunkel, U.; Schulz, W.; Guillon, A.; Noyon, N.; Leroy, G.; Bados, P.; Bogialli, S.; Stipanicev, D.; Rostkowski, P.; Hollender, J. Non-target screening with high-resolution mass spectrometry: critical review using a collaborative trial on water analysis. *Anal. Bioanal. Chem.* **2015**, *407*, 6237.

(14) Schymanski, E. L.; Jeon, J.; Gulde, R.; Fenner, K.; Ruff, M.; Singer, H. P.; Hollender, J. Identifying Small Molecules via High Resolution Mass Spectrometry: Communicating Confidence. *Environ. Sci. Technol.* **2014**, *48* (4), 2097−2098.

(15) Nakayama, S.; Strynar, M. J.; Helfant, L.; Egeghy, P.; Ye, X.; Lindstrom, A. B. Perfluorinated compounds in the Cape Fear Drainage Basin in North Carolina. *Environ. Sci. Technol.* **2007**, *41* (15), 5271−6.

(16) Nakayama, S. F.; Strynar, M. J.; Reiner, J. L.; Delinsky, A. D.; Lindstrom, A. B. Determination of Perfluorinated Compounds in the Upper Mississippi River Basin. *Environ. Sci. Technol.* **2010**, *44* (11), 4103−4109.

(17) Trier, X.; Granby, K.; Christensen, J. H. Tools to discover anionic and nonionic polyfluorinated alkyl surfactants by liquid chromatography electrospray ionisation mass spectrometry. *J. Chromatogr. A* **2011**, *1218* (40), 7094−104.

(18) Ferrer, I.; Thurman, E. M. *Liquid Chromatography Time-of-Flight Mass Spectrometry*; Wiley: Hoboken, NJ, 2009.

(19) Kind, T.; Fiehn, O. Seven Golden Rules for heuristic filtering of molecular formulas obtained by accurate mass spectrometry. *BMC Bioinf.* **2007**, *8* (1), 105.

(20) Wang, Z.; Cousins, I. T.; Scheringer, M.; Hungerbühler, K. Fluorinated alternatives to long-chain perfluoroalkyl carboxylic acids (PFCAs), perfluoroalkane sulfonic acids (PFSAs) and their potential precursors. *Environ. Int.* **2013**, *60* (0), 242−248.

(21) NCDENR. *Onsite PFOA Groundwater Monitoring Report 12-9-13*; p 6. https://edm.nc.gov/DENR-Portal/; full text search HW_F_NCD047368642_12-09-2013_GW_GMR.

(22) USEPA. Envirofacts. http://iaspub.epa.gov/enviro/tsca.get_chem_info?v_registry_id=110000559609. 2015.

(23) D'Agostino, L. A.; Mabury, S. A. Identification of novel fluorinated surfactants in aqueous film forming foams and commercial surfactant concentrates. *Environ. Sci. Technol.* **2014**, *48* (1), 121−9.

(24) Scheringer, M.; Trier, X.; Cousins, I. T.; de Voogt, P.; Fletcher, T.; Wang, Z.; Webster, T. F. Helsingør Statement on poly- and perfluorinated alkyl substances (PFASs). *Chemosphere* **2014**, *114* (0), 337−339.

(25) Blum, A.; Balan, S.A.; Scheringer, M.; Goldenman, G.; Trier, X.; Cousins, I.; Diamond, M.; Fletcher, T.; Higgins, C.; Lindeman, A. A.; Peaslee, G.; de Voogt, P.; Wang, Z.; Weber, R. Madrid Statement. *Environ. Health Perspect.* **2015**, *123*, A107.

(26) Lau, C.; Anitole, K.; Hodes, C.; Lai, D.; Pfahles-Hutchens, A.; Seed, J. Perfluoroalkyl acids: a review of monitoring and toxicological findings. *Toxicol. Sci.* **2007**, *99* (2), 366−94.

(27) European Chemical Agency (ECHA). Registered Substances. http://echa.europa.eu/information-on-chemicals/registered-substances. 2015.

DOI: 10.1021/acs.est.5b01215
Environ. Sci. Technol. 2015, 49, 11622−11630

Supporting Information for:

Identification of novel perfluoroalkyl ether carboxylic acids (PFECAs) and sulfonic acids (PFESAs) in natural waters using accurate mass time-of-flight mass spectrometry (TOFMS)

Mark Strynar[1], Sonia Dagnino[2], Rebecca McMahen[2], Shuang Liang[2], Andrew Lindstrom[1], Erik Andersen[1], Larry McMillan[3], Michael Thurman[4], Imma Ferrer[4], Carol Ball[5]

1. National Exposure Research Laboratory, U.S. Environmental Protection Agency, Research Triangle Park, NC;

2. ORISE fellow at the United States Environmental Protection Agency, National Exposure Research Laboratory, Research Triangle Park, North Carolina;

3. National Caucus and Center on Black Aged, Inc, Durham, NC;

4. Center for Environmental Mass Spectrometry, University of Colorado in Boulder CO;

5. Agilent Technologies Inc., Wilmington, DE

This document includes one table, and 12 SI figures, on 13 pages.

Table S1. Water samples description and GPS coordinates.

Sample ID	Description	Latitude	Longitude
CFR 001	Cape Fear river Tar Heel, NC	34.74525	-78.78574
CFR 002	Cape Fear river below Huske lock and dam #3	34.83026	-78.82246
CFR 003	unnamed tributary	34.83179	-78.82375
CFR 004	Cape Fear river above Huske lock and dam #3	34.83544	-78.82347
CFR 005	Cape Fear river below Rockfish creek	34.96820	-78.81579
CFR 006	Rockfish Creek	34.95610	-78.84424
CFR 007	Rockfish Creek WWTP effluent	34.96834	-78.82765
CFR 008	Cape Fear River at Fayetteville boat ramp access	34.99669	-78.85076
CFR 009	Regional drinking water sample	34.94199	-78.92422

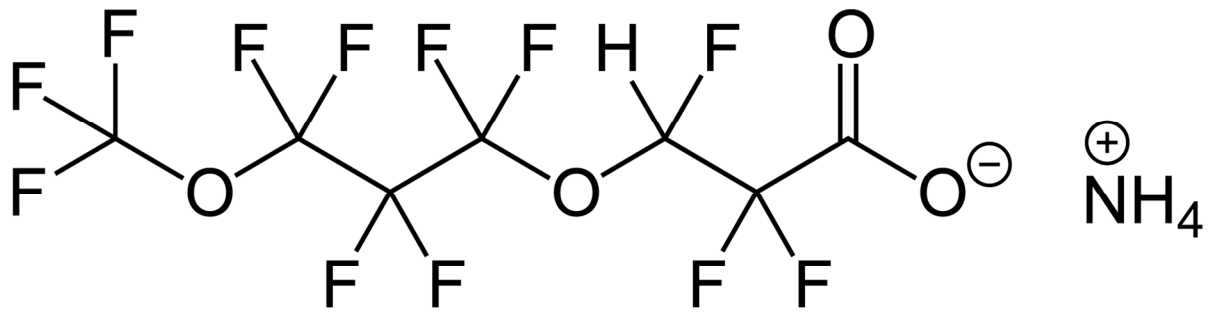

Figure S1. The structure of ADONA (4,8-dioxa-3H-perfluorononanoate) a polyfluorinated compounds used to replace classic perfluorinated compounds such as APFO.

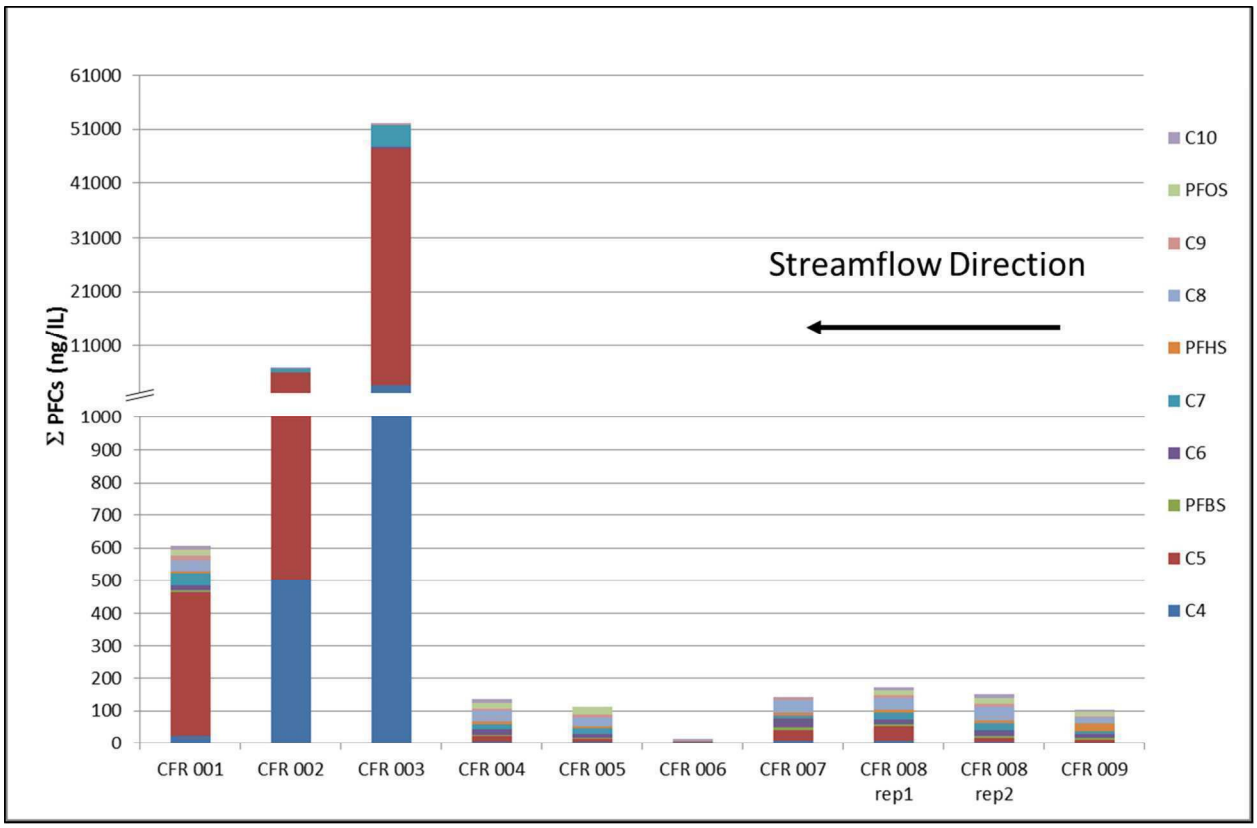

Figure S2. PFAAs found in water samples from the Cape Fear River. Note the y-axis is a split scale.

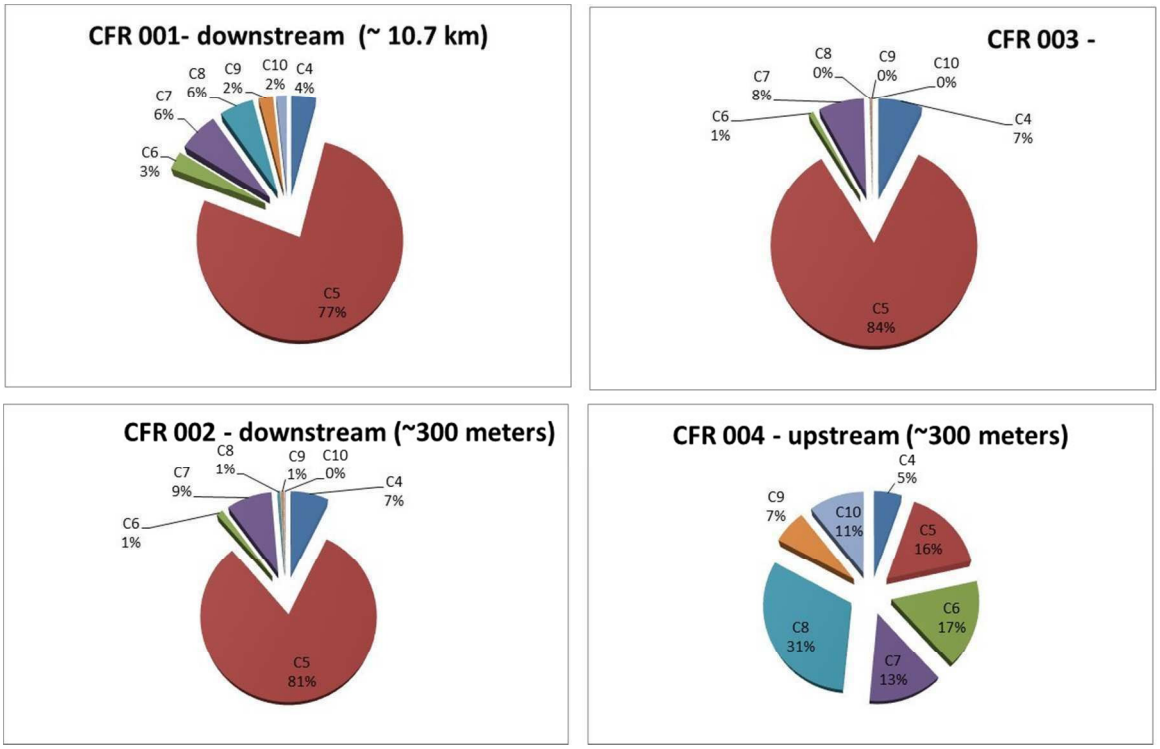

Figure S3. Proportion of PFAAs contribution to the total for select water samples from the Cape Fear River.

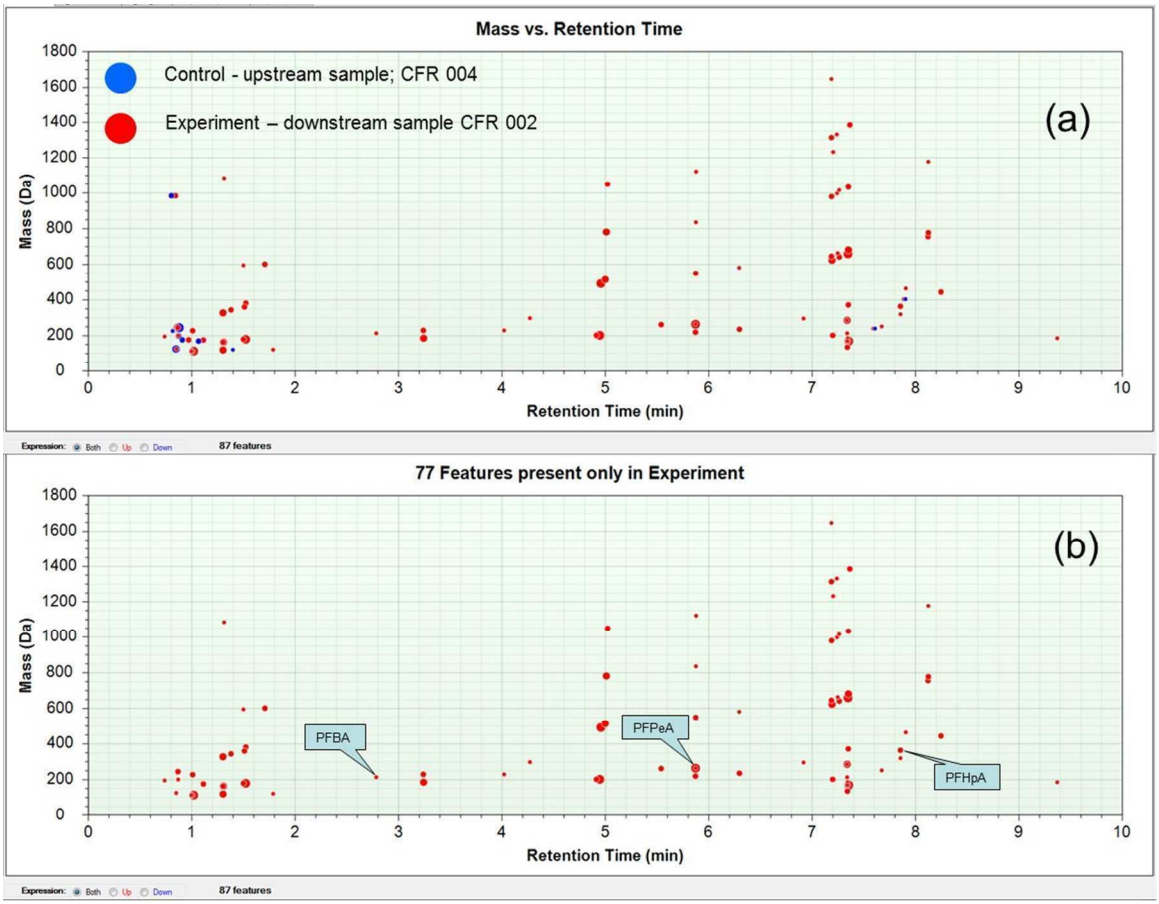

Figure S4. Mass Profiler visualization of molecular features found in (a) control and experimental sample and (b) 77 features unique only to experimental sample, with select peaks previously identified (PFBA, PFPeA and PFHpA). Note: The size of the symbol in this plot is proportional to the area of the peak. Pronounced co-eluting peaks that appear as vertical lines are likely related (i.e. fragments, M-H-, *n-mers*).

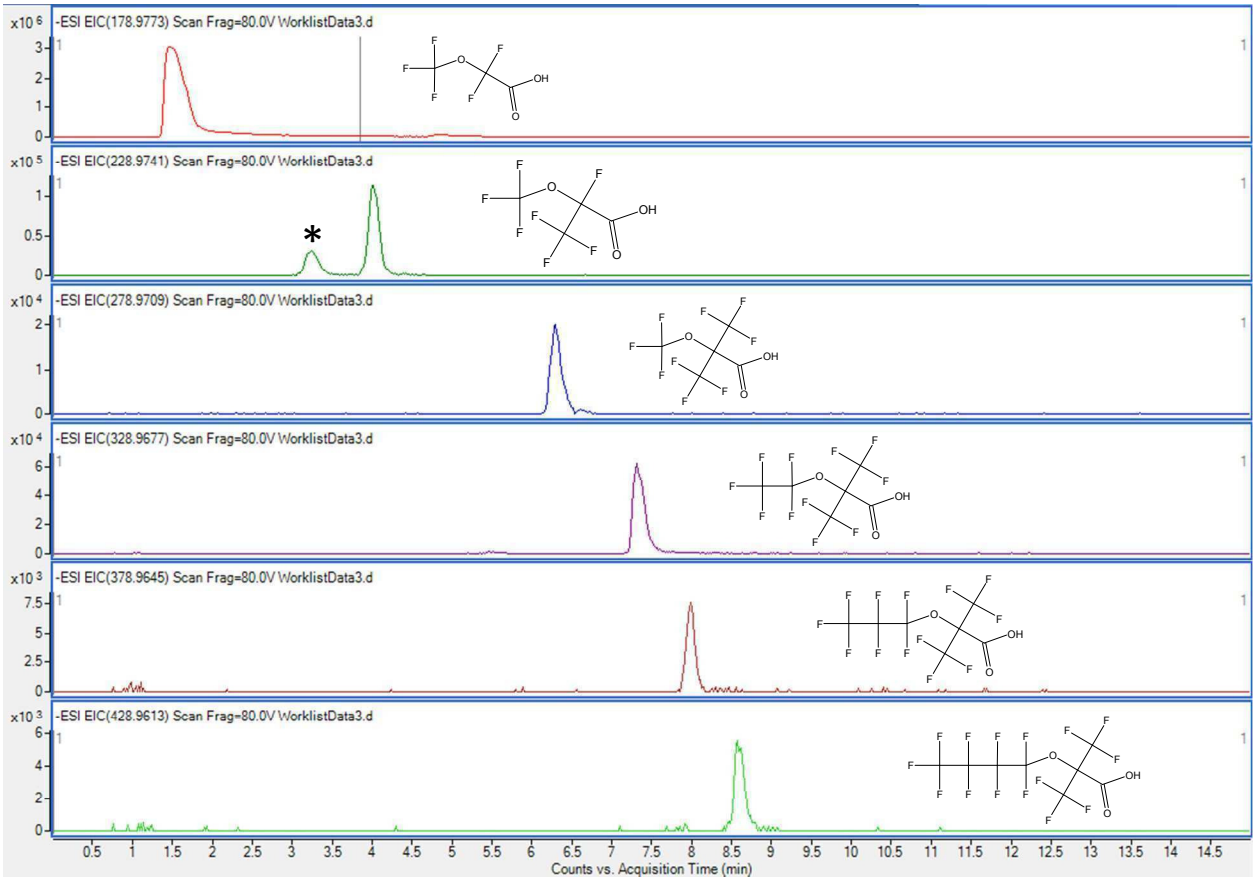

Figure S5. Extracted Ion Chromatogram (EIC) of a suspected homologous series of perfluorinated ether carboxylic acids. Note: The chromatographic peak indicated by an * is the substance associated with this homologous series based on the H^+ and Na^+ dimer co-elution at this retention time. The second later eluting peak in this chromatogram is a similar m/z, possibly an isomer.

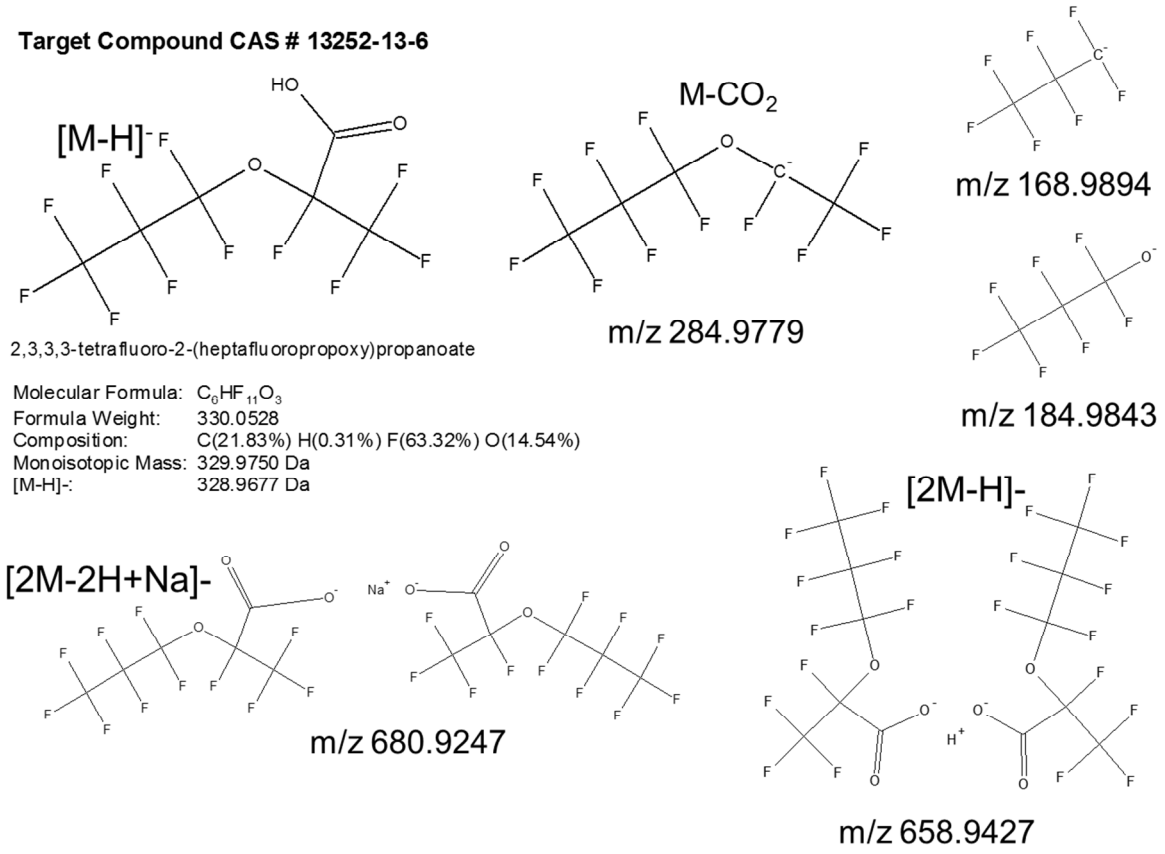

87

88

89 Figure S6. Identified perfluorinated ether carboxylic acid and diagnostic fragment and dimer

90 ions.

91

92

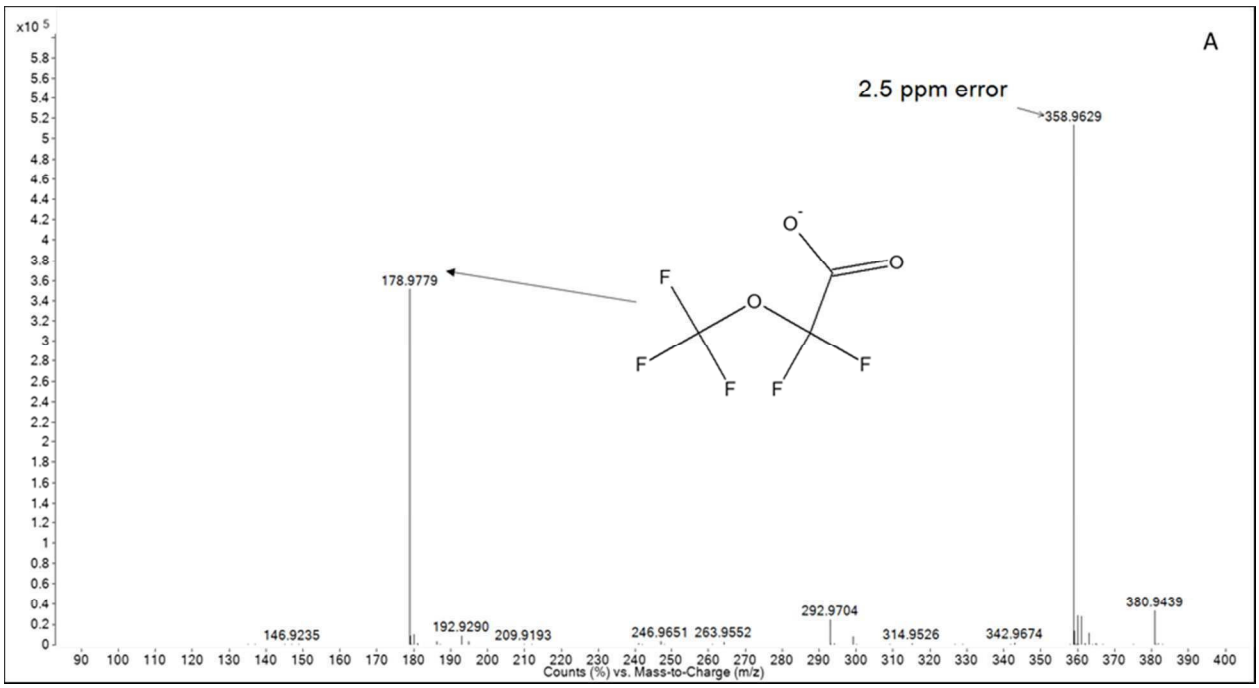
A
2.5 ppm error
358.9629
178.9779
146.9235
192.9290
209.9193
246.9651
263.9552
292.9704
314.9526
342.9674
380.9439
Counts (%) vs. Mass-to-Charge (m/z)

93

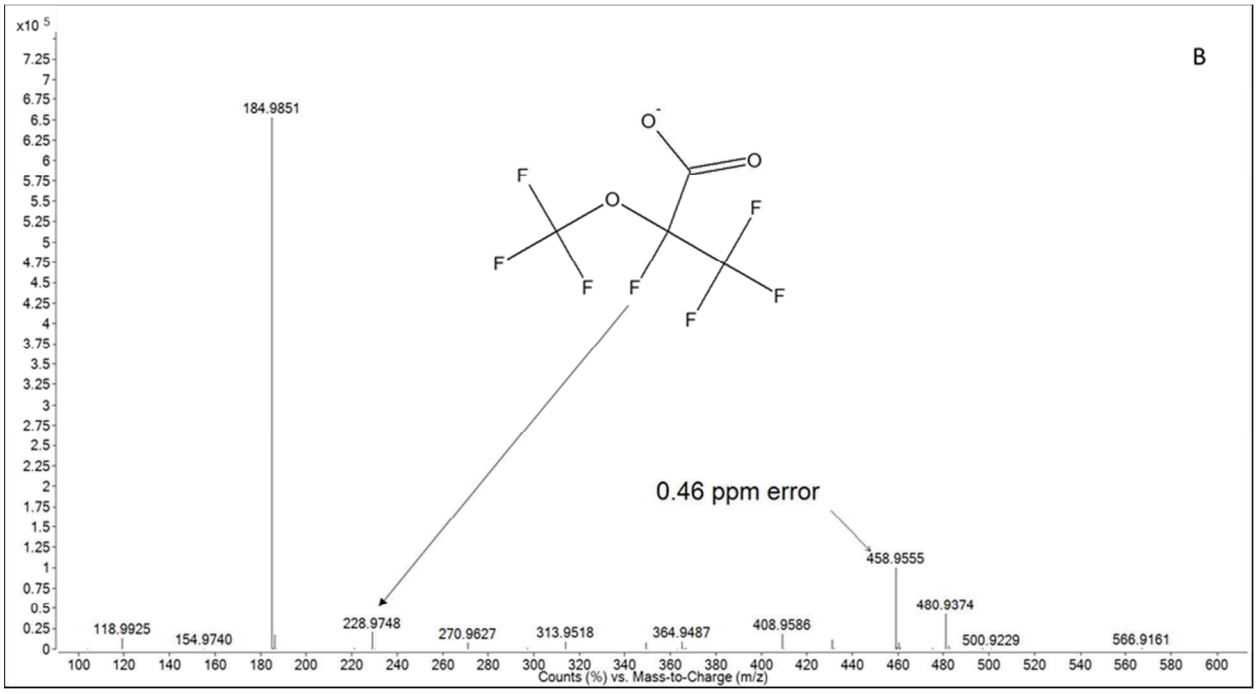
B
184.9851
0.46 ppm error
458.9555
118.9925
154.9740
228.9748
270.9627
313.9518
364.9487
408.9586
480.9374
500.9229
566.9161
Counts (%) vs. Mass-to-Charge (m/z)

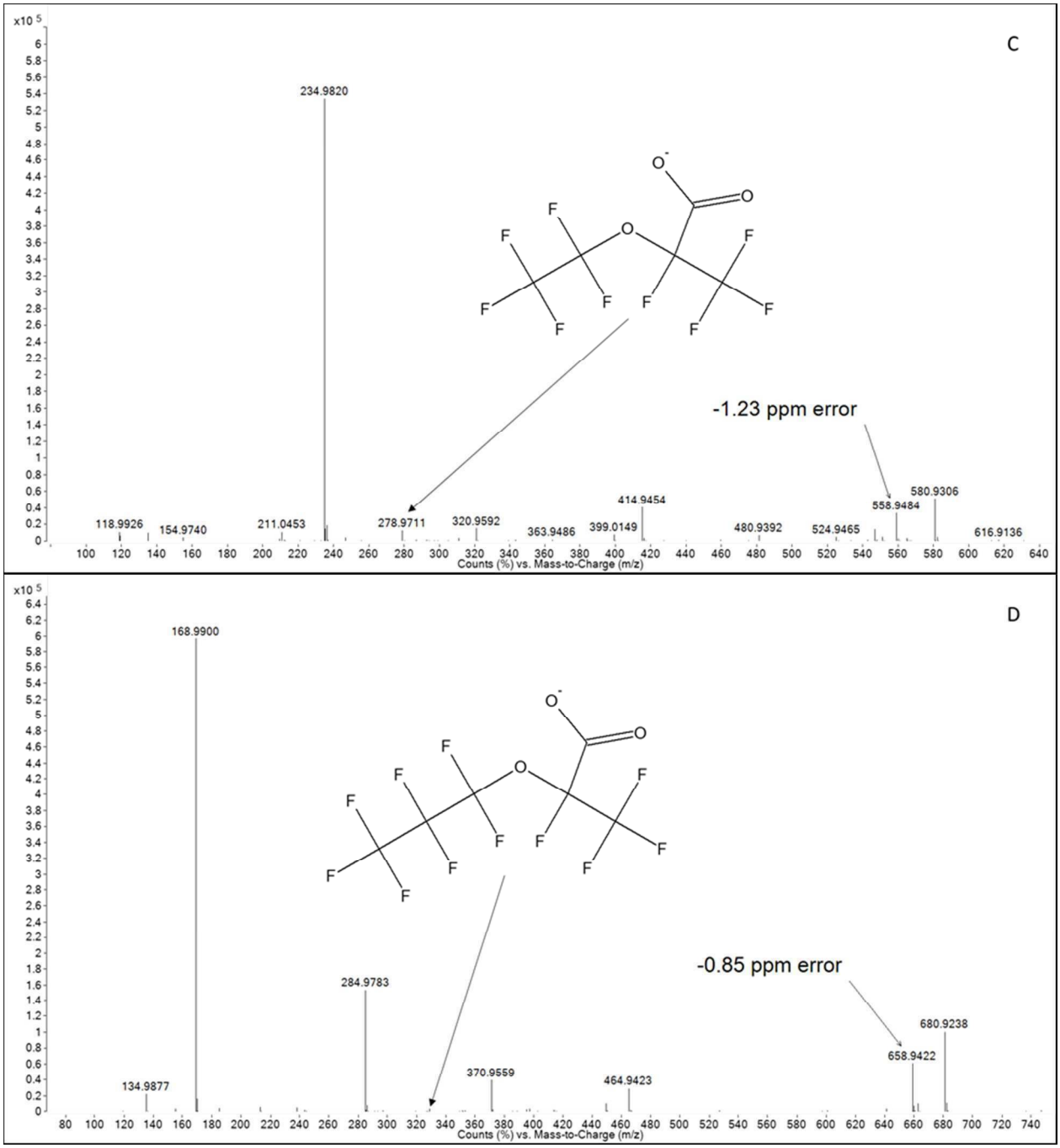

Figure S7 Spectra for Figure S5 chromatographic plot EICs. The spectra shown are for the first four eluting mono ether PFECAs shown in Figure S5. Plot A corresponds to m/z 178.9773; Plot B corresponds to m/z 228.9741; Plot C corresponds to m/z 278.9709; Plot D corresponds to m/z 328.9677. Error values shown are for the corresponding $[2M-H]^-$ (Table 1)

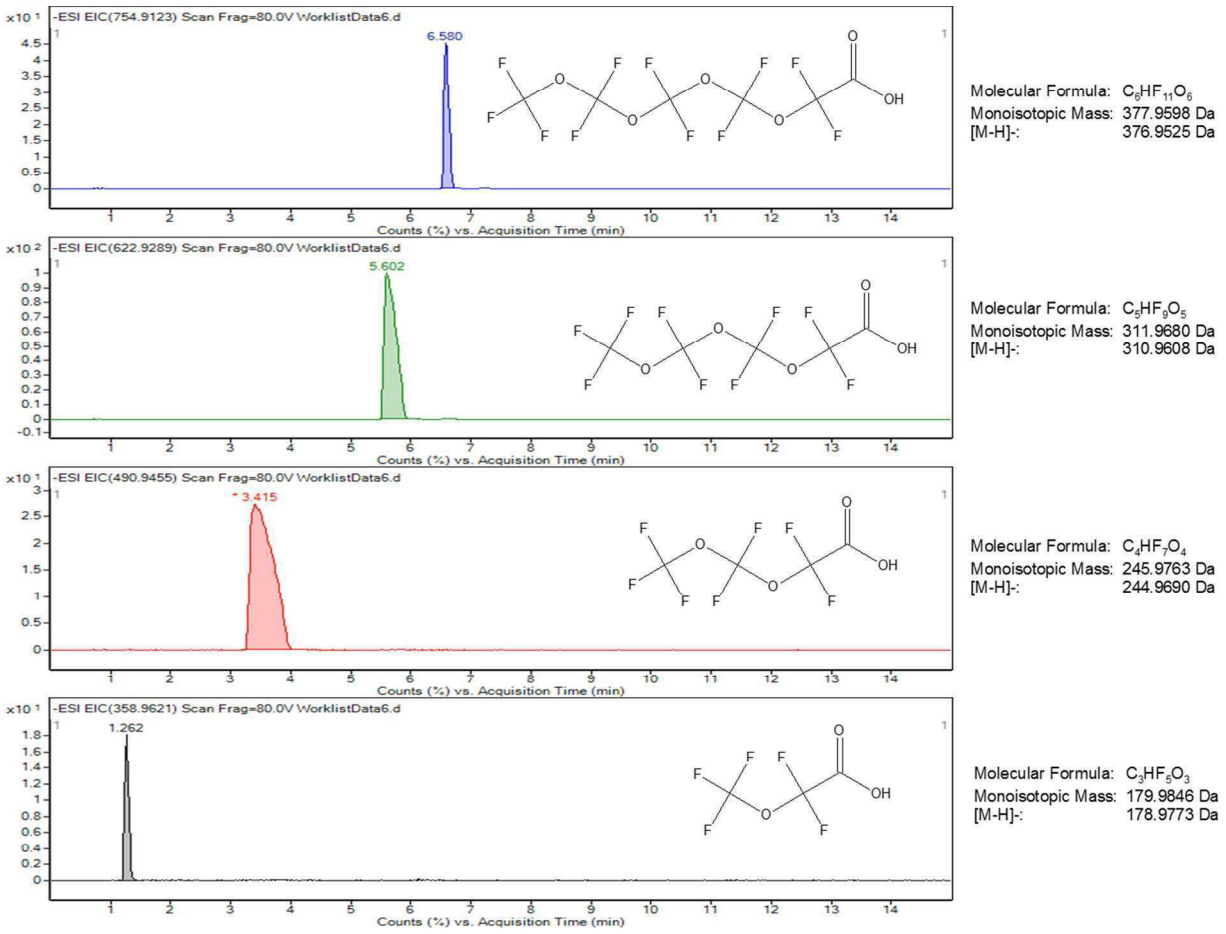

Figure S8. Extracted ion chromatogram of additional perfluorinated ether carboxylic acids homologous series. Proton bound dimer EIC shown for chromatogram. Monomer structure and exact mass shown

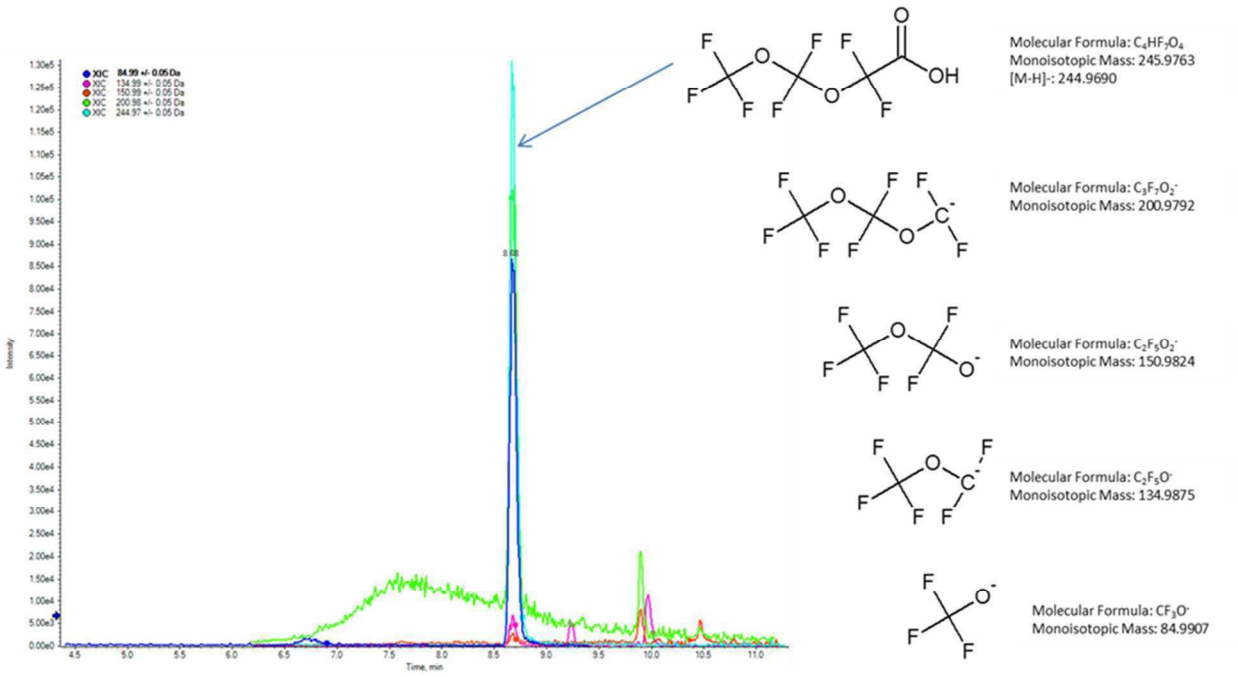

Figure S9. QTOF fragment ions for $C_4HF_7O_4$ (m/z 244.9691) pefluoroether carboxylic acid.

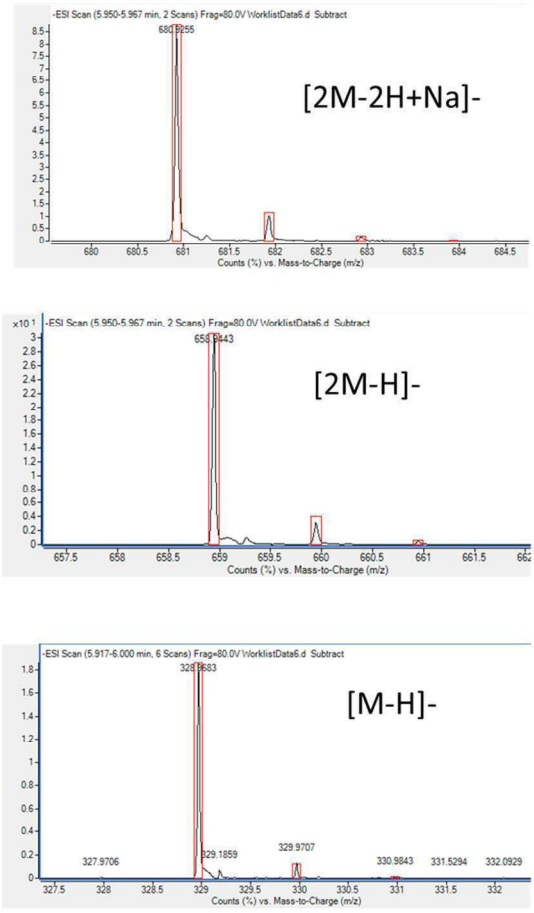

	Formula	Measured m/z	Exact m/z	Error (ppm)	Score
[2M-2H+Na]-	$C_{12}F_{22}NaO_6^-$	680.9255	680.9247	-1.2	98.11
[2M-H]-	$C_{12}HF_{22}O_6^-$	658.9433	658.9427	-2.36	92.96
[M-H]-	$C_6F_{11}O_3^-$	328.9683	328.9677	-1.8	97.85
Fragment 1	$C_5F_{11}O^-$	284.9789	284.9779	-3.49	96.35
Fragment 2	$C_3F_7^-$	168.9902	168.9894	-4.75	84.41

Figure S10. Spectrum, isotope pattern matching and identified adducts and fragment of molecular feature (m/z 328.9683) found in water. The table shows the formula, measured m/z, the exact m/z, the error associated with the measurement and the software scoring of the isotope cluster. The red boxes around each spectrum peak indicate the agreement between the measured and theoretical isotope cluster. The scoring is a bundled measurement of the accurate mass of the monoisotopic peak versus theoretical, the isotope abundance and the isotope spacing.

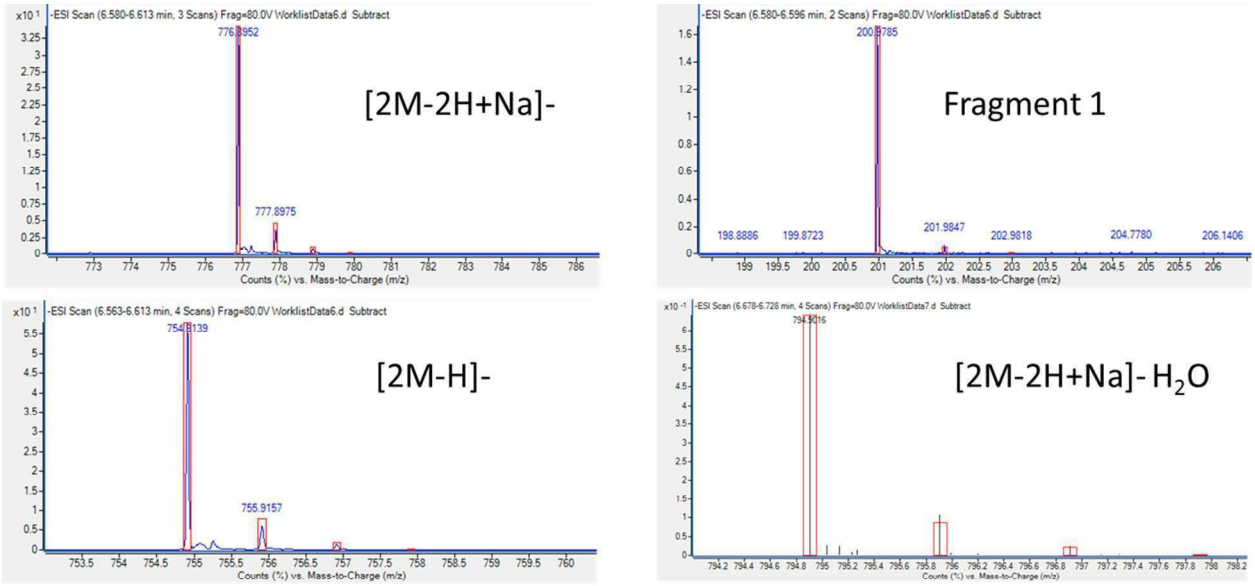

	Formula	Measured m/z	Exact m/z	Error (ppm)	Score
[2M-2H+Na]-	$C_{12}F_{22}NaO_{12}^-$	776.8952	776.8942	-1.31	95.92
[2M-H]-	$C_{12}HF_{22}O_{12}^-$	754.9139	754.9122	-2.22	92.66
[M-H]-	$C_6F_{11}O_6^-$	Not Observed	376.9525	---	---
Fragment 1	$C_3F_7O_2^-$	200.9785	200.9792	3.71	95.18
[2M-2H+Na]- H_2O	$C_{12}H_3F_{22}NaO_{13}^-$	794.9016	794.9047	3.95	84.15

Figure S11. Spectrum, isotope pattern matching and identified adducts and fragment of molecular feature (m/z 376.9525) found in water. The table shows the formula, measured m/z, the exact m/z, the error associated with the measurement and the software scoring of the isotope cluster. The red boxes around each spectrum peak indicate the agreement between the measured and theoretical isotope cluster. The scoring is a bundled measurement of the accurate mass of the monoisotopic peak versus theoretical, the isotope abundance and the isotope spacing.

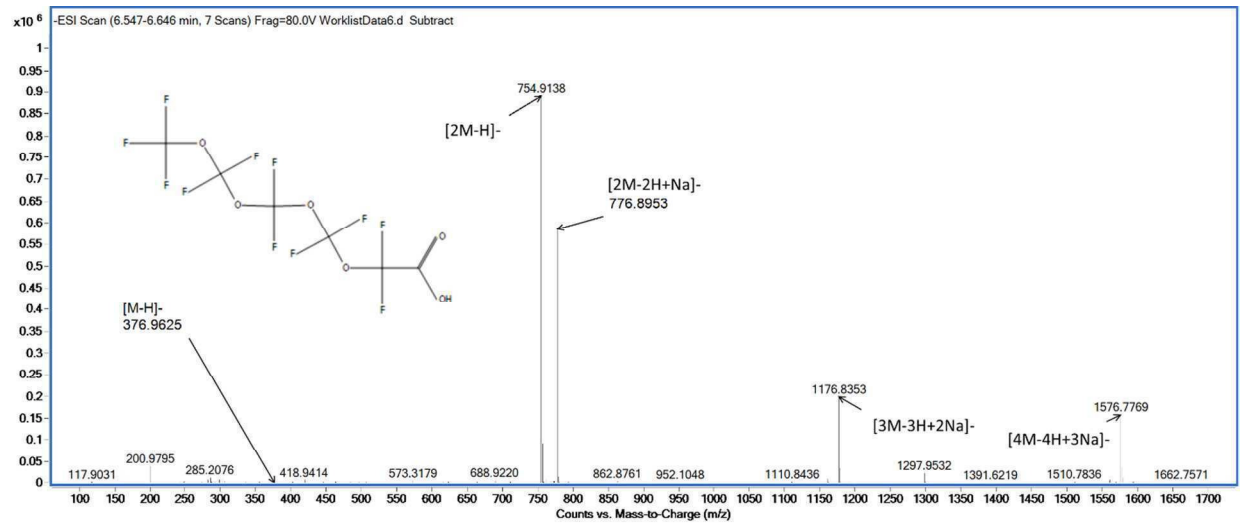

Figure S12. Spectrum of novel perfluorinated ether carboxylic acids showing proton bound and sodium bound *n*-mers found. The structure shown is the parent compound. The various in-source n-mers formed are shown with shorthand nomenclature for dimers, trimers and tetramers.

SUPPORTING INFORMATION

Validation of Quantitative Measurements and Semi-Quantitative Estimates of Emerging Perfluoroethercarboxylic Acids (PFECAs) and Hexfluoroprolyene Oxide Acids (HFPOAs)

James McCord[1], Seth Newton[2], Mark Strynar[2,]*

1 Oak Ridge Institute for Science and Education, National Exposure Research Laboratory, U.S. Environmental Protection Agency, Research Triangle Park, NC

2 National Exposure Research Laboratory, U.S. Environmental Protection Agency, Research Triangle Park, North Carolina 27711, United States

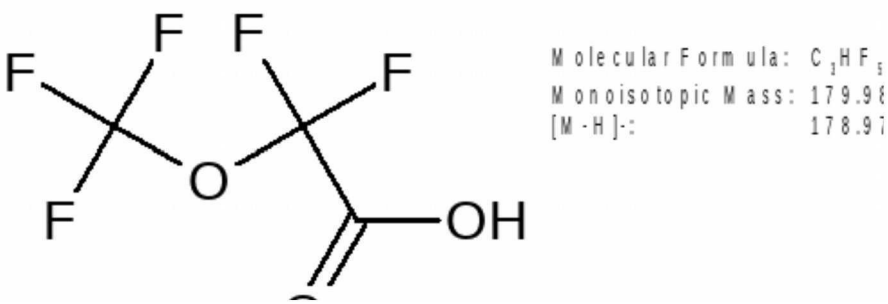

Figure 1. PFMOAA - 2,2-difluoro-2-(trifluoromethoxy)acetic acid

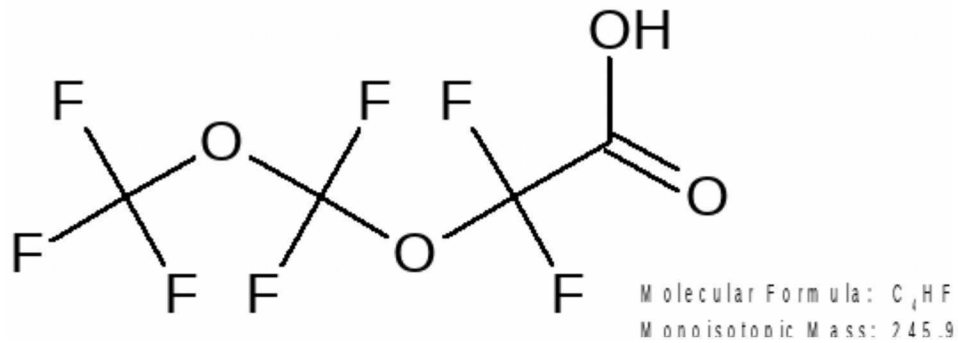

Figure 2. PFO2HxA - perfluoro-3,5-dioxahexanoic acid

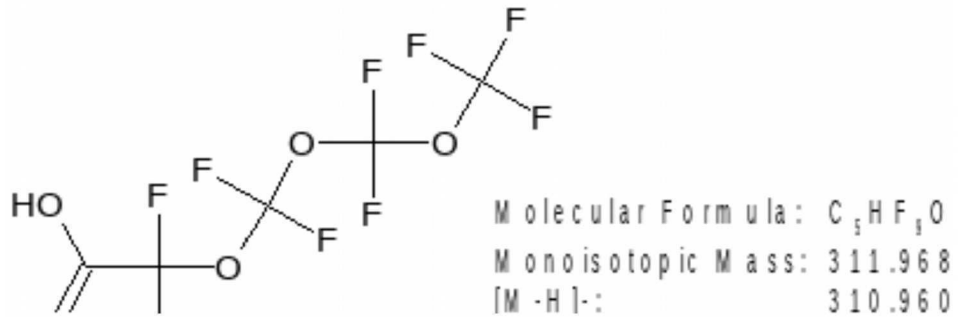

Figure 3. PFO3OA - perfluoro-3,5,7-trioxaoctanoic acid

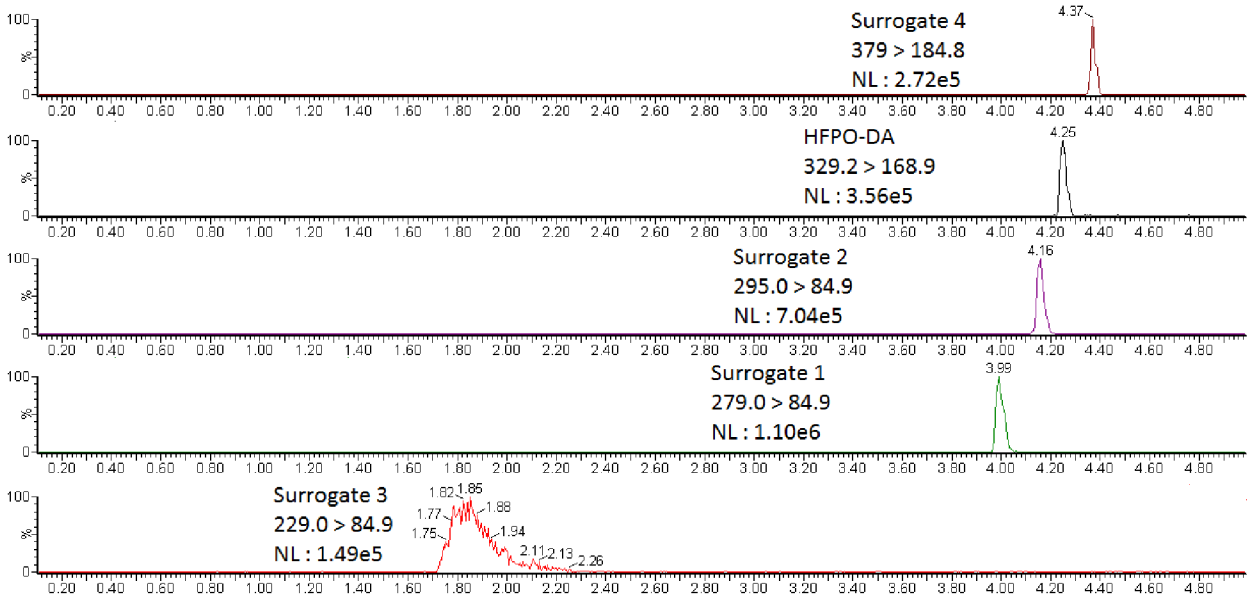

Figure 4. Representative extracted ion chromatograms for the quantitative transitions of the four PFECA surrogates and HFPO-DA in DI water

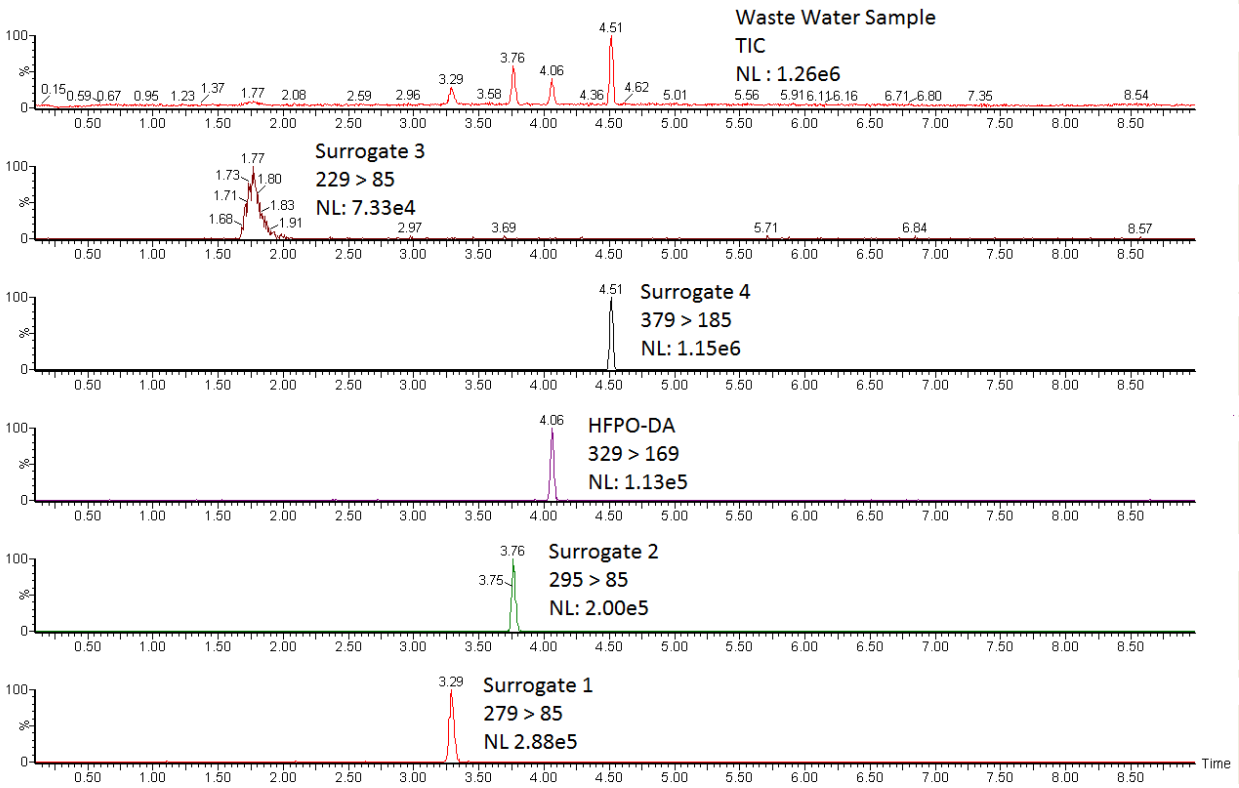

Figure 5. Representative extracted ion chromatograms for quantitative transitions of four PFECA surrogates and HFPO-DA in Waste Water

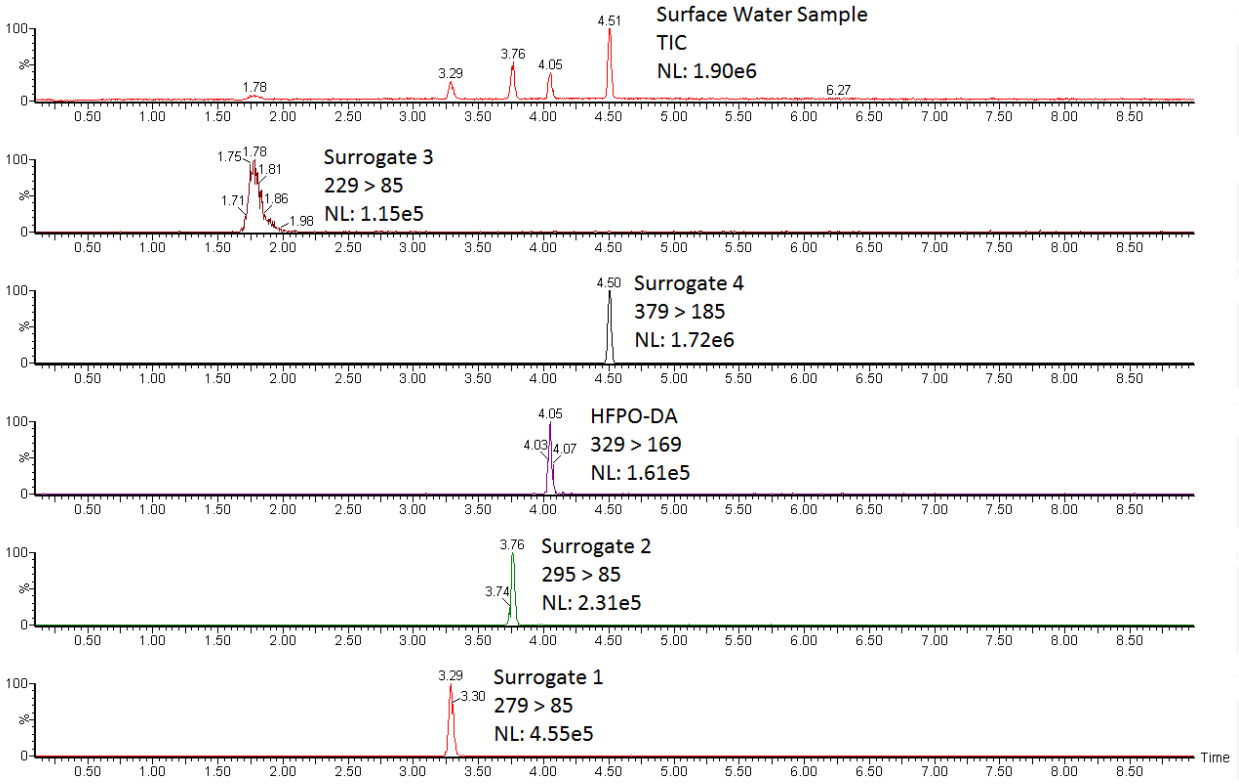

Figure 6. Representative extracted Ion Chromatograms for quantitative transitions of four PFECA surrogates and HFPO-DA in Waste Water

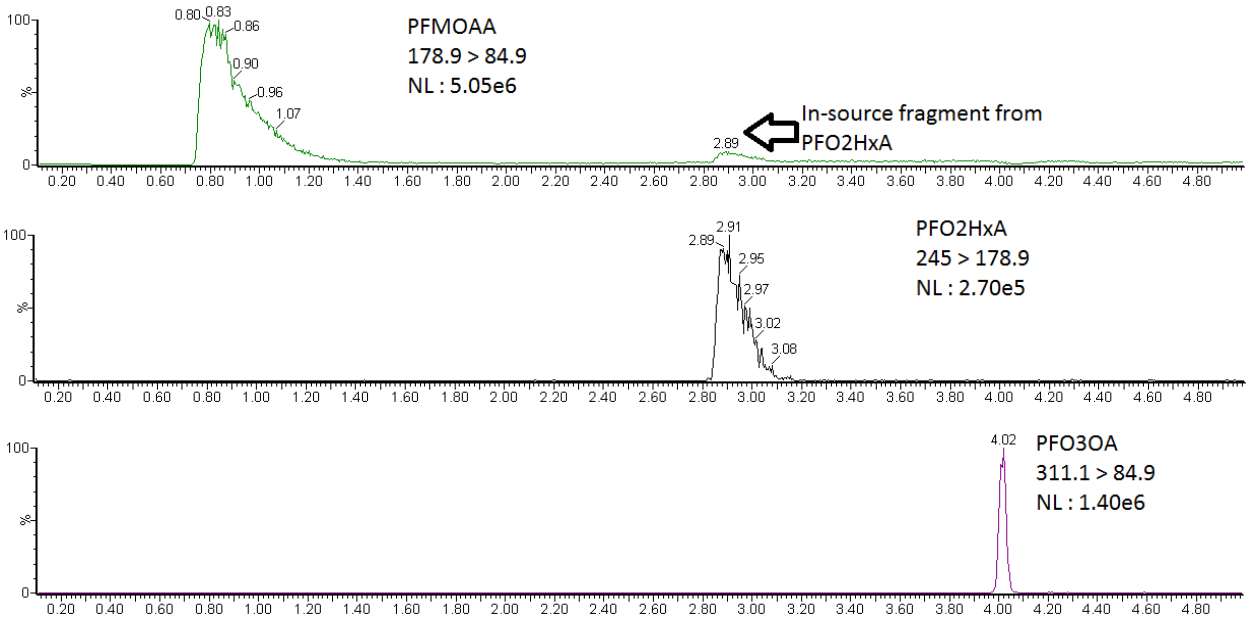

Figure 7. Representative extracted ion chromatograms for three emerging PFECA compounds extracted from surface water

Table 1. LC-MS Source Parameters

ESI Mode	Negative
ESI Voltage	1.97kV
Cone Voltage	15 V
Extractor Voltage	3 V
RF Lens	0.3
ESI Source Temp	150
Desolvation Flow	350 L/hr
Cone Gas Flow	2 L/hr

Journal of Chromatography A, 1551 (2018) 52–58

Contents lists available at ScienceDirect

Journal of Chromatography A

journal homepage: www.elsevier.com/locate/chroma

Validation of quantitative measurements and semi-quantitative estimates of emerging perfluoroethercarboxylic acids (PFECAs) and hexfluoroprolyene oxide acids (HFPOAs)

James McCord[a], Seth Newton[b], Mark Strynar[b,*]

[a] Oak Ridge Institute for Science and Education, National Exposure Research Laboratory, U.S. Environmental Protection Agency, Research Triangle Park, NC, United States

[b] National Exposure Research Laboratory, U.S. Environmental Protection Agency, Research Triangle Park, NC, 27711, United States

ARTICLE INFO

Article history:
Received 11 January 2018
Received in revised form 20 March 2018
Accepted 22 March 2018
Available online 23 March 2018

Keywords:
Perfluoroalkyl substances
HFPO-DA
GenX
Cape fear river
LC–MS

ABSTRACT

Legacy perfluorinated compounds exhibit significant environmental persistence and bioaccumulation potential, which has spawned an ongoing effort to introduce replacement compounds with reduced toxicological risk profiles. Many of these emerging chemical species lack validated quantitative methods, and, frequently, appropriate analytical standards for accurate monitoring and identification. To fill this knowledge gap, a general method for the quantitative determination of perfluoroether carboxylic acids (PFECAs) by LC–MS/MS was single-lab validated on spike-recovery samples in surface, drinking, and wastewater for a variety of perfluorinated ether standards. Relative error measurements for spike-recovery samples in each matrix ranged from 0.36% to 25.9%, with an average error of 10% overall. Coefficient of variation (CV) for each compound ranged from 10 to 28% with an average of 17%. The quantitative methodology was applied during repeated weekly monitoring of the Cape Fear River during remediation of PFECA hexafluoropropyloxide dimer-acid (HFPO-DA), known by the brand name "GenX." Semi-quantitative concentration estimates for emerging PFECA compounds lacking analytical standards was also carried out using surrogate calibration curves and mass labeled HFPO-DA as an internal standard. Estimates of the emerging compounds were possible using matched standards, but application of the estimation methodology to compounds with known concentration revealed that such estimates may possess up to an order of magnitude, or more, in uncertainty due to the difficulty of matching with an appropriate standard. Nevertheless, the estimation biases are primarily systematic (extraction efficiency and instrument response) rather than stochastic, enabling the collection of time-course data; both HFPO-DA and the emerging compounds were reduced in surface water and drinking water concentration of several orders of magnitude after removal of the source waste stream.

Published by Elsevier B.V.

1. Introduction

Per- and polyfluoroalkyl substances (PFASs) are recalcitrant environmental pollutants which have become a focus of significant public health interest in recent years [1]. In particular, the widely used compounds perfluorooctanoic acid (PFOA) and perfluorooctanesulfonate (PFOS) were found to have a negative toxicological profile and bioaccumulation potential [2,3], resulting in publication of a drinking water health advisory by the EPA [3,4], international restrictions [5], and pressure for banning under the Stockholm Convention on Persistent Organic Pollutants [6]. The primary manufacturers of these molecules phased out US production of PFOS/PFOA and related chemical species in the 2000s [7,8]. However, fluorinated surfactants, such as PFOA and PFOS, as well as the fluorinated polymer products whose production they support, exhibit unique chemical properties that are of substantial value in the textiles and consumer products industries [9]. As a consequence, numerous alternative chemistries have emerged to replace the discontinued species [10–12], with estimates as high as several thousand species [13].

One broad class of the replacement chemicals are fluorinated ether compounds [11], which consist of a series of short chain perfluorinated carbons linked by ether oxygens and capped with an acidic head group (Table 1). Many species demonstrating this general fluorinated ether structure have been detected in locations where fluorochemical manufacturing

* Corresponding author.
E-mail address: strynar.mark@epa.gov (M. Strynar).

https://doi.org/10.1016/j.chroma.2018.03.047
0021-9673/Published by Elsevier B.V.

Table 1
A) Reference perfluoro-ether carboxylic acids included in the PFECA standard mixture and B) emerging perfluorinated ether species lacking analytical standards.

A) Perfluorinated Ether Standards			
Compound Name	CAS	Formula	Structure
Perfluoro(4-oxapentanoic acid) ("Surrogate 1")	863090–89-5	$C_5HF_9O_3$	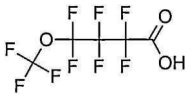
Perfluoro(3,6-dioxaheptanoic acid) ("Surrogate 2")	151772–58-6	$C_5HF_9O_4$	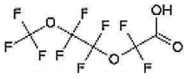
Perfluoro(3-oxabutanoic acid) ("Surrogate 3")	377–73-1	$C_4HF_7O_3$	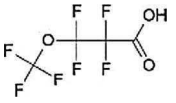
Perfluro(5-oxa-6-dimethylhexanoic) acid ("Surrogate 4")	801212–59-9	$C_7HF_{13}O_3$	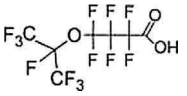
Perfluoro(2-methyl-3-oxahexanoic) acid ("HFPO-DA")	13252–13-6	$C_6HF_{11}O_3$	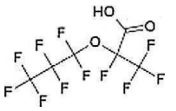
B) Emerging Compounds			
Compound Name	CAS	Formula	Structure
Perfluoro-methoxyacetic acid (PFMOAA)	674–13-5	$C_3HF_5O_3$	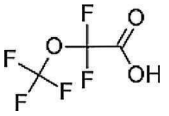
Perfluoro-3,5-dioxahexanoic acid (PFO2HxA)	39492–88-1	$C_4HF_7O_4$	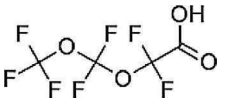
Perfluoro-3,5,7-trioxaoctanoic acid (PFO3OA)	39492–89-2	$C_5HF_9O_5$	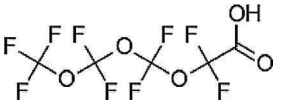

impacts the water supply [14,17], but toxicological data of these emerging compounds are limited. One particular chemical, 2,3,3,3-Tetrafluoro-2-(heptafluoropropoxy) propanoic acid, also known as hexafluoropropylene oxide dimer acid (HFPO-DA), or the trade name of its ammonium salt, GenX, [18] was designed as a fluorochemical processing surfactant that meets the requirements of the EPA PFASs management program [18,19]. HFPO-DA, and other HFPO related products have been found in significant concentrations in the discharge from certain fluorochemical manufacturing sites [14,16,20]. The limited toxicological studies of the HFPO-DA compound indicate that *acute* toxicity and metabolism are of limited concern for the replacement chemical, [21–24] but long-term exposure effects require additional study. [23–27] The detection of the compound in the Cape Fear River in North Carolina sparked an intensive investigation and establishment of a statewide health goal [28] amid concerns over its potential long-term effects.

HFPO-DA is but one of an amalgamation of related fluorochemical compounds emerging as pollutants of interest in surface, ground, and drinking water, and, while existing non-targeted methodologies have allowed for the detection of novel structures, [12–16] quantitative methods will be necessary for long term environmental monitoring and health effects studies regarding new fluorochemicals like HFPO-DA/GenX. Existing methodologies, such as EPA method 537, were developed for the analysis of legacy compounds, straight chain perfluorinated carboxylic acids and sulfonates, in drinking water, but there is substantial need for general methods sufficient to analyze known and emerging compounds in environmental matrices. Further, as emerging contaminants frequently lack authenticated standards, methods for tracking and estimating fluorochemical concentrations are needed for monitoring environmental levels of unknown contaminants. Here we demonstrate a quantitative sample preparation and LC–MS/MS method suitable for emerging perfluoroether compounds, validate it in multiple water source matrices, and apply it to the ongoing monitoring of an impacted watershed. Further, we estimate concentrations and conduct time course monitoring of perfluoroether compounds with no existing standards by using closely related surrogate species to model instrument responses and construct non-matched calibration curves.

2. Materials and methods

2.1. Preparation of PFECA standards

Reference standards of perfluoroether carboxylic acids were obtained from Synquest Laboratories (Table 1) along with $13C_3$ labeled 2,3,3,3-Tetrafluoro-2-(heptafluoropropoxy) propanoic acid (HFPO-DA) for use as an internal standard (Wellington Labs).

A stock solution of each standard was prepared in 95:5 methanol:2.5 M NaOH to prevent the formation of the methyl ester. From these stocks, a mixed PFECA standard was prepared containing equal mass of each native species and diluted to the desired final concentrations in methanol.

Standard PFECA solution mixtures were prepared using water sourced from three locations as the background matrices. Background matrix water was sourced as followed: surface water collected from Discovery Lake, Research Triangle Park, NC, waste water collected from Jacksonville Wastewater Treatment facility effluent, Jacksonville, NC, and drinking water collected from a laboratory faucet in the Environmental Protection Agency office in Research Triangle Park, NC. Each source sample was collected into one liter pre-cleaned high-density polyethyelene (HDPE) Nalgene bottles and spiked with a standard mixture of PFECAs (Table 1) at either 0, 50, or 200 ng/L. Five replicates of these matrix spiked samples were prepared for each combination of background matrix (Surface Water, Waste Water, Drinking Water) and PFECA level (Blank, Low Spike, High Spike) resulting in 45 samples. The prepared spiked samples were stabilized by pH adjustment to pH ~ 2 with the addition of 5 mL of 35% nitric acid. A set of samples of the PFECA mixture at 0, 10, 25, 50, 100, 150, 200, and 250 ng/L was also prepared in deionized water (DI) and processed immediately in tandem to construct calibration curves.

2.2. Environmental sampling

Fluorochemical contaminated water samples were acquired from North Carolina Department of Environmental Quality (NCDEQ) at a location near the industrial waste outfall for a local fluorochemical manufacturer, as well as from downstream drinking water treatment plants. Location 1 was the source water drawn from the Cape Fear River for a downstream water treatment facility and Location 2 was finished drinking water delivered to Wilmington, NC. Each sample was collected in a one liter HDPE bottle and stabilized by pH adjustment with nitric acid as previously described [29]. Samples were stored at room temperature, extracted and analyzed within five days of the sampling date.

2.3. Solid phase extraction of PFECAs from aqueous matrix

The previously prepared, stabilized samples were decanted into a 1000 mL HDPE graduated cylinder and their total volume recorded; water in excess of 1000 mL was discarded. The maximum oversampling possible in a one liter HDPE bottle is ~10%, allowing a worst case 10% bias if 100% of in-solution PFASs bind to the bottle surface and the maximum amount of excess water is discarded. This scenario can be avoided by not filling bottles completely; the maximum sample collection overfill was <10 mL in this sample set. The sample bottle was then rinsed with 10 mL of methanol to remove any compounds that partially adhere during sample processing and storage; the retained water was returned to the bottle alongside the methanol. An internal standard of $^{13}C_3$ labeled HFPO-DA was added to each water sample at a concentration of 100 ng/L of sample, and shaken vigorously before being vacuum filtered through a Whatman GF/A glass filter.

Oasis weak anion exchange (WAX) Plus (225 mg) solid phase extraction (SPE) cartridges (Waters Corporation) were conditioned according to the manufacturer instructions, as follows: the SPE cartridges were equilibrated under 10 mL/min methanol flow for 2.5 min, followed by 2.5 min of deionized water (DI) at 10 mL/min; flow was maintained through a SPC10-P Sep-Pak concentrator binary piston pump (Waters Corporation). Samples were concentrated at a flow rate of 10 mL/min for 50 min (500 mL total volume) and SPE cartridges were removed for later elution. The Sep-Pak system was flushed with 25 mL of methanol (2.5 min at 10 mL/min) between sample cartridges to prevent sample carryover.

After sample concentration, the SPE cartridges were washed with 4 mL of 25 mM pH 4.0 acetate/acetic acid buffer, followed by a wash of 4 mL of neutral methanol. Compounds of interest were then eluted with 4 mL of freshly prepared 0.1% ammonium hydroxide in methanol and evaporated in a polypropylene tube at 40°C under a dry nitrogen stream to a final volume of ~ 1 mL. The evaporated samples were diluted 4-fold in 2.5 mM ammonium acetate to match the starting conditions for liquid chromatography.

2.4. LC–MS/MS data acquisition and quantification

LC–MS/MS quantification took place on a Waters Acquity ultra performance liquid chromatograph which had been modified to replace OEM PTFE filters and solvent plumbing with stainless steel or PEEK tubing and incorporate a PFC isolation column (Waters P/N 176001744). The chromatographic separation was carried out using a Waters ACQUITY UPLC BEH C18 column (2.1 mm × 50 mm, 1.7 μm), a flow rate of 500 μL/min, 50 μL injection volume, and a binary mobile phase gradient with mobile phases A (95:5, 2.5 mM ammonium acetate: Methanol) and B (95:5, Methanol: 2.5 mM ammonium acetate). The gradient program was a follows: 10–85% B (5 min), 85–100% (0.1 min), 100% (hold for 1.9 min), 100–10% (0.1 min), 10% (hold for 1.9 min). Detection and quantitation was performed with an interfaced Waters Quattro Premier XE triple quadrupole mass spectrometer in negative mode (Supplemental Table 1) with individual transition parameters for each PFECA species analyzed (Table 2). Stable isotope labeled (SIL) HFPO-DA was used as an internal standard for all measured compounds.

MRM transitions were previously optimized for the four surrogate perfluoroether compounds and HFPO-DA using available standards. Additional transitions for three emerging PFECAs previously described (Table 1, Supplemental Fig. 1–3), [16] but currently lacking analytical standards, were selected using direct infusion of extracts prepared from the Cape Fear River. For method validation, the MRM method contained only the surrogate and HFPO-DA transitions, while environmental samples included the three MRM transitions for the emerging PFECAs as well.

The PFECA mixture was used to prepare an eight-point calibration curve for each constituent PFECA standard for quantitation. Ion abundances were normalized to the HFPO-DA internal standard intensity and curves were fitted as a concentration weighted (1/x) quadratic curve with two injections per concentration. For spike recovery experiments, quantitation was derived from the matching standard curve. For quantitative measurements of HFPO-DA and semi-quantitative estimates for the emerging PFECAs in environmental samples, systematic application of each surrogate standard curve was used to calculate estimated concentrations.

3. Results and discussion

3.1. Spike-recovery validation

Representative figures of merit were calculated for the quantitative spike recovery assessment based on the five sample preparations for each combination of background matrix and concentration (Fig. 1). For each replicate, the relative percentage error (RE) ranges from 0.36% to 25.9%, with an average of ~10% when aggregated across compounds and background matrices (Table 3). Sample precision was calculated with average coefficient of variation of 17% across matrices and spike levels (Table 3). A method limit of detection (LOD) for PFECAs was estimated at 16 ng/L using a 3X signal-to-noise cutoff. The method noise was estimated as the standard deviation of repeated injections of the 10 ng/L calibration

Table 2
Multiple reaction monitoring (MRM) transition table for surrogate and emerging PFECAs analyzed in this study.

Species	Molecular Formula	Precursor Mass (Da)	Product Mass (Da)	Cone Voltage (V)	Collision Energy (eV)
Surrogate 1	$C_5HF_9O_3$	279.0	84.9	14	22
			134.8	22	24
Surrogate 2	$C_5HF_9O_4$	295.0	84.9	10	26
			200.9	10	10
Surrogate 3	$C_4HF_7O_3$	229.0	84.9	10	10
			184.9	22	18
Surrogate 4	$C_7HF_{13}O_3$	379.0	184.8	16	12
			134.9	16	34
HFPO-DA	$C_6HF_{11}O_3$	329.2	168.9	10	12
			286.9	10	6
HFPO-DA IS	$[13C]_3C_3HF_{11}O_3$	332.2	168.9	10	12
			286.9	10	6
PFMOAA	$C_3HF_9O_5$	178.9	84.9	10	12
PFO2HxA	$C_4HF_7O_4$	245.0	84.9	22	18
			178.8	22	4
PFO3OA	$C_5HF_9O_5$	311.1	84.9	22	20
			150.8	22	4

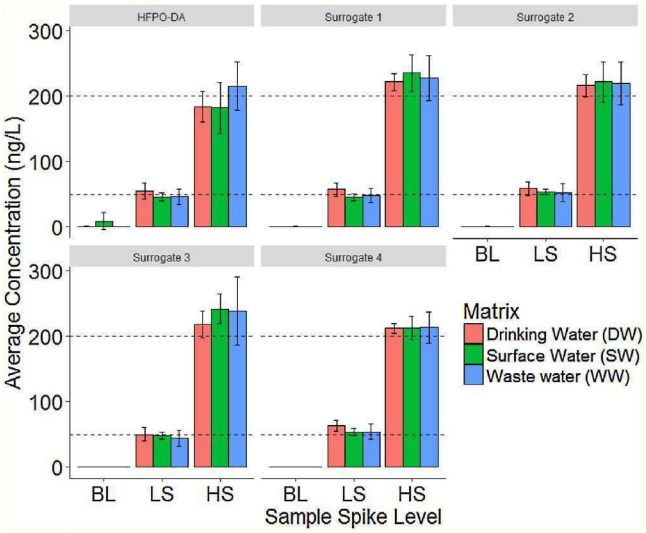

Fig. 1. Measured PFECA concentrations for a synthetic PFECA mixture in varying matrices at 200 ng/L (HS), 50 ng/L (LS), and 0 ng/L (BL) spike levels, with 95% confidence intervals.

Table 3
Calculated relative percentage error (RE) and coefficient of variation (CV) for measurements (n = 5) in waste water (WW), surface water (SW) and drinking water (DW) matrices for a series of PFECA compounds.

Compound	Matrix	RE (%)	CV (%)
HFPO-DA	DW	9.2	20%
	SW	8.6	20%
	WW	7.4	25%
Surrogate 1	DW	12.9	14%
	SW	13.4	14%
	WW	9.1	22%
Surrogate 2	DW	13.0	14%
	SW	9.2	12%
	WW	7.5	23%
Surrogate 3	DW	4.7	17%
	SW	12.2	12%
	WW	15.6	28%
Surrogate 4	DW	15.9	10%
	SW	7.0	10%
	WW	7.5	19%

curve point. This reported LOD value is not a physical limitation, and can be reduced through modifications to the SPE concentration step, sample blowdown, or injection volume to increase the on-column analyte load and improve sensitivity, or use of an MS platform with better intrinsic sensitivity.

For the HFPO-DA compound, the measurement retains accuracy regardless of matrix or sample concentration within the range of the calibration curve; all measurements correspond to their theoretical values within the 95% confidence interval and demonstrate acceptable RE (<10%) and CV (<30%) values. However, the other PFECA compounds demonstrate a small, systemic overestimation of their concentration in some background matrices. This effect is attributable to a non-matched internal standard, and can be corrected in the future as appropriate stable isotope labeled species become available. The reproducibility of the assay is still high; CVs of the surrogate compounds are equivalent or better than HFPO-DA with one exception, and the RE remains under 20% in all cases, with results from each matrix being statistically indistinguishable from each other. Thus, the methodology can be generally applied even in absence of matched internal standards. Of note, a single replicate of waste water – high spike was excluded from the collection sample set due to a significant contaminant in the preparation. Investigation of the sample revealed significant (>5-fold) signal suppression of HFPO-DA and the SIL HFPO-DA standard in only that prep. HFPO-DA quantification was unaffected due to the matched internal standard, but surrogate concentration estimates were >3.5 standard deviation outliers due to the suppressed SIL used for normalization. This event demonstrates that caution remains necessary when using non-matched internal standards, especially in heterogeneous matrices such as waste water.

3.2. Application in longitudinal monitoring of HFPO-DA

Initial environmental samples obtained in June 2017 from fluorochemical manufacturing outfall, surface, and drinking water far exceeded the designated calibration range and required significant dilution to enter the calibration curve range for accurate quantitation. Following this sampling, the manufacturer ceased waste stream emissions from one of their manufacturing lines and the measured concentrations of all monitored species dramatically declined in both the direct outfall and downstream locations (Figs. 2 and 3). Of note, local contamination from pumps and piping at the manufacturing site are hypothesized to be the cause of the persistently high concentrations in the waste outfall through the third sampling week in spite of the immediate decline observed at downstream locations. Continuous monitoring of both outfall and impacted drinking water sites demonstrated minor daily variation but consistent reduction below North Carolina's targeted health goal of 140 ng/L [28].

Blank, low spike, and high spiked standard mixtures were carried to the sampling site as field blanks each week and returned for QC analysis. Throughout the sampling course, QC samples mea-

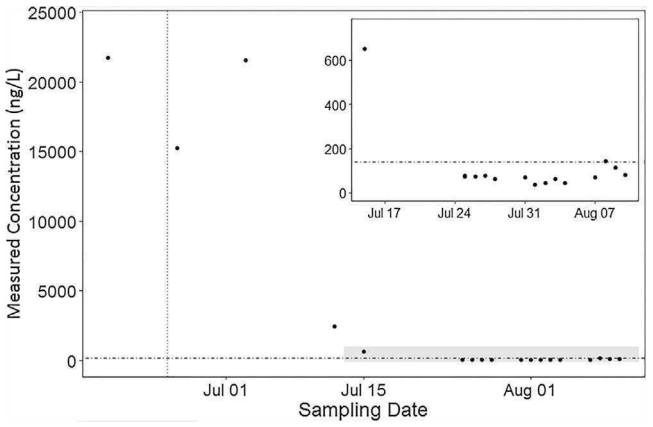

Fig. 2. Measured HFPO-DA concentrations in manufacturing outfall over time. The vertical line indicates diversion of PFECA generating waste stream, the horizontal line indicates targeted HFPO-DA health goal (140 ng/L), inset shows shaded region.

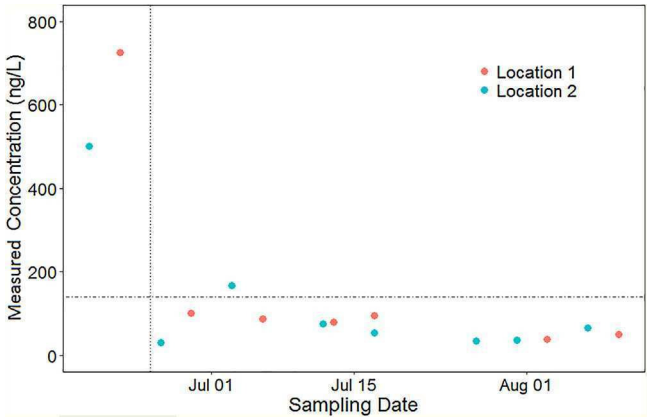

Fig. 3. Measured HFPO-DA concentrations at drinking water treatment plants located in the Cape Fear River basin. Vertical line indicates diversion of PFECA generating waste stream, horizontal line indicates targeted health goal (140 ng/L).

sured were quantified with an average RE of 22%. Each week, a randomly selected 10% subset of the environmental samples were replicated and inter-replicate CVs were <10%, demonstrating long term method stability and precision.

3.3. Semi-quantitative estimates of emerging PFECAs

For compounds tentatively identified as PFMOAA, PFO2HxA, and PFO3OA [16], the lack of a matched standard and reliance on a surrogate internal standard limits the potential accuracy of quantitative efforts. Nevertheless, semi-quantitative estimates can inform public health decisions and provide focus for further development of analytical methods [30]. The PFECA mixture was used to prepare an eight-point calibration curve for each constituent PFECA standard. Ion abundances were normalized to the HFPO-DA internal standard intensity and calibration curves were fitted as a concentration weighted (1/x) quadratic curve. Estimated concentrations for the three emerging compounds, which lack standards, and HFPO-DA were obtained using each of the five calibration curves each sampling week, as well as a global estimate curve built from the response of all five individual surrogates.

To establish an estimate of the level of error when using surrogate compounds for concentration estimates, the HFPO-DA value from its matched calibration curve was compared to values obtained using the calibration curves from the four surrogate compounds. The surrogate estimated concentrations yielded average errors of 1.3%, 0.6%, 48%, and 0.3% for Surrogates 1–4 respectively. The three closely matching surrogates, 1, 2 and 4, elute within a 1-min window, very near the HFPO-DA peak (Supplemental Fig. 4–7). As a consequence, they demonstrate remarkably little bias in estimated concentrations for HFPO-DA, unlike Surrogate 3, which elutes much earlier in the chromatographic run, and has significant peak distortions resulting from its more hydrophilic character than the other species. Surrogate 3 however, does have a more similar chromatographic profile to PFMOAA and PFO2HXA. For the HFPO-DA, a best case scenario of a closely matched chemical structure for the calibration curve and internal standard yields accurate results within the error margins of the matched curve and standard, while a poorly matched species yields a several-fold, but still manageable, level of bias in estimation. Matching of surrogates can be performed empirically, by selecting similar chemical structures and confirming similar chromatographic and MS performance, but a general solution to determining “good” surrogate matches is beyond the scope of this paper.

The emerging species exhibit significantly more variability in estimated concentrations compared to the surrogate standards (Fig. 4). Structurally, the emerging compounds appear similar to the surrogate PFECA compounds, however, their elution time indicates substantially higher hydrophilicity consistent with their low molecular weight and increased oxygen content; PFMOAA elutes nearly in the void volume, and PFO2HxA falls somewhere between the PFMOAA and surrogate standards (Supplemental Fig. 5). Further, the extraction efficiency of non-targeted species in SPE is currently unknown, and can contribute to significant variability, but we assume the binding to be consistently high when using anion exchange phases with easily ionized species such as perfluoroacids [31].

The systematic dissimilarity between the lower molecular weight emerging compounds and the surrogate standards impacts the concentration estimates. The predicted concentrations are

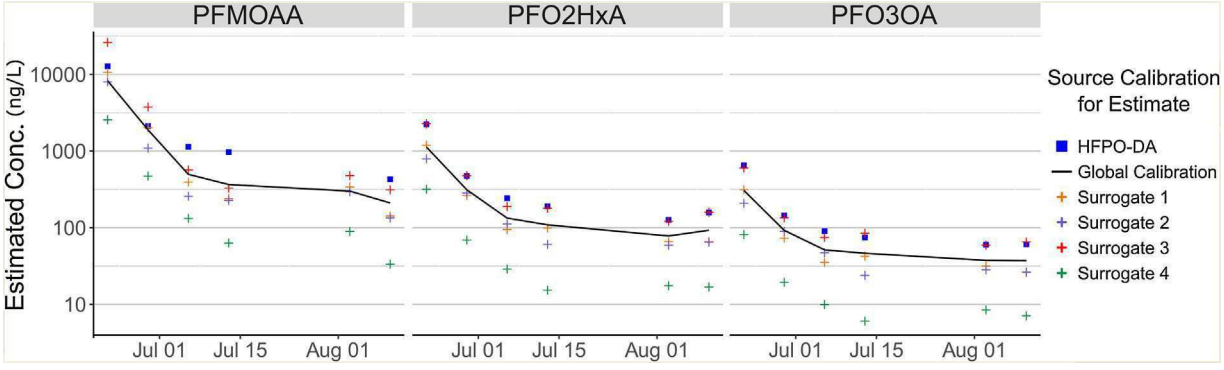

Fig. 4. Estimated concentrations of three emerging PFECA compounds at Location 2, using five surrogate calibration curves and a global calibration of all species.

consistent in their ordering, with HFPO-DA estimate being the highest value and Surrogate 4 underestimating that value by ~10-fold.

The systematic bias of estimated concentration is consistent across sampling location and date, implying it is intrinsic to the process, likely the result of hydrophobic bias in the chromatography and/or electrospray that cannot be corrected for without more closely matched calibration curve and/or internal standard. A conservative application of the variation between the five closely related PFECA standards suggests the error of the global average is on the order of ten-fold and can be considered semi-quantitative at best. Regardless, using the global average calibration curve of the PFECA standards provides a rough estimate of concentration that can be useful for directing further work. The most recent PFMOAA estimate range still falls partially above the health goal for HFPO-DA and it is worthy of further scrutiny, while the other compounds have been reduced below that target level, even when using the highest estimate of the concentration.

Nevertheless, all three of the non-standard PFECA compounds demonstrated substantial reduction over time as the result of halted upstream emission, similarly to the behavior of the HFPO-DA compound. This signifies that all the related PFECA compounds likely derive from the single fluoropolymer manufacturing process whose waste was diverted. Further, time trends indicate that the overall concentration has dropped ~2 orders of magnitude, similar to the HFPO-DA, regardless of the calibration source used. This methodology is therefore suitable for tracking temporal changes in compounds lacking standards even though the specific estimation of concentrations remains highly uncertain, presuming that such species can be detected by LC–MS.

4. Conclusion

The ongoing proliferation of new perfluorinated species to serve industrial chemical need in absence of the legacy compounds PFOA and PFOS is a burgeoning topic in environmental and public health with substantial interest. Monitoring efforts for these new species require a robust, generalized method for quantitative determinations of exposure. The availability of a SIL internal standard for HFPO-DA allows for robust analysis of this species, and allows its use as a surrogate internal standard for other compounds barring the production of matching SIL perfluoroethers. The methodology presented here is robust to variations in the environmental matrix (tap, surface, and waste water) and offers an extended range of sensitivity through the use of multiple concentration steps. Nevertheless, the calibration range utilized, with a method limit of detection ~10 ng/L, is sufficient for exposure monitoring, as the existing health advisory/goal levels for both the legacy and emerging perfluorinated compounds are around an order of magnitude higher. Lower health targets for legacy species exist in some states [32], and increased concentration factors or improved instrument sensitivity would be necessary to achieve the necessary lower method detection limits.

The same sample preparation technique can be applied to the analysis of only partially characterized species assuming chemically similar standards are available for purchase. Using one or more related species to construct calibration curves, even with surrogate internal standards, allows for an estimation of concentrations that can inform future research and policy efforts in environmental exposure. This can act as supplemental and supporting information to other mass spectrometry related monitoring efforts in non-targeted analysis. For species with some available structural information and a closely related standard, the error is on the same order as the method variation and theoretically suitable for quantitative work. However, this should be consisted a stop-gap technique prior to the acquisition of standards or validation of the assumption of similar extraction efficiency and instrument response. suitable for quantitative work. The estimates from less closely matched calibrations curves vary by >10-fold depending on the selected calibration species, but nevertheless can reveal accurate time-trend data for determining the impact of systemic changes and determining whether multiple species have correlated behaviors in response to an intervention.

Acknowledgements

The United States Environmental Protection Agency, through its Office of Research and Development, funded and managed the research described here. It has been subjected to Agency administrative review and approved for publication. James McCord was supported by an appointment to the Internship/Research Participation Program at the Office of Research and Development, U.S. Environmental Protection Agency, administered by the Oak Ridge Institute for Science and Education through an interagency agreement between the U.S. Department of Energy and EPA. Thanks are extended to the North Carolina Department of Environmental Quality for collecting the water samples used for the longitudinal monitoring application.

Appendix A. Supplementary data

Supplementary data associated with this article can be found, in the online version, at https://doi.org/10.1016/j.chroma.2018.03.047.

References

[1] A.B. Lindstrom, M.J. Strynar, E.L. Libelo, Polyfluorinated Compounds: past, present, and future, Environ. Sci. Technol. 45 (19) (2011) 7954.
[2] T. Stahl, D. Mattern, H. Brunn, Toxicology of perfluorinated compounds, Environ. Sci. Eur. 23 (1) (2011) 38.
[3] Lifetime Health Advisories and Health Effects Support Documents for Perfluorooctanoic Acid and Perfluorooctane Sulfonate, E. P. A., Ed. Federal Register, United States, 2016, pp 33250–33251.
[4] Provisional Health Advisories for Perfluorooctanoic Acid (PFOA) and Perfluorooctane Sulfonate (PFOS), United States Environmental Protection Agency, Washington DC, 2009.
[5] Report of the Conference of the Parties of the Stockholm Convention on Persistent Organic Pollutants on the Work of Its Fourth Meeting, 2009.
[6] Proposal for a COUNCIL DECISION on the Submission, on Behalf of the European Union, of a Proposal for the Listing of Additional Chemicals in Annex A to the Stockholm Convention on Persistent Organic Pollutants, Council of the European Union, 2016.
[7] Fact Sheet: 2010/ PFOA Stewardship Program, 2015 https://www.epa.gov/assessing-and-managing-chemicals-under-tsca/fact-sheet-20102015-pfoa-stewardship-program.
[8] EPA and 3 M Announce Phase Out of PFOS, 2018 https://yosemite.epa.gov/opa/admpress.nsf/0/33aa946e6cb11f35852568e1005246b4.
[9] E. Kissa, Fluorinated Surfactants and Repellents, vol. 97, CRC Press, 2001.
[10] M. Scheringer, X. Trier, I. Cousins, P. T.; de Voogt, T. Fletcher, Z. Wang, T.F. Webster, Helsingør Statement on poly- and perfluorinated alkyl substances (PFASs), Chemosphere 114 (2014) 337–339.
[11] Z. Wang, I.T. Cousins, M. Scheringer, K. Hungerbühler, Fluorinated alternatives to long-chain perfluoroalkyl carboxylic acids (PFCAs), perfluoroalkane sulfonic acids (PFSAs) and their potential precursors, Environ. Int. 60 (2013) 242.
[12] F. Xiao, Emerging poly- and perfluoroalkyl substances in the aquatic environment: a review of current literature, Water Res. 124 (2017) 482–495.
[13] Z. Wang, J.C. DeWitt, C.P. Higgins, I.T. Cousins, A never-Ending story of per- and polyfluoroalkyl substances (PFASs), Environ. Sci. Technol. 51 (5) (2017) 2508–2518.
[14] M. Sun, E. Arevalo, M. Strynar, A. Lindstrom, M. Richardson, B. Kearns, A. Pickett, C. Smith, D.R.U. Knappe, Legacy and emerging perfluoroalkyl substances are important drinking water contaminants in the cape fear river watershed of north carolina, Environ. Sci. Technol. Lett. 3 (12) (2016) 415–419.
[15] S. Newton, R. McMahen, J.A. Stoeckel, M. Chislock, A. Lindstrom, M. Strynar, Novel polyfluorinated compounds identified using high resolution mass spectrometry downstream of manufacturing facilities near Decatur, alabama, Environ. Sci. Technol. 51 (3) (2017) 1544–1552.
[16] M. Strynar, S. Dagnino, R. McMahen, S. Liang, A. Lindstrom, E. Andersen, L. McMillan, M. Thurman, I. Ferrer, C. Ball, Identification of novel perfluoroalkyl ether carboxylic acids (PFECAs) and sulfonic acids (PFESAs) in natural waters

using accurate mass time-of-flight mass spectrometry (TOFMS), Environ. Sci. Technol. 49 (19) (2015) 11622.
[17] F. Heydebreck, J. Tang, Z. Xie, R. Ebinghaus, Alternative and legacy perfluoroalkyl substances: differences between european and chinese River/Estuary systems, Environ. Sci. Technol. 49 (14) (2015) 8386–8395.
[18] DuPont™ GenX Processing Aid for Making Fluoropolymer Resins, Chemours, 2010.
[19] Risk Management for Per- and Polyfluoroalkyl Substances (PFASs) Under TSCA, United States Environmental Protection Agency, Washington DC, 2015.
[20] Y. Pan, H. Zhang, Q. Cui, N. Sheng, L.W. Yeung, Y. Guo, Y. Sun, J. Dai, First report on the occurrence and bioaccumulation of hexafluoropropylene oxide trimer acid: an emerging concern, Environ. Sci. Technol. 51 (17) (2017) 9553–9560.
[21] S.A. Gannon, W.J. Fasano, M.P. Mawn, D.L. Nabb, R.C. Buck, L.W. Buxton, G.W. Jepson, S. Frame, R. Absorption, distribution, metabolism, excretion, and kinetics of 2,3,3,3-tetrafluoro-2-(heptafluoropropoxy)propanoic acid ammonium salt following a single dose in rat, mouse, and cynomolgus monkey, Toxicology 340 (2016) 1–9.
[22] J.M. Caverly Rae, L. Craig, T.W. Slone, S.R. Frame, L.W. Buxton, G.L. Kennedy, Evaluation of chronic toxicity and carcinogenicity of ammonium 2,3,3,3-tetrafluoro-2-(heptafluoropropoxy)-propanoate in Sprague–Dawley rats, Toxicol. Rep. 2 (2015) 939–949.
[23] R.A. Hoke, B.D. Ferrell, T.L. Sloman, R.C. Buck, L. Buxton, W. Aquatic hazard, bioaccumulation and screening risk assessment for ammonium 2,3,3, 3-tetrafluoro-2-(heptafluoropropoxy)-propanoate, Chemosphere 149 (2016) 336–342.
[24] B.R. Rushing, Q. Hu, J.N. Franklin, R.L. McMahen, S. Dagnino, C.P. Higgins, M.J. Strynar, J.C. DeWitt, Evaluation of the immunomodulatory effects of 2,3,3,3-Tetrafluoro-2-(Heptafluoropropoxy)-Propanoate in C57BL/6 mice, Toxicol. Sci. 156 (1) (2017) 179–189.
[25] E.C. Agency, Ammonium 2,3,3,3-tetrafluoro-2-(heptafluoropropoxy)propanoate Acute Toxicity Endpoint Summary, 2018 https://echa.europa.eu/registration-dossier/-/registered-dossier/2679/7/3/1.
[26] M.Z.P. Beekman, A. Muler, W. de Vriew, P. Janssen, M. Zeilmaker, Evaluation of Substances Used in the GenX Technology by Chemours, The Dutch National Institute for Public Health and the Environment (RIVM), Dordrecht, 2016.
[27] C. Smit, Research into Indicative Water Quality Standards for Substances Used in the GenX Technology, The Dutch National Institute for Public Health and the Environment (RIVM), 2017.
[28] NC DHHS Preliminary Risk Assessment FAQ for GenX (Perfluoro2-propoxypropanoic Acid), North Carolina Department of Health and Human Services, 2017.
[29] S.F. Nakayama, M.J. Strynar, J.L. Reiner, A.D. Delinsky, A.B. Lindstrom, Determination of perfluorinated compounds in the upper mississippi river basin, Environ. Sci. Technol. 44 (11) (2010) 4103.
[30] Environmental Decisions in the Face of Uncertainty, National Research Council, 2013.
[31] K.-U. Goss, The pKa values of PFOA and other highly fluorinated carboxylic acids, Environ. Sci. Technol. 42 (2) (2008) 456–458.
[32] Maximum Contamination Level Recommendation for Perfluorooctanoic Acid in Drinking Water, Drinking Water Quality Institute, New Jersey, 2017.

Environmental Science & Technology

Article

Cite This: Environ. Sci. Technol. 2019, 53, 4717−4727

pubs.acs.org/est

Identification of Per- and Polyfluoroalkyl Substances in the Cape Fear River by High Resolution Mass Spectrometry and Nontargeted Screening

James McCord[†] and Mark Strynar*[,‡]

[†]National Exposure Research Laboratory, U.S. Environmental Protection Agency, Oak Ridge Institute for Science and Education, Research Triangle Park, Durham, North Carolina 27711, United States

[‡]National Exposure Research Laboratory, U.S. Environmental Protection Agency, Research Triangle Park, Durham, North Carolina 27711, United States

Supporting Information

ABSTRACT: Ongoing chemical development in response to regulation of historical perfluorinated compounds, (i.e., perfluorooctanoic acid (PFOA) and perfluorooctanesulfonic acid (PFOS)) has resulted in a proliferation of novel per- and polyfluorinated species. Screening and monitoring for these emerging chemicals benefit from a nontargeted approach due to a lack of necessary standards and a paucity of information about the replacement chemistries. In this paper, we apply nontargeted screening to the Cape Fear River of North Carolina, a fluorochemically impacted watershed. The continued presence of perfluorinated ether acids was confirmed, with a total of 37 unique chemical formulas comprising 58 isomers detected. Structural determination was carried out by LC-MS/MS to determine isomeric structures where possible. Novel structures determined included perfluorinated ether acid species containing two acidic sites, polyfluorinated ether acids containing a single hydrogenation, and previously unreported perfluorinated ether acids. Compounds identified by an initial nontargeted screen were monitored over repeated sampling to track long-term reductions in PFAS content during emission source control. Hierarchical clustering of the time course data was used to associate groups of chemicals based on their trends over time. Six clusters were identified and showed some similarity in chemical class; they are believed to represent the byproducts of different fluorochemical production lines.

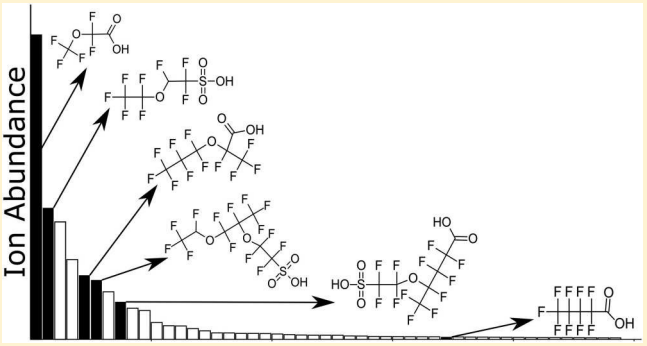

INTRODUCTION

Fluorinated polymers and fluorosurfactants are constantly evolving due to in-demand consumer and industrial products with a long and complicated history of environmental impacts.[1] A consequence of the ubiquity of per- and polyfluoroalkyl substances (PFASs) in industry is their extensive environmental infiltration due to their use as manufacturing aids, production as waste, and release as degradations and side-products of manufactured products. PFASs possess exemplary thermochemical inertness, and fluorinated carbons are resistant to biological breakdown,[2] which is the cause of their persistent nature in the environment[3] and was the driving rationale for the erroneous assumption of biological inertness for over 25 years.[4]

The most historically dominant PFAS species, perfluorooctanesulfonate (PFOS) and perfluorooctanoic acid (PFOA), were used extensively before triggering domestic and international action due to concerns about their negative toxicological effects and bioaccumulation potential.[5−7] Long-term toxicological studies demonstrated that these species have broad spectrum influence and require exposure controls.[8,9] Coinciding with the environmental studies in the previous decade, domestic manufacturing began phasing out PFOA and PFOS,[10,11] but the chemical qualities of fluorochemicals are difficult, or impossible, to replicate using nonfluorinated species.[12,13] Consequently, industries developed fluorinated alternatives, including short-chain PFASs and perfluoroalkyl ether acids, to replace legacy long-chain PFASs.[14,15]

A chief difficulty with chemical phase-out is the assurance that replacement chemicals from the same class demonstrate improved environmental and human health profiles. Historically, reliance on chemicals within a single chemical class has not markedly overcome fundamental issues presented by the original compounds (e.g., the replacement of polychlorinated biphenyls with short-chain chlorinated paraffins or the

Received: October 25, 2018
Revised: February 25, 2019
Accepted: March 14, 2019
Published: April 17, 2019

Downloaded via US EPA OFFICE OF ENVIRONMENTAL INFO on April 29, 2020 at 12:41:52 (UTC).
See https://pubs.acs.org/sharingguidelines for options on how to legitimately share published articles.

ACS Publications © 2019 American Chemical Society

DOI: 10.1021/acs.est.8b06017
Environ. Sci. Technol. 2019, 53, 4717−4727

emerging replacements for brominated flame retardants).[16,17] Due to the aforementioned uniqueness of fluorinated compounds, there may be challenges to the prospect of alleviating the toxicological effects associated with PFOA/PFOS or legacy PFASs by using related chemistries.[13,18] One company has introduced a new line of "short-chain" PFOS replacements which exhibit nearly identical structures but potentially better biological clearance rates.[19] Others have introduced branched polymeric surfactants with "low-bioaccumulation potential".[20] Still, more manufacturers have created species with interspersed ether-oxygen linkages[21] or partial hydrogenation.[22] The net result is a proliferation of product chemicals, precursors, and degradation products with limited publicly available toxicological and physical data due to the proprietary nature of these compounds. Monitoring this vast new chemical landscape requires the development of new analytical methodologies.

High-resolution mass spectrometry (HRMS) has a proven track record in compound elucidation and environmental screening that is well suited to the task of identifying and monitoring emerging pollutants through accurate chemical prediction and structural elucidation.[23−28] HRMS approaches have been applied to numerous environmental samples collected around fluorochemical point sources to identify new unregulated compounds. For example, new structures were resolved in water located around Chinese manufacturing facilities[28] and in river water from domestic sites.[29] Potential structures were assigned to numerous PFASs in Alabama[26] and previously in the Cape Fear River of North Carolina.[29,30] In each case, spatial and/or temporal sampling was used to compare impacted and baseline water samples, while identifying molecular features associated with the fluorochemical waste stream.

In North Carolina, discovery of the chemical hexafluoropropylene oxide dimer acid (HFPO-DA) sparked intense scrutiny of its long-term effects, resulting in the establishment of a preliminary NC state drinking water health goal.[31] Since initial reporting by media outlets,[32] the "chemical" GenX has been used as a public synonym for HFPO-DA. While GenX has occupied the center of the debate regarding fluorochemical contamination in the Cape Fear River, the presence of other fluorinated chemicals of related classes is also of interest. We combine the previously demonstrated nontargeted approach with techniques for structural assignment by tandem mass spectrometry (MS/MS) to identify the additional fluorochemical species affecting the Cape Fear watershed.

METHODS

Sample Collection. Surface water grab samples were collected in May 2017 from the main flow of the Cape Fear River and its tributaries at the William O. Huske Lock and Dam. An "upstream" sample was collected approximately 2 miles upstream of the dam, representative of the background contents of the river. A "downstream" sample was collected immediately above the dam, representative of the impacts of nearby (<1 mile) manufacturing outfall (Supporting Information Figure 91). Longitudinal grab samples of the manufacturing outfall were collected weekly by the North Carolina Department of Environmental Quality (NCDEQ) throughout the summer of 2017,[33] and follow-up samples were collected at the original sampling locations in February 2018. At each site, water was collected in a precleaned one liter high-density polyethyelene (HDPE) Nalgene bottle according to an established procedure.[34]

The collected water was processed as previously described, after stabilization with the addition of 5 mL 35% nitric acid.[26] In brief, one liter of water was measured in an HDPE graduated cylinder, and the sample bottle was washed with 10 mL of methanol to desorb analytes adhered to the interior of the bottle. The water and methanol were pooled in the bottle and filtered using a Whatman GF/A glass fiber filter. From this filtered sample, 500 mL of liquid was concentrated using a SPC10-P Sep-Pak concentrator onto an Oasis WAX Plus SPE cartridge (225 mg sorbent, 60 μm particle size) that had been preconditioned with methanol (MeOH) and water per manufacturer instructions. SPE cartridges were washed with 4 mL of pH 4 acetate buffer, followed by 4 mL of neutral methanol, and then compounds were eluted in 4 mL of 0.1% NH_4OH in MeOH. The methanol wash fraction could have contained nonacidic PFAS, but preliminary experiments did not detect these in samples from the Cape Fear, so they were discarded in the work for this manuscript. The eluent was evaporated under a nitrogen stream at 40 °C to a final volume of 1 mL and diluted 4-fold with 2.5 mM ammonium formate. A method blank was prepared in parallel using laboratory deionized water.

Sample Analysis and Data Processing. Initial mass spectrometry (MS) analysis on the collected water samples was carried out by liquid chromatography coupled to time-of-flight (TOF) in a fashion previously described;[29] instrument details are located in the Supporting Information. MS sample data was postprocessed using a software workflow of Agilent ProFinder, MassHunter, and Mass Profiler. Samples were subjected to batch recursive molecular feature extraction (MFE) in ProFinder using previously determined thresholds for this instrument and separation gradient (Supporting Information Table 3). A molecular feature, as defined by the software, consists of a specific isotopic distribution with a distinct extracted ion chromatogram peak abundance and is assigned a monoisotopic mass and retention time. Molecular features identified in the method blank were removed from the sample data, and the remaining values were exported for comparison in Mass Profiler. Samples collected downstream of the known fluorochemical point source were compared to upstream samples, which should be free of species introduced by the intervening facility. Pairwise comparison was used to identify features unique to the downstream samples as well as species which were significantly increased (>3-fold increase in integrated peak area). The list of the top 100 most abundant unique and statistically significant species was exported and prepared as an inclusion list for further MS/MS investigation.

Structural investigation of the molecular features was performed using an Agilent 1260 Infinity UPLC coupled to an Agilent 6530 quadrupole time-of-flight (QTOF). Parameters for LC separation were the same as the initial TOF analysis, but MS settings were adjusted to allow collection of MS/MS fragmentation spectra of the targeted inclusion list from the TOF analysis. Modifications to the MS collection are detailed in the Supporting Information.

The raw data collected from QTOF MS/MS experiments was processed using ProFinder, followed by filtering to isolate features for closer inspection. Comparison of precursor and fragment masses allowed a maximum 5 ppm precursor and 20 ppm fragment mass error; average mass error was ∼1 ppm, consistent with the performance specifications of the instru-

DOI: 10.1021/acs.est.8b06017
Environ. Sci. Technol. 2019, 53, 4717−4727

ment. Features were individually examined to determine structures where possible. For each mass-to-charge (m/z) identified at the formula level or better (Confidence 4+), an ±10 ppm extracted ion chromatogram of the theoretical precursor mass was generated to determine retention times (Supporting Information Figures 1−83). Composite MS/MS spectra consisting of multiple averaged MS/MS scans at collision induced dissociation (CID) energies of 10 and 25 V; spectrawere generated for individual isomers of each precursor, where possible.

The list of molecular features was sorted by integrated peak area and the isotopic distributions for each of the molecular features; a putative empirical formula was assigned using MassHunter's formula generator tool. This assignment is a score obtained by matching the feature's accurate mass and isotopic distribution with theoretical values calculated using known isotopic distributions of a potential formula's constituent elements (i.e., 1.1% ^{13}C, 0.4% ^{15}N, etc.). Allowed atoms included C, H, N, O, S, F, Cl, Br, and P. For compounds with only poorly scoring isotopic matches (e.g., <70%), background subtraction of the precursor spectrum was carried out against a background of the 0.2 min regions immediately preceding and following the chromatographic peak, and a second attempt at formula assignment was made.

The MS/MS spectra collected for each molecular feature were manually examined to ascertain the accuracy of the precursor formula and attempt to resolve molecular structures. Emphasis was placed on chemicals demonstrating a negative mass defect—the difference between the exact and nominal mass of the compound, a common signature of halogenation.[22] It is worth noting that this is only a rough proxy for the inclusion of critical atoms of interest (i.e F, Cl, Br) in small molecules and significant supporting data is necessary to classify an unknown as a PFAS.[35] Fragment ions were assigned partial empirical formulas based on exact monoisotopic mass using a similar process to the precursor mass but using the precursor formula as the list of allowed atoms. Potential formulas were compared against the existing EPA's Comptox Chemicals Dashboard,[36] an internally maintained PFAS database, and extant literature, including publications, patents, and the CAS registry, to obtain known potential structures. Potential structures were also generated *de novo* based on observed fragments and related chemicals. A degree-of-confidence assessment for each chemical feature was assigned based on the Schymanski classification.[37] Briefly, where verified standards existed for a proposed structure, comparison with the retention time and MS/MS structure of the standard was carried out; matches were assigned a confidence level of 1. In the absence of a confirmed standard, fragment ions were compared to available standards with similar substructures and empirical or *in silico* library spectra; probable structures were assigned a confidence level of 2. Where structures could not be completely resolved by MS/MS, partial elucidation of chemical class/structure was based on diagnostic fragments and relationship to identified compounds; tentative candidates were assigned a confidence level of 3. In absence of quality MS/MS spectra or where incompatible tentative candidates could not be resolved, only a molecular formula was determined; molecular formula level assignments were given a confidence level of 4. Features with lower confidence were not reported here.

Clustering of Non-Targeted Chemical Features by Time Trend. The samples collected in May 2017 and February 2018 bracketed significant changes to the Cape Fear River as the result of regulatory actions by NCDEQ against the Chemours company.[33] As part of their ongoing monitoring, the state collected water samples proximate to the waste outfall into the Cape Fear River over several months during the summer of 2017. These samples were acquired from NCDEQ, analyzed by TOF-MS as described, and the ion abundances for the species were monitored over the sampling time points. Abundance measurements for each chemical were normalized to the highest abundance for the feature across all sampling points for that chemical. Time trends of chemical features were hierarchical clustered for similarity with *hclust* in R (3.4.4) using Euclidean distance and the "Ward.D2" clustering criterion;[38] cluster p-values were calculated using *pvclust*[39] with 10000 bootstrap iterations and filtered to $p < 0.05$.

RESULTS AND DISCUSSION

Feature extraction from surface water collected upstream of a fluorochemical manufacturing site yielded ∼120 distinct molecular features. Features with PFAS-like MS signatures were all from the legacy perfluorinated acids (PFBA, PFPeA, PFHxA, PFHpA, PFHxS, PFOA, and PFOS). No additional PFAS species were detected in the samples. The existence of these fluorinated compounds in the surface water is expected, because of their persistent nature and ubiquitous use in preceding years, and has been previously reported.[40−44]

Feature extraction from the sample immediately downstream from the fluorochemical manufacturer yielded a significantly larger amount of ∼260 distinct molecular features of which nearly 200 possess the negative mass defect marker indicative of potential halogenation (Supporting Information Table 1). A comparison of the total signal intensity of species with a negative mass defect in the upstream and downstream samples indicates that while ∼15% of the total ion current for the upstream sample is resultant from perfluorinated acids above, the downstream sample is, by total ion intensity, >90% composed of species with a negative mass defect. Further, the ambient PFASs detected upstream make up <1% of the total ion intensity in the downstream sample. Clearly, wastewater discharge from the fluorochemical manufacture introduces a significant number of compounds to the river besides the legacy perfluorinated acids detailed in EPA 537[45] (Supporting Information Table 1).

Manual curation of detected chemical features yielded 58 distinct chromatographically resolved PFAS peaks, corresponding to 38 unique molecular formulas. Recent efforts have been made to identify novel contaminant species in fluorochemically impacted water supplies by the US EPA and other groups.[26,46−49] Cross-referencing literature lists of expected monoisotopic masses and their hypothetical structures against the molecular features observed in this study accounts for roughly half of the unique features, with the remainder being unidentified based on literature comparison.

The features were individually examined to determine novel structures as described in the Methods section (Supporting Information Table 2). For each mass-to-charge (m/z) identified at the formula level or better, an extracted ion chromatogram of the precursor mass was generated to determine retention times (Supporting Information Figures 1−83). Composite MS/MS spectra consisting of multiple averaged MS/MS scans at 10 and 25 CID settings were

DOI: 10.1021/acs.est.8b06017
Environ. Sci. Technol. 2019, 53, 4717−4727

Table 1. Identified Perfluorinated Ether Acids

ID	Conf	Formula	Theoretical [M]	ppm error	Isomers	CAS	Ref
1	1	$C_3HF_5O_3$	179.9846	1.68	1	674-13-5	29
2	1	$C_4HF_7O_3$	229.9814	2.18	2	13140-29-9, 377-73-1	29
3	1/2b	$C_4HF_7O_4$	245.9763	0.41	1	39492-88-1	29
4	2b	$C_5HF_9O_3$	279.9782	1.43	1	267239-61-2	29
5	3	$C_5HF_9O_4$	295.9731	2.71	1		
6	1	$C_5HF_9O_5$	311.968	0.96	1	39492-89-2	29
7	1	$C_6HF_{11}O_3$	329.975	1.22	1	13252-13-6	29
8	3	$C_6HF_{11}O_4$	345.9699	0.58	1		
9	3	$C_6HF_{11}O_5$	361.9648	0.83	1		
10	1	$C_6HF_{11}O_6$	377.9597	1.59	1		29
11	4	$C_8HF_{13}O_4$	407.9667	0.25	1		
12	3	$C_7HF_{13}O_5$	411.9616	1.46	1		
13	1	$C_7HF_{13}O_7$	443.9515	0.90	1		29
14	2b	$C_4HF_9O_4S$	315.94518	1.97	1	113507-82-7	29
15	3	$C_5HF_{11}O_4S$	365.94199	0.85	1		
16	1	$C_7HF_{13}O_5S$	443.93371	0.20	1	29311-67-9	29
17	3	$C_8HF_{15}O_5S$	493.93052	0.04	1		

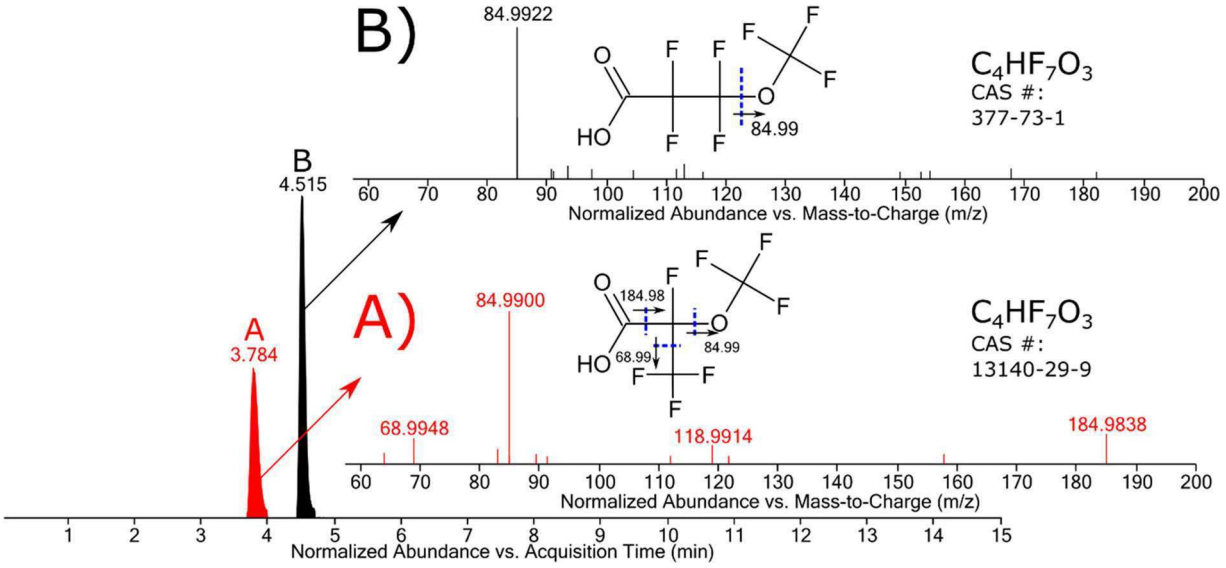

Figure 1. Determination of isomeric branching of perfluorinated ether compounds based on MS/MS fragmentation patterns. Compound 2A elutes at 3.8 min and has multiple major mass fragments. Compound 2B elutes later at 4.5 min and fragments only at the terminal ether linkage.

generated for individual isomers of each precursor, where possible (Supporting Information Figures 1−83).

Group A: Perfluorinated Ether Acids. A frequently observed PFAS class is that of fluoroether acids (here Group A), which exist with a general formula $CF_3(CF_2)_n(CF_2O)_m(R_1)$, where the headgroup, R_1, is an acidic moiety such as −COOH or $-SO_3H$.[29,30] These were expected to be the primary contaminants identified in the survey, given that nearby production includes perfluorinated polyvinyl ethers, empirical formula $(CF_2)_n(CF_2O)_m$. The production of the ammonium salt of 2,3,3,3-tetrafluoro-2-(heptafluoropropoxy) propanoic acid,[21] where $n = 3$, $m = 1$, R1 = COOH is shown in the above scheme, and "Nafion", a copolymer of tetrafluoroethylene and perfluoro(4-methyl-3,6-dioxaoct-7-ene)sulfonic acid, a monomer where $n = 3$, $m = 2$, $R_1 = SO_3H$ is shown as above.[50] Numerous molecules in this series were found during this sampling event (Table 1).

Compound 2 was identified previously in historical sampling in the river basin;[29] however, the UPLC separation resolved two isomeric structures with different MS/MS fragmentation patterns (Figure 1), which was not observed for other Group A species. The more abundant isomer of compound 2 (2B) is available as a standard, and its MS/MS fragmentation pattern and retention were confirmed to match the tentative assignment. The additional isomer is currently not commercially available and was assigned on the basis of MS/MS fragmentation and the shift in reverse phase retention time, indicative of increased branching (Schymanski Level 2b).[51]

The primary fragments for perfluorinated ether carboxylic acids are typically decarboxylation (neutral loss of 43.9898 Da) and production of the terminal ether fragment (here CF_3O^-, 84.99067 Da). Sulfonated acids produce a sulfonate (SO_3^-, 79.9568 Da) fragment instead of a decarboxylation, but the primary structural fragment remains the terminal ether. These patterns were observed across all Group A compounds, but the lack of significant internal fragmentation makes it difficult to assign complete linkage isomerization of longer perfluorinated

DOI: 10.1021/acs.est.8b06017
Environ. Sci. Technol. 2019, 53, 4717−4727

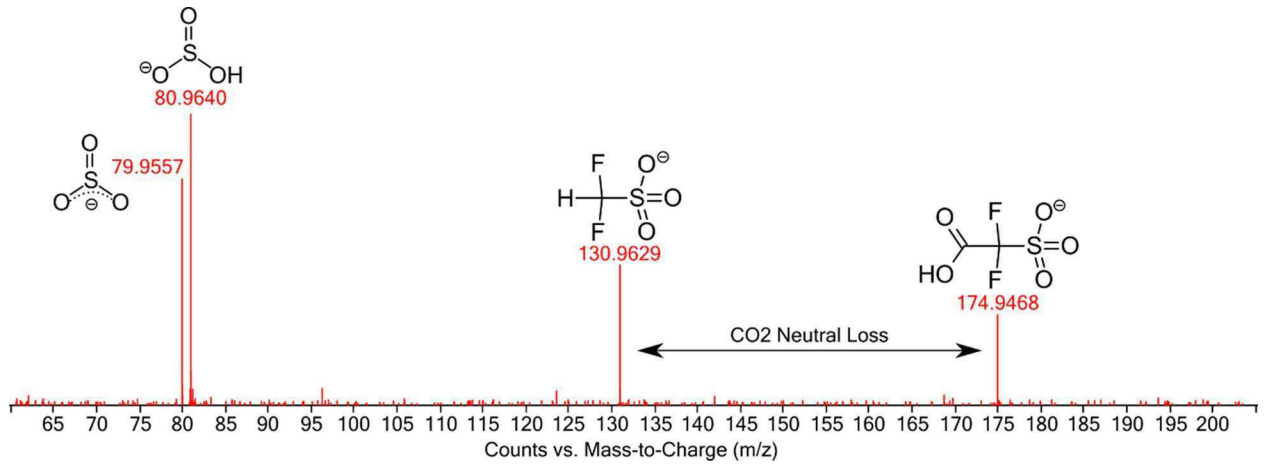

Figure 2. Annotated MS/MS spectrum of precursor m/z 174.9496 (compound 18), assigned the molecular formula $C_2H_2F_2O_5S$.

Table 2. Identified Perfluorinated Ether Acids with Multiple Acidic Sites

ID	Conf	Formula	Theoretical [M]	ppm error	Isomers	CAS	Ref
18	2b	$C_2H_2F_2O_5S$	175.9591	0.57	1	422-67-3	55
19	2b/3	$C_5H_2F_8O_6S$	341.9444	2.35	2	790642-73-8	55
20	3	$C_6H_2F_{10}O_5$	343.9743	2.33	1	919005-07-5	56
21	4	$C_7H_3F_{11}O_7S$	439.9424	0.68	2		
22	2b/3	$C_7H_2F_{12}O_6S$	441.938	0.23	2	852157-01-8	57
23	2b/3	$C_8H_2F_{14}O_7S$	507.9298	1.18	2	1235024-21-1	57
24	2b/3	$C_7H_3F_{13}O_8S_2$	525.9062	0.19	2	916340-65-3	58

ethers based on MS/MS alone, and many compounds remain level 3 identifications.

The initial patent description of the polyvinyl ether process refers to the creation of multiple competing side reactions and low molecular weight polyfluoro-ether byproducts,[52,53] which have been used as reactants and starting materials in more complicated copolymer production schemes.[54] Without further information about manufacturing processes, it is not immediately clear which reactions and waste streams yield the perfluoroether compounds detected and whether they are primary or secondary waste products. Further, broader nontargeted efforts would be necessary to determine whether they are contained in finished products directly impacting consumers or only in the nearby environment; however, the spatial and temporal correlation of detected species is highly suggestive of the point source (i.e., manufacturing outfall).

Group B: Multi-Headed Perfluoroether Species. Perfluoroether species previously described can be thought of in a more general sense as compounds with the form R_1-$(CF_2)_n(CF_2O)_m$-R_2, where R_1 and R_2 are both variable head groups. While R_1 is CF_3 for the Group A perfluorinated acids previously discussed, some compounds were observed with multiple acidic groups (R_1, R_2 = −COOH or $-SO_3H$). This group of compounds was identified in both −1 and −2 charge states and had initial predicted formulas suggesting an overabundance of oxygens which could only be structurally supported by multiple acidic sites on the perfluorinated backbone. Further, diagnostic ions for CO_2 and/or SO_3 were observed (Figure 2). We grouped these species as Group B, multiply sulfonated and/or carboxylated perfluorinated ether acids (Table 2).

While these species have not been previously reported in environmental media, to the best of our knowledge, the literature of fluorochemical manufacturers proposes a few possible structures in this group, primarily as side products in fluoropolymer production and degradation.[55−57] The formation of short chain fluorosulfonyl ($-SO_2F$) and acyl fluoride (−COF) fluoroethers formed as byproducts or intermediate steps in fluoropolymer synthesis is the likely source of precursor compounds that degrade into the observed compounds.[52] Aqueous hydrolysis of the acid fluoride intermediates during production or water treatment yields the familiar carboxylic acid (−COOH) and sulfonic acid moieties ($-SO_3H$), while more basic conditions (e.g., KOH, Na_2CO_3, etc.) yield further hydrolysis products (Scheme 1). These full and partial hydrolysis reactions are well-known steps in fluoropolymer production and in the abatement of fluoroether salts.[59−61]

Scheme 1. Transformation of a Fluorosulfonyl/Acyl Fluoride Fluoroether to Sulfonate End Products by Hydroloysis

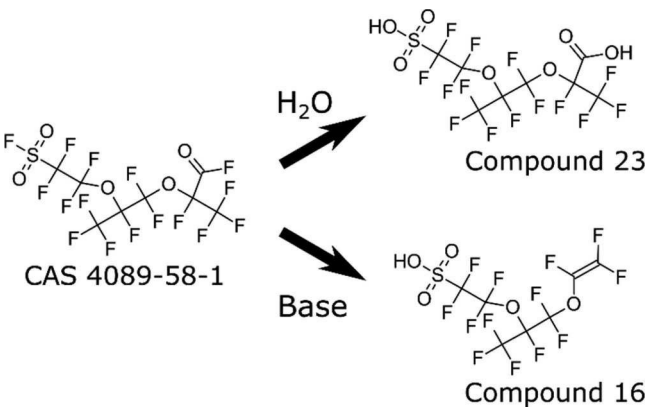

DOI: 10.1021/acs.est.8b06017
Environ. Sci. Technol. 2019, 53, 4717−4727

Table 3. Identified Polyfluorinated Ether Acids with a Single Hydrogen Substitution

ID	Conf	Formula	Theoretical [M]	ppm error	Isomers	CAS	Ref
25	2b/3	$C_3H_2F_6O_4S$	247.9578	1.62	3	905363-45-3	58
26	1	$C_4H_2F_8O_4S$	297.9546	1.35	1	905363-44-2	58
27	2b/3	$C_5H_2F_{10}O_4S$	347.9514	1.15	3	935443-55-3	58
28	3	$C_6H_2F_{12}O_4S$	397.9482	1.51	2		
29	3	$C_8H_2F_{14}O_4S$	459.9450	0.00	3		
30	2b/3	$C_5H_2F_8O_3$	261.9876	1.15	3	919005-00-8, 919005-13-3	56
31	2b/3	$C_6H_2F_{10}O_3$	311.9844	1.61	3	919005-19-9	56
32	3	$C_7H_2F_{12}O_3$	361.9812	3.05	1	919005-26-8	56
33	3	$C_6H_2F_{12}O_5S$	413.9431	0.00	2		
34	1	$C_7H_2F_{14}O_5S$	463.9399	1.30	2	749836-20-2	29
35	4	$C_9H_2F_{16}O_6S$	541.9317	0.00	1		
36	1	$C_8H_2F_{14}O_4$	427.9730	2.11	1	773804-62-9	
37	4	$C_8H_2F_{14}O_7$	475.9577	4.42	2		

Group C: Single-H Containing Polyfluorinated Acids. Another subset of fluorinated compounds, Group C, was identified with molecular formulas containing a single F → H substitution compared to that in the Group A perfluorinated ether compounds (Table 3). For example, compound 14 ($C_4HO_4SF_9$) and compound 26 ($C_4H_2O_4SF_8$) differ by the substitution of a hydrogen for a fluorine. These compounds are highly isomerized, and MS/MS fragmentation is frequently insufficient to unequivocally assign the structure; the structures presented in the Supporting Information (Table S-2) are representative of a single observed isomer.

The production of polyfluorosulfonic acid ethers of the form R-OCF**H**−CF_2−SO_3 was described in early patent filings,[58] and their use as fluoropolymer surfactants was mentioned in a follow up.[62] The use and production of these chemicals as part of Nafion manufacturing is assumed to be responsible for at least some of the observed species. In contrast to the previously mentioned literature structures, MS/MS fragmentation of some polyether sulfonate isomers indicates that the single hydrogen substitution occurs on the tail ether rather than adjacent to the head; for example, the fragment C_2HF_4O− (116.9969 Da) from one isomer of compound 30 (Supporting Information Figure 64) is derived from a two carbon polyfluorinated ether unit (Supporting Information Table S-4). These species are assumed to be products of the fluorosulfonyl and/or acyl fluoride species which produced Group B but further decomposed. The complete loss of a headgroup (e.g., decarboxylation) during production, waste treatment, or naturally in surface water would yield a compound with a single hydrogen in that site (Scheme 2). Thermally decarboxylated perfluoroether species are noted as potentially undesirable byproducts of fluoropolymer production in the patent literature of fluoropolymer production,[60] and partially decarboxylated species are noted as possible products from multiply acidic species such as Group B chemicals.[63]

Scheme 2. Transformation by Decarboxylation of Sulfonated Carboxylic Acid Perfluoroether to Yield the Polyfluorosulfonic Acid

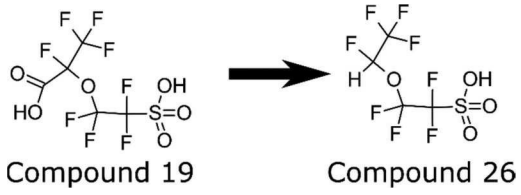

Presence and Prevalence of Novel Species. The lack of authentic standards limits the potential for quantitative measurements of novel compounds; relative abundance and semiquantitative estimates of emerging compounds are all that are available. However, this information remains useful for targeting individual chemicals for follow-up study and for monitoring environmental changes in response to systemic actions. Our examination of the May 2017 downstream sample could assign 35 of the top 50 most abundant features, corresponding to ∼90% of the total ion current in the sample (Figure 3). While ion abundances are sensitive to many aspects of the sample matrix and molecules, the structural similarity of the fluoroethers would suggest some similarity in instrument response, and that species can be roughly compared. At least one species of each of the three major chemical groups outlined (groups A, B, and C) exhibited a higher ion abundance than the HFPO-DA species with a targeted health goal. Further, of the targeted compounds detailed in EPA 537,[45] only perfluoropentanoic acid (PFPeA) is present in the top 50; thus, the fluorochemical load in the system would be greatly underestimated by traditional targeted approaches. Additionally, including the compounds previously detailed in studies of the Cape Fear River[29,30] accounts for only ∼50% of the total ion intensity in the initial sample, suggesting that even single-time-point nontargeted survey can fail to sufficiently capture the chemical complexity of a location.

An advantage of nontargeted analysis is the historical data banking of samples and the ability to perform relative quantification across disparate sample sets. The comparison of chemical species abundance over the time period from May 2017 to February 2018 revealed several distinct abundance patterns from simple visual inspection (Figure 4). Many fluoroether species exhibited exponential decline in concentration (Figure 4, left) while others showed lagging or even temporarily increased abundances (Figure 4, center and right).

Matrices of the weekly relative ion abundance of each of the identified chemical features over the eight sampling points were clustered for similarity using Ward's clustering criterion implemented in R *hclust*;[38] *p*-value calculations for clusters were performed using multiscale bootstrap resampling implemented in the *pvclust* package. Clustering of the time-trend data yielded six distinct chemical clusters (Figure 5, Supporting Information Figures 84−89).

DOI: 10.1021/acs.est.8b06017
Environ. Sci. Technol. 2019, 53, 4717−4727

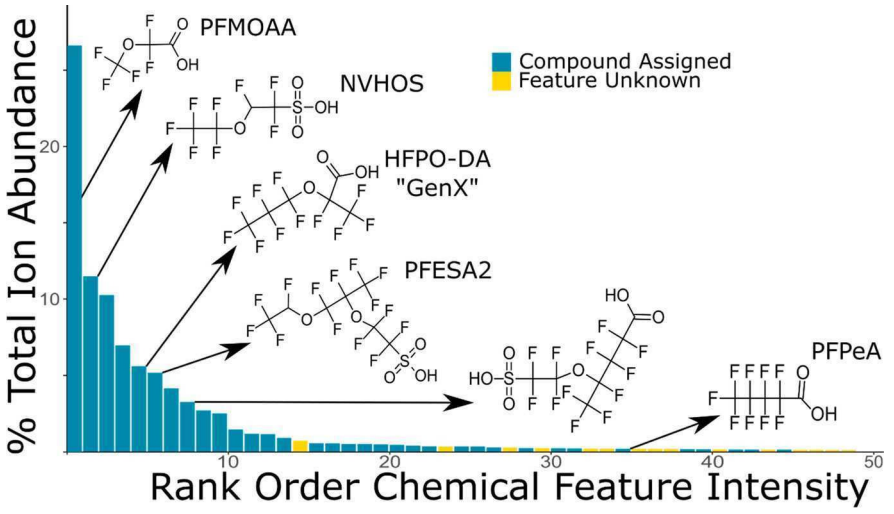

Figure 3. Total ion abundance as a percentage of the sum of all chemical features for compounds identified in a May 2017 sample of the Cape Fear River downstream of a fluorochemical manufacturer. Selected highly abundant compounds confirmed by standards obtained from and labeled by Chemours include: compounds 1 (PFMOAA), 26 (NVHOS), 7 (HFPO-DA), 34 (PFESA2), 22 (PFESA4), and perfluoropentanoic acid (PFPeA).

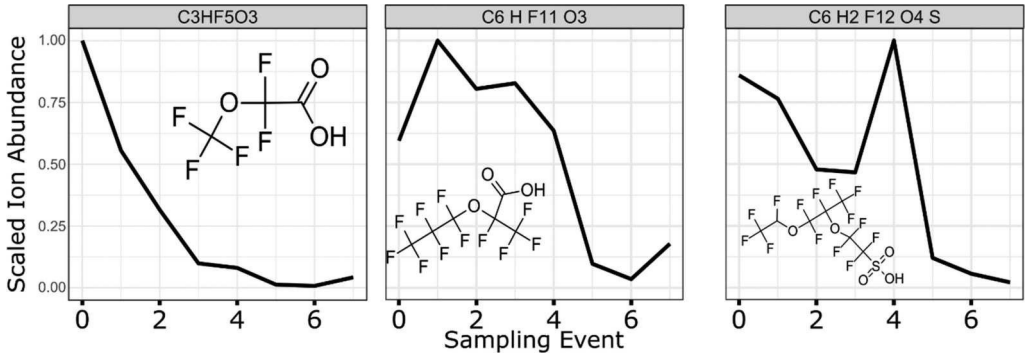

Figure 4. Scaled ion abundance of three chemical features confirmed by standard and detected in the Cape Fear River over a time course sample. Time points one to six were taken weekly beginning June 19, 2017 with time points zero and seven being collected in May 2017 and February 2018, respectively.

These clusters support the hypothesis that multiple production processes generate distinct groups of the chemicals observed in the Cape Fear River, as the compound abundances are correlated over time and are chemically similar based on naive classification. For example, the cluster at branch 16 (Figure 5) contains the H-substituted sulfonic acid ethers from Group C. These compounds abruptly and almost uniformly vanish following the initial sampling event (Supporting Information Figure 86), while the clusters at branches 13 and 18 contain the perfluoroether carboxylic acids and their associated H substituted versions; both classes exponentially and smoothly decrease from the early sampling events (Supporting Information Figures 84,87). Other clusters contain more chemical variation, as well as more complex time-trend patterns, that may be reflective of species with multiple sources or processes involving multiple PFAS classes.

It is worth noting that the chemical assignment provided to each feature is not required for clustering. Application of the clustering approach reveals chemical feature relationships that could be used to target unidentified species for follow-up analysis based on their close association with compounds of interest (e.g., HFPO-DA), and occurs before the assignment of formulas or structures.

Environmental Impact. The phase-out of PFOA/PFOS and longer-chain PFAS materials has led to an increased prevalence of replacement chemicals. The chemical groups detailed here are derived from processes and procedures that are over 20 years old within the fluorochemical production industry but are only now becoming apparent due to increased scrutiny of environmental media and the proliferation of nontargeted methodologies. Fluorinated ethers such as those described here have been reported in the Cape Fear River previously.[29,30] Similar structures have been reported in numerous locations worldwide, indicating that emerging PFAS are every bit as ubiquitous as their PFOA/PFOS antecedents.[64,65] Physiochemical characteristics of similar perfluorinated ether compounds suggest that the fluoroether substances are of reduced health impact compared to similarly sized perfluorinated acids, but retain some degree of health risk.[66] Further, longer-chain perfluorinated ethers are not currently regulated similarly to long chain perfluorinated acids and exhibit similar bioaccumulation potential, as evidenced by the preliminary reporting in human blood in spite of their relative low abundance in surface water.[67] Efforts to determine reasonable health levels for these emerging compounds are ongoing. During the preparation of this manuscript, the state of North Carolina set a drinking water health goal for a single perfluorinated ether acid (PFECA) compound, HFPO-DA, at 140 ng/L, based on their assessment of human health risk from available data submitted in the European Union.[31,68,69]

DOI: 10.1021/acs.est.8b06017
Environ. Sci. Technol. 2019, 53, 4717−4727

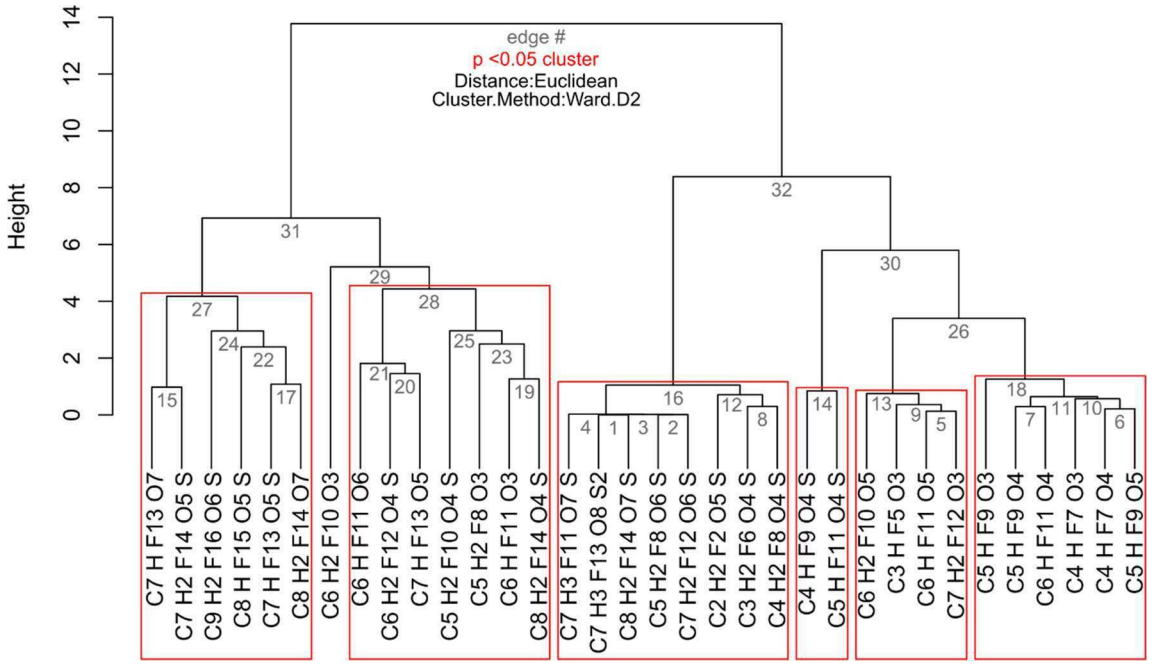

Figure 5. Clustering of identified chemical features from scaled ion-abundance of features detected in the Cape Fear River in eight sampling events between May 2017 and February 2018.

Sulfonated ether substances in this measurement series are primarily associated with sulfonated fluoropolymer production, specifically the Nafion polymer, and are of lesser widespread concern due to the limited manufacture of such polymers and their primary application being energy-related technologies, such as fuel cells.[50] Nevertheless, for locations that are exposed to such manufacturing waste streams, sulfonated fluorinated acids have shown higher accumulation potential and toxicological effects than equivalent carboxylic acids.[19] Further, other sulfonated ether acids, such as F-53B, have shown equivalent bioaccumulation potential as the regulated perfluorinated sulfonic acid PFOS.[70,71] Other sulfonated fluoroether species have begun to be detected by other groups, but they exhibit different structural elements and likely have different origins that need to be examined independently.[64,72] The continued appearance of new PFAS species necessitates an increase in the generation of toxicological profiling and monitoring efforts to assess human risk from exposure to these novel chemicals.

With regards to human exposure, it has been demonstrated that perfluoroether compounds are poorly cleared by water treatment processes, including activated carbon, and the most effective method of removal is through source control.[30,73] Long-term monitoring of impacted watersheds remains an important tool for both detecting new chemical species over multiyear time scales and for determining shorter-term changes in local chemical load. An application of this approach to other watersheds has been effective for other chemical classes, such as surfactants.[23,47] During the course of this study, our monitoring activities resulted in the cessation of discharge from the vinyl ether production at the source manufacturing location, which resulted in a concomitant decrease in PFECAs hypothesized to derive from that process, but not in the immediate reduction of the perfluorinated ether sulfonic acid (PFESAs) species since they derive from a different source than the PFECAs.[33] Targeted methods and single time-point nontargeted surveys can easily miss transient chemicals or underestimate chemical loads for exposure assessment; some species spiked as much as 5-fold during the sampling period (cluster branch 27, Supporting Information Figure 88), even as other compounds were declining. The proactive application of a nontargeted screening approach is capable of identifying and monitoring chemicals present in the water, even prior to complete structural elucidation or toxicological analysis and provides a useful tool toward those ends.

■ ASSOCIATED CONTENT

Supporting Information

The Supporting Information is available free of charge on the ACS Publications website at DOI: 10.1021/acs.est.8b06017.

All detected chemical features, assigned chemical species, software settings for molecular feature extraction, common MS/MS fragments of PFAS compounds, chromatographic traces for molecular ions of chemical features, composite MS/MS fragmentation spectra of chemical features, scaled abundance time trends for chemical features, statistical validation of chemical feature clustering, sampling map (PDF)

Cape Fear upstream and downstream data (XLSX)

■ AUTHOR INFORMATION

Corresponding Author

*Phone: 919-541-3706. E-mail: strynar.mark@epa.gov.

ORCID

James McCord: 0000-0002-1780-4916

Mark Strynar: 0000-0003-3472-7921

Author Contributions

The manuscript was written through contributions of all authors. All authors have given approval to the final version of the manuscript.

Notes

The authors declare no competing financial interest.

DOI: 10.1021/acs.est.8b06017
Environ. Sci. Technol. 2019, 53, 4717−4727

■ ACKNOWLEDGMENTS

The U.S. Environmental Protection Agency, through its Office of Research and Development, funded and managed the research described here. This document has been reviewed by the U.S. Environmental Protection Agency, Office of Research and Development, and approved for publication. The views expressed in this article are those of the authors and do not necessarily represent the views or policies of the U.S. Environmental Protection Agency. This research was supported in part by an appointment to the Postdoctoral Research Program at the National Exposure Research Laboratory administered by the Oak Ridge Institute for Science and Education through Interagency Agreement DW89992431601 between the U.S. Department of Energy and the U.S. Environmental Protection Agency.

■ REFERENCES

(1) Lindstrom, A. B.; Strynar, M. J.; Libelo, E. L. Polyfluorinated Compounds: Past, Present, and Future. *Environ. Sci. Technol.* **2011**, *45* (19), 7954.

(2) Sargent, J. W.; Seffl, R. In *Properties of perfluorinated liquids, Federation proceedings*, 1970; pp 1699−1703.

(3) Rahman, M. F.; Peldszus, S.; Anderson, W. B. Behaviour and fate of perfluoroalkyl and polyfluoroalkyl substances (PFASs) in drinking water treatment: A review. *Water Res.* **2014**, *50*, 318−340.

(4) Grandjean, P.; Clapp, R. Changing Interpretation of Human Health Risks from Perfluorinated Compounds. *Public Health Rep.* **2014**, *129* (6), 482−485.

(5) *Provisional Health Advisories for Perfluorooctanoic Acid (PFOA) and Perfluorooctane Sulfonate (PFOS)*. In United States Environmental Protection Agency: Washington DC, 2009.

(6) Report of the Conference of the Parties of the Stockholm Convention on Persistent Organic Pollutants on the work of its fourth meeting 2009.

(7) Proposal for a COUNCIL DECISION on the submission, on behalf of the European Union, of a proposal for the listing of additional chemicals in Annex A to the Stockholm Convention on Persistent Organic Pollutants. In Council of the European Union: 2016.

(8) MacNeil, J.; Steenland, N. K.; Shankar, A.; Ducatman, A. A cross-sectional analysis of type II diabetes in a community with exposure to perfluorooctanoic acid (PFOA). *Environ. Res.* **2009**, *109* (8), 997−1003.

(9) Steenland, K.; Fletcher, T.; Savitz, D. A. Epidemiologic Evidence on the Health Effects of Perfluorooctanoic Acid (PFOA). *Environ. Health Perspect.* **2010**, *118* (8), 1100−1108.

(10) Fact Sheet: 2010/2015 PFOA Stewardship Program. https://www.epa.gov/assessing-and-managing-chemicals-under-tsca/fact-sheet-20102015-pfoa-stewardship-program.

(11) EPA and 3M Announce phase out of PFOS. https://yosemite.epa.gov/opa/admpress.nsf/0/33aa946e6cb11f35852568e1005246b4.

(12) Kissa, E. *Fluorinated surfactants and repellents*. CRC Press: 2001; Vol. 97.

(13) Bowman, J. S. Fluorotechnology is critical to modern life: the FluoroCouncil counterpoint to the Madrid Statement. *Environ. Health Perspect.* **2015**, *123* (5), A112.

(14) Scheringer, M.; Trier, X.; Cousins, I. T.; de Voogt, P.; Fletcher, T.; Wang, Z.; Webster, T. F. Helsingør Statement on poly- and perfluorinated alkyl substances (PFASs). *Chemosphere* **2014**, *114*, 337−339.

(15) Wang, Z.; Cousins, I. T.; Scheringer, M.; Hungerbühler, K. Fluorinated alternatives to long-chain perfluoroalkyl carboxylic acids (PFCAs), perfluoroalkane sulfonic acids (PFSAs) and their potential precursors. *Environ. Int.* **2013**, *60*, 242.

(16) Strempel, S.; Scheringer, M.; Ng, C. A.; Hungerbühler, K. Screening for PBT Chemicals among the "Existing" and "New" Chemicals of the EU. *Environ. Sci. Technol.* **2012**, *46* (11), 5680−5687.

(17) Fantke, P.; Weber, R.; Scheringer, M. From incremental to fundamental substitution in chemical alternatives assessment. *Sustainable Chemistry and Pharmacy* **2015**, *1*, 1−8.

(18) Blum, A.; Balan, S. A.; Scheringer, M.; Trier, X.; Goldenman, G.; Cousins, I. T.; Diamond, M.; Fletcher, T.; Higgins, C.; Lindeman, A. E. The Madrid statement on poly-and perfluoroalkyl substances (PFASs). *Environ. Health Perspect.* **2015**, *123* (5), A107.

(19) DeWitt, J. C. *Toxicological Effects of Perfluoroalkyl and Polyfluoroalkyl Substances*. 2015.

(20) Marchionni, G.; Tortelli, V.; Wlassics, I.; Kapeliouchko, V. Method for manufacturing fluoropolymers. US8703889B2, 2014.

(21) DuPont GenX Processing Aid for Making Fluoropolymer Resins. In *Chemours*: 2010.

(22) Trier, X.; Granby, K.; Christensen, J. H. Polyfluorinated surfactants (PFS) in paper and board coatings for food packaging. *Environ. Sci. Pollut. Res.* **2011**, *18* (7), 1108−1120.

(23) Schymanski, E. L.; Singer, H. P.; Slobodnik, J.; Ipolyi, I. M.; Oswald, P.; Krauss, M.; Schulze, T.; Haglund, P.; Letzel, T.; Grosse, S.; Thomaidis, N. S.; Bletsou, A.; Zwiener, C.; Ibáñez, M.; Portolés, T.; de Boer, R.; Reid, M. J.; Onghena, M.; Kunkel, U.; Schulz, W.; Guillon, A.; Noyon, N.; Leroy, G.; Bados, P.; Bogialli, S.; Stipaničev, D.; Rostkowski, P.; Hollender, J. Non-target screening with high-resolution mass spectrometry: critical review using a collaborative trial on water analysis. *Anal. Bioanal. Chem.* **2015**, *407* (21), 6237−6255.

(24) Chibwe, L.; Titaley, I. A.; Hoh, E.; Simonich, S. L. M. Integrated framework for identifying toxic transformation products in complex environmental mixtures. *Environ. Sci. Technol. Lett.* **2017**, *4* (2), 32−43.

(25) Knolhoff, A. M.; Croley, T. R. Non-targeted screening approaches for contaminants and adulterants in food using liquid chromatography hyphenated to high resolution mass spectrometry. *Journal of Chromatography A* **2016**, *1428*, 86−96.

(26) Newton, S.; McMahen, R.; Stoeckel, J. A.; Chislock, M.; Lindstrom, A.; Strynar, M. Novel Polyfluorinated Compounds Identified Using High Resolution Mass Spectrometry Downstream of Manufacturing Facilities near Decatur, Alabama. *Environ. Sci. Technol.* **2017**, *51* (3), 1544−1552.

(27) Ferrer, I.; Thurman, E. M. Liquid chromatography/time-of-flight/mass spectrometry (LC/TOF/MS) for the analysis of emerging contaminants. *TrAC, Trends Anal. Chem.* **2003**, *22* (10), 750.

(28) Liu, Y.; Pereira, A. D. S.; Martin, J. W. Discovery of C5−C17 Poly-and Perfluoroalkyl Substances in Water by In-Line SPE-HPLC-Orbitrap with In-Source Fragmentation Flagging. *Anal. Chem.* **2015**, *87* (8), 4260.

(29) Strynar, M.; Dagnino, S.; McMahen, R.; Liang, S.; Lindstrom, A.; Andersen, E.; McMillan, L.; Thurman, M.; Ferrer, I.; Ball, C. Identification of novel perfluoroalkyl ether carboxylic acids (PFECAs) and sulfonic acids (PFESAs) in natural waters using accurate mass time-of-flight mass spectrometry (TOFMS). *Environ. Sci. Technol.* **2015**, *49* (19), 11622.

(30) Sun, M.; Arevalo, E.; Strynar, M.; Lindstrom, A.; Richardson, M.; Kearns, B.; Pickett, A.; Smith, C.; Knappe, D. R. U. Legacy and Emerging Perfluoroalkyl Substances Are Important Drinking Water Contaminants in the Cape Fear River Watershed of North Carolina. *Environ. Sci. Technol. Lett.* **2016**, *3* (12), 415−419.

(31) *NC DHHS Preliminary Risk Assessment FAQ for GenX (Perfluoro2-propoxypropanoic acid)*. In North Carolina Department of Health and Human Services: 2017.

(32) Hagerty, V., Toxin taints CFPUA drinking water. *StarNews* 2017.

(33) NC Department of Environmental Quality GenX Investigation. https://deq.nc.gov/news/hot-topics/genx-investigation/.

(34) Nakayama, S. F.; Strynar, M. J.; Reiner, J. L.; Delinsky, A. D.; Lindstrom, A. B. Determination of perfluorinated compounds in the Upper Mississippi River Basin. *Environ. Sci. Technol.* **2010**, *44* (11), 4103.

DOI: 10.1021/acs.est.8b06017
Environ. Sci. Technol. 2019, 53, 4717−4727

(35) Sleno, L. The use of mass defect in modern mass spectrometry. *J. Mass Spectrom.* **2012**, *47* (2), 226−36.
(36) McEachran, A. D.; Sobus, J. R.; Williams, A. J. Identifying known unknowns using the US EPA's CompTox Chemistry Dashboard. *Anal. Bioanal. Chem.* **2017**, *409* (7), 1729−1735.
(37) Schymanski, E. L.; Jeon, J.; Gulde, R.; Fenner, K.; Ruff, M.; Singer, H. P.; Hollender, J. Identifying small molecules via high resolution mass spectrometry: communicating confidence. *Environ. Sci. Technol.* **2014**, *48* (4), 2097.
(38) Murtagh, F.; Legendre, P. Ward's Hierarchical Agglomerative Clustering Method: Which Algorithms Implement Ward's Criterion? *Journal of Classification* **2014**, *31* (3), 274−295.
(39) Suzuki, R.; Shimodaira, H. Pvclust: an R package for assessing the uncertainty in hierarchical clustering. *Bioinformatics* **2006**, *22* (12), 1540−1542.
(40) Hu, X. C.; Andrews, D. Q.; Lindstrom, A. B.; Bruton, T. A.; Schaider, L. A.; Grandjean, P.; Lohmann, R.; Carignan, C. C.; Blum, A.; Balan, S. A.; Higgins, C. P.; Sunderland, E. M. Detection of Poly- and Perfluoroalkyl Substances (PFASs) in U.S. Drinking Water Linked to Industrial Sites, Military Fire Training Areas, and Wastewater Treatment Plants. *Environ. Sci. Technol. Lett.* **2016**, *3* (10), 344−350.
(41) Arsenault, G.; Chittim, B.; McAlees, A.; McCrindle, R.; Riddell, N.; Yeo, B. Some issues relating to the use of perfluorooctanesulfonate (PFOS) samples as reference standards. *Chemosphere* **2008**, *70* (4), 616−25.
(42) Hansen, K. J.; Clemen, L. A.; Ellefson, M. E.; Johnson, H. O. Compound-specific, quantitative characterization of organic fluorochemicals in biological matrices. *Environ. Sci. Technol.* **2001**, *35* (4), 766−70.
(43) Giesy, J. P.; Kannan, K. Global distribution of perfluorooctane sulfonate in wildlife. *Environ. Sci. Technol.* **2001**, *35* (7), 1339−42.
(44) Buck, R. C.; Franklin, J.; Berger, U.; Conder, J. M.; Cousins, I. T.; de Voogt, P.; Jensen, A. A.; Kannan, K.; Mabury, S. A.; van Leeuwen, S. P. J. Perfluoroalkyl and Polyfluoroalkyl Substances in the Environment: Terminology, Classification, and Origins. *Integr. Environ. Assess. Manage.* **2011**, *7* (4), 513−541.
(45) Shoemaker, J.; Grimmett, P.; Boutin, B. *Method 537. Determination of selected perfluorinated alkyl acids in drinking water by solid phase extraction and liquid chromatography/tandem mass spectrometry (LC/MS/MS)*. U.S. Environmental Protection Agency: Washington, DC, 2009.
(46) J Place, B.; Field, J. *Identification of Novel Fluorochemicals in Aqueous Film-Forming Foams Used by the US Military*. 2012; Vol. *46*, p 7120−7.
(47) Hollender, J.; Schymanski, E. L.; Singer, H. P.; Ferguson, P. L. Nontarget Screening with High Resolution Mass Spectrometry in the Environment: Ready to Go? *Environ. Sci. Technol.* **2017**, *51* (20), 11505−11512.
(48) Gebbink, W. A.; van Asseldonk, L.; van Leeuwen, S. P. J. Presence of Emerging Per- and Polyfluoroalkyl Substances (PFASs) in River and Drinking Water near a Fluorochemical Production Plant in the Netherlands. *Environ. Sci. Technol.* **2017**, *51* (19), 11057−11065.
(49) Xiao, F.; Golovko, S. A.; Golovko, M. Y. Identification of novel non-ionic, cationic, zwitterionic, and anionic polyfluoroalkyl substances using UPLC−TOF−MSE high-resolution parent ion search. *Anal. Chim. Acta* **2017**, *988*, 41−49.
(50) Mauritz, K. A.; Moore, R. B. State of understanding of Nafion. *Chem. Rev.* **2004**, *104* (10), 4535−4586.
(51) Burda, J.; Kuraš, M.; Kříž, J.; Vodička, L. Relationship between retention behaviour and molecular structure of alkanes in reversed phase high performance liquid chromatography. *Fresenius' Z. Anal. Chem.* **1985**, *321* (6), 549−552.
(52) Franklin, G. W.; James, C. D. Fluorocarbon vinyl ether polymers. 3,282,875, 1966.
(53) Milian, J. A. S.; Moore, J. E. P.; Sousa, E. H. Fluorocarbon ethers derived from hexafluoropropylene epoxide. 3,250,808, 1966.
(54) Liang, B.; Hung, M. H.; Resnick, P. R. Co-production of perfluoromethyl perfluorovinyl ether and perfluoroethyl perfluorovinyl ether. US5777179A, 1998.
(55) Takasaki, M.; Nakagawa, Y.; Sakiyama, Y.; Tanabe, K.; Ookubo, K.; Sato, N.; Minamide, T.; Nakayama, H.; Hori, M. Degradation Study of Perfluorosulfonic Acid Polymer Electrolytes: Approach from Decomposition Product Analysis. *J. Electrochem. Soc.* **2013**, *160* (4), F413−F416.
(56) Hintzer, K.; Jürgens, M.; Kaspar, H.; Koenigsmann, H.; Lochhaas, K. H.; Maurer, A. R.; Schwertfeger, W.; Zipplies, T.; Mayer, L.; Dadalas, M. C. Method of making fluoropolymer dispersion. 7,671,112 B2, 2010.
(57) Zhou, C.; Guerra, M. A.; Qiu, Z.-M.; Zawodzinski, T. A.; Schiraldi, D. A. Chemical Durability Studies of Perfluorinated Sulfonic Acid Polymers and Model Compounds under Mimic Fuel Cell Conditions. *Macromolecules* **2007**, *40* (24), 8695−8707.
(58) Junk, C.; Harmer, M.; Feiring, A.; Schadt, F.; Schnepp, Z. Hydrofluoroalkanesulfonic acids from fluorovinyl ethers. 7,834,209, 2005−06−07, 2006.
(59) Brothers, P. D.; Leung, L. H.; Gangal, S. V. Abatement of Fluoroether Carboxylic Acids or Salts Employed in Fluoropolymer Resin Manufacture. 2015/0203427 A1 2009−11−12, 2009.
(60) Nappa Mario, J. Improved Process For Preparing Fluorocarbon Polyethers. EP 0337743 B1, 1989/04/12, 1994.
(61) Ezzell Bobby, R.; Carl William, P.; Mod William, A. Preparation, Decarboxylation And Polymerization Of Novel Acid Fluorides And Resulting Monomers. US 4687821 A, 1983/07/05, 1987.
(62) Peng, S.; Hung, M. H.; Junk, C. P.; Tang, P. L. Fluoroalkyl ether sulfonate surfactants. US 7,977,426 B2, 2010.
(63) Marchionni, G.; Petricci, S.; Spataro, G.; Pezzin, G. A study of the thermal decarboxylation of three perfluoropolyether salts. *J. Fluorine Chem.* **2003**, *124* (2), 123−130.
(64) Pan, Y.; Zhang, H.; Cui, Q.; Sheng, N.; Yeung, L. W. Y.; Sun, Y.; Guo, Y.; Dai, J. Worldwide Distribution of Novel Perfluoroether Carboxylic and Sulfonic Acids in Surface Water. *Environ. Sci. Technol.* **2018**, *52* (14), 7621−7629.
(65) Wang, Z.; DeWitt, J. C.; Higgins, C. P.; Cousins, I. T. A Never-Ending Story of Per- and Polyfluoroalkyl Substances (PFASs)? *Environ. Sci. Technol.* **2017**, *51* (5), 2508−2518.
(66) Wang, Z.; Cousins, I. T.; Scheringer, M.; Hungerbuehler, K. Hazard assessment of fluorinated alternatives to long-chain perfluoroalkyl acids (PFAAs) and their precursors: status quo, ongoing challenges and possible solutions. *Environ. Int.* **2015**, *75*, 172−9.
(67) Hoppin, J.; Knappe, D.; Smart, R.; May, K.; Collier, D.; DeWitt, J. The GenX Exposure Study: Center for Human Health and the Environment. https://chhe.research.ncsu.edu/the-genx-exposure-study/.
(68) *NC DHHS Risk Assessment FAQ, July 2017*. In North Carolina Department of Health and Human Services: 2017.
(69) Agency, E. C. Ammonium 2,3,3,3-tetrafluoro-2-(heptafluoropropoxy)propanoate Acute Toxicity Endpoint Summary. https://echa.europa.eu/registration-dossier/-/registered-dossier/2679/7/3/1.
(70) Shi, Y.; Vestergren, R.; Zhou, Z.; Song, X.; Xu, L.; Liang, Y.; Cai, Y. Tissue Distribution and Whole Body Burden of the Chlorinated Polyfluoroalkyl Ether Sulfonic Acid F-53B in Crucian Carp (Carassius carassius): Evidence for a Highly Bioaccumulative Contaminant of Emerging Concern. *Environ. Sci. Technol.* **2015**, *49* (24), 14156−14165.
(71) Briels, N.; Ciesielski, T. M.; Herzke, D.; Jaspers, V. L. B. Developmental Toxicity of Perfluorooctanesulfonate (PFOS) and Its Chlorinated Polyfluoroalkyl Ether Sulfonate Alternative F-53B in the Domestic Chicken. *Environ. Sci. Technol.* **2018**, *52* (21), 12859−12867.
(72) Rotander, A.; Kärrman, A.; Toms, L.-M. L.; Kay, M.; Mueller, J. F.; Gómez Ramos, M. J. Novel Fluorinated Surfactants Tentatively Identified in Firefighters Using Liquid Chromatography Quadrupole

DOI: 10.1021/acs.est.8b06017
Environ. Sci. Technol. 2019, 53, 4717−4727

Time-of-Flight Tandem Mass Spectrometry and a Case-Control Approach. *Environ. Sci. Technol.* **2015**, *49* (4), 2434−2442.
(73) Hopkins, Z. R.; Sun, M.; DeWitt, J. C.; Knappe, D. R. U. Recently Detected Drinking Water Contaminants: GenX and Other Per- and Polyfluoroalkyl Ether Acids. *J. - Am. Water Works Assoc.* **2018**, *110* (7), 13−28.

DOI: 10.1021/acs.est.8b06017
Environ. Sci. Technol. 2019, 53, 4717−4727

Table of Contents

General_Authors_Publications.....2
LI-266273_Summers_et_al_NaHRSI.....19
LI-266274_Summers_et_al_ResilienceToNaturalHazards-2018.....42
LI-266275_Buck_-_PRISM_2019_Publication.....59
Summers_STAA_2020_Bundle_-_percent_contribution_concurrence.....80
Summers_STAA_2020_Bundle_-_Journal_Statistics_Supplemental_Information.....83
Summers_et_al_NaHRSI.....84
Summers_et_al_ResilienceToNaturalHazards-2018.....107
Buck_-_PRISM_2019_Publication.....124

STAA REPORT FOR THE SCIENTIST NOMINATIONS

General Information:

Nomination ID/App ID:	20-109
Research Category Primary:	Sustainability and Innovation (SI)
Research Category Secondary:	Other Environmental Research (OR)
Laboratory/Office Name:	ORD
Nomination Entered By:	Matthew Harwell

Eligibility Checklist:

[Y] The nominated publication(s) has not been submitted to a previous STAA competition.

[Y] The nominated publication(s) was published on or before January 1, 2017 and on or after January 1,2012

[Y] The principal author was an EPA employee or a PHS employee assigned to EPA when the research was performed

[Y] The EPA authors (includes PHS employees assigned to EPA) contributed collectively a minimum of 50% toward the publication(s)

Nominating Official Name:	Susan George
Nominating Official Title:	DIRECTOR, GULF ECOLOGY DIVISION
Nominating OfficialEmail:	george.elizabeth@epa.gov
STAA Coordinator Name:	Kathleen Wiser
STAA Coordinator Email:	wiser.kathi@epa.gov

Justifications:

Justification 1:

1) The conceptualization, development and application of the Climate Resilience Screening Index (CRSI) (also referred to as NaHRSI – Natural Hazard Resilience Screening Index and after 2020 as CRSI – Cumulative Resilience Screening Index) was requested by the EPA Administrator through the ORD Assistant Administrator (previous administration) to provide a mechanism for the comparative evaluation of the climate/natural hazard resilience capacity of counties/communities throughout the United States. This index was designed to be used examine the strength of resilience to natural hazards, identify the contributing factors to that resilience, assess the local shortcomings in order the provide guidance for capacity building and to rank locales for Agency investment for capacity building. The index is the first approach to integrate environmental, economic and social attributes affecting resilience into a single representation. Other approaches examine a single attribute type or possibly two. The index provides direct support to the Office of Land and Emergency Management (OLEM) for emergency preparedness and response and to the Agency's mission of protecting human health and the environment. Similarly, CRSI provides support for the Agency Strategic Goals #1 (Core Mission) and #2 (Cooperative Federalism). CRSI provides information the results that enhance a county's or community's ability to protect its land, air and water resources and ensure chemical safety as well as provides counties and communities with the means to assess their resilience and create tangible improvements to that resilience.

The applications of the index demonstrate its utility at the national (Summers et al. 2018a) and regional (Summers et al 2018b) levels. Both applications provide the Agency with important information concerning the potential resilience of counties, states, regions and the nation to natural hazard events individually and combined. The first manuscript (Summers et al. 2018a) provides national level information of importance to EPA's Office of Land and Emergency Management (OLEM) for preparedness and responsiveness to natural hazards. The second manuscript (Summers et al. 2018b) provides regional level information that can be useful for EPA regions for preparedness and responsiveness to these events. The third manuscript provides the basis for the development of the risk domain used in CRSI that represents exposure and loss levels for each type of natural hazard.

Justification 2A:

The applications of the index demonstrate its utility at the national (Summers et al. 2018a) and regional (Summers et al 2018b) levels. Both applications provide the Agency with important information concerning the potential resilience of counties, states, regions and the nation to natural hazard events individually and combined. The first manuscript (Summers et al. 2018a) provides national level information of importance to EPA's Office of Land and Emergency Management (OLEM) for preparedness and responsiveness to natural hazards. The second manuscript (Summers et al. 2018b) provides regional level information that can be useful for EPA regions for preparedness and responsiveness to these events. The third manuscript provides the basis for the development of the risk domain used in CRSI that represents exposure and loss levels for each type of natural hazard.

Justification 2B:

J. Kevin Summers:

Summers, K. M. McCullough E. Smith, M. Gwinn, F. Kremer, M. Sjogren, A. Geller and M. Slimak. 2014. The Sustainable and Healthy Communities Research Program: The Environmental Protection Agency's Research Approach to Assisting Community Decision-Making. Sustainability 6: 306-318.

Summers, J.K., L.M. Smith, L.C. Harwell, J.C. Case, K.M. Wade, K.R. Straub, and H.M. Smith. 2014. An index of human well-being for the U.S.: A TRIO approach. Sustainability 6:3916-3935. (Received Honorable Mention Award – 2014)

Summers, J.K. and L.M. Smith. 2014. The roles of social and intergenerational equity in making changes in human well-being sustainable. Ambio 43: 718-728. (Submitted 2015)

Smith, L. M., Wade, C. M., Case, J. L., Harwell, L. C., Straub, K. R., & Summers, J. K. (2015). Evaluating the transferability of a US human well-being index (HWBI) framework to Native American populations. Social Indicators Research, 124(1), 157-182. (Nominated 2019)

Summers, J.K., L.C. Harwell and L.M. Smith. 2016. A model for change: An approach for forecasting well-being from service-based decisions. Ecological Indicators 69:295-309. (Nominated 2019)

Buck, K.D., J.K. Summers, L.M. Smith and L.C. Harwell. 2017. Application of the Human Well-Being Index to Sensitive Population Divisions: A Children's Well-Being Index Development. Children's Indicator Research 11(4): 1249-1280. (Nominated 2019)

Summers, J.K., L. M. Smith, L. C. Harwell, K. D. Buck, E. M. Hunter, S. F. Hafner and D. M. Nelson. 2017. Conceptualizing Holistic Climate Resilience: Foundation for the Climate Resilience Screening Index. GeoHealth 1: 151-164. (Nominated 2019; Awarded Level 1)

Hecht, A., A. Ferster and K. Summers. 2017**.** EPA Leadership on Science, Innovation, and Decision Support Tools for Addressing Current and Future Challenge. Jacobs Journal of Environmental Sciences 3:21

Summers, J.K. and D. N. Vivian. 2018. Ecotherapy: An unrealized ecosystem service. Frontiers in Psychology. 9: 1389. Doi: 10.3389/fpsyg.2018.01389 (Nominated 2019)

Summers, J.K., L.M. Smith, L.C. Harwell, K.D. Buck. 2018. Measuring community resilience to natural hazards; The Natural Hazard Resilience Screening Index (NaHRSI) – Development and Application to the United States. GeoHealth 2: 372-394. (Nominated 2020)

Summers, K., L. Harwell, L. Smith and K. Buck. 2018. Regionalizing resilience to acute meteorological events: Comparison of regions in the U.S. Frontiers in Environmental Science https://doi.org/10.3389/fenvs.2018.00147 (Nominated 2020)

Summers, J.K., L.M. Smith, R. Fulford and R. de Jesus Crespo. 2018. The Role of Ecosystem Services in Community Well-Being. In: L. Hufnagel (ed.) Ecosystem Services and Global Ecology. In-Tech Publishing. DOI:10.5772/intechopen.74068. (Nominated 2020)

Buck, K.D., J.K. Summers, S.F. Hafner, L.C. Harwell, and L.M. Smith. 2019. Development of a Multi-Hazard Landscape for Exposure and Risk Interpretation: The PRISM Approach. Current Environmental Engineering 6: doi: 10.2174/2212717806666190204103455 (Nominated 2020)

Smith, L.M., L.C. Harwell, J.K. Summers, J. Bousquin, J. Harvey and K.D. Buck. 2019. Using Re-Scaled Resilience Screening Index Results and Location Quotients for Socio-Ecological Characterizations in U.S. Coastal Regions**.** Frontiers in Environmental Science. doi: 10.3389/fenvs.2019.00096.

Summers, J.K., L.M. Smith and K.D. Buck. 2019. (eds.) Special Issue: Resilience (6 articles) Frontiers in Environmental Science.

Summers, J.K. 2019. (ed.) Special Issue: Ecosystem Services (25 articles). International Journal of Environmental Research and Public Health.

Summers, J.K., D.N. Vivian and J.T. Summers. 2019. The Role of Interaction with Nature in Childhood Development: An Under-Appreciated Ecosystem Service. Psychology and Behavioral Sciences 8: 142-150.

Lisa M. Smith

Summers, J.K., L.M. Smith, L.C. Harwell, J.C. Case, K.M. Wade, K.R. Straub, and H.M. Smith. 2014. An index of human well-being for the U.S.A. TRIO approach. Sustainability 6:3916-3935. (Received Honorable Mention Award – 2014)

Summers, J.K. and L.M. Smith. 2014. The roles of social and intergenerational equity in making changes in human well-being sustainable. Ambio 43: 718-728. (Submitted 2015)

Smith, L. M., Wade, C. M., Case, J. L., Harwell, L. C., Straub, K. R., & Summers, J. K. (2015). Evaluating the transferability of a US human well-being index (HWBI) framework to Native American populations. Social Indicators Research, 124(1), 157-182. (Nominated 2019)

Summers, J.K., L.C. Harwell and L.M. Smith. 2016. A model for change: An approach for forecasting well-being from service-based decisions. Ecological Indicators 69:295-309. (Nominated 2019)

Buck, K.D., J.K. Summers, L.M. Smith and L.C. Harwell. 2017. Application of the Human Well-Being Index to Sensitive Population Divisions: A Children's Well-Being Index Development. Children's Indicator Research 11(4): 1249-1280. (Nominated 2019)

Summers, J.K., L. M. Smith, L. C. Harwell, K. D. Buck, E. M. Hunter, S. F. Hafner and D. M. Nelson. 2017. Conceptualizing Holistic Climate Resilience: Foundation for the Climate Resilience Screening Index. GeoHealth 1: 151-164. (Nominated 2019 – Awarded Level 1)

Summers, J.K., L.M. Smith, L.C. Harwell, K.D. Buck. 2018. Measuring community resilience to natural hazards; The Natural Hazard Resilience Screening Index (NaHRSI) – Development and Application to the United States. GeoHealth 2: 372-394. (Nominated 2020)

Summers, K., L. Harwell, L. Smith and K. Buck. 2018. Regionalizing resilience to acute meteorological events: Comparison of regions in the U.S. Frontiers in Environmental Science https://doi.org/10.3389/fenvs.2018.00147 (Nominated 2020)

Summers, J.K., L.M. Smith, R. Fulford and R. de Jesus Crespo. 2018. The Role of Ecosystem Services in Community Well-Being. In: L. Hufnagel (ed.) Ecosystem Services and Global Ecology. In-Tech Publishing. DOI:10.5772/intechopen.74068. (Nominated 2020)

Buck, K.D., J.K. Summers, S.F. Hafner, L.C. Harwell, and L.M. Smith. 2019. Development of a Multi-Hazard Landscape for Exposure and Risk Interpretation: The PRISM Approach. Current Environmental Engineering 6: doi: 10.2174/2212717806666190204103455 (Nominated 2020)

Linda C. Harwell

Summers, J.K., L.M. Smith, L.C. Harwell, J.C. Case, K.M. Wade, K.R. Straub, and H.M. Smith. 2014. An index of human well-being for the U.S.: A TRIO approach. Sustainability 6:3916-3935. (Received Honorable Mention Award – 2014)

Smith, L. M., Wade, C. M., Case, J. L., Harwell, L. C., Straub, K. R., & Summers, J. K. (2015). Evaluating the transferability of a US human well-being index (HWBI) framework to Native American populations. Social Indicators Research, 124(1), 157-182. (Nominated 2019)

Ignatius, A. R., Wolfe, K., Parmar, R., Flaishans, J., Harwell, L., Yee, S., Purucker, T., and Galvin, M. (2016). Design and Implementation of a REST API for the Human Well Being Index (HWBI). 8th International Congress on Environmental Modelling and Software—Toulouse, France. July,2016. https://scholarsarchive.byu.edu/iemssconference/2016/Stream-A/17/

Summers, J.K., L.C. Harwell and L.M. Smith. 2016. A model for change: An approach for forecasting well-being from service-based decisions. Ecological Indicators 69:295-309. (Nominated 2019)

Buck, K.D., J.K. Summers, L.M. Smith and L.C. Harwell. 2017. Application of the Human Well-Being Index to Sensitive Population Divisions: A Children's Well-Being Index Development. Children's Indicator Research 11(4): 1249-1280. (Nominated 2019)

Summers, J.K., L. M. Smith, L. C. Harwell, K. D. Buck, E. M. Hunter, S. F. Hafner and D. M. Nelson. 2017. Conceptualizing Holistic Climate Resilience: Foundation for the Climate Resilience Screening Index. GeoHealth 1: 151-164. (Nominated 2019 – Won Level 1)

Summers, J.K., L.M. Smith, L.C. Harwell, K.D. Buck. 2018. Measuring community resilience to natural hazards; The Natural Hazard Resilience Screening Index (NaHRSI) – Development and Application to the United States. GeoHealth 2: 372-394. (Nominated 2020)

Summers, K., L. Harwell, L. Smith and K. Buck. 2018. Regionalizing resilience to acute meteorological events: Comparison of regions in the U.S. Frontiers in Environmental Science https://doi.org/10.3389/fenvs.2018.00147 (Nominated 2020)

Harwell Linda C., D. Vivian, M. McLaughlin, AND S. Hafner. 2018. Scientific Data Management in the Age of Big Data: An Approach Supporting a Resilience Index Development Effort. Frontiers in Environmental Science, Special Topic Area: Resilience to Natural Hazards – Concepts, Ecosystems and Communities. 04 June 2018.

Buck, K.D., J.K. Summers, S.F. Hafner, L.C. Harwell, and L.M. Smith. 2019. Development of a Multi-Hazard Landscape for Exposure and Risk Interpretation: The PRISM Approach. Current Environmental Engineering 6: doi: 10.2174/2212717806666190204103455 (Nominated 2020)

Yee, S.H., E. Paulukonis, M. Russell, R. Fulford, L.M. Smith, L. Harwell, C. Simmons. Forecasting effects of climate and land-use change on human well-being through changes in ecosystem services. (in review at Ecological Modelling)

Nestlerode, J. A., Murrell, M. C., Hagy, J. D., **Harwell, L.**, & Lisa, J. A. (2019). Bioassessment of a Northwest Florida Estuary Using Benthic Macroinvertebrates. *Integrated environmental assessment and management*, 16(2), 245-256.

Kyle D. Buck

Buck, K.D., J.K. Summers, L.M. Smith and L.C. Harwell. 2017. Application of the Human Well-Being Index to Sensitive Population Divisions: A Children's Well-Being Index Development. Children's Indicator Research 11(4): 1249-1280. (Nominated 2019)

Summers, J.K., L. M. Smith, L. C. Harwell, K. D. Buck, E. M. Hunter, S. F. Hafner and D. M. Nelson. 2017. Conceptualizing Holistic Climate Resilience: Foundation for the Climate Resilience Screening Index. GeoHealth 1: 151-164. (Nominated 2019)

Summers, J.K., L.M. Smith, L.C. Harwell, K.D. Buck. 2018. Measuring community resilience to natural hazards; The Natural Hazard Resilience Screening Index (NaHRSI) – Development and Application to the United States. GeoHealth 2: 372-394. (Nominated 2020)

Summers, K., L. Harwell, L. Smith and K. Buck. 2018. Regionalizing resilience to acute meteorological events: Comparison of regions in the U.S. Frontiers in Environmental Science https://doi.org/10.3389/fenvs.2018.00147 (Nominated 2020)

Buck, K.D., J.K. Summers, S.F. Hafner, L.C. Harwell, and L.M. Smith. 2019. Development of a Multi-Hazard Landscape for Exposure and Risk Interpretation: The PRISM Approach. Current Environmental Engineering 6: doi: 10.2174/2212717806666190204103455 (Nominated 2020)

Stephen Hafner:

Summers, Kevin, L. Harwell, K. Buck, L. Smith, D. Vivian, J. Bousquin, J. Harvey, S. Hafner, AND M.

McLaughlin. Development of a Climate Resilience Screening Index (CRSI): An Assessment of Resilience to Acute Meteorological Events and Selected Natural Hazards. U.S. Environmental Protection Agency, Washington, DC, EPA/600/R-17/238, 2017.

Buck, K., Kevin Summers, S. Hafner, L. Smith, AND L. Harwell. Development of a Multi-Hazard Landscape for Exposure and Risk Interpretation: The PRISM Approach. Current Environmental Engineering, 2019, Vol. 6, No. 1. (Nominated)

Harwell Linda C., D. Vivian, M. McLaughlin, AND S. Hafner. 2018. Scientific Data Management in the Age of Big Data: An Approach Supporting a Resilience Index Development Effort. Frontiers in Environmental Science, Special Topic Area: Resilience to Natural Hazards – Concepts, Ecosystems and Communities. 04 June 2018.

Justification 2C:

The present nominations represent applications of index and the previous submission (2019) represented the conceptualization of the index.

Justification 2D:

n/a

Justification 2E:

n/a

Justification 3A:

Record of Percentage Agreement attached.

The impact of this research includes invited presentations at national/international societies:

(1) Summers et al. 2018a invited to present at Fourteenth International Conference on Environmental, Cultural, Economic & Social Sustainability, Cairns, Australia, January 17-19, 2018

(2) Summers et al. 2018b invited to present at Fifteen International Conference on Environmental, Cultural, Economic & Social Sustainability, Vancouver, British Columbia, Canada, January 17-19, 2019 (unable to attend due to government shutdown)

(3) Buck et al. 2019 invited to present at Society for Conservation GIS (SCGIS) conference, Monterey, CA, July 2017.

Number of times the publication has been downloaded/viewed:

Summers et al. 2018a: 2197

Summers et al. 2018b: 1333

Buck et al. 2019: 177

And the number of times the publication has been downloaded/viewed (Google Scholar)

Summers et al. 2018a: 6

Summers et al. 2018b: 1

Buck et al. 2019: 2

Justification 3B:

The manuscripts were reviewed by an external reviewer, branch management and division management according to the ORD STICs process prior to submission to the journals, GeoHealth, Frontiers in Environment, and Current Environmental Engineering. The publications were further peer reviewed by two or more anonymous reviewers (for each manuscript) and the associate editor for each journal review.

AUTHORS

Contributing Author

Author Name:	J Kevin Summers		
Professional Title:		Salutation:	
Email:	summers.kevin@epa.gov	Organization:	
Mailing Address:			
Street Line 1:	Office of Research and Development, U.S. EPA 1 Sabine Island Drive		
City:	Gulf Breeze		
Zip Code:	32561	State:	FL
At time of research was:	EPA Employee		

Separation Date:			
% of Effort:	33		

Contributing Author

Author Name:	Lisa M Smith		
Professional Title:		Salutation:	
Email:	smith.lisam@epa.gov	Organization:	
Mailing Address:			
Street Line 1:	Office of Research and Development, U.S. EPA 1 Sabine Island Drive		
City:	Gulf Breeze		
Zip Code:	32561	State:	FL
At time of research was:	EPA Employee		
Separation Date:			
% of Effort:	17		

Contributing Author

Author Name:	Linda Harwell		
Professional Title:		Salutation:	
Email:	harwell.linda@epa.gov	Organization:	
Mailing Address:			
Street Line 1:	Office of Research and Development, U.S. EPA 1 Sabine Island Drive		
City:	Gulf Breeze		
Zip Code:	32561	State:	FL

At time of research was:	EPA Employee		
Separation Date:			
% of Effort:	18		

Contributing Author

Author Name:	Kyle Buck		
Professional Title:		Salutation:	
Email:	buck.kyle@epa.gov	Organization:	
Mailing Address:			
Street Line 1:	Office of Research and Development, U.S. EPA 1 Sabine Island Drive		
City:	Gulf Breeze		
Zip Code:	32561	State:	FL
At time of research was:	EPA Employee		
Separation Date:			
% of Effort:	26		

Contributing Author

Author Name:	Stephen Hafner		
Professional Title:		Salutation:	
Email:	stevehafner1@gmail.com	Organization:	
Mailing Address:			
Street Line 1:	Office of Research and Development, U.S. EPA 1 Sabine Island Drive		
City:	Gulf Breeze		

Zip Code:	32561	State:	FL
At time of research was:	Non EPA Personnel		
Separation Date:	Sat Sep 01 00:00:00 GMT 2018		
% of Effort:	6		

PUBLICATIONS

Publication 1:

Publication Title:	Measuring community resilience to natural hazards; The Natural Hazard Resilience Screening Index (Na		
Publication Date:	Fri Dec 07 00:00:00 GMT 2018		
Journal/Publication Method:	GeoHealth		
All Author(s):			
Volume:	2	Number:	*
Pages:	372-394	Immediately Index:	Immediately Index:
Citation ½ Life:	see note	Impact Factor:	see note

Publication 2:

Publication Title:	Regionalizing resilience to acute meteorological events: Comparison of regions in the U.S		
Publication Date:	Fri Nov 30 00:00:00 GMT 2018		
Journal/Publication Method:	Frontiers in Environmental Science		
All Author(s):			
Volume:	https://doi.org/10.3389/fenvs.2018.00147	Number:	*

Pages:	*	Immediately Index:	Immediately Index:
Citation ½ Life:	see note	Impact Factor:	see note

Publication 3:

Publication Title:	Development of a Multi-Hazard Landscape for Exposure and Risk Interpretation: The PRISM Approach		
Publication Date:	Sat Jan 19 00:00:00 GMT 2019		
Journal/Publication Method:	Current Environmental Engineering		
All Author(s):			
Volume:	6., doi: 10.2174/2212717806666190204103455	Number:	*
Pages:	*	Immediately Index:	Immediately Index:
Citation ½ Life:	see note	Impact Factor:	see note

GeoHealth

RESEARCH ARTICLE
10.1029/2018GH000160

Key Points:
- An index of resilience to acute weather events has been developed
- The index has been applied to all counties in the United States
- The application allows the comparison of resilience of counties and the selections of counties provided best lessons learned for county resilience improvement

Measuring Community Resilience to Natural Hazards: The Natural Hazard Resilience Screening Index (NaHRSI)—Development and Application to the United States

J. Kevin Summers[1], Linda C. Harwell[1], Lisa M. Smith[1], and Kyle D. Buck[1]

[1]Gulf Ecology Division, National Health and Environmental Effects Research Laboratory, U.S. Environmental Protection Agency, Gulf Breeze, FL, USA

Correspondence to:
J. K. Summers,
summers.kevin@epa.gov

Citation:
Summers, J. K., Harwell, L. C., Smith, L. M., & Buck, K. D. (2018). Measuring community resilience to natural hazards: The Natural Hazard Resilience Screening Index (NaHRSI)—Development and application to the United States. *GeoHealth*, *2*, 372–394. https://doi.org/10.1029/2018GH000160

Received 11 JUL 2018
Accepted 12 NOV 2018
Accepted article online 16 NOV 2018
Published online 7 DEC 2018

Author Contributions:
Conceptualization: J. Kevin Summers, Linda C. Harwell
Formal analysis: J. Kevin Summers, Linda C. Harwell
Investigation: J. Kevin Summers
Methodology: J. Kevin Summers, Linda C. Harwell
Validation: J. Kevin Summers
Visualization: J. Kevin Summers
Writing - original draft: J. Kevin Summers
Writing – review & editing: J. Kevin Summers, Linda C. Harwell

©2018. The Authors.
This is an open access article under the terms of the Creative Commons Attribution-NonCommercial-NoDerivs License, which permits use and distribution in any medium, provided the original work is properly cited, the use is non-commercial and no modifications or adaptations are made.

Abstract Natural disasters often impose significant and long-lasting stress on financial, social, and ecological systems. From Atlantic hurricanes to Midwest tornadoes to Western wildfires, no corner of the United States is immune from the threat of a devastating natural hazard event. Across the nation, there is a recognition that the benefits of creating environments resilient to adverse natural hazard events help promote and sustain county and community success over time. The challenge for communities is in finding ways to balance the need to preserve the socioecological systems on which they depend in the face of constantly changing natural hazard threats. The Natural Hazard Resilience Screening Index (NaHRSI; previously entitled Climate Resilience Screening Index) has been developed as an endpoint for characterizing county resilience outcomes that are based on risk profiles and responsive to changes in governance, societal, built, and natural system characteristics. The NaHRSI framework serves as a conceptual roadmap showing how natural hazard events impact resilience after factoring in county characteristics. By evaluating the factors that influence vulnerability and recoverability, an estimation of resilience can quantify how changes in these characteristics will impact resilience given specific hazard profiles. Ultimately, this knowledge will help communities identify potential areas to target for increasing resilience to natural hazard events.

Plain Language Summary NaHRSI (Natural Hazard Resilience Screening Index) is a tool for communities to evaluate their likely vulnerability and resilience acute meteorological events like hurricanes, tornadoes, droughts, floods, etc. The index has been applied to all counties of the United States and is comprised of five major parts examining risk of events, governance to address events, societal, built environment and natural environment attributes that will enhance recoverability for these types of events.

1. Introduction

Natural disasters can impose long-lasting and significant stress on social, financial, and ecological systems. From Western wildfires to Midwest tornadoes to Atlantic hurricanes, no portion of the United States is immune from the threat of a devastating meteorological event. Throughout the nation, the benefits of creating environments resilient to adverse weather or weather-related events are recognized as helping to promote and sustain county and community success. The true challenge is in finding ways to balance the preservation of socioecological systems on which communities depend in the face of the constant barrage of natural hazard threats.

The U.S. National Security Strategy suggests that impacts from adverse meteorological events represent a credible national security concern (National Security Strategy, 2015). By one accounting, the federal government has incurred more than $357 billion in direct costs due to extreme weather and fire events alone over the last 10 years (Office of Management and Budget and Council on Environmental Quality, 2016). With the tempo and magnitude of natural disasters experienced in 2017, it is likely that a considerable spike will be observed in the federal expenditure for recovery and response efforts. Since 2013, the U.S. Government Accountability Office monitors the high-risk fiscal exposure to the federal government because of natural hazard-related events. Recognizing the sweeping impacts of natural disasters across the infrastructure, defense, agriculture, health, and local economies, the U.S. government is challenged with taking steps to better manage this fiscal risk (Government Accountability Office, 2017).

The concept of resilience has evolved from its initial emphasis on the general persistence of ecological system functions in a world that is subject to ongoing change (Holling, 1973), through an orientation

toward coupled socioecological systems and questions of adaptation of humans in nature (Carpenter et al., 1999, 2001; Walker, 1993; Walker et al., 2002). In general terms, resilience is a characteristic of human (or social/societal) and natural systems exhibiting a capacity to withstand and recover from an adverse shock or event Keck & Sakdapolrak, 2013). In towns and cities, resilience is promoted through planning while in nature, this trait is assumed inherent (Meadows, 2008; National Research Council, 2012). While societal and ecological resilience are highly dependent on one another, an examination of resilience literature reveals that one is often described without appreciation of the other or in the context of their opposing roles (Handmer et al., 2012). Similarly, previous research suggests that positive aspects of county and community quality of life are linked to not only built environments but natural ones as well (Smith et al., 2012; Summers et al., 2012). Any discussion of resilience would be incomplete without considering the role of natural ecosystems, as they could influence many of a county's and community's vulnerability and recoverability characteristics (Summers et al., 2016, 2012, 2014).

In the context of the research presented here, vulnerability describes the propensity or predisposition to be adversely affected while resilience describes the ability of a system and its component parts to anticipate, absorb, accommodate, or recover from the effects of a hazardous event in a timely and efficient manner (Intergovernmental Panel on Climate Change, 2012). Much of the existing resilience literature focuses on either vulnerability (risk) or recovery (e.g., Cutter et al., 2003; Frazier et al., 2014) as independent constructs of resilience. Summers, Smith, et al. (2017) suggest that a more holistic relationship exists, where an intersection of vulnerability and recoverability sits along a spectrum of resilience. The position of human and natural systems along this gradient reflects their ability or capacity for resilience. In terms of natural hazards, for example, both people and nature can absorb, recover from, and adapt to adverse events (Berkes & Ross, 2013; Gunderson, 2010); however, the degree of resilience is reflected in their mechanisms for recovery. This leads to the concept of basic resilience and recovery potential. Basic resilience can be determined by a direct relationship between risk of a natural hazard occurring and planning, regulation, and training by a community to be ready to face that risk (governance). Thus, basic resilience could be characterized by ratio of level of governance to the likelihood of risk (governance/risk). Similarly, a community's ability to recover from the realization of a natural, hazard event can be exacerbated or diminished by local factors relating to the social structure of the community, the natural environment, and the built environment (Berkes et al., 2003; O'Brien et al., 2009; Pelling & Manuel-Navarette, 2011). These concepts of basic resilience, adaptation, and transformation are included in the development of Natural Hazard Resilience Screening Index (NaHRSI) below.

Ecosystems have innate structures and functions (such as diversity and redundancy) to facilitate recovery from an adverse event (Holling, 1986; Melillo et al., 2014; National Fish, Wildlife and Plants Climate Adaptation Partnership, 2012). Human systems rely on planning and preparation to mitigate known natural hazard exposures and reduce vulnerabilities (Magus, 2010; Tobin, 1999). In both systems, the success of the recovery process is dependent on the robustness of the mechanism. This robustness refers to the system's ability to resist or tolerate change without adapting its initial stable configuration (Meadows, 2008). In the case of nature, ecological conditions may be the factor determining robustness of resilience while the depth and breadth in resilience planning or governance are pillars for resilience in built environments. In the context of governance and risk, the intersection of the status of society and the natural and built environments can modify actual local area resilience to natural hazard events. Understanding how different aspects of resilience reflect a community's capacity for adaptive management is critical for envisioning urban systems and natural ecosystems that can persist through extreme weather events.

A community's ability to endure and recover from abrupt system shocks is an important factor for sustainability. Natural hazard events (e.g., droughts, hurricanes, and floods) can impose long-lasting and significant effects that can impact people and the natural systems on which they depend for sustenance, protection, livelihoods, and recreation. As losses stemming from these events have continued to rise, there has been a notable increase in communities seeking economic, social, and ecological solutions to improve both their sustainability and resilience. The concepts of sustainability and resilience are closely tied as more county and community decision makers recognize that recurring and anomalous weather events may impede achieving their sustainability goals without appropriate and actionable preparation. Therefore, it is not surprising that interest in the subject of resilience related to natural disasters, both cyclic and evolving, is growing.

The concept of resilience has evolved over the past several decades, particularly given the increased interest in preparing for and addressing the current and future challenges we (nations, states, and cities) face, including threats posed by major meteorological events. However, the topic of resilience is a disputed and heavily debated subject regarding anthropogenic and natural systems (Patel et al., 2017). The varying ideas about community resilience generally align, but they are applied differently across the field of resilience research. These differences in application have historically made it difficult for policy makers to identify priorities for improving resilience (e.g., increased governance vs. enhancement of training and economic development, natural resource conservation versus enhancement of social services, and investment in the built environment vs. investment in risk reduction). Despite the differences in conception and application, there are well-understood elements that are widely proposed as important for a resilient community, agreeing that community resilience relates to the sustained ability of a community (a socioecological system) to utilize available resources to respond to, withstand, and recover from adverse difficulties or perturbations (Federal Emergency Management Agency, FEMA, 2011, 2012, 2017; RAND Corporation, 2017).

The NaHRSI was developed using publicly accessible data (e.g., databases available through websites) to help decision makers identify the characteristics that make resilience stronger and weaker. NaHRSI integrates the various viewpoints regarding resilience in terms of potential exposures to natural hazards, governance practices, and the conditions observed in societal, built, and natural systems to inform resilience planning efforts. The index focuses on county-scale measures, the policy action level that is most broadly applicable. While disaster event planning occurs at smaller spatial scales for some urban areas and communities, these data are generally not available for all areas of the Nation. The NaHRSI framework (Summers et al., 2017) serves as a conceptual roadmap to describe the potential impact of natural hazard events impact on a community in the context of exposures and county characteristics. By addressing the factors that influence vulnerability and recoverability, an estimate of resilience can gauge how changes in these characteristics could potentially impact a community's ability to recover from given specific hazard profiles. Ultimately, this knowledge can help communities identify areas to target for improvement to increase their resilience to natural hazard events.

2. Approach

2.1. Conceptualizing Resilience

As part of the conceptualization of NaHRSI, existing community resilience characterization methods and approaches were reviewed with the intent to identify mainstream resilience indicators and indices and determine the applicability of each within the scope of the development of NaHRSI (Summers, Smith, et al., 2017). In summary, an initial search produced 369 print and web publications, which was further reduced by using selected criteria (e.g., quantifiable, integrated, and focus on natural disasters). The resulting pool of 27 published indices representing 57 candidate indicators from this review demonstrated measures that favored an integrated socioeconomic and ecological development approach and showed notable trends toward the use of composite indices for the characterization of community resilience. The 27 published indices and their indicators, in relation to the likely NaHRSI domains, are shown in Table 1.

2.2. Determination of Natural Hazard Event Factors to Be Included in NaHRSI

The National Climate Assessment summarized the current and future impacts of climate change in the United States (http://sca2014.globalchange.gov/report). In the construction of this index, the likely changes in natural hazard events associated with geographic regions throughout the United States were assessed, as well as the infrastructure challenges these changes would likely create. Extended heat waves (with associated drought), more frequent heavy downpours (with associated flooding), sea level rise, enhanced insect outbreaks, increased wildfires, altered timing of streamflow, increased and faster sea ice and glacial loss, and increased major storm events (including hurricanes, tornadoes, and superstorms) were identified as impacts likely to be seen in the coming decade. Similarly, infrastructure issues were identified as likely contributors to the impacts of these weather-related events. Discussions with climate and natural hazard experts in each of the 10 Environmental Protection Agency regions, in conjunction with the information provided by the National Climate Assessment (Melillo et al., 2014) and the 100 Resilient Cities report (ARUP, 2014), yielded 12 natural hazards that would be included in NaHRSI:

GeoHealth

10.1029/2018GH000160

Table 1

Summary of Literature Reviewed Index by Topical Areas of Interest for Development of NaHRSI

NaHRSI Relevance			Literature Review - Selected Index/Framework
Domains of Resilience	Topic of Interest	Candidate Measurement Categories	ARI, AWRVI, BRIC, CRI, CRISLR, CDRI1, CDRI2, CResI, CRIG, CRiskI, MCCR, MCR, MRR, M-RD, M-EI, DRI, EJSI, EPI, ESI, EVI, FRI, FVI, HRI, M-CRD, RFI, RIMM, SSI
Natural Environment	Extent of Natural Areas	• Managed Lands • Ecosystem Type	
	Integrity	• Condition	
Society	Economy	• Economic Diversity • Employment • Insurance	
	Critical Services	• Safety and Security • Social • Labor/Trade	
	Characteristics	• Demographics • Health	
Built Environment	Infrastructure Integrity / Continuity	• Communication • Transportation • Utilities	
	Structure / Housing Characteristics	• Non-Residential • Residential • Shelter	
Governance	Preparedness	• Planning • Investment	
	Response	• Expenditure • Time	
Risk	Losses	• Property • Human	
	Hazard Exposure	• Geophysical • Technology Hazards	

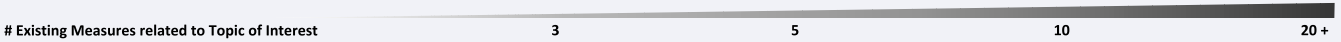

Note. Intensity of color represents the number of potential indicators and metrics (lighter color—lower number to darker color—higher number). The numbers refer to the existing measures related to topic of interest. ARI = Agricultural Resilience Index (Ciani, 2012); AWRVI = Arctic Water Resource Vulnerability Index (Alessa et al., 2008); BRIC = Baseline Resilience Indicators for Communities (Cutter et al., 2014); CRI = City Resilience Index (ARUP, 2014); CRISLR = City Resilience Index to Sea Level Rise (Abdrabo & Hassaan, 2014); CDRI1 = Climate Disaster Resilience Index 2011 (Joerin & Shaw, 2011); CDRI2 = Community Disaster Resilience Index 2010 (Peacock et al., 2010); CResI = Community Resilience Index (Kafle, 2012, Renschler et al., 2010); CRIG = Community Resilience Index for the Gulf of Mexico (Baker, 2009); CRiskI = Community Risk Index (Daniell et al., 2010); MCCR = Composite measure of coastal community resilience (K. Li, 2011); MCR = Composite measure of community resilience (Meher et al., 2011); MRR = Composite measure of regional resilience (Martini, 2014); M-RD = Composite measure of resilience to disasters (Kusumastuti et al., 2014); M-EI = Composite measures of ecological integrity (Vickerman & Kagan, 2014); DRI = Displacement Risk Index (Esnard et al., 2011); EJSI-EJ SCREEN Index (U.S. Environmental Protection Agency, 2015); EPI = Environmental Performance Index (Hsu et al., 2016); ESI = Environmental Sustainability Index (Esty et al., 2005); EVI = Environmental Vulnerability Index (Pratt et al., 2004); FRI = Flood Resilience Index (Batica, 2015); FVI = Flood Vulnerability Index (Balica, 2012); HRI = Household Resilience Index (Cassidy & Barnes, 2012); M-CRD = Metrics for community resilience to disasters (Burton, 2015); RFI = Resilience Factor Index (Ainuddin & Routray, 2012); RIMM = Resilience Inference Measurement model (Lam et al., 2016; C. Li, 2013); SSI = Sustainable Society Index (van de Kerk & Manual, 2014).

1. Hurricanes
2. Tornadoes
3. Inland floods
4. Coastal flooding
5. Earthquakes
6. Wildfires
7. drought
8. High winds
9. Hail
10. Landslides
11. Low-temperature extremes
12. High-temperature extremes

2.3. The NaHRSI Conceptual Framework

No singular approach from the literature survey existing composite measures of natural hazard resilience met all of the expected needs for developing NaHRSI. Collectively, however, the reviewed literature provided many of the building blocks (e.g., suites of indicators, indicator groupings, and domains). A heat map table (Table 1) depicts the distribution of metrics used in the final 27 indices across resilience topics of interest to NaHRSI. To varying degrees, all of the existing indices offered patterns of indicator groupings, which were allocated into five domains to describe overall resilience: natural environment, built environment, society, governance, and risk. None of the indices reviewed provided all possible indicators necessary for the construction of NaHRSI. However, 10 of the reviewed publications included information relevant for describing the NaHRSI domains. Information pertaining to the Natural Environment, governance, and risk domains were most frequently excluded from existing indices. Five indices—BRIC, CDRI1, CDRI2, M-RD, and M-CRD (Burton, 2015; Cutter et al., 2014; Joerin & Shaw, 2011; Kafle, 2012; Kusumastuti et al., 2014; Peacock et al., 2010; Renschler et al., 2010)—offered fairly comprehensive descriptions of indicators relevant for quantifying NaHRSI domains. The Climate Disaster Resilience Index 2011 (CRDI1) contributed the most to the proposed NaHRSI structure, addressing all domains based on a suite of 18 indicators.

The final conceptualization of NaHRSI is discussed in Summers, Smith, et al. (2017) and includes five domains composed of 10 indicators, which, in turn, were derived from 117 unique metrics. Figure 1 depicts the final NaHRSI conceptual framework including the domains and indicators of the index. A summary of the domains, indicators, and types of metrics used in NaHRSI is provided in Table 2. The selection of the domains and indicators are completely described in Summers, Harwell, et al. (2017) and are summarized here for completeness. The domains included in NaHRSI include risk, governance, society, built environment, and natural environment. In accordance with the concept of basic community resilience to natural hazards being driven by the likelihood of an event occurring and the community's preparation for such an event, the domains of risk and governance are included at the base of the conceptual model (Figure 1) to denote basic resilience as some relationship between risk and preparedness. Exposure and losses comprise the indicators for risk (discussed below) and community and personal preparedness (Adager et al., 2005; Linnenluecke et al., 2012; Paton & Johnston 2001) and natural resource conservation (Strickland-Munro et al., 2010; Tompkins & Adger, 2004) represent the indicators for governance. Twenty metrics contribute to the two indicators for the risk domain and five metrics contribute to the three indicators for the governance domain (Table 2).

The remaining domains include elements that could exacerbate or diminish the vulnerability and recovery potentials of a community to an event or postevent. These include society, built environment, and natural environment. Societal indicators that can modify vulnerability or recovery include availability of social services (Dominelli, 2013), the type of available labor or trades within the community (Kirrane et al., 2013), safety and security requirements (Christopher & Peck, 2004; Keim, 2008), the socioeconomics and economic diversity of the community (Klein et al., 2003, Linnenluecke et al., 2012), the health characteristics and availability of health care access in the community (Ebi, 2011; Oven et al., 2012), basic demographic information concerning the community (Balbus & Malina, 2009), and the cohesiveness of the community (Baldwin & King, 2018; Meitzen et al., 2018; Sanchez et al., 2017). Fifty metrics are utilized to describe these indicators of society (Table 2). Built environment indicators that can modify vulnerability or recovery include multiple

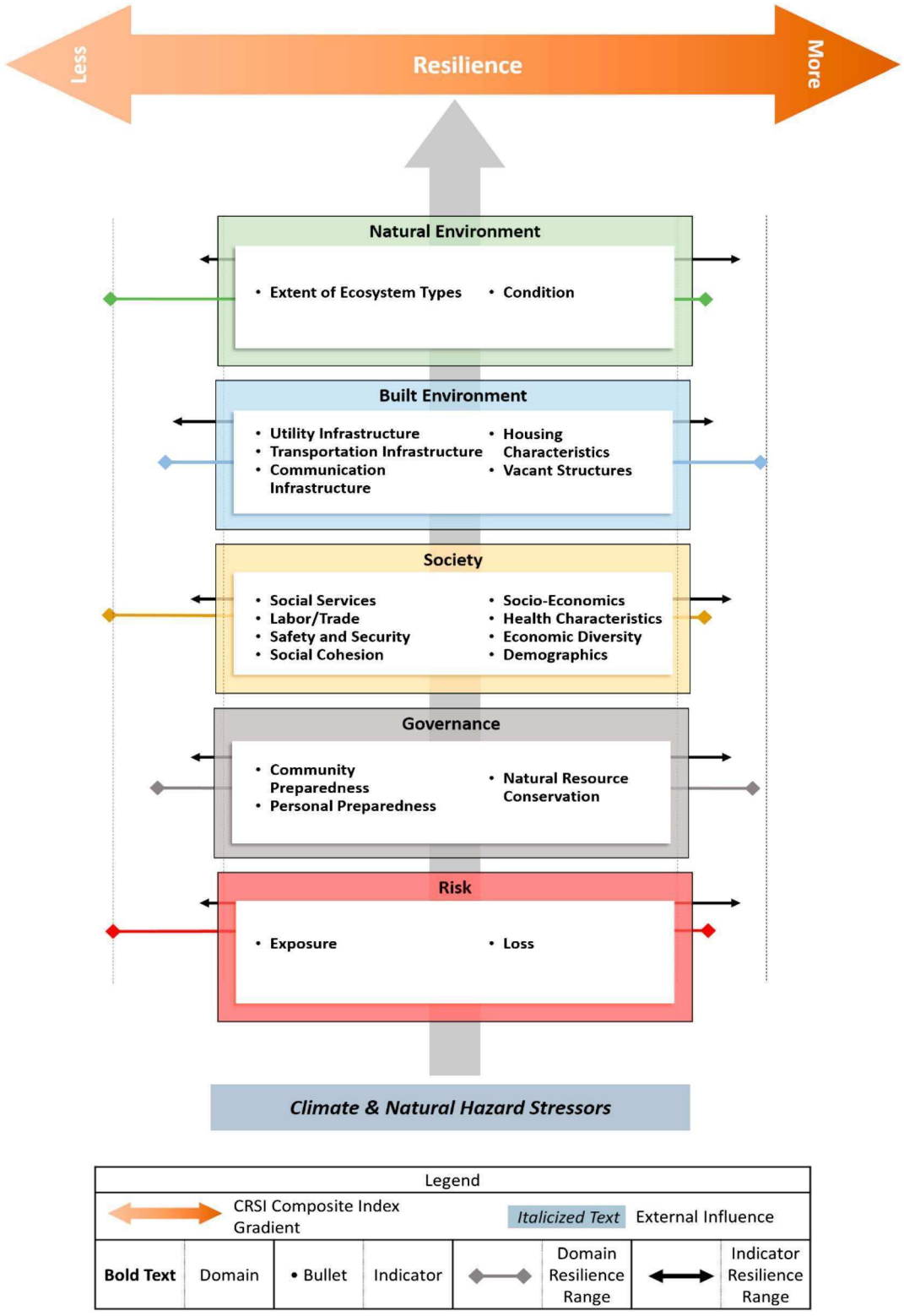

Figure 1. Final Natural Hazard Resilience Screening Index conceptual framework. Arrows projected from boxes to the left and right represent hypothetical increases and decreases in ranges for indicators (black arrows) and domains (colored arrows). CRSI = Climate Resilience Screening Index.

Table 2
List of NaHRSI Domains, Indicators, Scope, and Number of Metrics

Domain	Indicator(s)	Metric(s)
Built Environment (5/24)	Communication Infrastructure	Communication continuity (7)
	Housing characteristics	Structure vulnerability (5)
	Transportation infrastructure	Transportation flow continuity (6)
	Utility infrastructure	Utility continuity (3)
	Vacant structures	Structure vulnerability (3)
Governance (3/5)	Community preparedness	Community resilience strengthening (2)
	Natural resource conservation	Natural Resource Recovery (1)
	Personal preparedness	Personal property hazard protection (2)
Natural Environment (2/18)	Condition	Biodiversity, using birds as a proxy (1)
		Coastal condition (1)
		Forest condition (1)
		Inland lake condition (1)
		Percentage of clean air days (1)
		Rivers and streams condition (1)
		Soil growth suitability (1)
		Soil productivity (1)
		Wetlands condition (1)
	Extent of ecosystem types	Agriculture area (1)
		Forested area (1)
		Grassland area (1)
		Inland surface water area (1)
		Marine/estuarine area (1)
		Perennial ice/snow area (1)
		Protected areas (1)
		Tundra area (1)
		Wetland area (1)
Risk (2/20)	Exposure	Earthquake probability (1)
		Extreme high temperature incidents (1)
		Extreme low temperature incidents (1)
		Flood probability (2)
		Hailstorm probability (1)
		Tornado probability (2)
		Hurricane probability (2)
		Landslide probability (1)
		Major toxics presence (1)
		Non-storm damaging wind incidents (1)
		Nuclear presence (1)
		RCRA sites (1)
		Superfund sites (1)
		Toxic release presence (1)
		Wildfire probability (1)
	Loss	Developed area loss (includes human and property measures) (1)
		Natural area loss (1)
		Dual-benefit area loss (includes cropland and managed area measures) (1)
Society (8/50)	Demographics	Vulnerable population (5)
	Economic diversity	Economic stability/recovery (2)
	Health characteristics	Health problems that may impact personal Resilience (9)
	Labor and trade services	Construction recovery (8)
	Safety and security	Provisioning of emergency and civil services (4)
	Social cohesion	Access to social support (4)
	Social services	Access provisioning to critical services (15)
	Socioeconomics	Employment opportunity (1)
		Personal economics (2)
Built Environment (5/24)	Communication infrastructure	Communication continuity (7)
	Housing characteristics	Structure vulnerability (5)
	Transportation infrastructure	Transportation flow continuity (6)
	Utility infrastructure	Utility continuity (3)
	Vacant structures	Structure vulnerability (3)
Governance (3/5)	Community preparedness	Community resilience strengthening (2)
	Natural resource conservation	Natural resource recovery (1)

Table 2 *(continued)*

Domain	Indicator(s)	Metric(s)
	Personal preparedness	Personal property hazard protection (2)
Natural Environment (2/18)	Condition	Biodiversity, using birds as a proxy (1)
		Coastal condition (1)
		Forest condition (1)
		Inland lake condition (1)
		Percentage of clean air days (1)
		Rivers and streams condition (1)
		Soil growth suitability (1)
		Soil productivity (1)
		Wetlands condition (1)
	Extent of ecosystem types	Agriculture area (1)
		Forested area (1)
		Grassland area (1)
		Inland surface water area (1)
		Marine/estuarine area (1)
		Perennial ice/snow area (1)
		Protected areas (1)
		Tundra area (1)
		Wetland area (1)
Risk (2/20)	Exposure	Earthquake probability (1)
		Extreme high temperature incidents (1)
		Extreme low temperature incidents (1)
		Flood probability (2)
		Hailstorm probability (1)
		Tornado probability (2)
		Hurricane probability (2)
		Landslide probability (1)
		Major toxics presence (1)
		Non-storm damaging wind incidents (1)
		Nuclear presence (1)
		RCRA sites (1)
		Superfund sites (1)
		Toxic release presence (1)
		Wildfire probability (1)
	Loss	Developed area loss (includes human and property measures) (1)
		Natural area loss (1)
		Dual-benefit area loss (includes cropland and managed area measures) (1)
Society (8/50)	Demographics	Vulnerable population (5)
	Economic diversity	Economic stability/recovery (2)
	Health characteristics	Health problems that may impact personal Resilience (9)
	Labor and trade services	Construction recovery (8)
	Safety and security	Provisioning of emergency and civil services (4)
	Social cohesion	Access to social support (4)
	Social services	Access provisioning to critical services (15)
	Socioeconomics	Employment opportunity (1)
		Personal economics (2)

Note. Numbers in parentheses for domains show the total number of indicators/total metrics in the domain. Numbers in parentheses for metrics for number of metrics. RCRA = Resource Conservation and Recovery Act.

infrastructure elements—communications (Martins et al., 2017; Wang & Wang, 2017; Zimmerman, 2017), utilities (Ma et al., 2018; Panteli & Mancarella, 2017; Zimmerman et al., 2017), and transportation (Linnenluecke et al., 2012; Wedawatta et al., 2010)—and housing characteristics (Cutter et al., 2008; Dominelli, 2013; Henstra, 2012; Smoyer, 1998). Twenty-four metrics are compiled to represent the built environment (Table 2). The natural environment domain describes the resilience of natural and managed ecosystems through measures of ecosystem extent (Adager et al., 2005; Foley et al., 2005; Smit et al., 2000) and condition (Foley et al., 2005; Stenseth et al., 2002; Walther et al., 2002). Eighteen metrics are combined to represent the indicators within the natural environment domain (Table 2).

Metric data are documented in Appendix A of Summers, Harwell, et al. (2017). This appendix characterizes the sources of the metric data, their ranges, and their directional relationship to the indicator and provided box-and-whisker plots of the county-level data.

2.4. Data Collection and Preparation

Secondary data from established, publicly accessible sources served as the data foundation in the development of NaHRSI. Nationally consistent, county-level, or equivalent-scale data available within the 2000–2015 time frame were targeted for culling. Where county-level data were not available (i.e., condition of ecological systems by county), imputed values were calculated to achieve desired spatial unit representation. In short, ecosystem condition data were only available from national probabilistic surveys. These data were imputed to provide an estimate of condition of each ecosystem type in each county. Metadata were reviewed to ascertain appropriateness for use in NaHRSI. Collected data were age, population, or land area weighted, as appropriate.

Ecological and distance-factored metrics were interpolated using the inverse distance weighting method to arrive at the spatial unit of interest (county). Distance weighted values were derived using preset distance buffers. Buffer values varied from 50 to 100 miles (roughly 80 to 160 km) depending on the ecological resource or attribute the data represented.

Finally, all standardized values were geolocated to county. Because contributed data were not annually consistent, standardized values were averaged across years within each county or county-equivalent unit. Mean data were normalized on a 0 to 1.0 scale to form the metric basis for NaHRSI. The complement of data represents 3,135 of 3,143 counties and county equivalents, excluding eight boroughs from Alaska that were not represented from secondary data sources.

2.5. Calculations

2.5.1. Risk Domain

The risk domain is a probabilistic calculation based on data provided by a partially derived multihazard model using proportional land area exposure extent and accompanying losses data described in Buck et al. (2018) and Summers et al. (2017). The metrics include historical and modeled exposures, basic likelihood of proximal exposures, potential anthropogenic exposures, and losses. All standardized exposure metrics summed for each county or county equivalent to calculate the exposure indicator. The loss indicator was derived from the sum of standardized loss values stemming from natural hazard events that included human, property, and crop monetary losses plus losses of natural lands to human development. Other sources of potential losses occur (e.g., costs of business activities lost and tourism dollars lost), but no broadly applicable data exist for these potential sources of loss. The risk domain measures were calculated for each county as the exposure indicator value multiplied by the loss indicator value. The approach used to calculate the risk domain scores is presented in Figure 2.

2.5.2. Built Environment, Governance, Natural Environment, and Society Domains

Indicators and domains, with the exception of risk (discussed separately), were derived using the following approach:

1. Metric data were adjusted for age, population, or spatial area, as appropriate, prior to standardization (e.g., number of hospitals in a county adjusted by the population of the county).
2. Indicator scores were determined using the average of related standardized metric values, and each indicator was standardized using the calculated range of the indicator.
3. Domain scores were determined from the average of appropriate standardized indicator values and then standardized in preparation for the final NaHRSI calculation.

2.5.3. The Final Steps to NaHRSI

All domains for each county, parish, and borough (all referred to as county below) were min-max standardized on a scale from 0.01 to 0.99. The final NaHRSI calculation begins as a scaled value for recoverability/vulnerability derived from governance and risk (basic resilience) with the basic resilience value being adjusted by the remaining domain scores for social, built environment, and natural environment to represent enhancement of or diminution of basic resilience to complete the calculation of NaHRSI as shown below:

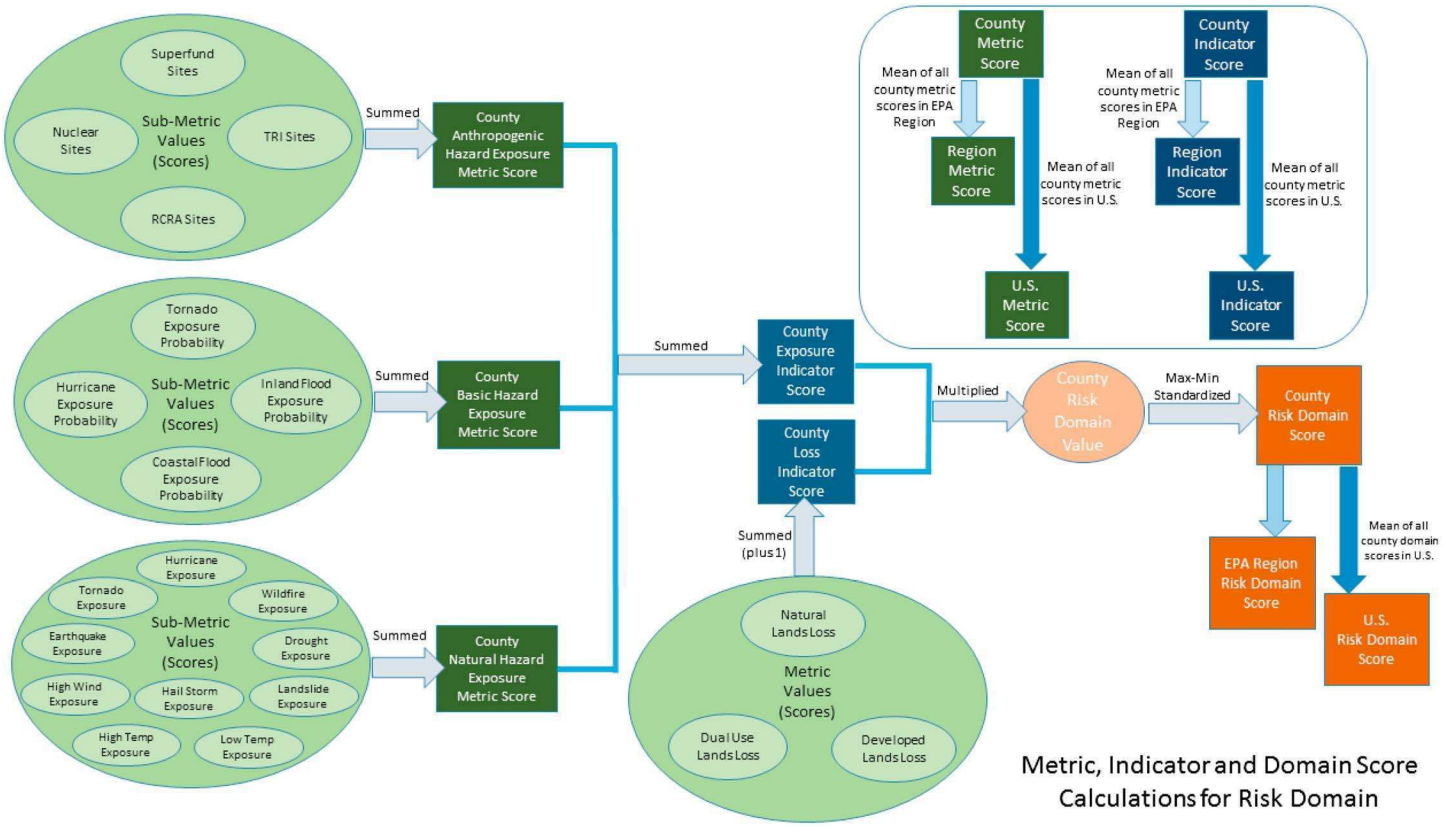

Figure 2. Representation of the metric, indicator, and domain scores for risk domain of Natural Hazard Resilience Screening Index.

$$CRSI(B)i = {}^{Ri}/_{Vi} = {}^{Govi}/_{Riski}$$

where NaHRSI$(B)_i$ = value of basic resilience (recovery/vulnerability or R_i/V_i) and R_i/V_i = governance in county *i*/risk in county *i*. The overall NaHRSI score is calculated as follows:

$$CRSIi = (\text{Gov}i + \text{Soc}(a)i\text{Gov}i + \text{BE}(a)i\text{Gov}i + \text{NE}(a)i\text{Gov}i)/\text{Risk}i$$

where NaHRSI$_i$ = the value of NaHRSI or adjusted resilience for county *i* and Soc$(a)_i$, BE$(a)_i$, and NE$(a)_i$ are the adjustment multipliers for society, built environment, and natural environment in each county *i* and Risk$_i$ is the risk score for county *i*. The adjust factors are calculated as follows:

$$Soc(a)i = {}^{(Soci-Socm)}/_{Socm}$$

where $Soc(a)_i$ is the adjustment multiplier for society in county *i*, Soc_i is the social domain score for county *i*, and Soc_m is the median social domain score for all counties:

$$BE(a)i = {}^{(BEi-BEm)}/_{BEm}$$

where $BE(a)_I$ is the adjustment multiplier for built environment in county *i*, BE_i is the built environment domain score for county *i*, and BE_m is the median built environment domain score for all counties:

$$NE(a)i = {}^{(NEi-NEm)}/_{NEm}$$

and where $NE(a)_I$ is the adjustment multiplier for natural environment in county *i*, NE_i is the natural environment domain score for county *I*, and NE_m is the median natural environment domain score for all counties.

The domains were weighted equally in the calculation of NaHRSI. An initial analysis was performed to assess whether the NaHRSI results associated with basic resilience (governance and risk) varied in a predictable way. Plotting the domain values of risk versus governance would, from a policy standpoint, be expected to have a positive relationship—greater risk should be accompanied by greater governance. This examination of a positive relationship between risk and governance was tested in three ways: (1) assessment analysis of risk domain versus governance domain scores, (2) examination of the cumulative distribution function of basic resilience (governance/risk), and (3) mapping basic resilience to examine potential patterns.

3. Results

3.1. Analyses of Basic Resilience (Governance/Risk)

An assessment of basic resilience is represented by the ratio of governance domain score to the risk domain score (governance/risk). The expected result of the assessment is a 45° angle from low risk-low governance to high risk-high governance. This finding would demonstrate that governance is developed in proportion to risk. Significant deviation from this finding could reflect an underreaction or overreaction to risk in terms of governance activities. Placing results into quantiles allows characterization of clusters of counties as overreacting or underreacting to risk in terms of governance. In this categorical relationship, generally any combination of risk and governance along the 45° angle (slope = 1.0) plus or minus one category would be in the expected range. A combination of high risk and low governance would suggest underreacting, whereas low risk and high governance would suggest overreacting. Mapping these risk-governance ratio categories by county demonstrates any clustering throughout the United States to detect spatial trends.

The assessment results based on normalized risk and governance domains are shown in Figure 3. These results indicate that the governance score is generally higher than the risk score. Only 181 counties (5.8% of the U.S. counties) have risk scores greater than their governance scores. This suggests that governance activities in the vast majority of counties outweigh the risk of exposure to extreme natural hazard events. This high governance to risk ratio is largely driven by a large number of counties with lower levels of risk to devastating natural hazard events. Figure 4 depicts four management action types: low risk-high governance (A), high risk-high governance (B), low risk-low governance (C), and high risk-low governance (D). Types B and C likely represent situations where the level of governance is commensurate with the level of risk. Type A represents the largest number of counties and indicates a level of governance that exceeds the probable level of risk. Type D indicates a level of governance that is significantly less than the level of risk. Type D counties are those most likely to demonstrate poor basic resilience to natural hazard events and would benefit from increased governance measures.

The distribution of basic resilience for the counties was examined using a ratio of the governance-risk domain scores to determine the roughly 500–1,000 counties with the largest risk to governance disparities. Figure 4 shows the county data from the assessment as a cumulative distribution function of basic resilience (governance/risk). Roughly 6% of counties have a basic level of resilience less than 1.0 indicating that risk is greater than governance suggesting that these counties could be poorly resilient to a natural hazard event. About 56% of counties have basic resilience scores of greater than 2.0 basic resilience suggesting clearly sufficient governance for the likely level of risk. While this result suggests that most counties in the United States would be resilient to natural hazard events, it can be misleading as will be discussed in the next section. The remaining percentage of counties (38%) with basic resilience values between 1 and 2 represent counties with a greater potential to demonstrate inadequate planning given their likely risk. Counties in this category (basic risk scores between 1 and 2) are characterized as more likely to depend on their community and natural resources to provide the adequate services to improve overall resilience.

These county basic resilience scores were mapped to explore the spatial distribution of the quintiles for any potential trends (Figure 5). Areas with the highest basic resilience scores tend to be in the northeast and scattered through Midwest. Areas with the lowest basic resilience scores appear along the West Coast in the southeast and Appalachia. Four counties ($<$1% of total) showed very low basic resilience scores of $<$0.25. All of these counties are located in the southeast. Twenty-three counties demonstrated risk scores that were twice their governance scores (i.e., $<$0.5) and again were predominantly located in southeast and lower Midwest. Eighty counties had basic resilience scores $<$0.75 where the southeast contained 90% of the

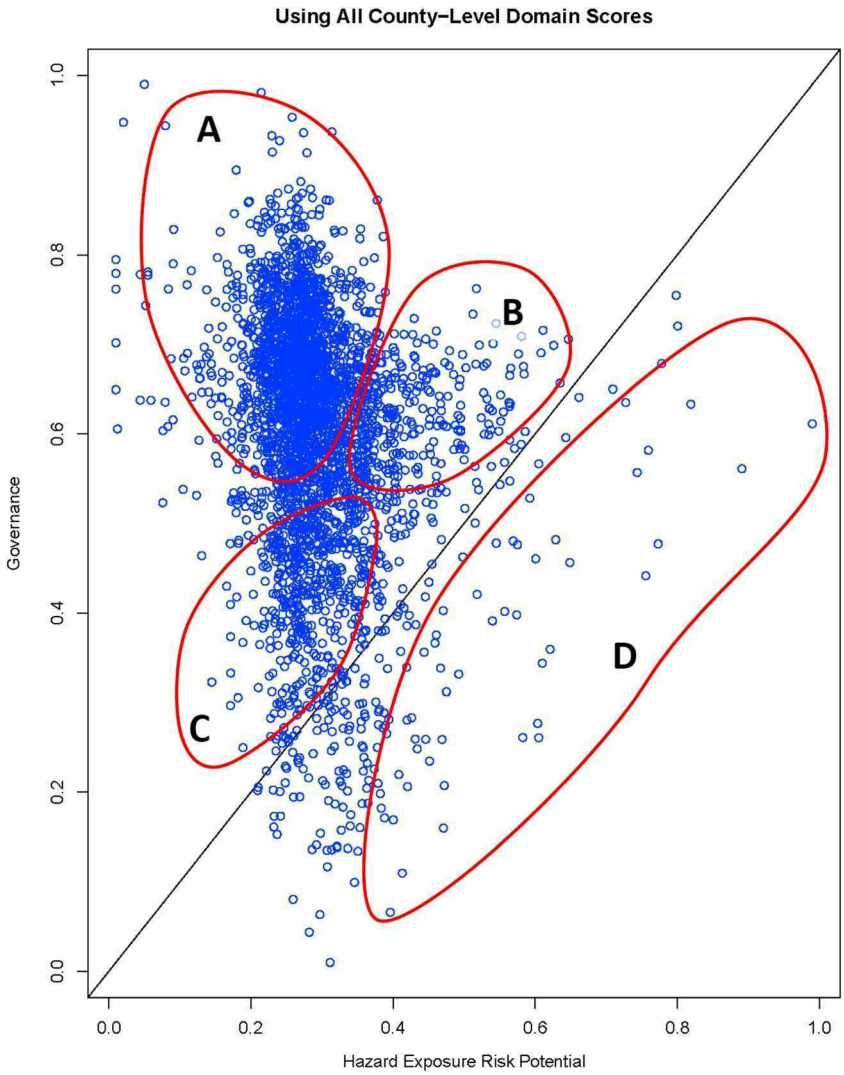

Figure 3. Linear assessment of risk versus governance based on domain scores. Ellipses represent differing management implications with A: low risk-high governance (little increased governance necessary other than improvements for selected below-average indicators; B: high risk-high governance (likely appropriate governance but any improvement in below-average indicators a likely improvement to resilience); C: low risk-low governance (likely appropriate governance for level of potential risk; D: high risk-low governance (improvements to governance and indicator of the Natural Hazard Resilience Screening Index domains necessary).

counties with the remaining counties in far west and southwest. Of all the counties in the United States with basic resilience scores <1 (risk exceeded governance), 85% were in the southeast), 9% the south central and southwest, 4% in the west, and $<$ 1% in the Midwest.

3.2. National NaHRSI Results

Basic resilience is modified by social aspects and structures, the built environment, and the natural environment to represent overall resilience (the NaHRSI score). If these attributes are strong, then resilience (mainly through recoverability) is enhanced. If these attributes are weak, then resilience for an area is reduced. The following national results sections examine basic resilience as modified by societal, natural environment, and built environment factors to determine an overall NaHRSI score. These scores were examined both including and excluding the boroughs of Alaska. This modification was deemed prudent given the mixed levels of data available for the Alaskan boroughs (some boroughs had all levels of data while others did not).

The U.S. NaHRSI score is 2.71 based on the average of NaHRSI scores for all counties in the United States, excluding Alaska, ranging from -2.13 to 14.10 (including Alaska increases the max to 189.17). The NaHRSI

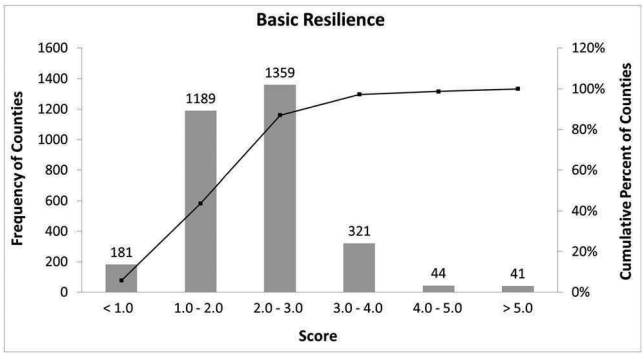

Figure 4. Distribution of county basic resilience scores (governance/risk). Bars equal frequency of basic resilience score for counties. Line indicates cumulative percentage of counties. Number represents number of counties in the basic resilience score range.

and domain scores for the nation are shown in Table 3. The distribution of overall NaHRSI values and the domain scores by county for the United States are shown in Figure 6. Examples of inferences that can be made from the maps are the following:

1. The western United States (east of the Rockies), the Great Lakes area, and the upper northeast have higher NaHRSI values (higher resilience to natural hazard events).
2. The western Midwest, the southeast, the southwest, and Appalachian region have lower NaHRSI values.
3. The lower northeastern coastal area, southeast/Gulf coasts, a small area associated with southern Lake Michigan, and southern far west have the highest risk domain scores albeit for different types of natural hazard events. Lower risk scores for natural hazard events are seen in the west and upper Midwest, Alaska, and Hawaii.
4. Higher governance scores are seen in the northeast, Mid-Atlantic, and Great Lakes areas of the U.S. lower governance scores related to natural hazards were observed in Appalachia, the deep south, and selected counties in the far west.
5. Higher society scores are seen in the upper Midwest and mountain west. Lower society scores are seen in Appalachia and the deep south.
6. Both built and natural environment domain scores were higher in the west, parts of deep south, and lower in the western Midwest and parts of the southeast.

Examining the 150 counties in the United States with the highest NaHRSI values, the Pacific Northwest, and Alaska have the most counties (48 counties of which 19 are in Alaska) followed by the upper west (44), the upper Midwest (23), and the northeast (14). Only the southeast and Mid-Atlantic areas do not have any counties in the top 150 NaHRSI county list. This provides state and counties with lower NaHRSI scores with several example counties to use as role models for the improvement of their scores. The 150 counties with the lowest NaHRSI scores are predominated by the southeast (86 counties) followed by the Mid-Atlantic (33), the south central United States, (13), the Midwest (9), and the Rocky Mountain states (7).

Risk due to natural hazard events across the United States is examined in more detail in Figure 7. The lowest risk domain scores all occur in Alaska, but if Alaska is excluded, the five lowest risk scores occur in the northwest (Montana, Idaho, and Washington). The highest risk scores occur throughout the United States, with two counties in Texas and one each in Colorado, Georgia, and Virginia. Natural exposures due to natural hazard

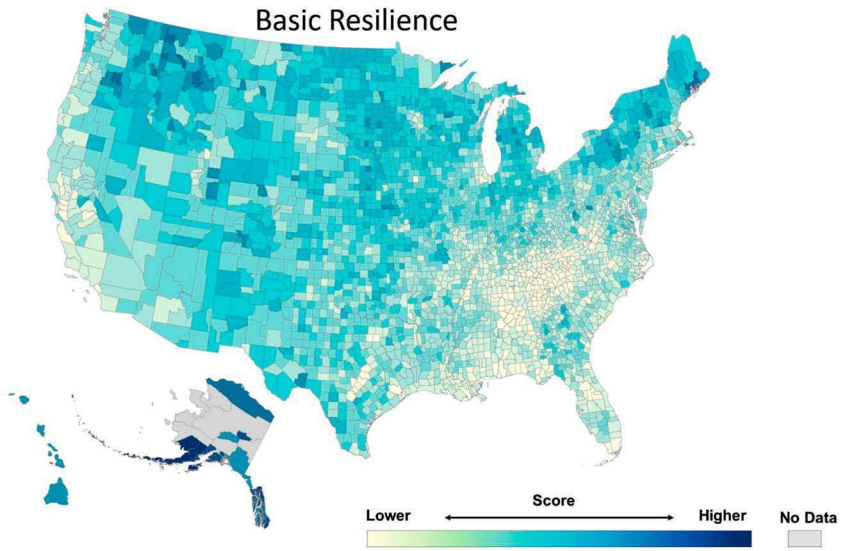

Figure 5. Map of the distribution of county scores for basic resilience.

Table 3
Summary of NaHRSI and Domain Scores for the United States, Both With and Without Alaska

Region	Inclusions and Exclusions	Risk	Governance	Built environment	Natural environment	Society	NaHRSI
National Average	Including Alaska	0.29590	0.59674	0.39320	0.41333	0.51561	2.71349
	Excluding Alaska	0.29758	0.59575	0.39262	0.41182	0.51587	2.37534

Note. NaHRSI = Natural Hazard Resilience Screening Index.

events are predominated by drought (99% of counties experiencing drought), extreme high and low temperatures (100%), inland flooding (99%), high winds (98%), and hail (98%). In short, the meteorological events depicted in NaHRSI, for the 2000–2015 period, are experienced largely throughout the United States with the exceptions of wildfires (52% of counties), landslides (39%), earthquakes (12%), coastal flooding (11%), and hurricanes (8%). Other types of anthropogenic exposure that could exacerbate natural hazard events impact most counties. Resource Conservation and Recovery Act sites and Toxic Release Inventory sites dominate the technological exposure indicator at 71% and 87%, respectively. Superfund sites were seen in 28% of counties, while nuclear facilities were located in 5% of counties. Losses due to natural hazard events of human life, property, and natural ecosystems occur in almost all counties, while losses of crops have occurred in 73% of counties.

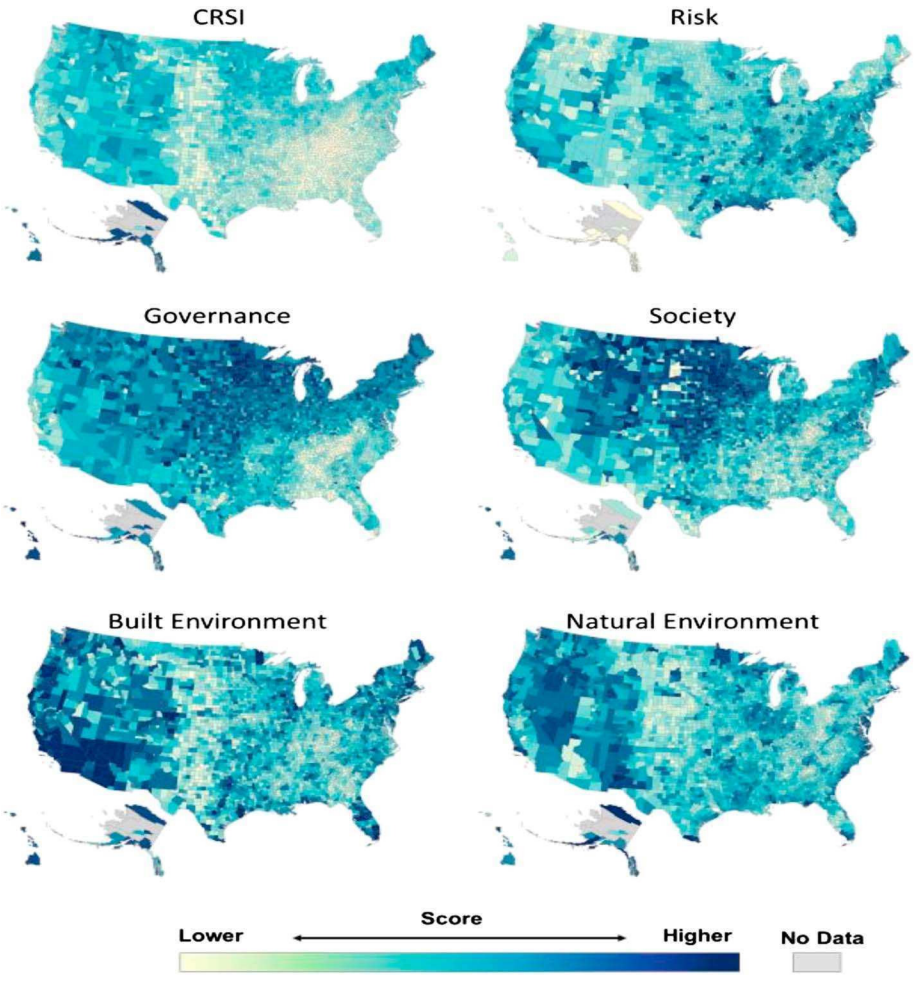

Figure 6. National Natural Hazard Resilience Screening Index values and domain scores (risk, governance, society, built environment, and natural environment). CRSI = Climate Resilience Screening Index.

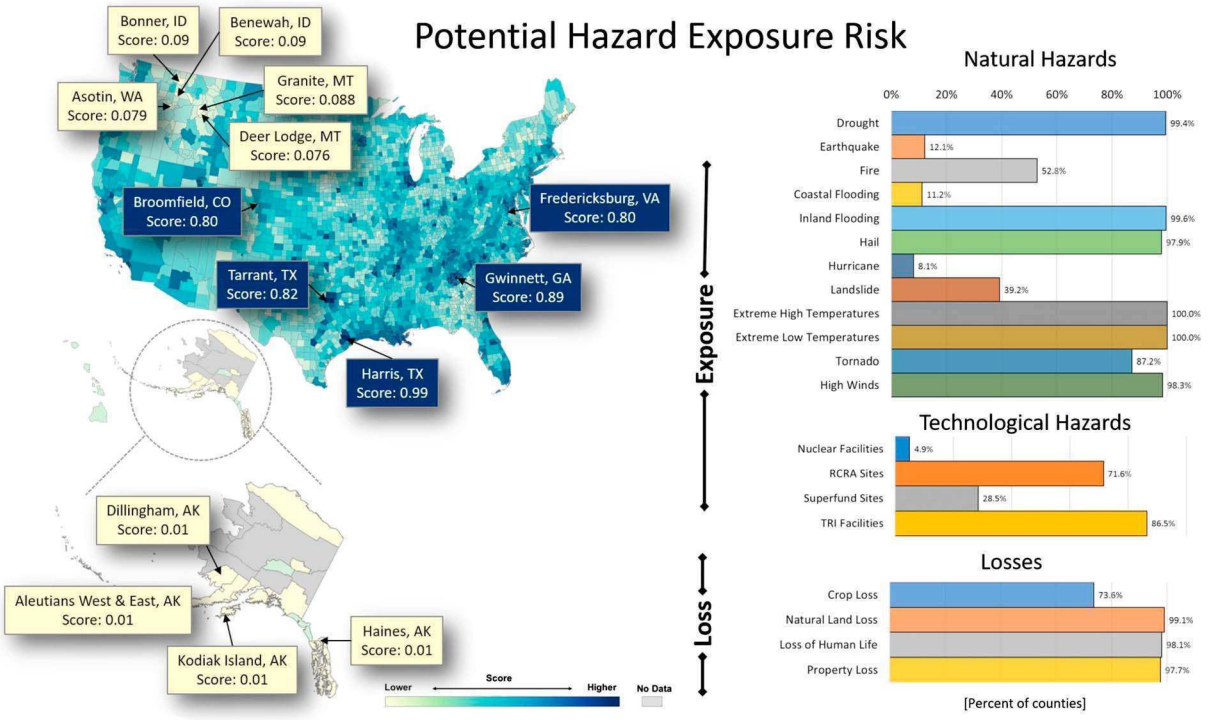

Figure 7. Map of risk domain scores delineating the five counties with the highest risk domain scores and the four lowest risk domain scores (all in Alaska) and the five lowest scores excluding Alaska. The percentage of counties experiencing each of the 11 natural hazard event types, the 4 technological hazards, and losses of human life and property. RCRA = Resource Conservation and Recovery Act; TRI = Toxic Release Inventory.

The contributions of the 20 indicators to the national domain scores are shown in Figure 8. Natural resource conservation (governance), number of vacant structures and housing characteristics (built environment), as well as demographic characteristics (society) most strongly influenced national domain scores. Secondary influences included levels of exposure (risk), socioeconomic characteristics, social cohesion, and economic diversity in the society domain, community, and personal preparedness (governance) and acreage of ecosystem types (natural environment).

4. Discussion

Every year, U.S. counties and communities face devastating losses caused by weather-related disasters. Fires, floods, storms, other hazards, and their associated consequences have significant impacts on counties and communities, especially, their economies, infrastructures, and the environments. The United States has recently experienced a number of large-scale and devastating natural disasters, including catastrophic wildfires, far-reaching floods, and damaging storms. The increasing prominence of extreme weather events makes it critical for governments, businesses, and individuals to examine their anticipatory adaptation and organizational resilience to these events (Linnenluecke et al., 2012). The private sector and all levels of government are embracing resilience as a holistic, proactive framework to reduce vulnerabilities, improve services, adapt to changing conditions, and empower citizens (e.g., National Disaster Resilience Competition; Housing and Urban Development, 2017; Leadership in Community Resilience; National League of Cities, 2016, 2017).

Unlike other resilience estimates, NaHRSI integrates all the major aspects of resilience through its five domains. Overall, NaHRSI values, domain scores, and indicator contributions all paint a picture for the United States of reasonable resilience to natural hazard events. However, the distribution of these scores is broad. While there are many relatively resilient counties in the United States, there are a number of counties in which overall resilience to natural hazard events is low or one or more of the domain scores are low. Therefore, more specific results and analyses should be examined for each of the regions.

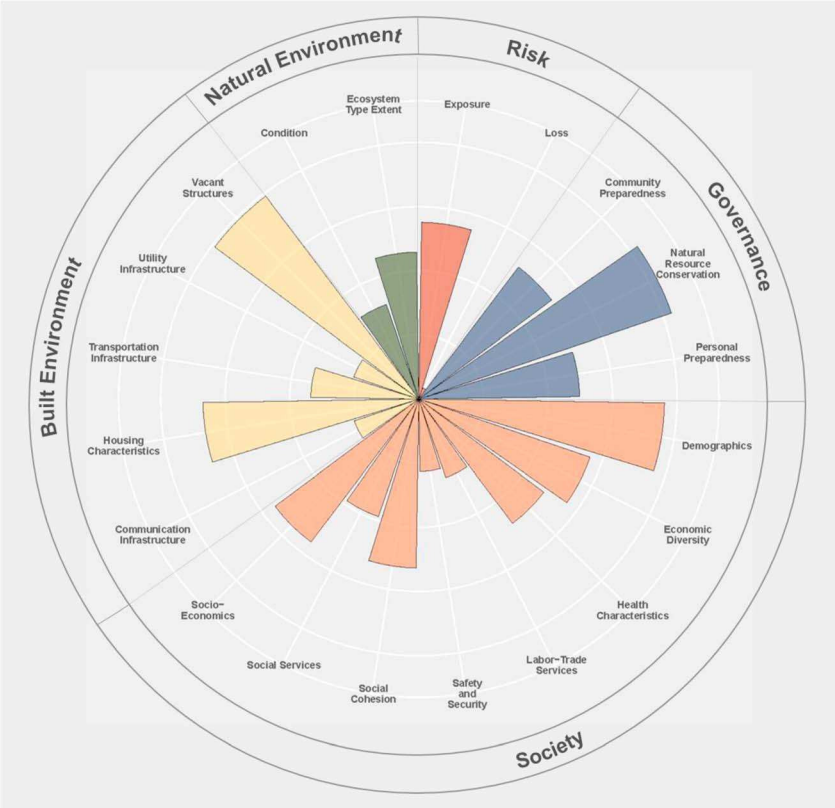

Figure 8. Polar plot showing the contribution of the 20 indicators associated with the domain scores for the nation. The length of the bars corresponds to the indicator score. Within a domain, the higher indicator scores show a greater contribution to the domain.

4.1. Potential Utility of NaHRSI

For over 50 years, hazards researchers have focused on a series of fundamental questions relating to "How do people respond to environmentgal hazard and what factors influence their choice of adjustments" (Cutter 1996, 2012). There are few examples of comparative measures of community health, well-being, resilience, or condition at the county level (Miringhoff & Miringhoff, 1999). The Social Vulnerability Index in one of the few county-level measures of social vulnerability to environmental hazards (Cutter, 2003).

This present paper outlines the approach and application of an index to examine the resilience of U.S. counties, regions, and the overall nation to natural hazard events, holistically, examining not only risk but including governance, social attributes, the built environment, and aspects of the natural environment. No other efforts to quantify county-level resilience have examined all five of these component domains. A number of studies have examined one or two of the domains, while a few have examined as many as three or four of the domains (see Table 1). BRIC (Baseline Resilience Indicators for communities, Cutter et al., 2014) provides the closest effort that includes all five of the domains. BRIC does not include a probability of risk event measure but does include measures associated with society (social, economic, and community capital indicators), the built, and natural environments and governance.

The highlights of BRIC (Cutter et al., 2014) suggest that inherent resilience and its drivers are spatially variable. Similarly, NaHRSI shows basic resilience (governance and risk) to be spatially variable as well as the recovery potential domains of society, built environment, and natural environment. BRIC demonstrates higher level of inherent resilience in the Midwest and northeast. NaHRSI shows the highest resilience in Alaska and Hawaii (not included in the BRIC assessment), the upper Midwest, northeast, and selected parts of the northwest (in contrast to BRIC). Some of these minor differences are likely due to the inclusion of risk in NaHRSI but not in BRIC. The lowest levels of resilience in BRIC are identified as Texas border counties, Appalachia, and the interior western United States. In NaHRSI, poorest resilience occurs in

Appalachia, much of the southeast, the Western Plains including border and west Texas counties. The extension of lower resilience scores into the southeast in NaHRSI appears to be driven by higher risk scores and lower society scores in this area.

BRIC found that resilience (defined in NaHRSI as the nonrisk domains) and vulnerability (defined in NaHRSI as the risk domain and by Cutter et al., 2008, as Social Vulnerability Index) were statistically related but not the obverse of one another. Clearly, social vulnerability and physical risk are not the same measure but a similar observation can be made for physical risk of a disaster event and resilience to such an event in NaHRSI. The concept used in NaHRSI of basic resilience being the ratio of governance and risk permits some high risk areas to offset that risk by increased governance to enhance resilience, while areas with high risk but lower governance display lower basic resilience.

Further research and application efforts to adapt NaHRSI for use within individual counties and communities would clearly be useful for the development of community-specific resilience plans. The potential of using NaHRSI-related information by state and local staff tasked with assessing resilience in their areas of the counties seems particularly useful. Supporting state and counties to assess risk, governance, societal attributes, the built environment, and natural environment in a holistic manner will be important in further development of local and county-level, and even state, resilience plans. Similarly, at the county level, states and counties can

1. Assess relative risks of differing weather-related events
2. Disassemble NaHRSI to determine why the resilience of certain counties is projected to be low and that of others are projected to be high
3. Provide lessons learned from one county to the next on governance and other activities that have increased local resilience to weather-related events
4. Provide a comparative database permitting one way to assess where investments might have the greatest return in terms of improved resilience
5. Provide a database that can be updated to include the most recent information on the NaHRSI metrics, indicators, and domains so that improvements can be tracked.

4.2. Example of NaHRSI Use—Hurricane Harvey

In August, 2017, Hurricane Harvey had two landfalls in Texas—Rockport, TX, in Aransas County and Port Aransas, TX, in Nueces County. In addition to wind damage, rainfall from Hurricane Harvey resulted in massive flooding in Houston and surrounding areas (Galveston, Harris, and Brazoria Counties) and Beaumont and surrounding areas (Jefferson and Chambers Counties). Some of the worst damage appeared to be in Rockport, a coastal city of about 10,000 that was directly in the storm's path. Many structures were destroyed and Rockport's roads were littered with toppled power poles. Extensive damage was also registered in Port Aransas, TX (site of the second Texas landfall). It is estimated that it will be a long time before the storm's catastrophic damage is repaired. Flooding in the Houston/Beaumont areas is the worst in history, displacing millions of people and with flood waters taking weeks to months to recede. As an exercise, NaHRSI results were examined (after the fact) to determine the magnitude and likely locations of extensive damage and low resilience along the Texas Gulf Coast (Table 4).

Of these counties, NaHRSI scores for Aransas, Calhoun, Chambers, Galveston, Harris, Jackson, Jefferson, and Refugio Counties are significantly below the national average for NaHRSI suggesting lower resilience to natural hazard events. All of these counties, plus Brazoria, Fort Bend, Jefferson, and Nueces, display risk domain scores greater than the national average suggesting a history that includes exposure and potential losses stemming from of major natural hazard events. Aransas, Jackson, and Refugio Counties have significantly reduced built environment domain scores suggesting that if an event were to strike these counties, they would be more likely to suffer significant structural damages as a result of reduced public infrastructure and large proportions of vacant buildings. These three counties also possess society scores below the national average. This could indicate a lack of skills diversity to easily rebuild along with deficient security and security infrastructures. Hurricane Harvey also devastated Port Aransas, TX, in Nueces County. Nueces County has a significantly higher risk domain score than the national average associated primarily with historical hurricane paths. The county is dominated by Corpus Christi, TX, which avoided much of the devastation associated with the hurricane; however, Port Aransas suffered extensive structural damage. Port Aransas

Table 4
NaHRSI and Domain Scores for Select Counties Along the Texas Gulf Coast and National Average Scores (Excluding Alaska)

County		Risk	Governance	Built environment	Natural environment	Society	NaHRSI
Aransas		**0.32889**	0.57259	**0.33419**	**0.52163**	**0.40423**	**1.68467**
Brazoria		**0.38408**	**0.66188**	**0.77630**	**0.54926**	0.52368	**4.22022**
Calhoun		**0.33956**	**0.50474**	**0.43549**	**0.49039**	**0.42868**	**1.79703**
Chambers		**0.41971**	0.61495	**0.51116**	**0.50005**	**0.43950**	**2.13280**
Fort Bend		**0.55134**	**0.64353**	**0.78479**	0.42022	**0.58024**	2.64409
Galveston		**0.47067**	0.61040	**0.60782**	0.40844	0.47196	**2.01258**
Harris		**0.99000**	0.61143	**0.83741**	**0.19155**	0.49091	**1.03005**
Jackson		0.31103	0.58578	**0.33742**	**0.48061**	0.53769	**2.14238**
Jefferson		**0.46213**	**0.53399**	**0.69823**	0.44851	0.52149	2.29798
Matagorda		0.29963	**0.54478**	**0.43992**	**0.50342**	**0.43102**	2.28617
Nueces		**0.32810**	**0.63902**	**0.69866**	0.41923	0.47736	**3.56655**
Refugio		0.31287	**0.63050**	**0.26566**	0.46778	**0.44307**	**1.46869**
San Patricio		0.26694	0.61545	**0.48926**	0.44391	**0.40174**	2.73226
Victoria		**0.23454**	**0.53276**	**0.51231**	**0.51035**	0.54069	**3.82251**
National	Including Alaska	0.29590	0.59674	0.39320	0.41333	0.51561	2.71349
Average	Excluding Alaska	0.29758	0.59575	0.39262	0.41182	0.51587	2.37534

Note. Bold denotes significantly below national average for NaHRSI and above national average for domains. NaHRSI = Natural Hazard Resilience Screening Index.

is likely much more similar to Rockport, TX, in Aransas County, which demonstrates a significantly lower than average NaHRSI score.

The other counties with lower NaHRSI scores—Harris (1.03), Calhoun (1.79), Galveston (2.01), Chambers (2.13), and Jefferson (2.29)—all show high risk domain scores well above the national average. The Harris County risk score (the highest in the United States) is exacerbated by significant anthropologic risks located there (e.g., chemical and oil refinery facilities and Superfund sites). Chambers County, located southeast of Harris county, has a lower than average NaHRSI score but a significantly higher than average risk domain score. Four of these counties are at significant risk for flooding and all four counties significantly flooded due to the intense rainfall associated with Hurricane Harvey. Houston (in Harris County) is reported to have had historic flooding that did not recede for weeks or months in some areas. The region's flat topography, hard clay soil, and sprawl of new development combine to make for a drainage nightmare.

Resilience from the flooding in these counties appears to be driven by differing factors based on the NaHRSI and domain scores. Brazoria County has a higher than average resilience score that appears to be the result simply of a high risk, but all the remaining factors tend to reduce the risk and increase the resilience score to 4.22 (well above the national average). Harris County, on the other hand, has the highest risk scores in Texas (0.99) again associated with flooding and several exacerbating factors. The NaHRSI score for this county in significantly below the national average at 1.03 suggesting recovery from a major event could be a very long process. This lower resilience seems to be driven by a very low natural environment score (0.192) suggesting that increasing development in the last decade and loss of natural lands is significant (particularly to the north and west of Houston). Natural and open lands often provide a buffering impact to natural hazard events. They are usually damaged but tend to recover quickly while reducing the impact of the event on surrounding populated areas. This low level of natural ecosystems in the Houston area (often replaced by impervious surfaces) would enhance the impact of flooding. Chambers and Jefferson Counties also have high risks levels associated with flooding with both counties displaying significantly lower than average resilience scores (Chambers County—2.13 and Jefferson—2.29). However, the remaining domain scores in both counties suggest more rapid recovery than Harris County with Chambers County recovering at a slower rate than Jefferson County.

4.3. Where Can We Go From Here?

Our desire to have counties and communities that are minimally impacted by natural hazard events is nearly impossible without a strong recoverability plan and its execution following an event. These plans and their

execution maintain a community at a significant distance from ecological, economic, and social tipping points (e.g., stability, sustainability, joblessness, social inequity, and ecosystem condition). Little attention has been given to the interconnectedness of the vulnerability and recoverability—the basic aspects of resilience (Summers et al., 2014) as they relate to a community's natural hazard resilience. A community may be naturally vulnerable to natural hazard events or vulnerable through anthropogenic activities, but its resilience to these vulnerabilities is guided by the combination of environmental, social, economic, and governance drivers.

U.S. national, state, and local governments have recognized that an integrated, coordinated, and cooperative effort is required to enhance their capacities to withstand and recover from weather-related disasters and emergencies. A disaster-resilient community is one that works together to understand and manage the risks that it may confront. Resilience to disasters is the joint responsibility of all elements of society, including all levels of business, government, the nongovernment sector and individuals. If all these sectors work together with a shared focus and sense of responsibility, they will be much more effective in developing disaster resilience than the individual efforts of any one sector.

4.3.1. Potential Role of Governments

Governments, at all levels, must play a significant role in improving the nation's resilience to disasters:

1. Developing and implementing effective and useful land management and planning arrangements and other mitigation activities based on risk;
2. Having effective plans and policies in place to provide information to people about how to assess risks and reduce their vulnerability to hazards;
3. Having effective and clear education systems so people understand what choices are available and what the best course of action could be for responding to an approaching hazard;
4. Supporting counties and communities, as well as individuals, to prepare for extreme events;
5. Ensuring the most effective, well-coordinated response from our emergency services and volunteers when disaster hits; and
6. Working in a swift, compassionate and pragmatic way to help counties and communities recover from devastation and to learn, innovate and adapt in the aftermath of disastrous events.

Local, state, and national governments are working collectively to incorporate the principle of disaster resilience into aspects of natural disaster arrangements, including preventing, preparing, responding to, and recovering from disasters. Further future enhancements and local applications of NaHRSI can provide advancements in these disaster-related resilience activities.

The FEMA established the Strategic Foresight Initiative (FEMA 2012) to address the need. This initiative brings together significant elements of the emergency management community to discuss important future issues, trends, and other issues and to work through their implications. Working collaboratively, these groups are beginning to understand the full range of changes they might encounter and the nature of their likely future needs. Therefore, they can begin to develop and execute a shared action agenda for action. One of the first tasks of this initiative group should be to bring together the representative views of all governments, business, nongovernment sector and the community into a comprehensive National Disaster Resilience Strategy. This group should also be tasked with considering further those lessons arising from the recent bushfires, floods, tornadoes, and superstorms that could benefit from national collaboration.

4.3.2. Role of Business

Businesses can and do play a critical role in supporting a community's resilience to disasters. Businesses provide expertise, resources, and many essential services upon which the community depends. Businesses, particularly important infrastructure providers, contribute to understanding the risks that they face and ensuring that they can continue providing services during or soon after a disaster.

Insurance and reinsurance businesses are particularly important to county and community resilience (both planning and after an event). If insurance is not available for an area because of higher risk of a meteorological event or the has not been purchased to cover potential damage due to cost, negative impacts of events to communities and individuals become magnified and extended. Working with the insurance industry so that they more fully accept community resilience approaches could be a major influence for improving overall resilience. Having insurers take into account the efforts that governments take at all levels to enhance resilience to natural disasters could reduce overall costs, impacts, and losses.

4.3.3. Role of Individuals

Community disaster resilience is largely based on individuals taking their share of responsibility for preparing for, preventing, responding to, and recovering from natural hazard disasters. A community's constituents can do this by drawing on the resources, guidance, and policies of local government and community organizations. Individuals' resilience to these types of disasters is significantly increased by active planning and preparation for protecting life and property, including purchasing insurance at reasonable rates to cover potential losses. This planning and preparation should be based on an awareness of the threats relevant to their locality as well as being involved in local community disaster or emergency management arrangements. This involvement can often take the form of volunteerism.

4.3.4. Role of Nongovernment Organizations and Volunteers

Nongovernment and community organizations are at the forefront of strengthening disaster resilience in the United States. It is to them that Americans often turn for support or advice, and the dedicated work of these agencies and organizations is critical to helping counties and communities to cope with, and recover from, a disaster. Building and fostering partnerships between U.S. national, state, and local governments and these agencies and organizations is essential to communicate the disaster resilience message and to explore practical ways to strengthen resilience to natural disasters in the counties and communities they serve. Strengthening the disaster resilience of the United States is not a stand-alone activity that can be achieved in the short term. Similarly, it cannot be achieved without a common commitment and concerted effort by all sectors of society. But it is an effort that is worth making because building a more disaster resilient nation is an investment in our future.

5. Conclusions

The United States has and continues to cope well with natural disasters, through cooperative and established emergency management policies and plans, effective capabilities, and dedicated volunteer and professional personnel. Americans are renowned for their resilience to natural hazard events, including the ability to adapt and innovate a strong community spirit that supports those in need and the self-reliance to recover from disasters. Joint, collective responsibility is needed to build capacities for resilience at multiple scales effectively.

We believe that the use of NaHRSI can help the United States and its regions and counties to promote and address capacity building of resilience to natural hazard events by comparatively examining each county's resilience to these events and the deconstructed make-up of these county NaHRSI scores. Furthermore, using the overall and deconstructed scores can allow government entities charged with resilience capacity building to understand their specific strengths and shortcomings and locate others who have successfully addressed similar shortcomings.

Acknowledgments

The authors would like to acknowledge the remaining members of the NaHRSI team—James Harvey, Justin Bousquin, and Deborah Vivian. All are located at the Gulf Ecology Division, and all have played instrumental roles in the development and application of NaHRSI. The data used to develop NaHRSI are numerous and varied. Over six million data points comprise the characterization of individual metrics, indicators, domains, and eventually the NaHRSI scores. It is impractical to deposit these data in a single location for use by other researchers, and, in fact, some data are proprietary and cannot be posted. However, the sources of all data used in the construction and application of NaHRSI can be found in the NaHRSI (CRSI) report compiled by Summers, Harwell, et al. (2017) as Appendix A. This appendix provides the metadata for all metrics including the original source locations of all data. The views expressed in this article are those of the author(s) and do not necessarily reflect the views or policies of the U.S. Environmental Protection Agency.

References

Abdrabo, M., & Hassaan, M. (2014). *Assessing resilience of the Nile Delta urban centers to sea level rise impacts*. 5th Global Forum on Urban Resilience and Adaptation, Bonn, Germany. http://hdl.handle.net/10625/53873

Adager, W. N., Hughes, T. P., Folke, C., Carpenter, S. R., & Rockstrom, J. (2005). Social-ecological resilience to coastal disasters. *Science*, *309*, 1036–1039.

Ainuddin, S., & Routray, J. K. (2012). Earthquake hazards and community resilience in Baluchistan. *Natural Hazards*, *63*(2), 909–937.

Alessa, L., Kliskey, A., Lammers, R., Arp, C., White, D., Hinzman, L., & Busey, R. (2008). The arctic water resource vulnerability index: an integrated assessment tool for community resilience and vulnerability with respect to freshwater. *Environmental Management*, *42*(3), 523–541.

ARUP. (2014). *City Resilience Framework*. The Rockefeller Foundation, ARUP Development International. https://www.rockefellerfoundation.org/report/city-resilience-framework/

Baker, A. (2009). *Creating an empirically derived community resilience index of the Gulf of Mexico region* (Master of Science Thesis in Department of Environmental Sciences, Louisiana State University, Baton Rouge, LA). Retrieved from https://digitalcommons.lsu.edu/gradschool_theses/1046

Balbus, J. M., & Malina, C. (2009). Identifying vulnerable subpopulations for climate change health effects in the United States. *Journal of Occupational and Environmental Medicine*, *51*, 33–37.

Baldwin, C., & King, R. (2018). *Social sustainability, climate resilience and community-based urban development* (p. 198). London: Routledge.

Balica, S. F. (2012). *Applying the flood vulnerability index as a knowledge base for flood risk assessments* (PhD Thesis, Delft University of Technology, Delft, The Netherlands).

Batica, J. (2015). *Methodology for flood resilience assessment in urban environments and mitigation strategy development* (PhD Thesis, Universite Nice Sophia Antipolis, Nice, France).

Berkes, F., Colding, J., & Folke, C. (2003). *Navigating social-ecological systems. Building resilience for complexity and change*. Cambridge: Cambridge University Press. https://doi.org/10.1017/CBO9780511541957

Berkes, F., & Ross, H. (2013). Community resilience: Toward an integrated approach. *Society and Natural Resources*, *26*(1), 5–20.

Buck, K., Summers, J. K., Hafner, S., Harwell, L., & Smith, L. (2018). Development of a multi-hazard landscape for exposure and risk interpretation: The PRISM approach. *Sustainability and Disaster Risk Management*. https://doi.org/10.2174/2542614101666180514123146

Burton, C. G. (2015). A validation of metrics for community resilience to natural hazards and disasters using the recovery from Hurricane Katrina as a case study. *Annals of the Association of American Geographers*, *105*(1), 67–86.

Carpenter, S., Brock, W., & Hanson, P. (1999). Ecological and social dynamics in simple models of ecosystem management. *Conservation Ecology*, *3*, 4. http://www.consecol.org/vol3/iss2/art4/

Carpenter, S., Walker, B., Anderies, J. M., & Abel, N. (2001). From metaphor to measurement: resilience of what to what. *Ecosystems*, *4*, 765–781.

Cassidy, L., & Barnes, G. D. (2012). Understanding household connectivity and resilience in marginal rural communities through social network analysis in the village of Habu, Botswana. *Ecology and Society*, *17*(4), 11.

Christopher, M., & Peck, H. (2004). Building the resilient supply chain. *International Journal of Logistics Management*, *15*, 1–13.

Ciani, F. (2012). A resilience-based approach to food insecurity: the impact of Mitch Hurricane on rural households in Nicaragua. University of Florence, Department of economics, PhD programme in development economics.

Cutter, S. L. (1996). Vulnerability to environmental hazards. *Progress in Human Geography*, *20*, 529–539.

Cutter, S. L. (2003). The vulnerability of science and the science of vulnerability. *Annals of the Association of American Geographers*, *93*, 1–12.

Cutter, S. L. (2012). Vulnerability to environmental hazards. In S. L. Cutter (Ed.), *Hazards vulnerability and environmental justice* (Chap 6, pp. 71-82). London: Routledge.

Cutter, S. L., Ash, K. D., & Emrich, C. T. (2014). The geographies of community disaster resilience. *Global Environmental Change*, *29*, 65–77.

Cutter, S. L., Barnes, L., Berry, M., Burton, C., Evans, E., Tate, E., & Webb, J. (2008). A place-based model for understanding community resilience to natural disasters. *Global Environmental Change*, *18*, 598–606.

Cutter, S. L., Boruff, B. J., & Shirley, W. L. (2003). Social vulnerability to environmental hazards. *Social Science Quarterly*, *84*(2), 242–261.

Daniell, J. E., Daniell, K. A., Daniell, T. M., & Khazai, B. (2010). *A country level physical and community risk index in the Asia-Pacific region for earthquakes and floods*. Karlsruhe. Germany: Karlsruhe Institute of Technology.

Dominelli, N. (2013). Mind the gap: Built infrastructures, sustainable caring relations, and resilient communities in extreme weather events. *Australian Social Work*, *66*, 204–217.

Ebi, K. L. (2011). Resilience to the health risks of extreme weather events in a changing climate in the United States. *International Journal of Environmental Research and Public Health*, *8*, 4582–4595.

Esnard, A. M., Sapat, A., & Mitsova, D. (2011). An index of relative displacement risk to hurricanes. *Natural Hazards*, *59*, 833–859.

Esty, D. C., Levy, M., Srebotnjak, T., & De Sherbinin, A. (2005). *Environmental sustainability index: Benchmarking national environmental stewardship* (pp. 47–60). New Haven: Yale Center for Environmental Law and Policy.

FEMA (Federal Emergency Management Agency) (2011). A whole community approach to emergency management: Principles, themes, and pathways for action. Department of Homeland Security, FDOC 104–008-1, December 2011. Retrieved from https://www.fema.gov/media-library-data/20130726-1813-25045-0649/whole_community_dec2011__2_.pdf

FEMA (Federal Emergency Management Agency) (2012). Crisis response and disaster resilience 2030: Forging strategic action in an age of uncertainty. Retrieved from https://www.fema.gov/media-library-data/20130726-1816-25045-5167/sfi_report_13.jan.2012_final.docx.pdf

FEMA (Federal Emergency Management Agency) (2017). Draft interagency concept for community resilience indicators and national-level measures. Retrieved from https://www.fema.gov/community-resilience-indicators

Foley, J. A., DeFries, R., Asner, G. P., Barford, C., Bonan, G., Carpenter, S. R., et al. (2005). Global consequences of land use. *Science*, *309*, 570–574.

Frazier, T. G., Thompson, C. M., & Dezzani, R. J. (2014). A framework for the development of the SERV model: A Spatially Explicit Resilience-Vulnerability model. *Applied Geography*, *51*, 158–172.

Government Accountability Office (2017). High-risk series: An update. Report to Congressional Committees. Government Printing Office, GAO-17-317. Retrieved from http://www.gao.gov/assets/690/682765.pdf

Gunderson, L. (2010). Ecological and human community resilience in response to natural disasters. *Ecology and Society*, *15*(2), 18.

Handmer, J., Honda, Y., Kundzewicz, Z. W., & Mechler, R. (2012). Changes in impacts of climate extremes: human systems and ecosystems. In J. Handmer et al. (Eds.), *Managing the risks of extreme events and disasters to advance climate change adaptation* (pp. 231–290). Cambridge, UK and New York, NY: Cambridge University Press.

Henstra, D. (2012). Toward the climate-resilient city: Extreme weather and urban climate adaptation policies in two Canadian provinces. *Journal of Comparative Policy Analysis; Research and Practice*, *14*, 175–194.

Holling, C. S. (1973). Resilience and stability of ecological systems. *Annual Review of Ecology and Systematics*, *4*, 1–23.

Holling, C. S. (1986). The resilience of terrestrial ecosystems: Local surprise and global change. In W. C. Clark & R. E. Munn (Eds.), *Sustainable development of the biosphere* (pp. 292–317). New York: John Wiley.

Hsu, A., Esty, D. C., Levy, M. A., & de Sherbinin, A. (2016). *2016 environmental performance index*. New Haven, CT: Yale University.

Housing and Urban Development (2017). National Disaster Resilience Competition.

Intergovernmental Panel on Climate Change (2012). *Managing the risks of extreme events and disasters to advance climate change adaptation. A special report of Working Groups I and II of the Intergovernmental Panel on Climate Change* (p. 582). Cambridge, UK, and New York, NY: Cambridge University Press.

Joerin, J., & Shaw, R. (2011). Climate and disaster resilience in cities. *Community, Environment and Disaster Risk Management*, *6*, 47–61.

Kafle, S. K. (2012). Measuring disaster-resilient communities: A case study of coastal communities in Indonesia. *Journal of Business Continuity & Emergency Planning*, *5*, 316–326.

Keck, M., & Sakdapolrak, P. (2013). What is social resilience? Lessons learned and ways forward. *Erkunde*, *67*, 5–19.

Keim, M. E. (2008). Building human resilience: the role of public health preparedness and response as an adaptation to climate change. *American Journal of Preventive Medicine*, *35*, 508–516.

Kirrane, C., Sharkey, C., & Naess, L. O. (2013). Shaping strategies: Factors and actors in climate change adaptation. In A. Carrapatoso & E. Kurzinger (Eds.), *Climate-resilient development: Participatory solutions from developing countries* (pp. 43–59). London: Routledge.

Klein, R. J. T., Nicholls, R. J., & Thomalla, F. (2003) Resilience to natural hazards: How useful is this concept? EVA Working Paper No. 9, DINAS-COAST Working Paper No. 14, Potsdam Institute for Climate Impact Research, Potsdam, Germany. Retrieved from http://temis.documentation.developpement-durable.gouv.fr/docs/Temis/0075/Temis-0075362/20080.pdfww

Kusumastuti, R., Husodo, Z. A., Suardi, L., & Danarsari, D. N. (2014). Developing a resilience index towards natural disasters in Indonesia. *International Journal of Disaster Risk Reduction*, *10*, 327–340.

Lam, N., Reams, M., Li, K., Li, C., & Mata, L. (2016). Measuring community resilience to coastal hazards along the northern Gulf of Mexico. *Natural Hazards Review*, *17*(1). https://doi.org/10.1061/(ASCE)NH.1527-6996.0000193

Li, C. (2013). *Community resilience to coastal hazards: An analysis of two geographical scales in Louisiana* (Master of Science Thesis, Louisiana State University, Baton Rouge, LA).
Li, K. (2011). *Temporal changes of coastal community resilience in the Gulf of Mexico region* (Master of Science Thesis, Louisiana State University, Baton Rouge, LA). Baton Rouge: LA.
Linnenluecke, M. K., Griffiths, A., & Winn, M. (2012). Extreme weather events and the critical importance of anticipatory adaptation and organizational resilience in responding to impact. *Business Strategy and the Environment*, *21*, 17–32.
Ma, S., Chen, B., & Wang, Z. (2018). Resilience enhancement strategy for distribution systems under extreme weather events. *IEEE Transactions on Smart Grid*, *9*, 1442–1451.
Magus, K. (2010). Community resilience: An indicator of social sustainability. *Society and Natural Resources*, *23*(5), 401–416.
Martini, B. (2014). *Economic, social and environmental resilience: An analysis for the Italians Regions after 2007. University of Rome Tor Vergata*. Italy: Rome.
Martins, L., Girao-Silva, R., Jorge, L., Gomes, A., Musumeci, F., & Rak, J. (2017). Interdependence between power grids and communications networks: A resilience perspective. DRCN 2017 – Design of Reliable Communications Networks; 13th International Conference, March 8–10, 2017, Munich, Germany.
Meadows, D. H. (2008). *Thinking in systems* (p. 218). White River Junction, VT: Chelsea Breen Publishing.
Meher, M., Patra, H., & Sethy, K. (2011). Creating an empirically derived community resilience index for disaster prone area: A case study from Orissa. Disaster, Risk and Vulnerability Conference, Mahatma Gandhi University. Meghalaya, India.
Meitzen, K. M., Phillips, J. N., Perkins, T., Manning, A., & Julian, J. P. (2018). Catastrophic flood disturbance and a community's response to plant resilience in the heart of the Texas Hill Country. *Geomorphology*, *305*, 20–32.
Melillo, J. M., Richmond, T., & Yohe, G. W. (2014). Climate change impacts in the 11 United States: The third national climate assessment. U.S. Global Change Research Program, 12. Retrieved from http://nca2014.globalchange.gov/report%5d/
Miringhoff, M., & Miringhoff, M. L. (1999). *The Social Health of the Nation* (248 pp.). Oxford: Oxford University Press.
National Fish, Wildlife and Plants Climate Adaptation Partnership (2012). *National fish, wildlife and plants climate adaptation strategy. Association of fish and wildlife agencies, Council on environmental quality*. Washington, DC: Great Lakes Indian Fish and Wildlife Commission, national oceanic and atmospheric administration, and U.S. Fish and Wildlife Service. https://www.wildlifeadaptationstrategy.gov/
National League of Cities (2016). Leadership in community resilience program.
National League of Cities (2017). Webinar: Leadership in community resilience.
National Research Council (2012). *Disaster resilience: A national imperative*. Washington, DC: The National Academies Press.
O'Brien, K. (2011). Responding to environmental change: A new age for human geography? *Progress in Human Geography*, *35*, 542–549.
O'Brien, K., Hayward, B., & Berkes, F. (2009). Rethinking social contracts: building resilience in a changing climate. *Ecology and Society* 14(2), 12. http://www.ecologyandsociety.org/vol14/iss2/art12/
Office of Management and Budget and Council on Environmental Quality (2016). Memorandum for executive departments and agencies: Strengthening climate adaptation planning in fiscal year 2016 and beyond. Memorandum.M-16-09. Retrieved from https://www.whitehouse.gov/sites/whitehouse.gov/files/omb/memoranda/2016/m-16-09.pdf
Oven, K. J., Curtis, S. E., Reaney, S., Riva, M., Stewart, M. G., Ohlemuller, R., et al. (2012). Climate change and health and social care: Defining future hazard, vulnerability and risk for infrastructure systems supporting older people's health care in England. *Applied Geography*, *33*, 16–24.
Panteli, M., & Mancarella, P. (2017). Modeling and evaluating the resilience of critical electrical power infrastructure to extreme weather events. *IEEE Systems Journal*, *11*, 1733–1742.
Patel, S. S., Rogers, M. B., Amlot, R., & Rubin, G. J. (2017). What do we mean by 'community resilience'? A systematic literature review of how it is defined in the literature. *PLOS Currents Disasters*, *1*. https://doi.org/10.1371/currents.dis.db775aff25efc5ac4f0660ad9c9f7db2
Paton, D., & Johnston, D. (2001). Disasters and communities: Vulnerability, resilience and preparedness. *Disaster Prevention and Management: An International Journal*, *10*, 270–277.
Peacock, W. G., Brody, S., Seitz, W., Merrell, W., Vedlitz, A., Zahran, S., et al. (2010). *Advancing resilience of coastal localities: Developing, implementing, and sustaining the use of coastal resilience indicators: A final report*. College Station, TX: Hazard Reduction and Recovery Center, Texas A & M University.
Pelling, M., & Manuel-Navarette, D. (2011). From resilience to transformation: The adaptive cycle in two Mexican urban centers. *Ecology and Society*, *6*, 11. http://www.ecologyandsociety.org/vol16/iss2/art11/
Pratt, C., Kaly U., & Mitchell J. (2004). Manual: How to use the environment vulnerability index. SOPAC Technical Report 383.60 pp. United Nations Environmental Programme (UNEP), South Pacific Applied Geoscience Commission (SOPAC).
RAND Corporation (2017). Community resilience. https://www.rand.org/topics/community-resilience.html
Renschler, C. S., Frazier, A. E., & Miles, S. (2010). *Assessing community resilience: A remote sensing approach to evaluate post-disaster ecosystem recovery*. Buffalo, NY: University of Buffalo.
Sanchez, A. X., Osmund, P., & van der Heijden, J. (2017). Resilient policies for wicked problems: Increasing resilience in a complex and uncertain world through information integration. In A. X. Sanchez, K. Hampson, & G. London (Eds.), *Integrating information in built environments* (p. 36–53). London: Routledge.
Smit, B., Burton, I., Klein, R. T., & Wandel, J. (2000). An anatomy of adaptation to climate change and variability. *Climatic Change*, *45*, 223–251.
Smith, L. M., Case, J. L., Smith, H. M., Harwell, L. C., & Summers, J. K. (2012). Relating ecosystem services to domains of human well-being: Foundation for a U.S. index. *Ecological Indicators*, *28*, 79–90.
Smoyer, K. E. (1998). Putting risk in its place: methodological considerations for investigating extreme health risk. *Social Science & Medicine*, *47*, 1809–1824.
Stenseth, N. C., Mysterud, A., Ottersen, G., Hurrell, J. W., Chan, K., & Lima, M. (2002). Ecological effects of climate fluctuations. *Science*, *297*, 1292–1296.
Strickland-Munro, J. K., Allison, H. E., & Moore, S. A. (2010). Using resilience concepts to investigate the impacts of protected area tourism on communities. *Annals of Tourism Research*, *37*, 499–519.
Summers, J. K., Harwell, L. C., Buck, K. D., Smith, L. M., Vivian, D. N., Bousquin, J. J., et al. (2017). *Development of a Climate Resilience Screening Index (CRSI): An assessment of resilience to acute meteorological events and selected natural hazards*. U.S. Environmental Protection Agency, Washington, DC, EPA600/R-17/238. https://cfpub.epa.gov/si/si_public_record_report.cfm?dirEntryId=337914
Summers, J. K., Harwell, L. C., & Smith, L. M. (2016). A model for change: An approach for forecasting resilience from service-based decisions. *Ecological Indicators*, *69*, 295–309.
Summers, J. K., Smith, L. M., Case, J. L., & Linthurst, R. A. (2012). A review of the elements of human resilience with an emphasis on the contribution of ecosystem services. *Ambio*, *41*, 327–340.

Summers, J. K., Smith, L. M., Harwell, L. C., & Buck, K. D. (2017). Conceptualizing holistic community resilience to climate events: Foundation for a climate resilience screening index. *GeoHealth*, *1*, 151–164.

Summers, J. K., Smith, L. M., Harwell, L. C., Case, J. L., Wade, C. M., Straub, K. R., & Smith, H. M. (2014). An index of human resilience for the US: A TRIO approach. *Sustainability*, *6*(6), 3915–3935.

Tobin, G. A. (1999). Sustainability and community resilience: The holy grail of hazards planning? *Global Environmental Change Part B: Environmental Hazards*, *1*(1), 13–25.

Tompkins, E. L., & Adger, W. N. (2004). Does adaptive management of natural resources enhance resilience to climate change? *Ecology and Society*, *9*, 10. http://www.ecologyandsociety.org/vol9/iss2/art10/

U.S. Environmental Protection Agency (2015). EJSCREEN: Environmental Justice Screening Tool.

U.S. National Security Strategy (2015). National Security Strategy. Retrieved from http://nssarchive.us/wp-content/uploads/2015/02/2015.pdf

van de Kerk, G., & Manuel, A. (2014). *Sustainable Society Index 2014 Report* (Vol. 90). The Hague, Netherlands: Sustainable Society Foundation.

Vickerman, S., & Kagan, J. S. (2014). Assessing ecological integrity across jurisdictions and scales. Institutes for Natural Resources, Oregon Biodiversity Information Center, Portland State University, Portland, Oregon.

Walker, B. (1993). Rangeland ecology: Understanding and managing change. *Ambio*, *22*, 80–87.

Walker, B. H., Carpenter, S. R., Anderies, J. M., Abel, N., Cumming, G. S., Janssen, M. A., et al. (2002). Resilience management in social-ecological systems: A working hypothesis for a participatory approach. *Conservation Ecology*, *6*, 14. http://www.consecol.org/vol16/iss1/art14

Walther, G., Post, E., Convey, P., Menzel, A., Parmesani, C., Beebee, T. J. C., et al. (2002). Ecological responses to recent climate change. *Nature*, *416*, 389–395.

Wang, Z., & Wang, J. (2017). Service restoration based on AMI and networked MGs under extreme weather conditions. *IET Generation Transmission and Distribution*, *11*, 401–408.

Wedawatta, G., Ingirige, B., & Amaratunga, D. (2010). Building up resilience of construction sector SMEs and their supply chains to extreme weather events. *International Journal of Strategic Property Management*, *14*, 362–372.

Zimmerman, R. (2017). Effective public service communication networks for climate change adaptation. In W. L. Filho & J. M. Keenan (Eds.), *Climate change adaptation in North America: Experiences, case studies and best practice* (pp. 241–259). Berlin: Springer.

Zimmerman, R., Zhu, Q., de Leon, F., & Guo, Z. (2017). Conceptual modeling framework to integrate resilient and interdependent infrastructure in extreme weather. *Journal of Infrastructure Systems*, *23*, 04017034.

frontiers in Environmental Science

ORIGINAL RESEARCH
published: 30 November 2018
doi: 10.3389/fenvs.2018.00147

Regionalizing Resilience to Acute Meteorological Events: Comparison of Regions in the U.S.

Kevin Summers, Linda Harwell, Lisa M. Smith and Kyle D. Buck*

Gulf Ecology Division, National Health and Environmental Effects Research Laboratory Office of Research and Development U.S. Environmental Protection Agency, Gulf Breeze, FL, United States

Using a Climate Resilience Screening Index (CRSI) that was developed to represent resilience to acute weather events at multiple scales for the United States, nine regions of the United States are compared for resilience for these types of natural hazards. The comparison examines the domains, indicators, and metrics of CRSI addressing environmental, economic, and societal aspects of resilience to acute climate events at county scales. The index was applied at the county scale and aggregated to represent select regions of the United States. Comparisons showed higher levels of resilience in the Northeast and West, including Alaska, (>4.0) while counties in the South Atlantic and South-Central regions exhibited lower resilience (<2.0) to acute climate events. Northeast, West and Mountain regions of the US are characterized by relatively low levels of risk (<0.26), higher levels of governance (>0.60), and above national median scores for society, built environment and natural environment domains which enhances their resilience scores. South Atlantic and South-Central regions of the US are characterized by higher risk scores (>0.31) accompanied by lower levels of governance (<0.48) and below national median scores for society and built environment domains reducing the region's overall resilience.

Keywords: climate events, resilience, vulnerability, recoverability, natural hazards

OPEN ACCESS

Edited by:
Yang Liu,
Emory University, United States

Reviewed by:
Sofia Kottou,
National and Kapodistrian University of Athens, Greece
Gulnihal Ozbay,
Delaware State University, United States

****Correspondence:***
Kevin Summers
summers.kevin@epa.gov

Specialty section:
This article was submitted to Environmental Health, a section of the journal Frontiers in Environmental Science

Received: *16 August 2018*
Accepted: *08 November 2018*
Published: *30 November 2018*

Citation:
Summers K, Harwell L, Smith LM and Buck KD (2018) Regionalizing Resilience to Acute Meteorological Events: Comparison of Regions in the U.S. Front. Environ. Sci. 6:147. doi: 10.3389/fenvs.2018.00147

INTRODUCTION

Natural hazards can result in disasters without proper governance and mitigating systems (Chandra et al., 2007). In the recent past, the United States has witnessed several natural disasters including major hurricanes, earthquakes, tornadoes, and wildfires. While some governance and mitigation measures have been taken, future natural hazards disasters cannot be prevented due to the fact these events can hit random locations, have varying magnitudes, and can take unexpected forms. Therefore, the enhancement of the capacity of communities to resist and recover from these types of natural hazard disasters is paramount. Several global, national, and local agencies are confronted with this situation and have developed frameworks to address these issues (e.g., UN/ISDR, 2002; FEMA, 2012, 2017a,b; NRC, 2012; FDH, 2016; FDEM, 2018).

Resilience is increasingly used as a pathway for understanding the actions of natural hazard disasters. Resilience was originally an ecological concept (Holling, 1973) that was adapted to social

systems (Adger, 2000) and eventually to joint human-environmental systems (Folke, 2006). What natural disasters have taught us is that resilience to these disasters needs to be discussed within the framework of integrated socio-ecological systems (Berkes et al., 2003). Similarly, the temporal scale of these disaster events can be short-term (Bruneau et al., 2003; Rose, 2004) associated with specific acute meteorological events or longer-term associated with global change (Dovers and Handmer, 1992). Regardless, there is no common conceptualization for resilience. This manuscript uses a conceptualization for resilience to short-term meteorological hazards (Summers et al., 2017a, 2018) and analyses the results to depict regional comparisons.

CLIMATE RESILIENCE SCREENING INDEX—CONCEPTUALIZATION, APPROACH AND STRUCTURE

The conceptualization, approach and structure of the Climate Resilience Screening Index (CRSI) for acute meteorological events has been described in detail in Summers et al. (2017a,b). A short synopsis of this index is provided here.

In the construction of the CRSI index, the historical occurrence of acute meteorological events associated with geographic regions throughout the United States were assessed as well as the infrastructure challenges these events created. Discussions with climate experts, in conjunction with the information provided by the National Climate Assessment (Melillo et al., 2014) and the 100 Resilient Cities report (ARUP, 2014) yielded twelve (12) acute meteorological events and natural hazards that were included in CRSI:

- Hurricanes
- Tornadoes
- Inland Floods
- Coastal Flooding
- Earthquakes
- Wildfires
- Drought
- High winds
- Hail
- Landslides
- Extreme high temperatures
- Extreme low temperatures.

No singular approach among existing composite measures of climate resilience met all of the expected needs for developing CRSI. Collectively, however, the reviewed literature provided many of the building blocks (e.g., suites of indicators, indicator groupings, domains). To varying degrees, all of the existing indices offered patterns of indicator groupings. In the final conceptualization of CRSI, five domains were comprised of twenty indicators that were derived from 117 unique metrics. **Figure 1** depicts the final CRSI conceptual framework including the domains and indicators of the index. A summary and discussion of the domains, indicators and types of metrics used in CRSI can be found in Summers et al. (2017b, 2018) and are listed in **Table 1**.

All domains for each county, parish and borough (all referred to as county below) were min-max standardized on a scale from 0.01 to 0.99. The final CRSI calculation begins as a scaled value for recoverability/vulnerability derived from Governance and Risk (basic CRSI) with the Governance value being adjusted by the remaining domain scores for social, built environment and natural environment to complete the calculation of CRSI as shown below:

$$CRSI(B)_i = {}^{R_i}\!/_{V_i} = {}^{Gov_i}\!/_{Risk_i}$$

where $CRSI(B)_i$ = value of basic resilience (Recovery/Vulnerability or R_i/V_i) and R_i/V_i = Governance in county i/Risk in county i. The overall CRSI score is calculated as:

$$CRSI_i = (Gov_i + Soc(a)_i Gov_i + BE(a)_i Gov_i + NE(a)_i Gov_i)/Risk_i$$

where $CRSI_i$ = the value of CRSI or adjusted resilience for county i and $Soc(a)_i$, $BE(a)_i$, and $NE(a)_i$ are the adjustment multipliers for Society, Built Environment, and Natural Environment in each county i, and $Risk_i$ is the Risk score for county i. The adjustment factors are calculated as:

$$Soc(a)_i = {}^{(Soc_i - Soc_m)}\!/_{Soc_m}$$

where Soc(a)i is the adjustment multiplier for society in county i, Soc_i is the social domain score for county i and Soc_m is the median social domain score (median is used rather than mean to match the skewed distribution of the data) for all counties;

$$BE(a)_i = {}^{(BE_i - BE_m)}\!/_{BE_m}$$

where $BE(a)_I$ is the adjustment multiplier for built environment in county i, BE_i is the built environment domain score for county i and BE_m is the median built environment domain score for all counties;

$$NE(a)_i = {}^{(NE_i - NE_m)}\!/_{NE_m}$$

and where $NE(a)_i$ is the adjustment multiplier for natural environment in county i, NE_i is the natural environment domain score for county i and NE_m is the median natural environment domain score for all counties.

The national results of CRSI have been provided elsewhere (Summers et al., 2017b, 2018) as well as a regionalization providing direct utility to the U.S. Environmental Protection Agency (EPA)—a regionalization by EPA Regions (the U.S. is divided into 10 EPA regions). However, such a regionalization is of limited utility to non-EPA decision makers. Therefore, the national data has been regionalized by geographic region based on Census Divisions (U.S. Department of Commerce, 2018) and by state to be of better use for these decision-makers as presented in **Figure 2**. This regionalization separates the United States into nine areas:

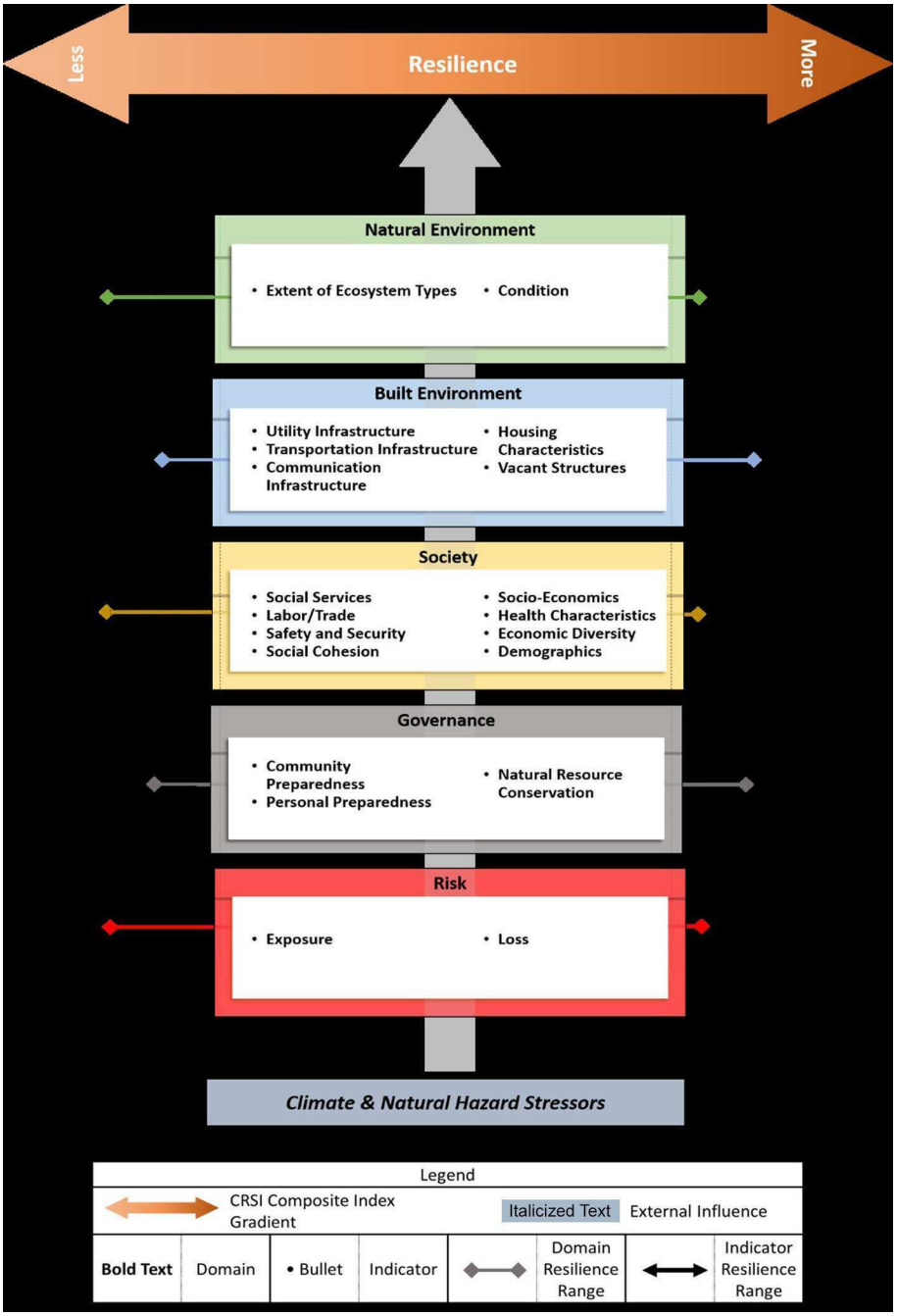

FIGURE 1 | Final CRSI conceptual framework. Arrows projected from boxes to the left and right represent hypothetical increases and decreases in ranges for indicators (black arrows) and domains (colored arrows).

1) New England—Connecticut, Maine, Massachusetts, New Hampshire, Rhode Island, and Vermont
2) Middle Atlantic—New Jersey, New York, and Pennsylvania
3) East North Central—Illinois, Indiana, Michigan, Ohio, and Wisconsin
4) West North Central—Iowa, Kansas, Minnesota, Missouri, Nebraska, North Dakota, and South Dakota
5) South Atlantic—Delaware, District of Columbia, Florida, Georgia, Maryland, North Carolina, South Carolina, Virginia, and West Virginia
6) East South Central—Alabama, Kentucky, Mississippi, and Tennessee
7) West South Central—Arkansas, Louisiana, Oklahoma, and Texas

TABLE 1 | List of CRSI domains, indicators, scope, and number of metrics.

Domain (# indicators/ #metrics)	Indicator(s)	Metric category (number of specific metrics)
Built environment (5/24)	Communication infrastructure	Communication continuity (7)
	Housing characteristics	Structure vulnerability (5)
	Transportation infrastructure	Transportation flow continuity (6)
	Utility infrastructure	Utility continuity (3)
	Vacant structures	Structure vulnerability (3)
Governance (3/5)	Community preparedness	Community resilience strengthening (2)
	Natural resource conservation	Natural resource recovery (1)
	Personal preparedness	Personal property hazard protection (2)
Natural environment (2/18)	Condition	Biodiversity, using birds as a proxy (1)
		Coastal condition (1)
		Forest condition (1)
		Inland lake condition (1)
		Percentage of clean air days (1)
		Rivers and streams condition (1)
		Soil growth suitability (1)
		Soil productivity (1)
		Wetlands condition (1)
	Extent of ecosystem types	Agriculture area (1)
		Forested area (1)
		Grassland area (1)
		Inland surface water area (1)
		Marine/estuarine area (1)
		Perennial ice/snow area (1)
		Protected areas (1)
		Tundra area (1)
		Wetland area (1)
Risk (2/20)	Exposure	Earthquake probability (1)
		Extreme high temperature incidents (1)
		Extreme low temperature incidents (1)
		Flood probability (2)
		Hailstorm probability (1)
		Tornado probability (2)
		Hurricane probability (2)
		Landslide probability (1)
		Major toxics presence (1)
		Non-storm damaging wind incidents (1)
		Nuclear presence (1)
		Location of RCRA sites (1)*
		Location of Superfund sites (1)**
		Toxic release presence (1)
		Wildfire probability (1)
	Loss	Developed area loss (includes human and property measures) (1)
		Natural area loss (1)
		Dual-benefit area loss (includes cropland and managed area measures) (1)
Society (8/50)	Demographics	Vulnerable populations (5)
	Economic diversity	Economic stability/recovery (2)
	Health characteristics	Health problems that may impact personal resilience (9)
	Labor and trade services	Construction recovery (8)
	Safety and security	Provisioning of emergency and civil services (4)
	Social cohesion	Access to social support (4)
	Social services	Access provisioning to critical services (15)
	Socio-economics	Employment opportunity (1)
		Personal economics (2)

*Numbers in parentheses for domains show the total number of indicators/total metrics in the domain. Numbers in parentheses for metrics indicate number of individual metrics used to represent the metric category. *RCRA, Resource Conservation and Recovery Act – RCRA is a U.S. public law that creates the framework for the proper management of hazardous and non-hazardous solid waste. The metric represents the number and locations of RCRA sites; **Superfund, EPA's Superfund Program is responsible for cleaning up some of the nation's most contaminated sites. The metric represents the number and location of Superfund sites.*

8) Mountain—Arizona, Colorado, Idaho, Nevada, New Mexico, Utah, and Wyoming
9) Pacific—Alaska, California, Hawaii, Oregon, and Washington.

Data from Alaska is only partially available with about 50% of its boroughs not represented. Due to both missing data and very low risk domain scores for Alaska (risk to acute meteorological events), use of Alaska data skews the scores for the Pacific region. To better represent issues associated with the Pacific region, results will be discussed both including and excluding Alaska.

REGIONALIZATION RESULTS

The overall CRSI regionalized results are depicted in **Figure 2**. These scores show that the Pacific (with or without Alaska), New England, and Mountain Regions display the highest overall resilience while the East South Central, South Atlantic, and West South Central display the lowest overall resilience. This distribution of overall scores is the result of specific regional domain scores (**Figure 3**). One of the primary domains affecting the overall CRSI score for a region is risk. Risk is comprised of 12 types of meteorological events and is adjusted based on losses due to those events and potential anthropogenic hazard exposures. **Figure 4** shows the comparative levels of risk for the events, losses, and anthropogenic risks by U.S. region. In all regions the risk domain is driven by historical exposure with minimal contributions from historical losses. The highlights of the domain

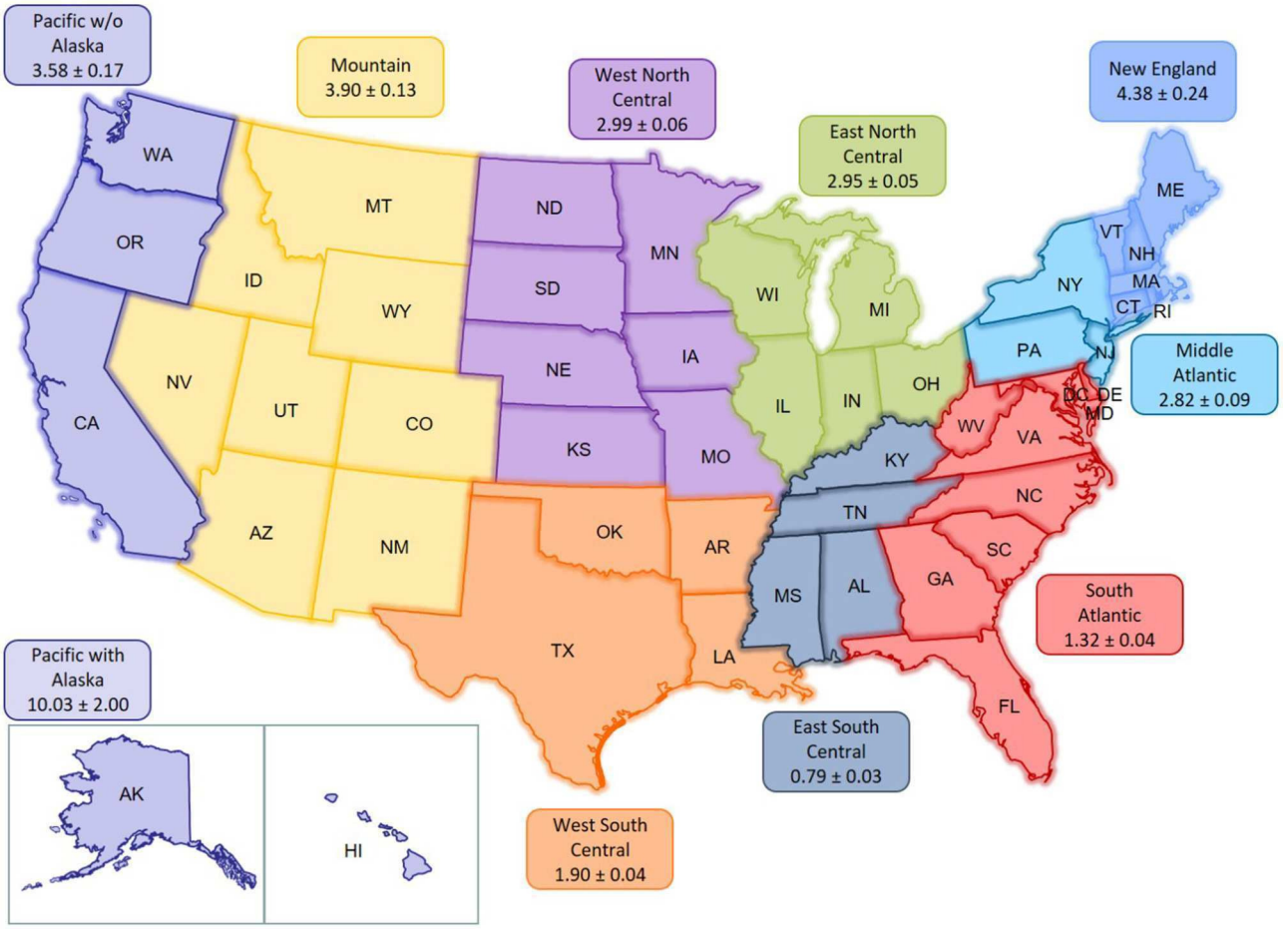

FIGURE 2 | Regionalized CRSI results with estimate of uncertainty.

scores for each region and its comprising states will be discussed below by individual region.

New England

The New England region is comprised of five states and is characterized by the second highest CRSI score in the U.S. (4.375) or the highest score if Alaska is excluded from the Pacific region (**Table 2**). All states in the New England region are either near the national CRSI average (Rhode Island) or significantly above the national averages (all remaining states in the region). All New England states are characterized by lower than average risk to meteorological events and significantly higher than average governance. All states have average or higher than average built environment scores except Rhode Island which is significantly lower than average (0.302). Similarly, all states have higher than average society scores with Vermont demonstrated among the highest state society scores in the nation (0.671). All New England states have natural environment scores either close to the national average or significantly greater than the average (Rhode Island, 0.511, and Maine, 0.484).

Meteorological risks in New England (**Figure 4**) are characterized by extreme high and low temperatures (49% of events and well-above the national average) and drought (23% of events but well-below the national average). Inland flooding, high winds and hailstorms comprise the remaining secondary risks at 9, 9, and 3%, respectively, with high wind events being significantly above the national average. These types of events result in minimal loss of life and physical property (about 1% of the loss in New England), although losses to agricultural and silvicultural lands, as well as natural ecosystem, comprise about 99% of losses. Potential anthropogenic hazards existing near sites of meteorological events are dominated by Superfund sites (47%) and general toxic release sites (e.g., industrial outflows) at 36% (both at the national average).

CRSI scores can be deconstructed to assess which indicators are the primary contributors to the score and which indicators contribute weakly to the score. Using polar plots (**Figures 5**–**7**), these contributions can be quantified visually for each region of the United States. **Figure 5A** shows the deconstruction of the New England CRSI score by domains. Risk domains simply reflect histories of exposure and cannot theoretically be altered by human actions to reduce risks. The major contributors to the CRSI score in the New England region are natural resource conservation

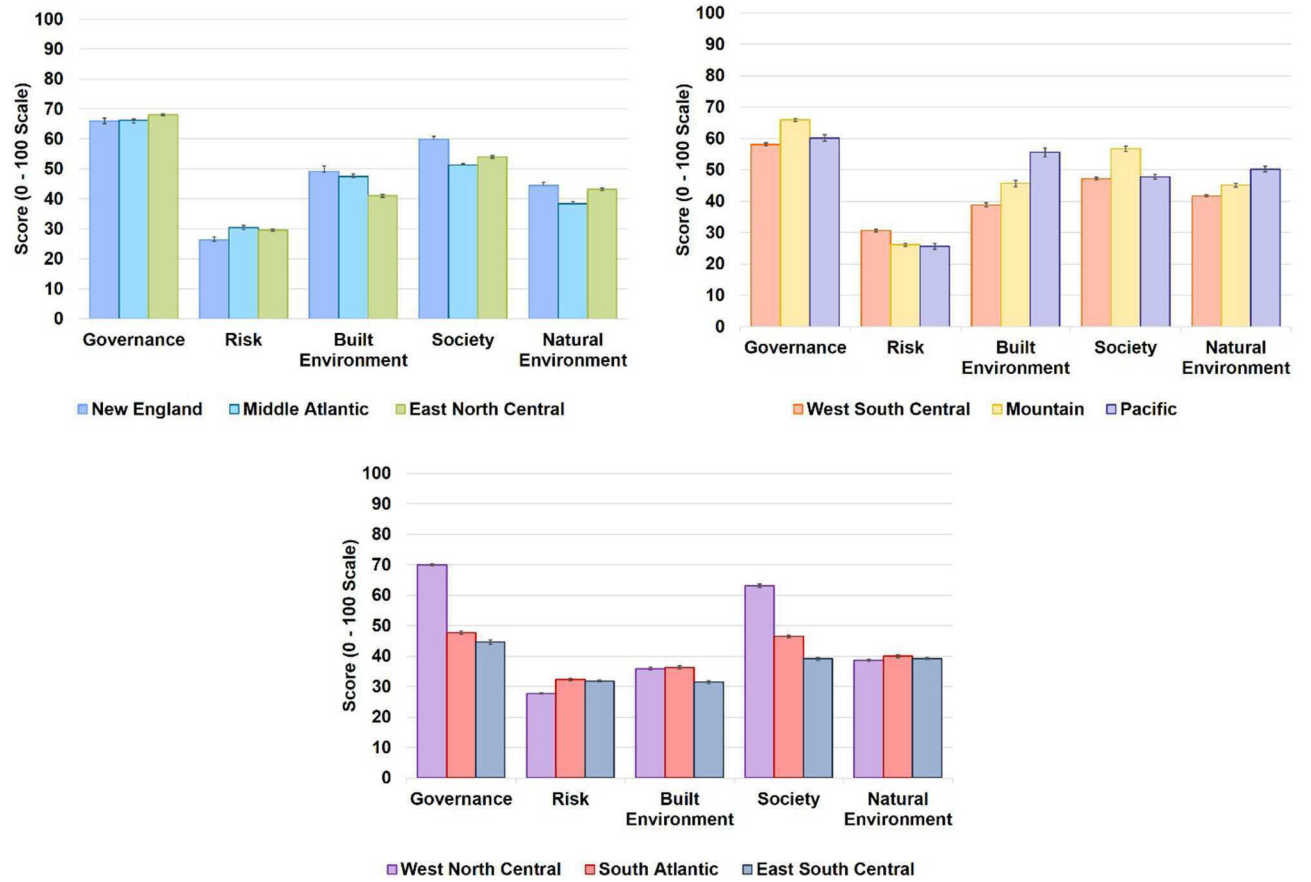

FIGURE 3 | Domain scores by U.S. Region (vertical bars represent uncertainty).

contributions to governance; demographic characteristics, economic diversity, and socio-economics to society; the number of vacant structures and general housing characteristics to the built environment; and, the extent or acreage of natural ecosystems (not built environments) in the natural environment.

Of the 67 counties in the New England region, the top 10% of CRSI scores (scores = 6.95 to 12.7) were seen in Maine (3 counties), Vermont (2 counties), and Massachusetts and New Hampshire (1 county each). Only two New England counties (both in Rhode Island) have resilience scores significantly below the national average.

Middle Atlantic

The Middle Atlantic region is comprised of three states and is characterized a moderate CRSI score (2.823) (**Table 2**). All states in the Middle Atlantic region are near the national CRSI average with New York demonstrating an overall CRSI score slightly above the national average (3.103). Most Middle Atlantic states are characterized by average risk to meteorological events with New Jersey showing elevated risks (0.379) and all states in the region showed significantly higher than average governance scores. All states have higher than average built environment scores and average society scores. All Middle Atlantic states have natural environment scores slightly lower than the national average.

Meteorological risks in the Middle Atlantic region (**Figure 4**) are characterized by extreme high and low temperatures (46% of events and well-above the national average) and drought (19% of events but well-below the national average). The region is exposed to three other types of meteorological events—landslides (13%), high wind events (9%), and inland flooding (8%). Landslides and high wind events are about twice the national average. These types of events result in minimal loss of life and physical property (<1% of the loss in the Middle Atlantic) although losses to agricultural and silvicultural lands, as well as natural ecosystem, comprise about 99% of losses (equally divided). Potential anthropogenic hazards existing near sites of meteorological events are dominated by Superfund sites (54%, significantly above the national average), general toxic release sites (e.g., industrial outflows) at 26% (significantly below the national average) and RCRA sites (12% at twice the national average).

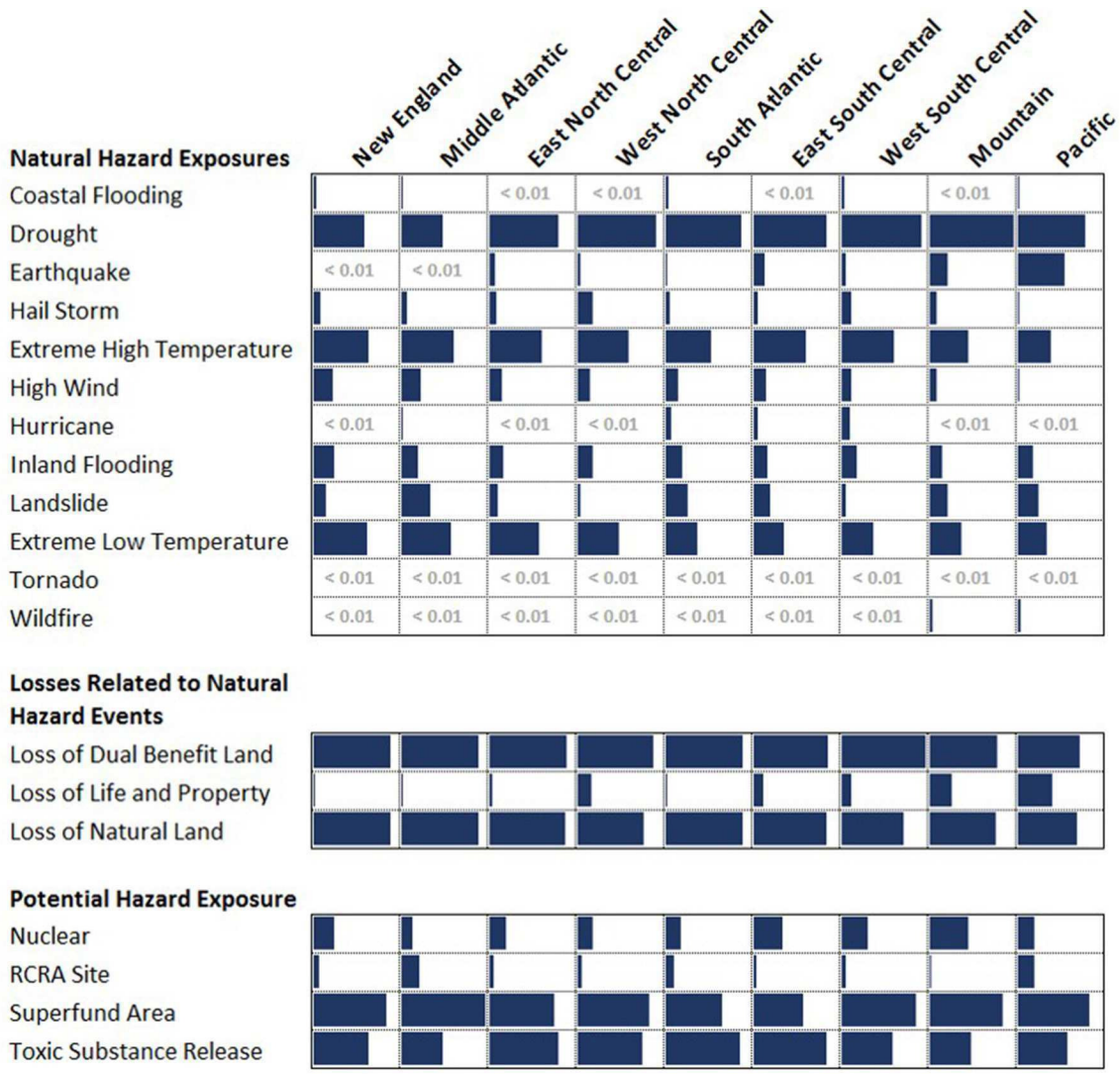

FIGURE 4 | Relative comparison of risk of meteorological events, losses due to those events and potential anthropogenic hazard exposures by region. Sum of each column associated with the three risk subsets equals 1 (or multiplied by 100 equals 100%).

The major contributors to the CRSI score in the Middle Atlantic region are natural resource conservation contributions to governance; demographic characteristics, economic diversity, socio-economics and social cohesion to society; the number of vacant structures to the built environment; and, the extent and condition of natural ecosystems in the natural environment (**Figure 5B**).

Of the 150 counties in the Middle Atlantic region, the top 10% of CRSI scores (scores = 4.35 to 5.61) were seen in New York (12 counties) and Pennsylvania (3 counties). Nearly 25% of counties in the Middle Atlantic region has overall CRSI scores significantly below the national average of 2. 375 (excluding Alaska). The 10% of Middle Atlantic counties with the lowest CRSI scores equitably split among the three states with 4–6 counties in each state.

East North Central

The East North Central region of the United States is comprised of five states and is characterized an above average CRSI score (2.948) (**Table 2**). All states in the East North Central region are either near the national CRSI average or significantly higher than the average with Wisconsin and Michigan demonstrating the highest CRSO scores (4.145 and 3.066, respectively). Most East North Central states are characterized by average risk to meteorological events with Illinois showing elevated risks (0.335) and all states in the region showed significantly higher than average governance scores. All states, except Indiana, have average built environment scores and all states, except Wisconsin, have average, or slightly below average society scores. Indiana's built environment score (0.360) is significantly below the national average while Wisconsin's society score (0.623) is significantly above the national average. All East North Central states, except

TABLE 2 | Regionalized CRSI scores and domain scores by region and state.

Region	State	Governance	Risk	Built	Society	Natural	CRSI
DOMAINS							
Northeast		**0.660**	**0.263**	**0.492**	**0.599**	**0.445**	**4.375**
	Connecticut	0.654	0.308	0.520	0.547	0.398	3.106
	Maine	0.677	0.228	0.499	0.565	0.484	5.368
	Massachusetts	0.602	0.311	0.557	0.601	0.447	3.802
	New Hampshire	0.670	0.250	0.519	0.596	0.421	4.448
	Rhode Island	0.627	0.305	0.302	0.586	0.511	2.653
	Vermont	0.708	0.223	0.450	0.671	0.417	5.102
Middle Atlantic		**0.662**	**0.305**	**0.475**	**0.513**	**0.384**	**2.823**
	New Jersey	0.639	0.379	0.471	0.518	0.397	2.280
	New York	0.665	0.276	0.469	0.521	0.381	3.103
	Pennsylvania	0.667	0.307	0.481	0.503	0.383	2.733
East North Central		**0.681**	**0.295**	**0.410**	**0.540**	**0.433**	**2.948**
	Illinois	0.662	0.338	0.414	0.515	0.489	2.703
	Indiana	0.659	0.286	0.360	0.570	0.452	2.857
	Michigan	0.705	0.258	0.412	0.492	0.418	3.066
	Ohio	0.651	0.307	0.421	0.514	0.352	2.237
	Wisconsin	0.746	0.279	0.457	0.623	0.441	4.145
West North Central		**0.699**	**0.277**	**0.359**	**0.631**	**0.386**	**2.988**
	Iowa	0.704	0.280	0.382	0.653	0.419	3.397
	Kansas	0.698	0.291	0.332	0.651	0.369	2.595
	Minnesota	0.772	0.289	0.389	0.735	0.442	4.345
	Missouri	0.626	0.286	0.399	0.530	0.389	2.395
	Nebraska	0.714	0.268	0.311	0.613	0.340	2.387
	North Dakota	0.704	0.234	0.374	0.662	0.354	3.503
	South Dakota	0.703	0.268	0.314	0.608	0.377	2.677
South Atlantic		**0.477**	**0.323**	**0.363**	**0.465**	**0.400**	**1.321**
	Delaware	0.606	0.361	0.586	0.472	0.547	3.197
	District of Columbia	0.610	0.470	0.402	0.506	0.200	0.721
	Florida	0.427	0.309	0.485	0.434	0.426	1.607
	Georgia	0.442	0.300	0.282	0.420	0.395	0.846
	Maryland	0.622	0.352	0.494	0.518	0.463	2.733
	North Carolina	0.435	0.341	0.419	0.463	0.431	1.440
	South Carolina	0.462	0.319	0.393	0.437	0.420	1.347
	Virginia	0.520	0.351	0.331	0.548	0.378	1.482
	West Virginia	0.555	0.293	0.324	0.435	0.328	1.104
East South Central		**0.446**	**0.318**	**0.315**	**0.392**	**0.392**	**0.787**
	Alabama	0.335	0.303	0.408	0.385	0.397	0.901
	Kentucky	0.534	0.307	0.255	0.388	0.371	0.642
	Mississippi	0.494	0.308	0.337	0.382	0.444	1.151
	Tennessee	0.370	0.350	0.305	0.409	0.370	0.577
West South Central		**0.581**	**0.306**	**0.388**	**0.472**	**0.417**	**1.895**
	Arkansas	0.533	0.302	0.393	0.451	0.445	1.865
	Louisiana	0.570	0.372	0.430	0.479	0.457	1.914
	Oklahoma	0.649	0.287	0.384	0.530	0.401	2.436
	Texas	0.577	0.297	0.377	0.459	0.403	1.735

(Continued)

TABLE 2 | Continued

Region	State	Governance	Risk	Built	Society	Natural	CRSI
Mountain		**0.659**	**0.261**	**0.456**	**0.567**	**0.451**	**3.898**
	Arizona	0.613	0.280	0.710	0.458	0.410	3.997
	Colorado	0.673	0.277	0.453	0.555	0.396	3.216
	Idaho	0.666	0.233	0.423	0.545	0.537	4.873
	Montana	0.676	0.231	0.381	0.638	0.402	4.090
	Nevada	0.623	0.291	0.485	0.446	0.548	3.263
	New Mexico	0.621	0.267	0.472	0.505	0.498	3.571
	Utah	0.670	0.302	0.495	0.617	0.463	3.983
	Wyoming	0.659	0.253	0.464	0.658	0.433	4.231
Pacific		**0.602**	**0.256**	**0.556**	**0.478**	**0.503**	**10.034**
	Alaska	0.736	0.058	0.475	0.479	0.627	50.546
	California	0.498	0.322	0.641	0.485	0.461	2.852
	Hawaii	0.739	0.182	0.570	0.589	0.479	8.431
	Oregon	0.618	0.278	0.499	0.465	0.517	3.561
	Washington	0.648	0.259	0.524	0.465	0.485	4.044
Pacific w/o Alaska		**0.580**	**0.288**	**0.568**	**0.478**	**0.483**	**2.375**
United States		**0.597**	**0.296**	**0.393**	**0.516**	**0.413**	**2.713**
United States w/o Alaska		**0.596**	**0.298**	**0.393**	**0.516**	**0.412**	**2.375**

Bold, Regional Scores; Built, Built Environment, Natural, Natural Environment.

Ohio (0.352), have natural environment scores higher than the national average.

Meteorological risks in the East North Central region (**Figure 4**) are characterized by extreme high and low temperatures (47% of events and well-above the national average) and drought (32% of events but at the national average). The region is exposed to five other types of meteorological events—inland flooding (7%), high wind events (6%), landslides (4%), hailstorms (3%), and earthquakes (3%). These five risk exposures were at about the national average. Tornadoes and wildfire exposures (<1%) were comparable to the national average. These types of events result in lower than average loss of life and physical property (1.4% of the loss in the East North Central) although losses to agricultural and silvicultural lands, as well as natural ecosystem, comprise about 98% of losses (equally divided). Potential anthropogenic hazards existing near sites of meteorological events are dominated by general toxic release sites (e.g., industrial outflows) at 44% (slightly above the national average), Superfund sites at 42% (slightly below the national average) and nuclear facilities (11% at the national average).

The major contributors to the CRSI score in the East North Central region are natural resource conservation contributions to governance; demographic characteristics, economic diversity, socio-economics, and social cohesion to society; the number of vacant structures and general housing characteristics to the built environment; and, the extent and condition of natural ecosystems in the natural environment (**Figure 5C**).

Of the 437 counties in the East North Central region, the top 5% of CRSI scores (scores = 4.75 to 6.00) were seen in Wisconsin (20 counties), Michigan (3), and Illinois and Indiana (1 each). Nearly 15% of counties in the East North Central region have overall CRSI scores significantly below the national average of 2.375 (excluding Alaska). The 5% of East North Central counties with the lowest CRSI scores were largely seen in Ohio (15 counties), with Illinois (6), Indiana (3) and Michigan (1) comprising the remainder.

West North Central

The West North Central region of the United States is comprised of seven states and is characterized an above average CRSI score (2.988) (**Table 2**). All states in the West North Central region are either near the national CRSI average or significantly higher than the average with Minnesota and North Dakota demonstrating the highest CRSO scores (4.345 and 3.503, respectively). Most West North Central states are characterized by below average risk to meteorological events with North Dakota characterized by significantly below average risks (0.234). All states in the region showed significantly higher than average governance scores with Minnesota demonstrating the highest governance score in the nation (0.772). In fact, five of the seven West North Central states had governance scores >0.7. All states, except Missouri, have below average built environment scores and all West North Central states have slightly or significantly above average society scores. Nebraska, South Dakota and Kansas had society scores that are significantly below the national average (0.311, 0.314, and 0.332, respectively) while Minnesota's society score (0.735) is the highest in the U.S. All West North Central states, except Minnesota and Iowa, have natural environment scores significantly lower than the national average.

Meteorological risks in the West North Central region (**Figure 4**) are characterized by extreme high and low temperatures (41% of events and slightly above the national

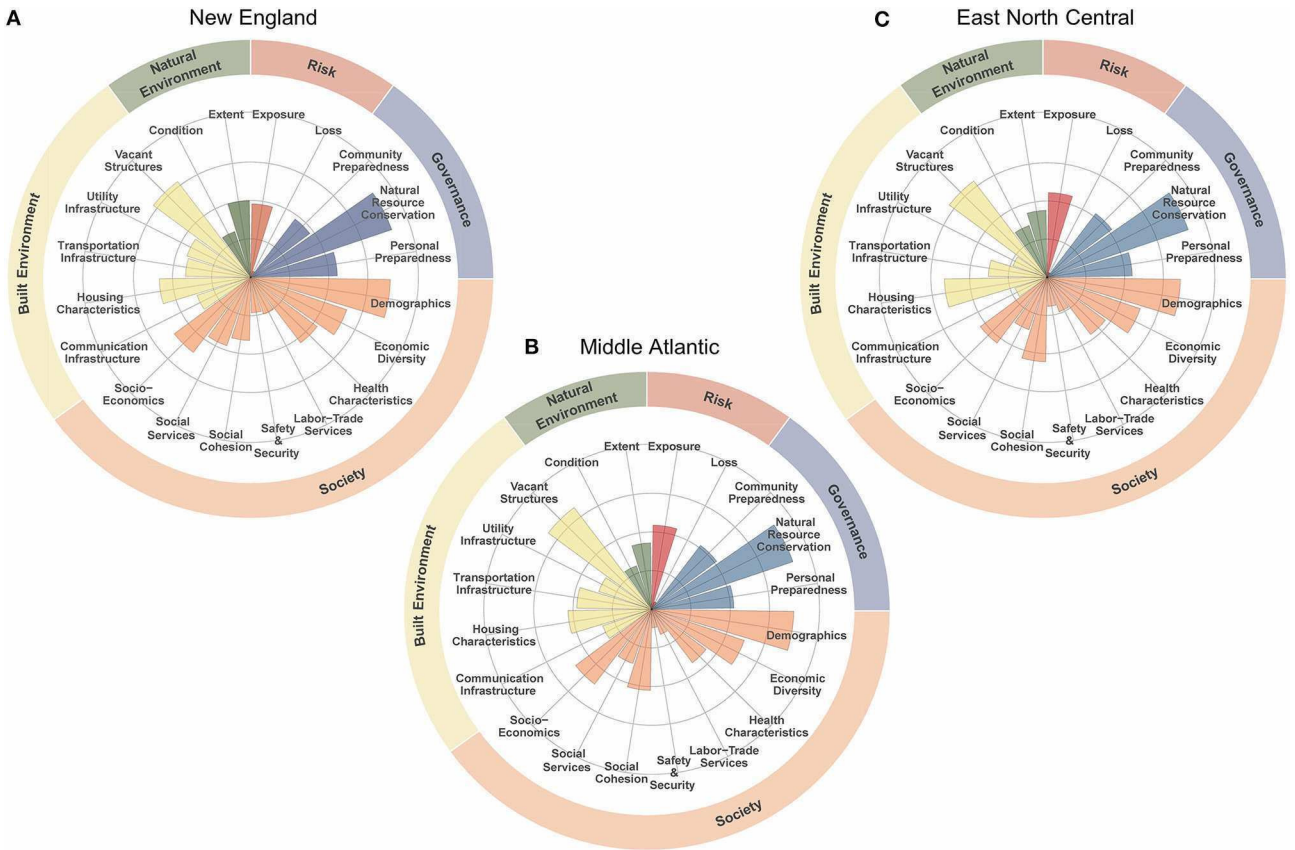

FIGURE 5 | Polar plots of the **(A)** New England, **(B)** Middle Atlantic, and **(C)** East North Central regions.

average) and drought (36% of events but at the national average). The region is exposed to five other types of meteorological events—hailstorms (7%), inland flooding (7%), high wind events (5%), landslides (1%), and earthquakes (1%). Of these five risk exposures, hailstorms were at about twice the national average while inland flooding and high wind events were at about the national average and landslides and earthquakes were significantly below the national average. Wildfires (0.12%) and tornadoes (0.11%) were slightly above the national average. These types of events result in about twice the national average for loss of life and physical property (9% of the loss in the West North Central) although losses to agricultural and silvicultural lands, as well as natural ecosystem, comprise about 91% of losses (49% for dual use lands and 42% for natural lands). Potential anthropogenic hazards existing near sites of meteorological events are dominated by Superfund sites (46%) being at about the national average, general toxic release sites (e.g., industrial outflows) at 41% (slightly above the national average) and nuclear facilities (10% at the national average).

The major contributors to the CRSI score in the West North Central region are natural resource conservation contributions to governance; demographic characteristics, social cohesion, health characteristics, economic diversity and socio-economics to society; the number of vacant structures and general housing characteristics to the built environment; and, the extent and condition of natural ecosystems in the natural environment (**Figure 6A**).

Of the 618 counties in the West North Central region, the top 5% of CRSI scores (scores = 5.32 to 8.12) were seen in Minnesota (14 counties), South and North Dakota (4 each), Iowa (2) and Nebraska (1). Nearly 25% of counties in the West North Central region have overall CRSI scores significantly below the national average of 2.375 (excluding Alaska). The 5% of West North Central counties with the lowest CRSI scores were largely seen in Nebraska (15 counties), with South Dakota (6), Kansas (2), and North Dakota and Missouri (1 each) comprising the remainder.

South Atlantic

The South Atlantic region of the United States is comprised of eight states and the District of Columbia and is characterized by a significant below average CRSI score (1.321) (**Table 2**). All states in the South Atlantic region are significantly below the national average except for Delaware (3.179) with the District of Columbia and Georgia displaying the lowest overall CRSI scores (0.721 and 0.846, respectively). The South Atlantic region has the highest risk to acute meteorological events in the nation (0.323). All South Atlantic states, except West

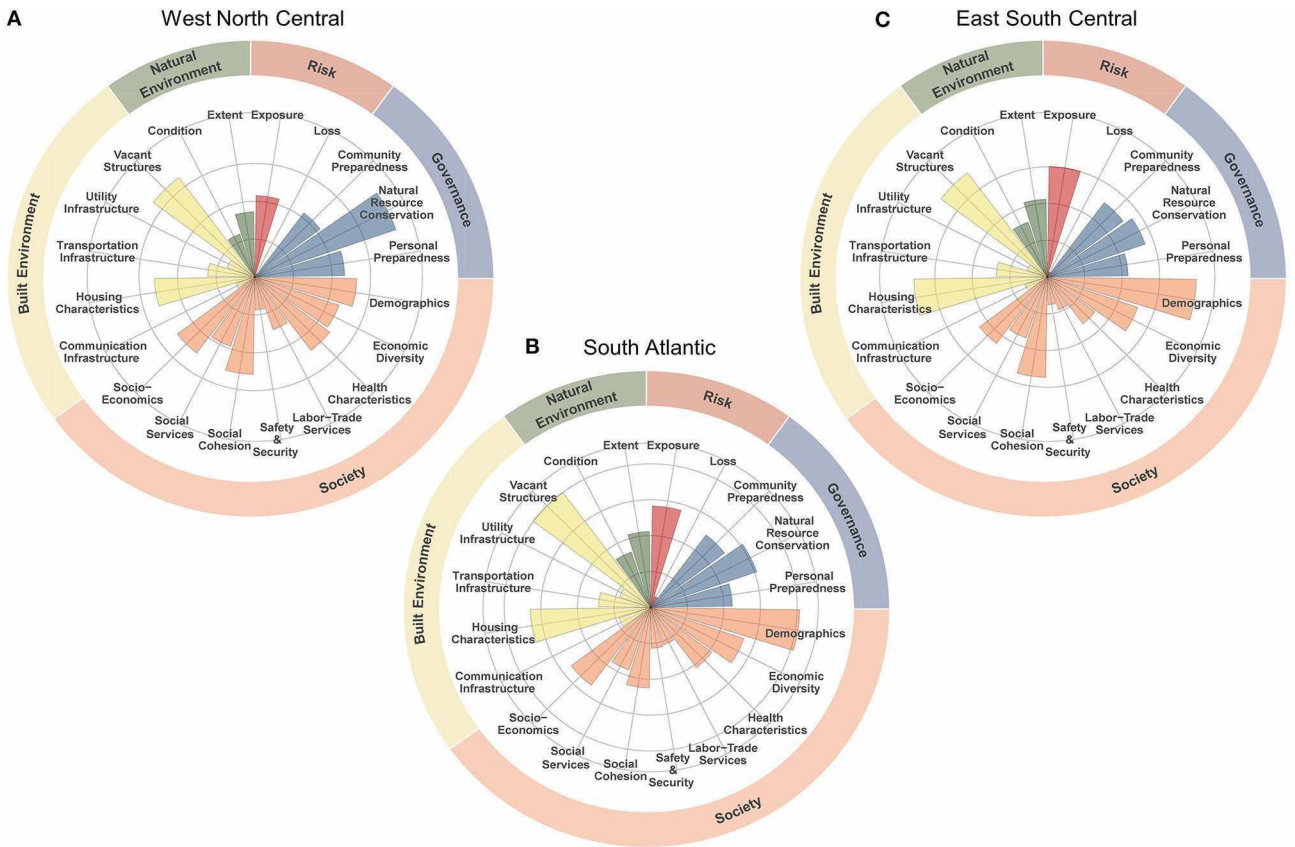

FIGURE 6 | Polar plots of the **(A)** West North Central, **(B)** South Atlantic, and **(C)** East South Central regions.

Virginia (0.293), are characterized by above to significantly above average risk to meteorological events with the District of Columbia and Delaware characterized by the highest risk scores (0.470 and 0.361, respectively). All states in the region showed significantly lower than average governance scores except for Maryland, Delaware and the District of Columbia (ranging between 0.610 and 0.622). Half of the eight South Atlantic states had governance scores <0.5. States in the South Atlantic region widely spanned the range of national built environment scores with four states (Delaware, Florida, Maryland, and North Carolina) and the District of Columbia being significantly above the average, one state (South Carolina) being at about the average and three states (Georgia, Virginia, and West Virginia) being significantly below the average. All South Atlantic states, except Virginia and Maryland, had society scores well-below the national average. Most South Atlantic states (Delaware, Florida, Maryland, North Carolina, and South Carolina) were either at or above the national average for their natural environment scores. The District of Columbia demonstrated the lowest natural environment score (0.200) while Georgia, Virginia and West Virginia have natural environment scores significantly below the national average.

Meteorological risks in the South Atlantic region (**Figure 4**) are characterized by extreme high and low temperatures (35% of events and slightly below the national average) and drought (35% of events but at the national average). The region is exposed to six other types of meteorological events – landslides (10%), inland flooding (7%), high wing events (6%), hurricanes (3%), hailstorms (3%), and coastal flooding (1%). Of these six risk exposures, landslides were about 50% above the national average while coastal and inland flooding as well as high wind events were at about the national average. Hurricanes were three times more prevalent than the national average while hailstorms were at about half the national average. Earthquakes (0.70%) were about 30% of the national average while wildfires (0.18%) were twice the national average. These types of events result in minimal loss of life and physical property (1% of the loss in the South Atlantic) although losses to agricultural and silvicultural lands, as well as natural ecosystem, comprise about 99% of losses (equitably distributed). Potential anthropogenic hazards existing near sites of meteorological events are dominated by general toxic release sites (e.g., industrial outflows) at 48% (significantly above the national average) Superfund sites (36%) being significantly below the national average, and nuclear facilities (10% at the national average).

The major contributors to the CRSI score in the South Atlantic region are natural resource conservation and community

preparedness contributions to governance; demographic characteristics, economic diversity, socio-economics, social cohesion, and health characteristics to society; the number of vacant structures and general housing characteristics to the built environment; and, the extent and condition of natural ecosystems in the natural environment (**Figure 6B**).

Of the 588 counties in the South Atlantic region, the top 5% of CRSI scores (scores = 3.10 to 4.8) were seen in Virginia (10 counties), Maryland (9), West Virginia (2) and Florida, Delaware, and North Carolina (1 each). Over 50% of counties in the South Atlantic region have overall CRSI scores significantly below the national average of 2.375. The 5% of South Atlantic counties with the lowest CRSI scores were largely seen in Virginia (16 counties), Georgia (8) and West Virginia (1).

East South Central

The East South Central region of the United States is comprised of four states and is characterized by the lowest overall CRSI score (0.787) (**Table 2**). All states in the East South Central region are significantly below the national average with only Mississippi showing an overall CRSI score >1.0 (1.151). The East South Central region has the second highest risk to acute meteorological events in the nation (0.318) and the lowest national governance domain score (0.446) with half the states (Alabama and Tennessee) having scores <0.4. States in the East South Central region has the lowest built environment score in the nation (0.315) with three of its states (Kentucky, Mississippi, and Tennessee) with significantly lower than the national average built environment scores. The East South Central region has the lowest society score in the nation (0.392) with all four states significantly below the national average. Most East South Central states (Alabama, Kentucky and Tennessee) were below the national average for their natural environment scores.

Meteorological risks in the East South Central region (**Figure 4**) are characterized by extreme high and low temperatures (37% of events and slightly below the national average) and drought (33% of events but at the national average). The region is exposed to seven other types of meteorological events—landslides (8%), inland flooding (7%), high wing events (6%), earthquakes (5%), hailstorms (2%), hurricanes (2%), and tornadoes (0.3%). Of these seven risk exposures, landslides, and high wind events were slightly above the national average while inland flooding events were at about the national average. Hurricanes were three times more prevalent than the national average while hailstorms were at about half the national average. Earthquakes (0.70%) and hailstorms (2%) were about 50% above and 50% below the national averages, respectively. Hurricanes were twice as prevalent in the East South Central region and

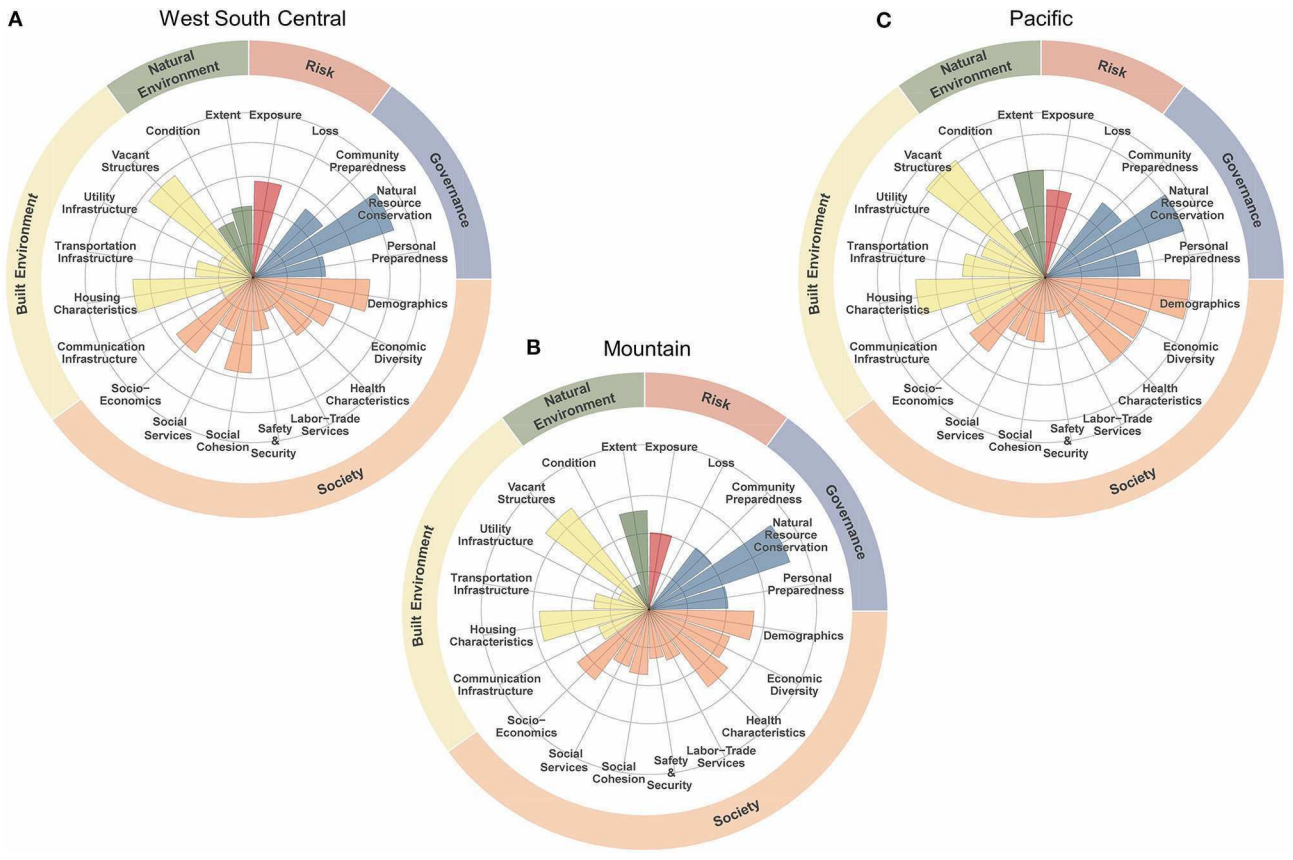

FIGURE 7 | Polar plots of the **(A)** West South Central, **(B)** Mountain, and **(C)** Pacific regions.

wildfires were about three times more prevalent. These types of events resulted in about a 50% higher prevalence of loss of life and physical property (6% of the loss in the South Atlantic) than that seen for the nation, while losses to agricultural and silvicultural lands, as well as natural ecosystems, comprise about 94% of losses (equitably distributed). Potential anthropogenic hazards existing near sites of meteorological events are dominated by general toxic release sites (e.g., industrial outflows) at 47% (significantly above the national average), Superfund sites (32%) being significantly below the national average, and nuclear facilities (18% at roughly twice the national average).

The major contributors to the CRSI score in the East South Central region are natural resource conservation, community preparedness, and personal preparedness contributions to governance; demographic characteristics, social cohesion, economic diversity and socio-economics to society; general housing characteristics and the number of vacant structures to the built environment; and, the extent and condition of natural ecosystems in the natural environment (**Figure 6C**).

Of the 364 counties in the East South Central region, all but two counties were significantly below the national average. The only two counties with overall CRSI scores equal to the national average are in Kentucky and Mississippi. Nearly 10% of the counties in this region have negative CRSI scores with the lowest scores being in Kentucky (21 counties), and Tennessee and Mississippi (2 each). Ninety-nine percent of counties in the East South Central region have overall CRSI scores significantly below the national average of 2.375.

West South Central

The West South Central region of the United States is comprised of four states and is characterized by an overall CRSI score (1.895) that is significantly below the national average (**Table 2**). Seventy-five percent of the states in the West South Central region (Arkansas, Louisiana, and Texas) are significantly below the national average with only Oklahoma showing an overall CRSI score >2.0 (2.436). The risk of acute meteorological events in the West South Central region is about average (0.306) and the regional governance score is also about at the national average. The West South Central region has an average built environment score in the nation (0.388) with only Texas being significantly below the national average. The West South Central region has a below average society score (0.497) with only one state (Oklahoma) being slightly above the national average. All West South Central states were about at the national average for their natural environment scores.

Meteorological risks in the West South Central region (**Figure 4**) are characterized by extreme high and low temperatures (37% of events and slightly below the national average) and drought (33% of events but at the national average). The region is exposed to eight other types of meteorological events – inland flooding (7%), high wind events (5%), hailstorms (4%), hurricanes (4%), landslides (2%), earthquakes (2%), coastal flooding (1%), and wildfire exposure (0.2%). Of these eight risk exposures, inland flooding, high wind events and hailstorms occurred at about the national average while hurricanes occurred at about four times the national average, wildfires occurred at twice the national average and coastal flooding happened at about 25% above the national average. Earthquakes (2%) and landslides (2%) were about 50% below the national averages. These types of events resulted in about a 50% higher prevalence of loss of life and physical property (6% of the loss in the West South Central) than that seen for the nation, while losses to agricultural and silvicultural lands, as well as natural ecosystems, comprised about 94% of losses (with most of these losses observed in dual benefit lands, 54% and the reminder in natural lands, 40%). Potential anthropogenic hazards existing near sites of meteorological events are dominated by Superfund sites (47%, about the national average), general toxic release sites (e.g., industrial outflows) at 33% (about the national average) and nuclear facilities (17%, at roughly twice the national average).

The major contributors to the CRSI score in the West South Central region are natural resource conservation contributions to governance; demographic characteristics, social cohesion and socio-economics to society; general housing characteristics and the number of vacant structures to the built environment; and, the extent and condition of natural ecosystems in the natural environment (**Figure 7A**).

Of the 470 counties in the West South Central region, the top 5% of CRSI scores (scores = 3.41–5.72) were seen in Texas (15 counties), Oklahoma (7), Arkansas (2), and Louisiana (1). Nearly 50% of counties in the West South Central region have overall CRSI scores significantly below the national average of 2.375. The 5% of West South Central counties with the lowest CRSI scores were seen almost completely in Texas (24 counties) with one county in Oklahoma.

Mountain

The Mountain region of the United States is comprised of eight states and is characterized by the overall CRSI score (3.898) that is among the highest in the nation (**Table 2**). All the states in the Mountain region are significantly above the national average with three states (Idaho, Montana and Wyoming) with overall CRSI scores >4.0. The risk of acute meteorological events in the Mountain region is less than average (0.261) and the regional governance score is significantly greater than the national average. The Mountain region has a significantly above average built environment score (0.456) with Arizona having the highest score in the U.S. (0.710) and only Montana being slightly below the national average. The Mountain region has a significantly above average society score (0.567) with only one state (Arizona) being significantly below the national average. All Mountain states were at or significantly above the national average for their natural environment scores.

Meteorological risks in the Mountain region (**Figure 4**) are characterized by drought (38%) that is significantly higher than the national average and extreme high and low temperatures (32% of events and significantly below the national average). The region is exposed to seven other types of meteorological events—landslides (8%), earthquakes (8%), inland flooding (6%), hailstorms (3%), high wind events (3%), wildfires (1%), and tornadoes (0.1%). Of these seven risk exposures, wildfires exposure is about ten times the national average and earthquake exposure is about 2.5 times the national average. Landslide

occurrences are at about 30% above the national average and high wind events are about 50% below the national average. Exposures to inland flooding, hailstorms and tornadoes occur at about the national average. These types of events resulted in about a 300% higher prevalence of loss of life and physical property (14% of the loss in the Mountain) than that seen for the nation, while losses to agricultural and silvicultural lands, as well as natural ecosystems, comprised about 86% of losses (equitably distributed between dual benefit and natural lands). Potential anthropogenic hazards existing near sites of meteorological events are dominated by Superfund sites (47%, about the national average), general toxic release sites (e.g., industrial outflows) at 27% (somewhat less than the national average) and nuclear facilities (25%, at roughly 2.5 times the national average).

The major contributors to the CRSI score in the Mountain region are natural resource conservation contributions to governance; health characteristics, demographic characteristics and socio-economics to society; the number of vacant structures and general housing characteristics to the built environment; and, the extent of natural ecosystems in the natural environment (**Figure 7B**).

Of the 281 counties in the Mountain region, the top 10% of CRSI scores (scores = 6.59–14.60) were seen in Montana (9 counties), Idaho (9), Colorado (2), New Mexico (2), Wyoming (2), and Utah (1). Three counties in this region have overall CRSI scores that are >10.0. Nearly 20% of counties in the Mountain region have overall CRSI scores significantly below the national average of 2.375. The 10% of Mountain counties with the lowest CRSI scores were seen in Colorado (9), Montana (8), New Mexico (3), Idaho (3) and Wyoming (1).

Pacific

The Pacific region of the United States is comprised of five states and is characterized by the overall CRSI score (10.034 with Alaska and 3.576 without Alaska) that is among the highest in the nation (**Table 2**). All the states in the Pacific region are significantly above the national average with three states (Alaska, Hawaii, and Washington) with overall CRSI scores >4.0. The risk of acute meteorological events in the Pacific region is less than average (0.256) with Alaska having a risk score of <0.1. Almost half of the boroughs in Alaska have insufficient data to complete CRSO scoring but including the counties with adequate data shows very low risk (0.058) and very high governance (0.736). CRSI does not include chronic, long-term climate changes like sea-level rise and Alaskan topography minimizes coastal flooding and high winds events. The regional governance score including Alaska (0.602) is significantly greater than the national average but excluding Alaska reduces the score to 0.580 which is slightly lower than the national average. The Pacific region has a significantly above average built environment score (0.556 with Alaska and 0.568 without Alaska) with California having among highest scores in the U.S. (0.641) and no states being at or below the national average. The Pacific region has a slightly below average society score (0.478 with or without Alaska) with only one state (Hawaii) being significantly below the national average. All Pacific states were significantly above the national average for their natural environment scores with Alaska having the highest score in the nation (0.627) and Oregon having a score of 0.517.

Meteorological risks in the Pacific region (**Figure 4**) are characterized by drought (31%) that is about at the national average, earthquakes (22%) that are seven times the national average and extreme high and low temperatures (28% of events and significantly below the national average). The region is exposed to three other types of meteorological events—landslides (9%), inland flooding (7%), hailstorms (3%), and wildfires (1%). Of these three risk exposures, wildfires exposure is about twelve times the national average and landslide exposure is about 50% above the national average. Exposures to inland flooding occur at about the national average. These types of events resulted in about a five times higher prevalence of loss of life and physical property (21% of the loss in the Pacific) than that seen for the nation, while losses to agricultural and silvicultural lands, as well as natural ecosystems, comprised about 78% of losses (equitably distributed between dual benefit and natural lands). Potential anthropogenic hazards existing near sites of meteorological events are dominated by Superfund sites (47%, about the national average), general toxic release sites (e.g., industrial outflows) at 32% (somewhat less than the national average), RCRA exposure at 11% (about twice the national average) and nuclear facilities at 11% (at the national average).

The major contributors to the CRSI score in the Pacific region are natural resource conservation contributions to governance; demographic characteristics, health characteristics and economic diversity to society; the number of vacant structures and general housing characteristics to the built environment; and, the extent of natural ecosystems in the natural environment (**Figure 7C**).

Of the 160 counties in the Pacific region, the top 10% of CRSI scores (scores = 8.89 to 148.07) were seen in Alaska (20 boroughs), Hawaii (4 counties) and Washington (1). Twenty-one boroughs/counties in this region have overall CRSI scores that are >10.0. Nearly 25% of counties in the region have overall CRSI scores significantly below the national average of 2.375. The 10% of counties with the lowest CRSI scores were seen in California (16), Oregon (6), Washington (2) and Hawaii (1).

DISCUSSION

The results for the regionalization of CRSI can be used for capacity building regardless of CRSI score. The domain and indicator scores, as well as the polar plots, can be used to identify areas where improvements can be made to enhance overall resilience. The only domain in CRSI that cannot be improved *per se* is the risk domain. This domain is driven by historical observations relating to the tracked meteorological events. If CRSI included long-term climate events, then perhaps human activities could be developed to minimize long-term change which could impact the risk domain of CRSI (Rahmstorf, 2007; Nichols and Cazenave, 2010; Sweet et al., 2017). The remaining CRSI domains—governance, society, built environment, and natural environment—are driven by indicators and metrics that can be modified to improve resilience to acute climate events.

In the New England region, general CRSI scores are high (>3.8) and well-above the national average. However, one state in this region has an overall CRSI score below the regional average—Rhode Island with a CRSI score of 2.653. Rhode Island has suffered from multiple coastal and inland flooding events, winter storms, Superstorm Sandy, and Tropical Storm Irene in the last decade. An evaluation of the New England region, using the polar plot of indicator contribution to domains, show that increases in community preparedness and personal preparedness would enhance regional governance. Enhancements of labor-trade services, safety and security and social cohesion would enhance the society modifier. Improvements in infrastructure would enhance the built environment modifier and increases in natural ecosystem extents and condition would alter the natural environment modifier. Our review of the domain scores for Rhode Island suggest the area for greatest improvement could be in the domain representing the built environment where the Rhode Island score (0.320) is significantly below the national average and hence reducing the state's CRSI score.

Recently, Rhode Island drafted a new statewide climate resilience action strategy (RI-STAB, 2018). The results of the Rhode Island CRSI data were provided to a member the Rhode Island Science and Technical Advisory Board. These results targeted a lower overall CRSI score likely driven by lower built environment scores characterized by critical infrastructure and utilities and building characteristics and average governance scores (lower than most of New England) representing potential issues with emergency preparedness as well as emergency shelters and services. Like the CRSI approach, the Rhode Island Strategy defines climate resilience as "the capacity of individuals, institutions, businesses and natural systems within Rhode Island to survive, adapt, and grow regardless of chronic stresses and weather events they experience" (RI-STAB, 2018, p. 3). Also, like the CRSI results, Rhode Island recognizes that it primary acute meteorological risk events are extreme cold and heat, droughts, and extreme rainfall and flooding. The new strategy addresses built environment issues to reduce vulnerability and improve infrastructure for drinking water and wastewater systems; dam and storm-water systems; power grid and fuel supply issues; and transportation. Realizing the importance of natural systems for community resilience, Rhode Island (already with the highest natural environment domain scores in New England) is planning to increase its efforts to protect and conserve its coastal and inland natural systems. Rhode Island is already experiencing the effects of coastal flooding on buildings, infrastructure, evacuation shelters, and emergency services. The new strategy plan targets enhancements to address these issues. Realization of the actions and activities planned in the new Rhode Island strategy should increase its overall CRSI score to levels similar to other New England states.

The Middle Atlantic state with the lowest overall CRSI score (New Jersey-−2.28) is characterized by the highest risk factors to acute weather events (0.379) which is 20–40% higher than the other states in the region. These events include coastal and inland flooding, Superstorm Sandy, and a variety of high temperature and low temperature events. Because it cannot impact its risk to these events, New Jersey can do little to increase its overall CRSI score other than improve its already above-average governance and built environment scores and average society and natural environment scores. New Jersey Governor's Office of Recovery Rebuilding (2018) is actively developing plans to modify risks by developing governance associated with flood rebuilding standards, and the state's Department of Community Affairs ((NJDCA), 2018) has provided grants post-Sandy to enable development of strategic recovery plans and practices to facilitate smart and efficient rebuilding processes at the local level. Similarly, New Jersey's Office of Emergency Management (NJOEM, 2018) is identifying resiliency opportunities to modify the locations and characteristics of critical infrastructures including drinking water, wastewater, transportation, transit, energy, and communication systems. These infrastructure issues were observed as potential areas of improvement for the Middle Atlantic Region through CRSI analyses.

However, the greatest potential area of improvement for the overall New Jersey CRSI score would be enhancement of ecosystem type extent, and condition. For example, only 31 miles of New Jersey's 130 miles of shoreline are undeveloped (Headland, 2017; Stockton and Hafner, 2018). While some Post-Sandy activities in New Jersey seem to be addressing these resilience enhancements (NJOCM, 2010), few major efforts seem to be occurring in this area. Small efforts like dune reconstruction and vegetation planting are being undertaken, but no larger efforts directed at natural shoreline stabilization, wetland protection, and ecosystem condition improvements are included.

In the South Atlantic region, both Georgia and the District of Columbia displayed overall CRSI scores of less than one. The District of Columbia is characterized by high risk (0.470, nearly 50% above the US average) and is prone to frequent inland and coastal flooding (flash flooding, river flooding, tropical systems, dam breaks, and heavy snow melts). The District of Columbia showed a very low Natural Environment domain score (0.200) compared to the national average of 0.413. Enhancing the natural environment might be difficult for the District as it is surrounded on multiple sides by the Potomac and Anacostia Rivers and is characterized by extensive areas of impervious surface. Minimizing impervious surfaces and maximizing the conservation and re-development of riparian corridors, wetlands, and greenspaces are likely the areas where improvements would be anticipated to enhance the District's CRSI score. Similar improvements in infrastructure (e.g., transportation and water systems) would enhance the District's already above average built environment domain score.

On the other hand, Georgia (CRSI score of 0.846) has an average risk score but below average domain scores for governance, built environment, society and natural environment. Improvement in any of these domains would increase Georgia's CRSI score. Georgia's risks can be easily characterized by inland flooding, high wind events, hailstorms and tornadoes ((NWS), 2018). Governance improvements in the South Atlantic

region could focus more on holistic and catchment-oriented flood risk management rather than the emphasis on structure measures and construction which have dominated the past. Similar efforts in Germany have shown some success in reducing the adverse consequences of flooding for human health, the environment, cultural heritage and economic activity (Heintz et al., 2012). Georgia has a few large urban centers with diverse work forces where flooding occurs regularly. However, much of Georgia is comprised of small communities and counties where labor and trade services are not diverse and rebuilding after a meteorological event (e.g., tornado, flood) can be very difficult without construction labor pools. Creating enticements to develop these labor pools even if shared by several proximal counties would increase the CRSI scores of these counties. Finally, improvements in housing characteristics through upgrading building codes and reducing the number of vacant structures should increase a presently very low building environment domain score for Georgia (0.282). Homes and businesses throughout Georgia and the South Atlantic region would benefit from enhanced building codes and standard resulting in increased resilience (FEMA, 2017a). Georgia's neighboring state, Florida, has demonstrated how to enhance its building code to create greater resilience to storm events (PDH Academy, 2017). Florida building codes change in response to new technology and knowledge about weather events. Codes affecting the built environment should be modified or updated in response to changes in technology and procedures, growing and maturing with the times. With the increased storm activity of 2017, recently updated building codes guided by storms of the past were put to the test and demonstrated Florida community's enhanced resilience. These codes utilized more information about code strengths and weaknesses, building practices, and new building materials that helped homes and commercial properties withstand weather events.

California demonstrates an above average risk domain (0.322) dominated by drought and temperature extremes. The increased incidence of wildfires (10 times the national average), earthquakes (7 times the national average) and landslides (50% above the national average) contribute to a major portion of human life and dollar losses resulting from acute meteorological events. According to CRSI domain scores, California has the lowest governance domain score in the Pacific region (0.498); this is significantly below the national average and 50–75% below the remaining states in the region. While having among the highest built environment scores in the nation, California has increased building code requirements to withstand at least minimal to moderate earthquake impacts. California's seismic construction requirements are designed to protect the lives of those inside. But even with the most modern codes, building to the state's minimum requirements still leave some new buildings severely damaged in a major earthquake to the point of being a complete loss. Further enhancing these types of building codes would increase the state's CRSI scores but governance enhancement designed to increase personal and community preparedness would likely modify the governance score for California positively.

Wildfires, another type of event of increasing frequency and magnitude, in 2017 were the most destructive fires on record. A total of 9.133 fires burned over 1.3 million acres including 5 of the 20 most devastating wildland-urban interface fires in California history (CDFFP, 2018). Enhanced personal and community preparedness for wildfires would likely modify the governance score for California significantly. For example, the Tubbs fire in Napa and Sonoma counties, which ignited on October 8, 2017, killed 22 people, damaged 5,643 structures, and burned 36,807 acres, making it the single most destructive fire in California history. Interviews with personnel of the California Department of Forestry and Fire Protection demonstrated that little could be done to contain the fire but the lack of personal preparedness was demonstrated by the number of vehicles still parked in their driveways after calls for mandatory evacuations (Irfan, 2017). Fires are becoming more damaging because Californians keep building in harm's way much the same way homebuilders in flood plains rebuild homes after flood destruction. Deliberate decisions and unintended consequences of urban development over decades have turned many parts of California into tinderboxes (Irfan, 2017). This is also reflected in the Environmental Domain score for California (0.461), which is the lowest in the Pacific region, where natural habitats that might have reduced human life and property losses have become part of or consumed by suburban and urban sprawl (Irfan, 2017).

As evidenced by the data and examples above, direct enhancement in governance, environment, and even building codes and reduction of vacant structures would increase the resilience score for states like California. Georgia, New Jersey, Rhode Island, and the District of Columbia. Using CRSI scores and interpreting the deconstruction of those scores, can be critical elements to consider in resilience capacity building in these states and the District of Columbia. Using the Climate Recovery Screening Index to inform capacity building can enrich the dialogue and contribute to decision making that results in stronger community resilience to acute climate events.

AUTHOR CONTRIBUTIONS

All authors listed have made a substantial, direct and intellectual contribution to the work, and approved it for publication.

REFERENCES

Adger, W. N. (2000). Social and ecological resilience: are they related? *Prog. Hum. Geogr.* 24, 347–364. doi: 10.1191/030913200701540465

ARUP (2014). *City Resilience Framework*. The Rockefeller Foundation, ARUP Development International.

Berkes, F., Colding, J., and Folke, C. (eds.). (2003). *Navigating Social-Ecological Systems: Building Resilience for Complexity and Change*. Cambridge: Cambridge University Press.

Bruneau, M., Chang, S., Eguchi, R., Lee, G., O'Rourke, T., Reinhorn, A., et al. (2003). A framework to quantitatively assess and enhance seismic resilience of communities. *Earthquake Spectra* 19, 733–752. doi: 10.1193/1.1623497

CDFFP (California Department of Forestry and Fire Protection) (2018). *Incident Information*. Available online at: http://cdfdata.fire.ca.gov/incidents/incidents_stats?year=2017

Chandra, R. K., Papadopoulos, G. A., and Karanci, A. N. (2007). Disasters due to natural hazards. *Nat. Hazards* 40, 501–502. doi: 10.1007/s11069-006-9010-4

Dovers, S. R., and Handmer, J. W. (1992). Uncertainty, sustainability and change. *Global Environ. Change* 2, 262–276.

FDEM (Florida Department of Emergency Management) (2018). *Florida's Severe Weather Awareness Guide*. Available online at: https://www.floridadisaster.org/globalassets/library/2018-guidefinal.pdf

FDH (Florida Department of Health) (2016). *Florida Emergency Preparedness Guide*. Available online at: http://www.floridahealth.gov/programs-and-services/emergency-preparedness-and-response/_documents/preparedness-guide-large-print.pdf

FEMA (Federal Emergency Management Agency) (2012). *Crisis Response and Disaster Resilience 2030: Forging Strategic Action in an Age of Uncertainty*. Available online at: https://www.fema.gov/media-library-data/20130726-1816-25045-5167/sfi_report_13.jan.2012_final.docx.pdf

FEMA (Federal Emergency Management Agency) (2017a). *Draft Interagency Concept for Community Resilience Indicators and National-Level Measures*. Available online at: https://www.fema.gov/community-resilience-indicators

FEMA (Federal Emergency Management Agency) (2017b). *Building Science Branch Brochure – Wind Hazards*. Available online at: https://www.fema.gov/media-library-data/1496953980230-d52857ef8919276187b3c57d7c851239/Wind_508.pdf

Folke, C. (2006). Resilience: the emergence of a perspective for social-ecological systems analyses. *Glob. Environ. Change* 16, 253–267. doi: 10.1016/j.gloenvcha.2006.04.002

Headland, J. R. (2017). "Quantifying resilience: coastal structure and nourished beaches," in *Coastal Structures and Solutions to Coastal Disasters Joint Conference, 2015*. Available online at: https://ascelibrary.org/doi/pdf/10.1061/9780784480304.062

Heintz, M. D., Hagemeier-Klose, M., and Wagner, K. (2012). Towards a risk governance culture in flood policy – findings from the implementation of the "floods directive" in Germany. *Water* 4, 135–156. doi: 10.3390/w4010135

Holling, C. S. (1973). Resilience and stability of ecological systems. *Annu Rev. Ecol. Syst.* 4, 1–23.

Irfan, U. (2017). *California's Wildfires Are Not "Natural" – Humans Made Them Worse at Every Step*. Vox. Available online at: https://www.vox.com/energy-and-environment/2017/10/12/16458242/risk-wildfires-worse-climate-change-california-san-francisco-los-angeles (Accessed December 8, 2017).

Melillo, J. M., Richmond, T., and Yohe, G. W. (2014). *Climate Change Impacts in the 11 United States: The Third National Climate Assessment*. U.S. Global Change Research Program, 12. Available online at: http://nca2014.globalchange.gov/report

New Jersey Governor's Office of Recovery and Rebuilding (2018). *Planning for Resiliency*. Available online at: http://nj.gov/gorr/resiliency/

Nichols, R. J., and Cazenave, A. (2010). Sea-level rise and its impact on coastal zones. *Science* 328, 1517–1520. doi: 10.1126/science.1185782

NJDCA (New Jersey Department of Community Affairs) (2018). *Planning for Resiliency*. Available online at: http://nj.gov/gorr/resiliency/

NJOCM (New Jersey Office of Coastal Management. New Jersey Department of Environmental Protection) (2010). *Getting to Resilience: A Coastal Community Resilience Evaluation Tool*. Available online at: http://www.state.nj.us/dep/cmp/docs/gtr-resilience.pdf

NJOEM (New Jersey Office of Emergency Management) (2018). *Planning for Resiliency*. Available online at: http://nj.gov/gorr/resiliency/

NRC (National Research Council). (2012). *Disaster Resilience: A National Imperative*. Washington, DC: The National Academies Press.

NWS (National Weather Service) (2018) *Severe Storm Climatology for North and Central Georgia*. Available online at: https://www.weather.gov/ffc/svrclimo

PDH Academy (2017). *How Severe Weather Affects the Future of Building Codes*. Available online at: https://pdhacademy.com/2017/12/21/severe-weather-affects-future-building-codes/

Rahmstorf, S. (2007). A semi-empirical approach to projecting future sea-level rise. *Science* 315, 368–370. doi: 10.1126/science.1135456

RI-STAB (Rhode Island Science and Technical Advisory Board) (2018). *"Resilient Rhody" – Statewide Climate Resilience Action Plan, Draft. Providence, Rhode Island*. Available online at: http://climatechange.ri.gov/documents/rev-resstrategy.pdf

Rose, A. (2004). Defining and measuring economic resilience to disasters. *Disaster Prevent Manage.* 13, 307–314. doi: 10.1108/09653560410556528

Stockton, R., and Hafner, S. (2018). *Beach Stabilization: Structure and Beach Nourishment Alternatives*. Available online at: https://intraweb.stockton.edu/eyos/coastal/25yrConference/Beach-Stabilization.pdf

Summers, J. K., Harwell, L. C., Buck, K. D., Smith, L. M., Vivian, D. N., Bousquin, J. J., et al. (2017a). *Resilience Screening Index (CRSI): An Assessment of Resilience to Acute Meteorological Events and Selected Natural Hazards*. Washington, DC: Protection Agency. EPA600/R-17/238.

Summers, J. K., Harwell, L. C., Smith, L. M., and Buck, K. D. (2018). *Climate Resilience Screening Index (CRSI): Development and Application to the U.S. Submitted to GeoHealth*. Minneapolis, MN: Community Indicator Consortium.

Summers, J. K., Smith, L. M., Harwell, L. C., and, Buck, K. D. (2017b). Conceptualizing holistic community resilience to climate events: foundation for a climate resilience screening index. *GeoHealth* 1, 151–164. doi: 10.1002/2016GH000047

Sweet, W. V., Kopp, R. E., Weaver, C. P., Obeysekera, J., Horton, R. M., Thieler, E. R., et al. (2017). *Global and Regional Sea Level Rise Scenarios for the United States*. NOAA Technical Report, NOS CO-OPS 083. Available online at: https://ntrs.nasa.gov/archive/nasa/casi.ntrs.nasa.gov/20180001857.pdf

U.S. Department of Commerce, Economics and Statistics Administration and U.S. Census Bureau (2018). *Census Regions and Divisions of the United States*. Available online at: https://www2.census.gov/geo/pdfs/maps-data/maps/reference/us_regdiv.pdf

UN/ISDR (United Nations International Strategy for Disaster Reduction). (2002). *Living With Risk: A Global Review of Disaster Reduction Initiatives. Prepared as an Interagency Effort Coordinated by the ISDR Secretariat*. Geneva. Available online at: http://www.adrc.asia/publications/LWR/LWR_pdf/index.pdf

Disclaimer: The views expressed in this manuscript are those of the authors and do not necessarily represent the views or policies of the U.S. Environmental Protection Agency. Any mention of trade names, products, or services does not imply an endorsement by the U.S. Government or the U.S. Environmental Protection Agency. The EPA does not endorse any commercial products, services, or enterprises.

Conflict of Interest Statement: The authors declare that the research was conducted in the absence of any commercial or financial relationships that could be construed as a potential conflict of interest.

Copyright © 2018 Summers, Harwell, Smith and Buck. This is an open-access article distributed under the terms of the Creative Commons Attribution License (CC BY). The use, distribution or reproduction in other forums is permitted, provided the original author(s) and the copyright owner(s) are credited and that the original publication in this journal is cited, in accordance with accepted academic practice. No use, distribution or reproduction is permitted which does not comply with these terms.

Send Orders for Reprints to reprints@benthamscience.net

Current Environmental Engineering, 2019, *6*, 000-000

RESEARCH ARTICLE

Development of a Multi-Hazard Landscape for Exposure and Risk Interpretation: The PRISM Approach

Kyle D. Buck*, J. Kevin Summers, Stephen Hafner, Lisa M. Smith and Linda C. Harwell

United States Environmental Protection Agency, Gulf Ecology Division, 1 Sabine Island Drive, Gulf Breeze, FL 32561

ARTICLE HISTORY

Received: December 12, 2017
Revised: April 26, 2018
Accepted: January 19, 2019

DOI:
10.2174/2212717806666190204103455

Abstract: Multi-hazard risk assessment has long been centered on small scale needs, whereby a single community or group of communities' exposures are assessed to determine potential mitigation strategies. While this approach has advanced the understanding of hazard interactions, it is limiting on larger scales or when significantly different hazard types are present. In order to address some of these issues, an approach is developed where multiple hazards coalesce with losses into an index representing the risk landscape. Exposures are assessed as a proportion of land-area, allowing for multiple hazards to be combined in a single calculation. Risk calculations are weighted by land-use types (built, dual-benefit, natural) in each county. This allows for a more detailed analysis of land impacts and removes some of the bias introduced by monetary losses in heavily urbanized counties. The results of the quantitative analysis show a landscape where the risk to natural systems is high and the western United States is exposed to a bulk of the risk. Land-use and temporal profiles exemplify a dynamic risk-scape. The calculation of risk is meant to inform community decisions based on the unique set of hazards in that area over time.

Keywords: Climate, spatial, exposures, multi-hazard, index, land-use.

1. INTRODUCTION

The goal of reducing impacts from hazard exposure has never been more important. According to the United Nations 2012 Report on Development Agenda, the global increase in hazard exposures from 1970 to 2010 was between 114 and 192 percent, depending on the hazard. These exposures resulted in over 1.1 million deaths and $1.3 trillion in property losses, with an additional 2.7 billion people adversely impacted in that same time (UN 2012). As populations continue to grow, urbanize and shift into areas with greater exposure potential, the impact will only continue to grow (Chester *et al*. 2000, Lall and Deichmann 2010, Garschagen and Romero-Lankao 2015, Güneralp *et al*. 2015). On top of this, the severity and location of hazards continue to change, yielding a dynamic landscape requiring continual reassessment and long-term mitigation solutions (Miletti 1999).

The hazard landscape or "hazard-scape" is complex and difficult to fully represent in a comprehensive manner without some form of model by which exposures are tallied and assigned to locations (Cutter, Burton, & Emrich, 2010). In order to effectively reduce risks, communities must assess their unique hazard-scape by using integrated, holistic, multi-hazard assessments intended to represent the full range of past, present and future exposures. In this context, the International Panel on Climate Change (IPCC) considers disaster risk to be "the possibility of adverse effects in the future" (Fields 2012). The starting point is a hazard, de-

*Address correspondence to this author at the United States Environmental Protection Agency, Gulf Ecology Division, 1 Sabine Island Drive, Gulf Breeze, FL 32561; Tel: 850-934-9233; E-mail: Buck.Kyle@epa.gov

2212-7178/19 $58.00+.00 © 2019 Bentham Science Publishers

fined as a phenomena caused by the onset of events, whether acute or chronic, that are perceived to cause harm (Burton and Kates 1964). Hazards can be natural (geophysical, hydrological, climatological, or biological) or technological (environmental degradation, pollution, or accidents). An exposure occurs when a hazard intersects with the landscape, whether a living population or the natural or built environment. In the event of an exposure, there is a potential for loss, defined here as a risk. Losses are incorporated as a measure of consequences associated with hazard from exposure. They serve as a proxy for vulnerability in the calculation of risk.

While integration of multiple hazards is not a new concept, there has been a push to include more refined multi-hazard models into community planning for risk reduction. Hewitt and Burton first discussed the concept of "hazardousness of place", whereby a specified geographic unit is assessed for all hazards impacting it (1971). Their theoretical framework suggests a need for more location-specific work, as opposed to hazard-specific analysis, to inform policy decisions. Cutter takes this a step further with a "hazards of place" conceptual model through which location-dependent risk, or vulnerability, is defined by the complex interaction of hazards caused by natural, societal, and technological events (Cutter and Solecki 1989, Cutter 1996). The place-based approach allows for the combination of multiple hazards and mitigation activities. More recent research in multi-hazard risk assessments has attempted such analyses, focusing on either small geographic areas or looking at a cascade of hazards resulting from a single source (e.g. volcano) (Bell and Glade 2011, Thierry 2008). There are also examples of hazard integration using spatial tools for loss estimation, planning and mitigation purposes (FEMA 2013, Schmidt *et al*. 2011, Tate *et al*. 2011). Other attempts at multi-hazard integration use spatial assessment with the assignment of ordinal classification schemes for intensity (Batista *et al* 2004, Schmidy-Thome 2005, Greives *et al*. 2006). This is necessary due to the vast array of impacts stemming from natural and technological hazards, but forces decisions on weighting and lacks consideration of outcomes. While these methods present a robust way to integrate and assess multiple hazards, they do not lend as well to the construction of an index value for comparison across larger spaces.

In addition to simply combining hazards, temporal interactions between hazards are a significant consideration, where the potential exists for hazards to interact and amplify one another through both proximity and timing of occurrences. In the event that multiple hazards occur close in proximity and timeframe, disaster fatigue can occur, leaving the landscape more susceptible to harm from subsequent exposures (Kappes *et al*. 2012). There are additional psychologic impacts from repeated exposures and exacerbating effects stemming from hazardous facilities via chemical releases, explosions, or epidemics (Reser 2007, Watson *et al*. 2007). Consideration of these "cascading" impacts is important, and a primary reason for the use of multi-hazard assessment (Miletti 1999, Marzocchi *et al*. 2012). The goal is to operationalize an approach that will enable the merger of multiple hazards into a meaningful measure for communities to assess strategies and limit future vulnerabilities. This feat is challenged as a result of patchwork landscapes, differences in hazard size and intensity, and the enormity of data that must be processed to retain a useful level of resolution. Despite the difficulty, developing a scalable multi-hazard assessment for the entire U.S. at the county scale is important and necessary to establish a baseline risk profile for all areas of the country.

2. METHODS

The Patterns of Risk using an Integrated Spatial Multi-Hazard (PRISM) approach allows risk to be

assessed at the county level across states or regions and facilitates the integration of any hazard type provided it has an associated spatial component. Risk, in this approach, is represented as the probability of a hazard exposure (identified as proportional land area) multiplied by the degree of vulnerability (identified hazard losses). Exposure probability entails both historic and proximity-based measures of hazards responsible for risk. Losses provide a measure of the lives lost/ impacted, monetary losses in crops and property, and losses of natural land integrity. Data inclusion, conceptual development and processing of the risk parameters is described in this section. A conceptual overview, provided in Fig. (**1**), demonstrates the breakdowns of each risk component.

To address the spatial extent of hazard exposure and cope with the varied landscapes (e.g. hazard proximities and level of development) across the country, counties are used as the foundation for risk calculation. Though use of smaller spatial units is possible, the utility of the method better aligns with a larger aggregation for the purposes of county and regional governance. In addition, there is lack of certain metrics at finer scales, making calculation of risk based on land extent challenging. Loss data, for example, uses counties as its finest level of data aggregation, and in 15 years of data, only 3 major boundary changes have occurred (US Census 2010). Assessment of land-type distribution within each county is used to weigh exposure and loss values and account for differences in development and economic drivers. Proportional county exposure values allow different hazard types to be combined in a consistent manner, regardless of intensity or temporal variation.

2.1. Data Refinement

In the formulation of a hazard-scape, three inputs are utilized: a land-use layer, a natural hazard

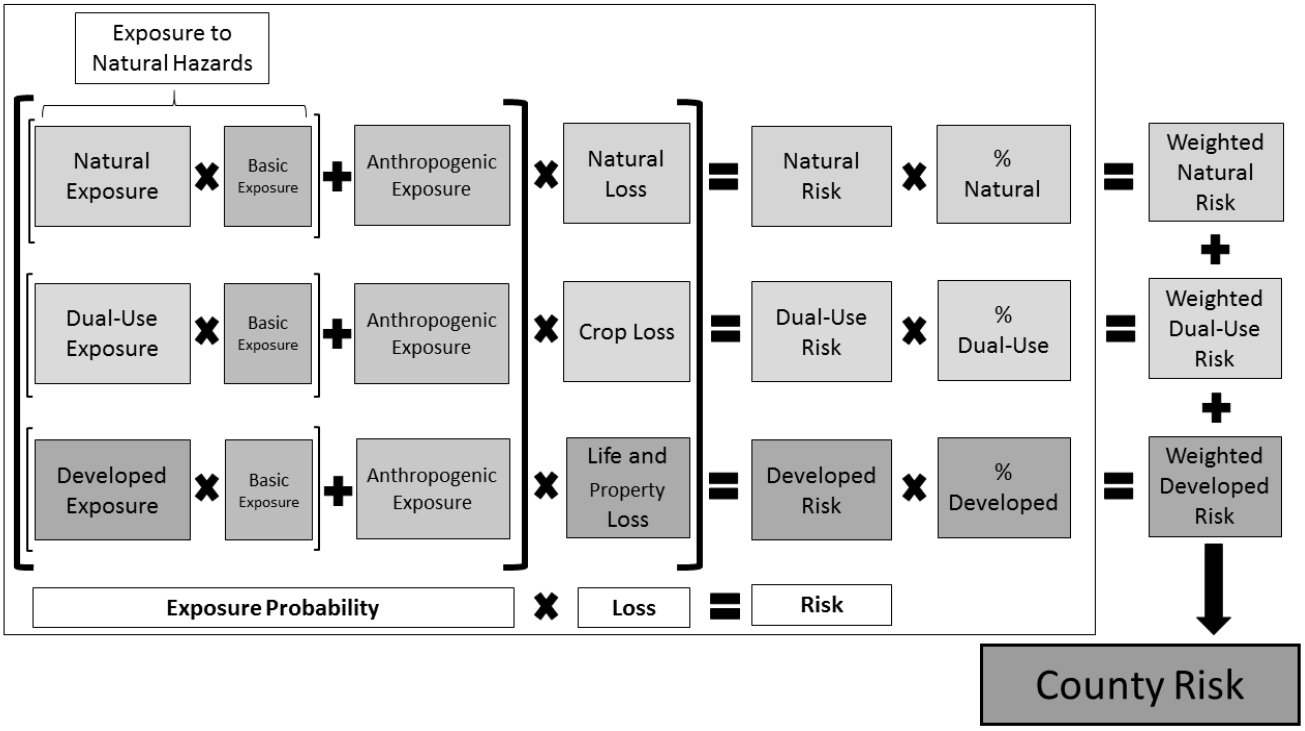

Fig. (1). PRISM Approach conceptual overview. Showing breakdown of exposures and land categories along with the inclusion of land-type weighting values used to derive a final risk value for all hazards in a county. Components of risk are identified in top and bottom bars to demonstrate steps in calculation of final score. Color codes: Green = Natural Risk components, Blue = Dual-Use components, and Grey = Developed components. Basic exposure and anthropogenic exposures are the same across all land-type categories.

layer, and technological hazard layer. The land-use layer is used to weight hazard exposures according to the landscape types present in a county; Natural, Dual-Benefit, or Developed (Table **1**). The natural hazard layer is used to define historic and proximity-based exposure probabilities. The technological hazard layer is used to add potential exposures resulting from man-made facilities. Each of these are calculated in units of total acreage and assigned to county boundaries using ArcGIS 10.3, where exposure size is calculated as a proportion of the county acreage in each land-use class.

2.1.1. Land Use Classifications

The land-use surface is developed using data from the 2011 version of the Multi-Resolution Land Characteristics Consortium (MRLC) National Land Cover Database (NLCD), which is based on LandSat imagery covering the entirety of the conterminous U.S. (Homer *et al*. 2015). The reason for this choice is two-fold. Firstly, the data was satellite-derived, spatially-referenced, and at a 30 x 30-meter resolution for the entire U.S. Although higher resolution alternatives existed, using those would have meant gathering multiple, disparate data sources and yielded a surface with high levels of inconsistency. The second advantage of using NLCD for surface exposure data is due to its well documented and regular collection, being compiled every 5 years and closely corresponding to the social data.

Land coverage classification in the NLCD falls into one of 20 different categories, making the data highly detailed. For the purposes of this approach, however, the original 20 classifications are compressed into 3 categories, developed lands, dual-benefit lands, and natural lands (Table **1**). Exposure extents are assigned to each land-type and calculated as a proportion. This allows exposure to be calculated for a specific land or aggregated up to a land-type weighted county value.

Table 1. Compression of 2011 NLCD categories from 20 down to 3 for use in exposure calculations. * data only available in Alaska. Left column represents original classification of land and right column represents new classification.

NLCD Classification (20 Categories)	PRISM Classification (3 Categories)
Developed, Open Space	Developed Land
Developed, Low Intensity	
Developed, Medium Intensity	
Developed, High Intensity	
Deciduous Forest	Dual-Benefit Environment
Evergreen Forest	
Mixed Forest	
Pasture/Hay	
Cultivated Crops	
Woody Wetlands	
Emergent Herbaceous Wetlands	
Open Water	Natural Environment (non-human)
Perennial Ice/Snow	
Barren Land (Rock/Sand/Clay)	
Dwarf Scrub*	
Shrub/Scrub	
Grassland/Herbaceous	
Sedge/Herbaceous*	
Lichens*	
Moss*	

2.1.2. Natural Hazards Exposure

There are a total of 8 (9 if high and low temperature extremes are counted separately) natural hazard types assessed using historical events along with an additional 4 proximity-based exposure potentials that use modeled data or location to approximate exposure probability (Table **2**). Points, areas or tracks of each hazard are collected for each hazard and geo-referenced. Depending on the hazard, further processing is

carried out to estimate the spatial extent of impacts. These extents are converted to proportional land-type areas by county and hazard type to represent exposure. In the case of droughts, for instance, the data is represented as an aerial extent. Other hazards are represented by path data only, such as hurricanes and tornadoes. In these instances, a buffer is used to estimate exposure extent. Table **2** provides a summary of all 11 natural hazards and the methods utilized for determination of spatial extent.

For each hazard type, the impact of the event is dependent on land-type and extent. Measuring hazards is typically accomplished through some form of index based on features of the hazard. The challenge in combining hazards thus centers on how to make the diverse indices equivalent numerically for combination in a summary index. An example of this challenge would come from hurricanes and tornadoes, for instance. Hurricanes are measured based on maximum wind speed. While related, this does not consider the accompanying threats of flooding or tornadoes that typically cause damage in the wake of a storm. Tornadoes are similarly measured using wind speed as a baseline for index development. Though both are wind-based storms, the indices for hurricanes and tornados are not directly relatable and do not capture the differences in other characteristics. Tornadoes are much more focused in their paths and intensity, while hurricanes are vaster in extent. The distinction between these two storm types is clear in the characteristics of impact. Hurricanes, because of their extent and necessity for water, have a more probable impact on larger populations and fragile coastal ecosystems. Tornadoes, with narrower path widths and higher probability inland, do not possess the same population threat as hurricanes. Due to the differential impacts and methods of measurement for these storm types, along with many other hazards, combining them through measures of intensity scale is not very enlightening. Measuring the exact location and extent of exposure to assess impact creates a much better assessment.

Extent decisions are established for each hazard based on data and physical characteristics. Hurricane wind exposure calculations use a buffer distance of 100 miles for all storms exceeding the Category 1 (winds > 74 mph) rating. This cut point is shown from previous research to be the most robust in relation to damages experienced and corresponds to additional research on hurricane and typhoon eye wall structure (Simpson and Riehl 1981, Weatherford and Gray 1988, Zhu 2008).

Data from the National Oceanic and Atmospheric Administration (NOAA) Storm Events Database was used to estimate tornado extents (NOAA 2010). Spatial information related to the tornado, including the path coordinates, length, and width were used to create an adaptive buffer around every tornado occurrence between 2000 and 2015. Since wider and longer paths are typically associated with more severe storms this method translates well as a severity proxy (Brooks 2004).

Earthquake exposure is assessed using data available from the USGS that models and maps earthquake magnitude probability based on proximity to fault lines, substrate existing in the area, and historic events. In order to predict ground movement for a specified ground composition, the USGS Earthquake Hazards Program uses the Peak Ground Acceleration (PGA), presented as a percentage of gravity (USGS 2003). Forecast models are created by USGS for areas with historic or potential exposure to earthquakes exceeding the 0.1 g PGA threshold. According to research conducted by FEMA, a PGA of greater than 10% (0.1 g) is considered of significant velocity to cause damage to buildings not up to code or older in age (FEMA 2009). While all three land-use types are calculated for PRISM, only developed land factors into

Table 2. Summary of Natural Hazard Calculations. For each natural hazard type, the class of data is either historic (based on previous exposures to land area) or modeled (some combination of historic or land-characteristic data used to create exposure probabilities). Spatial extent explains the methods used to create data for the exposure calculations.

Natural Hazard Type	Class	Spatial Extent	Exposure Calculation
Hurricane	Historic and Modeled	Buffer of 100 miles surrounding tracks for storms > Category 1.	Proportion of each land-use classification used to estimate exposure extent.
Tornado	Historic and Modeled	Adaptive buffer based on path width data and mapped tornado tracks.	Proportion of each land-use classification used to estimate exposure extent.
Earthquake	Modeled w/Historic	USGS Modeled data -historic events and probability of event exceeding 0.1g PGA.	Proportion of each land-use classification used to estimate exposure extent.
Fire	Historic	Ignition sites of historic fires with adaptive buffer using total burn acreage.	Proportion of each land-use classification used to estimate exposure extent.
Drought	Historic	U.S. Drought monitor database extents for 5-year period in four categories (D1-D4)	Proportion of each land-use classification used to estimate exposure extent.
Wind	Historic	Entire county used as extent.	Avg. number of damaging wind events (>50 mph) per year within the county.
Hail	Historic	Entire county used as extent.	Avg. number of damaging hail events (0.75") per year within the county.
Landslide	Modeled w/Historic	USGS historic landslide incidence and susceptibility based on slope and terrain types.	Proportion of each land-use classification used to estimate exposure extent.
Temperature Extremes (high and low temperature deviations)	Historic	Entire county used as extent.	The avg. deviation of annual min and max val. from the 32-year average high and low temps.
Inland Flood	Modeled	0.5-mile buffer around inland waterways (rivers, streams, lakes, ponds, etc.)	Proportion of each land-use classification used to estimate exposure extent.
Coastal Flood (SLR/Storm)	Modeled	Buffer along all coastal counties for land within 2 feet of current sea level at mean high tide.	Proportion of each land-use classification used to estimate exposure extent.

the final calculations for the index because of the limited or non-existent damage to predominantly natural systems exposed to earthquakes.

Fire data from 2000-2010 were collected from the U.S. Geologic Survey (USGS) Wildland Fire Information database (Hawbaker *et al*. 2017). Each fire occurrence has a point of ignition, identified with a latitude and longitude, as well as the total acreage burned. This value is used to create an adaptive buffer by back-calculating a buffer radius around the points. The circular burn buffers are then used to estimate land proportions exposed to fire in each county.

Drought exposure is based on data from the U.S. Drought Monitor Database (NDMC 2017). This dataset contains shapefiles of drought extent collected on a weekly basis since 2000, categorized into 5 levels of severity ranging from D0

(abnormally dry) to D4 (exceptional drought). For the purposes of this research, only categories D1-D4 were used. Due to the frequency of data collection, four samples, one representing drought conditions in each season (winter-first week of January, spring- first week of April, summer-first week of July, fall- first week of October), were taken from each year between 2005 and 2010. Annual and 5-year averages were tabulated for each county within each of the 4 drought categories (D1-D4) to represent total exposures as well as the severity of exposures.

Damaging hail and wind events exposures are assessed for the entire county using data from the NOAA Storm Prediction Center Historic Climatic Database (NWS 2016). A spatial buffer could not be used due to the lack of specific information on the spatial extent of hail and wind events. To calculate risk for the hail and wind events, the annual hail events within each county boundary are averaged over a 10-year span, from 2000-2010. The thresholds for damage-inducing events, a hail diameter of greater than 0.75 inches and wind gusts exceeding 50 miles per hour, are based on NOAA research (NWS 2007).

Landslide data comes from USGS incidence and susceptibility data, modelled and mapped based for locations of past landslides along with data on slope and terrain types that cause higher landslide risk (Radbruch-Hall *et al*. 1982; King and Beikman 1974). For the purposes of exposure likelihood, only the first four classes are used: High landslide incidence (>15% area involved in land-sliding), moderate landslide incidence (1.5-15% area involved in land-sliding), high susceptibility to land-sliding with low incidence, and moderate susceptibility with low incidence. The percentage of land falling into each of these four categories is summed to determine a probability extent for exposure to landslides.

Temperature extremes are assessed based on a 32-year record of maximum and minimum annual temperatures recorded in each county. Using this record, the annual average high and low temperatures are compared to establish and average deviation value above or below what is considered "normal" for the 3 decades. This is done by subtracting the annual high and low average temperatures from the 32-year mean values and inverting the result. Similar to the wind and hail data, the values for this metric represent the entire county and are not split into three land-type classifications. Both a deviation from annual low temperatures and annual high temperatures are calculated and used as individual metrics.

2.1.3. Proximity-Based Hazard Exposure

While tornadoes and hurricanes both have a documented historic risk based on events of the past 15 years in this study, it is important to also consider the inherent, or "basic" risk to locations based on their proximity to hazardous areas. This is very similar to the probability or susceptibility models done for earthquakes and landslide. Coastal counties along the Atlantic and Gulf of Mexico are at risk during any given hurricane season. Lack of occurrence data over the past 15 years does not exclude these counties from possessing future hurricane risk. The same applies to counties located in areas of higher tornado probability. Lack of impact in past does not preclude future incidents. Both hurricanes and tornadoes were assigned to counties as a basic risk established by location.

A proximity-based hurricane exposure probability score of 0.15% was assigned to all counties within 75 miles of the Atlantic or Gulf of Mexico coastlines. This percentage is created using the average probability of hurricane landfall in each, non-El Nino year (48%), divided 305, which is the number of coastal counties where hurricanes could strike (Bove *et al*. 1998). Proximity-based tornado

exposure probability was assigned using historic tornado data to select all counties with any tornadic activity in past 15 years. Each of these counties was assigned a basic risk score of 0.06% based on past climatological models (Schaefer *et al*. 1986).

Flood exposure is also quantified as a basic exposure in this research due to its calculation and the inherent risk present as a result of proximity to defined features. It is measured within two categories, inland exposure and coastal exposure. For the inland category, all rivers, streams, lakes and ponds were mapped using a ½ mile buffer to represent a potential exposure to flooding from these sources. Coastal flooding calculations use the NOAA Sea Level Rise predictions (Parris *et al*. 2012). These are based on height (mean high water) above sea level and derived from digital elevation maps (DEMs) along the coast. All land 2 feet or less above sea level are categorized as at risk.

2.1.4. Technological Hazards

In addition to natural hazards, a place may have additional exposure potential because of proximity to technological hazards. Technological hazards, such as nuclear power plants, Superfund sites, or toxic release sites, can have the potential to impact nearby populations regardless of natural exposure; however, natural hazards can exacerbate the technological risk. Table **3** shows the technological hazards used in this approach.

The Federal Emergency Management Agency (FEMA) tracks limited technological hazards through the Radiological Emergency Preparedness Program (REPP), for commercial power plants, and the Army chemical weapons stockpiles in the Chemical Stockpile Emergency Preparedness Program (CSEPP), for military chemical weapons stockpiles. In each of these preparedness programs, the concern is focused on potential human exposure to these hazards. However, many of the technological hazards could have a serious negative impact on plants and animals, suggesting this definition of technological risk needs to be expanded to encompass non-human ecosystems as well. In the case of crop land, even if human settlements are not directly impacted an exposure could still directly impact the food supply. For this reason, the point data for nuclear and chemical sites are assessed here for their impact on all land-use types and the data are expanded to include Superfund sites and sites on the Toxic Release Inventory (TRI).

Nuclear reactors or storage facilities in an area present additional hazards in the event of a leak. While most of these facilities are designed and built to withstand geologic and meteorological events common to their area, accidents are still possible and the underlying risk is still elevated because of their presence. The U.S. Nuclear Regulatory Commission (USNRC) designates an official Emergency Planning Zone (EPZ) based on the

Table 3. Technological Hazards metrics used in the PRISM approach and the methods used to collect and assess.

Technological Hazard Type	Spatial Extent	Exposure Calculation
Nuclear Facilities	All nuclear reactors and storage facilities in US identified and given a 10-mile buffer.	Proportion of each land-use classification used to estimate exposure extent.
Superfund Sites	Superfund sites - proposed or active in the US identified and given a 5-mile buffer.	Proportion of each land-use classification used to estimate exposure extent.
Toxic Release Inventory (TRI) Sites	TRI facilities identified when threshold chemical release criteria are met and given a ¼-mile buffer.	Proportion of each land-use classification used to estimate exposure extent.
Resource Conservation and Recovery (RCRA) Sites	All RCRA Site (LQGs, TSDs, and TRANSs) point data from EPA FRS Geodatabase are given a ¼-mmile buffer.	Proportion of each land-use classification used to estimate exposure extent.

plume exposure pathway distance of 10-miles. This distance is designed to limit exposure to radioactive materials through sheltering, evacuation, or the use of potassium iodide, if necessary (USNRC 2014). Nuclear facilities are mapped by point location and given a 10-mile buffer to designate their EPZ. Using methods described for natural hazards, risk is assigned to each county with percentages of risk distributed across each of the three land-use categories.

In contrast to nuclear facilities, superfund sites are slightly more complicated than nuclear facilities since they are not all the same. The sites can be in one of four conditions: proposed, active, completed, or deleted, depending on how far along the site is in the clean-up process. In addition, the chemicals present at a site can vary in their toxicity and range of potential travel. Generally, the impact of these sites will be localized, regardless of the chemical(s) present. Therefore, a buffer of one mile is created around each site that has been active during the past ten years and percentages of land covered are calculated for each of the three land-use types.

Toxic Release Inventory (TRI) and Resource Conservation and Recovery (RCRA) sites are by far the most numerous and varied of the technological hazards. Their potential to increase risk in the event of another hazard makes their inclusion important. TRI and RCRA sites have the capacity to impact air, water, and land quality and exist within both highly populated and more sparsely populated areas. TRI data was gathered from the TRI Explorer, which catalogs over 53,000 facilities that have been tracked in the past 20 years. To remain temporally consistent, only TRI sites logged within the 2000-2010 timeframe were used here. Data for RCRA sites was obtained from the EPAs Facility Registry Service (FRS) and only includes sites with greater exposure potential than TRIs, classified as Large Quantity Generators (LQGs), Hazardous Waste Transportation Services (TRANS) and Treatment, Storage and Disposal facilities (TSDs). To calculate the risk to each land type, a simple count of TRI and RCRA sites without a buffer in each county is used. TRI and RCRA density (count per area) with each land type in a county will represent the potential exposure.

2.1.4. Losses

Historic losses give exposure metrics the context needed to become a measure of intensity and impact across the landscape. In this approach, losses are combined into three categories, property, crop, and human, using data compiled from the Hazard and Vulnerability Research Institute's (HVRI) Spatial Hazard Events and Losses in the U.S (SHELDUS) database (HVRI 2017). Property and crop losses both serve as severity measures inbuilt and managed ecosystems, while human losses encompassing both fatalities and injuries, represent the social severity of the hazards. Losses are reported as per capita in 5-year segments. Losses are assigned to specific land classifications based on the type. Human and property losses are assigned to the built environment and crop losses are assigned to the dual-benefit environment. Natural losses are assessed using additional data from the NLCD on land cover change. This dataset identified land-use pixels that have changed to pervious surfaces (indicating built environment) between 2006 and 2011. The percentage of total county land converted to the built environment is used as a proxy for natural lands lost. The damage posed to natural systems resulting from population stresses or other anthropogenic influences, represented by the natural land loss, foreshadows potential reductions in ecosystem services (Hey and Philippi 1995).

2.2. Risk Calculation

While the specific issues related to collection and development of each risk exposure layer have

been described, the primary challenge comes in combining these to represent an overall risk landscape. In other words, how do the risks, both natural and technological, interact to create exposure likelihoods? A simple additive calculation cannot adequately answer this question. Instead, the calculation is more complicated, and a nuanced structure that accounts for not only each exposure, but the likelihood of loss that stems from the occurrence frequencies and the hazard severity.

Combining hazards in a meaningful way requires blending of spatial exposures and losses. Using the methods described, every hazard can be addressed by calculating a proportion of county land both impacted historically and land that could be impacted based on proximity to hazard zones (i.e. coastal Atlantic counties and hurricanes).

The complexity of the hazard-scape is represented in the final calculations, where the interplay of natural hazards, technological hazards, losses, and county landscape are used to create a risk score. This process, as shown in Fig. (**1**), is much more nuanced than a simple additive index. The combination of exposure extents, land-type distributions, and the associated losses are demonstrated in detail within section 3.3 with a regional analysis and break out of calculations for the high, medium, and low-risk counties in that area. Hazards are combined in steps based on the spatial extents, characteristics and land type first, then hazard type second. The first step modifies the historical exposures by weighting them with proximity-based hazards. Spatial extents for each hazard are based on the proportion of land area and added within land-types before modification. Proximity-based hazards are proportional as well, based on hazard probability, and added to one prior to being multiplied by the historic exposure.

The combined historic and proximity-based exposure value is added to the land-type proportion of technological hazards to create the final exposure probability. There will be three of these probability scores for each county, one for each land type. The exposure probability is then multiplied by the land specific loss (e.g. crop and structural loss for dual-benefit lands) to create a land-type risk score. Each county will have three risk scores following this step along with proportional land area types. These values are used to weight the risk scores and create a single risk value for the county. By weighting the historic exposure scores using both land types and proximity measures, the resulting PRISM score can capture the changes in risk resulting from locational and landscape-derived differences. The final score is thus dependent not only on direct hazard impacts, but also the changes occurring to the surrounding landscape.

3. RESULTS

The primary goal of the PRISM approach is to create a national landscape that accounts for a full suite of hazard exposures spatially. Along with losses, the data created from PRISM forms the risk domain of the Climate Resilience Screening Index (CRSI). However, the potential applications of the PRISM approach are much broader than inclusion in CRSI. In addition to creating an integrated risk value, the results can also be broken out into many categories for analysis. Some of the potential analyses enabled by PRISM include the examination of (1) temporal trends, (2) natural versus anthropogenic risks, (3) separate risk values for major land categories, and (4) multiple spatial scales ranging from county up to states and EPA regions. Prior to these type of specific analyses, a summary of the data is presented here to provide an overview of the results from the CRSI Risk domain as well as some specific spatial results.

3.1. National Results

The overall results, shown as a map in Fig. (**2**), and their variation across each land type are com-

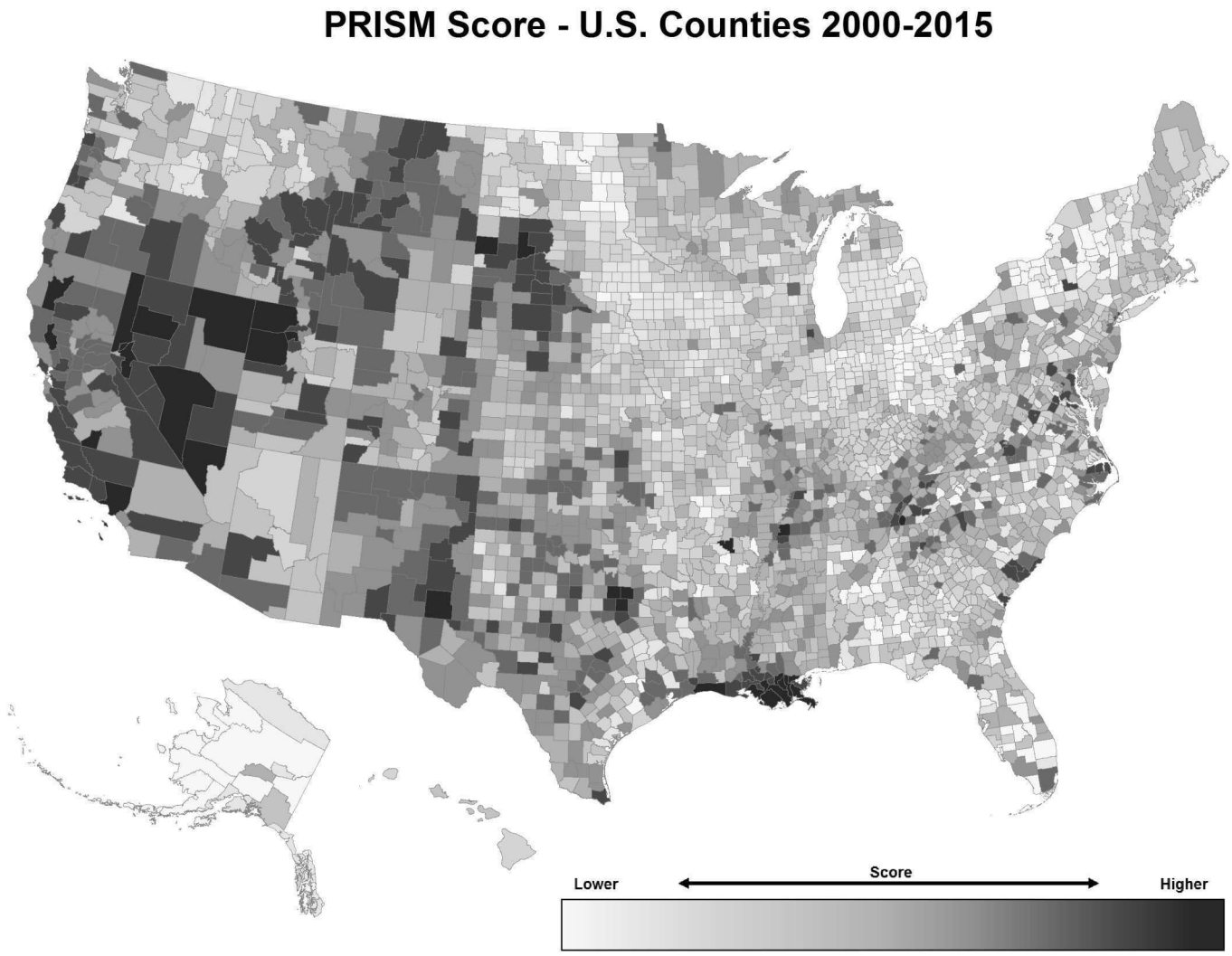

Fig. (2). PRISM Overall County Scores for all land types and entire 16-year period of measurement.

pared using a boxplot in Fig. (**3**). There are clear regional patterns in the data, with much of the Southwest, Louisiana, and plains states exhibiting higher risk levels. In addition, areas in the Appalachians and along the Eastern coastline display higher risk values. The Southeast, despite exposure to tornados and hurricanes, exhibits a comparatively low overall risk score. This could be due to the high exposure to drought and wildfires in the Western U.S. Interestingly, dual-benefit lands seem to drive much of the risk across the U.S. over the 15-year span. Risks to these lands are significantly higher than those in natural or developed lands, and the median falls closer to that of the overall score.

Analyzing the distribution of land types in the U.S., it is evident that much of the weight attributable to dual-benefit lands is due to the percentage of land in this category. Over 50 percent of U.S lands are classified as dual-benefit, with a bulk of those falling into either crop land in the middle of the country, and wetlands along the coast. Each of these land types provides a major service to urban communities and higher risk values to these lands is a significant concern. In addition to explaining the overall weighting as a function of percent coverage, this overall land distribution also highlights the importance of county-specific calculations for each category. While most of the U.S. is either natural or dual-benefit land, there are many coun-

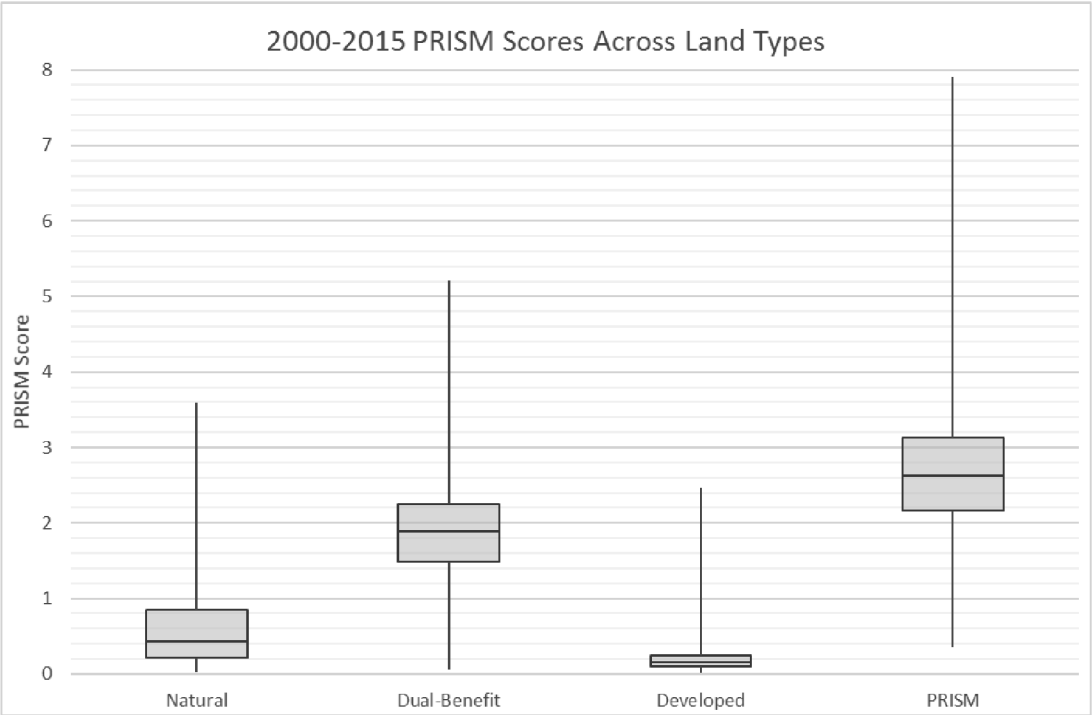

Fig. (3). Box Plots of Overall PRISM Score along with Land-type scores. Data represented in this graph are from 2000 - 2015.

ties that have a very small amount of this land type. Each county, state and region will have a very different land coverage, and thus a very different risk profile that must be managed. This distribution is shown in Fig. (**5**).

Temporal trends for PRISM across the three 5-year time periods (Fig. **4**) show that risk to dual-benefit lands consistently encompasses a majority of the overall score. Through each time period, both natural and developed land risk scores remain relatively low and unchanged. This is relatively surprising given the rise in sprawl and increased population in urban areas. Dual-benefit, however, experiences a spike in the 2005-2010 period. This spike is also evident in the overall score, despite both natural and developed lands experiencing a slight risk decrease over the same period. Reasons for this increase could be tied to changes in extent and severity of drought and wildfires, which impact much of the dual-benefit lands during this time period.

In addition to temporal patterns, there are clear patterns of risk distribution among the three land types both at a regional and county level. Regionally, both dual-benefit and natural lands dominate different parts of the country. Most of the Western U.S is predominantly natural, while the Midwest and up into portions of the Northeast is primarily dual-benefit. As suspected, the developed lands, except a few pockets of the interior, exists almost entirely along the coastline. Few counties are homogeneous, instead of having a mix of the three land-types.

Using a risk measure weighted by land-type distribution it is possible to adjust for county and regional patterns and better assess the extent of threat without exaggerating the impact of hazards on developed areas where monetary losses may be higher. The two forms of analysis, hazard-exposures and land-use types, are examined here using exposure and loss layers for the U.S. between 2000 and 2015. First, we will examine land-type changes and the accompanying shift in risk profiles that occur as the result of development and exposure types. Second, we conduct a temporal analysis that examines changes in the natural and techno-

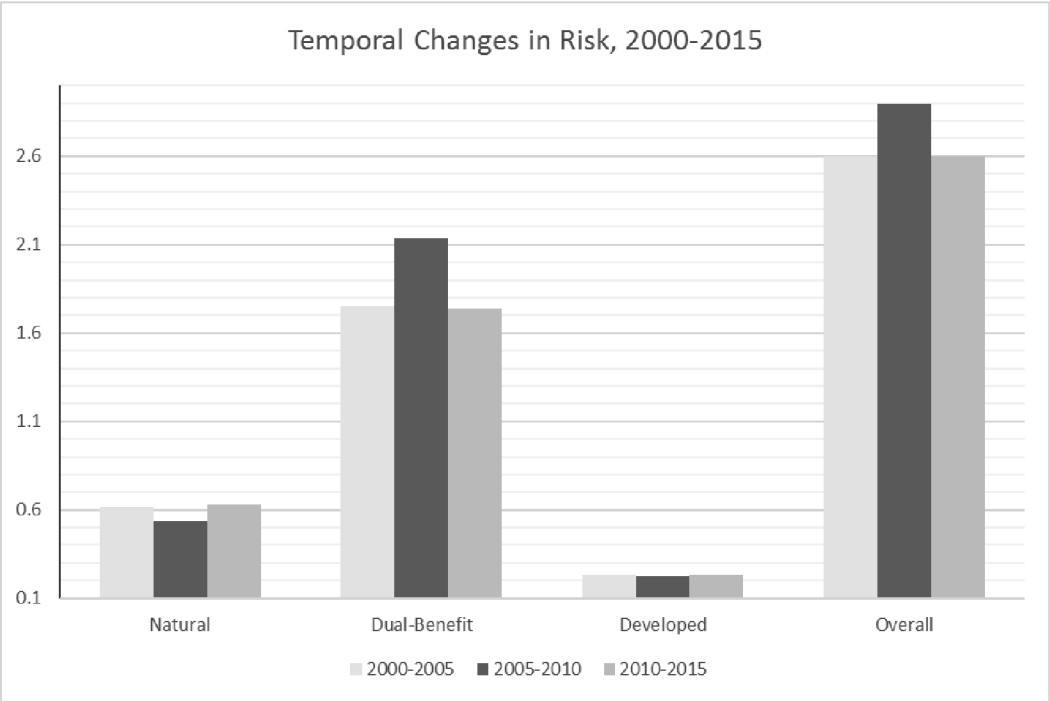

Fig. (4). Graph of Temporal Risk Changes across each land type and the overall PRISM Score.

logical risks. In each of these examples, the goal is to demonstrate flexibility and display the unique data produced for the analysis of multiple hazards.

The effects of county land-type composition are demonstrated through a series of maps (Fig. **5**), showing risk scores by land-use type for each of the three time-periods. Comparing this to the date in Fig. (**3**) can be used to address the distribution of risk versus the overall risk values, especially in the case of dual-benefit lands. While some increases in the spatial distribution of risk to developed lands occurs over the fifteen years, natural risk seems unchanged. While this matches up with the overall scores through time, the dual-benefit lands seem to exhibit a drastic spatial shift in risk from Eastern counties to Western counties. In the first time-period, risk in this category is primarily observed in the Eastern portions of the country. As time progresses, the areas of higher risk move Westward and appear to increase substantially along the West coast by the final time period.

Large spatial shifts like this are important to look at in more detail. Despite a relatively unchanged overall risk profile for the country, the land-type specific burden does appear to have shifted regionally. With regards to planning, a shift of this magnitude could also indicate that areas not normally exposed to hazards are now experiencing impacts, and could be potentially unprepared.

This national analysis is important from the perspective of regional and temporal changes in risk, however, it is a compilation of multiple values across many geographies and years. To showcase the value of an integrated multi-hazard approach, a more in-depth investigation of the risk components is also conducted using smaller geographic areas with higher risk scores. There are two that stand out in the overall approach; segments of the Southwest and the Gulf Coast of Louisiana, which are analyzed in more detail. This break down of risk components from the final score will call out specific hazards and risk areas and demonstrate why single risk values are valuable, yet require decomposition. Using a smaller number, the top 100 counties in overall risk, will allow for better analysis of their unique risk profiles.

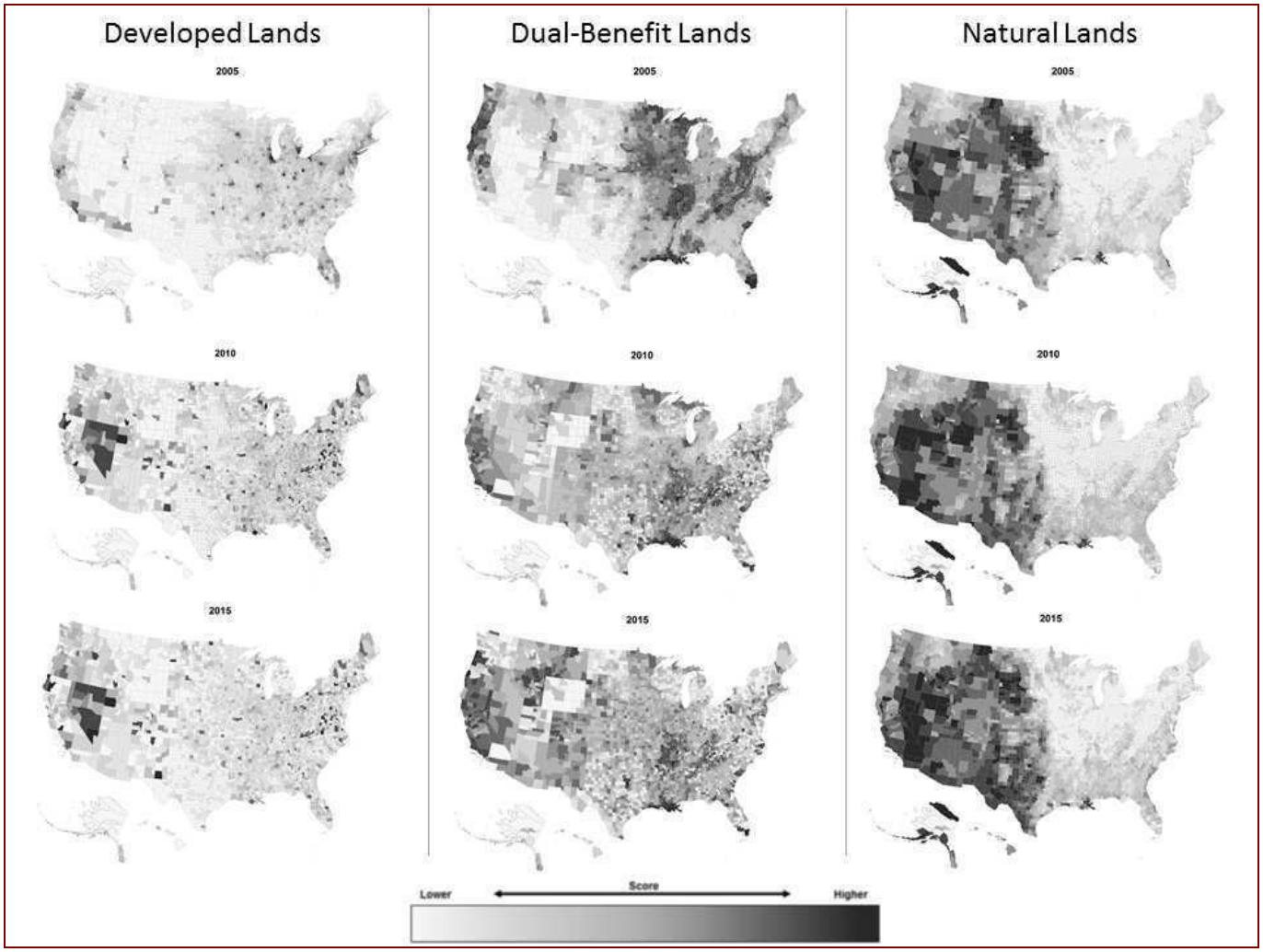

Fig. (5). Land-type Risk values break-down by time span. Each panel represents a specific land type within the counties over the same 5-year blocks of time. The left column represents risk to developed lands alone, the middle column represents risk to dual-benefit lands alone, and the right column represents risk to natural lands alone. In each map, darker colors indicate higher risk values, or a combination of exposure and losses for each land-type.

3.2. High-Risk County Analysis

The top 100 risk counties in the US represent twenty-three states, yet four states account for over fifty-percent of this group. Included in these four are, in order from most to least counties, Louisiana, Nevada, California, and Texas. Despite the similar overall risk scores, the two highest risk states, Nevada and Louisiana, have considerably different exposure profiles. In Louisiana, exposures from anthropogenic hazards are considerably higher than Nevada, with an average score of 0.067 versus 0.005. This is especially true in dual-benefit lands, where the exposure is more than 30 times greater (0.003 in NV and 0.103 in LA). Basic exposure in Louisiana (2.47) is also more than double that of Nevada (1.20). Driving the anthropogenic hazards in Louisiana is a significantly higher exposure to Superfund sites along the coast along with higher exposures to nuclear and RCRA sites. Elevated basic exposure in Louisiana is based on low-lying land threatened by both coastal and inland flooding. This produces a potentially dangerous combination in the event of natural hazard exposures exacerbating risk due to chemical or other toxic contamination related to these sites. In Nevada, the exposure from natural hazards (2.68) is larger than Louisiana (2.08), driven largely by

fire and drought, which are both closely related and cover a majority of the state's land area.

While the counties examined in these two states are similar in overall risk, it is helpful to examine the exposure metrics driving this risk. Changing patterns in risk drivers may require considerably different strategies when it comes to mitigation efforts. In Nevada, for instance, wildfires and drought would be handled through efforts such as prescribed burns, removal of undergrowth and potential fuel sources, and treatment of surfaces to minimize combustion. Louisiana would take a very different approach to mitigation by cleaning up hazardous waste sites, building flood control structures, and managing development in flood zones. In each instance, the end goal is the same, yet funding and policy would be handled in a different manner.

3.3. Regional and Hazard Specific Applications

In addition to the inspection of the broader risk profiles, PRISM can also be used to analyze regional patterns or investigate hazard-specific spatio-temporal changes. A subset consisting of Gulf Coast Counties is analyzed first to demonstrate the regional utility of PRISM. In this example, the representative sub-set consists of fifty-four coastal counties from five states bordering the Gulf of Mexico. Over the sixteen-year study period, the average PRISM score of these counties is 3.21, which is considerably higher than the national average of 2.7. From this set of counties, Plaquemines Parish, LA has the highest PRISM score (5.41) of the subset (second highest of the entire U.S), while Charlotte County, FL has the lowest (2.39).

The PRISM scores in this example are deconstructed by land-type and risk domain (exposure and loss) to better analyze and compare patterns of risk. Looking first at the mean land-type risk, there are distinction between counties that become apparent. Developed land risk is low (mean = 0.22) apart from a few counties with significantly higher scores. Dual-benefit land appears to drive much of the overall risk with a mean of 2.21 and maximum of 5.21. Natural lands fall in between the two with a mean risk score of 0.76. From an exposure perspective, the dual-benefit risk is likely driven by a reliance on saltwater marshes and other land-types associated with flood and storm protection in these coastal counties. With urban development and sea level rise threatening the hazard mitigation function of natural and dual-benefit lands, the risk of loss resulting from future exposures to spreading urban environments should be expected to increase. The trend toward higher risk in heavily urbanizing counties is already evident (Figure along the Gulf coast, where rapidly developing counties from the past decade also possess high risk values across all three land-type categories.

A deconstruction of the risk domains, exposure and loss, reveals yet more detail and another layer on top of the land-type analysis. Exposure measures are assessed independently to determine the extent of impact in an area and assess the relative distribution of exposure probabilities. An example of this can be seen in Fig. (**6**), with three pie charts that show the distribution of exposure and loss across each of the hazards and how these translate to losses by land type. What is striking about this graphic is both the sizeable amount of natural hazard exposure to drought and temperature extremes and the comparatively small amount of loss to developed lands. Despite these counties having higher populations and infrastructure, the primary drivers of risk are related to temperature and rainfall events that impact crops, forests, marshes, and other natural lands not primarily related to the built environment. This is contrary to the standard measures of risk that focus on built environments and report monetary losses.

Putting the two analyses together paints a more holistic picture of risk in a region presented with a number of potential exposures. Risk location is explained through closer analysis of exposure

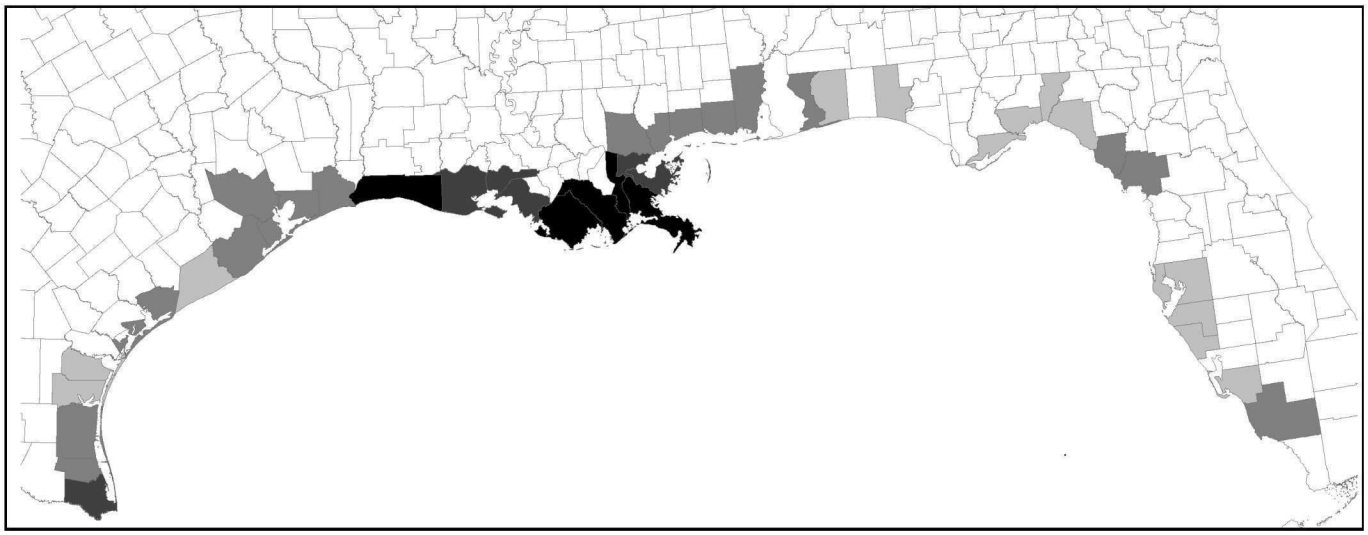

Fig. (6). Gulf Coast Counties overall PRISM score. 54 counties in 5 states with risk estimate calculated from 16-year period (2000-2015). Darker colors indicate higher risk probability across all land-types for all hazard types.

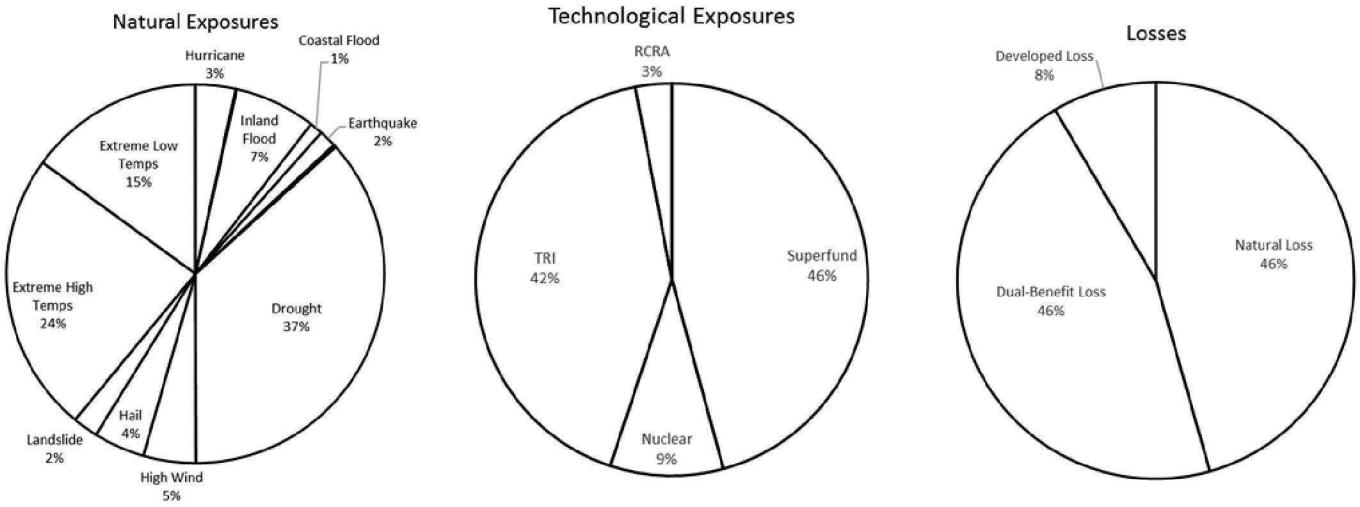

Fig. (7). Three pie charts showing distribution of exposure and loss across fifty-four counties bordering the Gulf of Mexico. The percentages represent the distribution of average exposure probability for each hazard type between 2000 – 2015.

types along with land-type characteristics. Many areas of the Gulf coast are sparsely populated, yet have numerous vulnerable natural resources. This vulnerability shows up in the deconstruction of PRISM exposure where a bulk of the losses occur in dual-benefit lands as a result of temperature and rainfall events. In a location where hurricanes are what most people would consider the primary risk concern, the actual exposure threats are quite different when compared alongside the full spectrum of exposures and losses.

To best capture the influence of exposure extents, land types, and losses, Table **4** shows the land weighted, scaled values associated with three of the Gulf Coast counties: Terrebonne Parish (highest), Charlotte County, FL (lowest), and Hillsborough County, FL (middle). The numbers represent exposure and loss values already weighted by land-use type. Land use percentages are shown under the county names to provide some insight into the differences between the counties. Interestingly, the county with the least developed land, Plaquemines, has the highest level of exposure to natural hazards and the highest loss values.

There are a few key measures easily identifiable and responsible for the differences in the final risk

Table 4. Example of PRISM calculation for Plaquemines Parish, Hillsborough County, and Charlotte County to display the influence of exposure and loss changes on the final score. Land-use percentages are shown in left column with county names. Bolded natural exposures represent basic exposures in the model. All exposures and losses are land-weighted prior to entry in this example.

	Land-Weighted Natural Exposures		Land-Weighted Technological Exposures	Land-Weighted Losses	Risk
Plaquemines Parish, LA: Natural Land – 47% Dual Land – 51% Developed Land – 2%	Hurricane - 0.5085 **Basic Hurr. -0.0015** Tornado- 0.000075 **Basic Torn. 0.0006** **Inland Flood- 0.975** **Coastal Flood- 0.97** Earthquake - 0 Fire - 0	Drought – 1 Wind – 0.0592 Hail – 0.0073 Landslide -0 High Temp. -0.50 Low Temp. -0.59 Sum – 4.6104	+ Superfund-0 TRI-0.006 RCRA-0.005 Sum-0.00652	× Nat.-0.0083 Dual-0.0085 Dev.-0.171 (Sum+1)-1.17267 =	5.41
Hillsborough County, FL: Natural Land – 13% Dual Land – 49% Developed Land – 38%	Hurricane - 0.50 **Basic Hurr. -0.0015** Tornado- 0.000411 **Basic Torn. 0.0006** **Inland Flood- 0.109** **Coastal Flood- 0.034** Earthquake - 0 Fire - 0	Drought – 1 Wind – 0.0216 Hail – 0.1605 Landslide -0 High Temp. -0.44 Low Temp. -0.11 Sum – 2.5779	+ Superfund-0.23 TRI-0.0732 RCRA-0.00324 Sum-0.3058	× Nat.-0.03086 Dual-0.03087 Dev.-0.0000995 (Sum+1)-1.0618 =	3.06
Charlotte County, FL: Natural Land – 15% Dual Land – 65% Developed Land – 20%	Hurricane - 0.50 **Basic Hurr. -0.0015** Tornado- 0.000143 **Basic Torn. 0.0006** **Inland Flood- 0.0754** **Coastal Flood- 0.12** Earthquake - 0 Fire - 0	Drought – 1 Wind – 0.0254 Hail – 0.030 Landslide -0 High Temp. -0.46 Low Temp. -0.10 Sum – 0.3267	+ Superfund-0 TRI-0.00371 RCRA-0 Sum-0.00371	× Nat.-0.00809 Dual-0.00853 Dev.-0.0069 (Sum+1)-1.0235 =	2.39

scores between these three examples. What separates Plaquemines Parish from the other two counties is both the flood risk and losses in developed lands. Whereas Hillsborough and Charlotte counties have similarly intermediate levels of exposure, they are relatively small in comparison. This is largely the result of Plaquemines' situation along the Mississippi River delta and the Gulf of Mexico. This Parish encompasses most of the delta and is experiencing significant losses due to both rising sea levels and land subsidence (Zou *et al*. 2016). These losses put most land in the parish at great risk from both riverine floods and coastal flooding as a result of decreased buffers provided by the marsh. Developed loss values for Plaquemine parish also stand out as significant compared to the other two counties. This is remarkable due to the small land percentage designated as developed. Losses to both human life and property are significantly higher than most other counties. Knowing this helps focus efforts by highlighting the intersections of exposure and loss.

The other key difference, and a feature that distinguishes the PRISM method, is the handling of losses as a function of exposure. High exposure potential can be tempered by low losses; just as

lower exposure potential can be greatly inflated by high losses. For example, if losses comparable to Charlotte county (1.02 instead of 1.17), were experienced in Plaquemines Parish, the resulting risk would be 4.7. Similarly, if Charlotte county were to increase losses to a level comparable to Plaquemines, the overall risk score would be 2.72. These examples provide some evidence of the utility of PRISM in the identification of highest exposure risks and more importantly in the determination of causal relationships driving the losses. Information gleaned from this analysis can be applied to more targeted mitigation actions.

4. DISCUSSION

While there are existing multi-hazard approaches, a surface based exposure approach melding multiple natural and technological hazards is novel and produces results that are highly adaptive and scalable. In a decision-making context, this makes the data useful for planning and analysis at the county, state and regional level. Resilience is defined through a regional ecology approach, where external forces act on a community, and the interactions with neighboring places for support are significant in recovery (Holling 1986). In this context, it makes sense to expand the reach of hazards integration across the entirety of the United States. From a policy standpoint as well, it is logical to analyze hazards at the minimum of a regional scale. Many disasters far exceed local capacity to rebound, and regional or national resources are needed to aid recovery in both the short and long terms. As development in areas of high exposure probability increase (e.g. coastal areas), the losses will continue to rise and strain development goals and the ability to mitigate (Miletti 1999).

In addition to policy concerns, there is also the consideration of rapidly changing landscapes and shifting hazard-scapes, making it critical to have an approach that can be updated on a regular basis. A good example of this would be through examination of county losses. Knowing that per capita human or property loss numbers increase over time only tells part of the story. The other part is told by the change in land-use or hazard exposure. Without a more detailed analysis, there is no way to know whether the increased losses are the result of expanding urban areas where hazards occur, increased exposure to hazards due to a change in patterns, or simply the existence of a new hazard. By accounting for each of these factors, the PRISM approach allows for a more detailed examination of all exposure types, and is capable of answering these types of questions.

PRISM results can also facilitate decisions at the county, state or regional level through use of a comparative value system that is consistent across the United States. For a large-scale multi-hazard approach, this is an incredibly important step that removes conflicts arising due to qualitative or region specific assessments of hazard severity. In PRISM exposure is calculated along with other hazard parameters, where applicable (e.g. wind speed, earthquake magnitude, etc.), to assess magnitude, which allows for comparability across hazard types. Because of this uniform exposure assessment, regional disparities in exposure type do not impact the analysis. Impact in the form of spatial extent and loss, not severity of the event, matters. It does not matter if a category 2 or a category 5 hurricane hits a county. What matters is how many people, structures, and other environments are in the path along with losses sustained as a result of the exposure. If a county is well prepared for the hazard, it would be expected that losses are less. It is very possible, following this logic, for a county exposed to a category 3 storm to have greater losses than another county exposed to a category 5 storm. In the end, the strength of the storm is of secondary concern to the extent and type of losses endured. For this reason, the storm severity is only used as a threshold value to deter-

mine risk. It is not used to categorize the exposures.

While the probability of hazard recurrence is not solely based on historical frequencies, it does aid in the discussion both from an exposure standpoint and in the determination of disaster fatigue. The impact of multiple events over a relatively short period of time can also have a major impact on a communities' recovery and future resilience (Bobrowski 2013). People are likely to be worn down, resulting in loss of business and potential emigration from the area. Long term impacts to the economy and social networks may take years to recover; if they ever do.

While the PRISM model was developed with a specific purpose, the final product can yield much greater use in general hazards planning. Aside from the consideration of potential hazard-type exposure to an area, it is equally important to consider the land types being impacted. All places are different, and this makes for differences in their vulnerabilities. In most cases, risk is assessed solely with regards to developed lands. People worry about impacts to lives, jobs, and structures primarily, while risk models fail to separate out the landscape to account for different land uses. The PRISM model uses three land classification categories to look at risk in the context of management decisions. The three choices for land use were meant to distinguish and call attention to places where conflicts of interest may arise. These dual-benefit lands are defined by their combined value to both humans and to ecosystem health. These lands typically do not hold many people and are neglected in most discussions of risk, whether it be natural or anthropogenic. Much of this land type is threatened, however, and this threat appears to be on the increase. Looking at the descriptive statistics for each land type, it is also clear that dual-benefit lands are the driver behind the overall risk value.

Given the challenges discussed here, a new approach to multi-hazard assessment is outlined with an intent to create a single measure of hazard risk for a location to be incorporated into further assessments of resilience, namely the Climate Resilience Screening Index (CRSI; Summers *et al*. 2017). This model uses an integrated spatial approach to assess multi-hazard exposure of a landscape to distill a single value representing a cross-section of this exposure with the vulnerabilities across counties. This is a novel approach meant to streamline the assessment of multi-hazard risks via the removal of both subjective impact measures and complicated hazard maps.

ETHICS APPROVAL AND CONSENT TO PARTICIPATE

Not applicable.

HUMAN AND ANIMAL RIGHTS

No Animals/Humans were used for studies that are the basis of this research.

CONSENT FOR PUBLICATION

Not applicable.

CONFLICT OF INTEREST

The authors declare no conflict of interest, financial or otherwise.

ACKNOWLEDGEMENTS

Declared none.

REFERENCES

[1] Batista, M.J., Martins, L., Costa, C., Relv, A.M., Schmidt-Thome, P., Greiving, S., Fleishauer, M., Peltonen, L. 2004. Preliminary results of a risk assessment study for uranium contamination in central Portugal. Proceedings of the Internation Workshop on Environmental Contamination from Uranium Production Facilities and Remediation Measures, ITN/DPRSN, Lisboa. February 11-13, 2004.

[2] Bell, R., and Glade, T. 2011. Multi-hazard analysis in natural risk assessments. *WIT Transactions on State of the Art in Science and Engineering* 53: 1-10.

[3] Bobrowski, P., ed. 2013. *Encyclopedia of Natural Hazards*. 1135 p. Springer.

[4] Bove, M., O'Brien, J., Eisner, J., Landsea, C., and Niu, X. 1998. Effect of El Nino on U.S. Landfalling Hurricanes, Revisited. *Bulletin of the American Meteorological Society* 79(11): 2477-2482.

[5] Brooks, H. 2004. On the Relationship of Tornado Path Length and Width to Intensity. *Weather and Forecasting* 19: 310-319.

[6] Burton, I., and Kates, R.W. 1964. The Perception of Natural Hazards in Resource Management. *Natural Resources Journal* 3(3): 412-441.

[7] Chester, D.K., Degg, M., Duncan, A.M., Guest, J.E. 2000. The increasing exposure of cities to the effects of volcanic eruptions: a global survey. *Global Environmental Change Part B: Environmental Hazards* 2(3): 89-103.

[8] Cutter, S.L., and Solecki, W.D. 1989. The national pattern of airborne toxic releases. *Professional Geographer* 41(2): 149-161.

[9] Cutter, S.L. 1996. Vulnerability to environmental hazards. *Progress in Human Geography* 20(4): 529-539.

[10] Cutter, S., Burton, C., and Emrich, C. 2010. Disaster Resilience Indicators for Benchmarking Baseline Conditions. *Journal of Homeland Security and Emergency Management* 7(1): 51-51.

[11] Federal Emergency Management Agency (FEMA). 2009. *National Earthquake Hazards Reduction Program Recommended Seismic Provisions for New Buildings and Other Structures* (FEMA P-750).

[12] Federal Emergency Management Agency (FEMA). 2013. *Multi-hazard Loss Estimation Methodology: Flood Model Hazus-MH Technical Manual.* Department of Homeland Security, Federal Emergency Management Agency Mitigation Division. Washington, D.C.

[13] Garschagen, M., and Romero-Lankao, P. 2015. Exploring the relationships between urbanization trends and climate change vulnerability. *Climate Change* 133(1): 37-52.

[14] Greiving, S., Fleischhauer, M., Lückenkötter, J. 2006. A methodology for an integrated risk assessment of spatially relevant hazards. *Journal of Environmental Planning and Management* 49(1): 1–19.

[15] Güneralp, B., Güneralp, I., Liu, Y. 2015. Changing global patterns of urban exposure to flood and drought hazards. *Global Environmental Change* 31: 217-225.

[16] Hawbaker, T., Vanderhoof, M., Beal, Y., Takacs, J., Schmidt, G., Falgout, J., Williams, B., Brunner, N., Caldwell, M., Picotte, J., Howard, S., Stitt, S., and Dwyer, J.L. 2017. *Landsat Burned Area Essential Climate Variable products for the conterminous United States (1984 - 2015): U.S. Geological Survey data release*, https://doi.org/10.5066/F73B5X76.

[17] Hazards and Vulnerability Research Institute (HVRI). 2016. *Spatial Hazard Events and Losses Database for the United States, Version 15.2*. [Online Database]. Columbia, SC: Hazards and Vulnerability Research Institute, University of South Carolina.

[18] Hewitt, K., and Burton, I. 1971. *The Hazardousness of a Place: A Regional Ecology of Damaging Events.* University of Toronto Press.

[19] Hey, D., and Philippi, N. 1995. Flood Reduction through Wetland Restoration: The Upper Mississippi River Basin as a Case History. *Restoration Ecology* 3(1): 4-17.

[20] Holling, C.S. 1986. The resilience of terrestrial ecosystems; local surprise and global change. *eds*. W.C. Clark and R.E. Munn. *Sustainable Development of the Biosphere*. Cambridge University Press, Cambridge, U.K.

[21] Homer, C., Dewitz, J., Yang, L., Jin, S., Danielson, P., Xian, G., Coulston, J., Herold, N., Wickham, J., and Megown, K. 2015. Completion of the 2011 National Land Cover Database for the conterminous United States-Representing a decade of land cover change information. *Photogrammetric Engineering and Remote Sensing* 81(5): 345-354.

[22] Field, C., Barros, V., Stocker, B., Qin, D., Dokken, K., Mastrandrea, M., Mach, K., Plattner, S., Allen, M., Tignor, M., and Midgley, P. eds. 2012. Managing the Risks of Extreme Events and Disasters to Advance Climate Change Adaptation. *A Special Report of Working Groups I and II of the Intergovernmental Panel on Climate Change.* Cambridge University Press, Cambridge, UK, and New York, NY, USA.

[23] Kappes, M., Keiler, M., Elverfeldt, K., and Glade, T. 2012. Challenges of analyzing multi-hazard risk: a review. *Natural Hazards* 64: 1925-1958.

[24] King, P., and Beikman, H. 1974. Geologic map of the United States (exclusive of Alaska and Hawaii) U.S. Geological Survey, scale 1:2,500,000, 2 sheets.

[25] Lall, S.V., Deichmann, W. 2010. Density and Disasters: Economics of Urban Hazard Risk. *The World Bank Research Observer* 27(1): 74-105.

[26] Marzocchi, W., Garcia-Aristizabal, A., Gasparini, P., Mastellone, M., and Di Ruocco, A. 2012. Basic principles of multi-risk assessment: a case study in Italy. *Natural Hazards* 62: 551-573.

[27] Miletti, D. 1999. *Disasters by design: A reassessment of Natural Hazards in the United States.* Joseph Henry Press. Washington, D.C.

[28] National Drought Mitigation Center (NDMC), U.S. Department of Agriculture (USDA), National Oceanic and Atmospheric Administration (NOAA). 2017. United States Drought Monitor Database. http://droughtmonitor.unl.edu/MapsAndData/GISData.aspx.

[29] National Weather Service (NWS). 2007. Storm Data Preparation. Directive National Weather Service Instruction 10-1605. National Weather Service.

[30] National Weather Service (NWS). 2016. Severe Weather Database Files (1950-2016). NOAA NWS. http://www.spc.noaa.gov/wcm/#data .

[31] Parris, A., Bromirski, P., Burkett, V., Cayan, D., Culver, M., Hall, J., Horton, R., Knuuti, K., Moss, R., Obeysekera, J., Sallenger, A., and Weiss, J. 2012. Global Sea Level Rise Scenarios for the US National Climate Assessment. *NOAA Tech Memo OAR CPO-1*. http://cpo.noaa.gov/sites/cpo/Reports/2012/NOAA_SLR_r3.pdf.

[32] Radbruch-Hall, D., Colton, R., Davies, W., Lucchitta, I., Skipp, B., and Varnes, D. 1982. Landslide Overview Map of the Conterminous United States, *Geological Survey Professional Paper 1183*. U.S. Geological Survey, Washington.

[33] Reser J.P. 2007 The Experience of Natural Disasters: Psychological Perspectives and Understandings. In: Lidstone J., Dechano L.M., Stoltman J.P. eds. *International Perspectives on Natural Disasters: Occurrence, Mitigation, and Consequences. Advances in Natural and Technological Hazards Research* vol 21. Springer, Dordrecht

[34] Schaefer, J., Kelly, D., and Abbey R. 1986. A minimum assumption tornado-hazard probability model. *Journal of Climate and Applied Meteorology* 25: 1934-1945.

[35] Schmidt-Thome, P. (Ed.) 2006. ESPON Project 1.3.1 – Natural and technological hazards and risks affecting the spatial development of European regions. Geological Survey of Finland.

[36] Simpson, R., and Reihl, H. 1981. *The Hurricane and Its Impact.* Louisiana State University Press: Baton Rouge and London.

[37] Tate, E., Burton, C., Berry, M., Emrich, C., and Cutter, S. 2011. Integrated Hazards Mapping Tool. *Transaction in GIS* 15(5): 689-706.

[38] Thierry, P. 2008. Multi-hazard risk mapping and assessment on an active volcano: the GRINP project at Mount Cameroon. *Natural Hazards*. 45(3): 429-456.

[39] U.S. Geological Survey. 2003. Earthquake Hazards Program: U.S. Seismic Design Maps: U.S. Geological Survey, https://doi.org/10.5066/F7MC8X8S.

[40] U.S. Nuclear Regulatory Committee (USNRC). 2014. Emergency Preparedness at Nuclear Power Plants. www.nrc.gov.

[41] Watson, J.T., Gayer, M., and Connolly, M.A. 2007. Epidemics after Natural Disasters. *Emerging Infectious Diseases* 13(1): 1-5.

[42] Weatherford, C., and Gray, W. 1988. Typhoon structure as revealed by aircraft reconnaissance. Part II: Structural variability. *Monthly Weather Review* 116: 1044–1056.

[43] Zhu, P. 2008. A multiple scale modeling system for coastal hurricane wind damage mitigation. *Natural Hazards* 47: 577. doi:10.1007/s11069-008-9240-8.

[44] Zou, L., Kent, J., Lam, N.S., Cai, H., Qiang, Yi., Li, K. 2016. Evaluating Land Subsidence Rates and Their Implications for Land Loss in the Lower Mississippi River Basin. *Water* 8(1): 10-25.

EMAIL CONCURRENCES FOR Summers et al and Buck et al. STAA submissions:

Original:

From: Summers, Kevin <Summers.Kevin@epa.gov>
Sent: Friday, April 17, 2020 9:55 AM
To: Smith, LisaM <Smith.Lisam@epa.gov>; Harwell, Linda <Harwell.Linda@epa.gov>; Buck, Kyle <buck.kyle@epa.gov>; stevehafner1@gmail.com
Subject: STAA 2020 Submission

I am preparing a submission for the 2020 STAA awards for three manuscripts for which each of you contributed. A requirement of the submission is an assessment of the contribution of each author to the publications. My assessment is listed below. If you agree with my assessment please send a return email to me stated

that you agree with the assessment. Thanks in advance.

(1) Summers, J.K., L.M. Smith, L.C. Harwell, K.D. Buck. 2018a. Measuring community resilience to natural hazards; The Natural Hazard Resilience Screening Index (NaHRSI) – Development and Application to the United States. GeoHealth 2: 372-394.

Summers: 40%
Smith: 20%
Harwell: 20%
Buck: 20%

(2) Summers, K., L. Harwell, L. Smith and K. Buck. 2018b. Regionalizing resilience to acute meteorological events: Comparison of regions in the U.S. Frontiers in Environmental Science https://doi.org/10.3389/fenvs.2018.00147

Summers: 40%

Harwell: 20%

Smith: 20%

Buck: 20%

(3) Buck, K.D., J.K. Summers, S.F. Hafner, L.C. Harwell, and L.M. Smith. 2019. Development of a Multi-Hazard Landscape for Exposure and Risk Interpretation: The PRISM Approach. Current Environmental Engineering 6: doi: 10.2174/2212717806666190204103455

Buck: 40%

Summers: 15%

Hafner: 20%

Harwell: 15%

Smith: 10%

J. Kevin Summers

Senior Research Ecologist

Gulf Ecosystem Measurement and Modeling Division

Center for Environmental Measurement and Modeling

Summers Response: Summers to Summers 4/17/20 @ 10:23am

I concur

Smith Response: Lisa Smith to K. Summers 4/17/20 @ 10:24am

I'm ok with the allocations. If someone feels they need to increase their contibution% please deduct it from mine.

Buck Response: Kyle Buck to K. Summers 4/17/20 @ 10:19am

Sent from my iPhone Agreed.

Kyle

Hafner Response: Hafner to K. Summers 4/20/20 @ 1:17pm

Oh sorry, I thought I had that at the end of the email, but yes I do concur with the assessment of my work on the PRISM project. My phone number is 850-221-0335. Thanks-

Linda Harwell Response: Harwell to K. Summers 4/20/20 @ 4:14 pm

I concur with contribution assignment.

Supporting Documentation – 2019 STAA Nomination

Summers et. al "For applications of resilience indices and tools to enhance capacity"

Journal statistics information (Immediacy Index; Citation of Life; Impact Factor) for the 3 papers in this STAA nomination:

(1) Summers, J.K., L.M. Smith, L.C. Harwell, K.D. Buck. 2018a. Measuring community resilience to natural hazards; The Natural Hazard Resilience Screening Index (NaHRSI) – Development and Application to the United States. *GeoHealth* 2: 372-394. (Published 12/7/2018)

> Statistics (Immediacy Index; Citation of Life; Impact Factor) do not yet exist for the journal *GeoHealth*. The journal does not have 5 years of publication to qualify for these statistics.

(2) Summers, K., L. Harwell, L. Smith and K. Buck. 2018b. Regionalizing resilience to acute meteorological events: Comparison of regions in the U.S. *Frontiers in Environmental Science* https://doi.org/10.3389/fenvs.2018.00147 (Published 11/30/2018)

> Statistics (Immediacy Index; Citation of Life; Impact Factor) do not yet exist for the journal *Frontiers in Environmental Science*. The journal does not have 5 years of publication to qualify for these statistics.

Buck, K.D., J.K. Summers, S.F. Hafner, L.C. Harwell, and L.M. Smith. 2019. Development of a Multi-Hazard Landscape for Exposure and Risk Interpretation: The PRISM Approach. *Current Environmental Engineering* 6: doi: 10.2174/2212717806666190204103455

> Statistics (Immediacy Index; Citation of Life; Impact Factor) do not yet exist for the journal *Current Environmental Engineering*. The journal does not have 5 years of publication to qualify for these statistics.

GeoHealth

RESEARCH ARTICLE
10.1029/2018GH000160

Key Points:
- An index of resilience to acute weather events has been developed
- The index has been applied to all counties in the United States
- The application allows the comparison of resilience of counties and the selections of counties provided best lessons learned for county resilience improvement

Measuring Community Resilience to Natural Hazards: The Natural Hazard Resilience Screening Index (NaHRSI)—Development and Application to the United States

J. Kevin Summers[1], Linda C. Harwell[1], Lisa M. Smith[1], and Kyle D. Buck[1]

[1]Gulf Ecology Division, National Health and Environmental Effects Research Laboratory, U.S. Environmental Protection Agency, Gulf Breeze, FL, USA

Correspondence to:
J. K. Summers,
summers.kevin@epa.gov

Citation:
Summers, J. K., Harwell, L. C., Smith, L. M., & Buck, K. D. (2018). Measuring community resilience to natural hazards: The Natural Hazard Resilience Screening Index (NaHRSI)—Development and application to the United States. *GeoHealth*, *2*, 372–394. https://doi.org/10.1029/2018GH000160

Received 11 JUL 2018
Accepted 12 NOV 2018
Accepted article online 16 NOV 2018
Published online 7 DEC 2018

Author Contributions:
Conceptualization: J. Kevin Summers, Linda C. Harwell
Formal analysis: J. Kevin Summers, Linda C. Harwell
Investigation: J. Kevin Summers
Methodology: J. Kevin Summers, Linda C. Harwell
Validation: J. Kevin Summers
Visualization: J. Kevin Summers
Writing - original draft: J. Kevin Summers
Writing – review & editing: J. Kevin Summers, Linda C. Harwell

©2018. The Authors.
This is an open access article under the terms of the Creative Commons Attribution-NonCommercial-NoDerivs License, which permits use and distribution in any medium, provided the original work is properly cited, the use is non-commercial and no modifications or adaptations are made.

Abstract Natural disasters often impose significant and long-lasting stress on financial, social, and ecological systems. From Atlantic hurricanes to Midwest tornadoes to Western wildfires, no corner of the United States is immune from the threat of a devastating natural hazard event. Across the nation, there is a recognition that the benefits of creating environments resilient to adverse natural hazard events help promote and sustain county and community success over time. The challenge for communities is in finding ways to balance the need to preserve the socioecological systems on which they depend in the face of constantly changing natural hazard threats. The Natural Hazard Resilience Screening Index (NaHRSI; previously entitled Climate Resilience Screening Index) has been developed as an endpoint for characterizing county resilience outcomes that are based on risk profiles and responsive to changes in governance, societal, built, and natural system characteristics. The NaHRSI framework serves as a conceptual roadmap showing how natural hazard events impact resilience after factoring in county characteristics. By evaluating the factors that influence vulnerability and recoverability, an estimation of resilience can quantify how changes in these characteristics will impact resilience given specific hazard profiles. Ultimately, this knowledge will help communities identify potential areas to target for increasing resilience to natural hazard events.

Plain Language Summary NaHRSI (Natural Hazard Resilience Screening Index) is a tool for communities to evaluate their likely vulnerability and resilience acute meteorological events like hurricanes, tornadoes, droughts, floods, etc. The index has been applied to all counties of the United States and is comprised of five major parts examining risk of events, governance to address events, societal, built environment and natural environment attributes that will enhance recoverability for these types of events.

1. Introduction

Natural disasters can impose long-lasting and significant stress on social, financial, and ecological systems. From Western wildfires to Midwest tornadoes to Atlantic hurricanes, no portion of the United States is immune from the threat of a devastating meteorological event. Throughout the nation, the benefits of creating environments resilient to adverse weather or weather-related events are recognized as helping to promote and sustain county and community success. The true challenge is in finding ways to balance the preservation of socioecological systems on which communities depend in the face of the constant barrage of natural hazard threats.

The U.S. National Security Strategy suggests that impacts from adverse meteorological events represent a credible national security concern (National Security Strategy, 2015). By one accounting, the federal government has incurred more than $357 billion in direct costs due to extreme weather and fire events alone over the last 10 years (Office of Management and Budget and Council on Environmental Quality, 2016). With the tempo and magnitude of natural disasters experienced in 2017, it is likely that a considerable spike will be observed in the federal expenditure for recovery and response efforts. Since 2013, the U.S. Government Accountability Office monitors the high-risk fiscal exposure to the federal government because of natural hazard-related events. Recognizing the sweeping impacts of natural disasters across the infrastructure, defense, agriculture, health, and local economies, the U.S. government is challenged with taking steps to better manage this fiscal risk (Government Accountability Office, 2017).

The concept of resilience has evolved from its initial emphasis on the general persistence of ecological system functions in a world that is subject to ongoing change (Holling, 1973), through an orientation

toward coupled socioecological systems and questions of adaptation of humans in nature (Carpenter et al., 1999, 2001; Walker, 1993; Walker et al., 2002). In general terms, resilience is a characteristic of human (or social/societal) and natural systems exhibiting a capacity to withstand and recover from an adverse shock or event Keck & Sakdapolrak, 2013). In towns and cities, resilience is promoted through planning while in nature, this trait is assumed inherent (Meadows, 2008; National Research Council, 2012). While societal and ecological resilience are highly dependent on one another, an examination of resilience literature reveals that one is often described without appreciation of the other or in the context of their opposing roles (Handmer et al., 2012). Similarly, previous research suggests that positive aspects of county and community quality of life are linked to not only built environments but natural ones as well (Smith et al., 2012; Summers et al., 2012). Any discussion of resilience would be incomplete without considering the role of natural ecosystems, as they could influence many of a county's and community's vulnerability and recoverability characteristics (Summers et al., 2016, 2012, 2014).

In the context of the research presented here, vulnerability describes the propensity or predisposition to be adversely affected while resilience describes the ability of a system and its component parts to anticipate, absorb, accommodate, or recover from the effects of a hazardous event in a timely and efficient manner (Intergovernmental Panel on Climate Change, 2012). Much of the existing resilience literature focuses on either vulnerability (risk) or recovery (e.g., Cutter et al., 2003; Frazier et al., 2014) as independent constructs of resilience. Summers, Smith, et al. (2017) suggest that a more holistic relationship exists, where an intersection of vulnerability and recoverability sits along a spectrum of resilience. The position of human and natural systems along this gradient reflects their ability or capacity for resilience. In terms of natural hazards, for example, both people and nature can absorb, recover from, and adapt to adverse events (Berkes & Ross, 2013; Gunderson, 2010); however, the degree of resilience is reflected in their mechanisms for recovery. This leads to the concept of basic resilience and recovery potential. Basic resilience can be determined by a direct relationship between risk of a natural hazard occurring and planning, regulation, and training by a community to be ready to face that risk (governance). Thus, basic resilience could be characterized by ratio of level of governance to the likelihood of risk (governance/risk). Similarly, a community's ability to recover from the realization of a natural, hazard event can be exacerbated or diminished by local factors relating to the social structure of the community, the natural environment, and the built environment (Berkes et al., 2003; O'Brien et al., 2009; Pelling & Manuel-Navarette, 2011). These concepts of basic resilience, adaptation, and transformation are included in the development of Natural Hazard Resilience Screening Index (NaHRSI) below.

Ecosystems have innate structures and functions (such as diversity and redundancy) to facilitate recovery from an adverse event (Holling, 1986; Melillo et al., 2014; National Fish, Wildlife and Plants Climate Adaptation Partnership, 2012). Human systems rely on planning and preparation to mitigate known natural hazard exposures and reduce vulnerabilities (Magus, 2010; Tobin, 1999). In both systems, the success of the recovery process is dependent on the robustness of the mechanism. This robustness refers to the system's ability to resist or tolerate change without adapting its initial stable configuration (Meadows, 2008). In the case of nature, ecological conditions may be the factor determining robustness of resilience while the depth and breadth in resilience planning or governance are pillars for resilience in built environments. In the context of governance and risk, the intersection of the status of society and the natural and built environments can modify actual local area resilience to natural hazard events. Understanding how different aspects of resilience reflect a community's capacity for adaptive management is critical for envisioning urban systems and natural ecosystems that can persist through extreme weather events.

A community's ability to endure and recover from abrupt system shocks is an important factor for sustainability. Natural hazard events (e.g., droughts, hurricanes, and floods) can impose long-lasting and significant effects that can impact people and the natural systems on which they depend for sustenance, protection, livelihoods, and recreation. As losses stemming from these events have continued to rise, there has been a notable increase in communities seeking economic, social, and ecological solutions to improve both their sustainability and resilience. The concepts of sustainability and resilience are closely tied as more county and community decision makers recognize that recurring and anomalous weather events may impede achieving their sustainability goals without appropriate and actionable preparation. Therefore, it is not surprising that interest in the subject of resilience related to natural disasters, both cyclic and evolving, is growing.

The concept of resilience has evolved over the past several decades, particularly given the increased interest in preparing for and addressing the current and future challenges we (nations, states, and cities) face, including threats posed by major meteorological events. However, the topic of resilience is a disputed and heavily debated subject regarding anthropogenic and natural systems (Patel et al., 2017). The varying ideas about community resilience generally align, but they are applied differently across the field of resilience research. These differences in application have historically made it difficult for policy makers to identify priorities for improving resilience (e.g., increased governance vs. enhancement of training and economic development, natural resource conservation versus enhancement of social services, and investment in the built environment vs. investment in risk reduction). Despite the differences in conception and application, there are well-understood elements that are widely proposed as important for a resilient community, agreeing that community resilience relates to the sustained ability of a community (a socioecological system) to utilize available resources to respond to, withstand, and recover from adverse difficulties or perturbations (Federal Emergency Management Agency, FEMA, 2011, 2012, 2017; RAND Corporation, 2017).

The NaHRSI was developed using publicly accessible data (e.g., databases available through websites) to help decision makers identify the characteristics that make resilience stronger and weaker. NaHRSI integrates the various viewpoints regarding resilience in terms of potential exposures to natural hazards, governance practices, and the conditions observed in societal, built, and natural systems to inform resilience planning efforts. The index focuses on county-scale measures, the policy action level that is most broadly applicable. While disaster event planning occurs at smaller spatial scales for some urban areas and communities, these data are generally not available for all areas of the Nation. The NaHRSI framework (Summers et al., 2017) serves as a conceptual roadmap to describe the potential impact of natural hazard events impact on a community in the context of exposures and county characteristics. By addressing the factors that influence vulnerability and recoverability, an estimate of resilience can gauge how changes in these characteristics could potentially impact a community's ability to recover from given specific hazard profiles. Ultimately, this knowledge can help communities identify areas to target for improvement to increase their resilience to natural hazard events.

2. Approach

2.1. Conceptualizing Resilience

As part of the conceptualization of NaHRSI, existing community resilience characterization methods and approaches were reviewed with the intent to identify mainstream resilience indicators and indices and determine the applicability of each within the scope of the development of NaHRSI (Summers, Smith, et al., 2017). In summary, an initial search produced 369 print and web publications, which was further reduced by using selected criteria (e.g., quantifiable, integrated, and focus on natural disasters). The resulting pool of 27 published indices representing 57 candidate indicators from this review demonstrated measures that favored an integrated socioeconomic and ecological development approach and showed notable trends toward the use of composite indices for the characterization of community resilience. The 27 published indices and their indicators, in relation to the likely NaHRSI domains, are shown in Table 1.

2.2. Determination of Natural Hazard Event Factors to Be Included in NaHRSI

The National Climate Assessment summarized the current and future impacts of climate change in the United States (http://sca2014.globalchange.gov/report). In the construction of this index, the likely changes in natural hazard events associated with geographic regions throughout the United States were assessed, as well as the infrastructure challenges these changes would likely create. Extended heat waves (with associated drought), more frequent heavy downpours (with associated flooding), sea level rise, enhanced insect outbreaks, increased wildfires, altered timing of streamflow, increased and faster sea ice and glacial loss, and increased major storm events (including hurricanes, tornadoes, and superstorms) were identified as impacts likely to be seen in the coming decade. Similarly, infrastructure issues were identified as likely contributors to the impacts of these weather-related events. Discussions with climate and natural hazard experts in each of the 10 Environmental Protection Agency regions, in conjunction with the information provided by the National Climate Assessment (Melillo et al., 2014) and the 100 Resilient Cities report (ARUP, 2014), yielded 12 natural hazards that would be included in NaHRSI:

GeoHealth

10.1029/2018GH000160

Table 1

Summary of Literature Reviewed Index by Topical Areas of Interest for Development of NaHRSI

NaHRSI Relevance			Literature Review - Selected Index/Framework
Domains of Resilience	Topic of Interest	Candidate Measurement Categories	ARI, AWRVI, BRIC, CRI, CRISLR, CDRI1, CDRI2, CResI, CRIG, CRiskI, MCCR, MCR, MRR, M-RD, M-EI, DRI, EJSI, EPI, ESI, EVI, FRI, FVI, HRI, M-CRD, RFI, RIMM, SSI
Natural Environment	Extent of Natural Areas	• Managed Lands • Ecosystem Type	
	Integrity	• Condition	
Society	Economy	• Economic Diversity • Employment • Insurance	
	Critical Services	• Safety and Security • Social • Labor/Trade	
	Characteristics	• Demographics • Health	
Built Environment	Infrastructure Integrity / Continuity	• Communication • Transportation • Utilities	
	Structure / Housing Characteristics	• Non-Residential • Residential • Shelter	
Governance	Preparedness	• Planning • Investment	
	Response	• Expenditure • Time	
Risk	Losses	• Property • Human	
	Hazard Exposure	• Geophysical • Technology Hazards	

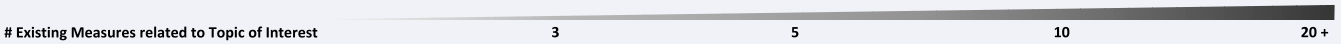

Note. Intensity of color represents the number of potential indicators and metrics (lighter color—lower number to darker color—higher number). The numbers refer to the existing measures related to topic of interest. ARI = Agricultural Resilience Index (Ciani, 2012); AWRVI = Arctic Water Resource Vulnerability Index (Alessa et al., 2008); BRIC = Baseline Resilience Indicators for Communities (Cutter et al., 2014); CRI = City Resilience Index (ARUP, 2014); CRISLR = City Resilience Index to Sea Level Rise (Abdrabo & Hassaan, 2014); CDRI1 = Climate Disaster Resilience Index 2011 (Joerin & Shaw, 2011); CDRI2 = Community Disaster Resilience Index 2010 (Peacock et al., 2010); CResI = Community Resilience Index (Kafle, 2012, Renschler et al., 2010); CRIG = Community Resilience Index for the Gulf of Mexico (Baker, 2009); CRiskI = Community Risk Index (Daniell et al., 2010); MCCR = Composite measure of coastal community resilience (K. Li, 2011); MCR = Composite measure of community resilience (Meher et al., 2011); MRR = Composite measure of regional resilience (Martini, 2014); M-RD = Composite measure of resilience to disasters (Kusumastuti et al., 2014); M-EI = Composite measures of ecological integrity (Vickerman & Kagan, 2014); DRI = Displacement Risk Index (Esnard et al., 2011); EJSI-EJ SCREEN Index (U.S. Environmental Protection Agency, 2015); EPI = Environmental Performance Index (Hsu et al., 2016); ESI = Environmental Sustainability Index (Esty et al., 2005); EVI = Environmental Vulnerability Index (Pratt et al., 2004); FRI = Flood Resilience Index (Batica, 2015); FVI = Flood Vulnerability Index (Balica, 2012); HRI = Household Resilience Index (Cassidy & Barnes, 2012); M-CRD = Metrics for community resilience to disasters (Burton, 2015); RFI = Resilience Factor Index (Ainuddin & Routray, 2012); RIMM = Resilience Inference Measurement model (Lam et al., 2016; C. Li, 2013); SSI = Sustainable Society Index (van de Kerk & Manual, 2014).

1. Hurricanes
2. Tornadoes
3. Inland floods
4. Coastal flooding
5. Earthquakes
6. Wildfires
7. drought
8. High winds
9. Hail
10. Landslides
11. Low-temperature extremes
12. High-temperature extremes

2.3. The NaHRSI Conceptual Framework

No singular approach from the literature survey existing composite measures of natural hazard resilience met all of the expected needs for developing NaHRSI. Collectively, however, the reviewed literature provided many of the building blocks (e.g., suites of indicators, indicator groupings, and domains). A heat map table (Table 1) depicts the distribution of metrics used in the final 27 indices across resilience topics of interest to NaHRSI. To varying degrees, all of the existing indices offered patterns of indicator groupings, which were allocated into five domains to describe overall resilience: natural environment, built environment, society, governance, and risk. None of the indices reviewed provided all possible indicators necessary for the construction of NaHRSI. However, 10 of the reviewed publications included information relevant for describing the NaHRSI domains. Information pertaining to the Natural Environment, governance, and risk domains were most frequently excluded from existing indices. Five indices—BRIC, CDRI1, CDRI2, M-RD, and M-CRD (Burton, 2015; Cutter et al., 2014; Joerin & Shaw, 2011; Kafle, 2012; Kusumastuti et al., 2014; Peacock et al., 2010; Renschler et al., 2010)—offered fairly comprehensive descriptions of indicators relevant for quantifying NaHRSI domains. The Climate Disaster Resilience Index 2011 (CRDI1) contributed the most to the proposed NaHRSI structure, addressing all domains based on a suite of 18 indicators.

The final conceptualization of NaHRSI is discussed in Summers, Smith, et al. (2017) and includes five domains composed of 10 indicators, which, in turn, were derived from 117 unique metrics. Figure 1 depicts the final NaHRSI conceptual framework including the domains and indicators of the index. A summary of the domains, indicators, and types of metrics used in NaHRSI is provided in Table 2. The selection of the domains and indicators are completely described in Summers, Harwell, et al. (2017) and are summarized here for completeness. The domains included in NaHRSI include risk, governance, society, built environment, and natural environment. In accordance with the concept of basic community resilience to natural hazards being driven by the likelihood of an event occurring and the community's preparation for such an event, the domains of risk and governance are included at the base of the conceptual model (Figure 1) to denote basic resilience as some relationship between risk and preparedness. Exposure and losses comprise the indicators for risk (discussed below) and community and personal preparedness (Adager et al., 2005; Linnenluecke et al., 2012; Paton & Johnston 2001) and natural resource conservation (Strickland-Munro et al., 2010; Tompkins & Adger, 2004) represent the indicators for governance. Twenty metrics contribute to the two indicators for the risk domain and five metrics contribute to the three indicators for the governance domain (Table 2).

The remaining domains include elements that could exacerbate or diminish the vulnerability and recovery potentials of a community to an event or postevent. These include society, built environment, and natural environment. Societal indicators that can modify vulnerability or recovery include availability of social services (Dominelli, 2013), the type of available labor or trades within the community (Kirrane et al., 2013), safety and security requirements (Christopher & Peck, 2004; Keim, 2008), the socioeconomics and economic diversity of the community (Klein et al., 2003, Linnenluecke et al., 2012), the health characteristics and availability of health care access in the community (Ebi, 2011; Oven et al., 2012), basic demographic information concerning the community (Balbus & Malina, 2009), and the cohesiveness of the community (Baldwin & King, 2018; Meitzen et al., 2018; Sanchez et al., 2017). Fifty metrics are utilized to describe these indicators of society (Table 2). Built environment indicators that can modify vulnerability or recovery include multiple

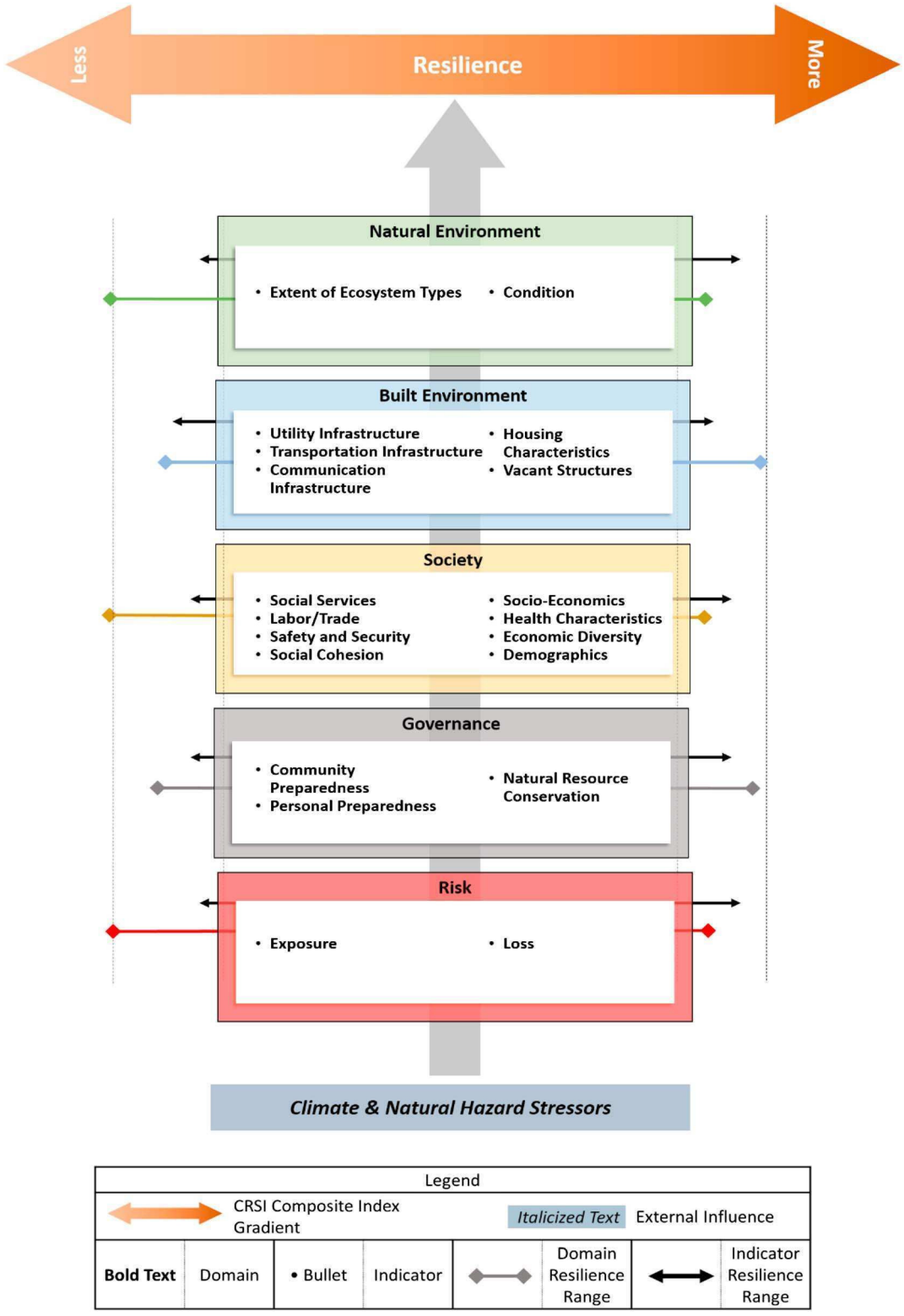

Figure 1. Final Natural Hazard Resilience Screening Index conceptual framework. Arrows projected from boxes to the left and right represent hypothetical increases and decreases in ranges for indicators (black arrows) and domains (colored arrows). CRSI = Climate Resilience Screening Index.

Table 2
List of NaHRSI Domains, Indicators, Scope, and Number of Metrics

Domain	Indicator(s)	Metric(s)
Built Environment (5/24)	Communication Infrastructure	Communication continuity (7)
	Housing characteristics	Structure vulnerability (5)
	Transportation infrastructure	Transportation flow continuity (6)
	Utility infrastructure	Utility continuity (3)
	Vacant structures	Structure vulnerability (3)
Governance (3/5)	Community preparedness	Community resilience strengthening (2)
	Natural resource conservation	Natural Resource Recovery (1)
	Personal preparedness	Personal property hazard protection (2)
Natural Environment (2/18)	Condition	Biodiversity, using birds as a proxy (1)
		Coastal condition (1)
		Forest condition (1)
		Inland lake condition (1)
		Percentage of clean air days (1)
		Rivers and streams condition (1)
		Soil growth suitability (1)
		Soil productivity (1)
		Wetlands condition (1)
	Extent of ecosystem types	Agriculture area (1)
		Forested area (1)
		Grassland area (1)
		Inland surface water area (1)
		Marine/estuarine area (1)
		Perennial ice/snow area (1)
		Protected areas (1)
		Tundra area (1)
		Wetland area (1)
Risk (2/20)	Exposure	Earthquake probability (1)
		Extreme high temperature incidents (1)
		Extreme low temperature incidents (1)
		Flood probability (2)
		Hailstorm probability (1)
		Tornado probability (2)
		Hurricane probability (2)
		Landslide probability (1)
		Major toxics presence (1)
		Non-storm damaging wind incidents (1)
		Nuclear presence (1)
		RCRA sites (1)
		Superfund sites (1)
		Toxic release presence (1)
		Wildfire probability (1)
	Loss	Developed area loss (includes human and property measures) (1)
		Natural area loss (1)
		Dual-benefit area loss (includes cropland and managed area measures) (1)
Society (8/50)	Demographics	Vulnerable population (5)
	Economic diversity	Economic stability/recovery (2)
	Health characteristics	Health problems that may impact personal Resilience (9)
	Labor and trade services	Construction recovery (8)
	Safety and security	Provisioning of emergency and civil services (4)
	Social cohesion	Access to social support (4)
	Social services	Access provisioning to critical services (15)
	Socioeconomics	Employment opportunity (1)
		Personal economics (2)
Built Environment (5/24)	Communication infrastructure	Communication continuity (7)
	Housing characteristics	Structure vulnerability (5)
	Transportation infrastructure	Transportation flow continuity (6)
	Utility infrastructure	Utility continuity (3)
	Vacant structures	Structure vulnerability (3)
Governance (3/5)	Community preparedness	Community resilience strengthening (2)
	Natural resource conservation	Natural resource recovery (1)

Table 2 *(continued)*

Domain	Indicator(s)	Metric(s)
	Personal preparedness	Personal property hazard protection (2)
Natural Environment (2/18)	Condition	Biodiversity, using birds as a proxy (1)
		Coastal condition (1)
		Forest condition (1)
		Inland lake condition (1)
		Percentage of clean air days (1)
		Rivers and streams condition (1)
		Soil growth suitability (1)
		Soil productivity (1)
		Wetlands condition (1)
	Extent of ecosystem types	Agriculture area (1)
		Forested area (1)
		Grassland area (1)
		Inland surface water area (1)
		Marine/estuarine area (1)
		Perennial ice/snow area (1)
		Protected areas (1)
		Tundra area (1)
		Wetland area (1)
Risk (2/20)	Exposure	Earthquake probability (1)
		Extreme high temperature incidents (1)
		Extreme low temperature incidents (1)
		Flood probability (2)
		Hailstorm probability (1)
		Tornado probability (2)
		Hurricane probability (2)
		Landslide probability (1)
		Major toxics presence (1)
		Non-storm damaging wind incidents (1)
		Nuclear presence (1)
		RCRA sites (1)
		Superfund sites (1)
		Toxic release presence (1)
		Wildfire probability (1)
	Loss	Developed area loss (includes human and property measures) (1)
		Natural area loss (1)
		Dual-benefit area loss (includes cropland and managed area measures) (1)
Society (8/50)	Demographics	Vulnerable population (5)
	Economic diversity	Economic stability/recovery (2)
	Health characteristics	Health problems that may impact personal Resilience (9)
	Labor and trade services	Construction recovery (8)
	Safety and security	Provisioning of emergency and civil services (4)
	Social cohesion	Access to social support (4)
	Social services	Access provisioning to critical services (15)
	Socioeconomics	Employment opportunity (1)
		Personal economics (2)

Note. Numbers in parentheses for domains show the total number of indicators/total metrics in the domain. Numbers in parentheses for metrics for number of metrics. RCRA = Resource Conservation and Recovery Act.

infrastructure elements—communications (Martins et al., 2017; Wang & Wang, 2017; Zimmerman, 2017), utilities (Ma et al., 2018; Panteli & Mancarella, 2017; Zimmerman et al., 2017), and transportation (Linnenluecke et al., 2012; Wedawatta et al., 2010)—and housing characteristics (Cutter et al., 2008; Dominelli, 2013; Henstra, 2012; Smoyer, 1998). Twenty-four metrics are compiled to represent the built environment (Table 2). The natural environment domain describes the resilience of natural and managed ecosystems through measures of ecosystem extent (Adager et al., 2005; Foley et al., 2005; Smit et al., 2000) and condition (Foley et al., 2005; Stenseth et al., 2002; Walther et al., 2002). Eighteen metrics are combined to represent the indicators within the natural environment domain (Table 2).

Metric data are documented in Appendix A of Summers, Harwell, et al. (2017). This appendix characterizes the sources of the metric data, their ranges, and their directional relationship to the indicator and provided box-and-whisker plots of the county-level data.

2.4. Data Collection and Preparation

Secondary data from established, publicly accessible sources served as the data foundation in the development of NaHRSI. Nationally consistent, county-level, or equivalent-scale data available within the 2000–2015 time frame were targeted for culling. Where county-level data were not available (i.e., condition of ecological systems by county), imputed values were calculated to achieve desired spatial unit representation. In short, ecosystem condition data were only available from national probabilistic surveys. These data were imputed to provide an estimate of condition of each ecosystem type in each county. Metadata were reviewed to ascertain appropriateness for use in NaHRSI. Collected data were age, population, or land area weighted, as appropriate.

Ecological and distance-factored metrics were interpolated using the inverse distance weighting method to arrive at the spatial unit of interest (county). Distance weighted values were derived using preset distance buffers. Buffer values varied from 50 to 100 miles (roughly 80 to 160 km) depending on the ecological resource or attribute the data represented.

Finally, all standardized values were geolocated to county. Because contributed data were not annually consistent, standardized values were averaged across years within each county or county-equivalent unit. Mean data were normalized on a 0 to 1.0 scale to form the metric basis for NaHRSI. The complement of data represents 3,135 of 3,143 counties and county equivalents, excluding eight boroughs from Alaska that were not represented from secondary data sources.

2.5. Calculations

2.5.1. Risk Domain

The risk domain is a probabilistic calculation based on data provided by a partially derived multihazard model using proportional land area exposure extent and accompanying losses data described in Buck et al. (2018) and Summers et al. (2017). The metrics include historical and modeled exposures, basic likelihood of proximal exposures, potential anthropogenic exposures, and losses. All standardized exposure metrics summed for each county or county equivalent to calculate the exposure indicator. The loss indicator was derived from the sum of standardized loss values stemming from natural hazard events that included human, property, and crop monetary losses plus losses of natural lands to human development. Other sources of potential losses occur (e.g., costs of business activities lost and tourism dollars lost), but no broadly applicable data exist for these potential sources of loss. The risk domain measures were calculated for each county as the exposure indicator value multiplied by the loss indicator value. The approach used to calculate the risk domain scores is presented in Figure 2.

2.5.2. Built Environment, Governance, Natural Environment, and Society Domains

Indicators and domains, with the exception of risk (discussed separately), were derived using the following approach:

1. Metric data were adjusted for age, population, or spatial area, as appropriate, prior to standardization (e.g., number of hospitals in a county adjusted by the population of the county).
2. Indicator scores were determined using the average of related standardized metric values, and each indicator was standardized using the calculated range of the indicator.
3. Domain scores were determined from the average of appropriate standardized indicator values and then standardized in preparation for the final NaHRSI calculation.

2.5.3. The Final Steps to NaHRSI

All domains for each county, parish, and borough (all referred to as county below) were min-max standardized on a scale from 0.01 to 0.99. The final NaHRSI calculation begins as a scaled value for recoverability/vulnerability derived from governance and risk (basic resilience) with the basic resilience value being adjusted by the remaining domain scores for social, built environment, and natural environment to represent enhancement of or diminution of basic resilience to complete the calculation of NaHRSI as shown below:

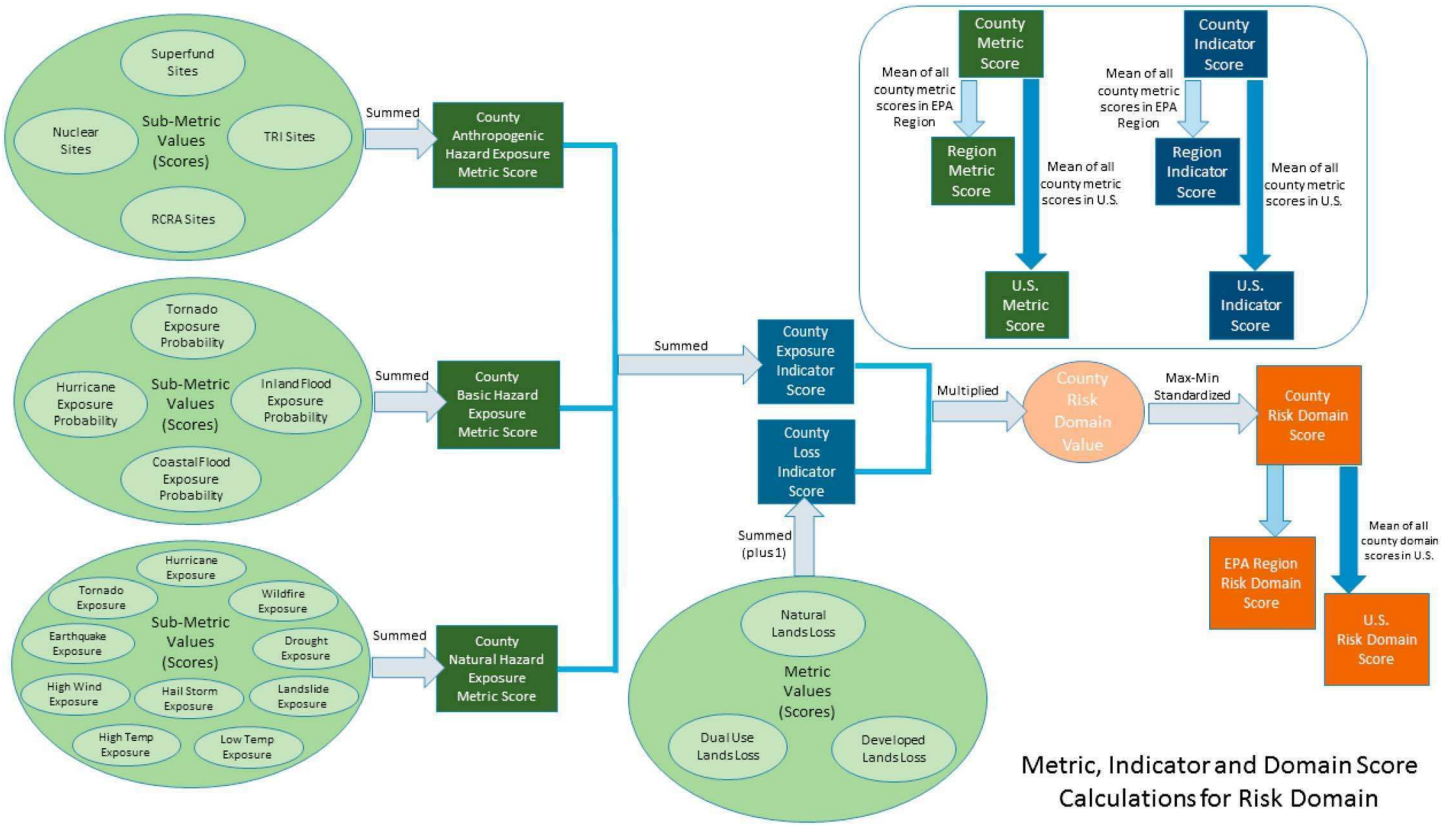

Figure 2. Representation of the metric, indicator, and domain scores for risk domain of Natural Hazard Resilience Screening Index.

$$CRSI(B)i = {}^{Ri}/_{Vi} = {}^{Govi}/_{Riski}$$

where NaHRSI$(B)_i$ = value of basic resilience (recovery/vulnerability or R_i/V_i) and R_i/V_i = governance in county *i*/risk in county *i*. The overall NaHRSI score is calculated as follows:

$$CRSIi = (\text{Gov}i + \text{Soc}(a)i\text{Gov}i + \text{BE}(a)i\text{Gov}i + \text{NE}(a)i\text{Gov}i)/\text{Risk}i$$

where NaHRSI$_i$ = the value of NaHRSI or adjusted resilience for county *i* and Soc$(a)_i$, BE$(a)_i$, and NE$(a)_i$ are the adjustment multipliers for society, built environment, and natural environment in each county *i* and Risk$_i$ is the risk score for county *i*. The adjust factors are calculated as follows:

$$Soc(a)i = {}^{(Soci-Socm)}/_{Socm}$$

where $Soc(a)_i$ is the adjustment multiplier for society in county *i*, Soc_i is the social domain score for county *i*, and Soc_m is the median social domain score for all counties:

$$BE(a)i = {}^{(BEi-BEm)}/_{BEm}$$

where $BE(a)_I$ is the adjustment multiplier for built environment in county *i*, BE_i is the built environment domain score for county *i*, and BE_m is the median built environment domain score for all counties:

$$NE(a)i = {}^{(NEi-NEm)}/_{NEm}$$

and where $NE(a)_I$ is the adjustment multiplier for natural environment in county *i*, NE_i is the natural environment domain score for county *I*, and NE_m is the median natural environment domain score for all counties.

The domains were weighted equally in the calculation of NaHRSI. An initial analysis was performed to assess whether the NaHRSI results associated with basic resilience (governance and risk) varied in a predictable way. Plotting the domain values of risk versus governance would, from a policy standpoint, be expected to have a positive relationship—greater risk should be accompanied by greater governance. This examination of a positive relationship between risk and governance was tested in three ways: (1) assessment analysis of risk domain versus governance domain scores, (2) examination of the cumulative distribution function of basic resilience (governance/risk), and (3) mapping basic resilience to examine potential patterns.

3. Results

3.1. Analyses of Basic Resilience (Governance/Risk)

An assessment of basic resilience is represented by the ratio of governance domain score to the risk domain score (governance/risk). The expected result of the assessment is a 45° angle from low risk-low governance to high risk-high governance. This finding would demonstrate that governance is developed in proportion to risk. Significant deviation from this finding could reflect an underreaction or overreaction to risk in terms of governance activities. Placing results into quantiles allows characterization of clusters of counties as overreacting or underreacting to risk in terms of governance. In this categorical relationship, generally any combination of risk and governance along the 45° angle (slope = 1.0) plus or minus one category would be in the expected range. A combination of high risk and low governance would suggest underreacting, whereas low risk and high governance would suggest overreacting. Mapping these risk-governance ratio categories by county demonstrates any clustering throughout the United States to detect spatial trends.

The assessment results based on normalized risk and governance domains are shown in Figure 3. These results indicate that the governance score is generally higher than the risk score. Only 181 counties (5.8% of the U.S. counties) have risk scores greater than their governance scores. This suggests that governance activities in the vast majority of counties outweigh the risk of exposure to extreme natural hazard events. This high governance to risk ratio is largely driven by a large number of counties with lower levels of risk to devastating natural hazard events. Figure 4 depicts four management action types: low risk-high governance (A), high risk-high governance (B), low risk-low governance (C), and high risk-low governance (D). Types B and C likely represent situations where the level of governance is commensurate with the level of risk. Type A represents the largest number of counties and indicates a level of governance that exceeds the probable level of risk. Type D indicates a level of governance that is significantly less than the level of risk. Type D counties are those most likely to demonstrate poor basic resilience to natural hazard events and would benefit from increased governance measures.

The distribution of basic resilience for the counties was examined using a ratio of the governance-risk domain scores to determine the roughly 500–1,000 counties with the largest risk to governance disparities. Figure 4 shows the county data from the assessment as a cumulative distribution function of basic resilience (governance/risk). Roughly 6% of counties have a basic level of resilience less than 1.0 indicating that risk is greater than governance suggesting that these counties could be poorly resilient to a natural hazard event. About 56% of counties have basic resilience scores of greater than 2.0 basic resilience suggesting clearly sufficient governance for the likely level of risk. While this result suggests that most counties in the United States would be resilient to natural hazard events, it can be misleading as will be discussed in the next section. The remaining percentage of counties (38%) with basic resilience values between 1 and 2 represent counties with a greater potential to demonstrate inadequate planning given their likely risk. Counties in this category (basic risk scores between 1 and 2) are characterized as more likely to depend on their community and natural resources to provide the adequate services to improve overall resilience.

These county basic resilience scores were mapped to explore the spatial distribution of the quintiles for any potential trends (Figure 5). Areas with the highest basic resilience scores tend to be in the northeast and scattered through Midwest. Areas with the lowest basic resilience scores appear along the West Coast in the southeast and Appalachia. Four counties ($<$1% of total) showed very low basic resilience scores of $<$0.25. All of these counties are located in the southeast. Twenty-three counties demonstrated risk scores that were twice their governance scores (i.e., $<$0.5) and again were predominantly located in southeast and lower Midwest. Eighty counties had basic resilience scores $<$0.75 where the southeast contained 90% of the

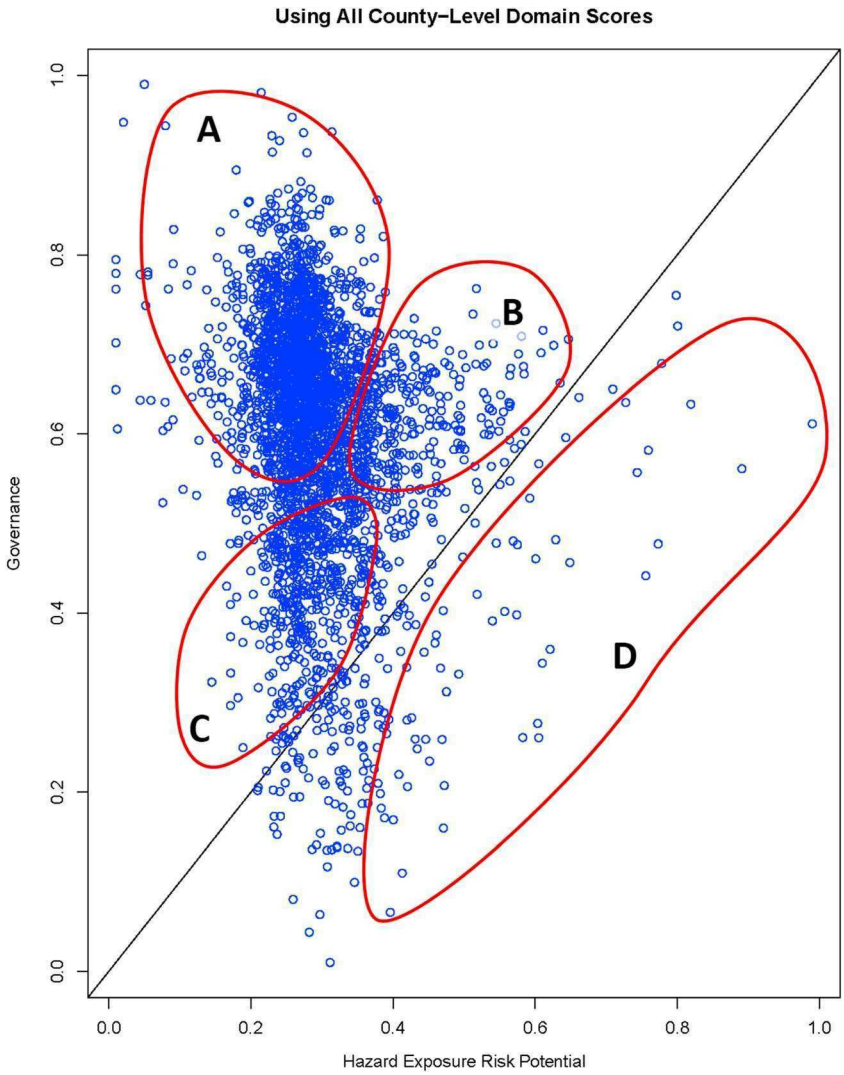

Figure 3. Linear assessment of risk versus governance based on domain scores. Ellipses represent differing management implications with A: low risk-high governance (little increased governance necessary other than improvements for selected below-average indicators; B: high risk-high governance (likely appropriate governance but any improvement in below-average indicators a likely improvement to resilience); C: low risk-low governance (likely appropriate governance for level of potential risk; D: high risk-low governance (improvements to governance and indicator of the Natural Hazard Resilience Screening Index domains necessary).

counties with the remaining counties in far west and southwest. Of all the counties in the United States with basic resilience scores <1 (risk exceeded governance), 85% were in the southeast), 9% the south central and southwest, 4% in the west, and $<$ 1% in the Midwest.

3.2. National NaHRSI Results

Basic resilience is modified by social aspects and structures, the built environment, and the natural environment to represent overall resilience (the NaHRSI score). If these attributes are strong, then resilience (mainly through recoverability) is enhanced. If these attributes are weak, then resilience for an area is reduced. The following national results sections examine basic resilience as modified by societal, natural environment, and built environment factors to determine an overall NaHRSI score. These scores were examined both including and excluding the boroughs of Alaska. This modification was deemed prudent given the mixed levels of data available for the Alaskan boroughs (some boroughs had all levels of data while others did not).

The U.S. NaHRSI score is 2.71 based on the average of NaHRSI scores for all counties in the United States, excluding Alaska, ranging from -2.13 to 14.10 (including Alaska increases the max to 189.17). The NaHRSI

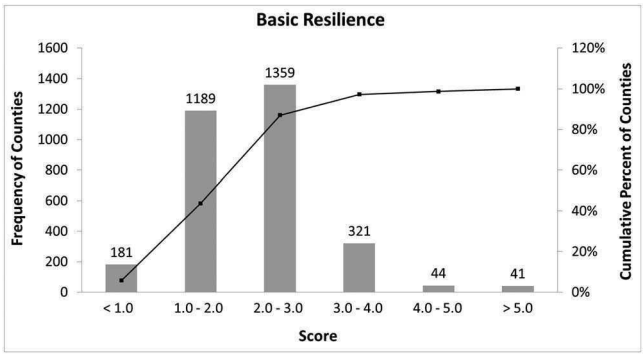

Figure 4. Distribution of county basic resilience scores (governance/risk). Bars equal frequency of basic resilience score for counties. Line indicates cumulative percentage of counties. Number represents number of counties in the basic resilience score range.

and domain scores for the nation are shown in Table 3. The distribution of overall NaHRSI values and the domain scores by county for the United States are shown in Figure 6. Examples of inferences that can be made from the maps are the following:

1. The western United States (east of the Rockies), the Great Lakes area, and the upper northeast have higher NaHRSI values (higher resilience to natural hazard events).
2. The western Midwest, the southeast, the southwest, and Appalachian region have lower NaHRSI values.
3. The lower northeastern coastal area, southeast/Gulf coasts, a small area associated with southern Lake Michigan, and southern far west have the highest risk domain scores albeit for different types of natural hazard events. Lower risk scores for natural hazard events are seen in the west and upper Midwest, Alaska, and Hawaii.
4. Higher governance scores are seen in the northeast, Mid-Atlantic, and Great Lakes areas of the U.S. lower governance scores related to natural hazards were observed in Appalachia, the deep south, and selected counties in the far west.
5. Higher society scores are seen in the upper Midwest and mountain west. Lower society scores are seen in Appalachia and the deep south.
6. Both built and natural environment domain scores were higher in the west, parts of deep south, and lower in the western Midwest and parts of the southeast.

Examining the 150 counties in the United States with the highest NaHRSI values, the Pacific Northwest, and Alaska have the most counties (48 counties of which 19 are in Alaska) followed by the upper west (44), the upper Midwest (23), and the northeast (14). Only the southeast and Mid-Atlantic areas do not have any counties in the top 150 NaHRSI county list. This provides state and counties with lower NaHRSI scores with several example counties to use as role models for the improvement of their scores. The 150 counties with the lowest NaHRSI scores are predominated by the southeast (86 counties) followed by the Mid-Atlantic (33), the south central United States, (13), the Midwest (9), and the Rocky Mountain states (7).

Risk due to natural hazard events across the United States is examined in more detail in Figure 7. The lowest risk domain scores all occur in Alaska, but if Alaska is excluded, the five lowest risk scores occur in the northwest (Montana, Idaho, and Washington). The highest risk scores occur throughout the United States, with two counties in Texas and one each in Colorado, Georgia, and Virginia. Natural exposures due to natural hazard

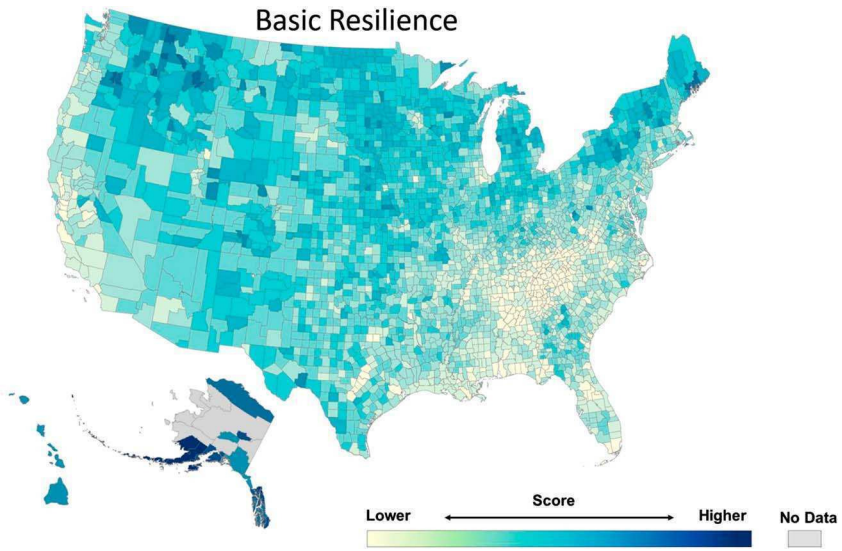

Figure 5. Map of the distribution of county scores for basic resilience.

Table 3
Summary of NaHRSI and Domain Scores for the United States, Both With and Without Alaska

Region	Inclusions and Exclusions	Risk	Governance	Built environment	Natural environment	Society	NaHRSI
National Average	Including Alaska	0.29590	0.59674	0.39320	0.41333	0.51561	2.71349
	Excluding Alaska	0.29758	0.59575	0.39262	0.41182	0.51587	2.37534

Note. NaHRSI = Natural Hazard Resilience Screening Index.

events are predominated by drought (99% of counties experiencing drought), extreme high and low temperatures (100%), inland flooding (99%), high winds (98%), and hail (98%). In short, the meteorological events depicted in NaHRSI, for the 2000–2015 period, are experienced largely throughout the United States with the exceptions of wildfires (52% of counties), landslides (39%), earthquakes (12%), coastal flooding (11%), and hurricanes (8%). Other types of anthropogenic exposure that could exacerbate natural hazard events impact most counties. Resource Conservation and Recovery Act sites and Toxic Release Inventory sites dominate the technological exposure indicator at 71% and 87%, respectively. Superfund sites were seen in 28% of counties, while nuclear facilities were located in 5% of counties. Losses due to natural hazard events of human life, property, and natural ecosystems occur in almost all counties, while losses of crops have occurred in 73% of counties.

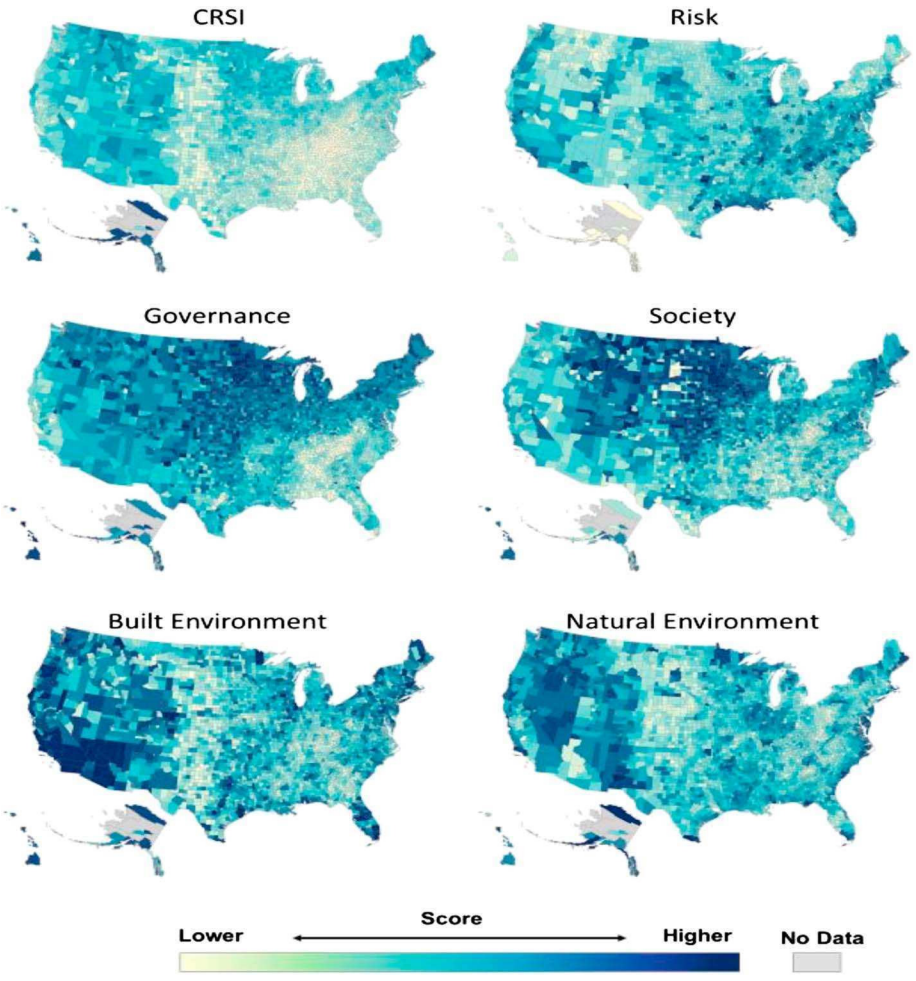

Figure 6. National Natural Hazard Resilience Screening Index values and domain scores (risk, governance, society, built environment, and natural environment). CRSI = Climate Resilience Screening Index.

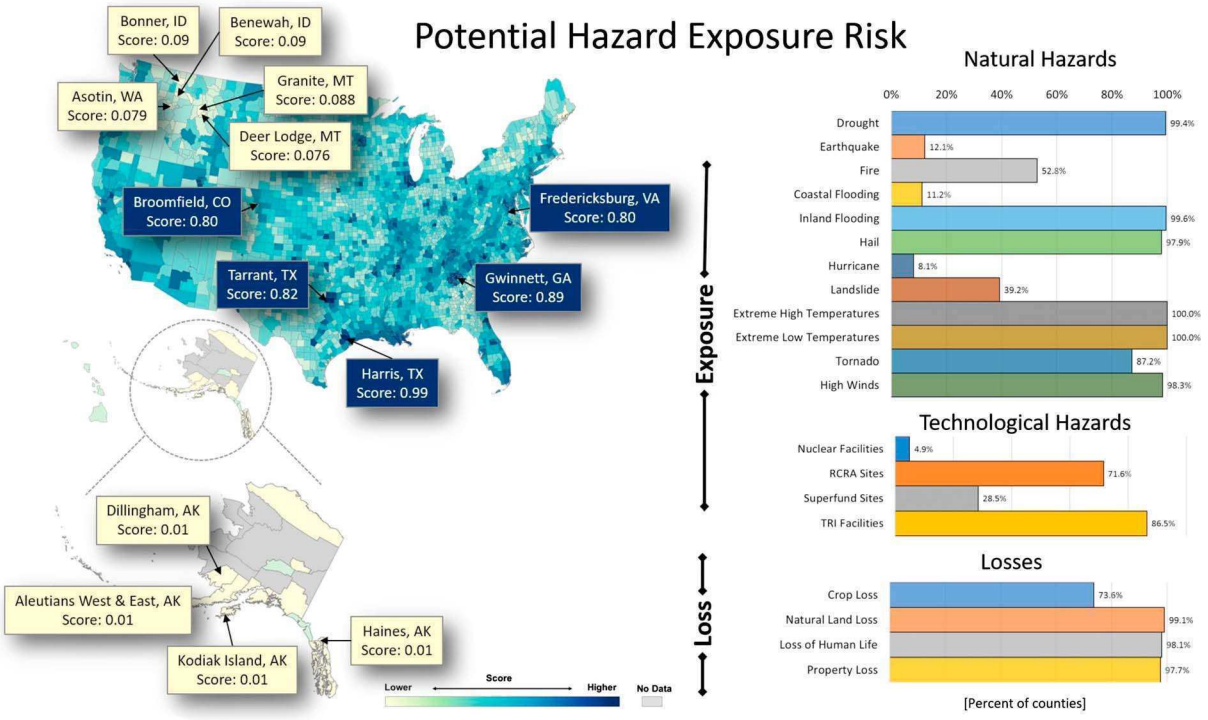

Figure 7. Map of risk domain scores delineating the five counties with the highest risk domain scores and the four lowest risk domain scores (all in Alaska) and the five lowest scores excluding Alaska. The percentage of counties experiencing each of the 11 natural hazard event types, the 4 technological hazards, and losses of human life and property. RCRA = Resource Conservation and Recovery Act; TRI = Toxic Release Inventory.

The contributions of the 20 indicators to the national domain scores are shown in Figure 8. Natural resource conservation (governance), number of vacant structures and housing characteristics (built environment), as well as demographic characteristics (society) most strongly influenced national domain scores. Secondary influences included levels of exposure (risk), socioeconomic characteristics, social cohesion, and economic diversity in the society domain, community, and personal preparedness (governance) and acreage of ecosystem types (natural environment).

4. Discussion

Every year, U.S. counties and communities face devastating losses caused by weather-related disasters. Fires, floods, storms, other hazards, and their associated consequences have significant impacts on counties and communities, especially, their economies, infrastructures, and the environments. The United States has recently experienced a number of large-scale and devastating natural disasters, including catastrophic wildfires, far-reaching floods, and damaging storms. The increasing prominence of extreme weather events makes it critical for governments, businesses, and individuals to examine their anticipatory adaptation and organizational resilience to these events (Linnenluecke et al., 2012). The private sector and all levels of government are embracing resilience as a holistic, proactive framework to reduce vulnerabilities, improve services, adapt to changing conditions, and empower citizens (e.g., National Disaster Resilience Competition; Housing and Urban Development, 2017; Leadership in Community Resilience; National League of Cities, 2016, 2017).

Unlike other resilience estimates, NaHRSI integrates all the major aspects of resilience through its five domains. Overall, NaHRSI values, domain scores, and indicator contributions all paint a picture for the United States of reasonable resilience to natural hazard events. However, the distribution of these scores is broad. While there are many relatively resilient counties in the United States, there are a number of counties in which overall resilience to natural hazard events is low or one or more of the domain scores are low. Therefore, more specific results and analyses should be examined for each of the regions.

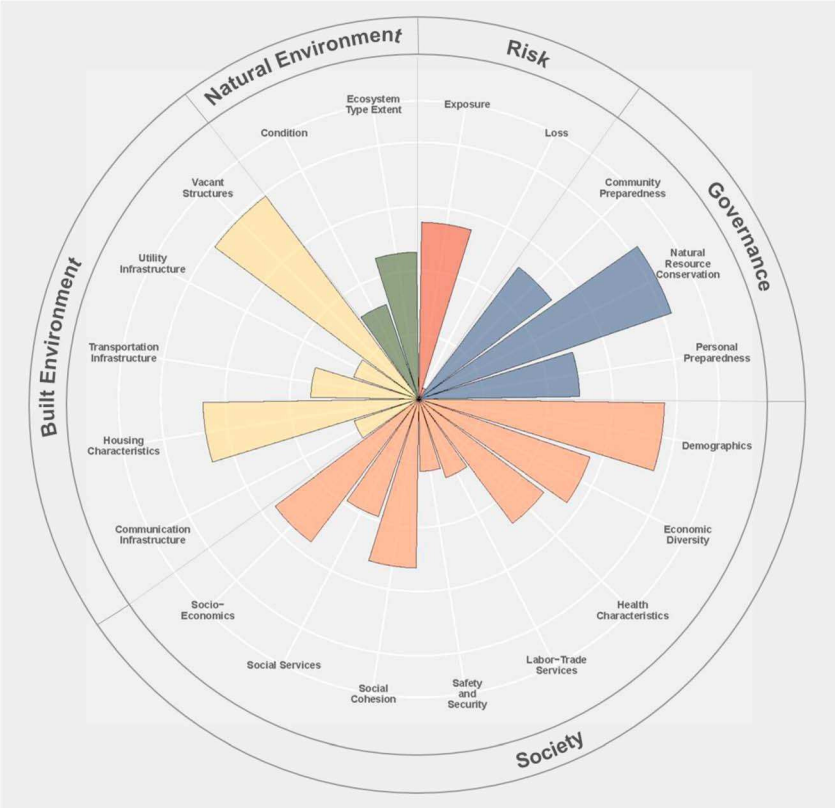

Figure 8. Polar plot showing the contribution of the 20 indicators associated with the domain scores for the nation. The length of the bars corresponds to the indicator score. Within a domain, the higher indicator scores show a greater contribution to the domain.

4.1. Potential Utility of NaHRSI

For over 50 years, hazards researchers have focused on a series of fundamental questions relating to "How do people respond to environmentgal hazard and what factors influence their choice of adjustments" (Cutter 1996, 2012). There are few examples of comparative measures of community health, well-being, resilience, or condition at the county level (Miringhoff & Miringhoff, 1999). The Social Vulnerability Index in one of the few county-level measures of social vulnerability to environmental hazards (Cutter, 2003).

This present paper outlines the approach and application of an index to examine the resilience of U.S. counties, regions, and the overall nation to natural hazard events, holistically, examining not only risk but including governance, social attributes, the built environment, and aspects of the natural environment. No other efforts to quantify county-level resilience have examined all five of these component domains. A number of studies have examined one or two of the domains, while a few have examined as many as three or four of the domains (see Table 1). BRIC (Baseline Resilience Indicators for communities, Cutter et al., 2014) provides the closest effort that includes all five of the domains. BRIC does not include a probability of risk event measure but does include measures associated with society (social, economic, and community capital indicators), the built, and natural environments and governance.

The highlights of BRIC (Cutter et al., 2014) suggest that inherent resilience and its drivers are spatially variable. Similarly, NaHRSI shows basic resilience (governance and risk) to be spatially variable as well as the recovery potential domains of society, built environment, and natural environment. BRIC demonstrates higher level of inherent resilience in the Midwest and northeast. NaHRSI shows the highest resilience in Alaska and Hawaii (not included in the BRIC assessment), the upper Midwest, northeast, and selected parts of the northwest (in contrast to BRIC). Some of these minor differences are likely due to the inclusion of risk in NaHRSI but not in BRIC. The lowest levels of resilience in BRIC are identified as Texas border counties, Appalachia, and the interior western United States. In NaHRSI, poorest resilience occurs in

Appalachia, much of the southeast, the Western Plains including border and west Texas counties. The extension of lower resilience scores into the southeast in NaHRSI appears to be driven by higher risk scores and lower society scores in this area.

BRIC found that resilience (defined in NaHRSI as the nonrisk domains) and vulnerability (defined in NaHRSI as the risk domain and by Cutter et al., 2008, as Social Vulnerability Index) were statistically related but not the obverse of one another. Clearly, social vulnerability and physical risk are not the same measure but a similar observation can be made for physical risk of a disaster event and resilience to such an event in NaHRSI. The concept used in NaHRSI of basic resilience being the ratio of governance and risk permits some high risk areas to offset that risk by increased governance to enhance resilience, while areas with high risk but lower governance display lower basic resilience.

Further research and application efforts to adapt NaHRSI for use within individual counties and communities would clearly be useful for the development of community-specific resilience plans. The potential of using NaHRSI-related information by state and local staff tasked with assessing resilience in their areas of the counties seems particularly useful. Supporting state and counties to assess risk, governance, societal attributes, the built environment, and natural environment in a holistic manner will be important in further development of local and county-level, and even state, resilience plans. Similarly, at the county level, states and counties can

1. Assess relative risks of differing weather-related events
2. Disassemble NaHRSI to determine why the resilience of certain counties is projected to be low and that of others are projected to be high
3. Provide lessons learned from one county to the next on governance and other activities that have increased local resilience to weather-related events
4. Provide a comparative database permitting one way to assess where investments might have the greatest return in terms of improved resilience
5. Provide a database that can be updated to include the most recent information on the NaHRSI metrics, indicators, and domains so that improvements can be tracked.

4.2. Example of NaHRSI Use—Hurricane Harvey

In August, 2017, Hurricane Harvey had two landfalls in Texas—Rockport, TX, in Aransas County and Port Aransas, TX, in Nueces County. In addition to wind damage, rainfall from Hurricane Harvey resulted in massive flooding in Houston and surrounding areas (Galveston, Harris, and Brazoria Counties) and Beaumont and surrounding areas (Jefferson and Chambers Counties). Some of the worst damage appeared to be in Rockport, a coastal city of about 10,000 that was directly in the storm's path. Many structures were destroyed and Rockport's roads were littered with toppled power poles. Extensive damage was also registered in Port Aransas, TX (site of the second Texas landfall). It is estimated that it will be a long time before the storm's catastrophic damage is repaired. Flooding in the Houston/Beaumont areas is the worst in history, displacing millions of people and with flood waters taking weeks to months to recede. As an exercise, NaHRSI results were examined (after the fact) to determine the magnitude and likely locations of extensive damage and low resilience along the Texas Gulf Coast (Table 4).

Of these counties, NaHRSI scores for Aransas, Calhoun, Chambers, Galveston, Harris, Jackson, Jefferson, and Refugio Counties are significantly below the national average for NaHRSI suggesting lower resilience to natural hazard events. All of these counties, plus Brazoria, Fort Bend, Jefferson, and Nueces, display risk domain scores greater than the national average suggesting a history that includes exposure and potential losses stemming from of major natural hazard events. Aransas, Jackson, and Refugio Counties have significantly reduced built environment domain scores suggesting that if an event were to strike these counties, they would be more likely to suffer significant structural damages as a result of reduced public infrastructure and large proportions of vacant buildings. These three counties also possess society scores below the national average. This could indicate a lack of skills diversity to easily rebuild along with deficient security and security infrastructures. Hurricane Harvey also devastated Port Aransas, TX, in Nueces County. Nueces County has a significantly higher risk domain score than the national average associated primarily with historical hurricane paths. The county is dominated by Corpus Christi, TX, which avoided much of the devastation associated with the hurricane; however, Port Aransas suffered extensive structural damage. Port Aransas

Table 4
NaHRSI and Domain Scores for Select Counties Along the Texas Gulf Coast and National Average Scores (Excluding Alaska)

County		Risk	Governance	Built environment	Natural environment	Society	NaHRSI
Aransas		**0.32889**	0.57259	**0.33419**	**0.52163**	**0.40423**	**1.68467**
Brazoria		**0.38408**	**0.66188**	**0.77630**	**0.54926**	0.52368	**4.22022**
Calhoun		**0.33956**	**0.50474**	**0.43549**	**0.49039**	**0.42868**	**1.79703**
Chambers		**0.41971**	0.61495	**0.51116**	**0.50005**	**0.43950**	**2.13280**
Fort Bend		**0.55134**	**0.64353**	**0.78479**	0.42022	**0.58024**	2.64409
Galveston		**0.47067**	0.61040	**0.60782**	0.40844	0.47196	**2.01258**
Harris		**0.99000**	0.61143	**0.83741**	**0.19155**	0.49091	**1.03005**
Jackson		0.31103	0.58578	**0.33742**	**0.48061**	0.53769	**2.14238**
Jefferson		**0.46213**	**0.53399**	**0.69823**	0.44851	0.52149	2.29798
Matagorda		0.29963	**0.54478**	**0.43992**	**0.50342**	**0.43102**	2.28617
Nueces		**0.32810**	**0.63902**	**0.69866**	0.41923	0.47736	**3.56655**
Refugio		0.31287	**0.63050**	**0.26566**	0.46778	**0.44307**	**1.46869**
San Patricio		0.26694	0.61545	**0.48926**	0.44391	**0.40174**	2.73226
Victoria		**0.23454**	**0.53276**	**0.51231**	**0.51035**	0.54069	**3.82251**
National	Including Alaska	0.29590	0.59674	0.39320	0.41333	0.51561	2.71349
Average	Excluding Alaska	0.29758	0.59575	0.39262	0.41182	0.51587	2.37534

Note. Bold denotes significantly below national average for NaHRSI and above national average for domains. NaHRSI = Natural Hazard Resilience Screening Index.

is likely much more similar to Rockport, TX, in Aransas County, which demonstrates a significantly lower than average NaHRSI score.

The other counties with lower NaHRSI scores—Harris (1.03), Calhoun (1.79), Galveston (2.01), Chambers (2.13), and Jefferson (2.29)—all show high risk domain scores well above the national average. The Harris County risk score (the highest in the United States) is exacerbated by significant anthropologic risks located there (e.g., chemical and oil refinery facilities and Superfund sites). Chambers County, located southeast of Harris county, has a lower than average NaHRSI score but a significantly higher than average risk domain score. Four of these counties are at significant risk for flooding and all four counties significantly flooded due to the intense rainfall associated with Hurricane Harvey. Houston (in Harris County) is reported to have had historic flooding that did not recede for weeks or months in some areas. The region's flat topography, hard clay soil, and sprawl of new development combine to make for a drainage nightmare.

Resilience from the flooding in these counties appears to be driven by differing factors based on the NaHRSI and domain scores. Brazoria County has a higher than average resilience score that appears to be the result simply of a high risk, but all the remaining factors tend to reduce the risk and increase the resilience score to 4.22 (well above the national average). Harris County, on the other hand, has the highest risk scores in Texas (0.99) again associated with flooding and several exacerbating factors. The NaHRSI score for this county in significantly below the national average at 1.03 suggesting recovery from a major event could be a very long process. This lower resilience seems to be driven by a very low natural environment score (0.192) suggesting that increasing development in the last decade and loss of natural lands is significant (particularly to the north and west of Houston). Natural and open lands often provide a buffering impact to natural hazard events. They are usually damaged but tend to recover quickly while reducing the impact of the event on surrounding populated areas. This low level of natural ecosystems in the Houston area (often replaced by impervious surfaces) would enhance the impact of flooding. Chambers and Jefferson Counties also have high risks levels associated with flooding with both counties displaying significantly lower than average resilience scores (Chambers County—2.13 and Jefferson—2.29). However, the remaining domain scores in both counties suggest more rapid recovery than Harris County with Chambers County recovering at a slower rate than Jefferson County.

4.3. Where Can We Go From Here?

Our desire to have counties and communities that are minimally impacted by natural hazard events is nearly impossible without a strong recoverability plan and its execution following an event. These plans and their

execution maintain a community at a significant distance from ecological, economic, and social tipping points (e.g., stability, sustainability, joblessness, social inequity, and ecosystem condition). Little attention has been given to the interconnectedness of the vulnerability and recoverability—the basic aspects of resilience (Summers et al., 2014) as they relate to a community's natural hazard resilience. A community may be naturally vulnerable to natural hazard events or vulnerable through anthropogenic activities, but its resilience to these vulnerabilities is guided by the combination of environmental, social, economic, and governance drivers.

U.S. national, state, and local governments have recognized that an integrated, coordinated, and cooperative effort is required to enhance their capacities to withstand and recover from weather-related disasters and emergencies. A disaster-resilient community is one that works together to understand and manage the risks that it may confront. Resilience to disasters is the joint responsibility of all elements of society, including all levels of business, government, the nongovernment sector and individuals. If all these sectors work together with a shared focus and sense of responsibility, they will be much more effective in developing disaster resilience than the individual efforts of any one sector.

4.3.1. Potential Role of Governments

Governments, at all levels, must play a significant role in improving the nation's resilience to disasters:

1. Developing and implementing effective and useful land management and planning arrangements and other mitigation activities based on risk;
2. Having effective plans and policies in place to provide information to people about how to assess risks and reduce their vulnerability to hazards;
3. Having effective and clear education systems so people understand what choices are available and what the best course of action could be for responding to an approaching hazard;
4. Supporting counties and communities, as well as individuals, to prepare for extreme events;
5. Ensuring the most effective, well-coordinated response from our emergency services and volunteers when disaster hits; and
6. Working in a swift, compassionate and pragmatic way to help counties and communities recover from devastation and to learn, innovate and adapt in the aftermath of disastrous events.

Local, state, and national governments are working collectively to incorporate the principle of disaster resilience into aspects of natural disaster arrangements, including preventing, preparing, responding to, and recovering from disasters. Further future enhancements and local applications of NaHRSI can provide advancements in these disaster-related resilience activities.

The FEMA established the Strategic Foresight Initiative (FEMA 2012) to address the need. This initiative brings together significant elements of the emergency management community to discuss important future issues, trends, and other issues and to work through their implications. Working collaboratively, these groups are beginning to understand the full range of changes they might encounter and the nature of their likely future needs. Therefore, they can begin to develop and execute a shared action agenda for action. One of the first tasks of this initiative group should be to bring together the representative views of all governments, business, nongovernment sector and the community into a comprehensive National Disaster Resilience Strategy. This group should also be tasked with considering further those lessons arising from the recent bushfires, floods, tornadoes, and superstorms that could benefit from national collaboration.

4.3.2. Role of Business

Businesses can and do play a critical role in supporting a community's resilience to disasters. Businesses provide expertise, resources, and many essential services upon which the community depends. Businesses, particularly important infrastructure providers, contribute to understanding the risks that they face and ensuring that they can continue providing services during or soon after a disaster.

Insurance and reinsurance businesses are particularly important to county and community resilience (both planning and after an event). If insurance is not available for an area because of higher risk of a meteorological event or the has not been purchased to cover potential damage due to cost, negative impacts of events to communities and individuals become magnified and extended. Working with the insurance industry so that they more fully accept community resilience approaches could be a major influence for improving overall resilience. Having insurers take into account the efforts that governments take at all levels to enhance resilience to natural disasters could reduce overall costs, impacts, and losses.

4.3.3. Role of Individuals

Community disaster resilience is largely based on individuals taking their share of responsibility for preparing for, preventing, responding to, and recovering from natural hazard disasters. A community's constituents can do this by drawing on the resources, guidance, and policies of local government and community organizations. Individuals' resilience to these types of disasters is significantly increased by active planning and preparation for protecting life and property, including purchasing insurance at reasonable rates to cover potential losses. This planning and preparation should be based on an awareness of the threats relevant to their locality as well as being involved in local community disaster or emergency management arrangements. This involvement can often take the form of volunteerism.

4.3.4. Role of Nongovernment Organizations and Volunteers

Nongovernment and community organizations are at the forefront of strengthening disaster resilience in the United States. It is to them that Americans often turn for support or advice, and the dedicated work of these agencies and organizations is critical to helping counties and communities to cope with, and recover from, a disaster. Building and fostering partnerships between U.S. national, state, and local governments and these agencies and organizations is essential to communicate the disaster resilience message and to explore practical ways to strengthen resilience to natural disasters in the counties and communities they serve. Strengthening the disaster resilience of the United States is not a stand-alone activity that can be achieved in the short term. Similarly, it cannot be achieved without a common commitment and concerted effort by all sectors of society. But it is an effort that is worth making because building a more disaster resilient nation is an investment in our future.

5. Conclusions

The United States has and continues to cope well with natural disasters, through cooperative and established emergency management policies and plans, effective capabilities, and dedicated volunteer and professional personnel. Americans are renowned for their resilience to natural hazard events, including the ability to adapt and innovate a strong community spirit that supports those in need and the self-reliance to recover from disasters. Joint, collective responsibility is needed to build capacities for resilience at multiple scales effectively.

We believe that the use of NaHRSI can help the United States and its regions and counties to promote and address capacity building of resilience to natural hazard events by comparatively examining each county's resilience to these events and the deconstructed make-up of these county NaHRSI scores. Furthermore, using the overall and deconstructed scores can allow government entities charged with resilience capacity building to understand their specific strengths and shortcomings and locate others who have successfully addressed similar shortcomings.

Acknowledgments

The authors would like to acknowledge the remaining members of the NaHRSI team—James Harvey, Justin Bousquin, and Deborah Vivian. All are located at the Gulf Ecology Division, and all have played instrumental roles in the development and application of NaHRSI. The data used to develop NaHRSI are numerous and varied. Over six million data points comprise the characterization of individual metrics, indicators, domains, and eventually the NaHRSI scores. It is impractical to deposit these data in a single location for use by other researchers, and, in fact, some data are proprietary and cannot be posted. However, the sources of all data used in the construction and application of NaHRSI can be found in the NaHRSI (CRSI) report compiled by Summers, Harwell, et al. (2017) as Appendix A. This appendix provides the metadata for all metrics including the original source locations of all data. The views expressed in this article are those of the author(s) and do not necessarily reflect the views or policies of the U.S. Environmental Protection Agency.

References

Abdrabo, M., & Hassaan, M. (2014). *Assessing resilience of the Nile Delta urban centers to sea level rise impacts*. 5th Global Forum on Urban Resilience and Adaptation, Bonn, Germany. http://hdl.handle.net/10625/53873

Adager, W. N., Hughes, T. P., Folke, C., Carpenter, S. R., & Rockstrom, J. (2005). Social-ecological resilience to coastal disasters. *Science*, *309*, 1036–1039.

Ainuddin, S., & Routray, J. K. (2012). Earthquake hazards and community resilience in Baluchistan. *Natural Hazards*, *63*(2), 909–937.

Alessa, L., Kliskey, A., Lammers, R., Arp, C., White, D., Hinzman, L., & Busey, R. (2008). The arctic water resource vulnerability index: an integrated assessment tool for community resilience and vulnerability with respect to freshwater. *Environmental Management*, *42*(3), 523–541.

ARUP. (2014). *City Resilience Framework*. The Rockefeller Foundation, ARUP Development International. https://www.rockefellerfoundation.org/report/city-resilience-framework/

Baker, A. (2009). *Creating an empirically derived community resilience index of the Gulf of Mexico region* (Master of Science Thesis in Department of Environmental Sciences, Louisiana State University, Baton Rouge, LA). Retrieved from https://digitalcommons.lsu.edu/gradschool_theses/1046

Balbus, J. M., & Malina, C. (2009). Identifying vulnerable subpopulations for climate change health effects in the United States. *Journal of Occupational and Environmental Medicine*, *51*, 33–37.

Baldwin, C., & King, R. (2018). *Social sustainability, climate resilience and community-based urban development* (p. 198). London: Routledge.

Balica, S. F. (2012). *Applying the flood vulnerability index as a knowledge base for flood risk assessments* (PhD Thesis, Delft University of Technology, Delft, The Netherlands).

Batica, J. (2015). *Methodology for flood resilience assessment in urban environments and mitigation strategy development* (PhD Thesis, Universite Nice Sophia Antipolis, Nice, France).

Berkes, F., Colding, J., & Folke, C. (2003). *Navigating social-ecological systems. Building resilience for complexity and change*. Cambridge: Cambridge University Press. https://doi.org/10.1017/CBO9780511541957

Berkes, F., & Ross, H. (2013). Community resilience: Toward an integrated approach. *Society and Natural Resources*, *26*(1), 5–20.

Buck, K., Summers, J. K., Hafner, S., Harwell, L., & Smith, L. (2018). Development of a multi-hazard landscape for exposure and risk interpretation: The PRISM approach. *Sustainability and Disaster Risk Management*. https://doi.org/10.2174/2542614101666180514123146

Burton, C. G. (2015). A validation of metrics for community resilience to natural hazards and disasters using the recovery from Hurricane Katrina as a case study. *Annals of the Association of American Geographers*, *105*(1), 67–86.

Carpenter, S., Brock, W., & Hanson, P. (1999). Ecological and social dynamics in simple models of ecosystem management. *Conservation Ecology*, *3*, 4. http://www.consecol.org/vol3/iss2/art4/

Carpenter, S., Walker, B., Anderies, J. M., & Abel, N. (2001). From metaphor to measurement: resilience of what to what. *Ecosystems*, *4*, 765–781.

Cassidy, L., & Barnes, G. D. (2012). Understanding household connectivity and resilience in marginal rural communities through social network analysis in the village of Habu, Botswana. *Ecology and Society*, *17*(4), 11.

Christopher, M., & Peck, H. (2004). Building the resilient supply chain. *International Journal of Logistics Management*, *15*, 1–13.

Ciani, F. (2012). A resilience-based approach to food insecurity: the impact of Mitch Hurricane on rural households in Nicaragua. University of Florence, Department of economics, PhD programme in development economics.

Cutter, S. L. (1996). Vulnerability to environmental hazards. *Progress in Human Geography*, *20*, 529–539.

Cutter, S. L. (2003). The vulnerability of science and the science of vulnerability. *Annals of the Association of American Geographers*, *93*, 1–12.

Cutter, S. L. (2012). Vulnerability to environmental hazards. In S. L. Cutter (Ed.), *Hazards vulnerability and environmental justice* (Chap 6, pp. 71-82). London: Routledge.

Cutter, S. L., Ash, K. D., & Emrich, C. T. (2014). The geographies of community disaster resilience. *Global Environmental Change*, *29*, 65–77.

Cutter, S. L., Barnes, L., Berry, M., Burton, C., Evans, E., Tate, E., & Webb, J. (2008). A place-based model for understanding community resilience to natural disasters. *Global Environmental Change*, *18*, 598–606.

Cutter, S. L., Boruff, B. J., & Shirley, W. L. (2003). Social vulnerability to environmental hazards. *Social Science Quarterly*, *84*(2), 242–261.

Daniell, J. E., Daniell, K. A., Daniell, T. M., & Khazai, B. (2010). *A country level physical and community risk index in the Asia-Pacific region for earthquakes and floods*. Karlsruhe. Germany: Karlsruhe Institute of Technology.

Dominelli, N. (2013). Mind the gap: Built infrastructures, sustainable caring relations, and resilient communities in extreme weather events. *Australian Social Work*, *66*, 204–217.

Ebi, K. L. (2011). Resilience to the health risks of extreme weather events in a changing climate in the United States. *International Journal of Environmental Research and Public Health*, *8*, 4582–4595.

Esnard, A. M., Sapat, A., & Mitsova, D. (2011). An index of relative displacement risk to hurricanes. *Natural Hazards*, *59*, 833–859.

Esty, D. C., Levy, M., Srebotnjak, T., & De Sherbinin, A. (2005). *Environmental sustainability index: Benchmarking national environmental stewardship* (pp. 47–60). New Haven: Yale Center for Environmental Law and Policy.

FEMA (Federal Emergency Management Agency) (2011). A whole community approach to emergency management: Principles, themes, and pathways for action. Department of Homeland Security, FDOC 104–008-1, December 2011. Retrieved from https://www.fema.gov/media-library-data/20130726-1813-25045-0649/whole_community_dec2011__2_.pdf

FEMA (Federal Emergency Management Agency) (2012). Crisis response and disaster resilience 2030: Forging strategic action in an age of uncertainty. Retrieved from https://www.fema.gov/media-library-data/20130726-1816-25045-5167/sfi_report_13.jan.2012_final.docx.pdf

FEMA (Federal Emergency Management Agency) (2017). Draft interagency concept for community resilience indicators and national-level measures. Retrieved from https://www.fema.gov/community-resilience-indicators

Foley, J. A., DeFries, R., Asner, G. P., Barford, C., Bonan, G., Carpenter, S. R., et al. (2005). Global consequences of land use. *Science*, *309*, 570–574.

Frazier, T. G., Thompson, C. M., & Dezzani, R. J. (2014). A framework for the development of the SERV model: A Spatially Explicit Resilience-Vulnerability model. *Applied Geography*, *51*, 158–172.

Government Accountability Office (2017). High-risk series: An update. Report to Congressional Committees. Government Printing Office, GAO-17-317. Retrieved from http://www.gao.gov/assets/690/682765.pdf

Gunderson, L. (2010). Ecological and human community resilience in response to natural disasters. *Ecology and Society*, *15*(2), 18.

Handmer, J., Honda, Y., Kundzewicz, Z. W., & Mechler, R. (2012). Changes in impacts of climate extremes: human systems and ecosystems. In J. Handmer et al. (Eds.), *Managing the risks of extreme events and disasters to advance climate change adaptation* (pp. 231–290). Cambridge, UK and New York, NY: Cambridge University Press.

Henstra, D. (2012). Toward the climate-resilient city: Extreme weather and urban climate adaptation policies in two Canadian provinces. *Journal of Comparative Policy Analysis; Research and Practice*, *14*, 175–194.

Holling, C. S. (1973). Resilience and stability of ecological systems. *Annual Review of Ecology and Systematics*, *4*, 1–23.

Holling, C. S. (1986). The resilience of terrestrial ecosystems: Local surprise and global change. In W. C. Clark & R. E. Munn (Eds.), *Sustainable development of the biosphere* (pp. 292–317). New York: John Wiley.

Hsu, A., Esty, D. C., Levy, M. A., & de Sherbinin, A. (2016). *2016 environmental performance index*. New Haven, CT: Yale University.

Housing and Urban Development (2017). National Disaster Resilience Competition.

Intergovernmental Panel on Climate Change (2012). *Managing the risks of extreme events and disasters to advance climate change adaptation. A special report of Working Groups I and II of the Intergovernmental Panel on Climate Change* (p. 582). Cambridge, UK, and New York, NY: Cambridge University Press.

Joerin, J., & Shaw, R. (2011). Climate and disaster resilience in cities. *Community, Environment and Disaster Risk Management*, *6*, 47–61.

Kafle, S. K. (2012). Measuring disaster-resilient communities: A case study of coastal communities in Indonesia. *Journal of Business Continuity & Emergency Planning*, *5*, 316–326.

Keck, M., & Sakdapolrak, P. (2013). What is social resilience? Lessons learned and ways forward. *Erkunde*, *67*, 5–19.

Keim, M. E. (2008). Building human resilience: the role of public health preparedness and response as an adaptation to climate change. *American Journal of Preventive Medicine*, *35*, 508–516.

Kirrane, C., Sharkey, C., & Naess, L. O. (2013). Shaping strategies: Factors and actors in climate change adaptation. In A. Carrapatoso & E. Kurzinger (Eds.), *Climate-resilient development: Participatory solutions from developing countries* (pp. 43–59). London: Routledge.

Klein, R. J. T., Nicholls, R. J., & Thomalla, F. (2003) Resilience to natural hazards: How useful is this concept? EVA Working Paper No. 9, DINAS-COAST Working Paper No. 14, Potsdam Institute for Climate Impact Research, Potsdam, Germany. Retrieved from http://temis.documentation.developpement-durable.gouv.fr/docs/Temis/0075/Temis-0075362/20080.pdfww

Kusumastuti, R., Husodo, Z. A., Suardi, L., & Danarsari, D. N. (2014). Developing a resilience index towards natural disasters in Indonesia. *International Journal of Disaster Risk Reduction*, *10*, 327–340.

Lam, N., Reams, M., Li, K., Li, C., & Mata, L. (2016). Measuring community resilience to coastal hazards along the northern Gulf of Mexico. *Natural Hazards Review*, *17*(1). https://doi.org/10.1061/(ASCE)NH.1527-6996.0000193

Li, C. (2013). *Community resilience to coastal hazards: An analysis of two geographical scales in Louisiana* (Master of Science Thesis, Louisiana State University, Baton Rouge, LA).
Li, K. (2011). *Temporal changes of coastal community resilience in the Gulf of Mexico region* (Master of Science Thesis, Louisiana State University, Baton Rouge, LA). Baton Rouge: LA.
Linnenluecke, M. K., Griffiths, A., & Winn, M. (2012). Extreme weather events and the critical importance of anticipatory adaptation and organizational resilience in responding to impact. *Business Strategy and the Environment*, *21*, 17–32.
Ma, S., Chen, B., & Wang, Z. (2018). Resilience enhancement strategy for distribution systems under extreme weather events. *IEEE Transactions on Smart Grid*, *9*, 1442–1451.
Magus, K. (2010). Community resilience: An indicator of social sustainability. *Society and Natural Resources*, *23*(5), 401–416.
Martini, B. (2014). *Economic, social and environmental resilience: An analysis for the Italians Regions after 2007. University of Rome Tor Vergata*. Italy: Rome.
Martins, L., Girao-Silva, R., Jorge, L., Gomes, A., Musumeci, F., & Rak, J. (2017). Interdependence between power grids and communications networks: A resilience perspective. DRCN 2017 – Design of Reliable Communications Networks; 13th International Conference, March 8–10, 2017, Munich, Germany.
Meadows, D. H. (2008). *Thinking in systems* (p. 218). White River Junction, VT: Chelsea Breen Publishing.
Meher, M., Patra, H., & Sethy, K. (2011). Creating an empirically derived community resilience index for disaster prone area: A case study from Orissa. Disaster, Risk and Vulnerability Conference, Mahatma Gandhi University. Meghalaya, India.
Meitzen, K. M., Phillips, J. N., Perkins, T., Manning, A., & Julian, J. P. (2018). Catastrophic flood disturbance and a community's response to plant resilience in the heart of the Texas Hill Country. *Geomorphology*, *305*, 20–32.
Melillo, J. M., Richmond, T., & Yohe, G. W. (2014). Climate change impacts in the 11 United States: The third national climate assessment. U.S. Global Change Research Program, 12. Retrieved from http://nca2014.globalchange.gov/report%5d/
Miringhoff, M., & Miringhoff, M. L. (1999). *The Social Health of the Nation* (248 pp.). Oxford: Oxford University Press.
National Fish, Wildlife and Plants Climate Adaptation Partnership (2012). *National fish, wildlife and plants climate adaptation strategy. Association of fish and wildlife agencies, Council on environmental quality*. Washington, DC: Great Lakes Indian Fish and Wildlife Commission, national oceanic and atmospheric administration, and U.S. Fish and Wildlife Service. https://www.wildlifeadaptationstrategy.gov/
National League of Cities (2016). Leadership in community resilience program.
National League of Cities (2017). Webinar: Leadership in community resilience.
National Research Council (2012). *Disaster resilience: A national imperative*. Washington, DC: The National Academies Press.
O'Brien, K. (2011). Responding to environmental change: A new age for human geography? *Progress in Human Geography*, *35*, 542–549.
O'Brien, K., Hayward, B., & Berkes, F. (2009). Rethinking social contracts: building resilience in a changing climate. *Ecology and Society* 14(2), 12. http://www.ecologyandsociety.org/vol14/iss2/art12/
Office of Management and Budget and Council on Environmental Quality (2016). Memorandum for executive departments and agencies: Strengthening climate adaptation planning in fiscal year 2016 and beyond. Memorandum.M-16-09. Retrieved from https://www.whitehouse.gov/sites/whitehouse.gov/files/omb/memoranda/2016/m-16-09.pdf
Oven, K. J., Curtis, S. E., Reaney, S., Riva, M., Stewart, M. G., Ohlemuller, R., et al. (2012). Climate change and health and social care: Defining future hazard, vulnerability and risk for infrastructure systems supporting older people's health care in England. *Applied Geography*, *33*, 16–24.
Panteli, M., & Mancarella, P. (2017). Modeling and evaluating the resilience of critical electrical power infrastructure to extreme weather events. *IEEE Systems Journal*, *11*, 1733–1742.
Patel, S. S., Rogers, M. B., Amlot, R., & Rubin, G. J. (2017). What do we mean by 'community resilience'? A systematic literature review of how it is defined in the literature. *PLOS Currents Disasters*, *1*. https://doi.org/10.1371/currents.dis.db775aff25efc5ac4f0660ad9c9f7db2
Paton, D., & Johnston, D. (2001). Disasters and communities: Vulnerability, resilience and preparedness. *Disaster Prevention and Management: An International Journal*, *10*, 270–277.
Peacock, W. G., Brody, S., Seitz, W., Merrell, W., Vedlitz, A., Zahran, S., et al. (2010). *Advancing resilience of coastal localities: Developing, implementing, and sustaining the use of coastal resilience indicators: A final report*. College Station, TX: Hazard Reduction and Recovery Center, Texas A & M University.
Pelling, M., & Manuel-Navarette, D. (2011). From resilience to transformation: The adaptive cycle in two Mexican urban centers. *Ecology and Society*, *6*, 11. http://www.ecologyandsociety.org/vol16/iss2/art11/
Pratt, C., Kaly U., & Mitchell J. (2004). Manual: How to use the environment vulnerability index. SOPAC Technical Report 383.60 pp. United Nations Environmental Programme (UNEP), South Pacific Applied Geoscience Commission (SOPAC).
RAND Corporation (2017). Community resilience. https://www.rand.org/topics/community-resilience.html
Renschler, C. S., Frazier, A. E., & Miles, S. (2010). *Assessing community resilience: A remote sensing approach to evaluate post-disaster ecosystem recovery*. Buffalo, NY: University of Buffalo.
Sanchez, A. X., Osmund, P., & van der Heijden, J. (2017). Resilient policies for wicked problems: Increasing resilience in a complex and uncertain world through information integration. In A. X. Sanchez, K. Hampson, & G. London (Eds.), *Integrating information in built environments* (p. 36–53). London: Routledge.
Smit, B., Burton, I., Klein, R. T., & Wandel, J. (2000). An anatomy of adaptation to climate change and variability. *Climatic Change*, *45*, 223–251.
Smith, L. M., Case, J. L., Smith, H. M., Harwell, L. C., & Summers, J. K. (2012). Relating ecosystem services to domains of human well-being: Foundation for a U.S. index. *Ecological Indicators*, *28*, 79–90.
Smoyer, K. E. (1998). Putting risk in its place: methodological considerations for investigating extreme health risk. *Social Science & Medicine*, *47*, 1809–1824.
Stenseth, N. C., Mysterud, A., Ottersen, G., Hurrell, J. W., Chan, K., & Lima, M. (2002). Ecological effects of climate fluctuations. *Science*, *297*, 1292–1296.
Strickland-Munro, J. K., Allison, H. E., & Moore, S. A. (2010). Using resilience concepts to investigate the impacts of protected area tourism on communities. *Annals of Tourism Research*, *37*, 499–519.
Summers, J. K., Harwell, L. C., Buck, K. D., Smith, L. M., Vivian, D. N., Bousquin, J. J., et al. (2017). *Development of a Climate Resilience Screening Index (CRSI): An assessment of resilience to acute meteorological events and selected natural hazards*. U.S. Environmental Protection Agency, Washington, DC, EPA600/R-17/238. https://cfpub.epa.gov/si/si_public_record_report.cfm?dirEntryId=337914
Summers, J. K., Harwell, L. C., & Smith, L. M. (2016). A model for change: An approach for forecasting resilience from service-based decisions. *Ecological Indicators*, *69*, 295–309.
Summers, J. K., Smith, L. M., Case, J. L., & Linthurst, R. A. (2012). A review of the elements of human resilience with an emphasis on the contribution of ecosystem services. *Ambio*, *41*, 327–340.

Summers, J. K., Smith, L. M., Harwell, L. C., & Buck, K. D. (2017). Conceptualizing holistic community resilience to climate events: Foundation for a climate resilience screening index. *GeoHealth*, *1*, 151–164.

Summers, J. K., Smith, L. M., Harwell, L. C., Case, J. L., Wade, C. M., Straub, K. R., & Smith, H. M. (2014). An index of human resilience for the US: A TRIO approach. *Sustainability*, *6*(6), 3915–3935.

Tobin, G. A. (1999). Sustainability and community resilience: The holy grail of hazards planning? *Global Environmental Change Part B: Environmental Hazards*, *1*(1), 13–25.

Tompkins, E. L., & Adger, W. N. (2004). Does adaptive management of natural resources enhance resilience to climate change? *Ecology and Society*, *9*, 10. http://www.ecologyandsociety.org/vol9/iss2/art10/

U.S. Environmental Protection Agency (2015). EJSCREEN: Environmental Justice Screening Tool.

U.S. National Security Strategy (2015). National Security Strategy. Retrieved from http://nssarchive.us/wp-content/uploads/2015/02/2015.pdf

van de Kerk, G., & Manuel, A. (2014). *Sustainable Society Index 2014 Report* (Vol. 90). The Hague, Netherlands: Sustainable Society Foundation.

Vickerman, S., & Kagan, J. S. (2014). Assessing ecological integrity across jurisdictions and scales. Institutes for Natural Resources, Oregon Biodiversity Information Center, Portland State University, Portland, Oregon.

Walker, B. (1993). Rangeland ecology: Understanding and managing change. *Ambio*, *22*, 80–87.

Walker, B. H., Carpenter, S. R., Anderies, J. M., Abel, N., Cumming, G. S., Janssen, M. A., et al. (2002). Resilience management in social-ecological systems: A working hypothesis for a participatory approach. *Conservation Ecology*, *6*, 14. http://www.consecol.org/vol16/iss1/art14

Walther, G., Post, E., Convey, P., Menzel, A., Parmesani, C., Beebee, T. J. C., et al. (2002). Ecological responses to recent climate change. *Nature*, *416*, 389–395.

Wang, Z., & Wang, J. (2017). Service restoration based on AMI and networked MGs under extreme weather conditions. *IET Generation Transmission and Distribution*, *11*, 401–408.

Wedawatta, G., Ingirige, B., & Amaratunga, D. (2010). Building up resilience of construction sector SMEs and their supply chains to extreme weather events. *International Journal of Strategic Property Management*, *14*, 362–372.

Zimmerman, R. (2017). Effective public service communication networks for climate change adaptation. In W. L. Filho & J. M. Keenan (Eds.), *Climate change adaptation in North America: Experiences, case studies and best practice* (pp. 241–259). Berlin: Springer.

Zimmerman, R., Zhu, Q., de Leon, F., & Guo, Z. (2017). Conceptual modeling framework to integrate resilient and interdependent infrastructure in extreme weather. *Journal of Infrastructure Systems*, *23*, 04017034.

frontiers in Environmental Science

ORIGINAL RESEARCH
published: 30 November 2018
doi: 10.3389/fenvs.2018.00147

Regionalizing Resilience to Acute Meteorological Events: Comparison of Regions in the U.S.

Kevin Summers, Linda Harwell, Lisa M. Smith and Kyle D. Buck*

Gulf Ecology Division, National Health and Environmental Effects Research Laboratory Office of Research and Development U.S. Environmental Protection Agency, Gulf Breeze, FL, United States

Using a Climate Resilience Screening Index (CRSI) that was developed to represent resilience to acute weather events at multiple scales for the United States, nine regions of the United States are compared for resilience for these types of natural hazards. The comparison examines the domains, indicators, and metrics of CRSI addressing environmental, economic, and societal aspects of resilience to acute climate events at county scales. The index was applied at the county scale and aggregated to represent select regions of the United States. Comparisons showed higher levels of resilience in the Northeast and West, including Alaska, (>4.0) while counties in the South Atlantic and South-Central regions exhibited lower resilience (<2.0) to acute climate events. Northeast, West and Mountain regions of the US are characterized by relatively low levels of risk (<0.26), higher levels of governance (>0.60), and above national median scores for society, built environment and natural environment domains which enhances their resilience scores. South Atlantic and South-Central regions of the US are characterized by higher risk scores (>0.31) accompanied by lower levels of governance (<0.48) and below national median scores for society and built environment domains reducing the region's overall resilience.

Keywords: climate events, resilience, vulnerability, recoverability, natural hazards

OPEN ACCESS

Edited by:
Yang Liu,
Emory University, United States

Reviewed by:
Sofia Kottou,
National and Kapodistrian University of Athens, Greece
Gulnihal Ozbay,
Delaware State University, United States

****Correspondence:***
Kevin Summers
summers.kevin@epa.gov

Specialty section:
This article was submitted to Environmental Health, a section of the journal Frontiers in Environmental Science

Received: *16 August 2018*
Accepted: *08 November 2018*
Published: *30 November 2018*

Citation:
Summers K, Harwell L, Smith LM and Buck KD (2018) Regionalizing Resilience to Acute Meteorological Events: Comparison of Regions in the U.S. Front. Environ. Sci. 6:147. doi: 10.3389/fenvs.2018.00147

INTRODUCTION

Natural hazards can result in disasters without proper governance and mitigating systems (Chandra et al., 2007). In the recent past, the United States has witnessed several natural disasters including major hurricanes, earthquakes, tornadoes, and wildfires. While some governance and mitigation measures have been taken, future natural hazards disasters cannot be prevented due to the fact these events can hit random locations, have varying magnitudes, and can take unexpected forms. Therefore, the enhancement of the capacity of communities to resist and recover from these types of natural hazard disasters is paramount. Several global, national, and local agencies are confronted with this situation and have developed frameworks to address these issues (e.g., UN/ISDR, 2002; FEMA, 2012, 2017a,b; NRC, 2012; FDH, 2016; FDEM, 2018).

Resilience is increasingly used as a pathway for understanding the actions of natural hazard disasters. Resilience was originally an ecological concept (Holling, 1973) that was adapted to social

systems (Adger, 2000) and eventually to joint human-environmental systems (Folke, 2006). What natural disasters have taught us is that resilience to these disasters needs to be discussed within the framework of integrated socio-ecological systems (Berkes et al., 2003). Similarly, the temporal scale of these disaster events can be short-term (Bruneau et al., 2003; Rose, 2004) associated with specific acute meteorological events or longer-term associated with global change (Dovers and Handmer, 1992). Regardless, there is no common conceptualization for resilience. This manuscript uses a conceptualization for resilience to short-term meteorological hazards (Summers et al., 2017a, 2018) and analyses the results to depict regional comparisons.

CLIMATE RESILIENCE SCREENING INDEX—CONCEPTUALIZATION, APPROACH AND STRUCTURE

The conceptualization, approach and structure of the Climate Resilience Screening Index (CRSI) for acute meteorological events has been described in detail in Summers et al. (2017a,b). A short synopsis of this index is provided here.

In the construction of the CRSI index, the historical occurrence of acute meteorological events associated with geographic regions throughout the United States were assessed as well as the infrastructure challenges these events created. Discussions with climate experts, in conjunction with the information provided by the National Climate Assessment (Melillo et al., 2014) and the 100 Resilient Cities report (ARUP, 2014) yielded twelve (12) acute meteorological events and natural hazards that were included in CRSI:

- Hurricanes
- Tornadoes
- Inland Floods
- Coastal Flooding
- Earthquakes
- Wildfires
- Drought
- High winds
- Hail
- Landslides
- Extreme high temperatures
- Extreme low temperatures.

No singular approach among existing composite measures of climate resilience met all of the expected needs for developing CRSI. Collectively, however, the reviewed literature provided many of the building blocks (e.g., suites of indicators, indicator groupings, domains). To varying degrees, all of the existing indices offered patterns of indicator groupings. In the final conceptualization of CRSI, five domains were comprised of twenty indicators that were derived from 117 unique metrics. **Figure 1** depicts the final CRSI conceptual framework including the domains and indicators of the index. A summary and discussion of the domains, indicators and types of metrics used in CRSI can be found in Summers et al. (2017b, 2018) and are listed in **Table 1**.

All domains for each county, parish and borough (all referred to as county below) were min-max standardized on a scale from 0.01 to 0.99. The final CRSI calculation begins as a scaled value for recoverability/vulnerability derived from Governance and Risk (basic CRSI) with the Governance value being adjusted by the remaining domain scores for social, built environment and natural environment to complete the calculation of CRSI as shown below:

$$CRSI(B)_i = {}^{R_i}\!/_{V_i} = {}^{Gov_i}\!/_{Risk_i}$$

where $CRSI(B)_i$ = value of basic resilience (Recovery/Vulnerability or R_i/V_i) and R_i/V_i = Governance in county i/Risk in county i. The overall CRSI score is calculated as:

$$CRSI_i = (Gov_i + Soc(a)_i Gov_i + BE(a)_i Gov_i + NE(a)_i Gov_i)/Risk_i$$

where $CRSI_i$ = the value of CRSI or adjusted resilience for county i and $Soc(a)_i$, $BE(a)_i$, and $NE(a)_i$ are the adjustment multipliers for Society, Built Environment, and Natural Environment in each county i, and $Risk_i$ is the Risk score for county i. The adjustment factors are calculated as:

$$Soc(a)_i = {}^{(Soc_i - Soc_m)}\!/_{Soc_m}$$

where Soc(a)i is the adjustment multiplier for society in county i, Soc_i is the social domain score for county i and Soc_m is the median social domain score (median is used rather than mean to match the skewed distribution of the data) for all counties;

$$BE(a)_i = {}^{(BE_i - BE_m)}\!/_{BE_m}$$

where $BE(a)_I$ is the adjustment multiplier for built environment in county i, BE_i is the built environment domain score for county i and BE_m is the median built environment domain score for all counties;

$$NE(a)_i = {}^{(NE_i - NE_m)}\!/_{NE_m}$$

and where $NE(a)_i$ is the adjustment multiplier for natural environment in county i, NE_i is the natural environment domain score for county i and NE_m is the median natural environment domain score for all counties.

The national results of CRSI have been provided elsewhere (Summers et al., 2017b, 2018) as well as a regionalization providing direct utility to the U.S. Environmental Protection Agency (EPA)—a regionalization by EPA Regions (the U.S. is divided into 10 EPA regions). However, such a regionalization is of limited utility to non-EPA decision makers. Therefore, the national data has been regionalized by geographic region based on Census Divisions (U.S. Department of Commerce, 2018) and by state to be of better use for these decision-makers as presented in **Figure 2**. This regionalization separates the United States into nine areas:

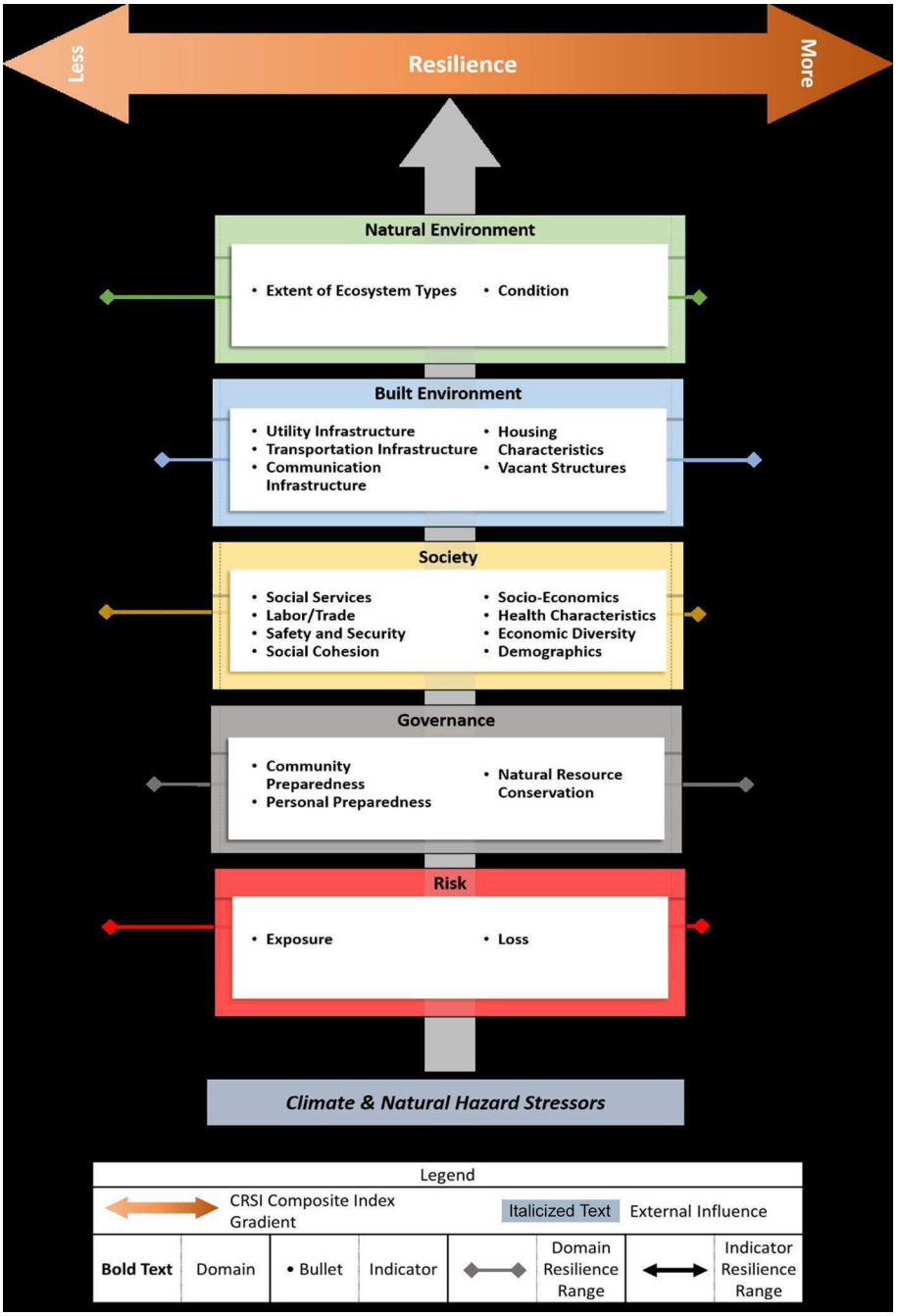

FIGURE 1 | Final CRSI conceptual framework. Arrows projected from boxes to the left and right represent hypothetical increases and decreases in ranges for indicators (black arrows) and domains (colored arrows).

1) New England—Connecticut, Maine, Massachusetts, New Hampshire, Rhode Island, and Vermont
2) Middle Atlantic—New Jersey, New York, and Pennsylvania
3) East North Central—Illinois, Indiana, Michigan, Ohio, and Wisconsin
4) West North Central—Iowa, Kansas, Minnesota, Missouri, Nebraska, North Dakota, and South Dakota
5) South Atlantic—Delaware, District of Columbia, Florida, Georgia, Maryland, North Carolina, South Carolina, Virginia, and West Virginia
6) East South Central—Alabama, Kentucky, Mississippi, and Tennessee
7) West South Central—Arkansas, Louisiana, Oklahoma, and Texas

TABLE 1 | List of CRSI domains, indicators, scope, and number of metrics.

Domain (# indicators/ #metrics)	Indicator(s)	Metric category (number of specific metrics)
Built environment (5/24)	Communication infrastructure	Communication continuity (7)
	Housing characteristics	Structure vulnerability (5)
	Transportation infrastructure	Transportation flow continuity (6)
	Utility infrastructure	Utility continuity (3)
	Vacant structures	Structure vulnerability (3)
Governance (3/5)	Community preparedness	Community resilience strengthening (2)
	Natural resource conservation	Natural resource recovery (1)
	Personal preparedness	Personal property hazard protection (2)
Natural environment (2/18)	Condition	Biodiversity, using birds as a proxy (1)
		Coastal condition (1)
		Forest condition (1)
		Inland lake condition (1)
		Percentage of clean air days (1)
		Rivers and streams condition (1)
		Soil growth suitability (1)
		Soil productivity (1)
		Wetlands condition (1)
	Extent of ecosystem types	Agriculture area (1)
		Forested area (1)
		Grassland area (1)
		Inland surface water area (1)
		Marine/estuarine area (1)
		Perennial ice/snow area (1)
		Protected areas (1)
		Tundra area (1)
		Wetland area (1)
Risk (2/20)	Exposure	Earthquake probability (1)
		Extreme high temperature incidents (1)
		Extreme low temperature incidents (1)
		Flood probability (2)
		Hailstorm probability (1)
		Tornado probability (2)
		Hurricane probability (2)
		Landslide probability (1)
		Major toxics presence (1)
		Non-storm damaging wind incidents (1)
		Nuclear presence (1)
		Location of RCRA sites (1)*
		Location of Superfund sites (1)**
		Toxic release presence (1)
		Wildfire probability (1)
	Loss	Developed area loss (includes human and property measures) (1)
		Natural area loss (1)
		Dual-benefit area loss (includes cropland and managed area measures) (1)
Society (8/50)	Demographics	Vulnerable populations (5)
	Economic diversity	Economic stability/recovery (2)
	Health characteristics	Health problems that may impact personal resilience (9)
	Labor and trade services	Construction recovery (8)
	Safety and security	Provisioning of emergency and civil services (4)
	Social cohesion	Access to social support (4)
	Social services	Access provisioning to critical services (15)
	Socio-economics	Employment opportunity (1)
		Personal economics (2)

*Numbers in parentheses for domains show the total number of indicators/total metrics in the domain. Numbers in parentheses for metrics indicate number of individual metrics used to represent the metric category. *RCRA, Resource Conservation and Recovery Act – RCRA is a U.S. public law that creates the framework for the proper management of hazardous and non-hazardous solid waste. The metric represents the number and locations of RCRA sites; **Superfund, EPA's Superfund Program is responsible for cleaning up some of the nation's most contaminated sites. The metric represents the number and location of Superfund sites.*

8) Mountain—Arizona, Colorado, Idaho, Nevada, New Mexico, Utah, and Wyoming
9) Pacific—Alaska, California, Hawaii, Oregon, and Washington.

Data from Alaska is only partially available with about 50% of its boroughs not represented. Due to both missing data and very low risk domain scores for Alaska (risk to acute meteorological events), use of Alaska data skews the scores for the Pacific region. To better represent issues associated with the Pacific region, results will be discussed both including and excluding Alaska.

REGIONALIZATION RESULTS

The overall CRSI regionalized results are depicted in **Figure 2**. These scores show that the Pacific (with or without Alaska), New England, and Mountain Regions display the highest overall resilience while the East South Central, South Atlantic, and West South Central display the lowest overall resilience. This distribution of overall scores is the result of specific regional domain scores (**Figure 3**). One of the primary domains affecting the overall CRSI score for a region is risk. Risk is comprised of 12 types of meteorological events and is adjusted based on losses due to those events and potential anthropogenic hazard exposures. **Figure 4** shows the comparative levels of risk for the events, losses, and anthropogenic risks by U.S. region. In all regions the risk domain is driven by historical exposure with minimal contributions from historical losses. The highlights of the domain

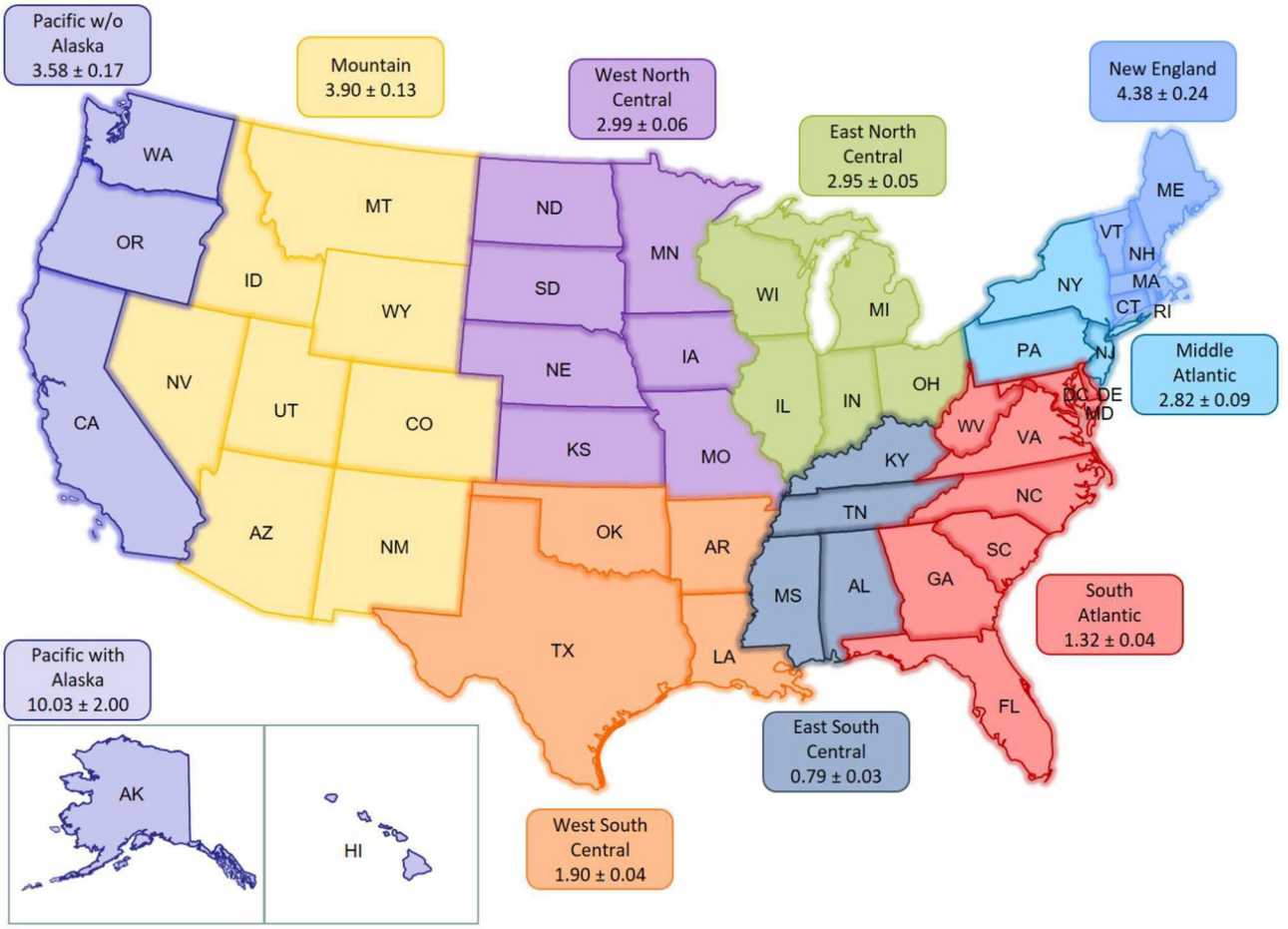

FIGURE 2 | Regionalized CRSI results with estimate of uncertainty.

scores for each region and its comprising states will be discussed below by individual region.

New England

The New England region is comprised of five states and is characterized by the second highest CRSI score in the U.S. (4.375) or the highest score if Alaska is excluded from the Pacific region (**Table 2**). All states in the New England region are either near the national CRSI average (Rhode Island) or significantly above the national averages (all remaining states in the region). All New England states are characterized by lower than average risk to meteorological events and significantly higher than average governance. All states have average or higher than average built environment scores except Rhode Island which is significantly lower than average (0.302). Similarly, all states have higher than average society scores with Vermont demonstrated among the highest state society scores in the nation (0.671). All New England states have natural environment scores either close to the national average or significantly greater than the average (Rhode Island, 0.511, and Maine, 0.484).

Meteorological risks in New England (**Figure 4**) are characterized by extreme high and low temperatures (49% of events and well-above the national average) and drought (23% of events but well-below the national average). Inland flooding, high winds and hailstorms comprise the remaining secondary risks at 9, 9, and 3%, respectively, with high wind events being significantly above the national average. These types of events result in minimal loss of life and physical property (about 1% of the loss in New England), although losses to agricultural and silvicultural lands, as well as natural ecosystem, comprise about 99% of losses. Potential anthropogenic hazards existing near sites of meteorological events are dominated by Superfund sites (47%) and general toxic release sites (e.g., industrial outflows) at 36% (both at the national average).

CRSI scores can be deconstructed to assess which indicators are the primary contributors to the score and which indicators contribute weakly to the score. Using polar plots (**Figures 5**–**7**), these contributions can be quantified visually for each region of the United States. **Figure 5A** shows the deconstruction of the New England CRSI score by domains. Risk domains simply reflect histories of exposure and cannot theoretically be altered by human actions to reduce risks. The major contributors to the CRSI score in the New England region are natural resource conservation

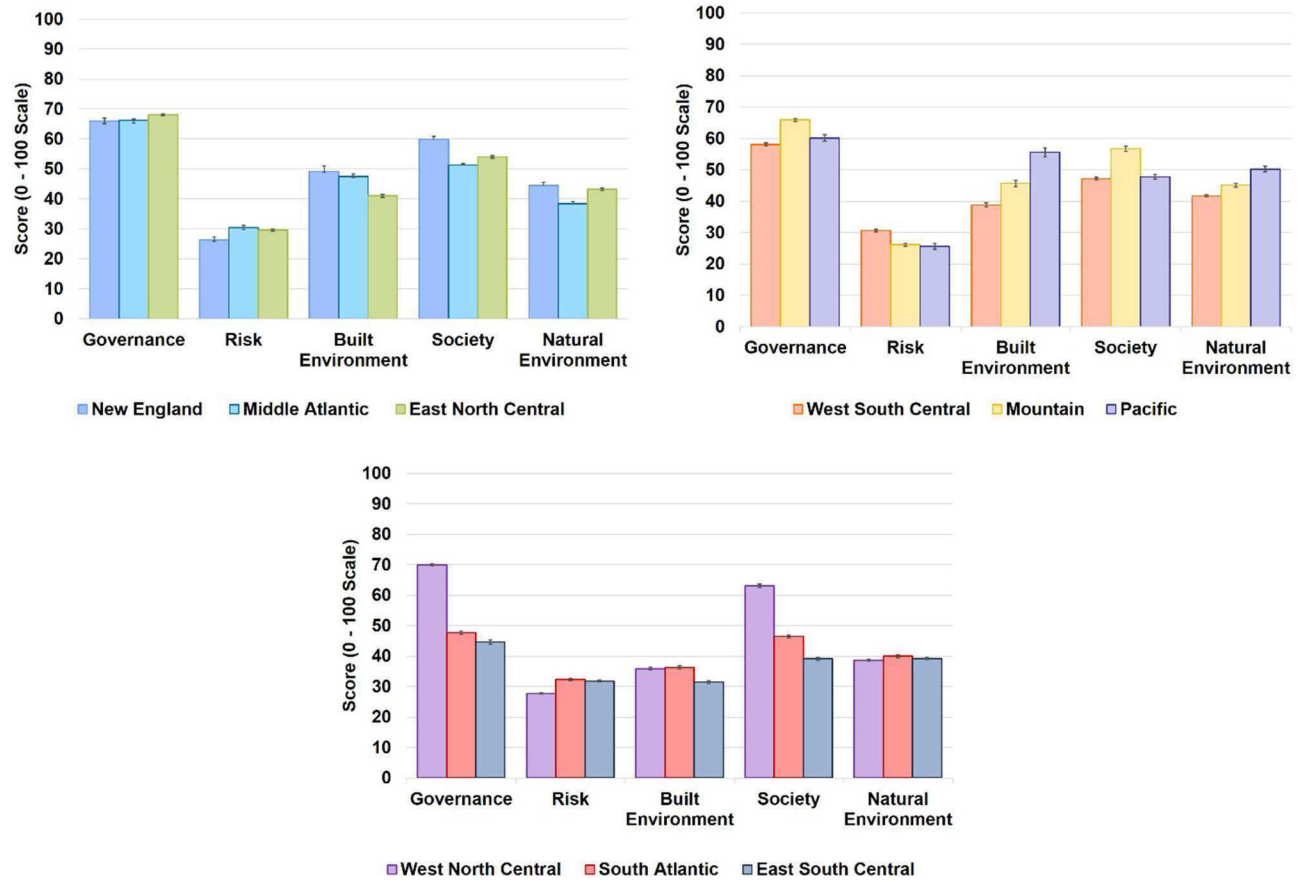

FIGURE 3 | Domain scores by U.S. Region (vertical bars represent uncertainty).

contributions to governance; demographic characteristics, economic diversity, and socio-economics to society; the number of vacant structures and general housing characteristics to the built environment; and, the extent or acreage of natural ecosystems (not built environments) in the natural environment.

Of the 67 counties in the New England region, the top 10% of CRSI scores (scores = 6.95 to 12.7) were seen in Maine (3 counties), Vermont (2 counties), and Massachusetts and New Hampshire (1 county each). Only two New England counties (both in Rhode Island) have resilience scores significantly below the national average.

Middle Atlantic

The Middle Atlantic region is comprised of three states and is characterized a moderate CRSI score (2.823) (**Table 2**). All states in the Middle Atlantic region are near the national CRSI average with New York demonstrating an overall CRSI score slightly above the national average (3.103). Most Middle Atlantic states are characterized by average risk to meteorological events with New Jersey showing elevated risks (0.379) and all states in the region showed significantly higher than average governance scores. All states have higher than average built environment scores and average society scores. All Middle Atlantic states have natural environment scores slightly lower than the national average.

Meteorological risks in the Middle Atlantic region (**Figure 4**) are characterized by extreme high and low temperatures (46% of events and well-above the national average) and drought (19% of events but well-below the national average). The region is exposed to three other types of meteorological events—landslides (13%), high wind events (9%), and inland flooding (8%). Landslides and high wind events are about twice the national average. These types of events result in minimal loss of life and physical property (<1% of the loss in the Middle Atlantic) although losses to agricultural and silvicultural lands, as well as natural ecosystem, comprise about 99% of losses (equally divided). Potential anthropogenic hazards existing near sites of meteorological events are dominated by Superfund sites (54%, significantly above the national average), general toxic release sites (e.g., industrial outflows) at 26% (significantly below the national average) and RCRA sites (12% at twice the national average).

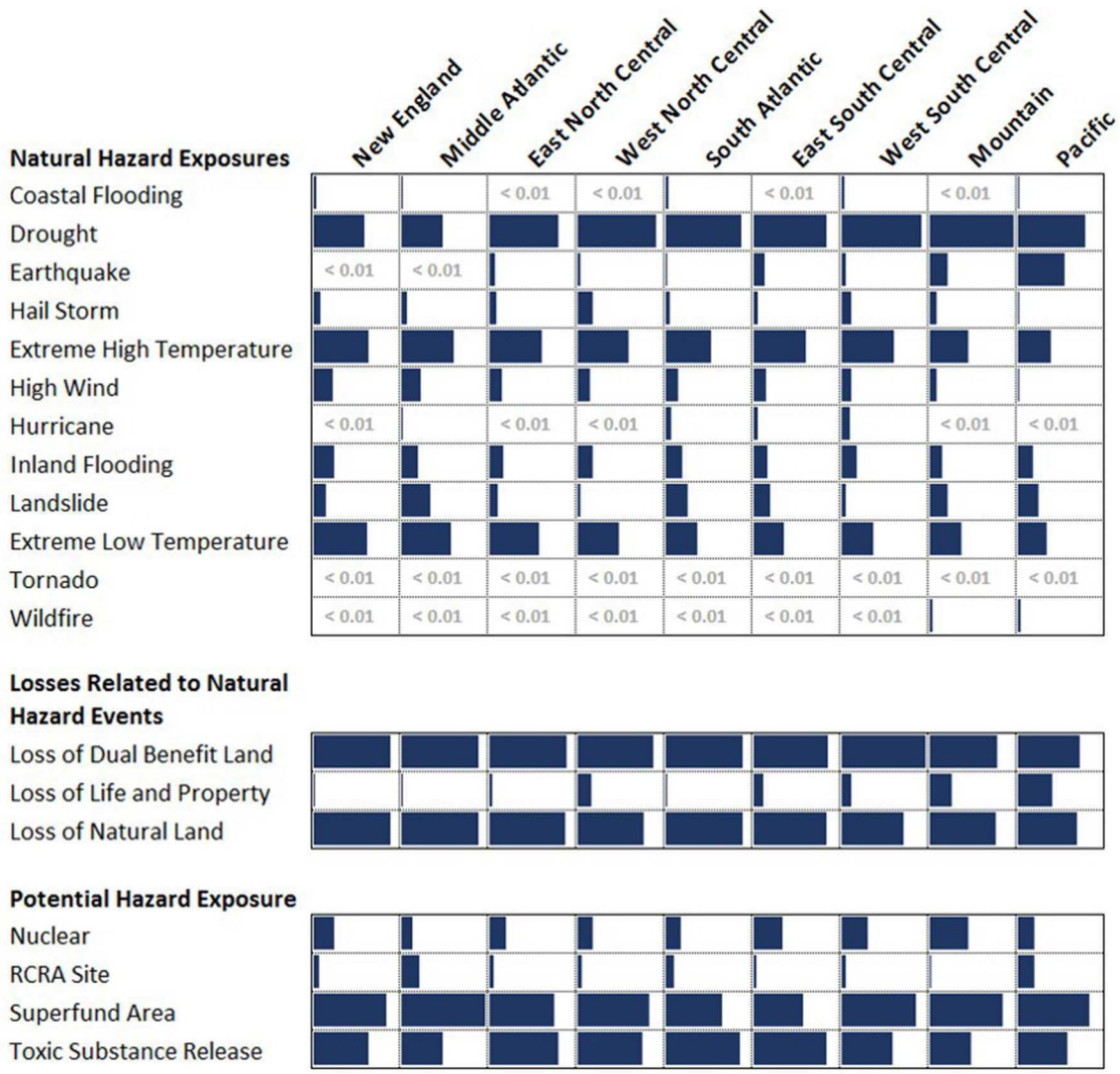

FIGURE 4 | Relative comparison of risk of meteorological events, losses due to those events and potential anthropogenic hazard exposures by region. Sum of each column associated with the three risk subsets equals 1 (or multiplied by 100 equals 100%).

The major contributors to the CRSI score in the Middle Atlantic region are natural resource conservation contributions to governance; demographic characteristics, economic diversity, socio-economics and social cohesion to society; the number of vacant structures to the built environment; and, the extent and condition of natural ecosystems in the natural environment (**Figure 5B**).

Of the 150 counties in the Middle Atlantic region, the top 10% of CRSI scores (scores = 4.35 to 5.61) were seen in New York (12 counties) and Pennsylvania (3 counties). Nearly 25% of counties in the Middle Atlantic region has overall CRSI scores significantly below the national average of 2. 375 (excluding Alaska). The 10% of Middle Atlantic counties with the lowest CRSI scores equitably split among the three states with 4–6 counties in each state.

East North Central

The East North Central region of the United States is comprised of five states and is characterized an above average CRSI score (2.948) (**Table 2**). All states in the East North Central region are either near the national CRSI average or significantly higher than the average with Wisconsin and Michigan demonstrating the highest CRSO scores (4.145 and 3.066, respectively). Most East North Central states are characterized by average risk to meteorological events with Illinois showing elevated risks (0.335) and all states in the region showed significantly higher than average governance scores. All states, except Indiana, have average built environment scores and all states, except Wisconsin, have average, or slightly below average society scores. Indiana's built environment score (0.360) is significantly below the national average while Wisconsin's society score (0.623) is significantly above the national average. All East North Central states, except

TABLE 2 | Regionalized CRSI scores and domain scores by region and state.

Region	State	Governance	Risk	Built	Society	Natural	CRSI
DOMAINS							
Northeast		**0.660**	**0.263**	**0.492**	**0.599**	**0.445**	**4.375**
	Connecticut	0.654	0.308	0.520	0.547	0.398	3.106
	Maine	0.677	0.228	0.499	0.565	0.484	5.368
	Massachusetts	0.602	0.311	0.557	0.601	0.447	3.802
	New Hampshire	0.670	0.250	0.519	0.596	0.421	4.448
	Rhode Island	0.627	0.305	0.302	0.586	0.511	2.653
	Vermont	0.708	0.223	0.450	0.671	0.417	5.102
Middle Atlantic		**0.662**	**0.305**	**0.475**	**0.513**	**0.384**	**2.823**
	New Jersey	0.639	0.379	0.471	0.518	0.397	2.280
	New York	0.665	0.276	0.469	0.521	0.381	3.103
	Pennsylvania	0.667	0.307	0.481	0.503	0.383	2.733
East North Central		**0.681**	**0.295**	**0.410**	**0.540**	**0.433**	**2.948**
	Illinois	0.662	0.338	0.414	0.515	0.489	2.703
	Indiana	0.659	0.286	0.360	0.570	0.452	2.857
	Michigan	0.705	0.258	0.412	0.492	0.418	3.066
	Ohio	0.651	0.307	0.421	0.514	0.352	2.237
	Wisconsin	0.746	0.279	0.457	0.623	0.441	4.145
West North Central		**0.699**	**0.277**	**0.359**	**0.631**	**0.386**	**2.988**
	Iowa	0.704	0.280	0.382	0.653	0.419	3.397
	Kansas	0.698	0.291	0.332	0.651	0.369	2.595
	Minnesota	0.772	0.289	0.389	0.735	0.442	4.345
	Missouri	0.626	0.286	0.399	0.530	0.389	2.395
	Nebraska	0.714	0.268	0.311	0.613	0.340	2.387
	North Dakota	0.704	0.234	0.374	0.662	0.354	3.503
	South Dakota	0.703	0.268	0.314	0.608	0.377	2.677
South Atlantic		**0.477**	**0.323**	**0.363**	**0.465**	**0.400**	**1.321**
	Delaware	0.606	0.361	0.586	0.472	0.547	3.197
	District of Columbia	0.610	0.470	0.402	0.506	0.200	0.721
	Florida	0.427	0.309	0.485	0.434	0.426	1.607
	Georgia	0.442	0.300	0.282	0.420	0.395	0.846
	Maryland	0.622	0.352	0.494	0.518	0.463	2.733
	North Carolina	0.435	0.341	0.419	0.463	0.431	1.440
	South Carolina	0.462	0.319	0.393	0.437	0.420	1.347
	Virginia	0.520	0.351	0.331	0.548	0.378	1.482
	West Virginia	0.555	0.293	0.324	0.435	0.328	1.104
East South Central		**0.446**	**0.318**	**0.315**	**0.392**	**0.392**	**0.787**
	Alabama	0.335	0.303	0.408	0.385	0.397	0.901
	Kentucky	0.534	0.307	0.255	0.388	0.371	0.642
	Mississippi	0.494	0.308	0.337	0.382	0.444	1.151
	Tennessee	0.370	0.350	0.305	0.409	0.370	0.577
West South Central		**0.581**	**0.306**	**0.388**	**0.472**	**0.417**	**1.895**
	Arkansas	0.533	0.302	0.393	0.451	0.445	1.865
	Louisiana	0.570	0.372	0.430	0.479	0.457	1.914
	Oklahoma	0.649	0.287	0.384	0.530	0.401	2.436
	Texas	0.577	0.297	0.377	0.459	0.403	1.735

(Continued)

TABLE 2 | Continued

Region	State	Governance	Risk	Built	Society	Natural	CRSI
Mountain		**0.659**	**0.261**	**0.456**	**0.567**	**0.451**	**3.898**
	Arizona	0.613	0.280	0.710	0.458	0.410	3.997
	Colorado	0.673	0.277	0.453	0.555	0.396	3.216
	Idaho	0.666	0.233	0.423	0.545	0.537	4.873
	Montana	0.676	0.231	0.381	0.638	0.402	4.090
	Nevada	0.623	0.291	0.485	0.446	0.548	3.263
	New Mexico	0.621	0.267	0.472	0.505	0.498	3.571
	Utah	0.670	0.302	0.495	0.617	0.463	3.983
	Wyoming	0.659	0.253	0.464	0.658	0.433	4.231
Pacific		**0.602**	**0.256**	**0.556**	**0.478**	**0.503**	**10.034**
	Alaska	0.736	0.058	0.475	0.479	0.627	50.546
	California	0.498	0.322	0.641	0.485	0.461	2.852
	Hawaii	0.739	0.182	0.570	0.589	0.479	8.431
	Oregon	0.618	0.278	0.499	0.465	0.517	3.561
	Washington	0.648	0.259	0.524	0.465	0.485	4.044
Pacific w/o Alaska		**0.580**	**0.288**	**0.568**	**0.478**	**0.483**	**2.375**
United States		**0.597**	**0.296**	**0.393**	**0.516**	**0.413**	**2.713**
United States w/o Alaska		**0.596**	**0.298**	**0.393**	**0.516**	**0.412**	**2.375**

Bold, Regional Scores; Built, Built Environment, Natural, Natural Environment.

Ohio (0.352), have natural environment scores higher than the national average.

Meteorological risks in the East North Central region (**Figure 4**) are characterized by extreme high and low temperatures (47% of events and well-above the national average) and drought (32% of events but at the national average). The region is exposed to five other types of meteorological events—inland flooding (7%), high wind events (6%), landslides (4%), hailstorms (3%), and earthquakes (3%). These five risk exposures were at about the national average. Tornadoes and wildfire exposures (<1%) were comparable to the national average. These types of events result in lower than average loss of life and physical property (1.4% of the loss in the East North Central) although losses to agricultural and silvicultural lands, as well as natural ecosystem, comprise about 98% of losses (equally divided). Potential anthropogenic hazards existing near sites of meteorological events are dominated by general toxic release sites (e.g., industrial outflows) at 44% (slightly above the national average), Superfund sites at 42% (slightly below the national average) and nuclear facilities (11% at the national average).

The major contributors to the CRSI score in the East North Central region are natural resource conservation contributions to governance; demographic characteristics, economic diversity, socio-economics, and social cohesion to society; the number of vacant structures and general housing characteristics to the built environment; and, the extent and condition of natural ecosystems in the natural environment (**Figure 5C**).

Of the 437 counties in the East North Central region, the top 5% of CRSI scores (scores = 4.75 to 6.00) were seen in Wisconsin (20 counties), Michigan (3), and Illinois and Indiana (1 each). Nearly 15% of counties in the East North Central region have overall CRSI scores significantly below the national average of 2.375 (excluding Alaska). The 5% of East North Central counties with the lowest CRSI scores were largely seen in Ohio (15 counties), with Illinois (6), Indiana (3) and Michigan (1) comprising the remainder.

West North Central

The West North Central region of the United States is comprised of seven states and is characterized an above average CRSI score (2.988) (**Table 2**). All states in the West North Central region are either near the national CRSI average or significantly higher than the average with Minnesota and North Dakota demonstrating the highest CRSO scores (4.345 and 3.503, respectively). Most West North Central states are characterized by below average risk to meteorological events with North Dakota characterized by significantly below average risks (0.234). All states in the region showed significantly higher than average governance scores with Minnesota demonstrating the highest governance score in the nation (0.772). In fact, five of the seven West North Central states had governance scores >0.7. All states, except Missouri, have below average built environment scores and all West North Central states have slightly or significantly above average society scores. Nebraska, South Dakota and Kansas had society scores that are significantly below the national average (0.311, 0.314, and 0.332, respectively) while Minnesota's society score (0.735) is the highest in the U.S. All West North Central states, except Minnesota and Iowa, have natural environment scores significantly lower than the national average.

Meteorological risks in the West North Central region (**Figure 4**) are characterized by extreme high and low temperatures (41% of events and slightly above the national

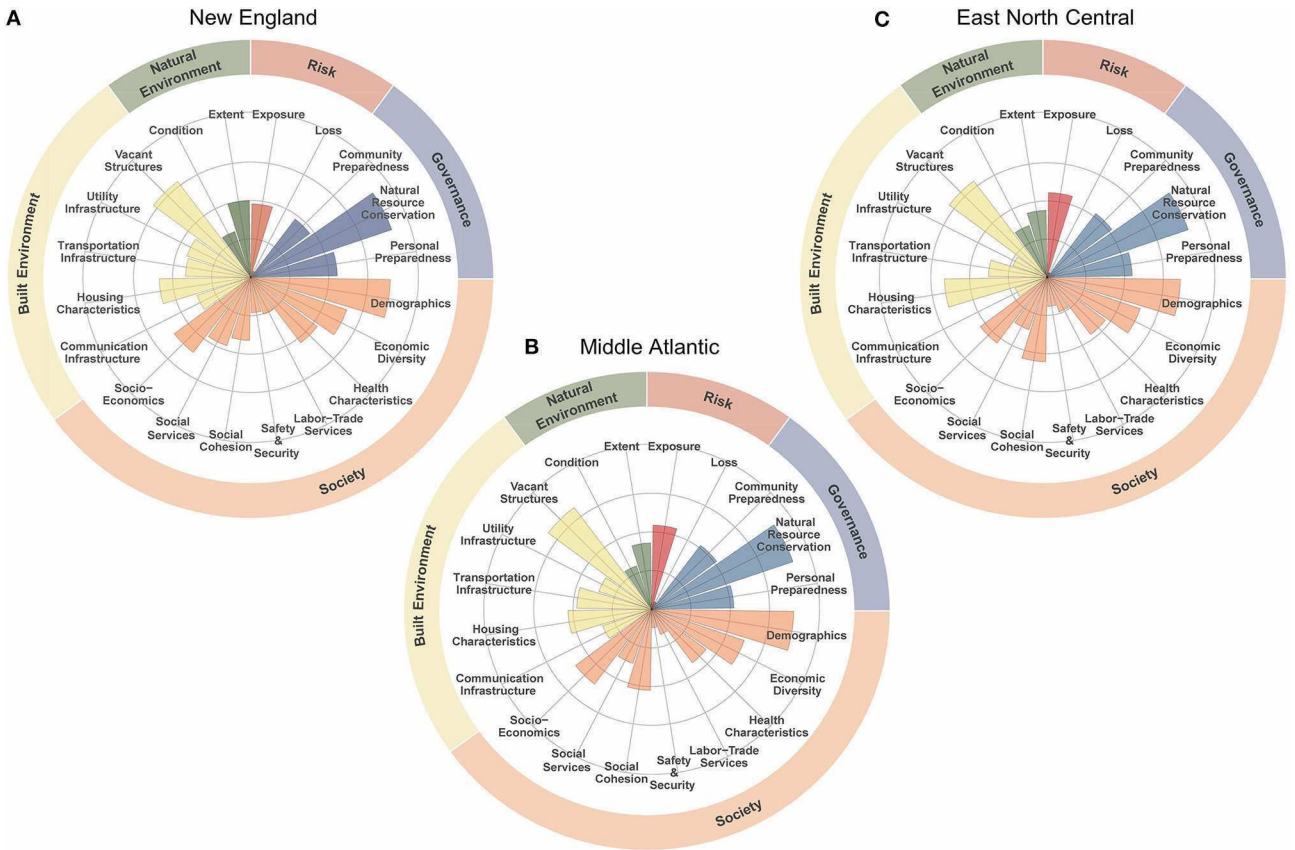

FIGURE 5 | Polar plots of the **(A)** New England, **(B)** Middle Atlantic, and **(C)** East North Central regions.

average) and drought (36% of events but at the national average). The region is exposed to five other types of meteorological events—hailstorms (7%), inland flooding (7%), high wind events (5%), landslides (1%), and earthquakes (1%). Of these five risk exposures, hailstorms were at about twice the national average while inland flooding and high wind events were at about the national average and landslides and earthquakes were significantly below the national average. Wildfires (0.12%) and tornadoes (0.11%) were slightly above the national average. These types of events result in about twice the national average for loss of life and physical property (9% of the loss in the West North Central) although losses to agricultural and silvicultural lands, as well as natural ecosystem, comprise about 91% of losses (49% for dual use lands and 42% for natural lands). Potential anthropogenic hazards existing near sites of meteorological events are dominated by Superfund sites (46%) being at about the national average, general toxic release sites (e.g., industrial outflows) at 41% (slightly above the national average) and nuclear facilities (10% at the national average).

The major contributors to the CRSI score in the West North Central region are natural resource conservation contributions to governance; demographic characteristics, social cohesion, health characteristics, economic diversity and socio-economics to society; the number of vacant structures and general housing characteristics to the built environment; and, the extent and condition of natural ecosystems in the natural environment (**Figure 6A**).

Of the 618 counties in the West North Central region, the top 5% of CRSI scores (scores = 5.32 to 8.12) were seen in Minnesota (14 counties), South and North Dakota (4 each), Iowa (2) and Nebraska (1). Nearly 25% of counties in the West North Central region have overall CRSI scores significantly below the national average of 2.375 (excluding Alaska). The 5% of West North Central counties with the lowest CRSI scores were largely seen in Nebraska (15 counties), with South Dakota (6), Kansas (2), and North Dakota and Missouri (1 each) comprising the remainder.

South Atlantic

The South Atlantic region of the United States is comprised of eight states and the District of Columbia and is characterized by a significant below average CRSI score (1.321) (**Table 2**). All states in the South Atlantic region are significantly below the national average except for Delaware (3.179) with the District of Columbia and Georgia displaying the lowest overall CRSI scores (0.721 and 0.846, respectively). The South Atlantic region has the highest risk to acute meteorological events in the nation (0.323). All South Atlantic states, except West

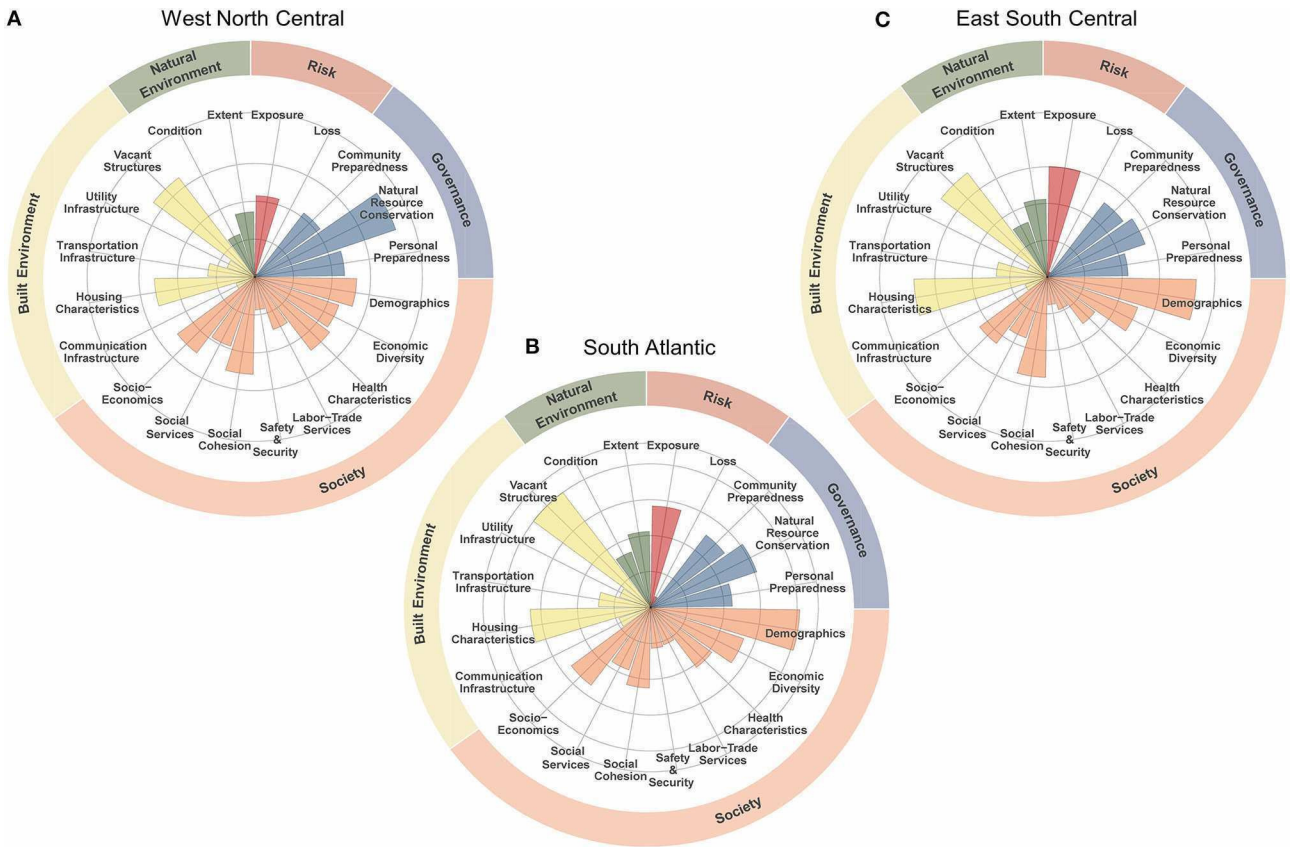

FIGURE 6 | Polar plots of the **(A)** West North Central, **(B)** South Atlantic, and **(C)** East South Central regions.

Virginia (0.293), are characterized by above to significantly above average risk to meteorological events with the District of Columbia and Delaware characterized by the highest risk scores (0.470 and 0.361, respectively). All states in the region showed significantly lower than average governance scores except for Maryland, Delaware and the District of Columbia (ranging between 0.610 and 0.622). Half of the eight South Atlantic states had governance scores <0.5. States in the South Atlantic region widely spanned the range of national built environment scores with four states (Delaware, Florida, Maryland, and North Carolina) and the District of Columbia being significantly above the average, one state (South Carolina) being at about the average and three states (Georgia, Virginia, and West Virginia) being significantly below the average. All South Atlantic states, except Virginia and Maryland, had society scores well-below the national average. Most South Atlantic states (Delaware, Florida, Maryland, North Carolina, and South Carolina) were either at or above the national average for their natural environment scores. The District of Columbia demonstrated the lowest natural environment score (0.200) while Georgia, Virginia and West Virginia have natural environment scores significantly below the national average.

Meteorological risks in the South Atlantic region (**Figure 4**) are characterized by extreme high and low temperatures (35% of events and slightly below the national average) and drought (35% of events but at the national average). The region is exposed to six other types of meteorological events – landslides (10%), inland flooding (7%), high wing events (6%), hurricanes (3%), hailstorms (3%), and coastal flooding (1%). Of these six risk exposures, landslides were about 50% above the national average while coastal and inland flooding as well as high wind events were at about the national average. Hurricanes were three times more prevalent than the national average while hailstorms were at about half the national average. Earthquakes (0.70%) were about 30% of the national average while wildfires (0.18%) were twice the national average. These types of events result in minimal loss of life and physical property (1% of the loss in the South Atlantic) although losses to agricultural and silvicultural lands, as well as natural ecosystem, comprise about 99% of losses (equitably distributed). Potential anthropogenic hazards existing near sites of meteorological events are dominated by general toxic release sites (e.g., industrial outflows) at 48% (significantly above the national average) Superfund sites (36%) being significantly below the national average, and nuclear facilities (10% at the national average).

The major contributors to the CRSI score in the South Atlantic region are natural resource conservation and community

preparedness contributions to governance; demographic characteristics, economic diversity, socio-economics, social cohesion, and health characteristics to society; the number of vacant structures and general housing characteristics to the built environment; and, the extent and condition of natural ecosystems in the natural environment (**Figure 6B**).

Of the 588 counties in the South Atlantic region, the top 5% of CRSI scores (scores = 3.10 to 4.8) were seen in Virginia (10 counties), Maryland (9), West Virginia (2) and Florida, Delaware, and North Carolina (1 each). Over 50% of counties in the South Atlantic region have overall CRSI scores significantly below the national average of 2.375. The 5% of South Atlantic counties with the lowest CRSI scores were largely seen in Virginia (16 counties), Georgia (8) and West Virginia (1).

East South Central

The East South Central region of the United States is comprised of four states and is characterized by the lowest overall CRSI score (0.787) (**Table 2**). All states in the East South Central region are significantly below the national average with only Mississippi showing an overall CRSI score >1.0 (1.151). The East South Central region has the second highest risk to acute meteorological events in the nation (0.318) and the lowest national governance domain score (0.446) with half the states (Alabama and Tennessee) having scores <0.4. States in the East South Central region has the lowest built environment score in the nation (0.315) with three of its states (Kentucky, Mississippi, and Tennessee) with significantly lower than the national average built environment scores. The East South Central region has the lowest society score in the nation (0.392) with all four states significantly below the national average. Most East South Central states (Alabama, Kentucky and Tennessee) were below the national average for their natural environment scores.

Meteorological risks in the East South Central region (**Figure 4**) are characterized by extreme high and low temperatures (37% of events and slightly below the national average) and drought (33% of events but at the national average). The region is exposed to seven other types of meteorological events—landslides (8%), inland flooding (7%), high wing events (6%), earthquakes (5%), hailstorms (2%), hurricanes (2%), and tornadoes (0.3%). Of these seven risk exposures, landslides, and high wind events were slightly above the national average while inland flooding events were at about the national average. Hurricanes were three times more prevalent than the national average while hailstorms were at about half the national average. Earthquakes (0.70%) and hailstorms (2%) were about 50% above and 50% below the national averages, respectively. Hurricanes were twice as prevalent in the East South Central region and

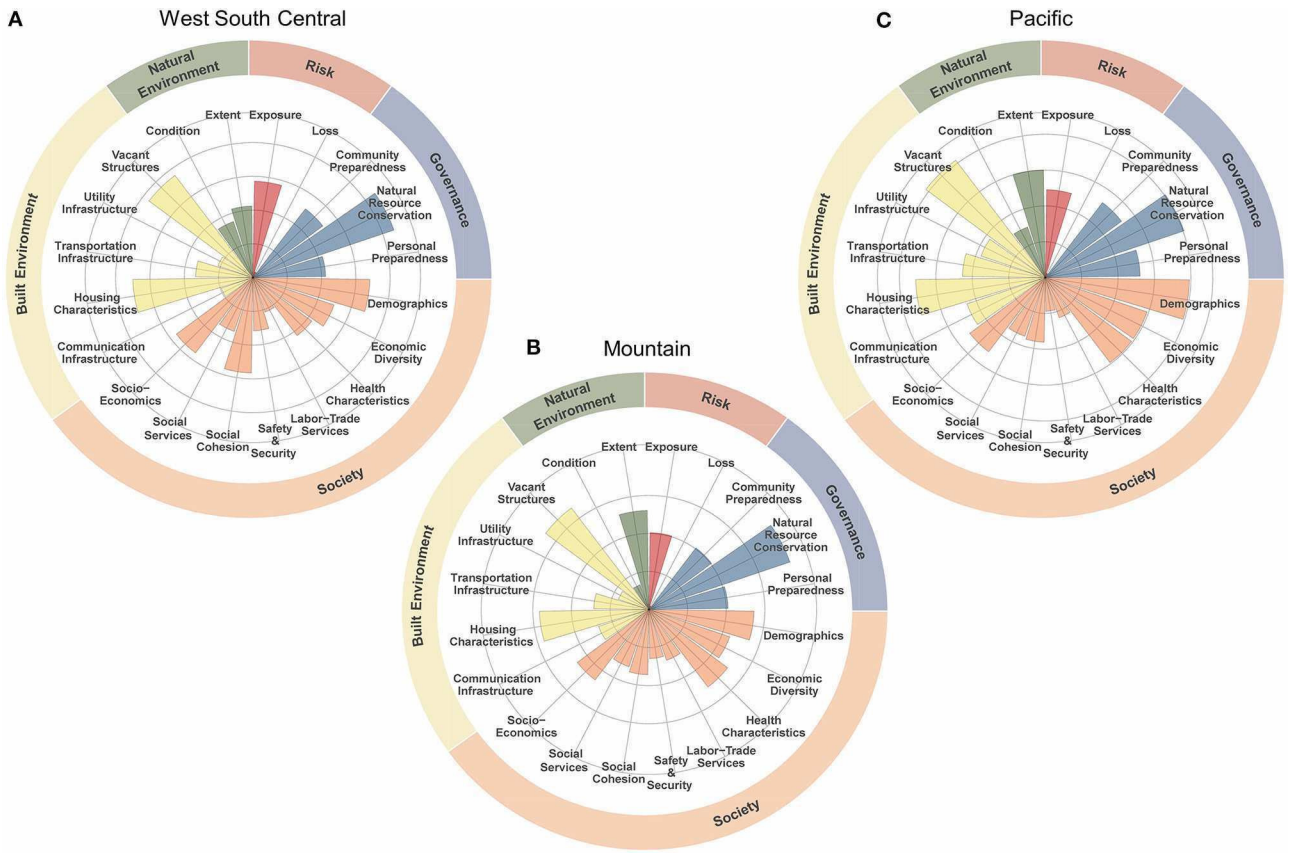

FIGURE 7 | Polar plots of the **(A)** West South Central, **(B)** Mountain, and **(C)** Pacific regions.

wildfires were about three times more prevalent. These types of events resulted in about a 50% higher prevalence of loss of life and physical property (6% of the loss in the South Atlantic) than that seen for the nation, while losses to agricultural and silvicultural lands, as well as natural ecosystems, comprise about 94% of losses (equitably distributed). Potential anthropogenic hazards existing near sites of meteorological events are dominated by general toxic release sites (e.g., industrial outflows) at 47% (significantly above the national average), Superfund sites (32%) being significantly below the national average, and nuclear facilities (18% at roughly twice the national average).

The major contributors to the CRSI score in the East South Central region are natural resource conservation, community preparedness, and personal preparedness contributions to governance; demographic characteristics, social cohesion, economic diversity and socio-economics to society; general housing characteristics and the number of vacant structures to the built environment; and, the extent and condition of natural ecosystems in the natural environment (**Figure 6C**).

Of the 364 counties in the East South Central region, all but two counties were significantly below the national average. The only two counties with overall CRSI scores equal to the national average are in Kentucky and Mississippi. Nearly 10% of the counties in this region have negative CRSI scores with the lowest scores being in Kentucky (21 counties), and Tennessee and Mississippi (2 each). Ninety-nine percent of counties in the East South Central region have overall CRSI scores significantly below the national average of 2.375.

West South Central

The West South Central region of the United States is comprised of four states and is characterized by an overall CRSI score (1.895) that is significantly below the national average (**Table 2**). Seventy-five percent of the states in the West South Central region (Arkansas, Louisiana, and Texas) are significantly below the national average with only Oklahoma showing an overall CRSI score >2.0 (2.436). The risk of acute meteorological events in the West South Central region is about average (0.306) and the regional governance score is also about at the national average. The West South Central region has an average built environment score in the nation (0.388) with only Texas being significantly below the national average. The West South Central region has a below average society score (0.497) with only one state (Oklahoma) being slightly above the national average. All West South Central states were about at the national average for their natural environment scores.

Meteorological risks in the West South Central region (**Figure 4**) are characterized by extreme high and low temperatures (37% of events and slightly below the national average) and drought (33% of events but at the national average). The region is exposed to eight other types of meteorological events – inland flooding (7%), high wind events (5%), hailstorms (4%), hurricanes (4%), landslides (2%), earthquakes (2%), coastal flooding (1%), and wildfire exposure (0.2%). Of these eight risk exposures, inland flooding, high wind events and hailstorms occurred at about the national average while hurricanes occurred at about four times the national average, wildfires occurred at twice the national average and coastal flooding happened at about 25% above the national average. Earthquakes (2%) and landslides (2%) were about 50% below the national averages. These types of events resulted in about a 50% higher prevalence of loss of life and physical property (6% of the loss in the West South Central) than that seen for the nation, while losses to agricultural and silvicultural lands, as well as natural ecosystems, comprised about 94% of losses (with most of these losses observed in dual benefit lands, 54% and the reminder in natural lands, 40%). Potential anthropogenic hazards existing near sites of meteorological events are dominated by Superfund sites (47%, about the national average), general toxic release sites (e.g., industrial outflows) at 33% (about the national average) and nuclear facilities (17%, at roughly twice the national average).

The major contributors to the CRSI score in the West South Central region are natural resource conservation contributions to governance; demographic characteristics, social cohesion and socio-economics to society; general housing characteristics and the number of vacant structures to the built environment; and, the extent and condition of natural ecosystems in the natural environment (**Figure 7A**).

Of the 470 counties in the West South Central region, the top 5% of CRSI scores (scores = 3.41–5.72) were seen in Texas (15 counties), Oklahoma (7), Arkansas (2), and Louisiana (1). Nearly 50% of counties in the West South Central region have overall CRSI scores significantly below the national average of 2.375. The 5% of West South Central counties with the lowest CRSI scores were seen almost completely in Texas (24 counties) with one county in Oklahoma.

Mountain

The Mountain region of the United States is comprised of eight states and is characterized by the overall CRSI score (3.898) that is among the highest in the nation (**Table 2**). All the states in the Mountain region are significantly above the national average with three states (Idaho, Montana and Wyoming) with overall CRSI scores >4.0. The risk of acute meteorological events in the Mountain region is less than average (0.261) and the regional governance score is significantly greater than the national average. The Mountain region has a significantly above average built environment score (0.456) with Arizona having the highest score in the U.S. (0.710) and only Montana being slightly below the national average. The Mountain region has a significantly above average society score (0.567) with only one state (Arizona) being significantly below the national average. All Mountain states were at or significantly above the national average for their natural environment scores.

Meteorological risks in the Mountain region (**Figure 4**) are characterized by drought (38%) that is significantly higher than the national average and extreme high and low temperatures (32% of events and significantly below the national average). The region is exposed to seven other types of meteorological events—landslides (8%), earthquakes (8%), inland flooding (6%), hailstorms (3%), high wind events (3%), wildfires (1%), and tornadoes (0.1%). Of these seven risk exposures, wildfires exposure is about ten times the national average and earthquake exposure is about 2.5 times the national average. Landslide

occurrences are at about 30% above the national average and high wind events are about 50% below the national average. Exposures to inland flooding, hailstorms and tornadoes occur at about the national average. These types of events resulted in about a 300% higher prevalence of loss of life and physical property (14% of the loss in the Mountain) than that seen for the nation, while losses to agricultural and silvicultural lands, as well as natural ecosystems, comprised about 86% of losses (equitably distributed between dual benefit and natural lands). Potential anthropogenic hazards existing near sites of meteorological events are dominated by Superfund sites (47%, about the national average), general toxic release sites (e.g., industrial outflows) at 27% (somewhat less than the national average) and nuclear facilities (25%, at roughly 2.5 times the national average).

The major contributors to the CRSI score in the Mountain region are natural resource conservation contributions to governance; health characteristics, demographic characteristics and socio-economics to society; the number of vacant structures and general housing characteristics to the built environment; and, the extent of natural ecosystems in the natural environment (**Figure 7B**).

Of the 281 counties in the Mountain region, the top 10% of CRSI scores (scores = 6.59–14.60) were seen in Montana (9 counties), Idaho (9), Colorado (2), New Mexico (2), Wyoming (2), and Utah (1). Three counties in this region have overall CRSI scores that are >10.0. Nearly 20% of counties in the Mountain region have overall CRSI scores significantly below the national average of 2.375. The 10% of Mountain counties with the lowest CRSI scores were seen in Colorado (9), Montana (8), New Mexico (3), Idaho (3) and Wyoming (1).

Pacific

The Pacific region of the United States is comprised of five states and is characterized by the overall CRSI score (10.034 with Alaska and 3.576 without Alaska) that is among the highest in the nation (**Table 2**). All the states in the Pacific region are significantly above the national average with three states (Alaska, Hawaii, and Washington) with overall CRSI scores >4.0. The risk of acute meteorological events in the Pacific region is less than average (0.256) with Alaska having a risk score of <0.1. Almost half of the boroughs in Alaska have insufficient data to complete CRSO scoring but including the counties with adequate data shows very low risk (0.058) and very high governance (0.736). CRSI does not include chronic, long-term climate changes like sea-level rise and Alaskan topography minimizes coastal flooding and high winds events. The regional governance score including Alaska (0.602) is significantly greater than the national average but excluding Alaska reduces the score to 0.580 which is slightly lower than the national average. The Pacific region has a significantly above average built environment score (0.556 with Alaska and 0.568 without Alaska) with California having among highest scores in the U.S. (0.641) and no states being at or below the national average. The Pacific region has a slightly below average society score (0.478 with or without Alaska) with only one state (Hawaii) being significantly below the national average. All Pacific states were significantly above the national average for their natural environment scores with Alaska having the highest score in the nation (0.627) and Oregon having a score of 0.517.

Meteorological risks in the Pacific region (**Figure 4**) are characterized by drought (31%) that is about at the national average, earthquakes (22%) that are seven times the national average and extreme high and low temperatures (28% of events and significantly below the national average). The region is exposed to three other types of meteorological events—landslides (9%), inland flooding (7%), hailstorms (3%), and wildfires (1%). Of these three risk exposures, wildfires exposure is about twelve times the national average and landslide exposure is about 50% above the national average. Exposures to inland flooding occur at about the national average. These types of events resulted in about a five times higher prevalence of loss of life and physical property (21% of the loss in the Pacific) than that seen for the nation, while losses to agricultural and silvicultural lands, as well as natural ecosystems, comprised about 78% of losses (equitably distributed between dual benefit and natural lands). Potential anthropogenic hazards existing near sites of meteorological events are dominated by Superfund sites (47%, about the national average), general toxic release sites (e.g., industrial outflows) at 32% (somewhat less than the national average), RCRA exposure at 11% (about twice the national average) and nuclear facilities at 11% (at the national average).

The major contributors to the CRSI score in the Pacific region are natural resource conservation contributions to governance; demographic characteristics, health characteristics and economic diversity to society; the number of vacant structures and general housing characteristics to the built environment; and, the extent of natural ecosystems in the natural environment (**Figure 7C**).

Of the 160 counties in the Pacific region, the top 10% of CRSI scores (scores = 8.89 to 148.07) were seen in Alaska (20 boroughs), Hawaii (4 counties) and Washington (1). Twenty-one boroughs/counties in this region have overall CRSI scores that are >10.0. Nearly 25% of counties in the region have overall CRSI scores significantly below the national average of 2.375. The 10% of counties with the lowest CRSI scores were seen in California (16), Oregon (6), Washington (2) and Hawaii (1).

DISCUSSION

The results for the regionalization of CRSI can be used for capacity building regardless of CRSI score. The domain and indicator scores, as well as the polar plots, can be used to identify areas where improvements can be made to enhance overall resilience. The only domain in CRSI that cannot be improved *per se* is the risk domain. This domain is driven by historical observations relating to the tracked meteorological events. If CRSI included long-term climate events, then perhaps human activities could be developed to minimize long-term change which could impact the risk domain of CRSI (Rahmstorf, 2007; Nichols and Cazenave, 2010; Sweet et al., 2017). The remaining CRSI domains—governance, society, built environment, and natural environment—are driven by indicators and metrics that can be modified to improve resilience to acute climate events.

In the New England region, general CRSI scores are high (>3.8) and well-above the national average. However, one state in this region has an overall CRSI score below the regional average—Rhode Island with a CRSI score of 2.653. Rhode Island has suffered from multiple coastal and inland flooding events, winter storms, Superstorm Sandy, and Tropical Storm Irene in the last decade. An evaluation of the New England region, using the polar plot of indicator contribution to domains, show that increases in community preparedness and personal preparedness would enhance regional governance. Enhancements of labor-trade services, safety and security and social cohesion would enhance the society modifier. Improvements in infrastructure would enhance the built environment modifier and increases in natural ecosystem extents and condition would alter the natural environment modifier. Our review of the domain scores for Rhode Island suggest the area for greatest improvement could be in the domain representing the built environment where the Rhode Island score (0.320) is significantly below the national average and hence reducing the state's CRSI score.

Recently, Rhode Island drafted a new statewide climate resilience action strategy (RI-STAB, 2018). The results of the Rhode Island CRSI data were provided to a member the Rhode Island Science and Technical Advisory Board. These results targeted a lower overall CRSI score likely driven by lower built environment scores characterized by critical infrastructure and utilities and building characteristics and average governance scores (lower than most of New England) representing potential issues with emergency preparedness as well as emergency shelters and services. Like the CRSI approach, the Rhode Island Strategy defines climate resilience as "the capacity of individuals, institutions, businesses and natural systems within Rhode Island to survive, adapt, and grow regardless of chronic stresses and weather events they experience" (RI-STAB, 2018, p. 3). Also, like the CRSI results, Rhode Island recognizes that it primary acute meteorological risk events are extreme cold and heat, droughts, and extreme rainfall and flooding. The new strategy addresses built environment issues to reduce vulnerability and improve infrastructure for drinking water and wastewater systems; dam and storm-water systems; power grid and fuel supply issues; and transportation. Realizing the importance of natural systems for community resilience, Rhode Island (already with the highest natural environment domain scores in New England) is planning to increase its efforts to protect and conserve its coastal and inland natural systems. Rhode Island is already experiencing the effects of coastal flooding on buildings, infrastructure, evacuation shelters, and emergency services. The new strategy plan targets enhancements to address these issues. Realization of the actions and activities planned in the new Rhode Island strategy should increase its overall CRSI score to levels similar to other New England states.

The Middle Atlantic state with the lowest overall CRSI score (New Jersey-−2.28) is characterized by the highest risk factors to acute weather events (0.379) which is 20–40% higher than the other states in the region. These events include coastal and inland flooding, Superstorm Sandy, and a variety of high temperature and low temperature events. Because it cannot impact its risk to these events, New Jersey can do little to increase its overall CRSI score other than improve its already above-average governance and built environment scores and average society and natural environment scores. New Jersey Governor's Office of Recovery Rebuilding (2018) is actively developing plans to modify risks by developing governance associated with flood rebuilding standards, and the state's Department of Community Affairs ((NJDCA), 2018) has provided grants post-Sandy to enable development of strategic recovery plans and practices to facilitate smart and efficient rebuilding processes at the local level. Similarly, New Jersey's Office of Emergency Management (NJOEM, 2018) is identifying resiliency opportunities to modify the locations and characteristics of critical infrastructures including drinking water, wastewater, transportation, transit, energy, and communication systems. These infrastructure issues were observed as potential areas of improvement for the Middle Atlantic Region through CRSI analyses.

However, the greatest potential area of improvement for the overall New Jersey CRSI score would be enhancement of ecosystem type extent, and condition. For example, only 31 miles of New Jersey's 130 miles of shoreline are undeveloped (Headland, 2017; Stockton and Hafner, 2018). While some Post-Sandy activities in New Jersey seem to be addressing these resilience enhancements (NJOCM, 2010), few major efforts seem to be occurring in this area. Small efforts like dune reconstruction and vegetation planting are being undertaken, but no larger efforts directed at natural shoreline stabilization, wetland protection, and ecosystem condition improvements are included.

In the South Atlantic region, both Georgia and the District of Columbia displayed overall CRSI scores of less than one. The District of Columbia is characterized by high risk (0.470, nearly 50% above the US average) and is prone to frequent inland and coastal flooding (flash flooding, river flooding, tropical systems, dam breaks, and heavy snow melts). The District of Columbia showed a very low Natural Environment domain score (0.200) compared to the national average of 0.413. Enhancing the natural environment might be difficult for the District as it is surrounded on multiple sides by the Potomac and Anacostia Rivers and is characterized by extensive areas of impervious surface. Minimizing impervious surfaces and maximizing the conservation and re-development of riparian corridors, wetlands, and greenspaces are likely the areas where improvements would be anticipated to enhance the District's CRSI score. Similar improvements in infrastructure (e.g., transportation and water systems) would enhance the District's already above average built environment domain score.

On the other hand, Georgia (CRSI score of 0.846) has an average risk score but below average domain scores for governance, built environment, society and natural environment. Improvement in any of these domains would increase Georgia's CRSI score. Georgia's risks can be easily characterized by inland flooding, high wind events, hailstorms and tornadoes ((NWS), 2018). Governance improvements in the South Atlantic

region could focus more on holistic and catchment-oriented flood risk management rather than the emphasis on structure measures and construction which have dominated the past. Similar efforts in Germany have shown some success in reducing the adverse consequences of flooding for human health, the environment, cultural heritage and economic activity (Heintz et al., 2012). Georgia has a few large urban centers with diverse work forces where flooding occurs regularly. However, much of Georgia is comprised of small communities and counties where labor and trade services are not diverse and rebuilding after a meteorological event (e.g., tornado, flood) can be very difficult without construction labor pools. Creating enticements to develop these labor pools even if shared by several proximal counties would increase the CRSI scores of these counties. Finally, improvements in housing characteristics through upgrading building codes and reducing the number of vacant structures should increase a presently very low building environment domain score for Georgia (0.282). Homes and businesses throughout Georgia and the South Atlantic region would benefit from enhanced building codes and standard resulting in increased resilience (FEMA, 2017a). Georgia's neighboring state, Florida, has demonstrated how to enhance its building code to create greater resilience to storm events (PDH Academy, 2017). Florida building codes change in response to new technology and knowledge about weather events. Codes affecting the built environment should be modified or updated in response to changes in technology and procedures, growing and maturing with the times. With the increased storm activity of 2017, recently updated building codes guided by storms of the past were put to the test and demonstrated Florida community's enhanced resilience. These codes utilized more information about code strengths and weaknesses, building practices, and new building materials that helped homes and commercial properties withstand weather events.

California demonstrates an above average risk domain (0.322) dominated by drought and temperature extremes. The increased incidence of wildfires (10 times the national average), earthquakes (7 times the national average) and landslides (50% above the national average) contribute to a major portion of human life and dollar losses resulting from acute meteorological events. According to CRSI domain scores, California has the lowest governance domain score in the Pacific region (0.498); this is significantly below the national average and 50–75% below the remaining states in the region. While having among the highest built environment scores in the nation, California has increased building code requirements to withstand at least minimal to moderate earthquake impacts. California's seismic construction requirements are designed to protect the lives of those inside. But even with the most modern codes, building to the state's minimum requirements still leave some new buildings severely damaged in a major earthquake to the point of being a complete loss. Further enhancing these types of building codes would increase the state's CRSI scores but governance enhancement designed to increase personal and community preparedness would likely modify the governance score for California positively.

Wildfires, another type of event of increasing frequency and magnitude, in 2017 were the most destructive fires on record. A total of 9.133 fires burned over 1.3 million acres including 5 of the 20 most devastating wildland-urban interface fires in California history (CDFFP, 2018). Enhanced personal and community preparedness for wildfires would likely modify the governance score for California significantly. For example, the Tubbs fire in Napa and Sonoma counties, which ignited on October 8, 2017, killed 22 people, damaged 5,643 structures, and burned 36,807 acres, making it the single most destructive fire in California history. Interviews with personnel of the California Department of Forestry and Fire Protection demonstrated that little could be done to contain the fire but the lack of personal preparedness was demonstrated by the number of vehicles still parked in their driveways after calls for mandatory evacuations (Irfan, 2017). Fires are becoming more damaging because Californians keep building in harm's way much the same way homebuilders in flood plains rebuild homes after flood destruction. Deliberate decisions and unintended consequences of urban development over decades have turned many parts of California into tinderboxes (Irfan, 2017). This is also reflected in the Environmental Domain score for California (0.461), which is the lowest in the Pacific region, where natural habitats that might have reduced human life and property losses have become part of or consumed by suburban and urban sprawl (Irfan, 2017).

As evidenced by the data and examples above, direct enhancement in governance, environment, and even building codes and reduction of vacant structures would increase the resilience score for states like California. Georgia, New Jersey, Rhode Island, and the District of Columbia. Using CRSI scores and interpreting the deconstruction of those scores, can be critical elements to consider in resilience capacity building in these states and the District of Columbia. Using the Climate Recovery Screening Index to inform capacity building can enrich the dialogue and contribute to decision making that results in stronger community resilience to acute climate events.

AUTHOR CONTRIBUTIONS

All authors listed have made a substantial, direct and intellectual contribution to the work, and approved it for publication.

REFERENCES

Adger, W. N. (2000). Social and ecological resilience: are they related? *Prog. Hum. Geogr.* 24, 347–364. doi: 10.1191/030913200701540465

ARUP (2014). *City Resilience Framework*. The Rockefeller Foundation, ARUP Development International.

Berkes, F., Colding, J., and Folke, C. (eds.). (2003). *Navigating Social-Ecological Systems: Building Resilience for Complexity and Change*. Cambridge: Cambridge University Press.

Bruneau, M., Chang, S., Eguchi, R., Lee, G., O'Rourke, T., Reinhorn, A., et al. (2003). A framework to quantitatively assess and enhance seismic resilience of communities. *Earthquake Spectra* 19, 733–752. doi: 10.1193/1.1623497

CDFFP (California Department of Forestry and Fire Protection) (2018). *Incident Information*. Available online at: http://cdfdata.fire.ca.gov/incidents/incidents_stats?year=2017

Chandra, R. K., Papadopoulos, G. A., and Karanci, A. N. (2007). Disasters due to natural hazards. *Nat. Hazards* 40, 501–502. doi: 10.1007/s11069-006-9010-4

Dovers, S. R., and Handmer, J. W. (1992). Uncertainty, sustainability and change. *Global Environ. Change* 2, 262–276.

FDEM (Florida Department of Emergency Management) (2018). *Florida's Severe Weather Awareness Guide*. Available online at: https://www.floridadisaster.org/globalassets/library/2018-guidefinal.pdf

FDH (Florida Department of Health) (2016). *Florida Emergency Preparedness Guide*. Available online at: http://www.floridahealth.gov/programs-and-services/emergency-preparedness-and-response/_documents/preparedness-guide-large-print.pdf

FEMA (Federal Emergency Management Agency) (2012). *Crisis Response and Disaster Resilience 2030: Forging Strategic Action in an Age of Uncertainty*. Available online at: https://www.fema.gov/media-library-data/20130726-1816-25045-5167/sfi_report_13.jan.2012_final.docx.pdf

FEMA (Federal Emergency Management Agency) (2017a). *Draft Interagency Concept for Community Resilience Indicators and National-Level Measures*. Available online at: https://www.fema.gov/community-resilience-indicators

FEMA (Federal Emergency Management Agency) (2017b). *Building Science Branch Brochure – Wind Hazards*. Available online at: https://www.fema.gov/media-library-data/1496953980230-d52857ef8919276187b3c57d7c851239/Wind_508.pdf

Folke, C. (2006). Resilience: the emergence of a perspective for social-ecological systems analyses. *Glob. Environ. Change* 16, 253–267. doi: 10.1016/j.gloenvcha.2006.04.002

Headland, J. R. (2017). "Quantifying resilience: coastal structure and nourished beaches," in *Coastal Structures and Solutions to Coastal Disasters Joint Conference, 2015*. Available online at: https://ascelibrary.org/doi/pdf/10.1061/9780784480304.062

Heintz, M. D., Hagemeier-Klose, M., and Wagner, K. (2012). Towards a risk governance culture in flood policy – findings from the implementation of the "floods directive" in Germany. *Water* 4, 135–156. doi: 10.3390/w4010135

Holling, C. S. (1973). Resilience and stability of ecological systems. *Annu Rev. Ecol. Syst.* 4, 1–23.

Irfan, U. (2017). *California's Wildfires Are Not "Natural" – Humans Made Them Worse at Every Step*. Vox. Available online at: https://www.vox.com/energy-and-environment/2017/10/12/16458242/risk-wildfires-worse-climate-change-california-san-francisco-los-angeles (Accessed December 8, 2017).

Melillo, J. M., Richmond, T., and Yohe, G. W. (2014). *Climate Change Impacts in the 11 United States: The Third National Climate Assessment*. U.S. Global Change Research Program, 12. Available online at: http://nca2014.globalchange.gov/report

New Jersey Governor's Office of Recovery and Rebuilding (2018). *Planning for Resiliency*. Available online at: http://nj.gov/gorr/resiliency/

Nichols, R. J., and Cazenave, A. (2010). Sea-level rise and its impact on coastal zones. *Science* 328, 1517–1520. doi: 10.1126/science.1185782

NJDCA (New Jersey Department of Community Affairs) (2018). *Planning for Resiliency*. Available online at: http://nj.gov/gorr/resiliency/

NJOCM (New Jersey Office of Coastal Management. New Jersey Department of Environmental Protection) (2010). *Getting to Resilience: A Coastal Community Resilience Evaluation Tool*. Available online at: http://www.state.nj.us/dep/cmp/docs/gtr-resilience.pdf

NJOEM (New Jersey Office of Emergency Management) (2018). *Planning for Resiliency*. Available online at: http://nj.gov/gorr/resiliency/

NRC (National Research Council). (2012). *Disaster Resilience: A National Imperative*. Washington, DC: The National Academies Press.

NWS (National Weather Service) (2018) *Severe Storm Climatology for North and Central Georgia*. Available online at: https://www.weather.gov/ffc/svrclimo

PDH Academy (2017). *How Severe Weather Affects the Future of Building Codes*. Available online at: https://pdhacademy.com/2017/12/21/severe-weather-affects-future-building-codes/

Rahmstorf, S. (2007). A semi-empirical approach to projecting future sea-level rise. *Science* 315, 368–370. doi: 10.1126/science.1135456

RI-STAB (Rhode Island Science and Technical Advisory Board) (2018). *"Resilient Rhody" – Statewide Climate Resilience Action Plan, Draft. Providence, Rhode Island*. Available online at: http://climatechange.ri.gov/documents/rev-resstrategy.pdf

Rose, A. (2004). Defining and measuring economic resilience to disasters. *Disaster Prevent Manage.* 13, 307–314. doi: 10.1108/09653560410556528

Stockton, R., and Hafner, S. (2018). *Beach Stabilization: Structure and Beach Nourishment Alternatives*. Available online at: https://intraweb.stockton.edu/eyos/coastal/25yrConference/Beach-Stabilization.pdf

Summers, J. K., Harwell, L. C., Buck, K. D., Smith, L. M., Vivian, D. N., Bousquin, J. J., et al. (2017a). *Resilience Screening Index (CRSI): An Assessment of Resilience to Acute Meteorological Events and Selected Natural Hazards*. Washington, DC: Protection Agency. EPA600/R-17/238.

Summers, J. K., Harwell, L. C., Smith, L. M., and Buck, K. D. (2018). *Climate Resilience Screening Index (CRSI): Development and Application to the U.S. Submitted to GeoHealth*. Minneapolis, MN: Community Indicator Consortium.

Summers, J. K., Smith, L. M., Harwell, L. C., and, Buck, K. D. (2017b). Conceptualizing holistic community resilience to climate events: foundation for a climate resilience screening index. *GeoHealth* 1, 151–164. doi: 10.1002/2016GH000047

Sweet, W. V., Kopp, R. E., Weaver, C. P., Obeysekera, J., Horton, R. M., Thieler, E. R., et al. (2017). *Global and Regional Sea Level Rise Scenarios for the United States*. NOAA Technical Report, NOS CO-OPS 083. Available online at: https://ntrs.nasa.gov/archive/nasa/casi.ntrs.nasa.gov/20180001857.pdf

U.S. Department of Commerce, Economics and Statistics Administration and U.S. Census Bureau (2018). *Census Regions and Divisions of the United States*. Available online at: https://www2.census.gov/geo/pdfs/maps-data/maps/reference/us_regdiv.pdf

UN/ISDR (United Nations International Strategy for Disaster Reduction). (2002). *Living With Risk: A Global Review of Disaster Reduction Initiatives. Prepared as an Interagency Effort Coordinated by the ISDR Secretariat*. Geneva. Available online at: http://www.adrc.asia/publications/LWR/LWR_pdf/index.pdf

Disclaimer: The views expressed in this manuscript are those of the authors and do not necessarily represent the views or policies of the U.S. Environmental Protection Agency. Any mention of trade names, products, or services does not imply an endorsement by the U.S. Government or the U.S. Environmental Protection Agency. The EPA does not endorse any commercial products, services, or enterprises.

Conflict of Interest Statement: The authors declare that the research was conducted in the absence of any commercial or financial relationships that could be construed as a potential conflict of interest.

Copyright © 2018 Summers, Harwell, Smith and Buck. This is an open-access article distributed under the terms of the Creative Commons Attribution License (CC BY). The use, distribution or reproduction in other forums is permitted, provided the original author(s) and the copyright owner(s) are credited and that the original publication in this journal is cited, in accordance with accepted academic practice. No use, distribution or reproduction is permitted which does not comply with these terms.

Send Orders for Reprints to reprints@benthamscience.net

Current Environmental Engineering, 2019, *6*, 000-000

RESEARCH ARTICLE

Development of a Multi-Hazard Landscape for Exposure and Risk Interpretation: The PRISM Approach

Kyle D. Buck*, J. Kevin Summers, Stephen Hafner, Lisa M. Smith and Linda C. Harwell

United States Environmental Protection Agency, Gulf Ecology Division, 1 Sabine Island Drive, Gulf Breeze, FL 32561

ARTICLE HISTORY

Received: December 12, 2017
Revised: April 26, 2018
Accepted: January 19, 2019

DOI:
10.2174/2212717806666190204103455

Abstract: Multi-hazard risk assessment has long been centered on small scale needs, whereby a single community or group of communities' exposures are assessed to determine potential mitigation strategies. While this approach has advanced the understanding of hazard interactions, it is limiting on larger scales or when significantly different hazard types are present. In order to address some of these issues, an approach is developed where multiple hazards coalesce with losses into an index representing the risk landscape. Exposures are assessed as a proportion of land-area, allowing for multiple hazards to be combined in a single calculation. Risk calculations are weighted by land-use types (built, dual-benefit, natural) in each county. This allows for a more detailed analysis of land impacts and removes some of the bias introduced by monetary losses in heavily urbanized counties. The results of the quantitative analysis show a landscape where the risk to natural systems is high and the western United States is exposed to a bulk of the risk. Land-use and temporal profiles exemplify a dynamic risk-scape. The calculation of risk is meant to inform community decisions based on the unique set of hazards in that area over time.

Keywords: Climate, spatial, exposures, multi-hazard, index, land-use.

1. INTRODUCTION

The goal of reducing impacts from hazard exposure has never been more important. According to the United Nations 2012 Report on Development Agenda, the global increase in hazard exposures from 1970 to 2010 was between 114 and 192 percent, depending on the hazard. These exposures resulted in over 1.1 million deaths and $1.3 trillion in property losses, with an additional 2.7 billion people adversely impacted in that same time (UN 2012). As populations continue to grow, urbanize and shift into areas with greater exposure potential, the impact will only continue to grow (Chester *et al*. 2000, Lall and Deichmann 2010, Garschagen and Romero-Lankao 2015, Güneralp *et al*. 2015). On top of this, the severity and location of hazards continue to change, yielding a dynamic landscape requiring continual reassessment and long-term mitigation solutions (Miletti 1999).

The hazard landscape or "hazard-scape" is complex and difficult to fully represent in a comprehensive manner without some form of model by which exposures are tallied and assigned to locations (Cutter, Burton, & Emrich, 2010). In order to effectively reduce risks, communities must assess their unique hazard-scape by using integrated, holistic, multi-hazard assessments intended to represent the full range of past, present and future exposures. In this context, the International Panel on Climate Change (IPCC) considers disaster risk to be "the possibility of adverse effects in the future" (Fields 2012). The starting point is a hazard, de-

*Address correspondence to this author at the United States Environmental Protection Agency, Gulf Ecology Division, 1 Sabine Island Drive, Gulf Breeze, FL 32561; Tel: 850-934-9233; E-mail: Buck.Kyle@epa.gov

2212-7178/19 $58.00+.00 © 2019 Bentham Science Publishers

fined as a phenomena caused by the onset of events, whether acute or chronic, that are perceived to cause harm (Burton and Kates 1964). Hazards can be natural (geophysical, hydrological, climatological, or biological) or technological (environmental degradation, pollution, or accidents). An exposure occurs when a hazard intersects with the landscape, whether a living population or the natural or built environment. In the event of an exposure, there is a potential for loss, defined here as a risk. Losses are incorporated as a measure of consequences associated with hazard from exposure. They serve as a proxy for vulnerability in the calculation of risk.

While integration of multiple hazards is not a new concept, there has been a push to include more refined multi-hazard models into community planning for risk reduction. Hewitt and Burton first discussed the concept of "hazardousness of place", whereby a specified geographic unit is assessed for all hazards impacting it (1971). Their theoretical framework suggests a need for more location-specific work, as opposed to hazard-specific analysis, to inform policy decisions. Cutter takes this a step further with a "hazards of place" conceptual model through which location-dependent risk, or vulnerability, is defined by the complex interaction of hazards caused by natural, societal, and technological events (Cutter and Solecki 1989, Cutter 1996). The place-based approach allows for the combination of multiple hazards and mitigation activities. More recent research in multi-hazard risk assessments has attempted such analyses, focusing on either small geographic areas or looking at a cascade of hazards resulting from a single source (e.g. volcano) (Bell and Glade 2011, Thierry 2008). There are also examples of hazard integration using spatial tools for loss estimation, planning and mitigation purposes (FEMA 2013, Schmidt *et al*. 2011, Tate *et al*. 2011). Other attempts at multi-hazard integration use spatial assessment with the assignment of ordinal classification schemes for intensity (Batista *et al* 2004, Schmidy-Thome 2005, Greives *et al*. 2006). This is necessary due to the vast array of impacts stemming from natural and technological hazards, but forces decisions on weighting and lacks consideration of outcomes. While these methods present a robust way to integrate and assess multiple hazards, they do not lend as well to the construction of an index value for comparison across larger spaces.

In addition to simply combining hazards, temporal interactions between hazards are a significant consideration, where the potential exists for hazards to interact and amplify one another through both proximity and timing of occurrences. In the event that multiple hazards occur close in proximity and timeframe, disaster fatigue can occur, leaving the landscape more susceptible to harm from subsequent exposures (Kappes *et al*. 2012). There are additional psychologic impacts from repeated exposures and exacerbating effects stemming from hazardous facilities via chemical releases, explosions, or epidemics (Reser 2007, Watson *et al*. 2007). Consideration of these "cascading" impacts is important, and a primary reason for the use of multi-hazard assessment (Miletti 1999, Marzocchi *et al*. 2012). The goal is to operationalize an approach that will enable the merger of multiple hazards into a meaningful measure for communities to assess strategies and limit future vulnerabilities. This feat is challenged as a result of patchwork landscapes, differences in hazard size and intensity, and the enormity of data that must be processed to retain a useful level of resolution. Despite the difficulty, developing a scalable multi-hazard assessment for the entire U.S. at the county scale is important and necessary to establish a baseline risk profile for all areas of the country.

2. METHODS

The Patterns of Risk using an Integrated Spatial Multi-Hazard (PRISM) approach allows risk to be

assessed at the county level across states or regions and facilitates the integration of any hazard type provided it has an associated spatial component. Risk, in this approach, is represented as the probability of a hazard exposure (identified as proportional land area) multiplied by the degree of vulnerability (identified hazard losses). Exposure probability entails both historic and proximity-based measures of hazards responsible for risk. Losses provide a measure of the lives lost/ impacted, monetary losses in crops and property, and losses of natural land integrity. Data inclusion, conceptual development and processing of the risk parameters is described in this section. A conceptual overview, provided in Fig. (**1**), demonstrates the breakdowns of each risk component.

To address the spatial extent of hazard exposure and cope with the varied landscapes (e.g. hazard proximities and level of development) across the country, counties are used as the foundation for risk calculation. Though use of smaller spatial units is possible, the utility of the method better aligns with a larger aggregation for the purposes of county and regional governance. In addition, there is lack of certain metrics at finer scales, making calculation of risk based on land extent challenging. Loss data, for example, uses counties as its finest level of data aggregation, and in 15 years of data, only 3 major boundary changes have occurred (US Census 2010). Assessment of land-type distribution within each county is used to weigh exposure and loss values and account for differences in development and economic drivers. Proportional county exposure values allow different hazard types to be combined in a consistent manner, regardless of intensity or temporal variation.

2.1. Data Refinement

In the formulation of a hazard-scape, three inputs are utilized: a land-use layer, a natural hazard

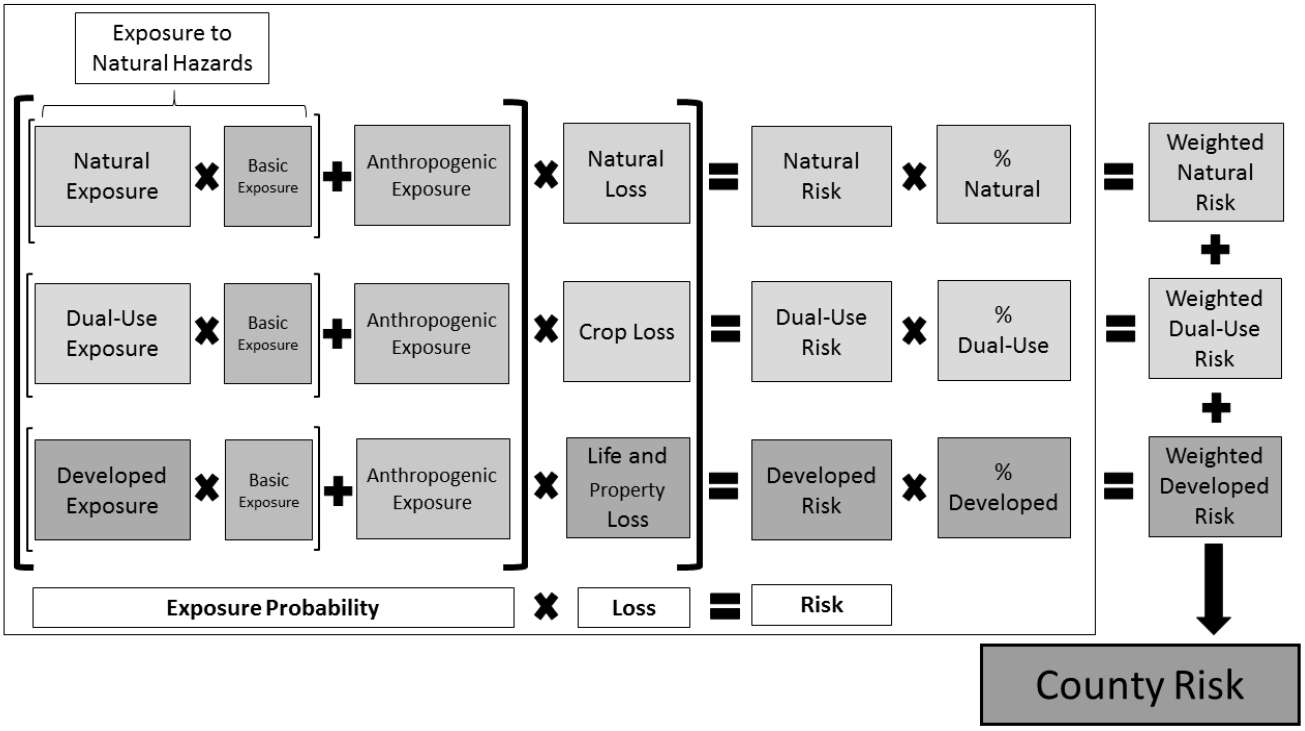

Fig. (1). PRISM Approach conceptual overview. Showing breakdown of exposures and land categories along with the inclusion of land-type weighting values used to derive a final risk value for all hazards in a county. Components of risk are identified in top and bottom bars to demonstrate steps in calculation of final score. Color codes: Green = Natural Risk components, Blue = Dual-Use components, and Grey = Developed components. Basic exposure and anthropogenic exposures are the same across all land-type categories.

layer, and technological hazard layer. The land-use layer is used to weight hazard exposures according to the landscape types present in a county; Natural, Dual-Benefit, or Developed (Table **1**). The natural hazard layer is used to define historic and proximity-based exposure probabilities. The technological hazard layer is used to add potential exposures resulting from man-made facilities. Each of these are calculated in units of total acreage and assigned to county boundaries using ArcGIS 10.3, where exposure size is calculated as a proportion of the county acreage in each land-use class.

2.1.1. Land Use Classifications

The land-use surface is developed using data from the 2011 version of the Multi-Resolution Land Characteristics Consortium (MRLC) National Land Cover Database (NLCD), which is based on LandSat imagery covering the entirety of the conterminous U.S. (Homer *et al*. 2015). The reason for this choice is two-fold. Firstly, the data was satellite-derived, spatially-referenced, and at a 30 x 30-meter resolution for the entire U.S. Although higher resolution alternatives existed, using those would have meant gathering multiple, disparate data sources and yielded a surface with high levels of inconsistency. The second advantage of using NLCD for surface exposure data is due to its well documented and regular collection, being compiled every 5 years and closely corresponding to the social data.

Land coverage classification in the NLCD falls into one of 20 different categories, making the data highly detailed. For the purposes of this approach, however, the original 20 classifications are compressed into 3 categories, developed lands, dual-benefit lands, and natural lands (Table **1**). Exposure extents are assigned to each land-type and calculated as a proportion. This allows exposure to be calculated for a specific land or aggregated up to a land-type weighted county value.

Table 1. Compression of 2011 NLCD categories from 20 down to 3 for use in exposure calculations. * data only available in Alaska. Left column represents original classification of land and right column represents new classification.

NLCD Classification (20 Categories)	PRISM Classification (3 Categories)
Developed, Open Space	Developed Land
Developed, Low Intensity	
Developed, Medium Intensity	
Developed, High Intensity	
Deciduous Forest	Dual-Benefit Environment
Evergreen Forest	
Mixed Forest	
Pasture/Hay	
Cultivated Crops	
Woody Wetlands	
Emergent Herbaceous Wetlands	
Open Water	Natural Environment (non-human)
Perennial Ice/Snow	
Barren Land (Rock/Sand/Clay)	
Dwarf Scrub*	
Shrub/Scrub	
Grassland/Herbaceous	
Sedge/Herbaceous*	
Lichens*	
Moss*	

2.1.2. Natural Hazards Exposure

There are a total of 8 (9 if high and low temperature extremes are counted separately) natural hazard types assessed using historical events along with an additional 4 proximity-based exposure potentials that use modeled data or location to approximate exposure probability (Table **2**). Points, areas or tracks of each hazard are collected for each hazard and geo-referenced. Depending on the hazard, further processing is

carried out to estimate the spatial extent of impacts. These extents are converted to proportional land-type areas by county and hazard type to represent exposure. In the case of droughts, for instance, the data is represented as an aerial extent. Other hazards are represented by path data only, such as hurricanes and tornadoes. In these instances, a buffer is used to estimate exposure extent. Table **2** provides a summary of all 11 natural hazards and the methods utilized for determination of spatial extent.

For each hazard type, the impact of the event is dependent on land-type and extent. Measuring hazards is typically accomplished through some form of index based on features of the hazard. The challenge in combining hazards thus centers on how to make the diverse indices equivalent numerically for combination in a summary index. An example of this challenge would come from hurricanes and tornadoes, for instance. Hurricanes are measured based on maximum wind speed. While related, this does not consider the accompanying threats of flooding or tornadoes that typically cause damage in the wake of a storm. Tornadoes are similarly measured using wind speed as a baseline for index development. Though both are wind-based storms, the indices for hurricanes and tornados are not directly relatable and do not capture the differences in other characteristics. Tornadoes are much more focused in their paths and intensity, while hurricanes are vaster in extent. The distinction between these two storm types is clear in the characteristics of impact. Hurricanes, because of their extent and necessity for water, have a more probable impact on larger populations and fragile coastal ecosystems. Tornadoes, with narrower path widths and higher probability inland, do not possess the same population threat as hurricanes. Due to the differential impacts and methods of measurement for these storm types, along with many other hazards, combining them through measures of intensity scale is not very enlightening. Measuring the exact location and extent of exposure to assess impact creates a much better assessment.

Extent decisions are established for each hazard based on data and physical characteristics. Hurricane wind exposure calculations use a buffer distance of 100 miles for all storms exceeding the Category 1 (winds > 74 mph) rating. This cut point is shown from previous research to be the most robust in relation to damages experienced and corresponds to additional research on hurricane and typhoon eye wall structure (Simpson and Riehl 1981, Weatherford and Gray 1988, Zhu 2008).

Data from the National Oceanic and Atmospheric Administration (NOAA) Storm Events Database was used to estimate tornado extents (NOAA 2010). Spatial information related to the tornado, including the path coordinates, length, and width were used to create an adaptive buffer around every tornado occurrence between 2000 and 2015. Since wider and longer paths are typically associated with more severe storms this method translates well as a severity proxy (Brooks 2004).

Earthquake exposure is assessed using data available from the USGS that models and maps earthquake magnitude probability based on proximity to fault lines, substrate existing in the area, and historic events. In order to predict ground movement for a specified ground composition, the USGS Earthquake Hazards Program uses the Peak Ground Acceleration (PGA), presented as a percentage of gravity (USGS 2003). Forecast models are created by USGS for areas with historic or potential exposure to earthquakes exceeding the 0.1 g PGA threshold. According to research conducted by FEMA, a PGA of greater than 10% (0.1 g) is considered of significant velocity to cause damage to buildings not up to code or older in age (FEMA 2009). While all three land-use types are calculated for PRISM, only developed land factors into

Table 2. Summary of Natural Hazard Calculations. For each natural hazard type, the class of data is either historic (based on previous exposures to land area) or modeled (some combination of historic or land-characteristic data used to create exposure probabilities). Spatial extent explains the methods used to create data for the exposure calculations.

Natural Hazard Type	Class	Spatial Extent	Exposure Calculation
Hurricane	Historic and Modeled	Buffer of 100 miles surrounding tracks for storms > Category 1.	Proportion of each land-use classification used to estimate exposure extent.
Tornado	Historic and Modeled	Adaptive buffer based on path width data and mapped tornado tracks.	Proportion of each land-use classification used to estimate exposure extent.
Earthquake	Modeled w/Historic	USGS Modeled data -historic events and probability of event exceeding 0.1g PGA.	Proportion of each land-use classification used to estimate exposure extent.
Fire	Historic	Ignition sites of historic fires with adaptive buffer using total burn acreage.	Proportion of each land-use classification used to estimate exposure extent.
Drought	Historic	U.S. Drought monitor database extents for 5-year period in four categories (D1-D4)	Proportion of each land-use classification used to estimate exposure extent.
Wind	Historic	Entire county used as extent.	Avg. number of damaging wind events (>50 mph) per year within the county.
Hail	Historic	Entire county used as extent.	Avg. number of damaging hail events (0.75") per year within the county.
Landslide	Modeled w/Historic	USGS historic landslide incidence and susceptibility based on slope and terrain types.	Proportion of each land-use classification used to estimate exposure extent.
Temperature Extremes (high and low temperature deviations)	Historic	Entire county used as extent.	The avg. deviation of annual min and max val. from the 32-year average high and low temps.
Inland Flood	Modeled	0.5-mile buffer around inland waterways (rivers, streams, lakes, ponds, etc.)	Proportion of each land-use classification used to estimate exposure extent.
Coastal Flood (SLR/Storm)	Modeled	Buffer along all coastal counties for land within 2 feet of current sea level at mean high tide.	Proportion of each land-use classification used to estimate exposure extent.

the final calculations for the index because of the limited or non-existent damage to predominantly natural systems exposed to earthquakes.

Fire data from 2000-2010 were collected from the U.S. Geologic Survey (USGS) Wildland Fire Information database (Hawbaker *et al*. 2017). Each fire occurrence has a point of ignition, identified with a latitude and longitude, as well as the total acreage burned. This value is used to create an adaptive buffer by back-calculating a buffer radius around the points. The circular burn buffers are then used to estimate land proportions exposed to fire in each county.

Drought exposure is based on data from the U.S. Drought Monitor Database (NDMC 2017). This dataset contains shapefiles of drought extent collected on a weekly basis since 2000, categorized into 5 levels of severity ranging from D0

(abnormally dry) to D4 (exceptional drought). For the purposes of this research, only categories D1-D4 were used. Due to the frequency of data collection, four samples, one representing drought conditions in each season (winter-first week of January, spring- first week of April, summer-first week of July, fall- first week of October), were taken from each year between 2005 and 2010. Annual and 5-year averages were tabulated for each county within each of the 4 drought categories (D1-D4) to represent total exposures as well as the severity of exposures.

Damaging hail and wind events exposures are assessed for the entire county using data from the NOAA Storm Prediction Center Historic Climatic Database (NWS 2016). A spatial buffer could not be used due to the lack of specific information on the spatial extent of hail and wind events. To calculate risk for the hail and wind events, the annual hail events within each county boundary are averaged over a 10-year span, from 2000-2010. The thresholds for damage-inducing events, a hail diameter of greater than 0.75 inches and wind gusts exceeding 50 miles per hour, are based on NOAA research (NWS 2007).

Landslide data comes from USGS incidence and susceptibility data, modelled and mapped based for locations of past landslides along with data on slope and terrain types that cause higher landslide risk (Radbruch-Hall *et al*. 1982; King and Beikman 1974). For the purposes of exposure likelihood, only the first four classes are used: High landslide incidence (>15% area involved in land-sliding), moderate landslide incidence (1.5-15% area involved in land-sliding), high susceptibility to land-sliding with low incidence, and moderate susceptibility with low incidence. The percentage of land falling into each of these four categories is summed to determine a probability extent for exposure to landslides.

Temperature extremes are assessed based on a 32-year record of maximum and minimum annual temperatures recorded in each county. Using this record, the annual average high and low temperatures are compared to establish and average deviation value above or below what is considered "normal" for the 3 decades. This is done by subtracting the annual high and low average temperatures from the 32-year mean values and inverting the result. Similar to the wind and hail data, the values for this metric represent the entire county and are not split into three land-type classifications. Both a deviation from annual low temperatures and annual high temperatures are calculated and used as individual metrics.

2.1.3. Proximity-Based Hazard Exposure

While tornadoes and hurricanes both have a documented historic risk based on events of the past 15 years in this study, it is important to also consider the inherent, or "basic" risk to locations based on their proximity to hazardous areas. This is very similar to the probability or susceptibility models done for earthquakes and landslide. Coastal counties along the Atlantic and Gulf of Mexico are at risk during any given hurricane season. Lack of occurrence data over the past 15 years does not exclude these counties from possessing future hurricane risk. The same applies to counties located in areas of higher tornado probability. Lack of impact in past does not preclude future incidents. Both hurricanes and tornadoes were assigned to counties as a basic risk established by location.

A proximity-based hurricane exposure probability score of 0.15% was assigned to all counties within 75 miles of the Atlantic or Gulf of Mexico coastlines. This percentage is created using the average probability of hurricane landfall in each, non-El Nino year (48%), divided 305, which is the number of coastal counties where hurricanes could strike (Bove *et al*. 1998). Proximity-based tornado

exposure probability was assigned using historic tornado data to select all counties with any tornadic activity in past 15 years. Each of these counties was assigned a basic risk score of 0.06% based on past climatological models (Schaefer *et al*. 1986).

Flood exposure is also quantified as a basic exposure in this research due to its calculation and the inherent risk present as a result of proximity to defined features. It is measured within two categories, inland exposure and coastal exposure. For the inland category, all rivers, streams, lakes and ponds were mapped using a ½ mile buffer to represent a potential exposure to flooding from these sources. Coastal flooding calculations use the NOAA Sea Level Rise predictions (Parris *et al*. 2012). These are based on height (mean high water) above sea level and derived from digital elevation maps (DEMs) along the coast. All land 2 feet or less above sea level are categorized as at risk.

2.1.4. Technological Hazards

In addition to natural hazards, a place may have additional exposure potential because of proximity to technological hazards. Technological hazards, such as nuclear power plants, Superfund sites, or toxic release sites, can have the potential to impact nearby populations regardless of natural exposure; however, natural hazards can exacerbate the technological risk. Table **3** shows the technological hazards used in this approach.

The Federal Emergency Management Agency (FEMA) tracks limited technological hazards through the Radiological Emergency Preparedness Program (REPP), for commercial power plants, and the Army chemical weapons stockpiles in the Chemical Stockpile Emergency Preparedness Program (CSEPP), for military chemical weapons stockpiles. In each of these preparedness programs, the concern is focused on potential human exposure to these hazards. However, many of the technological hazards could have a serious negative impact on plants and animals, suggesting this definition of technological risk needs to be expanded to encompass non-human ecosystems as well. In the case of crop land, even if human settlements are not directly impacted an exposure could still directly impact the food supply. For this reason, the point data for nuclear and chemical sites are assessed here for their impact on all land-use types and the data are expanded to include Superfund sites and sites on the Toxic Release Inventory (TRI).

Nuclear reactors or storage facilities in an area present additional hazards in the event of a leak. While most of these facilities are designed and built to withstand geologic and meteorological events common to their area, accidents are still possible and the underlying risk is still elevated because of their presence. The U.S. Nuclear Regulatory Commission (USNRC) designates an official Emergency Planning Zone (EPZ) based on the

Table 3. Technological Hazards metrics used in the PRISM approach and the methods used to collect and assess.

Technological Hazard Type	Spatial Extent	Exposure Calculation
Nuclear Facilities	All nuclear reactors and storage facilities in US identified and given a 10-mile buffer.	Proportion of each land-use classification used to estimate exposure extent.
Superfund Sites	Superfund sites - proposed or active in the US identified and given a 5-mile buffer.	Proportion of each land-use classification used to estimate exposure extent.
Toxic Release Inventory (TRI) Sites	TRI facilities identified when threshold chemical release criteria are met and given a ¼-mile buffer.	Proportion of each land-use classification used to estimate exposure extent.
Resource Conservation and Recovery (RCRA) Sites	All RCRA Site (LQGs, TSDs, and TRANSs) point data from EPA FRS Geodatabase are given a ¼-mmile buffer.	Proportion of each land-use classification used to estimate exposure extent.

plume exposure pathway distance of 10-miles. This distance is designed to limit exposure to radioactive materials through sheltering, evacuation, or the use of potassium iodide, if necessary (USNRC 2014). Nuclear facilities are mapped by point location and given a 10-mile buffer to designate their EPZ. Using methods described for natural hazards, risk is assigned to each county with percentages of risk distributed across each of the three land-use categories.

In contrast to nuclear facilities, superfund sites are slightly more complicated than nuclear facilities since they are not all the same. The sites can be in one of four conditions: proposed, active, completed, or deleted, depending on how far along the site is in the clean-up process. In addition, the chemicals present at a site can vary in their toxicity and range of potential travel. Generally, the impact of these sites will be localized, regardless of the chemical(s) present. Therefore, a buffer of one mile is created around each site that has been active during the past ten years and percentages of land covered are calculated for each of the three land-use types.

Toxic Release Inventory (TRI) and Resource Conservation and Recovery (RCRA) sites are by far the most numerous and varied of the technological hazards. Their potential to increase risk in the event of another hazard makes their inclusion important. TRI and RCRA sites have the capacity to impact air, water, and land quality and exist within both highly populated and more sparsely populated areas. TRI data was gathered from the TRI Explorer, which catalogs over 53,000 facilities that have been tracked in the past 20 years. To remain temporally consistent, only TRI sites logged within the 2000-2010 timeframe were used here. Data for RCRA sites was obtained from the EPAs Facility Registry Service (FRS) and only includes sites with greater exposure potential than TRIs, classified as Large Quantity Generators (LQGs), Hazardous Waste Transportation Services (TRANS) and Treatment, Storage and Disposal facilities (TSDs). To calculate the risk to each land type, a simple count of TRI and RCRA sites without a buffer in each county is used. TRI and RCRA density (count per area) with each land type in a county will represent the potential exposure.

2.1.4. Losses

Historic losses give exposure metrics the context needed to become a measure of intensity and impact across the landscape. In this approach, losses are combined into three categories, property, crop, and human, using data compiled from the Hazard and Vulnerability Research Institute's (HVRI) Spatial Hazard Events and Losses in the U.S (SHELDUS) database (HVRI 2017). Property and crop losses both serve as severity measures inbuilt and managed ecosystems, while human losses encompassing both fatalities and injuries, represent the social severity of the hazards. Losses are reported as per capita in 5-year segments. Losses are assigned to specific land classifications based on the type. Human and property losses are assigned to the built environment and crop losses are assigned to the dual-benefit environment. Natural losses are assessed using additional data from the NLCD on land cover change. This dataset identified land-use pixels that have changed to pervious surfaces (indicating built environment) between 2006 and 2011. The percentage of total county land converted to the built environment is used as a proxy for natural lands lost. The damage posed to natural systems resulting from population stresses or other anthropogenic influences, represented by the natural land loss, foreshadows potential reductions in ecosystem services (Hey and Philippi 1995).

2.2. Risk Calculation

While the specific issues related to collection and development of each risk exposure layer have

been described, the primary challenge comes in combining these to represent an overall risk landscape. In other words, how do the risks, both natural and technological, interact to create exposure likelihoods? A simple additive calculation cannot adequately answer this question. Instead, the calculation is more complicated, and a nuanced structure that accounts for not only each exposure, but the likelihood of loss that stems from the occurrence frequencies and the hazard severity.

Combining hazards in a meaningful way requires blending of spatial exposures and losses. Using the methods described, every hazard can be addressed by calculating a proportion of county land both impacted historically and land that could be impacted based on proximity to hazard zones (i.e. coastal Atlantic counties and hurricanes).

The complexity of the hazard-scape is represented in the final calculations, where the interplay of natural hazards, technological hazards, losses, and county landscape are used to create a risk score. This process, as shown in Fig. (**1**), is much more nuanced than a simple additive index. The combination of exposure extents, land-type distributions, and the associated losses are demonstrated in detail within section 3.3 with a regional analysis and break out of calculations for the high, medium, and low-risk counties in that area. Hazards are combined in steps based on the spatial extents, characteristics and land type first, then hazard type second. The first step modifies the historical exposures by weighting them with proximity-based hazards. Spatial extents for each hazard are based on the proportion of land area and added within land-types before modification. Proximity-based hazards are proportional as well, based on hazard probability, and added to one prior to being multiplied by the historic exposure.

The combined historic and proximity-based exposure value is added to the land-type proportion of technological hazards to create the final exposure probability. There will be three of these probability scores for each county, one for each land type. The exposure probability is then multiplied by the land specific loss (e.g. crop and structural loss for dual-benefit lands) to create a land-type risk score. Each county will have three risk scores following this step along with proportional land area types. These values are used to weight the risk scores and create a single risk value for the county. By weighting the historic exposure scores using both land types and proximity measures, the resulting PRISM score can capture the changes in risk resulting from locational and landscape-derived differences. The final score is thus dependent not only on direct hazard impacts, but also the changes occurring to the surrounding landscape.

3. RESULTS

The primary goal of the PRISM approach is to create a national landscape that accounts for a full suite of hazard exposures spatially. Along with losses, the data created from PRISM forms the risk domain of the Climate Resilience Screening Index (CRSI). However, the potential applications of the PRISM approach are much broader than inclusion in CRSI. In addition to creating an integrated risk value, the results can also be broken out into many categories for analysis. Some of the potential analyses enabled by PRISM include the examination of (1) temporal trends, (2) natural versus anthropogenic risks, (3) separate risk values for major land categories, and (4) multiple spatial scales ranging from county up to states and EPA regions. Prior to these type of specific analyses, a summary of the data is presented here to provide an overview of the results from the CRSI Risk domain as well as some specific spatial results.

3.1. National Results

The overall results, shown as a map in Fig. (**2**), and their variation across each land type are com-

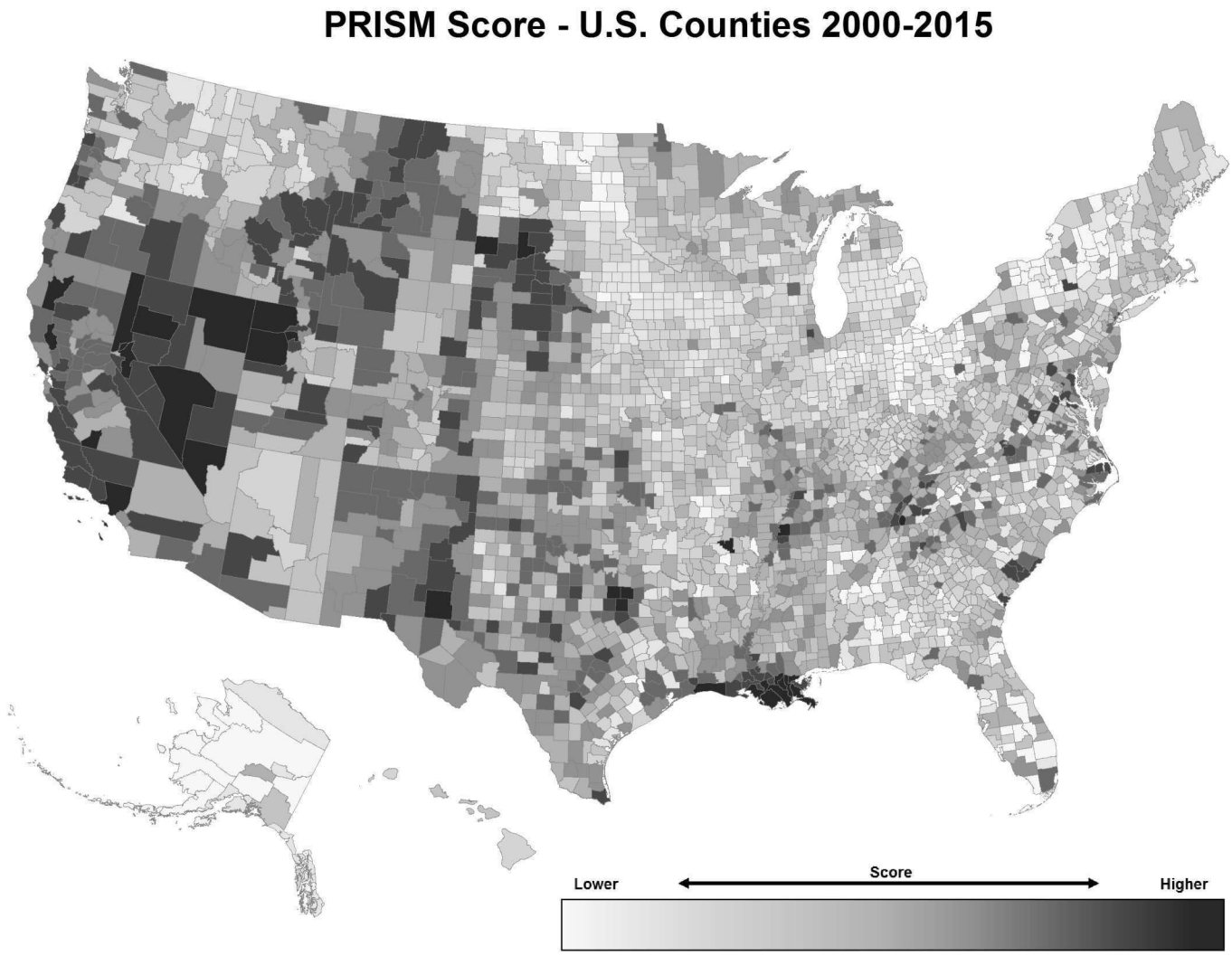

Fig. (2). PRISM Overall County Scores for all land types and entire 16-year period of measurement.

pared using a boxplot in Fig. (**3**). There are clear regional patterns in the data, with much of the Southwest, Louisiana, and plains states exhibiting higher risk levels. In addition, areas in the Appalachians and along the Eastern coastline display higher risk values. The Southeast, despite exposure to tornados and hurricanes, exhibits a comparatively low overall risk score. This could be due to the high exposure to drought and wildfires in the Western U.S. Interestingly, dual-benefit lands seem to drive much of the risk across the U.S. over the 15-year span. Risks to these lands are significantly higher than those in natural or developed lands, and the median falls closer to that of the overall score.

Analyzing the distribution of land types in the U.S., it is evident that much of the weight attributable to dual-benefit lands is due to the percentage of land in this category. Over 50 percent of U.S lands are classified as dual-benefit, with a bulk of those falling into either crop land in the middle of the country, and wetlands along the coast. Each of these land types provides a major service to urban communities and higher risk values to these lands is a significant concern. In addition to explaining the overall weighting as a function of percent coverage, this overall land distribution also highlights the importance of county-specific calculations for each category. While most of the U.S. is either natural or dual-benefit land, there are many coun-

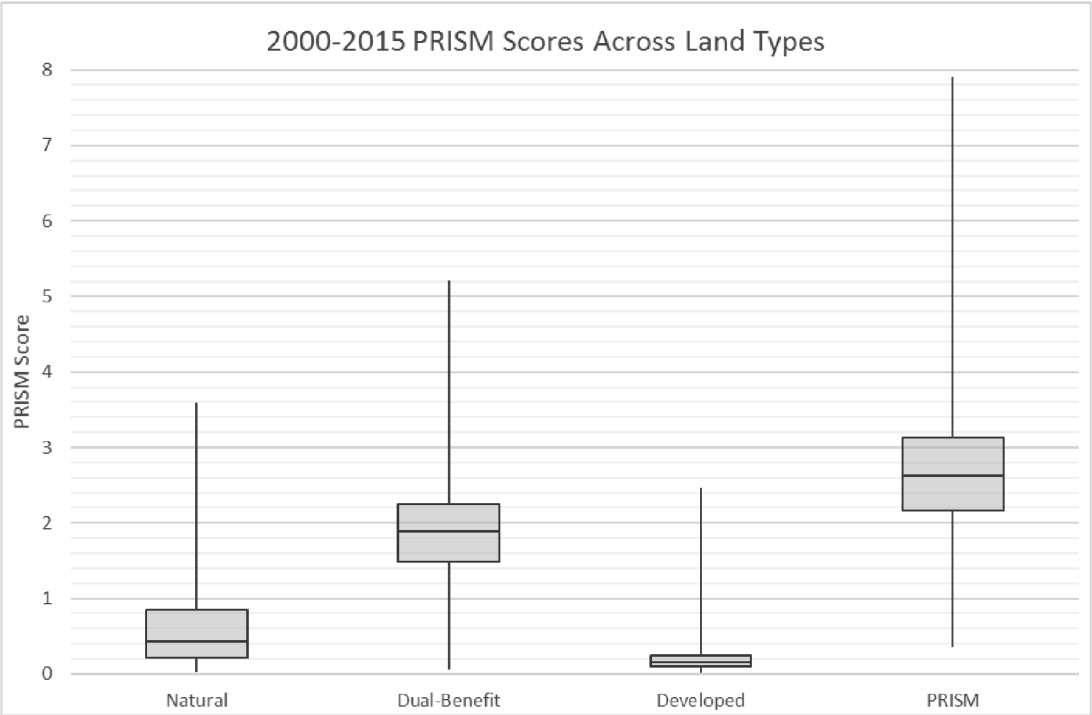

Fig. (3). Box Plots of Overall PRISM Score along with Land-type scores. Data represented in this graph are from 2000 - 2015.

ties that have a very small amount of this land type. Each county, state and region will have a very different land coverage, and thus a very different risk profile that must be managed. This distribution is shown in Fig. (**5**).

Temporal trends for PRISM across the three 5-year time periods (Fig. **4**) show that risk to dual-benefit lands consistently encompasses a majority of the overall score. Through each time period, both natural and developed land risk scores remain relatively low and unchanged. This is relatively surprising given the rise in sprawl and increased population in urban areas. Dual-benefit, however, experiences a spike in the 2005-2010 period. This spike is also evident in the overall score, despite both natural and developed lands experiencing a slight risk decrease over the same period. Reasons for this increase could be tied to changes in extent and severity of drought and wildfires, which impact much of the dual-benefit lands during this time period.

In addition to temporal patterns, there are clear patterns of risk distribution among the three land types both at a regional and county level. Regionally, both dual-benefit and natural lands dominate different parts of the country. Most of the Western U.S is predominantly natural, while the Midwest and up into portions of the Northeast is primarily dual-benefit. As suspected, the developed lands, except a few pockets of the interior, exists almost entirely along the coastline. Few counties are homogeneous, instead of having a mix of the three land-types.

Using a risk measure weighted by land-type distribution it is possible to adjust for county and regional patterns and better assess the extent of threat without exaggerating the impact of hazards on developed areas where monetary losses may be higher. The two forms of analysis, hazard-exposures and land-use types, are examined here using exposure and loss layers for the U.S. between 2000 and 2015. First, we will examine land-type changes and the accompanying shift in risk profiles that occur as the result of development and exposure types. Second, we conduct a temporal analysis that examines changes in the natural and techno-

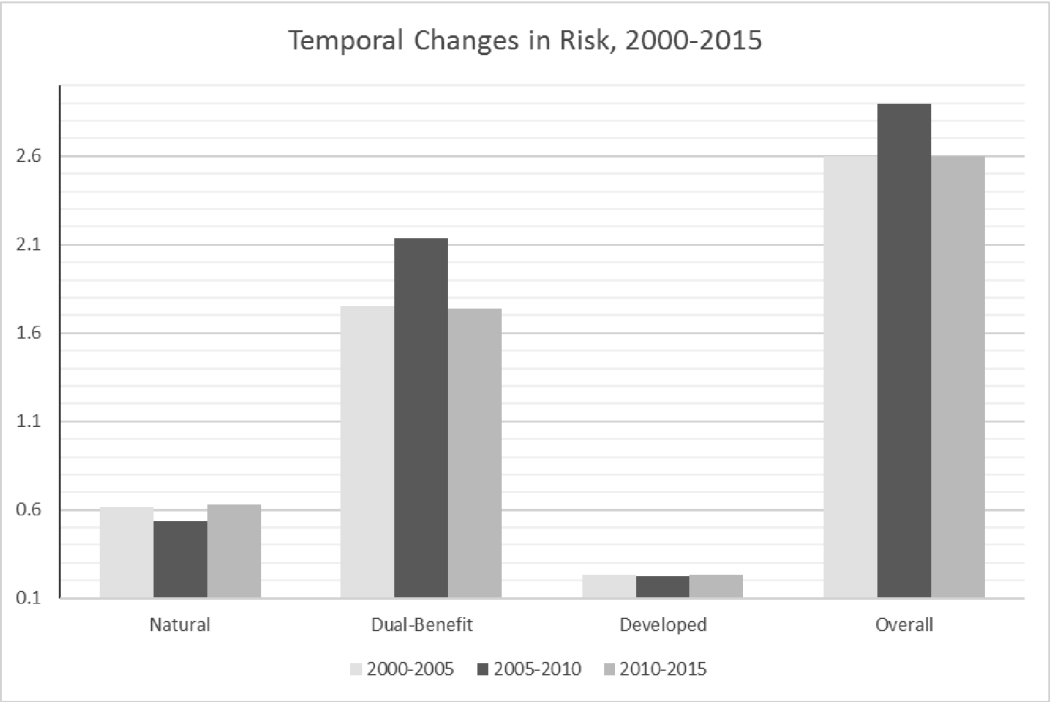

Fig. (4). Graph of Temporal Risk Changes across each land type and the overall PRISM Score.

logical risks. In each of these examples, the goal is to demonstrate flexibility and display the unique data produced for the analysis of multiple hazards.

The effects of county land-type composition are demonstrated through a series of maps (Fig. **5**), showing risk scores by land-use type for each of the three time-periods. Comparing this to the date in Fig. (**3**) can be used to address the distribution of risk versus the overall risk values, especially in the case of dual-benefit lands. While some increases in the spatial distribution of risk to developed lands occurs over the fifteen years, natural risk seems unchanged. While this matches up with the overall scores through time, the dual-benefit lands seem to exhibit a drastic spatial shift in risk from Eastern counties to Western counties. In the first time-period, risk in this category is primarily observed in the Eastern portions of the country. As time progresses, the areas of higher risk move Westward and appear to increase substantially along the West coast by the final time period.

Large spatial shifts like this are important to look at in more detail. Despite a relatively unchanged overall risk profile for the country, the land-type specific burden does appear to have shifted regionally. With regards to planning, a shift of this magnitude could also indicate that areas not normally exposed to hazards are now experiencing impacts, and could be potentially unprepared.

This national analysis is important from the perspective of regional and temporal changes in risk, however, it is a compilation of multiple values across many geographies and years. To showcase the value of an integrated multi-hazard approach, a more in-depth investigation of the risk components is also conducted using smaller geographic areas with higher risk scores. There are two that stand out in the overall approach; segments of the Southwest and the Gulf Coast of Louisiana, which are analyzed in more detail. This break down of risk components from the final score will call out specific hazards and risk areas and demonstrate why single risk values are valuable, yet require decomposition. Using a smaller number, the top 100 counties in overall risk, will allow for better analysis of their unique risk profiles.

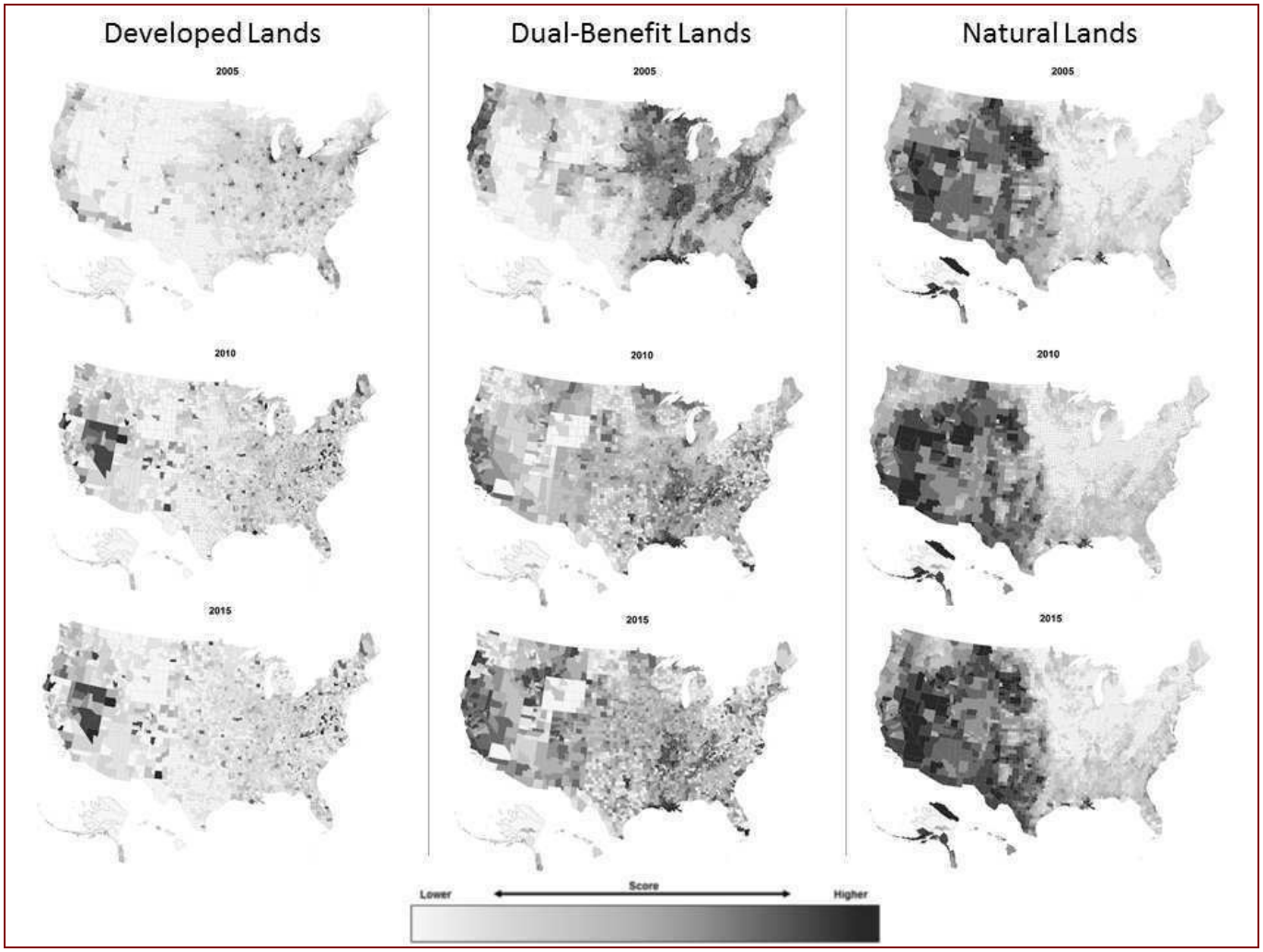

Fig. (5). Land-type Risk values break-down by time span. Each panel represents a specific land type within the counties over the same 5-year blocks of time. The left column represents risk to developed lands alone, the middle column represents risk to dual-benefit lands alone, and the right column represents risk to natural lands alone. In each map, darker colors indicate higher risk values, or a combination of exposure and losses for each land-type.

3.2. High-Risk County Analysis

The top 100 risk counties in the US represent twenty-three states, yet four states account for over fifty-percent of this group. Included in these four are, in order from most to least counties, Louisiana, Nevada, California, and Texas. Despite the similar overall risk scores, the two highest risk states, Nevada and Louisiana, have considerably different exposure profiles. In Louisiana, exposures from anthropogenic hazards are considerably higher than Nevada, with an average score of 0.067 versus 0.005. This is especially true in dual-benefit lands, where the exposure is more than 30 times greater (0.003 in NV and 0.103 in LA). Basic exposure in Louisiana (2.47) is also more than double that of Nevada (1.20). Driving the anthropogenic hazards in Louisiana is a significantly higher exposure to Superfund sites along the coast along with higher exposures to nuclear and RCRA sites. Elevated basic exposure in Louisiana is based on low-lying land threatened by both coastal and inland flooding. This produces a potentially dangerous combination in the event of natural hazard exposures exacerbating risk due to chemical or other toxic contamination related to these sites. In Nevada, the exposure from natural hazards (2.68) is larger than Louisiana (2.08), driven largely by

fire and drought, which are both closely related and cover a majority of the state's land area.

While the counties examined in these two states are similar in overall risk, it is helpful to examine the exposure metrics driving this risk. Changing patterns in risk drivers may require considerably different strategies when it comes to mitigation efforts. In Nevada, for instance, wildfires and drought would be handled through efforts such as prescribed burns, removal of undergrowth and potential fuel sources, and treatment of surfaces to minimize combustion. Louisiana would take a very different approach to mitigation by cleaning up hazardous waste sites, building flood control structures, and managing development in flood zones. In each instance, the end goal is the same, yet funding and policy would be handled in a different manner.

3.3. Regional and Hazard Specific Applications

In addition to the inspection of the broader risk profiles, PRISM can also be used to analyze regional patterns or investigate hazard-specific spatio-temporal changes. A subset consisting of Gulf Coast Counties is analyzed first to demonstrate the regional utility of PRISM. In this example, the representative sub-set consists of fifty-four coastal counties from five states bordering the Gulf of Mexico. Over the sixteen-year study period, the average PRISM score of these counties is 3.21, which is considerably higher than the national average of 2.7. From this set of counties, Plaquemines Parish, LA has the highest PRISM score (5.41) of the subset (second highest of the entire U.S), while Charlotte County, FL has the lowest (2.39).

The PRISM scores in this example are deconstructed by land-type and risk domain (exposure and loss) to better analyze and compare patterns of risk. Looking first at the mean land-type risk, there are distinction between counties that become apparent. Developed land risk is low (mean = 0.22) apart from a few counties with significantly higher scores. Dual-benefit land appears to drive much of the overall risk with a mean of 2.21 and maximum of 5.21. Natural lands fall in between the two with a mean risk score of 0.76. From an exposure perspective, the dual-benefit risk is likely driven by a reliance on saltwater marshes and other land-types associated with flood and storm protection in these coastal counties. With urban development and sea level rise threatening the hazard mitigation function of natural and dual-benefit lands, the risk of loss resulting from future exposures to spreading urban environments should be expected to increase. The trend toward higher risk in heavily urbanizing counties is already evident (Figure along the Gulf coast, where rapidly developing counties from the past decade also possess high risk values across all three land-type categories.

A deconstruction of the risk domains, exposure and loss, reveals yet more detail and another layer on top of the land-type analysis. Exposure measures are assessed independently to determine the extent of impact in an area and assess the relative distribution of exposure probabilities. An example of this can be seen in Fig. (**6**), with three pie charts that show the distribution of exposure and loss across each of the hazards and how these translate to losses by land type. What is striking about this graphic is both the sizeable amount of natural hazard exposure to drought and temperature extremes and the comparatively small amount of loss to developed lands. Despite these counties having higher populations and infrastructure, the primary drivers of risk are related to temperature and rainfall events that impact crops, forests, marshes, and other natural lands not primarily related to the built environment. This is contrary to the standard measures of risk that focus on built environments and report monetary losses.

Putting the two analyses together paints a more holistic picture of risk in a region presented with a number of potential exposures. Risk location is explained through closer analysis of exposure

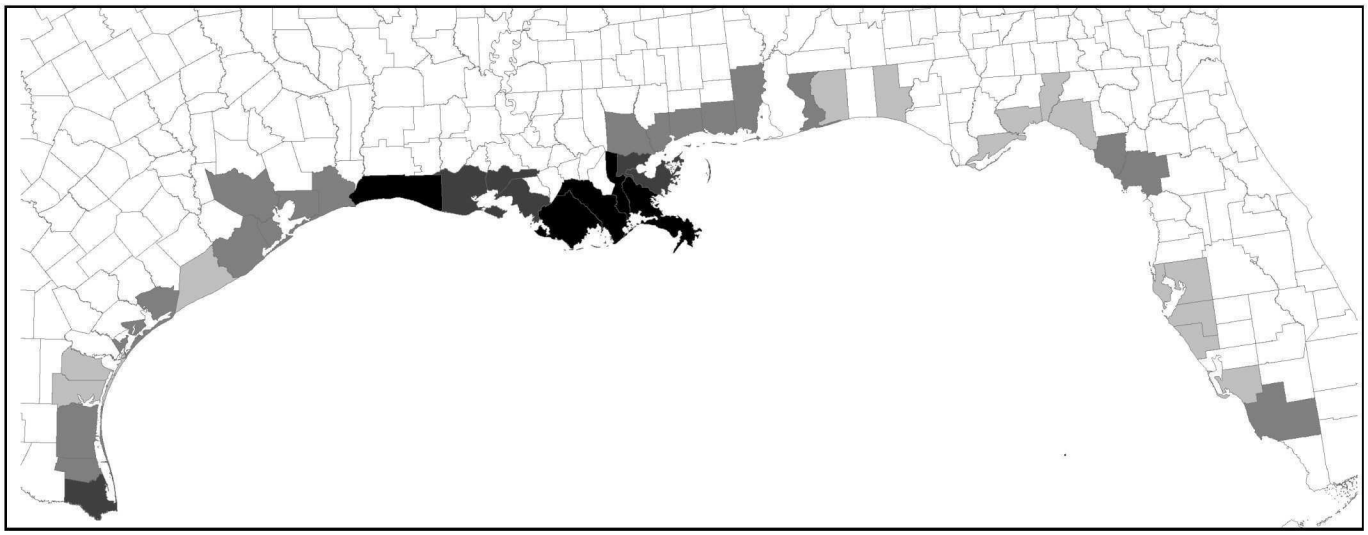

Fig. (6). Gulf Coast Counties overall PRISM score. 54 counties in 5 states with risk estimate calculated from 16-year period (2000-2015). Darker colors indicate higher risk probability across all land-types for all hazard types.

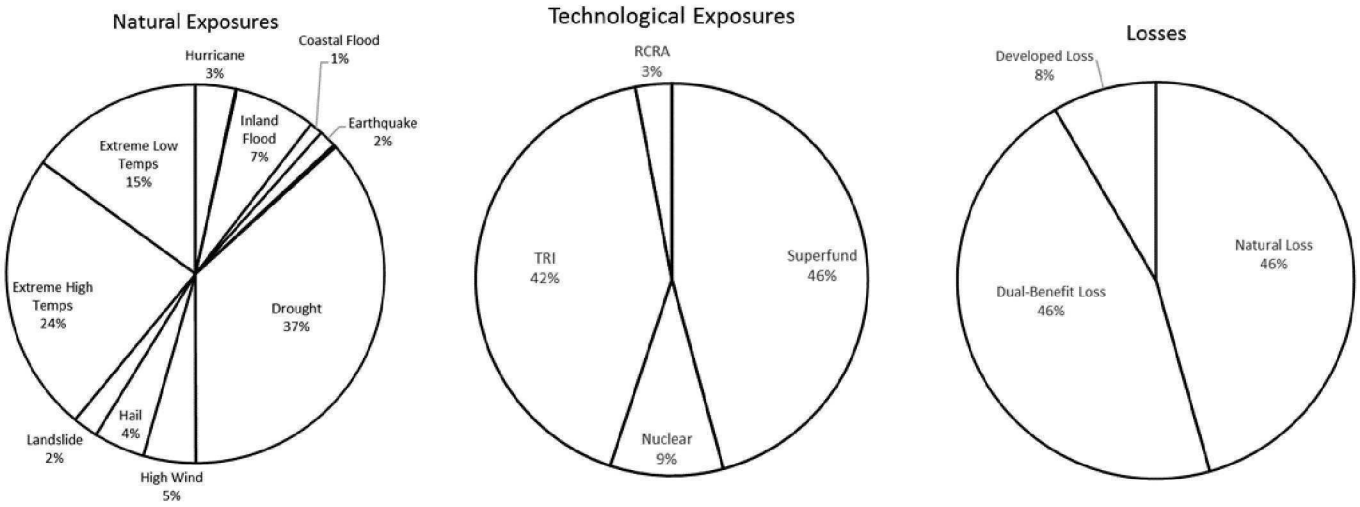

Fig. (7). Three pie charts showing distribution of exposure and loss across fifty-four counties bordering the Gulf of Mexico. The percentages represent the distribution of average exposure probability for each hazard type between 2000 – 2015.

types along with land-type characteristics. Many areas of the Gulf coast are sparsely populated, yet have numerous vulnerable natural resources. This vulnerability shows up in the deconstruction of PRISM exposure where a bulk of the losses occur in dual-benefit lands as a result of temperature and rainfall events. In a location where hurricanes are what most people would consider the primary risk concern, the actual exposure threats are quite different when compared alongside the full spectrum of exposures and losses.

To best capture the influence of exposure extents, land types, and losses, Table **4** shows the land weighted, scaled values associated with three of the Gulf Coast counties: Terrebonne Parish (highest), Charlotte County, FL (lowest), and Hillsborough County, FL (middle). The numbers represent exposure and loss values already weighted by land-use type. Land use percentages are shown under the county names to provide some insight into the differences between the counties. Interestingly, the county with the least developed land, Plaquemines, has the highest level of exposure to natural hazards and the highest loss values.

There are a few key measures easily identifiable and responsible for the differences in the final risk

Table 4. Example of PRISM calculation for Plaquemines Parish, Hillsborough County, and Charlotte County to display the influence of exposure and loss changes on the final score. Land-use percentages are shown in left column with county names. Bolded natural exposures represent basic exposures in the model. All exposures and losses are land-weighted prior to entry in this example.

	Land-Weighted Natural Exposures		Land-Weighted Technological Exposures	Land-Weighted Losses	Risk
Plaquemines Parish, LA: Natural Land – 47% Dual Land – 51% Developed Land – 2%	Hurricane - 0.5085 **Basic Hurr. -0.0015** Tornado- 0.000075 **Basic Torn. 0.0006** **Inland Flood- 0.975** **Coastal Flood- 0.97** Earthquake - 0 Fire - 0	Drought – 1 Wind – 0.0592 Hail – 0.0073 Landslide -0 High Temp. -0.50 Low Temp. -0.59 Sum – 4.6104	+ Superfund-0 TRI-0.006 RCRA-0.005 Sum-0.00652	× Nat.-0.0083 Dual-0.0085 Dev.-0.171 (Sum+1)-1.17267 =	5.41
Hillsborough County, FL: Natural Land – 13% Dual Land – 49% Developed Land – 38%	Hurricane - 0.50 **Basic Hurr. -0.0015** Tornado- 0.000411 **Basic Torn. 0.0006** **Inland Flood- 0.109** **Coastal Flood- 0.034** Earthquake - 0 Fire - 0	Drought – 1 Wind – 0.0216 Hail – 0.1605 Landslide -0 High Temp. -0.44 Low Temp. -0.11 Sum – 2.5779	+ Superfund-0.23 TRI-0.0732 RCRA-0.00324 Sum-0.3058	× Nat.-0.03086 Dual-0.03087 Dev.-0.0000995 (Sum+1)-1.0618 =	3.06
Charlotte County, FL: Natural Land – 15% Dual Land – 65% Developed Land – 20%	Hurricane - 0.50 **Basic Hurr. -0.0015** Tornado- 0.000143 **Basic Torn. 0.0006** **Inland Flood- 0.0754** **Coastal Flood- 0.12** Earthquake - 0 Fire - 0	Drought – 1 Wind – 0.0254 Hail – 0.030 Landslide -0 High Temp. -0.46 Low Temp. -0.10 Sum – 0.3267	+ Superfund-0 TRI-0.00371 RCRA-0 Sum-0.00371	× Nat.-0.00809 Dual-0.00853 Dev.-0.0069 (Sum+1)-1.0235 =	2.39

scores between these three examples. What separates Plaquemines Parish from the other two counties is both the flood risk and losses in developed lands. Whereas Hillsborough and Charlotte counties have similarly intermediate levels of exposure, they are relatively small in comparison. This is largely the result of Plaquemines' situation along the Mississippi River delta and the Gulf of Mexico. This Parish encompasses most of the delta and is experiencing significant losses due to both rising sea levels and land subsidence (Zou *et al*. 2016). These losses put most land in the parish at great risk from both riverine floods and coastal flooding as a result of decreased buffers provided by the marsh. Developed loss values for Plaquemine parish also stand out as significant compared to the other two counties. This is remarkable due to the small land percentage designated as developed. Losses to both human life and property are significantly higher than most other counties. Knowing this helps focus efforts by highlighting the intersections of exposure and loss.

The other key difference, and a feature that distinguishes the PRISM method, is the handling of losses as a function of exposure. High exposure potential can be tempered by low losses; just as

lower exposure potential can be greatly inflated by high losses. For example, if losses comparable to Charlotte county (1.02 instead of 1.17), were experienced in Plaquemines Parish, the resulting risk would be 4.7. Similarly, if Charlotte county were to increase losses to a level comparable to Plaquemines, the overall risk score would be 2.72. These examples provide some evidence of the utility of PRISM in the identification of highest exposure risks and more importantly in the determination of causal relationships driving the losses. Information gleaned from this analysis can be applied to more targeted mitigation actions.

4. DISCUSSION

While there are existing multi-hazard approaches, a surface based exposure approach melding multiple natural and technological hazards is novel and produces results that are highly adaptive and scalable. In a decision-making context, this makes the data useful for planning and analysis at the county, state and regional level. Resilience is defined through a regional ecology approach, where external forces act on a community, and the interactions with neighboring places for support are significant in recovery (Holling 1986). In this context, it makes sense to expand the reach of hazards integration across the entirety of the United States. From a policy standpoint as well, it is logical to analyze hazards at the minimum of a regional scale. Many disasters far exceed local capacity to rebound, and regional or national resources are needed to aid recovery in both the short and long terms. As development in areas of high exposure probability increase (e.g. coastal areas), the losses will continue to rise and strain development goals and the ability to mitigate (Miletti 1999).

In addition to policy concerns, there is also the consideration of rapidly changing landscapes and shifting hazard-scapes, making it critical to have an approach that can be updated on a regular basis. A good example of this would be through examination of county losses. Knowing that per capita human or property loss numbers increase over time only tells part of the story. The other part is told by the change in land-use or hazard exposure. Without a more detailed analysis, there is no way to know whether the increased losses are the result of expanding urban areas where hazards occur, increased exposure to hazards due to a change in patterns, or simply the existence of a new hazard. By accounting for each of these factors, the PRISM approach allows for a more detailed examination of all exposure types, and is capable of answering these types of questions.

PRISM results can also facilitate decisions at the county, state or regional level through use of a comparative value system that is consistent across the United States. For a large-scale multi-hazard approach, this is an incredibly important step that removes conflicts arising due to qualitative or region specific assessments of hazard severity. In PRISM exposure is calculated along with other hazard parameters, where applicable (e.g. wind speed, earthquake magnitude, etc.), to assess magnitude, which allows for comparability across hazard types. Because of this uniform exposure assessment, regional disparities in exposure type do not impact the analysis. Impact in the form of spatial extent and loss, not severity of the event, matters. It does not matter if a category 2 or a category 5 hurricane hits a county. What matters is how many people, structures, and other environments are in the path along with losses sustained as a result of the exposure. If a county is well prepared for the hazard, it would be expected that losses are less. It is very possible, following this logic, for a county exposed to a category 3 storm to have greater losses than another county exposed to a category 5 storm. In the end, the strength of the storm is of secondary concern to the extent and type of losses endured. For this reason, the storm severity is only used as a threshold value to deter-

mine risk. It is not used to categorize the exposures.

While the probability of hazard recurrence is not solely based on historical frequencies, it does aid in the discussion both from an exposure standpoint and in the determination of disaster fatigue. The impact of multiple events over a relatively short period of time can also have a major impact on a communities' recovery and future resilience (Bobrowski 2013). People are likely to be worn down, resulting in loss of business and potential emigration from the area. Long term impacts to the economy and social networks may take years to recover; if they ever do.

While the PRISM model was developed with a specific purpose, the final product can yield much greater use in general hazards planning. Aside from the consideration of potential hazard-type exposure to an area, it is equally important to consider the land types being impacted. All places are different, and this makes for differences in their vulnerabilities. In most cases, risk is assessed solely with regards to developed lands. People worry about impacts to lives, jobs, and structures primarily, while risk models fail to separate out the landscape to account for different land uses. The PRISM model uses three land classification categories to look at risk in the context of management decisions. The three choices for land use were meant to distinguish and call attention to places where conflicts of interest may arise. These dual-benefit lands are defined by their combined value to both humans and to ecosystem health. These lands typically do not hold many people and are neglected in most discussions of risk, whether it be natural or anthropogenic. Much of this land type is threatened, however, and this threat appears to be on the increase. Looking at the descriptive statistics for each land type, it is also clear that dual-benefit lands are the driver behind the overall risk value.

Given the challenges discussed here, a new approach to multi-hazard assessment is outlined with an intent to create a single measure of hazard risk for a location to be incorporated into further assessments of resilience, namely the Climate Resilience Screening Index (CRSI; Summers *et al*. 2017). This model uses an integrated spatial approach to assess multi-hazard exposure of a landscape to distill a single value representing a cross-section of this exposure with the vulnerabilities across counties. This is a novel approach meant to streamline the assessment of multi-hazard risks via the removal of both subjective impact measures and complicated hazard maps.

ETHICS APPROVAL AND CONSENT TO PARTICIPATE

Not applicable.

HUMAN AND ANIMAL RIGHTS

No Animals/Humans were used for studies that are the basis of this research.

CONSENT FOR PUBLICATION

Not applicable.

CONFLICT OF INTEREST

The authors declare no conflict of interest, financial or otherwise.

ACKNOWLEDGEMENTS

Declared none.

REFERENCES

[1] Batista, M.J., Martins, L., Costa, C., Relv, A.M., Schmidt-Thome, P., Greiving, S., Fleishauer, M., Peltonen, L. 2004. Preliminary results of a risk assessment study for uranium contamination in central Portugal. Proceedings of the Internation Workshop on Environmental Contamination from Uranium Production Facilities and Remediation Measures, ITN/DPRSN, Lisboa. February 11-13, 2004.

[2] Bell, R., and Glade, T. 2011. Multi-hazard analysis in natural risk assessments. *WIT Transactions on State of the Art in Science and Engineering* 53: 1-10.

[3] Bobrowski, P., ed. 2013. *Encyclopedia of Natural Hazards*. 1135 p. Springer.

[4] Bove, M., O'Brien, J., Eisner, J., Landsea, C., and Niu, X. 1998. Effect of El Nino on U.S. Landfalling Hurricanes, Revisited. *Bulletin of the American Meteorological Society* 79(11): 2477-2482.

[5] Brooks, H. 2004. On the Relationship of Tornado Path Length and Width to Intensity. *Weather and Forecasting* 19: 310-319.

[6] Burton, I., and Kates, R.W. 1964. The Perception of Natural Hazards in Resource Management. *Natural Resources Journal* 3(3): 412-441.

[7] Chester, D.K., Degg, M., Duncan, A.M., Guest, J.E. 2000. The increasing exposure of cities to the effects of volcanic eruptions: a global survey. *Global Environmental Change Part B: Environmental Hazards* 2(3): 89-103.

[8] Cutter, S.L., and Solecki, W.D. 1989. The national pattern of airborne toxic releases. *Professional Geographer* 41(2): 149-161.

[9] Cutter, S.L. 1996. Vulnerability to environmental hazards. *Progress in Human Geography* 20(4): 529-539.

[10] Cutter, S., Burton, C., and Emrich, C. 2010. Disaster Resilience Indicators for Benchmarking Baseline Conditions. *Journal of Homeland Security and Emergency Management* 7(1): 51-51.

[11] Federal Emergency Management Agency (FEMA). 2009. *National Earthquake Hazards Reduction Program Recommended Seismic Provisions for New Buildings and Other Structures* (FEMA P-750).

[12] Federal Emergency Management Agency (FEMA). 2013. *Multi-hazard Loss Estimation Methodology: Flood Model Hazus-MH Technical Manual.* Department of Homeland Security, Federal Emergency Management Agency Mitigation Division. Washington, D.C.

[13] Garschagen, M., and Romero-Lankao, P. 2015. Exploring the relationships between urbanization trends and climate change vulnerability. *Climate Change* 133(1): 37-52.

[14] Greiving, S., Fleischhauer, M., Lückenkötter, J. 2006. A methodology for an integrated risk assessment of spatially relevant hazards. *Journal of Environmental Planning and Management* 49(1): 1–19.

[15] Güneralp, B., Güneralp, I., Liu, Y. 2015. Changing global patterns of urban exposure to flood and drought hazards. *Global Environmental Change* 31: 217-225.

[16] Hawbaker, T., Vanderhoof, M., Beal, Y., Takacs, J., Schmidt, G., Falgout, J., Williams, B., Brunner, N., Caldwell, M., Picotte, J., Howard, S., Stitt, S., and Dwyer, J.L. 2017. *Landsat Burned Area Essential Climate Variable products for the conterminous United States (1984 - 2015): U.S. Geological Survey data release*, https://doi.org/10.5066/F73B5X76.

[17] Hazards and Vulnerability Research Institute (HVRI). 2016. *Spatial Hazard Events and Losses Database for the United States, Version 15.2*. [Online Database]. Columbia, SC: Hazards and Vulnerability Research Institute, University of South Carolina.

[18] Hewitt, K., and Burton, I. 1971. *The Hazardousness of a Place: A Regional Ecology of Damaging Events.* University of Toronto Press.

[19] Hey, D., and Philippi, N. 1995. Flood Reduction through Wetland Restoration: The Upper Mississippi River Basin as a Case History. *Restoration Ecology* 3(1): 4-17.

[20] Holling, C.S. 1986. The resilience of terrestrial ecosystems; local surprise and global change. *eds*. W.C. Clark and R.E. Munn. *Sustainable Development of the Biosphere*. Cambridge University Press, Cambridge, U.K.

[21] Homer, C., Dewitz, J., Yang, L., Jin, S., Danielson, P., Xian, G., Coulston, J., Herold, N., Wickham, J., and Megown, K. 2015. Completion of the 2011 National Land Cover Database for the conterminous United States-Representing a decade of land cover change information. *Photogrammetric Engineering and Remote Sensing* 81(5): 345-354.

[22] Field, C., Barros, V., Stocker, B., Qin, D., Dokken, K., Mastrandrea, M., Mach, K., Plattner, S., Allen, M., Tignor, M., and Midgley, P. eds. 2012. Managing the Risks of Extreme Events and Disasters to Advance Climate Change Adaptation. *A Special Report of Working Groups I and II of the Intergovernmental Panel on Climate Change.* Cambridge University Press, Cambridge, UK, and New York, NY, USA.

[23] Kappes, M., Keiler, M., Elverfeldt, K., and Glade, T. 2012. Challenges of analyzing multi-hazard risk: a review. *Natural Hazards* 64: 1925-1958.

[24] King, P., and Beikman, H. 1974. Geologic map of the United States (exclusive of Alaska and Hawaii) U.S. Geological Survey, scale 1:2,500,000, 2 sheets.

[25] Lall, S.V., Deichmann, W. 2010. Density and Disasters: Economics of Urban Hazard Risk. *The World Bank Research Observer* 27(1): 74-105.

[26] Marzocchi, W., Garcia-Aristizabal, A., Gasparini, P., Mastellone, M., and Di Ruocco, A. 2012. Basic principles of multi-risk assessment: a case study in Italy. *Natural Hazards* 62: 551-573.

[27] Miletti, D. 1999. *Disasters by design: A reassessment of Natural Hazards in the United States.* Joseph Henry Press. Washington, D.C.

[28] National Drought Mitigation Center (NDMC), U.S. Department of Agriculture (USDA), National Oceanic and Atmospheric Administration (NOAA). 2017. United States Drought Monitor Database. http://droughtmonitor.unl.edu/MapsAndData/GISData.aspx.

[29] National Weather Service (NWS). 2007. Storm Data Preparation. Directive National Weather Service Instruction 10-1605. National Weather Service.

[30] National Weather Service (NWS). 2016. Severe Weather Database Files (1950-2016). NOAA NWS. http://www.spc.noaa.gov/wcm/#data .

[31] Parris, A., Bromirski, P., Burkett, V., Cayan, D., Culver, M., Hall, J., Horton, R., Knuuti, K., Moss, R., Obeysekera, J., Sallenger, A., and Weiss, J. 2012. Global Sea Level Rise Scenarios for the US National Climate Assessment. *NOAA Tech Memo OAR CPO-1*. http://cpo.noaa.gov/sites/cpo/Reports/2012/NOAA_SLR_r3.pdf.

[32] Radbruch-Hall, D., Colton, R., Davies, W., Lucchitta, I., Skipp, B., and Varnes, D. 1982. Landslide Overview Map of the Conterminous United States, *Geological Survey Professional Paper 1183*. U.S. Geological Survey, Washington.

[33] Reser J.P. 2007 The Experience of Natural Disasters: Psychological Perspectives and Understandings. In: Lidstone J., Dechano L.M., Stoltman J.P. eds. *International Perspectives on Natural Disasters: Occurrence, Mitigation, and Consequences. Advances in Natural and Technological Hazards Research* vol 21. Springer, Dordrecht

[34] Schaefer, J., Kelly, D., and Abbey R. 1986. A minimum assumption tornado-hazard probability model. *Journal of Climate and Applied Meteorology* 25: 1934-1945.

[35] Schmidt-Thome, P. (Ed.) 2006. ESPON Project 1.3.1 – Natural and technological hazards and risks affecting the spatial development of European regions. Geological Survey of Finland.

[36] Simpson, R., and Reihl, H. 1981. *The Hurricane and Its Impact.* Louisiana State University Press: Baton Rouge and London.

[37] Tate, E., Burton, C., Berry, M., Emrich, C., and Cutter, S. 2011. Integrated Hazards Mapping Tool. *Transaction in GIS* 15(5): 689-706.

[38] Thierry, P. 2008. Multi-hazard risk mapping and assessment on an active volcano: the GRINP project at Mount Cameroon. *Natural Hazards*. 45(3): 429-456.

[39] U.S. Geological Survey. 2003. Earthquake Hazards Program: U.S. Seismic Design Maps: U.S. Geological Survey, https://doi.org/10.5066/F7MC8X8S.

[40] U.S. Nuclear Regulatory Committee (USNRC). 2014. Emergency Preparedness at Nuclear Power Plants. www.nrc.gov.

[41] Watson, J.T., Gayer, M., and Connolly, M.A. 2007. Epidemics after Natural Disasters. *Emerging Infectious Diseases* 13(1): 1-5.

[42] Weatherford, C., and Gray, W. 1988. Typhoon structure as revealed by aircraft reconnaissance. Part II: Structural variability. *Monthly Weather Review* 116: 1044–1056.

[43] Zhu, P. 2008. A multiple scale modeling system for coastal hurricane wind damage mitigation. *Natural Hazards* 47: 577. doi:10.1007/s11069-008-9240-8.

[44] Zou, L., Kent, J., Lam, N.S., Cai, H., Qiang, Yi., Li, K. 2016. Evaluating Land Subsidence Rates and Their Implications for Land Loss in the Lower Mississippi River Basin. *Water* 8(1): 10-25.

Table of Contents

General_Authors_Publications.....2
LI-266824_Farraj_et_al_2015_Cardiac_effects_Seasonal_CAPs&O3.....23
LI-266830_Hazari_et_al_2018_Comparative_effects_of_Smog.....43
LI-266831_Thompson_et_al_2019-CAPs_Acrolein_Trpa1.....53
Cascio_agreement_letter_STAA2020.....67
Davies_agreement_letter_STAA2020.....70
Duvall_agreement_letter_STAA2020.....73
Gilmour_agreement_letter_STAA2020.....75
Haykal-Coates_agreement_letter_STAA2020.....77
Hazari_agreement_letter_STAA2020.....79
Higuchi_agreement_letter_STAA2020.....81
King_agreement_letter_STAA2020.....85
Kovalcik_agreement_letter_STAA2020.....87
Krantz_agreement_letter_STAA2020.....89
Krug_agreement_letter_STAA2020.....91
Ledbetter_agreement_letter_STAA2020.....93
Malik_agreement_letter_STAA2020.....95
Martin_agreement_letter_STAA2020.....98
McGee_agreement_letter_STAA2020.....100
Pancras_agreement_letter_STAA2020.....102
Stratford_agreement_letter_STAA2020.....105
Thompson_agreement_letter_STAA2020.....107
Walsh_agreement_letter_STAA2020.....110
Wood_agreement_letter_STAA2020.....112
Farraj_et_al_2015_Cardiac_effects_Seasonal_CAPs&O3.....116
Hazari_et_al_2018_Comparative_effects_of_Smog.....136
Thompson_et_al_2019-CAPs_Acrolein_Trpa1.....146

United States Environmental Protection Agency
Washington, DC 20460

STAA REPORT FOR THE SCIENTIST NOMINATIONS

General Information:

Nomination ID/App ID:	20-110
Research Category Primary:	Health Effects Research and Human Health Risk Assessment (HE)
Research Category Secondary:	
Laboratory/Office Name:	ORD
Nomination Entered By:	Aimen Farraj

Eligibility Checklist:

[Y] The nominated publication(s) has not been submitted to a previous STAA competition.

[Y] The nominated publication(s) was published on or before January 1, 2017 and on or after January 1,2012

[Y] The principal author was an EPA employee or a PHS employee assigned to EPA when the research was performed

[Y] The EPA authors (includes PHS employees assigned to EPA) contributed collectively a minimum of 50% toward the publication(s)

Nominating Official Name:	David Diazsanchez
Nominating Official Title:	
Nominating OfficialEmail:	diaz-sanchez.david@epa.gov
STAA Coordinator Name:	Kathleen Wiser
STAA Coordinator Email:	wiser.kathi@epa.gov

Justifications:

Justification 1:

The association between air pollution exposure and adverse cardiovascular outcomes is well established. Yet, efforts to quantify the cardiovascular health burden of a given ambient air shed have been hampered by the uncertainty relating to the potential biological responses resulting from the interaction of various constituents within that air shed and the identity of the components that drive toxicity. The publications described herein present the results of a systematic effort to disentangle the effects of components within mixtures by comparing the cardiovascular impacts of exposure to simple combinations of NAAQS and hazardous air pollutants in rodents. The first study (Farraj et al. 2015) examined impacts of co-exposure to ambient PM and O_3 during winter and summer seasons in hypertensive rats. Although there was a marked effect of season on PM mass, size, composition, and contributing sources, ambient PM and O_3 co-exposure caused more cardiac electrical disturbances and autonomic responses than exposure to either pollutant alone during both seasons. The second study (i.e. Thompson et al. 2019; Note: this study, although published last was conducted before the Hazari et al study) examined the impacts of co-exposure to ambient PM and the hazardous air pollutant acrolein in mice. Intermittent co-exposure to ambient PM and acrolein, but not exposure to either alone, caused myocardial dyssynchrony, indicating impaired coordination of heart muscle contraction. Furthermore, this co-exposure effect was absent in mice lacking expression of the transient receptor potential cation channel A1 (TRPA1), a prominent sensor of environmental irritants in the lung, potentially indicating a plausible mechanism of action common across air pollution mixtures. The results from these two studies demonstrate that exposure to binary combinations of pollutants elicits cardiovascular effects that are unique and perhaps more serious than effects caused by exposure to individual pollutants alone. We subsequently compared the effects of two air pollution mixtures that, although differing in levels of key constituents, had similar air quality health indices (AQHI), an index of health risk based on ambient pollutant levels. Mice were exposed to photochemical smog mixtures with either high PM and low O_3 levels or low PM and high O_3 levels. Smog rich in O_3 and other irritant gases caused more cardiac electrical disturbances and breathing changes than high PM smog, illustrating that levels of specific components influence health responses. Collectively, these studies provide 1) strong biological plausibility for more severe health effects from air pollution mixtures compared to single pollutants and 2) evidence that the composition of the mixture is a key determinant of toxicity.

The work described in these publications were part of research projects (ACE Task 035, PEP 1.2, and PEP1.3) outlined in ORD's Air and Energy Strategic Research Action Plans including 1) characterization of additive and synergistic health effects and associated mechanisms resulting from exposure to simple mixtures of pollutants including hazardous air pollutants and 2) comparison of health outcomes of complex mixtures with contrasting levels of NAAQS pollutants, but similar AQHI levels. Taken together, the findings from these studies increase our understanding of true multipollutant health effects. Greater than additive effects with mixtures may explain phenomena frequently observed at low ambient exposure levels, including those at and below national standards for single pollutants. Furthermore, health responses are determined by the unique chemistry of air pollution mixtures. Awareness of the potential for interactive effects and the importance of air pollution chemistry as part of a larger multipollutant approach to air pollution health assessment may reduce uncertainty, improve risk assessment efforts, and assist the Office of Air and Radiation in its efforts to strengthen

single pollutant standard determinations. Furthermore, these findings will inform local and national public health and air policy officials by providing a science-based framework to target the most toxic sources.

Justification 2A:

The studies described in these publications were part of a concerted effort to characterize the additive and synergistic effects of simple mixtures as well as compare more complex mixtures that varied in composition and were done in parallel. The first study (Farraj et al. 2015) examined the impacts of co-exposure to ambient PM and O_3 during winter and summer seasons in hypertensive rats. PM and O_3 were selected as the first pollutants to be studied because in addition to being co-localized in most air sheds, they are also the most prominent air pollutants associated with cardiovascular responses. To build on the first study with PM and O_3, we realized that other air pollutants co-localize with PM including the hazardous air pollutant acrolein, which is a ubiquitous aldehyde produced during the combustion of organic material like tobacco, wood, fats, and other fuels. Acrolein is an upper airway irritant that causes well-documented adverse cardiopulmonary effects on its own. Thus, the second study (i.e. Thompson et al. 2019) examined the impacts of co-exposure to ambient PM and acrolein in mice. Finally, up to this point we had focused on simple binary combinations of air pollutants to demonstrate "proof-of-concept," but in reality, air pollution is much more complex. Primary emissions undergo photochemical aging and transformation in the atmosphere giving rise to a complex smog mixture of multiple secondary reaction products. Moreover, the potency of a mixture may depend on the relative quantity of specific constituents within a mixture. Therefore, the third study (Hazari et al. 2018), using a novel photochemical reaction chamber to generate smog, compared the cardiovascular health effects of two photochemical smog mixtures with similar AQHI's, but that differed in levels of PM and O_3 among other components, in mice. The findings from the three studies collectively provide evidence for effects of air pollution mixtures that are distinct from effects of single pollutants and that are dependent on the levels of specific constituents within a mixture.

Justification 2B:

Wayne Cascio: Researching the role of neuroendocrine stress axes activation in systemic and pulmonary health effects of air pollutants. Miller DB, Ghio AJ, Karoly ED, Bell LN, Snow SJ, Madden MC, Soukup J, Cascio WE, Gilmour MI, Kodavanti UP. Ozone Exposure Increases Circulating Stress Hormones and Lipid Metabolites in Humans. Am J Respir Crit Care Med. 2016 Jun 15;193(12):1382-91. 2017, STAA Level II.

Wayne Cascio: Demonstrating the effects of air pollution on individuals with prior cardiac complications. 2017, STAA Level II.

Wayne Cascio: Dietary supplementation with olive oil or fish oil and vascular effects of concentrated ambient particulate matter" published in Environmental Health Perspectives, and Dietary and pharmacological intervention to mitigate the health effects of air pollution toxicity" published in Biochim Biophs Acta-General Subjects. 2017, STAA Honorable Mention.

Wayne Cascio: Ozone induces glucose intolerance and systemic metabolic effects in young and aged Brown Norway rats. Toxicology and Applied Pharmacology, December 2013, 273(3):551–560; and Episodic ozone exposure in adult and senescent Brown Norway rats: acute and delayed effect on heart rate, core temperature and motor activity. Toxicology, June 2014, 26(7):380-90. 2016, STAA Honorable Mention

Wayne Cascio: "Research Informing How Omega-3 Fatty Acids Can Protect People From Effects of Air Pollution". Awarded for the paper, Omega- 3 Fatty Acid Supplementation Attenuates Particulate Air Pollution Induced Cardiac Effects and Lipid Changes in Healthy Middle-Aged Adult Volunteers. Environmental Health Perspectives, 120(7):952-7 (2012). 2015, STAA Level III.

Ian Gilmour: "Development of a system for assessing the health impact of wildfire smoke." Kim YH, King C, Krantz T, Hargrove MM, George IJ, McGee J, Copeland L, Hays MD, Landis MS, Higuchi M, Gavett SH, Gilmour MI. The role of fuel type and combustion phase on the toxicity of biomass smoke following inhalation exposure in mice. Arch Toxicol. 2019. doi: 10.1007/s00204-019-02450-5. 2019, STAA Level III

Ian Gilmour: "Researching the role of neuroendocrine stress axes activation in health effects of air pollutants."

Miller DB, Ghio AJ, Karoly ED, Bell LN, Snow SJ, Madden MC, Soukup J, Cascio WE, Gilmour MI, Kodavanti UP. Ozone Exposure Increases Circulating Stress Hormones and Lipid Metabolites in Humans. Am J Respir Crit Care Med. 2016 Jun 15;193(12):1382-91. 2017 STAA Level II.

Ian Gilmour: "Mutagenicity and pollutant emissions factors for solid-fuel cookstoves." Mutlu E, Warren SH, Ebersviller SM, Kooter IM, Schmid JE, Dye JA, Linak WP, Gilmour MI, Jetter JJ, Higuchi M, DeMarini DM. Mutagenicity and Pollutant Emission Factors of Solid-Fuel Cookstoves: Comparison with Other Combustion Sources. Environ Health Perspect. 2016 Jul;124(7):974-82. 2017, STAA Honorable mention.

Ian Gilmour: “Comparative toxicity of wildfire smoke.” Kim YH., Yong H., Daniels, M., Boykin E.., Krantz, T., Gilmour MI. Cardiopulmonary toxicity of peat wildfire particulate matter and the predictive utility of precision cut lung slices. Particle and Fiber Toxicology 11 (Article 29). 2014. 2015, STAA Level II.

Ian Gilmour: “Near road modeling and measurement of cerium containing particles generated by diesel fuel additives.

Snow SJ, McGee J, Miller DB, Bass V, Schladweiler MC, Thomas RF, Krantz T, King C, Ledbetter AD, Richards J, Weinstein JP, Conner T, Willis R, Linak WP, Nash D, Wood CE, Elmore SA, Morrison JP, Johnson CL, Gilmour MI, Kodavanti UP. Inhaled diesel emissions generated with cerium oxide nanoparticle fuel additive induce adverse pulmonary and systemic effects. Toxicol Sci. 2014 Dec;142(2):403-17. 2015, STAA Level III.

Aimen Farraj, Mehdi Hazari, and Leslie Thompson: For following publications: Uterine Artery Flow and Offspring Growth in Long-Evans Rats following Maternal Exposure to Ozone during Implantation. Published in Environmental Health Perspectives. Aspirin Pre-Treatment Modulates Ozone-Induced Fetal Growth Restriction and Alterations in Uterine blood flow in rats. Published in Reproductive Toxicology. 2019, STAA Honorable mention.

Mark Higuchi: “Development of a system for assessing the health impact of wildfire smoke.” Kim YH, King C, Krantz T, Hargrove MM, George IJ, McGee J, Copeland L, Hays MD, Landis MS, Higuchi M, Gavett SH, Gilmour MI. The role of fuel type and combustion phase on the toxicity of biomass smoke following inhalation exposure in mice. Arch Toxicol. 2019. doi: 10.1007/s00204-019-02450-5. 2019, STAA Level III.

Mark Higuchi: “Mutagenicity and pollutant emissions factors for solid-fuel cookstoves.” Mutlu E, Warren SH, Ebersviller SM, Kooter IM, Schmid JE, Dye JA, Linak WP, Gilmour MI, Jetter JJ, Higuchi M, DeMarini DM. Mutagenicity and Pollutant Emission Factors of Solid-Fuel Cookstoves: Comparison with Other Combustion Sources. Environ Health Perspect. 2016 Jul;124(7):974-82. 2017, STAA Honorable mention.

Kacey Kovalcik: Cardiopulmonary Toxicity of Peat Wildfire Particulate Matter and the Predictive Utility of Precision Cut Lung Slices. Particle and Fibre Toxicology, 11(29):1-17 (2014). 2015, STAA Level II.

Kacey Kovalcik: Near Road Modeling and Measurement of Cerium Containing Particles Generated by Nanoparticle Diesel Fuel Additive Use; Environmental Science & Technology, 48(18):10607-10613 (2014). Inhaled Diesel Emissions Generated with Cerium Oxide Nanoparticle Fuel Additive Induce Adverse Pulmonary and Systemic Effects; Toxicological Sciences, 142(2):403-417 (2014). Predicting the Effects of Nanoscale Cerium Additives in Diesel Fuel on Regional Scale Air Quality; Environmental Science & Technology, 48(21):12775-12782 (2014). 2015, STAA Level III.

Todd Krantz: “Development of a system for assessing the health impact of wildfire smoke.” Kim YH, King C, Krantz T, Hargrove MM, George IJ, McGee J, Copeland L, Hays MD, Landis MS, Higuchi M, Gavett SH, Gilmour MI. The role of fuel type and combustion phase on the toxicity of biomass smoke following inhalation exposure in mice. Arch Toxicol. 2019. doi: 10.1007/s00204-019-02450-5. 2019, STAA Level III.

Todd Krantz: “Comparative toxicity of wildfire smoke.” Kim YH., Yong H., Daniels, M., Boykin E.., Krantz, T., Gilmour MI. Cardiopulmonary toxicity of peat wildfire particulate matter and the predictive utility of precision cut lung slices. Particle and Fiber Toxicology 11 (Article 29). 2014. 2015, STAA Level II.

Todd Krantz: “Near road modeling and measurement of cerium containing particles generated by diesel fuel additives.” Snow SJ, McGee J, Miller DB, Bass V, Schladweiler MC, Thomas RF, Krantz T, King C, Ledbetter AD, Richards J, Weinstein JP, Conner T, Willis R, Linak WP, Nash D, Wood CE, Elmore SA, Morrison JP, Johnson CL, Gilmour MI, Kodavanti UP. Inhaled diesel emissions generated with cerium oxide nanoparticle fuel additive induce adverse pulmonary and systemic effects. Toxicol Sci. 2014 Dec;142(2):403-17. 2015, STAA Level III.

John McGee: Cardiopulmonary Toxicity of Peat Wildfire Particulate Matter and the Predictive Utility of Precision Cut Lung Slices Particle and Fibre Toxicology, 11(29):1-17. 2015, STAA Level II.

John McGee: Inhaled Diesel Emissions Generated with Cerium Oxide Nanoparticle Fuel Additive Induce Adverse Pulmonary and Systemic Effects Toxicological Sciences/Peer Reviewed Journal Article, 142(2):403-417. 2015, STAA Level III.

Charles Wood: “Environmental Stress During a Critical Window in Pregnancy Impairs Fetal Growth Reference”: Miller CN, Ledbetter AD, Schladweiler MC, Richards JE, Wood CE, Snow S, Johnstone A, Jaskot R, Henriquez A, Thompson LA, Farraj A, Hazari M, Dye JA, Kodavanti U. Uterine Artery Flow and Offspring Growth in Long-Evans Rats Following Maternal Exposure to Ozone During Implantation. Environ Health Perspect 2017;125(12):127005. 2019, STAA Honorable Mention.

Charles Wood: “Development of a Novel Experimental System to Evaluate Predictive Toxicity Signatures.” Reference: Tal TL, McCollum CW, Harris PS, Olin J, Kleinstreuer N, Wood CE, Hans C, Shah S, Merchant FA, Bondesson M, Knudsen TB, Padilla S, Hemmer MJ. Immediate and long-term consequences of vascular toxicity during zebrafish development. Reprod Toxicol 2014;48:51-61. 2015, STAA Honorable Mention.

Justification 2C:

I (Aimen Farraj) have not submitted any STAA nomination in the past 5 years. This is the only nomination being submitted this year. I was a co-author on the publication “Uterine Artery Flow and Offspring Growth in Long-Evans Rats Following Maternal Exposure to Ozone During Implantation. Environ Health Perspect 2017;125(12):127005” that received an honorable mention in 2019. That publication looked at responses after exposure to ozone alone, whereas the present publications examined impacts after to exposures to 2 or more air pollutants simultaneously, an approach that we had not explored previously.

Justification 2D:

n/a

Justification 2E:

Not aware of any concurrent nominations.

Justification 3A:

The Farraj et al. (2015) manuscript has received high visibility as evidenced by the 3345 unique accesses (as of April 30, 2020) since publication. Furthermore, according to Google Scholar, the manuscript has been cited 27 times. In addition, work leading up to this manuscript was selected for a platform presentation at the 2014 Annual meeting of the Society of Toxicology. The Thompson et al (2019) manuscript has received high visibility on several fronts. Firstly, it was featured in the Editor's Highlights section in the journal issue in which it was published (https://academic.oup.com/toxsci/article/167/2/305/5305814). In addition, despite being a relatively new manuscript, it has already been accessed 992 times and, according to Google Scholar, cited 3 times. It has also received plenty of online attention as well as evidenced by its altimetric score of 7, which is due to social media interest (10 Tweets and one Facebook post). Furthermore, the lead author of this work (Leslie Thompson) won the Best Post-doctoral award for his abstract based on this work from the Cardiovascular Specialty Section of the Society of Toxicology. The Hazari et al (2018) manuscript has also been recognized on several fronts. The entire team responsible for this study received two internal awards for this work: 1) the Bronze Medal for Commendable Service for the effort entitled "Comparative Chemistry and Toxicity of Photochemical Air Pollution Mixtures" conferred by the Office of Research & Development of the U.S. EPA in November 2019 and 2) the National Exposure Research Laboratory Exposure Science Excellence Award awarded for work related to smog atmosphere characterization and health effects, also awarded in November 2019. Furthermore, this manuscript has already been accessed 426 times and, according to Google Scholar, cited 7 times. In addition, the journal in which it was published (Environmental Science and Technology) dedicated a special issue to work from our group.

Justification 3B:

These manuscripts were peer-reviewed internally by non-contributing Principal Investigators, Branch Chiefs and Division Directors within NHEERL and were approved for NHEERL clearance by the Cardiopulmonary and Immunotoxicology Branch chief and Environmental Public Health Division director at the time. Additionally, the journals Particle & Fibre Toxicology, Toxicological Sciences and Environmental Science and Technology have established rigorous, blinded, and independent peer review processes that ensure thorough review of technical quality and scientific merit by experts in the field as well as journal editors before acceptance.

AUTHORS

Principal Author

Author Name:	Aimen K. Farraj		
Professional Title:		Salutation:	
Email:	farraj.aimen@epa.gov	Organization:	
Mailing Address:			
Street Line 1:	109 TW Alexander Drive		
City:			
Zip Code:	27711	State:	NC
At time of research was:	EPA Employee		
Separation Date:			
% of Effort:	12		

Contributing Author

Author Name:	Mehdi S Hazari		
Professional Title:		Salutation:	
Email:	hazari.mehdi@epa.gov	Organization:	
Mailing Address:			
Street Line 1:			
City:			
Zip Code:		State:	
At time of research was:	EPA Employee		

Separation Date:		
% of Effort:	12	

Contributing Author

Author Name:	Wayne E. Cascio	
Professional Title:		Salutation:
Email:	cascio.wayne@epa.gov	Organization:
Mailing Address:		
Street Line 1:		
City:		
Zip Code:		State:
At time of research was:	EPA Employee	
Separation Date:		
% of Effort:	3	

Contributing Author

Author Name:	David Davies	
Professional Title:		Salutation:
Email:	davies.david@epa.gov	Organization:
Mailing Address:		
Street Line 1:		
City:		
Zip Code:		State:
At time of research was:	EPA Employee	

Separation Date:		
% of Effort:	3	

Contributing Author

Author Name:	Rachelle Duvall	
Professional Title:		Salutation:
Email:	duvall.rachelle@epa.gov	Organization:
Mailing Address:		
Street Line 1:		
City:		
Zip Code:		State:
At time of research was:	EPA Employee	
Separation Date:		
% of Effort:	3	

Contributing Author

Author Name:	Ian Gilmour	
Professional Title:		Salutation:
Email:	gilmour.ian@epa.gov	Organization:
Mailing Address:		
Street Line 1:		
City:		
Zip Code:		State:
At time of research was:	EPA Employee	

Separation Date:		
% of Effort:	4	

Contributing Author

Author Name:	Todd Krantz	
Professional Title:		Salutation:
Email:	krantz.todd@epa.gov	Organization:
Mailing Address:		
Street Line 1:		
City:		
Zip Code:		State:
At time of research was:	EPA Employee	
Separation Date:		
% of Effort:	4	

Contributing Author

Author Name:	Jonathan Krug	
Professional Title:		Salutation:
Email:	krug.jonathan@epa.gov	Organization:
Mailing Address:		
Street Line 1:		
City:		
Zip Code:		State:
At time of research was:	EPA Employee	

Separation Date:			
% of Effort:	3		

Contributing Author

Author Name:	Najwa Haykal-Coates		
Professional Title:		Salutation:	
Email:	coates.najwa@epa.gov	Organization:	
Mailing Address:			
Street Line 1:			
City:			
Zip Code:		State:	
At time of research was:	EPA Employee		
Separation Date:			
% of Effort:	7		

Contributing Author

Author Name:	Mark Higuchi		
Professional Title:		Salutation:	
Email:	higuchi.mark@epa.gov	Organization:	
Mailing Address:			
Street Line 1:			
City:			
Zip Code:		State:	
At time of research was:	EPA Employee		

Separation Date:			
% of Effort:	4		

Contributing Author

Author Name:	Kasey Kovalcik		
Professional Title:		Salutation:	
Email:	kovalcik.kasey@epa.gov	Organization:	
Mailing Address:			
Street Line 1:			
City:			
Zip Code:		State:	
At time of research was:	EPA Employee		
Separation Date:			
% of Effort:	4		

Contributing Author

Author Name:	Fatiha Malik		
Professional Title:		Salutation:	
Email:	fatihamlk1@gmail.com	Organization:	
Mailing Address:			
Street Line 1:			
City:			
Zip Code:		State:	
At time of research was:	Non EPA Personnel		

Separation Date:		
% of Effort:	2	

Contributing Author

Author Name:	John McGee	
Professional Title:		Salutation:
Email:	mcgee.john@epa.gov	Organization:
Mailing Address:		
Street Line 1:		
City:		
Zip Code:		State:
At time of research was:	EPA Employee	
Separation Date:		
% of Effort:	5	

Contributing Author

Author Name:	Charly King	
Professional Title:		Salutation:
Email:	king.charly@epa.gov	Organization:
Mailing Address:		
Street Line 1:		
City:		
Zip Code:		State:
At time of research was:	EPA Employee	

Separation Date:			
% of Effort:	4		

Contributing Author

Author Name:	Allen Ledbetter		
Professional Title:		Salutation:	
Email:	hawbob23@gmail.com	Organization:	
Mailing Address:			
Street Line 1:			
City:			
Zip Code:		State:	
At time of research was:	EPA Employee		
Separation Date:	Mon Sep 30 00:00:00 GMT 2019		
% of Effort:	3		

Contributing Author

Author Name:	Brandi Martin		
Professional Title:		Salutation:	
Email:	blmartin@live.unc.edu	Organization:	
Mailing Address:			
Street Line 1:			
City:			
Zip Code:		State:	
At time of research was:	Non EPA Personnel		

Separation Date:			
% of Effort:	2		

Contributing Author

Author Name:	Joseph Patrick Pancras		
Professional Title:		Salutation:	
Email:	pancras.patrick@epa.gov	Organization:	
Mailing Address:			
Street Line 1:			
City:			
Zip Code:		State:	
At time of research was:	EPA Employee		
Separation Date:			
% of Effort:	3		

Contributing Author

Author Name:	Kimberly Stratford		
Professional Title:		Salutation:	
Email:	kimberly.stratford@fda.hhs.gov	Organization:	
Mailing Address:			
Street Line 1:			
City:			
Zip Code:		State:	
At time of research was:	Non EPA Personnel		

Separation Date:		
% of Effort:	3	

Contributing Author

Author Name:	Leslie Thomspon	
Professional Title:		Salutation:
Email:	leslie.thompson@nih.gov	Organization:
Mailing Address:		
Street Line 1:		
City:		
Zip Code:		State:
At time of research was:	EPA Employee	
Separation Date:	Sat Aug 04 00:00:00 GMT 2018	
% of Effort:	7	

Contributing Author

Author Name:	Leon Walsh	
Professional Title:		Salutation:
Email:	lcwalsh@nc.rr.com	Organization:
Mailing Address:		
Street Line 1:		
City:		
Zip Code:		State:
At time of research was:	EPA Employee	

Separation Date:	Fri Dec 30 00:00:00 GMT 2016	
% of Effort:	7	

Contributing Author

Author Name:	Charles Wood	
Professional Title:		Salutation:
Email:	charleswood99@gmail.com	Organization:
Mailing Address:		
Street Line 1:		
City:		
Zip Code:		State:
At time of research was:	EPA Employee	
Separation Date:	Fri Jun 08 00:00:00 GMT 2018	
% of Effort:	3	

Contributing Author

Author Name:	Darrell Winsett (Deceased)	
Professional Title:		Salutation:
Email:	winsett.darrell@epa.gov	Organization:
Mailing Address:		
Street Line 1:		
City:		
Zip Code:		State:
At time of research was:	EPA Employee	

Separation Date:	Sat Jan 02 00:00:00 GMT 2016
% of Effort:	2

PUBLICATIONS

Publication 1:

Publication Title:	Cardiac effects of seasonal ambient particulate matter and ozone co-exposure in rats		
Publication Date:	Wed May 06 00:00:00 GMT 2015		
Journal/Publication Method:	Particle and Fibre Toxicology		
All Author(s):			
Volume:	12	Number:	12
Pages:	1-20	Immediately Index:	Immediately Index:
Citation ½ Life:	4.20	Impact Factor:	8.397

Publication 2:

Publication Title:	Comparative Cardiopulmonary Effects of Particulate Matter- And Ozone-Enhanced Smog Atmospheres in...		
Publication Date:	Thu Feb 01 00:00:00 GMT 2018		
Journal/Publication Method:	Environmental Science & Technology		
All Author(s):			
Volume:	52	Number:	5
Pages:	3071-3080	Immediately Index:	Immediately Index:

Citation ½ Life:	0.79	Impact Factor:	7.149

Publication 3:

Publication Title:	Ambient Particulate Matter and Acrolein Co-Exposure Increases Myocardial Dyssynchrony in Mice via...		
Publication Date:	Tue Oct 23 00:00:00 GMT 2018		
Journal/Publication Method:	Toxicological Sciences		
All Author(s):			
Volume:	167	Number:	2
Pages:	559–572	Immediately Index:	Immediately Index:
Citation ½ Life:	7.10	Impact Factor:	4.081

Farraj et al. Particle and Fibre Toxicology (2015) 12:12
DOI 10.1186/s12989-015-0087-3

PARTICLE AND FIBRE TOXICOLOGY

RESEARCH Open Access

Cardiac effects of seasonal ambient particulate matter and ozone co-exposure in rats

Aimen K Farraj[1*], Leon Walsh[1], Najwa Haykal-Coates[1], Fatiha Malik[1], John McGee[1], Darrell Winsett[1], Rachelle Duvall[2], Kasey Kovalcik[2], Wayne E Cascio[1], Mark Higuchi[1] and Mehdi S Hazari[1]

Abstract

Background: The potential for seasonal differences in the physicochemical characteristics of ambient particulate matter (PM) to modify interactive effects with gaseous pollutants has not been thoroughly examined. The purpose of this study was to compare cardiac responses in conscious hypertensive rats co-exposed to concentrated ambient particulates (CAPs) and ozone (O_3) in Durham, NC during the summer and winter, and to analyze responses based on particle mass and chemistry.

Methods: Rats were exposed once for 4 hrs by whole-body inhalation to fine CAPs alone (target concentration: 150 μg/m^3), O_3 (0.2 ppm) alone, CAPs plus O_3, or filtered air during summer 2011 and winter 2012. Telemetered electrocardiographic (ECG) data from implanted biosensors were analyzed for heart rate (HR), ECG parameters, heart rate variability (HRV), and spontaneous arrhythmia. The sensitivity to triggering of arrhythmia was measured in a separate cohort one day after exposure using intravenously administered aconitine. PM elemental composition and organic and elemental carbon fractions were analyzed by high-resolution inductively coupled plasma–mass spectrometry and thermo-optical pyrolytic vaporization, respectively. Particulate sources were inferred from elemental analysis using a chemical mass balance model.

Results: Seasonal differences in CAPs composition were most evident in particle mass concentrations (summer, 171 μg/m^3; winter, 85 μg/m^3), size (summer, 324 nm; winter, 125 nm), organic:elemental carbon ratios (summer, 16.6; winter, 9.7), and sulfate levels (summer, 49.1 μg/m^3; winter, 16.8 μg/m^3). Enrichment of metals in winter PM resulted in equivalent summer and winter metal exposure concentrations. Source apportionment analysis showed enrichment for anthropogenic and marine salt sources during winter exposures compared to summer exposures, although only 4% of the total PM mass was attributed to marine salt sources. Single pollutant cardiovascular effects with CAPs and O_3 were present during both summer and winter exposures, with evidence for unique effects of co-exposures and associated changes in autonomic tone.

Conclusions: These findings provide evidence for a pronounced effect of season on PM mass, size, composition, and contributing sources, and exposure-induced cardiovascular responses. Although there was inconsistency in biological responses, some cardiovascular responses were evident only in the co-exposure group during both seasons despite variability in PM physicochemical composition. These findings suggest that a single ambient PM metric alone is not sufficient to predict potential for interactive health effects with other air pollutants.

Keywords: Ambient particulate matter, Ozone, Season, Cardiac, Health effects, Co-exposure, Electrocardiogram, Rats, Source apportionment, Elements

* Correspondence: farraj.aimen@epa.gov
[1]Environmental Public Health Division, US EPA, 109 TW Alexander Drive, Research Triangle Park, Durham, NC 27711, USA
Full list of author information is available at the end of the article

BioMed Central

© 2015 Farraj et al.; licensee BioMed Central. This is an Open Access article distributed under the terms of the Creative Commons Attribution License (http://creativecommons.org/licenses/by/4.0), which permits unrestricted use, distribution, and reproduction in any medium, provided the original work is properly credited. The Creative Commons Public Domain Dedication waiver (http://creativecommons.org/publicdomain/zero/1.0/) applies to the data made available in this article, unless otherwise stated.

Background

Attempts to quantify the cardiovascular health burden resulting from exposure to particulate matter air pollution and identify biologically plausible mechanisms of action have been encumbered by the variability in PM composition. The physical and chemical properties of ambient PM in a given air shed are dependent on a number of factors including local geography, proximity to emission sources, time of day, and meteorology. Recent studies point to a pronounced seasonal pattern in fine PM (PM with an aerodynamic diameter less than 2.5 microns; $PM_{2.5}$) composition across the U.S. with higher levels of sulfate, aluminum and magnesium in the summer and higher levels of nitrate, zinc and nickel in the winter [1]. Time-series data from 202 U.S. counties [2] point to a commensurate seasonal impact on health effects including stronger $PM_{2.5}$ associations with same day cardiovascular and respiratory hospital admissions during the winter than in the summer. By contrast, Goldberg et al. [3] found carbon particle-related mortality was higher during the summer than in winter. In mouse studies, exposure to winter ambient PM caused greater pulmonary neutrophil influx [4] and greater systemic pro-inflammatory and procoagulant responses [5] than exposure to summer PM. In contrast, Happo et al. [6] found that PM collected in spring produced greater inflammatory responses in mouse lung than PM samples collected in the fall. Divergent responses have also been noted using *in vitro* models [7,8]. Components and/or properties of PM that vary across season and that drive season-dependent health effects of exposure need to be defined.

While the characteristics of PM are critical, PM is only one component of a complex air pollution mixture that also includes gases and volatile compounds. Assessment of the health effects of exposure at a given ambient air shed, therefore, must account for non-PM components and the potential for additive, synergistic or antagonistic responses resulting from gas-particle interactions. A growing body of evidence is pointing to interactive effects of exposure with a variety of air pollutants, including nitrogen dioxide (NO_2), ambient PM, and O_3 [9]. PM and O_3 co-exposure has been linked to more pronounced cardiovascular responses including increased diastolic blood pressure [10] and dispersion of ventricular repolarization [11] in humans and decreased HRV [12], and epicardial adipose tissue inflammation in rats [13]. The unique physicochemical characteristics of PM within each season may determine interaction between components within an air pollution mixture and serve as an important contributing factor in health outcomes.

Like other regions of the U.S., central North Carolina is subject to seasonal shifts in $PM_{2.5}$ composition with summer PM dominated by sulfate, and winter by nitrates [14]. Little is known about the influence of season on both ambient PM chemistry and cardiovascular responses within this region, particularly in the context of co-pollutant exposures. We have previously shown that exposure to various air pollutants causes exaggerated cardiovascular responses in rats [15-18]. The purpose of this study was to compare the impacts of a single summer exposure to CAPs with or without O_3 on cardiovascular responses in rats to similar exposures during the winter and relate the responses to differences in seasonal PM composition. ECG intervals and amplitudes, HR, spontaneous arrhythmia and HRV, an indicator of autonomic tone, were measured. In addition, sensitivity to myocardial calcium loading, an index of latent vulnerability to cardiac arrhythmia, and pulmonary and systemic indicators of inflammation were assessed one day after exposure. PM exposure characteristics and meteorological conditions were documented. Finally, elemental analysis data were used to quantify PM sources using a chemical mass balance model.

Results

Weather patterns

Summer and winter local weather patterns during exposures were unstable with unusually low ambient PM concentrations. Wind patterns shifted up to 180 degrees each day and were never consistent long enough to establish stable ambient PM levels. A map of superimposed backward trajectories (Figure 1) was created using the Hybrid Single Particle Lagrangian Integrated Trajectory Model (HYSPLIT; web version; Draxler, RR et al.) at the Real-Time Environmental Applications and Display sYstem (READY; Rolph, DG) website developed by the Air Resources Laboratory of the NOAA. Archived meteorological data (online) was utilized to model the direction and location of the test air mass in 6 hr increments for the previous 24 hr before 10 am local time of each exposure day. The trajectories terminated at the exposure facility in A-Building of the CRF in RTP, NC. (Latitude: 35.88350; Longitude: −78.87460). The tracings shown in Figure 1 illustrate how a uniform pattern of exposure sources was precluded because the direction of the air mass source changed for each daily exposure. Trajectories plotted do not follow air mass chronological fate after an exposure day, but rather, show how new air masses replaced current from day to day.

Exposure concentrations

Due to unusually low ambient PM levels and unseasonably small PM sizes for the winter test days, coupled with splitting CAPs system output between 2 chambers, target PM concentrations were not achievable during the winter exposures. The protocol was revised such that

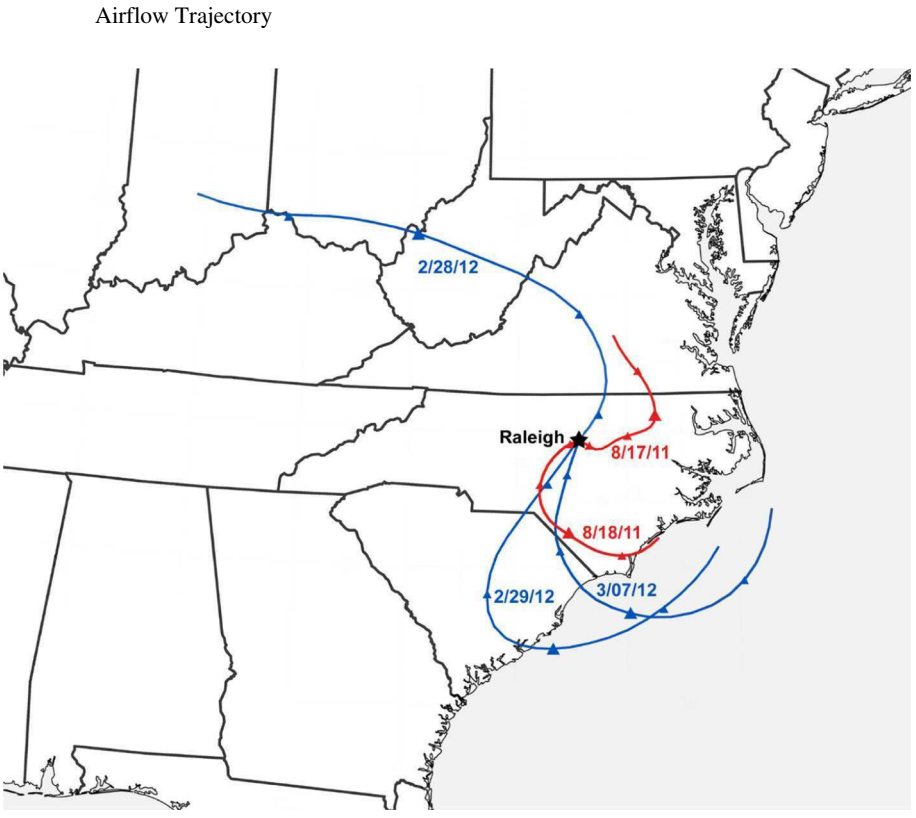

Figure 1 A map of superimposed backward trajectories using the Hybrid Single Particle Lagrangian Integrated Trajectory Model (HYSPLIT) at the Real-Time Environmental Applications and Display sYstem (READY) website developed by the Air Resources Laboratory of the National Oceanic and Atmospheric Administration. Archived meteorological data was utilized to model the direction and location of the test air mass for the previous 24 hr before 10 am local time (2 pm UTC (Universal Time Coordinated)) of each exposure day. Each trajectory represents a different air mass for each winter exposure day (2/28/12, and 2/29/12, and 3/07/12 and blue in color) and each summer exposure day (8/17/11 and 8/18/11 and red in color) and terminates at the exposure facility in A-Building of the US EPA campus in Durham, NC (indicated by a star). Triangle symbols indicate time of day (UTC) in 6 hour increments with larger symbols corresponding to midnight UTC (8 pm local time) in each path.

for the initial PM exposures of each group, maximum achievable concentration was provided. For the subsequent exposures, we attempted to match the first day's PM levels by including dilution air to regulate chamber PM levels. Filter samples were collected from each chamber and the system inlet for the PM exposures only as sampling the filtered air chambers (O_3 only and air controls) provided insufficient sample mass for either accurate weighing or detectable levels for chemical analysis. One filter, 37 mm Teflon for mass concentration in the CAPs + O_3 chamber on 8/17/11 failed during the exposure so that gravimetric sample was lost. The loss of the 37 mm Teflon mass sample did not affect PM chemical analysis or source apportionment modeling, which were performed using data derived from 47 mm Teflon, Nylasorb, and quartz filter samples. Chamber PM mass concentration for that exposure was determined by computing an average DustTrak (DT) calibration factor (DT cal factor = Filter conc/Avg DT conc) for other runs of PM filters vs average DT indicated concentrations and applying the factor to DT data for the run with the failed filter sample. Average ambient PM levels from filter samples were ~13.7 ug/m^3 for summer and ~8.4 ug/m^3 for winter PM exposure days. Summer ambient source PM size was larger than winter PM size producing better concentrating effects in the CAPs system during summer exposure days (Table 1). Background O_3 levels measured in the CAPs only and air control chambers ranged from 2.5 to 10.5 ppb in the summer and winter. Chamber CAPs and O_3 concentrations and environmental conditions for each group are reported in Table 1.

Chemical composition of CAPs

Group-averaged PM elemental and carbon fraction composition for summer and winter exposures are shown in Tables 2 and 3. Two sets of units are required to describe the aerosol: μg PM component per g PM (Table 2) shows seasonal differences in PM composition, and μg PM component per cubic meter chamber air (Table 3) shows chamber concentrations during exposures. When

Table 1 Exposures concentrations, particle size and chamber and ambient weather conditions

Exposure dates	Summer exposures				Winter exposures			
	Air	CAPs	O_3	CAPs + O_3	Air	CAPs	O_3	CAPs + O_3
	23 Aug11	17 Aug11	23 Aug11	17 Aug11	5 Mar12	28 Feb12	05 Mar12	28 Feb12
	2 Aug11	18 Aug11	24 Aug11	18 Aug11	6 Mar12	29 Feb12	06 Mar12	29 Feb12
						7 Mar12		7 Mar12
O3 (ppb)	5.8	4.8	197.1	203.1	2.5	10.5	199.4	198.3
PM Mass (μg/m^3)	—	168.7	—	174.9	—	78.5	—	91.3
Particle Size (nm)	—	333.4	—	315.0	—	125.5	—	125.0
Geometric Mean	—	316.1	—	295.8	—	125.5	—	125.0
Mode	—	316.1	—	295.8	—	125.5	—	125.0
Geometric SD	—	1.96	—	1.97	—	1.95	—	2.02
Chamber Temp (F)	72.6	72.5	70.8	70.4	73.6	72.3	71.2	69.6
Chamber RH (%)	51.3	50.3	51.3	56.5	46.7	42.6	51.0	47.1
Ambient Temp (F)	77.5	80	77.5	80	44.8	55.5	44.8	55.5
Ambient RH (%)	55	69.5	55	69.5	45.8	68.2	45.8	68.2

expressed as μg/g, PM composition differences between summer and winter were pronounced. No elements were enriched in summer relative to winter. Relative to summer, sodium, magnesium, and calcium were enriched at levels of 4–6 times higher in winter PM, and levels of another 15 elements were enriched by 2- 3-fold. However, expressing PM concentration in units of μg/m^3 exposure atmosphere takes into account the PM mass concentrations, which were approximately 2 times greater in summer. Table 3 shows that the overall elemental levels in the inhalation chambers were largely the same for both seasons' exposures, with a few exceptions. Chromium and sulfate levels were 2 to 3 times higher in summer, while alkali elements sodium, magnesium, and calcium were 2 to 3 times higher in winter.

Source apportionment analysis

Average source contributions to the CAPS and CAPS + O_3 mixtures are displayed in Figure 2 (Additional file 1: Table S1 and Additional file 2: Figure S1, respectively, show the same data in tabular and bar chart format); daily samples used to calculate averages are also found in Additional file 3: Table S2 and Additional file 4: Table S3, respectively. Across both seasons and pollutant mixtures, the CMB model explained between 60-100% of the particle mass (R^2 ranged from 0.76 to 0.92). The fit statistics including percent mass explained, R^2, chi Square, and T-statistic were within the recommended values [19]. Nitrate data were not available for inclusion in the CMB runs; therefore, some of the unresolved mass may be due to secondary nitrate (Aneja et al. [14] showed that nitrate levels in PM peak during winter months in North Carolina). The largest sources during both the summer and winter exposures included mobile sources (14-17% by mass), wood combustion (12-30%), and secondary sulfate (24-40%). Higher contributions of wood combustion were found during the winter exposures. Road dust and marine salt contributions were also higher during the winter exposures. In particular for marine salt, air flow trajectories (Figure 1) show that air masses originated from the ocean on 2/29/12 and 3/7/12. These observations are supported by the CMB results in which marine salt contributions were elevated on those two days for both the CAPS and CAPS + O_3 mixtures (Table S2).

Heart rate

Despite being acclimated to the exposure chambers on non-exposure days, rats routinely demonstrate elevated HR during baseline pre-exposure periods on exposure days. This was evident in rats exposed to filtered air during both summer and winter months. Figure 3 shows group averages normalized to baseline pre-exposure values (i.e. Exposure minus Pre-exposure Baseline). In the summer, rats during exposure to O_3, had a greater decrease in HR than rats exposed to filtered air ($p < 0.05$). There were no significant effects of CAPS or CAPS + O_3 exposure relative to filtered air controls.

In the winter, unlike O_3 exposure during the summer, O_3 did not cause a significant decrease in HR during exposure. By contrast, CAPs exposure caused a greater decrease in HR than filtered air exposure ($p < 0.05$). CAPS + O_3 caused the opposite effect resulting in an increase in HR relative to filtered air ($p < 0.05$).

HR did not change after exposure (i.e. 6-hour period after exposure) when compared to baseline in any exposure group during either season.

Table 2 Group-averaged PM elemental composition in μg/g

	Summer		Winter		Winter/Summer
Element (μg/g)	CAPs	CAPs + O_3	CAPs	CAPs + O_3	Enrichment factor
Al	951	622	2303	2250	2.9
As	14.8	14.2	20.3	15.5	1.2
Ba	304	101	335	239	1.4
Ca	1159	1033	4548	4200	4.0
Cd	2.4	2.3	9.2	6.9	3.5
Co	7.6	1.9	3.6	5.3	0.9
Cr	39.6	44.8	56.6	38.4	1.1
Cu	848	360	683	540	1.0
Fe	5053	4695	14946	10027	2.6
K	3637	5018	10392	7128	2.0
Li	6.3	11.6	32.6	21.3	3.0
Mg	386	271	2304	1690	6.1
Mn	442	688	2273	1481	3.3
Mo	10.3	6.7	17.7	7.8	1.5
Na	2404	3899	17638	13795	5.0
Ni	17.8	18.0	48.2	31.3	2.2
P	312	78	234	494	1.9
Pb	133	79	220	157	1.8
SO_4	276531	294486	240898	160234	0.7
Sb	39.8	27.9	88.8	63.4	2.2
Se	29.0	37.4	50.3	40.8	1.4
SiO_2	3822	1705	11341	6179	3.2
Sn	33.7	18.2	66.3	48.3	2.2
Sr	14.1	7.5	38.4	29.6	3.1
Ti	140	80	279	242	2.4
V	9.8	12.6	43.0	32.5	3.4
Zn	367	534	1475	1128	2.9
Organic C	287078	341624	448280	357174	1.3
Elemental C	14582	25329	49299	34830	2.1

Electrocardiographic parameters

In the summer, O_3 exposure significantly increased PR interval relative to filtered air controls ($p < 0.05$) (Figure 4). By contrast CAPS exposure significantly decreased the PR interval relative to filtered air controls ($p < 0.05$). CAPS + O_3 exposure produced no effect. During winter, no exposure affected the PR interval. In addition, PR interval did not change after exposure in any exposure group during either season.

In the summer, there were no effects of CAPs or O_3 exposure on QT_c interval relative to filtered air (Figure 5). By contrast, CAPS + O_3 exposure caused a significant increase in QT_c interval relative to filtered air ($p < 0.05$). There was no significant effect in QT_c interval in the winter during exposure. However, CAPS + O_3 exposure caused a significant increase in QT_c interval relative to filtered air in the winter after exposure.

Heart rate variability

During both summer and winter, there were no effects of CAPs or O_3 exposure alone on SDNN relative to the response in filtered air controls during both seasonal exposures (Figure 6). By contrast, CAPs + O_3 exposure during both summer and winter caused a significant decrease in SDNN during exposure relative to filtered air ($p < 0.05$). CAPs + O_3 exposure during the winter also caused a significant decrease in SDNN after exposure relative to filtered air ($p < 0.05$), although the magnitude change was smaller compared to the effect of co-exposure during the summer.

Table 3 Group-averaged PM elemental levels in μg/m³

	Summer		Winter		Winter/Summer
Element (μg/m³)	CAPs	CAPs + O_3	CAPs	CAPs + O_3	Enrichment factor
Al	0.160	0.109	0.181	0.205	1.4
As	0.00249	0.00248	0.00159	0.00142	0.6
Ba	0.0513	0.0176	0.0263	0.0218	0.7
Ca	0.195	0.181	0.357	0.383	2.0
Cd	0.00041	0.00040	0.00072	0.00063	1.7
Co	0.00128	0.00034	0.00028	0.00048	0.5
Cr	0.00669	0.00784	0.00444	0.00351	0.5
Cu	0.143	0.0630	0.0536	0.0493	0.5
Fe	0.852	0.821	1.173	0.915	1.2
K	0.614	0.878	0.816	0.651	1.0
Li	0.00107	0.00204	0.00256	0.00194	1.4
Mg	0.0651	0.0475	0.1809	0.1543	3.0
Mn	0.0745	0.1203	0.1784	0.1352	1.6
Mo	0.00174	0.00117	0.00139	0.00071	0.7
Na	0.406	0.682	1.385	1.259	2.4
Ni	0.00301	0.00316	0.00378	0.00285	1.1
P	0.0526	0.0136	0.0184	0.0451	1.0
Pb	0.0225	0.0138	0.0173	0.0144	0.9
SO_4	46.7	51.5	18.9	14.6	0.3
Sb	0.00671	0.00488	0.00697	0.00579	1.1
Se	0.00488	0.00654	0.00395	0.00373	0.7
SiO_2	0.645	0.298	0.890	0.564	1.5
Sn	0.00568	0.00318	0.00521	0.00441	1.1
Sr	0.00238	0.00132	0.00301	0.00270	1.5
Ti	0.0237	0.0140	0.0219	0.0221	1.2
V	0.00165	0.00220	0.00337	0.00297	1.6
Zn	0.0619	0.0933	0.1158	0.1030	1.4
Organic C	48.43	59.75	35.19	32.61	0.6
Elemental C	2.46	4.43	3.87	3.18	1.0
OC/EC ratio	16.6		9.7		

CAPs + O_3 exposure during the winter also caused a significant decrease in RMSSD and a significant increase in LF/HF after exposure relative to filtered air controls ($p < 0.05$; Additional file 5: Table S4). O_3 exposure alone also caused an increase in LF/HF relative to filtered air ($p < 0.05$).

Cardiac arrhythmia

There was no significant effect of exposure on the total number of arrhythmias relative to filtered air exposed controls with any exposure group during either season (data not shown).

Sensitivity to aconitine One Day after exposure

During the summer, exposure to CAPs alone or O_3 alone significantly increased sensitivity to triggering of arrhythmia by escalating doses of aconitine as evidenced by a decrease of the total dose of aconitine necessary to elicit the first ventricular premature beat relative to filtered air exposed controls ($p < 0.05$, Figure 7). CAPs, O_3, and CAPS + O_3 each significantly decreased the total dose of aconitine necessary to elicit the first episode of ventricular tachycardia relative to filtered air exposed controls ($p < 0.05$). There was no significant effect of exposure on the total dose of aconitine necessary to elicit

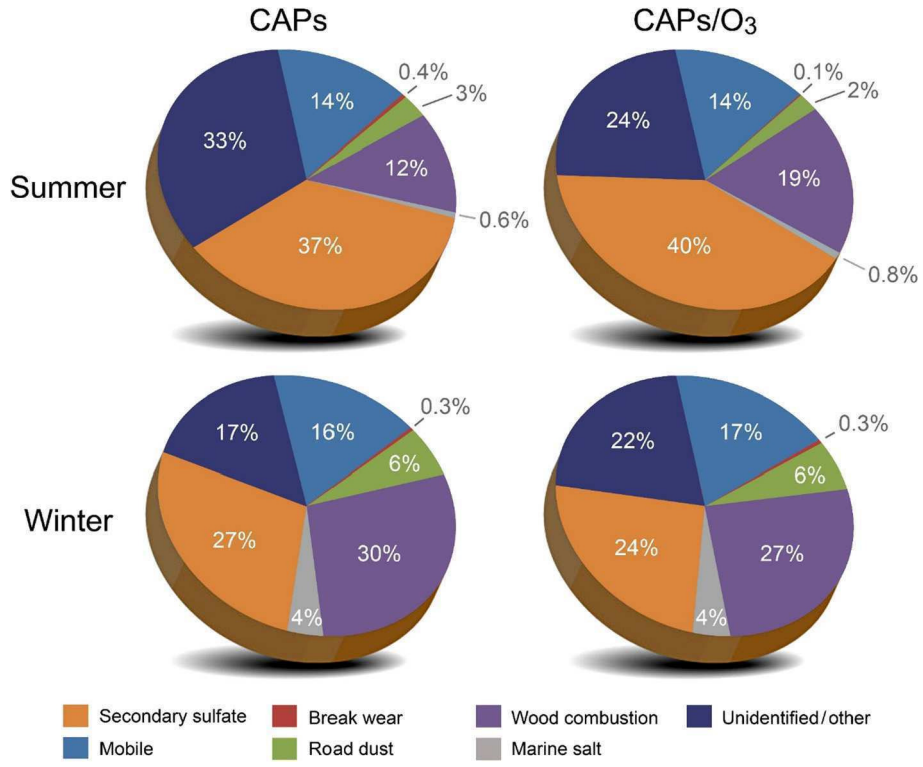

Figure 2 Pie Charts illustrating sources contributing to the concentrated ambient particulate (CAPs) and CAPs + ozone (O_3) mixtures during the summer and winter exposures. Sources for each season were quantified using the EPA Chemical Mass Balance Model.

the first episode of ventricular fibrillation or cardiac arrest relative to air exposed controls.

There was no significant effect of exposure on acontine arrhythmia sensitivity with any exposure group during the winter. Interestingly, in a comparison of the aconitine doses required to assess vulnerability to arrhythmia across season, the dose required to trigger arrhythmias in air-exposed rats during the winter was significantly lower than air-exposed rats during the summer.

Indicators of inflammation and injury in serum, plasma, and bronchoalveolar lavage fluid one day after exposure

Exposure to CAPs + O_3 during the winter significantly increased N-Acety-D-glucosaminidase (NAG) and lactate dehydrogenase (LDH) levels in the lung ling fluid ($p < 0.05$) relative to filtered air (Figure 8). There were no such changes in NAG in any of the exposure groups during the summer. In addition, exposure to CAPS or CAPs + O_3 during the summer significantly decreased lung LDH levels ($p < 0.05$) relative to filtered air. CAPs + O_3 exposure during the winter also significantly increased lung CuZn super oxide dismutase (CuZn SOD) levels ($p < 0.05$) relative to filtered air. There was no effect of co-exposure on CuZn SOD during the summer, whereas, CAPs exposure alone significantly decreased CuZn SOD levels ($p < 0.05$) relative to filtered air. Exposure to CAPs alone significantly decreased Glutathione S-Transferase (GST) levels during the summer ($p < 0.05$) relative to filtered air, whereas O_3 alone significantly increased lung GST levels ($p < 0.05$) relative to filtered air. There were no such changes in GST in any of the exposure groups during the winter. There was no significant effect of exposure in any other indicator of inflammation in the lung, serum, or plasma or number of infiltrated inflammatory cells in the lung lining fluid (data not shown).

Discussion

Here we present evidence that season and ozone are effect modifiers for ambient PM-induced cardiovascular responses in Spontaneous Hypertensive (SH) rats, a strain of rat known to demonstrate exaggerated cardiovascular effects in response to inhaled ambient PM, diesel exhaust particles, and acrolein [20-22]. Seasonal differences in PM were consistent with earlier findings [14], with new evidence of enrichment for anthropogenic emissions and marine salt sources during winter season

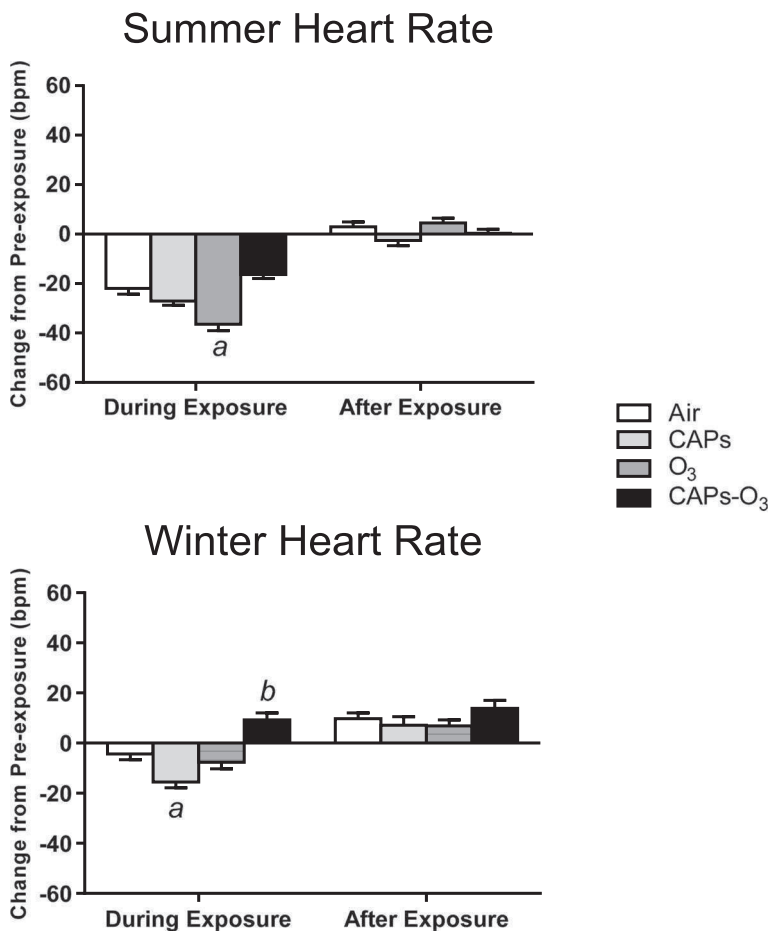

Figure 3 Mean change in Heart rate (HR) from pre-exposure values during summer and winter exposures. HR values for each animal at each time point during exposure or after exposure were subtracted from corresponding time-matched pre-exposure baseline data, which was recorded while the animals were either in the chamber (for "during exposure" data) or in their home cages (for "after exposure" data). Values represent mean change in HR in beats per minute ± standard error of the mean (n = 6). a - significantly less than filtered air control ($p < 0.05$). b - significantly greater than filtered air control ($p < 0.05$).

exposures compared to summer exposures in central North Carolina. Single pollutant cardiovascular effects with CAPs and O_3 were present during both summer and winter exposures, with evidence of unique effects of co-exposures with associated changes in autonomic tone during both seasons.

Biogenic emissions, agricultural activity, vehicular traffic, production of secondary organic aerosols and local weather conditions largely determine the concentration and chemical composition of North Carolina's particulate pollution [14]. The physiochemical characteristics of PM from the Research Triangle Park, NC air shed were highly variable between summer and winter seasons. Differences included particle mass concentrations, size, organic:elemental carbon ratios, and sulfate levels and are consistent with previous measurements [14]. Although winter exposures had 50% less total PM mass than summer exposures (85 vs. 171 μg/m^3), enrichment of metals on a μg/g basis in winter PM resulted in equivalent summer and winter metal exposure concentrations. These findings were based on data from a limited number of exposure days (two summer CAPs exposure days and three winter CAPs exposure days); future studies will need to include more PM exposure sampling days to increase robustness of analysis. Nevertheless, subsequent source apportionment analysis revealed that winter exposures were enriched primarily by wood combustion and to a lesser extent by road dust and marine salt sources compared to summer exposures. The relative impact of the enrichment of marine salt sources is unclear given that only 4% of the total PM mass was attributed to marine salt sources. PM within or near the ultrafine range (0.1 to 0.6 μm) dominates emissions from residential wood combustion while the composition of the PM is dependent on combustion conditions and furnace type, with multiple elements

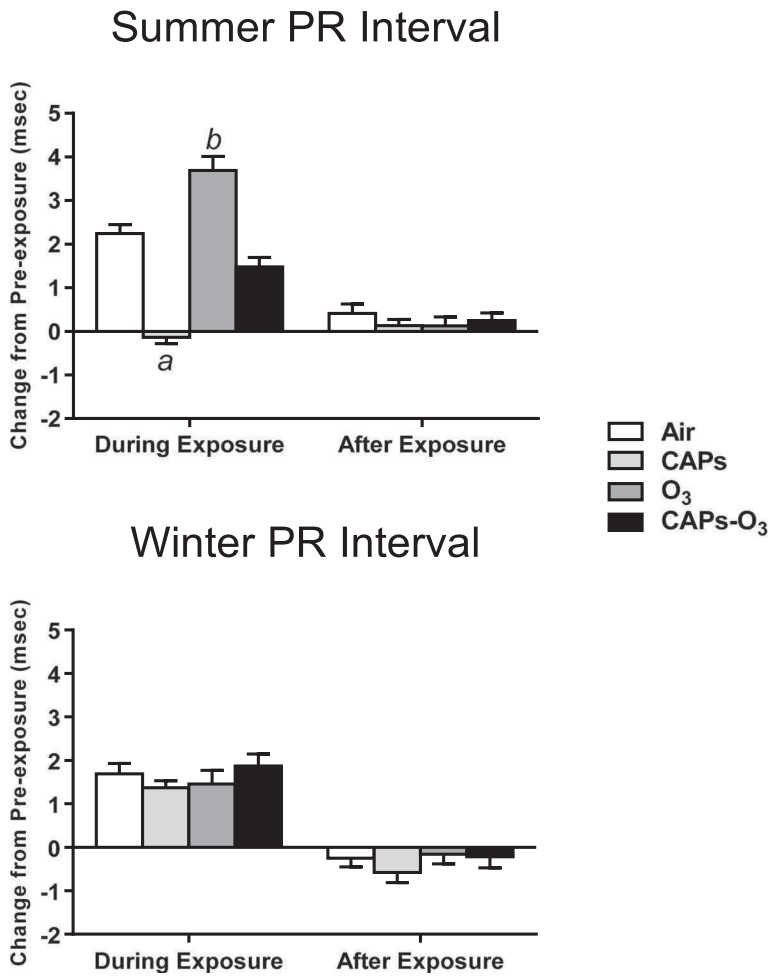

Figure 4 Mean change in PR interval from pre-exposure values during summer and winter exposures. PR values for each animal at each time point during exposure or after exposure were subtracted from corresponding time-matched pre-exposure baseline data, which was recorded while the animals were either in the chamber (for "during exposure" data) or in their home cages (for "after exposure" data). Values represent mean change in PR interval in msec ± standard error of the mean (n = 6). a - significantly less than filtered air control ($p < 0.05$). b - significantly greater than filtered air control ($p < 0.05$).

including potassium, sodium, magnesium, aluminum, and zinc, and transition metals like chromium and nickel present in appreciable quantities [23,24]. Exposure to PM rich in transition metals has been associated with increased cardiovascular mortality [25]. Moreover, the proportion of anthropogenic metals is a critical determinant of biological responses to PM including increased pulmonary effects on days with higher metal concentrations [26-28]. As well, summer PM, although having higher mass, may have been diluted by less bioactive compounds such as sulfates, which were present at higher concentrations during the summer. In addition, winter particle size was roughly one-third the size of summer particles (125 vs. 324 nm). Smaller, near-ultrafine particles have greater relative surface area than larger particles at any given mass concentration and have the capacity to penetrate deep into the lung and also permeate plasma membranes of cells including alveolar epithelial cells and capillary endothelium [29]. Furthermore, ultrafine PM may initiate inflammatory responses in the lung or systemic circulation or enter the blood stream and directly trigger vascular responses, either of which may trigger downstream cardiac responses [29]. In mice exposed to ambient PM collected near a highway [30] and a peat wildfire [31], size-segregated, ambient ultrafine PM caused cardiac changes, while coarse and fine PM from the same PM sample affected primarily pulmonary endpoints.

Single pollutant cardiac effects were mostly observed with summer exposures. With summer O_3 exposure, the effects included decreased HR, increased PR interval, an increase in the HRV parameter LF/HF and increased sensitivity to myocardial calcium loading, consistent with our previous findings [16]. Summer CAPs exposure

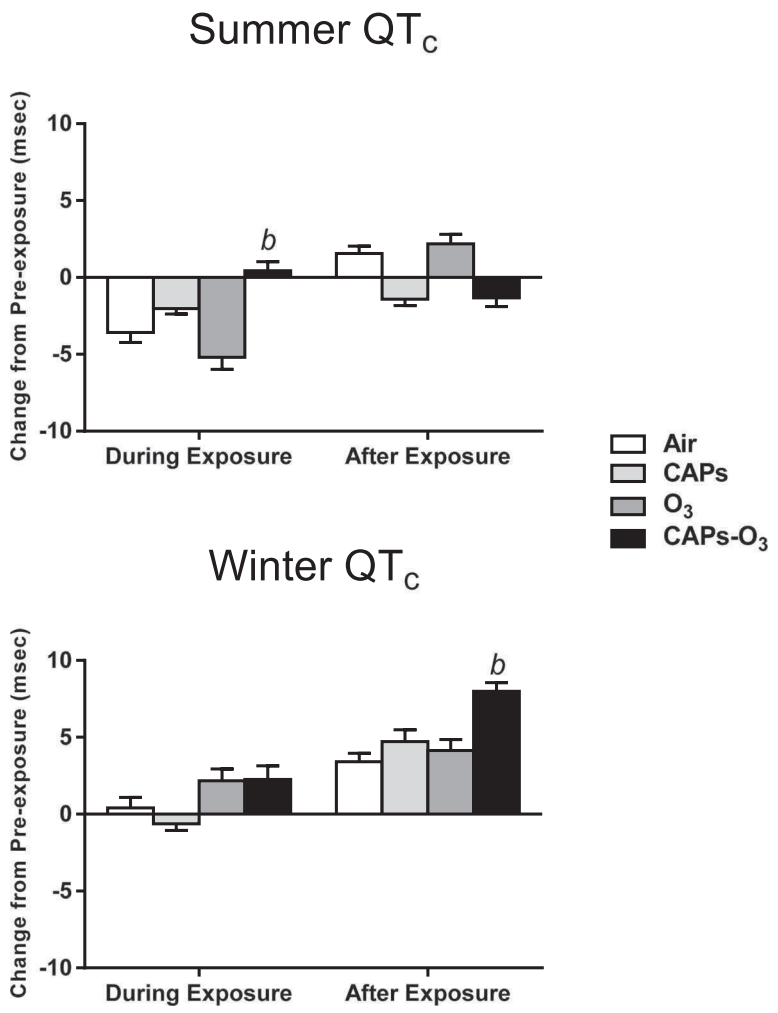

Figure 5 Mean change in QT_c interval from pre-exposure values during summer and winter exposures. QT_c values for each animal at each time point during exposure or after exposure were subtracted from corresponding time-matched pre-exposure baseline data, which was recorded while the animals were either in the chamber (for "during exposure" data) or in their home cages (for "after exposure" data). Values represent mean change in QT_c interval in msec ± standard error of the mean (n = 6). b - significantly greater than filtered air control ($p < 0.05$).

decreased PR interval and elevated sensitivity to myocardial calcium loading. The opposing PR response with summer CAPs exposure compared to summer O_3 exposure implicates pollutant specific disparate effects on atrioventricular conduction, although each pollutant ultimately caused increased vulnerability to ventricular arrhythmia. The relevance of the increased responses to aconitine during the summer is uncertain given that exposures to CAPs and/or O_3 during the winter had no effect on this endpoint, the precise reason of which is unclear. Nevertheless, winter time exposures caused a CAPs-induced decrease in HR, and a CAPs + O_3-induced increase in lung lactate dehydrogenase and n-acetyl B-D glucosaminidase and increased Cu-Zn superoxide dismutase, although the relevance of these findings are also uncertain given the decrease in some of these endpoints with single pollutant exposure. The decrease in HR with CAPs alone during the winter is similar to the findings of Rohr et al. [32] who compared the cardiac effects of winter and summer CAPS exposures in Michigan in the same rat strain used in the present study. Their study had additional effects that were not found in the present study with CAPs alone including linkage of the winter HR response with increased HRV and opposing summer effects characterized by increased HR and decreased HRV. The differences between the Rohr et al. study and the present study may reflect in part the differences in study design (the Rohr et al. study consisted of thirteen 8-hour exposure days vs. a single 4-hour exposure in the present study), exposure concentrations (e.g. summer CAPs concentrations in Rohr et al. averaged ~518 μg/m^3; in present study, ~170 μg/m^3) and/or local contributing air pollution sources, among other factors. Moreover, the variability

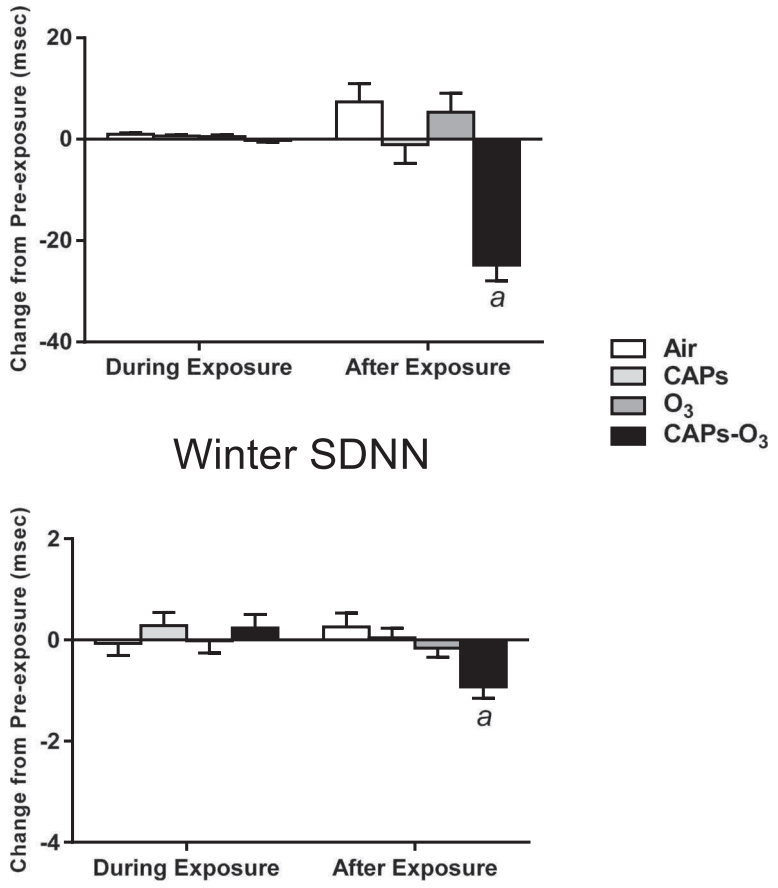

Figure 6 Mean change in SDNN from pre-exposure values during summer and winter exposures. SDNN values for each animal at each time point during exposure or after exposure were subtracted from corresponding time-matched pre-exposure baseline data, which was recorded while the animals were either in the chamber (for "during exposure" data) or in their home cages (for "after exposure" data). Values represent mean change in SDNN in msec ± standard error of the mean (n = 6). a - significantly less than filtered air control ($p < 0.05$).

in the single pollutant responses in the present study may reflect an insufficient short-term exposure required to elicit a significant inflammatory response in the SH rat. This possibility is consistent with epidemiological and human exposure data that suggest that cardiovascular effects to short-term exposures are more likely triggered by autonomic responses while long-term exposures increase the likelihood of persistent inflammatory responses [29].

With some parameters during both the summer and winter seasons, CAPs + O_3 exposure elicited unique responses that were not evident with exposure to either pollutant alone. These included changes in SDNN, RMSSD and QT_c, during the summer, and changes in HR, SDNN, QT_c, and lung injury and oxidative responses during the winter. The changes in QT_c and HR during summer and winter exposures, respectively, were each accompanied by a decrease in SDNN, which reflects overall heart rate variability, and indicates a decrease in parasympathetic tone. In addition, summer co-exposures caused post-exposure decreases in SDNN and RMSSD, another indicator of parasympathetic tone. Thus, decreased parasympathetic tone with co-exposure to CAPs and O_3 during both seasons reflects a shift in autonomic balance towards increased sympathetic tone. Summertime CAPs plus O_3 co-exposure in a recently conducted study in Michigan [12], characterized by greater ambient concentrations of SO4, Ni, V, Zn, and organic and elemental carbon than the present study, yielded similar HRV findings in rats. The present findings are also consistent and with other reports linking low HRV with exposure to PM [33-36] and O_3 [37,38]. Much of the evidence on the prognostic significance of HRV points to increased cardiovascular risk

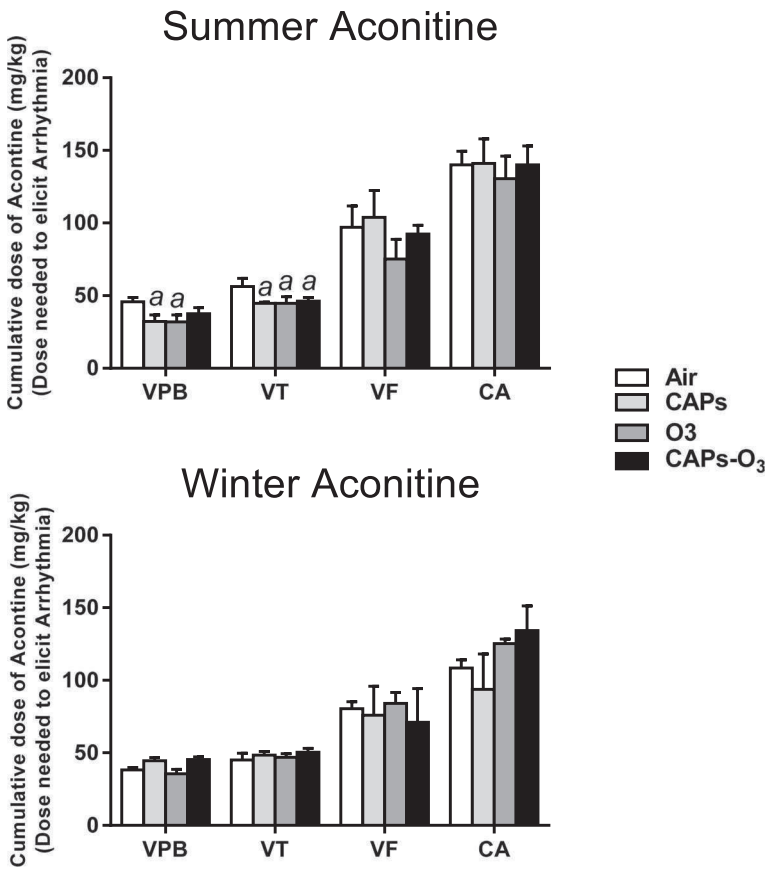

Figure 7 Cumulative dose of infused aconitine necessary to trigger ventricular premature beats (VPB), ventricular tachycardia (VT), ventricular fibrillation (VF), and cardiac arrest (CA) in rats one day after a single exposure. Values represent mean dose ± standard error of the mean (n = 5). a - significantly less than filtered air control ($p < 0.05$).

with low HRV, including increased risk of arrhythmia [39] and an increased mortality rate in people with heart disease [40,41].

The autonomic responses with co-exposure may have been triggered by activation of irritant nerve fibers, including pulmonary C fibers, which trigger reflex cardiopulmonary responses via transient receptor potential (TRP) channels. We recently showed that TRPA1 mediates the increased sensitivity to aconitine-induced arrhythmia after diesel exhaust exposure [22]. In addition, Taylor-Clark and Undem [42] demonstrated that O_3 exposure activates airway C fibers expressing TRPA1. Summer and winter CAPs exposures were rich in adsorbed elements including Fe and Ni, which have been linked to production of reactive oxygen species [7]. The potential involvement of TRP receptors in biological responses induced by transition metals should be examined in future studies given that reactive oxygen species are known activators of TRP receptors [43].

While the specific class of components that drove the observed cardiopulmonary responses is not certain, the similarity in elemental levels in the winter and summer PM due to elemental enrichment presents a plausible explanation for the physiological responses observed. More proinflammatory or irritating byproducts generated through atmospheric interaction between PM, its components, and gases might potentiate cardiovascular effects directly or via the alteration of dose distribution in the lung. For example, Fe and V salts increase the pulmonary irritancy of SO_2 via formation of the more irritating sulfate [44]. Moreover, PM including zinc oxide and inert carbon black, when mixed with gases such as SO_2 or O_3, cause greater than additive pulmonary effects by potentially serving as a carrier for the reactive gases enabling greater distribution into the deep lung [44]. Further research is required to define plausible mechanisms and identify the nature of interactions between specific components like metals and gases.

Seasonal differences in PM mass concentration and size in this study precludes a direct comparison of the physiological responses to ambient PM exposure between seasons. Although air flow patterns likely had little influence, low ambient PM levels and a lower ratio of fine to ultrafine particles during the winter prevented

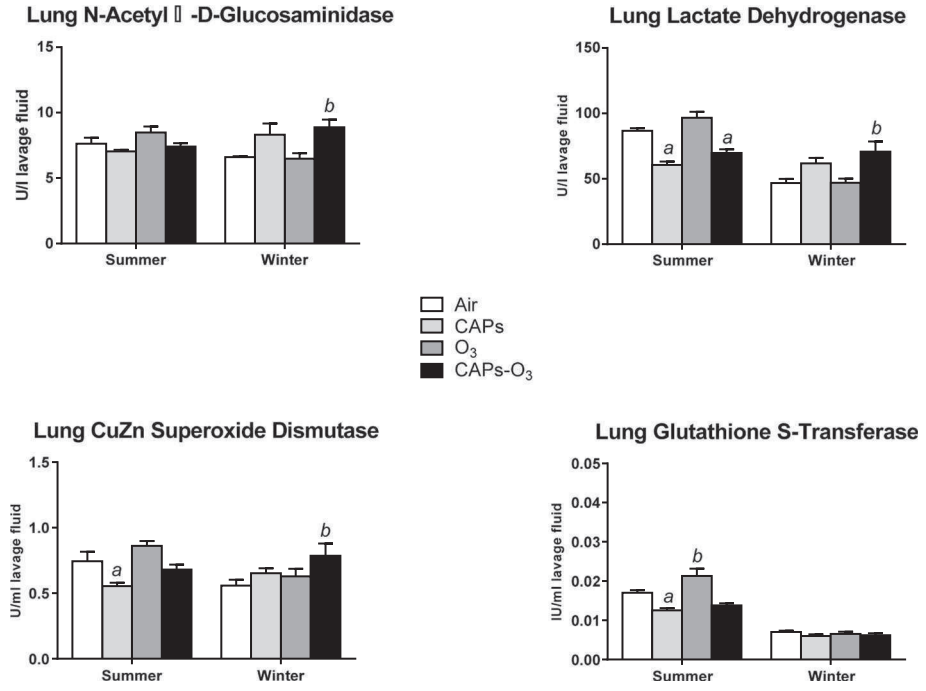

Figure 8 N-acetyl B-D glucosaminidase, lactate dehydrogenase, CuZn superoxide dismutase, and glutathione S-transferase in lung lining fluid one day after summer or winter exposures to concentrated ambient particulate (CAPs), ozone (O_3), CAPs + O_3, or filtered air. Bars represent means ± SEM for each marker shown (n = 6/group). a - significantly less than filtered air control $p < 0.05$). b - significantly greater than filtered air control ($p < 0.05$).

achievement of target concentrations comparable to summer levels with our concentration system. Therefore, one approach to control for seasonal differences in mass is to lower target concentrations. Moreover, the size of the particle is naturally an outcome of the type of local air pollution sources, the level of air pollution and weather conditions. Future studies that focus on exposure to ultrafine PM alone can obviate this concern.

Conclusions

These findings collectively point to marked seasonal effects on PM sources, mass, size, composition, and corresponding impacts on cardiovascular responses. While there was variability in some responses in this study, particularly sensitivity to aconitine-induced arrhythmia and indicators of inflammation/injury, there was evidence of electrocardiographic and autonomic responses that were unique to the CAPs and O_3 co-exposure group. This study, however, was limited by the small number of PM sampling and exposure days, which precluded drawing conclusions about effects of entire seasons. This is especially relevant given that winter conditions often induce stable inversions that increase levels of ambient PM. Moreover, because PM composition data was obtained from only a few samples in the present study, an analysis of a potential association between cardiovascular responses and specific components of PM was not possible. In addition, the absence of nitrogen species data provides some uncertainty in the source apportionment analysis. Future studies that examine the interactive effects of CAPs and O_3 should also mirror realistic seasonal O_3 concentrations. Nevertheless, some evidence of unique co-pollutant effects during both seasons suggests that a multipollutant approach to health effects assessment is warranted. Furthermore, seasonal variability in sources of anthropogenic emissions and evidence for winter elemental enrichment and smaller particle size suggest that PM size and composition may be as important as mass in determining its potential for interactive health effects with other pollutants.

Methods

Animals

Twelve week-old male SH rats (Charles River, Raleigh, NC) were housed in plastic cages (one per cage), maintained on a 12-hr light/dark cycle at approximately 22°C and 50% relative humidity in our Association for Assessment and Accreditation of Laboratory Animal Care-approved facility, and held for a minimum of 1 week before telemeter implantation. The Institutional Animal Care and Use Committee of the U.S. Environmental Protection Agency approved all protocols. Food (Prolab RMH 3000; PMI Nutrition International, St. Louis, MO)

and water were provided ad libitum, and all rats were grouped by weight. SH rats were selected because previous studies demonstrated exaggerated sensitivity to the effects of air pollution compared to rats with normal blood pressure [20,45,46].

Telemeter implantation

Animals (SH rats; n = 7 per group) were anesthetized with ketamine/xylazine (80 mg/ml ketamine HCL and 12 mg/ml xylazine HCL; 1 ml/kg i.p.; Sigma Chemical Co., St. Louis, MO), and were implanted with radiotelemeters (Model TA11CTA-F40; Data Science International, Inc., St. Paul, MN) in the abdominal cavity as previously described [47]. Electrode leads were guided through incisions made in the abdominal musculature. Leads were tunneled subcutaneously and secured in a lead II configuration. Body heat was maintained during and after surgery using a heating pad. Animals recovered for two weeks after surgery before inhalation studies.

Experimental design

SH rats (n = 6/group) surgically implanted with biopotential telemeters were exposed once for 4 hours to concentrated ambient particulate matter (target concentration 150 μg/m^3) with or without 0.2 ppm ozone. To compare the effects of season on health effects of this multipollutant mixture, exposures were conducted in the summer (August, 2011) and winter (February and March, 2012) seasons. Telemetered signals included body temperature, ECG, heart rate, and activity and were monitored before, during, and after exposure in conscious, unrestrained rats. All telemetered rats were euthanized one day after final exposure. Aconitine challenge was performed to assess sensitivity to the triggering of arrhythmia in a separate cohort of concurrently exposed rats one day after exposure.

Exposure schedule

A series of particulate matter and O_3 exposures were conducted in summer of 2011 and winter 2011–12. The study protocol included single 4-hour exposures for CAPs only, CAPs + O_3, O_3 only, and filtered air control groups. Upstream of the CAPs only chamber, air passed through a silica gel dryer that reacted with ambient O_3 and helped keep background O_3 levels in the CAPs only chamber at levels similar to the filtered air control chamber O_3 levels. Animals were allowed 15 to 30 minutes to acclimate to the system's noise and chamber environment then telemetry background measurements were performed for ~45 min. Exposures were initiated at about 7:30 am and continued until 11:30 am for each animal group. For all exposures, initial target $PM_{2.5}$ concentration was ~150 to 200 ug/m^3 while the O_3 target concentration was 200 ppb. To facilitate telemetric monitoring within each chamber CAPs and CAPs + O_3 groups during the summer exposures were split into two cohorts and exposed on either 8/17/11 or 8/18/11. The O_3 only and air groups were also split into two cohorts and exposed on either 8/23/11 or 8/24/11. Winter CAPs and CAPs + O_3 exposures were carried out on 2/17/12, 2/18/12, and 3/7/12. Winter O_3 only and air exposures took place on 2/23/12 and 2/24/12. Each animal group was acclimated to the exposure system and laboratory environmental noises by housing in an exposure chamber with room and CAPs systems operated to produce background noise for a minimum of 1 hour a day for 2 days prior to the exposures.

Ambient weather patterns

Studies involving exposures of animals to concentrated ambient air particles involve sampling outside air in real-time. Local weather conditions and patterns can have a dramatic effect on these real time studies. Ambient weather conditions were monitored during each exposure using a weather station mounted on the roof (Vantage Pro II, Davis Instruments, Hayward, CA) of the U.S. EPA exposure facility in Durham, NC. Data collected included temperature, relative humidity, dew point, barometric pressure, wind speed and direction, rainfall, and other variables providing information about the air mass being drawn from outside into the system during exposures. Data recorded during the times animals were resident in chambers were averaged to produce individual exposure values. Daily values were then averaged to generate group average ambient weather conditions. Exposure group averages are included in Table 1. Additionally, backward trajectory air mass plots were obtained from on-line resources developed by the National Oceanic and Atmospheric Administration (NOAA). Models queried included Hybrid Single Particle Lagrangian Integrated Trajectory Model (HYSPLIT) using the Real-Time Environmental Applications and Display sYstem (READY) [48], which utilized archived meteorological data to model direction and temporal air mass location. The resultant models indicate the path and location of an air mass in 6 hour increments for the 24 hours local time leading up to each PM exposure.

Chamber systems

All exposures were conducted in the U. S. EPA's Research Triangle Park, NC Consolidated Research Facility (CRF), Concentrated Air Particles (CAPs) Laboratory located at 179 T.W. Alexander Dr., RTP, NC. EPA's CAPs exposure facility accommodated 3 Hinners style, stainless steel and glass, 0.3 m^3 whole body chambers (Figure 9). Each chamber was modified to expose animals to ozone and clean air as well as CAPs. The wire mesh animal cages were modified and receivers positioned within each chamber to maximize telemeter signal transmission and

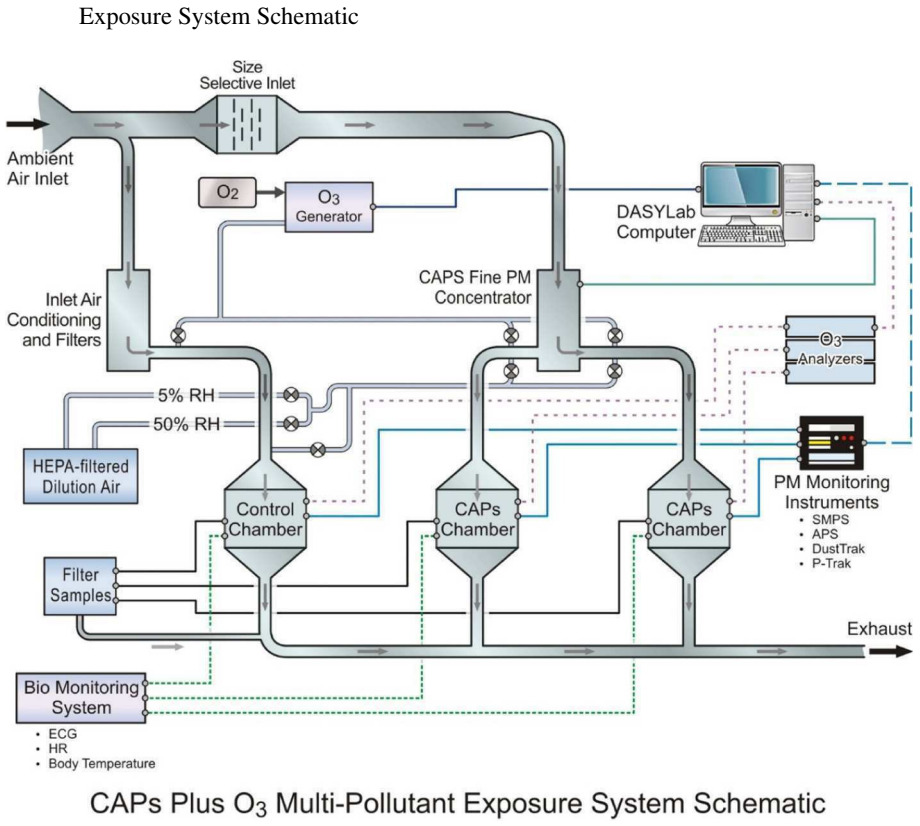

Figure 9 Schematic of concentrated ambient particulates (CAPs) and ozone (O_3) co-exposure system showing concentrator, O_3 generator, exposure chambers, and particulate matter (PM) and O_3 monitoring systems. Receivers were placed within each chamber to monitor electrocardiogram, heart rate and body temperature. Particle concentration and sizing were tracked in real-time using a scanning mobility particle sizer and an aerodynamic particle sizer. Additional aerosol monitors (DustTrak and P-Trak) were used to track PM levels in real-time.

minimize effects on chamber PM distribution. Two CAPs chambers were connected to the outlet of a $PM_{2.5}$ fine particle concentrator (Harvard Fine Particle Concentrator, Harvard University, Boston, MA; HFPC) [49]. Stainless steel tubing (3" diameter) with quick connecting joints was used to transport Air/PM from the concentrator outlet to the designated chamber(s). Transport tubing was configured to deliver all CAPs to a single chamber, split concentrated PM between two chambers, or to totally bypass chambers allowing for gas pollutant or clean air operation. Chamber temperature, relative humidity, air flow, and static pressure and test agent concentrations for PM and O_3 were continuously monitored, displayed, and recorded by the lab's computerized electronic data acquisition system. Clean, charcoal and HEPA filtered, and conditioned dilution air was available from two sources (Core Inhalator System (CIS) supply air, DP = ~55 F, 50% relative humidity (RH), and Medical Grade Air, DP = ~ −20 F, ~5% RH). The two dilution air streams were blended to regulate chamber RH and peak PM concentrations. Chamber environmental data, PM, and O_3 concentrations from multiple exposures within each group were averaged to produce mean values for each exposure group.

PM concentrating system and PM monitoring and control

Outside ambient air containing PM was drawn into the system inlet via a stainless steel duct. The air/PM mixture passed through a custom Size Selective Inlet (SSI) (2 sizing stages: 10 μm and 2.5 μm) (Harvard School of Public Health, Boston, Ma) [50] which removed PM > 2.5 μm. The resulting mixture of Air/$PM_{2.5}$ was transported to the exposure laboratory where it passed through the HFPC operating with 3 stages of slit virtual impactors and outputting ~50 Lpm of Air/CAPs as previously described [28].

CAPs chamber PM concentrations were monitored using both filter weights and real-time electronic instrumentation. Filter samples were collected for all PM exposures to provide gravimetric mass concentrations and for subsequent chemical analysis. Samples included: Teflon 47 mm (Pall Corp., TeFlo, R2PJ047, 2 μm pore) and 37 mm (Pall Corp., TeFlo, R2PJ037, 2 μm pore), Quartz

(Millipore, Quartz, AQFA04700, 47 mm), and Nylon (PALL, Nylasorb, 66509, 47 mm) filters. Particle concentration and sizing were tracked in real-time using scanning mobility particle sizer (SMPS, TSI Inc., St. Paul, MN) and aerodynamic particle sizer (APS, model 3321, TSI Inc., St. Paul, MN). PM data were analyzed and combined using particle data analytical software (Data Merge, ver. 1.0.1, TSI Inc, St. Paul, MN) to provide composite concentrations and particle size distributions representative of the average chamber PM. Data from multiple exposures was combined and averaged to provide concentrations and particle size distributions for each group. Additional aerosol monitors (DustTrak (DT), model 8520, TSI Inc., St. Paul, MN and P-Trak, model 8525, TSI Inc., St. Paul, MN) were used to track PM levels in real time. Peak PM concentrations, chamber pressures, and RH were controlled by regulating injection of conditioned, filtered dilution air upstream of the chamber inlets. Filtered and conditioned air supplied to the O_3 and Air Control groups contained only trace levels of PM with insufficient sample available for weighing or chemical analysis, therefore, no PM samples were collected from those exposures.

Ozone generation, monitoring, and control

Source O_3 was generated using O_2 from compressed gas cylinders fed through a silent arc O_3 generator (OREC, Osmonics Corp.). All wetted surfaces of the O_3 generating and monitoring systems were either stainless steel or Teflon. Flow through the generator was modulated so an excess of gas was always flowing to keep stock O_3 concentrations stable during exposures. Excess O_3 gas was continuously vented into the lab fume hood exhaust. Chamber O_3 supply flow was controlled to establish and maintain target O_3 concentration. Mass flow controllers (MFC) (Tylan Corp., model FC260) were used to control both excess and chamber O_3 flows. Manual and automated MFC command signals were regulated by the CAPs lab data acquisition system (DAS) running data acquisition and control software (DASYLab Pro, version 9, MCC). O_3 was injected counter current into the chamber inlet air duct upstream of the dilution air inlet to enhance mixing prior to entering the chamber. O_3 concentration was manually and/or automatically regulated via a feedback loop. Real-time O_3 concentrations for each group, including Air Controls, were monitored during all exposures. A continuous O_3 analyzer (TECO, model 49, Thermo Electron Co.,) measured chamber O_3 levels in the animal breathing zone and provided concentration signals to the laboratory's data system. Our laboratory operated under a strict quality assurance plan for all exposures. For the duration of the study, O_3 monitoring was performed to manufacturer's and EPA guidelines and under non-condensing conditions. The O_3 Gas analyzer was calibrated using a certified EPA/National Institute of Standards and Technology O_3 transfer standard prior to each study segment with routine zero and span checks and post study calibration verifications. The analyzer was preconditioned by continuous sampling of lab air at 72 F / 50% RH. Clean, conditioned dilution air regulated chamber RH and PM levels (therefore, O3 sample RH) which measured in the range 42.6% to 56.5% daily average during all exposures (Table 1). O_3 sampling system included an inline PM filter (Teflon 47 mm, Pall Corp., TeFlo, R2PJ047, 2 μm pore). The DAS monitored, displayed, recorded, and controlled chamber O_3 concentration and other system operating variables such as temperature, RH, static pressure, and chamber exhaust flow. Chamber O_3 concentration was controlled for the duration of each exposure to provide a target final average concentration of ~200 ppb for each run. During exposures, O_3 flow control was periodically set to manual and maintained at steady state while the O_3 analyzer was briefly cycled to monitor background O_3 chambers (CAPs only or Air Controls). After background levels were determined, O_3 monitoring returned to the O_3 (or CAPs + O_3) exposure chamber under DAS automated control. Outside air passing through the HFPC/CAPs PM concentrator contained naturally occurring ambient O_3. During CAPs only exposures it was desirable to eliminate this naturally occurring O_3 to the extent possible without affecting CAPs chamber PM levels. Upstream of the CAPs only chamber, air passed through a silica gel dryer that reacted with ambient O_3 and helped keep background O_3 levels in the CAPs only chamber at levels similar to the filtered air control chamber O_3 levels.

PM organic and elemental chemical analysis

Organic and elemental carbon contents of CAPs PM collected on quartz filters during exposure were measured using National Institute of Occupational Health (NIOSH) Method 5040 [51]. NIOSH 5040 is a thermo-optical method, based on sequential pyrolytic vaporization and detection of the carbon fractions. Elemental analysis was performed on aqua regia digests of CAP collected on Teflon filters. Prior to digestion, filter media were removed from their polymethylpentene support rings using Teflon blades. Filters were then submerged in 1 mL of concentrated hydrochloric acid (Optima grade, Fisher Scientific) in cleaned 15-ml polypropylene centrifuge tubes (part number 05-539-5, Fisher Scientific; washed in 1% Triton X-100, rinsed with ultrapure deionized water (Milli-Q, Millipore Corporation) and dried in a Class 100 cleanbench). Tubes were sonicated three times in an ultrasonic bath (Model TI-H15, Elma GmbH&Co, Singen Germany) at a frequency of 25 kHz at 200 W for 30 min at 50C°. After each sonication, tubes were cooled to room

temperature and vented in a fume hood. After the third sonication and venting, tubes were heated in an oven overnight at 60C°. The next morning, 0.33 mL of concentrated nitric acid (Optima grade, Fisher Scientific) was added to the tubes to form 3:1 aqua regia, and the same sonication and overnight heating procedure was performed as the preceding day. The following morning, 10 ml of ultrapure water was added, and the teflon filters removed from the tubes using cleaned Teflon forceps. Samples were then analyzed by high-resolution inductively coupled plasma-mass spectrometry (HR-ICP-MS, Element 2, Thermo Scientific).

Source apportionment analysis

Sources contributing to the CAPS and CAPS + O3 mixtures during the summer and winter exposures were quantified using the EPA Chemical Mass Balance Model (CMB 8.2; US EPA, 2004) [19]. The CMB estimates PM sources using a weighted least squares regression. Input data included elements, sulfate, organic carbon and elemental carbon concentrations and uncertainties as well as measured source profile concentrations and uncertainties. The road dust and brake wear profiles were obtained from Hildemann et al. [52] and the mobile source profile (which includes gasoline and diesel emissions) was obtained from Maykut et al. [53]. The wood combustion profile was obtained from Fine et al. [54]. The secondary sulfate and marine salt profiles were obtained from the EPA SPECIATE 4.4 Database. The same profiles and species were used for the summer and winter exposure mixtures.

Radiotelemetry data acquisition

Radiotelemetry methodology (Data Sciences International, Inc.) allowed constant monitoring of electrocardiographic data in conscious and unrestrained rats from implantation until sacrifice. Electrocardiographic data was monitored by remote receivers (DataART3.01; Data Sciences International, Inc.) positioned under the home cages within the animal facility, and under the exposure cages within the exposure chambers. In home cages, sixty-second segments of ECG waveforms were acquired and saved at 15-minute intervals from surgical recovery through sacrifice not including the exposure period. Pre-exposure baseline data was collected from home cages, as well as a 45 min baseline in exposure cages after acclimation for one hour. During the 4 hr exposure, sixty-second segments were acquired and saved at 5-minute intervals. After exposure, rats were monitored in home cages until the next exposure. All rats were monitored until the beginning of necropsy, approximately 18 hrs after exposure. HR was automatically obtained from the ECG waveforms with data acquisition software (DataART3.01; Data Sciences International, Inc.).

Electrocardiogram, arrhythmia identification and heart rate variability analysis

ECGAuto software (EMKA Technologies, Falls Church, VA) was used for automated analyses of ECG wave amplitudes and segment durations and areas, as well as for the visual identification and enumeration of arrhythmias and HRV analysis. Several parameters were determined for each ECG waveform: heart rate; PR interval; R amplitude; QRS duration, amplitude, and area; ST interval, amplitude, and area; and T-wave amplitude and area; QT interval, Bazett's heart rate–corrected QT interval (QTc). ECG and HRV parameters were quantified in the immediate 6-hour period after exposure and compared to time-matched data before exposure while the rats were unrestrained in their home cages. ECG parameters during exposure were analyzed relative to baseline (45 min recordings while in the exposure chambers immediately before the beginning of exposure).

Cardiac arrhythmic events were identified in part by using the Lambeth conventions [55] as a guideline for the identification of arrhythmias in rats. Arrhythmias were identified as atrial premature beats (APB), ventricular premature beats (VPB), sinoatrial block (SAB), atrioventricular block (AVB), or ventricular tachycardia (VT). Arrhythmias were quantified and totaled during the 4 hour exposure period and during the 6 hour period after exposure and compared to pre-exposure counts. Total arrhythmia counts during exposure were quantified (total of 48 one-minute segments during 4 h exposure period).

For the analysis of HRV, rhythms were thoroughly inspected to identify and exclude arrhythmias, artifacts, and 1-min ECG waveforms lacking distinguishable R waves for more than 30 sec. The analysis of HRV generated HR and time-domain measures, including mean time between adjacent QRS complex peaks (the RR interval), a standard deviation of the RR interval (SDNN), SDNN normalized for the effects of heart rate [SDNN/(RR interval x 100)], and the square root of the mean of squared differences of adjacent RR intervals (RMSSD). The SDNN represents overall HRV, whereas RMSSD represents parasympathetic influence over HR. The analysis of HRV also calculated frequency domain parameters including the LF and HF, and the ratio of these two frequency domains (LF/HF). LF is generally believed to represent a combination of sympathetic and parasympathetic tones, whereas HF indicates cardiac vagal (parasympathetic) tone, and LF/HF serves as an index of sympathovagal balance.

Aconitine challenge

One day after exposure to CAPs, O_3, CAPs + O_3, or filtered air, a separate cohort of animals were anesthetized with urethane (1.5 g/kg, *ip*) and underwent the aconitine challenge; supplemental doses of the anesthetic were administered intravenously when necessary to abolish pain reflex. Animal body temperature was maintained at ~36°C with a heating pad. The left jugular vein was cannulated with P.E. 50 polyethylene tubing for the administration of aconitine. Ten μg/ml aconitine was continuously infused at a speed of 0.2 ml/min while ECG was continuously monitored and timed. Sensitivity to arrhythmia was measured as the threshold dose of aconitine required to produce VPBs, VT, and VF, and was calculated using the following formula:

$$\begin{aligned}&\text{Threshold dose (μg/kg) for arrhythmia}\\&= 10\mu g/ml \text{ x } 0.2ml/\text{ min}\\&\quad \times \text{ time required for inducing arrhythmia (min)}\\&\quad /\text{body weight (kg)}\end{aligned}$$

Necropsy, blood collection and lung lavage

Rats were deeply anesthetized with i.p. injection of Euthasol (200 mg/kg sodium pentobarbital and 25 mg/kg phenytoin; Virbac Animal Health, Ft. Worth Texas) one day after exposure. Blood samples were collected from the abdominal aorta. The trachea was cannulated and the right lung (except for the caudal lobe) was lavaged with a total volume of 20 ml/kg of Ca^{2+}, Mg^{2+}, and phenol red-free Dulbecco's phosphate buffered saline (SAFC Biosciences, Lenexa MD) divided into 2 equal aliquots. The caudal lobe was collected for RNA analysis. Cytospins and cells differentials on lavaged cell samples, assays for total protein (Thermo Fisher Diagnostics, Rockford, IL), albumin (Diasorin, Stillwater, MN), LDH (Thermo DMA, Louisville, CO), NAG (Roche Diagnostics, Mannheim, Germany) superoxide dismutase (Randox Laboratories LTD Crumlin, CO), glutathione peroxidase, and glutathione S-transferase (Glathione peroxidase and transferase were based on an in-house automated analysis [56]) on lavage supernatants, serum C-reactive protein and fibrinogen (Diasorin, Stillwater, MN), creatine kinase (Fisher Diagnostics, Middletown, VA), sorbitol dehyrdogenase and creatinine (Sekisui Diagnostics, Charlottetown Prince Edward Island, Canada), high density (HDL) and low density (LDL) lipoprotein cholesterol and plasma angiotensin converting enzyme (Fisher Diagnostics, Middletown, VA) were conducted as previously described [20].

Statistics

The statistical analyses of ECG, HRV, and biochemical and inflammatory data in this study were performed using SAS software version 9.2 (SAS Institute Inc, Cary, NC). We used PROC MIXED of SAS because it offers greater flexibility for the modeling of repeated measures data than PROC GLM. It is also suitable for analysis of large, unbalanced data with missing data at random. A linear mixed model with restricted maximum-likelihood estimation analysis, least squares means and repeated measures ANOVA (analysis of variance) was used to determine which TIME*TRT interactions were statistically significant between baseline and exposure. Multiple comparison adjustment for the p values and confidence limits for the differences between the least squares means was done using adjust = Tukey HSD (Honest Significant Difference) test.

Additional files

Additional file 1: Table S1. Average source contributions for summer and winter exposures in μg/m^3. Percent of mass in parenthesis.

Additional file 2: Figure S1. Average source contributions for summer and winter Exposures.

Additional file 3: Table S2. Source contributions for summer exposures by exposure day in μg/m^3 (standard deviation in parenthesis).

Additional file 4: Table S3. Source contributions for winter exposures by exposure day in μg/m^3 (standard deviation in parenthesis).

Additional file 5: Table S4. Heart Rate Variability data before and after exposure.

Abbreviations

ANOVA: Analysis of variance; APB: Atrial premature beat; AVB: Atrioventricular block; Cal factor: Calibration factor; CAPs: Concentrated ambient particulates; CIS: Core inhalation system; CMB: Chemical mass balance; CRF: Consolidated research facility; CuZn SOD: Copper zinc superoxide dismutase; DAS: Data acquisition system; DP: Dew point; ECG: Electrocardiogram; GST: Glutathione S-transferase; HDL: High density lipoprotein; HF: High frequency; HFPC: Harvard fine particle concentrator; HR: Heart rate; HRV: Heart rate variability; HSD: Honest significant difference; HYSPLIT: Hybrid single particle lagrangian integrated trajectory; LDH: Lactate dehydrogenase; LDL: Low density lipoprotein; LF: Low frequency; LF/HF: Ratio of low frequency domain to high frequency domain; MFC: Mass flow controller; NAG: N-Acetyl-D-glucosaminidase; NIOSH: National Institute of Occupational Safety and Health; NOAA: National Oceanic and Atmospheric Administration; O_3: Ozone; PM: Particulate matter; $PM_{2.5}$: Particulate matter with an aerodynamic diameter less than 2.5 microns; READY: Real-time environmental applications and display sYstem; RH: Relative humidity; RMSSD: Root means squared of successive differences; SDNN: Standard deviation of the time between normal-to-normal beats; SH: Spontaneously hypertensive; SSI: Size selective inlet; TRP: Transient receptor potential; US EPA: United States Environmental Protection Agency; UTC: Universal Time Coordinated; VF: Ventricular fibrillation; VPB: Ventricular premature beat; VT: Ventricular tachycardia.

Competing interests

The authors declare that they have no competing interests.

Authors' contributions

AF conceived of, designed and managed the study and drafted the manuscript, LW engineered the exposure system, carried out all exposures, monitored various exposure parameters, and collected PM filters for elemental analysis, NHC participated in the design of the study, data acquisition, surgeries, and performed the statistical analysis, FM performed all electrocardiogram and heart rate variability analyses, JM and KK performed the organic and elemental analysis, DW participated in the telemetry set-up, data acquisition, and surgeries, RD performed the source apportionment analysis, MH assisted with the design of the exposure system, WC helped

draft the manuscript and assist with data interpretation, MSH participated in the design, conception and coordination of the study and performed the aconitine challenge tests. All authors read and approved the final manuscript.

Acknowledgements
The authors would like to thank David Davies of the U.S. EPA for his derivation of airflow trajectories, Judy Richards of the U.S. EPA for her excellent technical assistance, Drs. M. Ian Gilmour, Jan Dye, Daniel L. Costa, and William Linak, also of the U.S. EPA, for their thorough review of this manuscript, John Havel and Keith Tarpley of SRA International, Inc. for producing the illustrations, and the Air Resources Laboratory of the NOAA for use of their airflow trajectory models.

Disclaimer
This paper has been reviewed and approved for release by the National Health and Environmental Effects Research Laboratory, U.S. Environmental Protection Agency. Approval does not signify that the contents necessarily reflect the views and policies of the U.S. EPA, nor does mention of trade names or commercial products constitute endorsement or recommendation for use.

Author details
[1]Environmental Public Health Division, US EPA, 109 TW Alexander Drive, Research Triangle Park, Durham, NC 27711, USA. [2]Human Exposure and Atmospheric Sciences Division, US EPA, 109 TW Alexander Drive, Research Triangle Park, Durham, NC 27711, USA.

Received: 5 December 2014 Accepted: 26 March 2015
Published online: 06 May 2015

References

1. Bell ML, Dominici F, Ebisu K, Zeger SL, Samet KM. Spatial and temporal variation in PM2.5 chemical composition in the United States for health effects studies. Environ Health Perspect. 2007;115:989–95.
2. Bell ML, Ebisu K, Peng RD, Walker J, Samet JM, Zeger SL, et al. Seasonal and regional short-term effects of fine particles on hospital admissions in 202 US Counties, 1999–2005. Am J Epidemiol. 2008;168:1301–10.
3. Goldberg MS, Burnett RT, Valois MF, Flegel K, Bailar III JC, Brook J, et al. Associations between ambient air pollution and daily mortality among persons with congestive heart failure. Environ Res. 2003;91:8–20.
4. Plummer LE, Ham W, Kleeman MJ, Wexler A, Pinkerton KE. Influence of season and location on pulmonary response to California's San Joaquin Valley airborne particulate matter. J Toxicol Environ Health A. 2012;75(5):253–71.
5. Tablin F, den Hartigh LJ, Aung HH, Lame MW, Kleeman MJ, Ham W, et al. Seasonal influences on CAPs exposures: differential responses in platelet activation, serum cytokines and xenobiotic gene expression. Inhal Toxicol. 2012;24(8):506–17.
6. Happo MS, Hirvonen MR, Hälinen AI, Jalava PI, Pennanen AS, Sillanpää M, et al. Seasonal variation in chemical composition of size-segregated urban air particles and the inflammatory activity in the mouse lung. Inhal Toxicol. 2010;22(1):17–32.
7. Becker S, Dailey LA, Soukup JM, Grambow SC, Devlin RB, Huang YC. Seasonal variations in air pollution particle-induced inflammatory mediator release and oxidative stress. Environ Health Perspect. 2005;113(8):1032–8.
8. Happo M, Markkanen A, Markkanen P, Jalava P, Kuuspalo K, Leskinen A, et al. Seasonal variation in the toxicological properties of size-segregated indoor and outdoor air particulate matter. Toxicol In Vitro. 2013;7(5):1550–61.
9. Mauderly JL, Samet JM. Is there evidence for synergy among air pollutants in causing health effects? Environ Health Perspect. 2009;117(1):1–6.
10. Fakhri AA, Ilic LM, Wellenius GA, Urch B, Silverman F, Gold DR, et al. Autonomic effects of controlled fine particulate exposure in young health adults: effect modification by ozone. Environ Health Perspect. 2009;117(8):1287–92.
11. Sivagangabalan G, Spears D, Masse S, Urch B, Brook RD, Silverman F, et al. The effect of air pollution on spatial dispersion of myocardial repolarization in healthy human volunteers. J Am Coll Cardiol. 2011;57(2):198–206.
12. Wagner JG, Allen K, Yang HY, Nan B, Morishita M, Mukherjee B, et al. Cardiovascular depression in rats exposed to inhaled particulate matter and ozone: effects of diet-induced metabolic syndrome. Environ Health Perspect. 2014;122:27–33.
13. Sun L, Liu C, Xu X, Ying Z, Maiseyeu A, Wang A, et al. Ambient fine particulate matter and ozone exposures induce inflammation in epicardial and perirenal adipose tissues in rats fed a high fructose diet. Part Fibre Toxicol. 2013;10:43.
14. Aneja VP, Wang B, Tong DQ, Kimball H, Steger J. Characterization of major chemical components of fine particulate matter in North Carolina. J Air Waste Manag Assoc. 2006;56(8):1099–107.
15. Carll AP, Lamb C, Hazari MS, Winsett DW, Krantz QT, Costa DL KC, et al. Whole and particle-free diesel exhausts differentially affect cardiac electrophysiology, blood pressure, and autonomic balance in heart failure-prone rats. Toxicol Sci. 2012;128:490–9.
16. Farraj AK, Hazari MS, Winsett DW, Kulukulualani A, Carll AP, Haykal-Coates N, et al. Overt and Latent Cardiac Effects of Ozone Inhalation in Rats: Evidence for Autonomic Modulation and Increased Myocardial Vulnerability. Environ Health Perspect. 2012;120:348–54.
17. Hazari MS, Haykal-Coates N, Winsett DW, Costa DL, Farraj AK. A single exposure to particulate or gaseous air pollution increases the risk of aconitine-induced cardiac arrhythmia in hypertensive rats. Toxicol Sci. 2009;112(2):532–42.
18. Lamb CM, Hazari MS, Haykal-Coates N, Carll AP, Krantz QT, King C, et al. Divergent electrocardiographic responses to whole and particle-free diesel exhaust inhalation in spontaneously hypertensive rats. Toxicol Sci. 2012;125:558–68.
19. US EPA, 2004. EPA-CMB8.2 User's Manual. EPA-452/R-04-011. Research Triangle Park, NC.
20. Farraj AK, Haykal-Coates N, Winsett DW, Hazari MS, Carll AP, Rowan III WH, et al. Increased Non-conducted P-wave arrhythmias after a single Oil Fly Ash inhalation exposure in hypertensive rats. Environ Health Perspect. 2009;117(5):709–15.
21. Farraj AK, Hazari MS, Haykal-Coates N, Lamb C, Winsett DW, Ge Y, et al. ST depression, arrhythmia, vagal dominance, and reduced cardiac micro-RNA in particulate-exposed rats. Am J Respir Cell Mol Biol. 2011;44(2):185–96.
22. Hazari MS, Haykal-Coates N, Winsett DW, Krantz QT, King C, Costa DL, et al. TRPA1 and sympathetic activation contribute to increased risk of triggered cardiac arrhythmias in hypertensive rats exposed to diesel exhaust. Environ Health Perspect. 2011;119(7):951–7.
23. Boman BC, Forsberg AB, Järvholm BG. Adverse health effects from ambient air pollution in relation to residential wood combustion in modern society. Scand J Work Environ Health. 2003;29(4):251–60.
24. Boman BC, Nordin A, Boström D, Öhman M. Characterization of inorganic particulate matter from residential combustion of pelletized biomass fuels. Energ Fuels. 2004;18:338–48.
25. Ostro B, Feng W-Y, Broadwin R, Green S, Lipsett M. The effects of components of fine particulate air pollution on mortality in California: results from CALFINE. Environ Health Perspect. 2007;114:13–9.
26. Ghio AJ, Devlin RB. Inflammatory lung injury after bronchial instillation of air pollution particles. Am J Respir Crit Care Med. 2001;164(4):704–8.
27. Huang YC, Ghio AJ, Stonehuerner J, McGee J, Carter JD, Grambow SC, et al. The role of soluble components in ambient fine particles-induced changes in human lungs and blood. Inhal Toxicol. 2003;15(4):327–42.
28. Kodavanti UP, Schladweiler MC, Ledbetter AD, McGee JK, Walsh L, Gilmour PS, et al. Consistent pulmonary and systemic responses from inhalation of fine concentrated ambient particles: roles of rat strains used and physicochemical properties. Environ Health Perspect. 2005;113(11):1561–8.
29. Brook RD, Rajagopalan S, Pope III CA, Brook JR, Bhatnagar A, Diez-Roux AV, et al. Particulate matter air pollution and cardiovascular disease: An update to the scientific statement from the American Heart Association. Circulation. 2010;121:2331–78.
30. Cho SH, Tong H, McGee JK, Baldauf RW, Krantz QT, Gilmour MI. Comparative toxicity of size-fractionated airborne particulate matter collected at different distances from an urban highway. Environ Health Perspect. 2009;117(11):1682–9.
31. Kim YH, Tong H, Daniels M, Boykin E, Krantz QT, McGee J, et al. Cardiopulmonary toxicity of peat wildfire particulate matter and the predictive utility of precision cut lung slices. Part Fibre Toxicol. 2014;11:29.
32. Rohr AC, Kamal A, Morishita M, Mukherjee B, Keeler GJ, Harkema JR, et al. Altered heart rate variability in spontaneously hypertensive rats is associated with specific particulate matter components in Detroit, Michigan. Environ Health Perspect. 2011;119:474–80.

33. Chuang K-J, Chan C-C, Chen N-T, Su T-C, Lin L-Y. Effects of particle size fractions on reducing heart rate variability in cardiac and hypertensive patients. Environ Health Perspect. 2005;113:1693–7.
34. Muggenburg BA, Barr EB, Cheng YS, Seagrave JC, Tilley LP, Mauderley JL. Effect of inhaled residual oil fly ash on the electrocardiogram of dogs. Inhal Toxicol. 2000;12 Suppl 4:189–208.
35. Schulz H, Harder V, Ibald-Mulli A, Khandoga A, Koenig W, Krombach F, et al. Cardiovascular effects of fine and ultrafine particles. J Aeros Med. 2005;18(1):1–22.
36. Vallejo M, Ruiz S, Hermosillo AG, Borja-Aburto VH, Cardenas M. Ambient fine particles modify heart rate variability in young healthy adults. J Expos Sci Environ Epid. 2006;16:125–30.
37. Schwartz J, Litonjua A, Suh H, Verrier M, Zanobetti A, Syring M, et al. Traffic related pollution and heart rate variability in a panel of elderly subjects. Thorax. 2005;60(6):455–61.
38. Zanobetti A, Gold DR, Stone PH, Suh HH, Schwartz J, Coull BA, et al. Reduction in heart rate variability with traffic and air pollution in patients with coronary artery disease. Environ Health Perspect. 2010;118(3):324–30.
39. Corey LM, Baker C, Luchtel DL. Heart-rate variability in the Apo lipoprotein E knockout transgenic mouse following exposure to Seattle particulate matter. J Toxicol Environ Health Part A. 2006;69:953–65.
40. Bigger Jr JT, Fleiss JL, Rolnitzky LM, Steinman RC. Frequency domain measures of heart period variability to assess risk late after myocardial infarction. J Am Coll Cardiol. 1993;21:729–36.
41. Fauchier L, Babuty D, Melin A, Bonnet P, Cosnay P, Fauchier JP. Heart rate variability in severe right or left heart failure: the role of pulmonary hypertension and resistances. Eur J Heart Failure. 2004;1(6):181–5.
42. Taylor-Clark TE, Undem BJ. Ozone activates airway nerves via the selective stimulation of TRPA1 ion channels. J Physiol. 2010;588(3):423–33.
43. Takahashi N, Mori Y. TRP channels as sensors and signal integrators of redox status changes. Front Pharmacol. 2011;2:58.
44. Costa DL: Air Pollution. In Casarett & Doull's Toxicology: The Basic Science of Poison. 6th edition. Edited by Klaassen CD. New York: McGraw-Hill Companies, Inc; 2001:979–1012.
45. Perez CM, Hazari MS, Haykal-Coates N, Carll AP, Krantz QT, King C, et al. Hypoxia stress test reveals exaggerated cardiovascular effects in hypertensive rats after exposure to the Air pollutant acrolein. Toxicol Sci. 2013;132:467–77.
46. Carll AP, Lamb C, Hazari MS, Winsett DW, Krantz QT, Costa DL KC, et al. Diesel exhaust inhalation increases cardiac output, bradyarrhythmias, and parasympathetic tone in aged heart failure-prone rats. Toxicol Sci. 2013;131:583–95.
47. Watkinson WP, Campen MJ, Costa DL. Cardiac arrhythmia after exposure to residual oil fly ash particles in a rodent model of pulmonary hypertension. Toxicol Sci. 1998;41:209–16.
48. The READY system: [https://www.arl.noaa.gov/]
49. Sioutas C, Koutrakis P, Burton RM. A technique to expose animals to concentrated fine ambient aerosols. Environ Health Perspect. 1995;103(2):172–7.
50. Gupta T, Demokritou P, Koutrakis P. Development and performance evaluation of a high-volume ultrafine particle concentrator for inhalation toxicological studies. Inhal Toxicol. 2004;16(13):851–62.
51. The NIOSH Manual of Analytical Methods: [http://www.cdc.gov/niosh/docs/2003-154/pdfs/5040.pdf].
52. Hildemann LM, Markowski GR, Cass GR. Chemical composition of emissions from urban sources of fine organic aerosol. Environ Sci Technol. 1991;25:744–59.
53. Maykut NN, Lewtas J, Kim E, Larson TV. Source apportionment of PM2.5 at an urban IMPROVE site in Seattle, Washington. Sci Technol. 2003;37:5135–42.
54. Fine PM, Cass GR, Simoneit BRT. Chemical characterization of fine particle emissions from the wood stove combustion of prevalent United States tree species. Environ Eng Sci. 2004;21:705–21.
55. Walker MJA, Curtis MJ, Hearse DJ, Campbell RWF, Janse MJ, Yellon DM, et al. The Lambeth Conventions: guidelines for the study of arrhythmias in ischaemia, infarction, and reperfusion. Cardiovasc Res. 1988;22:447–55.
56. Jaskot RH, Charlet EG, Grose EC, Grady MA, Roycroft JH. An automated analysis of gluthione peroxidase, S-Transferase, and reductase activity in animal tissue. J Anal Tox. 1983;7:86–8.

Submit your next manuscript to BioMed Central and take full advantage of:

- **Convenient online submission**
- **Thorough peer review**
- **No space constraints or color figure charges**
- **Immediate publication on acceptance**
- **Inclusion in PubMed, CAS, Scopus and Google Scholar**
- **Research which is freely available for redistribution**

Submit your manuscript at
www.biomedcentral.com/submit

BioMed Central

Environmental Science & Technology

Article

Cite This: Environ. Sci. Technol. 2018, 52, 3071−3080

pubs.acs.org/est

Comparative Cardiopulmonary Effects of Particulate Matter- And Ozone-Enhanced Smog Atmospheres in Mice

Mehdi S. Hazari,*[,†] Kimberly M. Stratford,[‡] Q. Todd Krantz,[§] Charly King,[§] Jonathan Krug,[∥] Aimen K. Farraj,[†] and M. Ian Gilmour[†]

[†]Cardiopulmonary and Immunotoxicology Branch, Environmental Public Health Division, National Health and Environmental Effects Research Laboratory, U.S. Environmental Protection Agency, Research Triangle Park, North Carolina 27711, United States

[‡]Curriculum in Toxicology, University of North Carolina − Chapel Hill, Chapel Hill, North Carolina 27599, United States

[§]Inhalation Toxicology Facilities Branch, Environmental Public Health Division, National Health and Environmental Effects Research Laboratory, U.S. Environmental Protection Agency, Research Triangle Park, North Carolina 27711, United States

[∥]Exposure Methods and Measurement Division, National Exposure Research Laboratory, U.S. Environmental Protection Agency, Research Triangle Park, North Carolina 27711, United States

Downloaded via US EPA OFFICE OF ENVIRONMENTAL INFO on April 30, 2020 at 15:58:47 (UTC).
See https://pubs.acs.org/sharingguidelines for options on how to legitimately share published articles.

ABSTRACT: This study was conducted to compare the cardiac effects of particulate matter (PM)- (SA-PM) and ozone(O_3)-enhanced (SA-O_3) smog atmospheres in mice. Based on our previous findings of filtered diesel exhaust we hypothesized that SA-O_3 would cause greater cardiac dysfunction than SA-PM. Radiotelemetered mice were exposed to either SA-PM, SA-O_3, or filtered air (FA) for 4 h. Heart rate (HR) and electrocardiogram were recorded continuously before, during and after exposure. Both SA-PM and SA-O_3 increased heart rate variability (HRV) but only SA-PM increased HR. Normalization of responses to total hydrocarbons, gas-only hydrocarbons and PM concentration were performed to assess the relative contribution of each phase given the compositional variability. Normalization to PM concentration revealed that SA-O_3 was more potent in increasing HRV, arrhythmogenesis, and causing ventilatory changes. However, there were no differences when the responses were normalized to total or gas-phase only hydrocarbons. Thus, this study demonstrates that a single exposure to smog causes cardiac effects in mice. Although the responses of SA-PM and SA-O_3 are similar, the latter is more potent in causing electrical disturbances and breathing changes potentially due to the effects of irritant gases, which should therefore be accounted for more rigorously in health assessments.

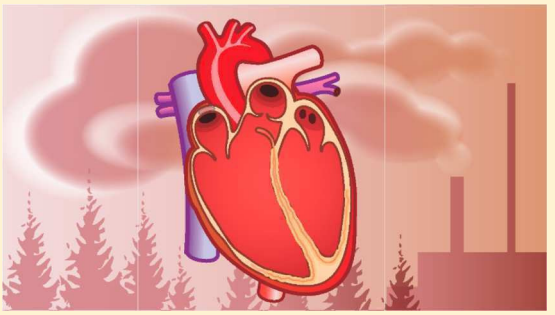

INTRODUCTION

The association between air pollution exposure and cardiovascular disease is well-established, particularly in people with certain risk factors like high blood pressure or those with pre-existing conditions.[1] The picture is less clear for healthy individuals and indeed there are still several unknowns with regards to how air pollution mediates cardiovascular dysfunction in this group, especially when there are no observable symptoms. In addition, nationwide variations in air pollution composition make it difficult to determine exactly which components, or combination of components, drive the response. This is the case for complex air pollution mixtures like smog, which originates as a set of primary pollutants (e.g., nitrogen oxides, volatile organic compounds) that are released from vehicles or industrial sources but thereafter transform after reacting with ultraviolet light to produce secondary pollutants like ozone and certain organic aerosols. Given these uncertainties, research studies need to address the comparative effects of multiple smog atmospheres and focus on determining which compositions, and hence components, cause the most serious health effects.

The American Heart Association cites several pathways by which air pollution, especially particulate matter (PM), leads to decrements in cardiovascular function.[2,3] These include elicitation of oxidative stress and inflammation, alteration of vasomotor properties, translocation of certain pollutants into the systemic circulation and modulation of autonomic controls which regulate the heart and vasculature. Some of these may not manifest as overt symptoms, especially in young healthy individuals, but instead as shifts in normal physiological function which render a person susceptible to subsequent stressors or triggers of adverse responses. We previously showed that exposure to a relatively low concentration of diesel exhaust, which contains many of the same pollutants as smog, caused increased arrhythmias and other cardiovascular effects when healthy rats were challenged with an exercise-like stressor.[4,5] The insight gained from these and other studies is

Received: September 20, 2017
Revised: December 19, 2017
Accepted: February 1, 2018
Published: February 1, 2018

ACS Publications © 2018 American Chemical Society

DOI: 10.1021/acs.est.7b04880
Environ. Sci. Technol. 2018, 52, 3071−3080

that exposure to complex air pollution mixtures results in latent autonomic shifts which cause a decrease in cardiac performance during exposure and even up to 1 day later.

Although many epidemiological studies point to PM as the main cause of air pollution's impacts on the cardiovascular system,[6−8] there are numerous human and rodent studies that implicate ubiquitous gaseous irritants like ozone as well.[9−11] In fact, our previous studies have shown that cardiovascular dysfunction occurs, sometimes at comparable levels or even after PM is removed from a multipollutant mixture like diesel exhaust.[12−14] Furthermore, the magnitude of the response is not just determined by the relative levels of PM and ozone but also by the resulting physical and chemical interactions that occur in the mixture. Therefore, the objective of this study was to examine and compare the cardiovascular responses of mice exposed to either a simulated high PM/low ozone (SA-PM) or low PM/high ozone (SA-O_3) smog atmosphere. These photo-oxidized mixtures approximated urban and regional evaporative pollutant emissions with similar Air Quality Health Index values. We previously determined that filtered diesel exhaust causes greater acute cardiac effects than whole diesel exhaust, and so we hypothesized that although both smog mixtures would elicit cardiac changes in mice, the atmosphere dominated by gaseous irritants would be more potent, particularly in causing electrical disturbances like arrhythmia.

MATERIALS AND METHODS

Animals. Female C57BL/6 (21 ± 1.1 g) mice between 13 and 15 weeks of age were used in this study (Jackson Laboratory, Bar Harbor, ME). Mice were initially housed five per cage and maintained on a 12 h light/dark cycle at approximately 22 °C and 50% relative humidity in an AAALAC−approved facility. Food (Prolab RMH 3000; PMI Nutrition International, St. Louis, MO) and water were provided ad libitum. All protocols were approved by the Institutional Animal Care and Use Committee of the U.S. Environmental Protection Agency and are in accordance with the National Institutes of Health Guides for the Care and Use of Laboratory Animals. Animals were randomly assigned to one of the following groups after implantation of radiotelemeters: (1) filtered air (FA), (2) SA-PM, or (3) SA-O_3.

Surgical Implantation of Radiotelemeters. Mice were implanted with radiotelemeters as previously described.[15] Animals were anesthetized using inhaled isoflurane (Isothesia, Butler Animal Health Supply, Dublin OH). Anesthesia was induced by spontaneous breathing of 2.5% isoflurane in pure oxygen at a flow rate of 1 L/min and then maintained by 1.5% isoflurane in pure oxygen at a flow rate of 0.5 L/min; all animals received the analgesic buprenorphrine (0.03 mg/kg, i.p. manufacturer). Briefly, using aseptic technique, each animal was implanted subcutaneously with a radiotelemeter (ETA-F10, Data Sciences International, St Paul, MN), the transmitter was placed under the skin to the right of the midline on the dorsal side. The two electrode leads were then tunneled subcutaneously across the lateral dorsal sides, and the distal portions were fixed in positions that approximated those of the lead II of a standard electrocardiogram (ECG). Body heat was maintained both during and immediately after the surgery. Animals were given food and water postsurgery and were housed individually. All animals were allowed 7−10 days to recover from the surgery and reestablish circadian rhythms.

Radiotelemetery Data Acquistion. Radiotelemetry methodology (Data Sciences International, Inc., St. Paul, MN) was used to track changes in cardiovascular function by monitoring heart rate (HR), and ECG waveforms immediately following telemeter implantation, through exposure until 24 hours postexposure. This methodology provided continuous monitoring and collection of physiologic data from individual mice to a remote receiver. Sixty-second ECG segments were recorded every 15 min during the pre- and postexposure periods and every 5 min during exposure (baseline and hours 1−4); HR was automatically obtained from the waveforms (Dataquest ART Software, version 3.01, Data Sciences International, St. Paul, MN). All animals were acclimated to the exposure chambers on two separate occasions, even then, an increase in HR was always observed when animals were placed in the chamber on the day of exposure.

Electrocardiogram Analysis. ECGAuto software (EMKA Technologies USA, Falls Church VA) was used to visualize individual ECG waveforms, analyze and quantify ECG segment durations and areas, as well as identify cardiac arrhythmias as previously described (Kurhanewicz et al. 2014). Briefly, using ECGAuto, Pwave, QRS complex, and T-wave were identified for individual ECG waveforms and compiled into a library. Analysis of all experimental ECG waveforms was then based on established libraries. The following parameters were determined for each ECG waveform: PR interval (P_{start}-R), QRS complex duration (Q_{start}-S), ST segment interval (S-T_{end}) and QT interval (Q_{start}-Tend). QT interval was corrected for HR using the correction formula for mice QTc = QT/(RR/100)1/2.[16] Pre-exposure assessments were measured as the exposure time-matched 4 h of data from 24 h before exposure for each animal. Immediately postexposure assessments were the 4 h of data taken immediately postexposure. Twenty-four postexposure assessments were the exposure time-matched 4 h of data taken 24 h after exposure.

Heart Rate Variability Analysis. Heart rate variability (HRV) was calculated as the mean of the differences between sequential RRs for the complete set of ECG waveforms using ECGAuto. For each 1 min stream of ECG waveforms, mean time between successive QRS complex peaks (RR interval), mean HR, and mean HRV-analysis−generated time-domain measures were acquired. The time-domain measures included standard deviation of the time between normal-to-normal beats (SDNN), and root mean squared of successive differences (RMSSD). HRV analysis was also conducted in the frequency domain using a Fast-Fourier transform. The spectral power obtained from this transformation represents the total harmonic variability for the frequency range being analyzed. In this study, the spectrum was divided into low-frequency (LF) and high-frequency (HF) regions. The ratio of these two frequency domains (LF/HF) provides an estimate of the relative balance between sympathetic (LF) and vagal (HF) activity.

Whole-Body Plethysmography. Ventilatory function was assessed in awake, unrestrained mice using a whole-body plethysmograph (Buxco, Wilmington, NC). Assessments were performed 1 day before exposure, immediately postexposure and 24 h after exposure. The plethysmograph pressure was monitored using Biosystems XA software (Buxco Electronics Inc., Wilmington, NC). Using respiratory-induced fluctuations in ambient pressure, ventilatory parameters including tidal volume (V_T), breathing frequency (f), inspiratory time (Ti), and expiratory time (Te), were calculated and recorded on a breath-by-breath basis.

DOI: 10.1021/acs.est.7b04880
Environ. Sci. Technol. 2018, 52, 3071−3080

Table 1. Concentrations of Criteria Pollutants and Air Quality Indexes[a]

	$PM_{2.5}$ (mg/m^3) AQI	NO_x/AQI (ppm) AQI	O_3/AQI (ppm) AQI	total hydrocarbons (ppmc)	gas-phase (mgC/m^3)	AQHI
	0.009		0.002			
filtered air	37 (green)	ND	1 (green)	ND	ND	<1
SA-PM	1.0362	0.380	0.190	5.5	3.847	92.5
	>500 (brown)	154 (orange)	287(red)			
SA-O_3	0.0523	0.647	0.448	6.1	3.125	102.6
	142 (orange)	199 (red)	>300 (purple)			

[a]ND, none detected. Green, AQ is satisfactory—little or no risk. Yellow, AQ is acceptable—moderate health concern for a very small number of people who are unusually sensitive to air pollution. Orange, Sensitive people may experience health effects. Red, Everyone may experience health effects; sensitive people at greater risk. Purple, Everyone may experience serious health effects. Brown, Health warnings at emergency conditions; entire population will be affected.

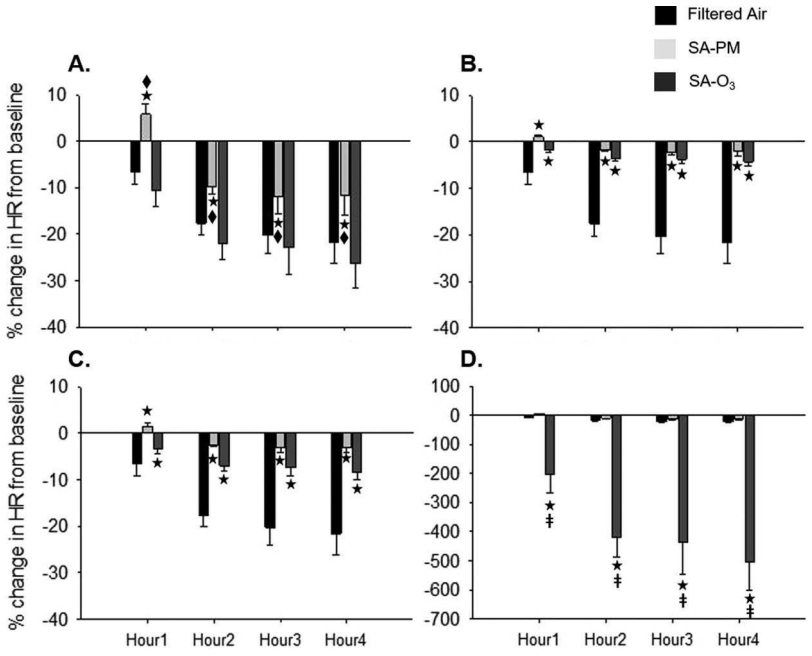

Figure 1. Exposure to smog alters heart rate responses in mice. In general, mice experienced a steady decrease in HR (from baseline) over the first 2 h of exposure, which then leveled off in hours three and four. Mice exposed to SA-PM experienced a significant increase in HR during the first hour and had less decrease in HR thereafter when compared to FA and SA-O_3 (A.). However, there was no difference between SA-PM and SA-O_3 when the change in HR during exposure was normalized to total hydrocarbons (B.) or gas-phase hydrocarbons only (C.). In contrast, decrease in HR during SA-O_3 exposure was significantly greater than SA-PM when responses were normalized to PM concentration (D.). significantly different from FA; • significantly different from SA-O_3; ǂ significantly different from SA-PM. $p < 0.05$.

Photochemical Smog Exposures. A gasoline blend was combined with either α-pinene or isoprene to produce a hydrocarbon mixture that was enhanced for particulate matter (PM) or ozone (O_3) during irradiation, respectively. Thus, photochemical smog atmospheres with either high $PM_{2.5}$ and low O_3/nitrogen oxide (NO_x) concentrations (SA-PM) or low $PM_{2.5}$ and high O_3/NO_x (SA-O_3) were generated in the Mobile Reaction Chamber (MRC). Briefly, SA-PM was artificially generated with 0.491 ppm nitrogen oxide (NO), 0.528 ppm of NO_x, 29.9 ppmC total hydrocarbons (THC), 24 ppmC gasoline and 5.3 ppmC α -pinene as the initial conditions, whereas SA-O_3 was generated from 0.794 ppm of NO, 0.912 ppm of NO_x, 12.4 ppmC THC, 5.2 ppmC isoprene and 7.21 ppmC gasoline. Each of the initial smog mixtures was then irradiated with ultraviolet light. Smog was then transported under vacuum to 0.3 m^3 whole body inhalation chambers where mice were exposed once for 4 h. Continuous gas and aerosol sampling for carbon monoxide (CO), O_3, NO_x, THC and particle mass concentration were conducted at both the MRC unit as well as from the inhalation exposure systems. All PM was formed as secondary organic aerosol (SOA) from the photochemical reactions in the MRC. Particle size distributions and gravimetric mass sampling was measured, and filter sampling for gravimetric analysis were conducted for the entire exposure time. Volatile organic compound (VOC) summa cannisters were periodically collected and analyzed by gas chromatography off-line to determine concentrations of various volatile organic compounds (VOCs) in the exposure atmosphere. Animals exposed to FA received room air, which was transported to the chambers after being HEPA filtered. Please refer to Krug et al. in this issue for complete exposure details.

Statistics. All data are expressed as means ± SEM. Statistical analyses were performed using Sigmaplot 13.0 (Systat Software, San Jose, CA) software. The delta values (i.e., change during exposure from baseline) of HR, HRV and

DOI: 10.1021/acs.est.7b04880
Environ. Sci. Technol. 2018, 52, 3071−3080

the ventilatory parameters were used and a two-way analysis of variance (ANOVA) for repeated-measures was employed with Bonferroni post hoc tests to determine statistical differences. Raw ECG and arrhythmia count data were analyzed by two-way ANOVA. Raw HR, HRV, ventilatory parameters, and arrhythmia counts were also normalized to total hydrocarbons (both particle and gas phases), gas-phase hydrocarbons only or PM concentration by dividing the physiological parameters by the pollutant concentrations. Normalizations were done to compare the relative contribution of these components to the physiological response to Smog A versus B and their relative potencies; no statistical comparisons were made to FA postnormalization. The statistical significance was set at $P < 0.05$.

RESULTS

Exposure Characteristics. Table 1 shows the inhalation chamber concentrations of $PM_{2.5}$ (i.e., secondary organic aerosols), NO_x, O_3, as well as total hydrocarbons in the complete smog mixture (particle and gas phases) and in the gas-phase only for both SA-PM (enhanced $PM_{2.5}$) and SA-O_3 (enhanced O_3). In addition, the respective air quality health indexes (AQHI) and air quality indexes (AQI) along with their color codes are also included to provide a health-risk comparison between these atmospheres. These indices describe the health risks from polluted air on individual days throughout the year, either from independent pollutants as in the case of AQI, or from a cumulative $PM_{2.5}$, O_3, and NO_x perspective as with AQHI. Refer to Krug et al. in this issue for a more comprehensive comparison of SA-PM (MR044) and SA-O_3 (MR059).

Heart Rate. There was no difference in the baseline HR, which was the resting level measured in the home cages, between any of the groups (FA = 588.0 ± 19.8 bpm; SA-PM = 568.6 ± 7.5 bpm; SA-O_3 = 565.9 ± 9.4 bpm). In general, all animals experienced a decrease in HR during the exposure; although, SA-PM caused a significant increase in HR during Hour1 and less HR decrease over the remaining exposure period when compared to FA and SA-O_3 (Figure 1A). However, there was no difference between SA-PM and SA-O_3 when the responses were normalized to THC (Figure 1B) or gas-phase hydrocarbons only (Figure 1C). On the other hand, HR decrease was significantly greater during SA-O_3 when compared to SA-PM after normalization to PM concentration (Figure 1D).

Arrhythmia. None of the animals experienced cardiac arrhythmias during the pre-exposure period. Figure 2 shows the raw arrhythmia counts during the 4 h exposure. Overall, exposure to SA-O_3 increased the incidence of arrhythmias when compared to FA (Figure 2A–D) but there was no difference with respect to SA-PM in the denormalized (Figure 2A) and THC normalized (Figure 2B) responses. In contrast, SA-O_3 caused significantly more arrhythmias than SA-PM when the responses were normalized to gas-phase hydrocarbons (Figure 2C) or PM concentrations (Figure 2D).

Heart Rate Variability. Figures 3-5 show the changes in HRV during exposure. There were no significant differences in the baseline HRV measures between any of the groups (FA − SDNN = 7.4 ± 0.7 ms, RMSSD = 4.0 ± 0.5 ms, LF/HF = 8.4 ± 0.7 ms^2; SA-PM − SDNN = 7.9 ± 0.7 mscec, RMSSD = 5.3 ± 0.6 ms, LF/HF = 7.1 ± 0.6 ms^2; SA-O_3−SDNN = 8.7 ± 0.7 ms, RMSSD = 5.5 ± 0.7 ms, LF/HF = 6.7 ± 0.6 ms^2). SDNN decreased in the first hour of exposure in control animals; this

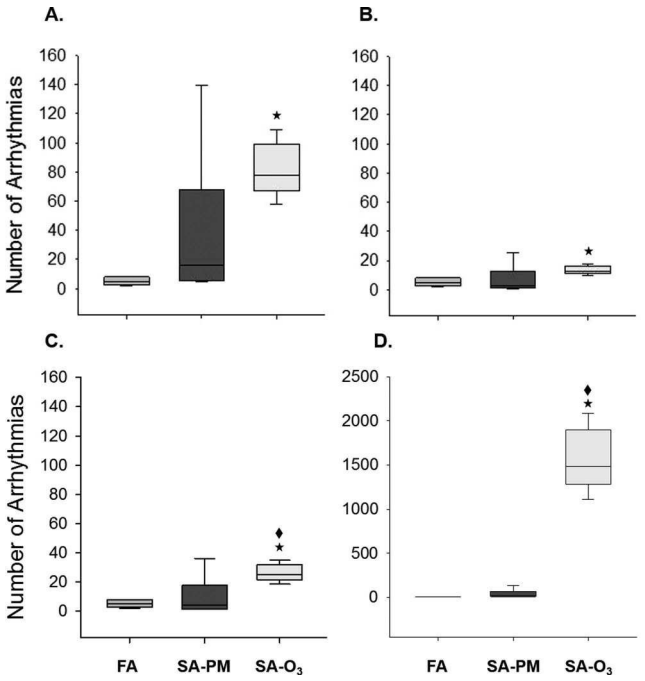

Figure 2. Exposure to O_3-enhanced smog increases cardiac arrhythmias in mice. Overall, exposure to SA-O_3 caused a significant increase in the number of cardiac arrhythmias in mice when compared to FA. There was no difference between SA-O_3 and SA-PM in the denormalized (A.) and THC-normalized (B.) responses; however, SA-O_3 caused significantly more arrhythmias than SA-PM when the responses were normalized to gas-phase hydrocarbons (C.) or PM concentration (D.). significantly different from FA; • significantly different from SA-PM. $p < 0.05$.

was likely due to sympathetic modulation from the stress of handling and placement in the chamber. Animals exposed to either SA-PM or SA-O_3 had a significant increase in SDNN (Figure 3A) when compared to FA and a similar trend was observed for RMSSD (Figure 4A). Both time-domain measures showed minimal to no effects for either SA-PM or SA-O_3 when the responses were normalized to THC (Figure 3B and 4B) or gas-phase hydrocarbons only (Figure 3C and 4C). However, the increase in SDNN and RMSSD during SA-O_3 exposure was significantly greater than SA-PM when the data were normalized to PM concentration (Figure 3D and 4D). On the other hand, there were no significant effects in the frequency-domain measures (i.e., LF/HF) for either smog atmosphere with or without normalization of responses (Figure 5).

Ventilatory Function. Whole-body plethysmography was performed on all animals during the baseline period as well as immediately and 1 day after exposure; results shown in Figure 6 compare the changes in ventilatory parameters from baseline between the groups. Baseline values did not differ between the groups (FA − f = 475.1 ± 13.1 breaths/min, V_T = 0.24 ± 0.01 mL, Ti = 0.06 ± 0.002 s, Te = 0.08 ± 0.002 s; SA-PM − f = 509.8 ± 6.3 breaths/min, V_T = 0.24 ± 0.01 mL, Ti = 0.05 ± 0.001 s, Te = 0.07 ± 0.001 s; SA-O_3 − f = 499.7 ± 12.1 breaths/min, V_T = 0.25 ± 0.01 mL, Ti = 0.06 ± 0.002 s, Te = 0.07 ± 0.002 s). There were no differences in f, V_T, Ti or Te between any of the groups in the unnormalized results (Figure 6A). However, normalizing to THC (Figure 6B) or gas-phase only hydrocarbons (Figure 6C) revealed a significant decrease in f, and increase in V_T and Ti in SA-PM and SA-O_3

DOI: 10.1021/acs.est.7b04880
Environ. Sci. Technol. 2018, 52, 3071−3080

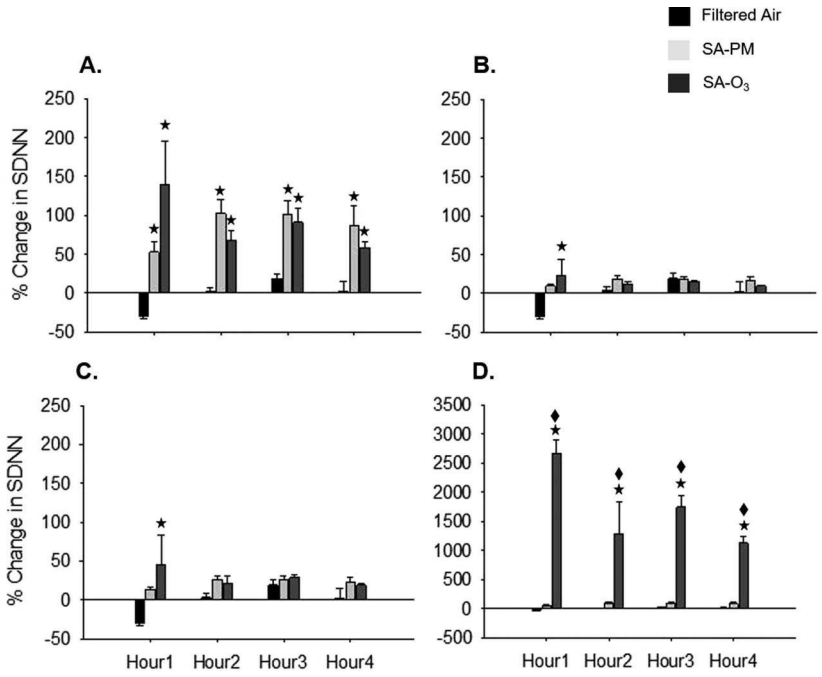

Figure 3. Exposure to smog increases SDNN in mice. SDNN decreased during the first hour of FA exposure probably due to stress. On the other hand, mice exposed to either SA-PM or SA-O_3 experienced a significant increase in SDNN (A.) when compared to FA. There was no difference in SDNN between SA-PM and SA-O_3 in the denormalized (A.), THC- (B.) or gas-phase only hydrocarbon (C.) normalized responses. In contrast, SDNN was significantly increased during SA-O_3 exposure when compared to SA-PM when responses were normalized to PM concentration (D.). significantly different from FA; • significantly different from SA-PM. $p < 0.05$.

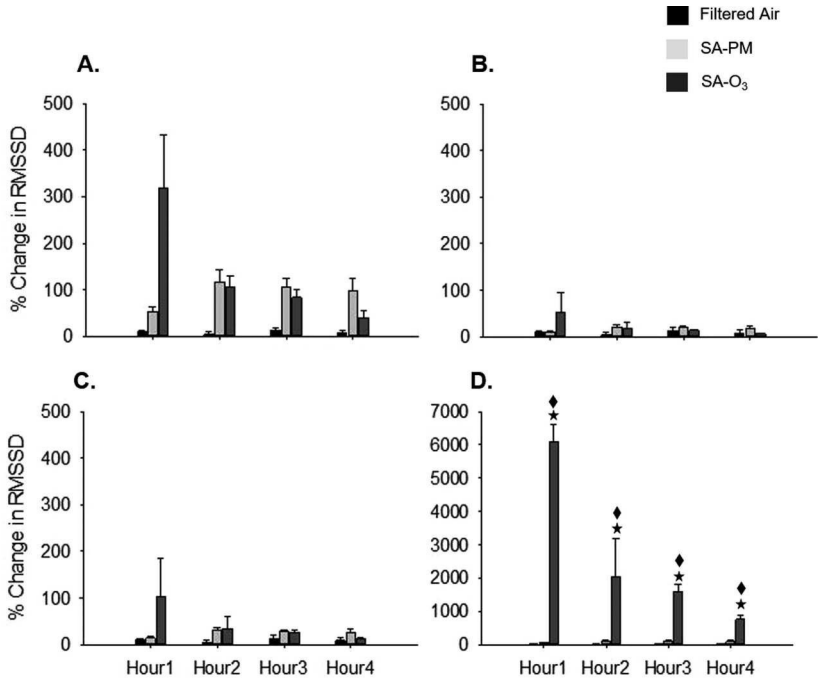

Figure 4. Exposure to O_3-enhanced smog increases RMSSD in mice. There was no effect of SA-PM or SA-O_3 on RMSSD when compared to FA although a trend of increase was observed for both (A.). There was no difference in RMSSD between SA-PM and SA-O_3 in the THC- (B.) or gas-phase only hydrocarbon (C.) normalized responses. On the other hand, RMSSD was significantly increased during SA-O_3 exposure when compared to SA-PM when responses were normalized to PM concentration (D.). significantly different from FA; • significantly different from SA-PM. $p < 0.05$.

immediately after exposure when compared to controls. Some of these responses relative to FA persisted 1 day after exposure but there was no difference between SA-PM and SA-O_3. In contrast, normalization to PM concentrations revealed a significant increase in *f*, and decrease in V_T and Ti immediately after exposure in SA-O_3-exposed animals when compared to SA-PM (Figure 6D); only the changes in *f* and V_T persisted 24 h later.

Electrocardiogram. There were no baseline differences in any ECG parameters between any of the groups. Changes in

DOI: 10.1021/acs.est.7b04880
Environ. Sci. Technol. 2018, 52, 3071−3080

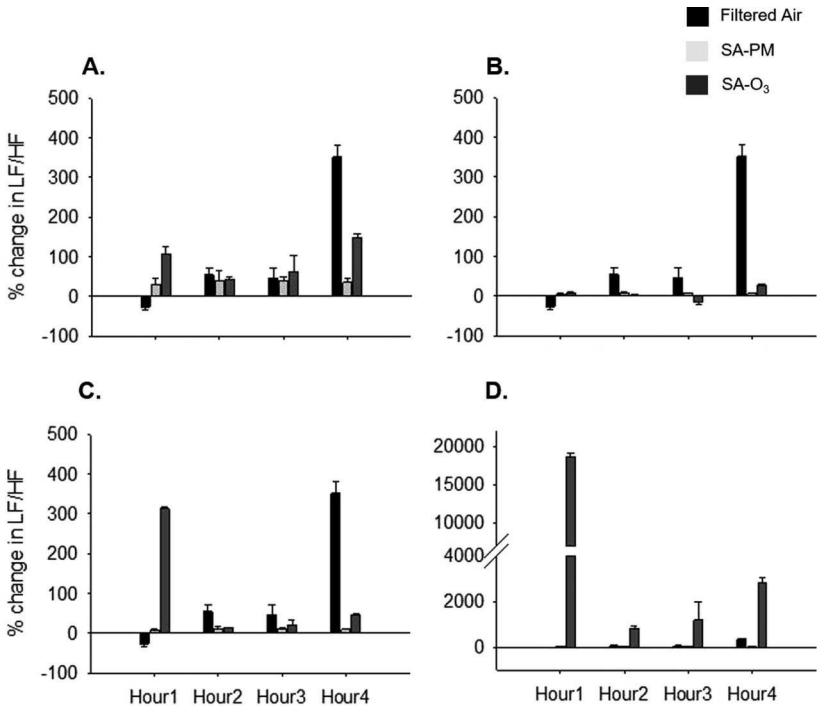

Figure 5. Change in LF/HF during smog exposure. There were no significant effects of SA-PM or SA-O_3 on LF/HF when compared to FA or when either smog atmosphere was compared to the other (A.). Normalization of the responses to THC- (B.), gas-phase only hydrocarbons (C.), or PM concentrations (D.) did not reveal any significant difference between SA-PM and SA-O_3 except in (D.) where a trend of increase was observed in SA-O_3-exposed mice.

ECG during exposure were restricted to a PR interval prolongation in mice exposed to SA-PM, which were significantly higher than FA and SA-O_3 (Table 2).

DISCUSSION

The results of this study demonstrate that a single inhalation exposure to atmospheric smog causes acute cardiovascular dysfunction in mice, irrespective of whether it is comprised predominantly of PM or O_3. Our findings also suggest that multipollutant mixtures which have a higher irritant gas composition are likely to cause more potent acute cardiac effects than those with higher PM/lower gases. Unfortunately, the relative toxicity of only the SOA in each of the atmospheres was not assessed, this would have provided greater information about their contributions to the differential health effects we observed. In either case, it is not possible to firmly conclude whether PM in general plays a greater role in causing cardiac effects or not because SOA is not necessarily the same as ambient PM. However, in an effort to compare the effects of SA-PM and SA-O_3 relative to their whole compositions, we normalized the data from this study to total hydrocarbons, gas-phase hydrocarbons only and PM concentration. Normalization of the results showed that there was no difference in heart rate, heart rate variability or cardiac arrhythmias between SA-PM and SA-O_3 when differences in total hydrocarbons or gas-phase only hydrocarbons were taken into account. In contrast, SA-O_3 caused significantly greater cardiac effects than SA-PM when results were normalized to PM concentration indicating that the difference in response was mediated by the gaseous components. Thus, these findings point to the complexity of interactions between air pollution components and the reactions that determine the composition of the final mixture and the resulting cardiovascular response.

Real-time cardiovascular measurements and responses to exposure as derived here from radiotelemetry often include stress-related effects (e.g., from handling, noise, etc). This was observed in all animals as a transient increase in heart rate upon placement in the exposure chamber, which occurred despite two separate one-hour acclimatizations. In controls, the overall heart rate progressively decreased per hour of exposure as the animals calmed down in the chambers. Similar responses were observed with SA-O_3 but with a trend of greater decrease in heart rate. Although this result was not statistically significant, it is not entirely surprising that SA-O_3 would have this effect given it was rich in irritant gases like O_3, NO_x and reactive aldehydes, which have the ability to activate airway sensory nerves, elicit autonomic reflexes and modulate parasympathetic function.[17−19] On the other hand, SA-PM caused a significant increase in heart rate in the first hour of exposure and less decrease (i.e., HR remained elevated above normal) over the remaining exposure period when compared to controls and SA-O_3. These disparate effects of SA-PM and SA-O_3 are not unusual. We previously showed that exposure to particle-filtered diesel exhaust caused greater decrements in heart rate than whole diesel exhaust while particle-rich air pollution has been shown to increase heart rate.[13,20,21] Thus, it appears from our data that decreases in heart rate during such exposures are related to the composition and concentration of gases in the complex air pollution mixture. Notice that normalization of the heart rate to total or gas-phase only hydrocarbons did not reveal any difference between SA-PM and SA-O_3, yet when the "effects" of PM were eliminated through normalization SA-O_3 caused a significant decrease in heart rate when compared to SA-PM.

The composition of the smog atmospheres may not have been the only determinant of this response, variations in the

DOI: 10.1021/acs.est.7b04880
Environ. Sci. Technol. 2018, 52, 3071−3080

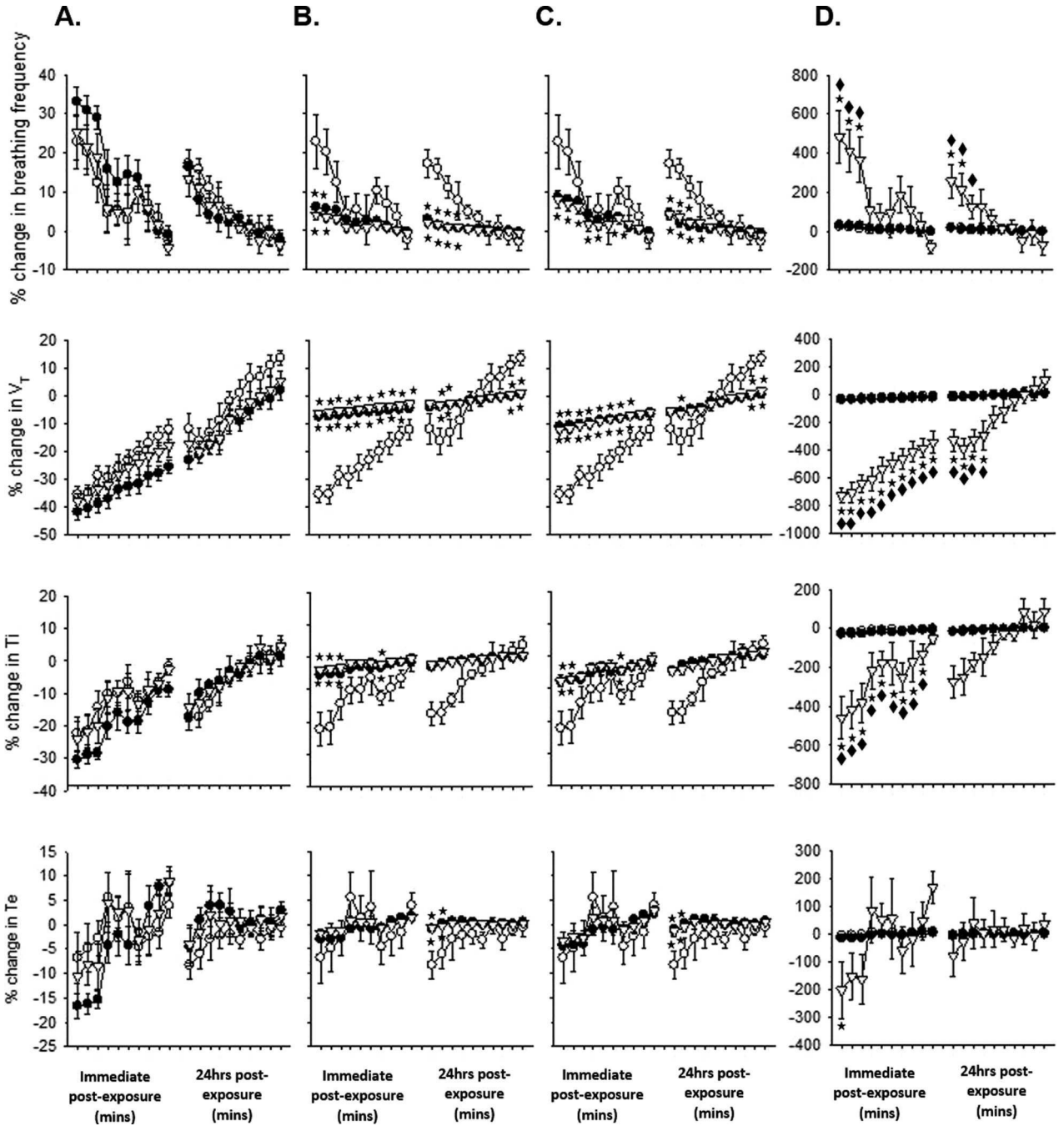

Figure 6. O_3-enhanced smog alters breathing in mice immediately after exposure. There was no effect of SA-PM (filled circles) or SA-O_3 (open triangles) on any ventilatory parameters when compared to FA (open circles) (A.) and there were no differences observed between SA-PM and SA-O_3 in the THC- (B.) or gasphase only hydrocarbon (C.) normalized responses. However, f was increased, and VT and Ti were significantly decreased after SA-O_3 exposure when compared to SA-PM when responses were normalized to PM concentration (D.). significantly different from FA; • significantly different from SA-PM. $p < 0.05$.

smell of SA-PM and SA-O_3 could have contributed as well. SA-PM had a very potent smell when compared to SA-O_3 and this may have caused an increase in the heart rate. This effect has been demonstrated previously, particularly with burnt or unpleasant smells,[22] and appears to be mediated by an increase in sympathetic modulation or decrease in heart rate variability. It is likely that in addition to smell, several smog factors could have triggered responses and altered autonomic function simultaneously, particularly given the complexity of the atmosphere (e.g., potent "burnt" smell + chemical airway irritation + secondary activation due to inflammation). The autonomic nervous system controls the heart and vasculature through a dynamic ebb and flow of both parasympathetic and sympathetic influence and tends to lean in the direction of one or the other based on the physiological circumstances. Thus, returning to the issue of composition, the difference in response between a predominantly gaseous mixture and one that is high in particles would depend on the sum of all the factors that impact autonomic function, and hence the resulting direction would be determined by which factor(s) dominates.

Although our data do not necessarily demonstrate this (i.e., parasympathetic/sympathetic activation) directly, it is possible

DOI: 10.1021/acs.est.7b04880
Environ. Sci. Technol. 2018, 52, 3071−3080

Table 2. Electrocardiographic Parameters

air	PR interval (msec)	QRS duration (msec)	QTc (msec)
baseline	36.1 ± 0.5	14.7 ± 1.9	94.2 ± 3.0
hour 1	33.4 ± 1.8	13.9 ± 0.5	92.7 ± 1.5
hour 2	35.7 ± 1.4	14.6 ± 0.4	92.9 ± 1.5
hour 3	35.9 ± 0.6	14.8 ± 0.4	94.9 ± 3.0
hour 4	37.5 ± 1.0	15.3 ± 0.4	94.5 ± 2.0
24 h postexp	36.0 ± 0.7	16.3 ± 0.3	94.6 ± 4.0
SA-PM			
baseline	32.8 ± 0.6	14.6 ± 0.3	88.2 ± 1.5
hour 1	40.7 ± 1.0*♦	13.3 ± 0.2	91.0 ± 4.6
hour 2	42.3 ± 1.1*♦	13.4 ± 0.4	93.3 ± 4.1
hour 3	43.3 ± 0.9*♦	13.7 ± 0.2	91.7 ± 2.6
hour 4	42.8 ± 1.2*♦	13.6 ± 0.3	99.3 ± 7.0
24 h postexp	33.4 ± 0.5	14.4 ± 0.2	81.5 ± 1.4
SA-O_3			
baseline	33.6 ± 0.9	13.4 ± 1.1	89.9 ± 1.8
hour 1	34.4 ± 1.1	11.8 ± 2.2	95.9 ± 3.4
hour 2	36.3 ± 0.8	11.0 ± 2.4	91.5 ± 3.6
hour 3	36.6 ± 0.7	9.6 ± 3.2	92.7 ± 4.9
hour 4	37.1 ± 0.7	10.1 ± 2.8	92.4 ± 2.9
24 h postexp	34.2 ± 0.6	14.4 ± 0.8	88.9 ± 0.8

that irritant gases drove a predominantly parasympathetic response whereas the PM-rich mixture caused a stress-induced sympathetic modulation. We observed a greater increase in SDNN and RMSSD, which is indicative of parasympathetic modulation, during SA-O_3 exposure when compared to SA-PM. This response was due to the effects of the gas-phase components given the difference in these parameters between the two smog atmospheres became evident when we normalized to PM concentration. As far as PM is concerned, studies have demonstrated, as stated previously, that it not only increases heart rate, blood pressure, low frequency blood pressure variability and noradrenalin release (i.e., stress), but also causes a decrease in heart rate variability.[3,23] All of these changes point to sympathetic modulation and a perceived increase in cardiac risk. However, we observed an increase in SDNN and RMSSD even with the PM-enhanced SA-PM mixture. This might be explained by the fact that SA-PM also contained irritant gases, some of which were present in high concentrations (see Krug et al. in this issue) and could have opposed the sympathetic modulatory effect of the PM. A lack of response in the LF/HF ratio suggests this parasympathetic-sympathetic push and pull.[24]

Comparisons between SA-PM and SA-O_3 also included the air quality health index or AQHI, which indicates the health risk of both atmospheres. The equation for this index provides the relative contribution of the $PM_{2.5}$ and the oxidant gases toward the health metric. In the case of SA-O_3, oxidant gases contributed to 97% of the AQHI with a negligible amount coming from PM, once again pointing to the fact that it is effects were predominantly mediated by irritant gases. In contrast, PM contributed to almost 70% of the AQHI of SA-PM, yet it also had a fairly significant contribution (30%) from the oxidant gases as well (see Krug et al. this issue). These results seem to confirm our conclusions that although the effects of SA-O_3, which included a significant decrease in heart rate and increase in heart rate variability, were almost entirely driven by gases, SA-PM's effects were likely driven by both. The implications for human health are important, particularly given most of the research over the past decade has focused on PM-driven cardiovascular effects. For example, both an increase of 6 ug/m^3 in fine PM and 20 ppb O_3 resulted in a significant increase in the risk of out of hospital heart attacks.[25] Furthermore, exposure to 0.3 ppm of O_3 caused similar HRV changes in healthy young individuals to what we observed in this study, suggesting gases like O_3 may not cause overt symptoms but rather underlying changes.[26]

While an increasing or decreasing heart rate or heart rate variability during exposure merely indicates a physiological change, one could potentially infer cardiac dysfunction when it is a deviation from the control response. It represents fluctuations that can normally happen in mammals (e.g., exercise or physical exertion). Sometimes these responses reflect adverse cardiac issues more strongly when observed in conjunction with cardinal signs of dysfunction like arrhythmia. This may be the case for what we observed in the mice exposed to these smog atmospheres. We have shown that gaseous air pollution is more arrhythmogenic than one with a high concentration of PM and the same appears to be the case in this study.[12,27] SA-O_3, particularly when normalized to PM concentration, caused a significantly greater number of sinoatrial (SA) node dysfunction than SA-PM. Furthermore, we found that SA-O_3 was more arrhythmogenic than SA-PM even when normalized to gas-phase hydrocarbons suggesting PM had very little effect. This form of arrhythmia or dysrhythmia, which can increase the risk of escape beats and cardiac insufficiency in humans, is due to an abnormal delay in the firing of the SA node and manifests as blocked p-waves and alternating runs of bradycardia followed by tachycardia.. Interestingly, some of the causes behind this phenomenon include an increase in vagal tone and airway irritation which leads to dyspneic breathing and airway spasm, both of which were observed in our animals.[28,29]

Exposure to SA-PM did cause a prolongation of the PR interval, which in some cases is normal but also can indicate a cardiac conduction abnormality. However, in the absence of other effects (e.g., arrhythmia) it would be hard to say that there was any real dysfunction in these mice. Indeed, even changes in breathing impact the heart on a breath-by-breath basis and through this physiological coupling the heart is able to maintain proper function.[30] Thus, alterations in breathing due to airway irritation and airflow obstruction have the potential to cause adverse cardiac events. Yet, we did not observe any remarkable differences in ventilatory parameters either immediately following the exposure or 1 day later for either SA-PM or SA-O_3. Normalization to total or only gas-phase hydrocarbons did not reveal any differences but SA-O_3 caused a significant increase in breathing frequency, and decreases in tidal volume and inspiratory time when the results were normalized to PM concentration. Thus, once again it appears that the gases in SA-O_3 caused a rapid shallow breathing in mice possibly due to irritation.

In conclusion, the results of this study demonstrate that inhalation exposure to a complex smog atmosphere causes acute cardiac effects in mice, and that the composition of the pollution mixture likely plays a key role in determining the degree of responsiveness. Although the PM-enhanced smog caused a change in cardiac function, it is likely that a single exposure was not enough to elicit worsening symptoms in our relatively young healthy animals. This is particularly true for the relatively low number of cardiac arrhythmias observed in those animals. It is entirely likely however that repeated exposures would have had a more pronounced impact. In contrast, the

DOI: 10.1021/acs.est.7b04880
Environ. Sci. Technol. 2018, 52, 3071−3080

O_3-enhanced smog caused a set of physiological changes which if considered with the increased incidence of arrhythmia suggest an acute irritant gas-mediated autonomic modulation and electrical disturbance. Even though the former is not considered a "toxicological" response, it does reflect a change from the homeostatic normal state of the body. These short-lived reversible effects probably do not pose a serious hazard to the body on their own, but when combined with an additional stressor could predispose the heart to dysfunction, particularly during in the 24 h following exposure.

AUTHOR INFORMATION

Corresponding Author

*Phone: 919-541-4588; fax: 919-541-0034; e-mail: hazari.mehdi@epa.gov.

ORCID

Mehdi S. Hazari: 0000-0003-0280-9690
Kimberly M. Stratford: 0000-0001-7076-9753
Jonathan Krug: 0000-0002-7045-7650

Notes

The authors declare no competing financial interest.

ACKNOWLEDGMENTS

We are grateful to Drs. Wayne Cascio, Christopher Gordon and Colette Miller for their careful reviews of this manuscript. This paper has been reviewed and approved for release by the National Health and Environmental Effects Research Laboratory, U.S. Environmental Protection Agency. Approval does not signify that the contents necessarily reflect the views and policies of the U.S. EPA, nor does mention of trade names. All funding for this study is from U.S. Environmental Protection Agency.

REFERENCES

(1) Langrish, J. P.; Bosson, J.; Unosson, J.; Muala, A.; Newby, D. E.; Mills, N. L.; Blomberg, A.; Sandström, T. Cardiovascular effects of particulate air pollution exposure: time course and underlying mechanisms. *J. Intern. Med.* **2012**, *272* (3), 224−39.

(2) Brook, R. D.; Urch, B.; Dvonch, J. T.; Bard, R. L.; Speck, M.; Keeler, G.; Morishita, M.; Marsik, F. J.; Kamal, A. S.; Kaciroti, N.; Harkema, J.; Corey, P.; Silverman, F.; Gold, D. R.; Wellenius, G.; Mittleman, M. A.; Rajagopalan, S.; Brook, J. R. Insights into the mechanisms and mediators of the effects of air pollution exposure on blood pressure and vascular function in healthy humans. *Hypertension* **2009**, *54* (3), 659−667.

(3) Brook, R. D.; Rajagopalan, S.; Pope, C. A.; Brook, J. R.; Bhatnagar, A.; Diez-Roux, A. V.; Holguin, F.; Hong, Y.; Luepker, R. V.; Mittleman, M. A.; Peters, A.; Siscovick, D.; Smith, S. C., Jr; Whitsel, L.; Kaufman, J. D. Particulate matter air pollution and cardiovascular disease: An update to the scientific statement from the American Heart Association. *Circulation* **2010**, *121* (21), 2331−78.

(4) Hazari, M. S.; Callaway, J.; Winsett, D. W.; Lamb, C.; Haykal-Coates, N.; Krantz, Q. T.; King, C.; Costa, D. L.; Farraj, A. K. Dobutamine "stress" test and latent cardiac susceptibility to inhaled diesel exhaust in normal and hypertensive rats. *Environ. Health Perspect.* **2012**, *120* (8), 1088−93.

(5) Carll, A. P.; Hazari, M. S.; Perez, C. M.; Krantz, Q. T.; King, C. J.; Haykal-Coates, N.; Cascio, W. E.; Costa, D. L.; Farraj, A. K. An autonomic link between inhaled diesel exhaust and impaired cardiac performance: insight from treadmill and dobutamine challenges in heart failure-prone rats. *Toxicol. Sci.* **2013**, *135* (2), 425−36.

(6) Peters, A. Particulate matter and heart disease: evidence from epidemiological studies. *Toxicol. Appl. Pharmacol.* **2005**, *207* (2 Suppl), 477−82.

(7) Pope, C. A., 3rd; Burnett, R. T.; Thurston, G. D.; Thun, M. J.; Calle, E. E.; Krewski, D.; Godleski, J. J. Cardiovascular mortality and long-term exposure to particulate air pollution: epidemiological evidence of general pathophysiological pathways of disease. *Circulation* **2004**, *109* (1), 71−7.

(8) Samet, J. M.; Rappold, A.; Graff, D.; Cascio, W. E.; Berntsen, J. H.; Huang, Y-C.T.; Herbst, M.; Bassett, M.; Montilla, T.; Hazucha, M. J.; Bromberg, P. A.; Devlin, R. B. Concentrated ambient ultrafine particle exposure induces cardiac changes in young healthy volunteers. *Am. J. Respir. Crit. Care Med.* **2009**, *179* (11), 1034−42.

(9) Ruidavets, J. B.; Cournot, M.; Cassadou, S.; Giroux, M.; Meybeck, M.; Ferrières, J. Ozone air pollution is associated with acute myocardial infarction. *Circulation* **2005**, *111* (5), 563−9.

(10) Farraj, A. K.; Hazari, M. S.; Winsett, D. W.; Kulukulualani, A.; Carll, A. P.; Haykal-Coates, N.; Lamb, C. M.; Lappi, E.; Terrell, D.; Cascio, W. E.; Costa, D. L. Overt and latent cardiac effects of ozone inhalation in rats: evidence for autonomic modulation and increased myocardial vulnerability. *Environ. Health Perspect.* **2012**, *120* (3), 348−54.

(11) Jerrett, M.; Burnett, R. T.; Beckerman, B. S.; Turner, M. C.; Krewski, D.; Thurston, G.; Martin, R. V.; van Donkelaar, A.; Hughes, E.; Shi, Y.; Gapstur, S. M.; Thun, M.; Pope, C. A. Spatial Analysis of Air Pollution and Mortality in California. *Am. J. Respir. Crit. Care Med.* **2013**, *188* (5), 593−600.

(12) Hazari, M. S.; Haykal-Coates, N.; Winsett, D. W.; Krantz, Q. T.; King, C.; Costa, D. L.; Farraj, A. K. TRPA1 and sympathetic activation contribute to increased risk of triggered cardiac arrhythmias in hypertensive rats exposed to diesel exhaust. *Environ. Health Perspect.* **2012**, *119* (7), 951−7.

(13) Lamb, C. M.; Hazari, M. S.; Haykal-Coates, N.; Carll, A. P.; Krantz, Q. T.; King, C.; Winsett, D. W.; Cascio, W. E.; Costa, D. L.; Farraj, A. K. Divergent electrocardiographic responses to whole and particle-free diesel exhaust inhalation in spontaneously hypertensive rats. *Toxicol. Sci.* **2012**, *125* (2), 558−68.

(14) Carll, A. P.; Hazari, M. S.; Perez, C. M.; Krantz, Q. T.; King, C. J.; Winsett, D. W.; Costa, D. L.; Farraj, A. K. Whole and particle-free diesel exhausts differentially affect cardiac electrophysiology, blood pressure, and autonomic balance in heart failure-prone rats. *Toxicol. Sci.* **2012**, *128* (2), 490−9.

(15) Kurhanewicz, N.; McIntosh-Kastrinsky, R.; Tong, H.; Walsh, L.; Farraj, A. K.; Hazari, M. S. Ozone co-exposure modifies cardiac responses to fine and ultrafine ambient particulate matter in mice: concordance of electrocardiogram and mechanical responses. *Part. Fibre Toxicol.* **2014**, *11*, 54.

(16) Mitchell, G. F.; Jeron, A.; Koren, G. Measurement of heart rate and Q-T interval in the conscious mouse. *Am. J. Physiol.* **1998**, *274* (3), 274 Pt 2.

(17) Widdicombe, J.; Lee, L. Y. Airway reflexes, autonomic function, and cardiovascular responses. *Environ. Health Perspect.* **2001**, *109*, 579−584.

(18) Taylor-Clark, T. E.; Undem, B. J. Ozone activates airway nerves via the selective stimulation of TRPA1 ion channels. *J. Physiol.* **2006**, *588*, 423−433.

(19) Kurhanewicz, N.; McIntosh-Kastrinsky, R.; Tong, H.; Ledbetter, A.; Walsh, L.; Farraj, A.; Hazari, M. S. TRPA1 mediates changes in heart rate variability and cardiac mechanical function in mice exposed to acrolein. *Toxicol. Appl. Pharmacol.* **2016**, *324*, 51−60.

(20) Peters, A.; Perz, S.; Dfiring, A.; Stieber, J.; Koenig, W.; Wichmann, H. E. Increases in Heart Rate during an Air Pollution Episode. *Am. J. Epidemiol.* **1999**, *150*, 1094−1099.

(21) Unosson, J.; Blomberg, A.; Sandström, T.; Muala, A.; Boman, C.; Nyström, R.; Westerholm, R.; Mills, N. L.; Newby, D. E.; Langrish, J. P.; Bosson, J. A. Exposure to wood smoke increases arterial stiffness and decreases heart rate variability in humans. *Part. Fibre Toxicol.* **2013**, *6*, 10−20.

(22) Glass, S. T.; Lingg, E.; Heuberger, E. Do ambient urban odors evoke basic emotions? *Front. Psychol* **2014**, *5*, 340.

(23) Ying, Z.; Xu, X.; Bai, Y.; Zhong, J.; Chen, M.; Liang, Y.; Zhao, J.; Liu, D.; Morishita, M.; Sun, Q.; Spino, C.; Brook, R. D.; Harkema, J.

DOI: 10.1021/acs.est.7b04880
Environ. Sci. Technol. 2018, 52, 3071−3080

R.; Rajagopalan, S. Long-term exposure to concentrated ambient PM2.5 increases mouse blood pressure through abnormal activation of the sympathetic nervous system: a role for hypothalamic inflammation. *Environ. Health Perspect* **2014**, *122* (1), 79−86.
(24) Billman, G. E. The LF/HF ratio does not accurately measure cardiac sympatho-vagal balance. *Front. Physiol.* **2013**, *4*, 26.
(25) Ensor, K. B.; Raun, L. H.; Persse, D. A case-crossover analysis of out-of-hospital cardiac arrest and air pollution. *Circulation* **2013**, *127*, 1192−1199.
(26) Devlin, R. B.; Duncan, K. E.; Jardim, M.; Schmitt, M. T.; Rappold, A. G.; Diaz-Sanchez, D. Controlled exposure of healthy young volunteers to ozone causes cardiovascular effects. *Circulation* **2012**, *126* (1), 104−111.
(27) Hazari, M. S.; Haykal-Coates, N.; Winsett, D. W.; Costa, D. L.; Farraj, A. K. A single exposure to particulate or gaseous air pollution increases the risk of aconitine-induced cardiac arrhythmia in hypertensive rats. *Toxicol. Sci.* **2009**, *112* (2), 532−42.
(28) Benditt, D. G.; Sakaguchi, S.; Lurie, K. G.; Lu, F. Sinus node dysfunction. In *Cardiovascular Medicine*; Willerson, J. T., Wellens, H. J. J., Cohn, J. N., Holmes, D. R., Jr, Eds.; Springer: London, 2007.
(29) Haqqani, H. M.; Kalman, J. M. Aging and sinoatrial dysfunction. *Circulation* **2007**, *115*, 1178−1179.
(30) Ben-Tal, A.; Shamailov, S. S.; Paton, J. F. R. Evaluating the physiological significance of respiratory sinus arrhythmia: looking beyond ventilation−perfusion efficiency. *J. Physiol.* **2012**, *590*, 1980−2008.

DOI: 10.1021/acs.est.7b04880
Environ. Sci. Technol. 2018, 52, 3071−3080

OXFORD

SOT | Society of Toxicology
www.toxsci.oxfordjournals.org

TOXICOLOGICAL SCIENCES, 167(2), 2019, 559–572

doi: 10.1093/toxsci/kfy262
Advance Access Publication Date: October 23, 2018
Research Article

Downloaded from https://academic.oup.com/toxsci/article-abstract/167/2/559/5142835 by EPA-RTP Main Library user on 15 January 2020

Ambient Particulate Matter and Acrolein Co-Exposure Increases Myocardial Dyssynchrony in Mice via TRPA1

Leslie C. Thompson,* Leon Walsh,* Brandi L. Martin,† John McGee,* Charles Wood,‡ Kasey Kovalcik,§ Joseph Patrick Pancras,* Najwa Haykal-Coates,* Allen D. Ledbetter,* David Davies,* Wayne E. Cascio,* Mark Higuchi,* Mehdi S. Hazari,* and Aimen K. Farraj*,[1]

*Environmental Public Health Division, National Health and Environmental Effects Research Laboratory; †Oak Ridge Institute for Science and Education, Oak Ridge, TN 37830; ‡Integrated Systems Toxicology Division, National Health and Environmental Effects Research Laboratory; and §Exposure Methods & Measurements Division, National Exposure Research Laboratory, United States Environmental Protection Agency, Research Triangle Park, North Carolina 27711

[1]To whom correspondence should be addressed at US Environmental Protection Agency, Environmental Public Health Division, 109 T.W. Alexander Drive, Mail Code: B105-02, Research Triangle Park, NC 27709. Fax: (919) 541-0034. E-mail: farraj.aimen@epa.gov.

Disclaimer: The research presented in the article was reviewed and approved for publication by the National Health and Environmental Effects Research Laboratory at the U.S. Environmental Protection Agency. The contents of this manuscript do not necessarily reflect the views and policies of the agency nor does mention of trade names or commercial products signify endorsement or recommendation for use.

ABSTRACT

Air pollution is a complex mixture of particulate matter and gases linked to adverse clinical outcomes. As such, studying responses to individual pollutants does not account for the potential biological responses resulting from the interaction of various constituents within an ambient air shed. We previously reported that exposure to high levels of the gaseous pollutant acrolein perturbs myocardial synchrony. Here, we examined the effects of repeated, intermittent co-exposure to low levels of concentrated ambient particulates (CAPs) and acrolein on myocardial synchrony and the role of transient receptor potential cation channel A1 (TRPA1), which we previously linked to air pollution-induced sensitization to triggered cardiac arrhythmia. Female B6129 and *Trpa1*−/− mice ($n = 6$/group) were exposed to filtered air (FA), CAPs (46 μg/m^3 of $PM_{2.5}$), Acrolein (0.42 ppm), or CAPs+Acrolein for 3 h/day, 2 days/week for 4 weeks. Cardiac ultrasound was conducted to assess cardiac synchronicity and function before and after the first exposure and after the final exposure. Heart rate variability (HRV), an indicator of autonomic tone, was assessed after the final exposure. Strain delay (time between peak strain in adjacent cardiac wall segments), an index of myocardial dyssynchrony, increased by 5-fold after the final CAPs+Acrolein exposure in B6129 mice compared with FA, CAPs, or Acrolein-exposed B6129 mice, and CAPs+Acrolein-exposed *Trpa1*−/− mice. Only exposure to acrolein alone increased the HRV high frequency domain (5-fold) in B6129 mice, but not in *Trpa1*−/− mice. Thus, repeated inhalation of pollutant mixtures may increase risk for cardiac responses compared with single or multiple exposures to individual pollutants through TRPA1 activation.

Key words: air pollution; particulate matter; acrolein; TRPA1; myocardial synchrony; heart rate variability.

Poor air quality is an important modifiable risk factor for cardiovascular morbidity and mortality (Argacha *et al.*, 2018; Bhatnagar, 2017; Brook and Rajagopalan, 2017; Cohen *et al.*, 2017; Newby *et al.*, 2015). However, attempts to quantify the cardiovascular health burden of air pollution is difficult given the complexity of particulate matter (PM), gas, and volatile organic

Published by Oxford University Press on behalf of the Society of Toxicology 2018.
This work is written by US Government employees and is in the public domain in the US.

compound mixtures, the relative quantities of which depend on local geography, proximity to emission sources, time of day, and weather conditions. Furthermore, the colocalization of pollutants promotes gas-particle interactions, potentially yielding additive, synergistic, or even antagonistic biological responses that may underlie the health effects of air pollution (Mauderly and Samet, 2009). For example, co-exposure to PM and ozone (O_3) has been linked to dispersion of ventricular repolarization in humans (Sivagangabalan *et al.*, 2011), as well as decreased heart rate variability (HRV) (Farraj *et al.*, 2015; Wagner *et al.*, 2014) and epicardial adipose inflammation in rats (Sun *et al.*, 2013). PM co-exposure with NO_2 has been shown to alter T-wave amplitude and low-frequency components of HRV in healthy volunteers, which were not present with exposure to either pollutant alone (Huang *et al.*, 2012).

Less is known about potential interactive effects between PM and acrolein (C═C─C═O), a ubiquitous aldehyde produced during the combustion of organic material like tobacco, wood, fats, and fuels (Henning *et al.*, 2017). Acrolein is an upper airway irritant with reactive electrophilic properties and well-documented adverse cardiopulmonary effects, some of which are mediated by transient receptor potential cation channel A1 (TRPA1) (ATSDR, 2007; Bautista *et al.*, 2006; Conklin, 2016; Henning *et al.*, 2017). Due to the colocalization of PM and acrolein in ambient airsheds, PM and acrolein may interact in a way that modifies the health effects of either pollutant alone, especially given that PM-adsorbed electrophiles have been shown to activate TRPA1 (Deering-Rice *et al.*, 2011; Fariss *et al.*, 2013; Ghelfi *et al.*, 2008). TRP channels are expressed on pulmonary C-fibers (Lee *et al.*, 2015; Lin *et al.*, 2010) and when activated in the nose and lung trigger autonomic reflexes that drive cardiopulmonary effects like apnea, bronchospasm, hypotension, and bradycardia (Pozsgai *et al.*, 2010). TRPA1 involvement in acute air pollution-induced sensory nerve activation, initiation of autonomic reflexes, and cardiovascular dysfunction has been extensively described in Conklin *et al.* (2017), Henning *et al.* (2017), Hooper *et al.* (2016), and Kurhanewicz *et al.* (2017). TRPA1-mediated effects have been reported with aerosol mixtures known to contain both PM and acrolein, including cigarette smoke-induced alteration of mouse tracheal ring responses (Kichko *et al.*, 2015) and diesel exhaust-induced increased sensitivity to triggered cardiac arrhythmia in rats (Hazari *et al.*, 2011).

In our previous work, we determined that acrolein inhalation (3.0 ppm) in mice decreased myocardial synchrony when measured 1 and 24 h after exposure (Thompson *et al.*, 2017). Myocardial synchrony is a measure of heart muscle contractile coordination, which we have proposed as a potentially sensitive indicator of air pollution health effects. Moreover, myocardial synchrony requires coordinated propagation of membrane depolarization, excitation-contraction coupling, and contraction mechanics, all of which are heavily influenced by changes in autonomic tone (Gimelli *et al.*, 2014). Given (a) the reports linking air pollution, altered cardiac autonomic activity and TRPA1 (Conklin *et al.*, 2017; Hazari *et al.*, 2011; Kunkler *et al.*, 2015; Kurhanewicz *et al.*, 2017) and (b) the lack of information regarding the interactive health effects of particulates and aldehydes, the purpose of this study was to compare the cardiovascular impacts of intermittent, repeated exposure to low levels of concentrated ambient particulate matter (CAPs), acrolein, or CAPs plus acrolein in wild-type and TRPA1 knockout mice. We hypothesized that co-exposure to CAPs and acrolein would increase myocardial dyssynchrony and alter cardiac autonomic tone when compared with exposure to either pollutant alone, and that such responses would be absent in TRPA1 knockout mice. Cardiac strain data, heart function and dimensions, and transmitral blood flow were investigated using high-frequency ultrasound before exposures, 1 day after the first exposure, and 1 day after the final exposure. Exposure-induced functional changes were coupled with measures of HRV for assessment of cardiac autonomic responses. Furthermore, because the effects of CAPS and acrolein co-exposure on overall cardiopulmonary well-being have not been reported before, we also measured several indicators of pulmonary and systemic inflammation and injury and examined for nasal, lung, and heart histopathology. Effects were related to PM composition and contributing sources by analysis of PM elemental data and quantification of PM sources using a chemical mass balance model.

MATERIALS AND METHODS

Sample size analysis. Sample size analysis was conducted using R Studio software (version 3.1.2) with the "pwr" package (https://cran.r-project.org/web/packages/pwr/pwr.pdf, last accessed November 14, 2018) and "pwr.anova.test" command. Data from a previous study of myocardial synchronicity after acrolein inhalation in mice was used to calculate sample size (Thompson *et al.*, 2017). The expected effect size for this study was an increase in myocardial strain delay by 5% of the cardiac cycle, which was the approximate increase observed in the previous study with acrolein inhalation. Also, the largest control group standard deviation (SD) from the multiple time points assessed in the previous study was 3.4%. Cohen's equation for effect size (d) and effect size index (f) was calculated as follows (Cohen, 1988):

d = effect range/control SD
$d = 5/3.4$
$d = 1.47$
$f = 0.5 * (d)$
$f = 0.5 * (1.47)$
$f = 0.74$

For group size (n) determinations, we set k (number of groups) = 4 because we were planning for 3 experimental groups and 1 air control group in each mouse strain, significance level = .05, and power = .8. The sample size analysis yielded $n = 6$.

Animals. Twenty-four female B6129PF2/J mice (B6129), strain code 100903, and 24 female B6; 129P-*Trpa1*^{tm1Kykw}/J (*Trpa1*−/−), strain code 006401 (Jackson Laboratories, Bar Harbor, Maine), were housed in plastic cages (three per cage), maintained on a 12-h light/dark cycle at approximately 22°C and 50% relative humidity (RH) in our Association for Assessment and Accreditation of Laboratory Animal Care-approved facility, and held for a minimum of 2 weeks before exposures. The Institutional Animal Care and Use Committee of the U.S. Environmental Protection Agency approved all protocols. Female mice were used in accordance with a previous study (Kurhanewicz *et al.*, 2017). The age range for the B6129 mice was 19–21 weeks and that for the *Trpa1*−/− mice, 21–28 weeks. Two 42-week-old *Trpa1*−/− mice were also used due to limited availability of younger mice. The two 42-week old mice, were, however, split into separate groups. That is, one of these mice was placed in the Acrolein-exposed *Trpa1*−/− group and one was placed in the CAPS-exposed *Trpa1*−/− group.

Experimental design. Mouse inhalation exposures were conducted within the U.S. Environmental Protection Agency's Concentrated

Downloaded from https://academic.oup.com/toxsci/article-abstract/167/2/559/5142835 by EPA-RTP Main Library user on 15 January 2020

Air Particles Laboratory at the Consolidated Research Facility in Research Triangle Park, North Carolina. To avoid restraint-stress we selected a whole-body inhalation method. Fine CAPs concentrations were targeted to be low enough to approximate peak concentrations in a typical urban environment (100 $\mu g/m^3$). We targeted an acrolein concentration of 0.300 ppm because it is only three times the recommended exposure limit established by the National Institute of Occupational Safety and Health of the United States Center for Disease Control and Prevention (ie, 0.1 ppm 10-h time weighted average; NIOSH, 2005) and is a concentration that can be reliably measured by our gas chromatograph. To reflect natural short-term and repeated, intermittent exposure to spikes in air pollution as experienced in the ambient environment by humans, mice were exposed for 3-h each day, 2 days per week (Monday and Wednesday or Tuesday and Thursday) for 4 consecutive weeks for a total of 8 exposures during November and December of 2014. Cardiac ultrasounds were performed on each mouse 1 week prior to beginning exposures, 1 day after the first exposure, and 1 day after the final exposure. Mice were necropsied immediately after the last ultrasound.

PM concentrating system. Ambient air (5000 L/min) was drawn into the exposure laboratory through a 2 stage, size selective inlet restricting PM larger than 10 μm and 2.5 μm diameters. Air with the resulting fine mode $PM_{2.5}$ fraction exited the size selective inlet and was transported via stainless steel ductwork to the CAPs laboratory where it entered a 3 stage Harvard Fine Particle Concentrator (HFPC) (Gupta *et al*., 2004). The HFPC was configured with 3 concentrating stages of slit virtual impactors and was operated at a vacuum of −9 to −10 inH_2O, producing 50 L/min of CAPs air as previously described in Kodavanti *et al.* (2005). Plumbing was configured to allow the HFPC to function in "chamber exposure" or "chamber bypass" modes (see Figure 1). For FA and Acrolein exposure groups, the HFPC was operated in "chamber bypass" mode so that all mice experienced the same level of noise generated by the HFPC, thus eliminating system noise as a potential experimental confounder.

Exposure chambers. During operation of the HFPC in chamber exposure mode, 50 L/min CAPs air at −9 to −10 in H_2O static pressure was split and 20 L/min were directed toward each of two Cannon nose-only chambers. The remaining 10 L/min were used for PM monitoring. Mice were exposed in rat-sized nose-only tubes with rear stoppers mounted to chamber ports, allowing for "whole-body" exposure conditions. More details are provided in the Supplementary material.

Acrolein supply. Acrolein gas was injected upstream of the chamber supply air inlet of one chamber. Gas was metered from a cylinder of known acrolein concentration (537 ppm acrolein, balance N2) and the gas flow rate was precisely monitored. CAPs DAS (Data acquisition software) regulated and monitored gas flow continuously as well as providing safety cutoff control of acrolein if necessary. The gas supply line included a solenoid valve and manual valves to isolate gas supply from the chamber and allowed operators to purge the supply line with breathing grade air for safety.

Chamber monitoring. HFPC and Cannon exposure chamber air parameters were monitored and recorded using CAPs lab DAS. Various analytical instruments, filter collections, GC sampling, and real-time monitors were utilized for analyses of chamber PM size and concentration, acrolein concentration, temperature, RH, airflow, and other system parameters, allowing for continuous control of chamber conditions. More details are provided in the Supplementary material.

$PM_{2.5}$ elemental, organic, and ion analysis. Due to limited airflow and low PM concentrations filters were collected after 4 weeks of exposure (1 filter per month), to collect sufficient PM mass for extraction and analysis. This allowed us to assess potential differences in PM content between November and December. Elemental analysis was performed on aqua regia digests of PM collected on Teflon filters as previously described in Farraj *et al.* (2015). Samples were analyzed by high-resolution inductively coupled plasma-mass spectrometry (HR-ICP-MS, Element 2, Thermo Fisher Scientific, Waltham, Massachusetts).

Chemical mass balance (CMB) source apportionment. To predict potential sources and estimates of their contributions to the $PM_{2.5}$ collected on filters during November and December of 2014, we tested sample chemical analysis profiles against the EPA Chemical Mass Balance Model (CMB8.2; US EPA, 2004). PM chemical composition data at the inlet of CAPs system alone were used for this source-receptor modeling. Source profiles to represent motor vehicles, biomass burning, secondary aerosol production, road dust, and marine aerosol were taken from EPA SPECIATE 4.3 Database (https://cfpub.epa.gov/speciate).

Echocardiography and electrocardiogram data collection. ECG waveform acquisition was performed using a Vevo 2100 ultrasound system immediately prior to ultrasound sonography (FujiFilm VisualSonics, Inc, Toronto, Canada). Isoflurane-anesthetized mice were placed in dorsal recumbency with paws grounded to the electrodes of a heated Vevo Mouse Handling Table (FujiFilm VisualSonics, Inc). Four cineloops optimized to collect approximately 12–13 s of ECG data each (approximately 50 s total) were recorded from each subject. Ultrasound scans were performed as previously described in Thompson *et al.* (2017) in accordance with the guidelines of the American Society of Echocardiography (Lang *et al*., 2005; Quinones *et al*., 2002). The sonographer was blinded to experimental groups. Scans were made using a Vevo 2100 ultrasound system (FujiFilm VisualSonics, Inc) and a MS550D transducer set to a 40 MHz sample rate in B-mode and M-mode, and 32 MHz for pulsed wave Doppler measurements. Data were collected at baseline (the week before exposures), 1 day after the first exposure, and 1 day after the final (8th) exposure. Parasternal short-axis views at the level of the left ventricular papillary muscles were collected in B-mode and M-mode. The apical 4-chamber view was used for pulsed wave Doppler measurements of transmitral valve blood flow. Three cineloops from each view were collected for data analysis. Anesthesia induction, subject preparation, data collection, and recovery from anesthesia ranged from 15 to 20 min per animal.

Ultrasound analysis and heart rate variability assessment. Ultrasound data analyses were also performed under blinded conditions, as previously described in Thompson *et al.* (2017). Circumferential strain delay, peak circumferential strain, time to peak (TPk) strain, peak diastolic circumferential strain rate, and TPk diastolic strain rate were each evaluated using B-mode data. Left ventricular stroke volume, cardiac output, ejection fraction, fractional shortening, end diastolic volume, end systolic volume, as well as wall and chamber dimensions were calculated from M-mode data. Left ventricular isovolumic contraction time (IVCT), aortic ejection time (AET), and isovolumic

Downloaded from https://academic.oup.com/toxsci/article-abstract/167/2/559/5142835 by EPA-RTP Main Library user on 15 January 2020

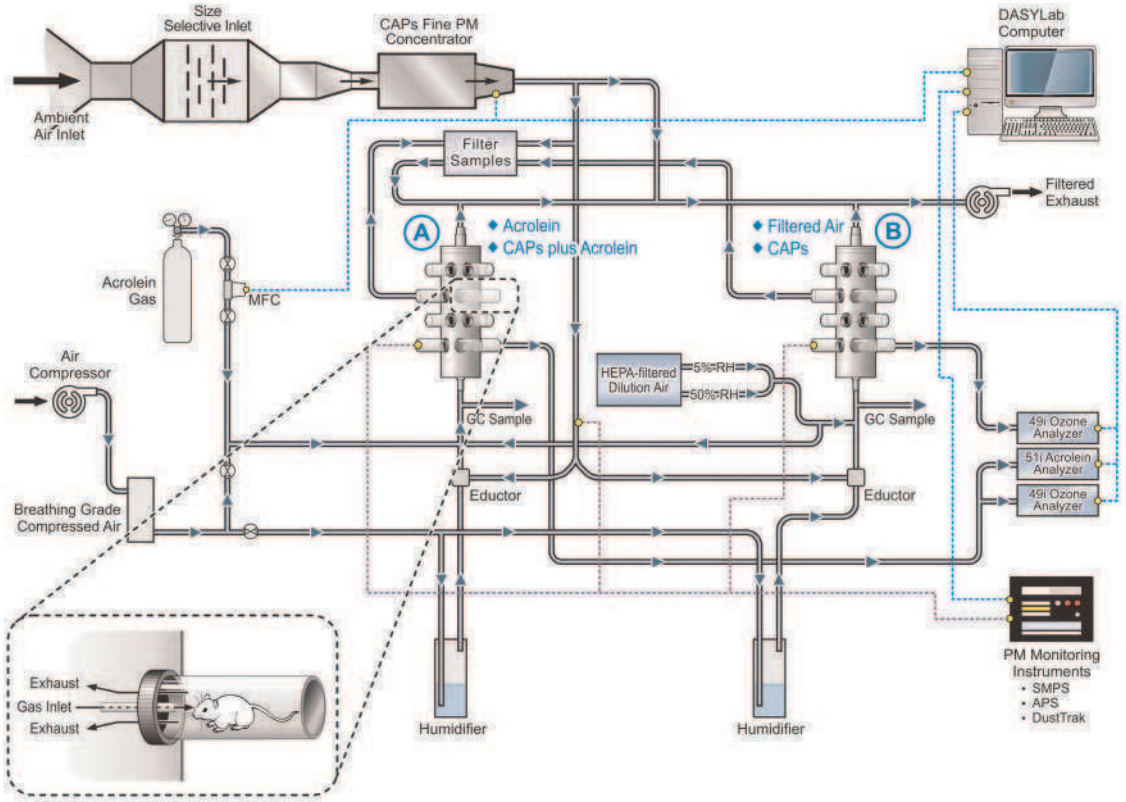

Figure 1. CAPs plus acrolein multipollutant exposure system. Particles entered via size selective inlet for 2.5 μm diameters or less and concentrated with a Harvard Fine Mode Particle Concentrator. Mice were exposed in rat-sized nose-only tubes providing a whole-body exposure system. CAPs lab DAS and various analytical instruments plus filters and GC sampling were utilized to monitor chamber PM concentration and size, Acrolein concentration, temperature and RH, chamber airflow, and other system parameters. Acrolein gas flow was also monitored and controlled by the DAS and a mass flow controller (MFC). Due to inhalation chamber airflow requirements, analytical sampling was carefully planned to get maximum $PM_{2.5}$ composition information from minimum amount of airflow. PM mass concentrations and inorganic elemental composition were measured using filters from the CAPs inlet, CAPs outlet, and both chambers. "A" marks the chamber used for acrolein only and CAPs plus acrolein exposures. "B" marks the chamber used for filtered air only and CAPs only exposures.

relaxation time (IVRT) were calculated form pulsed wave Doppler recordings. Myocardial performance Tei index was calculated with the following equation: (IVCT+IVRT)/AET (Tei *et al.*, 1995).

HRV was measured and calculated as previously described in Kurhanewicz *et al.* (2017). Briefly, the mean of the differences between sequential RRs for each set of ECG waveforms were calculated using ECGAuto (v3.3.5.10; EMKA Technologies S.A.S., Paris, France). Time-domain measures of HRV included standard deviation of the time between normal-to-normal beats (SDNN) and root mean squared of successive differences (RMSSD). SDNN represents overall HRV, whereas RMSSD represents parasympathetic influence over HR (Rowan *et al.*, 2007). The frequency domain of HRV was also analyzed including low-frequency (LF: 0.15–1.5 Hz), representing a combination of sympathetic and parasympathetic tone, and high-frequency (HF: 1.5–5 Hz), indicating parasympathetic tone, and the ratio of these two (LF/HF), indicating sympathovagal balance (Rowan *et al.*, 2007). Thorough visual inspection was conducted to identify and exclude arrhythmias and artifacts.

Necropsy, bronchoalveolar lavage, tissue collection, and analyses. Mice were anesthetized with pentobarbital (200 mg/kg) and phenytoin (25 mg/kg) given by intraperitoneal injection (Euthasol, Virbac Animal Health, Fort Worth, Texas). Blood was collected from the abdominal vena cava, placed in serum separator tubes, and after centrifugation serum was stored at −80°C. The trachea was cannulated and the right lung minus the caudal lobe was lavaged with cold Hanks' balanced salt solution (GIBCO HBSS, Thermo Fisher Scientific). The caudal lobe was tied off before lavage and snap frozen for tissue banking. Cytospins were used for cell differentials and supernatants were stored at −80°C. A transverse midsection of the left ventricle, the left lung, and nose was collected for histological examination. Bronchoalveolar lavage (BAL) cell pellets were resuspended in fresh HBSS, 500 μl were used for cytospins and 500 μl were used to determine total cell counts using a Beckman Coulter Z2 (Beckman Coulter Life Sciences, Brea, California). Cytospins were stained with modified Wright-Giemsa stain (#036-221, Fisher Scientific, Hampton, New Hampshire) and were counted microscopically to 300 cells per slide, with percentages multiplied by total cell counts to calculate final cell numbers.

Histopathology. Hearts, lungs, and heads (for nasal airway) were fixed in 4% fresh paraformaldehyde for histopathological evaluation (see additional detail in Supplementary Methods). The heart was sectioned transversely at the level of the mid-ventricle. The left lung lobe was first perfused intratracheally at a pressure of 30 cm of fixative and sectioned longitudinally. The nasal cavity of each mouse was transversely sectioned at three specific anatomic locations. Fixed tissues were paraffin-embedded, sectioned at approximately 5 μm, and stained with

Downloaded from https://academic.oup.com/toxsci/article-abstract/167/2/559/5142835 by EPA-RTP Main Library user on 15 January 2020

hematoxylin and eosin (H&E) using standard histologic procedures at Experimental Pathology Laboratories (Research Triangle Park, North Carolina). Stained sections were evaluated via light microscopy by a certified pathologist (CW). Differences in lesion incidence between treatment group and genotype were evaluated using a two-sided Fisher's exact test.

Statistical analyses. Data are reported as mean ± SD or presented as boxplots with all data points shown. Box edges identify the interquartile range, the middle line identifies the median, the "+" identifies the mean, and the whiskers identify the minimum and maximum data values. Data were analyzed and graphed with Graphpad Prism 6 software version 6.07 (La Jolla, California). For histopathology, differences in lesion incidence among treatment group or genotype were evaluated using a Fisher's exact test. For single time point biological data, one-way ANOVA with Tukey's post-test and multiplicity adjusted *p*-values were conducted. For repeated ultrasound assessments two-way repeated measures ANOVA with Tukey's post-test and multiplicity adjusted *p*-values were conducted across exposure groups within strain at each time point; Bonferroni's post-test was run across time and strain within exposure groups. For these data, *p*-values are reported except for those $< .0001$ in Figure 4. In Tables 3 and 4, *p*-values $< .05$ are denoted with * versus FA, # versus Acrolein, † versus CAPs, and ‡ versus B6129.

RESULTS

Exposure Concentrations and Environmental Conditions

Chamber exposure conditions for each group are provided in Table 1. Due to low ambient levels of PM, particle concentrations achieved were only 46.3 and 45.4 μg/m^3 for CAPs and CAPs+Acrolein, respectively. Mean particle sizes were 168 and 172 nm in diameter in the CAPs and CAPs+Acrolein exposures, respectively. In the acrolein alone and CAPs+Acrolein exposures, acrolein concentrations were stable at around 0.42 ppm and below the level of detection in the Filtered Air and CAPs alone exposures. Chamber temperatures were stable at approximately 22°C and RH ranged from 30% to 50%. Lower humidity in the CAPs and CAPs+Acrolein chambers was due to mixing of dry eductor motive air with outside ambient air drawn into the HFPC. Bubbler humidifiers in the eductor compressed motive air supply helped raise the RH levels to achieve approximately 30% chamber RH levels. Background O3 levels were less than 5.0 ppb.

Wind Trajectories

The airshed origin, wind direction, and airflow elevation for each CAPs exposure day during the study were obtained as previously described (Farraj *et al.*, 2015) and are shown in Figure 2. These were analyzed to identify contributing airsheds for particulate matter in Research Triangle Park, NC, USA in November and December of 2014. For both the November and December exposures, winds originated predominately from southwest to northwest, at elevations of < 2000 m in the atmospheric boundary layer of the lower troposphere (Figure 2A). Some of the PM delivered to the Raleigh/Durham area originated from the Chicago/Cincinnati airsheds (Figure 2B), and on some other days originated from the Cleveland/Columbus area and the Birmingham/Atlanta/Charlotte areas. The tracings presented in Figure 2A also illustrate that there was no uniform pattern of exposure sources because the direction of the air mass source changed daily.

Chemical Composition of CAPs

Table 2 compares the elemental compositions of $PM_{2.5}$ collected at the air inlet during November and December of 2014. The predominant components of the PM collected during this study were organic carbon (OC) and ammonium sulfate (SO_4). To improve the mass balance estimations, we expressed elements as oxides of the most common oxidation state. Also, the elemental OC was multiplied by 1.6 to account for associated hydrogens, oxygens, and nitrogens usually associated with the carbon fraction (Turpin and Lim, 2001). In general, November and December $PM_{2.5}$ compositions were very similar regarding both the total mass and constituents with the exception of cadmium in November, which was still low overall. The ratio of November/December microgram per cubic meter gravimetric ratios is 1.14 and the averaged analytes ratio is 1.18. Supplementary Table 1 also provides a comparison of CAPs elemental analyses of inlet PM, outlet PM, CAPS chamber PM, and CAPs+Acrolein chamber PM, thus verifying that the PM delivered to each CAPs exposure chamber was consistent in chemical composition to ambient PM in both November and December.

Source Apportionment Analysis

Source apportionment results for $PM_{2.5}$ mass concentrations on both exposure collections are displayed in Figure 3 (5-source CMB model) and Supplementary Figure 1 (6-source CMB model), which reveals marginal differences in secondary sulfate level, motor vehicle exhaust, and biomass combustion sources between the November and December samples collected in 2014. The CMB model explained up to 83%–85% of the $PM_{2.5}$ mass collected from the November and December PM filters. The fraction of measured concentration variance (R^2) was greater than 0.84 and the Chi square value was less than 2.5 for both samples, indicating a good fit between measured and modeled concentrations for both samples. Motor Vehicle Exhaust (26.4%, 31.3% by mass for November and December PM collections, respectively), biomass combustion (22.1%, 16.2%), and secondary sulfate (27.8%, 32.1%) were found to be the major sources of both PM samples. Together, these 3 source types accounted for

Table 1. Exposures Concentrations, Particle Size and Chamber and Ambient Weather Conditions

		Exposure and Weather Conditions				
		Filtered Air	Acrolein	CAPs	CAPs+Acrolein	HFPC Inlet
[PM mass]	μg/m^3	Below detection	Below detection	46.3 ± 0.2	45.4 ± 2.3	6.4 ± 0.6
Particle number	Count/cc	—	—	6580	6900	4890
PM diameter	nm	—	—	169 ± 134	172 ± 139	76 ± 84
[Acrolein]	ppm	Below detection	0.42 ± 0.02	Below detection	0.42 ± 0.01	Below detection
Temperature	°C	21.8 ± 0.2	22 ± 0.4	21.6 ± 0.3	22.3 ± 0.4	24.6 ± 13.3
Rel. humidity	%	50 ± 2.0	51 ± 2.0	30 ± 10	29 ± 9.0	65 ± 19

Downloaded from https://academic.oup.com/toxsci/article-abstract/167/2/559/5142835 by EPA-RTP Main Library user on 15 January 2020

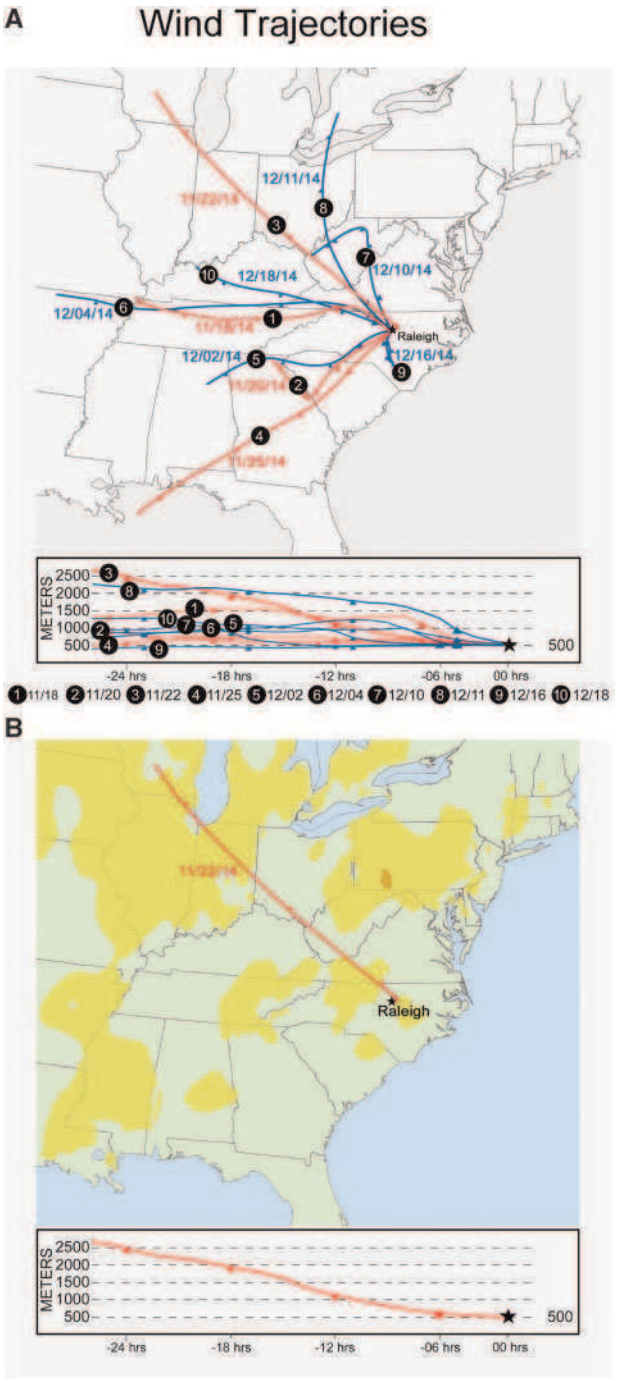

Figure 2. Wind trajectories. For both the November and December 2014 exposures, winds originated predominately from southwest to northwest, at elevations of < 2000 m in the atmospheric boundary layer of the lower troposphere. Panel A shows back trajectory analysis for each day, including elevation in meters (box). Lines 1–4 correspond to exposure days that occurred in November and lines 5–10 correspond to exposure days in December. Triangles on each line mark 6 h intervals of −24, −18, −12, and −6 h prior to exposure with the star marking the time and location of the U.S. Environmental Protection Agency's Concentrated Air Particles Laboratory in Research Triangle Park, NC, USA (Latitude: 35.88350; Longitude: −78.87460). Panel B shows an example of how air flow can drift through various PM airsheds. This map was modified from the PM air quality index map from Airnow.gov archives for November 22, 2014 with the back trajectory overlaid. Shaded areas were determined to be of moderate 24 h PM-based ambient air quality (12.1–35.4 μg/m^3).

76.2% and 79.7% of the fine PM during November and December, respectively. Though minor, marine aerosol and wind-blown crustal material were still consistent source contributors, accounting for 2.4% and 3.9% $PM_{2.5}$ mass, respectively.

Overt Toxicity

We found no evidence of overt toxicity (eg, lethargy, respiratory distress, and/or > 10% weight loss) during the study in virtually all animals. One B6129 mouse in the CAPs+Acrolein exposure group did, however, present indications of lethargy and respiratory distress during the third week of exposure and, consequently, was removed from the study. Prior to euthanasia, a cardiac ultrasound was performed on this moribund mouse, which indicated left ventricular hypertrophy (see Supplementary Figure 2). Interestingly, this mouse presented no clear evidence of health abnormalities at the beginning of the study so data from the first two ultrasound scans were included in the study. Mouse age and size related data at the time of necropsy for all other mice are provided in Table 3. We found no exposure related changes in food and water intake, body mass, or heart weight. *Trpa1*−/− mice were significantly smaller than B6129 mice and due to limited availability from the supplier were also older by about 7 weeks on average (26 weeks old vs 19 weeks old by the end of the study, respectively).

Bronchoalveolar Lavage Fluid Analysis and Cell Differentials

We compared potential pulmonary responses between the exposure groups by collecting and analyzing bronchoalveolar lavage fluid collected after the study. Overall cellularity in bronchoalveolar lavage was stable between groups. CAPs+Acrolein exposure groups from both strains had the most neutrophil and lymphocyte infiltration but the values were highly variable and not statistically significant from FA controls (Supplementary Table 2). There were also no significant differences in any biochemical indicators measured in bronchoalveolar lavage fluid (Supplementary Table 3).

Serum Biochemical Analysis

Assays for biomolecule targets in serum revealed minimal differences between exposure groups with two exceptions: HDL was significantly lower in all *Trpa1*−/− groups compared with the respective B6129 groups and LDL was significantly lower in the B6129 CAPs group relative to the *Trpa1*−/− CAPs group (Supplementary Table 4).

Histopathology

We found no histological evidence of lesions that would support the possibility that co-exposure to PM with acrolein altered the exposure distribution in the airway, at least at the concentrations tested (Supplementary Tables 5–7). In the nasal cavity, the incidence of minimal neutrophilic inflammation was modestly higher following acrolein exposure in *Trpa1*−/− mice ($p = .03$ vs filtered air) but not in B6129 mice. Conversely, there was higher incidence of cytoplasmic vacuolation in the nasal gland epithelium surrounding the vomeronasal organ following CAPs exposure in B6129 mice ($p = .03$ vs filtered air) but not *Trpa1*−/− mice. More details are provided in the Supplementary Results.

Cardiac Function and Dimensions and Myocardial Performance

Analysis results, including cardiac function and heart wall dimensions, of parasternal short axis M-mode views at the level

Downloaded from https://academic.oup.com/toxsci/article-abstract/167/2/559/5142835 by EPA-RTP Main Library user on 15 January 2020

Table 2. CAPs Chemical Composition Analysis

CAPs Chemical Composition Analysis						
Analyte	November $\mu g/m^3$	December $\mu g/m^3$	November/December Ratio	November $\mu g/g$	December $\mu g/g$	November/December Ratio
Inorganics						
Ag_2O	6.87e-6	6.55e-6	1.05	1.00	1.09	0.92
Al_2O_3	8.56e-2	9.32e-2	0.92	1.25e4	1.55e4	0.80
As_2O_3	<DL	4.23e-4	—	<DL	70.4	—
BaO	1.79e-3	3.05e-3	0.59	2.61e2	5.08e2	0.51
CaO	5.48e-2	3.41e-2	1.61	8.00e3	5.68e3	1.41
CdO	2.32e-3	0.05e-3	48.7	3.39e2	7.94	42.7
Ce_2O_3	4.46e-5	4.58e-5	0.97	6.51	7.63	0.85
Cr_2O_3	8.61e-4	6.58e-4	1.31	1.26e2	1.10e2	1.15
Cs_2O	3.32e-5	0.98e-5	3.40	4.85	1.63	2.98
CuO	1.41e-3	3.27e-3	0.43	2.05e2	5.45e2	0.38
FeO	5.79e-2	4.66e-2	1.24	8.45e3	7.77e3	1.09
K_2O	6.60e-2	4.36e-2	1.51	9.62e3	7262	1.32
MgO	1.75e-2	1.13e-2	1.55	2.55e3	1878	1.36
MnO	1.87e-3	1.48e-3	1.26	2.72e2	247	1.10
MoO_3	1.34e-4	2.28e-4	0.59	1.95e1	0.38e2	0.51
Na_2O	0.11	0.10	1.10	1.65e4	1.71e4	0.96
NiO	5.28e-4	4.14e-4	1.28	0.77e2	6.89e1	1.12
P_2O_5	1.93e-2	0.01	1.94	2.81e3	1.66e3	1.70
PbO	1.26e-3	0.94e-3	1.34	1.83e2	1.57e2	1.17
Rb_2O	1.65e-4	1.40e-4	1.18	2.40e1	2.32e1	1.03
SO_4	2.03	1.62	1.26	2.97e5	2.70e5	1.10
Sb_2O_5	4.78e-4	8.52e-4	0.56	6.97e1	1.42e2	0.49
SeO_3	1.60e-3	1.36e-3	1.18	2.34e2	2.26e2	1.03
SiO_2	8.54e-2	5.25e-2	1.63	1.25e4	8.75e3	1.42
SnO_2	3.45e-4	9.16e-4	0.38	5.04e1	1.53e2	0.33
SrO	2.64e-4	2.65e-4	1.0	3.85e1	4.41e1	0.87
TiO_2	1.66e-3	1.96e-3	0.85	2.42e2	3.27e2	0.74
V_2O_5	3.19e-4	2.87e-4	1.11	4.66e1	4.79e1	0.97
ZnO	0.01.03e-2	0.98e-2	1.05	1.50e3	1.63e3	0.92
Carbon						
[a]Organic C	4.53	3.02	1.50	6.60e5	5.04e5	1.31
Elemental C	0.13	0.18	0.72	1.88e4	3.06e4	0.61
Ions						
SO_4-	1.21	1.205	1.00	1.76e5	2.01e5	0.88
Na^+	5.55e-2	0.0351	1.58	8.10e3	5.86e3	1.38
NH_4^+	0.41	0.44	0.93	6.03e4	73 728	0.82
K^+	3.86e-2	0.03	1.29	5.63e3	5.00e3	1.13
Ca^{++}	6.40e-2	2.52e-2	2.54	9.34e3	4.20e3	2.22
Sum	7.63	5.68		1.11e6	9.48e5	
Mass ($\mu g/m^3$)	6.86	6.00			Analyte ratio	1.08
Ratio (sum/mass)	1.11	0.95				
	Analyte ratio		1.18			
	Mass ratio		1.14			

[a]CwHxOyNz (empirical formula = 1.6 • Organic C).
DL, detection limit.

of the papillary muscles, are reported in Table 4 and Supplementary Table 8, respectively. In addition, myocardial performance metrics derived from Doppler transmitral blood flow measures are presented in Supplementary Table 9 and Supplementary Figure 3. We found no differences in any cardiac function, heart wall dimensions, or myocardial performance parameters that were indicative of an exposure effect. In accordance with the guidelines of the American Society of Echocardiography (Lang *et al.*, 2005; Quinones *et al.*, 2002), we verified blinded interobserver variability for M-mode data analyses at 7.7% coefficient of variation.

Myocardial Synchronicity

The results of ultrasound analysis of myocardial synchronicity are displayed in Figure 4, Supplementary Table 10 and Supplementary Figure 4. Strain delay is a result of dyssynchronous systolic contraction within the heart wall, in this case between two adjacent wall segments, the anterior free wall and lateral wall. We found an increase in strain delay in B6129 mice when measured 1 day after the final exposure to CAPs+Acrolein; this increase ranged from around 3% of the cardiac cycle to over 10% of the cardiac cycle within this group. The increase in strain delay in the B6129 CAPs+Acrolein group was

Downloaded from https://academic.oup.com/toxsci/article-abstract/167/2/559/5142835 by EPA-RTP Main Library user on 15 January 2020

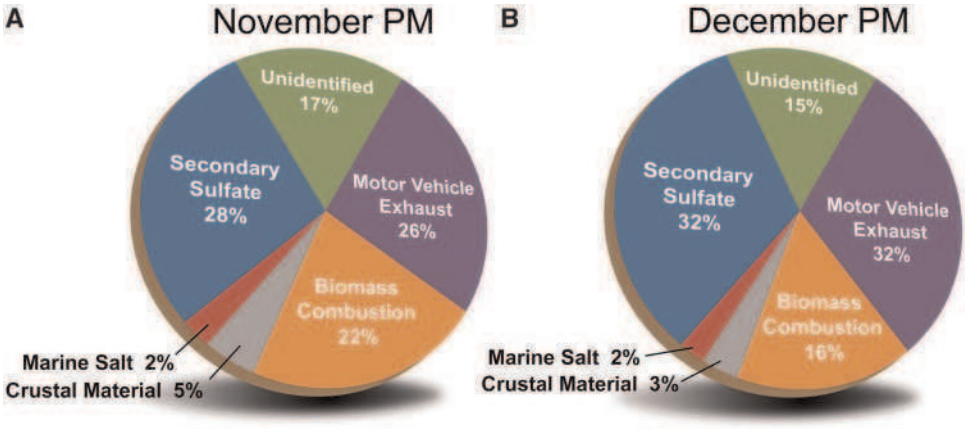

Figure 3. PM source apportionment. $PM_{2.5}$ samples from CAPs inlet filters collected in November and December of 2014 were analyzed using the 5-source chemical mass balance model (U.S. EPA). The results from our 5-source apportionment revealed 4%–6% differences in secondary sulfate, motor vehicle exhaust, and biomass combustion sources between November (A) and December (B).

Table 3. Body Weight and Heart Mass After Final Exposure

			Mouse Age and Size Statistics at the Time of Necropsy			
			Filtered Air	Acrolein	CAPs	CAPs+Acrolein
Age	Weeks	B6129	19.7 ± 0.5	18.6 ± 0.4	19.9 ± 0.5	*a*19.1 ± 0.6
		Trpa1−/−	24.0 ± 3.6 ‡	28.2 ± 5.8 ‡	27.5 ± 1.5 ‡	25.5 ± 1.6 ‡
Body mass	g	B6129	25.6 ± 2.3	24.1 ± 2.8	24.3 ± 2.4	*a*25.1 ± 2.7
		Trpa1−/−	19.2 ± 1.1 ‡	19.8 ± 1.7 ‡	20.6 ± 1.5 ‡	20.1 ± 2.3 ‡
Tibia length	mm	B6129	21.8 ± 0.4	20.7 ± 0.3	20.8 ± 1.2	*a*20.9 ± 0.9
		Trpa1−/−	20.2 ± 0.5	20.6 ± 0.6	20.0 ± 1.0	20.7 ± 0.4
Heart mass	mg	B6129	106.7 ± 20.7	91.8 ± 3.9	98.0 ± 17.9	*a*99.2 ± 1.3
		Trpa1−/−	89.0 ± 9.7 ‡	88.7 ± 7.5	100.0 ± 31.2	86.2 ± 6.5
			Mean ± SD ($n = 6$ unless denoted with *a* for $n = 5$)			

$p < .05$ noted with ‡ versus B6129.

significantly different from all other B6129 exposure groups and all *Trpa1*−/− exposed groups including the *Trpa1*−/− CAPs+Acrolein group. Strain delay in the B6129 CAPs+Acrolein group was also significantly different than earlier time points in the same group.

Heart Rate Variability

Results from HRV analysis of ECG signals collected from anesthetized B6129 and *Trpa1*−/− mice 1 day after the 8th exposure to Filtered Air, Acrolein, CAPs, or CAPs+Acrolein are presented in Figure 5. No significant differences in SDNN were found (Figure 5A). Whereas no significant differences in RMSSD were found (Figure 5B), the difference in means between B6129 mice exposed to Acrolein and B6129 mice exposed to Filtered Air yielded a $p = .07$. The high frequency domain of HRV increased in B6129 mice exposed to Acrolein compared with B6129 mice exposed to Filtered Air (Figure 5C). There was no such effect of acrolein in *Trpa1*−/− mice, and the difference in means between B6129 mice exposed to Acrolein and *Trpa1*−/− mice exposed to Acrolein yielded a $p = .10$.

DISCUSSION

This study shows for the first time that intermittent co-exposure to ambient PM and acrolein in mice, using a novel CAPs and acrolein co-exposure system, results in myocardial dyssynchrony through a mechanism involving TRPA1. The loss of myocardial synchrony after repeated, intermittent PM and acrolein co-exposure is unique from the response to a single exposure and from exposure to either pollutant alone, pointing to interactive effects of the two pollutants. The absence of concurrent changes in HRV in CAPs+Acrolein-exposed B6129 mice may point to molecular and cellular changes within the myocardium, but do not necessarily preclude autonomic activity that may have occurred earlier in the exposure regimen. Interestingly, although acrolein had no impact on myocardial synchronicity when measured, it did in fact increase an HRV index of parasympathetic tone in B6129 mice, an effect that was absent in acrolein-exposed *Trpa1*−/− mice. Such a stark qualitative difference in response pattern points to physiochemical and/or biological mechanisms in PM and acrolein mixtures that are either absent or activated to a lesser degree with exposure to either alone. Whereas the physicochemical properties that may underlie such exaggerated effects are unclear, activation of pulmonary TRPA1, a prominent sensor of environmental irritants, may have triggered the cascade of events leading to myocardial dyssynchrony.

Elemental analysis showed that organic carbon and ammonium sulfate were the predominant constituents of PM in this study, along with alkalis sodium, calcium, potassium, silicon, aluminum, and iron. Source apportionment found the majority of sources to be attributable to secondary sulfates, motor vehicle

Downloaded from https://academic.oup.com/toxsci/article-abstract/167/2/559/5142835 by EPA-RTP Main Library user on 15 January 2020

Table 4. Echocardiography (M-Mode)—Cardiac Function

			SAX M-Mode Evaluation at Baseline			
			Filtered Air	Acrolein	CAPs	CAPs+Acrolein
Heart rate	Beats/min	B6129	443 ± 27	392 ± 33	410 ± 41	420 ± 42
		Trpa1−/−	456 ± 33	468 ± 37 ‡	463 ± 29 #	437 ± 38
ESV	µl	B6129	26.5 ± 12.1	25.7 ± 9.8	21.3 ± 7.8	24.7 ± 7.5
		Trpa1−/−	19.3 ± 7.9	18.7 ± 6.7	27.1 ± 7.3	21.9 ± 8.6
EDV	µl	B6129	63.4 ± 22.9	58.9 ± 9.9	55.2 ± 12.9	54.7 ± 9.1
		Trpa1−/−	45.8 ± 12.0	45.7 ± 11.3	61.7 ± 20.2	47.4 ± 9.9
SV	µl	B6129	36.9 ± 11.1	33.2 ± 4.3	33.9 ± 9.0	30.1 ± 5.1
		Trpa1−/−	26.5 ± 8.3	26.9 ± 5.6	34.6 ± 13.9	25.5 ± 4.6
EF	%	B6129	59.1 ± 4.9	57.3 ± 9.7	61.9 ± 11.2	55.5 ± 7.4
		Trpa1−/−	58.3 ± 10.6	60.0 ± 7.3	55.3 ± 5.8	54.6 ± 9.6
FS	%	B6129	30.9 ± 3.2	29.8 ± 6.3	33.2 ± 8.5	28.5 ± 4.7
		Trpa1−/−	30.5 ± 8.1	31.2 ± 5.0	28.3 ± 3.9	27.8 ± 6.0
CO	ml/min	B6129	16.3 ± 4.9	13.0 ± 2.0	14.0 ± 4.4	12.8 ± 3.4
		Trpa1−/−	12.0 ± 3.7	12.5 ± 2.1	16.2 ± 7.6	11.1 ± 2.0
			Mean ± SD ($n = 6$)			
			SAX M-Mode Evaluation 1 Day After 1st Exposure			
Heart rate	Beats/min	B6129	447 ± 23	425 ± 61	445 ± 32	448 ± 38
		Trpa1−/−	500 ± 31	480 ± 48	476 ± 33	459 ± 21
ESV	µl	B6129	32.9 ± 18.1	25.1 ± 9.6	20.2 ± 6.7	24.9 ± 6.7
		Trpa1−/−	17.7 ± 4.4 ‡	28.2 ± 10.4	26.4 ± 9.0	24.8 ± 5.0
EDV	µl	B6129	66.1 ± 25.0	52.4 ± 14.7	50.6 ± 11.3	57.6 ± 11.9
		Trpa1−/−	41.7 ± 9.0 ‡	57.1 ± 11.9	57.1 ± 16.1	52.0 ± 8.5
SV	µl	B6129	33.2 ± 7.1	27.4 ± 7.3	30.4 ± 7.8	32.7 ± 7.0
		Trpa1−/−	24.0 ± 6.3	28.9 ± 4.0	30.7 ± 8.9	27.2 ± 4.7
EF	%	B6129	52.7 ± 8.4	53.3 ± 9.1	60.4 ± 8.9	57.1 ± 6.1
		Trpa1−/−	57.7 ± 7.5	51.8 ± 8.5	54.2 ± 6.1	52.4 ± 4.9
FS	%	B6129	26.8 ± 5.0	27.0 ± 5.5	31.8 ± 6.4	29.5 ± 4.0
		Trpa1−/−	29.6 ± 4.9	26.2 ± 5.1	27.6 ± 3.9	26.3 ± 3.1
CO	ml/min	B6129	14.7 ± 2.4	11.6 ± 3.7	13.6 ± 3.9	14.8 ± 4.1
		Trpa1−/−	12.1 ± 3.6	13.9 ± 2.5	14.6 ± 4.5	12.5 ± 2.2
			Mean ± SD ($n = 6$)			
			SAX M-Mode Evaluation 1 Day After Final Exposure			
Heart rate	Beats/min	B6129	454 ± 33	401 ± 31 *,†	453 ± 40 #	*a*431 ± 28
		Trpa1−/−	485 ± 26	475 ± 24 ‡	486 ± 15	477 ± 40
ESV	µl	B6129	25.0 ± 12.3	25.0 ± 4.9	19.7 ± 12.4	*a*24.2 ± 10.0
		Trpa1−/−	19.5 ± 4.4	17.2 ± 3.9	20.7 ± 11.7	20.5 ± 6.9
EDV	µl	B6129	57.6 ± 18.6	55.0 ± 7.7	55.0 ± 27.2	*a*53.9 ± 10.3
		Trpa1−/−	47.6 ± 6.9	44.3 ± 9.1	54.0 ± 21.5	47.1 ± 7.8
SV	µl	B6129	32.6 ± 7.9	30.0 ± 4.8	35.4 ± 15.7	*a*29.7 ± 2.2
		Trpa1−/−	28.1 ± 3.9	27.1 ± 5.7	33.4 ± 11.1	26.5 ± 3.2
EF	%	B6129	57.7 ± 7.5	54.6 ± 5.6	65.6 ± 9.3	*a*56.5 ± 9.0
		Trpa1−/−	59.3 ± 5.9	61.1 ± 3.5	63.3 ± 9.5	57.3 ± 9.1
FS	%	B6129	29.9 ± 5.1	27.7 ± 3.6	35.8 ± 7.7	*a*29.1 ± 5.5
		Trpa1−/−	30.9 ± 4.1	31.9 ± 2.4	34.0 ± 7.7	29.6 ± 6.1
CO	ml/min	B6129	14.9 ± 4.2	11.9 ± 1.5	16.2 ± 7.8	*a*12.9 ± 1.3
		Trpa1−/−	13.6 ± 1.9	12.9 ± 2.9	16.3 ± 5.9	12.6 ± 1.5
			Mean ± SD ($n = 6$ unless denoted with *a* for $n = 5$)			

$p < .05$ noted with *versus FA, #versus Acrolein, †versus CAPs, and ‡ versus B6129.
CO, cardiac output; EDV, end diastolic volume; EF, ejection fraction; ESV, end systolic volume; FS, fractional shortening; SAX, short axis view; SV, stroke volume.

emissions, and biomass combustion. The physicochemical characteristics of PM in this study were similar throughout the November and December exposure days in 2014. During that time, winds originated mostly from southwest to northwest at elevations of < 2000 m in the atmospheric boundary layer of the lower troposphere, bringing atmospheres derived from wind that originated, or passed through, metropolitan airsheds en route to Research Triangle Park, North Carolina. These derivative or supplemental airsheds included Chicago IL, Cincinnati/Cleveland/Columbus OH, Birmingham AL, Atlanta GA, and Charlotte NC. Lower-elevation airsheds have historically brought higher levels of particulates to North Carolina from regional combustion sources like biomass burning and power plants (Aneja *et al.*, 2006). The airshed of Research Triangle Park, North Carolina has been

Downloaded from https://academic.oup.com/toxsci/article-abstract/167/2/559/5142835 by EPA-RTP Main Library user on 15 January 2020

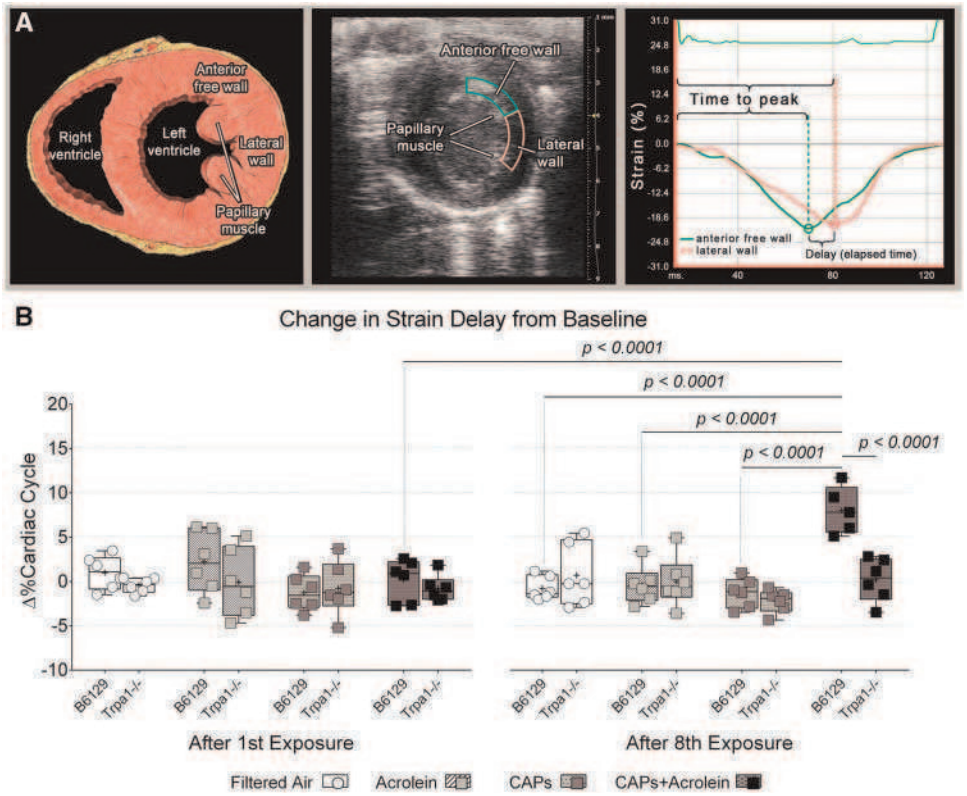

Figure 4. Myocardial synchrony. Panel A illustrates the derivation of circumferential strain delay including a schematic of a mouse heart oriented in the short axis view at the level of the papillary muscles, modified from Lynch and Jaffe (2006) with the regions of the anterior free wall and lateral wall denoted, a representative image of an echocardiographic short-axis view with the anterior free wall endocardium and the lateral wall endocardium, and software output for speckle-strain analysis depicting circumferential strain in the anterior free wall endocardium and the lateral wall endocardium. Delay was calculated as the difference in time to peak strain between the two regions or the time that elapsed between the occurrences of peak strain in the two regions. For reporting (%Cardiac Cycle), the ms value of strain delay was then converted to a percent of the cardiac cycle. Panel B shows the quantified data indicating that a significant increase in myocardial strain delay between the lateral and anterior free wall was found after the 8th exposure to CAPs+Acrolein in B6129 mice. Increases were not found with any other exposure group when compared with baseline and was also not found in *Trpa1−/−* mice. Elapsed time between peak strain in the lateral and anterior free wall are reported as a percentage of the cardiac cycle and normalized to baseline values. Data were compared by two-way ANOVA with Tukey (within strain) or Bonferroni (across strain) post-test. The *p*-values for significant findings are $< .0001$.

characterized by pollutants from biogenic emissions, agricultural activity, vehicular traffic, and secondary organic aerosols (Aneja *et al.*, 2006; Farraj *et al.*, 2015).

Co-exposure to CAPs and acrolein, but not exposure to either alone, in B6129 mice increased circumferential strain delay between the lateral and anterior free wall of the left ventricle, which we use as a measure of myocardial dyssynchrony. Regional contractile dyssynchrony in the myocardium has been linked to clinical regional cardiac ischemia (Chen *et al.*, 2012), with cardiac ischemia-related hospitalizations being a documented effect of air pollution exposure (Cox, 2017; McGuinn *et al.*, 2017; Pope *et al.*, 2015). Myocardial dyssynchrony could result from autonomic effects as repeated exposure to PM2.5 in combination with organic aerosols has recently been reported to influence autonomic nervous system regulation of heart function (Carll *et al.*, 2017). We have also reported autonomic cardiovascular effects with PM2.5 alone (Carll *et al.*, 2015) and acrolein alone (Hazari *et al.*, 2014; Kurhanewicz *et al.*, 2017; Perez *et al.*, 2013, 2015), and have linked exposure to 3.0 ppm acrolein alone with myocardial dyssynchrony (Thompson *et al.*, 2017). However, in this study, acrolein exposure alone at 0.4 ppm was not sufficient to elicit myocardial dyssynchrony and B6129 mice exposed to CAPs+Acrolein had myocardial dyssynchrony without accompanying changes in HRV. The absence of altered autonomic activity at the time heart function was assessed at the end of the study does not preclude a role for autonomic nervous system activity earlier in the exposure regimen, which, if present, could have "programmed" the myocardium for dyssynchronous contraction. For example, β-adrenergic stimulation alters myocardial gap junction conductance and expression of subtypes of connexins, key gap junction proteins involved in inter-cardiomyocyte signal transduction, which can result in electrical instability and predisposition to arrhythmia (Xia *et al.*, 2009). Alternatively, the loss of cardiac synchrony may have resulted from variable distribution of local regulation of contractile function within the myocardium secondary to oxidative stress (Kelly and Fussell, 2017) and/or altered myocardial autocrine/paracrine signaling (Chan *et al.*, 2016).

Although the precise physiological mechanism at play is unclear, this study suggests that myocardial dyssynchrony in CAPs+Acrolein-exposed B6129 mice resulted from activation of TRPA1, given the absence of such responses in similarly exposed *Trpa1−/−* mice. TRPA1 channels are expressed throughout the airways on vagal afferent C-fibers (Achanta and Jordt, 2017) and are activated by oxidizing agents (Bessac *et al.*, 2008), environmental toxicants like acrolein (Bautista *et al.*, 2006), and sulfur-containing compounds (Stenger *et al.*, 2017; Terada *et al.*, 2014). Previous reports describing exposure to single air pollutants have linked TRPA1 to altered autonomic function (Hazari *et al.*, 2011; Kurhanewicz *et al.*, 2017) and other cardiovascular

Downloaded from https://academic.oup.com/toxsci/article-abstract/167/2/559/5142835 by EPA-RTP Main Library user on 15 January 2020

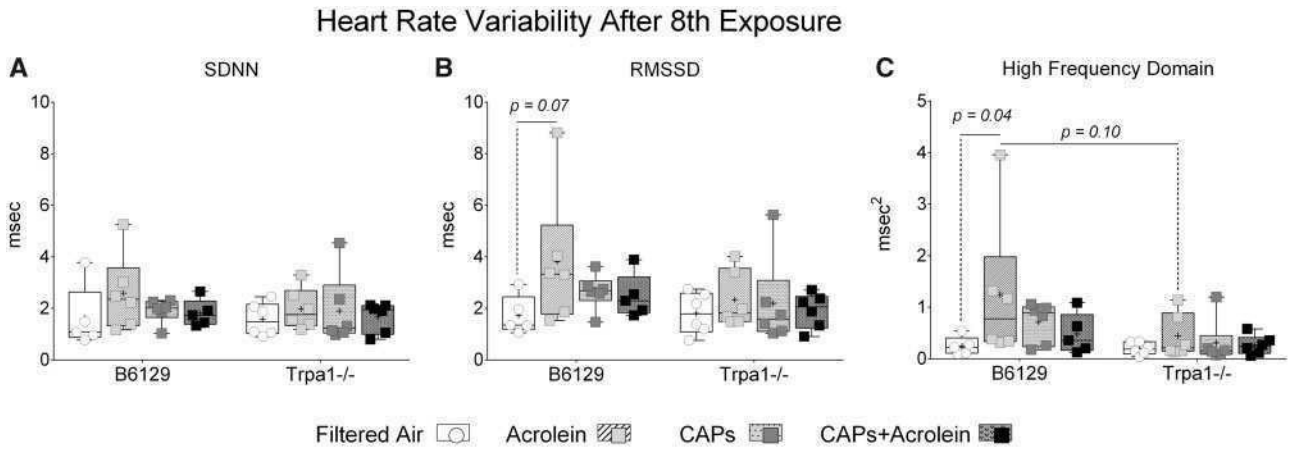

Figure 5. Heart rate variability. We analyzed HRV using ECG signals recorded in anesthetized B6129 and *Trpa1−/−* mice 1 day after the 8th exposure to Filtered Air, Acrolein, CAPs, or CAPs+Acrolein. A, No changes in SDNN were found. B, No significant differences in RMSSD were found but the change in mean between B6129 mice exposed to Filtered Air and B6129 mice exposed to Acrolein produced a $p = .07$. C, The high frequency domain of HRV increased in B6129 mice exposed to Acrolein compared with B6129 mice exposed to Filtered Air. No other differences in High Frequency were found. Data were compared by two-way ANOVA with Tukey (within strain) or Bonferroni (across strain) post-test. The *p*-values for significant differences and others near .05 are provided for clarity.

effects (Conklin, 2016; Conklin *et al.*, 2017). We have also recently reported that organic fractions of diesel exhaust particulate matter containing high levels of polar compounds, including oxy- and nitro-polyaromatic hydrocarbons, caused concentration-dependent irritant responses mediated by TRPA1 in an *in vivo* model (Stevens *et al.*, 2018). In other reports, delivery of TRPA1 agonists into the airways has been shown to produce cardiovascular responses through autonomic reflexes (Hooper *et al.*, 2016; Pozsgai *et al.*, 2010). Unsurprisingly, TRPA1 drove the acrolein-induced increases in HRV in B6129 mice, as such effects were absent in *Trpa1−/−* mice. However, this finding further highlights the qualitative divergence in single-pollutant versus co-pollutant effects, as the HRV effect with acrolein alone was not evident in CAPs+Acrolein-exposed B6129 mice. Although the precise reasons for this divergence are unclear, these data are consistent with our previous findings that compared effects of single and multiple pollutant exposures, which found that whole and particle-free diesel exhaust elicit varying physiological and autonomic responses (Carll *et al.*, 2012; Lamb *et al.*, 2012).

The unique co-pollutant effects in this study may have been driven by physicochemical interactions that modified the biological responses compared with exposure to either pollutant alone. Fine PM usually reaches the deep lung and the reactive properties of acrolein generally restrict it to the upper airways. However, the addition of PM may allow acrolein to penetrate the deep lung (Jakab, 1993) by serving as an acrolein preconcentrator and delivery agent, which as has been demonstrated by use of surrogate organic PM samples, ie, mineral oil aerosols (Ebersviller *et al.*, 2012). Although it is unclear if this took place during co-exposure in this study, measures of acrolein adducts in lung tissue in future studies would help assess this possibility (Conklin *et al.*, 2017). Alternatively, atmospheric interaction between PM and acrolein could lead to the formation of more proinflammatory and irritating byproducts as has been demonstrated with SO_2 in the presence of various metals (Amdur and Underhill, 1968; Vadjic *et al.*, 1991).

Several limitations should be considered in this study. First, low airflow and PM concentrations reduced the opportunity for PM sample collection. The 4 weeks required to collect enough PM mass to extract and analyze limited the temporal resolution of PM elemental analysis and source apportionment, and contributed to a loss of volatile PM constituents (eg, nitrate ions). Organic speciation of PM in future studies could also reduce the percentage of unidentified sources found in this study. In addition, the limited availability of *Trpa1−/−* mice required the use of a larger subject age range than expected. In fact, two of the *Trpa1−/−* mice were substantially older (ie, 3–4 months older) than the remaining mice and had significantly higher baseline strain delay. These two mice were, however, split into separate groups to minimize any potential age-related impacts. Moreover, given the use of female mice, estrous cycles among the mice were not synched presenting some uncertainty with respect to any potential impacts estrous had on the cardiovascular responses in this study. Although others have noted that cardiac function is in fact impacted by estrous (MacDonald *et al.*, 2014), the length of the exposure regimen (ie, 4 weeks), may have diminished any such impact. Furthermore, assessing HRV while under anesthesia may have dampened the degree of activation of the autonomic nervous system. In particular, isoflurane induces bradycardia and although we targeted HR to 450 beats/min by adjusting the level of isoflurane anesthesia, HR itself demonstrated wide variation. Whether this variability in HR played a role in the lower average HR and higher HRV in acrolein-exposed B6129 mice compared with all other groups is unclear. The HRV analysis was also limited by the short segment duration of data analyzed, which was due to the limited capacity to acquire electrocardiogram data using the ultrasound system. Although HRV segment length recommendations have not been espoused for rodents, guidelines for human clinical assessments recommend at least 5 min of continuous heart rate data (Task Force, 1996). Nonetheless, the recordings were nearly concurrent with measures of cardiac function, which allowed for inferences about potential relationships between the functional data and autonomic tone.

In conclusion, this study provides evidence that PM may interact with gaseous air toxicants like acrolein to produce unique health effects via TRPA1 activation. Moreover, this study lends support to the possibility that exposure to air pollution mixtures that include PM and volatile organics, like aldehydes, could increase the severity of health effects beyond that resulting from exposure to single pollutants alone, especially with repeated

Downloaded from https://academic.oup.com/toxsci/article-abstract/167/2/559/5142835 by EPA-RTP Main Library user on 15 January 2020

intermittent exposure. The finding that co-exposure to PM and acrolein in this study caused regional myocardial dyssynchrony in the absence of any overt pathophysiology highlights the capacity for exposure to air pollution mixtures to produce subclinical and latent effects, which may not register in conventional measures, but may nonetheless have serious health ramifications. Thus, evaluation of myocardial synchronicity in human populations prone to air pollution exposure or during controlled human exposure studies may provide data that indicates early manifestations of cardiovascular disease proclivity. Finally, further elucidation of the precise mode of TRPA1 activation and downstream effects including autonomic responses will increase the plausibility for greater than additive effects with co-pollutant exposure.

SUPPLEMENTARY DATA

Supplementary data are available at *Toxicological Sciences* online.

ACKNOWLEDGMENTS

We would like to thank various scientists at U.S. Environmental Protection Agency in Research Triangle Park, NC, USA for important contributions to this work: Paul Evansky for technical assistance with the acrolein analyzer, John Sullivan and Charly King for helping with exposure system setup and running exposures, George Hudson for collecting the particulate matter filters, Earl Puckett for exposure system component fabrication, and Judy Richards for serum and lavage fluid analysis. We also thank Dr Elizabeth A.W. Chan and Dr M. Ian Gilmour for thorough reviews of the manuscript. John Havel and Keith Tarpley of SRA International, Inc generated the graphics in Figures 1–4. The authors have no conflicts of interest to disclose.

REFERENCES

Achanta, S., and Jordt, S. E. (2017). TRPA1: Acrolein meets its target. *Toxicol. Appl. Pharmacol.* **324**, 45–50.

Amdur, M. O., and Underhill, D. (1968). The effect of various aerosols on the response of guinea pigs to sulfur dioxide. *Arch. Environ. Health* **16**, 460–468.

Aneja, V. P., Wang, B., Tong, D. Q., Kimball, H., and Steger, J. (2006). Characterization of major chemical components of fine particulate matter in North Carolina. *J. Air Waste Manag. Assoc.* **56**, 1099–1107.

Argacha, J. F., Bourdrel, T., and van de Borne, P. (2018). Ecology of the cardiovascular system: A focus on air-related environmental factors. *Trends Cardiovasc. Med.* **28**, 112–126.

ATSDR. (2007). *Toxicological Profile for Acrolein*. U.S. Department of Health and Human Services, Public Health Service, Atlanta, GA.

Bautista, D. M., Jordt, S. E., Nikai, T., Tsuruda, P. R., Read, A. J., Poblete, J., Yamoah, E. N., Basbaum, A. I., and Julius, D. (2006). TRPA1 mediates the inflammatory actions of environmental irritants and proalgesic agents. *Cell* **124**, 1269–1282.

Bessac, B. F., Sivula, M., von Hehn, C. A., Escalera, J., Cohn, L., and Jordt, S. E. (2008). TRPA1 is a major oxidant sensor in murine airway sensory neurons. *J. Clin. Invest.* **118**, 1899–1910.

Bhatnagar, A. (2017). Environmental determinants of cardiovascular disease. *Circ. Res.* **121**, 162–180.

Brook, R. D., and Rajagopalan, S. (2017). "Stressed" about air pollution: Time for personal action. *Circulation* **136**, 628–631.

Carll, A. P., Crespo, S. M., Filho, M. S., Zati, D. H., Coull, B. A., Diaz, E. A., Raimundo, R. D., Jaeger, T. N. G., Ricci-Vitor, A. L., and Papapostolou, V. (2017). Inhaled ambient-level traffic-derived particulates decrease cardiac vagal influence and baroreflexes and increase arrhythmia in a rat model of metabolic syndrome. *Part. Fibre Toxicol.* **14**, 16.

Carll, A. P., Haykal-Coates, N., Winsett, D. W., Hazari, M. S., Ledbetter, A. D., Richards, J. H., Cascio, W. E., Costa, D. L., and Farraj, A. K. (2015). Cardiomyopathy confers susceptibility to particulate matter-induced oxidative stress, vagal dominance, arrhythmia and pulmonary inflammation in heart failure-prone rats. *Inhal. Toxicol.* **27**, 100–112.

Carll, A. P., Hazari, M. S., Perez, C. M., Krantz, Q. T., King, C. J., Winsett, D. W., Costa, D. L., and Farraj, A. K. (2012). Whole and particle-free diesel exhausts differentially affect cardiac electrophysiology, blood pressure, and autonomic balance in heart failure-prone rats. *Toxicol. Sci.* **128**, 490–499.

Chan, E. A., Buckley, B., Farraj, A. K., and Thompson, L. C. (2016). The heart as an extravascular target of endothelin-1 in particulate matter-induced cardiac dysfunction. *Pharmacol. Ther.* **165**, 63–78.

Chen, C. C., Shen, T. Y., Chang, M. C., Hung, G. U., Chen, W. C., Kao, C. H., and Chen, J. (2012). Stress-induced myocardial ischemia is associated with early post-stress left ventricular mechanical dyssynchrony as assessed by phase analysis of 201tl gated spect myocardial perfusion imaging. *Eur. J. Nucl. Med. Mol. Imaging* **39**, 1904–1909.

Cohen, J. (1988). *Statistical Power Analysis for the Behavioral Sciences*. L. Erlbaum Associates, Hillsdale, NJ.

Cohen, A. J., Brauer, M., Burnett, R., Anderson, H. R., Frostad, J., Estep, K., Balakrishnan, K., Brunekreef, B., Dandona, L., Dandona, R., *et al.* (2017). Estimates and 25-year trends of the global burden of disease attributable to ambient air pollution: An analysis of data from the global burden of diseases study 2015. *Lancet* **389**, 1907–1918.

Conklin, D. J. (2016). Acute cardiopulmonary toxicity of inhaled aldehydes: Role of TRPA1. *Ann. N.Y. Acad. Sci.* **1374**, 59–67.

Conklin, D. J., Haberzettl, P., Jagatheesan, G., Kong, M., and Hoyle, G. W. (2017). Role of TRPA1 in acute cardiopulmonary toxicity of inhaled acrolein. *Toxicol. Appl. Pharmacol.* **324**, 61–72.

Cox, L. A., Jr. (2017). Socioeconomic and air pollution correlates of adult asthma, heart attack, and stroke risks in the United States, 2010–2013. *Environ. Res.* **155**, 92–107.

Deering-Rice, C. E., Romero, E. G., Shapiro, D., Hughen, R. W., Light, A. R., Yost, G. S., Veranth, J. M., and Reilly, C. A. (2011). Electrophilic components of diesel exhaust particles (DEP) activate transient receptor potential ankyrin-1 (TRPA1): A probable mechanism of acute pulmonary toxicity for DEP. *Chem. Res. Toxicol.* **24**, 950–959.

Ebersviller, S., Lichtveld, K., Sexton, K. G., Zavala, J., Lin, Y. H., Jaspers, I., and Jeffries, H. E. (2012). Gaseous VOCs rapidly modify particulate matter and its biological effects—Part 1: Simple VOCs and model PM. *Atmos. Chem. Phys. Discuss.* **12**, 5065–5105.

Fariss, M. W., Gilmour, M. I., Reilly, C. A., Liedtke, W., and Ghio, A. J. (2013). Emerging mechanistic targets in lung injury induced by combustion-generated particles. *Toxicol. Sci.* **132**, 253–267.

Farraj, A. K., Walsh, L., Haykal-Coates, N., Malik, F., McGee, J., Winsett, D., Duvall, R., Kovalcik, K., Cascio, W. E., Higuchi, M., *et al.* (2015). Cardiac effects of seasonal ambient particulate

Downloaded from https://academic.oup.com/toxsci/article-abstract/167/2/559/5142835 by EPA-RTP Main Library user on 15 January 2020

matter and ozone co-exposure in rats. *Part. Fibre Toxicol.* **12**, 12.

Ghelfi, E., Rhoden, C. R., Wellenius, G. A., Lawrence, J., and Gonzalez-Flecha, B. (2008). Cardiac oxidative stress and electrophysiological changes in rats exposed to concentrated ambient particles are mediated by TRP-dependent pulmonary reflexes. *Toxicol. Sci.* **102**, 328–336.

Gimelli, A., Liga, R., Genovesi, D., Giorgetti, A., Kusch, A., and Marzullo, P. (2014). Association between left ventricular regional sympathetic denervation and mechanical dyssynchrony in phase analysis: A cardiac CZT study. *Eur. J. Nucl. Med. Mol. Imaging* **41**, 946–955.

Gupta, T., Demokritou, P., and Koutrakis, P. (2004). Development and performance evaluation of a high-volume ultrafine particle concentrator for inhalation toxicological studies. *Inhal. Toxicol.* **16**, 851–862.

Hazari, M. S., Griggs, J., Winsett, D. W., Haykal-Coates, N., Ledbetter, A., Costa, D. L., and Farraj, A. K. (2014). A single exposure to acrolein desensitizes baroreflex responsiveness and increases cardiac arrhythmias in normotensive and hypertensive rats. *Cardiovasc. Toxicol.* **14**, 52–63.

Hazari, M. S., Haykal-Coates, N., Winsett, D. W., Krantz, Q. T., King, C., Costa, D. L., and Farraj, A. K. (2011). TRPA1 and sympathetic activation contribute to increased risk of triggered cardiac arrhythmias in hypertensive rats exposed to diesel exhaust. *Environ. Health Perspect.* **119**, 951–957.

Henning, R. J., Johnson, G. T., Coyle, J. P., and Harbison, R. D. (2017). Acrolein can cause cardiovascular disease: A review. *Cardiovasc. Toxicol.* **17**, 227–236.

Hooper, J. S., Hadley, S. H., Morris, K. F., Breslin, J. W., Dean, J. B., and Taylor-Clark, T. E. (2016). Characterization of cardiovascular reflexes evoked by airway stimulation with allylisothiocyanate, capsaicin, and ATP in Sprague-Dawley rats. *J. Appl. Physiol. (Bethesda, MD: 1985)* **120**, 580–591.

Huang, Y. C., Rappold, A. G., Graff, D. W., Ghio, A. J., and Devlin, R. B. (2012). Synergistic effects of exposure to concentrated ambient fine pollution particles and nitrogen dioxide in humans. *Inhal. Toxicol.* **24**, 790–797.

Jakab, G. J. (1993). The toxicologic interactions resulting from inhalation of carbon black and acrolein on pulmonary antibacterial and antiviral defenses. *Toxicol. Appl. Pharmacol.* **121**, 167–175.

Kelly, F. J., and Fussell, J. C. (2017). Role of oxidative stress in cardiovascular disease outcomes following exposure to ambient air pollution. *Free Radic. Biol. Med.* **110**, 345–367.

Kichko, T. I., Kobal, G., and Reeh, P. W. (2015). Cigarette smoke has sensory effects through nicotinic and TRPA1 but not TRPV1 receptors on the isolated mouse trachea and larynx. *Am. J. Physiol. Lung Cell. Mol. Physiol.* **309**, L812–L820.

Kodavanti, U. P., Schladweiler, M. C., Ledbetter, A. D., McGee, J. K., Walsh, L., Gilmour, P. S., Highfill, J. W., Davies, D., Pinkerton, K. E., Richards, J. H., *et al.* (2005). Consistent pulmonary and systemic responses from inhalation of fine concentrated ambient particles: Roles of rat strains used and physicochemical properties. *Environ. Health Perspect.* **113**, 1561–1568.

Kunkler, P. E., Zhang, L., Pellman, J. J., Oxford, G. S., and Hurley, J. H. (2015). Sensitization of the trigeminovascular system following environmental irritant exposure. *Cephalalgia* **35**, 1192–1201.

Kurhanewicz, N., McIntosh-Kastrinsky, R., Tong, H., Ledbetter, A., Walsh, L., Farraj, A., and Hazari, M. (2017). TRPA1 mediates changes in heart rate variability and cardiac mechanical function in mice exposed to acrolein. *Toxicol. Appl. Pharmacol.* **324**, 51–60.

Lamb, C. M., Hazari, M. S., Haykal-Coates, N., Carll, A. P., Krantz, Q. T., King, C., Winsett, D. W., Cascio, W. E., Costa, D. L., and Farraj, A. K. (2012). Divergent electrocardiographic responses to whole and particle-free diesel exhaust inhalation in spontaneously hypertensive rats. *Toxicol. Sci.* **125**, 558–568.

Lang, R. M., Bierig, M., Devereux, R. B., Flachskampf, F. A., Foster, E., Pellikka, P. A., Picard, M. H., Roman, M. J., Seward, J., Shanewise, J. S., *et al.* (2005). Recommendations for chamber quantification: A report from the American Society of Echocardiography's Guidelines and Standards Committee and the Chamber Quantification Writing Group, developed in conjunction with the European Association of Echocardiography, a branch of the European Society of Cardiology. *J. Am. Soc. Echocardiogr.* **18**, 1440–1463.

Lee, L. Y., Hsu, C. C., Lin, Y. J., Lin, R. L., and Khosravi, M. (2015). Interaction between TRPA1 and TRPV1: Synergy on pulmonary sensory nerves. *Pulm. Pharmacol. Ther.* **35**, 87–93.

Lin, Y. S., Hsu, C. C., Bien, M. Y., Hsu, H. C., Weng, H. T., and Kou, Y. R. (2010). Activations of TRPA1 and P2X receptors are important in ROS-mediated stimulation of capsaicin-sensitive lung vagal afferents by cigarette smoke in rats. *J. Appl. Physiol. (Bethesda, MD: 1985).* **108**, 1293–1303.

Lynch, P. J., and Jaffe, C. C. (2006). *Heart Normal Short Axis Section.*Creative Commons, New Haven, CT.

MacDonald, J. K., Pyle, W. G., Reitz, C. J., and Howlett, S. E. (2014). Cardiac contraction, calcium transients, and myofilament calcium sensitivity fluctuate with the estrous cycle in young adult female mice. *Am. J. Physiol. Heart Circ. Physiol.* **306**, H938–H953.

Mauderly, J. L., and Samet, J. M. (2009). Is there evidence for synergy among air pollutants in causing health effects? *Environ. Health Perspect.* **117**, 1–6.

McGuinn, L. A., Ward-Caviness, C., Neas, L. M., Schneider, A., Di, Q., Chudnovsky, A., Schwartz, J., Koutrakis, P., Russell, A. G., Garcia, V., *et al.* (2017). Fine particulate matter and cardiovascular disease: Comparison of assessment methods for long-term exposure. *Environ. Res.* **159**, 16–23.

National Institute for Occupational Safety and Health (NIOSH). (2005). *Pocket Guide to Chemical Hazards*. U.S. Department of Health and Human Services, Public Health Service, Centers for Disease Controland Prevention, Cincinnati, OH.

Newby, D. E., Mannucci, P. M., Tell, G. S., Baccarelli, A. A., Brook, R. D., Donaldson, K., Forastiere, F., Franchini, M., Franco, O. H., Graham, I., *et al.* (2015). Expert position paper on air pollution and cardiovascular disease. *Eur. Heart J.* **36**, 83–93b.

Perez, C. M., Hazari, M. S., Ledbetter, A. D., Haykal-Coates, N., Carll, A. P., Cascio, W. E., Winsett, D. W., Costa, D. L., and Farraj, A. K. (2015). Acrolein inhalation alters arterial blood gases and triggers carotid body-mediated cardiovascular responses in hypertensive rats. *Inhal. Toxicol.* **27**, 54–63.

Perez, C. M., Ledbetter, A. D., Hazari, M. S., Haykal-Coates, N., Carll, A. P., Winsett, D. W., Costa, D. L., and Farraj, A. K. (2013). Hypoxia stress test reveals exaggerated cardiovascular effects in hypertensive rats after exposure to the air pollutant acrolein. *Toxicol. Sci.* **132**, 467–477.

Pope, C. A., Muhlestein, J. B., Anderson, J. L., Cannon, J. B., Hales, N. M., Meredith, K. G., Le, V., and Horne, B. D. (2015). Short-term exposure to fine particulate matter air pollution is preferentially associated with the risk of ST-segment elevation acute coronary events. *J. Am. Heart Assoc.* **4**, e002506.

Pozsgai, G., Bodkin, J. V., Graepel, R., Bevan, S., Andersson, D. A., and Brain, S. D. (2010). Evidence for the pathophysiological

Downloaded from https://academic.oup.com/toxsci/article-abstract/167/2/559/5142835 by EPA-RTP Main Library user on 15 January 2020

relevance of TRPA1 receptors in the cardiovascular system *in vivo*. *Cardiovasc. Res.* **87**, 760–768.

Quinones, M. A., Otto, C. M., Stoddard, M., Waggoner, A., Zoghbi, W. A., and Doppler Quantification Task Force of the N, Standards Committee of the American Society of E. (2002). Recommendations for quantification of Doppler echocardiography: A report from the Doppler Quantification Task Force of the Nomenclature and Standards Committee of the American Society of Echocardiography. *J. Am. Soc. Echocardiogr.* **15**, 167–184.

Rowan, W. H., 3rd, Campen, M. J., Wichers, L. B., and Watkinson, W. P. (2007). Heart rate variability in rodents: Uses and caveats in toxicological studies. *Cardiovasc. Toxicol.* **7**, 28–51.

Sivagangabalan, G., Spears, D., Masse, S., Urch, B., Brook, R. D., Silverman, F., Gold, D. R., Lukic, K. Z., Speck, M., Kusha, M., *et al.* (2011). The effect of air pollution on spatial dispersion of myocardial repolarization in healthy human volunteers. *J. Am. Coll. Cardiol.* **57**, 198–206.

Stenger, B., Popp, T., John, H., Siegert, M., Tsoutsoulopoulos, A., Schmidt, A., Muckter, H., Gudermann, T., Thiermann, H., and Steinritz, D. (2017). *N*-acetyl-L-cysteine inhibits sulfur mustard-induced and TRPA1-dependent calcium influx. *Arch. Toxicol.* **91**, 2179–2189.

Stevens, J. S., Padilla, S., DeMarini, D. M., Hunter, D. L., Martin, W. K., Thompson, L. C., Gilmour, M. I., Hazari, M. S., and Farraj, A. K. (2018). Zebrafish locomotor responses reveal irritant effects of fine PM extracts and a role for TRPA1. *Toxicol. Sci.* **161**, 290–299.

Sun, L., Liu, C., Xu, X., Ying, Z., Maiseyeu, A., Wang, A., Allen, K., Lewandowski, R. P., Bramble, L. A., Morishita, M., *et al.* (2013). Ambient fine particulate matter and ozone exposures induce inflammation in epicardial and perirenal adipose tissues in rats fed a high fructose diet. *Part. Fibre Toxicol.* **10**, 43.

Task Force of the European Society of Cardiology and the North American Society of Pacing and Electrophysiology. (1996). Heart rate variability. Standards of measurement, physiological interpretation, and clinical use. *Eur. Heart J.* **17**, 354–381.

Tei, C., Ling, L. H., Hodge, D. O., Bailey, K. R., Oh, J. K., Rodeheffer, R. J., Tajik, A. J., and Seward, J. B. (1995). New index of combined systolic and diastolic myocardial performance: A simple and reproducible measure of cardiac function—A study in normals and dilated cardiomyopathy. *J. Cardiol.* **26**, 357–366.

Terada, Y., Hosono, T., Seki, T., Ariga, T., Ito, S., Narukawa, M., and Watanabe, T. (2014). Sulphur-containing compounds of durian activate the thermogenesis-inducing receptors TRPA1 and TRPV1. *Food Chem.* **157**, 213–220.

Thompson, L. C., Ledbetter, A. D., Haykal-Coates, N., Cascio, W. E., Hazari, M. S., and Farraj, A. K. (2017). Acrolein inhalation alters myocardial synchrony and performance at and below exposure concentrations that cause ventilatory responses. *Cardiovasc. Toxicol.* **17**, 97–108.

Turpin, B. J., and Lim, H.-J. (2001). Species contributions to PM2.5 mass concentrations: Revisiting common assumptions for estimating organic mass. *Aerosol Sci. Technol.* **35**, 602–610.

US EPA. (2004). EPA-CMB8.2 Users Manual. EPA-452/R-04-011. Research Triangle Park, NC.

Vadjic, V., Gentilizza, M., Hrsak, J., and Eskinja, I. (1991). The effect of metals and ammonia on SO_2 oxidation to sulphates in the ambient air. *Environ. Monit. Assess.* **18**, 163–171.

Wagner, J. G., Allen, K., Yang, H. Y., Nan, B., Morishita, M., Mukherjee, B., Dvonch, J. T., Spino, C., Fink, G. D., Rajagopalan, S., *et al.* (2014). Cardiovascular depression in rats exposed to inhaled particulate matter and ozone: Effects of diet-induced metabolic syndrome. *Environ. Health Perspect.* **122**, 27–33.

Xia, Y., Gong, K. Z., Xu, M., Zhang, Y. Y., Guo, J. H., Song, Y., and Zhang, P. (2009). Regulation of gap-junction protein connexin 43 by beta-adrenergic receptor stimulation in rat cardiomyocytes. *Acta Pharmacol. Sin.* **30**, 928–934.

Downloaded from https://academic.oup.com/toxsci/article-abstract/167/2/559/5142835 by EPA-RTP Main Library user on 15 January 2020

Farraj, Aimen

From: Cascio, Wayne
Sent: Wednesday, April 29, 2020 11:18 AM
To: Farraj, Aimen
Subject: RE: Need agreement letter for STAA award application

Follow Up Flag: Follow up
Flag Status: Flagged

Aimen – Thank you for including me on the application. I agree with the designation of 3%. I'll have Linda address your other request by COB. Hope all is well with you and yours. Stay well. Wayne

Wayne E. Cascio, MD, FACC | Director | Center for Public Health and Environmental Assessment | Office of Research and Development | U.S. Environmental Protection Agency | Research Triangle Park, NC 27711 | Phone: 919.541.2508 | Cell: 919.627.3762|

From: Farraj, Aimen <Farraj.Aimen@epa.gov>
Sent: Wednesday, April 29, 2020 10:21 AM
To: Cascio, Wayne <Cascio.Wayne@epa.gov>; Gilmour, Ian <Gilmour.Ian@epa.gov>; Hazari, Mehdi <Hazari.Mehdi@epa.gov>; Thompson, Leslie (NIH/OD) [E] <leslie.thompson@nih.gov>; Krug, Jonathan D. <Krug.Jonathan@epa.gov>; Kovalcik, Kasey <Kovalcik.Kasey@epa.gov>; McGee, John <Mcgee.John@epa.gov>; Higuchi, Mark <Higuchi.Mark@epa.gov>; Davies, David <Davies.David@epa.gov>; Coates, Najwa Haykal <Coates.Najwa@epa.gov>; King, Charly <King.Charly@epa.gov>; Duvall, Rachelle <Duvall.Rachelle@epa.gov>; Krantz, Todd <Krantz.Todd@epa.gov>; Pancras, Joseph <Pancras.Patrick@epa.gov>; Charles Wood <charleswood99@gmail.com>; Allen Ledbetter <hawbob23@gmail.com>; Lenny Walsh <lcwalsh@nc.rr.com>
Subject: FW: Need agreement letter for STAA award application
Importance: High

Good morning,

In addition to sending agreement letters (see email below), the STAA nomination process also requires that we list the previous 5 years of STAA nominations and associated publications for each EPA author. I know this is onerous (sorry), but please send me publication titles, year of award, and type of award (e.g. STAA level I, II, III, or honorable mention). I would appreciate it if you would send me this information by COB today if possible. Thanks.

Aimen Farraj, PhD, DABT
Research Biologist
U.S Environmental Protection Agency
Center for Public Health and Environmental Assessment
Public Health and Integrated Toxicology Division
109 TW Alexander Drive
Research Triangle Park, NC 27711
Mail Code: B105-02
Tele: (919) 541-5027; Fax: (919) 541-0034

From: Farraj, Aimen
Sent: Tuesday, April 28, 2020 1:49 PM
To: Cascio, Wayne <Cascio.Wayne@epa.gov>; Gilmour, Ian <Gilmour.Ian@epa.gov>; Hazari, Mehdi <Hazari.Mehdi@epa.gov>; Thompson, Leslie (NIH/OD) [E] <leslie.thompson@nih.gov>; Krug, Jonathan D. <Krug.Jonathan@epa.gov>; Kovalcik, Kasey <Kovalcik.Kasey@epa.gov>; McGee, John <Mcgee.John@epa.gov>; Higuchi,

Mark <Higuchi.Mark@epa.gov>; Davies, David <Davies.David@epa.gov>; Martin, Brandi Lee <blmartin@live.unc.edu>; Coates, Najwa Haykal <Coates.Najwa@epa.gov>; King, Charly <King.Charly@epa.gov>; Duvall, Rachelle <Duvall.Rachelle@epa.gov>; Krantz, Todd <Krantz.Todd@epa.gov>; Pancras, Joseph <Pancras.Patrick@epa.gov>; Charles Wood <charleswood99@gmail.com>; Fatiha Malik <fatihamlk1@gmail.com>; Allen Ledbetter <hawbob23@gmail.com>; Lenny Walsh <lcwalsh@nc.rr.com>; kmstrat0402@yahoo.com
Subject: Need agreement letter for STAA award application
Importance: High

Hello,

Mehdi and I are drafting an STAA submission based on the three publications listed below that focus on the unique health effects resulting from concurrent exposure to 2 or more air pollutants, including ambient PM + O_3, ambient PM + the HAP acrolein, and smog with either high PM and low O3 or low PM and high O3 (publications are also attached). Awareness of the potential for such interactive effects as part of a larger multipollutant approach to air pollution health assessment may strengthen the agency's single pollutant standard determinations. One of the requirements of the STAA nomination process is a letter from each author stating that he/she agrees with the percent effort/contribution attributed to him/her. I have assigned percent efforts for all authors in the table below - this is really challenging with 22 total authors. Once I finalize a draft of the STAA application, I will forward it along. In the meantime, please send me an email response indicating you agree with the percent effort attributed to you as soon as possible (by tomorrow afternoon). Thank you so much for your awesome collaboration. Thanks.

Ambient Particulate Matter and Acrolein Co-Exposure Increases Myocardial Dyssynchrony in Mice via TRPA1.
Thompson LC, Walsh L, Martin BL, McGee J, Wood C, Kovalcik K, Pancras JP, Haykal-Coates N, Ledbetter AD, Davies D, Cascio WE, Higuchi M, Hazari MS, Farraj AK.
Toxicol Sci. 2019 Feb 1;167(2):559-572. doi: 10.1093/toxsci/kfy262.

Comparative Cardiopulmonary Effects of Particulate Matter- And Ozone-Enhanced Smog Atmospheres in Mice.
Hazari MS, Stratford KM, Krantz QT, King C, Krug J, Farraj AK, Gilmour MI.
Environ Sci Technol. 2018 Mar 6;52(5):3071-3080. doi: 10.1021/acs.est.7b04880. Epub 2018 Feb 8.

Cardiac effects of seasonal ambient particulate matter and ozone co-exposure in rats.
Farraj AK, Walsh L, Haykal-Coates N, Malik F, McGee J, Winsett D, Duvall R, Kovalcik K, Cascio WE, Higuchi M, Hazari MS.
Part Fibre Toxicol. 2015 May 6;12:12. doi: 10.1186/s12989-015-0087-3.

Author	% Contribution
Cascio, Wayne	3
Davies, David	3
Duvall, Rachelle	3
Farraj, Aimen	12
Gilmour, M. Ian	4
Haykal-Coates, Najwa	7
Hazari, Mehdi	12
Higuchi, Mark	4
King, Charly	4
Kovalcik, Kacey	4
Krantz, Todd	4
Krug, Jonathan	3
Ledbetter, Allen	3
Malik, Fatiha	2
Martin, Brandi	2

McGee, John	5
Pancras, Joseph	3
Stratford, Kimberly	3
Thompson, Leslie	7
Walsh, Leon	7
Winsett, Darrell	2
Wood, Charles	3
Total	100

Aimen Farraj, PhD, DABT
Research Biologist
U.S Environmental Protection Agency
Center for Public Health and Environmental Assessment
Public Health and Integrated Toxicology Division
109 TW Alexander Drive
Research Triangle Park, NC 27711
Mail Code: B105-02
Tele: (919) 541-5027; Fax: (919) 541-0034

Farraj, Aimen

From: Davies, David
Sent: Tuesday, April 28, 2020 3:05 PM
To: Farraj, Aimen
Subject: RE: Need agreement letter for STAA award application

Follow Up Flag: Follow up
Flag Status: Flagged

Aimen, the % contribution is fine, and thank you.
Hope you & family are well and stay well.
D2

David W. Davies
Environmental Engineer
Inhalation Toxicology Facilities Branch
Public Health & Inhalation Toxicology Division
Center for Public Health & Environmental Assessment
Office of Research & Development
USEPA, RTP, NC 27711
Ph: (919) 541-4700
Fax: (919) 541-0204
email: davies.david@epa.gov

From: Farraj, Aimen <Farraj.Aimen@epa.gov>
Sent: Tuesday, April 28, 2020 1:49 PM
To: Cascio, Wayne <Cascio.Wayne@epa.gov>; Gilmour, Ian <Gilmour.Ian@epa.gov>; Hazari, Mehdi <Hazari.Mehdi@epa.gov>; Thompson, Leslie (NIH/OD) [E] <leslie.thompson@nih.gov>; Krug, Jonathan D. <Krug.Jonathan@epa.gov>; Kovalcik, Kasey <Kovalcik.Kasey@epa.gov>; McGee, John <Mcgee.John@epa.gov>; Higuchi, Mark <Higuchi.Mark@epa.gov>; Davies, David <Davies.David@epa.gov>; Martin, Brandi Lee <blmartin@live.unc.edu>; Coates, Najwa Haykal <Coates.Najwa@epa.gov>; King, Charly <King.Charly@epa.gov>; Duvall, Rachelle <Duvall.Rachelle@epa.gov>; Krantz, Todd <Krantz.Todd@epa.gov>; Pancras, Joseph <Pancras.Patrick@epa.gov>; Charles Wood <charleswood99@gmail.com>; Fatiha Malik <fatihamlk1@gmail.com>; Allen Ledbetter <hawbob23@gmail.com>; Lenny Walsh <lcwalsh@nc.rr.com>; kmstrat0402@yahoo.com
Subject: Need agreement letter for STAA award application
Importance: High

Hello,

Mehdi and I are drafting an STAA submission based on the three publications listed below that focus on the unique health effects resulting from concurrent exposure to 2 or more air pollutants, including ambient PM + O_3, ambient PM + the HAP acrolein, and smog with either high PM and low O3 or low PM and high O3 (publications are also attached). Awareness of the potential for such interactive effects as part of a larger multipollutant approach to air pollution health assessment may strengthen the agency's single pollutant standard determinations. One of the requirements of the STAA nomination process is a letter from each author stating that he/she agrees with the percent effort/contribution attributed to him/her. I have assigned percent efforts for all authors in the table below - this is really challenging with 22 total authors. Once I finalize a draft of the STAA application, I will forward it along. In the meantime, please send me an email response indicating you agree with the percent effort attributed to you as soon as possible (by tomorrow afternoon). Thank you so much for your awesome collaboration. Thanks.

Ambient Particulate Matter and Acrolein Co-Exposure Increases Myocardial Dyssynchrony in Mice via TRPA1.
Thompson LC, Walsh L, Martin BL, McGee J, Wood C, Kovalcik K, Pancras JP, Haykal-Coates N, Ledbetter AD, Davies D, Cascio WE, Higuchi M, Hazari MS, Farraj AK.
Toxicol Sci. 2019 Feb 1;167(2):559-572. doi: 10.1093/toxsci/kfy262.

Comparative Cardiopulmonary Effects of Particulate Matter- And Ozone-Enhanced Smog Atmospheres in Mice.
Hazari MS, Stratford KM, Krantz QT, King C, Krug J, Farraj AK, Gilmour MI.
Environ Sci Technol. 2018 Mar 6;52(5):3071-3080. doi: 10.1021/acs.est.7b04880. Epub 2018 Feb 8.

Cardiac effects of seasonal ambient particulate matter and ozone co-exposure in rats.
Farraj AK, Walsh L, Haykal-Coates N, Malik F, McGee J, Winsett D, Duvall R, Kovalcik K, Cascio WE, Higuchi M, Hazari MS.
Part Fibre Toxicol. 2015 May 6;12:12. doi: 10.1186/s12989-015-0087-3.

Author	% Contribution
Cascio, Wayne	3
Davies, David	3
Duvall, Rachelle	3
Farraj, Aimen	12
Gilmour, M. Ian	4
Haykal-Coates, Najwa	7
Hazari, Mehdi	12
Higuchi, Mark	4
King, Charly	4
Kovalcik, Kacey	4
Krantz, Todd	4
Krug, Jonathan	3
Ledbetter, Allen	3
Malik, Fatiha	2
Martin, Brandi	2
McGee, John	5
Pancras, Joseph	3
Stratford, Kimberly	3
Thompson, Leslie	7
Walsh, Leon	7
Winsett, Darrell	2
Wood, Charles	3
Total	100

Aimen Farraj, PhD, DABT
Research Biologist
U.S Environmental Protection Agency
Center for Public Health and Environmental Assessment
Public Health and Integrated Toxicology Division
109 TW Alexander Drive
Research Triangle Park, NC 27711
Mail Code: B105-02

Tele: (919) 541-5027; Fax: (919) 541-0034

Farraj, Aimen

From: Duvall, Rachelle
Sent: Tuesday, April 28, 2020 2:32 PM
To: Farraj, Aimen
Subject: RE: Need agreement letter for STAA award application

Follow Up Flag: Follow up
Flag Status: Flagged

Hi Aimen,
Great to hear! Yes I agree with the percent effort/contribution you listed for me. Good luck on the submission and hope all is well.

Best,
Rachelle

From: Farraj, Aimen <Farraj.Aimen@epa.gov>
Sent: Tuesday, April 28, 2020 1:49 PM
To: Cascio, Wayne <Cascio.Wayne@epa.gov>; Gilmour, Ian <Gilmour.Ian@epa.gov>; Hazari, Mehdi <Hazari.Mehdi@epa.gov>; Thompson, Leslie (NIH/OD) [E] <leslie.thompson@nih.gov>; Krug, Jonathan D. <Krug.Jonathan@epa.gov>; Kovalcik, Kasey <Kovalcik.Kasey@epa.gov>; McGee, John <Mcgee.John@epa.gov>; Higuchi, Mark <Higuchi.Mark@epa.gov>; Davies, David <Davies.David@epa.gov>; Martin, Brandi Lee <blmartin@live.unc.edu>; Coates, Najwa Haykal <Coates.Najwa@epa.gov>; King, Charly <King.Charly@epa.gov>; Duvall, Rachelle <Duvall.Rachelle@epa.gov>; Krantz, Todd <Krantz.Todd@epa.gov>; Pancras, Joseph <Pancras.Patrick@epa.gov>; Charles Wood <charleswood99@gmail.com>; Fatiha Malik <fatihamlk1@gmail.com>; Allen Ledbetter <hawbob23@gmail.com>; Lenny Walsh <lcwalsh@nc.rr.com>; kmstrat0402@yahoo.com
Subject: Need agreement letter for STAA award application
Importance: High

Hello,

Mehdi and I are drafting an STAA submission based on the three publications listed below that focus on the unique health effects resulting from concurrent exposure to 2 or more air pollutants, including ambient PM + O_3, ambient PM + the HAP acrolein, and smog with either high PM and low O3 or low PM and high O3 (publications are also attached). Awareness of the potential for such interactive effects as part of a larger multipollutant approach to air pollution health assessment may strengthen the agency's single pollutant standard determinations. One of the requirements of the STAA nomination process is a letter from each author stating that he/she agrees with the percent effort/contribution attributed to him/her. I have assigned percent efforts for all authors in the table below - this is really challenging with 22 total authors. Once I finalize a draft of the STAA application, I will forward it along. In the meantime, please send me an email response indicating you agree with the percent effort attributed to you as soon as possible (by tomorrow afternoon). Thank you so much for your awesome collaboration. Thanks.

Ambient Particulate Matter and Acrolein Co-Exposure Increases Myocardial Dyssynchrony in Mice via TRPA1.
Thompson LC, Walsh L, Martin BL, McGee J, Wood C, Kovalcik K, Pancras JP, Haykal-Coates N, Ledbetter AD, Davies D, Cascio WE, Higuchi M, Hazari MS, Farraj AK.
Toxicol Sci. 2019 Feb 1;167(2):559-572. doi: 10.1093/toxsci/kfy262.

Comparative Cardiopulmonary Effects of Particulate Matter- And Ozone-Enhanced Smog Atmospheres in Mice.
Hazari MS, Stratford KM, Krantz QT, King C, Krug J, Farraj AK, Gilmour MI.
Environ Sci Technol. 2018 Mar 6;52(5):3071-3080. doi: 10.1021/acs.est.7b04880. Epub 2018 Feb 8.

Cardiac effects of seasonal ambient particulate matter and ozone co-exposure in rats.
Farraj AK, Walsh L, Haykal-Coates N, Malik F, McGee J, Winsett D, Duvall R, Kovalcik K, Cascio WE, Higuchi M, Hazari MS. Part Fibre Toxicol. 2015 May 6;12:12. doi: 10.1186/s12989-015-0087-3.

Author	% Contribution
Cascio, Wayne	3
Davies, David	3
Duvall, Rachelle	3
Farraj, Aimen	12
Gilmour, M. Ian	4
Haykal-Coates, Najwa	7
Hazari, Mehdi	12
Higuchi, Mark	4
King, Charly	4
Kovalcik, Kacey	4
Krantz, Todd	4
Krug, Jonathan	3
Ledbetter, Allen	3
Malik, Fatiha	2
Martin, Brandi	2
McGee, John	5
Pancras, Joseph	3
Stratford, Kimberly	3
Thompson, Leslie	7
Walsh, Leon	7
Winsett, Darrell	2
Wood, Charles	3
Total	100

Aimen Farraj, PhD, DABT
Research Biologist
U.S Environmental Protection Agency
Center for Public Health and Environmental Assessment
Public Health and Integrated Toxicology Division
109 TW Alexander Drive
Research Triangle Park, NC 27711
Mail Code: B105-02
Tele: (919) 541-5027; Fax: (919) 541-0034

Farraj, Aimen

From: Gilmour, Ian
Sent: Tuesday, April 28, 2020 2:21 PM
To: Farraj, Aimen
Subject: RE: Need agreement letter for STAA award application

Follow Up Flag: Follow up
Flag Status: Flagged

I agree with the percent effort.
Thankyou for nominating this important work

M Ian Gilmour Ph.D DABT
Chief, Cardiopulmonary and Immunotoxicology Branch
Public Health Integrated Toxicology Division, Center for Public Health and Environmental Assessment, Office of Research and Development. U.S. Environmental Protection Agency.

Tel 919-541-0015

From: Farraj, Aimen <Farraj.Aimen@epa.gov>
Sent: Tuesday, April 28, 2020 1:49 PM
To: Cascio, Wayne <Cascio.Wayne@epa.gov>; Gilmour, Ian <Gilmour.Ian@epa.gov>; Hazari, Mehdi <Hazari.Mehdi@epa.gov>; Thompson, Leslie (NIH/OD) [E] <leslie.thompson@nih.gov>; Krug, Jonathan D. <Krug.Jonathan@epa.gov>; Kovalcik, Kasey <Kovalcik.Kasey@epa.gov>; McGee, John <Mcgee.John@epa.gov>; Higuchi, Mark <Higuchi.Mark@epa.gov>; Davies, David <Davies.David@epa.gov>; Martin, Brandi Lee <blmartin@live.unc.edu>; Coates, Najwa Haykal <Coates.Najwa@epa.gov>; King, Charly <King.Charly@epa.gov>; Duvall, Rachelle <Duvall.Rachelle@epa.gov>; Krantz, Todd <Krantz.Todd@epa.gov>; Pancras, Joseph <Pancras.Patrick@epa.gov>; Charles Wood <charleswood99@gmail.com>; Fatiha Malik <fatihamlk1@gmail.com>; Allen Ledbetter <hawbob23@gmail.com>; Lenny Walsh <lcwalsh@nc.rr.com>; kmstrat0402@yahoo.com
Subject: Need agreement letter for STAA award application
Importance: High

Hello,

Mehdi and I are drafting an STAA submission based on the three publications listed below that focus on the unique health effects resulting from concurrent exposure to 2 or more air pollutants, including ambient PM + O_3, ambient PM + the HAP acrolein, and smog with either high PM and low O3 or low PM and high O3 (publications are also attached). Awareness of the potential for such interactive effects as part of a larger multipollutant approach to air pollution health assessment may strengthen the agency's single pollutant standard determinations. One of the requirements of the STAA nomination process is a letter from each author stating that he/she agrees with the percent effort/contribution attributed to him/her. I have assigned percent efforts for all authors in the table below - this is really challenging with 22 total authors. Once I finalize a draft of the STAA application, I will forward it along. In the meantime, please send me an email response indicating you agree with the percent effort attributed to you as soon as possible (by tomorrow afternoon). Thank you so much for your awesome collaboration. Thanks.

Ambient Particulate Matter and Acrolein Co-Exposure Increases Myocardial Dyssynchrony in Mice via TRPA1.
Thompson LC, Walsh L, Martin BL, McGee J, Wood C, Kovalcik K, Pancras JP, Haykal-Coates N, Ledbetter AD, Davies D, Cascio WE, Higuchi M, Hazari MS, Farraj AK.
Toxicol Sci. 2019 Feb 1;167(2):559-572. doi: 10.1093/toxsci/kfy262.

Comparative Cardiopulmonary Effects of Particulate Matter- And Ozone-Enhanced Smog Atmospheres in Mice.
Hazari MS, Stratford KM, Krantz QT, King C, Krug J, Farraj AK, Gilmour MI.
Environ Sci Technol. 2018 Mar 6;52(5):3071-3080. doi: 10.1021/acs.est.7b04880. Epub 2018 Feb 8.

Cardiac effects of seasonal ambient particulate matter and ozone co-exposure in rats.
Farraj AK, Walsh L, Haykal-Coates N, Malik F, McGee J, Winsett D, Duvall R, Kovalcik K, Cascio WE, Higuchi M, Hazari MS.
Part Fibre Toxicol. 2015 May 6;12:12. doi: 10.1186/s12989-015-0087-3.

Author	% Contribution
Cascio, Wayne	3
Davies, David	3
Duvall, Rachelle	3
Farraj, Aimen	12
Gilmour, M. Ian	4
Haykal-Coates, Najwa	7
Hazari, Mehdi	12
Higuchi, Mark	4
King, Charly	4
Kovalcik, Kacey	4
Krantz, Todd	4
Krug, Jonathan	3
Ledbetter, Allen	3
Malik, Fatiha	2
Martin, Brandi	2
McGee, John	5
Pancras, Joseph	3
Stratford, Kimberly	3
Thompson, Leslie	7
Walsh, Leon	7
Winsett, Darrell	2
Wood, Charles	3
Total	100

Aimen Farraj, PhD, DABT
Research Biologist
U.S Environmental Protection Agency
Center for Public Health and Environmental Assessment
Public Health and Integrated Toxicology Division
109 TW Alexander Drive
Research Triangle Park, NC 27711
Mail Code: B105-02
Tele: (919) 541-5027; Fax: (919) 541-0034

Farraj, Aimen

From: Coates, Najwa Haykal
Sent: Wednesday, April 29, 2020 8:30 AM
To: Farraj, Aimen
Subject: RE: Need agreement letter for STAA award application

Follow Up Flag: Follow up
Flag Status: Flagged

Hello Aimen,
I agree .
Sorry I was having issues signing in remotely

From: Farraj, Aimen <Farraj.Aimen@epa.gov>
Sent: Tuesday, April 28, 2020 1:49 PM
To: Cascio, Wayne <Cascio.Wayne@epa.gov>; Gilmour, Ian <Gilmour.Ian@epa.gov>; Hazari, Mehdi <Hazari.Mehdi@epa.gov>; Thompson, Leslie (NIH/OD) [E] <leslie.thompson@nih.gov>; Krug, Jonathan D. <Krug.Jonathan@epa.gov>; Kovalcik, Kasey <Kovalcik.Kasey@epa.gov>; McGee, John <Mcgee.John@epa.gov>; Higuchi, Mark <Higuchi.Mark@epa.gov>; Davies, David <Davies.David@epa.gov>; Martin, Brandi Lee <blmartin@live.unc.edu>; Coates, Najwa Haykal <Coates.Najwa@epa.gov>; King, Charly <King.Charly@epa.gov>; Duvall, Rachelle <Duvall.Rachelle@epa.gov>; Krantz, Todd <Krantz.Todd@epa.gov>; Pancras, Joseph <Pancras.Patrick@epa.gov>; Charles Wood <charleswood99@gmail.com>; Fatiha Malik <fatihamlk1@gmail.com>; Allen Ledbetter <hawbob23@gmail.com>; Lenny Walsh <lcwalsh@nc.rr.com>; kmstrat0402@yahoo.com
Subject: Need agreement letter for STAA award application
Importance: High

Hello,

Mehdi and I are drafting an STAA submission based on the three publications listed below that focus on the unique health effects resulting from concurrent exposure to 2 or more air pollutants, including ambient PM + O_3, ambient PM + the HAP acrolein, and smog with either high PM and low O3 or low PM and high O3 (publications are also attached). Awareness of the potential for such interactive effects as part of a larger multipollutant approach to air pollution health assessment may strengthen the agency's single pollutant standard determinations. One of the requirements of the STAA nomination process is a letter from each author stating that he/she agrees with the percent effort/contribution attributed to him/her. I have assigned percent efforts for all authors in the table below - this is really challenging with 22 total authors. Once I finalize a draft of the STAA application, I will forward it along. In the meantime, please send me an email response indicating you agree with the percent effort attributed to you as soon as possible (by tomorrow afternoon). Thank you so much for your awesome collaboration. Thanks.

Ambient Particulate Matter and Acrolein Co-Exposure Increases Myocardial Dyssynchrony in Mice via TRPA1.
Thompson LC, Walsh L, Martin BL, McGee J, Wood C, Kovalcik K, Pancras JP, Haykal-Coates N, Ledbetter AD, Davies D, Cascio WE, Higuchi M, Hazari MS, Farraj AK.
Toxicol Sci. 2019 Feb 1;167(2):559-572. doi: 10.1093/toxsci/kfy262.

Comparative Cardiopulmonary Effects of Particulate Matter- And Ozone-Enhanced Smog Atmospheres in Mice.
Hazari MS, Stratford KM, Krantz QT, King C, Krug J, Farraj AK, Gilmour MI.
Environ Sci Technol. 2018 Mar 6;52(5):3071-3080. doi: 10.1021/acs.est.7b04880. Epub 2018 Feb 8.

Cardiac effects of seasonal ambient particulate matter and ozone co-exposure in rats.
Farraj AK, Walsh L, Haykal-Coates N, Malik F, McGee J, Winsett D, Duvall R, Kovalcik K, Cascio WE, Higuchi M, Hazari MS.

Part Fibre Toxicol. 2015 May 6;12:12. doi: 10.1186/s12989-015-0087-3.

Author	% Contribution
Cascio, Wayne	3
Davies, David	3
Duvall, Rachelle	3
Farraj, Aimen	12
Gilmour, M. Ian	4
Haykal-Coates, Najwa	7
Hazari, Mehdi	12
Higuchi, Mark	4
King, Charly	4
Kovalcik, Kacey	4
Krantz, Todd	4
Krug, Jonathan	3
Ledbetter, Allen	3
Malik, Fatiha	2
Martin, Brandi	2
McGee, John	5
Pancras, Joseph	3
Stratford, Kimberly	3
Thompson, Leslie	7
Walsh, Leon	7
Winsett, Darrell	2
Wood, Charles	3
Total	100

Aimen Farraj, PhD, DABT
Research Biologist
U.S Environmental Protection Agency
Center for Public Health and Environmental Assessment
Public Health and Integrated Toxicology Division
109 TW Alexander Drive
Research Triangle Park, NC 27711
Mail Code: B105-02
Tele: (919) 541-5027; Fax: (919) 541-0034

Farraj, Aimen

From: Hazari, Mehdi
Sent: Tuesday, April 28, 2020 1:51 PM
To: Farraj, Aimen
Subject: RE: Need agreement letter for STAA award application

Follow Up Flag: Follow up
Flag Status: Flagged

Thank you Aimen for putting this together.

I agree with the percent contribution attributed to me.

Mehdi

Mehdi Saeed Hazari, M.Sc., Ph.D., MT-ASCP
Physiologist
Center for Public Health and Environmental Assessment
Public Health and Integrated Toxicology Division
United States Environmental Protection Agency
919.541.4588

From: Farraj, Aimen <Farraj.Aimen@epa.gov>
Sent: Tuesday, April 28, 2020 1:49 PM
To: Cascio, Wayne <Cascio.Wayne@epa.gov>; Gilmour, Ian <Gilmour.Ian@epa.gov>; Hazari, Mehdi <Hazari.Mehdi@epa.gov>; Thompson, Leslie (NIH/OD) [E] <leslie.thompson@nih.gov>; Krug, Jonathan D. <Krug.Jonathan@epa.gov>; Kovalcik, Kasey <Kovalcik.Kasey@epa.gov>; McGee, John <Mcgee.John@epa.gov>; Higuchi, Mark <Higuchi.Mark@epa.gov>; Davies, David <Davies.David@epa.gov>; Martin, Brandi Lee <blmartin@live.unc.edu>; Coates, Najwa Haykal <Coates.Najwa@epa.gov>; King, Charly <King.Charly@epa.gov>; Duvall, Rachelle <Duvall.Rachelle@epa.gov>; Krantz, Todd <Krantz.Todd@epa.gov>; Pancras, Joseph <Pancras.Patrick@epa.gov>; Charles Wood <charleswood99@gmail.com>; Fatiha Malik <fatihamlk1@gmail.com>; Allen Ledbetter <hawbob23@gmail.com>; Lenny Walsh <lcwalsh@nc.rr.com>; kmstrat0402@yahoo.com
Subject: Need agreement letter for STAA award application
Importance: High

Hello,

Mehdi and I are drafting an STAA submission based on the three publications listed below that focus on the unique health effects resulting from concurrent exposure to 2 or more air pollutants, including ambient PM + O_3, ambient PM + the HAP acrolein, and smog with either high PM and low O3 or low PM and high O3 (publications are also attached). Awareness of the potential for such interactive effects as part of a larger multipollutant approach to air pollution health assessment may strengthen the agency's single pollutant standard determinations. One of the requirements of the STAA nomination process is a letter from each author stating that he/she agrees with the percent effort/contribution attributed to him/her. I have assigned percent efforts for all authors in the table below - this is really challenging with 22 total authors. Once I finalize a draft of the STAA application, I will forward it along. In the meantime, please send me an email response indicating you agree with the percent effort attributed to you as soon as possible (by tomorrow afternoon). Thank you so much for your awesome collaboration. Thanks.

Ambient Particulate Matter and Acrolein Co-Exposure Increases Myocardial Dyssynchrony in Mice via TRPA1.

Thompson LC, Walsh L, Martin BL, McGee J, Wood C, Kovalcik K, Pancras JP, Haykal-Coates N, Ledbetter AD, Davies D, Cascio WE, Higuchi M, Hazari MS, Farraj AK.
Toxicol Sci. 2019 Feb 1;167(2):559-572. doi: 10.1093/toxsci/kfy262.

Comparative Cardiopulmonary Effects of Particulate Matter- And Ozone-Enhanced Smog Atmospheres in Mice.
Hazari MS, Stratford KM, Krantz QT, King C, Krug J, Farraj AK, Gilmour MI.
Environ Sci Technol. 2018 Mar 6;52(5):3071-3080. doi: 10.1021/acs.est.7b04880. Epub 2018 Feb 8.

Cardiac effects of seasonal ambient particulate matter and ozone co-exposure in rats.
Farraj AK, Walsh L, Haykal-Coates N, Malik F, McGee J, Winsett D, Duvall R, Kovalcik K, Cascio WE, Higuchi M, Hazari MS.
Part Fibre Toxicol. 2015 May 6;12:12. doi: 10.1186/s12989-015-0087-3.

Author	% Contribution
Cascio, Wayne	3
Davies, David	3
Duvall, Rachelle	3
Farraj, Aimen	12
Gilmour, M. Ian	4
Haykal-Coates, Najwa	7
Hazari, Mehdi	12
Higuchi, Mark	4
King, Charly	4
Kovalcik, Kacey	4
Krantz, Todd	4
Krug, Jonathan	3
Ledbetter, Allen	3
Malik, Fatiha	2
Martin, Brandi	2
McGee, John	5
Pancras, Joseph	3
Stratford, Kimberly	3
Thompson, Leslie	7
Walsh, Leon	7
Winsett, Darrell	2
Wood, Charles	3
Total	100

Aimen Farraj, PhD, DABT
Research Biologist
U.S Environmental Protection Agency
Center for Public Health and Environmental Assessment
Public Health and Integrated Toxicology Division
109 TW Alexander Drive
Research Triangle Park, NC 27711
Mail Code: B105-02
Tele: (919) 541-5027; Fax: (919) 541-0034

Farraj, Aimen

From: Higuchi, Mark
Sent: Wednesday, April 29, 2020 6:53 PM
To: Farraj, Aimen
Subject: RE: Need agreement letter for STAA award application

Follow Up Flag: Follow up
Flag Status: Flagged

Aimen,

Sorry I agree with the level of effort you have indicated.

Thanks & stay safe!,

Mark Higuchi, M.Sc., Ph.D.
Chief, Inhalation Toxicology Facilities Branch
Public Health and Integrated Toxicology Division
Center for Public Health and Environmental Assessment
Office of Research and Development
United States Environmental Protection Agency
109 T.W. Alexander Drive
Mail Drop: B105-02, Room B-131I
Research Triangle Park, NC 27711
Telephone: 919-541-4167
Mobile: 919-451-7832
Fax: 919-541-0026
Email: Higuchi.Mark@EPA.Gov

From: Farraj, Aimen <Farraj.Aimen@epa.gov>
Sent: Wednesday, April 29, 2020 6:48 PM
To: Higuchi, Mark <Higuchi.Mark@epa.gov>
Subject: RE: Need agreement letter for STAA award application

Hi Mark,

I'm sorry to be a stickler and a pain, but may you please respond to the original request for agreement email indicating that you agree to the percent effort attributed to you. Thanks so much.

Aimen Farraj, PhD, DABT
Research Biologist
U.S Environmental Protection Agency
Center for Public Health and Environmental Assessment
Public Health and Integrated Toxicology Division
109 TW Alexander Drive
Research Triangle Park, NC 27711
Mail Code: B105-02
Tele: (919) 541-5027; Fax: (919) 541-0034

From: Higuchi, Mark <Higuchi.Mark@epa.gov>
Sent: Wednesday, April 29, 2020 6:46 PM

To: Farraj, Aimen <Farraj.Aimen@epa.gov>
Subject: RE: Need agreement letter for STAA award application

Aimen,

I appreciate your patient and inclusion in this effort. I believe the only previous STAA award nominations are the ones that Ian included. Let me know if you need anything else.

Thanks & stay safe!,

Mark Higuchi, M.Sc., Ph.D.
Chief, Inhalation Toxicology Facilities Branch
Public Health and Integrated Toxicology Division
Center for Public Health and Environmental Assessment
Office of Research and Development
United States Environmental Protection Agency
109 T.W. Alexander Drive
Mail Drop: B105-02, Room B-131I
Research Triangle Park, NC 27711
Telephone: 919-541-4167
Mobile: 919-451-7832
Fax: 919-541-0026
Email: Higuchi.Mark@EPA.Gov

From: Farraj, Aimen <Farraj.Aimen@epa.gov>
Sent: Wednesday, April 29, 2020 4:53 PM
To: Higuchi, Mark <Higuchi.Mark@epa.gov>
Subject: FW: Need agreement letter for STAA award application
Importance: High

Hi Mark,
Just resending this. If you don't mind, may you please respond as soon as possible. The deadline is tomorrow. Thanks.

Aimen Farraj, PhD, DABT
Research Biologist
U.S Environmental Protection Agency
Center for Public Health and Environmental Assessment
Public Health and Integrated Toxicology Division
109 TW Alexander Drive
Research Triangle Park, NC 27711
Mail Code: B105-02
Tele: (919) 541-5027; Fax: (919) 541-0034

From: Farraj, Aimen
Sent: Wednesday, April 29, 2020 10:21 AM
To: Cascio, Wayne <Cascio.Wayne@epa.gov>; Gilmour, Ian <Gilmour.Ian@epa.gov>; Hazari, Mehdi <Hazari.Mehdi@epa.gov>; Thompson, Leslie (NIH/OD) [E] <leslie.thompson@nih.gov>; Krug, Jonathan D. <Krug.Jonathan@epa.gov>; Kovalcik, Kasey <Kovalcik.Kasey@epa.gov>; McGee, John <Mcgee.John@epa.gov>; Higuchi, Mark <Higuchi.Mark@epa.gov>; Davies, David <Davies.David@epa.gov>; Coates, Najwa Haykal <Coates.Najwa@epa.gov>; King, Charly <King.Charly@epa.gov>; Duvall, Rachelle <Duvall.Rachelle@epa.gov>; Krantz, Todd <Krantz.Todd@epa.gov>; Pancras, Joseph <Pancras.Patrick@epa.gov>; Charles Wood <charleswood99@gmail.com>; Allen Ledbetter <hawbob23@gmail.com>; Lenny Walsh <lcwalsh@nc.rr.com>

Subject: FW: Need agreement letter for STAA award application
Importance: High

Good morning,

In addition to sending agreement letters (see email below), the STAA nomination process also requires that we list the previous 5 years of STAA nominations and associated publications for each EPA author. I know this is onerous (sorry), but please send me publication titles, year of award, and type of award (e.g. STAA level I, II, III, or honorable mention). I would appreciate it if you would send me this information by COB today if possible. Thanks.

Aimen Farraj, PhD, DABT
Research Biologist
U.S Environmental Protection Agency
Center for Public Health and Environmental Assessment
Public Health and Integrated Toxicology Division
109 TW Alexander Drive
Research Triangle Park, NC 27711
Mail Code: B105-02
Tele: (919) 541-5027; Fax: (919) 541-0034

From: Farraj, Aimen
Sent: Tuesday, April 28, 2020 1:49 PM
To: Cascio, Wayne <Cascio.Wayne@epa.gov>; Gilmour, Ian <Gilmour.Ian@epa.gov>; Hazari, Mehdi <Hazari.Mehdi@epa.gov>; Thompson, Leslie (NIH/OD) [E] <leslie.thompson@nih.gov>; Krug, Jonathan D. <Krug.Jonathan@epa.gov>; Kovalcik, Kasey <Kovalcik.Kasey@epa.gov>; McGee, John <Mcgee.John@epa.gov>; Higuchi, Mark <Higuchi.Mark@epa.gov>; Davies, David <Davies.David@epa.gov>; Martin, Brandi Lee <blmartin@live.unc.edu>; Coates, Najwa Haykal <Coates.Najwa@epa.gov>; King, Charly <King.Charly@epa.gov>; Duvall, Rachelle <Duvall.Rachelle@epa.gov>; Krantz, Todd <Krantz.Todd@epa.gov>; Pancras, Joseph <Pancras.Patrick@epa.gov>; Charles Wood <charleswood99@gmail.com>; Fatiha Malik <fatihamlk1@gmail.com>; Allen Ledbetter <hawbob23@gmail.com>; Lenny Walsh <lcwalsh@nc.rr.com>; kmstrat0402@yahoo.com
Subject: Need agreement letter for STAA award application
Importance: High

Hello,

Mehdi and I are drafting an STAA submission based on the three publications listed below that focus on the unique health effects resulting from concurrent exposure to 2 or more air pollutants, including ambient PM + O_3, ambient PM + the HAP acrolein, and smog with either high PM and low O3 or low PM and high O3 (publications are also attached). Awareness of the potential for such interactive effects as part of a larger multipollutant approach to air pollution health assessment may strengthen the agency's single pollutant standard determinations. One of the requirements of the STAA nomination process is a letter from each author stating that he/she agrees with the percent effort/contribution attributed to him/her. I have assigned percent efforts for all authors in the table below - this is really challenging with 22 total authors. Once I finalize a draft of the STAA application, I will forward it along. In the meantime, please send me an email response indicating you agree with the percent effort attributed to you as soon as possible (by tomorrow afternoon). Thank you so much for your awesome collaboration. Thanks.

Ambient Particulate Matter and Acrolein Co-Exposure Increases Myocardial Dyssynchrony in Mice via TRPA1.
Thompson LC, Walsh L, Martin BL, McGee J, Wood C, Kovalcik K, Pancras JP, Haykal-Coates N, Ledbetter AD, Davies D, Cascio WE, Higuchi M, Hazari MS, Farraj AK.
Toxicol Sci. 2019 Feb 1;167(2):559-572. doi: 10.1093/toxsci/kfy262.

Comparative Cardiopulmonary Effects of Particulate Matter- And Ozone-Enhanced Smog Atmospheres in Mice.
Hazari MS, Stratford KM, Krantz QT, King C, Krug J, Farraj AK, Gilmour MI.
Environ Sci Technol. 2018 Mar 6;52(5):3071-3080. doi: 10.1021/acs.est.7b04880. Epub 2018 Feb 8.

Cardiac effects of seasonal ambient particulate matter and ozone co-exposure in rats.
Farraj AK, Walsh L, Haykal-Coates N, Malik F, McGee J, Winsett D, Duvall R, Kovalcik K, Cascio WE, Higuchi M, Hazari MS. Part Fibre Toxicol. 2015 May 6;12:12. doi: 10.1186/s12989-015-0087-3.

Author	% Contribution
Cascio, Wayne	3
Davies, David	3
Duvall, Rachelle	3
Farraj, Aimen	12
Gilmour, M. Ian	4
Haykal-Coates, Najwa	7
Hazari, Mehdi	12
Higuchi, Mark	4
King, Charly	4
Kovalcik, Kacey	4
Krantz, Todd	4
Krug, Jonathan	3
Ledbetter, Allen	3
Malik, Fatiha	2
Martin, Brandi	2
McGee, John	5
Pancras, Joseph	3
Stratford, Kimberly	3
Thompson, Leslie	7
Walsh, Leon	7
Winsett, Darrell	2
Wood, Charles	3
Total	100

Aimen Farraj, PhD, DABT
Research Biologist
U.S Environmental Protection Agency
Center for Public Health and Environmental Assessment
Public Health and Integrated Toxicology Division
109 TW Alexander Drive
Research Triangle Park, NC 27711
Mail Code: B105-02
Tele: (919) 541-5027; Fax: (919) 541-0034

Farraj, Aimen

From: King, Charly
Sent: Tuesday, April 28, 2020 3:02 PM
To: Farraj, Aimen
Subject: RE: Need agreement letter for STAA award application

Follow Up Flag: Follow up
Flag Status: Flagged

Agreed

Thanks

Charly

From: Farraj, Aimen <Farraj.Aimen@epa.gov>
Sent: Tuesday, April 28, 2020 1:49 PM
To: Cascio, Wayne <Cascio.Wayne@epa.gov>; Gilmour, Ian <Gilmour.Ian@epa.gov>; Hazari, Mehdi <Hazari.Mehdi@epa.gov>; Thompson, Leslie (NIH/OD) [E] <leslie.thompson@nih.gov>; Krug, Jonathan D. <Krug.Jonathan@epa.gov>; Kovalcik, Kasey <Kovalcik.Kasey@epa.gov>; McGee, John <Mcgee.John@epa.gov>; Higuchi, Mark <Higuchi.Mark@epa.gov>; Davies, David <Davies.David@epa.gov>; Martin, Brandi Lee <blmartin@live.unc.edu>; Coates, Najwa Haykal <Coates.Najwa@epa.gov>; King, Charly <King.Charly@epa.gov>; Duvall, Rachelle <Duvall.Rachelle@epa.gov>; Krantz, Todd <Krantz.Todd@epa.gov>; Pancras, Joseph <Pancras.Patrick@epa.gov>; Charles Wood <charleswood99@gmail.com>; Fatiha Malik <fatihamlk1@gmail.com>; Allen Ledbetter <hawbob23@gmail.com>; Lenny Walsh <lcwalsh@nc.rr.com>; kmstrat0402@yahoo.com
Subject: Need agreement letter for STAA award application
Importance: High

Hello,

Mehdi and I are drafting an STAA submission based on the three publications listed below that focus on the unique health effects resulting from concurrent exposure to 2 or more air pollutants, including ambient PM + O_3, ambient PM + the HAP acrolein, and smog with either high PM and low O3 or low PM and high O3 (publications are also attached). Awareness of the potential for such interactive effects as part of a larger multipollutant approach to air pollution health assessment may strengthen the agency's single pollutant standard determinations. One of the requirements of the STAA nomination process is a letter from each author stating that he/she agrees with the percent effort/contribution attributed to him/her. I have assigned percent efforts for all authors in the table below - this is really challenging with 22 total authors. Once I finalize a draft of the STAA application, I will forward it along. In the meantime, please send me an email response indicating you agree with the percent effort attributed to you as soon as possible (by tomorrow afternoon). Thank you so much for your awesome collaboration. Thanks.

Ambient Particulate Matter and Acrolein Co-Exposure Increases Myocardial Dyssynchrony in Mice via TRPA1.
Thompson LC, Walsh L, Martin BL, McGee J, Wood C, Kovalcik K, Pancras JP, Haykal-Coates N, Ledbetter AD, Davies D, Cascio WE, Higuchi M, Hazari MS, Farraj AK.
Toxicol Sci. 2019 Feb 1;167(2):559-572. doi: 10.1093/toxsci/kfy262.

Comparative Cardiopulmonary Effects of Particulate Matter- And Ozone-Enhanced Smog Atmospheres in Mice.
Hazari MS, Stratford KM, Krantz QT, King C, Krug J, Farraj AK, Gilmour MI.
Environ Sci Technol. 2018 Mar 6;52(5):3071-3080. doi: 10.1021/acs.est.7b04880. Epub 2018 Feb 8.

Cardiac effects of seasonal ambient particulate matter and ozone co-exposure in rats.
Farraj AK, Walsh L, Haykal-Coates N, Malik F, McGee J, Winsett D, Duvall R, Kovalcik K, Cascio WE, Higuchi M, Hazari MS. Part Fibre Toxicol. 2015 May 6;12:12. doi: 10.1186/s12989-015-0087-3.

Author	% Contribution
Cascio, Wayne	3
Davies, David	3
Duvall, Rachelle	3
Farraj, Aimen	12
Gilmour, M. Ian	4
Haykal-Coates, Najwa	7
Hazari, Mehdi	12
Higuchi, Mark	4
King, Charly	4
Kovalcik, Kacey	4
Krantz, Todd	4
Krug, Jonathan	3
Ledbetter, Allen	3
Malik, Fatiha	2
Martin, Brandi	2
McGee, John	5
Pancras, Joseph	3
Stratford, Kimberly	3
Thompson, Leslie	7
Walsh, Leon	7
Winsett, Darrell	2
Wood, Charles	3
Total	100

Aimen Farraj, PhD, DABT
Research Biologist
U.S Environmental Protection Agency
Center for Public Health and Environmental Assessment
Public Health and Integrated Toxicology Division
109 TW Alexander Drive
Research Triangle Park, NC 27711
Mail Code: B105-02
Tele: (919) 541-5027; Fax: (919) 541-0034

Farraj, Aimen

From: Kovalcik, Kasey
Sent: Tuesday, April 28, 2020 4:16 PM
To: Farraj, Aimen
Subject: RE: Need agreement letter for STAA award application

Follow Up Flag: Follow up
Flag Status: Flagged

I agree.

Kasey

From: Farraj, Aimen <Farraj.Aimen@epa.gov>
Sent: Tuesday, April 28, 2020 1:49 PM
To: Cascio, Wayne <Cascio.Wayne@epa.gov>; Gilmour, Ian <Gilmour.Ian@epa.gov>; Hazari, Mehdi <Hazari.Mehdi@epa.gov>; Thompson, Leslie (NIH/OD) [E] <leslie.thompson@nih.gov>; Krug, Jonathan D. <Krug.Jonathan@epa.gov>; Kovalcik, Kasey <Kovalcik.Kasey@epa.gov>; McGee, John <Mcgee.John@epa.gov>; Higuchi, Mark <Higuchi.Mark@epa.gov>; Davies, David <Davies.David@epa.gov>; Martin, Brandi Lee <blmartin@live.unc.edu>; Coates, Najwa Haykal <Coates.Najwa@epa.gov>; King, Charly <King.Charly@epa.gov>; Duvall, Rachelle <Duvall.Rachelle@epa.gov>; Krantz, Todd <Krantz.Todd@epa.gov>; Pancras, Joseph <Pancras.Patrick@epa.gov>; Charles Wood <charleswood99@gmail.com>; Fatiha Malik <fatihamlk1@gmail.com>; Allen Ledbetter <hawbob23@gmail.com>; Lenny Walsh <lcwalsh@nc.rr.com>; kmstrat0402@yahoo.com
Subject: Need agreement letter for STAA award application
Importance: High

Hello,

Mehdi and I are drafting an STAA submission based on the three publications listed below that focus on the unique health effects resulting from concurrent exposure to 2 or more air pollutants, including ambient PM + O_3, ambient PM + the HAP acrolein, and smog with either high PM and low O3 or low PM and high O3 (publications are also attached). Awareness of the potential for such interactive effects as part of a larger multipollutant approach to air pollution health assessment may strengthen the agency's single pollutant standard determinations. One of the requirements of the STAA nomination process is a letter from each author stating that he/she agrees with the percent effort/contribution attributed to him/her. I have assigned percent efforts for all authors in the table below - this is really challenging with 22 total authors. Once I finalize a draft of the STAA application, I will forward it along. In the meantime, please send me an email response indicating you agree with the percent effort attributed to you as soon as possible (by tomorrow afternoon). Thank you so much for your awesome collaboration. Thanks.

Ambient Particulate Matter and Acrolein Co-Exposure Increases Myocardial Dyssynchrony in Mice via TRPA1.
Thompson LC, Walsh L, Martin BL, McGee J, Wood C, Kovalcik K, Pancras JP, Haykal-Coates N, Ledbetter AD, Davies D, Cascio WE, Higuchi M, Hazari MS, Farraj AK.
Toxicol Sci. 2019 Feb 1;167(2):559-572. doi: 10.1093/toxsci/kfy262.

Comparative Cardiopulmonary Effects of Particulate Matter- And Ozone-Enhanced Smog Atmospheres in Mice.
Hazari MS, Stratford KM, Krantz QT, King C, Krug J, Farraj AK, Gilmour MI.
Environ Sci Technol. 2018 Mar 6;52(5):3071-3080. doi: 10.1021/acs.est.7b04880. Epub 2018 Feb 8.

Cardiac effects of seasonal ambient particulate matter and ozone co-exposure in rats.
Farraj AK, Walsh L, Haykal-Coates N, Malik F, McGee J, Winsett D, Duvall R, Kovalcik K, Cascio WE, Higuchi M, Hazari MS.

Part Fibre Toxicol. 2015 May 6;12:12. doi: 10.1186/s12989-015-0087-3.

Author	% Contribution
Cascio, Wayne	3
Davies, David	3
Duvall, Rachelle	3
Farraj, Aimen	12
Gilmour, M. Ian	4
Haykal-Coates, Najwa	7
Hazari, Mehdi	12
Higuchi, Mark	4
King, Charly	4
Kovalcik, Kacey	4
Krantz, Todd	4
Krug, Jonathan	3
Ledbetter, Allen	3
Malik, Fatiha	2
Martin, Brandi	2
McGee, John	5
Pancras, Joseph	3
Stratford, Kimberly	3
Thompson, Leslie	7
Walsh, Leon	7
Winsett, Darrell	2
Wood, Charles	3
Total	100

Aimen Farraj, PhD, DABT
Research Biologist
U.S Environmental Protection Agency
Center for Public Health and Environmental Assessment
Public Health and Integrated Toxicology Division
109 TW Alexander Drive
Research Triangle Park, NC 27711
Mail Code: B105-02
Tele: (919) 541-5027; Fax: (919) 541-0034

Farraj, Aimen

From: Krantz, Todd
Sent: Tuesday, April 28, 2020 4:21 PM
To: Farraj, Aimen; Hazari, Mehdi
Subject: RE: Need agreement letter for STAA award application

Follow Up Flag: Follow up
Flag Status: Flagged

Thanks for the effort! Hope you all are doing well through this mess, Todd

I agree with the percent effort/contribution attributed to me.

From: Farraj, Aimen <Farraj.Aimen@epa.gov>
Sent: Tuesday, April 28, 2020 1:49 PM
To: Cascio, Wayne <Cascio.Wayne@epa.gov>; Gilmour, Ian <Gilmour.Ian@epa.gov>; Hazari, Mehdi <Hazari.Mehdi@epa.gov>; Thompson, Leslie (NIH/OD) [E] <leslie.thompson@nih.gov>; Krug, Jonathan D. <Krug.Jonathan@epa.gov>; Kovalcik, Kasey <Kovalcik.Kasey@epa.gov>; McGee, John <Mcgee.John@epa.gov>; Higuchi, Mark <Higuchi.Mark@epa.gov>; Davies, David <Davies.David@epa.gov>; Martin, Brandi Lee <blmartin@live.unc.edu>; Coates, Najwa Haykal <Coates.Najwa@epa.gov>; King, Charly <King.Charly@epa.gov>; Duvall, Rachelle <Duvall.Rachelle@epa.gov>; Krantz, Todd <Krantz.Todd@epa.gov>; Pancras, Joseph <Pancras.Patrick@epa.gov>; Charles Wood <charleswood99@gmail.com>; Fatiha Malik <fatihamlk1@gmail.com>; Allen Ledbetter <hawbob23@gmail.com>; Lenny Walsh <lcwalsh@nc.rr.com>; kmstrat0402@yahoo.com
Subject: Need agreement letter for STAA award application
Importance: High

Hello,

Mehdi and I are drafting an STAA submission based on the three publications listed below that focus on the unique health effects resulting from concurrent exposure to 2 or more air pollutants, including ambient PM + O_3, ambient PM + the HAP acrolein, and smog with either high PM and low O3 or low PM and high O3 (publications are also attached). Awareness of the potential for such interactive effects as part of a larger multipollutant approach to air pollution health assessment may strengthen the agency's single pollutant standard determinations. One of the requirements of the STAA nomination process is a letter from each author stating that he/she agrees with the percent effort/contribution attributed to him/her. I have assigned percent efforts for all authors in the table below - this is really challenging with 22 total authors. Once I finalize a draft of the STAA application, I will forward it along. In the meantime, please send me an email response indicating you agree with the percent effort attributed to you as soon as possible (by tomorrow afternoon). Thank you so much for your awesome collaboration. Thanks.

Ambient Particulate Matter and Acrolein Co-Exposure Increases Myocardial Dyssynchrony in Mice via TRPA1.
Thompson LC, Walsh L, Martin BL, McGee J, Wood C, Kovalcik K, Pancras JP, Haykal-Coates N, Ledbetter AD, Davies D, Cascio WE, Higuchi M, Hazari MS, Farraj AK.
Toxicol Sci. 2019 Feb 1;167(2):559-572. doi: 10.1093/toxsci/kfy262.

Comparative Cardiopulmonary Effects of Particulate Matter- And Ozone-Enhanced Smog Atmospheres in Mice.
Hazari MS, Stratford KM, Krantz QT, King C, Krug J, Farraj AK, Gilmour MI.
Environ Sci Technol. 2018 Mar 6;52(5):3071-3080. doi: 10.1021/acs.est.7b04880. Epub 2018 Feb 8.

Cardiac effects of seasonal ambient particulate matter and ozone co-exposure in rats.
Farraj AK, Walsh L, Haykal-Coates N, Malik F, McGee J, Winsett D, Duvall R, Kovalcik K, Cascio WE, Higuchi M, Hazari MS.

Part Fibre Toxicol. 2015 May 6;12:12. doi: 10.1186/s12989-015-0087-3.

Author	% Contribution
Cascio, Wayne	3
Davies, David	3
Duvall, Rachelle	3
Farraj, Aimen	12
Gilmour, M. Ian	4
Haykal-Coates, Najwa	7
Hazari, Mehdi	12
Higuchi, Mark	4
King, Charly	4
Kovalcik, Kacey	4
Krantz, Todd	4
Krug, Jonathan	3
Ledbetter, Allen	3
Malik, Fatiha	2
Martin, Brandi	2
McGee, John	5
Pancras, Joseph	3
Stratford, Kimberly	3
Thompson, Leslie	7
Walsh, Leon	7
Winsett, Darrell	2
Wood, Charles	3
Total	100

Aimen Farraj, PhD, DABT
Research Biologist
U.S Environmental Protection Agency
Center for Public Health and Environmental Assessment
Public Health and Integrated Toxicology Division
109 TW Alexander Drive
Research Triangle Park, NC 27711
Mail Code: B105-02
Tele: (919) 541-5027; Fax: (919) 541-0034

Farraj, Aimen

From: Krug, Jonathan D.
Sent: Wednesday, April 29, 2020 9:05 AM
To: Farraj, Aimen
Subject: Re: Need agreement letter for STAA award application

Follow Up Flag: Follow up
Flag Status: Flagged

Hi Aimen,

I concur with your assessment of my contribution. Thanks for your efforts in putting together a STAA submission.

Jonathan

From: Farraj, Aimen <Farraj.Aimen@epa.gov>
Sent: Tuesday, April 28, 2020 1:49 PM
To: Cascio, Wayne <Cascio.Wayne@epa.gov>; Gilmour, Ian <Gilmour.Ian@epa.gov>; Hazari, Mehdi <Hazari.Mehdi@epa.gov>; Thompson, Leslie (NIH/OD) [E] <leslie.thompson@nih.gov>; Krug, Jonathan D. <Krug.Jonathan@epa.gov>; Kovalcik, Kasey <Kovalcik.Kasey@epa.gov>; McGee, John <Mcgee.John@epa.gov>; Higuchi, Mark <Higuchi.Mark@epa.gov>; Davies, David <Davies.David@epa.gov>; Martin, Brandi Lee <blmartin@live.unc.edu>; Coates, Najwa Haykal <Coates.Najwa@epa.gov>; King, Charly <King.Charly@epa.gov>; Duvall, Rachelle <Duvall.Rachelle@epa.gov>; Krantz, Todd <Krantz.Todd@epa.gov>; Pancras, Joseph <Pancras.Patrick@epa.gov>; Charles Wood <charleswood99@gmail.com>; Fatiha Malik <fatihamlk1@gmail.com>; Allen Ledbetter <hawbob23@gmail.com>; Lenny Walsh <lcwalsh@nc.rr.com>; kmstrat0402@yahoo.com <kmstrat0402@yahoo.com>
Subject: Need agreement letter for STAA award application

Hello,

Mehdi and I are drafting an STAA submission based on the three publications listed below that focus on the unique health effects resulting from concurrent exposure to 2 or more air pollutants, including ambient PM + O_3, ambient PM + the HAP acrolein, and smog with either high PM and low O3 or low PM and high O3 (publications are also attached). Awareness of the potential for such interactive effects as part of a larger multipollutant approach to air pollution health assessment may strengthen the agency's single pollutant standard determinations. One of the requirements of the STAA nomination process is a letter from each author stating that he/she agrees with the percent effort/contribution attributed to him/her. I have assigned percent efforts for all authors in the table below - this is really challenging with 22 total authors. Once I finalize a draft of the STAA application, I will forward it along. In the meantime, please send me an email response indicating you agree with the percent effort attributed to you as soon as possible (by tomorrow afternoon). Thank you so much for your awesome collaboration. Thanks.

Ambient Particulate Matter and Acrolein Co-Exposure Increases Myocardial Dyssynchrony in Mice via TRPA1.
Thompson LC, Walsh L, Martin BL, McGee J, Wood C, Kovalcik K, Pancras JP, Haykal-Coates N, Ledbetter AD, Davies D, Cascio WE, Higuchi M, Hazari MS, Farraj AK.
Toxicol Sci. 2019 Feb 1;167(2):559-572. doi: 10.1093/toxsci/kfy262.

Comparative Cardiopulmonary Effects of Particulate Matter- And Ozone-Enhanced Smog Atmospheres in Mice.
Hazari MS, Stratford KM, Krantz QT, King C, Krug J, Farraj AK, Gilmour MI.
Environ Sci Technol. 2018 Mar 6;52(5):3071-3080. doi: 10.1021/acs.est.7b04880. Epub 2018 Feb 8.

Cardiac effects of seasonal ambient particulate matter and ozone co-exposure in rats.
Farraj AK, Walsh L, Haykal-Coates N, Malik F, McGee J, Winsett D, Duvall R, Kovalcik K, Cascio WE, Higuchi M, Hazari MS. Part Fibre Toxicol. 2015 May 6;12:12. doi: 10.1186/s12989-015-0087-3.

Author	% Contribution
Cascio, Wayne	3
Davies, David	3
Duvall, Rachelle	3
Farraj, Aimen	12
Gilmour, M. Ian	4
Haykal-Coates, Najwa	7
Hazari, Mehdi	12
Higuchi, Mark	4
King, Charly	4
Kovalcik, Kacey	4
Krantz, Todd	4
Krug, Jonathan	3
Ledbetter, Allen	3
Malik, Fatiha	2
Martin, Brandi	2
McGee, John	5
Pancras, Joseph	3
Stratford, Kimberly	3
Thompson, Leslie	7
Walsh, Leon	7
Winsett, Darrell	2
Wood, Charles	3
Total	100

Aimen Farraj, PhD, DABT
Research Biologist
U.S Environmental Protection Agency
Center for Public Health and Environmental Assessment
Public Health and Integrated Toxicology Division
109 TW Alexander Drive
Research Triangle Park, NC 27711
Mail Code: B105-02
Tele: (919) 541-5027; Fax: (919) 541-0034

Farraj, Aimen

From: Allen Ledbetter <hawbob23@gmail.com>
Sent: Tuesday, April 28, 2020 2:00 PM
To: Farraj, Aimen
Subject: Re: Need agreement letter for STAA award application

Follow Up Flag: Follow up
Flag Status: Flagged

I agree with the percent effort attributed to me.

Allen Ledbetter

On April 28, 2020, at 1:49 PM, "Farraj, Aimen" <Farraj.Aimen@epa.gov> wrote:

Hello,

Mehdi and I are drafting an STAA submission based on the three publications listed below that focus on the unique health effects resulting from concurrent exposure to 2 or more air pollutants, including ambient PM + O_3, ambient PM + the HAP acrolein, and smog with either high PM and low O3 or low PM and high O3 (publications are also attached). Awareness of the potential for such interactive effects as part of a larger multipollutant approach to air pollution health assessment may strengthen the agency's single pollutant standard determinations. One of the requirements of the STAA nomination process is a letter from each author stating that he/she agrees with the percent effort/contribution attributed to him/her. I have assigned percent efforts for all authors in the table below - this is really challenging with 22 total authors. Once I finalize a draft of the STAA application, I will forward it along. In the meantime, please send me an email response indicating you agree with the percent effort attributed to you as soon as possible (by tomorrow afternoon). Thank you so much for your awesome collaboration. Thanks.

Ambient Particulate Matter and Acrolein Co-Exposure Increases Myocardial Dyssynchrony in Mice via TRPA1.
Thompson LC, Walsh L, Martin BL, McGee J, Wood C, Kovalcik K, Pancras JP, Haykal-Coates N, Ledbetter AD, Davies D, Cascio WE, Higuchi M, Hazari MS, Farraj AK.
Toxicol Sci. 2019 Feb 1;167(2):559-572. doi: 10.1093/toxsci/kfy262.

Comparative Cardiopulmonary Effects of Particulate Matter- And Ozone-Enhanced Smog Atmospheres in Mice.
Hazari MS, Stratford KM, Krantz QT, King C, Krug J, Farraj AK, Gilmour MI.
Environ Sci Technol. 2018 Mar 6;52(5):3071-3080. doi: 10.1021/acs.est.7b04880. Epub 2018 Feb 8.

Cardiac effects of seasonal ambient particulate matter and ozone co-exposure in rats.
Farraj AK, Walsh L, Haykal-Coates N, Malik F, McGee J, Winsett D, Duvall R, Kovalcik K, Cascio WE, Higuchi M, Hazari MS.
Part Fibre Toxicol. 2015 May 6;12:12. doi: 10.1186/s12989-015-0087-3.

Author	% Contribution
Cascio, Wayne	3
Davies, David	3
Duvall, Rachelle	3
Farraj, Aimen	12
Gilmour, M. Ian	4

Haykal-Coates, Najwa	7
Hazari, Mehdi	12
Higuchi, Mark	4
King, Charly	4
Kovalcik, Kacey	4
Krantz, Todd	4
Krug, Jonathan	3
Ledbetter, Allen	3
Malik, Fatiha	2
Martin, Brandi	2
McGee, John	5
Pancras, Joseph	3
Stratford, Kimberly	3
Thompson, Leslie	7
Walsh, Leon	7
Winsett, Darrell	2
Wood, Charles	3
Total	100

Aimen Farraj, PhD, DABT
Research Biologist
U.S Environmental Protection Agency
Center for Public Health and Environmental Assessment
Public Health and Integrated Toxicology Division
109 TW Alexander Drive
Research Triangle Park, NC 27711
Mail Code: B105-02
Tele: (919) 541-5027; Fax: (919) 541-0034

Farraj, Aimen

From: Fatiha Malik <fatihamlk1@gmail.com>
Sent: Tuesday, April 28, 2020 6:19 PM
To: Farraj, Aimen
Subject: Re: Need agreement letter for STAA award application

Follow Up Flag: Follow up
Flag Status: Flagged

Hi Aimen,

Thanks for reaching out regarding this. I agree to the percent attributed to me.

Regards,

Fatiha Malik-Adams

On Tuesday, April 28, 2020, Farraj, Aimen <Farraj.Aimen@epa.gov> wrote:

> Hello,
>
> Mehdi and I are drafting an STAA submission based on the three publications listed below that focus on the unique health effects resulting from concurrent exposure to 2 or more air pollutants, including ambient PM + O_3, ambient PM + the HAP acrolein, and smog with either high PM and low O3 or low PM and high O3 (publications are also attached). Awareness of the potential for such interactive effects as part of a larger multipollutant approach to air pollution health assessment may strengthen the agency's single pollutant standard determinations. One of the requirements of the STAA nomination process is a letter from each author stating that he/she agrees with the percent effort/contribution attributed to him/her. I have assigned percent efforts for all authors in the table below - this is really challenging with 22 total authors. Once I finalize a draft of the STAA application, I will forward it along. In the meantime, please send me an email response indicating you agree with the percent effort attributed to you as soon as possible (by tomorrow afternoon). Thank you so much for your awesome collaboration. Thanks.
>
> **Ambient Particulate Matter and Acrolein Co-Exposure Increases Myocardial Dyssynchrony in Mice via TRPA1**.
>
> Thompson LC, Walsh L, Martin BL, McGee J, Wood C, Kovalcik K, Pancras JP, Haykal-Coates N, Ledbetter AD, Davies D, Cascio WE, Higuchi M, Hazari MS, Farraj AK.
>
> Toxicol Sci. 2019 Feb 1;167(2):559-572. doi: 10.1093/toxsci/kfy262.
>
> **Comparative Cardiopulmonary Effects of Particulate Matter- And Ozone-Enhanced Smog Atmospheres in Mice.**
>
> Hazari MS, Stratford KM, Krantz QT, King C, Krug J, Farraj AK, Gilmour MI.
>
> Environ Sci Technol. 2018 Mar 6;52(5):3071-3080. doi: 10.1021/acs.est.7b04880. Epub 2018 Feb 8.

Cardiac effects of seasonal ambient particulate matter and ozone co-exposure in rats.

Farraj AK, Walsh L, Haykal-Coates N, Malik F, McGee J, Winsett D, Duvall R, Kovalcik K, Cascio WE, Higuchi M, Hazari MS.

Part Fibre Toxicol. 2015 May 6;12:12. doi: 10.1186/s12989-015-0087-3.

Author	% Contribution
Cascio, Wayne	3
Davies, David	3
Duvall, Rachelle	3
Farraj, Aimen	12
Gilmour, M. Ian	4
Haykal-Coates, Najwa	7
Hazari, Mehdi	12
Higuchi, Mark	4
King, Charly	4
Kovalcik, Kacey	4
Krantz, Todd	4
Krug, Jonathan	3
Ledbetter, Allen	3
Malik, Fatiha	2
Martin, Brandi	2
McGee, John	5
Pancras, Joseph	3
Stratford, Kimberly	3
Thompson, Leslie	7
Walsh, Leon	7
Winsett, Darrell	2
Wood, Charles	3
Total	100

Aimen Farraj, PhD, DABT

Research Biologist

U.S Environmental Protection Agency

Center for Public Health and Environmental Assessment

Public Health and Integrated Toxicology Division

109 TW Alexander Drive

Research Triangle Park, NC 27711

Mail Code: B105-02

Tele: (919) 541-5027; Fax: (919) 541-0034

Farraj, Aimen

From: Martin, Brandi Lee <blmartin@live.unc.edu>
Sent: Tuesday, April 28, 2020 5:17 PM
To: Farraj, Aimen
Subject: Re: Need agreement letter for STAA award application

Follow Up Flag: Follow up
Flag Status: Flagged

Hi Aimen,

I agree to this percentage contribution.

Thank you!

Brandi Martin, MSPH
Doctoral Student
Environmental Science and Engineering
University of North Carolina Gillings School of Global Public Health
[Cell]: 828.275.7630

From: Farraj, Aimen <Farraj.Aimen@epa.gov>
Sent: Tuesday, April 28, 2020 2:49 PM
To: Cascio, Wayne <Cascio.Wayne@epa.gov>; Gilmour, Ian <Gilmour.Ian@epa.gov>; Hazari, Mehdi <Hazari.Mehdi@epa.gov>; Thompson, Leslie (NIH/OD) [E] <leslie.thompson@nih.gov>; Krug, Jonathan D. <Krug.Jonathan@epa.gov>; Kovalcik, Kasey <Kovalcik.Kasey@epa.gov>; McGee, John <Mcgee.John@epa.gov>; Higuchi, Mark <Higuchi.Mark@epa.gov>; Davies, David <Davies.David@epa.gov>; Martin, Brandi Lee <blmartin@live.unc.edu>; Coates, Najwa Haykal <Coates.Najwa@epa.gov>; King, Charly <King.Charly@epa.gov>; Duvall, Rachelle <Duvall.Rachelle@epa.gov>; Krantz, Todd <Krantz.Todd@epa.gov>; Pancras, Joseph <Pancras.Patrick@epa.gov>; Charles Wood <charleswood99@gmail.com>; Fatiha Malik <fatihamlk1@gmail.com>; Allen Ledbetter <hawbob23@gmail.com>; Lenny Walsh <lcwalsh@nc.rr.com>; kmstrat0402@yahoo.com <kmstrat0402@yahoo.com>
Subject: Need agreement letter for STAA award application

Hello,

Mehdi and I are drafting an STAA submission based on the three publications listed below that focus on the unique health effects resulting from concurrent exposure to 2 or more air pollutants, including ambient PM + O_3, ambient PM + the HAP acrolein, and smog with either high PM and low O3 or low PM and high O3 (publications are also attached). Awareness of the potential for such interactive effects as part of a larger multipollutant approach to air pollution health assessment may strengthen the agency's single pollutant standard determinations. One of the requirements of the STAA nomination process is a letter from each author stating that he/she agrees with the percent effort/contribution attributed to him/her. I have assigned percent efforts for all authors in the table below - this is really challenging with 22 total authors. Once I finalize a draft of the STAA application, I will forward it along. In the meantime, please send me an email response indicating you agree with the percent effort attributed to you as soon as possible (by tomorrow afternoon). Thank you so much for your awesome collaboration. Thanks.

Ambient Particulate Matter and Acrolein Co-Exposure Increases Myocardial Dyssynchrony in Mice via TRPA1.
Thompson LC, Walsh L, Martin BL, McGee J, Wood C, Kovalcik K, Pancras JP, Haykal-Coates N, Ledbetter AD, Davies D, Cascio WE, Higuchi M, Hazari MS, Farraj AK.

Toxicol Sci. 2019 Feb 1;167(2):559-572. doi: 10.1093/toxsci/kfy262.

Comparative Cardiopulmonary Effects of Particulate Matter- And Ozone-Enhanced Smog Atmospheres in Mice.
Hazari MS, Stratford KM, Krantz QT, King C, Krug J, Farraj AK, Gilmour MI.
Environ Sci Technol. 2018 Mar 6;52(5):3071-3080. doi: 10.1021/acs.est.7b04880. Epub 2018 Feb 8.

Cardiac effects of seasonal ambient particulate matter and ozone co-exposure in rats.
Farraj AK, Walsh L, Haykal-Coates N, Malik F, McGee J, Winsett D, Duvall R, Kovalcik K, Cascio WE, Higuchi M, Hazari MS.
Part Fibre Toxicol. 2015 May 6;12:12. doi: 10.1186/s12989-015-0087-3.

Author	% Contribution
Cascio, Wayne	3
Davies, David	3
Duvall, Rachelle	3
Farraj, Aimen	12
Gilmour, M. Ian	4
Haykal-Coates, Najwa	7
Hazari, Mehdi	12
Higuchi, Mark	4
King, Charly	4
Kovalcik, Kacey	4
Krantz, Todd	4
Krug, Jonathan	3
Ledbetter, Allen	3
Malik, Fatiha	2
Martin, Brandi	2
McGee, John	5
Pancras, Joseph	3
Stratford, Kimberly	3
Thompson, Leslie	7
Walsh, Leon	7
Winsett, Darrell	2
Wood, Charles	3
Total	100

Aimen Farraj, PhD, DABT
Research Biologist
U.S Environmental Protection Agency
Center for Public Health and Environmental Assessment
Public Health and Integrated Toxicology Division
109 TW Alexander Drive
Research Triangle Park, NC 27711
Mail Code: B105-02
Tele: (919) 541-5027; Fax: (919) 541-0034

Farraj, Aimen

From: McGee, John
Sent: Wednesday, April 29, 2020 9:00 AM
To: Farraj, Aimen
Subject: RE: Need agreement letter for STAA award application

Follow Up Flag: Follow up
Flag Status: Flagged

Good morning Aimen,

Yes, I agree with the percent level-of-effort assigned. Thank you for including me in this STAA application.

And a little bit more – thank you, Mehdi, and all your work team for everything you've done on these projects with ITFB. It's been a pleasure working with you.

And on a personal note – I hope you and all yours are safe and hanging in there during these strange days. We share Michigan, New York City, and Middle East connections, and I know you are staying in touch with them as we are. Wishing y'all all the best. Hopefully we meet again soon in RTP; it will be a joy to work there safely together,

John

From: Farraj, Aimen <Farraj.Aimen@epa.gov>
Sent: Tuesday, April 28, 2020 1:49 PM
To: Cascio, Wayne <Cascio.Wayne@epa.gov>; Gilmour, Ian <Gilmour.Ian@epa.gov>; Hazari, Mehdi <Hazari.Mehdi@epa.gov>; Thompson, Leslie (NIH/OD) [E] <leslie.thompson@nih.gov>; Krug, Jonathan D. <Krug.Jonathan@epa.gov>; Kovalcik, Kasey <Kovalcik.Kasey@epa.gov>; McGee, John <Mcgee.John@epa.gov>; Higuchi, Mark <Higuchi.Mark@epa.gov>; Davies, David <Davies.David@epa.gov>; Martin, Brandi Lee <blmartin@live.unc.edu>; Coates, Najwa Haykal <Coates.Najwa@epa.gov>; King, Charly <King.Charly@epa.gov>; Duvall, Rachelle <Duvall.Rachelle@epa.gov>; Krantz, Todd <Krantz.Todd@epa.gov>; Pancras, Joseph <Pancras.Patrick@epa.gov>; Charles Wood <charleswood99@gmail.com>; Fatiha Malik <fatihamlk1@gmail.com>; Allen Ledbetter <hawbob23@gmail.com>; Lenny Walsh <lcwalsh@nc.rr.com>; kmstrat0402@yahoo.com
Subject: Need agreement letter for STAA award application
Importance: High

Hello,

Mehdi and I are drafting an STAA submission based on the three publications listed below that focus on the unique health effects resulting from concurrent exposure to 2 or more air pollutants, including ambient PM + O_3, ambient PM + the HAP acrolein, and smog with either high PM and low O3 or low PM and high O3 (publications are also attached). Awareness of the potential for such interactive effects as part of a larger multipollutant approach to air pollution health assessment may strengthen the agency's single pollutant standard determinations. One of the requirements of the STAA nomination process is a letter from each author stating that he/she agrees with the percent effort/contribution attributed to him/her. I have assigned percent efforts for all authors in the table below - this is really challenging with 22 total authors. Once I finalize a draft of the STAA application, I will forward it along. In the meantime, please send me an email response indicating you agree with the percent effort attributed to you as soon as possible (by tomorrow afternoon). Thank you so much for your awesome collaboration. Thanks.

Ambient Particulate Matter and Acrolein Co-Exposure Increases Myocardial Dyssynchrony in Mice via TRPA1.

Thompson LC, Walsh L, Martin BL, McGee J, Wood C, Kovalcik K, Pancras JP, Haykal-Coates N, Ledbetter AD, Davies D, Cascio WE, Higuchi M, Hazari MS, Farraj AK.
Toxicol Sci. 2019 Feb 1;167(2):559-572. doi: 10.1093/toxsci/kfy262.

Comparative Cardiopulmonary Effects of Particulate Matter- And Ozone-Enhanced Smog Atmospheres in Mice.
Hazari MS, Stratford KM, Krantz QT, King C, Krug J, Farraj AK, Gilmour MI.
Environ Sci Technol. 2018 Mar 6;52(5):3071-3080. doi: 10.1021/acs.est.7b04880. Epub 2018 Feb 8.

Cardiac effects of seasonal ambient particulate matter and ozone co-exposure in rats.
Farraj AK, Walsh L, Haykal-Coates N, Malik F, McGee J, Winsett D, Duvall R, Kovalcik K, Cascio WE, Higuchi M, Hazari MS.
Part Fibre Toxicol. 2015 May 6;12:12. doi: 10.1186/s12989-015-0087-3.

Author	% Contribution
Cascio, Wayne	3
Davies, David	3
Duvall, Rachelle	3
Farraj, Aimen	12
Gilmour, M. Ian	4
Haykal-Coates, Najwa	7
Hazari, Mehdi	12
Higuchi, Mark	4
King, Charly	4
Kovalcik, Kacey	4
Krantz, Todd	4
Krug, Jonathan	3
Ledbetter, Allen	3
Malik, Fatiha	2
Martin, Brandi	2
McGee, John	5
Pancras, Joseph	3
Stratford, Kimberly	3
Thompson, Leslie	7
Walsh, Leon	7
Winsett, Darrell	2
Wood, Charles	3
Total	100

Aimen Farraj, PhD, DABT
Research Biologist
U.S Environmental Protection Agency
Center for Public Health and Environmental Assessment
Public Health and Integrated Toxicology Division
109 TW Alexander Drive
Research Triangle Park, NC 27711
Mail Code: B105-02
Tele: (919) 541-5027; Fax: (919) 541-0034

Farraj, Aimen

From: Pancras, Joseph
Sent: Wednesday, April 29, 2020 10:37 AM
To: Farraj, Aimen
Subject: RE: Need agreement letter for STAA award application

Follow Up Flag: Follow up
Flag Status: Flagged

Hi Aimen,
I agree with the percent effort of 3% attributed to my contribution to your health effects research.
None of my earlier publications have been nominated for STAA award in the last 5 years.
Wish you success with the award application. Let me know if I can help in any other ways.

Regards,
J Patrick Pancras

J Patrick Pancras | Quality Assurance Manager | US EPA/ORD/CPHEA/PHID
919-966-0625 (Chapel Hill) | 919-541-4543 (RTP)

Mailing address: EPA Human Studies Facility | Attn: J.P. Pancras | 104 Mason Farm Rd | CB7315, Mail Drop #58A | Chapel Hill, NC 27599-7315

https://usepa.sharepoint.com/sites/ORD_Work/EPHD/QA_Corner/

From: Farraj, Aimen <Farraj.Aimen@epa.gov>
Sent: Tuesday, April 28, 2020 1:49 PM
To: Cascio, Wayne <Cascio.Wayne@epa.gov>; Gilmour, Ian <Gilmour.Ian@epa.gov>; Hazari, Mehdi <Hazari.Mehdi@epa.gov>; Thompson, Leslie (NIH/OD) [E] <leslie.thompson@nih.gov>; Krug, Jonathan D. <Krug.Jonathan@epa.gov>; Kovalcik, Kasey <Kovalcik.Kasey@epa.gov>; McGee, John <Mcgee.John@epa.gov>; Higuchi, Mark <Higuchi.Mark@epa.gov>; Davies, David <Davies.David@epa.gov>; Martin, Brandi Lee <blmartin@live.unc.edu>; Coates, Najwa Haykal <Coates.Najwa@epa.gov>; King, Charly <King.Charly@epa.gov>; Duvall, Rachelle <Duvall.Rachelle@epa.gov>; Krantz, Todd <Krantz.Todd@epa.gov>; Pancras, Joseph <Pancras.Patrick@epa.gov>; Charles Wood <charleswood99@gmail.com>; Fatiha Malik <fatihamlk1@gmail.com>; Allen Ledbetter <hawbob23@gmail.com>; Lenny Walsh <lcwalsh@nc.rr.com>; kmstrat0402@yahoo.com
Subject: Need agreement letter for STAA award application
Importance: High

Hello,

Mehdi and I are drafting an STAA submission based on the three publications listed below that focus on the unique health effects resulting from concurrent exposure to 2 or more air pollutants, including ambient PM + O_3, ambient PM + the HAP acrolein, and smog with either high PM and low O3 or low PM and high O3 (publications are also attached). Awareness of the potential for such interactive effects as part of a larger multipollutant approach to air pollution health assessment may strengthen the agency's single pollutant standard determinations. One of the requirements of the STAA nomination process is a letter from each author stating that he/she agrees with the percent effort/contribution attributed to him/her. I have assigned percent efforts for all authors in the table below - this is really challenging with 22 total authors. Once I finalize a draft of the STAA application, I will forward it along. In the meantime,

please send me an email response indicating you agree with the percent effort attributed to you as soon as possible (by tomorrow afternoon). Thank you so much for your awesome collaboration. Thanks.

Ambient Particulate Matter and Acrolein Co-Exposure Increases Myocardial Dyssynchrony in Mice via TRPA1.
Thompson LC, Walsh L, Martin BL, McGee J, Wood C, Kovalcik K, Pancras JP, Haykal-Coates N, Ledbetter AD, Davies D, Cascio WE, Higuchi M, Hazari MS, Farraj AK.
Toxicol Sci. 2019 Feb 1;167(2):559-572. doi: 10.1093/toxsci/kfy262.

Comparative Cardiopulmonary Effects of Particulate Matter- And Ozone-Enhanced Smog Atmospheres in Mice.
Hazari MS, Stratford KM, Krantz QT, King C, Krug J, Farraj AK, Gilmour MI.
Environ Sci Technol. 2018 Mar 6;52(5):3071-3080. doi: 10.1021/acs.est.7b04880. Epub 2018 Feb 8.

Cardiac effects of seasonal ambient particulate matter and ozone co-exposure in rats.
Farraj AK, Walsh L, Haykal-Coates N, Malik F, McGee J, Winsett D, Duvall R, Kovalcik K, Cascio WE, Higuchi M, Hazari MS.
Part Fibre Toxicol. 2015 May 6;12:12. doi: 10.1186/s12989-015-0087-3.

Author	% Contribution
Cascio, Wayne	3
Davies, David	3
Duvall, Rachelle	3
Farraj, Aimen	12
Gilmour, M. Ian	4
Haykal-Coates, Najwa	7
Hazari, Mehdi	12
Higuchi, Mark	4
King, Charly	4
Kovalcik, Kacey	4
Krantz, Todd	4
Krug, Jonathan	3
Ledbetter, Allen	3
Malik, Fatiha	2
Martin, Brandi	2
McGee, John	5
Pancras, Joseph	3
Stratford, Kimberly	3
Thompson, Leslie	7
Walsh, Leon	7
Winsett, Darrell	2
Wood, Charles	3
Total	100

Aimen Farraj, PhD, DABT
Research Biologist
U.S Environmental Protection Agency
Center for Public Health and Environmental Assessment
Public Health and Integrated Toxicology Division
109 TW Alexander Drive

Research Triangle Park, NC 27711
Mail Code: B105-02
Tele: (919) 541-5027; Fax: (919) 541-0034

Farraj, Aimen

From: Kim <kmstrat0402@yahoo.com>
Sent: Tuesday, April 28, 2020 3:01 PM
To: Farraj, Aimen
Subject: Re: Need agreement letter for STAA award application

Follow Up Flag: Follow up
Flag Status: Flagged

Good Afternoon Aimen,
I agree with the percent contribution.

Hope you and your family are well and staying safe!

Best,
Kim Stratford

On Apr 28, 2020, at 1:49 PM, Farraj, Aimen <Farraj.Aimen@epa.gov> wrote:

Hello,

Mehdi and I are drafting an STAA submission based on the three publications listed below that focus on the unique health effects resulting from concurrent exposure to 2 or more air pollutants, including ambient PM + O_3, ambient PM + the HAP acrolein, and smog with either high PM and low O3 or low PM and high O3 (publications are also attached). Awareness of the potential for such interactive effects as part of a larger multipollutant approach to air pollution health assessment may strengthen the agency's single pollutant standard determinations. One of the requirements of the STAA nomination process is a letter from each author stating that he/she agrees with the percent effort/contribution attributed to him/her. I have assigned percent efforts for all authors in the table below - this is really challenging with 22 total authors. Once I finalize a draft of the STAA application, I will forward it along. In the meantime, please send me an email response indicating you agree with the percent effort attributed to you as soon as possible (by tomorrow afternoon). Thank you so much for your awesome collaboration. Thanks.

Ambient Particulate Matter and Acrolein Co-Exposure Increases Myocardial Dyssynchrony in Mice via TRPA1.
Thompson LC, Walsh L, Martin BL, McGee J, Wood C, Kovalcik K, Pancras JP, Haykal-Coates N, Ledbetter AD, Davies D, Cascio WE, Higuchi M, Hazari MS, Farraj AK.
Toxicol Sci. 2019 Feb 1;167(2):559-572. doi: 10.1093/toxsci/kfy262.

Comparative Cardiopulmonary Effects of Particulate Matter- And Ozone-Enhanced Smog Atmospheres in Mice.
Hazari MS, Stratford KM, Krantz QT, King C, Krug J, Farraj AK, Gilmour MI.
Environ Sci Technol. 2018 Mar 6;52(5):3071-3080. doi: 10.1021/acs.est.7b04880. Epub 2018 Feb 8.

Cardiac effects of seasonal ambient particulate matter and ozone co-exposure in rats.

Farraj AK, Walsh L, Haykal-Coates N, Malik F, McGee J, Winsett D, Duvall R, Kovalcik K, Cascio WE, Higuchi M, Hazari MS.
Part Fibre Toxicol. 2015 May 6;12:12. doi: 10.1186/s12989-015-0087-3.

Author	% Contribution
Cascio, Wayne	3
Davies, David	3
Duvall, Rachelle	3
Farraj, Aimen	12
Gilmour, M. Ian	4
Haykal-Coates, Najwa	7
Hazari, Mehdi	12
Higuchi, Mark	4
King, Charly	4
Kovalcik, Kacey	4
Krantz, Todd	4
Krug, Jonathan	3
Ledbetter, Allen	3
Malik, Fatiha	2
Martin, Brandi	2
McGee, John	5
Pancras, Joseph	3
Stratford, Kimberly	3
Thompson, Leslie	7
Walsh, Leon	7
Winsett, Darrell	2
Wood, Charles	3
Total	100

Aimen Farraj, PhD, DABT
Research Biologist
U.S Environmental Protection Agency
Center for Public Health and Environmental Assessment
Public Health and Integrated Toxicology Division
109 TW Alexander Drive
Research Triangle Park, NC 27711
Mail Code: B105-02
Tele: (919) 541-5027; Fax: (919) 541-0034

<Thompson_2019-CAPs_Acrolein_Trpa1.pdf>
<Hazari et al 2018 EST_PM and O3 enhanced smog in mice.pdf>
<Farraj et al, 2015 - Cardiac effects_Seasonal_CAPs&O3.pdf>

Farraj, Aimen

From: Thompson, Leslie (NIH/OD) [E] <leslie.thompson@nih.gov>
Sent: Wednesday, April 29, 2020 3:10 PM
To: Farraj, Aimen
Subject: RE: Need agreement letter for STAA award application

Greetings Dr. Farraj,

Sorry for my late reply. I humbly agree with your assignment of 7% contribution to me in this outstanding work. Please give my regards to all involved.

As for previous awards, my name was associated with

1) Uterine Artery Flow and Offspring Growth in Long-Evans Rats following Maternal Exposure to Ozone during Implantation. Published in Environmental Health Perspectives – STAA Honorable Mention, 2019

Please let me know if you need anything else or if your records indicate other STAA mentions.

Sincerely,

Dr. Leslie C. Thompson

Leslie C. Thompson, Ph.D.
Health Science Policy Analyst
-
Environmental influences on Child Health Outcomes (ECHO)
National Institutes of Health, Office of the Director
11601 Landsdown Street | Office 03D12
North Bethesda, MD 20852
[p] 301-435-5239 | [f] 301-496-4357
leslie.thompson@nih.gov

From: Farraj, Aimen <Farraj.Aimen@epa.gov>
Sent: Wednesday, April 29, 2020 10:21 AM
To: Cascio, Wayne <Cascio.Wayne@epa.gov>; gilmour ian <gilmour.ian@epa.gov>; Hazari, Mehdi <Hazari.Mehdi@epa.gov>; Thompson, Leslie (NIH/OD) [E] <leslie.thompson@nih.gov>; Krug, Jonathan D. <Krug.Jonathan@epa.gov>; Kovalcik, Kasey <Kovalcik.Kasey@epa.gov>; McGee, John <Mcgee.John@epa.gov>; Higuchi, Mark <Higuchi.Mark@epa.gov>; Davies, David <Davies.David@epa.gov>; Coates, Najwa Haykal <Coates.Najwa@epa.gov>; King, Charly <King.Charly@epa.gov>; Duvall, Rachelle <Duvall.Rachelle@epa.gov>; Krantz, Todd <Krantz.Todd@epa.gov>; Pancras, Joseph <Pancras.Patrick@epa.gov>; Charles Wood <charleswood99@gmail.com>; Allen Ledbetter <hawbob23@gmail.com>; Lenny Walsh <lcwalsh@nc.rr.com>
Subject: FW: Need agreement letter for STAA award application
Importance: High

Good morning,

In addition to sending agreement letters (see email below), the STAA nomination process also requires that we list the previous 5 years of STAA nominations and associated publications for each EPA author. I know this is onerous (sorry), but please send me publication titles, year of award, and type of award (e.g. STAA level I, II, III, or honorable mention). I would appreciate it if you would send me this information by COB today if possible. Thanks.

Aimen Farraj, PhD, DABT
Research Biologist
U.S Environmental Protection Agency
Center for Public Health and Environmental Assessment
Public Health and Integrated Toxicology Division
109 TW Alexander Drive
Research Triangle Park, NC 27711
Mail Code: B105-02
Tele: (919) 541-5027; Fax: (919) 541-0034

From: Farraj, Aimen
Sent: Tuesday, April 28, 2020 1:49 PM
To: Cascio, Wayne <Cascio.Wayne@epa.gov>; Gilmour, Ian <Gilmour.Ian@epa.gov>; Hazari, Mehdi <Hazari.Mehdi@epa.gov>; Thompson, Leslie (NIH/OD) [E] <leslie.thompson@nih.gov>; Krug, Jonathan D. <Krug.Jonathan@epa.gov>; Kovalcik, Kasey <Kovalcik.Kasey@epa.gov>; McGee, John <Mcgee.John@epa.gov>; Higuchi, Mark <Higuchi.Mark@epa.gov>; Davies, David <Davies.David@epa.gov>; Martin, Brandi Lee <blmartin@live.unc.edu>; Coates, Najwa Haykal <Coates.Najwa@epa.gov>; King, Charly <King.Charly@epa.gov>; Duvall, Rachelle <Duvall.Rachelle@epa.gov>; Krantz, Todd <Krantz.Todd@epa.gov>; Pancras, Joseph <Pancras.Patrick@epa.gov>; Charles Wood <charleswood99@gmail.com>; Fatiha Malik <fatihamlk1@gmail.com>; Allen Ledbetter <hawbob23@gmail.com>; Lenny Walsh <lcwalsh@nc.rr.com>; kmstrat0402@yahoo.com
Subject: Need agreement letter for STAA award application
Importance: High

Hello,

Mehdi and I are drafting an STAA submission based on the three publications listed below that focus on the unique health effects resulting from concurrent exposure to 2 or more air pollutants, including ambient PM + O_3, ambient PM + the HAP acrolein, and smog with either high PM and low O3 or low PM and high O3 (publications are also attached). Awareness of the potential for such interactive effects as part of a larger multipollutant approach to air pollution health assessment may strengthen the agency's single pollutant standard determinations. One of the requirements of the STAA nomination process is a letter from each author stating that he/she agrees with the percent effort/contribution attributed to him/her. I have assigned percent efforts for all authors in the table below - this is really challenging with 22 total authors. Once I finalize a draft of the STAA application, I will forward it along. In the meantime, please send me an email response indicating you agree with the percent effort attributed to you as soon as possible (by tomorrow afternoon). Thank you so much for your awesome collaboration. Thanks.

Ambient Particulate Matter and Acrolein Co-Exposure Increases Myocardial Dyssynchrony in Mice via TRPA1.
Thompson LC, Walsh L, Martin BL, McGee J, Wood C, Kovalcik K, Pancras JP, Haykal-Coates N, Ledbetter AD, Davies D, Cascio WE, Higuchi M, Hazari MS, Farraj AK.
Toxicol Sci. 2019 Feb 1;167(2):559-572. doi: 10.1093/toxsci/kfy262.

Comparative Cardiopulmonary Effects of Particulate Matter- And Ozone-Enhanced Smog Atmospheres in Mice.
Hazari MS, Stratford KM, Krantz QT, King C, Krug J, Farraj AK, Gilmour MI.
Environ Sci Technol. 2018 Mar 6;52(5):3071-3080. doi: 10.1021/acs.est.7b04880. Epub 2018 Feb 8.

Cardiac effects of seasonal ambient particulate matter and ozone co-exposure in rats.
Farraj AK, Walsh L, Haykal-Coates N, Malik F, McGee J, Winsett D, Duvall R, Kovalcik K, Cascio WE, Higuchi M, Hazari MS.
Part Fibre Toxicol. 2015 May 6;12:12. doi: 10.1186/s12989-015-0087-3.

Author	% Contribution
Cascio, Wayne	3
Davies, David	3
Duvall, Rachelle	3
Farraj, Aimen	12
Gilmour, M. Ian	4
Haykal-Coates, Najwa	7
Hazari, Mehdi	12
Higuchi, Mark	4
King, Charly	4
Kovalcik, Kacey	4
Krantz, Todd	4
Krug, Jonathan	3
Ledbetter, Allen	3
Malik, Fatiha	2
Martin, Brandi	2
McGee, John	5
Pancras, Joseph	3
Stratford, Kimberly	3
Thompson, Leslie	7
Walsh, Leon	7
Winsett, Darrell	2
Wood, Charles	3
Total	100

Aimen Farraj, PhD, DABT
Research Biologist
U.S Environmental Protection Agency
Center for Public Health and Environmental Assessment
Public Health and Integrated Toxicology Division
109 TW Alexander Drive
Research Triangle Park, NC 27711
Mail Code: B105-02
Tele: (919) 541-5027; Fax: (919) 541-0034

Farraj, Aimen

From: Lenny Walsh <lcwalsh@nc.rr.com>
Sent: Tuesday, April 28, 2020 3:32 PM
To: Farraj, Aimen; Lenny Walsh
Subject: Re: Need agreement letter for STAA award application

Follow Up Flag: Follow up
Flag Status: Flagged

Hello Aimen,

Greetings! I hope this message finds you and your family safe and healthy in these interesting and turbulent times. Debra and I are doing well sequestered at Carolina Beach. We'll catch up more at a later date. I have reviewed your suggested percent efforts/contributions table and concur with your values as assigned. Thank you and Mehdi (Hello also!) for putting together this submission and for including me. This was truly interesting and challenging work which hopefully has expanded our knowledge base with lasting positive effects. STAA recognition would serve as additional validation of everyone's dedication to these projects!

Hello to all!

Sincerely,

Leon Walsh

On 4/28/2020 1:49 PM, Farraj, Aimen wrote:

> Hello,
>
> Mehdi and I are drafting an STAA submission based on the three publications listed below that focus on the unique health effects resulting from concurrent exposure to 2 or more air pollutants, including ambient PM + O_3, ambient PM + the HAP acrolein, and smog with either high PM and low O3 or low PM and high O3 (publications are also attached). Awareness of the potential for such interactive effects as part of a larger multipollutant approach to air pollution health assessment may strengthen the agency's single pollutant standard determinations. One of the requirements of the STAA nomination process is a letter from each author stating that he/she agrees with the percent effort/contribution attributed to him/her. I have assigned percent efforts for all authors in the table below - this is really challenging with 22 total authors. Once I finalize a draft of the STAA application, I will forward it along. In the meantime, please send me an email response indicating you agree with the percent effort attributed to you as soon as possible (by tomorrow afternoon). Thank you so much for your awesome collaboration. Thanks.
>
> **Ambient Particulate Matter and Acrolein Co-Exposure Increases Myocardial Dyssynchrony in Mice via TRPA1**.
> Thompson LC, Walsh L, Martin BL, McGee J, Wood C, Kovalcik K, Pancras JP, Haykal-Coates N, Ledbetter AD, Davies D, Cascio WE, Higuchi M, Hazari MS, Farraj AK.
> Toxicol Sci. 2019 Feb 1;167(2):559-572. doi: 10.1093/toxsci/kfy262.
>
> **Comparative Cardiopulmonary Effects of Particulate Matter- And Ozone-Enhanced Smog Atmospheres in Mice.**

Hazari MS, Stratford KM, Krantz QT, King C, Krug J, Farraj AK, Gilmour MI.
Environ Sci Technol. 2018 Mar 6;52(5):3071-3080. doi: 10.1021/acs.est.7b04880. Epub 2018 Feb 8.

Cardiac effects of seasonal ambient particulate matter and ozone co-exposure in rats.
Farraj AK, Walsh L, Haykal-Coates N, Malik F, McGee J, Winsett D, Duvall R, Kovalcik K, Cascio WE, Higuchi M, Hazari MS.
Part Fibre Toxicol. 2015 May 6;12:12. doi: 10.1186/s12989-015-0087-3.

Author	% Contribution
Cascio, Wayne	3
Davies, David	3
Duvall, Rachelle	3
Farraj, Aimen	12
Gilmour, M. Ian	4
Haykal-Coates, Najwa	7
Hazari, Mehdi	12
Higuchi, Mark	4
King, Charly	4
Kovalcik, Kacey	4
Krantz, Todd	4
Krug, Jonathan	3
Ledbetter, Allen	3
Malik, Fatiha	2
Martin, Brandi	2
McGee, John	5
Pancras, Joseph	3
Stratford, Kimberly	3
Thompson, Leslie	7
Walsh, Leon	7
Winsett, Darrell	2
Wood, Charles	3
Total	100

Aimen Farraj, PhD, DABT
Research Biologist
U.S Environmental Protection Agency
Center for Public Health and Environmental Assessment
Public Health and Integrated Toxicology Division
109 TW Alexander Drive
Research Triangle Park, NC 27711
Mail Code: B105-02
Tele: (919) 541-5027; Fax: (919) 541-0034

Farraj, Aimen

From: Charles Wood <charleswood99@gmail.com>
Sent: Wednesday, April 29, 2020 12:20 PM
To: Farraj, Aimen; Hazari, Mehdi
Subject: Re: FW: Need agreement letter for STAA award application

Follow Up Flag: Follow up
Flag Status: Flagged

Hi Aimen,
Hope all is well with you and your family. Thanks for putting this submission together.
(1) I agree with the percent effort/contribution attributed to me (3%).
(2) Below are two STAAs from last 5 yrs that I am listed on, along with relevant publications.
Let me know if you need anything else.
Best regards,
Charles

2015 U.S. EPA ORD Scientific and Technological Achievement Award – Honorable Mention, Development of a Novel Experimental System to Evaluate Predictive Toxicity Signatures
Reference: Tal TL, McCollum CW, Harris PS, Olin J, Kleinstreuer N, Wood CE, Hans C, Shah S, Merchant FA, Bondesson M, Knudsen TB, Padilla S, Hemmer MJ. Immediate and long-term consequences of vascular toxicity during zebrafish development. Reprod Toxicol 2014;48:51-61. PMID: 24907688

2019 U.S. EPA ORD Scientific and Technological Achievement Award – Honorable Mention, Environmental Stress During a Critical Window in Pregnancy Impairs Fetal Growth
Reference: Miller CN, Ledbetter AD, Schladweiler MC, Richards JE, Wood CE, Snow S, Johnstone A, Jaskot R, Henriquez A, Thompson LA, Farraj A, Hazari M, Dye JA, Kodavanti U. Uterine Artery Flow and Offspring Growth in Long-Evans Rats Following Maternal Exposure to Ozone During Implantation. Environ Health Perspect 2017;125(12):127005. PMID: 29269335

On Wed, Apr 29, 2020 at 10:20 AM Farraj, Aimen <Farraj.Aimen@epa.gov> wrote:

> Good morning,
>
> In addition to sending agreement letters (see email below), the STAA nomination process also requires that we list the previous 5 years of STAA nominations and associated publications for each EPA author. I know this is onerous (sorry), but please send me publication titles, year of award, and type of award (e.g. STAA level I, II, III, or honorable mention). I would appreciate it if you would send me this information by COB today if possible. Thanks.
>
> Aimen Farraj, PhD, DABT
>
> Research Biologist
>
> U.S Environmental Protection Agency
>
> Center for Public Health and Environmental Assessment

Public Health and Integrated Toxicology Division

109 TW Alexander Drive

Research Triangle Park, NC 27711

Mail Code: B105-02

Tele: (919) 541-5027; Fax: (919) 541-0034

From: Farraj, Aimen
Sent: Tuesday, April 28, 2020 1:49 PM
To: Cascio, Wayne <Cascio.Wayne@epa.gov>; Gilmour, Ian <Gilmour.Ian@epa.gov>; Hazari, Mehdi <Hazari.Mehdi@epa.gov>; Thompson, Leslie (NIH/OD) [E] <leslie.thompson@nih.gov>; Krug, Jonathan D. <Krug.Jonathan@epa.gov>; Kovalcik, Kasey <Kovalcik.Kasey@epa.gov>; McGee, John <Mcgee.John@epa.gov>; Higuchi, Mark <Higuchi.Mark@epa.gov>; Davies, David <Davies.David@epa.gov>; Martin, Brandi Lee <blmartin@live.unc.edu>; Coates, Najwa Haykal <Coates.Najwa@epa.gov>; King, Charly <King.Charly@epa.gov>; Duvall, Rachelle <Duvall.Rachelle@epa.gov>; Krantz, Todd <Krantz.Todd@epa.gov>; Pancras, Joseph <Pancras.Patrick@epa.gov>; Charles Wood <charleswood99@gmail.com>; Fatiha Malik <fatihamlk1@gmail.com>; Allen Ledbetter <hawbob23@gmail.com>; Lenny Walsh <lcwalsh@nc.rr.com>; kmstrat0402@yahoo.com
Subject: Need agreement letter for STAA award application
Importance: High

Hello,

Mehdi and I are drafting an STAA submission based on the three publications listed below that focus on the unique health effects resulting from concurrent exposure to 2 or more air pollutants, including ambient PM + O_3, ambient PM + the HAP acrolein, and smog with either high PM and low O3 or low PM and high O3 (publications are also attached). Awareness of the potential for such interactive effects as part of a larger multipollutant approach to air pollution health assessment may strengthen the agency's single pollutant standard determinations. One of the requirements of the STAA nomination process is a letter from each author stating that he/she agrees with the percent effort/contribution attributed to him/her. I have assigned percent efforts for all authors in the table below - this is really challenging with 22 total authors. Once I finalize a draft of the STAA application, I will forward it along. In the meantime, please send me an email response indicating you agree with the percent effort attributed to you as soon as possible (by tomorrow afternoon). Thank you so much for your awesome collaboration. Thanks.

Ambient Particulate Matter and Acrolein Co-Exposure Increases Myocardial Dyssynchrony in Mice via TRPA1.

Thompson LC, Walsh L, Martin BL, McGee J, Wood C, Kovalcik K, Pancras JP, Haykal-Coates N, Ledbetter AD, Davies D, Cascio WE, Higuchi M, Hazari MS, Farraj AK.

Toxicol Sci. 2019 Feb 1;167(2):559-572. doi: 10.1093/toxsci/kfy262.

Comparative Cardiopulmonary Effects of Particulate Matter- And Ozone-Enhanced Smog Atmospheres in Mice.

Hazari MS, Stratford KM, Krantz QT, King C, Krug J, Farraj AK, Gilmour MI.

Environ Sci Technol. 2018 Mar 6;52(5):3071-3080. doi: 10.1021/acs.est.7b04880. Epub 2018 Feb 8.

Cardiac effects of seasonal ambient particulate matter and ozone co-exposure in rats.

Farraj AK, Walsh L, Haykal-Coates N, Malik F, McGee J, Winsett D, Duvall R, Kovalcik K, Cascio WE, Higuchi M, Hazari MS.

Part Fibre Toxicol. 2015 May 6;12:12. doi: 10.1186/s12989-015-0087-3.

Author	% Contribution
Cascio, Wayne	3
Davies, David	3
Duvall, Rachelle	3
Farraj, Aimen	12
Gilmour, M. Ian	4
Haykal-Coates, Najwa	7
Hazari, Mehdi	12
Higuchi, Mark	4
King, Charly	4
Kovalcik, Kacey	4
Krantz, Todd	4
Krug, Jonathan	3
Ledbetter, Allen	3
Malik, Fatiha	2
Martin, Brandi	2
McGee, John	5
Pancras, Joseph	3
Stratford, Kimberly	3
Thompson, Leslie	7
Walsh, Leon	7
Winsett, Darrell	2
Wood, Charles	3
Total	100

Aimen Farraj, PhD, DABT

Research Biologist

U.S Environmental Protection Agency

Center for Public Health and Environmental Assessment

Public Health and Integrated Toxicology Division

109 TW Alexander Drive

Research Triangle Park, NC 27711

Mail Code: B105-02

Tele: (919) 541-5027; Fax: (919) 541-0034

Farraj et al. Particle and Fibre Toxicology (2015) 12:12
DOI 10.1186/s12989-015-0087-3

PARTICLE AND FIBRE TOXICOLOGY

RESEARCH Open Access

Cardiac effects of seasonal ambient particulate matter and ozone co-exposure in rats

Aimen K Farraj[1*], Leon Walsh[1], Najwa Haykal-Coates[1], Fatiha Malik[1], John McGee[1], Darrell Winsett[1], Rachelle Duvall[2], Kasey Kovalcik[2], Wayne E Cascio[1], Mark Higuchi[1] and Mehdi S Hazari[1]

Abstract

Background: The potential for seasonal differences in the physicochemical characteristics of ambient particulate matter (PM) to modify interactive effects with gaseous pollutants has not been thoroughly examined. The purpose of this study was to compare cardiac responses in conscious hypertensive rats co-exposed to concentrated ambient particulates (CAPs) and ozone (O_3) in Durham, NC during the summer and winter, and to analyze responses based on particle mass and chemistry.

Methods: Rats were exposed once for 4 hrs by whole-body inhalation to fine CAPs alone (target concentration: 150 μg/m^3), O_3 (0.2 ppm) alone, CAPs plus O_3, or filtered air during summer 2011 and winter 2012. Telemetered electrocardiographic (ECG) data from implanted biosensors were analyzed for heart rate (HR), ECG parameters, heart rate variability (HRV), and spontaneous arrhythmia. The sensitivity to triggering of arrhythmia was measured in a separate cohort one day after exposure using intravenously administered aconitine. PM elemental composition and organic and elemental carbon fractions were analyzed by high-resolution inductively coupled plasma–mass spectrometry and thermo-optical pyrolytic vaporization, respectively. Particulate sources were inferred from elemental analysis using a chemical mass balance model.

Results: Seasonal differences in CAPs composition were most evident in particle mass concentrations (summer, 171 μg/m^3; winter, 85 μg/m^3), size (summer, 324 nm; winter, 125 nm), organic:elemental carbon ratios (summer, 16.6; winter, 9.7), and sulfate levels (summer, 49.1 μg/m^3; winter, 16.8 μg/m^3). Enrichment of metals in winter PM resulted in equivalent summer and winter metal exposure concentrations. Source apportionment analysis showed enrichment for anthropogenic and marine salt sources during winter exposures compared to summer exposures, although only 4% of the total PM mass was attributed to marine salt sources. Single pollutant cardiovascular effects with CAPs and O_3 were present during both summer and winter exposures, with evidence for unique effects of co-exposures and associated changes in autonomic tone.

Conclusions: These findings provide evidence for a pronounced effect of season on PM mass, size, composition, and contributing sources, and exposure-induced cardiovascular responses. Although there was inconsistency in biological responses, some cardiovascular responses were evident only in the co-exposure group during both seasons despite variability in PM physicochemical composition. These findings suggest that a single ambient PM metric alone is not sufficient to predict potential for interactive health effects with other air pollutants.

Keywords: Ambient particulate matter, Ozone, Season, Cardiac, Health effects, Co-exposure, Electrocardiogram, Rats, Source apportionment, Elements

* Correspondence: farraj.aimen@epa.gov
[1]Environmental Public Health Division, US EPA, 109 TW Alexander Drive, Research Triangle Park, Durham, NC 27711, USA
Full list of author information is available at the end of the article

BioMed Central

© 2015 Farraj et al.; licensee BioMed Central. This is an Open Access article distributed under the terms of the Creative Commons Attribution License (http://creativecommons.org/licenses/by/4.0), which permits unrestricted use, distribution, and reproduction in any medium, provided the original work is properly credited. The Creative Commons Public Domain Dedication waiver (http://creativecommons.org/publicdomain/zero/1.0/) applies to the data made available in this article, unless otherwise stated.

Background

Attempts to quantify the cardiovascular health burden resulting from exposure to particulate matter air pollution and identify biologically plausible mechanisms of action have been encumbered by the variability in PM composition. The physical and chemical properties of ambient PM in a given air shed are dependent on a number of factors including local geography, proximity to emission sources, time of day, and meteorology. Recent studies point to a pronounced seasonal pattern in fine PM (PM with an aerodynamic diameter less than 2.5 microns; $PM_{2.5}$) composition across the U.S. with higher levels of sulfate, aluminum and magnesium in the summer and higher levels of nitrate, zinc and nickel in the winter [1]. Time-series data from 202 U.S. counties [2] point to a commensurate seasonal impact on health effects including stronger $PM_{2.5}$ associations with same day cardiovascular and respiratory hospital admissions during the winter than in the summer. By contrast, Goldberg et al. [3] found carbon particle-related mortality was higher during the summer than in winter. In mouse studies, exposure to winter ambient PM caused greater pulmonary neutrophil influx [4] and greater systemic pro-inflammatory and procoagulant responses [5] than exposure to summer PM. In contrast, Happo et al. [6] found that PM collected in spring produced greater inflammatory responses in mouse lung than PM samples collected in the fall. Divergent responses have also been noted using *in vitro* models [7,8]. Components and/or properties of PM that vary across season and that drive season-dependent health effects of exposure need to be defined.

While the characteristics of PM are critical, PM is only one component of a complex air pollution mixture that also includes gases and volatile compounds. Assessment of the health effects of exposure at a given ambient air shed, therefore, must account for non-PM components and the potential for additive, synergistic or antagonistic responses resulting from gas-particle interactions. A growing body of evidence is pointing to interactive effects of exposure with a variety of air pollutants, including nitrogen dioxide (NO_2), ambient PM, and O_3 [9]. PM and O_3 co-exposure has been linked to more pronounced cardiovascular responses including increased diastolic blood pressure [10] and dispersion of ventricular repolarization [11] in humans and decreased HRV [12], and epicardial adipose tissue inflammation in rats [13]. The unique physicochemical characteristics of PM within each season may determine interaction between components within an air pollution mixture and serve as an important contributing factor in health outcomes.

Like other regions of the U.S., central North Carolina is subject to seasonal shifts in $PM_{2.5}$ composition with summer PM dominated by sulfate, and winter by nitrates [14]. Little is known about the influence of season on both ambient PM chemistry and cardiovascular responses within this region, particularly in the context of co-pollutant exposures. We have previously shown that exposure to various air pollutants causes exaggerated cardiovascular responses in rats [15-18]. The purpose of this study was to compare the impacts of a single summer exposure to CAPs with or without O_3 on cardiovascular responses in rats to similar exposures during the winter and relate the responses to differences in seasonal PM composition. ECG intervals and amplitudes, HR, spontaneous arrhythmia and HRV, an indicator of autonomic tone, were measured. In addition, sensitivity to myocardial calcium loading, an index of latent vulnerability to cardiac arrhythmia, and pulmonary and systemic indicators of inflammation were assessed one day after exposure. PM exposure characteristics and meteorological conditions were documented. Finally, elemental analysis data were used to quantify PM sources using a chemical mass balance model.

Results

Weather patterns

Summer and winter local weather patterns during exposures were unstable with unusually low ambient PM concentrations. Wind patterns shifted up to 180 degrees each day and were never consistent long enough to establish stable ambient PM levels. A map of superimposed backward trajectories (Figure 1) was created using the Hybrid Single Particle Lagrangian Integrated Trajectory Model (HYSPLIT; web version; Draxler, RR et al.) at the Real-Time Environmental Applications and Display sYstem (READY; Rolph, DG) website developed by the Air Resources Laboratory of the NOAA. Archived meteorological data (online) was utilized to model the direction and location of the test air mass in 6 hr increments for the previous 24 hr before 10 am local time of each exposure day. The trajectories terminated at the exposure facility in A-Building of the CRF in RTP, NC. (Latitude: 35.88350; Longitude: −78.87460). The tracings shown in Figure 1 illustrate how a uniform pattern of exposure sources was precluded because the direction of the air mass source changed for each daily exposure. Trajectories plotted do not follow air mass chronological fate after an exposure day, but rather, show how new air masses replaced current from day to day.

Exposure concentrations

Due to unusually low ambient PM levels and unseasonably small PM sizes for the winter test days, coupled with splitting CAPs system output between 2 chambers, target PM concentrations were not achievable during the winter exposures. The protocol was revised such that

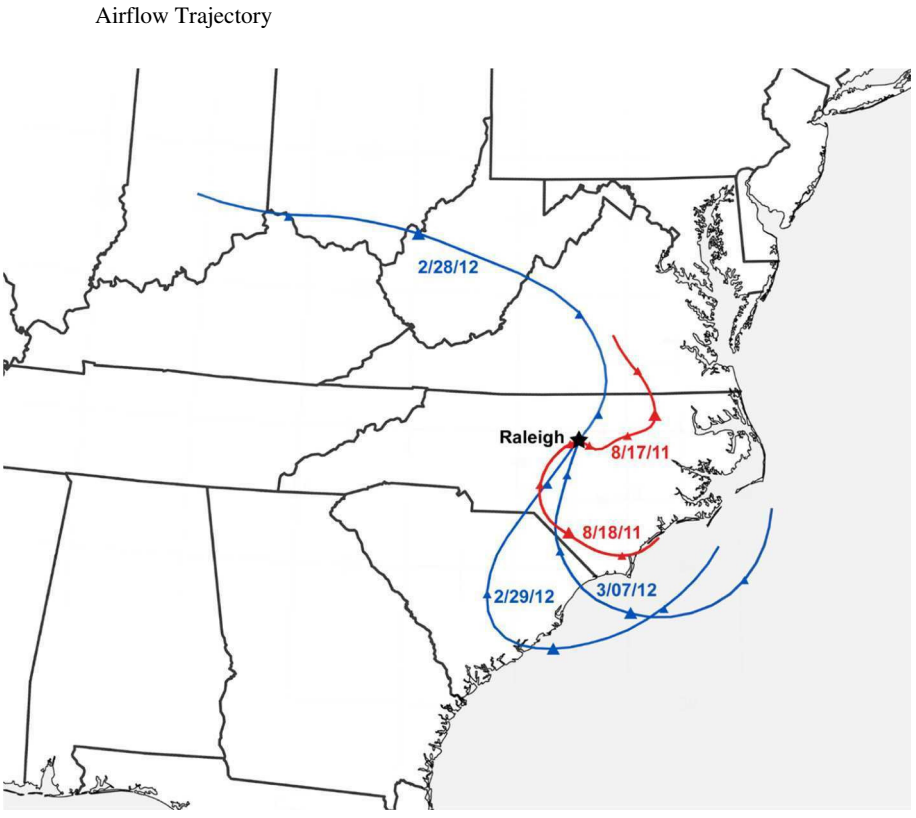

Figure 1 A map of superimposed backward trajectories using the Hybrid Single Particle Lagrangian Integrated Trajectory Model (HYSPLIT) at the Real-Time Environmental Applications and Display sYstem (READY) website developed by the Air Resources Laboratory of the National Oceanic and Atmospheric Administration. Archived meteorological data was utilized to model the direction and location of the test air mass for the previous 24 hr before 10 am local time (2 pm UTC (Universal Time Coordinated)) of each exposure day. Each trajectory represents a different air mass for each winter exposure day (2/28/12, and 2/29/12, and 3/07/12 and blue in color) and each summer exposure day (8/17/11 and 8/18/11 and red in color) and terminates at the exposure facility in A-Building of the US EPA campus in Durham, NC (indicated by a star). Triangle symbols indicate time of day (UTC) in 6 hour increments with larger symbols corresponding to midnight UTC (8 pm local time) in each path.

for the initial PM exposures of each group, maximum achievable concentration was provided. For the subsequent exposures, we attempted to match the first day's PM levels by including dilution air to regulate chamber PM levels. Filter samples were collected from each chamber and the system inlet for the PM exposures only as sampling the filtered air chambers (O_3 only and air controls) provided insufficient sample mass for either accurate weighing or detectable levels for chemical analysis. One filter, 37 mm Teflon for mass concentration in the CAPs + O_3 chamber on 8/17/11 failed during the exposure so that gravimetric sample was lost. The loss of the 37 mm Teflon mass sample did not affect PM chemical analysis or source apportionment modeling, which were performed using data derived from 47 mm Teflon, Nylasorb, and quartz filter samples. Chamber PM mass concentration for that exposure was determined by computing an average DustTrak (DT) calibration factor (DT cal factor = Filter conc/Avg DT conc) for other runs of PM filters vs average DT indicated concentrations and applying the factor to DT data for the run with the failed filter sample. Average ambient PM levels from filter samples were ~13.7 ug/m^3 for summer and ~8.4 ug/m^3 for winter PM exposure days. Summer ambient source PM size was larger than winter PM size producing better concentrating effects in the CAPs system during summer exposure days (Table 1). Background O_3 levels measured in the CAPs only and air control chambers ranged from 2.5 to 10.5 ppb in the summer and winter. Chamber CAPs and O_3 concentrations and environmental conditions for each group are reported in Table 1.

Chemical composition of CAPs

Group-averaged PM elemental and carbon fraction composition for summer and winter exposures are shown in Tables 2 and 3. Two sets of units are required to describe the aerosol: μg PM component per g PM (Table 2) shows seasonal differences in PM composition, and μg PM component per cubic meter chamber air (Table 3) shows chamber concentrations during exposures. When

Table 1 Exposures concentrations, particle size and chamber and ambient weather conditions

Exposure dates	Summer exposures				Winter exposures			
	Air	CAPs	O_3	CAPs + O_3	Air	CAPs	O_3	CAPs + O_3
	23 Aug11	17 Aug11	23 Aug11	17 Aug11	5 Mar12	28 Feb12	05 Mar12	28 Feb12
	2 Aug11	18 Aug11	24 Aug11	18 Aug11	6 Mar12	29 Feb12	06 Mar12	29 Feb12
						7 Mar12		7 Mar12
O3 (ppb)	5.8	4.8	197.1	203.1	2.5	10.5	199.4	198.3
PM Mass (μg/m^3)	—	168.7	—	174.9	—	78.5	—	91.3
Particle Size (nm)	—	333.4	—	315.0	—	125.5	—	125.0
Geometric Mean	—	316.1	—	295.8	—	125.5	—	125.0
Mode	—	316.1	—	295.8	—	125.5	—	125.0
Geometric SD	—	1.96	—	1.97	—	1.95	—	2.02
Chamber Temp (F)	72.6	72.5	70.8	70.4	73.6	72.3	71.2	69.6
Chamber RH (%)	51.3	50.3	51.3	56.5	46.7	42.6	51.0	47.1
Ambient Temp (F)	77.5	80	77.5	80	44.8	55.5	44.8	55.5
Ambient RH (%)	55	69.5	55	69.5	45.8	68.2	45.8	68.2

expressed as μg/g, PM composition differences between summer and winter were pronounced. No elements were enriched in summer relative to winter. Relative to summer, sodium, magnesium, and calcium were enriched at levels of 4–6 times higher in winter PM, and levels of another 15 elements were enriched by 2- 3-fold. However, expressing PM concentration in units of μg/m^3 exposure atmosphere takes into account the PM mass concentrations, which were approximately 2 times greater in summer. Table 3 shows that the overall elemental levels in the inhalation chambers were largely the same for both seasons' exposures, with a few exceptions. Chromium and sulfate levels were 2 to 3 times higher in summer, while alkali elements sodium, magnesium, and calcium were 2 to 3 times higher in winter.

Source apportionment analysis

Average source contributions to the CAPS and CAPS + O_3 mixtures are displayed in Figure 2 (Additional file 1: Table S1 and Additional file 2: Figure S1, respectively, show the same data in tabular and bar chart format); daily samples used to calculate averages are also found in Additional file 3: Table S2 and Additional file 4: Table S3, respectively. Across both seasons and pollutant mixtures, the CMB model explained between 60-100% of the particle mass (R^2 ranged from 0.76 to 0.92). The fit statistics including percent mass explained, R^2, chi Square, and T-statistic were within the recommended values [19]. Nitrate data were not available for inclusion in the CMB runs; therefore, some of the unresolved mass may be due to secondary nitrate (Aneja et al. [14] showed that nitrate levels in PM peak during winter months in North Carolina). The largest sources during both the summer and winter exposures included mobile sources (14-17% by mass), wood combustion (12-30%), and secondary sulfate (24-40%). Higher contributions of wood combustion were found during the winter exposures. Road dust and marine salt contributions were also higher during the winter exposures. In particular for marine salt, air flow trajectories (Figure 1) show that air masses originated from the ocean on 2/29/12 and 3/7/12. These observations are supported by the CMB results in which marine salt contributions were elevated on those two days for both the CAPS and CAPS + O_3 mixtures (Table S2).

Heart rate

Despite being acclimated to the exposure chambers on non-exposure days, rats routinely demonstrate elevated HR during baseline pre-exposure periods on exposure days. This was evident in rats exposed to filtered air during both summer and winter months. Figure 3 shows group averages normalized to baseline pre-exposure values (i.e. Exposure minus Pre-exposure Baseline). In the summer, rats during exposure to O_3, had a greater decrease in HR than rats exposed to filtered air ($p < 0.05$). There were no significant effects of CAPS or CAPS + O_3 exposure relative to filtered air controls.

In the winter, unlike O_3 exposure during the summer, O_3 did not cause a significant decrease in HR during exposure. By contrast, CAPs exposure caused a greater decrease in HR than filtered air exposure ($p < 0.05$). CAPS + O_3 caused the opposite effect resulting in an increase in HR relative to filtered air ($p < 0.05$).

HR did not change after exposure (i.e. 6-hour period after exposure) when compared to baseline in any exposure group during either season.

Table 2 Group-averaged PM elemental composition in μg/g

	Summer		Winter		Winter/Summer
Element (μg/g)	CAPs	CAPs + O_3	CAPs	CAPs + O_3	Enrichment factor
Al	951	622	2303	2250	2.9
As	14.8	14.2	20.3	15.5	1.2
Ba	304	101	335	239	1.4
Ca	1159	1033	4548	4200	4.0
Cd	2.4	2.3	9.2	6.9	3.5
Co	7.6	1.9	3.6	5.3	0.9
Cr	39.6	44.8	56.6	38.4	1.1
Cu	848	360	683	540	1.0
Fe	5053	4695	14946	10027	2.6
K	3637	5018	10392	7128	2.0
Li	6.3	11.6	32.6	21.3	3.0
Mg	386	271	2304	1690	6.1
Mn	442	688	2273	1481	3.3
Mo	10.3	6.7	17.7	7.8	1.5
Na	2404	3899	17638	13795	5.0
Ni	17.8	18.0	48.2	31.3	2.2
P	312	78	234	494	1.9
Pb	133	79	220	157	1.8
SO_4	276531	294486	240898	160234	0.7
Sb	39.8	27.9	88.8	63.4	2.2
Se	29.0	37.4	50.3	40.8	1.4
SiO_2	3822	1705	11341	6179	3.2
Sn	33.7	18.2	66.3	48.3	2.2
Sr	14.1	7.5	38.4	29.6	3.1
Ti	140	80	279	242	2.4
V	9.8	12.6	43.0	32.5	3.4
Zn	367	534	1475	1128	2.9
Organic C	287078	341624	448280	357174	1.3
Elemental C	14582	25329	49299	34830	2.1

Electrocardiographic parameters

In the summer, O_3 exposure significantly increased PR interval relative to filtered air controls ($p < 0.05$) (Figure 4). By contrast CAPS exposure significantly decreased the PR interval relative to filtered air controls ($p < 0.05$). CAPS + O_3 exposure produced no effect. During winter, no exposure affected the PR interval. In addition, PR interval did not change after exposure in any exposure group during either season.

In the summer, there were no effects of CAPs or O_3 exposure on QT_c interval relative to filtered air (Figure 5). By contrast, CAPS + O_3 exposure caused a significant increase in QT_c interval relative to filtered air ($p < 0.05$). There was no significant effect in QT_c interval in the winter during exposure. However, CAPS + O_3 exposure caused a significant increase in QT_c interval relative to filtered air in the winter after exposure.

Heart rate variability

During both summer and winter, there were no effects of CAPs or O_3 exposure alone on SDNN relative to the response in filtered air controls during both seasonal exposures (Figure 6). By contrast, CAPs + O_3 exposure during both summer and winter caused a significant decrease in SDNN during exposure relative to filtered air ($p < 0.05$). CAPs + O_3 exposure during the winter also caused a significant decrease in SDNN after exposure relative to filtered air ($p < 0.05$), although the magnitude change was smaller compared to the effect of co-exposure during the summer.

Table 3 Group-averaged PM elemental levels in μg/m³

	Summer		Winter		Winter/Summer
Element (μg/m³)	CAPs	CAPs + O_3	CAPs	CAPs + O_3	Enrichment factor
Al	0.160	0.109	0.181	0.205	1.4
As	0.00249	0.00248	0.00159	0.00142	0.6
Ba	0.0513	0.0176	0.0263	0.0218	0.7
Ca	0.195	0.181	0.357	0.383	2.0
Cd	0.00041	0.00040	0.00072	0.00063	1.7
Co	0.00128	0.00034	0.00028	0.00048	0.5
Cr	0.00669	0.00784	0.00444	0.00351	0.5
Cu	0.143	0.0630	0.0536	0.0493	0.5
Fe	0.852	0.821	1.173	0.915	1.2
K	0.614	0.878	0.816	0.651	1.0
Li	0.00107	0.00204	0.00256	0.00194	1.4
Mg	0.0651	0.0475	0.1809	0.1543	3.0
Mn	0.0745	0.1203	0.1784	0.1352	1.6
Mo	0.00174	0.00117	0.00139	0.00071	0.7
Na	0.406	0.682	1.385	1.259	2.4
Ni	0.00301	0.00316	0.00378	0.00285	1.1
P	0.0526	0.0136	0.0184	0.0451	1.0
Pb	0.0225	0.0138	0.0173	0.0144	0.9
SO_4	46.7	51.5	18.9	14.6	0.3
Sb	0.00671	0.00488	0.00697	0.00579	1.1
Se	0.00488	0.00654	0.00395	0.00373	0.7
SiO_2	0.645	0.298	0.890	0.564	1.5
Sn	0.00568	0.00318	0.00521	0.00441	1.1
Sr	0.00238	0.00132	0.00301	0.00270	1.5
Ti	0.0237	0.0140	0.0219	0.0221	1.2
V	0.00165	0.00220	0.00337	0.00297	1.6
Zn	0.0619	0.0933	0.1158	0.1030	1.4
Organic C	48.43	59.75	35.19	32.61	0.6
Elemental C	2.46	4.43	3.87	3.18	1.0
OC/EC ratio	16.6		9.7		

CAPs + O_3 exposure during the winter also caused a significant decrease in RMSSD and a significant increase in LF/HF after exposure relative to filtered air controls ($p < 0.05$; Additional file 5: Table S4). O_3 exposure alone also caused an increase in LF/HF relative to filtered air ($p < 0.05$).

Cardiac arrhythmia

There was no significant effect of exposure on the total number of arrhythmias relative to filtered air exposed controls with any exposure group during either season (data not shown).

Sensitivity to aconitine One Day after exposure

During the summer, exposure to CAPs alone or O_3 alone significantly increased sensitivity to triggering of arrhythmia by escalating doses of aconitine as evidenced by a decrease of the total dose of aconitine necessary to elicit the first ventricular premature beat relative to filtered air exposed controls ($p < 0.05$, Figure 7). CAPs, O_3, and CAPS + O_3 each significantly decreased the total dose of aconitine necessary to elicit the first episode of ventricular tachycardia relative to filtered air exposed controls ($p < 0.05$). There was no significant effect of exposure on the total dose of aconitine necessary to elicit

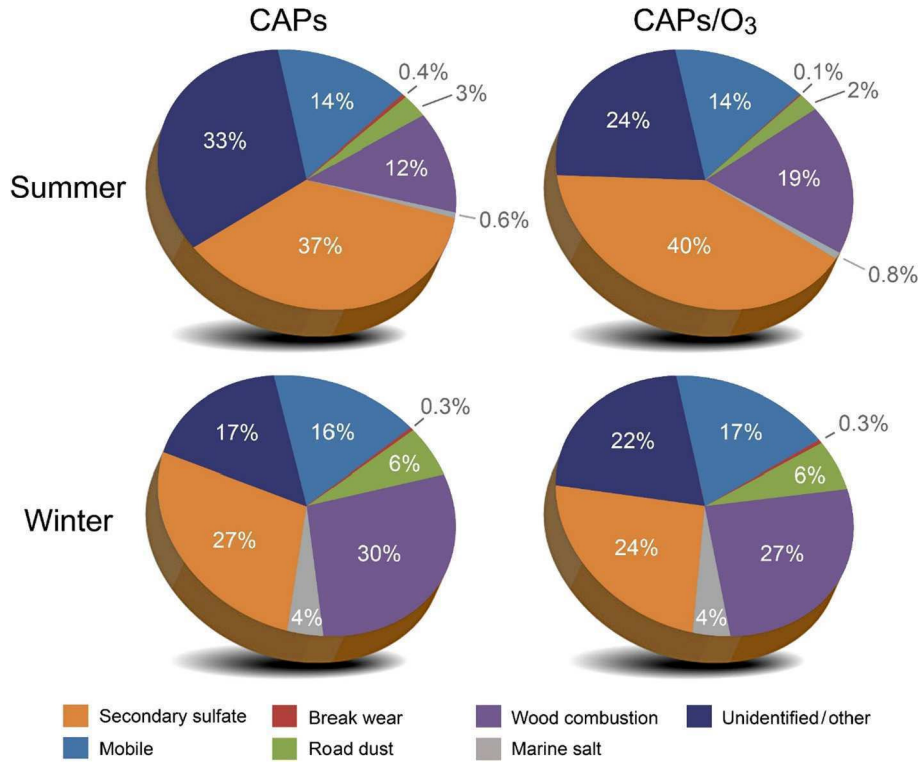

Figure 2 Pie Charts illustrating sources contributing to the concentrated ambient particulate (CAPs) and CAPs + ozone (O_3) mixtures during the summer and winter exposures. Sources for each season were quantified using the EPA Chemical Mass Balance Model.

the first episode of ventricular fibrillation or cardiac arrest relative to air exposed controls.

There was no significant effect of exposure on acontine arrhythmia sensitivity with any exposure group during the winter. Interestingly, in a comparison of the aconitine doses required to assess vulnerability to arrhythmia across season, the dose required to trigger arrhythmias in air-exposed rats during the winter was significantly lower than air-exposed rats during the summer.

Indicators of inflammation and injury in serum, plasma, and bronchoalveolar lavage fluid one day after exposure

Exposure to CAPs + O_3 during the winter significantly increased N-Acety-D-glucosaminidase (NAG) and lactate dehydrogenase (LDH) levels in the lung ling fluid ($p < 0.05$) relative to filtered air (Figure 8). There were no such changes in NAG in any of the exposure groups during the summer. In addition, exposure to CAPS or CAPs + O_3 during the summer significantly decreased lung LDH levels ($p < 0.05$) relative to filtered air. CAPs + O_3 exposure during the winter also significantly increased lung CuZn super oxide dismutase (CuZn SOD) levels ($p < 0.05$) relative to filtered air. There was no effect of co-exposure on CuZn SOD during the summer, whereas, CAPs exposure alone significantly decreased CuZn SOD levels ($p < 0.05$) relative to filtered air. Exposure to CAPs alone significantly decreased Glutathione S-Transferase (GST) levels during the summer ($p < 0.05$) relative to filtered air, whereas O_3 alone significantly increased lung GST levels ($p < 0.05$) relative to filtered air. There were no such changes in GST in any of the exposure groups during the winter. There was no significant effect of exposure in any other indicator of inflammation in the lung, serum, or plasma or number of infiltrated inflammatory cells in the lung lining fluid (data not shown).

Discussion

Here we present evidence that season and ozone are effect modifiers for ambient PM-induced cardiovascular responses in Spontaneous Hypertensive (SH) rats, a strain of rat known to demonstrate exaggerated cardiovascular effects in response to inhaled ambient PM, diesel exhaust particles, and acrolein [20-22]. Seasonal differences in PM were consistent with earlier findings [14], with new evidence of enrichment for anthropogenic emissions and marine salt sources during winter season

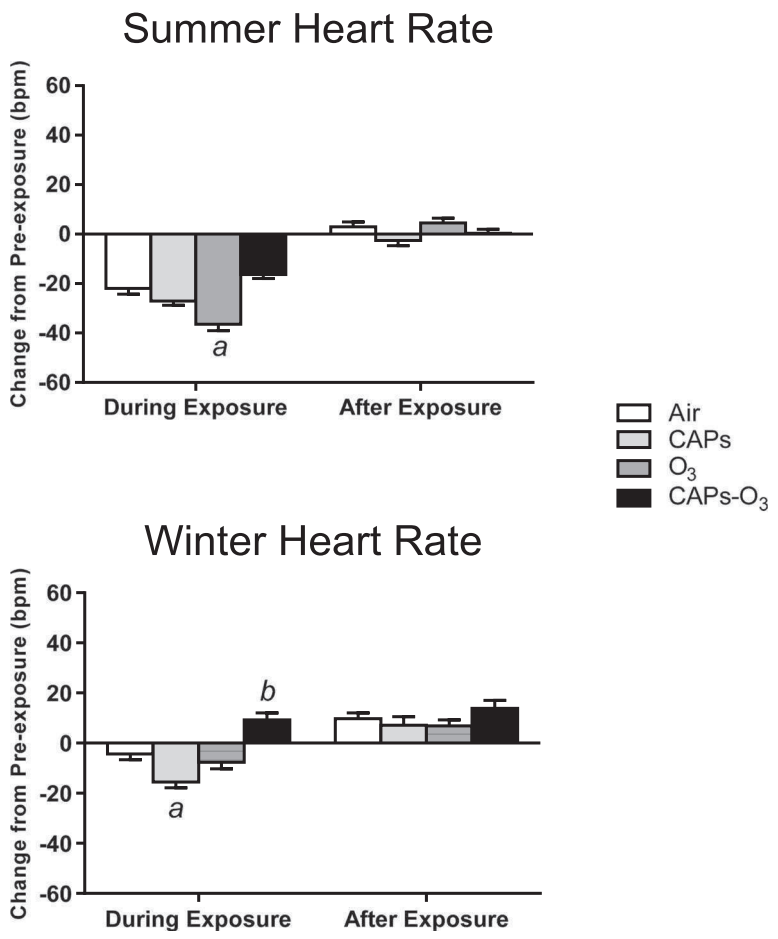

Figure 3 Mean change in Heart rate (HR) from pre-exposure values during summer and winter exposures. HR values for each animal at each time point during exposure or after exposure were subtracted from corresponding time-matched pre-exposure baseline data, which was recorded while the animals were either in the chamber (for "during exposure" data) or in their home cages (for "after exposure" data). Values represent mean change in HR in beats per minute ± standard error of the mean (n = 6). a - significantly less than filtered air control ($p < 0.05$). b - significantly greater than filtered air control ($p < 0.05$).

exposures compared to summer exposures in central North Carolina. Single pollutant cardiovascular effects with CAPs and O_3 were present during both summer and winter exposures, with evidence of unique effects of co-exposures with associated changes in autonomic tone during both seasons.

Biogenic emissions, agricultural activity, vehicular traffic, production of secondary organic aerosols and local weather conditions largely determine the concentration and chemical composition of North Carolina's particulate pollution [14]. The physiochemical characteristics of PM from the Research Triangle Park, NC air shed were highly variable between summer and winter seasons. Differences included particle mass concentrations, size, organic:elemental carbon ratios, and sulfate levels and are consistent with previous measurements [14]. Although winter exposures had 50% less total PM mass than summer exposures (85 vs. 171 μg/m^3), enrichment of metals on a μg/g basis in winter PM resulted in equivalent summer and winter metal exposure concentrations. These findings were based on data from a limited number of exposure days (two summer CAPs exposure days and three winter CAPs exposure days); future studies will need to include more PM exposure sampling days to increase robustness of analysis. Nevertheless, subsequent source apportionment analysis revealed that winter exposures were enriched primarily by wood combustion and to a lesser extent by road dust and marine salt sources compared to summer exposures. The relative impact of the enrichment of marine salt sources is unclear given that only 4% of the total PM mass was attributed to marine salt sources. PM within or near the ultrafine range (0.1 to 0.6 μm) dominates emissions from residential wood combustion while the composition of the PM is dependent on combustion conditions and furnace type, with multiple elements

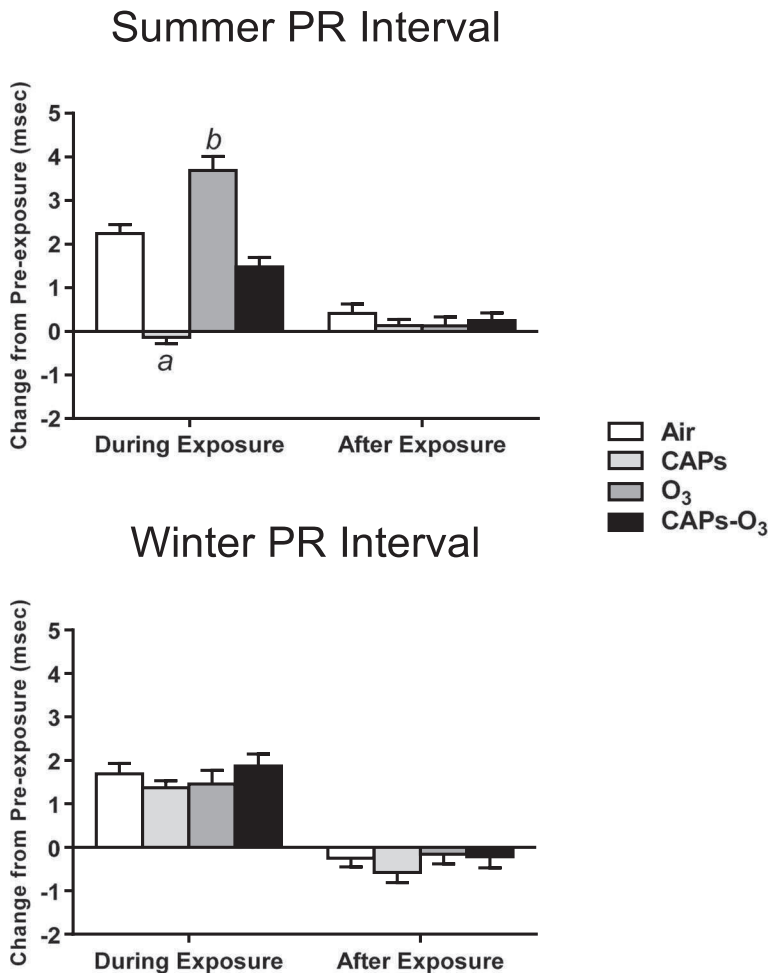

Figure 4 Mean change in PR interval from pre-exposure values during summer and winter exposures. PR values for each animal at each time point during exposure or after exposure were subtracted from corresponding time-matched pre-exposure baseline data, which was recorded while the animals were either in the chamber (for "during exposure" data) or in their home cages (for "after exposure" data). Values represent mean change in PR interval in msec ± standard error of the mean (n = 6). a - significantly less than filtered air control ($p < 0.05$). b - significantly greater than filtered air control ($p < 0.05$).

including potassium, sodium, magnesium, aluminum, and zinc, and transition metals like chromium and nickel present in appreciable quantities [23,24]. Exposure to PM rich in transition metals has been associated with increased cardiovascular mortality [25]. Moreover, the proportion of anthropogenic metals is a critical determinant of biological responses to PM including increased pulmonary effects on days with higher metal concentrations [26-28]. As well, summer PM, although having higher mass, may have been diluted by less bioactive compounds such as sulfates, which were present at higher concentrations during the summer. In addition, winter particle size was roughly one-third the size of summer particles (125 vs. 324 nm). Smaller, near-ultrafine particles have greater relative surface area than larger particles at any given mass concentration and have the capacity to penetrate deep into the lung and also permeate plasma membranes of cells including alveolar epithelial cells and capillary endothelium [29]. Furthermore, ultrafine PM may initiate inflammatory responses in the lung or systemic circulation or enter the blood stream and directly trigger vascular responses, either of which may trigger downstream cardiac responses [29]. In mice exposed to ambient PM collected near a highway [30] and a peat wildfire [31], size-segregated, ambient ultrafine PM caused cardiac changes, while coarse and fine PM from the same PM sample affected primarily pulmonary endpoints.

Single pollutant cardiac effects were mostly observed with summer exposures. With summer O_3 exposure, the effects included decreased HR, increased PR interval, an increase in the HRV parameter LF/HF and increased sensitivity to myocardial calcium loading, consistent with our previous findings [16]. Summer CAPs exposure

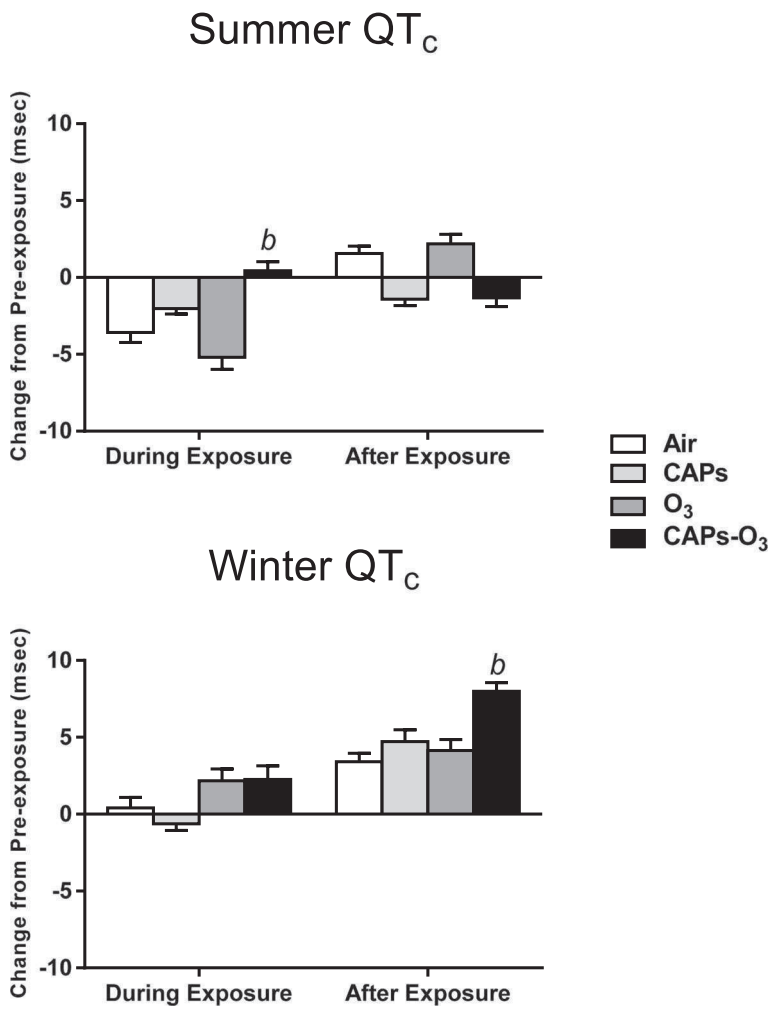

Figure 5 Mean change in QT_c interval from pre-exposure values during summer and winter exposures. QT_c values for each animal at each time point during exposure or after exposure were subtracted from corresponding time-matched pre-exposure baseline data, which was recorded while the animals were either in the chamber (for "during exposure" data) or in their home cages (for "after exposure" data). Values represent mean change in QT_c interval in msec ± standard error of the mean (n = 6). b - significantly greater than filtered air control ($p < 0.05$).

decreased PR interval and elevated sensitivity to myocardial calcium loading. The opposing PR response with summer CAPs exposure compared to summer O_3 exposure implicates pollutant specific disparate effects on atrioventricular conduction, although each pollutant ultimately caused increased vulnerability to ventricular arrhythmia. The relevance of the increased responses to aconitine during the summer is uncertain given that exposures to CAPs and/or O_3 during the winter had no effect on this endpoint, the precise reason of which is unclear. Nevertheless, winter time exposures caused a CAPs-induced decrease in HR, and a CAPs + O_3-induced increase in lung lactate dehydrogenase and n-acetyl B-D glucosaminidase and increased Cu-Zn superoxide dismutase, although the relevance of these findings are also uncertain given the decrease in some of these endpoints with single pollutant exposure. The decrease in HR with CAPs alone during the winter is similar to the findings of Rohr et al. [32] who compared the cardiac effects of winter and summer CAPS exposures in Michigan in the same rat strain used in the present study. Their study had additional effects that were not found in the present study with CAPs alone including linkage of the winter HR response with increased HRV and opposing summer effects characterized by increased HR and decreased HRV. The differences between the Rohr et al. study and the present study may reflect in part the differences in study design (the Rohr et al. study consisted of thirteen 8-hour exposure days vs. a single 4-hour exposure in the present study), exposure concentrations (e.g. summer CAPs concentrations in Rohr et al. averaged ~518 μg/m^3; in present study, ~170 μg/m^3) and/or local contributing air pollution sources, among other factors. Moreover, the variability

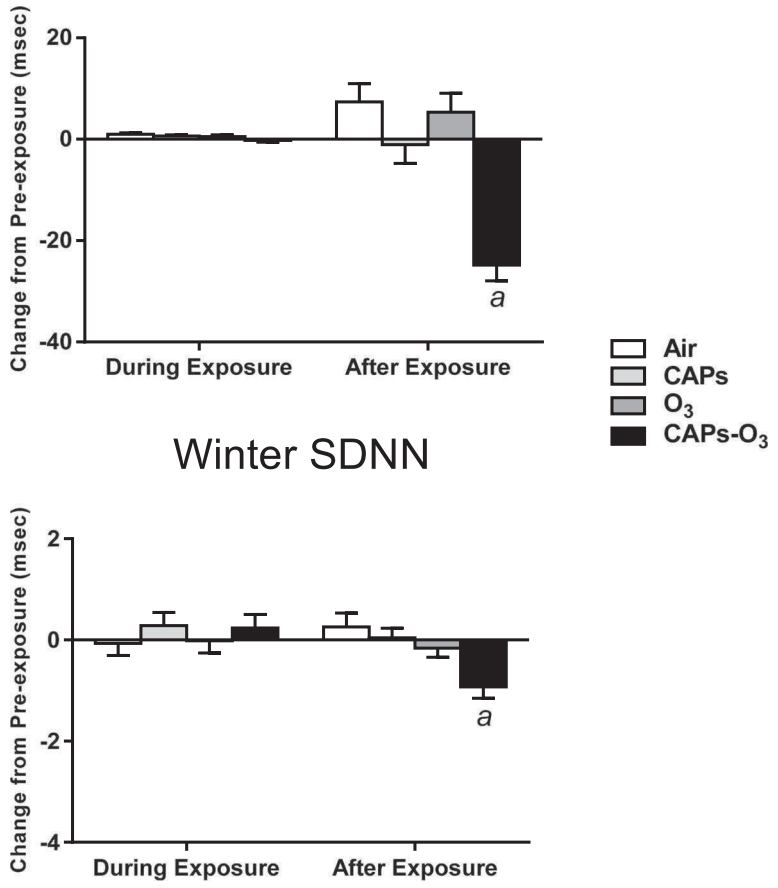

Figure 6 Mean change in SDNN from pre-exposure values during summer and winter exposures. SDNN values for each animal at each time point during exposure or after exposure were subtracted from corresponding time-matched pre-exposure baseline data, which was recorded while the animals were either in the chamber (for "during exposure" data) or in their home cages (for "after exposure" data). Values represent mean change in SDNN in msec ± standard error of the mean (n = 6). a - significantly less than filtered air control ($p < 0.05$).

in the single pollutant responses in the present study may reflect an insufficient short-term exposure required to elicit a significant inflammatory response in the SH rat. This possibility is consistent with epidemiological and human exposure data that suggest that cardiovascular effects to short-term exposures are more likely triggered by autonomic responses while long-term exposures increase the likelihood of persistent inflammatory responses [29].

With some parameters during both the summer and winter seasons, CAPs + O_3 exposure elicited unique responses that were not evident with exposure to either pollutant alone. These included changes in SDNN, RMSSD and QT_c, during the summer, and changes in HR, SDNN, QT_c, and lung injury and oxidative responses during the winter. The changes in QT_c and HR during summer and winter exposures, respectively, were each accompanied by a decrease in SDNN, which reflects overall heart rate variability, and indicates a decrease in parasympathetic tone. In addition, summer co-exposures caused post-exposure decreases in SDNN and RMSSD, another indicator of parasympathetic tone. Thus, decreased parasympathetic tone with co-exposure to CAPs and O_3 during both seasons reflects a shift in autonomic balance towards increased sympathetic tone. Summertime CAPs plus O_3 co-exposure in a recently conducted study in Michigan [12], characterized by greater ambient concentrations of SO4, Ni, V, Zn, and organic and elemental carbon than the present study, yielded similar HRV findings in rats. The present findings are also consistent and with other reports linking low HRV with exposure to PM [33-36] and O_3 [37,38]. Much of the evidence on the prognostic significance of HRV points to increased cardiovascular risk

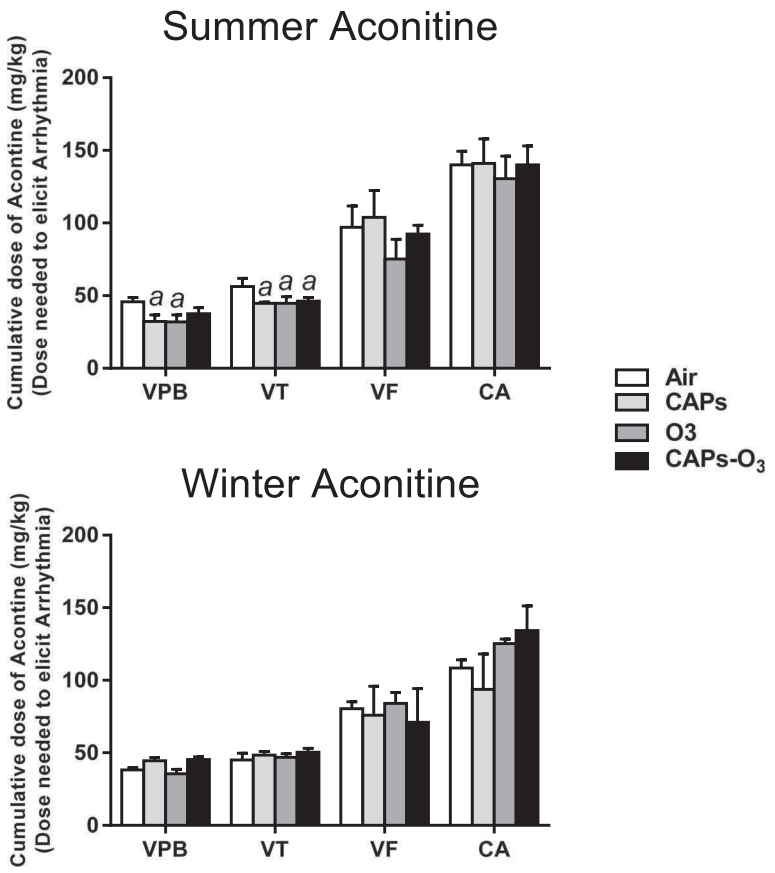

Figure 7 Cumulative dose of infused aconitine necessary to trigger ventricular premature beats (VPB), ventricular tachycardia (VT), ventricular fibrillation (VF), and cardiac arrest (CA) in rats one day after a single exposure. Values represent mean dose ± standard error of the mean (n = 5). a - significantly less than filtered air control ($p < 0.05$).

with low HRV, including increased risk of arrhythmia [39] and an increased mortality rate in people with heart disease [40,41].

The autonomic responses with co-exposure may have been triggered by activation of irritant nerve fibers, including pulmonary C fibers, which trigger reflex cardiopulmonary responses via transient receptor potential (TRP) channels. We recently showed that TRPA1 mediates the increased sensitivity to aconitine-induced arrhythmia after diesel exhaust exposure [22]. In addition, Taylor-Clark and Undem [42] demonstrated that O_3 exposure activates airway C fibers expressing TRPA1. Summer and winter CAPs exposures were rich in adsorbed elements including Fe and Ni, which have been linked to production of reactive oxygen species [7]. The potential involvement of TRP receptors in biological responses induced by transition metals should be examined in future studies given that reactive oxygen species are known activators of TRP receptors [43].

While the specific class of components that drove the observed cardiopulmonary responses is not certain, the similarity in elemental levels in the winter and summer PM due to elemental enrichment presents a plausible explanation for the physiological responses observed. More proinflammatory or irritating byproducts generated through atmospheric interaction between PM, its components, and gases might potentiate cardiovascular effects directly or via the alteration of dose distribution in the lung. For example, Fe and V salts increase the pulmonary irritancy of SO_2 via formation of the more irritating sulfate [44]. Moreover, PM including zinc oxide and inert carbon black, when mixed with gases such as SO_2 or O_3, cause greater than additive pulmonary effects by potentially serving as a carrier for the reactive gases enabling greater distribution into the deep lung [44]. Further research is required to define plausible mechanisms and identify the nature of interactions between specific components like metals and gases.

Seasonal differences in PM mass concentration and size in this study precludes a direct comparison of the physiological responses to ambient PM exposure between seasons. Although air flow patterns likely had little influence, low ambient PM levels and a lower ratio of fine to ultrafine particles during the winter prevented

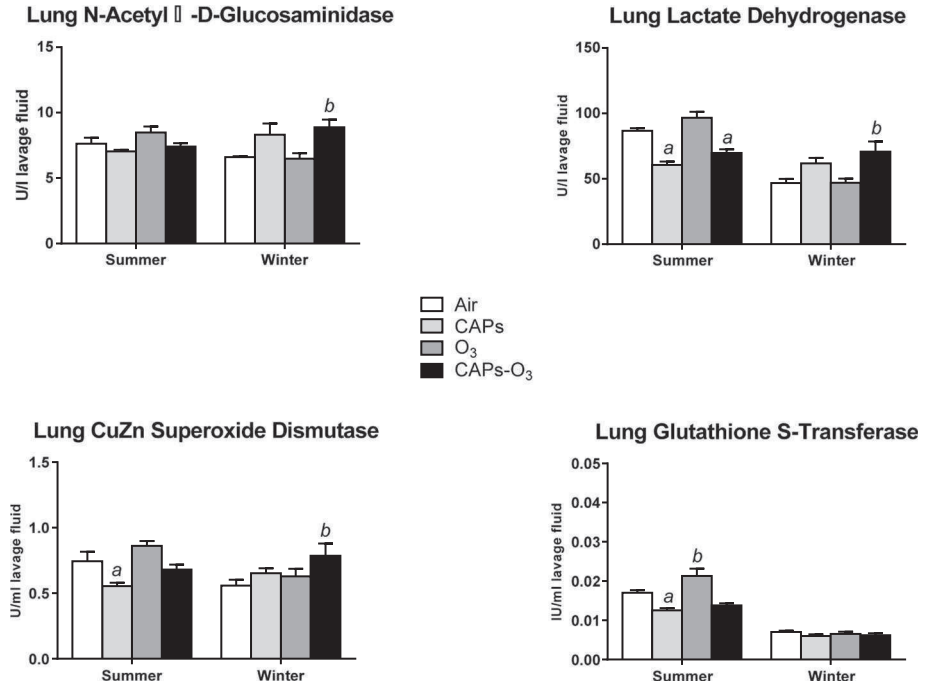

Figure 8 N-acetyl B-D glucosaminidase, lactate dehydrogenase, CuZn superoxide dismutase, and glutathione S-transferase in lung lining fluid one day after summer or winter exposures to concentrated ambient particulate (CAPs), ozone (O_3), CAPs + O_3, or filtered air. Bars represent means ± SEM for each marker shown (n = 6/group). a - significantly less than filtered air control $p < 0.05$). b - significantly greater than filtered air control ($p < 0.05$).

achievement of target concentrations comparable to summer levels with our concentration system. Therefore, one approach to control for seasonal differences in mass is to lower target concentrations. Moreover, the size of the particle is naturally an outcome of the type of local air pollution sources, the level of air pollution and weather conditions. Future studies that focus on exposure to ultrafine PM alone can obviate this concern.

Conclusions

These findings collectively point to marked seasonal effects on PM sources, mass, size, composition, and corresponding impacts on cardiovascular responses. While there was variability in some responses in this study, particularly sensitivity to aconitine-induced arrhythmia and indicators of inflammation/injury, there was evidence of electrocardiographic and autonomic responses that were unique to the CAPs and O_3 co-exposure group. This study, however, was limited by the small number of PM sampling and exposure days, which precluded drawing conclusions about effects of entire seasons. This is especially relevant given that winter conditions often induce stable inversions that increase levels of ambient PM. Moreover, because PM composition data was obtained from only a few samples in the present study, an analysis of a potential association between cardiovascular responses and specific components of PM was not possible. In addition, the absence of nitrogen species data provides some uncertainty in the source apportionment analysis. Future studies that examine the interactive effects of CAPs and O_3 should also mirror realistic seasonal O_3 concentrations. Nevertheless, some evidence of unique co-pollutant effects during both seasons suggests that a multipollutant approach to health effects assessment is warranted. Furthermore, seasonal variability in sources of anthropogenic emissions and evidence for winter elemental enrichment and smaller particle size suggest that PM size and composition may be as important as mass in determining its potential for interactive health effects with other pollutants.

Methods

Animals

Twelve week-old male SH rats (Charles River, Raleigh, NC) were housed in plastic cages (one per cage), maintained on a 12-hr light/dark cycle at approximately 22°C and 50% relative humidity in our Association for Assessment and Accreditation of Laboratory Animal Care-approved facility, and held for a minimum of 1 week before telemeter implantation. The Institutional Animal Care and Use Committee of the U.S. Environmental Protection Agency approved all protocols. Food (Prolab RMH 3000; PMI Nutrition International, St. Louis, MO)

and water were provided ad libitum, and all rats were grouped by weight. SH rats were selected because previous studies demonstrated exaggerated sensitivity to the effects of air pollution compared to rats with normal blood pressure [20,45,46].

Telemeter implantation

Animals (SH rats; n = 7 per group) were anesthetized with ketamine/xylazine (80 mg/ml ketamine HCL and 12 mg/ml xylazine HCL; 1 ml/kg i.p.; Sigma Chemical Co., St. Louis, MO), and were implanted with radiotelemeters (Model TA11CTA-F40; Data Science International, Inc., St. Paul, MN) in the abdominal cavity as previously described [47]. Electrode leads were guided through incisions made in the abdominal musculature. Leads were tunneled subcutaneously and secured in a lead II configuration. Body heat was maintained during and after surgery using a heating pad. Animals recovered for two weeks after surgery before inhalation studies.

Experimental design

SH rats (n = 6/group) surgically implanted with biopotential telemeters were exposed once for 4 hours to concentrated ambient particulate matter (target concentration 150 μg/m^3) with or without 0.2 ppm ozone. To compare the effects of season on health effects of this multipollutant mixture, exposures were conducted in the summer (August, 2011) and winter (February and March, 2012) seasons. Telemetered signals included body temperature, ECG, heart rate, and activity and were monitored before, during, and after exposure in conscious, unrestrained rats. All telemetered rats were euthanized one day after final exposure. Aconitine challenge was performed to assess sensitivity to the triggering of arrhythmia in a separate cohort of concurrently exposed rats one day after exposure.

Exposure schedule

A series of particulate matter and O_3 exposures were conducted in summer of 2011 and winter 2011–12. The study protocol included single 4-hour exposures for CAPs only, CAPs + O_3, O_3 only, and filtered air control groups. Upstream of the CAPs only chamber, air passed through a silica gel dryer that reacted with ambient O_3 and helped keep background O_3 levels in the CAPs only chamber at levels similar to the filtered air control chamber O_3 levels. Animals were allowed 15 to 30 minutes to acclimate to the system's noise and chamber environment then telemetry background measurements were performed for ~45 min. Exposures were initiated at about 7:30 am and continued until 11:30 am for each animal group. For all exposures, initial target $PM_{2.5}$ concentration was ~150 to 200 ug/m^3 while the O_3 target concentration was 200 ppb. To facilitate telemetric monitoring within each chamber CAPs and CAPs + O_3 groups during the summer exposures were split into two cohorts and exposed on either 8/17/11 or 8/18/11. The O_3 only and air groups were also split into two cohorts and exposed on either 8/23/11 or 8/24/11. Winter CAPs and CAPs + O_3 exposures were carried out on 2/17/12, 2/18/12, and 3/7/12. Winter O_3 only and air exposures took place on 2/23/12 and 2/24/12. Each animal group was acclimated to the exposure system and laboratory environmental noises by housing in an exposure chamber with room and CAPs systems operated to produce background noise for a minimum of 1 hour a day for 2 days prior to the exposures.

Ambient weather patterns

Studies involving exposures of animals to concentrated ambient air particles involve sampling outside air in real-time. Local weather conditions and patterns can have a dramatic effect on these real time studies. Ambient weather conditions were monitored during each exposure using a weather station mounted on the roof (Vantage Pro II, Davis Instruments, Hayward, CA) of the U.S. EPA exposure facility in Durham, NC. Data collected included temperature, relative humidity, dew point, barometric pressure, wind speed and direction, rainfall, and other variables providing information about the air mass being drawn from outside into the system during exposures. Data recorded during the times animals were resident in chambers were averaged to produce individual exposure values. Daily values were then averaged to generate group average ambient weather conditions. Exposure group averages are included in Table 1. Additionally, backward trajectory air mass plots were obtained from on-line resources developed by the National Oceanic and Atmospheric Administration (NOAA). Models queried included Hybrid Single Particle Lagrangian Integrated Trajectory Model (HYSPLIT) using the Real-Time Environmental Applications and Display sYstem (READY) [48], which utilized archived meteorological data to model direction and temporal air mass location. The resultant models indicate the path and location of an air mass in 6 hour increments for the 24 hours local time leading up to each PM exposure.

Chamber systems

All exposures were conducted in the U. S. EPA's Research Triangle Park, NC Consolidated Research Facility (CRF), Concentrated Air Particles (CAPs) Laboratory located at 179 T.W. Alexander Dr., RTP, NC. EPA's CAPs exposure facility accommodated 3 Hinners style, stainless steel and glass, 0.3 m^3 whole body chambers (Figure 9). Each chamber was modified to expose animals to ozone and clean air as well as CAPs. The wire mesh animal cages were modified and receivers positioned within each chamber to maximize telemeter signal transmission and

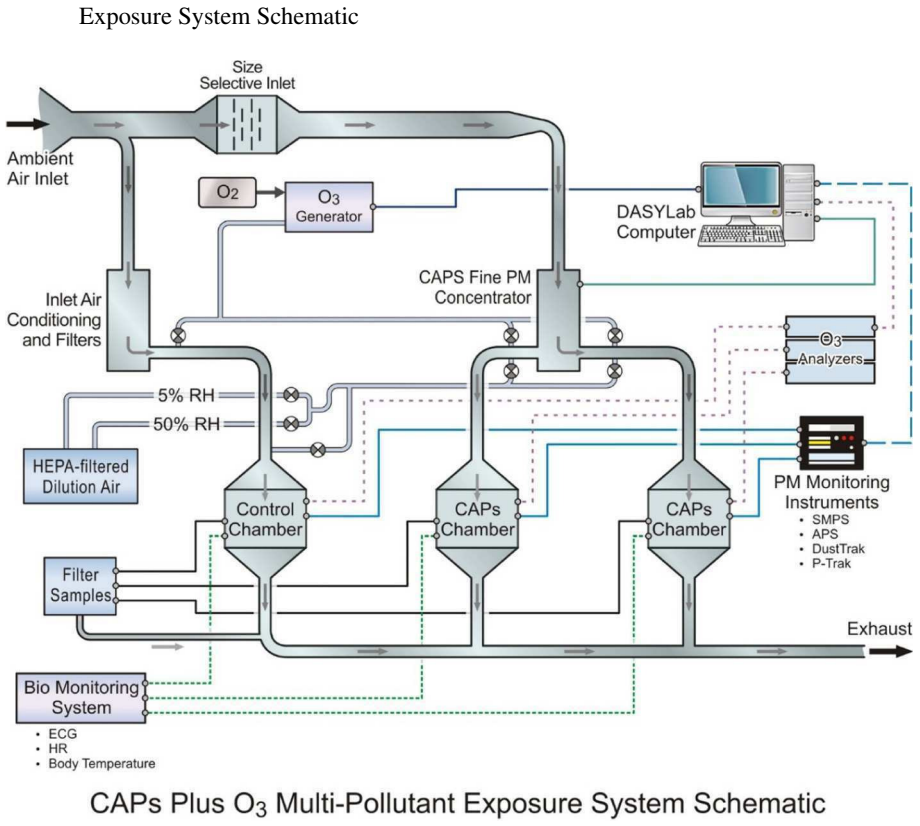

Figure 9 Schematic of concentrated ambient particulates (CAPs) and ozone (O_3) co-exposure system showing concentrator, O_3 generator, exposure chambers, and particulate matter (PM) and O_3 monitoring systems. Receivers were placed within each chamber to monitor electrocardiogram, heart rate and body temperature. Particle concentration and sizing were tracked in real-time using a scanning mobility particle sizer and an aerodynamic particle sizer. Additional aerosol monitors (DustTrak and P-Trak) were used to track PM levels in real-time.

minimize effects on chamber PM distribution. Two CAPs chambers were connected to the outlet of a $PM_{2.5}$ fine particle concentrator (Harvard Fine Particle Concentrator, Harvard University, Boston, MA; HFPC) [49]. Stainless steel tubing (3" diameter) with quick connecting joints was used to transport Air/PM from the concentrator outlet to the designated chamber(s). Transport tubing was configured to deliver all CAPs to a single chamber, split concentrated PM between two chambers, or to totally bypass chambers allowing for gas pollutant or clean air operation. Chamber temperature, relative humidity, air flow, and static pressure and test agent concentrations for PM and O_3 were continuously monitored, displayed, and recorded by the lab's computerized electronic data acquisition system. Clean, charcoal and HEPA filtered, and conditioned dilution air was available from two sources (Core Inhalator System (CIS) supply air, DP = ~55 F, 50% relative humidity (RH), and Medical Grade Air, DP = ~ −20 F, ~5% RH). The two dilution air streams were blended to regulate chamber RH and peak PM concentrations. Chamber environmental data, PM, and O_3 concentrations from multiple exposures within each group were averaged to produce mean values for each exposure group.

PM concentrating system and PM monitoring and control

Outside ambient air containing PM was drawn into the system inlet via a stainless steel duct. The air/PM mixture passed through a custom Size Selective Inlet (SSI) (2 sizing stages: 10 μm and 2.5 μm) (Harvard School of Public Health, Boston, Ma) [50] which removed PM > 2.5 μm. The resulting mixture of Air/$PM_{2.5}$ was transported to the exposure laboratory where it passed through the HFPC operating with 3 stages of slit virtual impactors and outputting ~50 Lpm of Air/CAPs as previously described [28].

CAPs chamber PM concentrations were monitored using both filter weights and real-time electronic instrumentation. Filter samples were collected for all PM exposures to provide gravimetric mass concentrations and for subsequent chemical analysis. Samples included: Teflon 47 mm (Pall Corp., TeFlo, R2PJ047, 2 μm pore) and 37 mm (Pall Corp., TeFlo, R2PJ037, 2 μm pore), Quartz

(Millipore, Quartz, AQFA04700, 47 mm), and Nylon (PALL, Nylasorb, 66509, 47 mm) filters. Particle concentration and sizing were tracked in real-time using scanning mobility particle sizer (SMPS, TSI Inc., St. Paul, MN) and aerodynamic particle sizer (APS, model 3321, TSI Inc., St. Paul, MN). PM data were analyzed and combined using particle data analytical software (Data Merge, ver. 1.0.1, TSI Inc, St. Paul, MN) to provide composite concentrations and particle size distributions representative of the average chamber PM. Data from multiple exposures was combined and averaged to provide concentrations and particle size distributions for each group. Additional aerosol monitors (DustTrak (DT), model 8520, TSI Inc., St. Paul, MN and P-Trak, model 8525, TSI Inc., St. Paul, MN) were used to track PM levels in real time. Peak PM concentrations, chamber pressures, and RH were controlled by regulating injection of conditioned, filtered dilution air upstream of the chamber inlets. Filtered and conditioned air supplied to the O_3 and Air Control groups contained only trace levels of PM with insufficient sample available for weighing or chemical analysis, therefore, no PM samples were collected from those exposures.

Ozone generation, monitoring, and control

Source O_3 was generated using O_2 from compressed gas cylinders fed through a silent arc O_3 generator (OREC, Osmonics Corp.). All wetted surfaces of the O_3 generating and monitoring systems were either stainless steel or Teflon. Flow through the generator was modulated so an excess of gas was always flowing to keep stock O_3 concentrations stable during exposures. Excess O_3 gas was continuously vented into the lab fume hood exhaust. Chamber O_3 supply flow was controlled to establish and maintain target O_3 concentration. Mass flow controllers (MFC) (Tylan Corp., model FC260) were used to control both excess and chamber O_3 flows. Manual and automated MFC command signals were regulated by the CAPs lab data acquisition system (DAS) running data acquisition and control software (DASYLab Pro, version 9, MCC). O_3 was injected counter current into the chamber inlet air duct upstream of the dilution air inlet to enhance mixing prior to entering the chamber. O_3 concentration was manually and/or automatically regulated via a feedback loop. Real-time O_3 concentrations for each group, including Air Controls, were monitored during all exposures. A continuous O_3 analyzer (TECO, model 49, Thermo Electron Co.,) measured chamber O_3 levels in the animal breathing zone and provided concentration signals to the laboratory's data system. Our laboratory operated under a strict quality assurance plan for all exposures. For the duration of the study, O_3 monitoring was performed to manufacturer's and EPA guidelines and under non-condensing conditions. The O_3 Gas analyzer was calibrated using a certified EPA/National Institute of Standards and Technology O_3 transfer standard prior to each study segment with routine zero and span checks and post study calibration verifications. The analyzer was preconditioned by continuous sampling of lab air at 72 F / 50% RH. Clean, conditioned dilution air regulated chamber RH and PM levels (therefore, O3 sample RH) which measured in the range 42.6% to 56.5% daily average during all exposures (Table 1). O_3 sampling system included an inline PM filter (Teflon 47 mm, Pall Corp., TeFlo, R2PJ047, 2 μm pore). The DAS monitored, displayed, recorded, and controlled chamber O_3 concentration and other system operating variables such as temperature, RH, static pressure, and chamber exhaust flow. Chamber O_3 concentration was controlled for the duration of each exposure to provide a target final average concentration of ~200 ppb for each run. During exposures, O_3 flow control was periodically set to manual and maintained at steady state while the O_3 analyzer was briefly cycled to monitor background O_3 chambers (CAPs only or Air Controls). After background levels were determined, O_3 monitoring returned to the O_3 (or CAPs + O_3) exposure chamber under DAS automated control. Outside air passing through the HFPC/CAPs PM concentrator contained naturally occurring ambient O_3. During CAPs only exposures it was desirable to eliminate this naturally occurring O_3 to the extent possible without affecting CAPs chamber PM levels. Upstream of the CAPs only chamber, air passed through a silica gel dryer that reacted with ambient O_3 and helped keep background O_3 levels in the CAPs only chamber at levels similar to the filtered air control chamber O_3 levels.

PM organic and elemental chemical analysis

Organic and elemental carbon contents of CAPs PM collected on quartz filters during exposure were measured using National Institute of Occupational Health (NIOSH) Method 5040 [51]. NIOSH 5040 is a thermo-optical method, based on sequential pyrolytic vaporization and detection of the carbon fractions. Elemental analysis was performed on aqua regia digests of CAP collected on Teflon filters. Prior to digestion, filter media were removed from their polymethylpentene support rings using Teflon blades. Filters were then submerged in 1 mL of concentrated hydrochloric acid (Optima grade, Fisher Scientific) in cleaned 15-ml polypropylene centrifuge tubes (part number 05-539-5, Fisher Scientific; washed in 1% Triton X-100, rinsed with ultrapure deionized water (Milli-Q, Millipore Corporation) and dried in a Class 100 cleanbench). Tubes were sonicated three times in an ultrasonic bath (Model TI-H15, Elma GmbH&Co, Singen Germany) at a frequency of 25 kHz at 200 W for 30 min at 50C°. After each sonication, tubes were cooled to room

temperature and vented in a fume hood. After the third sonication and venting, tubes were heated in an oven overnight at 60C°. The next morning, 0.33 mL of concentrated nitric acid (Optima grade, Fisher Scientific) was added to the tubes to form 3:1 aqua regia, and the same sonication and overnight heating procedure was performed as the preceding day. The following morning, 10 ml of ultrapure water was added, and the teflon filters removed from the tubes using cleaned Teflon forceps. Samples were then analyzed by high-resolution inductively coupled plasma-mass spectrometry (HR-ICP-MS, Element 2, Thermo Scientific).

Source apportionment analysis

Sources contributing to the CAPS and CAPS + O3 mixtures during the summer and winter exposures were quantified using the EPA Chemical Mass Balance Model (CMB 8.2; US EPA, 2004) [19]. The CMB estimates PM sources using a weighted least squares regression. Input data included elements, sulfate, organic carbon and elemental carbon concentrations and uncertainties as well as measured source profile concentrations and uncertainties. The road dust and brake wear profiles were obtained from Hildemann et al. [52] and the mobile source profile (which includes gasoline and diesel emissions) was obtained from Maykut et al. [53]. The wood combustion profile was obtained from Fine et al. [54]. The secondary sulfate and marine salt profiles were obtained from the EPA SPECIATE 4.4 Database. The same profiles and species were used for the summer and winter exposure mixtures.

Radiotelemetry data acquisition

Radiotelemetry methodology (Data Sciences International, Inc.) allowed constant monitoring of electrocardiographic data in conscious and unrestrained rats from implantation until sacrifice. Electrocardiographic data was monitored by remote receivers (DataART3.01; Data Sciences International, Inc.) positioned under the home cages within the animal facility, and under the exposure cages within the exposure chambers. In home cages, sixty-second segments of ECG waveforms were acquired and saved at 15-minute intervals from surgical recovery through sacrifice not including the exposure period. Pre-exposure baseline data was collected from home cages, as well as a 45 min baseline in exposure cages after acclimation for one hour. During the 4 hr exposure, sixty-second segments were acquired and saved at 5-minute intervals. After exposure, rats were monitored in home cages until the next exposure. All rats were monitored until the beginning of necropsy, approximately 18 hrs after exposure. HR was automatically obtained from the ECG waveforms with data acquisition software (DataART3.01; Data Sciences International, Inc.).

Electrocardiogram, arrhythmia identification and heart rate variability analysis

ECGAuto software (EMKA Technologies, Falls Church, VA) was used for automated analyses of ECG wave amplitudes and segment durations and areas, as well as for the visual identification and enumeration of arrhythmias and HRV analysis. Several parameters were determined for each ECG waveform: heart rate; PR interval; R amplitude; QRS duration, amplitude, and area; ST interval, amplitude, and area; and T-wave amplitude and area; QT interval, Bazett's heart rate–corrected QT interval (QTc). ECG and HRV parameters were quantified in the immediate 6-hour period after exposure and compared to time-matched data before exposure while the rats were unrestrained in their home cages. ECG parameters during exposure were analyzed relative to baseline (45 min recordings while in the exposure chambers immediately before the beginning of exposure).

Cardiac arrhythmic events were identified in part by using the Lambeth conventions [55] as a guideline for the identification of arrhythmias in rats. Arrhythmias were identified as atrial premature beats (APB), ventricular premature beats (VPB), sinoatrial block (SAB), atrioventricular block (AVB), or ventricular tachycardia (VT). Arrhythmias were quantified and totaled during the 4 hour exposure period and during the 6 hour period after exposure and compared to pre-exposure counts. Total arrhythmia counts during exposure were quantified (total of 48 one-minute segments during 4 h exposure period).

For the analysis of HRV, rhythms were thoroughly inspected to identify and exclude arrhythmias, artifacts, and 1-min ECG waveforms lacking distinguishable R waves for more than 30 sec. The analysis of HRV generated HR and time-domain measures, including mean time between adjacent QRS complex peaks (the RR interval), a standard deviation of the RR interval (SDNN), SDNN normalized for the effects of heart rate [SDNN/(RR interval x 100)], and the square root of the mean of squared differences of adjacent RR intervals (RMSSD). The SDNN represents overall HRV, whereas RMSSD represents parasympathetic influence over HR. The analysis of HRV also calculated frequency domain parameters including the LF and HF, and the ratio of these two frequency domains (LF/HF). LF is generally believed to represent a combination of sympathetic and parasympathetic tones, whereas HF indicates cardiac vagal (parasympathetic) tone, and LF/HF serves as an index of sympathovagal balance.

Aconitine challenge

One day after exposure to CAPs, O_3, CAPs + O_3, or filtered air, a separate cohort of animals were anesthetized with urethane (1.5 g/kg, *ip*) and underwent the aconitine challenge; supplemental doses of the anesthetic were administered intravenously when necessary to abolish pain reflex. Animal body temperature was maintained at ~36°C with a heating pad. The left jugular vein was cannulated with P.E. 50 polyethylene tubing for the administration of aconitine. Ten μg/ml aconitine was continuously infused at a speed of 0.2 ml/min while ECG was continuously monitored and timed. Sensitivity to arrhythmia was measured as the threshold dose of aconitine required to produce VPBs, VT, and VF, and was calculated using the following formula:

$$\begin{aligned}&\text{Threshold dose (μg/kg) for arrhythmia}\\&= 10\mu g/ml \text{ x } 0.2ml/\text{ min}\\&\quad \times \text{ time required for inducing arrhythmia (min)}\\&\quad /\text{body weight (kg)}\end{aligned}$$

Necropsy, blood collection and lung lavage

Rats were deeply anesthetized with i.p. injection of Euthasol (200 mg/kg sodium pentobarbital and 25 mg/kg phenytoin; Virbac Animal Health, Ft. Worth Texas) one day after exposure. Blood samples were collected from the abdominal aorta. The trachea was cannulated and the right lung (except for the caudal lobe) was lavaged with a total volume of 20 ml/kg of Ca^{2+}, Mg^{2+}, and phenol red-free Dulbecco's phosphate buffered saline (SAFC Biosciences, Lenexa MD) divided into 2 equal aliquots. The caudal lobe was collected for RNA analysis. Cytospins and cells differentials on lavaged cell samples, assays for total protein (Thermo Fisher Diagnostics, Rockford, IL), albumin (Diasorin, Stillwater, MN), LDH (Thermo DMA, Louisville, CO), NAG (Roche Diagnostics, Mannheim, Germany) superoxide dismutase (Randox Laboratories LTD Crumlin, CO), glutathione peroxidase, and glutathione S-transferase (Glathione peroxidase and transferase were based on an in-house automated analysis [56]) on lavage supernatants, serum C-reactive protein and fibrinogen (Diasorin, Stillwater, MN), creatine kinase (Fisher Diagnostics, Middletown, VA), sorbitol dehyrdogenase and creatinine (Sekisui Diagnostics, Charlottetown Prince Edward Island, Canada), high density (HDL) and low density (LDL) lipoprotein cholesterol and plasma angiotensin converting enzyme (Fisher Diagnostics, Middletown, VA) were conducted as previously described [20].

Statistics

The statistical analyses of ECG, HRV, and biochemical and inflammatory data in this study were performed using SAS software version 9.2 (SAS Institute Inc, Cary, NC). We used PROC MIXED of SAS because it offers greater flexibility for the modeling of repeated measures data than PROC GLM. It is also suitable for analysis of large, unbalanced data with missing data at random. A linear mixed model with restricted maximum-likelihood estimation analysis, least squares means and repeated measures ANOVA (analysis of variance) was used to determine which TIME*TRT interactions were statistically significant between baseline and exposure. Multiple comparison adjustment for the p values and confidence limits for the differences between the least squares means was done using adjust = Tukey HSD (Honest Significant Difference) test.

Additional files

Additional file 1: Table S1. Average source contributions for summer and winter exposures in μg/m^3. Percent of mass in parenthesis.

Additional file 2: Figure S1. Average source contributions for summer and winter Exposures.

Additional file 3: Table S2. Source contributions for summer exposures by exposure day in μg/m^3 (standard deviation in parenthesis).

Additional file 4: Table S3. Source contributions for winter exposures by exposure day in μg/m^3 (standard deviation in parenthesis).

Additional file 5: Table S4. Heart Rate Variability data before and after exposure.

Abbreviations

ANOVA: Analysis of variance; APB: Atrial premature beat; AVB: Atrioventricular block; Cal factor: Calibration factor; CAPs: Concentrated ambient particulates; CIS: Core inhalation system; CMB: Chemical mass balance; CRF: Consolidated research facility; CuZn SOD: Copper zinc superoxide dismutase; DAS: Data acquisition system; DP: Dew point; ECG: Electrocardiogram; GST: Glutathione S-transferase; HDL: High density lipoprotein; HF: High frequency; HFPC: Harvard fine particle concentrator; HR: Heart rate; HRV: Heart rate variability; HSD: Honest significant difference; HYSPLIT: Hybrid single particle lagrangian integrated trajectory; LDH: Lactate dehydrogenase; LDL: Low density lipoprotein; LF: Low frequency; LF/HF: Ratio of low frequency domain to high frequency domain; MFC: Mass flow controller; NAG: N-Acetyl-D-glucosaminidase; NIOSH: National Institute of Occupational Safety and Health; NOAA: National Oceanic and Atmospheric Administration; O_3: Ozone; PM: Particulate matter; $PM_{2.5}$: Particulate matter with an aerodynamic diameter less than 2.5 microns; READY: Real-time environmental applications and display sYstem; RH: Relative humidity; RMSSD: Root means squared of successive differences; SDNN: Standard deviation of the time between normal-to-normal beats; SH: Spontaneously hypertensive; SSI: Size selective inlet; TRP: Transient receptor potential; US EPA: United States Environmental Protection Agency; UTC: Universal Time Coordinated; VF: Ventricular fibrillation; VPB: Ventricular premature beat; VT: Ventricular tachycardia.

Competing interests

The authors declare that they have no competing interests.

Authors' contributions

AF conceived of, designed and managed the study and drafted the manuscript, LW engineered the exposure system, carried out all exposures, monitored various exposure parameters, and collected PM filters for elemental analysis, NHC participated in the design of the study, data acquisition, surgeries, and performed the statistical analysis, FM performed all electrocardiogram and heart rate variability analyses, JM and KK performed the organic and elemental analysis, DW participated in the telemetry set-up, data acquisition, and surgeries, RD performed the source apportionment analysis, MH assisted with the design of the exposure system, WC helped

draft the manuscript and assist with data interpretation, MSH participated in the design, conception and coordination of the study and performed the aconitine challenge tests. All authors read and approved the final manuscript.

Acknowledgements
The authors would like to thank David Davies of the U.S. EPA for his derivation of airflow trajectories, Judy Richards of the U.S. EPA for her excellent technical assistance, Drs. M. Ian Gilmour, Jan Dye, Daniel L. Costa, and William Linak, also of the U.S. EPA, for their thorough review of this manuscript, John Havel and Keith Tarpley of SRA International, Inc. for producing the illustrations, and the Air Resources Laboratory of the NOAA for use of their airflow trajectory models.

Disclaimer
This paper has been reviewed and approved for release by the National Health and Environmental Effects Research Laboratory, U.S. Environmental Protection Agency. Approval does not signify that the contents necessarily reflect the views and policies of the U.S. EPA, nor does mention of trade names or commercial products constitute endorsement or recommendation for use.

Author details
[1]Environmental Public Health Division, US EPA, 109 TW Alexander Drive, Research Triangle Park, Durham, NC 27711, USA. [2]Human Exposure and Atmospheric Sciences Division, US EPA, 109 TW Alexander Drive, Research Triangle Park, Durham, NC 27711, USA.

Received: 5 December 2014 Accepted: 26 March 2015
Published online: 06 May 2015

References

1. Bell ML, Dominici F, Ebisu K, Zeger SL, Samet KM. Spatial and temporal variation in PM2.5 chemical composition in the United States for health effects studies. Environ Health Perspect. 2007;115:989–95.
2. Bell ML, Ebisu K, Peng RD, Walker J, Samet JM, Zeger SL, et al. Seasonal and regional short-term effects of fine particles on hospital admissions in 202 US Counties, 1999–2005. Am J Epidemiol. 2008;168:1301–10.
3. Goldberg MS, Burnett RT, Valois MF, Flegel K, Bailar III JC, Brook J, et al. Associations between ambient air pollution and daily mortality among persons with congestive heart failure. Environ Res. 2003;91:8–20.
4. Plummer LE, Ham W, Kleeman MJ, Wexler A, Pinkerton KE. Influence of season and location on pulmonary response to California's San Joaquin Valley airborne particulate matter. J Toxicol Environ Health A. 2012;75(5):253–71.
5. Tablin F, den Hartigh LJ, Aung HH, Lame MW, Kleeman MJ, Ham W, et al. Seasonal influences on CAPs exposures: differential responses in platelet activation, serum cytokines and xenobiotic gene expression. Inhal Toxicol. 2012;24(8):506–17.
6. Happo MS, Hirvonen MR, Hälinen AI, Jalava PI, Pennanen AS, Sillanpää M, et al. Seasonal variation in chemical composition of size-segregated urban air particles and the inflammatory activity in the mouse lung. Inhal Toxicol. 2010;22(1):17–32.
7. Becker S, Dailey LA, Soukup JM, Grambow SC, Devlin RB, Huang YC. Seasonal variations in air pollution particle-induced inflammatory mediator release and oxidative stress. Environ Health Perspect. 2005;113(8):1032–8.
8. Happo M, Markkanen A, Markkanen P, Jalava P, Kuuspalo K, Leskinen A, et al. Seasonal variation in the toxicological properties of size-segregated indoor and outdoor air particulate matter. Toxicol In Vitro. 2013;7(5):1550–61.
9. Mauderly JL, Samet JM. Is there evidence for synergy among air pollutants in causing health effects? Environ Health Perspect. 2009;117(1):1–6.
10. Fakhri AA, Ilic LM, Wellenius GA, Urch B, Silverman F, Gold DR, et al. Autonomic effects of controlled fine particulate exposure in young health adults: effect modification by ozone. Environ Health Perspect. 2009;117(8):1287–92.
11. Sivagangabalan G, Spears D, Masse S, Urch B, Brook RD, Silverman F, et al. The effect of air pollution on spatial dispersion of myocardial repolarization in healthy human volunteers. J Am Coll Cardiol. 2011;57(2):198–206.
12. Wagner JG, Allen K, Yang HY, Nan B, Morishita M, Mukherjee B, et al. Cardiovascular depression in rats exposed to inhaled particulate matter and ozone: effects of diet-induced metabolic syndrome. Environ Health Perspect. 2014;122:27–33.
13. Sun L, Liu C, Xu X, Ying Z, Maiseyeu A, Wang A, et al. Ambient fine particulate matter and ozone exposures induce inflammation in epicardial and perirenal adipose tissues in rats fed a high fructose diet. Part Fibre Toxicol. 2013;10:43.
14. Aneja VP, Wang B, Tong DQ, Kimball H, Steger J. Characterization of major chemical components of fine particulate matter in North Carolina. J Air Waste Manag Assoc. 2006;56(8):1099–107.
15. Carll AP, Lamb C, Hazari MS, Winsett DW, Krantz QT, Costa DL KC, et al. Whole and particle-free diesel exhausts differentially affect cardiac electrophysiology, blood pressure, and autonomic balance in heart failure-prone rats. Toxicol Sci. 2012;128:490–9.
16. Farraj AK, Hazari MS, Winsett DW, Kulukulualani A, Carll AP, Haykal-Coates N, et al. Overt and Latent Cardiac Effects of Ozone Inhalation in Rats: Evidence for Autonomic Modulation and Increased Myocardial Vulnerability. Environ Health Perspect. 2012;120:348–54.
17. Hazari MS, Haykal-Coates N, Winsett DW, Costa DL, Farraj AK. A single exposure to particulate or gaseous air pollution increases the risk of aconitine-induced cardiac arrhythmia in hypertensive rats. Toxicol Sci. 2009;112(2):532–42.
18. Lamb CM, Hazari MS, Haykal-Coates N, Carll AP, Krantz QT, King C, et al. Divergent electrocardiographic responses to whole and particle-free diesel exhaust inhalation in spontaneously hypertensive rats. Toxicol Sci. 2012;125:558–68.
19. US EPA, 2004. EPA-CMB8.2 User's Manual. EPA-452/R-04-011. Research Triangle Park, NC.
20. Farraj AK, Haykal-Coates N, Winsett DW, Hazari MS, Carll AP, Rowan III WH, et al. Increased Non-conducted P-wave arrhythmias after a single Oil Fly Ash inhalation exposure in hypertensive rats. Environ Health Perspect. 2009;117(5):709–15.
21. Farraj AK, Hazari MS, Haykal-Coates N, Lamb C, Winsett DW, Ge Y, et al. ST depression, arrhythmia, vagal dominance, and reduced cardiac micro-RNA in particulate-exposed rats. Am J Respir Cell Mol Biol. 2011;44(2):185–96.
22. Hazari MS, Haykal-Coates N, Winsett DW, Krantz QT, King C, Costa DL, et al. TRPA1 and sympathetic activation contribute to increased risk of triggered cardiac arrhythmias in hypertensive rats exposed to diesel exhaust. Environ Health Perspect. 2011;119(7):951–7.
23. Boman BC, Forsberg AB, Järvholm BG. Adverse health effects from ambient air pollution in relation to residential wood combustion in modern society. Scand J Work Environ Health. 2003;29(4):251–60.
24. Boman BC, Nordin A, Boström D, Öhman M. Characterization of inorganic particulate matter from residential combustion of pelletized biomass fuels. Energ Fuels. 2004;18:338–48.
25. Ostro B, Feng W-Y, Broadwin R, Green S, Lipsett M. The effects of components of fine particulate air pollution on mortality in California: results from CALFINE. Environ Health Perspect. 2007;114:13–9.
26. Ghio AJ, Devlin RB. Inflammatory lung injury after bronchial instillation of air pollution particles. Am J Respir Crit Care Med. 2001;164(4):704–8.
27. Huang YC, Ghio AJ, Stonehuerner J, McGee J, Carter JD, Grambow SC, et al. The role of soluble components in ambient fine particles-induced changes in human lungs and blood. Inhal Toxicol. 2003;15(4):327–42.
28. Kodavanti UP, Schladweiler MC, Ledbetter AD, McGee JK, Walsh L, Gilmour PS, et al. Consistent pulmonary and systemic responses from inhalation of fine concentrated ambient particles: roles of rat strains used and physicochemical properties. Environ Health Perspect. 2005;113(11):1561–8.
29. Brook RD, Rajagopalan S, Pope III CA, Brook JR, Bhatnagar A, Diez-Roux AV, et al. Particulate matter air pollution and cardiovascular disease: An update to the scientific statement from the American Heart Association. Circulation. 2010;121:2331–78.
30. Cho SH, Tong H, McGee JK, Baldauf RW, Krantz QT, Gilmour MI. Comparative toxicity of size-fractionated airborne particulate matter collected at different distances from an urban highway. Environ Health Perspect. 2009;117(11):1682–9.
31. Kim YH, Tong H, Daniels M, Boykin E, Krantz QT, McGee J, et al. Cardiopulmonary toxicity of peat wildfire particulate matter and the predictive utility of precision cut lung slices. Part Fibre Toxicol. 2014;11:29.
32. Rohr AC, Kamal A, Morishita M, Mukherjee B, Keeler GJ, Harkema JR, et al. Altered heart rate variability in spontaneously hypertensive rats is associated with specific particulate matter components in Detroit, Michigan. Environ Health Perspect. 2011;119:474–80.

33. Chuang K-J, Chan C-C, Chen N-T, Su T-C, Lin L-Y. Effects of particle size fractions on reducing heart rate variability in cardiac and hypertensive patients. Environ Health Perspect. 2005;113:1693–7.
34. Muggenburg BA, Barr EB, Cheng YS, Seagrave JC, Tilley LP, Mauderley JL. Effect of inhaled residual oil fly ash on the electrocardiogram of dogs. Inhal Toxicol. 2000;12 Suppl 4:189–208.
35. Schulz H, Harder V, Ibald-Mulli A, Khandoga A, Koenig W, Krombach F, et al. Cardiovascular effects of fine and ultrafine particles. J Aeros Med. 2005;18(1):1–22.
36. Vallejo M, Ruiz S, Hermosillo AG, Borja-Aburto VH, Cardenas M. Ambient fine particles modify heart rate variability in young healthy adults. J Expos Sci Environ Epid. 2006;16:125–30.
37. Schwartz J, Litonjua A, Suh H, Verrier M, Zanobetti A, Syring M, et al. Traffic related pollution and heart rate variability in a panel of elderly subjects. Thorax. 2005;60(6):455–61.
38. Zanobetti A, Gold DR, Stone PH, Suh HH, Schwartz J, Coull BA, et al. Reduction in heart rate variability with traffic and air pollution in patients with coronary artery disease. Environ Health Perspect. 2010;118(3):324–30.
39. Corey LM, Baker C, Luchtel DL. Heart-rate variability in the Apo lipoprotein E knockout transgenic mouse following exposure to Seattle particulate matter. J Toxicol Environ Health Part A. 2006;69:953–65.
40. Bigger Jr JT, Fleiss JL, Rolnitzky LM, Steinman RC. Frequency domain measures of heart period variability to assess risk late after myocardial infarction. J Am Coll Cardiol. 1993;21:729–36.
41. Fauchier L, Babuty D, Melin A, Bonnet P, Cosnay P, Fauchier JP. Heart rate variability in severe right or left heart failure: the role of pulmonary hypertension and resistances. Eur J Heart Failure. 2004;1(6):181–5.
42. Taylor-Clark TE, Undem BJ. Ozone activates airway nerves via the selective stimulation of TRPA1 ion channels. J Physiol. 2010;588(3):423–33.
43. Takahashi N, Mori Y. TRP channels as sensors and signal integrators of redox status changes. Front Pharmacol. 2011;2:58.
44. Costa DL: Air Pollution. In Casarett & Doull's Toxicology: The Basic Science of Poison. 6th edition. Edited by Klaassen CD. New York: McGraw-Hill Companies, Inc; 2001:979–1012.
45. Perez CM, Hazari MS, Haykal-Coates N, Carll AP, Krantz QT, King C, et al. Hypoxia stress test reveals exaggerated cardiovascular effects in hypertensive rats after exposure to the Air pollutant acrolein. Toxicol Sci. 2013;132:467–77.
46. Carll AP, Lamb C, Hazari MS, Winsett DW, Krantz QT, Costa DL KC, et al. Diesel exhaust inhalation increases cardiac output, bradyarrhythmias, and parasympathetic tone in aged heart failure-prone rats. Toxicol Sci. 2013;131:583–95.
47. Watkinson WP, Campen MJ, Costa DL. Cardiac arrhythmia after exposure to residual oil fly ash particles in a rodent model of pulmonary hypertension. Toxicol Sci. 1998;41:209–16.
48. The READY system: [https://www.arl.noaa.gov/]
49. Sioutas C, Koutrakis P, Burton RM. A technique to expose animals to concentrated fine ambient aerosols. Environ Health Perspect. 1995;103(2):172–7.
50. Gupta T, Demokritou P, Koutrakis P. Development and performance evaluation of a high-volume ultrafine particle concentrator for inhalation toxicological studies. Inhal Toxicol. 2004;16(13):851–62.
51. The NIOSH Manual of Analytical Methods: [http://www.cdc.gov/niosh/docs/2003-154/pdfs/5040.pdf].
52. Hildemann LM, Markowski GR, Cass GR. Chemical composition of emissions from urban sources of fine organic aerosol. Environ Sci Technol. 1991;25:744–59.
53. Maykut NN, Lewtas J, Kim E, Larson TV. Source apportionment of PM2.5 at an urban IMPROVE site in Seattle, Washington. Sci Technol. 2003;37:5135–42.
54. Fine PM, Cass GR, Simoneit BRT. Chemical characterization of fine particle emissions from the wood stove combustion of prevalent United States tree species. Environ Eng Sci. 2004;21:705–21.
55. Walker MJA, Curtis MJ, Hearse DJ, Campbell RWF, Janse MJ, Yellon DM, et al. The Lambeth Conventions: guidelines for the study of arrhythmias in ischaemia, infarction, and reperfusion. Cardiovasc Res. 1988;22:447–55.
56. Jaskot RH, Charlet EG, Grose EC, Grady MA, Roycroft JH. An automated analysis of gluthione peroxidase, S-Transferase, and reductase activity in animal tissue. J Anal Tox. 1983;7:86–8.

Submit your next manuscript to BioMed Central and take full advantage of:

- **Convenient online submission**
- **Thorough peer review**
- **No space constraints or color figure charges**
- **Immediate publication on acceptance**
- **Inclusion in PubMed, CAS, Scopus and Google Scholar**
- **Research which is freely available for redistribution**

Submit your manuscript at
www.biomedcentral.com/submit

BioMed Central

Environmental Science & Technology

Article

Cite This: Environ. Sci. Technol. 2018, 52, 3071−3080

pubs.acs.org/est

Comparative Cardiopulmonary Effects of Particulate Matter- And Ozone-Enhanced Smog Atmospheres in Mice

Mehdi S. Hazari,*[,†] Kimberly M. Stratford,[‡] Q. Todd Krantz,[§] Charly King,[§] Jonathan Krug,[∥] Aimen K. Farraj,[†] and M. Ian Gilmour[†]

[†]Cardiopulmonary and Immunotoxicology Branch, Environmental Public Health Division, National Health and Environmental Effects Research Laboratory, U.S. Environmental Protection Agency, Research Triangle Park, North Carolina 27711, United States

[‡]Curriculum in Toxicology, University of North Carolina − Chapel Hill, Chapel Hill, North Carolina 27599, United States

[§]Inhalation Toxicology Facilities Branch, Environmental Public Health Division, National Health and Environmental Effects Research Laboratory, U.S. Environmental Protection Agency, Research Triangle Park, North Carolina 27711, United States

[∥]Exposure Methods and Measurement Division, National Exposure Research Laboratory, U.S. Environmental Protection Agency, Research Triangle Park, North Carolina 27711, United States

Downloaded via US EPA OFFICE OF ENVIRONMENTAL INFO on April 30, 2020 at 15:58:47 (UTC).
See https://pubs.acs.org/sharingguidelines for options on how to legitimately share published articles.

ABSTRACT: This study was conducted to compare the cardiac effects of particulate matter (PM)- (SA-PM) and ozone(O_3)-enhanced (SA-O_3) smog atmospheres in mice. Based on our previous findings of filtered diesel exhaust we hypothesized that SA-O_3 would cause greater cardiac dysfunction than SA-PM. Radiotelemetered mice were exposed to either SA-PM, SA-O_3, or filtered air (FA) for 4 h. Heart rate (HR) and electrocardiogram were recorded continuously before, during and after exposure. Both SA-PM and SA-O_3 increased heart rate variability (HRV) but only SA-PM increased HR. Normalization of responses to total hydrocarbons, gas-only hydrocarbons and PM concentration were performed to assess the relative contribution of each phase given the compositional variability. Normalization to PM concentration revealed that SA-O_3 was more potent in increasing HRV, arrhythmogenesis, and causing ventilatory changes. However, there were no differences when the responses were normalized to total or gas-phase only hydrocarbons. Thus, this study demonstrates that a single exposure to smog causes cardiac effects in mice. Although the responses of SA-PM and SA-O_3 are similar, the latter is more potent in causing electrical disturbances and breathing changes potentially due to the effects of irritant gases, which should therefore be accounted for more rigorously in health assessments.

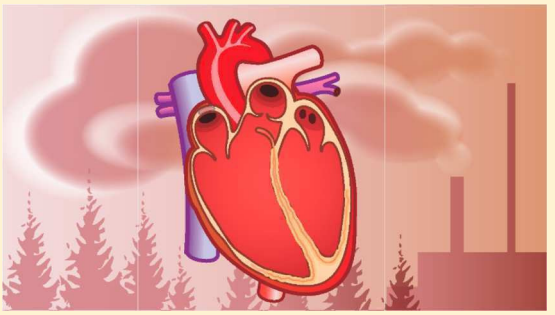

INTRODUCTION

The association between air pollution exposure and cardiovascular disease is well-established, particularly in people with certain risk factors like high blood pressure or those with pre-existing conditions.[1] The picture is less clear for healthy individuals and indeed there are still several unknowns with regards to how air pollution mediates cardiovascular dysfunction in this group, especially when there are no observable symptoms. In addition, nationwide variations in air pollution composition make it difficult to determine exactly which components, or combination of components, drive the response. This is the case for complex air pollution mixtures like smog, which originates as a set of primary pollutants (e.g., nitrogen oxides, volatile organic compounds) that are released from vehicles or industrial sources but thereafter transform after reacting with ultraviolet light to produce secondary pollutants like ozone and certain organic aerosols. Given these uncertainties, research studies need to address the comparative effects of multiple smog atmospheres and focus on determining which compositions, and hence components, cause the most serious health effects.

The American Heart Association cites several pathways by which air pollution, especially particulate matter (PM), leads to decrements in cardiovascular function.[2,3] These include elicitation of oxidative stress and inflammation, alteration of vasomotor properties, translocation of certain pollutants into the systemic circulation and modulation of autonomic controls which regulate the heart and vasculature. Some of these may not manifest as overt symptoms, especially in young healthy individuals, but instead as shifts in normal physiological function which render a person susceptible to subsequent stressors or triggers of adverse responses. We previously showed that exposure to a relatively low concentration of diesel exhaust, which contains many of the same pollutants as smog, caused increased arrhythmias and other cardiovascular effects when healthy rats were challenged with an exercise-like stressor.[4,5] The insight gained from these and other studies is

Received: September 20, 2017
Revised: December 19, 2017
Accepted: February 1, 2018
Published: February 1, 2018

ACS Publications © 2018 American Chemical Society

DOI: 10.1021/acs.est.7b04880
Environ. Sci. Technol. 2018, 52, 3071−3080

that exposure to complex air pollution mixtures results in latent autonomic shifts which cause a decrease in cardiac performance during exposure and even up to 1 day later.

Although many epidemiological studies point to PM as the main cause of air pollution's impacts on the cardiovascular system,[6−8] there are numerous human and rodent studies that implicate ubiquitous gaseous irritants like ozone as well.[9−11] In fact, our previous studies have shown that cardiovascular dysfunction occurs, sometimes at comparable levels or even after PM is removed from a multipollutant mixture like diesel exhaust.[12−14] Furthermore, the magnitude of the response is not just determined by the relative levels of PM and ozone but also by the resulting physical and chemical interactions that occur in the mixture. Therefore, the objective of this study was to examine and compare the cardiovascular responses of mice exposed to either a simulated high PM/low ozone (SA-PM) or low PM/high ozone (SA-O_3) smog atmosphere. These photo-oxidized mixtures approximated urban and regional evaporative pollutant emissions with similar Air Quality Health Index values. We previously determined that filtered diesel exhaust causes greater acute cardiac effects than whole diesel exhaust, and so we hypothesized that although both smog mixtures would elicit cardiac changes in mice, the atmosphere dominated by gaseous irritants would be more potent, particularly in causing electrical disturbances like arrhythmia.

MATERIALS AND METHODS

Animals. Female C57BL/6 (21 ± 1.1 g) mice between 13 and 15 weeks of age were used in this study (Jackson Laboratory, Bar Harbor, ME). Mice were initially housed five per cage and maintained on a 12 h light/dark cycle at approximately 22 °C and 50% relative humidity in an AAALAC−approved facility. Food (Prolab RMH 3000; PMI Nutrition International, St. Louis, MO) and water were provided ad libitum. All protocols were approved by the Institutional Animal Care and Use Committee of the U.S. Environmental Protection Agency and are in accordance with the National Institutes of Health Guides for the Care and Use of Laboratory Animals. Animals were randomly assigned to one of the following groups after implantation of radiotelemeters: (1) filtered air (FA), (2) SA-PM, or (3) SA-O_3.

Surgical Implantation of Radiotelemeters. Mice were implanted with radiotelemeters as previously described.[15] Animals were anesthetized using inhaled isoflurane (Isothesia, Butler Animal Health Supply, Dublin OH). Anesthesia was induced by spontaneous breathing of 2.5% isoflurane in pure oxygen at a flow rate of 1 L/min and then maintained by 1.5% isoflurane in pure oxygen at a flow rate of 0.5 L/min; all animals received the analgesic buprenorphrine (0.03 mg/kg, i.p. manufacturer). Briefly, using aseptic technique, each animal was implanted subcutaneously with a radiotelemeter (ETA-F10, Data Sciences International, St Paul, MN), the transmitter was placed under the skin to the right of the midline on the dorsal side. The two electrode leads were then tunneled subcutaneously across the lateral dorsal sides, and the distal portions were fixed in positions that approximated those of the lead II of a standard electrocardiogram (ECG). Body heat was maintained both during and immediately after the surgery. Animals were given food and water postsurgery and were housed individually. All animals were allowed 7−10 days to recover from the surgery and reestablish circadian rhythms.

Radiotelemetery Data Acquistion. Radiotelemetry methodology (Data Sciences International, Inc., St. Paul, MN) was used to track changes in cardiovascular function by monitoring heart rate (HR), and ECG waveforms immediately following telemeter implantation, through exposure until 24 hours postexposure. This methodology provided continuous monitoring and collection of physiologic data from individual mice to a remote receiver. Sixty-second ECG segments were recorded every 15 min during the pre- and postexposure periods and every 5 min during exposure (baseline and hours 1−4); HR was automatically obtained from the waveforms (Dataquest ART Software, version 3.01, Data Sciences International, St. Paul, MN). All animals were acclimated to the exposure chambers on two separate occasions, even then, an increase in HR was always observed when animals were placed in the chamber on the day of exposure.

Electrocardiogram Analysis. ECGAuto software (EMKA Technologies USA, Falls Church VA) was used to visualize individual ECG waveforms, analyze and quantify ECG segment durations and areas, as well as identify cardiac arrhythmias as previously described (Kurhanewicz et al. 2014). Briefly, using ECGAuto, Pwave, QRS complex, and T-wave were identified for individual ECG waveforms and compiled into a library. Analysis of all experimental ECG waveforms was then based on established libraries. The following parameters were determined for each ECG waveform: PR interval (P_{start}-R), QRS complex duration (Q_{start}-S), ST segment interval (S-T_{end}) and QT interval (Q_{start}-Tend). QT interval was corrected for HR using the correction formula for mice QTc = QT/(RR/100)1/2.[16] Pre-exposure assessments were measured as the exposure time-matched 4 h of data from 24 h before exposure for each animal. Immediately postexposure assessments were the 4 h of data taken immediately postexposure. Twenty-four postexposure assessments were the exposure time-matched 4 h of data taken 24 h after exposure.

Heart Rate Variability Analysis. Heart rate variability (HRV) was calculated as the mean of the differences between sequential RRs for the complete set of ECG waveforms using ECGAuto. For each 1 min stream of ECG waveforms, mean time between successive QRS complex peaks (RR interval), mean HR, and mean HRV-analysis−generated time-domain measures were acquired. The time-domain measures included standard deviation of the time between normal-to-normal beats (SDNN), and root mean squared of successive differences (RMSSD). HRV analysis was also conducted in the frequency domain using a Fast-Fourier transform. The spectral power obtained from this transformation represents the total harmonic variability for the frequency range being analyzed. In this study, the spectrum was divided into low-frequency (LF) and high-frequency (HF) regions. The ratio of these two frequency domains (LF/HF) provides an estimate of the relative balance between sympathetic (LF) and vagal (HF) activity.

Whole-Body Plethysmography. Ventilatory function was assessed in awake, unrestrained mice using a whole-body plethysmograph (Buxco, Wilmington, NC). Assessments were performed 1 day before exposure, immediately postexposure and 24 h after exposure. The plethysmograph pressure was monitored using Biosystems XA software (Buxco Electronics Inc., Wilmington, NC). Using respiratory-induced fluctuations in ambient pressure, ventilatory parameters including tidal volume (V_T), breathing frequency (f), inspiratory time (Ti), and expiratory time (Te), were calculated and recorded on a breath-by-breath basis.

DOI: 10.1021/acs.est.7b04880
Environ. Sci. Technol. 2018, 52, 3071−3080

Table 1. Concentrations of Criteria Pollutants and Air Quality Indexes[a]

	$PM_{2.5}$ (mg/m^3) AQI	NO_x/AQI (ppm) AQI	O_3/AQI (ppm) AQI	total hydrocarbons (ppmc)	gas-phase (mgC/m^3)	AQHI
	0.009		0.002			
filtered air	37 (green)	ND	1 (green)	ND	ND	<1
SA-PM	1.0362	0.380	0.190	5.5	3.847	92.5
	>500 (brown)	154 (orange)	287(red)			
SA-O_3	0.0523	0.647	0.448	6.1	3.125	102.6
	142 (orange)	199 (red)	>300 (purple)			

[a]ND, none detected. Green, AQ is satisfactory—little or no risk. Yellow, AQ is acceptable—moderate health concern for a very small number of people who are unusually sensitive to air pollution. Orange, Sensitive people may experience health effects. Red, Everyone may experience health effects; sensitive people at greater risk. Purple, Everyone may experience serious health effects. Brown, Health warnings at emergency conditions; entire population will be affected.

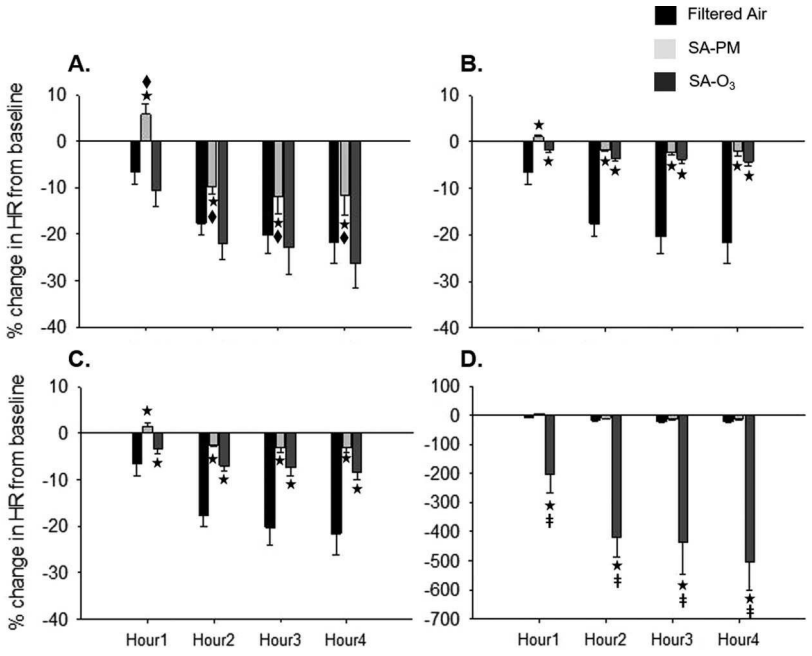

Figure 1. Exposure to smog alters heart rate responses in mice. In general, mice experienced a steady decrease in HR (from baseline) over the first 2 h of exposure, which then leveled off in hours three and four. Mice exposed to SA-PM experienced a significant increase in HR during the first hour and had less decrease in HR thereafter when compared to FA and SA-O_3 (A.). However, there was no difference between SA-PM and SA-O_3 when the change in HR during exposure was normalized to total hydrocarbons (B.) or gas-phase hydrocarbons only (C.). In contrast, decrease in HR during SA-O_3 exposure was significantly greater than SA-PM when responses were normalized to PM concentration (D.). significantly different from FA; • significantly different from SA-O_3; ǂ significantly different from SA-PM. $p < 0.05$.

Photochemical Smog Exposures. A gasoline blend was combined with either α-pinene or isoprene to produce a hydrocarbon mixture that was enhanced for particulate matter (PM) or ozone (O_3) during irradiation, respectively. Thus, photochemical smog atmospheres with either high $PM_{2.5}$ and low O_3/nitrogen oxide (NO_x) concentrations (SA-PM) or low $PM_{2.5}$ and high O_3/NO_x (SA-O_3) were generated in the Mobile Reaction Chamber (MRC). Briefly, SA-PM was artificially generated with 0.491 ppm nitrogen oxide (NO), 0.528 ppm of NO_x, 29.9 ppmC total hydrocarbons (THC), 24 ppmC gasoline and 5.3 ppmC α -pinene as the initial conditions, whereas SA-O_3 was generated from 0.794 ppm of NO, 0.912 ppm of NO_x, 12.4 ppmC THC, 5.2 ppmC isoprene and 7.21 ppmC gasoline. Each of the initial smog mixtures was then irradiated with ultraviolet light. Smog was then transported under vacuum to 0.3 m^3 whole body inhalation chambers where mice were exposed once for 4 h. Continuous gas and aerosol sampling for carbon monoxide (CO), O_3, NO_x, THC and particle mass concentration were conducted at both the MRC unit as well as from the inhalation exposure systems. All PM was formed as secondary organic aerosol (SOA) from the photochemical reactions in the MRC. Particle size distributions and gravimetric mass sampling was measured, and filter sampling for gravimetric analysis were conducted for the entire exposure time. Volatile organic compound (VOC) summa cannisters were periodically collected and analyzed by gas chromatography off-line to determine concentrations of various volatile organic compounds (VOCs) in the exposure atmosphere. Animals exposed to FA received room air, which was transported to the chambers after being HEPA filtered. Please refer to Krug et al. in this issue for complete exposure details.

Statistics. All data are expressed as means ± SEM. Statistical analyses were performed using Sigmaplot 13.0 (Systat Software, San Jose, CA) software. The delta values (i.e., change during exposure from baseline) of HR, HRV and

DOI: 10.1021/acs.est.7b04880
Environ. Sci. Technol. 2018, 52, 3071−3080

the ventilatory parameters were used and a two-way analysis of variance (ANOVA) for repeated-measures was employed with Bonferroni post hoc tests to determine statistical differences. Raw ECG and arrhythmia count data were analyzed by two-way ANOVA. Raw HR, HRV, ventilatory parameters, and arrhythmia counts were also normalized to total hydrocarbons (both particle and gas phases), gas-phase hydrocarbons only or PM concentration by dividing the physiological parameters by the pollutant concentrations. Normalizations were done to compare the relative contribution of these components to the physiological response to Smog A versus B and their relative potencies; no statistical comparisons were made to FA postnormalization. The statistical significance was set at $P < 0.05$.

RESULTS

Exposure Characteristics. Table 1 shows the inhalation chamber concentrations of $PM_{2.5}$ (i.e., secondary organic aerosols), NO_x, O_3, as well as total hydrocarbons in the complete smog mixture (particle and gas phases) and in the gas-phase only for both SA-PM (enhanced $PM_{2.5}$) and SA-O_3 (enhanced O_3). In addition, the respective air quality health indexes (AQHI) and air quality indexes (AQI) along with their color codes are also included to provide a health-risk comparison between these atmospheres. These indices describe the health risks from polluted air on individual days throughout the year, either from independent pollutants as in the case of AQI, or from a cumulative $PM_{2.5}$, O_3, and NO_x perspective as with AQHI. Refer to Krug et al. in this issue for a more comprehensive comparison of SA-PM (MR044) and SA-O_3 (MR059).

Heart Rate. There was no difference in the baseline HR, which was the resting level measured in the home cages, between any of the groups (FA = 588.0 ± 19.8 bpm; SA-PM = 568.6 ± 7.5 bpm; SA-O_3 = 565.9 ± 9.4 bpm). In general, all animals experienced a decrease in HR during the exposure; although, SA-PM caused a significant increase in HR during Hour1 and less HR decrease over the remaining exposure period when compared to FA and SA-O_3 (Figure 1A). However, there was no difference between SA-PM and SA-O_3 when the responses were normalized to THC (Figure 1B) or gas-phase hydrocarbons only (Figure 1C). On the other hand, HR decrease was significantly greater during SA-O_3 when compared to SA-PM after normalization to PM concentration (Figure 1D).

Arrhythmia. None of the animals experienced cardiac arrhythmias during the pre-exposure period. Figure 2 shows the raw arrhythmia counts during the 4 h exposure. Overall, exposure to SA-O_3 increased the incidence of arrhythmias when compared to FA (Figure 2A–D) but there was no difference with respect to SA-PM in the denormalized (Figure 2A) and THC normalized (Figure 2B) responses. In contrast, SA-O_3 caused significantly more arrhythmias than SA-PM when the responses were normalized to gas-phase hydrocarbons (Figure 2C) or PM concentrations (Figure 2D).

Heart Rate Variability. Figures 3-5 show the changes in HRV during exposure. There were no significant differences in the baseline HRV measures between any of the groups (FA − SDNN = 7.4 ± 0.7 ms, RMSSD = 4.0 ± 0.5 ms, LF/HF = 8.4 ± 0.7 ms^2; SA-PM − SDNN = 7.9 ± 0.7 mscec, RMSSD = 5.3 ± 0.6 ms, LF/HF = 7.1 ± 0.6 ms^2; SA-O_3−SDNN = 8.7 ± 0.7 ms, RMSSD = 5.5 ± 0.7 ms, LF/HF = 6.7 ± 0.6 ms^2). SDNN decreased in the first hour of exposure in control animals; this

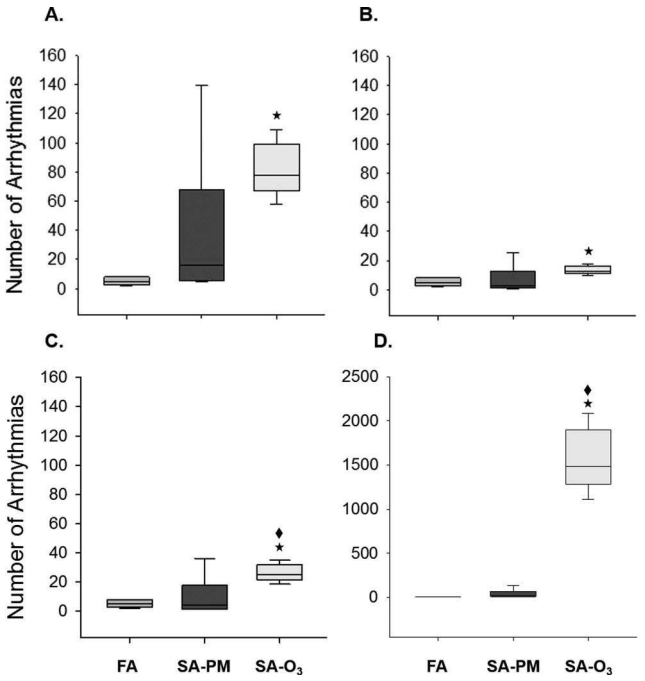

Figure 2. Exposure to O_3-enhanced smog increases cardiac arrhythmias in mice. Overall, exposure to SA-O_3 caused a significant increase in the number of cardiac arrhythmias in mice when compared to FA. There was no difference between SA-O_3 and SA-PM in the denormalized (A.) and THC-normalized (B.) responses; however, SA-O_3 caused significantly more arrhythmias than SA-PM when the responses were normalized to gas-phase hydrocarbons (C.) or PM concentration (D.). significantly different from FA; • significantly different from SA-PM. $p < 0.05$.

was likely due to sympathetic modulation from the stress of handling and placement in the chamber. Animals exposed to either SA-PM or SA-O_3 had a significant increase in SDNN (Figure 3A) when compared to FA and a similar trend was observed for RMSSD (Figure 4A). Both time-domain measures showed minimal to no effects for either SA-PM or SA-O_3 when the responses were normalized to THC (Figure 3B and 4B) or gas-phase hydrocarbons only (Figure 3C and 4C). However, the increase in SDNN and RMSSD during SA-O_3 exposure was significantly greater than SA-PM when the data were normalized to PM concentration (Figure 3D and 4D). On the other hand, there were no significant effects in the frequency-domain measures (i.e., LF/HF) for either smog atmosphere with or without normalization of responses (Figure 5).

Ventilatory Function. Whole-body plethysmography was performed on all animals during the baseline period as well as immediately and 1 day after exposure; results shown in Figure 6 compare the changes in ventilatory parameters from baseline between the groups. Baseline values did not differ between the groups (FA − f = 475.1 ± 13.1 breaths/min, V_T = 0.24 ± 0.01 mL, Ti = 0.06 ± 0.002 s, Te = 0.08 ± 0.002 s; SA-PM − f = 509.8 ± 6.3 breaths/min, V_T = 0.24 ± 0.01 mL, Ti = 0.05 ± 0.001 s, Te = 0.07 ± 0.001 s; SA-O_3 − f = 499.7 ± 12.1 breaths/min, V_T = 0.25 ± 0.01 mL, Ti = 0.06 ± 0.002 s, Te = 0.07 ± 0.002 s). There were no differences in f, V_T, Ti or Te between any of the groups in the unnormalized results (Figure 6A). However, normalizing to THC (Figure 6B) or gas-phase only hydrocarbons (Figure 6C) revealed a significant decrease in f, and increase in V_T and Ti in SA-PM and SA-O_3

DOI: 10.1021/acs.est.7b04880
Environ. Sci. Technol. 2018, 52, 3071−3080

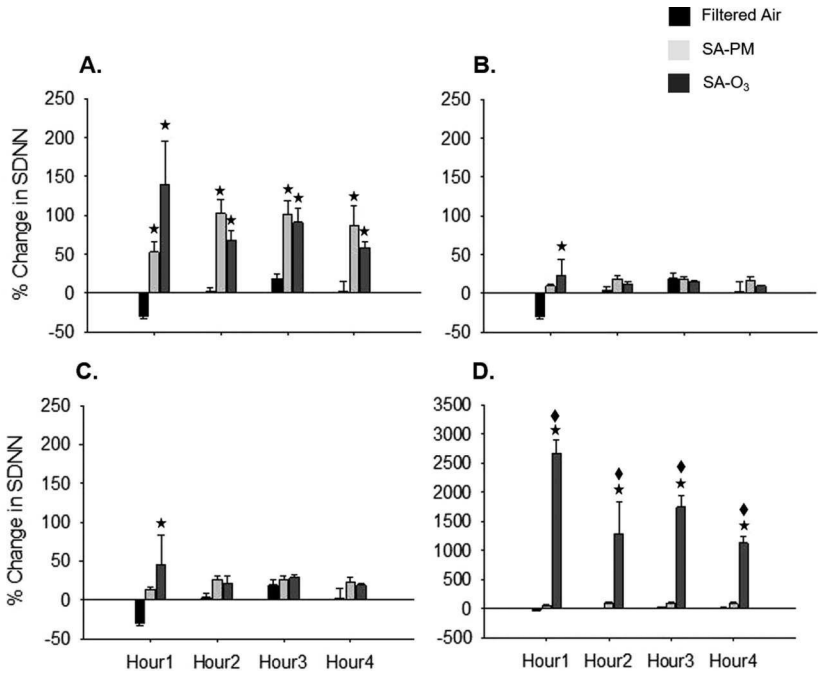

Figure 3. Exposure to smog increases SDNN in mice. SDNN decreased during the first hour of FA exposure probably due to stress. On the other hand, mice exposed to either SA-PM or SA-O_3 experienced a significant increase in SDNN (A.) when compared to FA. There was no difference in SDNN between SA-PM and SA-O_3 in the denormalized (A.), THC- (B.) or gas-phase only hydrocarbon (C.) normalized responses. In contrast, SDNN was significantly increased during SA-O_3 exposure when compared to SA-PM when responses were normalized to PM concentration (D.). significantly different from FA; • significantly different from SA-PM. $p < 0.05$.

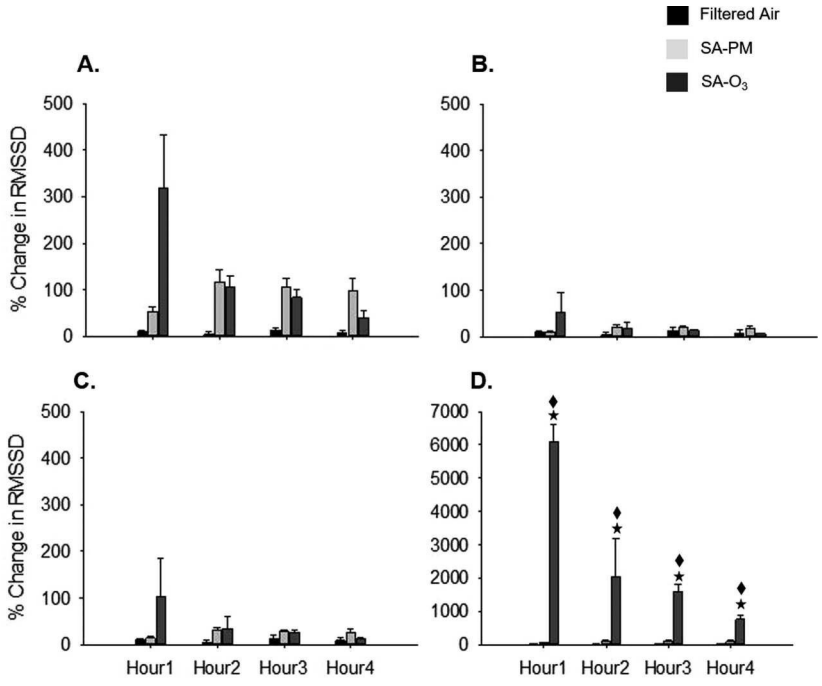

Figure 4. Exposure to O_3-enhanced smog increases RMSSD in mice. There was no effect of SA-PM or SA-O_3 on RMSSD when compared to FA although a trend of increase was observed for both (A.). There was no difference in RMSSD between SA-PM and SA-O_3 in the THC- (B.) or gas-phase only hydrocarbon (C.) normalized responses. On the other hand, RMSSD was significantly increased during SA-O_3 exposure when compared to SA-PM when responses were normalized to PM concentration (D.). significantly different from FA; • significantly different from SA-PM. $p < 0.05$.

immediately after exposure when compared to controls. Some of these responses relative to FA persisted 1 day after exposure but there was no difference between SA-PM and SA-O_3. In contrast, normalization to PM concentrations revealed a significant increase in *f*, and decrease in V_T and Ti immediately after exposure in SA-O_3-exposed animals when compared to SA-PM (Figure 6D); only the changes in *f* and V_T persisted 24 h later.

Electrocardiogram. There were no baseline differences in any ECG parameters between any of the groups. Changes in

DOI: 10.1021/acs.est.7b04880
Environ. Sci. Technol. 2018, 52, 3071−3080

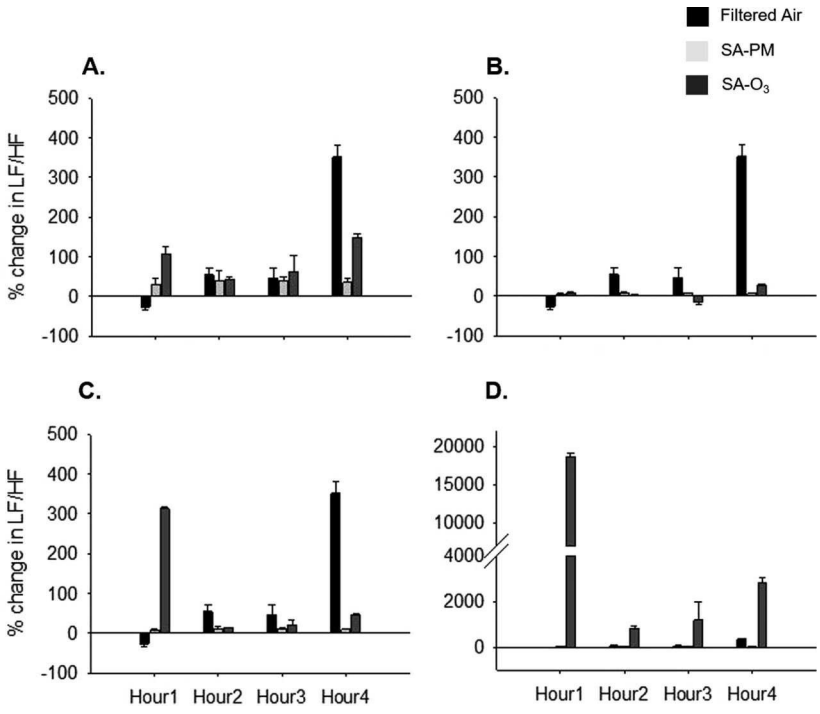

Figure 5. Change in LF/HF during smog exposure. There were no significant effects of SA-PM or SA-O_3 on LF/HF when compared to FA or when either smog atmosphere was compared to the other (A.). Normalization of the responses to THC- (B.), gas-phase only hydrocarbons (C.), or PM concentrations (D.) did not reveal any significant difference between SA-PM and SA-O_3 except in (D.) where a trend of increase was observed in SA-O_3-exposed mice.

ECG during exposure were restricted to a PR interval prolongation in mice exposed to SA-PM, which were significantly higher than FA and SA-O_3 (Table 2).

DISCUSSION

The results of this study demonstrate that a single inhalation exposure to atmospheric smog causes acute cardiovascular dysfunction in mice, irrespective of whether it is comprised predominantly of PM or O_3. Our findings also suggest that multipollutant mixtures which have a higher irritant gas composition are likely to cause more potent acute cardiac effects than those with higher PM/lower gases. Unfortunately, the relative toxicity of only the SOA in each of the atmospheres was not assessed, this would have provided greater information about their contributions to the differential health effects we observed. In either case, it is not possible to firmly conclude whether PM in general plays a greater role in causing cardiac effects or not because SOA is not necessarily the same as ambient PM. However, in an effort to compare the effects of SA-PM and SA-O_3 relative to their whole compositions, we normalized the data from this study to total hydrocarbons, gas-phase hydrocarbons only and PM concentration. Normalization of the results showed that there was no difference in heart rate, heart rate variability or cardiac arrhythmias between SA-PM and SA-O_3 when differences in total hydrocarbons or gas-phase only hydrocarbons were taken into account. In contrast, SA-O_3 caused significantly greater cardiac effects than SA-PM when results were normalized to PM concentration indicating that the difference in response was mediated by the gaseous components. Thus, these findings point to the complexity of interactions between air pollution components and the reactions that determine the composition of the final mixture and the resulting cardiovascular response.

Real-time cardiovascular measurements and responses to exposure as derived here from radiotelemetry often include stress-related effects (e.g., from handling, noise, etc). This was observed in all animals as a transient increase in heart rate upon placement in the exposure chamber, which occurred despite two separate one-hour acclimatizations. In controls, the overall heart rate progressively decreased per hour of exposure as the animals calmed down in the chambers. Similar responses were observed with SA-O_3 but with a trend of greater decrease in heart rate. Although this result was not statistically significant, it is not entirely surprising that SA-O_3 would have this effect given it was rich in irritant gases like O_3, NO_x and reactive aldehydes, which have the ability to activate airway sensory nerves, elicit autonomic reflexes and modulate parasympathetic function.[17−19] On the other hand, SA-PM caused a significant increase in heart rate in the first hour of exposure and less decrease (i.e., HR remained elevated above normal) over the remaining exposure period when compared to controls and SA-O_3. These disparate effects of SA-PM and SA-O_3 are not unusual. We previously showed that exposure to particle-filtered diesel exhaust caused greater decrements in heart rate than whole diesel exhaust while particle-rich air pollution has been shown to increase heart rate.[13,20,21] Thus, it appears from our data that decreases in heart rate during such exposures are related to the composition and concentration of gases in the complex air pollution mixture. Notice that normalization of the heart rate to total or gas-phase only hydrocarbons did not reveal any difference between SA-PM and SA-O_3, yet when the "effects" of PM were eliminated through normalization SA-O_3 caused a significant decrease in heart rate when compared to SA-PM.

The composition of the smog atmospheres may not have been the only determinant of this response, variations in the

DOI: 10.1021/acs.est.7b04880
Environ. Sci. Technol. 2018, 52, 3071−3080

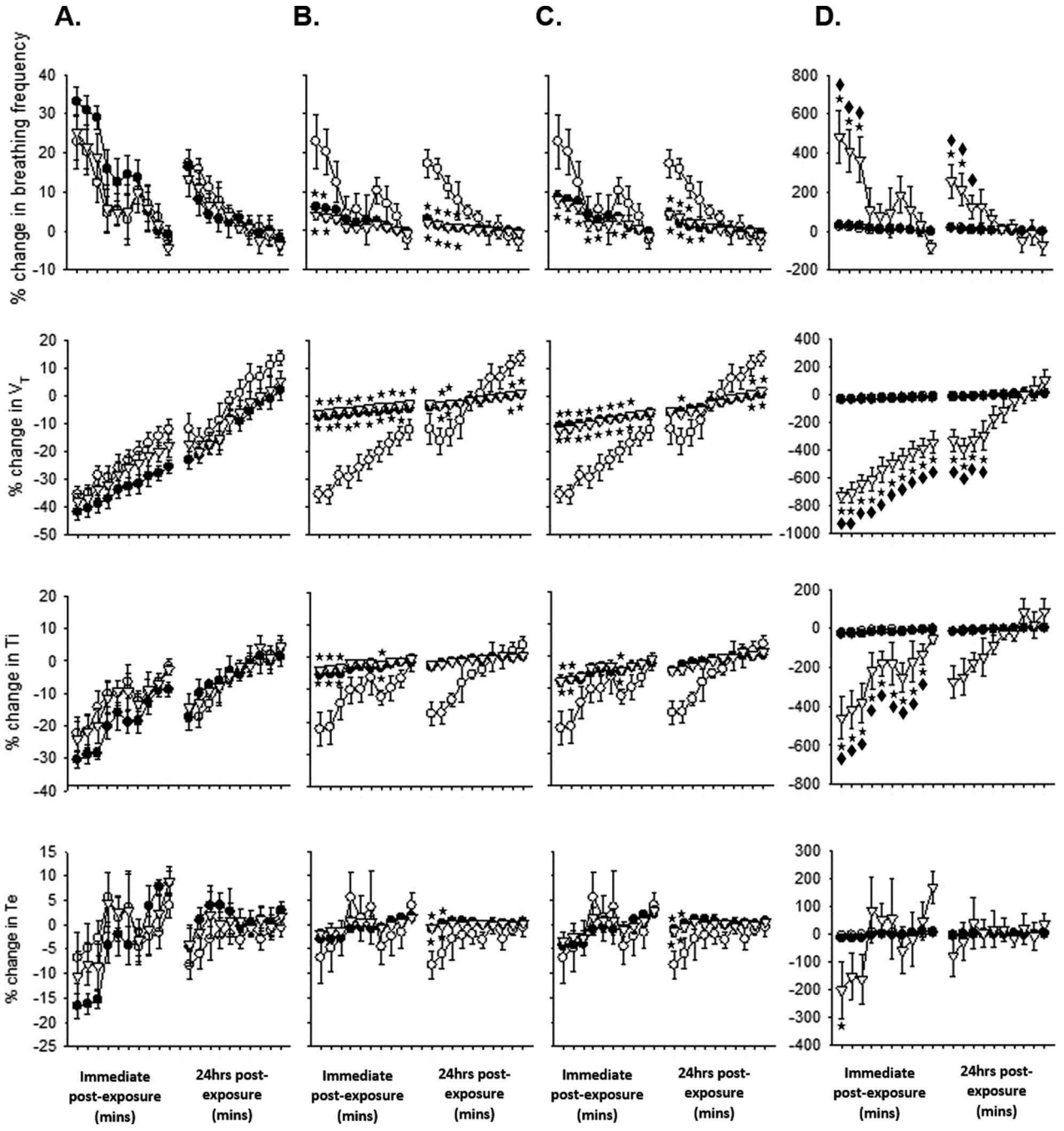

Figure 6. O_3-enhanced smog alters breathing in mice immediately after exposure. There was no effect of SA-PM (filled circles) or SA-O_3 (open triangles) on any ventilatory parameters when compared to FA (open circles) (A.) and there were no differences observed between SA-PM and SA-O_3 in the THC- (B.) or gasphase only hydrocarbon (C.) normalized responses. However, f was increased, and VT and Ti were significantly decreased after SA-O_3 exposure when compared to SA-PM when responses were normalized to PM concentration (D.). significantly different from FA; • significantly different from SA-PM. $p < 0.05$.

smell of SA-PM and SA-O_3 could have contributed as well. SA-PM had a very potent smell when compared to SA-O_3 and this may have caused an increase in the heart rate. This effect has been demonstrated previously, particularly with burnt or unpleasant smells,[22] and appears to be mediated by an increase in sympathetic modulation or decrease in heart rate variability. It is likely that in addition to smell, several smog factors could have triggered responses and altered autonomic function simultaneously, particularly given the complexity of the atmosphere (e.g., potent "burnt" smell + chemical airway irritation + secondary activation due to inflammation). The autonomic nervous system controls the heart and vasculature through a dynamic ebb and flow of both parasympathetic and sympathetic influence and tends to lean in the direction of one or the other based on the physiological circumstances. Thus, returning to the issue of composition, the difference in response between a predominantly gaseous mixture and one that is high in particles would depend on the sum of all the factors that impact autonomic function, and hence the resulting direction would be determined by which factor(s) dominates.

Although our data do not necessarily demonstrate this (i.e., parasympathetic/sympathetic activation) directly, it is possible

DOI: 10.1021/acs.est.7b04880
Environ. Sci. Technol. 2018, 52, 3071−3080

Table 2. Electrocardiographic Parameters

air	PR interval (msec)	QRS duration (msec)	QTc (msec)
baseline	36.1 ± 0.5	14.7 ± 1.9	94.2 ± 3.0
hour 1	33.4 ± 1.8	13.9 ± 0.5	92.7 ± 1.5
hour 2	35.7 ± 1.4	14.6 ± 0.4	92.9 ± 1.5
hour 3	35.9 ± 0.6	14.8 ± 0.4	94.9 ± 3.0
hour 4	37.5 ± 1.0	15.3 ± 0.4	94.5 ± 2.0
24 h postexp	36.0 ± 0.7	16.3 ± 0.3	94.6 ± 4.0
SA-PM			
baseline	32.8 ± 0.6	14.6 ± 0.3	88.2 ± 1.5
hour 1	40.7 ± 1.0*♦	13.3 ± 0.2	91.0 ± 4.6
hour 2	42.3 ± 1.1*♦	13.4 ± 0.4	93.3 ± 4.1
hour 3	43.3 ± 0.9*♦	13.7 ± 0.2	91.7 ± 2.6
hour 4	42.8 ± 1.2*♦	13.6 ± 0.3	99.3 ± 7.0
24 h postexp	33.4 ± 0.5	14.4 ± 0.2	81.5 ± 1.4
SA-O_3			
baseline	33.6 ± 0.9	13.4 ± 1.1	89.9 ± 1.8
hour 1	34.4 ± 1.1	11.8 ± 2.2	95.9 ± 3.4
hour 2	36.3 ± 0.8	11.0 ± 2.4	91.5 ± 3.6
hour 3	36.6 ± 0.7	9.6 ± 3.2	92.7 ± 4.9
hour 4	37.1 ± 0.7	10.1 ± 2.8	92.4 ± 2.9
24 h postexp	34.2 ± 0.6	14.4 ± 0.8	88.9 ± 0.8

that irritant gases drove a predominantly parasympathetic response whereas the PM-rich mixture caused a stress-induced sympathetic modulation. We observed a greater increase in SDNN and RMSSD, which is indicative of parasympathetic modulation, during SA-O_3 exposure when compared to SA-PM. This response was due to the effects of the gas-phase components given the difference in these parameters between the two smog atmospheres became evident when we normalized to PM concentration. As far as PM is concerned, studies have demonstrated, as stated previously, that it not only increases heart rate, blood pressure, low frequency blood pressure variability and noradrenalin release (i.e., stress), but also causes a decrease in heart rate variability.[3,23] All of these changes point to sympathetic modulation and a perceived increase in cardiac risk. However, we observed an increase in SDNN and RMSSD even with the PM-enhanced SA-PM mixture. This might be explained by the fact that SA-PM also contained irritant gases, some of which were present in high concentrations (see Krug et al. in this issue) and could have opposed the sympathetic modulatory effect of the PM. A lack of response in the LF/HF ratio suggests this parasympathetic-sympathetic push and pull.[24]

Comparisons between SA-PM and SA-O_3 also included the air quality health index or AQHI, which indicates the health risk of both atmospheres. The equation for this index provides the relative contribution of the $PM_{2.5}$ and the oxidant gases toward the health metric. In the case of SA-O_3, oxidant gases contributed to 97% of the AQHI with a negligible amount coming from PM, once again pointing to the fact that it is effects were predominantly mediated by irritant gases. In contrast, PM contributed to almost 70% of the AQHI of SA-PM, yet it also had a fairly significant contribution (30%) from the oxidant gases as well (see Krug et al. this issue). These results seem to confirm our conclusions that although the effects of SA-O_3, which included a significant decrease in heart rate and increase in heart rate variability, were almost entirely driven by gases, SA-PM's effects were likely driven by both. The implications for human health are important, particularly given most of the research over the past decade has focused on PM-driven cardiovascular effects. For example, both an increase of 6 ug/m^3 in fine PM and 20 ppb O_3 resulted in a significant increase in the risk of out of hospital heart attacks.[25] Furthermore, exposure to 0.3 ppm of O_3 caused similar HRV changes in healthy young individuals to what we observed in this study, suggesting gases like O_3 may not cause overt symptoms but rather underlying changes.[26]

While an increasing or decreasing heart rate or heart rate variability during exposure merely indicates a physiological change, one could potentially infer cardiac dysfunction when it is a deviation from the control response. It represents fluctuations that can normally happen in mammals (e.g., exercise or physical exertion). Sometimes these responses reflect adverse cardiac issues more strongly when observed in conjunction with cardinal signs of dysfunction like arrhythmia. This may be the case for what we observed in the mice exposed to these smog atmospheres. We have shown that gaseous air pollution is more arrhythmogenic than one with a high concentration of PM and the same appears to be the case in this study.[12,27] SA-O_3, particularly when normalized to PM concentration, caused a significantly greater number of sinoatrial (SA) node dysfunction than SA-PM. Furthermore, we found that SA-O_3 was more arrhythmogenic than SA-PM even when normalized to gas-phase hydrocarbons suggesting PM had very little effect. This form of arrhythmia or dysrhythmia, which can increase the risk of escape beats and cardiac insufficiency in humans, is due to an abnormal delay in the firing of the SA node and manifests as blocked p-waves and alternating runs of bradycardia followed by tachycardia.. Interestingly, some of the causes behind this phenomenon include an increase in vagal tone and airway irritation which leads to dyspneic breathing and airway spasm, both of which were observed in our animals.[28,29]

Exposure to SA-PM did cause a prolongation of the PR interval, which in some cases is normal but also can indicate a cardiac conduction abnormality. However, in the absence of other effects (e.g., arrhythmia) it would be hard to say that there was any real dysfunction in these mice. Indeed, even changes in breathing impact the heart on a breath-by-breath basis and through this physiological coupling the heart is able to maintain proper function.[30] Thus, alterations in breathing due to airway irritation and airflow obstruction have the potential to cause adverse cardiac events. Yet, we did not observe any remarkable differences in ventilatory parameters either immediately following the exposure or 1 day later for either SA-PM or SA-O_3. Normalization to total or only gas-phase hydrocarbons did not reveal any differences but SA-O_3 caused a significant increase in breathing frequency, and decreases in tidal volume and inspiratory time when the results were normalized to PM concentration. Thus, once again it appears that the gases in SA-O_3 caused a rapid shallow breathing in mice possibly due to irritation.

In conclusion, the results of this study demonstrate that inhalation exposure to a complex smog atmosphere causes acute cardiac effects in mice, and that the composition of the pollution mixture likely plays a key role in determining the degree of responsiveness. Although the PM-enhanced smog caused a change in cardiac function, it is likely that a single exposure was not enough to elicit worsening symptoms in our relatively young healthy animals. This is particularly true for the relatively low number of cardiac arrhythmias observed in those animals. It is entirely likely however that repeated exposures would have had a more pronounced impact. In contrast, the

DOI: 10.1021/acs.est.7b04880
Environ. Sci. Technol. 2018, 52, 3071−3080

O_3-enhanced smog caused a set of physiological changes which if considered with the increased incidence of arrhythmia suggest an acute irritant gas-mediated autonomic modulation and electrical disturbance. Even though the former is not considered a "toxicological" response, it does reflect a change from the homeostatic normal state of the body. These short-lived reversible effects probably do not pose a serious hazard to the body on their own, but when combined with an additional stressor could predispose the heart to dysfunction, particularly during in the 24 h following exposure.

AUTHOR INFORMATION

Corresponding Author

*Phone: 919-541-4588; fax: 919-541-0034; e-mail: hazari.mehdi@epa.gov.

ORCID

Mehdi S. Hazari: 0000-0003-0280-9690
Kimberly M. Stratford: 0000-0001-7076-9753
Jonathan Krug: 0000-0002-7045-7650

Notes

The authors declare no competing financial interest.

ACKNOWLEDGMENTS

We are grateful to Drs. Wayne Cascio, Christopher Gordon and Colette Miller for their careful reviews of this manuscript. This paper has been reviewed and approved for release by the National Health and Environmental Effects Research Laboratory, U.S. Environmental Protection Agency. Approval does not signify that the contents necessarily reflect the views and policies of the U.S. EPA, nor does mention of trade names. All funding for this study is from U.S. Environmental Protection Agency.

REFERENCES

(1) Langrish, J. P.; Bosson, J.; Unosson, J.; Muala, A.; Newby, D. E.; Mills, N. L.; Blomberg, A.; Sandström, T. Cardiovascular effects of particulate air pollution exposure: time course and underlying mechanisms. *J. Intern. Med.* **2012**, *272* (3), 224−39.

(2) Brook, R. D.; Urch, B.; Dvonch, J. T.; Bard, R. L.; Speck, M.; Keeler, G.; Morishita, M.; Marsik, F. J.; Kamal, A. S.; Kaciroti, N.; Harkema, J.; Corey, P.; Silverman, F.; Gold, D. R.; Wellenius, G.; Mittleman, M. A.; Rajagopalan, S.; Brook, J. R. Insights into the mechanisms and mediators of the effects of air pollution exposure on blood pressure and vascular function in healthy humans. *Hypertension* **2009**, *54* (3), 659−667.

(3) Brook, R. D.; Rajagopalan, S.; Pope, C. A.; Brook, J. R.; Bhatnagar, A.; Diez-Roux, A. V.; Holguin, F.; Hong, Y.; Luepker, R. V.; Mittleman, M. A.; Peters, A.; Siscovick, D.; Smith, S. C., Jr; Whitsel, L.; Kaufman, J. D. Particulate matter air pollution and cardiovascular disease: An update to the scientific statement from the American Heart Association. *Circulation* **2010**, *121* (21), 2331−78.

(4) Hazari, M. S.; Callaway, J.; Winsett, D. W.; Lamb, C.; Haykal-Coates, N.; Krantz, Q. T.; King, C.; Costa, D. L.; Farraj, A. K. Dobutamine "stress" test and latent cardiac susceptibility to inhaled diesel exhaust in normal and hypertensive rats. *Environ. Health Perspect.* **2012**, *120* (8), 1088−93.

(5) Carll, A. P.; Hazari, M. S.; Perez, C. M.; Krantz, Q. T.; King, C. J.; Haykal-Coates, N.; Cascio, W. E.; Costa, D. L.; Farraj, A. K. An autonomic link between inhaled diesel exhaust and impaired cardiac performance: insight from treadmill and dobutamine challenges in heart failure-prone rats. *Toxicol. Sci.* **2013**, *135* (2), 425−36.

(6) Peters, A. Particulate matter and heart disease: evidence from epidemiological studies. *Toxicol. Appl. Pharmacol.* **2005**, *207* (2 Suppl), 477−82.

(7) Pope, C. A., 3rd; Burnett, R. T.; Thurston, G. D.; Thun, M. J.; Calle, E. E.; Krewski, D.; Godleski, J. J. Cardiovascular mortality and long-term exposure to particulate air pollution: epidemiological evidence of general pathophysiological pathways of disease. *Circulation* **2004**, *109* (1), 71−7.

(8) Samet, J. M.; Rappold, A.; Graff, D.; Cascio, W. E.; Berntsen, J. H.; Huang, Y-C.T.; Herbst, M.; Bassett, M.; Montilla, T.; Hazucha, M. J.; Bromberg, P. A.; Devlin, R. B. Concentrated ambient ultrafine particle exposure induces cardiac changes in young healthy volunteers. *Am. J. Respir. Crit. Care Med.* **2009**, *179* (11), 1034−42.

(9) Ruidavets, J. B.; Cournot, M.; Cassadou, S.; Giroux, M.; Meybeck, M.; Ferrières, J. Ozone air pollution is associated with acute myocardial infarction. *Circulation* **2005**, *111* (5), 563−9.

(10) Farraj, A. K.; Hazari, M. S.; Winsett, D. W.; Kulukulualani, A.; Carll, A. P.; Haykal-Coates, N.; Lamb, C. M.; Lappi, E.; Terrell, D.; Cascio, W. E.; Costa, D. L. Overt and latent cardiac effects of ozone inhalation in rats: evidence for autonomic modulation and increased myocardial vulnerability. *Environ. Health Perspect.* **2012**, *120* (3), 348−54.

(11) Jerrett, M.; Burnett, R. T.; Beckerman, B. S.; Turner, M. C.; Krewski, D.; Thurston, G.; Martin, R. V.; van Donkelaar, A.; Hughes, E.; Shi, Y.; Gapstur, S. M.; Thun, M.; Pope, C. A. Spatial Analysis of Air Pollution and Mortality in California. *Am. J. Respir. Crit. Care Med.* **2013**, *188* (5), 593−600.

(12) Hazari, M. S.; Haykal-Coates, N.; Winsett, D. W.; Krantz, Q. T.; King, C.; Costa, D. L.; Farraj, A. K. TRPA1 and sympathetic activation contribute to increased risk of triggered cardiac arrhythmias in hypertensive rats exposed to diesel exhaust. *Environ. Health Perspect.* **2012**, *119* (7), 951−7.

(13) Lamb, C. M.; Hazari, M. S.; Haykal-Coates, N.; Carll, A. P.; Krantz, Q. T.; King, C.; Winsett, D. W.; Cascio, W. E.; Costa, D. L.; Farraj, A. K. Divergent electrocardiographic responses to whole and particle-free diesel exhaust inhalation in spontaneously hypertensive rats. *Toxicol. Sci.* **2012**, *125* (2), 558−68.

(14) Carll, A. P.; Hazari, M. S.; Perez, C. M.; Krantz, Q. T.; King, C. J.; Winsett, D. W.; Costa, D. L.; Farraj, A. K. Whole and particle-free diesel exhausts differentially affect cardiac electrophysiology, blood pressure, and autonomic balance in heart failure-prone rats. *Toxicol. Sci.* **2012**, *128* (2), 490−9.

(15) Kurhanewicz, N.; McIntosh-Kastrinsky, R.; Tong, H.; Walsh, L.; Farraj, A. K.; Hazari, M. S. Ozone co-exposure modifies cardiac responses to fine and ultrafine ambient particulate matter in mice: concordance of electrocardiogram and mechanical responses. *Part. Fibre Toxicol.* **2014**, *11*, 54.

(16) Mitchell, G. F.; Jeron, A.; Koren, G. Measurement of heart rate and Q-T interval in the conscious mouse. *Am. J. Physiol.* **1998**, *274* (3), 274 Pt 2.

(17) Widdicombe, J.; Lee, L. Y. Airway reflexes, autonomic function, and cardiovascular responses. *Environ. Health Perspect.* **2001**, *109*, 579−584.

(18) Taylor-Clark, T. E.; Undem, B. J. Ozone activates airway nerves via the selective stimulation of TRPA1 ion channels. *J. Physiol.* **2006**, *588*, 423−433.

(19) Kurhanewicz, N.; McIntosh-Kastrinsky, R.; Tong, H.; Ledbetter, A.; Walsh, L.; Farraj, A.; Hazari, M. S. TRPA1 mediates changes in heart rate variability and cardiac mechanical function in mice exposed to acrolein. *Toxicol. Appl. Pharmacol.* **2016**, *324*, 51−60.

(20) Peters, A.; Perz, S.; Dfiring, A.; Stieber, J.; Koenig, W.; Wichmann, H. E. Increases in Heart Rate during an Air Pollution Episode. *Am. J. Epidemiol.* **1999**, *150*, 1094−1099.

(21) Unosson, J.; Blomberg, A.; Sandström, T.; Muala, A.; Boman, C.; Nyström, R.; Westerholm, R.; Mills, N. L.; Newby, D. E.; Langrish, J. P.; Bosson, J. A. Exposure to wood smoke increases arterial stiffness and decreases heart rate variability in humans. *Part. Fibre Toxicol.* **2013**, *6*, 10−20.

(22) Glass, S. T.; Lingg, E.; Heuberger, E. Do ambient urban odors evoke basic emotions? *Front. Psychol* **2014**, *5*, 340.

(23) Ying, Z.; Xu, X.; Bai, Y.; Zhong, J.; Chen, M.; Liang, Y.; Zhao, J.; Liu, D.; Morishita, M.; Sun, Q.; Spino, C.; Brook, R. D.; Harkema, J.

DOI: 10.1021/acs.est.7b04880
Environ. Sci. Technol. 2018, 52, 3071−3080

R.; Rajagopalan, S. Long-term exposure to concentrated ambient PM2.5 increases mouse blood pressure through abnormal activation of the sympathetic nervous system: a role for hypothalamic inflammation. *Environ. Health Perspect* **2014**, *122* (1), 79−86.
(24) Billman, G. E. The LF/HF ratio does not accurately measure cardiac sympatho-vagal balance. *Front. Physiol.* **2013**, *4*, 26.
(25) Ensor, K. B.; Raun, L. H.; Persse, D. A case-crossover analysis of out-of-hospital cardiac arrest and air pollution. *Circulation* **2013**, *127*, 1192−1199.
(26) Devlin, R. B.; Duncan, K. E.; Jardim, M.; Schmitt, M. T.; Rappold, A. G.; Diaz-Sanchez, D. Controlled exposure of healthy young volunteers to ozone causes cardiovascular effects. *Circulation* **2012**, *126* (1), 104−111.
(27) Hazari, M. S.; Haykal-Coates, N.; Winsett, D. W.; Costa, D. L.; Farraj, A. K. A single exposure to particulate or gaseous air pollution increases the risk of aconitine-induced cardiac arrhythmia in hypertensive rats. *Toxicol. Sci.* **2009**, *112* (2), 532−42.
(28) Benditt, D. G.; Sakaguchi, S.; Lurie, K. G.; Lu, F. Sinus node dysfunction. In *Cardiovascular Medicine*; Willerson, J. T., Wellens, H. J. J., Cohn, J. N., Holmes, D. R., Jr, Eds.; Springer: London, 2007.
(29) Haqqani, H. M.; Kalman, J. M. Aging and sinoatrial dysfunction. *Circulation* **2007**, *115*, 1178−1179.
(30) Ben-Tal, A.; Shamailov, S. S.; Paton, J. F. R. Evaluating the physiological significance of respiratory sinus arrhythmia: looking beyond ventilation−perfusion efficiency. *J. Physiol.* **2012**, *590*, 1980−2008.

DOI: 10.1021/acs.est.7b04880
Environ. Sci. Technol. 2018, 52, 3071−3080

OXFORD

SOT | Society of Toxicology
www.toxsci.oxfordjournals.org

TOXICOLOGICAL SCIENCES, 167(2), 2019, 559–572

doi: 10.1093/toxsci/kfy262
Advance Access Publication Date: October 23, 2018
Research Article

Downloaded from https://academic.oup.com/toxsci/article-abstract/167/2/559/5142835 by EPA-RTP Main Library user on 15 January 2020

Ambient Particulate Matter and Acrolein Co-Exposure Increases Myocardial Dyssynchrony in Mice via TRPA1

Leslie C. Thompson,* Leon Walsh,* Brandi L. Martin,† John McGee,* Charles Wood,‡ Kasey Kovalcik,§ Joseph Patrick Pancras,* Najwa Haykal-Coates,* Allen D. Ledbetter,* David Davies,* Wayne E. Cascio,* Mark Higuchi,* Mehdi S. Hazari,* and Aimen K. Farraj*,[1]

*Environmental Public Health Division, National Health and Environmental Effects Research Laboratory; †Oak Ridge Institute for Science and Education, Oak Ridge, TN 37830; ‡Integrated Systems Toxicology Division, National Health and Environmental Effects Research Laboratory; and §Exposure Methods & Measurements Division, National Exposure Research Laboratory, United States Environmental Protection Agency, Research Triangle Park, North Carolina 27711

[1]To whom correspondence should be addressed at US Environmental Protection Agency, Environmental Public Health Division, 109 T.W. Alexander Drive, Mail Code: B105-02, Research Triangle Park, NC 27709. Fax: (919) 541-0034. E-mail: farraj.aimen@epa.gov.

Disclaimer: The research presented in the article was reviewed and approved for publication by the National Health and Environmental Effects Research Laboratory at the U.S. Environmental Protection Agency. The contents of this manuscript do not necessarily reflect the views and policies of the agency nor does mention of trade names or commercial products signify endorsement or recommendation for use.

ABSTRACT

Air pollution is a complex mixture of particulate matter and gases linked to adverse clinical outcomes. As such, studying responses to individual pollutants does not account for the potential biological responses resulting from the interaction of various constituents within an ambient air shed. We previously reported that exposure to high levels of the gaseous pollutant acrolein perturbs myocardial synchrony. Here, we examined the effects of repeated, intermittent co-exposure to low levels of concentrated ambient particulates (CAPs) and acrolein on myocardial synchrony and the role of transient receptor potential cation channel A1 (TRPA1), which we previously linked to air pollution-induced sensitization to triggered cardiac arrhythmia. Female B6129 and *Trpa1*−/− mice ($n = 6$/group) were exposed to filtered air (FA), CAPs (46 μg/m^3 of $PM_{2.5}$), Acrolein (0.42 ppm), or CAPs+Acrolein for 3 h/day, 2 days/week for 4 weeks. Cardiac ultrasound was conducted to assess cardiac synchronicity and function before and after the first exposure and after the final exposure. Heart rate variability (HRV), an indicator of autonomic tone, was assessed after the final exposure. Strain delay (time between peak strain in adjacent cardiac wall segments), an index of myocardial dyssynchrony, increased by 5-fold after the final CAPs+Acrolein exposure in B6129 mice compared with FA, CAPs, or Acrolein-exposed B6129 mice, and CAPs+Acrolein-exposed *Trpa1*−/− mice. Only exposure to acrolein alone increased the HRV high frequency domain (5-fold) in B6129 mice, but not in *Trpa1*−/− mice. Thus, repeated inhalation of pollutant mixtures may increase risk for cardiac responses compared with single or multiple exposures to individual pollutants through TRPA1 activation.

Key words: air pollution; particulate matter; acrolein; TRPA1; myocardial synchrony; heart rate variability.

Poor air quality is an important modifiable risk factor for cardiovascular morbidity and mortality (Argacha *et al.*, 2018; Bhatnagar, 2017; Brook and Rajagopalan, 2017; Cohen *et al.*, 2017; Newby *et al.*, 2015). However, attempts to quantify the cardiovascular health burden of air pollution is difficult given the complexity of particulate matter (PM), gas, and volatile organic

Published by Oxford University Press on behalf of the Society of Toxicology 2018.
This work is written by US Government employees and is in the public domain in the US.

compound mixtures, the relative quantities of which depend on local geography, proximity to emission sources, time of day, and weather conditions. Furthermore, the colocalization of pollutants promotes gas-particle interactions, potentially yielding additive, synergistic, or even antagonistic biological responses that may underlie the health effects of air pollution (Mauderly and Samet, 2009). For example, co-exposure to PM and ozone (O_3) has been linked to dispersion of ventricular repolarization in humans (Sivagangabalan *et al.*, 2011), as well as decreased heart rate variability (HRV) (Farraj *et al.*, 2015; Wagner *et al.*, 2014) and epicardial adipose inflammation in rats (Sun *et al.*, 2013). PM co-exposure with NO_2 has been shown to alter T-wave amplitude and low-frequency components of HRV in healthy volunteers, which were not present with exposure to either pollutant alone (Huang *et al.*, 2012).

Less is known about potential interactive effects between PM and acrolein (C═C─C═O), a ubiquitous aldehyde produced during the combustion of organic material like tobacco, wood, fats, and fuels (Henning *et al.*, 2017). Acrolein is an upper airway irritant with reactive electrophilic properties and well-documented adverse cardiopulmonary effects, some of which are mediated by transient receptor potential cation channel A1 (TRPA1) (ATSDR, 2007; Bautista *et al.*, 2006; Conklin, 2016; Henning *et al.*, 2017). Due to the colocalization of PM and acrolein in ambient airsheds, PM and acrolein may interact in a way that modifies the health effects of either pollutant alone, especially given that PM-adsorbed electrophiles have been shown to activate TRPA1 (Deering-Rice *et al.*, 2011; Fariss *et al.*, 2013; Ghelfi *et al.*, 2008). TRP channels are expressed on pulmonary C-fibers (Lee *et al.*, 2015; Lin *et al.*, 2010) and when activated in the nose and lung trigger autonomic reflexes that drive cardiopulmonary effects like apnea, bronchospasm, hypotension, and bradycardia (Pozsgai *et al.*, 2010). TRPA1 involvement in acute air pollution-induced sensory nerve activation, initiation of autonomic reflexes, and cardiovascular dysfunction has been extensively described in Conklin *et al.* (2017), Henning *et al.* (2017), Hooper *et al.* (2016), and Kurhanewicz *et al.* (2017). TRPA1-mediated effects have been reported with aerosol mixtures known to contain both PM and acrolein, including cigarette smoke-induced alteration of mouse tracheal ring responses (Kichko *et al.*, 2015) and diesel exhaust-induced increased sensitivity to triggered cardiac arrhythmia in rats (Hazari *et al.*, 2011).

In our previous work, we determined that acrolein inhalation (3.0 ppm) in mice decreased myocardial synchrony when measured 1 and 24 h after exposure (Thompson *et al.*, 2017). Myocardial synchrony is a measure of heart muscle contractile coordination, which we have proposed as a potentially sensitive indicator of air pollution health effects. Moreover, myocardial synchrony requires coordinated propagation of membrane depolarization, excitation-contraction coupling, and contraction mechanics, all of which are heavily influenced by changes in autonomic tone (Gimelli *et al.*, 2014). Given (a) the reports linking air pollution, altered cardiac autonomic activity and TRPA1 (Conklin *et al.*, 2017; Hazari *et al.*, 2011; Kunkler *et al.*, 2015; Kurhanewicz *et al.*, 2017) and (b) the lack of information regarding the interactive health effects of particulates and aldehydes, the purpose of this study was to compare the cardiovascular impacts of intermittent, repeated exposure to low levels of concentrated ambient particulate matter (CAPs), acrolein, or CAPs plus acrolein in wild-type and TRPA1 knockout mice. We hypothesized that co-exposure to CAPs and acrolein would increase myocardial dyssynchrony and alter cardiac autonomic tone when compared with exposure to either pollutant alone, and that such responses would be absent in TRPA1 knockout mice. Cardiac strain data, heart function and dimensions, and transmitral blood flow were investigated using high-frequency ultrasound before exposures, 1 day after the first exposure, and 1 day after the final exposure. Exposure-induced functional changes were coupled with measures of HRV for assessment of cardiac autonomic responses. Furthermore, because the effects of CAPS and acrolein co-exposure on overall cardiopulmonary well-being have not been reported before, we also measured several indicators of pulmonary and systemic inflammation and injury and examined for nasal, lung, and heart histopathology. Effects were related to PM composition and contributing sources by analysis of PM elemental data and quantification of PM sources using a chemical mass balance model.

MATERIALS AND METHODS

Sample size analysis. Sample size analysis was conducted using R Studio software (version 3.1.2) with the "pwr" package (https://cran.r-project.org/web/packages/pwr/pwr.pdf, last accessed November 14, 2018) and "pwr.anova.test" command. Data from a previous study of myocardial synchronicity after acrolein inhalation in mice was used to calculate sample size (Thompson *et al.*, 2017). The expected effect size for this study was an increase in myocardial strain delay by 5% of the cardiac cycle, which was the approximate increase observed in the previous study with acrolein inhalation. Also, the largest control group standard deviation (SD) from the multiple time points assessed in the previous study was 3.4%. Cohen's equation for effect size (d) and effect size index (f) was calculated as follows (Cohen, 1988):

d = effect range/control SD
$d = 5/3.4$
$d = 1.47$
$f = 0.5 * (d)$
$f = 0.5 * (1.47)$
$f = 0.74$

For group size (n) determinations, we set k (number of groups) = 4 because we were planning for 3 experimental groups and 1 air control group in each mouse strain, significance level = .05, and power = .8. The sample size analysis yielded $n = 6$.

Animals. Twenty-four female B6129PF2/J mice (B6129), strain code 100903, and 24 female B6; 129P-*Trpa1*^{tm1Kykw}/J (*Trpa1*−/−), strain code 006401 (Jackson Laboratories, Bar Harbor, Maine), were housed in plastic cages (three per cage), maintained on a 12-h light/dark cycle at approximately 22°C and 50% relative humidity (RH) in our Association for Assessment and Accreditation of Laboratory Animal Care-approved facility, and held for a minimum of 2 weeks before exposures. The Institutional Animal Care and Use Committee of the U.S. Environmental Protection Agency approved all protocols. Female mice were used in accordance with a previous study (Kurhanewicz *et al.*, 2017). The age range for the B6129 mice was 19–21 weeks and that for the *Trpa1*−/− mice, 21–28 weeks. Two 42-week-old *Trpa1*−/− mice were also used due to limited availability of younger mice. The two 42-week old mice, were, however, split into separate groups. That is, one of these mice was placed in the Acrolein-exposed *Trpa1*−/− group and one was placed in the CAPS-exposed *Trpa1*−/− group.

Experimental design. Mouse inhalation exposures were conducted within the U.S. Environmental Protection Agency's Concentrated

Downloaded from https://academic.oup.com/toxsci/article-abstract/167/2/559/5142835 by EPA-RTP Main Library user on 15 January 2020

Air Particles Laboratory at the Consolidated Research Facility in Research Triangle Park, North Carolina. To avoid restraint-stress we selected a whole-body inhalation method. Fine CAPs concentrations were targeted to be low enough to approximate peak concentrations in a typical urban environment (100 $\mu g/m^3$). We targeted an acrolein concentration of 0.300 ppm because it is only three times the recommended exposure limit established by the National Institute of Occupational Safety and Health of the United States Center for Disease Control and Prevention (ie, 0.1 ppm 10-h time weighted average; NIOSH, 2005) and is a concentration that can be reliably measured by our gas chromatograph. To reflect natural short-term and repeated, intermittent exposure to spikes in air pollution as experienced in the ambient environment by humans, mice were exposed for 3-h each day, 2 days per week (Monday and Wednesday or Tuesday and Thursday) for 4 consecutive weeks for a total of 8 exposures during November and December of 2014. Cardiac ultrasounds were performed on each mouse 1 week prior to beginning exposures, 1 day after the first exposure, and 1 day after the final exposure. Mice were necropsied immediately after the last ultrasound.

PM concentrating system. Ambient air (5000 L/min) was drawn into the exposure laboratory through a 2 stage, size selective inlet restricting PM larger than 10 μm and 2.5 μm diameters. Air with the resulting fine mode $PM_{2.5}$ fraction exited the size selective inlet and was transported via stainless steel ductwork to the CAPs laboratory where it entered a 3 stage Harvard Fine Particle Concentrator (HFPC) (Gupta *et al*., 2004). The HFPC was configured with 3 concentrating stages of slit virtual impactors and was operated at a vacuum of −9 to −10 inH_2O, producing 50 L/min of CAPs air as previously described in Kodavanti *et al.* (2005). Plumbing was configured to allow the HFPC to function in "chamber exposure" or "chamber bypass" modes (see Figure 1). For FA and Acrolein exposure groups, the HFPC was operated in "chamber bypass" mode so that all mice experienced the same level of noise generated by the HFPC, thus eliminating system noise as a potential experimental confounder.

Exposure chambers. During operation of the HFPC in chamber exposure mode, 50 L/min CAPs air at −9 to −10 in H_2O static pressure was split and 20 L/min were directed toward each of two Cannon nose-only chambers. The remaining 10 L/min were used for PM monitoring. Mice were exposed in rat-sized nose-only tubes with rear stoppers mounted to chamber ports, allowing for "whole-body" exposure conditions. More details are provided in the Supplementary material.

Acrolein supply. Acrolein gas was injected upstream of the chamber supply air inlet of one chamber. Gas was metered from a cylinder of known acrolein concentration (537 ppm acrolein, balance N2) and the gas flow rate was precisely monitored. CAPs DAS (Data acquisition software) regulated and monitored gas flow continuously as well as providing safety cutoff control of acrolein if necessary. The gas supply line included a solenoid valve and manual valves to isolate gas supply from the chamber and allowed operators to purge the supply line with breathing grade air for safety.

Chamber monitoring. HFPC and Cannon exposure chamber air parameters were monitored and recorded using CAPs lab DAS. Various analytical instruments, filter collections, GC sampling, and real-time monitors were utilized for analyses of chamber PM size and concentration, acrolein concentration, temperature, RH, airflow, and other system parameters, allowing for continuous control of chamber conditions. More details are provided in the Supplementary material.

$PM_{2.5}$ elemental, organic, and ion analysis. Due to limited airflow and low PM concentrations filters were collected after 4 weeks of exposure (1 filter per month), to collect sufficient PM mass for extraction and analysis. This allowed us to assess potential differences in PM content between November and December. Elemental analysis was performed on aqua regia digests of PM collected on Teflon filters as previously described in Farraj *et al.* (2015). Samples were analyzed by high-resolution inductively coupled plasma-mass spectrometry (HR-ICP-MS, Element 2, Thermo Fisher Scientific, Waltham, Massachusetts).

Chemical mass balance (CMB) source apportionment. To predict potential sources and estimates of their contributions to the $PM_{2.5}$ collected on filters during November and December of 2014, we tested sample chemical analysis profiles against the EPA Chemical Mass Balance Model (CMB8.2; US EPA, 2004). PM chemical composition data at the inlet of CAPs system alone were used for this source-receptor modeling. Source profiles to represent motor vehicles, biomass burning, secondary aerosol production, road dust, and marine aerosol were taken from EPA SPECIATE 4.3 Database (https://cfpub.epa.gov/speciate).

Echocardiography and electrocardiogram data collection. ECG waveform acquisition was performed using a Vevo 2100 ultrasound system immediately prior to ultrasound sonography (FujiFilm VisualSonics, Inc, Toronto, Canada). Isoflurane-anesthetized mice were placed in dorsal recumbency with paws grounded to the electrodes of a heated Vevo Mouse Handling Table (FujiFilm VisualSonics, Inc). Four cineloops optimized to collect approximately 12–13 s of ECG data each (approximately 50 s total) were recorded from each subject. Ultrasound scans were performed as previously described in Thompson *et al.* (2017) in accordance with the guidelines of the American Society of Echocardiography (Lang *et al*., 2005; Quinones *et al*., 2002). The sonographer was blinded to experimental groups. Scans were made using a Vevo 2100 ultrasound system (FujiFilm VisualSonics, Inc) and a MS550D transducer set to a 40 MHz sample rate in B-mode and M-mode, and 32 MHz for pulsed wave Doppler measurements. Data were collected at baseline (the week before exposures), 1 day after the first exposure, and 1 day after the final (8th) exposure. Parasternal short-axis views at the level of the left ventricular papillary muscles were collected in B-mode and M-mode. The apical 4-chamber view was used for pulsed wave Doppler measurements of transmitral valve blood flow. Three cineloops from each view were collected for data analysis. Anesthesia induction, subject preparation, data collection, and recovery from anesthesia ranged from 15 to 20 min per animal.

Ultrasound analysis and heart rate variability assessment. Ultrasound data analyses were also performed under blinded conditions, as previously described in Thompson *et al.* (2017). Circumferential strain delay, peak circumferential strain, time to peak (TPk) strain, peak diastolic circumferential strain rate, and TPk diastolic strain rate were each evaluated using B-mode data. Left ventricular stroke volume, cardiac output, ejection fraction, fractional shortening, end diastolic volume, end systolic volume, as well as wall and chamber dimensions were calculated from M-mode data. Left ventricular isovolumic contraction time (IVCT), aortic ejection time (AET), and isovolumic

Downloaded from https://academic.oup.com/toxsci/article-abstract/167/2/559/5142835 by EPA-RTP Main Library user on 15 January 2020

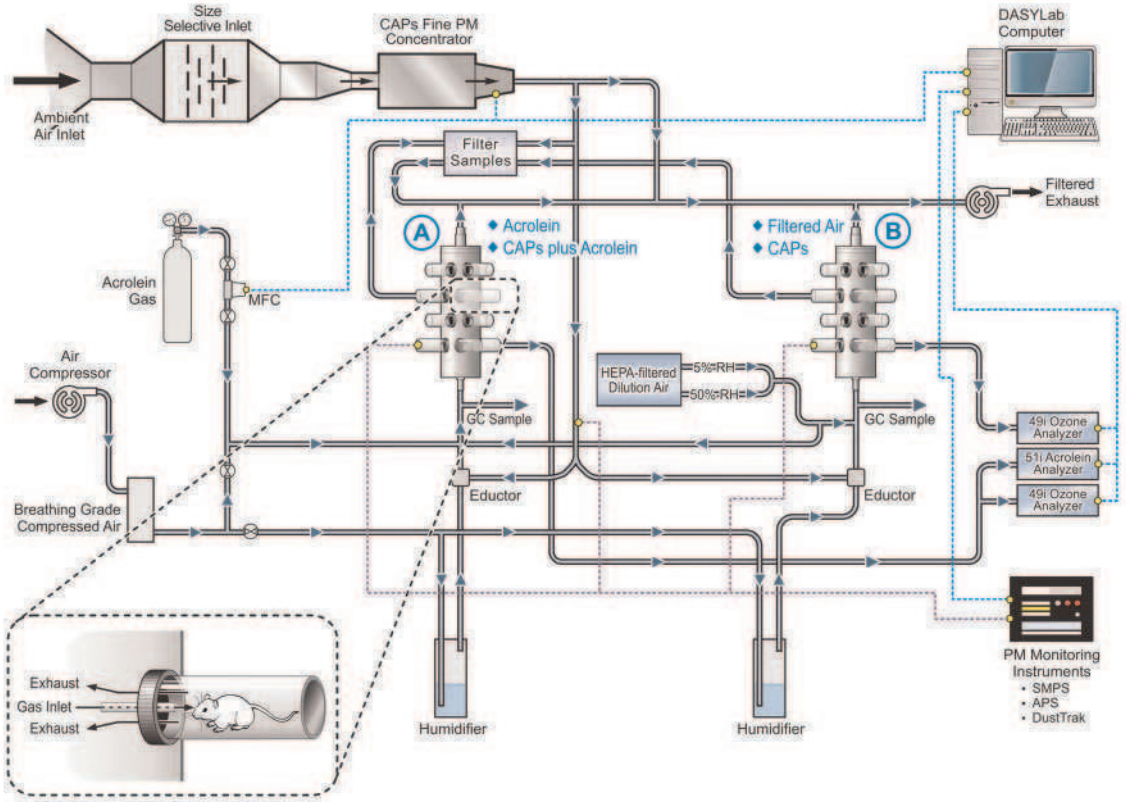

Figure 1. CAPs plus acrolein multipollutant exposure system. Particles entered via size selective inlet for 2.5 μm diameters or less and concentrated with a Harvard Fine Mode Particle Concentrator. Mice were exposed in rat-sized nose-only tubes providing a whole-body exposure system. CAPs lab DAS and various analytical instruments plus filters and GC sampling were utilized to monitor chamber PM concentration and size, Acrolein concentration, temperature and RH, chamber airflow, and other system parameters. Acrolein gas flow was also monitored and controlled by the DAS and a mass flow controller (MFC). Due to inhalation chamber airflow requirements, analytical sampling was carefully planned to get maximum $PM_{2.5}$ composition information from minimum amount of airflow. PM mass concentrations and inorganic elemental composition were measured using filters from the CAPs inlet, CAPs outlet, and both chambers. "A" marks the chamber used for acrolein only and CAPs plus acrolein exposures. "B" marks the chamber used for filtered air only and CAPs only exposures.

relaxation time (IVRT) were calculated form pulsed wave Doppler recordings. Myocardial performance Tei index was calculated with the following equation: (IVCT+IVRT)/AET (Tei *et al.*, 1995).

HRV was measured and calculated as previously described in Kurhanewicz *et al.* (2017). Briefly, the mean of the differences between sequential RRs for each set of ECG waveforms were calculated using ECGAuto (v3.3.5.10; EMKA Technologies S.A.S., Paris, France). Time-domain measures of HRV included standard deviation of the time between normal-to-normal beats (SDNN) and root mean squared of successive differences (RMSSD). SDNN represents overall HRV, whereas RMSSD represents parasympathetic influence over HR (Rowan *et al.*, 2007). The frequency domain of HRV was also analyzed including low-frequency (LF: 0.15–1.5 Hz), representing a combination of sympathetic and parasympathetic tone, and high-frequency (HF: 1.5–5 Hz), indicating parasympathetic tone, and the ratio of these two (LF/HF), indicating sympathovagal balance (Rowan *et al.*, 2007). Thorough visual inspection was conducted to identify and exclude arrhythmias and artifacts.

Necropsy, bronchoalveolar lavage, tissue collection, and analyses. Mice were anesthetized with pentobarbital (200 mg/kg) and phenytoin (25 mg/kg) given by intraperitoneal injection (Euthasol, Virbac Animal Health, Fort Worth, Texas). Blood was collected from the abdominal vena cava, placed in serum separator tubes, and after centrifugation serum was stored at −80°C. The trachea was cannulated and the right lung minus the caudal lobe was lavaged with cold Hanks' balanced salt solution (GIBCO HBSS, Thermo Fisher Scientific). The caudal lobe was tied off before lavage and snap frozen for tissue banking. Cytospins were used for cell differentials and supernatants were stored at −80°C. A transverse midsection of the left ventricle, the left lung, and nose was collected for histological examination. Bronchoalveolar lavage (BAL) cell pellets were resuspended in fresh HBSS, 500 μl were used for cytospins and 500 μl were used to determine total cell counts using a Beckman Coulter Z2 (Beckman Coulter Life Sciences, Brea, California). Cytospins were stained with modified Wright-Giemsa stain (#036-221, Fisher Scientific, Hampton, New Hampshire) and were counted microscopically to 300 cells per slide, with percentages multiplied by total cell counts to calculate final cell numbers.

Histopathology. Hearts, lungs, and heads (for nasal airway) were fixed in 4% fresh paraformaldehyde for histopathological evaluation (see additional detail in Supplementary Methods). The heart was sectioned transversely at the level of the mid-ventricle. The left lung lobe was first perfused intratracheally at a pressure of 30 cm of fixative and sectioned longitudinally. The nasal cavity of each mouse was transversely sectioned at three specific anatomic locations. Fixed tissues were paraffin-embedded, sectioned at approximately 5 μm, and stained with

Downloaded from https://academic.oup.com/toxsci/article-abstract/167/2/559/5142835 by EPA-RTP Main Library user on 15 January 2020

hematoxylin and eosin (H&E) using standard histologic procedures at Experimental Pathology Laboratories (Research Triangle Park, North Carolina). Stained sections were evaluated via light microscopy by a certified pathologist (CW). Differences in lesion incidence between treatment group and genotype were evaluated using a two-sided Fisher's exact test.

Statistical analyses. Data are reported as mean ± SD or presented as boxplots with all data points shown. Box edges identify the interquartile range, the middle line identifies the median, the "+" identifies the mean, and the whiskers identify the minimum and maximum data values. Data were analyzed and graphed with Graphpad Prism 6 software version 6.07 (La Jolla, California). For histopathology, differences in lesion incidence among treatment group or genotype were evaluated using a Fisher's exact test. For single time point biological data, one-way ANOVA with Tukey's post-test and multiplicity adjusted *p*-values were conducted. For repeated ultrasound assessments two-way repeated measures ANOVA with Tukey's post-test and multiplicity adjusted *p*-values were conducted across exposure groups within strain at each time point; Bonferroni's post-test was run across time and strain within exposure groups. For these data, *p*-values are reported except for those $< .0001$ in Figure 4. In Tables 3 and 4, *p*-values $< .05$ are denoted with * versus FA, # versus Acrolein, † versus CAPs, and ‡ versus B6129.

RESULTS

Exposure Concentrations and Environmental Conditions

Chamber exposure conditions for each group are provided in Table 1. Due to low ambient levels of PM, particle concentrations achieved were only 46.3 and 45.4 μg/m^3 for CAPs and CAPs+Acrolein, respectively. Mean particle sizes were 168 and 172 nm in diameter in the CAPs and CAPs+Acrolein exposures, respectively. In the acrolein alone and CAPs+Acrolein exposures, acrolein concentrations were stable at around 0.42 ppm and below the level of detection in the Filtered Air and CAPs alone exposures. Chamber temperatures were stable at approximately 22°C and RH ranged from 30% to 50%. Lower humidity in the CAPs and CAPs+Acrolein chambers was due to mixing of dry eductor motive air with outside ambient air drawn into the HFPC. Bubbler humidifiers in the eductor compressed motive air supply helped raise the RH levels to achieve approximately 30% chamber RH levels. Background O3 levels were less than 5.0 ppb.

Wind Trajectories

The airshed origin, wind direction, and airflow elevation for each CAPs exposure day during the study were obtained as previously described (Farraj *et al.*, 2015) and are shown in Figure 2. These were analyzed to identify contributing airsheds for particulate matter in Research Triangle Park, NC, USA in November and December of 2014. For both the November and December exposures, winds originated predominately from southwest to northwest, at elevations of < 2000 m in the atmospheric boundary layer of the lower troposphere (Figure 2A). Some of the PM delivered to the Raleigh/Durham area originated from the Chicago/Cincinnati airsheds (Figure 2B), and on some other days originated from the Cleveland/Columbus area and the Birmingham/Atlanta/Charlotte areas. The tracings presented in Figure 2A also illustrate that there was no uniform pattern of exposure sources because the direction of the air mass source changed daily.

Chemical Composition of CAPs

Table 2 compares the elemental compositions of $PM_{2.5}$ collected at the air inlet during November and December of 2014. The predominant components of the PM collected during this study were organic carbon (OC) and ammonium sulfate (SO_4). To improve the mass balance estimations, we expressed elements as oxides of the most common oxidation state. Also, the elemental OC was multiplied by 1.6 to account for associated hydrogens, oxygens, and nitrogens usually associated with the carbon fraction (Turpin and Lim, 2001). In general, November and December $PM_{2.5}$ compositions were very similar regarding both the total mass and constituents with the exception of cadmium in November, which was still low overall. The ratio of November/December microgram per cubic meter gravimetric ratios is 1.14 and the averaged analytes ratio is 1.18. Supplementary Table 1 also provides a comparison of CAPs elemental analyses of inlet PM, outlet PM, CAPS chamber PM, and CAPs+Acrolein chamber PM, thus verifying that the PM delivered to each CAPs exposure chamber was consistent in chemical composition to ambient PM in both November and December.

Source Apportionment Analysis

Source apportionment results for $PM_{2.5}$ mass concentrations on both exposure collections are displayed in Figure 3 (5-source CMB model) and Supplementary Figure 1 (6-source CMB model), which reveals marginal differences in secondary sulfate level, motor vehicle exhaust, and biomass combustion sources between the November and December samples collected in 2014. The CMB model explained up to 83%–85% of the $PM_{2.5}$ mass collected from the November and December PM filters. The fraction of measured concentration variance (R^2) was greater than 0.84 and the Chi square value was less than 2.5 for both samples, indicating a good fit between measured and modeled concentrations for both samples. Motor Vehicle Exhaust (26.4%, 31.3% by mass for November and December PM collections, respectively), biomass combustion (22.1%, 16.2%), and secondary sulfate (27.8%, 32.1%) were found to be the major sources of both PM samples. Together, these 3 source types accounted for

Table 1. Exposures Concentrations, Particle Size and Chamber and Ambient Weather Conditions

		Exposure and Weather Conditions				
		Filtered Air	Acrolein	CAPs	CAPs+Acrolein	HFPC Inlet
[PM mass]	μg/m^3	Below detection	Below detection	46.3 ± 0.2	45.4 ± 2.3	6.4 ± 0.6
Particle number	Count/cc	—	—	6580	6900	4890
PM diameter	nm	—	—	169 ± 134	172 ± 139	76 ± 84
[Acrolein]	ppm	Below detection	0.42 ± 0.02	Below detection	0.42 ± 0.01	Below detection
Temperature	°C	21.8 ± 0.2	22 ± 0.4	21.6 ± 0.3	22.3 ± 0.4	24.6 ± 13.3
Rel. humidity	%	50 ± 2.0	51 ± 2.0	30 ± 10	29 ± 9.0	65 ± 19

Downloaded from https://academic.oup.com/toxsci/article-abstract/167/2/559/5142835 by EPA-RTP Main Library user on 15 January 2020

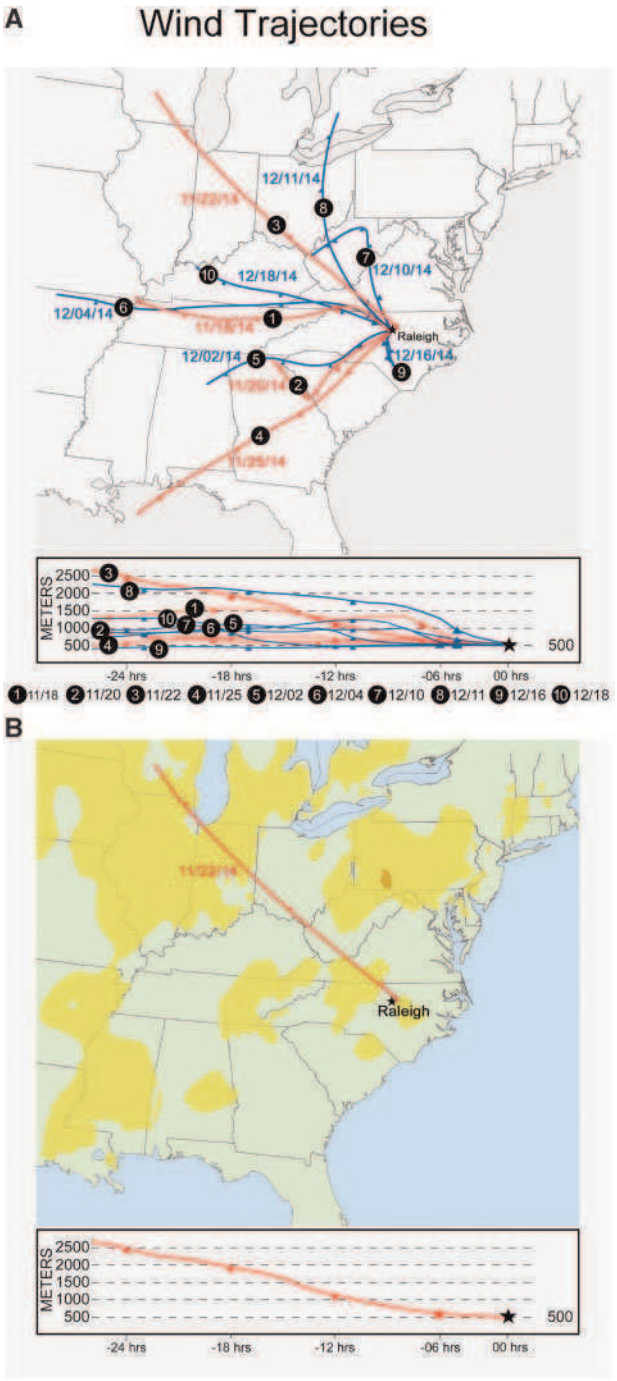

Figure 2. Wind trajectories. For both the November and December 2014 exposures, winds originated predominately from southwest to northwest, at elevations of < 2000 m in the atmospheric boundary layer of the lower troposphere. Panel A shows back trajectory analysis for each day, including elevation in meters (box). Lines 1–4 correspond to exposure days that occurred in November and lines 5–10 correspond to exposure days in December. Triangles on each line mark 6 h intervals of −24, −18, −12, and −6 h prior to exposure with the star marking the time and location of the U.S. Environmental Protection Agency's Concentrated Air Particles Laboratory in Research Triangle Park, NC, USA (Latitude: 35.88350; Longitude: −78.87460). Panel B shows an example of how air flow can drift through various PM airsheds. This map was modified from the PM air quality index map from Airnow.gov archives for November 22, 2014 with the back trajectory overlaid. Shaded areas were determined to be of moderate 24 h PM-based ambient air quality (12.1–35.4 μg/m^3).

76.2% and 79.7% of the fine PM during November and December, respectively. Though minor, marine aerosol and wind-blown crustal material were still consistent source contributors, accounting for 2.4% and 3.9% $PM_{2.5}$ mass, respectively.

Overt Toxicity

We found no evidence of overt toxicity (eg, lethargy, respiratory distress, and/or > 10% weight loss) during the study in virtually all animals. One B6129 mouse in the CAPs+Acrolein exposure group did, however, present indications of lethargy and respiratory distress during the third week of exposure and, consequently, was removed from the study. Prior to euthanasia, a cardiac ultrasound was performed on this moribund mouse, which indicated left ventricular hypertrophy (see Supplementary Figure 2). Interestingly, this mouse presented no clear evidence of health abnormalities at the beginning of the study so data from the first two ultrasound scans were included in the study. Mouse age and size related data at the time of necropsy for all other mice are provided in Table 3. We found no exposure related changes in food and water intake, body mass, or heart weight. *Trpa1*−/− mice were significantly smaller than B6129 mice and due to limited availability from the supplier were also older by about 7 weeks on average (26 weeks old vs 19 weeks old by the end of the study, respectively).

Bronchoalveolar Lavage Fluid Analysis and Cell Differentials

We compared potential pulmonary responses between the exposure groups by collecting and analyzing bronchoalveolar lavage fluid collected after the study. Overall cellularity in bronchoalveolar lavage was stable between groups. CAPs+Acrolein exposure groups from both strains had the most neutrophil and lymphocyte infiltration but the values were highly variable and not statistically significant from FA controls (Supplementary Table 2). There were also no significant differences in any biochemical indicators measured in bronchoalveolar lavage fluid (Supplementary Table 3).

Serum Biochemical Analysis

Assays for biomolecule targets in serum revealed minimal differences between exposure groups with two exceptions: HDL was significantly lower in all *Trpa1*−/− groups compared with the respective B6129 groups and LDL was significantly lower in the B6129 CAPs group relative to the *Trpa1*−/− CAPs group (Supplementary Table 4).

Histopathology

We found no histological evidence of lesions that would support the possibility that co-exposure to PM with acrolein altered the exposure distribution in the airway, at least at the concentrations tested (Supplementary Tables 5–7). In the nasal cavity, the incidence of minimal neutrophilic inflammation was modestly higher following acrolein exposure in *Trpa1*−/− mice ($p = .03$ vs filtered air) but not in B6129 mice. Conversely, there was higher incidence of cytoplasmic vacuolation in the nasal gland epithelium surrounding the vomeronasal organ following CAPs exposure in B6129 mice ($p = .03$ vs filtered air) but not *Trpa1*−/− mice. More details are provided in the Supplementary Results.

Cardiac Function and Dimensions and Myocardial Performance

Analysis results, including cardiac function and heart wall dimensions, of parasternal short axis M-mode views at the level

Downloaded from https://academic.oup.com/toxsci/article-abstract/167/2/559/5142835 by EPA-RTP Main Library user on 15 January 2020

Table 2. CAPs Chemical Composition Analysis

CAPs Chemical Composition Analysis						
Analyte	November $\mu g/m^3$	December $\mu g/m^3$	November/December Ratio	November $\mu g/g$	December $\mu g/g$	November/December Ratio
Inorganics						
Ag_2O	6.87e-6	6.55e-6	1.05	1.00	1.09	0.92
Al_2O_3	8.56e-2	9.32e-2	0.92	1.25e4	1.55e4	0.80
As_2O_3	<DL	4.23e-4	—	<DL	70.4	—
BaO	1.79e-3	3.05e-3	0.59	2.61e2	5.08e2	0.51
CaO	5.48e-2	3.41e-2	1.61	8.00e3	5.68e3	1.41
CdO	2.32e-3	0.05e-3	48.7	3.39e2	7.94	42.7
Ce_2O_3	4.46e-5	4.58e-5	0.97	6.51	7.63	0.85
Cr_2O_3	8.61e-4	6.58e-4	1.31	1.26e2	1.10e2	1.15
Cs_2O	3.32e-5	0.98e-5	3.40	4.85	1.63	2.98
CuO	1.41e-3	3.27e-3	0.43	2.05e2	5.45e2	0.38
FeO	5.79e-2	4.66e-2	1.24	8.45e3	7.77e3	1.09
K_2O	6.60e-2	4.36e-2	1.51	9.62e3	7262	1.32
MgO	1.75e-2	1.13e-2	1.55	2.55e3	1878	1.36
MnO	1.87e-3	1.48e-3	1.26	2.72e2	247	1.10
MoO_3	1.34e-4	2.28e-4	0.59	1.95e1	0.38e2	0.51
Na_2O	0.11	0.10	1.10	1.65e4	1.71e4	0.96
NiO	5.28e-4	4.14e-4	1.28	0.77e2	6.89e1	1.12
P_2O_5	1.93e-2	0.01	1.94	2.81e3	1.66e3	1.70
PbO	1.26e-3	0.94e-3	1.34	1.83e2	1.57e2	1.17
Rb_2O	1.65e-4	1.40e-4	1.18	2.40e1	2.32e1	1.03
SO_4	2.03	1.62	1.26	2.97e5	2.70e5	1.10
Sb_2O_5	4.78e-4	8.52e-4	0.56	6.97e1	1.42e2	0.49
SeO_3	1.60e-3	1.36e-3	1.18	2.34e2	2.26e2	1.03
SiO_2	8.54e-2	5.25e-2	1.63	1.25e4	8.75e3	1.42
SnO_2	3.45e-4	9.16e-4	0.38	5.04e1	1.53e2	0.33
SrO	2.64e-4	2.65e-4	1.0	3.85e1	4.41e1	0.87
TiO_2	1.66e-3	1.96e-3	0.85	2.42e2	3.27e2	0.74
V_2O_5	3.19e-4	2.87e-4	1.11	4.66e1	4.79e1	0.97
ZnO	0.01.03e-2	0.98e-2	1.05	1.50e3	1.63e3	0.92
Carbon						
[a]Organic C	4.53	3.02	1.50	6.60e5	5.04e5	1.31
Elemental C	0.13	0.18	0.72	1.88e4	3.06e4	0.61
Ions						
SO_4-	1.21	1.205	1.00	1.76e5	2.01e5	0.88
Na^+	5.55e-2	0.0351	1.58	8.10e3	5.86e3	1.38
NH_4^+	0.41	0.44	0.93	6.03e4	73 728	0.82
K^+	3.86e-2	0.03	1.29	5.63e3	5.00e3	1.13
Ca^{++}	6.40e-2	2.52e-2	2.54	9.34e3	4.20e3	2.22
Sum	7.63	5.68		1.11e6	9.48e5	
Mass ($\mu g/m^3$)	6.86	6.00			Analyte ratio	1.08
Ratio (sum/mass)	1.11	0.95				
	Analyte ratio		1.18			
	Mass ratio		1.14			

[a]CwHxOyNz (empirical formula = 1.6 • Organic C).
DL, detection limit.

of the papillary muscles, are reported in Table 4 and Supplementary Table 8, respectively. In addition, myocardial performance metrics derived from Doppler transmitral blood flow measures are presented in Supplementary Table 9 and Supplementary Figure 3. We found no differences in any cardiac function, heart wall dimensions, or myocardial performance parameters that were indicative of an exposure effect. In accordance with the guidelines of the American Society of Echocardiography (Lang *et al.*, 2005; Quinones *et al.*, 2002), we verified blinded interobserver variability for M-mode data analyses at 7.7% coefficient of variation.

Myocardial Synchronicity

The results of ultrasound analysis of myocardial synchronicity are displayed in Figure 4, Supplementary Table 10 and Supplementary Figure 4. Strain delay is a result of dyssynchronous systolic contraction within the heart wall, in this case between two adjacent wall segments, the anterior free wall and lateral wall. We found an increase in strain delay in B6129 mice when measured 1 day after the final exposure to CAPs+Acrolein; this increase ranged from around 3% of the cardiac cycle to over 10% of the cardiac cycle within this group. The increase in strain delay in the B6129 CAPs+Acrolein group was

Downloaded from https://academic.oup.com/toxsci/article-abstract/167/2/559/5142835 by EPA-RTP Main Library user on 15 January 2020

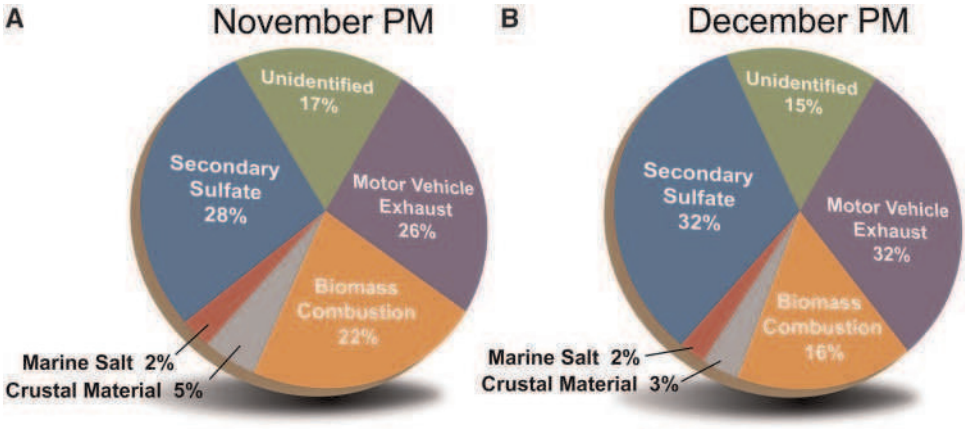

Figure 3. PM source apportionment. $PM_{2.5}$ samples from CAPs inlet filters collected in November and December of 2014 were analyzed using the 5-source chemical mass balance model (U.S. EPA). The results from our 5-source apportionment revealed 4%–6% differences in secondary sulfate, motor vehicle exhaust, and biomass combustion sources between November (A) and December (B).

Table 3. Body Weight and Heart Mass After Final Exposure

			Mouse Age and Size Statistics at the Time of Necropsy			
			Filtered Air	Acrolein	CAPs	CAPs+Acrolein
Age	Weeks	B6129	19.7 ± 0.5	18.6 ± 0.4	19.9 ± 0.5	*a*19.1 ± 0.6
		Trpa1−/−	24.0 ± 3.6 ‡	28.2 ± 5.8 ‡	27.5 ± 1.5 ‡	25.5 ± 1.6 ‡
Body mass	g	B6129	25.6 ± 2.3	24.1 ± 2.8	24.3 ± 2.4	*a*25.1 ± 2.7
		Trpa1−/−	19.2 ± 1.1 ‡	19.8 ± 1.7 ‡	20.6 ± 1.5 ‡	20.1 ± 2.3 ‡
Tibia length	mm	B6129	21.8 ± 0.4	20.7 ± 0.3	20.8 ± 1.2	*a*20.9 ± 0.9
		Trpa1−/−	20.2 ± 0.5	20.6 ± 0.6	20.0 ± 1.0	20.7 ± 0.4
Heart mass	mg	B6129	106.7 ± 20.7	91.8 ± 3.9	98.0 ± 17.9	*a*99.2 ± 1.3
		Trpa1−/−	89.0 ± 9.7 ‡	88.7 ± 7.5	100.0 ± 31.2	86.2 ± 6.5
			Mean ± SD ($n = 6$ unless denoted with *a* for $n = 5$)			

$p < .05$ noted with ‡ versus B6129.

significantly different from all other B6129 exposure groups and all *Trpa1*−/− exposed groups including the *Trpa1*−/− CAPs+Acrolein group. Strain delay in the B6129 CAPs+Acrolein group was also significantly different than earlier time points in the same group.

Heart Rate Variability

Results from HRV analysis of ECG signals collected from anesthetized B6129 and *Trpa1*−/− mice 1 day after the 8th exposure to Filtered Air, Acrolein, CAPs, or CAPs+Acrolein are presented in Figure 5. No significant differences in SDNN were found (Figure 5A). Whereas no significant differences in RMSSD were found (Figure 5B), the difference in means between B6129 mice exposed to Acrolein and B6129 mice exposed to Filtered Air yielded a $p = .07$. The high frequency domain of HRV increased in B6129 mice exposed to Acrolein compared with B6129 mice exposed to Filtered Air (Figure 5C). There was no such effect of acrolein in *Trpa1*−/− mice, and the difference in means between B6129 mice exposed to Acrolein and *Trpa1*−/− mice exposed to Acrolein yielded a $p = .10$.

DISCUSSION

This study shows for the first time that intermittent co-exposure to ambient PM and acrolein in mice, using a novel CAPs and acrolein co-exposure system, results in myocardial dyssynchrony through a mechanism involving TRPA1. The loss of myocardial synchrony after repeated, intermittent PM and acrolein co-exposure is unique from the response to a single exposure and from exposure to either pollutant alone, pointing to interactive effects of the two pollutants. The absence of concurrent changes in HRV in CAPs+Acrolein-exposed B6129 mice may point to molecular and cellular changes within the myocardium, but do not necessarily preclude autonomic activity that may have occurred earlier in the exposure regimen. Interestingly, although acrolein had no impact on myocardial synchronicity when measured, it did in fact increase an HRV index of parasympathetic tone in B6129 mice, an effect that was absent in acrolein-exposed *Trpa1*−/− mice. Such a stark qualitative difference in response pattern points to physiochemical and/or biological mechanisms in PM and acrolein mixtures that are either absent or activated to a lesser degree with exposure to either alone. Whereas the physicochemical properties that may underlie such exaggerated effects are unclear, activation of pulmonary TRPA1, a prominent sensor of environmental irritants, may have triggered the cascade of events leading to myocardial dyssynchrony.

Elemental analysis showed that organic carbon and ammonium sulfate were the predominant constituents of PM in this study, along with alkalis sodium, calcium, potassium, silicon, aluminum, and iron. Source apportionment found the majority of sources to be attributable to secondary sulfates, motor vehicle

Downloaded from https://academic.oup.com/toxsci/article-abstract/167/2/559/5142835 by EPA-RTP Main Library user on 15 January 2020

Table 4. Echocardiography (M-Mode)—Cardiac Function

			SAX M-Mode Evaluation at Baseline			
			Filtered Air	Acrolein	CAPs	CAPs+Acrolein
Heart rate	Beats/min	B6129	443 ± 27	392 ± 33	410 ± 41	420 ± 42
		Trpa1−/−	456 ± 33	468 ± 37 ‡	463 ± 29 #	437 ± 38
ESV	µl	B6129	26.5 ± 12.1	25.7 ± 9.8	21.3 ± 7.8	24.7 ± 7.5
		Trpa1−/−	19.3 ± 7.9	18.7 ± 6.7	27.1 ± 7.3	21.9 ± 8.6
EDV	µl	B6129	63.4 ± 22.9	58.9 ± 9.9	55.2 ± 12.9	54.7 ± 9.1
		Trpa1−/−	45.8 ± 12.0	45.7 ± 11.3	61.7 ± 20.2	47.4 ± 9.9
SV	µl	B6129	36.9 ± 11.1	33.2 ± 4.3	33.9 ± 9.0	30.1 ± 5.1
		Trpa1−/−	26.5 ± 8.3	26.9 ± 5.6	34.6 ± 13.9	25.5 ± 4.6
EF	%	B6129	59.1 ± 4.9	57.3 ± 9.7	61.9 ± 11.2	55.5 ± 7.4
		Trpa1−/−	58.3 ± 10.6	60.0 ± 7.3	55.3 ± 5.8	54.6 ± 9.6
FS	%	B6129	30.9 ± 3.2	29.8 ± 6.3	33.2 ± 8.5	28.5 ± 4.7
		Trpa1−/−	30.5 ± 8.1	31.2 ± 5.0	28.3 ± 3.9	27.8 ± 6.0
CO	ml/min	B6129	16.3 ± 4.9	13.0 ± 2.0	14.0 ± 4.4	12.8 ± 3.4
		Trpa1−/−	12.0 ± 3.7	12.5 ± 2.1	16.2 ± 7.6	11.1 ± 2.0
			Mean ± SD ($n = 6$)			
			SAX M-Mode Evaluation 1 Day After 1st Exposure			
Heart rate	Beats/min	B6129	447 ± 23	425 ± 61	445 ± 32	448 ± 38
		Trpa1−/−	500 ± 31	480 ± 48	476 ± 33	459 ± 21
ESV	µl	B6129	32.9 ± 18.1	25.1 ± 9.6	20.2 ± 6.7	24.9 ± 6.7
		Trpa1−/−	17.7 ± 4.4 ‡	28.2 ± 10.4	26.4 ± 9.0	24.8 ± 5.0
EDV	µl	B6129	66.1 ± 25.0	52.4 ± 14.7	50.6 ± 11.3	57.6 ± 11.9
		Trpa1−/−	41.7 ± 9.0 ‡	57.1 ± 11.9	57.1 ± 16.1	52.0 ± 8.5
SV	µl	B6129	33.2 ± 7.1	27.4 ± 7.3	30.4 ± 7.8	32.7 ± 7.0
		Trpa1−/−	24.0 ± 6.3	28.9 ± 4.0	30.7 ± 8.9	27.2 ± 4.7
EF	%	B6129	52.7 ± 8.4	53.3 ± 9.1	60.4 ± 8.9	57.1 ± 6.1
		Trpa1−/−	57.7 ± 7.5	51.8 ± 8.5	54.2 ± 6.1	52.4 ± 4.9
FS	%	B6129	26.8 ± 5.0	27.0 ± 5.5	31.8 ± 6.4	29.5 ± 4.0
		Trpa1−/−	29.6 ± 4.9	26.2 ± 5.1	27.6 ± 3.9	26.3 ± 3.1
CO	ml/min	B6129	14.7 ± 2.4	11.6 ± 3.7	13.6 ± 3.9	14.8 ± 4.1
		Trpa1−/−	12.1 ± 3.6	13.9 ± 2.5	14.6 ± 4.5	12.5 ± 2.2
			Mean ± SD ($n = 6$)			
			SAX M-Mode Evaluation 1 Day After Final Exposure			
Heart rate	Beats/min	B6129	454 ± 33	401 ± 31 *,†	453 ± 40 #	*a*431 ± 28
		Trpa1−/−	485 ± 26	475 ± 24 ‡	486 ± 15	477 ± 40
ESV	µl	B6129	25.0 ± 12.3	25.0 ± 4.9	19.7 ± 12.4	*a*24.2 ± 10.0
		Trpa1−/−	19.5 ± 4.4	17.2 ± 3.9	20.7 ± 11.7	20.5 ± 6.9
EDV	µl	B6129	57.6 ± 18.6	55.0 ± 7.7	55.0 ± 27.2	*a*53.9 ± 10.3
		Trpa1−/−	47.6 ± 6.9	44.3 ± 9.1	54.0 ± 21.5	47.1 ± 7.8
SV	µl	B6129	32.6 ± 7.9	30.0 ± 4.8	35.4 ± 15.7	*a*29.7 ± 2.2
		Trpa1−/−	28.1 ± 3.9	27.1 ± 5.7	33.4 ± 11.1	26.5 ± 3.2
EF	%	B6129	57.7 ± 7.5	54.6 ± 5.6	65.6 ± 9.3	*a*56.5 ± 9.0
		Trpa1−/−	59.3 ± 5.9	61.1 ± 3.5	63.3 ± 9.5	57.3 ± 9.1
FS	%	B6129	29.9 ± 5.1	27.7 ± 3.6	35.8 ± 7.7	*a*29.1 ± 5.5
		Trpa1−/−	30.9 ± 4.1	31.9 ± 2.4	34.0 ± 7.7	29.6 ± 6.1
CO	ml/min	B6129	14.9 ± 4.2	11.9 ± 1.5	16.2 ± 7.8	*a*12.9 ± 1.3
		Trpa1−/−	13.6 ± 1.9	12.9 ± 2.9	16.3 ± 5.9	12.6 ± 1.5
			Mean ± SD ($n = 6$ unless denoted with *a* for $n = 5$)			

$p < .05$ noted with *versus FA, #versus Acrolein, †versus CAPs, and ‡ versus B6129.
CO, cardiac output; EDV, end diastolic volume; EF, ejection fraction; ESV, end systolic volume; FS, fractional shortening; SAX, short axis view; SV, stroke volume.

emissions, and biomass combustion. The physicochemical characteristics of PM in this study were similar throughout the November and December exposure days in 2014. During that time, winds originated mostly from southwest to northwest at elevations of < 2000 m in the atmospheric boundary layer of the lower troposphere, bringing atmospheres derived from wind that originated, or passed through, metropolitan airsheds en route to Research Triangle Park, North Carolina. These derivative or supplemental airsheds included Chicago IL, Cincinnati/Cleveland/Columbus OH, Birmingham AL, Atlanta GA, and Charlotte NC. Lower-elevation airsheds have historically brought higher levels of particulates to North Carolina from regional combustion sources like biomass burning and power plants (Aneja *et al.*, 2006). The airshed of Research Triangle Park, North Carolina has been

Downloaded from https://academic.oup.com/toxsci/article-abstract/167/2/559/5142835 by EPA-RTP Main Library user on 15 January 2020

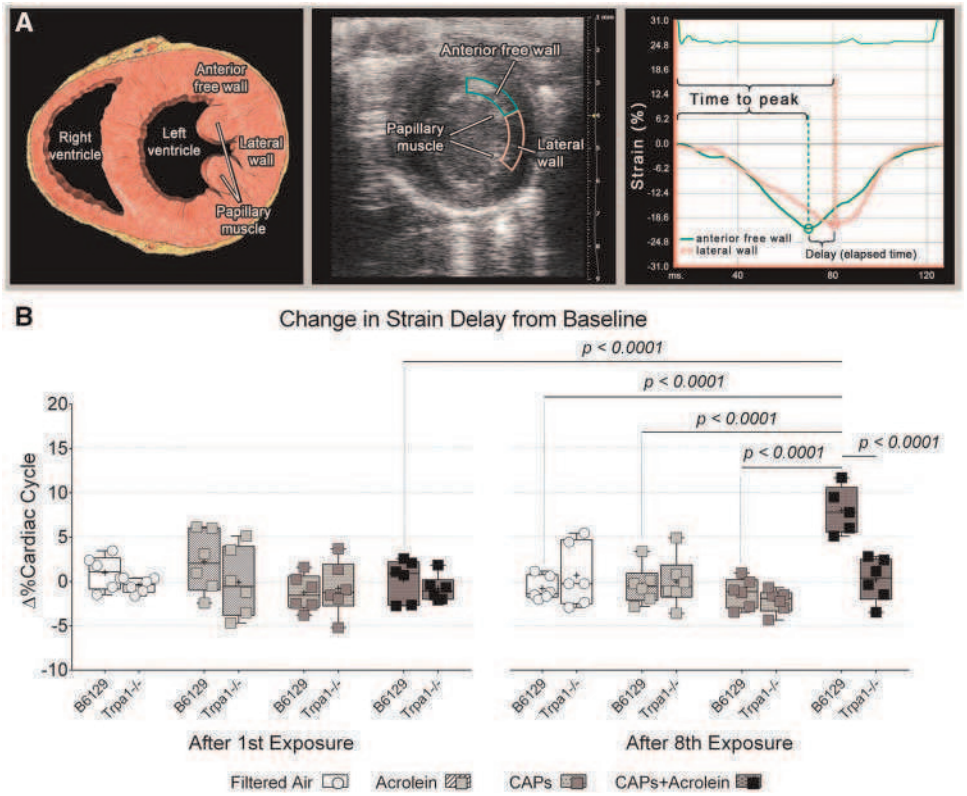

Figure 4. Myocardial synchrony. Panel A illustrates the derivation of circumferential strain delay including a schematic of a mouse heart oriented in the short axis view at the level of the papillary muscles, modified from Lynch and Jaffe (2006) with the regions of the anterior free wall and lateral wall denoted, a representative image of an echocardiographic short-axis view with the anterior free wall endocardium and the lateral wall endocardium, and software output for speckle-strain analysis depicting circumferential strain in the anterior free wall endocardium and the lateral wall endocardium. Delay was calculated as the difference in time to peak strain between the two regions or the time that elapsed between the occurrences of peak strain in the two regions. For reporting (%Cardiac Cycle), the ms value of strain delay was then converted to a percent of the cardiac cycle. Panel B shows the quantified data indicating that a significant increase in myocardial strain delay between the lateral and anterior free wall was found after the 8th exposure to CAPs+Acrolein in B6129 mice. Increases were not found with any other exposure group when compared with baseline and was also not found in *Trpa1−/−* mice. Elapsed time between peak strain in the lateral and anterior free wall are reported as a percentage of the cardiac cycle and normalized to baseline values. Data were compared by two-way ANOVA with Tukey (within strain) or Bonferroni (across strain) post-test. The *p*-values for significant findings are $< .0001$.

characterized by pollutants from biogenic emissions, agricultural activity, vehicular traffic, and secondary organic aerosols (Aneja *et al.*, 2006; Farraj *et al.*, 2015).

Co-exposure to CAPs and acrolein, but not exposure to either alone, in B6129 mice increased circumferential strain delay between the lateral and anterior free wall of the left ventricle, which we use as a measure of myocardial dyssynchrony. Regional contractile dyssynchrony in the myocardium has been linked to clinical regional cardiac ischemia (Chen *et al.*, 2012), with cardiac ischemia-related hospitalizations being a documented effect of air pollution exposure (Cox, 2017; McGuinn *et al.*, 2017; Pope *et al.*, 2015). Myocardial dyssynchrony could result from autonomic effects as repeated exposure to PM2.5 in combination with organic aerosols has recently been reported to influence autonomic nervous system regulation of heart function (Carll *et al.*, 2017). We have also reported autonomic cardiovascular effects with PM2.5 alone (Carll *et al.*, 2015) and acrolein alone (Hazari *et al.*, 2014; Kurhanewicz *et al.*, 2017; Perez *et al.*, 2013, 2015), and have linked exposure to 3.0 ppm acrolein alone with myocardial dyssynchrony (Thompson *et al.*, 2017). However, in this study, acrolein exposure alone at 0.4 ppm was not sufficient to elicit myocardial dyssynchrony and B6129 mice exposed to CAPs+Acrolein had myocardial dyssynchrony without accompanying changes in HRV. The absence of altered autonomic activity at the time heart function was assessed at the end of the study does not preclude a role for autonomic nervous system activity earlier in the exposure regimen, which, if present, could have "programmed" the myocardium for dyssynchronous contraction. For example, β-adrenergic stimulation alters myocardial gap junction conductance and expression of subtypes of connexins, key gap junction proteins involved in inter-cardiomyocyte signal transduction, which can result in electrical instability and predisposition to arrhythmia (Xia *et al.*, 2009). Alternatively, the loss of cardiac synchrony may have resulted from variable distribution of local regulation of contractile function within the myocardium secondary to oxidative stress (Kelly and Fussell, 2017) and/or altered myocardial autocrine/paracrine signaling (Chan *et al.*, 2016).

Although the precise physiological mechanism at play is unclear, this study suggests that myocardial dyssynchrony in CAPs+Acrolein-exposed B6129 mice resulted from activation of TRPA1, given the absence of such responses in similarly exposed *Trpa1−/−* mice. TRPA1 channels are expressed throughout the airways on vagal afferent C-fibers (Achanta and Jordt, 2017) and are activated by oxidizing agents (Bessac *et al.*, 2008), environmental toxicants like acrolein (Bautista *et al.*, 2006), and sulfur-containing compounds (Stenger *et al.*, 2017; Terada *et al.*, 2014). Previous reports describing exposure to single air pollutants have linked TRPA1 to altered autonomic function (Hazari *et al.*, 2011; Kurhanewicz *et al.*, 2017) and other cardiovascular

Downloaded from https://academic.oup.com/toxsci/article-abstract/167/2/559/5142835 by EPA-RTP Main Library user on 15 January 2020

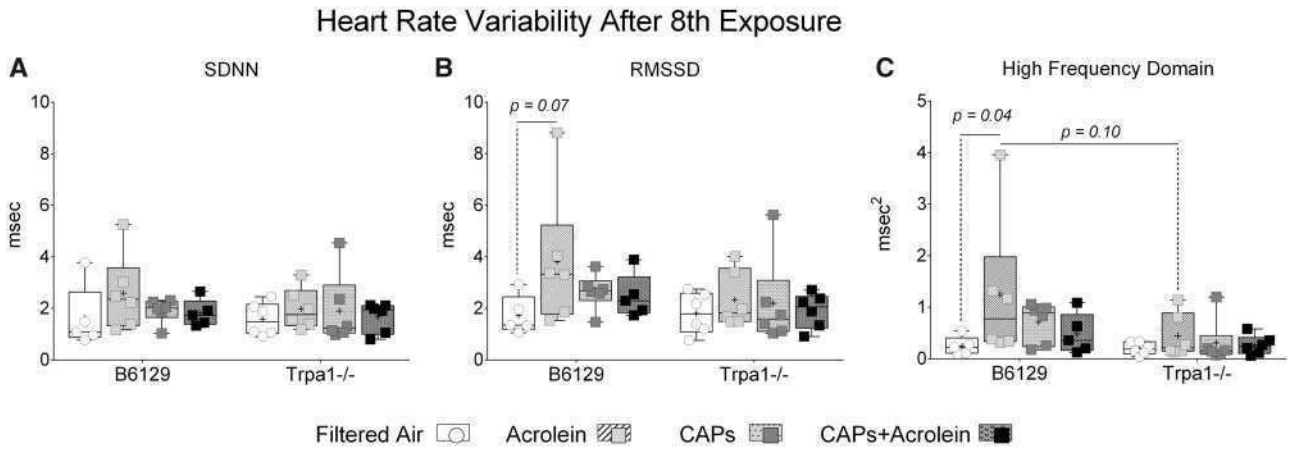

Figure 5. Heart rate variability. We analyzed HRV using ECG signals recorded in anesthetized B6129 and *Trpa1−/−* mice 1 day after the 8th exposure to Filtered Air, Acrolein, CAPs, or CAPs+Acrolein. A, No changes in SDNN were found. B, No significant differences in RMSSD were found but the change in mean between B6129 mice exposed to Filtered Air and B6129 mice exposed to Acrolein produced a $p = .07$. C, The high frequency domain of HRV increased in B6129 mice exposed to Acrolein compared with B6129 mice exposed to Filtered Air. No other differences in High Frequency were found. Data were compared by two-way ANOVA with Tukey (within strain) or Bonferroni (across strain) post-test. The *p*-values for significant differences and others near .05 are provided for clarity.

effects (Conklin, 2016; Conklin *et al.*, 2017). We have also recently reported that organic fractions of diesel exhaust particulate matter containing high levels of polar compounds, including oxy- and nitro-polyaromatic hydrocarbons, caused concentration-dependent irritant responses mediated by TRPA1 in an *in vivo* model (Stevens *et al.*, 2018). In other reports, delivery of TRPA1 agonists into the airways has been shown to produce cardiovascular responses through autonomic reflexes (Hooper *et al.*, 2016; Pozsgai *et al.*, 2010). Unsurprisingly, TRPA1 drove the acrolein-induced increases in HRV in B6129 mice, as such effects were absent in *Trpa1−/−* mice. However, this finding further highlights the qualitative divergence in single-pollutant versus co-pollutant effects, as the HRV effect with acrolein alone was not evident in CAPs+Acrolein-exposed B6129 mice. Although the precise reasons for this divergence are unclear, these data are consistent with our previous findings that compared effects of single and multiple pollutant exposures, which found that whole and particle-free diesel exhaust elicit varying physiological and autonomic responses (Carll *et al.*, 2012; Lamb *et al.*, 2012).

The unique co-pollutant effects in this study may have been driven by physicochemical interactions that modified the biological responses compared with exposure to either pollutant alone. Fine PM usually reaches the deep lung and the reactive properties of acrolein generally restrict it to the upper airways. However, the addition of PM may allow acrolein to penetrate the deep lung (Jakab, 1993) by serving as an acrolein preconcentrator and delivery agent, which as has been demonstrated by use of surrogate organic PM samples, ie, mineral oil aerosols (Ebersviller *et al.*, 2012). Although it is unclear if this took place during co-exposure in this study, measures of acrolein adducts in lung tissue in future studies would help assess this possibility (Conklin *et al.*, 2017). Alternatively, atmospheric interaction between PM and acrolein could lead to the formation of more proinflammatory and irritating byproducts as has been demonstrated with SO_2 in the presence of various metals (Amdur and Underhill, 1968; Vadjic *et al.*, 1991).

Several limitations should be considered in this study. First, low airflow and PM concentrations reduced the opportunity for PM sample collection. The 4 weeks required to collect enough PM mass to extract and analyze limited the temporal resolution of PM elemental analysis and source apportionment, and contributed to a loss of volatile PM constituents (eg, nitrate ions). Organic speciation of PM in future studies could also reduce the percentage of unidentified sources found in this study. In addition, the limited availability of *Trpa1−/−* mice required the use of a larger subject age range than expected. In fact, two of the *Trpa1−/−* mice were substantially older (ie, 3–4 months older) than the remaining mice and had significantly higher baseline strain delay. These two mice were, however, split into separate groups to minimize any potential age-related impacts. Moreover, given the use of female mice, estrous cycles among the mice were not synched presenting some uncertainty with respect to any potential impacts estrous had on the cardiovascular responses in this study. Although others have noted that cardiac function is in fact impacted by estrous (MacDonald *et al.*, 2014), the length of the exposure regimen (ie, 4 weeks), may have diminished any such impact. Furthermore, assessing HRV while under anesthesia may have dampened the degree of activation of the autonomic nervous system. In particular, isoflurane induces bradycardia and although we targeted HR to 450 beats/min by adjusting the level of isoflurane anesthesia, HR itself demonstrated wide variation. Whether this variability in HR played a role in the lower average HR and higher HRV in acrolein-exposed B6129 mice compared with all other groups is unclear. The HRV analysis was also limited by the short segment duration of data analyzed, which was due to the limited capacity to acquire electrocardiogram data using the ultrasound system. Although HRV segment length recommendations have not been espoused for rodents, guidelines for human clinical assessments recommend at least 5 min of continuous heart rate data (Task Force, 1996). Nonetheless, the recordings were nearly concurrent with measures of cardiac function, which allowed for inferences about potential relationships between the functional data and autonomic tone.

In conclusion, this study provides evidence that PM may interact with gaseous air toxicants like acrolein to produce unique health effects via TRPA1 activation. Moreover, this study lends support to the possibility that exposure to air pollution mixtures that include PM and volatile organics, like aldehydes, could increase the severity of health effects beyond that resulting from exposure to single pollutants alone, especially with repeated

Downloaded from https://academic.oup.com/toxsci/article-abstract/167/2/559/5142835 by EPA-RTP Main Library user on 15 January 2020

intermittent exposure. The finding that co-exposure to PM and acrolein in this study caused regional myocardial dyssynchrony in the absence of any overt pathophysiology highlights the capacity for exposure to air pollution mixtures to produce subclinical and latent effects, which may not register in conventional measures, but may nonetheless have serious health ramifications. Thus, evaluation of myocardial synchronicity in human populations prone to air pollution exposure or during controlled human exposure studies may provide data that indicates early manifestations of cardiovascular disease proclivity. Finally, further elucidation of the precise mode of TRPA1 activation and downstream effects including autonomic responses will increase the plausibility for greater than additive effects with co-pollutant exposure.

SUPPLEMENTARY DATA

Supplementary data are available at *Toxicological Sciences* online.

ACKNOWLEDGMENTS

We would like to thank various scientists at U.S. Environmental Protection Agency in Research Triangle Park, NC, USA for important contributions to this work: Paul Evansky for technical assistance with the acrolein analyzer, John Sullivan and Charly King for helping with exposure system setup and running exposures, George Hudson for collecting the particulate matter filters, Earl Puckett for exposure system component fabrication, and Judy Richards for serum and lavage fluid analysis. We also thank Dr Elizabeth A.W. Chan and Dr M. Ian Gilmour for thorough reviews of the manuscript. John Havel and Keith Tarpley of SRA International, Inc generated the graphics in Figures 1–4. The authors have no conflicts of interest to disclose.

REFERENCES

Achanta, S., and Jordt, S. E. (2017). TRPA1: Acrolein meets its target. *Toxicol. Appl. Pharmacol.* **324**, 45–50.

Amdur, M. O., and Underhill, D. (1968). The effect of various aerosols on the response of guinea pigs to sulfur dioxide. *Arch. Environ. Health* **16**, 460–468.

Aneja, V. P., Wang, B., Tong, D. Q., Kimball, H., and Steger, J. (2006). Characterization of major chemical components of fine particulate matter in North Carolina. *J. Air Waste Manag. Assoc.* **56**, 1099–1107.

Argacha, J. F., Bourdrel, T., and van de Borne, P. (2018). Ecology of the cardiovascular system: A focus on air-related environmental factors. *Trends Cardiovasc. Med.* **28**, 112–126.

ATSDR. (2007). *Toxicological Profile for Acrolein*. U.S. Department of Health and Human Services, Public Health Service, Atlanta, GA.

Bautista, D. M., Jordt, S. E., Nikai, T., Tsuruda, P. R., Read, A. J., Poblete, J., Yamoah, E. N., Basbaum, A. I., and Julius, D. (2006). TRPA1 mediates the inflammatory actions of environmental irritants and proalgesic agents. *Cell* **124**, 1269–1282.

Bessac, B. F., Sivula, M., von Hehn, C. A., Escalera, J., Cohn, L., and Jordt, S. E. (2008). TRPA1 is a major oxidant sensor in murine airway sensory neurons. *J. Clin. Invest.* **118**, 1899–1910.

Bhatnagar, A. (2017). Environmental determinants of cardiovascular disease. *Circ. Res.* **121**, 162–180.

Brook, R. D., and Rajagopalan, S. (2017). "Stressed" about air pollution: Time for personal action. *Circulation* **136**, 628–631.

Carll, A. P., Crespo, S. M., Filho, M. S., Zati, D. H., Coull, B. A., Diaz, E. A., Raimundo, R. D., Jaeger, T. N. G., Ricci-Vitor, A. L., and Papapostolou, V. (2017). Inhaled ambient-level traffic-derived particulates decrease cardiac vagal influence and baroreflexes and increase arrhythmia in a rat model of metabolic syndrome. *Part. Fibre Toxicol.* **14**, 16.

Carll, A. P., Haykal-Coates, N., Winsett, D. W., Hazari, M. S., Ledbetter, A. D., Richards, J. H., Cascio, W. E., Costa, D. L., and Farraj, A. K. (2015). Cardiomyopathy confers susceptibility to particulate matter-induced oxidative stress, vagal dominance, arrhythmia and pulmonary inflammation in heart failure-prone rats. *Inhal. Toxicol.* **27**, 100–112.

Carll, A. P., Hazari, M. S., Perez, C. M., Krantz, Q. T., King, C. J., Winsett, D. W., Costa, D. L., and Farraj, A. K. (2012). Whole and particle-free diesel exhausts differentially affect cardiac electrophysiology, blood pressure, and autonomic balance in heart failure-prone rats. *Toxicol. Sci.* **128**, 490–499.

Chan, E. A., Buckley, B., Farraj, A. K., and Thompson, L. C. (2016). The heart as an extravascular target of endothelin-1 in particulate matter-induced cardiac dysfunction. *Pharmacol. Ther.* **165**, 63–78.

Chen, C. C., Shen, T. Y., Chang, M. C., Hung, G. U., Chen, W. C., Kao, C. H., and Chen, J. (2012). Stress-induced myocardial ischemia is associated with early post-stress left ventricular mechanical dyssynchrony as assessed by phase analysis of 201tl gated spect myocardial perfusion imaging. *Eur. J. Nucl. Med. Mol. Imaging* **39**, 1904–1909.

Cohen, J. (1988). *Statistical Power Analysis for the Behavioral Sciences*. L. Erlbaum Associates, Hillsdale, NJ.

Cohen, A. J., Brauer, M., Burnett, R., Anderson, H. R., Frostad, J., Estep, K., Balakrishnan, K., Brunekreef, B., Dandona, L., Dandona, R., *et al.* (2017). Estimates and 25-year trends of the global burden of disease attributable to ambient air pollution: An analysis of data from the global burden of diseases study 2015. *Lancet* **389**, 1907–1918.

Conklin, D. J. (2016). Acute cardiopulmonary toxicity of inhaled aldehydes: Role of TRPA1. *Ann. N.Y. Acad. Sci.* **1374**, 59–67.

Conklin, D. J., Haberzettl, P., Jagatheesan, G., Kong, M., and Hoyle, G. W. (2017). Role of TRPA1 in acute cardiopulmonary toxicity of inhaled acrolein. *Toxicol. Appl. Pharmacol.* **324**, 61–72.

Cox, L. A., Jr. (2017). Socioeconomic and air pollution correlates of adult asthma, heart attack, and stroke risks in the United States, 2010–2013. *Environ. Res.* **155**, 92–107.

Deering-Rice, C. E., Romero, E. G., Shapiro, D., Hughen, R. W., Light, A. R., Yost, G. S., Veranth, J. M., and Reilly, C. A. (2011). Electrophilic components of diesel exhaust particles (DEP) activate transient receptor potential ankyrin-1 (TRPA1): A probable mechanism of acute pulmonary toxicity for DEP. *Chem. Res. Toxicol.* **24**, 950–959.

Ebersviller, S., Lichtveld, K., Sexton, K. G., Zavala, J., Lin, Y. H., Jaspers, I., and Jeffries, H. E. (2012). Gaseous VOCs rapidly modify particulate matter and its biological effects—Part 1: Simple VOCs and model PM. *Atmos. Chem. Phys. Discuss.* **12**, 5065–5105.

Fariss, M. W., Gilmour, M. I., Reilly, C. A., Liedtke, W., and Ghio, A. J. (2013). Emerging mechanistic targets in lung injury induced by combustion-generated particles. *Toxicol. Sci.* **132**, 253–267.

Farraj, A. K., Walsh, L., Haykal-Coates, N., Malik, F., McGee, J., Winsett, D., Duvall, R., Kovalcik, K., Cascio, W. E., Higuchi, M., *et al.* (2015). Cardiac effects of seasonal ambient particulate

Downloaded from https://academic.oup.com/toxsci/article-abstract/167/2/559/5142835 by EPA-RTP Main Library user on 15 January 2020

matter and ozone co-exposure in rats. *Part. Fibre Toxicol.* **12**, 12.

Ghelfi, E., Rhoden, C. R., Wellenius, G. A., Lawrence, J., and Gonzalez-Flecha, B. (2008). Cardiac oxidative stress and electrophysiological changes in rats exposed to concentrated ambient particles are mediated by TRP-dependent pulmonary reflexes. *Toxicol. Sci.* **102**, 328–336.

Gimelli, A., Liga, R., Genovesi, D., Giorgetti, A., Kusch, A., and Marzullo, P. (2014). Association between left ventricular regional sympathetic denervation and mechanical dyssynchrony in phase analysis: A cardiac CZT study. *Eur. J. Nucl. Med. Mol. Imaging* **41**, 946–955.

Gupta, T., Demokritou, P., and Koutrakis, P. (2004). Development and performance evaluation of a high-volume ultrafine particle concentrator for inhalation toxicological studies. *Inhal. Toxicol.* **16**, 851–862.

Hazari, M. S., Griggs, J., Winsett, D. W., Haykal-Coates, N., Ledbetter, A., Costa, D. L., and Farraj, A. K. (2014). A single exposure to acrolein desensitizes baroreflex responsiveness and increases cardiac arrhythmias in normotensive and hypertensive rats. *Cardiovasc. Toxicol.* **14**, 52–63.

Hazari, M. S., Haykal-Coates, N., Winsett, D. W., Krantz, Q. T., King, C., Costa, D. L., and Farraj, A. K. (2011). TRPA1 and sympathetic activation contribute to increased risk of triggered cardiac arrhythmias in hypertensive rats exposed to diesel exhaust. *Environ. Health Perspect.* **119**, 951–957.

Henning, R. J., Johnson, G. T., Coyle, J. P., and Harbison, R. D. (2017). Acrolein can cause cardiovascular disease: A review. *Cardiovasc. Toxicol.* **17**, 227–236.

Hooper, J. S., Hadley, S. H., Morris, K. F., Breslin, J. W., Dean, J. B., and Taylor-Clark, T. E. (2016). Characterization of cardiovascular reflexes evoked by airway stimulation with allylisothiocyanate, capsaicin, and ATP in Sprague-Dawley rats. *J. Appl. Physiol. (Bethesda, MD: 1985)* **120**, 580–591.

Huang, Y. C., Rappold, A. G., Graff, D. W., Ghio, A. J., and Devlin, R. B. (2012). Synergistic effects of exposure to concentrated ambient fine pollution particles and nitrogen dioxide in humans. *Inhal. Toxicol.* **24**, 790–797.

Jakab, G. J. (1993). The toxicologic interactions resulting from inhalation of carbon black and acrolein on pulmonary antibacterial and antiviral defenses. *Toxicol. Appl. Pharmacol.* **121**, 167–175.

Kelly, F. J., and Fussell, J. C. (2017). Role of oxidative stress in cardiovascular disease outcomes following exposure to ambient air pollution. *Free Radic. Biol. Med.* **110**, 345–367.

Kichko, T. I., Kobal, G., and Reeh, P. W. (2015). Cigarette smoke has sensory effects through nicotinic and TRPA1 but not TRPV1 receptors on the isolated mouse trachea and larynx. *Am. J. Physiol. Lung Cell. Mol. Physiol.* **309**, L812–L820.

Kodavanti, U. P., Schladweiler, M. C., Ledbetter, A. D., McGee, J. K., Walsh, L., Gilmour, P. S., Highfill, J. W., Davies, D., Pinkerton, K. E., Richards, J. H., *et al.* (2005). Consistent pulmonary and systemic responses from inhalation of fine concentrated ambient particles: Roles of rat strains used and physicochemical properties. *Environ. Health Perspect.* **113**, 1561–1568.

Kunkler, P. E., Zhang, L., Pellman, J. J., Oxford, G. S., and Hurley, J. H. (2015). Sensitization of the trigeminovascular system following environmental irritant exposure. *Cephalalgia* **35**, 1192–1201.

Kurhanewicz, N., McIntosh-Kastrinsky, R., Tong, H., Ledbetter, A., Walsh, L., Farraj, A., and Hazari, M. (2017). TRPA1 mediates changes in heart rate variability and cardiac mechanical function in mice exposed to acrolein. *Toxicol. Appl. Pharmacol.* **324**, 51–60.

Lamb, C. M., Hazari, M. S., Haykal-Coates, N., Carll, A. P., Krantz, Q. T., King, C., Winsett, D. W., Cascio, W. E., Costa, D. L., and Farraj, A. K. (2012). Divergent electrocardiographic responses to whole and particle-free diesel exhaust inhalation in spontaneously hypertensive rats. *Toxicol. Sci.* **125**, 558–568.

Lang, R. M., Bierig, M., Devereux, R. B., Flachskampf, F. A., Foster, E., Pellikka, P. A., Picard, M. H., Roman, M. J., Seward, J., Shanewise, J. S., *et al.* (2005). Recommendations for chamber quantification: A report from the American Society of Echocardiography's Guidelines and Standards Committee and the Chamber Quantification Writing Group, developed in conjunction with the European Association of Echocardiography, a branch of the European Society of Cardiology. *J. Am. Soc. Echocardiogr.* **18**, 1440–1463.

Lee, L. Y., Hsu, C. C., Lin, Y. J., Lin, R. L., and Khosravi, M. (2015). Interaction between TRPA1 and TRPV1: Synergy on pulmonary sensory nerves. *Pulm. Pharmacol. Ther.* **35**, 87–93.

Lin, Y. S., Hsu, C. C., Bien, M. Y., Hsu, H. C., Weng, H. T., and Kou, Y. R. (2010). Activations of TRPA1 and P2X receptors are important in ROS-mediated stimulation of capsaicin-sensitive lung vagal afferents by cigarette smoke in rats. *J. Appl. Physiol. (Bethesda, MD: 1985).* **108**, 1293–1303.

Lynch, P. J., and Jaffe, C. C. (2006). *Heart Normal Short Axis Section.*Creative Commons, New Haven, CT.

MacDonald, J. K., Pyle, W. G., Reitz, C. J., and Howlett, S. E. (2014). Cardiac contraction, calcium transients, and myofilament calcium sensitivity fluctuate with the estrous cycle in young adult female mice. *Am. J. Physiol. Heart Circ. Physiol.* **306**, H938–H953.

Mauderly, J. L., and Samet, J. M. (2009). Is there evidence for synergy among air pollutants in causing health effects? *Environ. Health Perspect.* **117**, 1–6.

McGuinn, L. A., Ward-Caviness, C., Neas, L. M., Schneider, A., Di, Q., Chudnovsky, A., Schwartz, J., Koutrakis, P., Russell, A. G., Garcia, V., *et al.* (2017). Fine particulate matter and cardiovascular disease: Comparison of assessment methods for long-term exposure. *Environ. Res.* **159**, 16–23.

National Institute for Occupational Safety and Health (NIOSH). (2005). *Pocket Guide to Chemical Hazards*. U.S. Department of Health and Human Services, Public Health Service, Centers for Disease Controland Prevention, Cincinnati, OH.

Newby, D. E., Mannucci, P. M., Tell, G. S., Baccarelli, A. A., Brook, R. D., Donaldson, K., Forastiere, F., Franchini, M., Franco, O. H., Graham, I., *et al.* (2015). Expert position paper on air pollution and cardiovascular disease. *Eur. Heart J.* **36**, 83–93b.

Perez, C. M., Hazari, M. S., Ledbetter, A. D., Haykal-Coates, N., Carll, A. P., Cascio, W. E., Winsett, D. W., Costa, D. L., and Farraj, A. K. (2015). Acrolein inhalation alters arterial blood gases and triggers carotid body-mediated cardiovascular responses in hypertensive rats. *Inhal. Toxicol.* **27**, 54–63.

Perez, C. M., Ledbetter, A. D., Hazari, M. S., Haykal-Coates, N., Carll, A. P., Winsett, D. W., Costa, D. L., and Farraj, A. K. (2013). Hypoxia stress test reveals exaggerated cardiovascular effects in hypertensive rats after exposure to the air pollutant acrolein. *Toxicol. Sci.* **132**, 467–477.

Pope, C. A., Muhlestein, J. B., Anderson, J. L., Cannon, J. B., Hales, N. M., Meredith, K. G., Le, V., and Horne, B. D. (2015). Short-term exposure to fine particulate matter air pollution is preferentially associated with the risk of ST-segment elevation acute coronary events. *J. Am. Heart Assoc.* **4**, e002506.

Pozsgai, G., Bodkin, J. V., Graepel, R., Bevan, S., Andersson, D. A., and Brain, S. D. (2010). Evidence for the pathophysiological

Downloaded from https://academic.oup.com/toxsci/article-abstract/167/2/559/5142835 by EPA-RTP Main Library user on 15 January 2020

relevance of TRPA1 receptors in the cardiovascular system *in vivo*. *Cardiovasc. Res.* **87**, 760–768.

Quinones, M. A., Otto, C. M., Stoddard, M., Waggoner, A., Zoghbi, W. A., and Doppler Quantification Task Force of the N, Standards Committee of the American Society of E. (2002). Recommendations for quantification of Doppler echocardiography: A report from the Doppler Quantification Task Force of the Nomenclature and Standards Committee of the American Society of Echocardiography. *J. Am. Soc. Echocardiogr.* **15**, 167–184.

Rowan, W. H., 3rd, Campen, M. J., Wichers, L. B., and Watkinson, W. P. (2007). Heart rate variability in rodents: Uses and caveats in toxicological studies. *Cardiovasc. Toxicol.* **7**, 28–51.

Sivagangabalan, G., Spears, D., Masse, S., Urch, B., Brook, R. D., Silverman, F., Gold, D. R., Lukic, K. Z., Speck, M., Kusha, M., *et al.* (2011). The effect of air pollution on spatial dispersion of myocardial repolarization in healthy human volunteers. *J. Am. Coll. Cardiol.* **57**, 198–206.

Stenger, B., Popp, T., John, H., Siegert, M., Tsoutsoulopoulos, A., Schmidt, A., Muckter, H., Gudermann, T., Thiermann, H., and Steinritz, D. (2017). *N*-acetyl-L-cysteine inhibits sulfur mustard-induced and TRPA1-dependent calcium influx. *Arch. Toxicol.* **91**, 2179–2189.

Stevens, J. S., Padilla, S., DeMarini, D. M., Hunter, D. L., Martin, W. K., Thompson, L. C., Gilmour, M. I., Hazari, M. S., and Farraj, A. K. (2018). Zebrafish locomotor responses reveal irritant effects of fine PM extracts and a role for TRPA1. *Toxicol. Sci.* **161**, 290–299.

Sun, L., Liu, C., Xu, X., Ying, Z., Maiseyeu, A., Wang, A., Allen, K., Lewandowski, R. P., Bramble, L. A., Morishita, M., *et al.* (2013). Ambient fine particulate matter and ozone exposures induce inflammation in epicardial and perirenal adipose tissues in rats fed a high fructose diet. *Part. Fibre Toxicol.* **10**, 43.

Task Force of the European Society of Cardiology and the North American Society of Pacing and Electrophysiology. (1996). Heart rate variability. Standards of measurement, physiological interpretation, and clinical use. *Eur. Heart J.* **17**, 354–381.

Tei, C., Ling, L. H., Hodge, D. O., Bailey, K. R., Oh, J. K., Rodeheffer, R. J., Tajik, A. J., and Seward, J. B. (1995). New index of combined systolic and diastolic myocardial performance: A simple and reproducible measure of cardiac function—A study in normals and dilated cardiomyopathy. *J. Cardiol.* **26**, 357–366.

Terada, Y., Hosono, T., Seki, T., Ariga, T., Ito, S., Narukawa, M., and Watanabe, T. (2014). Sulphur-containing compounds of durian activate the thermogenesis-inducing receptors TRPA1 and TRPV1. *Food Chem.* **157**, 213–220.

Thompson, L. C., Ledbetter, A. D., Haykal-Coates, N., Cascio, W. E., Hazari, M. S., and Farraj, A. K. (2017). Acrolein inhalation alters myocardial synchrony and performance at and below exposure concentrations that cause ventilatory responses. *Cardiovasc. Toxicol.* **17**, 97–108.

Turpin, B. J., and Lim, H.-J. (2001). Species contributions to PM2.5 mass concentrations: Revisiting common assumptions for estimating organic mass. *Aerosol Sci. Technol.* **35**, 602–610.

US EPA. (2004). EPA-CMB8.2 Users Manual. EPA-452/R-04-011. Research Triangle Park, NC.

Vadjic, V., Gentilizza, M., Hrsak, J., and Eskinja, I. (1991). The effect of metals and ammonia on SO_2 oxidation to sulphates in the ambient air. *Environ. Monit. Assess.* **18**, 163–171.

Wagner, J. G., Allen, K., Yang, H. Y., Nan, B., Morishita, M., Mukherjee, B., Dvonch, J. T., Spino, C., Fink, G. D., Rajagopalan, S., *et al.* (2014). Cardiovascular depression in rats exposed to inhaled particulate matter and ozone: Effects of diet-induced metabolic syndrome. *Environ. Health Perspect.* **122**, 27–33.

Xia, Y., Gong, K. Z., Xu, M., Zhang, Y. Y., Guo, J. H., Song, Y., and Zhang, P. (2009). Regulation of gap-junction protein connexin 43 by beta-adrenergic receptor stimulation in rat cardiomyocytes. *Acta Pharmacol. Sin.* **30**, 928–934.

Downloaded from https://academic.oup.com/toxsci/article-abstract/167/2/559/5142835 by EPA-RTP Main Library user on 15 January 2020

United States Environmental Protection Agency
Washington, DC 20460

STAA REPORT FOR THE SCIENTIST NOMINATIONS

General Information:

Nomination ID/App ID:	20-112
Research Category Primary:	Ecological Research (ER)
Research Category Secondary:	Sustainability and Innovation (SI)
Laboratory/Office Name:	ORD
Nomination Entered By:	Matthew Harwell

Eligibility Checklist:

[Y] The nominated publication(s) has not been submitted to a previous STAA competition.

[Y] The nominated publication(s) was published on or before January 1, 2017 and on or after January 1,2012

[Y] The principal author was an EPA employee or a PHS employee assigned to EPA when the research was performed

[Y] The EPA authors (includes PHS employees assigned to EPA) contributed collectively a minimum of 50% toward the publication(s)

Nominating Official Name:	Susan George
Nominating Official Title:	DIRECTOR, GULF ECOLOGY DIVISION
Nominating OfficialEmail:	george.elizabeth@epa.gov
STAA Coordinator Name:	Kathleen Wiser
STAA Coordinator Email:	wiser.kathi@epa.gov

Justifications:

Justification 1:

This research supports US EPA's goals to understand connections between healthy ecosystems, healthy people, and healthy communities, including protecting and building upon public health benefits associated with protecting environmental resources. The Sustainable and Healthy Communities Research Program, in particular, has identified a need to evaluate the causal relationships between ecosystem goods and services and human health (EPA 2018-2022 Strategic Plan). This nomination presents two research studies designed to 1) develop a conceptual framework and conduct a literature review to describe the causal relationships between ecosystem services and human health outcomes, and 2) apply this framework for a specific application in Puerto Rico to demonstrate how evidence for eco-health linkages can be applied and developed.

Ecosystem goods and services (EGS) are thought to play a role in protecting human health, but the empirical evidence directly linking EGS to human health outcomes is limited, and our ability to detect linkages is confounded by socio-economic factors. These limitations hinder opportunities to develop greening and restoration strategies to complement existing health promoting efforts at the community level. In order to better inform Eco-Health initiatives, the first nominated study (De Jesus Crespo and Fulford 2018) conducted a "weight of evidence" analysis to identify: i) which Eco-Health linkages are empirically supported and should be considered for management, ii) which are theoretically plausible but need further research, and iii) which socio-economic confounding factors should be accounted for when designing management plans. The results help to establish an agenda to shape future Eco-Health research and define priorities for managing green spaces to provide benefits to human health.

In a follow-up study, the research team applied the Eco-Health framework and evidence developed in the literature review to investigate the role of natural infrastructure in minimizing flood impacts and human health effects in Puerto Rico (De Jesus et al. 2019). Impoverished communities in Puerto Rico have and continue to be exposed to frequent flooding and flood related illnesses. The extensive flood impacts caused by Hurricane Maria on the Island in 2017 further underscore the potential for weather hazards to severely impact human health, especially among vulnerable sectors. Having a better understanding of the extent to which ecosystem services may help buffer environmental hazards and protect human health, would help guide community-based management of flood prone neighborhoods and justify conservation and restoration efforts focused on natural infrastructure. To inform this effort, the research team used the previously described literature review to accumulate evidence for the role of ecosystem services in relation to one of the most common health outcomes

associated to flooding - acute gastrointestinal (GI) illness. From the literature review, however, it was identified that no study had attempted to determine if the impact of floods on GI illness could be prevented with flood protection ecosystem services. The research team therefore conducted a statistical modeling study to evaluate the relationships between ecosystem services (i.e., rainfall retention), flood claims, and GI symptoms in Medicare claims. The roles of socio-economic factors and built infrastructure in mitigating flood claims and illness occurrence were also considered. The results support a linkage between the ability of ecosystems to promote rainfall infiltration, flood events, and GI illness. The results help inform planning strategies for future weather hazards, accounting for the role of natural and built infrastructure on minimizing flood impacts and human health effects.

Taken together, the two studies expand the evidence-base for relationships between ecosystem services and benefits to human health. The literature review provides evidence for causal relationships between ecosystem services and human health outcomes, in support of EPA's strategic goals. The second study demonstrates an application of how evidence of eco-health linkages can be applied to support environmental management and community decision-making in vulnerable communities, including improving their resilience to natural hazards. This research supports EPA's strategic goal of improving our understanding of waterborne threats to human health, and providing resources to help states and territories prevent harmful exposures (EPA 2018-2022 Strategic Plan).

https://www.epa.gov/sites/production/files/2019-09/documents/fy-2018-2022-epa-strategic-plan.pdf

Justification 2A:

This research supported efforts in EPA's Sustainable and Healthy Communities Research Program to quantify linkages between ecosystem services and human health and well-being through coordinated case studies in a number of locations across the U.S. The literature review (De Jesus Crespo and Fulford 2018) was conducted to identify relationships between ecosystem services and human health with potential for use and transferability across a variety of decision contexts and locations by using a "weight of evidence" analysis to identify: i) which Eco-Health linkages are empirically supported and should be considered for management, ii) which are theoretically plausible but need further research, and iii) which socio-economic confounding factors should be accounted for when designing management plans. The framework and evidence developed in this review were applied to a specific example of how greenspace might mitigate health impacts from coastal flooding for one of the coordinated case studies in Puerto Rico (De Jesus Crespo et al. 2019). The research team used the literature review to accumulate evidence for the role of ecosystem services in relation to one of the most common health

outcomes associated to flooding in Puerto Rico - acute gastrointestinal (GI) illness. From the literature review, however, it was identified that no study had attempted to determine if the impact of floods on GI illness could be prevented with flood protection ecosystem services. The research team therefore conducted a statistical modeling study to evaluate the relationships between ecosystem services (i.e., rainfall retention), flood claims, and GI symptoms in Medicare claims. Lessons from both studies were integrated into two EPA reports describing how EcoHealth evidence can be more broadly applied in community decision-making (Yee et al. 2017; Johnston et al. 2017).

Justification 2B:

Richard Fulford; 2017 EPA Scientific and Technological Achievement Level III Award; R. Fulford, D. Yoskowitz, M. Russell, D. Dantin, J. Rogers. Measuring sustainability through ecosystem service-based valuation of coastal restoration projects. Fulford, R., D. Yoskowitz, M. Russell, D. Dantin, AND Johne Rogers. Habitat and Recreational Fishing Opportunity in Tampa Bay: Linking Ecological and Ecosystem Services to Human Beneficiaries. Ecosystem Services. Elsevier Online, New York, NY, 17:64-74, (2016).

Susan Yee; 2015 EPA Scientific and Technological Achievement Award, Honorable Mention; Yee, S.H., J.A. Dittmar, L.M. Oliver. 2014. Comparison of methods for quantifying reef ecosystem services: a case study mapping services for St. Croix, USVI. Ecosystem Services 8:1-15. http://dx.doi.org/10.1016/j.ecoser.2014.01.001

Susan Yee; 2015 EPA Scientific and Technological Achievement Award, Honorable Mention; Yee, S.H., J. Carriger, W.S. Fisher, P. Bradley, B. Dyson. 2015. Developing scientific information to support decisions for sustainable reef ecosystem services. Ecological Economics 115:39-50. http://dx.doi.org/10.1016/j.ecolecon.2014.02.016

Justification 2C:

This nomination advances previously nominated work (Yee et al. 2014; Yee et al. 2015; Fulford et al. 2017), which developed approaches to model ecosystem services production, by connecting ecosystem services production to benefits on a human health through a literature review and a specific application for coastal flooding in Puerto Rico. In addition to building upon previous work, this effort to incorporate quantitative “weight-of-evidence” approaches to synthesize scientific literature represents a novel contribution to the field of Eco-Health research.

Justification 2D:

n/a

Justification 2E:

Some of the authors (Rebeca de Jesus Crespo, Susan Yee) have submitted a concurrent nomination (De Jesus Crespo et al. 2018; Yee et al. 2019), which uses a field study and statistical modeling to investigate the impacts of ecosystem services on vector-borne illness in the San Juan Bay estuary watershed of Puerto Rico. Both nominations are similar in building the evidence base for relationships between ecosystem services and benefits to human health. However, the concurrent nomination demonstrates through a specific application for the San Juan Bay estuary how an improved understanding of the relationships between environmental quality, ecosystem services, and vector-borne illness can help inform decision-making in vulnerable communities.

Justification 3A:

In 2019, Dr. De Jesus Crespo was invited to present this research as the keynote speaker at the Puerto Rico Watershed Symposium. As a result of this presentation, Dr. De Jesus Crespo was contacted by the West Puerto Rico Watershed Initiative requesting additional information to help inform management efforts in the Rio Grande de Anasco watershed (Supplement B1). Efforts to improve Puerto Rico's resilience to flooding were particularly heightened after 2017, when Hurricane Maria devastated the entire island of Puerto Rico.

· De Jesus Crespo, R. Watershed Symposium Puerto Rico 2019: Keynote Speaker/Agricultura, Urbanización y Plástico: Impacto y Manejo de Cuencas Tropicales Para la Salud y el Bienestar Público.

The research was highlighted as part of EPA's "Science Matters" newsletter (Supplement B2).

https://www.epa.gov/sciencematters/are-greenspaces-good-your-heart

The authors collaborated with EPA's EnviroAtlas to incorporate recent years from the literature review into an update of the EcoHealth Browser. The Eco-Health Relationship Browser illustrates scientific evidence for

linkages between human health and ecosystem services. This interactive tool provides information about several of our nation's major ecosystems, the services they provide, and how those services, or their degradation and loss, may affect people.

· https://www.epa.gov/enviroatlas/enviroatlas-eco-health-relationship-browser

The authors of this work have been invited to present this work at numerous conferences or symposiums. Two of the co-authors (Fulford and de Jesus Crespo) organized a special session at A Community on Ecosystem Services conference (ACES 2016, Jacksonville, FL) on “Evidence-based approaches for linkg ecosystem services and human health”. The research was also included as part of a 2018 invited session on “Governance Barriers and Opportunities for Integrating Ecosystem Services into Estuary and Coastal Management” at A Community on Ecosystem Services conference (ACES, 2018, Washington DC), where environmental effects on gastrointestinal illnesses were described alongside potential effects on asthma and vector-borne illness as part of a broader description of potential health benefits of estuary management. Dr. de Jesus Crespo was invited to present as the keynote speaker at the Odum School of Ecology Graduate Student Symposium (Supplement B3).

· Fulford, R. and R. DeJesus-Crespo. Applying eco-health science in environmental governance. A Community on Ecosystem Services (ACES) Conference, Jacksonville, FL, December 05 - 09, 2016. https://conference.ifas.ufl.edu/aces16/presentations.html

· Yee, S.H., R. de Jesus Crespo, D. Betancourt, T. Dean. 2018. Linking Ecosystem Services to Human Health to Inform Estuary Management in Puerto Rico. A Community of Ecosystem Services 2018 Conference, Washington D.C. https://conference.ifas.ufl.edu/aces18/speaker-presentations.html

· De Jesus Crespo, R. 2020. Zooming out and in: applying geo-spatial technology and stakeholder engagement to study eco-health linkages in coastal communities. Odum School of Ecology Graduate Student Symposium, Athens, Georgia, 2020. http://gsa.ecology.uga.edu/wp-content/uploads/2020/02/GSSProgram-2020.pdf

This research contributed to Dr. de Jesus Crespo being awarded an Early Career Fellowship from the National Academies of Science Gulf Research Program (Supplement B4).

.
https://www.nationalacademies.org/gulf/fellowships-and-grants/current-and-past-early-career-research-fellows

According to Google Scholar, these two articles have been cited 11 times in the past two years. Approaches and lessons from the literature review were integrated into two EPA reports describing how EcoHealth evidence can be applied in community decision-making (Yee et al. 2017 Supplement A1; Johnston et al. 2017 Supplement A2).

· Ares, Á., Brisbin, M. M., Sato, K. N., Martín, J. P., Iinuma, Y., & Mitarai, S. (2019). Extreme storm-induced run-off causes rapid, context-dependent shifts in nearshore subtropical bacterial communities. BioRxiv, 801886.

· Yu, Q., LI, N., DING, L., & WANG, Y. A New Methodology Developed to Assess the Impacts of Floods on Environment.

· Cochran, F., Jackson, L., Neale, A., Lovette, J., & Tran, L. (2019). A Community EcoHealth Index from EnviroAtlas Ecosystem Services Metrics. *International journal of environmental research and public health*, *16*(15), 2760.

· Wu, J., Rappazzo, K. M., Simpson Jr, R. J., Joodi, G., Pursell, I. W., Mounsey, J. P., ... & Jackson, L. E. (2018). Exploring links between greenspace and sudden unexpected death: A spatial analysis. Environment international, 113, 114-121.

· Xu, Z., Wei, H., Fan, W., Wang, X., Zhang, P., Ren, J., ... & Kong, W. (2019). Relationships between ecosystem services and human well-being changes based on carbon flow—A case study of the Manas River Basin, Xinjiang, China. *Ecosystem Services*, *37*, 100934.

· Summers, J. K., Smith, L. M., Fulford, R. S., & de Jesus Crespo, R. (2018). The Role of Ecosystem Services in Community Well-Being. Ecosystem Services and Global Ecology, 145.

· Yee, S. H., Yee, D. A., de Jesus Crespo, R., Oczkowski, A., Bai, F., & Friedman, S. (2019). Linking ewater quality to Aedes aegypti and Zika in flood-prone neighborhoods. *EcoHealth*, *16*(2), 191-209.

· Harwell, M.C. and C. Jackson. (2019) FY18 Output – SHC 2.61.3 – Incorporation of Ecosystem Goods and Services into Community-Level Decision Support Using EnviroAtlas and Other Tools. U.S. Environmental Protection Agency, Gulf Breeze, FL, EPA/600/R-19/087.

· Johnston, J.M. (2019) Quantitative and Qualitative Linkages Between Final Ecosystem Goods and Services and Human Health. Sustainable and Healthy Communities Research Program Fact Sheet 2.61.4.

· Yee, S., J. Bousquin, R. Bruins, T.J. Canfield, T.H. DeWitt, R. de Jesús-Crespo, B. Dyson, R. Fulford, M. Harwell, J. Hoffman, C.J. Littles, J.M. Johnston, R.B. McKane, L. Green, M. Russell, L. Sharpe, N. Seeteram, A. Tashie, and K. Williams. 2017. Practical Strategies for Integrating Final Ecosystem Goods and Services into Community Decision-Making. U.S. Environmental Protection Agency, Gulf Breeze, FL, EPA/600/R-17/266.

· Johnston, J.M., R. de Jesus Crespo, M. Harwell, C. Jackson, M. Myer, N. Seeteram, K. Williams, S. Yee, J. Hoffman. 2017. Valuing Community Benefits of Final Ecosystem Goods and Services: Human Health and Ethnographic Approaches as Complements to Economic Valuation. US Environmental Protection Agency, Washington, DC. EPA/600/R-17/309.

Justification 3B:

De Jesus and Fulford 2018 was submitted and accepted by the International Journal of Public Health. The article followed EPA's management clearance process, as well as journal editorial and peer-review processes. The EPA review included the Branch Chief and Division Director internal reviews, as well as an external review by Laura Jackson, an expert on EcoHealth science and key developer of the EnviroAtlas EcoHealth Browser. The journal reviews were performed by the editor, and two anonymous peer reviewers.

De Jesus et al. 2019 was submitted and accepted by the journal Science of the Total Environment. The article followed EPA's management clearance process, as well as journal editorial and peer-review processes. The EPA review included the Branch Chief and Division Director internal reviews, as well as an external review by Tim Wade, an expert on health science with the US EPA. The journal reviews were performed by the editor, and two anonymous peer reviewers.

AUTHORS

Contributing Author

Author Name:	Rebeca de Jesus Crespo		
Professional Title:		Salutation:	
Email:	rdejesuscrespo1@lsu.edu	Organization:	
Mailing Address:			
Street Line 1:			
City:			
Zip Code:		State:	
At time of research was:	EPA Employee		
Separation Date:	Sat Dec 01 00:00:00 GMT 2018		
% of Effort:	55		

Contributing Author

Author Name:	Jianyong Wu		
Professional Title:		Salutation:	
Email:	wu.jianyong@epa.gov	Organization:	
Mailing Address:			
Street Line 1:			
City:			
Zip Code:		State:	
At time of research was:	Non EPA Personnel		
Separation Date:			
% of Effort:	10		

Contributing Author

Author Name:	Richard Fulford		
Professional Title:		Salutation:	
Email:	fulford.richard@epa.gov	Organization:	
Mailing Address:			
Street Line 1:	Office of Research and Development, U.S. EPA 1 Sabine Island Drive		
City:	Gulf Breeze		
Zip Code:	32561	State:	FL
At time of research was:	EPA Employee		
Separation Date:			
% of Effort:	20		

Contributing Author

Author Name:	Mark Myer		
Professional Title:		Salutation:	
Email:	myermarkh@gmail.com	Organization:	
Mailing Address:			
Street Line 1:			
City:			
Zip Code:		State:	
At time of research was:	Non EPA Personnel		
Separation Date:	Fri Aug 23 00:00:00 GMT 2019		
% of Effort:	10		

Contributing Author

Author Name:	Susan Yee		
Professional Title:		Salutation:	
Email:	yee.susan@epa.gov	Organization:	
Mailing Address:			
Street Line 1:			
City:			
Zip Code:		State:	
At time of research was:	EPA Employee		
Separation Date:			
% of Effort:	5		

PUBLICATIONS

Publication 1:

Publication Title:	Eco-Health linkages: assessing the role of ecosystem goods and services on human health using causal		
Publication Date:	Tue Aug 01 00:00:00 GMT 2017		
Journal/Publication Method:	International Journal of Public Health		
All Author(s):			
Volume:	63	Number:	*
Pages:	81-92	Immediately Index:	Immediately Index:
Citation ½ Life:	5.4	Impact Factor:	2.373

Publication 2:

Publication Title:	Flood protection ecosystem services in the coast of Puerto Rico: Associations between extreme weathe		
Publication Date:	Thu Aug 01 00:00:00 GMT 2019		
Journal/Publication Method:	Science of the Total Environment		
All Author(s):			
Volume:	676	Number:	*
Pages:	343-355	Immediately Index:	Immediately Index:
Citation ½ Life:	4.4	Impact Factor:	5.589

Int J Public Health (2018) 63:81–92
https://doi.org/10.1007/s00038-017-1020-3

REVIEW

Eco-Health linkages: assessing the role of ecosystem goods and services on human health using causal criteria analysis

Rebeca de Jesus Crespo[1] · **Richard Fulford**[1]

Received: 9 February 2017 / Revised: 11 July 2017 / Accepted: 12 July 2017 / Published online: 1 August 2017
© Swiss School of Public Health (SSPH+) (outside the USA) 2017

Abstract
Objectives In the last decade, we saw an upsurge of studies evaluating the role of ecosystem goods and services (EGS) on human health (Eco-Health). Most of this work consists of observational research of intermediate processes and few address the full pathways from ecosystem to EGS to human health, limiting our ability to assess causality.
Methods We conducted a causal criteria analysis of Eco-Health literature using Eco-Evidence, a software tool that helps evaluate evidence of cause–effect relationships. We focus on the context of green spaces providing "buffering" EGS that may influence disease.
Results We found support for a causal linkage between green spaces and all of the EGS tested, and sufficient evidence linking EGS to gastro intestinal disease and heat morbidities. Inconsistencies were found when assessing the link between EGS to cardiovascular and respiratory diseases. Few studies directly link green spaces to health. Those that do, support a connection to cardiovascular disease, and heat morbidities, but provide inconsistent evidence regarding respiratory illness.
Conclusions Our results help establish an agenda to shape future Eco-Health research and define priorities for managing green spaces to provide human health benefits.

Keywords Ecosystem goods and services · Green spaces · Disease · Causal criteria analysis

Introduction

Ecosystem goods and services (EGS) are the outputs of ecological processes that directly or indirectly contribute to social welfare (Munns et al. 2015). One of the key uncertainties limiting the protection of EGS is the limited knowledge of how they may relate to human health (Corvalan et al. 2005). Since the Millennium Ecosystem Assessment (MEA 2005), there has been increasing interest in addressing this information gap, and an upsurge in the number of studies on the subject (Hartig et al. 2014).

The emerging body of literature relating EGS to human health has been compiled in over fifty review articles (Hartig et al. 2014), and captured in interactive tools, such as the US-EPA's Eco-Health Relationship Browser (Jackson et al. 2013). Although these compilations highlight empirical evidence, the references to date do not necessarily support causality, but rather focus on establishing plausible associations (Jackson et al. 2013). Moreover, the field is dominated by observational research and there is a dearth of primary studies to establish causal associations between EGS and health in a consistent and rigorous manner (Hartig et al. 2014).

Notably, there are few studies directly linking the presence of ecosystems to physical health and disease by means of buffering EGS. Buffering EGS refers to the ecosystem's capacity to "buffer" against health impacts

Electronic supplementary material The online version of this article (doi:10.1007/s00038-017-1020-3) contains supplementary material, which is available to authorized users.

✉ Rebeca de Jesus Crespo
Dejesus-crespo.rebeca@epa.gov

Richard Fulford
Fulford.Richard@epa.gov

[1] Gulf Ecology Division, National Health and Environmental Effects Research Laboratory, US EPA, Office of Research and Development, 1 Sabine Island Drive, Gulf Breeze, FL 32561-5299, USA

by, for example, removing pollutants from air and water, and mitigating heat and water hazards (Jackson et al. 2013). Most existing research links disease to intermediate processes (e.g., air pollution, floods), which may be attributed to anthropogenic impacts and not necessarily to buffering EGS by ecosystems. Given that the ecosystem is the operable management unit in the conservation of buffering EGS for human health, a lack of empirical evidence supporting a direct association could undermine the effectiveness (and public support) of conservation plans. There are few papers tracing the full pathways from ecosystem, to EGS processes, to health outcomes, which further limit our ability to demonstrate causality (Hartig et al. 2014).

One solution to these limitations is the collective analysis of existing Eco-Health literature using causal criteria analysis (CSA). CSA emerged in the field of epidemiology due to the need for decision-making based on relatively weak independent pieces of evidence (Weed 1997). Bradford Hill's criteria represent the most widely used guide for assessing causality, and consist of standards, summarized by Russo and Williamson (2007), into two categories: (1) probabilistic evidence, or consistent cause–effect association; and (2) mechanistic evidence, or a logical explanation of how the causal association occurs. Norris et al. (2011) subsequently applied causality criteria to develop a framework for assessing cause–effect relationships in environmental research. The premise is that isolated studies may not offer a strong case for causality, but they may do so if considered collectively.

We focus our CSA on the context of green spaces, its effects on buffering EGS, and the impact of these on human diseases. We address the following questions: (1) which linkages are theoretically plausible but need further research, (2) which diseases have been associated directly with presence/absence of green spaces, and (3) which Eco-Health linkages are best supported and should be considered for management. Addressing these questions will better characterize the current state of knowledge, define management priorities, and identify pending Eco-Health research topics.

Methods

To conduct our CSA, we applied a numerical technique that combines individual studies, weighted by research design, into a single score for or against a given hypothesis (Norris et al. 2011; Table 1). This method helps determine whether the composite of existing research supports the cause and effect relationship, or suggests inconsistent evidence, or support for an alternative hypothesis. This approach differs from meta-analysis as it is not meant to measure effect sizes. Instead it helps determine the evidence for a given causal linkage. It also allows consideration of studies that do not report summary statistics, which are needed for quantitative reviews (Norris et al. 2011). This method represents an alternative to narrative reviews as it allows for succinct literature synthesis and a systematic assessment of relative weight of evidence (Norris et al. 2011). This approach has been incorporated into an online tool called Eco-Evidence, summarized here in four sections: context definition; cause and effect mechanism; literature review; and weighting the evidence (Webb et al. 2015).

Table 1 Factors considered and weight of evidence scores for causal criteria analysis. Modified from Norris et al. (2011)

Factors considered	Weight applied
Study design type	
BACI or BARI MBACI	4
Gradient response model	3
Before vs after (no reference/control)	2
Reference vs control (no before)	2
After impact only	1
Number of independent control locations	
0	0
1	2
1+	3
Number of independent impact locations	
1	0
2	2
2+	3
Locations for gradient response model	
3	0
4	2
5	4
5+	6

BACI before–after-control-impact, *BARI* before–after-reference-impact, *MBACI* multiple before–after-control (or reference)-impact

Context definition

Our analysis focuses on diseases linked to buffering EGS provided by green spaces (Fig. 1). Here, the term green space refers to any vegetation within a human dominated environment (Kabisch and Haase 2013). This includes urban trees, green roofs, and wetlands.

We did not consider health promoting services (physical activity, engagement with nature), or mental health outcomes. Recent reviews describes the state of knowledge regarding these topics (Lee and Maheswaran 2011; Shanahan et al. 2015), while there is relatively less

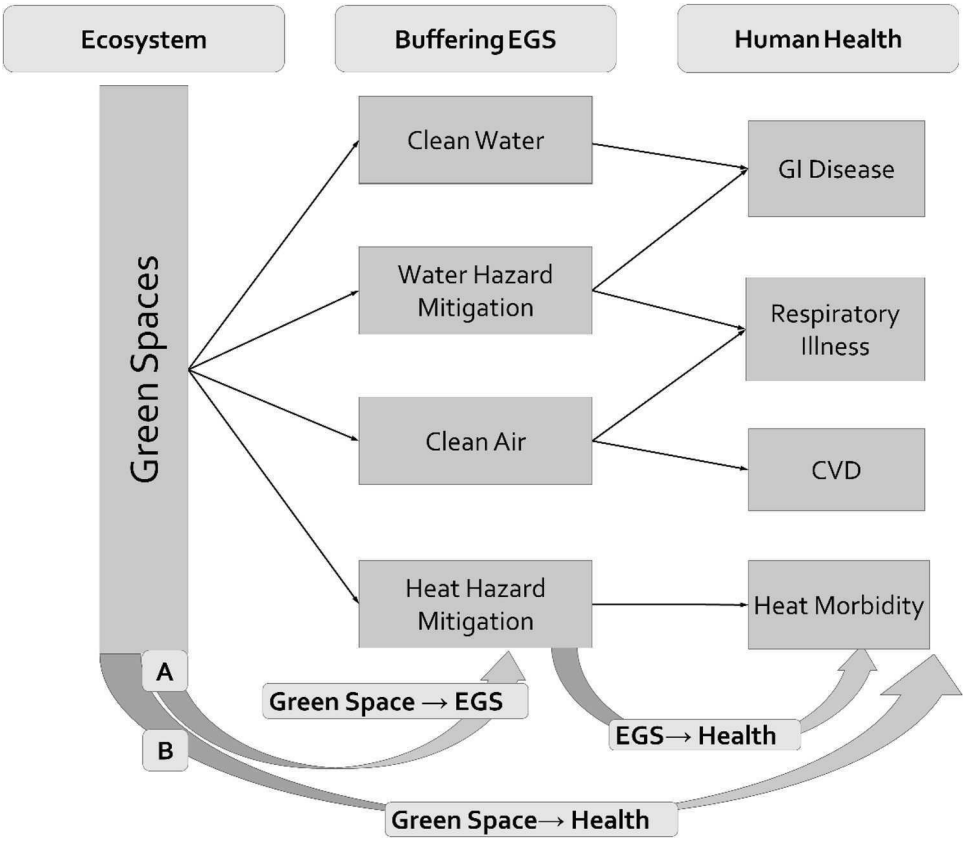

Fig. 1 Selected Eco-Health linkages for causal criteria analysis. We followed two approaches for our analysis: **a** Evaluating the intermediate steps linking green spaces to human health; **b** evaluating the evidence linking green spaces directly to human health. *EGS* ecosystem goods and services, *GI disease* gastro intestinal disease, *CVD* cardio vascular disease

information on the weight of evidence linking acute morbidities such as gastrointestinal disease, respiratory illness, cardiovascular disease, and heat morbidities to green-space–EGS (Hartig et al. 2014). We selected these four health endpoints for our assessment which followed two approaches:

1. Evaluating intermediate linkages:
   (a) Green space → EGS (i.e., green spaces providing buffering EGS)
   (b) EGS → Health (i.e., exposure to environmental hazards leading to disease).
2. Evaluating direct linkages:
   (a) Green space → Health (i.e., health benefits associated to presence/extent of the ecosystem).

This approach allowed us to fully characterize the cause–effect model (Fig. 1), and identify the greatest data gaps and the strongest support.

Cause and effect mechanisms

Green spaces mitigate water hazards (e.g., floods, storm surge) by increasing rainfall interception and infiltration and by acting as a physical barrier to waves and storm surges (Brody and Highfield 2013; Costanza et al. 2008). Water hazard mitigation lowers exposure to polluted flood waters that cause GI disease, and prevents flood prone homes from harboring conditions that lead to mold growth and asthma (Wade et al. 2004; Chew et al. 2006). Green spaces remove infectious and toxic pollutants (Silva et al. 1990; Karim et al. 2004), helping to prevent GI disease from drinking and recreational water (Araya et al. 2004; Katukiza et al. 2014). They trap air contaminants (Räsänen et al. 2013), which may otherwise lead to respiratory illness and cardiovascular disease (Peters et al. 1997; Brook et al. 2004). Green spaces mitigate extreme temperatures through shade and evapotranspiration, lowering heat morbidities during heat waves (Bouchama and Knochel 2002). Table 2 summarizes these cause–effect mechanisms.

Literature review

We examined 2756 publications regarding Eco-Health linkages [(ESM 1) from years 2000 to 2016. First, we searched within an existing Eco-Health database (Jackson et al. 2013), $N = 1434$] and selected papers relevant to our focal Eco-Health relationships ($N = 112$). We expanded this database with a targeted keyword search (ESM 2). We examined the titles and abstracts of all articles from the first 50 non-duplicative results per key-word combination

Table 2 Cause and effect mechanisms for the intermediate steps of the selected Eco-Health linkages

Eco-Health linkages	Cause–effect mechanism	Mechanistic references	# Studies
Green spaces and EGS			
Green spaces–clean water	Green spaces provide physical barriers to the movement of pollutants in water, change the soil's condition to promote pollutant immobilization, or capture pollutants in plant biomass	Silva et al. (1990), Karim et al. (2004)	44
Green spaces–water hazard mitigation	Green spaces reduce surface runoff by increasing rainfall interception and infiltration. They also act as physical barriers to waves and storm surges	Brody and Highfield (2013), Costanza et al. (2008)	19
Green spaces–clean air	Green spaces provide physical barriers to the movement of pollutants in air and absorb pollutants	Räsänen et al. (2013)	22
Green spaces–heat hazard mitigation	Green spaces provide cooling through shade and evapotranspiration	Pokorný et al. (2010), Kong et al. (2014)	19
EGS and health			
Clean water–GI disease	Pathogenic microbes cause toxicity and infection, heavy metals like copper cause vagal nerve stimulations which triggers GI symptoms	Araya et al. (2004), Katukiza et al. (2014)	6
Water hazard mitigation–GI disease	Flood water mixes with waste water discharged into rivers, or other polluted sources. Individuals in flood prone areas come in contact with contaminated flood waters	Wade et al. (2004)	7
Water hazard mitigation–respiratory illness	The humidity and dampness in flood prone households lead to indoor mold growth. Mold endotoxins cause respiratory conditions like asthma	Chew et al. (2006)	4
Clean air–respiratory illness	Outdoor air pollutants (i.e., PM, O_3, SO_2 and NO_2) cause oxidative stress and airway inflammation. Other mechanisms causing respiratory illness include increased susceptibility to infections and disruptions in oxygen transport	Kagawa (1985), Nel et al. (2006) Reno et al. (2015)	28
Clean air–cardiovascular disease (CVD)	Airway inflammation and obstruction in oxygen transport caused by $PM_{2.5}$ and PM_{10}), O_3, SO_2 and NO_2 leads to plaque formation and atherosclerosis. Pollutants may also affect blood coagulation	Peters et al. (1997), Brook et al. (2004)	23
Heat hazard mitigation–heat morbidities	Heated blood is transferred towards the surface of the body, increasing blood output and activating sweating. This leads to dehydration, increases in heart rate, and affects kidneys, liver and digestive systems as blood circulation is transferred away from the organs and towards the skin	Bouchama and Knochel (2002)	18

EGS ecosystem goods and services, *GI disease* gastrointestinal disease

($N = 950$), and eliminated non-relevant results (e.g., review articles) for a total of 208 papers. We then evaluated study methodology for all papers selected [$N = 320$ (112 + 208)] and excluded papers that were not primary research papers. For example, we excluded papers that used modeling techniques such as i-Tree (Nowak et al. 2008) as these tend to infer provision of EGS from estimates made by previous studies, and thus may not add new evidence. When available we assessed articles that helped informed model development (e.g., Pope et al. 2002). We also excluded articles that looked at the green space–human health link through the lens of physical activity or restorative theories, as our focus was buffering EGS. Our final selection ($N = 212$, ESM 4) was evaluated using CSA.

Weighting the evidence

Selected articles were classified using the weights described in Table 1. We summed these weights to calculate an evidence score for each cause and effect linkage. A score of 20 was the threshold for rejecting or supporting the causal linkage. This threshold implies that at least three high-quality studies are needed to provide evidence for causality, whereas in the case of low-quality research studies, more articles may be needed to obtain the same level of support (Norris et al. 2011). A score of 20 or more for articles contradicting the hypothesis serves as basis for rejecting the cause–effect relationship. Norris et al. 2011 chose this threshold after expert consultation and multiple trials; however, Eco-Evidence allows modifying these values if necessary. For our study, we applied the suggested score of 20, with the following possible scenarios:

1. In Favor ≥ 20 + Not in Favor ≤ 20 = Support for Hypothesis.
2. In Favor < 20 + Not in Favor ≥ 20 = Support for Alternate Hypothesis.
3. In Favor < 20 + Not in Favor < 20 = Insufficient Evidence.
4. In Favor ≥ 20 + Not in Favor ≥ 20 = Inconsistent Evidence.

To determine the sensitivity of our conclusions to the chosen threshold, we examined results at 5, 10, 15 and 20% of the base value (e.g., when using a 20% variation in threshold, scores of 16 and 24 were applied instead of 20).

Results

Weighting the evidence: intermediate linkages

Green spaces and buffering EGS

We reviewed 105 articles linking green spaces to clean water, water hazard mitigation, clean air, and heat hazard mitigation (Fig. 2; ESM 3).

We found 44 papers supporting the green spaces–clean water linkage. Most of the studies assessed the role of wetlands in removing copper and fecal coliform; we found fewer studies assessing the capacity of other types of green spaces (riparian vegetation, green roofs, urban trees) for removing pollutants (ESM 3). We found 20 papers supporting the role of green spaces in mitigating water hazards. Studies linked this EGS to several types of green spaces, including green roofs, wetlands and open spaces. Indicators used to assess water hazard mitigation included wave energy, surface runoff, and flood-related property damages, in the presence and absence of green spaces (ESM 3).

Our assessment supports the linkage between green spaces and clean air. We reviewed 22 articles, where urban trees (canopy cover, tree cover) were consistently shown to remove air pollutants, most frequently particulate matter (PM_{10} and $PM_{2.5}$). We also found support for the role of green spaces in heat hazard mitigation in 19 studies on the subject. The indicators to assess Heat Hazard were mostly temperature change and heat waves, while NDVI (Normalized Difference Vegetation Index) and tree cover were commonly used to measure green spaces.

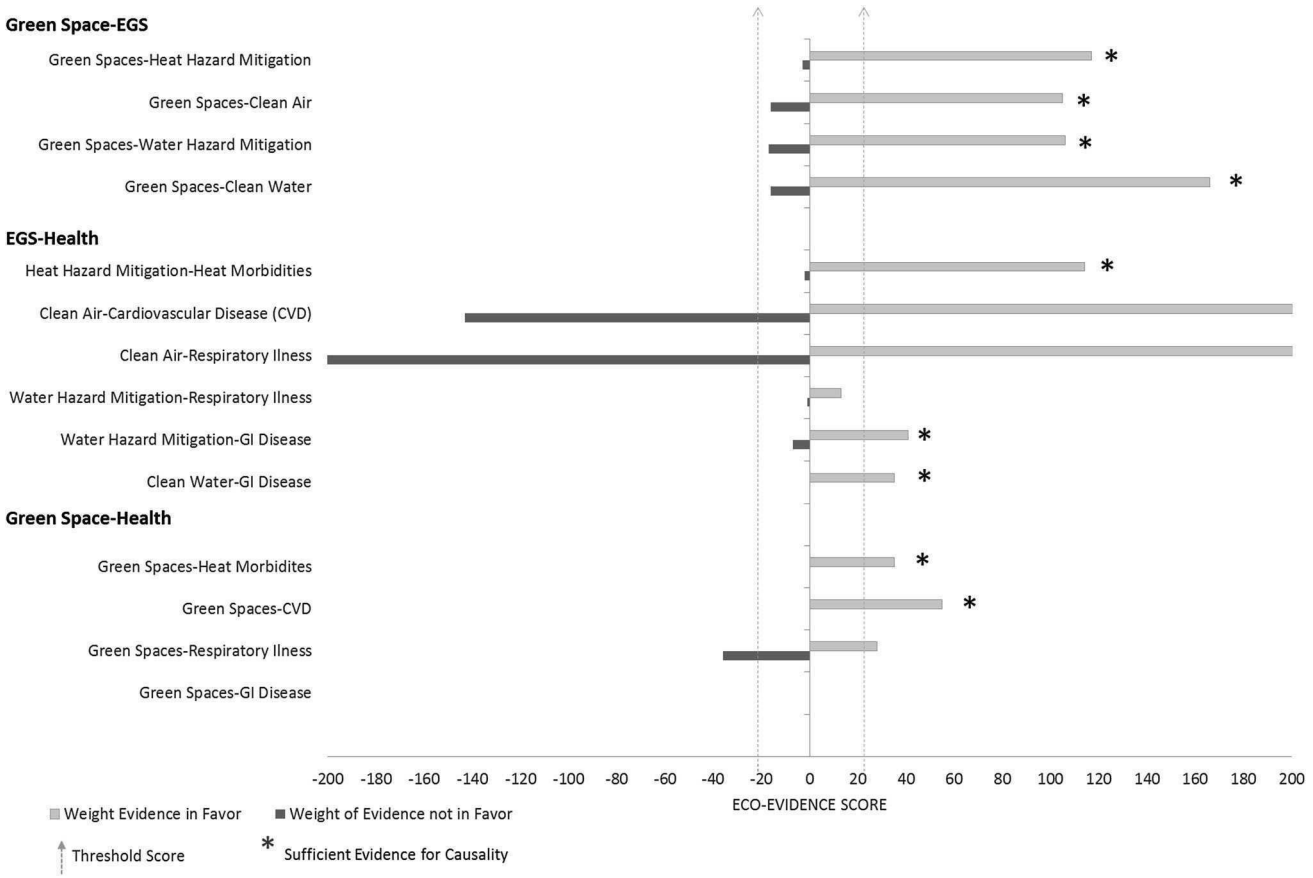

Fig. 2 Results from causal criteria analysis. Interpreting possible outcomes: (1) In Favor ≥ 20 + Not in Favor ≤ 20 = Support for Hypothesis; (2) In Favor <20 + Not in Favor ≥ 20 = Support for alternate Hypothesis; (3) In Favor <20 + Not in Favor <20 = Insufficient Evidence; (4) In Favor ≥ 20 + Not in Favor ≥ 20 = Inconsistent Evidence. *Negative values* here represent evidence not in favor, while *positive values* represent evidence in favor. *EGS* ecosystem goods and services, *GI disease* gastro intestinal disease, *CVD* cardiovascular disease

EGS and health

GI disease We reviewed 6 papers providing sufficient support for clean water–GI disease linkage. Swimming and consumption were the two mechanisms of exposure in the papers assessed, while surveys were used to characterize GI disease occurrences.

For the water hazard mitigation–GI disease linkage, we found 7 papers providing sufficient evidence in favor (Fig. 2). Most studies correlated flood events to GI disease, except for one which focused on rainfall. In this case, GI disease occurrences were assessed using hospital admissions or surveys.

Respiratory illness We found only 4 studies evaluating the linkage between water hazard mitigation and respiratory illness (ESM 3). Three of the papers assessed asthma as a response, and the fourth assessed bronchitis and cough. To measure water hazards, authors looked at flood and severe rainfall events, while health impacts were assessed using surveys or insurance claims. These papers provided insufficient evidence of a causal relationship (Fig. 2).

The linkage between respiratory illness and clean air has been studied extensively ($N = 27$ papers reviewed). Of the respiratory conditions assessed (bronchitis, cough, wheezing, asthma) we found more evidence against the correlation between air pollutants and asthma (not in favor = 93) than the evidence in favor (in favor = 79; ESM 3). In terms of indicators, most of the studies measured air pollutants using data from monitoring stations, while hospital admissions and surveys were commonly used to assess health outcomes.

Cardiovascular disease (CVD) The link between clean air and CVD had inconsistent evidence (Fig. 2). The studies reviewed ($N = 22$) used a variety of indicators to assess CVD, from blood pressure, to hospital admissions, to indicators of inflammation. This variability in methods may explain our inconsistent results. In terms of the air pollution variables, studies mostly used data from monitoring stations, and indicators like PM_{10}, $PM_{2.5}$, and NO_2.

Heat morbidities We reviewed 18 papers linking heat hazards to health, which provided strong support for causality. To measure heat hazards the authors used either temperature fluctuations or specific heat wave events. The health indicators used were hospital admissions and emergency room visits, particularly those related to heat (e.g., heat stroke), the renal system, or the circulatory system.

Weighing the evidence: direct Eco-Health linkages The evidence directly linking green spaces to health included 5 papers on Respiratory Conditions, 3 papers on heat morbidities, and 2 papers on CVD (Fig. 2). We found sufficient support for the role of green spaces in reducing heat morbidities and CVD, with most papers reporting correlations between green space cover and hospital admissions or mortality related to these conditions. The evidence linking green spaces to respiratory illness was inconsistent; most of the inconsistencies were associated with the response of asthma and/or allergies to green space cover (ESM 3). We did not find papers associating green spaces with GI disease, so our results indicate insufficient evidence to support this direct linkage (Fig. 2).

Sensitivity analysis Most relationships remained unchanged when varying the threshold value by 5–20%, with a few exceptions. Varying the threshold by 15% (i.e., a threshold of 17, or 23, instead of 20) would have changed the conclusion regarding the green spaces–water hazard mitigation and clean water linkage, from "sufficient" evidence, to "inconsistent" evidence as we found a few studies that found no support for the relationship. Varying the threshold by 20% (i.e., threshold of 16, or 24) would have changed the evidence supporting the green space linkage to clean air from "sufficient" to "inconsistent" with two well-designed studies falsifying the hypothesis. A 20% threshold decrease would have altered the conclusions regarding the water hazard mitigation–respiratory illness relationship, going from "insufficient evidence" to "sufficient evidence" as we found two well-designed studies and a relatively poor study in support of the linkage. See ESM3 for details of the studies reviewed.

Discussion

Evidence for causality: Eco-Health linkages

GI disease

Green spaces are causally linked to clean water and water hazard mitigation. Wetlands have been particularly well studied for their role in providing clean water. Factors determining their effectiveness include wetland type (De Lacerda and Abrao 1984), the species involved (Yang et al. 2008), hydrological residence time, and season (Reinelt and Horner 1995). For water hazard mitigation, several types of urban vegetation, including open spaces and green roofs, help reduce surface runoff and flooding (Bliss et al. 2009; Brody and Highfield 2013). Marshes and mangroves have been linked mainly to storm surge reduction and wave attenuation (Granek and Ruttenberg 2007; Möller et al. 2014); we found no papers assessing their role in mitigating urban floods. Our results correspond to findings by

Shepard et al. (2011), and suggest this is an area that remains unexplored.

Our review found sufficient evidence linking clean water and water hazard mitigation to GI disease. The impacts of water pollutants depend on exposure time, concentration of pollutants, extent of exposure, and sensitivity of exposed individuals (Araya et al. 2004; Wade et al. 2004; Collier et al. 2015). Most of the papers assessing these linkages used self-reporting to characterize health response. More objective indicators, such as medical records, or hospital visitations, are less common and could provide further support for this linkage.

We did not find studies addressing direct linkage between Green-Space and GI disease, even though there is sufficient evidence supporting intermediate processes leading to this association, as detailed above. Future research should focus on determining the effectiveness of green spaces to mitigate environmental exposure to toxic and pathogenic water pollutants in diverse contexts, such as recreation, consumption and hazard events.

Respiratory illness

We found support for the role of green spaces in water hazard mitigation (see "GI disease") and clean air, both of which protect from respiratory illness. Urban trees have been the focus of most studies assessing clean air EGS (e.g., Cavanagh et al. 2009; Grundström and Pleijel 2014), with evergreens showing greater effectiveness because of year-long foliage retention and more complex leaf structures (Beckett et al. 2000; Nguyen et al. 2015). Hairiness, stomatal density and leaf wettability are also factors that seem to increase pollutant capture by trees and that should be maximized for clean air EGS (Räsänen et al. 2013; Weber et al. 2014).

The evidence linking water hazards to respiratory illness was less clear. We found few papers linking floods to asthma. Only three of the four papers reviewed supported the linkage, while the fourth paper found a negative association (Park et al. 2013). Of the supporting papers, one found that response was partially mediated by psychological distress, and that asthma negatively correlated to flooding depth, which contradicts their findings (Reacher et al. 2004). The other two studies convincingly connected flood, mold and asthma, but only one followed an experimental approach (Dales et al. 1991), while the other consisted of a single case study (Makaryus et al. 2015). Therefore, the hypothesized linkage between flooding and asthma, mediated by mold growth, remains to be explored.

From the studies assessing linkage between clean air and respiratory illness, those using asthma as a response showed inconsistent evidence for causality (ESM 3). The inconsistencies are likely due to the types of indicators used to measure cause and effect. For example, a widely used clean air indicator is $PM_{2.5}$ mass (e.g., $\mu g/m^3$), while the mechanism that links air pollutants to asthma is in part mediated by oxidative stress and inflammation (Li et al. 2008). Certain particles have greater oxidative capacity than others, and their relative concentration may be a better indicator to assess respiratory impact than mass alone. Only one paper assessed oxidative potential in the air as an explanatory variable (Delfino et al. 2013); it found this was a better predictor of asthma than $PM_{2.5}$ mass. Other inconsistencies were related to season, with more respiratory susceptibility in the winter months. This trend may be related to more indoor pollutant exposure during winter (Walters et al. 1994), differences in pollution sources due to heating, or meteorological patterns in winter (e.g., less rainfall) that affect diffusion of pollutants (Zhen et al. 2013).

Accordingly, we found inconsistent evidence linking green spaces to asthma and allergies. Some studies report positive association between green space and asthma, pointing toward the negative influence of pollen and other allergens (Lovasi et al. 2013). Previous studies have found that while trees help remove pollutants, sometimes these pollutants get recirculated depending on location of buildings, wind direction and flow dynamics (Wania et al. 2012). Therefore, careful selections of tree species, and the use of flow dynamics modeling, are important considerations for designing green space configurations as part of restoration initiatives.

Cardio vascular disease (CVD)

We found inconsistent evidence for the link between clean air and CVD. We can hypothesize potential reasons, such as the use of various indicators in different studies and the presence of confounding natural and demographic factors. For example, in an experimental study by Hajat et al. (2015), different pollutants were tested against indicators of inflammation and blood clot formation with inconsistent results among the combinations tested (ESM 3). This signals a need for better characterizing the physiological mechanisms linking clean air to CVD to determine the best indicators to detect this connection. Another study found that age is an important factor, with the elderly showing greater CVD response to pollution (Prescott et al. 2000). Season may also play a role; in some instances, correlations were observed in cold but not warm months (Chang et al. 2015). Moreover, when looking at relationships that have many associated studies (e.g., CVD–clean air), the likelihood of finding inconsistencies increases (Norris et al. 2011). This does not imply that "inconsistent" connections are not real; rather, the inconsistencies help refine

hypotheses and future research questions (Norris et al. 2011).

We found support for a direct link between green space and CVD. Although we tried to avoid papers focusing on the health promoting benefits of green spaces, the studies we used were correlative, without explicit assessments of the mechanisms involved. The findings may in part be related to promotion of physical activity, engagement with nature, and the stress reducing potential of green spaces. In one of the papers, Pereira et al. (2013) found that neighborhood variability of greenness had a stronger association to CVD than absolute greenness, a finding that points toward physical activity as a mediating factor, since non-green areas (e.g., sidewalks, parking lots) were also important. Donovan et al. (2015) found that correlations between green space loss and CVD were significant after controlling for exercise, indicating that factors other than physical activity were important. Nevertheless, these other factors could include stress reduction from promotion of social engagement (EGS that also reduce CVD risk) and not necessarily air quality. Based on our review, we hypothesize that the benefits of trees to CVD could be attributed to mechanisms other than supporting air quality. In Fig. 3, we present this hypothesis by illustrating risk factors for CVD, and the role of green spaces using previous studies. Green spaces have been shown to promote a 44% increase in physical activity, but provide on average 0.11% air quality improvement via reduction of PM (Richardson et al. 2013; Nowak et al. 2013). Although these values come from studies with different methodologies, and quantitative comparisons are not justified, the differences in magnitude illustrate the relative influence of green spaces via these two EGS. Moreover, a study by Lim et al. (2013) showed that PM corresponds to 22% of the risk for CVD, while physical activity accounts for 31% and influences other important CVD drivers like stress and body mass index. Considering the relative importance of green spaces for physical activity vs clean air, and the relative importance of physical activity vs clean air in CVD, we propose that green spaces mainly influence CVD by promoting physical activity. This is not suggesting that clean air is unimportant for CVD, rather that green spaces likely play a modest pollutant buffering role, and that emphasis should be placed primarily on reducing pollution. In turn, management of green spaces for health promoting services should align with aspects of the built environment, such as access and safety features. This is especially important for low income communities, which face higher CVD risks (Fig. 3).

Heat morbidities

The link between green spaces and heat hazard mitigation is unequivocal, both for direct health outcomes and for the intermediate steps. Heat mitigation by trees has been reported for cities with different types of green space and ecosystems, and at multiple scales (Hou et al. 2013; Vailshery et al. 2013). Likewise, the protective value of green cover on heat morbidities has been well-documented in relation to heat waves and within arid environments at risk of heat extremes (Vandentorren et al. 2006; Harlan et al. 2013). Consistently, studies confirm increased risk from heat for vulnerable populations, such as elderly individuals and those with impaired mobility (Vandentorren et al. 2006; Burkart et al. 2016). Although correlations have been observed when documenting green cover at lower resolutions (e.g., 30 m resolution, using indicators such as NDVI), vegetation is most likely to be protective when it is strategically placed near exposed households within the urban context (Li et al. 2013).

In terms of management for heat hazard mitigation, the amount of green space is the most important factor, but there are other design considerations. Mixing tree species along street corridors to avoid continuous canopies that trap heat, and designing green roofs to have high leaf area index and adequate irrigation, are strategies to enhance the cooling effect (Norton et al. 2015). Urban greening not only buffers against heat islands and heat waves, but may also provide economic services to sectors that cannot rely on air conditioning, while supporting efficient energy use.

Limitations and recommendations

Limitations of the Eco-Evidence tool are discussed in detail in Norris et al. (2011). The authors address criticisms regarding the threshold value of 20, and advise that expert judgement should always be included. From our sensitivity analysis, we found that we would need to change the threshold by 15–20% to alter our conclusions. Because Norris et al. (2011) used trials and expert advice to develop the threshold of 20, we feel compelled to adhere to this value to maintain consistency, but we encourage readers to consider these alternative results when interpreting our findings. Another limitation is that the approach does not differentiate studies by their attention to confounding factors, which in the case of Eco-Health studies could be influential. Weighting studies by environmental or socioeconomic confounders would be a much-needed revision to the method (Norris et al. 2011). Lastly, while Eco-Evidence is not a substitute for strictly quantitative approaches such as meta-analyses, it allows weighting evidence from a variety of studies, including those that do not report summary statistics or cannot be combined due to fundamental differences in datasets. The contribution of Eco-Evidence is to help evaluate the knowledge base in support of a given relationship, not the effect size of that relationship, as in meta-analyses.

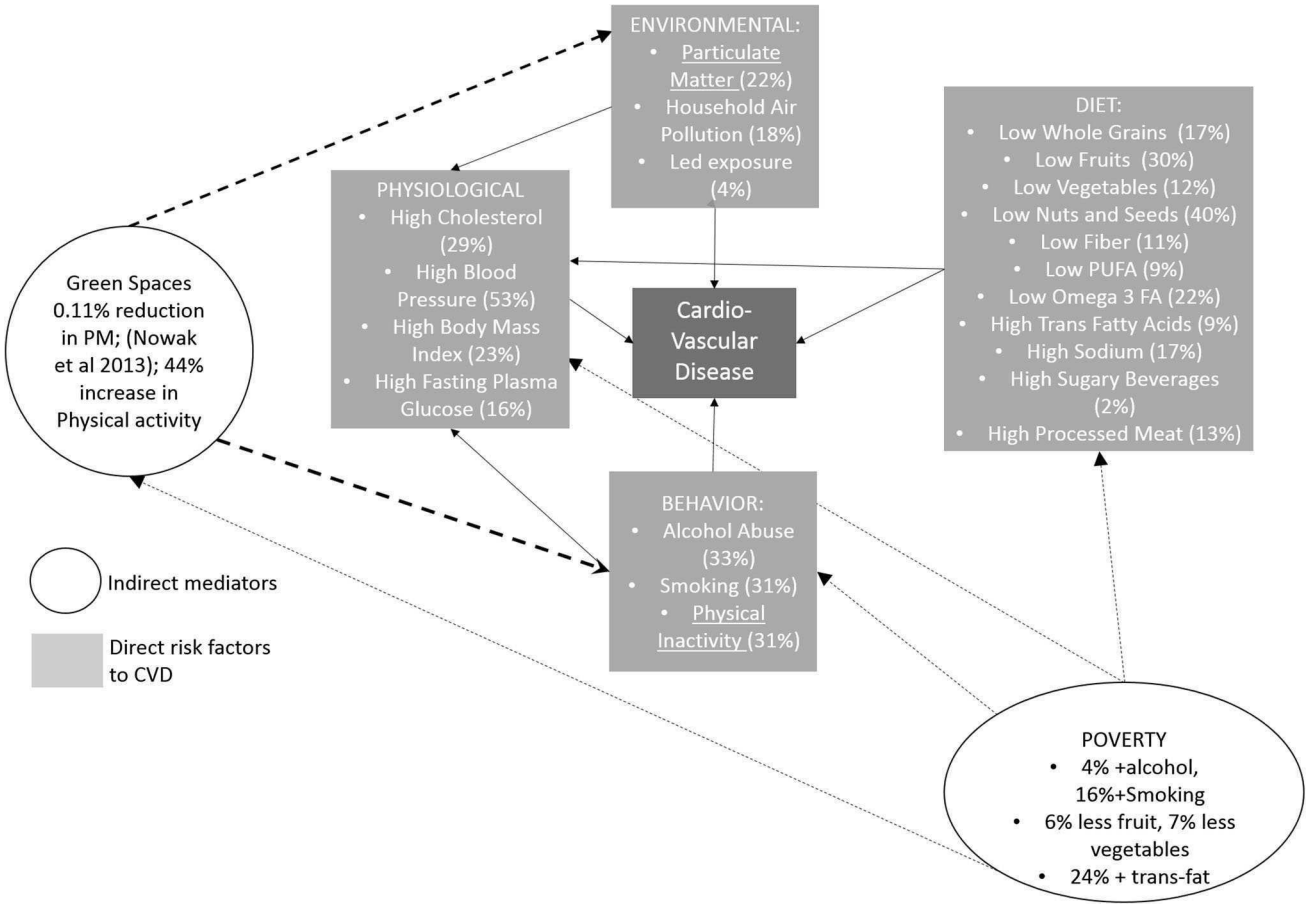

Fig. 3 Direct risk factors for cardiovascular disease (CVD, *gray boxes*) and indirect mediators (*white circles*, green spaces and poverty). The percentages represent the proportion of the effect attributed to the cause. The causes for CVD or risk factors (environmental, diet, behavior and physiological) were adapted from Lim et al. (2013), who looked at ischemic heart disease, a common type of CVD. The % of air quality improvement from trees was adapted from Nowak et al. (2013), by averaging the estimates for the ten US cities they assessed in their study. The percent in promotion of physical activity comes from Richardson et al. (2013); Poverty percentages come from Hulshof et al. (1991), and Galobardes et al. (2001)

Our results are partly determined by our strategy to identify relevant scientific studies (ESM 2). We invite readers to evaluate our review method and account for potentially missing keywords when interpreting our conclusions. In addition, to maintain consistency in the quality of material included, we only considered peer-reviewed publications, and excluded book chapters and gray literature. Despite these limitations, our review allowed us to make consistent comparisons, determine their relative state of knowledge, refine hypotheses and define areas of research need. Our findings support a proposed research agenda (Table 3) to advance the management of EGS for human health benefits.

Conclusions

We conducted a CSA to characterize Eco-Health literature. Our study fills a void that previous reviews had identified as crucial for valuing Eco-Health evidence: namely reviewing the evidence for the full pathways between ecosystem, ecosystem processes (e.g., EGS) and health outcomes (Hartig et al. 2014).

Our work confirms that most current Eco-Health literature supports the intermediate steps of these pathways (e.g., Ecosystem–EGS, EGS–Health), but few studies trace linkages from ecosystem to disease. Of these, few simultaneously address the pathways by which these direct connections occur. Research that fully determines if/how greening strategies deliver health benefits through buffering EGS is generally lacking, and in need of attention.

Despite identifying research needs, our review found consistent evidence of a connection between green spaces and buffering EGS, and between green spaces and certain health outcomes such as cardiovascular disease and heat morbidities. The role of green spaces in providing health

Table 3 Summary of causality assessment and priority questions for an Eco-Health research agenda

Eco-Health linkages	Evidence for causality		Priority questions
	Intermediate linkages	Direct linkages	
Green spaces–clean water/polluted water–GI disease	Support for Hypothesis	Insufficient	Is GI disease prevalence related to green space measures (presence, % cover, etc.) in areas exposed to water pollution?
Green spaces–water hazard mitigation/water hazards–GI disease	Support for hypothesis	Insufficient	Is GI disease prevalence related to green space measures (presence, % cover, etc.) in flood prone areas?
Green spaces–water hazard mitigation/water hazards–respiratory illness	Insufficient for EGS–health linkage	Insufficient	Is mold more common in houses prone to natural flooding? Does household mold correlate to asthma?
Green spaces–clean air/polluted air respiratory illness	Inconsistent for EGS–health linkage	Inconsistent	What are the best indicators to detect the impact of air quality on respiratory illnesses (e.g., oxidative potential vs pollutant mass)?
			Are there consistent confounding factors (demographics, seasonality) determining the impact of air pollutants?
			Could we define transferable green space restoration guidelines to enhance pollution removal and reduce allergen potential?
			How can we incorporate flow dynamic principles into the design of green space restoration?
Green spaces–clean air/polluted air–CVD	Inconsistent for Eco-Health linkage	Support for hypothesis	What are the best indicators to detect the impact of air quality on CVD (e.g., inflammatory response, coagulation, CVD prevalence)?
			Are there consistent confounding factors (demographics, seasonality) determining the impact of air pollutants on CVD?
			What is the main mediator between green spaces and CVD–physical activity or clean air?
Green spaces–heat hazard mitigation/heat hazard–heat morbidities	Support for hypothesis	Support for hypothesis	What are the barriers to establishing green space policy for heat morbidity prevention in cities?

GI disease gastrointestinal disease, *CVD* cardiovascular disease, *EGS* ecosystem goods and services

benefits is enhanced in cities if considered alongside design aspects such as selection of tree species, attention to placement and configuration of trees, and aspects of the built environment that encourage use of green spaces. This evidence should encourage green space planning within cities by showing human health is an achievable objective of restoration investments.

Acknowledgements We thank Laura Jackson, Mathew Harwell, Susan Yee, Marc Russell and anonymous reviewers for comments that greatly improved this manuscript. The views expressed in this paper are those of the authors and do not necessarily reflect the views or policies of the US Environmental Protection Agency. Any mention of trade names, products or services does not imply an endorsement by the US Government or the US Environmental Protection Agency (EPA). The EPA does not endorse any commercial products, services, or enterprises.

Compliance with ethical standards

Conflict of interest There is no conflict of interest to declare.

Human or animal rights Our work did not involve human subjects or third party funding sources.

References

Araya M, Olivares M, Pizarro F, Llanos A, Figueroa G, Uauy R (2004) Community-based randomized double-blind study of gastrointestinal effects and copper exposure in drinking water. Environ Health Perspect 112(10):1068–1073. doi:10.1289/ehp.6913

Beckett KP, Freer-Smith PH, Taylor G (2000) Particulate pollution capture by urban trees: effect of species and windspeed. Glob Change Biol 6(8):995–1003. doi:10.1046/j.1365-2486.2000.00376.x

Bliss DJ, Neufeld RD, Ries RJ (2009) Storm water runoff mitigation using a green roof. Environ Eng Sci 26(2):407–418. doi:10.1089/ees.2007.0186

Bouchama A, Knochel JP (2002) Heat stroke. N Engl J Med 346(25):1978–1988. doi:10.1056/NEJMra011089

Brody SD, Highfield WE (2013) Open space protection and flood mitigation: a national study. Land Use Policy 32:89–95. doi:10.1016/j.landusepol.2012.10.017

Brook RD, Franklin B, Cascio W, Hong Y, Howard G, Lipsett M, Luepker R, Mittleman M, Samet J, Smith SC, Tager I (2004) Air pollution and cardiovascular disease. Circulation 109(21):2655–2671. doi:10.1161/01.CIR.0000128587.30041.C8

Burkart K, Meier F, Schneider A, Breitner S, Canário P, Alcoforado MJ, Scherer D, Endlicher W (2016) Modification of heat-related mortality in an elderly urban population by vegetation (urban green) and proximity to water (urban blue): evidence from

Lisbon, Portugal. Environ Health Perspect 124(7):927. doi:10.1289/ehp.1409529

Cavanagh JA, Zawar-Reza P, Wilson JG (2009) Spatial attenuation of ambient particulate matter air pollution within an urbanised native forest patch. Urban For Urban Greening 8(1):21–30. doi:10.1016/j.ufug.2008.10.002

Chang CC, Chen PS, Yang CY (2015) Short-term effects of fine particulate air pollution on hospital admissions for cardiovascular diseases: a case-crossover study in a tropical city. J Toxicol Environ Health Part A 78(4):267–277. doi:10.1080/15287394.2014.960044

Chew GL, Wilson J, Rabito FA, Grimsley F, Iqbal S, Reponen T, Muilenberg ML, Thorne PS, Dearborn DG, Morley RL (2006) Mold and endotoxin levels in the aftermath of Hurricane Katrina: a pilot project of homes in New Orleans undergoing renovation. Environ Health Perspect 114(12):1883–1889. doi:10.1289/ehp.9258

Collier SA, Wade TJ, Sams EA, Hlavsa MC, Dufour AP, Beach MJ (2015) Swimming in the USA: beachgoer characteristics and health outcomes at US marine and freshwater beaches. J Water Health 13(2):531–543. doi:10.2166/wh.2014.095

Corvalan C, Hales S, McMichael AJ (2005) Ecosystems and human well-being: health synthesis. World Health Organization, Geneva

Costanza R, Pérez-Maqueo O, Martinez ML, Sutton P, Anderson SJ, Mulder K (2008) The value of coastal wetlands for hurricane protection. AMBIO J Human Environ 37(4):241–248. doi:10.1579/0044-7447(2008)37[241:TVOCWF]2.0.CO;2

Dales RE, Zwanenburg H, Burnett R, Franklin CA (1991) Respiratory health effects of home dampness and molds among Canadian children. Am J Epidemiol 134(2):196–203. doi:10.1093/oxfordjournals.aje.a116072

De Lacerda LD, Abrao JJ (1984) Heavy metal accumulation by mangrove and saltmarsh intertidal sediments. Rvta Brasil Bot 7:49–52

Delfino RJ, Staimer N, Tjoa T, Gillen DL, Schauer JJ, Shafer MM (2013) Airway inflammation and oxidative potential of air pollutant particles in a pediatric asthma panel. J Eposure Sci Environ Epidemiol 23(5):466–473. doi:10.1038/jes.2013.25

Donovan GH, Michael YL, Gatziolis D, Prestemon JP, Whitsel EA (2015) Is tree loss associated with cardiovascular-disease risk in the Women's Health Initiative? A natural experiment. Health Place 36:1–7. doi:10.1016/j.healthplace.2015.08.007

Galobardes B, Morabia A, Bernstein MS (2001) Diet and socioeconomic position: does the use of different indicators matter? Int J Epidemiol 30(2):334–340. doi:10.1093/ije/30.2.334

Granek EF, Ruttenberg BI (2007) Protective capacity of mangroves during tropical storms: a case study from 'Wilma'and 'Gamma'in Belize. Mar Ecol Prog Ser 343:101–105. doi:10.3354/meps07141

Grundström M, Pleijel H (2014) Limited effect of urban tree vegetation on NO_2 and O_3 concentrations near a traffic route. Environ Pollut 189:73–76. doi:10.1016/j.envpol.2014.02.026

Hajat A, Allison M, Diez-Roux AV, Jenny NS, Jorgensen NW, Szpiro AA, Vedal S, Kaufman JD (2015) Long-term exposure to air pollution and markers of inflammation, coagulation, and endothelial activation: a repeat-measures analysis in the Multi-Ethnic Study of Atherosclerosis (MESA). Epidemiology 26(3):310–320. doi:10.1097/EDE.0000000000000267

Harlan SL, Declet-Barreto JH, Stefanov WL, Petitti DB (2013) Neighborhood effects on heat deaths: social and environmental predictors of vulnerability in Maricopa County, Arizona. Environ Health Perspect 121(2):197. doi:10.1289/ehp.1104625

Hartig T, Mitchell R, De Vries S, Frumkin H (2014) Nature and health. Annu Rev Public Health 18(35):207–228. doi:10.1146/annurev-publhealth-032013-182443

Hou P, Chen Y, Qiao W, Cao G, Jiang W, Li J (2013) Near-surface air temperature retrieval from satellite images and influence by wetlands in urban region. Theor Appl Climatol 111(1–2):109–118. doi:10.1007/s00704-012-0629-7

Hulshof KF, Löwik MR, Kok FJ, Wedel M, Brants HA, Hermus RJ, Ten Hoor F (1991) Diet and other life-style factors in high and low socio-economic groups (Dutch Nutrition Surveillance System). Eur J Clin Nutr 45(9):441–450

Jackson LE, Daniel J, McCorkle B, Sears A, Bush KF (2013) Linking ecosystem services and human health: the Eco-Health Relationship Browser. Int J Public Health 58(5):747–755. doi:10.1007/s00038-013-0482-1

Kabisch N, Haase D (2013) Green spaces of European cities revisited for 1990–2006. Landsc Urban Plan 110:113–122. doi:10.1016/j.landurbplan.2012.10.017

Kagawa J (1985) Evaluation of biological significance of nitrogen oxides exposure. Tokai J Exp Clin Med 10(4):348–53

Karim MR, Manshadi FD, Karpiscak MM, Gerba CP (2004) The persistence and removal of enteric pathogens in constructed wetlands. Water Res 38(7):1831–1837. doi:10.1016/j.watres.2003.12.029

Katukiza AY, Ronteltap M, Steen P, Foppen JW, Lens PN (2014) Quantification of microbial risks to human health caused by waterborne viruses and bacteria in an urban slum. J Appl Microbiol 116(2):447–463. doi:10.1111/jam.12368

Kong F, Yin H, Wang C, Cavan G, James P (2014) A satellite image-based analysis of factors contributing to the green-space cool island intensity on a city scale. Urban For Urban Greening 13(4):846–853

Lee AC, Maheswaran R (2011) The health benefits of urban green spaces: a review of the evidence. J Public Health 33(2):212–222. doi:10.1093/pubmed/fdq068

Li N, Xia T, Nel AE (2008) The role of oxidative stress in ambient particulate matter-induced lung diseases and its implications in the toxicity of engineered nanoparticles. Free Radic Biol Med 44(9):1689–1699. doi:10.1016/j.freeradbiomed.2008.01.028

Li X, Zhou W, Ouyang Z (2013) Relationship between land surface temperature and spatial pattern of greenspace: what are the effects of spatial resolution? Landsc Urban Plan 114:1–8. doi:10.1016/j.freeradbiomed.2008.01.028

Lim SS, Vos T, Flaxman AD, Danaei G, Shibuya K, Adair-Rohani H, AlMazroa MA, Amann M, Anderson HR, Andrews KG, Aryee M (2013) A comparative risk assessment of burden of disease and injury attributable to 67 risk factors and risk factor clusters in 21 regions, 1990–2010: a systematic analysis for the Global Burden of Disease Study 2010. Lancet 380(9859):2224–2260. doi:10.1016/S0140-6736(12)61766-8

Lovasi GS, O'Neil-Dunne JP, Lu JW, Sheehan D, Perzanowski MS, MacFaden SW, King KL, Matte T, Miller RL, Hoepner LA, Perera FP (2013) Urban tree canopy and asthma, wheeze, rhinitis, and allergic sensitization to tree pollen in a New York City birth cohort. Environ Health Perspect 121(4):494. doi:10.1289/ehp.1205513

Makaryus M, Iakovou A, Lisker G (2015) A case of severe asthma with fungal sensitization (safs) due to Aureobasidium Pullulans following Hurricane Sandy. In: Interesting cases in allergy and immunology. American Thoracic Society, pp A5644–A5644

Millennium Ecosystem Assessment (MEA) (2005) Ecosystems and human well-being: synthesis. Island Press, Washington, DC. ISBN 1-59726-040-1

Möller I, Kudella M, Rupprecht F, Spencer T, Paul M, Van Wesenbeeck BK, Wolters G, Jensen K, Bouma TJ, Miranda-Lange M, Schimmels S (2014) Wave attenuation over coastal salt marshes under storm surge conditions. Nat Geosci 7(10):727–731. doi:10.1038/ngeo2251

Munns WR, Rea AW, Mazzotta MJ, Wainger LA, Saterson K (2015) Toward a standard lexicon for ecosystem services. Integr Environ Assess Manag 11(4):666–673. doi:10.1002/ieam.1631

Nel A, Xia T, Mädler L, Li N (2006) Toxic potential of materials at the nanolevel. Science 311(5761):622–627

Nguyen T, Yu X, Zhang Z, Liu M, Liu X (2015) Relationship between types of urban forest and PM 2.5 capture at three growth stages of leaves. J Environ Sci 27:33–41. doi:10.1016/j.jes.2014.04.019

Norris RH, Webb JA, Nichols SJ, Stewardson MJ, Harrison ET (2011) Analyzing cause and effect in environmental assessments: using weighted evidence from the literature. Freshw Sci 31(1):5–21. doi:10.1899/11-027.1

Norton BA, Coutts AM, Livesley SJ, Harris RJ, Hunter AM, Williams NS (2015) Planning for cooler cities: a framework to prioritise green infrastructure to mitigate high temperatures in urban landscapes. Landsc Urban Plan 134:127–138. doi:10.1016/j.landurbplan.2014.10.018

Nowak DJ, Crane DE, Stevens JC, Hoehn RE, Walton JT, Bond J (2008) A ground-based method of assessing urban forest structure and ecosystem services. Arboric Urban For 34(6):347–358

Nowak DJ, Hirabayashi S, Bodine A, Hoehn R (2013) Modeled $PM_{2.5}$ removal by trees in ten US cities and associated health effects. Environ Pollut 178:395–402. doi:10.1016/j.envpol.2013.03.050

Park KJ, Moon JY, Ha JS, Kim SD, Pyun BY, Min TK, Park YH (2013) Impacts of heavy rain and typhoon on allergic disease. Osong Public Health Res Perspect 4(3):140–145. doi:10.1016/j.phrp.2013.04.009

Pereira G, Christian H, Foster S, Boruff BJ, Bull F, Knuiman M, Giles-Corti B (2013) The association between neighborhood greenness and weight status: an observational study in Perth Western Australia. Environ Health 12(1):49. doi:10.1186/1476-069X-12-49

Peters A, Döring A, Wichmann HE, Koenig W (1997) Increased plasma viscosity during an air pollution episode: a link to mortality? Lancet 349(9065):1582–1587. doi:10.1016/S0140-6736(97)01211-7

Pope CA III, Burnett RT, Thun MJ, Calle EE, Krewski D, Ito K, Thurston GD (2002) Lung cancer, cardiopulmonary mortality, and long-term exposure to fine particulate air pollution. JAMA 287(9):1132–1141. doi:10.1001/jama.287.9.1132

Pokorný J, Květ J, Rejšková A, Brom J (2010) Wetlands as energy-dissipating systems. J Ind Microbiol biotechnol 37(12):1299–305

Prescott GJ, Lee RJ, Cohen GR, Elton RA, Lee AJ, Fowkes FG, Agius RM (2000) Investigation of factors which might indicate susceptibility to particulate air pollution. Occup Environ Med 57(1):53–57. doi:10.1136/oem.57.1.53

Räsänen JV, Holopainen T, Joutsensaari J, Ndam C, Pasanen P, Rinnan Å, Kivimäenpää M (2013) Effects of species-specific leaf characteristics and reduced water availability on fine particle capture efficiency of trees. Environ Pollut 183:64–70. doi:10.1016/j.envpol.2013.05.015

Reacher M, McKenzie K, Lane C, Nichols T, Kedge I, Iversen A, Hepple P, Walter T, Laxton C, Simpson J (2004) Health impacts of flooding in Lewes: a comparison of reported gastrointestinal and other illness and mental health in flooded and non-flooded households. Commun Dise Public Health 7(1):39–46

Reinelt LE, Horner RR (1995) Pollutant removal from stormwater runoff by palustrine wetlands based on comprehensive budgets. Ecol Eng 4(2):77–97. doi:10.1016/0925-8574(94)00002-M

Reno AL, Brooks EG, Ameredes BT (2015) Mechanisms of heightened airway sensitivity and responses to inhaled SO_2 in asthmatics. Environ Health Insights 9(Suppl 1):13

Richardson EA, Pearce J, Mitchell R, Kingham S (2013) Role of physical activity in the relationship between urban green space and health. Public Health 127(4):318–324. doi:10.1016/j.puhe.2013.01.004

Russo F, Williamson J (2007) Interpreting causality in the health sciences. Int Stud Philos Sci 21(2):157–170. doi:10.1080/02698590701498084

Shanahan DF, Lin BB, Bush R, Gaston KJ, Dean JH, Barber E, Fuller RA (2015) Toward improved public health outcomes from urban nature. Am J Public Health 105(3):470–477

Shepard CC, Crain CM, Beck MW (2011) The protective role of coastal marshes: a systematic review and meta-analysis. PLoS One 6(11):1–11. doi:10.1371/journal.pone.0027374

Silva CA, Lacerda LD, Rezende CE (1990) Metals reservoir in a red mangrove forest. Biotropica 22(4):339–345. doi:10.2307/2388551

Vailshery LS, Jaganmohan M, Nagendra H (2013) Effect of street trees on microclimate and air pollution in a tropical city. Urban For Urban Green 12(3):408–415. doi:10.1016/j.ufug.2013.03.002

Vandentorren S, Bretin P, Zeghnoun A, Mandereau-Bruno L, Croisier A, Cochet C, Ribéron J, Siberan I, Declercq B, Ledrans M (2006) August 2003 heat wave in France: risk factors for death of elderly people living at home. Eur J Public Health 16(6):583–591. doi:10.1093/eurpub/ckl063

Wade TJ, Sandhu SK, Levy D, Lee S, LeChevallier MW, Katz L, Colford JM Jr (2004) Did a severe flood in the Midwest cause an increase in the incidence of gastrointestinal symptoms? Am J Epidemiol 159(4):398–405. doi:10.1093/aje/kwh050

Walters S, Griffiths RK, Ayres JG (1994) Temporal association between hospital admissions for asthma in Birmingham and ambient levels of sulphur dioxide and smoke. Thorax 49(2):133–140. doi:10.1136/thx.49.10.1042

Wania A, Bruse M, Blond N, Weber C (2012) Analysing the influence of different street vegetation on traffic-induced particle dispersion using microscale simulations. J Environ Manag 94(1):91–101. doi:10.1016/j.jenvman.2011.06.036

Webb JA, Miller KA, Stewardson MJ, de Little SC, Nichols SJ, Wealands SR (2015) An online database and desktop assessment software to simplify systematic reviews in environmental science. Environ Model Softw 64:72–79. doi:10.1016/j.envsoft.2014.11.011

Weber F, Kowarik I, Säumel I (2014) Herbaceous plants as filters: immobilization of particulates along urban street corridors. Environ Pollut 186:234–240. doi:10.1016/j.envpol.2013.12.011

Weed DL (1997) On the use of causal criteria. Int J Epidemiol 26(6):1137–1141. doi:10.1093/ije/26.6.1137

Yang Q, Tam NF, Wong YS, Luan TG, Su WS, Lan CY, Shin PK, Cheung SG (2008) Potential use of mangroves as constructed wetland for municipal sewage treatment in Futian, Shenzhen, China. Mar Pollut Bull 57(6):735–743. doi:10.1016/j.marpolbul.2008.01.037

Zhen WM, Shan ZH, Gong WS, Yan TA, Zheng SK (2013) The weather temperature and air pollution interaction and its effect on hospital admissions due to respiratory system diseases in western China. Biomed Environ Sci 26:403–407. doi:10.3967/0895-3988.2013.05.011

Science of the Total Environment 676 (2019) 343–355

Contents lists available at ScienceDirect

Science of the Total Environment

journal homepage: www.elsevier.com/locate/scitotenv

Flood protection ecosystem services in the coast of Puerto Rico: Associations between extreme weather, flood hazard mitigation and gastrointestinal illness

R. De Jesus Crespo [a,*], J. Wu [b], M. Myer [c], S. Yee [a], R. Fulford [a]

[a] USEPA, ORD, NHERL, GED, United States of America
[b] USEPA, ORD, NHERL, RTP, United States of America
[c] USEPA, ORD, NERL, Athens, GA, United States of America

HIGHLIGHTS

- Extreme rain events in Puerto Rico correlate with spikes in Gastro Intestinal (GI) illness.
- Permeable karst soils help reduce flood impacts and GI illnesses according to FEMA and Medicare claims data.
- The benefits of karst soils are lost in areas with a high percentage of people living in flood zones.

GRAPHICAL ABSTRACT

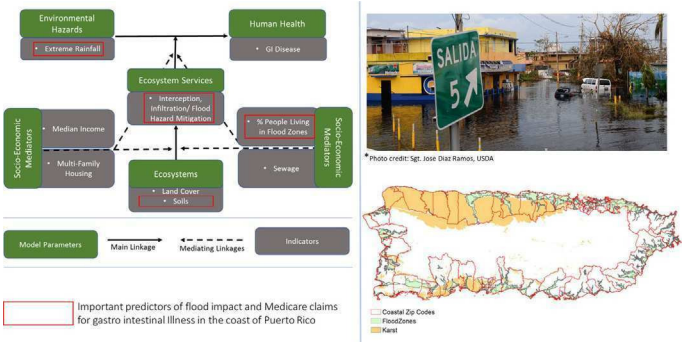

ARTICLE INFO

Article history:
Received 17 January 2019
Received in revised form 22 March 2019
Accepted 19 April 2019
Available online 24 April 2019

Editor: SCOTT SHERIDAN

Keywords:
Ecosystem services
Flooding
Gastro intestinal illness
Coastal communities

ABSTRACT

Floods are becoming increasingly influential in coastal cities due to the intensification of extreme weather events. The impacts of flooding go beyond damages to infrastructure, it also affects human health. During floods, discharge of sewage into streets increases exposure to pathogens causing gastrointestinal (GI) illnesses. A potential strategy for coastal protection during weather hazards is the use of flood protection ecosystem services, but their effectiveness at ameliorating the impact of floods on GI illnesses remain understudied. Here we explore the relationship between extreme rainfall, flood protection ecosystem services, and the occurrence of Medicare claims for gastrointestinal (GI) illnesses in Puerto Rico. We first conducted model averaging to detect variables explaining flood impact for the years (1999–2014), and then used these variables as predictors in a spatio-temporal analysis of GI illness in the same period (1999–2013). Our results show that flood impact varies proportionally with extreme rainfall, and inversely with flood protection ecosystem services, particularly due to the presence of karst soils. The protective effect of karst soils is lost when there is a high percentage of people living in flood prone areas, as suggested by a significant interaction effect between these two variables. In support of our hypotheses, cases of GI illness also spike after extreme rainfall events and are affected by the interaction effect of karst soils and people living in flood prone areas. Our results support the linkage between extreme weather events, flood damages and GI illnesses, and suggests a buffering role of ecosystem services that promote rainfall infiltration. The relevance of these ecosystem services, however, is affected by planning decisions such as

* Corresponding author.
E-mail address: rdejesuscrespo1@lsu.edu (R. De Jesus Crespo).

https://doi.org/10.1016/j.scitotenv.2019.04.287
0048-9697/© 2019 Elsevier B.V. All rights reserved.

residential development in flood prone areas. Our results help inform planning strategies for future weather hazards, accounting for the role of natural and built infrastructure on minimizing flood impacts and human health effects.

© 2019 Elsevier B.V. All rights reserved.

1. Introduction

Flood events are an increasingly important stressor in coastal communities due to projected sea level rise, and frequent exposure to weather hazards, particularly in the tropics (Vitousek et al., 2017). In Latin America and the Caribbean, it is estimated that there are over 7.5 million people currently exposed to flooding, and around 300 billion USD in built capital vulnerable to flood loss (Reguero et al., 2015). Island nations are expected to suffer the greatest impact due to direct exposure to tropical storms, and a strong dependency on coastal resources for tourism and other economic sectors (Reguero et al., 2015; Vitousek et al., 2017). Aside from property damages and impacts to the economy, flood hazards also have been associated to a variety of human health impacts such as vector borne illnesses, gastrointestinal infections, and mental health effects such as PTSD (Post Traumatic Stress Disorder) and Depression (Ahern et al., 2005). It is well established that the impacts of natural disasters such as floods disproportionately affect impoverished communities who are at higher risk of exposure (Winsemius et al., 2015) and who lack access to adequate services and resources to respond (Cutter et al., 2003). In this context, the need for low cost, community driven alternatives to flood hazard protection, including natural infrastructure and ecosystem services becomes particularly important.

Here we explore the role of ecosystem services in relation to one of the most common health outcomes associated to flooding, which is acute gastrointestinal (GI) illness. During floods, untreated sewage often mixes with storm water runoff, contaminating crops and household surfaces (Wade et al., 2014). Contaminated runoff may also come into direct contact with people within flooded residences or those wading through flooded streets to reach higher grounds during an event. Floods can also damage water treatment infrastructure, affecting the availability of safe and potable water for drinking (Wade et al., 2014). Families displaced by flooding often relocate to public shelters, where unsanitary conditions and overcrowding often leads to disease outbreaks (Wade et al., 2014; Huang et al., 2016).

Due to the multitude of pathways exposing people to pathogens during and after floods, many studies have effectively documented this linkage in a variety of settings (Curriero et al., 2001; Reacher et al., 2004; Wade et al., 2004; Wade et al., 2014; Huang et al., 2016). Yet, to date, no study has attempted to determine if the impact of floods on GI illness could be prevented with flood protection ecosystem services (De Jesus Crespo et al., 2018 A). Flood protection ecosystem services include rainfall interception and infiltration by natural land cover, which results in reductions in surface runoff and flood impact (Brody and Highfield, 2013a, 2013b, Xiao and McPherson, 2016). Interception and infiltration also help filter runoff, reducing concentrations of disease-causing pathogens available in storm water (Mallin et al., 2001; Yang et al., 2008). If natural infrastructure helps purify water and reduce surface runoff, and these flood related hazards are associated to GI illness, then we hypothesize that there will be lower occurrences of GI illness in flood prone regions that have flood protection ecosystem services.

We address this hypothesis in coastal neighborhoods in Puerto Rico. The extensive flood impacts caused by Hurricane Maria on the Island in 2017 underscores the potential for weather hazards to severely impact human health, especially among vulnerable sectors. Even before this event, impoverished communities in Puerto Rico had historically been exposed to frequent flooding and flood related illnesses (Azar and Rain, 2007, Briskin, 2016, De Jesus Crespo et al., 2018 B). Puerto Rico's economic downturn over the last decade has also increased unemployment and poverty around the Island, leading to mass migration of younger generations, and an increase in the median age of the remaining residents (Abel and Deitz, 2014; Castro-Prieto et al., 2017), exacerbating the vulnerability of the Island's population.

Focusing on the elderly, here we look at Medicare claims data over a 14-year period (1999–2013) to assess the associations between extreme rainfall, flood impact, and ecosystem services on GI illness (Fig. 1). We predicted that the impact of extreme rainfall on human health would be mitigated by flood protection ecosystem services, resulting in lower cases of GI illness. The role of ecosystems at providing ecosystem services, and of flood protection ecosystem services at ameliorating GI illness occurrences, would be mediated by socio-economic factors that determine the level of exposure to hazards and the adaptations available through built infrastructure for preventing flood impact and health effects (Fig. 1). Having a better understanding of the extent to which ecosystem services may help buffer environmental hazards and protect human health, would help guide community-based management of flood prone neighborhoods and justify conservation and restoration efforts focused on natural infrastructure.

2. Methods

2.1. Study site

Puerto Rico (PR) is a US territory located in the Northeastern Caribbean Sea. It is the smallest Island of the Greater Antilles archipelago, but also the most urbanized and densely populated (Lugo et al., 2012). Most of its population is located along the coast, while the center mountain range is more sparsely urbanized, and more heavily forested (Fig. 2B and C, Parés-Ramos et al., 2008). Around 55% of Puerto Rico's area is vegetation cover (USDA, 2017), most of which is secondary forest resulting from a shift from intense farming up until the mid-20th century, to an industrial economy (Larsen, 2017).

The maximum elevation in the central mountain range is 1338 m (Fig. 2B, Larsen, 2017), and rainfall averages 1651 mm annually, with the mountains receiving much greater precipitation than the coast (Yuan et al., 2015). Due to orographic factors, rainfall is unevenly distributed through the island (Fig. 2A, Hernández Ayala et al., 2017). These differences, driven by the configuration of the central mountain range, lead to four distinct climatic regions in the north, south, east and west (Warne et al., 2005). While the north and east receive abundant orographic rainfall, influenced by the northeast trade winds, the southern portion is relatively dry due to a rain shadow effect (Warne et al., 2005). The western portion is rainy as well, driven by an eastward flow of air from the sea onto the land producing abundant afternoon rainfall (Warne et al., 2005).

Around 55% of the Island is currently served by the Puerto Rico Aqueduct and Sewer Authority (PRASA) waste water system (Government of Puerto Rico, 2018). Many of PRASA's waste water infrastructure was developed in the 1950's, often making it obsolete to manage modern demands (Hunter and Arbona, 1995). Lack of financial resources has limited infrastructure improvement projects, leading PRASA to be the subject of multiple federal fines for failure to meet water quality regulations from its waste water treatment facilities (PRASA, 2014).

We focused this study on the PR coast, where higher population densities, lower elevations, and the potential for storm surges increase flood risk, and potential GI pathogen exposure. We included all coastal zip

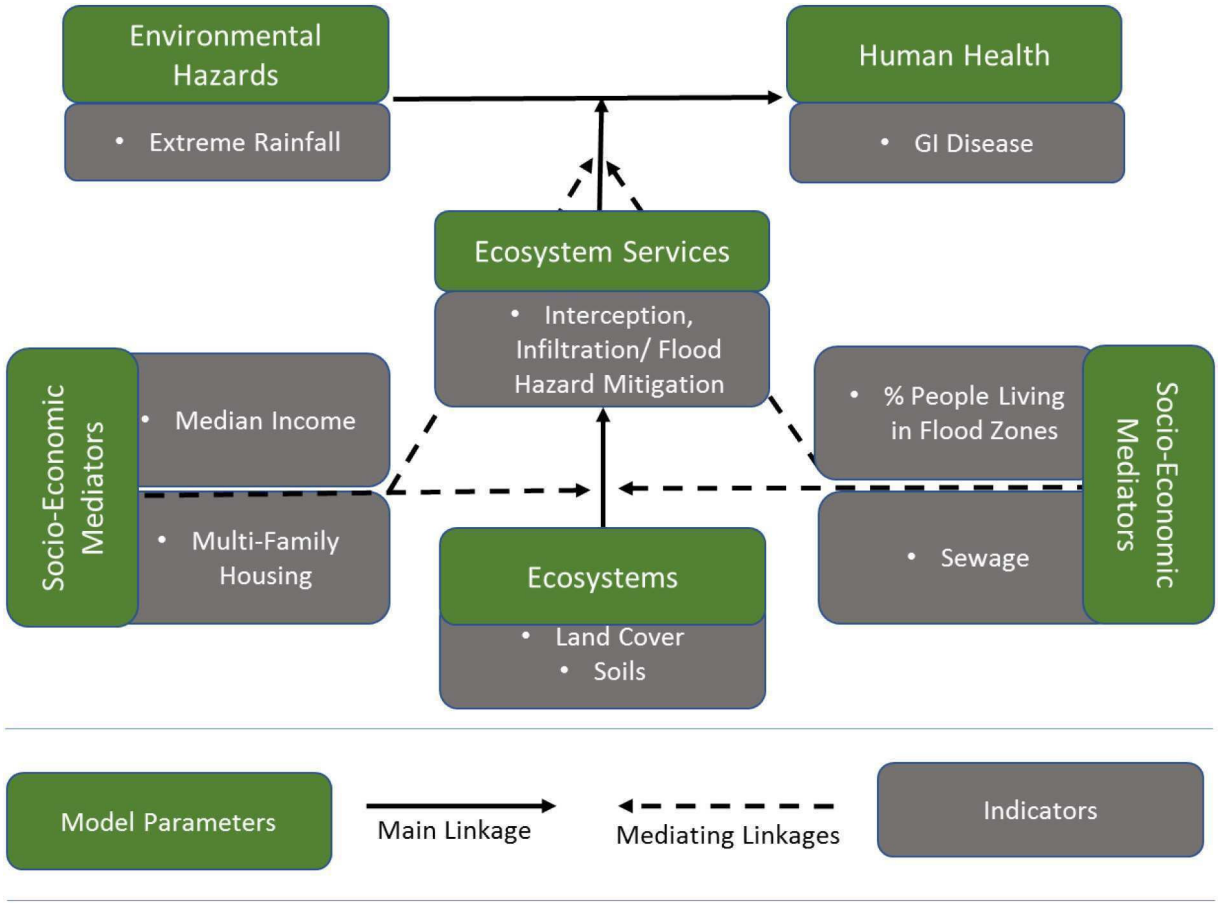

Fig. 1. Conceptual model describing the association between extreme rainfall and GI disease. We predict that the impact of extreme rainfall on human health would be mitigated by flood protection ecosystem services, resulting in lower cases of GI disease. The relationship between weather, floods, ecosystem services and GI disease would also be mediated by socio-economic factors that determine the level of exposure to hazards, the adaptations available through built infrastructure to manage flood impacts, the effectiveness with which ecosystems can deliver ecosystem services, and the relative importance of these ecosystem services to human health and well-being. See also Myers et al., 2013, and Crimmins et al., 2016.

codes ($N = 73$) except for the municipalities of Vieques and Culebra. These municipalities are separate islands, with distinct hydrological traits that make their comparison to other sites more challenging.

2.2. Data sources and processing

We selected indicators from available datasets (Table 1) for each component of our conceptual model (Fig. 1). Most estimates were done at the zip-code level, but when feasible, we also estimated indicators at the HUC-10 watershed levels (USGS, 2017), especially for predictor variables associated to hydrological patterns (e.g. rainfall, rain retention, vegetation cover, and slope).

Prior to analysis, all predictor variables were centered by subtracting the sample mean and dividing by the sample's standard deviation (Becker et al., 1988). Collinearity was examined using Pearson correlation coefficients (Supplementary material 1; SM1). Any correlation between explanatory variables of >0.60 was considered important and accounted for in subsequent analysis.

2.2.1. Extreme weather

Daily rainfall in Puerto Rico was estimated for the years 1999–2014 using the NASA Daymet surface weather and climatological summary dataset (Thornton et al., 1997). We generated 1 km spaced points through the island and used these as coordinates for data extraction with the "daymetr" R-package (Hufkens, 2014). Data were summarized by zip code, and analyzed longitudinally, calculating 7-day moving averages (allocated daily), and daily extreme events (90th, 95th and 99th percentile rainfall). These rainfall extremes were classified with a 1, 2, or 3 (representing 90, 95, 99% respectively), other days with a "0". For evaluating GI illness response, we assessed extreme rain events at a 7-day lag to capture the incubation period for most GI illnesses caused by waterborne pathogens (Jagai et al., 2015). Other studies have assessed GI response to rainfall at different lag periods and found one week lags to be representative (Jagai et al., 2015). To classify extreme rain with lag periods, we used the *rollapllyr* function of the package zoo in R. Since daily extreme events were classified as 1, 2, or 3, we calculated a moving maximum using the previous 7 days as a basis. This resulted in "1, 2, or 3" being applied to days that experienced any of these events in the previous seven days (the maximum of these three values) and "0" otherwise.

To model flood claim response, we used zip-code aggregated weather data for the entire study period as predictor variables, including average annual rainfall, as well as the magnitude of the 90th, 95th or 99th rainfall percentiles. In this part of the analysis, we explored rainfall trends at different spatial scales. The same 1 km spaced point file used to extract data at the zip code level, was used to summarize data at the HUC-10 watershed level. We then created estimates of HUC-10 level rainfall for each zip code. In the case were multiple HUC-10 watersheds intersected a single zip code, a weighted average was calculated so the rainfall in the watershed with greater spatial overlap with the zip code would have higher influence (SM2).

2.2.2. Ecosystem services

We estimated flood protection ecosystem services using the EPA H20 tool (Russell et al., 2015), which uses curve numbers (CN) to estimate a rain retention index. The curve number method incorporates

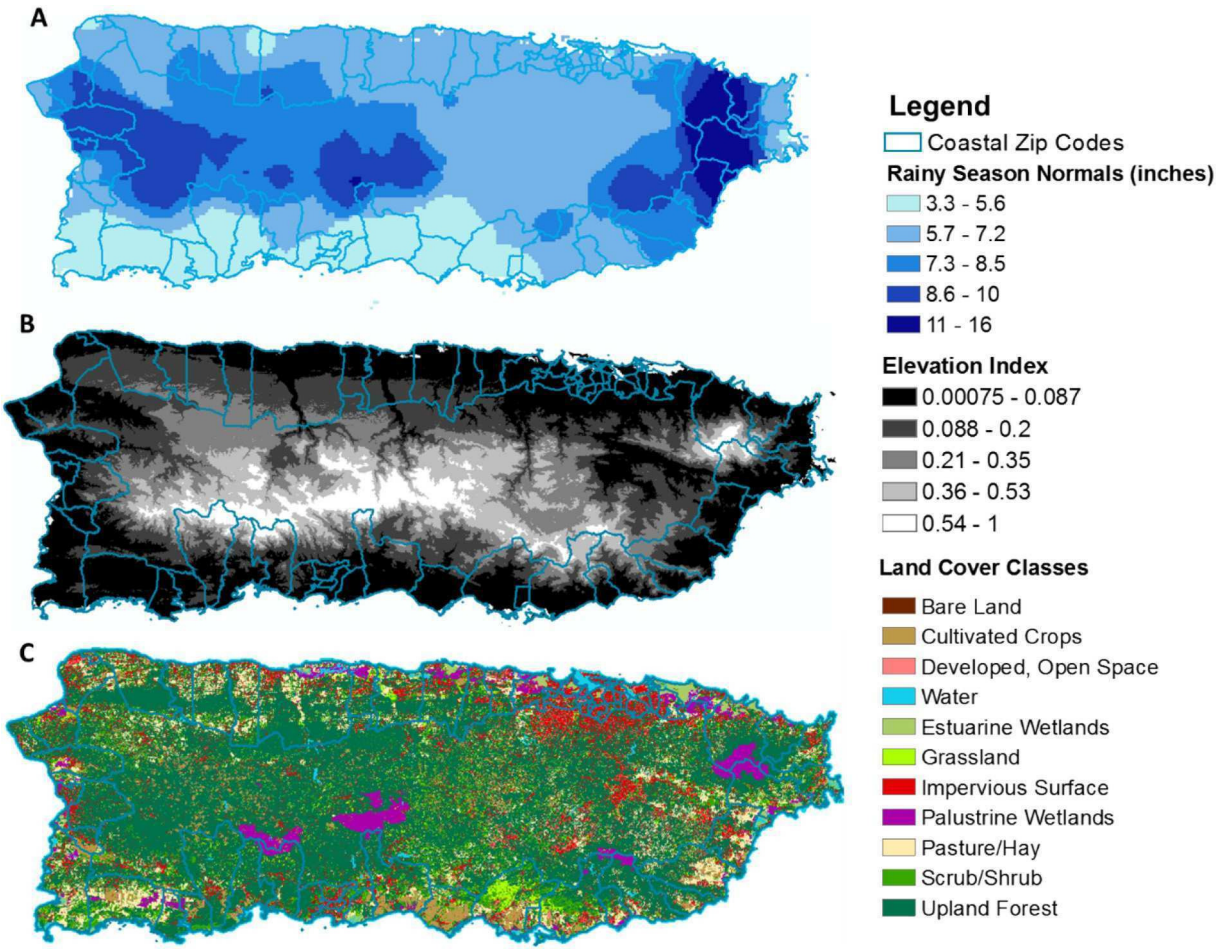

Fig. 2. Study site, coastal zip codes in Puerto Rico. A) Rainy season (May-Nov) normal precipitation (inches). This map is derived from NOAA 1981–2010 U.S. Climate Normals, by interpolating point data from weather stations through Puerto Rico (Arguez et al., 2012) using Inverse Distance Weighting in Arc GIS; B) Elevation index, derived from Digital Elevation Model values (CRIM 1998), presented as a fraction of the maximum elevation in Puerto Rico (i.e. value/max elevation); C) Land cover classes adapted from the Coastal Change Analysis Program C-CAP (DOC 2017).

soil infiltration characteristics and land cover water retention capacity through infiltration, interception and evapotranspiration (USDA, 1986). For the context of this paper, the CN rain retention index is used as an indicator of a reduction in surface runoff, which should result in flood mitigation, and consequently lower exposure of individuals to polluted waters.

Here we used SSURGO (USDA NRCS, 2004) layer for soil characterization and the Coastal Change Analysis Program C-CAP (DOC, 2010) land cover layer to create a CN index at 100 m cell sizes. A table with the CN values used for each land cover- soil combination can be found in the supplemental material (SM3). Rain retention was summarized at the zip code and the HUC-10 watershed scale. The HUC-10 estimates were allocated to zip codes using area weighted averages (SM2).

In addition to the rain retention index, we also calculated % karst soils (Alemán González, 2010), and % vegetation (i.e. combining the vegetation categories defined in Puerto Rico CCAP categories, 11/Mixed Forest and 12/Scrub/Shrub) in ArcGIS (ver. 10.3), as individual model predictor variables. These land cover and soils classes represent the land use/soil categories with higher retention values when calculating the CN index (USDA, 1986), and it was of our interest to determine which component of the index was more predictive of flood impact and/or GI illness. Percent vegetation was calculated at the HUC-10 watershed level, to account for the location of most of the vegetated areas at high elevations and in headwater areas. Percent karst was calculated at the zip code level only as most of the karst geology is located along the coast rather than at higher elevations (Fig. 3). For the same reason, percent wetlands (CCAP categories 13–18) was also estimated as a predictor at the zip code level. While in the CN method wetlands are considered as having low retention capacity due to water saturation, we know from previous studies that they can play a role in flood protection ecosystem services (Broody, 2006; Brody et al., 2012) as well as removal of pathogens that can cause GI illness (Yang et al., 2008). Topography is another factor that could affect rainfall retention dynamics. We calculated slope averages and maximums at the zip code and HUC-10 watershed levels, using Digital Elevation Models (DEM, CRIM, 1998) in ArcGIS.

2.2.3. Socio-economic variables

We characterized socio-economic indicators that could mediate the benefits derived from ecosystem services. Flood risk is influenced by the proportion of people living in flood prone areas (Fig. 3). We calculated this variable using population estimates (Sorichetta et al., 2015) and the Federal Emergency Management Agency (FEMA) flood zone layer (FEMA, 2009) in ArcGIS (ver 10.3). Sewage infrastructure alters the fate and transfer of waste water, potentially influencing the level of exposure to pathogens during flood events. While the sewage infrastructure in Puerto Rico has suffered from poor maintenance in the past (PRASA, 2014), we infer that exposure to waste water pathogens during floods would be greater in un-sewered areas of the Island. We estimated sewage cover density for each zip code using data from the Puerto Rico Aqueduct and Sewage Authority (PRASA, 2015).

Whenever there is high population density in a flood prone area, the type of housing could determine how many people are affected. For people living in high rises and multi-family buildings, exposure may

Table 1
Variables assessed, main indicators and sources.

Predictor variables evaluated (spatial scale)	Sources
Weather hazards	
90, 95, 99% Rainfall (Huc-10 Watershed and Zip Code); Average Annual Rainfall (Huc-10 Watershed and Zip Code)	NASA Daymet; https://daac.ornl.gov/cgi-bin/dsviewer.pl?ds_id=1328
Ecosystem goods and services	
Rain Retention (Huc-10 Watershed and Zip Code)	CCAP 2010 (NOAA, 2010); SSURGO (USDA NRSC, 2004); EPA H20 tool (Russell et al., 2015)
% Watershed Vegetation (Huc-10 Watershed)	CCAP 2010 (NOAA, 2010)
% Watershed Woody Wetlands (Zip Code)	CCAP 2010 (NOAA, 2010
% Watershed Grassy Wetlands (Zip Code)	CCAP 2010 (NOAA, 2010)
% Karst (Zip Code)	Karst raster (Alemán González, 2010)
Natural controls	
Average and Maximum Slopes (Huc-10 Watershed and Zip Code)	DEM (CRIM, 1998)
Socio-economic variables	
Sewage Density (Zip Code)	Sewer Lines PR Aqueduct and Sewer Authority (PRASA, 2015)
% Multifamily Housing (5 households or more); (Zip Code)	ACS 5-year estimates (2008–2012) https://www.census.gov/programs-surveys/acs/
Median Income (Zip Code)	ACS 5-year estimates (2008–2012) https://www.census.gov/programs-surveys/acs/
% People living in flood zones (Zip Code)	FEMA Flood Zones (FEMA, 2009); Dasymetric Population (Sorichetta et al., 2015)
Significant interactions	
% Karst *% People living in flood zones	
Huc-10 Watershed Rain Retention *% People living in flood zones	
Huc-10 Watershed Rain Retention Watershed Rain Retention *% Woody Wetlands	
Huc-10 Watershed Rain Retention *% Grassy Wetlands	
% Karst *%Woody Wetlands	
% Karst *%Grassy Wetlands	
Response variables	
FEMA flood claims (1999–2014) (Zip Code)	National Flood Insurance Data/FEMA National Flood Insurance Programs; Data not publicly available.
Medicare GI disease claims (1999–2013) (Zip Code)	The Centers for Medicare and Medicaid Services Hospitalization Data; Data not publicly available.

be limited to those in the ground floors who experience the flooding directly. To account for this, we calculated the proportion of people living in multi-family units (5+ families in a building) using the American Community Survey 5-year estimates (2008–2012; https://www.census.gov/programs-surveys/acs/). This same dataset was used to estimate median income as another socio-economic indicator, as it has been shown that wealthy communities tend to be less vulnerable to environmental hazards and the loss of ecosystem services (Myers et al., 2013).

2.2.4. Response variables

To estimate flood impact, we used data from the FEMA National Flood Insurance Program. Flood claims were obtained from the agency for the years 1999–2014. The agency summarized the data at the zip code level to remove any personal identifiable information (PII).

To estimate GI illness, we used hospitalization data from the Centers for Medicare and Medicaid Services (CMS), for the years 1999–2013. We summarized weekly claims associated to infectious GI illnesses for the selected zip codes and years, using the International Classification of Illnesses, Ninth Revision, Clinical Modification coding system (ICD-CM 9) for the following diagnosis: Cholera (ICD9-001), Salmonella (ICD9-003), Shigella (ICD9-004), Other bacterial poisoning (ICD9-005), Intestinal infection by other organisms (ICD9-008), and Ill-defined intestinal infections (ICD9-009). We intentionally did not include ICD codes for broad symptoms of GI illnesses (e.g., nausea, vomiting) as these could result from other types of illnesses and would add unexplained noise to statistical analysis. Because the data acquisition did not involve interaction with any individuals, and the data did not contain PII, it was determined by the U.S. Environmental Protection Agency's Human Subjects Research Protocol Officer that this research was exempt from Institutional Review Board review.

2.3. Data analysis

2.3.1. Flood protection EGS: FEMA flood claims

We evaluated the role of ecosystem services, and other variables on FEMA flood claims per zip code. Flood claim data consisted of integers ranging from 0 to over 400, and its distribution was heavily skewed towards zero. Data was therefore modeled as counts, using quasi-Poisson generalized linear models, which account for over dispersion. We developed a global quasi-Poisson model including all variables from each category (Table 1), significant interactions among variables ($Pr(>|z|) < 0.05$; Table 1), and households per zip code (American Community Survey Summary, 2008–2012) as a model offset. For variables that were indicators of the same predictor, but at two different scales (e.g. zip code 99% rainfall vs HUC-10 99% rainfall), we only used the best predictor of flood claims for inclusion in the model averaging procedure. Highly correlated variables that were not indicators of the same phenomena (e.g. %woody wetlands vs % people in flood zones), were kept in the global model.

We used this global model for model averaging (Grueber et al., 2011), which tested all possible variable combinations, and selected the top models explaining flood claim response (R package MuMin, Barton, 2009). To prevent overfitting, we limited the possible number of variable combinations to 5 factors, including interaction effects. This allowed us to have 10+ replicates per variable in accordance with recommended sample sizes for regressions (Vittinghoff and McCulloch, 2007; Austin and Steyerberg, 2015). The model averaging procedure was set up to prevent having highly correlated variables, that were not excluded from the global model (e.g. %woody wetlands vs % people in flood zones), to be featured together on any given 5-variable model. We used delta AICc>2 as a cut-off criterion for sub-model selection (Burnham and Anderson, 2002) and then calculated the conditional average effect of each variable after accounting for all the best models where that variable was included (Grueber et al., 2011). Variables were considered 'important' if their inclusion improved model fit in at least one of the selected sub-models. Results from model averaging were used to generate predicted flood claim values per zip code. These values were then regressed against observed FEMA claims to estimate the model's effectiveness at detecting flood impact.

2.3.2. Flood protection EGS and GI illness: Medicare claims

The variables that were selected as important predictors of flood claims were also used to evaluate spatio-temporal trends in GI illness response, with a few modifications. First, while the FEMA claims were standardized by the estimated zip code households, Medicare claims were analyzed controlling for the number of Medicare beneficiaries per zip code for each year of the study period. Second, weather parameters used to analyze FEMA claims were summarized for the entire study period, while Medicare Claims were analyzed in relation to daily estimates of 7-day lag extreme events (see *extreme weather* section for details), aggregated as weekly counts of 90, 95, or 99% rainfalls.

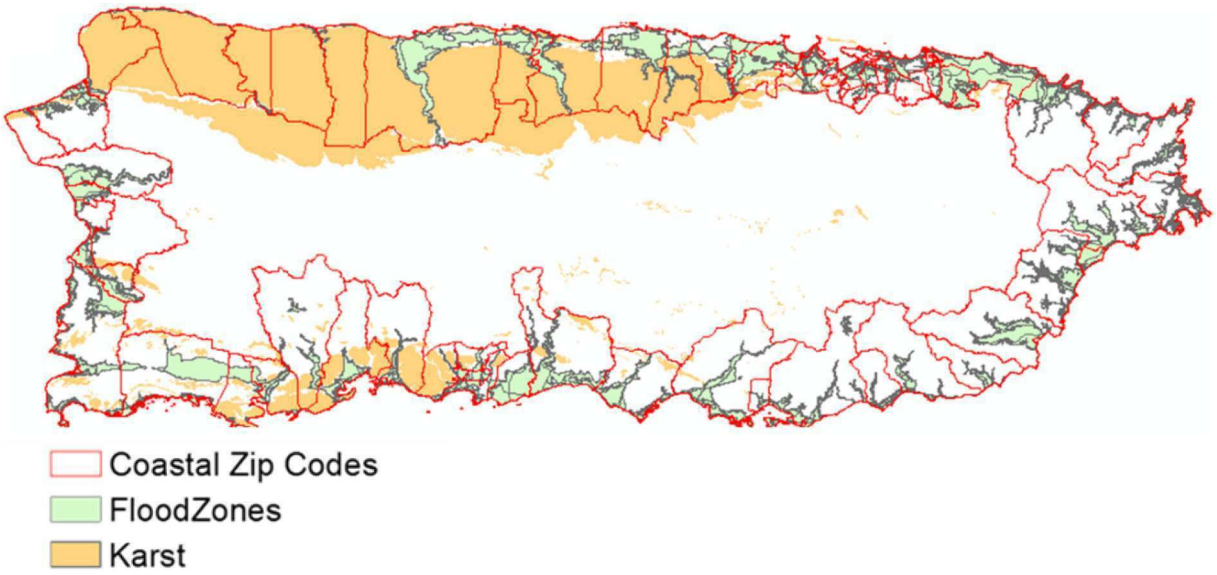

Fig. 3. Location of karst areas, and flood prone areas across Puerto Rico. The interaction of these two variables was a significant predictors of FEMA flood claims, and improved model fit for Medicare claims. The sources for these layers can be found in Table 1.

To evaluate the relationship between extreme weather events, flood impact predictors and GI illness, we used a Bayesian Integrated Nested Laplace Approximation (INLA) and Stochastic Partial Differential Equation (SPDE) approach. INLA-SPDE has been shown to be an efficient approach to assess spatio-temporal trends of relatively rare disease occurrences and develop robust models that are less computationally demanding than commonly used approaches (Myer et al., 2017).

Our response, presence/absence of GI illness in Medicare beneficiaries in a zip code each week, was coded as a binary outcome, with a 1 representing at least one case of GI illness reported among Medicare beneficiaries in a zip code that week, and a 0 representing no reported GI cases. Reports of more than one GI case were too sparse to justify modeling GI illness as a count response, so we elected to model the presence/absence of at least one GI illness. Logistic regression is typically used to model binary responses and produces a logit-linear measure of the probability of a positive outcome, and we elected to use binary logistic regression for this dataset.

The observational model for the spatiotemporal INLA SPDE model can be written as follows:

$$y(s,t) \mid \eta(s,t) \sim Bernoulli(\pi(s,t)),$$

where the presence of GI illness $y(s,t)$ at a particular location s and week t, given a vector of linear predictors $\eta(s,t)$, is a binary outcome with probability vector $\pi(s,t)$. The linear predictor has the general form

$$\eta(s,t) = \beta_1 X_1 + \ldots + \beta_n X_n + m_s + w_t$$

where $(\beta_1, \ldots, \beta_n)$ are the regression coefficients for the predictor variables $(X_1, \ldots, X_n)$, m_s is the spatial random effect at location s, w_t is the temporal random effect at week t, and the relationship between the linear predictor $\eta(s,t)$ and the GI illness probability $\pi(s,t)$ is the logit link

$$\pi(s,t) = log\frac{\eta(s,t)}{1-\eta(s,t)}$$

Spatial covariance m_s was addressed in the SPDE model using a Gaussian Markov random field based on a triangulation mesh represented as a labeled, undirected graph over the selected zip codes (SM5), which estimates spatial effects on GI illness probability across the study area using the Matérn covariance function (Musenge et al., 2013; Cosandey-Godin et al., 2014).

Temporal covariance was addressed using a first-order random walk process (RW1), which models the effect of time as a function of presence in the previous week plus a random error term. The conceptual model for the change in the ordinal vector of temporal coefficients $(w_1, \ldots, w_t)$ is of the form

$$\Delta w_i = w_i - w_{i-1} \sim N(0, \tau^{-1})$$

where τ is the precision parameter, estimated as a hyperparameter in the INLA model.

Diffuse normal priors (precision = 0.001) were chosen for variables in the linear predictor, reflecting no prior knowledge of their coefficients. For the spatial and temporal effects, we assigned the penalized complexity prior, which is a weakly informative prior that accounts for model complexity and has improved performance in SPDE models (Fuglstad et al., 2015; Simpson et al., 2017).

Building from the set of important variables and interactions in the flood claim analysis, we used model comparison approaches to evaluate whether models with ecosystem services variables provided significantly better fit in predicting GI illness outcomes than models with just weather hazards (counts of 90%, 95%, or 99% rainfall events), or socio-economic variables (sewage infrastructure). Models with only underlying spatial covariance (m_s) and temporal covariance (w_t), or with the number of Medicare beneficiaries as a control variable were used as baselines for comparing model fit.

Model ranking was conducted using Watanabe-Akaike Information Criterion (WAIC) which is a preferred approach for comparing fully Bayesian models (Gelman et al., 2014). Predictive fit was evaluated by generating a receiver-operating characteristic (ROC) curve, using the R package ROCR, (Sing et al., 2005), which plots the sensitivity (true positive rate) against 1-specificity (false positive rate), across all possible cutoff points. The area under curve (AUC) value was computed to determine predictive fit, by integrating the ROC curve. The AUC value represents the probability that a randomly chosen GI illness positive observation will have a higher modeled value than a randomly chosen GI illness negative observation. An AUC value higher than 0.5 indicates that the model is better than chance at predicting the outcome. The optimized cutoff point to minimize false positives and maximize true positives was determined by maximizing Youden's index (i.e., sensitivity + specificity -1).

All analyses were performed using the R package 'INLA' and R version 3.4.4 statistical software.

3. Results

3.1. Flood protection EGS and flood claims

Details of the model parameters by zip code and as averages are included in SM6. During our study period, a total of 4349 flood claims were filed to FEMA's National Flood Insurance Program. The variables best explaining FEMA claims were the magnitude of 99% rainfall at the HUC-10 watershed level ($p = 0.002$), the proportion of people living in multi-family units ($p = 0.014$), and average zip code slope ($p = 0.009$). The zip codes with the highest number of flood claims were in the towns of Santa Isabel (00757, 407 claims) and Salinas (00751, 413 claims), both within the Coamo River watershed, and in San Juan (00920, 333 claims), at the mouth of the Rio Puerto Nuevo, in the San Juan Bay. These zip codes had >1.6 times as many flood claims as the next largest zipcode, despite having comparable number of households and population sizes to other study sites. Zip codes 00751 and 00757 also showed a high level of influence on final model selection, leading to inflated residuals. Because of this, we repeated the analysis without these zip codes (see SM4 for more details), and removed them from sub-sequent analysis.

For the remaining study sites ($N = 70$) the variables best explaining flood claims were the magnitude of the 99% rainfall at the HUC-10 watershed level ($p < 0.001$), % karst ($p = 0.02$), % people living in flood zones ($p < 0.001$), and the interaction effect of these latter two variables ($p < 0.001$, Table 2). When exploring the significant interaction effect, karst soils appear to help lower the number of flood claims per household, but this relationship is lost in places with a greater number people living in flood prone areas (Fig. 4). In terms of rainfall, the magnitude of the 99% rainfall events at the watershed level, led, as expected to a higher number of FEMA claims per household. This model was the only one selected through the model averaging process, as no other model was comparable in terms of AIC model fit. The ability of the model to predict flood cases was significant ($R^2 = 0.578$, $p < 0.001$, Fig. 5), and we found no evidence of significant spatial autocorrelation of the model's residuals (Table 2).

3.2. Flood protection EGS and GI illness

For this part of the study we also focused on the zip codes that were not considered as outliers. For these zip codes ($N = 70$), a total of 1917 Medicare claims were submitted to the CMS for the selected GI illnesses between 1999 and 2013 (Table 3). The most common claims filed were for Intestinal infection due to other organisms (ICD9–008), and Ill-defined intestinal infections (ICD9-009).

There was a distinct temporal trend in the number of claims filed, with a sharp drop observed after week 400, which roughly corresponds to the year 2006 (Fig. 6A). Spatially, we observe higher than average effect of location on GI illness in the Southwest area of the Island, followed by the rest of the West coast, (Fig. 6B). The East coast overall seems to have a lower-than-average effect of location (Fig. 6B).

Controlling for these spatial and temporal covariances, we used the variables selected as best predictors in the FEMA claims assessment to evaluate GI illness trends. Controlling for the number of Medicare beneficiaries, the best model explaining GI illness claims included 7-day lag rainfall (90–99% events) and the interaction effect between % Karst and % People in flood zones. The strongest predictor of GI illness claims was the count of 90% + rainfall events within the last week (i.e. confidence interval for model coefficient did not overlap zero). When converting the coefficient of this relationship (see Table 4) from log odds ratio to percentage, we see a 17% modeled increase in the odds of GI Illness following 90% and above rainfall events. The best model's WAIC weight was close to two times higher than the next best model with other variable combinations (Table 4).

In general, we found that models with weather hazards performed better (lower WAIC) than the baseline models with only spatial and temporal covariance or the models that only control for the number of Medicare beneficiaries (Table 4). GI illness claims tended to increase with the number of beneficiaries and increase with the number of extreme weather events. Model fit improved when adding % karst and its interaction with the percentage of people living in flood zones but decreased when adding sewage density (Table 4). In terms of predictive accuracy, the best model's AUC value was 0.70 (Fig. 7), indicating that the model has a better than random chance at predicting GI illness. The optimal cutoff point for classifying the response obtained by maximizing Youden's index was 0.03, resulting in a sensitivity of 0.66 and a specificity of 0.63.

Table 2
Important variables selected through model averaging, with conditional averages of estimated effects and *p* values.

Selected variables	Estimate	Std. Error	t value	Pr (>|t|)
(Intercept)	−5.3011	0.1154	−45.934	<2e-16 ***
Huc-10 99Rain	0.4314	0.1138	3.789	0.000333 ***
% Karst	0.3699	0.1563	2.367	0.020922 *
% People living in flood zones	0.7395	0.1656	4.466	3.25e-05 ***
% Karst *% People living in flood zones	0.9182	0.21843	2.406	0.001719 **
Dispersion parameter for quasipoisson	32.8638			
Null deviance	2894.2			
Residual deviance	1613.0			
df	65			
Moran's Index (z-score; p value)[a]	0.1818; 0.8587			

[a] Moran's Index was calculated in Arc GIS (ver. 10.3) to determine spatial autocorrelation of model residuals.

4. Discussion

Rainfall extremes in the coast of Puerto Rico (PR) have historically caused property damages, and human health impacts that disproportionally affect neighborhoods in flood prone areas. This study is the first to document this trend empirically on an Island wide basis. In the aftermath of the most extreme natural disaster to strike PR in generations, Hurricane Maria, the importance of flooding, and weather-related illnesses has gained more attention. Here we provide evidence that some of the health problems associated to weather events on the Island are not new and deserve sustained attention in the face of potential increases on extreme rainfall in the future.

4.1. Flood protection ecosystem services and flood claims

Flood claims in Puerto Rico for the years 1999–2014 are closely tied to the average magnitude of the most extreme rainfall events (99%). Our final model predicted observed FEMA flood claims with reasonable accuracy, and a strong model fit was found once we accounted for the role of three outlier zip codes (SM4). The number of flood claims on these locations was particularly high around two important rainfall events. The first was a tropical storm in September of 2008 that resulted in around 20 million dollars in damages (Puerto Rico Science Museum, 2011). The second was a historical rainfall event in November of 2009, which caused record breaking river heights, and severe flooding in the San Juan metropolitan area (NOAA NWS, 2009). Our estimated rainfall values for these zip codes, however, was not any greater than that for other nearby study sites. Therefore, unaccounted factors that have been previously reported on these locations, such as housing quality and the capacity of local water infrastructure to handle events of high

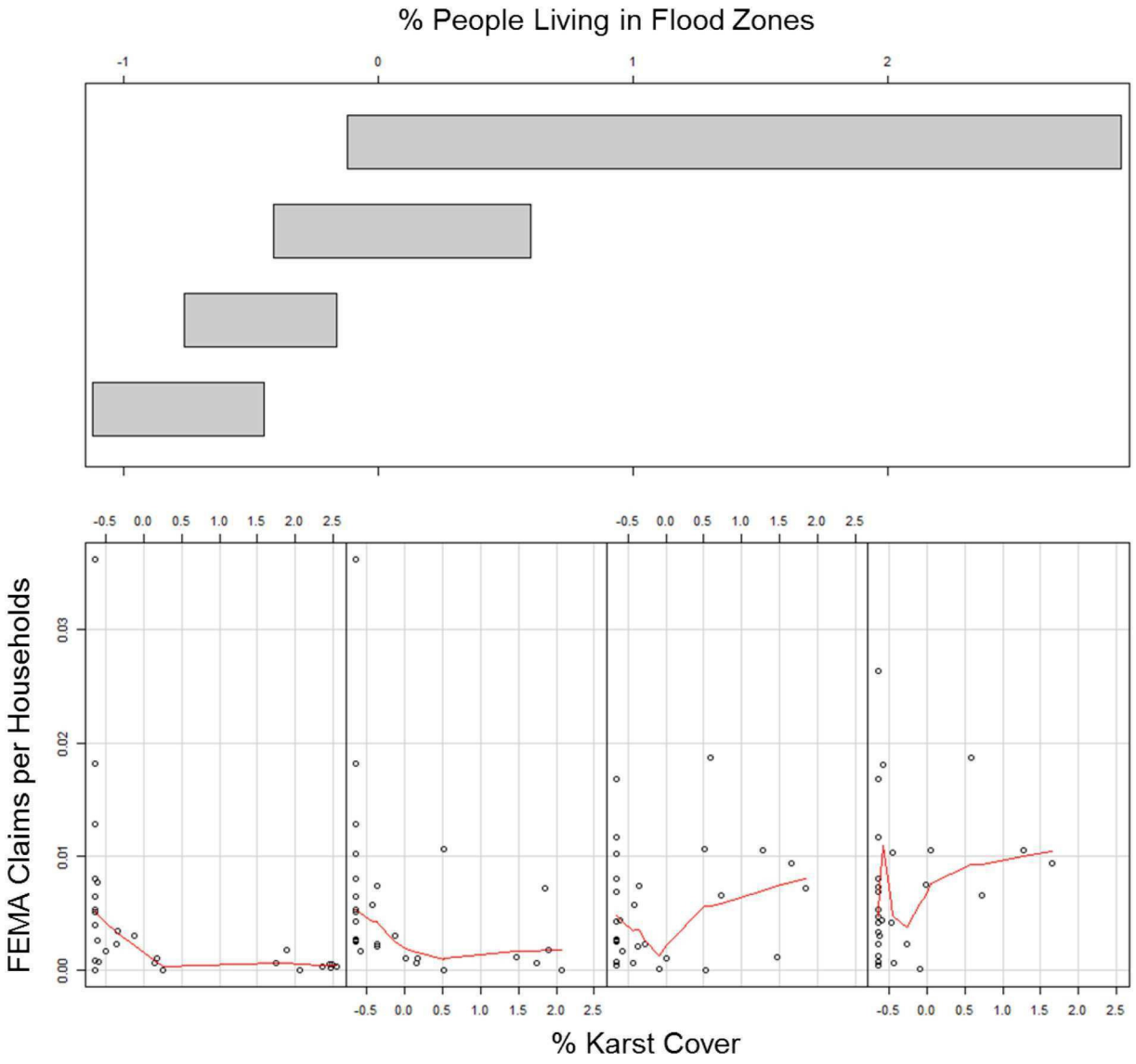

Fig. 4. Visualization of the interaction effects between %Karst * % People in Flood Zones, on FEMA flood claims (cases per household per zip code). The top panel shows different levels of the % people in flood zones, the bottom panel represents the relationship between % karst and claims per household at each of these levels. The red line represents a locally weighted scatterplot smoother (Cleveland, 1981).

magnitude (Stockstill and Leech, 1990; Bush et al., 1995), may have led to the observed trends, and should be determined through more extensive studies on these zip codes.

As we predicted, the relationship observed between extreme rainfall and floods is to some extent mitigated by natural structures, such as karst soils (Fig. 3, Fig. 4). The karst formations in Puerto Rico promote rapid infiltration of rainwater to underground conduits (Torres-González et al., 1996), potentially contributing to flood risk reduction, especially if rainfall retention features such as caves and sinkholes are protected from debris accumulation or urbanization (Zhou, 2007). The observed protective effect of karst soils is lost in areas where a high percentage of people live in flood zones (Fig. 4). Naturally infiltrated waters in karst soils re-emerge as surface water in springs, or wetlands, which may cause flooding further downstream under certain conditions. Therefore, flood protection services provided by karst soils may not protect neighborhoods located in the very same areas were infiltrated waters are naturally expected to re-surface. The role of karst hydrology and its relationship to flood dynamics is still a subject in need of more research (Gutiérrez et al., 2014; Naughton et al., 2018), and was not the focus of the present work, so we encourage further analysis of these observed trends.

Aside from its infiltration capacity, the karst region is one of the few areas of the Island with a firm legal basis for protection, as contained in Law 292, Law to Protect the Karst Physiography of Puerto Rico (Vale-Nieves, 2018). This law led to the establishment of a strict land use framework, where around 33% of the karst extent fell under the highest degree of protection possible (Vale-Nieves, 2018). This implies complete restriction of activities such as landfills, and waste disposal sites, prohibitions on the use of agrochemicals, and strict control of development projects (Garcia-Padilla et al., 2013). Law 292's regulations however, are not equally restrictive across the entire karst extent, including some karst municipalities with a high percentage of people living in flood prone areas (e.g., Vega Baja, Vega Alta, Dorado, Toa Baja, (Fig. 4, also see SM4, and CLCC, 2016). Therefore, the associations observed between karst and flood claims, moderated by people living in flood zones could also reflect regulatory disparities regarding hydrological alteration and water resource pollution. More studies are needed to establish a clear mechanism to explain these trends.

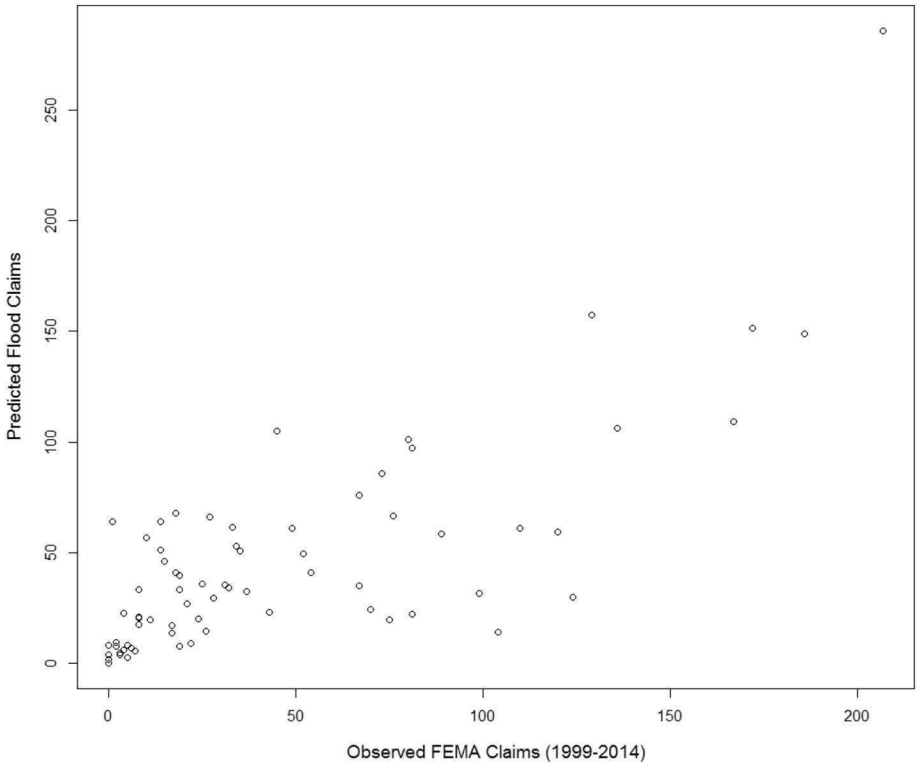

Fig. 5. Predicted flood claims vs observed flood claims from model averaging results excluding outlier zip codes ($R = 0.57$, $p < 0.001$).

4.2. Flood protection EGS and GI illness

Extreme rainfall events were a strong predictor of GI illnesses, with Medicare claims showing a 17% modeled increase in the odds of a GI-related illness following a 90% (and above) rainfall event. The interaction effect between % karst soils * % people living in flood zones greatly improved the fit of the model linking GI illness to extreme rainfall events. Because this interaction was also shown to be a good predictor of FEMA flood claims, these results lend some support to our hypothesis linking flood protection ecosystem services to a reduction in flood related health effects. This protective effect, however, seems very limited and what the interaction effect suggests is that these natural features are not effective at counteracting the level of exposure some communities face when located in flood prone neighborhoods.

Built adaptations, such as adequate sewage infrastructure should provide protection from GI illness occurrences, but this parameter, did not improve the fit of models linking GI illness to extreme weather events. Our models did not control for factors that could determine sewage system effectiveness, such as date of construction, maintenance levels, or the capacity of the infrastructure relative to the magnitude of the population served. In PR, these factors have been shown to affect the performance of waste management in the past (Hunter and Arbona, 1995; PRASA, 2014), and therefore, future studies could address in more detail which systems across the island are performing adequately with respect to their influence on public health issues such as GI illness.

Aside from flooding, an alternative pathway of exposure to untreated sewage is recreational swimming. Previous studies in Puerto Rico have shown correlations between rainfall and GI illness pathogens in public beaches (Cordero et al., 2012; Laureano-Rosario et al., 2017). Exposure to GI illness pathogens was also shown to be linked to recreational swimming and sewage infrastructure in one of the most important beaches in Southwest Puerto Rico (Wade et al., 2018). As seen in Fig. 6, the southwest of PR is the main region with a higher than average odds of having spatially associated cases of GI illness. This area's economy is closely tied to marine recreational opportunities, and our study supports previous research documenting public health concerns in this important tourism destination that should be addressed.

Aside from the spatial patterns observed, we also detected a prominent temporal pattern, where Medicare claims for GI illness dropped after the year 2006. The influence of this pattern was accounted for in our analysis. This drop in Medicare claims was not a reflection of any changes in rainfall trends as far as we can tell from our weather data. A potential explanation to this effect could be changes in Medicare policy affecting claim filing processes. For example, the Deficit Reduction Act of 2005, led to a reduction in the number of claims filed for certain hospital acquired infections (Kawai et al., 2015) and radiology referrals (Levin et al., 2009), but it is not clear whether this would have also led to a decrease in reported GI illnesses in Puerto Rico. Another potential factor could be associated to improvements in storm and waste water management in Puerto Rico around this time. Coincidentally, in 2006, the EPA fined the Puerto Rico Sewage and Aqueduct Authority (PRASA) for 15 violations to the Clean Water Act on wastewater and drinking treatment plants, for the unprecedented amount of 9 million dollars (USEPA, 2006). Remedial measures in the most polluting waste

Table 3
GI diseases examined for coastal zip codes in PR International Classification of Disease, Version 9 (ICD9).

Period	Gastro intestinal diseases (ICD 9 Codes)	Total Medicare claims
1999–2013	Cholera (ICD9-001)	0
	Salmonella (ICD9-003)	273
	Shigella (ICD9-004)	4
	Other Bacterial Poisoning (ICD9-005)	113
	Intestinal Infections due to Other Organisms (ICD9-008)	788
	Gastroenteritis (ICD9-009)	739
	Total	1917

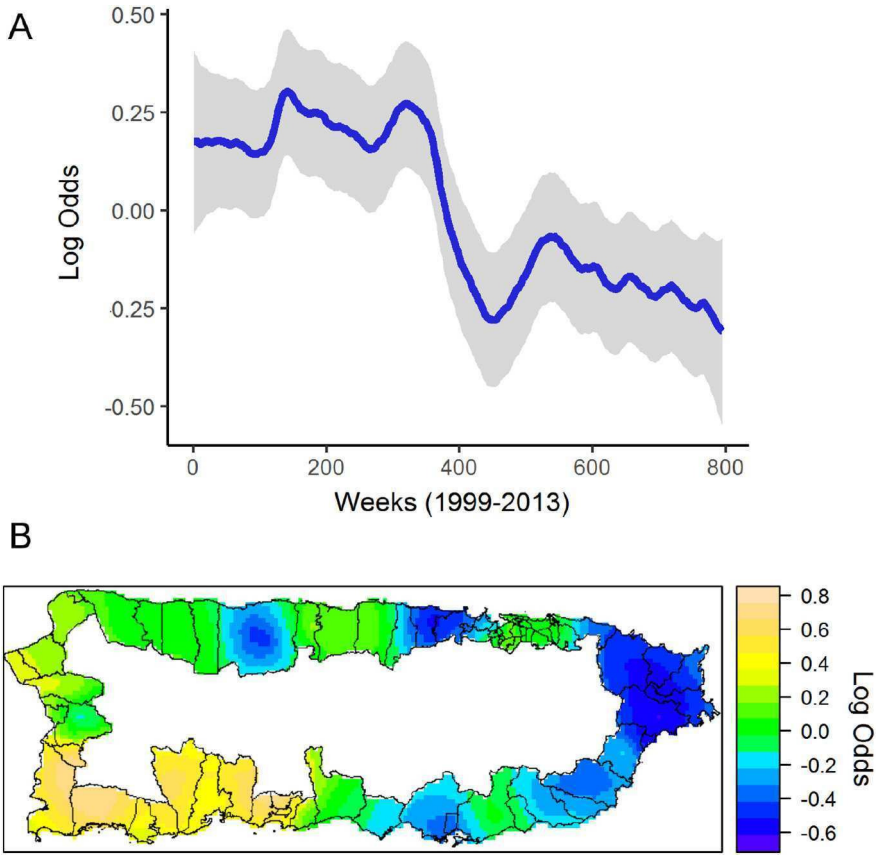

Fig. 6. Temporal and spatial trends in GI disease claims over the study period. The y axis in Fig. 6A shows the coefficient of the temporal effect in log-odds for the selected study weeks between the years 1999–2013. Fig. 6B shows the spatial coefficient, in log-odds, for coastal ZIP codes in Puerto Rico.

Table 4
Spatio-temporal regressions looking at the effect selected parameters on gastro-intestinal diseases in Puerto Rico (1999–2013).

Parameters*	0	1	2	3	4	5
Medicare beneficiaries		0.58 (0.51: 0.66)	0.58 (0.51: 0.66)	0.58 (0.51: 0.66)	0.58 (0.51–0.66)	0.58 (0.51: 0.66)
Weather hazards						
90%$^{+}$ Rainfall event			0.16 (0.03: 0.29)	0.16 (0.03: 0.29)	0.16 (0.04–0.29)	0.16 (0.04:0.29)
95%$^{+}$ Rainfall event			0.03 (−0.09: 0.15)	0.03 (−0.09: 0.15)	0.03 (−0.09–0.15)	0.03 (−0.09: 0.15)
99%$^{+}$ Rainfall event			0.07 (−0.11: 0.24)	0.07 (−0.11: 0.23)	0.07 (−0.11–0.23)	0.07 (−0.11: 0.24)
Sewage density				0.005 (−0.14: 0.15)		−0.0001 (−0.15: 0.15)
Ecosystem goods and services						
(1) %Karst[b] ppl_FldPer[a]					0.15 (−0.08–0.38)	0.15 (−0.08: 0.38)
%Karst					−0.10 (−0.32–0.11)	−0.10 (−0.33: 0.12)
ppl_FldPer[a]					0.14 (−0.01–0.29)	0.14 (−0.02: 0.29)
Hyperparameters						
Range spatial effect	4.47 (2.8: 6.7)	32.04 (15.91:61.18)	32.58 (16.03:62.46)	32.13 (15.71:62.29)	32.58 (16.62–60.57)	32.01 (16.26:59.76)
STDEV spatial effect	1.29 (0.98:1.67)	0.47 (0.34:0.66)	0.48 (0.34:0.66)	0.48 (0.34:0.66)	0.48 (0.32–0.68)	0.48 (0.33–0.68)
Precision temporal effect	36.97 (6.85:133.27)	22.42 (5.70:65.28)	23.20 (5.94:67.89)	23.58 (6.00:68.92)	23.18 (5.92–67.62)	23.43 (5.97–67.94)
Number of Parameters	65.81	46.76	49.66	50.35	50.7	51.09
WAIC	14,767.43	14,751.14	14,750.9	14,752.14	14,745.18	14,746.49
WAIC weights	0.00	0.03	0.03	0.02	**0.60**	0.31

[a] Percentage of people living in flood areas. Variables with 95% CI not encompassing zero are considered as best predictors. Best model's WAIC weight is in bold. The range for spatial refers to the distance in km at which spatial correlation becomes negligible. The precision for temporal effect refers to the inverse standard deviation for the RW1 error between week values.

[b] Values for the model parameters are in log odds ratio units.

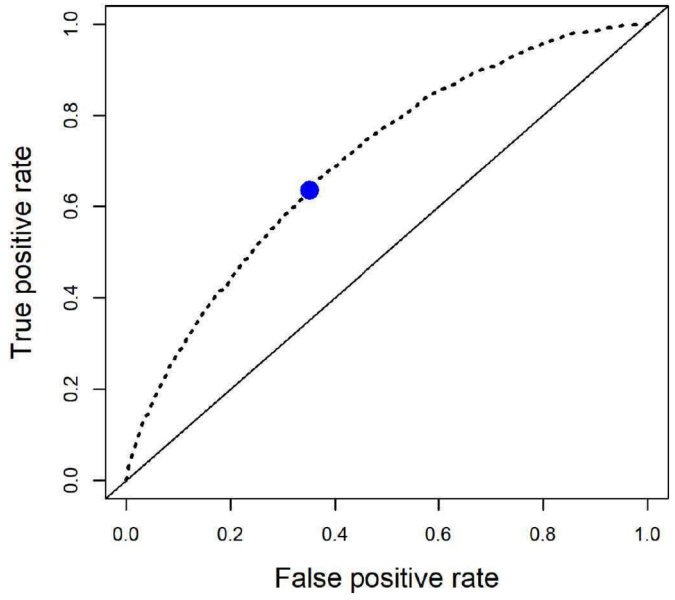

Fig. 7. Receiver operating characteristic curve illustrating the tradeoff between true positive rate and false positive rate for a range of cutoff values with the best INLA model. The blue dot indicates the optimal cutoff value calculated by Youden's index, 0.03, at which sensitivity (true positive rate) = 0.66 and specificity (1 – false positive rate) = 0.63. Overall area under curve = 0.70. Youden's index is (sensitivity + specificity −1), and the optimal cutoff point that minimizes misclassification is determined by maximizing the index along the ROC curve.

water treatment facilities may have quickly ensued after this incident, as PRASA was required to do so under the consent decree (USEPA, 2006). These potential explanations, however, are speculative and this temporal pattern in GI illness should be further assessed.

4.3. Study limitations

Our study has several limitations. First, the weather estimates are based on extrapolated data from existing meteorological stations, which may be more representative in some parts of the island than others. Studies assessing weather at a finer resolution could help provide more details to the trends observed. Likewise, the scale at which we analyzed our disease and flood claims (e.g. zip code) is still very coarse and is not able to capture relationships that may occur at the neighborhood level, in association to local rain retention management initiatives. Unfortunately, disease data is rarely publicly available at the neighborhood scale, so similar studies, using survey instruments for example, could help supplement our results. Moreover, while the Medicare claims system provides consistent data through the states GI illnesses, for the most part, are under reported, and we may have under estimated their occurrence. Incorrect reporting, and misclassification of Medicare claims, as well as omission of certain ICD-9 codes from our analysis should also be considered as potential sources of bias in our results. Furthermore, because we used Medicare claims as an indicator of GI illness trends, our study was mainly representative for the elderly demographic (~19.7% of PR's current population, US Census, 2018), and should be interpreted taking this factor into consideration. Previous studies suggest that the elderly is the most sensitive group to weather related GI illnesses (Jagai et al., 2015). However, the associations between rainfall and GI illness among other sensitive groups, such as young children, may need to be evaluated further.

In terms of our modeling approach, we tested parameters at multiple scales, and the selection of these scales were meant to respond to our study objectives. However, estimating more landscape parameters at the watershed level, or in association to health responses at the census tract or block group level, may help further address the linkage between flooding, ecosystem services and GI illness in the future. While our study did not find a statistically significant relationship between vegetation cover, the rain retention index and flood claims, we think this is still a question that needs to be researched further, looking at more study locations, and assessing this relationship at different spatial resolutions. At smaller spatial scales, such as census blocks, it is possible that the presence of rain retention gardens, riparian buffers and other locally managed green spaces provide a level of small scale protection that would have been difficult to capture in our study looking at zip codes. Moreover, a potential mismatch between the supply and demand of ecosystem services also needs to be considered, as places that are more at risk of flooding tend to be more urbanized and located within sprawling areas that are more likely to have lost more vegetation cover within their watersheds (Stürck et al., 2014). The context of coastal zip codes in Puerto Rico, where a large proportion of the population in flood zones are also downstream of the highly urbanized San Juan metropolitan area (Fig. 2, Fig. 3), provides a limited opportunity to test this hypothesis fully. Repeating this analysis in a larger context, such as across coastal counties in the mainland US could help address these questions further.

5. Conclusions

To our knowledge, this study is the first to explore the role of flood protection ecosystem services on preventing GI illnesses. We found that GI illnesses in PR spike after rain events, and that the natural infiltration provided by karst soils may help prevent floods and GI illness occurrences. The role of this ecosystem service is affected by planning decisions in coastal communities, such as residential development in flood prone areas, which undermines the protective effect of rainfall retention from natural features. Built adaptations, such as adequate sewage infrastructure, are expected to provide a protective role on GI illness occurrences, but we did not find evidence for this in our study. Factors such as the age and capacity of sewage infrastructure across the island needs to be accounted for in future research to better assess its effectiveness on protecting from GI illness associated to weather events. Aside from flooding, environmental exposure to disease pathogens after extreme weather events have been linked to recreational swimming in PR. This relationship may be related to the observed spatial association of GI illness to Southwest PR (a popular beach destination). This is a finding that supports previous studies and highlights the importance of effective waste water management and public health protection on this location.

Supplementary data to this article can be found online at https://doi.org/10.1016/j.scitotenv.2019.04.287.

Acknowledgements

Matthew Harwell, Marc Russell and Justin Bousquin provided advice on study design and the assessment flood protection ecosystem services. Lucas Neas, Laura Jackson, and John Johnston provided advise on the design and analysis of the Medicare claims data. In accordance with CMS data use agreement, this dataset was processed an analyzed at a single, secured workstation located at the USEPA Environmental and Public Health Division's Human Studies Facility, at the University of North Carolina, Chapel Hill. Special thanks to Lucas Neas for facilitating this process. The views expressed in this paper are those of the authors and do not necessarily reflect the views or policies of the U.S. Environmental Protection Agency. Any mention of trade names, products or services does not imply an endorsement by the U.S. Government or the U.S. Environmental Protection Agency (EPA). The EPA does not endorse any commercial products, services, or enterprises.

References

Abel, J., Deitz, R., 2014. The causes and consequences of Puerto Rico's declining population. Curr. Issues Econ. Financ. 20 (4). https://papers.ssrn.com/sol3/papers.cfm?abstract_id=2477891, Accessed date: 22 June 2018.

Ahern, M., Kovats, R.S., Wilkinson, P., Few, R., Matthies, F., 2005. Global health impacts of floods: epidemiologic evidence. Epidemiol. Rev. 27 (1), 36–46.

Alemán González, W.B., 2010. Karst map of Puerto Rico. U.S. geological survey open-file report, 2010-1104. http://pubs.usgs.gov/of/2010/1104/, Accessed date: 11 June 2018.

Arguez, A., Durre, I., Applequist, S., Vose, R.S., Squires, M.F., Yin, X., Owen, T.W., 2012. NOAA's 1981–2010 US climate normals: an overview. Bull. Am. Meteorol. Soc. 93 (11), 1687–1697.

Austin, P.C., Steyerberg, E.W., 2015. The number of subjects per variable required in linear regression analyses. J. Clin. Epidemiol. 68 (6), 627–636.

Azar, D., Rain, D., 2007. Identifying population vulnerable to hydrological hazards in San Juan, Puerto Rico. GeoJournal 69 (1–2), 23–43.

Barton, K., 2009. Mu-MIn: Multi-model inference. R Package Version 0.12.2/r18. http://R-Forge.R-project.org/projects/mumin/., Accessed date: 23 April 2019

Becker, R.A., Chambers, J.M., Wilks, A.R., 1988. The New S Language. Wadsworth & Brooks/Cole.

Briskin, E.A., 2016. Seroprevalence and Risk Factors for Leptospirosis in an Urban Community of Puerto Rico. https://elischolar.library.yale.edu/ysphtdl/1026/, Accessed date: 22 June 2018.

Brody, S.D., Highfield, W.E., 2013a. Open space protection and flood mitigation: a national study. Land Use Policy 32, 89–95.

Brody, S.D., Highfield, W.E., 2013b. Open space protection and flood mitigation: a national study. Land Use Policy 32, 89–95. https://doi.org/10.1016/j.landusepol.2012.10.017.

Brody, S.D., Peacock, W.G., Gunn, J., 2012. Ecological indicators of flood risk along the Gulf of Mexico. Ecol. Indic. 18, 493–500. https://doi.org/10.1016/j.ecolind.2012.01.004.

Broody, H.a., 2006. Price of permits: measuring the economic impacts of wetland development on flood damages in Florida. Nat. Hazards Rev. 7 (3), 123–130. https://doi.org/10.1061/(ASCE)1527-6988(2006)7:3(123).

Burnham, K.P., Anderson, D.R., 2002. Model Selection and Multimodel Inference: A Practical Information-theoretic Approach. 2nd edn. Springer, Berlin.

Bush, D.M., Webb, R.M., Liboy, J.G., 1995. Living with the Puerto Rico Shore. Duke University Press.

Caribbean Landscape Conservation Cooperative (CLCC), 2016. Puerto Rico Protected Areas Database (version of December, 2016]. GIS data. San Juan, PR).

Castro-Prieto, J., Martinuzzi, S., Radeloff, V.C., Helmers, D.P., Quiñones, M., Gould, W.A., 2017. Declining human population but increasing residential development around protected areas in Puerto Rico. Biol. Conserv. 209, 473–481.

Centro de Recaudación de Ingresos Municipales (CRIM) PR Office of Management and Budget, 1998. Puerto Rico Basemap Project: derived contours from CRIM Digital Elevation Model (1996–98). http://www.esri.com/metadata/esriprof80.html, Accessed date: 11 June 2018.

Cleveland, W.S., 1981. LOWESS: a program for smoothing scatterplots by robust locally weighted regression. Am. Stat. 35, 54.

Cordero, L., Norat, J., Mattei, H., Nazario, C., 2012. Seasonal variations in the risk of gastrointestinal illness on a tropical recreational beach. J. Water Health 10 (4), 579–593.

Cosandey-Godin, A., Krainski, E., Worm, B., Flemming, J.M., 2014. Applying Bayesian spatiotemporal to fisheries bycatch in the Canadian Arctic. Can. J. Fish. Aquat. Sci. 72, 186–19.

Crimmins, A., Balbus, J., Gamble, J.L., Beard, C.B., Bell, J.E., Dodgen, D., Eisen, R.J., Fann, N., Hawkins, M., Herring, S.C., Jantarasami, L., Mills, D.M., Saha, S., Sarofim, M.C., Trtanj, J., Ziska, L., 2016. Executive Summary. The Impacts of Climate Change on Human Health in the United States: A Scientific Assessment. U.S. Global Change Research Program, Washington, DC https://doi.org/10.7930/J00P0WXS 24 pp.

Curriero, F.C., Patz, J.A., Rose, J.B., Lele, S., 2001. The association between extreme precipitation and waterborne disease outbreaks in the United States, 1948–1994. Am. J. Public Health 91 (8), 1194–1199.

Cutter, S.L., Boruff, B.J., Shirley, W.L., 2003. Social vulnerability to environmental hazards. Soc. Sci. Q. 84 (2), 242–261.

De Jesus Crespo, R., Lázaro, P.M., Yee, S.H., 2018. Linking wetland ecosystem services to vector-borne disease: dengue fever in the San Juan Bay estuary, Puerto Rico. Wetlands 1–13.

Department of Commerce (DOC), 2010. C-CAP Land Cover. NOAA Ocean Service https://coast.noaa.gov/ccapftp/#/, Accessed date: 11 June 2018.

Federal Emergency Management Agency (FEMA), 2009. Digital Flood Insurance Rate Map Database. Commonwealth of Puerto Rico Available at. http://gis.otg.pr.gov/download_gis_files.htm.

Fuglstad, G.A., Simpson, D., Lindgren, F., Rue, H., 2015. Constructing Priors that Penalize the Complexity of Gaussian Random Fields. arXiv Statistics – Methodology (1503.00256v4).

Garcia-Padilla, A., Garcia-Pelatti, L., Perez, C. Guerrero, 2013. Plan y reglamento del area de planificacion especial del carso. Estado Libre Asociado de Puerto Ricohttp://gis.jp.pr.gov/Externo_Econ/Otras%20Areas%20-%20Vistas%20Publicas/Plan%20y%20Reglamento%20Area%20de%20Planificacion%20Especial%20del%20Carso.pdf, Accessed date: 22 June 2018.

Gelman, A., Carlin, J.B., Stern, H.S., Rubin, D.B., 2014. Bayesian data analysis. Chapman & Hall/CRC Boca Raton, FL, USA.

Government of Puerto Rico, 2018. Investor resources: Puerto Rico Aqueduct and Sewer Authority (PRASA). http://www.gdb.pr.gov/investors_resources/prasa.html, Accessed date: 1 October 2018.

Grueber, C.E., Nakagawa, S., Laws, R.J., Jamieson, I.G., 2011. Multimodel inference in ecology and evolution: challenges and solutions. J. Evol. Biol. 24 (4), 699–711.

Gutiérrez, F., Parise, M., De Waele, J., Jourde, H., 2014. A review on natural and human-induced geohazards and impacts in karst. Earth Sci. Rev. 138, 61–88.

Hernández Ayala, J.J., Keellings, D., Waylen, P.R., Matyas, C.J., 2017. Extreme floods and their relationship with tropical cyclones in Puerto Rico. Hydrol. Sci. J. 62 (13), 2103–2119.

Huang, L.Y., Wang, Y.C., Wu, C.C., Chen, Y.C., Huang, Y.L., 2016. Risk of flood-related illnesses of eyes, skin and gastrointestinal tract in Taiwan: a retrospective cohort study. PLoS One 11 (5), e0155166.

Hufkens, K., 2014. Daymetr – R package to download tiled and single pixel daymet data from the ORNL DAAC. https://doi.org/10.5281/zenodo.437886 Version 1.0. Zenodo.

Hunter, J.M., Arbona, S.I., 1995. Paradise lost: an introduction to the geography of water pollution in Puerto Rico. Soc. Sci. Med. 40 (10), 1331–1355.

Jagai, J.S., Li, Q., Wang, S., Messier, K.P., Wade, T.J., Hilborn, E.D., 2015. Extreme precipitation and emergency room visits for gastrointestinal illness in areas with and without combined sewer systems: an analysis of Massachusetts data, 2003–2007. Environ. Health Perspect. 123 (9), 873.

Kawai, A.T., Calderwood, M.S., Jin, R., Soumerai, S.B., Vaz, L.E., Goldmann, D., Lee, G.M., 2015. Impact of the Centers for Medicare and Medicaid Services hospital-acquired conditions policy on billing rates for 2 targeted healthcare-associated infections. Infect. Control Hosp. Epidemiol. 36 (8), 871–877.

Larsen, M.C., 2017. Forested watersheds, water resources, and ecosystem services, with examples from the United States, Panama, and Puerto Rico. Chemistry and Water, pp. 161–182.

Laureano-Rosario, A.E., Symonds, E.M., Rueda-Roa, D., Otis, D., Muller-Karger, F.E., 2017. Environmental factors correlated with culturable enterococci concentrations in tropical recreational waters: a case study in Escambron Beach, San Juan, Puerto Rico. Int. J. Environ. Res. Public Health 14 (12), 1602.

Levin, D.C., Rao, V.M., Parker, L., Frangos, A.J., 2009. The disproportionate effects of the Deficit Reduction Act of 2005 on radiologists' private office MRI and CT practices compared with those of other physicians. J. Am. Coll. Radiol. 6 (9), 620–625.

Lugo, A.E., Carlo, T.A., Wunderle, J.M., 2012. Natural mixing of species: novel plant-animal communities on Caribbean Islands. Anim. Conserv. 15, 233–241. https://doi.org/10.1111/j.1469-1795.2012.00523.x.

Mallin, M.A., Ensign, S.H., McIver, M.R., Shank, G.C., Fowler, P.K., 2001. Demographic, landscape, and meteorological factors controlling the microbial pollution of coastal waters. Hydrobiologia 460 (1), 185–193. https://doi.org/10.1023/a:1013169401211.

Musenge, E., Chirwa, T.F., Kahn, K., Vounatsou, P., 2013. Bayesian analysis of zero inflated spatiotemporal HIV/TB child mortality data through the INLA and SPDE approaches: applied to data observed between 1992 and 2010 in rural North East South Africa. Int. J. Appl. Earth Obs. Geoinf. 22, 86–98.

Myer, M.H., Campbell, S.R., Johnston, J.M., 2017. Spatiotemporal modeling of ecological and sociological predictors of West Nile virus in Suffolk County, NY, mosquitoes. Ecosphere 8 (6), e01854. https://doi.org/10.1002/ecs2.1854.

Myers, S.S., Gaffikin, L., Golden, C.D., Ostfeld, R.S., Redford, K.H., Ricketts, T.H., et al., 2013. Human health impacts of ecosystem alteration. Proc. Natl. Acad. Sci. 110 (47), 18753–18760. https://doi.org/10.1073/pnas.1218656110.

National Oceanic and Atmospheric Administration, 2010. Office for Coastal Management. "2010 Puerto Rico C-CAP 30m Land Cover." Coastal Change Analysis Program (C-CAP) Regional Land Cover.NOAA Office for Coastal Management, Charleston, SC www.coast.noaa.gov/ccapftp, Accessed date: 23 April 2019

National Oceanic and Atmospheric Administration (NOAA), National Weather Service (NWS), 2009. Monthly report of hydrologic conditions. https://www.weather.gov/media/sju/hydrology/E5/2009/E5nov09.pdf, Accessed date: 19 June 2018.

Naughton, O., McCormack, T., Gill, L., Johnston, P., 2018. Groundwater flood hazards and mechanisms in lowland karst terrains. Geol. Soc. Lond., Spec. Publ. 466 (1), 397–410.

Parés-Ramos, I., Gould, W., Aide, T., 2008. Agricultural abandonment, suburban growth, and forest expansion in Puerto Rico between 1991 and 2000. Ecol. Soc. 13 (2).

Puerto Rico Aqueduct and Sewage Authority (PRASA), 2014. Strategic Plan 2014–2018. http://www.acueductospr.com/planestrategico/2014/download/PLAN_ESTRATEGICO_2014-2018b.pdf, Accessed date: 1 October 2018.

Puerto Rico Aqueduct and Sewage Authority (PRASA), 2015. Sewer network. http://www.agencias.pr.gov/agencias/gis/descargaGeodatos/Infraestructuras/Pages/Agua.aspx, Accessed date: 11 June 2018.

Puerto Rico Science Museum, 2011. Puerto Rico Flooding. http://ecoexploratorio.org/amenazas-naturales/inundaciones/inundaciones-en-puerto-rico/, Accessed date: 19 June 2018.

Reacher, M., McKenzie, K., Lane, C., Nichols, T., Kedge, I., Iversen, A., ... Simpson, J., 2004. Lewes Flood Action Recovery Team. Health impacts of flooding in Lewes: a comparison of reported gastrointestinal and other illness and mental health in flooded and non-flooded households. Commun. Dis. Public Health 7 (1), 39–46.

Reguero, B.G., Losada, I.J., Diaz-Simal, P., Mendez, F.J., Beck, M.W., 2015. Effects of climate change on exposure to coastal flooding in Latin America and the Caribbean. PLoS One 10 (7), e0133409.

Russell, M., Harvey, J., Ranade, P., Murphy, K., 2015. EPA H2O User Manual. US EPA Office of Research and Development, Washington, DC (EPA/600/R-15/090).

Simpson, D., Rue, H., Riebler, A., Martins, T.G., Sørbye, S.H., 2017. Penalising model component complexity: a principled, practical approach to constructing priors. Stat. Sci. 32 (1), 1–28.

Sing, T., Sander, O., Beerenwinkel, N., Lengauer, T., 2005. ROCR: visualizing classifier performance in R. Bioinformatics 21, 7881.

Sorichetta, A., Hornby, G.M., Stevens, F.R., Gaughan, A.E., Linard, C., Tatem, A.J., 2015. High-resolution gridded population datasets for Latin America and the Caribbean in 2010, 2015, and 2020. Sci. Data 2, 150045.

Stockstill, R.L., Leech, J.R., 1990. Rio Puerto Nuevo Flood-Control Project. Hydraulic Model Investigation (No. WES/TR/HL-90-18), San Juan, Puerto Rico (ARMY ENGINEER WATERWAYS EXPERIMENT STATION VICKSBURG MS HYDRAULICS DIV).

Stürck, J., Poortinga, A., Verburg, P.H., 2014. Mapping ecosystem services: the supply and demand of flood regulation services in Europe. Ecol. Indic. 38, 198–211.
Thornton, P., Hasenauer, H., White, M., 1997. Generating surfaces of daily meteorological variables over large regions of complex terrain. J. Hydrol. 190, 204–251.
Torres-González, S., Planert, M., Rodríguez, M.J., 1996. Hydrogeology and simulation of ground-water flow in the upper aquifer of the Río Camuy to Río Grande de Manatí area, Puerto Rico. US Geol Surv Water Resour Invest Rep 95-4286, p. 102.
U.S. Census Bureau, 2018. Quick facts: Puerto Rico. https://www.census.gov/quickfacts/pr, Accessed date: 18 March 2019.
U.S. Department of Agriculture, Natural Resources Conservation Service, 2004. Soil Survey Geographic (SSURGO) Database for Puerto Rico, all Regions. http://SoilDataMart.nrcs.usda.gov/, Accessed date: 11 June 2018.
United States Department of Agriculture, 1986. Urban hydrology for small watersheds (PDF). Technical Release 55 (TR-55), Second ed. Natural Resources Conservation Service, Conservation Engineering Division.
United States Department of Agriculture, 2017. Forest inventory and analysis database. Available at. Forest Servicehttp://apps.fs.fed.us/fiadbdownloads/datamart.html, Accessed date: 11 June 2018.
United States Environmental Protection Agency (USEPA), 2006. Consent Decree: Puerto Rico Aqueduct and Sewer Authority Clean Water Act Settlement. https://www.epa.gov/enforcement/consent-decree-puerto-rico-aqueduct-and-sewer-authority-clean-water-act-settlement, Accessed date: 22 June 2018.
United States Geologic Survey (USGS), 2017. National Hydrography Dataset. https://nhd.usgs.gov/, Accessed date: 11 June 2018.
Vale-Nieves, A., 2018. Puerto Rico's karst protection—Beyond the Laws and Regulations. Karst Groundwater Contamination and Public Health. Springer, Cham, pp. 51–54.
Vitousek, S., Barnard, P.L., Fletcher, C.H., Frazer, N., Erikson, L., Storlazzi, C.D., 2017. Doubling of coastal flooding frequency within decades due to sea-level rise. Sci. Rep. 7 (1), 1399.
Vittinghoff, E., McCulloch, C.E., 2007. Relaxing the rule of ten events per variable in logistic and Cox regression. Am. J. Epidemiol. 165 (6), 710–718.
Wade, T. J., Sandhu, S. K., Levy, D., Lee, S., LeChevallier, M. W., Katz, L., & Colford Jr, J. M. (2004). Did a severe flood in the Midwest cause an increase in the incidence of gastrointestinal symptoms? Am. J. Epidemiol., 159(4), 398–405.
Wade, T.J., Lin, C.J., Jagai, J.S., Hilborn, E.D., 2014. Flooding and emergency room visits for gastrointestinal illness in Massachusetts: a case-crossover study. PLoS One 9 (10), e110474.
Wade, T.J., Augustine, S.A., Griffin, S.M., Sams, E.A., Oshima, K.H., Egorov, A.I., ... Dufour, A.P., 2018. Asymptomatic norovirus infection associated with swimming at a tropical beach: a prospective cohort study. PLoS One 13 (3), e0195056.
Warne, A.G., Webb, R.M.T., Larsen, M.C., 2005. Water, Sediment, and Nutrient Discharge Characteristics of Rivers in Puerto Rico, and their Potential Influence on Coral Reefs: U.S. Geological Survey Scientific Investigations Report 2005–5206 (58 p).
Winsemius, H. C., Jongman, B., Veldkamp, T. I., Hallegatte, S., Bangalore, M., & Ward, P. J. (2015). Disaster Risk, Climate Change, and Poverty: Assessing the Global Exposure of Poor People to Floods and Droughts. https://elibrary.worldbank.org/doi/abs/10.1596/1813-9450-7480. Accessed 07/10/2018.
Xiao, Q., McPherson, E.G., 2016. Surface water storage capacity of twenty tree species in Davis, California. J. Environ. Qual. 45, 188–198. https://doi.org/10.2134/jeq2015.02.0092.
Yang, Q., Tam, N.F., Wong, Y.S., Luan, T.G., Su, W.S., Lan, C.Y., Shin, P.K., Cheung, S.G., 2008. Potential use of mangroves as constructed wetland for municipal sewage treatment in Futian, Shenzhen, China. Mar. Pollut. Bull. 57 (6), 735–743. https://doi.org/10.1016/j.marpolbul.2008.01.037.
Yuan, Y., Jiang, Y., Taguas, E.V., Mbonimpa, E.G., Hu, W., 2015. Sediment loss and its cause in Puerto Rico watersheds. Soil 1 (2), 595–602.
Zhou, Wanfang, 2007. Drainage and flooding in karst terranes. Environ. Geol. 51 (6), 963–973.

Yee, Susan

From: Rebeca De Jesus Crespo <rdejesuscrespo1@lsu.edu>
Sent: Thursday, April 23, 2020 9:24 AM
To: Yee, Susan
Subject: Re: Record of Percent Agreement: R de Jesus Crespo

I concur

Thanks!

Rebeca de Jesús
Assistant Professor, Department of Environmental Sciences
Louisiana State University
College of Coast and the Environment
93 South Quad Drive
Baton Rouge, LA 70803

From: Yee, Susan <Yee.Susan@epa.gov>
Sent: Thursday, April 23, 2020 9:12 AM
To: Rebeca De Jesus Crespo <rdejesuscrespo1@lsu.edu>
Subject: Record of Percent Agreement: R de Jesus Crespo

Hi everyone.
Two of our journal articles are being nominated for a US EPA award for Science and Technical Achievement. As part of the nomination, I need a concurrence from each of you on your Percent Contribution to both articles. Note below I just took the Average across both papers for each article.
If you are ok with your percentage, **please just Reply to Me with an "I concur"**. If you'd like more information on the award nomination or to discuss further, let me know.

R. de Jesús Crespo 55%
R. Fulford 20%
M. Myer 10%
S. Yee 5%
J. Wu 10%

de Jesús Crespo, R., & Fulford, R. (2018). Eco-Health linkages: assessing the role of ecosystem goods and services on human health using causal criteria analysis. International journal of public health, 1-12.
de Jesús Crespo, R., J. Wu, M. Myer, S. Yee, and R. Fulford. Flood protection ecosystem services in the coast of Puerto Rico: Associations between extreme weather, flood hazard mitigation and gastrointestinal illness. SCIENCE OF THE TOTAL ENVIRONMENT. Elsevier BV, AMSTERDAM, NETHERLANDS, 676: 343-355, (2019).

	Eco-Evidence	GI Paper	Combined
Rebeca de Jesus Crespo	70	40	55

Richard Fulford	30	10	20
Mark Myer	0	20	10
Susan Yee	0	10	5
Jianyong Wu	0	20	10

Susan Yee
Gulf Ecosystem Measurement and Modeling
U.S. Environmental Protection Agency
1 Sabine Island Drive
Gulf Breeze, FL 32561
850-934-9397

Yee, Susan

From: Yee, Susan
Sent: Monday, April 20, 2020 10:10 AM
To: Yee, Susan
Subject: RE: Record of Percent Agreement: Yee, Susan

I concur.

From: Yee, Susan <Yee.Susan@epa.gov>
Sent: Monday, April 20, 2020 10:07 AM
To: Yee, Susan <Yee.Susan@epa.gov>
Subject: Record of Percent Agreement: Yee, Susan

Hi everyone.
Two of our journal articles are being nominated for a US EPA award for Science and Technical Achievement. As part of the nomination, I need a concurrence from each of you on your Percent Contribution to both articles. Note below I just took the Average across both papers for each article.
If you are ok with your percentage, **please just Reply to Me with an "I concur"**. If you'd like more information on the award nomination or to discuss further, let me know.

R. de Jesús Crespo 55%
R. Fulford 20%
M. Myer 10%
S. Yee 5%
J. Wu 10%

de Jesús Crespo, R., & Fulford, R. (2018). Eco-Health linkages: assessing the role of ecosystem goods and services on human health using causal criteria analysis. International journal of public health, 1-12.
de Jesús Crespo, R., J. Wu, M. Myer, S. Yee, and R. Fulford. Flood protection ecosystem services in the coast of Puerto Rico: Associations between extreme weather, flood hazard mitigation and gastrointestinal illness. SCIENCE OF THE TOTAL ENVIRONMENT. Elsevier BV, AMSTERDAM, NETHERLANDS, 676: 343-355, (2019).

	Eco-Evidence	GI Paper	Combined
Rebeca de Jesus Crespo	70	40	55
Richard Fulford	30	10	20
Mark Myer	0	20	10
Susan Yee	0	10	5
Jianyong Wu	0	20	10

Susan Yee
Gulf Ecosystem Measurement and Modeling
U.S. Environmental Protection Agency
1 Sabine Island Drive
Gulf Breeze, FL 32561

850-934-9397

Yee, Susan

From: Wu, Jianyong
Sent: Monday, April 20, 2020 1:51 PM
To: Yee, Susan
Subject: Re: record of Percent agreement: Wu, Jianyong

I concur.

Good luck,

Jianyong

From: Yee, Susan <Yee.Susan@epa.gov>
Sent: Monday, April 20, 2020 11:07 AM
To: Wu, Jianyong <wu.jianyong@epa.gov>
Subject: record of Percent agreement: Wu, Jianyong

Hi everyone.
Two of our journal articles are being nominated for a US EPA award for Science and Technical Achievement. As part of the nomination, I need a concurrence from each of you on your Percent Contribution to both articles. Note below I just took the Average across both papers for each article.
If you are ok with your percentage, **please just Reply to Me with an "I concur"**. If you'd like more information on the award nomination or to discuss further, let me know.

R. de Jesús Crespo 55%
R. Fulford 20%
M. Myer 10%
S. Yee 5%
J. Wu 10%

de Jesús Crespo, R., & Fulford, R. (2018). Eco-Health linkages: assessing the role of ecosystem goods and services on human health using causal criteria analysis. International journal of public health, 1-12.
de Jesús Crespo, R., J. Wu, M. Myer, S. Yee, and R. Fulford. Flood protection ecosystem services in the coast of Puerto Rico: Associations between extreme weather, flood hazard mitigation and gastrointestinal illness. SCIENCE OF THE TOTAL ENVIRONMENT. Elsevier BV, AMSTERDAM, NETHERLANDS, 676: 343-355, (2019).

	Eco-Evidence	GI Paper	Combined
Rebeca de Jesus Crespo	70	40	55
Richard Fulford	30	10	20
Mark Myer	0	20	10
Susan Yee	0	10	5
Jianyong Wu	0	20	10

Susan Yee
Gulf Ecosystem Measurement and Modeling
U.S. Environmental Protection Agency
1 Sabine Island Drive
Gulf Breeze, FL 32561
850-934-9397

Yee, Susan

From: Mark Myer <myermarkh@gmail.com>
Sent: Monday, April 20, 2020 10:11 AM
To: Yee, Susan
Subject: Re: Record of Percent Agreement: Myer, Mark

Hi Susan,

I concur.

Best,
Mark Myer

On Mon, Apr 20, 2020, 10:09 AM Yee, Susan <Yee.Susan@epa.gov> wrote:

> Hi everyone.
>
> Two of our journal articles are being nominated for a US EPA award for Science and Technical Achievement. As part of the nomination, I need a concurrence from each of you on your Percent Contribution to both articles. Note below I just took the Average across both papers for each article.
>
> If you are ok with your percentage, **please just Reply to Me with an "I concur"**. If you'd like more information on the award nomination or to discuss further, let me know.
>
> R. de Jesús Crespo 55%
>
> R. Fulford 20%
>
> M. Myer 10%
>
> S. Yee 5%
>
> J. Wu 10%
>
> de Jesús Crespo, R., & Fulford, R. (2018). Eco-Health linkages: assessing the role of ecosystem goods and services on human health using causal criteria analysis. International journal of public health, 1-12.
> de Jesús Crespo, R., J. Wu, M. Myer, S. Yee, and R. Fulford. Flood protection ecosystem services in the coast of Puerto Rico: Associations between extreme weather, flood hazard mitigation and gastrointestinal illness. SCIENCE OF THE TOTAL ENVIRONMENT. Elsevier BV, AMSTERDAM, NETHERLANDS, 676: 343-355, (2019).

	Eco-Evidence	GI Paper	Combined
Rebeca de Jesus Crespo	70	40	55
Richard Fulford	30	10	20

Mark Myer	0	20	10
Susan Yee	0	10	5
Jianyong Wu	0	20	10

Susan Yee

Gulf Ecosystem Measurement and Modeling

U.S. Environmental Protection Agency

1 Sabine Island Drive

Gulf Breeze, FL 32561

850-934-9397

Yee, Susan

From: Fulford, Richard
Sent: Monday, April 20, 2020 10:36 AM
To: Yee, Susan
Subject: RE: Record of Percent Agreement: Fulford, Richard

I concur

From: Yee, Susan <Yee.Susan@epa.gov>
Sent: Monday, April 20, 2020 10:08 AM
To: Fulford, Richard <Fulford.Richard@epa.gov>
Subject: Record of Percent Agreement: Fulford, Richard

Hi everyone.
Two of our journal articles are being nominated for a US EPA award for Science and Technical Achievement. As part of the nomination, I need a concurrence from each of you on your Percent Contribution to both articles. Note below I just took the Average across both papers for each article.
If you are ok with your percentage, **please just Reply to Me with an "I concur"**. If you'd like more information on the award nomination or to discuss further, let me know.

R. de Jesús Crespo 55%
R. Fulford 20%
M. Myer 10%
S. Yee 5%
J. Wu 10%

de Jesús Crespo, R., & Fulford, R. (2018). Eco-Health linkages: assessing the role of ecosystem goods and services on human health using causal criteria analysis. International journal of public health, 1-12.
de Jesús Crespo, R., J. Wu, M. Myer, S. Yee, and R. Fulford. Flood protection ecosystem services in the coast of Puerto Rico: Associations between extreme weather, flood hazard mitigation and gastrointestinal illness. SCIENCE OF THE TOTAL ENVIRONMENT. Elsevier BV, AMSTERDAM, NETHERLANDS, 676: 343-355, (2019).

	Eco-Evidence	GI Paper	Combined
Rebeca de Jesus Crespo	70	40	55
Richard Fulford	30	10	20
Mark Myer	0	20	10
Susan Yee	0	10	5
Jianyong Wu	0	20	10

Susan Yee
Gulf Ecosystem Measurement and Modeling
U.S. Environmental Protection Agency
1 Sabine Island Drive
Gulf Breeze, FL 32561

850-934-9397

Int J Public Health (2018) 63:81–92
https://doi.org/10.1007/s00038-017-1020-3

REVIEW

Eco-Health linkages: assessing the role of ecosystem goods and services on human health using causal criteria analysis

Rebeca de Jesus Crespo[1] · **Richard Fulford**[1]

Received: 9 February 2017 / Revised: 11 July 2017 / Accepted: 12 July 2017 / Published online: 1 August 2017
© Swiss School of Public Health (SSPH+) (outside the USA) 2017

Abstract
Objectives In the last decade, we saw an upsurge of studies evaluating the role of ecosystem goods and services (EGS) on human health (Eco-Health). Most of this work consists of observational research of intermediate processes and few address the full pathways from ecosystem to EGS to human health, limiting our ability to assess causality.
Methods We conducted a causal criteria analysis of Eco-Health literature using Eco-Evidence, a software tool that helps evaluate evidence of cause–effect relationships. We focus on the context of green spaces providing "buffering" EGS that may influence disease.
Results We found support for a causal linkage between green spaces and all of the EGS tested, and sufficient evidence linking EGS to gastro intestinal disease and heat morbidities. Inconsistencies were found when assessing the link between EGS to cardiovascular and respiratory diseases. Few studies directly link green spaces to health. Those that do, support a connection to cardiovascular disease, and heat morbidities, but provide inconsistent evidence regarding respiratory illness.
Conclusions Our results help establish an agenda to shape future Eco-Health research and define priorities for managing green spaces to provide human health benefits.

Keywords Ecosystem goods and services · Green spaces · Disease · Causal criteria analysis

Introduction

Ecosystem goods and services (EGS) are the outputs of ecological processes that directly or indirectly contribute to social welfare (Munns et al. 2015). One of the key uncertainties limiting the protection of EGS is the limited knowledge of how they may relate to human health (Corvalan et al. 2005). Since the Millennium Ecosystem Assessment (MEA 2005), there has been increasing interest in addressing this information gap, and an upsurge in the number of studies on the subject (Hartig et al. 2014).

The emerging body of literature relating EGS to human health has been compiled in over fifty review articles (Hartig et al. 2014), and captured in interactive tools, such as the US-EPA's Eco-Health Relationship Browser (Jackson et al. 2013). Although these compilations highlight empirical evidence, the references to date do not necessarily support causality, but rather focus on establishing plausible associations (Jackson et al. 2013). Moreover, the field is dominated by observational research and there is a dearth of primary studies to establish causal associations between EGS and health in a consistent and rigorous manner (Hartig et al. 2014).

Notably, there are few studies directly linking the presence of ecosystems to physical health and disease by means of buffering EGS. Buffering EGS refers to the ecosystem's capacity to "buffer" against health impacts

Electronic supplementary material The online version of this article (doi:10.1007/s00038-017-1020-3) contains supplementary material, which is available to authorized users.

✉ Rebeca de Jesus Crespo
Dejesus-crespo.rebeca@epa.gov

Richard Fulford
Fulford.Richard@epa.gov

[1] Gulf Ecology Division, National Health and Environmental Effects Research Laboratory, US EPA, Office of Research and Development, 1 Sabine Island Drive, Gulf Breeze, FL 32561-5299, USA

by, for example, removing pollutants from air and water, and mitigating heat and water hazards (Jackson et al. 2013). Most existing research links disease to intermediate processes (e.g., air pollution, floods), which may be attributed to anthropogenic impacts and not necessarily to buffering EGS by ecosystems. Given that the ecosystem is the operable management unit in the conservation of buffering EGS for human health, a lack of empirical evidence supporting a direct association could undermine the effectiveness (and public support) of conservation plans. There are few papers tracing the full pathways from ecosystem, to EGS processes, to health outcomes, which further limit our ability to demonstrate causality (Hartig et al. 2014).

One solution to these limitations is the collective analysis of existing Eco-Health literature using causal criteria analysis (CSA). CSA emerged in the field of epidemiology due to the need for decision-making based on relatively weak independent pieces of evidence (Weed 1997). Bradford Hill's criteria represent the most widely used guide for assessing causality, and consist of standards, summarized by Russo and Williamson (2007), into two categories: (1) probabilistic evidence, or consistent cause–effect association; and (2) mechanistic evidence, or a logical explanation of how the causal association occurs. Norris et al. (2011) subsequently applied causality criteria to develop a framework for assessing cause–effect relationships in environmental research. The premise is that isolated studies may not offer a strong case for causality, but they may do so if considered collectively.

We focus our CSA on the context of green spaces, its effects on buffering EGS, and the impact of these on human diseases. We address the following questions: (1) which linkages are theoretically plausible but need further research, (2) which diseases have been associated directly with presence/absence of green spaces, and (3) which Eco-Health linkages are best supported and should be considered for management. Addressing these questions will better characterize the current state of knowledge, define management priorities, and identify pending Eco-Health research topics.

Methods

To conduct our CSA, we applied a numerical technique that combines individual studies, weighted by research design, into a single score for or against a given hypothesis (Norris et al. 2011; Table 1). This method helps determine whether the composite of existing research supports the cause and effect relationship, or suggests inconsistent evidence, or support for an alternative hypothesis. This approach differs from meta-analysis as it is not meant to measure effect sizes. Instead it helps determine the evidence for a given causal linkage. It also allows consideration of studies that do not report summary statistics, which are needed for quantitative reviews (Norris et al. 2011). This method represents an alternative to narrative reviews as it allows for succinct literature synthesis and a systematic assessment of relative weight of evidence (Norris et al. 2011). This approach has been incorporated into an online tool called Eco-Evidence, summarized here in four sections: context definition; cause and effect mechanism; literature review; and weighting the evidence (Webb et al. 2015).

Table 1 Factors considered and weight of evidence scores for causal criteria analysis. Modified from Norris et al. (2011)

Factors considered	Weight applied
Study design type	
BACI or BARI MBACI	4
Gradient response model	3
Before vs after (no reference/control)	2
Reference vs control (no before)	2
After impact only	1
Number of independent control locations	
0	0
1	2
1+	3
Number of independent impact locations	
1	0
2	2
2+	3
Locations for gradient response model	
3	0
4	2
5	4
5+	6

BACI before–after-control-impact, *BARI* before–after-reference-impact, *MBACI* multiple before–after-control (or reference)-impact

Context definition

Our analysis focuses on diseases linked to buffering EGS provided by green spaces (Fig. 1). Here, the term green space refers to any vegetation within a human dominated environment (Kabisch and Haase 2013). This includes urban trees, green roofs, and wetlands.

We did not consider health promoting services (physical activity, engagement with nature), or mental health outcomes. Recent reviews describes the state of knowledge regarding these topics (Lee and Maheswaran 2011; Shanahan et al. 2015), while there is relatively less

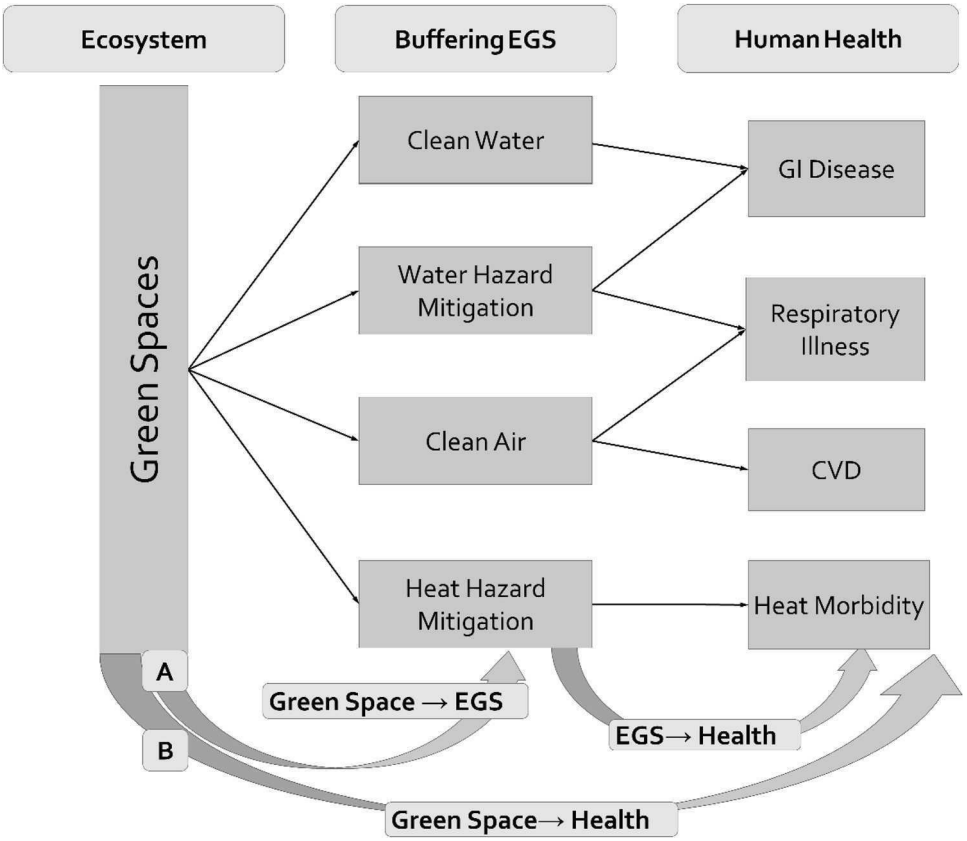

Fig. 1 Selected Eco-Health linkages for causal criteria analysis. We followed two approaches for our analysis: **a** Evaluating the intermediate steps linking green spaces to human health; **b** evaluating the evidence linking green spaces directly to human health. *EGS* ecosystem goods and services, *GI disease* gastro intestinal disease, *CVD* cardio vascular disease

information on the weight of evidence linking acute morbidities such as gastrointestinal disease, respiratory illness, cardiovascular disease, and heat morbidities to green-space–EGS (Hartig et al. 2014). We selected these four health endpoints for our assessment which followed two approaches:

1. Evaluating intermediate linkages:
   (a) Green space → EGS (i.e., green spaces providing buffering EGS)
   (b) EGS → Health (i.e., exposure to environmental hazards leading to disease).
2. Evaluating direct linkages:
   (a) Green space → Health (i.e., health benefits associated to presence/extent of the ecosystem).

This approach allowed us to fully characterize the cause–effect model (Fig. 1), and identify the greatest data gaps and the strongest support.

Cause and effect mechanisms

Green spaces mitigate water hazards (e.g., floods, storm surge) by increasing rainfall interception and infiltration and by acting as a physical barrier to waves and storm surges (Brody and Highfield 2013; Costanza et al. 2008). Water hazard mitigation lowers exposure to polluted flood waters that cause GI disease, and prevents flood prone homes from harboring conditions that lead to mold growth and asthma (Wade et al. 2004; Chew et al. 2006). Green spaces remove infectious and toxic pollutants (Silva et al. 1990; Karim et al. 2004), helping to prevent GI disease from drinking and recreational water (Araya et al. 2004; Katukiza et al. 2014). They trap air contaminants (Räsänen et al. 2013), which may otherwise lead to respiratory illness and cardiovascular disease (Peters et al. 1997; Brook et al. 2004). Green spaces mitigate extreme temperatures through shade and evapotranspiration, lowering heat morbidities during heat waves (Bouchama and Knochel 2002). Table 2 summarizes these cause–effect mechanisms.

Literature review

We examined 2756 publications regarding Eco-Health linkages [(ESM 1) from years 2000 to 2016. First, we searched within an existing Eco-Health database (Jackson et al. 2013), $N = 1434$] and selected papers relevant to our focal Eco-Health relationships ($N = 112$). We expanded this database with a targeted keyword search (ESM 2). We examined the titles and abstracts of all articles from the first 50 non-duplicative results per key-word combination

Table 2 Cause and effect mechanisms for the intermediate steps of the selected Eco-Health linkages

Eco-Health linkages	Cause–effect mechanism	Mechanistic references	# Studies
Green spaces and EGS			
Green spaces–clean water	Green spaces provide physical barriers to the movement of pollutants in water, change the soil's condition to promote pollutant immobilization, or capture pollutants in plant biomass	Silva et al. (1990), Karim et al. (2004)	44
Green spaces–water hazard mitigation	Green spaces reduce surface runoff by increasing rainfall interception and infiltration. They also act as physical barriers to waves and storm surges	Brody and Highfield (2013), Costanza et al. (2008)	19
Green spaces–clean air	Green spaces provide physical barriers to the movement of pollutants in air and absorb pollutants	Räsänen et al. (2013)	22
Green spaces–heat hazard mitigation	Green spaces provide cooling through shade and evapotranspiration	Pokorný et al. (2010), Kong et al. (2014)	19
EGS and health			
Clean water–GI disease	Pathogenic microbes cause toxicity and infection, heavy metals like copper cause vagal nerve stimulations which triggers GI symptoms	Araya et al. (2004), Katukiza et al. (2014)	6
Water hazard mitigation–GI disease	Flood water mixes with waste water discharged into rivers, or other polluted sources. Individuals in flood prone areas come in contact with contaminated flood waters	Wade et al. (2004)	7
Water hazard mitigation–respiratory illness	The humidity and dampness in flood prone households lead to indoor mold growth. Mold endotoxins cause respiratory conditions like asthma	Chew et al. (2006)	4
Clean air–respiratory illness	Outdoor air pollutants (i.e., PM, O_3, SO_2 and NO_2) cause oxidative stress and airway inflammation. Other mechanisms causing respiratory illness include increased susceptibility to infections and disruptions in oxygen transport	Kagawa (1985), Nel et al. (2006) Reno et al. (2015)	28
Clean air–cardiovascular disease (CVD)	Airway inflammation and obstruction in oxygen transport caused by $PM_{2.5}$ and PM_{10}), O_3, SO_2 and NO_2 leads to plaque formation and atherosclerosis. Pollutants may also affect blood coagulation	Peters et al. (1997), Brook et al. (2004)	23
Heat hazard mitigation–heat morbidities	Heated blood is transferred towards the surface of the body, increasing blood output and activating sweating. This leads to dehydration, increases in heart rate, and affects kidneys, liver and digestive systems as blood circulation is transferred away from the organs and towards the skin	Bouchama and Knochel (2002)	18

EGS ecosystem goods and services, *GI disease* gastrointestinal disease

($N = 950$), and eliminated non-relevant results (e.g., review articles) for a total of 208 papers. We then evaluated study methodology for all papers selected [$N = 320$ (112 + 208)] and excluded papers that were not primary research papers. For example, we excluded papers that used modeling techniques such as i-Tree (Nowak et al. 2008) as these tend to infer provision of EGS from estimates made by previous studies, and thus may not add new evidence. When available we assessed articles that helped informed model development (e.g., Pope et al. 2002). We also excluded articles that looked at the green space–human health link through the lens of physical activity or restorative theories, as our focus was buffering EGS. Our final selection ($N = 212$, ESM 4) was evaluated using CSA.

Weighting the evidence

Selected articles were classified using the weights described in Table 1. We summed these weights to calculate an evidence score for each cause and effect linkage. A score of 20 was the threshold for rejecting or supporting the causal linkage. This threshold implies that at least three high-quality studies are needed to provide evidence for causality, whereas in the case of low-quality research studies, more articles may be needed to obtain the same level of support (Norris et al. 2011). A score of 20 or more for articles contradicting the hypothesis serves as basis for rejecting the cause–effect relationship. Norris et al. 2011 chose this threshold after expert consultation and multiple trials; however, Eco-Evidence allows modifying these values if necessary. For our study, we applied the suggested score of 20, with the following possible scenarios:

1. In Favor ≥ 20 + Not in Favor ≤ 20 = Support for Hypothesis.
2. In Favor < 20 + Not in Favor ≥ 20 = Support for Alternate Hypothesis.
3. In Favor < 20 + Not in Favor < 20 = Insufficient Evidence.
4. In Favor ≥ 20 + Not in Favor ≥ 20 = Inconsistent Evidence.

To determine the sensitivity of our conclusions to the chosen threshold, we examined results at 5, 10, 15 and 20% of the base value (e.g., when using a 20% variation in threshold, scores of 16 and 24 were applied instead of 20).

Results

Weighting the evidence: intermediate linkages

Green spaces and buffering EGS

We reviewed 105 articles linking green spaces to clean water, water hazard mitigation, clean air, and heat hazard mitigation (Fig. 2; ESM 3).

We found 44 papers supporting the green spaces–clean water linkage. Most of the studies assessed the role of wetlands in removing copper and fecal coliform; we found fewer studies assessing the capacity of other types of green spaces (riparian vegetation, green roofs, urban trees) for removing pollutants (ESM 3). We found 20 papers supporting the role of green spaces in mitigating water hazards. Studies linked this EGS to several types of green spaces, including green roofs, wetlands and open spaces. Indicators used to assess water hazard mitigation included wave energy, surface runoff, and flood-related property damages, in the presence and absence of green spaces (ESM 3).

Our assessment supports the linkage between green spaces and clean air. We reviewed 22 articles, where urban trees (canopy cover, tree cover) were consistently shown to remove air pollutants, most frequently particulate matter (PM_{10} and $PM_{2.5}$). We also found support for the role of green spaces in heat hazard mitigation in 19 studies on the subject. The indicators to assess Heat Hazard were mostly temperature change and heat waves, while NDVI (Normalized Difference Vegetation Index) and tree cover were commonly used to measure green spaces.

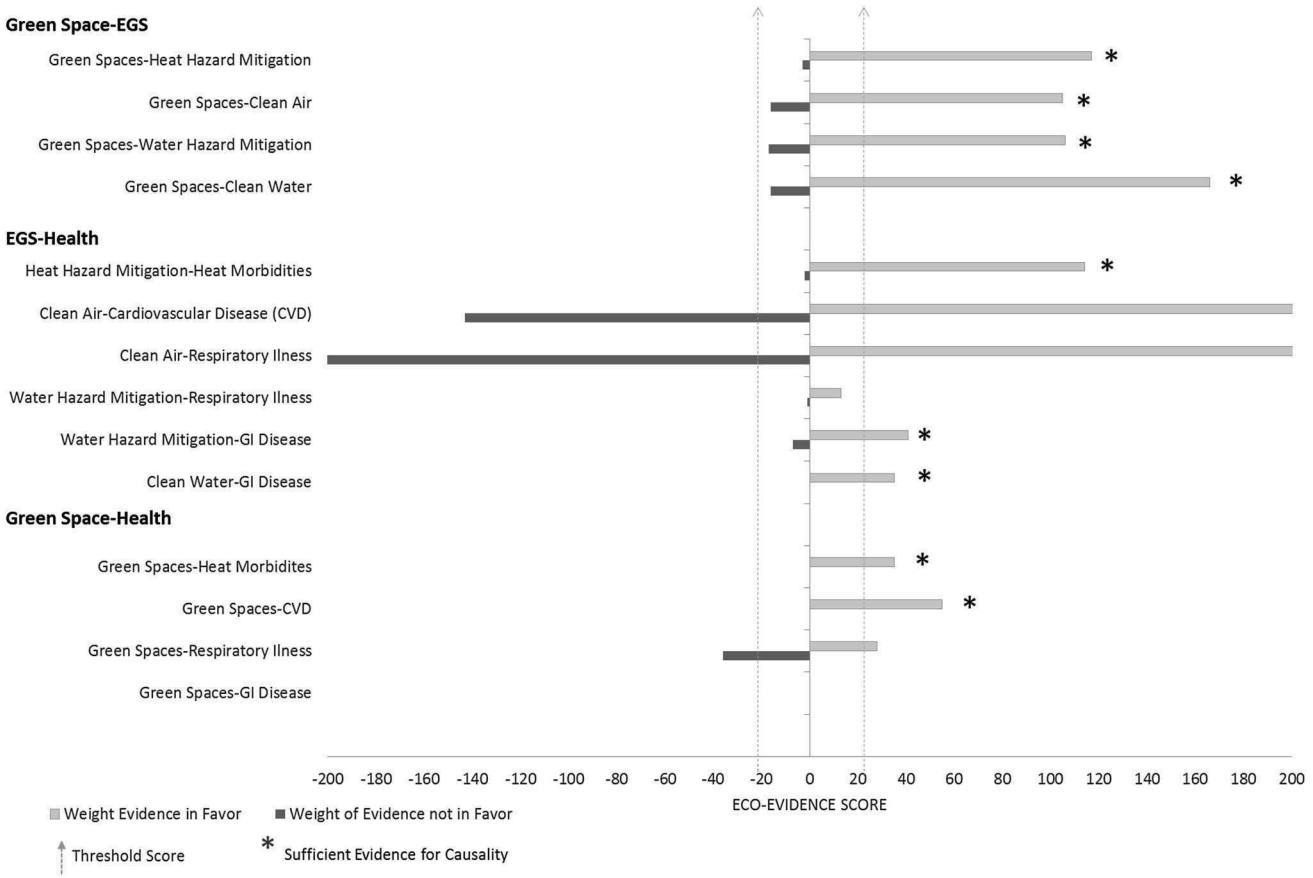

Fig. 2 Results from causal criteria analysis. Interpreting possible outcomes: (1) In Favor ≥ 20 + Not in Favor ≤ 20 = Support for Hypothesis; (2) In Favor <20 + Not in Favor ≥ 20 = Support for alternate Hypothesis; (3) In Favor <20 + Not in Favor <20 = Insufficient Evidence; (4) In Favor ≥ 20 + Not in Favor ≥ 20 = Inconsistent Evidence. *Negative values* here represent evidence not in favor, while *positive values* represent evidence in favor. *EGS* ecosystem goods and services, *GI disease* gastro intestinal disease, *CVD* cardiovascular disease

EGS and health

GI disease We reviewed 6 papers providing sufficient support for clean water–GI disease linkage. Swimming and consumption were the two mechanisms of exposure in the papers assessed, while surveys were used to characterize GI disease occurrences.

For the water hazard mitigation–GI disease linkage, we found 7 papers providing sufficient evidence in favor (Fig. 2). Most studies correlated flood events to GI disease, except for one which focused on rainfall. In this case, GI disease occurrences were assessed using hospital admissions or surveys.

Respiratory illness We found only 4 studies evaluating the linkage between water hazard mitigation and respiratory illness (ESM 3). Three of the papers assessed asthma as a response, and the fourth assessed bronchitis and cough. To measure water hazards, authors looked at flood and severe rainfall events, while health impacts were assessed using surveys or insurance claims. These papers provided insufficient evidence of a causal relationship (Fig. 2).

The linkage between respiratory illness and clean air has been studied extensively ($N = 27$ papers reviewed). Of the respiratory conditions assessed (bronchitis, cough, wheezing, asthma) we found more evidence against the correlation between air pollutants and asthma (not in favor = 93) than the evidence in favor (in favor = 79; ESM 3). In terms of indicators, most of the studies measured air pollutants using data from monitoring stations, while hospital admissions and surveys were commonly used to assess health outcomes.

Cardiovascular disease (CVD) The link between clean air and CVD had inconsistent evidence (Fig. 2). The studies reviewed ($N = 22$) used a variety of indicators to assess CVD, from blood pressure, to hospital admissions, to indicators of inflammation. This variability in methods may explain our inconsistent results. In terms of the air pollution variables, studies mostly used data from monitoring stations, and indicators like PM_{10}, $PM_{2.5}$, and NO_2.

Heat morbidities We reviewed 18 papers linking heat hazards to health, which provided strong support for causality. To measure heat hazards the authors used either temperature fluctuations or specific heat wave events. The health indicators used were hospital admissions and emergency room visits, particularly those related to heat (e.g., heat stroke), the renal system, or the circulatory system.

Weighing the evidence: direct Eco-Health linkages The evidence directly linking green spaces to health included 5 papers on Respiratory Conditions, 3 papers on heat morbidities, and 2 papers on CVD (Fig. 2). We found sufficient support for the role of green spaces in reducing heat morbidities and CVD, with most papers reporting correlations between green space cover and hospital admissions or mortality related to these conditions. The evidence linking green spaces to respiratory illness was inconsistent; most of the inconsistencies were associated with the response of asthma and/or allergies to green space cover (ESM 3). We did not find papers associating green spaces with GI disease, so our results indicate insufficient evidence to support this direct linkage (Fig. 2).

Sensitivity analysis Most relationships remained unchanged when varying the threshold value by 5–20%, with a few exceptions. Varying the threshold by 15% (i.e., a threshold of 17, or 23, instead of 20) would have changed the conclusion regarding the green spaces–water hazard mitigation and clean water linkage, from "sufficient" evidence, to "inconsistent" evidence as we found a few studies that found no support for the relationship. Varying the threshold by 20% (i.e., threshold of 16, or 24) would have changed the evidence supporting the green space linkage to clean air from "sufficient" to "inconsistent" with two well-designed studies falsifying the hypothesis. A 20% threshold decrease would have altered the conclusions regarding the water hazard mitigation–respiratory illness relationship, going from "insufficient evidence" to "sufficient evidence" as we found two well-designed studies and a relatively poor study in support of the linkage. See ESM3 for details of the studies reviewed.

Discussion

Evidence for causality: Eco-Health linkages

GI disease

Green spaces are causally linked to clean water and water hazard mitigation. Wetlands have been particularly well studied for their role in providing clean water. Factors determining their effectiveness include wetland type (De Lacerda and Abrao 1984), the species involved (Yang et al. 2008), hydrological residence time, and season (Reinelt and Horner 1995). For water hazard mitigation, several types of urban vegetation, including open spaces and green roofs, help reduce surface runoff and flooding (Bliss et al. 2009; Brody and Highfield 2013). Marshes and mangroves have been linked mainly to storm surge reduction and wave attenuation (Granek and Ruttenberg 2007; Möller et al. 2014); we found no papers assessing their role in mitigating urban floods. Our results correspond to findings by

Shepard et al. (2011), and suggest this is an area that remains unexplored.

Our review found sufficient evidence linking clean water and water hazard mitigation to GI disease. The impacts of water pollutants depend on exposure time, concentration of pollutants, extent of exposure, and sensitivity of exposed individuals (Araya et al. 2004; Wade et al. 2004; Collier et al. 2015). Most of the papers assessing these linkages used self-reporting to characterize health response. More objective indicators, such as medical records, or hospital visitations, are less common and could provide further support for this linkage.

We did not find studies addressing direct linkage between Green-Space and GI disease, even though there is sufficient evidence supporting intermediate processes leading to this association, as detailed above. Future research should focus on determining the effectiveness of green spaces to mitigate environmental exposure to toxic and pathogenic water pollutants in diverse contexts, such as recreation, consumption and hazard events.

Respiratory illness

We found support for the role of green spaces in water hazard mitigation (see "GI disease") and clean air, both of which protect from respiratory illness. Urban trees have been the focus of most studies assessing clean air EGS (e.g., Cavanagh et al. 2009; Grundström and Pleijel 2014), with evergreens showing greater effectiveness because of year-long foliage retention and more complex leaf structures (Beckett et al. 2000; Nguyen et al. 2015). Hairiness, stomatal density and leaf wettability are also factors that seem to increase pollutant capture by trees and that should be maximized for clean air EGS (Räsänen et al. 2013; Weber et al. 2014).

The evidence linking water hazards to respiratory illness was less clear. We found few papers linking floods to asthma. Only three of the four papers reviewed supported the linkage, while the fourth paper found a negative association (Park et al. 2013). Of the supporting papers, one found that response was partially mediated by psychological distress, and that asthma negatively correlated to flooding depth, which contradicts their findings (Reacher et al. 2004). The other two studies convincingly connected flood, mold and asthma, but only one followed an experimental approach (Dales et al. 1991), while the other consisted of a single case study (Makaryus et al. 2015). Therefore, the hypothesized linkage between flooding and asthma, mediated by mold growth, remains to be explored.

From the studies assessing linkage between clean air and respiratory illness, those using asthma as a response showed inconsistent evidence for causality (ESM 3). The inconsistencies are likely due to the types of indicators used to measure cause and effect. For example, a widely used clean air indicator is $PM_{2.5}$ mass (e.g., $\mu g/m^3$), while the mechanism that links air pollutants to asthma is in part mediated by oxidative stress and inflammation (Li et al. 2008). Certain particles have greater oxidative capacity than others, and their relative concentration may be a better indicator to assess respiratory impact than mass alone. Only one paper assessed oxidative potential in the air as an explanatory variable (Delfino et al. 2013); it found this was a better predictor of asthma than $PM_{2.5}$ mass. Other inconsistencies were related to season, with more respiratory susceptibility in the winter months. This trend may be related to more indoor pollutant exposure during winter (Walters et al. 1994), differences in pollution sources due to heating, or meteorological patterns in winter (e.g., less rainfall) that affect diffusion of pollutants (Zhen et al. 2013).

Accordingly, we found inconsistent evidence linking green spaces to asthma and allergies. Some studies report positive association between green space and asthma, pointing toward the negative influence of pollen and other allergens (Lovasi et al. 2013). Previous studies have found that while trees help remove pollutants, sometimes these pollutants get recirculated depending on location of buildings, wind direction and flow dynamics (Wania et al. 2012). Therefore, careful selections of tree species, and the use of flow dynamics modeling, are important considerations for designing green space configurations as part of restoration initiatives.

Cardio vascular disease (CVD)

We found inconsistent evidence for the link between clean air and CVD. We can hypothesize potential reasons, such as the use of various indicators in different studies and the presence of confounding natural and demographic factors. For example, in an experimental study by Hajat et al. (2015), different pollutants were tested against indicators of inflammation and blood clot formation with inconsistent results among the combinations tested (ESM 3). This signals a need for better characterizing the physiological mechanisms linking clean air to CVD to determine the best indicators to detect this connection. Another study found that age is an important factor, with the elderly showing greater CVD response to pollution (Prescott et al. 2000). Season may also play a role; in some instances, correlations were observed in cold but not warm months (Chang et al. 2015). Moreover, when looking at relationships that have many associated studies (e.g., CVD–clean air), the likelihood of finding inconsistencies increases (Norris et al. 2011). This does not imply that "inconsistent" connections are not real; rather, the inconsistencies help refine

hypotheses and future research questions (Norris et al. 2011).

We found support for a direct link between green space and CVD. Although we tried to avoid papers focusing on the health promoting benefits of green spaces, the studies we used were correlative, without explicit assessments of the mechanisms involved. The findings may in part be related to promotion of physical activity, engagement with nature, and the stress reducing potential of green spaces. In one of the papers, Pereira et al. (2013) found that neighborhood variability of greenness had a stronger association to CVD than absolute greenness, a finding that points toward physical activity as a mediating factor, since non-green areas (e.g., sidewalks, parking lots) were also important. Donovan et al. (2015) found that correlations between green space loss and CVD were significant after controlling for exercise, indicating that factors other than physical activity were important. Nevertheless, these other factors could include stress reduction from promotion of social engagement (EGS that also reduce CVD risk) and not necessarily air quality. Based on our review, we hypothesize that the benefits of trees to CVD could be attributed to mechanisms other than supporting air quality. In Fig. 3, we present this hypothesis by illustrating risk factors for CVD, and the role of green spaces using previous studies. Green spaces have been shown to promote a 44% increase in physical activity, but provide on average 0.11% air quality improvement via reduction of PM (Richardson et al. 2013; Nowak et al. 2013). Although these values come from studies with different methodologies, and quantitative comparisons are not justified, the differences in magnitude illustrate the relative influence of green spaces via these two EGS. Moreover, a study by Lim et al. (2013) showed that PM corresponds to 22% of the risk for CVD, while physical activity accounts for 31% and influences other important CVD drivers like stress and body mass index. Considering the relative importance of green spaces for physical activity vs clean air, and the relative importance of physical activity vs clean air in CVD, we propose that green spaces mainly influence CVD by promoting physical activity. This is not suggesting that clean air is unimportant for CVD, rather that green spaces likely play a modest pollutant buffering role, and that emphasis should be placed primarily on reducing pollution. In turn, management of green spaces for health promoting services should align with aspects of the built environment, such as access and safety features. This is especially important for low income communities, which face higher CVD risks (Fig. 3).

Heat morbidities

The link between green spaces and heat hazard mitigation is unequivocal, both for direct health outcomes and for the intermediate steps. Heat mitigation by trees has been reported for cities with different types of green space and ecosystems, and at multiple scales (Hou et al. 2013; Vailshery et al. 2013). Likewise, the protective value of green cover on heat morbidities has been well-documented in relation to heat waves and within arid environments at risk of heat extremes (Vandentorren et al. 2006; Harlan et al. 2013). Consistently, studies confirm increased risk from heat for vulnerable populations, such as elderly individuals and those with impaired mobility (Vandentorren et al. 2006; Burkart et al. 2016). Although correlations have been observed when documenting green cover at lower resolutions (e.g., 30 m resolution, using indicators such as NDVI), vegetation is most likely to be protective when it is strategically placed near exposed households within the urban context (Li et al. 2013).

In terms of management for heat hazard mitigation, the amount of green space is the most important factor, but there are other design considerations. Mixing tree species along street corridors to avoid continuous canopies that trap heat, and designing green roofs to have high leaf area index and adequate irrigation, are strategies to enhance the cooling effect (Norton et al. 2015). Urban greening not only buffers against heat islands and heat waves, but may also provide economic services to sectors that cannot rely on air conditioning, while supporting efficient energy use.

Limitations and recommendations

Limitations of the Eco-Evidence tool are discussed in detail in Norris et al. (2011). The authors address criticisms regarding the threshold value of 20, and advise that expert judgement should always be included. From our sensitivity analysis, we found that we would need to change the threshold by 15–20% to alter our conclusions. Because Norris et al. (2011) used trials and expert advice to develop the threshold of 20, we feel compelled to adhere to this value to maintain consistency, but we encourage readers to consider these alternative results when interpreting our findings. Another limitation is that the approach does not differentiate studies by their attention to confounding factors, which in the case of Eco-Health studies could be influential. Weighting studies by environmental or socioeconomic confounders would be a much-needed revision to the method (Norris et al. 2011). Lastly, while Eco-Evidence is not a substitute for strictly quantitative approaches such as meta-analyses, it allows weighting evidence from a variety of studies, including those that do not report summary statistics or cannot be combined due to fundamental differences in datasets. The contribution of Eco-Evidence is to help evaluate the knowledge base in support of a given relationship, not the effect size of that relationship, as in meta-analyses.

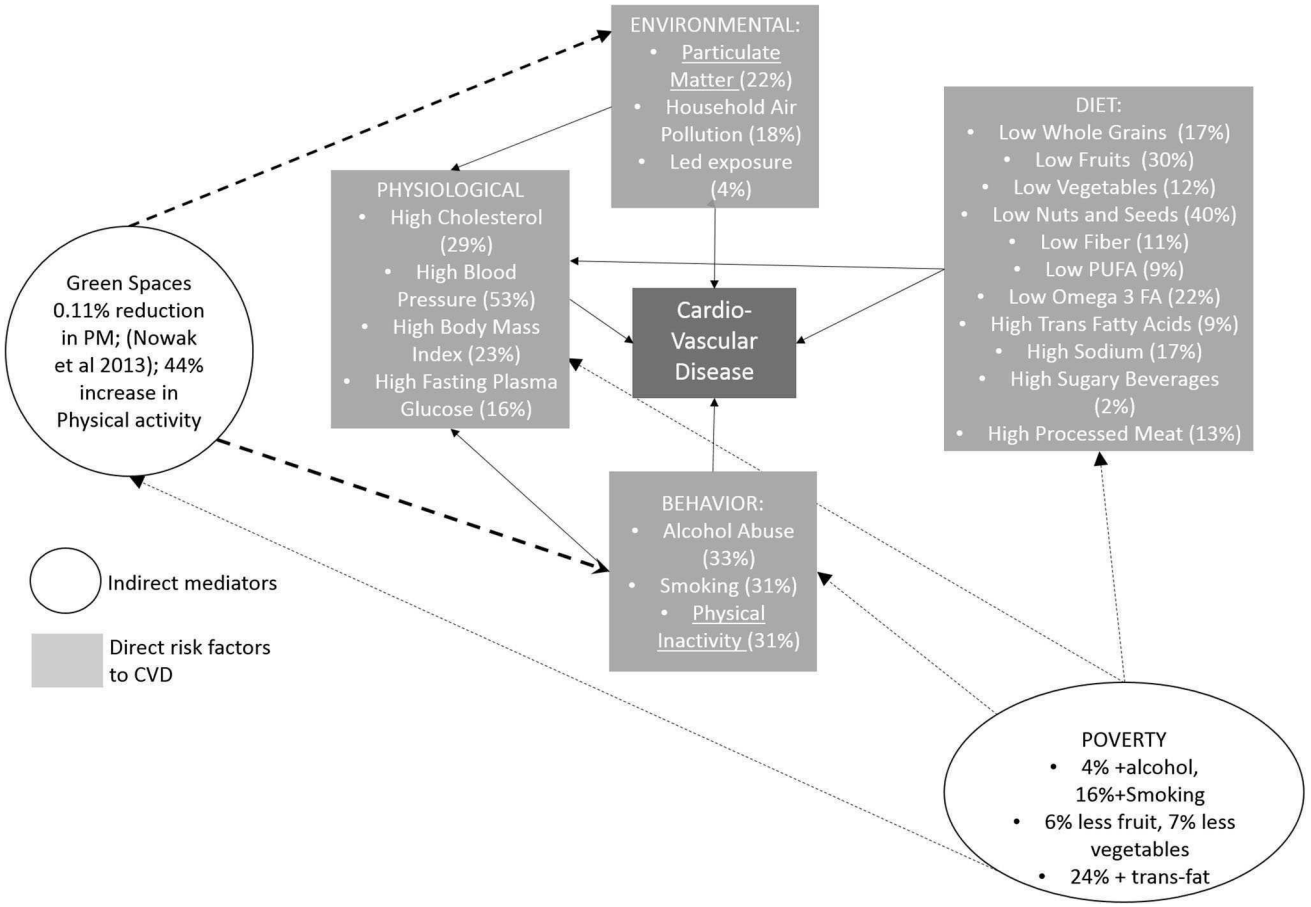

Fig. 3 Direct risk factors for cardiovascular disease (CVD, *gray boxes*) and indirect mediators (*white circles*, green spaces and poverty). The percentages represent the proportion of the effect attributed to the cause. The causes for CVD or risk factors (environmental, diet, behavior and physiological) were adapted from Lim et al. (2013), who looked at ischemic heart disease, a common type of CVD. The % of air quality improvement from trees was adapted from Nowak et al. (2013), by averaging the estimates for the ten US cities they assessed in their study. The percent in promotion of physical activity comes from Richardson et al. (2013); Poverty percentages come from Hulshof et al. (1991), and Galobardes et al. (2001)

Our results are partly determined by our strategy to identify relevant scientific studies (ESM 2). We invite readers to evaluate our review method and account for potentially missing keywords when interpreting our conclusions. In addition, to maintain consistency in the quality of material included, we only considered peer-reviewed publications, and excluded book chapters and gray literature. Despite these limitations, our review allowed us to make consistent comparisons, determine their relative state of knowledge, refine hypotheses and define areas of research need. Our findings support a proposed research agenda (Table 3) to advance the management of EGS for human health benefits.

Conclusions

We conducted a CSA to characterize Eco-Health literature. Our study fills a void that previous reviews had identified as crucial for valuing Eco-Health evidence: namely reviewing the evidence for the full pathways between ecosystem, ecosystem processes (e.g., EGS) and health outcomes (Hartig et al. 2014).

Our work confirms that most current Eco-Health literature supports the intermediate steps of these pathways (e.g., Ecosystem–EGS, EGS–Health), but few studies trace linkages from ecosystem to disease. Of these, few simultaneously address the pathways by which these direct connections occur. Research that fully determines if/how greening strategies deliver health benefits through buffering EGS is generally lacking, and in need of attention.

Despite identifying research needs, our review found consistent evidence of a connection between green spaces and buffering EGS, and between green spaces and certain health outcomes such as cardiovascular disease and heat morbidities. The role of green spaces in providing health

Table 3 Summary of causality assessment and priority questions for an Eco-Health research agenda

Eco-Health linkages	Evidence for causality		Priority questions
	Intermediate linkages	Direct linkages	
Green spaces–clean water/polluted water–GI disease	Support for Hypothesis	Insufficient	Is GI disease prevalence related to green space measures (presence, % cover, etc.) in areas exposed to water pollution?
Green spaces–water hazard mitigation/water hazards–GI disease	Support for hypothesis	Insufficient	Is GI disease prevalence related to green space measures (presence, % cover, etc.) in flood prone areas?
Green spaces–water hazard mitigation/water hazards–respiratory illness	Insufficient for EGS–health linkage	Insufficient	Is mold more common in houses prone to natural flooding? Does household mold correlate to asthma?
Green spaces–clean air/polluted air respiratory illness	Inconsistent for EGS–health linkage	Inconsistent	What are the best indicators to detect the impact of air quality on respiratory illnesses (e.g., oxidative potential vs pollutant mass)?
			Are there consistent confounding factors (demographics, seasonality) determining the impact of air pollutants?
			Could we define transferable green space restoration guidelines to enhance pollution removal and reduce allergen potential?
			How can we incorporate flow dynamic principles into the design of green space restoration?
Green spaces–clean air/polluted air–CVD	Inconsistent for Eco-Health linkage	Support for hypothesis	What are the best indicators to detect the impact of air quality on CVD (e.g., inflammatory response, coagulation, CVD prevalence)?
			Are there consistent confounding factors (demographics, seasonality) determining the impact of air pollutants on CVD?
			What is the main mediator between green spaces and CVD–physical activity or clean air?
Green spaces–heat hazard mitigation/heat hazard–heat morbidities	Support for hypothesis	Support for hypothesis	What are the barriers to establishing green space policy for heat morbidity prevention in cities?

GI disease gastrointestinal disease, *CVD* cardiovascular disease, *EGS* ecosystem goods and services

benefits is enhanced in cities if considered alongside design aspects such as selection of tree species, attention to placement and configuration of trees, and aspects of the built environment that encourage use of green spaces. This evidence should encourage green space planning within cities by showing human health is an achievable objective of restoration investments.

Acknowledgements We thank Laura Jackson, Mathew Harwell, Susan Yee, Marc Russell and anonymous reviewers for comments that greatly improved this manuscript. The views expressed in this paper are those of the authors and do not necessarily reflect the views or policies of the US Environmental Protection Agency. Any mention of trade names, products or services does not imply an endorsement by the US Government or the US Environmental Protection Agency (EPA). The EPA does not endorse any commercial products, services, or enterprises.

Compliance with ethical standards

Conflict of interest There is no conflict of interest to declare.

Human or animal rights Our work did not involve human subjects or third party funding sources.

References

Araya M, Olivares M, Pizarro F, Llanos A, Figueroa G, Uauy R (2004) Community-based randomized double-blind study of gastrointestinal effects and copper exposure in drinking water. Environ Health Perspect 112(10):1068–1073. doi:10.1289/ehp.6913

Beckett KP, Freer-Smith PH, Taylor G (2000) Particulate pollution capture by urban trees: effect of species and windspeed. Glob Change Biol 6(8):995–1003. doi:10.1046/j.1365-2486.2000.00376.x

Bliss DJ, Neufeld RD, Ries RJ (2009) Storm water runoff mitigation using a green roof. Environ Eng Sci 26(2):407–418. doi:10.1089/ees.2007.0186

Bouchama A, Knochel JP (2002) Heat stroke. N Engl J Med 346(25):1978–1988. doi:10.1056/NEJMra011089

Brody SD, Highfield WE (2013) Open space protection and flood mitigation: a national study. Land Use Policy 32:89–95. doi:10.1016/j.landusepol.2012.10.017

Brook RD, Franklin B, Cascio W, Hong Y, Howard G, Lipsett M, Luepker R, Mittleman M, Samet J, Smith SC, Tager I (2004) Air pollution and cardiovascular disease. Circulation 109(21):2655–2671. doi:10.1161/01.CIR.0000128587.30041.C8

Burkart K, Meier F, Schneider A, Breitner S, Canário P, Alcoforado MJ, Scherer D, Endlicher W (2016) Modification of heat-related mortality in an elderly urban population by vegetation (urban green) and proximity to water (urban blue): evidence from

Lisbon, Portugal. Environ Health Perspect 124(7):927. doi:10.1289/ehp.1409529

Cavanagh JA, Zawar-Reza P, Wilson JG (2009) Spatial attenuation of ambient particulate matter air pollution within an urbanised native forest patch. Urban For Urban Greening 8(1):21–30. doi:10.1016/j.ufug.2008.10.002

Chang CC, Chen PS, Yang CY (2015) Short-term effects of fine particulate air pollution on hospital admissions for cardiovascular diseases: a case-crossover study in a tropical city. J Toxicol Environ Health Part A 78(4):267–277. doi:10.1080/15287394.2014.960044

Chew GL, Wilson J, Rabito FA, Grimsley F, Iqbal S, Reponen T, Muilenberg ML, Thorne PS, Dearborn DG, Morley RL (2006) Mold and endotoxin levels in the aftermath of Hurricane Katrina: a pilot project of homes in New Orleans undergoing renovation. Environ Health Perspect 114(12):1883–1889. doi:10.1289/ehp.9258

Collier SA, Wade TJ, Sams EA, Hlavsa MC, Dufour AP, Beach MJ (2015) Swimming in the USA: beachgoer characteristics and health outcomes at US marine and freshwater beaches. J Water Health 13(2):531–543. doi:10.2166/wh.2014.095

Corvalan C, Hales S, McMichael AJ (2005) Ecosystems and human well-being: health synthesis. World Health Organization, Geneva

Costanza R, Pérez-Maqueo O, Martinez ML, Sutton P, Anderson SJ, Mulder K (2008) The value of coastal wetlands for hurricane protection. AMBIO J Human Environ 37(4):241–248. doi:10.1579/0044-7447(2008)37[241:TVOCWF]2.0.CO;2

Dales RE, Zwanenburg H, Burnett R, Franklin CA (1991) Respiratory health effects of home dampness and molds among Canadian children. Am J Epidemiol 134(2):196–203. doi:10.1093/oxfordjournals.aje.a116072

De Lacerda LD, Abrao JJ (1984) Heavy metal accumulation by mangrove and saltmarsh intertidal sediments. Rvta Brasil Bot 7:49–52

Delfino RJ, Staimer N, Tjoa T, Gillen DL, Schauer JJ, Shafer MM (2013) Airway inflammation and oxidative potential of air pollutant particles in a pediatric asthma panel. J Eposure Sci Environ Epidemiol 23(5):466–473. doi:10.1038/jes.2013.25

Donovan GH, Michael YL, Gatziolis D, Prestemon JP, Whitsel EA (2015) Is tree loss associated with cardiovascular-disease risk in the Women's Health Initiative? A natural experiment. Health Place 36:1–7. doi:10.1016/j.healthplace.2015.08.007

Galobardes B, Morabia A, Bernstein MS (2001) Diet and socioeconomic position: does the use of different indicators matter? Int J Epidemiol 30(2):334–340. doi:10.1093/ije/30.2.334

Granek EF, Ruttenberg BI (2007) Protective capacity of mangroves during tropical storms: a case study from 'Wilma'and 'Gamma'in Belize. Mar Ecol Prog Ser 343:101–105. doi:10.3354/meps07141

Grundström M, Pleijel H (2014) Limited effect of urban tree vegetation on NO_2 and O_3 concentrations near a traffic route. Environ Pollut 189:73–76. doi:10.1016/j.envpol.2014.02.026

Hajat A, Allison M, Diez-Roux AV, Jenny NS, Jorgensen NW, Szpiro AA, Vedal S, Kaufman JD (2015) Long-term exposure to air pollution and markers of inflammation, coagulation, and endothelial activation: a repeat-measures analysis in the Multi-Ethnic Study of Atherosclerosis (MESA). Epidemiology 26(3):310–320. doi:10.1097/EDE.0000000000000267

Harlan SL, Declet-Barreto JH, Stefanov WL, Petitti DB (2013) Neighborhood effects on heat deaths: social and environmental predictors of vulnerability in Maricopa County, Arizona. Environ Health Perspect 121(2):197. doi:10.1289/ehp.1104625

Hartig T, Mitchell R, De Vries S, Frumkin H (2014) Nature and health. Annu Rev Public Health 18(35):207–228. doi:10.1146/annurev-publhealth-032013-182443

Hou P, Chen Y, Qiao W, Cao G, Jiang W, Li J (2013) Near-surface air temperature retrieval from satellite images and influence by wetlands in urban region. Theor Appl Climatol 111(1–2):109–118. doi:10.1007/s00704-012-0629-7

Hulshof KF, Löwik MR, Kok FJ, Wedel M, Brants HA, Hermus RJ, Ten Hoor F (1991) Diet and other life-style factors in high and low socio-economic groups (Dutch Nutrition Surveillance System). Eur J Clin Nutr 45(9):441–450

Jackson LE, Daniel J, McCorkle B, Sears A, Bush KF (2013) Linking ecosystem services and human health: the Eco-Health Relationship Browser. Int J Public Health 58(5):747–755. doi:10.1007/s00038-013-0482-1

Kabisch N, Haase D (2013) Green spaces of European cities revisited for 1990–2006. Landsc Urban Plan 110:113–122. doi:10.1016/j.landurbplan.2012.10.017

Kagawa J (1985) Evaluation of biological significance of nitrogen oxides exposure. Tokai J Exp Clin Med 10(4):348–53

Karim MR, Manshadi FD, Karpiscak MM, Gerba CP (2004) The persistence and removal of enteric pathogens in constructed wetlands. Water Res 38(7):1831–1837. doi:10.1016/j.watres.2003.12.029

Katukiza AY, Ronteltap M, Steen P, Foppen JW, Lens PN (2014) Quantification of microbial risks to human health caused by waterborne viruses and bacteria in an urban slum. J Appl Microbiol 116(2):447–463. doi:10.1111/jam.12368

Kong F, Yin H, Wang C, Cavan G, James P (2014) A satellite image-based analysis of factors contributing to the green-space cool island intensity on a city scale. Urban For Urban Greening 13(4):846–853

Lee AC, Maheswaran R (2011) The health benefits of urban green spaces: a review of the evidence. J Public Health 33(2):212–222. doi:10.1093/pubmed/fdq068

Li N, Xia T, Nel AE (2008) The role of oxidative stress in ambient particulate matter-induced lung diseases and its implications in the toxicity of engineered nanoparticles. Free Radic Biol Med 44(9):1689–1699. doi:10.1016/j.freeradbiomed.2008.01.028

Li X, Zhou W, Ouyang Z (2013) Relationship between land surface temperature and spatial pattern of greenspace: what are the effects of spatial resolution? Landsc Urban Plan 114:1–8. doi:10.1016/j.freeradbiomed.2008.01.028

Lim SS, Vos T, Flaxman AD, Danaei G, Shibuya K, Adair-Rohani H, AlMazroa MA, Amann M, Anderson HR, Andrews KG, Aryee M (2013) A comparative risk assessment of burden of disease and injury attributable to 67 risk factors and risk factor clusters in 21 regions, 1990–2010: a systematic analysis for the Global Burden of Disease Study 2010. Lancet 380(9859):2224–2260. doi:10.1016/S0140-6736(12)61766-8

Lovasi GS, O'Neil-Dunne JP, Lu JW, Sheehan D, Perzanowski MS, MacFaden SW, King KL, Matte T, Miller RL, Hoepner LA, Perera FP (2013) Urban tree canopy and asthma, wheeze, rhinitis, and allergic sensitization to tree pollen in a New York City birth cohort. Environ Health Perspect 121(4):494. doi:10.1289/ehp.1205513

Makaryus M, Iakovou A, Lisker G (2015) A case of severe asthma with fungal sensitization (safs) due to Aureobasidium Pullulans following Hurricane Sandy. In: Interesting cases in allergy and immunology. American Thoracic Society, pp A5644–A5644

Millennium Ecosystem Assessment (MEA) (2005) Ecosystems and human well-being: synthesis. Island Press, Washington, DC. ISBN 1-59726-040-1

Möller I, Kudella M, Rupprecht F, Spencer T, Paul M, Van Wesenbeeck BK, Wolters G, Jensen K, Bouma TJ, Miranda-Lange M, Schimmels S (2014) Wave attenuation over coastal salt marshes under storm surge conditions. Nat Geosci 7(10):727–731. doi:10.1038/ngeo2251

Munns WR, Rea AW, Mazzotta MJ, Wainger LA, Saterson K (2015) Toward a standard lexicon for ecosystem services. Integr Environ Assess Manag 11(4):666–673. doi:10.1002/ieam.1631

Nel A, Xia T, Mädler L, Li N (2006) Toxic potential of materials at the nanolevel. Science 311(5761):622–627

Nguyen T, Yu X, Zhang Z, Liu M, Liu X (2015) Relationship between types of urban forest and PM 2.5 capture at three growth stages of leaves. J Environ Sci 27:33–41. doi:10.1016/j.jes.2014.04.019

Norris RH, Webb JA, Nichols SJ, Stewardson MJ, Harrison ET (2011) Analyzing cause and effect in environmental assessments: using weighted evidence from the literature. Freshw Sci 31(1):5–21. doi:10.1899/11-027.1

Norton BA, Coutts AM, Livesley SJ, Harris RJ, Hunter AM, Williams NS (2015) Planning for cooler cities: a framework to prioritise green infrastructure to mitigate high temperatures in urban landscapes. Landsc Urban Plan 134:127–138. doi:10.1016/j.landurbplan.2014.10.018

Nowak DJ, Crane DE, Stevens JC, Hoehn RE, Walton JT, Bond J (2008) A ground-based method of assessing urban forest structure and ecosystem services. Arboric Urban For 34(6):347–358

Nowak DJ, Hirabayashi S, Bodine A, Hoehn R (2013) Modeled $PM_{2.5}$ removal by trees in ten US cities and associated health effects. Environ Pollut 178:395–402. doi:10.1016/j.envpol.2013.03.050

Park KJ, Moon JY, Ha JS, Kim SD, Pyun BY, Min TK, Park YH (2013) Impacts of heavy rain and typhoon on allergic disease. Osong Public Health Res Perspect 4(3):140–145. doi:10.1016/j.phrp.2013.04.009

Pereira G, Christian H, Foster S, Boruff BJ, Bull F, Knuiman M, Giles-Corti B (2013) The association between neighborhood greenness and weight status: an observational study in Perth Western Australia. Environ Health 12(1):49. doi:10.1186/1476-069X-12-49

Peters A, Döring A, Wichmann HE, Koenig W (1997) Increased plasma viscosity during an air pollution episode: a link to mortality? Lancet 349(9065):1582–1587. doi:10.1016/S0140-6736(97)01211-7

Pope CA III, Burnett RT, Thun MJ, Calle EE, Krewski D, Ito K, Thurston GD (2002) Lung cancer, cardiopulmonary mortality, and long-term exposure to fine particulate air pollution. JAMA 287(9):1132–1141. doi:10.1001/jama.287.9.1132

Pokorný J, Květ J, Rejšková A, Brom J (2010) Wetlands as energy-dissipating systems. J Ind Microbiol biotechnol 37(12):1299–305

Prescott GJ, Lee RJ, Cohen GR, Elton RA, Lee AJ, Fowkes FG, Agius RM (2000) Investigation of factors which might indicate susceptibility to particulate air pollution. Occup Environ Med 57(1):53–57. doi:10.1136/oem.57.1.53

Räsänen JV, Holopainen T, Joutsensaari J, Ndam C, Pasanen P, Rinnan Å, Kivimäenpää M (2013) Effects of species-specific leaf characteristics and reduced water availability on fine particle capture efficiency of trees. Environ Pollut 183:64–70. doi:10.1016/j.envpol.2013.05.015

Reacher M, McKenzie K, Lane C, Nichols T, Kedge I, Iversen A, Hepple P, Walter T, Laxton C, Simpson J (2004) Health impacts of flooding in Lewes: a comparison of reported gastrointestinal and other illness and mental health in flooded and non-flooded households. Commun Dise Public Health 7(1):39–46

Reinelt LE, Horner RR (1995) Pollutant removal from stormwater runoff by palustrine wetlands based on comprehensive budgets. Ecol Eng 4(2):77–97. doi:10.1016/0925-8574(94)00002-M

Reno AL, Brooks EG, Ameredes BT (2015) Mechanisms of heightened airway sensitivity and responses to inhaled SO_2 in asthmatics. Environ Health Insights 9(Suppl 1):13

Richardson EA, Pearce J, Mitchell R, Kingham S (2013) Role of physical activity in the relationship between urban green space and health. Public Health 127(4):318–324. doi:10.1016/j.puhe.2013.01.004

Russo F, Williamson J (2007) Interpreting causality in the health sciences. Int Stud Philos Sci 21(2):157–170. doi:10.1080/02698590701498084

Shanahan DF, Lin BB, Bush R, Gaston KJ, Dean JH, Barber E, Fuller RA (2015) Toward improved public health outcomes from urban nature. Am J Public Health 105(3):470–477

Shepard CC, Crain CM, Beck MW (2011) The protective role of coastal marshes: a systematic review and meta-analysis. PLoS One 6(11):1–11. doi:10.1371/journal.pone.0027374

Silva CA, Lacerda LD, Rezende CE (1990) Metals reservoir in a red mangrove forest. Biotropica 22(4):339–345. doi:10.2307/2388551

Vailshery LS, Jaganmohan M, Nagendra H (2013) Effect of street trees on microclimate and air pollution in a tropical city. Urban For Urban Green 12(3):408–415. doi:10.1016/j.ufug.2013.03.002

Vandentorren S, Bretin P, Zeghnoun A, Mandereau-Bruno L, Croisier A, Cochet C, Ribéron J, Siberan I, Declercq B, Ledrans M (2006) August 2003 heat wave in France: risk factors for death of elderly people living at home. Eur J Public Health 16(6):583–591. doi:10.1093/eurpub/ckl063

Wade TJ, Sandhu SK, Levy D, Lee S, LeChevallier MW, Katz L, Colford JM Jr (2004) Did a severe flood in the Midwest cause an increase in the incidence of gastrointestinal symptoms? Am J Epidemiol 159(4):398–405. doi:10.1093/aje/kwh050

Walters S, Griffiths RK, Ayres JG (1994) Temporal association between hospital admissions for asthma in Birmingham and ambient levels of sulphur dioxide and smoke. Thorax 49(2):133–140. doi:10.1136/thx.49.10.1042

Wania A, Bruse M, Blond N, Weber C (2012) Analysing the influence of different street vegetation on traffic-induced particle dispersion using microscale simulations. J Environ Manag 94(1):91–101. doi:10.1016/j.jenvman.2011.06.036

Webb JA, Miller KA, Stewardson MJ, de Little SC, Nichols SJ, Wealands SR (2015) An online database and desktop assessment software to simplify systematic reviews in environmental science. Environ Model Softw 64:72–79. doi:10.1016/j.envsoft.2014.11.011

Weber F, Kowarik I, Säumel I (2014) Herbaceous plants as filters: immobilization of particulates along urban street corridors. Environ Pollut 186:234–240. doi:10.1016/j.envpol.2013.12.011

Weed DL (1997) On the use of causal criteria. Int J Epidemiol 26(6):1137–1141. doi:10.1093/ije/26.6.1137

Yang Q, Tam NF, Wong YS, Luan TG, Su WS, Lan CY, Shin PK, Cheung SG (2008) Potential use of mangroves as constructed wetland for municipal sewage treatment in Futian, Shenzhen, China. Mar Pollut Bull 57(6):735–743. doi:10.1016/j.marpolbul.2008.01.037

Zhen WM, Shan ZH, Gong WS, Yan TA, Zheng SK (2013) The weather temperature and air pollution interaction and its effect on hospital admissions due to respiratory system diseases in western China. Biomed Environ Sci 26:403–407. doi:10.3967/0895-3988.2013.05.011

EPA/600/R-17/266
August 2017
http://www.epa.gov/si

United States
Environmental Protection Agency

Practical Strategies for Integrating Final Ecosystem Goods and Services into Community Decision-Making

U.S. Environmental Protection Agency
Office of Research and Development

EPA/600/R-17/266
August 2017

Practical Strategies for Integrating Final Ecosystem Goods and Services into Community Decision-Making

By

Susan Yee[1], Justin Bousquin[1], Randy Bruins[2], Timothy J. Canfield[3], Theodore H. DeWitt[4], Rebeca de Jesús-Crespo[1], Brian Dyson[5], Richard Fulford[1], Matthew Harwell[1], Joel Hoffman[6], Chanda J. Littles[7], John M. Johnston[8], Robert B. McKane[9], Lauri Green[7], Marc Russell[1], Leah Sharpe[1], Nadia Seeteram[10], Arik Tashie[11], Kathleen Williams[6]

Office of Research and Development
U.S. Environmental Protection Agency

1. Gulf Ecology Division, National Health and Environmental Effects Research Laboratory, Gulf Breeze, FL 32561
2. Systems Exposure Division, National Exposure Research Laboratory, Cincinnati, OH 45268
3. Ground Water and Ecosystems Restoration Division, National Risk Management Research Laboratory, Ada, OK 74820
4. Western Ecology Division, National Health and Environmental Effects Research Laboratory, Newport, OR 97365
5. Land and Materials Management Division, National Risk Management Research Laboratory, Cincinnati, OH 45268
6. Mid-Continent Ecology Division, National Health and Environmental Effects Research Laboratory, Duluth, MN 55804
7. Oak Ridge Institute for Science Education (ORISE) Postdoctoral Fellow, Western Ecology Division, National Health and Environmental Effects Research Laboratory, Newport, OR 97365
8. Computational Exposure Division, National Exposure Research Laboratory, Athens, GA 30605
9. Western Ecology Division, National Health and Environmental Effects Research Laboratory, Corvallis, OR 97333
10. ORISE Fellow, Computational Exposure Division, National Exposure Research Laboratory, Athens, GA 30605
11. ORISE Fellow, Environmental and Public Health Division, National Health and Environmental Effects Research Laboratory, Research Triangle Park, NC 27709

5.4. Ecological Benefits Functions

In most cases, estimating the consequences of decisions on ecosystem services should include a direct connection from those services to human beneficiaries (EPFs to EBFs; **Figure 5.1**). This connection allows for more direct and meaningful assessments of impacts when production of FEGS may be affected by a decision. While benefits can be universally understood through a multi-dimensional concept of well-being (Munns et al. 2015a), impacts of ecosystem services on well-being may be measured in a number of different ways (see **Chapter 4.2**), and numerous approaches have been applied to quantify well-being.

In this section we summarize ecological benefits functions from three dominant benefit viewpoints:

- monetary value;
- human health; and
- human well-being.

Note, these approaches are not independent and have significant overlap. Monetary values can be placed on human health (e.g., costs of health care), and environmental economists often consider Total Economic Value (TEV) as a way to quantify well-being. Human health endpoints (e.g., mortality or disease rates) are also commonly assessed as a measure of well-being for outcomes that are difficult to monetize (Reacher et al. 2004; Gariepy et al. 2014). The final approach, human well-being, attempts to provide a comprehensive non-monetary measure by integrating metrics of health and wealth with other factors such as culture, safety, and social cohesion (Summers et al. 2014; Dyrbye et al. 2016). All three approaches have strengths and weaknesses worth considering, and could be used individually or in combination when assessing benefits from FEGS.

Strategy:	**Let objectives drive choice of methods for FEGS benefits analyses**
	Choice of methods to estimate ecosystem services benefits (EBFs) should primarily be driven by 1) the benefits endpoints under consideration as objectives and 2) the depth of analysis required to make a decision. Tool assumptions and input data needs also influence whether implementation of a method is practical.

The development of predictive or descriptive tools is similar across all three benefit categories, but the resulting tools are dependent on different assumptions and input data. Tools in general can be categorized across a continuum from:

- conceptual tools that elucidate connections between ecosystem services and benefits (Eco-Health Relationship Browser; Jackson et al. 2013), but do not attempt to estimate outcomes; to
- semi-quantitative tools that make predictions based on associative relationships (e.g., i-Tree, www.itreetools.org); to
- fully quantitative models that predict outcomes (NOAA 2009; Dorn et al. 2014) optimally with some estimate of uncertainty appropriate for assessment of risk (Miller et al. 2005).

These are similar to ecological production functions discussed in the previous section (**Section 5.3**), but have human benefit metrics as their output. The type of tool selected will depend on the specific benefits and management actions under consideration. Here we focus on data needs and outputs to compare different approaches for benefit functions.

Monetary endpoints are by far the most dominant category in terms of available tools (Birol et al. 2006; Johnston and Wainger 2015; Yoskowitz et al. 2016). This also includes endpoints that clearly represent economic markets (e.g., commercial fish harvest) from which a monetary value could easily be calculated or inferred. Aside from the plethora of choices, these tools are also useful for comparing benefit across disparate issues, as they focus on a common endpoint measure (e.g., monetary value). However, available valuation tools tend to be biased towards assessing benefits from consumptive services, as values of market goods are often more straightforward to quantify (Tuya et al. 2014). In cases of marketable commodities (e.g., natural resource products) this is a relatively straight forward exercise involving economic models of supply and demand (Ronnback 1999; Samonte-Tan et al. 2007; Fulford et al. 2015b). Yet, many ecosystem goods and services, such as habitat or carbon storage, are hard to monetize, as people do not buy and sell them directly. Instead, they provide non-consumptive services to a set of beneficiaries that is difficult to define. In the latter case, value is typically estimated based on preference models (Beaumont et al. 2008; Mangi et al. 2011; **Appendix E5**) that substitute stated or revealed preference of stakeholders for a more direct estimate of cost.

An extensive literature exists on the subject of preference models and the application of such models to general monetary valuation is well-supported (Castro et al. 2016; Irvine et al. 2016; Romo-Lozano et al. 2017). However, these models can be controversial as a predictive tool, because of underlying assumptions and the large potential for bias resulting from an often inadequate beneficiary sampling frame (Brouwer 2006; Christie and Gibbons 2011). Beneficiaries are asked to convert their perceived preference for a good or service into monetary terms. However, many unstated or unmeasurable factors can influence the outcome, including proximity of respondents to the good or service, demographics of respondents, or even state of mind of respondents during the survey. Despite these issues, stated preference models remain a common tool for estimating value of ecosystem services to beneficiaries because they allow straightforward comparison of the results across beneficiary groups and decision contexts.

Measures of health benefits from ecosystem goods and services are another prolific area of research and policy (**Appendix E6**). Human health endpoints bridge the gap between consumptive (e.g. diet) and non-consumptive (environmental quality) services (Reacher et al. 2004; Gariepy et al. 2014). Health outcomes can be divided into two broad categories (Jackson et al. 2013):

- acute or chronic health problems that could be buffered by natural ecosystems (Reacher et al. 2004; Wade et al. 2014); or
- the health promotional role of nature on physical activity, mental health, and general healthiness (Gariepy et al. 2014; Lee and Duk-Chul. 2014).

Most progress in development of health benefit functions has occurred in the former category where integrated public health and environmental research has generated abundant data linking environmental quality to health outcomes. Examples include the relationship between access to

green space and reductions in heat morbidity (Harlan et al. 2013). Here, the impact of preserving shading/transpiration capacity of greenspace can be clearly connected to changes in incidence of heat morbidity in urban ecosystems. A number of models and tools (e.g., i-Tree, BenMap[†]) exist to predict effects of ecosystem services on health outcomes, including respiratory diseases, heat-related morbidity, cardiovascular diseases, and mortality (reviewed in Oosterbroek et al. 2016). However, many tools rely on proxies to quantify health impacts, and while some ecosystem services (i.e., air purification, natural hazard protection) are fairly well represented, there are few, if any, tools available for other kinds of health outcomes (e.g., mental disorders, injuries, infectious diseases) or other kinds of health-related ecosystem services, including biological control of infectious diseases and promotion of social interactions (Oosterbroek et al. 2016).

Promotional benefits of the natural environment on general healthiness may be particularly hard to quantify (Breslow et al. 2016). Ecosystem services, such as swimmable water, clean air, and accessible green space, have well-accepted relationships to beneficiary activity level, fitness, and quality of life (Bryce et al. 2016), but data to effectively link these to measurable health benefits, particularly given the numerous social, economic, and behavioral correlates (e.g., regional differences in the popularity of outdoor activities), are challenging to collect. Some models and tools use proxies, such as reductions in the frequency of doctor visits or reduced healthcare costs, to quantify such promotional benefits (Oosterbroek et al. 2016). As a result, predictions of promotional health benefits to evaluate decision options are often based on qualitative relationships or educated guesses. Their quantification as causal relationships (or atleast robust correlations) is a promising area of research for development of benefit production functions.

In cases where tools to link ecosystem services to health outcomes are lacking, approaches that leverage more general evidence-based assessments or expert opinion may be better suited. Health Impact Assessments (HIA; **Appendix E7**) are conducted on a community by community basis, and rely on expert opinions to predict likely health outcomes across a suite of decision options (Rhodus et al. 2013). A formal analysis, such as a metadata analysis, can be used to assess the degree of scientific evidence for potential health outcomes (Norris et al. 2011; de Jesús-Crespo and Fulford 2017).

The final and most general category of ecological benefits functions includes functions that attempt to predict or quantify human well-being using non-monetary measures of well-being. Measures of well-being are typically composite indices of multiple metrics across a suite of categories developed based on expert opinion (Smith et al. 2013; Ferrara and Nistico 2015; Dyrbye et al. 2016). Measures of well-being are used globally to assess and summarize benefit in a consistent way across spatial areas or over time (e.g., Gallup Healthways Well-being Index, http://www.well-beingindex.com/; Canadian Index of Well-being, http://uwaterloo.ca/canadian-index-well-being).

Human well-being is a broad concept covering multiple benefits, including the monetary and health benefits previously discussed. The advantage of considering multiple types of well-being benefits is that it

[†] See List of Abbreviations and Symbols for full names of models.

- may be more closely aligned with what stakeholders value about their community than monetary measures (Fulford et al. 2016b; **Appendix C5**);
- provides a method to quantify well-being holistically as a single objective – enabling comparisons with other types of objectives (e.g., cost of a project); and
- provides a flexible approach for examining trade-offs across multiple objectives and their metrics of well-being that may not be amenable to standard cost-benefit analyses (e.g., living standards vs. connection to nature vs. social cohesion).

Several efforts have been undertaken to connect the provisioning of ecosystem services to measures of well-being, paving the way for a well-being benefit function (Gordon and Folke 2000; Pereira et al. 2005; Pinto et al. 2014). One example is the Human Well-Being Index (HWBI, Smith et al. 2013, **Appendix E8**), a compilation of metrics across eight domains of well-being. Recently developed models relate measures of economic, social, and ecosystem services to changes in HWBI, and can be applied to investigate how changes in ecosystem services might impact different domains of well-being, or well-being as a whole (Summers et al. 2016). Though based on nationally consistent county-scale metrics, these models may be informative for predicting potential qualitative outcomes for well-being under different decision scenarios (e.g., an increase in greenspace), and provide a transferable approach for development of finer scale models, with alternative metrics where needed, if community-scale data is available.

5.5. Data Availability and Model Transferability

Developing models and techniques for quantifying impacts on FEGS and their benefits can be a complex, highly technical process that is time-consuming and data-intensive. Often, the timeline of decisions is faster than the pace of ecosystem services research (Granek et al. 2010). Decision-makers are often faced with insufficient time to collect data specific to their site or develop models specific to their needs.

Practitioners and researchers may need to be willing and ready to work with available data on projects. Appropriate information or technical data may be limited regarding the future biophysical state of the ecosystem (e.g., preferred land use, topography or bathymetry), and the ability to control a future biophysical state adds uncertainty to the FEGS assessment. Further, ecological and decision-scales may be poorly matched (e.g, fish habitat may function on a spatial scale far larger than the decision scale regarding future ecological restoration; Angradi et al. 2016).

Practitioners can explore the potential of transferring existing measurements or models from the original site for which they were collected or developed, to their current site. Inappropriately transferring models or measurements between sites can lead to inaccurate estimates of FEGS, and consequently, decisions based on inaccurate information. While benefit-transfer methods exist to transfer economic models and measurements (e.g., Johnston and Rosenberger 2010), a formal methodology for transferring ecological models and measurements has only recently been developed. That methodology is detailed in **Appendix E9**.

Appendix E6
Measuring Health Outcomes

Background

Ecosystem services have been linked to a variety of physical and mental health benefits. For example, the recreation opportunities provided by nature promote greater physical activity and stress reduction, leading to lower rates of obesity and depression (Bell et al. 2008; Gariepy et al. 2014). The removal of air and water pollutants by trees and wetlands helps protect urban communities from respiratory, cardiovascular and gastrointestinal diseases (Yang et al. 2008; Nowak et al. 2013). Trees and wetlands also help mitigate weather hazards, ameliorating the impact of heat waves and flood events on human health (Reacher et al. 2004; Harlan et al. 2013). Many of these connections have been well studied and as a result, there is a growing number of resources available for communities to incorporate ecosystem services into decision-making for the benefit of human health. Here we list some of these resources and provide examples of how to apply these tools at the community level.

Available Tools

To understand the role of ecosystem services on human health, a good starting point is the Eco-Health Relationship Browser (Jackson et al. 2013), which compiles the evidence currently available, and displays linkages in a user friendly interface (**Fig.E6.1**).

Figure E6.1. The Eco-Health Browser visualizes linkages between ecosystems and human health, and provides literature. Urban Ecosystems → Obesity, used in an example below, is highlighted.

Next, communities may be interested in knowing what environmental stressors they are exposed to, and what natural assets may protect them from these stressors. This type of information can be found in the EnviroAtlas at the National Level and for around 50 communities through the US. In addition, understanding the current health status of your community is key for establishing priorities, and assessing the impact of management decisions. The CDC's Community Health Status Indicators (CHSI) provides information about disease trends at the county level, and visualization tools that help define how a specific place compares to the rest of the nation. For higher resolution, the CDC foundation recently launched the 500 cities project, which provides census block group health data, allowing communities to access information specific to their neighborhoods. For neighborhoods not featured in the 500 cities project, but that need information at a fine resolution, conducting Health Impact Assessments (HIA) may be the best alternative (see **Appendix E7**). The Eco-Health Browser and EnviroAtlas as well as CDC's Healthy Places Initiative provide tools, conceptual models, and educational material to help guide this process. Lastly, modelling approaches such as i-Tree Eco and BenMap are useful for communities interested in quantitatively estimating health benefits/impacts at present conditions and under different scenarios. These modelling tools are mainly available for the most studied Eco-Health linkages such as the role of trees in preventing respiratory and cardiovascular diseases, as well as heat hazards.

Example: Tree cover in Tampa Florida and Obesity Rate

Tampa Florida, is featured in both the EnviroAtlas Community datasets and the 500 Cities Project, which allows for low scale visualizations of Eco-Health linkages. In this example, we used block group data from EnviroAtlas showing the percentage of tree cover within walkable streets. We compared this map layer with data on obesity rates from the 500 cities project (**Figure E6.2**).

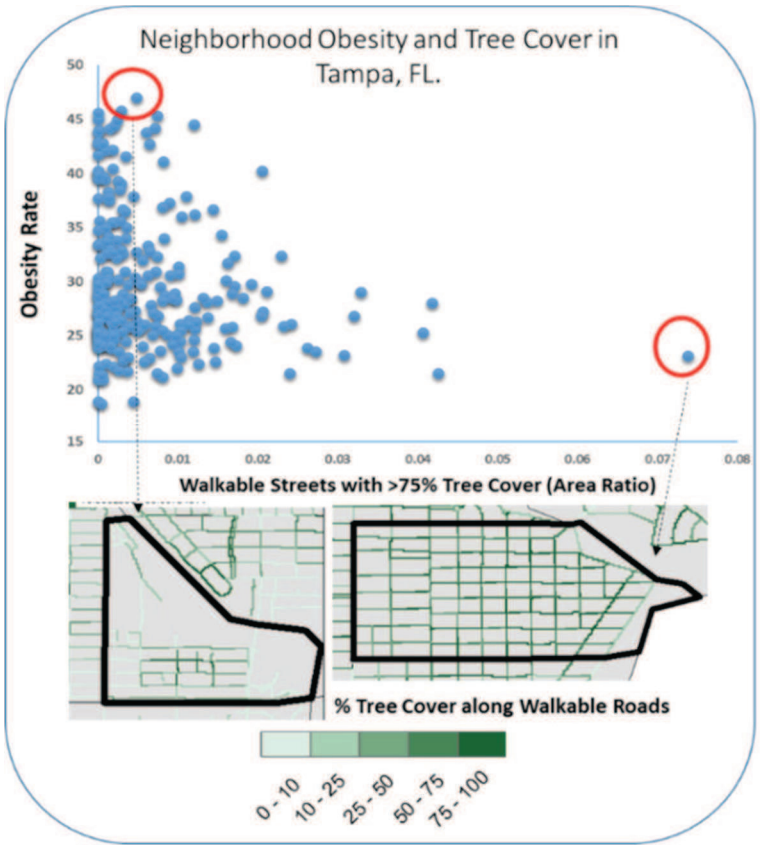

Figure E6.2. Descriptive analysis of obesity trends in relation to tree cover at the neighborhood scale. Data on tree cover comes from EnviroAtlas. Obesity data comes from the 500 Cities Project.

The resulting scatterplot suggests lower obesity rates on block groups with a high percentage of trees bordering walkable streets. This trend corresponds to the relationships shown in the Eco-Health browser, and may be used to set research priorities. For example, a follow up research question would be to ask if the relationship is driven more by walkability, by greenness or by the interaction of both elements. This and similar questions would help communities prioritize ecosystem service management for health promoting services.

Transferability of Approach

Many communities are not included on the high resolution datasets used for the example above. In such cases, County data may bring to attention larger trends to guide prioritization for research and management. For example, CHSI data for counties in Tampa, FL suggests lower physical in-activity and obesity rate for Pinellas vs Hillsborough County (**Fig. E6.3**). This finding may lead communities in Hillsborough to investigate potential drivers, such as the difference in proximity to green spaces observed in the same two counties at lower resolutions (**Fig. E6.3**).

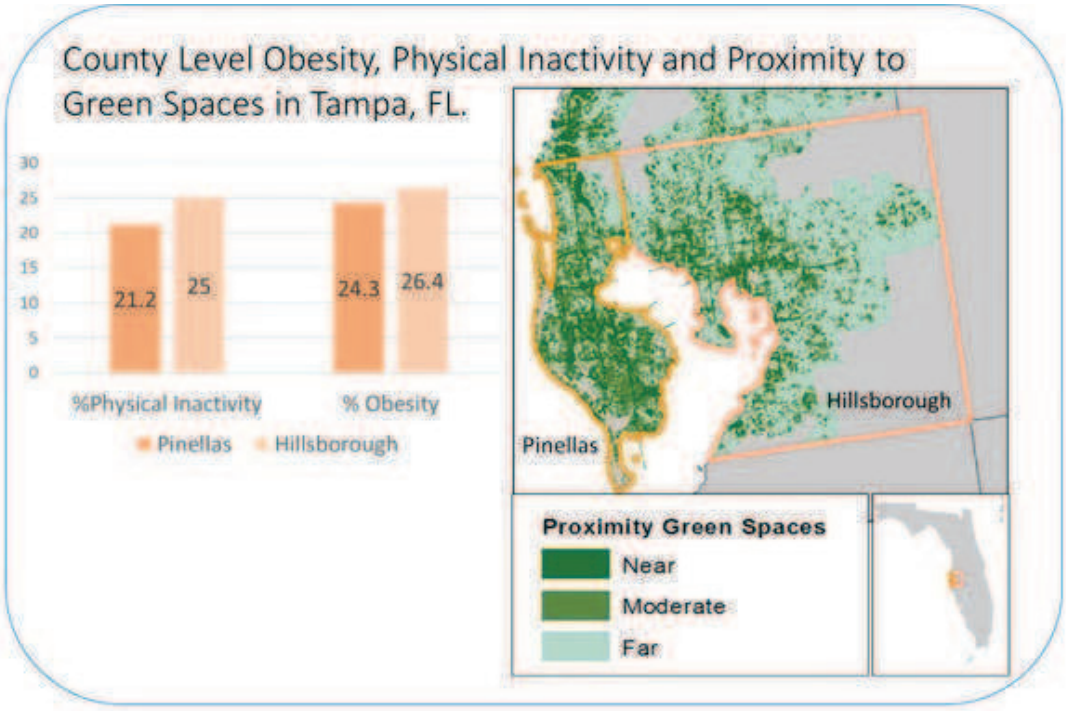

Figure E6.3. County level analysis. Data on Green Spaces comes from EnviroAtlas. Data on Obesity and Physical Inactivity comes from CHSI.

Transferability may also be affected by socio-economic and behavioral differences among exposed populations, which may either exacerbate or ameliorate the impact of ecosystem services on health. Incorporating data from the U.S census or CDC's behavioral risk factor surveillance system (BRFSS) could assist in identifying important confounding factors that may alter Eco-Health linkages.

Summary

Practical strategies discussed here for measuring health outcomes associated to Ecosystem Services are summarized in **Table E6.1**.

Table E6.1. Examples of potential steps in measuring community level health outcomes. Not all steps need to be followed, and the list is not comprehensive.

Steps	Useful Tools*	Scale
Understand Eco-Health Linkages	Eco-Health Browser	All
Evaluate Exposure to Environmental Stressors	EnviroAtlas	National-HUC/Community
Determine Health Priorities	CDC-500 Cities HIA** CDC-CHSI***	Community Community National-County
Model Current and Future Impact to Health	BenMap I-Tree	All All

*These are just examples of practical tools, and not a comprehensive list
**Health Impact Assessment (HIA)
***Center for Disease Control (CDC) Community Health Status Indicators (CHSI).

For More Information

500 Cities Project https://www.cdc.gov/500cities/

Bell, J.F., J.S. Wilson, G.C. Liu. 2008. Neighborhood greenness and 2-year changes in Body Mass Index of children and youth. American Journal of Preventive Medicine 35(6):547-553

BenMap Model: https://www.epa.gov/benmap

Centers for Disease Control and Prevention (CDC) Behavioral Risk Factor Surveillance System (BRFSS): https://www.cdc.gov/brfss/

CDC Community Health Status Indicators (CHSI) https://www.cdc.gov/CommunityHealth/home

Gariepy, G., A. Blair, Y. Kestens, N. Schmitz. 2014. Neighborhood characteristics and 10-year risk of depression in Canadian adults with and without a chronic illness. Health and Place 30:279-86

Harlan, S.L., J.H. Declet-Barreto, W.L. Stefanov, D.B. Petitti. 2013. Neighborhood effects on heat deaths: social and environmental predictors of vulnerability in Maricopa County, Arizona. Environmental Health Perspectives (Online) 121(2):197.

I-Tree Model: http://www.itreetools.org/

Jackson L.E., J. Daniel, B. McCorkle, A. Sears, K.F. Bush. 2013. Linking ecosystem services and human health: The Eco-Health Relationship Browser. International Journal of Public Health 58:747-755.

Nowak, D.J., S. Hirabayashi, A. Bodine, R. Hoehn.. 2013. Modeled PM 2.5 removal by trees in ten US cities and associated health effects. Environmental Pollution 178:395-402.

Reacher, M., K. McKenzie, C. Lane, T. Nichols, I. Kedge, A. Iversen, J. Simpson. 2004. Health impacts of flooding in Lewes: a comparison of reported gastrointestinal and other illness and mental health in flooded and non-flooded households. Communicable Disease and Public Health, 7(1):39-46.

U.S. Census: https://www.census.gov/

U.S. Environmental Protection Agency. 2015. Health Impact Assessment & EnviroAtlas: Integrating Ecosystem Services into the Decision Making Process. Office of Research and Development, National Health and Environmental Effects Research Laboratory, Research Triangle Park, NC. EPA/600/RR-15/128.

Yang, Q., N.F. Tam, Y.S. Wong, T.G. Luan, W.S. Su, C.Y. Lan, S.G. Cheung. 2008. Potential use of mangroves as constructed wetland for municipal sewage treatment in Futian, Shenzhen, China. Marine Pollution Bulletin 57(6):735-743.

EPA/600/R-17/309 | August 2017 | www.epa.gov/research

United States
Environmental Protection
Agency

Valuing Community Benefits of Final Ecosystem Goods and Services: Human Health and Ethnographic Approaches as Complements to Economic Valuation

SHC PROJECT 2.61

EPA/600/R-17/309
August 2017

Valuing Community Benefits of Final Ecosystem Goods and Services: Human Health and Ethnographic Approaches as Complements to Economic Valuation

SHC Project 2.61

by

John M. Johnston[1], Rebeca de Jesus Crespo[1], Matt Harwell[1], Chloe Jackson[1], Mark Myer[2], Nadia Seeteram[2], Kathleen Williams[2], Susan Yee[1], Joel Hoffman[1]
[1]U.S. Environmental Protection Agency
[2]Oak Ridge Institute for Science and Education
Washington, DC

Project Officer John M. Johnston

Computational Exposure Division
National Exposure Research Laboratory
Athens, GA 30605

2. Human Health Approaches – Causal Inference

2.1. Causal Criteria Analysis

In epidemiology, observed associations between human health and environmental, social, or behavioral variables are applied to inform causal inference about potential drivers of disease (Merrill et al. 2008). The principles of causal inference, consistency, strength of association, temporality, biological plausibility, and specificity[3] (Merrill et al. 2008), need to be met in order for cause-effect relationships to be supported. Causal criteria analysis applies these principles to determine the weight of evidence towards causal connections in terms of: 1) probabilistic evidence (i.e., consistent cause-effect association); and 2) mechanistic evidence (i.e., logical explanation of how the causal association occurs) (Russo and Williamson 2007). A classic example of the application of this approach is the Surgeon General's 1964 report on smoking and health, which has become a landmark of how science can be effectively applied in decision making for the benefit of human health (Parascandola et al. 2006).

Regarding ecosystem services, U.S. EPA's Eco-Health browser provides a comprehensive inventory of the best available science supporting the complex relationships between different ecosystems, human health and well-being. This tool provides a starting point to construct a causal criteria analysis on this context and better understand which linkages have enough evidence to be used as a basis for management applications and which should be regarded as working hypotheses in need of more research.

2.2. Application of Causal Criteria Analysis to Evaluate the Role of Green Space EGS on Human Health

Building on U.S. EPA's Eco-Health browser, a causal criteria analysis was conducted using Eco Evidence an open source software tool that incorporates causal inference principles (Eco-Evidence tool; accessed 20, July 2017) (Norris et al. 2011). The focus of this analysis were linkages between diseases and the buffering EGS provided by green spaces (de Jesus Crespo and Fulford 2017; Figure 2.1). Buffering EGS refers to the ecosystem's capacity to buffer against health impacts by removing pollutants from air and water, and mitigating heat and water hazards (Jackson et al. 2013). The term green space refers to any vegetation within a human dominated environment (Kabisch and Haase 2013). This includes urban trees, green roofs, and natural or constructed wetlands, all of which provide EGS that influence health (GI – gastrointestinal, CVD - cardiovascular disease). Green spaces intercept water,

[3] Consistency: the association has been replicated by different research projects; Strength of association: the association is not due to bias or confounding factors, and is statistically significant; Temporality: exposure to a suspected cause precedes the disease; Biological plausibility: a logical biological mechanism for the association exists; Specificity: the exposure and disease are specific to one another (this condition is not always needed in order to support causality) (Merrill et al. 2008).

promote infiltration, and serve as barriers to storm surges, leading to water hazard mitigation (Brody and Highfield 2013, Costanza et al. 2008). Mitigation of water hazards reduces exposure risk to polluted flood waters and GI disease (Wade et al. 2004). It also reduces the risk of post-flood household dampness, which could lead to mold growth and asthma (Chew et al. 2006). Green spaces also promote clean water by immobilizing and absorbing infectious and toxic pollutants (Karim et al. 2004, Silva et al. 1990) and reducing the risk of GI disease from contact or consumption (Araya et al. 2004, Katukiza et al. 2014). In addition, green spaces filter air pollutants (Räsänen et al. 2013) that cause respiratory illness and cardiovascular disease (Brook et al. 2004, Peters et al. 1997). They also provide shade and evapotranspiration, lowering the risk of heat wave induced morbidities (Bouchama and Knochel 2002).

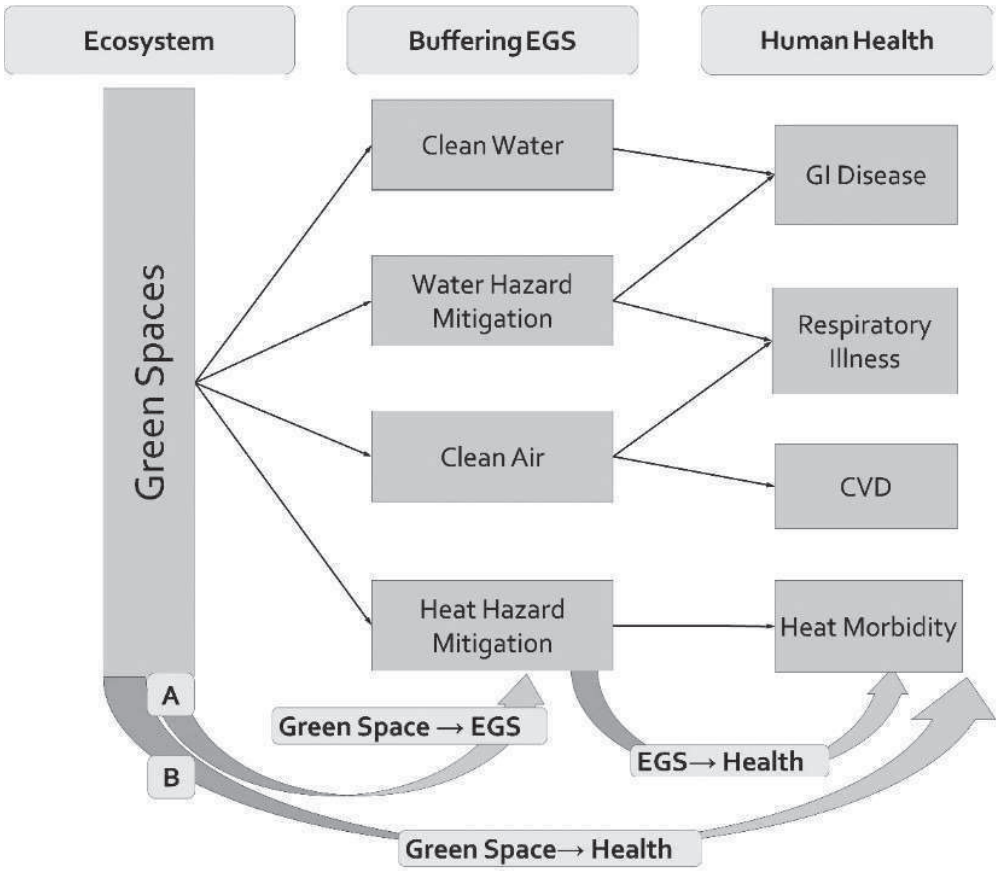

Figure 2.1 Eco-health pathways connecting the ecosystem attribute, green spaces, to human health endpoints through indirect ("A"; buffering EGS) and direct ("B"; human health) pathways. Figure from de Jesus Crespo and Fulford (2017).

While all these linkages are mechanistically plausible, our results showed that the weight of evidence supporting each of them varies as shown in Table 2.1. Notably, most of the current eco-health literature supports findings of intermediate steps (e.g., ecosystem to buffering EGS and buffering EGS to human health), but there is limited support for direct linkages from ecosystem (green spaces) to human health (disease endpoints) (Table 2.1). For example, while there is sufficient evidence supporting water pollution removal by vegetation, and sufficient evidence supporting a connection between certain water pollutants and GI disease, there is insufficient evidence supporting a direct connection between vegetation and GI disease (Table 8.3). Studies including all the components of the causal relationships are much needed as they would help provide clear management recommendations, such as the effectiveness of different plant species, relationships to the built environment and expected effect sizes of restoration initiatives. For more details of these results and the methods used see Appendix 3, and de

Jesus Crespo and Fulford (2017).

Table 2.1 Results of causal criteria analysis of eco-health linkages. (For more details, see Appendix 3; adapted from de Jesus Crespo and Fulford 2017).

Linkage	Total Studies Found	Total Studies Reviewed	Weight of Evidence in Favor	Weight of Evidence not in Favor	Conclusion
Green Spaces and Buffering EGS					
Green Spaces-Clean Water	60	44	166	16	Support for Hypothesis
Green Spaces-Water Hazard Mitigation	28	19	106	16	Support for Hypothesis
Green Spaces-Clean Air	44	22	105	16	Support for Hypothesis
Green Spaces-Heat Hazard Mitigation	31	19	117	3	Support for Hypothesis
Buffering EGS and Human Health					
Clean Water-GI Disease	11	6	35	0	Support for Hypothesis
Water Hazard Mitigation-GI Disease	9	7	41	7	Support for Hypothesis
Water Hazard Mitigation-Respiratory Illness	4	4	16	5	Insufficient Evidence
Clean Air-Respiratory Illness	37	28	247	178	Inconsistent Evidence*
Clean Air-Cardiovascular Disease (CVD)	27	23	206	143	Inconsistent Evidence*
Heat Hazard Mitigation-Heat Morbidities	22	18	114	2	Support for Hypothesis
Green Spaces and Human Health-Direct					
Green Spaces-GI Disease	0	0	0	0	Insufficient Evidence
Green Spaces-Respiratory Illness	9	7	28	27	Inconsistent Evidence*
Green Spaces-CVD	9	3	27	0	Support for Hypothesis
Green Spaces-Heat Morbidities	10	4	35	0	Support for Hypothesis

* Note: the finding of "inconsistent evidence" may indicate potential confounding factors that play a mediating role, or highlight the role that context and the types of indicators used could play in detecting a given cause and effect relationship. See Nichols et al. (2011) for more details on interpreting this and other conclusions derived using this approach.

2.3. Empirical Approaches for Eco-Health Research

Causal criteria analysis allowed identifying a research agenda (Appendix 3) to advance our

understanding of eco-health linkages. Conceptual models, such as the Final Ecosystem Goods and Services framework (Figure 2.2), have been developed to guide research on this topic, and may be applied to address research needs. The FEGS framework includes four key components: Ecosystem state metrics, EGS indicators, Health benefit indicators, and Socio-economic factors, which are essential to fully characterize eco-health relationship pathways.

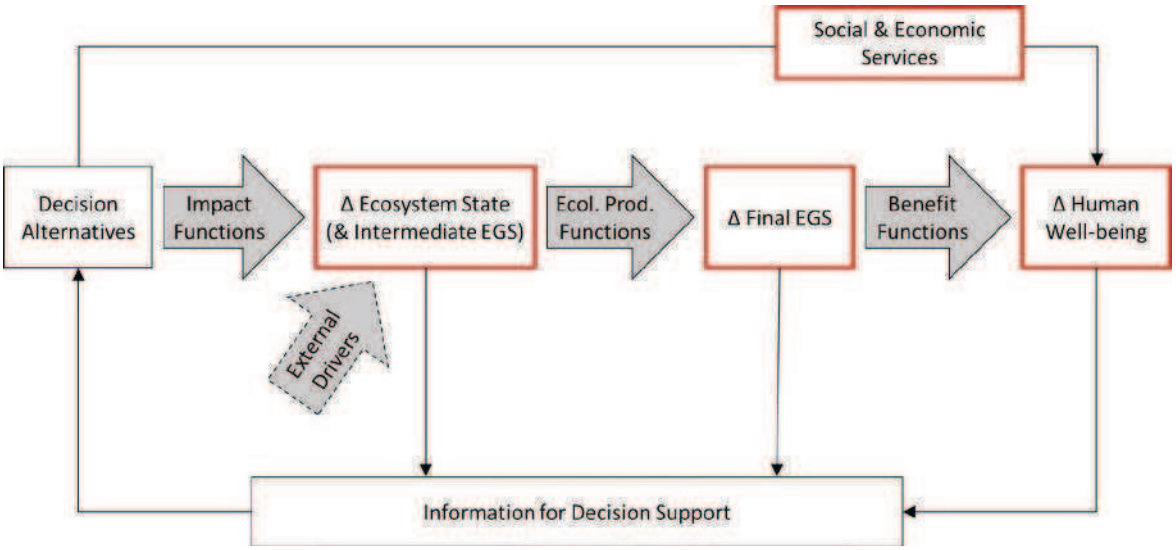

Figure 2.2 Conceptual Model for measuring Final Ecosystem Goods and Services. Areas measured through studies linking ecosystem services to health and well-being outcomes are highlighted in red.

Conducting spatially explicit correlation analyses is a logical first step towards testing eco-health conceptual models such as FEGS. Mapping platforms provide a way to test the spatial relationship between EGS and disease, contingent on the existence of suitable datasets to characterize the extent and quality of ecosystem services, to understand the socio-economic context, and to locate disease hotspots. Appendix 4 explores issues of data accessibility and granularity in mapping human health outcomes for spatially explicit correlation analyses approaches in eco-health studies.

For indicators that help map EGS, useful approaches include (but are not limited to) habitat suitability assessments, locations of trails or other recreational facilities, and modeling natural viewscapes. Angradi et al. (2016) mapped EGS in the Great Lakes region; the study provides a useful example of how to use existing datasets for EGS mapping, incorporating factors such as data uncertainty and tradeoffs into the analysis. Available sources for mapping EGS include the U.S. Geological Survey's National Gap Analysis Program, which helps estimate the distribution of species and ecosystems of interest, and the U.S. EPA EnviroAtlas (EnviroAtlas; accessed 20, July 2017) (Jackson et al. 2013), which helps visualize the extent of ecosystem services, among others.

Defining the spatial distribution of EGS is only the first step to modeling eco-health linkages. Socio-economic factors may exacerbate or decrease vulnerability to EGS loss and certain communities may be protected from the impacts of degrading EGS due to behavioral adaptations, technological adaptations, or access to EGS from other regions (Figure 2.3). These factors have been termed insulating layers (Myers et al. 2013), and are generally associated with wealth and access to information. Incorporating socio-economic indicators that reflect the potential for certain communities to benefit more than others from EGS provision (e.g., U.S. Census datasets) should be an essential part of studies assessing eco-health linkages.

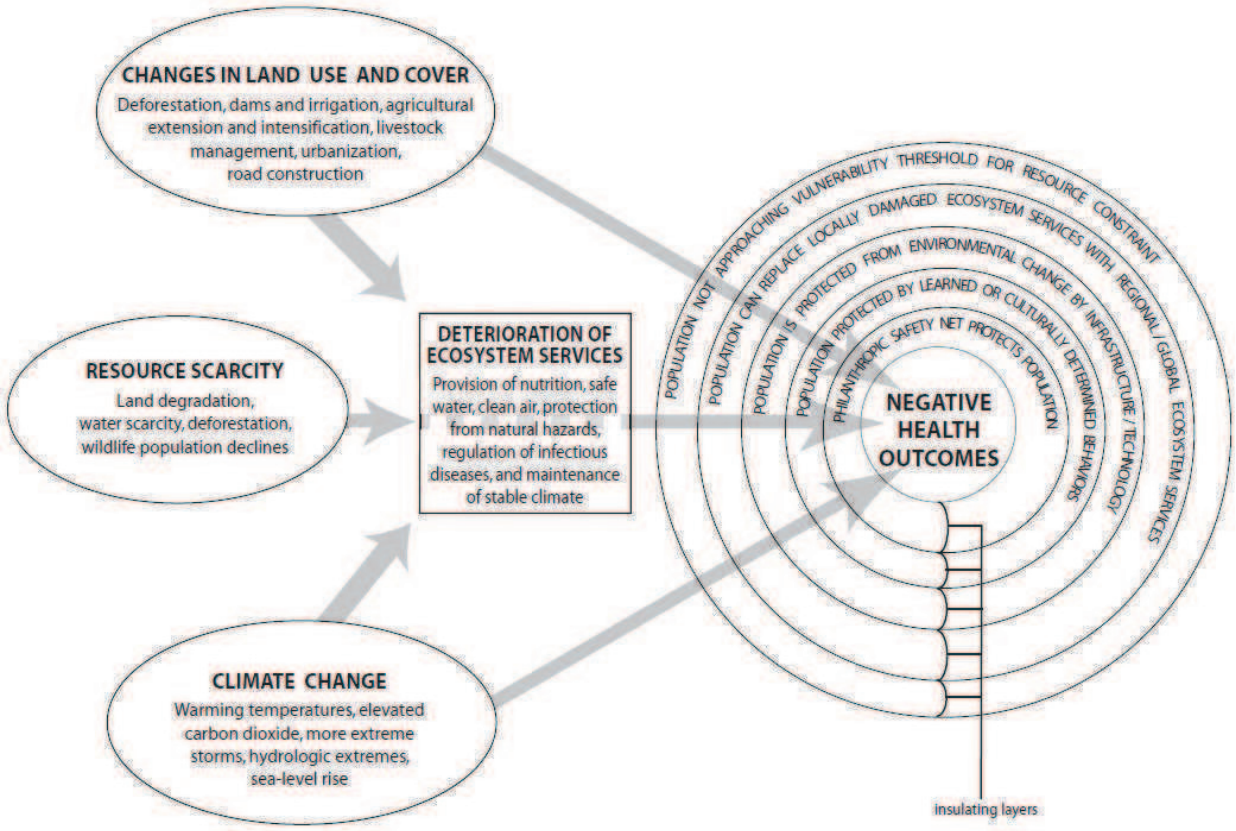

Figure 2.3 Schematic of the complex relationships between altered environmental conditions and human health. The impact of ecosystem goods and services loss is modified by socio-economic factors, termed insulating layers, which can ameliorate potential negative outcomes. Adapted from Myers et al. (2013).

Aside from health benefits, there are other human benefits associated with ecosystem services, such as safety, culture, and living standards. EPA's Human Well-Being Index (HWBI) provides a conceptual framework for mapping well-being at multiple scales in the United States (Smith et al. 2012, Smith et al. 2014), as well as forecasting changes due to loss of EGS (Summers et al. 2016). The HWBI is a tool that can be used to complement Eco-Health studies for a more general understanding of EGS benefits at the county and state levels.

Similar to economic benefit valuation (Figure 2.4; Wainger and Mazzotta 2011), research approaches for assessing health benefits could fall within a gradient of complexity, from the empirical analysis of conceptual models, as we propose here, to the use of simulation tools that predict loss of benefit from changes in EGS. Most conceptual models that describe eco-health linkages need more empirical evidence to develop quantitative relationships. Therefore, the use of simulation models is limited in this context to the few associations that have been studied extensively. A discussion of the use of data-derived models for simulating eco-health benefits is presented in Appendix 2.

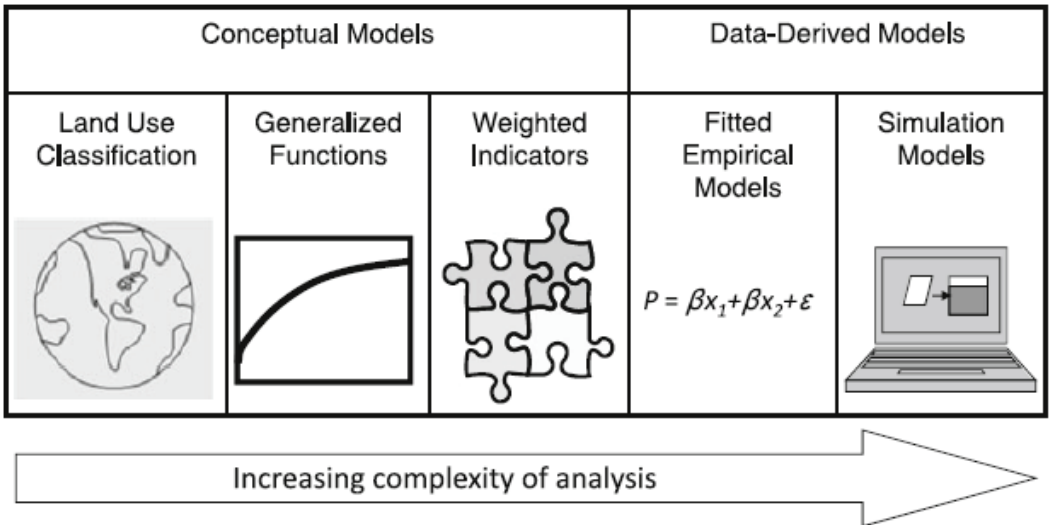

Figure 2.4 The gradient of modeling complexity shows different types of analysis used to generate the functional relations that estimate benefits of ecosystem goods and services management. From Wainger and Mazzotta (2011).

2.4. Upcoming Application of Empirical Approaches for Eco-Health Research in the San Juan Bay Estuary, PR

The communities in the SJBE, have identified many key health concerns associated with environmental stressors (Sheffield et al. 2014, Méndez-Lázaro et al. 2015). To help mitigate these stressors, the restoration of green spaces has been suggested a potential management strategy to improve health and well-being for SJBE residents (SJEB Management Plan 2017; accessed 26, July 2017). However, more studies are need to address the expected effectiveness of these practices. This case study seeks to quantify health outcomes associated with green space cover and buffering EGS using the FEGS framework (Figure 2.2) as a conceptual model. Using this approach entails identifying key ecosystems, ecosystem services, and socio-economic variables that are likely to influence health outcomes in the SJBE (Table 2.2), and then using statistical approaches to establish whether there is quantitative evidence for relationships between these key variables. Existing publicly available data sources could serve as indicators for each of these elements, in order to address the complex relationships in a cost-effective manner.

Some challenges to consider include disparate spatial scales of datasets to be included in the model, and restrictions on the availability of fine-scale human health information due to privacy considerations. Mechanisms to access detailed health data include establishing collaborations with health organizations, purchasing licenses to insurance claims or hospital data, or collecting information directly through surveys. All of these processes require consideration of PII and IRB restrictions. Appendix 5 presents a discussion on the challenges of collecting these types of data. To address limitations on the use of restricted health data, the SJBE case study will leverage collaborations with laboratories that have a health focus and the expertise in epidemiological research. This would not only allow access to data, but also foster cross-disciplinary dialogue to better inform the design and interpretation of a multidisciplinary topic such as eco-health linkages.

Table 2.2 Variables within the FEGS framework to evaluate Eco-Health linkages for the SJBE between green spaces or coastal wetlands and heat morbidities, GI disease, and Dengue fever.

ECOSYSTEM STATE		ECOSYSTEM GOODS AND SERVICES		Δ HUMAN HEALTH BENEFITS		SOCIO-ECONOMIC FACTORS	
NAME	Indicator	Name	Indicator	Name	Indicator	Name	Indicator
GREEN SPACES	% Green Space Cover	Heat Hazard mitigation	Surface temperature derived from satellite images (Landsat 8); Heat Wave Event time period	Heat Morbidities	Medicare Claims for heat related morbidities:	Wealth (influences air conditioning use, housing quality)	Median Income
COASTAL WETLANDS	% Wetland cover	Water Hazard Mitigation	FEMA[1] Flood Claims, Rainfall, Extreme flood event time period	Gastro-Intestinal Disease	Medicare Claims data for gastro-intestinal diseases	Infrastructure (influences storm water management effectiveness)	Sewage density
COASTAL WETLANDS	% Wetland cover	Habitat for Species (i.e., Biological Control)	Vertebrate Species Richness (Gould et al. 2008)	Dengue fever	Dengue prevalence (CDC[2])	Wealth (influences air conditioning use, housing quality)	Median Income
		Clean Water	Nitrogen Concentration (SJBE 2015)			Demographics (influences susceptibility to disease)	%Teenagers
		Heat Hazard mitigation	Surface temperature derived from satellite images (Landsat 8)			Infrastructure (influences vector habitat availability)	Sewage and road density

[1]FEMA: Federal Emergency Management Agency
[2]CDC: Center for Disease Control

As an example, ongoing studies in the SJBE are evaluating the role of wetland ecosystem services (e.g., biological control, clean water, and heat hazard mitigation) on Dengue fever (Figure 2.5). Heat hazard mitigation EGS may help reduce mosquito biting, ovi-position rate, and viral load; clean surface water provides habitat for wildlife and healthier ecosystems, favoring bio-control of mosquitoes (Araujo et al. 2015, Ibarra et al. 2013, Cox et al. 2007, Morin et al. 2015). Preliminary findings suggest that wetlands are negatively associated to Dengue cases even after controlling for potentially confounding variables (Table 2.2). They were also found to help reduce temperature (Figure 2.6), which is an environmental driver of Dengue transmission (Morin et al. 2015). These findings help support a connection between an important ecosystem in the SJBE, and an ecosystem service that directly influences human health. In the future, this and other eco-health research may help inform predictive models to estimate changes in health benefits under different decision scenarios.

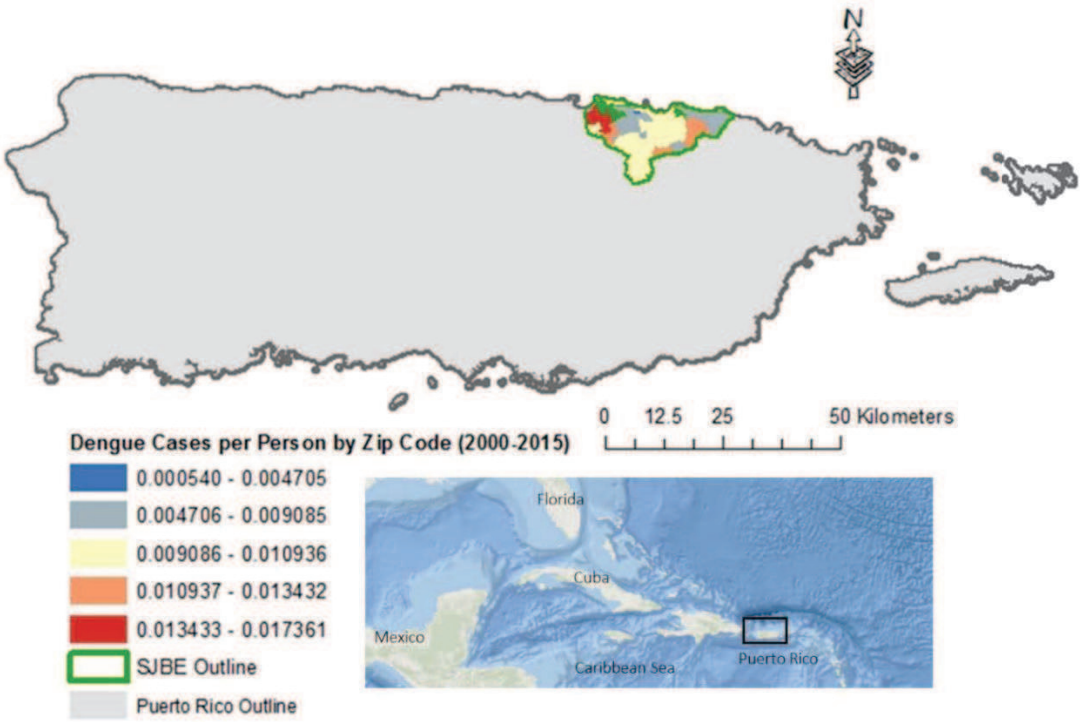

Figure 2.5 Dengue cases per person by zip code in the SJBE. Dengue data was provided by the CDC Dengue branch; Puerto Rico outline (United States Postal Service); Caribbean Map (DeLorme, MapmyIndia, © OpenStreetMap contributors, and the GIS community).

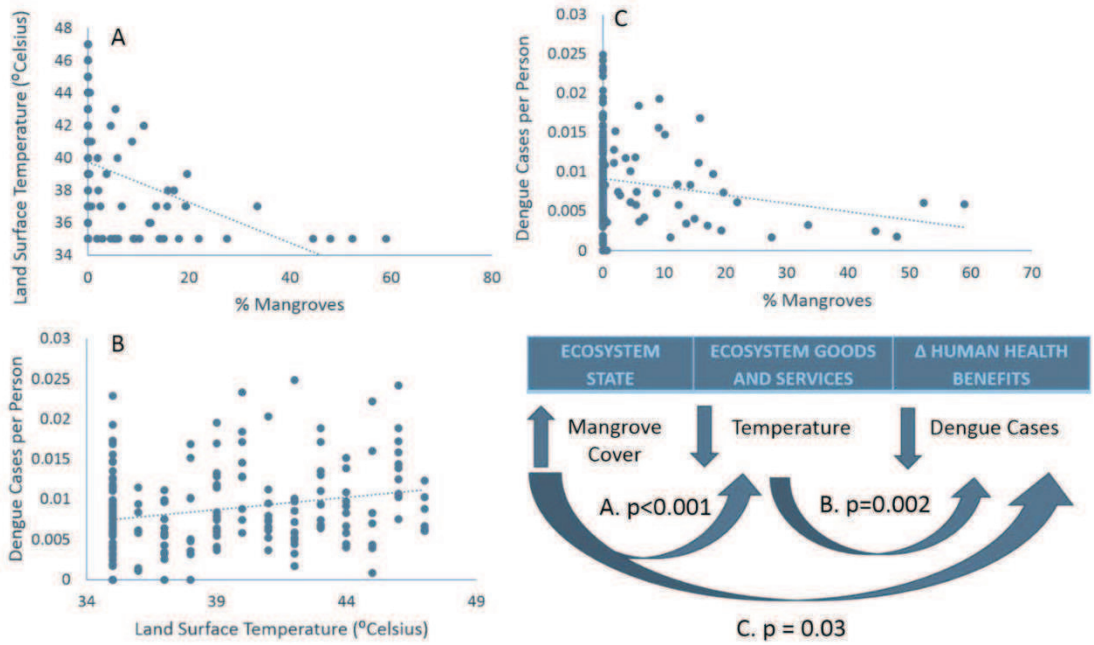

Figure 2.6 Preliminary findings of our study linking Dengue cases to wetland ecosystem services in the San Juan Bay Estuary (de Jesus Crespo et al. 2017). The p values for the linkages described in panel A and C were derived from Beta-binomial regressions including socio-economic confounding factors (Table 2.7). The p values from the link between mangroves and temperature were derived from simple linear regressions.

Work in the SJBE case study will link eco-health research to a decision context, which is the monitoring and management scenarios already proposed by the National Estuary Program (NEP). Aligning research objectives with those of the NEP will facilitate working with volunteers to collect data efficiently, promote educational opportunities, and improve the likelihood that the accumulating body of eco-health evidence (Table 2.2) is relevant and useful for decision makers.

2.5. Conclusions and Future Research Needs

Causal inference approaches allow researchers to use the best available science to inform evidence base decisions making. The principles of causal inference were applied to evaluate the weight of evidence linking green space EGS to human health and identify research needs. Results revealed that the evidence linking EGS to human health mainly supports intermediate steps, and very few published studies link the full pathways from ecosystem to disease. Establishing these linkages would be necessary to provide accurate non-monetary valuation of FEGS for community-based decision making. Specific research needs identified for the context of green space ecosystem services are summarized in Appendix 4 and include:

- Evaluating the association between green spaces on diseases such as GI disease and asthma by means of water hazard mitigation and clean water EGS;
- Defining the predominant mechanism driving the link between green spaces and cardiovascular benefits (i.e., physical activity or recreation versus air pollution removal);
- Better understanding the factors that determine if green spaces promote or prevent respiratory illness considering factors such as plant allergens, and re-circulation of pollutants trapped by foliage, among others.

For additional information on eco-health research needs involving ecosystems and health outcomes not discussed here, see Lee and Maheswaran (2011), Myers et al. (2013), Hartig et al. (2014), Hough (2014), and Sandifer and Sutton Grier (2014).

Addressing identified research needs could be facilitated by the application of conceptual models and using spatially explicit methods to empirically test these conceptual models. Studies evaluating eco-health linkages should take into consideration: 1) other aspects closely tied to human health and captured in conceptual models such as the FEGS framework; 2) the multidisciplinary nature of eco-health research; and 3) the importance of aligning research objectives to a decision context. In addition, issues of data accessibility and granularity in mapping human health outcomes as part of eco-health studies should also be considered (Appendix 4).

Examples were provided of the approach to incorporate these insights as part of ongoing research in the San Juan Bay Estuary, PR. Collaborating with local stakeholders and researchers across disciplines has facilitated progress in terms of identifying secondary data sources and defining priority questions to better inform non-monetary valuation of FEGS in this case study community.

Electronic Supplementary Material 1. Keyword search specifications**.** We searched in Google Scholar for a combination of all keywords in column 1 with the keywords in column 2 to assess Green Space-Ecosystem Goods and Services (EGS) linkages. We used a combination of keywords in column 2 and column 3 to assess EGS-Health linkages, and a combination of keywords in column 1 and column 3 to assess Green Space-Health direct linkages. The keywords selected were based on indicators that we found to be associated to Eco-Health linkages after revising the USEPA Eco Health browser (https://www.epa.gov/enviroatlas/enviroatlas-eco-health-relationship-browser)

1.Green Spaces	***2.Ecosystem Goods and Services***	***3.Physical Health***
trees	Clean Water	*GI Disease
vegetation	fecal coliform	gastro-intestinal
green spaces	copper	diarrhea
green-roofs	Clean Air	vomit
urban forest	*$PM_{2.5,10}$	Respiratory Illness
wetlands	*NO_2	respiratory
mangroves	*SO_2	bronchitis
marshes	*CO	asthma
	Water Hazard Mitigation	cough
	flood	wheeze
	urban runoff	Cardio Vascular Disease
	storm-surge	cardiovascular
	hurricane	heart
	wave attenuation	circulatory
	Heat Hazard Mitigation	Heat Morbidities
	heat	excess hospital admissions
	heat-wave	

*Abbreviations: $PM_{2.5,10}$= particulate matter smaller than 2.5µm, or 10µm; NO_2= Nitrogen dioxide; SO_2= Sulfur dioxide; CO=Carbon monoxide

Electronic Supplementary Material 2. Literature Review Process

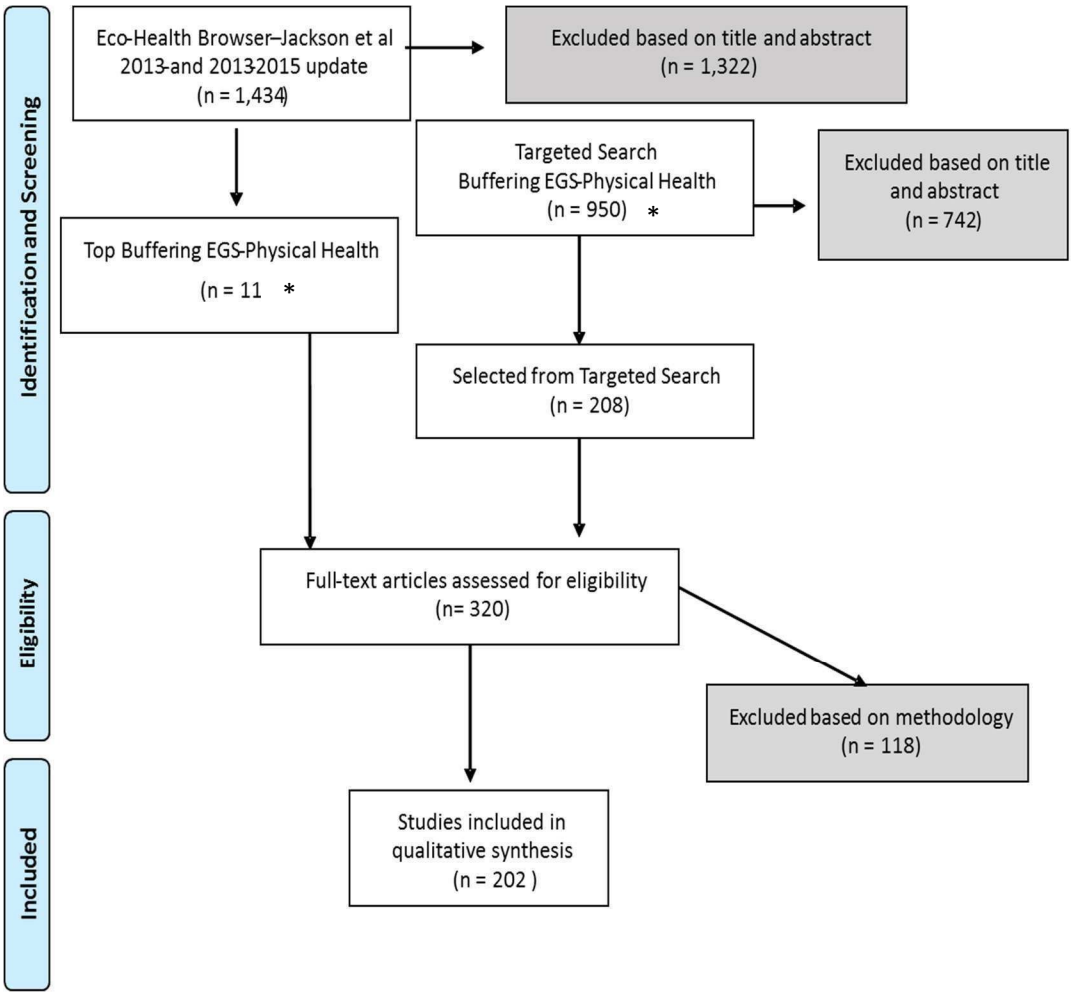

* EGS=Ecosystem Goods and Services

Supplementary Material 3. Details of articles evaluated and Eco-Evidence scores. Abbreviations: GI Disease= Gastro Intestinal Disease; CVD=Cardiovascular disease; EGS=Ecosystem Goods and Services; Y=Yes; N=No.

Linkage	Reference	Cause	Effect	Supports Linkage?	Design	Score	Controls	score	Impacted	Score	Total
Green Space-EGS											
Green Space-Clean Water	Allen 2003	bioretention facilities	copper removal	Y	Before/After	2	0	0	4	3	5
	Allen 2007	bioretention facilities	copper removal	Y	Before/After	2	0	0	2	2	4
	Ayaz et al 2008	constructed wetlands	fecal bacteria	Y	Before/after	2	0	0	3	3	5
	Birch et al 2004	constructed wetlands	fecal bacteria	Y	Before/after	2	0	0	1	0	2
	Birch et al 2005	stormwater infiltration basin	fecal bacteria removal	Y	Before/After	2	0	0	1	0	2
	Casteel et al 2005	riparian buffer	fecal bacteria removal	Y	Before/After	2	0	0	1	0	2
	Cheng et al 2002	constructed wetlandss	copper removal	Y	Before/After	2	0	0	1	0	2
	Coleman et al 2001	constructed wetlands	fecal bacteria	Y	Before/after	2	1	2	4	3	7
	Coyne et al 1995	grass filter strips	fecal Bacteria Removal	Y	Before/After	2	0	0	2	2	4
	Dallas et al 2004	reedbeds	fecal bacteria	Y	Before/after	2	0	0	1	0	2
	Davies and Bavor 2000	constructed wetlands	fecal bacteria	Y	Before/after	2	1	2	1	0	5
	Diaz et al 2010	constructed wetlands	fecal bacteria	Y	Before/after	2	0	0	4	3	5
	Dorsey et al 2010	urban salt marsh	fecal bacteria	N	Before/after	2	0	0	1	0	2
	Eger and Lapakko 1988	natural wetlands	copper removal	Y	Before/After	2	0	0	1	0	2
	Gerba et al 1999	constructed wetlands	fecal bacteria	Y	Before/after	2	0	0	2	1	3
	Hill and Sobsey 2001	constructed wetlands	fecal bacteria	Y	Before/after	2	0	0	3	3	5
	Johnston et al 1990	landscape wetland cover	fecal bacteria	Y	Gradient	3	0	0	15	6	9
	Karathanasis et al 2003	constructed wetlands	fecal bacteria	Y	Before/after	2	0	0	3	3	7
	Karpiscak et al 1996	constructed wetlands	fecal bacteria	Y	Before/after	2	0	0	2	1	3
	Khan et al 2009	constructed wetlandss	copper removal	Y	Before/After	2	0	0	1	0	2
	KNx et al 2008	natural wetlandss	fecal bacteria	Y	Before/after	2	0	0	1	0	2
	Knox et al 2009	impacted wetland	fecal bacteria	N	Before/after	2	0	0	1	0	2
	Lau and Chu 2000	wetland enclosures	fecal bacteria	Y	Before/after	2	0	0	2	1	3

	Li and Allen 2009	bioretention facilities	Copper removal	Y	Before/After	2	0	0	0	0	0
	Mahenge 2014	constructed mangroves	fecal bacteria	Y	Before/after	2	0	0	1	0	2
	Mallin et al 2001	wetland cover	correlation between rain and fecal coliform counts	Y	Gradient	3	0	0	11	6	9
	Mantovi et al 2003	reedbeds	fecal bacteria	Y	Before/after	2	0	0	2	1	3
	Murray-Gulde et al 2005	constructed wetlandss	copper removal	Y	Before/After	2	0	0	1	0	2
	Myers and Ambrose 2015	urban salt marsh	fecal bacteria	Y	Before/after	2	0	0	1	0	2
	Nelson et al 2006	constructed wetlandss	copper removal	Y	Before/After	2	0	0	1	0	2
	Neralla et al 2000	constructed wetlands	fecal bacteria	Y	Before/after	2	0	0	8	3	5
	Perkins and Hunter 2000	constructed wetlands	fecal bacteria	Y	Before/after	2	0	0	4	3	5
	Quiñónez-Dìaz	constructed wetlands	fecal bacteria	N	Before/after	2	1	2	1	0	4
	Rea et al 2015	coastal wetland	fecal bacteria	Y	Gradient	3	0	0	4	2	5
	Reinelt and Horner 1995	palustrine wetland	fecal bacteria	Y	Before/after	2	0	0	2	1	3
	Scholz et al 2002	constructed wetlandss	copper removal	Y	Before/After	2	0	0	1	0	2
	Shutes et al 2001	constructed wetlandss	copper removal	N	Before/After	2	0	0	1	0	2
	Sleytr et al 2007	constructed wetlands	fecal bacteria	N	Before/after	2	2	3	8	3	8
	Song et al 2006	constructed wetlands	fecal bacteria	Y	Before/after	2	0	0	1	0	2
	Steer et al 2002	constructed wetlands	fecal bacteria	Y	Before/after	2	0	0	21	3	5
	Tam and Wong 1995	mangrove mesocosms	copper concentration	Y	Before/after	4	6	3	6	3	10
	Thurston et al 2001	constructed wetlands	fecal bacteria	Y	Before/after	2	1	2	1	0	4
	Vijayaraghavan and Joshi 2014	green roof	Copper removal	Y	Before/After	2	1	2	1	0	4
	Yang et al 2008	constructed mangroves	fecal bacteria	Y	Before/after	2	0	0	3	3	5
Green Spaces-Clean Air	Hill 1971	alfalfa canopy	SO2 removal	Y	Before and After	2	0	0	1	0	2
	Martin and Barber 1967	hedge	SO2 removal	Y	Before and After	2	4	3	1	0	5
	Chaparro-Suarez et al 2011	tree cover	NO2	Y	BACI	4	1	2	1	0	6
	Cohen et al 2014	tree cover	NOx	Y	Gradient	3	0	0	3	0	3
	Grundström and Pleijel 2014	urban trees	NO2	Y	Before and After	2	0	0	1	0	2
	Setala et al 2012	tree canopy	NO2	N	Impact Reference	2	20	3	20	3	8
	Takahashi et al 2005	trees	NO2	Y	Before and After	2	0	0	70	3	5
	Beckettt et al 2000	trees	PM10, 2.5	Y	Reference control	2	5	3	5	3	8

	Cavanagh et al 2009	urban forest	PM10	Y	Gradient	3	0	0	8	6	9
	Cohen et al 2014	tree cover	PM10	Y	Gradient	3	0	0	3	0	3
	Dadvand et al 2015	greenness	TrafficRelated AirPollution	Y	Gradient	3	0	0	39	6	9
	Islam et al 2012	crown density	TSP removal	Y	Gradient	3	0		11	6	9
	Manes et al 2014	urban trees	PM 10	Y	Reference/Control	2	1	2	1	0	4
	Mori et al 2015	shrub species	Traffic Related Air Pollution	Y	Before and After	2	0	0	6	3	5
	Nguyen et al 2014	urban forest	PM 2.5	Y	Impact Reference		1	2	5	3	5
	Rasanen et al 2013	coniferous vs broadleaf	PM	Y	Before and After	2	4	3	4	3	8
	Sæbø et al 2012	woody Species	PM 10, 2.5	Y	Before and After	2	0	0	2	1	3
	Setala et al 2012	tree canopy	PM	N	Impact Reference	2	20	3	20	3	8
	Speak et al 2012	green roof	PM	Y	Impact Reference	2	1	2	2	1	5
	Sternberg et al 2010	green wall/Ivy	PM	Y	Impact Reference	2	2	3	2	1	6
	Weber et al 2014	herbaceous plants	PM	Y	Gradient	3	0	0	3	0	3
	Choi et al 2012	proximity to green space	urban Heat	Y	Gradient	3	0	0	5	4	7
Green Space-Heat Hazard Mitigation	Gromke et al 2015	green space	Heat	Y	Before/After	2	0	0	1	0	2
	Jenerette et al 2011	NDVI	Surface Temperature	Y	Gradient	3	0	0	5000	6	9
	Oliveira et al 2011	green space	Surface Temperature	Y	Reference/Control	2	?	?	1	0	
	Shashua-Bar et al 2011	trees,grass	Thermal Stress	Y	Reference/Control	2	2	3	2	2	7
	Simmons et al 2008	green roof	Surface Temperature	Y	Reference/Control	2	6	3	18	3	8
	Vandertorren et al 2006	green spaces	Heat	Y	Reference/Control	2	257	3	257	3	8
	Dvorak et al 2013	succulent roof tops	Temperature	Y	Reference/Control	2	3	3	9	3	8
	Akbari et al 1997	green space	Cooling Energy	Y	Before/After	2	0	0	2	2	4
	Amson et al 2012	grass and trees	Surface Temperature	Y	Reference/Control	2	1	2	3	3	7
	Chang and Li 2014	cool island parks	Temperature	Y	Gradient	3	0	0	60	6	9
	Chen et al 2014	cool island parks	Temperature	Y	Gradient	3	0	0	1089	6	9
	Feyisa and Milby 2014	NDVI and park area	Cooling	Y	Gradient	3	0	0	21	6	9

	Kong et al 2014	area of forest vegetation	urban Cool Island Intensity	Y	Gradient	3	0	0	153	6	9
	Tan et al 2007	Increased urban green space	Heat wave mortality	Y	Reference/Control	2	1	2	1	0	3
	Vailshery et al 2013	street trees	Temperature	Y	Reference/Control	2	1	2	3	2	8
	Yang et al 2010	percent greening	urban Heat Island	N	Gradient	3	0	0	3	0	3
	Hou et al 2013	distance to urban wetlands	Near Surface air temperature	Y	Gradient	3	0	0	7	6	9
	Song et al 2013	rooftop-wetlands	Temperature	Y	Reference/Control	2	1	2	1	0	4
	Costanza et al 2008	coastal wetlands	storm surge damage	Y	Gradient	3	0	0	34	6	9
Greenspace-WaterHazard Mitigation	Granek and Ruttenberg 2007	mangrove	storm surge damage	Y	BACI	4	7	3	7	3	10
	Krauss et al 2009	coastal wetlands	water level	Y	Before and After	2	0	0	4	3	5
	Moller et al 2016	salt marshes	wave attenuation	Y	Reference-Control	2	1	2	1	0	4
	Moller et al 1999	salt marshes	wave energy	Y	Reference-Control	2	1	2	1	0	4
	Quang 2011	mangrove	wave height	Y	Gradient	3	0	0	32	6	9
	Moller et al 2014	marshes	storm surge	Y	BACI	4	1	2	1	0	6
	Highfield and Broody 2006	inland wetlands	floods	Y	Gradient	3	0	0	67	6	9
	Broody etal 2012	inland wetlands	floods	Y	Gradient	3	0	0	144	6	9
	Broody et al 2008	inland wetlands	flood damage	Y	Gradient	3	0	0	423	6	9
	Carlton et al 2000	inland wetlands	changes in flow	N	Reference-Impact	2	3	3	33	3	8
	Broody and Highfield 2013	open spaces	flood damages	Y	Gradient	3	0	0	450	6	9
	Xiao and McPherson 2016	trees	surface runoff	Y	Before and After	2	0	0	20	3	5
	Lee et al 2013	green spaces	surface runoff	Y	Before and After	2	0	0	1	0	2
	Stovin 2009	green spaces	surface runoff	Y	Before and After	2	0	0	1	0	2
	Mentens et al 2006	green roofs	surface runoff	N	Gradient	3	0	0	18	6	9
	Simmons et al 2008	green roos	surface runoff	Y	Before and After	2	0	0	5	3	5
	VanWoert et al 2005	green roofs	surface runoff	Y	BACI	4	2	3	1	0	7
	Denardo 2005	green roofs	surface runoff	Y	Before and After	2	0	0	3	3	5
	Bliss et al 2008	green spaces	surface runoff	Y	BACI	4	1	2	1	0	6

EGS-Human Health											
Clean Water-GI Disease	Araya et al 2004	Copper	Gi symptoms	Y	Reference/Impact	2	124	3	317	3	8
	Collier et al 2015	waste water in beaches	GI disease	Y	Reference/Impact	2	14539	3	39711	3	8
	Jagai 2014	rainfall/combinedsewer-overflows/drinking water	GI disease	Y	Reference/Impact	2	1	2	2	2	6
	Knobeloch et al 1994	copper	GI upsets	Y	After impact only	1	0	0	5	3	4
	Qasim et al 2014	waterborne pathogens	GI disease	Y	Reference/Impact	2	13	3	252	3	8
	Tyagi et al 2013	fecal coliforms	Water Borne Infections	Y	After impact only	1	0	0	1	0	1
WaterHazard Mitigation-GI Disease	Wade et al 2004	flood	GI disease	Y	Control/ Reference	2	1110	3	1110	3	8
	Reacher et al 2004	flood	GI disease	Y	Reference/Control	2	104	3	103	3	8
	Yusof et al 1991	flood	GI disease	Y	After Impact	1	0	0	46740	3	4
	De Man et al 2015	flood	GI disease	Y	Reference/Control	2	1	2	149	3	7
	Masakazu et al 2016	flood	GI disease	Y	Gradient	3	0	0	10	6	9
	Jagai 2014	rainfall	GI disease	N	BACI	4	1	3	1	0	7
	Hashimoto et al 2014	flood depth	GI disease	Y	Before/After	2	0	0	10	3	5
WaterHazard Mitigation-Respiratory Disease	Dales et al 1991	flood/dampness	bronchitis and cough	Y	Reference-Control	2	10250	3	3238	3	8
	Lakovou et al 2015	flood	asthma	Y	After impact	1	0	0	1	0	1
	park et al 2013	rainfall	asthma	N	Before/After	2	0	0	16	3	5
	Reacher et al 2004	flood	asthma exacerbations	Y	Reference-Control	2	104	3	103	3	8
Clean Air-Respiratory Illness	Adam et al 2015	NO2, PM10	Forced Expiatory Volume and Forced Vital Capacity	Y	Gradient	3	0	0	5	4	7
	Adam et al 2015	PM2.5	Forced Expiatory Volume and Forced Vital Capacity	N	Gradient	3	0	0	5	4	7
	Bayer-Oglesby et al 2005	PM10	Bronchitis, Chronic Cough, Common Cold	Y	Before-After	2	0	0	10	3	5
	Bayer-Oglesby et al 2005	PM10	Asthma, Sneezing, Hay Fever	N	Before-After	2	0	0	10	3	5
	Braun-Fahrländer et al 1997	PM10, NO2, SO2	Chronic Cough, Bronchitis, Night cough	Y	Gradient	3	0	0	10	5	8

	Braun-Fahrländer et al 1997	PM10, NO2, SO3	Asthma, Allergies	N	Gradient	3	0	0	10	5	8
	Burnett et al 1997	Ozone	Respiratory Admissions	Y	Gradient	3	0	0	16	5	8
	Delfino et al 2013	PM2.5 Oxidative potential , NO2	Asthma (fractional exhaled nitric oxide)	Y	Gradient	3	0	0	45	5	8
	Delfino et al 2013	PM2.5 Mass	Asthma (fractional exhaled nitric oxide)	N	Gradient	3	0	0	45	5	8
	Dockery et al 1996	Acid Aerosols	bronchitis,	Y	Gradient	3	0	0	24	5	8
	Dockery et al 1996	Acid Aerosols	Asthma, Chronic Coungh, chronic Phlegm	N	Gradient	3	0	0	24	5	8
	Faustini et al 2013	PM 10, 2.5, and NO2	Respiratory hospitalizations	Y	Gradient	3	0	0	6	5	8
	Gao et al 2014	PM 10, 2.5, SO2, NO2, O3	Wheezing Boys	Y	Impact-Reference	2	1	2	1	0	4
	Gao et al 2014	PM 10, 2.5, SO2, NO2, O3	Wheezing Girls	N	Impact-Reference	2	1	2	1	0	4
	Gao et al 2014	PM 10, 2.5, SO2, NO2, O3	Cough, Phlegm with Cold, Boys, Girls	Y	Impact-Reference	2	1	2	1	0	4
	Gao et al 2014	PM 10, 2.5, SO2, NO2, O3	Allergies Boys and Girls	N	Impact-Reference	2	1	2	1	0	4
	Gonzales-Barcala et al 2013	proximity to Truck Traffic	Asthma in young Boys	Y	Gradient	3	0	0	>14 K	5	8
	Gonzales-Barcala et al 2013	proximity to Truck Traffic	Asthma in Adolescent Boys and Girls	N	Gradient	3	0	0	>14 K	5	8
	Gorai et al 2014	PM 2.5, SO2	Asthma Admissions	Y	Gradient	3	0	0	62	6	9
	Gorai et al 2014	O3	Asthma Admissions	N	Gradient	3	0	0	62	6	9
	Goudarzi et al 2013	O3	COPD	Y	Before and After	2	0	0	1	0	1
	Hasunuma et al 2014	PM, Nox	Asthma	Y	Gradient	3	0	0	28	6	9
	Hasunuma et al 2014	PM, Nox	Allergic Rhinitis	N	Gradient	3	0	0	28	6	9
	Jacquemin et al 2015	PM, Nox	Asthma	N	Gradient	3	0	0	24	6	9
	Kim et al 2015	proximity to Trafic Roads	Airway Hyperresponsiveness	Y	Gradient	3	0	0	4	2	5
	Liu et al 2013	PM 10, 2.5 Nox	Allergic Rhinitis, Persistent Cough and Phlegm, Wheezing in Girls	Y	Gradient	3	0	0	25	6	9
	Liu et al 2013	PM 10, 2.5 Nox	Allergic Rhinitis, Persistent Cough and Phlegm, Wheezing in Boys	N	Gradient	3	0	0	25	6	9
	Liu et al 2013	Exposure to roads and indoor pollution	Respiratory symptoms	Y	Gradient	3	0	0	6730	6	9
	Morales et al 2015	prenatal NO2 exposure	lung function-preschool children	Y	Gradient	3	0	0	620	6	9
	park et al 2013	PM 10, NO2	Asthmatic Hospital Admissions-Elderly	Y	Gradient	3	0	0	7	6	9
	park et al 2013	NO2	Asthmatic Hospital Admissions-Adults and Children	N	Gradient	3	0	0	7	6	9

	Ponka and Virtanen 1994	NO2, SO2	exacerbation of chronic bronchitis or emphysema-elderly	N	Gradient	3	0	0	1096	6	9
	Ponka and Virtanen 1994	NO2	exacerbation of chronic bronchitis or emphysema-adults	Y	Gradient	3	0	0	1096	6	9
	Ponka and Virtanen 1994	SO2	exacerbation of chronic bronchitis or emphysema-adults	Y	Gradient	3	0	0	1096	6	9
	Prescott et al 1998	Black Smoke, PM10, NO2	Respiratory Mortality elderly	Y	Gradient	3	0	0	33	6	9
	Prescott et al 1998	SO2, CO, O3, Black smoke, NO2	Respiratory Mortality elderly and adults	N	Gradient	3	0	0	33	6	9
	Puett et al 2014	PM10. 2.5	Lung Cancer-Nurses health study	Y	Gradient	3	0	0	72	6	9
	Segala et al 1998	PM, SO2, NO2	Prevalent and Incident Asthma, Respiratory infections all	Y	Gradient	3	0	0	84	6	9
	Segala et al 1998	PM, NO2	Incident and Prevalent Wheeze Mild Asthmatics	N	Gradient	3	0	0	43	6	9
	Segala et al 1998	PM, NO2, SO2	Incident and Prevalent Wheeze	Y	Gradient	3	0	0	43	6	9
	Vandini et al 2013	PM10	RSV	Y	Gradient	3	0	0	84	6	9
	Vandini et al 2013	PM2.5	RSV	N	Gradient	3	0	0	84	6	9
	Walter et al 1994	SO2	Asthma in Spring and Summer	N	Gradient	3	0	0	>5	6	9
	Walter et al 1994	SO2	Asthma in Winter and Fall	Y	Gradient	3	0	0	>5	6	9
	Walter et al 1994	Smoke	Respiratory All/All seasons	Y	Gradient	3	0	0	>5	6	9
	Wang et al 2013	PM10, NO2, SO2	Respiratory Admissions Low and Moderate Temperatures	Y	Gradient	3	0	0	>5	6	9
	Wang et al 2013	PM10, SO2,NO2	Respiratory Admissions Hot Temperatures	N	Gradient	3	0	0	>5	6	9
	Winquist et al 2014	PM2.5, NO2, O3 warm season	Pediatric Asthma admissions	Y	Gradient	3	0	0	1196	6	9
	Winquist et al 2014	PM2.5, NO2, O3 cold season	Pediatric Asthma admissions	N	Gradient	3	0	0	1148	6	9
	Yamazaki et al 2013	PM2.5, O3, NO2	Pediatric Asthma visits and Pediatric Hospital Admissions	N	Gradient	3	0	0	124-243	6	9
	Yamazaki et al 2014	O3	Hospital admissions asthma	Y	Gradient	3	0	0	210	6	9
	Zhou et al 2015	PM10	Respirstory mortality adults	N	Gradient	3	0	0	32	6	9
	Zhou et al 2015	PM10	Respirstory mortality elderly	Y	Gradient	3	0	0	32	6	9
	Pope etal 2002	SO2, PM	Lung Cancer	Y	Gradient	3	0	0	51	6	9
Clean Air-CVD	Babish et al 2014	PM2.5	Hypertension	Y	Gradient	3	0	0	4166	3	9
	Bilenko et al 2015	PM10,2.5, SO2	Blood Pressure	N	Gradient	3	0	0	1432	3	9
	Chang et al 2015	PM2.5	CVD admissions on cool days	Y	Gradient	3	0	0	>1500	3	9
	Chang et al 2015	PM2.5	CVD admissions on warm days	N	Gradient	3	0	0	>1501	3	9
	Chang et al 2013	PM 2.5	Myocardial infarction	Y	Gradient	3	0	0	>1500	3	9
	Dong et al 2013	PM10, SO2	CVD survey	N	Gradient	3	0	0	24845	3	9
	forester et al 2014	NO2	Blood Pressure	Y	Reference-Control	2	12 22	3	704	3	8

	Fuks et al 2014	Traffic load 100m from residence	Blood Pressure	Y	Gradient	3	0	0	113 000	6	9
	Hajat et al 2012	NOx	Blood Clots (fibrinogen)	Y	Gradient	3	0	0	>2k	3	9
	Hajat et al 2013	NOx	Inflamation (CRP, IL6, E-selecting, SICam), Blood Clots (D-Dimer)	N	Gradient	3	0	0	>2k	3	9
	Hajat et al 2015	PM2.5	Inflamation (CRP, IL6, E-selecting) and Blood Clots (fibrinogen)	Y	Gradient	3	0	0	>2k	3	9
	Hajat et al 2015	PM2.5	Inflamation (SiCam) and Blood Clots (D-Dimer)	N	Gradient	3	0	0	>2k	3	9
	Hajat et al 2015	NO2	Inflamation (CRP, IL6, E-selecting, SICam) and Blood Clots (fibrinogen)	N	Gradient	3	0	0	>2k	3	9
	Hajat et al 2015	NO2	Blood Clots (D-dimer)	Y	Gradient	3	0	0	>2k	3	9
	Henning et al 2014	PM2.5, 10	Inflamation (CRP)C.Reactive Protein	Y	Before-After	2	0	0	>4k	3	5
	Kajbafzadeh et al 2015	PM2.5 Traffic	Systemic inflamation:CVD morbidity	N	Reference-Control	2	48	3	48	3	8
	Kajbafzadeh et al 2015	PM2.5 WoodSmoke	Systemic inflamation:CVD morbidity	Y	Reference-Control	2	20	3	20	3	8
	Kalsch et al 2014	PM	Toracic Aortic Calcification (artherosclerosis indicator)	Y	Gradient	3	0	0	>4k	6	9
	Link et al 2013	PM 2.5 2 hr prior	Atrial Fibrilation	Y	Gradient	3	0	0	4	2	5
	Liu et al 2014	PM2.5, NO2	Blood Pressure	N	Gradient	3	0	0	2368	6	9
	Miller et al 2007	PM 2.5	Cardivascular Event	Y	Gradient	3	0	0	36	6	9
	Nuvolone et al 2013	O3	acute coronary event	N	Gradient	3	0	0	>500	6	9
	Nuvolone et al 2014	O3	out of hospital coronary death	Y	Gradient	3	0	0	>501	6	9
	Poloniecki et al 1997	O3	acute myocardial infarction	N	Gradient	3	0	0	>2k	6	9
	Poloniecki et al 1997	Black Smoke, CO, SO2	acute myocardial infarction	Y	Gradient	3	0	0	>2k	6	9
	Poloniecki et al 1997	Black Smoke, CO, SO2, O3	Cardiac Arrhytmias	N	Gradient	3	0	0	>2k	6	9
	Poloniecki et al 1997	NO2	Cardiac Arrhytmias	Y	Gradient	3	0	0	>2k	6	9
	Poloniecki et al 1997	CO	Angina Pectoris	Y	Gradient	3	0	0	>2k	6	9
	Poloniecki et al 1997	Black Smoke, SO2, O3, N02	Angina Pectoris	N	Gradient	3	0	0	>2k	6	9
	Poloniecki et al 1997	Black Smoke, CO, SO2, NO2	Combined Circulatory Diseases	Y	Gradient	3	0	0	>2k	6	9
	Poloniecki et al 1997	O3	Combined Circulatory Diseases	N	Gradient	3	0	0	>2k	6	9
	Poloniecki et al 1998	Black Smoke, CO, SO2, NO2, O3	Heart Failure	N	Gradient	3	0	0	>2k	6	9
	Prescott et al 1998	PM10 >65	cardio admissions	Y	Gradient	3	0	0	>36	6	9
	Prescott et al 1999	PM10 <65	cardio admissions	no	Gradient	3	0	0	>36	6	9
	Prescott et al 1999	O3, Black Smoke, So2, NO2 all	cardio admissions	no	Gradient	3	0	0	>36	6	9
	Schwartz et al 1999	CO and PM10	cardio admissions medicare	Y	Gradient	3	0	0	>600	6	9
	Tonne and Wilkinson 2013	PM 2.5	cardiac mortality	Y	Gradient	3	0	0	>6	6	9

	Tonne and Wilkinson 2013	PM 10, Nox	cardiac mortality	no	Gradient	3	0	0	>7	6	9
	Zhang et al 2014	PM 10	cardio mortality (especially IHD)	Y	Gradient	3	0	0	~11	6	9
Heat Hazard-Heat Morbidities	Mamou et al 2013	Heat	Sunburn, Dehydration, Heat Stroke	Y	BACI	4	4	3	4	3	10
	Chan et al 2013	Heat	Respiratory/Infectious disease in hot season	Y	Reference/Control	2	1	2	1	0	4
	Guirguis et al 2014	Heat	Hospital Admissions	Y	Before/After	2	1	2	19	3	7
	Bishop et al 2015	Heat	Hospital Admissions	Y	BACI	4	6	3	3	3	10
	Nitschke et al 2011	Heat	Hospital Admissions	Y	Reference-Control	2	2	3	1	0	5
	Jones etal 1982	1980 Heat Wave	Heat Stroke	Y	Before/After	2	2	3	2	2	7
	Knowlton et al 2008	Heat Wave	Hospital Admissions	Y	Before/After	2	0	0	6	3	5
	Semenza et al 1999	Heat Wave	Dehydration, Heat Stroke, Heat Exhaustion	no	Before/After	2	0	0	1	0	2
	Brunetti et al 2013	Heat Wave	Telecardiology	Y	Reference/Control	2	24	3	6	3	8
	Grolund et al 2014	Heat Wave	Hospital Admissions Medicare	Y	Gradient	3	0	0	114	6	9
	Hess et al 2014	Temperature Anomalies	Emergency Department Visits	Y	Gradient	3	0	0	5	4	7
	Jones et al 1982	1980 Heat Wave	Hospital Visits	Y	Before/After	2	0	0	2	2	4
	kingsley etal 2016	Teperature change	Hospital admissions	Y	Gradient	3	0	0	1260	6	9
	Smith et al 2012	Heat Wave	ED Visits	Y	Reference/Control	2	3	3	1	0	5
	Stotz et al 2014	Temperature Increase	Blood Pressure-Heart Rate	Y	Before/After	2	0	0	26	3	5
	Tasian et al 2014	Temperature	Kidney Stones	Y	Gradient	3	0	0	>2190	6	9
	Xu et al 2014	Extreme Temperatures	Pediatric ED visits	Y	Gradient	3	0	0	>2190	6	9
	Zhang et al 2014	Temperature	Cardiac-Senile Mice	Y	Reference/Control	2	6	3	6	3	8
green space-Human Health											
Green Space-Respiratory Illness	Donovan et al 2013	green space	Mortality-Lower Respiratory Tract	Y	Gradient	3	0	0	1296	6	9
	Lee et al 2014	forest vs City Walking	Respiratory Risk-Pulmonary Function Decrease	Y	BACI	4	19	3	43	3	10
	Lovasi et al 2013	tree canopy cover	Asthma/Allergies	N	Gradient	3	0	0	549	6	9
	Dadvand et al 2014	proximity to parks	Asthma	N	Gradient	3	0	0	3178	6	9
	Fuertes et al 2014	Residential greenness	Allergies	N	Gradient	3	0	0	2531	6	9
	Fuertes et al 2015	Residential greenness	Allergies	Y	Gradient	3	0	0	2007	6	9

Green Space-Heat Morbidities	Harlan et al 2013	Vegetation	Heat Mortality	Y	Gradient	3	0	0	2081	6	9
	Vandertorren et al 2006	green space	Heat Mortality	Y	BACI	4	262	3	315	3	8
	Burkart et al 2015	NDVI	Heat Mortality	Y	Gradient	3	0	0	203	6	9
Green Space-CVD	Donovan et al 2013	green space	CVD Mortality	Y	Gradient	3	0	0	1296	6	9
	Donovan et al 2013	green space	CV Disease	Y	Gradient	3	0	0	534891	6	9
	Pereira et al 2012	green space/NDVI	Coronary Heart Disease	Y	Gradient	3	0	0	11404	6	9

Electronic Supplementary Material 4: Full Bibliography

Green Spaces-EGS

Alongi, D. M., Clough, B. F., Dixon, P., & Tirendi, F. (2003). Nutrient partitioning and storage in arid-zone forests of the mangroves Rhizophora stylosa and Avicennia marina. Trees, 17(1), 51-60. doi: 10.1007/s00468-002-0206-2

Amorim, J. H., Valente, J., Cascão, P., Rodrigues, V., Pimentel, C., Miranda, A. I., & Borrego, C. (2013). Pedestrian Exposure to Air Pollution in Cities: Modeling the Effect of Roadside Trees. Advances in Meteorology, 2013, 1-7. doi: 10.1155/2013/964904

Ayaz, S. Ç. (2008). Post-treatment and reuse of tertiary treated wastewater by constructed wetlands. Desalination, 226(1–3), 249-255. doi: http://dx.doi.org/10.1016/j.desal.2007.02.110

Baker, A. J. M. (1981). Accumulators and excluders -strategies in the response of plants to heavy metals. Journal of Plant Nutrition, 3(1-4), 643-654. doi: 10.1080/01904168109362867

Baker, D. B., Richards, R. P., Loftus, T. T., & Kramer, J. W. (2004). A new flashiness index: Characteristics and applications to midwestern rivers and streams1: Wiley Online Library.

Barbier, E. B., Georgiou, I. Y., Enchelmeyer, B., & Reed, D. J. (2013). The value of wetlands in protecting southeast Louisiana from hurricane storm surges. PloS one, 8(3), e58715.

Baró, F., Chaparro, L., Gómez-Baggethun, E., Langemeyer, J., Nowak, D. J., & Terradas, J. (2014). Contribution of Ecosystem Services to Air Quality and Climate Change Mitigation Policies: The Case of Urban Forests in Barcelona, Spain. Ambio, 43(4), 466-479. doi: 10.1007/s13280-014-0507-x

Baumgardner, D., Varela, S., Escobedo, F. J., Chacalo, A., & Ochoa, C. (2012). The role of a peri-urban forest on air quality improvement in the Mexico City megalopolis. Environmental Pollution, 163, 174-183.

Bealey, W., McDonald, A., Nemitz, E., Donovan, R., Dragosits, U., Duffy, T., & Fowler, D. (2007). Estimating the reduction of urban PM 10 concentrations by trees within an environmental information system for planners. J Environ Manage, 85(1), 44-58.

Beckett, K. P., Freer Smith, P., & Taylor, G. (2000). Effective tree species for local air quality management. Journal of arboriculture, 26(1), 12-19.

Beckett, K. P., Freer-Smith, P. H., & Taylor, G. (2000). THE CAPTURE OF PARTICULATE POLLUTION BY TREES AT FIVE CONTRASTING URBAN SITES. Arboricultural Journal, 24(2-3), 209-230. doi: 10.1080/03071375.2000.9747273

Berland, A., & Hopton, M. E. (2014). Comparing street tree assemblages and associated stormwater benefits among communities in metropolitan Cincinnati, Ohio, USA. Urban Forestry & Urban Greening, 13(4), 734-741. doi: http://dx.doi.org/10.1016/j.ufug.2014.06.004

Birch, G. F., Matthai, C., Fazeli, M. S., & Suh, J. (2004). EFFICIENCY OF A CONSTRUCTED WETLAND IN REMOVING CONTAMINANTS FROM STORMWATER. Wetlands, 24(2), 459-466. doi: 10.1672/0277-5212(2004)024[0459:EOACWI]2.0.CO;2

Birch, G., Fazeli, M., & Matthai, C. (2005). Efficiency of an infiltration basin in removing contaminants from urban stormwater. Environmental monitoring and assessment, 101(1-3), 23-38.

Bliss, D. J., Neufeld, R. D., & Ries, R. J. (2008). Storm Water Runoff Mitigation Using a Green Roof. Environmental Engineering Science, 26(2), 407-418. doi: 10.1089/ees.2007.0186

Bolund, P., & Hunhammar, S. (1999). Ecosystem services in urban areas. Ecological economics, 29(2), 293-301.

Brody, S. D., & Highfield, W. E. (2013). Open space protection and flood mitigation: A national study. Land Use Policy, 32, 89-95. doi: http://dx.doi.org/10.1016/j.landusepol.2012.10.017

Brody, S. D., Peacock, W. G., & Gunn, J. (2012). Ecological indicators of flood risk along the Gulf of Mexico. Ecological Indicators, 18, 493-500. doi: http://dx.doi.org/10.1016/j.ecolind.2012.01.004

Brody, S. D., Zahran, S., Highfield, W. E., Grover, H., & Vedlitz, A. (2008). Identifying the impact of the built environment on flood damage in Texas. Disasters, 32(1), 1-18. doi: 10.1111/j.1467-7717.2007.01024.x

Broody, H. a. (2006). Price of Permits: Measuring the Economic Impacts of Wetland Development on Flood Damages in Florida. Natural Hazards Review, 7(3), 123-130. doi: doi:10.1061/(ASCE)1527-6988(2006)7:3(123)

Burkart, K., Meier, F., Schneider, A., Breitner, S., Canário, P., Joao Alcoforado, M., ... & Endlicher, W. (2015). Modification of heat-related mortality in an elderly urban population by vegetation (Urban Green) and proximity to water (Urban Blue): Evidence from Lisbon, Portugal. Environ. Health Perspect.

Carinanos, P., Casares-Porcel, M., & Quesada-Rubio, J.-M. (2014). Estimating the allergenic potential of urban green spaces: A case-study in Granada, Spain. Landscape and Urban Planning, 123, 134-144.

Carleton, J. N., Grizzard, T. J., Godrej, A. N., Post, H. E., Lampe, L., & Kenel, P. P. (2000). Performance of a Constructed Wetlands in Treating Urban Stormwater Runoff. Water Environment Research, 72(3), 295-304. doi: 10.2175/106143000X137518

Casteel, M., Bartow, G., Taylor, S., & Sweetland, P. (2005). Removal of bacterial indicators of fecal contamination in urban stormwater using a natural riparian buffer. Paper presented at the International Conference on Urban Drainage.

Cavanagh, J.-A. E., Zawar-Reza, P., & Wilson, J. G. (2009). Spatial attenuation of ambient particulate matter air pollution within an urbanised native forest patch. Urban Forestry & Urban Greening, 8(1), 21-30. doi: http://dx.doi.org/10.1016/j.ufug.2008.10.002

Chaparro-Suarez, I. G., Meixner, F. X., & Kesselmeier, J. (2011). Nitrogen dioxide (NO2) uptake by vegetation controlled by atmospheric concentrations and plant stomatal aperture. Atmospheric Environment, 45(32), 5742-5750. doi: http://dx.doi.org/10.1016/j.atmosenv.2011.07.021

Cheng, S., Grosse, W., Karrenbrock, F., & Thoennessen, M. (2002). Efficiency of constructed wetlands in decontamination of water polluted by heavy metals. Ecological Engineering, 18(3), 317-325. doi: http://dx.doi.org/10.1016/S0925-8574(01)00091-X

Chiu, C.-Y., & Chou, C.-H. (1991). The distribution and influence of heavy metals in mangrove forests of the Tamshui Estuary in Taiwan. Soil Science and Plant Nutrition, 37(4), 659-669. doi: 10.1080/00380768.1991.10416934

Cohen, P., Potchter, O., & Schnell, I. (2014). The impact of an urban park on air pollution and noise levels in the Mediterranean city of Tel-Aviv, Israel. Environmental Pollution, 195, 73-83.

Coleman, J., Hench, K., Garbutt, K., Sexstone, A., Bissonnette, G., & Skousen, J. (2001). Treatment of Domestic Wastewater by Three Plant Species in Constructed Wetlands. Water, Air, and Soil Pollution, 128(3), 283-295. doi: 10.1023/a:1010336703606

Costanza, R., Pérez-Maqueo, O., Martinez, M. L., Sutton, P., Anderson, S. J., & Mulder, K. (2008). The Value of Coastal Wetlands for Hurricane Protection. AMBIO: A Journal of the Human Environment, 37(4), 241-248. doi: 10.1579/0044-7447(2008)37[241:TVOCWF]2.0.CO;2

Coyne, M., Gilfillen, R., Rhodes, R., & Blevins, R. (1995). Soil and fecal coliform trapping by grass filter strips during simulated rain. Journal of Soil and Water Conservation, 50(4), 405-408.

Currie, B. A., & Bass, B. (2008). Estimates of air pollution mitigation with green plants and green roofs using the UFORE model. Urban Ecosystems, 11(4), 409-422. doi: 10.1007/s11252-008-0054-y

Dadvand, P., Rivas, I., Basagaña, X., Alvarez-Pedrerol, M., Su, J., Pascual, M. D. C., . . . Sunyer, J. (2015). The association between greenness and traffic-related air pollution at schools. Science of The Total Environment, 523, 59-63.

Dallas, S., Scheffe, B., & Ho, G. (2004). Reedbeds for greywater treatment—case study in Santa Elena-Monteverde, Costa Rica, Central America. Ecological Engineering, 23(1), 55-61. doi: http://dx.doi.org/10.1016/j.ecoleng.2004.07.002

Davies, C., & Bavor, H. (2000). The fate of stormwater-associated bacteria in constructed wetland and water pollution control pond systems. Journal of Applied Microbiology, 89(2), 349-360.

Davis, A. P. (2007). Field Performance of Bioretention: Water Quality. Environmental Engineering Science, 24(8), 1048-1064. doi: 10.1089/ees.2006.0190

Davis, A. P., Shokouhian, M., Sharma, H., Minami, C., & Winogradoff, D. (2003). Water quality improvement through bioretention: Lead, copper, and zinc removal. Water Environment Research, 73-82.

Defew, L. H., Mair, J. M., & Guzman, H. M. (2005). An assessment of metal contamination in mangrove sediments and leaves from Punta Mala Bay, Pacific Panama. Mar Pollut Bull, 50(5), 547-552. doi: 10.1016/j.marpolbul.2004.11.047

De Lacerda, L. D., & Abrao, J. J. (1984). Heavy metal accumulation by mangrove and saltmarsh intertidal sediments. Rvta. Brasil Bot, 7, 49-52..

DENARDO, J., JARRETT, A., MANBECK, H., BEATTIE, D., & BERGHAGE, R. (2005). Stormwater mitigation and surface temperature reduction by green roofs. Transactions of the ASAE, 48(4), 1491-1496.

Díaz, F. J., O'Geen, A. T., & Dahlgren, R. A. (2010). Efficacy of constructed wetlands for removal of bacterial contamination from agricultural return flows. Agricultural Water Management, 97(11), 1813-1821.

Dorsey, J. H., Carter, P. M., Bergquist, S., & Sagarin, R. (2010). Reduction of fecal indicator bacteria (FIB) in the Ballona Wetlands saltwater marsh (Los Angeles County, California, USA) with implications for restoration actions. Water Research, 44(15), 4630-4642. doi: http://dx.doi.org/10.1016/j.watres.2010.06.012

Dussaillant, A. R., Wu, C. H., & Potter, K. W. (2004). Richards equation model of a rain garden. Journal of Hydrologic Engineering, 9(3), 219-225.

Dzierżanowski, K., Popek, R., Gawrońska, H., Sæbø, A., & Gawroński, S. W. (2011). Deposition of Particulate Matter of Different Size Fractions on Leaf Surfaces and in Waxes of Urban Forest Species. International Journal of Phytoremediation, 13(10), 1037-1046. doi: 10.1080/15226514.2011.552929

Eger, P., & Lapakko, K. (1988). NICKEL AND COPPER REMOVAL FROM MINE DRAINAGE BY A NATURAL WETLAND. gas, 3, 7.

Entry, J. A., Hubbard, R. K., Thies, J. E., & Fuhrmann, J. J. (2000). The influence of vegetation in riparian filterstrips on coliform bacteria: II. Survival in soils. Journal of Environmental Quality, 29(4), 1215-1224.

Escobedo, F. J., & Nowak, D. J. (2009). Spatial heterogeneity and air pollution removal by an urban forest. Landscape and Urban Planning, 90(3–4), 102-110. doi: http://dx.doi.org/10.1016/j.landurbplan.2008.10.021

Gearheart, R. A. (1992). Use of Constructed Wetlands to Treat Domestic Wastewater, City of Arcata, California. Water Science and Technology, 26(7-8), 1625-1637.

Gerba, C. P., Thurston, J. A., Falabi, J. A., Watt, P. M., & Karpiscak, M. M. (1999). Optimization of artificial wetland design for removal of indicator microorganisms and pathogenic protozoa. Water Science and Technology, 40(4–5), 363-368. doi: http://dx.doi.org/10.1016/S0273-1223(99)00519-3

Granek, E. F., & Ruttenberg, B. I. (2007). Protective capacity of mangroves during tropical storms: a case study from 'Wilma'and 'Gamma'in Belize. MEPS, 343, 101-105.

Greenway, M. (2005). The role of constructed wetlands in secondary effluent treatment and water reuse in subtropical and arid Australia. Ecological Engineering, 25(5), 501-509. doi: http://dx.doi.org/10.1016/j.ecoleng.2005.07.008

Grundström, M., & Pleijel, H. (2014). Limited effect of urban tree vegetation on NO 2 and O 3 concentrations near a traffic route. Environmental Pollution, 189, 73-76.

Harlan, S. L., Declet-Barreto, J. H., Stefanov, W. L., & Petitti, D. B. (2013). Neighborhood effects on heat deaths: social and environmental predictors of vulnerability in Maricopa County, Arizona. Environmental Health Perspectives (Online), 121(2), 197.

Hill, A. C. (1971). Vegetation: A Sink for Atmospheric Pollutants. Journal of the Air Pollution Control Association, 21(6), 341-346. doi: 10.1080/00022470.1971.10469535

Hill, V. R., & Sobsey, M. D. (2001). Removal of Salmonella and microbial indicators in constructed wetlands treating swine wastewater. Water Sci Technol, 44(11-12), 215-222.

Hofman, J., Wuyts, K., Van Wittenberghe, S., Brackx, M., & Samson, R. (2014). On the link between biomagnetic monitoring and leaf-deposited dust load of urban trees: relationships and spatial variability of different particle size fractions. Environmental Pollution, 189, 63-72.

Hollis, G., & Thompson, J. (1993). Water resource developments and their hydrological impacts.

Islam, M. N., Rahman, K.-S., Bahar, M. M., Habib, M. A., Ando, K., & Hattori, N. (2012). Pollution attenuation by roadside greenbelt in and around urban areas. Urban Forestry & Urban Greening, 11(4), 460-464.

Jeong, Y., Sanders, B. F., McLaughlin, K., & Grant, S. B. (2008). Treatment of Dry Weather Urban Runoff in Tidal Saltwater Marshes: A Longitudinal Study of the Talbert Marsh in Southern California. Environmental Science & Technology, 42(10), 3609-3614. doi: 10.1021/es7026778

Jim, C. Y., & Chen, W. Y. (2008). Assessing the ecosystem service of air pollutant removal by urban trees in Guangzhou (China). J Environ Manage, 88(4), 665-676. doi: 10.1016/j.jenvman.2007.03.035

Johnston, C. A., Detenbeck, N. E., & Niemi, G. J. The cumulative effect of wetlands on stream water quality and quantity. A landscape approach. Biogeochemistry, 10(2), 105-141. doi: 10.1007/bf00002226

Johnston, K. K., Dorsey, J. H., & Saez, J. A. (2015). Stratification and loading of fecal indicator bacteria (FIB) in a tidally muted urban salt marsh. Environmental monitoring and assessment, 187(3), 58.

Kansiime, F., & van Bruggen, J. J. A. (2001). Distribution and retention of faecal coliforms in the Nakivubo wetland in Kampala, Uganda. Water Science and Technology, 44(11-12), 199-206.

Karathanasis, A. D., Potter, C. L., & Coyne, M. S. (2003). Vegetation effects on fecal bacteria, BOD, and suspended solid removal in constructed wetlands treating domestic wastewater. 20(2), 157-169. doi: 10.1016/S0925-8574(03)00011-9

Karim, M. R., Manshadi, F. D., Karpiscak, M. M., & Gerba, C. P. (2004). The persistence and removal of enteric pathogens in constructed wetlands. Water Research, 38(7), 1831-1837. doi: http://dx.doi.org/10.1016/j.watres.2003.12.029

Karpiscak, M. M., Gerba, C. P., Watt, P. M., Foster, K. E., & Falabi, J. A. (1996). Multi-species plant systems for wastewater quality improvements and habitat enhancement. Water Science and Technology, 33(10–11), 231-236. doi: http://dx.doi.org/10.1016/0273-1223(96)00424-6

Khambete, A. K., & Jagdish, S. N. (2010, 2-4 Nov. 2010). Role of Mangroves on domestic wastewater discharge: Case study at Jamnagar costal region, India. Paper presented at the 2010 2nd International Conference on Chemical, Biological and Environmental Engineering.

Khan, S., Ahmad, I., Shah, M. T., Rehman, S., & Khaliq, A. (2009). Use of constructed wetland for the removal of heavy metals from industrial wastewater. J Environ Manage, 90(11), 3451-3457. doi: http://dx.doi.org/10.1016/j.jenvman.2009.05.026

Knight, R. L., Payne Jr, V. W. E., Borer, R. E., Clarke Jr, R. A., & Pries, J. H. (2000). Constructed wetlands for livestock wastewater management. Ecological Engineering, 15(1–2), 41-55. doi: http://dx.doi.org/10.1016/S0925-8574(99)00034-8

Knox, A. K., Dahlgren, R. A., Tate, K. W., & Atwill, E. R. (2008). Efficacy of Natural Wetlands to Retain Nutrient, Sediment and Microbial Pollutants All rights reserved. No part of this periodical may be reproduced or transmitted in any form or by any means, electronic or mechanical, including photocopying, recording, or any information storage and retrieval system, without permission in writing from the publisher. Journal of Environmental Quality, 37(5). doi: 10.2134/jeq2007.0067

Krauss, K. W., Doyle, T. W., Doyle, T. J., Swarzenski, C. M., From, A. S., Day, R. H., & Conner, W. H. (2009). Water level observations in mangrove swamps during two hurricanes in Florida. Wetlands, 29(1), 142-149. doi: 10.1672/07-232.1

Lau, S. S. S., & Chu, L. M. (2000). Nutrient and faecal contamination and retention in wetland enclosures (gei wais) in the Mai Po Marshes, Hong Kong. Hydrobiologia, 431(1), 81-92. doi: 10.1023/a:1004058523243

Lee, J. Y., Moon, H. J., Kim, T. I., Kim, H. W., & Han, M. Y. (2013). Quantitative analysis on the urban flood mitigation effect by the extensive green roof system. Environmental Pollution, 181, 257-261. doi: http://dx.doi.org/10.1016/j.envpol.2013.06.039

Li, H. a. A. D. (2009). Water Quality Improvement through Reductions of Pollutant Loads Using Bioretention. Journal of Environmental Engineering, 135(8), 567-576. doi: doi:10.1061/(ASCE)EE.1943-7870.0000026

Li, X., Zhou, W., & Ouyang, Z. (2013). Relationship between land surface temperature and spatial pattern of greenspace: What are the effects of spatial resolution?. Landscape and Urban Planning, 114, 1-8.

Lindau, C. W., & Hossner, L. R. (1982). Sediment Fractionation of Cu, Ni, Zn, Cr, Mn, and Fe in One Experimental and Three Natural Marshes1. Journal of Environmental Quality, 11, 540-545. doi: 10.2134/jeq1982.00472425001100030041x

Liu, H., Zhang, K., Li, Y., & Xie, L. (2013). Numerical study of the sensitivity of mangroves in reducing storm surge and flooding to hurricane characteristics in southern Florida. Continental Shelf Research, 64, 51-65. doi: http://dx.doi.org/10.1016/j.csr.2013.05.015

Machado, W., Silva-Filho, E., Oliveira, R., & Lacerda, L. (2002). Trace metal retention in mangrove ecosystems in Guanabara Bay, SE Brazil. Marine Pollution Bulletin, 44(11), 1277-1280.

MAHENGE, A. S. (2014). PERFORMANCE OF HORIZONTAL SURFACE FLOW CONSTRUCTED MANGROVES WETLAND IN FAECAL COLIFORM REMOVAL. Journal of Applied Phytotechnology in Environmental Sanitation, 30(2).

Mallin, M. A., Ensign, S. H., McIver, M. R., Shank, G. C., & Fowler, P. K. (2001). Demographic, landscape, and meteorological factors controlling the microbial pollution of coastal waters. Hydrobiologia, 460(1), 185-193. doi: 10.1023/a:1013169401211

Manes, F. S., V;Salvatori, E;Incerti, G;Galante, G;Fusaro, L;Perrino, C. (2014). URBAN ECOSYSTEM SERVICES: TREE DIVERSITY AND STABILITY OF PM10 REMOVAL IN THE METROPOLITAN AREA OF ROME. Annali di Botanica, 4, 19-26.

Mantovi, P., Marmiroli, M., Maestri, E., Tagliavini, S., Piccinini, S., & Marmiroli, N. (2003). Application of a horizontal subsurface flow constructed wetland on treatment of dairy parlor wastewater. Bioresource Technology, 88(2), 85-94. doi: http://dx.doi.org/10.1016/S0960-8524(02)00291-2

Martin, A., & Barber, F. R. (1971). Some measurements of loss of atmospheric sulphur dioxide near foliage. Atmospheric Environment (1967), 5(5), 345-352. doi: http://dx.doi.org/10.1016/0004-6981(71)90106-5

McAllister, L. S., Peniston, B. E., Leibowitz, S. G., Abbruzzese, B., & Hyman, J. B. (2000). A synoptic assessment for prioritizing wetland restoration efforts to optimize flood attenuation. Wetlands, 20(1), 70-83. doi: 10.1672/0277-5212(2000)020[0070:asafpw]2.0.co;2

McIvor, A., Möller, I., Spencer, T., & Spalding, M. (2012). Reduction of wind and swell waves by mangroves: The Nature Conservancy and Wetlands International.

McPherson, E. G., Simpson, J. R., Peper, P. J., & Xiao, Q. TITLE: BENEFIT-COST ANALYSIS OF MODESTO'S MUNICIPAL URBAN FOREST.

Mentens, J., Raes, D., & Hermy, M. (2006). Green roofs as a tool for solving the rainwater runoff problem in the urbanized 21st century? Landscape and Urban Planning, 77(3), 217-226.

Ming, J., Xian-Guo, L., Lin-Shu, X., Li-juan, C., & Shouzheng, T. (2007). Flood mitigation benefit of wetland soil—A case study in Momoge National Nature Reserve in China. Ecological economics, 61(2), 217-223.

Möller, I. (2006). Quantifying saltmarsh vegetation and its effect on wave height dissipation: Results from a UK East coast saltmarsh. Estuarine, Coastal and Shelf Science, 69(3–4), 337-351. doi: http://dx.doi.org/10.1016/j.ecss.2006.05.003

Moller, I., Kudella, M., Rupprecht, F., Spencer, T., Paul, M., van Wesenbeeck, B. K., . . . Schimmels, S. (2014). Wave attenuation over coastal salt marshes under storm surge conditions. Nature Geosci, 7(10), 727-731. doi: 10.1038/ngeo2251

Möller, I., Spencer, T., French, J. R., Leggett, D. J., & Dixon, M. (1999). Wave Transformation Over Salt Marshes: A Field and Numerical Modelling Study from North Norfolk, England. Estuarine, Coastal and Shelf Science, 49(3), 411-426. doi: http://dx.doi.org/10.1006/ecss.1999.0509

Mori, J., Sæbø, A., Hanslin, H. M., Teani, A., Ferrini, F., Fini, A., & Burchi, G. (2015). Deposition of traffic-related air pollutants on leaves of six evergreen shrub species during a Mediterranean summer season. Urban Forestry & Urban Greening, 14(2), 264-273. doi: http://dx.doi.org/10.1016/j.ufug.2015.02.008

Murray-Gulde, C. L., Bearr, J., & Rodgers, J. H. (2005). Evaluation of a constructed wetland treatment system specifically designed to decrease bioavailable copper in a wastestream. Ecotoxicology and Environmental Safety, 61(1), 60-73. doi: http://dx.doi.org/10.1016/j.ecoenv.2004.12.020

Myers, M. R., & Ambrose, R. F. (2015). Salt Marsh Reduces Fecal Indicator Bacteria Input to Coastal Waters in Southern California. Bulletin, Southern California Academy of Sciences, 114(2), 76-88. doi: 10.3160/0038-3872-114.2.76

NARAYAN, S., BECK, M. W., REGUERO, B. G., & INGRAM, J. C. (2015). REVIEWING THE EVIDENCE FOR RISK REDUCTION BY NATURAL COASTAL HABITATS WORLD-WIDE: WHEN AND WHERE THEY HAVE WORKED.

Nelson, E. A., Specht, W. L., & Knox, A. S. (2006). Metal Removal from Water Discharges by a Constructed Treatment Wetland. Engineering in Life Sciences, 6(1), 26-30. doi: 10.1002/elsc.200620112

Neralla, S., Weaver, R. W., Lesikar, B. J., & Persyn, R. A. (2000). Improvement of domestic wastewater quality by subsurface flow constructed wetlands. Bioresource Technology, 75(1), 19-25. doi: http://dx.doi.org/10.1016/S0960-8524(00)00039-0

Ngugi, F. (2015). Adsorption of heavy metals from aqueous solutions using mangroves from Kenyan coast. University of Nairobi.

Nguyen, T., Yu, X., Zhang, Z., Liu, M., & Liu, X. (2015). Relationship between types of urban forest and PM2.5 capture at three growth stages of leaves. Journal of Environmental Sciences, 27, 33-41. doi: http://dx.doi.org/10.1016/j.jes.2014.04.019

Noor, M. J., Sultana, S., Fatima, S., Ahmad, M., Zafar, M., Sarfraz, M., . . . Ashraf, M. A. (2014). Estimation of Anticipated Performance Index and Air Pollution Tolerance Index and of vegetation around the marble industrial areas of Potwar region: bioindicators of plant pollution response. Environmental Geochemistry and Health, 37(3), 441-455. doi: 10.1007/s10653-014-9657-9

Nowak, D. J. (1994). Air Pollution Removal by Chicago's Urban Forest. Chicago's Urban Forest Ecosystem: Results of the Chicago Urban Forest Climate Project, 63.

Nowak, D. J. (2002). The effects of urban trees on air quality. USDA Forest Service, 96-102.

Nowak, D. J., Crane, D. E., & Stevens, J. C. (2006). Air pollution removal by urban trees and shrubs in the United States. Urban Forestry & Urban Greening, 4(3–4), 115-123. doi: http://dx.doi.org/10.1016/j.ufug.2006.01.007

Nowak, D. J., Crane, D. E., Stevens, J. C., Hoehn, R. E., Walton, J. T., & Bond, J. (2008). A ground-based method of assessing urban forest structure and ecosystem services.

Nowak, D. J., Hirabayashi, S., Bodine, A., & Hoehn, R. (2013). Modeled PM2.5 removal by trees in ten U.S. cities and associated health effects. Environmental Pollution, 178(0), 395-402. doi: http://dx.doi.org/10.1016/j.envpol.2013.03.050

Ogawa, H., and James W. Male. (1986). Simulating the Flood Mitigation Role of Wetlands. Journal of Water Resources Planning and Management, 112(1), 114-128. doi: doi:10.1061/(ASCE)0733-9496(1986)112:1(114)

Ong Che, R. G. (1999). Concentration of 7 Heavy Metals in Sediments and Mangrove Root Samples from Mai Po, Hong Kong. Marine Pollution Bulletin, 39(1–12), 269-279. doi: http://dx.doi.org/10.1016/S0025-326X(99)00056-9

Paz-Alberto, A. M., Vizmonte, J. L. D., & Sigua, G. C. (2015). Volume-5, Issue-4, Oct-Dec-2015 Coden: IJPAJX-CAS-USA, Copyrights@ 2015 ISSN-2231-4490 Received: 12 th Aug-2015 Revised: 26 th Aug-2015 Accepted: 27 th Aug-2015 Research article ASSESSING DIVERSITY AND PHYTOREMEDIATION POTENTIAL OF MANGROVES FOR COPPER CONTAMINATED SEDIMENTS IN SUBIC BAY, PHILIPPINES.

Perkins, J., & Hunter, C. (2000). Removal of enteric bacteria in a surface flow constructed wetland in Yorkshire, England. Water Research, 34(6), 1941-1947. doi: http://dx.doi.org/10.1016/S0043-1354(99)00333-4

Popek, R., Gawrońska, H., Wrochna, M., Gawroński, S. W., & Sæbø, A. (2013). Particulate matter on foliage of 13 woody species: Deposition on surfaces and phytostabilisation in waxes–a 3-year study. International Journal of Phytoremediation, 15(3), 245-256.

Quang Bao, T. (2011). Effect of mangrove forest structures on wave attenuation in coastal Vietnam. Oceanologia, 53(3), 807-818. doi: http://dx.doi.org/10.5697/oc.53-3.807

Quiñónez-Dìaz, M. d. J., Karpiscak, M. M., Ellman, E. D., & Gerba, C. P. (2001). REMOVAL OF PATHOGENIC AND INDICATOR MICROORGANISMS BY A CONSTRUCTED WETLAND RECEIVING UNTREATED DOMESTIC WASTEWATER. Journal of Environmental Science and Health, Part A, 36(7), 1311-1320. doi: 10.1081/ESE-100104880

Räsänen, J. V., Holopainen, T., Joutsensaari, J., Ndam, C., Pasanen, P., Rinnan, Å., & Kivimäenpää, M. (2013). Effects of species-specific leaf characteristics and reduced water availability on fine particle capture efficiency of trees. Environmental Pollution, 183, 64-70.

Rea, C. L., Bisesi, M. S., Mitsch, W., Andridge, R., & Lee, J. (2015). Human Health-Related Ecosystem Services of Avian-Dense Coastal Wetlands Adjacent to a Western Lake Erie Swimming Beach. EcoHealth, 12(1), 77-87. doi: 10.1007/s10393-014-1007-y

Reinelt, L. E., & Horner, R. R. (1995). Pollutant removal from stormwater runoff by palustrine wetlands based on comprehensive budgets. Ecological Engineering, 4(2), 77-97. doi: http://dx.doi.org/10.1016/0925-8574(94)00002-M

Rogers, H. H., Jeffries, H. E., & Witherspoon, A. M. (1979). Measuring Air Pollutant Uptake by Plants: Nitrogen Dioxide1. Journal of Environmental Quality, 8(4). doi: 10.2134/jeq1979.00472425000800040022x

Sæbø, A., Popek, R., Nawrot, B., Hanslin, H. M., Gawronska, H., & Gawronski, S. W. (2012). Plant species differences in particulate matter accumulation on leaf surfaces. Science of The Total Environment, 427–428, 347-354. doi: http://dx.doi.org/10.1016/j.scitotenv.2012.03.084

Sanders, R. A. (1986). Special Issue Ecology of the Urban Forest IIUrban vegetation impacts on the hydrology of Dayton, Ohio. Urban Ecology, 9(3), 361-376. doi: http://dx.doi.org/10.1016/0304-4009(86)90009-4

Scholz, M., & Xu, J. (2002). Comparison of constructed reed beds with different filter media and macrophytes treating urban stream water contaminated with lead and copper. Ecological Engineering, 18(3), 385-390. doi: http://dx.doi.org/10.1016/S0925-8574(01)00100-8

Scholz, M., Höhn, P., & Minall, R. (2002). Mature Experimental Constructed Wetlands Treating Urban Water Receiving High Metal Loads. Biotechnology Progress, 18(6), 1257-1264. doi: 10.1021/bp0200503

Setälä, H., Viippola, V., Rantalainen, A.-L., Pennanen, A., & Yli-Pelkonen, V. (2013). Does urban vegetation mitigate air pollution in northern conditions? Environmental Pollution, 183, 104-112.

Shutes, R. B. E., Revitt, D. M., Scholes, L. N. L., Forshaw, M., & Winter, B. (2001). An experimental constructed wetland system for the treatment of highway runoff in the UK. Water Science and Technology, 44(11-12), 571-578.

Silva, C., Lacerda, L., & Rezende, C. (1990). Metals reservoir in a red mangrove forest. Biotropica, 22(4), 339-345.

Simmons, M. T., Gardiner, B., Windhager, S., & Tinsley, J. (2008). Green roofs are not created equal: the hydrologic and thermal performance of six different extensive green roofs and reflective and non-reflective roofs in a sub-tropical climate. Urban Ecosystems, 11(4), 339-348. doi: 10.1007/s11252-008-0069-4

Sleytr, K., Tietz, A., Langergraber, G., & Haberl, R. (2007). Investigation of bacterial removal during the filtration process in constructed wetlands. Science of The Total Environment, 380(1–3), 173-180. doi: http://dx.doi.org/10.1016/j.scitotenv.2007.03.001

Song, Z., Zheng, Z., Li, J., Sun, X., Han, X., Wang, W., & Xu, M. (2006). Seasonal and annual performance of a full-scale constructed wetland system for sewage treatment in China. Ecological Engineering, 26(3), 272-282. doi: http://dx.doi.org/10.1016/j.ecoleng.2005.10.008

Speak, A. F., Rothwell, J. J., Lindley, S. J., & Smith, C. L. (2012). Urban particulate pollution reduction by four species of green roof vegetation in a UK city. Atmospheric Environment, 61, 283-293. doi: http://dx.doi.org/10.1016/j.atmosenv.2012.07.043

Steer, D., Fraser, L., Boddy, J., & Seibert, B. (2002). Efficiency of small constructed wetlands for subsurface treatment of single-family domestic effluent. Ecological Engineering, 18(4), 429-440. doi: http://dx.doi.org/10.1016/S0925-8574(01)00104-5

Sternberg, T., Viles, H., Cathersides, A., & Edwards, M. (2010). Dust particulate absorption by ivy (Hedera helix L) on historic walls in urban environments. Science of The Total Environment, 409(1), 162-168. doi: http://dx.doi.org/10.1016/j.scitotenv.2010.09.022

Stovin, V. (2010). The potential of green roofs to manage Urban Stormwater. Water and Environment Journal, 24(3), 192-199. doi: 10.1111/j.1747-6593.2009.00174.x

Takahashi, M., Higaki, A., Nohno, M., Kamada, M., Okamura, Y., Matsui, K., . . . Morikawa, H. (2005). Differential assimilation of nitrogen dioxide by 70 taxa of roadside trees at an urban pollution level. Chemosphere, 61(5), 633-639. doi: http://dx.doi.org/10.1016/j.chemosphere.2005.03.033

Tallis, M., Taylor, G., Sinnett, D., & Freer-Smith, P. (2011). Estimating the removal of atmospheric particulate pollution by the urban tree canopy of London, under current and future environments. Landscape and Urban Planning, 103(2), 129-138.

Tam, N. F. Y., & Wong, Y. S. (1995). Mangrove soils as sinks for wastewater-borne pollutants. Hydrobiologia, 295(1), 231-241. doi: 10.1007/bf00029130

Tam, N. F. Y., & Wong, Y. S. (1996). Retention and distribution of heavy metals in mangrove soils receiving wastewater. Environmental Pollution, 94(3), 283-291. doi: http://dx.doi.org/10.1016/S0269-7491(96)00115-7

Thurston, J. A., Foster, K. E., Karpiscak, M. M., & Gerba, C. P. (2001). Fate of indicator microorganisms, giardia and cryptosporidium in subsurface flow constructed wetlands. Water Research, 35(6), 1547-1551. doi: http://dx.doi.org/10.1016/S0043-1354(00)00414-0

Trinh, D. H., & Chui, T. F. M. (2013). Assessing the hydrologic restoration of an urbanized area via an integrated distributed hydrological model. Hydrol. Earth Syst. Sci., 17(12), 4789-4801. doi: 10.5194/hess-17-4789-2013.

Vandentorren, S., Bretin, P., Zeghnoun, A., Mandereau-Bruno, L., Croisier, A., Cochet, C., ... & Ledrans, M. (2006). August 2003 heat wave in France: risk factors for death of elderly people living at home. The European Journal of Public Health, 16(6), 583-591.

VanWoert, N. D., Rowe, D. B., Andresen, J. A., Rugh, C. L., Fernandez, R. T., & Xiao, L. (2005). Green Roof Stormwater Retention This paper is a portion of a thesis submitted by N.D. VanWoert. Journal of Environmental Quality, 34(3). doi: 10.2134/jeq2004.0364

Vijayaraghavan, K., & Joshi, U. M. (2014). Can green roof act as a sink for contaminants? A methodological study to evaluate runoff quality from green roofs. Environmental Pollution, 194, 121-129. doi: http://dx.doi.org/10.1016/j.envpol.2014.07.021

Wamsley, T. V., Cialone, M. A., Smith, J. M., Atkinson, J. H., & Rosati, J. D. (2010). The potential of wetlands in reducing storm surge. Ocean Engineering, 37(1), 59-68. doi: http://dx.doi.org/10.1016/j.oceaneng.2009.07.018

Wania, A., Bruse, M., Blond, N., & Weber, C. (2012). Analysing the influence of different street vegetation on traffic-induced particle dispersion using microscale simulations. J Environ Manage, 94(1), 91-101.

Warhurst, J. R., Parks, K. E., McCulloch, L., & Hudson, M. D. (2014). Front gardens to car parks: Changes in garden permeability and effects on flood regulation. Science of The Total Environment, 485–486, 329-339. doi: http://dx.doi.org/10.1016/j.scitotenv.2014.03.035

Weber, F., Kowarik, I., & Säumel, I. (2014). Herbaceous plants as filters: Immobilization of particulates along urban street corridors. Environmental Pollution, 186, 234-240.

Wong, Y. S., Tam, N. F. Y., & Lan, C. Y. (1997). Mangrove wetlands as wastewater treatment facility: a field trial. Hydrobiologia, 352(1), 49-59. doi: 10.1023/a:1003040920173

Wu, Y., Chung, A., Tam, N. F. Y., Pi, N., & Wong, M. H. (2008). Constructed mangrove wetland as secondary treatment system for municipal wastewater. Ecological Engineering, 34(2), 137-146. doi: http://dx.doi.org/10.1016/j.ecoleng.2008.07.010

Xiao, Q., & McPherson, E. G. (2016). Surface Water Storage Capacity of Twenty Tree Species in Davis, California. Journal of Environmental Quality, 45, 188-198. doi: 10.2134/jeq2015.02.0092

Xiao, Q., & McPherson, E. G. Rainfall interception by Santa Monica's municipal urban forest. Urban Ecosystems, 6(4), 291-302. doi: 10.1023/b:ueco.0000004828.05143.67

Yang, J., Yu, Q., & Gong, P. (2008). Quantifying air pollution removal by green roofs in Chicago. Atmospheric Environment, 42(31), 7266-7273. doi: http://dx.doi.org/10.1016/j.atmosenv.2008.07.003

Yang, Q., Tam, N., Wong, Y. S., Luan, T., Su, W., Lan, C., . . . Cheung, S. G. (2008). Potential use of mangroves as constructed wetland for municipal sewage treatment in Futian, Shenzhen, China. Marine Pollution Bulletin, 57(6), 735-743.

Yao, L., Chen, L., Wei, W., & Sun, R. (2015). Potential reduction in urban runoff by green spaces in Beijing: A scenario analysis. Urban Forestry & Urban Greening, 14(2), 300-308. doi: http://dx.doi.org/10.1016/j.ufug.2015.02.014

Ye, Y., Tam, N. F. Y., & Wong, Y. S. (2001). Livestock Wastewater Treatment by a Mangrove Pot-cultivation System and the Effect of Salinity on the Nutrient Removal Efficiency. Marine Pollution Bulletin, 42(6), 512-520. doi: http://dx.doi.org/10.1016/S0025-326X(00)00196-X

Zhang, B., Xie, G., Zhang, C., & Zhang, J. (2012). The economic benefits of rainwater-runoff reduction by urban green spaces: A case study in Beijing, China. J Environ Manage, 100, 65-71. doi: http://dx.doi.org/10.1016/j.jenvman.2012.01.015

Zhang, K., Liu, H., Li, Y., Xu, H., Shen, J., Rhome, J., & Smith Iii, T. J. (2012). The role of mangroves in attenuating storm surges. Estuarine, Coastal and Shelf Science, 102–103, 11-23. doi: http://dx.doi.org/10.1016/j.ecss.2012.02.021

EGS-Health

Adam, M., Schikowski, T., Carsin, A. E., Cai, Y., Jacquemin, B., Sanchez, M., . . . Probst-Hensch, N. (2015). Adult lung function and long-term air pollution exposure. ESCAPE: a multicentre cohort study and meta-analysis. European Respiratory Journal, 45(1), 38-50. doi: 10.1183/09031936.00130014

Aggarwal, P., & Jain, S. (2015). Impact of air pollutants from surface transport sources on human health: A modeling and epidemiological approach. Environment International, 83, 146-157.

Aggarwal, P., & Jain, S. (2015). Impact of air pollutants from surface transport sources on human health: A modeling and epidemiological approach. Environment International, 83, 146-157.

Araya, M., Olivares, M., Pizarro, F., Llanos, A., Figueroa, G., & Uauy, R. (2004). Community-Based Randomized Double-Blind Study of Gastrointestinal Effects and Copper Exposure in Drinking Water. Environmental Health Perspectives, 112(10), 1068-1073.

Babisch, W., Wolf, K., Petz, M., Heinrich, J., Cyrys, J., & Peters, A. (2014). Associations between traffic noise, particulate air pollution, hypertension, and isolated systolic hypertension in adults: the KORA study. Environmental Health Perspectives, 122(5), 492-498. doi: 10.1289/ehp.1306981

Bayer-Oglesby, L., Grize, L., Gassner, M., Takken-Sahli, K., Sennhauser, F. H., Neu, U., . . . nder, C. (2005). Decline of Ambient Air Pollution Levels and Improved Respiratory Health in Swiss Children. Environmental Health Perspectives, 113(11), 1632-1637.

Bilenko, N., Rossem, L. v., Brunekreef, B., Beelen, R., Eeftens, M., Hoek, G., . . . Gehring, U. (2015). Traffic-related air pollution and noise and children's blood pressure: Results from the PIAMA birth cohort study. European Journal of Preventive Cardiology, 22(1), 4-12. doi: 10.1177/2047487313505821

Bishop-Williams, K. E., Berke, O., Pearl, D. L., & Kelton, D. F. (2015). A spatial analysis of heat stress related emergency room visits in rural Southern Ontario during heat waves. BMC Emergency Medicine, 15, 17. doi: 10.1186/s12873-015-0043-4

Braun-Fahrländer, C., Vuille, J. C., Sennhauser, F. H., Neu, U., Künzle, T., Grize, L., . . . Wüthrich, B. (1997). Respiratory health and long-term exposure to air pollutants in Swiss schoolchildren. SCARPOL Team. Swiss Study on Childhood Allergy and Respiratory Symptoms with Respect to Air Pollution, Climate and Pollen. American Journal of Respiratory and Critical Care Medicine, 155(3), 1042-1049. doi: 10.1164/ajrccm.155.3.9116984

Brunetti, N., Amoruso, D., De Gennaro, L., Dellegrottaglie, G., Di Giuseppe, G., Antonelli, G., & Di Biase, M. (2013). Hot Spot: impact of July 2011 heat-wave in southern Italy (Apulia) on cardiovascular disease assessed by Emergency Medical Service and tele-medicine support. European Heart Journal, 34(suppl 1), P2504.

Burnett, R. T., Brook, J. R., Yung, W. T., Dales, R. E., & Krewski, D. (1997). Association between Ozone and Hospitalization for Respiratory Diseases in 16 Canadian Cities. Environmental Research, 72(1), 24-31. doi: http://dx.doi.org/10.1006/enrs.1996.3685

Bush, K. F., O'Neill, M. S., Shi, L., Mukherjee, B., Hu, H., Ghosh, S., & Balakrishnan, K. (2014). Associations between extreme precipitation and gastrointestinal-related hospital admissions in Chennai, India. Environmental Health Perspectives (Online), 122(3), 249.

Chan, E. Y. Y., Goggins, W. B., Yue, J. S. K., & Lee, P. (2013). Hospital admissions as a function of temperature, other weather phenomena and pollution levels in an urban setting in China. Bulletin of the World Health Organization, 91(8), 576-584. doi: 10.2471/BLT.12.113035

Chang, C. C., Chen, P. S., & Yang, C. Y. (2015). Short-term effects of fine particulate air pollution on hospital admissions for cardiovascular diseases: a case-crossover study in a tropical city. Journal of toxicology and environmental health. Part A, 78(4), 267-277. doi: 10.1080/15287394.2014.960044

Chang, C.-C., Kuo, C.-C., Liou, S.-H., & Yang, C.-Y. (2013). Fine particulate air pollution and hospital admissions for myocardial infarction in a subtropical city: Taipei, Taiwan. Journal of toxicology and environmental health. Part A, 76(7), 440-448. doi: 10.1080/15287394.2013.771559

Charan, P., & Sahel, H. (2014). Study of Respirable Dust in Ambient Air of Bikaner City and Its Impact on Human Health.

Chiu, H.-F., Tsai, S.-S., Weng, H.-H., & Yang, C.-Y. (2013). Short-Term Effects of Fine Particulate Air Pollution on Emergency Room Visits for Cardiac Arrhythmias: A Case-Crossover Study in Taipei. Journal of Toxicology and Environmental Health, Part A, 76(10), 614-623. doi: 10.1080/15287394.2013.801763

Chuang, W.-C., & Gober, P. (2015). Predicting hospitalization for heat-related illness at the census-tract level: Accuracy of a generic heat vulnerability index in phoenix, Arizona (USA). Environmental Health Perspectives (Online), 123(6), 606.

Chung, Y., Dominici, F., Wang, Y., Coull, B. A., & Bell, M. L. (2015). Associations between long-term exposure to chemical constituents of fine particulate matter (PM2. 5) and mortality in Medicare enrollees in the eastern United States.

Collier, S. A., Wade, T. J., Sams, E. A., Hlavsa, M. C., Dufour, A. P., & Beach, M. J. (2015). Swimming in the USA: beachgoer characteristics and health outcomes at US marine and freshwater beaches. Journal of water and health, 13(2), 531-543.

Dales, R. E., Zwanenburg, H., Burnett, R., & Franklin, C. A. (1991). Respiratory Health Effects of Home Dampness and Molds among Canadian Children. American Journal of Epidemiology, 134(2), 196-203.

De Man, H., Mughini Gras, L., Schimmer, B., Friesema, I. H. M., De Roda Husman, A. M., & Van Pelt, W. (2015). Gastrointestinal, influenza-like illness and dermatological complaints following exposure to floodwater: a cross-sectional survey in The Netherlands. Epidemiology and infection, 1-10.

Delfino, R. J., Staimer, N., Tjoa, T., Gillen, D. L., Schauer, J. J., & Shafer, M. M. (2013). Airway inflammation and oxidative potential of air pollutant particles in a pediatric asthma panel. J Expos Sci Environ Epidemiol, 23(5), 466-473. doi: 10.1038/jes.2013.25

Di Novi, C. (2013). The indirect effect of fine particulate matter on health through individuals' life-style. The Journal of Socio-Economics, 44, 27-36.

Dockery, D. W., Cunningham, J., Damokosh, A. I., Neas, L. M., Spengler, J. D., Koutrakis, P., . . . Speizer, F. E. (1996). Health Effects of Acid Aerosols on North American Children: Respiratory Symptoms. Environmental Health Perspectives, 104(5), 500-505. doi: 10.2307/3432990

Dong, G.-H., Qian, Z., Wang, J., Chen, W., Ma, W., Trevathan, E., . . . Ren, W.-H. (2013). Associations between ambient air pollution and prevalence of stroke and cardiovascular diseases in 33 Chinese communities. Atmospheric Environment, 77, 968-973. doi: http://dx.doi.org/10.1016/j.atmosenv.2013.06.034

Evans, J., van Donkelaar, A., Martin, R. V., Burnett, R., Rainham, D. G., Birkett, N. J., & Krewski, D. (2013). Estimates of global mortality attributable to particulate air pollution using satellite imagery. Environmental Research, 120, 33-42. doi: http://dx.doi.org/10.1016/j.envres.2012.08.005

Faustini, A., Stafoggia, M., Colais, P., Berti, G., Bisanti, L., Cadum, E., . . . Forastiere, F. (2013). Air pollution and multiple acute respiratory outcomes. European Respiratory Journal, 42(2), 304-313. doi: 10.1183/09031936.00128712

Foraster, M., Künzli, N., Aguilera, I., Rivera, M., Agis, D., Vila, J., . . . Ramos, R. (2014). High blood pressure and long-term exposure to indoor noise and air pollution from road traffic. Environmental Health Perspectives (Online), 122(11), 1193.

Fuks, K. B., Weinmayr, G., Foraster, M., Dratva, J., Hampel, R., Houthuijs, D., . . . Penell, J. (2014). Arterial blood pressure and long-term exposure to traffic-related air pollution: an analysis in the European Study of Cohorts for Air Pollution Effects (ESCAPE).

Gao, Y., Chan, E. Y., Li, L., Lau, P. W., & Wong, T. W. (2014). Chronic effects of ambient air pollution on respiratory morbidities among Chinese children: a cross-sectional study in Hong Kong. BMC Public Health, 14, 105. http://europepmc.org/abstract/MED/24484614

Gonzalez-Barcala, F. J., Pertega, S., Garnelo, L., Castro, T. P., Sampedro, M., Lastres, J. S., . . . Silvarrey, A. L. (2013). Truck traffic related air pollution associated with asthma symptoms in young boys: a cross-sectional study. Public Health, 127(3), 275-281. doi: http://dx.doi.org/10.1016/j.puhe.2012.12.028

Gorai, A. K., Tuluri, F., & Tchounwou, P. B. (2014). A GIS based approach for assessing the association between air pollution and asthma in New York State, USA. International journal of environmental research and public health, 11(5), 4845-4869. http://europepmc.org/abstract/MED/24806193

Goudarzi, G., Zallaghi, E., Neissi, A., Ankali, K. A., Saki, A., Babaei, A. A., . . . Mohammadi, M. J. (2013). Cardiopulmonary mortalities and chronic obstructive pulmonary disease attributed to ozone air pollution. Archives of Hygiene sciences, 2(2).

Gronlund, C. J., Zanobetti, A., Schwartz, J. D., Wellenius, G. A., & O'Neill, M. S. (2014). Heat, heat waves, and hospital admissions among the elderly in the United States, 1992–2006.

Guirguis, K., Gershunov, A., Tardy, A., & Basu, R. (2014). The impact of recent heat waves on human health in California. Journal of Applied Meteorology and Climatology, 53(1), 3-19.

Hajat, A., Allison, M., Diez-Roux, A. V., Jenny, N. S., Jorgensen, N. W., Szpiro, A. A., . . . Kaufman, J. D. (2015). Long-term Exposure to Air Pollution and Markers of Inflammation, Coagulation, and Endothelial Activation: A Repeat-measures Analysis in the Multi-Ethnic Study of Atherosclerosis (MESA). Epidemiology, 26(3), 310-320. doi: 10.1097/ede.0000000000000267

Hansen, A. L., Bi, P., Nitschke, M., Ryan, P., Pisaniello, D., & Tucker, G. (2008). The Effect of Heatwaves on Mental Health in a Temperate Australian City. Epidemiology, 19(6), S85. doi: 10.1097/01.ede.0000339795.05175.c2

Hashimoto, M., Suetsugi, T., Ichikawa, Y., Sunada, K., Nishida, K., Kondo, N., & Ishidaira, H. (2014). Assessing the relationship between inundation and diarrhoeal cases by flood simulations in low-income communities of Dhaka City, Bangladesh. Hydrological Research Letters, 8(3), 96-102. doi: 10.3178/hrl.8.96

Hasunuma, H., Ishimaru, Y., Yoda, Y., & Shima, M. (2014). Decline of ambient air pollution levels due to measures to control automobile emissions and effects on the prevalence of respiratory and allergic disorders among children in Japan. Environmental Research, 131, 111-118. doi: http://dx.doi.org/10.1016/j.envres.2014.03.007

Hennig, F., Fuks, K., Moebus, S., Weinmayr, G., Memmesheimer, M., Jakobs, H., . . . Erbel, R. (2014). Association between source-specific particulate matter air pollution and hs-CRP: local traffic and industrial emissions. Environmental Health Perspectives (Online), 122(7), 703.

Hess, J. J., Saha, S., & Luber, G. (2014). Summertime acute heat illness in US Emergency Departments from 2006 through 2010: analysis of a nationally representative sample. Environmental Health Perspectives (Online), 122(11), 1209.

Hou, P., Chen, Y., Qiao, W., Cao, G., Jiang, W., & Li, J. (2013). Near-surface air temperature retrieval from satellite images and influence by wetlands in urban region. Theoretical and applied climatology, 111(1-2), 109-118.

Hsieh, Y.-L., Tsai, S.-S., & Yang, C.-Y. (2013). Fine particulate air pollution and hospital admissions for congestive heart failure: a case-crossover study in Taipei. Inhalation Toxicology, 25(8), 455-460. doi: 10.3109/08958378.2013.804609

Jacquemin, B., Siroux, V., Sanchez, M., Carsin, A.-E., Schikowski, T., Adam, M., . . . Brunekreef, B. (2015). Ambient Air Pollution and Adult Asthma Incidence in Six European horts ESCAPE). Journal of Environmental Health Perspectives, 123(6), 613-621.

Jagai, J. (2014). Association between gastrointestinal illness and precipitation in areas impacted by combined sewer systems: utilizing a distributed lag model. Paper presented at the 142nd APHA Annual Meeting and Exposition (November 15-November 19, 2014).

Jagai, J. (2014). Association between gastrointestinal illness and precipitation in areas impacted by combined sewer systems: utilizing a distributed lag model. Paper presented at the 142nd APHA Annual Meeting and Exposition (November 15-November 19, 2014).

Jones, T. S., Liang, A. P., Kilbourne, E. M., Griffin, M. R., Patriarca, P. A., Wassilak, S. G., . . . Thacker, S. B. (1982). Morbidity and mortality associated with the July 1980 heat wave in St Louis and Kansas City, Mo. Jama, 247(24), 3327-3331.

Kajbafzadeh, M., Brauer, M., Karlen, B., Carlsten, C., van Eeden, S., & Allen, R. W. (2015). The impacts of traffic-related and woodsmoke particulate matter on measures of cardiovascular health: a HEPA filter intervention study. Occupational and Environmental Medicine, 72(6), 394-400. doi: 10.1136/oemed-2014-102696

Kälsch, H., Hennig, F., Moebus, S., Möhlenkamp, S., Dragano, N., Jakobs, H., . . . Heinz Nixdorf Recall Study Investigative, G. (2014). Are air pollution and traffic noise independently associated with atherosclerosis: the Heinz Nixdorf Recall Study. European Heart Journal, 35(13), 853-860. doi: 10.1093/eurheartj/eht426

Katukiza, A., Ronteltap, M., Steen, P., Foppen, J., & Lens, P. (2014). Quantification of microbial risks to human health caused by waterborne viruses and bacteria in an urban slum. Journal of Applied Microbiology, 116(2), 447-463.

Ketterer, C., & Matzarakis, A. (2014). Human-biometeorological assessment of heat stress reduction by replanning measures in Stuttgart, Germany. Landscape and Urban Planning, 122, 78-88.

Kim, B.-J., Lee, S.-Y., Kwon, J.-W., Jung, Y.-H., Lee, E., Yang, S. I., . . . Hong, S.-J. (2014). Traffic-related air pollution is associated with airway hyperresponsiveness. The Journal of allergy and clinical immunology, 133(6), 1763-1765.e1762. doi: 10.1016/j.jaci.2014.01.020

Kingsley, S., Eliot, M., Gold, J., Vanderslice, R., & Wellenius, G. (2016). Current and projected heat-related morbidity and mortality in Rhode Island. Environ Health Perspect, 124, 460-467.

Knobeloch, L., Ziarnik, M., Howard, J., Theis, B., Farmer, D., Anderson, H., & Proctor, M. (1994). Gastrointestinal upsets associated with ingestion of copper-contaminated water. Environmental Health Perspectives, 102(11), 958-961.

Knowlton, K., Rotkin-Ellman, M., King, G., Margolis, H. G., Smith, D., Solomon, G., . . . English, P. (2008). The 2006 California Heat Wave: Impacts on Hospitalizations and Emergency Department Visits. Epidemiology, 19(6), S323. doi: 10.1097/01.ede.0000340508.25106.ed

Lin, C. J., Wade, T. J., & Hilborn, E. D. Flooding and intestinal illness due to Clostridium difficile infection: a case-crossover analysis of Massachusetts data, 2003-2007.

Link, M. S., Luttmann-Gibson, H., Schwartz, J., Mittleman, M. A., Wessler, B., Gold, D. R., . . . Laden, F. (2013). Acute Exposure to Air Pollution Triggers Atrial Fibrillation. Journal of the American College of Cardiology, 62(9), 816-825. doi: http://dx.doi.org/10.1016/j.jacc.2013.05.043

Liu, C., Fuertes, E., Tiesler, C. M. T., Birk, M., Babisch, W., Bauer, C.-P., . . . Heinrich, J. (2014). The associations between traffic-related air pollution and noise with blood pressure in children: Results

from the GINIplus and LISAplus studies. International Journal of Hygiene and Environmental Health, 217(4–5), 499-505. doi: http://dx.doi.org/10.1016/j.ijheh.2013.09.008

Liu, M.-M., Wang, D., Zhao, Y., Liu, Y.-Q., Huang, M.-M., Liu, Y., . . . Dong, G.-H. (2013). Effects of Outdoor and Indoor Air Pollution on Respiratory Health of Chinese Children from 50 Kindergartens. Journal of Epidemiology, 23(4), 280-287. doi: 10.2188/jea.JE20120175

Mamou, F., & Henderson, T. (2013). Analysis of Heat Illness using Michigan Emergency Department Syndromic Surveillance. Online Journal of Public Health Informatics, 5(1), e139.

Mauderly, J. L., Barrett, E. G., Day, K. C., Gigliotti, A. P., McDonald, J. D., Harrod, K. S., . . . Seilkop, S. K. (2014). The National Environmental Respiratory Center (NERC) experiment in multi-pollutant air quality health research: II. Comparison of responses to diesel and gasoline engine exhausts, hardwood smoke and simulated downwind coal emissions. Inhalation Toxicology, 26(11), 651-667. doi: 10.3109/08958378.2014.925523

Miller , K. A., Siscovick , D. S., Sheppard , L., Shepherd , K., Sullivan , J. H., Anderson , G. L., & Kaufman , J. D. (2007). Long-Term Exposure to Air Pollution and Incidence of Cardiovascular Events in Women. New England Journal of Medicine, 356(5), 447-458. doi: doi:10.1056/NEJMoa054409

Mina, M., Annamaria, I., & Gita, L. (2015). A Case of Severe Asthma With Fungal Sensitization (SAFS) due to Aureobasidium Pullulans Following Hurricane Sandy D32. INTERESTING CASES IN ALLERGY AND IMMUNOLOGY (pp. A5644-A5644): American Thoracic Society.

Mohammadi, M. J., Godini, H., Tobeh Khak, M., Daryanoosh, S. M., Dobaradaran, S., & Goudarzi, G. (2015). An Association Between Air Quality and COPD in Ahvaz, Iran. Jundishapur J Chronic Dis Care, 4(1), e26621. doi: 10.5812/jjcdc.26621

Mohsin, M., Safdar, S., Asghar, F., & Jamal, F. (2013). Assessment of drinking water quality and its impact on residents health in Bahawalpur city. International Journal of Humanities and Social Science, 3(15), 114-128.

Monteiro, A., Carvalho, V., Oliveira, T., & Sousa, C. (2013). Excess mortality and morbidity during the July 2006 heat wave in Porto, Portugal. Int J Biometeorol, 57(1), 155-167. doi: 10.1007/s00484-012-0543-9

Morales, E., Garcia-Esteban, R., Asensio de la Cruz, O., Basterrechea, M., Lertxundi, A., Martinez López de Dicastillo, M. D., . . . Sunyer, J. (2015). Intrauterine and early postnatal exposure to outdoor air pollution and lung function at preschool age. Thorax, 70(1), 64-73. doi: 10.1136/thoraxjnl-2014-205413

Nuvolone, D., Balzi, D., Pepe, P., Chini, M., Scala, D., Giovannini, F., . . . Barchielli, A. (2013). Ozone short-term exposure and acute coronary events: A multicities study in Tuscany (Italy). Environmental Research, 126, 17-23.

Ostro, B. (1994). Estimating health effects of air pollution: A methodology with an application to Jakarta. Policy Research Working Paper, 1301, 32-54.

Ostro, B. D. (1990). Associations between morbidity and alternative measures of particulate matter. Risk Anal, 10(3), 421-427.

Park, K. J., Moon, J. Y., Ha, J. S., Kim, S. D., Pyun, B. Y., Min, T. K., & Park, Y. H. (2013). Impacts of Heavy Rain and Typhoon on Allergic Disease. Osong Public Health and Research Perspectives, 4(3), 140-145. doi: http://dx.doi.org/10.1016/j.phrp.2013.04.009

Park, M., Luo, S., Kwon, J., Stock, T. H., Delclos, G., Kim, H., & Yun-Chul, H. (2013). Effects of air pollution on asthma hospitalization rates in different age groups in metropolitan cities of Korea. Air Quality, Atmosphere & Health, 6(3), 543-551. doi: 10.1007/s11869-013-0195-x

Pillai, S. K., Noe, R. S., Murphy, M. W., Vaidyanathan, A., Young, R., Kieszak, S., . . . Wolkin, A. F. (2014). Heat illness: predictors of hospital admissions among emergency department visits-Georgia, 2002-2008. J Community Health, 39(1), 90-98. doi: 10.1007/s10900-013-9743-4

Pirani, M., Best, N., Blangiardo, M., Liverani, S., Atkinson, R. W., & Fuller, G. W. (2015). Analysing the health effects of simultaneous exposure to physical and chemical properties of airborne particles. Environment International, 79, 56-64.

Poloniecki, J. D., Atkinson, R. W., de Leon, A. P., & Anderson, H. R. (1997). Daily time series for cardiovascular hospital admissions and previous day's air pollution in London, UK. Occupational and Environmental Medicine, 54(8), 535-540.

Pönkä, A., & Virtanen, M. (1994). Chronic bronchitis, emphysema, and low-level air pollution in Helsinki, 1987-1989. Environmental Research, 65(2), 207-217. doi: 10.1006/enrs.1994.1032

Prescott, G. J., Cohen, G. R., Elton, R. A., Fowkes, F. G., & Agius, R. M. (1998). Urban air pollution and cardiopulmonary ill health: a 14.5 year time series study. Occupational and Environmental Medicine, 55(10), 697-704. doi: 10.1136/oem.55.10.697

Prescott, G. J., Cohen, G. R., Elton, R. A., Fowkes, F. G., & Agius, R. M. (1998). Urban air pollution and cardiopulmonary ill health: a 14.5 year time series study. Occupational and Environmental Medicine, 55(10), 697-704. doi: 10.1136/oem.55.10.697

Prevost, B., Lucas, F. S., Goncalves, A., Richard, F., Moulin, L., & Wurtzer, S. (2015). Large scale survey of enteric viruses in river and waste water underlines the health status of the local population. Environment International, 79, 42-50. doi: http://dx.doi.org/10.1016/j.envint.2015.03.004

Puett, R. C., Hart, J. E., Yanosky, J. D., Spiegelman, D., Wang, M., Fisher, J. A., . . . Laden, F. (2014). Particulate matter air pollution exposure, distance to road, and incident lung cancer in the nurses' health study cohort. Environmental Health Perspectives (Online), 122(9), 926.

Qasim, M., Anees, M. M., & Bashir, A. (2014). Unhygienic water is the cause of water borne disease among villagers: A case of Gujrat-Pakistan. World Applied Sciences Journal, 29(12), 1484-1491.

Reacher, M., McKenzie, K., Lane, C., Nichols, T., Kedge, I., Iversen, A., . . . Lewes Flood Action Recovery, T. (2004). Health impacts of flooding in Lewes: a comparison of reported gastrointestinal and other illness and mental health in flooded and non-flooded households. Communicable disease and public health / PHLS, 7(1), 39-46.

Reacher, M., McKenzie, K., Lane, C., Nichols, T., Kedge, I., Iversen, A., . . . Lewes Flood Action Recovery, T. (2004). Health impacts of flooding in Lewes: a comparison of reported gastrointestinal

and other illness and mental health in flooded and non-flooded households. Communicable disease and public health / PHLS, 7(1), 39-46.

Schwartz, J. (1999). Air Pollution and Hospital Admissions for Heart Disease in Eight U.S. Counties. Epidemiology, 10(1), 17-22.

Segala, C., Fauroux, B., Just, J., Pascual, L., Grimfeld, A., & Neukirch, F. (1998). Short-term effect of winter air pollution on respiratory health of asthmatic children in Paris. European Respiratory Journal, 11(3), 677-685.

Semenza, J. C., McCullough, J. E., Flanders, W. D., McGeehin, M. A., & Lumpkin, J. R. (1999). Excess hospital admissions during the July 1995 heat wave in Chicago. American Journal of Preventive Medicine, 16(4), 269-277. doi: http://dx.doi.org/10.1016/S0749-3797(99)00025-2

Siddique, A. K., Baqui, A. H., Eusof, A., & Zaman, K. (1991). 1988 floods in Bangladesh: pattern of illness and causes of death. J Diarrhoeal Dis Res, 9(4), 310-314.

Smith, S., Elliot, A. J., Hajat, S., Bone, A., Smith, G. E., & Kovats, S. (2016). Estimating the burden of heat illness in England during the 2013 summer heatwave using syndromic surveillance. Journal of epidemiology and community health, jech-2015-206079.

Soller, J., Bartrand, T., Ravenscroft, J., Molina, M., Whelan, G., Schoen, M., & Ashbolt, N. (2015). Estimated human health risks from recreational exposures to stormwater runoff containing animal faecal material. Environmental Modelling & Software, 72, 21-32. doi: http://dx.doi.org/10.1016/j.envsoft.2015.05.018

Stotz, A., Rapp, K., Oksa, J., Skelton, D. A., Beyer, N., Klenk, J., . . . Lindemann, U. (2014). Effect of a brief heat exposure on blood pressure and physical performance of older women living in the community—a pilot-study. International journal of environmental research and public health, 11(12), 12623-12631.

Tasian, G. E., Pulido, J. E., Gasparrini, A., Saigal, C. S., Horton, B. P., Landis, J. R., . . . Project, U. D. i. A. (2014). Daily mean temperature and clinical kidney stone presentation in five US metropolitan areas: a time-series analysis. Environmental Health Perspectives, 122(10), 1081.

Tonne, C., & Wilkinson, P. (2013). Long-term exposure to air pollution is associated with survival following acute coronary syndrome. European Heart Journal, 34(17), 1306-1311. doi: 10.1093/eurheartj/ehs480

Tyagi, V. K., Bhatia, A., Gaur, R. Z., Khan, A. A., Ali, M., Khursheed, A., . . . Lo, S.-L. (2013). Impairment in water quality of Ganges River and consequential health risks on account of mass ritualistic bathing. Desalination and Water Treatment, 51(10-12), 2121-2129. doi: 10.1080/19443994.2013.734677

Vailshery, L. S., Jaganmohan, M., & Nagendra, H. (2013). Effect of street trees on microclimate and air pollution in a tropical city. Urban forestry & urban greening, 12(3), 408-415.

Vandini, S., Corvaglia, L., Alessandroni, R., Aquilano, G., Marsico, C., Spinelli, M., . . . Faldella, G. (2013). Respiratory syncytial virus infection in infants and correlation with meteorological factors and air pollutants. Italian Journal of Pediatrics, 39, 1-1. doi: 10.1186/1824-7288-39-1

Vedal, S., Campen, M. J., McDonald, J. D., Larson, T. V., Sampson, P. D., Sheppard, L., . . . Szpiro, A. A. (2013). National Particle Component Toxicity (NPACT) initiative report on cardiovascular effects. Research report (Health Effects Institute)(178), 5-8.

von Clemm, E. M. (2014). Environmental Drivers of Diarrheal Disease Risk in Ho Chi Minh City, Vietnam.

Wade, T. J., Sandhu, S. K., Levy, D., Lee, S., LeChevallier, M. W., Katz, L., & Colford, J. M. (2004). Did a Severe Flood in the Midwest Cause an Increase in the Incidence of Gastrointestinal Symptoms? American Journal of Epidemiology, 159(4), 398-405. doi: 10.1093/aje/kwh050

Walters, S., Griffiths, R. K., & Ayres, J. G. (1994). Temporal association between hospital admissions for asthma in Birmingham and ambient levels of sulphur dioxide and smoke. Thorax, 49(2), 133-140. doi: 10.1136/thx.49.2.133

Wang, M. Z., Zheng, S., Wang, S. G., Tao, Y., & Shang, K. Z. (2013). The weather temperature and air pollution interaction and its effect on hospital admissions due to respiratory system diseases in western China. Biomedical and environmental sciences : BES, 26(5), 403-407. doi: 10.3967/0895-3988.2013.05.011

Wang, T.-N., Ko, Y.-C., Chao, Y.-Y., Huang, C.-C., & Lin, R.-S. (1999). Association between Indoor and Outdoor Air Pollution and Adolescent Asthma from 1995 to 1996 in Taiwan. Environmental Research, 81(3), 239-247. doi: http://dx.doi.org/10.1006/enrs.1999.3985

Winquist, A., Kirrane, E., Klein, M., Strickland, M., Darrow, L. A., Sarnat, S. E., . . . Tolbert, P. (2014). Joint Effects of Ambient Air Pollutants on Pediatric Asthma Emergency Department Visits in Atlanta, 1998–2004. Epidemiology, 25(5), 666-673. doi: 10.1097/ede.0000000000000146

Xiaoxue, Z., Yajuan, Z., & Xiaochuan, P. (2013). Study on Relationship of Incidence of Gastrointestinal Disorders with Drinking Water Quality and Personal Hygienic Habit in Part Rural Residents of Beijing. Journal of Environmental Hygiene, 3, 007.

Xu, Z., Hu, W., Su, H., Turner, L. R., Ye, X., Wang, J., & Tong, S. (2014). Extreme temperatures and paediatric emergency department admissions. Journal of epidemiology and community health, 68(4), 304-311.

Yamazaki, S., Shima, M., Yoda, Y., Oka, K., Kurosaka, F., Shimizu, S., . . . Yamamoto, N. (2013). Association of ambient air pollution and meteorological factors with primary care visits at night due to asthma attack. Environmental Health and Preventive Medicine, 18(5), 401-406. doi: 10.1007/s12199-013-0339-5

Yamazaki, S., Shima, M., Yoda, Y., Oka, K., Kurosaka, F., Shimizu, S., . . . Yamamoto, N. (2014). Association between PM2.5 and primary care visits due to asthma attack in Japan: relation to Beijing's air pollution episode in January 2013. Environmental Health and Preventive Medicine, 19(2), 172-176. doi: 10.1007/s12199-013-0371-5

Zahran, H. S., & Bailey, C. (2013). Factors Associated with Asthma Prevalence among Racial and Ethnic Groups—United States, 2009–2010 Behavioral Risk Factor Surveillance System. Journal of Asthma, 50(6), 583-589. doi: 10.3109/02770903.2013.794238

Zhang, L.-w., Chen, X., Xue, X.-d., Sun, M., Han, B., Li, C.-p., . . . Tang, N.-j. (2014). Long-term exposure to high particulate matter pollution and cardiovascular mortality: A 12-year cohort study in four cities in northern China. Environment International, 62, 41-47. doi: http://dx.doi.org/10.1016/j.envint.2013.09.012

Zhang, X., Lu, J., Zhang, S., Wang, C., Wang, B., Guo, P., & Dong, L. (2014). Effects of simulated heat waves on cardiovascular functions in senile mice. International journal of environmental research and public health, 11(8), 7841-7855.

Zhang, Y., Nitschke, M., & Bi, P. (2013). Risk factors for direct heat-related hospitalization during the 2009 Adelaide heatwave: A case crossover study. Science of The Total Environment, 442, 1-5. doi: http://dx.doi.org/10.1016/j.scitotenv.2012.10.042

Zhou, M., He, G., Liu, Y., Yin, P., Li, Y., Kan, H., . . . Fan, M. (2015). The associations between ambient air pollution and adult respiratory mortality in 32 major Chinese cities, 2006–2010. Environmental Research, 137, 278-286. doi: http://dx.doi.org/10.1016/j.envres.2014.12.016

Eco-Health-Direct

Barrett, M. A. M., Daphne;Frumkin, Howard. (2014). Parks and Health: Aligning Incentives to Create Innovations in Chronic Disease Prevention. Preventing Chronic Disease, 11, E63. doi: 10.5888/pcd11.130407

Beale, L., Hodgson, S., Abellan, J. J., Lefevre, S., & Jarup, L. (2010). Evaluation of spatial relationships between health and the environment: the rapid inquiry facility. Environ Health Perspect, 118(9), 1306-1312. doi: 10.1289/ehp.0901849

Beil, K., & Hanes, D. (2013). The Influence of Urban Natural and Built Environments on Physiological and Psychological Measures of Stress— A Pilot Study. International journal of environmental research and public health, 10(4), 1250-1267.

Coutts, C., Horner, M., & Chapin, T. (2010). Using geographical information system to model the effects of green space accessibility on mortality in Florida. Geocarto International, 25(6), 471-484. doi: 10.1080/10106049.2010.505302

de Vries, S., van Dillen, S. M. E., Groenewegen, P. P., & Spreeuwenberg, P. (2013). Streetscape greenery and health: Stress, social cohesion and physical activity as mediators. Social Science & Medicine, 94, 26-33. doi: http://dx.doi.org/10.1016/j.socscimed.2013.06.030

Donovan, G. H., Michael, Y. L., Gatziolis, D., Prestemon, J. P., & Whitsel, E. A. (2015). Is tree loss associated with cardiovascular-disease risk in the Women's Health Initiative? A natural experiment. Health & Place, 36, 1-7. doi: http://dx.doi.org/10.1016/j.healthplace.2015.08.007

Harlan, S. L., Declet-Barreto, J. H., Stefanov, W. L., & Petitti, D. B. (2013). Neighborhood Effects on Heat Deaths: Social and Environmental Predictors of Vulnerability in Maricopa County, Arizona. Environmental Health Perspectives, 121(2), 197-204. doi: 10.1289/ehp.1104625

Jenerette, G. D., Harlan, S. L., Stefanov, W. L., & Martin, C. A. (2011). Ecosystem services and urban heat riskscape moderation: water, green spaces, and social inequality in Phoenix, USA. Ecological Applications, 21(7), 2637-2651. doi: 10.1890/10-1493.1

Johnson, K. B., Jacob, A., & Brown, M. E. (2013). Forest cover associated with improved child health and nutrition: evidence from the Malawi Demographic and Health Survey and satellite data. Global Health: Science and Practice, 1(2), 237-248. doi: 10.9745/ghsp-d-13-00055

Laurent, O., Wu, J., Li, L., & Milesi, C. (2013). Green spaces and pregnancy outcomes in Southern California. Health & Place, 24(0), 190-195. doi: http://dx.doi.org/10.1016/j.healthplace.2013.09.016

Lee, J.-Y., & Lee, D.-C. (2014). Cardiac and pulmonary benefits of forest walking versus city walking in elderly women: A randomised, controlled, open-label trial. European Journal of Integrative Medicine, 6(1), 5-11. doi: http://dx.doi.org/10.1016/j.eujim.2013.10.006

Li, X., Zhou, W., & Ouyang, Z. (2013). Relationship between land surface temperature and spatial pattern of greenspace: What are the effects of spatial resolution? Landscape and Urban Planning, 114(0), 1-8. doi: http://dx.doi.org/10.1016/j.landurbplan.2013.02.005

Lovasi, G. S., O'Neil-Dunne, J. P., Lu, J. W., Sheehan, D., Perzanowski, M. S., Macfaden, S. W., . . . Rundle, A. (2013). Urban tree canopy and asthma, wheeze, rhinitis, and allergic sensitization to tree pollen in a New York City birth cohort. Environ Health Perspect, 121(4), 494-500, 500e491-496. doi: 10.1289/ehp.1205513

Lovasi, G. S., O'Neil-Dunne, J. P., Lu, J. W., Sheehan, D., Perzanowski, M. S., Macfaden, S. W., . . . Rundle, A. (2013). Urban tree canopy and asthma, wheeze, rhinitis, and allergic sensitization to tree pollen in a New York City birth cohort. Environ Health Perspect, 121(4), 494-500, 500e491-496. doi: 10.1289/ehp.1205513

Lovasi, G. S., Schwartz-Soicher, O., Quinn, J. W., Berger, D. K., Neckerman, K., Jaslow, R., . . . Rundle, A. (2013). Neighborhood safety and green space as predictors of obesity among preschool children from low-income families in New York City. Preventive Medicine, 57(3), 189-193. doi: 10.1016/j.ypmed.2013.05.012

Markevych, I. T., Elisabeth;Fuertes, Elaine;Sugiri, Dorothea;Berdel, Dietrich;Koletzko, Sibylle;von Berg, Andrea;Bauer, Carl-Peter;Heinrich, Joachim. (2014). A cross-sectional analysis of the effects of residential greenness on blood pressure in 10-year old children: results from the GINIplus and LISAplus studies. BMC Public Health, 14(1), 477.

Nowak, D. J., Hirabayashi, S., Bodine, A., & Hoehn, R. (2013). Modeled PM2.5 removal by trees in ten U.S. cities and associated health effects. Environmental Pollution, 178(0), 395-402. doi: http://dx.doi.org/10.1016/j.envpol.2013.03.050

Paquet, C., Orschulok, T. P., Coffee, N. T., Howard, N. J., Hugo, G., Taylor, A. W., . . . Daniel, M. (2013). Are accessibility and characteristics of public open spaces associated with a better cardiometabolic health? Landscape and Urban Planning, 118(0), 70-78. doi: http://dx.doi.org/10.1016/j.landurbplan.2012.11.011

Pereira, G., Christian, H., Foster, S., Boruff, B. J., Bull, F., Knuiman, M., & Giles-Corti, B. (2013). The association between neighborhood greenness and weight status: an observational study in Perth Western Australia. Environ Health, 12. doi: 10.1186/1476-069X-12-49

Richardson, E., Pearce, J., Mitchell, R., Day, P., & Kingham, S. (2010). The association between green space and cause-specific mortality in urban New Zealand: an ecological analysis of green space utility. BMC Public Health, 10(1), 1-14. doi: 10.1186/1471-2458-10-240

Richardson, E. A., Pearce, J., Mitchell, R., & Kingham, S. (2013). Role of physical activity in the relationship between urban green space and health. Public Health, 127(4), 318-324. doi: http://dx.doi.org/10.1016/j.puhe.2013.01.004

Stark, J. H., Neckerman, K., Lovasi, G. S., Quinn, J., Weiss, C. C., Bader, M. D. M., . . . Rundle, A. (2014). The impact of neighborhood park access and quality on body mass index among adults in New York City. Preventive Medicine, 64, 63-68. doi: http://dx.doi.org/10.1016/j.ypmed.2014.03.026

Tamosiunas, A., Grazuleviciene, R., Luksiene, D., Dedele, A., Reklaitiene, R., Baceviciene, M., . . . Nieuwenhuijsen, M. J. (2014). Accessibility and use of urban green spaces, and cardiovascular health: findings from a Kaunas cohort study. Environmental Health, 13(1), 1-11. doi: 10.1186/1476-069x-13-20

Tan, J., Zheng, Y., Song, G., Kalkstein, L. S., Kalkstein, A. J., & Tang, X. (2007). Heat wave impacts on mortality in Shanghai, 1998 and 2003. International Journal of Biometeorology, 51(3), 193-200. doi: 10.1007/s00484-006-0058-3

Uejio, C. K., Wilhelmi, O. V., Golden, J. S., Mills, D. M., Gulino, S. P., & Samenow, J. P. (2011). Intra-urban societal vulnerability to extreme heat: The role of heat exposure and the built environment, socioeconomics, and neighborhood stability. Health & Place, 17(2), 498-507. doi: http://dx.doi.org/10.1016/j.healthplace.2010.12.005

Vandentorren, S., Bretin, P., Zeghnoun, A., Mandereau-Bruno, L., Croisier, A., Cochet, C., . . . Ledrans, M. (2006). August 2003 Heat Wave in France: Risk Factors for Death of Elderly People Living at Home. The European Journal of Public Health, 16(6), 583-591. doi: 10.1093/eurpub/ckl063

Villeneuve, P. J., Jerrett, M., G. Su, J., Burnett, R. T., Chen, H., Wheeler, A. J., & Goldberg, M. S. (2012). A cohort study relating urban green space with mortality in Ontario, Canada. Environmental Research, 115, 51-58. doi: http://dx.doi.org/10.1016/j.envres.2012.03.003

Votsi, N.-E. P., Mazaris, A. D., Kallimanis, A. S., Drakou, E. G., & Pantis, J. D. (2013). Landscape structure and diseases profile: associating land use type composition with disease distribution. International Journal of Environmental Health Research, 24(2), 176-187. doi: 10.1080/09603123.2013.800965

Wilker, E. H. W., Chih-Da;McNeely, Eileen;Mostofsky, Elizabeth;Spengler, John;Wellenius, Gregory A.;Mittleman, Murray A. (2014). Green space and mortality following ischemic stroke. Environmental Research, 133(0), 42-48. doi: http://dx.doi.org/10.1016/j.envres.2014.05.005

Yamaguchi Dobbert, L., Ferreira da Silva Filho, D., & Polizel, J. L. (2013). Urban tree cover and human comfort in Campinas, Brazil. PROCEEDINGS of the Protected Areas and Place Making Conference 2013, 69-72.

Science of the Total Environment 676 (2019) 343–355

Contents lists available at ScienceDirect

Science of the Total Environment

journal homepage: www.elsevier.com/locate/scitotenv

Flood protection ecosystem services in the coast of Puerto Rico: Associations between extreme weather, flood hazard mitigation and gastrointestinal illness

R. De Jesus Crespo [a,*], J. Wu [b], M. Myer [c], S. Yee [a], R. Fulford [a]

[a] USEPA, ORD, NHERL, GED, United States of America
[b] USEPA, ORD, NHERL, RTP, United States of America
[c] USEPA, ORD, NERL, Athens, GA, United States of America

HIGHLIGHTS

- Extreme rain events in Puerto Rico correlate with spikes in Gastro Intestinal (GI) illness.
- Permeable karst soils help reduce flood impacts and GI illnesses according to FEMA and Medicare claims data.
- The benefits of karst soils are lost in areas with a high percentage of people living in flood zones.

GRAPHICAL ABSTRACT

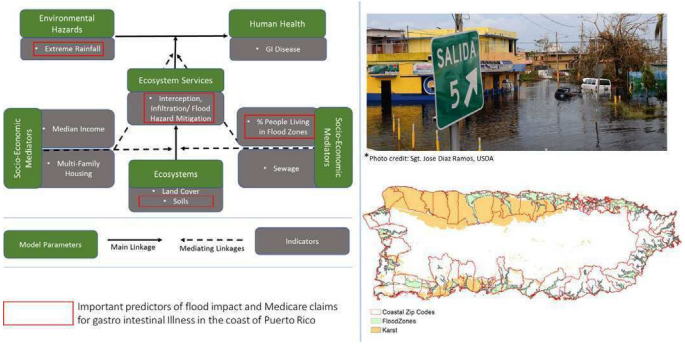

ARTICLE INFO

Article history:
Received 17 January 2019
Received in revised form 22 March 2019
Accepted 19 April 2019
Available online 24 April 2019

Editor: SCOTT SHERIDAN

Keywords:
Ecosystem services
Flooding
Gastro intestinal illness
Coastal communities

ABSTRACT

Floods are becoming increasingly influential in coastal cities due to the intensification of extreme weather events. The impacts of flooding go beyond damages to infrastructure, it also affects human health. During floods, discharge of sewage into streets increases exposure to pathogens causing gastrointestinal (GI) illnesses. A potential strategy for coastal protection during weather hazards is the use of flood protection ecosystem services, but their effectiveness at ameliorating the impact of floods on GI illnesses remain understudied. Here we explore the relationship between extreme rainfall, flood protection ecosystem services, and the occurrence of Medicare claims for gastrointestinal (GI) illnesses in Puerto Rico. We first conducted model averaging to detect variables explaining flood impact for the years (1999–2014), and then used these variables as predictors in a spatio-temporal analysis of GI illness in the same period (1999–2013). Our results show that flood impact varies proportionally with extreme rainfall, and inversely with flood protection ecosystem services, particularly due to the presence of karst soils. The protective effect of karst soils is lost when there is a high percentage of people living in flood prone areas, as suggested by a significant interaction effect between these two variables. In support of our hypotheses, cases of GI illness also spike after extreme rainfall events and are affected by the interaction effect of karst soils and people living in flood prone areas. Our results support the linkage between extreme weather events, flood damages and GI illnesses, and suggests a buffering role of ecosystem services that promote rainfall infiltration. The relevance of these ecosystem services, however, is affected by planning decisions such as

* Corresponding author.
E-mail address: rdejesuscrespo1@lsu.edu (R. De Jesus Crespo).

https://doi.org/10.1016/j.scitotenv.2019.04.287
0048-9697/© 2019 Elsevier B.V. All rights reserved.

residential development in flood prone areas. Our results help inform planning strategies for future weather hazards, accounting for the role of natural and built infrastructure on minimizing flood impacts and human health effects.

© 2019 Elsevier B.V. All rights reserved.

1. Introduction

Flood events are an increasingly important stressor in coastal communities due to projected sea level rise, and frequent exposure to weather hazards, particularly in the tropics (Vitousek et al., 2017). In Latin America and the Caribbean, it is estimated that there are over 7.5 million people currently exposed to flooding, and around 300 billion USD in built capital vulnerable to flood loss (Reguero et al., 2015). Island nations are expected to suffer the greatest impact due to direct exposure to tropical storms, and a strong dependency on coastal resources for tourism and other economic sectors (Reguero et al., 2015; Vitousek et al., 2017). Aside from property damages and impacts to the economy, flood hazards also have been associated to a variety of human health impacts such as vector borne illnesses, gastrointestinal infections, and mental health effects such as PTSD (Post Traumatic Stress Disorder) and Depression (Ahern et al., 2005). It is well established that the impacts of natural disasters such as floods disproportionately affect impoverished communities who are at higher risk of exposure (Winsemius et al., 2015) and who lack access to adequate services and resources to respond (Cutter et al., 2003). In this context, the need for low cost, community driven alternatives to flood hazard protection, including natural infrastructure and ecosystem services becomes particularly important.

Here we explore the role of ecosystem services in relation to one of the most common health outcomes associated to flooding, which is acute gastrointestinal (GI) illness. During floods, untreated sewage often mixes with storm water runoff, contaminating crops and household surfaces (Wade et al., 2014). Contaminated runoff may also come into direct contact with people within flooded residences or those wading through flooded streets to reach higher grounds during an event. Floods can also damage water treatment infrastructure, affecting the availability of safe and potable water for drinking (Wade et al., 2014). Families displaced by flooding often relocate to public shelters, where unsanitary conditions and overcrowding often leads to disease outbreaks (Wade et al., 2014; Huang et al., 2016).

Due to the multitude of pathways exposing people to pathogens during and after floods, many studies have effectively documented this linkage in a variety of settings (Curriero et al., 2001; Reacher et al., 2004; Wade et al., 2004; Wade et al., 2014; Huang et al., 2016). Yet, to date, no study has attempted to determine if the impact of floods on GI illness could be prevented with flood protection ecosystem services (De Jesus Crespo et al., 2018 A). Flood protection ecosystem services include rainfall interception and infiltration by natural land cover, which results in reductions in surface runoff and flood impact (Brody and Highfield, 2013a, 2013b, Xiao and McPherson, 2016). Interception and infiltration also help filter runoff, reducing concentrations of disease-causing pathogens available in storm water (Mallin et al., 2001; Yang et al., 2008). If natural infrastructure helps purify water and reduce surface runoff, and these flood related hazards are associated to GI illness, then we hypothesize that there will be lower occurrences of GI illness in flood prone regions that have flood protection ecosystem services.

We address this hypothesis in coastal neighborhoods in Puerto Rico. The extensive flood impacts caused by Hurricane Maria on the Island in 2017 underscores the potential for weather hazards to severely impact human health, especially among vulnerable sectors. Even before this event, impoverished communities in Puerto Rico had historically been exposed to frequent flooding and flood related illnesses (Azar and Rain, 2007, Briskin, 2016, De Jesus Crespo et al., 2018 B). Puerto Rico's economic downturn over the last decade has also increased unemployment and poverty around the Island, leading to mass migration of younger generations, and an increase in the median age of the remaining residents (Abel and Deitz, 2014; Castro-Prieto et al., 2017), exacerbating the vulnerability of the Island's population.

Focusing on the elderly, here we look at Medicare claims data over a 14-year period (1999–2013) to assess the associations between extreme rainfall, flood impact, and ecosystem services on GI illness (Fig. 1). We predicted that the impact of extreme rainfall on human health would be mitigated by flood protection ecosystem services, resulting in lower cases of GI illness. The role of ecosystems at providing ecosystem services, and of flood protection ecosystem services at ameliorating GI illness occurrences, would be mediated by socio-economic factors that determine the level of exposure to hazards and the adaptations available through built infrastructure for preventing flood impact and health effects (Fig. 1). Having a better understanding of the extent to which ecosystem services may help buffer environmental hazards and protect human health, would help guide community-based management of flood prone neighborhoods and justify conservation and restoration efforts focused on natural infrastructure.

2. Methods

2.1. Study site

Puerto Rico (PR) is a US territory located in the Northeastern Caribbean Sea. It is the smallest Island of the Greater Antilles archipelago, but also the most urbanized and densely populated (Lugo et al., 2012). Most of its population is located along the coast, while the center mountain range is more sparsely urbanized, and more heavily forested (Fig. 2B and C, Parés-Ramos et al., 2008). Around 55% of Puerto Rico's area is vegetation cover (USDA, 2017), most of which is secondary forest resulting from a shift from intense farming up until the mid-20th century, to an industrial economy (Larsen, 2017).

The maximum elevation in the central mountain range is 1338 m (Fig. 2B, Larsen, 2017), and rainfall averages 1651 mm annually, with the mountains receiving much greater precipitation than the coast (Yuan et al., 2015). Due to orographic factors, rainfall is unevenly distributed through the island (Fig. 2A, Hernández Ayala et al., 2017). These differences, driven by the configuration of the central mountain range, lead to four distinct climatic regions in the north, south, east and west (Warne et al., 2005). While the north and east receive abundant orographic rainfall, influenced by the northeast trade winds, the southern portion is relatively dry due to a rain shadow effect (Warne et al., 2005). The western portion is rainy as well, driven by an eastward flow of air from the sea onto the land producing abundant afternoon rainfall (Warne et al., 2005).

Around 55% of the Island is currently served by the Puerto Rico Aqueduct and Sewer Authority (PRASA) waste water system (Government of Puerto Rico, 2018). Many of PRASA's waste water infrastructure was developed in the 1950's, often making it obsolete to manage modern demands (Hunter and Arbona, 1995). Lack of financial resources has limited infrastructure improvement projects, leading PRASA to be the subject of multiple federal fines for failure to meet water quality regulations from its waste water treatment facilities (PRASA, 2014).

We focused this study on the PR coast, where higher population densities, lower elevations, and the potential for storm surges increase flood risk, and potential GI pathogen exposure. We included all coastal zip

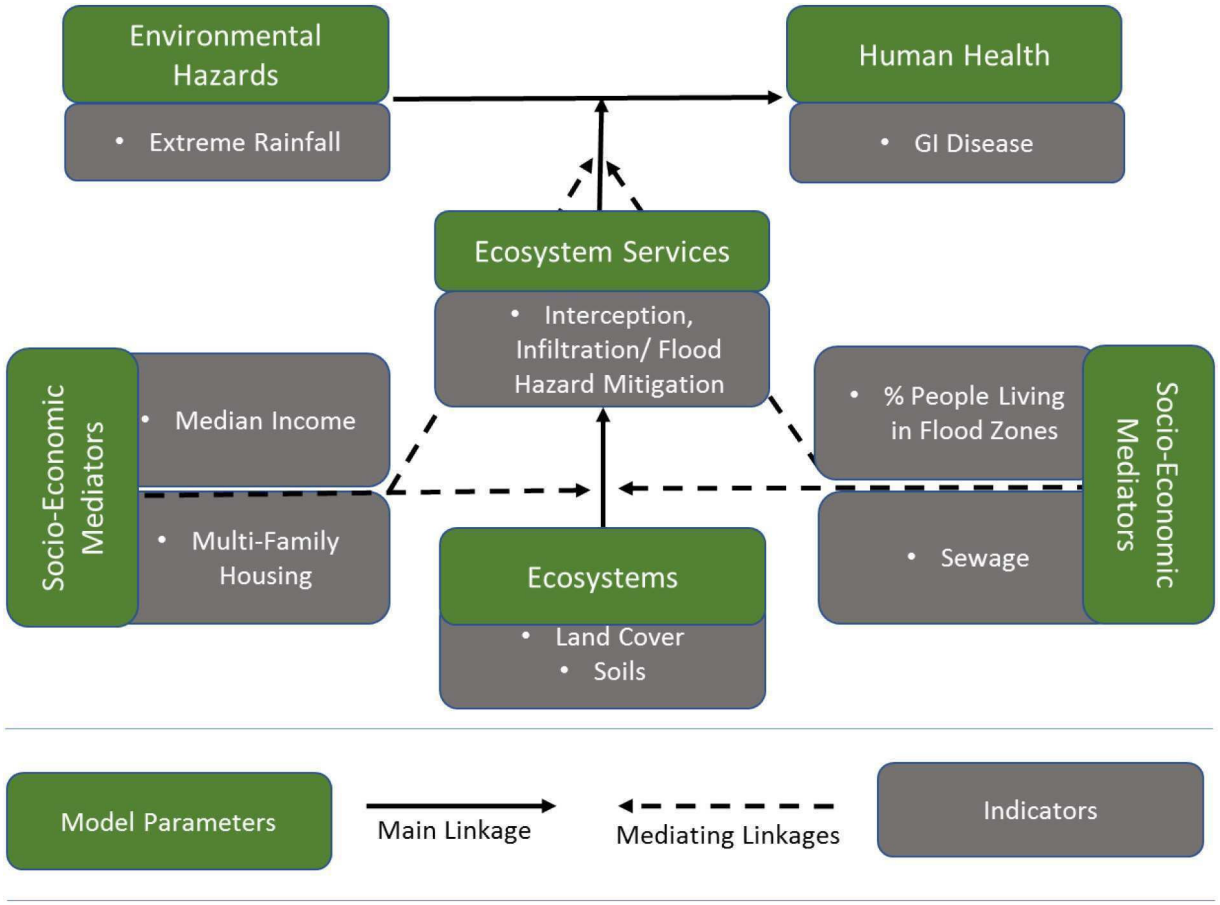

Fig. 1. Conceptual model describing the association between extreme rainfall and GI disease. We predict that the impact of extreme rainfall on human health would be mitigated by flood protection ecosystem services, resulting in lower cases of GI disease. The relationship between weather, floods, ecosystem services and GI disease would also be mediated by socio-economic factors that determine the level of exposure to hazards, the adaptations available through built infrastructure to manage flood impacts, the effectiveness with which ecosystems can deliver ecosystem services, and the relative importance of these ecosystem services to human health and well-being. See also Myers et al., 2013, and Crimmins et al., 2016.

codes ($N = 73$) except for the municipalities of Vieques and Culebra. These municipalities are separate islands, with distinct hydrological traits that make their comparison to other sites more challenging.

2.2. Data sources and processing

We selected indicators from available datasets (Table 1) for each component of our conceptual model (Fig. 1). Most estimates were done at the zip-code level, but when feasible, we also estimated indicators at the HUC-10 watershed levels (USGS, 2017), especially for predictor variables associated to hydrological patterns (e.g. rainfall, rain retention, vegetation cover, and slope).

Prior to analysis, all predictor variables were centered by subtracting the sample mean and dividing by the sample's standard deviation (Becker et al., 1988). Collinearity was examined using Pearson correlation coefficients (Supplementary material 1; SM1). Any correlation between explanatory variables of >0.60 was considered important and accounted for in subsequent analysis.

2.2.1. Extreme weather

Daily rainfall in Puerto Rico was estimated for the years 1999–2014 using the NASA Daymet surface weather and climatological summary dataset (Thornton et al., 1997). We generated 1 km spaced points through the island and used these as coordinates for data extraction with the "daymetr" R-package (Hufkens, 2014). Data were summarized by zip code, and analyzed longitudinally, calculating 7-day moving averages (allocated daily), and daily extreme events (90th, 95th and 99th percentile rainfall). These rainfall extremes were classified with a 1, 2, or 3 (representing 90, 95, 99% respectively), other days with a "0". For evaluating GI illness response, we assessed extreme rain events at a 7-day lag to capture the incubation period for most GI illnesses caused by waterborne pathogens (Jagai et al., 2015). Other studies have assessed GI response to rainfall at different lag periods and found one week lags to be representative (Jagai et al., 2015). To classify extreme rain with lag periods, we used the *rollapllyr* function of the package zoo in R. Since daily extreme events were classified as 1, 2, or 3, we calculated a moving maximum using the previous 7 days as a basis. This resulted in "1, 2, or 3" being applied to days that experienced any of these events in the previous seven days (the maximum of these three values) and "0" otherwise.

To model flood claim response, we used zip-code aggregated weather data for the entire study period as predictor variables, including average annual rainfall, as well as the magnitude of the 90th, 95th or 99th rainfall percentiles. In this part of the analysis, we explored rainfall trends at different spatial scales. The same 1 km spaced point file used to extract data at the zip code level, was used to summarize data at the HUC-10 watershed level. We then created estimates of HUC-10 level rainfall for each zip code. In the case were multiple HUC-10 watersheds intersected a single zip code, a weighted average was calculated so the rainfall in the watershed with greater spatial overlap with the zip code would have higher influence (SM2).

2.2.2. Ecosystem services

We estimated flood protection ecosystem services using the EPA H20 tool (Russell et al., 2015), which uses curve numbers (CN) to estimate a rain retention index. The curve number method incorporates

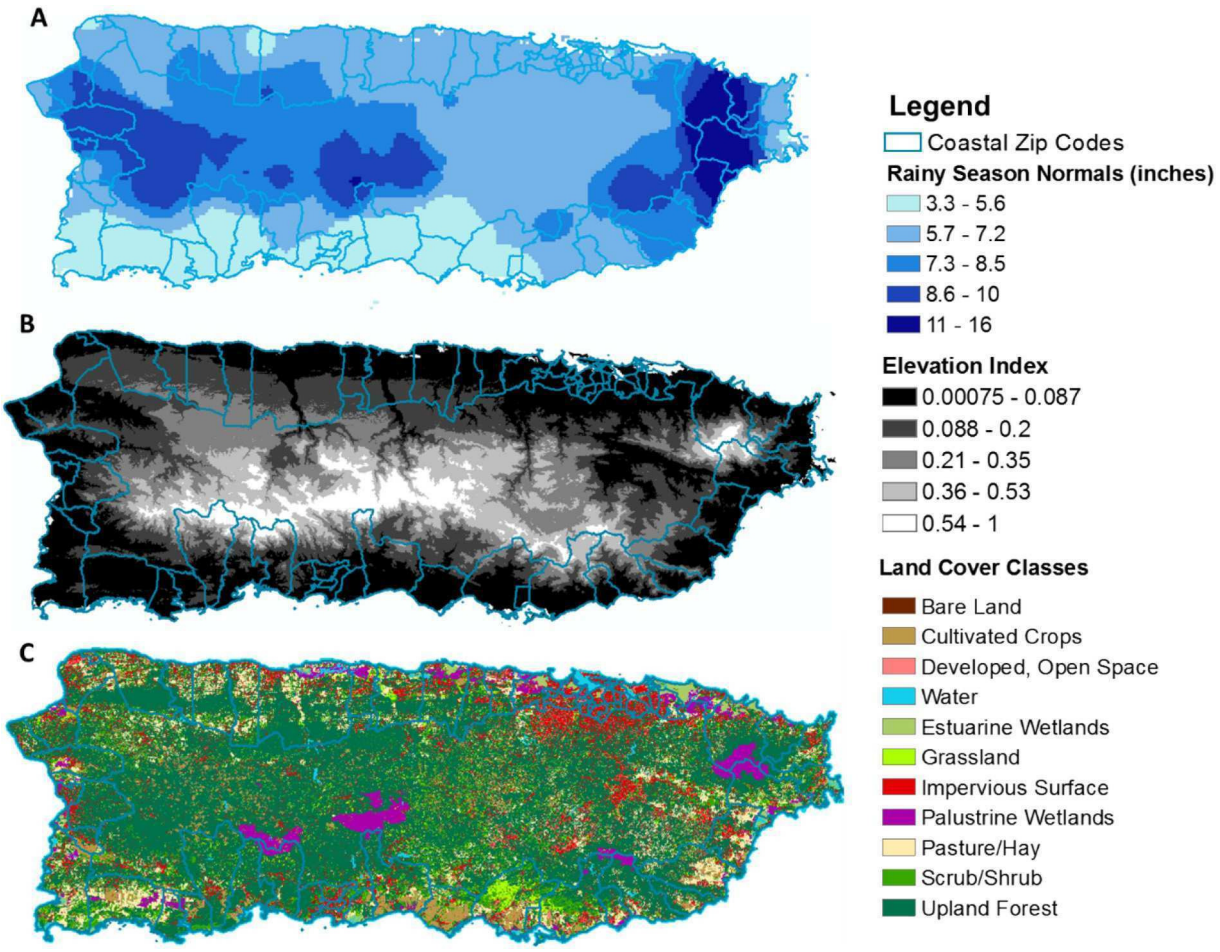

Fig. 2. Study site, coastal zip codes in Puerto Rico. A) Rainy season (May-Nov) normal precipitation (inches). This map is derived from NOAA 1981–2010 U.S. Climate Normals, by interpolating point data from weather stations through Puerto Rico (Arguez et al., 2012) using Inverse Distance Weighting in Arc GIS; B) Elevation index, derived from Digital Elevation Model values (CRIM 1998), presented as a fraction of the maximum elevation in Puerto Rico (i.e. value/max elevation); C) Land cover classes adapted from the Coastal Change Analysis Program C-CAP (DOC 2017).

soil infiltration characteristics and land cover water retention capacity through infiltration, interception and evapotranspiration (USDA, 1986). For the context of this paper, the CN rain retention index is used as an indicator of a reduction in surface runoff, which should result in flood mitigation, and consequently lower exposure of individuals to polluted waters.

Here we used SSURGO (USDA NRCS, 2004) layer for soil characterization and the Coastal Change Analysis Program C-CAP (DOC, 2010) land cover layer to create a CN index at 100 m cell sizes. A table with the CN values used for each land cover- soil combination can be found in the supplemental material (SM3). Rain retention was summarized at the zip code and the HUC-10 watershed scale. The HUC-10 estimates were allocated to zip codes using area weighted averages (SM2).

In addition to the rain retention index, we also calculated % karst soils (Alemán González, 2010), and % vegetation (i.e. combining the vegetation categories defined in Puerto Rico CCAP categories, 11/Mixed Forest and 12/Scrub/Shrub) in ArcGIS (ver. 10.3), as individual model predictor variables. These land cover and soils classes represent the land use/soil categories with higher retention values when calculating the CN index (USDA, 1986), and it was of our interest to determine which component of the index was more predictive of flood impact and/or GI illness. Percent vegetation was calculated at the HUC-10 watershed level, to account for the location of most of the vegetated areas at high elevations and in headwater areas. Percent karst was calculated at the zip code level only as most of the karst geology is located along the coast rather than at higher elevations (Fig. 3). For the same reason, percent wetlands (CCAP categories 13–18) was also estimated as a predictor at the zip code level. While in the CN method wetlands are considered as having low retention capacity due to water saturation, we know from previous studies that they can play a role in flood protection ecosystem services (Broody, 2006; Brody et al., 2012) as well as removal of pathogens that can cause GI illness (Yang et al., 2008). Topography is another factor that could affect rainfall retention dynamics. We calculated slope averages and maximums at the zip code and HUC-10 watershed levels, using Digital Elevation Models (DEM, CRIM, 1998) in ArcGIS.

2.2.3. Socio-economic variables

We characterized socio-economic indicators that could mediate the benefits derived from ecosystem services. Flood risk is influenced by the proportion of people living in flood prone areas (Fig. 3). We calculated this variable using population estimates (Sorichetta et al., 2015) and the Federal Emergency Management Agency (FEMA) flood zone layer (FEMA, 2009) in ArcGIS (ver 10.3). Sewage infrastructure alters the fate and transfer of waste water, potentially influencing the level of exposure to pathogens during flood events. While the sewage infrastructure in Puerto Rico has suffered from poor maintenance in the past (PRASA, 2014), we infer that exposure to waste water pathogens during floods would be greater in un-sewered areas of the Island. We estimated sewage cover density for each zip code using data from the Puerto Rico Aqueduct and Sewage Authority (PRASA, 2015).

Whenever there is high population density in a flood prone area, the type of housing could determine how many people are affected. For people living in high rises and multi-family buildings, exposure may

Table 1
Variables assessed, main indicators and sources.

Predictor variables evaluated (spatial scale)	Sources
Weather hazards	
90, 95, 99% Rainfall (Huc-10 Watershed and Zip Code); Average Annual Rainfall (Huc-10 Watershed and Zip Code)	NASA Daymet; https://daac.ornl.gov/cgi-bin/dsviewer.pl?ds_id=1328
Ecosystem goods and services	
Rain Retention (Huc-10 Watershed and Zip Code)	CCAP 2010 (NOAA, 2010); SSURGO (USDA NRSC, 2004); EPA H20 tool (Russell et al., 2015)
% Watershed Vegetation (Huc-10 Watershed)	CCAP 2010 (NOAA, 2010)
% Watershed Woody Wetlands (Zip Code)	CCAP 2010 (NOAA, 2010
% Watershed Grassy Wetlands (Zip Code)	CCAP 2010 (NOAA, 2010)
% Karst (Zip Code)	Karst raster (Alemán González, 2010)
Natural controls	
Average and Maximum Slopes (Huc-10 Watershed and Zip Code)	DEM (CRIM, 1998)
Socio-economic variables	
Sewage Density (Zip Code)	Sewer Lines PR Aqueduct and Sewer Authority (PRASA, 2015)
% Multifamily Housing (5 households or more); (Zip Code)	ACS 5-year estimates (2008–2012) https://www.census.gov/programs-surveys/acs/
Median Income (Zip Code)	ACS 5-year estimates (2008–2012) https://www.census.gov/programs-surveys/acs/
% People living in flood zones (Zip Code)	FEMA Flood Zones (FEMA, 2009); Dasymetric Population (Sorichetta et al., 2015)
Significant interactions	
% Karst *% People living in flood zones	
Huc-10 Watershed Rain Retention *% People living in flood zones	
Huc-10 Watershed Rain Retention Watershed Rain Retention *% Woody Wetlands	
Huc-10 Watershed Rain Retention *% Grassy Wetlands	
% Karst *%Woody Wetlands	
% Karst *%Grassy Wetlands	
Response variables	
FEMA flood claims (1999–2014) (Zip Code)	National Flood Insurance Data/FEMA National Flood Insurance Programs; Data not publicly available.
Medicare GI disease claims (1999–2013) (Zip Code)	The Centers for Medicare and Medicaid Services Hospitalization Data; Data not publicly available.

be limited to those in the ground floors who experience the flooding directly. To account for this, we calculated the proportion of people living in multi-family units (5+ families in a building) using the American Community Survey 5-year estimates (2008–2012; https://www.census.gov/programs-surveys/acs/). This same dataset was used to estimate median income as another socio-economic indicator, as it has been shown that wealthy communities tend to be less vulnerable to environmental hazards and the loss of ecosystem services (Myers et al., 2013).

2.2.4. Response variables

To estimate flood impact, we used data from the FEMA National Flood Insurance Program. Flood claims were obtained from the agency for the years 1999–2014. The agency summarized the data at the zip code level to remove any personal identifiable information (PII).

To estimate GI illness, we used hospitalization data from the Centers for Medicare and Medicaid Services (CMS), for the years 1999–2013. We summarized weekly claims associated to infectious GI illnesses for the selected zip codes and years, using the International Classification of Illnesses, Ninth Revision, Clinical Modification coding system (ICD-CM 9) for the following diagnosis: Cholera (ICD9-001), Salmonella (ICD9-003), Shigella (ICD9-004), Other bacterial poisoning (ICD9-005), Intestinal infection by other organisms (ICD9-008), and Ill-defined intestinal infections (ICD9-009). We intentionally did not include ICD codes for broad symptoms of GI illnesses (e.g., nausea, vomiting) as these could result from other types of illnesses and would add unexplained noise to statistical analysis. Because the data acquisition did not involve interaction with any individuals, and the data did not contain PII, it was determined by the U.S. Environmental Protection Agency's Human Subjects Research Protocol Officer that this research was exempt from Institutional Review Board review.

2.3. Data analysis

2.3.1. Flood protection EGS: FEMA flood claims

We evaluated the role of ecosystem services, and other variables on FEMA flood claims per zip code. Flood claim data consisted of integers ranging from 0 to over 400, and its distribution was heavily skewed towards zero. Data was therefore modeled as counts, using quasi-Poisson generalized linear models, which account for over dispersion. We developed a global quasi-Poisson model including all variables from each category (Table 1), significant interactions among variables ($Pr(>|z|) < 0.05$; Table 1), and households per zip code (American Community Survey Summary, 2008–2012) as a model offset. For variables that were indicators of the same predictor, but at two different scales (e.g. zip code 99% rainfall vs HUC-10 99% rainfall), we only used the best predictor of flood claims for inclusion in the model averaging procedure. Highly correlated variables that were not indicators of the same phenomena (e.g. %woody wetlands vs % people in flood zones), were kept in the global model.

We used this global model for model averaging (Grueber et al., 2011), which tested all possible variable combinations, and selected the top models explaining flood claim response (R package MuMin, Barton, 2009). To prevent overfitting, we limited the possible number of variable combinations to 5 factors, including interaction effects. This allowed us to have 10+ replicates per variable in accordance with recommended sample sizes for regressions (Vittinghoff and McCulloch, 2007; Austin and Steyerberg, 2015). The model averaging procedure was set up to prevent having highly correlated variables, that were not excluded from the global model (e.g. %woody wetlands vs % people in flood zones), to be featured together on any given 5-variable model. We used delta AICc>2 as a cut-off criterion for sub-model selection (Burnham and Anderson, 2002) and then calculated the conditional average effect of each variable after accounting for all the best models where that variable was included (Grueber et al., 2011). Variables were considered 'important' if their inclusion improved model fit in at least one of the selected sub-models. Results from model averaging were used to generate predicted flood claim values per zip code. These values were then regressed against observed FEMA claims to estimate the model's effectiveness at detecting flood impact.

2.3.2. Flood protection EGS and GI illness: Medicare claims

The variables that were selected as important predictors of flood claims were also used to evaluate spatio-temporal trends in GI illness response, with a few modifications. First, while the FEMA claims were standardized by the estimated zip code households, Medicare claims were analyzed controlling for the number of Medicare beneficiaries per zip code for each year of the study period. Second, weather parameters used to analyze FEMA claims were summarized for the entire study period, while Medicare Claims were analyzed in relation to daily estimates of 7-day lag extreme events (see *extreme weather* section for details), aggregated as weekly counts of 90, 95, or 99% rainfalls.

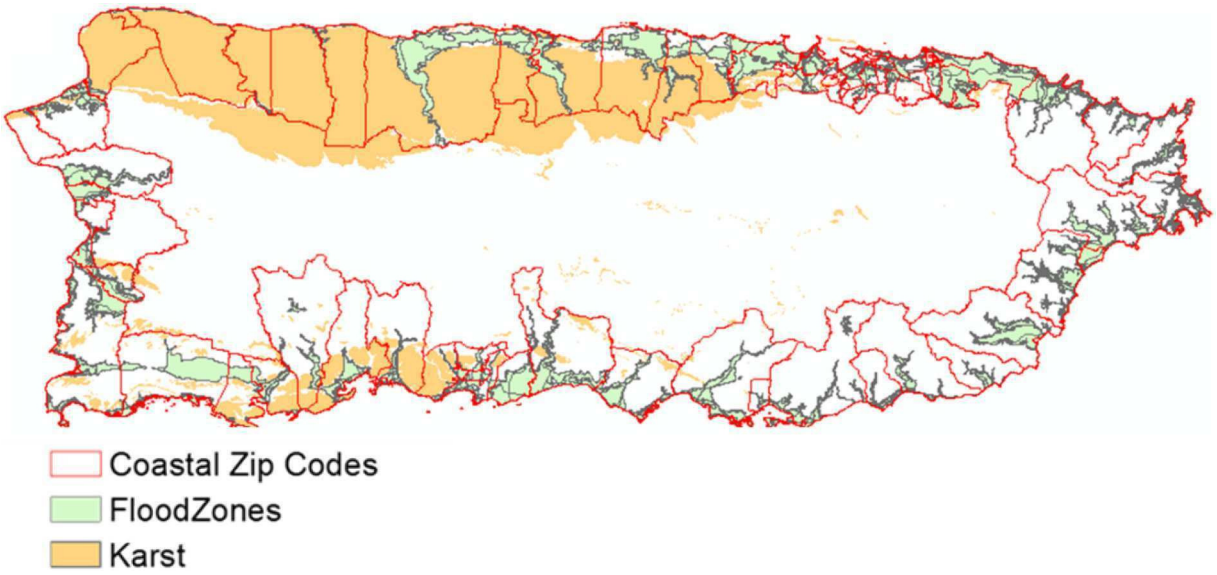

Fig. 3. Location of karst areas, and flood prone areas across Puerto Rico. The interaction of these two variables was a significant predictors of FEMA flood claims, and improved model fit for Medicare claims. The sources for these layers can be found in Table 1.

To evaluate the relationship between extreme weather events, flood impact predictors and GI illness, we used a Bayesian Integrated Nested Laplace Approximation (INLA) and Stochastic Partial Differential Equation (SPDE) approach. INLA-SPDE has been shown to be an efficient approach to assess spatio-temporal trends of relatively rare disease occurrences and develop robust models that are less computationally demanding than commonly used approaches (Myer et al., 2017).

Our response, presence/absence of GI illness in Medicare beneficiaries in a zip code each week, was coded as a binary outcome, with a 1 representing at least one case of GI illness reported among Medicare beneficiaries in a zip code that week, and a 0 representing no reported GI cases. Reports of more than one GI case were too sparse to justify modeling GI illness as a count response, so we elected to model the presence/absence of at least one GI illness. Logistic regression is typically used to model binary responses and produces a logit-linear measure of the probability of a positive outcome, and we elected to use binary logistic regression for this dataset.

The observational model for the spatiotemporal INLA SPDE model can be written as follows:

$$y(s,t) \mid \eta(s,t) \sim Bernoulli(\pi(s,t)),$$

where the presence of GI illness $y(s,t)$ at a particular location s and week t, given a vector of linear predictors $\eta(s,t)$, is a binary outcome with probability vector $\pi(s,t)$. The linear predictor has the general form

$$\eta(s,t) = \beta_1 X_1 + \ldots + \beta_n X_n + m_s + w_t$$

where $(\beta_1, \ldots, \beta_n)$ are the regression coefficients for the predictor variables $(X_1, \ldots, X_n)$, m_s is the spatial random effect at location s, w_t is the temporal random effect at week t, and the relationship between the linear predictor $\eta(s,t)$ and the GI illness probability $\pi(s,t)$ is the logit link

$$\pi(s,t) = log\frac{\eta(s,t)}{1-\eta(s,t)}$$

Spatial covariance m_s was addressed in the SPDE model using a Gaussian Markov random field based on a triangulation mesh represented as a labeled, undirected graph over the selected zip codes (SM5), which estimates spatial effects on GI illness probability across the study area using the Matérn covariance function (Musenge et al., 2013; Cosandey-Godin et al., 2014).

Temporal covariance was addressed using a first-order random walk process (RW1), which models the effect of time as a function of presence in the previous week plus a random error term. The conceptual model for the change in the ordinal vector of temporal coefficients $(w_1, \ldots, w_t)$ is of the form

$$\Delta w_i = w_i - w_{i-1} \sim N(0, \tau^{-1})$$

where τ is the precision parameter, estimated as a hyperparameter in the INLA model.

Diffuse normal priors (precision = 0.001) were chosen for variables in the linear predictor, reflecting no prior knowledge of their coefficients. For the spatial and temporal effects, we assigned the penalized complexity prior, which is a weakly informative prior that accounts for model complexity and has improved performance in SPDE models (Fuglstad et al., 2015; Simpson et al., 2017).

Building from the set of important variables and interactions in the flood claim analysis, we used model comparison approaches to evaluate whether models with ecosystem services variables provided significantly better fit in predicting GI illness outcomes than models with just weather hazards (counts of 90%, 95%, or 99% rainfall events), or socio-economic variables (sewage infrastructure). Models with only underlying spatial covariance (m_s) and temporal covariance (w_t), or with the number of Medicare beneficiaries as a control variable were used as baselines for comparing model fit.

Model ranking was conducted using Watanabe-Akaike Information Criterion (WAIC) which is a preferred approach for comparing fully Bayesian models (Gelman et al., 2014). Predictive fit was evaluated by generating a receiver-operating characteristic (ROC) curve, using the R package ROCR, (Sing et al., 2005), which plots the sensitivity (true positive rate) against 1-specificity (false positive rate), across all possible cutoff points. The area under curve (AUC) value was computed to determine predictive fit, by integrating the ROC curve. The AUC value represents the probability that a randomly chosen GI illness positive observation will have a higher modeled value than a randomly chosen GI illness negative observation. An AUC value higher than 0.5 indicates that the model is better than chance at predicting the outcome. The optimized cutoff point to minimize false positives and maximize true positives was determined by maximizing Youden's index (i.e., sensitivity + specificity -1).

All analyses were performed using the R package 'INLA' and R version 3.4.4 statistical software.

3. Results

3.1. Flood protection EGS and flood claims

Details of the model parameters by zip code and as averages are included in SM6. During our study period, a total of 4349 flood claims were filed to FEMA's National Flood Insurance Program. The variables best explaining FEMA claims were the magnitude of 99% rainfall at the HUC-10 watershed level ($p = 0.002$), the proportion of people living in multi-family units ($p = 0.014$), and average zip code slope ($p = 0.009$). The zip codes with the highest number of flood claims were in the towns of Santa Isabel (00757, 407 claims) and Salinas (00751, 413 claims), both within the Coamo River watershed, and in San Juan (00920, 333 claims), at the mouth of the Rio Puerto Nuevo, in the San Juan Bay. These zip codes had >1.6 times as many flood claims as the next largest zipcode, despite having comparable number of households and population sizes to other study sites. Zip codes 00751 and 00757 also showed a high level of influence on final model selection, leading to inflated residuals. Because of this, we repeated the analysis without these zip codes (see SM4 for more details), and removed them from sub-sequent analysis.

For the remaining study sites ($N = 70$) the variables best explaining flood claims were the magnitude of the 99% rainfall at the HUC-10 watershed level ($p < 0.001$), % karst ($p = 0.02$), % people living in flood zones ($p < 0.001$), and the interaction effect of these latter two variables ($p < 0.001$, Table 2). When exploring the significant interaction effect, karst soils appear to help lower the number of flood claims per household, but this relationship is lost in places with a greater number people living in flood prone areas (Fig. 4). In terms of rainfall, the magnitude of the 99% rainfall events at the watershed level, led, as expected to a higher number of FEMA claims per household. This model was the only one selected through the model averaging process, as no other model was comparable in terms of AIC model fit. The ability of the model to predict flood cases was significant ($R^2 = 0.578$, $p < 0.001$, Fig. 5), and we found no evidence of significant spatial autocorrelation of the model's residuals (Table 2).

3.2. Flood protection EGS and GI illness

For this part of the study we also focused on the zip codes that were not considered as outliers. For these zip codes ($N = 70$), a total of 1917 Medicare claims were submitted to the CMS for the selected GI illnesses between 1999 and 2013 (Table 3). The most common claims filed were for Intestinal infection due to other organisms (ICD9–008), and Ill-defined intestinal infections (ICD9-009).

There was a distinct temporal trend in the number of claims filed, with a sharp drop observed after week 400, which roughly corresponds to the year 2006 (Fig. 6A). Spatially, we observe higher than average effect of location on GI illness in the Southwest area of the Island, followed by the rest of the West coast, (Fig. 6B). The East coast overall seems to have a lower-than-average effect of location (Fig. 6B).

Controlling for these spatial and temporal covariances, we used the variables selected as best predictors in the FEMA claims assessment to evaluate GI illness trends. Controlling for the number of Medicare beneficiaries, the best model explaining GI illness claims included 7-day lag rainfall (90–99% events) and the interaction effect between % Karst and % People in flood zones. The strongest predictor of GI illness claims was the count of 90% + rainfall events within the last week (i.e. confidence interval for model coefficient did not overlap zero). When converting the coefficient of this relationship (see Table 4) from log odds ratio to percentage, we see a 17% modeled increase in the odds of GI Illness following 90% and above rainfall events. The best model's WAIC weight was close to two times higher than the next best model with other variable combinations (Table 4).

In general, we found that models with weather hazards performed better (lower WAIC) than the baseline models with only spatial and temporal covariance or the models that only control for the number of Medicare beneficiaries (Table 4). GI illness claims tended to increase with the number of beneficiaries and increase with the number of extreme weather events. Model fit improved when adding % karst and its interaction with the percentage of people living in flood zones but decreased when adding sewage density (Table 4). In terms of predictive accuracy, the best model's AUC value was 0.70 (Fig. 7), indicating that the model has a better than random chance at predicting GI illness. The optimal cutoff point for classifying the response obtained by maximizing Youden's index was 0.03, resulting in a sensitivity of 0.66 and a specificity of 0.63.

Table 2
Important variables selected through model averaging, with conditional averages of estimated effects and *p* values.

Selected variables	Estimate	Std. Error	t value	Pr (>|t|)
(Intercept)	−5.3011	0.1154	−45.934	<2e-16 ***
Huc-10 99Rain	0.4314	0.1138	3.789	0.000333 ***
% Karst	0.3699	0.1563	2.367	0.020922 *
% People living in flood zones	0.7395	0.1656	4.466	3.25e-05 ***
% Karst *% People living in flood zones	0.9182	0.21843	2.406	0.001719 **
Dispersion parameter for quasipoisson	32.8638			
Null deviance	2894.2			
Residual deviance	1613.0			
df	65			
Moran's Index (z-score; p value)[a]	0.1818; 0.8587			

[a] Moran's Index was calculated in Arc GIS (ver. 10.3) to determine spatial autocorrelation of model residuals.

4. Discussion

Rainfall extremes in the coast of Puerto Rico (PR) have historically caused property damages, and human health impacts that disproportionally affect neighborhoods in flood prone areas. This study is the first to document this trend empirically on an Island wide basis. In the aftermath of the most extreme natural disaster to strike PR in generations, Hurricane Maria, the importance of flooding, and weather-related illnesses has gained more attention. Here we provide evidence that some of the health problems associated to weather events on the Island are not new and deserve sustained attention in the face of potential increases on extreme rainfall in the future.

4.1. Flood protection ecosystem services and flood claims

Flood claims in Puerto Rico for the years 1999–2014 are closely tied to the average magnitude of the most extreme rainfall events (99%). Our final model predicted observed FEMA flood claims with reasonable accuracy, and a strong model fit was found once we accounted for the role of three outlier zip codes (SM4). The number of flood claims on these locations was particularly high around two important rainfall events. The first was a tropical storm in September of 2008 that resulted in around 20 million dollars in damages (Puerto Rico Science Museum, 2011). The second was a historical rainfall event in November of 2009, which caused record breaking river heights, and severe flooding in the San Juan metropolitan area (NOAA NWS, 2009). Our estimated rainfall values for these zip codes, however, was not any greater than that for other nearby study sites. Therefore, unaccounted factors that have been previously reported on these locations, such as housing quality and the capacity of local water infrastructure to handle events of high

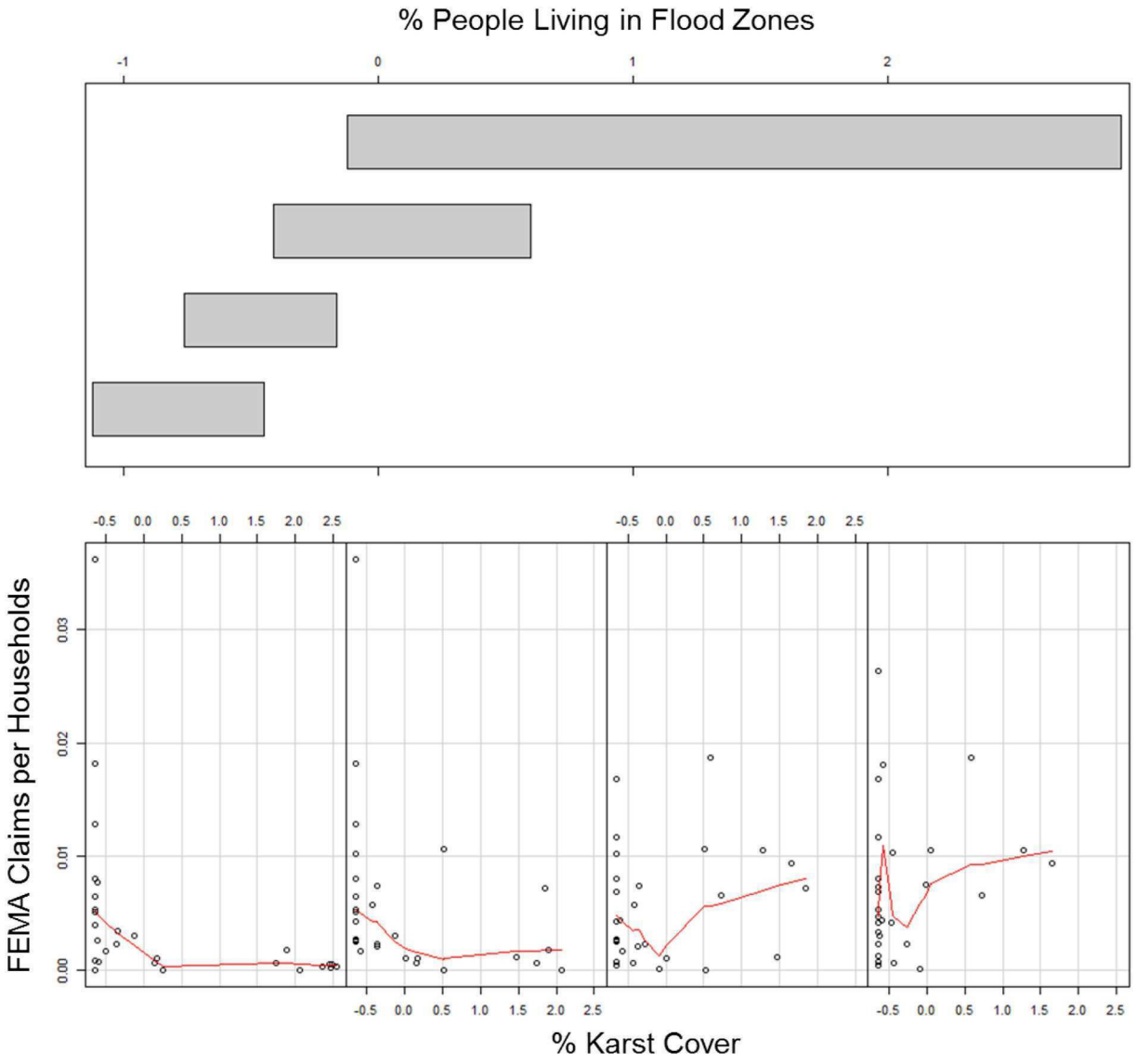

Fig. 4. Visualization of the interaction effects between %Karst * % People in Flood Zones, on FEMA flood claims (cases per household per zip code). The top panel shows different levels of the % people in flood zones, the bottom panel represents the relationship between % karst and claims per household at each of these levels. The red line represents a locally weighted scatterplot smoother (Cleveland, 1981).

magnitude (Stockstill and Leech, 1990; Bush et al., 1995), may have led to the observed trends, and should be determined through more extensive studies on these zip codes.

As we predicted, the relationship observed between extreme rainfall and floods is to some extent mitigated by natural structures, such as karst soils (Fig. 3, Fig. 4). The karst formations in Puerto Rico promote rapid infiltration of rainwater to underground conduits (Torres-González et al., 1996), potentially contributing to flood risk reduction, especially if rainfall retention features such as caves and sinkholes are protected from debris accumulation or urbanization (Zhou, 2007). The observed protective effect of karst soils is lost in areas where a high percentage of people live in flood zones (Fig. 4). Naturally infiltrated waters in karst soils re-emerge as surface water in springs, or wetlands, which may cause flooding further downstream under certain conditions. Therefore, flood protection services provided by karst soils may not protect neighborhoods located in the very same areas were infiltrated waters are naturally expected to re-surface. The role of karst hydrology and its relationship to flood dynamics is still a subject in need of more research (Gutiérrez et al., 2014; Naughton et al., 2018), and was not the focus of the present work, so we encourage further analysis of these observed trends.

Aside from its infiltration capacity, the karst region is one of the few areas of the Island with a firm legal basis for protection, as contained in Law 292, Law to Protect the Karst Physiography of Puerto Rico (Vale-Nieves, 2018). This law led to the establishment of a strict land use framework, where around 33% of the karst extent fell under the highest degree of protection possible (Vale-Nieves, 2018). This implies complete restriction of activities such as landfills, and waste disposal sites, prohibitions on the use of agrochemicals, and strict control of development projects (Garcia-Padilla et al., 2013). Law 292's regulations however, are not equally restrictive across the entire karst extent, including some karst municipalities with a high percentage of people living in flood prone areas (e.g., Vega Baja, Vega Alta, Dorado, Toa Baja, (Fig. 4, also see SM4, and CLCC, 2016). Therefore, the associations observed between karst and flood claims, moderated by people living in flood zones could also reflect regulatory disparities regarding hydrological alteration and water resource pollution. More studies are needed to establish a clear mechanism to explain these trends.

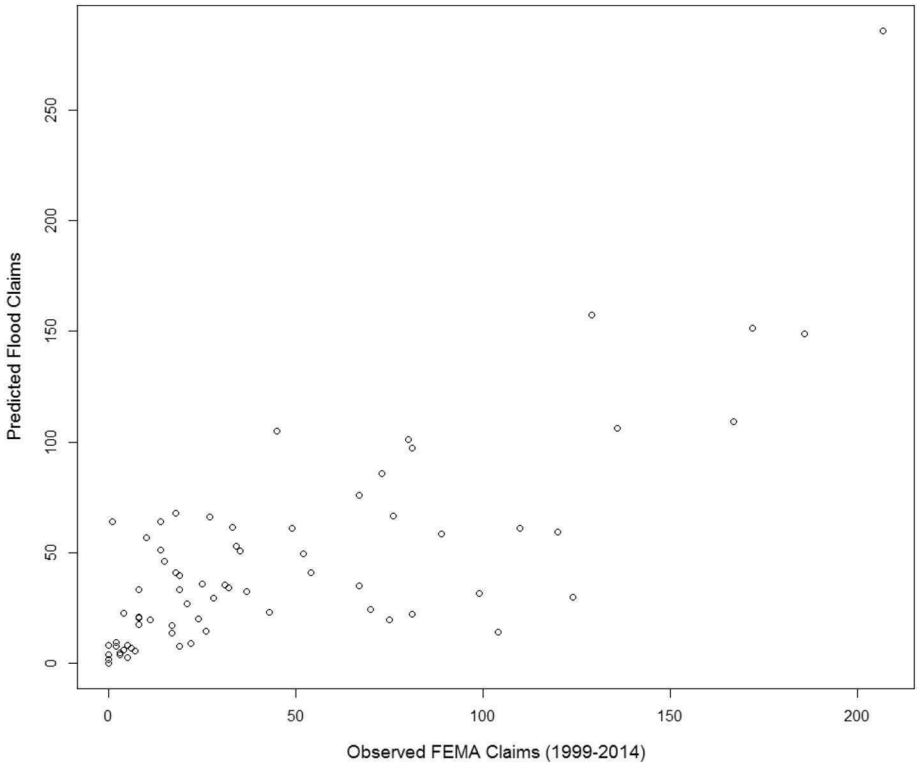

Fig. 5. Predicted flood claims vs observed flood claims from model averaging results excluding outlier zip codes ($R = 0.57$, $p < 0.001$).

4.2. Flood protection EGS and GI illness

Extreme rainfall events were a strong predictor of GI illnesses, with Medicare claims showing a 17% modeled increase in the odds of a GI-related illness following a 90% (and above) rainfall event. The interaction effect between % karst soils * % people living in flood zones greatly improved the fit of the model linking GI illness to extreme rainfall events. Because this interaction was also shown to be a good predictor of FEMA flood claims, these results lend some support to our hypothesis linking flood protection ecosystem services to a reduction in flood related health effects. This protective effect, however, seems very limited and what the interaction effect suggests is that these natural features are not effective at counteracting the level of exposure some communities face when located in flood prone neighborhoods.

Built adaptations, such as adequate sewage infrastructure should provide protection from GI illness occurrences, but this parameter, did not improve the fit of models linking GI illness to extreme weather events. Our models did not control for factors that could determine sewage system effectiveness, such as date of construction, maintenance levels, or the capacity of the infrastructure relative to the magnitude of the population served. In PR, these factors have been shown to affect the performance of waste management in the past (Hunter and Arbona, 1995; PRASA, 2014), and therefore, future studies could address in more detail which systems across the island are performing adequately with respect to their influence on public health issues such as GI illness.

Aside from flooding, an alternative pathway of exposure to untreated sewage is recreational swimming. Previous studies in Puerto Rico have shown correlations between rainfall and GI illness pathogens in public beaches (Cordero et al., 2012; Laureano-Rosario et al., 2017). Exposure to GI illness pathogens was also shown to be linked to recreational swimming and sewage infrastructure in one of the most important beaches in Southwest Puerto Rico (Wade et al., 2018). As seen in Fig. 6, the southwest of PR is the main region with a higher than average odds of having spatially associated cases of GI illness. This area's economy is closely tied to marine recreational opportunities, and our study supports previous research documenting public health concerns in this important tourism destination that should be addressed.

Aside from the spatial patterns observed, we also detected a prominent temporal pattern, where Medicare claims for GI illness dropped after the year 2006. The influence of this pattern was accounted for in our analysis. This drop in Medicare claims was not a reflection of any changes in rainfall trends as far as we can tell from our weather data. A potential explanation to this effect could be changes in Medicare policy affecting claim filing processes. For example, the Deficit Reduction Act of 2005, led to a reduction in the number of claims filed for certain hospital acquired infections (Kawai et al., 2015) and radiology referrals (Levin et al., 2009), but it is not clear whether this would have also led to a decrease in reported GI illnesses in Puerto Rico. Another potential factor could be associated to improvements in storm and waste water management in Puerto Rico around this time. Coincidentally, in 2006, the EPA fined the Puerto Rico Sewage and Aqueduct Authority (PRASA) for 15 violations to the Clean Water Act on wastewater and drinking treatment plants, for the unprecedented amount of 9 million dollars (USEPA, 2006). Remedial measures in the most polluting waste

Table 3
GI diseases examined for coastal zip codes in PR International Classification of Disease, Version 9 (ICD9).

Period	Gastro intestinal diseases (ICD 9 Codes)	Total Medicare claims
1999–2013	Cholera (ICD9-001)	0
	Salmonella (ICD9-003)	273
	Shigella (ICD9-004)	4
	Other Bacterial Poisoning (ICD9-005)	113
	Intestinal Infections due to Other Organisms (ICD9-008)	788
	Gastroenteritis (ICD9-009)	739
	Total	1917

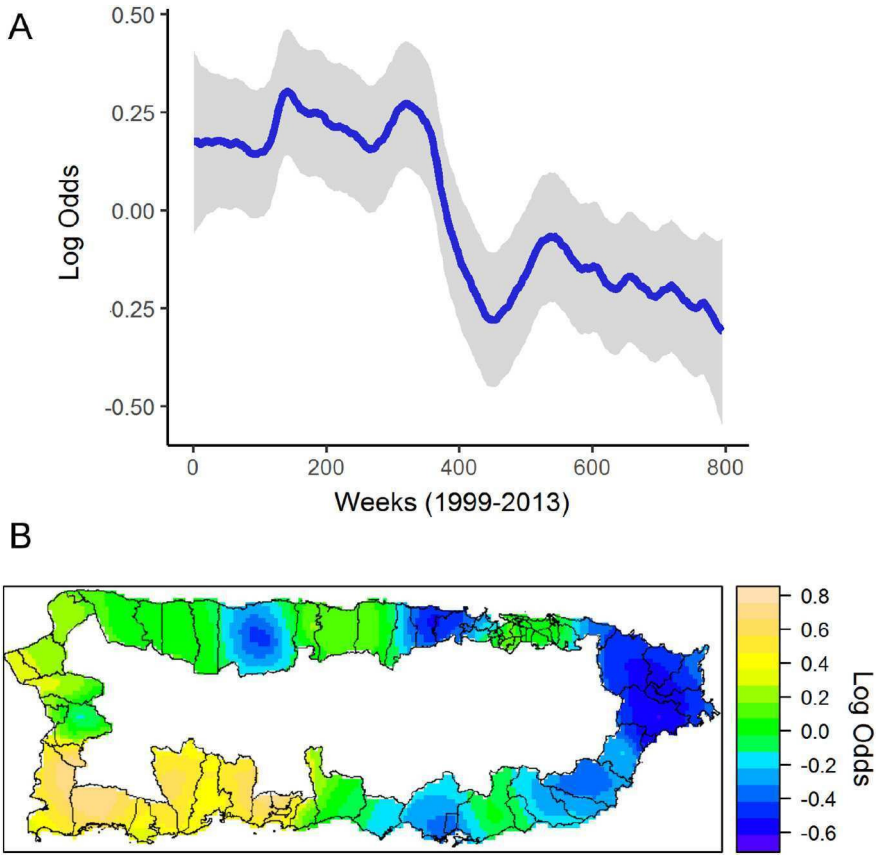

Fig. 6. Temporal and spatial trends in GI disease claims over the study period. The y axis in Fig. 6A shows the coefficient of the temporal effect in log-odds for the selected study weeks between the years 1999–2013. Fig. 6B shows the spatial coefficient, in log-odds, for coastal ZIP codes in Puerto Rico.

Table 4
Spatio-temporal regressions looking at the effect selected parameters on gastro-intestinal diseases in Puerto Rico (1999–2013).

Parameters*	0	1	2	3	4	5
Medicare beneficiaries		0.58 (0.51: 0.66)	0.58 (0.51: 0.66)	0.58 (0.51: 0.66)	0.58 (0.51–0.66)	0.58 (0.51: 0.66)
Weather hazards						
90%$^{+}$ Rainfall event			0.16 (0.03: 0.29)	0.16 (0.03: 0.29)	0.16 (0.04–0.29)	0.16 (0.04:0.29)
95%$^{+}$ Rainfall event			0.03 (−0.09: 0.15)	0.03 (−0.09: 0.15)	0.03 (−0.09–0.15)	0.03 (−0.09: 0.15)
99%$^{+}$ Rainfall event			0.07 (−0.11: 0.24)	0.07 (−0.11: 0.23)	0.07 (−0.11–0.23)	0.07 (−0.11: 0.24)
Sewage density				0.005 (−0.14: 0.15)		−0.0001 (−0.15: 0.15)
Ecosystem goods and services						
(1) %Karst[b] ppl_FldPer[a]					0.15 (−0.08–0.38)	0.15 (−0.08: 0.38)
%Karst					−0.10 (−0.32–0.11)	−0.10 (−0.33: 0.12)
ppl_FldPer[a]					0.14 (−0.01–0.29)	0.14 (−0.02: 0.29)
Hyperparameters						
Range spatial effect	4.47 (2.8: 6.7)	32.04 (15.91:61.18)	32.58 (16.03:62.46)	32.13 (15.71:62.29)	32.58 (16.62–60.57)	32.01 (16.26:59.76)
STDEV spatial effect	1.29 (0.98:1.67)	0.47 (0.34:0.66)	0.48 (0.34:0.66)	0.48 (0.34:0.66)	0.48 (0.32–0.68)	0.48 (0.33–0.68)
Precision temporal effect	36.97 (6.85:133.27)	22.42 (5.70:65.28)	23.20 (5.94:67.89)	23.58 (6.00:68.92)	23.18 (5.92–67.62)	23.43 (5.97–67.94)
Number of Parameters	65.81	46.76	49.66	50.35	50.7	51.09
WAIC	14,767.43	14,751.14	14,750.9	14,752.14	14,745.18	14,746.49
WAIC weights	0.00	0.03	0.03	0.02	**0.60**	0.31

[a] Percentage of people living in flood areas. Variables with 95% CI not encompassing zero are considered as best predictors. Best model's WAIC weight is in bold. The range for spatial refers to the distance in km at which spatial correlation becomes negligible. The precision for temporal effect refers to the inverse standard deviation for the RW1 error between week values.

[b] Values for the model parameters are in log odds ratio units.

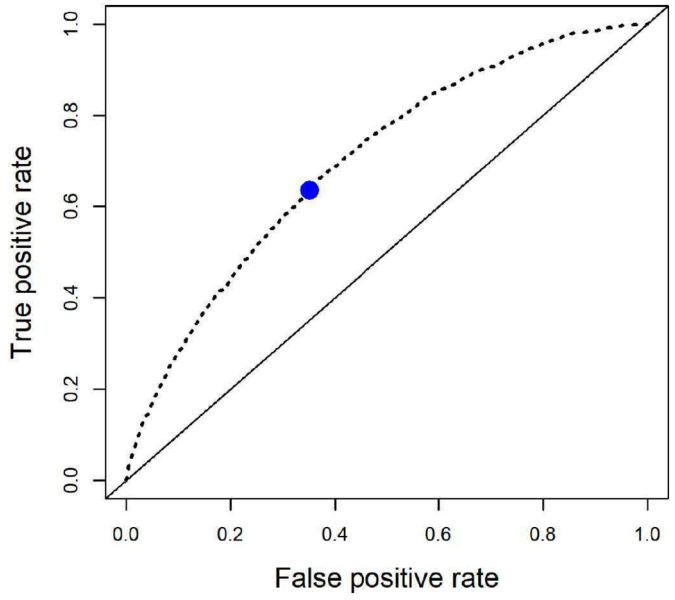

Fig. 7. Receiver operating characteristic curve illustrating the tradeoff between true positive rate and false positive rate for a range of cutoff values with the best INLA model. The blue dot indicates the optimal cutoff value calculated by Youden's index, 0.03, at which sensitivity (true positive rate) = 0.66 and specificity (1 – false positive rate) = 0.63. Overall area under curve = 0.70. Youden's index is (sensitivity + specificity −1), and the optimal cutoff point that minimizes misclassification is determined by maximizing the index along the ROC curve.

water treatment facilities may have quickly ensued after this incident, as PRASA was required to do so under the consent decree (USEPA, 2006). These potential explanations, however, are speculative and this temporal pattern in GI illness should be further assessed.

4.3. Study limitations

Our study has several limitations. First, the weather estimates are based on extrapolated data from existing meteorological stations, which may be more representative in some parts of the island than others. Studies assessing weather at a finer resolution could help provide more details to the trends observed. Likewise, the scale at which we analyzed our disease and flood claims (e.g. zip code) is still very coarse and is not able to capture relationships that may occur at the neighborhood level, in association to local rain retention management initiatives. Unfortunately, disease data is rarely publicly available at the neighborhood scale, so similar studies, using survey instruments for example, could help supplement our results. Moreover, while the Medicare claims system provides consistent data through the states GI illnesses, for the most part, are under reported, and we may have under estimated their occurrence. Incorrect reporting, and misclassification of Medicare claims, as well as omission of certain ICD-9 codes from our analysis should also be considered as potential sources of bias in our results. Furthermore, because we used Medicare claims as an indicator of GI illness trends, our study was mainly representative for the elderly demographic (~19.7% of PR's current population, US Census, 2018), and should be interpreted taking this factor into consideration. Previous studies suggest that the elderly is the most sensitive group to weather related GI illnesses (Jagai et al., 2015). However, the associations between rainfall and GI illness among other sensitive groups, such as young children, may need to be evaluated further.

In terms of our modeling approach, we tested parameters at multiple scales, and the selection of these scales were meant to respond to our study objectives. However, estimating more landscape parameters at the watershed level, or in association to health responses at the census tract or block group level, may help further address the linkage between flooding, ecosystem services and GI illness in the future. While our study did not find a statistically significant relationship between vegetation cover, the rain retention index and flood claims, we think this is still a question that needs to be researched further, looking at more study locations, and assessing this relationship at different spatial resolutions. At smaller spatial scales, such as census blocks, it is possible that the presence of rain retention gardens, riparian buffers and other locally managed green spaces provide a level of small scale protection that would have been difficult to capture in our study looking at zip codes. Moreover, a potential mismatch between the supply and demand of ecosystem services also needs to be considered, as places that are more at risk of flooding tend to be more urbanized and located within sprawling areas that are more likely to have lost more vegetation cover within their watersheds (Stürck et al., 2014). The context of coastal zip codes in Puerto Rico, where a large proportion of the population in flood zones are also downstream of the highly urbanized San Juan metropolitan area (Fig. 2, Fig. 3), provides a limited opportunity to test this hypothesis fully. Repeating this analysis in a larger context, such as across coastal counties in the mainland US could help address these questions further.

5. Conclusions

To our knowledge, this study is the first to explore the role of flood protection ecosystem services on preventing GI illnesses. We found that GI illnesses in PR spike after rain events, and that the natural infiltration provided by karst soils may help prevent floods and GI illness occurrences. The role of this ecosystem service is affected by planning decisions in coastal communities, such as residential development in flood prone areas, which undermines the protective effect of rainfall retention from natural features. Built adaptations, such as adequate sewage infrastructure, are expected to provide a protective role on GI illness occurrences, but we did not find evidence for this in our study. Factors such as the age and capacity of sewage infrastructure across the island needs to be accounted for in future research to better assess its effectiveness on protecting from GI illness associated to weather events. Aside from flooding, environmental exposure to disease pathogens after extreme weather events have been linked to recreational swimming in PR. This relationship may be related to the observed spatial association of GI illness to Southwest PR (a popular beach destination). This is a finding that supports previous studies and highlights the importance of effective waste water management and public health protection on this location.

Supplementary data to this article can be found online at https://doi.org/10.1016/j.scitotenv.2019.04.287.

Acknowledgements

Matthew Harwell, Marc Russell and Justin Bousquin provided advice on study design and the assessment flood protection ecosystem services. Lucas Neas, Laura Jackson, and John Johnston provided advise on the design and analysis of the Medicare claims data. In accordance with CMS data use agreement, this dataset was processed an analyzed at a single, secured workstation located at the USEPA Environmental and Public Health Division's Human Studies Facility, at the University of North Carolina, Chapel Hill. Special thanks to Lucas Neas for facilitating this process. The views expressed in this paper are those of the authors and do not necessarily reflect the views or policies of the U.S. Environmental Protection Agency. Any mention of trade names, products or services does not imply an endorsement by the U.S. Government or the U.S. Environmental Protection Agency (EPA). The EPA does not endorse any commercial products, services, or enterprises.

References

Abel, J., Deitz, R., 2014. The causes and consequences of Puerto Rico's declining population. Curr. Issues Econ. Financ. 20 (4). https://papers.ssrn.com/sol3/papers.cfm?abstract_id=2477891, Accessed date: 22 June 2018.

Ahern, M., Kovats, R.S., Wilkinson, P., Few, R., Matthies, F., 2005. Global health impacts of floods: epidemiologic evidence. Epidemiol. Rev. 27 (1), 36–46.

Alemán González, W.B., 2010. Karst map of Puerto Rico. U.S. geological survey open-file report, 2010-1104. http://pubs.usgs.gov/of/2010/1104/, Accessed date: 11 June 2018.

Arguez, A., Durre, I., Applequist, S., Vose, R.S., Squires, M.F., Yin, X., Owen, T.W., 2012. NOAA's 1981–2010 US climate normals: an overview. Bull. Am. Meteorol. Soc. 93 (11), 1687–1697.

Austin, P.C., Steyerberg, E.W., 2015. The number of subjects per variable required in linear regression analyses. J. Clin. Epidemiol. 68 (6), 627–636.

Azar, D., Rain, D., 2007. Identifying population vulnerable to hydrological hazards in San Juan, Puerto Rico. GeoJournal 69 (1–2), 23–43.

Barton, K., 2009. Mu-MIn: Multi-model inference. R Package Version 0.12.2/r18. http://R-Forge.R-project.org/projects/mumin/., Accessed date: 23 April 2019

Becker, R.A., Chambers, J.M., Wilks, A.R., 1988. The New S Language. Wadsworth & Brooks/Cole.

Briskin, E.A., 2016. Seroprevalence and Risk Factors for Leptospirosis in an Urban Community of Puerto Rico. https://elischolar.library.yale.edu/ysphtdl/1026/, Accessed date: 22 June 2018.

Brody, S.D., Highfield, W.E., 2013a. Open space protection and flood mitigation: a national study. Land Use Policy 32, 89–95.

Brody, S.D., Highfield, W.E., 2013b. Open space protection and flood mitigation: a national study. Land Use Policy 32, 89–95. https://doi.org/10.1016/j.landusepol.2012.10.017.

Brody, S.D., Peacock, W.G., Gunn, J., 2012. Ecological indicators of flood risk along the Gulf of Mexico. Ecol. Indic. 18, 493–500. https://doi.org/10.1016/j.ecolind.2012.01.004.

Broody, H.a., 2006. Price of permits: measuring the economic impacts of wetland development on flood damages in Florida. Nat. Hazards Rev. 7 (3), 123–130. https://doi.org/10.1061/(ASCE)1527-6988(2006)7:3(123).

Burnham, K.P., Anderson, D.R., 2002. Model Selection and Multimodel Inference: A Practical Information-theoretic Approach. 2nd edn. Springer, Berlin.

Bush, D.M., Webb, R.M., Liboy, J.G., 1995. Living with the Puerto Rico Shore. Duke University Press.

Caribbean Landscape Conservation Cooperative (CLCC), 2016. Puerto Rico Protected Areas Database (version of December, 2016]. GIS data. San Juan, PR).

Castro-Prieto, J., Martinuzzi, S., Radeloff, V.C., Helmers, D.P., Quiñones, M., Gould, W.A., 2017. Declining human population but increasing residential development around protected areas in Puerto Rico. Biol. Conserv. 209, 473–481.

Centro de Recaudación de Ingresos Municipales (CRIM) PR Office of Management and Budget, 1998. Puerto Rico Basemap Project: derived contours from CRIM Digital Elevation Model (1996–98). http://www.esri.com/metadata/esriprof80.html, Accessed date: 11 June 2018.

Cleveland, W.S., 1981. LOWESS: a program for smoothing scatterplots by robust locally weighted regression. Am. Stat. 35, 54.

Cordero, L., Norat, J., Mattei, H., Nazario, C., 2012. Seasonal variations in the risk of gastrointestinal illness on a tropical recreational beach. J. Water Health 10 (4), 579–593.

Cosandey-Godin, A., Krainski, E., Worm, B., Flemming, J.M., 2014. Applying Bayesian spatiotemporal to fisheries bycatch in the Canadian Arctic. Can. J. Fish. Aquat. Sci. 72, 186–19.

Crimmins, A., Balbus, J., Gamble, J.L., Beard, C.B., Bell, J.E., Dodgen, D., Eisen, R.J., Fann, N., Hawkins, M., Herring, S.C., Jantarasami, L., Mills, D.M., Saha, S., Sarofim, M.C., Trtanj, J., Ziska, L., 2016. Executive Summary. The Impacts of Climate Change on Human Health in the United States: A Scientific Assessment. U.S. Global Change Research Program, Washington, DC https://doi.org/10.7930/J00P0WXS 24 pp.

Curriero, F.C., Patz, J.A., Rose, J.B., Lele, S., 2001. The association between extreme precipitation and waterborne disease outbreaks in the United States, 1948–1994. Am. J. Public Health 91 (8), 1194–1199.

Cutter, S.L., Boruff, B.J., Shirley, W.L., 2003. Social vulnerability to environmental hazards. Soc. Sci. Q. 84 (2), 242–261.

De Jesus Crespo, R., Lázaro, P.M., Yee, S.H., 2018. Linking wetland ecosystem services to vector-borne disease: dengue fever in the San Juan Bay estuary, Puerto Rico. Wetlands 1–13.

Department of Commerce (DOC), 2010. C-CAP Land Cover. NOAA Ocean Service https://coast.noaa.gov/ccapftp/#/, Accessed date: 11 June 2018.

Federal Emergency Management Agency (FEMA), 2009. Digital Flood Insurance Rate Map Database. Commonwealth of Puerto Rico Available at. http://gis.otg.pr.gov/download_gis_files.htm.

Fuglstad, G.A., Simpson, D., Lindgren, F., Rue, H., 2015. Constructing Priors that Penalize the Complexity of Gaussian Random Fields. arXiv Statistics – Methodology (1503.00256v4).

Garcia-Padilla, A., Garcia-Pelatti, L., Perez, C. Guerrero, 2013. Plan y reglamento del area de planificacion especial del carso. Estado Libre Asociado de Puerto Ricohttp://gis.jp.pr.gov/Externo_Econ/Otras%20Areas%20-%20Vistas%20Publicas/Plan%20y%20Reglamento%20Area%20de%20Planificacion%20Especial%20del%20Carso.pdf, Accessed date: 22 June 2018.

Gelman, A., Carlin, J.B., Stern, H.S., Rubin, D.B., 2014. Bayesian data analysis. Chapman & Hall/CRC Boca Raton, FL, USA.

Government of Puerto Rico, 2018. Investor resources: Puerto Rico Aqueduct and Sewer Authority (PRASA). http://www.gdb.pr.gov/investors_resources/prasa.html, Accessed date: 1 October 2018.

Grueber, C.E., Nakagawa, S., Laws, R.J., Jamieson, I.G., 2011. Multimodel inference in ecology and evolution: challenges and solutions. J. Evol. Biol. 24 (4), 699–711.

Gutiérrez, F., Parise, M., De Waele, J., Jourde, H., 2014. A review on natural and human-induced geohazards and impacts in karst. Earth Sci. Rev. 138, 61–88.

Hernández Ayala, J.J., Keellings, D., Waylen, P.R., Matyas, C.J., 2017. Extreme floods and their relationship with tropical cyclones in Puerto Rico. Hydrol. Sci. J. 62 (13), 2103–2119.

Huang, L.Y., Wang, Y.C., Wu, C.C., Chen, Y.C., Huang, Y.L., 2016. Risk of flood-related illnesses of eyes, skin and gastrointestinal tract in Taiwan: a retrospective cohort study. PLoS One 11 (5), e0155166.

Hufkens, K., 2014. Daymetr – R package to download tiled and single pixel daymet data from the ORNL DAAC. https://doi.org/10.5281/zenodo.437886 Version 1.0. Zenodo.

Hunter, J.M., Arbona, S.I., 1995. Paradise lost: an introduction to the geography of water pollution in Puerto Rico. Soc. Sci. Med. 40 (10), 1331–1355.

Jagai, J.S., Li, Q., Wang, S., Messier, K.P., Wade, T.J., Hilborn, E.D., 2015. Extreme precipitation and emergency room visits for gastrointestinal illness in areas with and without combined sewer systems: an analysis of Massachusetts data, 2003–2007. Environ. Health Perspect. 123 (9), 873.

Kawai, A.T., Calderwood, M.S., Jin, R., Soumerai, S.B., Vaz, L.E., Goldmann, D., Lee, G.M., 2015. Impact of the Centers for Medicare and Medicaid Services hospital-acquired conditions policy on billing rates for 2 targeted healthcare-associated infections. Infect. Control Hosp. Epidemiol. 36 (8), 871–877.

Larsen, M.C., 2017. Forested watersheds, water resources, and ecosystem services, with examples from the United States, Panama, and Puerto Rico. Chemistry and Water, pp. 161–182.

Laureano-Rosario, A.E., Symonds, E.M., Rueda-Roa, D., Otis, D., Muller-Karger, F.E., 2017. Environmental factors correlated with culturable enterococci concentrations in tropical recreational waters: a case study in Escambron Beach, San Juan, Puerto Rico. Int. J. Environ. Res. Public Health 14 (12), 1602.

Levin, D.C., Rao, V.M., Parker, L., Frangos, A.J., 2009. The disproportionate effects of the Deficit Reduction Act of 2005 on radiologists' private office MRI and CT practices compared with those of other physicians. J. Am. Coll. Radiol. 6 (9), 620–625.

Lugo, A.E., Carlo, T.A., Wunderle, J.M., 2012. Natural mixing of species: novel plant-animal communities on Caribbean Islands. Anim. Conserv. 15, 233–241. https://doi.org/10.1111/j.1469-1795.2012.00523.x.

Mallin, M.A., Ensign, S.H., McIver, M.R., Shank, G.C., Fowler, P.K., 2001. Demographic, landscape, and meteorological factors controlling the microbial pollution of coastal waters. Hydrobiologia 460 (1), 185–193. https://doi.org/10.1023/a:1013169401211.

Musenge, E., Chirwa, T.F., Kahn, K., Vounatsou, P., 2013. Bayesian analysis of zero inflated spatiotemporal HIV/TB child mortality data through the INLA and SPDE approaches: applied to data observed between 1992 and 2010 in rural North East South Africa. Int. J. Appl. Earth Obs. Geoinf. 22, 86–98.

Myer, M.H., Campbell, S.R., Johnston, J.M., 2017. Spatiotemporal modeling of ecological and sociological predictors of West Nile virus in Suffolk County, NY, mosquitoes. Ecosphere 8 (6), e01854. https://doi.org/10.1002/ecs2.1854.

Myers, S.S., Gaffikin, L., Golden, C.D., Ostfeld, R.S., Redford, K.H., Ricketts, T.H., et al., 2013. Human health impacts of ecosystem alteration. Proc. Natl. Acad. Sci. 110 (47), 18753–18760. https://doi.org/10.1073/pnas.1218656110.

National Oceanic and Atmospheric Administration, 2010. Office for Coastal Management. "2010 Puerto Rico C-CAP 30m Land Cover." Coastal Change Analysis Program (C-CAP) Regional Land Cover.NOAA Office for Coastal Management, Charleston, SC www.coast.noaa.gov/ccapftp, Accessed date: 23 April 2019

National Oceanic and Atmospheric Administration (NOAA), National Weather Service (NWS), 2009. Monthly report of hydrologic conditions. https://www.weather.gov/media/sju/hydrology/E5/2009/E5nov09.pdf, Accessed date: 19 June 2018.

Naughton, O., McCormack, T., Gill, L., Johnston, P., 2018. Groundwater flood hazards and mechanisms in lowland karst terrains. Geol. Soc. Lond., Spec. Publ. 466 (1), 397–410.

Parés-Ramos, I., Gould, W., Aide, T., 2008. Agricultural abandonment, suburban growth, and forest expansion in Puerto Rico between 1991 and 2000. Ecol. Soc. 13 (2).

Puerto Rico Aqueduct and Sewage Authority (PRASA), 2014. Strategic Plan 2014–2018. http://www.acueductospr.com/planestrategico/2014/download/PLAN_ESTRATEGICO_2014-2018b.pdf, Accessed date: 1 October 2018.

Puerto Rico Aqueduct and Sewage Authority (PRASA), 2015. Sewer network. http://www.agencias.pr.gov/agencias/gis/descargaGeodatos/Infraestructuras/Pages/Agua.aspx, Accessed date: 11 June 2018.

Puerto Rico Science Museum, 2011. Puerto Rico Flooding. http://ecoexploratorio.org/amenazas-naturales/inundaciones/inundaciones-en-puerto-rico/, Accessed date: 19 June 2018.

Reacher, M., McKenzie, K., Lane, C., Nichols, T., Kedge, I., Iversen, A., ... Simpson, J., 2004. Lewes Flood Action Recovery Team. Health impacts of flooding in Lewes: a comparison of reported gastrointestinal and other illness and mental health in flooded and non-flooded households. Commun. Dis. Public Health 7 (1), 39–46.

Reguero, B.G., Losada, I.J., Diaz-Simal, P., Mendez, F.J., Beck, M.W., 2015. Effects of climate change on exposure to coastal flooding in Latin America and the Caribbean. PLoS One 10 (7), e0133409.

Russell, M., Harvey, J., Ranade, P., Murphy, K., 2015. EPA H2O User Manual. US EPA Office of Research and Development, Washington, DC (EPA/600/R-15/090).

Simpson, D., Rue, H., Riebler, A., Martins, T.G., Sørbye, S.H., 2017. Penalising model component complexity: a principled, practical approach to constructing priors. Stat. Sci. 32 (1), 1–28.

Sing, T., Sander, O., Beerenwinkel, N., Lengauer, T., 2005. ROCR: visualizing classifier performance in R. Bioinformatics 21, 7881.

Sorichetta, A., Hornby, G.M., Stevens, F.R., Gaughan, A.E., Linard, C., Tatem, A.J., 2015. High-resolution gridded population datasets for Latin America and the Caribbean in 2010, 2015, and 2020. Sci. Data 2, 150045.

Stockstill, R.L., Leech, J.R., 1990. Rio Puerto Nuevo Flood-Control Project. Hydraulic Model Investigation (No. WES/TR/HL-90-18), San Juan, Puerto Rico (ARMY ENGINEER WATERWAYS EXPERIMENT STATION VICKSBURG MS HYDRAULICS DIV).

Stürck, J., Poortinga, A., Verburg, P.H., 2014. Mapping ecosystem services: the supply and demand of flood regulation services in Europe. Ecol. Indic. 38, 198–211.
Thornton, P., Hasenauer, H., White, M., 1997. Generating surfaces of daily meteorological variables over large regions of complex terrain. J. Hydrol. 190, 204–251.
Torres-González, S., Planert, M., Rodríguez, M.J., 1996. Hydrogeology and simulation of ground-water flow in the upper aquifer of the Río Camuy to Río Grande de Manatí area, Puerto Rico. US Geol Surv Water Resour Invest Rep 95-4286, p. 102.
U.S. Census Bureau, 2018. Quick facts: Puerto Rico. https://www.census.gov/quickfacts/pr, Accessed date: 18 March 2019.
U.S. Department of Agriculture, Natural Resources Conservation Service, 2004. Soil Survey Geographic (SSURGO) Database for Puerto Rico, all Regions. http://SoilDataMart.nrcs.usda.gov/, Accessed date: 11 June 2018.
United States Department of Agriculture, 1986. Urban hydrology for small watersheds (PDF). Technical Release 55 (TR-55), Second ed. Natural Resources Conservation Service, Conservation Engineering Division.
United States Department of Agriculture, 2017. Forest inventory and analysis database. Available at. Forest Servicehttp://apps.fs.fed.us/fiadbdownloads/datamart.html, Accessed date: 11 June 2018.
United States Environmental Protection Agency (USEPA), 2006. Consent Decree: Puerto Rico Aqueduct and Sewer Authority Clean Water Act Settlement. https://www.epa.gov/enforcement/consent-decree-puerto-rico-aqueduct-and-sewer-authority-clean-water-act-settlement, Accessed date: 22 June 2018.
United States Geologic Survey (USGS), 2017. National Hydrography Dataset. https://nhd.usgs.gov/, Accessed date: 11 June 2018.
Vale-Nieves, A., 2018. Puerto Rico's karst protection—Beyond the Laws and Regulations. Karst Groundwater Contamination and Public Health. Springer, Cham, pp. 51–54.
Vitousek, S., Barnard, P.L., Fletcher, C.H., Frazer, N., Erikson, L., Storlazzi, C.D., 2017. Doubling of coastal flooding frequency within decades due to sea-level rise. Sci. Rep. 7 (1), 1399.
Vittinghoff, E., McCulloch, C.E., 2007. Relaxing the rule of ten events per variable in logistic and Cox regression. Am. J. Epidemiol. 165 (6), 710–718.
Wade, T. J., Sandhu, S. K., Levy, D., Lee, S., LeChevallier, M. W., Katz, L., & Colford Jr, J. M. (2004). Did a severe flood in the Midwest cause an increase in the incidence of gastrointestinal symptoms? Am. J. Epidemiol., 159(4), 398–405.
Wade, T.J., Lin, C.J., Jagai, J.S., Hilborn, E.D., 2014. Flooding and emergency room visits for gastrointestinal illness in Massachusetts: a case-crossover study. PLoS One 9 (10), e110474.
Wade, T.J., Augustine, S.A., Griffin, S.M., Sams, E.A., Oshima, K.H., Egorov, A.I., ... Dufour, A.P., 2018. Asymptomatic norovirus infection associated with swimming at a tropical beach: a prospective cohort study. PLoS One 13 (3), e0195056.
Warne, A.G., Webb, R.M.T., Larsen, M.C., 2005. Water, Sediment, and Nutrient Discharge Characteristics of Rivers in Puerto Rico, and their Potential Influence on Coral Reefs: U.S. Geological Survey Scientific Investigations Report 2005–5206 (58 p).
Winsemius, H. C., Jongman, B., Veldkamp, T. I., Hallegatte, S., Bangalore, M., & Ward, P. J. (2015). Disaster Risk, Climate Change, and Poverty: Assessing the Global Exposure of Poor People to Floods and Droughts. https://elibrary.worldbank.org/doi/abs/10.1596/1813-9450-7480. Accessed 07/10/2018.
Xiao, Q., McPherson, E.G., 2016. Surface water storage capacity of twenty tree species in Davis, California. J. Environ. Qual. 45, 188–198. https://doi.org/10.2134/jeq2015.02.0092.
Yang, Q., Tam, N.F., Wong, Y.S., Luan, T.G., Su, W.S., Lan, C.Y., Shin, P.K., Cheung, S.G., 2008. Potential use of mangroves as constructed wetland for municipal sewage treatment in Futian, Shenzhen, China. Mar. Pollut. Bull. 57 (6), 735–743. https://doi.org/10.1016/j.marpolbul.2008.01.037.
Yuan, Y., Jiang, Y., Taguas, E.V., Mbonimpa, E.G., Hu, W., 2015. Sediment loss and its cause in Puerto Rico watersheds. Soil 1 (2), 595–602.
Zhou, Wanfang, 2007. Drainage and flooding in karst terranes. Environ. Geol. 51 (6), 963–973.

	Zip99Rain	Zip95Rain	Zip90Rain	ZipRainYr	ZipRainMn	ZipRainMa	ZipRainMa	Huc10_99F
Zip99Rain	1	0.195298	-0.000872	0.40048	0.39465	0.818808	0.532417	0.900109
Zip95Rain	0.195298	1	0.893738	0.869628	0.869837	0.055169	0.745537	0.307465
Zip90Rain	-0.000872	0.893738	1	0.755373	0.75688	-0.08766	0.619088	0.1219
ZipRainYr	0.40048	0.869628	0.755373	1	0.999918	0.377959	0.945665	0.551066
ZipRainMn	0.39465	0.869837	0.75688	0.999918	1	0.373976	0.945183	0.545747
ZipRainMa	0.818808	0.055169	-0.08766	0.377959	0.373976	1	0.470438	0.785521
ZipRainMa	0.532417	0.745537	0.619088	0.945665	0.945183	0.470438	1	0.676506
Huc10_99F	0.900109	0.307465	0.1219	0.551066	0.545747	0.785521	0.676506	1
Huc10_95F	0.281013	0.899499	0.802664	0.846538	0.844749	0.176681	0.733246	0.447339
Huc10_90F	0.050108	0.892182	0.868838	0.781188	0.780967	0.007941	0.596264	0.180843
Huc10Rain	0.396632	0.834959	0.730452	0.948061	0.946194	0.359117	0.865151	0.551839
Huc10Rain	0.379405	0.843028	0.745878	0.948778	0.947024	0.344843	0.860222	0.529704
FloodPerc	0.007	-0.093427	-0.086857	0.019435	0.019987	0.087137	0.040504	0.106458
KarstPerc	-0.332135	0.063636	0.138231	-0.191504	-0.195677	-0.516788	-0.308682	-0.38288
ppl_FldPer	0.023476	-0.073745	-0.068735	0.041081	0.041761	0.117854	0.057066	0.124933
MedIncom	-0.064082	0.124888	0.116201	0.236888	0.239089	-0.03135	0.26003	0.036395
Per5PlsHo	-0.079242	0.095708	0.078994	0.180755	0.184871	-0.061038	0.205706	-0.046224
ZipSlopeAv	0.332915	0.177396	0.130015	0.098027	0.097087	0.303552	0.05683	0.256664
ZipMaxSlo	0.25378	0.140873	0.091162	0.032379	0.029394	0.151646	-0.016553	0.172592
Ave_HucSl	0.288247	-0.130462	-0.158032	-0.271086	-0.274089	0.17941	-0.3109	0.182393
MaxHucSlp	0.323076	-0.085001	-0.152558	-0.205289	-0.210506	0.19969	-0.28919	0.192138
PercWood	0.203784	0.079184	0.042233	0.246653	0.245588	0.321324	0.287411	0.31579
PercGrass	0.034926	0.116523	0.188698	0.180274	0.17984	0.060455	0.195822	0.19574
mmhaHuc	-0.222951	0.153525	0.150309	-0.087494	-0.093173	-0.426524	-0.180651	-0.269535
mmhaZip_	-0.168813	0.19433	0.212463	-0.012505	-0.016574	-0.433937	-0.059632	-0.242068
PercVegeta	0.025541	-0.084383	-0.069399	-0.350063	-0.353864	-0.090067	-0.449036	-0.099026
SwgDen	-0.12036	0.025664	0.013673	0.136428	0.140426	-0.082703	0.180833	-0.065871

Huc10_95F	Huc10_90F	Huc10Rain	Huc10Rain	FloodPerc	KarstPerc	ppl_FldPer	MedIncom	Per5PlsHo
0.281013	0.050108	0.396632	0.379405	0.007	-0.332135	0.023476	-0.064082	-0.079242
0.899499	0.892182	0.834959	0.843028	-0.093427	0.063636	-0.073745	0.124888	0.095708
0.802664	0.868838	0.730452	0.745878	-0.086857	0.138231	-0.068735	0.116201	0.078994
0.846538	0.781188	0.948061	0.948778	0.019435	-0.191504	0.041081	0.236888	0.180755
0.844749	0.780967	0.946194	0.947024	0.019987	-0.195677	0.041761	0.239089	0.184871
0.176681	0.007941	0.359117	0.344843	0.087137	-0.516788	0.117854	-0.03135	-0.061038
0.733246	0.596264	0.865151	0.860222	0.040504	-0.308682	0.057066	0.26003	0.205706
0.447339	0.180843	0.551839	0.529704	0.106458	-0.38288	0.124933	0.036395	-0.046224
1	0.941008	0.906546	0.901356	0.098025	-0.007088	0.107298	0.120519	0.076145
0.941008	1	0.854917	0.85871	0.04662	0.093572	0.057629	0.108555	0.089811
0.906546	0.854917	1	0.992476	0.124607	-0.150341	0.134444	0.210211	0.173778
0.901356	0.85871	0.992476	1	0.090794	-0.130788	0.103304	0.210799	0.172282
0.098025	0.04662	0.124607	0.090794	1	-0.332755	0.98241	-0.046327	0.124634
-0.007088	0.093572	-0.150341	-0.130788	-0.332755	1	-0.335569	-0.109954	-0.331874
0.107298	0.057629	0.134444	0.103304	0.98241	-0.335569	1	-0.094478	0.083738
0.120519	0.108555	0.210211	0.210799	-0.046327	-0.109954	-0.094478	1	0.3065
0.076145	0.089811	0.173778	0.172282	0.124634	-0.331874	0.083738	0.3065	1
0.05242	0.032302	-0.022039	0.006627	-0.517994	0.094713	-0.441205	-0.242238	-0.456098
0.05674	0.034575	-0.055326	-0.037837	-0.449205	0.348892	-0.391309	-0.28197	-0.602419
-0.078917	-0.100733	-0.215201	-0.205685	-0.099477	0.068287	-0.06374	-0.376685	-0.59672
-9.46E-06	-0.023154	-0.107774	-0.10992	-0.076582	0.282838	-0.057063	-0.367845	-0.604831
0.264673	0.188971	0.329601	0.284482	0.624733	-0.249978	0.605164	0.016918	-0.060622
0.290017	0.234959	0.276003	0.254831	0.62352	-0.10091	0.619499	-0.056083	-0.221303
0.088316	0.135676	-0.055282	-0.041828	-0.294565	0.8487	-0.300502	-0.218067	-0.363212
0.125321	0.18689	0.02129	0.031851	-0.363025	0.708407	-0.38445	-0.057821	-0.267464
-0.076442	-0.031663	-0.291577	-0.277757	-0.220113	0.423166	-0.188046	-0.447069	-0.685383
-0.016974	-0.005143	0.122563	0.118008	0.102201	-0.348307	0.067604	0.146673	0.744837

ZipSlopeAv	ZipMaxSlo	Ave_HucSl	MaxHucSlp	PercWood	PercGrass	mmhaHuc	mmhaZip_	PercVegeta
0.332915	0.25378	0.288247	0.323076	0.203784	0.034926	-0.222951	-0.168813	0.025541
0.177396	0.140873	-0.130462	-0.085001	0.079184	0.116523	0.153525	0.19433	-0.084383
0.130015	0.091162	-0.158032	-0.152558	0.042233	0.188698	0.150309	0.212463	-0.069399
0.098027	0.032379	-0.271086	-0.205289	0.246653	0.180274	-0.087494	-0.012505	-0.350063
0.097087	0.029394	-0.274089	-0.210506	0.245588	0.17984	-0.093173	-0.016574	-0.353864
0.303552	0.151646	0.17941	0.19969	0.321324	0.060455	-0.426524	-0.433937	-0.090067
0.05683	-0.016553	-0.3109	-0.28919	0.287411	0.195822	-0.180651	-0.059632	-0.449036
0.256664	0.172592	0.182393	0.192138	0.31579	0.19574	-0.269535	-0.242068	-0.099026
0.05242	0.05674	-0.078917	-9.46E-06	0.264673	0.290017	0.088316	0.125321	-0.076442
0.032302	0.034575	-0.100733	-0.023154	0.188971	0.234959	0.135676	0.18689	-0.031663
-0.022039	-0.055326	-0.215201	-0.107774	0.329601	0.276003	-0.055282	0.02129	-0.291577
0.006627	-0.037837	-0.205685	-0.10992	0.284482	0.254831	-0.041828	0.031851	-0.277757
-0.517994	-0.449205	-0.099477	-0.076582	0.624733	0.62352	-0.294565	-0.363025	-0.220113
0.094713	0.348892	0.068287	0.282838	-0.249978	-0.10091	0.8487	0.708407	0.423166
-0.441205	-0.391309	-0.06374	-0.057063	0.605164	0.619499	-0.300502	-0.38445	-0.188046
-0.242238	-0.28197	-0.376685	-0.367845	0.016918	-0.056083	-0.218067	-0.057821	-0.447069
-0.456098	-0.602419	-0.59672	-0.604831	-0.060622	-0.221303	-0.363212	-0.267464	-0.685383
1	0.856854	0.645685	0.518028	-0.270252	-0.278031	0.138364	0.116863	0.608914
0.856854	1	0.649442	0.654604	-0.180456	-0.177703	0.370215	0.318886	0.723405
0.645685	0.649442	1	0.882644	-0.028817	0.019653	0.071332	0.041087	0.887001
0.518028	0.654604	0.882644	1	0.030265	0.029012	0.247943	0.143577	0.855778
-0.270252	-0.180456	-0.028817	0.030265	1	0.623964	-0.173268	-0.221924	-0.130786
-0.278031	-0.177703	0.019653	0.029012	0.623964	1	-0.05286	-0.104359	-0.026619
0.138364	0.370215	0.071332	0.247943	-0.173268	-0.05286	1	0.798039	0.438259
0.116863	0.318886	0.041087	0.143577	-0.221924	-0.104359	0.798039	1	0.330718
0.608914	0.723405	0.887001	0.855778	-0.130786	-0.026619	0.438259	0.330718	1
-0.562821	-0.725049	-0.643793	-0.653548	-0.134932	-0.188049	-0.392	-0.288344	-0.75683

SwgDen
-0.12036
0.025664
0.013673
0.136428
0.140426
-0.082703
0.180833
-0.065871
-0.016974
-0.005143
0.122563
0.118008
0.102201
-0.348307
0.067604
0.146673
0.744837
-0.562821
-0.725049
-0.643793
-0.653548
-0.134932
-0.188049
-0.392
-0.288344
-0.75683
1

Variables	Definitions
Zip99Rain	99% rainfall event magnitude at the zip code level
Zip95Rain	95% rainfall event magnitude at the zip code level
Zip90Rain	90% rainfall event magnitude at the zip code level
ZipRainYr	Average Annual Rainfall at the Zip Code Level
ZipRainMnth	Average Monthly Rainfall at the Zip Code Level
ZipRainMaxMnth	Maximum Annual Rainfall at the Zip Code Level
ZipRainMaxYr	Maximum Monthly Rainfall at the Zip Code Level
Huc10_99Rain	99% rainfall event magnitude at the Huc-10 watershed level
Huc10_95Rain	95% rainfall event magnitude at the Huc-10 watershedlevel
Huc10_90Rain	90% rainfall event magnitude at the Huc-10 watershed level
Huc10RainYr	Average Annual Rainfall at the Huc-10 Watershed Level
Huc10RainMnth	Average Monthly Rainfall at the Huc-10 Watershed Level
FloodPerc	Percentage of flood area
KarstPerc	Percentage of karst at the zip code level ((karst area/zip code area) *100)
ppl_FldPer	Percentage of people living in flood areas
MedIncome	Median Income
Per5PlsHou	Percentage of housing units with more than 5 households
ZipSlopeAvg	Average slope at the zip code level
ZipMaxSlope	Maximum slope at the zip code level
Ave_HucSlo	Average slope at the Huc-10 level
MaxHucSlpe	Maximum slope at the Huc-10 level
PercWoodyWet	Percentage of woody wetlands at the zip code level
PercGrassWet	Percentage of grassy wetlands at the zip code level
mmhaHuc10_2010	Rain retained at the Huc 10 level
mmhaZip_2010	Rain retained at the zip code level
PercVegetation	Percentage of vegetation at the Huc-10 level
SwgDen	Sewage density (sewage m /zip code m2)

C-CAP Value	C-CAP Class	Group A	Group B	Group C	Group D
2	High-Intensity Developed	89	92	94	95
3	Medium-Intensity Developed	77	85	90	92
4	Low-Intensity Developed	61	75	83	87
5	Developed Open Space	49	69	79	84
6	Cultivated Land	67	78	85	89
7	Pasture/Hay	39	61	74	80
8	Grassland	30	58	71	78
9	Deciduous Forest	30	55	70	77
10	Evergreen Forest	30	55	70	77
11	Mixed Forest	30	55	70	77
12	Scrub/Shrub	30	48	65	73
13	Palustrine Forested Wetland	0	0	0	0
14	Palustrine Scrub/Shrub Wetland	0	0	0	0
15	Palustrine Emergent Wetland	0	0	0	0
16	Estuarine Forested Wetland	0	0	0	0
17	Estuarine Scrub/Shrub Wetland	0	0	0	0
18	Estuarine Emergent Wetland	0	0	0	0
19	Unconsolidated Shore	0	0	0	0
20	Bare Land	77	86	91	94
21	Water	0	0	0	0
22	Palustrine Aquatic Bed	0	0	0	0
23	Estuarine Aquatic Bed	0	0	0	0

Supplementary Material 3. C-CAP Land Cover Classes to Curve Numbers

Adapted from file:///C:/Users/RDejesus/Desktop/opennspect-technical-guide.pdf

Source: USDA NRCS (U.S. Department of Agriculture, Natural Resources Conservation Service). 1986. Urban Hydrology for Small Watersheds: Technical Release 55 (TR-55). Second Edition. Washington, DC. Accessed at www.cpesc.org/reference/tr55.pdf.

I. Location of outliers

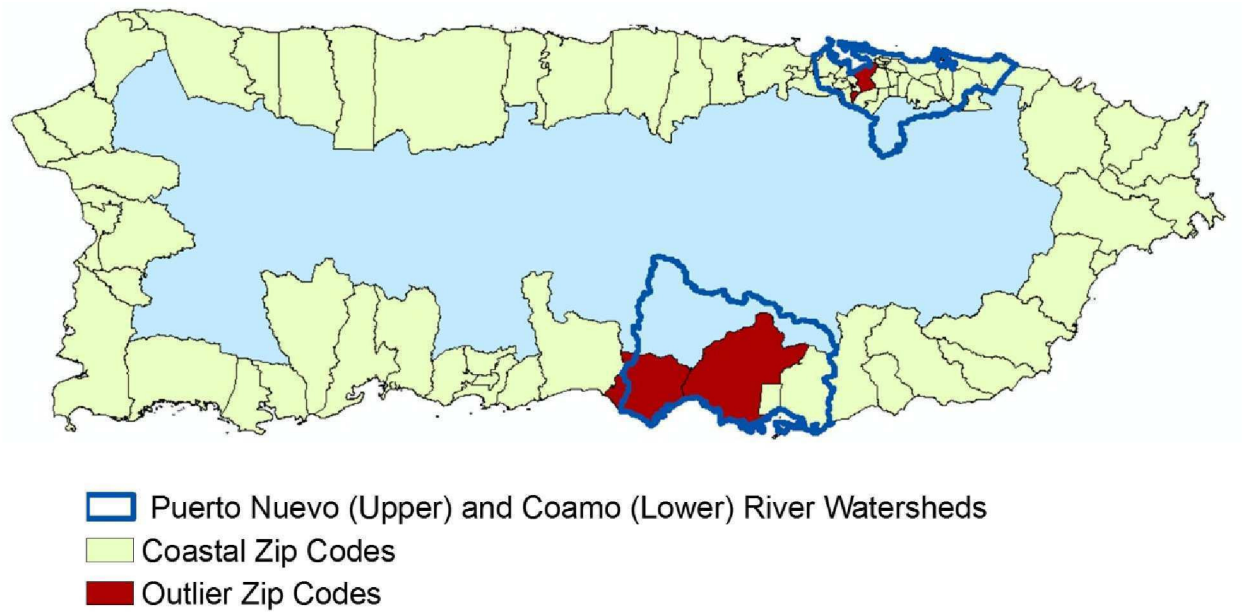

Location of outlier zip codes in terms of FEMA Claims, and their associated Huc-10 watersheds

II. Outlier detection process:

In the Poisson regression, FEMA claims where treated as counts, with households on each zip code as an offset, under the assumption that zip codes with more households would inherently have more flood claims. Looking at the relationship between claims and population, we see that this pattern is generally true except for three zip codes (00751 (obs 40), 00757 (obs41), 00920 (obs 56). See plots below and refer to http://strata.uga.edu/8370/rtips/regressionPlots.html for plot interpretation:

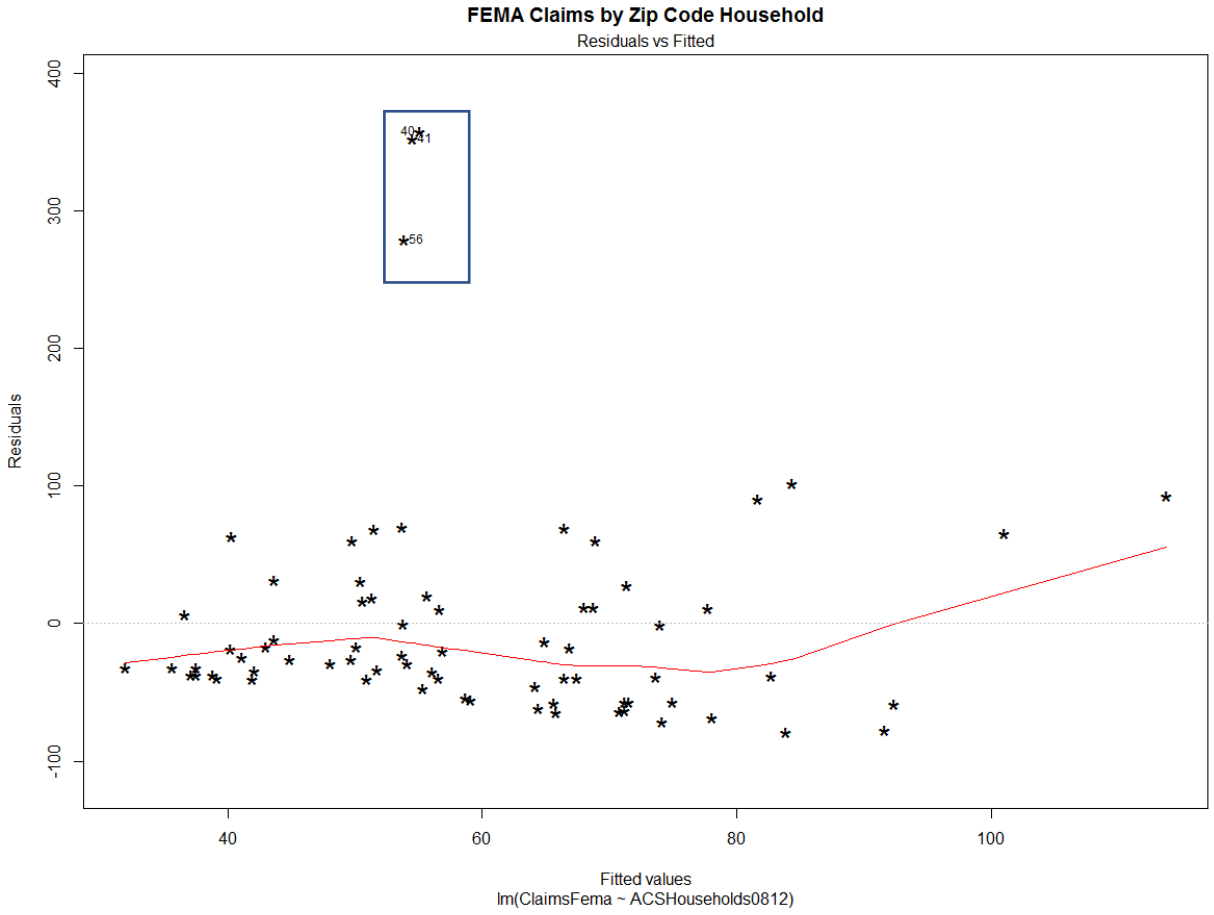
FEMA Claims by Zip Code Household
Residuals vs Fitted
Residuals
400
300
200
100
0
-100
40
60
80
100
Fitted values
lm(ClaimsFema ~ ACSHouseholds0812)

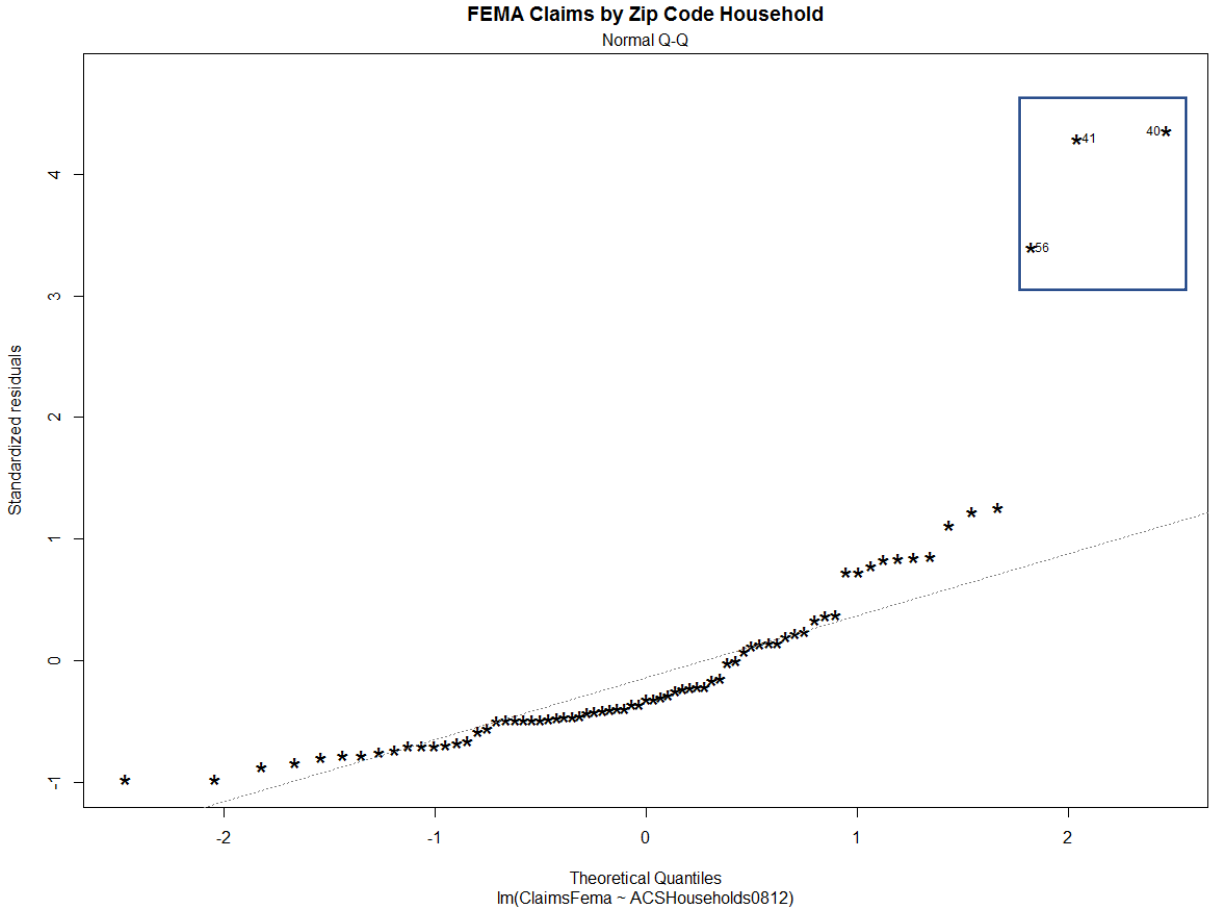

Influence Analysis

High influence is considered as having studentized residuals above 2.
https://onlinecourses.science.psu.edu/stat501/node/339/

	StudRes	Hat	CookD
4	0.8401713	0.10026991	0.03949725
40	5.0597499	0.01470811	0.14191082
41	4.9578988	0.01501166	0.14061071
63	1.2364530	0.16203860	0.14672260

Because of the potential role of these outliers, the analysis was conducted keeping track of these outliers to determine if they were too influential in the model selection.

III. Quasi-poisson model averaging results with outliers in:

Call:
model.avg(object = top.modelsglobal.modelQPoisson_N73_offsetCOVHouse)

Component models:

‘12456’ ‘13456’

Coefficients:
```
       (Intercept) Huc10_99Rain  KarstPerc Per5PlsHou ZipSlopeAvg mmhaHuc10_2010
full     -5.241588    0.4086784 -0.2523500 -0.6894223  -0.4787281    -0.09067435
subset   -5.241588    0.4086784 -0.3664714 -0.6894223  -0.4787281    -0.29117730
```
Model-averaged coefficients:
(full average)
```
                Estimate Std. Error Adjusted SE z value Pr(>|z|)
(Intercept)    -5.245e+00  1.729e-01   1.760e-01  29.803   <2e-16 ***
Huc10_99Rain    3.902e-01  1.674e-01   1.704e-01   2.290   0.0220 *
KarstPerc      -3.665e-01  2.071e-01   2.109e-01   1.738   0.0822 .
Per5PlsHou     -6.983e-01  2.798e-01   2.848e-01   2.451   0.0142 *
ZipSlopeAvg    -4.816e-01  1.813e-01   1.846e-01   2.608   0.0091 **
mmhaHuc10_2010 -1.259e-15  2.302e-08   2.315e-08   0.000   1.0000
```

(conditional average)
```
                Estimate Std. Error Adjusted SE z value Pr(>|z|)
(Intercept)     -5.2454     0.1729      0.1760  29.803   <2e-16 ***
Huc10_99Rain     0.3902     0.1674      0.1704   2.290   0.0220 *
KarstPerc       -0.3665     0.2071      0.2109   1.738   0.0822 .
Per5PlsHou      -0.6983     0.2798      0.2848   2.451   0.0142 *
ZipSlopeAvg     -0.4816     0.1813      0.1846   2.608   0.0091 **
mmhaHuc10_2010  -0.2912     0.1943      0.1978   1.472   0.1411
---
Signif. codes:  0 ‘***’ 0.001 ‘**’ 0.01 ‘*’ 0.05 ‘.’ 0.1 ‘ ’ 1
```

Relative variable importance:
```
     Huc10_99Rain offset(log(ACSHouseholds0812)) Per5PlsHou ZipSlopeAvg KarstPerc mmhaHuc10_2010
Importance:          1.00         1.00            1.00       1.00       0.69      0.31
N containing models:    2            2               2          2          1         1
```
> confint(Avg.ModGlobal_global.modelQPoisson_N73_offsetCOVHouse)
```
                  2.5 %      97.5 %
(Intercept)    -5.59031745 -4.90039934
Huc10_99Rain    0.05621311  0.72424957
KarstPerc      -0.77973310  0.04679034
Per5PlsHou     -1.25652982 -0.13999047
ZipSlopeAvg    -0.84340079 -0.11971340
mmhaHuc10_2010 -0.67892943  0.09657484
```

Call:
lm(formula = FP_EGSData$ClaimsFema ~ predicted_claimsQPoisson_N73_offsetCOVHouse)

Residuals:
```
   Min     1Q  Median     3Q    Max
-117.92  -32.01  -18.59    3.39  347.96
```

Coefficients:
```
                                    Estimate Std. Error t value Pr(>|t|)
(Intercept)                          12.9644    13.0621   0.993    0.324
predicted_claimsQPoisson_N73_offsetCOVHouse   0.7824     0.1650   4.743 1.06e-05 ***
---
Signif. codes:  0 ‘***’ 0.001 ‘**’ 0.01 ‘*’ 0.05 ‘.’ 0.1 ‘ ’ 1
```

Residual standard error: 73.51 on 71 degrees of freedom
Multiple R-squared: 0.2406,	Adjusted R-squared: 0.2299
F-statistic: 22.49 on 1 and 71 DF, p-value: 1.057e-05

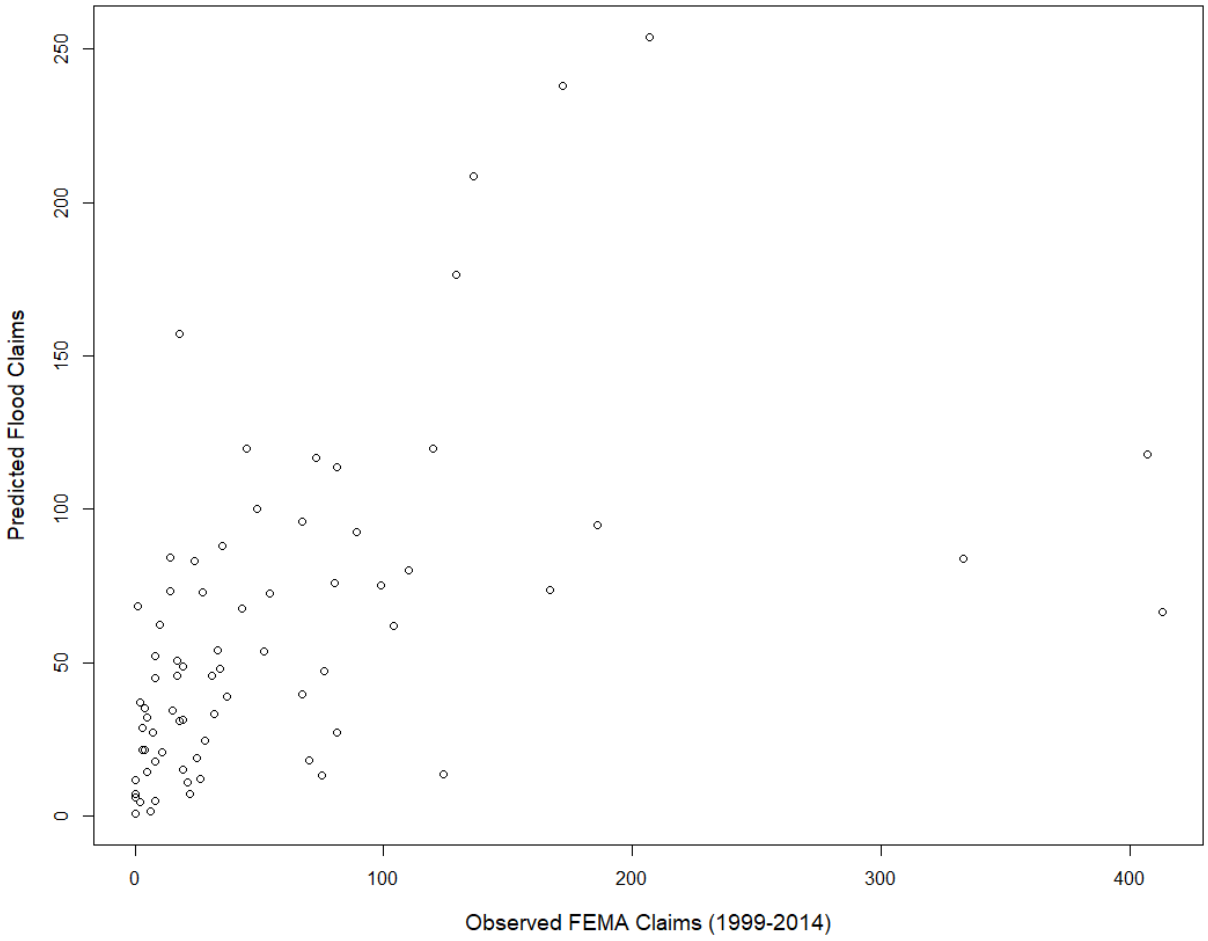

IV. Influence detecting in model averaging results:

We evaluated the individual models included in the model averaging results above to determine the influence of outliers. Influential places were highlighted for having > 2 Studentized Residuals (https://onlinecourses.science.psu.edu/stat501/node/339/)

mod1044<-glm(formula = ClaimsFema ~ Huc10_99Rain + KarstPerc + Per5PlsHou + ZipSlopeAvg + 1 + offset(log(ACSHouseholds0812)), family = "x.quasipoisson", data = FP_EGSData)

	StudRes	Hat	CookD
40	4.3504061	0.04279290	0.18953909
41	3.0110331	0.06791866	0.12463502
42	-0.7634534	0.18591744	0.01597649
46	-0.6465671	0.19823380	0.01276612
70	2.7331768	0.08136796	0.19582303

mod1050<-glm(formula = ClaimsFema ~ Huc10_99Rain + mmhaHuc10_2010 + Per5PlsHou +
ZipSlopeAvg + 1 + offset(log(ACSHouseholds0812)), family = "x.quasipoisson",
data = FP_EGSData)

	StudRes	Hat	CookD
24	1.965982	0.23447218	0.20822003
40	4.347858	0.04476542	0.20178832
41	2.992402	0.06960144	0.12786404
42	-0.904840	0.21562897	0.02682373

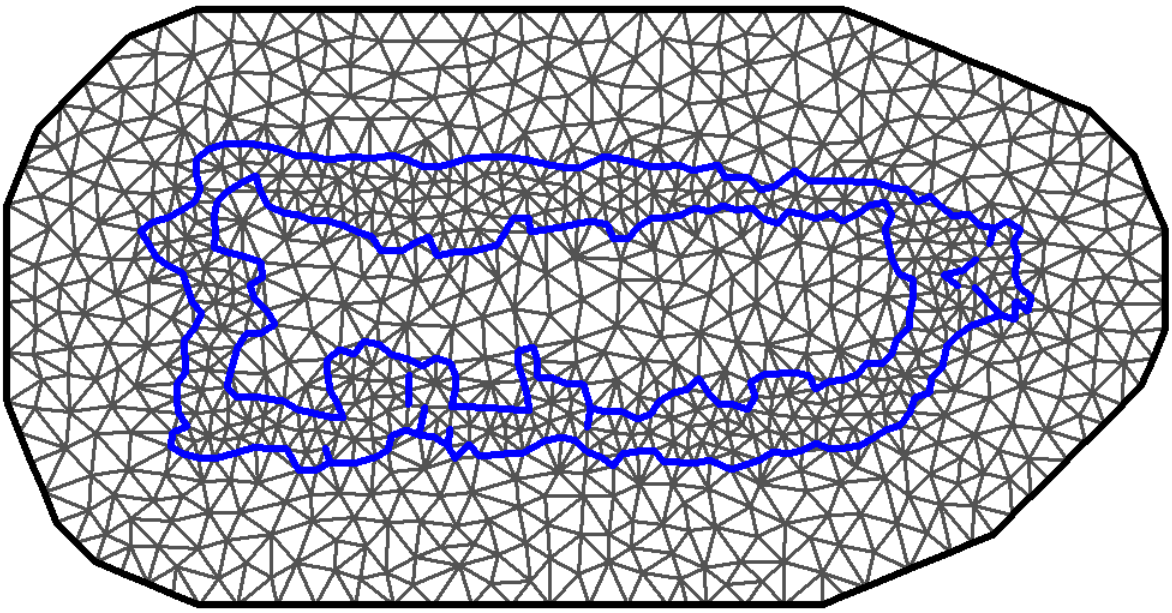

Supplementary material 5. Labeled undirected graph, or triangulation mesh, used by the SPDE to estimate spatial covariance. Blue line represents the border of the ZIP codes of interest, outside of which the mesh is extended at a low resolution to avoid boundary effects.

FEMA Flood Claims Analysis

Author: Rebeca de Jesus Crespo/2017-18

Objective: To evaluate predictors of FEMA flood claims in Puerto Rico

I. Get data scale and check for colinearity

```
Predictors<-read.csv("PredictorVariables_2018Revised_Summarized.csv")

Labels<-Predictors[ ,1:2]#to desginate the first 3 columns as labels

Labels

Predictors_Scaled<-scale(Predictors[ ,3:37])#to scale only predictor variables and not the labels

Predictors_Scaled

Predictors_corrmatrix<-cor(Predictors_Scaled)#to detect correlation among predictor variables

Predictors_corrmatrix

write.csv(Predictors_corrmatrix, file="Predictors2018_corrmatrix.csv")#to save in work directory above

Predictors<-cbind(Labels, Predictors_Scaled)#to attach the labels to predictors

Response<-read.csv("ResponseVariables_FPEGS.csv")

Response

FP_EGSData<-cbind(Response,Predictors)#attach scaled predictors to response variables


write.csv(FP_EGSData, file="FP_EGSDataScaled2018.csv")#to save in work directory above

names(FP_EGSData)


hist(FP_EGSData$ClaimsFema)#to see the distribution of the claims data. Claims are skewed toward zero, so a Poisson is desirable.


#II. Check if the response is influenced by outliers

#Our response is Fema Claims, corrected by the number of people in a zip code, so we first look at whether the relationship between fema claims and population is behaving as expected


#To see how claims relate to population, we see three potential outliers (00751, 00757, 00920)
```

```
FemaClaims_Households<-lm(ClaimsFema ~ ACSHouseholds0812, data=FP_EGSData)

FemaClaims_Households<-lm(ClaimsFema ~ ACSHouseholds0812, data=FP_EGSData)

summary(FemaClaims_Households)

plot(FemaClaims_Households, pch="*", cex=2, main="FEMA Claims by Zip Code Household")



#residual test #Potential outliers show up separated from other sites

predFemaClaimsHouses<-predict(FemaClaims_Households)

res_FemaClaims_Households<- residuals(FemaClaims_Households, type="pearson")

plot(predFemaClaimsHouses, res_FemaClaims_Households)

abline(h=0, lty=2)

qqnorm(res_FemaClaims_Households)

qqline(res_FemaClaims_Households)



#Two of them show up as high influence sites

library(car)

influencePlot(FemaClaims_Households)#influential sites numbers 41, 40 (zip codes 751, 757, based on high (~5) studentized residuals

plot(residuals(FemaClaims_Households))

abline(h=0, lty=2)


#Because of their potential role driving our model, we will keep track of sites 40,41,and 56 (zip codes 751,757,920) to see if they influence model results


#III. MODELS WITH ALL SITES IN, INCLUDING OUTLIERS


#Poisson regressions with Claims per population-------------------------OUTLIERS IN

#A. test which SIMILAR variables are better predictors of FLOOD CLAIMS
```

#1 Weather: rainzip90, rainzip95, rainzip99, rainHuc99, rainHuc90, rainHuc95 are all significant. 90-95 are correlated at both scales, while zip and huc 99 are correlated. 90 and 95 are not correlated to 99. I chose huc 90 and huc 99 to represent the two trends ***OUTLIERS IN

```
rainzipAvg<-glm(ClaimsFema~ZipRainYr+offset(log(ACSHouseholds0812)),family=quasipoisson, data=FP_EGSData)

anova(rainzipAvg, test="F")


rainzip90<-glm(ClaimsFema~Zip90Rain+offset(log(ACSHouseholds0812)),family=quasipoisson,data=FP_EGSData)

summary(rainzip90)#p= 0.00153 **

anova(rainzip90, test="F")


rainzip95<-glm(ClaimsFema~Zip95Rain+offset(log(ACSHouseholds0812)),family=quasipoisson,data=FP_EGSData)

summary(rainzip95)## 0.0016 **

anova(rainzip95, test="F")


rainzip99<-glm(ClaimsFema~Zip99Rain+offset(log(ACSHouseholds0812)),family=quasipoisson,data=FP_EGSData)

summary(rainzip99) # 0.0247 *

anova(rainzip99, test="F")


rainHuc99<-glm(ClaimsFema~Huc10_99Rain+offset(log(ACSHouseholds0812)),family=quasipoisson,data=FP_EGSData)

summary(rainHuc99) # 0.011 *

anova(rainHuc99, test="F")


rainHuc90<-glm(ClaimsFema~Huc10_90Rain+offset(log(ACSHouseholds0812)),family=quasipoisson,data=FP_EGSData)

summary(rainHuc90)#0.000216 ***

anova(rainHuc90, test="F")
```

```
rainHuc95<-glm(ClaimsFema~Huc10_95Rain+offset(log(ACSHouseholds0812)),family=quasipoisson,data
=FP_EGSData)

summary(rainHuc95) # 0.0209 *

anova(rainHuc95, test="F")


rainHucAvg<-glm(ClaimsFema~Huc10RainYr+offset(log(ACSHouseholds0812)),family=quasipoisson,data=
FP_EGSData)

summary(rainHucAvg)#0.256

anova(rainHucAvg, test="F")




#2 EGS: Best is mmHuc10_2010 #p==0.141 _____OUTLIERS IN


mmhaHuc102010<-glm(ClaimsFema~mmhaHuc10_2010+offset(log(ACSHouseholds0812)),family=quasip
oisson,data=FP_EGSData)

summary(mmhaHuc102010)#p=0.141

anova(mmhaHuc102010, test="F")#p=0.1101


mmhaZip2010<-glm(ClaimsFema~mmhaZip_2010+offset(log(ACSHouseholds0812)),family=quasipoisson,
data=FP_EGSData)

summary(mmhaZip2010)#p= 0.217

anova(mmhaZip2010, test="F")#p=0.1989




#3 Slope: Best is zip slope Avg p=0.4953_OUTLIERS IN


ZipSlopeAvg<-glm(ClaimsFema~ZipSlopeAvg+offset(log(ACSHouseholds0812)),family=quasipoisson,data=
FP_EGSData)
```

```
anova(ZipSlopeAvg, test="F")#p= 0.4953


ZipSlopeMax<-glm(ClaimsFema~ZipMaxSlope+offset(log(ACSHouseholds0812)),family=quasipoisson,data=FP_EGSData)

anova(ZipSlopeMax, test="F")#p= 0.7942


Ave_HucSlope<-glm(ClaimsFema~Ave_HucSlo+offset(log(ACSHouseholds0812)),family=quasipoisson,data=FP_EGSData)

anova(Ave_HucSlope, test="F")#p= 0.7531


Max_HucSlope<-glm(ClaimsFema~MaxHucSlpe+offset(log(ACSHouseholds0812)),family=quasipoisson,data=FP_EGSData)

anova(Max_HucSlope, test="F")#p=  0.9019




#B.Build a global model with all the variables  of interest.OUTLIERS IN

library(MuMIn)

options(na.action = "na.fail")


#1. Global Model wITH INTERACTIONS WITH ALL ZIPCODES #I tested all possible interactions among the selected variables and added the ones that were significant_OUTLIERS IN


global.modelQPoisson_offsetCOV_N73House<-glm(ClaimsFema~mmhaHuc10_2010+SwgDen+KarstPerc+ppl_FldPer+ZipSlopeAvg+Huc10_99Rain+Huc10_90Rain+MedIncome+PercVegetation+PercWoodyWet+Per5PlsHou+PercGrassWet+(Huc10_90Rain*mmhaHuc10_2010)+(PercWoodyWet*Huc10_90Rain)+(PercWoodyWet*ppl_FldPer)+offset(log(ACSHouseholds0812)), family=quasipoisson, data=FP_EGSData)

(chat <- deviance(global.modelQPoisson_offsetCOV_N73House) / df.residual(global.modelQPoisson_offsetCOV_N73House)) #chat = c^, the variance inflation factor


global.modelQPoisson_offsetCOV_N73House
```

```
global.modelQPoisson_offsetCOV_N73House<-glm(ClaimsFema~mmhaHuc10_2010+SwgDen+KarstPerc
+ppl_FldPer+ZipSlopeAvg+Huc10_99Rain+MedIncome+PercVegetation+PercWoodyWet+Per5PlsHou+Per
cGrassWet+(PercWoodyWet*ppl_FldPer)+offset(log(ACSHouseholds0812)), family=quasipoisson,
data=FP_EGSData)

(chat <- deviance(global.modelQPoisson_offsetCOV_N73House) /
df.residual(global.modelQPoisson_offsetCOV_N73House)) #chat = c^, the variance inflation factor
```

```
##2. Get ML estimator_____OUTLIERS IN

#because glm does not supply the log-likelihood for quasipiosson (and quasibinomial) regression, We
need to create a function that will trick glm into giving up the log likelihood, so we can use model
averaging. Here it is below.

#First create the function #See
https://sites.google.com/site/rforfishandwildlifegrads/home/mumin_usage_examples
```

```
x.quasipoisson <- function(...) {
  res <- quasipoisson(...)
  res$aic <- poisson(...)$aic
  res
}
```

```
#3. Update the global model to take in this function_____OUTLIERS IN

global.modelQPoisson_offsetCOV_N73House<-update(global.modelQPoisson_offsetCOV_N73House,
family = "x.quasipoisson")

(chat <- deviance(global.modelQPoisson_offsetCOV_N73House) /
df.residual(global.modelQPoisson_offsetCOV_N73House)) #chat = c^, the variance inflation factor

chat
```

global.modelQPoisson_offsetCOV_N73House

#4. Conduct Model averaging-testing all posible variable combinations to see which have a better fit_____OUTLIERS IN

library(MuMIn)

options(na.action = "na.fail") # prevent fitting models to different datasets

#DREDGE Global Model WITH INTERACTIONS NO OUTLIERS USING THE QUASI POISSON OPTION_____OUTLIERS IN

model.setglobal.modelQPoisson_N73_offsetCOVHouse<-dredge(global.modelQPoisson_offsetCOV_N73House, m.lim=c(1,5), fixed="offset(log(ACSHouseholds0812))", subset = !((KarstPerc && mmhaHuc10_2010)||(PercVegetation && mmhaHuc10_2010)||(PercGrassWet && ppl_FldPer)||(PercVegetation && Per5PlsHou)||(SwgDen && Per5PlsHou)||(SwgDen && ZipSlopeAvg)), rank = "QAICc", chat = chat) #the item !subset is to prevent two correlated variables from being together in any model (note that pplfldper and woody wetlands are correlated and not allowed, but their interaction is significant, i decided not to include them due to colinearity), the limit on 5 is to prevent model overfitting, the number can be changed to more or less explanatory variables if so wished

model.setglobal.modelQPoisson_N73_offsetCOVHouse

top.modelsglobal.modelQPoisson_N73_offsetCOVHouse<-get.models(model.setglobal.modelQPoisson_N73_offsetCOVHouse, subset=delta < 2) # TO SELECT just the models that are within 2 QaIC from each other

top.modelsglobal.modelQPoisson_N73_offsetCOVHouse

Avg.ModGlobal_global.modelQPoisson_N73_offsetCOVHouse<-model.avg(top.modelsglobal.modelQPoisson_N73_offsetCOVHouse)

Avg.ModGlobal_global.modelQPoisson_N73_offsetCOVHouse

Weights(Avg.ModGlobal_global.modelQPoisson_N73_offsetCOVHouse) <-jackknifeWeights(Avg.ModGlobal_global.modelQPoisson_N73_offsetCOVHouse, data =FP_EGSData)

summary(Avg.ModGlobal_global.modelQPoisson_N73_offsetCOVHouse)

confint(Avg.ModGlobal_global.modelQPoisson_N73_offsetCOVHouse)

```
#Predict

predicted_claimsQPoisson_N73_offsetCOVHouse<-exp(predict(Avg.ModGlobal_global.modelQPoisson_
N73_offsetCOVHouse))*FP_EGSData$ACSHouseholds0812

predicted_claimsQPoisson_N73_offsetCOVHouse


plot(FP_EGSData$ClaimsFema, predicted_claimsQPoisson_N73_offsetCOVHouse, xlab = "Observed
FEMA Claims (1999-2014)", ylab = "Predicted Flood Claims", cex.lab=1.2)


summary(lm(FP_EGSData$ClaimsFema~predicted_claimsQPoisson_N73_offsetCOVHouse)) #Note that
the resulting plot (above) has small values in the y axis, why? Maybe try the model again but asa Poisson




#5. Determine the influence of outliers


#model 1

mod1044<-glm(formula = ClaimsFema ~ Huc10_99Rain + KarstPerc + Per5PlsHou +

          ZipSlopeAvg + 1 + offset(log(ACSHouseholds0812)), family = "x.quasipoisson",

        data = FP_EGSData)


#Influence Points

library(car)

influencePlot(mod1044) #40,41,42,46,70


res_mod1044<-residuals(mod1044, type="deviance")

res_mod1044

plot(predict(mod1044), res_mod1044)

abline(h=0, lty=2)

qqnorm(res_mod1044)
```

```
qqline(res_mod1044)



#model 2
mod1050<-glm(formula = ClaimsFema ~ Huc10_99Rain + mmhaHuc10_2010 + Per5PlsHou +
               ZipSlopeAvg + 1 + offset(log(ACSHouseholds0812)), family = "x.quasipoisson",
             data = FP_EGSData)
#Influence Points
library(car)
influencePlot(mod1050)
#40,41,42,24



#D. conclusion: the models selected through model averaging are influenced by  the outliers detected (40-Salinas,41-Santa Isabel), according to studentized residuals >3
#We repeated the analysis without these outliers, and also removing 00920-56



#IV. REPEATE ANALYSIS WITHOUT OUTLIERS

#A. call data without outliers, scale and check for colinearity
Predictors2<-read.csv("PredictorVariables_2018Revised_Summarized_NoOutliers920751757.csv")
Labels2<-Predictors2[ ,1:2]#to desginate the first 3 columns as labels
Labels2
Predictors_Scaled2<-scale(Predictors2[ ,3:35])#to scale only predictor variables and not the labels
```

```
Predictors_Scaled2

Predictors_corrmatrix2<-cor(Predictors_Scaled2)#to detect correlation among predictor variables

Predictors_corrmatrix2 #this one is without outliers

write.csv(Predictors_corrmatrix2, file="Predictors2018_corrmatrix_NoOutliers.csv")#to save in work directory above

Predictors2<-cbind(Labels2, Predictors_Scaled2)#to attach the labels to predictors

Response2<-read.csv("ResponseVariables_FPEGS_noOutliers920_751_757.csv")

FP_EGSData2<-cbind(Response2,Predictors2)#attach scaled predictors to response variables

FP_EGSData2

write.csv(FP_EGSData2, file="FP_EGSDataScaled2018_NoOutliers.csv")#to save in work directory above

names(FP_EGSData2)



#B. MODELS WITHOUT THE OUTLIERS: test which SIMILAR variables are better predictors of FLOOD CLAIMS


#1 Weather:#1 Weather: rainzip90, rainzip95, rainzip99, rainHuc99, rainHuc90, rainHuc95 are all significant. 90-95 are correlated at both scales, while zip and huc 99 are correlated. 90 and 95 are not correlated to 99. I chose huc 90 and huc 99 to represent the two trends

rainzipAvg<-glm(ClaimsFema~ZipRainYr,family=quasipoisson, weights = offset(log(ACSHouseholds0812)), data=FP_EGSData2)

anova(rainzipAvg, test="F") #p= 0.3253


rainzip90<-glm(ClaimsFema~Zip90Rain+offset(log(ACSHouseholds0812)),family=quasipoisson,data=FP_EGSData2)

anova(rainzip90, test="F")#p=0.4207

summary(rainzip90)


rainzip95<-glm(ClaimsFema~Zip95Rain+offset(log(ACSHouseholds0812)),family=quasipoisson,data=FP_EGSData2)

anova(rainzip95, test="F")#p=0.5382
```

```
summary(rainzip95)

rainzip99<-glm(ClaimsFema~Zip99Rain+offset(log(ACSHouseholds0812)),family=quasipoisson,data=FP_EGSData2)

anova(rainzip99, test="F")### 0.003953*

rainHuc99<-glm(ClaimsFema~Huc10_99Rain+offset(log(ACSHouseholds0812)),family=quasipoisson,data=FP_EGSData2)

anova(rainHuc99, test="F")# 0.0006514 ***

summary(rainHuc99)

rainHuc90<-glm(ClaimsFema~Huc10_90Rain+offset(log(ACSHouseholds0812)),family=quasipoisson,data=FP_EGSData2)

anova(rainHuc90, test="F")#0.2906

summary(rainHuc90)

rainHuc95<-glm(ClaimsFema~Huc10_95Rain+offset(log(ACSHouseholds0812)),family=quasipoisson,data=FP_EGSData2)

anova(rainHuc95, test="F")# 0.6139

rainHucAvg<-glm(ClaimsFema~Huc10RainYr+offset(log(ACSHouseholds0812)),family=quasipoisson,data=FP_EGSData2)

anova(rainHucAvg, test="F")#0.4753

#2 EGS: Best is mmHuc10_2010 p=0.2404

mmhaHuc102010<-glm(ClaimsFema~mmhaHuc10_2010+offset(log(ACSHouseholds0812)),family=quasipoisson,data=FP_EGSData2)

anova(mmhaHuc102010, test="F")#p=0.2404

summary(mmhaHuc102010)
```

```
mmhaZip2010<-glm(ClaimsFema~mmhaZip_2010+offset(log(ACSHouseholds0812)),family=quasipoisson,
data=FP_EGSData2)

anova(mmhaZip2010, test="F")#p=0.3083

summary(mmhaZip2010)



#3 Slope: Best is zip slope Avg P=0.4018


ZipSlopeAvg<-glm(ClaimsFema~ZipSlopeAvg+offset(log(ACSHouseholds0812)),family=quasipoisson,data=
FP_EGSData2)

anova(ZipSlopeAvg, test="F")#P=0.4018

summary(ZipSlopeAvg)



ZipSlopeMax<-glm(ClaimsFema~ZipMaxSlope+offset(log(ACSHouseholds0812)),family=quasipoisson,dat
a=FP_EGSData2)

anova(ZipSlopeMax, test="F")#p= 0.7162

summary(ZipSlopeMax)


Ave_HucSlope<-glm(ClaimsFema/Population~Ave_HucSlo+offset(log(ACSHouseholds0812)),family=quasi
poisson,data=FP_EGSData2)

anova(Ave_HucSlope, test="F")#p=  0.7971

summary(Ave_HucSlope)



Max_HucSlope<-glm(ClaimsFema/Population~MaxHucSlpe+offset(log(ACSHouseholds0812)),family=qua
sipoisson,data=FP_EGSData2)

anova(Max_HucSlope, test="F")#p=0.6624

summary(Max_HucSlope)
```

```
#C.Build a global model with all the variables  of interest.

library(MuMIn)

options(na.action = "na.fail")



#1. Global Model without outliers and with offset in the covariates. Note that the interactions selected are different because now im working with a different dataset


global.modelQPoisson_offsetCOVHouse<-glm(ClaimsFema~mmhaHuc10_2010+SwgDen+KarstPerc+ppl_FldPer+ZipSlopeAvg+Huc10_99Rain+Huc10_90Rain+MedIncome+PercVegetation+PercWoodyWet+Per5PlsHou+PercGrassWet+(PercGrassWet*mmhaHuc10_2010)+(PercWoodyWet*mmhaHuc10_2010)+(PercGrassWet*KarstPerc)+(PercWoodyWet*KarstPerc)+(mmhaHuc10_2010*ppl_FldPer)+(KarstPerc*ppl_FldPer)+offset(log(ACSHouseholds0812)), family=quasipoisson,data=FP_EGSData2)

(chat <- deviance(global.modelQPoisson_offsetCOVHouse) / df.residual(global.modelQPoisson_offsetCOVHouse)) #chat = c^, the variance inflation factor



##2. Get ML estimator

#because glm does not supply the log-likelihood for quasipiosson (and quasibinomial) regression, We need to create a function that will trick glm into giving up the log likelihood, so we can use model averaging. Here it is below.

#First create the function #See https://sites.google.com/site/rforfishandwildlifegrads/home/mumin_usage_examples



x.quasipoisson <- function(...) {
  res <- quasipoisson(...)
  res$aic <- poisson(...)$aic
  res
}
```

#3. Update the global model to take in this function

global.modelQPoisson_offsetCOVHouse<-update(global.modelQPoisson_offsetCOVHouse, family = "x.quasipoisson")

(chat <- deviance(global.modelQPoisson_offsetCOVHouse) / df.residual(global.modelQPoisson_offsetCOVHouse)) #chat = c^, the variance inflation factor

#4. Conduct Model averaging-testing all posible variable combinations to see which have a better fit

library(MuMIn)

options(na.action = "na.fail") # prevent fitting models to different datasets

#DREDGE Global Model WITH INTERACTIONS NO OUTLIERS USING THE QUASI POISSON OPTION

model.setglobal.modelQPoisson_offsetCOVHouse<-dredge(global.modelQPoisson_offsetCOVHouse, m.lim=c(1,5), fixed="offset(log(ACSHouseholds0812))", subset = !((PercWoodyWet && ppl_FldPer) ||(KarstPerc && mmhaHuc10_2010)||(PercVegetation && mmhaHuc10_2010)||(SwgDen && Per5PlsHou)||(SwgDen && ZipSlopeAvg)), rank = "QAICc", chat = chat) #the item !subset is to prevent two correlated variables from being together in any model (the ones selected for subsetting were not the only correlated predictor variables, but only those that had shown to be important predictors in previous iterations of the dredge), the limit on 5 is to prevent model overfitting, the number can be changed to more or less explanatory variables if so wished

#Note that in this model I asked to incloude only models with offset(log(ACSHouseholds0812)) (fixed=offset(log(ACSHouseholds0812)))

top.modelsglobal.modelQPoisson_offsetCOVHouse<-get.models(model.setglobal.modelQPoisson_offsetCOVHouse, subset=delta < 2) # TO SELECT just the models that are within 2 QaIC from each other

top.modelsglobal.modelQPoisson_offsetCOVHouse

Avg.ModGlobal_global.modelQPoisson_offsetCOVHouse<-model.avg(top.modelsglobal.modelQPoisson_offsetCOVHouse)

```
summary(Avg.ModGlobal_global.modelQPoisson_offsetCOVHouse)# Error in
model.avg.default(top.modelsglobal.modelQPoisson_offsetCOV) :only one model supplied. Nothing to
do

Avg.ModGlobal_global.modelQPoisson_offsetCOVHouse

confint(Avg.ModGlobal_global.modelQPoisson_offsetCOVHouse) #

#Only one model, no average

topModel_offsetCOVHouse<-glm(formula = ClaimsFema ~ Huc10_99Rain + KarstPerc + ppl_FldPer +

                      KarstPerc:ppl_FldPer + 1 + offset(log(ACSHouseholds0812)),

                    family = "x.quasipoisson", data = FP_EGSData2)

summary(topModel_offsetCOVHouse)


#Predict


predicted_claimsQPoisson_OffsetCOVHouse<-exp(predict(topModel_offsetCOVHouse))

predicted_claimsQPoisson_OffsetCOVHouse

plot(FP_EGSData2$ClaimsFema, predicted_claimsQPoisson_OffsetCOVHouse, xlab = "Observed FEMA
Claims (1999-2014)", ylab = "Predicted Flood Claims", cex.lab=1.2)


summary(lm(FP_EGSData2$ClaimsFema~predicted_claimsQPoisson_OffsetCOVHouse))



#Verifying Residuals


res_topModel_offsetCOVHouse<- residuals(topModel_offsetCOVHouse, type="deviance")

res_topModel_offsetCOVHouse

plot(predicted_claimsQPoisson_OffsetCOVHouse, res_topModel_offsetCOVHouse)

abline(h=0, lty=2)

qqnorm(res_topModel_offsetCOVHouse)

qqline(res_topModel_offsetCOVHouse)
```

```
library(lattice)

#PercWoodyWet: KarstPerc

KarstPerc<-FP_EGSData2$KarstPerc

ppl_FldPer<-FP_EGSData2$ppl_FldPer

ClaimsPH<-FP_EGSData2$ClaimsPH

coplot(ClaimsPH~ KarstPerc | ppl_FldPer, number = 4, rows = 1,panel = panel.smooth, span = 2/3, iter = 3)

coplot(ClaimsPH ~ ppl_FldPer | KarstPerc, number = 4, rows = 1,panel = panel.smooth)
```

```
library(interplot)

devtools::install_github("sammo3182/interplot")

FloodKarst<-glm(ClaimsFema~(KarstPerc*ppl_FldPer)
+offset(log(ACSHouseholds0812)),family=quasipoisson,data=FP_EGSData2)
```

```
interplot(m = FloodKarst, var1 = 'KarstPerc', var2 = 'ppl_FldPer') +

  xlab('% Karst') +

  ylab('FEMA Claims per Household') +

  ggtitle('Claims per Household vs Percent Karst') +

  theme(plot.title = element_text(face='bold'))
```

#CONCLUSION: The model that resulted from the datset without outliers had a much lower AIC value than the model with the outliers in (1974 vs 3414).

#Also, the top models selected by the dredge with outliers in were all influenced by the outliers detected. The model fit (observed vs predicted) was also higher for the model without outliers (0.54, vs 0.45)

```
#V. Get residuals of best models to test autocorrelation with and without outliers
#Conclusion: No spatial autocorrelation was detected in the models


#Outliers in
mod2308.Res<-residuals(mod2308)###to get residuals of model including all scales and interactions
plot(mod2308)
ResidualTable_mod2308<-data.frame(mod2308.Res, FP_EGSData$ZIP_CODE)
write.csv(ResidualTable_mod2308, file = "ResidualTable_mod2308.csv")

mod8452.Res<-residuals(mod8452)###to get residuals of model including all scales and interactions
plot(mod8452)
ResidualTable_mod8452<-data.frame(mod8452.Res, FP_EGSData$ZIP_CODE)
write.csv(ResidualTable_mod8452, file = "ResidualTable_mod8452.csv")


mod2116.Res<-residuals(mod2116)###to get residuals of model including all scales and interactions
plot(mod2116)
ResidualTable_mod2116<-data.frame(mod2116.Res, FP_EGSData$ZIP_CODE)
write.csv(ResidualTable_mod2116, file = "ResidualTable_mod2116.csv")


mod2084.Res<-residuals(mod2084)###to get residuals of model including all scales and interactions
plot(mod2084)
ResidualTable_mod2084<-data.frame(mod2084.Res, FP_EGSData$ZIP_CODE)
write.csv(ResidualTable_mod2084, file = "ResidualTable_mod2084.csv")
```

```
mod2564.Res<-residuals(mod2564)###to get residuals of model including all scales and interactions

plot(mod2564)

ResidualTable_mod2564<-data.frame(mod2564.Res, FP_EGSData$ZIP_CODE)

write.csv(ResidualTable_mod2564, file = "ResidualTable_mod2564.csv")



#Outliers out


topModel_offsetCOVHouse.Res<-residuals(topModel_offsetCOVHouse)###to get residuals of model including all scales and interactions

plot(topModel_offsetCOVHouse)

ResidualTable_topModel_offsetCOVHouse<-data.frame(topModel_offsetCOVHouse.Res, FP_EGSData2$ZIP_CODE)

write.csv(ResidualTable_topModel_offsetCOVHouse, file = "ResidualTable_topModel_offsetCOVHouse.csv")
```

GI illness Medicare Claims Analysis

```
# PRMedicareGastroINLACodes.R

#

# Author: Mark Myer

#

# Purpose: To perform spatiotemporal analysis of gastrointestinal illness in coastal Puerto Rico Medicare recipients from 1999-2013 using R-INLA

#

# Revision: October 15, 2018

# R Version 3.4.4 Someone to Lean On

#####
```

```
#Required packages
library(readr)
library(INLA)
library(rgeos)
library(rgdal)
library(maptools)
library(splancs)
library(dplyr)
library(lubridate)

#Set a working drive
setwd("E:/mmyer")

#Import the aggregated dataset
MergedPRvars <- read_csv("E:/mmyer/all_vars.csv")
#Remove the last year, as initial analysis found it was abnormal
MergedPRvars <- subset(MergedPRvars, ordinalweek <= (max(ordinalweek) - 52))
#Quality check: Do we have 15 years of data with 53 epiweeks each?
max(MergedPRvars$ordinalweek) == 15 * 53

#Load the workspace with the Puerto Rico mesh
load("O:/Public/Myer/Puerto Rico Medicare Project/MeshCreate_Workspace.RData")

#Plot the mesh
tiff(filename="PRMesh.tiff",width=5,height=3,units="in",res=300,pointsize=8,compression="lzw")
plot(mesh,asp=1,main="")
dev.off()

#Get the coordinates of the observations
```

```
coords <- as.matrix(loc@coords)

#####Create the INLA SPDE and run the model
min.width <- min(c(diff(range(mesh$loc[, 1])), diff(range(mesh$loc[, 2])))) #Minimum width of the study area in km

spde <- inla.spde2.pcmatern(
  mesh=mesh, alpha=2, ### mesh and smoothness parameter
  prior.range=c(min.width/2, 0.5), ### P(range<(half the minimum width of study area in km)=0.5
  prior.sigma=c(1, 0.5) ### P(sigma>1)=0.5
)

#Define prior for precision (for zero-inflation)
prec.prior <- list(prior='pc.prec', param=c(1, 0.01))

#####
#Do the binomial model with outliers as identified by FEMA claims removed
#Remove ZIP codes considered outliers by flood claim analysis
MergedPRvars <- subset(MergedPRvars, zipcode != "751" & zipcode != "757" & zipcode != "920")
#Quality check: make sure the zip codes aren't in the dataset anymore
unique(MergedPRvars$zipcode)

#Replace the incorrect SwgPerc variable with the corrected one
MergedPRvars <- subset(MergedPRvars, select =c(-SwgPerc)) #Remove the old incorrect values
NewSwg <- read.csv("O:/Public/Myer/Puerto Rico Medicare Project/New_SwgValues_10122018.csv") #import the correct values
names(NewSwg)[1] = "zipcode"
NewSwg <- NewSwg[,-2] #The name isn't needed for matching
MergedPRvars <- merge(MergedPRvars, NewSwg, by="zipcode") #Merge the new values in by zipcode. It's now called SwgDen
```

```
#Get some descriptor variables
n <- nrow(MergedPRvars) #number of observations
s <- nrow(coords) #number of locations
t <- max(MergedPRvars$ordinalweek) #number of time steps
#Quality check: s*t should equal n
s*t == n

#Attach the responses
y.n <- MergedPRvars$gastro.case

#Get the covariates
vars.n <- data.frame(
  rlag99 = as.factor(MergedPRvars$rlag99),
  ppl_FldPer = (MergedPRvars$ppl_FldPer),
  SwgDen = (MergedPRvars$'SwgDen..m.m2.'),
  KarstPerc = (MergedPRvars$KarstPerc),
  X2010mmha_Huc10 = (MergedPRvars$X2010mmha_Huc10), #variable names can't start with a number so add an X
  population = (MergedPRvars$population),
  ClaimsPP_1 = (MergedPRvars$ClaimsPP_1),
  zipcode = (MergedPRvars$zipcode),
  wk = (MergedPRvars$ordinalweek)
)

vars.n[,2:7] <- scale(vars.n[,2:7])

#Create the projector matrix without week grouping
```

```
obs.locations.n <- data.frame(easting=MergedPRvars$easting,northing=MergedPRvars$northing)

obs.locations.n <- as.matrix (obs.locations.n)

A.n <- inla.spde.make.A(mesh, loc=obs.locations.n)


#Create the model matrix

mat.n <- model.matrix(~rlag99 + ppl_FldPer + SwgDen + KarstPerc + X2010mmha_Huc10 + population + ClaimsPP_1, vars.n)


#Create the stack

stack.n <- inla.stack(data=list(y=as.vector(y.n), Ntrials=length(y.n), link=1), #Note that y needs to be defined earlier

                      A=list(A.n,1),

                      effects=list(list(spatial = 1:spde$n.spde),data.frame(mu0=1, wk=vars.n$wk, mat.n)))


#Define the formula

formula.n <- y ~ -1 + mu0 + rlag991 + rlag992 + rlag993 + ppl_FldPer + SwgDen + KarstPerc + X2010mmha_Huc10 + population + ClaimsPP_1 +

  f(spatial, model=spde) +

  f(wk, model = 'rw1', scale.model= TRUE, hyper = list(theta=list(prior="pc.prec", param= c(0.5,0.01))))


gastro.result.bin.rw1.n<- inla(formula.n,

                               family="binomial",

                               data=inla.stack.data(stack.n),

                               control.predictor=list(compute=TRUE, A=inla.stack.A(stack.n), link = 1), #link = 1 scales the fitted values with the logit link

                               control.family=list(link='logit'),

                               control.inla=list(int.strategy='eb', correct=T),

                               control.fixed=list(expand.factor.strategy ='model.matrix'),

                               control.compute=list(dic=T,waic=T,cpo=T),

                               verbose = TRUE)
```

```
#Improve estimation of hyperparameters by rerunning the model, using the previous run's estimates as the starting point

#inla.rerun(gastro.result.bin.rw1.n)

summary(gastro.result.bin.rw1.n)


#Save the result locally in case of crash, since still contains privileged data

save.image(file="E:/mmyer/INLAModelComparisons_NewSwgValues.RData")


#Get the variance for the RW1 temporal effect

variance.temporal.n<- inla.tmarginal(function(x) 1/x,
gastro.result.bin.rw1.n$marginals.hyperpar$`Precision for wk`)

variance.temporal.m1.n<-inla.emarginal(function(x) x, variance.temporal.n)

variance.temporal.m2.n<-inla.emarginal(function(x) x^2, variance.temporal.n)

sd.variance.temporal.n<-sqrt(variance.temporal.m2.n - variance.temporal.m1.n^2)

variance.temporal.quants.n<- inla.qmarginal(c(0.025, 0.5, 0.975), variance.temporal.n)


#Obtain the posterior mean values for the Week effects:

weekvalues.n <- data.frame(week = 1:t, mean = gastro.result.bin.rw1.n$summary.random$wk$mean,
lower = gastro.result.bin.rw1.n$summary.random$wk$`0.025quant`, upper =
gastro.result.bin.rw1.n$summary.random$wk$`0.975quant`)

tiff(filename="gastroRW1RedoFig_n.tiff",width=4,height=3,units="in",res=300,pointsize=8,compression=
"lzw")

ggplot(weekvalues.n) +
  geom_line(aes(y=mean, x=week, colour= ""), size=1.5) +
  geom_ribbon(aes(ymin=lower, ymax=upper, x=week, fill=""), alpha=0.3) +
  scale_colour_manual("", values="blue") +
  scale_fill_manual("", values="grey50") +
  labs(x="Weeks (1999-2013)", y="Log Odds") +
  theme(panel.grid.major = element_blank(),
        panel.grid.minor = element_blank(),
```

```
      panel.background = element_blank(),
      axis.line = element_line(colour = "black"),
      legend.position="none",
      axis.title.x = element_text(size=rel(1.2)),#, face="bold"),
      axis.title.y = element_text(size=rel(1.2))#, face="bold")
      )
dev.off()

#Plot the spatial component of the model
stepsize <- 1 #This defines the grid as made of squares 1Km on a side
nxy <- round(c(diff(range(bound$loc[,1]))/stepsize, diff(range(bound$loc[,2]))/stepsize)) #Defines the number of pixels in each direction based on the size of the County
projgrid <- inla.mesh.projector(mesh, xlim=range(bound$loc[,1]), ylim=range(bound$loc[,2]), dims=nxy) #Define a projection grid over the dims of our study area

#Find the spatial mean values
logit2prob<- function(logit){ #This function turns logit output to probability
  odds <- exp(logit)
  prob <- odds / (1 + odds)
  return(prob)
}

study.area.mean.n<- mean(exp(gastro.result.bin.rw1.n$summary.random$spatial$mean))
spatial.mean.probability.n <- inla.mesh.project(projgrid, (gastro.result.bin.rw1.n$summary.random$spatial$mean))#/study.area.mean.n)) #Plot the spatial effect odds ratio over the study area
range((exp(gastro.result.bin.rw1.n$summary.random$spatial$mean)/study.area.mean.n))#Get the range of odds for the spatial effect

#NA out the areas of the grid that are outside the border
simplemesh <-inla.mesh.2d(boundary=bound, cutoff=1, max.edge=100)
```

```
ok = inla.mesh.projector(simplemesh, projgrid$lattice$loc)$proj$ok

spatial.mean.probability.n[!ok] <- NA

#tiff(filename="gastroSpatialTestFig_n_logodds.tiff",width=5,height=2,units="in",res=300,pointsize=8,compression="lzw")

library(lattice)

lattice::levelplot(spatial.mean.probability.n,
            par.settings=list(
              layout.widths=list(right.padding=2)),
            colorkey=list(space="right", labels=list(cex=0.7)),
            xlab='',
            ylab='',
            col.regions=topo.colors(16),
            scales=list(draw=F))
#dev.off()


#Check the CPO values to see that none of them are throwing an error. If they are, that means there are points not predicted well by the model

#The total here is the number of points that throw a CPO error and may be poorly fit by the model.

sum(gastro.result.bin.rw1.n$cpo$failure != 0)


#Check the predictive power of the model on observations

pred.responses.n<-gastro.result.bin.rw1.n$summary.fitted.values$mean[1:nrow(MergedPRvars)]

#Create an ROC curve, determine the optimal cutoff point using Youden's index, and then calculate AUC value with optimal cutoff

install.packages("ROCR")

library(ROCR)

roc.pred.n<-prediction(pred.responses.n,y.n)

roc.perf.n<-performance(roc.pred, measure="tpr", x.measure="fpr") #"tpr" means true positive rate, "fpr" is false positive rate

tiff(filename="gastroROC_Curve.tiff",width=4,height=4,units="in",res=300,pointsize=8,compression="lzw")
```

```
plot(roc.perf.n, colorize=F, lwd=2, lty=3, cex.lab=1.4)

points(x=1.01-opt.cut.n[1], y=opt.cut.n[2], cex=2, pch=19, col="blue") #0.01 is added to the x coordinate to scoot the point a little over so it's centered on the line

abline(a=0,b=1)

dev.off()


#This function finds the optimal cutoff point

opt.cut = function(perf, pred){
  cut.ind = mapply(FUN=function(x, y, p){
    d = (x - 0)^2 + (y-1)^2
    ind = which(d == min(d))
    c(sensitivity = y[[ind]], specificity = 1-x[[ind]],
      cutoff = p[[ind]])
  }, perf@x.values, perf@y.values, pred@cutoffs)
}

opt.cut.n <- print(opt.cut(roc.perf.n, roc.pred.n))


#Obtain the AUC value

auc.perf.n = performance(roc.pred.n, measure = "auc")

auc.perf.n@y.values



#####

#Run several incremental models to compare the relative fit based on DIC/CPO information-theoretic comparisons


#Model 1: Spatial and Temporal only (Null), no predictors

#Define the formula

formula.1 <- y ~ -1 + mu0 +
  f(spatial, model=spde) +
```

```
 f(wk, model = 'rw1', scale.model= TRUE, hyper = list(theta=list(prior="pc.prec", param= c(0.5,0.01))))


gastro.result.bin.rw1.1<- inla(formula.1,
                    family="binomial",
                    data=inla.stack.data(stack.n),
                    control.predictor=list(compute=TRUE, A=inla.stack.A(stack.n), link = 1), #link = 1 scales the fitted values with the logit link
                    control.family=list(link='logit'),
                    control.inla=list(int.strategy='eb', correct=T),
                    control.fixed=list(expand.factor.strategy ='model.matrix'),
                    control.compute=list(dic=T,waic=T,cpo=T),
                    verbose = TRUE)

#Save the result locally in case of crash, since still contains privileged data
save.image(file="E:/mmyer/INLAModelComparisons_NewSwgValues.RData")

#Check the CPO values to see that none of them are throwing an error. If they are, that means there are points not predicted well by the model
#The total here is the number of points that throw a CPO error and may be poorly fit by the model.
sum(gastro.result.bin.rw1.1$cpo$failure != 0)

#Check DIC, WAIC values
gastro.result.bin.rw1.1$waic
gastro.result.bin.rw1.1$dic

#Check the predictive power of the model on observations
pred.responses.1<-gastro.result.bin.rw1.1$summary.fitted.values$mean[1:nrow(MergedPRvars)]
#Create an ROC curve, determine the optimal cutoff point using Youden's index, and then calculate AUC value with optimal cutoff
roc.pred.1<-prediction(pred.responses.1,y.n)
```

```
roc.perf.1<-performance(roc.pred, measure="tpr", x.measure="fpr") #"tpr" means true positive rate, "fpr" is false positive rate

plot(roc.perf.1)

abline(a=0,b=1)


#Get the optimal cutoff

opt.cut.1 <- print(opt.cut(roc.perf.1, roc.pred.1))


#Obtain the AUC value

auc.perf.1 = performance(roc.pred.1, measure = "auc")

auc.perf.1@y.values


#####

#Model 2: Spatial and Temporal, with Population

#Define the formula

formula.2 <- y ~ -1 + mu0 + population +

  f(spatial, model=spde) +

  f(wk, model = 'rw1', scale.model= TRUE, hyper = list(theta=list(prior="pc.prec", param= c(0.5,0.01))))


gastro.result.bin.rw1.2<- inla(formula.2,

                               family="binomial",

                               data=inla.stack.data(stack.n),

                               control.predictor=list(compute=TRUE, A=inla.stack.A(stack.n), link = 1), #link = 1 scales the fitted values with the logit link

                               control.family=list(link='logit'),

                               control.inla=list(int.strategy='eb', correct=T),

                               control.fixed=list(expand.factor.strategy ='model.matrix'),

                               control.compute=list(dic=T,waic=T,cpo=T),

                               verbose = TRUE)
```

```
#Save the result locally in case of crash, since still contains privileged data

save.image(file="E:/mmyer/INLAModelComparisons_NewSwgValues.RData")


#Check the CPO values to see that none of them are throwing an error. If they are, that means there are points not predicted well by the model

#The total here is the number of points that throw a CPO error and may be poorly fit by the model.

sum(gastro.result.bin.rw1.2$cpo$failure != 0)


#Check DIC, WAIC values

gastro.result.bin.rw1.2$waic

gastro.result.bin.rw1.2$dic


#Check the predictive power of the model on observations

pred.responses.2<-gastro.result.bin.rw1.2$summary.fitted.values$mean[1:nrow(MergedPRvars)]

#Create an ROC curve, determine the optimal cutoff point using Youden's index, and then calculate AUC value with optimal cutoff

roc.pred.2<-prediction(pred.responses.2,y.n)

roc.perf.2<-performance(roc.pred, measure="tpr", x.measure="fpr") #"tpr" means true positive rate, "fpr" is false positive rate

plot(roc.perf.2)

abline(a=0,b=1)


#Get the optimal cutoff

opt.cut.2 <- print(opt.cut(roc.perf.2, roc.pred.2))


#Obtain the AUC value

auc.perf.2 = performance(roc.pred.2, measure = "auc")

auc.perf.2@y.values


#####
```

```
#Model 3: Spatial and Temporal, with Population + Rainfall

#Define the formula

formula.3 <- y ~ -1 + mu0 + population + rlag991 + rlag992 + rlag993 +

  f(spatial, model=spde) +

  f(wk, model = 'rw1', scale.model= TRUE, hyper = list(theta=list(prior="pc.prec", param= c(0.5,0.01))))


gastro.result.bin.rw1.3<- inla(formula.3,

                               family="binomial",

                               data=inla.stack.data(stack.n),

                               control.predictor=list(compute=TRUE, A=inla.stack.A(stack.n), link = 1), #link = 1 scales the fitted values with the logit link

                               control.family=list(link='logit'),

                               control.inla=list(int.strategy='eb', correct=T),

                               control.fixed=list(expand.factor.strategy ='model.matrix'),

                               control.compute=list(dic=T,waic=T,cpo=T),

                               verbose = TRUE)


#Save the result locally in case of crash, since still contains privileged data

save.image(file="E:/mmyer/INLAModelComparisons_NewSwgValues.RData")


#Check the CPO values to see that none of them are throwing an error. If they are, that means there are points not predicted well by the model

#The total here is the number of points that throw a CPO error and may be poorly fit by the model.

sum(gastro.result.bin.rw1.3$cpo$failure != 0)


#Check DIC, WAIC values

gastro.result.bin.rw1.3$waic

gastro.result.bin.rw1.3$dic


#Check the predictive power of the model on observations
```

```
pred.responses.3<-gastro.result.bin.rw1.3$summary.fitted.values$mean[1:nrow(MergedPRvars)]

#Create an ROC curve, determine the optimal cutoff point using Youden's index, and then calculate AUC value with optimal cutoff

roc.pred.3<-prediction(pred.responses.3,y.n)

roc.perf.3<-performance(roc.pred, measure="tpr", x.measure="fpr") #"tpr" means true positive rate, "fpr" is false positive rate

plot(roc.perf.3)

abline(a=0,b=1)


#Get the optimal cutoff

opt.cut.3 <- print(opt.cut(roc.perf.3, roc.pred.3))


#Obtain the AUC value

auc.perf.3 = performance(roc.pred.3, measure = "auc")

auc.perf.3@y.values


#####

#Model 4: Spatial and Temporal, with Population + Rainfall + Sewage

#Define the formula

formula.4 <- y ~ -1 + mu0 + population + rlag991 + rlag992 + rlag993 + SwgDen +

  f(spatial, model=spde) +

  f(wk, model = 'rw1', scale.model= TRUE, hyper = list(theta=list(prior="pc.prec", param= c(0.5,0.01))))


gastro.result.bin.rw1.4<- inla(formula.4,

                               family="binomial",

                               data=inla.stack.data(stack.n),

                               control.predictor=list(compute=TRUE, A=inla.stack.A(stack.n), link = 1), #link = 1 scales the fitted values with the logit link

                               control.family=list(link='logit'),

                               control.inla=list(int.strategy='eb', correct=T),
```

```
                control.fixed=list(expand.factor.strategy ='model.matrix'),
                control.compute=list(dic=T,waic=T,cpo=T),
                verbose = TRUE)

#Save the result locally in case of crash, since still contains privileged data
save.image(file="E:/mmyer/INLAModelComparisons_NewSwgValues.RData")

#Check the CPO values to see that none of them are throwing an error. If they are, that means there are points not predicted well by the model
#The total here is the number of points that throw a CPO error and may be poorly fit by the model.
sum(gastro.result.bin.rw1.4$cpo$failure != 0)

#Check DIC, WAIC values
gastro.result.bin.rw1.4$waic
gastro.result.bin.rw1.4$dic

#Check the predictive power of the model on observations
pred.responses.4<-gastro.result.bin.rw1.4$summary.fitted.values$mean[1:nrow(MergedPRvars)]
#Create an ROC curve, determine the optimal cutoff point using Youden's index, and then calculate AUC value with optimal cutoff
roc.pred.4<-prediction(pred.responses.4,y.n)
roc.perf.4<-performance(roc.pred, measure="tpr", x.measure="fpr") #"tpr" means true positive rate, "fpr" is false positive rate
plot(roc.perf.4)
abline(a=0,b=1)

#Get the optimal cutoff
opt.cut.4 <- print(opt.cut(roc.perf.4, roc.pred.4))

#Obtain the AUC value
```

```
auc.perf.4 = performance(roc.pred.4, measure = "auc")

auc.perf.4@y.values


#####

#Model 5: Spatial and Temporal, with Population + Rainfall + Karst + People in Flood Zones + (Karst * People in Flood Zones)

#Define the formula

formula.5 <- y ~ -1 + mu0 + population + rlag991 + rlag992 + rlag993 + KarstPerc + ppl_FldPer + KarstPerc*ppl_FldPer +

  f(spatial, model=spde) +

  f(wk, model = 'rw1', scale.model= TRUE, hyper = list(theta=list(prior="pc.prec", param= c(0.5,0.01))))


gastro.result.bin.rw1.5<- inla(formula.5,

                               family="binomial",

                               data=inla.stack.data(stack.n),

                               control.predictor=list(compute=TRUE, A=inla.stack.A(stack.n), link = 1), #link = 1 scales the fitted values with the logit link

                               control.family=list(link='logit'),

                               control.inla=list(int.strategy='eb', correct=T),

                               control.fixed=list(expand.factor.strategy ='model.matrix'),

                               control.compute=list(dic=T,waic=T,cpo=T),

                               verbose = TRUE)


#Save the result locally in case of crash, since still contains privileged data

save.image(file="E:/mmyer/INLAModelComparisons_NewSwgValues.RData")


#Check the CPO values to see that none of them are throwing an error. If they are, that means there are points not predicted well by the model

#The total here is the number of points that throw a CPO error and may be poorly fit by the model.

sum(gastro.result.bin.rw1.5$cpo$failure != 0)
```

```
#Check DIC, WAIC values

gastro.result.bin.rw1.5$waic

gastro.result.bin.rw1.5$dic


#Check the predictive power of the model on observations

pred.responses.5<-gastro.result.bin.rw1.5$summary.fitted.values$mean[1:nrow(MergedPRvars)]

#Create an ROC curve, determine the optimal cutoff point using Youden's index, and then calculate AUC value with optimal cutoff

roc.pred.5<-prediction(pred.responses.5,y.n)

roc.perf.5<-performance(roc.pred, measure="tpr", x.measure="fpr") #"tpr" means true positive rate, "fpr" is false positive rate


#Get the optimal cutoff

opt.cut.5 <- print(opt.cut(roc.perf.5, roc.pred.5))


#Obtain the AUC value

auc.perf.5 = performance(roc.pred.5, measure = "auc")

auc.perf.5@y.values


#Plot the ROC curve

tiff(filename="gastroROC_Curve_BestModel.tiff",width=4,height=4,units="in",res=300,pointsize=8,compression="lzw")

plot(roc.perf.5, colorize=F, lwd=2, lty=3, cex.lab=1.4)

points(x=1.01-opt.cut.5[1], y=opt.cut.5[2], cex=2, pch=19, col="blue") #0.01 is added to the x coordinate to scoot the point a little over so it's centered on the line

abline(a=0,b=1)

dev.off()


#Get the variance for the RW1 temporal effect
```

```
variance.temporal.5<- inla.tmarginal(function(x) 1/x,
gastro.result.bin.rw1.5$marginals.hyperpar$`Precision for wk`)

variance.temporal.m1.5<-inla.emarginal(function(x) x, variance.temporal.5)

variance.temporal.m2.5<-inla.emarginal(function(x) x^2, variance.temporal.5)

sd.variance.temporal.5<-sqrt(variance.temporal.m2.5 - variance.temporal.m1.5^2)

variance.temporal.quants.5<- inla.qmarginal(c(0.025, 0.5, 0.975), variance.temporal.5)


#Obtain the posterior mean values for the Week effects:

weekvalues.5 <- data.frame(week = 1:t, mean = gastro.result.bin.rw1.5$summary.random$wk$mean,
lower = gastro.result.bin.rw1.5$summary.random$wk$`0.025quant`, upper =
gastro.result.bin.rw1.5$summary.random$wk$`0.975quant`)

tiff(filename="gastroRW1Fig_BestModel.tiff",width=4,height=3,units="in",res=300,pointsize=8,compress
ion="lzw")

ggplot(weekvalues.5) +

 geom_line(aes(y=mean, x=week, colour= ""), size=1.5) +

 geom_ribbon(aes(ymin=lower, ymax=upper, x=week, fill=""), alpha=0.3) +

 scale_colour_manual("", values="blue") +

 scale_fill_manual("", values="grey50") +

 labs(x="Weeks (1999-2013)", y="Log Odds") +

 theme(panel.grid.major = element_blank(),

       panel.grid.minor = element_blank(),

       panel.background = element_blank(),

       axis.line = element_line(colour = "black"),

       legend.position="none",

       axis.title.x = element_text(size=rel(1.2)),#, face="bold"),

       axis.title.y = element_text(size=rel(1.2))#, face="bold")

 )

dev.off()


#Plot the spatial component of the model
```

```
stepsize <- 1 #This defines the grid as made of squares 1Km on a side

nxy <- round(c(diff(range(bound$loc[,1]))/stepsize, diff(range(bound$loc[,2]))/stepsize)) #Defines the number of pixels in each direction based on the size of the County

projgrid <- inla.mesh.projector(mesh, xlim=range(bound$loc[,1]), ylim=range(bound$loc[,2]), dims=nxy) #Define a projection grid over the dims of our study area


#Find the spatial mean values

logit2prob<- function(logit){ #This function turns logit output to probability

  odds <- exp(logit)

  prob <- odds / (1 + odds)

  return(prob)

}


study.area.mean.5<- mean(exp(gastro.result.bin.rw1.5$summary.random$spatial$mean))

spatial.mean.probability.5 <- inla.mesh.project(projgrid, (gastro.result.bin.rw1.5$summary.random$spatial$mean))#/study.area.mean.5)) #Plot the spatial effect odds ratio over the study area

range((exp(gastro.result.bin.rw1.5$summary.random$spatial$mean)/study.area.mean.5))#Get the range of odds for the spatial effect


#NA out the areas of the grid that are outside the border

simplemesh <-inla.mesh.2d(boundary=bound, cutoff=1, max.edge=100)

ok = inla.mesh.projector(simplemesh, projgrid$lattice$loc)$proj$ok

spatial.mean.probability.5[!ok] <- NA

tiff(filename="gastroSpatialTestFig_BestModel_logodds.tiff",width=5,height=2,units="in",res=300,pointsize=8,compression="lzw")

library(lattice)

lattice::levelplot(spatial.mean.probability.5,

                   par.settings=list(

                     layout.widths=list(right.padding=2)),

                   colorkey=list(space="right", labels=list(cex=0.7)),
```

```
            xlab='',
            ylab='',
            col.regions=topo.colors(16),
            scales=list(draw=F))
dev.off()

#Check the CPO values to see that none of them are throwing an error. If they are, that means there are points not predicted well by the model
#The total here is the number of points that throw a CPO error and may be poorly fit by the model.
sum(gastro.result.bin.rw1.5$cpo$failure != 0)

#####
#Model 6: Spatial and Temporal, with Population + Rainfall + HUC10 Retention + People in Flood Zones + (HUC10 Retention * People in Flood Zones)
#Define the formula
formula.6 <- y ~ -1 + mu0 + population + rlag991 + rlag992 + rlag993 + X2010mmha_Huc10 + ppl_FldPer + X2010mmha_Huc10 *ppl_FldPer +
  f(spatial, model=spde) +
  f(wk, model = 'rw1', scale.model= TRUE, hyper = list(theta=list(prior="pc.prec", param= c(0.5,0.01))))

gastro.result.bin.rw1.6<- inla(formula.6,
                    family="binomial",
                    data=inla.stack.data(stack.n),
                    control.predictor=list(compute=TRUE, A=inla.stack.A(stack.n), link = 1), #link = 1 scales the fitted values with the logit link
                    control.family=list(link='logit'),
                    control.inla=list(int.strategy='eb', correct=T),
                    control.fixed=list(expand.factor.strategy ='model.matrix'),
                    control.compute=list(dic=T,waic=T,cpo=T),
                    verbose = TRUE)
```

```
#Save the result locally in case of crash, since still contains privileged data

save.image(file="E:/mmyer/INLAModelComparisons_NewSwgValues.RData")


#Check the CPO values to see that none of them are throwing an error. If they are, that means there are points not predicted well by the model

#The total here is the number of points that throw a CPO error and may be poorly fit by the model.

sum(gastro.result.bin.rw1.6$cpo$failure != 0)


#Check DIC, WAIC values

gastro.result.bin.rw1.6$waic

gastro.result.bin.rw1.6$dic


#Check the predictive power of the model on observations

pred.responses.6<-gastro.result.bin.rw1.6$summary.fitted.values$mean[1:nrow(MergedPRvars)]

#Create an ROC curve, determine the optimal cutoff point using Youden's index, and then calculate AUC value with optimal cutoff

roc.pred.6<-prediction(pred.responses.6,y.n)

roc.perf.6<-performance(roc.pred, measure="tpr", x.measure="fpr") #"tpr" means true positive rate, "fpr" is false positive rate

plot(roc.perf.6)

abline(a=0,b=1)


#Get the optimal cutoff

opt.cut.6 <- print(opt.cut(roc.perf.6, roc.pred.6))


#Obtain the AUC value

auc.perf.6 = performance(roc.pred.6, measure = "auc")

auc.perf.6@y.values
```

```
#####

#Model 7: Spatial and Temporal, with Population + Rainfall + Sewage + Karst + People in Flood Zones + (Karst * People in Flood Zones)

#Define the formula

formula.7 <- y ~ -1 + mu0 + population + rlag991 + rlag992 + rlag993 + SwgDen + KarstPerc + ppl_FldPer + KarstPerc*ppl_FldPer +

  f(spatial, model=spde) +

  f(wk, model = 'rw1', scale.model= TRUE, hyper = list(theta=list(prior="pc.prec", param= c(0.5,0.01))))


gastro.result.bin.rw1.7<- inla(formula.7,

                        family="binomial",

                        data=inla.stack.data(stack.n),

                        control.predictor=list(compute=TRUE, A=inla.stack.A(stack.n), link = 1), #link = 1 scales the fitted values with the logit link

                        control.family=list(link='logit'),

                        control.inla=list(int.strategy='eb', correct=T),

                        control.fixed=list(expand.factor.strategy ='model.matrix'),

                        control.compute=list(dic=T,waic=T,cpo=T),

                        verbose = TRUE)


#Save the result locally in case of crash, since still contains privileged data

save.image(file="E:/mmyer/INLAModelComparisons_NewSwgValues.RData")


#Check the CPO values to see that none of them are throwing an error. If they are, that means there are points not predicted well by the model

#The total here is the number of points that throw a CPO error and may be poorly fit by the model.

sum(gastro.result.bin.rw1.7$cpo$failure != 0)


#Check DIC, WAIC values

gastro.result.bin.rw1.7$waic
```

```
gastro.result.bin.rw1.7$dic


#Check the predictive power of the model on observations

pred.responses.7<-gastro.result.bin.rw1.7$summary.fitted.values$mean[1:nrow(MergedPRvars)]

#Create an ROC curve, determine the optimal cutoff point using Youden's index, and then calculate AUC value with optimal cutoff

roc.pred.7<-prediction(pred.responses.7,y.n)

roc.perf.7<-performance(roc.pred, measure="tpr", x.measure="fpr") #"tpr" means true positive rate, "fpr" is false positive rate

plot(roc.perf.7)

abline(a=0,b=1)


#Get the optimal cutoff

opt.cut.7 <- print(opt.cut(roc.perf.7, roc.pred.7))


#Obtain the AUC value

auc.perf.7 = performance(roc.pred.7, measure = "auc")

auc.perf.7@y.values



#####

#Model 8: Spatial and Temporal, with Population + Rainfall + Sewage + HUC10 Retention + People in Flood Zones + (HUC10 Retention * People in Flood Zones)

#Define the formula

formula.8 <- y ~ -1 + mu0 + population + rlag991 + rlag992 + rlag993 + SwgDen + X2010mmha_Huc10 + ppl_FldPer + X2010mmha_Huc10*ppl_FldPer +

  f(spatial, model=spde) +

  f(wk, model = 'rw1', scale.model= TRUE, hyper = list(theta=list(prior="pc.prec", param= c(0.5,0.01))))


gastro.result.bin.rw1.8<- inla(formula.8,
```

```
                family="binomial",
                data=inla.stack.data(stack.n),
                control.predictor=list(compute=TRUE, A=inla.stack.A(stack.n), link = 1), #link = 1 scales the fitted values with the logit link
                control.family=list(link='logit'),
                control.inla=list(int.strategy='eb', correct=T),
                control.fixed=list(expand.factor.strategy ='model.matrix'),
                control.compute=list(dic=T,waic=T,cpo=T),
                verbose = TRUE)

#Save the result locally in case of crash, since still contains privileged data
save.image(file="E:/mmyer/INLAModelComparisons_NewSwgValues.RData")

#Check the CPO values to see that none of them are throwing an error. If they are, that means there are points not predicted well by the model
#The total here is the number of points that throw a CPO error and may be poorly fit by the model.
sum(gastro.result.bin.rw1.8$cpo$failure != 0)

#Check DIC, WAIC values
gastro.result.bin.rw1.8$waic
gastro.result.bin.rw1.8$dic

#Check the predictive power of the model on observations
pred.responses.8<-gastro.result.bin.rw1.8$summary.fitted.values$mean[1:nrow(MergedPRvars)]
#Create an ROC curve, determine the optimal cutoff point using Youden's index, and then calculate AUC value with optimal cutoff
roc.pred.8<-prediction(pred.responses.8,y.n)
roc.perf.8<-performance(roc.pred, measure="tpr", x.measure="fpr") #"tpr" means true positive rate, "fpr" is false positive rate
plot(roc.perf.8)
```

```
abline(a=0,b=1)

#Get the optimal cutoff
opt.cut.8 <- print(opt.cut(roc.perf.8, roc.pred.8))

#Obtain the AUC value
auc.perf.8 = performance(roc.pred.8, measure = "auc")
auc.perf.8@y.values

#####
#Remove the dataset, responses, and the stack, which contain privileged data
rm(MergedPRvars, y.n, stack.n)

#Save the result to my public drive, now that we have removed privileged data
save.image(file="O:/Public/Myer/Puerto Rico Medicare
Project/INLAModelComparisons_NewSwgValues.RData")
```

Yee, Susan

From: Rebeca De Jesus Crespo <rdejesuscrespo1@lsu.edu>
Sent: Friday, April 17, 2020 10:51 AM
To: Yee, Susan
Subject: Fw: Estudio Cuenca Hidrográfica del Río Grande de Añasco
Attachments: ATT00001.txt

Hi Susan,

Below the email thread from the West Puerto Rico Watershed Initiative (Iniciativa de Cuencas del Oeste de Puerto Rico), their leader Luis Villanueva Cubero works for FEMA.

Thanks!

Rebeca de Jesús
Assistant Professor, Department of Environmental Sciences
Louisiana State University
College of Coast and the Environment
93 South Quad Drive
Baton Rouge, LA 70803

From: Villanueva-Cubero, Luis <luis.villanueva-cubero@fema.dhs.gov>
Sent: Tuesday, April 14, 2020 9:50 AM
To: Rebeca De Jesus Crespo <rdejesuscrespo1@lsu.edu>
Cc: Edgardo Gonzalez <edgonz581@gmail.com>; Edgardo Gonzalez <edgardo@ccpaisaje.org>; Lisette Fas-Quiñones <lisettefas@gmail.com>
Subject: RE: Estudio Cuenca Hidrográfica del Río Grande de Añasco

Si, de mucha utilidad, igracias!

LUIS VILLANUEVA-CUBERO
NDRS – Community Planning Lead
Community Planning & Capacity Building
DR-4339-PR, Branch I (Aguadilla)
202-568-3542 iPhone
luis.villanueva-cubero@fema.dhs.gov

The mission of the Community Planning and Capacity Building Recovery Support Function (CPCB RSF) is to enable local governments to effectively and efficiently carry out community-based recovery planning and management in a post-disaster environment. The CPCB RSF also supports state or territorial governments in developing programs of support for local recovery planning and management.

From: Rebeca De Jesus Crespo <rdejesuscrespo1@lsu.edu>
Sent: Monday, March 30, 2020 12:43 PM
To: Villanueva-Cubero, Luis <luis.villanueva-cubero@fema.dhs.gov>
Cc: Edgardo Gonzalez <edgonz581@gmail.com>; Edgardo Gonzalez <edgardo@ccpaisaje.org>
Subject: Re: Estudio Cuenca Hidrográfica del Río Grande de Añasco

Saludos Luis y Edgardo,

Adjunto el artículo. El área Sur/Oeste (Cabo Rojo, Guanica...) es la de mayor probabilidad de infecciones. Sin embargo, la cuenca baja del RGA tiene también probabilidades relativamente altas en comparación con el resto de la isla (ver Figura 6b). Pueden leerlo y dejarme saber si tienen dudas. Espero les sirva.

Gracias,

Rebeca de Jesús
Assistant Professor, Department of Environmental Sciences
Louisiana State University
College of Coast and the Environment
93 South Quad Drive
Baton Rouge, LA 70803

From: Villanueva-Cubero, Luis <luis.villanueva-cubero@fema.dhs.gov>
Sent: Monday, March 30, 2020 11:13 AM
To: Rebeca De Jesus Crespo <rdejesuscrespo1@lsu.edu>
Cc: Edgardo Gonzalez <edgonz581@gmail.com>; Edgardo Gonzalez <edgardo@ccpaisaje.org>
Subject: Estudio Cuenca Hidrográfica del Río Grande de Añasco

Saludos, Rebeca:

Me acuerdo que en el simposio de cuencas hidrográficas, hiciste una presentación donde se correlacionaba la calidad del agua con enfermedades gastrointestinales en la Cuenca Hidrográfica del Rio Grande de Añasco después del Huracán María, y me pregunto si podrías compartir la información con Edgardo González (cc).

Lo que estamos buscando, para la Iniciativa de Cuencas del Oeste de PR es cualquier documento y/o estudio que establezca esta cuenca como prioritaria en la necesidad de reducir riesgos y aumentar su resiliencia. Cualquier cosa, ya sea del análisis que se hizo del grupo de GIS o también de estudios o documentos de agencias federales, y estatales que tengan que ver con esa cuenca.

Cordialmente,

LUIS VILLANUEVA-CUBERO
NDRS – Community Planning Lead
Community Planning & Capacity Building
DR-4339-PR, Branch I (Aguadilla)
202-568-3542 iPhone
luis.villanueva-cubero@fema.dhs.gov

FEMA

The mission of the Community Planning and Capacity Building Recovery Support Function (CPCB RSF) is to enable local governments to effectively and efficiently carry out community-based recovery planning and management in a post-disaster environment. The CPCB RSF also supports state or territorial governments in developing programs of support for local recovery planning and management.

Graduate Student Symposium

January 31– February 1, 2020

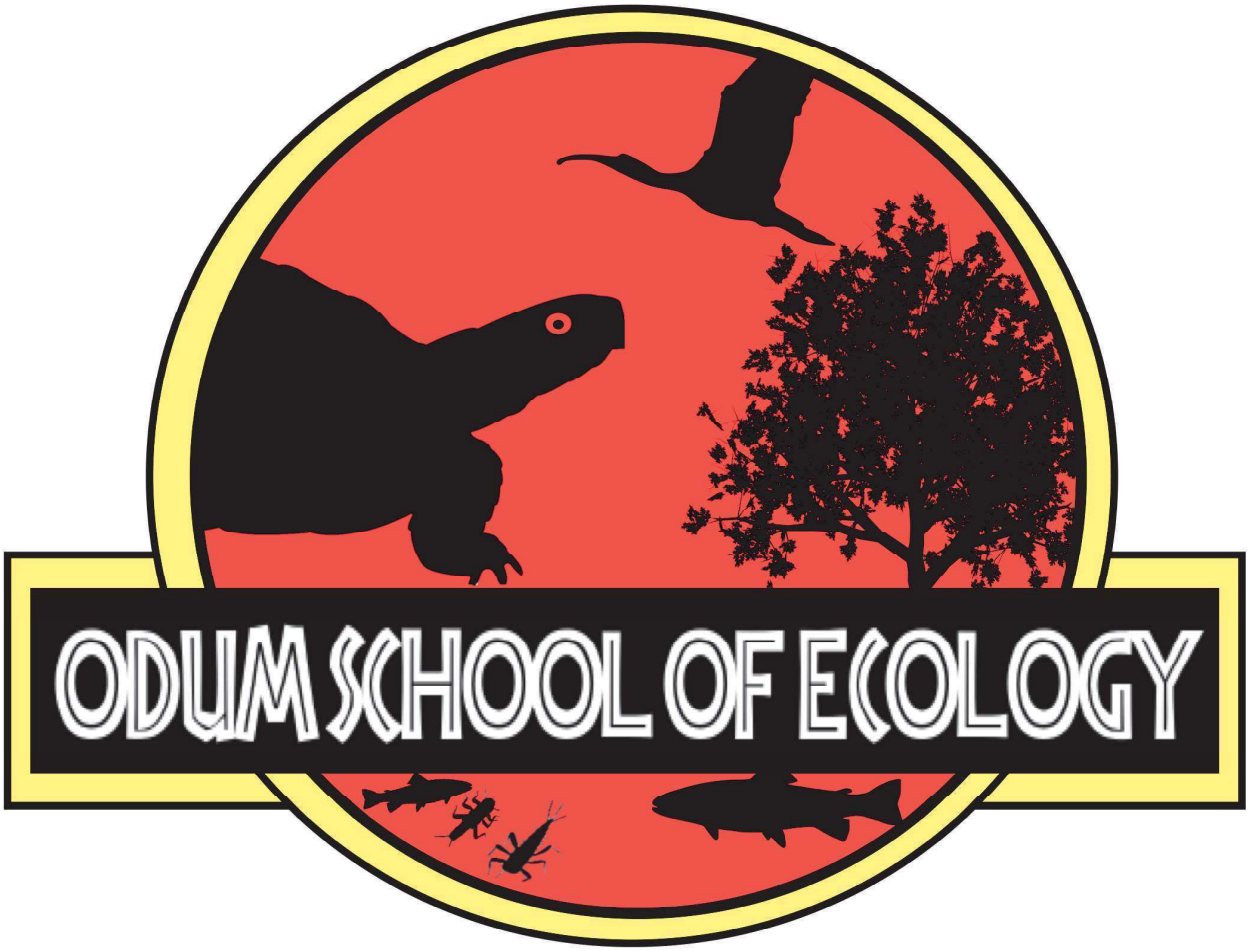

Graduate Student Symposium 2020
An Adventure 26 Years In The Making

Keynote Speaker

Rebeca de Jesús Crespo

Assistant Professor, Louisiana State University

Baton Rouge, Louisiana

Zooming out and in: applying geo-spatial technology and stakeholder engagement to study eco-health linkages in coastal communities

A common theme through my career has been the use of geo-spatial technologies to describe trends at the landscape level (zooming out) and engaging with stakeholders (zooming in) to help define research priorities and the practical implications of research findings. I have applied these approaches for the study of watershed management to improve stream integrity, and more recently, to study the linkages between ecosystem services with human health and well being. This seminar will describe projects developed for the US Environmental Protection Agency's Sustainable and Healthy communities program to better understand eco-health linkages. These projects characterized ecosystem service indicators at the landscape level in association to health outcomes identified as important by coastal communities in Puerto Rico, including gastrointestinal infections due to flooding, and mosquito borne diseases. Through ongoing projects on these topics, my work seeks to provide strategies at the community level to improve coastal resilience to environmental hazards, and manage ecosystem services for human health benefits.

Supplementary Material 2. Huc-10 Rain Retention by Zip Code

1. A rain retention raster (100m pixels) was developed for the entire area of Puerto Rico, using land cover (CCAP 2010), and soil layers (SSURGO), and applying the EPA H20 method (Russell et al 2015).
2. Rain retention was summarized at the zip code and Huc-10 watershed levels using the zonal statistics as table tool. Total rain retention was standardized by zip code or watershed area, resulting in mm/ha per unit.
3. Because the response variables are at the zip code level, we had to allocate upstream, rain retention (Huc-10) values to each zip code. We estimated the mm/ha of rain retained upstream by weighting the relative influence of each intersecting watershed. We followed the following steps:
    a. We created a point file through the entire Island at 1km intervals.
    b. We spatial joined each of these points to the zip code it intersects, and gave each point a label based on this zip code.
    c. We spatial joined this zip code-point layer to the Huc-10 watershed rain retention layer. This resulted on each point having a Huc-10 mm/ha value and a zip code label.
    d. With the Summarize function, we calculated the average Huc-10 rain retention per zip code. The relative importance of each watershed on rain retention upstream of the zip code is captured by the number of points that fall within each watershed, and that are then factored in the average.

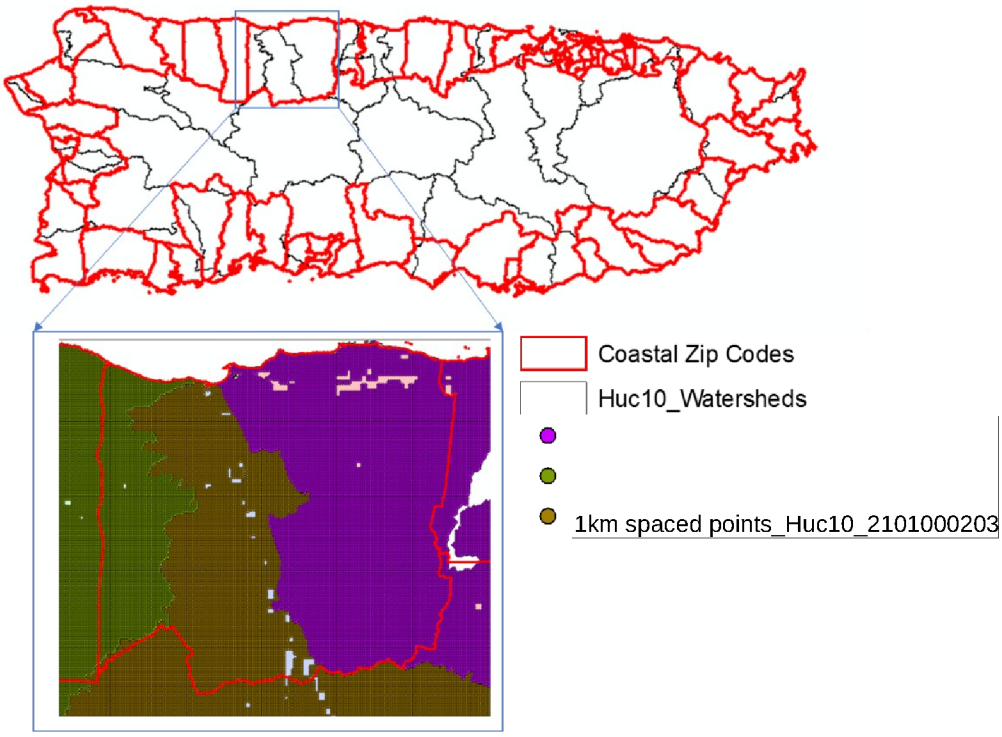

ZIP_CODE	NAME	Population	FEMAClaims_1999-2014	Zip99Rain	Zip95Rain	Zip90Rain	N99
602	Aguada	41520	8	35.24146	22.35	16.62022	59
603	Aguadilla	54689	5	35.96042	20.62656	14.10521	59
610	Anasco	29016	4	35.79467	22.9551	17.46075	59
612	Arecibo	67010	167	43.93883	24.07813	16.96212	59
617	Barceloneta	24597	76	43.70348	23.24638	22.94203	59
623	Cabo Rojo	43061	99	35.997	19.25123	11.45599	59
624	Penuelas	26241	8	45.93674	21.25795	14.81818	59
627	Camuy	35159	3	41.63758	24.00859	16.92266	59
646	Dorado	38199	80	41.88349	22.82698	15.14444	59
647	Ensenada	6172	0	39.49793	17.07069	10	59
653	Guanica	13307	75	40.2044	17.265	10.42	59
656	Guayanilla	21481	70	42.64798	18.49832	12.52941	59
659	Hatillo	41953	7	44.8933	25.1308	17.57321	59
660	Hormigueros	17250	67	38.48788	22.30606	15.12121	59
662	Isabela	43282	3	39.28619	21.45219	15.34125	59
667	Lajas	25968	17	36.9446	17.8819	11.06552	59
674	Manati	44457	10	43.44727	22.91484	14.98438	59
677	Rincon	15272	19	42.0561	23.41463	17.95366	59
678	Quebradillas	27819	5	41.4681	23.39683	16.32063	59
680	Mayaguez	58140	34	39.9322	24.20568	17.51667	59
682	Mayaguez	32615	8	40.71229	23.20143	16.11429	59
690	San Antonio	6255	0	38.675	20.50833	13.16667	59
692	Vega Alta	37511	19	42.91415	23.77195	15.64756	59
693	Vega Baja	61038	186	42.95128	22.99436	15.13534	59
698	Yauco	41782	28	39.33586	21.6337	15.42932	59
704	Aguirre	8577	104	51.948	17.6	9.866667	59
707	Maunabo	12225	32	54.88667	23.60083	15.7	59
714	Arroyo	19566	110	52.93488	21.11977	12.74651	59
715	Mercedita	3656	4	46.15022	18.20222	10.33778	59
716	Ponce	33779	27	47.41385	18.85192	10.69615	59
717	Ponce	18457	31	47.6	19.01	11.2	58
718	Naguabo	26606	67	52.35007	25.74049	17.80915	59
723	Patillas	19277	33	53.44879	22.7303	14.22652	59
728	Ponce	44908	15	46.3925	19.93636	12.41136	59
730	Ponce	35742	14	44.9675	19.21458	11.95833	59
735	Ceiba	13730	19	55.17947	25.90789	17.80421	59
738	Fajardo	34922	81	52.46949	25.63367	17.74694	59
741	Punta Santiago	4971	43	48.00122	24.15769	16.08462	59
745	Rio Grande	55062	45	48.00122	25.63415	17.99634	59
751	Salinas	23129	413	49.28455	17.29398	10.16911	59
757	Santa Isabel	23263	407	47.08	16.68775	9.152941	59
767	Yabucoa	38019	136	53.29632	23.22645	15.64	59
772	Loiza	23105	120	45.8544	22.00267	15.65333	59
773	Luquillo	20068	18	51.25729	26.08857	17.98857	59
784	Guayama	44637	73	53.92905	20.35079	11.83757	59
791	Humacao	53417	172	53.10068	23.71271	15.98305	59
795	Juana Diaz	43736	89	46.38923	19.19699	12.42131	59
907	San Juan	17458	21	42.95667	22.56111	15	59
909	San Juan	6230	2	43.61	23	15	59

911	San Juan	8623	26	45	22	15	51
912	San Juan	6801	0	43.61	23	15	59
913	San Juan	9312	8	44	22	15	55
915	San Juan	32820	49	43	22	15	55
917	San Juan	21053	37	43.25	21.75	15	56
918	San Juan	18056	25	42.70125	21.87	15	59
920	San Juan	17893	333	42.04067	22.2	14.86	59
921	San Juan	37763	35	43.42857	22	15	58
923	San Juan	29086	52	43.60167	21.5	14.83	59
924	San Juan	56691	14	43.41312	21.44375	14.9375	59
925	San Juan	8696	22	43	22	15	55
927	San Juan	14936	81	43.74571	21.85714	15.14286	59
934	Fort Buchanan	288	0	41.9025	22	15	59
949	Toa Baja	82278	207	40.84143	22.13182	14.74156	59
952	Sabana Seca	10008	2	41	22	15	56
961	Bayamon	32429	1	41.64864	21.95682	14.91364	59
962	Catano	22491	54	42	22.05833	14.61111	58
965	Guaynabo	9134	17	42	22.5	15	57
966	Guaynabo	16676	11	42.125	22	15	58
968	Guaynabo	3478	6	42	22	15	54
979	Carolina	17030	124	44.20125	21.4375	14.9375	59
982	Carolina	16428	24	44.122	21.01	14.8	59
983	Carolina	39234	18	44	21.1	14.8	58
985	Carolina	36553	129	44.21034	21.17586	14.96897	59

N95	N90	ZipRainYr	ZipRainMnth	Huc10_99Rain	Huc10_95Rain	Huc10_90Rain	Huc10RainYr
292	584	1727	146.7	32.164658	20.6005993	15.9303999	1826.044327
292	584	1567	132.5	36.929533	21.3327999	15.6148005	1858.308057
292	584	1849	156.7	37.545378	22.9153004	17.3152008	2000.140146
292	584	1957	165.6	42.929021	23.3146992	16.3871994	1985.209108
291	584	1730	146.4	44.856223	23.4848003	16.4682007	1949.416046
292	584	1213	104.2	37.133833	19.4629002	12.6886997	1260.330298
292	583	1680	143	41.620605	19.4946995	13.6828003	1535.525364
292	584	1873	158.3	38.211811	21.5300007	15.5299997	1867
292	584	1734	146.7	41.616641	21.8976994	14.7546997	1860.62659
292	579	992.1	85.04	36.534679	17.3999996	10.79	1078
292	583	1038	88.56	36.863509	17.5268002	10.9729996	1106.626812
292	583	1369	117	41.35107	19.2584991	13.4715996	1497.486418
292	583	1966	166.4	38.227041	21.5396004	15.5358	1868.135856
292	583	1401	119.1	37.885262	22.0499992	15.0699997	1489
292	584	1732	146	38.202452	21.5286007	15.5305996	1866.936559
292	584	1074	92.24	36.53791	17.4111004	10.8002005	1078.983123
292	583	1729	146.2	44.103267	23.7705002	16.4522991	1963.242847
292	584	1733	147.2	35.498209	22.0345993	16.7882996	1933.902989
291	584	1796	151.6	38.211811	21.5300007	15.5299997	1867
292	584	1757	149.5	38.940473	23.3405991	16.8628006	1764.282794
292	582	1549	131.6	38.791072	23.2479	16.8087006	1768.068571
292	582	1422	119.9	38.211811	21.5300007	15.5299997	1867
292	584	1808	152.6	42.110209	23.4099998	15.5292997	1822.511348
292	582	1727	145.9	42.12978	23.4699993	15.5600004	1821
292	583	1588	135.4	40.070456	19.1907005	13.2526999	1454.898623
291	582	1288	109	46.291599	17.3999996	10.4099998	1385
292	583	2097	176.6	52.43741	23.3255005	15.7339001	2219.961253
292	584	1666	140.6	54.25396	21.4699993	13.1899996	1790
292	584	1164	98.73	42.315781	20.0300007	13.3699999	1552
292	584	1190	101.1	42.269107	19.9871006	13.3837004	1549.759336
292	576	1193	101.4	42.315781	20.0300007	13.3699999	1552
292	584	2644	223.2	52.386557	25.2964001	17.5639992	2543.433592
292	584	1944	164.1	54.247116	21.4722996	13.1938	1790.69061
292	584	1328	113.1	42.100682	19.8320999	13.4330997	1541.673736
292	582	1313	111.5	42.315781	20.0300007	13.3699999	1552
292	584	2554	215.3	52.51466	25.3999996	17.6499996	2554
292	584	2481	209.6	51.422759	25.3698006	17.6574993	2549.220109
292	584	2323	195.8	52.51466	25.3999996	17.6499996	2554
291	584	2634	222.7	48.177143	25.1837006	17.5963001	2525.376792
292	584	1343	113.7	46.291599	17.3999996	10.4099998	1385
292	584	1118	94.65	45.681262	17.8036995	10.8643999	1410.636583
292	584	2215	186.6	52.432006	23.3285999	15.7384996	2220.805346
292	582	2069	175.1	46.288931	23.5627995	16.3062	2288.179206
292	584	2548	215.5	48.180317	25.2801991	17.6800003	2535.026035
292	584	1613	136.4	48.531109	19.6392002	12.1929998	1632.526465
292	583	2326	196.1	52.45916	24.1322002	16.4806995	2350.332421
292	584	1384	117.2	42.31645	20.0307999	13.3708	1552.112488
292	581	1858	157.6	42.58577	21.5400009	14.7799997	1939
266	564	1892	160.4	42.58577	21.5400009	14.7799997	1939

291	559	1860	157.9	42.58577	21.5400009	14.7799997	1939
266	564	1892	160.4	42.58577	21.5400009	14.7799997	1939
285	559	1858	157.6	42.58577	21.5400009	14.7799997	1939
283	555	1881	159.5	42.58577	21.5400009	14.7799997	1939
288	567	1889	160.1	42.58577	21.5400009	14.7799997	1939
287	577	1887	160	42.58577	21.5400009	14.7799997	1939
291	583	1893	160.5	42.58577	21.5400009	14.7799997	1939
290	583	1941	164.5	42.58577	21.5400009	14.7799997	1939
290	583	1905	161.4	42.58577	21.5400009	14.7799997	1939
292	578	1951	165.3	42.58577	21.5400009	14.7799997	1939
274	551	1924	163.1	42.58577	21.5400009	14.7799997	1939
288	579	1943	164.7	42.58577	21.5400009	14.7799997	1939
290	567	1898	160.9	42.58577	21.5400009	14.7799997	1939
292	584	1778	150.7	41.458943	21.0629005	14.3507004	1891.679844
287	560	1825	154.7	41.815402	21.2035007	14.4877996	1917.425352
292	584	1870	158.6	42.919816	21.6494007	14.9112997	1986.398876
291	581	1834	155.6	42.54118	21.5177994	14.7634001	1940.604895
288	562	1864	158.1	42.58577	21.5400009	14.7799997	1939
292	583	1935	164	42.658918	21.5639992	14.8086996	1949.379242
287	552	1891	160.3	42.58577	21.5400009	14.7799997	1939
288	579	1887	159.9	42.58577	21.5400009	14.7799997	1939
292	583	1915	162.3	42.58577	21.5400009	14.7799997	1939
290	581	1936	164	42.58577	21.5400009	14.7799997	1939
292	584	2000	169.3	44.586618	21.6501999	14.7516003	2028.967006

Huc10RainMnth	FloodPerc	SwgDen	ppl_FldPer	MedIncome	Per5PlsHou	ZipSlopeAvg
154.9173	20.3379	0.001033	24.9221	15106	0.0253428	9.6746721
156.9473	5.09422	0.002356	4.78549	15079	0.129103	5.043035
169.4569	23.0471	0.000737	30.5791	16923	0.0424478	13.8979435
168.478	17.3429	0.000838	19.5438	18111	0.0676923	9.3255844
163.81	25.3434	0.001272	23.8963	15114	0.0408227	5.6310949
104.4952	23.8955	0.000728	22.2113	16447	0.0847627	5.6585693
136.1563	8.252	0.000198	11.6065	15500	0.0167235	22.1327953
157.9	1.04564	0.000391	2.15113	17762	0.0244549	8.9469833
157.5423	38.7587	0.001785	32.9884	28530	0.0566767	5.2260327
91.0104	18.0914	0.000727	17.5977	14533	0.0284491	7.6681976
94.3215	25.0495	0.000451	32.7965	13292	0.0620595	8.5087957
126.3706	14.2633	0.000302	20.1013	14669	0.0198335	17.4253883
158.2073	1.97947	0.000505	3.3149	18669	0.0412378	7.9398556
126.9	46.0964	0.001662	43.6587	20428	0.041791	5.091948
157.8427	1.45789	0.000562	1.69538	14735	0.0384999	8.3872509
91.3986	25.5904	0.000234	16.9764	13843	0.0435406	5.8964353
166.0511	19.5027	0.000898	16.0071	17560	0.0896442	7.1704412
163.8833	1.78387	0.000687	1.43022	16590	0.135587	10.5831041
157.9	2.71834	0.000337	0.57491	13975	0.0713098	9.9975672
152.0488	11.988	0.00087	18.1121	14877	0.20263	14.3892956
147.2937	42.4001	0.004074	39.8437	15312	0.243677	4.7023363
157.9	8.40735	0.002289	8.76023	17208	0.0691469	3.7035067
153.0249	13.7872	0.000964	16.0879	18145	0.0768316	9.0273447
153.7	26.7648	0.000907	28.4288	16230	0.0359709	5.9505038
126.3392	4.54984	0.000547	8.57792	14810	0.0433573	22.8108311
117.3	17.4091	0.002161	15.4252	13327	0	3.3929234
186.9137	9.86155	0.000446	13.0879	16043	0.0374577	19.7772388
151.1	14.8547	0.001749	13.6117	16114	0.0440847	15.7005539
129.94	70.6233	0.00035	53.2083	15029	0.0323326	1.1961983
131.3088	42.7338	0.003688	41.0055	18845	0.241361	2.7970936
131.4	70.7555	0.009432	69.8925	14178	0.339155	0.6587558
214.0928	20.5231	0.000456	24.8642	16655	0.0532958	15.1943903
151.4379	7.53623	0.000199	12.3649	14777	0.0091533	22.2275372
130.7928	11.7469	0.001746	17.2441	18849	0.0627359	12.9336786
131.4	16.5193	0.004835	20.4524	16595	0.105206	8.7279911
205.9222	23.6007	0.000477	21.2239	20543	0.13531	12.3636742
204.7349	18.0377	0.001388	14.7323	21779	0.177731	11.8446236
202.3061	98.1768	0.002705	96.4267	17192	0.0293296	0.500012
211.028	18.6445	0.0006	22.8903	22931	0.110002	14.615098
114.8814	16.551	0.000412	24.9526	13323	0.0396776	12.9220428
118.6821	23.7615	0.000951	23.2031	18024	0.0479812	4.0729589
184.1537	19.35	0.000399	24.4816	17965	0.0188301	11.1668291
190.3014	91.9721	0.001348	86.2481	16151	0.111917	0.6327919
214.4054	14.5743	0.000571	22.6569	20084	0.219629	15.1708832
140.5491	12.9267	0.001088	15.3755	17680	0.0586085	15.0897655
193.6235	22.7156	0.001676	22.8991	20336	0.133853	9.2738724
131.4497	20.8275	0.00092	22.4955	17006	0.0235334	13.0731926
164.3	10.2722	0.016345	6.14004	32025	0.782895	1.2981566
164.3	2.22355	0.020931	0.68303	14912	0.634649	2.84886

146.0444	33.2139	0.020339	30.3824	28578	0.52971	1.0883653
164.3	5.83095	0.023075	3.26061	18934	0.351633	3.7857788
164.3	71.0158	0.018344	73.6872	7892	0.78415	0.6185822
164.3	50.5745	0.014719	46.2268	12926	0.207963	1.6758195
164.3	24.4991	0.01489	25.8232	17017	0.418475	1.0865688
164.3	66.1291	0.010655	65.3448	28710	0.608333	0.8132923
157.1565	51.8507	0.008078	51.7704	25191	0.132992	1.7419399
164.3	18.2758	0.015151	18.9415	19079	0.28323	3.1278498
164.3	57.8533	0.013179	53.2403	16164	0.401298	1.3966867
164.3	7.36384	0.012231	3.12304	19720	0.38068	3.7797222
164.3	0.95848	0.014824	1.51149	14209	0.562034	2.574697
164.3	15.4979	0.011068	15.5381	34633	0.401155	2.7348506
164.3	0	0.001592	0	64398	0	4.6555114
159.811	64.8273	0.003193	55.6188	25173	0.0674991	3.2099855
162.7098	9.55474	0.011163	11.7095	17856	0.0096008	3.256377
168.2644	32.6693	0.006654	32.3698	30952	0.214914	4.2990642
159.3215	86.7554	0.006166	89.6336	15565	0.213568	0.4152234
158.6345	38.79	0.003833	48.3003	14874	0.0979269	0.5027035
164.9601	3.22677	0.010754	1.88748	52813	0.450308	3.8745017
164.3	15.7584	0.005852	16.0642	40000	0.753704	5.8749399
159.7361	52.8252	0.00435	38.716	39747	0.714133	0.4017728
164.3	8.12336	0.00862	4.85415	25489	0.10318	0.8028896
164.3	66.2617	0.010896	61.8275	27121	0.176499	0.7562062
173.5782	93.6433	0.002959	95.4446	26653	0.108324	1.3988518

ZipMaxSlope	Ave_HucSlope	MaxHucSlpe	mmhaHuc10_2010	mmhaZip_2010	PercVegetation
44.6209717	10.2442	49.6834984	114.7929993	110.5530014	67.032
38.4337921	8.935	76.2769012	133.0090027	118.2249985	68.8365
63.9462662	18.8068	80.9162979	61.6273994	75.7585983	79.2965
110.9426956	12.6358	82.9504013	110.814003	135.4170074	71.6439
37.2575493	12.4998	74.7767029	103.5339966	115.2689972	69.1234
53.4614334	10.8378	69.0445023	75.6289978	81.6272964	65.5146
97.478363	20.9629	98.1460037	65.7303009	53.8081017	78.8538
67.9176865	8.5834	83.4335022	137.9060059	129.7250061	69.3229
41.4366989	13.6964	82.0177994	104.8079987	127.973999	65.06
49.7726097	8.0227	63.6968002	87.2721024	85.4774017	59.7554
51.0667458	8.8735	65.9047012	85.8072968	68.325798	61.0179
79.2464523	20.4846	96.0378036	65.8220978	107.9240036	78.2482
66.0371552	8.6245	83.5231018	137.7550049	165.1499939	69.3522
43.0130806	14.3683	75.7514038	61.0267982	48.6786995	72.7376
77.2352295	8.586	83.3813019	137.8699951	145.0189972	69.3193
48.3321838	8.0378	63.7256012	87.2092972	72.6649017	59.7864
57.9061737	14.6028	81.2024002	113.8000031	170.9340057	68.6104
47.4489861	15.5491	69.0334015	81.8548965	143.5469971	74.6303
83.4335403	8.5834	83.4335022	137.9060059	170.9349976	69.3229
56.2930374	16.3476	70.5044022	57.5172997	59.8888016	77.2811
27.7899494	16.4361	71.5457993	57.948101	67.5101013	77.2141
24.9562111	8.5834	83.4335022	137.9060059	153.3820038	69.3229
68.4847183	8.885	69.2734985	152.2660065	178.0110016	65.6884
50.3897324	8.6943	68.7682037	154.147995	152.5590057	65.7133
95.9630432	17.8454	88.3001022	69.7330017	63.5654984	74.6264
30.5951385	14.8132	79.6006012	66.7297974	103.8290024	60.7134
65.95121	12.1396	78.4030991	63.1553993	72.2562027	60.4297
64.5779572	19.6615	78.422699	92.5402985	61.2186012	70.6362
21.2867336	17.8922	109.3929977	71.0681992	91.1852036	71.4227
31.619812	18.0881	108.651001	70.6819	58.6576004	71.8988
2.5310571	17.8922	109.3929977	71.0681992	34.7736015	71.4227
95.7870331	12.9957	95.2994003	69.8411026	60.485199	55.3742
78.4227295	19.6496	78.4250031	92.490799	93.5895004	70.6208
54.1352463	18.7952	105.9749985	69.2878036	38.0365982	73.617
50.8828316	17.8922	109.3929977	71.0681992	44.901001	71.4227
79.05793	12.9687	95.7870026	70.0266037	67.8160019	55.0855
68.3945389	12.9515	92.0550003	72.7559967	112.163002	55.9589
17.4973221	12.9687	95.7870026	70.0266037	50.8633995	55.0855
80.9523392	12.9285	80.9138031	80.3823013	60.7490997	58.7347
79.1363525	14.8132	79.6006012	66.7297974	77.1523972	60.7134
60.881546	15.2859	84.1740036	67.3957977	70.5552979	62.3574
78.4030075	12.1254	78.4033966	63.0970001	62.9217987	60.4112
21.3490334	9.6577	67.1458969	72.5932999	89.6968994	48.7985
65.0864792	12.9006	80.972702	80.8612976	100.439003	58.5528
71.7748184	17.019	80.9007034	78.6737976	100.4950027	65.3139
45.5590286	12.453	85.1579971	65.7818985	58.1585999	58.3443
86.3910065	17.8931	109.3909988	71.069397	82.6187973	71.4227
5.648562	2.926	40.7527008	63.1856003	52.3708	27.23
6.1871843	2.926	40.7527008	63.1856003	65.2357025	27.23

4.0812068	2.926	40.7527008	63.1856003	97.2873001	27.23
7.1589108	2.926	40.7527008	63.1856003	61.0276985	27.23
1.3806701	2.926	40.7527008	63.1856003	114.7639999	27.23
7.9941382	2.926	40.7527008	63.1856003	46.2865982	27.23
3.7291086	2.926	40.7527008	63.1856003	60.5013008	27.23
3.5355339	2.926	40.7527008	63.1856003	54.7573013	27.23
25.3753071	2.926	40.7527008	63.1856003	54.2794991	27.23
9.4091043	2.926	40.7527008	63.1856003	64.1268005	27.23
5.2737556	2.926	40.7527008	63.1856003	63.4660988	27.23
24.4961739	2.926	40.7527008	63.1856003	74.433403	27.23
6.9574599	2.926	40.7527008	63.1856003	74.1580963	27.23
8.8969803	2.926	40.7527008	63.1856003	93.7003021	27.23
22.2941971	2.926	40.7527008	63.1856003	121.3529968	27.23
34.2550163	15.9724	87.7335968	76.0475998	82.4113007	63.6921
19.1450062	15.2143	85.7231979	74.0580978	93.5610962	63.4063
39.7668991	9.4911	66.6221008	65.8115997	84.8873978	51.2541
2.1578345	4.5294	46.7588005	64.3655014	57.0850983	32.3026
2.5739076	2.926	40.7527008	63.1856003	37.1162987	27.23
13.7044697	4.3636	46.4174995	63.760601	80.4097977	32.4907
30.044239	2.926	40.7527008	63.1856003	61.3320007	27.23
1.5103807	2.926	40.7527008	63.1856003	44.7985992	27.23
3.4865813	2.926	40.7527008	63.1856003	74.0655975	27.23
4.7565746	2.926	40.7527008	63.1856003	60.0517998	27.23
20.8865986	6.8272	54.4863014	63.2750015	38.3261986	40.6311

PercWoodyWet	PercGrassWet	KarstPerc
0.25525	1.26723	6.5696
0.47373	0	92.9997
0.00456	1.78884	0
0.48372	5.05096	77.1474
0.47323	15.4239	71.2315
3.49896	3.13481	8.96181
0.22061	0	25.1828
0.12595	0.43481	98.5864
1.00106	6.43964	42.3685
0.25558	1.5134	36.1145
0.99647	0.55764	38.1451
1.15304	1.37757	35.8035
0.13669	0.40924	96.0113
0.01839	0.09502	21.3478
0.12231	0.06178	96.1277
1.45691	0.89519	8.58973
0.44295	3.16567	73.7997
0.04666	0.46659	9.57761
0	0	96.7155
0.35391	1.13083	2.08473
5.85485	9.2162	0
0.97001	0	83.8026
0.28912	1.79002	78.4785
2.50266	6.5199	59.409
0.01314	0	8.8161
5.9343	0.20953	0
0.23614	0.53998	0
1.72256	4.91033	0
3.49061	13.5955	0.87426
4.14241	0.25117	11.6292
0	0	0
3.8081	4.05203	0
0.49098	0.00221	0
0.65948	0.06595	65.5947
0	0	20.2114
11.7774	1.75162	0
3.47076	0.85644	0
24.7228	20.2484	0
4.23988	6.66284	0
3.38444	0.98684	2.03722
2.83634	1.06172	5.45225
0.43901	1.21373	0
27.9366	23.8367	1.89471
1.18518	3.91648	0
2.05047	0.16654	0
0.92542	3.03093	0
0.5542	0.90969	7.0132
0	0	1.25054
0	0	0

0	0	0
0	0	0
0	0	0
1.56092	0	5.33715
0.63835	0.0532	1.49777
6.01539	0.29189	0
6.55495	5.32089	2.18788
0	0	0
0.51998	0.26787	0
0.79886	0.03687	1.71406
0	0	1.079
0.22246	0	0
0.71528	0	28.0189
3.18365	9.93699	19.5323
0.07442	0	24.5675
0.49737	5.21504	17.2017
3.68986	19.7595	0
6.41246	8.69486	0
0	0	4.29808
0.31845	0	16.2024
10.762	0.11758	0
2.67055	14.9752	0
8.52669	0	0
7.54361	21.0346	6.23116

	Definitions
Population	dasymetric population estimate
FEMAClaims_1999-2014	FEMA claims from 1999-2014
Zip99Rain	99% rainfall event magnitude at the zip code level
Zip95Rain	95% rainfall event magnitude at the zip code level
Zip90Rain	90% rainfall event magnitude at the zip code level
N99	Number of 99% events per zip code (1999-2014)
N95	Number of 95% events per zip code (1999-2014)
N90	Number of 90% events per zip code (1999-2014)
ZipRainYr	Average Annual Rainfall at the Zip Code Level
ZipRainMnth	Average Monthly Rainfall at the Zip Code Level
Huc10_99Rain	99% rainfall event magnitude at the Huc-10 watershed level
Huc10_95Rain	95% rainfall event magnitude at the Huc-10 watershedlevel
Huc10_90Rain	90% rainfall event magnitude at the Huc-10 watershed level
Huc10RainYr	Average Annual Rainfall at the Huc-10 Watershed Level
Huc10RainMnth	Average Monthly Rainfall at the Huc-10 Watershed Level
FloodPerc	Percentage of flood area
SwgPerc	Sewage density (sewage m /zip code m2)
ppl_FldPer	Percentage of people living in flood areas
MedIncome	Median Income
Per5PlsHou	Percentage of housing units with more than 5 households
ZipSlopeAvg	Average slope at the zip code level
ZipMaxSlope	Maximum slope at the zip code level
Ave_HucSlope	Average slope at the Huc-10 level
MaxHucSlpe	Maximum slope at the Huc-10 level
mmhaHuc10_2010	Rain retained at the Huc 10 level in mm
mmhaZip_2010	Rain retained at the zip code level in mm
PercVegetation	Percentage of vegetation at the Huc-10 level
PercWoodyWet	Percentage of woody wetlands at the zip code level
PercGrassWet	Percentage of grassy wetlands at the zip code level
KarstPerc	Percentage of karst at the zip code level ((karst area/zip code area)
Zip Code Area	Area in square kilometers

Average	Max	Min	Sdev
27754.67123	82278	288	17150.552429599
59.57534247	413	0	83.7691798615
44.28619753	55.17947	35.24146	4.7414817992
21.81780459	26.08857	16.68775	2.1728602677
14.72225093	22.94203	9.152941	2.3727155322
58.47945205	59	51	1.4152894192
290.1917808	292	266	4.9008432785
579.4109589	584	551	8.6551776675
1776.069863	2644	992.1	368.3343486732
150.4619178	223.2	85.04	30.8833248632
43.04269618	54.25396	32.16466	4.6992752515
21.54965228	25.3999996	17.4	1.9291671855
14.75543409	17.6800003	10.41	1.7568614295
1861.888563	2554	1078	327.7717373428
156.4470603	214.4054	91.0104	26.3863883347
27.112937	98.176804	0	24.556653
0.004833019	0.0230754	0.000198	0.0060079887
27.088891	96.426697	0	23.404106
20102.80822	64398	7892	8964.2949212379
18.015933	78.415001	0	20.655789
7.070422116	22.8108311	0.401773	5.9263115702
41.7512775	110.9426956	1.38067	29.8365390341
10.38944384	20.9629	2.926	5.853235409
69.87399385	109.3929977	40.7527	22.238878517
79.48011655	154.147995	57.5173	25.3612798541
85.01759051	178.0110016	34.7736	35.616401391
54.30170274	79.2965	27.23	18.8781023582
0.02546056	0.279366	0	0.0479895212
0.032152378	0.238367	0	0.0562852045
20.028844	98.586403	0	30.683324
61.842983	328.026001	0.905253	65.282064

An official website of the United States government.

Close

We've made some changes to EPA.gov. If the information you are looking for is not here, you may be able to find it on the EPA Web Archive or the January 19, 2017 Web Snapshot.

Are Greenspaces Good for Your Heart?

Published February 26, 2018

Sudden unexpected death (SUD), more commonly known as sudden cardiac death, is one of the leading causes of mortality in the United States, estimated to claim as many as 450,000 lives per year. People at risk for SUD can include those with conditions such as heart disease, hypertension, and diabetes. That is why identifying preventive measures is a major priority for local public health officials, and of EPA researchers working in partnership to support their work.

One promising area currently under investigation is exploring the links between a healthy environment and a healthy heart. Agency and other research has already made a strong scientific case for how reducing exposure to particulate matter and other forms of air pollution can reduce the risk of cardiac events, especially for those already suffering from the impacts of cardiovascular disease.

Now, they are turning their attention to another promising area: the link between greenspaces, such as neighborhood forests, and healthier communities. Agency researchers have recently published the results of two such studies.

In *Exploring links between greenspace and sudden expected death: A spatial analysis* (Wu, et al., 2018), they and their partners combined an examination of 396 SUDs recorded in Wake County, NC, between March 2013 and February 2015 with spatial analysis of multiple greenspace metrics (percent forest, grassland, average and near-road tree canopy, and diversity of tree canopy). "To our knowledge, this is the first study to examine the spatial patterns of SUD cases and explore potential associations between SUD incidence and greenspace," the authors report. Results showed increased levels of SUD in areas with lower percentages of forest.

The study concludes: "…we found that SUD incidence was inversely associated with greenway density and percent forest after controlling for confounding factors such as household income, population density and race."

The implication is clear: neighborhood forests may be good for our hearts. Illuminating the causes of why this might be the case is the subject of another recent EPA study: *Eco-Health linkages: assessing the role of ecosystem goods and services on human health using causal criteria analysis* (de Jesus Crespo, et al. 2018). In that study, Agency researchers used a software tool called "Eco-Evidence" to comb through some 16 years of published, peer-reviewed scientific research to find evidence of causal links between greenspaces and human health benefits.

Using a framework previously used more widely for epidemiological studies, the researchers applied a numerical approach that combines individual studies in a way that allows for more broad conclusions. "The premise is that isolated studies may not offer a strong case for causality, but they may do so if considered collectively," they state in their paper. "This approach allowed us to fully characterize the cause-effect model and identify the greatest data gaps and strongest support."

Using this novel approach for an eco-health study, they assessed 2,756 papers to hone in on those that offered causal relationships between greenspace and human health. They were then able to focus in on 212 papers for conducting a "causal criteria analysis," examining evidence of the links between healthy ecosystems and four categories important to public health: gastrointestinal disease, respiratory illness, heat morbidity, and cardiovascular disease.

The researchers found consistent evidence of links between the beneficial effects of natural ecosystems, namely the ability of "ecosystems goods and services" to buffer potential and known health impacts in those four health areas, "and between greenspaces and certain health outcomes such as cardiovascular disease and heat morbidities."

Both papers are adding to an emerging body of scientific research, much of it led by EPA scientists, showing direct links between the natural environments and human health. What they are learning is helping local communities better capture those benefits as it become increasingly clear that greenspaces can be good for the heart.

Sources and References Cited

Wu, J., Rappazzo, K. M., Simpson, R. J., Joodi, G., Pursell, I. W., Mounsey, J. P., ... & Jackson, L. E. (2018). Exploring links between greenspace and sudden unexpected death: a spatial analysis. *Environment international*, 113, 114-121. https://doi.org/10.1016/j.envint.2018.01.021

de Jesus Crespo, R., & Fulford, R. (2018). Eco-Health linkages: assessing the role of ecosystem goods and services on human health using causal criteria analysis. *International journal of public health,* 1-12. http://rdcu.be/HQar

LAST UPDATED ON FEBRUARY 27, 2018

The National Academies of SCIENCES ENGINEERING MEDICINE

SHARE

Current and Past Early-Career Research Fellows

Our Early-Career Research Fellows take risks on research ideas not yet tested, pursue unique collaborations, and build a network of colleagues who share their interest in improving offshore energy system safety and the well-being of coastal communities and ecosystems.

2019

Trisha Atwood
Utah State University
Dr. Atwood is an assistant professor in the Department of Watershed Sciences and the Ecology Center at Utah State University. Dr. Atwood earned her Ph.D. in aquatic ecology and conservation at the University of British Columbia and her B.A. and M.S. in marine science at the University of Hawaii at Hilo. Her research investigates factors that affect carbon accumulation and retention in marine sediments, as well as the distribution of carbon stocks in marine habitats. Her approach to science—which merges community ecology, ecosystem ecology, biogeochemistry, and conservation ecology—allows her to investigate novel questions in aquatic sciences with both pure and applied outcomes.

Shanondora Billiot
University of Illinois
Dr. Billiot (United Houma Nation) is an assistant professor in the School of Social Work at the University of Illinois. Prior to assuming this role, she was a pre-doctoral Henry Roe Cloud Dissertation Writing Fellow at Yale University. She earned a Ph.D. in social work from Washington University in St. Louis. She holds a master's of social work from the University of Michigan and both B.A. and B.S. degrees from Louisiana State University. Her research explores the intersection of health, environment, and culture among Indigenous peoples and is informed by post-graduate practice experience in disaster recovery community development and national policy analysis. Her current research uses mixed methods to explore Indigenous-specific sensitivities to global

This site uses cookies. For more information on cookies visit:
http://nas.edu/legal/privacy/index.html

Traci Birch
Louisiana State University
Dr. Birch became an assistant professor in the School of Architecture at Louisiana State University after three years of experience as a research faculty member at the same institution. She is also the interim managing director of the LSU Coastal Sustainability Studio. Her doctoral research focused on the ability and effectiveness of local communities to implement ecosystem management. Her post-doctoral research focuses on developing planning frameworks for coupled coastal-inland community resilience and well-being in the face of accelerated climate change. She holds a Ph.D. in urban studies and environmental management and a master's in urban and regional planning, both from the University of New Orleans. Her B.A. in graphic design is from Baldwin-Wallace University.

Edward Camp
University of Florida
Dr. Camp is an assistant professor of fisheries and aquaculture governance at the University of Florida. He received his Ph.D. and M.S. degrees in fisheries and aquatic sciences from the University of Florida, where he used quantitative socioecological models to study management strategies designed to improve economic and ecological outcomes for recreational fisheries. Dr. Camp employs similar inter- and multi-disciplinary approaches in his current work, which includes evaluating oyster fishery and aquaculture management strategies, understanding the effects of artificial reefs on fish populations and fishing-based economies, and developing decision tools for stock enhancement of freshwater fisheries. These projects all seek to forward the science of managing fish resources by creating greater understanding of how humans and fish populations affect each other and how both will be affected by different management actions. This understanding can be applied to decisions about how fish are used and to increase the resilience of fish-human systems.

Andia Chaves Fonnegra
Florida Atlantic University
Dr. Chaves Fonnegra is an assistant professor of biology in the Honors College and Harbor Branch Oceanographic Institute at Florida Atlantic University. She previously conducted postdoctoral research at the University of Mississippi, University of the Virgin Islands, and Nova Southeastern University. Dr. Chaves Fonnegra received her Ph.D. from Nova Southeastern University in oceanography and marine biology. She also holds an M.S. from Universidad Nacional de Colombia and a B.S. from Universidad Jorge Tadeo Lozano, both in marine biology. She was an UNESCO-L'Oréal Young Women in Science Fellow and a fellow at the Smithsonian Tropical Research Institute. Dr. Chaves Fonnegra runs the FAU Laboratory of Integrative Marine and Coastal Ecology, which focuses on understanding mechanisms that underlie changes in marine and coastal communities. Her own research focuses on enhancing management of marine ecosystems by determining how ecological

This site uses cookies. For more information on cookies visit:
http://nas.edu/legal/privacy/index.html

Rebeca de Jesus Crespo
Louisiana State University
Dr. De Jesús Crespo is an assistant professor in the Department of Environmental Sciences at Louisiana State University. She holds a Ph.D. in integrative conservation and ecology from the University of Georgia and M.S. and B.S. degrees in biology from the University of Puerto Rico (UPR). Awards from the UPR Center for Applied Tropical Ecology and Conservation, the Ford Foundation, and the Fulbright Program helped fund her graduate research. Dr. Jesús Crespo previously worked as a biologist for the Puerto Rico Department of Environmental and Natural Resources and as a postdoctoral researcher for the Environmental Protection Agency's National Health and Environmental Research Laboratory, where she earned the Gulf Ecology Division Scientist of the Year Award and the EPA Environmental Justice Award. Her research links landscape level patterns of anthropogenic activities, ecosystem services, and socio-economic factors to indicators of ecological integrity and human health.

Kim de Mutsert
George Mason University
Dr. de Mutsert is an assistant professor in the Department of Environmental Science and Policy at George Mason University and associate director of the Potomac Environmental Research and Education Center. She holds a Ph.D. in oceanography and coastal sciences from Louisiana State University and an M.S. in biology from the University of Amsterdam. Her research interests include ecosystem-based fisheries management and fish ecology in estuarine and coastal ecosystems. She studies the effects of environmental factors and anthropogenic impacts on fish abundance, biomass, community structure, and fisheries landings using end-to-end model simulations, large existing datasets, field surveys, and lab studies. Current projects in the Gulf of Mexico include evaluating effects of the hypoxic zone on fish and fisheries, incorporating ecosystem-based consideration in fisheries management, and assessing environmental impact of large sediment diversions on estuarine fisheries species.

Jessica Fitzsimmons
Texas A&M University
Dr. Fitzsimmons is an assistant professor in the Department of Oceanography at Texas A&M University. She received her Ph.D. in chemical oceanography from the Massachusetts Institute of Technology and Woods Hole Oceanographic Institute Joint Program and her B.A. in chemistry and biology with a specialization in marine science from Boston University. Dr. Fitzsimmons received the Carl-Gustaf Rossby Award, given for the best Ph.D. dissertation in MIT's Program in Atmospheres, Oceans, and Climate. She is an environmental analytical chemist whose research uses high precision, multi-element measurements of trace metal concentrations, isotope ratios, and speciation to understand how metals are transformed in marine waters. Recent projects have investigated open

This site uses cookies. For more information on cookies visit:
http://nas.edu/legal/privacy/index.html

projects in Galveston Bay and the Gulf of Mexico.

Mariana Fuentes
Florida State University
Dr. Fuentes is an assistant professor in the Department of Earth, Ocean, and Atmospheric Sciences at Florida State University. She received her Ph.D. in environmental sciences and marine biology from James Cook University. Previously she undertook a Super Science Postdoctoral Fellowship at the Australian Research Council Centre of Excellence for Coral Reef Studies, where she used an interdisciplinary approach to translate science to real-world application to advance marine species conservation planning. Her work has been recognized by the Australian Institute of Policy and Science and she was a recipient of the Young Tall Poppy Science Awards. Dr. Fuentes's expertise is in integrating field-based ecology with systematic conservation planning, decision-theory approaches, climate modeling, and applied qualitative and geographic spatial analysis. She uses these tools to explore how marine wildlife interact with environmental processes and how they are impacted by current and future threats.

Evan Goldstein
University of North Carolina at Greensboro
Dr. Goldstein is a research scientist in the Department of Geography, Environment, and Sustainability at the University of North Carolina at Greensboro. He earned a Ph.D. in earth and ocean sciences from Duke University and a B.A. in Geology from Colgate University. Previously he was a postdoctoral researcher and a research assistant professor at the University of North Carolina at Chapel Hill. Dr. Goldstein's research focuses on geomorphology and human-landscape interactions across the coastal zone. His recent work centers on the use of machine learning to study coastal geomorphology, studying developed coastal areas during and after storm events, and the dynamics of coastal dunes. He is an advocate for open science practices, specifically preprinting and open data.

James Nelson
University of Louisiana at Lafayette
Dr. Nelson is an assistant professor of biology at the University of Louisiana Lafayette. He completed his Ph.D. in chemical oceanography at Florida State University using stable isotope analysis to trace the major sources of energy in offshore food webs in the Gulf of Mexico. After completing his Ph.D., he received a Northeast Climate Science Center fellowship working at the Marine Biological Laboratory in Woods Hole, MA, where he researched linkages between long-term changes in climate and the marsh landscape to changes in the food webs and fish production. His current research uses a combination of field observation, experimental approaches, remote sensing, stable isotope analysis, and mathematical modeling to quantify how ecosystem change will alter energy flow

This site uses cookies. For more information on cookies visit:
http://nas.edu/legal/privacy/index.html

Kwame Owusu-Daaku
University of West Florida
Dr. Kwame Owusu-Daaku is an assistant professor in the Department of Earth and Environmental Sciences at the University of West Florida. He earned his Ph.D. in geography from the University of South Carolina, his M.S. in urban and regional planning from the University of Iowa, and his B.Sc. in development planning from the Kwame Nkrumah University of Science and Technology in Ghana. Dr. Owusu-Daaku's research focuses on the impacts of climate change and pollution on different groups in coastal communities in Northwest Florida and the efforts of these groups to build resilience to these impacts. He employs an interdisciplinary framework that engages multiple social science and humanities perspectives, including those of geography, planning, anthropology, and history. The goal of his research is to pair a focus on unequal impacts of socio-environmental change with strategies such as citizen science to build awareness of—and inspire action to improve—socio-environmental problems.

Allison Reilly
University of Maryland
Dr. Reilly is an assistant professor in the Department of Civil and Environmental Engineering at the University of Maryland. She is a civil engineer and risk analyst whose research explores the intersection of hazards, infrastructure, and policy. Dr. Reilly's work evaluates how coastal communities adapt infrastructure in response to repeated disasters, how disaster aid is used to fund infrastructure recovery projects, and how the built environment affects the livelihood of coastal residents. She is currently the PI on a National Science Foundation-sponsored research project exploring how to speed infrastructure recovery after disasters through improved information sharing. Dr. Reilly holds a Ph.D. and M.S. in civil engineering from Cornell University and a B.S. in civil engineering from Johns Hopkins University. Previously, she was a post-doctoral research associate at Johns Hopkins University and a research fellow at the University of Michigan.

Isabel Romero
University of South Florida
Dr. Romero is a research associate in the College of Marine Science at the University of South Florida (USF). Dr. Romero earned her Ph.D. in ocean sciences at the University of Southern California (USC) and her B.S. with a double major in biology and marine science at the Universidad del Valle in Colombia. Prior to joining USF, she was a postdoctoral fellow in the Earth Science Department and Biological Science Department at USC. Dr. Romero's research focuses on uncovering geochemical signatures in the ocean as archives of how marine systems function and respond to natural and anthropogenic events. Specifically, she studies the sources, transformation processes, and fate of molecules in the marine environment and biota to reveal temporal and spatial trends of physical and

This site uses cookies. For more information on cookies visit:
http://nas.edu/legal/privacy/index.html

The Ohio State University

Dr. Sawyer is an assistant professor in the School of Earth Sciences at The Ohio State University. He received his Ph.D. in geological sciences from the University of Texas at Austin, his M.S. in geosciences from Penn State University, and his B.S. in marine sciences from Eckerd College. Previously, Dr. Sawyer worked for ExxonMobil in offshore drilling in the Gulf of Mexico and other locations to plan and execute safe well designs and assess hazards for safe subsea development projects. At Ohio State, Dr. Sawyer's research focuses on natural hazards of submarine landslides, tsunami, earthquakes, and hurricanes. He examines them with indirect and direct methods, including geophysical data, borehole logs, sedimentary cores, numerical modeling, and physical experiments. Study sites span the range of shallow water coastal environments to deepwater continental margins and sedimentary basins in a range of tectonic settings.

Lauren Stadler

Rice University

Dr. Stadler is an assistant professor in the Department of Civil and Environmental Engineering at Rice University. Her research focuses on advancing sustainable and safe biological wastewater treatment, resource recovery, and bioremediation processes. Her group seeks to advance the control and engineering of microbial communities to improve the efficacy of treatment, understand the fate and removal of emerging contaminants, and advance resource recovery from waste. Her group integrates microbial ecology, environmental microbiology, and process engineering to study both engineered and natural systems. Before joining the faculty at Rice, Dr. Stadler earned her B.S. from Swarthmore College and M.S. and Ph.D. in environmental engineering from the University of Michigan, did a Fulbright scholarship in India, and worked in environmental consulting for several years.

Elaina Sutley

University of Kansas

Dr. Sutley is an assistant professor in the Department of Civil, Environmental and Architectural Engineering at the University of Kansas. She earned her Ph.D. in civil engineering from Colorado State University and B.S. and M.S. in civil engineering from the University of Alabama. Her research lies at the nexus of structural engineering, social science, and public policy with an emphasis on progressing interdisciplinary science for community disaster resilience. Dr. Sutley is a researcher for the National Institute of Standards and Technology Center of Excellence for Risk-Based Community Resilience Planning, where she leads a longitudinal community resilience-focused field study following Hurricanes Matthew and Florence. Dr. Sutley received the prestigious National Science Foundation CAREER award for integrated convergence research and education on community disaster resilience, and has on-going projects related to earthquake, hurricane, and tornado disasters, where she focuses on damage to residential buildings and modeling post-disaster housing

This site uses cookies. For more information on cookies visit:
http://nas.edu/legal/privacy/index.html

Florida Atlantic University

Dr. Tang is an assistant professor in the Department of Computer and Electrical Engineering and Computer Science at Florida Atlantic University. He received his Ph.D. in electrical engineering from the University of Rhode Island and his M.S. and B.Eng. in electrical engineering and automation from Hohai University. His research interests are in the general areas of computational intelligence and cyber-physical systems. His current research focuses on networked big data and system analytics and predictive maintenance of marine structures/systems. Dr. Tang has current collaborations with many research institutions, including the Southeast National Marine Renewable Energy Center, the Harbor Branch Oceanographic Institute, and the National Renewable Energy Laboratory. He is the recipient of the University of Rhode Island's Steve Bouley and Rhonda Wilson Graduate Fellowship, the Chinese Government Award for Outstanding Student Abroad, and Best Paper awards from the IEEE Power & Energy Society General Meeting and International Conference on Communications.

William Tarpeh

Stanford University

Dr. Tarpeh is an assistant professor in the Department of Chemical Engineering at Stanford University. The Tarpeh Lab develops and evaluates selective approaches to converting water pollutants into products by investigating molecular mechanisms of chemical transport and transformation; developing novel unit processes that increase resource efficiency; and conducting systems-level assessments that identify optimization opportunities. Most recently, Dr. Tarpeh has been studying selective nitrogen sensing and treatment using novel adsorbents and electrochemical separations. He completed his B.S. in chemical engineering at Stanford, M.S. and Ph.D. in environmental engineering at the University of California, Berkeley, and postdoctoral training at the University of Michigan in environmental engineering. Dr. Tarpeh is a member of the Bouchet Honor Society, NBCBLK's "28 Under 28" African-American Innovators, and Forbes' "30 Under 30" 2019 Science List.

Gabrielle Wong-Parodi

Stanford University

Dr. Wong-Parodi is an assistant professor in the Department of Earth System Science and a Center Fellow at the Woods Institute for the Environment at Stanford University. Her research focuses on applying behavioral decision research methods to address challenges associated with global environmental change. She uses behavioral decision science approaches to create evidence-based strategies for informed decision making, with a particular focus on building resilience and promoting sustainability in the face of a changing climate. Dr. Wong-Parodi has a background in energy resources, climate change adaptation and mitigation, and risk perceptions of emerging technologies. She recently served on the committee that produced the National Academies of Sciences, Engineering, and Medicine report Understanding the Long-Term Evolution of the Coupled Natural-

This site uses cookies. For more information on cookies visit:
http://nas.edu/legal/privacy/index.html

2018

Srijan Aggarwal
University of Alaska Fairbanks
Dr. Aggarwal is an assistant professor in the Department of Civil and Environmental Engineering at the University of Alaska Fairbanks. He completed a bachelor's in civil engineering from the Indian Institute of Technology-Delhi and an M.S. and Ph.D. in civil engineering with a focus in environmental engineering at the University of Minnesota-Twin Cities. He spent two-and-a-half years as a post-doctoral scholar in a joint appointment at the BioTechnology Institute and the Department of Civil, Environmental, and Geo-Engineering at the University of Minnesota-Twin Cities. Dr. Aggarwal specializes in the field of environmental biotechnology. He has specific interest in bacterial biofilms in environmental systems, expanding to biofilms at oil-water interface and resultant impacts on oil biodegradation in the marine environment. He is a recipient of the National Science Foundation CAREER award for his work on biofilms in drinking water.

Lauren Clay
D'Youville College
Dr. Clay is an assistant professor in the Health Services Administration Department at D'Youville College, an affiliated professor at the Disaster Research Center at the University of Delaware, and an affiliated professor in the College of Global Public Health at New York University. She has worked on studies of household and family recovery from Hurricane Katrina; the Deepwater Horizon oil spill; Superstorm Sandy; the 2013 tornadoes in Moore, Oklahoma; and Hurricane Harvey. She has also conducted international research on health and economic development as a Fulbright Fellow in Bangladesh. She has her M.P.H. from Drexel University and Ph.D. in disaster science and management from the University of Delaware. Dr. Clay utilizes social epidemiologic methods and interdisciplinary collaboration as tools for developing a deeper understanding of individual and ecological factors that influence how natural and environmental hazards affect family and community health and well-being. Currently, she is studying the post-disaster food environment and food insecurity.

Adrienne Simoes Correa
Rice University
Dr. Correa became an assistant professor in BioSciences at Rice University after five years of experience as a non-tenure track faculty member at the same institution. Her postdoctoral and

This site uses cookies. For more information on cookies visit:
http://nas.edu/legal/privacy/index.html

three years, Dr. Correa has helped advise management of coral reefs in the northwest Gulf of Mexico through her seat on the Flower Garden Banks National Marine Sanctuary Advisory Council. Dr. Correa's work monitors how marine microbial communities shift when human activities alter temperature, nutrient availability, and other conditions in coastal ecosystems. She is currently characterizing the impacts of viruses on coral reefs and is expanding these efforts into mangrove, salt marsh, and seagrass ecosystems.

Sarah Davies
Boston University
Dr. Davies is an assistant professor of Biology at Boston University, where she studies the ecophysiology and genomics of reef building corals. Although she has conducted research on corals reefs around the world, she has always maintained an active research program at the Flower Garden Banks in the Gulf of Mexico. Dr. Davies earned her M.S. in biology from the University of Calgary and her Ph.D. in ecology, evolution, and behavior from the University of Texas at Austin. During her M.S. and Ph.D. work, she was supported by fellowships with the Natural Sciences and Engineering Research Council and the National Science Foundation. She also worked as a postdoctoral researcher at the University of North Carolina at Chapel Hill, where she became a Simons Foundation Fellow of the Life Sciences Research Foundation. Research in the Davies lab focuses on the potential roles of acclimation, adaptation, and dispersal in an organism's response to rapid climate change.

Nicole Errett
University of Washington
Dr. Errett is a lecturer in the Department of Environmental and Occupational Health at the University of Washington. Her research interests and expertise are in the use of public policy to enhance health outcomes during and after disaster. Dr. Errett co-founded and co-directs the University of Washington Collaborative on Extreme Event Resilience (CEER), a network of public health researchers, practitioners, and community scientists who collaborate to address real world challenges that impact communities' resilience to disasters and the acute impacts of climate change. Dr. Errett holds a Ph.D. in health and public policy, an M.S.P.H. in health policy, and a B.A. in public health studies from the Johns Hopkins University. She completed post-doctoral training in coastal community resilience at the University of British Columbia's School of Community and Regional Planning. Dr. Errett is also a Robert Wood Johnson Foundation New Connections Scholar.

Ipsita Gupta
Louisiana State University
Dr. Gupta is an assistant professor in the Department of Petroleum Engineering at Louisiana State University. She received her Ph.D. from the University of South Carolina, M.Tech from the Indian

This site uses cookies. For more information on cookies visit:
http://nas.edu/legal/privacy/index.html

research is on integrated reservoir-wellbore multiphase flow and transport modeling, and numerical modeling of rock/fluid interaction across different spatial and temporal scales. Dr. Gupta's industry experience spans strategic research, technology development, and technical services, as well as large capital project maturation in the Gulf of Mexico. Besides research, Dr. Gupta enjoys teaching and uses her industry experience to mentor students on the real-life applications of petroleum engineering.

Pedram Hassanzadeh
Rice University
Dr. Hassanzadeh is an assistant professor in the Departments of Mechanical Engineering and Earth, Environmental, and Planetary Sciences at Rice University. Before joining Rice, he was at Harvard University as a Ziff Environmental Fellow with the Center for the Environment and a research associate with the Department of Earth and Planetary Sciences. Dr. Hassanzadeh received his Ph.D. in mechanical engineering and M.A. in mathematics from the University of California at Berkeley. Dr. Hassanzadeh's research is aimed at providing reliable scientific information with quantified uncertainties about the historical and future extreme events. Using fundamentals of atmospheric dynamics and hierarchies of idealized-to-comprehensive climate models, mathematical/statistical modeling, and advanced machine learning techniques, Dr. Hassanzadeh works on improving the understanding of extreme weather events and their dynamics, predictability, and response to climate change. His Environmental Fluid Dynamics Group at Rice studies fundamentals of geophysical/environmental turbulence and dynamics of large-scale atmospheric circulation and extreme weather events.

Marccus Hendricks
University of Maryland
Dr. Hendricks is an assistant professor in the School of Architecture, Planning, and Preservation and a faculty research affiliate with the Clark School of Engineering's Center for Disaster Resilience at the University of Maryland. He holds a Ph.D. in urban and regional science and a Master of Public Health, both from Texas A&M University. Dr. Hendricks' primary research interests include stormwater infrastructure resilience, social vulnerability to disaster, environmental justice, sustainable development, and participatory action. He utilizes a combined social vulnerability to disaster and environmental justice framework to explore the provision of green space, adequate sewer, community facilities, public works, and stormwater services by municipalities to marginalized neighborhoods, which can modify environmental outcomes and experiences related to infrastructure. Dr. Hendricks is a founding fellow of the William Averette Anderson Fund, the first national interdisciplinary organization working to increase the number of underrepresented persons of color in the field of disaster research, practice, and pedagogy.

This site uses cookies. For more information on cookies visit:
http://nas.edu/legal/privacy/index.html

Psychology at Boston College. She received her Ph.D. in clinical psychology from the University of Miami and completed her clinical internship at Stanford University School of Medicine. Dr. Lai's research focuses on how children and families respond to disasters and other traumatic stressors. Her work also examines how advanced statistical modeling strategies may be applied to better understand how to minimize the effects of disasters on children's functioning. She is the principal investigator on a project examining school recovery after disasters and a project to better understand how and why children differ in their distress responses following acute traumatic events. Dr. Lai was named a National Scholar for the Academy on Violence and Abuse and a Next Generation of Hazard and Disasters Researchers Fellow. Dr. Lai's work has been recognized with Early Career Awards from the American Psychological Association.

Vincent Lecours
University of Florida
Dr. Lecours is an assistant professor of Marine Remote Sensing & Geospatial Analysis at the University of Florida. He completed a B.S. in applied geomatics from the Université de Sherbrooke and received his Ph.D. in geography from Memorial University, where he studied the methods associated with the mapping of deep-water habitats. He worked with spatial data collected with a remotely operated vehicle between 650 and 10,000 feet deep in previously unexplored areas of the ocean. Dr. Lecours conducts cross-disciplinary research using geospatial technologies and spatial sciences. His research program bridges the spatial sciences with the marine sciences by studying ways to improve marine habitat mapping methods through a better integration of spatial concepts, such as spatial scale, autocorrelation, and spatial data quality, in the habitat mapping workflow. It is aimed at developing best practices in the application of geomatics-based marine habitat mapping to ecological and management questions.

Mark Losego
Georgia Tech
Dr. Losego is an assistant professor in the School of Materials Science and Engineering at the Georgia Institute of Technology (Georgia Tech). He received his B.S. from Penn State University and an M.S. and Ph.D. from North Carolina State University, all in materials science and engineering. Prior to joining the Georgia Tech faculty, he was a postdoctoral researcher at the University of Illinois and research faculty at NC State. At Georgia Tech, Dr. Losego runs a highly interdisciplinary research team that focuses on the science of vapor phase processing applied to unconventional materials sets for environmental protection, renewable energy, and national security technologies. His research spans from fundamental studies of surface chemistry and processing kinetics to the development of novel deposition equipment and manufacturing methods. He is also the faculty founder of the Materials Innovation and Learning Laboratory, an open-access make-and-measure space devoted to peer-to-peer, experiential education within the materials science discipline.

This site uses cookies. For more information on cookies visit:
http://nas.edu/legal/privacy/index.html

Dr. Mayo is an assistant professor in the Department of Civil, Environmental, and Construction Engineering at the University of Central Florida. She earned her B.S. in mathematics from Grambling State University, and she earned her M.S. and Ph.D. in computational sciences, engineering, and mathematics from The University of Texas at Austin. Dr. Mayo's research interests are interdisciplinary, but focus on numerical modeling of the coastal ocean. She develops mathematical tools to assess the risk of hurricane storm surges and to improve the hydrodynamic models required to do so, helping coastal communities strengthen their resilience to these hazards. Her research has the potential to greatly improve storm surge modeling for long term planning and emergency management.

Jill McDermott
Lehigh University

Dr. McDermott is a geochemist and an assistant professor in the Earth and Environmental Sciences Department at Lehigh University. She earned her B.A. in chemistry from Dartmouth College, an M.S. in geochemical systems from the University of New Hampshire, and a Ph.D. in chemical oceanography from the Massachusetts Institute of Technology and Woods Hole Oceanographic Institution Joint Program. Dr. McDermott received the Carl-Gustaf Rossby Award, given for the best Ph.D. thesis within MIT's Program in Atmospheres, Oceans, and Climate, and is a National Academy of Sciences Kavli Fellow. She investigates the aqueous and volatile geochemistry and biogeochemistry of seafloor hydrothermal vents and ancient terrestrial fracture waters tapped by deep mines. The multidisciplinary approach Dr. McDermott uses in her work carries over into her teaching and mentoring, where she engages students with fundamental and applied science in the classroom and in individual research projects in her lab.

Alejandra Ortiz
North Carolina State University
Dr. Ortiz is an assistant professor in the Department of Civil, Construction, and Environmental Engineering at North Carolina State University. She earned her B.A. in geosciences at Wellesley College with a double major in classical civilizations, and she completed an M.S. in civil and environmental engineering and a Ph.D. in marine geology from the Massachusetts Institute of Technology and Woods Hole Oceanographic Institution Joint Program. Dr. Ortiz's research is focused on coastal geomorphology and understanding the evolution of coasts under rising sea levels. She uses numerical models, satellite imagery, fieldwork, and a flume to study the evolution of coastal systems and predict their resiliency over the next century. Recent projects have looked at the impact of pond expansion on the Mississippi Delta coast resulting in large-scale land loss and the role of vegetation in delta resiliency with rising seas.

This site uses cookies. For more information on cookies visit:
http://nas.edu/legal/privacy/index.html

Dr. Patrick is an assistant professor at Texas A&M University-Corpus Christi, a research associate at the Smithsonian Environmental Research Center, and the director of MarineGEO Texas, a node in the Smithsonian Marine Global Earth Observatory. He received his B.S. in behavior, evolution, ecology, & systematics from the University of Maryland and his Ph.D. in ecology from the University of Notre Dame. He also performed post-doctoral research on Chesapeake Bay seagrass ecology at the Smithsonian Environmental Research Center and worked with the EPA Office of Water during his AAAS Science & Technology Policy Fellowship. His research program bridges freshwater and estuarine ecosystems to understand how anthropogenic stressors interact with natural environmental variation to drive spatio-temporal patterns in aquatic biodiversity and ecosystem functioning. This work both advances fundamental ecological theory and has direct applications in coastal ecosystem management and biomonitoring.

Kevin Smiley
University at Buffalo
Dr. Smiley is an assistant professor of Sociology at the University at Buffalo. He is also a core faculty member of the university's Research and Education in Energy, Environment, and Water (RENEW) Institute. He received his B.A. in history and sociology from Western Kentucky University, an M.A. in sociology from the University of Memphis, and a Ph.D. in sociology from Rice University. Dr. Smiley's research is at the intersection of environmental and urban issues, with foci including natural hazards, public space, and industrial air pollution. In particular, his research analyzes the social characteristics of human populations that are made more vulnerable because of land cover changes from vegetated landscapes to developed ones, as well as the characteristics of those who benefit from newly developed land. He is one of the authors, along with Michael Oluf Emerson, of Market Cities, People Cities.

Xingyong Song
Texas A&M University
Dr. Song is an assistant professor in the College of Engineering at Texas A&M University. He received his Ph.D. in mechanical engineering from the University of Minnesota. His research interests include drilling automation systems for more efficient and safe oil and gas production, mechatronic system design and dynamics control, and renewable energy systems enabled by advanced control technologies. Prior to appointment at Texas A&M University, he had industrial working experience at the General Motors Research Center and at the Halliburton Energy Service Company Innovation Center. While at Halliburton, he actively piloted control solutions to address advanced automation needs in the oil and gas industry, including drilling automation, well logging, and drilling fluid management and control. His novel control solution for the new Halliburton sonic logging tool won him the Halliburton Innovation of the Year Award.

Beth Stauffer

This site uses cookies. For more information on cookies visit:
http://nas.edu/legal/privacy/index.html

Lafayette. Prior to joining the UL Lafayette faculty, she was an AAAS Science & Technology Policy Fellow hosted by the U.S. Environmental Protection Agency and a Lamont-Doherty Postdoctoral Fellow at the Lamont-Doherty Earth Observatory of Columbia University. Dr. Stauffer's research focuses on understanding how dynamic physical environments and variable grazing interactions contribute to changing phytoplankton communities in coastal waters, and what those effects mean for estuarine and marine food webs. She is a fellow with the Louisiana Sea Grant Discovery, Integration and Application Program (LaDIA), a member of the Louisiana Universities Marine Consortium (LUMCON) Advisory Council, and the founder and organizer of the Science on the Bayou informal science communication series. Dr. Stauffer earned her B.S. with a double major in marine science and biology at University of Miami and her Ph.D. in marine environmental biology at the University of Southern California.

Courtney Thompson
Texas A&M University
Dr. Thompson is an assistant professor at Texas A&M University in the Department of Geography. Dr. Thompson received her Ph.D. in geography from the University of Idaho. She also holds an M.S. in geography from the University of Idaho and a B.S. in geography from New Mexico State University. Her research in human-environment interactions examines relationships between social systems and natural hazard impacts using a mix of qualitative and quantitative methods, including GIS, interviews, survey analysis, and spatial statistics. Specifically, she employs vulnerability and resilience assessment methodologies that empower local decision-makers to create and strategically implement resilience-enhancing mitigation and adaptation strategies. Her research also focuses on quantifying how the vulnerability and resilience of coastal communities interact with the social structuration of society, multi-scalar factors, and risk perceptions.

Hannah Vander Zanden
University of Florida
Dr. Vander Zanden is an assistant professor in the Department of Biology and the Archie Carr Center for Sea Turtle Research at the University of Florida. She holds a B.A. from Pomona College and a Ph.D. in zoology from the University of Florida. She also held postdoctoral appointments at the University of Utah and U.S. Geological Survey. The goal of Dr. Vander Zanden's research is to address critical knowledge gaps about where sea turtles are most abundant in the Gulf of Mexico. Much of her research program relies on the use of intrinsic markers called stable isotopes, which are naturally occurring forms of elements that are integrated from the environment through an organism's diet. By identifying where sea turtles forage via samples collected at the nesting beach, population hotspots can be identified and paired with information about threat severity and target restoration activities.

This site uses cookies. For more information on cookies visit:
http://nas.edu/legal/privacy/index.html

2017

Christoph Aeppli
Bigelow Laboratory for Ocean Sciences
Dr. Aeppli is an environmental chemist and a senior research scientist at Bigelow Laboratory for Ocean Sciences. Dr. Aeppli has studied oil weathering at natural oil seeps, in Arctic conditions, and after major oil spills, including the Deepwater Horizon oil spill. He received his master's degree in chemistry from the University of Bern, Switzerland, and his doctorate in environmental chemistry from the Swiss Federal Institute of Technology. Postdoctoral fellowships took him to Stockholm University, where he investigated the dynamics of halogenated compounds, and to Woods Hole Oceanographic Institution, where he studied biodegradation and photooxidation of petroleum hydrocarbons. Dr. Aeppli's research is helping to understand the formation, fate, and effects of oil transformation products. This knowledge will lead to an improved assessment of the impacts that oil spills have on humans and the environment.

Laura Bakkensen
University of Arizona
Dr. Bakkensen is an assistant professor at the University of Arizona's School of Government and Public Policy, where she uses applied microeconomic and econometric techniques to analyze the economics of natural disasters, identifying current hazard risks and evidence of adaptation to damages and fatalities across the globe. Dr. Bakkensen received her Ph.D. in environmental and natural resource economics from Yale University. She also holds an M.Phil. in environmental and natural resource economics from Yale University, an M.S. in environment and development from the London School of Economics and Political Science, and a B.A. in economics from Whitman College. As an economist, Dr. Bakkensen researches individual responses, overall community resilience, and policy responses in the face of natural disasters like hurricanes, tornadoes, and floods. Her research informs policy on public insurance and regulation, pre- and post-disaster aid, severe weather warnings, and public adaptation projects.

Paul Harnik
Franklin and Marshall College
Dr. Harnik is an assistant professor in the Department of Earth and Environment at Franklin and Marshall College. He received his B.A. in geology from Oberlin College and his Ph.D. in evolutionary biology from the University of Chicago. Dr. Harnik's doctoral and postdoctoral research focused on understanding extinction risk in the oceans through analyses of the marine fossil record. At Franklin and Marshall, his research has focused increasingly on the links between modern, historical, and ancient marine systems with the goal of advancing our understanding of the biological consequences of current and future anthropogenic environmental change. Most recently, Dr. Harnik and his

This site uses cookies. For more information on cookies visit:
http://nas.edu/legal/privacy/index.html

baselines for these communities and assess the effects of human activities on coastal ecosystems.

YeongAe Heo
Case Western Reserve University
Dr. Heo is an assistant professor in the Department of Civil Engineering at Case Western Reserve University. She received her Ph.D. in civil and environmental engineering from the University of California, Davis. She has expertise in modeling and simulation of probabilistic risk-based system-level performance for complex structures subjected to dynamic loads. Dr. Heo worked at the Offshore Technology R&D Center of Samsung Heavy Industries, where she examined diverse multi-hazard problems for offshore oil and gas process systems exposed to severe weather and operation conditions. She holds three patents for offshore structural systems and was the recipient of the 2012 American Society of Civil Engineers (ASCE) Norman Medal. Dr. Heo's research focuses on minimizing risks in on- and offshore oil and gas systems. As an engineer, she uses a variety of tools, including modeling and simulations, to investigate multi-hazard risks for the complex energy infrastructure systems that are subject to constantly changing stresses.

Michael Martínez-Colón
Florida A&M University
Dr. Martínez-Colón is an assistant professor in the School of the Environment at Florida Agricultural and Mechanical University, a Courtesy Professor in the Department of Environmental Science at the University of South Florida, and adjunct faculty at the Savannah River Field Station. He received his Ph.D. in oceanography from the University of South Florida and a B.S. and M.S. in geology from the University of Puerto Rico. His research expertise is in coastal ecosystems, specifically coastal and marine ecology and biogeochemistry. His research portfolio examines aspects of environmental micropaleontology, geochemistry, and pollutants in conjunction with bioindicators in short- and long-term monitoring efforts. Dr. Martínez-Colón takes a novel approach to studying anthropogenic stressors such as chemical pollutants and microplastics, focusing on a type of single-celled organisms called foraminifera, which have calcium carbonate skeletons and tend to live in sediments.

Ali Mostafavi
Texas A&M University
Dr. Mostafavi is an assistant professor in the Zachry Department of Civil Engineering at Texas A&M University. He received his Ph.D. in civil engineering at Purdue University. He also holds a Master of Science in industrial administration from the Krannert School of Management at Purdue University. Dr. Mostafavi supervises the Infrastructure System-of-Systems Research Group. He also works closely with community partners, such as the Southeast Florida Climate Compact, to extend the broader impacts of his research. Dr. Mostafavi takes a "system of systems" approach to studying chronic and acute stressors facing coastal communities all over the world. He bridges the boundaries

This site uses cookies. For more information on cookies visit:
http://nas.edu/legal/privacy/index.html

planning.

David Murphy
University of South Florida
Dr. Murphy is an assistant professor in the Department of Mechanical Engineering at the University of South Florida. He completed a double B.S. in mechanical and biomedical engineering from the University of Alabama at Birmingham, an M.Phil. in biological science from Cambridge University, and an M.S. in mechanical engineering from the Georgia Institute of Technology. He received his Ph.D. in civil and environmental engineering from Georgia Tech. He completed a postdoctoral fellowship in the Department of Mechanical Engineering at Johns Hopkins University. Dr. Murphy is an expert in fluid mechanics whose research has biological, ecological, and environmental applications. For example, he has worked on crude oil spill dispersion in marine environments and potential human health effects of exposure to oily marine aerosols. Through a variety of methods, including advanced flow visualization and measurement techniques, he has also investigated zooplankton swimming, insect flight, and prosthetic heart valves.

Ashley Ross
Texas A&M University, Galveston
Dr. Ross is an assistant professor in the Department of Marine Sciences and a faculty fellow with the Center for Texas Beaches and Shores at Texas A&M University at Galveston. She holds an M.A. in political science from Louisiana State University and a Ph.D. in political science from Texas A&M University. Dr. Ross studies the vulnerability of coastal communities to natural disasters and other hazards and how to make them more resilient. As a political scientist, she approaches these challenges from a public administration and policy perspective. She then uses this information to inform policies with the goal of enhancing community resilience. Her research examining coastal hazards has produced the book Local Disaster Resilience: Administrative and Political Perspectives. Dr. Ross was a 2014 National Science Foundation Next Generation of Hazard and Disasters Researchers Program fellow. Her work on Gulf Coast disaster resilience has also been supported by the Department of Homeland Security.

Wanyun Shao
University of Alabama
Dr. Shao is an assistant professor of Geography at the University of Alabama, where her primary research interests are the interaction between nature and society. She received her B.S. in geography from Jilin University (China) and M.P. in planning from the University of Wyoming. While pursuing her Ph.D in geography at Louisiana State University, Shao was a research assistant for the Southern Climate Impacts Planning Program, which is funded by the U.S. National Oceanic and Atmospheric Administration. After receiving her Ph.D., Dr. Shao worked as a Coastal Resources Scientist at the

This site uses cookies. For more information on cookies visit:
http://nas.edu/legal/privacy/index.html

policies and planning, and impacts of climate change on public health. The interdisciplinary nature of her research leads her to work across traditional disciplinary lines.

J. Cameron Thrash
University of Southern California
Dr. Thrash is an assistant professor in the Department of Biological Sciences at the University of Southern California. He received a B.S. in biology from the University of California, San Diego. He received his Ph.D. in microbiology from the University of California, Berkeley, where he studied microbial physiology. His graduate work included perchlorate bioremediation and isolation of novel perchlorate reducing microorganisms. He also studied anaerobic oxidation of iron and uranium. He was awarded a National Science Foundation Postdoctoral Fellowship to work at Oregon State University, where he focused on the evolution and genomics of SAR11, the most abundant marine bacteria. Dr. Thrash's research focuses on the function of microbes in the different interconnected aquatic systems within the Gulf of Mexico, including the coasts, estuaries, the shelf region, and the Mississippi River. He aims to predict which microbes contribute to the vital ecosystem services of nutrient and carbon processing to generate strategic options for pollutant remediation.

2016

Jordon Beckler
Florida Atlantic University Harbor Branch Oceanographic Institute
Dr. Beckler is an assistant research professor in the Geochemistry and Geochemical Sensing Lab at the Florida Atlantic University Harbor Branch Oceanographic Institute in Fort Pierce, Florida. He completed a Ph.D. in chemical oceanography with a minor in inorganic chemistry at the Georgia Institute of Technology. Dr. Beckler is currently working to understand the role of sediment-derived iron in serving as a nutrient source to Florida red tides and in enhancing the degradation of hydrocarbons; improve efforts to understand harmful algae bloom formation by developing optical techniques and autonomous measurement platforms; and develop in situ chromatographic techniques for remote detection of harmful algae bloom toxins. His work focuses on developing autonomous instrumentation to measure previously unidentified introductions of iron to coastal waters and will contribute to improved understanding of the influences on Gulf algal blooms.

Ann Cook

This site uses cookies. For more information on cookies visit:
http://nas.edu/legal/privacy/index.html

geophysics from Columbia University. Dr. Cook's research is focused on natural gas hydrates, an ice-like form of methane gas and solid water that forms in marine sediments. She uses analytical data like geophysical well logs, seismic data, and sediment cores along with mathematical models to investigate these natural gas hydrates. Since she arrived at Ohio State, Dr. Cook's research has been funded primarily through several grants from the U.S. Department of Energy, including an $81 million project focused on drilling and recovering natural gas hydrate in sand reservoirs from the Gulf of Mexico.

Brad Erisman
University of Texas at Austin
Dr. Erisman is an assistant professor of fisheries ecology at the University of Texas at Austin Marine Science Institute. He received his B.S. in aquatic biology from the University of California, Santa Barbara, his M.S. degree in biology from California State University Northridge, and his Ph.D. in marine biology from the Scripps Institution of Oceanography. After earning his doctorate, he remained at Scripps as a postdoctoral scholar and assistant research scientist for several years, during which time he co-founded the Gulf of California Marine Program. He currently leads several projects related to fishes and fisheries in the Gulf of Mexico, California, the Indo-Pacific, and Mexico. Dr. Erisman's research focuses on understanding interconnections among fish spawning aggregations (FSAs), ecosystems, fisheries, and climate. FSAs are productivity hotspots critical to marine food webs and ecosystem function. They also support the most productive and important commercial, recreational, and subsistence fisheries.

Diego Figueroa
University of Texas Rio Grande Valley
Dr. Figueroa is an assistant professor in the School of Earth, Environmental, and Marine Sciences at the University of Texas Rio Grande Valley. He received his B.S. in marine biology from the University of Alaska Southeast and his M.S. and Ph.D. in biological oceanography from Oregon State University. Dr. Figueroa's work focuses on establishing a baseline of oceanographic and biological characteristics of the near-shore region of the South Texas Gulf Coast, one of the least-studied areas in the entire Gulf of Mexico, to serve as a foundation for long-term oceanographic monitoring. His research focuses on how oceanographic processes, anthropogenic effects, and climate change impact the biodiversity and connectivity of marine habitats. Dr. Figueroa works with zooplankton in coastal and open ocean environments and with corals in the deep sea. Dr. Figueroa uses multivariate tools for community analyses and a wide range of molecular methods to answer ecological and evolutionary questions.

Huilin Gao
Texas A&M University

This site uses cookies. For more information on cookies visit:
http://nas.edu/legal/privacy/index.html

and are focused on several areas indispensable to protecting water and environmental resources—particularly those related to coastal ecosystem sustainability. Her expertise is centered on understanding the impacts of a changing environment on freshwater inflows and the effects of inflows on coastal ecosystems. Dr. Gao uses a combination of in situ observations, state-of-the-art remote sensing, and high-performance modeling approaches to investigate interactions between phytoplankton and oil in the marine ecosystem to provide a better understanding of the role phytoplankton play in altering oil compounds, which phytoplankton functional types are most affected by oil spills, and which functional types are most likely to aid oil decomposition.

Michelle Meyer
Louisiana State University
Dr. Meyer is an assistant professor of sociology at Louisiana State University. She completed her Ph.D. in sociology at Colorado State University and received a B.A. in sociology from Murray State University. Her research interests include environmental sociology and community sustainability, disaster resilience and mitigation, climate change displacement, environmental justice, and the interplay between environmental conditions and social vulnerability. She has worked on various projects, including analyzing organizational networks in long-term recovery; comparing disaster recovery following technological and natural disasters; assessing the inclusion of disability in emergency management planning; and analyzing social capital and collective efficacy for individual and community resilience; among others. Using her research findings, Dr. Meyer has helped community organizations understand demographics that contribute to vulnerability and then prepare disaster recovery plans. With increasing disaster frequency, everyday practices and relationships are crucial to supporting community resilience.

Jennifer Pazour
Rensselaer Polytechnic Institute
Dr. Pazour is an assistant professor of industrial and systems engineering at Rensselaer Polytechnic Institute. She holds three degrees in industrial engineering: a B.S. from South Dakota School of Mines and Technology, and a M.S. and Ph.D. from the University of Arkansas. She is an active member of the Institute for Operations Research and the Management Sciences and the Institute of Industrial and Systems Engineers, and she serves on the board of directors for the Warehousing Education and Research Council. Dr. Pazour's research explores how to make decisions in logistics and resource-sharing systems. She develops mathematical models and solution algorithms of complex systems as a way of understanding and quantifying trade-offs with operational and design decisions.

Kerri Pratt
University of Michigan
Dr. Pratt is currently the Seyhan N. Ege Assistant Professor of Chemistry at the University of

This site uses cookies. For more information on cookies visit:
http://nas.edu/legal/privacy/index.html

research laboratory studies atmospheric composition, clouds, and precipitation to understand key processes in air quality and climate change, particularly across the Alaska outer continental shelf. Her lab also examines air pollution contributions of oil extraction activities at coastal Prudhoe Bay, the third largest oilfield in North America. Recently, Dr. Pratt developed an innovative course featuring original Arctic snow chemistry research to introduce first- and second-year college students to scientific research to improve STEM retention.

Adam Skarke
Mississippi State University
Dr. Skarke is an assistant professor of Geology in the Department of Geosciences at Mississippi State University. He earned a B.A. in geology from Colgate University as well as an M.S. and Ph.D. in geology from the University of Delaware. Dr. Skarke conducts research focused on understanding the fundamental physical relationships between fluid dynamics, sediment transport processes, morphological expression, and the stratigraphic record in marine environments that span the continental margin from coastal waters to the deep sea. His technical approach is field-based and focused on the analysis of geological, geophysical, and oceanographic data collected with innovative environmental observing sensors and platforms. Results of Dr. Skarke's research may help scientists and environmental managers better understand and mitigate processes detrimental to the health and resilience of marine ecosystems, commercial fisheries, and coastal property and infrastructure.

Jill Trepanier
Louisiana State University
Dr. Trepanier is an assistant professor in the Department of Geography and Anthropology at Louisiana State University. She received her bachelor's degree in geography from the University of Wisconsin-Oshkosh and her master's and Ph.D. in geography from Florida State University. Dr. Trepanier's work focuses on the quantification of extreme hurricane wind and storm surge risks in coastal locations. This risk estimate provides planners and managers with an understanding of how often the most extreme events will occur in the region, which can help them better prepare structures for the worst-case scenario. Dr. Trepanier's main research focus is on quantifying tropical cyclones, for which she has two different statistical approaches. The first uses extreme value statistics to estimate wind speeds or storm surges to specific locations. The second utilizes a copula model to find the combined probability of joint wind and storm surge occurrence.

2015

This site uses cookies. For more information on cookies visit:
http://nas.edu/legal/privacy/index.html

Dr. Albert is an assistant professor and the Robert and Gayle Longmire Early Career Professor in Chemical Engineering at Tulane University. She received her B.S. in chemical engineering from the University of Florida and her Ph.D. in chemical engineering from the University of Delaware. Her doctoral and postdoctoral research focused on developing gradient methods for exploring the effects of surface interactions on block copolymer thin film self-assembly and tailoring the chemical and mechanical properties of silicone elastomer networks for cell mobility studies and peptide assembly. At Tulane, Dr. Albert's research is centered on the use of combinatorial methods to engineer nano- and micro-structured polymeric materials for applications in energy, health, and the environment. Specifically, she takes advantage of the phase separation processes responsible for self-assembly in block copolymers and polymer blends to produce materials in thin film geometries exhibiting desired morphologies.

Alberto Caban-Martinez
University of Miami
Dr. Caban-Martinez is an assistant professor of public health sciences and director of the Musculoskeletal Disorders and Occupational Health Lab at the University of Miami, Miller School of Medicine. He earned his B.S. in computer science from the University of Miami, his M.P.H. from Nova Southeastern University, and completed the osteopathic medicine program at Nova Southeastern University and the doctoral occupational epidemiology program at the University of Miami. He then completed a postdoctoral fellowship at the Harvard School of Public Health, where he learned to develop workplace interventions in the construction industry. Dr. Caban-Martinez's interdisciplinary program of research aims to conduct robust occupational and environmental health surveillance activities and provide rigorous scientific evidence about effective ways to reduce musculoskeletal disorders and improve the well-being of worker populations. He focuses on finding ways to promote safe work practices, healthy behaviors, and healthy work environments.

Zachary Darnell
University of Southern Mississippi
Dr. Darnell is an assistant professor in the Department of Coastal Sciences at the University of Southern Mississippi. Dr. Darnell earned a B.S. in biological sciences from Vanderbilt University and a Ph.D. in ecology from Duke University. Dr. Darnell's long-term research interests are centered on the environmental constraints imposed upon marine and estuarine invertebrate species. Specifically, his research focuses on physiological and behavioral responses to environmental change and environmental stress; environmental effects on life histories, distributions, and population dynamics; and anthropogenic impacts on organism-environment interactions. Focusing primarily on crustaceans, this research relies on a combination of field- and lab-based experimental work, complemented by quantitative and spatial analyses of long-term fishery-dependent and fishery-independent datasets to better understand patterns of abundance and distribution in relation to

This site uses cookies. For more information on cookies visit:
http://nas.edu/legal/privacy/index.html

Dauphin Island Sea Lab

Dr. Dorgan is a senior marine scientist at the Dauphin Island Sea Lab and an assistant professor of marine sciences at the University of South Alabama. She received her B.S. in marine biology from the University of California, Santa Cruz, and her Ph.D. in oceanography from the University of Maine. As part of her dissertation research, she showed that worms extend burrows through muddy sediments by fracture, a result that was published in Nature and for which she was awarded the Association for the Sciences of Limnology and Oceanography Lindeman Award. Dr. Dorgan's research program aims to develop a mechanistic understanding of the ecological and biogeochemical processes occurring in marine sediments. She is specifically interested in animal-sediment interactions, including the mechanics of burrowing and feeding and the impacts of these activities on the physical structure of sediments.

Joel Fodrie

University of North Carolina

Dr. Fodrie is an assistant professor of fisheries oceanography and ecology at the University of North Carolina, where he studies the population dynamics of fishes and shellfish. He has conducted research along all three major U.S. coastlines, as well as in the Baltic Sea and around the Galápagos Islands. Dr. Fodrie earned his Ph.D. in Oceanography from the Scripps Institution of Oceanography, where he was supported as a National Science Foundation Graduate Research Fellow and presented with the E. W. Fager Student Award. Dr. Fodrie's research focuses on four major themes: 1) how the movement of fishes connects landscapes and affects population dynamics; 2) linkages between coastal habitat abundance/quality and fishery production; 3) biogenic habitat restoration; and 4) how basin-scale perturbations such as harvest pressure, climate change, and oil pollution influence the long-term community ecology of coastal ecosystems.

Anna Michel

Woods Hole Oceanographic Institution

Dr. Michel earned B.S. degrees in biology and chemical engineering from the Massachusetts Institute of Technology (MIT). She then earned an M.S. in Ocean Engineering from MIT and a Ph.D. in Mechanical and Oceanographic Engineering from the MIT-Woods Hole Oceanographic Institution (WHOI) Joint Program. After receiving her Ph.D., Dr. Michel was a post-doctoral fellow and then an associate research scholar at the Center for Mid-Infrared Technologies for Health and the Environment at Princeton University. She returned to WHOI as an assistant scientist in applied ocean physics and engineering. Dr. Michel's research focus is on advancing environmental observation through the development and deployment of novel optical sensors for measurement of key chemical species. Dr. Michel designs, builds, and deploys advanced laser-based chemical sensors that are capable of measuring trace concentrations in gaseous and aqueous environments in locations ranging from the deep sea to Arctic environments, using remotely operated vehicles.

This site uses cookies. For more information on cookies visit:
http://nas.edu/legal/privacy/index.html

Dr. Wallace is an assistant professor in the Department of Marine Science at the University of Southern Mississippi. He is also currently a guest investigator at the Woods Hole Oceanographic Institution and a complimentary research scholar at Rice University. Dr. Wallace earned a B.S. degree from Tulane University, with a double major in geology and German. He earned a Ph.D. degree in earth science from Rice University. The aim of Dr. Wallace's research is to establish the response of coastal systems to global change over historic and geologic timescales. Specifically, Dr. Wallace is primarily a field geologist interested in understanding how variations in hurricanes, sediment supply, and relative sea-level shape and impact the coastlines of the world. He has worked in areas along the Gulf of Mexico, Japan, Bermuda, and the Philippines.

Helen White
Haverford College

Dr. White is an associate professor of chemistry and the director of the environmental studies program at Haverford College. She received a master's degree in chemistry from the University of Sussex, U.K., and a Ph.D. in chemical oceanography from the Massachusetts Institute of Technology and Woods Hole Oceanographic Institution (WHOI) Joint Program. Dr. White's research examines the persistence of oil and other organic contaminants in the marine environment. Her work seeks to examine how the chemical structure, physical associations, and bioavailability of specific compounds determine their cycling and eventual fate. Her research at Haverford College has been funded by an National Science Foundation RAPID grant to determine the impact of the Deepwater Horizon oil spill on a deep-water coral community in the Gulf of Mexico, as well as a grant from the Gulf of Mexico Research Initiative to examine the weathering of petroleum and dispersant components in the deep-sea, on Gulf Coast beaches, and in laboratory incubations.

The National Academies of SCIENCES ENGINEERING MEDICINE

NATIONAL ACADEMY OF SCIENCES
NATIONAL ACADEMY OF ENGINEERING
NATIONAL ACADEMY OF MEDICINE

About Us | Our Work
Events | Contact Us
Opportunities | Publications
Visit

Privacy Statement | DMCA Policy | Terms of Use | Site Map

Copyright © 2020 National Academy of Sciences. All Rights Reserved.

This site uses cookies. For more information on cookies visit:
http://nas.edu/legal/privacy/index.html

Table of Contents

General_Authors_Publications.....2
LI-266340_A_Yee2019_Article_LinkingWaterQualityToAedesAegy.....14
LI-266342_B_DeJes?sCrespo2019_Article_LinkingWetlandEcosystemService.....33
SupplementA1_CMP_Naled_Letter.....46
SupplementA2_Maria_Call.....53
SupplementA3_NEP_Support.....55
SupplementA4_RevealNews.....72
SupplementA5_2017_ord_honor_award_recipients.....102
A_Yee2019_Article_LinkingWaterQualityToAedesAegy.....112
B_DeJes?sCrespo2019_Article_LinkingWetlandEcosystemService.....131
B_Wetlands_Journal_SupplementaryMaterial.....144
SupplementB1_Dengue_Distribution.....147
SupplementB2_Keynote_Odum.....152
SupplementB3_LSUNewsArticles.....154
SupplementB5_Benefits_Ch2.....159
SupplementB4_EarlyCareerResearchFellows.....170
Yee_Mosquito_2020_RecordPercentageAgreement.....194

STAA REPORT FOR THE SCIENTIST NOMINATIONS

General Information:

Nomination ID/App ID:	20-113
Research Category Primary:	Sustainability and Innovation (SI)
Research Category Secondary:	Ecological Research (ER)
Laboratory/Office Name:	ORD
Nomination Entered By:	Matthew Harwell

Eligibility Checklist:

[Y] The nominated publication(s) has not been submitted to a previous STAA competition.

[Y] The nominated publication(s) was published on or before January 1, 2017 and on or after January 1,2012

[Y] The principal author was an EPA employee or a PHS employee assigned to EPA when the research was performed

[Y] The EPA authors (includes PHS employees assigned to EPA) contributed collectively a minimum of 50% toward the publication(s)

Nominating Official Name:	Susan George
Nominating Official Title:	DIRECTOR, GULF ECOLOGY DIVISION
Nominating OfficialEmail:	george.elizabeth@epa.gov
STAA Coordinator Name:	Kathleen Wiser
STAA Coordinator Email:	wiser.kathi@epa.gov

Justifications:

Justification 1:

This research supports US EPA's goals to revitalize vulnerable communities and understand connections between healthy ecosyste Additionally, the 2019-2022 EPA Strategic Plan recognizes that disease vectors carried by pests create challenges, and calls for wo officials and researchers to weigh risks and determine effective methods of pesticide use. In particular, mosquito borne diseases rep economic burden to communities around the world. The emergence of serious vector mediated viruses, such as Zika and dengue, u effective strategies for vector control and mosquito eradication. With growing concerns of how strategies such as aerial spraying m wildlife, researchers are increasingly interested in sustainable approaches for safe vector population management, including approa of the transmission cycle.

This research presents innovative work in the Caño Martín Peña (CMP) community in San Juan, Puerto Rico, linkir mosquito-vectored diseases. The CMP is an impoverished sector, historically prone to environmental hazards related to poor wa diseases. This collaborative research between EPA ORD, the University of Southern Mississippi, and local partners (e.g., EPA Re for Disease Control, the San Juan Bay Estuary, and University of Puerto Rico), targeted vector borne diseases, one of the most pr community. Habitat alterations and land-use development have disrupted the natural flow of water throughout the San Juan B neighborhoods to frequent flooding events, exacerbated by the effects of wastewater discharges and polluted runoff. The researc field work and statistical models to investigate the role of wetland ecosystem services, including temperature regulation, wa protection, in mediating vector capacity and disease occurrences.

The research team conducted spatial modelling studies using historical data on dengue fever to assess the relationship between envi the landscape level and vector borne disease control (de Jesús Crespo et al., 2018). Looking at the CMP community and other coas linked wetland ecosystem services to dengue occurrences during the largest dengue epidemic on the Island. According to the stud may help reduce dengue cases primarily by reducing surface temperature, a factor which has been shown to promote dengue in wetlands in mitigating vector-borne illness may include biological control of vectors, viral dilution through the presence of alte regulation. Dengue incidence was also associated with water quality. This supports the role of ecosystem services as an effective m diseases in an environmental justice (EJ) community.

A field study (Yee et al. 2019) was conducted during the 2016 Zika epidemic, which affected over 40,000 individuals in Puerto Ric undertook community engagement efforts to strategically place mosquito sampling traps in the CMP and other flood-zone commun and 2017. The study investigated whether flooding events and associated debris, in addition to creating mosquito breeding habitat, existing larval breeding sites depending on the water quality of adjacent waterbodies. Field data were used to identify whether there viral load and nutrient content of adult mosquitos with water quality in larval habitats to determine the potential effects of nutrient e transmission (Yee et al., 2019). The study provided preliminary evidence that environmental variability in nutrient inputs can influe

mosquito vectors. This suggests that management actions to reduce flooding and improve water quality could go hand-in-hand with aerial spraying, to help control spread of vector-borne diseases in EJ communities.

https://www.epa.gov/sites/production/files/2019-09/documents/fy-2018-2022-epa-strategic-plan.pdf

Justification 2A:

In 2016, the research team initiated the statistical modeling study, using secondary data on dengue incidence and environmental factors, to expl ecosystem services, socio-economic condition, and dengue incidence in humans (De Jesus Crespo et al. 2018). In summer of 2016, when Puert outbreak, the research team made a decision to leverage the unique short-term opportunity to gather field data on Zika infected mosquitos after Martín Peña community (Yee et al. 2019). Though less comprehensive than the statistical study, the field study afforded the opportunity to mec load in larval mosquito containers, larvae, and adults. The results of both studies supported a potential linkage between water quality (i.e., nitro disease incidence. However, results of the statistical study emphasize that other ecosystem services (e.g., temperature regulation) and protective income-level) also have strong influences on how infection rates in mosquitos ultimately translate to disease incidence in humans.

Justification 2B:

Susan Yee; 2015 EPA Scientific and Technological Achievement Award, Honorable Mention; Yee, S.H., J.A. Dittmar, L.M. Olive quantifying reef ecosystem services: a case study mapping services for St. Croix, USVI. Ecosystem Services 8:1-15. http://dx.doi.o

Susan Yee; 2015 EPA Scientific and Technological Achievement Award, Honorable Mention; Yee, S.H., J. Carriger, W.S. Fisher, Developing scientific information to support decisions for sustainable reef ecosystem services. Ecological Economics 115:39-50. http://dx.doi.org/10.1016/j.ecolecon.2014.02.016

Justification 2C:

This nomination advances previously nominated work (Yee et al. 2014; Yee et al. 2015), which developed approaches to model ec connecting ecosystem services production to benefits on a human health issue of major concern, vector-borne diseases, in a specific vulnerable communities of Puerto Rico.

Justification 2D:

n/a

Justification 2E:

Some of the authors (Rebeca de Jesus Crespo, Susan Yee) have submitted a concurrent nomination (De Jesus Crespo et al. 2018; D conducts a literature review assessing evidence for relationships between ecosystem services and human health outcomes, and then analysis for one understudied relationship of relevance to Puerto Rico, namely impacts of flood-regulation ecosystem services on G similar in building the evidence base for relationships between ecosystem services and benefits to human health. The current nomir through a specific application for the San Juan Bay estuary how an improved understanding of the relationships between environme and vector-borne illness can help inform decision-making in vulnerable communities.

Justification 3A:

During the Zika outbreak of 2016, the local Caño Martín Peña community group argued against using aerial spraying of Naled to th Health, citing discussions with the research team and some of the very early preliminary results of the field study to argue that effor remove debris that could be providing mosquito habitats were potentially more sustainable solutions (Supplement A1). In 2017, Hu island of Puerto Rico. Concerns over vector borne diseases increased island-wide due to deforestation, high accumulation of debris deteriorated housing infrastructure (Supplement A2). Members of the research team consulted with EPA Region 2 and local commu interventions to minimize the potential impacts of mosquito outbreaks on the local communities. The final journal articles were sha Bay Estuary Program, the Caño Martín Peña community group, and the San Juan Urban Long-term Research Area (Supplement B1 of Southern Mississippi have continued mosquito field sampling efforts in Caño Martín Peña after 2017 to further tease apart socio- incidence, impacts of Hurricane Maria on mosquito populations, and mechanistically understand relationships between mosquito st and vector capacity.

This research has been highlighted in a number of news articles. EPA profiled how this research is helping to support the National Estuary Prog simultaneously improve the health and sustainability of neighborhoods adjacent to the estuary. University of Southern Mississippi collaborator Reveal News shortly after field sampling in 2016, where he described the potential linkages between water quality and Zika, as well as the enga of the Martin Peña community to conduct sampling (Supplement A4).

- https://www.epa.gov/eco-research/epa-research-supports-national-estuary-program
- https://www.revealnews.org/episodes/from-a-to-zika/

The authors of this work have been invited to present this work at numerous conferences or symposiums. In an invited presentation to the "One Environmental Toxicology and Chemistry North America 39th Annual Meeting (SETAC, Sacramento, California 2018), the two studies were u

DPSIR (Driver-Pressure-State-Impact-Response) framework can be used to link influences of environment, society, and economic status in vec
actions to mitigate disease risk. The research was also included as part of an invited session on "Governance Barriers and Opportunities for Int
Estuary and Coastal Management" at A Community on Ecosystem Services conference (ACES, 2018, Washington DC), where environmental

described alongside potential effects on asthma and gastrointestinal illnesses as part of a broader description of potential health benefits of estua
was invited to present the research at the Society of Vector Ecology Conference in San Juan, Puerto Rico in 2019 as part of a special session on
mosquitoes in Puerto Rico", as well as being invited to present as the keynote speaker at the Odum School of Ecology Graduate Student Sympo

· Fisher, W., R. DeJesus-Crespo, and S. Yee. 2018. A Health and Ecological Systems Framework for Vector-Borne Diseases in Puerto Rico. S
and Chemistry North America 39th Annual Meeting, Sacramento, CA, November 04 - 08, 2018.

· Yee, S.H., R. de Jesus Crespo, D. Betancourt, T. Dean. 2018. Linking Ecosystem Services to Human Health to Inform Estuary M
Community of Ecosystem Services 2018 Conference, Washington D.C. https://conference.ifas.ufl.edu/aces18/speaker-presentations

· De Jesus Crespo, R. 2019. The role of ecosystem services on species assemblages and arbovirus disease transmission along urba
Society for Vector Ecology Conference, San Juan, Puerto Rico.

· De Jesus Crespo, R. 2020. Zooming out and in: applying geo-spatial technology and stakeholder engagement to study eco-health
Odum School of Ecology Graduate Student Symposium, Athens, Georgia, 2020. http://gsa.ecology.uga.edu/wp-content/uploads/20

Lessons learned from this study are being applied by researchers at Louisiana State University to the city of New Orleans, which lil
area with frequent flooding and water pollution problems. The relationships between the LSU effort and the nominated San Juan st
university news articles (Supplement B3).

· https://www.lsu.edu/cce/newsevents/news/2019/08/09-de-jesus-crespo-mosquitoes.php

·
https://www.lsureveille.com/news/lsu-professor-studies-virus-carrying-mosquitoes-conducting-research-in-new/article_72d49a9a-c

This research has received a number of awards, including the EPA ORD 2017 Environmental Justice Award (Supplement A5) for '
development of research to link wetland ecosystem services to mosquito-vectored diseases in Environmental Justice communities i
contributed to Dr. de Jesus Crespo being awarded an Early Career Fellowship from the National Academies of Science Gulf Resear

· https://www.nationalacademies.org/gulf/fellowships-and-grants/current-and-past-early-career-research-fellows

According to Google Scholar, these two articles have been cited 9 times in the past two years. Lessons from these studies were integrated i
EcoHealth evidence can be applied in community decision-making (Johnston et al. 2017 Supplement B5).

· Sutton-Grier, A. E., & Sandifer, P. A. (2018). Conservation of wetlands and other coastal ecosystems: a commentary on their value to protec and promote human health and well-being. *Wetlands*, 1-8.

· McFarlane, R. A., Horwitz, P., Arabena, K., Capon, A., Jenkins, A., Jupiter, S., ... & Saketa, S. H. (2019). Ecosystem services for human he (C).

· Luo, K., & Mornya, P. M. (2019). Fine Monitoring of Wetlands at Provincial Large-Scale Using Object-Based Technique and Medium-Res *Selected Topics in Applied Earth Observations and Remote Sensing*, *12*(8), 2878-2888.

· Summers, J. K., Smith, L. M., Fulford, R. S., & de Jesus Crespo, R. (2018). The Role of Ecosystem Services in Community Well-Being. *Ec* 145.

· Murry, B. A. (2019). Wetland Conservation Requires Transition toward Landscape-Scale Interdisciplinary Approaches. *Wetlands*, 1-6.

· Febles, N. Á., & Félix, G. F. (2020). HURRICANE MARÍA, AGROECOLOGY, AND CLIMATE CHANGE RESILIENCY. *Climate Justi Resistance and Grassroots Solutions*, 9.

· Crespo, R. D. J., Wu, J., Myer, M., Yee, S., & Fulford, R. (2019). Flood protection ecosystem services in the coast of Puerto Rico: Associati hazard mitigation and gastrointestinal illness. *Science of the total environment*, *676*, 343-355.

· Sukiato, F., Wasserman, R. J., Foo, S. C., Wilson, R. F., & Cuthbert, R. N. (2019). The effects of temperature and shading on mortality and (Diptera: Culicidae). *Journal of Vector Ecology*, *44*(2), 264-270.

· Johnston, J.M., R. de Jesus Crespo, M. Harwell, C. Jackson, M. Myer, N. Seeteram, K. Williams, S. Yee, J. Hoffman. 2017. Val Ecosystem Goods and Services: Human Health and Ethnographic Approaches as Complements to Economic Valuation. US Enviro Washington, DC. EPA/600/R-17/309.

Justification 3B:

De Jesus et al. 2018 was invited by Brent Murry (U.S. Fish and Wildlife Service) as an article contribution for a special issue on "L Management" for the journal Wetlands. The article followed EPA's management clearance process, as well as journal editorial and review included the Branch Chief and Division Director internal reviews, as well as an external review by the special issue organiz reviews were performed by the editor, and two anonymous peer reviewers.

Yee et al. 2019 was submitted and accepted by the journal EcoHealth. The article followed EPA's management clearance process, a peer-review processes. The EPA review included the Branch Chief and Division Director internal reviews, as well as an external re mosquito ecologist at the University of Maryland. The journal reviews were performed by the editor, one anonymous peer reviewer reviewer, Dr. John Drake, a distinguished research professor of infectious disease ecology at the University of Georgia.

AUTHORS

Contributing Author

Author Name:	Susan Yee		
Professional Title:		Salutation:	
Email:	yee.susan@epa.gov	Organization:	
Mailing Address:			
Street Line 1:			
City:			
Zip Code:		State:	
At time of research was:	EPA Employee		
Separation Date:			
% of Effort:	28		

Contributing Author

Author Name:	Rebeca de Jesus Crespo		
Professional Title:		Salutation:	
Email:	rdejesuscrespo1@lsu.edu	Organization:	
Mailing Address:			

Street Line 1:		
City:		
Zip Code:		State:
At time of research was:	EPA Employee	
Separation Date:	Sat Dec 01 00:00:00 GMT 2018	
% of Effort:	40	

Contributing Author

Author Name:	Stephanie Friedman	
Professional Title:		Salutation:
Email:	friedman.stephanie@epa.gov	Organization:
Mailing Address:		
Street Line 1:		
City:		
Zip Code:		State:
At time of research was:	EPA Employee	
Separation Date:		
% of Effort:	5	

Contributing Author

Author Name:	Donald Yee	
Professional Title:		Salutation:
Email:	donald.yee@usm.edu	Organization:
Mailing Address:		

Street Line 1:		
City:		
Zip Code:		State:
At time of research was:	Non EPA Personnel	
Separation Date:		
% of Effort:	10	

Contributing Author

Author Name:	Autumn Oczkowski	
Professional Title:		Salutation:
Email:	oczkowski.autumn@epa.gov	Organization:
Mailing Address:		
Street Line 1:		
City:		
Zip Code:		State:
At time of research was:	EPA Employee	
Separation Date:		
% of Effort:	5	

Contributing Author

Author Name:	Pablo Mendez Lazaro	
Professional Title:		Salutation:
Email:	pablo.mendez1@upr.edu	Organization:
Mailing Address:		

Street Line 1:		
City:		
Zip Code:		State:
At time of research was:	Non EPA Personnel	
Separation Date:		
% of Effort:	7	

Contributing Author

Author Name:	Fengwei Bai	
Professional Title:		Salutation:
Email:	fengwei.bai@usm.edu	Organization:
Mailing Address:		
Street Line 1:		
City:		
Zip Code:		State:
At time of research was:	Non EPA Personnel	
Separation Date:		
% of Effort:	5	

PUBLICATIONS

Publication 1:

Publication Title:	Linking Water Quality to Aedes aegypti and Zika in Flood-Prone Neighborhoods
Publication Date:	Wed Apr 03 00:00:00 GMT 2019
Journal/Publication Method:	EcoHealth

All Author(s):		
Volume:	16	Number:
Pages:	191-209	Immediately
Citation ½ Life:	7.1	Impact Facto

Publication 2:

Publication Title:	Linking wetland ecosystem services to vector borne disease: Dengue fever in San Juan Bay Estuary, Pu	
Publication Date:	Tue Jan 23 00:00:00 GMT 2018	
Journal/Publication Method:	Wetlands	
All Author(s):		
Volume:	39	Numb
Pages:	1281-1293	Immec
Citation ½ Life:	9.7	Impact

EcoHealth
https://doi.org/10.1007/s10393-019-01406-6

EcoHealth

© 2019 This is a U.S. government work and its text is not subject to copyright protection in the United States; however, its text may be subject to foreign copyright protection

Original Contribution

Linking Water Quality to *Aedes aegypti* and Zika in Flood-Prone Neighborhoods

Susan Harrell Yee,[1] Donald A. Yee,[2] Rebeca de Jesus Crespo,[1] Autumn Oczkowski,[3] Fengwei Bai,[2] and Stephanie Friedman[1]

[1]*Gulf Ecology Division, National Health and Environmental Effects Research Laboratory, U.S. Environmental Protection Agency, 1 Sabine Island Drive, Gulf Breeze, FL 32561*
[2]*Department of Biological Sciences, University of Southern Mississippi, Hattiesburg, MS 39406*
[3]*Atlantic Ecology Division, National Health and Environmental Effects Research Laboratory, U.S. Environmental Protection Agency, Narragansett, RI 02882*

Abstract: The ability of ecosystems to regulate water quality and flood events has been linked to health outcomes, including mosquito-borne illnesses. In the San Juan Bay Estuary watershed of Puerto Rico, habitat alterations and land-use development have disrupted watershed hydrology, exacerbating wastewater discharges and subjecting some neighborhoods to frequent flooding events. In 2016, the mosquito-borne illness Zika became a new cause for concern. We hypothesized that nutrient-enriched flood water could provide pulses of supplemental nutrients to local mosquito populations. We conducted a field study in six neighborhoods adjacent to the estuary to assess whether environmental variability of nutrient inputs could be linked to breeding habitat containers, *Aedes aegypti* larvae and adults, and the acquisition of Zika virus by adult mosquitoes. The most frequently flooded neighborhood had consistently higher levels of nitrogen in estuary water, leaf detritus, containers, and adult mosquitoes compared to other neighborhoods. Adult body nitrogen was significantly related to both nitrogen content of containers and leaf detritus from the local trapping area. Disseminated Zika concentration in adult *Ae. aegypti* tended to decrease as body carbon and nitrogen increased. Our study provides preliminary evidence that environmental variability in nutrient inputs can influence viral acquisition by mosquito vectors. This suggests that management actions to reduce flooding and improve water quality should go hand-in-hand with more traditional vector control methods, such as aerial spraying, to help control spread of vector-borne diseases.

Keywords: *Aedes aegypti*, Nitrogen, Carbon, Stable isotopes, Zika

Introduction

Decision makers are increasingly framing environmental management issues within the context of benefits to the health and well-being of stakeholders (Rhodus et al. 2013; Korfmacher et al. 2015; Oosterbroek et al. 2016). Land-use change, climate change, and point and nonpoint source

Susan Harrell Yee and Donald A. Yee have contributed equally to this manuscript.

Correspondence to: Susan Harrell Yee, e-mail: yee.susan@epa.gov

Published online: 03 April 2019

runoff alter the state of ecosystems and their services, including disservices, leading to subsequent effects on human health (Myers et al. 2013). The ability of ecosystems to regulate water quality and flood events has been linked to decreases in a number of health outcomes, including infectious and parasitic diseases, mental disorders, and respiratory illnesses (Hinga and Batchelor 2005; Ivers and Ryan 2006; Oosterbroek et al. 2016; De Jesus Crespo and Fulford 2017). In coastal communities, greenspaces such as wetlands may play a role in mitigating mosquito-borne illnesses by moderating flooding events or regulating water quality (Carver et al. 2015; De Jesus Crespo et al. 2018). With growing concerns about the health risks of aerial spraying for mosquitoes, alternative management strategies that leverage these natural ecosystem services may provide more sustainable approaches to managing mosquito vectors.

Estuary management programs, in particular, have been linking actions to improve the habitat and water quality of the estuary to goals of improving human health and public safety (SJBEP 2000). For example, the San Juan Bay estuary, Puerto Rico, comprises a connected system of bays, lagoons, and canals in a highly urbanized watershed of over half a million residents, with socioeconomic conditions varying widely across neighborhoods (Azar and Rain 2007). Habitat alterations and land-use development have disrupted the natural flow of water throughout the estuary system, subjecting some neighborhoods to frequent flooding events and exacerbating the effects of wastewater discharges, including untreated sewage and stormwater runoff into areas of the bay (SJBEP 2000). A recent Health Impact Assessment identified vector-borne illnesses, including dengue, as a major health concern for flood-impacted communities neighboring the estuary (Sheffield et al. 2014; Korfmacher et al. 2015), and supported efforts to reduce flooding and debris that create mosquito breeding sites (Ahern et al. 2005; Pires and Gleiser 2010).

Most recently, the mosquito-borne illness Zika has become a cause for concern. Zika virus (ZIKV) is a flavivirus, closely related to other arboviruses like dengue, West Nile, and yellow fever, and was originally isolated in Uganda, Africa (Dick et al. 1952; Musso and Gubler 2016). ZIKV was first detected in the Americas in Brazil in 2015 (Zanluca et al. 2015) and spread explosively throughout the Americas in 2016 (WHO 2016a). The first confirmed case of locally acquired Zika infection in Puerto Rico was reported in December 2015 (WHO 2016b), and Zika cases continued to increase rapidly, peaking in August 2016 with as many as 2500 confirmed cases per week (Puerto Rico Department of Health 2017). In North America, *Aedes aegypti* and *Ae. albopictus* are the only mosquitoes known to be competent vectors of ZIKV (Chouin-Carneiro et al. 2016), with only *Ae. aegypti* known to have an established distribution in Puerto Rico (Sharp et al. 2013).

Like other arboviruses, transmission of Zika virus is influenced by a complex array of interactions among humans, wildlife, mosquito vectors, and the environment (Thomas et al. 2017). Mosquitoes become exposed to virus when they take a blood meal from an infected person (Gratz 2004), or wildlife that may serve as pathogen reservoirs (Gonzalez-Salazar et al. 2017). The virus then replicates in the mosquito's midgut and salivary glands, and after an incubation period, may be spread when the infectious mosquito takes its next blood meal (Musso and Gubler 2016). The capacity of a mosquito vector to spread a virus depends on factors such as the probability of acquiring and transmitting the pathogen, the proportion of vectors acquiring the pathogen, and the density of vectors per human host (Anderson and Rico-Hesse 2006; Klempner et al. 2007). Environmental factors, such as larval nutrition (Nasci and Mitchell 1994), larval density (Alto et al. 2005; 2008a; Reiskind and Lounibos 2009), adult nutrition (Canyon et al. 1999), adult body size (Scott et al. 2000; Alto et al. 2008b), and seasonality and climate (Almeida et al. 2005), have all been shown to affect virus acquisition for mosquitoes. Moreover, a handful of studies have directly linked water quality factors, such as nutrient enhancement through fertilizer runoff (Mutero et al. 2004) or water chemistry in septic systems (Burke et al. 2010), to the abundance of mosquito larvae and adults. To our knowledge, however, no studies have assessed whether local variability in water quality can be linked to variability in the acquisition of virus by adult mosquitoes. As a result, the degree to which proposed actions in the San Juan Bay watershed to reduce sewage discharges, improve stormwater drainage, and restore natural flow could mitigate vector-borne illnesses (Sheffield et al. 2014; Korfmacher et al. 2015) is challenging to ascertain.

We hypothesized that variability in point and nonpoint source runoff creates variability in estuary water quality (Fig. 1). During extreme rainfall events, larval habitat containers, such as buckets, food containers, or discarded vehicle tires, may experience inputs of flood waters as rivers, canals, or lagoons overflow (Hashizume et al. 2012). Normally, larval containers are filled through precipitation events, and allochthonous inputs from leaf or animal

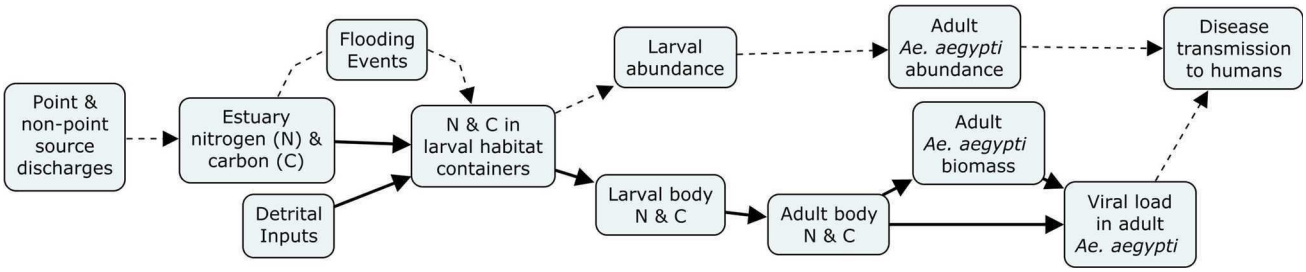

Figure 1. Causal flow diagram illustrating how nitrogen and carbon inputs into mosquito larval containers through flooding events and detrital inputs could influence viral load in adult mosquitoes and ultimately disease transmission to humans. Solid paths were tested with field data; dashed paths were inferred.

detritus are important sources of nutrients (Kling et al. 2007). In areas where waterbodies are subjected to runoff or wastewater discharges, flood water could provide pulses of supplemental nutrients to local mosquito populations, dependent on the frequency of flooding. In larval containers, nutrients such as nitrogen are often limiting, such that the growth, survival, and mass of larvae, and consequently of adults, are crucially affected by allochthonous inputs (Carpenter 1983; Yee and Juliano 2006). Nutrition and mass subsequently affect the acquisition and multiplication rates of virus within adult mosquitoes (Nasci and Mitchell 1994; Canyon et al. 1999; Scott et al. 2000; Alto et al. 2008b) and ultimately, along with the abundance of infected mosquitoes (Klempner et al. 2007), transmit to humans.

We conducted a field study in neighborhoods bordering water bodies within the San Juan Bay estuary system in June 2016, when confirmed Zika cases in Puerto Rico were approximately 672 per week and were rapidly increasing (Puerto Rico Department of Health 2016). In each neighborhood, we assessed the particulate nitrogen and carbon content of estuary water, leaf detritus, water from larval containers, *Ae. aegypti* larvae within containers, and local adult *Ae. aegypti* populations, to determine the degree to which environmental variability in nutrients is carried through to adult mosquitoes. Sampling locations were chosen to cover a range of variability in water quality, observed in periodic water quality monitoring data (SJBEP 2016), in order to maximize our potential to detect differences. Finally, we tested adults for ZIKV to determine whether adult nutrition affects acquisition of Zika virus. By simultaneously collecting field data on water quality, leaf detritus, larval habitat, mosquito larvae, mosquito adults, and virus, our study is one of the first to attempt to connect environmental variability to the capacity of mosquito vectors to spread disease.

Study Area

The San Juan Bay Estuary (SJBE) is an interconnected system of channels and lagoons, many of which have been severely altered by human activity (Brandeis et al. 2014). The SJBE is the only tropical estuary in the US National Estuary Program, and is the most highly urbanized, with approximately 82% of the watershed developed. The remaining watershed is dominated by moist forest and wetlands, including the most extensive contiguous mangrove forest in Puerto Rico (Brandeis et al. 2014). We selected neighborhoods adjacent to six waterbodies: La Malaria channel, Martin Peña channel, Suarez channel, Torrecilla Lagoon, Piñones Lagoon, and Rio Piedras (Fig. 2). Waterbodies were chosen to reflect a range of water quality parameters, including salinity (0.17–34.03 PSS; SJBEP 2016), nitrogen (0.23–35.6 Kjeldahl nitrogen mg/L; SJBEP 2016), and carbon (0.122–7.475 TOC mg/L; SJBEP 2016). Cumulative Zika cases up to June 2016 were comparable across the four municipios (i.e., county-equivalent areas) covered by the study area (Puerto Rico Department of Health 2016; Cataño municipio, 175 cases per 100,000 inhabitants; San Juan municipio, 293 cases per 100,000 inhabitants; Carolina municipio 156 cases per 100,000 inhabitants; Loiza municipio: 136 cases per 100,000 inhabitants).

We focused our most intensive sampling efforts on the Martin Peña neighborhood, with the five other waterbodies included for comparison. The Martin Peña neighborhood comprises eight distinct adjoining communities, but is referred to as a single neighborhood as the sampling unit for the purpose of this study. Decades of unregulated dumping and construction into the severely blocked Martin Peña Channel, along with deficient sewage infrastructure and direct discharges of untreated residential wastewater, has led to frequent flood events during which residents are

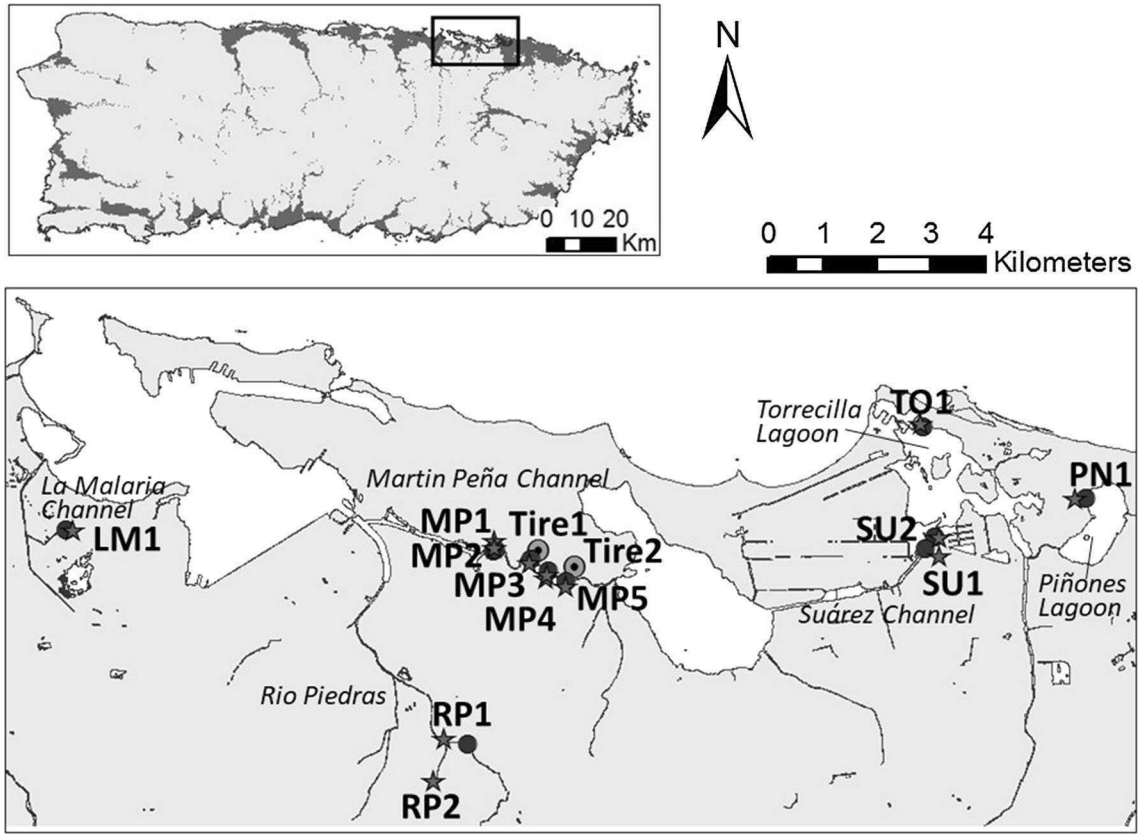

Figure 2. Water, larval habitats, and adult mosquitoes were sampled from FEMA flood zones (gray shaded areas) in and around San Juan, Puerto Rico. Mosquito trap locations (stars) and estuary sampling locations (solid circles) were sited within each of six sampled neighborhoods. Larval habitat containers were located and sampled within 150 meters of traps. Two tire piles (concentric circles) were also sampled for comparison to dispersed containers.

exposed to polluted surface waters in their homes and roadways (Korfmacher et al. 2015). As many as 70% of residents report flooding in or near their home in a given year, with some residents reporting their homes flooded upwards of 20 times per year (Sheffield et al. 2014). Flood waters often reach heights greater than 30 cm, sufficient to cover accumulated trash from illegal dumping or other containers. The Martin Peña neighborhood experienced such a flood event two weeks prior to our June 2016 sampling. Sampled neighborhoods from other waterbodies were also within established flood zones (FEMA 2009; Fig. 2), though it is unknown whether they had experienced flooding recent to our field sampling.

Study Design

A sampling site within each neighborhood was defined by the placement of an adult mosquito trap within 50–150 m of the adjacent waterbody and any sampled larval container habitats within 150 m of that trap (Fig. 2). All trap locations were adjacent to water sources within the estuarine watershed, with similar vegetation and canopy cover. With the exception of a state forest location near Piñones Lagoon (PN1), all trap locations were within the San Juan metropolitan area in neighborhoods with dense housing. Across the six neighborhoods, we placed a total of 12 adult mosquito traps, with between 1 and 5 traps placed per neighborhood. We searched for water-filled containers with larvae in the 150 m radial area surrounding each trap, with between 1 and 4 larval containers located and sampled per trap (Table 1). Container sampling was highly dependent on our ability to find containers in accessible areas (e.g., not in a private yard), and we cannot assume potential sources for adults were exhaustively sampled. However, adult *Ae. aegypti* typically disperse less than 150 m (Harrington et al. 2005), so larval containers at each sampling site were assumed to be a representative source of adult mosquitoes in that area. Sites were sampled on June 7 and

Table 1. Number of Estuary Water Samples and Mosquito Larvae Containers Sampled Corresponding to Each Trap Location, as Well as the Number of Adult *Aedes aegypti*.

Neighborhood	Trap location	Flood composite index	Estuary water samples	Leaf samples	Larval container samples	Female *Ae. aegypti* per trap	Fraction *Ae. aegypti* infected with ZIKV
Martin Peña Channel	MP1	3.25	3	4	1 Tire	18	0/18
	MP2	7.21	2[a]	3	3 Tires, 1 bucket	13	0/13
	MP3	7.65	3	4	1 Tire, 1 bucket, 1 small tub	0	–
	MP4	6.14	3	3	1 Tire, 1 small tub	16[c]	0/15
	MP5	2.50	3	4	2 Buckets	27[c]	0/12
Piñones Lagoon	PN1	8.90	3	5	1 Large boat, 1 large bin	7	0/7
Rio Piedras	RP1	3.00	3[b]	3	1 Tire	10	6/10
	RP2	1.03	0	0	0	4	1/4
La Malaria channel	LM1	3.18	3	0	1 Tire, 1 small boot, 1 small pan	*Trap malfunction*	
Suárez channel	SU1	2.48	1[a]	0	1 small bin	2	1/2
	SU2	3.00	3	4	0	3	1/3
Torrecilla Lagoon	TO1	5.21	3	4	0	30	9/30
Tire Pile 1	–	7.71	–	–	5 Tires	–	–
Tire Pile 2	–	2.93	–	–	5 Tires	–	–

[a]Additional samples with peak areas of < 0.5 nA were removed from analysis.
[b]All samples had peak areas < 0.5 nA, but were included in analysis to prevent total loss of data.
[c]Not all females were tested for virus due to methodological limitations.

8, 2016, with approximately half of the sites sampled each day.

To collect adult mosquitoes, we used BG-Sentinel traps (Biogents AG, Regensburg, Germany), baited with a human scent lure (BG-Lure; Biogents AG). BG-Sentinel traps are effective at capturing host-seeking adult *Ae. aegypti* (Maciel-de-Freitas et al. 2006), which are likely to have taken a blood meal and thus been exposed to virus. A battery-operated fan prevents adults from escaping after they have entered the trap. Efforts were made to centrally locate each trap among paired sampled containers, dependent on the ability to place traps in a secure location, such as the gated yard of a homeowner, to minimize disturbance. Traps were left out for a 48-h period before adults were collected. One trap malfunctioned (LM1; Fig. 2) and therefore did not capture any adults. Collected adults were identified to sex and species, with 0–30 female *Ae. aegypti* collected per trap (Table 1). Only adult female *Ae. aegypti* were used for subsequent analysis. Adults were frozen and transported to the respective laboratories for nutrient and ZIKV analysis.

For each trap location, we collected three 50 mL samples of surface water from each waterbody, within the shortest direct distance of the approximate center of that site. Water samples were filtered on site through 2.5-cm glass fiber filters (Whatman GF/F), with filters immediately placed on ice and then in a drying oven within a few hours of collection each day. Because water samples are highly dynamic, varying daily with recent precipitation, runoff, or waterflow, we also collected three leaf samples from the dominant vegetation (i.e., typically mangrove) directly adjacent to the water sampling location as a long-term, more stable proxy of local waterbody nutrients. Leaves were placed in a drying oven within a few hours of collection. For a few locations (RP2, LM1, SU1), leaf or water samples could not be collected due to accessibility issues. All samples were dried at 65°C for approximately 48 h before being transported to the continental USA.

We similarly filtered three 50 mL water samples from any accessible larval container habitats that could be located at each sampling site. Containers included discarded

plastic food containers, buckets, rubber boots, plant trays, and discarded vehicle tires, and had to contain live *Ae. aegypti* larvae to be included. Subsamples of approximately 5–10 *Ae. aegypti* larvae were collected from each container and placed on a filter in the drying oven at the end of each collection day. In addition to scattered containers, we also sampled water and larvae from tires from two tire shops within the Martin Peña neighborhoods (Table 1). Because tire shops experience frequent turnover, we treated them as separate sampling locations from scattered discarded containers which, based on visual inspection, likely spent a much longer time in the environment and had a greater likelihood of having received environmental inputs. For example, although used tires at the shop near MP3 (Tire 1; Fig. 2) had been flooded with water approximately 0.5 meters high in the week prior to our study, they had already been removed for recycling, with the more recent tires that we sampled having not been exposed to flood water (personal communication with shop employee).

Nutrient Analysis

Filtered contents from waterbody and container water, leaf samples, larvae samples, and adults were analyzed for particulate nitrogen (N) and carbon (C) content. Due to low body weight, 5–10 larvae were analyzed as a single sample. After removing heads for ZIKV analysis, individual adult mosquitoes were analyzed separately.

We hypothesize that nutrient content (%N, %C, C:N) of larval container habitats and subsequent adult mosquitoes would be similar to nutrient content of adjacent waterbodies, either directly via flood water or indirectly through detritus, such that containers or adults from the same trap location are more similar to one another than those from other locations. Additionally, nitrogen (δ^{15}N) and carbon (δ^{13}C) stable isotopes were used to track the unique source locations of nutrients. Stable isotopes provide a record of assimilation, processing, and recycling of nutrients, such that samples collected from different locations can have unique isotopic signatures, particularly from anthropogenic sources such as fertilizer or sewage discharges (Oczkowski et al. 2009, 2011). Similar isotope values between waterbodies and larval containers or adults would provide further support that local waterbodies were sources for nutrients, above and beyond any similarities in nutrient content.

Carbon and nitrogen stable isotopes were measured using an Elementar Vario Micro elemental analyzer connected to a continuous-flow Isoprime 100 isotope ratio mass spectrometer (Elementar Americas, Mt. Laurel, NJ) at the Environmental Protection Agency in Narragansett, Rhode Island. Replicate analyses of isotopic standard reference materials USGS 40 (δ^{13}C = − 26.39‰; δ^{15}N = − 4.52‰) and USGS 41 (δ^{13}C = 37.63‰; δ^{15}N = 47.57‰) were used to normalize isotopic values of working standards (blue mussel homogenate) to the air (δ^{15}N) and Vienna Pee Dee Belemnite (δ^{13}C) scales (Paul et al. 2007). Isotope values are expressed in δ notation following the formula $\delta X\ (‰) = [(R_{sample}/R_{standard}) - 1] \times 10^3$, where X is ^{13}C or ^{15}N and R is ^{13}C/^{12}C or ^{15}N/^{14}N isotopic ratio, respectively. Working standards were analyzed after every 24 samples to monitor instrument performance and check data normalization. The precision of the laboratory standards was better than ± 0.3‰ for C and N. A few samples with peaks less than 0.5 were excluded from analysis to improve accuracy, except where removal would result in the complete elimination of a sampling site (RP1). Analyses in which RP1 was included were consistent with those where it was removed.

The sample particulate N and C content was calculated from area/mass relationships, determined during stable isotope analysis, for replicate standards of known N and C (Oczkowski et al. 2009, 2011). The relationship between the N and C contents of the standards and their analytical peak areas were used to determine the N and C contents of the samples via the peak areas of the samples. For adult mosquitoes, larvae, and leaf detritus, sample N or C was divided by total sample mass to determine the %N or %C. For particulate matter, N and C content was expressed in mg/L by dividing the mg of N and C by the volume of water filtered (usually 50 mL).

ZIKV Processing

To quantify the level of infection with ZIKV, heads from individual adult females were analyzed to assess disseminated virus rather than viruses that might be within a blood meal in the midgut. Total RNA in individual mosquito heads was isolated using TRI-reagent (Molecular Research Center, Inc., Cincinnati, OH, USA). Complementary DNA (cDNA) was synthesized using the iSCRIPT cDNA Synthesis Kit (Bio-Rad Laboratories, Inc.), and RT-qPCR assays were performed in a CFX96 Real-Time System (Bio-Rad Laboratories, Inc.) using iTaq Universal Probe Supermix (Bio-Rad Laboratories, Inc.). The RT-qPCR procedure was performed twice for each sample. Primers

and a probe specific to the Envelope gene of ZIKV were designed and synthesized according to the previous work (Acharya et al. 2016). Due to methodological and cost restrictions, we were limited to testing two batches of 57 individual female adults for ZIKV, for a total of 114 tested adults. After 40 PCR cycles, zero or trace amounts of ZIKV near or below threshold detection limits were considered as zeros ($<$ 1.2 ZIKV E copies/ng total RNA), with values greater than 18 ZIKV E copies/ng total RNA considered as true positives for Zika.

In anticipation of a second Zika outbreak in summer 2017, we repeated the adult mosquito trapping in June 2017 (Appendix A) with the intention of comparing the relationships between adult body nutrients and ZIKV from 2016 to 2017. However, by then, confirmed Zika cases in humans had dropped to less than ten per week across all of Puerto Rico and were continuing to decline (Puerto Rico Department of Health 2017). We detected no virus in trapped adult *Ae. aegypti* from June 2017 (Appendix A). Therefore, here we focus our analysis solely on June 2016 data.

Statistical Analysis

To assess potential linkages between environmental variability in nutrients and ZIKV in adult mosquitoes (Fig. 1), we first assessed whether there was significant natural spatial variability in nutrients from either estuary water or potential leaf detritus, in body nutrients of larval or adult mosquitoes, and in ZIKV concentration. Second, we used multiple regressions to explore whether nutrient variability and ZIKV concentration in mosquitoes could be explained by nutrient variability in the local environment.

We used nested Multivariate Analysis of Variance (MANOVA) to test if trap locations or neighborhoods differed significantly in nutrients, including N, C, δ^{13}C, δ^{15}N, and the ratio of C to N, for waterbody water samples, leaf detritus samples, container water samples, larvae samples, or adult samples. Adult mass was included as an additional dependent variable along with nutrient variables in the adult MANOVA. Trap locations were nested within each neighborhood. If MANOVAs were significant, we followed up with univariate ANOVAs to determine which nutrient variables were most likely contributing to any significant differences. Due to unbalanced sampling design, with a variable number of replicates per location, we used Type II Sums of Squares to assess significance. The sampling units for each trap location were the individual 50 mL waterbody water samples (1–3 per location), individual leaves (1–3 per location), the average of the replicate water samples from each container (1–5 per location), the combined larval value per container (1–5 per location), or individual adults (2–30 per location). Data were tested for normality and Box–Cox-transformed as needed to normalize data prior to analysis. Significant differences between pairs of trap locations or neighborhoods were assessed using Tukey-adjusted least squares means. MANOVAs were conducted in R (www.r-project.org) using the "stats" and "lsmeans" libraries.

To test whether ZIKV concentration differed significantly across locations or neighborhoods, we used general linear models (GLMs) with a Tweedie distribution because ZIKV concentration data were not normal due to a high frequency of zeroes in non-infected mosquitoes. The Tweedie distributions describe a family of distributions characterized by a power parameter, p, which includes the special cases of Poisson or gamma distribution for $P = 1$ or $P = 2$, respectively. For $1 < P < 2$, the distribution is a compound Poisson-gamma distribution, which allows for bimodal distributions where variables are described by different underlying processes, namely a discrete Poisson distribution (e.g., the number of mosquitoes positive for ZIKV) with a continuous gamma distribution (e.g., ZIKV concentration levels within positive mosquitoes). The Tweedie distribution is a good choice for bimodal or zero-inflated data that contain a large number of zeros (Shono 2008). We first estimated the power parameter, p, of the Tweedie function for the ZIKV concentration data using maximum likelihood and then used this fitted distribution, with a log-link power function, in the GLM. The sampling unit was individual adult mosquitoes (2–30 per location), with trap locations nested within neighborhoods. Analyses were conducted in R (www.r-project.org) using the package "tweedie" within "statmod." Results were consistent with a standard logistic regression analysis on the fraction of Zika-positive adults per trap (GLM with a binomial distribution, not shown).

We used a series of multiple regressions to determine whether differences in container nutrients, larval nutrients, adult nutrients, adult mass, or ZIKV concentration could be explained by differences in the nutrient concentrations from potential nutrient sources. To minimize the number of possible explanatory variables under consideration, we limited fixed effects in each regression to the most proximate potential source for nutrients (Fig. 1): (1) waterbody nutrients or leaf detritus nutrients were considered as

explanatory variables for container nutrient content, (2) container nutrients were considered as explanatory variables for larval nutrient content, (3) larval nutrients were considered as explanatory variables for adult nutrient content, (4) adult nutrient content was considered as explanatory variables for adult mass, and (5) adult nutrient content or mass was considered as explanatory variables for ZIKV concentration. Because trapped adults did not directly originate from sampled larvae, we also included the average container nutrients, leaf detrital nutrients, and waterbody nutrients within each neighborhood as potential predictors of adult nutrient content.

In addition to nutrient sources, we considered the influence of flooding and container availability (i.e., type and number) on the dependent variables in regressions. Sampled containers were categorized as tires, 5-gallon buckets, small miscellaneous containers (e.g., boots, food tubs), and large miscellaneous containers (e.g., boat, plastic bin). Because we could not definitively know whether individual sampled containers had flooded recently, we instead used the Flood Hazard Composite Index (NOAA 2018) as a proxy for the likelihood of neighborhood flooding (Table 1). The Composite Index counts the number out of 10 flood hazard data sets, including FEMA flood zones, shallow coastal flooding, and storm surge, that intersect each pixel, which we then averaged to estimate a single value for a 150-m radius around each trap location. Because inputs of containers into nutrients are idiosyncratic and potential inputs from flooding would depend on waterbody nutrients, we did not expect that nutrient content would be significantly related to container type or flood risk (e.g., smaller containers have lower nitrogen; flooded sites have higher nitrogen). Indeed, preliminary analysis with these variables as fixed effects in regressions confirmed no significant relationships between container type or flood risk and nutrient content of containers, larvae, or adults. However, frequent flooding or container type could impact the variability in nutrient content across samples. For example, recently flooded containers may be similar to one another; small containers may be more variable than larger ones; adults emerging from sites with numerous container habitats may be more variable than adults originating from sites with few. Moreover, tires and recently flooded sites in Martin Peña were more heavily sampled than other sites or types of containers, contributing to heteroscedasticity in fitted models. Hence, we tested whether homogeneity of residuals significantly improved when model variance was allowed to vary with either container type, container count around each adult trapping site, or flood risk. Variance structure was modeled in R using "*varPower*" for continuous effects (flood risk, container count) and "*varIdent*" for categorical effects (i.e., container type).

Because there were multiple replicates (e.g., containers, adults per trap) within each sampling site, we accounted for repeated measures in regression analysis by treating trap location as a random effect. Replicates (e.g., waterbody water samples) were averaged to produce a single value to be paired with each sample (e.g., container) at each trap location. For sites MP3 and MP5, including nearby tire piles in container and larval averages as potential sources for adult nutrients did not change results (not shown). Locations with incomplete data (e.g., no leaf samples due to inaccessibility) were dropped from regressions. All variables were Box–Cox-transformed to adhere to assumptions of normality and minimize nonlinear relationships that can arise from non-normal data. Variables were then standardized (mean-centered and scaled by standard deviation) to facilitate the comparison of model coefficients for variables of different magnitude, such that mean relationships with each variable can be interpreted by setting other fixed effects in the fitted regression equation to their standardized mean of zero. Highly correlated variables (Pearson correlation coefficient, $r > 0.5$) were prohibited from simultaneously being allowed as predictor variables to prevent issues with collinearity (e.g., C or N with C:N ratio). Regressions were conducted in R using procedure "lme" within package "nlme" for nutrients and mass, assuming a normal distribution, and with procedure "glmer" within package "lme4" for ZIKV, assuming a Tweedie distribution. For regression analyses, we followed a basic mixed-effects modeling protocol (Zuur et al. 2009; Lima 2017): i) fit the full model with all fixed effects and random effect (location) using maximum likelihood (ML), ii) test for heteroscedasticity and the significance of variability weights (container type, container count, or flood risk) in improving homogeneity of residuals to optimize the variability structure in subsequent models, iii) test the significance of fixed effects using ML estimation and likelihood ratio tests, and iv) estimate the final optimal model coefficients using restricted maximum likelihood (REML) estimation, which are unbiased compared to ML, but are meaningless for comparing fixed effects. Goodness of fit for fixed effects in the final model were calculated using "r.squaredGLMM" of the package "MuMIN" in R;

regression lines and confidence intervals were plotted using "visreg."

Results

Nutrient Availability at Trapping Locations

Trap locations and neighborhoods differed significantly in nutrients in both estuarine water and leaf detritus, establishing that there was a range of potential availability of nitrogen and carbon to larval containers from different trap locations and neighborhoods (MANOVA; Table 2; Fig. 3a, b). Likewise, nutrient content of larval container water also differed significantly among neighborhoods, although containers within a neighborhood were similar to one another (MANOVA; Table 2; Fig. 3c). Despite significant neighborhood differences in container water nutrients, *Ae. aegypti* larvae inhabiting those containers were not significantly different in nutrient content between neighborhoods or trap locations (MANOVA; Table 2; Fig. 3d). However, earlier instar larvae grown on mixed resources tend to be most similar in nutrient content, with differential effects of nutrient availability not appearing until later developmental stages (D. Yee, unpublished laboratory data for different life stages grown on mixed resources: first instars: variance in %N = 0.11; fourth instars: variance in %N = 0.50; adults: variance in %N = 2.5). Indeed, similar to container habitats, adult *Ae. aegypti* did differ significantly across neighborhoods in nitrogen and C:N ratios (MANOVA; Table 2; Fig. 3e). Adults collected from different trapping locations also differed significantly in mass, with the largest adults collected from Martin Peña (MP5), Piñones (PN1), and Torrecilla (TO1).

Water samples from the neighborhood adjacent to the Martin Peña channel, particularly MP4 and MP5, had the highest concentrations of nitrogen and carbon in particulate matter compared to other locations (Fig. 3a). Martin Peña sites were also among locations with the highest concentrations of nitrogen and carbon in leaf detritus samples. Container water in the Martin Peña neighborhood also was significantly higher in N and C than most other neighborhoods, and adults were among the highest in N (Fig. 3e). Rio Piedras and Suarez Channel neighborhoods also had high levels of N in adults, larvae, and nearby leaf detritus. Adults collected from Piñones and Torrecilla had the lowest %N values (Fig. 3e), comparable to lower values

Table 2. MANOVA Results, Followed by Univariate Tests, Evaluating Whether Particulate Carbon and Nitrogen Variables Differed Among Trap Locations or Between Neighborhoods in San Juan, Puerto Rico, 2016.

Factor	Estuary water		Leaf sample		Larval container		Larval *Ae. aegypti*		Adult *Ae. aegypti*	
	df	Pillai	*df*	Pillai	*df*	Pillai	*df*	Pillai	*df*	Pillai
Trap location	5,19	**1.77*****	4,25	**1.06***	4,18	1.08	4,17	0.83	5102	**0.45***
Neighborhood	5,19	**2.05*****	4,25	**1.97*****	6,18	**1.86***	6,17	1.35	4102	**0.46****
	Variable	*F* value	Variable	*F* value	Variable	*F* value	Variable	*F* value	Variable	*F* value
Trap location	N mg/L	**3.05***	N%	0.16	N mg/L	0.46	N%	1.36	N%	0.48
Neighborhood		**8.56*****		**4.22****		**2.79***		0.93		**7.28*****
Trap location	C mg/L	**2.76***	C%	**3.65***	C mg/L	0.44	C%	1.22	C%	1.69
Neighborhood		**9.11*****		**27.69*****		2.02		0.92		1.23
Trap location	δ^{15}N	**2.32**@	δ^{15}N	**6.48****	δ^{15}N	1.72	δ^{15}N	1.19	δ^{15}N	1.03
Neighborhood		**2.48**@		**8.02*****		**2.38**@		1.44		0.70
Trap location	δ^{13}C	**3.21***	δ^{13}C	0.49	δ^{13}C	0.80	δ^{13}C	0.75	δ^{13}C	1.70
Neighborhood		**2.77***		**4.30****		1.01		0.62		0.78
Trap location	C:N	**3.10***	C:N	0.08	C:N	**3.55***	C:N	1.06	C:N	0.66
Neighborhood		**9.02*****		1.63		**6.12****		1.74		**6.35*****
Trap location		–	–	–	–	–	–	–	Mass	**6.30*****
Neighborhood		–	–	–	–	–	–	–		**3.28***

Significance indicated in bold, where ***$P < 0.001$; **$0.001 \leq P < 0.01$; *$0.01 \leq P < 0.05$; @ $0.05 \leq P < 0.1$.

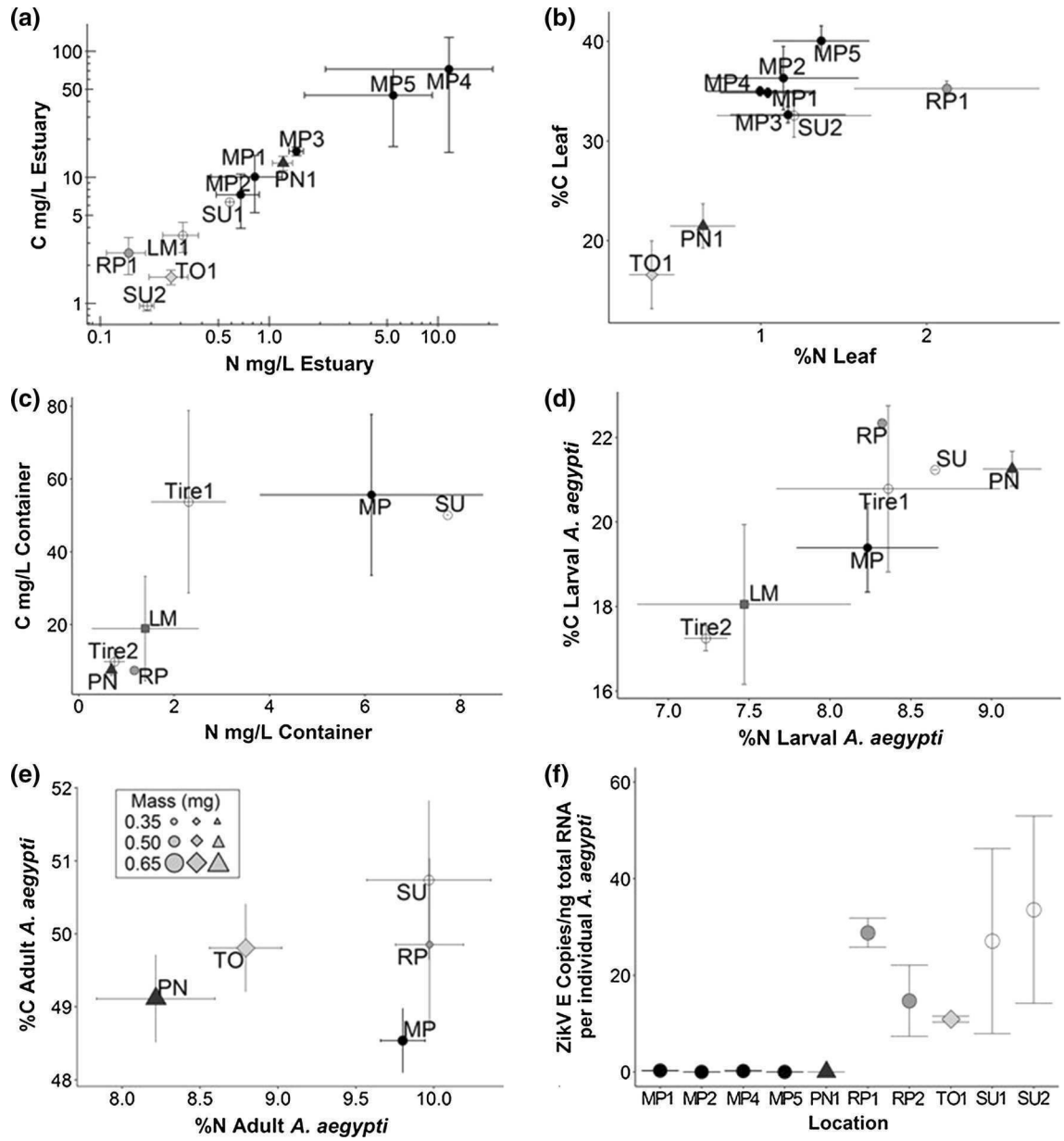

Figure 3. Mean particulate carbon and nitrogen, ± SE, across trapping locations for, **a** estuary water samples (log-scale) and **b** leaf samples, and across neighborhoods for **c** larval containers, **d** larval *Ae. aegypti*, and **e** adult *Ae. aegypti*. Symbol sizes indicate mean individual adult mass in **e**. Mean ZIKV concentration, ± SE, per individual adult *Ae. aegypti* at each trap location is also given (**f**). Symbol shapes and colors visually distinguish different neighborhoods (e.g., MP black circles; PN dark gray triangles).

for nearby estuarine water, leaf samples, and containers (Fig. 3a, b, c).

Relationships Between Nutrient Content and Nutrient Sources

Particulate nitrogen and carbon content of larval container water was significantly related to the nitrogen and carbon content of leaf detritus at sampling locations (Table 3; Fig. 4a). Larval nutrient content also tended to increase with increasing nitrogen content of water from their natal container habitats (Table 3; Fig. 4b). Adult nitrogen content was significantly related to the mean nitrogen content of containers, as well as nitrogen content of leaf detritus at the sampling location (Table 3; Fig. 4c). Differences in adult mass across locations were not significantly explained by adult nutrient content (Table 3).

Table 3. Significant Coefficients from Regression Analyses Comparing Relationships Between Most Proximate Source Nitrogen or Carbon Variables on Container, Larval, or Adult *Ae. aegypti* Nitrogen or Carbon, Adult Mass, and ZIKV Concentration.

Variable	N	Variance structure		Intercept	Fixed-effects variables				Fixed effect
Container		Flood	Container type		Estuary	Leaf			R^2
N mg/L	15	NS	**T > B > S > L****	− 0.11^{NS}	NS	**0.61 × %N****			**0.16**
C mg/L	15	NS	NS	0.00^{NS}	NS	**0.49 × %C***			**0.23**
δ^{15}N	15	NS	NS	0.00^{NS}	NS	NS			0.00
δ^{13}C	15	NS	**L > S > T > B***	0.02^{NS}	**0.36 × δ^{13}C***	NS			**0.25**
Larvae		Flood	Container type		Container				
%N	28	NS	NS	0.06^{NS}	**0.33** × mgN/L$^{@}$				**0.10**
%C	28	NS	NS	0.05 ^{NS}	NS				0.00
δ^{15}N	28	NS	NS	0.00^{NS}	**0.34** × δ^{15}N$^{@}$				**0.11**
δ^{13}C	28	NS	NS	0.04^{NS}	**0.75 × δ^{13}C*****				**0.52**
Adult		Flood	Container count		Estuary	Leaf	Container	Larvae	
%N	74	NS	NS	0.00^{NS}	NS	**0.38 × %N*****	**0.23** × mgN/L**	NS	**0.18**
%C	74	NS	**− 0.37****	0.05^{NS}	NS	NS	NS	NS	0.00
δ^{15}N	74	**0.38***	**− 0.34****	0.02^{NS}	NS	NS	NS	NS	0.00
δ^{13}C	74	**0.45***	NS	− 0.09^{NS}	NS	NS	NS	NS	0.00
Mass (mg)		Flood	Container count		Adult N	Adult C	Adult C/N		
	112	NS	NS	− 0.05^{NS}	NS	NS	–		0.00
	112	NS	NS	− 0.05^{NS}	–	–	NS		0.00
ZIKV		Flood	Container count		Adult N	Adult C	Adult C/N	Adult Mass	
	112	NS	NS	− 2.72^{NS}	**0.19 × %N*****	**0.14 × %C****	–	NS	**0.29**
	112	NS	NS	− 2.74^{NS}	–	–	NS	**0.16** × mg**	**0.26**

Dashed lines (—) indicate predictor variables not included in multiple regressions due to high covariance with other factors. Model variables are transformed to adhere to normality and standardized. Significance indicated in bold, where ***$P < 0.001$; **$0.001 \leq P < 0.01$; *$0.01 \leq P < 0.05$; @, $0.05 \leq P < 0.1$. Containers were classified as tires (T), buckets (B), small containers (S), or large containers (L).

Trap locations covered a range of stable isotope signatures (δ^{15}N, δ^{13}C) for both estuarine water and leaf detrital samples (Fig. 5a, b), with significant differences across locations and neighborhoods that could be used to track potential sources of inputs to containers (MANOVA; Table 2). However, we detected no corresponding significant differences in stable isotopes across neighborhoods or locations for container habitats, larvae, or adult *Ae. aegypti* (MANOVA; Table 2), although container water δ^{13}C was significantly positively correlated with nearby estuary δ^{13}C (Table 3). Within containers, larval stable isotopes were strongly correlated with the stable isotope signatures of their container water (Table 3; Fig. 5c, d), indicating that stable isotopes can effectively be used to link larval nutrient content to its most direct nutrient source. These differences did not appear to persist to adults, however, as stable isotopes in adults were not significantly related to those of potential estuary, leaf, container, or larval sources (Table 3).

In general, the explanatory power of regression models between nutrient content and nutrient sources did not depend on flood risk at the trap location, the number of sampled containers, or the variability in types of sampled containers (Table 3). There was significantly higher variability in nitrogen concentration in container water from tires than other types of containers, and accounting for this variance structure improved model fit between leaf and container nitrogen. Similarly, large containers from Piñones had significantly higher variability in δ^{13}C. Vari-

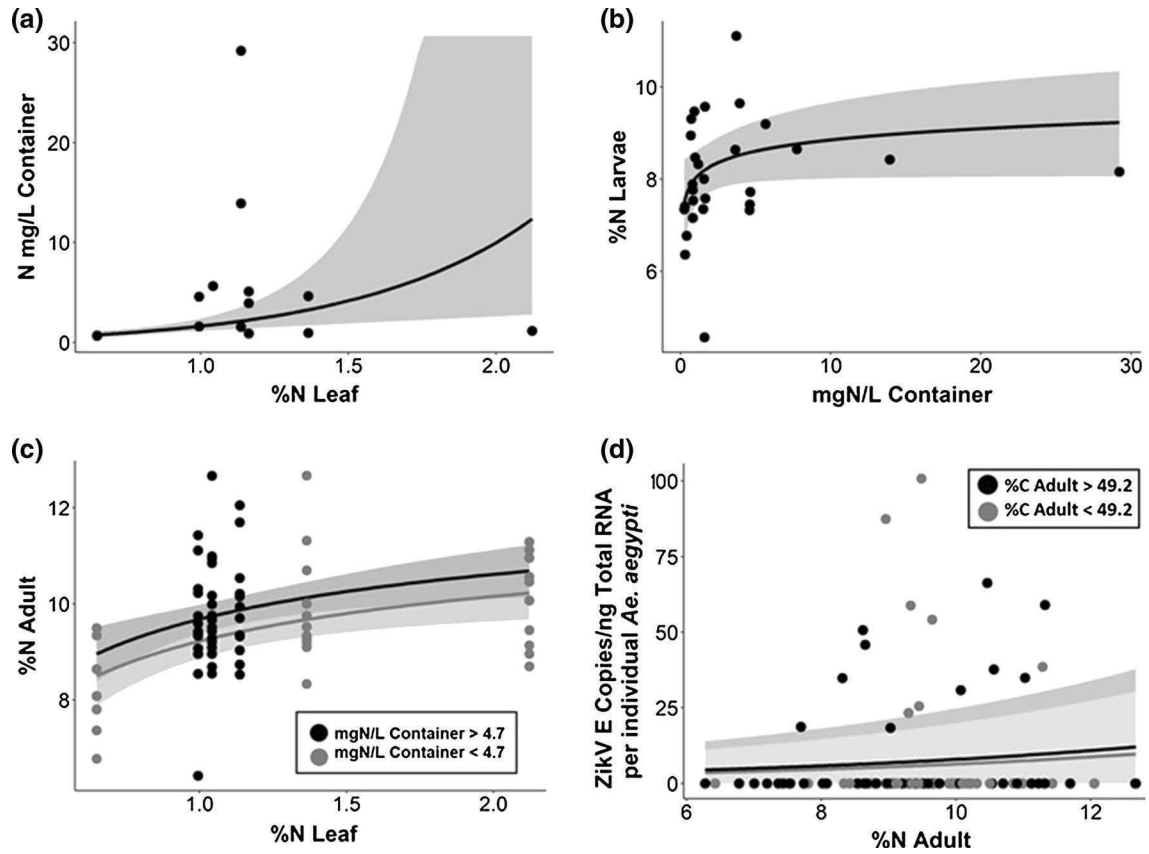

Figure 4. Relationships between source nutrients and particulate carbon or nitrogen for **a** containers, **b** larval, or **c** adult *Ae. aegypti,* and **d** ZIKV concentration, as determined by multiple regressions (see Table 3). Adults from each trap were paired with the average leaf nitrogen value for that trapping location (**c**). For regressions with more than one significant fixed effect (**c**, **d**), mean regression lines were plotted by fixing the second variable in the fitted regression equation (Table 3) to its mean value for data either above (black lines; black circles) or below (gray lines; gray circles) the standardized mean of zero (representing 4.7 mg N/L container in **c** or 49.2% C adult in **d**). Gray ribbons around regression lines indicate 95% confidence intervals.

ability in adult nutrient content tended to decrease with the number of sampled containers (%C, δ^{15}N) and increase at locations with higher flood risk (%C, δ^{13}C). Accounting for these higher variances, however, did not improve model fit with source nutrients (Table 3).

Zika Concentration in *Ae. aegypti*

In total, 130 adult *Ae. aegypti* were collected from 11 functioning traps at the 12 sampled trap locations (Table 1). Adult density per trap differed significantly across neighborhoods (Poisson GLM; Chisq = 48.74; $df = 4$; $P < 0.001$), with the Torrecilla trap TO1 having the highest density, followed by the traps in the Martin Peña neighborhood, and the Suárez channel traps having the lowest density per trap. Adult density per trap was somewhat higher the first sampling night than the second (mean of 13.2 adults per trap, first night; mean of 9.3 adults per trap, second night).

Eighteen of the 114 tested adult *Ae. aegypti* were infected with ZIKV in amounts ranging from 18 to 100 copies/ng total RNA, a rate of 15.7 infected (Table 1). Traps from San Juan municipio (MP, RP) had the lowest percentage of infected adult mosquitoes, about 9.7%, despite being the municipio with the highest density of reported human cases (293.2 per 100,000 people; Puerto Rico Department of Health 2016). Adult mosquitoes collected from Carolina municipio (SU) and Loiza municipio (PN, TO) were 40% or 24.3% positive for Zika, respectively, where the density of human cases was somewhat lower (Carolina: 156.9 cases per 100,000 persons; Loiza: 136.4 cases per 100,000 persons; Puerto Rico Department of Health 2016). No adults were collected from Cataño (LM) due to a trap malfunction.

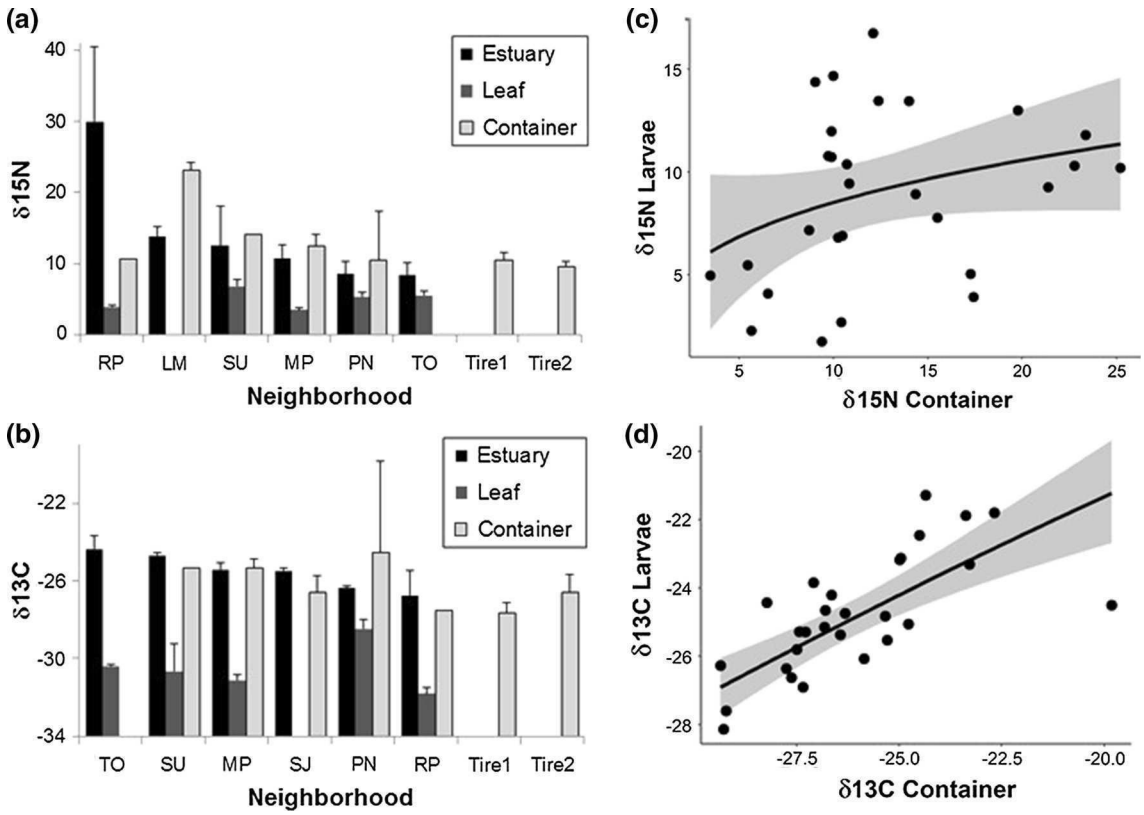

Figure 5. Nitrogen and carbon stable isotope values, ± SE, in each neighborhood for estuary, leaf, and larval container samples (**a**, **b**), as well as for larvae within each container (**c**, **d**) and corresponding fitted regression lines (see Table 3). Gray ribbons around regression lines indicate 95% confidence intervals.

ZIKV concentration in adult mosquitoes differed significantly across neighborhoods (Tweedie GLM; df = 4, 104; F value = 27.67; $P < 0.001$) but were consistent across locations within neighborhoods (Tweedie GLM; df = 5, 104; F value = 0.56; $P = 0.727$). Adult mosquitoes trapped adjacent to Rio Piedras, Torrecilla Lagoon, and Suárez Channel had significantly higher ZIKV concentration than individuals trapped near Martin Peña or Piñones Lagoon (Fig. 3f). Differences were both due to differences between neighborhoods in adults being positive or negative for zero (binomial GLM; $F = 19.4$; $P < 0.001$), as well as differences among locations in ZIKV concentration only within Zika-positive mosquitoes (normal GLM; $F = 3.80$; $P = 0.037$).

ZIKV concentration increased significantly with both adult C and N (Table 3; Fig. 4d). ZIKV concentration was also positively related to individual adult mass, but this variable did not explain significant variability when C and N were also included in the final model (Table 3). To confirm trap locations with Zika-negative mosquitoes were not dominating the observed relationships between C, N, and ZIKV, possibly due to an unmeasured location variable, we ran regressions again but limiting data to locations where Zika-positive mosquitoes were trapped. Regression results were consistent, with ZIKV concentration increasing significantly with both N and C (samples = 48; 2.95 + 0.17%N Adult + 0.16%C Adult; N: $P < 0.001$; C: $P < 0.001$).

Discussion

Although flooding events are widely perceived as creating aquatic breeding sites for mosquito larvae (Ahern et al. 2005; Pires and Gleiser 2010), the role of floods as a potential source of nutrients and the consequences for disease outbreaks is largely underdeveloped. Our study found significant differences across neighborhoods in the nutrient content of larval habitat containers and ZIKV in adult *Ae. aegypti*, which may in part reflect significant environmental variability in estuary water from flooding events and leaf detritus as potential inputs to containers.

Containers can be highly variable in a number of factors, including type, size, detritus inputs, or age, that contribute to high variability in nutrient content (e.g., Murrell et al. 2011; Yee et al. 2015a, b). Despite this, we found significant differences in container nutrient content among neighborhoods, which was significantly correlated with the nitrogen and carbon content of leaf detritus in the local area. Moreover, containers tended to have similar δ^{13}C signatures as waterbodies in the local area. The lack of a significant relationship between container water and estuary water nutrient content (N or C) broadly across sampling locations may not be too surprising given the dynamic nature of water quality with precipitation events, wind, and runoff. Furthermore, even containers right next to each other may or may not receive flood water, depending on their specific height, orientation, and other factors, and over time, flooded containers may begin to diverge from one another through differential evaporation or additional allochthonous inputs. In this sense, leaf detritus may simply be a better proxy than estuarine water for longer-term trends in local environmental inputs.

Martin Peña was the only neighborhood known to have flooded in the weeks prior to sampling, and known to experience frequent, periodic flooding. Containers from neighborhoods adjacent to the Martin Peña channel had higher nitrogen and carbon content than most other neighborhoods, consistent with the higher nitrogen content in water from the channel and in leaf detritus in the local environment. Moreover, adult *Ae. aegypti* collected from the Martin Peña neighborhood had higher body nitrogen content relative to neighborhoods adjacent to other waterbodies. Adult *Ae. aegypti* nutrient content in Martin Peña was also remarkably consistent from 2016 to 2017, compared to other neighborhoods, which were more variable over time (Appendix A). These data provide tantalizing evidence for linkages among inputs from the surrounding environment, containers, and mosquitoes produced from those environments.

Nutrient content of larval *Ae. aegypti* was tightly linked to the nutrient content of their container habitats, particularly δ^{15}N and δ^{13}C. Adult *Ae. aegypti* nitrogen content was also positively related to both the nitrogen content of typical containers in each sampling location, and the nitrogen content of leaf detritus in each area. The relatively small amount of variability explained may indicate other unmeasured environmental factors, such as animal detritus, which are influencing the availability of nutrients to larval mosquitoes (Kling et al. 2007). Moreover, our inability to exhaustively sample larval containers in each area, nor conclusively determine whether adults trapped in a particular location originated from the sampled larval containers, also likely contributes to unexplained variability. Indeed, ''hidden'' containers such as underground septic systems can provide a significant source of adult *Ae. aegypti* in Puerto Rico (Barrera et al. 2008). Furthermore, while larval body nutrients were closely linked to the current nutrient content of container water, adult body nitrogen may be more closely related to the nutrient content of container water 7–10 days prior when they were developing as larvae. More extensive sampling, including changes in container nutrients over time, is needed to more dynamically link environmental variability in nutrients to that of mosquitoes.

In addition to neighborhood differences in environmental and mosquito nutrient content, we also found neighborhood differences in ZIKV concentration. At the time of sampling, the neighborhoods adjacent to Rio Piedras, Torrecilla Lagoon, and Suárez channel had the highest levels of ZIKV concentration in adult *Ae. aegypti*, with no infected adults collected near Martin Peña channel or Piñones lagoon. Higher levels of nitrogen and carbon content in adult bodies tended to be associated with higher ZIKV concentration. Furthermore, the higher ZIKV concentrations could not merely be attributed to a body size effect (i.e., bigger mosquitoes take a greater blood meal and consume more virus from infected hosts) because %N and %C, scaled per unit body mass, explained greater variability than adult body size. Moreover, in our field data, adult mass was not significantly related to adult body nutrients. Nitrogen has generally been associated with increased severity of disease in other systems, often by providing abundant building blocks needed for pathogen replication, but underlying mechanisms and results are inconsistent depending on the specific form of nitrogen and immunity-related responses (Dordas 2008). Laboratory studies, particularly those discerning viral uptake, dissemination, and infectiousness, are needed to tease apart the underlying mechanisms by which nitrogen or carbon may be impacting viral concentrations in mosquito vectors.

Our results are consistent with previous laboratory studies that have found that larval nutrition, adult nutrition, and body size can affect the ability of mosquitoes to acquire dengue or Ross River virus (Nasci and Mitchell 1994; Alto et al. 2008b), and with modeling studies indicating that environmental variability in nitrogen may influence dengue cases (De Jesus Crespo et al. 2018). Our

study, however, is one of the first field studies to identify a pathway by which environmental variability in potential nutrient inputs into container habitats can affect nutrient content in mosquito larvae and adults, leading to variable viral acquisition in adult mosquitoes.

It is important to note that higher levels of viral titer in individual adult mosquitoes do not necessarily confer higher rates of viral infection in humans. Our study focused on dissemination of the pathogen but not the interaction with vector density (Anderson and Rico-Hesse 2006, Klempner et al. 2007). Indeed, two of the neighborhoods with the highest ZIKV concentrations, Rio Piedras and Suárez channel, also had the lowest densities of mosquitoes caught per trap. Additionally, the lack of Zika-positive mosquitoes from Martin Peña is somewhat surprising, given the relatively high nitrogen levels in adults at this location, as well as the high density of human cases in the San Juan municipio (Puerto Rico Department of Health 2016). Although our study focused on nutrient availability from the local environment, other factors can influence the probability that a vector acquires a pathogen, including host density, pathogen density in hosts, and climatic or behavioral factors that influence host-seeking or biting behavior (LaDeau et al. 2015). More extensive sampling would be needed to more accurately assess mosquito density, host density, biting behavior, and other factors across the different neighborhoods, to be able to rigorously understand the role environmental nutrient variability plays on vectorial capacity.

Social and infrastructural factors can also buffer or enhance the susceptibility of people to health outcomes (Myers et al. 2013; Oosterbroek et al. 2016). Age, housing density, and access to air-conditioning are all factors that can influence transmission of dengue virus to humans (Méndez-Lázaro et al. 2014; Barrera et al. 2011; De Jesus Crespo et al. 2018). Even less is known about the complex suite of ecological and social factors influencing Zika transmission (Thomas et al. 2017). Indeed, our sampling was a single snapshot at a time when the spread of Zika was accelerating through the San Juan metropolitan area and throughout Puerto Rico. It is possible that the neighborhood differences in ZIKV infection in adult mosquitoes reflect local acquisition patterns from the human population, such that certain neighborhoods simply had not been affected yet. However, because the neighborhoods where mosquitoes were strongly positive for ZIKV (Torrecilla, Rio Piedras, Suárez channel) are adjacent to the two neighborhoods where mosquitoes were negative for ZIKV (Martin Peña, Piñones), we did not see a strong spatial pattern (e.g., radiating from a source point of local human acquisition) that would support this. Furthermore, cumulative Zika cases by June 2016 were reasonably similar across the three municipalities covered by the study area (Puerto Rico Department of Health 2016). More extensive temporal sampling is needed to tease apart the suite of ecological and social factors affecting the spread of the virus, and what role environmental variability in water and detrital quality might play in that spread.

Our study provides preliminary evidence that environmental variability in nutrient inputs can influence the acquisition of virus by mosquito vectors. In addition to the potential influence on viral titer, variability in leaf detrital inputs has been demonstrated to influence survival, growth, and competition among mosquito larvae (Yee et al. 2007; Muturi et al. 2012). This suggests a mechanism by which urban greenspaces, in addition to temperature regulation or biological control (De Jesus Crespo et al. 2018), may influence vector-borne illnesses through detrital resource inputs. Moreover, flooding events, in addition to providing pools of short-term breeding habitat (Ahern et al. 2005; Pires and Gleiser 2010), can also provide a pulse of nutrients to existing larval containers depending on the water quality of nearby waterbodies. This suggests that management actions to reduce flooding and improve water quality should go hand-in-hand to help control spread of vector-borne diseases. As such, environmental restoration of ecosystem services in the urban landscape could be part of a sustainable solution to help reduce vector disease transmission by mitigating flooding events and regulating water quality (Carver et al. 2015; De Jesus Crespo et al. 2018).

Acknowledgements

We thank Roberto Barrera and Gilberto Felix from the CDC Dengue Branch in Puerto Rico for assistance and access to mosquito traps. We are extremely grateful to Estrella Santiago at Enlace and Evelyn Huertas at EPA Region 2, as well as the numerous homeowners and communities, who helped us obtain access to neighborhoods and locations for setting traps. Alonso Ramirez provided access to laboratory space at the University of Puerto Rico during the time of the field survey. E. Ashley Thompson and Biswas Nepane, at the University of Southern Mississippi, and Candice Lavelle and Emilie Cooper of the US EPA Gulf Ecology Division, assisted with processing mosquito viral data. Emily Santos assisted with nutrient analyses at the US EPA Atlantic Ecology Division. Hunter Deerman, of the University of Southern

Table 4. Number of Adult Female *Ae. aegypti* Trapped and Processed in 2017, and Results of Viral Analysis.

Neighborhood	Trap location	Female *Ae. aegypti* per trap	*Ae. aegypti* infected with ZIKV	*Ae. aegypti* infected with chikungunya	*Ae. aegypti* infected with dengue
Martin Peña Channel	MP1	0	–	–	–
	MP2a	9	0	0	0
	MP2b	5	0	0	0
	MP3	7	0	0	0
	MP4a	4	0	0	0
	MP4b	4	0	0	0
	MP5	0	–	–	–
	MP6a	7	0	0	0
	MP6b	0	–	–	–
Piñones Lagoon	PN1	NS	NS	NS	NS
Rio Piedras	RP1	6	0	0	0
	RP2	0	–	–	–
La Malaria Channel	LM1a	16	0	0	0
	LM1b	9	0	0	0
Suárez Channel	SU1	7	0	0	0
	SU2a	2	0	0	0
	SU2b	2	0	0	0
	SU2c	5	0	0	0
	SU2d	8	0	0	0
Torrecilla Lagoon	TO1a	21	0	0	0
	TO1b	32	0	0	0

Traps were placed at the same locations as mapped in Figure 2, with more than one trap placed in some locations (e.g., front yard and back yard; labeled a–d). One new location, MP6, situated roughly halfway between the two tire locations (Fig. 2), was sampled in 2017 but not 2016.
NS: Location not sampled in 2017.

Mississippi, assisted with field collection. We are grateful for reviews by P. Leisnham and peer reviewers on earlier drafts of this manuscript. The views expressed in this paper are those of the authors and do not necessarily reflect the views or policies of the US Environmental Protection Agency. Any mention of trade names, products, or services does not imply an endorsement by the US Government or the US Environmental Protection Agency (EPA). The EPA does not endorse any commercial products, services, or enterprises.

Appendix A

In June 2017, we sampled adult mosquito populations at many of the same sampling locations to compare to the June 2016 field collection (Table 4). As in 2016, adult mosquitoes were collected using BG-Sentinel traps (Biogents AG, Regensburg, Germany) baited with a human scent lure (BG-Lure; Biogents AG). Traps were left out for a 48-h period before adults were collected. Collected adults were identified to sex and species, with 0–32 female *Ae. aegypti* collected per trap (Table 4). Only adult female *Ae. aegypti* were used for subsequent analysis.

For the 2017 sampling, individual adult heads were preserved in 1 mL RNAlater (Ambion, Austin, TX, USA) within 6 h of field collection. Heads and bodies were then frozen for transport to the continental USA. Adult mosquitoes were processed for particulate nutrient content (%N, %C, C:N) and stable isotopes (δ15 N, δ13C) as described in the main text. We used nested Multivariate Analysis of Variance (MANOVA) to test whether trap locations, neighborhoods, or years (2016 vs 2017) differed significantly in nutrients, including N, C, δ13C, δ15 N, the ratio of C to N, or adult mass.

In addition to ZIKV, we extended the viral analysis to include chikungunya and dengue using the 2017 collected mosquitoes. Following the removal of the RNAlater by gentle pipetting, 200 µL of DMEM media (Gibco, no glu-

Table 5. MANOVA Results, Followed by Univariate Tests, Evaluating Whether Particulate Carbon and Nitrogen Variables Differed Among Trap Locations or Between Neighborhoods from 2016 to 2017 in San Juan, Puerto Rico.

Factor	Adult *Ae. aegypti*	
	df	*Pillai*
Trap location	15,224	**0.47@**
Neighborhood	6224	**0.37*** **
Year	1224	**0.17*** **
Neighborhood × Year	3224	**0.16****
	Variable	*F* value
Trap location	N%	**1.87***
Neighborhood		**5.1*** **
Year		**4.98***
Neighborhood × Year		**5.46****
Trap location	C%	**1.82***
Neighborhood		**3****
Year		**25.35*** **
Neighborhood × Year		**2.91***
Trap location	d15N	0.52
Neighborhood		1.46
Year		0.01
Neighborhood × Year		0.39
Trap location	d13C	1.14
Neighborhood		**2.05@**
Year		0.58
Neighborhood × Year		1.04
Trap location	C:N	0.71
Neighborhood		**3.19****
Year		**20.51*** **
Neighborhood × Year		**5.8*** **
Trap location	Mass	**2.44****
Neighborhood		1.67
Year		**4.83***
Neighborhood × Year		1.1

Significance indicated in bold, where ***$P < 0.001$; **$0.001 \leq P < 0.01$; * $0.01 \leq P < 0.05$; @ $0.05 \leq P < 0.1$.

cose, no glutamine, no phenol red; Thermo Fisher Scientific, Waltham, MA) was added to each mosquito head in RNase-free tubes. Individual mosquito tissues were homogenized using sterile, RNase-free disposable tissue grinders, centrifuged for 5 min in the cold, and the supernatant was removed for subsequent RNA extraction. RNA extractions

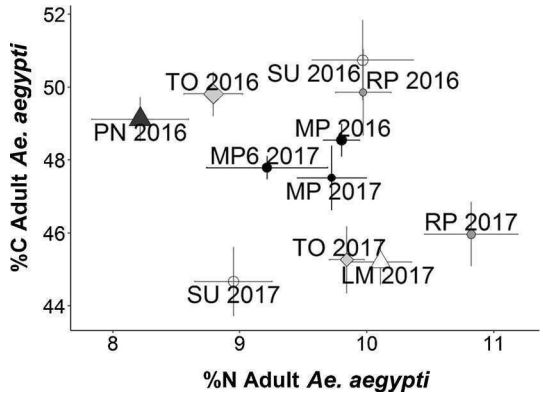

Figure 6. Mean particulate carbon and nitrogen values, ± SE, across neighborhoods for adult *Ae. Aegypti* in 2016 and 2017. Symbol sizes indicate mean individual adult mass.

were performed immediately following tissue homogenization using the QIAamp Viral RNA kit (Qiagen, Germantown, MD) according to manufacturer's instructions with minor modifications by adding additional washes with Buffer AW1 and AW2 (Mbanzulu et al. 2017). The purified RNA was analyzed for RNA integrity and concentration using the BioAnalyzer RNA 6000 Nano Reagent kit (Agilent, Santa Claire, CA) and stored at − 80°C. Real-time reverse transcription-PCR (RT-qPCR) was performed for dengue, chikungunya, and ZIKV using a multiplex viral kit (MyBioSource, San Diego, CA). All of the above procedures were performed aseptically using RNase-free materials.

In total, 144 adult female mosquitoes were collected in traps (Table 4). Of the 144 adults tested for virus, not a single individual was confirmed to have ZIKV, chikungunya, or dengue. Results were consistent with public health data that, in contrast to concerns of an anticipated second outbreak of Zika, rates of arboviral cases in Puerto Rico were quite low in June 2017, with less than 10 confirmed cases across all of Puerto Rico (Puerto Rico Department of Health 2017). Adult nutrient content differed significantly from 2016 to 2017, but the effect differed among neighborhoods (Neighborhood × Year; Table 5). Adult mosquitoes from Martin Pena were remarkably consistent in both %N and %C between 2016 and 2017, despite a general pattern of lower %C and higher %N in 2017 for most other neighborhoods. Adult mass tended to be lower in Martin Pena, consistently in both 2016 and 2017. There were no significant differences in stable isotopes across trap locations, neighborhoods, or years (Fig. 6).

References

Acharya D, Bastola P, Le L, Paul AM, Fernandez E, Diamond MS, Miao W, Bai F (2016) An ultrasensitive electrogenerated chemiluminescence-based immunoassay for specific detection of Zika virus. *Scientific Reports* 6:32227

Ahern M, Kovats RS, Wilkinson P, Few R, Matthies F (2005) Global health impacts of floods: epidemiologic evidence. *Epidemiologic Reviews* 27:36–46

Almeida APG, Baptista SSSG, Sousa CAGCC, Novo MTLM, Ramos HC, Panella NA, Godsey M, Simões MJ, Anselmo ML, Komar N, Mitchell CJ, Ribiero H (2005) Bioecology and vectorial capacity of *Aedes albopictus* (Diptera: Culicidae) in Macao, China, in relation to dengue virus transmission. *Journal of Medical Entomology* 42:419–428

Alto BW, Lounibos LP, Higgs S, Juliano SA (2005) Larval competition differentially affects arbovirus infection in *Aedes* mosquitoes. *Ecology* 86:3279–3288

Alto BW, Lounibos LP, Mores CN, Reiskind MH (2008) Larval competition alters susceptibility of adult *Aedes* mosquitoes to dengue infection. *Proceedings of the Royal Society B* 275:463–471

Alto BW, Reiskind MH, Lounibos LP (2008) Size alters susceptibility of vectors to dengue virus infection and dissemination. *American Journal of Tropical Medicine and Hygiene* 79:688–695

Anderson JR, Rico-Hesse R (2006) *Aedes aegypti* vectorial capacity is determined by the infecting genotype of dengue virus. *American Journal of Tropical Medicine and Hygiene* 75:886–892

Azar D, Rain D (2007) Identifying population vulnerable to hydrological hazards in San Juan, Puerto Rico. *GeoJournal* 69:23–43

Barrera R, Amador M, Diaz A, Smith J, Munoz-Jordan JL, Rosario Y (2008) Unusual productivity of *Aedes aegypti* in septic tanks and its implications for dengue control. *Medical and Veterinary Entomology* 22:62–69

Barrera R, Amador M, MacKay AJ (2011) Population dynamics of *Aedes aegypti* and dengue as influenced by weather and human behavior in San Juan, Puerto Rico. *PLoS Neglected Tropical Diseases* 5:e1378

Brandeis TJ, Escobedo FJ, Staudhammer CL, Nowak DJ, Zipperer WC (2014). *San Juan Bay Estuary watershed urban forest inventory*. US Forest Service, Asheville, NC. Technical Report SRS-190.

Burke R, Barrera R, Lewis M, Kluchinsky T, Claborn D (2010) Septic tanks as larval habitats for the mosquitoes *Aedes aegypti* and *Culex quinquefasciatus* in Playa-Playita, Puerto Rico. *Medical Veterinary Entomology* 24:117–123

Canyon DV, Hii JLK, Muller R (1999) Effect of diet on biting, oviposition, and survival of *Aedes aegypti* (Diptera: Culicidae). *Journal of Medical Entomology* 36:301–308

Carpenter SR (1983) Resource limitation of larval treehole mosquitoes subsisting on beech detritus. *Ecology* 64:219–223

Carver S, Slaney DP, Leisnham PT, Weinstein P (2015) Healthy wetlands, healthy people: mosquito borne disease. In: *Wetlands and human health*, Finlayson MC, Horwitz P, Weinstein P (editors), Dordrecht: Springer, pp 95–121

Chouin-Carneiro T, Vega-Rua A, Vazeille M, Yebakima A, Girod R, Goindin D, Dupont-Rouzeyrol M, Lourenco-de-Oliveira R, Failloux AB (2016) Differential susceptibilities of *Aedes aegypti* and *Aedes albopictus* from the Americas to Zika virus. *PLoS Neglected Tropical Diseases* 10:e0004543

De Jesus Crespo R, Fulford R (2017) Eco-health linkages: assessing the role of ecosystem goods and services on human health using causal criteria analysis. *International Journal of Public Health* 63:81–92

De Jesus Crespo R, Mendez Lazaro P, Yee SH (2018) Linking wetland ecosystem services to vector-borne disease: dengue fever in the San Juan Bay Estuary, Puerto Rico. *Wetlands* . https://doi.org/10.1007/s13157-017-0990-5

Dick GWA, Kitchen SF, Haddow AJ (1952) Zika virus (I). Isolations and serological specificity. *Transactions of the Royal Society of Tropical Medicine and Hygiene* 46:509–520

Dordas C (2008) Role of nutrients in controlling plant diseases in sustainable agriculture: a review. *Agronomy for Sustainable Development* 28:33–46

Federal Emergency Management Agency, FEMA (2009) Digital flood insurance rate map database, Commonwealth of Puerto Rico. http://gis.otg.pr.gov/download_gis_files.htm. Accessed 22 June 2017

Gonzalez-Salazar C, Stephens CR, Sanchez-Cordero V (2017) Predicting the potential role of non-human hosts in Zika virus maintenance. *EcoHealth* 14:171–177

Gratz NG (2004) Critical review of the vector status of *Aedes albopictus*. *Medical and Veterinary Entomology* 18:215–227

Harrington LC, Scott TW, Lerdthusnee K, Coleman RC, Costero A, Clark GG, Jones JJ, Kitthawee S, Kittayapong P, Sithiprasasna R, Edman JD (2005) Dispersal of the dengue vector *Aedes aegypti* within and between rural communities. *American Journal of Tropical Medicine and Hygiene* 72:209–220

Hashizume M, Dewan AM, Sunahara T, Rahman MZ, Yamamoto T (2012) Hydroclimatological variability and dengue transmission in Dhaka, Bangladesh: a time-series study. *BMC Infectious Diseases* 12(1):98

Hinga KR, Batchelor A (2005) Waste processing and detoxification. In: *Millennium ecosytem assessment, volume 1: conditions and trends working group report*, Hassan R, Scholes R, Ash N (editors), Washington, D.C.: Island Press, pp 417–439

Ivers LC, Ryan ET (2006) Infectious diseases of severe weather-related and flood-related natural disasters. *Current Opinion in Infectious Diseases* 19:408–414

Klempner MS, Unnasch TR, Hu LT (2007) Taking a bite out of vector-transmitted infectious diseases. *New England Journal of Medicine* 356:2567–2569

Kling LJ, Juliano SA, Yee DA (2007) Larval mosquito communities in discarded vehicle tires in a forested and unforested site: detritus type, amount, and water nutrient differences. *Journal of Vector Ecology* 32:207–217

Korfmacher KS, Aviles K, Cummings BJ, Daniell W, Erdmann J, Garrison V (2015) Health impact assessment of urban waterway decisions. *International Journal of Environmental Research and Public Health* 12:300–321

LaDeau SL, Allan BF, Leisnham PT, Levy MZ (2015) The ecological foundations of transmission potential and vector-borne disease in urban landscapes. *Functional Ecology* 29:889–901

Lima F (2017) Linear mixed-effects models in R. https://poissonisfish.wordpress.com/2017/12/11/linear-mixed-effect-models-in-r/. Accessed Nov 2018

Maciel-de-Freitas R, Eiras AE, Lourenco-de-Oliveira R (2006) Field evaluation of effectiveness of the BG-Sentinel, a new trap for capturing adult *Aedes aegypti* (Diptera: Culicidae). *Memorias do Instituto Oswaldo Cruz* 101:321–325

Mbanzulu KM, Wumba R, Mukendi J-PK, Zanga JK, Shija F, Bobanga TL, Aloni MN, Misinzo G (2017) Mosquito-borne viruses circulating in Kinshasa, Democratic Republic of the Congo. *International Journal of Infectious Diseases* 57:32–37

Méndez-Lázaro P, Muller-Karger FE, Otis D, McCarthy MJ, Peña-Orellana M (2014) Assessing climate variability effects on dengue incidence in San Juan, Puerto Rico. *International Journal of Environmental Research and Public Health* 11:9409–9428

Murrell EG, Damal K, Lounibos LP, Juliano SA (2011) Distributions of competing container mosquitoes depend on detritus types, nutrient ratios, and food availability. *Annals of the Entomological Society of America* 104:688–698

Musso D, Gubler DJ (2016) Zika virus. *Clinical Microbiology Reviews* 29:487–524

Mutero CM, Ng'ang'a PN, Wekoyela P, Githure J, Konradsen F (2004) Ammonium sulphate fertilizer increases larval populations of *Anopheles arabiensis* and culicine mosquitoes in rice fields. *Acta Tropical* 89:187–192

Muturi EJ, Allan BF, Ricci J (2012) Influence of leaf detritus type on production and longevity of container-breeding mosquitoes. *Environmental Entomology* 41:1062–1068

Myers SS, Gaffikin L, Golden CD, Ostfeld RS, Redford KH, Ricketts TH, Turner WR, Osofsky SA (2013) Human health impacts of ecosystem alteration. *Proceedings of the National Academy of Sciences* 110:18753–18760

Nasci RS, Mitchell CJ (1994) Larval diet, adult size, and susceptibility of *Aedes aegypti* (Diptera: Culicidae) to infection with Ross River virus. *Journal of Medical Entomology* 31:123–126

NOAA (National Oceanic and Atmospheric Administration) (2018) Coastal flood exposure mapper. https://coast.noaa.gov/floodexposure/. Accessed Nov 2018

Oczkowski AJ, Nixon SW, Granger SL, El-Sayed AFM, McKinney RA (2009) Anthropogenic enhancement of Egypt's Mediterranean fishery. *Proceedings of the National Academy of Sciences* 106:1364–1367

Oczkowski AJ, Flower RJ, Thompson JR, Ayache F, Ahmed MH, Ramdani M, Turner S (2011) Evidence of North Africa's green revolution preserved in sedimentary organic matter deposited in three coastal lagoons. *Ecological Applications* 21:1708–1717

Oosterbroek B, de Kraker J, Huynen MMTE, Martens P (2016) Assessing ecosystem impacts on health: a tool review. *Ecosystem Services* 17:237–254

Paul D, Skrzypek G, Fórizs I (2007) Normalization of measured stable isotopic compositions to isotope reference scales—a review. *Rapid Communications in Mass Spectrometry* 21:3006–3014

Pires DA, Gleiser RM (2010) Mosquito fauna inhabiting water bodies in the urban environment of Córdoba city, Argentina, following a St. Louis encephalitis outbreak. *Journal of Vector Ecology* 35:401–409

Puerto Rico Department of Health (2016) Informe Semanal de Enfermedades Arbovirales (ArboV): Semanal 23 (27 de mayo al 9 de junio de 2016). http://www.salud.gov.pr/Estadisticas-Registros-y-Publicaciones/Pages/VigilanciadeZika.aspx. Accessed Mar 2018

Puerto Rico Department of Health (2017) Informe Semanal de Enfermedades Arbovirales (ArboV): Semanal 52 (24 al 30 de diciembre de 2017). http://www.salud.gov.pr/Estadisticas-Registros-y-Publicaciones/Pages/VigilanciadeZika.aspx. Accessed Mar 2018

Reiskind MH, Lounibos LP (2009) Effects of intraspecific larval competition on adult longevity in the mosquitoes *Aedes aegypti* and *Aedes albopictus*. *Medical and Veterinary Entomology* 23:62–68

Rhodus J, Fulk F, Autrey B, O'Shea S, Roth A (2013) *A review of health impact assessment in the U.S.: current state-of-science, best practices, and areas for improvement*. U.S. Environmental Protection Agency, Cincinnati, OH, EPA/600/R-13/354

Scott TW, Amerasinghe PH, Morrison AC, Lorenz LH, Clark GG, Strickman D, Kittaypong P, Edman JD (2000) Longitudinal studies of *Aedes aegypti* (Diptera: Culicidae) in Thailand and Puerto Rico: blood feeding frequency. *Journal of Medical Entomology* 37:89–101

Sharp TM, Hunsperger E, Santiago GA, Muñoz-Jordan JL, Santiago LM, Rivera A, Rodríguez-Acosta RL, Gonzalez Feliciano L, Margolis HS, Tomashek KM (2013) Virus-specific differences in rates of disease during the 2010 Dengue epidemic in Puerto Rico. *PLoS Neglected Tropical Diseases* 7:e2159

Sheffield PE, Agu DP, Rowe M, Fischer K, Pérez AE, Rodríguez LN, Avilés KR (2014) *Health impact assessment of the proposed environmental restoration of Caño Martín Peña*. Icahn School of Medicine at Mount Sinai and Corporación del Proyecto ENLACE del Caño Martín Peña, San Juan, Puerto Rico

Shono H (2008) Application of the Tweedie distribution to zero-catch data in CPUE analysis. *Fisheries Research* 93:154–162

San Juan Bay Estuary Program, SJBEP (2000) *Program del Estuario de la Bahía de San Juan: Comprehensive conservation and management plan*. San Juan Bay Estuary Program, San Juan, Puerto Rico.

SJBEP (2016) Water quality monitoring data. www.estuario.org. Accessed 30 Mar 2018

Thomas SJ, Pearce JM, Ramey AM (2017) Vectors, hosts, and control measures for Zika virus in the Americas. *EcoHealth* 14:821–839

World Health Organization, WHO (2016a) Report Zika Situation Neurological Syndrome and Congenital Anomalies. http://www.who.int/emergencies/zika-virus/situation-report/5-february-2016/en/. Accessed Mar 2018

WHO (2016b) Zika virus infection—United States of America—Puerto Rico. http://www.who.int/csr/don/8-january-2016-zika-usa/en/. Accessed Mar 2018

Yee DA, Juliano SA (2006) Abundance matters: a field experiment testing the more individuals hypothesis for richness–productivity relationships. *Oecologia* 153:153–162

Yee DA, Kaufman MG, Juliano SA (2007) The significance of ratios of detritus types and micro-organism productivity to competitive interactions between aquatic insect detritivores. *Journal of Animal Ecology* 76:1105–1115

Yee DA, Abuzeineh AA, Ezeakacha NF, Schelble SS, Glasgow WC, Flanagan SD, Skiff JJ, Reeves A, Kuehn K (2015) Mosquito larvae in tires from Mississippi, U.S.A.: the efficacy of abiotic and biotic parameters in predicting spatial and temporal patterns of mosquito populations and communities. *Journal of Medical Entomology* 52:394–407

Yee DA, Kaufman MG, Ezeakacha NF (2015) How diverse detrital environments influence nutrient stoichiometry between males and females of the co-occurring container mosquitoes *Aedes albopictus*, *Ae. Aegypti*, and *Culex quinquefasciatus*. *PLOS ONE* 10:e0133734

Zanluca C, de Melo VCA, Mosimann ALP, dos Santos GIV, dos Santos CND, Luz K (2015) First report of autochthonous transmission of Zika virus in Brazil. *Memorias do Instituto Oswaldo Cruz* 110:569–572

Zuur A, Ieno EN, Walker N, Savelieve AA, Smith GM (2009) *Mixed Effects Models and Extensions in ecology with R*, New York: Springer

Wetlands (2019) 39:1281–1293
https://doi.org/10.1007/s13157-017-0990-5

Linking Wetland Ecosystem Services to Vector-borne Disease: Dengue Fever in the San Juan Bay Estuary, Puerto Rico

Rebeca de Jesús Crespo[1] · Pablo Méndez Lázaro[2] · Susan H. Yee[1]

Received: 22 September 2017 / Accepted: 19 December 2017 / Published online: 23 January 2018
© US Government 2018

Abstract

Mosquito-borne diseases are an increasingly important health concern, which pose great challenges for safe and sustainable control and eradication. This reality calls for management approaches that consider multiple aspects of the transmission cycle from a landscape and vector ecology perspective, to socio-economic elements that may increase exposure. This study seeks to better understand these pathways using dengue fever in the San Juan Bay Estuary (SJBE), Puerto Rico. Dengue is transmitted by *Aedes aegypti*, a species that thrives in cities. Here we ask which elements within the urban landscape could be managed to help prevent dengue outbreaks. We studied the potential of coastal wetlands in the SJBE to buffer vector proliferation, hypothesizing that wetland ecosystem services lead to lower dengue occurrence. We test this hypothesis using census-block level dengue data from 2010-13, including the largest epidemic in Puerto Rican history. Our analytical model includes socio-economic factors and environmental controls that may also affect dengue dynamics. Results from beta-binomial regressions and model averaging indicated that dengue occurrence was lower in neighborhoods with higher wetland cover even after controlling for population density and other socio-economic aspects. Our models suggest that heat hazard mitigation is partly responsible for the association between wetlands and dengue.

Keywords Ecosystem Goods and Services · Coastal wetlands · Dengue · "Vector-borne" diseases · Urban landscape · San Juan Bay Estuary

Introduction

Mosquito-borne diseases represent a significant health and economic burden to cities around the world. The emergence of serious vector mediated viruses, such as Zika, has recently sparked the interest to find safe and effective strategies for vector control and mosquito eradication. With growing concerns of how strategies such as aerial spraying may indirectly impact humans and wildlife, researchers are increasingly interested in sustainable approaches for safe vector population management. One of the most prominent mosquito vectors for diseases like dengue, chikungunya, and Zika is *Aedes aegypti*. *A. aegypti* thrives in the presence of water filled artificial containers, and mainly feeds on human blood, making the urban environment, with abundant trash and dense populations, particularly suitable for its proliferation.

The proliferation of mosquito vectors in cities, as well as vector disease transmission, is also intensified by other aspects of the urban environment. Flood prone areas, exacerbated in cities due to altered hydrology, may increase habitat availability. Flood waters from urban runoff or overflowing rivers may fill trash items such as discarded plastic containers, creating suitable breeding sites for mosquito larvae (Hashizume et al. 2012). Water chemistry, in turn, has been linked to *A. aegypti* nutrition and consequently pupal and adult productivity (Barrera et al. 2006; Couret et al. 2014). Urban waters that contribute to filling container habitat could therefore affect mosquito vectors indirectly through nutrition enhancement from wastewater inputs. In cities, high temperatures due to urban heat islands shorten pupal development time and viral incubation period, and increases

Electronic supplementary material The online version of this article (https://doi.org/10.1007/s13157-017-0990-5) contains supplementary material, which is available to authorized users.

✉ Rebeca de Jesús Crespo
dejesus-crespo.rebeca@epa.gov

[1] Gulf Ecology Division, National Health and Environmental Effects Research Laboratory, US EPA, Office of Research and Development, 1 Sabine Island Drive, Gulf Breeze, FL 32561-5299, USA

[2] University of Puerto Rico, Medical Sciences Campus, San Juan, Puerto Rico

female biting and oviposition rate, all factors that promote vector proliferation and dengue transmission ((Ibarra et al. 2013; Méndez-Lázaro et al. 2014), Chang et al. 2015, (Morin et al. 2015)). Urbanized environments may also present habitat limitations for predators and competitors which help control mosquito vector populations ((Barrera et al. 2006; Cox et al. 2007), Murugan et al. 2015).

The extent to which environmental factors such as heat islands, floods, habitat loss, and water pollution, impact urban environments may be determined, in part, by landscape management and design aspects, such as restoration and preservation of urban green spaces. Urban green spaces help control temperature extremes by providing shade, and increasing evapo-transpiration (Bouchama and Knochel 2002). They also promote rainfall interception and infiltration ameliorating the scale of urban flooding (Brody and Highfield 2013). Green spaces clean surface water in cities and provide habitat for wildlife, creating healthier ecosystems that may favor biocontrol of mosquitoes.

Ecosystem services in the urban landscape could help reduce vector disease transmission (Carver et al. 2015), but the data correlating vegetation cover to mosquitoes and its related diseases is conflicting. Some studies have found negative associations suggesting a protective role of vegetation against "mosquito-borne" disease ((Cox et al. 2007); Cheong et al. 2014; Tiong et al. 2015; Myer et al. 2017). Other studies, have found positive correlations (Sarfraz et al. 2012; Cheong et al. 2014; Stanforth et al. 2016) suggesting a disease promoting effect. Possible reasons for these inconsistencies include different vegetation types contributing differently to the provision of ecosystem services or difference in the role of ecosystem services for vector control in different environmental contexts. The relative importance of ecosystem services as a determinant of "vector-borne" disease occurrence can also vary depending on socio-economic factors. For example, vector abundance is likely a bigger concern for residences built with low quality construction material or lacking air conditioning (Mulligan et al. 2015) which is commonly observed in poor neighborhoods. Given these considerations, more studies are needed that evaluate the role of vegetation on "mosquito-borne" diseases while simultaneously measuring relevant ecosystem services and confounding socio-economic factors.

This study seeks to contribute by evaluating linkages between coastal wetlands and dengue fever occurrences on census block groups of the San Juan Bay Estuary (SJBE), Puerto Rico. Due to its high population density and favorable climate for mosquitoes, the SJBE, has been a hotspot for "vector-borne" diseases in Puerto Rico for decades, including a recent Zika epidemic that affected over 40,000 individuals in 2016 (Puerto Rico Department of Health (PRDH) 2017). Understanding how vectors and disease transmission vary across environmental and socio-economic gradients is needed to better guide the allocation of management resources among communities and habitats during epidemics in the SJBE. Moreover, as we now live in an interconnected world, were viruses and vectors spread more rapidly than in previous centuries, addressing these questions is of broader interest beyond the context of Puerto Rico and the US.

We present our hypothesized relationship between ecosystem services and dengue as a conceptual model in Fig. 1. We hypothesize that greater wetland cover will promote heat and water hazard mitigation, as well as cleaner water and more habitat for species that predate and/or compete with mosquitoes. These ecosystem services should in turn negatively affect dengue transmission, leading to a reduction in cases. We incorporate into our conceptual model socio-economic factors that may influence this relationship. In particular, we build on Myers et al.'s (Myers et al. 2013) concept of "insulating layers", where infrastructure, technology, behaviors, and other adaptations may protect certain groups from the potential health impacts of ecosystem service lost (Myers et al. 2013).

Study Site

The San Juan Bay Estuary (SJBE, Fig. 2) has an average temperature that ranges from 23.9 °C to 27.2 °C, and rainfall from 1500 and 1700 mm (Lugo et al. 2011). It lies within a "moist forest" ecological life zone according to Holdridge's classification (Torres-Valcárcel et al. 2014). The SJBE is part of the San Juan, Puerto Rico (PR) metropolitan area, encompassing the most densely urbanized and populated region on the Island, with an estimated population of 2.5 million people, according to the 2010 US Census (Brandeis et al. 2014). The SJBE comprises a total area of 216.58 km^2, of which around 82% is developed, and the rest is composed of mangroves (~7%), grassy wetlands and water bodies (~6%), and moist forest (~5%) (Brandeis et al. 2014). It is the only tropical estuary included in the US National Estuary Programs (NEP) and is characterized by a series of interconnected lagoons and channels, many of which have been severely altered by human activity (Brandeis et al. 2014). The most prominent natural features of the SJBE NEP are its coastal wetlands, which include the most extensive contiguous mangrove forest in Puerto Rico (Brandeis et al. 2014).

Here we focus on the role of these wetlands on ecosystem services and disease. Therefore, we limited our analysis to compare only neighborhoods that could potentially have had coastal wetlands in the past (N=170). For this we selected census block groups (United States Census Bureau 2015) that intersected flood zones (Federal Emergency Management Agency (FEMA) 2009) and that were below the 3m elevation line (U.S. Geological Survey 1944). This cutoff was selected based on historical maps from the SJBE showing the existence of mangroves and marshes mainly between 0-3 meters above sea level (masl) (U.S. Geological Survey 1941).

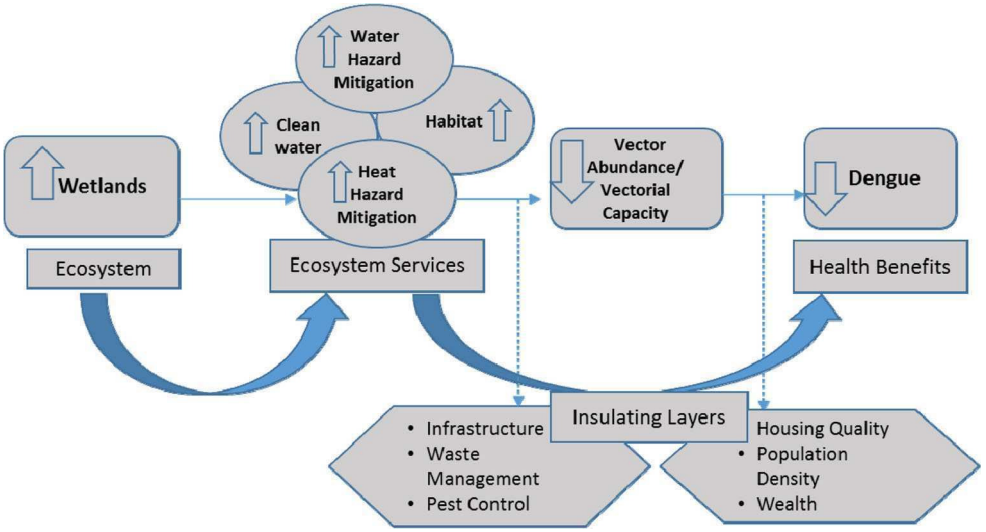

Fig. 1 Hypothesized linkage between wetlands and Dengue ocurrence through Ecosystem Services. Vectorial capacity refers to the mosquito's ability to spread disease accounting for host, virus, and vector interactions (Liu-(Helmersson 2012)). This can be influenced by factors such as mosquito growth rate, biting rate, the time it takes the virus to replicate within the vector, all of which are affected by temperature. In this case, it also incorporates the relative abundance of A. aegypti over other species of mosquitoes that are less effective at transmitting dengue and prefer more vegetated habitats (Cox et al.2007). Insulating factors refer to socio-economic elements which can insulate certain populations, generally the wealthy, from the impacts of a loss in Ecosystem Services (see (Myers et al. 2013))

Methods

To test our proposed Ecosystem Service-Dengue model (Fig. 1) we selected indicator variables from existing secondary data and estimated the spatial distribution of the selected variables in ArcGIS (version 10.3).

For the dengue response, we used laboratory confirmed dengue cases for the SJBE from the passive dengue surveillance system administered by the Center for Disease Control and Prevention (CDC) and the Puerto Rico Department of Health (years 2010-2013) (https://www.cdc.gov/dengue/about/inpuerto.html). Cases were summarized by census-block groups prior and standardized by population counts for analysis using 5-year population summaries from the American Community Survey (ACS 2011-2014, (United States Census Bureau 2015)). Block group area ranged from 0.04 to 21 km^2, with an average of 0.56km^2. The dispersal area of *A. aegypti* is estimated at less than 0.01 kilometers

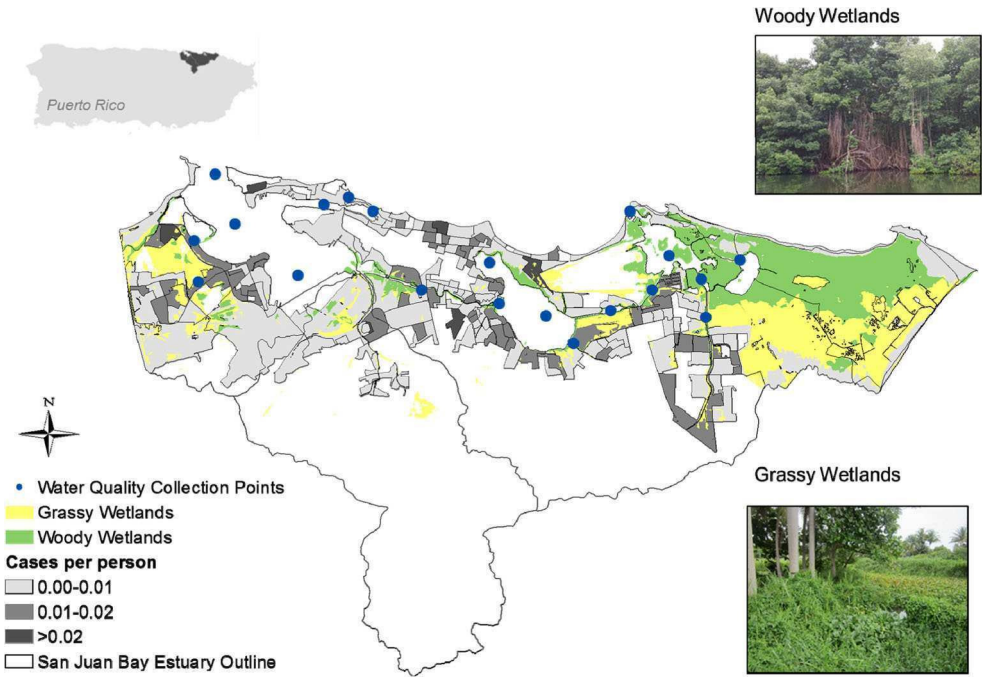

Fig. 2 Study sites in the San Juan Bay Estuary (SJBE), with water quality collection points (SJBE monitoring program), wetland areas (PR GAP analysis) and dengue cases per person by census block group (CDC dengue surveillance 2010-2013; ACS community survey 2011-2014). Pictures show examples of grassy and woody wetlands in the SJBE

(Harrington et al. 2005; Reiter et al. 1995). Therefore, it is reasonable to treat each block group as independent study units to assess disease trends.

To align our analysis with our conceptual model (Fig. 1) we divided our explanatory variables into three main categories: a) Ecosystem; b) Ecosystem Services; and c) Insulating Layers. We also included a fourth category, Environment, which characterizes natural variability unrelated to the ecosystem or ecosystem services categories, but which could affect dengue vectors.

Ecosystem

For the Ecosystem category we used the PR GAP project's land use layer (Gould et al. 2008). We extracted all wetlands within the SJBE and classified them as Woody or Grassy. Woody Wetlands consisted of all segments classified as Mangrove+Shrubland or as Pterocarpus forest. Grassy Wetlands consisted of segments classified as Emergent Herbaceous or Seasonally Flooded Herbaceous (Fig. 2). The percent of woody and grassy wetland cover was determined by dividing wetland area over total area by census block groups. The total area of each census block group was calculated excluding water bodies (Centro de Recaudación de Ingresos Municipales (CRIM) 2006), such as streams and lagoons, to more accurately represent the area occupied by people.

Ecosystem Services

The Ecosystem Services group included heat hazard mitigation, clean water, and habitat. We did not include the ecosystem service of water hazard mitigation because we could not get data on flood occurrences. Instead, we included georeferenced flood zones as part of our Environmental Controls sub-model (see below).

For heat hazard mitigation we used land surface temperature (LST; Fig. 3a) estimated from the Landsat 8 Operational Land Imager sensor's thermal infrared band (Band 10) on September 2013. The methods used to derive these estimates are described in Mendez-Lazaro et al. (2017). For each census block group, we calculated LST Mean, Minimum, and Maximum across 30 meter pixels using zonal statistics in ArcGIS (ver 10.3), and the block group area (revised as described above).

The ecosystem service of clean water was assessed using measures collected by the SJBE National Estuary Program (NEP) water monitoring initiative. This project measures water quality parameters through different areas of the SJBE (Fig. 2) several times per year, spanning from 2011-2014 (San Juan Bay Estuary (SJBE) 2015). In this case we focused on total nitrogen, as previous studies have shown that nitrogen enrichment can increase mosquito and midge production (Sanford et al. 2005). While the nitrogen concentrations used to evaluate this ecosystem service come from water bodies (e.g., streams, estuary) and not directly from *A. aegypti* habitat, we posit that nutrients from these water bodies may enter artificial containers in nearby block groups directly during floods (e.g., (Pires and Gleiser 2010)), or indirectly through allochthonous organic matter input from the associated vegetation (Kling et al. 2007). Here we selected the highest recorded total nitrogen per sampling station per year, and averaged the results to get a composite value per station (Fig. 3b). These composite values were used to create a raster surface of nitrogen levels using Inverse Distance Weighting (IDW) interpolation (Philip et al. 1982, Watson et al. 1985) in Arc GIS (ver 10.3). IDW interpolation estimates regional measures based on nearby sampling locations. In our case, we used a search radius of the nearest 3 points on 30m pixels, and assigned a weighting value of 3, on a scale of 0-3, where higher values suggest a greater influence of the closest vs farthest points. The resulting raster (30m pixel size) was then applied to calculate a mean value with zonal statistics, using the census block groups as the boundaries.

Lastly, vertebrate richness was used as our indicator of habitat provisioning (Fig. 3c). Here we hypothesize that healthy habitats should lead to bio-control of mosquito vectors by promoting healthier predator and competitor populations. We used the PRGAP vertebrate richness dataset, which includes estimates for amphibian, reptile, bat and bird richness using existing inventories, habitat suitability and expert opinion (Gould et al. 2008). We calculated median vertebrate richness by census block group using the PRGAP vertebrate richness layer (15m pixel size) and zonal statistics in Arc GIS.

Insulating Layers

The concept of insulating layers represents social elements that could moderate the influence of ecosystem services on health (Myers et al. 2013). We divided this group into two categories: a) infrastructure and b) socio-economic factors. Our infrastructure variables included sewage and road density, calculated from the road and sewage layers (source: *Portal Datos Geográficos Gubernamentales*http://www2.pr.gov/agencias/gis/Pages/default.aspx), divided over census block group area (excluding water bodies), resulting in a measure of linear meters over area per study unit. Sewage density was included as previous studies have linked the presence of septic tanks with vector mosquito habitat ((Burke et al. 2010; Mackay et al. 2009). (Myer et al. 2017)). We predicted that areas with lower sewage density would have higher number of septic tanks, increasing vector habitat availability and the potential for dengue transmission (Burke et al. 2010). Roads and the environmental modifications they cause were also

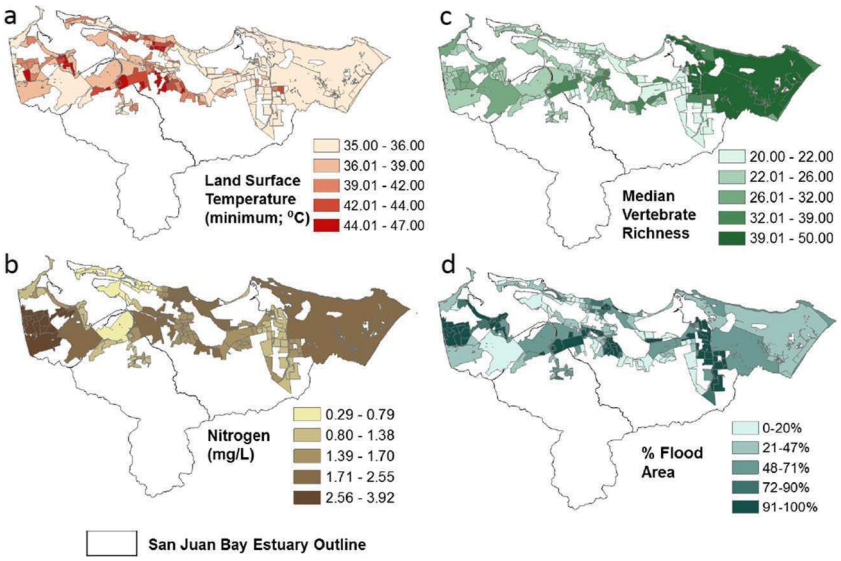

Fig. 3 Landscape scale patterns across SJBE coastal neighborhoods

explored, as they can alter hydro-dynamics by increasing surface runoff, potentially affecting water accumulation and habitat creation.

For our socio-economic variables, we focused on demographic characteristics and wealth indicators. Our demographic of choice was the percent of teenagers per block group because previous studies on Dengue in the SJBE have shown that this is the most vulnerable demographic (Méndez-Lázaro et al. 2014; Sharp et al. 2013). We calculate the proportion of people from the ages of 10-19 over total population using ACS data (ACS-2011-2014, (United States Census Bureau 2015)). Also using ACS data, we calculated median household income by census block group, as an umbrella measure potentially representing factors such as better housing quality, air conditioner use, waste management, and infrastructure. Finally, we included population density (population/m2) as a potential driver of higher dengue transmission rates. This variable was calculated excluding areas within the block group occupied by water bodies or wetlands.

Environment

Our Environment sub-model consists of environmental "control" variables that are not expected to be influenced by the presence of the wetland ecosystems, and not related directly to ecosystem services, but that are expected to influence Dengue. Here we include the flood area (Fig. 3d), which has been suggested to create breeding sites for mosquito vectors (World Health Organization (WHO) 2006). Our flood area indicator is derived from FEMA flood zone maps (Federal Emergency Management Agency (FEMA) 2009), which were used to calculate % flood area within populated segments of each block group, that is, excluding water bodies and areas covered by wetlands. Although water hazard mitigation (e.g. flood control) is an ecosystem service expected from wetlands, the flood zone map does not represent areas that get flooded most often, but rather areas with potential of flooding. Therefore, it cannot be used as an ecosystem services indicator, hence its inclusion as an environmental "control" instead. Our second environmental control is salinity. Our second environmental control is salinity. *A. aegypti* larvae can tolerate brackish waters (Ramasamy et al. 2011), but oviposition and larvae survival are limited at salinity levels above 12-13% (Navarro et al. 2003). Since there are differences in salinities in the different water bodies of the SJBE, we included it to account for its potential influence. To calculate salinity by block group, we followed the approach used for nitrogen (see above), using NEP water monitoring data and the IDW tool in ArcGIS. As with nitrogen, we focus on the premise that salinity from nearby water systems may influence chemistry in container habitat (Yee et al. 2014) via water inputs from flood events, or allochthonous organic matter inputs from vegetation.

Data Analysis

We evaluated the relationship between ecosystems and ecosystem services using linear regressions between woody or grassy wetlands and the ES indicators (nitrogen, richness, LST). We then evaluated the role of Ecosystems, Ecosystem Services, Insulating Layers and Environment on dengue prevalence (dengue cases per block group population) using beta-binomial generalized linear models, accounting for over-dispersion. Standard binomial regression (i.e. logistic regression) models the presence or absence of disease in an individual as a binary response variable (Quinn and Keough, 2002). Beta-binomial regression is a modified version of binomial regression that accounts for multiple samples (people) per

census block group (Venables and Ripley 2003). We developed a "global" beta-binomial model which included all variables from each category (Table 1), standardized around their means and 1 standard deviations (Becker et al. 1988). In this global model we also included significant interactions (Pr(>|z|)<0.05) between ecological variables with "Insulating Layers" indicators (with main effects included). For this we ran individual beta-binomial models between each factor included in the Insulating Layers category interacting with each of the other variables, to test the premise that these factors may mediate the role of the natural environment (Ecosystem, Ecosystem Services, Environment) on dengue occurrence.

We used this global model as basis for model averaging, following the steps described in Grueber et al. (Grueber et al. 2011). The goal of this approach was to select the top variable combinations that best explained dengue occurrence considering all possible combinations. Variable combinations were limited to 8 factors in order to have at least 20 replicates per explanatory variable, and prevent model overfitting. We used AICc > 4 as a cut-off criterion for sub model selection (Burnham and Anderson 2002) and then calculated the conditional average effect of each variable after accounting for all of the "best models" where it was featured (Grueber et al. 2011). Model averages were used to represent the relative importance of each variable, determine an average effect size and construct predictive models of dengue prevalence.

Variables included in the "best models" were further analyzed through a variation partitioning analysis. This analysis allowed us to determine the fractions of variability explained independently (pure effects) by each predictor, or jointly by the intersection of two or more predictors. In particular, we were interested in whether the effect of wetlands on dengue prevalence could be partly attributed to ecosystem services. We applied the subtraction approach described in detail in Ruiz-Fons et al. (Ruiz-Fons et al. 2013). Briefly, this approach calculates the deviance explained by all the variables featured in the "best models", and then fractures that into individual components representing the pure effects of each variable and the overlaid effects between variables. For example, a model that has both % wetlands and ecosystem service variables may not exhibit great reductions in deviance relative to one that only has % wetlands because part of the effect of ecosystem services is already captured by the %wetlands model. Here we wanted to test if there was such overlap, and if so, determine the relative magnitude.

Prior to analysis, all explanatory variables were tested for collinearity using Pearson correlation coefficients. If any important correlation was identified between explanatory variables (>0.60), we only selected the ones with a stronger relationship to the response variable for model selection (See supplementary Table 1). Prior to model averaging, the global model was tested for spatial autocorrelation applying the Global Moran's I procedure to residuals (supplementary Table 2).

Analyses were conducted in R studio (ver. 3.2.2) and/or ArcGIS (ver 10.3). The "Analysis of Overdispersed Data"(aod) package (ver 1.3, (Lesnoff and Lancelot 2012)) was used for beta-binomial model building, the MuMIn package (Bartoń 2009) was used for model averaging, and the "modEva" package (ver 1.3.2, Barbosa et al., 2013) for variation partitioning analysis.

Results

Relationship between Ecosystems and Ecosystem Services

Woody and grassy wetlands showed similar relationships to the ecosystem services indicators of temperature (heat hazard mitigation) and vertebrate richness (habitat). Increasing cover of both types of wetlands was associated with significant increases in vertebrate richness and significant reductions in land surface temperature (Fig. 4). The relationship to nitrogen, our "clean water" ecosystem services indicator differed. Both types of wetlands showed a positive association to nitrogen which is opposite to our prediction. This association was significant for grassy wetlands (p<0.001), but not woody wetlands.

Dengue Prevalence Model Selection

Model averaging resulted in five models with equal support following the AICc>4 criterion (Supplementary Table 3). The variables featured or excluded from these models, and their relative importance are listed in Table 1. From the "ecosystem" category, we found that higher percentage of woody wetlands associated significantly with lower dengue prevalence (p=0.03). Moreover, grassy wetlands significantly interacted with median income to explain dengue cases (p<0.001): while % grassy wetlands seem to inversely relate to dengue in low income neighborhoods, the trend is reversed in high income areas (Fig. 5). The significant "ecosystem service" indicators were Minimum Land Surface Temperature (LST, hereinafter minimum temperature) (p=0.002) and Nitrogen (p=0.01). Both variables showed a positive association to Dengue cases. Maximum LST (hereinafter maximum temperature) significantly interacted with population density to explain dengue cases (p=0.002), suggesting that in areas with high population density, higher maximum temperature was associated to higher number of cases, but that the effect is reversed in more sparsely populated neighborhoods (Fig. 5).

Both of the variables in the "environment" category significantly explained dengue occurrence. As predicted higher salinity was associated to lower dengue (p=0.02), while higher % flood area positively correlated to dengue (p=0.02). Salinity also interacted with the % of teenagers (p=0.003), suggesting that

Table 1 Descriptive statistics for treatment variables and their effect on dengue cases based on model averaging results (n=170)

Indicators		Descriptive Statistics				Model Averaging Results#				
Categories	Variables	max	min	mean	SD	Avg. Estimate	2.5%	97.5%	P (>z)	Relative Variable Importance
Ecosystem	%Woody Wetlands	58.98	0.00	3.35	9.23	-0.12	-0.23	-0.01	0.03	0.29
	% Grassy Wetlands	63.49	0.00	3.63	8.60	-0.04	-0.14	0.06	0.44	^0.00
Ecosystem Services	MinLST (^{0}C)	47.00	35.00	39.34	3.94	0.18	0.07	0.29	0.002	0.62
	MaxLST (^{0}C)	63.00	36.00	48.47	3.87	-0.08	-0.23	0.07	0.31	^0.00
	MeanLST (^{0}C)	52.54	35.25	44.06	3.40	n/a	n/a	n/a	n/a	n/a
	Nitrogen (mg/L)	3.92	0.29	1.62	0.68	0.12	0.03	0.21	0.01	0.17
	Vert.Rich.(Median)	50.00	20.00	26.21	6.29	n/a	n/a	n/a	n/a	n/a
Insulating Layers										
Infrastructure	Roads (m/m2)	0.04	0.00	0.02	0.01	n/a	n/a	n/a	n/a	n/a
	Sewage (m/m2)	0.06	0.00	0.01	0.01	n/a	n/a	n/a	n/a	n/a
Socio Economic	Median Income	83365.00	2499.00	24186.63	15373.27	-0.03	-0.13	0.08	0.60	^0.00
	% Teenagers	40.82	0.00	11.69	0.07	0.03	-0.06	0.12	0.51	^0.00
	Population per m^2	0.02	0.00	0.01	0.00	-0.12	-0.23	0.003	0.06	^0.00
Environment*	Salinity (ppm)	39.44	3.43	24.20	9.67	-0.10	-0.19	-0.02	0.02	0.70
	% Flood Area^	100.00	3.62	59.37	35.92	0.10	0.02	0.18	0.02	0.28
Interactions	GrassWetl*MedInc	n/a	n/a	n/a	n/a	0.26	0.15	0.38	<0.001	1.00
	MaxLST*Popm()	n/a	n/a	n/a	n/a	0.18	0.07	0.29	0.002	1.00
	Salinity*%Teens	n/a	n/a	n/a	n/a	-0.12	-0.19	-0.04	0.003	0.06

*Environmental control variables not necessarily related to the Ecosystem or to tested Ecosystem Services; ^represents flood prone zones, not actual flooded areas. ^ = This variable was only featured in models including it as part of an interaction term; see relative importance of its interaction term. # Model averaging results are "conditional averages", derived from the models that include the variable of interest out of all the "best models" (Supplementary Table 3). n/a (Not applicable; for model averaging results, it implies that the variable was never featured in the "best models"). LST (Land Surface Temperature); Vert.Rich (Vertebrate Richness)

in neighborhoods associated to higher salinities, the positive correlation between teenagers and dengue weakens (Fig. 5). The variables within the "insulating layers" category were not significantly associated to dengue, although we did find significant interaction effects with some of these variables as discussed above.

Variance partitioning analysis showed that the relationship between wetlands and dengue may in part be attributed to the ecosystem service of "heat hazard mitigation" (LST as indicator). About 19% of the deviance explained by woody wetlands and about 50% of that explained by the interaction of grassy wetlands and median income is also explained by minimum temperature (Fig. 6). There was no shared deviance between wetlands and the other variables featured in the "best models" (See Supplementary Fig. 1), including nitrogen, which was the other significant ecosystem service indicator (Fig. 6).

We used the resulting variable estimates from the model averaging procedure (Table 1) to develop predictive models of the role of wetland ecosystem services on dengue occurrence. For this we set all model variables to the mean, and varied woody and grassy wetland cover on increments of 2%. (Figure 7). Results suggest that at the current mean woody wetland cover of 3.4%, there are approximately 9.3 cases of Dengue per 1000 people. Increasing woody wetland cover by 10% would reduce Dengue cases by roughly 11%, resulting in around 8.3 cases per 1000 people during a timeframe similar to our dataset (3 years, one epidemic period). Closer to a 20% increase in grassy wetland cover would be needed to achieve the same effect. (Figure 7).

Discussion

To our knowledge, this is the first study to assess the role of wetlands in the urban landscape on dengue occurrence through the lens of ecosystem services. Wetlands in the San Juan Bay Estuary, and in particular mangroves seem to provide a protective effect, being negatively correlated to dengue. Part of that effect seems to be mediated by the ecosystem service of heat hazard mitigation, as lower temperatures are associated to higher mangrove cover and lower dengue. Our study suggests that variables such as median income, population density and demographics could play a mediating role in the relationship between dengue occurrence and the natural environment. These results support our hypothesis of a potential buffering effect of wetlands to "vector-borne" diseases in

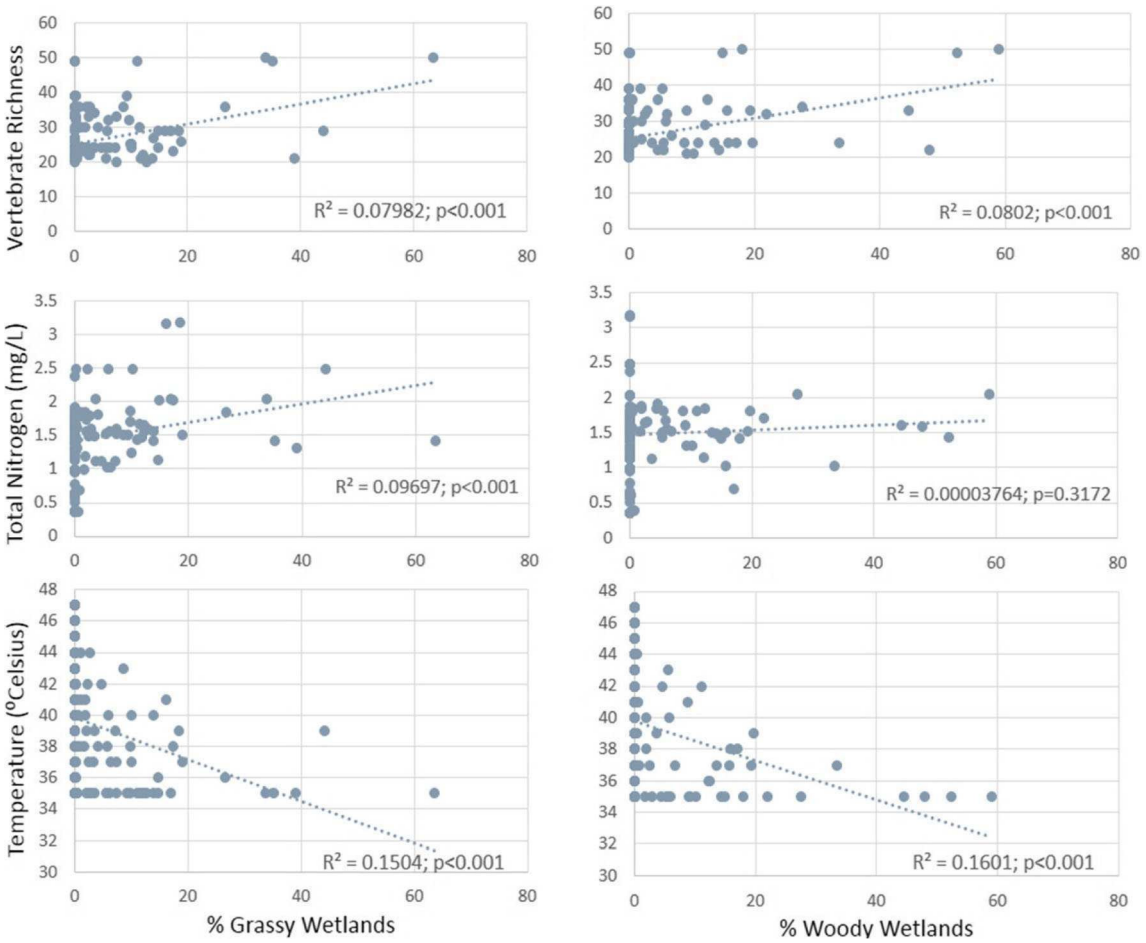

Fig. 4 Scatterplots displaying relationships between wetland ecosystems and selected ecosystem services. The temperature measure selected here was Minimum Land Surface Temperature, as it was the most closely related to dengue cases

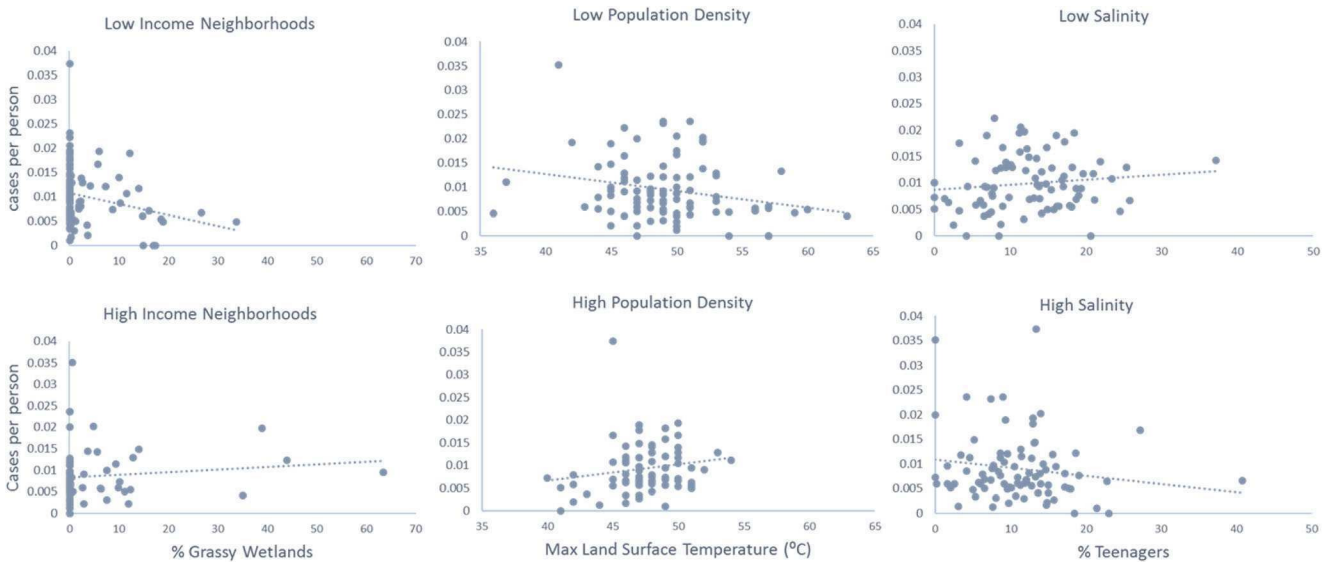

Fig. 5 Significant interactions explaining dengue cases in the SJBE. Breakpoints for the two figures on each panel were based on the average (above and below) of the variables: **a**) Median Income; **b**) Population Density; and C) Salinity See Supplementary Table 4 for more details

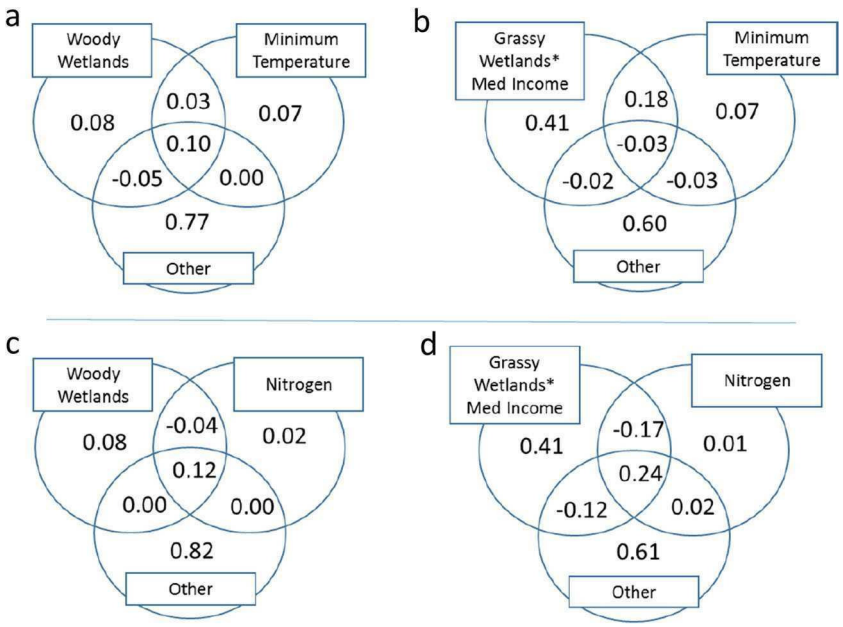

Fig. 6 Variation partitioning analysis of models explaining Dengue cases. Values represent the proportion of the deviance explained by the variables of interest individually and in combination to other model components. In this case, the variables of interest are the wetland ecosystems and the "ecosystem service" indicators Minimum Land Surface Temperature (**a**, **b**) and Nitrogen (**c**, **d**). The "other" circle represents all variables featured in the model averaging results aside from the single predictors concurrently being examined (Table 1; Supplementary Table 3). Negative explained variances are artifacts of the VP procedure, which mainly suggest no overlay in the amount of deviance explained. Tested individually, none of these other variables shared deviance with wetlands. Results from variation partitioning with different variables of the model and wetlands can be found in Supplementary Fig. 1

coastal urbanized neighborhoods, even after controlling for confounding environmental and socio-economic factors.

The role of temperature on dengue has been documented before in the SJBE. As in our study, Méndez-Lázaro et al. (Méndez-Lázaro et al. 2014) found that minimum temperatures were positively associated to dengue in the municipality of San Juan. Our study supports their findings at a lower spatial resolution. Previous studies have shown that higher temperatures promote dengue transmission, by means of reductions in viral incubation period, and mosquito development time, and increases in feeding and oviposition rate (Morin et al. 2013). This relationship however is non-linear

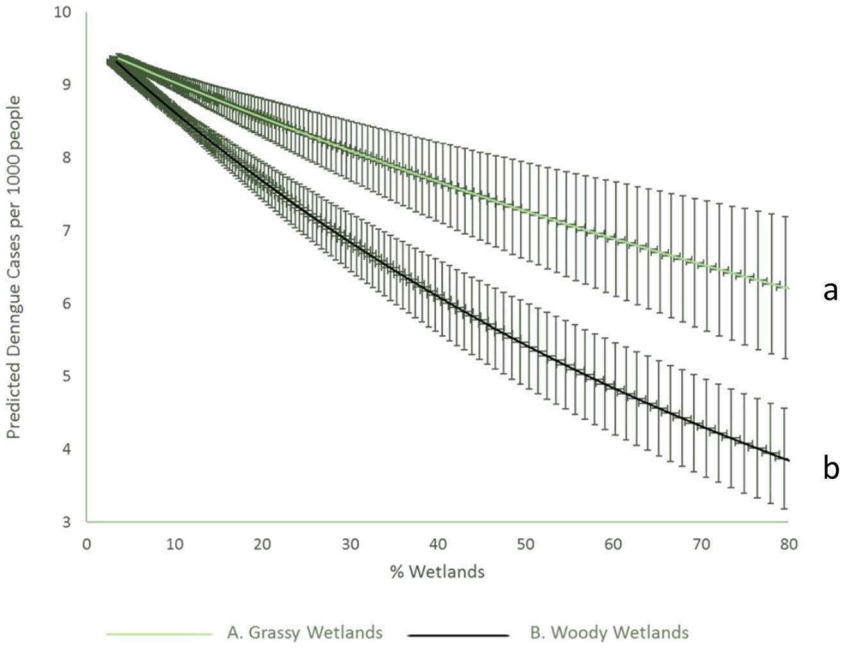

Fig. 7 Predicted relationship between grassy wetlands (**a**) and woody wetlands (**b**) and dengue cases in the SJBE

and at extremely high temperatures mosquito activity and survival becomes negatively affected (Carrington et al. 2013; Morin et al. 2013). This non-linearity became evident in our result of a significant interaction between maximum temperature and population density. We observe (Fig. 5) that areas that are more sparsely populated seem to reach much higher temperature extremes, therefore becoming less suitable for dengue transmission. These lower population densities could correspond to industrial zones, or sprawled development, with lower residential greenery and more concrete surfaces that promote temperatures above the vector-dengue threshold. The threshold for mosquito competence of dengue transmission seems to lie between 30-35^0 Celsius in air temperature (note here we used Land Surface Temperature, which tends to be higher) (Carrington et al. 2013; Morin et al. 2013). Above this temperature, different aspects of mosquito ecology become negatively affected (Carrington et al. 2013; Morin et al. 2013). The role that wetland ecosystem services play in promoting optimal temperature ranges may therefore vary by context. While in the SJBE it seems to be having a protective effect, in drier, hotter environments, the presence of vegetation may actually help bring temperatures down to more suitable ranges, and prevent evaporation of water from container habitats (Barrera et al. 2006). These considerations should be taken into account when applying these findings to other sites.

While temperature seems to partially describe the relationship between wetlands and dengue in the SJBE, a proportion of the deviance explained by wetlands remains un-attributed to any of the other ecosystem services tested, according to our variation partitioning analysis. A possible pathway may be flood control. We found a positive correlation between % flood area and dengue cases, and previous studies suggest that wetlands can mitigate floods in coastal cities (Brody et al. 2012). To determine the effect of wetlands on preventing flood and consequently on dengue, it would be necessary to document actual flood events. While we did not have flood indicator data for the scale of analysis of this study, this question may likely be addressed at coarser spatial resolutions in future studies, using for example flood claims data for the San Juan metropolitan area.

Another potential explanation of the role of wetlands on dengue may lie in bio-control pathways not evaluated through this study. For example, while we included estimates of vertebrate richness, we did not have an indicator of invertebrate distributions. Invertebrates may act as predators and competitors of *Aedes aegypti* (Quiroz-Martínez and Rodríguez-Castro 2007) and they may be positively affected by the presence of wetlands. For example, a closely related species, *Aedes mediovittatus,* potentially competes with *A. aegypti,* for resources but prefers to live in woody environments (Cox et al. 2007). While *A. mediovittatus* could also transmit dengue, it is a less competent vector because it is less susceptible to certain dengue serotypes (Poole-Smith et al. 2015). Moreover, contrary to *A. aegypti,* this mosquito commonly feeds on other mammals besides humans (Barrera et al. 2012) potentially diluting dengue transmission rates. The effect of this or other invertebrates within the SJBE wetlands on dengue could be the subject of future research.

The role that woody and grassy wetlands seem to play in dengue occurrence is not equal. Grassy wetlands had the same inverse correlation to dengue as woody wetlands but only in low income neighborhoods. This result supports previous studies showing that wealth moderates "vector-borne" disease exposure (LaDeau et al. 2013) as well as the ecosystem service-human health linkage (Myers et al. 2013). Like woody wetlands, grassy wetlands also seem to provide heat hazard mitigation, and so their presence could be preferentially benefitting households more exposed to vectors than those protected by air conditioning and better building material. The stronger effect of woody wetlands, which seems to affect all income classes, may be attributed to additional, unexplained factors such as the ones discussed above (e.g. bio-control, flood control).

Another factor differentiating woody and grassy wetlands may be their influence on water quality. We found that nitrogen levels were significantly associated to dengue, supporting our prediction that water quality degradation could have an effect mosquito vectors. However, contrary to our predictions, we observed no correlation between water nitrogen concentration and neighborhood woody wetland cover, and a positive and significant correlation between water nitrogen concentration and the percentage of grassy wetlands. This result may suggest that grassy wetlands are subjected to higher levels of pollution, or that they process pollutant loads differently than woody wetlands. Moreover, the role that other, un-measured, water quality indicators that vary concomitantly with nitrogen play, and their association to different wetland types needs further evaluation.

Aside from nitrogen, we also included salinity as a water quality "control" variable. As predicted salinity had a negative effect on dengue. High salinity concentrations seem to dampen the effect of dengue on certain vulnerable populations, as we observed a significant interaction between this variable and the % of teenagers (Fig. 5). As in previous studies (Méndez-Lázaro et al. 2014), we found that dengue occurrence positively relates to % teens, but that this relationship becomes weaker in areas of higher salinity. If brackish water enters artificial containers, then container salinity levels could rise, negatively affecting oviposition and larvae development. In neighborhoods associated to coastal ecosystems of higher salinity, it is plausible that high salinity levels in breeding habitat ameliorates vector emergence, providing a level of disease control among a vulnerable sector of the population. While we can expect this effect to be relatively small in magnitude (as we saw in our results), we also think it is plausible and worth exploring further through field validation. Hydrological alterations such as artificial drainage structures

and channelization tend to reduce salinity levels in coastal ecosystems (Lugo and Snedaker 1974), but sea level rise, is expected to expand the extent of estuarine area in the SJBE, promoting saltwater intrusion inland (Méndez-Lázaro et al. 2014). These altered salinity gradients could determine the distribution of mosquito vectors and Dengue occurrence across coastal neighborhoods of the SJBE and should de more closely examined in the future, as our understanding of these dynamics remains limited (Méndez-Lázaro et al. 2014).

Aside from the interactions cited in the preceding paragraphs, the variables in our "insulating layers" category were not significantly associated to dengue. Particularly noteworthy is the lack of correlation of dengue to population density as a main effect, suggesting that this variable is not mediating the observed role of wetlands. The SJBE is more or less densely populated through, and for the purpose of dengue transmission, the slight differences do not seem to have an impact. Moreover, even in neighborhoods with high wetland cover, we observe households congregating around densely developed zones, rather than scattered within or around the wetland area.

Our study had several limitations. Many of the variables used to assess ecosystem services were derived from extrapolations, either from point measurements or remotely sensed images. Therefore, there are uncertainties related to how these measures represent conditions of our study units both in spatial and temporal terms. The dengue cases used as a response come from official confirmed occurrences. People with limited access to health care are likely underrepresented by this dataset. We did not account for human mobility, and how this factor may affect the disease-environment associations. Accounting for block group employment rate, age structure, and human behaviors that affect transmission and exposure to dengue (see (Barrera et al. 2011)) could help contribute to better understanding these relationships in the future. Our results are based on disease occurrence, while many of the hypotheses we test are related to mosquito vector ecology. Future sampling of mosquito populations in the same neighborhoods should be developed to support our findings. These efforts should focus on monitoring adult female vectors, which are superior disease risk indicators than larvae or non-specific adult mosquito abundance ((Barrera et al. 2011), Bowman et al 2014).

Aside from mosquito vector abundance other factors may influence Dengue dynamics such as immunity due to previous exposure, vector to person contact rate, and current level of exposure risk. Our study attempted to include some indicators to account for these factors, such as teenagers (10-19yo), which are less likely to have acquired the immunity, median income, which may indicate level of exposure due to housing quality, waste management and access to air conditioning, and population density, which increases contact between infected individuals and vectors. Nevertheless, the path from vector to disease is complex and is affected by a multitude of dynamics which were not entirely captured by this analysis, so we encourage future studies to address our limitations to more accurately represent dengue trends in the SJBE.

In spite of these limitations, our results are consistent with our theoretical models and with previous studies on environmental drivers of dengue fever. Furthermore, our results and predictive models (Fig. 7) could be used as preliminary evidence to help justify wetland restoration strategies for the benefit of human health, and to evaluate potential gains and tradeoffs of different landscape management scenarios in the SJBE.

Acknowledgements We thank Roberto Barrera from the CDC Dengue Branch for providing data and advice in the development of this work. Matthew Harwell, Marc Russell and Richard Fulford provided suggestions that greatly helped improved this research. The views expressed in this paper are those of the authors and do not necessarily reflect the views or policies of the U.S. Environmental Protection Agency. Any mention of trade names, products or services does not imply an endorsement by the U.S. Government or the U.S. Environmental Protection Agency (EPA). The EPA does not endorse any commercial products, services, or enterprises.

References

Barbosa AM, Real R, Munoz AR, Brown JA (2013) New measures for assessing model equilibrium and prediction mismatch in species distribution models. Diversity and Distributions 19:1333–1338. https://doi.org/10.1111/ddi.12100

Barrera R, Amador M, Clark GG (2006) Ecological factors influencing Aedes aegypti (Diptera: Culicidae) productivity in artificial containers in Salinas, Puerto Rico. Journal of Medical Entomology 43(3):484–492. https://doi.org/10.1093/jmedent/43.3.484

Barrera R, Amador M, MacKay AJ (2011) Population dynamics of Aedes aegypti and dengue as influenced by weather and human behavior in San Juan, Puerto Rico. PLoS Neglected Tropical Diseases 5(12). https://doi.org/10.1371/journal.pntd.0001378

Barrera R, Bingham AM, Hassan HK, Amador M, Mackay AJ, Unnasch TR (2012) Vertebrate hosts of Aedes aegypti and Aedes mediovittatus (Diptera: Culicidae) in rural Puerto Rico. Journal of Medical Entomology 49(4):917–921. https://doi.org/10.1603/ME12046

Bartoń, K (2009) MuMIn: multi-model inference. R package, version 0.12.2. Available at: http://r-forge.r-project.org/projects/mumin/. Accessed 11/14/2017

Becker, R. A., Chambers, J. M. and Wilks, A. R. (1988) The New S Language. Wadsworth & Brooks/Cole

Bouchama A, Knochel JP (2002) Heat stroke. New England Journal of Medicine 346(25):1978–1988. https://doi.org/10.1056/NEJMra011089

Bowman LR, Runge-Ranzinger S, McCall PJ (2014) Assessing the relationship between vector indices and dengue transmission: a systematic review of the evidence. PLoS Negl Trop Dis 8(5):e2848 https://doi.org/10.1371/journal.pntd.0002848

Brandeis, T. J., Escobedo, F. J., Staudhammer, C. L., Nowak, D. J., & Zipperer, W. C. (2014). San Juan Bay Estuary watershed urban forest inventory. Available at: https://www.nrs.fs.fed.us/pubs/45759. Accessed 11/14/2017

Brody SD, Highfield WE (2013) Open space protection and flood mitigation: A national study. Land Use Policy 32:89–95. https://doi.org/10.1016/j.landusepol.2012.10.017

Brody SD, Peacock WG, Gunn J (2012) Ecological indicators of flood risk along the Gulf of Mexico. Ecological Indicators 18:493–500. https://doi.org/10.1016/j.ecolind.2012.01.004

Burke R, Barrera R, Lewis M, Kluchinsky T, Claborn D (2010) Septic tanks as larval habitats for the mosquitoes Aedes aegypti and Culex quinquefasciatus in Playa-Playita, Puerto Rico. Medical and Veterinary Entomology 24(2):117–123. https://doi.org/10.1111/j.1365-2915.2010.00864.x

Burnham KP, Anderson DR (2002) Model Selection and Multimodel Inference: A Practical Information-Theoretic Approach, 2nd edn. Springer, Berlin

Carrington LB, Armijos MV, Lambrechts L, Barker CM, Scott TW (2013) Effects of fluctuating daily temperatures at critical thermal extremes on Aedes aegypti life-history traits. PLoS One 8(3). https://doi.org/10.1371/journal.pone.0058824

Carver, S., Slaney, D. P., Leisnham, P. T., & Weinstein, P. (2015). Healthy wetlands, healthy people: "mosquito-borne" disease. In Wetlands and Human Health (pp. 95-121). Springer Netherlands

Centro de Recaudación de Ingresos Municipales (CRIM). (2006). Hydrography Revision, 2001-04 from CRIM Basemap, scale 1: 5000. Available at: http://gis.otg.pr.gov. Accessed 06/22/2017

Chang FS, Tseng YT, Hsu PS, Chen CD, Lian IB, Chao DY (2015) Re-assess vector indices threshold as an early warning tool for predicting dengue epidemic in a dengue non-endemic country. PLoS Negl Trop Dis 9(9):e0004043 https://doi.org/10.1371/journal.pntd.0004043

Cheong YL, Leitão PJ, Lakes T (2014) Assessment of land use factors associated with dengue cases in Malaysia using boosted regression trees. Spat Spatiotemporal Epidemiol 10:75–84 https://doi.org/10.1016/j.sste.2014.05.002

Couret J, Dotson E, Benedict MQ (2014) Temperature, larval diet, and density effects on development rate and survival of Aedes aegypti (Diptera: Culicidae). PLoS One 9(2):e87468

Cox J, Grillet ME, Ramos OM, Amador M, Barrera R (2007) Habitat segregation of dengue vectors along an urban environmental gradient. The American Journal of Tropical Medicine and Hygiene 76(5): 820–826. https://doi.org/10.4269/ajtmh.2007.76.820

Federal Emergency Management Agency (FEMA). (2009). Digital flood insurance rate map database, Commonwealth of Puerto Rico. Available at: http://gis.otg.pr.gov/download_gis_files.htm. Accessed 06/22/2017

Gould, W. A., Alarcón, C., Fevold, B., Jiménez, M. E., Martinuzzi, S., Potts, G., ... & Ventosa, E. (2008). The Puerto Rico Gap Analysis Project volume 1: land cover, vertebrate species distributions, and land stewardship. Gen. Tech. Rep. IITF-GTR-39. Río Piedras, PR: U.S. Department of Agriculture, Forest Service, International Institute of Tropical Forestry. 165 p

Grueber CE, Nakagawa S, Laws RJ, Jamieson IG (2011) Multimodel inference in ecology and evolution: challenges and solutions. Journal of Evolutionary Biology *24*(4):699–711. https://doi.org/10.1111/j.1420-9101.2010.02210.x

Harrington LC, Scott TW, Lerdthusnee K, Coleman RC, Costero A, Clark GG et al (2005) Dispersal of the dengue vector Aedes aegypti within and between rural communities. The American Journal of Tropical Medicine and Hygiene 72(2):209–220. https://doi.org/10.4269/ajtmh.2005.72.209

Hashizume M, Dewan AM, Sunahara T, Rahman MZ, Yamamoto T (2012) Hydroclimatological variability and dengue transmission in Dhaka, Bangladesh: a time-series study. BMC Infectious Diseases 12(1):98. https://doi.org/10.1186/1471-2334-12-9

Helmersson, J. (2012) Mathematical Modeling of Dengue-Temperature Effect on Vectorial Capacity. Universitet UMEA.. Master of Science Thesis. Available at: http://www.phmed.umu.se/digitalAssets/104/104555_jing-helmersson.pdf: Umeå University; 2012. 11/14/2017

Ibarra AMS, Ryan SJ, Beltrán E, Mejía R, Silva M, Muñoz Á (2013) Dengue vector dynamics (Aedes aegypti) influenced by climate and social factors in Ecuador: implications for targeted control. PLoS One 8(11). https://doi.org/10.1371/journal.pone.0078263

Kling LJ, Juliano SA, Yee DA (2007) Larval mosquito communities in discarded vehicle tires in a forested and unforested site: detritus type, amount, and water nutrient differences. Journal of Vector Ecology 32(2):207–217. https://doi.org/10.3376/1081-1710

LaDeau SL, Leisnham PT, Biehler D, Bodner D (2013) Higher mosquito production in low-income neighborhoods of Baltimore and Washington, DC: understanding ecological drivers and mosquito-borne disease risk in temperate cities. International Journal of Environmental Research and Public Health 10(4):1505–1526. https://doi.org/10.3390/ijerph10041505

Lesnoff M. and Lancelot R (2012) Analysis of Overdispersed Data (aod, ver 1.3). Available at: https://cran.r-project.org/web/packages/aod/index.html. Accessed 01/20/2017

Lugo AE, Snedaker SC (1974) The ecology of mangroves. Annual Review of Ecology and Systematics 5(1):39–64. https://doi.org/10.1146/annurev.es.05.110174.000351

Lugo, A. E., Ramos, O., & Rodriguez, C. (2011). The Río Piedras watershed and its surrounding environment. U.S. Department of Agriculture Forest Service, International Institute of Tropical Forestry. 48 p. Available at: https://www.researchgate.net/profile/Ariel_Lugo/publication/267236241_ThE_RiO_PiEdRAs_WATERshEd_and_Its_Surrounding_Environment_ACknOWLEdGMEnTs/links/548863900cf289302e30a35e.pdf. Accessed 11/14/2017

Mackay AJ, Amador M, Diaz A, Smith J, Barrera R (2009) Dynamics of Aedes aegypti and Culex quinquefasciatus in septic tanks. Journal of the American Mosquito Control Association 25(4):409–416. https://doi.org/10.2987/09-5888.1

Méndez-Lázaro P, Muller-Karger FE, Otis D, McCarthy MJ, Peña-Orellana M (2014) Assessing climate variability effects on dengue incidence in San Juan, Puerto Rico. International Journal of Environmental Research and Public Health 11(9):9409–9428. https://doi.org/10.3390/ijerph110909409

Méndez-Lázaro, P., Muller-Karger, F. E., Otis, D., McCarthy, M. J., & Rodríguez, E. (2017). A heat vulnerability index to improve urban public health management in San Juan, Puerto Rico. International journal of biometeorology, 1-14. https://doi.org/10.1007/s00484-017-1319-z

Morin CW, Comrie AC, Ernst K (2013) Climate and dengue transmission: evidence and implications. Environmental Health Perspectives 121(11-12):1264. https://doi.org/10.1289/ehp.1306556

Morin CW, Monaghan AJ, Hayden MH, Barrera R, Ernst K (2015) Meteorologically driven simulations of dengue epidemics in San Juan, PR. PLoS Neglected Tropical Diseases 9(8). https://doi.org/10.1371/journal.pntd.0004002

Mulligan K, Dixon J, Sinn CLJ, Elliott SJ (2015) Is dengue a disease of poverty? A systematic review. Pathogens and Global Health 109(1): 10. https://doi.org/10.1179/2047773214Y.0000000168

Murugan K, Priyanka V, Dinesh D, Madhiyazhagan P, Panneerselvam C, Subramaniam J et al (2015) Predation by Asian bullfrog tadpoles, Hoplobatrachus tigerinus, against the dengue vector, Aedes aegypti, in an aquatic environment treated with mosquitocidal nanoparticles. Parasitol Res 114(10):3601–3610 https://doi.org/10.1007/s00436-015-4582-0

Myer MH, Campbell SR, Johnston JM (2017) Spatiotemporal modeling of ecological and sociological predictors of West Nile virus in Suffolk County, NY, mosquitoes. Ecosphere 8(6) https://doi.org/10.1002/ecs2.1854

Myers SS, Gaffikin L, Golden CD, Ostfeld RS, Redford KH, Ricketts TH et al (2013) Human health impacts of ecosystem alteration.

Proceedings of the National Academy of Sciences 110(47):18753–18760. https://doi.org/10.1073/pnas.1218656110

Navarro DMAF, De Oliveira PES, Potting RPJ, Brito AC, Fital SJF, Sant'Ana AE (2003) The potential attractant or repellent effects of different water types on oviposition in Aedes aegypti L.(Dipt., Culicidae). Journal of Applied Entomology 127(1):46–50. https://doi.org/10.1046/j.1439-0418.2003.00690.x

Philip GM, Watson DF (1982) A precise method for determining contoured surfaces. APPEA J 22(1):205–212 https://doi.org/10.1071/AJ81016

Pires DA, Gleiser RM (2010) Mosquito fauna inhabiting water bodies in the urban environment of Córdoba city, Argentina, following a St. Louis encephalitis outbreak. Journal of Vector Ecology 35(2):401–409. https://doi.org/10.1111/j.1948-7134.2010.00099.x

Poole-Smith BK, Hemme RR, Delorey M, Felix G, Gonzalez AL, Amador M et al (2015) Comparison of vector competence of Aedes mediovittatus and Aedes aegypti for dengue virus: implications for dengue control in the Caribbean. PLoS Neglected Tropical Diseases *9*(2):e0003462. https://doi.org/10.1371/journal.%20pntd.0003462

Puerto Rico Department of Health (PRDH). (2017). Informe seminal de enfermedades arbovirales (Semana 4-10 de Junio de 2017). Available at: http://www.salud.gov.pr/Estadisticas-Registros-y-Publicaciones/Informes%20Arbovirales/Reporte%20ArboV%20semana%2023-2017.pdf/ Accessed 06/29/2017

Quinn GP, Keough MJ (2002) Experimental design and data analysis for biologists. Cambridge University Press

Quiroz-Martínez H, Rodríguez-Castro A (2007) Aquatic insects as predators of mosquito larvae. Journal of the American mosquito control association, 23(sp2), 110-117. https://doi.org/10.2987/8756-971X(2007)23%5B110:AIAPOM%5D2.0.CO;2

Ramasamy R, Surendran SN, Jude PJ, Dharshini S, Vinobaba M (2011) Larval development of Aedes aegypti and Aedes albopictus in peri-urban brackish water and its implications for transmission of arboviral diseases. PLoS Neglected Tropical Diseases *5*(11):e1369. https://doi.org/10.1371/journal.pntd.0001369

Reiter P, Amador MA, Anderson RA, Clark GG (1995) Dispersal of Aedes aegypti in an urban area after blood feeding as demonstrated by rubidium-marked eggs. The American Journal of Tropical Medicine and Hygiene 52(2):177–179. https://doi.org/10.4269/ajtmh.1995.52.177

Ruiz-Fons, F., Acevedo, P., Sobrino, R., Vicente, J., Fierro, Y., & Fernández-de-Mera, I. G. (2013). Sex-biased differences in the effects of host individual, host population and environmental traits driving tick parasitism in red deer. Frontiers in cellular and infection microbiology, 3. doi: https://doi.org/10.3389/fcimb.2013.00023

San Juan Bay Estuary (SJBE). (2015). Area cientifica: datos de monitoreo. Available at: http://www.estuario.org/index.php/datos/ciencia?limitstart=0. Accessed 01/30/2017

Sanford MR, Chan K, Walton WE (2005) Effects of inorganic nitrogen enrichment on mosquitoes (Diptera: Culicidae) and the associated aquatic community in constructed treatment wetlands. Journal of Medical Entomology 42(5):766–776. https://doi.org/10.1093/jmedent/42.5.766

Sarfraz MS, Tripathi NK, Tipdecho T, Thongbu T, Kerdthong P, Souris M (2012) Analyzing the spatio-temporal relationship between dengue vector larval density and land-use using factor analysis and spatial ring mapping. BMC Public Health 12(1):853 https://doi.org/10.1186/1471-2458-12-853

Sharp TM, Hunsperger E, Santiago GA, Muñoz-Jordan JL, Santiago LM, Rivera A et al (2013) Virus-specific differences in rates of disease during the 2010 Dengue epidemic in Puerto Rico. PLoS Neglected Tropical Diseases 7(4):e2159. https://doi.org/10.1371/journal.pntd.0002159

Stanforth A, Moreno-Madriñán MJ, Ashby J (2016) Exploratory analysis of dengue fever niche variables within the Río Magdalena watershed. Remote Sens 8(9):770 https://doi.org/10.3390/rs8090770

Tiong V, Abd-Jamil J, Zan MH, Abu-Bakar RS, Ew CL, Jafar FL et al (2015) Evaluation of land cover and prevalence of dengue in Malaysia. Trop Biomed 32(4):587–597

Torres-Valcárcel Á, Harbor J, González-Avilés C, Torres-Valcárcel A (2014) Impacts of Urban Development on Precipitation in the Tropical Maritime Climate of Puerto Rico. Climate 2(2):47–77. https://doi.org/10.3390/cli2020047

U.S. Geological Survey, (1941) A. USGS 1:30000-scale Quadrangle for San Juan, PR 1941: U.S. Geological Survey: Reston, Virginia. Available at: https://prd-tnm.s3.amazonaws.com/StagedProducts/Maps/HistoricalTopo/2/14619/4985332.pdf. Accessed 01/25/2017

U.S. Geological Survey. (1944). 1:20000 scale Topographic contours for Puerto Rico quadrangles converted form USGS Digital Line Graph data. Available at: http://gis.otg.pr.gov/download_gis_files.htm. Accessed 01/25/2017

United States Census Bureau. (2015). 2011-5-year summary American Community Survey. U.S. Census Bureau's American Community Survey Office. Available at: http://ftp2.census.gov/. Accessed 01/25/2017

Venables WN, Ripley BD (2003) Modern Applied Statistics with S, 4th edn. Springer-Verlag, New York

Watson DF, Philip GM (1985) A refinement of inverse distance weighted interpolation. Geoprocessing 2(4):315–327

World Health Organization (WHO). (2006). Communicable diseases following natural disasters: Risk assessment and priority interventions (WHO/CDS/NTD/DCE/2006.4). Available at: http://www.who.int/diseasecontrol_emergencies/guidelines/CD_Disasters_26_06.pdf Accessed 01/30/2017

Yee DA, Himel E, Reiskind MH, Vamosi SM (2014) Implications of saline concentrations for the performance and competitive interactions of the mosquitoes Aedes aegypti (Stegomyia aegypti) and Aedes albopictus (Stegomyia albopictus). Medical and Veterinary Entomology 28(1):60–69. https://doi.org/10.1111/mve.12007

From: Huertas, Evelyn
Sent: Wednesday, July 6, 2016 5:07 PM
To: Yee, Susan; Hanson, Alana; Wigand, Cathleen; Oczkowski, Autumn
Cc: Fisher, Bill; Patricia Bradley
Subject: FW: Caño Martín Peña: Preocupaciones sobre Naled
Attachments: c-ds-16-jul-05 LNR Asperjacion con Naled.pdf

Some of the results from your nitrogen study and the purpose of the mosquito's study have been used to empower the citizens to stand against spraying us with Naled. Citizens here are very furious (and have been several protests) against CDC that wants to spray the whole island with Naled.

Evelyn

From: Lyvia Rodriguez [mailto:lrodriguez@martinpena.org]
Sent: Wednesday, July 06, 2016 1:20 PM
To: Font, Jose <Font.Jose@epa.gov>; Huertas, Evelyn <Huertas.Evelyn@epa.gov>; Gutierrez, Claudia <Gutierrez.Claudia@epa.gov>
Subject: Caño Martín Peña: Preocupaciones sobre Naled

Saludos,

Se incluye copia de una carta enviada a la Secretaria de Salud de Puerto Rico en la que se expresan varias preocupaciones sobre el efecto de una potencial asperjación con Naled sobre la salud de los residentes de las comunidades aledañas al Caño Martín Peña. Gracias.

Lyvia N. Rodríguez Del Valle
Directora Ejecutiva
Corporación del Proyecto ENLACE del Caño Martín Peña
Apartado Postal 41308
San Juan, Puerto Rico 00940-1308

T.787.729.1594
F.787.725.2544
www.cano3punto7.org

caño 3.7
g-8 • enlace • fideicomiso

6 de julio de 2016

VIA CORREO ELECTRONICO: anarius@salud.gov.pr; brendarivera@salud.pr.gov

Hon. Ana Rius Armendáriz
Secretaria
Departamento de Salud
Apartado Postal 70184
San Juan, PR 00936-0184

Atención: Dra. Brenda Rivera García, Directora de la Oficina de Epidemiología e Investigación

ASPERJACION CON NALED

Estimada señora Secretaria:

Le expresamos nuestra preocupación con respecto a la asperjación aérea propuesta con el pesticida organofosfato Naled. Por años, las comunidades aledañas al Caño Martín Peña se han visto afectadas desproporcionalmente por el dengue y más recientemente, el chikungunya. Hemos visto a familias perder a sus seres queridos y a otros tantos incapacitarse durante varios meses. Al igual que usted, y por qué nos toca de cerca, nos preocupan los efectos que el virus del zika pueda tener en las personas afectadas. Es por ello que, a pesar de los recursos limitados, nos hemos movilizado junto a nuestros aliados y colaboradores para llevar a cabo actividades comunitarias de prevención y educación popular.

Nos preocupa el impacto que el Naled puede tener en la ya comprometida salud de nuestra población, muy particularmente en las personas que padecen de asma bronquial y dermatitis atópica, así como en las cosechas de nuestros huertos ecológicos comunitarios que nuestros residentes voluntarios trabajan como medida de prevención de vertederos clandestinos y seguridad alimentaria, en los insectos polinizadores y el medio ambiente en general. Por lo tanto, solicitamos que como alternativa, los fondos previstos para asperjar se utilicen para fortalecer los esfuerzos de prevención y control de criaderos de mosquitos.

Las comunidades aledañas al Caño Martín Peña, localizadas en el corazón del Área Metropolitana de San Juan, tienen cerca de 25,000 habitantes y constituyen el lugar más densamente poblado del país, con 22,257 habitantes por milla cuadrada en el Distrito de Planificación Especial del Caño Martín Peña,. La salud de los vecinos se ha afectado significativamente debido a los efectos de la degradación ambiental del Caño Martín Peña, lo que, entre otros, ha llevado a una lucha de más de una década en torno al derecho a la salud y la justicia ambiental.. Veamos:

- Estudios epidemiológicos[1,2] han correlacionado el impacto a la salud pública de las inundaciones y de vivir cerca del Caño Martín Peña, dada la pobre calidad del agua y el deterioro ambiental. La prevalencia de enfermedades gastrointestinales es el doble para los residentes expuestos a las aguas contaminadas que inundan casas y calles cuando llueve, comparado con el resto de los residentes. En un periodo de solo tres meses, el 31% de la población del Caño sufre de problemas estomacales, en contraste con el 22% de la población en Puerto Rico durante todo un año.

- **La prevalencia de asma bronquial entre los menores de 5 años de las comunidades del Caño es de 44.5%, es decir, más del doble del 21.5% que se ha reportado en Puerto Rico en este grupo de edad.** También se evidenció que entre los residentes menores de 18 años que viven más cerca del Caño hay una mayor prevalencia de asma bronquial y dermatitis atópica que entre los que viven en otros sectores de la comunidad. La Evaluación de Impacto a la Salud de la Rehabilitación Ambiental del Caño Martín Peña (HIA)[3] realizada en 2014 por la escuela de medicina Icahn del Hospital Mount Sinai en Nueva York, identifica la presencia de humedad y hongos en las viviendas, resultado de las inundaciones frecuentes, así como la exposición a vectores, como algunas de las causas de asma entre los residentes del Caño.

- La Agencia de Protección Ambiental de los EE.UU. (EPA) tomó muestras de las concentraciones de sulfuro de hidrógeno en el aire, encontrando 0.002 ppm y 0.062 ppm. El valor de referencia para la exposición crónica de H_2S en niños es de 0.001 ppm, que claramente se excede. La exposición crónica a H_2S está asociada a efectos negativos en el sistema respiratorio, letargia, falta de coordinación, dolores de cabeza, pérdida de memoria y disfunción motora, entre otros (ATSDR, 2006)

Como es de conocimiento de las autoridades sanitarias, el Naled es efectivo para matar el mosquito adulto. En zonas urbanas y densamente pobladas como la nuestra, donde el mosquito se desarrolla dentro de estructuras, el efecto del Naled sobre los mosquitos adultos pudiera ser limitado. Asimismo, este pesticida no afecta a los mosquitos en otras etapas de su ciclo de vida, por lo que es posible que las autoridades consideren asperjar en múltiples ocasiones, por lo que una dosis baja de Naled de una onza por cuerda se multiplicaría. También pudieran considerar combinar el Naled con larvicidas. La Dra. Cruz María Nazario, del Departamento de Bioestadística y Epidemiología de la Escuela Graduada de Salud Pública de la Universidad de Puerto Rico y miembro de nuestra Junta Asesora comenta que no conocemos el efecto de la mezcla de ambos, aunque es conocido que la acumulación de pesticidas en el cuerpo, desencadena efectos a largo plazo en condiciones crónicas. Comenta además lo siguiente:

> "La fumigación ha sido efectiva para eliminar otros insectos, por ejemplo, se ha usado en EEUU para eliminar el mosquito que transmite el Western Nyle Virus. Desde el 1999[1], hay evidencia que la fumigación no es efectiva para reducir la población de mosquitos del tipo Aedes aegypti ni el Aedes albopictus. Estos

---

[1] 2012, Vélez, Himilce, Mayra Roubert, et.al. Prevalencia de la sintomatología gastrointestinal entre los residentes de las comunidades aledañas al Caño Martín Peña en San Juan, Puerto Rico. Preparado por la Escuela de Medicina y Ciencias de la Salud de Ponce para la Agencia de Protección Ambiental de los Estados Unidos y la Corporación del Proyecto ENLACE del Caño Martín Peña.

[2] 2012, Suárez, Erick, Cynthia Pérez, et.al. Prevalencia de asma bronquial y dermatitis atópica en la población pediátrica residente en las comunidades adyacentes al Caño Martín Peña. Preparado por el Departamento de Epidemiología y Bioestadística de la Escuela Graduada de Salud Pública, Recinto de Ciencias Médicas de la Universidad de Puerto Rico para la Corporación del Proyecto ENLACE del Caño Martín Peña.

[3] Sheffield PE, Agu DP, Rowe M, Fischer K, Pérez AE, Rodríguez LN, Avilés KR. 2014. *Health Impact Assessment of the Proposed Environmental Restoration of Caño Martín Peña*, p.17. San Juan, Puerto Rico. Subvencionado por la *Robert Wood Johnson Foundation* y *The Pew Charitable Trust*.

> tipos de mosquitos están presentes en el Sur de EEUU desde Connecticut hasta California. En esos estados no se ha establecido campañas de fumigación en contra del tipo de mosquito Aedes, si para otros insectos. En 2005, dos renombrados médicos investigadores de Dengue del CDC en Puerto Rico, escribieron un artículo[4]que explicaba que la fumigación no era la forma más eficiente de eliminar el mosquito Aedes."

Al efecto limitado del Naled para controlar la población de los mosquitos *Aedes Aegypti* se suma el impacto acumulativo adverso por exposición directa o indirecta que puede tener en la salud, ya afectada, de los residentes de las comunidades aledañas al Caño. Nos preocupa además el impacto a los cultivos de agroecología urbana de nuestros residentes y la ingesta de cultivos rociados con Naled, así como el impacto al medio ambiente. Hemos tomado conocimiento de que en la Unión Europea, se ha prohibdo la asperjación con Naled desde 2012.

El HIA reconoce que ya hay motivo de preocupación con respecto al uso periódico de pesticidas, particularmente los organofosfatos, en las comunidades aledañas al Caño:

> *"Pesticide use – Any pesticide use represents a potential increase in pesticide exposure for the people – doing the spraying or living - nearby. Government spraying campaigns are informed by the systematic surveillance of dengue cases (as noted above) led by the Centers for Disease Control Dengue Branch located in San Juan. While specifics regarding frequency of spraying by the government were not available, in general, spraying is increased in areas where clusters are detected. Regarding use of pesticides by individual residents, focus group participants reported using pesticides to reduce mosquito populations. Specifically, they reported using a type of organophosphate pesticide called Malathion. A number of recent studies in other locations have highlighted potential negative effects of commonly used organophosphate pesticides. These health risks can occur even at low levels of pesticide exposure. In two New York City studies, children whose mothers were exposed to organophosphates during pregnancy were seen to have a decrease in neurobehavioral development starting at 12 months and a decrease in perceptual reasoning and Working Memory evaluated at 6-9 years of age (Engel et al., 2011; Rauh et al., 2011). Another study evaluating the effect of chronic exposure to low levels of organophosphates found that prenatal exposure was associated with poorer intellectual development in 7-year-old children (Bouchard et al., 2011)."*[5]

Es evidente que el uso del malathion no ha eliminado ni disminuido la población del Aedes Aegypti. Las características medioambientales que llevan a la alta presencia de mosquitos en las comunidades aledañas al Caño no serán atendidas por la asperjación con Naled. Veamos:

- Situaciones relacionadas a la degradación ambiental del Caño:
  - Según estudios realizados en el 2015 por la EPA, hay altas concentraciones de nitrógeno en el Caño. La EPA nos ha alertado de la correlación entre altas concentraciones de nitrógeno y una mayor población y tamaño del mosquito *Aedes Aegypti*. Asimismo, se prevé que a mayor tamaño de mosquito, mayor concentración de virus, o más tipos de virus, pueden contener. Recientemente, un grupo de investigadores de la EPA visitaron nuevamente las comunidades para tomar muestras de mosquitos adultos y larvas con el fin de estudiar de manera más detallada la presencia de virus en relación con el nitrógeno. Recientemente, visitaron la comunidad para tomar muestras de mosquitos y estudiar de manera más detallada la presencia de virus en relación con el nitrógeno.

---

[4] Rigau Pérez, José G. y Gary G. Clark, 2005. Como responder aa una epidemia de dengue: visión global y experiencia en Puerto Rico, en Revista Panamericana de Salud Pública/Pan Am J Public Health 17(4), 2005.

[5] Sheffield PE, et. al., p.17.

  - Presencia de criaderos de mosquitos en la basura, envases y otro material que hay en el Caño y que no puede extraerse con facilidad.
- Situaciones comunes en zonas urbanas:
  - Presencia de criaderos de mosquitos en la basura, envases y otro material que hay en el Caño y que no puede extraerse con facilidad en estructuras abandonadas; vertederos clandestinos y gomas de automóviles; envases en los patios de las residencias y acumulación de agua limpia en techos y alrededores; entre otros.

Proponemos que los recursos que se pondera invertir en la asperjación aérea con Naled se redirijan a fortalecer, de forma decidida y certera, iniciativas dirigidas a disminuir o eliminar los criaderos de mosquitos, proteger a la población contra las picaduras y otras formas de contagio, y educar para generar cambios duraderos y fomentar que las personas incorporen en su rutina diaria las medidas recomendadas. Ello es cónsono con lo dispuesto por el Gobernador en el Boletín Administrativo OE-2016-003, es cual establece que "las medidas de prevención y protección más importantes son la eliminación de los criaderos de mosquitos y evitar sus picaduras, especialmente en las mujeres embarazadas." Asimismo, proponemos que se consideren otras estrategias que han probado ser efectivas para el control de la población de mosquitos, como las trampas. En el caso del Caño, recomendamos además que se evalúe, en el marco de la emergencia de salud, invertir recursos para remover la basura superficial en el agua y en lugares de difícil acceso en las márgenes del cuerpo de agua. La Corporación del Proyecto ENLACE está disponible para coordinar estos trabajos, si se le asignan los recursos requeridos.

Estos procesos deben tomar en cuenta el contexto de los grupos sociales a los que se dirigen, y que deben ser actores principales en la atención de esta situación. . En el caso de nuestras comunidades, estimamos que solamente un 15% de las estructuras tiene mallas metálicas (*screens*) protegiendo puertas y ventanas. Asimismo, hay estructuras donde la instalación de mallas no cubre la totalidad de los orificios. Estamos disponibles para compartir los estimados de costos preliminares para subvencionar la colocación de mallas en puertas y ventanas.

De otra parte, el uso continuo de repelentes de mosquito autorizados, así como el uso de aire acondicionado, es costoso y no es accesible a gran parte de la población, 56% de la cual vive bajo los niveles de pobreza y con una mediana de ingresos de $13,523[6]. Debido al calor intenso de verano, hay resistencia al uso de manga larga. Por lo tanto, las medidas de prevención deben partir de esta realidad y abordarla.

Entre las gestiones que hemos realizado a la fecha, se encuentran:

- Con la colaboración de aliados, preparar y repartir casa a casa imanes que los vecinos puedan colocar en sus neveras, con consejos de lo que pueden hacer diariamente para prevenir los criaderos de mosquitos y las picaduras.
- Informar a la comunidad en medios comunitarios, y discutir el tema en actividades.
- Proveer talleres a todas las escuelas elementales del Distrito para educar a los niños y jóvenes sobre la importancia de eliminar los criaderos de mosquitos y protegerse de picaduras.
- Ayudar a las familias en sus casas a que identifiquen y eliminen los criaderos de mosquito en su entorno.

---

[6] *2010 American Community Survey 1-Year Estimates.*

- Trabajar junto al Municipio de San Juan refiriéndole los vertederos clandesdinos y lugares con concentración de gomas, para su remoción.

Asimismo, hemos recibido la visita de funcionarios de los Centros para el Control y la Prevención de Enfermedades (CDC) y de medios de comunicación de los Estados Unidos en torno al zika, y discutido alternativas, como la instalación de mallas. Además, en el caso de nuestras comunidades, queda claro que la prevalencia de dengue, chikungunya y zika son una alerta adicional sobre la urgencia de recuperar el Caño Martín Peña.

Le urgimos a que considere lo aquí planteado. El impacto acumulativo de la aplicación del Naled en una población vulnerable, cuya salud ya está afectada, habiendo otras alternativas que pudieran ser más efectivas, nos plantea una cuestión de justicia ambiental y mantiene en alerta a las organizaciones de base comunitaria. Confiamos en que usted será sensible a la preocupación de nuestras comunidades.

Estamos disponibles para seguir aportando al manejo de esta situación. De requerirlo, puede comunicarse a lrodriguez@martinpena.org. Sin más, queda,

Atentamente,

Carmen L. Febres Alméstica
Presidenta
G-8, Grupo de las Ocho Comunidades
Aledañas al Caño Martín Peña, Inc.

Lyvia N. Rodríguez Del Valle
Directora Ejecutiva
Corporación del Proyecto ENLACE
del Caño Martín Peña

María E. Hernández Torrales
Presidenta
Fideicomiso de la Tierra del Caño Martín Peña

c. Mariela Cruz, Asesora del Gobernador en Infraestructura
Angela Díaz, Asesora del Gobernador en Salud
Centers for Disease Control
Agencia Federal de Protección Ambiental
Junta de Acción Comunitaria de Bitumul e Israel, Inc.
Corporación Desarrolladora de Viviendas de Israel y Bitumul
Consejo Vecinal Pro Desarrollo de la Península de Cantera, Inc.
Residentes Unidos de Barrio Obrero Marina, Inc.
Las Monjas Renace, Inc.
Buena Vista Florece, Inc.
Junta de Residentes de Buena Vista Santurce, Inc.
Asociación Pro Bienestar Parada 27, Inc.
Vecinos Unidos por Nuestra Comunidad, Inc.
Asociación de Damas Salesianas, Inc.
Líderes Jóvenes en Acción
Coalición Martín Peña en Acción, Inc.

Yee, Susan

From: Estrella D. Santiago Perez <esantiago@martinpena.org>
Sent: Tuesday, November 07, 2017 9:13 AM
To: Huertas, Evelyn
Cc: Oczkowski, Autumn; Betancourt, Doris; Hanson, Alana; Wigand, Cathleen; Yee, Susan; Martin, Rose; Dejesus-Crespo, Rebeca; Lyvia N Rodríguez del Valle; Dean, Timothy
Subject: Re: Call with Estrella from Enlace

Hi all,

As discussed in our call, the G-8 suggests continuing research efforts after January 2018, as the communities are still recovering from Hurricane Maria's impact. Hopefully, by January '18 power has been restored in the communities, eliminating one of the main stressors that residents have, and we could be transitioning from immediate relief response to medium and long-term recovery efforts. I would be assisting in the coordination with the G-8.

We appreciate your continued support,

--
Lcda. Estrella D. Santiago Pérez
Gerente de Asuntos Ambientales | Environmental Affairs Manager
Corporación del Proyecto ENLACE del Caño Martín Peña
P.O. Box 41308 | San Juan, Puerto Rico 00940-1308
✉ esantiago@martinpena.org | ☎ (787) 729-1594 | 📱 (787) 689-1558 | 🖷 (787) 725-2544
| 🌎 www.cano3punto7.org / www.martinpena.org

AVISO DE CONFIDENCIALIDAD: Este correo electrónico y/o el material adjunto es para uso exclusivo de la persona o entidad a la que expresamente se le ha enviado, y puede contener información confidencial o material privilegiado. Si usted no es el destinatario legítimo del mismo, por favor repórtelo inmediatamente al remitente del correo y bórrelo. Cualquier revisión, retransmisión, difusión o cualquier otro uso de este correo, por personas o entidades distintas a las del destinatario legítimo, queda expresamente prohibido. Este correo electrónico no pretende ni debe ser considerado como constitutivo de ninguna relación legal, contractual o de otra índole.

CONFIDENTIALITY NOTICE: This email and/or accompanying material is for exclusive use of the person or entity to which it was expressly sent and may contain confidential or privileged material. If you are not the intended recipient of it, please report it immediately to the sender and delete the email. Any review, retransmission, dissemination or other use of this email, by persons other than the intended recipient entities, is expressly prohibited. This email is not intended nor should it be considered as constituting any legal relationship, contractual or otherwise.

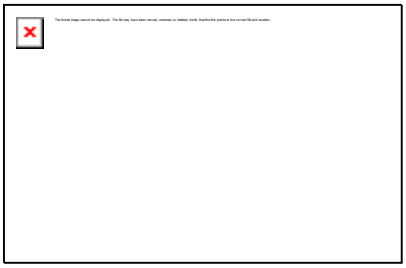

On Thu, Nov 2, 2017 at 2:33 PM, Huertas, Evelyn <Huertas.Evelyn@epa.gov> wrote:

We will be discussing with Estrella about any immediate research needs in CMP as consequence of the pass of Hurricane Maria and if there is any need of making any changes to the current studies in the area. Of course, we are not making any promises because it all depends on the available budget and the approval of ORD management.

Evelyn

~ ~

Evelyn Huertas, MS

Region 2 San Juan Bay Estuary Program Manager

US EPA, Caribbean Environmental Protection Division

Multimedia Permits and Compliance Branch

City View Plaza 2, Suite 7000, Guaynabo, Puerto Rico 00968

P. 787.977.5852

huertas.evelyn@epa.gov / www.epa.gov / www.estuario.org

An official website of the United States government.

We've made some changes to EPA.gov. If the information you are looking for is not here, you may be able to find it on the EPA Web Archive or the January 19, 2017 Web Snapshot.

Close ✕

EPA Research Supports National Estuary Program

Estuaries—those areas where freshwater rivers flow into oceans—serve as prime examples of how natural habitats provide benefits to people and local communities.

Such benefits, often referred to as ecosystem services, include serving as breeding and nursery areas for many commercially important fish and seafood, providing coveted spots for canoeing, kayaking, and other outdoor activities, and buffering the impacts of erosion and flooding from coastal storms.

EPA researchers are working closely with partners in the Agency's National Estuary Program (NEP) to help local communities improve the water quality, habitats, and living resources of estuaries.

A major focus is to provide the information, tools, and data needed to improve and protect estuaries and ensure these habitats continue to provide benefits that contribute to healthy, sustainable, and vibrant communities.

EPA National Estuary Program Research Across the Nation

Cool Science

Partner: Lower Columbia Estuary Partnership
Project: Cold Water Refuge for Endangered Salmon and Steelhead

Agency researchers are working with the Lower Columbia Estuary Partnership (LCEP) to prevent further decline in the area's iconic salmon and steelhead trout migrations. One of the major stressors for these now endangered species is rising stream temperatures.

Using temperature and population data from monitoring studies by the LCEP, EPA scientists are developing fish population models that link cold water microhabitats with fish survival rates. The cooler microhabitats provide areas of refuge for the fish during their long upriver journey to spawning grounds. The models will forecast whether the refuges are adequate for successful upstream migration and will guide actions to protect and restore the endangered populations.

Informing Decisions Across a Watershed

Partner: Tillamook Estuaries Partnership
Project: Sustaining the Natural Benefits of Tillamook Bay

Much of the local economy surrounding the Tillamook Bay estuary is provided by the coastal ecosystem: the area is a hotspot for coastal birding, home to a rich diversity of marine fish and wildlife, and a prized location for harvesting bay clams and culturing oysters. But these benefits are at increasing risk from environmental conditions that lead to algal blooms, reduced oxygen, and acidified water.

Agency researchers are working with the Tillamook Estuaries Partnership as well as stakeholders across the watershed on a suite of studies that identify sources of microbial pathogens and excess nutrients flowing into the estuary, quantify drivers of acidification, and assess recreational uses of the estuary. The goal of the research is to directly support environmental planning that balances the sustained health of the estuary with other, sometimes conflicting benefits and priorities.

A Framework for Setting Goals

Partner: Massachusetts Bays National Estuary Program
Project: Managing Multiple Bays and Estuaries

The Massachusetts Bays National Estuary Program (MassBays) has set out an ambitious goal: setting environmental targets and managing the 47 independent embayments—harbors, bays, and coves—that make up the coastline, each with different watershed, landscape, and ecosystem benefit characteristics to meet those targets.

MassBays has organized the individual embayments into ecological classes based on physical properties and biological resources such as seagrass, saltmarsh or shellfish beds. Now, EPA scientists are working with MassBays' science advisors and local stakeholders to develop a framework that highlights the benefits that accrue from these resources as well as the watershed stressors that threaten them.

MassBays will use the framework to inform management objectives and to communicate to local decisionmakers how estuaries provide social and economic benefits to communities across the watershed.

Holding Back the Tide: Exploring the Use of Living Shorelines

Partner: Partnership for the Delaware Estuary
Project: Living Shorelines for Increased Resiliency

The saltmarsh habitats that grow along the edges of estuaries provide essential refuge for fish and wildlife and protect shorelines from erosion by buffering wave action and trapping sediments. But rising sea levels, increased storm intensity, nutrient pollution, and other stressors linked to human activities on the surrounding land have sparked declines in saltmarshes across the globe.

EPA researchers worked with the Partnership for the Delaware Estuary on methods to better protect saltmarshes and the benefits they provide through construction of living shorelines—engineered habitat enhancements that reduce erosion while encouraging the growth of vegetation and shellfish.

They conducted a study that explored the effectiveness of coir logs (coconut fiber rolled in burlap) to protect the shoreline from erosion, along with planted mussel seedlings to filter algae and sediment from the water. The trial showed that coir logs could protect the shoreline and build up marsh in Delaware Bay because of high sediment supplies in that estuary, but were much less effective in Northeast estuaries where sediment supply was insufficient to build marshes. The effort provided key insights about how and where certain living shoreline types could restore saltmarsh habitat. This has informed decisions for estuary restoration and protection across National Estuary Programs.

Rising to the Challenge: Assessing Sediment Applications to Save Drowning Marshes

Partner: Narragansett Bay Estuary Program
Project: Restoring Saltmarshes

Saltmarsh habitats are critical to estuarine heath. They are nurseries, refuges, and feeding stations for estuarine life, protect shorelines, and clean water by trapping sediments. While saltmarshes face many stressors, sea level rise and marsh flooding are a particular concern across Rhode Island.

EPA scientists worked with the Narragansett Bay Estuary Program, the Rhode Island Coastal Resources Management Council, the Rhode Island Natural History Survey, and the National Estuarine Research Reserve in Rhode Island to design a sediment application project. The project consisted of placing clean dredge material on the surface of a drowning marsh thick enough to counter rising sea. With that in place, EPA is providing scientific support for monitoring the impacts, including vegetation growth, soils pH, salinity, percent organic matter, and more.

While a number of similar sediment application projects have taken place or are planned across the US, this work is one of only a few that have included scientific monitoring, making it a key contributor to future success.

Cultivating Science to Reduce Nutrient Pollution and Protect Seagrasses

Partner: Narragansett Bay Estuary Program
Project: Protecting Seagrasses

Too many nutrients flowing into estuaries can lead to increased algal growth that triggers a cascade of impacts—lower disolved oxygen levels, acidification, less sunlight penetrating the water column—impacts that ultimately reduce seagrass abundance, a key habitat for the health of the entire ecosystem.

To better assess the health of the seagrass in Narragansett Bay over time, EPA scientists, in partnership with the Narragansett Bay Estuary Program, and the University of Rhode Island compiled and analyzed photographs, early charts, and other historic documents. Using this information, they documented changes to the extent (area) of seagrass coverage across the Bay from 1776 to 2016, and then correlated this to nutrient inputs over that time period. Using this information, they documented the extent (area) of seagrass coverage across the Bay, and then correlated the changes they found with sources of nutrients entering the Bay.

The work has led to a better understanding of how wastewater treatment upgrades have contributed to lower nutrient levels and improved the environment—important information for local communities searching for effective, cost-efficient solutions.

Past, Present, and Future: Innovative Research for Tampa Bay

Partner: Tampa Bay Estuary Program
Project: Setting Water Quality Goals

The Tampa Bay Estuary Program (TBEP) has embraced the daunting challenge of protecting the water quality, habitat and benefits provided by Tampa Bay, Florida's largest open water estuary. To this end, EPA researchers have been working with TBEP and other State and local partners for more than 20 years. Projects have covered a wide range of subjects, including nutrient assessment and monitoring, aquatic habitats, assessing the benefits (ecosystem services) that the estuary provides, and setting management targets for recovery and restoration.

In one innovative project, Agency researchers used historic data to document and illustrate the loss of seagrass habitat over time, then worked with local partners to set seagrass restoration targets. The historic dataset was highly influential with stakeholders and, after almost two decades of highly collaborative work, the seagrass goals were met. The use of historic data as a community engagement tool was so successful it has been adopted for use in four other National Estuary Programs.

A common focus throughout EPA's collaboration with TBEP has been to provide information and develop tools that help the local community make decisions that meet short term goals while still protecting the long-term health of the estuary. A recent example is the EPA H2O Tool, a GIS-based, open-source support tool for exploring the impact of different land use scenarios and human population growth on the Bay. The tool has been used by regional planners and incorporated into a suite of community studies to inform decision-making in and around Tampa Bay.

Streaming Science: Quantifying the Benefits of Stream Restoration

Partners: Mobile Bay National Estuary Program
Project: Socio-economic Impacts of Stream Restoration

Stream restoration techniques—adding physical and biological elements to degraded streams—are widely used to stabilize streambanks, reduce erosion, upgrade aesthetics, and improve water quality. Over the past several years Alabama has used such approaches to restore streams in the Mobile Bay watershed.

EPA researchers are working with the Mobile Bay National Estuary Program (MBNEP) to characterize stream restoration activities and model how improved streams, as well as other attributes of the local environment (land use and cover, watershed conditions, and high-priority ecosystem services), contribute both economic and social benefits to local communities.

Their work has been incorporated into the MBNEP 2019-2023 Comprehensive Conservation and Management Plans for sites of interest. By finding ways to document the value of stream restoration, the MBNEP will have continued influence in stream restoration decisions affecting the Mobile Bay watershed.

Sound Science: Supporting the Long Island Sound Study

Partner: Long Island Sound Study
Project: Reducing Nutrient Pollution

In 1985 EPA worked cooperatively with the States of New York and Connecticut to establish the Long Island Sound Study (LISS). Since then, Agency researchers have been collaborating with LISS partners to support its vision to protect and restore the large estuary commonly known as Long Island Sound. One of the most serious threats to water quality in Long Island Sound is nutrient input from the surrounding watersheds. Excess nutrients lead to algal blooms, acidification and lower oxygen levels in the water.

Agency researcher have served key membership and leadership roles on numerous LISS working committees (Advisory Group for the new Long Island Sound nitrogen strategy; the Advisory Committee for Long Island; Niantic River Nitrogen Workgroup; LISS Management and Science Technical Advisory Committees) and have collaborated on a host of projects to inform the *LISS Comprehensive Conservation and Management Plan*. For example, in 2014 Agency scientists headed the editorial team that produced *Long Island Sound: Prospects for The Urban Sea*, the first synthesis of the science of Long Island Sound in more than 35 years.

Linking Healthy Ecosystems with Healthy Communities in Puerto Rico

Partners: San Juan Bay Estuary Program
Project: Supporting Water Quality for Stronger Communities

The San Juan Bay Estuary Program is the only member of EPA's National Estuary Program located in a tropical region. Agency researchers collaborate with partners on several topics, including water quality modeling, nutrient and contaminant pollution, carbon sequestration, green infrastructure and benefits provided by the estuary to surrounding communities.

A uniting theme of the research is to find environmental solutions that simultaneously improve the health and sustainability of neighborhoods adjacent to the estuary. For example, investigations are providing information to local managers who are considering dredging and other management options to restore flow to the nearly-stagnant Martin Pena Canal—advancing solutions that restore ecosystem functions and reduce public health risks.

Researchers are also using stable isotope methods and historical analysis to better understand the role of carbon and nitrogen pollution in ecosystem dynamics. EPA and SJBEP scientists are working closely to analyze isotopes samples and use the results to identify the most impaired areas for remediation and restoration. Moreover, the results are leading to formulation of a future workplan to employ molecular techniques for determining sources of nitrogen and indicator bacteria.

Supporting "The State of Narragansett Bay and its Watershed"

Partners: Narragansett Bay Estuary Program
Project: Nutrients and Seagrass Habitats

Excess nutrients flowing from the creeks, streams, and rivers of the surrounding watershed are adversely affecting the water quality of Narragansett Bay. Agency researchers have cultivated a strong working relationship with the Narragansett Bay Estuary Program on topics related to nutrient pollution and its effect on seagrass abundance, hypoxia, and algal blooms. They have also developed indicators than can be used to assess and monitor the biological condition of the estuary and its resources.

Agency scientists have made significant contributions to the 2017 *State of Narragansett Bay and Its Watershed*, a technical report that serves as a blueprint for the development of conservation and management activities outlined in the Narragansett Bay Estuary Program Comprehensive Conservation Management Plan.

Nutrient Reductions for a Northwest Estuary

Partners: Puget Sound Partnership
Project: Reducing Nutrient Pollution in Puget Sound

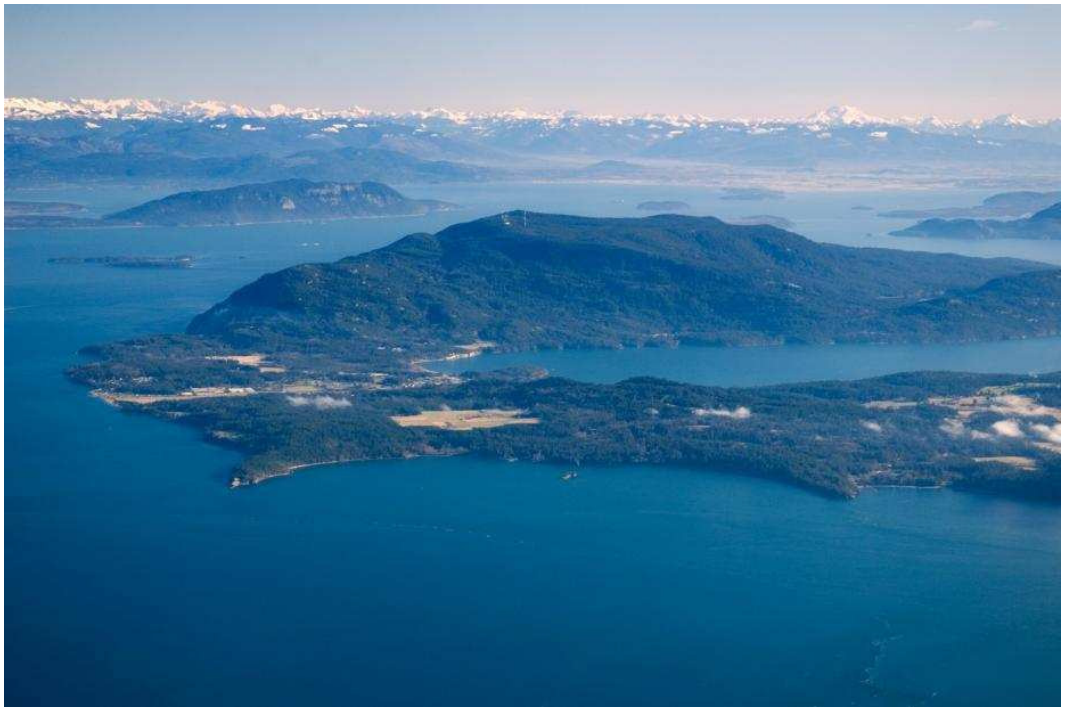

Increasing inputs of nitrogen and other nutrients are a threat to water quality and aquatic resources in Puget Sound.

EPA researchers are collaborating with regional, local, and state partners to develop strategies for identifying and reducing the sources of nitrogen. Collaboratively, they have constructed a detailed nitrogen budget that quantifies sources and fluxes of nitrogen in the transboundary Nooksack River Watershed (British Columbia, Canada and Washington, USA), which is an important contributor to nitrogen loads in Puget Sound. Local, state, tribal and federal planners are now using budget results to link human activities to environmental outcomes and help create effective and economically viable solutions.

Agency researchers are also working with multiple partners to support the development of a comprehensive, scientifically-backed approach that considers and informs environmental planning and decision making across the sprawling Puget Sound watershed. Their goal is to develop a framework that integrates models for land-based watersheds, ocean circulation and biogeochemistry, and marine food webs to simulate chemical and biophysical interactions of water movement, nutrients, and contaminants across large-scale land and water boundaries. Unification of these complex models will allow stakeholders to anticipate the effects of management actions on all parts of the system.

Shell Games: Studying the Complex Dynamics of Coastal Acidification

Partners: Multiple National Estuary Programs and Partnerships
Project: Combating Coastal Acidification

Ocean acidification is a growing global concern, and nutrient pollution can exacerbate acidification in coastal and estuarine waters. As these waters acidify, it takes more energy for developing oysters, clams, and other shellfish species to grow their shells. Other types of organisms are also affected, threatening not only healthy ecosystems but also local fishery-based economies.

EPA researchers are collaborating with nine National Estuary Programs to document patterns of acidification in estuarine environments, where the dynamics of river and ocean inputs and currents create complex water quality conditions that are challenging to understand.

EPA has provided environmental equipment to continuously monitor and measure spatial and temporal changes in coastal and estuarine pH and CO_2 levels (a measure of acidification). Agency researchers developed guidelines for monitoring and continue to provide technical assistance. The partnership is contributing to the characterization of coastal acidification at a national level, and the results are expected to predict patterns and severity of local acidification events that can inform ecosystem restoration and shellfish management.

Related Research

Collaborative Research

Articles and reports from EPA research conducted with NEP partners to achieve mutual goals, or initiated in direct response to a stated need or request from an NEP partner

Beck, M. and J. Hagy. 2015. Adaptation of a weighted regression approach to evaluate water quality trends in an estuary. *Environmental Modeling and Assessment* 20(6):637-655. (Tampa Bay Estuary Program)

Beck, M., J. Hagy, and C. Le. 2018. Quantifying seagrass light requirements using an algorithm to spatially resolve depth of colonization. *Estuaries and Coasts* 41(2):592-610 (Tampa Bay Estuary Program, Indian River Lagoon National Estuary Program)

Bernagros, J., M. E. Huertas, K. Pennino, Proyecto ENLACE, and Spackman Mossop Michaels. 2017. Smart Growth Implementation Assistance: Caño Martín Peña, San Juan, PR. U.S. EPA Office of Community Revitalization, Washington, DC. (San Juan Bay Estuary Program)

Cicchetti, G. and H. Greening. 2011. Estuarine biotope mosaics and habitat management goals: An application in Tampa Bay, Florida, USA. *Estuaries and Coasts* 34(6):1278-1292. (Tampa Bay Estuary Program)

Cicchetti, G., M. Pelletier, M. Pryor, S. Jackson, P. Bradley, S. Davies, C. Deacutis, K. Rocha, D. Santavy, and E. Shumchenia. 2017. Implementing the Biological Condition Gradient framework for Management of Estuaries and Coasts. US EPA Office of Research and Development, Washington, DC, EPA/600/R-15/287, 2017. (Mobile Bay National Estuary Program, Tampa Bay Estuary Program, Narragansett Bay Estuary Program)

De Jesus Crespo, R., P. Méndez Lázaro, and S. Yee. 2018. Linking Wetland Ecosystem Services to Vector-borne Disease: Dengue Fever in the San Juan Bay Estuary, Puerto Rico. *Wetlands*, published online - doi.org/10.1007/s13157-017-0990-5. (San Juan Bay Estuary Program)

De Jesus Crespo, R., J. Wub, M. Myer, S. Yee, and R. Fulford. 2019. Flood protection ecosystem services in the coast of Puerto Rico: Associations between extreme weather, flood hazard mitigation and gastrointestinal illness. *Science of the Total Environment* 676: 343–355. (San Juan Bay Estuary Program)

Latimer, J., M. Tedesco, R. Swanson, C. Yarish, and P. Stacey (eds). 2014. Long Island Sound: Prospects for the Urban Sea. Springer, New York NY. (Long Island Sound Study)

Oczkowski, A., C. Schmidt, E. Santos, K. Miller, A. Hanson, D. Cobb, J. Krumholz, A. Pimenta, L. Heffner, S. Robinson, J. Chaves, and R. McKinney. 2018. How the distribution of anthropogenic nitrogen has changed in Narragansett Bay (RI, USA) following major reductions in nutrient loads. *Estuaries and Coasts* 41(8):2260-2276. (Narragansett Bay Estuary Program)

Oczkowski, A., E. Santos, A. Gray, K. Miller, E. Huertas, A. Hanson, R. Martin, E. Watson, and C. Wigand. 2019. Tracking the dynamic ecological history of a tropical urban estuary as it responds to human pressures. *Ecosystems*, published online at https://doi.org/10.1007/s10021-019-00399-1. (San Juan Bay Estuary Program)

Russell, M. and H. Greening. 2015. Estimating benefits in a recovering estuary: Tampa Bay, Florida. *Estuaries and Coasts* 38 (Suppl 1):S9–S18. (Tampa Bay Estuary Program)

Russell, M., J. Rogers, S. Jordan, D. Dantin, J. Harvey, J. Nestledrode, and F. Alvarez. 2011. Prioritization of ecosystem services research: Tampa Bay Demonstration Project.

Narragansett Bay Estuary Program. 2017. State of Narragansett Bay and its Watershed: Summary Report and Technical Report. (Narragansett Bay Estuary Program) *Journal of Coastal Conservation* 15(4): 647-658. (Tampa Bay Estuary Program)

Tedesco, M., R. Swanson, P. Stacey, J. Latimer, C. Yarish, and C. Garza. Synthesis for Management. Chapter 7 in Latimer, J., M. Tedesco, R. Swanson, C. Yarish, and P. Stacey (eds). 2014. Long Island Sound: Prospects for the Urban Sea. Springer, New York NY. (Long Island Sound Study)

Thom, R., J. Gaeckle, K. Buenau, A. Borde, J. Vavrinec, L. Aston, D. Woodruff, T. Khangaonkar, and J. Kaldy. 2018. Eelgrass (*Zostera* marina L.) restoration in Puget Sound: development of a site suitability assessment process. *Restoration Ecology* 26(6) 1066-1074. (Puget Sound Partnership)

Yee, D., R. DeJesus-Crespo, F. Hunter, and F. Bai. 2018. Assessing natural infection with Zika virus in the southern house mosquito, *Culex* quinquefasciatus, during 2016 in Puerto Rico. *Medical and Veterinary Entomology* 32(2):255-258. (San Juan Bay Estuary Program)

Yee, S., D. Yee, R. de Jesus Crespo, A. Oczkowski, F. Bai, and S. Friedman. 2019. Linking water quality to *Aedes* aegypti and Zika in flood-prone neighborhoods. *EcoHealth*, published online - doi.org/10.1007/s10393-019-01406-6. (San Juan Bay Estuary Program)

Supporting Tools

EPA tools and resources developed to support NEP information and decision needs

Brown, C. and W. Nelson. 2015. A method to identify exceedances associated with ocean conditions. Environmental Monitoring and Assessment 187:133.

Detenbeck, N. and S. Rego. 2015. Predictive Seagrass Habitat Model. U.S. EPA, Office of Research and Development, Narragansett, RI. EPA/600/R-15/003.

Ferraro, S. and F. Cole. 2012. Ecological periodic tables for benthic macrofaunal usage of estuarine habitats: Insights from a case study in Tillamook Bay, Oregon, USA. *Estuarine, Coastal and Shelf Science* 102–103:70-83.

Jewhurst, S. and M. Mazzotta. 2016. Economic Tools for Managing Nitrogen in Coastal Watersheds. U.S. Environmental Protection Agency, Washington, DC, EPA/600/R-16/036. (Intended for NEPs)

Jewhurst, S., K. Mulvaney, and M. Mazzotta. 2017. The application and usefulness of economic analyses for water quality management in coastal areas. *Journal of Ocean and Coastal Economics* 4(1):Article 7.

Li, X., M. Sivaganesan, C. Kelty, A. Zimmer-Faust, P. Clinton, J. Reichman, Y. Johnson, W. Matthews, S. Bailey, and O. Shanks. 2019. Large-scale implementation of standardized quantitative real-time PCR fecal source identification procedures in the Tillamook Bay Watershed. *PLoS ONE* 14(6):e0216827.

Rossman, L.A. and J. Bernagos. 2019. National Stormwater Calculator. U.S. Environmental Protection Agency, Cincinnati, OH, EPA/600/R-19/076 and EPA/600/R-13/085g.

Zimmer-Faust, A., C. Brown, and A. Manderson. 2018. Statistical models of fecal coliform levels in Pacific Northwest estuaries for improved shellfish harvest area closure decision making**.** *Marine Pollution Bulletin* 137:360-369.

Research Partnerships Featured on This Page

- Lower Columbia Estuary
- Tillamook Estuaries Partnership
- Massachusetts Bays National Estuary Program
- Partnership for the Delaware Estuary
- Narragansett Bay Estuary Program: Marshes
- Narragansett Bay Estuary Program: Seagrasses
- Tampa Bay Estuary Program
- Mobile Bay National Estuary Program
- Long Island Sound Study
- San Juan Bay Estuary Program
- Narragansett Bay Estuary Program: Nutrients and Seagrass Habitats
- Puget Sound Partnership
- Multiple National Estuary Programs and Partnerships: Coastal Acidification

LAST UPDATED ON SEPTEMBER 16, 2019

EVEAL (HTTPS://CHECKOUT.FUNDJOURNALISM.ORG/MEMBERFORM?ORG_ID=CIR&AMOUNT=12&INSTALLMENTPERIOD=MONTHLY&CAMPAIGN=

(https://www.revealnews.org/)

Aug 6, 2016

From A to Zika

Co-produced with

(http://www.prx.org/)

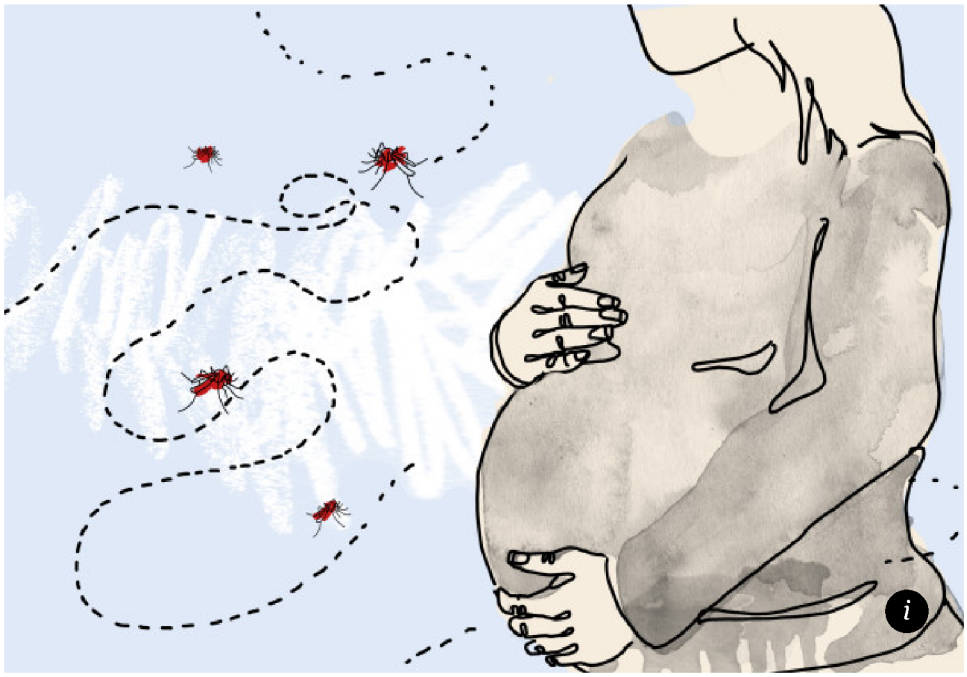

1es.apple.com/us/podcast/reveal/id886009669)

le
sts

tps://play.google.com/music/listen?
o#/ps/Iwzomzopcxsphh3qyvarhxecxye)

pp.stitcher.com/browse/feed/59279/episodes)

n.spotify.com/show/51CN011CgUdG7EUfm7cXF7?
QASompnf9XivlQ)

Public
ttps://play.radiopublic.com/07a47879-
07-4c88-a495-ae9236714b76)

p://feeds.revealradio.org/revealpodcast)

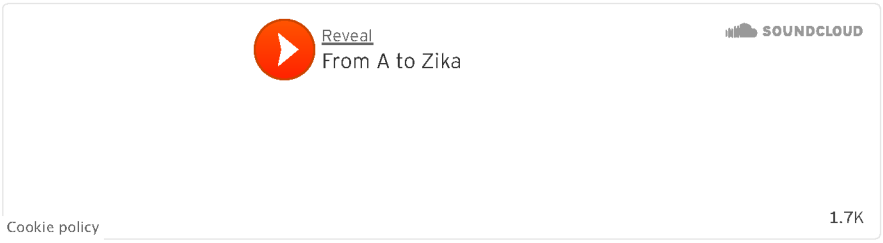

The Zika virus already has spread swiftly across the island territory of Puerto Rico. And now, Miami is reporting its first cases in people infected by local mosquitoes. This week, Reveal takes us to the front lines of the battle against the disease.

In Puerto Rico, about 1,000 miles southeast of Miami, we tour one of the poorest neighborhoods in San Juan. It borders a polluted river that serves as an ideal breeding ground for the Aedes aegypti mosquito, carrier of the Zika virus. We meet a woman living next to the river who has lost all hope of attempting to keep the bugs out of her house. Down the street, an 18-year-old neighbor is pregnant and Zika positive. We learn about her journey, from her diagnosis to her new treatment at the Hospital Universitario, Puerto Rico's public university hospital. There, one of the territory's most renowned doctors describes a crisis that's not just growing, but exploding.

Next, we head to a neighborhood called Wynwood, just north of downtown Miami, where more than a dozen people have been infected by local mosquitos. It's the first time the virus has been transmitted by insects domestically, and now this community is ground zero for Zika

at home. We talk with the head of mosquito control in Miami-Dade County, who's doing his best to keep Zika from spreading, and a virologist with more troubling facts to share.

Reporter Amy Walters (https://www.revealnews.org/author/amywalters) continues her Zika journey to one other high-risk area: Texas' Lower Rio Grande Valley, one of the poorest regions in the country. She meets one pregnant woman who's facing the possibility of Zika head on. The community clinics are ill-equipped to handle this crisis, and they aren't alone – Texas is short on doctors. According to one study, Texas needs 12,000 more physicians to meet our per-capita national average. And about half the state has no OB-GYNs. It's an ominous report. And Zika hasn't even arrived in Texas – yet.

DIG DEEPER

- Read (https://www.revealnews.org/blog/did-our-reporter-get-zika/): Did our reporter get Zika?

Credits

Support for Reveal is provided by The Reva and David Logan Foundation, the Ford Foundation, the John D. and Catherine T. MacArthur Foundation and Mary and Steven Swig.

Track list:

- Camerado, "True Game (Reveal show theme)" (Cut-Off Man Records)
- Dirty Three, "Rude (And Then Some Slight Return)" from "She Has No Strings Apollo" (Touch and Go Records)
- SUBSET, "NLD2016 SIDE B" from "SUBSET meets Netlabel Day 2016 at The Dub Factory"
- KILN, "Royal Peppermint Forest" from "Sunbox" (Ghostly International)
- SUBSET, "Chiloe" from "Series 70" (cCommunity)
- Shigeto, "Look At All the Smiling Faces" from "Full Circle" (Ghostly International)
- Shigeto, "Look At All the Smiling Faces" from "Full Circle" (Ghostly International)
- Dirty Three, "Indian Love Song" from "Dirty Three" (Touch and Go Records)
- Shigeto, "Field Trip" from "Lineage" (Ghostly International)
- SUBSET, "Taganga" from "Series 70" (cCommunity)
- Blue Dot Sessions, "In the Back Room" from "Studio J" (Blue Dot Sessions)
- KILN, "Hong" from "Sunbox" (Ghostly International)
- Jideh High, "Melodica Time (Sound System Style)" from "Melodica Time" (Angel Dust Records)
- Laszlo Harsanyi, "The Latin Lounge" from "Havana Heat" (Sound Tube)
- Ketsa, "Tree Tops" from "Subconscious Communications" (Ketsa Music)
- Minus, "Rooftops" from "Buzz.RO! 2011 [LCL11]" (Local Records)
- Robert Fripp + Brian Eno, "The Heavenly Music Corporation" from "No Pussyfooting" (Polydor Records)
- Cahill Locksmith, "Diamond Variety" from "Starter Kin" (Power Moves)
- Cahill Locksmith, "Rail in Window Nights" from "Starter Kin" (Power Moves)
- Cahill Locksmith, "Sentence Ends" from "Starter Kin" (Power Moves)

- Cahill Locksmith, “Sentence Ends” from “Starter Kin” (Power Moves)
- SUBSET, “NLD2016 SIDE B” from “SUBSET meets Netlabel Day 2016 at The Dub Factory” (The Dub Factory)

TRANSCRIPT:

Reveal transcripts are produced by a third-party transcription service and may contain errors. Please be aware that the official record for Reveal's radio stories is the audio.

Donald: The virus simply uses the mosquito in many cases, as a way to grow its numbers.

Fernanda: In May, Doctor Ye and a team of scientists from the environmental protection agency set a mosquito trap in Gladys's backyard. They collected and froze more than 100 Aedes aegypti females from the Martin Pena canal. The water may hold high levels of nitrogen gas from the human raw sewage. Scientists want to know how that nitrogen may affect mosquito's immune system.

Donald: Nitrogen is often times beneficial for the production of mosquitoes. In other words, if you put more nitrogen into the system, you often are able to grow more mosquitoes, and they're bigger too, which has a whole bunch of ramifications.

Fernanda: It's like the stream could be breeding super mosquitoes. Those bugs then fly into homes in Barrio Obero. Many Puerto Ricans do not have window screens or air conditioning. The Aedes aegypti buzz right in and bite. They also lay eggs in tiny pools of standing water around the house. In Gladys's kitchen, small puddles of water collect on the counter and in dirty pots and pans. Next to me, the inside of a coffee mug is lined with mosquitoes. The health department has been trying to educate Puerto Ricans about the importance of eliminating all

1400 65th St., Suite 200
Emeryville, CA 94608
510-809-3160 | info@revealnews.org (mailto:)

© Copyright 2020, The Center for Investigative Reporting

TRANSCRIPT

Section 1 of 3	[00:00:00 - 00:14:05] *(NOTE: speaker names may be different in each section)*
Al:	From the Center for Investigative Reporting and PRX, this is Reveal. I'm Al Letson. Consider 2016 the summer of Zika, the mosquito born virus that can cause birth defects in babies has landed in the US.
Female:	For many Americans, the excitement over this weekend's unofficial start of summer is mixed with fears of that Zika virus.
Female:	Thousands of people may have contracted the Zika virus before returning to the US. That's from the CDC Tuesday.
Male:	The Zika virus is spreading out of Florida, where the governor has declared a state of emergency in 4 counties, and ground zero for the outbreak Brazil is struggling to contain it with prominent voices now calling for this summer's Rio Olympics to be cancelled.
Male:	Utah health officials say an elderly patient who was infected with the virus has died.
Female:	It's what health officials have been preparing for for months. Investigators say they may have discovered the first cases of Zika being spread within the US mainland.
Male:	This morning, we learned that 4 people in our state likely have the Zika virus as a result of a mosquito bite. This means Florida has become the first state in our nation to have local transmission of the Zika virus.
Al:	Zika has been threatening to invade the US all summer long. Now, it's finally happened. The numbers are growing. The CDC reports over a dozen people in the Miami area who caught the disease from domestic mosquitoes. This is a huge development, and could quicken Zika's spread. Until now, all the roughly 1600 Zika cases in the continental US could be traced to people who caught it while traveling or who had sex with someone who had traveled. Adults who are affected might not even know it. Some people don't get any

	symptoms, or the symptoms are common complaints, like fever, rash, joint pain, and pink eye. For unborn babies, the virus can have devastating consequences, including microcephaly. It's a serious birth defect that causes children to be born with abnormally small heads and brains. We're going to visit Miami where mosquitoes are spreading Zika, and ask, "Is the US prepared to stop the disease?" First, we turn to Puerto Rico, where the outbreak has already infected about 7300 people. About 800 of them are pregnant women. Reveal's Fernanda Camarena joins us with more on that. Fernanda, tell me about what you saw in Puerto Rico.
Fernanda:	I visited Puerto Rico in June, which is their rainy season. It's easy to see how it's a perfect storm for Zika. It's humid, it's crowded, its economy is suffering a massive debt crisis. Its poverty rate is 45%. Put this all together and it lacks the resources to fight the crisis. The CDC is actually there, and they are working to learn more about how Zika is transmitted.
Al:	While they are trying to figure out how it's transmitted, the virus is continuing to spread, correct?
Fernanda:	Yes. The CDC says 25% of the population could be infected with Zika by the end of this year. That would mean 875,000 of the island's 3.5 million people.
Al:	Fernanda, what's the government doing to stop Zika.
Fernanda:	Al, I took a ride along with a team called Emergency Zika Management, which was created by the local government, and they from time to time do what they called local impact to address the Zika crisis. It's lead by [Guespo 00:03:24], and he told me that they go all around Puerto Rico every week. They pump up the salsa music through giant speakers on the back of a pick up truck, and take off to the streets with about 30 people. [inaudible 00:03:42] is in charge, and he goes from house to house handing out Zika care packages. It's basically a Ziploc bag with larvicide, bug repellent, and some informational brochures.
Guespo (?):	[Spanish 00:03:54]

Fernanda:	He asks people if they know about Zika, then explains what it is. People listen to him but don't appear to be alarmed. Like most Puerto Ricans, they don't really see the threats.
Al:	Is that pretty much all these teams do?
Fernanda:	Well they spend a lot of their time collecting discarded tires, where water can pool and attract mosquitoes. They also clean out abandoned homes that attract the insects, and they spray, too. It's a huge problem. In the back of another open bed truck, a contraption that resembles a cannon fires pesticide fog called [inaudible 00:04:36]. Now, this substance is recommended by the CDC as the most effective right now. The gas is strong. I could hardly breathe and had to interrupt my interview to run out for a second. I can only imagine what it does for kids playing outside.
Al:	That sounds like some seriously heavy stuff. The question I have is, is all of it working?
Fernanda:	I don't think it's making much of a difference. [inaudible 00:05:04] says fumigations happen daily, but residents say they're not happening everywhere, or as often as they should. I caught the sense that the health department is overwhelmed by Zika. Here's how [inaudible 00:05:17] puts it.
Guespo (?):	It's like a boxer. You're in a fight and you have your guard high, but in the middle of the fight, you get tired and you put your guard down.
Al:	Fernanda, it seems like Puerto Rico is the perfect storm for Zika as you said.
Fernanda:	Yeah, it is. I spent most of my time in a barrio that many consider the eye of the storm. Deep in San Juan, the air is sweet. Tall sugar cane plants sway in the breeze. This is Gladys's backyard. Her hands are brown, wrinkled, and weathered, a testament to a life of labor. Gladys rips away leaves and snaps a thick stock of sugar cane and she offers it to me. The plant is fragrant and fresh but it's the only thing sweet here. The houses are tightly packed and falling apart. Chickens roam the streets. I'm in Barrio Obero, one of the poorest neighborhoods in San Juan. Right behind Gladys's sugar cane patch, I

	see the banks of the Martin Pena canal, a murky 4-mile channel that cuts through San Juan villages in gentle curves. It's shaped like the line on a heart monitor that's barely beating. It's one of Puerto Rico's most polluted streams. I see that it's stagnant, clogged by trash, sludge, and human waste, a perfect breeding grounds for the Aedes aegypti mosquito, carrier of the Zika virus. The water is deep brown and reeks of sewage. During heavy rains, the banks overflow and flood Gladys's yard, along with their neighbor's.
Gladys:	[Spanish 00:07:06]
Fernanda:	She remembers a particular night when the flooding was so intense she felt like she was drowning on the Titanic. This channel like the Titanic, may soon become synonymous with tragedy. Doctor Donald Ye, an associate professor of the Department of Biological Sciences at the University of Southern Mississippi thinks this river and more specifically the trash in and around it may hold important answers about Zika and the mosquitoes that spread it.
Donald:	The virus simply uses the mosquito in many cases, as a way to grow its numbers.
Fernanda:	In May, Doctor Ye and a team of scientists from the environmental protection agency set a mosquito trap in Gladys's backyard. They collected and froze more than 100 Aedes aegypti females from the Martin Pena canal. The water may hold high levels of nitrogen gas from the human raw sewage. Scientists want to know how that nitrogen may affect mosquito's immune system.
Donald:	Nitrogen is often times beneficial for the production of mosquitoes. In other words, if you put more nitrogen into the system, you often are able to grow more mosquitoes, and they're bigger too, which has a whole bunch of ramifications.
Fernanda:	It's like the stream could be breeding super mosquitoes. Those bugs then fly into homes in Barrio Obero. Many Puerto Ricans do not have window screens or air conditioning. The Aedes aegypti buzz right in and bite. They also lay eggs in tiny pools of standing water around the house. In Gladys's kitchen, small puddles of water collect on the counter and in dirty pots and pans. Next to me, the inside of a coffee mug is lined with mosquitoes. The health department has been

	trying to educate Puerto Ricans about the importance of eliminating all standing water inside their homes. This is exactly where mosquitoes like to reproduce, but that message hasn't resonated with Gladys.
Gladys:	[Spanish 00:09:13]
Fernanda:	"I can't be scared of Zika," she says. The most important thing here is [Spanish 00:09:20], keep on moving, and get out of poverty. Any fear Gladys has about Zika sails out the door with the mosquitoes. For one of her neighbors, the threat hits home. About 5 doors down from Gladys sits a pink house with a white fence. On the front porch, I notice a young woman spraying bug repellent all over her body. She has fair skin, hair that hangs down to her hips, and delicate features. Her prized possession dangles around her neck, a rosary made out of gold. It's her only jewelry. I notice she has a small stomach popping from her white tank top. She's 5 months pregnant.
Carla:	[Spanish 00:10:14] I went to a CVS and bought the pregnancy test. I came back and dropped it in a bag so no one would see it. I then went upstairs. I was really nervous. I took the test and it came out positive. I thought, "What will my family say?" I felt like I let them down.
Fernanda:	We're calling this 18 year old woman Carla. She wants us to protect her privacy because we're discussing private health issues. She found out she was pregnant in February. One month later, she felt sick after a huge storm flooded the banks of Martin Pena, trapping people inside their homes for a few days. A doctor from WIC, a federally run program that aids women and children, passed through her neighborhood. The doctor was testing for Zika. It took Carla a week to get her results. She was positive.
Carla:	[Spanish 00:11:06] I wanted to cry, but I was trying to listen to her. When she left, that's when I started crying. I said, "God, why? I'm not a bad person. Please make my baby be okay."
Fernanda:	Many women have to wait up to 2 months to get results from overburdened local clinics. If they are positive, their children may have birth defects. The delay creates a huge problem for women who

	may wish to have an abortion. As for Carla, she decided against an abortion. She's having a girl.
Carla:	It's like, I don't know, an instinct. I feel like everything is okay. There's nothing wrong with her.
Child:	[Spanish 00:11:54]
Fernanda:	She now lives with her boyfriend and his family, including his little niece. It's a big support system. Since Carla was diagnosed with Zika, she started going to the high risk pregnancy unit at the university's hospital. Her boyfriend regularly joins her for weekly prenatal sessions here. I wanted to see how doctors are advising pregnant women about Zika, so I went to a prenatal session. About 12 pregnant women and their partners sit in a circle. A nurse gives them the latest Zika information and they take turns sharing their stories. She passes out goodie bags that include a mosquito net for their beds, repellent, and a pamphlet with more information. Each woman gets a sonogram, and the Zika positive patients meet Doctor Alberto De La Vega. According to the health department, there are more than 700 pregnant women diagnoses with Zika in Puerto Rico. Half of them come here.
Alberto:	Most of them are very worried when they come to us.
Fernanda:	De La Vega's an OB/GYN and chief of the ultrasound unit. He says he's treating 4 to 5 new Zika cases every day. That number doubles every month. He's already seen 3 cases of birth defects including microcephaly.
Alberto:	What you see is a normal appearing child except for the fact that the head is much smaller than expected. The forehead may be slanting backwards because there is a smaller degree of brain matter.
Fernanda:	He says sonograms can only tell you so much, and worries the most for babies born who don't appear to have microcephaly.
Alberto:	Defining the problem based on finding or not finding microcephaly is ignoring the fact that this infection may be much more severe and

	serious than we can even imagine, because it could produce learning disabilities and neurological problems.
Section 1 of 3	[00:00:00 - 00:14:05]
Section 2 of 3	[00:14:00 - 00:28:05] *(NOTE: speaker names may be different in each section)*
De La Vega:	Learning disabilities and neurological problems that will only be manifested in the future. That's the real problem.
Fernanda:	De La Vega told Carla that her ultrasound as of now appears to be fine. It's not a crystal ball into whether the child will be healthy. Like many patients, Carla doesn't know if she contracted Zika through a mosquito or her partner. Zika is very unusual for a mosquito born illness, because it can also be passed on by unprotected sex.
Rullan:	This becomes very difficult human problem, because of the fact that you get initially infected by a mosquito, but then you amplify it tremendously by sex.
Fernanda:	That's Doctor Johnny Rullan, an epidemiologist and former health secretary of Puerto Rico. He came out of retirement to advise the current governor. Officially, Puerto Rico has about 7,300 cases of Zika. Doctor Rullan believes that number is much higher. He says 9,000 people are getting infected every day. He is pushing for a public campaign about safe sex, but he says historically, it's been hard to get people on the island to follow that advice.
Rullan:	Puerto Rico in the past, we're okay at knowledge. We're pretty okay in attitude. It doesn't always translate change in behavior.
Fernanda:	He also says Puerto Rico needs to eliminate the places where mosquitoes breed. He initially advocated aerial spraying, but there was a public backlash over health concerns, and he has now backed off that idea. Rullan believes that old cemeteries need to be drained of standing water. Thousands of abandoned tires need to be collected, and millions of mosquito traps need to be set. It's an enormous and expensive plan.

Rullan:	Science drives it, but then you need to get policy management, and you need to then follow up and get it done.
Fernanda:	Puerto Rico hasn't been able to get it done. A few weeks after I interviewed Doctor Rullan, he quit his post. He was frustrated with the island's response to the virus. In a statement, he said the outbreak was now out of control. After months of fighting Zika, Doctor Rullan decided to go on vacation to Spain.
Al:	That was Reveal's Fernanda Camaraina. Next, we head back to the mainland ...
Captain:	Flight attendants prepare doors for departure. Stand by for roll call.
Al:	... where an understaffed and underfunded mosquito control program is struggling to contain the first locally transmitted cases of Zika.
Captain:	Ladies and gentlemen, we'd like to welcome you to Miami International Airport, where the local time is 9:45.
Al:	That's next on Reveal.
David:	Hey podcast listeners, I'm David Rodriguez, and I've been interning at Reveal this summer. If you want a behind the scenes look at how this hour in Zika came together, go ahead and open up Instagram on your phone right now. I'll wait. Search for Reveal News. We've uploaded photos and videos from the front lines of the battle against Zika. Check them out and give us a follow.
Al:	From the Center for Investigative Reporting and PRX, this is Reveal. I'm Al Letson. Before the break, we were in Puerto Rico, where officials are failing to control a full blown outbreak of Zika. Now, we head to Miami where the spread of the virus is picking up pace. Right now, Florida is home to about 400 travel related cases of Zika. People who either caught the disease while traveling or had sex with someone who was, and for the first time ever in the continental US, more than a dozen people have been diagnosed with catching Zika from local mosquitoes. It's been traced to one neighborhood in Miami, Wynwood, an artsy touristy part of town. Now the Center for Disease Control and Prevention has done something extraordinary.

	They're advising women who visited Wynwood after June 15th to avoid getting pregnant for 2 months. Reveal's Amy Walters was in Miami earlier in June. The city is a gateway to the US where every day people arrive from countries where the Zika virus has taken hold.
Amy:	When I got to Miami, I did what a lot of people do, hit the clubs. Not to party exactly, but to ask people or rather shout questions at people about Zika.
	[inaudible 00:18:56] Zika in Miami.
Female :	Oh no way.
Amy:	Can I ask? Do you mind?
Female :	I mean, I don't know anything about it. Sure.
Amy:	There's a bar, a dance floor, a bowling alley, and an ice rink here at Basement. You can see how not everybody has Zika on their mind.
	Do you mind if I ask you if you're worried about it?
Male:	She just got here from Zika Land.
Amy:	I'm not sure you caught that, but that guy told me his date just flew in from Columbia, what he called Zika Land. Other partiers I met were from New York, even Greenland, and at least one couple I talked to were from Brazil, where this recent outbreak got going. There was one woman who was really worried.
Female:	Yeah, I'm worried about that. I'm freaking scared. The fact that mosquitoes could just bite you whenever. They are everywhere, so it's not like you can really know which mosquito is good or not. It's not cool.
Amy:	Are you trying to get pregnant?
Female:	No. Not anytime soon, no baby.

Amy:	Miami is ground zero for Zika in the continental US. At least that's what [Charlmars Baskas 00:20:05] says.
Charlmars:	I know the mosquitoes transmit Zika. It's the most highly [inaudible 00:20:10] mosquito in this county. It's everywhere.
Amy:	Charlmars has a pretty good grasp on the Zika situation here. He runs mosquito control for Miami Dade. His accent's from Nicaragua, where he grew up with mosquitoes, lots of them. He remembers the health department fighting them off when he was a kid.
Charlmars:	I remember this from malaria, and spraying the walls of the houses with DDT at the time.
Amy:	Inside the house?
Charlmars:	Inside it. [inaudible 00:20:39] inside homes.
Amy:	It may sound extreme but it was actually pretty effective. Back in the 1950s, health officials also used DDT to eradicate the Aedes aegypti mosquito from Nicaragua, Ecuador, Brazil, and other Latin American countries. At the time, they were trying to stop the spread of yellow fever. Because they didn't eradicate that mosquito everywhere, including here in the US, it eventually came back. Now, it spreads Zika and other tropical diseases like dengue which can be deadly, chikungunya which causes fever and joint pain.
Charlmars:	My home town, only half the population was infected with chikungunya. They do have Zika cases. They're reporting Zika cases in Nicaragua. Most of the Central American countries, Caribbean, and South America. It's all over. It's all over.
Amy:	Small world, right? Now, Charlmars is doing what he can to keep Zika from spreading here in the United States. In 1972, the environmental protection agency banned DDT here. Armed with chemicals that are a little less damaging to the environment, and less effective at killing mosquitoes, Charlmars' team of 12 mosquito inspectors, plus some contractors, try to keep Zika at bay. They say they're trying to hire up the 8 more, but it's a poultry team compared to nearby counties like Lee and Key West. Their staffs top

	100, with a fraction of Miami's population. Each work day, Charlmars starts by pulling up facts from the health department.
Charlmars:	This is what we receive from the health department on a daily basis. This is Zika.
Amy:	This is a Zika case?
Charlmars:	This is a Zika case, all this. 1, 4, 5.
Amy:	These are 4 different addresses, 5 different addresses?
Charlmars:	4 different, 5 different addresses. We are not supposed to provide you with that.
Amy:	Right. He kept that list close to his chest. It has the addresses of people the Florida Health Department has identified as having Zika. Carlos Vargos, one of the inspectors, who goes out spraying.
Carlos:	The reason is that we need to eliminate the potential. You have mosquitoes around, and if a mosquito bites an infected person, or carrying the virus, that mosquito may be the carrier now.
Amy:	In early June, there was no evidence of that happening here. At the time, all confirmed cases were travel related. In addition to the list from the health department, Charlmars' team also responds to requests from the public. People can call in if they're worried about mosquitoes in their area. We ended up at one of those homes, a lovely Spanish style house in Coral Gables, a pretty upscale neighborhood.
Carlos:	As a matter of fact, the lady of this house, she called because she's now pregnant. She's kind of worried about the Zika virus, which is understandable. It's common, and it's something that is very worrisome, I would say.
Amy:	It rained the night before. There is puddles of water everywhere. Carlos drops granules of insecticide into the garden pots. You can actually see the bugs hovering. Then, Charlmars calls us over.

Charlmars:	Yeah, let me show you something across the street.
Amy:	The sound you're hearing is folks doing yard work at the neighbor's house next door. Charlmars takes me up to what seems to be the most innocent thing in the world, it's a child's tiny toy wheelbarrow with maybe a couple inches of water.
Charlmars:	Don't move. Let them start feeding. See how many there are flying around me?
Amy:	Just to let you know, mosquitoes are landing all over him. That toy has become a nursery for Aedes aegypti bugs.
	He's just eating lunch.
Charlmars:	Yes. They're hungry.
Amy:	1, 2, 3, 4. You got another one on your hand right now. They're everywhere.
Charlmars:	Yeah, this is getting full with blood. You see he's engorging with blood. This one here on this side.
Amy:	Oh my gosh, do you have 7 on you now?
Charlmars:	Yep. Hopefully they're not carrying the virus.
Amy:	When I was there, there were no cases of locally acquired Zika in Miami yet.
Charlmars:	You see how bad it is? This is real bad now.
Amy:	This is how these guys count mosquitoes. More and more just keep landing, puncturing his skin and sucking his blood.
	Are you going to get a Zika test?
Charlmars:	I should have, after I came back from Nicaragua, I should have been tested. I still have a chance you see?

Amy:	You actually don't know if you have Zika?
Charlmars:	Yep.
Amy:	Charlmars, the guy running mosquito control in Miami is telling me he could be infected himself. The thing is, even if Charlmars is infected right now, he probably wouldn't know it. Carlos explains.
Carlos:	One of the things that up to 80% of the people that may be infected with the virus, they don't show any symptoms.
Amy:	You don't know who has it.
Carlos:	Exactly.
Amy:	You don't know who is spreading it. Those mosquitoes that we saw, I mean, how do you know if they have it?
Carlos:	You don't.
Charlmars:	Well, we can ask them.
Amy:	We can ask them. That's it right now. All jokes aside, it really comes down to testing. Knowing which mosquitoes have the virus allows mosquito control to know where to spray. When I visited back in June, only 8 out of 67 counties in Florida were testing. Miami Dade wasn't one of them. Charlmars promised they'd start testing soon, and 2 weeks later, they did. Now 28 counties in Florida are testing, but back then when I was there, I thought, "Why don't I try to get some tested?" I was already noticing a couple of bites.
	Can you save some of these guys for me?
Charlmars:	It's going to be hard.
Amy:	I ended up with 2. I put them in a bottle cap, wrapped them up in a piece of paper, and drove away in the car. The fight against Zika in Miami gives you an idea of just how unprepared the United States is for this disease. The thing that's so surprising? We already have a

	system that was designed to protect us from mosquito born diseases like Zika.
Jeffrey:	This is Jeffrey Engel, MD. I am the Executive Director of the Council of State and Territorial Epidemiologists.
Amy:	To explain how this system got started, he took me way back to 1999, when another mosquito born virus landed in the US.
Jeffrey:	When West Nile hit New York City in 1999, several people had already died and it was a public health emergency as it spread rapidly over the continental United States.
Amy:	The best got the attention of Capitol Hill. Federal funding was freed up to set up a pretty fancy computer program called Arbonet. Ar for arthropod, that's a kind of bug a mosquito is, Bo for ...
Section 2 of 3	[00:14:00 - 00:28:05]
Section 3 of 3	[00:28:00 - 00:52:00] *(NOTE: speaker names may be different in each section)*
Amy:	Ar for Arthropod, that's a kind of bug a mosquito is, Bo for Borne and Net for Network. It tracks vector borne illnesses transmitted by mosquitoes but it's only as good at the data it collects so a lot of the federal funding went to state and local mosquito surveillance.
Scott:	The states had no capacity to do vector borne work related to this threat. The fact is that the money for the West Nile virus epidemic was used to built infrastructure for all vector borne disease threats. We hadn't even heard about Zika at the time.
Amy:	You can actually pull up maps based on ArboNET data on your computer right now to follow the spread of viruses like Dengue, Chikungunya and West Nile throughout the United States. It was really successful. Once ArboNET ramped up, deaths from West Nile plummeted. That's when federal funding slowed. It went for 24 million in 2004 to 9 million in 2012. As funding for ArboNET has gone down the number of deaths from West Nile has climbed back up.

	Her's where we are right now: With all these cut backs there are fewer people to monitor the mosquitoes, fewer people to test them for disease, and less overall mosquito control, so this ArboNET system that relies on data is handicapped and now has less data so it's harder to track mosquito borne diseases and squelch outbreaks before they take hold. Now with the spread of Zika one virologist, Sharon [Iscern 00:29:43], isn't willing to give up on collecting information.
Sharon:	If we could study how these disease outbreaks start and if we can get a better handle on how to control them as they're starting I think we could learn a lot of lessons on how we can handle this globally on a bigger scale.
Amy:	Sharon's volunteered to test Miami's mosquitoes for Zika for free.
Sharon:	It's just a small little sandbox and we can study it from the beginning.
Amy:	Sharon's a scientist at Florida Gulf Coast University and in 2010 she and her husband tested the mosquitoes from the first Dengue outbreak in Key West in half a century.
Sharon:	The mosquitoes come in and the first thing you've got to do is you have to grind them up. This is basically a blender that can take the mosquito bodies and puree them into a little sauce and we can then use ...
Amy:	With Zika, Miami hadn't [inaudible 00:30:33] any bugs yet, but remember those mosquitoes I got?
	I brought something for you. I know that you said that you have a contract with Miami but they hadn't brought you any mosquitoes.
Sharon:	You actually brought us some?
Amy:	I did.
	After rifling around in my purse for a minute I unfold the paper holding my mosquitoes.

	There's 2 Aedes Egyptis in here.
Scott:	These may be the key.
Amy:	That's Scott Michael, Sharon's husband, who's also a virologist.
Sharon:	Look at that. In a little ...
Scott:	In a bottle cap.
Sharon:	In a water ...
Amy:	it was a water bottle cap. There's no soda in there.
Sharon:	No soda in there, so these ...
Amy:	I'm not the scientist. They said they'd send me the results soon.
	The ArboNET system wasn't just set up to collect data about mosquitoes. It also gathers information on humans infected by them. It just so happened I noticed a couple of sizable welts swelling up on my left forearm. I got bitten by those mosquitoes the day before I Miami there were no local transmissions so it actually seemed unlikely that I had it, but just in case I called up Florida's Zika hotline to see how the system works.
	Hi Stan. My name's Amy Walters.
	Stan isn't a spokesperson so I only recorded my end of the conversation.
	I'm a journalist.
	Full disclosure.
	I'm in Florida and I went out with the mosquito control this morning and I guess I got a couple bites from the Aedes Egypti mosquitoes. I wanted to check if I have Zika.

	His response? You can't have Zika unless you've traveled outside the country. At that time in June there was no local transmission of Zika in Florida so they wouldn't test me.
	Right, by mosquitoes.
	But they don't test mosquitoes in Miami for Zika. The next week I got home to California and I wasn't feeling great. I had a fever, which is a symptom of Zika. Maybe I had Zika on the brain, but why take chances? I tried to get it checked out by calling my own health care provider.
	I was traveling in Miami reporting a story on Zika and I got some mosquito bites and I did sort of come down with a cold and maybe a bit of a fever this week so I wanted to see if it was possible to get tested?
	It wasn't. Again, unless I'd been out of the continental US, California wouldn't test me either. Until very recently, those were the guidelines from the CDC, so why did things change? What led the CDC to update it's guidelines? One proactive doctor who made the decision to test a patient who hadn't traveled. That's how the first locally acquired Zika cases were diagnosed. I asked Tom Skinner, the CDC spokesman how it happened. The interview was a little rushed. They're a bit busy now as you can imagine.
Tom:	They were sick, they actually had Zika virus so the went to their doctor and they were diagnosed.
Amy:	I've tried to call the hotline and they said unless I've traveled out of the country they can't test me.
Tom:	At the end of the day each doctor makes the call as to whether or not they're going to test somebody for Zika virus infection. We've put out our guidelines to who ought to be tested and the doctor makes a call on whether or not they're going to require a particular test be performed.
Amy:	Going beyond the CDC guidelines is what revealed that mosquitoes were already in the Wynwood neighborhood of Miami spreading the Zika virus and in less than a week the CDC uncovered more than a

	dozen cases of locally acquired Zika. That led the agency to issue a historic travel advisory warning pregnant women and their partners to avoid Wynwood. This is the first time the CDC has told people to avoid travel to a specific place inside the continental US.
	The CDCs also recommending that anyone, male or female, who's been to Wynwood wait at least 8 weeks before trying to conceive.
Tom:	Literally, we're making these decisions on a day by day basis based on information that we're gathering each day.
Amy:	They are gathering information. So far, clinicians have tested over 23 hundred people in Florida and they're doing more mosquito testing too. The bugs I took to the lab ended up coming back negative, but Zika was soon found where I'd been in Miami. Skinner says they'd be able to track Zika better if the federal government fully funded ArboNET, the system created to stop the spread of mosquito borne diseases.
Tom:	Hopefully if we can get the money that we've asked for from congress that will help us even better improve our ability to check these outbreaks when they occur.
Amy:	When I asked him how bad this is going to get he just didn't know.
Tom:	We don't have a crystal ball. It's mosquito season and the states where we're likely to see more cases of Zika from locally transmitted mosquitoes are on the alert.
Al:	That story was from Reveal's, Amy Walters.
	Month's ago, President Obama asked congress to approve 1.9 billion dollars to fight Zika but lawmakers were gridlocked and went on summer break without green-lighting new money to deal with the virus. Congress won't be back in DC until after labor day. As a stopgap measure, the CDC has freed up more than 40 million dollars to states fighting Zika.

	One other note from the CDCs Tom Skinner: That area of heightened alert for Zika stretches along the southern border of the United States to Alabama, Mississippi, Louisiana and Texas.
Speaker 6:	Ladies and gentlemen, welcome to Harlingen. We're going to be taxing for a few minutes.
Al:	That is where Amy heads next, the Lone Star State, when we come back on Reveal from the Center of Investigative Reporting and PRX.
Julia:	Hey there. Reveal's Julia B. Chan here. I want to tell you about this new fellowship we just launched. It's for journalists of color, specifically working journalists already employed by another media outlet or currently freelancing full time. Throughout the year our staff will work with the fellow to help them produce and report an investigative story. Fellows will be hooked up with skills training, coaching, and editing from mentors here in the Reveals newsroom. This deadline for applications is September 12th so think about applying, or help us spread the word. Go to RevealNews.org/diversity to apply and find out more. That's RevealNews.org/diversity.
Al:	For the Center of Investigative Reporting and PRX, this is Reveal. I'm Al Letson. The sound you're hearing comes from mosquitoes that carry the Zika virus. They're called Aedes Egypti. These were plucked from standing water in the very southern tip of Texas, the Rio Grande Valley, on the border with Mexico.
Dr. Imperial:	Huge, fat mosquitoes.
Al:	That's Dr. Henry [Imperial 00:38:07].
Dr. Imperial:	I wouldn't be surprised if we have a case of Zika in Brownsville. We might not even know.
Al:	He's lead doctor at the Brownsville Community Health Center. This part of the nation is a high risk area for the disease and also one of the poorest in the country. One third of the population is uninsured and the women have limited access to healthcare. Amy Walters went

	there to continue her Zika journey and met one pregnant woman facing the possibility of contracting the virus.
Amy:	When I showed up here it was a nice hot day, actually really hot and wet and buggy, the perfect conditions to find someone who's worried about these bugs and about them carrying Zika.
Speaker 9:	Lemonade for 50 cents ... Oh, 25 cents, okay.
Amy:	I ran into Bella and Corina, 11 and 8 respectively, over some lemonade at their family's garage sale. I explained the story I was working on and they pointed me to their aunt, Carolina.
Carolina:	Carolina Rocha and I'm from McAllen, Texas.
Amy:	She's tall with dark hair and when I met her, her belly was pleasantly round.
	How far along are you, do you know?
Carolina:	I am 5 months.
Amy:	Do you know if it's a boy or a girl yet?
Carolina:	Yes, it's a boy. Matthew.
Speaker 11:	I came home to show Daddy something.
Carolina:	That's Joshua.
Amy:	Joshua is 5 and getting used the idea of being an older brother. It turns out Carolina wasn't expecting to be expecting to be expecting either.
Carolina:	Since our oldest is already 5 we just thought it wasn't going to happen, but surprise, it happened.
Amy:	Pretty awesome, right?
Carolina:	I love kids.

Amy:	She works in a daycare, her life basically revolves around them and to have a second, she's thrilled, but she's also heard about Zika.
Carolina:	It's pretty scary, the fact that so many people come from South America and Mexico and into the United States, especially here in the Rio Grande Valley, not knowing of how at first how you could get it, but now that they say the mosquito carries it ... I love being outside. We like going to the beach, fishing. Now knowing that it might cause birth defects is even more scary and the mosquitoes down here are so huge.
Amy:	Have you had ultrasounds yet? Have you been tested?
Carolina:	I did have an ultrasound last month ...
Amy:	The ultrasound had her thinking about Zika. They saw some issues that are not likely Zika, but she just wants to be sure.
Carolina:	I think when I go I'm going to tell them to test me for it to be on the safe side.
Dr. Imperial:	We don't test. The state always says that we are ready to serve all women of Texas.
Amy:	That's Dr. Henry Imperial again, the Medical Director at the Brownsville Community Health Center. He says if a local outbreak gets going the clinic wouldn't be able to test all the pregnant women who have symptoms connected to Zika even thought that's what the CDC recommends. He said it would overwhelm the clinic.
Dr. Imperial:	It's just one of those, that sort of make the work that we do a lot more difficult and adding to already things that we do for pregnant women, you're going to have to add Zika among them.
Amy:	Many lower income women rely on these community clinics, but this system is starting to sound pretty fragile and Zika hasn't even arrived. Dr. Imperial's next available appointment is in January, next year, and that's normal.
	Exceptional circumstances like the outbreak of a new virus would crash the system. During the swine flu epidemic, Dr. Imperial's clinic

	abandoned at least 10 thousand samples without testing them for the disease.
Dr. Imperial:	No point in doing it. We run out of protective masks during the swine flu epidemic.
Amy:	It's not just public health clinics that would be overwhelmed. Texas is short on doctors, way short. According to a federally funded study, Texas needs another 12 thousand physicians to come close to the national average and about half the state has no OBGYNs. For me it was startling. For Carolina, not so much.
Carolina:	I know a lot of doctors don't take care of the women very here in the Valley.
Amy:	Women like her older sister it turns out.
Carolina:	My sister was pregnant and her doctor did not inform her that her child had a stroke while in the womb which is something very rare. It took a year after he was born, after his first birthday, to realize that there was something wrong.
Amy:	Because of her nephew's stroke he has seizures now and no one in this part of Texas can help, so every couple of months they drive at least 5 hours from McAllen to Houston for care. Carolina thinks about families like hers who could be dealing with the long term effects of a disease like Zika.
Carolina:	If the women end up getting the Zika virus here and they have babies, it's just going to cost so much all around and I don't think the state of Texas is ready for that.
Amy:	It's a good point. What about the babies? I went back to the Brownsville Clinic to ask Paula Gomez, the director, how well prepared they are to cope with the potential of babies with Zika, babies that could be born with abnormally small heads and brains. Some Zika babies are even stillborn.
Paula:	I think if you ask about the finances, no, we're not equipped. You can never really be prepared.

Amy:	They've never dealt with the consequences of Zika, but the clinic's seen a similar condition, a baby born without a brain.
Paula:	We weren't prepared for that either. I remember the young woman coming and asking why she was told that her child was in a bottle someplace in the back of a hospital. She wanted that child so she could give it a burial. It created a lot of very, very serious issues for them emotionally and spiritually. The community gets scared, it effects a lot of things. Obviously, this is a little bit different, but I think the devastation of a family is the same.
Amy:	I wondered, what are doctors here telling woman who are thinking about getting pregnant?
Dr. Imperial:	I honestly don't know what to tell women who would like to have babies.
Amy:	That's Dr. Henry Imperial again, who's also at the Brownsville Clinic.
Dr. Imperial:	That's a tough question to answer in terms of asking women not to get pregnant. I was hoping we could get rid of mosquitoes first.
Amy:	The truth is, there's been a lot of different messages about what women should do in all the countries where there's Zika. Back in January, El Salvador asked women to delay pregnancy for 2 years. Columbia and Ecuador urged women to put off getting pregnant for several months and one representative of the World Health Organization was quoted saying, "Delaying pregnancy was sound advice," but WHO policy leaves that decision to the individual.
	Here in the United States the Center for Disease Control and Prevention is not asking women to delay pregnancies across the board, only if they've traveled to places where mosquitoes are currently spreading Zika, but they are saying women should have access birth control. To be able to make that choice on their own.
Jose:	Responding to the Zika virus is going to take a new view of birth control because of Zika.

Amy:	Jose Camacho is the Executive Director of the Texas Association of Community Health Centers.
Jose:	We have to not only educate, but provide women the ability to prevent pregnancy.
Amy:	Maybe you remember the Texas legislature's fight with Planned Parenthood. In 2011 they restricted funding from clinics associated with abortion providers and shrank the state's family planning budget by 2 thirds. A New England Journal of Medicine study claimed that cutback led to more babies. A lot of that money has been restored, but bringing the system back on board takes time.
Jose:	Leave for just a second the issue of Planned Parenthood aside. There are fewer places where a woman can go to get birth control. When you go in and destroy capacity, it takes years to rebuild. We're still in a rebuilding mode that's showing up with preparedness on issues like Zika.
Amy:	According to John Hellerstedt, the Commissioner of the Texas Department of Health, there is a plan.
John:	Texas is ready. If we have local mosquito vector transmission of Zika in the state we have a plan. We're working with our partners at the national, state, regional and local level on how to respond.
Amy:	Back at the garage sale the heat won't let up. Carolina stands under the sun wearing shorts, not long pants and the long sleeve shirt like the CDC recommends. It's hot here, it's hard to blame her. She was already pregnant when she found out about Zika. She covers herself with repellent and stays inside, but apart from that, she doesn't really feel like there's a lot she can do, but she worries about other women here who are not pregnant yet.
Carolina:	It's kind of scary because the women here in the Valley can't get those birth control and I know my little sister, she's gone to Planned Parenthood and she wanted to get birth control but they were going to charge her 150 which I thought was nonsense.
Amy:	This is Carolina's younger sister, Christina.

Christina:	Why not just cross the border, go get birth control for 7 dollars which covers me for 3 months and I'm good?
Amy:	Did you do that?
Christina:	Yes.
Amy:	It's funny, we're so afraid of this virus coming across the border into the US and now Americans are going the other way into Mexico for birth control. Carolina picks up on that irony.
Carolina:	It would be better if the state of Texas could actually come up with a better system.
Al:	With 3 months of mosquito season left to go, it's not just Texas. The truth is, we could use a better system throughout the US and better funding of systems like ArboNET that we've already set up. The CDC is reporting more than 800 women are pregnant with Zika right now. There are likely more and there will definitely be more to come. It will take months, even years, before we know the effects on those babies, what we do know is the summer of Zika will stay with us long after this summer is gone.
	Next week we'll have the story of one woman's decades long quest for justice. More on that in a minute. First, today's show was reported and produced by Amy Walters, Fernanda Camarena and Katharine Mieszkowski. Our program was edited by Taki Telonidis. Our sound design team is The Wonder Twins, my man, J Breezy, Mr. Jim Briggs and Claire C Note Mullen. Our Head of Studio is Christa Scharfenberg. Amy Pyle is our Editor in Chief. Susanne Reber is our Executive Editor and our Executive Producer is Kevin Sullivan. Our theme music is by Camarado, Lightning. Support for Reveal is provided by the Reva and David Logan Foundation, the Ford Foundation, the John D and Catherine T MacArthur Foundation, the John S and James L Knight Foundation and the Ethics and Excellence in Journalism Foundation.
	Be sure to catch next weeks show. We bring you an incredibly intimate story of a woman who comes to terms with the abuse she suffered as a child at the hands of her gymnastics coach.

Speaker 16:	He had set up this mat, a floor mat, but that he could prop up, and he's explaining to me that because I had trouble concentrating and focusing and that he didn't want me to be distracted, that I had to stretch with him behind the mat.
Al:	We follow her story as she reports the crime to the police as a grown woman.
Amy:	At that moment did you feel uncomfortable at that age?
Speaker 16:	Yeah.
Amy:	You already felt like this was something that shouldn't have been happening.
Speaker 16:	Yeah, I remember having this sort of deeply shameful and, slash, sick feeling. Knowing it was wrong, not knowing exactly what to do.
Al:	We'll find out what happens when she tries to bring her abuser to justice. That's next week.
	Reveal is a co-production of The Center for Investigative Reporting and PRX. I'm Al Letson, and remember, there is always more to the story.
Section 3 of 3	[00:28:00 - 00:52:00]

2017 ORD HONOR AWARD RECIPIENTS

Administrative, Operations, and Support Services Award

National Center for Environmental Assessment

Collaborative ORD Space Consolidation Team
For exemplary administrative and operational support to major office moves for ORD.

Philip Baker, OARM
Shadawn Brooks, NCEA
Richard Callan, NCER
Shelia Davis, OSIM
Lisa Doucet, NCER
James Gentry, NCER
Michael Hiscock, NCERAbdel-Razak Kadry, NCEA
Keeley Dean, OSIM
Jay Kress, OSIM
Patrick Lau, NCER
Danielle Lewis, OSIM
Marieka Boyd, NCEA
Leslie Meadows, NCEA
Lenee Morina, OARM
Mel Peffers, NCER
Michael Perry, OARM
Brenda Randall, OARM
Chris Saint, NCEA
Crystal Samuels, NCEA
Janice Sanchez, NCEA
Helen Smith, OARM
Preston Turner, OARM
Luke Weber, NCER

For extraordinary administrative support to assure the NCEA-RTP program is highly efficient, effective and influential.

Maureen Johnson, NCEA
For exemplary support to the National Center for Environmental Assessment in developing the CADDIS website.

National Exposure Research Laboratory

Breanne Benton-Madonna, NERL
For exceptional support in improved efficiency in processing "cleared" peer-reviewed technical manuscripts across NERL and standardizing entry into ORD's Scientific Technical Information Clearance System.

Claudette W. Mitchell, NERL
For her exceptional professionalism and dedication in support of ORD.

National Health and Environmental Effects Research Laboratory

Barbara A. Sherman, NHEERL
In recognition of her sustained administrative excellence through efficiency, diligence, thrift, and skill in support of her division, colleagues, and research to protect the environment.

Linda D. Lassiter, NHEERL
For exceptional service in providing superior customer service to the National Health Environmental Effects Research Laboratory, and ORISE program.

National Risk Management Research Laboratory

EPA-Cincinnati Safety, Health, and Environmental Management Team (SHEM)
For the EPA-Cincinnati SHEM team's outstanding support services resulting in efficiency, infrastructure, safety, and environmental performance improvements at the Laboratory Support Center.

Gerard Henderson, NRMRL
Steve Musson, NRMRL
Jennifer Tant, NRMRL
Joshua Weber, NRMRL
Leslie Wilsong, NRMRL

Suzanne Jackson, NRMRL
In recognition of her exceptional operational administrative support for NRMRL and continued initiative to identify and solve issues before they arise.

Office of Administrative and Research Support

Agency Funds Control Officer (FCO) Workgroup
For outstanding efforts to form an agency FCO Workgroup to facilitate information exchange and support consistent implementation of financial management practices.

Katherine Berrey, OARM
Carmelita Chadwick-Gallo, OCFO
Jayna Alexander Cimonetti, OCFO
Brent Eischen, OARS
Donald Giamporcaro, OCFO
Timothy Hinds, OEI
Hamilton Humes, OCFO
Vonda Jennette, OCFO
Kennard Jones, OCFO
Joseph Layman, OCFO
Robin Lunsford, OARS
Regina Milbeck, OARS
Barbara Murphy, OEI
Sharon Ridings, OARM
Christine Robinson, OARM
Jason Ruehl, OCFO
Kelly Siegel, OCFO
Cindy Spadaro, OCFO
Shaun Trudeau, OGC
Brian Webb, OCFO

OARS Budget Execution Division's Services Branch
For extraordinary initiative and team efforts to create and effectively deliver innovative customer-driven budget training

Monica R. Brooks, OARS
Azuree J. Cooksey, OARS
Betty L. Hastings, OARS
Naneka M. Mason, OARS
Christine T. Snowden, OARS

ORD's Simplified Acquisition Contracting Officers Team
For outstanding acquisition results under the Simplified Acquisition Contracting Officers expansion program which mitigated an Agency enterprise risk and enabled accomplishment of ORD's research mission.

Kevin Broadnax, OARS
Renae Cochran, OARS
Pam Daggs, OARS
William Goins, OPARM
Robin Harris, OARS
Andrew Howe, OARS
Sonya Mitchell, OARS
Glennis Reslock, OARS
Lisa Rogers, OARS
William Sahli, OARS

Office of Science Information Management

ORD Computer Room Consolidation Team
For outstanding support working to close ORD computer rooms in Edison, NJ, Chapel Hill, NC and Grosse Ile, MI.

Brain Devir, OSIM
Steve Greenfield, OSIM
Craig Hammel, OSIM
Sarah Lopez, OSIM
Michael McDowell, OSIM
Elroy Seegars, OSIM
Barbara Sheedy, NHEERL
David Shoffner, NHEERL
Rick Smith, OSIM
Debra Taylor, NHEERL

ORD Virtual Computer Team
For outstanding support to transition ORD Staff and business partners to ORD's Virtual Computing environment.

Keeley Dean, OSIM
Craig Hammel, OSIM
Danielle Lewis, OSIM
Michael McDowell, OSIM
John Sykes, OSIM
Melissa Tracy, OSIM

Office of Science Policy

Shared Administrative Resources Group
For innovation in providing exceptional shared administrative support and ensuring consistency and creating efficiencies in administrative processes.

Danielle Branch, IOAA
Anna Champlin, IOAA
Robin Clarke, IOAA
Danielle Dixon, IOAA
Anthony Grimm, OSP
Tia Groves, IOAA
Irving Matchen, OSP
Rachel Matney, IOAA
Patricia McGhee, IOAA
Danielle Pope, OSA
Ashley Ramsey, OPARM
Brandon Walters, IOAA

Bronze Medal Award

National Center for Environmental Assessment

IRIS Benzo[a]pyrene and Trimethylbenzene Assessment Team
For exceptional and innovative scientific assessment work on the Benzo[a]pyrene and Trimethylbenzene IRIS Assessments.

Lyle Burgoon, NCEA
Christine Cai, NCEA
Vincent Cogliano, NCEA
Glinda Cooper, NCEA
John Cowden, NCCT
Allen Davis, NCEA
Gary Foureman, NCEA
Martin Gehlhaus, Region 3
Catherine Gibbons, NCEA
Kevin Hogan, NCEA
Andrew Kraft, NCEA
Eva McLanahan, ASTDR/CDC
Kathleen Newhouse, NCEA
Linda Phillips, NCEA
John Schaum, NCEA
Paul Schlosser, NCEA
Jamie Strong, OW

The Integrated Science Assessment Team

The Integrated Science Assessment Team is recognized for exceptional scientific support to the Administrator EPA decision making on the Primary NAAQS for Sulfur Oxides.

Breanna Alman, OAQPS
Renee Beardslee, NCEA
Marieka Boyd, NCEA
Michael Breen, NCEA
James Brown, NCEA
Barbara Buckley, NCEA
Evan Coffman, NCEA
Steven J. Dutton, NCEA
Rachelle Duvall, NCEA
Brooke L. Hemming, NCEA
Erin Hines, NCEA
Ryan Jones, NCEA
Ellen Kirrane, NCEA
Dennis Kotchmar, NCEA
Tom Long, NCEA
Thomas Luben, NCEA
Connie Meacham, NCEA
Jennifer Nichols, NCEA
Elizabeth Oesterling Owens, NCEA
Molini Patel, NCEA
Steven Perry, NCEA
Joseph P. Pinto, NCEA
Kristen Rappazzo, NCEA
Adam Reff, OAQPS
Jennifer Richmond-Bryant, NCEA
Jason Sacks, NCEA
Douglas A. Solomon, OAQPS
Lisa Vinikoor-Imler, NCEA
Debra Walsh, NCEA
Richard Wilson, NCEA

Urban Resilience Indicators Team

In recognition of the excellent work done on the development and application of an indicator-based framework to improve community resilience.

Curt Baranowski, OW
Megan Goold, Region 3
Cynthia Greene, Region 1
Verle Hansen, NRMRL
Laura Jackson, NHEERL
Susan Julius, NCEA
Linda Lawson, USDOT
Megan Susman, AO
Norman Willard, Region 1
Emma Zinsmeister, OAR

National Exposure Research Laboratory

Modeling Approaches for Lead in Drinking Water Team

For exemplary efforts in applying cutting-edge science, cross-agency collaboration and scientific leadership for a multimedia Lead exposure modeling analysis for children to inform public-health decisions.

Jim Brown, NCEA
Lisa Christ, OW
Rebecca Daniels, NERL
Andrew, Geller, IOAA
Ahmed Hafez, OW
Erik Helm, OW
Claudette Mitchell, NERL
Nicole Shao, OSP
Emily Smith, NERL
Brittany Stuart, NERL
Mike Tornero-Velez, NERL
Jim Xue, NERL
Valerie Zartarian, NERL

ORD FEMA Support Team

During an extremely active hurricane season in 2017, ORD employees volunteered with FEMA's Surge Capacity Force to help support response and recovery efforts.

Laurel Ajabi, OARS
Felicia Barnett, OSP

Chelsea Berg, NERL
Jason Bernagros, NRMRL
Nichole Brinkman, NERL
Dana Bruce, OPARM
Rebecca Daniels, NERL
Peter Evanko, OARS
Vicente Gomez-Alvarez, NRMRL
Maureen Hingeley, OPARM
Debra Hutchins, OPARM
Curtis Jackson, OSIM
Luanne Lasnier, NERL
Lahne Mattas-Curry, IOAA
Marcia McCain, OPARM
Michael Pirhalla, NHSRC
Matthew Richards, OPARM
Evan Schwend, OARS
Elroy Seegars, OSIM
Ramona Sherman, NHSRC
Toni Stern, NRMRL
Eva Tankersley, OARS
Joyce Terry, OARS
Greg Toth, NERL
Lisa Tychsen, OARS
Kelly Van Bronkhorst, OPARM
Andre Wade, OPARM

National Health and Environmental Effects Research Laboratory

Alejandro Almario, NHEERL and Kyle Buck, NHEERL
For excellence in educational outreach to the community on EPA's mission to protect human health and the environment

Earl Puckett, NHEERL
For designing, refining, and manufacturing the Cell Culture Exposure System (CCES) allowing EPA scientists to expose cells to gas, vapor, or aerosol.

ECOTOX Team
For updating the ECOTOX Knowledgebase with modernized web interface, improved functionality, and enhanced data mining capabilities improving its utility for risk assessors and other users.

Collene Elonen, NHEERL
Carlie LaLone, NHEERL
Jennifer Olker, NHEERL

Lake Huron Cooperative Science Monitoring Initiative Team
For implementing an innovative and technically-challenging field-based research program to support the science needs identified by the Lake Huron Action Management Plan.

Ted R. Angradi, NHEERL
Terry Brown, NHEERL
Tim Corry, NHEERL
Anne M. Cotter, NHEERL
Joel C. Hoffman, NHEERL
Thomas P. Hollenhorst, HHEERL
Samuel E. Miller, NHEERL
Mary F. Moffett, NHEERL
James Pauer, NHEERL
Gregory S. Peterson, NHEERL
Erik Pilgrim, NERL
Jill V. Scharold, NHEERL
Anett S. Trebitz, NHEERL

Peer Review Handbook Team
For outstanding leadership and steadfast commitment to improving business processes associated with peer review and advancing their implementation by developing essential guidance, tools and training.

Vincia Holloman, OEI
Virginia Houk, NHEERL

Cheryl Itkin, NCEA
Eric Koglin, NHSRC
Anand Mudambi, OSA
Tom O'Farrell, OSA
Stephanie Sanzone, AO

Rapid Benefit Indicators Team
For the Rapid Benefit Indicators approach and tools that allow users to quickly estimate and quantify human benefits resulting from alternative freshwater wetland restoration scenarios.

Walter Berry, NHEERL
Justin Bousquin, NHEERL
David Martin, NHEERL
Marisa Mazzotta, NHEERL

Thyroid Hormone-Based Developmental Neurotoxicity Team
For development of an adverse outcome pathway for neurodevelopmental effects of thyroid hormone deficiency.

Kevin Crofton, NCCT
Sigmund Degitz, NHEERL
Jeffrey Denny, NHEERL
Hisham El-Masri, NHEERL
Jermaine Ford, NHEERL
Mary Gilbert, NHEERL
Jonathan Haselman, NHEERL
Iman Hassan, NHEERL
Michael Hornung, NHEERL
Michelle Hotchkiss, NHEERL
Joseph Korte, NHEERL
Patricia Kosian, NHEERL
Jennifer Olker, NHEERL
Wendy Oshiro, NHEERL
Katie Paul-Friedman, NCCT
Carmen Wood, NHEERL

William D. Rugh, NHEERL
His technical expertise, can-do attitude, and selflessness have made NHEERL's Western Ecology Division an exceptional research facility, exemplifying the best of ORD.

National Homeland Security Research Center

Category A Infectious Waste Handling Guidance Team
For improving the Nation's resiliency to outbreaks involving the most dangerous infectious agents by developing original, interagency guidance for handling Category A waste.

Erica Canzler, OECA
Reggie Cheatham, OLEM
Nancy Cohen, OLEM
Betsy Devlin, OLEM
Ross Elliot, OLEM
Mario Ierardi, OLEM
Melissa Kaps, OLEM
Kim Kirkland, OLEM
Paul Lemieux, NHSRC
Mike Nalipinski, OLEM
Cayce Parrish, OA
Kathleen Salyer, OLEM
Gregory Sayles, NHSRC

EPA Representatives to the Interagency Validated Sampling Plan Working Group
For their significant contribution to addressing a critical and difficult gap in the Nation's ability to respond to a bioterrorism attack.

M. Worth Calfee, NHSRC
Romy Campisano, NHSRC
Erica Canzler, OECA
Shawn Ryan, NHSRC
Sanjiv Shaw, NHSRC
Erin Silvestri, NHSRC
Francisco J. Cruz, OLEM
Tonya Nichols, NHSRC

Sarah Taft, NHSRC

Flint, MI Drinking Water Quality Modeling Team
For protecting public health in Flint, MI by providing cutting-edge scientific expertise and water-system models to help improve water quality in real time.

Jonathan Burkhardt, NRMRL
Ruth Corn, OARS
Mark Durno, Region 5
John Hall, NHSRC
Terra Haxton, NHSRC
Rob Janke, NHSRC
Eric Koglin, NHSRC
Regan Murray, NRMRL
Tom Speth, NRMRL
Jeff Szabo, NHSRC
Dan Williams, NRMRL

ORD ReAChback for Emergency Response Team
For building and implementing an improved capability for ORD to deliver technical support to EPA, states and local agencies during emergency responses.

Charlena Bowling, NRMRL
Kelly Dipolt, NHSRC
Eric Koglin, NHSRC
Gregory Sayles, NHSRC

National Risk Management Research Laboratory

Coweeta Flux Tower Collaboration Team
In recognition of EPA and Forest Service collaboration establishing the Coweeta Flux Tower and studies of atmospheric deposition and nutrient cycling in high elevation forests.

Xi (Doris) Chen, NRMRL
Ryan Daly, NRMRL
Christopher Geron, NRMRL
John Iiames, NERL
Chelcy Miniat, USDA Forest Service
Andrew C. Oishi, USDA Forest Service
Melissa Puchalski, OAR
Donna B. Schwede, NERL
John T. Walker, NRMRL

Innovative Biological Treatment for Small Drinking Water Systems
For creating, patenting, piloting, and commercializing a new innovative drinking water treatment approach for the removal of contaminants from drinking water sources.

Sarah Bauer, OARS
Stephanie Brown, NRMRL
Kathleen Graham, OARS
Roy Haught, NRMRL
Darren Lytle, NRMRL
Christopher Parrett, NRMRL
Maily Pham, NRMRL
Eugenia Riddick, NRMRL
Christy Muhlen, NRMRL

The ORD Household Energy Research Team
In recognition of EPA employees whose research supports the high-priority initiative addressing global human health and environmental problems from household air pollution.

Bryan Bloomer, NCER
David DeMarini, NHEERL
Kathie Dionisio, NERL
Jan Dye, NHEERL
Terry Keating, NCER
Charly King, NHEERL
Todd Krantz, NHEERL
Bill Linak, NRMRL
Ingrid George, NRMRL
Ian Gilmour, NHEERL
Dale Greenwell, NRMRL
Michael Hays, NRMRL

Mark Higuchi, NHEERL
Amara Holder, NRMRL
Jim Jetter, NRMRL
Ozge Kaplan, NRMRL
John Mitchell, OAR
Laura Nessley, NRMRL
Carlos Nunez, NRMRL
Jacky Rosati Rowe, NRMRL
Bob Thompson, NRMRL
Susan Thorneloe, NRMRL
Sara Warren, NHEERL
Robert Wright, NRMRL

Office of Administrative and Research Support

ORD Data Analytics Team
The ORD Data Analytics Team transformed how ORD receives data/reports and its ability to visualize and manipulate data for the purposes of more informed decision-making.

Laurel Ajabi, OARS
Rebecca Clausen, OSIM
Christopher Dietz, OARS
Andrew Howe, OARS
Audrey Kanet, OARS
Desmond Mayes, OARS
Sonya Mitchell-Holmes, OARS
Sharon Moxley, OARS
Kami Nolte, OARS
Kathrine Park, OARS
Steve Vanhorn, OARS
John Steenbock, OARS

Office of Program Accountability and Resource Management

Lab Cost Data Team
ORD/OCFO collaboration on developing an IT module in the new Budget Formulation System for the collection and analysis of Laboratory Enterprise Study data.

Dana Bruce, OPARM
Eric Burman, OPARM
Michael Cocimano, OPARM
Jackye Herzfeld, OCFO
Jamie Lang, OPARM
Linda Schwaegerle, OPARM

Office of Science Information Management

John Sykes, OSIM
For outstanding voluntary public service to improve natural habitat and promote environmental education and awareness for the Wake County public schools.

Office of Science Policy

Board of Scientific Counselors Designated Federal Officers Team
For Outstanding and efficient work in reconstituting EPA's Board of Scientific Counselors to ensure ongoing scientific advice for ORD's research programs.

Timothy Benner, OSP
Jace Cuje, OSP
Megan Fleming, OSP
Noelle Green, OGC
Cynthia Roberts, OSP
Toni Rousey, OARM
Mya Sjogren, IOAA
Tanya Tharps, OARS
Maureen Gwinn, NCCT
Kevin Kuhn, IOAA
Melissa Tracy, OSIM
Thomas Tracy, OSP

Viktoriya Plotkin, NHSRC
Steve Watkins, OSP

ORD's Recreational Water Quality Criteria Research Team
ORD's Recreational Water Quality Criteria (RWQC) Research Team conducted and synthesized EPA's research results to support OW's 5-yr statutory review of the 2012 RWQC.

Mike Cyterski, NERL
Al Dufour, NERL
Richard Greene, IOAA
Ann Grimm, NERL
Richard Haugland, NERL
Asja Korajkic, NERL
Brian McMinn, NERL
Kevin Oshima, NERL
Orin Shanks, NRMRL
Nicole Shao, OSP
Eric Villegas, NERL
Timothy Wade, NHEER
Gene Whelan, NERL
Richard Zepp, NERL
Marirosa Molina, NERL

Excellence in Supervision Award

National Center for Environmental Assessment

Susan Rieth, NCEA
Demonstrated excellence in supervision of multi-disciplinary scientists delivering highly complex scientific assessments during a time of tremendous change and challenge for the IRIS Program.

Exceptional Support to ORD Award

National Health and Environmental Effects Research Laboratory

California Endangered Species Case Study Team
For outstanding support to the California Endangered Species Case Study, providing Programmatic and Regional expertise to ensure transferrable research products.

Debra Denton, Region 9
Kristina Garber, OPP
Andrew Kanarek, OPP

Exceptional Technical Assistance to the Regions or Program Offices

National Exposure Research Laboratory

Donna Schwede, NERL
For providing outstanding support to Programs and Regions by ensuring data from the National Atmospheric Deposition Program continues to be available to support EPA programs.

National Health and Environmental Effects Research Laboratory

Jana Compton, NHEERL
For helping to solve nutrient management problems with biogeochemistry.

National Risk Management Research Laboratory

Biomass Team
For outstanding technical support in developing emissions characterizations from co-firing various biomass and coal blends to inform decisions on cleaner burning and waste-to-energy options.

James Edward Brown, NRMRL
Peter Kariher, NRMRL
Jeffrey Ryan, NRMRL
Tiffany L.B. Yelverton, NRMRL

Flint, Michigan Crisis Support Team to Region 5
For the exceptional technical support given to Region 5 in wake of the Flint, Michigan water crisis.

Jonathan Burkhardt, NRMRL
Samuel Hayes, NRMRL
Robert Janke, NHSRC
Eric Koglin, NHSRC
Darren Lytle, NRMRL
Christy Muheln, NRMRL
Regan Murray, NRMRL
Chris Parrett, NRMRL
Sandhya Parshionikar, NRMRL
Jonathan Pressman, NRMRL
Mark Rodgers, NRMRL
Michael Schock, NRMRL
Kelly Dipolt, NHSRC
Cynthia Sonich-Mullin, NRMRL
Thomas Speth, NRMRL
Daniel Williams, NRMRL

ORD Diversity Leadership Award

National Risk Management Research Laboratory

Michael Gonzalez, NRMRL
For creating a dynamic and energetic environment for meeting scientific challenges.

ORD Environmental Justice Award

National Health and Environmental Effects Research Laboratory

Rebecca De Jesus Crespo, NHEERL, Autumn Oczkowski, NHEERL, and Susan YEE, NHEERL
For outstanding innovation and development of research to link wetland ecosystem services to mosquito-vectored diseases in Environmental Justice communities in Puerto Rico.

EcoHealth
https://doi.org/10.1007/s10393-019-01406-6

EcoHealth

© 2019 This is a U.S. government work and its text is not subject to copyright protection in the United States; however, its text may be subject to foreign copyright protection

Original Contribution

Linking Water Quality to *Aedes aegypti* and Zika in Flood-Prone Neighborhoods

Susan Harrell Yee,[1] Donald A. Yee,[2] Rebeca de Jesus Crespo,[1] Autumn Oczkowski,[3] Fengwei Bai,[2] and Stephanie Friedman[1]

[1]*Gulf Ecology Division, National Health and Environmental Effects Research Laboratory, U.S. Environmental Protection Agency, 1 Sabine Island Drive, Gulf Breeze, FL 32561*
[2]*Department of Biological Sciences, University of Southern Mississippi, Hattiesburg, MS 39406*
[3]*Atlantic Ecology Division, National Health and Environmental Effects Research Laboratory, U.S. Environmental Protection Agency, Narragansett, RI 02882*

Abstract: The ability of ecosystems to regulate water quality and flood events has been linked to health outcomes, including mosquito-borne illnesses. In the San Juan Bay Estuary watershed of Puerto Rico, habitat alterations and land-use development have disrupted watershed hydrology, exacerbating wastewater discharges and subjecting some neighborhoods to frequent flooding events. In 2016, the mosquito-borne illness Zika became a new cause for concern. We hypothesized that nutrient-enriched flood water could provide pulses of supplemental nutrients to local mosquito populations. We conducted a field study in six neighborhoods adjacent to the estuary to assess whether environmental variability of nutrient inputs could be linked to breeding habitat containers, *Aedes aegypti* larvae and adults, and the acquisition of Zika virus by adult mosquitoes. The most frequently flooded neighborhood had consistently higher levels of nitrogen in estuary water, leaf detritus, containers, and adult mosquitoes compared to other neighborhoods. Adult body nitrogen was significantly related to both nitrogen content of containers and leaf detritus from the local trapping area. Disseminated Zika concentration in adult *Ae. aegypti* tended to decrease as body carbon and nitrogen increased. Our study provides preliminary evidence that environmental variability in nutrient inputs can influence viral acquisition by mosquito vectors. This suggests that management actions to reduce flooding and improve water quality should go hand-in-hand with more traditional vector control methods, such as aerial spraying, to help control spread of vector-borne diseases.

Keywords: *Aedes aegypti*, Nitrogen, Carbon, Stable isotopes, Zika

Introduction

Decision makers are increasingly framing environmental management issues within the context of benefits to the health and well-being of stakeholders (Rhodus et al. 2013; Korfmacher et al. 2015; Oosterbroek et al. 2016). Land-use change, climate change, and point and nonpoint source

Susan Harrell Yee and Donald A. Yee have contributed equally to this manuscript.

Correspondence to: Susan Harrell Yee, e-mail: yee.susan@epa.gov

Published online: 03 April 2019

runoff alter the state of ecosystems and their services, including disservices, leading to subsequent effects on human health (Myers et al. 2013). The ability of ecosystems to regulate water quality and flood events has been linked to decreases in a number of health outcomes, including infectious and parasitic diseases, mental disorders, and respiratory illnesses (Hinga and Batchelor 2005; Ivers and Ryan 2006; Oosterbroek et al. 2016; De Jesus Crespo and Fulford 2017). In coastal communities, greenspaces such as wetlands may play a role in mitigating mosquito-borne illnesses by moderating flooding events or regulating water quality (Carver et al. 2015; De Jesus Crespo et al. 2018). With growing concerns about the health risks of aerial spraying for mosquitoes, alternative management strategies that leverage these natural ecosystem services may provide more sustainable approaches to managing mosquito vectors.

Estuary management programs, in particular, have been linking actions to improve the habitat and water quality of the estuary to goals of improving human health and public safety (SJBEP 2000). For example, the San Juan Bay estuary, Puerto Rico, comprises a connected system of bays, lagoons, and canals in a highly urbanized watershed of over half a million residents, with socioeconomic conditions varying widely across neighborhoods (Azar and Rain 2007). Habitat alterations and land-use development have disrupted the natural flow of water throughout the estuary system, subjecting some neighborhoods to frequent flooding events and exacerbating the effects of wastewater discharges, including untreated sewage and stormwater runoff into areas of the bay (SJBEP 2000). A recent Health Impact Assessment identified vector-borne illnesses, including dengue, as a major health concern for flood-impacted communities neighboring the estuary (Sheffield et al. 2014; Korfmacher et al. 2015), and supported efforts to reduce flooding and debris that create mosquito breeding sites (Ahern et al. 2005; Pires and Gleiser 2010).

Most recently, the mosquito-borne illness Zika has become a cause for concern. Zika virus (ZIKV) is a flavivirus, closely related to other arboviruses like dengue, West Nile, and yellow fever, and was originally isolated in Uganda, Africa (Dick et al. 1952; Musso and Gubler 2016). ZIKV was first detected in the Americas in Brazil in 2015 (Zanluca et al. 2015) and spread explosively throughout the Americas in 2016 (WHO 2016a). The first confirmed case of locally acquired Zika infection in Puerto Rico was reported in December 2015 (WHO 2016b), and Zika cases continued to increase rapidly, peaking in August 2016 with as many as 2500 confirmed cases per week (Puerto Rico Department of Health 2017). In North America, *Aedes aegypti* and *Ae. albopictus* are the only mosquitoes known to be competent vectors of ZIKV (Chouin-Carneiro et al. 2016), with only *Ae. aegypti* known to have an established distribution in Puerto Rico (Sharp et al. 2013).

Like other arboviruses, transmission of Zika virus is influenced by a complex array of interactions among humans, wildlife, mosquito vectors, and the environment (Thomas et al. 2017). Mosquitoes become exposed to virus when they take a blood meal from an infected person (Gratz 2004), or wildlife that may serve as pathogen reservoirs (Gonzalez-Salazar et al. 2017). The virus then replicates in the mosquito's midgut and salivary glands, and after an incubation period, may be spread when the infectious mosquito takes its next blood meal (Musso and Gubler 2016). The capacity of a mosquito vector to spread a virus depends on factors such as the probability of acquiring and transmitting the pathogen, the proportion of vectors acquiring the pathogen, and the density of vectors per human host (Anderson and Rico-Hesse 2006; Klempner et al. 2007). Environmental factors, such as larval nutrition (Nasci and Mitchell 1994), larval density (Alto et al. 2005; 2008a; Reiskind and Lounibos 2009), adult nutrition (Canyon et al. 1999), adult body size (Scott et al. 2000; Alto et al. 2008b), and seasonality and climate (Almeida et al. 2005), have all been shown to affect virus acquisition for mosquitoes. Moreover, a handful of studies have directly linked water quality factors, such as nutrient enhancement through fertilizer runoff (Mutero et al. 2004) or water chemistry in septic systems (Burke et al. 2010), to the abundance of mosquito larvae and adults. To our knowledge, however, no studies have assessed whether local variability in water quality can be linked to variability in the acquisition of virus by adult mosquitoes. As a result, the degree to which proposed actions in the San Juan Bay watershed to reduce sewage discharges, improve stormwater drainage, and restore natural flow could mitigate vector-borne illnesses (Sheffield et al. 2014; Korfmacher et al. 2015) is challenging to ascertain.

We hypothesized that variability in point and nonpoint source runoff creates variability in estuary water quality (Fig. 1). During extreme rainfall events, larval habitat containers, such as buckets, food containers, or discarded vehicle tires, may experience inputs of flood waters as rivers, canals, or lagoons overflow (Hashizume et al. 2012). Normally, larval containers are filled through precipitation events, and allochthonous inputs from leaf or animal

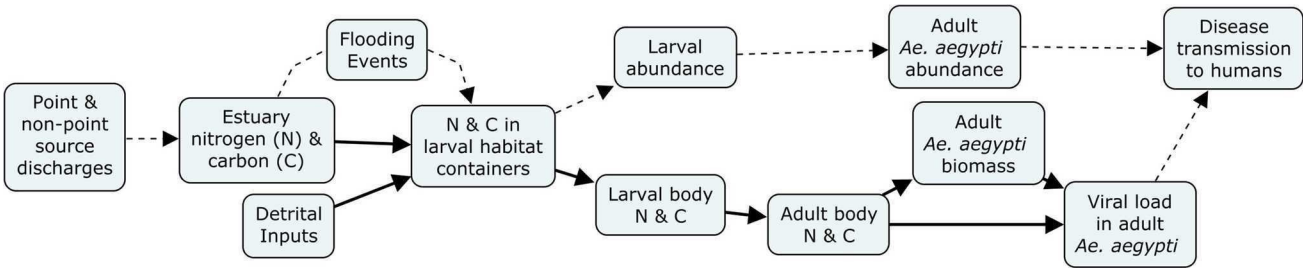

Figure 1. Causal flow diagram illustrating how nitrogen and carbon inputs into mosquito larval containers through flooding events and detrital inputs could influence viral load in adult mosquitoes and ultimately disease transmission to humans. Solid paths were tested with field data; dashed paths were inferred.

detritus are important sources of nutrients (Kling et al. 2007). In areas where waterbodies are subjected to runoff or wastewater discharges, flood water could provide pulses of supplemental nutrients to local mosquito populations, dependent on the frequency of flooding. In larval containers, nutrients such as nitrogen are often limiting, such that the growth, survival, and mass of larvae, and consequently of adults, are crucially affected by allochthonous inputs (Carpenter 1983; Yee and Juliano 2006). Nutrition and mass subsequently affect the acquisition and multiplication rates of virus within adult mosquitoes (Nasci and Mitchell 1994; Canyon et al. 1999; Scott et al. 2000; Alto et al. 2008b) and ultimately, along with the abundance of infected mosquitoes (Klempner et al. 2007), transmit to humans.

We conducted a field study in neighborhoods bordering water bodies within the San Juan Bay estuary system in June 2016, when confirmed Zika cases in Puerto Rico were approximately 672 per week and were rapidly increasing (Puerto Rico Department of Health 2016). In each neighborhood, we assessed the particulate nitrogen and carbon content of estuary water, leaf detritus, water from larval containers, *Ae. aegypti* larvae within containers, and local adult *Ae. aegypti* populations, to determine the degree to which environmental variability in nutrients is carried through to adult mosquitoes. Sampling locations were chosen to cover a range of variability in water quality, observed in periodic water quality monitoring data (SJBEP 2016), in order to maximize our potential to detect differences. Finally, we tested adults for ZIKV to determine whether adult nutrition affects acquisition of Zika virus. By simultaneously collecting field data on water quality, leaf detritus, larval habitat, mosquito larvae, mosquito adults, and virus, our study is one of the first to attempt to connect environmental variability to the capacity of mosquito vectors to spread disease.

Study Area

The San Juan Bay Estuary (SJBE) is an interconnected system of channels and lagoons, many of which have been severely altered by human activity (Brandeis et al. 2014). The SJBE is the only tropical estuary in the US National Estuary Program, and is the most highly urbanized, with approximately 82% of the watershed developed. The remaining watershed is dominated by moist forest and wetlands, including the most extensive contiguous mangrove forest in Puerto Rico (Brandeis et al. 2014). We selected neighborhoods adjacent to six waterbodies: La Malaria channel, Martin Peña channel, Suarez channel, Torrecilla Lagoon, Piñones Lagoon, and Rio Piedras (Fig. 2). Waterbodies were chosen to reflect a range of water quality parameters, including salinity (0.17–34.03 PSS; SJBEP 2016), nitrogen (0.23–35.6 Kjeldahl nitrogen mg/L; SJBEP 2016), and carbon (0.122–7.475 TOC mg/L; SJBEP 2016). Cumulative Zika cases up to June 2016 were comparable across the four municipios (i.e., county-equivalent areas) covered by the study area (Puerto Rico Department of Health 2016; Cataño municipio, 175 cases per 100,000 inhabitants; San Juan municipio, 293 cases per 100,000 inhabitants; Carolina municipio 156 cases per 100,000 inhabitants; Loiza municipio: 136 cases per 100,000 inhabitants).

We focused our most intensive sampling efforts on the Martin Peña neighborhood, with the five other waterbodies included for comparison. The Martin Peña neighborhood comprises eight distinct adjoining communities, but is referred to as a single neighborhood as the sampling unit for the purpose of this study. Decades of unregulated dumping and construction into the severely blocked Martin Peña Channel, along with deficient sewage infrastructure and direct discharges of untreated residential wastewater, has led to frequent flood events during which residents are

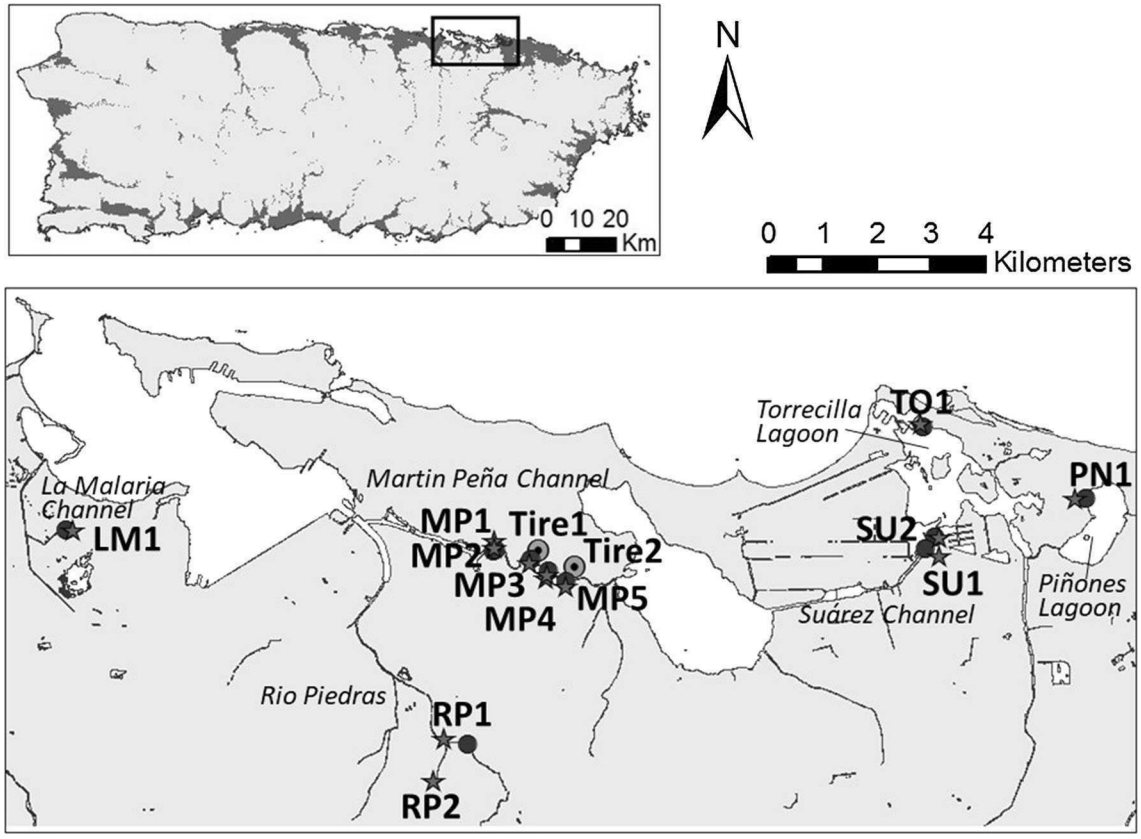

Figure 2. Water, larval habitats, and adult mosquitoes were sampled from FEMA flood zones (gray shaded areas) in and around San Juan, Puerto Rico. Mosquito trap locations (stars) and estuary sampling locations (solid circles) were sited within each of six sampled neighborhoods. Larval habitat containers were located and sampled within 150 meters of traps. Two tire piles (concentric circles) were also sampled for comparison to dispersed containers.

exposed to polluted surface waters in their homes and roadways (Korfmacher et al. 2015). As many as 70% of residents report flooding in or near their home in a given year, with some residents reporting their homes flooded upwards of 20 times per year (Sheffield et al. 2014). Flood waters often reach heights greater than 30 cm, sufficient to cover accumulated trash from illegal dumping or other containers. The Martin Peña neighborhood experienced such a flood event two weeks prior to our June 2016 sampling. Sampled neighborhoods from other waterbodies were also within established flood zones (FEMA 2009; Fig. 2), though it is unknown whether they had experienced flooding recent to our field sampling.

Study Design

A sampling site within each neighborhood was defined by the placement of an adult mosquito trap within 50–150 m of the adjacent waterbody and any sampled larval container habitats within 150 m of that trap (Fig. 2). All trap locations were adjacent to water sources within the estuarine watershed, with similar vegetation and canopy cover. With the exception of a state forest location near Piñones Lagoon (PN1), all trap locations were within the San Juan metropolitan area in neighborhoods with dense housing. Across the six neighborhoods, we placed a total of 12 adult mosquito traps, with between 1 and 5 traps placed per neighborhood. We searched for water-filled containers with larvae in the 150 m radial area surrounding each trap, with between 1 and 4 larval containers located and sampled per trap (Table 1). Container sampling was highly dependent on our ability to find containers in accessible areas (e.g., not in a private yard), and we cannot assume potential sources for adults were exhaustively sampled. However, adult *Ae. aegypti* typically disperse less than 150 m (Harrington et al. 2005), so larval containers at each sampling site were assumed to be a representative source of adult mosquitoes in that area. Sites were sampled on June 7 and

Table 1. Number of Estuary Water Samples and Mosquito Larvae Containers Sampled Corresponding to Each Trap Location, as Well as the Number of Adult *Aedes aegypti*.

Neighborhood	Trap location	Flood composite index	Estuary water samples	Leaf samples	Larval container samples	Female *Ae. aegypti* per trap	Fraction *Ae. aegypti* infected with ZIKV
Martin Peña Channel	MP1	3.25	3	4	1 Tire	18	0/18
	MP2	7.21	2[a]	3	3 Tires, 1 bucket	13	0/13
	MP3	7.65	3	4	1 Tire, 1 bucket, 1 small tub	0	–
	MP4	6.14	3	3	1 Tire, 1 small tub	16[c]	0/15
	MP5	2.50	3	4	2 Buckets	27[c]	0/12
Piñones Lagoon	PN1	8.90	3	5	1 Large boat, 1 large bin	7	0/7
Rio Piedras	RP1	3.00	3[b]	3	1 Tire	10	6/10
	RP2	1.03	0	0	0	4	1/4
La Malaria channel	LM1	3.18	3	0	1 Tire, 1 small boot, 1 small pan	*Trap malfunction*	
Suárez channel	SU1	2.48	1[a]	0	1 small bin	2	1/2
	SU2	3.00	3	4	0	3	1/3
Torrecilla Lagoon	TO1	5.21	3	4	0	30	9/30
Tire Pile 1	–	7.71	–	–	5 Tires	–	–
Tire Pile 2	–	2.93	–	–	5 Tires	–	–

[a]Additional samples with peak areas of < 0.5 nA were removed from analysis.
[b]All samples had peak areas < 0.5 nA, but were included in analysis to prevent total loss of data.
[c]Not all females were tested for virus due to methodological limitations.

8, 2016, with approximately half of the sites sampled each day.

To collect adult mosquitoes, we used BG-Sentinel traps (Biogents AG, Regensburg, Germany), baited with a human scent lure (BG-Lure; Biogents AG). BG-Sentinel traps are effective at capturing host-seeking adult *Ae. aegypti* (Maciel-de-Freitas et al. 2006), which are likely to have taken a blood meal and thus been exposed to virus. A battery-operated fan prevents adults from escaping after they have entered the trap. Efforts were made to centrally locate each trap among paired sampled containers, dependent on the ability to place traps in a secure location, such as the gated yard of a homeowner, to minimize disturbance. Traps were left out for a 48-h period before adults were collected. One trap malfunctioned (LM1; Fig. 2) and therefore did not capture any adults. Collected adults were identified to sex and species, with 0–30 female *Ae. aegypti* collected per trap (Table 1). Only adult female *Ae. aegypti* were used for subsequent analysis. Adults were frozen and transported to the respective laboratories for nutrient and ZIKV analysis.

For each trap location, we collected three 50 mL samples of surface water from each waterbody, within the shortest direct distance of the approximate center of that site. Water samples were filtered on site through 2.5-cm glass fiber filters (Whatman GF/F), with filters immediately placed on ice and then in a drying oven within a few hours of collection each day. Because water samples are highly dynamic, varying daily with recent precipitation, runoff, or waterflow, we also collected three leaf samples from the dominant vegetation (i.e., typically mangrove) directly adjacent to the water sampling location as a long-term, more stable proxy of local waterbody nutrients. Leaves were placed in a drying oven within a few hours of collection. For a few locations (RP2, LM1, SU1), leaf or water samples could not be collected due to accessibility issues. All samples were dried at 65°C for approximately 48 h before being transported to the continental USA.

We similarly filtered three 50 mL water samples from any accessible larval container habitats that could be located at each sampling site. Containers included discarded

plastic food containers, buckets, rubber boots, plant trays, and discarded vehicle tires, and had to contain live *Ae. aegypti* larvae to be included. Subsamples of approximately 5–10 *Ae. aegypti* larvae were collected from each container and placed on a filter in the drying oven at the end of each collection day. In addition to scattered containers, we also sampled water and larvae from tires from two tire shops within the Martin Peña neighborhoods (Table 1). Because tire shops experience frequent turnover, we treated them as separate sampling locations from scattered discarded containers which, based on visual inspection, likely spent a much longer time in the environment and had a greater likelihood of having received environmental inputs. For example, although used tires at the shop near MP3 (Tire 1; Fig. 2) had been flooded with water approximately 0.5 meters high in the week prior to our study, they had already been removed for recycling, with the more recent tires that we sampled having not been exposed to flood water (personal communication with shop employee).

Nutrient Analysis

Filtered contents from waterbody and container water, leaf samples, larvae samples, and adults were analyzed for particulate nitrogen (N) and carbon (C) content. Due to low body weight, 5–10 larvae were analyzed as a single sample. After removing heads for ZIKV analysis, individual adult mosquitoes were analyzed separately.

We hypothesize that nutrient content (%N, %C, C:N) of larval container habitats and subsequent adult mosquitoes would be similar to nutrient content of adjacent waterbodies, either directly via flood water or indirectly through detritus, such that containers or adults from the same trap location are more similar to one another than those from other locations. Additionally, nitrogen (δ^{15}N) and carbon (δ^{13}C) stable isotopes were used to track the unique source locations of nutrients. Stable isotopes provide a record of assimilation, processing, and recycling of nutrients, such that samples collected from different locations can have unique isotopic signatures, particularly from anthropogenic sources such as fertilizer or sewage discharges (Oczkowski et al. 2009, 2011). Similar isotope values between waterbodies and larval containers or adults would provide further support that local waterbodies were sources for nutrients, above and beyond any similarities in nutrient content.

Carbon and nitrogen stable isotopes were measured using an Elementar Vario Micro elemental analyzer connected to a continuous-flow Isoprime 100 isotope ratio mass spectrometer (Elementar Americas, Mt. Laurel, NJ) at the Environmental Protection Agency in Narragansett, Rhode Island. Replicate analyses of isotopic standard reference materials USGS 40 (δ^{13}C = − 26.39‰; δ^{15}N = − 4.52‰) and USGS 41 (δ^{13}C = 37.63‰; δ^{15}N = 47.57‰) were used to normalize isotopic values of working standards (blue mussel homogenate) to the air (δ^{15}N) and Vienna Pee Dee Belemnite (δ^{13}C) scales (Paul et al. 2007). Isotope values are expressed in δ notation following the formula $\delta X\ (‰) = [(R_{sample}/R_{standard}) - 1] \times 10^3$, where X is ^{13}C or ^{15}N and R is ^{13}C/^{12}C or ^{15}N/^{14}N isotopic ratio, respectively. Working standards were analyzed after every 24 samples to monitor instrument performance and check data normalization. The precision of the laboratory standards was better than ± 0.3‰ for C and N. A few samples with peaks less than 0.5 were excluded from analysis to improve accuracy, except where removal would result in the complete elimination of a sampling site (RP1). Analyses in which RP1 was included were consistent with those where it was removed.

The sample particulate N and C content was calculated from area/mass relationships, determined during stable isotope analysis, for replicate standards of known N and C (Oczkowski et al. 2009, 2011). The relationship between the N and C contents of the standards and their analytical peak areas were used to determine the N and C contents of the samples via the peak areas of the samples. For adult mosquitoes, larvae, and leaf detritus, sample N or C was divided by total sample mass to determine the %N or %C. For particulate matter, N and C content was expressed in mg/L by dividing the mg of N and C by the volume of water filtered (usually 50 mL).

ZIKV Processing

To quantify the level of infection with ZIKV, heads from individual adult females were analyzed to assess disseminated virus rather than viruses that might be within a blood meal in the midgut. Total RNA in individual mosquito heads was isolated using TRI-reagent (Molecular Research Center, Inc., Cincinnati, OH, USA). Complementary DNA (cDNA) was synthesized using the iSCRIPT cDNA Synthesis Kit (Bio-Rad Laboratories, Inc.), and RT-qPCR assays were performed in a CFX96 Real-Time System (Bio-Rad Laboratories, Inc.) using iTaq Universal Probe Supermix (Bio-Rad Laboratories, Inc.). The RT-qPCR procedure was performed twice for each sample. Primers

and a probe specific to the Envelope gene of ZIKV were designed and synthesized according to the previous work (Acharya et al. 2016). Due to methodological and cost restrictions, we were limited to testing two batches of 57 individual female adults for ZIKV, for a total of 114 tested adults. After 40 PCR cycles, zero or trace amounts of ZIKV near or below threshold detection limits were considered as zeros ($<$ 1.2 ZIKV E copies/ng total RNA), with values greater than 18 ZIKV E copies/ng total RNA considered as true positives for Zika.

In anticipation of a second Zika outbreak in summer 2017, we repeated the adult mosquito trapping in June 2017 (Appendix A) with the intention of comparing the relationships between adult body nutrients and ZIKV from 2016 to 2017. However, by then, confirmed Zika cases in humans had dropped to less than ten per week across all of Puerto Rico and were continuing to decline (Puerto Rico Department of Health 2017). We detected no virus in trapped adult *Ae. aegypti* from June 2017 (Appendix A). Therefore, here we focus our analysis solely on June 2016 data.

Statistical Analysis

To assess potential linkages between environmental variability in nutrients and ZIKV in adult mosquitoes (Fig. 1), we first assessed whether there was significant natural spatial variability in nutrients from either estuary water or potential leaf detritus, in body nutrients of larval or adult mosquitoes, and in ZIKV concentration. Second, we used multiple regressions to explore whether nutrient variability and ZIKV concentration in mosquitoes could be explained by nutrient variability in the local environment.

We used nested Multivariate Analysis of Variance (MANOVA) to test if trap locations or neighborhoods differed significantly in nutrients, including N, C, δ^{13}C, δ^{15}N, and the ratio of C to N, for waterbody water samples, leaf detritus samples, container water samples, larvae samples, or adult samples. Adult mass was included as an additional dependent variable along with nutrient variables in the adult MANOVA. Trap locations were nested within each neighborhood. If MANOVAs were significant, we followed up with univariate ANOVAs to determine which nutrient variables were most likely contributing to any significant differences. Due to unbalanced sampling design, with a variable number of replicates per location, we used Type II Sums of Squares to assess significance. The sampling units for each trap location were the individual 50 mL waterbody water samples (1–3 per location), individual leaves (1–3 per location), the average of the replicate water samples from each container (1–5 per location), the combined larval value per container (1–5 per location), or individual adults (2–30 per location). Data were tested for normality and Box–Cox-transformed as needed to normalize data prior to analysis. Significant differences between pairs of trap locations or neighborhoods were assessed using Tukey-adjusted least squares means. MANOVAs were conducted in R (www.r-project.org) using the "stats" and "lsmeans" libraries.

To test whether ZIKV concentration differed significantly across locations or neighborhoods, we used general linear models (GLMs) with a Tweedie distribution because ZIKV concentration data were not normal due to a high frequency of zeroes in non-infected mosquitoes. The Tweedie distributions describe a family of distributions characterized by a power parameter, p, which includes the special cases of Poisson or gamma distribution for $P = 1$ or $P = 2$, respectively. For $1 < P < 2$, the distribution is a compound Poisson-gamma distribution, which allows for bimodal distributions where variables are described by different underlying processes, namely a discrete Poisson distribution (e.g., the number of mosquitoes positive for ZIKV) with a continuous gamma distribution (e.g., ZIKV concentration levels within positive mosquitoes). The Tweedie distribution is a good choice for bimodal or zero-inflated data that contain a large number of zeros (Shono 2008). We first estimated the power parameter, p, of the Tweedie function for the ZIKV concentration data using maximum likelihood and then used this fitted distribution, with a log-link power function, in the GLM. The sampling unit was individual adult mosquitoes (2–30 per location), with trap locations nested within neighborhoods. Analyses were conducted in R (www.r-project.org) using the package "tweedie" within "statmod." Results were consistent with a standard logistic regression analysis on the fraction of Zika-positive adults per trap (GLM with a binomial distribution, not shown).

We used a series of multiple regressions to determine whether differences in container nutrients, larval nutrients, adult nutrients, adult mass, or ZIKV concentration could be explained by differences in the nutrient concentrations from potential nutrient sources. To minimize the number of possible explanatory variables under consideration, we limited fixed effects in each regression to the most proximate potential source for nutrients (Fig. 1): (1) waterbody nutrients or leaf detritus nutrients were considered as

explanatory variables for container nutrient content, (2) container nutrients were considered as explanatory variables for larval nutrient content, (3) larval nutrients were considered as explanatory variables for adult nutrient content, (4) adult nutrient content was considered as explanatory variables for adult mass, and (5) adult nutrient content or mass was considered as explanatory variables for ZIKV concentration. Because trapped adults did not directly originate from sampled larvae, we also included the average container nutrients, leaf detrital nutrients, and waterbody nutrients within each neighborhood as potential predictors of adult nutrient content.

In addition to nutrient sources, we considered the influence of flooding and container availability (i.e., type and number) on the dependent variables in regressions. Sampled containers were categorized as tires, 5-gallon buckets, small miscellaneous containers (e.g., boots, food tubs), and large miscellaneous containers (e.g., boat, plastic bin). Because we could not definitively know whether individual sampled containers had flooded recently, we instead used the Flood Hazard Composite Index (NOAA 2018) as a proxy for the likelihood of neighborhood flooding (Table 1). The Composite Index counts the number out of 10 flood hazard data sets, including FEMA flood zones, shallow coastal flooding, and storm surge, that intersect each pixel, which we then averaged to estimate a single value for a 150-m radius around each trap location. Because inputs of containers into nutrients are idiosyncratic and potential inputs from flooding would depend on waterbody nutrients, we did not expect that nutrient content would be significantly related to container type or flood risk (e.g., smaller containers have lower nitrogen; flooded sites have higher nitrogen). Indeed, preliminary analysis with these variables as fixed effects in regressions confirmed no significant relationships between container type or flood risk and nutrient content of containers, larvae, or adults. However, frequent flooding or container type could impact the variability in nutrient content across samples. For example, recently flooded containers may be similar to one another; small containers may be more variable than larger ones; adults emerging from sites with numerous container habitats may be more variable than adults originating from sites with few. Moreover, tires and recently flooded sites in Martin Peña were more heavily sampled than other sites or types of containers, contributing to heteroscedasticity in fitted models. Hence, we tested whether homogeneity of residuals significantly improved when model variance was allowed to vary with either container type, container count around each adult trapping site, or flood risk. Variance structure was modeled in R using "*varPower*" for continuous effects (flood risk, container count) and "*varIdent*" for categorical effects (i.e., container type).

Because there were multiple replicates (e.g., containers, adults per trap) within each sampling site, we accounted for repeated measures in regression analysis by treating trap location as a random effect. Replicates (e.g., waterbody water samples) were averaged to produce a single value to be paired with each sample (e.g., container) at each trap location. For sites MP3 and MP5, including nearby tire piles in container and larval averages as potential sources for adult nutrients did not change results (not shown). Locations with incomplete data (e.g., no leaf samples due to inaccessibility) were dropped from regressions. All variables were Box–Cox-transformed to adhere to assumptions of normality and minimize nonlinear relationships that can arise from non-normal data. Variables were then standardized (mean-centered and scaled by standard deviation) to facilitate the comparison of model coefficients for variables of different magnitude, such that mean relationships with each variable can be interpreted by setting other fixed effects in the fitted regression equation to their standardized mean of zero. Highly correlated variables (Pearson correlation coefficient, $r > 0.5$) were prohibited from simultaneously being allowed as predictor variables to prevent issues with collinearity (e.g., C or N with C:N ratio). Regressions were conducted in R using procedure "lme" within package "nlme" for nutrients and mass, assuming a normal distribution, and with procedure "glmer" within package "lme4" for ZIKV, assuming a Tweedie distribution. For regression analyses, we followed a basic mixed-effects modeling protocol (Zuur et al. 2009; Lima 2017): i) fit the full model with all fixed effects and random effect (location) using maximum likelihood (ML), ii) test for heteroscedasticity and the significance of variability weights (container type, container count, or flood risk) in improving homogeneity of residuals to optimize the variability structure in subsequent models, iii) test the significance of fixed effects using ML estimation and likelihood ratio tests, and iv) estimate the final optimal model coefficients using restricted maximum likelihood (REML) estimation, which are unbiased compared to ML, but are meaningless for comparing fixed effects. Goodness of fit for fixed effects in the final model were calculated using "r.squaredGLMM" of the package "MuMIN" in R;

regression lines and confidence intervals were plotted using "visreg."

Results

Nutrient Availability at Trapping Locations

Trap locations and neighborhoods differed significantly in nutrients in both estuarine water and leaf detritus, establishing that there was a range of potential availability of nitrogen and carbon to larval containers from different trap locations and neighborhoods (MANOVA; Table 2; Fig. 3a, b). Likewise, nutrient content of larval container water also differed significantly among neighborhoods, although containers within a neighborhood were similar to one another (MANOVA; Table 2; Fig. 3c). Despite significant neighborhood differences in container water nutrients, *Ae. aegypti* larvae inhabiting those containers were not significantly different in nutrient content between neighborhoods or trap locations (MANOVA; Table 2; Fig. 3d). However, earlier instar larvae grown on mixed resources tend to be most similar in nutrient content, with differential effects of nutrient availability not appearing until later developmental stages (D. Yee, unpublished laboratory data for different life stages grown on mixed resources: first instars: variance in %N = 0.11; fourth instars: variance in %N = 0.50; adults: variance in %N = 2.5). Indeed, similar to container habitats, adult *Ae. aegypti* did differ significantly across neighborhoods in nitrogen and C:N ratios (MANOVA; Table 2; Fig. 3e). Adults collected from different trapping locations also differed significantly in mass, with the largest adults collected from Martin Peña (MP5), Piñones (PN1), and Torrecilla (TO1).

Water samples from the neighborhood adjacent to the Martin Peña channel, particularly MP4 and MP5, had the highest concentrations of nitrogen and carbon in particulate matter compared to other locations (Fig. 3a). Martin Peña sites were also among locations with the highest concentrations of nitrogen and carbon in leaf detritus samples. Container water in the Martin Peña neighborhood also was significantly higher in N and C than most other neighborhoods, and adults were among the highest in N (Fig. 3e). Rio Piedras and Suarez Channel neighborhoods also had high levels of N in adults, larvae, and nearby leaf detritus. Adults collected from Piñones and Torrecilla had the lowest %N values (Fig. 3e), comparable to lower values

Table 2. MANOVA Results, Followed by Univariate Tests, Evaluating Whether Particulate Carbon and Nitrogen Variables Differed Among Trap Locations or Between Neighborhoods in San Juan, Puerto Rico, 2016.

Factor	Estuary water		Leaf sample		Larval container		Larval *Ae. aegypti*		Adult *Ae. aegypti*	
	df	Pillai	*df*	Pillai	*df*	Pillai	*df*	Pillai	*df*	Pillai
Trap location	5,19	**1.77*****	4,25	**1.06***	4,18	1.08	4,17	0.83	5102	**0.45***
Neighborhood	5,19	**2.05*****	4,25	**1.97*****	6,18	**1.86***	6,17	1.35	4102	**0.46****
	Variable	*F* value	Variable	*F* value	Variable	*F* value	Variable	*F* value	Variable	*F* value
Trap location	N mg/L	**3.05***	N%	0.16	N mg/L	0.46	N%	1.36	N%	0.48
Neighborhood		**8.56*****		**4.22****		**2.79***		0.93		**7.28*****
Trap location	C mg/L	**2.76***	C%	**3.65***	C mg/L	0.44	C%	1.22	C%	1.69
Neighborhood		**9.11*****		**27.69*****		2.02		0.92		1.23
Trap location	δ^{15}N	**2.32**@	δ^{15}N	**6.48****	δ^{15}N	1.72	δ^{15}N	1.19	δ^{15}N	1.03
Neighborhood		**2.48**@		**8.02*****		**2.38**@		1.44		0.70
Trap location	δ^{13}C	**3.21***	δ^{13}C	0.49	δ^{13}C	0.80	δ^{13}C	0.75	δ^{13}C	1.70
Neighborhood		**2.77***		**4.30****		1.01		0.62		0.78
Trap location	C:N	**3.10***	C:N	0.08	C:N	**3.55***	C:N	1.06	C:N	0.66
Neighborhood		**9.02*****		1.63		**6.12****		1.74		**6.35*****
Trap location		–	–	–	–	–	–	–	Mass	**6.30*****
Neighborhood		–	–	–	–	–	–	–		**3.28***

Significance indicated in bold, where ***$P < 0.001$; **$0.001 \leq P < 0.01$; *$0.01 \leq P < 0.05$; @ $0.05 \leq P < 0.1$.

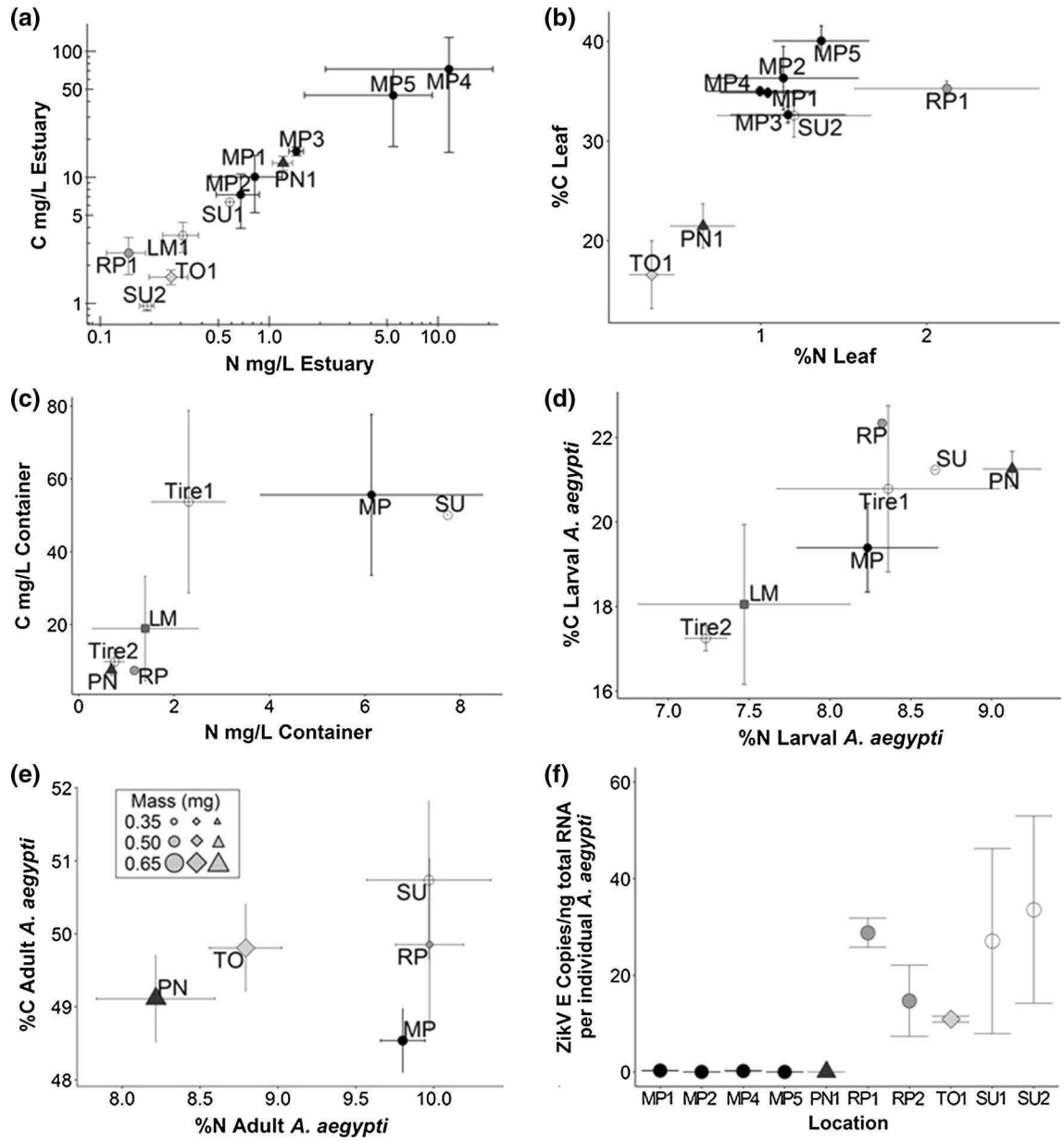

Figure 3. Mean particulate carbon and nitrogen, ± SE, across trapping locations for, **a** estuary water samples (log-scale) and **b** leaf samples, and across neighborhoods for **c** larval containers, **d** larval *Ae. aegypti*, and **e** adult *Ae. aegypti*. Symbol sizes indicate mean individual adult mass in **e**. Mean ZIKV concentration, ± SE, per individual adult *Ae. aegypti* at each trap location is also given (**f**). Symbol shapes and colors visually distinguish different neighborhoods (e.g., MP black circles; PN dark gray triangles).

for nearby estuarine water, leaf samples, and containers (Fig. 3a, b, c).

Relationships Between Nutrient Content and Nutrient Sources

Particulate nitrogen and carbon content of larval container water was significantly related to the nitrogen and carbon content of leaf detritus at sampling locations (Table 3; Fig. 4a). Larval nutrient content also tended to increase with increasing nitrogen content of water from their natal container habitats (Table 3; Fig. 4b). Adult nitrogen content was significantly related to the mean nitrogen content of containers, as well as nitrogen content of leaf detritus at the sampling location (Table 3; Fig. 4c). Differences in adult mass across locations were not significantly explained by adult nutrient content (Table 3).

Table 3. Significant Coefficients from Regression Analyses Comparing Relationships Between Most Proximate Source Nitrogen or Carbon Variables on Container, Larval, or Adult *Ae. aegypti* Nitrogen or Carbon, Adult Mass, and ZIKV Concentration.

Variable	N	Variance structure		Intercept	Fixed-effects variables				Fixed effect
Container		Flood	Container type		Estuary	Leaf			R^2
N mg/L	15	NS	**T > B > S > L****	− 0.11^{NS}	NS	**0.61 × %N****			**0.16**
C mg/L	15	NS	NS	0.00^{NS}	NS	**0.49 × %C***			**0.23**
δ^{15}N	15	NS	NS	0.00^{NS}	NS	NS			0.00
δ^{13}C	15	NS	**L > S > T > B***	0.02^{NS}	**0.36 × δ^{13}C***	NS			**0.25**
Larvae		Flood	Container type		Container				
%N	28	NS	NS	0.06^{NS}	**0.33** × mgN/L$^{@}$				**0.10**
%C	28	NS	NS	0.05 ^{NS}	NS				0.00
δ^{15}N	28	NS	NS	0.00^{NS}	**0.34** × δ^{15}N$^{@}$				**0.11**
δ^{13}C	28	NS	NS	0.04^{NS}	**0.75 × δ^{13}C*****				**0.52**
Adult		Flood	Container count		Estuary	Leaf	Container	Larvae	
%N	74	NS	NS	0.00^{NS}	NS	**0.38 × %N*****	**0.23** × mgN/L**	NS	**0.18**
%C	74	NS	**− 0.37****	0.05^{NS}	NS	NS	NS	NS	0.00
δ^{15}N	74	**0.38***	**− 0.34****	0.02^{NS}	NS	NS	NS	NS	0.00
δ^{13}C	74	**0.45***	NS	− 0.09^{NS}	NS	NS	NS	NS	0.00
Mass (mg)		Flood	Container count		Adult N	Adult C	Adult C/N		
	112	NS	NS	− 0.05^{NS}	NS	NS	–		0.00
	112	NS	NS	− 0.05^{NS}	–	–	NS		0.00
ZIKV		Flood	Container count		Adult N	Adult C	Adult C/N	Adult Mass	
	112	NS	NS	− 2.72^{NS}	**0.19 × %N*****	**0.14 × %C****	–	NS	**0.29**
	112	NS	NS	− 2.74^{NS}	–	–	NS	**0.16** × mg**	**0.26**

Dashed lines (—) indicate predictor variables not included in multiple regressions due to high covariance with other factors. Model variables are transformed to adhere to normality and standardized. Significance indicated in bold, where ***$P < 0.001$; **$0.001 \leq P < 0.01$; *$0.01 \leq P < 0.05$; @, $0.05 \leq P < 0.1$. Containers were classified as tires (T), buckets (B), small containers (S), or large containers (L).

Trap locations covered a range of stable isotope signatures (δ^{15}N, δ^{13}C) for both estuarine water and leaf detrital samples (Fig. 5a, b), with significant differences across locations and neighborhoods that could be used to track potential sources of inputs to containers (MANOVA; Table 2). However, we detected no corresponding significant differences in stable isotopes across neighborhoods or locations for container habitats, larvae, or adult *Ae. aegypti* (MANOVA; Table 2), although container water δ^{13}C was significantly positively correlated with nearby estuary δ^{13}C (Table 3). Within containers, larval stable isotopes were strongly correlated with the stable isotope signatures of their container water (Table 3; Fig. 5c, d), indicating that stable isotopes can effectively be used to link larval nutrient content to its most direct nutrient source. These differences did not appear to persist to adults, however, as stable isotopes in adults were not significantly related to those of potential estuary, leaf, container, or larval sources (Table 3).

In general, the explanatory power of regression models between nutrient content and nutrient sources did not depend on flood risk at the trap location, the number of sampled containers, or the variability in types of sampled containers (Table 3). There was significantly higher variability in nitrogen concentration in container water from tires than other types of containers, and accounting for this variance structure improved model fit between leaf and container nitrogen. Similarly, large containers from Piñones had significantly higher variability in δ^{13}C. Vari-

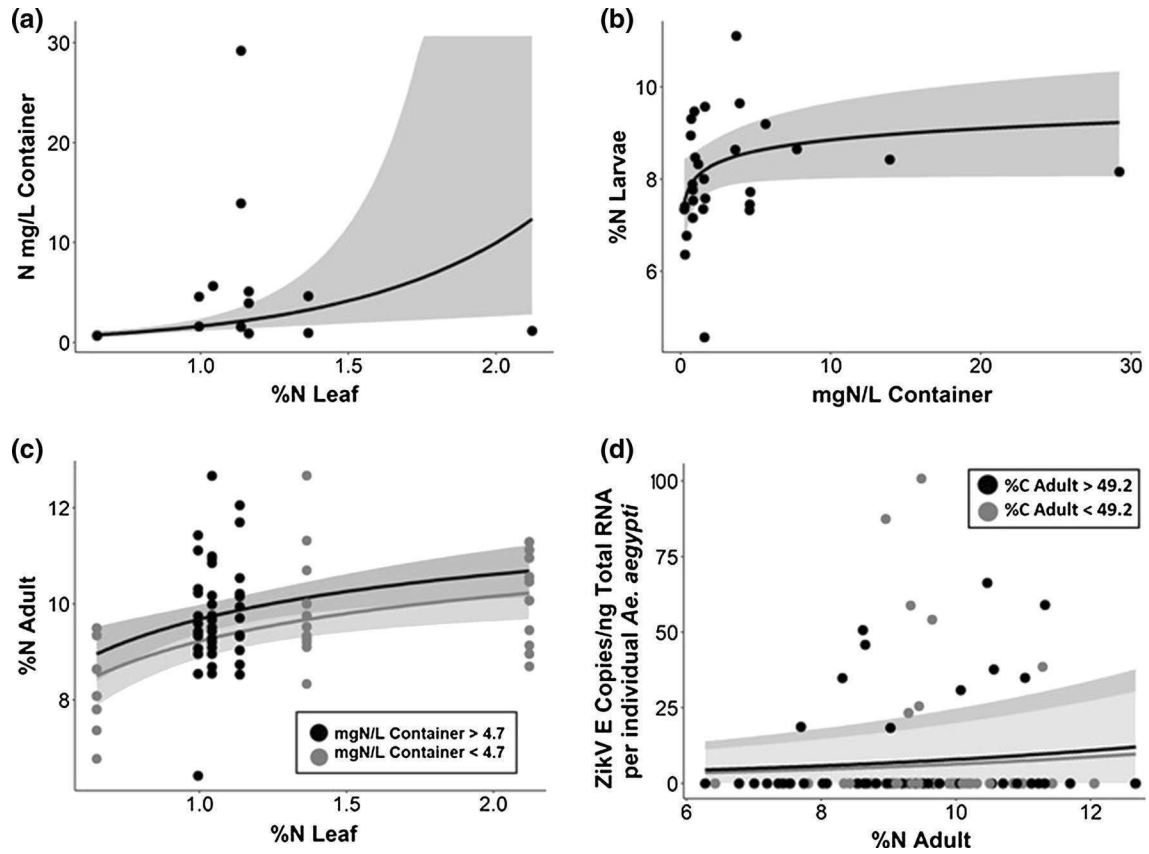

Figure 4. Relationships between source nutrients and particulate carbon or nitrogen for **a** containers, **b** larval, or **c** adult *Ae. aegypti,* and **d** ZIKV concentration, as determined by multiple regressions (see Table 3). Adults from each trap were paired with the average leaf nitrogen value for that trapping location (**c**). For regressions with more than one significant fixed effect (**c**, **d**), mean regression lines were plotted by fixing the second variable in the fitted regression equation (Table 3) to its mean value for data either above (black lines; black circles) or below (gray lines; gray circles) the standardized mean of zero (representing 4.7 mg N/L container in **c** or 49.2% C adult in **d**). Gray ribbons around regression lines indicate 95% confidence intervals.

ability in adult nutrient content tended to decrease with the number of sampled containers (%C, δ^{15}N) and increase at locations with higher flood risk (%C, δ^{13}C). Accounting for these higher variances, however, did not improve model fit with source nutrients (Table 3).

Zika Concentration in *Ae. aegypti*

In total, 130 adult *Ae. aegypti* were collected from 11 functioning traps at the 12 sampled trap locations (Table 1). Adult density per trap differed significantly across neighborhoods (Poisson GLM; Chisq = 48.74; $df = 4$; $P < 0.001$), with the Torrecilla trap TO1 having the highest density, followed by the traps in the Martin Peña neighborhood, and the Suárez channel traps having the lowest density per trap. Adult density per trap was somewhat higher the first sampling night than the second (mean of 13.2 adults per trap, first night; mean of 9.3 adults per trap, second night).

Eighteen of the 114 tested adult *Ae. aegypti* were infected with ZIKV in amounts ranging from 18 to 100 copies/ng total RNA, a rate of 15.7 infected (Table 1). Traps from San Juan municipio (MP, RP) had the lowest percentage of infected adult mosquitoes, about 9.7%, despite being the municipio with the highest density of reported human cases (293.2 per 100,000 people; Puerto Rico Department of Health 2016). Adult mosquitoes collected from Carolina municipio (SU) and Loiza municipio (PN, TO) were 40% or 24.3% positive for Zika, respectively, where the density of human cases was somewhat lower (Carolina: 156.9 cases per 100,000 persons; Loiza: 136.4 cases per 100,000 persons; Puerto Rico Department of Health 2016). No adults were collected from Cataño (LM) due to a trap malfunction.

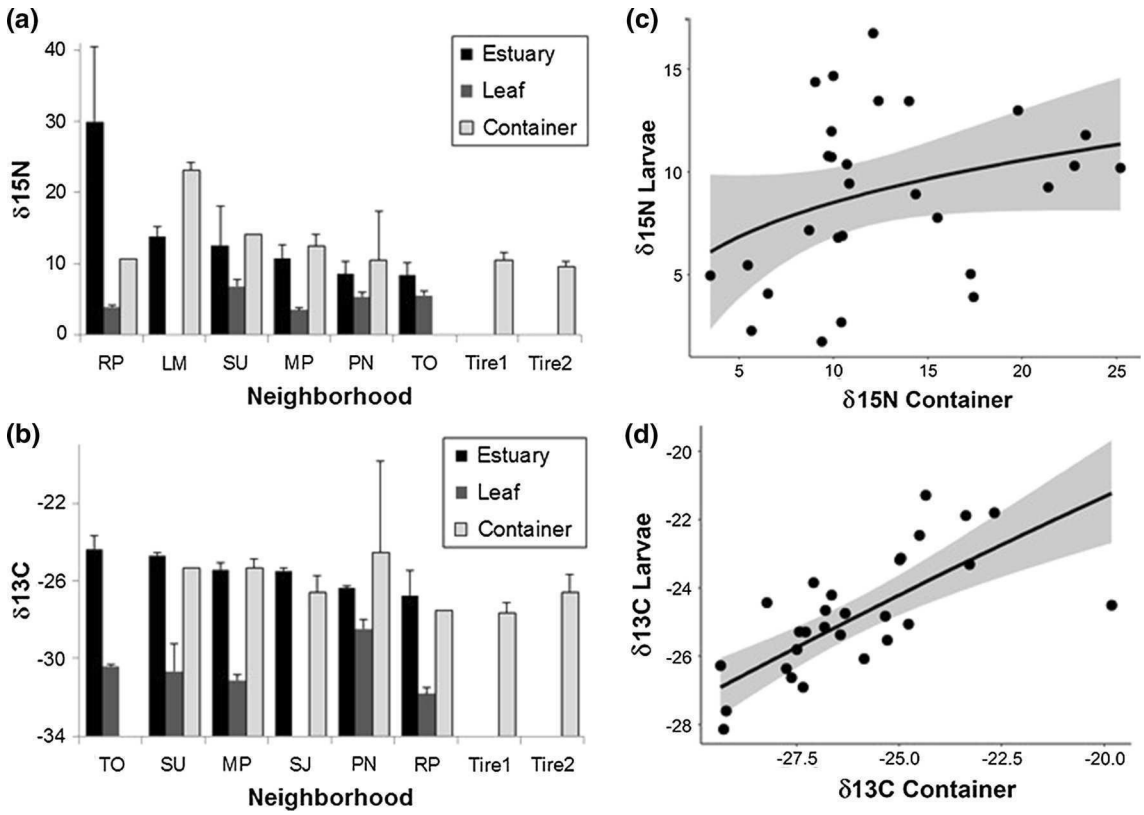

Figure 5. Nitrogen and carbon stable isotope values, ± SE, in each neighborhood for estuary, leaf, and larval container samples (**a**, **b**), as well as for larvae within each container (**c**, **d**) and corresponding fitted regression lines (see Table 3). Gray ribbons around regression lines indicate 95% confidence intervals.

ZIKV concentration in adult mosquitoes differed significantly across neighborhoods (Tweedie GLM; df = 4, 104; F value = 27.67; $P < 0.001$) but were consistent across locations within neighborhoods (Tweedie GLM; df = 5, 104; F value = 0.56; $P = 0.727$). Adult mosquitoes trapped adjacent to Rio Piedras, Torrecilla Lagoon, and Suárez Channel had significantly higher ZIKV concentration than individuals trapped near Martin Peña or Piñones Lagoon (Fig. 3f). Differences were both due to differences between neighborhoods in adults being positive or negative for zero (binomial GLM; $F = 19.4$; $P < 0.001$), as well as differences among locations in ZIKV concentration only within Zika-positive mosquitoes (normal GLM; $F = 3.80$; $P = 0.037$).

ZIKV concentration increased significantly with both adult C and N (Table 3; Fig. 4d). ZIKV concentration was also positively related to individual adult mass, but this variable did not explain significant variability when C and N were also included in the final model (Table 3). To confirm trap locations with Zika-negative mosquitoes were not dominating the observed relationships between C, N, and ZIKV, possibly due to an unmeasured location variable, we ran regressions again but limiting data to locations where Zika-positive mosquitoes were trapped. Regression results were consistent, with ZIKV concentration increasing significantly with both N and C (samples = 48; 2.95 + 0.17%N Adult + 0.16%C Adult; N: $P < 0.001$; C: $P < 0.001$).

Discussion

Although flooding events are widely perceived as creating aquatic breeding sites for mosquito larvae (Ahern et al. 2005; Pires and Gleiser 2010), the role of floods as a potential source of nutrients and the consequences for disease outbreaks is largely underdeveloped. Our study found significant differences across neighborhoods in the nutrient content of larval habitat containers and ZIKV in adult *Ae. aegypti*, which may in part reflect significant environmental variability in estuary water from flooding events and leaf detritus as potential inputs to containers.

Containers can be highly variable in a number of factors, including type, size, detritus inputs, or age, that contribute to high variability in nutrient content (e.g., Murrell et al. 2011; Yee et al. 2015a, b). Despite this, we found significant differences in container nutrient content among neighborhoods, which was significantly correlated with the nitrogen and carbon content of leaf detritus in the local area. Moreover, containers tended to have similar δ^{13}C signatures as waterbodies in the local area. The lack of a significant relationship between container water and estuary water nutrient content (N or C) broadly across sampling locations may not be too surprising given the dynamic nature of water quality with precipitation events, wind, and runoff. Furthermore, even containers right next to each other may or may not receive flood water, depending on their specific height, orientation, and other factors, and over time, flooded containers may begin to diverge from one another through differential evaporation or additional allochthonous inputs. In this sense, leaf detritus may simply be a better proxy than estuarine water for longer-term trends in local environmental inputs.

Martin Peña was the only neighborhood known to have flooded in the weeks prior to sampling, and known to experience frequent, periodic flooding. Containers from neighborhoods adjacent to the Martin Peña channel had higher nitrogen and carbon content than most other neighborhoods, consistent with the higher nitrogen content in water from the channel and in leaf detritus in the local environment. Moreover, adult *Ae. aegypti* collected from the Martin Peña neighborhood had higher body nitrogen content relative to neighborhoods adjacent to other waterbodies. Adult *Ae. aegypti* nutrient content in Martin Peña was also remarkably consistent from 2016 to 2017, compared to other neighborhoods, which were more variable over time (Appendix A). These data provide tantalizing evidence for linkages among inputs from the surrounding environment, containers, and mosquitoes produced from those environments.

Nutrient content of larval *Ae. aegypti* was tightly linked to the nutrient content of their container habitats, particularly δ^{15}N and δ^{13}C. Adult *Ae. aegypti* nitrogen content was also positively related to both the nitrogen content of typical containers in each sampling location, and the nitrogen content of leaf detritus in each area. The relatively small amount of variability explained may indicate other unmeasured environmental factors, such as animal detritus, which are influencing the availability of nutrients to larval mosquitoes (Kling et al. 2007). Moreover, our inability to exhaustively sample larval containers in each area, nor conclusively determine whether adults trapped in a particular location originated from the sampled larval containers, also likely contributes to unexplained variability. Indeed, ''hidden'' containers such as underground septic systems can provide a significant source of adult *Ae. aegypti* in Puerto Rico (Barrera et al. 2008). Furthermore, while larval body nutrients were closely linked to the current nutrient content of container water, adult body nitrogen may be more closely related to the nutrient content of container water 7–10 days prior when they were developing as larvae. More extensive sampling, including changes in container nutrients over time, is needed to more dynamically link environmental variability in nutrients to that of mosquitoes.

In addition to neighborhood differences in environmental and mosquito nutrient content, we also found neighborhood differences in ZIKV concentration. At the time of sampling, the neighborhoods adjacent to Rio Piedras, Torrecilla Lagoon, and Suárez channel had the highest levels of ZIKV concentration in adult *Ae. aegypti*, with no infected adults collected near Martin Peña channel or Piñones lagoon. Higher levels of nitrogen and carbon content in adult bodies tended to be associated with higher ZIKV concentration. Furthermore, the higher ZIKV concentrations could not merely be attributed to a body size effect (i.e., bigger mosquitoes take a greater blood meal and consume more virus from infected hosts) because %N and %C, scaled per unit body mass, explained greater variability than adult body size. Moreover, in our field data, adult mass was not significantly related to adult body nutrients. Nitrogen has generally been associated with increased severity of disease in other systems, often by providing abundant building blocks needed for pathogen replication, but underlying mechanisms and results are inconsistent depending on the specific form of nitrogen and immunity-related responses (Dordas 2008). Laboratory studies, particularly those discerning viral uptake, dissemination, and infectiousness, are needed to tease apart the underlying mechanisms by which nitrogen or carbon may be impacting viral concentrations in mosquito vectors.

Our results are consistent with previous laboratory studies that have found that larval nutrition, adult nutrition, and body size can affect the ability of mosquitoes to acquire dengue or Ross River virus (Nasci and Mitchell 1994; Alto et al. 2008b), and with modeling studies indicating that environmental variability in nitrogen may influence dengue cases (De Jesus Crespo et al. 2018). Our

study, however, is one of the first field studies to identify a pathway by which environmental variability in potential nutrient inputs into container habitats can affect nutrient content in mosquito larvae and adults, leading to variable viral acquisition in adult mosquitoes.

It is important to note that higher levels of viral titer in individual adult mosquitoes do not necessarily confer higher rates of viral infection in humans. Our study focused on dissemination of the pathogen but not the interaction with vector density (Anderson and Rico-Hesse 2006, Klempner et al. 2007). Indeed, two of the neighborhoods with the highest ZIKV concentrations, Rio Piedras and Suárez channel, also had the lowest densities of mosquitoes caught per trap. Additionally, the lack of Zika-positive mosquitoes from Martin Peña is somewhat surprising, given the relatively high nitrogen levels in adults at this location, as well as the high density of human cases in the San Juan municipio (Puerto Rico Department of Health 2016). Although our study focused on nutrient availability from the local environment, other factors can influence the probability that a vector acquires a pathogen, including host density, pathogen density in hosts, and climatic or behavioral factors that influence host-seeking or biting behavior (LaDeau et al. 2015). More extensive sampling would be needed to more accurately assess mosquito density, host density, biting behavior, and other factors across the different neighborhoods, to be able to rigorously understand the role environmental nutrient variability plays on vectorial capacity.

Social and infrastructural factors can also buffer or enhance the susceptibility of people to health outcomes (Myers et al. 2013; Oosterbroek et al. 2016). Age, housing density, and access to air-conditioning are all factors that can influence transmission of dengue virus to humans (Méndez-Lázaro et al. 2014; Barrera et al. 2011; De Jesus Crespo et al. 2018). Even less is known about the complex suite of ecological and social factors influencing Zika transmission (Thomas et al. 2017). Indeed, our sampling was a single snapshot at a time when the spread of Zika was accelerating through the San Juan metropolitan area and throughout Puerto Rico. It is possible that the neighborhood differences in ZIKV infection in adult mosquitoes reflect local acquisition patterns from the human population, such that certain neighborhoods simply had not been affected yet. However, because the neighborhoods where mosquitoes were strongly positive for ZIKV (Torrecilla, Rio Piedras, Suárez channel) are adjacent to the two neighborhoods where mosquitoes were negative for ZIKV (Martin Peña, Piñones), we did not see a strong spatial pattern (e.g., radiating from a source point of local human acquisition) that would support this. Furthermore, cumulative Zika cases by June 2016 were reasonably similar across the three municipalities covered by the study area (Puerto Rico Department of Health 2016). More extensive temporal sampling is needed to tease apart the suite of ecological and social factors affecting the spread of the virus, and what role environmental variability in water and detrital quality might play in that spread.

Our study provides preliminary evidence that environmental variability in nutrient inputs can influence the acquisition of virus by mosquito vectors. In addition to the potential influence on viral titer, variability in leaf detrital inputs has been demonstrated to influence survival, growth, and competition among mosquito larvae (Yee et al. 2007; Muturi et al. 2012). This suggests a mechanism by which urban greenspaces, in addition to temperature regulation or biological control (De Jesus Crespo et al. 2018), may influence vector-borne illnesses through detrital resource inputs. Moreover, flooding events, in addition to providing pools of short-term breeding habitat (Ahern et al. 2005; Pires and Gleiser 2010), can also provide a pulse of nutrients to existing larval containers depending on the water quality of nearby waterbodies. This suggests that management actions to reduce flooding and improve water quality should go hand-in-hand to help control spread of vector-borne diseases. As such, environmental restoration of ecosystem services in the urban landscape could be part of a sustainable solution to help reduce vector disease transmission by mitigating flooding events and regulating water quality (Carver et al. 2015; De Jesus Crespo et al. 2018).

Acknowledgements

We thank Roberto Barrera and Gilberto Felix from the CDC Dengue Branch in Puerto Rico for assistance and access to mosquito traps. We are extremely grateful to Estrella Santiago at Enlace and Evelyn Huertas at EPA Region 2, as well as the numerous homeowners and communities, who helped us obtain access to neighborhoods and locations for setting traps. Alonso Ramirez provided access to laboratory space at the University of Puerto Rico during the time of the field survey. E. Ashley Thompson and Biswas Nepane, at the University of Southern Mississippi, and Candice Lavelle and Emilie Cooper of the US EPA Gulf Ecology Division, assisted with processing mosquito viral data. Emily Santos assisted with nutrient analyses at the US EPA Atlantic Ecology Division. Hunter Deerman, of the University of Southern

Table 4. Number of Adult Female *Ae. aegypti* Trapped and Processed in 2017, and Results of Viral Analysis.

Neighborhood	Trap location	Female *Ae. aegypti* per trap	*Ae. aegypti* infected with ZIKV	*Ae. aegypti* infected with chikungunya	*Ae. aegypti* infected with dengue
Martin Peña Channel	MP1	0	–	–	–
	MP2a	9	0	0	0
	MP2b	5	0	0	0
	MP3	7	0	0	0
	MP4a	4	0	0	0
	MP4b	4	0	0	0
	MP5	0	–	–	–
	MP6a	7	0	0	0
	MP6b	0	–	–	–
Piñones Lagoon	PN1	NS	NS	NS	NS
Rio Piedras	RP1	6	0	0	0
	RP2	0	–	–	–
La Malaria Channel	LM1a	16	0	0	0
	LM1b	9	0	0	0
Suárez Channel	SU1	7	0	0	0
	SU2a	2	0	0	0
	SU2b	2	0	0	0
	SU2c	5	0	0	0
	SU2d	8	0	0	0
Torrecilla Lagoon	TO1a	21	0	0	0
	TO1b	32	0	0	0

Traps were placed at the same locations as mapped in Figure 2, with more than one trap placed in some locations (e.g., front yard and back yard; labeled a–d). One new location, MP6, situated roughly halfway between the two tire locations (Fig. 2), was sampled in 2017 but not 2016.
NS: Location not sampled in 2017.

Mississippi, assisted with field collection. We are grateful for reviews by P. Leisnham and peer reviewers on earlier drafts of this manuscript. The views expressed in this paper are those of the authors and do not necessarily reflect the views or policies of the US Environmental Protection Agency. Any mention of trade names, products, or services does not imply an endorsement by the US Government or the US Environmental Protection Agency (EPA). The EPA does not endorse any commercial products, services, or enterprises.

Appendix A

In June 2017, we sampled adult mosquito populations at many of the same sampling locations to compare to the June 2016 field collection (Table 4). As in 2016, adult mosquitoes were collected using BG-Sentinel traps (Biogents AG, Regensburg, Germany) baited with a human scent lure (BG-Lure; Biogents AG). Traps were left out for a 48-h period before adults were collected. Collected adults were identified to sex and species, with 0–32 female *Ae. aegypti* collected per trap (Table 4). Only adult female *Ae. aegypti* were used for subsequent analysis.

For the 2017 sampling, individual adult heads were preserved in 1 mL RNAlater (Ambion, Austin, TX, USA) within 6 h of field collection. Heads and bodies were then frozen for transport to the continental USA. Adult mosquitoes were processed for particulate nutrient content (%N, %C, C:N) and stable isotopes (δ15 N, δ13C) as described in the main text. We used nested Multivariate Analysis of Variance (MANOVA) to test whether trap locations, neighborhoods, or years (2016 vs 2017) differed significantly in nutrients, including N, C, δ13C, δ15 N, the ratio of C to N, or adult mass.

In addition to ZIKV, we extended the viral analysis to include chikungunya and dengue using the 2017 collected mosquitoes. Following the removal of the RNAlater by gentle pipetting, 200 µL of DMEM media (Gibco, no glu-

Table 5. MANOVA Results, Followed by Univariate Tests, Evaluating Whether Particulate Carbon and Nitrogen Variables Differed Among Trap Locations or Between Neighborhoods from 2016 to 2017 in San Juan, Puerto Rico.

Factor	Adult *Ae. aegypti*	
	df	*Pillai*
Trap location	15,224	**0.47@**
Neighborhood	6224	**0.37*** **
Year	1224	**0.17*** **
Neighborhood × Year	3224	**0.16****
	Variable	*F* value
Trap location	N%	**1.87***
Neighborhood		**5.1*** **
Year		**4.98***
Neighborhood × Year		**5.46****
Trap location	C%	**1.82***
Neighborhood		**3****
Year		**25.35*** **
Neighborhood × Year		**2.91***
Trap location	d15N	0.52
Neighborhood		1.46
Year		0.01
Neighborhood × Year		0.39
Trap location	d13C	1.14
Neighborhood		**2.05@**
Year		0.58
Neighborhood × Year		1.04
Trap location	C:N	0.71
Neighborhood		**3.19****
Year		**20.51*** **
Neighborhood × Year		**5.8*** **
Trap location	Mass	**2.44****
Neighborhood		1.67
Year		**4.83***
Neighborhood × Year		1.1

Significance indicated in bold, where ***$P < 0.001$; **$0.001 \leq P < 0.01$; * $0.01 \leq P < 0.05$; @ $0.05 \leq P < 0.1$.

cose, no glutamine, no phenol red; Thermo Fisher Scientific, Waltham, MA) was added to each mosquito head in RNase-free tubes. Individual mosquito tissues were homogenized using sterile, RNase-free disposable tissue grinders, centrifuged for 5 min in the cold, and the supernatant was removed for subsequent RNA extraction. RNA extractions

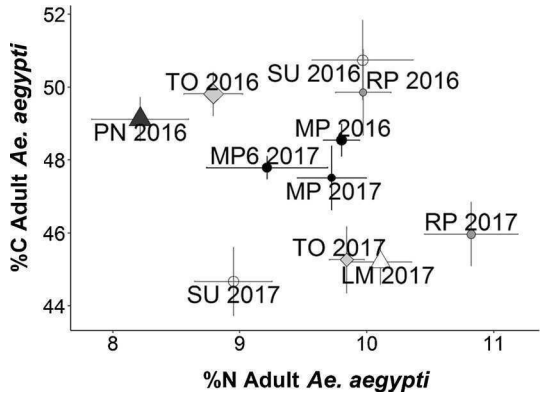

Figure 6. Mean particulate carbon and nitrogen values, ± SE, across neighborhoods for adult *Ae. Aegypti* in 2016 and 2017. Symbol sizes indicate mean individual adult mass.

were performed immediately following tissue homogenization using the QIAamp Viral RNA kit (Qiagen, Germantown, MD) according to manufacturer's instructions with minor modifications by adding additional washes with Buffer AW1 and AW2 (Mbanzulu et al. 2017). The purified RNA was analyzed for RNA integrity and concentration using the BioAnalyzer RNA 6000 Nano Reagent kit (Agilent, Santa Claire, CA) and stored at − 80°C. Real-time reverse transcription-PCR (RT-qPCR) was performed for dengue, chikungunya, and ZIKV using a multiplex viral kit (MyBioSource, San Diego, CA). All of the above procedures were performed aseptically using RNase-free materials.

In total, 144 adult female mosquitoes were collected in traps (Table 4). Of the 144 adults tested for virus, not a single individual was confirmed to have ZIKV, chikungunya, or dengue. Results were consistent with public health data that, in contrast to concerns of an anticipated second outbreak of Zika, rates of arboviral cases in Puerto Rico were quite low in June 2017, with less than 10 confirmed cases across all of Puerto Rico (Puerto Rico Department of Health 2017). Adult nutrient content differed significantly from 2016 to 2017, but the effect differed among neighborhoods (Neighborhood × Year; Table 5). Adult mosquitoes from Martin Pena were remarkably consistent in both %N and %C between 2016 and 2017, despite a general pattern of lower %C and higher %N in 2017 for most other neighborhoods. Adult mass tended to be lower in Martin Pena, consistently in both 2016 and 2017. There were no significant differences in stable isotopes across trap locations, neighborhoods, or years (Fig. 6).

References

Acharya D, Bastola P, Le L, Paul AM, Fernandez E, Diamond MS, Miao W, Bai F (2016) An ultrasensitive electrogenerated chemiluminescence-based immunoassay for specific detection of Zika virus. *Scientific Reports* 6:32227

Ahern M, Kovats RS, Wilkinson P, Few R, Matthies F (2005) Global health impacts of floods: epidemiologic evidence. *Epidemiologic Reviews* 27:36–46

Almeida APG, Baptista SSSG, Sousa CAGCC, Novo MTLM, Ramos HC, Panella NA, Godsey M, Simões MJ, Anselmo ML, Komar N, Mitchell CJ, Ribiero H (2005) Bioecology and vectorial capacity of *Aedes albopictus* (Diptera: Culicidae) in Macao, China, in relation to dengue virus transmission. *Journal of Medical Entomology* 42:419–428

Alto BW, Lounibos LP, Higgs S, Juliano SA (2005) Larval competition differentially affects arbovirus infection in *Aedes* mosquitoes. *Ecology* 86:3279–3288

Alto BW, Lounibos LP, Mores CN, Reiskind MH (2008) Larval competition alters susceptibility of adult *Aedes* mosquitoes to dengue infection. *Proceedings of the Royal Society B* 275:463–471

Alto BW, Reiskind MH, Lounibos LP (2008) Size alters susceptibility of vectors to dengue virus infection and dissemination. *American Journal of Tropical Medicine and Hygiene* 79:688–695

Anderson JR, Rico-Hesse R (2006) *Aedes aegypti* vectorial capacity is determined by the infecting genotype of dengue virus. *American Journal of Tropical Medicine and Hygiene* 75:886–892

Azar D, Rain D (2007) Identifying population vulnerable to hydrological hazards in San Juan, Puerto Rico. *GeoJournal* 69:23–43

Barrera R, Amador M, Diaz A, Smith J, Munoz-Jordan JL, Rosario Y (2008) Unusual productivity of *Aedes aegypti* in septic tanks and its implications for dengue control. *Medical and Veterinary Entomology* 22:62–69

Barrera R, Amador M, MacKay AJ (2011) Population dynamics of *Aedes aegypti* and dengue as influenced by weather and human behavior in San Juan, Puerto Rico. *PLoS Neglected Tropical Diseases* 5:e1378

Brandeis TJ, Escobedo FJ, Staudhammer CL, Nowak DJ, Zipperer WC (2014). *San Juan Bay Estuary watershed urban forest inventory*. US Forest Service, Asheville, NC. Technical Report SRS-190.

Burke R, Barrera R, Lewis M, Kluchinsky T, Claborn D (2010) Septic tanks as larval habitats for the mosquitoes *Aedes aegypti* and *Culex quinquefasciatus* in Playa-Playita, Puerto Rico. *Medical Veterinary Entomology* 24:117–123

Canyon DV, Hii JLK, Muller R (1999) Effect of diet on biting, oviposition, and survival of *Aedes aegypti* (Diptera: Culicidae). *Journal of Medical Entomology* 36:301–308

Carpenter SR (1983) Resource limitation of larval treehole mosquitoes subsisting on beech detritus. *Ecology* 64:219–223

Carver S, Slaney DP, Leisnham PT, Weinstein P (2015) Healthy wetlands, healthy people: mosquito borne disease. In: *Wetlands and human health*, Finlayson MC, Horwitz P, Weinstein P (editors), Dordrecht: Springer, pp 95–121

Chouin-Carneiro T, Vega-Rua A, Vazeille M, Yebakima A, Girod R, Goindin D, Dupont-Rouzeyrol M, Lourenco-de-Oliveira R, Failloux AB (2016) Differential susceptibilities of *Aedes aegypti* and *Aedes albopictus* from the Americas to Zika virus. *PLoS Neglected Tropical Diseases* 10:e0004543

De Jesus Crespo R, Fulford R (2017) Eco-health linkages: assessing the role of ecosystem goods and services on human health using causal criteria analysis. *International Journal of Public Health* 63:81–92

De Jesus Crespo R, Mendez Lazaro P, Yee SH (2018) Linking wetland ecosystem services to vector-borne disease: dengue fever in the San Juan Bay Estuary, Puerto Rico. *Wetlands* . https://doi.org/10.1007/s13157-017-0990-5

Dick GWA, Kitchen SF, Haddow AJ (1952) Zika virus (I). Isolations and serological specificity. *Transactions of the Royal Society of Tropical Medicine and Hygiene* 46:509–520

Dordas C (2008) Role of nutrients in controlling plant diseases in sustainable agriculture: a review. *Agronomy for Sustainable Development* 28:33–46

Federal Emergency Management Agency, FEMA (2009) Digital flood insurance rate map database, Commonwealth of Puerto Rico. http://gis.otg.pr.gov/download_gis_files.htm. Accessed 22 June 2017

Gonzalez-Salazar C, Stephens CR, Sanchez-Cordero V (2017) Predicting the potential role of non-human hosts in Zika virus maintenance. *EcoHealth* 14:171–177

Gratz NG (2004) Critical review of the vector status of *Aedes albopictus*. *Medical and Veterinary Entomology* 18:215–227

Harrington LC, Scott TW, Lerdthusnee K, Coleman RC, Costero A, Clark GG, Jones JJ, Kitthawee S, Kittayapong P, Sithiprasasna R, Edman JD (2005) Dispersal of the dengue vector *Aedes aegypti* within and between rural communities. *American Journal of Tropical Medicine and Hygiene* 72:209–220

Hashizume M, Dewan AM, Sunahara T, Rahman MZ, Yamamoto T (2012) Hydroclimatological variability and dengue transmission in Dhaka, Bangladesh: a time-series study. *BMC Infectious Diseases* 12(1):98

Hinga KR, Batchelor A (2005) Waste processing and detoxification. In: *Millennium ecosytem assessment, volume 1: conditions and trends working group report*, Hassan R, Scholes R, Ash N (editors), Washington, D.C.: Island Press, pp 417–439

Ivers LC, Ryan ET (2006) Infectious diseases of severe weather-related and flood-related natural disasters. *Current Opinion in Infectious Diseases* 19:408–414

Klempner MS, Unnasch TR, Hu LT (2007) Taking a bite out of vector-transmitted infectious diseases. *New England Journal of Medicine* 356:2567–2569

Kling LJ, Juliano SA, Yee DA (2007) Larval mosquito communities in discarded vehicle tires in a forested and unforested site: detritus type, amount, and water nutrient differences. *Journal of Vector Ecology* 32:207–217

Korfmacher KS, Aviles K, Cummings BJ, Daniell W, Erdmann J, Garrison V (2015) Health impact assessment of urban waterway decisions. *International Journal of Environmental Research and Public Health* 12:300–321

LaDeau SL, Allan BF, Leisnham PT, Levy MZ (2015) The ecological foundations of transmission potential and vector-borne disease in urban landscapes. *Functional Ecology* 29:889–901

Lima F (2017) Linear mixed-effects models in R. https://poissonisfish.wordpress.com/2017/12/11/linear-mixed-effect-models-in-r/. Accessed Nov 2018

Maciel-de-Freitas R, Eiras AE, Lourenco-de-Oliveira R (2006) Field evaluation of effectiveness of the BG-Sentinel, a new trap for capturing adult *Aedes aegypti* (Diptera: Culicidae). *Memorias do Instituto Oswaldo Cruz* 101:321–325

Mbanzulu KM, Wumba R, Mukendi J-PK, Zanga JK, Shija F, Bobanga TL, Aloni MN, Misinzo G (2017) Mosquito-borne viruses circulating in Kinshasa, Democratic Republic of the Congo. *International Journal of Infectious Diseases* 57:32–37

Méndez-Lázaro P, Muller-Karger FE, Otis D, McCarthy MJ, Peña-Orellana M (2014) Assessing climate variability effects on dengue incidence in San Juan, Puerto Rico. *International Journal of Environmental Research and Public Health* 11:9409–9428

Murrell EG, Damal K, Lounibos LP, Juliano SA (2011) Distributions of competing container mosquitoes depend on detritus types, nutrient ratios, and food availability. *Annals of the Entomological Society of America* 104:688–698

Musso D, Gubler DJ (2016) Zika virus. *Clinical Microbiology Reviews* 29:487–524

Mutero CM, Ng'ang'a PN, Wekoyela P, Githure J, Konradsen F (2004) Ammonium sulphate fertilizer increases larval populations of *Anopheles arabiensis* and culicine mosquitoes in rice fields. *Acta Tropical* 89:187–192

Muturi EJ, Allan BF, Ricci J (2012) Influence of leaf detritus type on production and longevity of container-breeding mosquitoes. *Environmental Entomology* 41:1062–1068

Myers SS, Gaffikin L, Golden CD, Ostfeld RS, Redford KH, Ricketts TH, Turner WR, Osofsky SA (2013) Human health impacts of ecosystem alteration. *Proceedings of the National Academy of Sciences* 110:18753–18760

Nasci RS, Mitchell CJ (1994) Larval diet, adult size, and susceptibility of *Aedes aegypti* (Diptera: Culicidae) to infection with Ross River virus. *Journal of Medical Entomology* 31:123–126

NOAA (National Oceanic and Atmospheric Administration) (2018) Coastal flood exposure mapper. https://coast.noaa.gov/floodexposure/. Accessed Nov 2018

Oczkowski AJ, Nixon SW, Granger SL, El-Sayed AFM, McKinney RA (2009) Anthropogenic enhancement of Egypt's Mediterranean fishery. *Proceedings of the National Academy of Sciences* 106:1364–1367

Oczkowski AJ, Flower RJ, Thompson JR, Ayache F, Ahmed MH, Ramdani M, Turner S (2011) Evidence of North Africa's green revolution preserved in sedimentary organic matter deposited in three coastal lagoons. *Ecological Applications* 21:1708–1717

Oosterbroek B, de Kraker J, Huynen MMTE, Martens P (2016) Assessing ecosystem impacts on health: a tool review. *Ecosystem Services* 17:237–254

Paul D, Skrzypek G, Fórizs I (2007) Normalization of measured stable isotopic compositions to isotope reference scales—a review. *Rapid Communications in Mass Spectrometry* 21:3006–3014

Pires DA, Gleiser RM (2010) Mosquito fauna inhabiting water bodies in the urban environment of Córdoba city, Argentina, following a St. Louis encephalitis outbreak. *Journal of Vector Ecology* 35:401–409

Puerto Rico Department of Health (2016) Informe Semanal de Enfermedades Arbovirales (ArboV): Semanal 23 (27 de mayo al 9 de junio de 2016). http://www.salud.gov.pr/Estadisticas-Registros-y-Publicaciones/Pages/VigilanciadeZika.aspx. Accessed Mar 2018

Puerto Rico Department of Health (2017) Informe Semanal de Enfermedades Arbovirales (ArboV): Semanal 52 (24 al 30 de diciembre de 2017). http://www.salud.gov.pr/Estadisticas-Registros-y-Publicaciones/Pages/VigilanciadeZika.aspx. Accessed Mar 2018

Reiskind MH, Lounibos LP (2009) Effects of intraspecific larval competition on adult longevity in the mosquitoes *Aedes aegypti* and *Aedes albopictus*. *Medical and Veterinary Entomology* 23:62–68

Rhodus J, Fulk F, Autrey B, O'Shea S, Roth A (2013) *A review of health impact assessment in the U.S.: current state-of-science, best practices, and areas for improvement*. U.S. Environmental Protection Agency, Cincinnati, OH, EPA/600/R-13/354

Scott TW, Amerasinghe PH, Morrison AC, Lorenz LH, Clark GG, Strickman D, Kittaypong P, Edman JD (2000) Longitudinal studies of *Aedes aegypti* (Diptera: Culicidae) in Thailand and Puerto Rico: blood feeding frequency. *Journal of Medical Entomology* 37:89–101

Sharp TM, Hunsperger E, Santiago GA, Muñoz-Jordan JL, Santiago LM, Rivera A, Rodríguez-Acosta RL, Gonzalez Feliciano L, Margolis HS, Tomashek KM (2013) Virus-specific differences in rates of disease during the 2010 Dengue epidemic in Puerto Rico. *PLoS Neglected Tropical Diseases* 7:e2159

Sheffield PE, Agu DP, Rowe M, Fischer K, Pérez AE, Rodríguez LN, Avilés KR (2014) *Health impact assessment of the proposed environmental restoration of Caño Martín Peña*. Icahn School of Medicine at Mount Sinai and Corporación del Proyecto ENLACE del Caño Martín Peña, San Juan, Puerto Rico

Shono H (2008) Application of the Tweedie distribution to zero-catch data in CPUE analysis. *Fisheries Research* 93:154–162

San Juan Bay Estuary Program, SJBEP (2000) *Program del Estuario de la Bahía de San Juan: Comprehensive conservation and management plan*. San Juan Bay Estuary Program, San Juan, Puerto Rico.

SJBEP (2016) Water quality monitoring data. www.estuario.org. Accessed 30 Mar 2018

Thomas SJ, Pearce JM, Ramey AM (2017) Vectors, hosts, and control measures for Zika virus in the Americas. *EcoHealth* 14:821–839

World Health Organization, WHO (2016a) Report Zika Situation Neurological Syndrome and Congenital Anomalies. http://www.who.int/emergencies/zika-virus/situation-report/5-february-2016/en/. Accessed Mar 2018

WHO (2016b) Zika virus infection—United States of America—Puerto Rico. http://www.who.int/csr/don/8-january-2016-zika-usa/en/. Accessed Mar 2018

Yee DA, Juliano SA (2006) Abundance matters: a field experiment testing the more individuals hypothesis for richness–productivity relationships. *Oecologia* 153:153–162

Yee DA, Kaufman MG, Juliano SA (2007) The significance of ratios of detritus types and micro-organism productivity to competitive interactions between aquatic insect detritivores. *Journal of Animal Ecology* 76:1105–1115

Yee DA, Abuzeineh AA, Ezeakacha NF, Schelble SS, Glasgow WC, Flanagan SD, Skiff JJ, Reeves A, Kuehn K (2015) Mosquito larvae in tires from Mississippi, U.S.A.: the efficacy of abiotic and biotic parameters in predicting spatial and temporal patterns of mosquito populations and communities. *Journal of Medical Entomology* 52:394–407

Yee DA, Kaufman MG, Ezeakacha NF (2015) How diverse detrital environments influence nutrient stoichiometry between males and females of the co-occurring container mosquitoes *Aedes albopictus*, *Ae. Aegypti*, and *Culex quinquefasciatus*. *PLOS ONE* 10:e0133734

Zanluca C, de Melo VCA, Mosimann ALP, dos Santos GIV, dos Santos CND, Luz K (2015) First report of autochthonous transmission of Zika virus in Brazil. *Memorias do Instituto Oswaldo Cruz* 110:569–572

Zuur A, Ieno EN, Walker N, Savelieve AA, Smith GM (2009) *Mixed Effects Models and Extensions in ecology with R*, New York: Springer

Wetlands (2019) 39:1281–1293
https://doi.org/10.1007/s13157-017-0990-5

Linking Wetland Ecosystem Services to Vector-borne Disease: Dengue Fever in the San Juan Bay Estuary, Puerto Rico

Rebeca de Jesús Crespo[1] · Pablo Méndez Lázaro[2] · Susan H. Yee[1]

Received: 22 September 2017 / Accepted: 19 December 2017 / Published online: 23 January 2018
© US Government 2018

Abstract

Mosquito-borne diseases are an increasingly important health concern, which pose great challenges for safe and sustainable control and eradication. This reality calls for management approaches that consider multiple aspects of the transmission cycle from a landscape and vector ecology perspective, to socio-economic elements that may increase exposure. This study seeks to better understand these pathways using dengue fever in the San Juan Bay Estuary (SJBE), Puerto Rico. Dengue is transmitted by *Aedes aegypti*, a species that thrives in cities. Here we ask which elements within the urban landscape could be managed to help prevent dengue outbreaks. We studied the potential of coastal wetlands in the SJBE to buffer vector proliferation, hypothesizing that wetland ecosystem services lead to lower dengue occurrence. We test this hypothesis using census-block level dengue data from 2010-13, including the largest epidemic in Puerto Rican history. Our analytical model includes socio-economic factors and environmental controls that may also affect dengue dynamics. Results from beta-binomial regressions and model averaging indicated that dengue occurrence was lower in neighborhoods with higher wetland cover even after controlling for population density and other socio-economic aspects. Our models suggest that heat hazard mitigation is partly responsible for the association between wetlands and dengue.

Keywords Ecosystem Goods and Services · Coastal wetlands · Dengue · "Vector-borne" diseases · Urban landscape · San Juan Bay Estuary

Introduction

Mosquito-borne diseases represent a significant health and economic burden to cities around the world. The emergence of serious vector mediated viruses, such as Zika, has recently sparked the interest to find safe and effective strategies for vector control and mosquito eradication. With growing concerns of how strategies such as aerial spraying may indirectly impact humans and wildlife, researchers are increasingly interested in sustainable approaches for safe vector population management. One of the most prominent mosquito vectors for diseases like dengue, chikungunya, and Zika is *Aedes aegypti*. *A. aegypti* thrives in the presence of water filled artificial containers, and mainly feeds on human blood, making the urban environment, with abundant trash and dense populations, particularly suitable for its proliferation.

The proliferation of mosquito vectors in cities, as well as vector disease transmission, is also intensified by other aspects of the urban environment. Flood prone areas, exacerbated in cities due to altered hydrology, may increase habitat availability. Flood waters from urban runoff or overflowing rivers may fill trash items such as discarded plastic containers, creating suitable breeding sites for mosquito larvae (Hashizume et al. 2012). Water chemistry, in turn, has been linked to *A. aegypti* nutrition and consequently pupal and adult productivity (Barrera et al. 2006; Couret et al. 2014). Urban waters that contribute to filling container habitat could therefore affect mosquito vectors indirectly through nutrition enhancement from wastewater inputs. In cities, high temperatures due to urban heat islands shorten pupal development time and viral incubation period, and increases

Electronic supplementary material The online version of this article (https://doi.org/10.1007/s13157-017-0990-5) contains supplementary material, which is available to authorized users.

✉ Rebeca de Jesús Crespo
dejesus-crespo.rebeca@epa.gov

[1] Gulf Ecology Division, National Health and Environmental Effects Research Laboratory, US EPA, Office of Research and Development, 1 Sabine Island Drive, Gulf Breeze, FL 32561-5299, USA

[2] University of Puerto Rico, Medical Sciences Campus, San Juan, Puerto Rico

female biting and oviposition rate, all factors that promote vector proliferation and dengue transmission ((Ibarra et al. 2013; Méndez-Lázaro et al. 2014), Chang et al. 2015, (Morin et al. 2015)). Urbanized environments may also present habitat limitations for predators and competitors which help control mosquito vector populations ((Barrera et al. 2006; Cox et al. 2007), Murugan et al. 2015).

The extent to which environmental factors such as heat islands, floods, habitat loss, and water pollution, impact urban environments may be determined, in part, by landscape management and design aspects, such as restoration and preservation of urban green spaces. Urban green spaces help control temperature extremes by providing shade, and increasing evapo-transpiration (Bouchama and Knochel 2002). They also promote rainfall interception and infiltration ameliorating the scale of urban flooding (Brody and Highfield 2013). Green spaces clean surface water in cities and provide habitat for wildlife, creating healthier ecosystems that may favor biocontrol of mosquitoes.

Ecosystem services in the urban landscape could help reduce vector disease transmission (Carver et al. 2015), but the data correlating vegetation cover to mosquitoes and its related diseases is conflicting. Some studies have found negative associations suggesting a protective role of vegetation against "mosquito-borne" disease ((Cox et al. 2007); Cheong et al. 2014; Tiong et al. 2015; Myer et al. 2017). Other studies, have found positive correlations (Sarfraz et al. 2012; Cheong et al. 2014; Stanforth et al. 2016) suggesting a disease promoting effect. Possible reasons for these inconsistencies include different vegetation types contributing differently to the provision of ecosystem services or difference in the role of ecosystem services for vector control in different environmental contexts. The relative importance of ecosystem services as a determinant of "vector-borne" disease occurrence can also vary depending on socio-economic factors. For example, vector abundance is likely a bigger concern for residences built with low quality construction material or lacking air conditioning (Mulligan et al. 2015) which is commonly observed in poor neighborhoods. Given these considerations, more studies are needed that evaluate the role of vegetation on "mosquito-borne" diseases while simultaneously measuring relevant ecosystem services and confounding socio-economic factors.

This study seeks to contribute by evaluating linkages between coastal wetlands and dengue fever occurrences on census block groups of the San Juan Bay Estuary (SJBE), Puerto Rico. Due to its high population density and favorable climate for mosquitoes, the SJBE, has been a hotspot for "vector-borne" diseases in Puerto Rico for decades, including a recent Zika epidemic that affected over 40,000 individuals in 2016 (Puerto Rico Department of Health (PRDH) 2017). Understanding how vectors and disease transmission vary across environmental and socio-economic gradients is needed to better guide the allocation of management resources among communities and habitats during epidemics in the SJBE. Moreover, as we now live in an interconnected world, were viruses and vectors spread more rapidly than in previous centuries, addressing these questions is of broader interest beyond the context of Puerto Rico and the US.

We present our hypothesized relationship between ecosystem services and dengue as a conceptual model in Fig. 1. We hypothesize that greater wetland cover will promote heat and water hazard mitigation, as well as cleaner water and more habitat for species that predate and/or compete with mosquitoes. These ecosystem services should in turn negatively affect dengue transmission, leading to a reduction in cases. We incorporate into our conceptual model socio-economic factors that may influence this relationship. In particular, we build on Myers et al.'s (Myers et al. 2013) concept of "insulating layers", where infrastructure, technology, behaviors, and other adaptations may protect certain groups from the potential health impacts of ecosystem service lost (Myers et al. 2013).

Study Site

The San Juan Bay Estuary (SJBE, Fig. 2) has an average temperature that ranges from 23.9 °C to 27.2 °C, and rainfall from 1500 and 1700 mm (Lugo et al. 2011). It lies within a "moist forest" ecological life zone according to Holdridge's classification (Torres-Valcárcel et al. 2014). The SJBE is part of the San Juan, Puerto Rico (PR) metropolitan area, encompassing the most densely urbanized and populated region on the Island, with an estimated population of 2.5 million people, according to the 2010 US Census (Brandeis et al. 2014). The SJBE comprises a total area of 216.58 km^2, of which around 82% is developed, and the rest is composed of mangroves (~7%), grassy wetlands and water bodies (~6%), and moist forest (~5%) (Brandeis et al. 2014). It is the only tropical estuary included in the US National Estuary Programs (NEP) and is characterized by a series of interconnected lagoons and channels, many of which have been severely altered by human activity (Brandeis et al. 2014). The most prominent natural features of the SJBE NEP are its coastal wetlands, which include the most extensive contiguous mangrove forest in Puerto Rico (Brandeis et al. 2014).

Here we focus on the role of these wetlands on ecosystem services and disease. Therefore, we limited our analysis to compare only neighborhoods that could potentially have had coastal wetlands in the past (N=170). For this we selected census block groups (United States Census Bureau 2015) that intersected flood zones (Federal Emergency Management Agency (FEMA) 2009) and that were below the 3m elevation line (U.S. Geological Survey 1944). This cutoff was selected based on historical maps from the SJBE showing the existence of mangroves and marshes mainly between 0-3 meters above sea level (masl) (U.S. Geological Survey 1941).

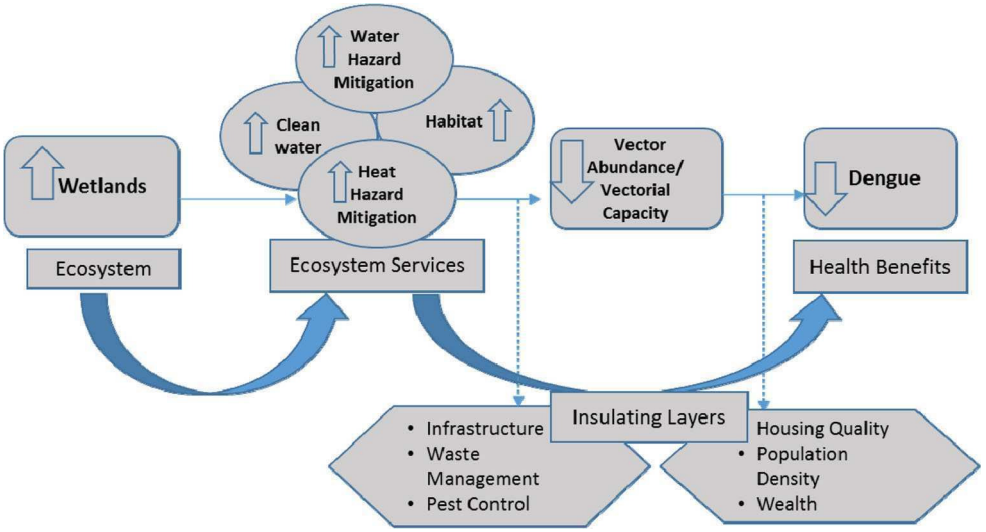

Fig. 1 Hypothesized linkage between wetlands and Dengue ocurrence through Ecosystem Services. Vectorial capacity refers to the mosquito's ability to spread disease accounting for host, virus, and vector interactions (Liu-(Helmersson 2012)). This can be influenced by factors such as mosquito growth rate, biting rate, the time it takes the virus to replicate within the vector, all of which are affected by temperature. In this case, it also incorporates the relative abundance of A. aegypti over other species of mosquitoes that are less effective at transmitting dengue and prefer more vegetated habitats (Cox et al.2007). Insulating factors refer to socio-economic elements which can insulate certain populations, generally the wealthy, from the impacts of a loss in Ecosystem Services (see (Myers et al. 2013))

Methods

To test our proposed Ecosystem Service-Dengue model (Fig. 1) we selected indicator variables from existing secondary data and estimated the spatial distribution of the selected variables in ArcGIS (version 10.3).

For the dengue response, we used laboratory confirmed dengue cases for the SJBE from the passive dengue surveillance system administered by the Center for Disease Control and Prevention (CDC) and the Puerto Rico Department of Health (years 2010-2013) (https://www.cdc.gov/dengue/about/inpuerto.html). Cases were summarized by census-block groups prior and standardized by population counts for analysis using 5-year population summaries from the American Community Survey (ACS 2011-2014, (United States Census Bureau 2015)). Block group area ranged from 0.04 to 21 km^2, with an average of 0.56km^2. The dispersal area of *A. aegypti* is estimated at less than 0.01 kilometers

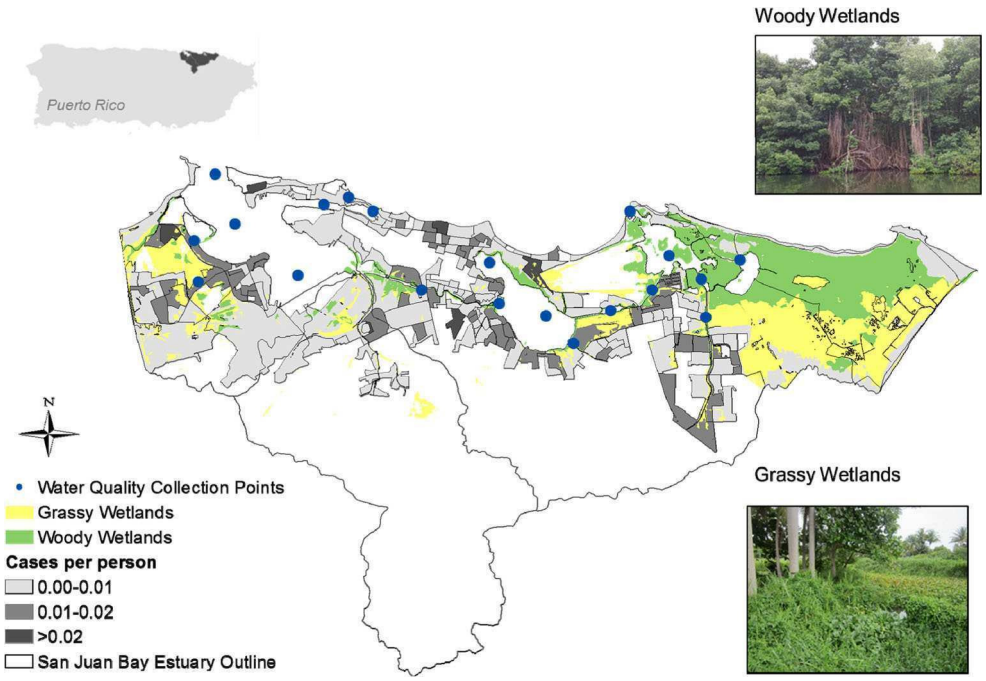

Fig. 2 Study sites in the San Juan Bay Estuary (SJBE), with water quality collection points (SJBE monitoring program), wetland areas (PR GAP analysis) and dengue cases per person by census block group (CDC dengue surveillance 2010-2013; ACS community survey 2011-2014). Pictures show examples of grassy and woody wetlands in the SJBE

(Harrington et al. 2005; Reiter et al. 1995). Therefore, it is reasonable to treat each block group as independent study units to assess disease trends.

To align our analysis with our conceptual model (Fig. 1) we divided our explanatory variables into three main categories: a) Ecosystem; b) Ecosystem Services; and c) Insulating Layers. We also included a fourth category, Environment, which characterizes natural variability unrelated to the ecosystem or ecosystem services categories, but which could affect dengue vectors.

Ecosystem

For the Ecosystem category we used the PR GAP project's land use layer (Gould et al. 2008). We extracted all wetlands within the SJBE and classified them as Woody or Grassy. Woody Wetlands consisted of all segments classified as Mangrove+Shrubland or as Pterocarpus forest. Grassy Wetlands consisted of segments classified as Emergent Herbaceous or Seasonally Flooded Herbaceous (Fig. 2). The percent of woody and grassy wetland cover was determined by dividing wetland area over total area by census block groups. The total area of each census block group was calculated excluding water bodies (Centro de Recaudación de Ingresos Municipales (CRIM) 2006), such as streams and lagoons, to more accurately represent the area occupied by people.

Ecosystem Services

The Ecosystem Services group included heat hazard mitigation, clean water, and habitat. We did not include the ecosystem service of water hazard mitigation because we could not get data on flood occurrences. Instead, we included georeferenced flood zones as part of our Environmental Controls sub-model (see below).

For heat hazard mitigation we used land surface temperature (LST; Fig. 3a) estimated from the Landsat 8 Operational Land Imager sensor's thermal infrared band (Band 10) on September 2013. The methods used to derive these estimates are described in Mendez-Lazaro et al. (2017). For each census block group, we calculated LST Mean, Minimum, and Maximum across 30 meter pixels using zonal statistics in ArcGIS (ver 10.3), and the block group area (revised as described above).

The ecosystem service of clean water was assessed using measures collected by the SJBE National Estuary Program (NEP) water monitoring initiative. This project measures water quality parameters through different areas of the SJBE (Fig. 2) several times per year, spanning from 2011-2014 (San Juan Bay Estuary (SJBE) 2015). In this case we focused on total nitrogen, as previous studies have shown that nitrogen enrichment can increase mosquito and midge production (Sanford et al. 2005). While the nitrogen concentrations used to evaluate this ecosystem service come from water bodies (e.g., streams, estuary) and not directly from *A. aegypti* habitat, we posit that nutrients from these water bodies may enter artificial containers in nearby block groups directly during floods (e.g., (Pires and Gleiser 2010)), or indirectly through allochthonous organic matter input from the associated vegetation (Kling et al. 2007). Here we selected the highest recorded total nitrogen per sampling station per year, and averaged the results to get a composite value per station (Fig. 3b). These composite values were used to create a raster surface of nitrogen levels using Inverse Distance Weighting (IDW) interpolation (Philip et al. 1982, Watson et al. 1985) in Arc GIS (ver 10.3). IDW interpolation estimates regional measures based on nearby sampling locations. In our case, we used a search radius of the nearest 3 points on 30m pixels, and assigned a weighting value of 3, on a scale of 0-3, where higher values suggest a greater influence of the closest vs farthest points. The resulting raster (30m pixel size) was then applied to calculate a mean value with zonal statistics, using the census block groups as the boundaries.

Lastly, vertebrate richness was used as our indicator of habitat provisioning (Fig. 3c). Here we hypothesize that healthy habitats should lead to bio-control of mosquito vectors by promoting healthier predator and competitor populations. We used the PRGAP vertebrate richness dataset, which includes estimates for amphibian, reptile, bat and bird richness using existing inventories, habitat suitability and expert opinion (Gould et al. 2008). We calculated median vertebrate richness by census block group using the PRGAP vertebrate richness layer (15m pixel size) and zonal statistics in Arc GIS.

Insulating Layers

The concept of insulating layers represents social elements that could moderate the influence of ecosystem services on health (Myers et al. 2013). We divided this group into two categories: a) infrastructure and b) socio-economic factors. Our infrastructure variables included sewage and road density, calculated from the road and sewage layers (source: *Portal Datos Geográficos Gubernamentales*http://www2.pr.gov/agencias/gis/Pages/default.aspx), divided over census block group area (excluding water bodies), resulting in a measure of linear meters over area per study unit. Sewage density was included as previous studies have linked the presence of septic tanks with vector mosquito habitat ((Burke et al. 2010; Mackay et al. 2009). (Myer et al. 2017)). We predicted that areas with lower sewage density would have higher number of septic tanks, increasing vector habitat availability and the potential for dengue transmission (Burke et al. 2010). Roads and the environmental modifications they cause were also

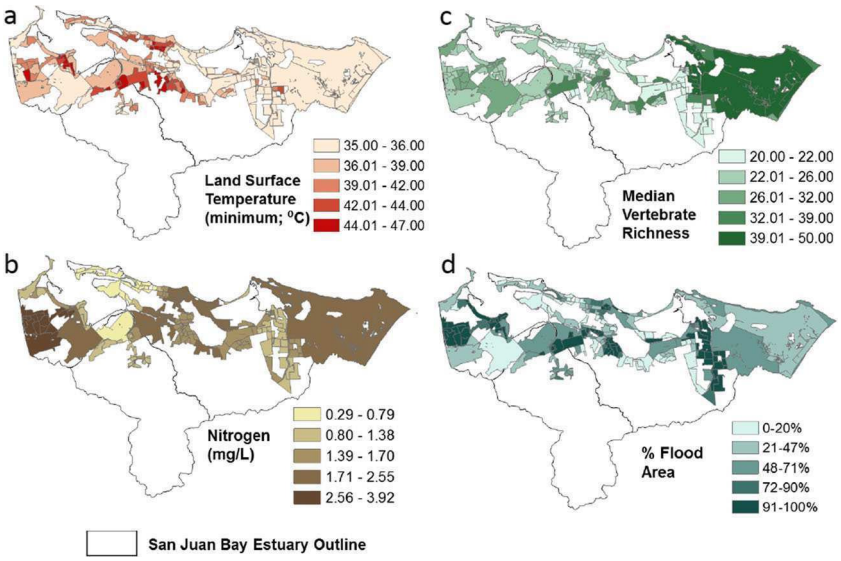

Fig. 3 Landscape scale patterns across SJBE coastal neighborhoods

explored, as they can alter hydro-dynamics by increasing surface runoff, potentially affecting water accumulation and habitat creation.

For our socio-economic variables, we focused on demographic characteristics and wealth indicators. Our demographic of choice was the percent of teenagers per block group because previous studies on Dengue in the SJBE have shown that this is the most vulnerable demographic (Méndez-Lázaro et al. 2014; Sharp et al. 2013). We calculate the proportion of people from the ages of 10-19 over total population using ACS data (ACS-2011-2014, (United States Census Bureau 2015)). Also using ACS data, we calculated median household income by census block group, as an umbrella measure potentially representing factors such as better housing quality, air conditioner use, waste management, and infrastructure. Finally, we included population density (population/m2) as a potential driver of higher dengue transmission rates. This variable was calculated excluding areas within the block group occupied by water bodies or wetlands.

Environment

Our Environment sub-model consists of environmental "control" variables that are not expected to be influenced by the presence of the wetland ecosystems, and not related directly to ecosystem services, but that are expected to influence Dengue. Here we include the flood area (Fig. 3d), which has been suggested to create breeding sites for mosquito vectors (World Health Organization (WHO) 2006). Our flood area indicator is derived from FEMA flood zone maps (Federal Emergency Management Agency (FEMA) 2009), which were used to calculate % flood area within populated segments of each block group, that is, excluding water bodies and areas covered by wetlands. Although water hazard mitigation (e.g. flood control) is an ecosystem service expected from wetlands, the flood zone map does not represent areas that get flooded most often, but rather areas with potential of flooding. Therefore, it cannot be used as an ecosystem services indicator, hence its inclusion as an environmental "control" instead. Our second environmental control is salinity. Our second environmental control is salinity. *A. aegypti* larvae can tolerate brackish waters (Ramasamy et al. 2011), but oviposition and larvae survival are limited at salinity levels above 12-13% (Navarro et al. 2003). Since there are differences in salinities in the different water bodies of the SJBE, we included it to account for its potential influence. To calculate salinity by block group, we followed the approach used for nitrogen (see above), using NEP water monitoring data and the IDW tool in ArcGIS. As with nitrogen, we focus on the premise that salinity from nearby water systems may influence chemistry in container habitat (Yee et al. 2014) via water inputs from flood events, or allochthonous organic matter inputs from vegetation.

Data Analysis

We evaluated the relationship between ecosystems and ecosystem services using linear regressions between woody or grassy wetlands and the ES indicators (nitrogen, richness, LST). We then evaluated the role of Ecosystems, Ecosystem Services, Insulating Layers and Environment on dengue prevalence (dengue cases per block group population) using beta-binomial generalized linear models, accounting for over-dispersion. Standard binomial regression (i.e. logistic regression) models the presence or absence of disease in an individual as a binary response variable (Quinn and Keough, 2002). Beta-binomial regression is a modified version of binomial regression that accounts for multiple samples (people) per

census block group (Venables and Ripley 2003). We developed a "global" beta-binomial model which included all variables from each category (Table 1), standardized around their means and 1 standard deviations (Becker et al. 1988). In this global model we also included significant interactions (Pr(>|z|)<0.05) between ecological variables with "Insulating Layers" indicators (with main effects included). For this we ran individual beta-binomial models between each factor included in the Insulating Layers category interacting with each of the other variables, to test the premise that these factors may mediate the role of the natural environment (Ecosystem, Ecosystem Services, Environment) on dengue occurrence.

We used this global model as basis for model averaging, following the steps described in Grueber et al. (Grueber et al. 2011). The goal of this approach was to select the top variable combinations that best explained dengue occurrence considering all possible combinations. Variable combinations were limited to 8 factors in order to have at least 20 replicates per explanatory variable, and prevent model overfitting. We used AICc > 4 as a cut-off criterion for sub model selection (Burnham and Anderson 2002) and then calculated the conditional average effect of each variable after accounting for all of the "best models" where it was featured (Grueber et al. 2011). Model averages were used to represent the relative importance of each variable, determine an average effect size and construct predictive models of dengue prevalence.

Variables included in the "best models" were further analyzed through a variation partitioning analysis. This analysis allowed us to determine the fractions of variability explained independently (pure effects) by each predictor, or jointly by the intersection of two or more predictors. In particular, we were interested in whether the effect of wetlands on dengue prevalence could be partly attributed to ecosystem services. We applied the subtraction approach described in detail in Ruiz-Fons et al. (Ruiz-Fons et al. 2013). Briefly, this approach calculates the deviance explained by all the variables featured in the "best models", and then fractures that into individual components representing the pure effects of each variable and the overlaid effects between variables. For example, a model that has both % wetlands and ecosystem service variables may not exhibit great reductions in deviance relative to one that only has % wetlands because part of the effect of ecosystem services is already captured by the %wetlands model. Here we wanted to test if there was such overlap, and if so, determine the relative magnitude.

Prior to analysis, all explanatory variables were tested for collinearity using Pearson correlation coefficients. If any important correlation was identified between explanatory variables (>0.60), we only selected the ones with a stronger relationship to the response variable for model selection (See supplementary Table 1). Prior to model averaging, the global model was tested for spatial autocorrelation applying the Global Moran's I procedure to residuals (supplementary Table 2).

Analyses were conducted in R studio (ver. 3.2.2) and/or ArcGIS (ver 10.3). The "Analysis of Overdispersed Data"(aod) package (ver 1.3, (Lesnoff and Lancelot 2012)) was used for beta-binomial model building, the MuMIn package (Bartoń 2009) was used for model averaging, and the "modEva" package (ver 1.3.2, Barbosa et al., 2013) for variation partitioning analysis.

Results

Relationship between Ecosystems and Ecosystem Services

Woody and grassy wetlands showed similar relationships to the ecosystem services indicators of temperature (heat hazard mitigation) and vertebrate richness (habitat). Increasing cover of both types of wetlands was associated with significant increases in vertebrate richness and significant reductions in land surface temperature (Fig. 4). The relationship to nitrogen, our "clean water" ecosystem services indicator differed. Both types of wetlands showed a positive association to nitrogen which is opposite to our prediction. This association was significant for grassy wetlands (p<0.001), but not woody wetlands.

Dengue Prevalence Model Selection

Model averaging resulted in five models with equal support following the AICc>4 criterion (Supplementary Table 3). The variables featured or excluded from these models, and their relative importance are listed in Table 1. From the "ecosystem" category, we found that higher percentage of woody wetlands associated significantly with lower dengue prevalence (p=0.03). Moreover, grassy wetlands significantly interacted with median income to explain dengue cases (p<0.001): while % grassy wetlands seem to inversely relate to dengue in low income neighborhoods, the trend is reversed in high income areas (Fig. 5). The significant "ecosystem service" indicators were Minimum Land Surface Temperature (LST, hereinafter minimum temperature) (p=0.002) and Nitrogen (p=0.01). Both variables showed a positive association to Dengue cases. Maximum LST (hereinafter maximum temperature) significantly interacted with population density to explain dengue cases (p=0.002), suggesting that in areas with high population density, higher maximum temperature was associated to higher number of cases, but that the effect is reversed in more sparsely populated neighborhoods (Fig. 5).

Both of the variables in the "environment" category significantly explained dengue occurrence. As predicted higher salinity was associated to lower dengue (p=0.02), while higher % flood area positively correlated to dengue (p=0.02). Salinity also interacted with the % of teenagers (p=0.003), suggesting that

Table 1 Descriptive statistics for treatment variables and their effect on dengue cases based on model averaging results (n=170)

Indicators		Descriptive Statistics				Model Averaging Results#				
Categories	Variables	max	min	mean	SD	Avg. Estimate	2.5%	97.5%	P (>z)	Relative Variable Importance
Ecosystem	%Woody Wetlands	58.98	0.00	3.35	9.23	-0.12	-0.23	-0.01	0.03	0.29
	% Grassy Wetlands	63.49	0.00	3.63	8.60	-0.04	-0.14	0.06	0.44	^0.00
Ecosystem Services	MinLST (^{0}C)	47.00	35.00	39.34	3.94	0.18	0.07	0.29	0.002	0.62
	MaxLST (^{0}C)	63.00	36.00	48.47	3.87	-0.08	-0.23	0.07	0.31	^0.00
	MeanLST (^{0}C)	52.54	35.25	44.06	3.40	n/a	n/a	n/a	n/a	n/a
	Nitrogen (mg/L)	3.92	0.29	1.62	0.68	0.12	0.03	0.21	0.01	0.17
	Vert.Rich.(Median)	50.00	20.00	26.21	6.29	n/a	n/a	n/a	n/a	n/a
Insulating Layers										
Infrastructure	Roads (m/m2)	0.04	0.00	0.02	0.01	n/a	n/a	n/a	n/a	n/a
	Sewage (m/m2)	0.06	0.00	0.01	0.01	n/a	n/a	n/a	n/a	n/a
Socio Economic	Median Income	83365.00	2499.00	24186.63	15373.27	-0.03	-0.13	0.08	0.60	^0.00
	% Teenagers	40.82	0.00	11.69	0.07	0.03	-0.06	0.12	0.51	^0.00
	Population per m^2	0.02	0.00	0.01	0.00	-0.12	-0.23	0.003	0.06	^0.00
Environment*	Salinity (ppm)	39.44	3.43	24.20	9.67	-0.10	-0.19	-0.02	0.02	0.70
	% Flood Area^	100.00	3.62	59.37	35.92	0.10	0.02	0.18	0.02	0.28
Interactions	GrassWetl*MedInc	n/a	n/a	n/a	n/a	0.26	0.15	0.38	<0.001	1.00
	MaxLST*Popm()	n/a	n/a	n/a	n/a	0.18	0.07	0.29	0.002	1.00
	Salinity*%Teens	n/a	n/a	n/a	n/a	-0.12	-0.19	-0.04	0.003	0.06

*Environmental control variables not necessarily related to the Ecosystem or to tested Ecosystem Services; ^represents flood prone zones, not actual flooded areas. ^ = This variable was only featured in models including it as part of an interaction term; see relative importance of its interaction term. # Model averaging results are "conditional averages", derived from the models that include the variable of interest out of all the "best models" (Supplementary Table 3). n/a (Not applicable; for model averaging results, it implies that the variable was never featured in the "best models"). LST (Land Surface Temperature); Vert.Rich (Vertebrate Richness)

in neighborhoods associated to higher salinities, the positive correlation between teenagers and dengue weakens (Fig. 5). The variables within the "insulating layers" category were not significantly associated to dengue, although we did find significant interaction effects with some of these variables as discussed above.

Variance partitioning analysis showed that the relationship between wetlands and dengue may in part be attributed to the ecosystem service of "heat hazard mitigation" (LST as indicator). About 19% of the deviance explained by woody wetlands and about 50% of that explained by the interaction of grassy wetlands and median income is also explained by minimum temperature (Fig. 6). There was no shared deviance between wetlands and the other variables featured in the "best models" (See Supplementary Fig. 1), including nitrogen, which was the other significant ecosystem service indicator (Fig. 6).

We used the resulting variable estimates from the model averaging procedure (Table 1) to develop predictive models of the role of wetland ecosystem services on dengue occurrence. For this we set all model variables to the mean, and varied woody and grassy wetland cover on increments of 2%. (Figure 7). Results suggest that at the current mean woody wetland cover of 3.4%, there are approximately 9.3 cases of Dengue per 1000 people. Increasing woody wetland cover by 10% would reduce Dengue cases by roughly 11%, resulting in around 8.3 cases per 1000 people during a timeframe similar to our dataset (3 years, one epidemic period). Closer to a 20% increase in grassy wetland cover would be needed to achieve the same effect. (Figure 7).

Discussion

To our knowledge, this is the first study to assess the role of wetlands in the urban landscape on dengue occurrence through the lens of ecosystem services. Wetlands in the San Juan Bay Estuary, and in particular mangroves seem to provide a protective effect, being negatively correlated to dengue. Part of that effect seems to be mediated by the ecosystem service of heat hazard mitigation, as lower temperatures are associated to higher mangrove cover and lower dengue. Our study suggests that variables such as median income, population density and demographics could play a mediating role in the relationship between dengue occurrence and the natural environment. These results support our hypothesis of a potential buffering effect of wetlands to "vector-borne" diseases in

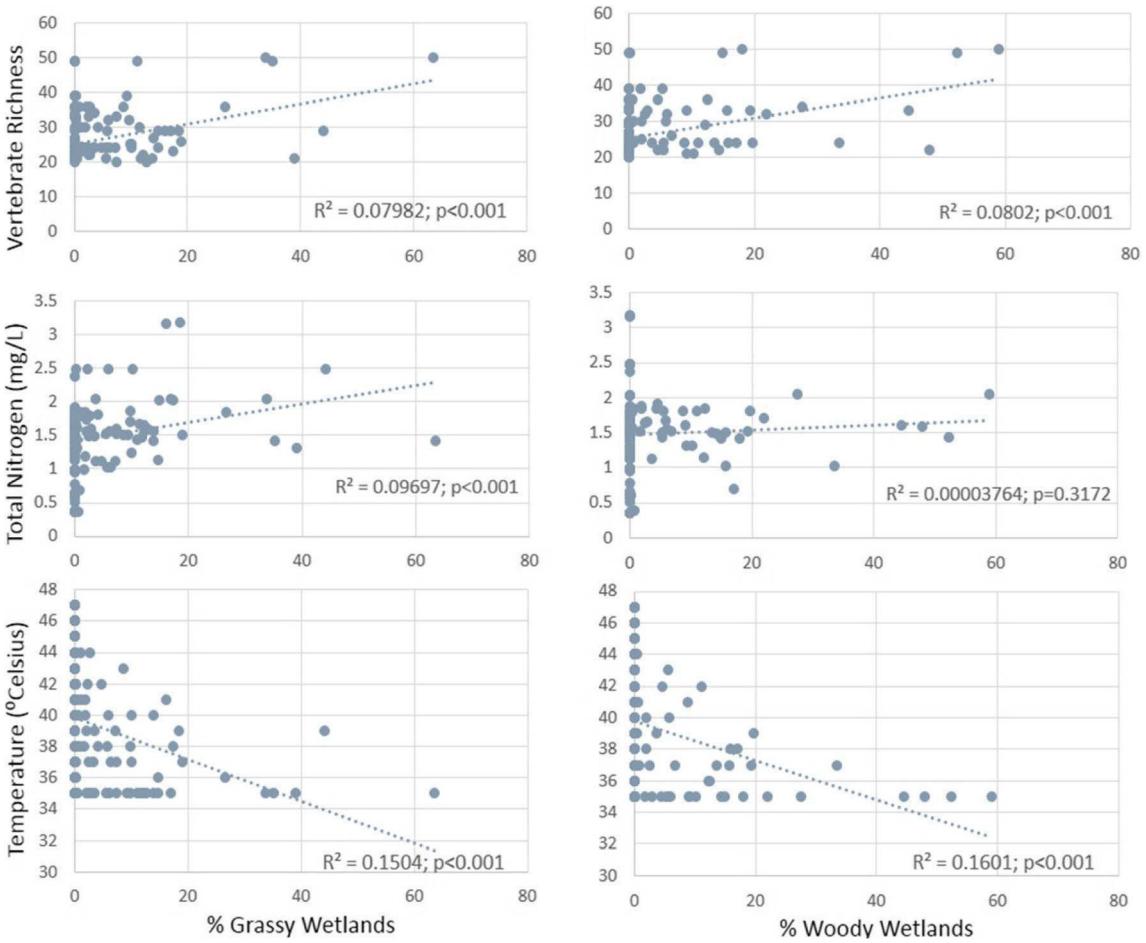

Fig. 4 Scatterplots displaying relationships between wetland ecosystems and selected ecosystem services. The temperature measure selected here was Minimum Land Surface Temperature, as it was the most closely related to dengue cases

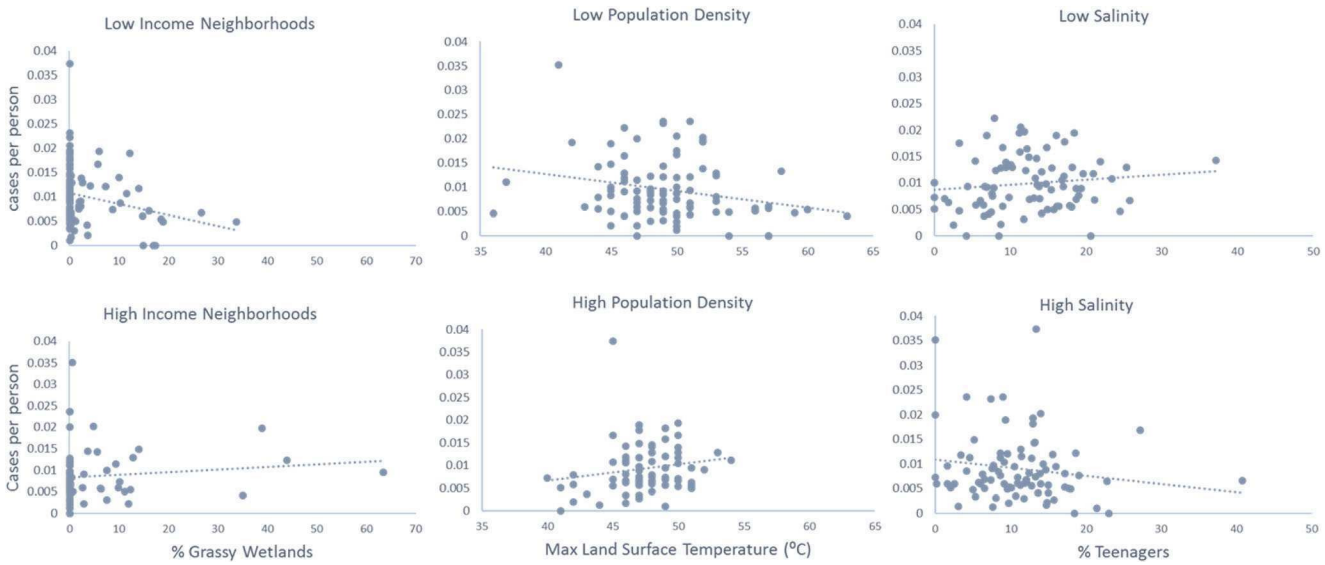

Fig. 5 Significant interactions explaining dengue cases in the SJBE. Breakpoints for the two figures on each panel were based on the average (above and below) of the variables: **a**) Median Income; **b**) Population Density; and C) Salinity See Supplementary Table 4 for more details

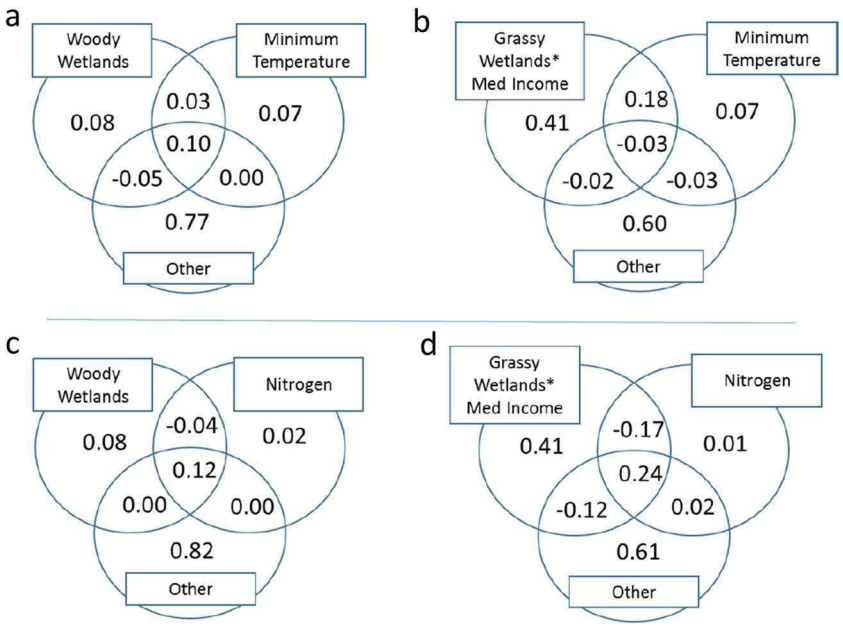

Fig. 6 Variation partitioning analysis of models explaining Dengue cases. Values represent the proportion of the deviance explained by the variables of interest individually and in combination to other model components. In this case, the variables of interest are the wetland ecosystems and the "ecosystem service" indicators Minimum Land Surface Temperature (**a**, **b**) and Nitrogen (**c**, **d**). The "other" circle represents all variables featured in the model averaging results aside from the single predictors concurrently being examined (Table 1; Supplementary Table 3). Negative explained variances are artifacts of the VP procedure, which mainly suggest no overlay in the amount of deviance explained. Tested individually, none of these other variables shared deviance with wetlands. Results from variation partitioning with different variables of the model and wetlands can be found in Supplementary Fig. 1

coastal urbanized neighborhoods, even after controlling for confounding environmental and socio-economic factors.

The role of temperature on dengue has been documented before in the SJBE. As in our study, Méndez-Lázaro et al. (Méndez-Lázaro et al. 2014) found that minimum temperatures were positively associated to dengue in the municipality of San Juan. Our study supports their findings at a lower spatial resolution. Previous studies have shown that higher temperatures promote dengue transmission, by means of reductions in viral incubation period, and mosquito development time, and increases in feeding and oviposition rate (Morin et al. 2013). This relationship however is non-linear

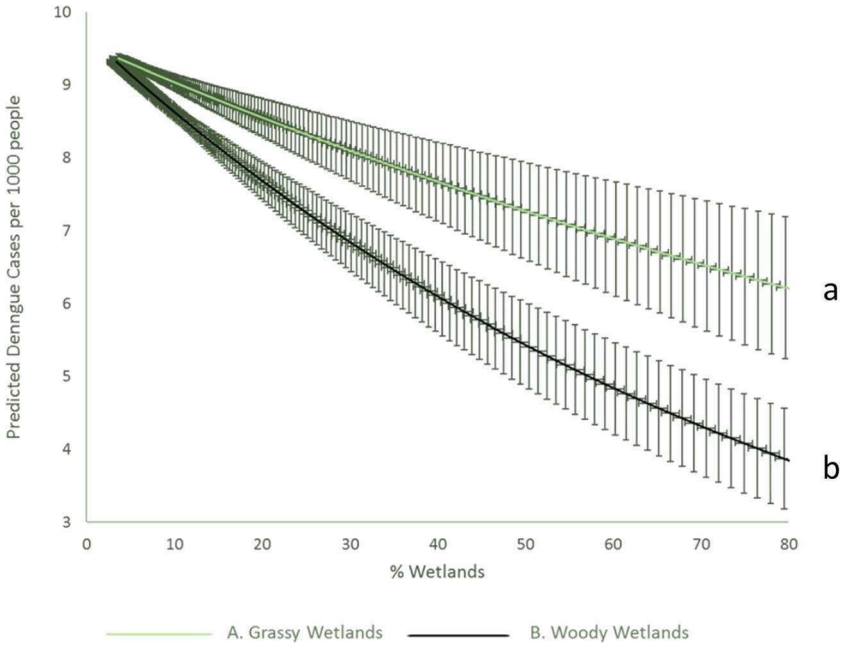

Fig. 7 Predicted relationship between grassy wetlands (**a**) and woody wetlands (**b**) and dengue cases in the SJBE

and at extremely high temperatures mosquito activity and survival becomes negatively affected (Carrington et al. 2013; Morin et al. 2013). This non-linearity became evident in our result of a significant interaction between maximum temperature and population density. We observe (Fig. 5) that areas that are more sparsely populated seem to reach much higher temperature extremes, therefore becoming less suitable for dengue transmission. These lower population densities could correspond to industrial zones, or sprawled development, with lower residential greenery and more concrete surfaces that promote temperatures above the vector-dengue threshold. The threshold for mosquito competence of dengue transmission seems to lie between 30-35^0 Celsius in air temperature (note here we used Land Surface Temperature, which tends to be higher) (Carrington et al. 2013; Morin et al. 2013). Above this temperature, different aspects of mosquito ecology become negatively affected (Carrington et al. 2013; Morin et al. 2013). The role that wetland ecosystem services play in promoting optimal temperature ranges may therefore vary by context. While in the SJBE it seems to be having a protective effect, in drier, hotter environments, the presence of vegetation may actually help bring temperatures down to more suitable ranges, and prevent evaporation of water from container habitats (Barrera et al. 2006). These considerations should be taken into account when applying these findings to other sites.

While temperature seems to partially describe the relationship between wetlands and dengue in the SJBE, a proportion of the deviance explained by wetlands remains un-attributed to any of the other ecosystem services tested, according to our variation partitioning analysis. A possible pathway may be flood control. We found a positive correlation between % flood area and dengue cases, and previous studies suggest that wetlands can mitigate floods in coastal cities (Brody et al. 2012). To determine the effect of wetlands on preventing flood and consequently on dengue, it would be necessary to document actual flood events. While we did not have flood indicator data for the scale of analysis of this study, this question may likely be addressed at coarser spatial resolutions in future studies, using for example flood claims data for the San Juan metropolitan area.

Another potential explanation of the role of wetlands on dengue may lie in bio-control pathways not evaluated through this study. For example, while we included estimates of vertebrate richness, we did not have an indicator of invertebrate distributions. Invertebrates may act as predators and competitors of *Aedes aegypti* (Quiroz-Martínez and Rodríguez-Castro 2007) and they may be positively affected by the presence of wetlands. For example, a closely related species, *Aedes mediovittatus,* potentially competes with *A. aegypti,* for resources but prefers to live in woody environments (Cox et al. 2007). While *A. mediovittatus* could also transmit dengue, it is a less competent vector because it is less susceptible to certain dengue serotypes (Poole-Smith et al. 2015). Moreover, contrary to *A. aegypti,* this mosquito commonly feeds on other mammals besides humans (Barrera et al. 2012) potentially diluting dengue transmission rates. The effect of this or other invertebrates within the SJBE wetlands on dengue could be the subject of future research.

The role that woody and grassy wetlands seem to play in dengue occurrence is not equal. Grassy wetlands had the same inverse correlation to dengue as woody wetlands but only in low income neighborhoods. This result supports previous studies showing that wealth moderates "vector-borne" disease exposure (LaDeau et al. 2013) as well as the ecosystem service-human health linkage (Myers et al. 2013). Like woody wetlands, grassy wetlands also seem to provide heat hazard mitigation, and so their presence could be preferentially benefitting households more exposed to vectors than those protected by air conditioning and better building material. The stronger effect of woody wetlands, which seems to affect all income classes, may be attributed to additional, unexplained factors such as the ones discussed above (e.g. bio-control, flood control).

Another factor differentiating woody and grassy wetlands may be their influence on water quality. We found that nitrogen levels were significantly associated to dengue, supporting our prediction that water quality degradation could have an effect mosquito vectors. However, contrary to our predictions, we observed no correlation between water nitrogen concentration and neighborhood woody wetland cover, and a positive and significant correlation between water nitrogen concentration and the percentage of grassy wetlands. This result may suggest that grassy wetlands are subjected to higher levels of pollution, or that they process pollutant loads differently than woody wetlands. Moreover, the role that other, un-measured, water quality indicators that vary concomitantly with nitrogen play, and their association to different wetland types needs further evaluation.

Aside from nitrogen, we also included salinity as a water quality "control" variable. As predicted salinity had a negative effect on dengue. High salinity concentrations seem to dampen the effect of dengue on certain vulnerable populations, as we observed a significant interaction between this variable and the % of teenagers (Fig. 5). As in previous studies (Méndez-Lázaro et al. 2014), we found that dengue occurrence positively relates to % teens, but that this relationship becomes weaker in areas of higher salinity. If brackish water enters artificial containers, then container salinity levels could rise, negatively affecting oviposition and larvae development. In neighborhoods associated to coastal ecosystems of higher salinity, it is plausible that high salinity levels in breeding habitat ameliorates vector emergence, providing a level of disease control among a vulnerable sector of the population. While we can expect this effect to be relatively small in magnitude (as we saw in our results), we also think it is plausible and worth exploring further through field validation. Hydrological alterations such as artificial drainage structures

and channelization tend to reduce salinity levels in coastal ecosystems (Lugo and Snedaker 1974), but sea level rise, is expected to expand the extent of estuarine area in the SJBE, promoting saltwater intrusion inland (Méndez-Lázaro et al. 2014). These altered salinity gradients could determine the distribution of mosquito vectors and Dengue occurrence across coastal neighborhoods of the SJBE and should de more closely examined in the future, as our understanding of these dynamics remains limited (Méndez-Lázaro et al. 2014).

Aside from the interactions cited in the preceding paragraphs, the variables in our "insulating layers" category were not significantly associated to dengue. Particularly noteworthy is the lack of correlation of dengue to population density as a main effect, suggesting that this variable is not mediating the observed role of wetlands. The SJBE is more or less densely populated through, and for the purpose of dengue transmission, the slight differences do not seem to have an impact. Moreover, even in neighborhoods with high wetland cover, we observe households congregating around densely developed zones, rather than scattered within or around the wetland area.

Our study had several limitations. Many of the variables used to assess ecosystem services were derived from extrapolations, either from point measurements or remotely sensed images. Therefore, there are uncertainties related to how these measures represent conditions of our study units both in spatial and temporal terms. The dengue cases used as a response come from official confirmed occurrences. People with limited access to health care are likely underrepresented by this dataset. We did not account for human mobility, and how this factor may affect the disease-environment associations. Accounting for block group employment rate, age structure, and human behaviors that affect transmission and exposure to dengue (see (Barrera et al. 2011)) could help contribute to better understanding these relationships in the future. Our results are based on disease occurrence, while many of the hypotheses we test are related to mosquito vector ecology. Future sampling of mosquito populations in the same neighborhoods should be developed to support our findings. These efforts should focus on monitoring adult female vectors, which are superior disease risk indicators than larvae or non-specific adult mosquito abundance ((Barrera et al. 2011), Bowman et al 2014).

Aside from mosquito vector abundance other factors may influence Dengue dynamics such as immunity due to previous exposure, vector to person contact rate, and current level of exposure risk. Our study attempted to include some indicators to account for these factors, such as teenagers (10-19yo), which are less likely to have acquired the immunity, median income, which may indicate level of exposure due to housing quality, waste management and access to air conditioning, and population density, which increases contact between infected individuals and vectors. Nevertheless, the path from vector to disease is complex and is affected by a multitude of dynamics which were not entirely captured by this analysis, so we encourage future studies to address our limitations to more accurately represent dengue trends in the SJBE.

In spite of these limitations, our results are consistent with our theoretical models and with previous studies on environmental drivers of dengue fever. Furthermore, our results and predictive models (Fig. 7) could be used as preliminary evidence to help justify wetland restoration strategies for the benefit of human health, and to evaluate potential gains and tradeoffs of different landscape management scenarios in the SJBE.

Acknowledgements We thank Roberto Barrera from the CDC Dengue Branch for providing data and advice in the development of this work. Matthew Harwell, Marc Russell and Richard Fulford provided suggestions that greatly helped improved this research. The views expressed in this paper are those of the authors and do not necessarily reflect the views or policies of the U.S. Environmental Protection Agency. Any mention of trade names, products or services does not imply an endorsement by the U.S. Government or the U.S. Environmental Protection Agency (EPA). The EPA does not endorse any commercial products, services, or enterprises.

References

Barbosa AM, Real R, Munoz AR, Brown JA (2013) New measures for assessing model equilibrium and prediction mismatch in species distribution models. Diversity and Distributions 19:1333–1338. https://doi.org/10.1111/ddi.12100

Barrera R, Amador M, Clark GG (2006) Ecological factors influencing Aedes aegypti (Diptera: Culicidae) productivity in artificial containers in Salinas, Puerto Rico. Journal of Medical Entomology 43(3):484–492. https://doi.org/10.1093/jmedent/43.3.484

Barrera R, Amador M, MacKay AJ (2011) Population dynamics of Aedes aegypti and dengue as influenced by weather and human behavior in San Juan, Puerto Rico. PLoS Neglected Tropical Diseases 5(12). https://doi.org/10.1371/journal.pntd.0001378

Barrera R, Bingham AM, Hassan HK, Amador M, Mackay AJ, Unnasch TR (2012) Vertebrate hosts of Aedes aegypti and Aedes mediovittatus (Diptera: Culicidae) in rural Puerto Rico. Journal of Medical Entomology 49(4):917–921. https://doi.org/10.1603/ME12046

Bartoń, K (2009) MuMIn: multi-model inference. R package, version 0.12.2. Available at: http://r-forge.r-project.org/projects/mumin/. Accessed 11/14/2017

Becker, R. A., Chambers, J. M. and Wilks, A. R. (1988) The New S Language. Wadsworth & Brooks/Cole

Bouchama A, Knochel JP (2002) Heat stroke. New England Journal of Medicine 346(25):1978–1988. https://doi.org/10.1056/NEJMra011089

Bowman LR, Runge-Ranzinger S, McCall PJ (2014) Assessing the relationship between vector indices and dengue transmission: a systematic review of the evidence. PLoS Negl Trop Dis 8(5):e2848 https://doi.org/10.1371/journal.pntd.0002848

Brandeis, T. J., Escobedo, F. J., Staudhammer, C. L., Nowak, D. J., & Zipperer, W. C. (2014). San Juan Bay Estuary watershed urban forest inventory. Available at: https://www.nrs.fs.fed.us/pubs/45759. Accessed 11/14/2017

Brody SD, Highfield WE (2013) Open space protection and flood mitigation: A national study. Land Use Policy 32:89–95. https://doi.org/10.1016/j.landusepol.2012.10.017

Brody SD, Peacock WG, Gunn J (2012) Ecological indicators of flood risk along the Gulf of Mexico. Ecological Indicators 18:493–500. https://doi.org/10.1016/j.ecolind.2012.01.004

Burke R, Barrera R, Lewis M, Kluchinsky T, Claborn D (2010) Septic tanks as larval habitats for the mosquitoes Aedes aegypti and Culex quinquefasciatus in Playa-Playita, Puerto Rico. Medical and Veterinary Entomology 24(2):117–123. https://doi.org/10.1111/j.1365-2915.2010.00864.x

Burnham KP, Anderson DR (2002) Model Selection and Multimodel Inference: A Practical Information-Theoretic Approach, 2nd edn. Springer, Berlin

Carrington LB, Armijos MV, Lambrechts L, Barker CM, Scott TW (2013) Effects of fluctuating daily temperatures at critical thermal extremes on Aedes aegypti life-history traits. PLoS One 8(3). https://doi.org/10.1371/journal.pone.0058824

Carver, S., Slaney, D. P., Leisnham, P. T., & Weinstein, P. (2015). Healthy wetlands, healthy people: "mosquito-borne" disease. In Wetlands and Human Health (pp. 95-121). Springer Netherlands

Centro de Recaudación de Ingresos Municipales (CRIM). (2006). Hydrography Revision, 2001-04 from CRIM Basemap, scale 1: 5000. Available at: http://gis.otg.pr.gov. Accessed 06/22/2017

Chang FS, Tseng YT, Hsu PS, Chen CD, Lian IB, Chao DY (2015) Re-assess vector indices threshold as an early warning tool for predicting dengue epidemic in a dengue non-endemic country. PLoS Negl Trop Dis 9(9):e0004043 https://doi.org/10.1371/journal.pntd.0004043

Cheong YL, Leitão PJ, Lakes T (2014) Assessment of land use factors associated with dengue cases in Malaysia using boosted regression trees. Spat Spatiotemporal Epidemiol 10:75–84 https://doi.org/10.1016/j.sste.2014.05.002

Couret J, Dotson E, Benedict MQ (2014) Temperature, larval diet, and density effects on development rate and survival of Aedes aegypti (Diptera: Culicidae). PLoS One 9(2):e87468

Cox J, Grillet ME, Ramos OM, Amador M, Barrera R (2007) Habitat segregation of dengue vectors along an urban environmental gradient. The American Journal of Tropical Medicine and Hygiene 76(5): 820–826. https://doi.org/10.4269/ajtmh.2007.76.820

Federal Emergency Management Agency (FEMA). (2009). Digital flood insurance rate map database, Commonwealth of Puerto Rico. Available at: http://gis.otg.pr.gov/download_gis_files.htm. Accessed 06/22/2017

Gould, W. A., Alarcón, C., Fevold, B., Jiménez, M. E., Martinuzzi, S., Potts, G., ... & Ventosa, E. (2008). The Puerto Rico Gap Analysis Project volume 1: land cover, vertebrate species distributions, and land stewardship. Gen. Tech. Rep. IITF-GTR-39. Río Piedras, PR: U.S. Department of Agriculture, Forest Service, International Institute of Tropical Forestry. 165 p

Grueber CE, Nakagawa S, Laws RJ, Jamieson IG (2011) Multimodel inference in ecology and evolution: challenges and solutions. Journal of Evolutionary Biology *24*(4):699–711. https://doi.org/10.1111/j.1420-9101.2010.02210.x

Harrington LC, Scott TW, Lerdthusnee K, Coleman RC, Costero A, Clark GG et al (2005) Dispersal of the dengue vector Aedes aegypti within and between rural communities. The American Journal of Tropical Medicine and Hygiene 72(2):209–220. https://doi.org/10.4269/ajtmh.2005.72.209

Hashizume M, Dewan AM, Sunahara T, Rahman MZ, Yamamoto T (2012) Hydroclimatological variability and dengue transmission in Dhaka, Bangladesh: a time-series study. BMC Infectious Diseases 12(1):98. https://doi.org/10.1186/1471-2334-12-9

Helmersson, J. (2012) Mathematical Modeling of Dengue-Temperature Effect on Vectorial Capacity. Universitet UMEA.. Master of Science Thesis. Available at: http://www.phmed.umu.se/digitalAssets/104/104555_jing-helmersson.pdf: Umeå University; 2012. 11/14/2017

Ibarra AMS, Ryan SJ, Beltrán E, Mejía R, Silva M, Muñoz Á (2013) Dengue vector dynamics (Aedes aegypti) influenced by climate and social factors in Ecuador: implications for targeted control. PLoS One 8(11). https://doi.org/10.1371/journal.pone.0078263

Kling LJ, Juliano SA, Yee DA (2007) Larval mosquito communities in discarded vehicle tires in a forested and unforested site: detritus type, amount, and water nutrient differences. Journal of Vector Ecology 32(2):207–217. https://doi.org/10.3376/1081-1710

LaDeau SL, Leisnham PT, Biehler D, Bodner D (2013) Higher mosquito production in low-income neighborhoods of Baltimore and Washington, DC: understanding ecological drivers and mosquito-borne disease risk in temperate cities. International Journal of Environmental Research and Public Health 10(4):1505–1526. https://doi.org/10.3390/ijerph10041505

Lesnoff M. and Lancelot R (2012) Analysis of Overdispersed Data (aod, ver 1.3). Available at: https://cran.r-project.org/web/packages/aod/index.html. Accessed 01/20/2017

Lugo AE, Snedaker SC (1974) The ecology of mangroves. Annual Review of Ecology and Systematics 5(1):39–64. https://doi.org/10.1146/annurev.es.05.110174.000351

Lugo, A. E., Ramos, O., & Rodriguez, C. (2011). The Río Piedras watershed and its surrounding environment. U.S. Department of Agriculture Forest Service, International Institute of Tropical Forestry. 48 p. Available at: https://www.researchgate.net/profile/Ariel_Lugo/publication/267236241_ThE_RiO_PiEdRAs_WATERshEd_and_Its_Surrounding_Environment_ACknOWLEdGMEnTs/links/548863900cf289302e30a35e.pdf. Accessed 11/14/2017

Mackay AJ, Amador M, Diaz A, Smith J, Barrera R (2009) Dynamics of Aedes aegypti and Culex quinquefasciatus in septic tanks. Journal of the American Mosquito Control Association 25(4):409–416. https://doi.org/10.2987/09-5888.1

Méndez-Lázaro P, Muller-Karger FE, Otis D, McCarthy MJ, Peña-Orellana M (2014) Assessing climate variability effects on dengue incidence in San Juan, Puerto Rico. International Journal of Environmental Research and Public Health 11(9):9409–9428. https://doi.org/10.3390/ijerph110909409

Méndez-Lázaro, P., Muller-Karger, F. E., Otis, D., McCarthy, M. J., & Rodríguez, E. (2017). A heat vulnerability index to improve urban public health management in San Juan, Puerto Rico. International journal of biometeorology, 1-14. https://doi.org/10.1007/s00484-017-1319-z

Morin CW, Comrie AC, Ernst K (2013) Climate and dengue transmission: evidence and implications. Environmental Health Perspectives 121(11-12):1264. https://doi.org/10.1289/ehp.1306556

Morin CW, Monaghan AJ, Hayden MH, Barrera R, Ernst K (2015) Meteorologically driven simulations of dengue epidemics in San Juan, PR. PLoS Neglected Tropical Diseases 9(8). https://doi.org/10.1371/journal.pntd.0004002

Mulligan K, Dixon J, Sinn CLJ, Elliott SJ (2015) Is dengue a disease of poverty? A systematic review. Pathogens and Global Health 109(1): 10. https://doi.org/10.1179/2047773214Y.0000000168

Murugan K, Priyanka V, Dinesh D, Madhiyazhagan P, Panneerselvam C, Subramaniam J et al (2015) Predation by Asian bullfrog tadpoles, Hoplobatrachus tigerinus, against the dengue vector, Aedes aegypti, in an aquatic environment treated with mosquitocidal nanoparticles. Parasitol Res 114(10):3601–3610 https://doi.org/10.1007/s00436-015-4582-0

Myer MH, Campbell SR, Johnston JM (2017) Spatiotemporal modeling of ecological and sociological predictors of West Nile virus in Suffolk County, NY, mosquitoes. Ecosphere 8(6) https://doi.org/10.1002/ecs2.1854

Myers SS, Gaffikin L, Golden CD, Ostfeld RS, Redford KH, Ricketts TH et al (2013) Human health impacts of ecosystem alteration.

Proceedings of the National Academy of Sciences 110(47):18753–18760. https://doi.org/10.1073/pnas.1218656110

Navarro DMAF, De Oliveira PES, Potting RPJ, Brito AC, Fital SJF, Sant'Ana AE (2003) The potential attractant or repellent effects of different water types on oviposition in Aedes aegypti L.(Dipt., Culicidae). Journal of Applied Entomology 127(1):46–50. https://doi.org/10.1046/j.1439-0418.2003.00690.x

Philip GM, Watson DF (1982) A precise method for determining contoured surfaces. APPEA J 22(1):205–212 https://doi.org/10.1071/AJ81016

Pires DA, Gleiser RM (2010) Mosquito fauna inhabiting water bodies in the urban environment of Córdoba city, Argentina, following a St. Louis encephalitis outbreak. Journal of Vector Ecology 35(2):401–409. https://doi.org/10.1111/j.1948-7134.2010.00099.x

Poole-Smith BK, Hemme RR, Delorey M, Felix G, Gonzalez AL, Amador M et al (2015) Comparison of vector competence of Aedes mediovittatus and Aedes aegypti for dengue virus: implications for dengue control in the Caribbean. PLoS Neglected Tropical Diseases *9*(2):e0003462. https://doi.org/10.1371/journal.%20pntd.0003462

Puerto Rico Department of Health (PRDH). (2017). Informe seminal de enfermedades arbovirales (Semana 4-10 de Junio de 2017). Available at: http://www.salud.gov.pr/Estadisticas-Registros-y-Publicaciones/Informes%20Arbovirales/Reporte%20ArboV%20semana%2023-2017.pdf/ Accessed 06/29/2017

Quinn GP, Keough MJ (2002) Experimental design and data analysis for biologists. Cambridge University Press

Quiroz-Martínez H, Rodríguez-Castro A (2007) Aquatic insects as predators of mosquito larvae. Journal of the American mosquito control association, 23(sp2), 110-117. https://doi.org/10.2987/8756-971X(2007)23%5B110:AIAPOM%5D2.0.CO;2

Ramasamy R, Surendran SN, Jude PJ, Dharshini S, Vinobaba M (2011) Larval development of Aedes aegypti and Aedes albopictus in peri-urban brackish water and its implications for transmission of arboviral diseases. PLoS Neglected Tropical Diseases *5*(11):e1369. https://doi.org/10.1371/journal.pntd.0001369

Reiter P, Amador MA, Anderson RA, Clark GG (1995) Dispersal of Aedes aegypti in an urban area after blood feeding as demonstrated by rubidium-marked eggs. The American Journal of Tropical Medicine and Hygiene 52(2):177–179. https://doi.org/10.4269/ajtmh.1995.52.177

Ruiz-Fons, F., Acevedo, P., Sobrino, R., Vicente, J., Fierro, Y., & Fernández-de-Mera, I. G. (2013). Sex-biased differences in the effects of host individual, host population and environmental traits driving tick parasitism in red deer. Frontiers in cellular and infection microbiology, 3. doi: https://doi.org/10.3389/fcimb.2013.00023

San Juan Bay Estuary (SJBE). (2015). Area cientifica: datos de monitoreo. Available at: http://www.estuario.org/index.php/datos/ciencia?limitstart=0. Accessed 01/30/2017

Sanford MR, Chan K, Walton WE (2005) Effects of inorganic nitrogen enrichment on mosquitoes (Diptera: Culicidae) and the associated aquatic community in constructed treatment wetlands. Journal of Medical Entomology 42(5):766–776. https://doi.org/10.1093/jmedent/42.5.766

Sarfraz MS, Tripathi NK, Tipdecho T, Thongbu T, Kerdthong P, Souris M (2012) Analyzing the spatio-temporal relationship between dengue vector larval density and land-use using factor analysis and spatial ring mapping. BMC Public Health 12(1):853 https://doi.org/10.1186/1471-2458-12-853

Sharp TM, Hunsperger E, Santiago GA, Muñoz-Jordan JL, Santiago LM, Rivera A et al (2013) Virus-specific differences in rates of disease during the 2010 Dengue epidemic in Puerto Rico. PLoS Neglected Tropical Diseases 7(4):e2159. https://doi.org/10.1371/journal.pntd.0002159

Stanforth A, Moreno-Madriñán MJ, Ashby J (2016) Exploratory analysis of dengue fever niche variables within the Río Magdalena watershed. Remote Sens 8(9):770 https://doi.org/10.3390/rs8090770

Tiong V, Abd-Jamil J, Zan MH, Abu-Bakar RS, Ew CL, Jafar FL et al (2015) Evaluation of land cover and prevalence of dengue in Malaysia. Trop Biomed 32(4):587–597

Torres-Valcárcel Á, Harbor J, González-Avilés C, Torres-Valcárcel A (2014) Impacts of Urban Development on Precipitation in the Tropical Maritime Climate of Puerto Rico. Climate 2(2):47–77. https://doi.org/10.3390/cli2020047

U.S. Geological Survey, (1941) A. USGS 1:30000-scale Quadrangle for San Juan, PR 1941: U.S. Geological Survey: Reston, Virginia. Available at: https://prd-tnm.s3.amazonaws.com/StagedProducts/Maps/HistoricalTopo/2/14619/4985332.pdf. Accessed 01/25/2017

U.S. Geological Survey. (1944). 1:20000 scale Topographic contours for Puerto Rico quadrangles converted form USGS Digital Line Graph data. Available at: http://gis.otg.pr.gov/download_gis_files.htm. Accessed 01/25/2017

United States Census Bureau. (2015). 2011-5-year summary American Community Survey. U.S. Census Bureau's American Community Survey Office. Available at: http://ftp2.census.gov/. Accessed 01/25/2017

Venables WN, Ripley BD (2003) Modern Applied Statistics with S, 4th edn. Springer-Verlag, New York

Watson DF, Philip GM (1985) A refinement of inverse distance weighted interpolation. Geoprocessing 2(4):315–327

World Health Organization (WHO). (2006). Communicable diseases following natural disasters: Risk assessment and priority interventions (WHO/CDS/NTD/DCE/2006.4). Available at: http://www.who.int/diseasecontrol_emergencies/guidelines/CD_Disasters_26_06.pdf Accessed 01/30/2017

Yee DA, Himel E, Reiskind MH, Vamosi SM (2014) Implications of saline concentrations for the performance and competitive interactions of the mosquitoes Aedes aegypti (Stegomyia aegypti) and Aedes albopictus (Stegomyia albopictus). Medical and Veterinary Entomology 28(1):60–69. https://doi.org/10.1111/mve.12007

Supplementary Table 1. Correlation matrix (Pearson coefficients) of explanatory variables used for model selection. In bold the variables that were carefully selected for the model averaging due to potential collinearity. For variables that had >0.60 correlation coefficient, we specified that they could not be featured together in any model during the model averaging procedure Salinity was not allowed together with Nitrogen; Minimum Temperature and Maximum Temperature were not allowed in combination with mean temperature.

VARIABLES	% Teens	Pop. Density	% Woody Wetl.	% Grassy Wetl.	Median Income	% Flood Area	Salinity	Nitrogen	Median Richness	Road Density	Sewage Density	Min Temp	Max Temp	Mean Temp
% Teenagers	1.00	0.26	0.06	0.16	-0.42	0.09	-0.18	0.25	0.10	-0.12	-0.01	0.06	0.11	0.07
Population Density	0.26	1.00	-0.20	-0.28	-0.32	0.20	-0.18	0.08	-0.18	-0.15	0.46	0.34	-0.31	0.09
% Woody Wetlands	0.06	-0.20	1.00	0.32	0.06	0.01	0.05	0.07	0.41	-0.06	-0.23	-0.29	-0.01	-0.36
% Grassy Wetlands	0.16	-0.28	0.32	1.00	0.00	0.01	0.03	0.25	0.39	-0.10	-0.30	-0.29	0.16	-0.28
Median Income	-0.42	-0.32	0.06	0.00	1.00	-0.15	0.33	-0.36	-0.03	0.16	-0.16	-0.27	-0.16	-0.27
% Flood	0.09	0.20	0.01	0.01	-0.15	1.00	-0.06	0.25	0.13	-0.22	-0.01	0.19	0.02	0.17
Salinity	-0.18	-0.18	0.05	0.03	0.33	-0.06	1.00	**-0.65**	0.09	0.16	-0.09	-0.01	0.04	-0.03
Nitrogen	0.25	0.08	0.07	0.25	-0.36	0.25	**-0.65**	1.00	0.19	-0.29	-0.11	-0.04	0.09	0.01
Median Richness	0.10	-0.18	0.41	0.39	-0.03	0.13	0.09	0.19	1.00	-0.18	-0.29	-0.17	0.11	-0.09
Road Density	-0.12	-0.15	-0.06	-0.10	0.16	-0.22	0.16	-0.29	-0.18	1.00	0.00	0.07	0.21	0.13
Sewage Density	-0.01	0.46	-0.23	-0.30	-0.16	-0.01	-0.09	-0.11	-0.29	0.00	1.00	0.31	-0.11	0.12
Min. Temp	0.06	0.34	-0.29	-0.29	-0.27	0.19	-0.01	-0.04	-0.17	0.07	0.31	1.00	0.34	**0.76**
Max. Temp	0.11	-0.31	-0.01	0.16	-0.16	0.02	0.04	0.09	0.11	0.21	-0.11	0.34	1.00	**0.72**
Mean. Temp	0.07	0.09	-0.36	-0.28	-0.27	0.17	-0.03	0.01	-0.09	0.13	0.12	**0.76**	**0.72**	1.00

Supplementary Table 2 Results from Global Moran's I to test for spatial autocorrelation (method: inverse distance, Euclidean, default neighborhood search threshold 3450.4072 Meters). This analysis was made for the residuals of the global model, including all variables on Table1 in relation to dengue cases by census block group.

Global Moran's I to test for spatial autocorrelation of global model residuals	
Moran's Index	-0.022309

Expected Index	-0.005917
Variance	0.000360
z-score	-0.863551*
p-value	0.387835*

Given the negative z value and non-significant p value, the pattern does not seem to be significantly different from random, and no spatial-autocorrelation was detected.

Supplementary Table 3. Best models resulting from model averaging procedure using the selection criterion of AIC>4.

Component Models	Variables in the Model*	df	logLik	AICc	delta	weight
1	1/2/3/5/7/10/11/12	10	-495.41	1012.20	0.00	0.39
2	1/2/3/4/5/7/11/12	10	-496.20	1013.78	1.58	0.17
3	1/2/5/7/8/10/11/12	10	-496.29	1013.96	1.76	0.16
4	1/2/5/6/7/8/11/12	10	-496.51	1014.40	2.20	0.13
4	1/2/5/6/7/10/11/12	10	-496.84	1015.06	2.87	0.09
6	1/3/5/6/9/10/11/13	10	-497.27	1015.92	3.72	0.06

*Term Codes: 1) MaxTemp; 2) Median Income; 3) MinTemp; 4) Nitrogen; 5) Population Density; 6) %Flood Area; 7) %Grassy Wetlands; 8) %Woody Wetlands; 9) % Teenagers; 10) Salinity; 11) MaxTemp*Population Density; 12) Median Income*Grassy Wetlands; 13) %Teenagers*Salinity

Supplementary Table 4. Results from beta-binomial regressions for significant interactions. We categorized data above and below the mean for each variable featured in a significant interaction. We then selected pairs (above, below) that showed significant correlation in one or both of the categories, and also had opposite signs for their estimate coefficient. Here the selected terms are classified with the symbol ^.

Significant Interaction Tests	*Beta-binonimal Model Results*			
*1. Grassy Wetlands * Median Income*	Estimate	Std.Error	Z value	Pr (> |z|)
*1.1 Grassy Wetlands in High Median Income Neighborhoods^*	0.72	0.49	1.48	0.14
*1.2 Grassy Wetlands in Low Income Neighborhoods^*	-3.28	1.14	-2.87	<0.01
1.3 Median Income in Neighborhoods with High Grassy Wetland	-0.27	0.99	-0.27	0.79
1.4 Median Income in Neighborhoods with Low Grassy Wetland	-6.18	7.99	-0.77	0.44
*2. Max Temp*Population Density*	Estimate	Std.Error	Z value	Pr (>|z|)
*2.1. Max Temp in Neighborhoods with High Population Density^*	0.06	0.02	2.68	<0.01
*2.2. Max Temp in Neighborhoods with Low Population Density^*	-0.03	0.01	-2.57	<0.01
2.3. Population Density in High Max Temp Neighborhoods	25.69	16.44	1.56	0.12
2.4. Population Density in Low Max Temp Neighborhoods	-16.97	17.20	-0.98	0.32
*3. Salinity * % Teenagers*	Estimate	Std.Error	Z value	Pr (>|z|)
3.1. Salinity in Neighborhoods with High % Teenagers	-0.05	0.02	-2.74	0.006
3.2. Salinity in Neighborhoods with Low % Teenagers	-0.004	0.01	-0.25	0.80

*3.3. % Teenagers in Neighborhoods with High Salinity^*	-1.86	1.16	-1.59	0.11
*3.4. % Teenagers in Neighborhoods with Low Salinity^*	1.81	0.82	2.19	0.03

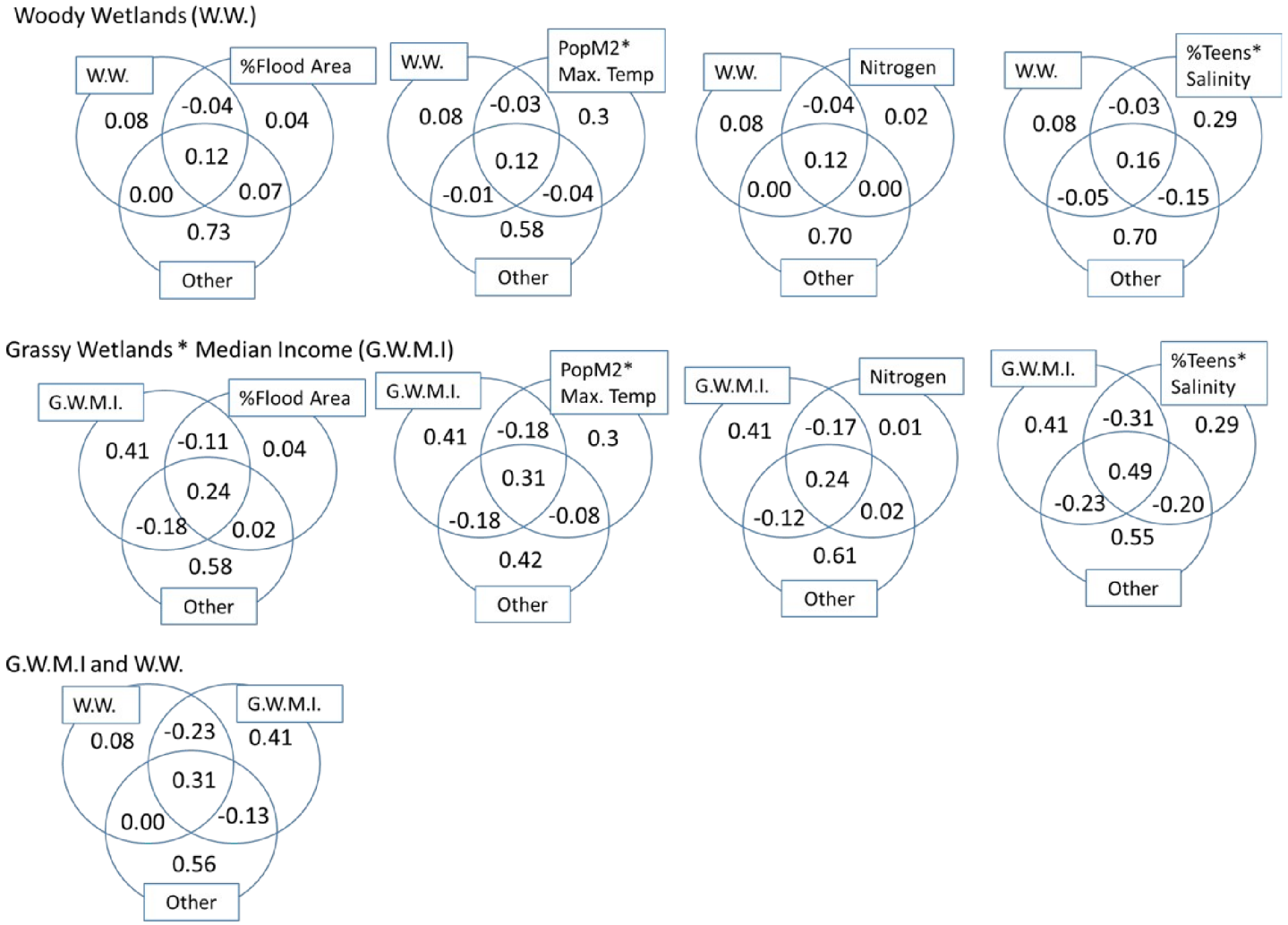

Supplementary Figure 1. Variation partitioning analysis between wetlands and other variables selected in the “best models.

Yee, Susan

From: Estrella D. Santiago Perez <esantiago@martinpena.org>
Sent: Friday, March 16, 2018 9:01 AM
To: Dejesus-Crespo, Rebeca
Cc: Balogh, Stephen; Wigand, Cathleen; Huertas, Evelyn; Fisher, Bill; Donald Yee (donald.yee@usm.edu); Wu, Jianyong; Jackson, Laura; Johnston, JohnM; Myer, Mark; tmunozerickson@gmail.com; Gladys Rivera; Jorge Bauzá; Christian Torres; benjamin.branoff@gmail.com; Elvia Melendez-Ackerman (elmelend@gmail.com); Alonso Ramirez; Alan Covich; Yee, Susan
Subject: Re: San Juan Wetland Ecosystem Services article available online

Thanks, Rebecca! I shared the article with ENLACE's staff and look forward to reading it!

Regards.

--
Lcda. Estrella D. Santiago Pérez
Gerente de Asuntos Ambientales | Environmental Affairs Manager
Corporación del Proyecto ENLACE del Caño Martín Peña
P.O. Box 41308 | San Juan, Puerto Rico 00940-1308
✉ esantiago@martinpena.org | ☎ (787) 729-1594 | 📱 (787) 689-1558 | 🖷 (787) 725-2544 | 🌎 www.cano3punto7.org / www.martinpena.org

AVISO DE CONFIDENCIALIDAD: Este correo electrónico y/o el material adjunto es para uso exclusivo de la persona o entidad a la que expresamente se le ha enviado, y puede contener información confidencial o material privilegiado. Si usted no es el destinatario legítimo del mismo, por favor repórtelo inmediatamente al remitente del correo y bórrelo. Cualquier revisión, retransmisión, difusión o cualquier otro uso de este correo, por personas o entidades distintas a las del destinatario legítimo, queda expresamente prohibido. Este correo electrónico no pretende ni debe ser considerado como constitutivo de ninguna relación legal, contractual o de otra índole.

CONFIDENTIALITY NOTICE: This email and/or accompanying material is for exclusive use of the person or entity to which it was expressly sent and may contain confidential or privileged material. If you are not the intended recipient of it, please report it immediately to the sender and delete the email. Any review, retransmission, dissemination or other use of this email, by persons other than the intended recipient entities, is expressly prohibited. This email is not intended nor should it be considered as constituting any legal relationship, contractual or otherwise.

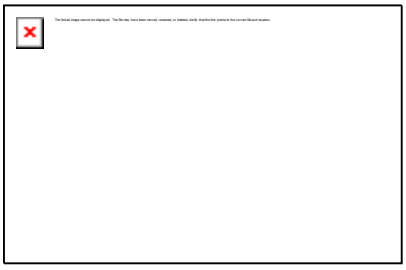

On Thu, Mar 15, 2018 at 9:31 AM, Dejesus-Crespo, Rebeca <dejesus-crespo.rebeca@epa.gov> wrote:

> Hi everyone,
>
> I wanted to share with you our article linking wetland ecosystem services to dengue fever in the San Juan Bay Estuary, which is now available online. Feel free to share it with others who might be interested.

Bests, Rebeca

https://link.springer.com/content/pdf/10.1007%2Fs13157-017-0990-5.pdf

Rebeca de Jesus Crespo, PhD

Ecologist

Gulf Ecology Division
National Health and Environmental Effects Research Laboratory
US EPA, Office of Research and Development
1 Sabine Island Drive, Gulf Breeze FL 32561-5299
tel: 850-934-9376

Yee, Susan

From: Jorge Bauzá <jbauza@estuario.org>
Sent: Monday, March 19, 2018 11:56 AM
To: Dejesus-Crespo, Rebeca
Cc: Balogh, Stephen; Wigand, Cathleen; Huertas, Evelyn; Fisher, Bill; esantiago@martinpena.org; Donald Yee (donald.yee@usm.edu); Wu, Jianyong; Jackson, Laura; Johnston, JohnM; Myer, Mark; tmunozerickson@gmail.com; Gladys Rivera; Christian Torres; benjamin.branoff@gmail.com; Elvia Melendez-Ackerman (elmelend@gmail.com); Alonso Ramirez; Alan Covich; Yee, Susan
Subject: Re: San Juan Wetland Ecosystem Services article available online

Excelente job!
Thank you,
Jorge

Jorge F Bauzá-Ortega, PhD; QEP
Science Director
San Juan Bay Estuary Program
Telephone: 787-725-8165
Fax: 787-723-8165
Website: www.estuario.org

2018-03-15 9:31 GMT-04:00 Dejesus-Crespo, Rebeca <dejesus-crespo.rebeca@epa.gov>:

> Hi everyone,
>
> I wanted to share with you our article linking wetland ecosystem services to dengue fever in the San Juan Bay Estuary, which is now available online. Feel free to share it with others who might be interested.
>
> Bests, Rebeca
>
> https://link.springer.com/content/pdf/10.1007%2Fs13157-017-0990-5.pdf
>
> Rebeca de Jesus Crespo, PhD
>
> Ecologist
>
> Gulf Ecology Division
> National Health and Environmental Effects Research Laboratory
> US EPA, Office of Research and Development
> 1 Sabine Island Drive, Gulf Breeze FL 32561-5299
> tel: 850-934-9376

Yee, Susan

From: Tischa Munoz-Erickson <tmunozerickson@gmail.com>
Sent: Friday, March 16, 2018 8:22 AM
To: Dejesus-Crespo, Rebeca; Pablo A Mendez Lazaro; Yee, Susan
Subject: Re: San Juan Wetland Ecosystem Services article available online

This is great Rebeca, congrats to you all!!

I will share with the ULTRA group. Susan, would it be alright if I also mention our new MOU with the EPA?

On Thu, Mar 15, 2018 at 6:31 AM, Dejesus-Crespo, Rebeca <dejesus-crespo.rebeca@epa.gov> wrote:

> Hi everyone,
>
> I wanted to share with you our article linking wetland ecosystem services to dengue fever in the San Juan Bay Estuary, which is now available online. Feel free to share it with others who might be interested.
>
> Bests, Rebeca
>
> https://link.springer.com/content/pdf/10.1007%2Fs13157-017-0990-5.pdf
>
> Rebeca de Jesus Crespo, PhD
>
> Ecologist
>
> Gulf Ecology Division
> National Health and Environmental Effects Research Laboratory
> US EPA, Office of Research and Development
> 1 Sabine Island Drive, Gulf Breeze FL 32561-5299
> tel: 850-934-9376

--
Tischa A. Muñoz-Erickson, Ph.D.

Research Social Scientist, USDA Forest Service, International Institute of Tropical Forestry,
http://www.fs.usda.gov/main/iitf/home

Principal Investigator, San Juan ULTRA, www.sanjuanultra.org

Principal Investigator, USAID CLIMA-IITF, Dominican Republic

Co-Principal Investigator, Urban Resilience SRN, www.urexsrn.net

Jardín Botánico Sur
1201 Calle Ceiba
Río Piedras, PR 00926-1119

cell phone: 928-600-1613
fax: 928-226-0056

Graduate Student Symposium

January 31– February 1, 2020

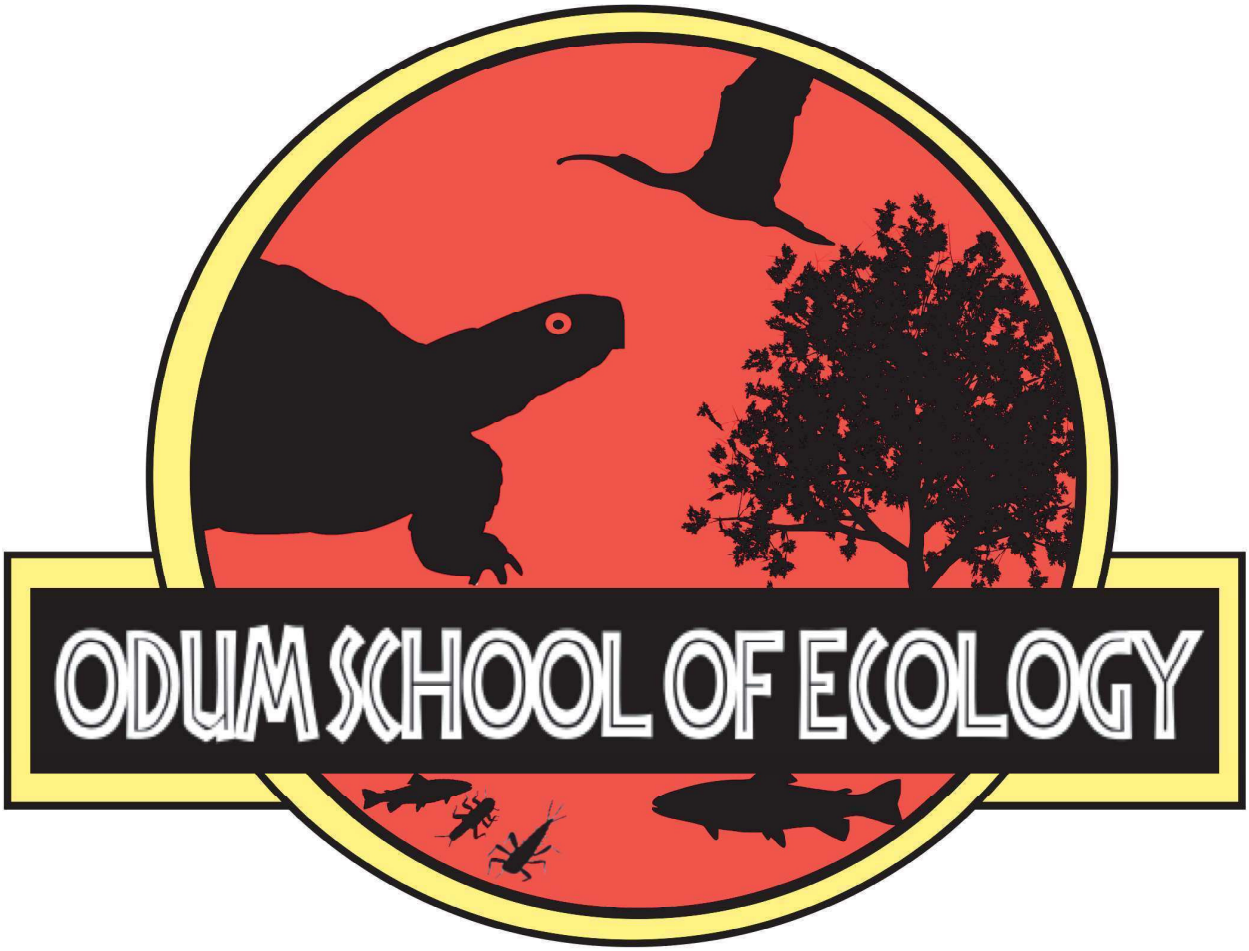

Graduate Student Symposium 2020
An Adventure 26 Years In The Making

Keynote Speaker

Rebeca de Jesús Crespo

Assistant Professor, Louisiana State University

Baton Rouge, Louisiana

Zooming out and in: applying geo-spatial technology and stakeholder engagement to study eco-health linkages in coastal communities

A common theme through my career has been the use of geo-spatial technologies to describe trends at the landscape level (zooming out) and engaging with stakeholders (zooming in) to help define research priorities and the practical implications of research findings. I have applied these approaches for the study of watershed management to improve stream integrity, and more recently, to study the linkages between ecosystem services with human health and well being. This seminar will describe projects developed for the US Environmental Protection Agency's Sustainable and Healthy communities program to better understand eco-health linkages. These projects characterized ecosystem service indicators at the landscape level in association to health outcomes identified as important by coastal communities in Puerto Rico, including gastrointestinal infections due to flooding, and mosquito borne diseases. Through ongoing projects on these topics, my work seeks to provide strategies at the community level to improve coastal resilience to environmental hazards, and manage ecosystem services for human health benefits.

Mosquito Misery: Can Environmental Changes Reduce Mosquito-Borne Disease?

By Christine Wendling

In autumn, as the heat becomes a bit more bearable and we enter football season, we begin to spend more time outdoors where we are sure to be plagued by that quintessential Louisiana nuisance—mosquitoes. And, mosquitoes are more than just an annual annoyance. Mosquitoes are common pests and vectors for diseases. But, what if more mosquitoes were actually the solution? Rebeca De Jesus Crespo is an assistant professor and landscape ecologist in LSU's College of the Coast & Environment who is exploring why virus-carrying mosquitoes proliferate in New Orleans and San Juan, Puerto Rico and how promoting mosquito diversity may reduce disease transmission. And, she is looking for New Orleans citizens who would like to assist in her research.

De Jesus Crespo was part of a team of scientists that explored how habitat alteration has led to flooding and water pollution problems in San Juan, Puerto Rico, and whether these factors could be related to increasingly common outbreaks of diseases such as dengue, Zika, and chikungunya (pronounced "CHIK-ən-GUN-yə") there. They found that unlike regular rainwater, flooding in these neighborhoods may have brought an influx of nutrients in the water, which were linked to higher virus concentrations in the mosquito vectors. In another study, De Jesus Crespo found that wetland cover helped to reduce temperatures in the city of San Juan, and that this was associated with lower cases of dengue in certain neighborhoods.

San Juan and New Orleans are similar in that both are metropolitan cities experiencing an increase in flooding, water pollution, and urban heat islands. And, both cities contain yellow fever mosquitoes, the main mosquito vectors of Zika. Other species that could carry Zika are also present, including Asian tiger mosquitoes in New Orleans and Caribbean treehole mosquitoes in Puerto Rico. While all three species can bite humans and other animals, yellow fever mosquitoes prefer to snack on humans while the other two species are more opportunistic and bite other animals more often. These mosquito species are natural competitors, and De Jesus Crespo believes that increasing the presence of Asian tiger mosquitoes (and Caribbean treehole mosquitoes) could reduce the population of yellow fever mosquitoes —the vector that is most likely to transmit viruses to humans. Currently, Asian tiger mosquitoes are the dominate species in North America and, presumably, New Orleans. De Jesus Crespo believes that may be why New Orleans does not experience Zika epidemics like those in San Juan, yet.

"New Orleans has more of a winter, unlike San Juan, and it gets too cold for yellow fever mosquitoes to survive that long here. But, the question is whether, in the future, hotter temperatures due to climate change would lead to more favorable conditions for transmission from any of these vectors," De Jesus Crespo said.

Yellow fever mosquitoes are better adapted to higher temperatures than Asian tiger mosquitoes. Therefore, if New Orleans were to become hotter and drier, that may tip the scales to favor yellow fever mosquitoes and increase the risk of Zika.

“If you combine that with other factors such as floods and water pollution, which also seem to favor the disease, then we may have an even bigger problem,” De Jesus Crespo said.

So, this August, De Jesus Crespo and her graduate student, Rachel Rogers, are going to visit local mosquito hot spots in New Orleans in order to map the mosquito populations of these two species.

“If we are able to say, ‘In this neighborhood the temperature gets really hot, there’s no tree cover, and it’s flood prone and so we got all these surges in nutrients and it just so happens that we have more abundance of yellow fever mosquitoes here than in other neighborhoods,” then that’s data that we can use to make projections into the future to see how the risk could change,” De Jesus Crespo said.

They will work closely with the New Orleans Mosquito, Termite and Rodent Control Board to define their study sites, particularly flood prone neighborhoods, and they are hoping to find residents who are willing to help. They plan to collect the mosquito data by placing traps in people’s homes that will help them characterize adult mosquito populations, and if the mosquitoes are feeding preferentially on humans or other animals. They will also collect data on nutrients, flood risk, temperature and tree cover around the homes to determine if any of these traits are associated with mosquito trends.

If you live in New Orleans, and are interested in participating, please contact Rebeca De Jesus Crespo at **rdejesuscrespo1@lsu.edu (mailto:rdejesuscrespo1@lsu.edu?subject=)**.

Additional Information

View De Jesus Crespo’s papers:

- **Linking Water Quality to Aedes aegypti and Zika in Flood-Prone Neighborhoods (https://www.ncbi.nlm.nih.gov/pubmed/30945160)**
- **Linking Wetland Ecosystem Services to Vector-borne Disease: Dengue Fever in the San Juan Bay Estuary, Puerto Rico (https://link.springer.com/article/10.1007/s13157-017-0990-5)**

-30-

Contact Christine Wendling

LSU College of the Coast & Environment

225-578-4984

christinew@lsu.edu (mailto:christinew@lsu.edu?subject=)

LSU (/index.php)

Louisiana State University (http://www.lsu.edu/index.php?utm_source=lsuhomepage&utm_medium=footer&utm_content=textlink&utm_campaign=internal_site_traffic)
Baton Rouge, Louisiana 70803
webmaster@lsu.edu (mailto:webmaster@lsu.edu)

Provide Website Feedback (/feedback/index.php)
Accessibility Statement (/accessibility/index.php)
Privacy Statement (/privacy/index.php)

(https://www.facebook.com/pages/LSU-School-of-the-Coast-Environment/432504395174)
(https://twitter.com/LSU_CCE)
College of the Coast and Environment
93 South Quad Drive
Suite 1002
Baton Rouge, LA 70803
Telephone: 225-578-6316
Fax: 225-578-5328

Email (mailto:kfalls1@lsu.edu?subject=)

Copyright **© (http://a.cms.omniupdate.com/10?skin=oucampus&account=lsu&site=www&action=de&path=/cce/newsevents/news/2019/08/09-de-jesus-crespo-mosquitoes.pcf)**
2020 **Louisiana State University (/index.php)**. All Rights Reserved.

https://www.lsureveille.com/news/lsu-professor-studies-virus-carrying-mosquitoes-conducting-research-in-new-orleans/article_72d49a9a-cdd4-11e9-a76b-37a549633101.html

LSU professor studies virus-carrying mosquitoes, conducting research in New Orleans

Sophie Liberto | @LibertoSophie
Sep 4, 2019

Environmental Sciences Assistant Professor Rebeca de Jesus Crespo conducts research.
Courtesy of Professor Rebecca de Jesus Crespo

It's no secret that mosquitoes run rampant in Louisiana, as anyone who tries to go outside may know.

Environmental Sciences Assistant Professor Rebeca de Jesus Crespo is exploring why virus-carrying mosquitoes are all over New Orleans.

De Jesus Crespo is interested in studying how ecosystems develop in relation to trees in urban areas, which often affects mosquito assemblages, the gathering of mosquitoes. Trees can change temperatures in the city, or microclimates, making temperatures cooler.

Some mosquitoes are more tolerant to high temperatures than others. The more tolerant mosquitoes are to high temperatures, the more likely they are to transmit diseases.

Because of global warming projections, conditions are expected to become more favorable for mosquitoes that can tolerate higher temperatures. De Jesus Crespo's team hopes by adding trees and creating shade, they will have less harmful mosquitoes. This will reduce the number of mosquito borne diseases in communities.

De Jesus Crespo has always been interested in environmental conservation. While studying insects' role in water quality conservation, she decided she wanted to learn more about insects' impact on the environment as a whole.

"I started studying water quality conservation and looking at insects as indicators of water quality," de Jesus Crespo said. "That made me really interested in insects in general and how they can tell us something about the environment."

This interest in water quality and insects led to her fascination with mosquitoes, which live in water as larvae.

This is de Jesus Crespo's first year at the University, but she started the project while she was in Puerto Rico. Due to similarities like urban sprawl and warm temperatures, she wants to compare her findings from San Juan, where she grew up, to her Louisiana research.

De Jesus Crespo's project is currently in the design phase. She plans to start collecting data in New Orleans in October. She said that anyone with a home in New Orleans can help participate in the study.

"My study requires me to put traps in people's homes in New Orleans," de Jesus Crespo said. "If anybody is interested in participating in the study and letting me put the trap in their home for mosquitoes, it would be great."

EPA/600/R-17/309 | August 2017 | www.epa.gov/research

United States
Environmental Protection
Agency

Valuing Community Benefits of Final Ecosystem Goods and Services: Human Health and Ethnographic Approaches as Complements to Economic Valuation

SHC PROJECT 2.61

EPA/600/R-17/309
August 2017

Valuing Community Benefits of Final Ecosystem Goods and Services: Human Health and Ethnographic Approaches as Complements to Economic Valuation

SHC Project 2.61

by

John M. Johnston[1], Rebeca de Jesus Crespo[1], Matt Harwell[1], Chloe Jackson[1], Mark Myer[2], Nadia Seeteram[2], Kathleen Williams[2], Susan Yee[1], Joel Hoffman[1]
[1]U.S. Environmental Protection Agency
[2]Oak Ridge Institute for Science and Education
Washington, DC

Project Officer John M. Johnston

Computational Exposure Division
National Exposure Research Laboratory
Athens, GA 30605

2. Human Health Approaches – Causal Inference

2.1. Causal Criteria Analysis

In epidemiology, observed associations between human health and environmental, social, or behavioral variables are applied to inform causal inference about potential drivers of disease (Merrill et al. 2008). The principles of causal inference, consistency, strength of association, temporality, biological plausibility, and specificity[3] (Merrill et al. 2008), need to be met in order for cause-effect relationships to be supported. Causal criteria analysis applies these principles to determine the weight of evidence towards causal connections in terms of: 1) probabilistic evidence (i.e., consistent cause-effect association); and 2) mechanistic evidence (i.e., logical explanation of how the causal association occurs) (Russo and Williamson 2007). A classic example of the application of this approach is the Surgeon General's 1964 report on smoking and health, which has become a landmark of how science can be effectively applied in decision making for the benefit of human health (Parascandola et al. 2006).

Regarding ecosystem services, U.S. EPA's Eco-Health browser provides a comprehensive inventory of the best available science supporting the complex relationships between different ecosystems, human health and well-being. This tool provides a starting point to construct a causal criteria analysis on this context and better understand which linkages have enough evidence to be used as a basis for management applications and which should be regarded as working hypotheses in need of more research.

2.2. Application of Causal Criteria Analysis to Evaluate the Role of Green Space EGS on Human Health

Building on U.S. EPA's Eco-Health browser, a causal criteria analysis was conducted using Eco Evidence an open source software tool that incorporates causal inference principles (Eco-Evidence tool; accessed 20, July 2017) (Norris et al. 2011). The focus of this analysis were linkages between diseases and the buffering EGS provided by green spaces (de Jesus Crespo and Fulford 2017; Figure 2.1). Buffering EGS refers to the ecosystem's capacity to buffer against health impacts by removing pollutants from air and water, and mitigating heat and water hazards (Jackson et al. 2013). The term green space refers to any vegetation within a human dominated environment (Kabisch and Haase 2013). This includes urban trees, green roofs, and natural or constructed wetlands, all of which provide EGS that influence health (GI – gastrointestinal, CVD - cardiovascular disease). Green spaces intercept water,

[3] Consistency: the association has been replicated by different research projects; Strength of association: the association is not due to bias or confounding factors, and is statistically significant; Temporality: exposure to a suspected cause precedes the disease; Biological plausibility: a logical biological mechanism for the association exists; Specificity: the exposure and disease are specific to one another (this condition is not always needed in order to support causality) (Merrill et al. 2008).

promote infiltration, and serve as barriers to storm surges, leading to water hazard mitigation (Brody and Highfield 2013, Costanza et al. 2008). Mitigation of water hazards reduces exposure risk to polluted flood waters and GI disease (Wade et al. 2004). It also reduces the risk of post-flood household dampness, which could lead to mold growth and asthma (Chew et al. 2006). Green spaces also promote clean water by immobilizing and absorbing infectious and toxic pollutants (Karim et al. 2004, Silva et al. 1990) and reducing the risk of GI disease from contact or consumption (Araya et al. 2004, Katukiza et al. 2014). In addition, green spaces filter air pollutants (Räsänen et al. 2013) that cause respiratory illness and cardiovascular disease (Brook et al. 2004, Peters et al. 1997). They also provide shade and evapotranspiration, lowering the risk of heat wave induced morbidities (Bouchama and Knochel 2002).

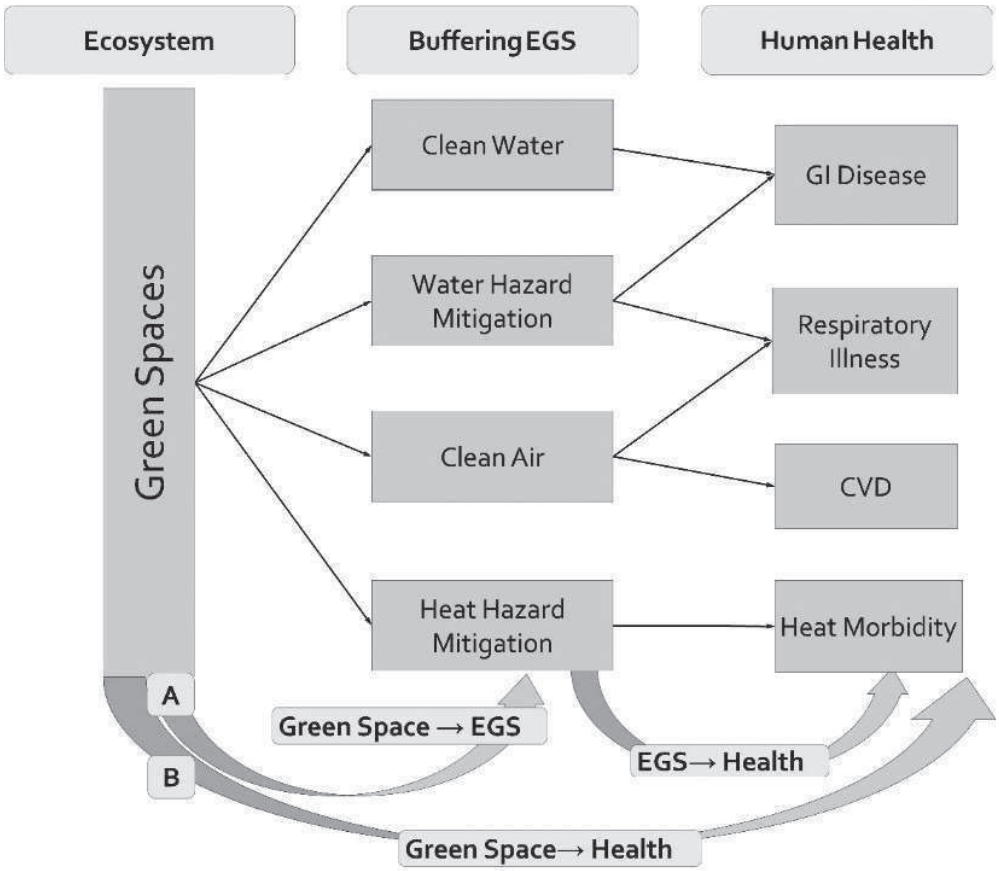

Figure 2.1 Eco-health pathways connecting the ecosystem attribute, green spaces, to human health endpoints through indirect ("A"; buffering EGS) and direct ("B"; human health) pathways. Figure from de Jesus Crespo and Fulford (2017).

While all these linkages are mechanistically plausible, our results showed that the weight of evidence supporting each of them varies as shown in Table 2.1. Notably, most of the current eco-health literature supports findings of intermediate steps (e.g., ecosystem to buffering EGS and buffering EGS to human health), but there is limited support for direct linkages from ecosystem (green spaces) to human health (disease endpoints) (Table 2.1). For example, while there is sufficient evidence supporting water pollution removal by vegetation, and sufficient evidence supporting a connection between certain water pollutants and GI disease, there is insufficient evidence supporting a direct connection between vegetation and GI disease (Table 8.3). Studies including all the components of the causal relationships are much needed as they would help provide clear management recommendations, such as the effectiveness of different plant species, relationships to the built environment and expected effect sizes of restoration initiatives. For more details of these results and the methods used see Appendix 3, and de

Jesus Crespo and Fulford (2017).

Table 2.1 Results of causal criteria analysis of eco-health linkages. (For more details, see Appendix 3; adapted from de Jesus Crespo and Fulford 2017).

Linkage	Total Studies Found	Total Studies Reviewed	Weight of Evidence in Favor	Weight of Evidence not in Favor	Conclusion
Green Spaces and Buffering EGS					
Green Spaces-Clean Water	60	44	166	16	Support for Hypothesis
Green Spaces-Water Hazard Mitigation	28	19	106	16	Support for Hypothesis
Green Spaces-Clean Air	44	22	105	16	Support for Hypothesis
Green Spaces-Heat Hazard Mitigation	31	19	117	3	Support for Hypothesis
Buffering EGS and Human Health					
Clean Water-GI Disease	11	6	35	0	Support for Hypothesis
Water Hazard Mitigation-GI Disease	9	7	41	7	Support for Hypothesis
Water Hazard Mitigation-Respiratory Illness	4	4	16	5	Insufficient Evidence
Clean Air-Respiratory Illness	37	28	247	178	Inconsistent Evidence*
Clean Air-Cardiovascular Disease (CVD)	27	23	206	143	Inconsistent Evidence*
Heat Hazard Mitigation-Heat Morbidities	22	18	114	2	Support for Hypothesis
Green Spaces and Human Health-Direct					
Green Spaces-GI Disease	0	0	0	0	Insufficient Evidence
Green Spaces-Respiratory Illness	9	7	28	27	Inconsistent Evidence*
Green Spaces-CVD	9	3	27	0	Support for Hypothesis
Green Spaces-Heat Morbidities	10	4	35	0	Support for Hypothesis

* Note: the finding of "inconsistent evidence" may indicate potential confounding factors that play a mediating role, or highlight the role that context and the types of indicators used could play in detecting a given cause and effect relationship. See Nichols et al. (2011) for more details on interpreting this and other conclusions derived using this approach.

2.3. Empirical Approaches for Eco-Health Research

Causal criteria analysis allowed identifying a research agenda (Appendix 3) to advance our

understanding of eco-health linkages. Conceptual models, such as the Final Ecosystem Goods and Services framework (Figure 2.2), have been developed to guide research on this topic, and may be applied to address research needs. The FEGS framework includes four key components: Ecosystem state metrics, EGS indicators, Health benefit indicators, and Socio-economic factors, which are essential to fully characterize eco-health relationship pathways.

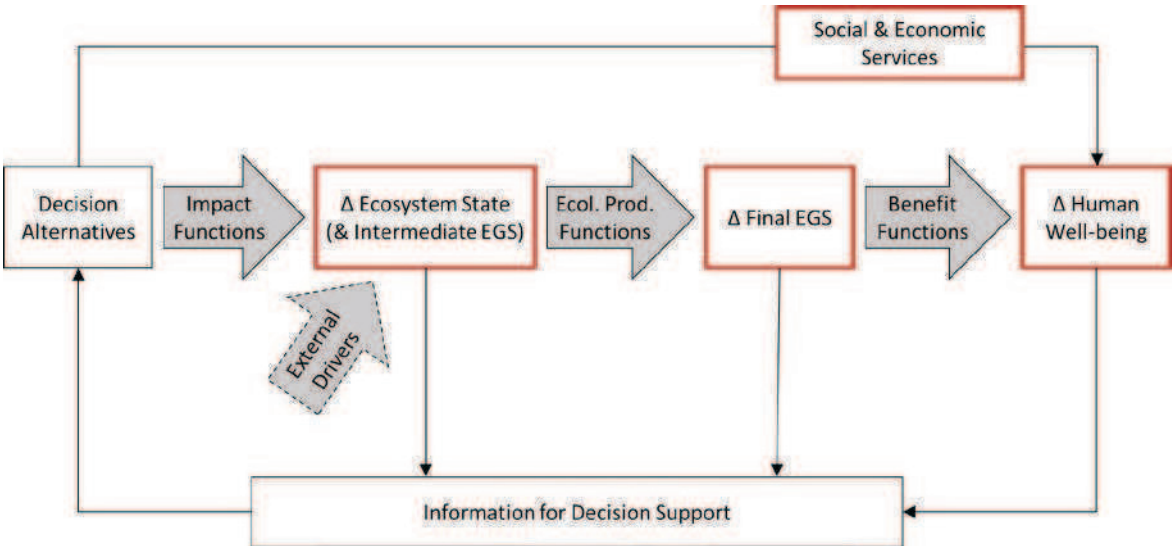

Figure 2.2 Conceptual Model for measuring Final Ecosystem Goods and Services. Areas measured through studies linking ecosystem services to health and well-being outcomes are highlighted in red.

Conducting spatially explicit correlation analyses is a logical first step towards testing eco-health conceptual models such as FEGS. Mapping platforms provide a way to test the spatial relationship between EGS and disease, contingent on the existence of suitable datasets to characterize the extent and quality of ecosystem services, to understand the socio-economic context, and to locate disease hotspots. Appendix 4 explores issues of data accessibility and granularity in mapping human health outcomes for spatially explicit correlation analyses approaches in eco-health studies.

For indicators that help map EGS, useful approaches include (but are not limited to) habitat suitability assessments, locations of trails or other recreational facilities, and modeling natural viewscapes. Angradi et al. (2016) mapped EGS in the Great Lakes region; the study provides a useful example of how to use existing datasets for EGS mapping, incorporating factors such as data uncertainty and tradeoffs into the analysis. Available sources for mapping EGS include the U.S. Geological Survey's National Gap Analysis Program, which helps estimate the distribution of species and ecosystems of interest, and the U.S. EPA EnviroAtlas (EnviroAtlas; accessed 20, July 2017) (Jackson et al. 2013), which helps visualize the extent of ecosystem services, among others.

Defining the spatial distribution of EGS is only the first step to modeling eco-health linkages. Socio-economic factors may exacerbate or decrease vulnerability to EGS loss and certain communities may be protected from the impacts of degrading EGS due to behavioral adaptations, technological adaptations, or access to EGS from other regions (Figure 2.3). These factors have been termed insulating layers (Myers et al. 2013), and are generally associated with wealth and access to information. Incorporating socio-economic indicators that reflect the potential for certain communities to benefit more than others from EGS provision (e.g., U.S. Census datasets) should be an essential part of studies assessing eco-health linkages.

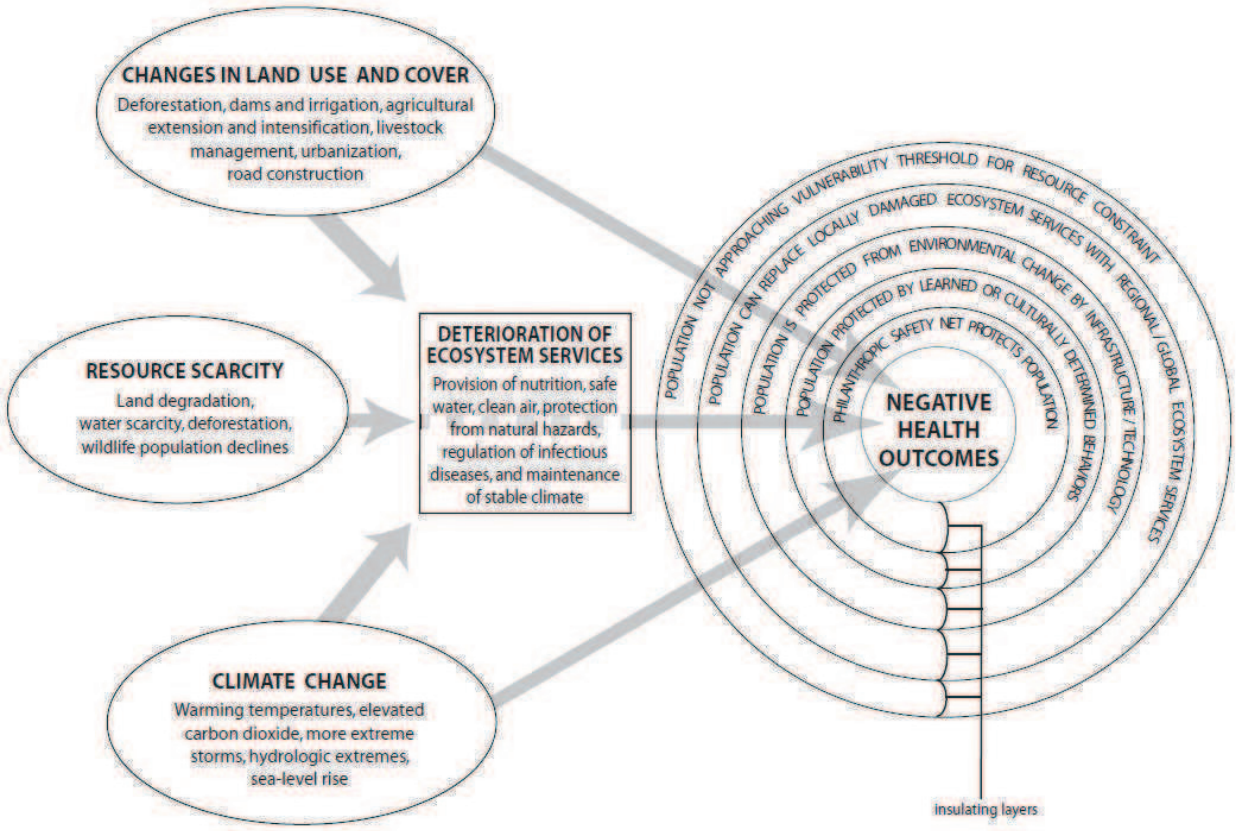

Figure 2.3 Schematic of the complex relationships between altered environmental conditions and human health. The impact of ecosystem goods and services loss is modified by socio-economic factors, termed insulating layers, which can ameliorate potential negative outcomes. Adapted from Myers et al. (2013).

Aside from health benefits, there are other human benefits associated with ecosystem services, such as safety, culture, and living standards. EPA's Human Well-Being Index (HWBI) provides a conceptual framework for mapping well-being at multiple scales in the United States (Smith et al. 2012, Smith et al. 2014), as well as forecasting changes due to loss of EGS (Summers et al. 2016). The HWBI is a tool that can be used to complement Eco-Health studies for a more general understanding of EGS benefits at the county and state levels.

Similar to economic benefit valuation (Figure 2.4; Wainger and Mazzotta 2011), research approaches for assessing health benefits could fall within a gradient of complexity, from the empirical analysis of conceptual models, as we propose here, to the use of simulation tools that predict loss of benefit from changes in EGS. Most conceptual models that describe eco-health linkages need more empirical evidence to develop quantitative relationships. Therefore, the use of simulation models is limited in this context to the few associations that have been studied extensively. A discussion of the use of data-derived models for simulating eco-health benefits is presented in Appendix 2.

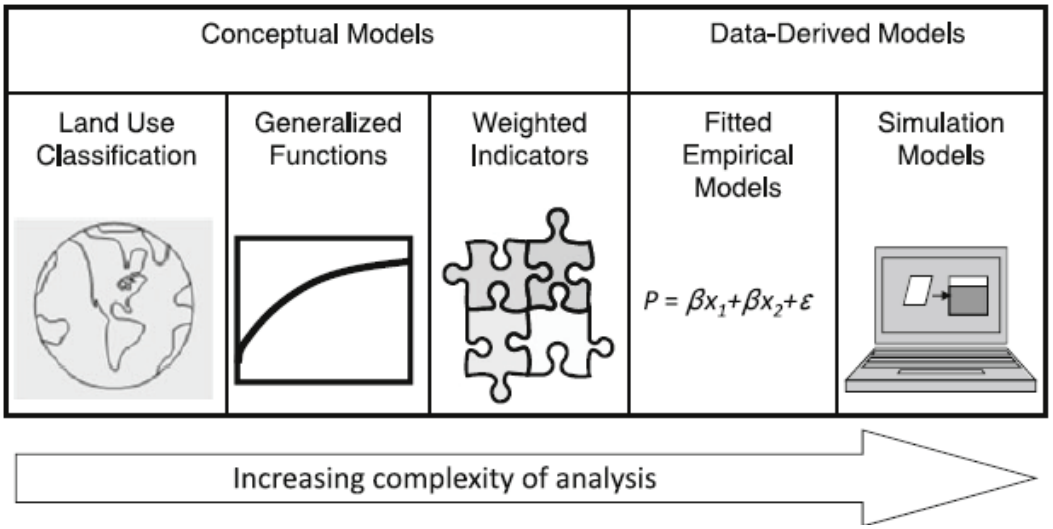

Figure 2.4 The gradient of modeling complexity shows different types of analysis used to generate the functional relations that estimate benefits of ecosystem goods and services management. From Wainger and Mazzotta (2011).

2.4. Upcoming Application of Empirical Approaches for Eco-Health Research in the San Juan Bay Estuary, PR

The communities in the SJBE, have identified many key health concerns associated with environmental stressors (Sheffield et al. 2014, Méndez-Lázaro et al. 2015). To help mitigate these stressors, the restoration of green spaces has been suggested a potential management strategy to improve health and well-being for SJBE residents (SJEB Management Plan 2017; accessed 26, July 2017). However, more studies are need to address the expected effectiveness of these practices. This case study seeks to quantify health outcomes associated with green space cover and buffering EGS using the FEGS framework (Figure 2.2) as a conceptual model. Using this approach entails identifying key ecosystems, ecosystem services, and socio-economic variables that are likely to influence health outcomes in the SJBE (Table 2.2), and then using statistical approaches to establish whether there is quantitative evidence for relationships between these key variables. Existing publicly available data sources could serve as indicators for each of these elements, in order to address the complex relationships in a cost-effective manner.

Some challenges to consider include disparate spatial scales of datasets to be included in the model, and restrictions on the availability of fine-scale human health information due to privacy considerations. Mechanisms to access detailed health data include establishing collaborations with health organizations, purchasing licenses to insurance claims or hospital data, or collecting information directly through surveys. All of these processes require consideration of PII and IRB restrictions. Appendix 5 presents a discussion on the challenges of collecting these types of data. To address limitations on the use of restricted health data, the SJBE case study will leverage collaborations with laboratories that have a health focus and the expertise in epidemiological research. This would not only allow access to data, but also foster cross-disciplinary dialogue to better inform the design and interpretation of a multidisciplinary topic such as eco-health linkages.

Table 2.2 Variables within the FEGS framework to evaluate Eco-Health linkages for the SJBE between green spaces or coastal wetlands and heat morbidities, GI disease, and Dengue fever.

ECOSYSTEM STATE		ECOSYSTEM GOODS AND SERVICES		Δ HUMAN HEALTH BENEFITS		SOCIO-ECONOMIC FACTORS	
NAME	Indicator	Name	Indicator	Name	Indicator	Name	Indicator
GREEN SPACES	% Green Space Cover	Heat Hazard mitigation	Surface temperature derived from satellite images (Landsat 8); Heat Wave Event time period	Heat Morbidities	Medicare Claims for heat related morbidities:	Wealth (influences air conditioning use, housing quality)	Median Income
COASTAL WETLANDS	% Wetland cover	Water Hazard Mitigation	FEMA[1] Flood Claims, Rainfall, Extreme flood event time period	Gastro-Intestinal Disease	Medicare Claims data for gastro-intestinal diseases	Infrastructure (influences storm water management effectiveness)	Sewage density
COASTAL WETLANDS	% Wetland cover	Habitat for Species (i.e., Biological Control)	Vertebrate Species Richness (Gould et al. 2008)	Dengue fever	Dengue prevalence (CDC[2])	Wealth (influences air conditioning use, housing quality)	Median Income
		Clean Water	Nitrogen Concentration (SJBE 2015)			Demographics (influences susceptibility to disease)	%Teenagers
		Heat Hazard mitigation	Surface temperature derived from satellite images (Landsat 8)			Infrastructure (influences vector habitat availability)	Sewage and road density

[1]FEMA: Federal Emergency Management Agency
[2]CDC: Center for Disease Control

As an example, ongoing studies in the SJBE are evaluating the role of wetland ecosystem services (e.g., biological control, clean water, and heat hazard mitigation) on Dengue fever (Figure 2.5). Heat hazard mitigation EGS may help reduce mosquito biting, ovi-position rate, and viral load; clean surface water provides habitat for wildlife and healthier ecosystems, favoring bio-control of mosquitoes (Araujo et al. 2015, Ibarra et al. 2013, Cox et al. 2007, Morin et al. 2015). Preliminary findings suggest that wetlands are negatively associated to Dengue cases even after controlling for potentially confounding variables (Table 2.2). They were also found to help reduce temperature (Figure 2.6), which is an environmental driver of Dengue transmission (Morin et al. 2015). These findings help support a connection between an important ecosystem in the SJBE, and an ecosystem service that directly influences human health. In the future, this and other eco-health research may help inform predictive models to estimate changes in health benefits under different decision scenarios.

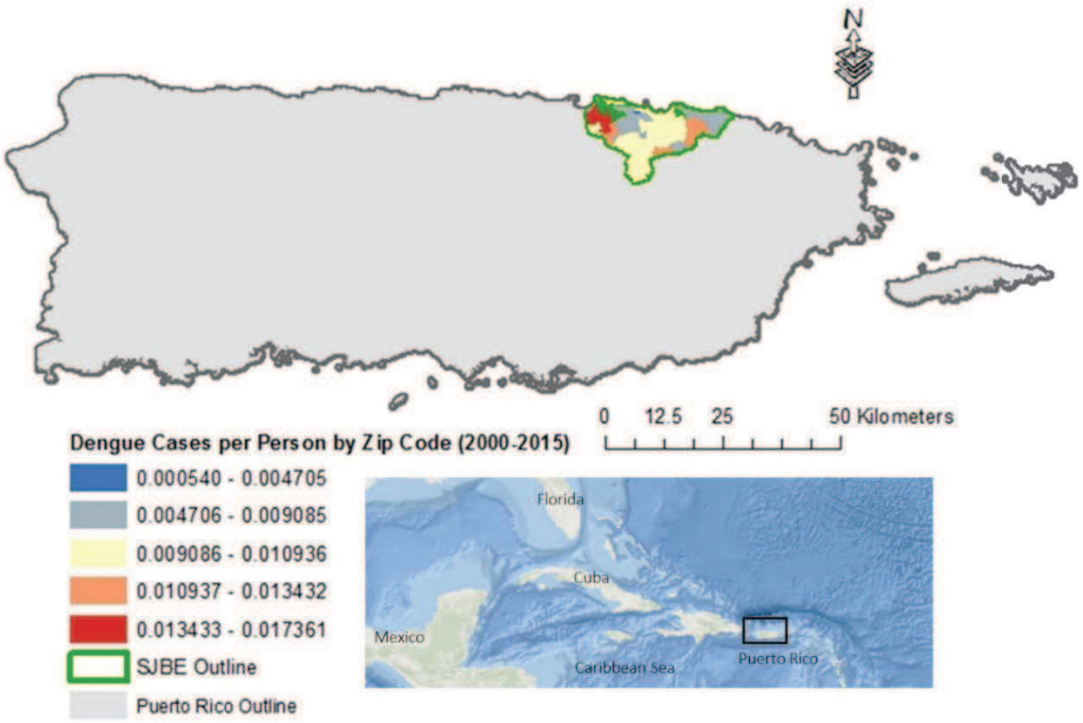

Figure 2.5 Dengue cases per person by zip code in the SJBE. Dengue data was provided by the CDC Dengue branch; Puerto Rico outline (United States Postal Service); Caribbean Map (DeLorme, MapmyIndia, © OpenStreetMap contributors, and the GIS community).

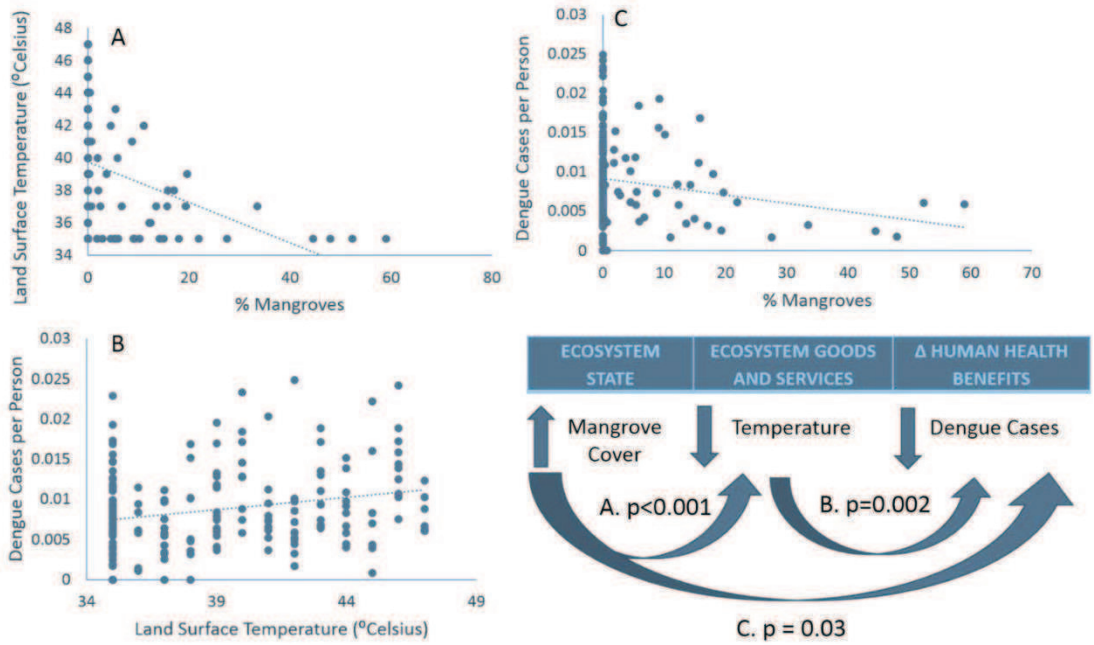

Figure 2.6 Preliminary findings of our study linking Dengue cases to wetland ecosystem services in the San Juan Bay Estuary (de Jesus Crespo et al. 2017). The p values for the linkages described in panel A and C were derived from Beta-binomial regressions including socio-economic confounding factors (Table 2.7). The p values from the link between mangroves and temperature were derived from simple linear regressions.

Work in the SJBE case study will link eco-health research to a decision context, which is the monitoring and management scenarios already proposed by the National Estuary Program (NEP). Aligning research objectives with those of the NEP will facilitate working with volunteers to collect data efficiently, promote educational opportunities, and improve the likelihood that the accumulating body of eco-health evidence (Table 2.2) is relevant and useful for decision makers.

2.5. Conclusions and Future Research Needs

Causal inference approaches allow researchers to use the best available science to inform evidence base decisions making. The principles of causal inference were applied to evaluate the weight of evidence linking green space EGS to human health and identify research needs. Results revealed that the evidence linking EGS to human health mainly supports intermediate steps, and very few published studies link the full pathways from ecosystem to disease. Establishing these linkages would be necessary to provide accurate non-monetary valuation of FEGS for community-based decision making. Specific research needs identified for the context of green space ecosystem services are summarized in Appendix 4 and include:

- Evaluating the association between green spaces on diseases such as GI disease and asthma by means of water hazard mitigation and clean water EGS;
- Defining the predominant mechanism driving the link between green spaces and cardiovascular benefits (i.e., physical activity or recreation versus air pollution removal);
- Better understanding the factors that determine if green spaces promote or prevent respiratory illness considering factors such as plant allergens, and re-circulation of pollutants trapped by foliage, among others.

For additional information on eco-health research needs involving ecosystems and health outcomes not discussed here, see Lee and Maheswaran (2011), Myers et al. (2013), Hartig et al. (2014), Hough (2014), and Sandifer and Sutton Grier (2014).

Addressing identified research needs could be facilitated by the application of conceptual models and using spatially explicit methods to empirically test these conceptual models. Studies evaluating eco-health linkages should take into consideration: 1) other aspects closely tied to human health and captured in conceptual models such as the FEGS framework; 2) the multidisciplinary nature of eco-health research; and 3) the importance of aligning research objectives to a decision context. In addition, issues of data accessibility and granularity in mapping human health outcomes as part of eco-health studies should also be considered (Appendix 4).

Examples were provided of the approach to incorporate these insights as part of ongoing research in the San Juan Bay Estuary, PR. Collaborating with local stakeholders and researchers across disciplines has facilitated progress in terms of identifying secondary data sources and defining priority questions to better inform non-monetary valuation of FEGS in this case study community.

The National Academies of SCIENCES ENGINEERING MEDICINE

SHARE

Current and Past Early-Career Research Fellows

Our Early-Career Research Fellows take risks on research ideas not yet tested, pursue unique collaborations, and build a network of colleagues who share their interest in improving offshore energy system safety and the well-being of coastal communities and ecosystems.

2019

Trisha Atwood
Utah State University
Dr. Atwood is an assistant professor in the Department of Watershed Sciences and the Ecology Center at Utah State University. Dr. Atwood earned her Ph.D. in aquatic ecology and conservation at the University of British Columbia and her B.A. and M.S. in marine science at the University of Hawaii at Hilo. Her research investigates factors that affect carbon accumulation and retention in marine sediments, as well as the distribution of carbon stocks in marine habitats. Her approach to science—which merges community ecology, ecosystem ecology, biogeochemistry, and conservation ecology—allows her to investigate novel questions in aquatic sciences with both pure and applied outcomes.

Shanondora Billiot
University of Illinois
Dr. Billiot (United Houma Nation) is an assistant professor in the School of Social Work at the University of Illinois. Prior to assuming this role, she was a pre-doctoral Henry Roe Cloud Dissertation Writing Fellow at Yale University. She earned a Ph.D. in social work from Washington University in St. Louis. She holds a master's of social work from the University of Michigan and both B.A. and B.S. degrees from Louisiana State University. Her research explores the intersection of health, environment, and culture among Indigenous peoples and is informed by post-graduate practice experience in disaster recovery community development and national policy analysis. Her current research uses mixed methods to explore Indigenous-specific sensitivities to global

This site uses cookies. For more information on cookies visit:
http://nas.edu/legal/privacy/index.html

Traci Birch
Louisiana State University
Dr. Birch became an assistant professor in the School of Architecture at Louisiana State University after three years of experience as a research faculty member at the same institution. She is also the interim managing director of the LSU Coastal Sustainability Studio. Her doctoral research focused on the ability and effectiveness of local communities to implement ecosystem management. Her post-doctoral research focuses on developing planning frameworks for coupled coastal-inland community resilience and well-being in the face of accelerated climate change. She holds a Ph.D. in urban studies and environmental management and a master's in urban and regional planning, both from the University of New Orleans. Her B.A. in graphic design is from Baldwin-Wallace University.

Edward Camp
University of Florida
Dr. Camp is an assistant professor of fisheries and aquaculture governance at the University of Florida. He received his Ph.D. and M.S. degrees in fisheries and aquatic sciences from the University of Florida, where he used quantitative socioecological models to study management strategies designed to improve economic and ecological outcomes for recreational fisheries. Dr. Camp employs similar inter- and multi-disciplinary approaches in his current work, which includes evaluating oyster fishery and aquaculture management strategies, understanding the effects of artificial reefs on fish populations and fishing-based economies, and developing decision tools for stock enhancement of freshwater fisheries. These projects all seek to forward the science of managing fish resources by creating greater understanding of how humans and fish populations affect each other and how both will be affected by different management actions. This understanding can be applied to decisions about how fish are used and to increase the resilience of fish-human systems.

Andia Chaves Fonnegra
Florida Atlantic University
Dr. Chaves Fonnegra is an assistant professor of biology in the Honors College and Harbor Branch Oceanographic Institute at Florida Atlantic University. She previously conducted postdoctoral research at the University of Mississippi, University of the Virgin Islands, and Nova Southeastern University. Dr. Chaves Fonnegra received her Ph.D. from Nova Southeastern University in oceanography and marine biology. She also holds an M.S. from Universidad Nacional de Colombia and a B.S. from Universidad Jorge Tadeo Lozano, both in marine biology. She was an UNESCO-L'Oréal Young Women in Science Fellow and a fellow at the Smithsonian Tropical Research Institute. Dr. Chaves Fonnegra runs the FAU Laboratory of Integrative Marine and Coastal Ecology, which focuses on understanding mechanisms that underlie changes in marine and coastal communities. Her own research focuses on enhancing management of marine ecosystems by determining how ecological

This site uses cookies. For more information on cookies visit:
http://nas.edu/legal/privacy/index.html

Rebeca de Jesus Crespo
Louisiana State University
Dr. De Jesús Crespo is an assistant professor in the Department of Environmental Sciences at Louisiana State University. She holds a Ph.D. in integrative conservation and ecology from the University of Georgia and M.S. and B.S. degrees in biology from the University of Puerto Rico (UPR). Awards from the UPR Center for Applied Tropical Ecology and Conservation, the Ford Foundation, and the Fulbright Program helped fund her graduate research. Dr. Jesús Crespo previously worked as a biologist for the Puerto Rico Department of Environmental and Natural Resources and as a postdoctoral researcher for the Environmental Protection Agency's National Health and Environmental Research Laboratory, where she earned the Gulf Ecology Division Scientist of the Year Award and the EPA Environmental Justice Award. Her research links landscape level patterns of anthropogenic activities, ecosystem services, and socio-economic factors to indicators of ecological integrity and human health.

Kim de Mutsert
George Mason University
Dr. de Mutsert is an assistant professor in the Department of Environmental Science and Policy at George Mason University and associate director of the Potomac Environmental Research and Education Center. She holds a Ph.D. in oceanography and coastal sciences from Louisiana State University and an M.S. in biology from the University of Amsterdam. Her research interests include ecosystem-based fisheries management and fish ecology in estuarine and coastal ecosystems. She studies the effects of environmental factors and anthropogenic impacts on fish abundance, biomass, community structure, and fisheries landings using end-to-end model simulations, large existing datasets, field surveys, and lab studies. Current projects in the Gulf of Mexico include evaluating effects of the hypoxic zone on fish and fisheries, incorporating ecosystem-based consideration in fisheries management, and assessing environmental impact of large sediment diversions on estuarine fisheries species.

Jessica Fitzsimmons
Texas A&M University
Dr. Fitzsimmons is an assistant professor in the Department of Oceanography at Texas A&M University. She received her Ph.D. in chemical oceanography from the Massachusetts Institute of Technology and Woods Hole Oceanographic Institute Joint Program and her B.A. in chemistry and biology with a specialization in marine science from Boston University. Dr. Fitzsimmons received the Carl-Gustaf Rossby Award, given for the best Ph.D. dissertation in MIT's Program in Atmospheres, Oceans, and Climate. She is an environmental analytical chemist whose research uses high precision, multi-element measurements of trace metal concentrations, isotope ratios, and speciation to understand how metals are transformed in marine waters. Recent projects have investigated open

This site uses cookies. For more information on cookies visit:
http://nas.edu/legal/privacy/index.html

projects in Galveston Bay and the Gulf of Mexico.

Mariana Fuentes
Florida State University
Dr. Fuentes is an assistant professor in the Department of Earth, Ocean, and Atmospheric Sciences at Florida State University. She received her Ph.D. in environmental sciences and marine biology from James Cook University. Previously she undertook a Super Science Postdoctoral Fellowship at the Australian Research Council Centre of Excellence for Coral Reef Studies, where she used an interdisciplinary approach to translate science to real-world application to advance marine species conservation planning. Her work has been recognized by the Australian Institute of Policy and Science and she was a recipient of the Young Tall Poppy Science Awards. Dr. Fuentes's expertise is in integrating field-based ecology with systematic conservation planning, decision-theory approaches, climate modeling, and applied qualitative and geographic spatial analysis. She uses these tools to explore how marine wildlife interact with environmental processes and how they are impacted by current and future threats.

Evan Goldstein
University of North Carolina at Greensboro
Dr. Goldstein is a research scientist in the Department of Geography, Environment, and Sustainability at the University of North Carolina at Greensboro. He earned a Ph.D. in earth and ocean sciences from Duke University and a B.A. in Geology from Colgate University. Previously he was a postdoctoral researcher and a research assistant professor at the University of North Carolina at Chapel Hill. Dr. Goldstein's research focuses on geomorphology and human-landscape interactions across the coastal zone. His recent work centers on the use of machine learning to study coastal geomorphology, studying developed coastal areas during and after storm events, and the dynamics of coastal dunes. He is an advocate for open science practices, specifically preprinting and open data.

James Nelson
University of Louisiana at Lafayette
Dr. Nelson is an assistant professor of biology at the University of Louisiana Lafayette. He completed his Ph.D. in chemical oceanography at Florida State University using stable isotope analysis to trace the major sources of energy in offshore food webs in the Gulf of Mexico. After completing his Ph.D., he received a Northeast Climate Science Center fellowship working at the Marine Biological Laboratory in Woods Hole, MA, where he researched linkages between long-term changes in climate and the marsh landscape to changes in the food webs and fish production. His current research uses a combination of field observation, experimental approaches, remote sensing, stable isotope analysis, and mathematical modeling to quantify how ecosystem change will alter energy flow

This site uses cookies. For more information on cookies visit:
http://nas.edu/legal/privacy/index.html

Kwame Owusu-Daaku
University of West Florida
Dr. Kwame Owusu-Daaku is an assistant professor in the Department of Earth and Environmental Sciences at the University of West Florida. He earned his Ph.D. in geography from the University of South Carolina, his M.S. in urban and regional planning from the University of Iowa, and his B.Sc. in development planning from the Kwame Nkrumah University of Science and Technology in Ghana. Dr. Owusu-Daaku's research focuses on the impacts of climate change and pollution on different groups in coastal communities in Northwest Florida and the efforts of these groups to build resilience to these impacts. He employs an interdisciplinary framework that engages multiple social science and humanities perspectives, including those of geography, planning, anthropology, and history. The goal of his research is to pair a focus on unequal impacts of socio-environmental change with strategies such as citizen science to build awareness of—and inspire action to improve—socio-environmental problems.

Allison Reilly
University of Maryland
Dr. Reilly is an assistant professor in the Department of Civil and Environmental Engineering at the University of Maryland. She is a civil engineer and risk analyst whose research explores the intersection of hazards, infrastructure, and policy. Dr. Reilly's work evaluates how coastal communities adapt infrastructure in response to repeated disasters, how disaster aid is used to fund infrastructure recovery projects, and how the built environment affects the livelihood of coastal residents. She is currently the PI on a National Science Foundation-sponsored research project exploring how to speed infrastructure recovery after disasters through improved information sharing. Dr. Reilly holds a Ph.D. and M.S. in civil engineering from Cornell University and a B.S. in civil engineering from Johns Hopkins University. Previously, she was a post-doctoral research associate at Johns Hopkins University and a research fellow at the University of Michigan.

Isabel Romero
University of South Florida
Dr. Romero is a research associate in the College of Marine Science at the University of South Florida (USF). Dr. Romero earned her Ph.D. in ocean sciences at the University of Southern California (USC) and her B.S. with a double major in biology and marine science at the Universidad del Valle in Colombia. Prior to joining USF, she was a postdoctoral fellow in the Earth Science Department and Biological Science Department at USC. Dr. Romero's research focuses on uncovering geochemical signatures in the ocean as archives of how marine systems function and respond to natural and anthropogenic events. Specifically, she studies the sources, transformation processes, and fate of molecules in the marine environment and biota to reveal temporal and spatial trends of physical and

This site uses cookies. For more information on cookies visit:
http://nas.edu/legal/privacy/index.html

The Ohio State University

Dr. Sawyer is an assistant professor in the School of Earth Sciences at The Ohio State University. He received his Ph.D. in geological sciences from the University of Texas at Austin, his M.S. in geosciences from Penn State University, and his B.S. in marine sciences from Eckerd College. Previously, Dr. Sawyer worked for ExxonMobil in offshore drilling in the Gulf of Mexico and other locations to plan and execute safe well designs and assess hazards for safe subsea development projects. At Ohio State, Dr. Sawyer's research focuses on natural hazards of submarine landslides, tsunami, earthquakes, and hurricanes. He examines them with indirect and direct methods, including geophysical data, borehole logs, sedimentary cores, numerical modeling, and physical experiments. Study sites span the range of shallow water coastal environments to deepwater continental margins and sedimentary basins in a range of tectonic settings.

Lauren Stadler

Rice University

Dr. Stadler is an assistant professor in the Department of Civil and Environmental Engineering at Rice University. Her research focuses on advancing sustainable and safe biological wastewater treatment, resource recovery, and bioremediation processes. Her group seeks to advance the control and engineering of microbial communities to improve the efficacy of treatment, understand the fate and removal of emerging contaminants, and advance resource recovery from waste. Her group integrates microbial ecology, environmental microbiology, and process engineering to study both engineered and natural systems. Before joining the faculty at Rice, Dr. Stadler earned her B.S. from Swarthmore College and M.S. and Ph.D. in environmental engineering from the University of Michigan, did a Fulbright scholarship in India, and worked in environmental consulting for several years.

Elaina Sutley

University of Kansas

Dr. Sutley is an assistant professor in the Department of Civil, Environmental and Architectural Engineering at the University of Kansas. She earned her Ph.D. in civil engineering from Colorado State University and B.S. and M.S. in civil engineering from the University of Alabama. Her research lies at the nexus of structural engineering, social science, and public policy with an emphasis on progressing interdisciplinary science for community disaster resilience. Dr. Sutley is a researcher for the National Institute of Standards and Technology Center of Excellence for Risk-Based Community Resilience Planning, where she leads a longitudinal community resilience-focused field study following Hurricanes Matthew and Florence. Dr. Sutley received the prestigious National Science Foundation CAREER award for integrated convergence research and education on community disaster resilience, and has on-going projects related to earthquake, hurricane, and tornado disasters, where she focuses on damage to residential buildings and modeling post-disaster housing

This site uses cookies. For more information on cookies visit:
http://nas.edu/legal/privacy/index.html

Florida Atlantic University

Dr. Tang is an assistant professor in the Department of Computer and Electrical Engineering and Computer Science at Florida Atlantic University. He received his Ph.D. in electrical engineering from the University of Rhode Island and his M.S. and B.Eng. in electrical engineering and automation from Hohai University. His research interests are in the general areas of computational intelligence and cyber-physical systems. His current research focuses on networked big data and system analytics and predictive maintenance of marine structures/systems. Dr. Tang has current collaborations with many research institutions, including the Southeast National Marine Renewable Energy Center, the Harbor Branch Oceanographic Institute, and the National Renewable Energy Laboratory. He is the recipient of the University of Rhode Island's Steve Bouley and Rhonda Wilson Graduate Fellowship, the Chinese Government Award for Outstanding Student Abroad, and Best Paper awards from the IEEE Power & Energy Society General Meeting and International Conference on Communications.

William Tarpeh

Stanford University

Dr. Tarpeh is an assistant professor in the Department of Chemical Engineering at Stanford University. The Tarpeh Lab develops and evaluates selective approaches to converting water pollutants into products by investigating molecular mechanisms of chemical transport and transformation; developing novel unit processes that increase resource efficiency; and conducting systems-level assessments that identify optimization opportunities. Most recently, Dr. Tarpeh has been studying selective nitrogen sensing and treatment using novel adsorbents and electrochemical separations. He completed his B.S. in chemical engineering at Stanford, M.S. and Ph.D. in environmental engineering at the University of California, Berkeley, and postdoctoral training at the University of Michigan in environmental engineering. Dr. Tarpeh is a member of the Bouchet Honor Society, NBCBLK's "28 Under 28" African-American Innovators, and Forbes' "30 Under 30" 2019 Science List.

Gabrielle Wong-Parodi

Stanford University

Dr. Wong-Parodi is an assistant professor in the Department of Earth System Science and a Center Fellow at the Woods Institute for the Environment at Stanford University. Her research focuses on applying behavioral decision research methods to address challenges associated with global environmental change. She uses behavioral decision science approaches to create evidence-based strategies for informed decision making, with a particular focus on building resilience and promoting sustainability in the face of a changing climate. Dr. Wong-Parodi has a background in energy resources, climate change adaptation and mitigation, and risk perceptions of emerging technologies. She recently served on the committee that produced the National Academies of Sciences, Engineering, and Medicine report Understanding the Long-Term Evolution of the Coupled Natural-

This site uses cookies. For more information on cookies visit:
http://nas.edu/legal/privacy/index.html

2018

Srijan Aggarwal
University of Alaska Fairbanks
Dr. Aggarwal is an assistant professor in the Department of Civil and Environmental Engineering at the University of Alaska Fairbanks. He completed a bachelor's in civil engineering from the Indian Institute of Technology-Delhi and an M.S. and Ph.D. in civil engineering with a focus in environmental engineering at the University of Minnesota-Twin Cities. He spent two-and-a-half years as a post-doctoral scholar in a joint appointment at the BioTechnology Institute and the Department of Civil, Environmental, and Geo-Engineering at the University of Minnesota-Twin Cities. Dr. Aggarwal specializes in the field of environmental biotechnology. He has specific interest in bacterial biofilms in environmental systems, expanding to biofilms at oil-water interface and resultant impacts on oil biodegradation in the marine environment. He is a recipient of the National Science Foundation CAREER award for his work on biofilms in drinking water.

Lauren Clay
D'Youville College
Dr. Clay is an assistant professor in the Health Services Administration Department at D'Youville College, an affiliated professor at the Disaster Research Center at the University of Delaware, and an affiliated professor in the College of Global Public Health at New York University. She has worked on studies of household and family recovery from Hurricane Katrina; the Deepwater Horizon oil spill; Superstorm Sandy; the 2013 tornadoes in Moore, Oklahoma; and Hurricane Harvey. She has also conducted international research on health and economic development as a Fulbright Fellow in Bangladesh. She has her M.P.H. from Drexel University and Ph.D. in disaster science and management from the University of Delaware. Dr. Clay utilizes social epidemiologic methods and interdisciplinary collaboration as tools for developing a deeper understanding of individual and ecological factors that influence how natural and environmental hazards affect family and community health and well-being. Currently, she is studying the post-disaster food environment and food insecurity.

Adrienne Simoes Correa
Rice University
Dr. Correa became an assistant professor in BioSciences at Rice University after five years of experience as a non-tenure track faculty member at the same institution. Her postdoctoral and

This site uses cookies. For more information on cookies visit:
http://nas.edu/legal/privacy/index.html

three years, Dr. Correa has helped advise management of coral reefs in the northwest Gulf of Mexico through her seat on the Flower Garden Banks National Marine Sanctuary Advisory Council. Dr. Correa's work monitors how marine microbial communities shift when human activities alter temperature, nutrient availability, and other conditions in coastal ecosystems. She is currently characterizing the impacts of viruses on coral reefs and is expanding these efforts into mangrove, salt marsh, and seagrass ecosystems.

Sarah Davies
Boston University
Dr. Davies is an assistant professor of Biology at Boston University, where she studies the ecophysiology and genomics of reef building corals. Although she has conducted research on corals reefs around the world, she has always maintained an active research program at the Flower Garden Banks in the Gulf of Mexico. Dr. Davies earned her M.S. in biology from the University of Calgary and her Ph.D. in ecology, evolution, and behavior from the University of Texas at Austin. During her M.S. and Ph.D. work, she was supported by fellowships with the Natural Sciences and Engineering Research Council and the National Science Foundation. She also worked as a postdoctoral researcher at the University of North Carolina at Chapel Hill, where she became a Simons Foundation Fellow of the Life Sciences Research Foundation. Research in the Davies lab focuses on the potential roles of acclimation, adaptation, and dispersal in an organism's response to rapid climate change.

Nicole Errett
University of Washington
Dr. Errett is a lecturer in the Department of Environmental and Occupational Health at the University of Washington. Her research interests and expertise are in the use of public policy to enhance health outcomes during and after disaster. Dr. Errett co-founded and co-directs the University of Washington Collaborative on Extreme Event Resilience (CEER), a network of public health researchers, practitioners, and community scientists who collaborate to address real world challenges that impact communities' resilience to disasters and the acute impacts of climate change. Dr. Errett holds a Ph.D. in health and public policy, an M.S.P.H. in health policy, and a B.A. in public health studies from the Johns Hopkins University. She completed post-doctoral training in coastal community resilience at the University of British Columbia's School of Community and Regional Planning. Dr. Errett is also a Robert Wood Johnson Foundation New Connections Scholar.

Ipsita Gupta
Louisiana State University
Dr. Gupta is an assistant professor in the Department of Petroleum Engineering at Louisiana State University. She received her Ph.D. from the University of South Carolina, M.Tech from the Indian

This site uses cookies. For more information on cookies visit:
http://nas.edu/legal/privacy/index.html

research is on integrated reservoir-wellbore multiphase flow and transport modeling, and numerical modeling of rock/fluid interaction across different spatial and temporal scales. Dr. Gupta's industry experience spans strategic research, technology development, and technical services, as well as large capital project maturation in the Gulf of Mexico. Besides research, Dr. Gupta enjoys teaching and uses her industry experience to mentor students on the real-life applications of petroleum engineering.

Pedram Hassanzadeh
Rice University
Dr. Hassanzadeh is an assistant professor in the Departments of Mechanical Engineering and Earth, Environmental, and Planetary Sciences at Rice University. Before joining Rice, he was at Harvard University as a Ziff Environmental Fellow with the Center for the Environment and a research associate with the Department of Earth and Planetary Sciences. Dr. Hassanzadeh received his Ph.D. in mechanical engineering and M.A. in mathematics from the University of California at Berkeley. Dr. Hassanzadeh's research is aimed at providing reliable scientific information with quantified uncertainties about the historical and future extreme events. Using fundamentals of atmospheric dynamics and hierarchies of idealized-to-comprehensive climate models, mathematical/statistical modeling, and advanced machine learning techniques, Dr. Hassanzadeh works on improving the understanding of extreme weather events and their dynamics, predictability, and response to climate change. His Environmental Fluid Dynamics Group at Rice studies fundamentals of geophysical/environmental turbulence and dynamics of large-scale atmospheric circulation and extreme weather events.

Marccus Hendricks
University of Maryland
Dr. Hendricks is an assistant professor in the School of Architecture, Planning, and Preservation and a faculty research affiliate with the Clark School of Engineering's Center for Disaster Resilience at the University of Maryland. He holds a Ph.D. in urban and regional science and a Master of Public Health, both from Texas A&M University. Dr. Hendricks' primary research interests include stormwater infrastructure resilience, social vulnerability to disaster, environmental justice, sustainable development, and participatory action. He utilizes a combined social vulnerability to disaster and environmental justice framework to explore the provision of green space, adequate sewer, community facilities, public works, and stormwater services by municipalities to marginalized neighborhoods, which can modify environmental outcomes and experiences related to infrastructure. Dr. Hendricks is a founding fellow of the William Averette Anderson Fund, the first national interdisciplinary organization working to increase the number of underrepresented persons of color in the field of disaster research, practice, and pedagogy.

This site uses cookies. For more information on cookies visit:
http://nas.edu/legal/privacy/index.html

Psychology at Boston College. She received her Ph.D. in clinical psychology from the University of Miami and completed her clinical internship at Stanford University School of Medicine. Dr. Lai's research focuses on how children and families respond to disasters and other traumatic stressors. Her work also examines how advanced statistical modeling strategies may be applied to better understand how to minimize the effects of disasters on children's functioning. She is the principal investigator on a project examining school recovery after disasters and a project to better understand how and why children differ in their distress responses following acute traumatic events. Dr. Lai was named a National Scholar for the Academy on Violence and Abuse and a Next Generation of Hazard and Disasters Researchers Fellow. Dr. Lai's work has been recognized with Early Career Awards from the American Psychological Association.

Vincent Lecours
University of Florida
Dr. Lecours is an assistant professor of Marine Remote Sensing & Geospatial Analysis at the University of Florida. He completed a B.S. in applied geomatics from the Université de Sherbrooke and received his Ph.D. in geography from Memorial University, where he studied the methods associated with the mapping of deep-water habitats. He worked with spatial data collected with a remotely operated vehicle between 650 and 10,000 feet deep in previously unexplored areas of the ocean. Dr. Lecours conducts cross-disciplinary research using geospatial technologies and spatial sciences. His research program bridges the spatial sciences with the marine sciences by studying ways to improve marine habitat mapping methods through a better integration of spatial concepts, such as spatial scale, autocorrelation, and spatial data quality, in the habitat mapping workflow. It is aimed at developing best practices in the application of geomatics-based marine habitat mapping to ecological and management questions.

Mark Losego
Georgia Tech
Dr. Losego is an assistant professor in the School of Materials Science and Engineering at the Georgia Institute of Technology (Georgia Tech). He received his B.S. from Penn State University and an M.S. and Ph.D. from North Carolina State University, all in materials science and engineering. Prior to joining the Georgia Tech faculty, he was a postdoctoral researcher at the University of Illinois and research faculty at NC State. At Georgia Tech, Dr. Losego runs a highly interdisciplinary research team that focuses on the science of vapor phase processing applied to unconventional materials sets for environmental protection, renewable energy, and national security technologies. His research spans from fundamental studies of surface chemistry and processing kinetics to the development of novel deposition equipment and manufacturing methods. He is also the faculty founder of the Materials Innovation and Learning Laboratory, an open-access make-and-measure space devoted to peer-to-peer, experiential education within the materials science discipline.

This site uses cookies. For more information on cookies visit:
http://nas.edu/legal/privacy/index.html

Dr. Mayo is an assistant professor in the Department of Civil, Environmental, and Construction Engineering at the University of Central Florida. She earned her B.S. in mathematics from Grambling State University, and she earned her M.S. and Ph.D. in computational sciences, engineering, and mathematics from The University of Texas at Austin. Dr. Mayo's research interests are interdisciplinary, but focus on numerical modeling of the coastal ocean. She develops mathematical tools to assess the risk of hurricane storm surges and to improve the hydrodynamic models required to do so, helping coastal communities strengthen their resilience to these hazards. Her research has the potential to greatly improve storm surge modeling for long term planning and emergency management.

Jill McDermott
Lehigh University

Dr. McDermott is a geochemist and an assistant professor in the Earth and Environmental Sciences Department at Lehigh University. She earned her B.A. in chemistry from Dartmouth College, an M.S. in geochemical systems from the University of New Hampshire, and a Ph.D. in chemical oceanography from the Massachusetts Institute of Technology and Woods Hole Oceanographic Institution Joint Program. Dr. McDermott received the Carl-Gustaf Rossby Award, given for the best Ph.D. thesis within MIT's Program in Atmospheres, Oceans, and Climate, and is a National Academy of Sciences Kavli Fellow. She investigates the aqueous and volatile geochemistry and biogeochemistry of seafloor hydrothermal vents and ancient terrestrial fracture waters tapped by deep mines. The multidisciplinary approach Dr. McDermott uses in her work carries over into her teaching and mentoring, where she engages students with fundamental and applied science in the classroom and in individual research projects in her lab.

Alejandra Ortiz
North Carolina State University
Dr. Ortiz is an assistant professor in the Department of Civil, Construction, and Environmental Engineering at North Carolina State University. She earned her B.A. in geosciences at Wellesley College with a double major in classical civilizations, and she completed an M.S. in civil and environmental engineering and a Ph.D. in marine geology from the Massachusetts Institute of Technology and Woods Hole Oceanographic Institution Joint Program. Dr. Ortiz's research is focused on coastal geomorphology and understanding the evolution of coasts under rising sea levels. She uses numerical models, satellite imagery, fieldwork, and a flume to study the evolution of coastal systems and predict their resiliency over the next century. Recent projects have looked at the impact of pond expansion on the Mississippi Delta coast resulting in large-scale land loss and the role of vegetation in delta resiliency with rising seas.

This site uses cookies. For more information on cookies visit:
http://nas.edu/legal/privacy/index.html

Dr. Patrick is an assistant professor at Texas A&M University-Corpus Christi, a research associate at the Smithsonian Environmental Research Center, and the director of MarineGEO Texas, a node in the Smithsonian Marine Global Earth Observatory. He received his B.S. in behavior, evolution, ecology, & systematics from the University of Maryland and his Ph.D. in ecology from the University of Notre Dame. He also performed post-doctoral research on Chesapeake Bay seagrass ecology at the Smithsonian Environmental Research Center and worked with the EPA Office of Water during his AAAS Science & Technology Policy Fellowship. His research program bridges freshwater and estuarine ecosystems to understand how anthropogenic stressors interact with natural environmental variation to drive spatio-temporal patterns in aquatic biodiversity and ecosystem functioning. This work both advances fundamental ecological theory and has direct applications in coastal ecosystem management and biomonitoring.

Kevin Smiley
University at Buffalo
Dr. Smiley is an assistant professor of Sociology at the University at Buffalo. He is also a core faculty member of the university's Research and Education in Energy, Environment, and Water (RENEW) Institute. He received his B.A. in history and sociology from Western Kentucky University, an M.A. in sociology from the University of Memphis, and a Ph.D. in sociology from Rice University. Dr. Smiley's research is at the intersection of environmental and urban issues, with foci including natural hazards, public space, and industrial air pollution. In particular, his research analyzes the social characteristics of human populations that are made more vulnerable because of land cover changes from vegetated landscapes to developed ones, as well as the characteristics of those who benefit from newly developed land. He is one of the authors, along with Michael Oluf Emerson, of Market Cities, People Cities.

Xingyong Song
Texas A&M University
Dr. Song is an assistant professor in the College of Engineering at Texas A&M University. He received his Ph.D. in mechanical engineering from the University of Minnesota. His research interests include drilling automation systems for more efficient and safe oil and gas production, mechatronic system design and dynamics control, and renewable energy systems enabled by advanced control technologies. Prior to appointment at Texas A&M University, he had industrial working experience at the General Motors Research Center and at the Halliburton Energy Service Company Innovation Center. While at Halliburton, he actively piloted control solutions to address advanced automation needs in the oil and gas industry, including drilling automation, well logging, and drilling fluid management and control. His novel control solution for the new Halliburton sonic logging tool won him the Halliburton Innovation of the Year Award.

Beth Stauffer

This site uses cookies. For more information on cookies visit:
http://nas.edu/legal/privacy/index.html

Lafayette. Prior to joining the UL Lafayette faculty, she was an AAAS Science & Technology Policy Fellow hosted by the U.S. Environmental Protection Agency and a Lamont-Doherty Postdoctoral Fellow at the Lamont-Doherty Earth Observatory of Columbia University. Dr. Stauffer's research focuses on understanding how dynamic physical environments and variable grazing interactions contribute to changing phytoplankton communities in coastal waters, and what those effects mean for estuarine and marine food webs. She is a fellow with the Louisiana Sea Grant Discovery, Integration and Application Program (LaDIA), a member of the Louisiana Universities Marine Consortium (LUMCON) Advisory Council, and the founder and organizer of the Science on the Bayou informal science communication series. Dr. Stauffer earned her B.S. with a double major in marine science and biology at University of Miami and her Ph.D. in marine environmental biology at the University of Southern California.

Courtney Thompson
Texas A&M University
Dr. Thompson is an assistant professor at Texas A&M University in the Department of Geography. Dr. Thompson received her Ph.D. in geography from the University of Idaho. She also holds an M.S. in geography from the University of Idaho and a B.S. in geography from New Mexico State University. Her research in human-environment interactions examines relationships between social systems and natural hazard impacts using a mix of qualitative and quantitative methods, including GIS, interviews, survey analysis, and spatial statistics. Specifically, she employs vulnerability and resilience assessment methodologies that empower local decision-makers to create and strategically implement resilience-enhancing mitigation and adaptation strategies. Her research also focuses on quantifying how the vulnerability and resilience of coastal communities interact with the social structuration of society, multi-scalar factors, and risk perceptions.

Hannah Vander Zanden
University of Florida
Dr. Vander Zanden is an assistant professor in the Department of Biology and the Archie Carr Center for Sea Turtle Research at the University of Florida. She holds a B.A. from Pomona College and a Ph.D. in zoology from the University of Florida. She also held postdoctoral appointments at the University of Utah and U.S. Geological Survey. The goal of Dr. Vander Zanden's research is to address critical knowledge gaps about where sea turtles are most abundant in the Gulf of Mexico. Much of her research program relies on the use of intrinsic markers called stable isotopes, which are naturally occurring forms of elements that are integrated from the environment through an organism's diet. By identifying where sea turtles forage via samples collected at the nesting beach, population hotspots can be identified and paired with information about threat severity and target restoration activities.

This site uses cookies. For more information on cookies visit:
http://nas.edu/legal/privacy/index.html

2017

Christoph Aeppli
Bigelow Laboratory for Ocean Sciences
Dr. Aeppli is an environmental chemist and a senior research scientist at Bigelow Laboratory for Ocean Sciences. Dr. Aeppli has studied oil weathering at natural oil seeps, in Arctic conditions, and after major oil spills, including the Deepwater Horizon oil spill. He received his master's degree in chemistry from the University of Bern, Switzerland, and his doctorate in environmental chemistry from the Swiss Federal Institute of Technology. Postdoctoral fellowships took him to Stockholm University, where he investigated the dynamics of halogenated compounds, and to Woods Hole Oceanographic Institution, where he studied biodegradation and photooxidation of petroleum hydrocarbons. Dr. Aeppli's research is helping to understand the formation, fate, and effects of oil transformation products. This knowledge will lead to an improved assessment of the impacts that oil spills have on humans and the environment.

Laura Bakkensen
University of Arizona
Dr. Bakkensen is an assistant professor at the University of Arizona's School of Government and Public Policy, where she uses applied microeconomic and econometric techniques to analyze the economics of natural disasters, identifying current hazard risks and evidence of adaptation to damages and fatalities across the globe. Dr. Bakkensen received her Ph.D. in environmental and natural resource economics from Yale University. She also holds an M.Phil. in environmental and natural resource economics from Yale University, an M.S. in environment and development from the London School of Economics and Political Science, and a B.A. in economics from Whitman College. As an economist, Dr. Bakkensen researches individual responses, overall community resilience, and policy responses in the face of natural disasters like hurricanes, tornadoes, and floods. Her research informs policy on public insurance and regulation, pre- and post-disaster aid, severe weather warnings, and public adaptation projects.

Paul Harnik
Franklin and Marshall College
Dr. Harnik is an assistant professor in the Department of Earth and Environment at Franklin and Marshall College. He received his B.A. in geology from Oberlin College and his Ph.D. in evolutionary biology from the University of Chicago. Dr. Harnik's doctoral and postdoctoral research focused on understanding extinction risk in the oceans through analyses of the marine fossil record. At Franklin and Marshall, his research has focused increasingly on the links between modern, historical, and ancient marine systems with the goal of advancing our understanding of the biological consequences of current and future anthropogenic environmental change. Most recently, Dr. Harnik and his

This site uses cookies. For more information on cookies visit:
http://nas.edu/legal/privacy/index.html

baselines for these communities and assess the effects of human activities on coastal ecosystems.

YeongAe Heo
Case Western Reserve University
Dr. Heo is an assistant professor in the Department of Civil Engineering at Case Western Reserve University. She received her Ph.D. in civil and environmental engineering from the University of California, Davis. She has expertise in modeling and simulation of probabilistic risk-based system-level performance for complex structures subjected to dynamic loads. Dr. Heo worked at the Offshore Technology R&D Center of Samsung Heavy Industries, where she examined diverse multi-hazard problems for offshore oil and gas process systems exposed to severe weather and operation conditions. She holds three patents for offshore structural systems and was the recipient of the 2012 American Society of Civil Engineers (ASCE) Norman Medal. Dr. Heo's research focuses on minimizing risks in on- and offshore oil and gas systems. As an engineer, she uses a variety of tools, including modeling and simulations, to investigate multi-hazard risks for the complex energy infrastructure systems that are subject to constantly changing stresses.

Michael Martínez-Colón
Florida A&M University
Dr. Martínez-Colón is an assistant professor in the School of the Environment at Florida Agricultural and Mechanical University, a Courtesy Professor in the Department of Environmental Science at the University of South Florida, and adjunct faculty at the Savannah River Field Station. He received his Ph.D. in oceanography from the University of South Florida and a B.S. and M.S. in geology from the University of Puerto Rico. His research expertise is in coastal ecosystems, specifically coastal and marine ecology and biogeochemistry. His research portfolio examines aspects of environmental micropaleontology, geochemistry, and pollutants in conjunction with bioindicators in short- and long-term monitoring efforts. Dr. Martínez-Colón takes a novel approach to studying anthropogenic stressors such as chemical pollutants and microplastics, focusing on a type of single-celled organisms called foraminifera, which have calcium carbonate skeletons and tend to live in sediments.

Ali Mostafavi
Texas A&M University
Dr. Mostafavi is an assistant professor in the Zachry Department of Civil Engineering at Texas A&M University. He received his Ph.D. in civil engineering at Purdue University. He also holds a Master of Science in industrial administration from the Krannert School of Management at Purdue University. Dr. Mostafavi supervises the Infrastructure System-of-Systems Research Group. He also works closely with community partners, such as the Southeast Florida Climate Compact, to extend the broader impacts of his research. Dr. Mostafavi takes a "system of systems" approach to studying chronic and acute stressors facing coastal communities all over the world. He bridges the boundaries

This site uses cookies. For more information on cookies visit:
http://nas.edu/legal/privacy/index.html

planning.

David Murphy
University of South Florida
Dr. Murphy is an assistant professor in the Department of Mechanical Engineering at the University of South Florida. He completed a double B.S. in mechanical and biomedical engineering from the University of Alabama at Birmingham, an M.Phil. in biological science from Cambridge University, and an M.S. in mechanical engineering from the Georgia Institute of Technology. He received his Ph.D. in civil and environmental engineering from Georgia Tech. He completed a postdoctoral fellowship in the Department of Mechanical Engineering at Johns Hopkins University. Dr. Murphy is an expert in fluid mechanics whose research has biological, ecological, and environmental applications. For example, he has worked on crude oil spill dispersion in marine environments and potential human health effects of exposure to oily marine aerosols. Through a variety of methods, including advanced flow visualization and measurement techniques, he has also investigated zooplankton swimming, insect flight, and prosthetic heart valves.

Ashley Ross
Texas A&M University, Galveston
Dr. Ross is an assistant professor in the Department of Marine Sciences and a faculty fellow with the Center for Texas Beaches and Shores at Texas A&M University at Galveston. She holds an M.A. in political science from Louisiana State University and a Ph.D. in political science from Texas A&M University. Dr. Ross studies the vulnerability of coastal communities to natural disasters and other hazards and how to make them more resilient. As a political scientist, she approaches these challenges from a public administration and policy perspective. She then uses this information to inform policies with the goal of enhancing community resilience. Her research examining coastal hazards has produced the book Local Disaster Resilience: Administrative and Political Perspectives. Dr. Ross was a 2014 National Science Foundation Next Generation of Hazard and Disasters Researchers Program fellow. Her work on Gulf Coast disaster resilience has also been supported by the Department of Homeland Security.

Wanyun Shao
University of Alabama
Dr. Shao is an assistant professor of Geography at the University of Alabama, where her primary research interests are the interaction between nature and society. She received her B.S. in geography from Jilin University (China) and M.P. in planning from the University of Wyoming. While pursuing her Ph.D in geography at Louisiana State University, Shao was a research assistant for the Southern Climate Impacts Planning Program, which is funded by the U.S. National Oceanic and Atmospheric Administration. After receiving her Ph.D., Dr. Shao worked as a Coastal Resources Scientist at the

This site uses cookies. For more information on cookies visit:
http://nas.edu/legal/privacy/index.html

policies and planning, and impacts of climate change on public health. The interdisciplinary nature of her research leads her to work across traditional disciplinary lines.

J. Cameron Thrash
University of Southern California
Dr. Thrash is an assistant professor in the Department of Biological Sciences at the University of Southern California. He received a B.S. in biology from the University of California, San Diego. He received his Ph.D. in microbiology from the University of California, Berkeley, where he studied microbial physiology. His graduate work included perchlorate bioremediation and isolation of novel perchlorate reducing microorganisms. He also studied anaerobic oxidation of iron and uranium. He was awarded a National Science Foundation Postdoctoral Fellowship to work at Oregon State University, where he focused on the evolution and genomics of SAR11, the most abundant marine bacteria. Dr. Thrash's research focuses on the function of microbes in the different interconnected aquatic systems within the Gulf of Mexico, including the coasts, estuaries, the shelf region, and the Mississippi River. He aims to predict which microbes contribute to the vital ecosystem services of nutrient and carbon processing to generate strategic options for pollutant remediation.

2016

Jordon Beckler
Florida Atlantic University Harbor Branch Oceanographic Institute
Dr. Beckler is an assistant research professor in the Geochemistry and Geochemical Sensing Lab at the Florida Atlantic University Harbor Branch Oceanographic Institute in Fort Pierce, Florida. He completed a Ph.D. in chemical oceanography with a minor in inorganic chemistry at the Georgia Institute of Technology. Dr. Beckler is currently working to understand the role of sediment-derived iron in serving as a nutrient source to Florida red tides and in enhancing the degradation of hydrocarbons; improve efforts to understand harmful algae bloom formation by developing optical techniques and autonomous measurement platforms; and develop in situ chromatographic techniques for remote detection of harmful algae bloom toxins. His work focuses on developing autonomous instrumentation to measure previously unidentified introductions of iron to coastal waters and will contribute to improved understanding of the influences on Gulf algal blooms.

Ann Cook

This site uses cookies. For more information on cookies visit:
http://nas.edu/legal/privacy/index.html

geophysics from Columbia University. Dr. Cook's research is focused on natural gas hydrates, an ice-like form of methane gas and solid water that forms in marine sediments. She uses analytical data like geophysical well logs, seismic data, and sediment cores along with mathematical models to investigate these natural gas hydrates. Since she arrived at Ohio State, Dr. Cook's research has been funded primarily through several grants from the U.S. Department of Energy, including an $81 million project focused on drilling and recovering natural gas hydrate in sand reservoirs from the Gulf of Mexico.

Brad Erisman
University of Texas at Austin
Dr. Erisman is an assistant professor of fisheries ecology at the University of Texas at Austin Marine Science Institute. He received his B.S. in aquatic biology from the University of California, Santa Barbara, his M.S. degree in biology from California State University Northridge, and his Ph.D. in marine biology from the Scripps Institution of Oceanography. After earning his doctorate, he remained at Scripps as a postdoctoral scholar and assistant research scientist for several years, during which time he co-founded the Gulf of California Marine Program. He currently leads several projects related to fishes and fisheries in the Gulf of Mexico, California, the Indo-Pacific, and Mexico. Dr. Erisman's research focuses on understanding interconnections among fish spawning aggregations (FSAs), ecosystems, fisheries, and climate. FSAs are productivity hotspots critical to marine food webs and ecosystem function. They also support the most productive and important commercial, recreational, and subsistence fisheries.

Diego Figueroa
University of Texas Rio Grande Valley
Dr. Figueroa is an assistant professor in the School of Earth, Environmental, and Marine Sciences at the University of Texas Rio Grande Valley. He received his B.S. in marine biology from the University of Alaska Southeast and his M.S. and Ph.D. in biological oceanography from Oregon State University. Dr. Figueroa's work focuses on establishing a baseline of oceanographic and biological characteristics of the near-shore region of the South Texas Gulf Coast, one of the least-studied areas in the entire Gulf of Mexico, to serve as a foundation for long-term oceanographic monitoring. His research focuses on how oceanographic processes, anthropogenic effects, and climate change impact the biodiversity and connectivity of marine habitats. Dr. Figueroa works with zooplankton in coastal and open ocean environments and with corals in the deep sea. Dr. Figueroa uses multivariate tools for community analyses and a wide range of molecular methods to answer ecological and evolutionary questions.

Huilin Gao
Texas A&M University

This site uses cookies. For more information on cookies visit:
http://nas.edu/legal/privacy/index.html

and are focused on several areas indispensable to protecting water and environmental resources—particularly those related to coastal ecosystem sustainability. Her expertise is centered on understanding the impacts of a changing environment on freshwater inflows and the effects of inflows on coastal ecosystems. Dr. Gao uses a combination of in situ observations, state-of-the-art remote sensing, and high-performance modeling approaches to investigate interactions between phytoplankton and oil in the marine ecosystem to provide a better understanding of the role phytoplankton play in altering oil compounds, which phytoplankton functional types are most affected by oil spills, and which functional types are most likely to aid oil decomposition.

Michelle Meyer
Louisiana State University
Dr. Meyer is an assistant professor of sociology at Louisiana State University. She completed her Ph.D. in sociology at Colorado State University and received a B.A. in sociology from Murray State University. Her research interests include environmental sociology and community sustainability, disaster resilience and mitigation, climate change displacement, environmental justice, and the interplay between environmental conditions and social vulnerability. She has worked on various projects, including analyzing organizational networks in long-term recovery; comparing disaster recovery following technological and natural disasters; assessing the inclusion of disability in emergency management planning; and analyzing social capital and collective efficacy for individual and community resilience; among others. Using her research findings, Dr. Meyer has helped community organizations understand demographics that contribute to vulnerability and then prepare disaster recovery plans. With increasing disaster frequency, everyday practices and relationships are crucial to supporting community resilience.

Jennifer Pazour
Rensselaer Polytechnic Institute
Dr. Pazour is an assistant professor of industrial and systems engineering at Rensselaer Polytechnic Institute. She holds three degrees in industrial engineering: a B.S. from South Dakota School of Mines and Technology, and a M.S. and Ph.D. from the University of Arkansas. She is an active member of the Institute for Operations Research and the Management Sciences and the Institute of Industrial and Systems Engineers, and she serves on the board of directors for the Warehousing Education and Research Council. Dr. Pazour's research explores how to make decisions in logistics and resource-sharing systems. She develops mathematical models and solution algorithms of complex systems as a way of understanding and quantifying trade-offs with operational and design decisions.

Kerri Pratt
University of Michigan
Dr. Pratt is currently the Seyhan N. Ege Assistant Professor of Chemistry at the University of

This site uses cookies. For more information on cookies visit:
http://nas.edu/legal/privacy/index.html

research laboratory studies atmospheric composition, clouds, and precipitation to understand key processes in air quality and climate change, particularly across the Alaska outer continental shelf. Her lab also examines air pollution contributions of oil extraction activities at coastal Prudhoe Bay, the third largest oilfield in North America. Recently, Dr. Pratt developed an innovative course featuring original Arctic snow chemistry research to introduce first- and second-year college students to scientific research to improve STEM retention.

Adam Skarke
Mississippi State University
Dr. Skarke is an assistant professor of Geology in the Department of Geosciences at Mississippi State University. He earned a B.A. in geology from Colgate University as well as an M.S. and Ph.D. in geology from the University of Delaware. Dr. Skarke conducts research focused on understanding the fundamental physical relationships between fluid dynamics, sediment transport processes, morphological expression, and the stratigraphic record in marine environments that span the continental margin from coastal waters to the deep sea. His technical approach is field-based and focused on the analysis of geological, geophysical, and oceanographic data collected with innovative environmental observing sensors and platforms. Results of Dr. Skarke's research may help scientists and environmental managers better understand and mitigate processes detrimental to the health and resilience of marine ecosystems, commercial fisheries, and coastal property and infrastructure.

Jill Trepanier
Louisiana State University
Dr. Trepanier is an assistant professor in the Department of Geography and Anthropology at Louisiana State University. She received her bachelor's degree in geography from the University of Wisconsin-Oshkosh and her master's and Ph.D. in geography from Florida State University. Dr. Trepanier's work focuses on the quantification of extreme hurricane wind and storm surge risks in coastal locations. This risk estimate provides planners and managers with an understanding of how often the most extreme events will occur in the region, which can help them better prepare structures for the worst-case scenario. Dr. Trepanier's main research focus is on quantifying tropical cyclones, for which she has two different statistical approaches. The first uses extreme value statistics to estimate wind speeds or storm surges to specific locations. The second utilizes a copula model to find the combined probability of joint wind and storm surge occurrence.

2015

This site uses cookies. For more information on cookies visit:
http://nas.edu/legal/privacy/index.html

Dr. Albert is an assistant professor and the Robert and Gayle Longmire Early Career Professor in Chemical Engineering at Tulane University. She received her B.S. in chemical engineering from the University of Florida and her Ph.D. in chemical engineering from the University of Delaware. Her doctoral and postdoctoral research focused on developing gradient methods for exploring the effects of surface interactions on block copolymer thin film self-assembly and tailoring the chemical and mechanical properties of silicone elastomer networks for cell mobility studies and peptide assembly. At Tulane, Dr. Albert's research is centered on the use of combinatorial methods to engineer nano- and micro-structured polymeric materials for applications in energy, health, and the environment. Specifically, she takes advantage of the phase separation processes responsible for self-assembly in block copolymers and polymer blends to produce materials in thin film geometries exhibiting desired morphologies.

Alberto Caban-Martinez
University of Miami
Dr. Caban-Martinez is an assistant professor of public health sciences and director of the Musculoskeletal Disorders and Occupational Health Lab at the University of Miami, Miller School of Medicine. He earned his B.S. in computer science from the University of Miami, his M.P.H. from Nova Southeastern University, and completed the osteopathic medicine program at Nova Southeastern University and the doctoral occupational epidemiology program at the University of Miami. He then completed a postdoctoral fellowship at the Harvard School of Public Health, where he learned to develop workplace interventions in the construction industry. Dr. Caban-Martinez's interdisciplinary program of research aims to conduct robust occupational and environmental health surveillance activities and provide rigorous scientific evidence about effective ways to reduce musculoskeletal disorders and improve the well-being of worker populations. He focuses on finding ways to promote safe work practices, healthy behaviors, and healthy work environments.

Zachary Darnell
University of Southern Mississippi
Dr. Darnell is an assistant professor in the Department of Coastal Sciences at the University of Southern Mississippi. Dr. Darnell earned a B.S. in biological sciences from Vanderbilt University and a Ph.D. in ecology from Duke University. Dr. Darnell's long-term research interests are centered on the environmental constraints imposed upon marine and estuarine invertebrate species. Specifically, his research focuses on physiological and behavioral responses to environmental change and environmental stress; environmental effects on life histories, distributions, and population dynamics; and anthropogenic impacts on organism-environment interactions. Focusing primarily on crustaceans, this research relies on a combination of field- and lab-based experimental work, complemented by quantitative and spatial analyses of long-term fishery-dependent and fishery-independent datasets to better understand patterns of abundance and distribution in relation to

This site uses cookies. For more information on cookies visit:
http://nas.edu/legal/privacy/index.html

Dauphin Island Sea Lab

Dr. Dorgan is a senior marine scientist at the Dauphin Island Sea Lab and an assistant professor of marine sciences at the University of South Alabama. She received her B.S. in marine biology from the University of California, Santa Cruz, and her Ph.D. in oceanography from the University of Maine. As part of her dissertation research, she showed that worms extend burrows through muddy sediments by fracture, a result that was published in Nature and for which she was awarded the Association for the Sciences of Limnology and Oceanography Lindeman Award. Dr. Dorgan's research program aims to develop a mechanistic understanding of the ecological and biogeochemical processes occurring in marine sediments. She is specifically interested in animal-sediment interactions, including the mechanics of burrowing and feeding and the impacts of these activities on the physical structure of sediments.

Joel Fodrie

University of North Carolina

Dr. Fodrie is an assistant professor of fisheries oceanography and ecology at the University of North Carolina, where he studies the population dynamics of fishes and shellfish. He has conducted research along all three major U.S. coastlines, as well as in the Baltic Sea and around the Galápagos Islands. Dr. Fodrie earned his Ph.D. in Oceanography from the Scripps Institution of Oceanography, where he was supported as a National Science Foundation Graduate Research Fellow and presented with the E. W. Fager Student Award. Dr. Fodrie's research focuses on four major themes: 1) how the movement of fishes connects landscapes and affects population dynamics; 2) linkages between coastal habitat abundance/quality and fishery production; 3) biogenic habitat restoration; and 4) how basin-scale perturbations such as harvest pressure, climate change, and oil pollution influence the long-term community ecology of coastal ecosystems.

Anna Michel

Woods Hole Oceanographic Institution

Dr. Michel earned B.S. degrees in biology and chemical engineering from the Massachusetts Institute of Technology (MIT). She then earned an M.S. in Ocean Engineering from MIT and a Ph.D. in Mechanical and Oceanographic Engineering from the MIT-Woods Hole Oceanographic Institution (WHOI) Joint Program. After receiving her Ph.D., Dr. Michel was a post-doctoral fellow and then an associate research scholar at the Center for Mid-Infrared Technologies for Health and the Environment at Princeton University. She returned to WHOI as an assistant scientist in applied ocean physics and engineering. Dr. Michel's research focus is on advancing environmental observation through the development and deployment of novel optical sensors for measurement of key chemical species. Dr. Michel designs, builds, and deploys advanced laser-based chemical sensors that are capable of measuring trace concentrations in gaseous and aqueous environments in locations ranging from the deep sea to Arctic environments, using remotely operated vehicles.

This site uses cookies. For more information on cookies visit:
http://nas.edu/legal/privacy/index.html

Dr. Wallace is an assistant professor in the Department of Marine Science at the University of Southern Mississippi. He is also currently a guest investigator at the Woods Hole Oceanographic Institution and a complimentary research scholar at Rice University. Dr. Wallace earned a B.S. degree from Tulane University, with a double major in geology and German. He earned a Ph.D. degree in earth science from Rice University. The aim of Dr. Wallace's research is to establish the response of coastal systems to global change over historic and geologic timescales. Specifically, Dr. Wallace is primarily a field geologist interested in understanding how variations in hurricanes, sediment supply, and relative sea-level shape and impact the coastlines of the world. He has worked in areas along the Gulf of Mexico, Japan, Bermuda, and the Philippines.

Helen White
Haverford College

Dr. White is an associate professor of chemistry and the director of the environmental studies program at Haverford College. She received a master's degree in chemistry from the University of Sussex, U.K., and a Ph.D. in chemical oceanography from the Massachusetts Institute of Technology and Woods Hole Oceanographic Institution (WHOI) Joint Program. Dr. White's research examines the persistence of oil and other organic contaminants in the marine environment. Her work seeks to examine how the chemical structure, physical associations, and bioavailability of specific compounds determine their cycling and eventual fate. Her research at Haverford College has been funded by an National Science Foundation RAPID grant to determine the impact of the Deepwater Horizon oil spill on a deep-water coral community in the Gulf of Mexico, as well as a grant from the Gulf of Mexico Research Initiative to examine the weathering of petroleum and dispersant components in the deep-sea, on Gulf Coast beaches, and in laboratory incubations.

The National Academies of SCIENCES ENGINEERING MEDICINE

NATIONAL ACADEMY OF SCIENCES
NATIONAL ACADEMY OF ENGINEERING
NATIONAL ACADEMY OF MEDICINE

About Us | Our Work
Events | Contact Us
Opportunities | Publications
Visit

Privacy Statement | DMCA Policy | Terms of Use | Site Map

Copyright © 2020 National Academy of Sciences. All Rights Reserved.

This site uses cookies. For more information on cookies visit:
http://nas.edu/legal/privacy/index.html

Yee, Susan

From: Friedman, Stephanie
Sent: Monday, April 20, 2020 10:46 AM
To: Yee, Susan
Subject: Re: Record of Percentage Agreement: Friedman, Stephanie

I concur.

Thank you!!

Great work, Susan!

From: Yee, Susan <Yee.Susan@epa.gov>
Sent: Monday, April 20, 2020 9:43 AM
To: Friedman, Stephanie <Friedman.Stephanie@epa.gov>
Subject: Record of Percentage Agreement: Friedman, Stephanie

Hi everyone.
Two of our journal articles are being nominated for a US EPA award for Science and Technical Achievement. As part of the nomination, I need a concurrence from each of you on your Percent Contribution to both articles. Note below I just took the Average across both papers for each article.
If you are ok with your percentage, **please just Reply to Me with an "I concur"**. If you'd like more information on the award nomination or to discuss further, let me know.

R De Jesús Crespo 40%
S Yee 30%
S Friedman 5%
D Yee 10%
F Bai 5%
P. Méndez Lázaro 5%
A Oczkowski 5%

Thank You!

Yee, S. H., D. A. Yee, R. de Jesús Crespo, A. Oczkowski, F. Bai, and S. Friedman (2019). Linking Water Quality to Aedes aegypti and Zika in Flood-Prone Neighborhoods. EcoHealth 16:191-209 https://doi.org/10.1007/s10393-019-01406-6
De Jesús Crespo, R., P. Méndez Lázaro, and S.H. Yee (2018) Linking wetland ecosystem services to vector borne disease: Dengue fever in San Juan Bay Estuary, Puerto Rico. Wetlands 39: 1281-1293. https://doi.org/10.1007%2Fs13157-017-0990-5

	Yee et al. 2019 (zika)	De Jesus Crespo et al. 2018 (dengue)	Combined
Rebeca de Jesus Crespo	10	70	40
Susan Yee	40	20	30

Stephanie Friedman	10	0	5
Donald Yee	20	0	10
Fengwei Bai	10	0	5
Pablo Mendez Lazaro	0	10	5
Autumn Oczkowski	10	0	5

Susan Yee
Gulf Ecosystem Measurement and Modeling
U.S. Environmental Protection Agency
1 Sabine Island Drive
Gulf Breeze, FL 32561
850-934-9397

Yee, Susan

From: Yee, Susan
Sent: Tuesday, April 21, 2020 8:59 AM
To: Yee, Susan
Subject: RE: Record of Percentage Agreement: Yee, Susan

I concur.

From: Yee, Susan <Yee.Susan@epa.gov>
Sent: Tuesday, April 21, 2020 8:58 AM
To: Yee, Susan <Yee.Susan@epa.gov>
Subject: FW: Record of Percentage Agreement: Mendez Lazaro, Pablo

I am adjusting Pablo's contribution to 15% for the one paper, giving him an average of 7.5%. I am reducing yours to 27.5% to make the balance.

	Yee et al. 2019 (zika)	De Jesus Crespo et al. 2018 (dengue)	Combined
Rebeca de Jesus Crespo	10	70	40
Susan Yee	40	15	27.5
Stephanie Friedman	10	0	5
Donald Yee	20	0	10
Fengwei Bai	10	0	5
Pablo Mendez Lazaro	0	15	7.5
Autumn Oczkowski	10	0	5

From: Yee, Susan
Sent: Tuesday, April 21, 2020 8:45 AM
To: Pablo A Mendez Lazaro <pablo.mendez1@upr.edu>
Subject: RE: Record of Percentage Agreement: Mendez Lazaro, Pablo

Yes, I can do that. Thanks!

From: Pablo A Mendez Lazaro <pablo.mendez1@upr.edu>
Sent: Monday, April 20, 2020 7:49 PM
To: Yee, Susan <Yee.Susan@epa.gov>
Subject: Re: Record of Percentage Agreement: Mendez Lazaro, Pablo

Hi Susan,

Congrats and thank you for sharing this we us. Could it be said that my component (Land Surface Temperature remote sensing techniques is around 15)?

Please stay safe with you and your family during this COVID19 situation.
Pablo

On Mon, Apr 20, 2020 at 10:43 AM Yee, Susan <Yee.Susan@epa.gov> wrote:

> Hi everyone.
>
> Two of our journal articles are being nominated for a US EPA award for Science and Technical Achievement. As part of the nomination, I need a concurrence from each of you on your Percent Contribution to both articles. Note below I just took the Average across both papers for each article.
>
> If you are ok with your percentage, **please just Reply to Me with an "I concur"**. If you'd like more information on the award nomination or to discuss further, let me know.
>
> R De Jesús Crespo 40%
>
> S Yee 30%
>
> S Friedman 5%
>
> D Yee 10%
>
> F Bai 5%
>
> P. Méndez Lázaro 5%
>
> A Oczkowski 5%
>
> Thank You!
>
> Yee, S. H., D. A. Yee, R. de Jesús Crespo, A. Oczkowski, F. Bai, and S. Friedman (2019). Linking Water Quality to Aedes aegypti and Zika in Flood-Prone Neighborhoods. EcoHealth 16:191-209 https://doi.org/10.1007/s10393-019-01406-6
>
> De Jesús Crespo, R., P. Méndez Lázaro, and S.H. Yee (2018) Linking wetland ecosystem services to vector borne disease: Dengue fever in San Juan Bay Estuary, Puerto Rico. Wetlands 39: 1281-1293. https://doi.org/10.1007%2Fs13157-017-0990-5

	Yee et al. 2019 (zika)	De Jesus Crespo et al. 2018 (dengue)	Combined
Rebeca de Jesus Crespo	10	70	40
Susan Yee	40	20	30
Stephanie Friedman	10	0	5
Donald Yee	20	0	10
Fengwei Bai	10	0	5
Pablo Mendez Lazaro	0	10	5
Autumn Oczkowski	10	0	5

Susan Yee

Gulf Ecosystem Measurement and Modeling

U.S. Environmental Protection Agency

1 Sabine Island Drive

Gulf Breeze, FL 32561

850-934-9397

--

Pablo A. Méndez Lázaro, Ph.D.
Principal Investigator: NASA--Early Warning of Synoptic Air Quality Events to Improve Health and Well Being in the Greater Caribbean Region (80NSSC19K0194)

Co-Principal Investigator: NIH--Impact of Hurricane-Related Stressors and Responses on Oncology Care and Health Outcomes of Women with Gynecologic Cancers from Puerto Rico and US Virgin Islands

City Co-lead: NSF--Urban Resilience to Extreme Weather Events-SRN, www.urexsrn.net

Environmental Health Department
Graduate School of Public Health
University of Puerto Rico-Medical Sciences Campus
PO BOX 365067
San Juan Puerto Rico 00936-5067
(001) 787 758 2525
ext 2928/1469

Yee, Susan

From: Oczkowski, Autumn
Sent: Monday, April 20, 2020 9:58 AM
To: Yee, Susan
Subject: RE: Record of Percentage Agreement: Oczkowski, Autumn

I concur.
Thanks and hope that all is well,
Autumn

From: Yee, Susan <Yee.Susan@epa.gov>
Sent: Monday, April 20, 2020 10:44 AM
To: Oczkowski, Autumn <Oczkowski.Autumn@epa.gov>
Subject: Record of Percentage Agreement: Oczkowski, Autumn

Hi everyone.
Two of our journal articles are being nominated for a US EPA award for Science and Technical Achievement. As part of the nomination, I need a concurrence from each of you on your Percent Contribution to both articles. Note below I just took the Average across both papers for each article.
If you are ok with your percentage, **please just Reply to Me with an "I concur"**. If you'd like more information on the award nomination or to discuss further, let me know.

R De Jesús Crespo 40%
S Yee 30%
S Friedman 5%
D Yee 10%
F Bai 5%
P. Méndez Lázaro 5%
A Oczkowski 5%

Thank You!

Yee, S. H., D. A. Yee, R. de Jesús Crespo, A. Oczkowski, F. Bai, and S. Friedman (2019). Linking Water Quality to Aedes aegypti and Zika in Flood-Prone Neighborhoods. EcoHealth 16:191-209 https://doi.org/10.1007/s10393-019-01406-6
De Jesús Crespo, R., P. Méndez Lázaro, and S.H. Yee (2018) Linking wetland ecosystem services to vector borne disease: Dengue fever in San Juan Bay Estuary, Puerto Rico. Wetlands 39: 1281-1293. https://doi.org/10.1007%2Fs13157-017-0990-5

	Yee et al. 2019 (zika)	De Jesus Crespo et al. 2018 (dengue)	Combined
Rebeca de Jesus Crespo	10	70	40
Susan Yee	40	20	30
Stephanie Friedman	10	0	5
Donald Yee	20	0	10

Fengwei Bai	10	0	5
Pablo Mendez Lazaro	0	10	5
Autumn Oczkowski	10	0	5

Susan Yee
Gulf Ecosystem Measurement and Modeling
U.S. Environmental Protection Agency
1 Sabine Island Drive
Gulf Breeze, FL 32561
850-934-9397

Yee, Susan

From: Donald Yee <Donald.Yee@usm.edu>
Sent: Monday, April 20, 2020 9:47 AM
To: Yee, Susan
Subject: Re: Record of Percentage Agreement: Yee, Donald

I concur.

Donald A. Yee
Associate Professor

Board Certified Entomologist in Medical Entomology

Subject Editor, Journal of Medical Entomology

Yee Mosquito Lab

Follow me on Twitter: @MosquitoLab
Lab Website
Google Scholar
LinkedIn
ResearchGate

School of Biological, Environmental, & Earth Sciences
The University of Southern Mississippi
TEC 104E, 2609 West 4th Street
Hattiesburg, MS 39406-0001

Johnson Science Tower 1014 (Office), 1016 (Research Lab) 601-266-4927

On 4/20/2020 9:44 AM, Yee, Susan wrote:

> Hi everyone.
> Two of our journal articles are being nominated for a US EPA award for Science and Technical Achievement. As part of the nomination, I need a concurrence from each of you on your Percent Contribution to both articles. Note below I just took the Average across both papers for each article. If you are ok with your percentage, **please just Reply to Me with an "I concur"**. If you'd like more information on the award nomination or to discuss further, let me know.
>
> R De Jesús Crespo 40%
> S Yee 30%
> S Friedman 5%
> D Yee 10%
> F Bai 5%
> P. Méndez Lázaro 5%

A Oczkowski 5%

Thank You!

Yee, S. H., D. A. Yee, R. de Jesús Crespo, A. Oczkowski, F. Bai, and S. Friedman (2019). Linking Water Quality to Aedes aegypti and Zika in Flood-Prone Neighborhoods. EcoHealth 16:191-209 https://doi.org/10.1007/s10393-019-01406-6

De Jesús Crespo, R., P. Méndez Lázaro, and S.H. Yee (2018) Linking wetland ecosystem services to vector borne disease: Dengue fever in San Juan Bay Estuary, Puerto Rico. Wetlands 39: 1281-1293. https://doi.org/10.1007%2Fs13157-017-0990-5

	Yee et al. 2019 (zika)	De Jesus Crespo et al. 2018 (dengue)	Combined
Rebeca de Jesus Crespo	10	70	40
Susan Yee	40	20	30
Stephanie Friedman	10	0	5
Donald Yee	20	0	10
Fengwei Bai	10	0	5
Pablo Mendez Lazaro	0	10	5
Autumn Oczkowski	10	0	5

Susan Yee
Gulf Ecosystem Measurement and Modeling
U.S. Environmental Protection Agency
1 Sabine Island Drive
Gulf Breeze, FL 32561
850-934-9397

Yee, Susan

From: Fengwei Bai <Fengwei.Bai@usm.edu>
Sent: Monday, April 20, 2020 10:34 AM
To: Yee, Susan
Subject: Re: Record of Percentage Agreement: Bai, Fengwei

I concur

Thank you.

Fengwei

--

Fengwei Bai Ph.D

Associate Professor

Cell and Molecular Biology

University of Southern Mississippi

118 College Dr. #5018

Hattiesburg, MS 39406

Office: (601)266-4755

Email: fengwei.bai@usm.edu

https://www.usm.edu/faculty-directory/profile.php?id=1936828

From: "Yee, Susan" <Yee.Susan@epa.gov>
Date: Monday, April 20, 2020 at 9:43 AM
To: Fengwei Bai <Fengwei.Bai@usm.edu>
Subject: Record of Percentage Agreement: Bai, Fengwei

Hi everyone.
Two of our journal articles are being nominated for a US EPA award for Science and Technical Achievement. As part of the nomination, I need a concurrence from each of you on your Percent Contribution to both articles. Note below I just took the Average across both papers for each article.
If you are ok with your percentage, **please just Reply to Me with an "I concur"**. If you'd like more information on the award nomination or to discuss further, let me know.

R De Jesús Crespo 40%
S Yee 30%
S Friedman 5%
D Yee 10%
F Bai 5%
P. Méndez Lázaro 5%
A Oczkowski 5%

Thank You!

Yee, S. H., D. A. Yee, R. de Jesús Crespo, A. Oczkowski, F. Bai, and S. Friedman (2019). Linking Water Quality to Aedes aegypti and Zika in Flood-Prone Neighborhoods. EcoHealth 16:191-209 https://doi.org/10.1007/s10393-019-01406-6

De Jesús Crespo, R., P. Méndez Lázaro, and S.H. Yee (2018) Linking wetland ecosystem services to vector borne disease: Dengue fever in San Juan Bay Estuary, Puerto Rico. Wetlands 39: 1281-1293. https://doi.org/10.1007%2Fs13157-017-0990-5

	Yee et al. 2019 (zika)	De Jesus Crespo et al. 2018 (dengue)	Combined
Rebeca de Jesus Crespo	10	70	40
Susan Yee	40	20	30
Stephanie Friedman	10	0	5
Donald Yee	20	0	10
Fengwei Bai	10	0	5
Pablo Mendez Lazaro	0	10	5
Autumn Oczkowski	10	0	5

Susan Yee
Gulf Ecosystem Measurement and Modeling
U.S. Environmental Protection Agency
1 Sabine Island Drive
Gulf Breeze, FL 32561
850-934-9397

Yee, Susan

From: Yee, Susan
Sent: Tuesday, April 21, 2020 8:45 AM
To: Pablo A Mendez Lazaro
Subject: RE: Record of Percentage Agreement: Mendez Lazaro, Pablo

Yes, I can do that. Thanks!

From: Pablo A Mendez Lazaro <pablo.mendez1@upr.edu>
Sent: Monday, April 20, 2020 7:49 PM
To: Yee, Susan <Yee.Susan@epa.gov>
Subject: Re: Record of Percentage Agreement: Mendez Lazaro, Pablo

Hi Susan,

Congrats and thank you for sharing this we us. Could it be said that my component (Land Surface Temperature remote sensing techniques is around 15)?

Please stay safe with you and your family during this COVID19 situation.
Pablo

On Mon, Apr 20, 2020 at 10:43 AM Yee, Susan <Yee.Susan@epa.gov> wrote:

> Hi everyone.
>
> Two of our journal articles are being nominated for a US EPA award for Science and Technical Achievement. As part of the nomination, I need a concurrence from each of you on your Percent Contribution to both articles. Note below I just took the Average across both papers for each article.
>
> If you are ok with your percentage, **please just Reply to Me with an "I concur"**. If you'd like more information on the award nomination or to discuss further, let me know.
>
> R De Jesús Crespo 40%
>
> S Yee 30%
>
> S Friedman 5%
>
> D Yee 10%
>
> F Bai 5%
>
> P. Méndez Lázaro 5%
>
> A Oczkowski 5%

Thank You!

Yee, S. H., D. A. Yee, R. de Jesús Crespo, A. Oczkowski, F. Bai, and S. Friedman (2019). Linking Water Quality to Aedes aegypti and Zika in Flood-Prone Neighborhoods. EcoHealth 16:191-209 https://doi.org/10.1007/s10393-019-01406-6

De Jesús Crespo, R., P. Méndez Lázaro, and S.H. Yee (2018) Linking wetland ecosystem services to vector borne disease: Dengue fever in San Juan Bay Estuary, Puerto Rico. Wetlands 39: 1281-1293. https://doi.org/10.1007%2Fs13157-017-0990-5

	Yee et al. 2019 (zika)	De Jesus Crespo et al. 2018 (dengue)	Combined
Rebeca de Jesus Crespo	10	70	40
Susan Yee	40	20	30
Stephanie Friedman	10	0	5
Donald Yee	20	0	10
Fengwei Bai	10	0	5
Pablo Mendez Lazaro	0	10	5
Autumn Oczkowski	10	0	5

Susan Yee

Gulf Ecosystem Measurement and Modeling

U.S. Environmental Protection Agency

1 Sabine Island Drive

Gulf Breeze, FL 32561

850-934-9397

--

Pablo A. Méndez Lázaro, Ph.D.
Principal Investigator: NASA--Early Warning of Synoptic Air Quality Events to Improve Health and Well Being in the Greater Caribbean Region (80NSSC19K0194)

Co-Principal Investigator: NIH--Impact of Hurricane-Related Stressors and Responses on Oncology Care and Health Outcomes of Women with Gynecologic Cancers from Puerto Rico and US Virgin Islands

City Co-lead: NSF--Urban Resilience to Extreme Weather Events-SRN, www.urexsrn.net

Environmental Health Department
Graduate School of Public Health
University of Puerto Rico-Medical Sciences Campus
PO BOX 365067
San Juan Puerto Rico 00936-5067
(001) 787 758 2525
ext 2928/1469

Yee, Susan

From: Rebeca De Jesus Crespo <rdejesuscrespo1@lsu.edu>
Sent: Wednesday, April 22, 2020 1:27 PM
To: Yee, Susan
Subject: Re: Record of Percentage Agreement: De Jesus Crespo, Rebeca

I concur

Thanks!

Rebeca de Jesús
Assistant Professor, Department of Environmental Sciences
Louisiana State University
College of Coast and the Environment
93 South Quad Drive
Baton Rouge, LA 70803

From: Yee, Susan <Yee.Susan@epa.gov>
Sent: Monday, April 20, 2020 9:44 AM
To: Rebeca De Jesus Crespo <rdejesuscrespo1@lsu.edu>
Subject: Record of Percentage Agreement: De Jesus Crespo, Rebeca

Hi everyone.
Two of our journal articles are being nominated for a US EPA award for Science and Technical Achievement. As part of the nomination, I need a concurrence from each of you on your Percent Contribution to both articles. Note below I just took the Average across both papers for each article.
If you are ok with your percentage, **please just Reply to Me with an "I concur"**. If you'd like more information on the award nomination or to discuss further, let me know.

R De Jesús Crespo 40%
S Yee 30%
S Friedman 5%
D Yee 10%
F Bai 5%
P. Méndez Lázaro 5%
A Oczkowski 5%

Thank You!

Yee, S. H., D. A. Yee, R. de Jesús Crespo, A. Oczkowski, F. Bai, and S. Friedman (2019). Linking Water Quality to Aedes aegypti and Zika in Flood-Prone Neighborhoods. EcoHealth 16:191-209 https://doi.org/10.1007/s10393-019-01406-6
De Jesús Crespo, R., P. Méndez Lázaro, and S.H. Yee (2018) Linking wetland ecosystem services to vector borne disease: Dengue fever in San Juan Bay Estuary, Puerto Rico. Wetlands 39: 1281-1293. https://doi.org/10.1007%2Fs13157-017-0990-5

	Yee et al. 2019 (zika)	De Jesus Crespo et al. 2018 (dengue)	Combined
Rebeca de Jesus Crespo	10	70	40
Susan Yee	40	20	30
Stephanie Friedman	10	0	5
Donald Yee	20	0	10
Fengwei Bai	10	0	5
Pablo Mendez Lazaro	0	10	5
Autumn Oczkowski	10	0	5

Susan Yee
Gulf Ecosystem Measurement and Modeling
U.S. Environmental Protection Agency
1 Sabine Island Drive
Gulf Breeze, FL 32561
850-934-9397

Table of Contents

General_Authors_Publications.....2
LI-266406_Hughes_and_Edwards_in_vivo_pyrethroids.....15
LI-266409_Xenobiotica_bifenpk_2016.....25
LI-266410_Toxicology_Vol_359_2016_pyrethroid_dose_response.....37
Crofton_Level_of_Effort_STAA_2020.....47
Devito_Level_of_Effort_STAA_2020.....49
Edwards_Level_of_Effort_STAA_2020.....51
Hughes_Level_of_Effort_STAA_2020.....53
Scollon_Level_of_Effort_STAA_2020.....55
Starr_Level_of_Effort_STAA_2020.....57
Wolansky_Level_of_Effort_STAA_2020.....59
Ross_level_of_Effort_STAA_2020.....62
In_vitro_dermal_absorption_of_pyethroids.....64

United States Environmental Protection Agency
Washington, DC 20460

STAA REPORT FOR THE SCIENTIST NOMINATIONS

General Information:

Nomination ID/App ID:	20-114
Research Category Primary:	Health Effects Research and Human Health Risk Assessment (HE)
Research Category Secondary:	Health Effects Research and Human Health Risk Assessment (HE)
Laboratory/Office Name:	ORD
Nomination Entered By:	Michael Hughes

Eligibility Checklist:

[Y] The nominated publication(s) has not been submitted to a previous STAA competition.

[Y] The nominated publication(s) was published on or before January 1, 2017 and on or after January 1,2012

[Y] The principal author was an EPA employee or a PHS employee assigned to EPA when the research was performed

[Y] The EPA authors (includes PHS employees assigned to EPA) contributed collectively a minimum of 50% toward the publication(s)

Nominating Official Name:	Reeder Sams
Nominating Official Title:	DEPUTY DIRECTOR FOR MANAGEMENT, NERL
Nominating OfficialEmail:	sams.reeder@epa.gov
STAA Coordinator Name:	Kathleen Wiser
STAA Coordinator Email:	wiser.kathi@epa.gov

Justifications:

Justification 1:

Pyrethroids are a class of synthetic pesticides with a chemical structure based on the pyrethrins, which are natural botanicals. The pyrethroids have greater insecticidal activity and are more stable in the environment than the pyrethrins. The use of pyrethroids is more common now as they are replacing organophosphate and carbamate pesticides, which are more acutely toxic classes of pesticides to mammals and birds than pyrethroids. There are about 20 pyrethroids that are registered with EPA for use on food crops. Exposure to pyrethroids may occur via inhalation or contact with the skin during spraying operations or ingestion when consuming food contaminated with pyrethroid residues. Studies have also shown that human exposure to multiple pyrethroids may occur. As EPA reregisters pyrethroids for use over time, our research goals were to provide our partners in the Office of Pesticide Programs with data from experimental studies to aid in the development of risk assessments for these compounds. In the studies nominated here, we examined 1) the bioavailability of bifenthrin in the rat; 2) the in vivo dermal absorption of 3 pyrethroids in the rat and using the parallelogram approach with in vitro data from a previous publication (see Supplemental Items) to estimate human dermal absorption of these compounds; and 3) correlate blood and brain concentrations of pyrethroids and neurobehavior, the latter measured as alteration in motor activity in rats, following an acute oral administration of five pyrethroids as a mixture. The research nominated provides information on the dosimetry and bioavailability of bifenthrin. Determination of bioavailability provides information on the extent that the parent compound bifenthrin, the presumed toxic species, reaches the systemic circulation and distributes to tissues following oral exposure. The dermal absorption research provides information on the distribution of pyrethroids to tissues and elimination following exposure to skin and penetration through it to reach the systemic circulation. The data from this research was used with previously published in vitro data to estimate human dermal absorption of the pyrethroid pesticides of which little is known. Correlating tissue concentrations of pyrethroids to neurotoxicity provides valuable information for toxicity assessments rather than solely relying on administered dose. Our results showed that blood concentrations of pyrethroids administered orally as a mixture can be a surrogate for brain concentrations of when assessing neurotoxic effect. Overall, this research has provided valuable data and information to our partners in the Office of Pesticide programs.

Justification 2A:

Two areas of research we have focused on is assessing the disposition of pyrethroid pesticides following oral, intravenous and dermal administration and correlating tissue dose of the pyrethroids to neurotoxic endpoint, for example, motor activity in rats. For our bifenthrin paper (published in Xenobiotica), we determined the disposition of the compound following oral and intravenous administration to rats in various tissues (blood, brain, etc.) and were able to estimate its bioavailability. For the in vivo dermal absorption paper (published in Journal of Toxicology and Environmental Health, Part A), we determined the disposition of 3 pyrethroids following dermal administration in rats. In addition, using data from our in vitro dermal absorption paper (see supplemental information), we were able to estimate human dermal absorption of these compounds using the parallelogram approach. A mathematical relationship is set up between the known in vitro dermal absorption values in rat and human skin and the values from the in vivo rat dermal absorption studies. Finally, in our pyrethroid tissue concentration and motor activity paper (published in Toxicology), we quantitated the levels of pyrethroids administered (multiple doses, one time point) orally to rat in blood and brain. From this information we were able to correlate motor activity of the rats with concentration of the pyrethroids in blood and brain (the target organ of the pyrethroids). We found that determination of blood concentrations of the pyrethroids could serve as a surrogate for pyrethroid concentration in brain. This may be an aid in future neurotoxicology studies of the pyrethroid pesticides.

Justification 2B:

Michael Hughes - two STAA nominations in the previous five years:

1) 2016, Level II 1) Independent Data Validation of an In Vitro Method for the Prediction of the Relative Bioavailability of Arsenic in Contaminated Soils; 2) Mouse Assay for Determination of Arsenic Bioavailability in Contaminated Soils

2) 2015, Level III 1) Biogeographical Analysis of Chemical Co-Occurrence Data to Identify Priorities for Mixtures Research, (2) Environmentally Relevant Mixtures in Cumulative Assessments: an Acute Study of Toxicokinetics and Effects on Motor Activity in Rats Exposed to a Mixture of Pyrethroids, and (3) A Pharmacokinetic Model of Cis-and Trans-Permethrin Disposition in Rats and Humans with Aggregate Exposure Application

Kevin Crofton- four STAA nominations in the previous five years:

1) 2019 Level I STAA: 1) Development of a Thyroperoxidase Inhibition Assay for High-Throughput Screening; 2) Tiered High-Throughput Screening Approach to Identify Thyroperoxidase Inhibitors within the ToxCast Phase I and II Chemical Libraries

2) 2019 Level III: A chemical and chemoinformatics foundation for ToxCast & Tox21 research programs.

3) 2017 Honorable Mention: Expanding the Test Set: Chemicals with Potential to Disrupt Mammalian Brain Development

4) 2015 Level III STAA: (1) Biogeographical Analysis of Chemical Co-Occurrence Data to Identify Priorities for Mixtures Research, (2) Environmentally Relevant Mixtures in Cumulative Assessments: an Acute Study of Toxicokinetics and Effects on Motor Activity in Rats Exposed to a Mixture of Pyrethroids, and (3) A Pharmacokinetic Model of Cis-and Trans-Permethrin Disposition in Rats and Humans with Aggregate Exposure Application

5) 2015 Honorable Mention: (1) An Animal Model of Marginal Iodine Deficiency During Development: The Thyroid Axis And Neurodevelopmental Outcome, and (2) Evaluation of Iodide Deficiency In The Lactating Rat and Pup Using A Biologically Based Dose-Response Model

Michael DeVito, James Starr, David Ross, Edward Scollon, Marcelo Wolansky - one STAA nomination in the last five years

1) 2015 Level III STAA: (1) Biogeographical Analysis of Chemical Co-Occurrence Data to Identify Priorities for Mixtures Research, (2) Environmentally Relevant Mixtures in Cumulative Assessments: an Acute Study of Toxicokinetics and Effects on Motor Activity in Rats Exposed to a Mixture of Pyrethroids, and (3) A Pharmacokinetic Model of Cis-and Trans-Permethrin Disposition in Rats and Humans with Aggregate Exposure Application

Brenda Edwards - no STAA nominations in the past five years

Justification 2C:

The awards for all of the participants except for the 2015 Level III STAA are not related to the current nomination. These awards are for the development of models to determine the bioavailability of soil-contaminated arsenic, the role of iodine and the thyroid axis in neurodevelopment, chemoinformatics for ToxCast and Tox21 research programs, and development of a high-throughput thyroperoxidaase inhibition screening assay. The 2015 award had a mixtures research theme using the pyrethroids as the example compounds. The overall outcomes of the studies nominated in the 2015 award showed that the co-occurrence of pesticides such as the pyrethroids in many settings is not random but highly structured resulting with specific pesticide combinations; supported the additive model of pyrethroid effect on motor activity in rats following an acute exposure (two doses, multiple time points) to a mixture of pyrethroids; and physiologically based pharmacokinetic models can be developed that simulate the disposition of cis- and trans-permethrin, basically a mixture of permethrin, in the rat. The present nomination has a theme of disposition of pyrethroid pesticides following oral, intravenous and dermal administration and correlation of tissue concentration of pyrethroid pesticides (multiple doses, one time point) administered as a mixture to motor activity, a neurotoxic endpoint.

Justification 2D:

One paper is added as supplemental information (In vitro dermal absorption of pyrethroid pesticides in human and rat skin). It is authored by Hughes and Edwards, published in 2010 in Toxicology and Applied Pharmacology. This study examined the in vitro dermal absorption of 3 pyrethroid pesticides using rat and human cadaver skin. The data from this study was used in the rat in vivo dermal absorption study (published in the Journal of Toxicology and Environmental Health, Part A) with the same 3 pyrethroid pesticides to estimate human in vivo absorption using the parallelogram approach.

Justification 2E:

No concurrent nominations have been submitted by any of the authors.

Justification 3A:

Citations:

Hughes, M.F. and Edwards, B.C. (2016) In vivo dermal absorption of pyrethroid pesticides in the rat. *Journal of Toxicology and Environmental Health, Part A* 79:83-91. Citations: 10 (Google Scholar)

Hughes, M.F., Ross, D.G., Edwards, B.C., DeVito, M.J. and Starr, J.M. (2016) Tissue time course and bioavailability of the pyrethroid insecticide bifenthrin in the Long-Evans rat. *Xenobiotica* 46:430-438. Citations: 6 (Google Scholar)

Hughes, M.F., Ross, D.G., Starr, J.M., Scollon, E.J., Wolansky, M.J., Crofton, K.M. and DeVito, M.J. (2016) Environmentally relevant pyrethroid mixtures: a study on the correlation of blood and brain concentration to motor activity of a mixture of pyrethroid insecticides administered to rats. *Toxicology* 359:19-28. Citations: 10 (Google Scholar)

Posters presented at the Society of Toxicology Annual Meetings:

Ross, D.G., Starr, J.M., Edwards, B.C., Hutchison, J., DeVito, M.J. and Hughes, M.F. (2012) Toxicokinetics of the pyrethroid pesticide bifenthrin in blood and brain of the rat. *Toxicological Sciences (The Toxicologist)* 126:404.

Hughes, M.F., Ross, D.G., Starr, J.M., Scollon, E.J., Wolansky, M.J., Crofton, K.M. and DeVito, M.J. (2013) Dose-response relationship of an environmental mixture of pyrethroids following acute oral administration in the rat. *Toxicological Sciences (The Toxicologist)* 132:104.

Justification 3B:

For the paper published in Journal of Toxicology and Environmental Health, Part A, Dr. Gabriel Knudsen of NIEHS, and Drs. Rogelio Tornero-Velez and Jane Ellen Simmons of EPA provided EPA internal reviews. For the paper published in Xeniobiotica, Drs. Elaina Kenyon, Jane Ellen Simmons and Rogelio Tornero-Velez of EPA provided EPA internal reviews. For the paper published in Toxicology, Drs. Nicole Tulve, Hisham El-Masri and Jane Ellen Simmons of EPA provided EPA internal reviews. All of the papers were edited based on comments from the various reviewers before submission to the journals. Each manuscript was submitted to a peer reviewed journal. There were four reviewers for the paper submitted to the Journal of Toxicology and Environmental Health, three reviewers for Xenobiotica and two reviewers for Toxicology. Comments from all reviewers were addressed, edits to the manuscripts were made and the papers were subsequently accepted for publication.

AUTHORS

Principal Author

Author Name: Michael F. Hughes

Professional Title: Salutation:

Email:	hughes.michaelf@epa.gov	Organization:	
Mailing Address:			
Street Line 1:	109 T.W. Alexander Dr. MD B105-03		
City:	Research Triangle Park		
Zip Code:	27711	State:	North Carolina
At time of research was:	EPA Employee		
Separation Date:			
% of Effort:	15		

Contributing Author

Author Name:	Michael J DeVito		
Professional Title:		Salutation:	
Email:	devito.michael@epa.gov	Organization:	
Mailing Address:			
Street Line 1:	109 T.W. Alexander Drive		
City:	Research Triangle Park		
Zip Code:	27711	State:	North Carolina
At time of research was:	EPA Employee		
Separation Date:			
% of Effort:	5		

Contributing Author

Author Name:	Brenda C Edwards		
Professional Title:		Salutation:	

Email:	edwards.brenda@epa.gov	Organization:	
Mailing Address:			
Street Line 1:	109 T.W. Alexander Dr.		
City:	Research Triangle Park		
Zip Code:	27711	State:	North Carolina
At time of research was:	EPA Employee		
Separation Date:			
% of Effort:	20		

Contributing Author

Author Name:	David Ross		
Professional Title:		Salutation:	
Email:	ross.david@epa.gov	Organization:	
Mailing Address:			
Street Line 1:	109 T.W. Alexander Dr.		
City:	Research Triangle Park		
Zip Code:	North Carolina	State:	North Carolina
At time of research was:	EPA Employee		
Separation Date:			
% of Effort:	20		

Contributing Author

Author Name:	James Starr		
Professional Title:		Salutation:	

Email:	starr.james@epa.gov	Organization:	
Mailing Address:			
Street Line 1:	109 T.W. Alexander Dr.		
City:	Research Triangle Park		
Zip Code:	North Carolina	State:	North Carolina
At time of research was:	EPA Employee		
Separation Date:			
% of Effort:	20		

Contributing Author

Author Name:	Kevin Crofton		
Professional Title:		Salutation:	
Email:	croftonwork@outlook.com	Organization:	
Mailing Address:			
Street Line 1:	2311 Willow St.		
City:	Durham		
Zip Code:	27705	State:	North Carolina
At time of research was:	EPA Employee		
Separation Date:	Sat Apr 28 00:00:00 GMT 2018		
% of Effort:	5		

Contributing Author

Author Name:	Edward Scollon Scollon		
Professional Title:		Salutation:	

Email:	ed.scollon@valent.com	Organization:	
Mailing Address:			
Street Line 1:	Valent Technical Center 6560 Trinity Court		
City:	Dublin		
Zip Code:	94568	State:	California
At time of research was:	EPA Employee		
Separation Date:	Sat Oct 11 00:00:00 GMT 2014		
% of Effort:	5		

Contributing Author

Author Name:	Marcelo Wolansky		
Professional Title:		Salutation:	
Email:	mhwolansky@gmail.com	Organization:	
Mailing Address:			
Street Line 1:	Department of Biological Chemistry Facultad de Ciencias Exactas y Naturales Ciudad Universitaria (UBA) Pabellon 2 - Piso 4		
City:	Buenos Aires		
Zip Code:	1428	State:	
At time of research was:	Non EPA Personnel		
Separation Date:			
% of Effort:	10		

PUBLICATIONS

Publication 1:

Publication Title:	In vivo dermal absorption of pyrethroid pesticides in the rat		
Publication Date:	Thu Jan 28 00:00:00 GMT 2016		
Journal/Publication Method:	Journal of Toxicology and Environmental Health, Part A		
All Author(s):			
Volume:	79	Number:	2
Pages:	83-71	Immediately Index:	Immediately Index:
Citation ½ Life:	9.0	Impact Factor:	2.649

Publication 2:

Publication Title:	Tissue time course and bioavailability of the pyrethroid insecticide bifenthrin in the Long-Evans ra		
Publication Date:	Mon Sep 14 00:00:00 GMT 2015		
Journal/Publication Method:	Xenobiotica 46:430-438.		
All Author(s):			
Volume:	46	Number:	5
Pages:	430-438	Immediately Index:	Immediately Index:
Citation ½ Life:	10	Impact Factor:	1.92

Publication 3:

Publication Title:	Environmentally relevant pyrethroid mixtures: a study on the correlation of blood and brain concentr
Publication Date:	Wed Jun 01 00:00:00 GMT 2016

Journal/Publication Method:	Toxicology		
All Author(s):			
Volume:	359	Number:	359
Pages:	19-28	Immediately Index:	Immediately Index:
Citation ½ Life:	10.9	Impact Factor:	3.547

Taylor & Francis
Taylor & Francis Group

Journal of Toxicology and Environmental Health, Part A
Current Issues

ISSN: 1528-7394 (Print) 1087-2620 (Online) Journal homepage: http://www.tandfonline.com/loi/uteh20

In vivo dermal absorption of pyrethroid pesticides in the rat

Michael F. Hughes & Brenda C. Edwards

To cite this article: Michael F. Hughes & Brenda C. Edwards (2016): In vivo dermal absorption of pyrethroid pesticides in the rat, Journal of Toxicology and Environmental Health, Part A, DOI: 10.1080/15287394.2015.1109571

To link to this article: http://dx.doi.org/10.1080/15287394.2015.1109571

Published online: 28 Jan 2016.

Submit your article to this journal

View related articles

View Crossmark data

Full Terms & Conditions of access and use can be found at
http://www.tandfonline.com/action/journalInformation?journalCode=uteh20

Download by: [US EPA Library] **Date:** 28 January 2016, At: 07:18

JOURNAL OF TOXICOLOGY AND ENVIRONMENTAL HEALTH, PART A
http://dx.doi.org/10.1080/15287394.2015.1109571

Taylor & Francis
Taylor & Francis Group

In vivo dermal absorption of pyrethroid pesticides in the rat

Michael F. Hughes and Brenda C. Edwards

U.S. Environmental Protection Agency, Research Triangle Park, North Carolina, USA

ABSTRACT

Exposure to pyrethroid pesticides is a potential cause for concern. The objective of this study was to examine the in vivo dermal absorption of bifenthrin, deltamethrin, and permethrin in the rat. Dorsal hair on adult male Long-Evans rats was removed. The next day, the skin was dosed with 1750 nmol (312.5 nmol/cm^2) of radiolabeled (5 μCi) bifenthrin, deltamethrin, or permethrin in acetone. A nonoccluding plastic cover was glued over the dosing site. The animals were placed in metabolism cages to collect excreta. At 24 h postdosing, the skin was washed with soap and water, and rats in one group were euthanized and their tissues were collected. The skin was removed and tape stripped. The remaining animals were returned to the metabolism cages after the wash for 4 d. These rats were then euthanized and handled as already described. Excreta, wash, tape strips, tissues, and carcass were analyzed for pyrethroid-derived radioactivity. The wash and tape strips removed >50% of the dose and skin retained 9–24%. Cumulative radioactivity in excreta was 0.5–7% at 24 h and 3–26% at 120 h. Radioactivity in tissues was <0.3% of the dose, while carcass retained 2 to 5%. Assuming absorption equals cumulative recovery in skin (washed and tape stripped), excreta, tissues, and carcass, absorption was permethrin ~ bifenthrin > deltamethrin at 24 h and permethrin > deltamethrin > bifenthrin at 120 h. Using the parallelogram approach with published in vitro data, human dermal absorption of these pyrethroids was estimated to be <10% of the dose.

ARTICLE HISTORY
Received 11 August 2015
Accepted 14 October 2015

Downloaded by [US EPA Library] at 07:18 28 January 2016

The use of pyrethroid pesticides is more commonplace today in the United States than that of other pesticide classes (Power and Sudakin, 2007). This is due in part to the phasing out of the organophosphate (OP) insecticides from residential uses. Pyrethroid exposure may occur during their manufacture, during their use in agricultural and residential settings, during their use as a veterinary or medicinal agent, or from the diet. Pyrethroids are detected in indoor surface wipes of child care centers (Tulve et al., 2006) and personal residences (Stout et al., 2009; Julien et al., 2008), indoor dusts (Harnly et al., 2009; Starr et al., 2008; Quivrós-Alcalá et al., 2011) and on fruits and vegetables (U.S. Department of Agriculture [USDA], 2013). Pyrethroid metabolites are found in urine at low levels in adults and children who are not occupationally exposed and who had not used them in the home (Heudorf and Angerer, 2001). Heudorf and Angerer (2001) suggested that absorption of pyrethroids and subsequent urinary elimination resulted from dietary exposure.

The human health effects of acute exposure to pyrethroids include respiratory, eye, and skin irritation and dermal paresthesia (Saillenfait et al., 2015). Hudson et al. (2014) assessed illnesses and injuries associated with acute exposures to pyrethrin and pyrethroids from 2000 to 2008 in 11 states within the United States and identified approximately 5000 cases of pyrethroid exposures. They reported that the incidence rate in 2008 was low, with 8 cases identified per million people. Eighty-five percent of cases were classified as low severity. Work-related effects of pyrethrin/pyrethroid exposure were 34% of the total identified effects. The most common illness of all reported cases from exposure to either pyrethrins or pyrethroids or both was respiratory effects such as cough, dyspnea, wheeze, or lower respiratory pain/irritation (Hudson et al. 2014). During this time period (2000–2008), five fatalities (approximately 0.01% of all cases examined) were associated with pyrethrin/pyrethroid exposure. Two cases were classified as definite (18-mo child and 76-yr-old woman),

CONTACT Michael Hughes, PhD hughes.michaelf@epa.gov Office of Research and Development, National Health and Environmental Effects Research Laboratory, U.S. Environmental Protection Agency, Research Triangle Park, NC 27711, USA.

© 2016 Taylor & Francis

Downloaded by [US EPA Library] at 07:18 28 January 2016

two cases were probable (64-yr-old woman and 35-yr-old man, both asthmatics), and the final case was classified as suspicious (10-mo-old child). The "definite" cases were a result of the child ingesting allethrin and the woman spraying permethrin/tetramethrin over her head. The other cases were a result of the individuals being in areas that had been sprayed with pyrethroids. Effects from low-level chronic exposure to pyrethroids are not well characterized. Epidemiological studies suggested that sperm quality, reproductive hormones, and pregnancy outcomes may be affected by this type of exposure to pyrethroids (Saillenfait et al., 2015). A mixture of permethrin/allethrin was found to produce cytotoxicity and genotoxicity in human peripheral blood lymphocytes (Ramos-Chaves et al., 2015). In an extensive review, Wolansky and Tornero-Velez (2013) described the neurotoxicity associated with pyrethroid exposure.

The three main routes of chemical exposure include oral, inhalation, and dermal are important to consider for chemical risk assessments. Regarding dermal exposure to pyrethroids, Zhang et al. (1991) reported that dermal exposure was the main route of absorption of the pyrethroids deltamethrin and fenvalerate sprayed by workers onto cotton fields. Military personnel and forestry workers wearing clothing impregnated with permethrin have an increased internal exposure to this pyrethroid, based on elevation of excreted permethrin urinary metabolites (Kegel et al., 2015; Rossbach et al., 2014). Permethrin is used medicinally for the treatment of scabies and lice (Taplin and Meinking, 1990; Tomalik-Scharte et al., 2005; van der Rhee et al., 1989) and was utilized in combination with *N,N*-diethyl-*m*-toluamide (DEET) during the first Gulf War (Abu-Qare and Abou-Donia, 2003). Permethrin is systemically absorbed by this medical use; approximately 0.5% of an applied dose (1250 mg) of permethrin cream to skin was excreted in urine over 48 h (van der Rhee et al., 1989). Woollen et al. (1992) reported that in human volunteers treated with cypermethrin on the back approximately 1% of the applied dose was excreted in urine following an 8-h exposure.

The objective of this study was to examine in vivo dermal absorption of three radiolabeled pyrethroids, bifenthrin, deltamethrin, and permethrin, in adult male Long-Evans (LE) rats. The treated skin was washed at 24 h to remove unabsorbed pyrethroid. One group of rats was euthanized and tissues and excreta were collected. A second group of similarly treated rats was maintained for 4 additional days for collection of daily excreta and tissues at 120 h post-exposure. Collected tissues, wash, tape strips, and excreta were analyzed for pyrethroid-derived radioactivity. Pyrethroid disposition data following dermal exposure might aid in more accurate risk assessment of this class of commonly used pesticides.

Materials and methods

Chemicals

[^{3}H(G)]-Bifenthrin (specific activity 317 mCi/mmol, radiochemical purity >98%) and [^{3}H(G)]-deltamethrin (specific activity 9 Ci/mmol, radiochemical purity >95%) were purchased from Perkin-Elmer Life and Analytical Sciences, Inc. (Waltham, MA). *cis*-[Cycloproprane-1-^{14}C]-permethrin (specific activity 54 mCi/mmol, radiochemical purity >98%) was purchased from Amersham Biosciences (Piscataway, NJ). Radiochemical purity of the radiolabeled pyrethroids was confirmed by high-performance liquid chromatography (HPLC) radio-flow analysis as described by Hughes and Edwards (2010). Unlabeled pyrethroids (purity >98%) were purchased from Chem Service (West Chester, PA). Ketamine hydrochloride was purchased from Fort Dodge Laboratories (Fort Dodge, IA), and xylazine was from Phoenix Scientific (St. Joseph, MO).

Animals

Adult male LE rats were purchased from Charles River Laboratories (Portage, MI). The LE rat was used because of collaborative neurotoxicology and pharmacokinetic studies that used this strain (Godin et al., 2010; Hughes and Edwards, 2010; Scollon et al., 2011; Tornero-Velez et al., 2012; Wolansky et al., 2006). Animals were housed individually in polycarbonate cages with heat-treated lab-grade pine shavings (Northeastern Products, Warrensburg, NY) in an Association for the Assessment and Accreditation of Laboratory Animal Care-approved facility. Animals were provided with feed (Purina Rodent Chow 5001, Barnes Supply Co., Durham, NC) and tap water

Downloaded by [US EPA Library] at 07:18 28 January 2016

for ad libitum consumption. Tap water (Durham, NC) used in the animal facility was filtered through sand and activated charcoal and rechlorinated to 4–5 ppm Cl^-. All animal procedures were approved by the Institutional Animal Care and Use Committee of the National Health and Environmental Effects Research Laboratory.

Experimental

Animals (approximately 70 d old; 270–326 g body weight) were placed in individual metabolism cages 2 d before the experiment. The day before the experiment, animals were anesthetized with isoflurane via inhalation, and hair on their dorsal surface was removed with an electric clipper (Oster Corp., Milwaukee, WI, size 40 blade). The skin was rinsed with distilled water to remove extraneous material and checked for abrasions and nicks. A Tygon tubing collar secured with wire was placed behind the forelegs of the rats. This was used to prevent the animal from licking the clipped area and plastic cover used once the chemical was applied. The following day, rats were anesthetized with ketamine (80 mg/kg) and xylazine (10 mg/kg) administered ip. Once animals were anesthetized, the collar was removed and a circular dosing site (area 5.6 cm^2) was drawn on the clipped skin with a felt tip pen. Pyrethroid (5 μCi radiolabeled and unlabeled pyrethroid were combined to prepare a dose of 1750 nmol) in acetone (250 μl) was applied within the dosing site (5.6 cm^2). Once the acetone dried, a clear plastic cover punched with a few holes to minimize occlusion was glued over the dosing site with cyanoacrylate adhesive. The collar was reattached behind the forelegs of the rats. Animals were returned to metabolism cages for collection of urine and feces. Twenty-four hours postexposure, rats were anesthetized with the ketamine/xylazine solution. Once the animal was anesthetized, the top of the plastic cover was cut away. The skin was washed with 1 ml Ivory liquid soap:water (50:50) mixture and a cotton ball three times, one wash with 1 ml of water and a cotton ball, and a dry wash with a cotton ball. The washes and cotton balls were placed in scintillation vials and mixed with 10 ml scintillant (Ultima Gold, PerkinElmer, Waltham, MA). Animals were then euthanized by cardiac puncture under CO_2-induced anesthesia. The following tissues were removed: treated skin, a piece of untreated skin, liver, lung, kidneys, brain, and perirenal fat. The blood, untreated skin, and organs were weighed, frozen in liquid nitrogen, and stored at –70°C until processing for combustion in a PerkinElmer model D307 oxidizer. These samples were then assayed for radioactivity in a PerkinElmer model 2560 liquid scintillation counter. The carcasses were weighed and stored at –70°C until processing. The carcasses were processed by homogenization in liquid nitrogen in an industrial blender (Waring Products Division, New Hartford, CT). Aliquots of the carcass homogenate were weighed, combusted, and analyzed for radioactivity. Urine and feces were collected from each metabolism cage at the time of euthanasia. Each metabolism cage was washed with approximately 75 ml 10% (v/v) Count-Off (PerkinElmer). The wash was mixed with urine and brought to a total volume of 100 ml with water. Aliquots of the combined urine and cage wash were mixed with scintillant and assayed for radioactivity. The feces were weighed and stored at –70°C until processing. The feces were processed by pulverizing each sample, weighing aliquots (approximately 250 mg), combustion, and assay for radioactivity. The treated skin was allowed to dry overnight at room temperature and then stripped with clear cellophane tape 10 times. Each tape strip was placed in a scintillation vial and mixed with scintillant before assay for radioactivity. The stripped skin was then immediately combusted and assayed for radioactivity.

In a second study, rats were treated with pyrethroid as already described. Their skin was washed 24 h postexposure under anesthesia. A second plastic cap was glued over the original cap and animals returned to metabolism cages for an additional 4 d. Urine and feces were collected daily. Five days postexposure, animals were euthanized by cardiac puncture under CO_2-induced anesthesia and the same tissues were removed as already described. The excreta, tissues, treated skin, and carcass were handled as already described.

Results

Pyrethroid-derived radioactivity was detected in urine and feces at 24 h and increased over the course of 120 h for the 3 pyrethroids (Table 1 and Figure 1).

Downloaded by [US EPA Library] at 07:18 28 January 2016

Table 1. Cumulative Percent Dose of Pyrethroid-Derived Radioactivity in Urine and Feces After Dermal Application of Pyrethroids to Rats.

Pyrethroid	Time (h)	Urine	Feces
Bifenthrin	24	0.6 ± 0.1	2.0 ± 0.7
	120	2.6 ± 2.1	7.5 ± 2.7
Deltamethrin	24	0.2 ± 0.03	0.3 ± 0.2
	120	1.4 ± 0.3	1.8 ± 1.0
Permethrin	24	3.5 ± 0.9	3.7 ± 1.6
	120	14.6 ± 2.8	11.3 ± 2.9

Note. Dose of pyrethroid was 1750 nmol on 5.6 cm^2 of skin; data displayed are from time of euthanasia. Data represent mean ± SD, $n = 4$, except for deltamethrin at 120 h, where $n = 3$.

For permethrin, total excretion was highest of the three pyrethroids examined. Total excretion was 7% at 24 h and rose to 26% at 120 h. Urinary excretion and fecal excretion of permethrin-derived radioactivity were the same at 24 h, but at 120 h urinary excretion was numerically higher. For bifenthrin, total excretion increased from 3% at 24 to 10% at 120 h and was greater in feces than urine at both time points. Total excretion of deltamethrin was lowest overall of the three pyrethroids examined. It was 0.5% at 24 h and rose to 3% at 120 h. The percentage excreted was similar in both urine and feces at these two time points. The skin was washed at 24 h post-exposure for all treated animals, and detection of radioactivity in excreta beyond this time indicates that pyrethroid-derived radioactivity in skin was available to diffuse into the systemic circulation and eventually excreted.

The highest percentage of the dose was recovered in the skin wash, ranging from 42 to 70% (Table 2). Treated skin that was washed and tape stripped displayed the second highest percentage, ranging from 9 to 24% (Table 2). Radioactivity removed by tape stripping the treated skin ranged from 3.3 to 6.2% of the dose (Table 2). For the organs collected and analyzed, pyrethroid-derived radioactivity was < 0.3%. The rank order of pyrethroid-derived radioactivity from highest to lowest percent distribution trended toward fat > liver > kidneys > lung > brain. Exceptions to this trend in this study of percent distribution were deltamethrin at 120 h and permethrin at 24 h, where liver > fat (Table 2). The percent dose in carcass ranged from 3 to 5% of the dose (Table 2). Recovery of pyrethroid-derived radioactivity in wash, tape strips, excreta, tissues, and carcass ranged from 87 to 98% (Table 2).

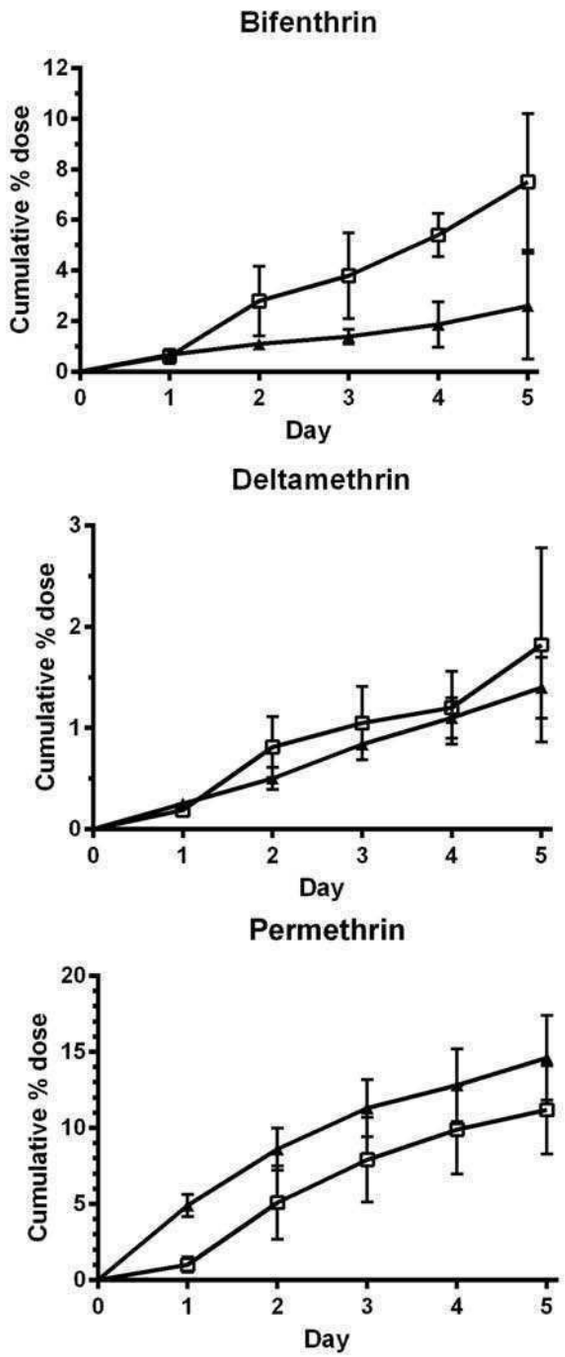

Figure 1. Cumulative percent excretion of the dose of bifenthrin, deltamethrin and permethrin in urine (▲) and feces (□) over 5 d after dermal exposure to male rats. The skin of the rats was washed on d 1. Data represent mean ± SD, $n = 4$ for bifenthrin and *cis*-permethrin, $n = 3$ for deltamethrin. Data displayed are only from animals euthanized at 120 h.

Concentration of pyrethroid-derived radioactivity was no greater than 0.01%/g for liver (bifenthrin) and kidneys (permethrin) at 24 h and fat (bifenthrin) at 120 h (Table 3). The lowest concentration of radioactivity was detected in brain

Downloaded by [US EPA Library] at 07:18 28 January 2016

Table 2. Distribution (Percent of Dose) Of Pyrethroid-Derived Radioactivity in Wash, Tape Strip, Carcass, and Tissues of Rats after Dermal Application.

Pyrethroid	Time (h)	Wash	Tape strip	Treated Skin	Carcass	Liver	Lung	Brain	Kidney	Fat[c]	Recovery[d]
Bifenthrin	24	52.3 ± 5.0	5.2 ± 2.0	24.1 ± 5.7	2.9 ± 2.2	0.08 ± 0.02	0.003 ± 0.003	0.002 ± 0.0003	0.006 ± 0.001	0.1 ± 0.03	87.3 ± 3.5%
	120	70.0 ± 3.0[a]	6.2 ± 2.9[b]	9.2 ± 4.2	2.0 ± 3.0	0.05 ± 0.05	0.002 ± 0.002	0.0001 ± 0.0001	0.005 ± 0.005	0.1 ± 0.1	97.5 ± 1.0%
Deltamethrin	24	62.6 ± 3.6	3.6 ± 0.7	20.1 ± 2.4	2.8 ± 4.5	0.02 ± 0.003	0.003 ± 0.002	0.0007 ± 0.0003	0.002 ± 0.0004	0.048 ± 0.009	89.7 ± 2.9%
	120	59.5 ± 4.9[a]	3.3 ± 1.2[b]	20.4 ± 6.1	2.6 ± 3.4	0.02 ± 0.02	0.0007 ± 0.0006	0.0002 ± 0.0001	0.003 ± 0.0004	0.014 ± 0.009	89.0 ± 5.3%
Permethrin	24	62.3 ± 4.2	5.1 ± 0.4	18.7 ± 3.8	4.9 ± 1.4	0.2 ± 0.08	0.004 ± 0.003	0.0001 ± 0.0002	0.02 ± 0.007	0.03 ± 0.01	98.4 ± 2.3%
	120	52.1 ± 5.0[a]	4.7 ± 1.0[b]	11.3 ± 6.2	4.1 ± 3.3	0.07 ± 0.04	0.003 ± 0.002	0.0009 ± 0.0004	0.006 ± 0.004	0.18 ± 0.08	98.1 ± 5.5%

Note. Dose of pyrethroid was 1750 nmol on 5.6 cm^2 of skin. Data represent mean ± SD, $n = 4$, except for deltamethrin at 120 h, where $n = 3$.
[a]Wash conducted at 24 h.
[b]Tape strip at 120 h.
[c]Estimated using 7.8% body fat (Simmons et al., 2002).
[d]Recovery includes data from Table 1.

Table 3. Concentration (Percent Dose/g Tissue) of Pyrethroid-Derived Radioactivity in Tissues of Rats After Dermal Application.

Pyrethroid	Time (h)	Blood	Brain	Fat	Kidney	Liver	Lung	Untreated skin
Bifenthrin	24	0.001 ± 0.0002	0.0009 ± 0.0001	0.004 ± 0.001	0.002 ± 0.0004	0.006 ± 0.001	0.003 ± 0.002	0.003 ± 0.002
	120	0.0005 ± 0.0004	0.00007 ± 0.00008	0.006 ± 0.005	0.002 ± 0.001	0.004 ± 0.004	0.001 ± 0.0006	0.003 ± 0.005
Deltamethrin	24	0.0003 ± 0.0001	0.0004 ± 0.0001	0.002 ± 0.0003	0.0007 ± 0.0001	0.001 ± 0.0002	0.002 ± 0.001	0.0009 ± 0.0002
	120	0.002 ± 0.00008	0.0001 ± 0.0001	0.0006 ± 0.0004	0.0009 ± 0.0002	0.002 ± 0.002	0.0005 ± 0.0001	0.003 ± 0.002
Permethrin	24	0.004 ± 0.003	0.00008 ± 0.00008	0.001 ± 0.0005	0.006 ± 0.002	0.01 ± 0.004	0.003 ± 0.002	0.002 ± 0.001
	120	0.001 ±.0.0007	0.0004 ± 0.0002	0.008 ± 0.004	0.002 ± 0.001	0.002 ± 0.001	0.002 ± 0.001	0.005 ± 0.007

Note. Dose of pyrethroid was 1750 nmol on 5.6 cm^2 of skin. Data represent mean ± SD, $n = 4$, except for deltamethrin at 120 h, where $n = 3$.

Table 4. Pyrethroid-Derived Radioactivity (Percent of Dose) in Excreta, Treated Skin, and Body of the LE rat 24 and 120 h Postadministration.

Pyrethroid	Time (h)	Excerta[a]	Treated skin[b]	Body burden[c]
Bifenthrin	24	2.7 ± 0.8[d]	24.1 ± 5.7	3.1 ± 2.3
	120	10.1 ± 4.8	9.2 ± 4.2	2.2 ± 3.1
Deltamethrin	24	0.5 ± 0.2	20.1 ± 2.4	2.8 ± 4.5
	120	3.2 ± 0.9	20.4 ± 6.1	2.6 ± 3.5
Permethrin	24	7.2 ± 2.4	18.7 ± 3.8	5.1 ± 1.5
	120	25.8 ± 5.3	11.3 ± 6.2	4.3 ± 3.5

[a]Sum of pyrethroid-derived radioactivity (% dose) in urine and feces.
[b]Sum of pyrethroid-derived radioactivity (% dose) in washed and tape-stripped treated skin.
[c]Sum of pyrethroid-derived radioactivity (% dose) in brain, carcass, fat (estimated), kidney, liver, and lung.
[d]Data represent mean ± SD, $n = 4$ except for deltamethrin at 120 h, where $n = 3$.

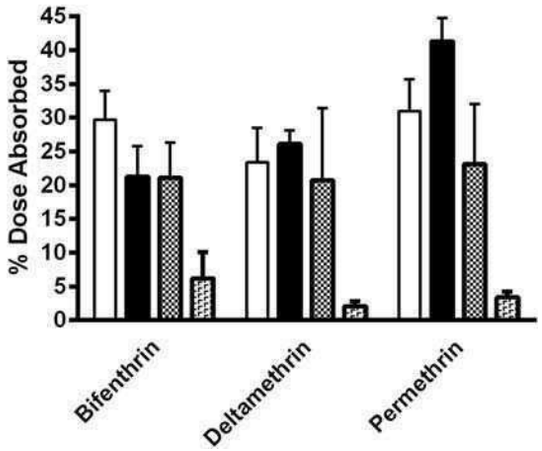

Figure 2. Percent absorption of pyrethroids at 24 h (□) and 120 h (■) post dermal exposure to rats in vivo and 24 h postexposure to rat (▒) and human (⁞) skin in vitro. All skins from the present and in vitro study received an equivalent pyrethroid dose of 312.5 nmol/cm^2. For in vivo data, absorption includes pyrethroid-derived radioactivity detected in urine, feces, skin (washed and tape stripped), carcass, liver, lung, kidneys, brain, and perirenal fat. For in vitro data, absorption includes pyrethroid-derived radioactivity in receptor fluid and skin (washed and tape stripped) (data from Hughes and Edwards, 2010). Data represents mean ± SD, $n = 4$, except for deltamethrin at 120 h where $n = 3$.

for all tissues, pyrethroids, and times, except for deltamethrin at 24 h. At this time, the concentration of deltamethrin in brain (0.0004% dose/g) was numerically higher than in blood (0.0003% dose/g).

A summary of the total percent pyrethroid-derived radioactivity in excreta, treated skin, and the body burden at 24 and 120 h postadministration is displayed in Table 4. A greater percentage of the bifenthrin dose decreased in treated skin than for permethrin and deltamethrin by 120 h. The percent of dose of deltamethrin in skin remained the same at 24 and 120 h. The body burden of pyrethroid-derived radioactivity was ≤5% of the dose and decreased only slightly relative to the percent of the dose excreted in urine and feces, suggesting fairly rapid clearance of pyrethroids from the systemic circulation.

Figure 2 shows the absorption data for the three pyrethroids at 24 and 120 h, as well as data from our in vitro study at 24 h in rat and human skin (Hughes and Edwards, 2010). An equivalent dose, 312.5 nmol/cm^2, was used in the present study and in the in vitro study. The term *absorption* includes chemical that (1) penetrated into the skin and could not be removed by washing and tape stripping, and (2) chemical that has completely penetrated the skin and detected in tissues, carcass, and excreta for in vivo studies or receptor fluid for in vitro studies. Absorption in vivo ranged from approximately 25 to 30% at 24 h and 20 to 40% at 120 h for the 3 pyrethroids. For deltamethrin and permethrin, absorption increased from 24 to 120 h. A portion of the pyrethroid in skin not removed by the wash at 24 h penetrated further into the skin to the systemic circulation. For bifenthrin, percent absorption was less at 120 than at 24 h. An explanation for this observation is that washing of the skin was less efficient for the 24- than for the 120-h group. Alternatively, bifenthrin in the epidermis may have diffused to the surface and was removed by the tape stripping. The rat in vitro absorption value at 24 h was 9–30% less than the comparable in vivo value at 24 h for the 3 pyrethroids (Figure 2). Human in vitro absorption was 80–90% less than rat in vivo absorption at 24 h. Using the parallelogram approach to estimate human dermal absorption of chemicals (% human absorption = (% rat in vivo/% rat in vitro) × % human in vitro; van Ravenzwaay and Leibold, 2004), the estimated absorption at 24 h was 8.7, 2.4, and 5.4% for bifenthrin, deltamethrin, and permethrin, respectively.

Discussion

Human exposure to pyrethroid pesticides is becoming a more common occurrence because of

Downloaded by [US EPA Library] at 07:18 28 January 2016

Downloaded by [US EPA Library] at 07:18 28 January 2016

their use for crop protection and in residences and child care centers (Wolansky and Tornero-Velez, 2013). Exposure to pyrethroids may occur via inhalation, ingestion, or dermal contact. The latter exposure route may occur when pyrethroids are sprayed or when humans come into contact with a contaminated surface. Data in the present study showed that pyrethroid pesticides bifenthrin, deltamethrin, and permethrin permeated rat skin and were systemically absorbed following a 24-h exposure. The pyrethroids distributed throughout the animal and were excreted. Washing the skin removed more than 50% of the dose for the 3 pyrethroids. A portion of the chemical that had permeated the skin and was not removed by the wash was available for absorption into the systemic circulation, as evidenced by pyrethroid-derived radioactivity detected in excreta out to 4 d post washing the skin. Of the three pyrethroids examined, permethrin was absorbed to the greatest extent in the rat. Absorption is defined as chemical in excreta, tissues, carcass, and skin that could not be removed by the wash and tape strips. Other than the wash, the skin displayed the highest percentage of the dose for the three pyrethroids. Evidence thus indicates the importance of including treated skin when accounting for the study compound in lab dermal exposure studies. It is noteworthy that 9–20% of the dose was detected in skin at 120 h. The results from the 5-d study suggest that some fraction of pyrethroid in rat skin may continue to be systemically absorbed past 5 d, because radioactivity in excreta was still increasing from d 4 to 5. However, not all of the chemical retained in skin may be available for entry into the systemic circulation. Highly lipophilic and high-molecular-weight chemicals such as pyrethroids that are retained in skin may be eliminated in part as the epidermis turns over by desquamation (Reddy et al., 2000).

Permethrin is commonly used as a mixture of its *cis* and *trans* isomers. The physicochemical parameters of *cis*- and *trans*-permethrin are fairly similar. In this study the *cis* isomer of permethrin was used. Because dermal absorption is a process of passive diffusion, there should be limited differences in dermal absorption between these two permethrin isomers. An in vitro study by Franz et al. (1996) that used guinea pig and human skin fractions and an in vivo study by Sidon et al. (1988) that used monkeys and rats confirmed the lack of a difference in the dermal absorption between *cis*- and *trans*-permethrin. However, once absorbed into the systemic circulation and distributed throughout the body, there may be differences in disposition of the two isomers. The *trans* isomer of permethrin is more easily hydrolyzed by esterases than the *cis* isomer (Soderlund and Casida, 1977). The *cis* isomer of permethrin is more persistent than the *trans* isomer in tissues of rats administered a mixture of *cis*/*trans*-permethrin by the oral route because it is less susceptible to hydrolysis by esterases (Tornero-Velez et al., 2012).

Sidon et al. (1988) examined the in vivo dermal absorption of *cis*- and *trans*-permethrin in monkeys and rats. There were no significant differences in total percent of the dose absorbed between *cis*- and *trans*-permethrin applied as each isomer to either the forearm and forehead of monkeys or the dorsal region of rats. In rats, following a 24-h exposure to permethrin (approximately 7 μg) in the dorsal region, approximately 45% of the dose was excreted in urine over 7 d. In monkeys, absorption was no greater than 28% of the dose (approximately 7 μg) and was dependent on the site of application (absorption greater in forehead than forearm). More recently, Reifenrath et al. (2011) studied in vivo dermal absorption of permethrin (*cis:trans*, 47:53) in male Sprague-Dawley (SD) rats. At a dose of 500 nmol/cm^2 (200 μg/cm^2), Reifenrath et al. (2011) reported 28% absorption of permethrin at 24 h and 30% absorption after 5 d. At a dose of 312.5 nmol/cm^2 absorption of 31% at 24 h and 41% at 5 d was noted in this investigation.

Human dermal absorption of permethrin, assessed indirectly by measuring permethrin metabolites excreted in urine, suggests absorption based on percent applied dose is low (van der Rhee et al., 1989; Tomalik-Scharte et al., 2005). For example, approximately 0.5% of the applied dose of permethrin (approximately 1.25 g) was absorbed through the skin of scabies patients (van der Rhee et al., 1989). Ross et al. (2011) estimated human dermal absorption of permethrin using the parallelogram approach based upon data from SD rat for in vivo and in vitro

studies. Using 3 dose levels (2–200 μg/cm^2), Ross et al. (2011) estimated human dermal absorption of permethrin ranged from 1.5 to 3.3% at 24 h. Our dose of permethrin was lower than the high dose of Ross et al. (2011), but our estimated human absorption values were similar (3.3 vs. 5.4%). Overall the human dermal absorption of pyrethroids would appear to be low based on percent of applied dose, but additional studies are required to confirm this assumption.

In conclusion, in vivo dermal absorption of the pyrethroids bifenthrin, deltamethrin, and permethrin in the LE rat ranged from 23 to 31% at 24 h. Greater than 50% of the dose of pyrethroid might be removed by skin wash at 24 h. At this same time, 19–24% of the dose was detected in the treated skin dose site. Chemical in skin not removed by the wash at 24 h ranged from 19 to 24%. Some of the dose in skin was absorbed into the systemic circulation over a 4-d period after the wash. The chemicals were widely distributed throughout the body of the animals. Fat and liver displayed the highest distribution of compound of the tissues examined, but overall were low (<0.2% of the dose). Of the organs examined, brain showed the lowest distribution and concentration of pyrethroid-derived radioactivity. Using these data and previous findings from our lab (Hughes and Edwards, 2010), human dermal absorption of the pyrethroids examined in this study is estimated to range from 5 to 9% of the applied dose at 24 h postexposure.

Disclaimer

This article has been reviewed in accordance with the policy of the National Health and Environmental Effects Research Laboratory, U.S. Environmental Protection Agency, and approved for publication. Approval does not signify that the contents necessarily reflect the views and policies of the agency, nor does mention of trade names or commercial products constitute endorsement or recommendation for use.

ORCID

Michael Hughes http://orcid.org/0000-0002-5571-5447

Acknowledgments

The authors thank Carol Mitchell and Frances McQuaid for their technical assistance with this study and Drs. Gabriel Knudsen, Jane Ellen Simmons, and Rogelio Tornero-Velez for their comments on an earlier version of this article.

References

Abu-Qare, A. W., and Abou-Donia, M.B. 2003. Combined exposure to DEET (*N,N*-diethyl-*m*-toluamide) and permethrin: Pharmacokinetic and toxicological effects. *J. Toxicol. Environ. Health B* 6: 41–53.

Franz, T. J., Lehman, P. A., Franz, S. F., and Guin, J. D. 1996. Comparative percutaneous absorption of lindane and permethrin. *Arch. Dermatol.* 123: 901–905.

Godin, S. J., DeVito, M. J., Hughes, M. F., Ross, D. G., Scollon, E. J., Starr, J. M., Setzer, R. W., Conolly, R. B., and Tornero-Velez, R. 2010. Physiologically-based pharmacokinetic modeling of deltamethrin: Development of a rat and human diffusion-limited model. *Toxicol. Sci.* 115: 330–343.

Harnly, M. E., Bradman, A., Nishioka, M., McKone, T. E., Smith, D., McLaughlin, R., Kavanagh-Baird, G., Castorina, R., and Eskenazi, B. 2009. Pesticides in dust from homes in an agricultural area. *Environ. Sci. Technol.* 43: 8767–8774.

Heudorf, U., and Angerer, J. 2001. Metabolites of pyrethroid insecticides in urine specimens: current exposure in an urban population in Germany. *Environ. Health Perspect.* 109: 213–217.

Hudson, N. L., Kasner, E.J., Beckman, J., Mehler, L., Schwartz, A., Higgins, S., Bonnar-Prado, J., Lackovic, M., Mulay, P., Mitchell, Y., Larios, L., Walker, R., Waltz, J., Moraga-McHaley, S., Roisman, R., and Calvert, G. M. 2014. Characteristics and magnitude of acute pesticide-related illnesses and injuries associated with pyrethrin and pyrethroid exposures—11 States, 2000–2008. *Am. J. Ind. Med.* 57: 15–30.

Hughes, M. F., and Edwards, B. C. 2010. In vitro dermal absorption of pyrethroids in human and rat skin. *Toxicol. Appl. Pharmacol.* 246: 29–37.

Julien, R., Adamkiewicz, G., Levy, J. I., Bennett, D., Nishioka, M., and Spengler, J. D. 2008. Pesticide loadings of select organophosphate and pyrethroid pesticides in urban public housing. *J. Expos. Sci. Environ. Epidemiol.* 18: 167–174.

Kegel, P., Letzel, S., and Rossbach, B. 2015. Biomonitoring in wearers of permethrin impregnated battle dress uniforms in Afghanistan and Germany. *Occup. Environ. Med.* 71: 112–117.

Power, L. E., and Sudakin, D. L. 2007. Pyrethrin and pyrethroid exposures in the United States: A longitudinal analysis of incidents reported to Poison Centers. *J. Med. Toxicol.* 3: 94–99.

Quivrós-Alcalá, L., Bradman, A., Nishioka, M., Harnly, M. E., Hubbard, A., McKone, T. E., Ferber, J., and Eskenazi, B. 2011 Pesticides in house dust from urban and farmworker

Downloaded by [US EPA Library] at 07:18 28 January 2016

Downloaded by [US EPA Library] at 07:18 28 January 2016

households in California: An observational measurement study. *Environ Health* 10: 19.

Ramos-Chavez, L. A., Sordo, M., Calderon-Aranda, E., Castañada-Saucedo, E., Ostroskky-Wegman, P., and Moreno-Godinez, M. E. 2015. A permethrin/allethrin mixture induces genotoxicity and cytotoxicity in human peripheral blood lymphocytes.. *J. Toxicol. Environ. Health A* 78: 7–14.

Reddy, M. B., Guy, R. H., and Bunge, A. L. 2000. Does epidermal turnover reduce percutaneous penetration? *Pharm. Res*. 17: 1414–1419.

Reifenrath, W. G., Ross, J. H., and Driver, J. H. 2011. Experimental methods for determining permethrin dermal absorption. *J. Toxicol. Environ. Health A* 74: 325–335.

Ross, J. H., Reifenrath, W. G., and Driver, J. H. 2011. Estimation of the percutaneous absorption of permethrin in humans using the parallelogram method. *J. Toxicol. Environ. Health A* 74: 351–363.

Rossbach, B., Niemietz, A., Kegel, P., and Letzel, S. 2014. Uptake and elimination of permethrin related to the use of permethrin treated clothing for forestry workers. *Toxicol. Lett*. 231: 147–153.

Saillenfait, A.-M., Ndiaye, D., and Sabaté, J.-P. 2015. Pyrethroids: exposure and health effects—An update. *Int. J. Hyg. Environ. Health* 218: 281–292.

Scollon, E. J., Starr, J. M., Crofton, K. M., Wolansky, M. J., DeVito, M. J., and Hughes, M. F. 2011. Correlation of tissue concentrations of the pyrethroid bifenthrin with neurotoxicity in the rat. *Toxicology* 290: 1–6.

Sidon, E. W., Moody, R. P., and Franklin, C. A. 1988. Percutaneous absorption of cis- and trans-permethrin in rhesus monkeys and rats: Anatomic site and interspecies variation. *J. Toxicol. Environ. Health* 23: 207–216.

Simmons, J. E., Boyes, W. K., Bushnell, P. J., Raymer, J. M., Limsakun, T., McDonald, A., Sey, Y. M., and Evans, M. V. 2002. A physiologically based pharmacokinetic model for trichloroethylene in the male Long-Evans rat. *Toxicol. Sci*. 69: 3–15.

Soderlund, D. M., and Casida, J. E. 1977. Effects of pyrethroid structure on rates of hydrolysis and oxidation by mouse liver microsomal enzymes. *Pestic. Biochem. Physiol*. 7: 391–401.

Starr, J., Graham, S., Stout, D. 2nd, Andrews, K., and Nishioka, M. 2008. Pyrethroid pesticides and their metabolites in vacuum cleaner dusts collected from homes and day-care centers. *Environ. Res*. 108: 271–279.

Stout, D. M. II, Bradham, K. D., Egeghy, P. P., Jones, P. A., Croghan, C. W., Ashley, P. A., Pinzer, E., Friedman, W., Brinkman, M. C., Nishioka, M. G., and Cox, D. C. 2009. American Healthy Homes Survey: A national study of residential pesticides measured from floor wipes. *Environ. Sci. Technol*. 43: 4294–4300.

Taplin, D., and Meinknig, T. L. 1990. Pyrethrins and pyrethroids in dermatology. *Arch. Dermatol*. 126: 213–221.

Tomalik-Scharte, D., Lazar, A., Meins, J., Bastian, B., Ihrig, M., Wachall, B., Jetter, A.,Tantcheva-Poor, I., Mahrle, G., and Fuhr, U. 2005. Dermal absorption of permethrin following topical administration. *Eur. J. Clin. Pharmacol*. 61: 399–404.

Tornero-Velez, R. Davis, J.,Scollon, E. J., Starr, J. M., Setzer, R. W., Goldsmith, M.-R., Chang, D. T., Xue, J., Zartarian, V., DeVito, M. J., and Hughes, M. F. 2012. A pharmacokinetic model of *cis*- and *trans*-permethrin disposition in rats and humans with aggregate exposure application. *Toxicol. Sci*. 130: 33–47.

Tulve, N. S., Jones, P. A., Nishioka, M. G., Fortmann, R. C., Croghan, C. W., Zhou, J. Y., Fraser, A., Cave, C., and Friedman, W. 2006. Pesticide measurements from the first national environmental health survey of child care centers using a multi-residue GC/MS analysis method. *Environ. Sci. Technol*. 40: 6269–6274.

U.S. Department of Agriculture. 2013. Pesticide data program. Annual summary calendar year 2011. U.S. Department of Agriculture, Agricultural Marketing Service, Science and Technology Program. http://www.ams.usda.gov/AMSv1.0/getfile?dDocName=stelprdc5102692 (accessed September 9, 2013).

van der Rhee, H. J., Farquhar, J. A., and Vermeulen, N. P. E. 1989. Efficacy and transdermal absorption of permethrin in scabies patients. *Acta Derm. Venereol*. 69: 170–182.

Van Ravenzwaay, B., and Leibold, E. 2004. The significance of in vitro rat skin absorption studies to human risk assessment. *Toxicol. In Vitro* 18: 219–225.

Wolansky, M. J., Gennings, C., and Crofton, K. M. 2006. Relative potencies for acute effects of pyrethroids on motor function in rats. *Toxicol. Sci*. 89: 271–277.

Wolansky, M. J., and Tornero-Velez, R. 2013. Critical considerations of the multiplicity of experimental and organismic determinants of pyrethroid neurotoxicity: A proof of concept. *J. Toxicol. Environ. Health B* 16: 453–490.

Woollen, B. H., Marsh, J. R., Laird, W. J. D., and Lesser, J. E. 1992. The metabolism of cypermethrin in man: Differences in urinary metabolite profiles following oral and dermal administration. *Xenobiotica* 22: 983–991.

Zhang, Z., Sun, J., Chen, S., Wu, Y., and He, F. 1991. Levels of exposure and biological monitoring of pyrethroids in spraymen. *Br. J. Ind. Med*. 48: 82–86.

Taylor & Francis
Taylor & Francis Group

Xenobiotica
the fate of foreign compounds in biological systems

ISSN: 0049-8254 (Print) 1366-5928 (Online) Journal homepage: http://www.tandfonline.com/loi/ixen20

Tissue time course and bioavailability of the pyrethroid insecticide bifenthrin in the Long-Evans rat

Michael F. Hughes, David G. Ross, Brenda C. Edwards, Michael J. DeVito & James M. Starr

To cite this article: Michael F. Hughes, David G. Ross, Brenda C. Edwards, Michael J. DeVito & James M. Starr (2016) Tissue time course and bioavailability of the pyrethroid insecticide bifenthrin in the Long-Evans rat, Xenobiotica, 46:5, 430-438, DOI: 10.3109/00498254.2015.1081710

To link to this article: http://dx.doi.org/10.3109/00498254.2015.1081710

View supplementary material

Published online: 14 Sep 2015.

Submit your article to this journal

Article views: 42

View related articles

View Crossmark data

Full Terms & Conditions of access and use can be found at
http://www.tandfonline.com/action/journalInformation?journalCode=ixen20

Download by: [US EPA Library] **Date:** 19 February 2016, At: 05:58

http://tandfonline.com/ixen
ISSN: 0049-8254 (print), 1366-5928 (electronic)

Xenobiotica

Xenobiotica, 2016; 46(5): 430–438
DOI: 10.3109/00498254.2015.1081710

Taylor & Francis
Taylor & Francis Group

RESEARCH ARTICLE

Tissue time course and bioavailability of the pyrethroid insecticide bifenthrin in the Long-Evans rat

Michael F. Hughes[1], David G. Ross[1], Brenda C. Edwards[1], Michael J. DeVito[2], and James M. Starr[3]

[1]U.S. Environmental Protection Agency, Office of Research and Development, National Health and Environmental Effects Research Laboratory, Research Triangle Park, NC, USA, [2]National Toxicology Program, National Institute of Environmental Health Sciences, Research Triangle Park, NC, USA, and [3]U.S. Environmental Protection Agency, Office of Research and Development, National Exposure Research Laboratory, Research Triangle Park, NC, USA

Downloaded by [US EPA Library] at 05:58 19 February 2016

Abstract

1. Pyrethroids are neurotoxic and parent pyrethroid appears to be toxic entity. This study evaluated the oral disposition and bioavailability of bifenthrin in the adult male Long-Evans rat.
2. In the disposition study, rats were administered bifenthrin (0.3 or 3 mg/kg) by oral gavage and serially sacrificed (0.25 h to 21 days). Blood, liver, brain and adipose tissue were removed. In the bioavailability study, blood was collected serially from jugular vein cannulated rats (0.25 to 24 h) following oral (0.3 or 3 mg/kg) or intravenous (0.3 mg/kg) administration of bifenthrin. Tissues were extracted and analyzed for bifenthrin by high-performance liquid chromatography-tandem mass spectrometry (HPLC-MS/MS).
3. Bifenthrin concentration in blood and liver peaked 1–2-h postoral administration and were approximately 90 ng/ml (or g) and 1000 ng/ml (or g) for both tissues at 0.3 and 3 mg/kg, respectively. Bifenthrin was rapidly cleared from both blood and liver. Brain concentrations peaked at 4–6 h and were lower than in blood at both doses (12 and 143 ng/g). Bifenthrin in adipose tissue peaked at the collected time points of 8 (157 ng/g) and 24 (1145 ng/g) h for the 0.3 and 3 mg/kg doses, respectively and was retained 21 days postoral administration. Following intravenous administration, the blood bifenthrin concentration decreased bi-exponentially, with a distribution half-life of 0.2 h and an elimination half-life of 8 h. Bifenthrin bioavailability was approximately 30%. These disposition and kinetic bifenthrin data may decrease uncertainties in the risk assessment for this pyrethroid insecticide.

Keywords

Bifenthrin, disposition, pharmacokinetics, pyrethroids

History

Received 26 June 2015
Revised 5 August 2015
Accepted 6 August 2015
Published online 11 September 2015

Introduction

Human exposure to pyrethroid insecticides has increased since 2000 in the United States principally due to the phase-out of organophosphate insecticides in residential and agricultural settings (Power & Sudakin, 2007). Tulve et al. (2006) detected pyrethroids in indoor surfaces of childcare centers and in surrounding soils of these facilities. Other investigators found pyrethroids on floor wipes of residential homes and apartments (Julien et al., 2008; Stout et al., 2009), indoor dust (Harnly et al., 2009; Quivrós-Alcalá et al., 2011) and on fruits and vegetables (USDA, 2013).

Address for correspondence: Michael F. Hughes, U.S Environmental Protection Agency, Office of Research and Development, National Health and Environmental Effects Research Laboratory, Research Triangle Park, NC 27711, USA. Tel: +919-541-2160. Fax: 919-541-4284. E-mail: hughes.michaelf@epa.gov

This work was authored as part of the Contributor's official duties as an Employee of the United States Government and is therefore a work of the United States Government. In accordance with 17 U.S.C. 105, no copyright protection is available for such works under U.S. Law.

Pyrethroid insecticides are synthetic chemicals and their structure is derived from the botanical insecticides, the pyrethrins (Soderlund et al., 2002). Allethrin, initially synthesized in 1949, was the first pyrethroid prepared for commercial use (Casida, 1980). Allethrin and other first-generation pyrethroids are sensitive to sunlight. Chemists synthetically modified the structures of these pyrethroids to generate others which are more photostable and have greater insecticidal activity. Thus, these later generation pyrethroids are more effective in agricultural applications (Casida, 1980). Among this later generation of pyrethroids is bifenthrin (Figure 1).

Pyrethroids are basically classified into one of two types (Soderlund et al., 2002). Type-I pyrethroids are distinguished from type-II pyrethroids based on the absence or presence, respectively, of an α-cyano group in the alcohol moiety and acute neurobehavioral activity of rats following oral or parenteral administration (Soderlund et al., 2002). Rats exposed to type-I pyrethroids, such as bifenthrin (Figure 1), display aggressive sparring, altered sensitivity to external stimuli and fine tremor progressing to whole-body tremor and prostration. Profuse salivation and writhing seizures are

Figure 1. Structure of bifenthrin.

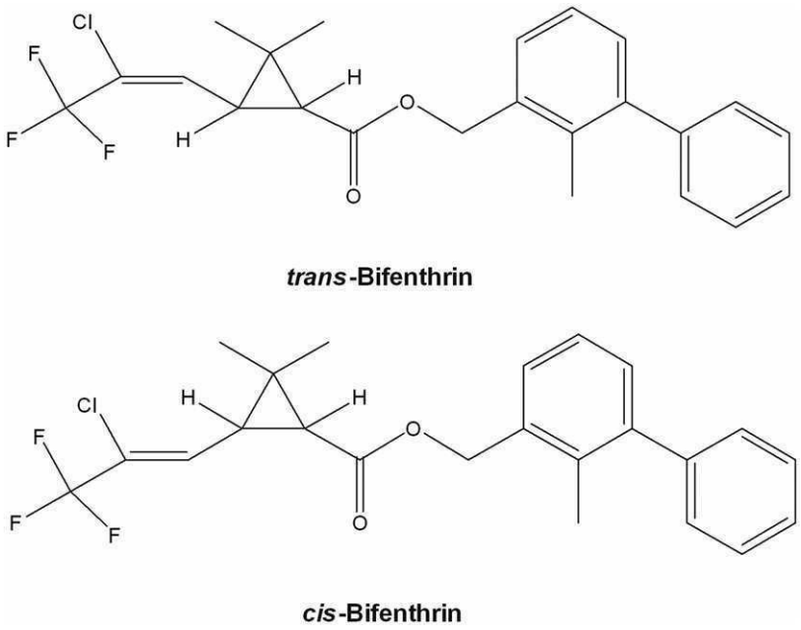

Downloaded by [US EPA Library] at 05:58 19 February 2016

displayed in rats exposed to type-II pyrethroids. An example of a type-II pyrethroid is deltamethrin.

It is important to understand the disposition and kinetics of pyrethroid insecticides to assess the potential risks of exposure to these compounds. Pyrethroids studied in rats include deltamethrin (Anadón et al., 1996; Godin et al., 2010; Gray & Rickard, 1982a; Kim et al., 2008; Mirfazaelian et al., 2006; Ruzo et al., 1978), permethrin (Anadón et al., 1991; Gaughan et al., 1977; Tornero-Velez et al., 2012), λ-cyhalothrin (Anadón et al., 2006) and more recently bifenthrin (Gammon et al., 2014). Oral bioavailability of pyrethroids ranges from 25% for deltamethrin (Godin et al., 2010) to 71% for λ-cyhalothrin (Anadón et al., 2006). Once systemically absorbed, pyrethroids are distributed rapidly and widely within the body, being detected in the brain, liver and adipose tissue (Kaneko, 2011; Soderlund et al., 2002). Pyrethroids are cleared from brain and liver but are retained in adipose tissue with half-lives nearing 2–3 weeks. Pyrethroids are metabolized by oxidation and hydrolysis, conjugated and excreted in urine and feces. Absorption, bioavailability and ultimately the neurotoxic effect of pyrethroids are influenced by the vehicle used (e.g. corn oil, glycerol formal) (Crofton et al., 1995; Kim et al., 2007) and vehicle volume (e.g. 1 vs. 5 mL) (Wolansky et al., 2007).

The objective of this study was to evaluate the oral pharmacokinetics including bioavailability of the pyrethroid insecticide bifenthrin in the Long-Evans rat. Our laboratory and collaborators used this rat strain in several neurotoxicology and disposition studies (Crofton et al., 1995; Godin et al., 2010; Scollon et al., 2011; Tornero-Velez et al., 2012; Wolansky et al., 2006, 2007). We administered bifenthrin by oral gavage at two dose levels and studied the tissue disposition of parent compound out to 21 days. Parent compound was measured because laboratory studies suggest it is the neurotoxic entity. Intracerebral administration of pyrethroids in mice and rats results in the classic neurobehavioral endpoints (Gray & Rickard, 1982b; Lawrence & Casida, 1982). The concentration of deltamethrin (Anand et al., 2006; Kim et al., 2010; Rickard & Brodie, 1985) and bifenthrin (Scollon et al., 2011) in brain correlate with neurobehavioral effects in rats. Also, tremors are not observed in rats administered pyrethroid metabolites (White et al., 1976).

Material and methods

Chemicals

All chemicals used in this study were of analytical grade or better unless otherwise specified. Bifenthrin (CAS no. 82657-0403, 2-methyl-1,1-biphenyl-3-yl-methyl-3-(2-chloro-3,3,3-trifluoro-1-propenyl)-2,2-dimethyl cyclopropanecarboxylate, 98% purity) used in dosing solutions and as an analytical standard was from Chem Service (West Chester, PA). The *cis* isomer of bifenthrin was used in the study, and it is the predominant stereoisomer found in the technical product. Other analytical standards that were used included *cis*- (99% purity) and *trans*-permethrin (3-phenoxybenzyl(1RS)-*cis*,-*trans*-3-(2,2-dichlorovinyl)-2,2-dimethylcyclopropanecarboxylate, 94% purity) and were also from Chem Service. Labeled *cis*- and *trans*-permethrin (phenoxy-$^{13}C_6$) were purchased from Cambridge Isotope Laboratories (Andover, MA) and used as internal and surrogate standards, respectively. Solvents including acetone, hexanes (Fisher Scientific, Pittsburgh, PA) and methanol (VWR, West Chester, PA) were pesticide grade quality. Corn oil, glycerol formal and dextrose were from Sigma (St. Louis, MO), heparin from Baxter Healthcare Corp. (Deerfield, IL) and saline from Abbott Laboratories (North Chicago, IL).

Animals

Male Long-Evans rats (Charles River Laboratories, Inc., Wilmington, MA) were obtained at 55–58 days of age and housed two per cage in standard polycarbonate hanging cages (45 cm × 24 cm × 20 cm) containing heat-sterilized pine

Downloaded by [US EPA Library] at 05:58 19 February 2016

shavings (Northeastern Products, Inc., Warrensburg, NY). Jugular-vein cannulated rats (Charles River) were housed singly in the standard cages with pine shavings. Animals were given a 5–9-day acclimation period and were maintained on a 12:12-h photoperiod (L/D, 0600:1800). Feed (Purina 5001 Lab Chow, Barnes Supply Co., Durham, NC) and tap water were provided *ad libitum*. Tap water (Durham, NC) used in the animal facility was filtered through sand and activated charcoal and rechlorinated to 4–5 ppm Cl^-. Animal-holding rooms were maintained at $22 \pm 2\,^{\circ}C$ and relative humidity at $50 \pm 10\%$ in an Association for Assessment and Accreditation of Laboratory Animal Care approved facility. The Institutional Animal Care and Use Committee of the US EPA's National Health and Environmental Effects Research Laboratory approved all experimental protocols in advance.

Experimental

There were two experiments in this study, a tissue time course (with serial sacrifice) and a serial blood sampling for bioavailability assessment following administration of bifenthrin. For both experiments, rats were administered bifenthrin at a dose of 0.3 or 3 mg/kg in corn oil (1 mL/kg) by oral (po) gavage. Our group has used corn oil as a vehicle for the oral administration of pyrethroids in several studies (Godin et al., 2010; Tornero-Velez et al., 2012; Wolansky et al., 2006, 2007). The high dose of bifenthrin is equivalent to an oral dose that decreases motor activity in a rat by 30% (Wolansky et al., 2006). As part of the bioavailability study, rats were also administered bifenthrin (0.3 mg/kg, 0.1 mL/kg) intravenously in glycerol formal via the jugular vein catheter. After intravenous dosing, the catheter was flushed with 300 µL saline and filled with a void volume of heparinized dextrose to maintain catheter patency. The weight of the rats on the day of dosing (po and iv) ranged from 306.2 to 400.6 gm.

For the tissue time-course study, the animals were sacrificed by cardiac puncture under CO_2-induced anesthesia at 0.25-, 0.5-, 1-, 2-, 4-, 6-, 8-, 12-, 24-, 48- (2 days), 168- (7 days), 336- (14 days) or 504 (21 days)-h postadministration. Tissues (whole brain, liver and abdominal fat) were collected, weighed and flash frozen in liquid nitrogen and stored at $-80\,^{\circ}C$. For the bioavailability study, serial blood samples were removed (300 µL) via the catheter and immediately flash frozen in liquid nitrogen. For the po-dosed animals, blood samples were taken at 0.25-, 0.5-, 1-, 2-, 3-, 4-, 6-, 8- 12- and 24-h postadministration. For the iv-dosed animals, blood samples were taken at 0.08-, 0.17-, 0.33-, 0.5-, 1-, 2-, 4-, 6-, 8-, 12- and 24-h postadministration. A predose blood sample was also withdrawn from all of the jugular vein cannulated rats. Following each sampling, the catheters were flushed with 300 µL of saline and filled with a void volume of heparinized dextrose to maintain catheter patency. For the tissue time course, there were 3–4 rats per time point and dose. For the bioavailability experiments, there were 3–4 rats per dose and route.

Tissue extraction

Tissue extraction of bifenthrin followed the procedure of Godin et al. (2010). Frozen whole brain, liver and adipose tissue were homogenized in a Spex CertiPrep 6850 freezer/mill (Metuchen, NJ) apparatus to form a fine homogenous powder. Replicate samples of pulverized tissue (300–500 mg) and thawed blood (2 mL for time-course study) from the serial sacrifice study were vortex extracted with 20:80 acetone/hexane. The whole sample of blood (0.3 mL) from the bioavailability study was similarly extracted. About 25 µL of 6 µM labeled *trans*-permethrin (phenoxy-$^{13}C_6$) in acetone was added prior to the extraction of all samples as a surrogate. Samples were vortexed for 10 min in 16×100-mm glass tubes with 5 mL solvent and centrifuged. The organic fraction was collected. The extraction was repeated two more times with 3 mL solvent. The pyrethroid-containing organic extracts were combined, dried under a stream of nitrogen and reconstituted in 1 mL hexane.

Reconstituted blood and brain extracts underwent solid-phase extraction (SPE) using Sep-pak 500 mg silica SPE columns (Waters, Inc., Milford, MA). The solid-phase cleanup was automated using a RapidTrace SPE Workstation (Hopkinton, MA). SPE columns were washed with 5 mL hexane before sample loading. Analytes were eluted with 5 mL 94:6 hexane/ethyl acetate. Column eluants were dried under a stream of nitrogen and reconstituted in 1 mL of 90:10 methanol/water with 25 µL of 6 µM labeled *cis*-permethrin (phenoxy-$^{13}C_6$) added as an internal standard of instrument efficiency for HPLC tandem mass spectrometry analysis.

Reconstituted liver and adipose tissue extracts were cleaned using styrene divinylbenzene gel permeation columns (OI Analytical, College Station, TX) with a 70% ethyl acetate and 30% cyclopentane mobile phase flowing at a rate of 5 mL/min. A 25 mL fraction containing the pyrethroids was collected with a fraction collector and then dried under a stream of nitrogen. Samples were reconstituted in 3 mL hexane. These extracts were partitioned 3x against equal volumes of hexane-saturated acetonitrile. The acetonitrile fractions were combined, dried under a stream of nitrogen and reconstituted in mobile phase with internal standard (25 µL of 6 µM labeled *cis*-permethrin (phenoxy-$^{13}C_6$)).

Analytical

Sample analysis was performed using an AB SCIEX (Framingham, MA) model API 4000^{TM}liquid chromatography-tandem mass spectrometer (LC/MS/MS) system configured with a Turbo Ion Spray. Conditions and settings were the same as those described by Scollon et al. (2011). The mobile phase consisted of methanol/5 mM ammonium acetate in water (98:2) and flowed at a rate of 400 µL/min. An analytical column (C18, 3.5 µm, 150×3 mm) from Agilent Technologies (Santa Clara, CA) was used. Two replicates from the tissue time-course study were processed and analyzed for each sample and the results were averaged.

When recovery of the surrogate (i.e. *trans*-permethrin (phenoxy-$^{13}C_6$)) was within 80–120% of the expected value, the value of the sample was considered acceptable. Samples with surrogate recoveries above or below the acceptable range were reanalyzed. If samples were still outside the acceptable range, additional tissue was extracted and analyzed.

For each type of tissue, bifenthrin and the surrogate *trans*-permethrin (phenoxy-$^{13}C_6$) were quantified using matrix matched six-point calibration curve with *cis*-permethrin

Downloaded by [US EPA Library] at 05:58 19 February 2016

(phenoxy-$^{13}C_6$) as the internal standard for both analytes. Matrices for the calibration standards were made by collecting and processing appropriate tissue masses, or volumes, from untreated rats. To provide more precise estimates of tissue concentrations, ranges of bifenthrin concentrations used for a calibration curve were generally limited to two orders of magnitude. All samples were run initially against a curve with bifenthrin concentrations ranging from 1 to 100 ng/mL. Samples with concentrations outside these values were reprocessed using relevant calibration curve concentrations and the minimum and maximum bifenthrin concentrations (all tissues) were 0.1 and 3000 ng/mL. After adjusting for the mass of each tissue that was collected during tissue harvesting (2 mL blood, 0.33 g brain, 0.11 g liver and 0.11 g adipose tissue), the limits of quantitation for bifenthrin were; 0.05 ng/mL blood, 0.3 ng/g brain, 0.88 ng/g liver and 0.93 ng/g adipose tissue.

Data analysis

The data in the graphs are displayed as mean ± SD ($N = 3$–4 rats). Concentration values > 0 but $<$ LOQ were assigned a value of ½ LOQ. Maximal concentration (C_{max}) and the time (T_{max}) occurred were determined by observation of the sampled time points (Supplemental Figures 1–4). Data from the tissue time course study were dose-normalized. Data from each dose and time point were averaged. These data were analyzed by a two-way analysis of variance (ANOVA) with time, dose and time × dose as factors (GraphPad Prism, version 6.0, San Diego, CA). The level of significance was $p < 0.05$. For a significant dose effect, differences in C_{max} were analyzed by a Tukey's multiple comparison test. The level of significance was $p < 0.05$. The kinetic parameters of this normalized data were determined using a noncompartmental method of analysis (PK Solutions, version 2.0, Summit Research Services, Montrose, CO). The following equation was used for this analysis:

$$\text{Concentration} = Ae^{-\alpha t} + De^{-\delta t} + Ee^{-\gamma t}$$

Where A, D, E represent the y-axis intercepts and α, δ and γ represent the respective rate constants for the phases of absorption, distribution and elimination, respectively.

The analysis for blood, brain and liver were truncated to 24, 48 and 12 h, respectively, in order to make dose comparisons. Area under the curve (AUC) was determined by the trapezoidal rule. Exponential terms were determined by the method of residuals (i.e. curve stripping). The slope of the apparent linear terminal phase was estimated using at least three data points. The elimination rate constant (k_{el} or γ) was determined by the following equation:

$$k_{el} = -2.303 \times \text{slope of the apparent linear terminal phase}$$

The elimination half-life ($t_{½}$) was determined by the following equation:

$$t_{½} = 0.693/k_{el}.$$

For the analysis of the data from serial blood sampling (i.e. bioavailability study), the kinetic parameters for each animal were determined and then averaged. The parameters were determined using noncompartmental method of analysis

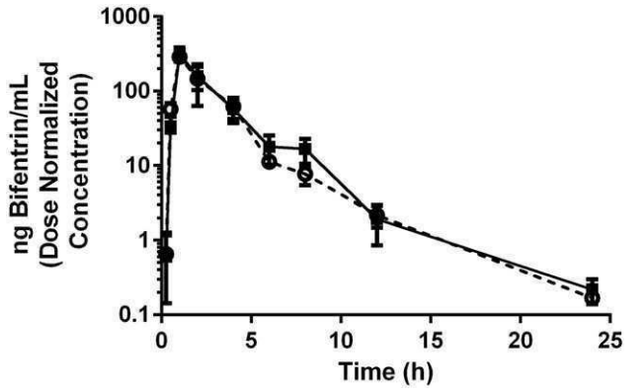

Figure 2. Dose-normalized concentration–time course of bifenthrin in blood following 0.3 (○) or 3 (■) mg/kg dose by oral gavage. Animals were serial sacrificed over time. Data points represent mean ± SD, $N = 3$–4 (animals).

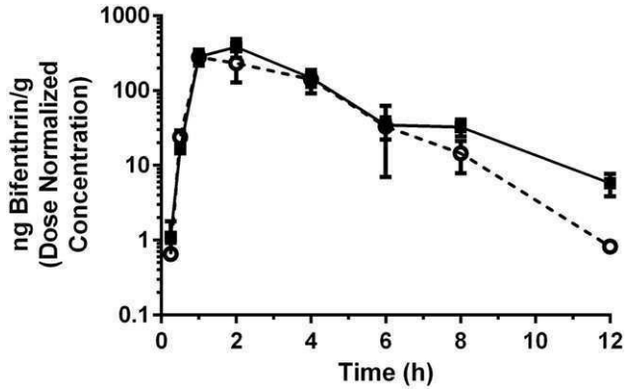

Figure 3. Dose-normalized concentration–time course of bifenthrin in liver following 0.3 (○) or 3 (■) mg/kg dose by oral gavage. Animals were serial sacrificed over time. Data points represent mean ± SD, $N = 4$ (animals).

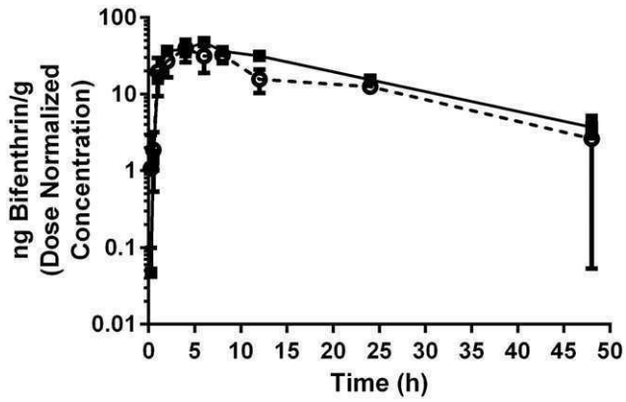

Figure 4. Dose-normalized concentration–time course of bifenthrin in brain following 0.3 (○) or 3 (■) mg/kg dose by oral gavage. Animals were serial sacrificed over time. Data points represent mean ± SD, $N = 3$–4 (animals).

(PK Solutions, version 2.0, Summit Research Services, Montrose, CO). The three-term equation described previously was used for the analysis of the oral data and the following equation was used for the intravenous data:

$$\text{Concentration} = Ae^{-\alpha t} + Be^{-\beta t},$$

where A and B equal the y-intercepts and α and β represent

the rate constants of the distribution and elimination phases, respectively. AUC and area under the moment curve (AUMC) were determined by the trapezoidal rule. Exponential terms were determined by the method of residuals (i.e. curve stripping). The volume of distribution at steadystate (V_{ss}) was determined by the following equation:

$$V_{ss} = \text{Dose x}(\text{AUMC})/(\text{AUC})^2.$$

Bioavailability was determined by the following equation:

$$\text{Bioavailability} = \left[\text{AUC}_{po}/\text{AUC}_{iv}\right] * \left[\text{Dose}_{iv}/\text{Dose}_{po}\right] \text{ x } 100.$$

Clearance (Cl) was determined by the following equation:

$$\text{Cl} = (\text{Bioavailability}/100) \times \text{Dose}/\text{AUC}.$$

Statistical analysis of the kinetic parameters of the oral dose bioavailability group was done using a *t*-test (GraphPad Prism ver.6.0, GraphPad Software, Inc., San Diego, CA) with a level of significance of $p < 0.05$.

Results

Tissue time course following oral administration and serial sacrifice

The absorption of bifenthrin into the blood following oral administration was rapid (detected within 15 min), peaked early (1 h) and then started to decrease over time (Supplemental Figure 1). Bifenthrin was not detected in blood after 48- and 336-h postadministration for the 0.3 and 3 mg/kg doses, respectively. There was an 11-fold difference in the maximal concentration (C_{max}) (Table 1). The dose-normalized concentration–time course of bifenthrin in blood is shown in Figure 2. The two-way ANOVA indicated that there were significant effects on time ($p < 0.0001$). The concentration of bifenthrin in blood for the two doses appears to be within the linear dose range out to 24-h postadministration. The elimination rate constants and half-lives were similar for both normalized doses of bifenthrin (Table 1) and showed the elimination of bifenthrin from blood was rapid. The dose-normalized $AUC_{0–24\,h}$ of bifenthrin in blood was 9% greater for the low than the high dose (Table 1).

Bifenthrin distributed rapidly to the liver as it was detected within 15-min postadministration by the oral route (Figure 3). The concentration of bifenthrin peaked 1–2 h postadministration for both doses (Table 1). There was an approximate 14-fold difference in bifenthrin C_{max} between the two doses. Bifenthrin in liver was not detected after 12- and 48-h postadministration for the low and high dose, respectively (Supplemental Figure 3). The dose-normalized concentration–time course of bifenthrin in liver is shown in Figure 3. The two-way ANOVA showed that there were significant effects of time ($p < 0.0001$) and the interaction of dose × time ($p = 0.044$). The concentration of bifenthrin in liver for the two normalized doses appears to be within the linear dose range out to 12-h postadministration. The elimination rate constant for the normalized low dose of bifenthrin was about 50% greater than the normalized high dose (Table 1). The elimination half-life for bifenthrin was 1–2 h, indicating elimination of bifenthrin from the liver was rapid. The dose-normalized $AUC_{0–12\,h}$ for the high dose of bifenthrin was about 30% greater than that for the low dose (Table 1).

Table 1. Pharmacokinetic parameters of bifenthrin in tissues of the rat after oral administration[a].

Tissue	Dose (mg/kg)	C_{max}[a] (ng/mL or ng/g)	T_{max}[a] (h)	k_{el}[b] (h^{-1})	$t_{½}$[b] (h)	$AUC_{0\text{ to }t}$[b] (ng-h/mL or ng-h/g)
Blood	0.3	86.1	1	0.25	2.8	702.4
	3	946.5	1	0.24	2.9	642.6
Liver	0.3	83.7	1	0.63	1.1	957.1
	3	1146.0	2	0.24	2.9	1264.9
Brain	0.3	11.9	4	0.05	13.9	677.5
	3	142.8	6	0.06	11.6	925.1
Adipose	0.3	157.1	8	1.0×10^{-3}	693	1.67×10^5
	3	1445.3	24	1.0×10^{-3}	693	1.82×10^5

[a]Maximum concentration in tissue and time it occurred from Supplemental Figures 1–4.
[b]Elimination rate, half-life and area under the curve data based on normalized dose in Figures 2–5. The AUC was truncated at: blood, 24 h; liver, 12 h; brain, 48 h; adipose, 506 h.

The maximal concentration of bifenthrin in brain after oral administration was lower and did not peak as early as in blood and liver for both doses (Table 1, Supplemental Figure 3). There was a 12-fold difference in bifenthrin C_{max} in the brain between the two doses. The dose-normalized concentration–time course of bifenthrin in brain is shown in Figure 4. The two-way ANOVA showed that there were significant effects on time ($p < 0.0001$), dose ($p = 0.0028$) and the interaction of dose × time ($p = 0.028$). However, there was no significant difference in the C_{max} between the two doses. The elimination rate constants of bifenthrin in brain were similar, and the elimination half-life was approximately 12–13 h (Table 1). The dose-normalized $AUC_{0–48\,h}$ for the high dose of bifenthrin in brain was about 35% greater than that for the low dose (Table 1).

Bifenthrin distributed more slowly to the adipose tissue after oral administration and was retained unlike the other tissues (Supplemental Figures 4A and 4B, Table 1). Peak concentrations of bifenthrin in adipose tissue were at the sampled time points of 8 and 24 h for the low and high dose, respectively, and were the highest for each dose level of the tissues analyzed. The dose-normalized concentration–time course of bifenthrin in adipose tissue is shown in Figure 5. The two-way ANOVA indicated that there were significant time effects ($p < 0.0001$). The concentration of bifenthrin in adipose tissue for the two doses appears to be within the linear range out to 506-h postadministration. The elimination rate constants for both normalized doses of bifenthrin were low at 0.001/h (Table 1). The half-life for both doses was high at 693 h, indicating elimination of bifenthrin from adipose tissue was slow. The dose-normalized $AUC_{0–506\,h}$ for the high dose of bifenthrin was about 9% greater than that for the normalized low dose (Table 1).

Serial blood sampling following oral and intravenous administration

Bifenthrin was not detected in the blood collected before dosing the rats with this insecticide. The bifenthrin blood concentration–time course (Figure 6) following iv

Downloaded by [US EPA Library] at 05:58 19 February 2016

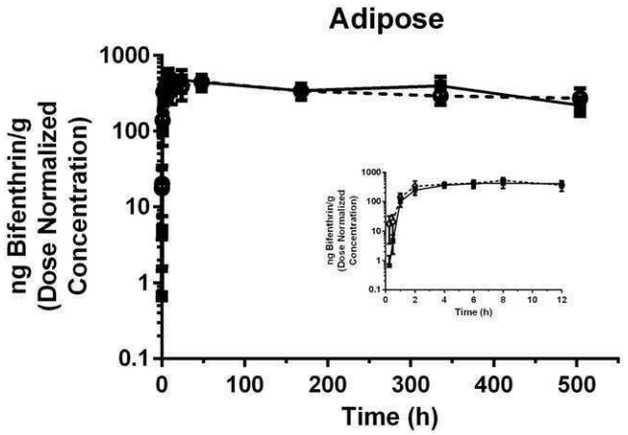

Figure 5. Dose-normalized concentration–time course of bifenthrin in adipose tissue following 0.3 (○) or 3 (■) mg/kg dose by oral gavage. The inset shows the concentration–time course to 12 h. Animals were serial sacrificed over time. Data points represent mean ± SD, $N = 3$–4 (animals).

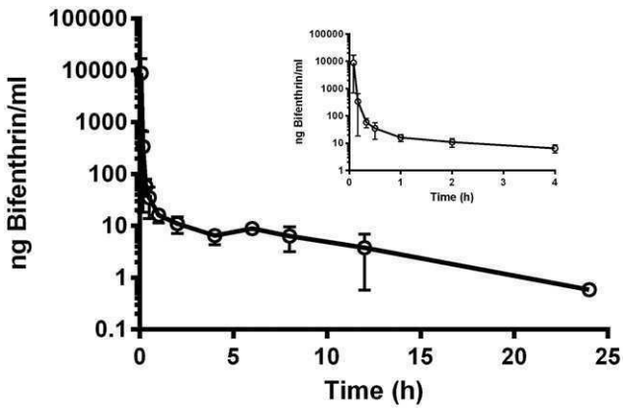

Figure 6. Time course of bifenthrin in serial-collected blood samples of jugular vein-cannulated rats following 0.3 mg/kg dose by intravenous administration. Data points represent mean ± SD, $N = 3$–4 (blood samples).

administration and serial blood sampling showed a rapid distribution ($t_{½\alpha} = 0.17 \pm 0.08$ h, mean ± SD) out to about 30-min postadministration followed by a slower elimination component with a half-life of approximately 8 h (Table 2). Clearance of bifenthrin was 203 mL/h and the volume of distribution at steady state was approximately 560 mL.

Following oral administration of bifenthrin and serial blood sampling, peak concentration (Figure 7) was 2 h for the 0.3 mg/kg dose and 1 h for the 3 mg/kg dose. The elimination half-life was about 3 times longer for the low dose than the high dose (Table 2). The clearance values were essentially the same, approximately 100 mL/h, but the volume of distribution at steady state was significantly greater for the low dose (3660 mL) than the high dose (1000 mL) of bifenthrin.

The AUC for bifenthrin in blood in the oral bioavailability study was approximately 266 and 4081 ng-h/mL for the 0.3 and 3 mg/kg doses, respectively (Table 2). There was an approximate 15-fold difference ($p < 0.05$) in the AUC between these two doses. The iv AUC for bifenthrin in blood was about 1078 ng-h/mL. The bioavailability for the low and high dose of bifenthrin was 25 and 38%, respectively.

Discussion

The mammalian disposition of several type-I and type-II pyrethroids such as permethrin (Anadón et al., 1991; Tornero-Velez et al., 2012) and deltamethrin (Anadón et al., 1996; Godin et al., 2010; Kim et al., 2008), respectively, have been studied. However, information regarding the disposition of many other pyrethroids that are also in use today, such as bifenthrin, are not well characterized. Gammon et al. (2014) recently compared the pharmacokinetics of bifenthrin in the male Sprague-Dawley rat following inhalation, iv and po administration. They analyzed plasma instead of blood for bifenthrin as we report, and after oral administration, they observed lower maximal levels in plasma (361 ng/ml) than with blood (947 ng/ml), but nearly the same levels in brain (83 ng/g) as we report (143 ng/g) in the present study. Data, such as dose to target tissue, which are obtained from chemical disposition and kinetic studies, are needed to allow risk assessors to make informed decisions when evaluating the potential health risk from exposure to pyrethroid insecticides.

Bifenthrin kinetics in the rat have many similarities with pyrethroids such as deltamethrin (Anadón et al., 1996; Godin et al., 2010; Kim et al., 2008), permethrin (Anadón et al., 1991; Tornero-Velez et al., 2012) and λ-cyhalothrin (Anadón et al., 2006) after oral administration. The similarities are prompt absorption into the systemic circulation and clearance from it. Pyrethroids, including bifenthrin, are rapidly distributed to tissues such as the liver and brain after oral administration. Bifenthrin was cleared fairly quickly from liver (elimination half-life <3 h). Tornero-Velez et al. (2012) reported lower elimination half-lives for *cis*- and *trans*-permethrin in liver (<1.5 h) of the rat after oral administration of a 40:60 mixture of *cis*:*trans*-permethrin (doses of 1 and 10 mg/kg). In brain, the elimination of bifenthrin was slower than observed in the liver; the levels of bifenthrin in brain were detected out to 14 days at the 3 mg/kg dose. Our tissue analysis of bifenthrin did not differentiate between compound in tissue and that in residual blood in tissue. The animals were euthanized by exsanguination under anesthesia, which would result in some blood being removed from the tissues. The area under the curve data (Table 1) indicates the concentration of bifenthrin was 36 to 100% higher in liver than in blood, suggesting that bifenthrin had been absorbed into these tissues. At the 3 mg/kg dose, the concentration of bifenthrin in brain exceeded the concentration in blood at 24-, 48- and 168-h postadministration (Supplemental Figure 5) suggesting that bifenthrin was absorbed into brain. Gammon et al. (2014) reported brain concentrations of bifenthrin after a po dose (3.1 mg/kg) out to 12-h postadministration, whereas we went out to 48 h for the low dose and 336 h (14 days) for the high dose. The brain concentration of bifenthrin at both doses was constant from 4 to 24 h in the present study. In contrast, the elimination of *cis*- and *trans*-permethrin from brain (elimination half-life <5 h) was faster than bifenthrin (Tornero et al., 2012), although levels of *cis*-permethrin were detected out to 48 h in this organ. Kim et al. (2008) also detected deltamethrin (10 mg/kg dose) in brain out to 48 h. The levels of bifenthrin in brain began to decrease 24-h postadministration. Peak motor activity effects of bifenthrin

Downloaded by [US EPA Library] at 05:58 19 February 2016

Table 2. Pharmacokinetic parameters of bifenthrin in serial collected blood over 24 h after intravenous or oral administration in jugular vein-cannulated rats.

Route	Dose (mg/kg)	k_{el} (h^{-1})	$t_{½}$ (h)	AUC (ng-h/ml)	AUMC (ng-h^2/ml)	V_{ss} (mL)	Cl (mL/h)
iv	0.3	0.11 ± 0.051	8.2 ± 5.9	1077.6 ± 865.3	2314.5 ± 2926.0	562.9 ± 728.3	202.6 ± 200.3
Oral	0.3	0.07 ± 0.02	10.9 ± 3.2	265.5 ± 43.4	2260.0 ± 561.1	3658.1 ± 2030.6[b]	96.6 ± 14.5
Oral	3	0.18 ± 0.02	3.9 ± 0.6	4080.6 ± 570.4[c]	14879.0 ± 2360.0	1001.1 ± 276.0	102.5 ± 11.2

Mean ± SD, $N = 3$–4.
[b] *t*-test, significantly greater than 3 mg/kg oral dose, $p < 0.05$.
[c] *t*-test, significantly greater than 0.3 mg/kg oral dose, $p < 0.0001$.

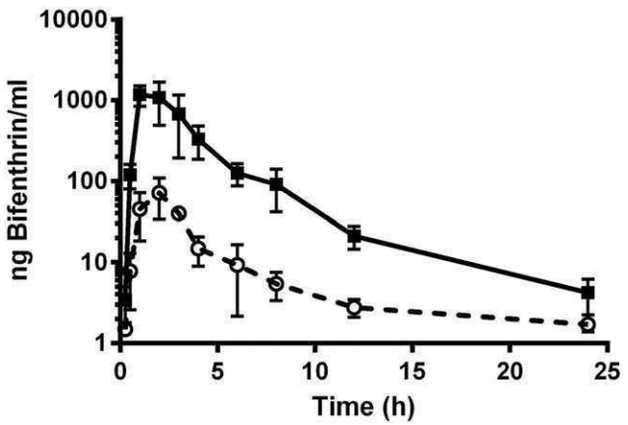

Figure 7. Time course of bifenthrin in serial-collected blood samples of jugular vein-cannulated rats following 0.3 (○) or 3 (■) mg/kg dose by oral gavage. Data points represent mean ± SD, $N = 3$–4 (blood samples).

in the rat occur at 4-h postadministration when the dosing volume is 1 mL/kg (Wolansky et al., 2006, 2007). This is the same volume used in this study. Although we did not measure motor activity in this study, we did not observe any overt signs of toxicity with the doses administered. Gammon et al. (2014) also reported no signs of toxicity in Sprague-Dawley rats after a similar oral dose (3.1 mg/kg) or an equivalent inhalation dose. Although bifenthrin was detected in brain out to 14 days postadministration in the present study, Wolansky et al. (2006) reported that the neurotoxic effects of orally administered pyrethroids in the rat subside 24–48 h postadministration. This suggests that there is a threshold dose of the pyrethroid that must be attained in the brain for an effect to occur. Distribution of bifenthrin and other pyrethroids to adipose tissue takes somewhat longer (up to 24 h) to attain peak concentrations (Godin et al., 2010; Kim et al., 2008; Tornero-Velez et al., 2012); pyrethroids, including bifenthrin, are retained in this tissue. Bifenthrin was detected in adipose tissue out to 21 days postadministration in the present study. Following iv administration, bifenthrin in blood shows a rapid distribution phase followed by a slower elimination phase, and these results are similar as reported by Gammon et al. (2014). Similar kinetic characteristics following iv administration are also observed in the rat with permethrin, deltamethrin and λ-cyhalothrin (Anadón et al., 1991, 1996, 2006).

Bifenthrin was persistent in adipose tissue out to at least 21 days, which was the final time point in our study. Pyrethroids such as deltamethrin, *cis*-permethrin and *cis*-cypermethrin following oral administration persist in adipose tissue of rats and mice (Crawford et al., 1981; Godin et al., 2010; Hutson et al., 1981; Kim et al., 2008; Marei et al., 1982; Tornero-Velez et al., 2012). Pyrethroids have fairly high log octanol/water (Log P) partition coefficients (Laskowski, 2002). Bifenthrin has a measured and calculated Log P of 6.4 and 7.2, respectively (Laskowski, 2002). With its physicochemical preference toward organic phases, it is reasonable that bifenthrin distributes to adipose tissue and accumulates to levels higher than observed in other organs or tissues. Pyrethroids that persist within adipose tissue most likely would not be metabolized, as lipases have no enzymatic activity toward these insecticides (Ross et al., 2006). The primary means of decreasing pyrethroid levels in adipose tissue would be redistribution into the systemic circulation. Once in the systemic circulation of the rat, pyrethroids could be hydrolyzed by serum esterases or taken up by the liver and metabolized by oxidation, hydrolysis or by both processes.

The persistence of pyrethroids in adipose tissue appears to be dependent on the rate of metabolism of the pyrethroid. Pyrethroids with the structure of a primary alcohol ester in the *trans* configuration tend to be more readily metabolized, particularly by hydrolysis, than their counterpart pyrethroids in the *cis* configuration (Soderlund & Casida, 1977). Analysis of rat adipose tissue following the administration of *cis*/*trans*-permethrin or *cis*/*trans*-cypermethrin shows that the *cis* isomer of these pyrethroids persists to a greater extent in this tissue than the *trans* isomer (Crawford et al., 1981; Rhodes et al., 1984; Tornero-Velez et al., 2012). In this study, the *cis* isomer of bifenthrin was used. Bifenthrin in the *cis* configuration is not hydrolyzed in rat hepatic microsomes (Scollon et al., 2009) and the hydrolytic activity of recombinant carboxylesterases is low toward this pyrethroid compared to *trans*-permethrin and *trans*-cypermethrin (Stok et al., 2004; Nishi et al., 2006). The lower rate of metabolism of pyrethroids in the *cis* configuration suggests that they are more likely to persist in the body, particularly in lipid rich tissues. The differences in metabolism and persistence of the *cis*/*trans* pyrethroid isomers could be important if exposures to pyrethroids are being reconstructed by analyzing adipose tissue. Exposure to pyrethroids in the *trans* configuration would be underestimated, and thus, the actual exposure to the pyrethroid would be underestimated. This would lead to misinformed health risk estimates from exposures to pyrethroid insecticides.

In previous work from our laboratory with deltamethrin (Godin et al., 2010), we observed an approximate twofold lower peak concentration of this pyrethroid in brain as in the present study with bifenthrin, using the same route of administration (oral) and dose (3 mg/kg; molar dose: bifenthrin, 7.1 μmole/kg; deltamethrin, 5.9 μmole/kg). The neurotoxic

Downloaded by [US EPA Library] at 05:58 19 February 2016

Downloaded by [US EPA Library] at 05:58 19 February 2016

effect of the pyrethroids appears to be related to their concentration in brain (Anand et al., 2006; Kim et al., 2010; Rickard & Brodie, 1985; Scollon et al., 2011). Wolansky et al. (2006) reported that bifenthrin had a higher effective $dose_{30}$ than deltamethrin for a comparable decrease in motor activity in the rat. Our bifenthrin brain concentration results support the hypothesis that brain concentrations of pyrethroids are related to neurotoxic effect. The differences in neurotoxic potency of bifenthrin and deltamethrin may be due to differences in pharmacokinetics, pharmacodynamics or both. In both studies, the *cis* isomer of bifenthrin and deltamethrin was used. This isomer is the predominant isomer found in insecticidal formulations for these two pyrethroids. The higher concentration of bifenthrin in the brain suggests that deltamethrin is more rapidly metabolized. Ghiasuddin and Soderlund (1984) reported on the hydrolysis activity in the soluble fraction of mouse brain homogenates. Greater activity was found in the soluble fraction than the nuclear and microsomal fractions of the brain. In their assays, Ghiasuddin and Soderlund examined seven pyrethroids including *cis*- and *trans*-permethrin and deltamethrin. Of these three pyrethroids, the hydrolysis rate of *trans*-permethrin was about 4- and 8-fold greater than *cis*-permethrin and deltamethrin, respectively. The liver is an important metabolizing organ of pyrethroids. The hydrolysis activity toward *trans*-permethrin in mouse liver is 57-fold greater than in brain (Ghiasuddin & Soderlund, 1984). The role of cytochrome P450s in metabolizing pyrethroids in brain is not well characterized. An alternative explanation is that deltamethrin is transported out of the brain more rapidly than bifenthrin, but whether pyrethroids are substrates for transporters in the brain is not known.

It does appear, however, that pyrethroids bind to transporter proteins located in areas outside of the brain. Permethrin and resmethrin, but not cypermethrin and deltamethrin, bind to and inhibit ATPase activity of the human breast cancer resistance protein efflux transporters (Bircsak et al., 2013). None of these same pyrethroids inhibit ATPase activity of the human multidrug resistance protein 1 (mdr1) efflux transporters (Bircsak et al., 2013). The transport of tetramethylrosamine by mdr1 isolated from plasma membrane of a Chinese hamster ovary cell line that is multidrug resistant was inhibited by cypermethrin and fenvalerate (Sreeramulu et al., 2007). Transport of doxorubicin by human mdr1 was weakly inhibited by fluvalinate and permethrin but not fenvalerate (Bain & LeBlanc, 1996). Intestinal transport studies by Zastre et al. (2013) using Caco-2 cells indicate that there is no efflux of deltamethrin or *cis*/*trans*-permethrin by mdr1. While some studies report that pyrethroids appear to bind to at least mdr1 and can inhibit this efflux transporter, it appears that pyrethroids are not transported by mdr1.

The bioavailability of bifenthrin is not extensive in the rat, as we observed values ranging from 25–38%. Similar values (25–28%) are reported for deltamethrin by Godin et al. (2010), whereas Anadón et al. (1996) and Kim et al. (2008) are reported lower bioavailability values (14–18%). Permethrin (61%) and λ-cyhalothrin (67–71%) have higher bioavailability values in the rat than bifenthrin and deltamethrin (Anadón et al., 1991, 2006). The lower bioavailability of bifenthrin than permethrin and λ-cyhalothrin could be due to first-pass hepatic metabolism. This would most likely be by cytochrome P450-dependent oxidative metabolism (Scollon et al., 2009). Bifenthrin is not as readily hydrolyzed by esterases (Nishi et al., 2006; Scollon et al., 2009; Stok et al., 2004) such as occurs with *trans*-permethrin and bioresmethrin (Ross et al., 2006). There is the possibility that bifenthrin is excreted intact in the bile following absorption. However, Kim et al. (2008) did not detect deltamethrin in feces following iv administration to rats suggesting limited biliary elimination of the parent compound. Kim et al. (2008) did however observe about 40% of the dose of deltamethrin in feces following oral administration, suggesting incomplete absorption of this pyrethroid. Mirfazaelian et al. (2006) proposed that deltamethrin is effluxed out of the gastrointestinal tract by transporters lining this organ. Zastre et al. (2013) report that there is no efflux of deltamethrin or *cis*/*trans*-permethrin by mdr1 in experiments with Caco-2 cells. Additional experiments by this group suggest a role for an unspecified influx transporter. However, the permeability coefficients of the pyrethroids tested by Zastre et al. (2013) in their *in vitro* model system were similar to that of mannitol, which is used as a marker for low permeability and low absorption. Zastre et al. (2013) interpret their results to indicate that deltamethrin and *cis*/*trans*-permethrin have low potential for gastrointestinal absorption. Whether this occurs with bifenthrin is not known and should be investigated.

Conclusions

Bifenthrin was rapidly absorbed by the rat following oral administration. It was detected in blood, liver, brain and adipose tissue. Bifenthrin was cleared rapidly from blood and liver, persisted out to about 14 days in brain and was retained in adipose tissue out to 21 days. Bioavailability of bifenthrin was 25–38%. These data will aid risk assessors when evaluating the potential for adverse health effects to humans following exposure to bifenthrin by decreasing uncertainties in the disposition of this pyrethroid pesticide.

Acknowledgements

The authors gratefully acknowledge Drs. E. Kenyon, J.E. Simmons and M. Tornero-Velez for their comments on a previous version of this manuscript. The authors thank Ms. J. Hutchison for her technical assistance in this study. All research was funded internally by the U.S. Environmental Protection Agency.

Declaration of interest

The authors declare that there is no conflict of interest. This article is reviewed in accordance with the policy of the National Health and Environmental Effects Research laboratory, U.S. Environmental Protection Agency and the National Institute of Environmental Health Sciences and approved for publication. Approval does not signify that the contents necessarily reflect the views and policies of the Agency, nor does mention of trade names or commercial products constitute endorsement or recommendation for use. This article may be the work product of an employee of the National Institute of Environmental Health Sciences (NIEHS), National Institutes of Health (NIH); however, the

statements opinions or conclusions contained therein do not necessarily represent the statements, opinions or conclusions of NIEHS, NIH or the United States government.

References

Anand SS, Kim KB, Padilla S, et al. (2006). Ontogeny of hepatic and plasma metabolism of deltamethrin in vitro: role in age-dependent acute neurotoxicity. Drug Metab Dispos 34:389–97.

Anadón A, Martinez-Larrañaga MR, Diaz MJ, et al. (1991). Toxicokinetics of permethrin in the rat. Toxicol Appl Pharmacol 110:1–8.

Anadón A, Martinez-Larrañaga MR, Fernandez-Cruz ML, et al. (1996). Toxicokinetics of deltamethrin and its 4′-HO-metabolite in the rat. Toxicol Appl Pharmacol 141:8–16.

Anadón A, Martínez M, Martínez MA, et al. (2006). Toxicokinetics of lambda-cyhalothrin in rats. Toxicol Lett 165:47–56.

Bain LJ, LeBlanc GA. (1996). Interaction of structurally diverse pesticides with the human MDR1 gene product P-glycoprotein. Toxicol Appl Pharmacol 141:288–98.

Bircsak KM, Richardson JR, Aleksunes LM. (2013). Inhibition of human MDR1 and BCRP transporter ATPase activity by organochlorine and pyrethroid insecticides. J Biochem Molec Toxicol 27:157–64.

Casida JE. (1980). Pyrethrum flowers and pyrethroid insecticides. Environ Health Perspect 34:189–202.

Crawford MJ, Croucher A, Hutson DH. (1981). Metabolism of cis- and trans-cypermethin in rats. Balance and tissue retention study. J Agric Food Chem 29:130–5.

Crofton KM, Kehn LS, Gilbert ME. (1995). Vehicle and route dependent effects of a pyrethroid insecticide, deltamethrin, on motor function in the rat. Neurotoxicol Teratol 17:489–95.

Gammon D, Liu Z, Chandraeskaran A, ElNaggar S. (2014). The pharmacokinetic properties of bifenthrin in the rat following multiple routes of exposure. Pestic Manag Sci. [Epub ahead of print]. DOI: 1 0.1002/ps.3883.

Gaughan LC, Unai T, Casida JE. (1977). Permethrin metabolism in rats. J Agric Food Chem 25:9–17.

Ghiasuddin SM, Soderlund DM. (1984). Hydrolysis of pyrethroid insecticides by soluble mouse brain esterases. Toxicol Appl Pharmacol 74:390–6.

Godin SJ, DeVito MJ, Hughes MF, et al. (2010). Physiologically based pharmacokinetic modeling of deltamethrin: development of a rat and human diffusion-limited model. Toxicol Sci 115:330–43.

Gray AJ, Rickard J. (1982a). The toxicokinetics of deltamethrin in rats after intravenous administration of a toxic dose. Pestic Biochem Physiol 18:205–15.

Gray AJ, Rickard J. (1982b). Toxicity of pyrethroids to rats after direct injection into the central nervous system. Neurotoxicology 3:25–35.

Harnly ME, Bradman A, Nishioka M, et al. (2009). Pesticides in dust from homes in an agricultural area. Environ Sci Technol 43:8767–74.

Hutson DH, Gaughan LC, Casida JE. (1981). Metabolism of the cis- and trans-isomers of cypermethrin in mice. Pestic Sci 12:385–95.

Julien R, Adamkiewicz G, Levy JI, et al. (2008). Pesticide loadings of select organophosphate and pyrethroid pesticides in urban public housing. J Expo Sci Environ Epidemiol 18:167–74.

Kaneko H. (2011). Pyrethroids: mammalian metabolism and toxicity. J Agric Food Chem 59:2786–91.

Kim KB, Anand SS, Kim HJ, et al. (2008). Toxicokinetics and tissue distribution of deltamethrin in adult Sprague-Dawley rats. Toxicol Sci 101:197–205.

Kim KB, Anand SS, Kim HJ, et al. (2010). Age, dose and time-dependency of plasma and tissue distribution of deltamethrin in immature rats. Toxicol Sci 115:354–68.

Kim KB, Anand SS, Muralidhara S, et al. (2007). Formulation-dependent toxicokinetics explains differences in the GI absorption, bioavailability and acute neurotoxicity of deltamethrin in rats. Toxicology 234:194–202.

Laskowski DA. (2002). Physical and chemical properties of pyrethroids. Rev Environ Contam Toxicol 174:49–170.

Lawrence LJ, Casida JE. (1982). Pyrethroids toxicology: mouse intracerebral structure-activity relationships. Pestic Biochem Physiol 18:9–14.

Marei AE, Ruzo LO, Casida JE. (1982). Analysis and persistence of permethrin, cypermethrin, deltamethrin, and fenvalerate in the fat and brain of treated rats. J Agric Food Chem 30:558–62.

Mirfazaelian A, Kim KB, Anand SS, et al. (2006). Development of a physiologically based pharmacokinetic model for deltamethrin in the adult male Sprague Dawley rat. Toxicol Sci 93:432–42.

Nishi K, Huang H, Kamita SG, et al. (2006). Characterization of pyrethroid hydrolysis by the human liver carboxylesterases hCE-1 and hCE-2. Arch Biochem Biophys 445:115–23.

Power LE, Sudakin DL. (2007). Pyrethrin and pyrethroid exposures in the United States: a longitudinal analysis of incidents reported to poison centers. J Med Toxicol 3:94–99.

Quivrós-Alcalá L, Bradman A, Nishioka M, et al. (2011). Pesticides in house dust from urban and farmworker households in California: an observational measurement study. Environ Health 10:19.

Rhodes C, Jones BK, Croucher A, et al. (1984). The bioaccumulation and biotransformation of *cis*, *trans*-cypermethrin in the rat. Pestic Sci 24:471–80.

Rickard J, Brodie ME. (1985). Correlation of blood and brain levels of the neurotoxic pyrethroid deltamethrin with the onset of symptoms in rats. Pestic Biochem Physiol 23:143–56.

Ross MK, Borazjani A, Edwards CC, et al. (2006). Hydrolytic metabolism of pyrethroids by human and other mammalian carboxylesterases. Biochem Pharmacol 71:657–69.

Ruzo LO, Unai T, Casida JE. (1978). Decamethrin metabolism in rats. J Agric Food Chem 27:918–25.

Scollon EJ, Starr JM, Crofton KM, et al. (2011). Correlation of tissue concentrations of the pyrethroid bifenthrin with neurotoxicity in the rat. Toxicology 290:1–6.

Scollon EJ, Starr JM, Godin SJ, et al. (2009). In vitro metabolism of pyrethroid pesticides by rat and human hepatic microsomes and cytochrome P450 isoforms. Drug Metab Dispos 37:221–8.

Soderlund DM, Casida JE. (1977). Effects of pyrethroid structure on rates of hydrolysis and oxidation by mouse liver microsomal enzymes. Pestic Biochem Physiol 7:391–401.

Soderlund DM, Clark JM, Sheets LP, et al. (2002). Mechanisms of pyrethroid neurotoxicity: implications for cumulative risk assessment. Toxicology 171:3–59.

Sreeramulu K, Liu R, Sharom FJ. (2007). Interaction of insecticides with mammalian P-glycoprotein and their effect on its transport function. Biochim Biophys Acta 1768:1750–7.

Stok JE, Huang H, Jones PD, et al. (2004). Identification, expression, and purification of a pyrethroid-hydrolyzing carboxylesterase from mouse liver microsomes. J Biol Chem 279:29863–9.

Stout II DM, Bradham KD, Egeghy PP, et al. (2009). American healthy homes survey: a national study of residential pesticides measured from floor wipes. Environ Sci Technol 43:4294–300.

Tornero-Velez R, Davis J, Scollon EJ, et al. (2012). A pharmacokinetic model of *cis*- and *trans*-permethrin disposition in rats and humans with aggregate exposure application. Toxicol Sci 130:33–47.

Tulve NS, Jones PA, Nishioka MG, et al. (2006). Pesticide measurements from the first national environmental health survey of child care centers using a multi-residue GC/MS analysis method. Environ Sci Technol 40:6269–74.

USDA. (2013). Pesticide data program. Annual Summary Calendar Year 2011. United States Department of Agriculture, Agricultural Marketing Service, Science and Technology Program. Available from: http://www.ams.usda.gov/AMSv1.0/getfile?dDocName=stelprdc5102692 [last accessed 9 Sep 2013].

White INH, Verschoyle RD, Moradian MH, et al. (1976). The relationship between brain levels of cismethrin and bioresmethrin in female rats and neurotoxic effects. Pestic Biochem Physiol 6: 491–500.

Wolansky MJ, Gennings C, Crofton KM. (2006). Relative potencies for acute effects of pyrethroids on motor function in rats. Toxicol Sci 89: 271–7.

Wolansky MJ, McDaniel KL, Moser VC, Crofton KM. (2007). Influence of dosing volume on the neurotoxicity of bifenthrin. Neurotoxicol Teratol 29:377–84.

Zastre J, Dowd C, Bruckner J, et al. (2013). Lack of P-glycoprotein-mediated efflux and the potential involvement of an influx transport process contributing to the intestinal uptake of deltamethrin, cis-permethrin, and trans-permethrin. Toxicol Sci 136: 284–93.

Supplementary materials available online

Supplemental Figures 1–5

Downloaded by [US EPA Library] at 05:58 19 February 2016

Toxicology 359 (2016) 19–28

Contents lists available at ScienceDirect

Toxicology

journal homepage: www.elsevier.com/locate/toxicol

Environmentally relevant pyrethroid mixtures: A study on the correlation of blood and brain concentrations of a mixture of pyrethroid insecticides to motor activity in the rat

Michael F. Hughes[a,*], David G. Ross[a], James M. Starr[b], Edward J. Scollon[a,1], Marcelo J. Wolansky[c,2], Kevin M. Crofton[a,3], Michael J. DeVito[a,4]

[a] U.S. Environmental Protection Agency, Office of Research and Development, National Health and Environmental Effects Research Laboratory, Research Triangle Park, NC, United States
[b] U.S. Environmental Protection Agency, Office of Research and Development, National Exposure Research Laboratory, Research Triangle Park, NC, United States
[c] National Research Council, Research Triangle Park, NC, United States

ARTICLE INFO

Article history:
Received 13 April 2016
Received in revised form 16 June 2016
Accepted 17 June 2016
Available online 18 June 2016

Keywords:
Pesticide
Pyrethroid
Neurotoxicity
Mixture
Dosimetry

ABSTRACT

Human exposure to multiple pyrethroid insecticides may occur because of their broad use on crops and for residential pest control. To address the potential health risk from co-exposure to pyrethroids, it is important to understand their disposition and toxicity in target organs such as the brain, and surrogates such as the blood when administered as a mixture. The objective of this study was to assess the correlation between blood and brain concentrations of pyrethroids and neurobehavioral effects in the rat following an acute oral administration of the pyrethroids as a mixture. Male Long-Evans rats were administered a mixture of β-cyfluthrin, cypermethrin, deltamethrin, esfenvalerate and *cis*- and *trans*-permethrin in corn oil at seven dose levels. The pyrethroid with the highest percentage in the dosing solution was *trans*-permethrin (31% of total mixture dose) while deltamethrin and esfenvalerate had the lowest percentage (3%). Motor activity of the rats was then monitored for 1 h. At 3.5 h post-dosing, the animals were euthanized and blood and brain were collected. These tissues were extracted and analyzed for parent pyrethroid using HPLC-tandem mass spectrometry. Cypermethrin and *cis*-permethrin were the predominate pyrethroids detected in blood and brain, respectively, at all dosage levels. The relationship of total pyrethroid concentration between blood and brain was linear ($r = 0.93$). The pyrethroids with the lowest fraction in blood were *trans*-permethrin and β-cyfluthrin and in brain were deltamethrin and esfenvalerate. The relationship between motor activity of the treated rats and summed pyrethroid blood and brain concentration was described using a sigmoidal E_{max} model with the Effective $Concentration_{50}$ being more sensitive for brain than blood. The data suggests summed pyrethroid rat blood concentration could be used as a surrogate for brain concentration as an aid to study the neurotoxic effects of pyrethroids administered as a mixture under the conditions used in this study.

Published by Elsevier Ireland Ltd.

1. Introduction

Pyrethroids are a class of synthetic insecticides with a structure based on the botanical pyrethrins. The structural commonality of pyrethrins and pyrethroids are the acid and alcohol moieties that are linked by an ester group. Another common feature of pyrethrins and pyrethroids is that they may have 1–3 chiral carbons and are isomeric (Soderlund et al., 2002). Consequently, there may be differences in the metabolism of the isomers (hydrolysis vs. oxidation) as well as insecticidal potency (Miyamoto, 1990; Soderlund et al., 2002). In general, pyrethroids tend to have greater insecticidal activity and are less susceptible to

* Corresponding author at: U.S. Environmental Protection Agency, MD B105-03, Research Triangle Park, NC 27709. United States.
E-mail address: hughes.michaelf@epa.gov (M.F. Hughes).
[1] Current address: Syngenta Crop Protection, Greensboro, NC, United States.
[2] Current address: University of Buenos Aires and Argentine NRC Institute IQUIBICEN, Buenos Aires, Argentina.
[3] Current address: U.S. Environmental Protection Agency, Office of Research and Development, National Center for Computational Toxicology, Research Triangle Park, NC, United States.
[4] Current address: National Institute of Environmental Health Sciences, National Toxicology Program, Research Triangle Park, NC, United States.

http://dx.doi.org/10.1016/j.tox.2016.06.013
0300-483X/Published by Elsevier Ireland Ltd.

environmental degradation than pyrethrins (Bradberry et al., 2005).

The many uses of pyrethroids including agricultural, commercial and residential pest control, and veterinary and medical practices (Amweg et al., 2005; Bradberry et al., 2005) may lead to human exposure. Residues of multiple pyrethroids are detected in surface wipe samples collected from child care centers (Tulve et al., 2006) and residential homes (Stout et al., 2009), indoor air and dust samples (Rudel et al., 2003), and on fruits and vegetables (USDA, 2014). A biological monitoring study in Canada of a metropolitan populace exposed to pyrethroids in the diet found that the study population was mainly exposed to permethrin and cypermethrin (Fortin et al., 2008). From their use in agriculture and pest management, humans can be exposed to multiple pyrethroids (Fortin et al., 2008; Heudorf and Angerer, 2001; Stout et al., 2009; Tulve et al., 2006; Tornero-Velez et al., 2012).

Most pyrethroids are commonly classified into two groups, termed Type I and II, based on chemical structure and neurotoxic effects in rodents (Soderlund et al., 2002; Soderlund, 2012). Type I pyrethroids (e.g., permethrin, bifenthrin) contain either a primary or secondary alcohol, and their neurotoxic syndrome hallmark is tremor. Type II pyrethroids (e.g., cypermethrin and deltamethrin) are primary alcohols with a cyano group on the alpha-carbon of the alcohol. Oral administration of exposure to Type II pyrethroids results in choreoathetosis and salivation.

The mode of action of Type I and II pyrethroids appears to be binding to and disruption of voltage-gated sodium channels in targeted neurons (Soderlund et al., 2002; Soderlund, 2012). Wolansky et al. (2006) conducted extensive dose-response assays using motor activity as a neurobehavioral endpoint in rats exposed to eleven pyrethroids administered by oral gavage individually; all compounds produced a dose-related decrease in motor activity, but the potency was variable, dependent upon the pyrethroid administered. In a later study, Wolansky et al. (2009) reported dose-additive effects in rats exposed to an eleven chemical mixture of Type I and II pyrethroids for a decrease in motor activity. An in vitro study by Cao et al. (2011) reported dose-additive effects in inducing sodium influx in primary cultures of murine cerebrocortical neurons with this same pyrethroid mixture. However, based on several other *in vivo* and *in vitro* studies, Breckenridge et al. (2009) proposed that Type I and Type II compounds have separate mechanisms of neurotoxicity. Nevertheless, the U.S. Environmental Protection Agency in 2011 determined the pyrethroids share a common mechanism of action for a cumulative risk assessment (US EPA, 2011).

The nervous system is the primary target tissue for the neurotoxicity produced soon after acute exposure to pyrethroids in laboratory animals. Mice and rats administered very low doses of pyrethroids by direct infusion into the brain display pyrethroid poisoning signs, including tremors (Lawrence and Casida, 1982; Gray and Rickard, 1982a). Neurotoxicological endpoints such as tremors and decreased motor activity in rats administered deltamethrin (i.v.) (Gray and Rickard, 1982b) and bifenthrin (p. o.) (Scollon et al., 2011), respectively, are correlated with brain concentrations of these pyrethroids. As humans are exposed to multiple pyrethroids (Fortin et al., 2008; Heudorf and Angerer, 2001; Stout et al., 2009; Tulve et al., 2006; Tornero-Velez et al., 2012), it is important to understand the disposition of these pesticides, particularly to target organs such as the brain. In the present work we examined the distribution to blood and brain of an environmentally-relevant mixture of five pyrethroid compounds after an acute oral gavage in adult rats (Table 1). The objectives of this study were to: (1) determine the blood and brain concentrations of the test chemicals to characterize the relationships between administered mixture dose and target tissue level; (2) assess the correlation of blood and brain concentrations of the administered pyrethroids to motor activity, a behavioral end point. Only the concentrations of parent pyrethroids were determined as metabolism is thought to be a principal detoxication mechanism in pyrethroid intoxications in mammals (Soderlund et al., 2002). Information on dose to target tissue of a mixture of pyrethroids and relating it to a behavioral effect may reduce uncertainties in the cumulative health risk assessment of this class of insecticides.

2. Materials and methods

2.1. Chemicals

The selection process for the five pyrethroids used in this study has been described by Tornero-Velez et al. (2012). The choice of pyrethroids used in this study was based on a national study of a randomly selected set of 168 child-care centers from across the United States (Tulve et al., 2006). Basically, the five pyrethroids had a greater frequency of occurrence and made up roughly 95% of the pyrethroid load found in the Tulve et al. (2006) study.

Each pyrethroid used in the dosing solution was provided by its respective manufacturer as follows: permethrin and cypermethrin (FMC Corporation, Philadelphia, PA); deltamethrin and β-cyfluthrin (Bayer CropScience, Research Triangle Park, NC); and esfenvalerate (DuPont Crop Protection, Wilmington, DE). The physical and chemical properties of the pyrethroids used in this study have been described previously (Wolansky et al., 2006).

The solvents used for processing samples included acetone, hexanes, ethyl acetate, methanol (Fisher Scientific, Pittsburgh, PA), cyclopentane and acetonitrile (Honeywell Burdick & Jackson, Muskegon, MI). These solvents were pesticide grade or better. The water used for all sample analysis had a resistance of 18 MΩ. Corn oil was purchased from Sigma (St. Louis, MO; Product Number C8267).

Primary calibration standards including *cis*-permethrin (99% purity), *trans*-permethrin (94%), deltamethrin (99%), cypermethrin (98%), β-cyfluthrin (98%) and esfenvalerate (98%) were purchased from Absolute Standards (Hamden, CT). Ring-labeled (phenoxy-$^{13}C_6$) pyrethroids, used as internal standards or surrogates, were purchased from Cambridge Isotope Laboratories (Andover, MA). These labeled standards included *cis*-permethrin, *trans*-permethrin, β-cyfluthrin and cypermethrin.

2.2. Animals

Male Long-Evans rats (Charles River Laboratories, Wilmington, MA) were obtained at 55–58 days of age, and housed two per cage

Table 1
Pyrethroid type, percentage of dose in mixture and potency of pyrethroids administered as a mixture to rats.

	β-Cyfluthrin	Cypermethrin	Deltamethrin	Esfenvalerate	Permethrin[b]
Type	II	II	II	I	I
% of total mixture dose	12.9	28.8	3.4	2.7	52.2
Relative potency[a]	1.136	0.235	1.000	2.092	0.059

[a] Relative potency based on a pyrethroid ED_{30} for effect on motor activity relative to deltamethrin as the index pyrethroid (Wolansky et al., 2006).
[b] Relative potency for permethrin determined from 40:60 *cis:trans*-permethrin.

in standard polycarbonate hanging cages (45 cm × 24 cm × 20 cm) containing heat-sterilized pine shavings (Northeastern Products, Inc., Warrensburg, NY). All animals were given a 1–2 week acclimation period and were maintained on a 12:12 h photoperiod (0600:1800). Feed (Purina 5001 Lab Chow) and tap water were provided *ad libitum*. Tap water (Durham, NC, city water) was filtered through sand and activated charcoal filters, and then re-chlorinated to 4–5 ppm Cl^- before use. Colony rooms were maintained at 22 ± 2 °C and relative humidity at 55 ± 20%. The facility is approved by the American Association for Accreditation of Laboratory Animal Care (AAALAC). All experimental protocols were approved in advance by the National Health and Environmental Effects Research Laboratory's Institutional Animal Care and Use Committee.

2.3. Experimental

The treatment groups consisted of a corn oil control and seven doses of the pyrethroid mixture prepared in corn oil. Concentrations of the pyrethroids for the highest or 1X dose in mg/kg were: permethrin (40% *cis*, 60% *trans*), 14.3; cypermethrin, 7.89; β-cyfluthrin, 3.54; deltamethrin, 0.93; esfenvalerate, 0.74. The total pyrethroid dose in the 1X stock mixture was 27.4 mg/kg. As a frame of reference, it is estimated that the daily exposure to permethrin in a human adult male (70 kg) is 3.2 μg/day (ATSDR, 2003). The percentage of each pyrethroid in the dose and their% potency for reduction in motor activity within the mixture are shown in Table 1. In addition to the 1X stock solution, dilutions of this stock included in the scheme were 0.01X, 0.04X, 0.1X, 0.33X, 0.5X and 0.66X (see Supplemental Table 1 for dose of pyrethroid at each dilution). Each individual pyrethroid in the 1X stock solution contributed low levels ranging from sub-threshold to low-effective doses based on previously reported Effective $Dose_{30}$ (ED_{30}) levels for motor activity in the rat computed by Wolansky et al. (2006). Except for β-cyfluthrin at 0.66X (5% higher) and 1X (60% higher), the doses of the individual pyrethroids examined in this study were less than the individual ED_{30}s determined by Wolansky et al. (2006). Fresh stock mixtures were prepared by dissolving the pyrethroids in corn oil before dosing. Mixture solutions were stirred with intermittent heating (max. 40–45 °C) for at least 15 min before administration. All doses were delivered at a dose volume rate of 1 mL/kg at room temperature. There were twelve animals in each dose group.

Beginning at two hours post-dosing, the motor activity of each animal was assessed for one hour (Wolansky et al., 2006). Previous studies showed that the time of peak effect for cypermethrin and permethrin was 1.5 h and 2 h for β-cyfluthrin, deltamethrin and esfenvalerate (Wolansky et al., 2006; Crofton and Reiter, 1984, 1988). The animals were euthanized at 3.5 h post-dosing by exsanguination (cardiac puncture) under CO_2-induced anesthesia. Whole blood was collected in 2 mL aliquots and frozen in a methanol/dry ice bath. The brain was then removed from the expired animals and placed in liquid nitrogen. Blood and brain samples were stored at −80 °C until processed for extraction.

The method of Godin et al. (2010) was used to process and extract the tissues for parent pyrethroids. Frozen brain was pulverized in a Spex CertiPrep 6850 freezer/mill (Metuchen, NJ) to form a fine homogeneous tissue powder. A portion of the powdered brain was weighed (350–400 mg) before extraction. For blood, two 2 mL aliquots were extracted. Prior to extraction, both brain and blood samples were spiked with $^{13}C_6$-*trans*-permethrin that served as a surrogate standard. Samples were extracted with acetone:hexane and the extracts were cleaned as described by Starr et al. (2012). Cleaned extracts were dried under nitrogen and reconstituted in 1 mL methanol:water (9:1, v:v). Internal standards ($^{13}C_6$-*cis*-permethrin, $^{13}C_6$-cyfluthrin and $^{13}C_6$-cypermethrin) were added and the samples were transferred to autosampler vials. All samples were stored at −20 °C until analysis.

2.4. Instrumental analysis

Sample analysis was performed using an AB SCIEX (Framingham, MA) model API 4000™ Liquid Chromatography-Tandem Mass Spectrometry (LC–MS/MS) system configured with a Turbo Ion Spray. Conditions and settings were the same as those described by Starr et al. (2012). The mobile phase consisted of methanol:5 mM ammonium acetate in water (98:2) and flowed at a rate of 400 μL/min. An analytical column (C18, 3.5 μm, 150 × 3 mm) from Agilent Technologies (Santa Clara, CA) was used. Under the conditions used, *cis*- and *trans*-permethrin were separated, but the isomers for cypermethrin and β-cyfluthrin were not resolved. Deltamethrin and esfenvalerate were essentially one isomer each in the dosing solutions, so there were no isomers to resolve for these two pyrethroids. The method of validation, limits of detection and quantitation and quality control and assurance procedures were the same as presented by Starr et al. (2012).\

2.5. Data analysis

Surrogate corrections were made to the calculated pyrethroid blood and brain concentrations by dividing the detected pyrethroid concentration by the recovered surrogate fraction. Several pyrethroid tissue concentration values were less than the level of quantitation (LOQ) (See Supplemental Table 2 for pyrethroid LOQs in blood and brain). These samples were not included in the data analysis.

The tissue response data were first analyzed by linear regression using GraphPad Prism 6 (GraphPad Software, La Jolla, CA). Analysis of dose effects on tissue concentrations was done after normalizing tissue levels by dividing the tissue concentration by the administered dose of pyrethroid. Normalized tissue concentration levels were analyzed using linear regression with a significance level of $p < 0.05$. Data were used in the dose effect analysis only if the $N \geq 3$.

In assessing the correlation between blood and brain concentrations of pyrethroid, the measured concentrations of the pyrethroids in each animal were summed to obtain a pyrethroid load in blood and brain. Linear regression analysis was used with a significance level of $p < 0.05$.

The effect of administered dose of total pyrethroid concentration on motor activity was assessed using a one-way analysis of variance (ANOVA) (GraphPad Prism 6) with a significance level of $p < 0.05$. The post-hoc test was a Dunnett's multiple comparison test with a significance level of $p < 0.05$.

Brain to blood concentration ratios for each pyrethroid were calculated by dividing each individual pyrethroid brain concentration by the respective blood concentration of each animal. The data were then averaged within each dose group.

Non-linear regression analysis (GraphPad Prism) was used to assess the relationship between blood or brain concentrations of the summed pyrethroid concentration (i.e., load) and motor activity. A sigmoidal E_{max} model was used for this analysis and is given as:

$$Y = E_0 - [E_{max} \times X^n]/[b^n + X^n].$$

For this analysis, X is the total pyrethroid concentration in the tissue, E_0 is the estimated motor activity when X is 0, E_{max} is the estimated maximum possible decrease in motor activity, b is the estimated Effective $Concentration_{50}$ (EC_{50}) and n is a shape parameter. When n equals 1, the dose-response relationship is linear. When n is greater than 1, the dose-response relationship

becomes threshold-like. The biologically important characteristics of this function are that it has lower and upper extremes that are determined by the biological response independent of the concentration. For this study, E_0 was constrained to be less than 130 and E_{max} was constrained to be less than 100 (Scollon et al., 2011).

The theoretical relative percent contributions (RPC) of individual pyrethroids in brain that reduces motor activity were estimated by the following equation:

$$RPC_i = (C_i \times RP_i)/(\sum_{i=1\ to\ n} C_i \times RP_i) \times 100$$

Where RPC_i is the relative percent contribution of pyrethroid *i* to motor activity response, C_i is the brain concentration of pyrethroid *i*, and RP_i represents relative potency of pyrethroid *i* (Table 1).

3. Results

The concentrations of pyrethroids in blood and brain increased with administered dose (Fig. 1). Other than β-cyfluthrin in blood ($r = 0.85$), the correlation coefficient values were ≥ 0.95 for all pyrethroids in both tissues (Fig. 1 and Table 2). The slopes of the regression lines of all pyrethroids in both tissues were significantly greater than zero (Table 2). While the slopes were all positive, in blood, they varied from a low of 1.8 for *trans*-permethrin to a high of 67.3 for deltamethrin; in brain, the slopes varied from a low of 2.4 for *trans*-permethrin to a high of 34.6 for *cis*-permethrin. In

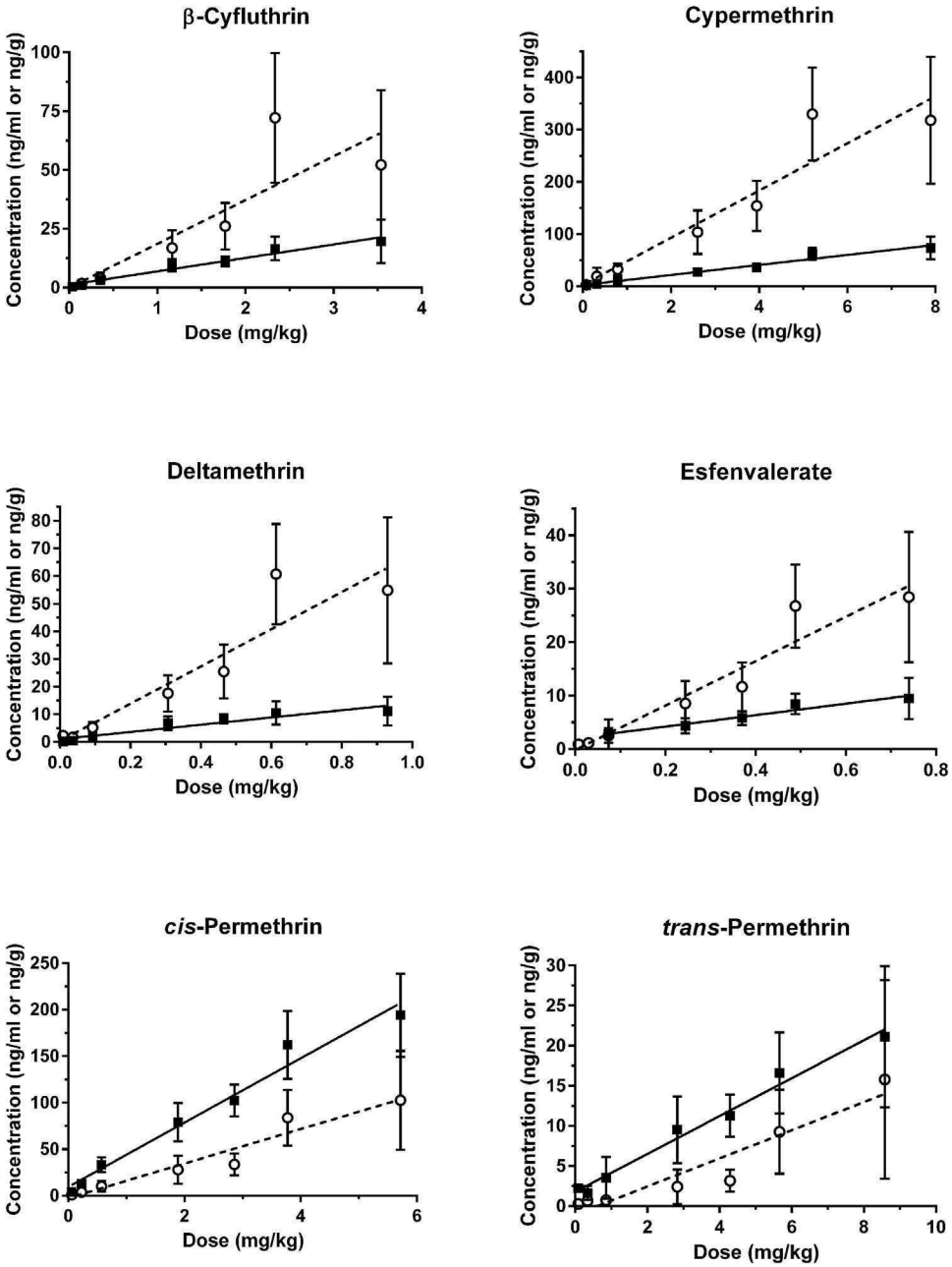

Fig. 1. Relationship between administered dose of pyrethroid and concentration in blood (○) and brain (■). Data represents mean ± SD, N = 1-12 (the N for each line can be found in Tables 3 and 4). The solid and dashed lines represent the linear regression of the blood and brain data, respectively.

Table 2
Level of significance of the slope (p value), F value, degrees of freedom (DF), correlation coefficient (r), and equation of the regression line of pyrethroid concentrations in blood and brain following oral administration of a mixture of pyrethroids.[a]

	β-Cyfluthrin	Cypermethrin	Deltamethrin	Esfenvalerate	*cis*-Permethrin	*trans*-Permethrin
Blood						
p value	0.0321	<0.0001	0.0023	0.0006	0.0003	0.001
F value	10.4	46.0	32.7	59.8	77.5	47.6
DF	1, 4	1, 5	1, 5	1, 5	1, 5	1, 5
r	0.85	0.95	0.98	0.96	0.97	0.95
equation	y = 18.6x − 0.03	y = 45.2x + 2.6	y = 67.3x + 0.4	y = 41.5x − 0.2	y = 18.6x − 2.5	y = 1.8x − 1.1
Brain						
p value	<0.0001	<0.0001	0.0011	0.0058	<0.0001	<0.0001
F value	133.8	160.7	46.2	50.0	195.8	306.1
DF	1, 5	1, 5	1, 5	1, 3	1, 5	1, 5
r	0.98	0.98	0.95	0.97	0.99	0.99
equation	y = 5.7x + 1.2	y = 9.6x + 2.5	y = 13.1x + 1.0	y = 10.7x + 2.1	y = 34x.6 + 9.5	y = 2.4x + 1.8

[a] Data from graphs in Fig. 1.

addition, the slopes for β-cyfluthrin, cypermethrin, deltamethrin and esfenvalerate were higher in blood than brain. For *trans*-permethrin, the slopes were similar in both tissues. In contrast, the slope was about 2-fold higher in brain than in blood for *cis*-permethrin. Adjusting the tissue concentrations by administered dose, showed that there were no significant dose effects on pyrethroid blood concentrations (Table 3). For brain, significant dose effects were detected for β-cyfluthrin, cypermethrin, and *cis*- and *trans*-permethrin (Table 4). The general trend was that the dose-adjusted pyrethroid brain concentration decreased with increased administered dose.

The slope of the line describing the relationship of summed pyrethroid concentration between blood and brain was significantly different from zero ($p < 0.0001$; F value = 536.7; degrees of freedom: 1, 82) and positively correlated (r = 0.93) (Fig. 2).

The fractional composition of the pyrethroid load (based on weight) in blood and brain relative to administered dose is shown in Fig. 3. There were differences between the pyrethroid fractions in blood and brain. Within each tissue, the general trend was the pyrethroid fractions were similar over the dose range administered. For blood, the rank order from highest fraction to lowest tended to be cypermethrin (approximate fraction of 0.6–0.8), *cis*-permethrin (0.09–0.18), β-cyfluthrin and deltamethrin (approximately 0.05–0.12), esfenvalerate (0.02–0.05) and *trans*-permethrin (0.01–0.02). The only exception was for β-cyfluthrin at the lowest dose, which was not quantifiable. For brain, the fraction was highest for *cis*-permethrin (0.6–0.7), followed by cypermethrin (0.2), β-cyfluthrin and *trans*-permethrin (0.02–0.07), deltamethrin (0.004–0.05) and esfenvalerate (0.03). Esfenvalerate was not quantifiable in brain at the two lowest administered doses.

The brain:blood ratios of the pyrethroids are shown in Table 5. There was preferential distribution of *cis*- and *trans*-permethrin in brain, with ratios exceeding 1 at all administered doses. For deltamethrin, the ratios were less than 1 for all doses, indicating preferential distribution in the blood except at the lowest dose, where the levels were below the LOQ. For β-cyfluthrin, cypermethrin and esfenvalerate, the lower doses had ratios of approximately 1 and decreased to less than 1 with increased dose, showing preferential distribution to the blood.

Motor activity of the rats was similar within the 0- (i.e., control)-to-0.33X mixture dose range, but declined at higher doses (Fig. 4). The motor activity of the rats administered the 1X dose decreased approximately 60%. The one-way ANOVA revealed a significant dose-related decrease ($p < 0.0001$; F value = 9.915; degrees of freedom: 7, 88) in motor activity with increased total pyrethroid administered dose. The motor activity of the 0.66X and 1X groups were significantly less than control ($p < 0.01$ and $p < 0.0001$, respectively). The relative percent contributions (RPC, see above for equation) of individual pyrethroids to decrease motor activity were determined by multiplying the relative potency of the specific pyrethroid by the brain concentration of that pyrethroid divided by the sum of the relative potency multiplied by the brain concentration for all pyrethroids. In the 0.66X group, the RPCs were: β-cyfluthrin, 27%; esfenvalerate, 22%; cypermethrin 21%; deltamethrin, 15%; *cis*-permethrin, 14%; and *trans*-permethrin, 1%. At the 1X dose, the RPCs were β-cyfluthrin, 26%; esfenvalerate, 24%; cypermethrin, 21%; *cis*-permethrin, 14%; deltamethrin, 14%; and *trans*-permethrin, 1%.

The effect of the pyrethroids on motor activity was assessed versus summed pyrethroid concentration in blood and brain (Fig. 5, Table 6). For concentrations less than approximately 100 ng/mL or ng/g in blood or brain, respectively, the sigmoidal E_{max} model computed a nearly 100% (i.e., control-like) level of motor activity, although there was variability among the animals at

Table 3
Dose normalized blood concentrations (ng/mL/dose) at 3.5 h post-administration of a mixture of pyrethroids by oral gavage in rats.

Dose group	β-Cyfluthrin	Cypermethrin	Deltamethrin	Esfenvalerate	*cis*-Permethrin	*trans*-Permethrin
0.01X	N.D.[a]	36.2 ± 26.3 (12)	251.0 ± 146.6 (4)	115.8, 126.8 (2)	14.6 ± 5.1 (7)	2.7, 3.2 (2)
0.04X	12.7 ± 8.7 (11)[b]	59.6 ± 52.6 (12)	46.9 ± 27.1 (10)	38.2 ± 12.5 (5)	17.1 ± 10.1 (12)	2.0 (1)
0.1X	11.2 ± 6.8 (12)	41.2 ± 14.5 (12)	56.3 ± 21.0 (12)	34.5 ± 19.0 (12)	17.6 ± 10.0 (12)	0.9 ± 0.4 (5)
0.33X	14.4 ± 6.4 (12)	39.8 ± 16.0 (12)	57.4 ± 21.5 (12)	34.9 ± 17.5 (12)	14.9 ± 7.9 (12)	0.9 ± 0.8 (9)
0.5X	14.8 ± 5.6 (12)	39.0 ± 12.2 (12)	54.7 ± 20.9 (12)	31.4 ± 12.4 (12)	11.7 ± 4.2 (12)	0.7 ± 0.4 (8)
0.66X	30.9 ± 11.8 (12)	63.3 ± 17.2 (12)	99.0 ± 29.6 (12)	54.8 ± 15.9 (12)	22.2 ± 7.9 (12)	1.6 ± 0.9 (11)
1X	14.7 ± 9.0 (12)	40.3 ± 15.4 (12)	59.0 ± 28.5 (12)	38.5 ± 16.5 (12)	18.0 ± 9.3 (12)	1.8 ± 1.4 (12)
Deviation from zero[c]	N.S.[d]	N.S.	N.S.	N.S.	N.S.	N.S.

[a] Not Determined (all values below LOQ).
[b] mean ± SD (N).
[c] Linear regression analysis on dose-normalized data for N ≥ 3.
[d] Not Significant (p > 0.05).

Table 4
Dose normalized pyrethroid brain concentrations (ng/g/dose) at 3.5 h post-administration of a mixture of pyrethroids by oral gavage in rats.

Dose group	β-Cyfluthrin	Cypermethrin	Deltamethrin	Esfenvalerate	*cis*-Permethrin	*trans*-Permethrin
0.01X	11.6 ± 2.3 (4)[a]	18.2 ± 11.7 (12)	28.4, 30.7 (2)	N.D.[b]	74.7 ± 30.9 (12)	17.3, 34.4 (2)
0.04X	7.8 ± 2.7 (12)	15.4 ± 4.7 (12)	13.3 ± 4.3 (11)	18.6 ± 9.0 (12)	57.0 ± 17.9 (12)	4.8 ± 2.6 (10)
0.1X	9.3 ± 2.3 (12)	14.3 ± 3.0 (12)	18.4 ± 7.5 (12)	37.7 ± 38.1 (9)	58.6 ± 13.9 (12)	4.1 ± 3.0 (12)
0.33X	8.2 ± 2.2 (12)	10.4 ± 3.2 (12)	22.2 ± 8.1 (12)	17.8 ± 5.9 (10)	41.9 ± 10.9 (12)	3.4 ± 1.5 (12)
0.5X	6.3 ± 1.2 (12)	9.2 ± 2.0 (12)	17.8 ± 3.7 (12)	14.3 ± 5.7 (10)	35.8 ± 6.0 (12)	2.6 ± 0.6 (12)
0.66X	7.1 ± 2.2 (12)	12.0 ± 2.2 (12)	17.1 ± 6.9 (12)	17.3 ± 3.9 (11)	43.0 ± 9.7 (12)	2.9 ± 0.9 (12)
1X	5.5 ± 2.6 (12)	9.3 ± 2.8 (12)	12.0 ± 5.6 (12)	12.8 ± 5.2 (12)	33.9 ± 7.8 (12)	2.5 ± 1.0 (12)
Deviation from zero[c]	p = 0.0344	p = 0.0306	N.S.[d]	N.S.	p = 0.019	p = 0.0163

[a] Mean ± SD (N).
[b] Not determined (all values below LOQ).
[c] Linear regression analysis on dose-normalized data for N ≥ 3.
[d] Not Significant (p > 0.05).

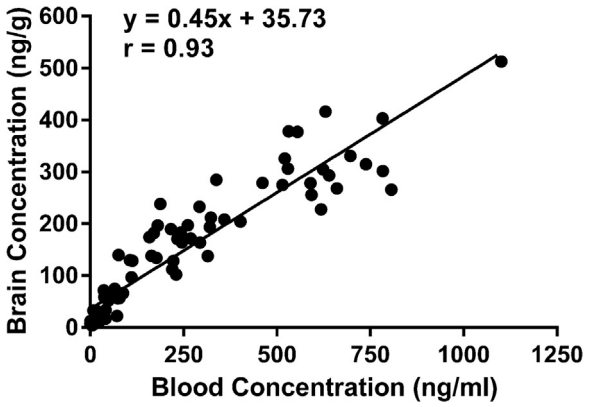

Fig. 2. The relationship between blood (ng/mL) and brain (ng/g) summed pyrethroid concentration following oral administration of an environmental mixture of pyrethroids in the rat. The closed circles represent individual data points and the solid line the best fit line using a linear equation.

concentrations below this level. With increasing tissue concentrations greater than 100 ng/mL or ng/g in blood or brain, respectively, the motor activity of the animals decreased. The shape parameters of the model for both blood (3.7 ± 2.2, mean ± SE) and brain (5.4 ± 2.9) were greater than 1, indicating a threshold-like effect of the pyrethroids on motor activity. The estimated EC_{50} for decrease in motor activity was slightly lower in brain (207 ± 25 ng/g) than in blood (246 ± 39 ng/g).

4. Discussion

Assessing the concentration of a toxicant in a target organ such as the brain or a surrogate biological matrix such as the blood may provide more valuable information for a toxicity assessment than solely considering administered dose (Meador et al., 2008). In the present paper the blood and brain concentrations of a mixture of pyrethroid insecticides administered by oral gavage to rats were determined. The concentrations of β-cyfluthrin, cypermethrin, deltamethrin, esfenvalerate, and *cis*- and *trans*-permethrin in rat blood and brain increased linearly with increased dose. However, the rates of these increases were not equivalent. The differences in slopes between the pyrethroids and tissues indicate that although the chemical structures are similar, being based on the natural pyrethrins, there are dispositional (absorption, distribution, metabolism and excretion) differences among them. The uptake into blood and brain of the pyrethroids did not correspond with the Type I and Type II groupings or relative potencies, as previously reported by Starr et al. (2012), who conducted a time course study with the same proportional mixture of pyrethroids. Dispositional differences may have an important influence on the neurotoxicity of the test chemicals of this work as ED_{30}s for decreased motor activity have been found to vary from 1.2 to 42.7 mg/kg in the rat (Wolansky et al., 2006).

The results presented here have several consistencies with two studies by Starr et al. (2012, 2014). Starr et al. (2012) examined the tissue (blood, brain, fat and liver) time course (2.5–24.5 h post-administration) of the same mixture of pyrethroids at doses of 0.4X and 1X. More recently, Starr et al. (2014) reported the time course of this mixture in blood and brain at doses of 0.4X and 1.3X. In both studies (Starr et al., 2012, 2014) no differences in the dose normalized blood concentrations of the pyrethroids at 3.5 h were reported as observed in the present study. In brain, no significant differences in the dose normalized pyrethroid brain concentrations at 2.5 h (3.5 h not reported) were observed by Starr et al. (2012) and at 3.5 h by Starr et al. (2014). For deltamethrin and esfenvalerate in the present study at 3.5 h, no significant differences in dose normalized brain concentrations were found. However, significant differences were observed for β-cyfluthrin, cypermethrin and *cis*- and *trans*-permethrin. The trend was for higher dose normalized concentrations at the low doses, which decreased as dose increased. Although significantly different ($p < 0.05$), the decreases in dose normalized brain concentrations were two-fold or less. Experimental variability may explain the differences between the studies. Starr et al. (2012, 2014) also reported that the relative concentrations of pyrethroids in brain reflected that in the administered dose if the permethrin isomer brain concentrations are summed. A similar finding was observed in the present study.

In the administered pyrethroid mixture, *trans*-permethrin changed the most with regard to fractional composition between the dosing solution and the tissues, as reported by Starr et al. (2012, 2014). The fraction of *trans*-permethrin decreased greatly in blood, but slightly less so in brain, relative to the dosing solution. One explanation for this considerable decrease of *trans*-permethrin in rat blood is that a serum carboxylesterase hydrolyzes *trans*-permethrin much faster than *cis*-permethrin, deltamethrin and esfenvalerate (Crow et al., 2007). Hydrolysis of pyrethroids by carboxylesterases is an important elimination pathway for this class of insecticides (Godin et al., 2006; Ross et al., 2006; Crow et al., 2007; Scollon et al., 2009). In addition, the *trans* configuration of pyrethroids with a primary alcohol, such as *trans*-permethrin, are in general more readily hydrolyzed by carboxylesterases than the *trans* isomers with a secondary alcohol (e.g., cypermethrin) and pyrethroids in the *cis* configuration (e.g., *cis*-permethrin) (Abernathy et al., 1973; Ross et al., 2006). While rat serum has carboxylesterase activity towards pyrethroids, human serum is devoid of such activity (Crow et al., 2007; Godin et al., 2007). This species difference in the metabolism of pyrethroids in serum has implications in species extrapolation of pyrethroid toxicity from rat to human. The rat serum carboxylesterase appears to be a single isozyme with differential pyrethroid hydrolyzing

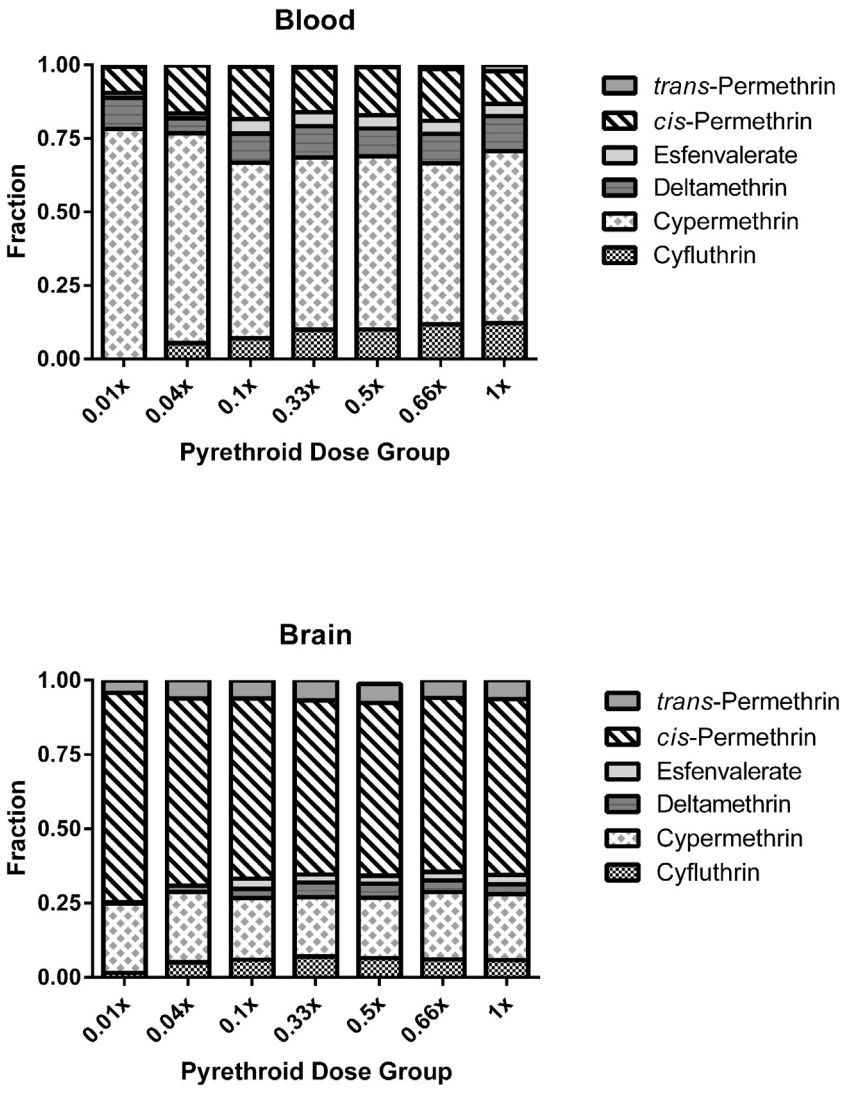

Fig. 3. Fractional composition of pyrethroids in blood and brain of rats administered a mixture of pyrethroids by oral gavage. Data extracted from Fig. 1. At 3.5 h post-administration, the animals were sacrificed and blood and brain were collected. The tissue were extracted and analyzed for parent pyrethroid. The dose bar in Figs. 4A and 4 B represents the fractional pyrethroid composition of the administered dose.

Table 5
Brain to blood ratio of pyrethroids in rats 3.5 h after administration of a mixture of pyrethroids by oral gavage.

Dose group	β-Cyfluthrin	Cypermethrin	Deltamethrin	Esfenvalerate	*cis*-Permethrin	*trans*-Permethrin
0.01X	N.D.[a]	1.1 ± 1.6 (12)	N.D.	N.D.	5.2 ± 2.8 (7)	N.D.
0.04X	1.0 ± 1.1 (8)[b]	0.4 ± 0.2 (12)	0.4 ± 0.3 (10)	N.D.	4.8 ± 3.3 (11)	N.D.
0.1X	1.1 ± 0.6 (12)	0.4 ± 0.1 (12)	0.4 ± 0.4 (12)	1.3 ± 1.2 (9)	4.1 ± 1.6 (12)	4.0 ± 2.6 (5)
0.33X	0.7 ± 0.4 (12)	0.3 ± 0.1 (12)	0.4 ± 0.2 (12)	0.6 ± 0.3 (10)	3.8 ± 2.4 (12)	8.9 ± 11.4 (9)
0.5X	0.5 ± 0.2 (12)	0.3 ± 0.1 (12)	0.4 ± 0.2 (12)	0.5 ± 0.1 (10)	3.5 ± 1.4 (12)	4.4 ± 1.9 (8)
0.66X	0.3 ± 0.2 (12)	0.2 ± 0.1 (12)	0.2 ± 0.1 (12)	0.4 ± 0.2 (11)	2.1 ± 0.7 (12)	2.2 ± 0.9 (11)
1X	0.5 ± 0.3 (12)	0.3 ± 0.1 (12)	0.2 ± 0.1 (12)	0.4 ± 0.3 (11)	2.3 ± 0.9 (12)	2.0 ± 1.2 (12)

[a] Not Determined (insufficient data to calculate a ratio).
[b] mean ± SD (N).

activity; *trans*-permethrin is hydrolyzed efficiently by this enzyme, whereas deltamethrin, esfenvalerate, cypermethrin (alpha isomer) and *cis*-permethrin are hydrolyzed to a lesser extent (Crow et al., 2007). The higher concentrations of the pyrethroids relative to that of *trans*-permethrin in blood in the present study may be explained by the higher activity of this enzyme towards *trans*-permethrin.

Pyrethroid-metabolizing carboxylesterases are also found in the liver and intestines (Nishi et al., 2006; Crow et al., 2007). In rat liver, hydrolase A and B are highly expressed carboxylesterase isozymes and are part of the carboxylesterase 1 (CES1) family (Hosokawa, 2008; Okura et al., 2014). These two isozymes have differential hydrolytic activity towards deltamethrin and esfenvalerate (Godin et al., 2006) and *cis*- and *trans*-permethrin (Ross et al., 2006). The hydrolysis of *trans*-permethrin measured as catalytic activity (k_{cat}) is 5- and 10-fold greater than *cis*-permethrin for hydrolase B and A, respectively (Ross et al., 2006). In human liver, two predominant and highly expressed carboxylesterases have been identified and are termed hepatic carboxylesterase-1

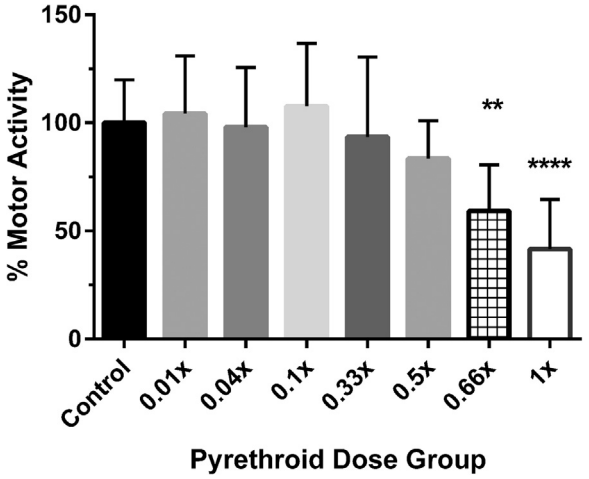

Fig. 4. % Motor activity in rats versus pyrethroid mixture dose group administered by oral gavage. Motor activity of the rats was monitored from 2 to 3 h post-administration. Data represents mean ± SD, N = 12 per dose group. **, $p < 0.01$; ****, $p < 0.0001$.

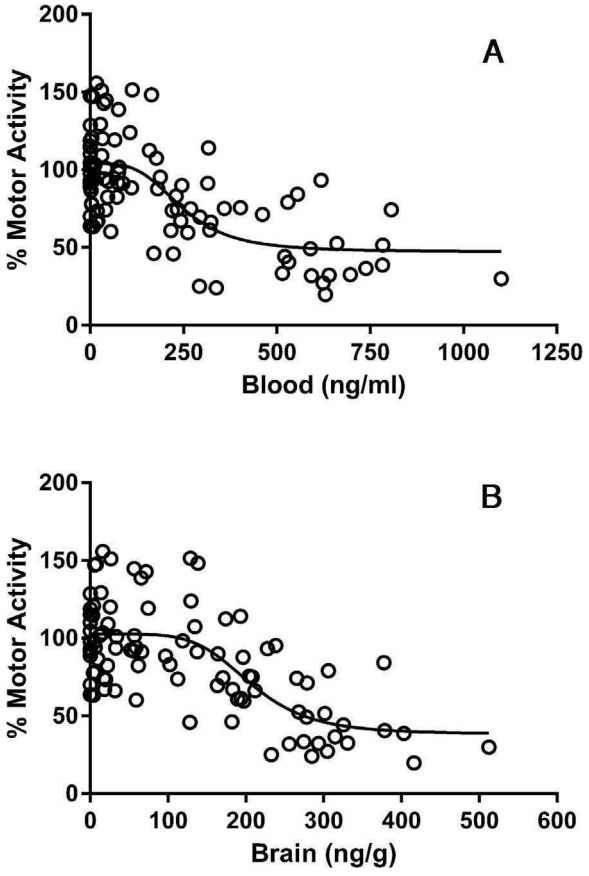

Fig. 5. Summed pyrethroid concentration in blood (A) and brain (B) with respect to % motor activity in rats. Animals were administered a mixture of pyrethroids at different doses and assessed for motor activity from 2 to 3 h post-administration. At 3.5 h, the animals were sacrificed and blood and brain were removed. Tissues were extracted and analyzed for parent pyrethroids by LC–MS/MS. Data points represent individual animals. The solid line represents the results from the sigmoidal E_{max} model analysis.

(hCE-1) and hepatic carboxylesterase-2 (hCE-2) (Brzezinski et al., 1994; Pindel et al., 1997). Differential activity between these two isozymes have been reported for deltamethrin and esfenvalerate, with hCE1 having a higher hydrolytic specific activity towards these two pyrethroids (Godin et al., 2006). Ross et al. (2006) observed both isozymes have a higher activity toward *trans*-permethrin than *cis*-permethrin.

Intestinal metabolism by rat carboxylesterases may also explain the lower fraction of *trans*-permethrin relative to the other pyrethroids in blood. Crow et al. (2007) incubated a pool of rat intestinal microsomes with deltamethrin and *trans*-permethrin. The specific activity for hydrolysis of *trans*-permethrin was ~0.2 nmole/min/mg protein and deltamethrin was not hydrolyzed. Nakamura et al. (2007) reported that the hydrolysis rate of *trans*-permethrin was 5-fold greater than that for *cis*-permethrin in rat intestinal microsomes. Rat intestinal carboxylesterases appear to contribute to the metabolic clearance of *trans*-permethrin to a greater extent than *cis*-permethrin and deltamethrin, and may explain in part for its low levels in blood relative to the other pyrethroids.

While all of the pyrethroids in the mixture were absorbed systemically into blood and brain, the role of uptake and efflux transporters is not known. For the gastrointestinal tract, Mirfazaelian et al. (2006) proposed intestinal efflux transporters for deltamethrin, based on modeling of fecal excretion data in the rat. However, Godin et al. (2010) did not observe dose-dependent bioavailability of deltamethrin in rats, suggesting that transporters are not involved in intestinal transport of this pyrethroid. In *in vitro* studies with Caco-2 cells, efflux of deltamethrin or *cis*/*trans*-permethrin by multidrug resistant protein 1 was not observed (Zastre et al., 2013). Exposure of resistant and sensitive ticks to acaricides showed no difference in the LC_{50} for cypermethrin in the presence and absence of ABC-transporter inhibitors (Pohl et al., 2012). Furthermore, within the administered dose range used, the fraction of each pyrethroid detected in the brain remained fairly constant. The finding of an overall constant fraction suggests that there was no interaction between the pyrethroids influencing absorption into the brain. The constant fraction also does not give any indication if transporters move pyrethroids into or out of the brain. Presently, it appears that transporters are not involved in intestinal and tissue uptake or efflux of pyrethroids. If transporters are involved, an effect may become apparent at higher doses of pyrethroids administered because of saturation of the transport process.

There was a difference in the distribution of the pyrethroids between blood and brain. The two permethrin isomers preferentially partitioned into brain, whereas cypermethrin, β-cyfluthrin, deltamethrin and esfenvalerate partitioned to a greater extent in blood. These partitioning results are similar to those reported by Starr et al. (2012, 2014), with one exception. The β-cyfluthrin brain to blood ratio was 2.4 in Starr et al. (2012) and approximately 1 or less (depending on the dose) in the present study. The test pyrethroids have a fairly high lipid solubility (Log P > 4.5) and contain no ionizable groups that could retard absorption. Brain to blood partition coefficients of the pyrethroids were calculated by Starr et al. (2012), with values ranging from 28.1 to 28.4. Thus high partitioning of the pyrethroids into brain could be predicted. However, the brain to blood partition values reported by Starr et al. (2012, 2014) and observed in the present study were >3-fold lower than those predicted. A potential reason for greater partitioning of a chemical into blood over a tissue is blood protein binding. Abu-Qare and Abou-Donia (2002) reported low binding of permethrin (isomer not specified) to human serum albumin. Sethi et al. (2014) more recently measured plasma protein and lipoprotein binding of deltamethrin and *cis*- and *trans*-permethrin in rats and humans. With increasing pyrethroid concentration (0.25–100 μM), they observed an increased unbound fraction of pyrethroid. The lowest concentration (0.25 μM) used by Sethi et al. (2014) corresponds approximately to the highest concentrations of deltamethrin

Table 6
Parameter estimates of the pyrethroid load in blood and brain of rats vs. motor activity (% control).[a]

Parameter	Blood	Brain
E_o	104.2 ± 3.6[b]	102.7 ± 3.5
E_{max}	56.9 ± 9.1	64.2 ± 13.3
Shape (n)	3.7 ± 2.2	5.4 ± 2.9
Effective Concentration$_{50}$ (b)	246.2 ± 39.2	207.2 ± 24.8
r^2	0.46	0.47
N[c]	96	96

[a] Data were fit with a sigmoidal E_{max} model. E_0 is the motor activity of the rats when the pyrethroid load is zero and E_{max} is the maximal change from control. E_0 was bound at <130 and E_{max} was bound at <100 in this analysis.
[b] Mean ± SE.
[c] Number of animals.

(0.16 μM) and *cis*- (0.26 μM) and *trans*-permethrin (0.04 μM) detected in blood in the present study. At 0.25 μM, Sethi et al. (2014) reported approximately 20% of deltamethrin and *cis*- and *trans*-permethrin were not bound to protein. If the observations of Sethi et al. (2014) are consistent with pyrethroid concentrations lower than 0.25 μM, the unbound fraction would be lower. This suggests that at the pyrethroid blood concentrations determined in this study, there would be less pyrethroid available for partitioning into the brain. However, Starr et al. (2012) reported a trend of higher partitioning of the pyrethroids into the brain for the lower dose as observed in this study; partitioning of the pyrethroids into brain decreased as dose increased. The reason for this partitioning observation is not known, but perhaps the physicochemical properties of the pyrethroids including their tertiary structure have an important role here or there is an unknown transporter involved in the uptake of the pyrethroids into the brain.

The correlation between summed pyrethroid tissue concentration and effect on motor activity in this study is consistent with the results of previous five-pyrethroid mixture studies (Starr et al., 2012, 2014). Similarly, β-cyfluthrin in brain had the highest estimated relative percent contribution to decrease in motor activity as reported by Starr et al. (2012, 2014). This study, those by Starr et al. (2012, 2014) and that of Wolansky et al. (2009), who studied an eleven pyrethroid mixture which contained the five pyrethroids studied here, produced comparable results in that the mixtures contained low effective concentrations of individual pyrethroids, yet significant dose-response decreases in motor activity were observed in rats administered the mixture. Furthermore, the present study shows that both blood and brain concentrations of the pyrethroid load are predictive of motor activity to a similar extent, although the results from brain appear to be more sensitive. The EC_{50} for the pyrethroid concentration in brain was lower than in blood, which supports the hypothesis that brain is a target organ for the neurotoxic effects of pyrethroids. The blood and brain concentrations of the pyrethroids were highly correlated at the 3.5 h time point, so it stands to reason that blood concentrations, as a surrogate for brain concentrations, could be an acceptable predictor of motor activity in the rat. However, over time, the concentration of pyrethroids in blood decrease and the ability for blood concentrations to predict motor activity most likely will decrease. For the pyrethroid bifenthrin, administered singly, there was a good correlation between bifenthrin blood concentration and motor activity at 4 h post-dosing (Scollon et al., 2011). However, by 7 h the correlation of bifenthrin blood concentration to motor activity decreased considerably. In the brain, the correlations were similar at 4 and 7 h, suggesting there was little efflux of bifenthrin out of the brain, minimal metabolism in this organ during this time frame or both. This is supported by the observation by Starr et al. (2012) that the pyrethroids have a longer half-life in brain relative to that in blood and liver.

In summary, pyrethroids administered as a mixture to rats by oral gavage were absorbed into blood and brain. With increased dose, there was an increase in the concentration of pyrethroid in blood and brain. There were differences between the fractions of each pyrethroid in the dosing solution with those detected in blood; the fractions in brain were very similar to the dosing solution provided the permethrin isomer concentrations were summed. The pyrethroids β-cyfluthrin, cypermethrin, deltamethrin and esfenvalerate primarily partitioned into blood, whereas *cis*- and *trans*-permethrin primarily partitioned into brain. There was a significant dose-dependent decrease in motor activity of the rats administered the pyrethroid mixture. Further research is clearly needed to explain this differential partitioning of the pyrethroids between blood and brain and its relationship to neurotoxicity and how it relates to the more than 35-fold range in relative potencies among these five pyrethroids.

Conflict of interest

The authors declare to have no competing conflicts of interest.

Disclaimer

The research described in this article has been reviewed by the National Health and Environmental Effects Research Laboratory, United States Environmental Protection Agency, and approved for publication. Approval does not signify that the contents necessarily reflect the views of the Agency nor the mention of trade names or commercial products constitute endorsement or recommendation for use.

This article may be a work product of an employee of the National Institute of Environmental Health Sciences (NIEHS), National Institutes of Health (NIH), however, the statements, opinions, or conclusions contained therein do not necessarily represent the statements, opinions, or conclusions of NIEHS, NIH, or the United States government.

Acknowledgements

The authors thank FMC Corporation, Bayer CropScience and DuPont Crop Protection for providing the pyrethroids used in this study. The authors also thank Drs. Hisham El-Masri, Jane Ellen Simmons and Nicole Tulve for their review of an earlier version of this manuscript. This research was supported by internal US Environmental Protection Agency, Office of Research and Development funds.

Appendix A. Supplementary data

Supplementary data associated with this article can be found, in the online version, at http://dx.doi.org/10.1016/j.tox.2016.06.013.

References

ATSDR, 2003. Public Health Statement. Pyrethrins and Pyrethroids. Agency for Toxic Substances and Disease Registry. . (accessed 06.03.14) http://www.atscr.cdc.gov/ToxProfiles/tp155-c1-b.pdf.
Abernathy, C.O., Ueda, K., Engel, J.L., Gaughan, L.C., Casida, J.E., 1973. Substrate-specificity and toxicological significance of pyrethroid-hydrolyzing esterases of mouse liver microsomes. Pestic. Biochem. Physiol. 3, 300–311.
Abu-Qare, A.W., Abou-Donia, M.B., 2002. Binding of pyridostigmine bromide, N,N-diethyl-m-toluamide and permethrin alone and in combinations, to human serum albumin. Arch. Toxicol. 26, 203–208.
Amweg, E.L., Weston, D.P., Ureda, N.M., 2005. Use and toxicity of pyrethroid pesticides in the Central Valley California, USA. Environ. Toxicol. Chem. 24, 966–972.
Bradberry, S.M., Cage, S.A., Proudfoot, A.T., Vale, J.A., 2005. Poisoning due to pyrethroids. Toxicol. Rev. 24, 93–106.

Breckenridge, C.B., Holden, L., Sturgess, N., Weinder, M., Sheets, L., et al., 2009. Evidence for separate mechanism of toxicity for the Type I and the Type II pyrethroid insecticides. Neurotoxicology 30S, S17–S31.
Brzezinski, M.R., Abraham, T.L., Stone, C.L., Dean, R.A., Bosron, W.F., 1994. Purification and characterization of a human liver cocaine carboxylesterase that catalyzed the production of benzoylecgonine and the formation of cocaethylene from alcohol and cocaine. Biochem. Pharmacol. 48, 1747–1755.
Cao, Z., Shafer, T.J., Crofton, K.M., Gennings, C., Murray, T.F., 2011. Additivity of pyrethroid actions on sodium influx in cerebrocortical neurons in primary culture. Environ. Health Perspect. 119, 1239–1246.
Crofton, K.M., Reiter, L.W., 1984. Effects of two pyrethroid insecticides on motor activity and the acoustic startle response in the rat. Toxicol. Appl. Pharmacol. 15, 318–328.
Crofton, K.M., Reiter, L.W., 1988. The effects of type I and II pyrethroids on motor activity and the acoustic startle response in the rat. Fundam. Appl. Toxicol. 10, 624–634.
Crow, J.A., Borazjani, A., Potter, P.M., Ross, M.K., 2007. Hydrolysis of pyrethroids by human and rat tissues: examination of intestinal: liver and serum carboxylesterases. Toxicol. Appl. Pharmacol. 221, 1–12.
Fortin, M.-C., Bouchard, M., Carrier, G., Dumas, P., 2008. Biological monitoring of exposure to pyrethrins and pyrethroids in a metropolitan population of the Province of Quebec, Canada. Environ. Res. 107, 343–350.
Godin, S.J., Scollon, E.J., Hughes, M.F., Potter, P.M., DeVito, M.J., et al., 2006. Species differences in the in vitro metabolism of deltamethrin and esfenvalerate: differential oxidative and hydrolytic metabolism by humans and rats. Drug Metab. Dispos. 34, 1764–1771.
Godin, S.J., Crow, J.A., Scollon, E.J., Hughes, M.F., DeVito, M.J., et al., 2007. Identification of rat and human cytochrome P450 isoforms and a rat serum esterase that metabolize the pyrethroid insecticides deltamethrin and esfenvalerate. Drug Metab. Dispos. 35, 1664–1671.
Godin, S.J., Devito, M.J., Hughes, M.F., Ross, D.G., Scollon, E.J., et al., 2010. Physiologically based pharmacokinetic modeling of deltamethrin: development of a rat and human diffusion-limited model. Toxicol. Sci. 115, 330–343.
Gray, A.J., Rickard, J., 1982a. Toxicity of pyrethroids to rats after direct injection into the central nervous system. Neurotoxicology 3, 25–35.
Gray, A.J., Rickard, J., 1982b. The toxicokinetics of deltamethrin in rats after intravenous administration of a toxic dose. Pestic. Biochem. Physiol. 18, 205–215.
Heudorf, U., Angerer, J., 2001. Metabolites of pyrethroid insecticides in urine specimens: current exposure in an urban population in Germany. Environ. Health Perspect. 109, 213–217.
Hosokawa, M., 2008. Structure and catalytic properties of carboxylesterase isozymes involved in the metabolic activation of prodrugs. Molecules 13, 412–431.
Lawrence, L.J., Casida, J.E., 1982. Pyrethroid toxicology: mouse intracerebral structure-activity relationships. Pestic. Biochem. Physiol. 18, 9–14.
Meador, J.P., McCarty, L.S., Escher, B.I., Adams, W.U., 2008. 10th Anniversary Critical Review: the tissue-residue approach for toxicity assessment: concepts, issues, application, and recommendations. J. Environ. Monit. 10, 1486–1498.
Mirfazaelian, A., Kim, K.-B., Anand, S.S., Kim, H.J., Tornero-Velez, R., et al., 2006. Development of a physiologically based pharmacokinetic model for deltamethrin in the adult male Sprague-Dawley rat. Toxicol. Sci. 92, 432–442.
Miyamoto, J., 1990. Stereoselective metabolism and toxicology of pyrethroids. In: Holmstedt, B., Frank, H., Testa, B. (Eds.), Chirality and Biological Activity. A.R. Liss, Inc., New York, pp. 153–168.
Nakamura, Y., Sugihara, K., Sone, T., Isobe, M., Ohta, S., et al., 2007. The in vitro metabolism of a pyrethroid insecticide, permethrin and its hydrolysis products in rats. Toxicology 235, 176–184.
Nishi, K., Huang, H., Kamita, S.G., Kim, I.-H., Morisseau, C., et al., 2006. Characterization of pyrethroid hydrolysis by the human liver carboxylesterases hCE-1 and hCE-2. Arch. Biochem. Biophys. 445, 115–123.
Okura, K., Tasaka, K., Hashimoto, M., Imai, T., 2014. Distinct patterns of aging effects and activity of carboxylesterase in rat liver and intestine. Drug Metab. Dispos. 42, 264–273.
Pindel, E.V., Kedishvili, N.Y., Abraham, T.L., Brzezinski, M.R., Zhang, J., et al., 1997. Purification and cloning of a broad substrate specificity human liver carboxylesterase that catalyzes the hydrolysis of cocaine and heroin. J. Biol. Chem. 272, 14769–14775.
Pohl, P.C., Klafke, G.M., Junior, J.R., Martins, J.R., da Silva Vas Jr., I., et al., 2012. ABC transporters as a multidrug detoxification mechanism in Rhipicephalus (Boophilus) microplus. Parasitol. Res. 111, 2345–2351.
Ross, M.K., Borazjani, A., Edwards, C.C., Potter, P.M., 2006. Hydrolytic metabolism of pyrethroids by human and other mammalian carboxylesterases. Biochem. Pharmacol. 71, 657–669.
Rudel, R.A., Camann, D.E., Spengler, J.D., Korn, L.R., Brody, J.G., 2003. Phthalates, alkylphenols, pesticides, polybrominated diphenyl ethers, and other endocrine-disrupting compounds in indoor air and dust. Environ. Sci. Technol. 72, 4543–4553.
Scollon, E.J., Starr, J.M., Godin, S.J., DeVito, M.J., Hughes, M.F., 2009. In vitro metabolism of pyrethroid pesticides by rat and human hepatic microsomes and cytochrome P450 isoforms. Drug Metab. Dispos. 37, 221–228.
Scollon, E.J., Starr, J.M., Crofton, K.M., Wolansky, M.J., DeVito, M.J., et al., 2011. Correlation of tissue concentrations of the pyrethroid bifenthrin with neurotoxicity in the rat. Toxicology 290, 1–6.
Sethi, P.K., Muralidhara, S., Bruckner, J.V., White, C.A., 2014. Measurement of plasma protein and lipoprotein binding of pyrethroids. J. Pharmacol. Toxicol. Methods 70, 106–111.
Soderlund, D.M., Clark, J., Sheets, L.P., Mullin, L.S., Piccirillo, V.J., et al., 2002. Mechanisms of pyrethroid neurotoxicity: implications for cumulative risk assessment. Toxicology 17, 3–59.
Soderlund, D.M., 2012. Molecular mechanisms of pyrethroid insecticide neurotoxicity: recent advances. Arch. Toxicol. 86, 165–181.
Starr, J.M., Scollon, E.J., Hughes, M.F., Ross, D.G., Graham, S.E., et al., 2012. Environmentally relevant mixtures in cumulative assessments: an acute study of toxicokinetics and effects on motor activity in rats exposed to a mixture of pyrethroids. Toxicol. Sci. 130, 309–318.
Starr, J.M., Graham, S.E., Ross, D.G., Tornero-Velez, R., Scollon, E.J., et al., 2014. Environmentally relevant mixing ratios in cumulative assessments: a study of the kinetics of pyrethroids and their ester cleavage metabolites in blood and brain; and the effect of a pyrethroid mixture on the motor activity of rats. Toxicology 310, 15–24.
Stout II, D.M., Bradham, K.D., Egeghy, P.P., Jones, P.A., Croghan, C.W., et al., 2009. American Healthy Homes Survey: a national study of residential pesticides measured from floor wipes. Environ. Sci. Technol. 43, 4294–4300.
Tornero-Velez, R., Egeghy, P.P., Cohen Hubal, E.A., 2012. Biogeographical analysis of chemical co-occurrence data to identify priorities for mixtures research. Risk Anal. 32, 224–236.
Tulve, N.S., Jones, P.A., Nishioka, M., Fortmann, R.C., Croghan, C.W., et al., 2006. Pesticide measurements from the first national environmental health survey of child care centers using a multi-residue GC/MS analysis method. Environ. Sci. Technol. 40, 6269–6274.
US EPA, 2011. Pyrethrins/Pyrethroid Cumulative Risk Assessment. United States Environmental Protection Agency. http://www.regulations.gov/#!documentDetail;D=EPA-HQ-OPP-2011-0746-0003. (accessed 15.01.16).
USDA, 2014. Pesticide Data Program. Annual Summary. Calendar Year 2014. United States Department of Agriculture. http://www.ams.usda.gov/sites/default/files/media/2014%20PDP%20Annual%20Summary.pdf (accessed 02.02.16)
Wolansky, M.J., Gennings, C., Crofton, K.M., 2006. Relative potencies for acute effects of pyrethroids on motor function in rats. Toxicol. Sci. 89, 271–277.
Wolansky, M.J., Gennings, C., DeVito, M.J., Crofton, K.M., 2009. Evidence for dose-additive effects of pyrethroids on motor activity in rats. Environ. Health Perspect. 117, 1563–1570.
Zastre, J., Dowd, C., Bruckner, J., Popovici, A., 2013. Lack of P-glycoprotein-mediated efflux and the potential involvement of an influx transport process contributing to the intestinal uptake of deltamethrin *cis*-permethrin, and *trans*-permethrin. Toxicol. Sci. 136, 284–293.

Hughes, MichaelF

From: Kevin Crofton <croftonwork@outlook.com>
Sent: Friday, April 24, 2020 11:05 AM
To: Hughes, MichaelF
Cc: Devito, Michael
Subject: RE: STAA - Level of Effort

Mike – I think you left a zero off my number! 😊

I'm fine with the numbers.

Kevin

From: Devito, Michael <Devito.Michael@epa.gov>
Sent: Friday, April 24, 2020 8:44 AM
To: Hughes, MichaelF <Hughes.MichaelF@epa.gov>; Ross, David <Ross.David@epa.gov>; Dr. Kevin Crofton <croftonwork@outlook.com>; Marcelo Wolansky <mjwolansky@gmail.com>; Edward Scollon (ed.scollon@syngenta.com) <ed.scollon@syngenta.com>; Starr, James <Starr.James@epa.gov>; edwards.brenda@hotmail.com
Subject: RE: STAA - Level of Effort

I am good with the numbers

thanks

Michael DeVito, Ph.D.
Director
Chemical Characterization and Exposure Division
Center for Computational Toxicology and Exposure
Office of Research and Development
US Environmental Protection Agency
MC-E205-C
109 T.W. Alexander Drive
Research Triangle Park, NC
27711

Phone: 919-541-4016
Email:devito.michael@epa.gov

From: Hughes, MichaelF <Hughes.MichaelF@epa.gov>
Sent: Friday, April 24, 2020 8:37 AM
To: Devito, Michael <Devito.Michael@epa.gov>; Ross, David <Ross.David@epa.gov>; Dr. Kevin Crofton <croftonwork@outlook.com>; Marcelo Wolansky <mjwolansky@gmail.com>; Edward Scollon (ed.scollon@syngenta.com) <ed.scollon@syngenta.com>; Starr, James <Starr.James@epa.gov>; edwards.brenda@hotmail.com; Hughes, MichaelF <Hughes.MichaelF@epa.gov>
Subject: STAA - Level of Effort

Hi everyone,

Can you please look over the level of effort below and send me an email that you concur (or not). I appreciate your help here.

Name	% Effort
Brenda Edwards	20
David Ross	20
Kevin Crofton	5
Ed Scollon	5
Mike DeVito	5
Mike Hughes	15
Jim Starr	20
Marcelo Wolansky	10

Marcelo – thank you for your suggestions as papers, but we are limited to 3 papers/submission. Also, there is a time limit. Only papers published since 2015 are permissible.

Best regards,
Mike

Michael F. Hughes, PhD, DABT
U.S. Environmental Protection Agency
ORD/CCTE/CCED/ETTB
MD B105-03
Research Triangle Park, NC 27711
(T): 919-541-2160; (F): 919-541-4284

Hughes, MichaelF

From: Devito, Michael
Sent: Friday, April 24, 2020 8:44 AM
To: Hughes, MichaelF; Ross, David; Dr. Kevin Crofton; Marcelo Wolansky; Edward Scollon (ed.scollon@syngenta.com); Starr, James; edwards.brenda@hotmail.com
Subject: RE: STAA - Level of Effort

I am good with the numbers

thanks

Michael DeVito, Ph.D.
Director
Chemical Characterization and Exposure Division
Center for Computational Toxicology and Exposure
Office of Research and Development
US Environmental Protection Agency
MC-E205-C
109 T.W. Alexander Drive
Research Triangle Park, NC
27711

Phone: 919-541-4016
Email:devito.michael@epa.gov

From: Hughes, MichaelF <Hughes.MichaelF@epa.gov>
Sent: Friday, April 24, 2020 8:37 AM
To: Devito, Michael <Devito.Michael@epa.gov>; Ross, David <Ross.David@epa.gov>; Dr. Kevin Crofton <croftonwork@outlook.com>; Marcelo Wolansky <mjwolansky@gmail.com>; Edward Scollon (ed.scollon@syngenta.com) <ed.scollon@syngenta.com>; Starr, James <Starr.James@epa.gov>; edwards.brenda@hotmail.com; Hughes, MichaelF <Hughes.MichaelF@epa.gov>
Subject: STAA - Level of Effort

Hi everyone,

Can you please look over the level of effort below and send me an email that you concur (or not). I appreciate your help here.

Name	% Effort
Brenda Edwards	20
David Ross	20
Kevin Crofton	5
Ed Scollon	5
Mike DeVito	5
Mike Hughes	15

Jim Starr	20
Marcelo Wolansky	10

Marcelo – thank you for your suggestions as papers, but we are limited to 3 papers/submission. Also, there is a time limit. Only papers published since 2015 are permissible.

Best regards,
Mike

Michael F. Hughes, PhD, DABT
U.S. Environmental Protection Agency
ORD/CCTE/CCED/ETTB
MD B105-03
Research Triangle Park, NC 27711
(T): 919-541-2160; (F): 919-541-4284

Hughes, MichaelF

From: edwards.brenda@hotmail.com
Sent: Friday, April 24, 2020 9:10 AM
To: Hughes, MichaelF
Subject: Re: STAA - Level of Effort

Hi Mike I concur with the number
.

Thanks Brenda Edwards

On Apr 24, 2020 8:37 AM, "Hughes, MichaelF" <Hughes.MichaelF@epa.gov> wrote:

> Hi everyone,
>
> Can you please look over the level of effort below and send me an email that you concur (or not). I appreciate your help here.
>
> | Name | % Effort |
> |---|---|
> | Brenda Edwards | 20 |
> | David Ross | 20 |
> | Kevin Crofton | 5 |
> | Ed Scollon | 5 |
> | Mike DeVito | 5 |
> | Mike Hughes | 15 |
> | Jim Starr | 20 |
> | Marcelo Wolansky | 10 |
>
> Marcelo – thank you for your suggestions as papers, but we are limited to 3 papers/submission. Also, there is a time limit. Only papers published since 2015 are permissible.
>
> Best regards,

Mike

Michael F. Hughes, PhD, DABT

U.S. Environmental Protection Agency

ORD/CCTE/CCED/ETTB

MD B105-03

Research Triangle Park, NC 27711

(T): 919-541-2160; (F): 919-541-4284

Hughes, MichaelF

From: Hughes, MichaelF
Sent: Wednesday, April 29, 2020 12:04 PM
To: Hughes, MichaelF
Subject: RE: STAA - Level of Effort

I concur with a 15% Level of Effort for this application.

Michael F. Hughes, PhD, DABT
U.S. Environmental Protection Agency
ORD/CCTE/CCED/ETTB
MD B105-03
Research Triangle Park, NC 27711
(T): 919-541-2160; (F): 919-541-4284

From: Hughes, MichaelF <Hughes.MichaelF@epa.gov>
Sent: Wednesday, April 29, 2020 12:03 PM
To: Hughes, MichaelF <Hughes.MichaelF@epa.gov>
Subject: FW: STAA - Level of Effort

Michael F. Hughes, PhD, DABT
U.S. Environmental Protection Agency
ORD/CCTE/CCED/ETTB
MD B105-03
Research Triangle Park, NC 27711
(T): 919-541-2160; (F): 919-541-4284

From: Hughes, MichaelF
Sent: Friday, April 24, 2020 8:37 AM
To: Devito, Michael <Devito.Michael@epa.gov>; Ross, David <Ross.David@epa.gov>; Dr. Kevin Crofton <croftonwork@outlook.com>; Marcelo Wolansky <mjwolansky@gmail.com>; Edward Scollon (ed.scollon@syngenta.com) <ed.scollon@syngenta.com>; James Starr <Starr.James@epa.gov>; edwards.brenda@hotmail.com; Hughes, MichaelF <Hughes.MichaelF@epa.gov>
Subject: STAA - Level of Effort

Hi everyone,

Can you please look over the level of effort below and send me an email that you concur (or not). I appreciate your help here.

Name	% Effort
Brenda Edwards	20
David Ross	20

Kevin Crofton	5
Ed Scollon	5
Mike DeVito	5
Mike Hughes	15
Jim Starr	20
Marcelo Wolansky	10

Marcelo – thank you for your suggestions as papers, but we are limited to 3 papers/submission. Also, there is a time limit. Only papers published since 2015 are permissible.

Best regards,
Mike

Michael F. Hughes, PhD, DABT
U.S. Environmental Protection Agency
ORD/CCTE/CCED/ETTB
MD B105-03
Research Triangle Park, NC 27711
(T): 919-541-2160; (F): 919-541-4284

Hughes, MichaelF

From: Scollon, Ed <Edward.Scollon@valent.com>
Sent: Friday, April 24, 2020 12:12 PM
To: Hughes, MichaelF
Subject: RE: STAA - Level of Effort

Thanks Mike. I concur with the recommendations.

From: Hughes, MichaelF <Hughes.MichaelF@epa.gov>
Sent: Friday, April 24, 2020 5:41 AM
To: Scollon, Ed <Edward.Scollon@valent.com>
Subject: FW: STAA - Level of Effort

Hi Ed,

I hope you and Tanya are well. I sent the message below to your Syngenta address.

Best regards,
Mike

Michael F. Hughes, PhD, DABT
U.S. Environmental Protection Agency
ORD/CCTE/CCED/ETTB
MD B105-03
Research Triangle Park, NC 27711
(T): 919-541-2160; (F): 919-541-4284

From: Hughes, MichaelF
Sent: Friday, April 24, 2020 8:37 AM
To: Devito, Michael <Devito.Michael@epa.gov>; Ross, David <Ross.David@epa.gov>; Dr. Kevin Crofton <croftonwork@outlook.com>; Marcelo Wolansky <mjwolansky@gmail.com>; Edward Scollon (ed.scollon@syngenta.com) <ed.scollon@syngenta.com>; James Starr <Starr.James@epa.gov>; edwards.brenda@hotmail.com; Hughes, MichaelF <Hughes.MichaelF@epa.gov>
Subject: STAA - Level of Effort

Hi everyone,

Can you please look over the level of effort below and send me an email that you concur (or not). I appreciate your help here.

Name	% Effort
Brenda Edwards	20
David Ross	20
Kevin Crofton	5
Ed Scollon	5

Mike DeVito	5
Mike Hughes	15
Jim Starr	20
Marcelo Wolansky	10

Marcelo – thank you for your suggestions as papers, but we are limited to 3 papers/submission. Also, there is a time limit. Only papers published since 2015 are permissible.

Best regards,
Mike

Michael F. Hughes, PhD, DABT
U.S. Environmental Protection Agency
ORD/CCTE/CCED/ETTB
MD B105-03
Research Triangle Park, NC 27711
(T): 919-541-2160; (F): 919-541-4284

Hughes, MichaelF

From: Starr, James
Sent: Friday, April 24, 2020 8:44 AM
To: Hughes, MichaelF
Subject: RE: STAA - Level of Effort

Thanks Mike,

I concur with my LOE. Also, while the limit is three in the last 5 years, additional papers can be cited as supplemental information. Kind of a backdoor way to get them in.

Jim

From: Hughes, MichaelF <Hughes.MichaelF@epa.gov>
Sent: Friday, April 24, 2020 8:37 AM
To: Devito, Michael <Devito.Michael@epa.gov>; Ross, David <Ross.David@epa.gov>; Dr. Kevin Crofton <croftonwork@outlook.com>; Marcelo Wolansky <mjwolansky@gmail.com>; Edward Scollon (ed.scollon@syngenta.com) <ed.scollon@syngenta.com>; Starr, James <Starr.James@epa.gov>; edwards.brenda@hotmail.com; Hughes, MichaelF <Hughes.MichaelF@epa.gov>
Subject: STAA - Level of Effort

Hi everyone,

Can you please look over the level of effort below and send me an email that you concur (or not). I appreciate your help here.

Name	% Effort
Brenda Edwards	20
David Ross	20
Kevin Crofton	5
Ed Scollon	5
Mike DeVito	5
Mike Hughes	15
Jim Starr	20
Marcelo Wolansky	10

Marcelo – thank you for your suggestions as papers, but we are limited to 3 papers/submission. Also, there is a time limit. Only papers published since 2015 are permissible.

Best regards,
Mike

Michael F. Hughes, PhD, DABT

U.S. Environmental Protection Agency
ORD/CCTE/CCED/ETTB
MD B105-03
Research Triangle Park, NC 27711
(T): 919-541-2160; (F): 919-541-4284

Hughes, MichaelF

From: Marcelo Wolansky <mjwolansky@gmail.com>
Sent: Tuesday, April 28, 2020 1:23 PM
To: Hughes, MichaelF
Subject: Re: FW: STAA - Level of Effort

Hi Michael, Yes, I do. I am quite happy with my memories of those times. Whatever you consider between 5 and 10% is fine to me. Make the equation as you consider more convenient for this particular application.
Thanks!!
Marcelo

El mar., 28 abr. 2020 14:05, Hughes, MichaelF <Hughes.MichaelF@epa.gov> escribió:

> Hello Marcelo,
>
> Hope you are well, including your family too! Can you please let me know if you agree with the level of effort listed below for you?
>
> Thanks,
>
> Mike
>
> Michael F. Hughes, PhD, DABT
>
> U.S. Environmental Protection Agency
>
> ORD/CCTE/CCED/ETTB
>
> MD B105-03
>
> Research Triangle Park, NC 27711
>
> (T): 919-541-2160; (F): 919-541-4284
>
> **From:** Hughes, MichaelF
> **Sent:** Friday, April 24, 2020 8:37 AM
> **To:** Devito, Michael <Devito.Michael@epa.gov>; Ross, David <Ross.David@epa.gov>; Dr. Kevin Crofton <croftonwork@outlook.com>; Marcelo Wolansky <mjwolansky@gmail.com>; Edward Scollon (ed.scollon@syngenta.com) <ed.scollon@syngenta.com>; James Starr <Starr.James@epa.gov>;

edwards.brenda@hotmail.com; Hughes, MichaelF <Hughes.MichaelF@epa.gov>
Subject: STAA - Level of Effort

Hi everyone,

Can you please look over the level of effort below and send me an email that you concur (or not). I appreciate your help here.

Name	% Effort
Brenda Edwards	20
David Ross	20
Kevin Crofton	5
Ed Scollon	5
Mike DeVito	5
Mike Hughes	15
Jim Starr	20
Marcelo Wolansky	10

Marcelo – thank you for your suggestions as papers, but we are limited to 3 papers/submission. Also, there is a time limit. Only papers published since 2015 are permissible.

Best regards,

Mike

Michael F. Hughes, PhD, DABT

U.S. Environmental Protection Agency

ORD/CCTE/CCED/ETTB

MD B105-03

Research Triangle Park, NC 27711

(T): 919-541-2160; (F): 919-541-4284

Hughes, MichaelF

From: Ross, David
Sent: Friday, April 24, 2020 8:43 AM
To: Hughes, MichaelF
Subject: RE: STAA - Level of Effort

Hi Mike,

I concur.

David

David G. Ross
Biologist
Office B456A
Advanced Experimental Toxicology Models Branch MD B105-03
Biomolecular & Computational Toxicology Division
Center for Computational Toxicology and Exposure
United States Environmental Protection Agency
109 T.W. Alexander Drive
Research Triangle Park, NC 27711
Phone: 919-541-3358
Fax: 919-541-9464
Email: ross.david@epa.gov

From: Hughes, MichaelF <Hughes.MichaelF@epa.gov>
Sent: Friday, April 24, 2020 8:37 AM
To: Devito, Michael <Devito.Michael@epa.gov>; Ross, David <Ross.David@epa.gov>; Dr. Kevin Crofton <croftonwork@outlook.com>; Marcelo Wolansky <mjwolansky@gmail.com>; Edward Scollon (ed.scollon@syngenta.com) <ed.scollon@syngenta.com>; Starr, James <Starr.James@epa.gov>; edwards.brenda@hotmail.com; Hughes, MichaelF <Hughes.MichaelF@epa.gov>
Subject: STAA - Level of Effort

Hi everyone,

Can you please look over the level of effort below and send me an email that you concur (or not). I appreciate your help here.

Name	% Effort
Brenda Edwards	20
David Ross	20
Kevin Crofton	5
Ed Scollon	5
Mike DeVito	5

Mike Hughes	15
Jim Starr	20
Marcelo Wolansky	10

Marcelo – thank you for your suggestions as papers, but we are limited to 3 papers/submission. Also, there is a time limit. Only papers published since 2015 are permissible.

Best regards,
Mike

Michael F. Hughes, PhD, DABT
U.S. Environmental Protection Agency
ORD/CCTE/CCED/ETTB
MD B105-03
Research Triangle Park, NC 27711
(T): 919-541-2160; (F): 919-541-4284

Provided for non-commercial research and education use.
Not for reproduction, distribution or commercial use.

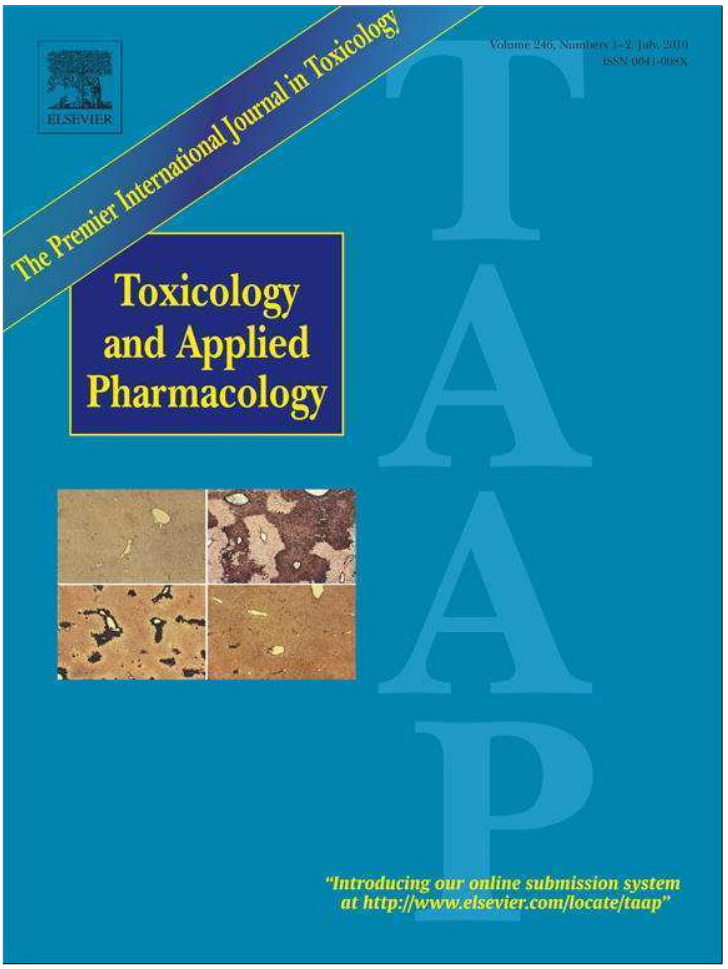

This article appeared in a journal published by Elsevier. The attached copy is furnished to the author for internal non-commercial research and education use, including for instruction at the authors institution and sharing with colleagues.

Other uses, including reproduction and distribution, or selling or licensing copies, or posting to personal, institutional or third party websites are prohibited.

In most cases authors are permitted to post their version of the article (e.g. in Word or Tex form) to their personal website or institutional repository. Authors requiring further information regarding Elsevier's archiving and manuscript policies are encouraged to visit:

http://www.elsevier.com/copyright

Author's personal copy

Toxicology and Applied Pharmacology 246 (2010) 29–37

Contents lists available at ScienceDirect

Toxicology and Applied Pharmacology

journal homepage: www.elsevier.com/locate/ytaap

In vitro dermal absorption of pyrethroid pesticides in human and rat skin

Michael F. Hughes *, Brenda C. Edwards

Integrated Systems Toxicology Division, National Health and Environmental Effects Research Laboratory, Office of Research and Development, U.S. Environmental Protection Agency, Research Triangle Park, NC, USA

ARTICLE INFO

Article history:
Received 6 January 2010
Revised 6 April 2010
Accepted 7 April 2010
Available online 14 April 2010

Keywords:
Dermal absorption
In vitro
Pyrethroids

ABSTRACT

Dermal exposure to pyrethroid pesticides can occur during manufacture and application. This study examined the *in vitro* dermal absorption of pyrethroids using rat and human skin. Dermatomed skin from adult male Long Evans rats or human cadavers was mounted in flow-through diffusion cells, and radiolabeled bifenthrin, deltamethrin or cis-permethrin was applied in acetone to the skin. Fractions of receptor fluid were collected every 4 h. At 24 h, the skins were washed with soap and water to remove unabsorbed chemical. The skin was then solubilized. Two additional experiments were performed after washing the skin; the first was tape-stripping the skin and the second was the collection of receptor fluid for an additional 24 h. Receptor fluid, skin washes, tape strips and skin were analyzed for radioactivity. For rat skin, the wash removed 53–71% of the dose and 26–43% remained in the skin. The cumulative percentage of the dose at 24 h in the receptor fluid ranged from 1 to 5%. For human skin, the wash removed 71–83% of the dose and 14–25% remained in the skin. The cumulative percentage of the dose at 24 h in the receptor fluid was 1–2%. Tape-stripping removed 50–56% and 79–95% of the dose in rat and human skin, respectively, after the wash. From 24–48 h, 1–3% and about 1% of the dose diffused into the receptor fluid of rat and human skin, respectively. The pyrethroids bifenthrin, deltamethrin and cis-permethrin penetrated rat and human skin following dermal application *in vitro*. However, a skin wash removed 50% or more of the dose from rat and human skin. Rat skin was more permeable to the pyrethroids than human skin. Of the dose in skin, 50% or more was removed by tape-stripping, suggesting that permeation of pyrethroids into viable tissue could be impeded. The percentage of the dose absorbed into the receptor fluid was considerably less than the dose in rat and human skin. Therefore, consideration of the skin type used and fractions analyzed are important when using *in vitro* dermal absorption data for risk assessment.

Published by Elsevier Inc.

Introduction

Pyrethroids are a class of synthetic pesticides that have applications in agriculture, medicine, forestry, horticulture, and veterinary practices. Exposure to pyrethroids has increased recently because of regulatory restrictions placed on other insecticides (Power and Sudakin, 2007). The American Association of Poison Control Centers reported slightly more than 20,000 pyrethroid exposures in 2006 compared to about 3000 and 5000 exposures for carbamates and organophosphates, respectively (Bronstein et al., 2007). Exposure to pyrethroids can occur by oral, inhalation, or dermal routes. Oral exposure to pyrethroids can occur by direct ingestion, either intentional or accidental, from ingestion of pyrethroid-treated food (e.g., fruit) (Schettgen et al., 2002) or hand-to-mouth activity of soil or dust bound with pyrethroids (Morgan et al., 2007). Inhalation and dermal exposure to pyrethroids may occur during their occupational or residential use (Adamis et al., 1984; Chen et al., 1991; Zhang et al., 1991; Chester et al., 1992; Hughes et al., 2008).

As a class of insecticides, the pyrethroids have relatively low mammalian toxicity, but high insecticidal activity (Soderlund et al., 2002; Bradberry et al., 2006). Pyrethroids are neurotoxicants and act by blocking the voltage-sensitive sodium channel and possibly other ion channels (Ray and Forshaw, 2000; Soderlund et al., 2002; Shafer and Meyer, 2004; Ray and Fry, 2006). There are two basic signs of pyrethroid toxicity in laboratory rodents (Ray and Forshaw, 2000; Soderlund et al., 2002). The first sign is Type I or T syndrome, which is characterized by whole-body tremor, aggressive behavior, hyperexcitation and ataxia. The second sign is Type II, or CS syndrome, which is characterized by choreoathetosis and profuse salivation. In general, pyrethroids without an α-cyano group (e.g., bifenthrin and permethrin, Fig. 1) produce Type I symptoms, and pyrethroids with this group (e.g., deltamethrin, Fig. 1) produce Type II symptoms. In humans, the symptoms that may arise from acute oral exposure to pyrethroids include dizziness, headache, nausea, anorexia, fatigue, vomiting, mild disturbance of consciousness, or muscular fasciculation in limbs (He et al., 1989). It is rare for an individual to die from pyrethroid poisoning, although pulmonary edema, convulsive attacks and coma have been recorded following

* Corresponding author. US EPA, MD B143-01, Research Triangle Park, NC 27711, USA. Fax: +1 919 541 4284.
E-mail address: hughes.michaelf@epa.gov (M.F. Hughes).

0041-008X/$ – see front matter. Published by Elsevier Inc.
doi:10.1016/j.taap.2010.04.003

Author's personal copy

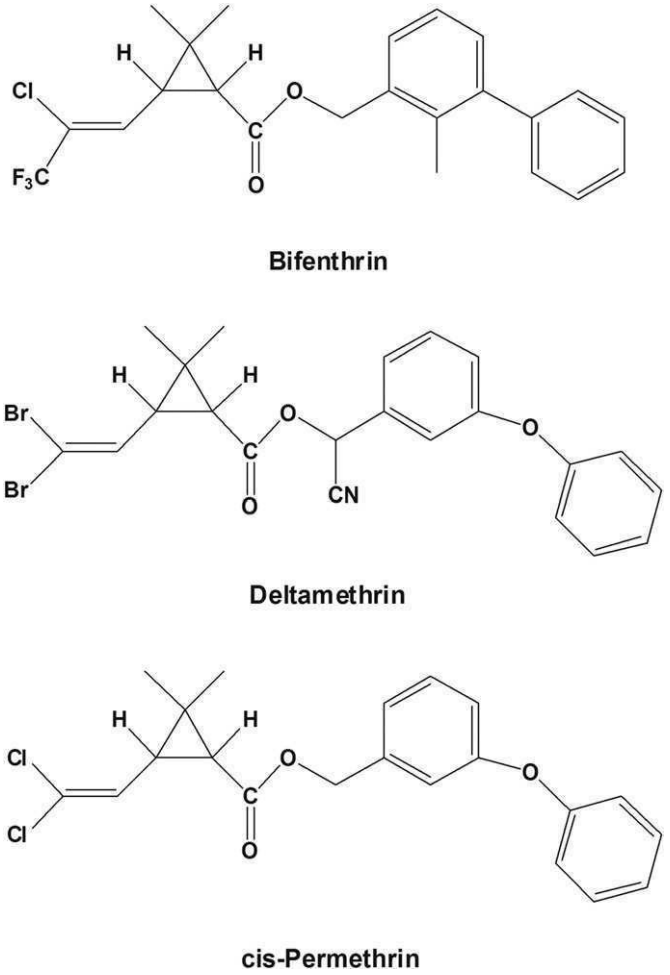

Fig. 1. Structure of pyrethroids used in this study.

exposure to high concentrations of pyrethroids (He et al., 1989). The signs of overt dermal exposure to pyrethroids in humans include burning, itching or tingling sensations of the skin (He et al., 1989).

One of the most studied pyrethroids with regard to dermal absorption is permethrin (Sidon et al., 1988; van der Rhee et al., 1989; Franz et al., 1996; Bast et al., 1997; Baynes et al., 1997; Riviere et al., 2002; Tomalik-Scharte et al., 2005). For *in vitro* studies, absorption of permethrin through human skin appears to be lower than for animal skin (Franz et al., 1996; Baynes et al., 1997; Riviere et al., 2002). After a 48 h exposure to permethrin *in vitro*, less than 0.1% of the dose (1.2 μmol) was absorbed through human skin (Franz et al., 1996). Correspondingly low levels were detected in epidermal and dermal fractions (Franz et al., 1996). About 5% of the dose of permethrin (1.2 μmol) was absorbed through guinea pig skin *in vitro* and similar percentages were found in dermal and epidermal fractions (Franz et al., 1996). Dermal absorption of permethrin is low in humans *in vivo* (van der Rhee et al., 1989; Tomalik-Scharte et al., 2005). For example, about 0.5% of the applied dose of permethrin (ca. 1.25 g) was absorbed through the skin of scabies patients (van der Rhee et al., 1989). Absorption in this case was assessed indirectly by measuring permethrin metabolites excreted in urine. Sidon et al. (1988) reported higher dermal absorption of permethrin in rats and monkeys. In rats, following a 24 h exposure to permethrin (ca. 7 μg) on the midlumbosacral region, approximately 45% of the dose was excreted in urine over 7 days. In monkeys, absorption was no greater than 28% of the dose (ca. 7 μg) and was dependent on the site of application (absorption greater in forehead than forearm).

Because pyrethroids are used occupationally and residentially, it is important to assess their dermal absorption. The objective of this study was to examine the *in vitro* dermal absorption of three pyrethroid insecticides, bifenthrin, deltamethrin, and permethrin, in rat and human cadaver skin. In addition, extracts of pyrethroid-treated skin were analyzed to determine if metabolism of the pyrethroids had occurred.

Materials and methods

Chemicals. [^{3}H(G)]-Bifenthrin (specific activity, 317 mCi/mmol, radiochemical purity>98%) and [^{3}H(G)]-deltamethrin (specific activity, 9 Ci/mmol, radiochemical purity >95%) were purchased from PerkinElmer Life and Analytical Sciences, Inc. (Waltham, MA, USA). cis-[cyclopropane-1-^{14}C]-Permethrin (specific activity, 54 mCi/mmol, radiochemical purity >98%) was purchased from Amersham Biosciences (Piscataway, NJ, USA). Unlabeled pyrethroids (purity >98% for pyrethroid) were purchased from Chem Service (West Chester, PA, USA). Ketamine hydrochloride was purchased from Fort Dodge Laboratories (Fort Dodge, IA, USA) and xylazine was from Phoenix Scientific (St. Joseph, MO, USA). Some relevant chemical and physical parameters of the pyrethroids used in this study are displayed in Table 1. Because pyrethroids contain chiral centers, stereoisomers of these pesticides exist. However, some of the pyrethroids sold in the market are enriched, in that specific isomers or enantiomers are isolated and used as the active ingredient to increase insecticidal potency. For bifenthrin in this study, its composition was 97% cis and 3% trans (note: this mixture consists of 4 enantiomers, two each at a 1:1 ratio for the cis and trans isomers of bifenthrin). For deltamethrin in this study, its composition was 99% of the cis enantiomer (S)-α-cyano-3-phenoxybenzyl-(1R,3R)-3-(2,2-dibromovinyl)-2,2-dimethylcyclopropanecarboxylate. For cis-permethrin, the composition consisted of a 1:1 ratio of the two cis enantiomers.

Animals. Adult male Long Evans rats were purchased from Charles River Laboratories (Raleigh, NC, USA). The rats were approximately 70 days old. The strain, sex and age of the rats used in this study were chosen because of their use in previous and on-going collaborative research on the pyrethroids with regard to their neurotoxicity (Crofton and Reiter, 1984, 1987, 1988; Peele and Crofton, 1987; Sheets et al., 1994; Crofton et al., 1995; Wolansky et al., 2006, 2007, 2009) and metabolism (Godin et al., 2006, 2007, 2010; Scollon et al., 2009). Our laboratory group has recently developed a diffusion-limited physiologically-based pharmacokinetic model for deltamethrin using data from *in vitro* metabolism and in vivo pharmacokinetic (following oral exposure) studies that used this same strain, sex and age of rat (Godin et al., 2010). Data from the present *in vitro* dermal absorption study can be used in the development of PBPK models of pyrethroids with a dermal route of exposure. The animals were housed in an Association for the Assessment and Accreditation of Laboratory Animal Care approved facility and maintained according to the National Institutes of Health *Guide for the Care and Use of Laboratory Animals* (1996). All animal procedures were approved by the Institutional Animal Care and Use Committee of the National Health and Environmental Effects Research Laboratory. The animals were housed individually in polycarbonate cages with heat-treated laboratory-grade pine shavings (Northeastern Products, Warrensburg, NY, USA). Animals were provided with feed (Purina Rodent Chow 5001, Barnes Supply Co., Durham, NC, USA) and tap water *ad libitum*.

Human skin. Dorsal skin was obtained from adult male cadavers (U. S. Tissue & Cell, Cincinnati, OH, USA and National Disease Research Interchange, Philadelphia, PA, USA). Human cadaver skin was obtained from two vendors because of its limited supply during the course of this study. The skin was dermatomed to a thickness of approximately 350–400 μm by the vendor. The skin was shipped and stored frozen (−70 °C) until use.

Author's personal copy

Table 1
Physical and chemical characteristics of bifenthrin, deltamethrin and permethrin[a].

Pyrethroid	CAS no.	MW	Melting point[d]	Log P	CLog P[e]	Vapor pressure (mm Hg)	Water solubility (ppm)	Hydrolysis $t_{1/2}$, pH 7
Bifenthrin	826057-04-3	422.9	68–70 °C	6.4	7.2	$1.8e^{-7}$	$1.5e^{-8}$	stable
Deltamethrin	52918-63-5	505.2	98–101 °C	4.5	6.5	$9.3e^{-11}$	$2.0e^{-4}$	stable
Permethrin[b]	52645-53-1[c]	391.3	35 °C	6.1	6.9	$1.5e^{-8}$	$5.5e^{-3}$	stable

[a] Information from Laskowski (2002), except for melting point data.
[b] Information only available for permethrin, which consists of a mixture of cis- and trans-permethrin.
[c] CAS No. for cis-permethrin is 61949-76-6.
[d] Data from Farm Chemicals Handbook (2002).
[e] Calculated Log P.

Chromatography. An Agilent Technologies (Palo Alto, CA, USA) Model 1100 high performance liquid chromatography system (HPLC) was used with a PerkinElmer Model A500 Flow Scintillation Analyzer (FSA) to analyze the purity of the radiolabeled pyrethroids. A Waters (Milford, MA, USA) C_{18} μBondapak column (3.9 mm × 150 mm, 10 μ) was used along with a pre-column packed with Perisorb RP-18 (Upchurch Scientific, Oak Harbor WA, USA). The solvents were water and methanol (10:90, water:methanol) flowing at a rate of 0.7 ml/min. The system was set isocratically. The size of the flow cell in the FSA was 0.5 ml. The flow rate of the scintillation fluid (Ultima Gold, PerkinElmer) was 4.2 ml/min. In this system, bifenthrin has a retention time of 4.8 min, deltamethrin a retention time of 3.7 min, and cis-permethrin a retention time of 4.6 min.

In vitro dermal absorption apparatus. A flow-through diffusion cell system (Crown Bio Scientific, Inc., Somerville, NJ, USA) and methodology as described by Bronaugh and Stewart (1985) and Bronaugh and Maibach (1991) were used. Teflon Flo-Thru diffusion cells with a diffusional area of 0.32 cm^2 were used. Each cell was placed in a PosiBloc Diffusion Cell Heater, which was heated by pumping water at a temperature of 35 °C through it. A peristaltic pump was used to pump receptor fluid at a rate of 1.5 ml/h from a reservoir through Tygon tubing (R-3603, Fisher Scientific Co., Fair Lawn, NJ, USA) to the flow-through cells. Scintillation vials (20 ml) were placed in a fraction collector to collect the receptor fluid. All components of the diffusional apparatus were sterilized with 70% ethanol solution and rinsed with sterile receptor solution before placing the skin samples in the flow-through cells.

Receptor fluid. HEPES-buffered Hanks' balanced salt solution, pH 7.4, with 10% fetal bovine serum, was used as the receptor fluid. This fluid has been shown by Collier et al. (1989) to maintain the viability of skin for up to 24 h. The chemical composition of the receptor fluid included sodium chloride, potassium chloride, calcium chloride (dihydrate), magnesium sulfate (heptahydrate), dextrose, sodium bicarbonate, and sodium hydroxide, which were purchased from Sigma Chemical Co. (St. Louis, MO, USA). Additional components were N-(2-hydroxyethyl) piperazine-N′-(2-ethanesulfonic acid, sodium salt) (HEPES), fetal bovine serum, and gentamicin sulfate, obtained from GIBCO (Grand Island, NY, USA), and disodium hydrogen phosphate and potassium dihydrogen phosphate, purchased from Scientific Products (McGraw Park, IL, USA) and Matheson Coleman and Bell (Norwood, OH, USA), respectively. The receptor fluid was prepared with distilled water and sterilized by filtration (0.2 μm filter, Nalgene disposable filterware, Sybron Corp., Rochester, NY, USA). A 10% solution (v/v) of fetal bovine serum was prepared with the sterile receptor fluid. The receptor fluid was continuously gassed with 100% oxygen throughout the experiment.

Experimental procedure. Twenty-four hours before the experiment, rats were anesthetized with a solution (0.1 ml) of ketamine (20 mg/ml) and xylazine (0.64 mg/ml) administered ip. Hair on the dorsal surface was removed from these animals with electric clippers (Oster Corp., Model A2, Milwaukee, WI, USA) using a size 40 blade. The clipped area was washed with distilled water to remove extraneous matter. The following day the rats were killed by CO_2 asphyxiation and the dorsal skin was removed immediately. Skin sections of approximately 350 μm thick were removed with a Padgett dermatome (Kansas City, MO, USA) and placed in receptor fluid. Skin discs were cut from each skin with a 0.75-inch diameter bow punch. The thickness of each skin was measured along its edge with microcalipers (Model D-1000, The Dyer Co., Lancaster, PA, USA). The mean (±SD) skin thickness was 350 (±30) μm. The discs were mounted epidermal side up in the flow-through cells. Once all of the skin discs were mounted, the receptor fluid pump was started. Each skin disc was rinsed with a small volume of water and dried with Kim Wipe® paper three times.

Cadaver skin was thawed, and skin discs were prepared with a 0.75-inch bow punch. The mean (±SD) cadaver skin thickness was 360 (±120) μm. Skin discs were mounted epidermal side up in the flow-through cells as described above. The receptor fluid and experimental conditions were as described above.

After an equilibration period of 30 min, the integrity of the skin's barrier was tested with [^{3}H]–H_2O (New England Nuclear, Boston, MA, USA). However, only skin to be treated with [^{14}C]-permethrin was tested. The procedure for skin integrity was as follows: [^{3}H]–H_2O (1 μCi, 100 μl) was applied to the skin with a Pipetman, the pump turned on, and the receptor fluid was collected. The [^{3}H]–H_2O was removed with Kim Wipe® paper 5 min after it was applied to the skin. The skin was rinsed with a small volume of nonradioactive water and dried with Kim Wipe® paper three times. Receptor fluid was collected for 1 h. The collected receptor fluid was mixed with 10 ml of scintillation fluid and analyzed for [^{3}H] in a PerkinElmer Model 2700 liquid scintillation analyzer. The mean percentage of the dose of [^{3}H]–H_2O detected in the receptor fluid for the rat skin was 0.21 ± 0.24% and for human cadaver skin was 0.32 ± 0.25%.

Each skin disc was treated with a pyrethroid in 15 μl acetone. At the end of the experiment (24–48 h post-dosing), the peristaltic pump was stopped. The epidermal surface (with the cell top in place) was washed six times with 0.5 ml of a mixture of soap:water (1:1) to remove unabsorbed chemical. A Pipetman® (Gilson, Middleton, WI, USA) was used to apply and remove each skin wash twenty times. The skin wash fractions were pooled into two vials and mixed with scintillation fluid. The cell top and cell body were individually washed three times with 0.5 ml ethanol. The cell top was placed in a small weigh boat and a Pipetman® was used to apply and remove each ethanol wash twenty times. Each ethanol wash of the interior of the cell body was applied and removed twenty times. The cell top and body washes and weigh boat were kept in separate vials. Skin washes, cell top and body washes, weigh boats and receptor fluid were mixed with scintillation fluid and analyzed for radioactivity in the liquid scintillation analyzer. An experiment was done to determine the wash efficiency using a 100 nmol dose of each of the three pyrethroids. Pyrethroid was applied to the skin and after allowing the acetone to evaporate (ca. 5 min), the skin was washed as described above. This wash procedure removed 72.8 ± 11.1% (mean ± SD, $N = 5$) of the dose for bifenthrin, 70.4 ± 8.0% for deltamethrin and 79.5 ± 3.0% for permethrin.

In the 24-h time course study, two and three dose levels of each pyrethroid were used for human (0.5 μCi, 10 and 100 nmol, 31.3 and 312.5 nmol/cm^2, respectively) and rat (0.5 μCi, 10, 30 and 100 nmol,

Author's personal copy

31.3, 93.8, 312.5 nmol/cm^2, respectively), respectively. In a second experiment, absorption was assessed for an additional 24 h following the skin wash at 24 h (total 48 h). The dose level for this study was 100 nmol pyrethroid (0.5 μCi, 312.5 nmol/cm^2) for both human and rat skin. In a tape strip study, rat and human skins were dosed with 100 nmol pyrethroid (0.5 μCi, 312.5 nmol/cm^2), washed at 24 h, and the epidermal side stripped with cellophane tape ten times.

Skin was solubilized in 1 ml of Soluene 350 (PerkinElmer) overnight in a water bath set at 37 °C. Hionic Fluor (PerkinElmer) was added to the dissolved skin solution, which was then analyzed for radioactivity in the liquid scintillation analyzer.

Skin disc analysis. In a skin metabolism study, rat skin was prepared and mounted in the cells as described above. The skin was treated with bifenthrin, deltamethrin or cis-permethrin (5 μCi, 100 nmol, 312.5 nmol/cm^2) in acetone. Following a 24 h exposure, the skin was washed as described above and then stored at −70 °C in a scintillation vial until analyzed. For analysis, the skin was thawed, tape-stripped ten times, and homogenized in 4 ml of receptor fluid (without fetal bovine serum) using a polytron homogenizer. Ten milliliters of methanol were added to the homogenate and then it was vortexed vigorously, followed by centrifugation. The supernatant was removed. Ten milliliters of methanol were added to the pellet, followed by vortexing and centrifugation. The supernatants were combined, taken to dryness under a stream of nitrogen, reconstituted in 0.5 ml HPLC mobile phase (water/methanol, 10/90) and centrifuged through a 0.2 μm filter. These samples were analyzed by HPLC as described above.

Data analysis. The data in the text, figures and tables are mean ± SD. Each *N* for the rat data represents an individual animal. Each *N* for the human data represents an individual donor. However, for the 24-h study, two skin samples from each donor were used for each dose and 4 skin samples from each donor were used for the 48-h exposure and the tape-stripping experiments. The data for these latter experiments were averaged for each individual.

The percent of the dose in the skin wash included the cell top wash and weigh boat data. The percent of the dose in the receptor fluid included the cell body washes. The maximal flux data was calculated by determining the time period of maximal absorption into the receptor fluid (e.g., 0–4 h), and converting the percent absorption for each dose into micrograms and dividing by the area of diffusion (0.32 cm^2) and the time period of sample collection (4 h). Rat data at 24 h were analyzed by a one-way analysis of variance with Tukey–Kramer Multiple Comparison (GraphPad Instat, v 3.05, San Diego, CA, USA) for the post-hoc test if significant differences ($p<0.05$) were detected. Human data at 24 h were analyzed by a two-tailed unpaired *t*-test with a significance level of $p<0.05$.

Results

The *in vitro* dermal absorption of the pyrethroids bifenthrin, deltamethrin and cis-permethrin were assessed in rat and human cadaver skin.

Bifenthrin

Less than 2% of the applied dose of bifenthrin was detected in receptor fluid 24 h after application to rat skin (Fig. 2, Table 2). Bifenthrin-derived radioactivity was detected at the earliest time point (4 h) of receptor fluid collection for all dose levels. No dose-dependent differences in cumulative percent dose in the receptor fluid were observed at 24 h. The skin wash removed 59–69% of the dose of bifenthrin. The percent of the dose removed by the skin wash for the 100 nmol dose of bifenthrin was significantly greater ($p<0.05$) than the wash for the 10 nmol dose. Following the wash, 33–43% of the dose of bifenthrin remained in the skin. The percent of the dose in the skin for the 10 nmol dose was significantly greater ($p<0.05$) than the 100 nmol dose. Slightly more than half of the dose of bifenthrin remaining in washed skin of the rat was removed by 10 tape strips (Table 3). The maximal flux increased with dose and ranged from about 6–56 μg/cm^2 h (Table 4). From 24 to 48 h, the percent of the dose of bifenthrin in the receptor fluid increased from 1 to 2% (Fig. 3). Analysis of the extracts of rat skin treated with bifenthrin detected the parent compound only (data not shown).

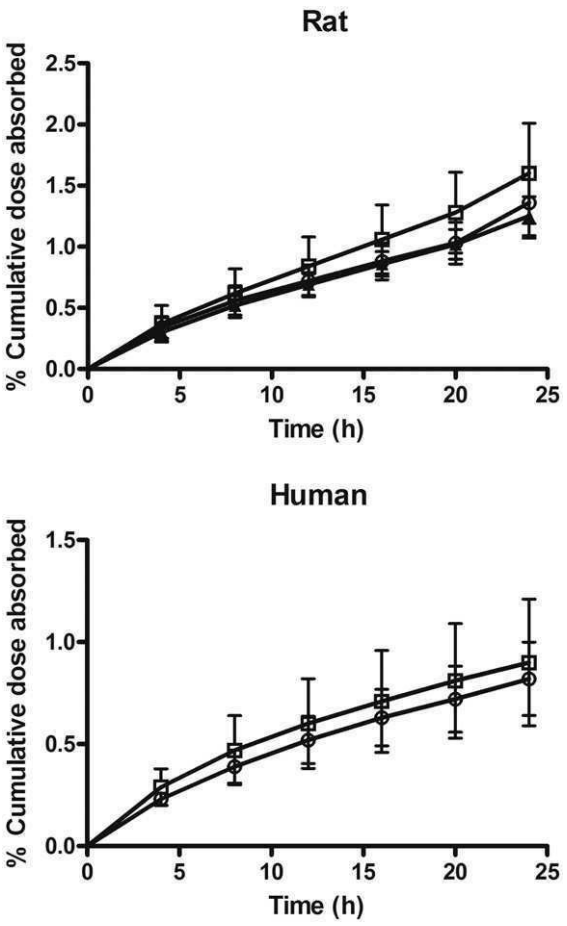

Fig. 2. Cumulative percent of the dose of [^{3}H]-bifenthrin detected in the receptor fluid over 24 h after application to rat or human skin. Doses of [^{3}H]-bifenthrin were 10 (□), 30 (▲) (rat only) and 100 (○) nmol and were applied in acetone. Data represents mean ± SD, $N=8$ for rat skin and $N=3$ for human skin.

Table 2
Distribution (% of applied dose) of chemical-derived radioactivity in the skin wash, skin and receptor fluid 24 h following application of radiolabeled pyrethroid to rat skin.

Pyrethroid	Dose (nmol)	Skin wash	Skin	Receptor fluid	Recovery
Bifenthrin	10	59.4 ± 6.9	42.6 ± 5.9[b]	1.6 ± 0.4	103.6 ± 2.6
	30	60.8 ± 7.9	41.2 ± 10.4	1.3 ± 0.2	103.3 ± 3.8
	100	68.8 ± 4.3[a]	32.9 ± 5.7	1.4 ± 0.3	103.1 ± 2.1
Deltamethrin	10	69.0 ± 6.1	26.0 ± 4.9	4.3 ± 1.9[c]	99.3 ± 2.8
	30	68.3 ± 4.8	27.6 ± 6.7	3.4 ± 1.2[b]	99.3 ± 3.5
	100	70.9 ± 3.2	26.9 ± 4.7	1.5 ± 0.7	99.3 ± 2.4
Permethrin	10	56.5 ± 4.8	36.6 ± 4.5	5.2 ± 1.7[c]	98.3 ± 2.7
	30	55.7 ± 7.3	35.9 ± 7.9	3.9 ± 1.2	95.5 ± 4.0
	100	52.5 ± 4.9	42.8 ± 4.8	2.7 ± 0.5	98.1 ± 1.3

Data represents mean ± SD, $N=8$. The specific doses for 10, 30 and 100 nmol are 31.3, 93.8 and 312.5 nmol/cm^2, respectively.
[a] Significantly greater than 10 nmol, $p<0.05$.
[b] Significantly greater than 100 nmol, $p<0.05$.
[c] Significantly greater than 100 nmol, $p<0.01$.

Author's personal copy

Table 3
Distribution (% of applied dose) of chemical-derived radioactivity in the skin wash, tape strip, skin and receptor fluid 24 h following application of 100 nmol of radiolabeled pyrethroid to rat skin.

Pyrethroid	Skin wash	Tape strip	Skin	Receptor fluid	Recovery
Bifenthrin	52.6 ± 12.7	24.4 ± 14.7	19.5 ± 5.1	1.6 ± 0.1	98.1 ± 1.6
Deltamethrin	53.2 ± 16.2	22.0 ± 17.5	18.6 ± 10.6	2.2 ± 0.4	95.9 ± 3.4
Permethrin	53.9 ± 6.2	19.1 ± 12.0	19.3 ± 8.5	3.6 ± 0.4	96.0 ± 0.8

Data represents mean ± SD, $N = 4$. The specific dose for 100 nmol is 312.5 nmol/cm^2.

For human skin, approximately 1% of the dose of bifenthrin was detected in the receptor fluid 24 h after application (Fig. 2, Table 5). The major portion of the dose (75–83%) was removed by the skin wash. Following the wash, the skin contained 14–21% of the applied dose, with the 10 nmol dose being significantly greater ($p<0.05$) than the 100 nmol dose of bifenthrin. The major portion of the dose (79%) that remained in human skin following the wash was removed by 10 tape strips (Table 6). The maximal flux increased from about 5–38 μg/cm^2 h with increased dose (Table 7). After the wash, the percent of the dose detected in the receptor fluid increased from about 0.6 to 1% during the 24–48 h collection period (Fig. 3).

Deltamethrin

Two to 4% of the dose of deltamethrin was detected in the receptor fluid 24 h after application to rat skin (Fig. 4, Table 2). Deltamethrin-derived radioactivity was detected in the receptor fluid at the earliest time point (4 h) for all dose levels. The percentage of the dose in the receptor fluid for the 10 and 30 nmol doses were significantly greater ($p<0.01$ and 0.05, respectively) than the 100 nmol dose of deltamethrin. The skin wash removed about 70% of the applied dose and about 27% remained in the skin (Table 2). Tape-stripping removed more than half of the dose that was in the skin following the wash (Table 3). The maximal flux increased with dose and ranged from about 17–64 μg/cm^2 h (Table 4). The percent of the dose of deltamethrin in the receptor fluid increased from 2 to 4% during the 24–48 h collection period after the skin wash (Fig. 3). Analysis of the extracts of rat skin treated with deltamethrin detected the parent compound only (data not shown).

Approximately 1% of the dose of deltamethrin was detected in the receptor fluid 24 h after application to human skin (Fig. 4, Table 5). The skin wash removed about 80% of the dose of deltamethrin and 14–15% remained in human skin. Tape-stripping removed most of the dose that could not be removed by the wash (Table 6). The maximal flux increased from about 14–76 μg/cm^2 h with increased dose (Table 7). The dose of deltamethrin in receptor fluid during the 24 to 48 h collection after the skin wash increased from about 0.5 to 1 % (Fig. 3).

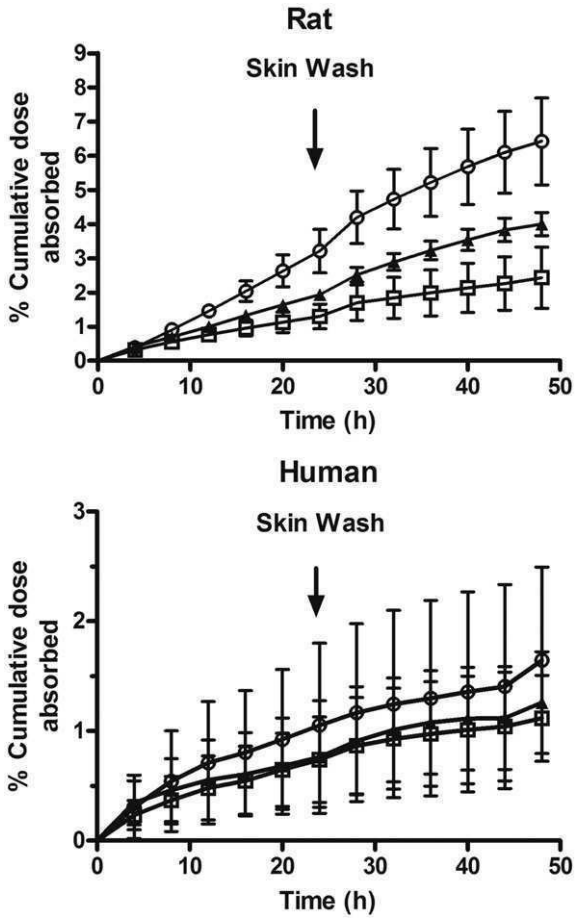

Fig. 3. Cumulative percent of the dose of [^{3}H]-bifenthrin (□), [^{3}H]-deltamethrin (▲) or [^{14}C]-permethrin (○) detected in receptor fluid over 48 h after application to rat or human skin. A dose of 100 nmol of each pyrethroid in acetone was applied to the skin. At 24 h, the epidermal surface of the skin was washed with a mixture of soap:water (1:1). After the wash, the cells were placed back in the holders and receptor fluid was collected for an additional 24 h. Data represents mean ± SD, $N = 8$ for rat skin and $N = 3$ for human skin.

Permethrin

At 24 h after application of permethrin to rat skin, approximately 3–5% of the dose was detected in the receptor fluid (Fig. 5, Table 2). Permethrin-derived radioactivity was detected in the receptor fluid at the earliest time point (4 h) for all dose levels. The percentage of the dose of permethrin in the receptor fluid was significantly greater ($p<0.05$) in the 10 than the 100 nmol dose group. Slightly greater than half of the applied dose was removed by the wash at 24 h. The

Table 4
Maximal flux and time of radiolabeled pyrethroids penetrating through rat skin.

Pyrethroid	Dose (nmol)	Maximum flux (μg/cm^2 h)	Time (h)
Bifenthrin	10	6.1 ± 2.6[a]	4
	30	14.9 ± 3.7	4
	100	56.0 ± 16.0	4
Deltamethrin	10	16.9 ± 6.3	24
	30	45.4 ± 16.9	24
	100	63.7 ± 17.7	24
Permethrin	10	14.6 ± 17.2	4
	30	36.8 ± 12.1	20
	100	67.8 ± 17.6	4

[a] Data represents mean ± SD, $N = 8$. The specific doses for 10, 30 and 100 nmol are 31.3, 93.8 and 312.5 nmol/cm^2, respectively.

Table 5
Distribution (% of applied dose) of chemical-derived radioactivity in the skin wash, skin and receptor fluid 24 h following application of radiolabeled pyrethroid to human skin.

Pyrethroid	Dose (nmol)	Skin wash	Skin	Receptor fluid	Recovery
Bifenthrin	10	75.4 ± 3.2	20.7 ± 3.8[a]	1.0 ± 0.2	97.1 ± 1.1
	100	82.6 ± 4.1	13.8 ± 2.0	1.2 ± 0.2	97.5 ± 2.0
Deltamethrin	10	78.7 ± 3.0	13.8 ± 1.1	1.4 ± 0.3	94.0 ± 3.5
	100	78.1 ± 9.6	14.8 ± 7.2	1.3 ± 0.3	94.1 ± 3.8
Permethrin	10	70.6 ± 7.3	24.6 ± 6.9	2.2 ± 1.4	97.3 ± 0.7
	100	72.0 ± 6.5	21.9 ± 5.9	2.1 ± 1.7	95.9 ± 1.6

Data represents mean ± SD, $N = 3$. The specific doses for 10 and 100 nmol are 31.3 and 312.5 nmol/cm^2, respectively.
[a] Significantly greater than 100 nmol dose ($p<0.05$).

Author's personal copy

Table 6
Distribution (% of applied dose) of chemical-derived radioactivity in the skin wash, tape strip, skin and receptor fluid 24 h following application of 100 nmol of radiolabeled pyrethroid to human skin.

Pyrethroid	Skin wash	Tape strip	Skin	Receptor fluid	Recovery
Bifenthrin	69.7 ± 6.3	19.8 ± 5.0	5.4 ± 3.6	1.0 ± 0.7	96.0 ± 1.0
Deltamethrin	68.1 ± 2.5	24.9 ± 1.0	1.2 ± 0.3	1.1 ± 0.7	95.3 ± 2.1
Permethrin	66.9 ± 7.5	24.9 ± 5.6	1.8 ± 0.4	2.1 ± 1.6	95.8 ± 1.2

Data represents mean ± SD, $N = 3$. The specific dose for 100 nmol is 312.5 nmol/cm^2.

Table 7
Maximal flux and time of radiolabeled pyrethroids penetrating through human skin.

Pyrethroid	Dose (nmol)	Maximal flux (μg/cm^2 h)	Time (h)
Bifenthrin	10	4.7 ± 1.5	4
	100	38.0 ± 8.4	4
Deltamethrin	10	13.4 ± 9.2	4
	100	75.5 ± 20.7	4
Permethrin	10	8.8 ± 11.8	4
	100	103.0 ± 102.7	4

Data represents mean ± SD, $N = 3$. The specific doses for 10 and 100 nmol are 31.3 and 312.5 nmol/cm^2, respectively.

percentage of the dose that remained in the skin ranged from 36–43%. Tape-stripping removed half of the dose that remained in rat skin following the skin wash (Table 3). The maximal flux increased with dose and ranged from 15–68 μg/cm^2 h (Table 4). The percentage of the dose

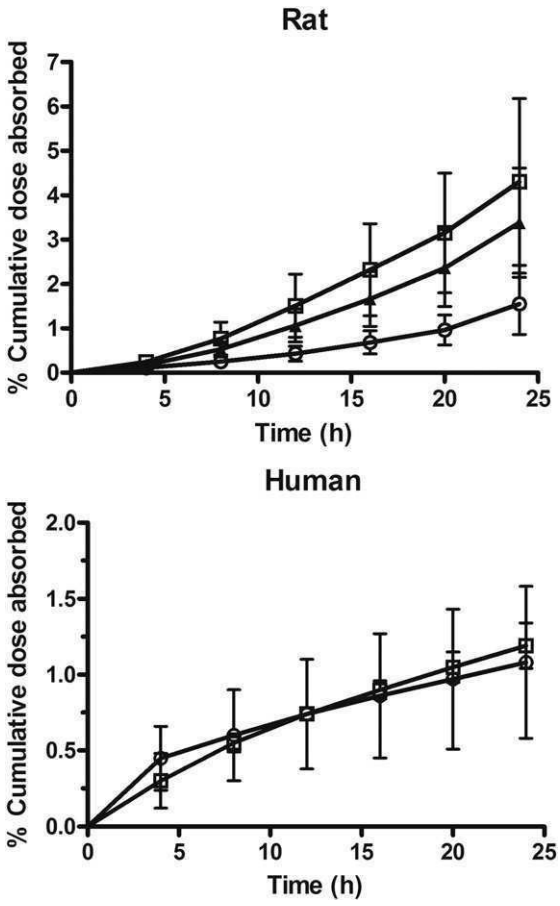

Fig. 4. Cumulative percent of the dose of [^{3}H]-deltamethrin detected in receptor fluid over 24 h after application to rat or human skin. Doses of [^{3}H]-deltamethrin were 10 (□), 30 (▲) (rat only) and 100 (○) nmol and were applied in acetone. Data represents mean ± SD, $N = 8$ for rat skin and $N = 3$ for human skin.

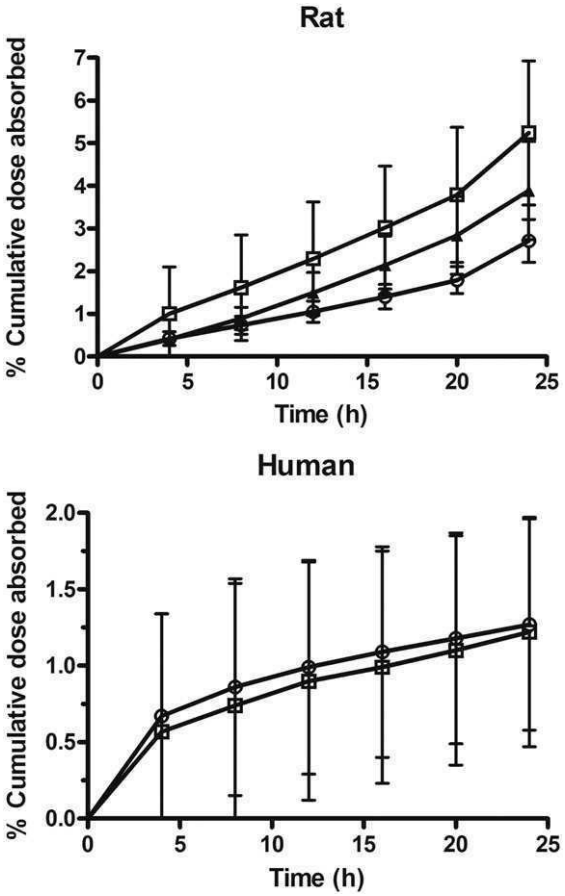

Fig. 5. Cumulative percent of the dose of [^{14}C]-permethrin detected in receptor fluid over 24 h after application to rat or human skin. Doses of [^{14}C]-permethrin were 10 (□), 30 (▲) (rat only) and 100 (○) nmol and were applied in acetone. Data represents mean ± SD, $N = 8$ for rat skin and $N = 3$ for human skin.

in the receptor fluid increased from 3 to 6% during the 24–48 h collection period following the skin wash (Fig. 3). Analysis of the extracts of rat skin treated with permethrin detected the parent compound only (data not shown).

In human skin, 2% of the dose of permethrin was detected in the receptor fluid for both dose levels at 24 h (Fig. 5, Table 5). About 70% of the dose was removed by the skin wash and 22–25% remained in the skin. Most of the dose in human skin could be removed by tape-stripping (Table 6). The maximal flux increased from about 9–103 μg/cm^2 h with increased dose (Table 7). During the collection period of 24–48 h after the skin wash, the percent of the dose in the receptor fluid increased from 1 to 1.4% (Fig. 3).

Discussion

Dermal exposure to pesticides such as pyrethroids can occur in occupational and residential settings. In the present study, *in vitro* exposure of rat and human skin to the pyrethroids bifenthrin, deltamethrin, and permethrin resulted in their detection in skin and receptor fluid, indicating that dermal absorption of these pesticides occurred. Although there are no published data on the *in vitro* dermal absorption of bifenthrin and deltamethrin, there are several studies on the absorption of permethrin. Franz et al. (1996) used a static diffusion system to investigate the *in vitro* absorption of permethrin (1.2 μmol, trans/cis ratio, ca. 2.8:1) in guinea pig and human skin. Guinea pig skin was more permeable than human skin, with about 5 and 1% of the dose, respectively, detected in receptor fluid 48 h after application. The skin was washed with isopropanol and sectioned into dermis and epidermis. For both human and guinea pig skin, the major

Author's personal copy

portion of the dose was in the wash (85–98%). In guinea pig skin, 5% of the dose was in each skin fraction. In human skin, 0.2% was in the dermis and 1.1% in the epidermis. Baynes et al. (1997), using a flow-through cell system with rat and guinea pig skin, did not detect permethrin (ca. 33 nmol, 102 nmol/cm^2) in the receptor fluid over 8 h following its application. However, using mouse skin, they did observe <2% of the dose in the receptor fluid over 24 h following its application in acetone or dimethylsulfoxide. They did not report on the percentage of the dose in the wash and skin. In another study by Baynes et al. (2002), using pig skin in a flow-through cell system, <1% of the dose (ca. 65 nmol, 102 nmol/cm^2) was detected in the receptor fluid after an 8 h exposure to permethrin. About 50–70% of the dose was removed by a skin wash (soap/water), 10–20% was in the stratum corneum (removed by tape-stripping), and 2–5% was in the tape-stripped skin. The results of the studies described above have a similar trend to those reported here with regard to permethrin, bifenthrin, and deltamethrin. Fifty percent or more of the dose of the pyrethroids was removed by skin washing. The next major percentage of the dose was in skin, but 50% or more of the dose in skin could be removed by tape-stripping the epidermal surface. A low percentage of the dose of each pyrethroid was in the receptor fluid. However, there are some differences in the absolute percentages between the previously published studies described above and those reported in the present study. Franz et al. (1996) reported a much higher percentage of the dose removed by the skin wash. They used an organic solvent, isopropanol, to wash the skin, whereas we used a soap and water mixture. Since the pyrethroids are lipophilic, with a log octanol:water partition coefficient (Log P) 4.5 or greater (Table 1), it seems reasonable that a wash with an organic solvent would remove a higher percentage of the dose than a wash with soap and water. Other variations can be attributed to the types of apparatus used (static vs. flow-through), species, vehicles and recovery of the applied dose. The recovery of the applied dose in our study and that of Franz et al. (1996) were essentially 100%, whereas that of Baynes et al. (2002) was around 70%. Low recovery of the applied dose makes it difficult to compare results across studies.

The *in vitro* absorption of these pyrethroids was 3- to 10-fold greater for rat than human skin, if absorption includes material in receptor fluid plus skin (or tape-stripped skin). The trend of greater permeability of chemicals other than pyrethroids in rat than human skin *in vitro* has been observed by several investigators (Sato et al., 1991; van Ravenzwaay and Leibold, 2004; Yourick et al., 2008). The reason for this difference between the *in vitro* dermal absorption of chemicals between rat and human skin is not clear. Of 14 chemicals tested by van Ravenzwaay and Leibold (2004), there was no physicochemical factor (e.g., molecular weight, lipophilicity or aqueous solubility) of the chemicals that could account for this difference between rat and human skin. Bronaugh et al. (1982) measured the thickness of stratum corneum, epidermis and whole skin of humans and rats. While the thickness of the stratum corneum was similar (rat, 18 μm; human, 17 μm), the epidermis (human, 47 μm; rat, 32 μm) and whole skin were thicker for human (human, 3 mm; rat, 2 mm). Because the stratum corneum is considered the predominant barrier to permeability (Scheuplein and Blank, 1971), and because there is no difference in the thickness of the stratum corneum between rats and humans, the greater permeability in rat skin may be due to differences in the composition of the lipids in the stratum corneum of these species. Also, follicular transport may be greater in rat than human skin, because rat has a higher density of hair follicles (Bronaugh et al., 1982).

The physicochemical properties of a chemical can affect the extent and rate of its dermal absorption (Guy and Hadgraft, 1991; Moss et al., 2002). Some of these properties include lipophilicity, hydrogen bonding and structural (e.g., molecular weight). The measured Log Ps of the pyrethroids studied, ranged from 4.5 to 6.4, while the calculated values ranged from 6.5 to 7.2 (Table 1). In both cases, deltamethrin had the lower value, whilst bifenthrin had the highest. There is a general trend in that chemicals with a Log P between 1 and 3 will have higher dermal absorption than chemicals outside of this range (Guy and Hadgraft, 1991). An example of a chemical class that displays this trend is the para-substituted phenols (Hinz et al., 1991; Hughes et al., 1993). Also, chemicals with a high Log P tend to be found to a greater extent in skin than in the receptor fluid. For example, heptyloxyphenol has a higher Log P than phenol (4.6 vs. 1.45, respectively). About 22–33% of the applied dose of heptyloxyphenol was in skin of rat and 46–63% in the receptor fluid (Hughes et al., 1993). The value was dependent on the diffusion system used (static vs. flow-through). In contrast, about 2% of the dose of phenol was in skin and 95–98% was in the receptor fluid. The pyrethroids have a high Lop P and this property is consistent with the higher levels found in skin than in the receptor fluid of this *in vitro* study. The differences in Log P between the pyrethroids used were not large enough to result in large differences in the extent of their absorption, which ranged from 21–23% for rat skin and 2–6% for human skin (absorption being the sum of dose in tape-stripped skin and receptor fluid). An increased ability of a chemical to hydrogen bond can result in a slower diffusion of it through skin. The pyrethroids do not have ionizable moieties that could participate in hydrogen bonding, but have some functional groups (e.g., carboxyl) that are available for this type of bonding. The differences in structure between bifenthrin, deltamethrin and cis-permethrin are the halogens (Cl for permethrin, Br for deltamethrin, Cl and F for bifenthrin), a cyano group in deltamethrin, and a different aromatic group for bifenthrin. These differences did not appear to affect the extent of dermal absorption of these pyrethroids. The diffusional resistance of the stratum corneum increases as the molecular weight of a chemical increases (Guy and Hadgraft, 1991). The molecular weight of permethrin was the lowest and that of deltamethrin the highest. But the differences in the molecular weight of the pyrethroids were not enough to impact their dermal absorption. Chemicals with a low melting point tend to be absorbed to a greater extent in skin relative to chemicals with a higher melting point (Guy and Hadgraft, 1991). Permethrin has the lowest melting point of the three pyrethroids, yet its absorption was not that much different from the other two chemicals examined.

Dose applied to skin can affect the dermal absorption of a chemical (Wester and Maibach, 1993). In the experiments that varied dose (10–100 nmol, 31.3–312.5 nmol/cm^2), and just considering the dose in receptor fluid, the percentage remained constant or decreased as dose increased. However, the amount of chemical increased with the dose applied to skin. This effect has been observed with testosterone, benzoic acid, parathion, lindane and many other chemicals in human and animal skin (Wester and Maibach, 1993).

Pyrethroids are marketed as single isomers or as a mixture of several isomers. Both bifenthrin and deltamethrin are single isomer pyrethroids. Permethrin is generally used as a mixture of its cis and trans isomers. This mixture would include the four enantiomers (two each for the cis and trans isomers) of permethrin. In the present study, only cis-permethrin was used. However, we would not expect any differences between cis- and trans-permethrin in their *in vitro* dermal absorption, which is a process of passive diffusion. Franz et al. (1996) found no difference in the trans:cis ratio of permethrin in guinea pig or human skin fractions or in receptor fluid to that of the dosing formulation. Sidon et al. (1988) examined the *in vivo* dermal absorption of cis- and trans-permethrin in monkeys and rats. There were no significant differences in the total percentage absorbed between cis- and trans-permethrin applied singly to either the forearm and forehead of monkeys or the dorsal region of rats.

Acetone was used as the vehicle to apply the pyrethroids to the skin in this study. Acetone is a good choice to use as a vehicle in dermal absorption studies because of its volatility and many chemicals are soluble in it. Typically, the volume of acetone used in dermal absorption studies ranges from 5–10 μl/cm^2, although a wider range has been used (5–36 μl/cm^2) (Feldmann and Maibach, 1974).

Author's personal copy

The volume of acetone used in this study was greater (47 μl/cm^2) than what is usually used. Deltamethrin was less soluble in acetone than bifenthrin and cis-permethrin, so a greater volume of it was needed. We decided to use the same volume of acetone for all three chemicals. Acetone could potentially damage skin, which could lead to greater penetration of chemical into the skin. For example, Bond and Barry (1988) reported that a 2-min exposure to acetone (160 μl/cm^2) damaged the permeability of hairless mouse skin to 5-fluorouracil, but not that of human skin. Based on the results of Bond and Barry (1988), the possibility exists that the absorption of the pyrethroids in rat skin was enhanced by the use of acetone as a vehicle with its increased volume. However, this same data suggests that the absorption of the pyrethroids in human skin would not be affected by the larger volume of acetone. Nevertheless, it is best to minimize the volume of volatile organic vehicles used in dermal absorption studies such that the penetration of the test chemical is not affected by its use.

A considerable percentage of the applied dose of the pyrethroids was detected in rat and human skin after the wash (26–43% for rat, 14–25% for human). Because the percentage of the dose of pyrethroids in the receptor fluid was low (1–5% for rat, 1–2% for human), the chemical in skin could represent a reservoir or depot. Other investigators have reported that the skin may act as a reservoir for chemicals after dermal exposure (Kemppainen et al., 1991; Yourick et al., 2004, 2008). It should be noted that the wash was not 100% effective as evidenced by the pilot wash experiment. The soap/water wash was chosen because this is a typical choice most people would use for cleanup after the use of insecticides. The amount of pyrethroid in skin was decreased by tape-stripping the epidermal surface, which removed 50% or more from rat skin and greater than 80% from human skin. This means a major portion of the dose in the skin was on top of or in the stratum corneum and had not penetrated into the viable regions of the epidermis. This material would not be considered absorbed. However, there was chemical in the skin after tape-stripping and could be a reservoir for further penetration. Potential mechanisms of this reservoir effect are the binding of a chemical to a macromolecule in skin or difficulties in partitioning from lipid regions of the skin to the aqueous receptor fluid. For example, dihydroxyacetone, a color additive in sunless tanning products, was retained in skin *in vitro* following its application (Yourick et al., 2004), probably as a result of its binding to amine groups of macromolecules (Kurz, 1994), making it unavailable for absorption. Kraeling and Bronaugh (1997) also noted that glycolic and lactic acid, which are polar chemicals, are strongly retained in skin *in vitro* after a 24-h study. Lipophilic compounds may be retained in skin artificially in *in vitro* studies because of difficulty in partitioning from lipid areas in the skin into aqueous receptor fluids. The pyrethroids examined in the present study are lipophilic with measured Log Ps ranging from 4.5 to 6.4. We did detect the pyrethroids in the receptor fluid during the 24–48 h collection following the skin wash. The overall diffusion of pyrethroid from skin to receptor fluid during this time was low (1–3% for rat skin, 0.5–1% for human skin). This was no more than the amount absorbed during the first 24-h collection period. Yourick et al. (2008) reported that for retinol, 6% of the dose was in receptor fluid and 23% in rat skin at 24 h, while at 72 h, 18% was in skin and 13% in receptor fluid. Thus a portion of the chemical in the skin that has been washed is still available for absorption.

In summary, the pyrethroids bifenthrin, deltamethrin and permethrin were absorbed *in vitro* into rat and human skin. The absorption was greater in rat than in human skin. For both skin types, more than 50% of the applied dose of the pyrethroids was removed by a soap and water wash at 24 h. A higher percentage of the dose was detected in rat and human skin than in the receptor fluid. For rat and human skin, about 50% and 80% of the dose in the skin, respectively, was removed by tape-stripping. A low percentage of the dose in skin was able to diffuse into the receptor fluid during the first 24 h post-exposure and the 24–48 h collection period following the wash. Only the parent chemical was detected in extracts of rat skins treated with the pyrethroids. Because the exposure of pyrethroids to skin is potentially high, examination of the dermal absorption of this class of insecticides is important so that the risk of their exposure can be adequately assessed.

Conflict of interest statement

The authors have no financial conflict of interest.

Acknowledgments

This article has been reviewed in accordance with the policy of the National Health and Environmental Effects Research Laboratory, U.S. Environmental Protection Agency, and approved publication. Approval does not signify that the contents necessarily reflect the views and policies of the Agency, nor does mention of trade names or commercial products constitute endorsement or recommendation for use.

The authors thank Ms. Carol Mitchell and Frances McQuaid for their technical assistance and Drs. David Thomas and Rogelio Tornero-Velez for their comments and suggestion on an earlier version of this manuscript.

References

Adamis, Z., Antal, A., Fuzesi, I., Molnar, J., Nagy, L., Susan, M., 1984. Occupational exposure to organophosphorous insecticides and synthetic pyrethroid. Int. Arch. Occup. Environ. Health 56, 299–305.

Bast, G.E., Taeschner, D., Kampffmeyer, H.G., 1997. Permethrin absorption not detected in single-pass perfused rabbit ear, and absorption with oxidation of 3-phenoxybenzyl alcohol. Arch. Toxicol. 71, 179–186.

Baynes, R.E., Halling, K.B., Riviere, J.E., 1997. The influence of diethyl-m-toluamide (DEET) on the percutaneous absorption of permethrin and carbaryl. Toxicol. Appl. Pharmacol. 144, 332–339.

Baynes, R.E., Monteiro-Riviere, N.A., Riviere, J.E., 2002. Pyridostigmine bromide modulates the dermal disposition of [^{14}C]permethrin. Toxicol. Appl. Pharmacol. 181, 164–173.

Bond, J.R., Barry, B.W., 1988. Damaging effect of acetone on the permeability barrier of hairless mouse skin compared with that of human skin. Int. J. Pharmaceut. 41, 91–93.

Bradberry, S.M., Cage, S.A., Proudfoot, A.T., Vale, J.A., 2006. Poisoning due to pyrethroids. Toxicol. Rev. 24, 93–106.

Bronaugh, R.L., Maibach, H.I., 1991. *In vitro* Percutaneous Absorption: Principles, Fundamentals, and Applications. CRC Press, Boca Raton, FL.

Bronaugh, R.L., Stewart, R.F., 1985. Methods for *in vitro* percutaneous absorption studies IV. The flow-through diffusion cell. J. Pharm. Sci. 74, 64–67.

Bronaugh, R.L., Stewart, R.F., Congdon, E.R., 1982. Methods for *in vitro* percutaneous absorption studies II. Animal models for human skin. Toxicol. Appl. Pharmacol. 62, 48–488.

Bronstein, A.C., Spyker, D.A., Cantilena, L.R., Green, J., Rumack, B.H., Heard, S.E., 2007. 2006 Annual Report of the American Association of Poison Control Centers' National Poison Data System (NPDS). Clin. Toxicol. 45, 815–917.

Chen, S., Zhang, He, F., Yao, P., Wu, Y., Sun, J., Liu, L., Li, Q., 1991. An epidemiological study on occupational acute pyrethroid poisoning in cotton farmers. Br. J. Ind. Med. 48, 77–81.

Chester, G., Sabapathy, N.N., Woollen, B.H., 1992. Exposure and health assessment during application of lambda-cyhalothrin for malaria vector control in Pakistan. Bull. World Health Organ. 70, 615–619.

Collier, S.W., Sheikh, N.M., Sakr, A., Litchin, J.L., Stewart, R.F., Bronaugh, R.L., 1989. Maintenance of skin viability during *in vitro* percutaneous absorption/metabolism studies. Toxicol. Appl. Pharmacol. 99, 522–533.

Crofton, K.M., Kehn, L.S., Gilbert, M.E., 1995. Vehicle and route dependent effects of a pyrethroid insecticide, deltamethrin, on motor function in the rat. Neurotoxicol. Teratol. 17, 489–495.

Crofton, K.J., Reiter, L.W., 1984. Effects of two pyrethroid insecticides on motor activity and the acoustic startle response in the rat. Toxicol. Appl. Pharmacol. 75, 318–328.

Crofton, K.M., Reiter, L.W., 1987. Pyrethroid insecticides and the gamma-aminobutyric acid A receptor complex: motor activity and the acoustic startle response in the rat. J. Pharmacol. Exp. Ther. 243, 946–954.

Crofton, K.M., Reiter, L.W., 1988. The effects of type I and II pyrethroids on motor activity and the acoustic startle response in the rat. Fundam. Appl. Toxicol. 10, 624–634.

Farm Chemicals Handbook, 2002. Meister Publishing Company. Willoughby, OH.

Feldmann, R.J., Maibach, H.J., 1974. Percutaneous penetration of some pesticides and herbicides in man. Toxicol. Appl. Pharmacol. 28, 126–132.

Franz, T.J., Lehman, P.A., Franz, S.F., Guin, J.D., 1996. Comparative percutaneous absorption of lindane and permethrin. Arch. Dermatol. 132, 901–905.

Godin, S.J., Crow, J.A., Scollon, E.J., Hughes, M.F., DeVito, M.J., Ross, M.K., 2007. Identification of rat and human cytochrome P450 isoforms and a rat serum esterase

Author's personal copy

that metabolize the pyrethroid insecticides deltamethrin and esfenvalerate. Drug Metab. Dispos. 35, 1664–1671.
Godin, S.J., DeVito, M.J., Hughes, M.F., Ross, D.G., Scollon, E.J., Starr, J.M., Setzer, R.W., Conolly, R.B., Tornero-Velez, R., 2010. Physiologically based pharmacokinetic modeling of deltamethrin: development of a rat and human diffusion-limited model. Toxicol. Sci.10.1093/toxsci/kfq051
Godin, S.J., Scollon, E.J., Hughes, M.F., Potter, P.M., DeVito, M.J., Ross, M.K., 2006. Species differences in the in vitro metabolism of deltamethrin and esfenvalerate: differential oxidative and hydrolytic metabolism by humans and rats. Drug Metab. Dispos. 34, 1764–1771.
Guy, R.H., Hadgraft, J., 1991. Principles of skin permeability relevant to chemical exposure. In: Hobson, D.W. (Ed.), Dermal and Ocular Toxicology: Fundamentals and Methods. CRC Press, Boca Raton, pp. 221–246.
He, F., Wang, S., Liu, L., Chen, S., Zhang, Z., Sun, J., 1989. Clinical manifestations and diagnosis of acute pyrethroid poisoning. Arch. Toxicol. 63, 54–58.
Hinz, R.S., Lorence, C.R., Hodson, C.D., Hansch, C., Hall, L.L., Guy, R.H., 1991. Percutaneous penetration of para-substituted phenols *in vitro*. Fundam. Appl. Pharmacol. 17, 573–583.
Hughes, E.A., Flores, A.P., Ramos, L.M., Zalts, A., Glass, C.R., Montserrat, J.M., 2008. Potential dermal exposure to deltamethrin and risk assessment for manual sprayers: influence of crop type. Sci. Total Environ. 391, 34–40.
Hughes, M.F., Shrivastava, S.P., Fisher, H.L., Hall, L.L., 1993. Comparative *in vitro* percutaneous absorption of p-substituted phenols through rat skin using static and flow-through diffusion systems. Toxicol. in Vitro 7, 221–227.
Kemppainen, B.W., Reifenrath, W.G., Stafford, R.G., Mehta, M., 1991. Methods for in vitro skin absorption studies of a lipophilic toxin produced by red tide. Toxicology 66, 1–17.
Kraeling, M.E.K., Bronaugh, R.L., 1997. In vitro percutaneous absorption of alpha hydroxyl acids in human skin. J. Soc. Cosmet. Chem. 48, 187–197.
Kurz, T., 1994. Formulating effective self-tanners with DHA. Cosmet. Toiletries 109, 55–61.
Laskowski, D.A., 2002. Physical and chemical properties of pyrethroids. Rev. Environ. Contam. Toxicol. 174, 49–170.
Morgan, M.K., Sheldon, L.S., Croghan, C.W., Jones, P.W., Chuang, J.C., Wilson, N.K., 2007. An observational study of 127 preschool children at their homes and daycare centers in Ohio: environmental pathways to cis- and trans-permethrin exposure. Environ. Res. 104, 266–274.
Moss, G.P., Dearden, J.C., Patel, H., Cronin, M.T.D., 2002. Quantitative structure-permeability relationships (QSPRs) for percutaneous absorption. Toxicol. in Vitro 16, 299–317.
Peele, D.B., Crofton, K.M., 1987. Pyrethroid effects on schedule-controlled behavior: time and dosage relationships. Neurotoxicol. Teratol. 9, 387–394.
Power, L.E., Sudakin, D.L., 2007. Pyrethrin and pyrethroid exposures in the United States: a longitudinal analysis of incidents reported to Poison Centers. J. Med. Toxicol. 3, 94–99.
Ray, D.E., Forshaw, P.J., 2000. Pyrethroid insecticides: poisoning syndromes, synergies, and therapy. Clin. Toxicol. 38, 95–101.
Ray, D.E., Fry, J.R., 2006. A reassessment of the neurotoxicity of pyrethroid insecticides. Pharmacol. Ther. 111, 174–193.
Riviere, J.E., Monteiro-Riviere, N.A., Baynes, R.E., 2002. Gulf War related exposure factors influencing topical absorption of ^{14}C-permethrin. Toxicol. Lett. 134, 61–71.
Sato, K., Sugibyashi, K., Morimoto, Y., 1991. Species differences in percutaneous absorption of nicorandil. J. Pharm. Sci. 80, 104–107.
Schettgen, T., Heudorf, U., Drexler, H., Angerer, J., 2002. Pyrethroid exposure of the general population — is this due to diet? Toxicol. Lett. 134, 141–145.
Scheuplein, R.J., Blank, I.H., 1971. Permeability of the skin. Physiol. Rev. 51, 702–747.
Scollon, E.J., Starr, J., Godin, S.J., DeVito, M.J., Hughes, M.F., 2009. In vitro metabolic clearance of pyrethroids by rat and human hepatic microsomes and cytochrome P450 isoforms. Drug Metab. Dispos. 37, 1–8.
Shafer, T.J., Meyer, D.A., 2004. Effects of pyrethroids on voltage-sensitive calcium channels: a critical evaluation of strengths, weaknesses, data needs and relationship to assessment of cumulative neurotoxicity. Toxicol. Appl. Pharmacol. 196, 303–318.
Sheets, L.P., Doherty, J.D., Law, M.W., Reiter, L.W., Crofton, K.M., 1994. Age-dependent differences in the susceptibility of rats to deltamethrin. Toxicol. Appl. Pharmacol. 126, 186–190.
Sidon, E.W., Moody, R.P., Franklin, C.A., 1988. Percutaneous absorption of cis- and trans-permethrin in rhesus monkeys and rats: anatomic site and interspecies variation. J. Toxicol. Environ. Health 23, 207–216.
Soderlund, D.M., Clark, J.M., Sheets, L.P., Mullin, L.S., Piccirillo, V.J., Sargent, D., Stevens, J.T., Weiner, M.L., 2002. Mechanisms of pyrethroid neurotoxicity: implications for cumulative risk assessment. Toxicology 171, 3–59.
Tomalik-Scharte, D., Lazar, A., Meins, J., Bastian, B., Ihrig, M., Wachall, B., Jetter, A., Tantcheva-Poor, I., Mahrle, G., Fuhr, U., 2005. Dermal absorption of permethrin following topical administration. Eur. J. Clin. Pharmacol. 61, 399–404.
van Ravenzwaay, B., Leibold, E., 2004. The significance of *in vitro* rat skin absorption studies to human risk assessment. Toxicol. in Vitro 18, 219–225.
van der Rhee, H.J., Farquhar, J.A., Vermeulen, N.P., 1989. Efficacy and transdermal absorption of permethrin in scabies patients. Acta Derm. Venereol. 69, 170–173.
Wester, R.C., Maibach, H.I., 1993. The dose response of percutaneous absorption. In: Wang, R.G.M., Knaak, J.B., Maibach, H.I. (Eds.), Health Risk Assessment: Dermal and Inhalation Exposure and Absorption of Toxicants. CRC Press, Boca Raton, pp. 217–228.
Wolansky, M.J., Gennings, C., Crofton, K.M., 2006. Relative potencies for acute effects of pyrethroids on motor function in rats. Toxicol. Sci. 89, 271–277.
Wolansky, M.J., Gennings, C., DeVito, M.J., Crofton, K.M., 2009. Evidence for dose-additive effects of pyrethroids on motor activity in rats. Environ. Health Perspect. 117, 1563–1570.
Wolansky, M.J., McDaniel, K.L., Moser, V.C., Crofton, K.M., 2007. Influence of dosing volume on the neurotoxicity of bifenthrin. Neurotoxicol. Teratol. 29, 377–384.
Yourick, J.J., Jung, C.T., Bronaugh, R.L., 2008. *In vitro* and *in vivo* percutaneous absorption of retinol from cosmetic formulations: significance of the skin reservoir and prediction of systemic absorption. Toxicol. Appl. Pharmacol. 231, 117–121.
Yourick, J.J., Koening, M.L., Yourick, D.L., Bronaugh, R.L., 2004. Fate of chemicals in skin after dermal application: does the *in vitro* skin reservoir affect the estimate of systemic absorption. Toxicol. Appl. Pharmacol. 195, 309–320.
Zhang, Z., Sun, J., Chen, S., Wu, Y., He, F., 1991. Levels of exposure and biological monitoring of pyrethroids in spraymen. Br. J. Ind. Med. 48, 82–86.

Table of Contents

General_Authors_Publications.....2
LI-266379_Sobus2016_AIR.....22
LI-266379_Rager_etal_2016_Supplemental_Figures.....27
LI-266380_Sobus2018_AIR.....31
Author_Contributions.....36

STAA REPORT FOR THE SCIENTIST NOMINATIONS

General Information:

Nomination ID/App ID:	20-115
Research Category Primary:	Health Effects Research and Human Health Risk Assessment (HE)
Research Category Secondary:	Monitoring and Measurement Methods (MM)
Laboratory/Office Name:	ORD
Nomination Entered By:	Jon Sobus

Eligibility Checklist:

[Y] The nominated publication(s) has not been submitted to a previous STAA competition.

[Y] The nominated publication(s) was published on or before January 1, 2017 and on or after January 1,2012

[Y] The principal author was an EPA employee or a PHS employee assigned to EPA when the research was performed

[Y] The EPA authors (includes PHS employees assigned to EPA) contributed collectively a minimum of 50% toward the publication(s)

Nominating Official Name:	Michael Devito
Nominating Official Title:	
Nominating OfficialEmail:	devito.michael@epa.gov
STAA Coordinator Name:	Kathleen Wiser
STAA Coordinator Email:	wiser.kathi@epa.gov

Justifications:

Justification 1:

Rager JE, Strynar MJ, Liang S, McMahen RL, Richard AM, Grulke CM, Wambaugh JF, Isaacs KK, Judson R, Williams AJ, Sobus JR. Linking high resolution mass spectrometry data with exposure and toxicity forecasts to advance high-throughput environmental monitoring. Environ Int. 2016 Mar;88:269-280.

Background: The US EPA is responsible for ensuring the safety of ten-of-thousands of chemicals used in commerce. Indeed, part of EPA's Strategic Plan is to "Ensure Safety of Chemicals in the Marketplace". Over the past decade, EPA's Office of Research and Development (ORD) has developed projects to much more rapidly assess chemical safety based on anticipated exposure and hazard. These projects, known as "ToxCast" and "ExpoCast", make use of high-throughput testing strategies and model-based predictions to rapidly prioritize thousands of chemicals based on anticipated risk. ExpoCast models suggest that most chemical exposure occurs in the near-field environment; that is, within the home and workplace through use of consumer products and contact with manufactured materials. Prior laboratory research has shown dust to be a sink for various consumer product chemicals present within the home. Research has further shown children to receive larger chemical exposures from dust owing to crawling and hand-to-mouth behaviors. Most laboratory analyses of dust, to date, have used targeted analytical methods, focusing on relatively few (tens) chemicals predetermined to be of high-interest. A need therefore exists to develop high-throughput monitoring methods to better characterize to totality of chemical exposures emanating from indoor dust. The goal of this work was to develop a non-targeted analysis (NTA) method, based on high-resolution mass spectrometry (HRMS), that would enable identification and prioritization of hundreds-to-thousands of poorly studied chemicals in house dust using samples from across the US.

Research Description: Samples were collected from 56 U.S. residences as part of the American Healthy Homes Survey. Dust samples were seived, extracted, cleaned, and analyzed using liquid chromatography (LC) time-of-flight (TOF) HRMS. Molecular feature data obtained via LC-TOF HRMS were used to first tentatively identify unknowns at the accurate mass and molecular formula levels. Predicted

molecular formula were matched against version 2 of EPA's Distributed Structure-Searchable Toxicity (DSSTox) Database to retrieve candidate structures. In total, more than 3,000 candidate structures were considered as being present in the dust samples. Further prioritization of these >3,000 candidates was necessary to produce a list of candidates that could be confirmed with authentic standards. Prioritization of candidates was performed using a novel algorithm (with supporting visualization software) that utilized experimental data about each candidate (i.e., detection frequency and mean intensity across the sample set), as well as existing exposure and bioactivity values made available from the ExpoCast and ToxCast/Tox21 programs, respectively. Standards were procured for 100 priority compounds, of which 33 were confirmed as being present in study samples using retention time and spectral matching. SciFinder searching of each confirmed

compound (identified by CASRN) was performed to determine if compounds had previously been reported in house dust, with 15 having not been reported in any prior studies.

Impact: The publication of this work was a watershed moment for EPA's ORD. A year after its publication it was twice featured in the National Academies of Science Report *Using 21st Century Science to Improve Risk-Related Evaluations*. Authors of the report commented that our method was an "…innovative approach for identifying and setting priorities among chemicals for additional exposure assessment, hazard testing, and risk assessment that complements the current hazard-oriented paradigm". The methods used in the article set the foundation for a burgeoning NTA program within ORD. Specifically, this work led to the creation of multiple dedicated research Outputs within two ORD National Research Programs (Chemical Safety for Sustainability [CSS] and Sustainable and Health Communities [SHC]), and further led to the creation of a dedicated Branch (i.e., the Advanced Analytical Chemistry Methods Branch) within ORD's Center for Computational Toxicology and Exposure (CCTE). The work also led to a Pathfinder Innovation Project Award to further develop and implement NTA methodologies. The impact of this groundbreaking work is difficult to fully capture, as it has influenced activities within and outside EPA, and has been cited in the peer-reviewed literature more than 100 times (see supplemental article impact report 'Sobus2016_AIR.pdf'. This work will certainly continue to be heavily utilized and referenced by the scientific community.

Sobus JR, Wambaugh JF, Isaacs KK, Williams AJ, McEachran AD, Richard AM, Grulke CM, Ulrich EM, Rager JE, Strynar MJ, Newton SR. Integrating tools for non-targeted analysis research and chemical safety evaluations at the US EPA. J Expo Sci Environ Epidemiol. 2018 Sep;28(5):411-426.

Background: At the core of public health research is the quandary surrounding the origins of long-term latency disease. For hundreds of years researchers have tried to

identify and mitigate causes of chronic illness. Efforts over the past quarter century have largely focused on genetic factors that influence disease incidence, but mysteries remain surrounding environmental causes of disease. These mysteries have driven research into the human exposome, which represents the totality of all exposures experienced by an individual over their lifetime. Much exposome research uses high-resolution mass spectrometry (HRMS) to identify important exposures within biological samples from patients with disease. Here, non-targeted analysis (NTA) techniques are the basis for identifying exposure of interest based on HRMS data. While these studies have proven informative, they are retrospective in nature, and thus work backwards from the diseased population to the causative exposures. The US EPA has a regulatory mandate to ensure the safety of man-made chemicals and must therefore prospectively consider possible deleterious effects of chemical exposures. Moreover, the agency must consider these possible effects across tens-of-thousands of chemicals (and non-chemical stressors), hundreds of biological endpoints, and within a reasonable time frame. To meet these demands, the US EPA's Office of Research and Development (ORD) developed the Toxicity Forecaster (ToxCast) and Exposure Forecaster (ExpoCast) projects, with the goal of performing high-throughput provisional safety assessments across thousands of potential stressors. Assessment decisions to date have been largely based on sparse training and test data, leading to large uncertainties risk-related predictions. NTA via HRMS has been proposed to drastically reduce these uncertainties by providing exposure data on thousands of stressors across various environmental (e.g., drinking water, consumer products) and biological media. Noting this opportunity, our team was explicitly asked by the current ORD Assistant Administrator to develop a framework showing the potential for integration between exposomics efforts,

activities within the ToxCast and ExpoCast programs, and HRMS-based NTA research. We produced this article in direct response to the Assistant Administrator's request.

Research Description: The article has four primary components: 1) a review of recent exposomic and HRMS-based NTA research efforts; 2) a review of chemical screening data, models, and tools developed and used within ORD; 3) a summary of an ORD-led NTA workshop and an introduction to an ORD-led NTA trial; and 4) a detailed description of the integrated research framework. The exposomics and NTA review section details the history of exposomics, the various types of analytical instruments used to support NTA experiments, strategies for communicating confidence in compound identifications, and databases and tools commonly used in the exposomics and NTA fields. The section on ORD data, models, and tools covers the history and applications of EPA's ToxCast project, ExpoCast project, Distributed Structure-Searchable Toxicity (DSSTox) database, and CompTox Chemistry Dashboard. Specific attention is given to the types of data that have been generated, stored, and made publicly available through each effort. The section on the ORD-led workshop and trial describes how authors of this article convened a two-day workshop in RTP, NC to: 1) discuss current efforts in exposomics, NTA, and high-throughput chemical screening; and 2) highlight opportunities for integration across the various related research domains. This section further describes the genesis and design of EPA's Non-Targeted Analysis Trial (ENTACT), a collaborative study developed by authors of this article to foster research integration and examine NTA performance capabilities. The final section of the article describes the integrated research framework, detailing how NTA experimental data can be prioritized using the CompTox Chemicals Dashboard (and underlying DSSTox database) and existing ToxCast and ExpoCast data. The final section further describes how the framework contains a feedback loop in which new discoveries from NTA experiments inform the ToxCast and ExpoCast projects, thus reducing uncertainty in risk-related decisions. The article concludes with an outlook for future integrated research that makes full use of NTA data to enhance exposomic studies and high-throughput chemical safety evaluations.

Impact: This work followed on the heels of the aforementioned publication and was a means of formalizing and communicating the relationships between multiple research enterprises within ORD. This article clearly showed ORD and EPA managers, as well as the larger scientific community, how NTA research can

integrate with ongoing efforts to rapidly screen known chemicals for potential risks. Internally, this work cemented NTA research as a viable and beneficial discipline and led to the creation of official research Products and Outputs within the Chemical Safety for Sustainability (CSS) and Sustainable and Healthy Communities (SHC) National Research Programs. It further led to the creation of the Advanced Analytical Chemistry Methods Branch (AACMB) within ORD's Center for Computational Toxicology and Exposure (CTTE). NTA research being performed within CSS and AACMS provide direct support to the ToxCast and ExpoCast projects, which in turn provide direct support to agency program offices conducting risk-based chemical prioritization under the Frank R. Lautenberg Chemical Safety for the 21st Century Act. This specific publication has been recognized as one of the Journal of Exposure Science and Environmental Epidemiology's 'Best Papers' of 2018-2019 and cited over 50 times in the literature (in only two years) (see supplemental article impact report 'Sobus2018_AIR.pdf'). The contents of this framework article will continue to provide the blueprint for NTA research within ORD for years to come.

Justification 2A:

The first paper was a proof-of-concept using samples of house dust collected from around the US. The article showed exactly what could be accomplished when integrating NTA monitoring data with exposure and toxicity forecasts for the sake of risk-based chemical prioritization. The second paper is very much an extension of the first paper, and provides much needed detail and context sounding the methods proposed in Paper 1. Importantly, the second paper provides a formalized framework that is now the blueprint for integrated NTA research within ORD.

Justification 2B:

Jon Sobus:

2016 STAA submission (not awarded) - Sobus JR, et al. Uses of NHANES biomarker data for chemical risk assessment: Trends, challenges, and opportunities. Environ Health Perspect. 2015 Oct;123(10):919-27.

2020 STAA Submission – “Temporal exposures of adults to pyrethroid insecticides, pyrethroid degradates, and bisphenol A”. Individual papers: (1) Morgan M et al. Distribution, variability, and predictors of urinary bisphenol-A levels in 50 North Carolina adults over a six-week monitoring period. Environment International. 2018:112: 85-99.; (2) Morgan et al. Pyrethroid insecticides and their environmental degradates in repeated duplicate-diet solid food samples of 50 adults. Journal of Exposure Science and Environmental Epidemiology. 2018: 28: 40-45. (3) Morgan M et al. Temporal variability of pyrethroid metabolite levels in bedtime, morning, and 24-hr urine samples for 50 adults in North Carolina. Environmental Research. 2016: 144; 81-91.

John Wambaugh:

2019 Level III Award - Biryol, Derya, et al. "High-throughput dietary exposure predictions for chemical migrants from food contact substances for use in chemical prioritization." Environment international 108 (2017): 185-194.

2019 Level III Award - Isaacs, Kristin K., et al. "SHEDS-HT: an integrated probabilistic exposure model for prioritizing exposures to chemicals with near-field and dietary sources." Environmental science & technology 48.21 (2014): 12750-12759.

2019 Level III Award - Isaacs, Kristin K., et al. "Characterization and prediction of chemical functions and weight fractions in consumer products." Toxicology reports 3 (2016): 723-732.

2019 Level III Award - Phillips, Katherine A., et al. "High-throughput screening of chemicals as functional substitutes using structure-based classification models." Green Chemistry 19.4 (2017): 1063-1074.

2014 Level II Award - Wambaugh, John F., et al. "High-throughput models for exposure-based chemical prioritization in the ExpoCast project." Environmental science & technology 47.15 (2013): 8479-8488.

2015 Level III Award - Wambaugh, John F., et al. "High throughput heuristics for prioritizing human exposure to environmental chemicals." Environmental science & technology 48.21 (2014): 12760-12767.

Kristin Isaacs:

2019 Level III Award: Advancing High-Throughput Chemical Exposure Models for Consumer and Dietary Pathways

2019- Level III Award: High-throughput screening of chemicals as functional substitutes using structure-based classification models

2016- Level III Award: (1) Air Pollution Exposure Model for Individuals (EMI) in Health Studies: Evaluation for Ambient PM2.5 in Central North Carolina, (2) GPS-based Microenvironment Tracker (MicroTrac) Model to Estimate Time-Location of Individuals for Air Pollution Exposure Assessments: Model Evaluation in Central North Carolina. (3) Modeling Spatial and Temporal Variability of Residential Air Exchange Rates for the Near-Road Exposures and Effects of Urban Air Pollutants Study (NEXUS)

Ann Richard:

2019 Level III Award - Richard, Ann M., et al. "ToxCast chemical landscape: paving the road to 21st century toxicology." Chemical research in toxicology 29.8 (2016): 1225-1251.

Richard Judson:

2019 Level I Award - Development and deployment of a high-throughput assay to detect chemical disruptors of thyroid hormone synthesis.

2019 Level III Award - A chemical and cheminformatics foundation for ToxCast & Tox21 research programs

Justification 2C:

The current nomination has nothing in common with prior submissions by Sobus, Isaacs, and Judson. Components of research discussed in Wambaugh et al. (2013 & 2014) and in Richard et al. (2016) inspired work in both articles of the current

submission. Yet, the specific work described in all former articles and the two current articles are complete distinct. That is, there is absolutely no overlap in the work performed.

Justification 2D:

n/a

Justification 2E:

The package submitted by Morgan et al. (*Temporal exposures of adults to pyrethroid insecticides, pyrethroid degradates, and bisphenol A* - for which Sobus is a coauthor) has nothing in common with the articles in the present submission. The work submitted by Morgan et al. details the findings of an observational study of 50 adult participants with focus on exposure to specific pyrethroids and bisphenol A.

Justification 3A:

The first article (Rager et al. 2016) was twice featured in the National Academies of Science Report Using 21st Century Science to Improve Risk-Related Evaluations. Authors of the report commented that our method was an "…innovative approach for identifying and setting priorities among chemicals for additional exposure assessment, hazard testing, and risk assessment that complements the current hazard-oriented paradigm". This work led to an EPA Pathfinder Innovation Project Award (3 separate competitive awards) to further develop and implement NTA methodologies within ORD. The impact of this groundbreaking work is difficult to fully capture, as it has influenced activities within and outside EPA, and has been cited in the peer-reviewed literature more than 100 times (see supplemental article impact report 'Sobus2016_AIR.pdf'). I have personally given more than 10 invited presentations (including international seminars) highlighting the methods and findings of this work.

The second article (Sobus et al. 2018) led to me being awarded the President's Early Career Award for Scientists and Engineers (PECASE). This is "…the highest honor bestowed by the U.S. government on outstanding scientists and engineers beginning their independent careers." This article has been recognized as one of the Journal of Exposure Science and Environmental Epidemiology's 'Best Papers' of 2018-2019 and cited over 50 times in the literature (in only two years) (see supplemental article impact report 'Sobus2018_AIR.pdf'). I have personally given more than 12 invited presentations (including international seminars) highlighting the methods and findings of this work.

Justification 3B:

These articles were individually subjected to *ad hoc* review by internal EPA science colleagues. Subsequently, they were subjected to the ORD internal peer review policy which includes official internal technical review via standard EPA-363 forms followed by policy review by the Division Director and the NERL Associate Director for Health resulting in pre-submission approval via EPA-362 clearance form. The articles were then submitted to their respective journals and were subjected to rigorous external peer-review. Upon successfully addressing several rounds of external peer-reviewers' comments, the authors received EPA approval for the final draft, and subject to further editorial review at the journal, received final acceptance for publication from the journal.

AUTHORS

Principal Author

Author Name: Jon R. Sobus

Professional Title: Salutation: Dr.

Email:	sobus.jon@epa.gov	Organization:	
Mailing Address:			
Street Line 1:			
City:			
Zip Code:		State:	
At time of research was:	EPA Employee		
Separation Date:			
% of Effort:	20		

Contributing Author

Author Name:	John Wambaugh		
Professional Title:		Salutation:	Dr.
Email:	wambaugh.john@epa.gov	Organization:	
Mailing Address:			
Street Line 1:			
City:			
Zip Code:		State:	
At time of research was:	EPA Employee		
Separation Date:			
% of Effort:	5		

Contributing Author

Author Name:	Antony Williams		
Professional Title:		Salutation:	Dr.

Email:	williams.antony@epa.gov	Organization:	
Mailing Address:			
Street Line 1:			
City:			
Zip Code:		State:	
At time of research was:	EPA Employee		
Separation Date:			
% of Effort:	5		

Contributing Author

Author Name:	Mark Strynar		
Professional Title:		Salutation:	Dr.
Email:	strynar.mark@epa.gov	Organization:	
Mailing Address:			
Street Line 1:			
City:			
Zip Code:		State:	
At time of research was:	EPA Employee		
Separation Date:			
% of Effort:	5		

Contributing Author

Author Name:	Julia Rager		
Professional Title:		Salutation:	Dr.

Email:	jrager@live.unc.edu	Organization:	
Mailing Address:			
Street Line 1:			
City:			
Zip Code:		State:	
At time of research was:	Non EPA Personnel		
Separation Date:			
% of Effort:	20		

Contributing Author

Author Name:	Kristin Isaacs		
Professional Title:		Salutation:	Dr.
Email:	isaacs.kristin@epa.gov	Organization:	
Mailing Address:			
Street Line 1:			
City:			
Zip Code:		State:	
At time of research was:	EPA Employee		
Separation Date:			
% of Effort:	5		

Contributing Author

Author Name:	Andrew McEachran		
Professional Title:		Salutation:	Dr.

Email:	andrew.mceachran@agilent.com	Organization:	
Mailing Address:			
Street Line 1:			
City:			
Zip Code:		State:	
At time of research was:	Non EPA Personnel		
Separation Date:			
% of Effort:	5		

Contributing Author

Author Name:	Elin Ulrich		
Professional Title:		Salutation:	Dr.
Email:	ulrich.elin@epa.gov	Organization:	
Mailing Address:			
Street Line 1:			
City:			
Zip Code:		State:	
At time of research was:	EPA Employee		
Separation Date:			
% of Effort:	5		

Contributing Author

Author Name:	Shuang Liang		
Professional Title:		Salutation:	Ms.

Email:	lsveracool@gmail.com	Organization:	
Mailing Address:			
Street Line 1:			
City:			
Zip Code:		State:	
At time of research was:	Non EPA Personnel		
Separation Date:			
% of Effort:	5		

Contributing Author

Author Name:	Rebecca McMahen		
Professional Title:		Salutation:	Ms.
Email:	rlmcmahen@gmail.com	Organization:	
Mailing Address:			
Street Line 1:			
City:			
Zip Code:		State:	
At time of research was:	Non EPA Personnel		
Separation Date:			
% of Effort:	5		

Contributing Author

Author Name:	Ann Richard		
Professional Title:		Salutation:	Dr.

Email:	richard.ann@epa.gov	Organization:	
Mailing Address:			
Street Line 1:			
City:			
Zip Code:		State:	
At time of research was:	EPA Employee		
Separation Date:			
% of Effort:	5		

Contributing Author

Author Name:	Christopher Grulke		
Professional Title:		Salutation:	Dr.
Email:	grulke.chris@epa.gov	Organization:	
Mailing Address:			
Street Line 1:			
City:			
Zip Code:		State:	
At time of research was:	EPA Employee		
Separation Date:			
% of Effort:	5		

Contributing Author

Author Name:	Seth Newton		
Professional Title:		Salutation:	Dr.

Email:	newton.seth@epa.gov	Organization:	
Mailing Address:			
Street Line 1:			
City:			
Zip Code:		State:	
At time of research was:	EPA Employee		
Separation Date:			
% of Effort:	5		

Contributing Author

Author Name:	Richard Judson		
Professional Title:		Salutation:	Dr.
Email:	judson.richard@epa.gov	Organization:	
Mailing Address:			
Street Line 1:			
City:			
Zip Code:		State:	
At time of research was:	EPA Employee		
Separation Date:			
% of Effort:	5		

PUBLICATIONS

Publication 1:

Linking high resolution mass spectrometry data with exposure and toxicity

Publication Title:	forecasts to advance high-		
Publication Date:	Sat Jan 23 00:00:00 GMT 2016		
Journal/Publication Method:	Environ Int.		
All Author(s):			
Volume:	88	Number:	n/a
Pages:	269-280	Immediately Index:	Immediately Index:
Citation ½ Life:	6.0	Impact Factor:	7.943

Publication 2:

Publication Title:	Integrating tools for non-targeted analysis research and chemical safety evaluations at the US EPA		
Publication Date:	Fri Dec 29 00:00:00 GMT 2017		
Journal/Publication Method:	J Expo Sci Environ Epidemiol.		
All Author(s):			
Volume:	28	Number:	5
Pages:	411-426	Immediately Index:	Immediately Index:
Citation ½ Life:	8.1	Impact Factor:	3.025

EPA-RTP LIBRARY

Article Impact Report

Linking High Resolution Mass Spectrometry Data With Exposure And Toxicity Forecasts To Advance High-Throughput Environmental Monitoring

ENVIRONMENT INTERNATIONAL

Rager, JE; Strynar, MJ; Liang, S; McMahen, RL; Richard, AM; Grulke, CM; Sobus, JR; et al.

Rager, JE, et al. (2016). Linking High Resolution Mass Spectrometry Data With Exposure And Toxicity Forecasts To Advance High-Throughput Environmental Monitoring. *Environment International*, 88. 269-280. PMID: 26812473. DOI: 10.1016/j.envint.2015.12.008

Highlights

Citations

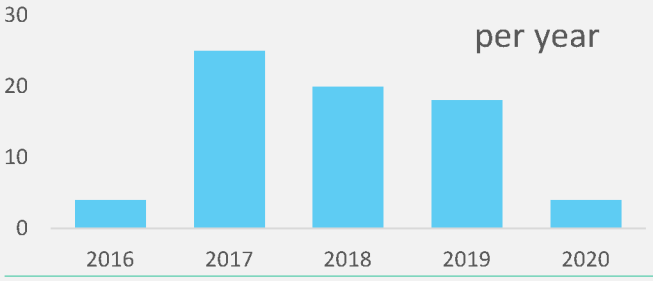

96 Google Scholar

75 Web of Science

111 Mendeley Readers

Top Citing Journal
Environmental Science & Technology

6 Articles

7.14 Impact Factor

Citations by Country

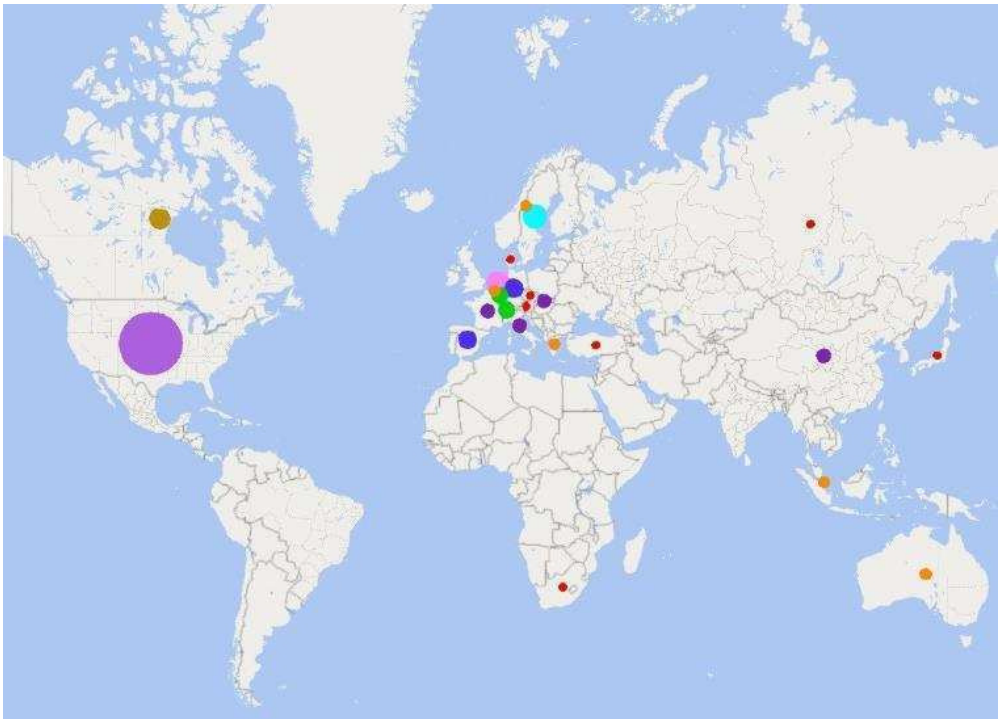

Countries	Papers
USA	55
SWEDEN	8
NETHERLANDS	7
CANADA	6
GERMANY	5
SPAIN	5
LUXEMBOURG	4
ENGLAND	4
SWITZERLAND	4
ITALY	3

Top Citing Organizations

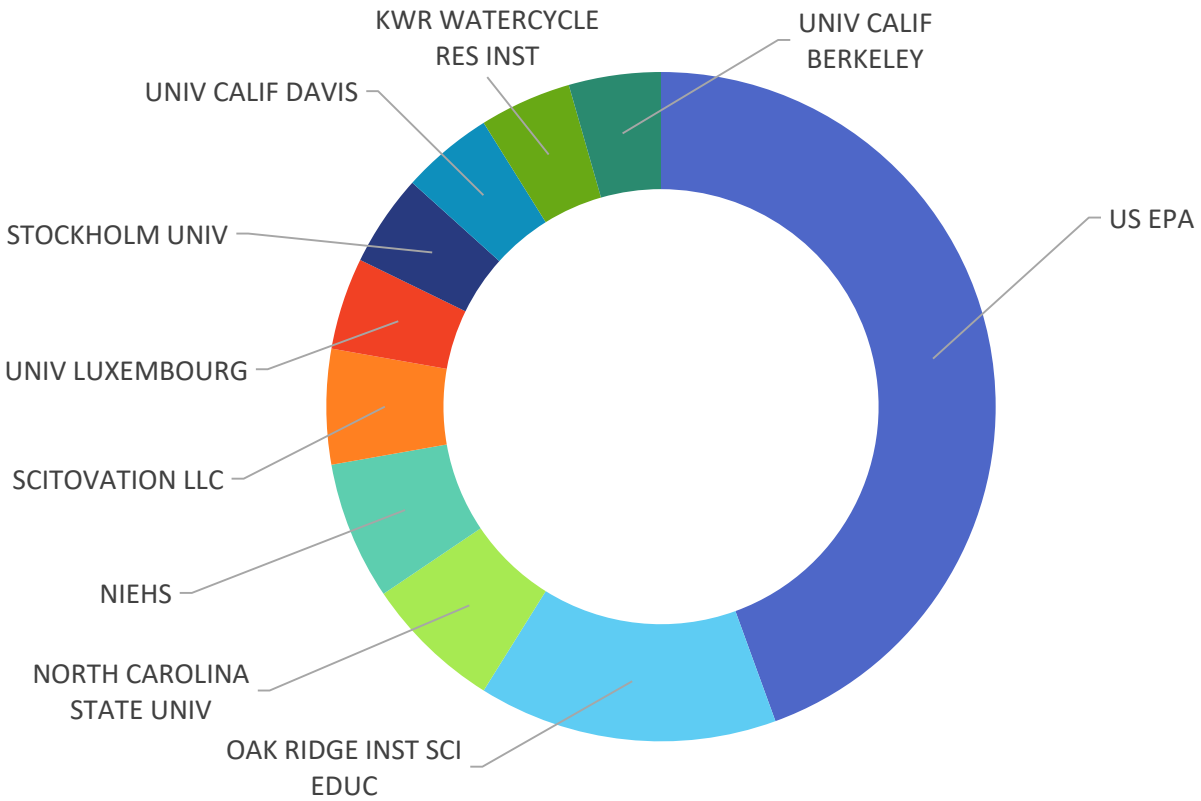

Citing Journals (Impact Factor)

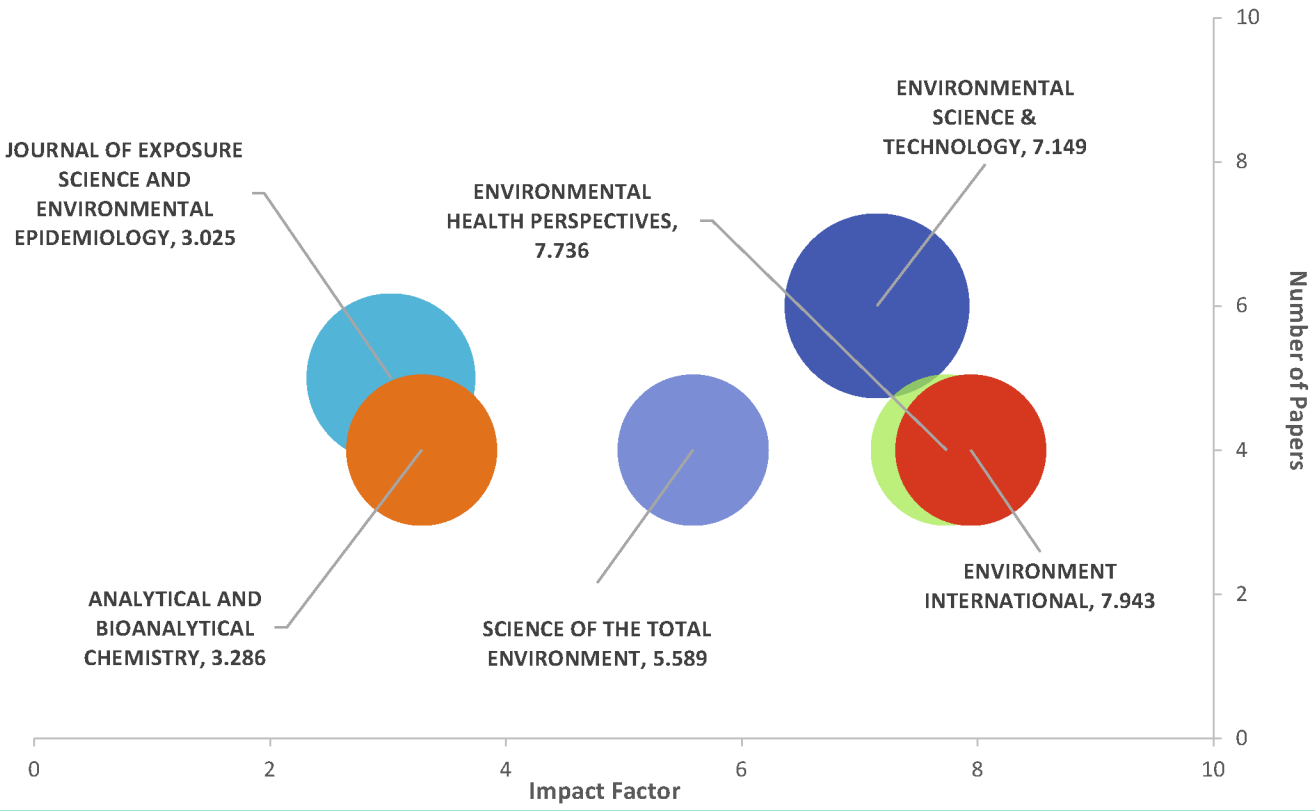

Research Areas

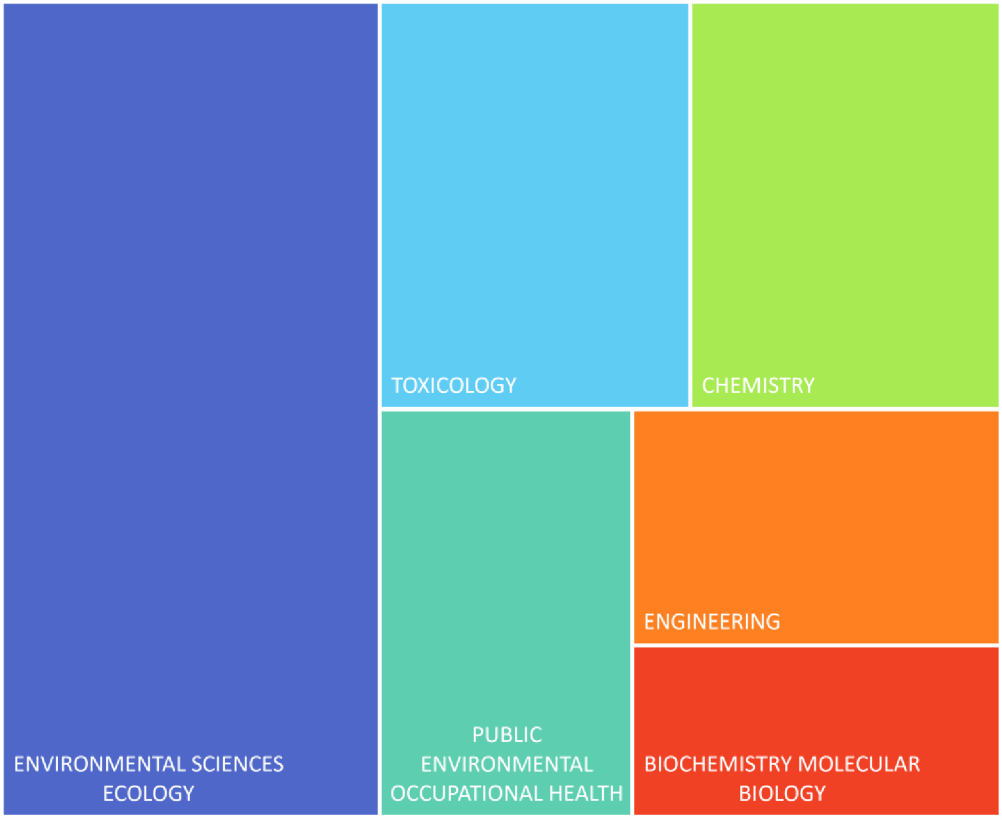

Research Areas	Papers
ENVIRONMENTAL SCIENCES ECOLOGY	39
TOXICOLOGY	16
CHEMISTRY	16
PUBLIC ENVIRONMENTAL OCCUPATIONAL HEALTH	13
ENGINEERING	11
BIOCHEMISTRY MOLECULAR BIOLOGY	8

Alternative Metrics

Altmetric

11

About this Attention Score

In the top 25% of all research outputs scored by Altmetric

High Attention Score compared to outputs of the same age (87th percentile)

Good Attention Score compared to outputs of the same age and source (67th percentile)

Mentioned by

1 policy source
13 tweeters
1 Redditor

Citations

75 Dimensions

Readers on

111 Mendeley
1 CiteULike

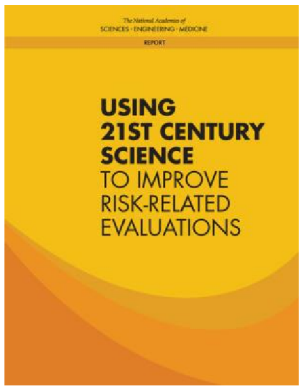

Using 21st Century Science to Improve Risk-Related Evaluations

National Academies of Sciences, Engineering, and Medicine
2017

Dimensions

15
Field Citation Ratio

This article features relative citation performance **15 times higher**, on average, than similarly aged articles in its subject field.

7.96
Relative Citation Ratio

This article has been cited at a rate that is **almost 8 times higher** than the average rate of articles normally cited alongside it.

As of April 2020,
this article was mentioned
in **25 tweets**
by **13 users**
with an upper bounds of
27,948 followers

Data collected 04/15/2020.
Current data may differ.

About the Report

This report was compiled using data from Web of Science, Google Scholar, Altmetric, and other databases when necessary. It is a snapshot of a particular article where the impact has been determined through analyzing various information about the papers citing that article. By collecting and organizing these statistics, a picture of reach, popularity, and value is created.

Citations by Country

The origin of the citing papers as determined by author addresses. All records are shown on the graphic, and the logical threshold is displayed in the accompanying table.

Top Citing Organizations

The listed author affiliations of citing articles. Percentage is determined using a logical threshold where the remaining percent of the whole would be considered "other."

Citing Journals

The volume of citing papers per the top ten journal titles compared to other titles citing the paper, displayed along with the journal's impact factor for the report year. In the graphic:

- position along the x axis is determined by the journal impact factor
- position along the y axis is determined by the number of citing papers published in the source title
- size is determined by the percentage of citing papers published in the specific source title compared to all other titles

Research Areas

The scientific category for each citing paper. A logical threshold is displayed in the graphic, and an expansion is shown in the accompanying table.

Alternative Metrics

Metrics gathered using the Altmetric database, PlumX Analytics, publisher website data, and other sources including but not limited to those listed in the Altmetric doughnut:

Source name	Definition
Twitter	Collection of tweets, retweets, and quoted tweets with links to scholarly content
Facebook	Monitors Public Facebook Pages and posts
Google+	Mentions from public posts (Coverage ended Jan. 2019 but historical data still available)
Policy documents	Scans and text-mines policy document PDFs for references; connected to CrossRef and PubMed for DOIs
Patents	Using data from IIFI CLAIMS®, tracks references found in patents filed with nine international patents offices
News	Manually curated data provided from third-parties and RSS feeds
Blogs	Manually curated list, attempts to gather posts linking to scholarly articles
Wikipedia	Mentions located in References section
Mendeley	Number of readers with the content in their library
CiteULike	Online reference manager counted similar to Mendeley (Coverage ended Dec. 2014 but historical data still available)

Supplementary Figure 1

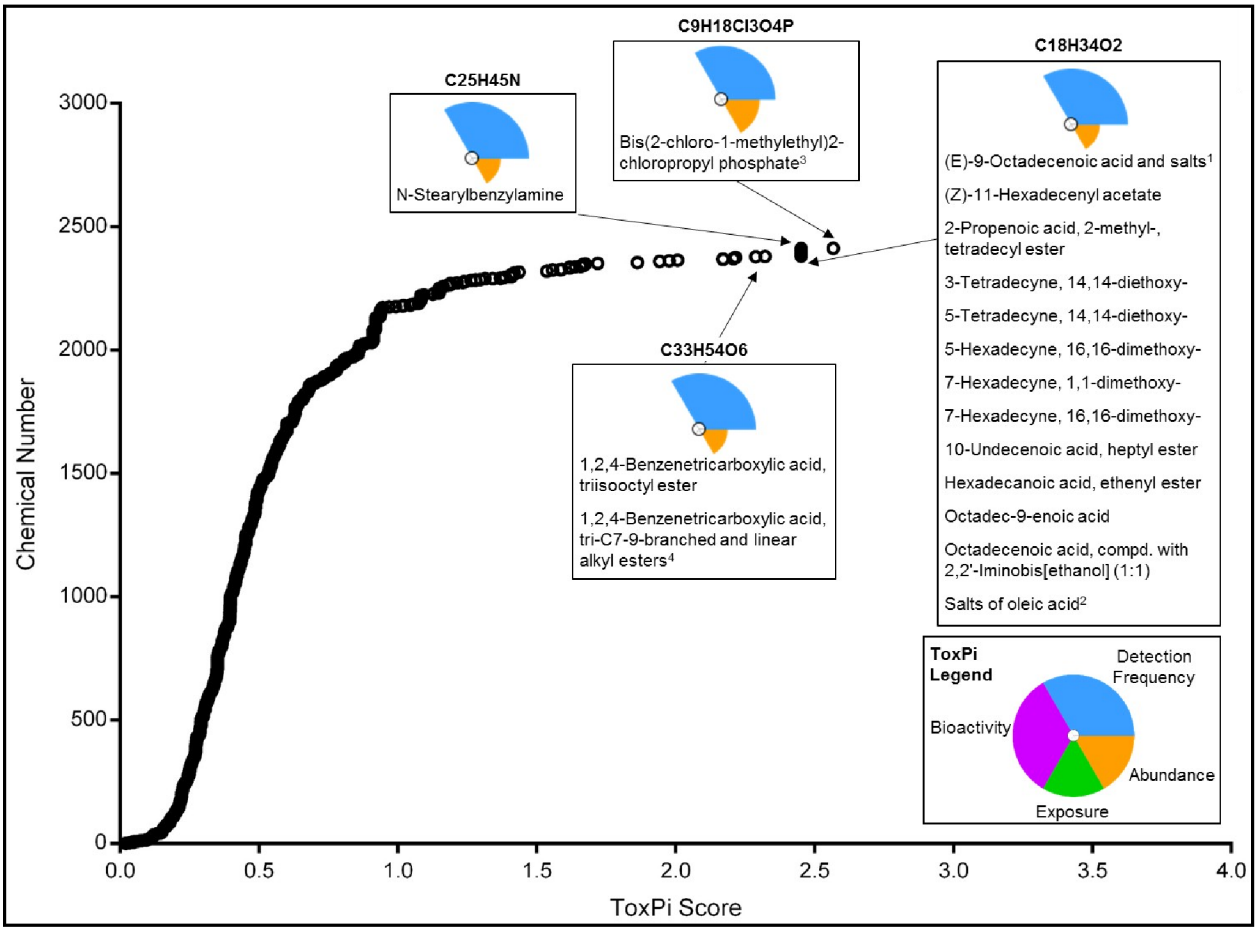

Supplementary Figure 1. Prioritization scoring for group B chemicals. ToxPi scores are plotted for the 2414 chemicals in group B that have yet to be evaluated for exposure and bioactivity (based on available ExpoCast and Tox21 data). Chemicals are organized according to ToxPi score, and ToxPi visualizations are displayed for the highest ranking chemicals. The desalted formulas associated with the listed chemicals are displayed above each ToxPi visualization.

[1](E)-9-Octadecenoic acid salt forms include 9-Octadecenoic acid (9Z)-, cadmium salt; 9-Octadecenoic acid (9Z)-, calcium salt; 9-Octadecenoic acid (9Z)-, compd. with (9Z)-9-octadecen-1-amine (1:1); 9-Octadecenoic acid (9Z)-, compd. with 1H-benzotriazole; 9-Octadecenoic acid (9Z)-, compd. with 2,2',2"-nitrilotris[2-propanol] (1:1); 9-Octadecenoic acid (9Z)-, compd. with 4-methylmorpholine (1:1); 9-Octadecenoic acid (9Z)-, compd. with N,N-dimethyl-1-hexadecanamine (1:1); 9-Octadecenoic acid (9Z)-, compd. with N,N-dimethylcyclohexanamine (1:1); 9-Octadecenoic acid (9Z)-, magnesium salt; 9-Octadecenoic acid (9Z)-, zinc salt; Cupric oleate; Mercuric oleate; Stannous oleate.

[2]Oleic acid salt forms include 9-Octadecenoic acid (9Z)-, cobalt salt; 9-Octadecenoic acid (9Z)-, copper salt; 9-Octadecenoic acid (9Z)-, compd. with 2,2',2"-nitrilotris[ethanol] (1:1); Ethanolamine oleate; Oleic acid Diethanolamine; Potassium oleate; Sodium oleate

[3]Chemical has the same formula as two other Group A chemicals (Tris(2-chloropropyl) phosphate and Tris(2-chloroisopropyl)phosphate)

[4]Chemicals have the same formula as two other Group A chemicals (Tris(2-ethylhexyl) trimellitate and Trioctyl trimellitate)

Supplementary Figure 2

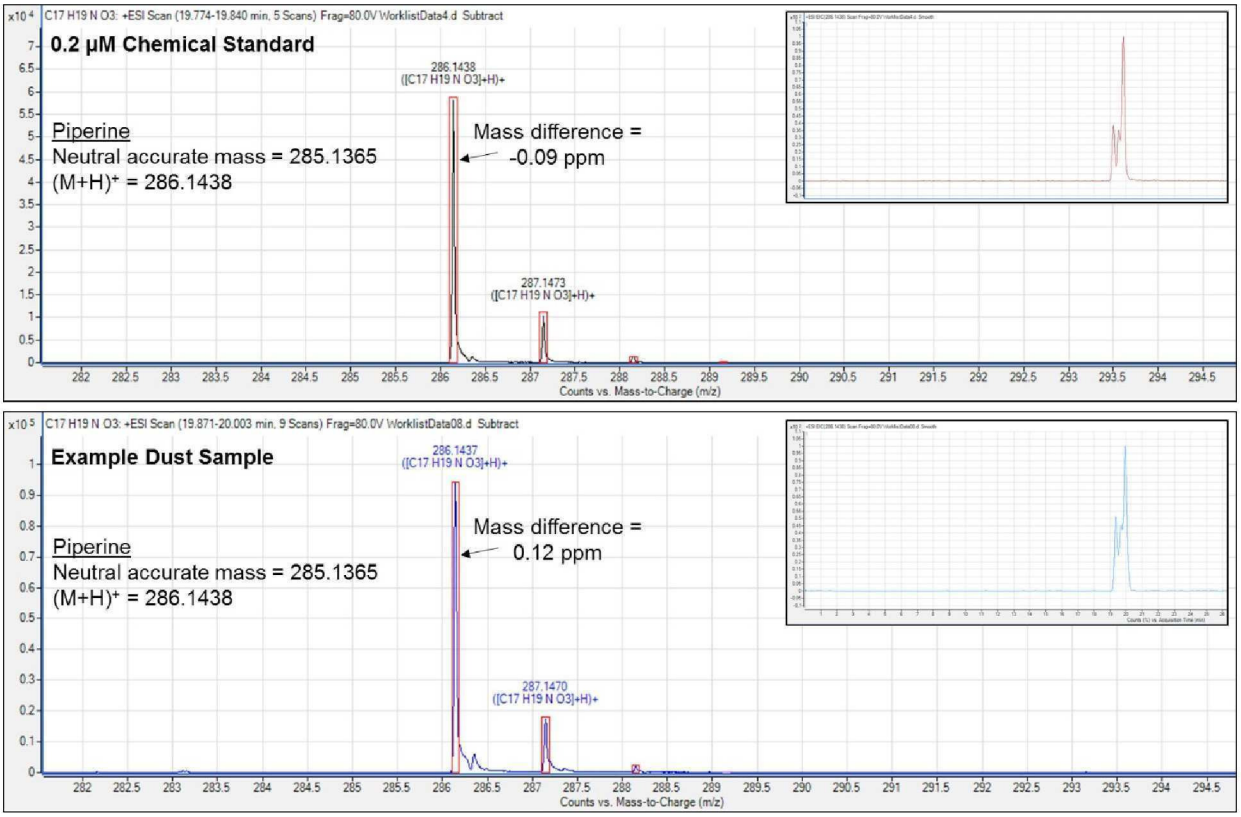

Supplementary Figure 2. Piperine extracted ion chromatograms from the chemical standard mixture (top) and an example dust sample (bottom). Chromatograms were extracted by searching for piperine's neutral accurate mass value plus a proton $(M+H)^+$. The mass difference between each spectral peak and the $(M+H)^+$ value is indicated in ppm (parts per million). Since its conjugated double bonds can each exist in either cis or trans configurations, there are multiple isomeric forms of piperine. These isomers separated chromatographically to show multiple peaks, as seen in the upper right corner of the spectrum. Note that these multiple peaks were also detected in the dust samples, but only one peak per dust sample passed the criteria for the database search match scoring. The results shown here were produced in positive ionization mode.

Supplementary Figure 3

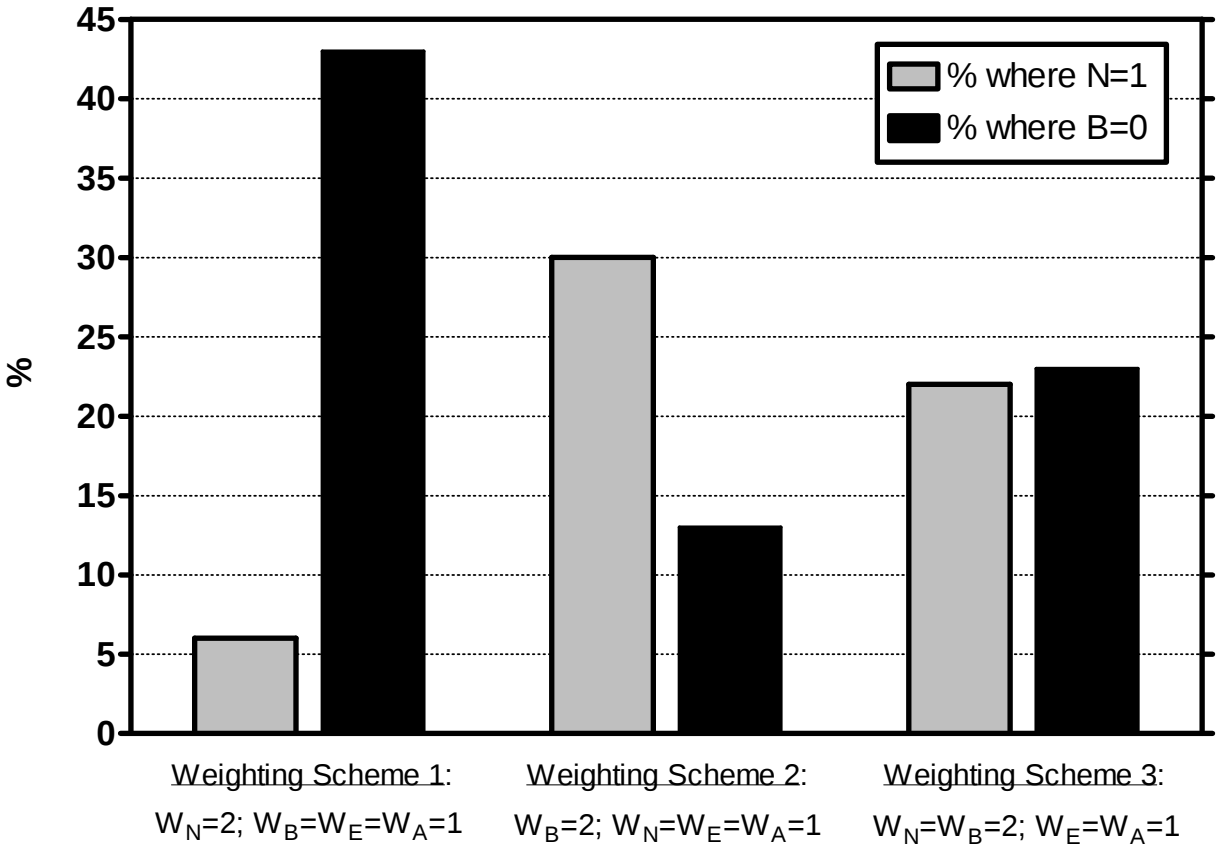

Supplementary Figure 3. Results of a ToxPi sensitivity analysis. Chemicals tentatively identified via suspect screening (based on formula match) were prioritized using the ToxPi framework. Three different ToxPi weighting schemes were evaluated for their impacts on chemical prioritization. For weighting scheme 1, ToxPi scores were calculated according to equation 2, where detection frequency (N) was given twice the weight of bioactivity (B), exposure (E), and abundance (A). For weighting scheme 2, ToxPi scores were recalculated with B given twice the weight of N, E, and A. For weighting scheme 3, ToxPi scores were recalculated with N and B given twice the weight of E and A. The top 100 chemicals, as prioritized according to schemes 1-3, were evaluated to inform the optimal weighting strategy. Specifically, the number of times (out of 100) that N=1 (chemical tentatively identified in one of 56 samples) and B=0 (no bioactivity across 16 assays) were tallied. Calculated values are shown as percentages in this figure.

Results and Discussion of Sensitivity Analysis.

Under weighting scheme 1, six of the top 100 chemicals were found in only one sample, and 43 showed no bioactivity. Under weighting scheme 2, 30 of the top 100 chemicals were found in

only one sample, and 13 showed no bioactivity. Under weighting scheme 3, 22 of the top 100 chemicals were found in only one sample, and 23 showed no bioactivity. Given these results, weighting scheme 3 is most appropriate for balancing occurrences where priority chemicals have an extreme (low) value of N or B.

When a priority chemical has one extreme value (or more), the investigator(s) must decide if and when that chemical is further considered in confirmatory analyses. For example, an investigator may choose to ignore a top-ranking chemical that shows little or no bioactivity. However, it may be more prudent to contemplate alternative scenarios before discounting a chemical. Consider hypothetical chemical A with formula $C_nH_nN_nO_nS_n$. Let us say that chemical A was tentatively identified (based on formula $C_nH_nN_nO_nS_n$) in all study samples at high abundance, but it isn't associated with bioactivity based on a set of high-throughput assays. It's entirely possible that the observed formula $C_nH_nN_nO_nS_n$ actually represents chemical B, which is not in our screening library (i.e., DSSTox_v2), and has not undergone *in vitro* testing as part of the ToxCast/Tox21 programs. Here, given extremely high N and A, it may be worthwhile determining whether formula $C_nH_nN_nO_nS_n$ represents chemical A or B (or neither) using additional resources (MS/MS spectra or authentic standards). Thus, the investigator must choose to first more carefully evaluate chemicals A and B, or move to other tentatively identified chemicals found in fewer samples but with higher bioactivity. This simple example highlights both the uncertainty and nuance in screening analyses, and underscores the need for balanced assessment methods that consider multiple data sources.

EPA-RTP LIBRARY

Article Impact Report

Integrating Tools for Non-Targeted Analysis Research and Chemical Safety Evaluations at the US EPA

JOURNAL OF EXPOSURE SCIENCE AND ENVIRONMENTAL EPIDEMIOLOGY

Sobus, JR; Wambaugh, JF; Isaacs, KK; Williams, AJ; McEachran, AD; Richard, AM; et al.

Sobus, JR, et al. (2018). Integrating Tools for Non-Targeted Analysis Research and Chemical Safety Evaluations at the US EPA. *Journal Of Exposure Science And Environmental Epidemiology, 28*(5), 411-426. PMID: 29288256. DOI: 10.1038/s41370-017-0012-y

Highlights

Citations

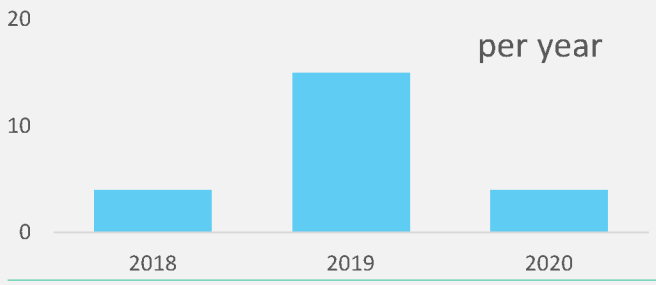

52 Google Scholar

36 Dimensions

25 Web of Science

by authors from
62 organizations
across
17 publication titles

Top Citing Journal
Analytical and Bioanalytical Chemistry

4 Articles

3.29 Impact Factor

3501
Total Downloads

Citations by Country

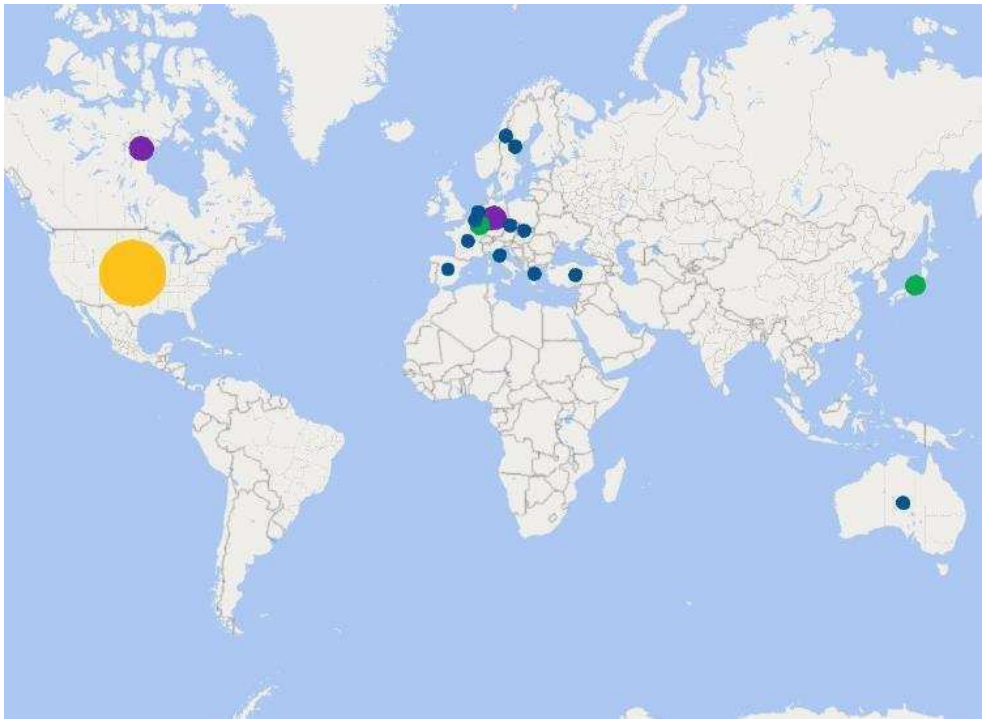

Countries	Papers
USA	22
CANADA	3
GERMANY	3
LUXEMBOURG	2
JAPAN	2
ITALY	1
ENGLAND	1
NORWAY	1
SWEDEN	1
GREECE	1

Top Citing Organizations

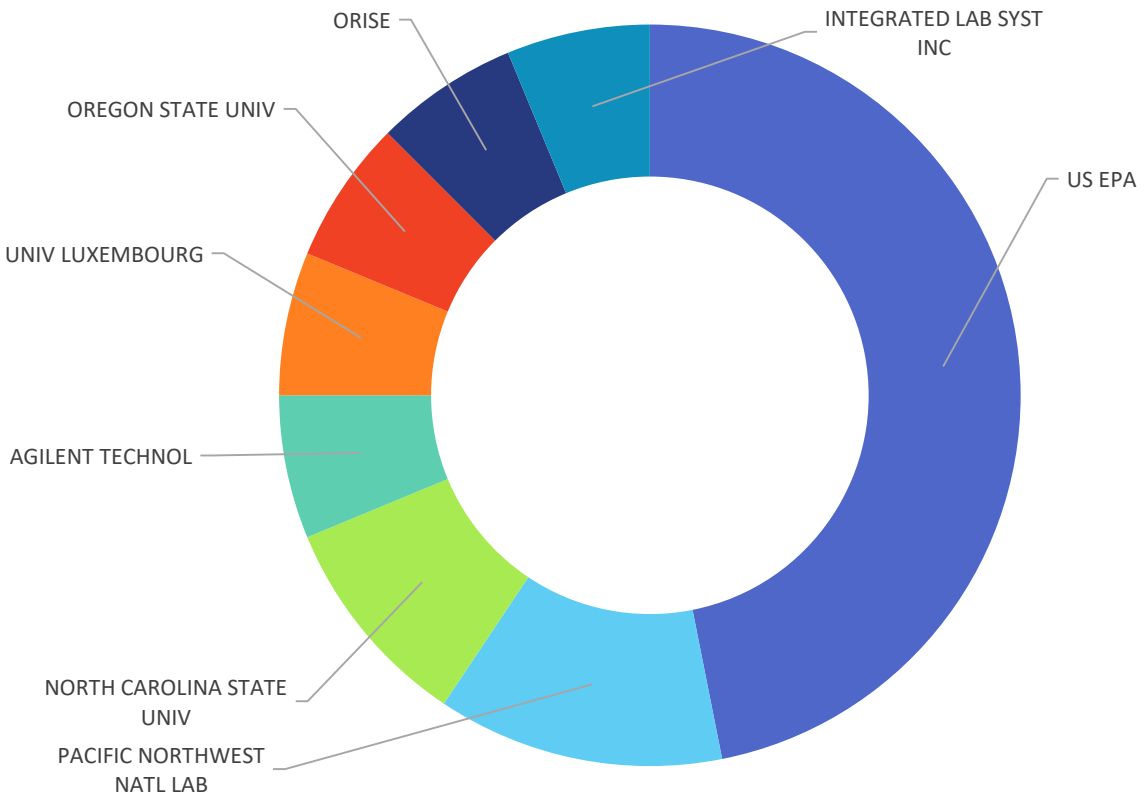

Citing Journals (Impact Factor)

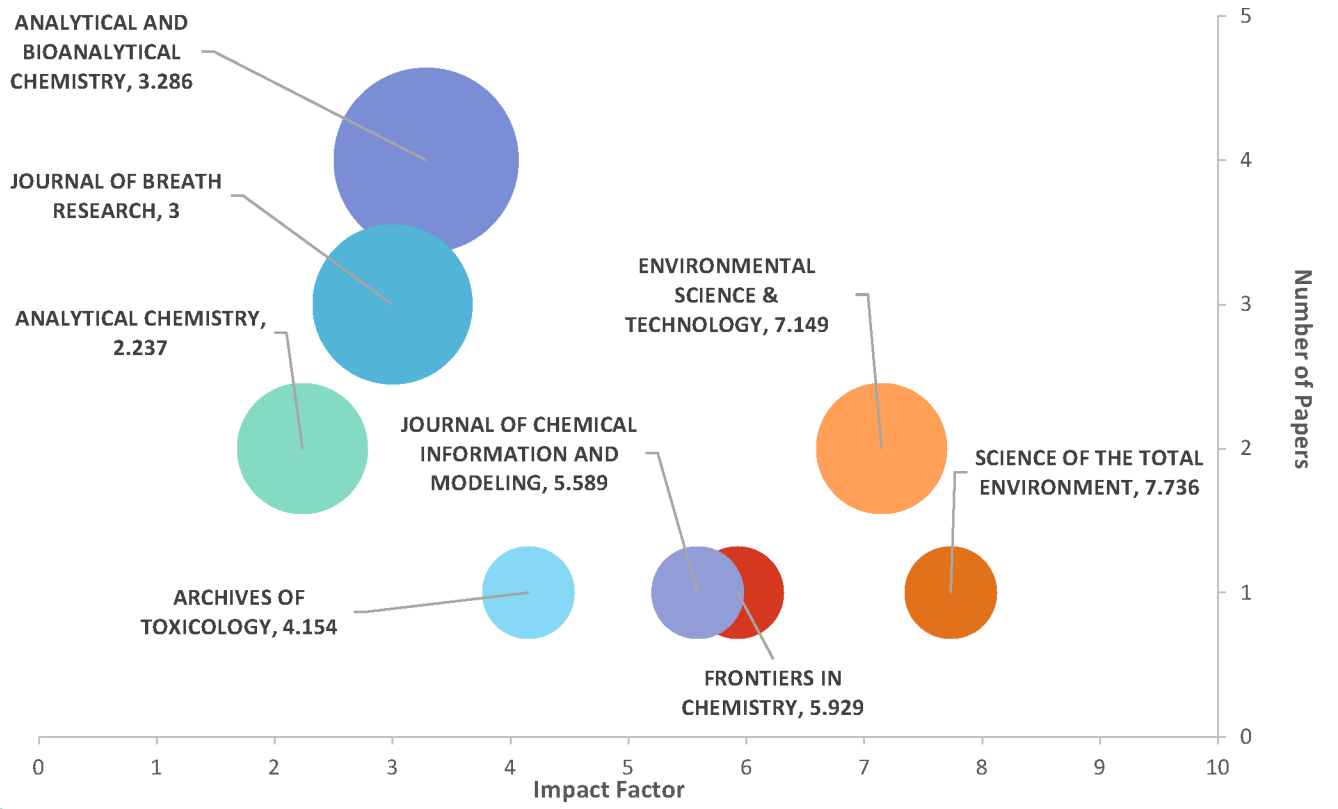

Research Areas

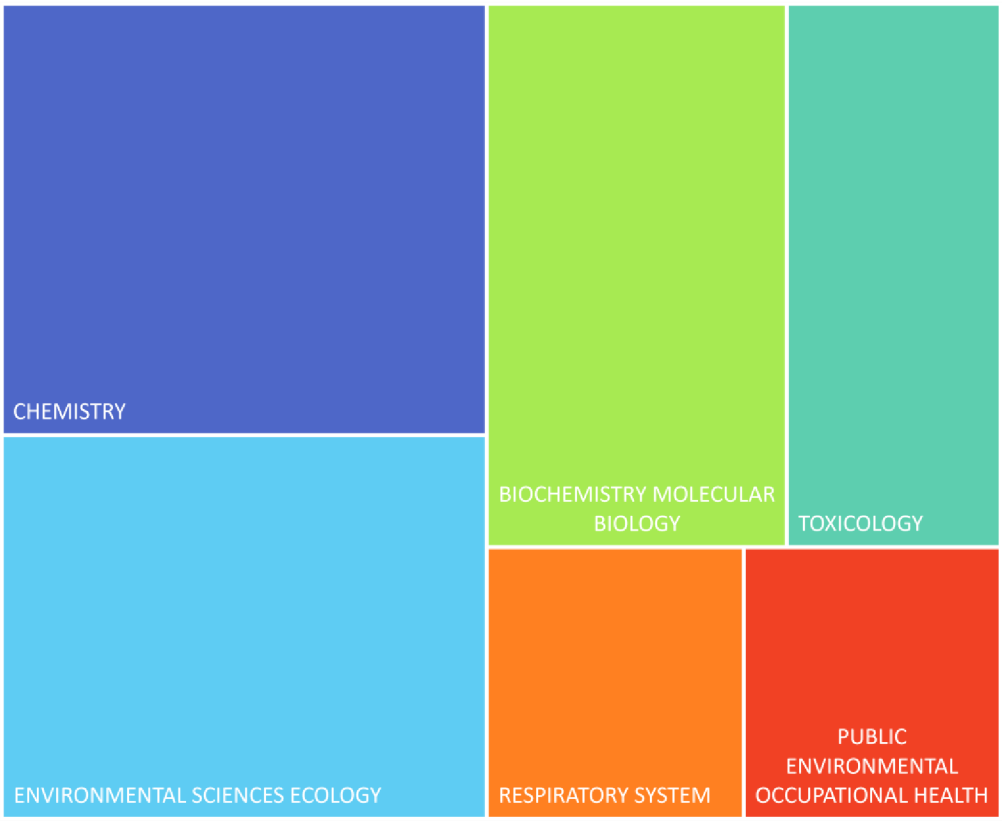

Research Areas	Papers
CHEMISTRY	9
ENVIRONMENTAL SCIENCES ECOLOGY	8
BIOCHEMISTRY MOLECULAR BIOLOGY	7
TOXICOLOGY	5
RESPIRATORY SYSTEM	3
PUBLIC ENVIRONMENTAL OCCUPATIONAL HEALTH	3

Alternative Metrics

Altmetric

Mendeley

Mendeley Readers' Disciplines

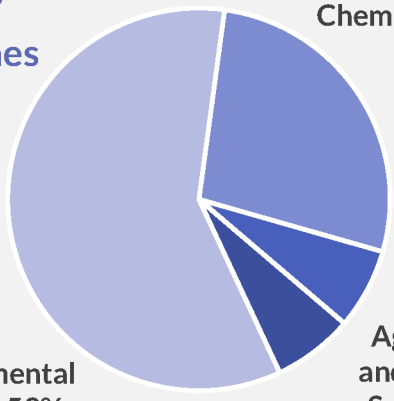

About this Attention Score

Good Attention Score compared to outputs of the same age (66th percentile)

Average Attention Score compared to outputs of the same age and source

Chosen as one of *The Journal of Exposure Science and Environmental Epidemiology's* '**Best Papers**' of 2018-2019

Mentioned by

5 tweeters

1 Facebook page

Citations

36 Dimensions

Readers on

74 Mendeley

As of April 2020, this article was mentioned in **6 tweets** by **5 users** with an upper bounds of **6,387 followers**

Data collected 17 April 2020.
Current data may differ.

About the Report

This report was compiled using data from Web of Science, Google Scholar, Altmetric, and other databases when necessary. It is a snapshot of a particular article where the impact has been determined through analyzing various information about the papers citing that article. By collecting and organizing these statistics, a picture of reach, popularity, and value is created.

Citations by Country

The origin of the citing papers as determined by author addresses. All records are shown on the graphic, and the logical threshold is displayed in the accompanying table.

Top Citing Organizations

The listed author affiliations of citing articles. Percentage is determined using a logical threshold where the remaining percent of the whole would be considered "other."

Citing Journals

The volume of citing papers per the top ten journal titles compared to other titles citing the paper, displayed along with the journal's impact factor for the report year. In the graphic:

- position along the x axis is determined by the journal impact factor
- position along the y axis is determined by the number of citing papers published in the source title
- size is determined by the percentage of citing papers published in the specific source title compared to all other titles

Research Areas

The scientific category for each citing paper. A logical threshold is displayed in the graphic, and an expansion is shown in the accompanying table.

Alternative Metrics

Metrics gathered using the Altmetric database, PlumX Analytics, publisher website data, and other sources including but not limited to those listed in the Altmetric doughnut:

Source name	Definition
Twitter	Collection of tweets, retweets, and quoted tweets with links to scholarly content
Facebook	Monitors Public Facebook Pages and posts
Google+	Mentions from public posts (Coverage ended Jan. 2019 but historical data still available)
Policy documents	Scans and text-mines policy document PDFs for references; connected to CrossRef and PubMed for DOIs
Patents	Using data from IIFI CLAIMS®, tracks references found in patents filed with nine international patents offices
News	Manually curated data provided from third-parties and RSS feeds
Blogs	Manually curated list, attempts to gather posts linking to scholarly articles
Wikipedia	Mentions located in References section
Mendeley	Number of readers with the content in their library
CiteULike	Online reference manager counted similar to Mendeley (Coverage ended Dec. 2014 but historical data still available)

Author Order - Paper 1	Author Order - Paper 2	Combined Author List
Rager JE	Sobus JR	Sobus JR
Strynar MJ	Wambaugh JF	Rager JE
Liang S	Isaacs KK	Strynar MJ
McMahen RL	Williams AJ	Wambaugh JF
Richard AM	McEachran AD	Isaacs KK
Grulke CM	Richard AM	Williams AJ
Wambaugh JF	Grulke CM	McEachran AD
Isaacs KK	Ulrich EM	Ulrich EM
Judson R	Rager JE	Liang S
Williams AJ	Strynar MJ	McMahen RL
Sobus JR	Newton SR	Richard AM
		Grulke CM
		Newton SR
		Judson R

Percent Contribution	Affiliation
20	EPA Staff Scientist
20	ORISE Participant
5	EPA Staff Scientist
5	EPA Staff Scientist
5	EPA Staff Scientist
5	EPA Title 42
5	ORISE Participant
5	EPA Staff Scientist
5	ORISE Participant
5	ORISE Participant
5	EPA Staff Scientist
5	EPA Title 42
5	EPA Staff Scientist
5	EPA Title 42

100

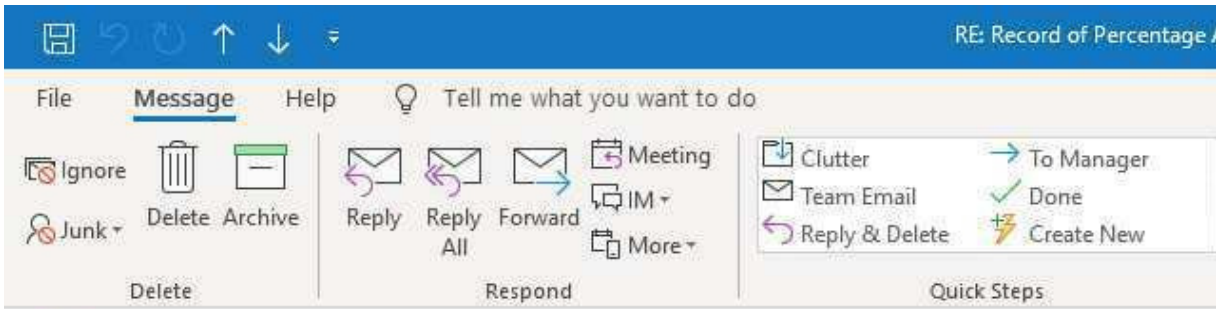

Tue 4/28/2020 11:44 AM

Sobus, Jon

RE: Record of Percentage Agreement - Jon Sobus

To Sobus, Jon

Dear Jon,

I confirm my position/organization and agree to the total percent level of effort.

Best regards,

Jon

From: Sobus, Jon <Sobus.Jon@epa.gov>
Sent: Tuesday, April 28, 2020 11:42 AM
To: Sobus, Jon <Sobus.Jon@epa.gov>
Subject: FW: Record of Percentage Agreement - Jon Sobus

Dear Jon,

I'm submitting two publications for consideration for a 2020 STAA award:

Rager JE, Strynar MJ, Liang S, McMahen RL, Richard AM, Grulke CM, Wambaugh JF, Isaacs KK, Judson R, advance high-throughput environmental monitoring. Environ Int. 2016 Mar;88:269-280. Impact Factor =

Sobus JR, Wambaugh JF, Isaacs KK, Williams AJ, McEachran AD, Richard AM, Grulke CM, Ulrich EM, Rage the US EPA. J Expo Sci Environ Epidemiol. 2018 Sep;28(5):411-426. Impact Factor = 3.025; Immediacy Ind

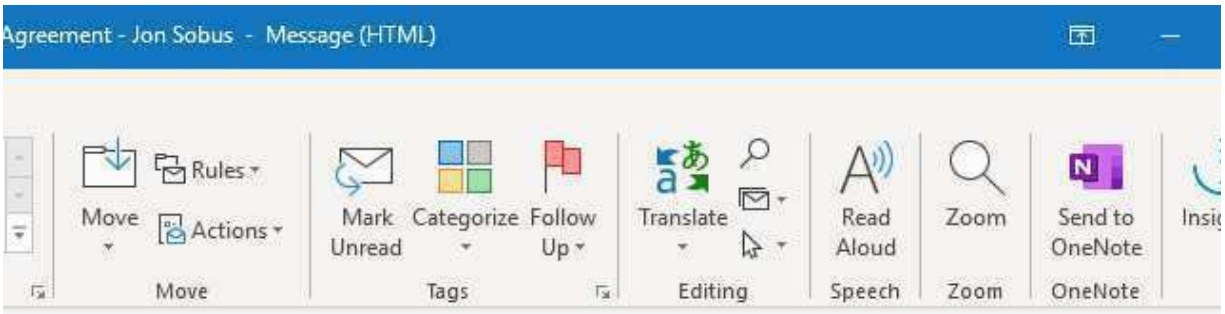

Williams AJ, Sobus JR. Linking high resolution mass spectrometry data with exposure and toxicity forecasts t
7.943; Immediacy Index = 1.108; Cited Half-Life = 6.0; Times Cited = 75.

r JE, Strynar MJ, Newton SR. Integrating tools for non-targeted analysis research and chemical safety evalua
ex = 1.277; Cited Half-Life = 8.1; Times Cited = 24.

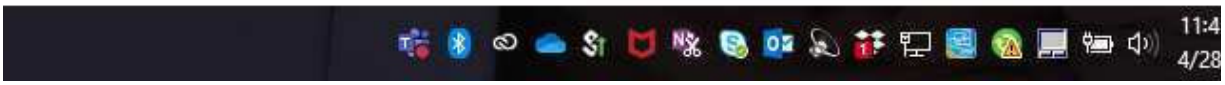

ghts
o
itions at
5 AM
/2020
21

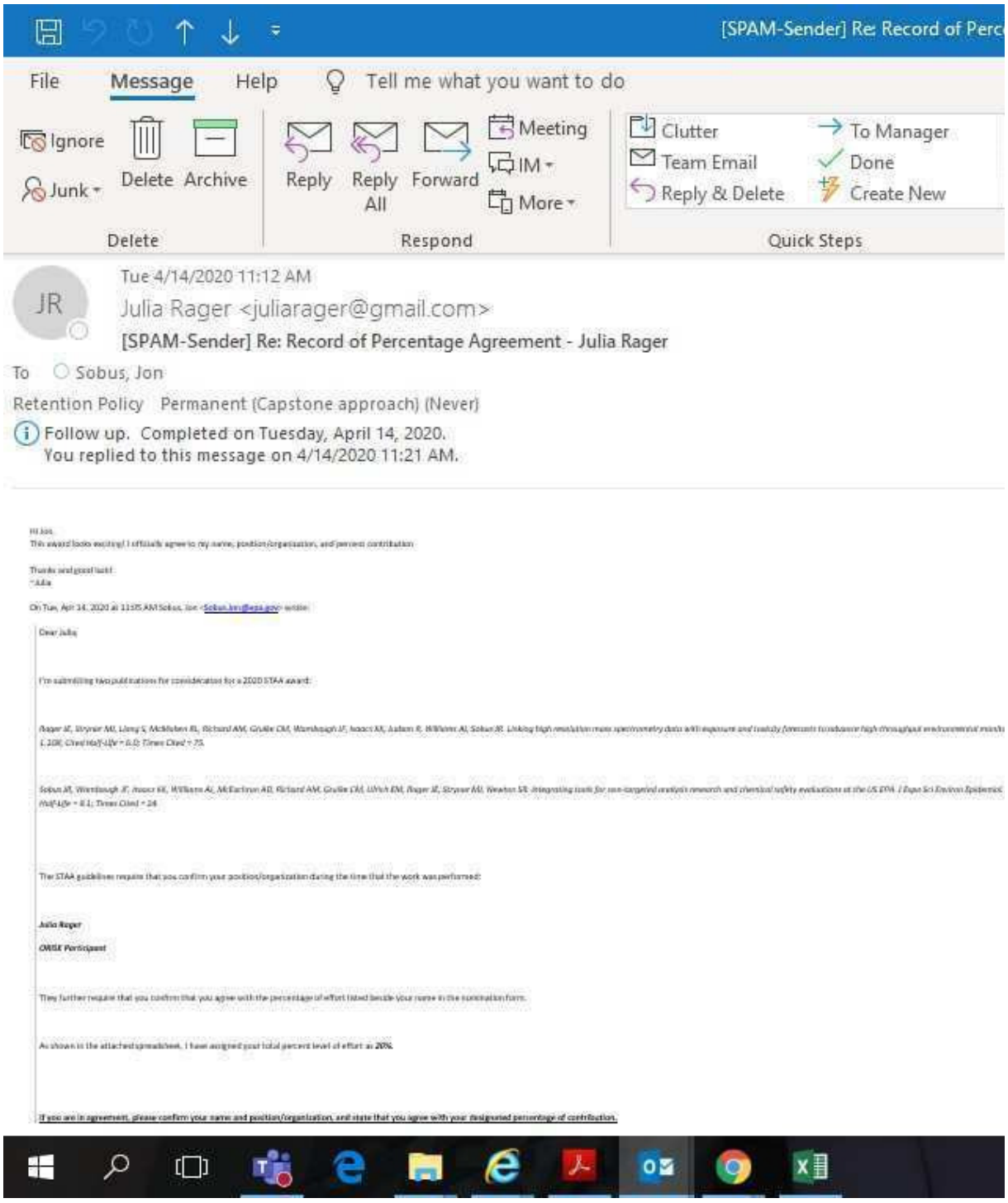
[SPAM-Sender] Re: Record of Perc
File
Message
Help
Tell me what you want to do
Ignore
Junk
Delete
Archive
Reply
Reply All
Forward
Meeting
IM
More
Clutter
Team Email
Reply & Delete
To Manager
Done
Create New
Delete
Respond
Quick Steps
JR
Tue 4/14/2020 11:12 AM
Julia Rager <juliarager@gmail.com>
[SPAM-Sender] Re: Record of Percentage Agreement - Julia Rager
To
Sobus, Jon
Retention Policy Permanent (Capstone approach) (Never)
Follow up. Completed on Tuesday, April 14, 2020.
You replied to this message on 4/14/2020 11:21 AM.
Hi Jon,
This award looks exciting! I officially agree to my name, position/organization, and percent contribution.
Thanks and good luck!
-Julia
On Tue, Apr 14, 2020 at 11:05 AM Sobus, Jon <Sobus.Jon@epa.gov> wrote:
Dear Julia,
I'm submitting two publications for consideration for a 2020 STAA award:
Rager JE, Strynar MJ, Liang S, McMahen RL, Richard AM, Grulke CM, Wambaugh JF, Isaacs KK, Judson R, Williams AJ, Sobus JR. Linking high resolution mass spectrometry data with exposure and toxicity forecasts to advance high-throughput environmental monito
1, 100, Cited Half-Life = 0.0; Times Cited = 75.
Sobus JR, Wambaugh JF, Isaacs KK, Williams AJ, McEachran AD, Richard AM, Grulke CM, Ulrich EM, Rager JE, Strynar MJ, Newton SR. Integrating tools for non-targeted analysis research and chemical safety evaluations at the US EPA. J Expo Sci Environ Epidemiol.
Half-Life = 0.1; Times Cited = 24
The STAA guidelines require that you confirm your position/organization during the time that the work was performed:
Julia Rager
ORISE Participant
They further require that you confirm that you agree with the percentage of effort listed beside your name in the nomination form.
As shown in the attached spreadsheet, I have assigned your total percent level of effort as 20%.
If you are in agreement, please confirm your name and position/organization, and state that you agree with your designated percentage of contribution.

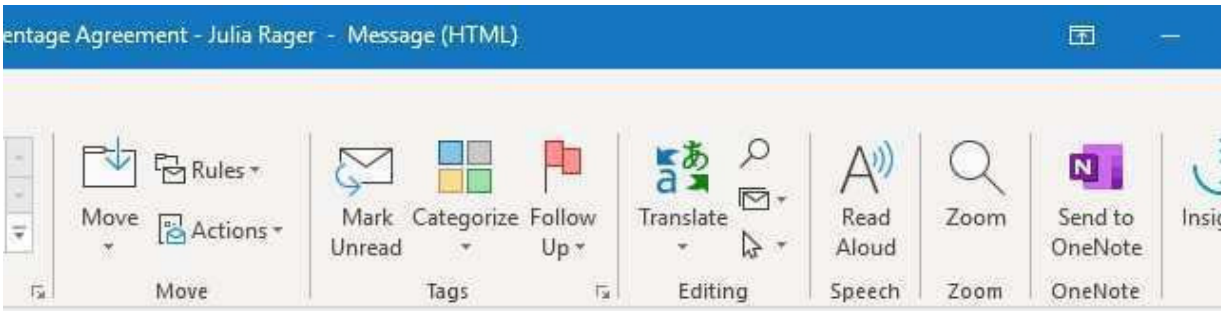

Expires Never

ning. Environ Int. 2016 Mar;88:269-280. Impact Factor = 7.982; Immediacy Index =

2018 Sep;24(5):422-426. Impact Factor = 3.025; Immediacy Index = 1.277; Cited

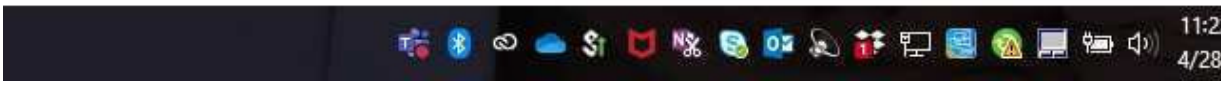

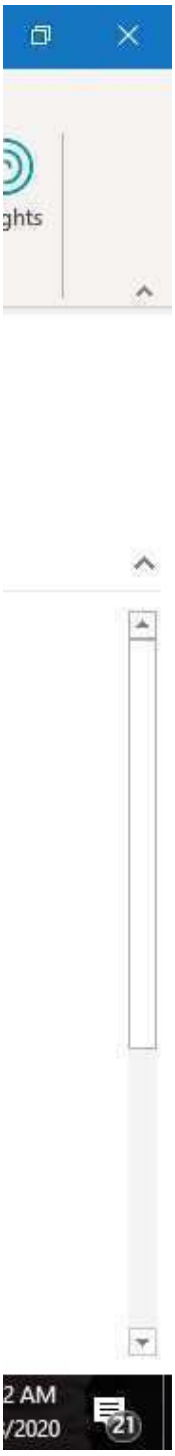
ghts
2 AM
/2020
21

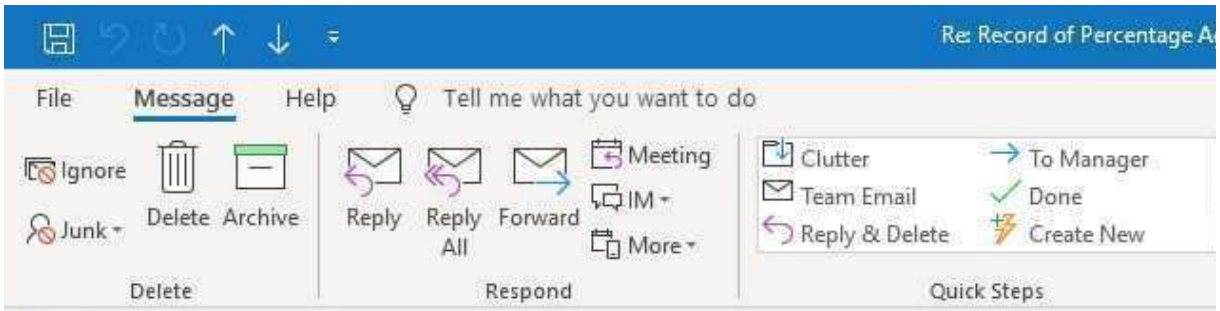

Tue 4/14/2020 3:04 PM

Strynar, Mark

Re: Record of Percentage Agreement - Mark Strynar

To Sobus, Jon

Retention Policy Permanent (Capstone approach) (Never)

You replied to this message on 4/14/2020 3:05 PM.

Hi Jon,

I agree to being assigned 5% effort for this STAA package. Additionally my last STAA package award was from 2013 so I think it is outside of the time window luck.

Mark

My pertinent info is:
Mark Strynar
Physical Scientist
US EPA/ORD/CEMM

Dr. Mark Strynar
US EPA/ORD/CEMM
strynar.mark@epa.gov
(office) 919-541-3706
(mobile) 919-606-6905

From: Sobus, Jon <Sobus.Jon@epa.gov>
Sent: Tuesday, April 14, 2020 1:19 PM
To: Strynar, Mark <Strynar.Mark@epa.gov>
Subject: FW: Record of Percentage Agreement - Mark Strynar

Dear Mark,

I'm submitting two publications for consideration for a 2020 STAA award:

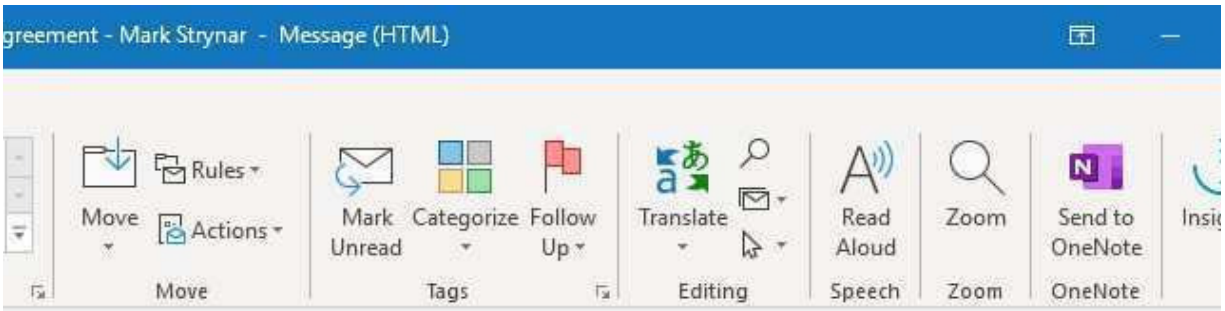

Expires Never

for this go round. However, I am intending to submit a package with James McCord and others for this go round. I dont expect that you need that info. Good

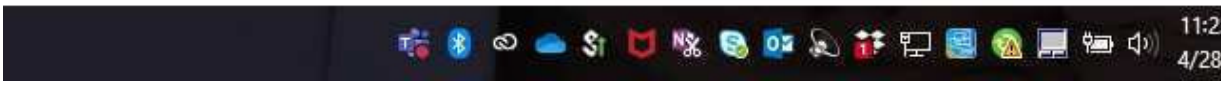

ghts
3 AM
/2020
21

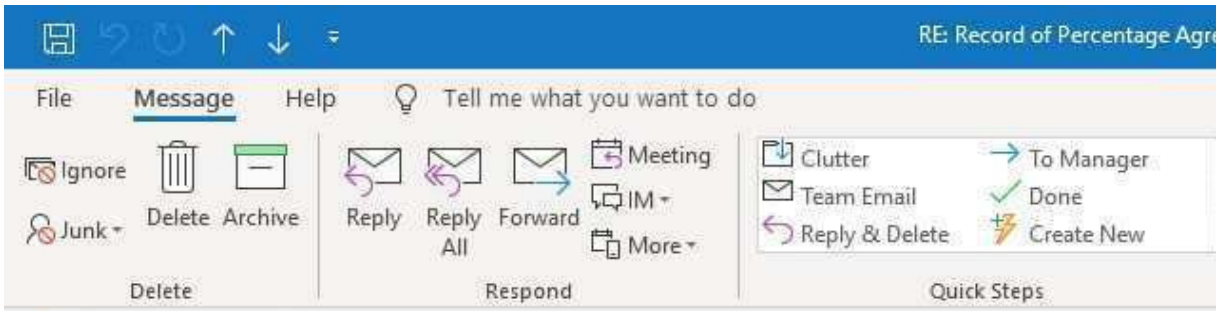

Tue 4/14/2020 1:53 PM

Wambaugh, John

RE: Record of Percentage Agreement - John Wambaugh

To Sobus, Jon

Retention Policy Permanent (Capstone approach) (Never)

You replied to this message on 4/14/2020 2:05 PM.

Thank you for including me! 5% is fair. I will pull the papers together.

John

From: Sobus, Jon <Sobus.Jon@epa.gov>
Sent: Tuesday, April 14, 2020 1:42 PM
To: Wambaugh, John <Wambaugh.John@epa.gov>
Subject: Record of Percentage Agreement - John Wambaugh

Dear John,

I'm submitting two publications for consideration for a 2020 STAA award:

Rager JE, Strynar MJ, Liang S, McMahen RL, Richard AM, Grulke CM, Wambaugh JF, Isaacs KK, Judson R, Williams AJ, Sobus JR. Linking high resolution mass spectrometry dat 1.108; Cited Half-Life = 6.0; Times Cited = 75.

Sobus JR, Wambaugh JF, Isaacs KK, Williams AJ, McEachran AD, Richard AM, Grulke CM, Ulrich EM, Rager JE, Strynar MJ, Newton SR. Integrating tools for non-targeted analy Life = 8.1; Times Cited = 24.

The STAA guidelines require that you confirm your position/organization during the time that the work was performed:

John Wambaugh
EPA Staff Scientist

They further require that you confirm that you agree with the percentage of effort listed beside your name in the nomination form.

As shown in the attached spreadsheet, I have assigned your total percent level of effort as ***5%***.

If you are in agreement, please confirm your name and position/organization, and state that you agree with your designated percentage of contribution.

Finally, I need you to list any papers that you've nominated for a STAA award over the past 6 years. Please include the publication title, year, and award level for each pu

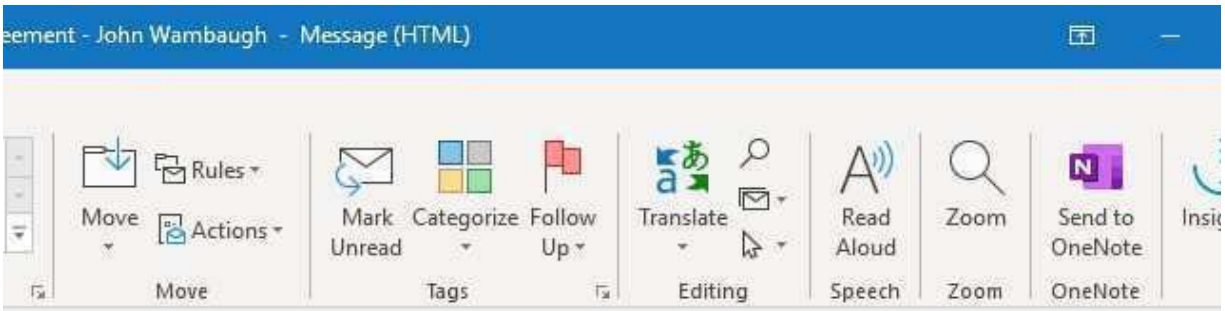

Expires Never

e with exposure and toxicity forecasts to advance high-throughput environmental monitoring. Environ Int. 2016 Mar;88:269-280. Impact Factor = 7.943; Immediacy Index =

sis research and chemical safety evaluations at the US EPA. J Expo Sci Environ Epidemiol. 2018 Sep;28(5):411-426. Impact Factor = 3.025; Immediacy Index = 1.277; Cited Half-

blication.

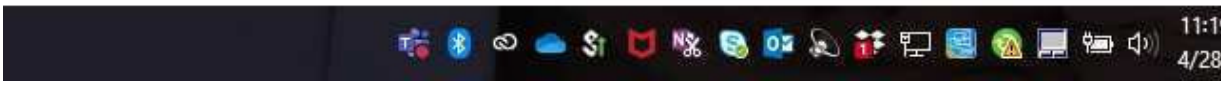

ghts
9 AM
/2020
21

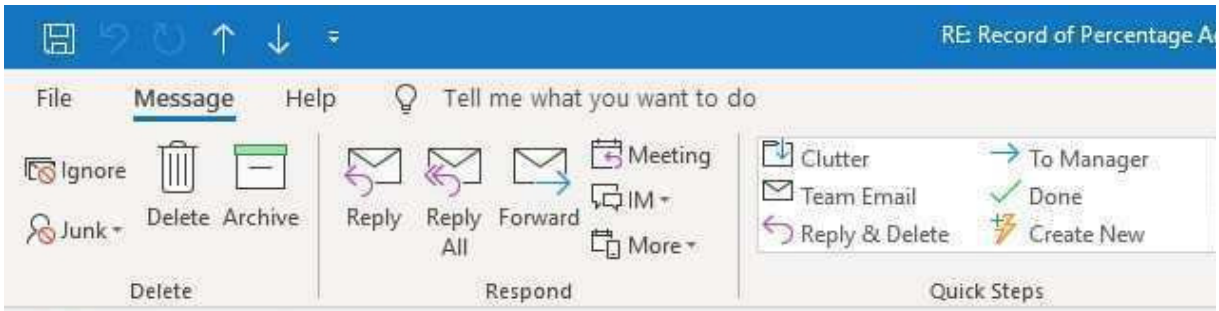

Tue 4/14/2020 2:09 PM

Isaacs, Kristin

RE: Record of Percentage Agreement - Kristin Isaacs

To Sobus, Jon

Retention Policy Permanent (Capstone approach) (Never)

You replied to this message on 4/14/2020 2:12 PM.

Sorry- organization associated with time the work was performed (assume you actually just need NERL):

Kristin Isaacs
Research Physical Scientist
NERL: HEASD,SED, and CED

From: Isaacs, Kristin
Sent: Tuesday, April 14, 2020 2:04 PM
To: Sobus, Jon <Sobus.Jon@epa.gov>
Subject: RE: Record of Percentage Agreement - Kristin Isaacs

Hi Jon-

Good luck with the submittal! I confirm the level of effort and here is my info (not sure if you needed nominations that I personally submitted or everything I have been on).

2019- Level III Award: Advancing High-Throughput Chemical Exposure Models for Consumer and Dietary Pathways

2019- Level III Award: High-throughput screening of chemicals as functional substitutes using structure-based classification models

2016- Level III Award: (1) Air Pollution Exposure Model for Individuals (EMI) in Health Studies: Evaluation for Ambient PM2.5 in Central North Carolina, (2) GPS-based Microe
Modeling Spatial and Temporal Variability of Residential Air Exchange Rates for the Near-Road Exposures and Effects of Urban Air Pollutants Study (NEXUS)

From: Sobus, Jon <Sobus.Jon@epa.gov>
Sent: Tuesday, April 14, 2020 1:44 PM
To: Isaacs, Kristin <Isaacs.Kristin@epa.gov>
Subject: Record of Percentage Agreement - Kristin Isaacs

Dear Kristin,

I'm submitting two publications for consideration for a 2020 STAA award:

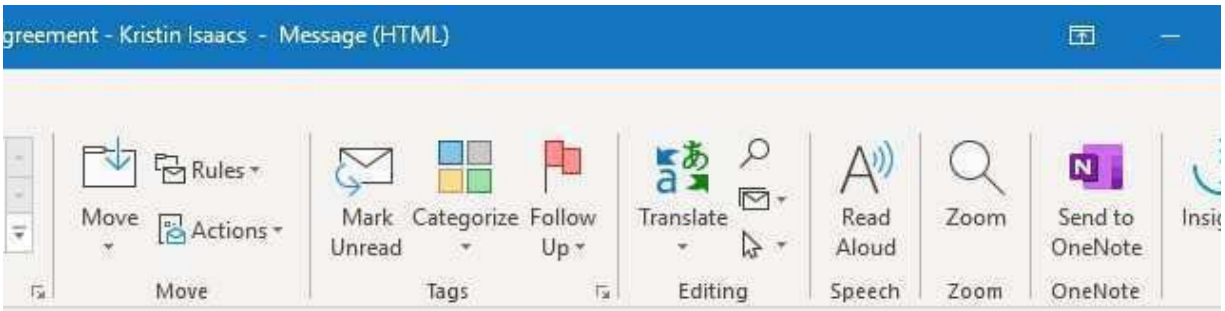

Expires Never

I was the actual submitter on only the first one listed below.

nvironment Tracker (MicroTrac) Model to Estimate Time-Location of Individuals for Air Pollution Exposure Assessments: Model Evaluation in Central North Carolina. (3)

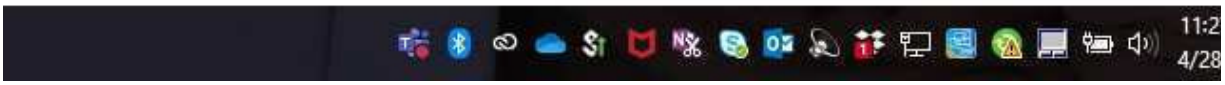

ghts
7 AM
/2020
21

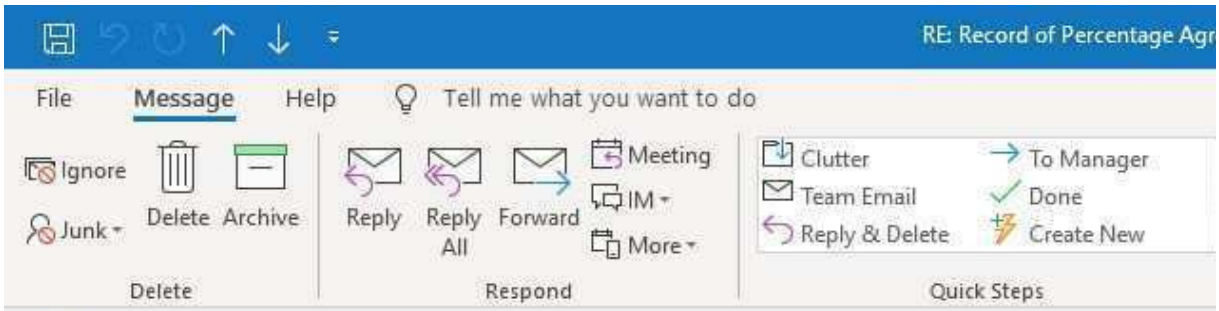

Tue 4/14/2020 2:36 PM

Williams, Antony

RE: Record of Percentage Agreement - Antony Williams

To Sobus, Jon

Retention Policy Permanent (Capstone approach) (Never)

You replied to this message on 4/14/2020 2:38 PM.

Dear Jon,

Thank you for the opportunity to contribute to the two papers listed. I agree with the designated percentage of contribution. My organizati

Antony J. Williams
Center for Computational Toxicology and Exposure
U.S. Environmental Protection Agency
109 T.W. Alexander Drive
Room D131I, Mail Drop D143-02
Research Triangle Park, NC 27711

Office Phone: 919-541-1033
Mobile Phone: 919-698-0526

Try out the **CompTox Chemicals Dashboard** and access data for almost 875,000 chemical substances

HOT OFF THE PRESS "Open-source QSAR models for pKa prediction using multiple machine learning approaches"

From: Sobus, Jon <Sobus.Jon@epa.gov>
Sent: Tuesday, April 14, 2020 1:46 PM
To: Williams, Antony <Williams.Antony@epa.gov>
Subject: Record of Percentage Agreement - Antony Williams

Dear Antony,

I'm submitting two publications for consideration for a 2020 STAA award:

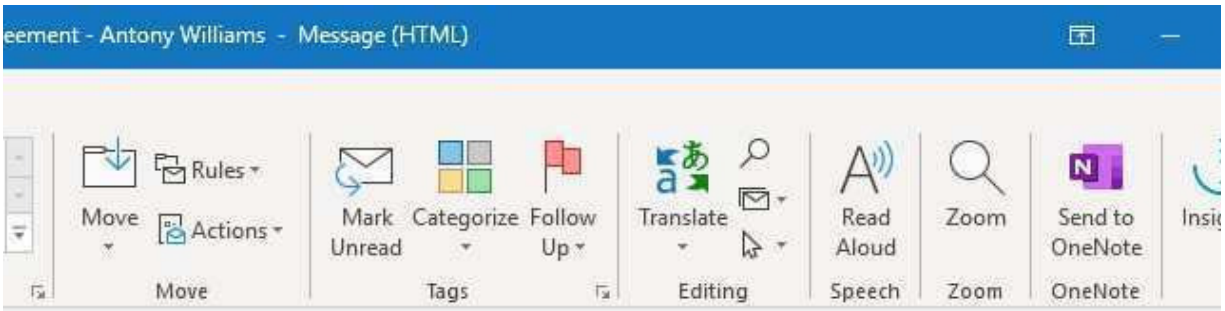

Expires Never

ional details are below. Best wishes.

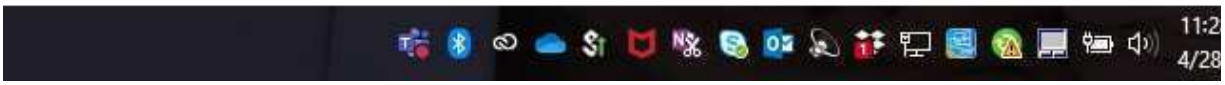

ghts
8 AM
/2020
21

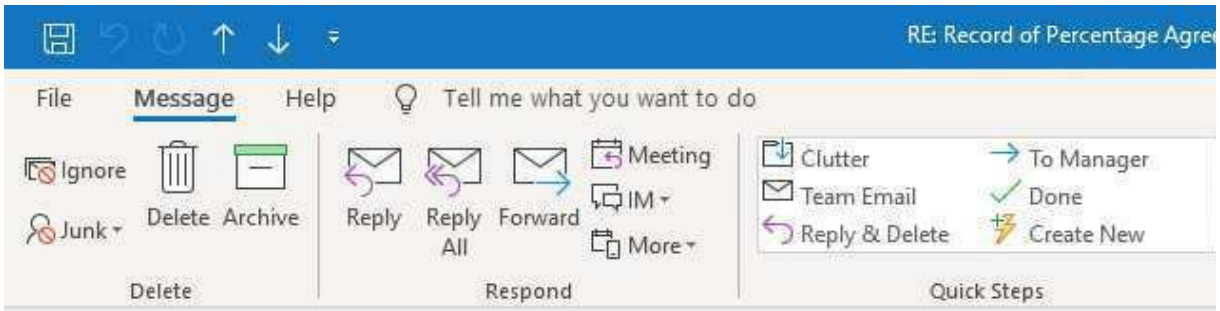

Tue 4/14/2020 4:09 PM

A

andrew.mceachran@agilent.com

RE: Record of Percentage Agreement - Andrew McEachran

To Sobus, Jon

Retention Policy Permanent (Capstone approach) (Never)

You replied to this message on 4/14/2020 4:33 PM.

Hi Jon-

I confirm my name and position as written and I agree with the designated percentage of contribution.

One thought- I know there can be discrepancies with citation numbers, but Google Scholar has 52 citatic

Best,
Andrew

From: Sobus, Jon <Sobus.Jon@epa.gov>
Sent: Tuesday, April 14, 2020 10:48 AM
To: MCEACHRAN,ANDREW (Agilent USA) <andrew.mceachran@agilent.com>
Subject: Record of Percentage Agreement - Andrew McEachran

Dear Andrew,

I'm submitting two publications for consideration for a 2020 STAA award:

Rager JE, Strynar MJ, Liang S, McMahen RL, Richard AM, Grulke CM, Wambaugh JF, Isaacs KK, Judson R, advance high-throughput environmental monitoring. Environ Int. 2016 Mar;88:269-280. Impact Factor =

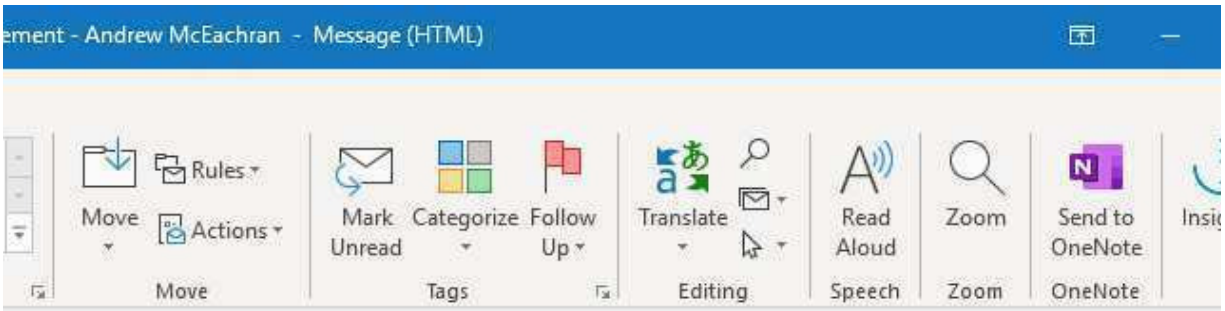

Expires Never

Good luck!

ons for the JESEE article.

Williams AJ, Sobus JR. Linking high resolution mass spectrometry data with exposure and toxicity forecasts t
7.943; Immediacy Index = 1.108; Cited Half-Life = 6.0; Times Cited = 75.

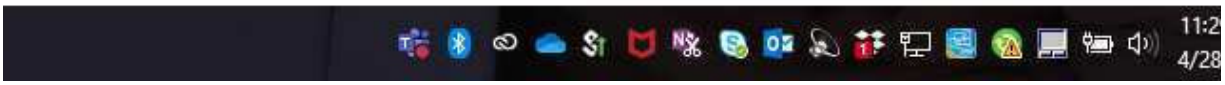

ghts
o
9 AM
/2020
21

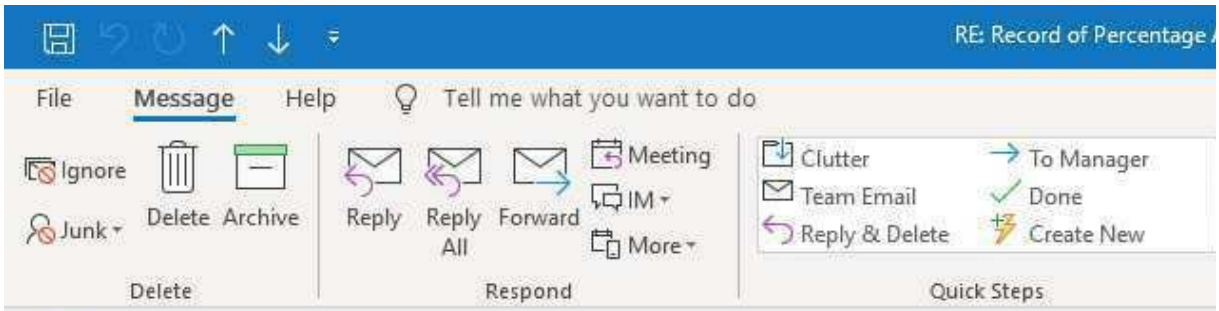

Tue 4/14/2020 2:06 PM
Ulrich, Elin
RE: Record of Percentage Agreement - Elin Ulrich

To Sobus, Jon

Retention Policy Permanent (Capstone approach) (Never)

You replied to this message on 4/14/2020 2:11 PM.

Jon,
I confirm that I was an EPA Research Chemist/Staff Scientist with NERL during the work being nominatec
I concur with my effort level of 5%.

2014 US EPA Level III Scientific and Technological Achievement Awards for Reviews of Chiral Pesticides:

E. M. Ulrich, C. N. Morrison, M. R. Goldsmith, and W. T. Foreman "Chirality in agrochemicals" *Reviews o*
E. M. Ulrich and R. L. Falconer "Chiral chlordane components in environmental matrices" In *Chiral Pestic*
Washington, DC, **2011**; *1085*, 11-43.

Let me know if you need any additional information and thanks for doing this.

****

Elin M. Ulrich, Ph.D.; Branch Chief
Advanced Analytical Chemistry Methods Branch
Email: ulrich.elin@epa.gov
Office Phone: 919-541-3717
Cell Phone (Tues/emergencies): 919-451-5988

U.S. Environmental Protection Agency
109 TW Alexander Dr.
Mail Drop D205-05
Research Triangle Park, NC 27711

****

SAVE THE DATE:

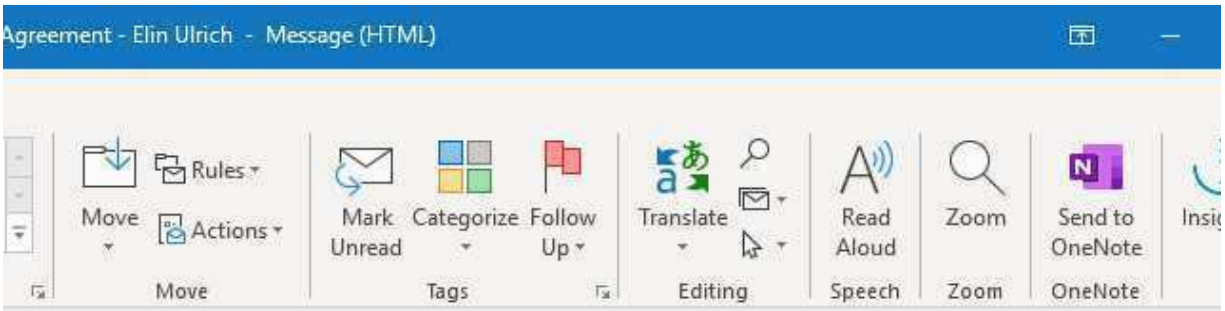

Expires Never

l.

f Environmental Contamination and Toxicology **2012,** *217*, 1-74.
ides: Stereoselectivity and Its Consequences, Garrison, A. W.; Gan, J.; Liu, W., Eds. American Chemical Societ

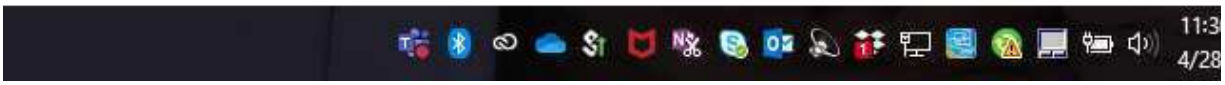

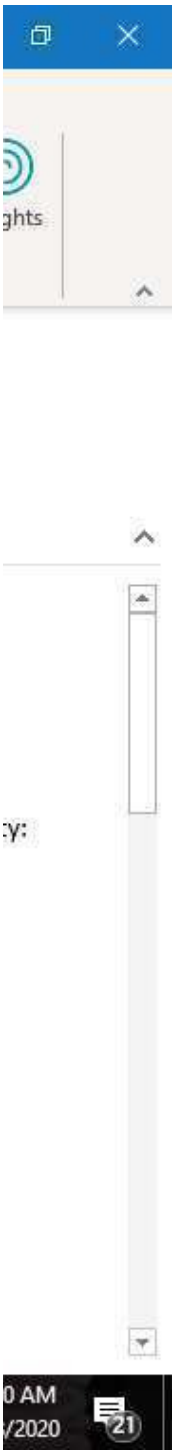
ghts
:y:
0 AM
/2020
21

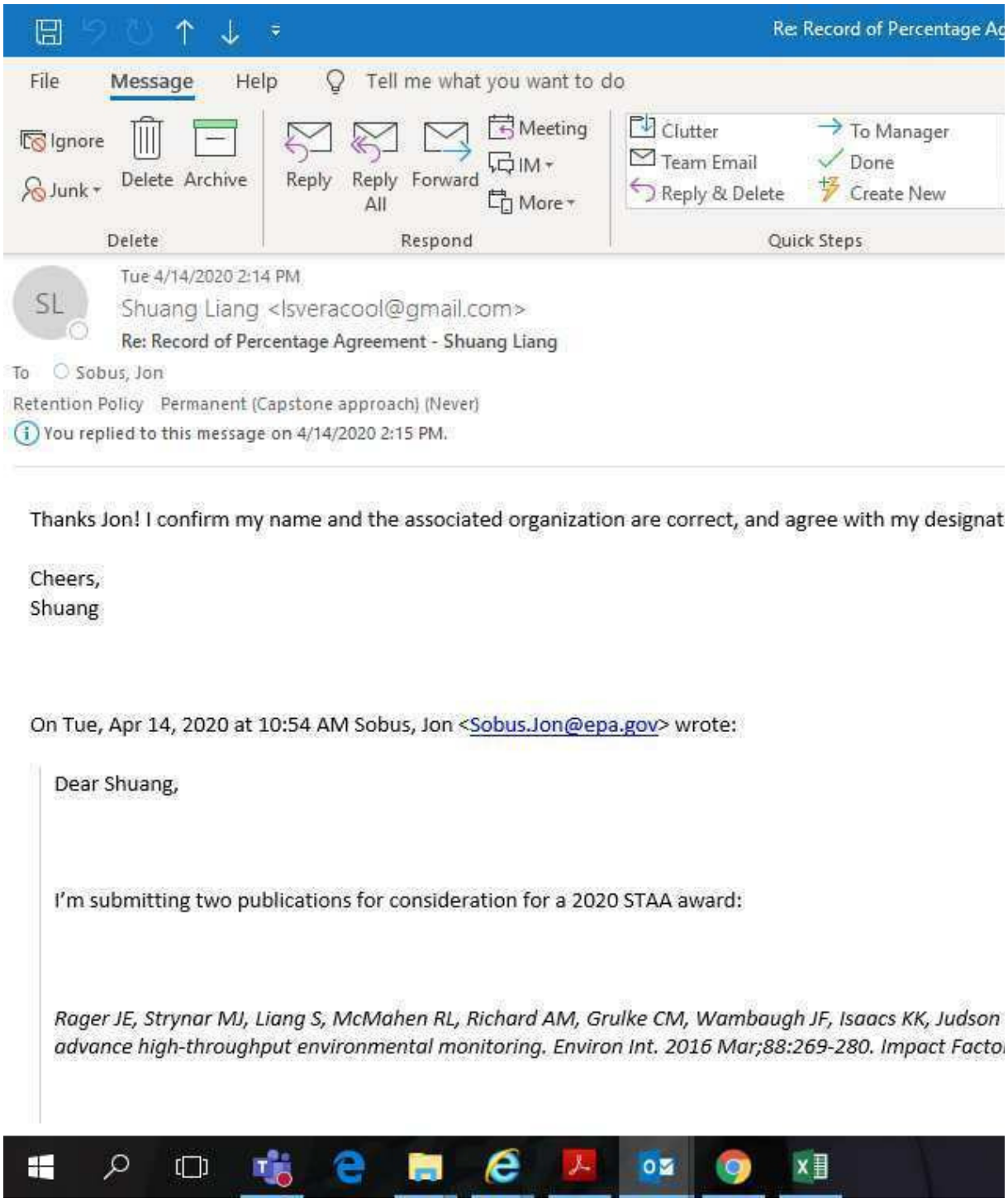
Re: Record of Percentage Ag
File
Message
Help
Tell me what you want to do
Ignore
Junk
Delete
Archive
Reply
Reply All
Forward
Meeting
IM
More
Clutter
Team Email
Reply & Delete
To Manager
Done
Create New
Delete
Respond
Quick Steps
SL
Tue 4/14/2020 2:14 PM
Shuang Liang <lsveracool@gmail.com>
Re: Record of Percentage Agreement - Shuang Liang
To Sobus, Jon
Retention Policy Permanent (Capstone approach) (Never)
You replied to this message on 4/14/2020 2:15 PM.
Thanks Jon! I confirm my name and the associated organization are correct, and agree with my designat
Cheers,
Shuang
On Tue, Apr 14, 2020 at 10:54 AM Sobus, Jon <Sobus.Jon@epa.gov> wrote:
Dear Shuang,
I'm submitting two publications for consideration for a 2020 STAA award:
Roger JE, Strynar MJ, Liang S, McMahen RL, Richard AM, Grulke CM, Wambaugh JF, Isaacs KK, Judson
advance high-throughput environmental monitoring. Environ Int. 2016 Mar;88:269-280. Impact Facto

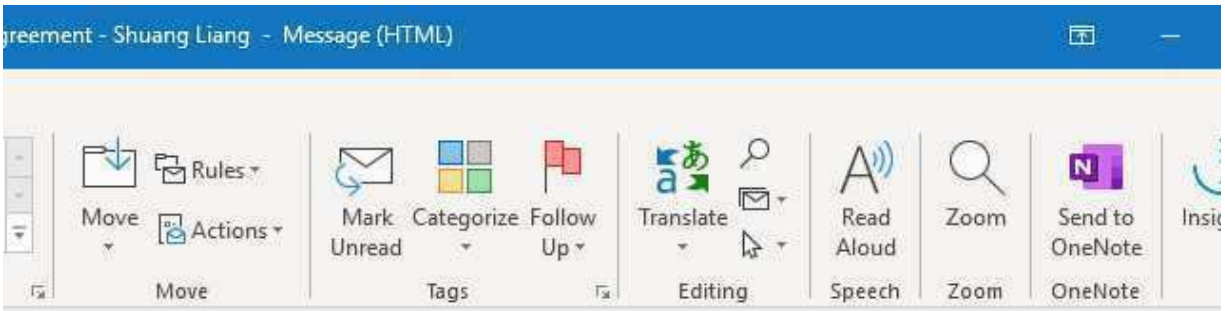

Expires Never

ed percentage of contribution!

R, Williams AJ, Sobus JR. Linking high resolution mass spectrometry data with exposure and toxicity forecast
r = 7.943; Immediacy Index = 1.108; Cited Half-Life = 6.0; Times Cited = 75.

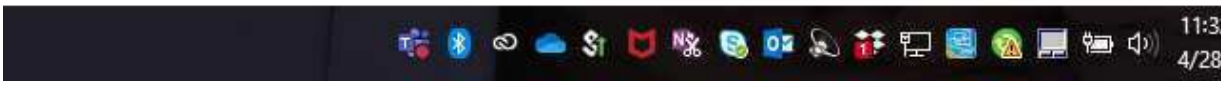

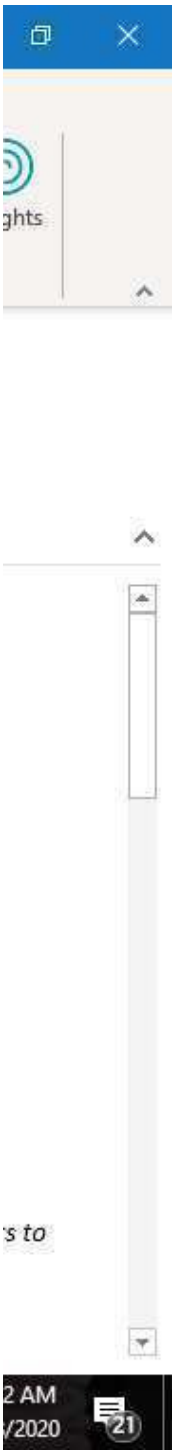
ghts
's to
2 AM
/2020
21

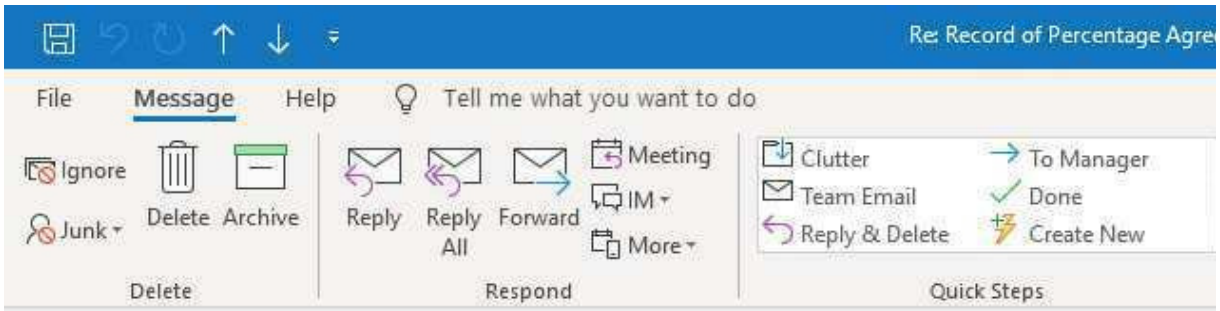

RM

Tue 4/14/2020 4:34 PM

Rebecca McMahen <rlmcmahen@gmail.com>

Re: Record of Percentage Agreement - Rebecca McMahen

To Sobus, Jon

Retention Policy Permanent (Capstone approach) (Never)

You replied to this message on 4/14/2020 7:44 PM.

Hi Jon,

I confirm my contributions and position. Thanks and hope all is well!

Rebecca

Sent from my iPhone

On Apr 14, 2020, at 1:56 PM, Sobus, Jon <Sobus.Jon@epa.gov> wrote:

> Dear Rebecca,
>
> I'm submitting two publications for consideration for a 2020 STAA award:
>
> *Rager JE, Strynar MJ, Liang S, McMahen RL, Richard AM, Grulke CM, Wambaugh JF, Isaacs KK, Ju forecasts to advance high-throughput environmental monitoring. Environ Int. 2016 Mar;88:269-*
>
> *Sobus JR, Wambaugh JF, Isaacs KK, Williams AJ, McEachran AD, Richard AM, Grulke CM, Ulrich E safety evaluations at the US EPA. J Expo Sci Environ Epidemiol. 2018 Sep;28(5):411-426. Impact F*

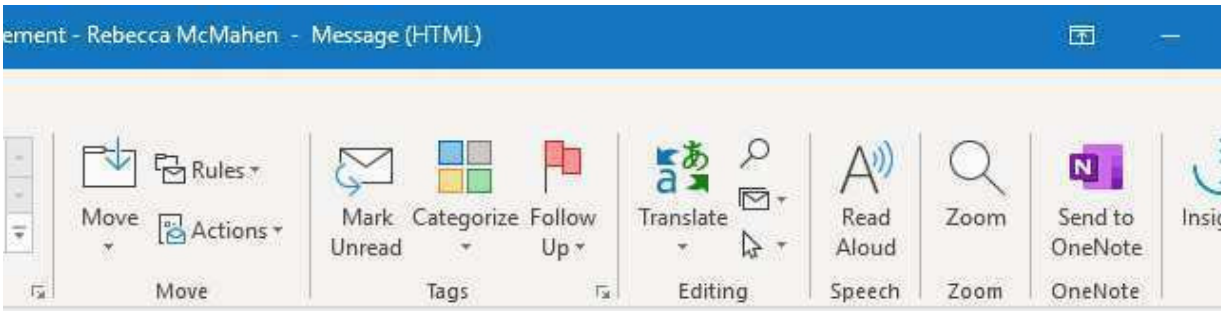

Expires Never

ıdson R, Williams AJ, Sobus JR. Linking high resolution mass spectrometry data with exposure and toxicity
280. Impact Factor = 7.943; Immediacy Index = 1.108; Cited Half-Life = 6.0; Times Cited = 75.

'M, Rager JE, Strynar MJ, Newton SR. Integrating tools for non-targeted analysis research and chemical
Factor = 3.025; Immediacy Index = 1.277; Cited Half-Life = 8.1; Times Cited = 24.

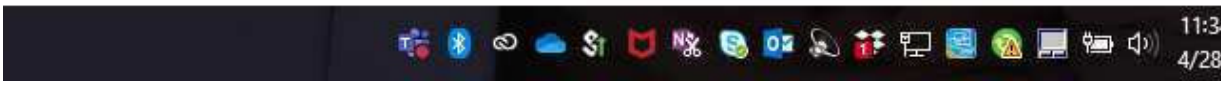

ghts
4 AM
/2020
21

Tue 4/14/2020 2:02 PM

Richard, Ann

RE: Record of Percentage Agreement - Ann Richard

To Sobus, Jon

Retention Policy Permanent (Capstone approach) (Never)

You replied to this message on 4/14/2020 2:09 PM.

Best of luck, Jon. I'm happy with the attribution and % contribution.

Also wanted to say I thought you did a great job presenting at the CSS mtg yesterday, as always. Very ir

Hope you're managing ok these days, staying busy and safe and sane. Strange new world we live in, eh?

Take care,
Ann

<><><><><><><><><><><><><><><><><><><><><>
Ann M Richard, PhD
Research Chemist
Mail Drop D143-02
Center for Computational Toxicology & Exposure (CCTE)
Computational Chemistry & Cheminformatics Branch
Office of Research & Development
US Environmental Protection Agency
Research Triangle Park, NC 27711
tel: 919-541-3934
email: richard.ann@epa.gov
office: EPA Main Facility, Rm D131C
<><><><><><><><><><><><><><><><><><><><><>

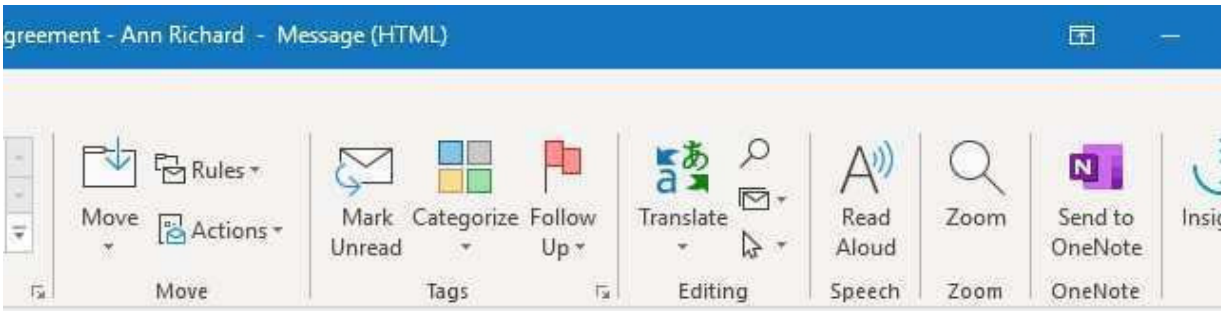

Expires Never

npressive body of work and effort.

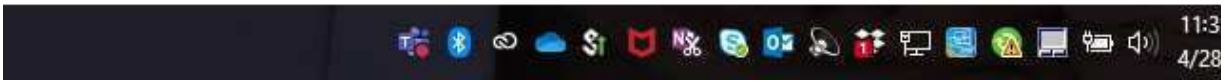

ghts
5 AM
/2020
21

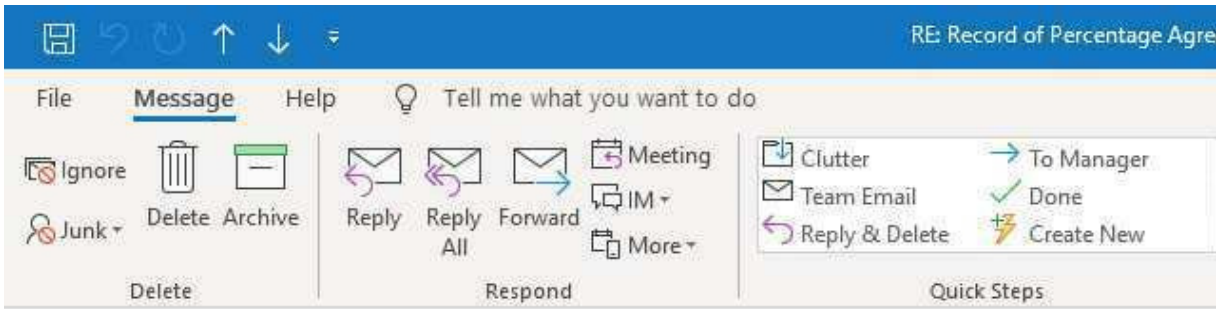

GC

Tue 4/14/2020 3:42 PM

Grulke, Chris

RE: Record of Percentage Agreement - Christopher Grulke

To Sobus, Jon

Retention Policy Permanent (Capstone approach) (Never)

You replied to this message on 4/14/2020 3:44 PM.

I confirm that is my name, position, and contribution percentage. I have not nominated any papers for a

C

From: Sobus, Jon <Sobus.Jon@epa.gov>
Sent: Tuesday, April 14, 2020 2:01 PM
To: Grulke, Chris <Grulke.Chris@epa.gov>
Subject: Record of Percentage Agreement - Christopher Grulke

Dear Christopher,

I'm submitting two publications for consideration for a 2020 STAA award:

Rager JE, Strynar MJ, Liang S, McMahen RL, Richard AM, Grulke CM, Wambaugh JF, Isaacs KK, Judson R, advance high-throughput environmental monitoring. Environ Int. 2016 Mar;88:269-280. Impact Factor =

Sobus JR, Wambaugh JF, Isaacs KK, Williams AJ, McEachran AD, Richard AM, Grulke CM, Ulrich EM, Rage the US EPA. J Expo Sci Environ Epidemiol. 2018 Sep;28(5):411-426. Impact Factor = 3.025; Immediacy Ind

The STAA guidelines require that you confirm your position/organization during the time that the work

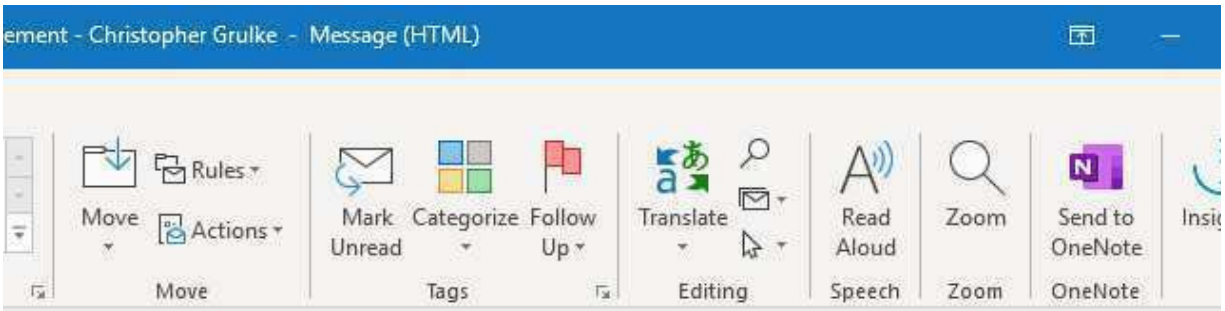

Expires Never

a STAA award ever.

Williams AJ, Sobus JR. Linking high resolution mass spectrometry data with exposure and toxicity forecasts t
7.943; Immediacy Index = 1.108; Cited Half-Life = 6.0; Times Cited = 75.

r JE, Strynar MJ, Newton SR. Integrating tools for non-targeted analysis research and chemical safety evalua
ex = 1.277; Cited Half-Life = 8.1; Times Cited = 24.

was performed:

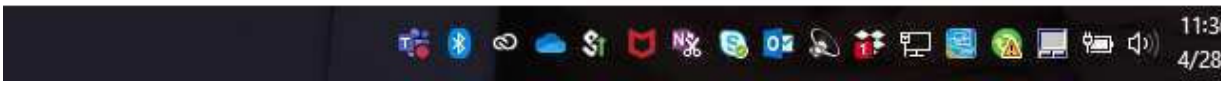

ghts
o
tions at
6 AM
/2020
21

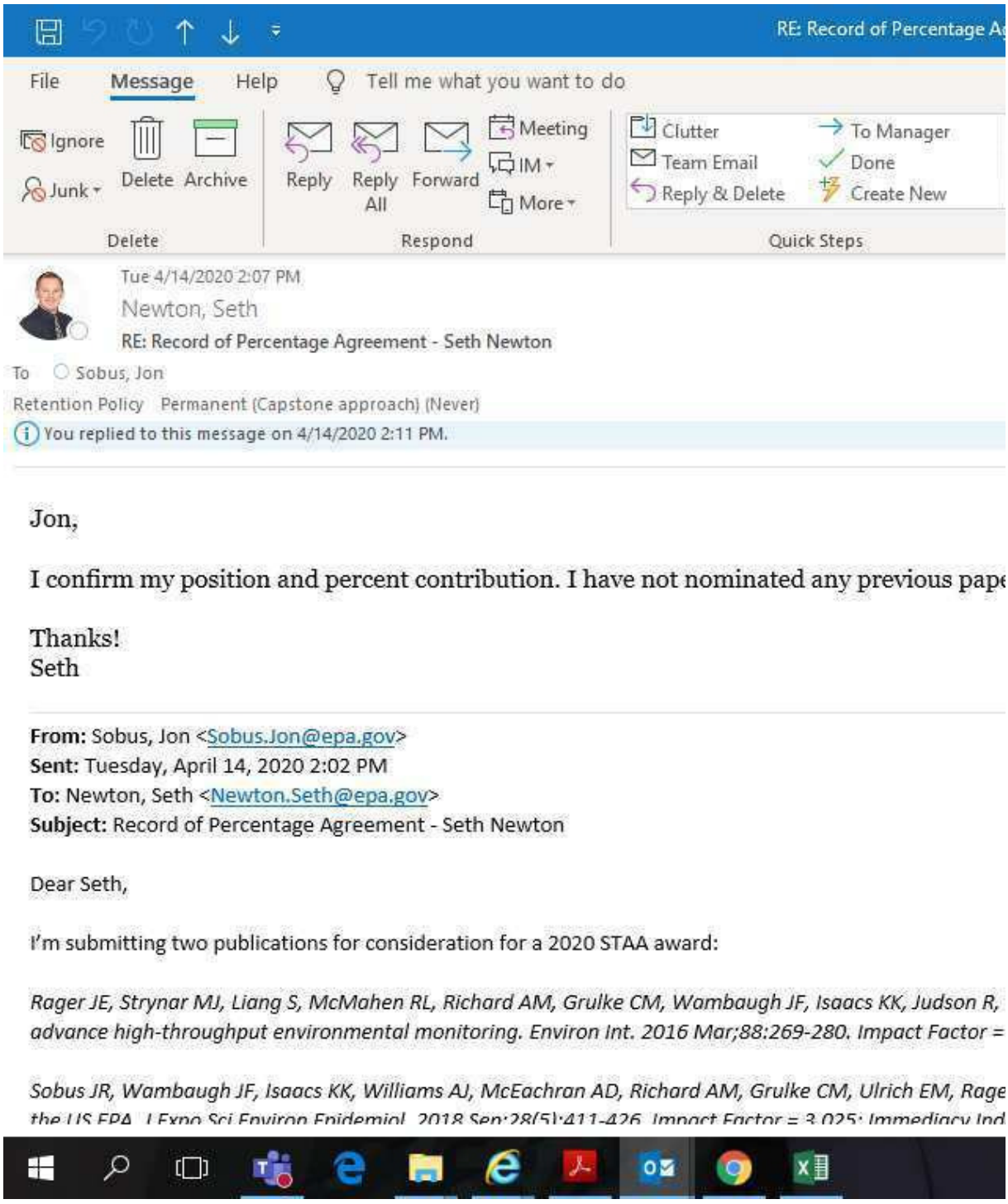
RE: Record of Percentage A
File
Message
Help
Tell me what you want to do
Ignore
Junk
Delete
Archive
Reply
Reply All
Forward
Meeting
IM
More
Clutter
Team Email
Reply & Delete
To Manager
Done
Create New
Delete
Respond
Quick Steps
Tue 4/14/2020 2:07 PM
Newton, Seth
RE: Record of Percentage Agreement - Seth Newton
To
Sobus, Jon
Retention Policy
Permanent (Capstone approach) (Never)
You replied to this message on 4/14/2020 2:11 PM.
Jon,
I confirm my position and percent contribution. I have not nominated any previous pape
Thanks!
Seth
From: Sobus, Jon <Sobus.Jon@epa.gov>
Sent: Tuesday, April 14, 2020 2:02 PM
To: Newton, Seth <Newton.Seth@epa.gov>
Subject: Record of Percentage Agreement - Seth Newton
Dear Seth,
I'm submitting two publications for consideration for a 2020 STAA award:
Rager JE, Strynar MJ, Liang S, McMahen RL, Richard AM, Grulke CM, Wambaugh JF, Isaacs KK, Judson R,
advance high-throughput environmental monitoring. Environ Int. 2016 Mar;88:269-280. Impact Factor =
Sobus JR, Wambaugh JF, Isaacs KK, Williams AJ, McEachran AD, Richard AM, Grulke CM, Ulrich EM, Rage

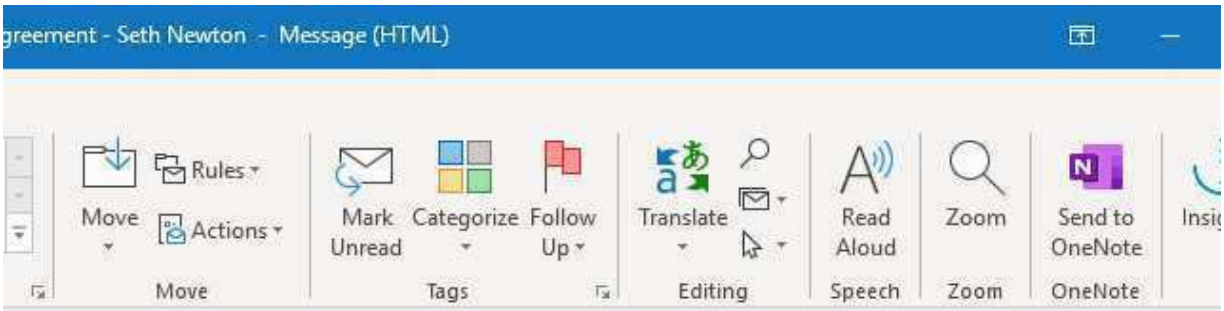

Expires Never

ers for STAA awards over the past 6 years.

Williams AJ, Sobus JR. Linking high resolution mass spectrometry data with exposure and toxicity forecasts t
7.943; Immediacy Index = 1.108; Cited Half-Life = 6.0; Times Cited = 75.

r JE, Strynar MJ, Newton SR. Integrating tools for non-targeted analysis research and chemical safety evalua
ex = 1.277; Cited Half-Life = 8.1; Times Cited = 24

ghts
o
tions at
7 AM
/2020
21

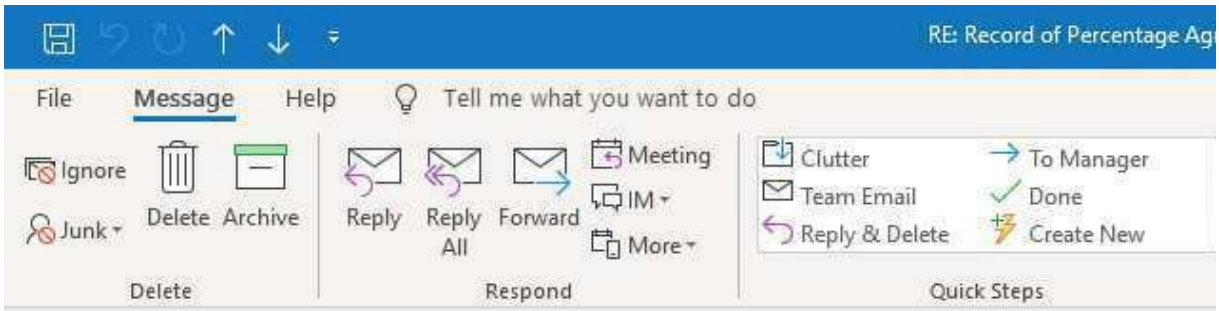

JR

Tue 4/14/2020 2:29 PM

Judson, Richard

RE: Record of Percentage Agreement - Richard Judson

To Sobus, Jon

Retention Policy Permanent (Capstone approach) (Never)

You replied to this message on 4/14/2020 2:31 PM.

Hi Jon.

I confirm my name, position and designated percentage of contribution

Here's my list of STAA nominations...

2017

- Concerning Estrogen receptor signaling (not clear if this was actually submitted)

2019

- Development and deployment of a high-throughput assay to detect chemical disruptors
- A chemical and Cheminformatics foundation for ToxCast & Tox21 research programs (le

By the way, great talk on the CSS call yesterday

Richard

From: Sobus, Jon <Sobus.Jon@epa.gov>

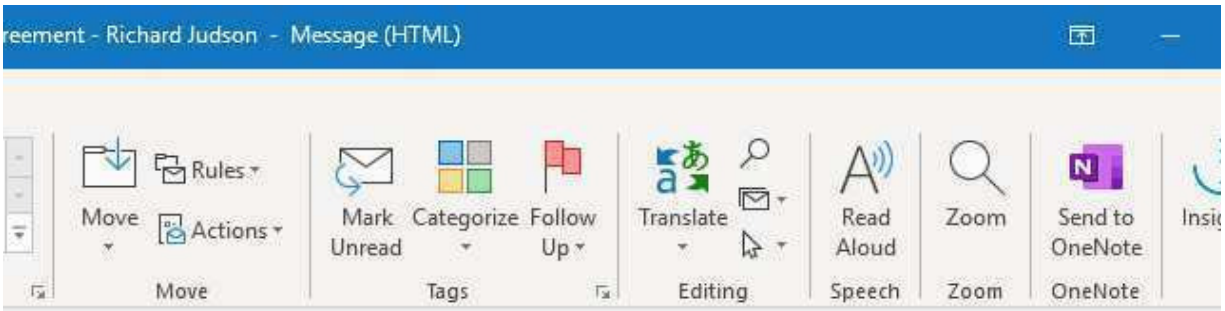

Expires Never

of thyroid hormone synthesis (level 1 award)
vel 3 award)

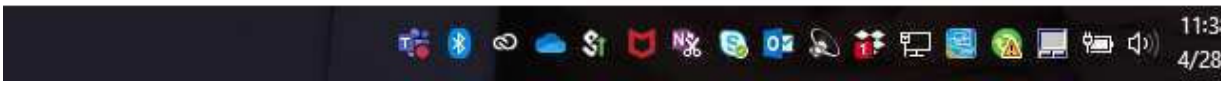

ghts
8 AM
/2020
21

Table of Contents

General_Authors_Publications.....2
LI-266382_Boyes_et_al_2017__A_comprehensive_framework_for_evaluating.....18
LI-266382_2020_STAA_Nomination_reviews.....63
LI-266382_Re__STAA_award_Nomination_Paul_R.....67
LI-266382_RE__STAA_nomination_for_review_article_andersen.....69
LI-266382_RE__STAA_nomination_for_review_article_Burgess.....71
LI-266382_RE__STAA_nomination_for_review_article_Hughes.....73
LI-266382_RE__STAA_nomination_for_review_article_rogers.....75
LI-266382_RE__STAA_nomination_for_review_article_Zucker.....77
LI-266382_Re__STAA_nomination_for_review_article_Thornton.....79
LI-266382_Boyes_et_al_2017__A_comprehensive_framework_for_evaluating.....81
LI-266382_FW__STAA_nomination_for_review_article_boyes.....126
LI-266382_RE__STAA_nomination_for_review_article_ho.....128
LI-266382_RE__STAA_nomination_for_review_article_Scheckel.....130
LI-266382_STAA_nomination_for_review_article_non-responders.....132
LI-266382_Submission_of_review_for_STAA_award_Zepp.....133
LI-266382_Record_of_Percentage_Agreement_?_Souhail_Al-Abed.....134
Re__STAA_award_Nomination_Paul_R.....135
RE__STAA_nomination_for_review_article_andersen.....137
RE__STAA_nomination_for_review_article_Burgess.....139
RE__STAA_nomination_for_review_article_Hughes.....141
RE__STAA_nomination_for_review_article_rogers.....143
RE__STAA_nomination_for_review_article_Zucker.....145
Re__STAA_nomination_for_review_article_Thornton.....147
FW__STAA_nomination_for_review_article_boyes.....149
Record_of_Percentage_Agreement_?_Souhail_Al-Abed.....151
STAA_nomination_for_review_article_non-responders.....152
RE__STAA_nomination_for_review_article_Scheckel.....153
Submission_of_review_for_STAA_award_Zepp.....155
RE__STAA_nomination_for_review_article_ho.....156
2020_STAA_Nomination_reviews.....158

STAA REPORT FOR THE SCIENTIST NOMINATIONS

General Information:

Nomination ID/App ID:	20-116
Research Category Primary:	Review Articles (RA)
Research Category Secondary:	Ecological Research (ER);Health Effects Research and Human Health Risk Assessment (HE)
Laboratory/Office Name:	ORD
Nomination Entered By:	William Boyes

Eligibility Checklist:

[Y] The nominated publication(s) has not been submitted to a previous STAA competition.

[Y] The nominated publication(s) was published on or before January 1, 2017 and on or after January 1,2012

[Y] The principal author was an EPA employee or a PHS employee assigned to EPA when the research was performed

[Y] The EPA authors (includes PHS employees assigned to EPA) contributed collectively a minimum of 50% toward the publication(s)

Nominating Official Name:	David Diazsanchez
Nominating Official Title:	
Nominating OfficialEmail:	diaz-sanchez.david@epa.gov
STAA Coordinator Name:	Kathleen Wiser
STAA Coordinator Email:	wiser.kathi@epa.gov

Justifications:

Justification 1:

Engineered nanomaterials (ENM) are a growing aspect of the global economy, and their safe and sustainable development, use, and eventual disposal requires the capability to forecast and avoid potential problems. This review provides a framework to evaluate the health and safety implications of ENM releases into the environment, including purposeful releases such as for antimicrobial sprays or nano-enabled pesticides, and inadvertent releases as a consequence of other intended applications. Considerations encompass product life cycles, environmental media, exposed populations, and possible adverse outcomes. This framework is presented as a series of compartmental flow diagrams that serve as a basis to help derive future quantitative predictive models, guide research, and support development of tools for making risk-based decisions. After use, ENM are not expected to remain in their original form due to reactivity and/or propensity for hetero-agglomeration in environmental media. Therefore, emphasis is placed on characterizing ENM as they occur in environmental or biological matrices. In addition, predicting the activity of ENM in the environment is difficult due to the multiple dynamic interactions between the physical/chemical aspects of ENM and similarly complex environmental conditions. Others have proposed the use of simple predictive functional assays as an intermediate step to address the challenge of using physical/chemical properties to predict environmental fate and behavior of ENM. The nodes and interactions of the framework presented here reflect phase transitions that could be targets for development of such assays to estimate kinetic reaction rates and simplify model predictions. Application, refinement, and demonstration of this framework, along with an associated knowledgebase that includes targeted functional assay data, will allow better de novo predictions of potential exposures and adverse outcomes.

Justification 2A:

n/a

Justification 2B:

Boyes, (2015) STAA level III. Evaluation of the developmental toxicity of inhaled ethanol as a component of renewable automotive fuels. Boyes, W.K., Degn L., Martin S.A., Lyke D. F., and Herr D.W. Neurophysiological assessment of auditory,

peripheral nerve, somatosensory, and visual system functions after developmental exposure to ethanol vapors. Neurotoxicology and Teratology 43(0): 1-10, 2014. (Unrelated to current nomination).

Hughes (2015) STAA Level III. Biogeographical Analysis of Chemical Co-Occurrence Data to Identify Priorities for Mixtures Research Risk Analysis/Peer Reviewed, 32(2):224-236 (2) Environmentally Relevant Mixtures in Cumulative Assessments: an Acute Study of Toxicokinetics and Effects on Motor Activity in Rats Exposed to a Mixture of Pyrethroids Toxicological Sciences/Peer Reviewed, 130(2):309-318 (3) A Pharmacokinetic Model of Cis-and Trans-Permethrin Disposition in Rats and Humans with Aggregate Exposure Application Toxicological Sciences/Peer Reviewed, 130(1):33-47. (Unrelated to current nomination).

Hughes (2016} STAA Level II. Bradham, K.D., Scheckel. K.G., Nelson, C.M., Seales, P.E., Lee, G.E., Hughes, M.F., Miller, B.W., Yeow, A., Gilmore, T., Harper, S., Thomas, D.J. (2011) Relative Bioavailability and Bioaccessibility and Speciation of Arsenic in Contaminated Soils. Environ. Health Perspect. 119(11): 1629–1634. (Unrelated to current nomination).

Justification 2C:

Current nomination is unrelated to previous submissions

Justification 2D:

n/a

Justification 2E:

Boyes, Zucker, Rogers and Hughes are also nominated for awards in other categories (Health effects). the current nomination is a comprehensive review article covering an expanse of issues related to the environmental and health effects of engineered nanomaterials. The other nominations are related to original laboratory

research covering very specific aspects of nanomaterials or other potential environmental contaminants.

Justification 3A:

1. . The following invited presentations resulted from this research:

· Boyes WK. A Decision Support Framework for Environmental Health and Safety Evaluation of Engineered Nanomaterials. Invited presentation to the American Public Health Association Meeting, Denver, Oct 29- Nov 2, 2016.

· Boyes, WK. Evaluating the Environmental Health and Safety Implications of Engineered Nanomaterials. Conference Keynote Speaker. Nanosafety 2017. Saarbrucken, Germany. Oct. 10-13, 2017.

· Boyes, WK . A Framework for Evaluation of Engineered Nanomaterials. Invited presentation to the Genetics and Environmental Mutagenesis Society, Research Triangle Park, NC. May 2. 2018

· Boyes, WK. A Comprehensive Framework for Evaluation of Engineered Nanomaterials. Invited webinar briefing for EPA Regional Science Liaisons. April 24. 2018

· Boyes, WK . Overview of EPA Office of Research and Development (ORD) Research Activities Related to Nanomaterials. Webinar presented to the Nanomaterial Environmental Health Implications (NEHI) subcommittee of the National Nanotechnology Initiative (NNI). May 24. 2018

· Boyes, WK . Evaluating the Environmental Health and Safety Impact of Engineered Nanomaterials. North East Nanomaterials Meeting (NENM2018), Lake Placid NY June 1-3. 2018. http://nny.sites.acs.org/2018nenanomeeting.htm

· Boyes, WK. Round Table Panel member. Connecting the Pieces: Linking Manufacture and Use of Nanomaterials or Nanotechnology-Enabled Products with Exposure, Outcome, and Risk. QEEN II: 2nd Quantifying Exposure to Engineered Nanomaterials from Manufactured Products Workshop, Washington DC, Oct. 9-10. 2018.

· Boyes, WK. Chair, Plenary Session. Exposure-Driven Risk Assessment for Nanosafety Research. QEEN II: 2nd Quantifying Exposure to Engineered Nanomaterials from Manufactured Products Workshop, Washington DC, Oct. 9-10. 2018.

· Sheckel K. Application of X-ray Absorption Spectroscopy for Monitoring Transformation of Nanomaterials. 2nd Quantifying Exposure to Engineered Nanomaterials (QEEN) from Manufactured Products Workshop, Washington, DC, 2018.

· K. Scheckel, E. Donner, R. Sekine, G. Brunetti, and E. Lombi. Environmental Transformations of Silver and Zinc Oxide Nanoparticles Drive Risk Assessment Understanding. 55th Annual Meeting of the Clay Minerals Society, Urbanna, IL, 2018.

· Boyes, WK. Nanosafety Research: The US EPA Perspective. Invited presentation to a workshop entitled "Fostering EU-US cooperation in Nanosafety Research" sponsored by the European Union. Harvard University, Boston Mass. March 5-6. 2019

· Boyes, WK. Invited Moderator, Respiratory Effects of Engineered Nanomaterials in Relation to Physiochemical Properties. NanoEHS Webinar Series, U.S. National Nanotechnology Initiative. September 10 , 2019.

· Boyes, WK. Update on Nanomaterial Research at EPA. Invited seminar. Annual meeting of the Center for Environmental Implications of Nanotechnology (CEINT), Duke Univ., September 13, 2019.

Publication	**Number of downloads/views**	**Number of citations (Google Scholar)**
Boyes et al., 2017	716	29

Justification 3B:

The manuscript was peer-reviewed internally within ORD prior to receiving clearance for journal submission . The internal peer review was conducted by two senior scientists with knowledge of nanomaterial environmental and toxicological actions. The manuscript was revised to address internal peer review, cleared for submission by EPA management, and submitted for publication to Critical Reviews in Toxicology. Extensive peer review comments were received from three anonymous journal peer reviewers. The manuscript was revised to address all reviewer comments and resubmitted to the journal along with a detailed accounting of the responses to reviewer comments. The revised manuscript was then accepted for publication.

AUTHORS

Principal Author

Author Name:	William K. (Will) Boyes		
Professional Title:		Salutation:	
Email:	boyes.william@epa.gov	Organization:	
Mailing Address:			
Street Line 1:			
City:			
Zip Code:		State:	
At time of research was:	EPA Employee		
Separation Date:			
% of Effort:	5		

Contributing Author

Author Name:	Kim Rogers		
Professional Title:		Salutation:	Dr.
Email:	rogers.kim@epa.gov	Organization:	
Mailing Address:			
Street Line 1:			
City:			
Zip Code:		State:	
At time of research was:	EPA Employee		
Separation Date:			
% of Effort:	5		

Contributing Author

Author Name:	Lila Thornton		
Professional Title:		Salutation:	Mrs.
Email:	lila.thornton@duke.edu	Organization:	
Mailing Address:			
Street Line 1:	Environmental Engineering Duke University, Durham NC		
City:	Durham		
Zip Code:		State:	North Carolina
At time of research was:	Non EPA Personnel		
Separation Date:			
% of Effort:	15		

Contributing Author

Author Name:	Elaine Cohen Hubel		
Professional Title:		Salutation:	
Email:	hubal.elaine@epa.gov	Organization:	
Mailing Address:			
Street Line 1:			
City:			
Zip Code:		State:	
At time of research was:	EPA Employee		
Separation Date:			
% of Effort:	5		

Contributing Author

Author Name:	Souhail Al-Abed		
Professional Title:		Salutation:	Dr.
Email:	al-abed.souhail@epa.gov	Organization:	
Mailing Address:			
Street Line 1:			
City:			
Zip Code:		State:	
At time of research was:	EPA Employee		
Separation Date:			
% of Effort:	5		

Contributing Author

Author Name:	Christian Andersen		
Professional Title:		Salutation:	Dr.
Email:	andersen.christian@epa.gov	Organization:	
Mailing Address:			
Street Line 1:			
City:			
Zip Code:		State:	
At time of research was:	EPA Employee		
Separation Date:			
% of Effort:	5		

Contributing Author

Author Name:	Robert Burgess		
Professional Title:		Salutation:	Dr.
Email:	burgess.robert@epa.gov	Organization:	
Mailing Address:			
Street Line 1:			
City:			
Zip Code:		State:	
At time of research was:	EPA Employee		
Separation Date:			
% of Effort:	5		

Contributing Author

Author Name:	Dermont Bouchard		
Professional Title:		Salutation:	Dr.
Email:	bouchard.dermont@epa.gov	Organization:	
Mailing Address:			
Street Line 1:	n/a		
City:			
Zip Code:		State:	
At time of research was:	EPA Employee		
Separation Date:			
% of Effort:	5		

Contributing Author

Author Name:	Kay Ho		
Professional Title:		Salutation:	Dr.
Email:	ho.kay@epa.gov	Organization:	
Mailing Address:			
Street Line 1:			
City:			
Zip Code:		State:	
At time of research was:	EPA Employee		
Separation Date:			
% of Effort:	5		

Contributing Author

Author Name:	Michael Hughes		
Professional Title:		Salutation:	Dr.
Email:	hughes.michaelf@epa.gov	Organization:	
Mailing Address:			
Street Line 1:			
City:			
Zip Code:		State:	
At time of research was:	EPA Employee		
Separation Date:			
% of Effort:	5		

Contributing Author

Author Name:	Kirk Kitchin		
Professional Title:		Salutation:	Dr.
Email:	kitchin.kirk@epa.gov	Organization:	
Mailing Address:			
Street Line 1:			
City:			
Zip Code:		State:	
At time of research was:	EPA Employee		
Separation Date:	Sat Mar 03 00:00:00 GMT 2018		
% of Effort:	5		

Contributing Author

Author Name:	Jeffrey Ross		
Professional Title:		Salutation:	Dr.
Email:	ross.jeff@epa.gov	Organization:	
Mailing Address:			
Street Line 1:			
City:			
Zip Code:		State:	
At time of research was:	EPA Employee		
Separation Date:			
% of Effort:	5		

Contributing Author

Author Name:	Jay Reichman		
Professional Title:		Salutation:	Dr.
Email:	reichman.jay@epa.gov	Organization:	
Mailing Address:			
Street Line 1:			
City:			
Zip Code:		State:	
At time of research was:	EPA Employee		
Separation Date:			
% of Effort:	5		

Contributing Author

Author Name:	Paul Rygiewicz		
Professional Title:		Salutation:	Dr.
Email:	ragspdxor@yahoo.com	Organization:	
Mailing Address:			
Street Line 1:			
City:			
Zip Code:		State:	
At time of research was:	EPA Employee		
Separation Date:			
% of Effort:	5		

Contributing Author

Author Name:	Richard Zepp		
Professional Title:		Salutation:	Dr.
Email:	zepp.richard@epa.gov	Organization:	
Mailing Address:			
Street Line 1:			
City:			
Zip Code:		State:	
At time of research was:	EPA Employee		
Separation Date:			
% of Effort:	5		

Contributing Author

Author Name:	Kirk Scheckel		
Professional Title:		Salutation:	Dr.
Email:	scheckel.kirk@epa.gov	Organization:	
Mailing Address:			
Street Line 1:			
City:			
Zip Code:		State:	
At time of research was:	EPA Employee		
Separation Date:			
% of Effort:	5		

Contributing Author

Author Name:	Sheau-Fung Thai		
Professional Title:		Salutation:	Dr.
Email:	thai.sheau-fung@epa.gov	Organization:	
Mailing Address:			
Street Line 1:			
City:			
Zip Code:		State:	
At time of research was:	EPA Employee		
Separation Date:			
% of Effort:	5		

Contributing Author

Author Name:	Robert Zucker		
Professional Title:		Salutation:	Dr.
Email:	zucker.robert@epa.gov	Organization:	
Mailing Address:			
Street Line 1:			
City:			
Zip Code:		State:	
At time of research was:	EPA Employee		
Separation Date:			
% of Effort:	5		

PUBLICATIONS

Publication 1:

Publication Title:	Comprehensive framework for evaluating the environmental health and safety implications of engineere		
Publication Date:	Thu Jun 29 00:00:00 GMT 2017		
Journal/Publication Method:	Critical Reviews in Toxicology		
All Author(s):			
Volume:	47	Number:	9
Pages:	767-810	Immediately Index:	Immediately Index:
Citation ½ Life:	8.6	Impact Factor:	4.771

Critical Reviews in Toxicology

ISSN: 1040-8444 (Print) 1547-6898 (Online) Journal homepage: http://www.tandfonline.com/loi/itxc20

A comprehensive framework for evaluating the environmental health and safety implications of engineered nanomaterials

William K. Boyes , Brittany Lila M. Thornton, Souhail R. Al-Abed , Christian P. Andersen , Dermont C. Bouchard , Robert M. Burgess , Elaine A. Cohen Hubal , Kay T. Ho , Michael F. Hughes , Kirk Kitchin , Jay R. Reichman, Kim R. Rogers, Jeffrey A. Ross , Paul T. Rygiewicz, Kirk G. Scheckel , Sheau-Fung Thai, Richard G. Zepp & Robert M. Zucker

To cite this article: William K. Boyes , Brittany Lila M. Thornton, Souhail R. Al-Abed , Christian P. Andersen , Dermont C. Bouchard , Robert M. Burgess , Elaine A. Cohen Hubal , Kay T. Ho , Michael F. Hughes , Kirk Kitchin , Jay R. Reichman, Kim R. Rogers, Jeffrey A. Ross , Paul T. Rygiewicz, Kirk G. Scheckel , Sheau-Fung Thai, Richard G. Zepp & Robert M. Zucker (2017): A comprehensive framework for evaluating the environmental health and safety implications of engineered nanomaterials, Critical Reviews in Toxicology

To link to this article: http://dx.doi.org/10.1080/10408444.2017.1328400

Published online: 29 Jun 2017.

Submit your article to this journal

View related articles

View Crossmark data

Full Terms & Conditions of access and use can be found at
http://www.tandfonline.com/action/journalInformation?journalCode=itxc20

Download by: [US EPA Library] **Date:** 29 June 2017, At: 10:33

CRITICAL REVIEWS IN TOXICOLOGY, 2017
https://doi.org/10.1080/10408444.2017.1328400

Taylor & Francis
Taylor & Francis Group

REVIEW ARTICLE

Check for updates

A comprehensive framework for evaluating the environmental health and safety implications of engineered nanomaterials

William K. Boyes[a], Brittany Lila M. Thornton[a]*, Souhail R. Al-Abed[b], Christian P. Andersen[c], Dermont C. Bouchard[d], Robert M. Burgess[e], Elaine A. Cohen Hubal[a], Kay T. Ho[e], Michael F. Hughes[a], Kirk Kitchin[a], Jay R. Reichman[c], Kim R. Rogers[f], Jeffrey A. Ross[a], Paul T. Rygiewicz[c], Kirk G. Scheckel[b], Sheau-Fung Thai[a], Richard G. Zepp[d] and Robert M. Zucker[a]†

[a]National Health and Environmental Effects Research Laboratory, Office of Research and Development, U.S. Environmental Protection Agency, Research Triangle Park, NC, USA; [b]National Risk Management Research Laboratory, Office of Research and Development, U.S. Environmental Protection Agency, Cincinnati, OH, USA; [c]National Health and Environmental Effects Research Laboratory, Office of Research and Development, U.S. Environmental Protection Agency, Corvallis, OR, USA; [d]National Exposure Research Laboratory, Office of Research and Development, U.S. Environmental Protection Agency, Athens, GA, USA; [e]National Health and Environmental Effects Research Laboratory, Office of Research and Development, U.S. Environmental Protection Agency, Narragansett, RI, USA; [f]National Exposure Research Laboratory, Office of Research and Development, U.S. Environmental Protection Agency, Research Triangle Park, NC, USA

ABSTRACT

Engineered nanomaterials (ENM) are a growing aspect of the global economy, and their safe and sustainable development, use, and eventual disposal requires the capability to forecast and avoid potential problems. This review provides a framework to evaluate the health and safety implications of ENM releases into the environment, including purposeful releases such as for antimicrobial sprays or nano-enabled pesticides, and inadvertent releases as a consequence of other intended applications. Considerations encompass product life cycles, environmental media, exposed populations, and possible adverse outcomes. This framework is presented as a series of compartmental flow diagrams that serve as a basis to help derive future quantitative predictive models, guide research, and support development of tools for making risk-based decisions. After use, ENM are not expected to remain in their original form due to reactivity and/or propensity for hetero-agglomeration in environmental media. Therefore, emphasis is placed on characterizing ENM as they occur in environmental or biological matrices. In addition, predicting the activity of ENM in the environment is difficult due to the multiple dynamic interactions between the physical/chemical aspects of ENM and similarly complex environmental conditions. Others have proposed the use of simple predictive functional assays as an intermediate step to address the challenge of using physical/chemical properties to predict environmental fate and behavior of ENM. The nodes and interactions of the framework presented here reflect phase transitions that could be targets for development of such assays to estimate kinetic reaction rates and simplify model predictions. Application, refinement, and demonstration of this framework, along with an associated knowledgebase that includes targeted functional assay data, will allow better *de novo* predictions of potential exposures and adverse outcomes.

ARTICLE HISTORY
Received 22 October 2016
Revised 25 April 2017
Accepted 5 May 2017

KEYWORDS
Engineered nanomaterials; nanoparticles; life cycle; environmental fate and transport; transformations; exposure; adverse outcome pathway; oxidative stress; inflammation; nanotoxicity; human health; ecotoxicity

Table of contents

Introduction ... 2
Comprehensive framework structure ... 4
Life cycle ... 5
Manufacture ... 6
Product use ... 7
Disposal ... 11
Landfills ... 11
Wastewater treatment ... 12
Incineration ... 14
Recycling and recovery ... 14
Fate, transport, and transformation ... 14
Air ... 14
Soil ... 15
Aquatic ... 16
Exposure and biodistribution ... 18
Human exposure ... 19
Human biodistribution (dosimetry) ... 20
Absorption: portals of entry ... 20
Distribution ... 21

CONTACT William K. Boyes boyes.william@epa.gov National Health and Environmental Effects Research Laboratory, Office of Research and Development, Mail Code B105-04, U.S. Environmental Protection Agency, 109 T.W. Alexander Drive, Research Triangle Park, NC 27711, USA
*Current address: Department of Civil and Environmental Engineering, Duke University, Durham NC, USA
†After first two, authors are listed alphabetically.

This article has been reviewed in accordance with the policy of the National Health and Environmental Effects Research Laboratory, U.S. Environmental Protection Agency and approved for publication. Approval does not signify that the contents necessarily reflect the views and policies of the Agency, nor does mention of trade names or commercial products constitute endorsement or recommendation for use.

© 2017 US Government author

Metabolism ... 21
Elimination and excretion ... 21
Physiologically based PK modeling ... 22
Extracellular interactions ... 22
Protein corona/opsonization ... 22
Biological barriers (e.g. BBB, placenta) ... 23
Cellular uptake and intracellular fate ... 24
Endocytosis ... 24
Pinocytosis ... 25
Phagocytosis ... 25
Intracellular destination ... 25
Exocytosis ... 25
Terrestrial exposure and biodistribution ... 25
Terrestrial plants and animals ... 26
Aquatic species exposure and biodistribution ... 26
Effects ... 28
MIE/cellular, organ response ... 28
Oxidative stress ... 28
Ion toxicity after dissolution of nanomaterials ... 29
Altered cell physiology: altered cell cycle, growth ... 29
Cytotoxicity ... 29
Genotoxicity ... 29
Inflammation ... 30
Cross-kingdom effects – MIE/cellular responses ... 30
Whole organism terrestrial and aquatic species effects 31
Terrestrial plants ... 32
Discussion ... 32
Conclusions ... 33
Acknowledgements ... 34
Declaration of interest ... 34
ORCID ... 34
References ... 34

Introduction

Engineered nanomaterials (ENM) are particles which are manufactured to have at least one dimension between approximately 1 and 100 nm, and have other desirable novel properties due to their size (Roco 1999). This classification includes materials that were designed and built from the ground up as well as those produced by other process, such as grinding powders to a nanoscale. When particles are in the nanometer size range they can develop a variety of unique properties that make them valuable in a number of commercial, industrial or biomedical applications. The production and use of ENM are anticipated to be substantial components of future global economic activity (PCAST 2014). As nanotechnologies advance and grow, it is essential to ensure that new products do not cause collateral adverse effects on human health or the environment. Responsible development should include an evaluation of the potential for release of ENM across the life cycle of nanomaterial-enabled products, transformations of these reactive materials in environmental media, and both exposures and adverse effects of exposures to humans and ecologically relevant or sensitive species.

Evaluating the effects of novel nanoscale materials and their transformation products in complex environmental matrices and biological media is extremely challenging. There are many non-ENM industrial chemicals with insufficient toxicological information, and the costs of performing traditional toxicological evaluations are too high to address the tens of thousands of materials now employed in commerce (NRC 2007). The increasing number and variety of ENM and ENM-enabled products compounds this issue, as the number and pace of ENM developments exceeds traditional testing capacity. Furthermore, materials are developed at the nanometer scale in order to take advantage of special nanoscale properties such as: elevated rates of reactivity caused by high surface area to mass ratios, high tensile strength and durability, and in some cases, added dispersion and mobility (Uskokovic 2013). These nanoscale properties may convey unique fate, transport, and toxic properties not observed with bulk-sized conventional materials. There is ongoing debate about whether ENM possess special toxicological properties in addition to those of the composite chemicals (Donaldson & Poland 2013; Maynard 2014). It is clear, however, that the biodistribution and enhanced biological activity of nanoparticles on a mass basis can differ from that of their bulk (i.e. micron-sized or larger) counterparts and lead to potential unique target sites and effects (García-Alonso et al. 2014; Wang et al. 2014b). For these reasons, novel approaches are required to determine whether there are concerns for present and future uses of ENM. These approaches must be efficient and predictive, so that applications of ENM with higher probability of exposure or hazard can be quickly identified. Rapid and efficient testing and predictive approaches could be mutually beneficial to many resource-constrained sectors of the nanotechnology community, including regulatory decision makers, industry, and other developers seeking opportunities for innovation and commercialization. Using a tiered approach would allow rapid and efficient screening of many materials to identify a smaller number that are most likely to pose a potential hazard. Those few materials could then be assessed using more traditional and thorough approaches. Data from the more extensive evaluations would then build the basis for risk assessments as described by the National Research Council (NRC 1983), with screening data becoming a component of the traditional Hazard Identification stage of the risk assessment process. The question is: what is the best approach for screening to efficiently consider a myriad of potential environmental effects across the life cycle of uses of diverse and numerous nano-enabled products? To answer this question will require a more comprehensive understanding of ENM across the life cycle of nano-enabled products, ENM movement in the environment, exposures, and effects, and the critical points along these pathways in which the fate and actions of ENM are determined.

Several strategies have been proposed in order to aid the assessment of ENM, such as grouping of materials for "read-across" risk assessment, and prioritization of toxicity testing (Som et al. 2012; Hansen et al. 2013; Arts et al. 2014; Oomen et al. 2014; Stone et al. 2014; Godwin et al. 2015).

Table 1. A list of supplementary models organized by evaluation area.

Model	Description	Reference
Life cycle emissions		
protégé	Models human near-field exposure across the life cycle	Royce et al. (2014)
Fate & transport		
NanoDUFLOW	Links ENM processes to hydrologic model	Quik et al. (2015)
WASP	Mechanistic model being adapted to assess ENM exposure in aquatic media	Knightes (2015)
	Transport of TiO_2 Nanoparticles into Leachate of Municipal Waste Landfills	de Castro et al. (2012)
Exposure		
PRoTEGE	Models human near-field exposure across the life cycle	Royce et al. (2014)
USEtox	Models human far-field and fresh-water ecotoxicity exposure; evaluated for organic chemicals (not ENM)	Rosenbaum et al. (2008)
SHEDS	Stochastic Human Exposure and Dose Simulation (SHEDS) Model	Isaacs et al. (2014)
NanoRiskCat	Decision support tool to estimate exposure and hazard ratings for consumer products containing ENM	Hansen et al. (2013)
Pharmacokinetic/dosimetric		
MPPD	Models particle deposition in the respiratory tract	Asgharian et al. (2001) and Cassee et al. (2002)
PBPK	Physiologically based pharmacokinetic models describe particle absorption, distribution and elimination based on physiological parameters; Models have been published for Ag and TiO_2 ENM, PLGA/mPEG particles	Bachler et al. (2013, 2015) and Li et al. (2012)
ISDD	*In vitro* Sedimentation, Diffusion and Dosimetry model; predicts particle dosimetry for adherent cells in tissue culture systems	Teeguarden et al. (2007), Hinderliter et al. (2010), and Cohen et al. (2014)
Effects		
NanoRiskCat	Decision support tool to estimate exposure and hazard ratings for consumer products containing ENM	Hansen et al. (2013)

For example, NanoRiskCat (Table 1) is a model that categorizes levels of potential risk and hazard in order to help decision makers even where data are lacking (Hansen et al. 2013). Grieger et al. (2012) reviewed and evaluated a number of frameworks for environmental health and safety risk analysis and concluded that most were primarily applicable to occupational settings with minor environmental considerations. In addition, there are differences among frameworks as to their threshold for concern. For example, one scheme considered fibrous ENM with aspect ratios greater than 3:1 as candidates for further testing (RCC-NI 2014), while another set the boundary at 100:1 (Som et al. 2012). Arts et al. (2014) reviewed the concept of grouping ENM as a means of streamlining nanomaterial testing, and concluded that none of the available approaches fully considered the nanomaterial life cycle, material properties and biophysical interactions, types of use, exposure, biokinetics, and early and apical toxicological effects. Thomas et al. (2009) also emphasized the need for evaluating potential exposure to ENM along with hazard in risk assessments. A framework for Comprehensive Environmental Assessment has been proposed that emphasizes a process for input from stakeholders and topical experts to set research priorities for evaluating ENM (Powers et al. 2016).

Environmental transformations or fate and transport of ENM across media are considered by few frameworks. Oomen et al. (2014) and Stone et al. (2014) provided approaches to tiered prioritizations of nanomaterial testing, but their foci were on testing materials and not on developing predictive capability. Cohen et al. (2013b) offered an approach that could become predictive based on high-throughput toxicity data and *in silico* quantitative structure activity relationships (QSAR) analyses. At this time, however, nano-QSAR are limited by the extent of quality data available for modeling (Ivask et al. 2013; Tantra et al. 2014; Oksel et al. 2015). Similarly, case study assessments of ENM risks to human health and the environment have limited data and are associated with high uncertainties (Aschberger et al. 2011). Toxicity testing strategies have been proposed based on *in vitro* systems, including high-throughput systems (Nel et al. 2013) or representing priority target tissues (Farcal et al. 2015) or toxic mechanisms (Costa & Fadeel 2016). Among the challenges of ENM alternative toxicity testing systems are selecting and characterizing ENM for study, preparation of adequate dispersions, determining dose to target cells or tissues, and potential interference of ENM suspensions with optical readouts (Johnston et al. 2013; Cohen et al. 2014). There is additional complexity when considering nanomaterial life cycles within a framework of higher level societal and economic systems (Tolaymat et al. 2015).

A recent review of frameworks and tools for risk assessment of nanomaterials developed eight criteria for evaluating frameworks that included: nano-specific requirements (such as physicochemical properties that may influence kinetics); life cycle thinking (including changes in nanomaterial characteristics across their life cycle); pre-assessment phase (screening to focus assessments); exposure driven approach (to prioritize toxicity testing); transparency of objectives and communication with stakeholders; documented applications; and allowing for grouping or read-across assessments (Hristozov et al. 2016). In their review, Hristozov et al. concluded that none of the nanomaterial risk assessment frameworks currently available satisfied all of these criteria.

The complexity of nanomaterial transformations, life cycles, and environmental interactions further complicates environmental health and safety assessments (Lowry et al. 2012;

Grassian et al. 2016). It is important to understand ENM in complex realistic environments (Murphy et al. 2015). For example, environmental transformations can potentially modulate the toxicity of silver nanoparticles (Ag ENM) by converting them to toxic silver ions, but Ag ENM may also be produced with the reduction of ionic silver by natural organic matter (Hou et al. 2013). TiO_2 in either bulk pigment grade or ENM forms may be coated with a substance such as $AlOH_3$ to improve dispersion and to prevent UV activation and subsequent product degradation (WHO-IARC 2010). When $AlOH_3$-coated TiO_2 ENM, as incorporated into cosmetics or sunscreens, is exposed to swimming pool water, however, the coating can degrade increasing the potential phototoxicity of the transformed ENM (Al-Abed et al. 2016). Thus, consideration of ENM transformations and release from products should play a central role in ascertaining and predicting how ENM propagate through environmental systems to reach important ecological and human receptors and their potential actions at those receptors. In all, we are not aware of any comprehensive frameworks to date that seek to build a quantitative and predictive capability using realistic environmental and biological compartments, and also consider: potential environmental release of ENM across product life cycles; ENM fate, transport, and transformation in environmental media; ENM exposure to receptor populations; and potential effects in susceptible species or humans.

Here we propose a framework for the evaluation which is organized to reflect the potential movement of ENM across realistic environmental or biological systems. We discuss the key phenomena captured in the framework and review the literature related to characterizing these phenomena. Finally, we identify key gaps in this knowledge and where we see potential for methods development to address these gaps. We believe that the consideration of environmental and biological compartments with associated parameters such as transfer rates, affinity coefficients, dissolution rates, and other relevant metrics, where applicable, will benefit the long-term ability to develop and demonstrate relevant, quantitative, predictive models of both ENM exposures and effects across product life cycles. Data to fill such a vision are currently far from complete. The framework will guide future research to design efficient approaches for characterizing potential impacts of ENM and ENM-enabled products and support risk-based decisions.

Comprehensive framework structure

The overall framework is divided into four separate, but linked, stages of assessment (Figure 1). The structure of these stages resembles the topical layout proposed for comprehensive environmental assessment (Powers et al. 2016), but here the emphasis is on understanding and predicting the movement, fate, and behavior of ENM across environmental compartments. The first of these evaluation stages addresses the potential release of ENM across the life cycle of nano-enabled products, including initial production of ENM, incorporation of ENM into products, product use, and final disposal. The second stage considers the movement, transformation, and fate of ENM in environmental media, specifically air, soil, and aquatic compartments. In the third stage, the focus is on exposure to receptor populations, comprising aquatic and terrestrial species, including humans. This includes biokinetic and biotransformation processes. The final stage concerns the development of adverse effects along an adverse outcome pathway (AOP) sequence, as recently suggested by Gerloff et al. (2017). The concept of an AOP begins with a molecular initiating event (MIE) and progresses to the generation of adverse health outcomes in an individual or a population (Ankley et al. 2010). An AOP is an analytical concept that enables linking mechanistic information into a predictive framework (OECD 2016). The concept is independent of the chemical or material that causes the MIE, and thus AOPs developed for toxic chemicals in theory could also be applicable to nanoparticles causing the same MIE (Gerloff et al. 2017). These four evaluation stages are intended to identify pathways of sequential compartments along which a nanomaterial might travel, and the considerations – including ENM physical and chemical properties – that might influence them to take one path or another.

Figure 1. An overview of the four over-arching evaluation areas considered in this evaluation framework for engineered nanomaterial (ENM) safety. Each of these evaluation areas – (1) life cycle emissions, (2) fate and transport, (3) exposure, and (4) effects – is broken down into focus areas that will be described in subsequent detail.

The framework, at present, is qualitative and reflects probable routes of potential concern. We hope to identify a few critical steps along these pathways that are key for predicting the fate and transport of materials. A strategy for nanomaterial assessment has been proposed by Hendren et al. (2015) in which a few functional assays could simplify attempts to use a complex set of physical and chemical ENM parameters to predict similarly complex environmental behaviors. For example, they propose surface affinity and dissolution rate as two examples of functional assays that would serve as critical determinants of the environmental fate of ENM. Similarly, Ivask et al. (2013) identified three factors determining the toxicity of silver, zinc oxide, and copper oxide ENM to relevant environmental test species. These factors were dissolution (in agreement with Hendren et al. 2015), organism-dependent cellular uptake, and induction of oxidative stress and consequent cellular damage. We propose a similar approach to identify a few critical parameters along the four stages of our framework. In this way, we hope that critical parameters measured by standardized functional assays can be identified that will serve as initial screening points for evaluating potential risks of novel materials.

The National Research Council has recommended development of models that link behavior of ENM to their

characteristics and to properties of systems into which they are released (NRC 2012, 2013). It may be possible to associate rate parameters with these transition points (represented by arrows in Figures 1–10), where applicable, so that the models can become more quantitative and predictive. A number of compartmental models for factors such as life cycle emissions, environmental fate and transport, exposure, dosimetry, and particle kinetics have been developed for chemicals or ambient particles that might be applied or adapted for ENM (Table 1). We hope that the conceptual framework proposed here will facilitate identification of needs for further model development to adequately describe important mechanisms unique to ENM so that resulting models can be applied and demonstrated to predict potential for impacts across the ENM life cycle.

With this manuscript, we hope to

- Establish a framework that could eventually be used to screen ENM based on a minimal set of measured information and then prioritize for more in depth testing and evaluation.
- Identify key nodes in the framework that are critical determinants of ENM behavior.
- Identify research needs where further information is necessary to develop the structure of the model and/or parameterize relevant functions.
- Evaluate knowledge gaps regarding nanomaterial environmental health and safety in a context that enables a value of information assessment to better prioritize needs for future research.

Additionally, with this framework, we hope in the future to

- Identify alternative testing methodologies for the key nodes at which development of simple functional predictive assays will be possible.
- Achieve the ability to quantify transitions and rate functions as a basis for development of quantitative predictive models.
- Develop quantitative predictive models for screening-level evaluations of novel ENM.
- Foster a process for demonstration and refinement of the framework and its associated knowledgebase.

The intended users of this framework include

- Regulatory authorities throughout the world who must evaluate submissions for registration of novel ENM or new uses of ENM in a short period of time and with little data.
- Research planners who need to determine where new research is most needed and would most efficiently refine and reduce uncertainties in the framework and its associated models and knowledgebase.
- Developers and engineers who are interested in designing materials likely to be sustainable and not associated with significant environmental impacts.

Life cycle

The potential for release of ENM into the environment should be considered across the successive stages of a product life cycle including manufacture, use, and disposal (Figure 2).

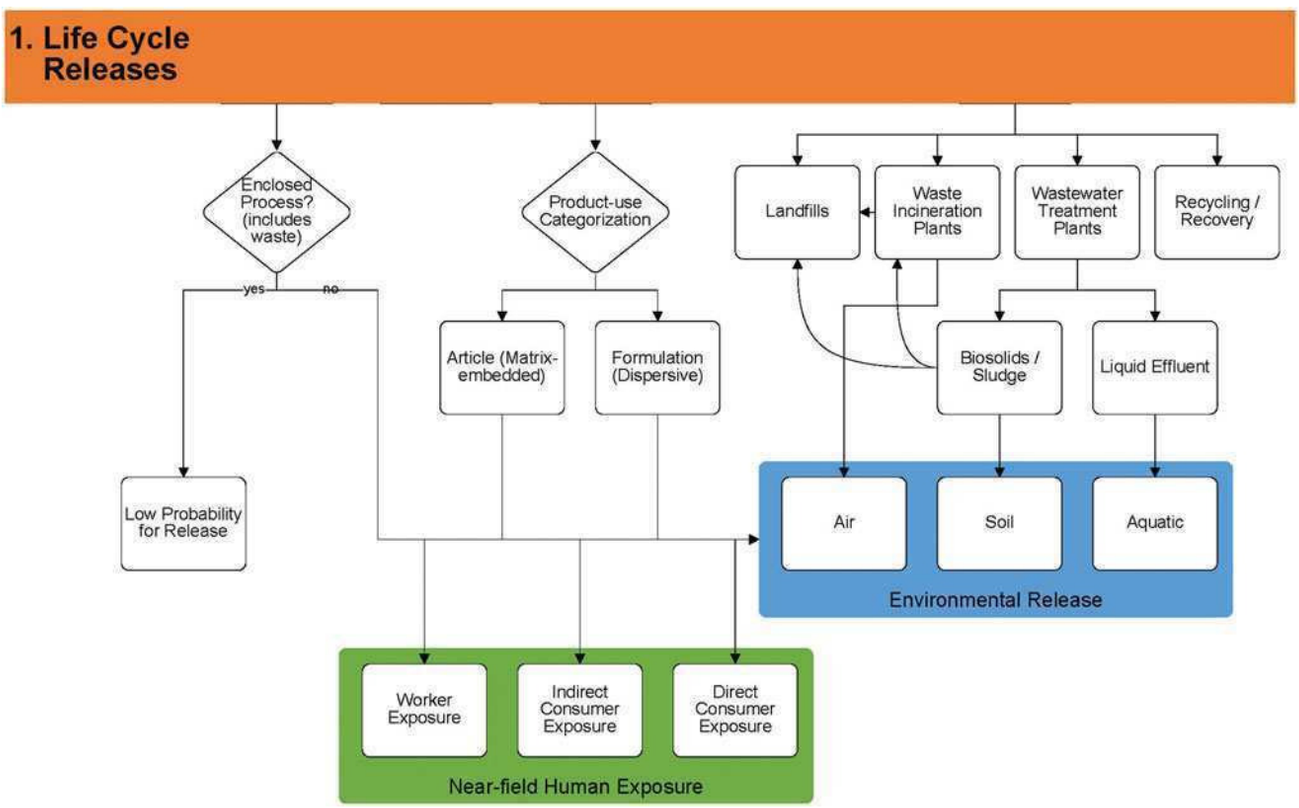

Figure 2. Potential pathways for ENM release across the ENM or product life cycle (manufacture, use, and disposal).

Manufacture

The manufacture of ENM and ENM-enabled products includes a risk of release of ENM into the workplace and exposure to workers and surrounding environment. ENM may be released inadvertently as a byproduct of synthesis, application, recycling, and disposal of nanoparticles or ENM enabled products. Manufacturing processes greatly influence the potential for release of ENM into the environment. Processes that are enclosed have low probability of releasing ENM during routine operations, although materials can be released during transport or handling, or during equipment maintenance or failure. Processes that are not enclosed have a greater potential for releasing materials into the workplace where near-field exposure to workers may occur. In addition, opened manufacturing has the potential to release ENM into air, soil or aquatic environmental media (Figure 2).

In the US, environmental concerns for the use of ENM are regulated primarily through the Toxics Substances Control Act (TSCA), which was recently updated as the Frank R. Lautenberg Chemical Safety for the Twenty-first Century Act, and under the Federal Insecticide, Rodenticide and Fungicide Act (FIFRA). Neither TSCA nor FIFRA has the authority to regulate commercial particles based solely on particle size. Novel chemical structures must be registered under TSCA prior to being manufactured or imported into the US, which applies to ENM such as carbon nanotubes, but not to materials such as TiO_2 in a nanomaterial form, because the chemical structure was previously registered and used as a bulk material. With regard to pesticides, ENM that are included in products for the express purpose of biocidal activity must be registered under FIFRA, but manufacturers who use Ag ENM in products without claiming a biocidal function are not legally required to register the product under FIFRA. Currently, it is unclear the extent to which non-registered ENM are being produced and perhaps released into environmental media. To attain information regarding broader application of ENM in commerce, EPA published a rule in January 2017 under TSCA (8a) that requests manufacturers and formulators to provide EPA with information regarding their use of chemical substances when manufactured or processed as nanoscale materials which were not previously reported to EPA (EPA 2017). The rule did not require companies to acquire data not currently available, and did not have direct implications for controlling the use of ENM in industry or commerce.

Inadvertent releases of registered or non-registered ENM could include accidental releases during manufacturing or plant maintenance, or spills from transportation or shipping accidents. Such inadvertent or accidental releases cannot be anticipated to any level of specificity, and the accuracy of data on the historical frequency of chemical spills is in question (McClure et al. 2013).

Although potential large scale transportation accidents involving ENM has not been addressed in the literature to our knowledge, modeling efforts for possible nanomaterial exposure due to accidental release in a manufacturing facility has been reported (Pilou et al. 2016).

Product use

Advancement in nanoparticle manufacturing, as well as a better understanding of the unique properties that these materials impart to products and processes, has significantly increased the number and scope of ENM-enabled products in recent years. Yet we know little concerning the number of ENM-enabled products (in the US and worldwide) and the amount and composition of ENM in these products. In the US, manufacturers and distributors of consumer products are not required to specify whether product ingredients are nano-sized. We also know little concerning the release of particles, particle–polymer fragments, or dissolved ions during typical use or misuse of ENM-enabled products. The ability to derive quantitative transfer coefficients that reflect release of ENM from products during their consumer usage is limited by the small proportion of products and exposure scenarios evaluated (Caballero-Guzman & Nowack 2016). This lack of information at the product-use stage represents a significant data gap in exposure and risk analyses.

There are a few publicly available international inventories that list consumer products with "nano-claims". These sources (Table 2) include the joint Wilson Center and Virginia Tech "[Nanotechnology] Consumer Products Inventory" (CPI) (Project on Emerging Nanotechnologies 2013); the 2010 and 2012 (nanosilver-only) inventories by the European Consumer Organization (BEUC) and the European Consumer Voice in Standardisation (ANEC) (ANEC & BEUC 2010, 2012); "The Nanodatabase" (Hansen et al. 2016); and the German BUND database (BUND). The CPI and The Nanodatabase are currently curated for the addition of new products and removal of discontinued products that are no longer commercially available. Reviews and analyses of these databases have been

Table 2. Publically available inventories and/or databases of consumer products that claim to contain nanomaterials or nanotechnology.

Inventory/database name	Organization	Scope	Source
Consumer Products Inventory (CPI)	Wilson Center; Virginia Tech	Global market; continuously updated through wiki-style platform	Project on Emerging Nanotechnologies (2013) and Vance et al. (2015)
The Nanodatabase	DTU Environment; Danish Ecological Council; Danish Consumer Council	European market; continuously updated; includes pictorial overviews of potential exposure and hazard	Hansen et al. (2016)
ANEC/BEUC 2010 inventory	European Consumer Voice in Standardisation (ANEC); European Consumer Organization (BEUC)	European market; last updated in 2010	ANEC and BEUC (2010)
ANEC/BEUC 2012 nanosilver inventory	ANEC; BEUC	European market (nanosilver only); last updated in 2010	ANEC and BEUC (2012)
Nanoprodukt-datenbank des BUND	BUND (Friends of the Earth Germany)	German market; "continuously updated and expanded"	BUND

recently published and describe the wide range of ENM-enabled or enhanced products (Yang & Westerhoff 2014; Vance et al. 2015; Hansen et al. 2016).

Although there is evidence for the presence of ENM in many products, most of these products do not advertise the composition or in many cases even the presence of ENM (Vance et al. 2015). Of those products where manufacturers have disclosed the presence of ENM, information other than composition is not often available. Consequently, information concerning particle size, concentration, distribution (within the product), and leaching of ENM during normal use is unavailable except where added by a third party. Analyses of products in the CPI with compositional information have suggested that metal particles (primarily silver and to a lesser extent titanium, zinc, and gold) were present in the greatest number followed by products containing carbon and silicon (Yang & Westerhoff 2014; Vance et al. 2015). The release of ENM from consumer products has not been well described for most common ENM in a wide range of products. In addition, information on the relative penetration of nano-enabled products in the marketplace, that is, what proportion of the products sold in a given category, such as sunscreen, would be those brands containing ENM, is not generally available.

Because there is considerable uncertainty regarding the potential future uses of ENM, one screening level approach to approximate potential release is to consider surrogate chemicals that serve the intended purpose in the product that will be assumed by the ENM. The potential for ENM-release from products might be different than for chemical releases from similar products, but a surrogate approach based on consumer product usage data can at least bound the estimates of the degree of use of ENM-enabled products. In general, consumer product categories can be condensed into (1) formulas, including liquids and sprays, where direct consumer exposure may be possible; and (2) articles, including hard surfaces and textiles such as furniture, where chemicals or nanoparticles might be a component of the product, but are typically less available for direct consumer exposure (Isaacs et al. 2014; Figure 2). For ENM applications in which the particles can be physically separated from their matrix (i.e. a suspension), exposure can be considered in two steps: the first being the release of particles from the product and the second the contact of ENM with the target organism. For ENM-enabled products intended to be ingested or applied to the skin (typically liquid, cream, or gel suspensions), these steps might be combined. Estimates of ENM exposure based on chemical surrogates could be considered as a first pass estimate of the potential levels of ENM usage.

Although there is minimal information concerning the characterization and release of ENM present in consumer products, research results have been reported for a limited number of consumer products. For example, characterization and release of nanosilver from a number of consumer products have been reported (Benn & Westerhoff 2008; Benn et al. 2010; Quadros & Marr 2011; Quadros et al. 2013; Tulve et al. 2015). Population-level exposure to silver nanoparticles present in consumer products was estimated on the basis of the Consumer Product Inventory of the US-based Project on Engineered Nanotechnologies (PEN) and a tiered life cycle analysis and exposure modeling approach referred to as Prioritization/Ranking of Toxic Exposures with GIS (geographic information system) Extension (PRoTEGE) (Royce et al. 2014; Table 1).

One of the subcategories for consumer products is personal care products. Depending on how they are categorized, these nano-enabled consumer products comprise 39% of the 505 health and fitness products listed in the US Nanotechnology Consumer Products Index (CPI) (Vance et al. 2015) or 233 out of 2231 products listed in the European Union Nanodatabase (Hansen et al. 2016). In both cases, nanoscale silver is the most commonly reported ENM. Consumer products typically include toothbrushes, lotions, mouthwashes, as well as hairstyling tools and products (Vance et al. 2015). Depending on the particular product, the most dominant exposure route is dermal followed by ingestion and inhalation (Hansen et al. 2016). Because CPI focuses on ENM-enabled consumer products, ENM-enabled industrial products used to improve construction materials or energy-sector products have not been typically covered by this database, but may be available elsewhere (West et al. 2016). These applications include the use of micronized copper in treated lumber (Santiago-Rodríguez et al. 2015; Platten III et al. 2016) and, for automobiles outside the U.S., nanoscale cerium oxide added to diesel fuel (Cassee et al. 2011; Gantt et al. 2014). The potential for release of carbon nanotubes (CNTs) from composite materials under a variety of usage scenarios has been the focus of a multi-institute research effort (Nowack et al. 2013; Froggett et al. 2014). There are a number of products in which CNTs are embedded in polymers or resins. This project evaluated the potential for CNT release either directly during manufacture or subsequently from the matrix during various usage scenarios, including those with substantial abrasion or other destructive conditions. The potential for release was present during manufacturing; however, this condition was best able to be controlled. For most of the life cycle stages evaluated, the potential for CNT release from a solid product matrix was low. One exception was the use of CNTs in tires where abrasion could result in their release into the environment. In addition, the proposed use of CNTs in textiles could also lead to consumer exposures. Another potential source of CNT release was identified during recycling operations if polymers containing CNTs were mixed for handling with other polymer materials.

Disposal

Landfills, waste incinerators, and wastewater treatment plants (WWTPs) giving rise to biosolids are important routes of disposal at the end of the ENM life cycle. These are, therefore, key intermediaries between the usage phase of nano-enabled products and the environment (Dale et al. 2015). Additional releases of ENMs, may occur during recycling and recovery processes.

Landfills

Landfills are the predominant global disposal option for ENM across all use categories. Based on a market study of global production rates and product life cycles, Keller et al. (2013a, 2013b) estimated that of 260,000–309,000 metric tons of

ENM used in commercial or industrial applications worldwide, 63–91% were eventually disposed of in landfills in 2010. Keller et al. incorporated high and low bound estimates for rates of ENM release into the environment during manufacture, use, and disposal of ENM enabled products. Materials released from ENM-enabled products would likely no longer be in their original nanoscale form, depending on the ENM, the product matrix, and use. Additionally, most of the ENM-containing waste released during manufacturing (up to 80%) ends up in landfills. It is likely that ENM would be affected (e.g. aggregated, dissolved, destabilized, oxidized or reduced, complexed with organic matter) by their interaction with landfill leachate. In particular, the coating could be altered, compromising the particles' stability and reducing the potential to migrate into other media. Several factors have been found to affect the surface charge and aggregation state of Ag nanoparticles: pH, oxygen concentration, organic matter content, chloride concentration, sulfide concentration, and type of coating agent (El Badawy et al. 2010; Gitipour et al. 2013). This is important because if the ENM coating is not affected by the landfill leachate, the particles would be stable in the aqueous phase, potentially endangering the surrounding municipal solid waste aquifers and surface waters. Bolyard et al. (2013) found that ZnO, TiO_2, and Ag ENM exposed to landfill leachate in a stirred reactor (humic acid concentrations from 300 to 6500 mg/L, pH 7.4–7.9) increased Zn, Ti, and Ag concentrations in the aqueous phase, and that released particles tended to agglomerate. Nevertheless, the concentrations of dissolved metals were minimal because of the small concentrations of ENM added onto the reactor and the low solubility of the ENM in water. The authors also concluded that ENM did not significantly change the ability of microorganisms under aerobic or anaerobic conditions tested to break down organic matter present in landfill leachate. Zhu et al. (2014) concluded that at high ionic concentrations, which is expected from landfill leachate, humic acid has a bridging effect and promotes the aggregation and sedimentation of TiO_2 nanoparticles.

More research is required on the interaction of ENM with landfill leachate, including high humic acid concentrations, and how these interactions affect their coating and stability (Bolyard et al. 2013). New and improved analytical techniques are needed to determine ENM fate in landfills because current methods do not allow ENM identification and quantification in complex heterogeneous matrices such as landfill leachate. This is an area of active research, however, and evolving capabilities (Badireddy et al. 2012; Huynh et al. 2016). Less than 1 mg/L of ENMs (ZnO, TiO_2, or Ag) added to leachate at a concentration of approximately 100 mg/L and incubated for 30 d under controlled experimental conditions, was predicted to be in the free ionized metal form (Bolyard et al. 2013). There is a need to standardize the sampling, separation and quantification methods used for ENM. One of the most challenging aspects of ENM determination is how to differentiate naturally occurring particles or those that are incidentally produced (such as in combustion) from purposefully manufactured ENM (Wiesner et al. 2011; Part et al. 2015).

Since many ENM transform during wastewater treatment, assessment of landfill disposal of biosolids or sludge produced during wastewater treatment must consider these transformed phases, which are distinctly different than pristine ENM. Chemical speciation in the aqueous phase of systems containing ENM is currently being modeled in literature using Visual Minteq or similar software (Bolyard et al. 2013; MINTEQ 2013). Since the coating materials used to stabilize ENM are not typically contained in software databases, research could be conducted to determine the equilibrium coefficients for these coating materials at different pH-Eh conditions to improve the accuracy of estimations.

de Castro et al. (2012) modeled the behavior of TiO_2 ENM in landfill leachate in a 5-year period using a Fortran-based code and evaluated the model with experimental data obtained in column experiments. The results showed that TiO_2 ENM were adsorbed onto the soil within the protection barriers of the landfill over the 5-year-simulated period.

Wastewater treatment

An inevitable pathway of ENM in consumer products is from the home to the local WWTP. Several studies have shown that ENM accumulate in biosolids during wastewater treatment; TiO_2 in particular has a high retention in sewage sludge – as high as 99% (Judy et al. 2012; Tourinho et al. 2012). Partitioning of Ag ENM in biosolids is typically greater than 90% and, in many cases, greater than 99% (Kaegi et al. 2011; Impellitteri et al. 2013). The distribution of ENM in WWTP primarily to solids is expected due to surface charges and reactive sites suitable to retain ENM; the small amount of particles that remain suspended during clarification may pass through to the effluent. Research on the impact of ENM in effluent beyond the WWTP is limited, likely due to high retention in biosolids, but the restricted continuation of ENM through WWTP to drinking water distribution systems warrants further research to be protective to drinking water supplies.

Upon entering the WWTP, ENM will encounter a unique chemical and physical environment that includes primary and secondary clarifiers where ENM will partition to other solids in wastewater, followed by anaerobic digestion. If not transformed to other phases by this point, anaerobic digestion likely will act on redox sensitive ENM to form sulfides. Some ENM, such as TiO_2, are resistant to transformation, whereas ENM like Ag, Zn, Cu, and Cd quantum dots are highly sensitive to sulfidation change. After anaerobic digestion, the sewage sludge is further processed by composting or stabilization to hinder microbial activity before being land applied as biosolids for fertilization. Some of the transformed ENM will remain unchanged during composting (i.e. Ag_2S), while others may transform again governed by the environmental conditions of composting and aging (i.e. Zn and Cu) (Table 3). It is important to note that this pathway begins in the home with a consumer product containing ENM traveling through home drains to a network of service lines connected to the WWTP, which means ENM are not added at the end of the process in the fresh or composted biosolids. In fact, convincing research shows that sulfidation reactions occur in the urban wastewater service line network prior to reaching the WWTP (Kaegi et al. 2013; Thalmann et al. 2014). The fact that ENM may be transformed in the sewage service line network

Table 3. Examples of transformations of metallic ENM in biosolids systems.

ENM	Study	Analysis	Transformation products	Citation
Ag	2009 TNSSS Report. Source of Ag in the sample is unknown	TEM-EDX	α-Ag_2S nano-clusters	Kim et al. (2010a)
Ag	Investigation of Ag ENM in a pilot scale WWTP observed	TEM and XAS	∼90% Ag ENM partitioned of to biosolids with transformation to Ag_2S	Kaegi et al. (2011)
Ag	Three Ag ENM (citrate, PVS, and MSA coated) and one AgCl ENM were exposed to a pilot scale WWTP along with a $AgNO_3$ positive control. Samples were evaluated as a function of time within the WWTP system and post-processing simulated composting up to 6 months	XAS	All ENM and $AgNO_3$ were transformed to Ag_2S	Lombi et al. (2013)
Ag	A full scale pilot WWTP consisting of a primary clarifier (PC), aeration basin, and secondary clarifier (SC) connected to a municipal WWTP feed was utilized to examine citrate coated Ag ENM, Ag_2S ENM, and $AgNO_3$ in solids from the PC and SC	XAS	Ag_2S in both the PC and SC.	Impellitteri et al. (2013)
Ag	Plasma polymerization employed to immobilize citrate, polyethylene glycol, and polyethyleneimine capped Ag ENM on a Kapton substrate (nanoparticle in-situ deployment devices – nIDDs) and deployed directly in a municipal WWTP's primary sewage sludge for 24 h	XAS, SEM/EDX	Full conversion to Ag sulfide phases was not observed; 14–60% of Ag was retained as metallic Ag	Sekine et al. (2013)
Ag	This study examines the speciation and lability of Ag in archived, stockpiled, and contemporary biosolids from the UK, USA and Australia, and indicated that biosolids Ag concentrations decreased significantly over recent decades. Reduced-sulfur binding environments was important for Ag speciation in materials ranging from freshly produced sludge to biosolids weathered under ambient environmental conditions for more than 50 years	XAS	Ag in biosolids was predominantly Ag sulfides and had low lability (0.0002–3.4%) upon land application.	Donner et al. (2015)
ZnO	Three ZnO ENM (OECD NM112, OECD NM112 capric/caprylic triglyceride capped, Co-doped ZnO) and $ZnCl_2$ control were exposed to a pilot scale WWTP. Samples were evaluated as a function of time within the WWTP system and post-processing simulated composting up to 6 months	XAS	ENM and $ZnCl_2$ were transformed to ZnS within the WWTP; however, upon composting ZnS was re-transformed to Zn-adsorbed to iron oxides, Zn phosphate, and Zn organic matter complexes	Lombi et al. (2012)
ZnO	Utilizing an established full pilot scale WWTP, ZnO nIDDs or $ZnCl_2$ were added to evaluate Zn transformations. Application of nIDDs permits usage of substrates with immobilized ENM in relevant environmental systems with recovery of the substrate for analytical analysis	XAS, TEM	Over the course of the study ZnO dissolved resulting in ZnS (∼90%) and Zn ligands (cysteine and citrate)	Brunetti et al. (2015)
CuO	There have been no studies of CuO nanoparticles in a pilot scale WWTP to date; however, related studies can provide potential insight. Ma et al. (2014) examined the sulfidation of CuO in sulfidized water. Donner et al. (2011) examined native Cu in fresh and aged (composted) biosolids from 5 WWTPs	XAS, XRD, and TEM	Covelite (CuS) and amorphous Cu_xS_y in sulfidized water Cu speciation in the fresh (direct from secondary treatment) sludge was identified as chalcocite (Cu2S), cubanite (CuFe2S3), and Cu sorbed to organic matter. However, upon aging, Cu was further altered to ∼70% Cu sorbed to organic matter followed by cubanite, covelite, and Cu phosphate	Ma et al. (2014) Donner et al. (2011)
TiO_2	Ti concentrations and Ti phase were examined in effluent samples from several WWTPs	SEM/EDX	Ti particles ranging from 10s nm to >0.7 μm. The particles comprised of primarily Ti and O presuming TiO_2; some larger particles also contained Si with Ti.	Kiser et al. (2009)
TiO_2	Nano and larger TiO_2 phases were identified in biosolids and biosolids amended soils	SEM, TEM	No phase transformations occur within a WWTP for TiO_2	Kim et al. (2012)

Table 4. Relevant concentrations of nano-based constituents in soils and biosolids, and predicted concentrations of ENM in biosolids.

Material	Common range in soil (mg/kg)[a]	Average in soil (mg/kg)[a]	Targeted National Sewage Sludge Survey Report (mg/kg)[b]				Predicted ENM contribution (mg/kg) range in biosolids[c]	Predicted ENM contribution (mg/kg) range in biosolids[d]
			Range	Average	50th Percentile	95th Percentile		
Silver/Ag ENM	0.01–3.15	0.27	1.94–856	31.6	13.6	63.6	10^{-4}–10^{1}	10^{-5}–10^{-1}
Zinc/ZnO ENM	3–2900	52	216–8550	994	784	2068	10^{1}	10^{-1}–10^{1}
Titanium/TiO_2 ENM	210–54500	5720	11.6–4805	286	12.7	915	10^{-2}–10^{4}	10°–10^{2}
Copper/CuO ENM	1–256	14	115–1720	558	463	1248	ND	ND
Cerium/CeO_2 ENM	15–100	50	ND				$10^{-5.5}$	ND
CNT			ND				10^{-1}	10^{-4}–10^{-1}
Fullerenes			ND				10^{-3}–10^{-1}	10^{-4}–10^{-1}

ND: not determined.
[a]Salminen et al. (2005).
[b]TNSSS Report (EPA 2009).
[c]Gottschalk et al. (2013).
[d]Sun et al. (2015).

(within hours) between the home and WWTP to species that are typically less toxic provides some protection during sewer overflow discharge resulting from excessive storm water and groundwater input, that may account for 2–10% of total inflow (Mueller & Nowack 2008).

In the US, 50–60% of biosolids are recycled for land-application and are applied on less than one percent of farmland (Gottschalk et al. 2009; EPA 2012). Land application of biosolids is regulated under Title 40 of the Code of Federal Regulations (US 1999) with the goal to protect human health and the environment from any reasonably anticipated adverse effects of certain pollutants, including metals, which might be present in biosolids. Table 4 shows documented distributions of Ag, Zn, Ti, Cu, Ce, CNT, and fullerenes for ranges and averages naturally in soils, results of the Targeted National Sewage Sludge Survey (TNSSS) Report (EPA 2009), and literature predictions of ENM concentrations in biosolids. Information from the TNSSS report shows the range, average, 50th percentile, and 95th percentile for Ag, Zn, Ti, and Cu in biosolids collected in 2006 and 2007 from 74 randomly selected WWTP. This information can be very helpful in designing experiments. For example, a number of studies of Ag in biosolids or soils have utilized a value close to 1000 mg/kg based on the maximum value of Ag (846 mg/kg; a documented outlier) in the TNSSS report. However, the average Ag concentration in biosolids measured for the report is only about 32 mg/kg and the 50th percentile (median) is approximately 14 mg/kg. Likewise, biosolids are often applied at a rate of 5–10 tonnes/hectare, which upon mixing in the top 15 cm of topsoil results in a dilution factor of 100–50, respectively. For example, while predicted contributions of ZnO ENM to total biosolids concentration may be on the order of 10 mg/kg, the effective increase in soil concentration from ZnO ENM would range from 0.1 to 0.2 mg/kg per application. Quantitation of rate parameters such as these will be essential for eventual quantitative modeling based on this framework. Also worth noting about the TNSSS report in relation to the predicted contribution of ENM to biosolids is the fact that some native metal concentrations in biosolids may be significantly higher than the input from ENM, making the distinction of ENM-associated risk difficult to assess with current procedures. Better methods for detection and characterization of ENM in complex matrices are critically needed.

Incineration

Alternative disposal methods of biosolids include landfill (see discussion above) and incineration. Approximately 20% of sludge from wastewater treatment facilities is incinerated in the US (Holder et al. 2013). Incineration of biosolids impacted by ENM has received little attention (Impellitteri et al. 2013; Meier et al. 2016), but historical research of metal-laden biosolids incineration is plentiful. One study examined the path of Ag ENM through a pilot scale WWTP along with a $AgNO_3$ control (Impellitteri et al. 2013). Samples were collected from the primary clarifier (fresh biosolids) and the secondary clarifier (aged biosolids) and in each case the transformed Ag species was primarily Ag_2S with some Ag sulfhydryl and metallic Ag phases as determined by X-ray absorption spectroscopy (XAS). The fresh and aged samples were then incinerated at 850 °C for 4 h and the residual ash examined by XAS to determine changes in Ag speciation. Incineration impacted Ag speciation by shifting Ag_2S → Ag sulfhydryl → metallic Ag in the fresh and aged biosolids to metallic Ag → Ag sulfhydryl → Ag sulfate in the ash. Scanning electron microscope images show accumulation of Ag clusters (1–3 μm) in the incineration ash; however, the stability of these clusters warrants further research. Since incineration ash is typically landfilled, the caution above related to assessing risk based on the transformed phases rather than the pristine ENM is applicable. Recently, it was shown that Fe_2O_3 nanofiller in thermoplastics altered the shape and composition of residual incinerator ash to be more brittle and have surface-exposed nanofillers when subjected to incinerator-like thermo decomposition, although with CNT-enabled products no carbon nanotubes were found to escape in the aerosol form (Sotiriou et al. 2016). These results illustrate that information on transformation products in the system being assessed is required for sound decision making.

Recycling and recovery

A number of ENM-containing consumer products (electronics, construction materials, batteries, textiles) may become

recycled. Caballero-Guzman et al. (2015) concluded that, during the recycling process in Switzerland, most of the nano-sized TiO_2, ZnO, or Ag was not recovered for returning to product re-manufacturing, but instead was subsequently transferred to be incinerated or landfilled. The only ENM-containing products that were traced back into the productive process were small quantities of ENM that are part of construction waste or plastics. Very small ENM release into wastewater was found in the recycling process. The authors also concluded that more research is needed focusing on occupational exposure, waste incineration, and landfills.

Fate, transport, and transformation

When ENMs are released into environmental media, these are likely to react or heteroaggregate with constituents of the environmental matrix (air, water, or soil), so that eventual exposures to environmental species or humans, for the most part, will not be to the original form of the material but instead to highly diluted ENM transformation or degredation products.

These environmental reactions will not occur under highly constrained laboratory or manufacturing conditions, but instead will be subject to a range of conditions and essentially stochastic forces which will dynamically change across time and location. Therefore, if exposures to environmental transformation products of ENM occur, the exposures will likely be to multiple forms of environmental transformations including a range of particle agglomerates, sizes, and coatings. Life cycle models for estimating chemical exposures from multiple routes and sources have been developed (e.g. USEtox, WASP; Table 1), and are beginning to be adapted to estimate exposures to ENM (Pu et al. 2016).

Air

A large body of literature describes the behavior of ambient air particles in the atmosphere that is largely applicable to ENM (Oberdörster et al. 2005; Bakand et al. 2012). When released into the air, aerosolized particles are subject to abiotic and biotic transformations, including agglomeration and photooxidation, and are transported with wind or air currents (Figure 3). Advective transport involves the movement of ENM by bulk movements of air, including indoor air currents, wind, up currents, down currents, etc. Particles with smaller aerodynamic diameter and lower mass remain suspended for longer periods of time and can lead to far-field inhalation exposures for humans or other breathing terrestrial species. Airborne particles may also become deposited onto soil, water and plant surfaces. It is estimated that only 0.1–1.5% of globally produced ENM mass is released into ambient air (Keller et al. 2013b). One potential source for the release of EMNs into ambient air involves the use of nanoscale CeO_2 as an automotive diesel fuel additive (Cassee et al. 2011). Nanoscale CeO_2 is widely used in both off-road and on-road vehicles in Europe but is currently only licensed for off-road use in the US (Erdakos et al. 2014). The use of CeO_2 as a fuel additive has been shown to increase fuel efficiency and

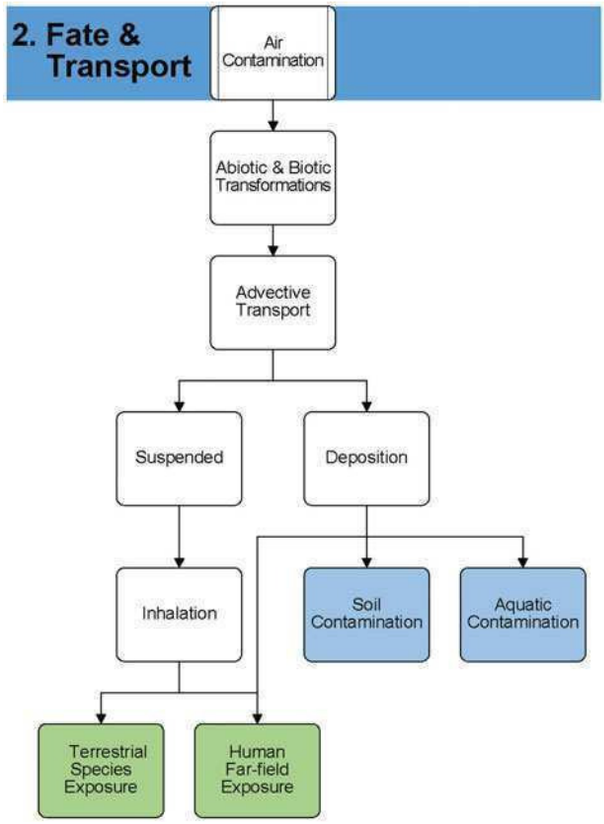

Figure 3. Potential pathways of ENM starting from release into ambient or indoor air. ENM may eventually be transported to another environmental compartment – either media or a human or ecological receptor.

decrease total particulate matter emissions. Despite a lower total mass of particulate emissions, the number of particles in the respirable size range increases, and the particles have greater adverse pulmonary effects in animal models (Snow et al. 2014).

Even though the release into ambient air represents only a small portion of the ENM production volume, there are several exposure scenarios where ENM release into air may pose a potential risk of direct inhalation for humans or local deposition for ecosystem exposure. These include occupational exposure during manufacture, formulation or modification of the ENM-enhanced polymer (through drilling, grinding, sanding, etc.), use of ENM-containing building materials, or formation of aerosols during spray applications (Figure 2). Although engineering control measures have been suggested to lower exposure to airborne EMNs in occupational settings, monitoring worker exposure and health effects remains a challenge (Evans et al. 2010). Exposures to ENMs during manufacture have presented a number of challenges to traditional approaches for protecting worker health. Significant challenges are also involved in relating exposure to risk and include issues such as small and often variable particulate size (within the nano-size range), lung deposition, as well as metrics that are used to measure exposure and effects (e.g. particle mass, surface area or number) (Liao et al. 2014; Eastlake et al. 2016a, 2016b). A battery of pulmonary and cardiovascular disease markers as well as inflammatory and oxidative stress markers, anti-oxidant enzymes, and genotoxicity

markers were compared in nanomaterial-handling and unexposed workers at 14 manufacturing plants in Taiwan (Liao et al. 2014). For this study, the ENM were associated with manufacturing, fabrication or use, and included Ag, TiO_2, SiO_2, Fe_2O_3, and CNT. Significant changes in several biomarkers including antioxidant enzymes (superoxide dismutase, glutathione peroxidase) and cardiovascular markers (vascular cell adhesion molecule, paraoxonase) were associated with exposure at the 6-month follow-up for handlers of carbon nanotubes, TiO_2, SiO_2, and Ag ENM. These results are relevant to the current framework, indicating that oxidative stress and inflammation represent key events along the AOP.

Another area where ENMs might be released into air is through the application and eventual weathering of coatings on building materials, or the remodeling or demolition of those structures (Shandilya et al. 2015). Photocatalytic TiO_2 ENM are released from ceramic building materials or coatings during weathering or abrasion, (Shandilya et al. 2015). West et al. (2016) documented over 450 construction products reported to be nano-enabled. The most frequently reported ENMs included TiO_2, silica, ZnO, and CNT. A case study using TiO_2-coated ENM tiles suggested that local exhaust ventilation during cutting and grinding of tiles significantly reduced Ti-containing respirable dust in the personal breathing zone and local construction areas. Recommendations also suggested better quantification of worker exposure and the effects of transformation and release over the product life cycles (West et al. 2016).

In addition to the aerosol application of coatings involved with building material surfaces, the use of ENM-enabled consumer spray products as coatings or disinfectants also show the potential for near-field human exposures. ENM-enabled products are quite diverse in terms of intended uses as well as the ENM employed. Examples of products that have been described in the literature include; antiperspirants, anti-odor shoe spray, and "plant-strengthening spray" (Lorenz et al. 2011) as well as anti-odor spray for hunters, surface disinfectant and throat spray (Quadros & Marr 2011). These exposures could be assessed according to the outline of Figure 2; Product Use; Dispersive Formulation; leading to Direct Consumer Exposures.

Soil

When ENM enter the soil environment, they are subject to biotic and abiotic transformations as in other environmental media, and they may either become bound and immobilized in the soil matrix, or remain unbound and relatively available for exposures or for transport to other environmental compartments (Figure 4). Assessing the fate and transport of ENM in soils is complex due to highly varying soil physical, chemical, and biological characteristics and processes, all of which can react spatially (angstroms to landscapes), temporally (instantaneous to geologic time steps), and biologically (across scales from prions to ecosystems). The biogeochemistry of a soil at any given locale results from continuous interactions among these characteristics and processes while the soil also reacts to ever changing environmental factors. Soil exposure to ENM may occur through direct deposition,

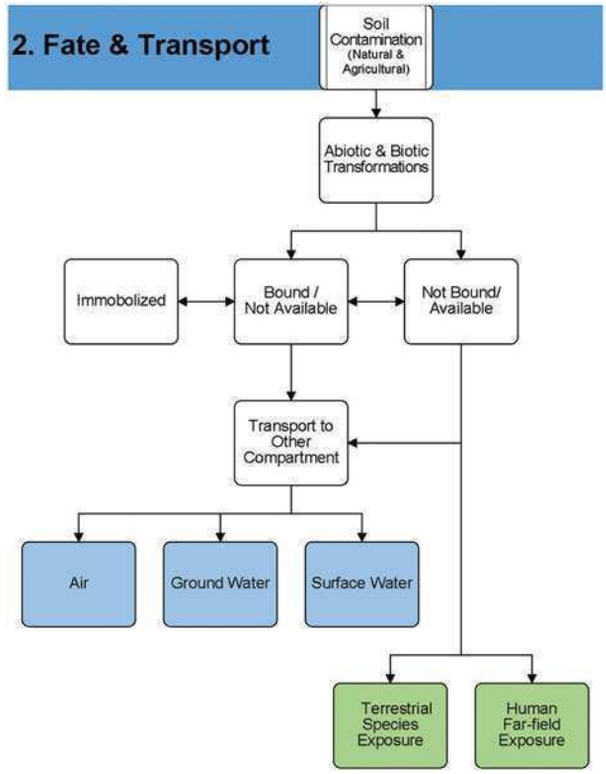

Figure 4. Potential pathways of ENM starting from release into natural or agricultural soil. ENM may eventually be transported to another environmental compartment – either media or a human or ecological receptor.

rainfall removal of excluded (non-bound) ENM from leaves, or from decomposition of vegetation containing ENM. Soils contain significant diversity in forms of organic matter, which may bind and influence aggregation and availability to soil flora and fauna.

Once in the soil, numerous transformations may occur, including physicochemical, macromolecular, or biological (Dwivedi et al. 2015). Other soil characteristics such as water content, pH, mineral content, and bulk density may influence chemical interactions in the soil, including homo- and hetero-aggregation (Dwivedi et al. 2015). In some cases, metal ENM such as Cu and Ag may solubilize and form other complexes. The extent to which an ENM is chemically transformed are constrained by the class and properties of the ENM, e.g. metals, metal oxides, carbon-based, quantum dots, ENM surface coatings, etc., and soil properties; see Dwivedi et al. (2015) for a more thorough discussion of the underlying mechanisms that initiate the abiotic and biotic transformations of ENM. Briefly, an assessment of ENM transformations in soil needs to include the physicochemical processes of aggregation, stability, dissolution, and deposition, and the potential for sunlight to induce photochemical reactions. Soil properties contributing to these processes and reactions include, but are not limited to, the relative and absolute amounts of organic matter of various qualities; soil inorganic particle size distribution; ionic strength; cation exchange capacity; relative soil hydrophobicity/hydrophilicity; type of salts; and the valence of the associated cation, base cation saturation ratio, water content, and pH.

Numerous substances are produced and released into the soil as carbon and nutrient resources (and ENM) that move

along the bidirectional pathway, e.g. ions, organic acids, amino acids, polypeptides, enzymes, and catalysts, all of which will influence the biotic and abiotic transformations of ENM.

Physical processes also contribute to the bound/unavailable and unbound/available status of ENM. Several factors contribute to the fate of ENM on any particular site, such as protocols for soil managment; soil particle size distribution; the absolute and relative quantities of various quality fractions of soil organic matter; and the uptake, translocation, and potential for re-release of ENM by organisms throughout the plant–soil food web. These factors will determine whether ENM remain on-site or will be transported to another environmental compartment. Reviews and more thorough discussions on the roles of soil organic matter, humic, and fulvic acids, and soil colloidal chemistry and physics are available (Hunter 2001; Kleber & Johnson 2010; Essington 2015). Examples of off-site transport include soil removal via actions of wind and water, consumption by mobile consumers [e.g. squirrels eating mushrooms, bird and mammal foraging, uptake of ENM into human food resources (plants and animals), etc.]. The myriad of ways ENM can be transported to another environmental compartment leads to the potential for ENM to be transferred to the atmosphere, ground and surface waters, thereby creating additional pathways of potential exposure to terrestrial species and humans.

The application of biosolids to land is estimated to be the main source of ENM emissions into soil (Tourinho et al. 2012; Gottschalk et al. 2013; Keller et al. 2013a, 2013b; Sun et al. 2014; Figure 4). As discussed earlier, many ENM will be chemically and physically altered during wastewater treatment. Sulfidation of metal and metal oxide ENM is generally the end-product in fresh biosolids, and some of these sulfidation products are further transformed during composting, aging, and stockpiling prior to land application. Pristine ENM are unlikely to enter the soil environment from the consumer → WWTP → soil pathway.

Direct application of ENM as nano-formulated pesticides, or some spray applications such as surface coatings, may result in direct exposure of ENM to soils. Additionally, direct release of ENM as a result of storage or transportation accidents should be considered. Exposure estimates that utilize broad averaging methods to divide nanomaterial potential releases over large geographical areas or environmental compartments may arrive at low estimated exposure concentrations. However, receptors might encounter pockets of higher concentrations of ENM due to latent chronic releases, concentrated intentional distribution, or spills. For these reasons, it is important to be mindful of the implicit assumptions behind exposure scenario descriptions, and assure that they are appropriate reflections of the cases being considered.

Several literature studies have attempted to examine ENM reactions in soils either through the consumer-to-WWTP-to-soil pathway or direct release. Unfortunately, many of these studies employ ENM concentrations that are disproportionately high in relation to probabilistic modeling of ENM release to soil systems, or spike ENM into processed biosolids without taking into account physiochemical reactions that occur in a WWTP (Priester et al. 2012; Colman et al. 2013). Historical research on biosolids application to soil, with particular emphasis on metal risks, highlights the complexity of understanding contaminant chemistry. Metal spiking in soils causes what is called the "salt effect". When metals (or ENM) work their way through a WWTP, the chemical reactions are buffered after the biosolids product has equilibrated for several months before land application. However, spiking a metal salt (i.e. Zn^{2+}) directly into soil or processed biosolids results in forms of Zn that are not similar to Zn phases in the WWTP-reacted, composted biosolid. Further, the spiked Zn^{2+} seeks equilibrium and, through hydrolysis ($Zn^{2+} + 2H_2O \rightarrow Zn(OH)_2 + 2H^+$), causes soil acidification that is not encountered in the equilibrated, composted biosolids. While spiking metal salts or ENM directly into soil would provide the worst case scenario for risk assessment, application, and interpretation of such results is challenging. There are limited examples examining the impact of ENM-influenced biosolids land application as well as realistic direct exposure of ENM in soils.

A case study of Ag salt and Ag ENM spiking directly in soil can be drawn from recent studies (Settimio et al. 2014; Sekine et al. 2015) which examined the lability of Ag_2S ENM represented in biosolids in comparison with labile $AgNO_3$ and metallic Ag ENM. Regardless of soil pH, $AgNO_3$ spiked soils observed more labile Ag than those treated with metallic Ag ENM. The Ag_2S ENM demonstrated virtually no Ag lability. Since the application of biosolids to land is estimated to be the main source of ENM emissions into soil and the primary form of Ag in biosolids is Ag_2S (Kim et al. 2010a; Kaegi et al. 2011; Impellitteri et al. 2013; Lombi et al. 2013), the chemical stability and low Ag lability from Ag_2S should drive the long-term risks of Ag toxicity in the soil environment.

Aquatic

Once an ENM is introduced into the aquatic environment, a series of processes begin that ultimately affect its fate and potential to cause adverse ecological and human health effects (Figure 5). Most fundamentally, and regardless of the source to the aquatic environment (e.g. soil groundwater intrusion, atmospheric deposition, and/or in-flow of surface waters), the ENM will distribute between the surface water and either suspended solids, dissolved organic carbon (DOC) or some other partitioning phase, and ultimately through depositional processes, may be deposited into sediments (Klaine et al. 2008; Praetorius et al. 2012; Dale et al. 2015; Velzeboer et al. 2014, Wang et al. 2014b). However, through competing dynamic processes, including resuspension, an ENM in the sediment may be returned to the surface waters only to be returned again to the sediments when the resuspension event ends. In the surface water or sediment, the ENM will be distributed between the aqueous phase and some form of particulate phase (i.e. heteroaggregation). Heteroaggregation is a process that occurs predominately between colloidal particles. By the time particles reach the microscale, they start to precipitate out in many systems. In the surface waters, this means the ENM will be either suspended in the aqueous phase or associated with suspended

colloids, DOC, or some other phase (Hyung et al. 2007; Klaine et al. 2008; Chang & Bouchard 2016). In the water located between sediment particles, the ENM will remain similarly suspended in the aqueous phase or associated with DOC, colloids, other ligands, and sediment particles.

For ENM in surface waters, transport and transformation will be governed by parameters such as ionic strength, temperature, pH, light intensity, and the concentrations of suspended particle matter (SPM), colloids, and DOC. These parameters affect ENM aggregation state, deposition on surfaces (Hyung et al. 2007; Saleh et al. 2008; Chang & Bouchard 2013), and transformation rates (Lowry et al. 2012; Hou et al. 2013, 2015; Chen & Zepp 2015; Chowdhury et al. 2015a; Mitrano et al. 2015). While the literature is well populated with reports of ENM–ENM interactions (i.e. homoaggregation), there is a growing consensus that heteroaggregation, the interaction of ENM with naturally occurring particles, will be the dominant particle interaction process in most natural systems (Koelmans et al. 2009; Praetorius et al. 2012; Bouchard et al. 2015). The reason for heteroaggregation dominance is that naturally occurring particles will greatly outnumber ENM in most environmental waters (Figure 5).

Relative to transport mechanisms, ENM released into a water body will interact with SPM, colloids and DOC and will then be subject to advective transport with water flow (e.g. stream and riverine flow, tidal motion) and to a lesser degree diffusive transport. Eventually ENM will be deposited to stream, lake or estuary bed with settleable SPM. Once deposited, the SMP-ENM aggregate may be buried in sediments or resuspended in the water column depending on water body

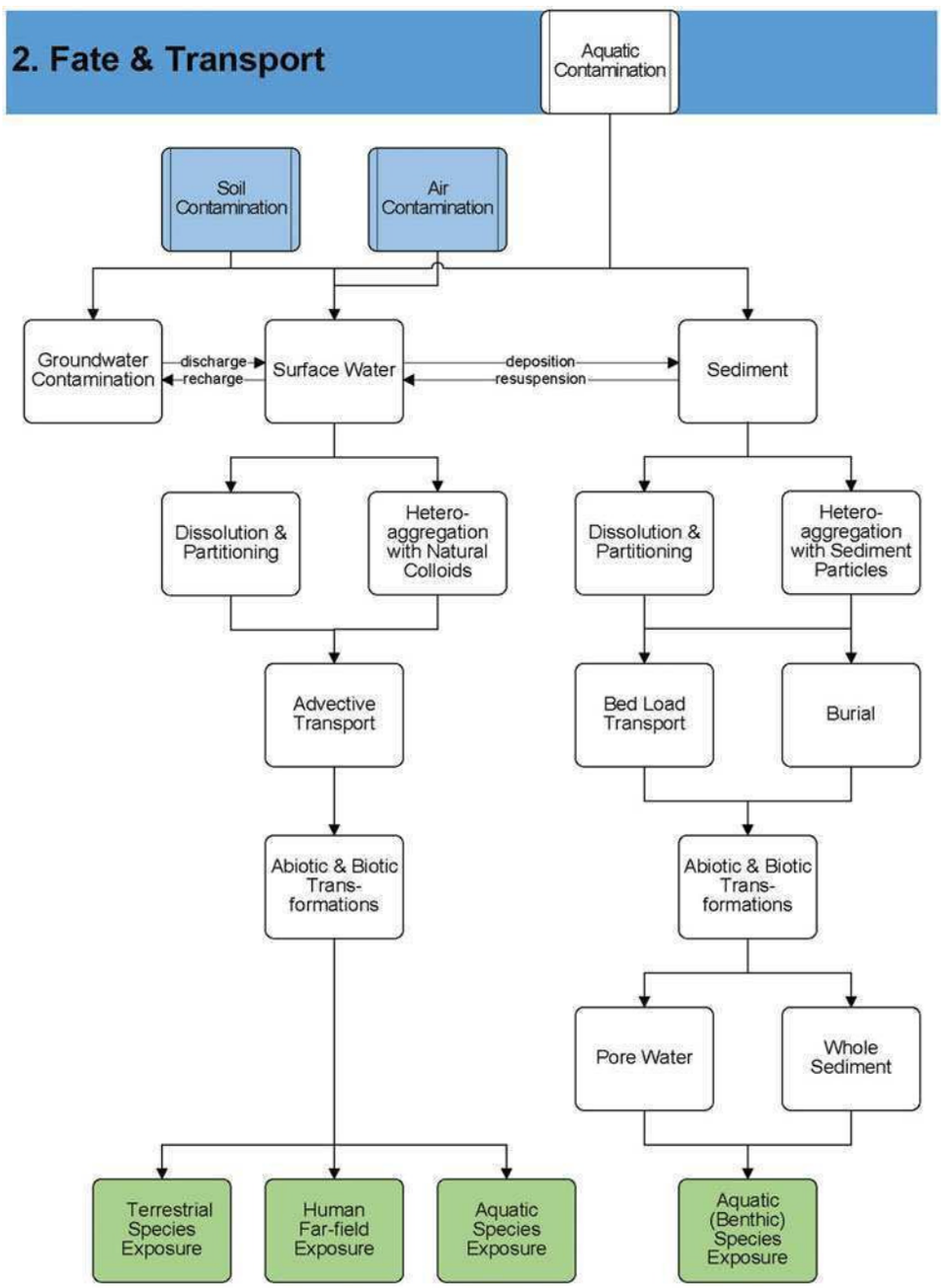

Figure 5. Potential pathways of ENM starting from release into surface water, groundwater, or sediment. ENM are less likely to transport to another form of environmental media. ENM will likely come into contact with an ecological receptor.

hydrodynamics. Within the sediment interstitial water, the aqueous phase ENM may also be transported by diffusive processes which may result in ENM exiting the interstitial water at the sediment water interface and entering the surface water. Along with the physicochemical and transport processes just discussed, there are also abiotic and biotic transformations (e.g. photodegradation, microbial degradation) that may affect ENM. For example, Chowdhury et al. (2013) reported that graphene oxide, a modified form of graphene, was stable and did not precipitate for days in natural and synthetic surface waters.

Given the extensive research and development that have produced the currently available contaminant transport and diffusive models (see Table 1 for examples), novel ENM models should not need to be developed. Rather, existing transport and diffusive parameters may be modified to address processes that differ between traditional dissolved contaminants (solutes) and ENM. One important difference is that most existing contaminant transport models use equilibrium solute partitioning to describe solute interactions with environmental particle surfaces, whereas ENM interactions are classically described using particle attachment kinetics. It is important to consider the complexity and interconnected nature of the various environmental compartments and the biota within them in determining fate (and toxicity) of the ENM. Sediments are the final sink for many anthropogenic contaminants including ENM. In many aquatic systems, particularly marine systems, ENM enter the water column and in a relatively short time frame move to the sediment phase via heteroaggregation and precipitation (Figure 5).

Hendren et al. (2013) have assessed the utility and limitations of existing contaminant transport and fate models for their application to ENM. There is a small but growing literature on ENM transport in surface waters. Streambed-water column exchange of TiO_2 nanoparticles has been modeled using particle–particle interactions and stream bed filtration processes (Boncagni et al. 2009) and ENM-specific processes have been linked to a spatially explicit hydrologic model (Quik et al. 2015). In an application of heteroaggregation attachment efficiencies, TiO_2–SPM interactions and TiO_2 concentrations in the water column and in sediments have been estimated (Praetorius et al. 2012). As these types of modeling approaches progress, data from ENM transformation and biota response studies should be incorporated into simulation models to provide more thorough estimates of the environmental distribution and potential for adverse effects from ENM released to water bodies.

In aquatic systems, as in other complex media, environmental transformations of ENM have important effects on their transport and toxicity (Lowry et al. 2012; Mitrano et al. 2015). Transformations are typically dependent on the chemical and biological conditions surrounding the ENM, so rates and products vary throughout the life cycles. Transformations are likely to be most varied during the use phase of life cycles due to the high variability of environmental conditions that apply during use. Mathematical models are one potentially useful tool for evaluating the variable effects of transformations on human and ecological exposures to ENM. For example, the Water Quality Analysis Simulation Program (WASP) is a mechanistic fate and transport water quality model that includes transformation processes (Table 1). WASP has been widely utilized for modeling the fate of traditional contaminants, but is now being updated to allow simulation of ENM exposures in aquatic environment (Knightes 2015). Process descriptors and data (e.g. for aggregation, deposition and transformations) and data inputs for conditions prevalent in aquatic environments are incorporated into WASP to provide improved understanding of the factors that influence exposure to ENM. Transformed (i.e. aged) ENM or ENM released during product use typically no longer have the same characteristics of their pristine counterparts (Lowry et al. 2012; Froggett et al. 2014; Kingston et al. 2014; Mitrano et al. 2015).

Considerations of carbon ENM illustrate the varied potential impacts of transformations on exposures and toxicity of ENM. These changes can be mediated by aggregation of the ENM. Increases in ionic strength alter the aggregation of CNTs and these changes may alter phototoxicity by increasing photoproduction of toxic singlet oxygen by the CNTs (Chen & Zepp 2015). Environmental transformation of the ENM released from products such as plastic composites can be initiated by sunlight (Froggett et al. 2014; Kingston et al. 2014; Mitrano et al. 2015). Direct and indirect processes are both competitively involved in the environmental phototransformation of ENM. For example, graphene oxide (GO) – a promising precursor to graphene-based materials – strongly absorbs sunlight in the ultraviolet and visible spectral regions, making direct photochemical reactions an important determinant of the persistence of these materials (Hou et al. 2015). Light-induced transformations of GO ENM produce much more hydrophobic, and likely more toxic, polycyclic aromatic hydrocarbons (Chowdhury et al. 2015a, Hou et al. 2015). Transformations can be driven by photochemical reactions, oxidation reactions, and biological processes, all of which affect their environmental transport (Chowdhury et al. 2015a). In the case of GO in natural waters, direct photoreaction likely dominates the initial phototransformation of GO into reduced graphene oxide species, low molecular weight (LMW) species and CO_2; these photoproducts are significantly less photoreactive, however, and persist under direct photolysis conditions. Thus, indirect photolysis initiated by natural organic matter is likely to dominate the secondary phototransformation process, ultimately converting reduced graphene oxide and LMW species into CO_2 (Hou et al. 2015). During this mineralization process, the intermediate species exhibit decreasing size and higher carboxyl group concentrations, and greater stability against aggregation and reduced surface deposition, indicating they would be more mobile than parent GO (Chowdhury et al. 2015a). This information combined with rate data can be used to model the fate of the GO ENM outlined in Figure 5.

Information on transformation processes can be used as inputs to water quality models such as WASP to evaluate the drivers of exposure concentrations in various compartments of aquatic environments such as rivers, ponds, lakes, estuaries, and coastal environments. Transformations can be responsible for evaluating exposure concentration changes in aquatic systems, including changes in the toxicity of ENM.

This information can be useful in designing monitoring and remediation strategies for contaminated systems. Also changes such as potential releases of ENM from plastics and related effects on ENM distribution and biological uptake can be evaluated using this modeling approach. Graphene oxide provides a good example of an ENM that can be evaluated using this modeling approach. Changes caused by photo-transformations can alter the persistence, mobility, and toxicity of graphene oxide residues (Hou et al. 2015, 2016).

CNT's have been shown to be stabilized in water by DOC, which acts like a surfactant to keep the CNT's suspended in the aqueous phase (Hyung et al. 2007; Kennedy et al. 2009). For graphene family materials, GO, with its substantial oxygen content is readily suspendable in water (Chowdhury et al. 2015b). In natural waters, particularly those with high DOC contents, carbon-based ENM can be stable in the water column resulting in organism exposures. Regarding transport and uptake of CNTs in water and soil, these materials are usually incorporated as composites with various matrices such as plastics in many commercial products and these composites have different fate and transport characteristics than pristine (pure) CNTs. It is now recognized that plastics have become widely distributed in aquatic environments and incorporated into food webs. Also, it has been shown that CNTs can be released from the composites by weathering and abrasion.

Some ENM release truly dissolved materials which are readily bioavailable, but arguably are no longer ENM. Nevertheless, because nano-scaled particles have a significantly larger surface area per unit mass and dissolve more rapidly than their micron-scale counterparts, the rapid release of toxic ions at the biological interface is a mechanistic consideration for ENM. A good example in consumer products is copper which is often in the chemical form of copper carbonates ($CuCO_3$) (e.g. pressure treated lumber), and releases the readily bioavailable and toxic Cu^{2+} (Parks et al. 2015). Silver ENM are often used in commercial products as vehicles for controlled release of silver ion at biological interfaces. Very low free Ag ion concentrations might be expected for fresh water or estuary environments that are likely to contain chloride, phosphate, and carbonate ions. Dissolution and transformation of Ag ENM in suspension compared with those interacting with bacteria and other aquatic organisms presents a significant uncertainty. Contact with aquatic organisms may increase the release of silver ions within the organism's local membrane environment (Fabrega et al. 2011). As a consequence, biotic as well as abiotic effects on dissolution and transformation should be considered in assessing risk of ENM to ecosystem targets (Navarro et al. 2008b).

Exposure and biodistribution

The determination of potential risk from ENM-enabled products requires assessments of exposure and hazard. As a simplistic example, a highly hazardous type of ENM may rarely be encountered by a target organism – or by contrast, a target organism may be chronically exposed to an ENM that shows only a moderate acute toxicological response. In any case, risk-based decisions will consider relative potential for exposure and hazard.

Exposure and biodistribution to terrestrial species, including humans, is depicted in Figure 6. Terrestrial fungi and microbes, as well as the roots of terrestrial plants, may become exposed to ENM in the soil. Terrestrial plants may also become exposed through the foliage after aerosol deposition or the application of nano-enabled agricultural products. Following such contact, the ENM may be absorbed, adsorbed, or excluded. Absorbed and adsorbed materials may be translocated to the interior of the organism leading to cellular level exposures, or they may be released or excreted causing a transfer to other environmental compartments. Exposures to terrestrial animals, including humans, through inhalation, oral, or dermal routes can lead to transformations at the point of contact, and perhaps either translocation across the biological barriers to the interior of the organism, or exclusion. Nanoparticles that reach pulmonary fluid, the gut, or the blood plasma typically will be coated with a protein corona, as discussed below. *In vitro* modeling of gastrointestinal digestion for polystyrene nanoparticles influenced the protein corona composition and increased translocation of these particles into Caco-2 and HT29-MTX cells. Variations in the protein corona and translocation rates were dependent on the biochemical surface modification of the polystyrene nanoparticles (Walczak et al. 2015). The composition of the corona may include opsonin or other proteins which can trigger macrophage phagocytosis leading to degredation or excretion. The protein corona also may influence distribution across biological barriers and cellular uptake. Modification of the surface of nanoparticles with polyethylene glycol (PEG) can alter binding of proteins to the nanoparticles, and thus impacts protein corona formation. This modification of the nanoparticles using PEG results in decreased uptake by macrophages and prolonged tissue residence time (Pearson et al. 2014). Such changes in particle coatings could change rate constants for nanoparticle transitions for systemic absorption, distribution, and clearance (Figure 6). Particle aerodynamic diameter influences the region of deposition in the respiratory tract, but the effect of particle size on macrophage uptake may not be a factor. Blank et al. (2013) have shown that there was no difference in murine alveolar macrophage uptake between 20 and 1000 nm sized polystyrene nanoparticles.

Human exposure

The exposure of humans or indicator organisms to ENM or ENM-enabled products may occur at numerous points along the product life cycle. One way to consider human exposure assessment is through analysis of activities along the nanomaterial life cycle that bring these materials into contact with receptors. In addition to estimating these activities, it is important to consider the magnitude, frequency and duration of exposure to an agent, along with the number and characteristics of the exposed population (Zartarian et al. 2004). These factors are part of the exposure assessment for a risk assessment for any chemical or physical agents. Two sources of human exposure to airborne ENM are during manufacturing and use of ENM-enabled construction products (coatings, cements, and concrete). Given the relatively high number

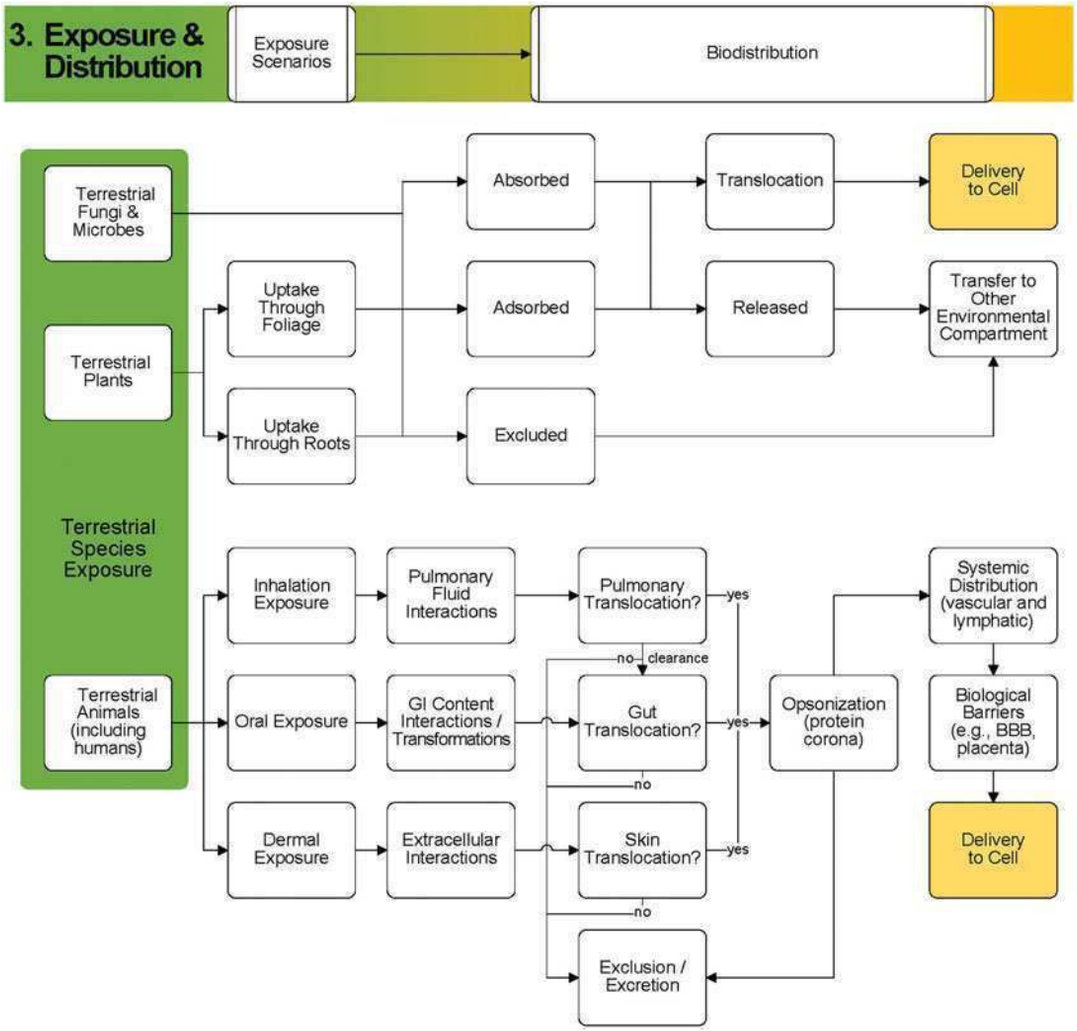

Figure 6. Potential terrestrial species exposure and biouptake pathways, including pharmacokinetic distribution routes that continue up to contact with cells.

(70–80%) of construction workers who are unaware of the presence of nanomaterials in the products that they routinely spray, cut, or sand, the potential use of personal protective equipment or use of engineering controls are likely to be limited (West et al. 2016).

Occupational exposure can occur during the synthesis, application, recycling and disposal of nanoparticles or ENM-enabled products. Workers may be among the first people exposed to new ENM, and may have higher levels of exposure than do other segments of the population (Schulte et al. 2014). Occupational safety and health achieved through limiting worker exposures to ENM is an area of focus for the responsible development and use of nanotechnology. One particular area of focus has been the potential for inhalation exposure to poorly soluble particles and fibers (Kuempel et al. 2012). As the current paper primarily concerns environmentally mediated exposures, interested readers may find detailed considerations of occupational safety issues elsewhere (Pietroiusti & Magrini 2014; Schulte et al. 2014; Thompson et al. 2015; Boonruksa et al. 2016; Brouwer et al. 2016; Larese Filon et al. 2016). Although occupational exposure concentrations may be higher than those of the general public, the number of individuals potentially exposed in the general population is larger than in the workplace, and includes individuals with greater potential susceptibility such as the young, elderly, or those with other compromising health conditions.

The main routes of exposure for particles from ENM-enabled products are shown in Figure 6. Due to the relatively limited total volumes of most manufactured ENM and the limited time that most ENM have been in production (in the absence of a large spill), human exposures from far-field sources (arising from environmental background) are not likely to become a significant contribution to overall exposure in the near future. Consequently, the most significant exposures for humans in a non-occupational setting are expected to be near-field (arising from interaction with ENM-enabled consumer products), as opposed to far-field scenarios. Where nanomaterial composition was identified, analysis of nano-enabled consumer product inventories suggested that the greatest number of currently listed products contain metal-based ENM (Ag or Ti), followed by Si- and carbon-based ENM (Vance et al. 2015; Hansen et al. 2016).

Estimation of an individual's exposure to ENM from the use of ENM-enabled consumer products requires information concerning the product composition (magnitude of

exposure), how often it is likely to be used (frequency of exposure events), the pattern of product use (duration and potential exposure route), and potential for ENM release from the product matrix. Population exposure modeling requires input on market penetration of the product. Modeling of cumulative exposure can be considered for target populations using multiple products containing similar ENM using integrated probabilistic techniques such as the Stochastic Human Exposure and Dose Simulation (SHEDS) Model (Isaacs et al. 2014). Human exposure pathways to ENM include dermal/ocular contact, inhalation, and oral ingestion. The dermal route has the highest probability of exposure to consumer products (Vance et al. 2015). Ingestion and inhalation routes follow, with about half of the number of reported products being metal-ENM, followed by silicon and carbon-based ENM. Inhalation exposure can result from occupational and environmental sources and, of the three pathways, is most likely to occur and poses the greatest risk of adverse outcomes. Oral ingestion could occur from dietary sources or drinking water contaminated with ENM, hand-to-mouth activity following dermal contact of ENM contaminated surfaces, or from swallowing mucous and macrophages containing inhaled ENM that were cleared from the lung by the mucociliary tract lining the conducting airways of this organ. Given the significant changes in matrix conditions that occur along the GI tract including the acidic environment in the stomach and complex intestinal components, transformation is an important consideration for ENM bioavailability (Alger et al. 2014). Silver nanoparticles have been shown to aggregate, react with chloride and sulfide as well as form protein aggregates and coronas (Mwilu et al. 2013; Walczak et al. 2013). In addition, copper carbonate nanoparticles associated with treated lumber have been shown to dissolute into ions in the presence of simulated stomach fluid (Santiago-Rodríguez et al. 2015). Dermal contact may occur through unintentional or intentional exposure – the latter from, for example, applying sunscreen that contains ENM. Although transport of ENM through skin is typically limited, damaged skin may facilitate increased rates of transdermal transport (Baroli 2010).

Human biodistribution (dosimetry)

The pharmacokinetics (PKs) of chemicals including ENM involves aspects of the rate and extent of their absorption, distribution, metabolism, and excretion (ADME) from the body (Figure 6). The role each process has in the disposition of an ENM is dependent on the route of exposure, characteristics of the individual exposed (e.g. age, health status), and properties of the ENM (e.g. size, surface properties, etc.) and exposure medium (e.g. water, soil, etc.). Publications by Elder et al. (2009), Hagens et al. (2007), Landsiedel et al. (2012), Lin et al. (2015), and Riviere (2009) review the PKs of ENM. Overall, exposure of ENM to terrestrial mammalian species can occur by inhalation, ingestion or contact with the skin (Figure 6). The Multiple-Path Particle Dosimetry Model (MPPD; Table 1) calculates deposition in the respiratory tract based on airway geometry and physical/chemical properties of aerosol or particle. Once exposed to the lung, gastrointestinal tract or skin, different extracellular interactions may occur with the ENM between proteins, lipids, and microbiota within the different fluids of each organ. Transformation of nanoparticles in biological fluids depends on the core particle composition, particle coating, and biological fluid. Simulated gastrointestinal exposure to CdSe-core/ZnS-shell quantum dots resulted in solublization of Zn and to a lesser extent Cd (Wiecinski et al. 2009). Similar treatment of Ag ENM resulted in aggregation and formation of a AgCl coating on the particle aggregates (Rogers et al. 2012). The extent of this transformation was dependent on the initial coating used to stabilize the Ag ENM (Mwilu et al. 2013). Biological fluids such as artificial sweat and urine solubilize Ag ions from Ag ENM-enabled fabrics to a greater extent than water or simulated saliva (Quadros et al. 2013).

Translocation of the ENM through each organ may or may not occur (Baroli et al. 2007; George et al. 2014). Translocation is the result of crossing an epithelial barrier and the ENM is absorbed systemically (Larese et al. 2009). The ENM may then interact with proteins and other biomolecules forming a protein corona. The ENM may then distribute to other organs, requiring crossing another barrier eventually being delivered to a cell within an organ (Baroli et al. 2007; George et al. 2014). Systemically absorbed ENM may also be excreted in the urine or bile for eventual fecal elimination.

The commonality of the exposure pathways described above leading to absorption of ENM is that these materials must cross an epithelial barrier. However, the epithelial barriers of the lungs, gastrointestinal (GI) tract and skin (Figure 6) are different in many ways (Elder et al. 2009). Epithelial cell types include columnar, cuboidal, squamous, and others which vary within each organ/system (GI tract consists of several organs) and each cell type has a different function. While the cells that line the lungs and gastrointestinal tract are viable, the outer layer of the skin, the stratum corneum is non-viable. The microenvironment of each organ system differs with respect to hydration, pH, air:surface interface and other factors. Immune cells are integrated differently within each organ system and provide unique means and abilities which may limit absorption of ENM.

Absorption: portals of entry

The outer layer of the skin, the stratum corneum, is non-viable epidermal tissue (Baroli 2010). The stratum corneum consists of keratinocytes filled with the protein keratin surrounded by a lipid membrane. The means of absorption through the skin is passive diffusion. The epidermis contains pores and shunts, which ENM may enter. ENM have been detected in the pores, cracks and hair shafts of skin (Baroli 2010). The results of most dermal absorption studies of ENM indicate that these materials may penetrate to lower levels of the epidermis, which are viable, but rarely penetrate into the dermis, which underlies the epidermis and is the vascularized tissue of the skin. With intact skin, most studies indicate ENM are excluded from entering the body (Pflucker et al. 2001; Monteiro-Riviere et al. 2011). However, if the stratum corneum is damaged from, for example, sunburn, cuts or

abrasions, further penetration of the ENM through the skin may occur with potential systemic absorption (Larese et al. 2009).

Inhalation of ENM can result in their deposition in conducting and respirable airways. The particle size determines the location of deposition in the respiratory tract. Inhaled particles of about 20 nm in size have the highest proportional deposition in the alveolar region (~50%) (Oberdörster et al. 2005; Elder et al. 2009). Conducting airways (bronchi) are lined with mucous and epithelial cells with cilia. Particles that deposit in the mucous are moved up (i.e. cleared) in the respiratory tract by action of the cilia to the trachea, where they are eventually swallowed and translocated to the gastrointestinal tract. ENM that deposit in the respirable region of the lungs can be absorbed through epithelium of the alveoli. The distance between the outer surface of the alveoli and the capillaries ranges from 0.36 to 2.5 μm (Elder et al. 2009). The ENM may enter the vascular or lymphatic system. The size of ENM particles is a determinant for systemic absorption, with particles <55 nm diameter having greater penetration through the alveoli than particles of 200 nm or greater (Elder et al. 2009). If the alveoli/blood vessel interface is inflamed, absorption of the ENM may be potentially increased (Elder et al. 2009). If not absorbed, ENM may be phagocytized by macrophages, which may be cleared by the mucociliary tract and eventually swallowed and translocated to the gastrointestinal tract. Multiwalled carbon nanotubes (MWCNT) that reach the alveoli may eventually translocate to the pleural cavity (Mercer et al. 2013), as has been found with asbestos fibers (Donaldson et al. 2010; Xu et al. 2014). Length and shape of the MWCNT appears to affect its translocation to the pleural cavity (Xu et al. 2014). There is also evidence of absorption of ENM via the olfactory nervous system following inhalation exposure, where particles may enter the brain without crossing the blood–brain barrier (BBB) (Oberdorster et al. 2004; De Lorenzo 2008).

The GI tract is the anatomical organ system exposed to ENM following their ingestion and includes esophagus, stomach, small and large intestine and colon. The cells lining the GI tract, even though epidermal, change in structure, and function as the GI tract progresses from the esophagus to the colon. The pH of the GI tract also changes from acidic conditions in the stomach to slightly basic in the intestine which can affect the physicochemical properties of the ENM (Elder et al. 2009). Surface charge of the ENM can affect GI absorption, as positively charged ENM seem to be absorbed to a greater extent than neutral or negatively charged ENM (Hagens et al. 2007). As for conventional chemicals, most absorption of ENM in the GI tract takes place in the intestine. This is due in part to the large surface area of the intestine, the longer residence time of the ENM within it than in other parts of the gastrointestinal tract, and the epithelial cell type favoring absorption. It appears the most common mechanism of uptake of ENM in intestinal epithelial cells is by endocytosis (Frohlich & Roblegg 2012). Paracellular uptake may also be involved, but may be less than endocytosis because the area available for the former uptake to occur is much less (Hagens et al. 2007). Particle size may affect intestinal absorption, as Desai et al. (Desai et al. 1996, 1997) have reported polylactic polyglycolic acid co-polymer particles of size 100 nm–10 μm show decreased absorption with increased size of particle *in vitro* whether in the rat *in situ* intestinal loop model or in Caco-2 cells (Desai et al. 1997).

Distribution

ENM absorbed into the systemic circulation are distributed to organs within the body (Figure 6) (Almeida et al. 2011; Stapleton & Nurkiewicz 2014). Studies have essentially found that systemically absorbed ENM are distributed to most, if not all, organs, but the levels detected in the organs vary greatly (Hillyer & Albrecht 2001; Oberdorster et al. 2002; Fabian et al. 2008; Landsiedel et al. 2012). Factors that influence the distribution of ENM include route of administration, physicochemical properties of the ENM, physiological environment where the ENM enters the systemic circulation and the morphology of the endothelium (i.e. blood vessel wall) within that organ. Because the physical flow of blood changes with the size of the blood vessel, when the vessel becomes <300 μm, the smaller solutes tend to move towards the vessel wall (Stapleton & Nurkiewicz 2014). Thus, the size of the ENM is an important determinant of its ability to pass through the endothelium of different morphologies. A continuous endothelium is essentially found in lung and muscle capillaries. The endothelium of kidneys is fenestrated, and that of liver and spleen discontinuous (Almeida et al. 2011).

Proteins and other biochemicals in blood may surround ENM to form a corona. The characteristics of the corona are dependent on the physicochemical properties of the ENM (e.g. size, surface properties) and the biochemicals and proteins that interact and bind to the ENM. As ENM are phagocytized by macrophages and monocytes, the blood and organs that possess macrophages such as liver, spleen, lymph nodes, and bone marrow are some of the first organs that sequester ENM (Almeida et al. 2011). ENM may also be absorbed into the lymphatic system and be distributed as well, although little is known about this aspect of ENM distribution. Stapleton and Nurkiewicz (2014) contend that ENM in lymphatics may contribute to inflammation to a greater degree than in the circulatory system. This is because ENM would be in higher concentrations in lymphatics than in blood, their residence time would be longer due to a lower flow rate, and they could interact with neutrophils and propagate inflammatory signals to a greater extent.

Metabolism

Mammalian biological transformations of ENM are not well characterized or known (Hagens et al. 2007). The available information on fullerenes and silica ENM indicates that these materials are not biotransformed (Landsiedel et al. 2012). Metal-based ENM can be in various oxidation states, so there is the potential that these materials could be oxidized or reduced *in situ* based on the pH and oxidation state of the tissue environment. Metal-based ENM taken up by cells via phagocytosis or endocytosis are exposed to enzymes and changes in pH within the endosome/lysosome. These enzymes may degrade corona proteins and the acidic environment of these vesicles may degrade a metal-based ENM

with release of metallic ions (Soenen et al. 2015). Functionalized single-walled carbon nanotubes (SWCNT) *in vitro* are susceptible to degradation by human myeloperoxidase and eosinophil peroxidase (Kagan et al. 2010; Andón et al. 2013). Overall, more studies are needed to understand the metabolism of ENMs.

Elimination and excretion

Systemically absorbed ENM are eliminated via urinary elimination, fecal excretion or both (Landsiedel et al. 2012). The extent of the elimination by these routes is dependent on the physicochemical characteristics such as size, surface chemistry, and charge of the ENM and the route of administration (Lin et al. 2015). Urinary elimination involves filtration of blood plasma through the glomerulus. Although ENM are found in urine, not all ENM are able to pass through the glomerulus. Choi et al. (2007) report that quantum dots (CdSe/ZnS core/shell) with a hydrodynamic diameter less than 5.5 nm, when administered i.v. to mice, are rapidly and efficiently eliminated via the urine. The adsorption of serum proteins to the quantum dots, which could be prevented by zwitterionic or neutral organic coatings on the dots, tended to increase the hydrodynamic diameter and thus retard their urinary elimination. Intravenous administration of Ag ENM (approximately 8 nm size) to rabbits was followed by low urinary excretion (Lee et al. 2012). This suggests that factors in addition to size of ENM can influence elimination of the particle from the body. Functionalized SWCNT and MWCNT have also been detected in urine of laboratory animals administered these carbon-based ENM (Landsiedel et al. 2012). Whether ENM are secreted or absorbed by the renal tubules is not known.

After being absorbed, ENM may be transported via the bile to the gastrointestinal tract and eliminated in the feces. For an ENM to be excreted into the bile, it would have to cross the cell membrane of the hepatocyte, and then be excreted into the biliary tract. Ag ENM were detected in feces of rabbits administered Ag ENM intravenously, suggesting biliary excretion of these particles (Lee et al. 2012). Low levels of polystyrene nanospheres (50 nm diameter) have been detected in rat bile following intravenous administration (Ogawara et al. 1999). The mechanism of the ENM entry into the bile is not known.

Some ENM dissolve to smaller constituents or ions over a time course of days, while other ENM can be strongly persistent. For example, 90 d after i.v. infusion of 30-nm sized CeO_2 in rats, there was little decrease in cerium concentration in any tissue (Yokel et al. 2012).

Physiologically based PK modeling

PK models use mathematical formulas to describe the movement of a chemical or drug in the body. A progression of PK models is the inclusion of physiological, anatomical, biochemical, and other specific aspects in mathematical terms (tissue volumes, flow rates, etc.) to build physiologically based PK (PBPK) models. PBPK models have several advantages over PK models in terms of extrapolating dose, exposure duration, route-to-route and species. A strength of PBPK models is that they can be used for hypothesis testing, to understand mechanisms of toxicity, and to make predictions of movement of a chemical in humans using *in vitro* and *in vivo* PK animal data. PBPK models are extremely useful for regulators because of the information they can gather from this predictive tool. PBPK models have been applied primarily to inorganic and organic compounds, such as drugs, with a MW less than approximately 900 Da. The PKs of small molecules are different from ENM in areas of diffusion, active transport, metabolism, and excretion. The physiological, biochemical, and metabolic processes that the body imposes upon ENM are generally different than those for non-particulate or small molecules (Li et al. 2012). For these reasons, only a few PBPK models have been published for ENM and include those on Ag (Bachler et al. 2013), ZnO (Chen et al. 2015), and TiO_2 (Bachler et al. 2015) (Table 1).

The Ag ENM PBPK model (Bachler et al. 2013) included structures for ionic and nanoparticulate Ag and were based on PK data from intravenous studies in rats. The modeling results, within the confines of particle sizes (15–150 nm) and coatings (polyvinylpyrrolidone and carboxymethyl cellulose), indicate that particle size and coating had minimal impact on the distribution and organ uptake of the Ag ENM; dissolution to Ag ions was not significant; the ENM were stored as insoluble salt particles; and uptake of Ag ENM by macrophages was of minimal significance for relevant human exposure levels. The ZnO PBPK model (Chen et al. 2015) was based on previous PK studies using ZnO ENM (10 and 71 nm) and $ZnNO_2$ (soluble) administered to mice. The modeling efforts showed that the tissue partition coefficients of ZnO ENM were greater than those of soluble zinc; the excretion and elimination rates in liver and gastrointestinal tract of 71 nm ZnO ENM and soluble Zn were important determinants of their PKs; ZnO ENM decomposed to soluble Zn after 1 week in the body. The TiO_2 PBPK model (Bachler et al. 2015) was based on published PK data of mice and rats administered TiO_2 ENM intravenously. The modeling results showed that particle size (15–150 nm) and crystalline structure of nano-TiO_2 had limited impact on the distribution; and the nanoparticles agglomerated at high concentrations and were engulfed by macrophages (Bachler et al. 2015). Extrapolating the results to human oral exposures to nano-TiO_2, Bachler et al. (2015) reported that the organ concentrations of titanium at the 95th percentile level were lower than concentrations in *in vitro* studies that resulted in toxic effects.

There has been a great research effort to understand the biodistribution and dosimetry of ENM over the past 10–15 years. Certainly the physical and chemical properties of the ENM, such as chemical composition, size, coatings, have a tremendous impact on how the body interacts with these particles regarding their absorption, distribution, metabolism, and excretion. But the most critical ENM property affecting biodistribution and dosimetry has not been clearly defined, and represents a significant data gap. With all of the different types of ENM (e.g. metals, metal oxides, SW-, and MWCNT) currently in use and with their transformation/degradation in the environment to a variety of products, it may not be possible delineate a specific property of the ENM that has the greatest impact on its biodistribution and dosimetry within the body.

Testing the potential toxicity of ENM frequently includes *in vitro* assessments as a component of the testing strategy. Understanding dosimetry to cells *in vitro* has become an important consideration (Teeguarden et al. 2007). Typically the cells to be tested are adherent to the bottom of a flash or well and the nanomaterial suspension is added to the media over the cells, with the dose expressed as the mass concentration per unit volume. However, the amount of nanoparticles reaching the cell layer can differ substantially from the added concentration. The behavior of ENM suspended in media is dependent on forces of diffusion, where particles tend to remain in suspension, and sedimentation, where particles tend to settle gravimetrically (Teeguarden et al. 2007; Hinderliter et al. 2010). Computational models (Table 1) have been developed to predict dose delivered over time to the celluar layer, including the *In vitro* Sedimentation, Diffusion and Dosimetry (ISDD) model (Hinderliter et al. 2010). Subsequently, procedures were standardized for preparations of particle suspensions (Cohen et al. 2013a, 2014), and estimating density of particle agglomerates (DeLoid et al. 2014) with corresponding model updates, to better estimate *in vitro* particle dosimetry.

Extracellular interactions

Protein corona/opsonization

Once introduced into a biological fluid such as blood, ENM interact with a variety of cells, proteins and other biochemicals. The interaction of ENM with proteins in blood *in vivo* or serum *in vitro* results in formation of a protein corona (Figure 7) (Nel et al. 2009; Zhu et al. 2012; Fleischer & Payne 2014; Pearson et al. 2014; Treuel et al. 2014). Proteins that have been found in the corona include albumin, immunoglobulins, apolipoproteins, and fibrinogen (Lundqvist et al. 2008). In some circumstances, over 80 proteins have been associated with citrate stabilized Ag ENM (Shannahan et al. 2015). The formation of these complexes is a dynamic process that is dependent on surface characteristics of the ENM, properties of the suspending media (e.g. salts and multivalent ions), the solid-liquid interface (e.g. surface hydration and dehydration) and the ENM–protein interface (e.g. conformational change in protein) (Nel et al. 2009; Ritz et al. 2015). The adsorption of proteins to ENM occurs at various rates because of differing affinities the proteins have towards the surface of the ENM (Ritz et al. 2015). It was proposed that eventually, a "hard" corona is formed with proteins that have a high affinity towards the surface of the ENM and an overlaying "soft" corona, consisting of proteins having a lower affinity to the ENM (Lynch et al. 2007). Others find the protein coronas to be unstable and reversible, similar to other forms of heteroaggregation (Liu et al. 2013). The forces controlling the interactions between ENM and protein include hydrodynamic, electrodynamic, electrostatic, solvent, steric, and polymer bridging (Nel et al. 2009). The formation of the ENM-protein corona complex may alter the physicochemical properties of

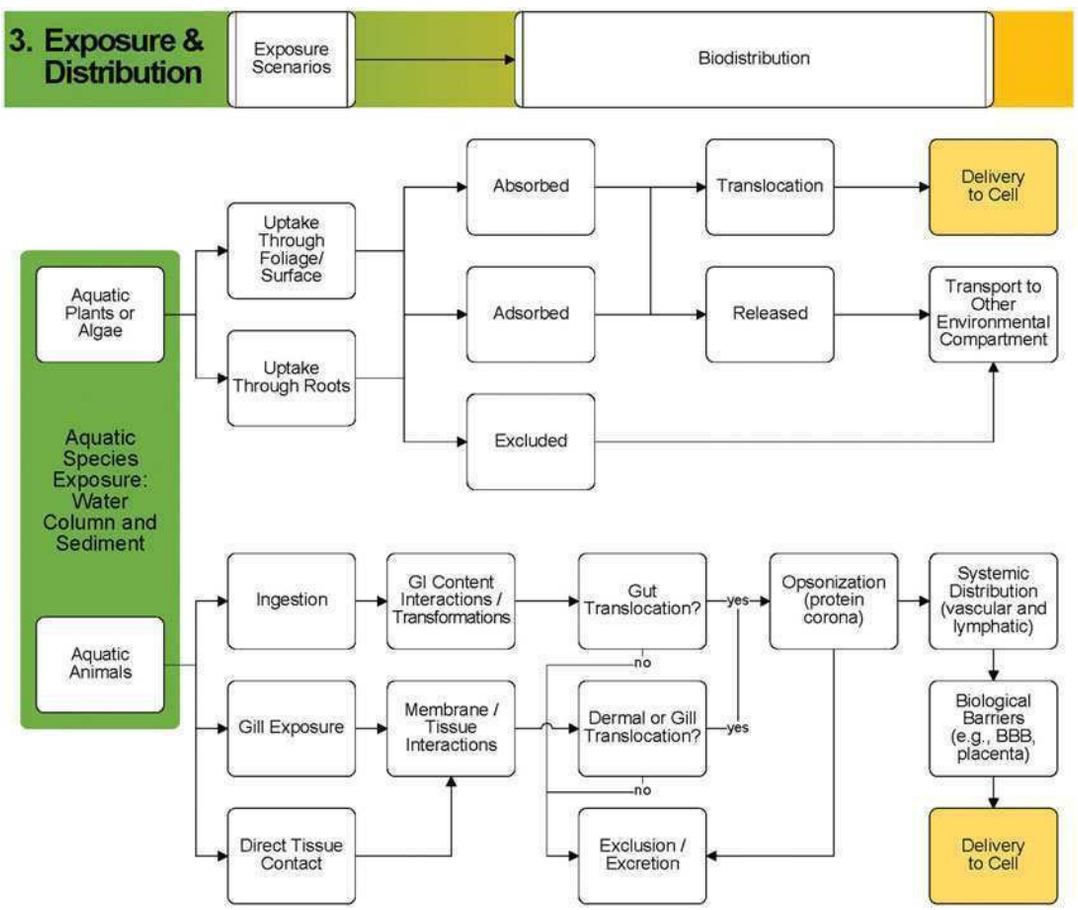

Figure 7. Potential aquatic species exposure and biouptake pathways, including pharmacokinetic distribution routes that continue up to contact with cells.

the ENM such as zeta potential and agglomeration of the ENM (Pearson et al. 2014; Treuel et al. 2014). Conformational changes in the protein as a result of this interaction with an ENM may result in exposure of new epitopes (leading to potential allergenicity), altered function (protein no longer recognized by cellular receptors), and changes in avidity (Nel et al. 2009; Shannahan et al. 2015). Knowledge of the ENM–protein corona complex and how it is formed will enable an understanding how ENM are internalized into cells, as these complexes can bind to specific receptors involved with cellular uptake.

Opsonization is a biological process that promotes, but does not always result in, clearance of ENM from the systemic circulation. Complement proteins adsorbed to the ENM are recognized by receptors on macrophages (Walkey et al. 2012). Macrophages internalize the ENM-protein corona complex via receptor mediated phagocytosis. Remarkably, modifying an ENM with polyethylene glycol (PEG) will reduce uptake of the ENM by macrophages (Pearson et al. 2014). The uptake of gold ENM by murine macrophages is decreased by 75% or more when the density of polyethylene glycol grafted on to the gold nanoparticles reaches 0.32 PEG/nm^2 (Walkey et al. 2012). This effectively increases the systemic circulation time of the ENM. PEGylation of ENM reduces binding of proteins to the ENM. Because of differences in the physicochemical properties of ENM, such as size, the effect of PEGylation on the ENM must be made on a case by case basis.

Biological barriers (e.g. BBB, placenta)

ENM that have reached the systemic circulation following oral, pulmonary, or dermal exposure have translocated through an epithelial barrier. To translocate from the systemic circulation into internal organs, ENM must pass through an endothelial barrier – the wall of the blood vessel. The lining of blood vessels by the endothelium, which varies from organ to organ, is continuous, fenestrated, or discontinuous. Organs such as the liver and spleen have a discontinuous endothelial cell lining and are more "leaky" than other organs. This allows for substances in the blood to be absorbed more easily by these organs. Other organs such as the brain have a continuous endothelium that is more specialized. This distinctive lining limits the absorption of many exogenous chemicals in these organs and provides a level of protection.

The brain is a unique and sensitive target organ for toxicants because of its limited ability to regenerate cells and tissue after toxic insult. The uptake of many exogenous chemicals including ENM from the systemic circulation into the brain may be limited due to its specialized barrier, the BBB (Bhaskar et al. 2010). The endothelial cells of the vasculature within the brain are connected by special protein complexes that form tight junctions between the cells (Pietroiusti et al. 2013). Efflux transporter proteins also line the endothelium that carries xenobiotics out of the brain (Tamai & Tsuji 2000). However, the role of transporters eliminating ENM out of the brain is not well defined. Despite the BBB, chemicals including ENM are still absorbed into this organ following oral administration or intra-tracheal instillation (He et al. 2010; Hu et al. 2010; Kim et al. 2010b; Park et al. 2010; Yang et al. 2010; Schleh et al. 2012). Molecules of low molecular mass (<400–500 Da) and lipophilic compounds may cross the BBB and enter the brain tissue by passive diffusion (Bhaskar et al. 2010). Although not quite clear, ENM may be absorbed into the brain by receptor-mediated endocytosis or pinocytosis (Bhaskar et al. 2010; Zhao et al. 2011). ENM from extravascular sources that enter the body are absorbed to a very limited extent if at all into the brain (<0.03% of the administered dose) (Pietroiusti et al. 2013). However, animal studies have shown damage to brain (e.g. inflammation, altered morphology of neurons, perturbations in neurotransmitter secretion) following administration of ENM such as carbon black, TiO_2, and SWCNT following intra-tracheal instillation, oral administration, and inhalation (Wang et al. 2007; Hu et al. 2010; Jackson et al. 2011; Pietroiusti et al. 2013; Karmakar et al. 2014). ENM are also being developed for intravascular administration targeting the brain for purposes of medical imaging or as a carrier of therapeutic drugs (Bhaskar et al. 2010; Domínguez et al. 2014), indicating that the BBB is not impermeable to ENM.

Male germ cells mature in the seminiferous tubules within the testes. The blood–testis barrier (BTB) protects these germ cells from exposure to potential toxicants. This epithelial barrier consists of Sertoli cells, with specialized proteins (tight junction, desmosome, basal ectoplasmic specialization, and gap junction) between adjacent cells (Cheng et al. 2011; Cheng & Mruk 2012). An anatomical feature that enhances protection to the seminiferous tubules is that they are not infiltrated by blood vessels, lymph vessels, or nerves. Nevertheless, despite this epithelial barrier, animal studies have shown translocation of several ENM (Ag, CeO_2, Fe_2O_3) from the systemic circulation to the testes and damage to this organ as well (carbon black, TiO_2, SiO_2) (Pietroiusti et al. 2013). Relative to the BBB, the BTB appears to be less effective as a long-term barrier to ENM. This may be due to damage to the Sertoli cells, decreased ability to translocate ENM out of the Sertoli cells, or both (Pietroiusti et al. 2013).

The developing fetus is extremely vulnerable and susceptible to toxic insults from a variety of toxicants. Toxicants in the mother's systemic circulation have the ability to distribute to the fetus. ENM that adversely interact with the placenta itself may affect the developing fetus. Knowledge on the ability of ENM to cross the placenta is limited. The placenta is a "short-term" barrier, unlike the BBB and BTB (Saunders 2009). It is present in the mother only for the term of the fetus. Nutrients from the mother are transferred through the placenta for the growth and development of the fetus. The placenta also metabolizes endogenous and exogenous compounds, exchanges gas between mother and fetus, plays a role in immune function and removes waste products from the fetus (Saunders 2009). The barrier is the trophoblast, a continuously fused non-replicating epithelial tissue derived from the fetus. The trophoblast is immersed in the maternal blood, and pores within it are thought to be no greater than 10 nm (Saunders 2009). To reach the fetal circulation, chemicals must traverse the trophoblast (which consists of two layers of cells), basement membrane, connective tissue, and endothelial wall of the fetal blood vessel. The placental barrier changes over time, from a hemodichorial architecture in

the first trimester to a hemomonochorial architecture during the second and third trimesters (Juch et al. 2013). The barrier thus becomes thinner and presumably more permeable as the fetus develops. Translocation of chemicals is thought to be primarily by diffusion, but mechanisms including receptor-mediated endocytosis, phagocytosis, and transporter proteins may also be involved (Saunders 2009). Several studies in which pregnant rodents were administered ENM (e.g. SiO_2, TiO_2, fullernes, Au, SWCNT) reported translocation and/or toxicity to the embryo/fetus/pup (Pietroiusti et al. 2013). These outcomes were dependent on the type of ENM used (metalloid, metal, metal oxide, carbon nanotube), dose administered, route of administration (sc, oral, iv), and day of gestation (single or multiple days) (Takahashi & Matsuoka 1981; Lim et al. 2011; Pietroiusti et al. 2011; Yamashita et al. 2011).

Cellular uptake and intracellular fate

A simple schematic depicting uptake and distribution of ENM at the cellular level is presented in Figure 8. The physical and chemical interactions among the nanoparticle, its protein corona, and the cell membrane surface determine the probability that the particle will enter the cell or be excluded from it (Verma & Stellacci 2010; Zhao et al. 2011; Zhu et al. 2012; Oh & Park 2014).

The uptake of ENM into cells has been an active area of drug development research because ENM may enable drugs to enter cells or cross biological barriers where they otherwise would not. Cellular uptake of ENM is also a key determinant of nanotoxicity (Ivask et al. 2013). Although studies of cellular uptake frequently use electron microscopy (e.g. Chithrani & Chan 2007) uptake of fluorescently labeled ENM has been observed using fluorescent or confocal microscopy (Davda & Labhasetwar 2002; Treuel et al. 2013). Cellular uptake of nanoparticles composed of materials that reflect light, such as Ag or Ti, can be observed with dark-field microscopy and quantified using flow cytometry (Zucker et al. 2010). Plasmonic resonance of Ag ENM in a cellular matrix also presents an opportunity to detect ENM with a larger signal to noise ratio than by using light scattering (Zucker et al. 2013). Much of the nano-pharmaceutical understanding of mechanisms through which cells internalize particles, and the influence of nanoparticle physical and chemical parameters, can be applied to considerations for nanotoxicology. Numerous factors influence cellular uptake pathways including particle size, shape, charge, hydrophobicity, surface modifications, and dissolution.

Mammalian cells have mechanisms for particle uptake, although different types of cells take up particles to different degrees. The uptake mechanisms are distinguished by the size of particles processed, the signaling and enzymatic pathways involved and the destination of the internalized materials. In addition to direct penetration through the membrane, which occurs primarily for very small particles, the following uptake pathways have been described: phagocytosis, through which macrophages and other phagocytic cells engulf foreign materials, including nanoparticles; pinocytosis, through which cells engulf fluids, nutrients and other materials; and endocytosis, membrane receptor-mediated processes involving either clathrin (clathrin-mediated endocytosis), caveolin (caveolin-mediated endocytosis), or neither (clathrin/caveolin-independent endocytosis). Detailed reviews and diagrams of these cellular uptake pathways are available elsewhere (Dobrovolskaia & McNeil 2007; Jin et al. 2009; Zhao et al. 2011; Canton & Battaglia 2012; Zhu et al. 2012; Adjei et al. 2014; Oh & Park 2014).

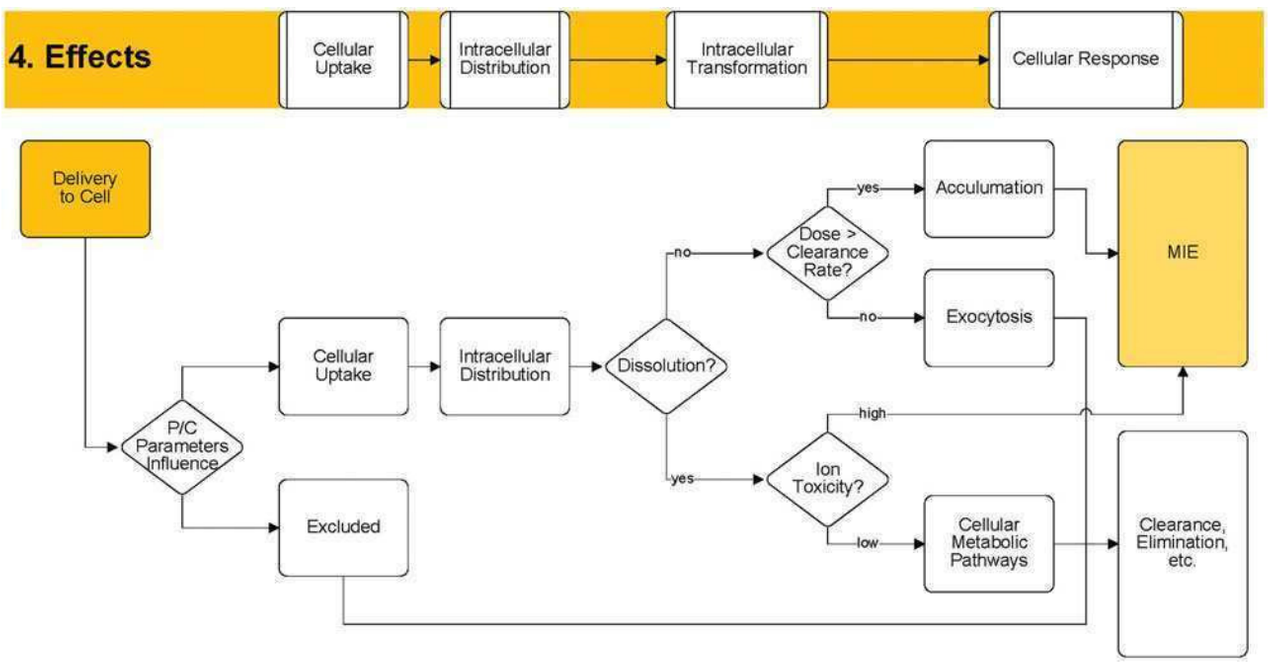

Figure 8. Potential pathways between cellular contact with a biologically transformed ENM and potential molecular perturbations, including molecular initiating events (MIE). Labelled branches indicate directional selectivity based on ENM physicochemical (P/C) properties.

Endocytosis

In clathrin-mediated endocytosis, clathrin is a membrane resident receptor protein that recognizes ligands for absorption, including opsonin-bound particles (Canton & Battaglia 2012; Oh & Park 2014). Caveolin-dependent endocytosis involves invaginations of the cell membrane that enclose primarily sphingolipids bound to cholesterol or the protein caveolin in the membrane (Nabi & Le 2003). The composition of the ENM and its coating influence which endocytic pathway are involved.

In clathrin-mediated endocytosis, biomechanical thermodynamic modeling indicates that ENM of around 55 nm have the fastest membrane wrapping time and are taken up more rapidly and efficiently than bigger or smaller particles (Gao et al. 2005). Gold ENM that were spherical and 50 nm in diameter were taken up to a greater extent than 14 nm spherical particles or rod shaped gold ENM (Chithrani et al. 2006; Chithrani & Chan 2007). Smaller ENM cluster on the cell membrane until there is sufficient thermodynamic energy to overcome membrane elastic resistance and the entropic energy barrier to form vesicles for endocytosis (Chithrani & Chan 2007; Jin et al. 2009). Smaller ENM are taken up by endocytosis more slowly and in batches that are then packaged together in membrane bound vesicles. These vessels fuse together after uptake to contain higher number of particles per vessel. This results in larger particle agglomerates inside of cells than outside.

Pinocytosis

Pinocytosis is a process by which cells intake fluids by extending the cell membrane to surround a portion of the extracellular space and engulf the fluids along with solutes and suspended materials as well including ENM (Buono et al. 2009). Pinocytosis can take up a wide range of particle sizes (up to 10 μm) (Adjei et al. 2014). Pinocytosis may be the primary uptake mechanism for small particles (<25 nm) where, at reasonable exposure concentrations, it is unlikely that sufficient numbers of the particles co-locate on proximate receptors to trigger clathrin-mediated endocytosis (Adjei et al. 2014). Nanoparticles taken up by pinocytosis do not need to interact with cell membrane receptors, but the amount taken up in this way is lower than that through receptor mediated endocytosis pathways.

Phagocytosis

Phagocytosis is a process present primarily in cells with immunological or similar functions to defend against pathogens or to cleanup waste and debris (Zhu et al. 2012). These cells include phagocytes such as macrophages, neutrophils, and monocytes. Particles that are first coated with opsonin, immunoglobulin, complement, or serum proteins are subject to phagocytosis. The opsonized nanoparticles bind to cell surface receptors; the cell membrane forms a cup-shaped extension and internalizes the material into membrane bound phagosomes. The phagosomes are transported internally and fuze with lysosomes, transferring the vesicle contents to the acidic environment of the lysosome that also contains enzymes to digest and destroy the contents. Phagocytosis of ENM by cells in the immune system may trigger production of inflammatory cytokines and inflammatory reactions (Dobrovolskaia & McNeil 2007; Kim & Choi 2012).

Intracellular destination

The intracellular destination of ENM is determined by several factors, as discussed subsequently, one of which is the potential for dissolution. Some metal or metal-oxide ENM are prone for dissolving and releasing metallic ions, where others are relatively insoluble and stable in the intracellular environment. Particles that dissolve can release toxic ions, such as Ag (Singh & Ramarao 2012) or Zn (Shen et al. 2013). Materials that are insoluble can be removed from the cell by exocytosis (Sakhtianchi et al. 2013; Wang et al. 2013; Oh & Park 2014). If the rate of uptake exceeds that of removal, ENM could bioaccumulate inside cells, however, feedback mechanisms may exist to reduce further cellular uptake when ENM accumulate in cells (Gunduz et al. 2017). The release of toxic soluble components, or bioaccumulation of persistent materials, could lead to a MIE which then begins a sequence of key events leading to an adverse outcome (Gerloff et al. 2017).

Nanomaterials packaged in endosomes may merge, leading to agglomeration into larger sized particles. Endosomes may be transferred to the endoplasmic reticulum or Golgi apparatus and the contents can become packaged in lysosomes. Over time nanoparticles accumulate in lysosomes where low pH and proteolytic enzymes digest opsonin coatings and soluble nanomaterial components. Nanoparticles composed of soluble metals, such as silver, iron, or zinc, may dissolve in a lysosomal environment and release ionic forms of the metals. Dissolution rates depend on both cellular and material factors. Cellular compartments vary in terms of pH, ionic strength, and concentration. Materials with core/shell composition dissolve layer by layer. Other factors influencing dissolution include surface area (smaller particles dissolve faster than larger), diffusion coefficient of the material; volume of solution, and thickness of diffusion layer. Nanoparticles composed of relatively insoluble materials, such as TiO_2 or CeO_2, may resist dissolution, even in an acidic lysosomal environment. Depending on rates of uptake and removal, particles may persist in cells for weeks or months and accumulate into large intracellular deposits (Zucker et al. 2010). Small particles may cross the nuclear membrane through the nuclear pore complex which is 20–50 nm in diameter (Tkachenko et al. 2003). ENM absorbed cellularly, if not retained, can be re-packaged for expulsion from the cell by exocytosis (Frohlich 2016).

Exocytosis

In comparison with the large number of studies on endocytosis and other uptake pathways, there has been relatively less research evaluating ENM exocytosis. Removal by exocytosis involves fusion of an exosomal vessel with the cell wall and expulsion of the vessel contents into the extracellular space. For transferrin-coated gold ENM, smaller particles were removed from HeLa cells by exocytosis at a faster rate than

larger particles, as the rate of exocytosis was inversely proportional to particle surface area (Chithrani & Chan 2007). The rate of exocytosis varies substantially across different types of cells (Sakhtianchi et al. 2013). Particle shape and coatings influence the rate of exocytosis; however, the literature is mixed as to the influence of rod shape and aspect ratios relative to spherical particles (Oh & Park 2014). In addition to exocytosis, the ENM content of cells may be reduced by cell death releasing nanomaterials into the extracellular space, cell division where daughter cells may inherit the parent cell ENM content, through dissolution or degredation of the ENM, or via transcytosis where ENM are transferred directly to another cell avoiding the extracellular space (Frohlich 2016).

Terrestrial exposure and biodistribution

ENM exposure to terrestrial ecosystems can occur through air, soil or water (see Figures 3–5 for illustrations of related fate and transport). In all cases, interactions in the soil, and on plant and animal surfaces, can influence the activity and likelihood of uptake into terrestrial organisms. The biological processes and ecology of soil organisms, viewed as a functioning ecosystem, also are complex (Coleman et al. 2004). Generally, soil biota can be organized by functional groups, and for some organisms within groups as guilds, all of which are situated along a multi-level trophic-gradient food web. Carbon produced through photosynthesis is transferred from primary producers (e.g. green plants) to an extensive array of consumers in the food web along a carbon utilization pathway whereby the end products of each sequential consumption step become more resistant to decomposition (Stevenson & Cole 1999). A nutrient utilization pathway processes resources in the opposite direction, i.e. from the soil biogeochemical matrix, along the pathway, to the primary producers. Once consumed, and depending on the niche and life history of the consumer, ENM may be transformed, sequestered, or re-released to the soil environment via internal physiological processes and/or turnover/food web consumption/decomposition processes. At each release of an ENM, it may be become bound again and unavailable (adsorbed/absorbed), or may it be transformed remaining unbound and available for further biological acquisition (Figure 4). It is anticipated that ENMs may be acquired internally (adsorbed and/or absorbed) by any of the innumerable species deployed throughout the food web, similar to other particles, however to our knowledge no studies have yet examined ENM fate and transfer in the soil food web organisms. Although the number of studies is currently limited, there are some examples of ENM being transferred through the food chain. Holbrook et al. (2008) showed quantum dots being transferred from protozoans to rotifers in a simple aquatic food chain. Biomagnification of cadmium selenide quantum dots was observed in an experimental microbial food chain (Werlin et al. 2011). In a terrestrial food chain, Judy et al. (2011) demonstrated the transfer of Au ENM from tobacco plants to the tobacco hornworm. Because of the small number of studies available on the dynamics of ENM in food chains, it is too soon to state definitively whether or not ENM move up food chains.

Release of ENM to soil can lead to exposure of soil microfauna and flora (Figure 6). Free-living fungi, micro- and macroinvertebrates, and bacteria in soil form a unique ecosystem comprised of high structural and functional diversity.

Terrestrial plants and animals

When ENM enter the environment, they may interact directly with plants via deposition to foliage, or to soil, wherein they may be taken up through roots (Dietz & Herth 2011). At the surface of roots, ENM uptake is a complex and poorly understood process, in large part due to the heterogeneity of soils and the complexity of rhizosphere interactions. Several studies have found differential uptake by plant species (Ma et al. 2010; Rico et al. 2011; Judy et al. 2012). Judy et al. (2011) suggested that differential uptake may be related to the types of root exudates present in the rhizosphere, an area where more research is needed. Many of these exudates play important roles in nutrient acquisition and sequestration by plants. For example, Manceau et al. (2008) found that Cu was transformed into metallic nanoparticles in the rhizosphere of wetland plants. They also found that arbuscular mycorrhizal (AM) fungi were involved in the chemical transformation. It is possible that root exudates and symbiotic AM associates have developed these rhizosphere compounds as a means to avoid copper toxicity. Given the range and surface chemistries of the ENM in production, additional research is needed to better elucidate how rhizosphere chemistry influences ENM transformation and exposure at the root surface.

Foliar deposition does not necessarily mean that the ENM will be taken up into the leaves; some particles may tightly bind to cell walls or lipophilic surface cuticles, but not move intracellularly across the plasmalemma (living cell membrane). They also may be actively excluded through various mechanisms. There may be uptake into the substomatal cavity through stomates, leading to direct exposure of internal mesophyll cells (Navarro et al. 2008a). Regardless of site of deposition, particles may be adsorbed, absorbed, or excluded (Figure 6).

If particles are not bound or taken up into cells (i.e. excluded), then they may move to another terrestrial compartment either through wind dispersal or by rainfall removal. They also may be transported to other terrestrial organisms or compartments following consumption by grazers (Figure 6).

Regardless of whether the particle is taken up through roots or through leaves, terrestrial organisms that feed on vegetation may be exposed to ENM. Recent studies have shown that there can be biomagnification of ENM by organisms feeding on plant foliage (Judy et al. 2011). For example, Majumdar et al. (2016) found significant biomagnification of CeO_2 from kidney bean plants to Mexican bean beetles to spined soldier bugs. Overall, however, there has been little research into biomagnification in terrestrial food webs or on the potential entry of ENM into the human food chain through various agricultural products (Rico et al. 2011). Wheat did not take up ENM CeO_2 via the plant roots, but barley did, although it was unclear whether uptake was in the particle or ionic form (Rico et al. 2017).

In addition to ingestion, terrestrial animals also may be exposed to ENM through inhalation and dermal absorption (Figure 6). Many of the studies examining routes of exposure to terrestrial animals have been done using species such as mice and rats as human analogs (Mitchell et al. 2009; Larsen et al. 2016). As a result, there is considerable understanding of ENM effects on mammals (i.e. typical laboratory study species), however information on the extent of exposure of native populations of animals in terrestrial ecosystems is lacking.

Aquatic species exposure and biodistribution

Once an ENM is introduced into the aquatic environment, a series of processes begin that ultimately affect its fate and potential to cause adverse ecological and human health effects (Figure 7). For aquatic and terrestrial species, including humans and plants, exposure to ENM may occur from surface waters directly, the sediment interstitial water, or whole sediment. Uptake may occur through foliage, roots, ingestion, gills, and direct contact with skin or tissues. Each of these processes is described in more detail below. Much of the bioavailability literature indicates that traditional contaminants associated with SPM, colloids, DOC, ligands related to ionic strength, and sediment are not as bioavailable as the aqueous form of the chemical (Di Toro et al. 1991). However, once associated with an environmental particle, an ENM may be more easily taken-up by filter- or deposit-feeding organisms (although not necessarily in a bioavailable form). Learning from existing traditional materials and understanding the differences in the relationships between the transport pathways of specific ENM in aquatic systems and observed ecological effects is critical. Ultimately, all these environmental processes will affect the likelihood of the ENM being exposed to organisms (e.g. aquatic and terrestrial species as well as humans) via the surface waters directly, the sediment interstitial water, or whole sediment.

Although sediments will be a primary route of aquatic exposure to ENM, water column exposure should not be overlooked as organisms can be exposed as ENM pass through the aqueous phase or remain suspended in the water column due to functionalization of the ENM, episodic discharges or pseudo-persistence (when concentrations of degradable or removable chemicals persist in the environment through continual input) (Holden et al. 2016). Such pseudo persistence could be modeled in the Framework as a chronic exposure.

When considering exposures to aquatic organisms, it is helpful to differentiate between carbon-based and metallic ENM. Exposure investigations with carbon-based ENM, specifically SWCNT and MWCNT, so far indicate that little actual exposure to aquatic organisms occurs before the CNTs precipitate from the overlying water and are buried in the sediments in a non-bioavailable form (Petersen et al. 2011; Parks et al. 2014). However, in fresh waters with significant DOC contents, CNTs may be quite stable and remain suspended in the water column. Furthermore, if the carbon-based ENM are ingested by an aquatic organism (e.g. associated with sediment particles), indirect evidence suggests that the carbon-based ENM pass through the organism's digestive tract, which are then deposited into the sediment as pseudo-feces (Parks et al. 2014). Little exposure research in the aquatic environment has been performed on non-functionalized fullerene and graphene carbon-based ENM, although it is likely they will behave in a similar fashion to the SWCNT and MWCNT.

A source of uncertainty regarding the exposure of aquatic organisms to carbon-based ENM is associated with the modified forms of SWCNT, MWCNT, fullerenes, and graphene. While most of the current research has been performed on pristine versions of carbon-based ENM, the materials used in products are often modified, altering their physicochemical behavior to make them more water soluble. This makes ENM less likely to associate with sediment particles and potentially increases exposures and bioavailability. A measure of heteroaggregation in natural water models might help quantify such behavior. Gaps in understanding of this aspect of aquatic organism exposure to carbon-based ENM remain.

In contrast to carbon-based ENM, metallic ENM have been shown to be bioavailable to aquatic organisms. Exposure can occur via skin (dermal), gill, or ingestion of contaminated prey or sediment. For many aquatic organisms, particularly invertebrates, internal organs are bathed directly by overlying water or pore-water. Compared with terrestrial organisms, this blurring of internal and external exposure results in less of a division for aquatic organisms between dermal and non-dermal exposure. For example, in bivalves the pericardial cavity, gonads and ganglion epidermis may be exposed directly to ENM in water that enters the shell. Uptake of ENM in mollusks also may occur through filtration or ingestion of suspended sediments to which ENM are associated. Bivalves can selectively filter particles sizes ranging from 2 to 10 μm (Kraeuter & Castagna 2001), and ENM heteroaggregation in marine waters can increase the size of individual nanoparticles to microparticles within hours of introduction to marine systems (Wang et al. 2014a). This increases the possibility of ENM exposure to bivalves and other invertebrate filter feeders. For fish and other vertebrates, exposure to suspended ENM can occur primarily via gills and ingestion. The occurrence of dermal exposure may be less than in terrestrial organisms as fish are often protected by a mucous layer that is difficult to penetrate (Handy et al. 2008).

In aquatic organisms, the gills are often a targeted tissue for ENM exposure. The gills necessarily have a high exposure to large volumes of water and nanoparticles can be entrapped in gill tissue. For example, exposure to TiO_2 ENM resulted in damage to fish gills including edema, thickening of the lamellae, decreases in Na^+K^+-ATPase activity, and increased levels of thiobarbituric acid reactive substances (TBARS) and glutathione (GSH) (Federici et al. 2007). There is also evidence that metal nanoparticles interact differently than metal ions in gills (Kádár et al. 2010; Gomes et al. 2011), and that gill damage from ENM particles goes beyond solubilization of metals from nano-copper or nano-silver particles (Griffitt et al. 2007, 2009; Shaw & Handy 2011; Trevisan et al. 2014).

Because of the difficulty in detecting ENM within organisms, there are many knowledge gaps in assessing exposure

to and distribution of ENM in aquatic organisms. In fish, the gills, gut, liver, and brain may be target organs, but streamlined methods of detecting ENM within organisms need to be developed. Not surprisingly, the surface properties of ENM affect the movement through the organism (Wang et al. 2014b, Zhu et al. 2010). Metallic ENM move through the walls of the digestive tract and into the body of organisms. Researchers have shown that Au ENM are internalized into the cytoplasm and co-localized with DNA in nuclei (Joubert et al. 2013). Titanium ENM have been found in bivalve hemocytes (Marisa et al. 2015) and Cu, Ag, and Ti ENM have been identified in the lysosomes and lumen of digestive glands (Jimeno-Romero et al. 2012). Overall, in mollusks, the digestive gland or hepatopancreas appears to be a target organ for metallic ENM (Gomes et al. 2012); however, more research is needed on the systemic biodistribution of ENM in aquatic organisms.

Uptake of ENM whether through ingestion or other processes, may increase the availability of ENM transferred through the food web. Researchers have shown that Au ENM can easily pass from the water column into the food web with mollusks taking up the majority of the ENM (Ferry et al. 2009). The bioavailability of ENM will be affected by environmental conditions, like suspended sediments, and will reduce exposures. In contrast, some ENM, depending on their physicochemical characteristics, will be bioavailable. If ENMs do not enter the body, either absorbed through the gut, skin or gills, they could pass through the digestive tract of aquatic organisms where they are also bioprocessed (i.e. repackaged into different sized metallo-organic molecules) (Hull et al. 2011; Pan et al. 2012) that will have varying fate pathways compared to pristine ENM. The fate of bioprocessed ENM is unknown, however, if ENM enter the mollusk body, there is a good chance they would enter the food web as the mollusk flesh is often consumed whole by predators including humans.

Effects

Consideration of adverse effects follows the potential for ENM exposures. A sequence of steps is described between external exposure to the material and the PK and pharmacodynamic steps that lead to the occurrence of a MIE (Figures 5–8). The AOP sequence, then, progresses from a MIE through a sequence of key events (KE) occurring at progressively higher levels of organization including cellular, organ level, and whole organism responses (Figure 9). The AOP sequence can continue to describe effects at the population level if ecosystem effects are of concern (Figure 10). Here we use AOP as a conceptual progression under which to organize information, and are not proposing specific AOP sequences for any particular adverse outcome. This prevents more specific delineation of an AOP pathway. The effects of ENM on organisms have been studied primarily in mammalian systems, with a few notable exceptions such as the relatively extensive testing of zebrafish (Fako & Furgeson 2009; Harper et al. 2011; Muller et al. 2015; Wehmas et al. 2015; Chakraborty et al. 2016), and a some other aquatic species (Petersen et al. 2015). The discussion below considers

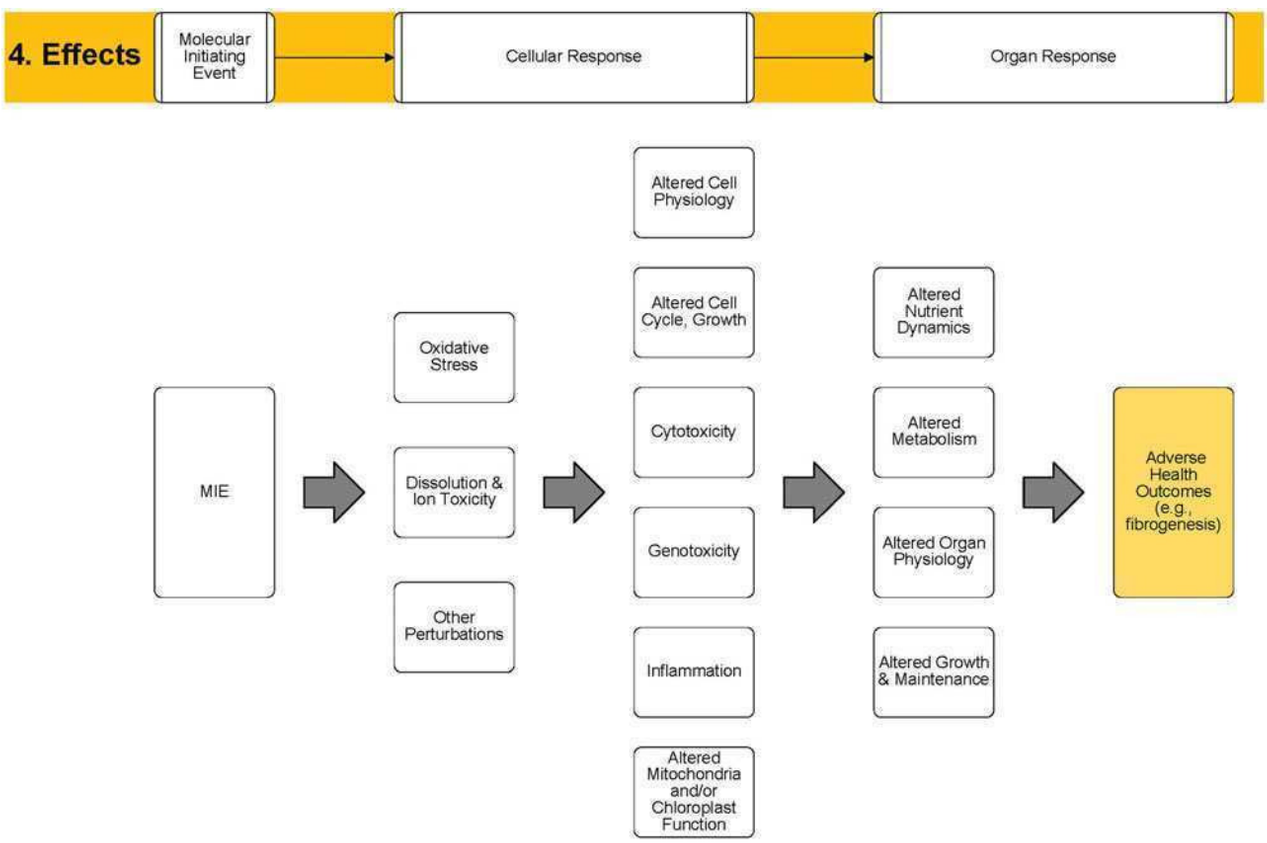

Figure 9. Potential ENM effects on organisms from the molecular initiating event (MIE) to individual adverse health outcomes.

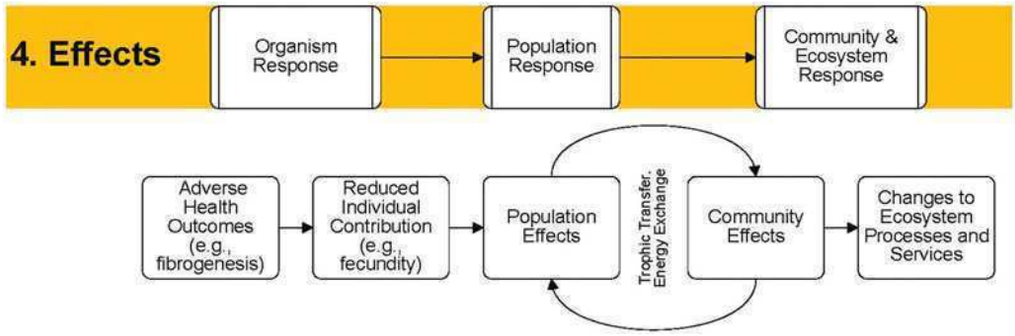

Figure 10. Cascade of potential effects from individual adverse health outcomes to greater potential subsequent effects on relevant populations, communities, and ecosystems.

primarily mammalian species where the majority of the mechanistic-level research has occurred.

MIE/cellular, organ response

A schematic concept of an AOP for the toxic effects of exposure to ENM at the cellular level is depicted in Figure 9. Ankley et al. (2010) produced a conceptual framework of an AOP leading to the production of a toxic or adverse event. The AOP concept is anchored by an MIE that is linked through a series of Key Events to an adverse outcome with significance to risk assessment. Conceptually, AOPs are independent of a specific chemical trigger, so that any potential toxicant causing a MIE would be expected to trigger the sequence of events in the AOP and potentially lead to the adverse outcome. In this way, observations of mechanistic or molecular toxic events can be projected to their potential adversity and aid in the support and interpretation of mechanistic data for risk assessment purposes (Gerloff et al. 2017). Because AOPs theoretically apply to multiple chemicals, it could be argued that development of AOPs for ENM are irrelevant if the ENM induces the same MIE as a toxic chemical. Here we limit the discussion to MIE or KE that have been attributed to ENM and AOP frameworks in which they have been applied.

Recently published studies on CuO ENM and MWCNT have included the concept of AOPs in their toxicological evaluation. Muller et al. (2015) examined the effect of CuO ENM on hatching in zebrafish and reported that CuO ENM elevated the Cu level in the hatchlings (the perivitelline space) at a greater rate relative to Cu salts. The MIE was considered to be inhibition of Zebrafish Hatching Enzyme 1 (ZHE1) by released Cu^{2+} ions.

Labib et al. (2016) applied toxicogenomics to the AOP framework for lung fibrosis in mice exposed to three individual MWCNT. The MWCNT had different physicochemical properties, yet comparable biological pathways were perturbed across dose and time. The transcriptional bench mark dose values for the MWCNT were similar to the values for lung fibrotic lesions induced by these materials. The authors concluded the genomic data in an AOP framework could be used to estimate levels of exposure that would be acceptable in the absence of epidemiological data (Labib et al. 2016). Multiple pathways leading to lung fibrosis were considered by which carbon nanotubes could induce fibrosis, including release of pro-inflammatory or pro-fibrotic mediators, oxidative stress, and direct effects on fibroblasts (Vietti et al. 2016).

In mammalian cells, changes in signaling pathways and microRNAs indicated effects of TiO_2 on a number of pathways including cell-cycle regulation, apoptosis, calcium signaling, Nrf2 responses, IGF1 signaling, RAS signaling, PI3K/AKT signaling, cytoskeleton remodeling, cell adhesion, BMP signaling, and inflammatory responses (Thai et al. 2015). Rat dopaminergic cells exposed to Ag ENM showed genomic response pathways generally indicative of mitochondrial disruption (Chorley et al. 2014). Gerloff et al. (2017) proposed an AOP framework for hepatic toxicity that could be suitable for metal oxide ENM. Gerloff et al. (2017) point out that MIEs for chemicals or ENM can vary widely and may not be completely understood, and, therefore, it may make more sense to use Key Events rather than MIEs as linking factors when trying to map ENMs to chemical-derived AOPs.

Oxidative stress

Nanomaterial exposures in biological systems are strongly linked to generation of reactive oxygen species (ROS) and, to a much lesser extent, reactive nitrogen species (RNS). For ENM exposures, higher degrees of positive association and/or causality are available for ROS species like superoxide, hydrogen peroxide and hydroxyl radical. One way ENM produce ROS is by a direct property of the nanomaterial itself, and another is via an interaction between the ENM and the biological system. Examples include electron donation from the nanomaterial to molecular oxygen to produce superoxide, redox cycling of quinones, semiquinones and other organics, Fenton chemistry, band gap (energy difference between conducting and valence bond electrons), and UV light producing electron hole pairs in ENM (Nel et al. 2006).

For ROS production by ENM, determinants of outcome include ENM chemical composition, surface area, surface reactivity, agglomerated size, and dose to target organ (Kitchin et al. 2011). ENM surface area was associated with depletion of lung cell GSH for four ENM (carbon black, TiO_2, Co, and Ni) as well as for four other larger particles (TiO_2, carbon black, $BaSO_4$, and alpha quartz) (Monteiller et al. 2007). In tissues or organisms with UVA exposure, photoactivation may be a dominant causal factor such as with photoactivatable forms of TiO_2 (Sanders et al. 2012; Ma & Diamond 2013).

There are many commonly used biomarkers for oxidative stress including molecular redox probes, such as 2′,7′-dichlorofluorescein diacetate, Mitosox, isoprostanes, lipid peroxidation markers, membrane damage (e.g. lactic dehydrogenase enzyme leakage), phagocytic oxidative bursts, and decreased antioxidant defenses (GSH concentration, superoxide dismutase, and glutathione peroxidase).

Associations between oxidative stress and adverse outcome have been made in many cases including DNA damage (Xie et al. 2011), mutation (Xie et al. 2011), cancer (Klaunig et al. 2011); and in multiple tissues: skin (Shukla et al. 2011), central nervous system (Sayre et al. 2008; Skalska et al. 2016), lung (Li et al. 2008; Madl et al. 2014), liver (Kim et al. 2009; Shukla et al. 2013), and kidney (Liang et al. 2009; Guan et al. 2012). For SWCNT or MWCNT in lung tissues, oxidative stress may be a mediator of inflammation and fibrosis, with a potential to progress to pleural malignant mesothelioma and lung tumors (Muller et al. 2005; Chou et al. 2008; Kim et al. 2014; Suzui et al. 2016).

Ion toxicity after dissolution of nanomaterials

Metal ions may be released from ENM that are composed of metals, metal oxides, or inorganic carbon containing residual metal catalysts (e.g. MWCNT). If this happens, a relatively high concentration of metal ions could occur near the site where the nanomaterial is located, with the ENM releasing toxic metal ions acting as a "Trojan horse". Enhanced uptake of CuO ENM, followed by local release of Cu^{2+} ions to inhibit Zebrafish Hatching Enzyme, was considered as the mechanism for impaired Zebrafish hatching (Muller et al. 2015). Similarly, adverse effects could result in a number of organ systems, including mammalian lungs and blood vessels (reviewed in Rodriguez-Yañez et al. 2013).

Metal responsive genes that can act as biomarkers of metal ion exposure include heme oxygenase-1, metallothioneins, and catalase. For reasons of specificity and sensitivity, analytical chemistry measures of metals (such as ICP-MS) are often used as measures of exposure.

Altered cell physiology: altered cell cycle, growth

ENM also may impair cell-cycle progression and proliferation, dependent on the chemical composition, particle size, and other physical/chemical properties (Mahmoudi et al. 2011; Marano et al. 2011; Asharani et al. 2012). At low concentrations, increased cell proliferation *in vitro* is dependent on the ENM chemical composition, size, surface reactivity, agglomerated size, dispersion medium, and activation of different signaling pathways. For example, Unfried et al. (2008) reported that carbon ENM (nano-particulate carbon black) and silica ENM (amorphous SiO_2), both with a median diameter of 14 nm, induced proliferation in a rat lung epithelial cell line. Huang et al. (2009) showed that exposure to non-toxic concentrations of TiO_2 ENM enhanced cell proliferation and growth of cultured fibroblast cells (NIH3T3).

When the concentrations of ENM are high enough to induce oxidative stress, they will generally alter many different stress response/metabolic/signaling pathways including inflammation, NRF-2 mediated stress response, and protein and lipid peroxidation. These alterations may in turn lead to changes in cell cycle progression/proliferation, some may even result in cell cycle arrest or cell death. These ENM include metals and metal oxides (Au, Ag, Cu, Zn, Ti, Fe, Pd, Ni, and Ce), SiO_2, and carbon nanotubes (Huang et al. 2010; Mahmoudi et al. 2011; Manke et al. 2013). There are also reports of cell-cycle alteration caused by SWCNT and MWCNT *in vitro* (Zhang & Yan 2012; Chen et al. 2012; Zeni et al. 2015). While both carboxylated and pristine MWCNT caused cell cycle arrest, carboxylated MWCNT seemed to induce less apoptosis (Liu et al. 2015).

Cytotoxicity

Cytotoxicity can be an outcome of ENM exposure either *in vitro* or *in vivo*. Either the necrotic or apoptotic pathways could be dominant depending on the exposure. ENM can exert toxicity either from outside or inside of cells. Generally, the most important factors in determining cytotoxicity are the ENM chemical composition, dose, dose rate, surface reactivity, surface area, and agglomerated size.

There are many approaches to quantifying a response to nanomaterial exposure such as the *in vitro* approaches of dye exclusion (trypan blue), dye uptake (neutral red, propidium iodide, and ethidium bromide), cellular reductive enzymes (calcein-AM, MTT, MTS, or alamar blue), ATP content, and DNA-based stains. Enzymes that are released from membrane damaged or dead cells can be useful indicators of effect such as lactate dehydrogenase, alanine aminotransferase, or aspartate aminotransferase. Cell-based assays that are reliant on fluorescent or luminance quantification may be subject to optical interference from nanoparticles in suspension, and should be used with appropriate controls (Kroll et al. 2009; Guadagnini et al. 2015).

Genotoxicity

Genotoxicity encompasses any change to cellular DNA that has the potential to interfere with the transmission of genetic information, either through impacts on replication or on transcription. Genotoxicity is important to assessing the potential health risks posed by exposure to ENM because it represents an important early molecular event in the induction of cancer, and is strongly associated with other adverse health outcomes such as atherosclerosis (Mercer et al. 2010). The ability to induce genotoxic effects has been well studied for a variety of ENM, and several recent reviews are available (Kumar & Dhawan 2013; Magdolenova et al. 2014; Golbamaki et al. 2015; Guo & Chen 2015). Genotoxicity studies on ENM have generally focused on the induction of DNA damage, the induction of mutations, or on induction of expression of DNA damage response genes or functional alteration of DNA damage response proteins in exposed cells.

The most frequently used approach for the assessment of ENM-induced DNA damage is the single-cell gel electrophoresis, or Comet assay. The assay is capable of detecting a variety of types of DNA damage, including single strand breaks,

double strand breaks, abasic sites, and other alkali-labile types of DNA damage. When the assay is modified by incorporating *in vitro* digestion with DNA-damage specific nucleases or glycosylases, the range of types of damage detectable can be extended. In general, the enzyme enhanced version of the assay yields a higher sensitivity for detecting DNA damage induced by ENM. Additional assays for DNA damage include the observation of chromosome level effects, such as the micronucleus (MN) assay, and the chromosomal aberration (CA) assay. *In vitro*, ENM have been found to induce MN in more cases than CA, while *in vivo* the situation appears to be reversed, although fewer ENM have been evaluated for CA (Guo & Chen 2015). The agglomeration state of ENM and treatment media may influence assays of genotoxicity differently (Prasad et al. 2013, 2014). Other approaches for directly measuring DNA damage, such as ^{32}P-postlabeling and ELISA, have also been used (Foldbjerg et al. 2011).

A recent review found that the most commonly used genotoxicity/mutagenicity tests for ENM were (a) Comet assay (19 studies), (b) micronucleus (14 studies), and the Ames test (6 studies) (Golbamaki et al. 2015). These authors offered seven recommendations for genotoxicity testing of ENM: (a) know what nanomaterial has been tested and in what form, (b) recognize that ENM are not all the same, (c) consider uptake and distribution of ENM, (d) take ENM-specific properties into account, (e) use standardized methods, (f) use *in vivo* studies to correlate *in vitro* results, and (g) learn about the mechanism of ENM genotoxic effects. The key difference between these recommendations for ENM and general recommendations for assessing the genotoxic effects of chemicals lies in the need for rigorous characterization of the physical properties of the ENM being tested in addition to their chemical properties. Relative to the uptake of various nanomaterial in the bacteria *Salmonella typhimurium* (Ames test), bacterial uptake was reported for ENM composed of ZnO and TiO_2 as measured by transmission electron microscopy (TEM), scanning electron microscopy (SEM), and flow cytometry (Kumar et al. 2011). In contrast, uptake of TiO_2 in *Salmonella typhimurium* was not demonstrated by others, who questioned the TEM results of Kumar et al. (2011) regarding mismatch of the reported particle sizes and lack of chemical component analysis (Woodruff et al. 2012). Further, Woodruff et al. argue that ENM cannot enter bacterial cells, probably due to a lack of endocytosis mechanisms, and have a cell wall unlike eukaryotic cells, and, therefore, the Ames assay may be an inappropriate assay for ENM genotoxicity. Subsequently, however, uptake of Au, CeO_2, SWCNT, and MWCNT by *Salmonella typhimurium* was reported, but without showing mutagenicity (Clift et al. 2013).

The inference of DNA damage from monitoring cellular DNA damage response pathways provides useful indirect evidence for the genotoxic potential of ENM. Focal accumulation of phosphorylated γ-H2AX is diagnostic for double strand breaks in DNA and has been documented for a variety of ENM (Petersen & Nelson 2010). Silica ENM have been shown to activate the Chk1-dependent G2/M checkpoint DNA damage response signaling pathway (Duan et al. 2013) and both SWCNT and MWCNT induce the Erk1/2 signaling pathway, which is involved in cell proliferation and is also induced by asbestos exposure (Pacurari et al. 2010).

Inflammation

ENM cause inflammation in many organs, with the lungs being the most studied. The biological purpose of inflammation is to eliminate the cause of cell injury (e.g. bacteria). With biopersistent ENM like CeO_2, there may be no "off" switch to stop the inflammation process and the inflammation would become persistent. Many potential determining factors for ENM-induced inflammation have been studied including dose, surface reactivity, surface area, pulmonary deposition and clearance, agglomerated size, chemical composition, surface charge, dissolution rate (solubility), hydrophobicity, hydrophilicity, shape, primary particle size, purity, and crystal structure (Braakhuis et al. 2014). Cells types mediating the inflammatory response include macrophages, mast cells, eosinophils, neutrophils, and dendritic cells. The infusion of neutrophils into tissues is a common measure of inflammation. Other commonly used inflammatory biomarkers are the cytokines (e.g. interferons, interleukins, TNF-alpha, IL-10, and TGF-beta), chemokines (e.g. IL-8 and MCP-1), NF-kB, and prostaglandins.

In normal aging, chronic inflammation may lead to many diseases, such as atherosclerosis, rheumatoid arthritis, and cancer. ENM exposures have been linked to inflammation in several organs, particularly in the lung, liver, and skin (Murray et al. 2009; Braakhuis et al. 2014; Sadeghi et al. 2015). Various degrees of organ effects have been observed in the central nervous system, lung, liver, gastrointestinal tract, heart, spleen, blood vessels, and skin following carbon nanotube exposures (Rodriguez-Yañez et al. 2013). In lungs, inflammation, granuloma formation, fibrosis, alveolitis, genotoxicity, and cancer have been observed; while in blood vessels, endothelial cell activation, platelet activation, thrombus formation, and changes in blood pressure have been seen (Morimoto et al. 2013; Rodriguez-Yañez et al. 2013; Kasai et al. 2015).

Cross-kingdom effects – MIE/cellular responses

Most of what is currently known about MIEs induced by ENM exposure has been developed through studies on human and animal systems. As described above, plants in a variety of habitats are also likely to be exposed to ENM inadvertently through aerial deposition and water runoff or purposefully by application of wastewater sludge to soils. Now, there is an increasing recognition that altered survival, development, and reproduction of plants may be affected by exposure to ENM. Furthermore, such impacts to plants could have economic, ecological, and health consequences for people as well. An understanding of ENM-induced MIEs in plants is only beginning to emerge and is an area where there is a clear need for more research.

Early studies evaluated changes in plant transcriptomes following exposures to ENM and dose levels required for toxicity (reviewed in Park et al. 2014). These papers, however, generally did not link exposure and gene expression change

MIEs to altered plant physiology/morphology. More recently, some of the first associations between transcriptomic responses and phenotypic development were established in TiO_2 and CeO_2 ENM exposed *Arabidopsis* plants (Tumburu et al. 2015). The authors reported significant EMN-induced regulation of genes that are responsive to abiotic and biotic stress and control DNA metabolism, hormone metabolism, tetrapyrrole synthesis, photosynthesis, and root development. They also demonstrated that the ENM exposures resulted in increased percentages of germinating seeds and early growth of leaves.

Surprising follow-up work showed CeO_2 ENM induction of *Arabidopsis* DREB transcription factor genes (Tumburu et al. 2017). These responses were remarkable because DREBs are known for initiating cascades of gene expression and cellular restructuring that results in cold-acclimation (Liu et al. 2000; Agarwal et al. 2006; Knight & Knight 2012). CeO_2 ENM up-regulation of DREBs was not expected. Within these experiments, development of exposed plants also mimicked cold-acclimatization responses with delayed growth and increased leaf number. Superficially, such changes might not seem like adverse outcomes; however, downstream effects could include reduced fecundity of exposed plants. Transcription of DREB genes is rapidly triggered by a transient increase in cytosolic Ca^{2+} (Knight & Knight 2012; Miura & Furumoto 2013), which suggests that the MIE of CeO_2 EMN exposure in plants affects Ca^{2+} signaling. Whether or not similar responses would be observed under more natural conditions or in more distantly related plant species or animals remains to be determined.

Identification of ENM that are capable of causing MIEs linked to adverse outcomes across large taxonomic groups is of high interest. The greater the conservation of molecular, cellular and structural features among organisms, the higher the likelihood of comparable MIEs and downstream responses. Plant and animal cells appear to have more characteristics in common than those that differentiate them, but the most recent common ancestor of plants and animals was a single celled organism that existed more than 1 billion years ago. It is accepted that multicellularity evolved independently within each lineage. So, there is substantial divergence between the plant and animal membrane-bound receptors and signaling pathways that affect homeostasis, development and reproduction (Alberts et al. 2002). This points to the possibility that ENM which bring about the same generalized MIEs in many species (e.g. photoactivated toxicity beginning with reactive singlet oxygen causing oxidative damage to a wide variety of biological molecules) could very well produce distinct adverse outcomes in plants and animals. Another scenario to consider is that mitochondria are found in both cell types, but chloroplasts are unique to phototrophs. Thus, if an ENM affects a mitochondrial-centric process, there may be a greater likelihood for "broad" cross species fidelity in MIEs. Conversely, if an ENM affects a chloroplast-centric process, at least among phototrophs there may be broad commonalities, but shared MIEs between phototrophs and non-phototrophs may not occur (Figure 9). The range of responses across species may become more important to consider in risk assessments of certain EMNs where there is potential for wide-spread exposure.

Whole organism terrestrial and aquatic species effects

The AOP concept is a sequence of events beginning with a MIE and acting at a cellular level (Figure 9), which continues to build until adverse effects occur at the levels of the organ, individual, population, and community or ecosystem level (Holden et al. 2013; Figure 10). Community-level effects can involve terrestrial or aquatic systems (or both). A search performed in August 2016 in the Web of Science database yielded 473 references when querying for titles, abstracts, and key words with the topical terms "aquatic", "environmental", "organism", "toxicity", and "nanomaterials" in publications released from 1990 to August 2016. This number of references suggests strongly that nanomaterials will cause adverse effects to whole organisms. Among the references were several recent review articles discussing responses to a range of ENM. For example, ENM described in the review articles include Ag (Walters et al. 2014; Xin et al. 2015), TiO_2 (in seawater) (Minetto et al. 2014), CNT (Petersen et al. 2011; Boncel et al. 2015), and nanowires (Kwak & An 2015), as well as all-inclusive reviews of multiple ENM (Nowack & Bucheli 2007; Handy et al. 2008; Klaine et al. 2008; Radhika et al. 2010; Kumar et al. 2015) and Canesi and Corsi's (2016) review of nanomaterial effects on marine invertebrates. In addition, Hou et al. (2013) reviewed the accumulation of ENM by organisms under the assumption that, in general, accumulation of the ENM must first occur before effects will be observed.

In their comprehensive review, Klaine et al. (2008) reported toxicity to bacteria caused by fullerenes, SWCNT, MWCNT, metallic Cu and Ag, and metal oxides including Ti, Ce, Zn, and Si. Specific toxic effects to bacteria were described as antibacterial and bactericidal impacts. Similarly, freshwater and marine plants, invertebrates, and vertebrates demonstrated toxicity from exposure to a range of ENM including fullerenes, SW- and MWCNT, metallic copper and silver, and the metal oxides titanium and zinc, and quantum dots (Handy et al. 2008; Klaine et al. 2008). Toxic effects included some increases in mortality and evidence of reductions in growth and development, as well as a wide range of sub-lethal cellular insults. The highly variable effects on bacteria suggest that their susceptibility needs to be examined in order to fully understand community and ecosystem-level effects (Figure 10). Reviews of the literature performed concurrently to Klaine et al. (2008) and those that were published later, demonstrated similar findings of evidence of toxic effects to a range of organisms resulting from exposure to multiple types of ENM. However, some of these findings have been modified. For example, for carbon nanotubes, most recent data suggest that because of their limited bioavailability, toxic effects are unlikely to occur in the environment except at very high and unrealistic concentrations, such as 1000 mg/kg and 100 mg/L (OECD 2000, 2004) for sediment and water, respectively (Petersen & Nelson 2010).

Relative to the exposure of ENM to aquatic plants and algae, there is a "moderate" amount of literature on algae and less so aquatic plants. Researchers have reported TiO_2 toxicity

of algae ranging from low mg/L to over 100 mg/L (Hund-Rinke & Simon 2006; Aruoja et al. 2009; Hall et al. 2009). Zn and CuO nanoparticles are also noted to elicit toxicity in algae in the low mg/L range (Aruoja et al. 2009). In addition, trophic transfer of Cd-based quantum dots has been observed between algae and *Cerodaphnia dubia* (Bouldin et al. 2008). Much of this work has focused on short-term studies, often with traditional toxicity tests in monoculture. These tests offer little aid in evaluating how ENM affect complex aquatic systems (i.e. food chain, competitive interactions, carbon and nitrogen cycling, etc.). Overall, how ENM affect algae and aquatic plants in an ecological context is not well known.

Terrestrial plants

If ENM are bound on the surface or in the cuticle (e.g. adsorbed), they may not alter cellular properties but they may influence light harvesting properties of leaves through either photoactivity or reflection of specific light wavelengths. Yang et al. (2006, 2007) found that TiO_2 on spinach leaves may interact with N_2 to form reduced nitrogen compounds that can be subsequently taken up and increase plant growth. ENM may also be taken into internal plant organs but remain in the apoplast (non-living) portion of the plant, where additional binding and dissolution may occur. Bound particles also may influence cell wall chemistry and interact with other surface particles to influence uptake of other materials and gasses. Finally, certain particles may alter cuticular waxes, which may affect the hydrodynamics of the leaf.

If ENM are taken up into living cells into the symplast (e.g. absorption), there may be further interactions that alter the characteristics of the particle, such as binding or dissolution. Once in the symplast or living portion of the plant, particles may initiate a cascade of events leading to altered biochemistry, physiology, and growth (Figure 8). There is currently very little information regarding the fate and effects of ENM taken up through foliage (Rico et al. 2011; Chichiriccò & Poma 2015).

Plant studies have shown a variety of responses to ENM including growth reductions, increases, or no effect at all, depending on the nanomaterial and plant species being studied (Ma et al. 2010; Kumar et al. 2013). Klaine et al. (2008) reported toxicity to terrestrial plants (e.g. corn, cucumber, lettuce, radish, mustard rape, radish, and ryegrass) from ENM including fullerenes and MWCNT, metallic aluminum and zinc, aluminum, titanium and zinc oxides. Alternatively, CNTs, Au, CeO_2, and TiO_2 have been found to enhance seed germination and early plant development in some studies (Zheng et al. 2005; Kumar et al. 2013; Tumburu et al. 2015), but not others (López-Moreno et al. 2010). In some cases, the variable responses may be due to the composition of the ENM and whether or not it is soluble: ENM forms of Fe, Cu, and Zn, for example, may enhance growth via improved plant nutrition since they are required plant nutrients. In other cases, the presence of ENM forms of Ag and Cu, for example, may provide some plant protection from pathogens in the root zone, resulting in enhanced growth. Interpreting the conflicting results is often complicated by differences in methodology, poor characterization, or unrealistically high doses of ENM exposure. In order to better understand effects on plant growth and development, there is a need for longer-term studies with ENMs that incorporate natural soil microbial communities (Ge et al. 2016).

Whole-organism effects can also lead to changes in how individuals interact as members of an ecosystem. Disruption of specific structural or functional groups by ENM may lead to changes in community structure and function, altering important ecosystem processes such as nutrient cycling (Dinesh et al. 2012; Rodrigues et al. 2013; Simonin & Richaume 2015). Organisms compete for resources throughout their life cycle, and differential sensitivity to ENM may alter the competitive nature of interspecies interactions. There is currently insufficient information available for most species to be able to predict effects at larger scales.

Discussion

Some general conclusions drawn from the literature that may become starting places for further research are as follows:

1. If ENM are released into environmental media, they will likely react or heteroaggregate with constituents of the environmental matrix (air, water, or soil), and be dispersed into a relatively large receiving compartment, so that eventual exposures to environmental species or humans, for the most part, will not be to the original form of the material but instead to highly diluted ENM transformation or degredation products.
2. These environmental reactions will not occur under highly constrained laboratory or manufacturing conditions, but instead will be subject to a range of conditions and stochastic forces which will dynamically change across time and location. Therefore, if exposures to environmental transformation products of ENM occur, the exposures will likely be to multiple forms of these products including a range of particle agglomerates, sizes and coatings.
3. We currently have insufficient information regarding (i) the uses of ENM in industry and commerce, (ii) the penetration of ENM-enabled products into the marketplace, (iii) the potential for release of ENM from products, or (iv) the form of ENM that may be released. Notably, these limitations are also characteristic of the uses of standard industrial chemicals. Such uncertainties hamper accurate assessments of ENM exposure as they do for conventional materials.
4. For the general population, near-field exposures from consumer use of ENM products, particularly with dispersive applications, will likely be higher than far-field exposures.
5. The predominant destiny of ENM emitted into wastewater systems will likely be biosolids, over half of which may be recycled through land application.
6. The predominant destiny of ENM emitted into solid waste systems will be landfills.
7. The predominant destiny of ENM emitted into aquatic ecosystems will be to become complexed with natural organic matter or other constituents of the aquatic system and subsequent deposition into sediments. An

exception may be polarizable materials such as graphene oxide that may have the ability to remain suspended in the water column for long term transport. In a decision framework, such polarizable suspended materials may be considered a higher risk exposure to organisms in the water column, as opposed to those residing in the sediment.

8. Aquatic organisms residing in the sediments including filter feeding organisms will likely experience higher levels of exposure to ENM than will other aquatic species.
9. Soluble and reactive metal-based ENM, such as those composed of silver, will likely react with constituents such as sulfides in the environment to form less soluble metallic salts. This is particularly relevant in wastewater systems.
10. Rates of uptake of ENM may be low by oral and dermal of exposure, but elimination rates of systemically absorbed ENM may be even lower. By inhalation exposure, ENM deposition in the respiratory tract may cause local oxidative stress and inflammation, and systemic absorption may become significant.
11. In biologic media, ENM will be coated with a protein corona or similar biomolecules that influence the biokinetics of particles and reactions with cellular receptors.
12. Uptake and penetration barriers at the portal of entry and within the body at important organs, such as the brain and placenta, may limit the biodistribution of absorbed ENM. Typically, these barriers are not absolute, and serve to reduce, but not eliminate, diffusion or translocation of materials.
13. Most mammalian cells have the ability to uptake particles through several pathways, although the rates of uptake vary across cell types and are dependent on numerous physical and chemical factors of the particles such as size, coatings, surface charge, and biological transformations.
14. ENM may initiate molecular events associated with adverse outcomes such as induction of reactive oxygen species, dissolution to toxic metal ions, or initiation of inflammation.
15. The greater the conservation of molecular, cellular, and structural features among organisms exposed to EMNs, the higher the likelihood of comparable MIEs and downstream responses.
16. Because there is substantial divergence between the plant and animal membrane-bound receptors and signaling pathways that affect homeostasis, development and reproduction, ENM which bring about the same generalized MIEs in many species could very well produce distinct adverse outcomes in plants and animals.
17. Potential adverse outcomes are not limited to effects within cells or organs. They extend to whole organisms, communities and ecosystems.

Conclusions

Nanotechnology and the production of ENM have the potential to significantly enhance future economic development and to produce advanced capabilities that will benefit many segments of society (PCAST 2014). We are at a time where the informed development and use of these new materials can be done in a way that avoids many of the mishaps of the past such as those associated with the early development of the chemical industry. The ability to forecast and avoid potential environmental problems across the life cycle of material development, including use and disposal, is required if we are to achieve sustainable development of nanotechnology. Here we propose a series of compartmental stages that encompass the full life cycle of ENM, their potential release into environmental media, their fate, transport, and transformation in the environment, potential exposures to sensitive species including humans, and the possibility to cause adverse effects in those species. There are currently large numbers of ENM used in industrial and commercial applications, but there is insufficient information about the potential for those materials to enter the environment. Many potential scenarios involve release of dissolved ions rather than nanoparticles, such as copper ions leaching from pressure treated lumber or silver ions released from children's clothing or other products. Other scenarios of potential release, such as sawing or sanding nano-enabled solid materials, are likely to release ENM that are still attached to parts of the original product matrix rather than release ENM in their originally manufactured form. In other cases, the release of ENM in nanoparticle form is possible, such as for nanoparticles suspended in liquid or cream formulations including spray cleaners, personal care products, or as nano-formulated pesticides. A potential for a large release of ENM into the environment may be from road or rail accidents involving ENM transporting vehicles. In recognition of the difficulty of modeling the complex networks of ENM with novel physical and chemical properties, we propose that critical nodes along these pathways should be considered as the targets to develop simple functional assays that can be used to efficiently determine the likely behavior of ENM in these systems. The diagrams presented here may serve as guidance for targeted assay development. In addition, this compartmental framework will assist in placing the results of specific investigations into context for interpretation of broader environmental implications. These diagrams may also assist in development of quantitative modeling as rates and transformation functions for movement of particles across compartments are developed.

The framework described here currently addresses some, but not all, of the criteria listed by Hristozov et al. (2016). The framework can be said to consider their criteria in that it includes nano-specific requirements, life cycle thinking, an exposure-driven approach, an iterative and adaptive structure, and transparency of objectives. The current framework is not completed, however. At this point, it provides guidance for development of functional assays and models that will eventually lead to a simplification of ENM evaluations, but does not yet identify specific assays or models. Future implementation of the framework also should be amendable to grouping, read across or other simplifying approaches to risk assessment. The development of documented applications should

await the definition of the critical nodes and functional assays.

Although ENMs share a common size range, many of their properties are as unique as the elements from which they are composed. The properties they provide for a wide variety of products vary greatly, as well as their potential release, exposure, and mechanism of effect. Consequently knowledge gaps with respect to release, exposure, and effects are often ENM- and product specific. Never-the-less, there are broad and general gaps of data and predictive modeling which include: incomplete information regarding ENM composition, concentration and potential releases from ENM-enabled products; measuring and predicting affinity of ENM for environmental substrates; dissolution rates of metal-based ENM in environmental and biological media; environmental transformation and degredation products; influence of environmental transformations on biodistribution and toxicity; AOP specifications; as well as species differences in uptake, biodistribution, and susceptibility. Future research addressing these data gaps can be incorporated into the growing exposition of the pathways outlined in the framework presented here.

Acknowledgements

The authors thank Dr. Christine Hendren (Duke University, Center for Environmental Implications of Nanotechnology) and Maureen Gwinn (U.S. EPA Office of Research of Development, National Center for Environmental Assessment) for their extremely helpful reviews of an earlier version of the manuscript. The authors also are very appreciative of the extensive review comments from peer-reviewers selected by the Editor and anonymous to the authors. This input served to greatly strengthen the manuscript.

Declaration of interest

The authors declare that there are no financial conflicts of interest. The author's affiliations are as shown on the cover page. The authors have sole responsibility for the writing and content of the paper. The work was conducted under the EPA Office of Research and Development Chemical Safety for Sustainability Research Program. This article was reviewed in accordance with the policy of the National Health and Environmental Effects Research Laboratory, U.S. Environmental Protection Agency and approved for publication. Approval does not signify that the contents necessarily reflect the views and policies of the Agency, nor does mention of trade names or commercial products constitute endorsement or recommendation for use.

All of the authors, with one exception, were employees of the U.S. Environmental Protection Agency, and development of this document was a portion of their job responsibilities. The exception was Ms. B. L. Thornton, who was an independent student services contractor to the EPA, and preparation of this manuscript was a portion of her assigned work duties (Contract no. EP-13-C-000164).

None of the authors, with one exception, have participated in legal or regulatory proceedings regarding the content of this manuscript within the last 5 years. The exception was Dr. W. K. Boyes, who served on workgroups related to the issuance of a Toxics Substances Control Act (TSCA) Section 8(a) action: "Chemical Substances When Manufactured or Processed as Nanoscale Materials; TSCA Reporting and Recordkeeping Requirements", and in responding to public comments related to this action (40 CFR Part 704; Fed. Reg.82 (8) 3641–3655, 2017).

This work was supported by the U.S. Environmental Protection Agency.

ORCID

William K. Boyes http://orcid.org/0000-0002-3598-0032
Souhail R. Al-Abed http://orcid.org/0000-0002-5595-1300
Christian P. Andersen http://orcid.org/0000-0003-2169-2520
Dermont C. Bouchard http://orcid.org/0000-0002-7467-0248
Robert M. Burgess http://orcid.org/0000-0003-4504-5125
Elaine A. Cohen Hubal http://orcid.org/0000-0002-9650-3483
Kay T. Ho http://orcid.org/0000-0002-6750-4487
Michael F. Hughes http://orcid.org/0000-0002-5571-5447
Kirk Kitchin http://orcid.org/0000-003-0693-8967
Jeffrey A. Ross http://orcid.org/0000-0002-7002-4548
Kirk G. Scheckel http://orcid.org/0000-0001-9326-9241

References

Adjei IM, Sharma B, Labhasetwar V. 2014. Nanoparticles: cellular uptake and cytotoxicity. In: Capco DG, Chen Y, editor. Nanomaterial. Netherlands: Springer; p. 73–91.

Agarwal PK, Agarwal P, Reddy MK, Sopory SK. 2006. Role of DREB transcription factors in abiotic and biotic stress tolerance in plants. Plant Cell Rep. 25:1263–1274.

Al-Abed SR, Virkutyte J, Ortenzio JNR, McCarrick RM, Degn LL, Zucker R, Coates NH, Childs K, Ma H, Diamond S, et al. 2016. Environmental aging alters Al(OH)3 coating of TiO2 nanoparticles enhancing their photocatalytic and phototoxic activities. Environ Sci: Nano. 2016;3:593–601.

Alberts B, Johnson A, Lewis J, Raff M, Roberts K, Walter P. 2002. Molecular biology of the cell. New York: Garland Science.

Alger H, Momcilovic D, Carlander D, Duncan TV. 2014. Methods to evaluate uptake of engineered nanomaterials by the alimentary tract. Compr Rev Food Sci Food Saf. 13:705–729.

Almeida JPM, Chen AL, Foster A, Drezek R. 2011. *In vivo* biodistribution of nanoparticles. Nanomedicine (Lond). 6:815–835.

Andón FT, Kapralov AA, Yanamala N, Feng W, Baygan A, Chambers BJ, Hultenby K, Ye F, Toprak MS, Brandner BD, et al. 2013. Biodegradation of Single-Walled Carbon Nanotubes by Eosinophil Peroxidase. Small. 9:2721–2729.

ANEC, BEUC. 2010. ANEC/BEUC inventory of products claiming to contain nanoparticles available on the EU market. European Consumers Organization and the European Consumer Voice in Standardization.

ANEC, BEUC. 2012. ANEC/BEUC inventory of products claiming to contain nano-silver particles available on the EU market. European Consumers Organization; European Consumer Voice in Standardization.

Ankley GT, Bennett RS, Erickson RJ, Hoff DJ, Hornung MW, Johnson RD, Mount DR, Nichols JW, Russom CL, Schmieder PK, et al. 2010. Adverse outcome pathways: a conceptual framework to support ecotoxicology research and risk assessment. Environ Toxicol Chem. 29:730–741.

Arts JHE, Hadi M, Keene AM, Kreiling R, Lyon D, Maier M, Michel K, Petry T, Sauer UG, Warheit D, et al. 2014. A critical appraisal of existing concepts for the grouping of nanomaterials. Regul Toxicol Pharmacol. 70:492–506.

Aruoja V, Dubourguier H-C, Kasemets K, Kahru A. 2009. Toxicity of nanoparticles of CuO, ZnO and TiO2 to microalgae Pseudokirchneriella subcapitata. Sci Total Environ. 407:1461–1468.

Aschberger K, Micheletti C, Sokull-Klüttgen B, Christensen FM. 2011. Analysis of currently available data for characterising the risk of engineered nanomaterials to the environment and human health—lessons learned from four case studies. Environ Int. 37:1143–1156.

Asgharian B, Hofmann W, Bergmann R. 2001. Particle deposition in a multiple-path model of the human lung. Aerosol Sci Technol. 34:332–339.

Asharani P, Sethu S, Lim HK, Balaji G, Valiyaveettil S, Hande MP. 2012. Differential regulation of intracellular factors mediating cell cycle, DNA

repair and inflammation following exposure to silver nanoparticles in human cells. Genome Integr. 3:2.
Bachler G, von Goetz N, Hungerbuhler K. 2015. Using physiologically based pharmacokinetic (PBPK) modeling for dietary risk assessment of titanium dioxide (TiO2) nanoparticles. Nanotoxicology. 9:373–380.
Bachler G, von Goetz N, Hungerbühler K. 2013. A physiologically based pharmacokinetic model for ionic silver and silver nanoparticles. Int J Nanomedicine. 8:3365–3382.
Badireddy AR, Wiesner MR, Liu J. 2012. Detection, characterization, and abundance of engineered nanoparticles in complex waters by hyperspectral imagery with enhanced darkfield microscopy. Environ Sci Technol. 46:10081–10088.
Bakand S, Hayes A, Dechsakulthorn F. 2012. Nanoparticles: a review of particle toxicology following inhalation exposure. Inhal Toxicol. 24:125–135.
Baroli B. 2010. Penetration of nanoparticles and nanomaterials in the skin: Fiction or reality? J Pharm Sci. 99:21–50.
Baroli B, Ennas MG, Loffredo F, Isola M, Pinna R, Lopez-Quintela MA. 2007. Penetration of metallic nanoparticles in human full-thickness skin. J Invest Dermatol. 127:1701–1712.
Benn T, Cavanagh B, Hristovski K, Posner JD, Westerhoff P. 2010. The release of nanosilver from consumer products used in the home. J Environ Qual. 39:1875–1882.
Benn TM, Westerhoff P. 2008. Nanoparticle silver released into water from commercially available sock fabrics. Environ Sci Technol. 42:4133–4139.
Bhaskar S, Tian F, Stoeger T, Kreyling W, de la Fuente JM, Grazú V, Borm P, Estrada G, Ntziachristos V, Razansky D. 2010. Multifunctional Nanocarriers for diagnostics, drug delivery and targeted treatment across blood–brain barrier: perspectives on tracking and neuroimaging. Part Fibre Toxicol. 7:3–3.
Blank F, Stumbles PA, Seydoux E, Holt PG, Fink A, Rothen-Rutishauser B, Strickland DH, von Garnier C. 2013. Size-dependent uptake of particles by pulmonary antigen-presenting cell populations and trafficking to regional lymph nodes. Am J Respir Cell Mol Biol. 49:67–77.
Bolyard SC, Reinhart DR, Santra S. 2013. Behavior of engineered nanoparticles in landfill leachate. Environ Sci Technol. 47:8114–8122.
Boncagni NT, Otaegui JM, Warner E, Curran T, Ren J, Fidalgo de Cortalezzi MM. 2009. Exchange of TiO2 nanoparticles between streams and streambeds. Environ Sci Technol. 43:7699–7705.
Boncel S, Kyzioł-Komosińska J, Krzyżewska I, Czupioł J. 2015. Interactions of carbon nanotubes with aqueous/aquatic media containing organic/inorganic contaminants and selected organisms of aquatic ecosystems – a review. Chemosphere. 136:211–221.
Boonruksa P, Bello D, Zhang J, Isaacs JA, Mead JL, Woskie SR. 2016. Characterization of potential exposures to nanoparticles and fibers during manufacturing and recycling of carbon nanotube reinforced polypropylene composites. Ann Occup Hyg. 60:40–55.
Bouchard D, Chang X, Chowdhury I. 2015. Heteroaggregation of multiwalled carbon nanotubes with sediments. Environ Nanotechnol Monit Manag. 4:42–50.
Bouldin JL, Ingle TM, Sengupta A, Alexander R, Hannigan RE, Buchanan RA. 2008. Aqueous toxicity and food chain transfer of quantum dots™ in freshwater algae and *Ceriodaphnia dubia*. Environ Toxicol Chem. 27:1958–1963.
Braakhuis HM, Park MV, Gosens I, D, Jong WH, Cassee FR. 2014. Physicochemical characteristics of nanomaterials that affect pulmonary inflammation. Part Fibre Toxicol. 11:1–25.
Brouwer DH, Spaan S, Roff M, Sleeuwenhoek A, Tuinman I, Goede H, van Duuren-Stuurman B, Filon FL, Bello D, Cherrie JW. 2016. Occupational dermal exposure to nanoparticles and nano-enabled products: Part 2, exploration of exposure processes and methods of assessment. Int J Hyg Environ Health. 219:503–512.
Brunetti G, Donner E, Laera G, Sekine R, Scheckel KG, Khaksar M, Vasilev K, De Mastro G, Lombi E. 2015. Fate of zinc and silver engineered nanoparticles in sewerage networks. Water Res. 77:72–84.
BUND. Nanoproduktdatenbank Des BUND. Germany: Der Bund für Umwelt und Naturschutz Deutschland [Friends of the Earth Germany].
Buono C, Anzinger JJ, Amar M, Kruth HS. 2009. Fluorescent pegylated nanoparticles demonstrate fluid-phase pinocytosis by macrophages in mouse atherosclerotic lesions. J Clin Invest. 119:1373–1381.
Caballero-Guzman A, Nowack B. 2016. A critical review of engineered nanomaterial release data: are current data useful for material flow modeling? Environ Pollut. 213:502–517.
Caballero-Guzman A, Sun T, Nowack B. 2015. Flows of engineered nanomaterials through the recycling process in Switzerland. Waste Manag. 36:33–43.
Canesi L, Corsi I. 2016. Effects of nanomaterials on marine invertebrates. Sci Total Environ. 565:933–940.
Canton I, Battaglia G. 2012. Endocytosis at the nanoscale. Chem Soc Rev. 41:2718–2739.
Cassee F, Muijser H, Duistermaat E, Freijer J, Geerse K, Marijnissen JC, Arts JH. 2002. Particle size-dependent total mass deposition in lungs determines inhalation toxicity of cadmium chloride aerosols in rats. Application of a multiple path dosimetry model. Arch Toxicol. 76:277–286.
Cassee FR, van Balen EC, Singh C, Green D, Muijser H, Weinstein J, Dreher K. 2011. Exposure, health- and ecological effects review of engineered nanoscale cerium and cerium oxide associated with its use as a fuel additive. Crit Rev Toxicol. 41:213–229.
Chakraborty C, Sharma AR, Sharma G, Lee S-S. 2016. Zebrafish: a complete animal model to enumerate the nanoparticle toxicity. J Nanobiotechnol. 14:1–13.
Chang X, Bouchard DC. 2013. Multiwalled carbon nanotube deposition on model environmental surfaces. Environ Sci Technol. 47:10372–10380.
Chang X, Bouchard DC. 2016. Surfactant-wrapped multiwalled carbon nanotubes in aquatic systems: surfactant displacement in the presence of humic acid. Environ Sci Technol. 50:9214–9222.
Chen C-Y, Zepp RG. 2015. Probing photosensitization by functionalized carbon nanotubes. Environ Sci Technol. 49:13835–13843.
Chen W-Y, Cheng Y-H, Hsieh N-H, Wu B-C, Chou W-C, Ho CC, Chen JK, Liao CM, Lin P. 2015. Physiologically based pharmacokinetic modeling of zinc oxide nanoparticles and zinc nitrate in mice. Int J Nanomed. 10:6277–6292.
Chen Y, Qu K, Zhao C, Wu L, Ren J, Wang J, Qu X. 2012. Insights into the biomedical effects of carboxylated single-wall carbon nanotubes on telomerase and telomeres. Nat Commun. 3:1074.
Cheng CY, Mruk DD. 2012. The blood–testis barrier and its implications for male contraception. Pharmacol Rev. 64:16–64.
Cheng CY, Wong EWP, Lie PPY, Li MWM, Mruk DD, Yan HH, Mok KW, Mannu J, Mathur PP, Lui WY, et al. 2011. Regulation of blood–testis barrier dynamics by desmosome, gap junction, hemidesmosome and polarity proteins. Spermatogenesis. 1:105–115.
Chichiriccò G, Poma A. 2015. Penetration and toxicity of nanomaterials in higher plants. Nanomaterials (Basel). 5:851.
Chithrani BD, Chan WCW. 2007. Elucidating the mechanism of cellular uptake and removal of protein-coated gold nanoparticles of different sizes and shapes. Nano Lett. 7:1542–1550.
Chithrani BD, Ghazani AA, Chan WCW. 2006. Determining the size and shape dependence of gold nanoparticle uptake into mammalian cells. Nano Lett. 6:662–668.
Choi HS, Liu W, Misra P, Tanaka E, Zimmer JP, Ipe BI, Bawendi M, Frangioni JV. 2007. Renal clearance of quantum dots. Nat Biotechnol. 25:1165–1170.
Chorley B, Ward W, Simmons SO, Vallanat B, Veronesi B. 2014. The cellular and genomic response of rat dopaminergic neurons (N27) to coated nanosilver. NeuroToxicology. 45:12–21.
Chou C-C, Hsiao H-Y, Hong Q-S, Chen C-H, Peng Y-W, Chen HW, Yang PC. 2008. Single-walled carbon nanotubes can induce pulmonary injury in mouse model. Nano Lett. 8:437–445.
Chowdhury I, Duch MC, Mansukhani ND, Hersam MC, Bouchard D. 2013. Colloidal properties and stability of graphene oxide nanomaterials in the aquatic environment. Environ Sci Technol. 47:6288–6296.
Chowdhury I, Hou WC, Goodwin D, Henderson M, Zepp RG, Bouchard D. 2015a. Sunlight affects aggregation and deposition of graphene oxide in the aquatic environment. Water Res. 78:37–46.

Chowdhury I, Mansukhani ND, Guiney LM, Hersam MC, Bouchard D. 2015b. Aggregation and stability of reduced graphene oxide: complex roles of divalent cations, pH, and natural organic matter. Environ Sci Technol. 49:10886–10893.

Clift MJD, Raemy DO, Endes C, Ali Z, Lehmann AD, Brandenberger C, Petri-Fink A, Wick P, Parak WJ, Gehr P, et al. 2013. Can the Ames test provide an insight into nano-object mutagenicity? Investigating the interaction between nano-objects and bacteria. Nanotoxicology. 7:1373–1385.

Cohen J, Deloid G, Pyrgiotakis G, Demokritou P. 2013a. Interactions of engineered nanomaterials in physiological media and implications for *in vitro* dosimetry. Nanotoxicology. 7:417–431.

Cohen JM, Teeguarden JG, Demokritou P. 2014. An integrated approach for the *in vitro* dosimetry of engineered nanomaterials. Part Fibre Toxicol. 11:20–20.

Cohen Y, Rallo R, Liu R, Liu HH. 2013b. In silico analysis of nanomaterials: hazard and risk. Acc Chem Res. 46:802–812.

Coleman DC, Crossley DA, Hendrix PF. 2004. Fundamentals of soil ecology. New York: Elsevier Academic Press.

Colman BP, Arnaout CL, Anciaux S, Gunsch CK, Hochella MF Jr., Kim B, Lowry GV, McGill BM, Reinsch BC, Richardson CJ, et al. 2013. Low concentrations of silver nanoparticles in biosolids cause adverse ecosystem responses under realistic field scenario. PLoS One. 8:e57189.

Costa PM, Fadeel B. 2016. Emerging systems biology approaches in nanotoxicology: towards a mechanism-based understanding of nanomaterial hazard and risk. Toxicol Appl Pharmacol. 299:101–111.

Dale AL, Casman EA, Lowry GV, Lead JR, Viparelli E, Baalousha M. 2015. Modeling nanomaterial environmental fate in aquatic systems. Environ Sci Technol. 49:2587–2593.

Davda J, Labhasetwar V. 2002. Characterization of nanoparticle uptake by endothelial cells. Int J Pharm. 233:51–59.

de Castro JA, Pereira BA, Tassi E, Pini R, Araujo ASF, Valadão ICP. 2012. Modeling the transport phenomena of TiO2 nanoparticles into Leachate of Municipal Waste Landfills. In: Salgado L, Filho FA, editors. Materials science forum. Switzerland: Trans Tech Publications; p. 1695–1700.

De Lorenzo AJD. 2008. The olfactory neuron and the blood-brain barrier. In: Ciba Foundation Symposium: internal secretions of the pancreas (Colloquia on Endocrinology). New York: John Wiley & Sons, Ltd.; p. 151–176.

DeLoid G, Cohen JM, Darrah T, Derk R, Rojanasakul L, Pyrgiotakis G, Wohlleben W, Philip Demokritou P. 2014. Estimating the effective density of engineered nanomaterials for *in vitro* dosimetry. Nat Commun. 5:3514.

Desai MP, Labhasetwar V, Amidon GL, Levy RJ. 1996. Gastrointestinal uptake of biodegradable microparticles: effect of particle size. Pharm Res. 13:1838–1845.

Desai MP, Labhasetwar V, Walter E, Levy RJ, Amidon GL. 1997. The mechanism of uptake of biodegradable microparticles in Caco-2 cells is size dependent. Pharm Res. 14:1568–1573.

Di Toro DM, Zarba CS, Hansen DJ, Berry WJ, Swartz RC, Cowan C, Pavlou S, Allen H. 1991. Technical basis for establishing sediment quality criteria for nonionic organic chemicals using equilibrium partitioning. Environ Toxicol Chem. 10:1541–1583.

Dietz K-J, Herth S. 2011. Plant nanotoxicology. Trends Plant Sci. 16:582–589.

Dinesh R, Anandaraj M, Srinivasan V, Hamza S. 2012. Engineered nanoparticles in the soil and their potential implications to microbial activity. Geoderma. 173:19–27.

Dobrovolskaia MA, McNeil SE. 2007. Immunological properties of engineered nanomaterials. Nat Nanotechnol. 2:469–478.

Domínguez A, Suárez-Merino B, Goñi-de-Cerio F. 2014. Nanoparticles and blood-brain barrier: the key to central nervous system diseases. J Nanosci Nanotechnol. 14:766–779.

Donaldson K, Murphy FA, Duffin R, Poland CA. 2010. Asbestos, carbon nanotubes and the pleural mesothelium: a review of the hypothesis regarding the role of long fibre retention in the parietal pleura, inflammation and mesothelioma. Part Fibre Toxicol. 7:5.

Donaldson K, Poland CA. 2013. Nanotoxicity: challenging the myth of nano-specific toxicity. Curr Opin Biotechnol. 24:724–734.

Donner E, Howard DL, Jonge MDd, Paterson D, Cheah MH, Naidu R, Lombi E. 2011. X-ray absorption and micro X-ray fluorescence spectroscopy investigation of copper and zinc speciation in biosolids. Environ Sci Technol. 45:7249–7257.

Donner E, Scheckel K, Sekine R, Popelka-Filcoff RS, Bennett JW, Brunetti G, Naidu R, McGrath SP, Lombi E. 2015. Non-labile silver species in biosolids remain stable throughout 50 years of weathering and ageing. Environ Pollut. 205:78–86.

Duan J, Yu Y, Li Y, Yu Y, Li Y, Zhou X, Huang P, Sun Z. 2013. Toxic effect of silica nanoparticles on endothelial cells through DNA damage response via Chk1-dependent G2/M checkpoint. PLoS One. 8:e62087.

Dwivedi AD, Dubey SP, Sillanpää M, Kwon Y-N, Lee C, Varma RS. 2015. Fate of engineered nanoparticles: implications in the environment. Coord Chem Rev. 287:64–78.

Eastlake A, Zumwalde R, Geraci C. 2016a. Can control banding be useful for the safe handling of nanomaterials? A systematic review. J Nanopart Res: Interdiscip Forum Nanoscale Sci Technol. 18:169.

Eastlake AC, Beaucham C, Martinez KF, Dahm MM, Sparks C, Hodson LL, Geraci CL. 2016b. Refinement of the nanoparticle emission assessment technique into the Nanomaterial Exposure Assessment Technique (NEAT 2.0). J Occup Environ Hygiene. 13:708–717.

El Badawy AM, Luxton TP, Silva RG, Scheckel KG, Suidan MT, Tolaymat TM. 2010. Impact of environmental conditions (pH, ionic strength, and electrolyte type) on the surface charge and aggregation of silver nanoparticles suspensions. Environ Sci Technol. 44:1260–1266.

Elder A, Vidyasagar S, DeLouise L. 2009. Physicochemical factors that affect metal and metal oxide nanoparticle passage across epithelial barriers. Wiley Interdiscip Rev Nanomed Nanobiotechnol. 1:434–450.

EPA. 2009. *Targeted National Sewage Sludge Survey Sampling and Analysis Technical Report*. Washington (DC): U.S. Environmental Protection Agency, Office of Water.

EPA. 2012. Water: Sewage Sludge (Biosolids): Frequently Asked Questions. U.S. Environmental Protection Agency.

EPA. 2017. Chemical Substances When Manufactured or Processed as Nanoscale Materials; TSCA Reporting and Recordkeeping Requirements ed. OoPPa Toxics. Washington (DC): Federal Register; p. 3641–3655.

Erdakos GB, Bhave PV, Pouliot GA, Simon H, Mathur R. 2014. Predicting the effects of nanoscale cerium additives in diesel fuel on regional-scale air quality. Environ Sci Technol. 48:12775–12782.

Essington ME. 2015. Soil and water chemistry: an integrative approach. 2nd ed. Boca Raton (FL): CRC Press, Taylor and Francis Group.

Evans DE, Ku BK, Birch ME, Dunn KH. 2010. Aerosol monitoring during carbon nanofiber production: mobile direct-reading sampling. Ann Occup Hyg. 54:514–531.

Fabian E, Landsiedel R, Ma-Hock L, Wiench K, Wohlleben W, van Ravenzwaay B. 2008. Tissue distribution and toxicity of intravenously administered titanium dioxide nanoparticles in rats. Arch Toxicol. 82.

Fabrega J, Luoma SN, Tyler CR, Galloway TS, Lead JR. 2011. Silver nanoparticles: behaviour and effects in the aquatic environment. Environ Int. 37:517–531.

Fako VE, Furgeson DY. 2009. Zebrafish as a correlative and predictive model for assessing biomaterial nanotoxicity. Adv Drug Deliv Rev. 61:478–486.

Farcal L, Torres Andón F, Di Cristo L, Rotoli BM, Bussolati O, Bergamaschi E, Mech A, Hartmann NB, Rasmussen K, Riego-Sintes J, et al. 2015. Comprehensive *in vitro* toxicity testing of a panel of representative oxide nanomaterials: first steps towards an intelligent testing strategy. PLoS One. 2015;10:e0127174.

Federici G, Shaw BJ, Handy RD. 2007. Toxicity of titanium dioxide nanoparticles to rainbow trout (*Oncorhynchus mykiss*): gill injury, oxidative stress, and other physiological effects. Aquat Toxicol. 84:415–430.

Ferry JL, Craig P, Hexel C, Sisco P, Frey R, Paul LP, Michael HF, Geoff SI, Alan WD, Shosaku K, et al. 2009. Transfer of gold nanoparticles from the water column to the estuarine food web. Nat Nano. 4:441–444.

Fleischer CC, Payne CK. 2014. Nanoparticle–cell interactions: molecular structure of the protein corona and cellular outcomes. Accounts Chem Res. 47:2651–2659.

Foldbjerg R, Dang DA, Autrup H. 2011. Cytotoxicity and genotoxicity of silver nanoparticles in the human lung cancer cell line, A549. Arch Toxicol. 85:743–750.

Froggett SJ, Clancy SF, Boverhof DR, Canady RA. 2014. A review and perspective of existing research on the release of nanomaterials from solid nanocomposites. Part Fibre Toxicol. 11:1–28.

Frohlich E. 2016. Cellular elimination of nanoparticles. Environ Toxicol Pharmacol. 46:90–94.

Frohlich E, Roblegg E. 2012. Models for oral uptake of nanoparticles in consumer products. Toxicology. 291:10–17.

Gantt B, Hoque S, Willis RD, Fahey KM, Delgado-Saborit JM, Harrison RM, Erdakos GB, Bhave PV, Zhang KM, Kovalcik K, Pye HO. 2014. Near-road modeling and measurement of cerium-containing particles generated by nanoparticle diesel fuel additive use. Environ Sci Technol. 48:10607–10613.

Gao H, Shi W, Freund LB. 2005. Mechanics of receptor-mediated endocytosis. Proc Natl Acad Sci USA. 102:9469–9474.

García-Alonso J, Rodriguez-Sanchez N, Misra SK, Valsami-Jones E, Croteau M-N, Luoma SN, Rainbow PS. 2014. Toxicity and accumulation of silver nanoparticles during development of the marine polychaete *Platynereis dumerilii*. Sci Total Environ. 476–477:688–695.

Ge Y, Priester JH, Mortimer M, Chang CH, Ji Z, Schimel JP, Holden PA. 2016. Long-term effects of multiwalled carbon nanotubes and graphene on microbial communities in dry soil. Environ Sci Technol. 50:3965–3974.

George R, Merten S, Wang TT, Kennedy P, Maitz P. 2014. *In vivo* analysis of dermal and systemic absorption of silver nanoparticles through healthy human skin. Australas J Dermatol. 55:185–190.

Gerloff K, Landesmann B, Worth A, Munn S, Palosaari T, Whelan M. 2017. The adverse outcome pathway approach in nanotoxicology. Comput Toxicol. 1:3–11.

Gitipour A, El Badawy A, Arambewela M, Miller B, Scheckel K, Elk M, Ryu H, Gomez-Alvarez V, Domingo JS, Thiel S, et al. 2013. The impact of silver nanoparticles on the composting of municipal solid waste. Environ Sci Technol. 47:14385–14393.

Godwin H, Nameth C, Avery D, Bergeson LL, Bernard D, Beryt E, Boyes W, Brown S, Clippinger AJ, Cohen Y, et al. 2015. Nanomaterial categorization for assessing risk potential to facilitate regulatory decision-making. ACS Nano. 9:3409–3417.

Golbamaki N, Rasulev B, Cassano A, Marchese Robinson RL, Benfenati E, Leszczynski J, Cronin MT. 2015. Genotoxicity of metal oxide nanomaterials: review of recent data and discussion of possible mechanisms. Nanoscale. 7:2154–2198.

Gomes T, Pereira CG, Cardoso C, Pinheiro JP, Cancio I, Bebianno MJ. 2012. Accumulation and toxicity of copper oxide nanoparticles in the digestive gland of *Mytilus galloprovincialis*. Aquat Toxicol. 118–119:72–79.

Gomes T, Pinheiro JP, Cancio I, Pereira CG, Cardoso C, Bebianno MJ. 2011. Effects of copper nanoparticles exposure in the Mussel *Mytilus galloprovincialis*. Environ Sci Technol. 45:9356–9362.

Gottschalk F, Sonderer T, Scholz RW, Nowack B. 2009. Modeled environmental concentrations of engineered nanomaterials (TiO2, ZnO, Ag, CNT, fullerenes) for different regions. Environ Sci Technol. 43:9216–9222.

Gottschalk F, Sun T, Nowack B. 2013. Environmental concentrations of engineered nanomaterials: review of modeling and analytical studies. Environ Pollut. 181:287–300.

Grassian VH, Haes AJ, Mudunkotuwa IA, Demokritou P, Kane AB, Murphy CJ, Hutchinson JE, Issacs JA, Jun Y-S, Karn B, et al. 2016. NanoEHS: defining fundamental science needs: no easy feat when the simple itself is complex. Environ Sci: Nano. 3:15–27.

Grieger KD, Linkov I, Hansen SF, Baun A. 2012. Environmental risk analysis for nanomaterials: review and evaluation of frameworks. Nanotoxicology. 6:196–212.

Griffitt RJ, Hyndman K, Denslow ND, Barber DS. 2009. Comparison of molecular and histological changes in zebrafish gills exposed to metallic nanoparticles. Toxicol Sci. 107:404–415.

Griffitt RJ, Weil R, Hyndman KA, Denslow ND, Powers K, Taylor D, Barber DS. 2007. Exposure to copper nanoparticles causes gill injury and acute lethality in zebrafish (Danio rerio). Environ Sci Technol. 41:8178–8186.

Guadagnini R, Halamoda Kenzaoui B, Walker L, Pojana G, Magdolenova Z, Bilanicova D, Saunders M, Juillerat-Jeanneret L, Marcomini A, Huk A, et al. 2015. Toxicity screenings of nanomaterials: challenges due to interference with assay processes and components of classic *in vitro* tests. Nanotoxicology. 9:13–24.

Guan R, Kang T, Lu F, Zhang Z, Shen H, Liu M. 2012. Cytotoxicity, oxidative stress, and genotoxicity in human hepatocyte and embryonic kidney cells exposed to ZnO nanoparticles. Nanoscale Res Lett. 7:602.

Gunduz N, Ceylan H, Guler MO, Tekinay AB. 2017. Intracellular accumulation of gold nanoparticles leads to inhibition of macropinocytosis to reduce the endoplasmic reticulum stress. Sci Rep. 7:40493.

Guo X, Chen T. 2015. Chapter 7. Progress in genotoxicity evaluation of engineered nanomaterials. In: Soloneski S, Larramendy ML, editors. Nanomaterials: toxicity and risk assessment. Rijeka: Intech.

Hagens WI, Oomen AG, de Jong WH, Cassee FR, Sips AJ. 2007. What do we (need to) know about the kinetic properties of nanoparticles in the body? Regul Toxicol Pharmacol. 49:217–229.

Hall S, Bradley T, Moore JT, Kuykindall T, Minella L. 2009. Acute and chronic toxicity of nano-scale TiO2 particles to freshwater fish, cladocerans, and green algae, and effects of organic and inorganic substrate on TiO2 toxicity. Nanotoxicology. 3:91–97.

Handy R, Henry T, Scown T, Johnston B, Tyler C. 2008. Manufactured nanoparticles: their uptake and effects on fish – a mechanistic analysis. Ecotoxicology. 17:396–409.

Hansen S, Jensen K, Baun A. 2013. NanoRiskCat: a conceptual tool for categorization and communication of exposure potentials and hazards of nanomaterials in consumer products. J Nanopart Res. 16:1–25.

Hansen SF, Heggelund LR, Revilla Besora P, Mackevica A, Boldrin A, Baun A. 2016. Nanoproducts -what is actually available to European consumers? Environ Sci: Nano. 3:169–180.

Harper SL, Carriere JL, Miller JM, Hutchison JE, Maddux BL, Tanguay RL. 2011. Systematic evaluation of nanomaterial toxicity: utility of standardized materials and rapid assays. ACS Nano. 5.

He X, Zhang H, Ma Y, Bai W, Zhang Z, Lu K, Ding Y, Zhao Y, Chai Z. 2010. Lung deposition and extrapulmonary translocation of nano-ceria after intratracheal instillation. Nanotechnology. 21:285103.

Hendren CO, Lowry GV, Unrine JM, Wiesner MR. 2015. A functional assay-based strategy for nanomaterial risk forecasting. Sci Total Environ. 536:1029–1037.

Hendren CO, Lowry M, Grieger KD, Money ES, Johnston JM, Wiesner MR, Beaulieu SM. 2013. Modeling approaches for characterizing and evaluating environmental exposure to engineered nanomaterials in support of risk-based decision making. Environ Sci Technol. 47:1190–1205.

Hillyer JF, Albrecht RM. 2001. Gastrointestinal persorption and tissue distribution of differently sized colloidal gold nanoparticles. J Pharm Sci. 90:1927–1936.

Hinderliter PM, Minard KR, Orr G, Chrisler WB, Thrall BD, Pounds JG, Teeguarden JG. 2010. ISDD: a computational model of particle sedimentation, diffusion and target cell dosimetry for *in vitro* toxicity studies. Part Fibre Toxicol. 7:36.

Holbrook RD, Murphy KE, Morrow JB, Cole KD. 2008. Trophic transfer of nanoparticles in a simplified invertebrate food web. Nat Nano. 3:352–355.

Holden PA, Gardea-Torresdey JL, Klaessig F, Turco RF, Mortimer M, Hund-Rinke K, Cohen Hubal EA, Avery D, Barceló D, Behra R, et al. 2016. Considerations of environmentally relevant test conditions for improved evaluation of ecological hazards of engineered nanomaterials. Environ Sci Technol. 50:6124–6145.

Holden PA, Nisbet RM, Lenihan HS, Miller RJ, Cherr GN, Schimel JP, Gardea-Torresdey JL. 2013. Ecological nanotoxicology: integrating nanomaterial hazard considerations across the subcellular, population, community, and ecosystems levels. Acc Chem Res. 46:813–822.

Holder AL, Vejerano EP, Zhou X, Marr LC. 2013. Nanomaterial disposal by incineration. Environ Sci Process Impacts. 15:1652–1664.

Hou W-C, Chowdhury I, Goodwin DG, Henderson WM, Fairbrother DH, Bouchard D, Zepp RG. 2015. Photochemical transformation of graphene oxide in sunlight. Environ Sci Technol. 49:3435–3443.

Hou W-C, Henderson WM, Chowdhury I, Goodwin DG Jr., Chang X, Martinf S, Fairbrotherd DH, Boucharde D, Zepp RG. 2016. The contribution of indirect photolysis to the degradation of graphene oxide in sunlight. Carbon. 110:426–437.

Hou WC, Stuart B, Howes R, Zepp RG. 2013. Sunlight-driven reduction of silver ions by natural organic matter: formation and transformation of silver nanoparticles. Environ Sci Technol. 47:7713–7721.

Hristozov D, Gottardo S, Semenzin E, Oomen A, Bos P, Peijnenburg W, van Tongeren M, Nowack B, Hunt N, Brunelli A, et al. 2016. Frameworks and tools for risk assessment of manufactured nanomaterials. Environ Int. 95:36–53.

Hu R, Gong X, Duan Y, Li N, Che Y, Cui Y, Zhou M, Liu C, Wang H, Hong F. 2010. Neurotoxicological effects and the impairment of spatial recognition memory in mice caused by exposure to TiO2 nanoparticles. Biomaterials. 31:8043–8050.

Huang S, Chueh PJ, Lin YW, Shih TS, Chuang SM. 2009. Disturbed mitotic progression and genome segregation are involved in cell transformation mediated by nano-TiO2 long-term exposure. Toxicol Appl Pharmacol. 241:182–194.

Huang YW, Wu C, Aronstam RS. 2010. Toxicity of transition metal oxide nanoparticles: recent insights from *in vitro* studies. Materials. 3:4842–4859.

Hull MS, Chaurand P, Rose J, Auffan M, Bottero J-Y, Jones JC, Schultz IR, Vikesland PJ. 2011. Filter-feeding bivalves store and biodeposit colloidally stable gold nanoparticles. Environ Sci Technol. 45:6592–6599.

Hund-Rinke K, Simon M. 2006. Ecotoxic effect of photocatalytic active nanoparticles (TiO2) on algae and daphnids (8 pp). Environ Sci Pollut Res Int. 13:225–232.

Hunter RJ. 2001. Foundations of colloid science. Oxford (UK): Oxford University Press.

Huynh KA, Siska E, Heithmar E, Tadjiki S, Pergantis SA. 2016. Detection and quantification of silver nanoparticles at environmentally relevant concentrations using asymmetric flow field–flow fractionation online with single particle inductively coupled plasma mass spectrometry. Anal Chem. 88:4909–4916.

Hyung H, Fortner JD, Hughes JB, Kim J-H. 2007. Natural organic matter stabilizes carbon nanotubes in the aqueous phase. Environ Sci Technol. 41:179–184.

Impellitteri CA, Harmon S, Silva RG, Miller BW, Scheckel KG, Luxtona TP, Schuppb D, Panguluri S. 2013. Transformation of silver nanoparticles in fresh, aged, and incinerated biosolids. Water Res. 47:3878–3886.

Isaacs KK, Glen WG, Egeghy P, Goldsmith M-R, Smith L, Vallero D, Brooks R, Grulke CM, Özkaynak H. 2014. SHEDS-HT: an integrated probabilistic exposure model for prioritizing exposures to chemicals with near-field and dietary sources. Environ Sci Technol. 48:12750–12759.

Ivask A, Juganson K, Bondarenko O, Mortimer M, Aruoja V, Kasemets K, Blinova I, Heinlaan M, Slaveykova V, Kahru A. 2013. Mechanisms of toxic action of Ag, ZnO and CuO nanoparticles to selected ecotoxicological test organisms and mammalian cells *in vitro*: a comparative review. Nanotoxicology. 8:57–71.

Jackson P, Vogel U, Wallin H, Hougaard KS. 2011. Prenatal exposure to carbon black (printex 90): effects on sexual development and neurofunction. Basic Clin Pharmacol Toxicol. 109:434–437.

Jimeno-Romero A, Berhanu D, Reip P, Oron M, Gilliland D, Valsami-Jones E, Cajaraville MP, Warley A, Marigómez I, Soto M. 2012. Down the rabbit hole: Subcellular localization and x-ray microanalysis of a set of metallic nanoparticles in mussels. Comp Biochem Physiol A: Mol Integr Physiol. 163:S23–S24.

Jin H, Heller DA, Sharma R, Strano MS. 2009. Size-dependent cellular uptake and expulsion of single-walled carbon nanotubes: single particle tracking and a generic uptake model for nanoparticles. ACS Nano. 3:149–158.

Johnston H, Pojana G, Zuin S, Jacobsen NR, Moller P, Loft S, Semmler-Behnke M, McGuiness C, Balharry D, Marcomini A, et al. 2013. Engineered nanomaterial risk. Lessons learnt from completed nanotoxicology studies: potential solutions to current and future challenges. Crit Rev Toxicol. 43:1–20.

Joubert Y, Pan J-F, Buffet P-E, Pilet P, Gilliland D, Valsami-Jones E, Mouneyrac C, Amiard-Triquet C. 2013. Subcellular localization of gold nanoparticles in the estuarine bivalve *Scrobicularia plana* after exposure through the water. Gold Bull. 46:47–56.

Juch H, Nikitina L, Debbage P, Dohr G, Gauster M. 2013. Nanomaterial interference with early human placenta: sophisticated matter meets sophisticated tissues. Reprod Toxicol. 41:73–79.

Judy JD, Unrine JM, Bertsch PM. 2011. Evidence for biomagnification of gold nanoparticles within a terrestrial food chain. Environ Sci Technol. 45:776–781.

Judy JD, Unrine JM, Rao W, Wirick S, Bertsch PM. 2012. Bioavailability of gold nanomaterials to plants: importance of particle size and surface coating. Environ Sci Technol. 46:8467–8474.

Kádár E, Lowe D, Solé M, Fisher A, Jha A, Readman JW, Hutchinson TH. 2010. Uptake and biological responses to nano-Fe versus soluble FeCl3 in excised mussel gills. Anal Bioanal Chem. 396:657–666.

Kaegi R, Voegelin A, Ort C, Sinnet B, Thalmann B, Krismerb J, Hagendorferc H, Elumelua M, Mueller E. 2013. Fate and transformation of silver nanoparticles in urban wastewater systems. Water Res. 47:3866–3877.

Kaegi R, Voegelin A, Sinnet B, Zuleeg S, Hagendorfer H, Burkhardt M, Siegrist H. 2011. Behavior of metallic silver nanoparticles in a pilot wastewater treatment plant. Environ Sci Technol. 45:3902–3908.

Kagan VE, Konduru NV, Feng W, Allen BL, Conroy J, Volkov Y, Vlasova II, Belikova NA, Yanamala N, Kapralov A, et al. 2010. Carbon nanotubes degraded by neutrophil myeloperoxidase induce less pulmonary inflammation. Nat Nano. 5:354–359.

Karmakar A, Zhang Q, Zhang Y. 2014. Neurotoxicity of nanoscale materials. J Food Drug Anal. 22:147–160.

Kasai T, Umeda Y, Ohnishi M, Mine T, Kondo H, Takeuchi T, Matsumoto M, Fukushima S. 2015. Lung carcinogenicity of inhaled multi-walled carbon nanotube in rats. Part Fibre Toxicol. 13:53.

Keller A, McFerran S, Lazareva A, Suh S. 2013a. Global life cycle releases of engineered nanomaterials. J Nanopart Res. 15:1–17.

Keller AA, McFerran S, Lazareva A, Suh S. 2013b. Global life cycle releases of engineered nanomaterials. J Nanopart Res. 15:1692.

Kennedy AJ, Gunter JC, Chappell MA, Goss JD, Hull MS, Kirgan RA, Steevens JA. 2009. Influence of nanotube preparation in aquatic bioassays. Environ Toxicol Chem. 28:1930–1938.

Kim B, Murayama M, Colman BP, Hochella MF. 2012. Characterization and environmental implications of nano- and larger TiO2 particles in sewage sludge, and soils amended with sewage sludge. J Environ Monit. 14:1128–1136.

Kim B, Park C-S, Murayama M, Hochella MF. 2010a. Discovery and characterization of silver sulfide nanoparticles in final sewage sludge products. Environ Sci Technol. 44:7509–7514.

Kim JS, Sung JH, Choi BG, Ryu HY, Song KS, Shin JH, Lee JS, Hwang JH, Lee JH, Lee GH, et al. 2014. *In vivo* genotoxicity evaluation of lung cells from Fischer 344 rats following 28 days of inhalation exposure to MWCNTs, plus 28 days and 90 days post-exposure. Inhal Toxicol. 26:222–234.

Kim S, Choi I-H. 2012. Phagocytosis and endocytosis of silver nanoparticles induce interleukin-8 production in human macrophages. Yonsei Med J. 53:654–657.

Kim S, Choi JE, Choi J, Chung KH, Park K, Yi J, Ryu DY. 2009. Oxidative stress-dependent toxicity of silver nanoparticles in human hepatoma cells. Toxicol In Vitro. 23:1076–1084.

Kim YS, Song MY, Park JD, Song KS, Ryu HR, Chung YH, Chang HK, Lee JH, Oh KH, Kelman BJ, et al. 2010b. Subchronic oral toxicity of silver nanoparticles. Part Fibre Toxicol. 7:20.

Kingston C, Zepp R, Andrady A, Boverhof D, Fehir R, Hawkins D, Roberts J, Sayre P, Shelton B, Sultan Y, et al. 2014. Release characteristics of selected carbon nanotube polymer composites. Carbon. 68:33–57.

Kiser MA, Westerhoff P, Benn T, Wang Y, Pérez-Rivera J, Hristovski K. 2009. Titanium nanomaterial removal and release from wastewater treatment plants. Environ Sci Technol. 43:6757–6763.

Kitchin KT, Prasad RY, Wallace K. 2011. Oxidative stress studies of six TiO2 and two CeO2 nanomaterials: immuno-spin trapping results with DNA. Nanotoxicology. 5:546–556.

Klaine SJ, Alvarez PJJ, Batley GE, Fernandes TF, Handy RD, Lyon DY, Mahendra S, McLaughlin MJ, Lead JR. 2008. Nanomaterials in the

environment: behavior, fate, bioavailability, and effects. Environ Toxicol Chem. 27:1825–1851.
Klaunig JE, Wang Z, Pu X, Zhou S. 2011. Oxidative stress and oxidative damage in chemical carcinogenesis. Toxicol Appl Pharmacol. 254:86–99.
Kleber M, Johnson MG. 2010. Advances in understanding the molecular structure of soil organic matter: implications for interactions in the environment. Adv Agronomy. 106:77–142.
Knight MR, Knight H. 2012. Low-temperature perception leading to gene expression and cold tolerance in higher plants. New Phytol. 195:737–751.
Knightes C. 2015. Simulating the fate and transport of nanomaterials in surface waters. In: Quantifying exposure to engineered nanomaterials from manufactured products: addressing environmental, health, and safety implications, consumer products safety commission. Washington, DC: National Nanotechnology Initiative.
Koelmans AA, Nowack B, Wiesner MR. 2009. Comparison of manufactured and black carbon nanoparticle concentrations in aquatic sediments. Environ Pollut. 157:1110–1116.
Kraeuter JN, Castagna M. 2001. Biology of the hard clam. Amsterdam: Elsevier.
Kroll A, Pillukat MH, Hahn D, Schnekenburger J. 2009. Current *in vitro* methods in nanoparticle risk assessment: limitations and challenges. Eur J Pharm Biopharm. 72:370–377.
Kuempel ED, Castranova V, Geraci CL, Schulte PA. 2012. Development of risk-based nanomaterial groups for occupational exposure control. J Nanopart Res. 14:1029.
Kumar A, Dhawan A. 2013. Genotoxic and carcinogenic potential of engineered nanoparticles: an update. Arch Toxicol. 87:1883–1900.
Kumar A, Pandey AK, Singh SS, Shanker R, Dhawan A. 2011. Cellular uptake and mutagenic potential of metal oxide nanoparticles in bacterial cells. Chemosphere. 83:1124–1132.
Kumar A, Shanker R, Alok D. 2015. Nanotoxicity: aquatic organisms and ecosystems. In: Reisner D, editor. Aquananotechnology: global prospects. London: CRC Press; p. 97–106.
Kumar V, Guleria P, Kumar V, Yadav SK. 2013. Gold nanoparticle exposure induces growth and yield enhancement in Arabidopsis thaliana. Sci Total Environ. 461–462:462–468.
Kwak JI, An Y-J. 2015. A review of the ecotoxicological effects of nanowires. Int J Environ Sci Technol. 12:1163–1172.
Labib S, Williams A, Yauk CL, Nikota JK, Wallin H, Vogel U, Halappanavar S. 2016. Nano-risk science: application of toxicogenomics in an adverse outcome pathway framework for risk assessment of multi-walled carbon nanotubes. Part Fibre Toxicol. 13:1–17.
Landsiedel R, Fabian E, Ma-Hock L, Wohlleben W, Wiench K, Oesch F. 2012. Toxico-/biokinetics of nanomaterials. Arch Toxicol. 86:1021–1060.
Larese FF, D'Agostin F, Crosera M, Adami G, Renzi N, Bovenzi M, Maina G. 2009. Human skin penetration of silver nanoparticles through intact and damaged skin. Toxicology. 255:33–37.
Larese Filon F, Bello D, Cherrie JW, Sleeuwenhoek A, Spaan S, Brouwer DH. 2016. Occupational dermal exposure to nanoparticles and nano-enabled products: Part I. Factors affecting skin absorption. Int J Hyg Environ Health. 219:536–544.
Larsen ST, Jackson P, Poulsen SS, Levin M, Jensen KA, Wallin H, Nielsen GD, Koponen IK. 2016. Airway irritation, inflammation, and toxicity in mice following inhalation of metal oxide nanoparticles. Nanotoxicology. 10:1254–1262.
Lee Y, Kim P, Yoon J, Lee B, Choi K, Kil KH, Park K. 2012. Serum kinetics, distribution and excretion of silver in rabbits following 28 days after a single intravenous injection of silver nanoparticles. Nanotoxicology. 7:1120–1130.
Li M, Panagi Z, Avgoustakis K, Reineke J. 2012. Physiologically based pharmacokinetic modeling of PLGA nanoparticles with varied mPEG content. Int J Nanomedicine. 7:1345–1356.
Li N, Xia T, Nel AE. 2008. The role of oxidative stress in ambient particulate matter-induced lung diseases and its implications in the toxicity of engineered nanoparticles. Free Radic Biol Med. 44:1689–1699.
Liang G, Pu Y, Yin L, Liu R, Ye B, Su Y, Li Y. 2009. Influence of different sizes of titanium dioxide nanoparticles on hepatic and renal functions in rats with correlation to oxidative stress. J Toxicol Environ Health Part A. 72:740–745.
Liao H-Y, Chung Y-T, Lai C-H, Wang S-L, Chiang H-C, Li LA, Tsou TC, Li WF, Lee HL, Wu WT, et al. 2014. Six-month follow-up study of health markers of nanomaterials among workers handling engineered nanomaterials. Nanotoxicology. 8:100–110.
Lim JH, Kim SH, Shin IS, Park NH, Moon C, Kang SS, Kim SH, Park SC, Kim JC. 2011. Maternal exposure to multi-wall carbon nanotubes does not induce embryo-fetal developmental toxicity in rats. Birth Defects Res Part B Dev Reprod Toxicol. 92:69–76.
Lin Z, Monteiro-Riviere NA, Riviere JE. 2015. Pharmacokinetics of metallic nanoparticles. Wiley Interdiscip Rev Nanomed Nanobiotechnol. 7:189–217.
Liu Q, Zhao N, Yamaguch-Shinozaki K, Shinozaki K. 2000. Regulatory role of DREB transcription factors in plant drought, salt and cold tolerance. Chin Sci Bull. 45:970–975.
Liu W, Rose J, Plantevin S, Auffan M, Bottero J-Y, Vidaud C. 2013. Protein corona formation for nanomaterials and proteins of a similar size: hard or soft corona? Nanoscale. 5:1658–1668.
Liu Z, Liu Y, Peng D. 2015. Carboxylation of multiwalled carbon nanotube attenuated the cytotoxicity by limiting the oxidative stress initiated cell membrane integrity damage, cell cycle arrestment, and death receptor mediated apoptotic pathway. J Biomed Mater Res Part A. 103:2770–2777.
Lombi E, Donner E, Taheri S, Tavakkoli E, Jämting ÅK, McClure S, Naidu R, Miller BW, Scheckel KG, Vasilev K. 2013. Transformation of four silver/silver chloride nanoparticles during anaerobic treatment of wastewater and post-processing of sewage sludge. Environ Pollut. 176:193–197.
Lombi E, Donner E, Tavakkoli E, Turney TW, Naidu R, Miller BW, Scheckel KG. 2012. Fate of zinc oxide nanoparticles during anaerobic digestion of wastewater and post-treatment processing of sewage sludge. Environ Sci Technol. 46:9089–9096.
López-Moreno ML, de la Rosa G, Hernández-Viezcas JA, Peralta-Videa JR, Gardea-Torresdey JL. 2010. X-ray absorption spectroscopy (XAS) corroboration of the uptake and storage of CeO2 nanoparticles and assessment of their differential toxicity in four edible plant species. J Agric Food Chem. 58:3689–3693.
Lorenz C, Hagendorfer H, von Goetz N, Kaegi R, Gehrig R, Ulrich A, Scheringer M, Hungerbühler K. 2011. Nanosized aerosols from consumer sprays: experimental analysis and exposure modeling for four commercial products. J Nanopart Res. 13:3377–3391.
Lowry GV, Gregory KB, Apte SC, Lead JR. 2012. Transformations of nanomaterials in the environment. Environ Sci Technol. 46:6893–6899.
Lundqvist M, Stigler J, Elia G, Lynch I, Cedervall T, Dawson KA. 2008. Nanoparticle size and surface properties determine the protein corona with possible implications for biological impacts. Proc Natl Acad Sci. 105:14265–14270.
Lynch I, Cedervall T, Lundqvist M, Cabaleiro-Lago C, Linse S, Dawson KA. 2007. The nanoparticle–protein complex as a biological entity; a complex fluids and surface science challenge for the 21st century. Adv Colloid Interface Sci. 134–135:167–174.
Ma H, Diamond SA. 2013. Phototoxicity of TiO2 nanoparticles to zebrafish (Danio rerio) is dependent on life stage. Environ Toxicol Chem. 32:2139–2143.
Ma R, Stegemeier J, Levard C, Dale JG, Noack CW, Yang T, Brown G, Lowry GV. 2014. Sulfidation of copper oxide nanoparticles and properties of resulting copper sulfide. Environ Sci: Nano. 1:347–357.
Ma X, Geiser-Lee J, Deng Y, Kolmakov A. 2010. Interactions between engineered nanoparticles (ENPs) and plants: phytotoxicity, uptake and accumulation. Sci Total Environ. 408:3053–3061.
Madl AK, Plummer LE, Carosino C, Pinkerton KE. 2014. Nanoparticles, lung injury, and the role of oxidant stress. Annu Rev Physiol. 76:447–465.
Magdolenova Z, Collins A, Kumar A, Dhawan A, Stone V, Dusinska M. 2014. Mechanisms of genotoxicity. A review of *in vitro* and *in vivo* studies with engineered nanoparticles. Nanotoxicology. 8:233–278.
Mahmoudi M, Azadmanesh K, Shokrgozar MA, Journeay WS, Laurent S. 2011. Effect of nanoparticles on the cell life cycle. Chem Rev. 111:3407–3432.
Majumdar S, Trujillo-Reyes J, Hernandez-Viezcas JA, White JC, Peralta-Videa JR, Gardea-Torresdey JL. 2016. Cerium biomagnification in a

terrestrial food chain: influence of particle size and growth stage. Environ Sci Technol. 50:6782–6792.
Manceau A, Nagy KL, Marcus MA, Lanson M, Geoffroy N, Jacquet T, Kirpichtchikova T. 2008. Formation of metallic copper nanoparticles at the soil–root interface. Environ Sci Technol. 42:1766–1772.
Manke A, Wang L, Rojanasakul Y. 2013. Mechanisms of nanoparticle-induced oxidative stress and toxicity. BioMed Res Int. 2013:942916.
Marano F, Hussain S, Rodrigues-Lima F, Baeza-Squiban A, Boland S. 2011. Nanoparticles: molecular targets and cell signalling. Arch Toxicol. 85:733–741.
Marisa I, Marin MG, Caicci F, Franceschinis E, Martucci A, Matozzo V. 2015. *In vitro* exposure of haemocytes of the clam Ruditapes philippinarum to titanium dioxide (TiO2) nanoparticles: nanoparticle characterisation, effects on phagocytic activity and internalisation of nanoparticles into haemocytes. Mar Environ Res. 103:11–17.
Maynard AD. 2014. Is novelty overrated? Nat Nanotechnol. 9:409–410.
McClure J, Lathrop D, Jacob M. 2013. After West disaster, News study finds U.S. chemical safety data about 90 percent wrong. The Dallas Morning News. Aug 24, 2013.
Meier C, Voegelin A, Pradas del Real A, Sarret G, Mueller CR, Kaegi R. 2016. Transformation of silver nanoparticles in sewage sludge during incineration. Environ Sci Technol. 50:3503–3510.
Mercer JR, Cheng KK, Figg N, Gorenne I, Mahmoudi M, Griffin J, Vidal-Puig A, Logan A, Murphy MP, Bennett M. 2010. DNA damage links mitochondrial dysfunction to atherosclerosis and the metabolic syndrome. Circ Res. 107:1021–1031.
Mercer RR, Scabilloni JF, Hubbs AF, Wang L, Battelli LA, McKinney W, Castranova V, Porter DW. 2013. Extrapulmonary transport of MWCNT following inhalation exposure. Part Fibre Toxicol. 10:38.
Minetto D, Libralato G, Volpi Ghirardini A. 2014. Ecotoxicity of engineered TiO2 nanoparticles to saltwater organisms: an overview. Environ Int. 66:18–27.
MINTEQ V. 2013. [Cited 2017 Feb 15]. Available from: https://vminteq.lwr.kth.se/
Mitchell LA, Lauer FT, Burchiel SW, McDonald JD. 2009. Mechanisms for how inhaled multiwalled carbon nanotubes suppress systemic immune function in mice. Nat Nano. 4:451–456.
Mitrano DM, Motellier S, Clavaguera S, Nowack B. 2015. Review of nanomaterial aging and transformations through the life cycle of nano-enhanced products. Environ Int. 77:132–147.
Miura K, Furumoto T. 2013. Cold signaling and cold response in plants. Int J Mol Sci. 14:5312–5337.
Monteiller C, Tran L, MacNee W, Faux S, Jones A, Miller B, Donaldson K. 2007. The pro-inflammatory effects of low-toxicity low-solubility particles, nanoparticles and fine particles, on epithelial cells *in vitro*: the role of surface area. Occup Environ Med. 64:609–615.
Monteiro-Riviere NA, Wiench K, Landsiedel R, Schulte S, Inman AO, Riviere JE. 2011. Safety evaluation of sunscreen formulations containing titanium dioxide and zinc oxide nanoparticles in UVB sunburned skin: an *in vitro* and *in vivo* study. Toxicol Sci. 123:264–280.
Morimoto Y, Horie M, Kobayashi N, Shinohara N, Shimada M. 2013. Inhalation toxicity assessment of carbon-based nanoparticles. Acc Chem Res. 46:770–781.
Mueller NC, Nowack B. 2008. Exposure modeling of engineered nanoparticles in the environment. Environ Sci Technol. 42:4447–4453.
Muller EB, Lin S, Nisbet RM. 2015. Quantitative adverse outcome pathway analysis of hatching in zebrafish with CuO nanoparticles. Environ Sci Technol. 49:11817–11824.
Muller J, Huaux F, Moreau N, Misson P, Heilier JF, Delos M, Arras M, Fonseca A, Nagy JB, Lison D. 2005. Respiratory toxicity of multi-wall carbon nanotubes. Toxicol Appl Pharmacol. 207:221–231.
Murphy CJ, Vartanian AM, Geiger FM, Hamers RJ, Pedersen J, Cui Q, Haynes CL, Carlson EE, Hernandez R, Klaper RD, et al. 2015. Biological responses to engineered nanomaterials: needs for the next decade. ACS Cent Sci. 1:117–123.
Murray AR, Kisin E, Leonard SS, Young SH, Kommineni C, Kagan VE, Castranova V, Shvedova AA. 2009. Oxidative stress and inflammatory response in dermal toxicity of single-walled carbon nanotubes. Toxicology. 257:161–171.
Mwilu SK, El Badawy AM, Bradham K, Nelson C, Thomas D, Scheckel KG, Tolaymat T, Ma L, Rogers KR. 2013. Changes in silver nanoparticles exposed to human synthetic stomach fluid: effects of particle size and surface chemistry. Sci Total Environ. 447:90–98.
Nabi IR, Le PU. 2003. Caveolae/raft-dependent endocytosis. J Cell Biol. 161:673–677.
Navarro E, Baun A, Behra R, Hartmann NB, Filser J, Miao AJ, Quigg A, Santschi PH, Sigg L. 2008a. Environmental behavior and ecotoxicity of engineered nanoparticles to algae, plants, and fungi. Ecotoxicology. 17:372–386.
Navarro E, Piccapietra F, Wagner B, Marconi F, Kaegi R, Odzak N, Sigg L, Behra R. 2008b. Toxicity of silver nanoparticles to *Chlamydomonas reinhardtii*. Environ Sci Technol. 42:8959–8964.
Nel A, Xia T, Mädler L, Li N. 2006. Toxic potential of materials at the nanolevel. Science. 311:622–627.
Nel A, Xia T, Meng H, Wang X, Lin S, Ji Z, Zhang H. 2013. Nanomaterial toxicity testing in the 21st century: use of a predictive toxicological approach and high throughput screening. Acc Chem Res. 46:607–621.
Nel AE, Madler L, Velegol D, Xia T, Hoek EMV, Somasundaran P, Klaessig F, Castranova V, Thompson M. 2009. Understanding biophysicochemical interactions at the nano-bio interface. Nat Mater. 8:543–557.
Nowack B, Bucheli TD. 2007. Occurrence, behavior and effects of nanoparticles in the environment. Environ Pollut. 150:5–22.
Nowack B, David RM, Fissan H, Morris H, Shatkin JA, Stintzf M, Zeppg R, Brouwer D. 2013. Potential release scenarios for carbon nanotubes used in composites. Environ Int. 59:1–11.
NRC. 1983. Risk assessment in the federal government: managing the process. Washington (DC): The National Academies Press. 191 p.
NRC. 2007. Toxicity testing in the 21st century: a vision and a strategy. Washington, DC: The National Academies Press. 216 p.
NRC. 2012. A research strategy for environmental, health, and safety aspects of engineered nanomaterials. Washington (DC): The National Academies Press. 212 p.
NRC. 2013. Research progress on environmental, health, and safety aspects of engineered nanomaterials. Washington (DC): The National Academies Press. 162 p.
Oberdörster G, Oberdörster E, Oberdörster J. 2005. Nanotoxicology: an emerging discipline evolving from studies of ultrafine particles. Environ Health Perspect. 113:823–839.
Oberdorster G, Sharp Z, Atudorei V, Elder A, Gelein R, Kreyling W, Cox C. 2004. Translocation of inhaled ultrafine particles to the brain. Inhal Toxicol. 16:437–445.
Oberdorster G, Sharp Z, Atudorei V, Elder A, Gelein R, Lunts A, Kreyling W, Cox C. 2002. Extrapulmonary translocation of ultrafine carbon particles following whole-body inhalation exposure of rats. J Toxicol Environ Health Part A. 65:1531–1543.
OECD OfEC-oaD. 2000. Guidance document on aquatic toxicity testing of difficult substances and mixtures. ed. Paris: OfEC-oa Development.
OECD OfEC-oaD. 2004. Test No. 218: sediment water chironomid toxicity using spiked sediment. ed. Paris: OfEC-oa Development.
OECD OfEC-oaD. 2016. Adverse outcome pathways, molecular screening and toxicogenomics. Organisation for Economic Co-operation and Development.
Ogawara K-I, Yoshida M, Furumoto K, Takakura Y, Hashida M, Higaki K, Kimura T. 1999. Uptake by hepatocytes and biliary excretion of intravenously administered polystyrene microspheres in rats. J Drug Target. 7:213–221.
Oh N, Park J-H. 2014. Endocytosis and exocytosis of nanoparticles in mammalian cells. Int J Nanomedicine. 9:51–63.
Oksel C, Ma CY, Wang XZ. 2015. Current situation on the availability of nanostructure – biological activity data. SAR QSAR Environ Res. 26:79–94.
Oomen AG, Bos PMJ, Fernandes TF, Hund-Rinke K, Boraschi D, Byrne HJ, Aschberger K, Gottardo S, von der Kammer F, Kühnel D, et al. 2014. Concern-driven integrated approaches to nanomaterial testing and assessment – report of the NanoSafety Cluster Working Group 10. Nanotoxicology. 8:334–348.
Pacurari M, Castranova V, Vallyathan V. 2010. Single- and multi-wall carbon nanotubes versus asbestos: are the carbon nanotubes a new health risk to humans? J Toxicol Environ Health A. 73:378–395.

Pan J-F, Buffet P-E, Poirier L, Amiard-Triquet C, Gilliland D, Joubert Y, Pilet P, Guibbolini M, Risso de Faverney C, Roméo M, et al. 2012. Size dependent bioaccumulation and ecotoxicity of gold nanoparticles in an endobenthic invertebrate: the Tellinid clam *Scrobicularia plana*. Environ Poll. 168:37–43.

Park EJ, Bae E, Yi J, Kim Y, Choi K, Lee SH, Yoon J, Lee BC, Park K. 2010. Repeated-dose toxicity and inflammatory responses in mice by oral administration of silver nanoparticles. Environ Toxicol Pharmacol. 30:162–168.

Park S, Woodhall J, Ma G, Veinot JGC, Cresser MS, Boxall ABA. 2014. Regulatory ecotoxicity testing of engineered nanoparticles: are the results relevant to the natural environment? Nanotoxicology. 8:583–592.

Parks AN, Chandler GT, Ho KT, Burgess RM, Ferguson PL. 2015. Environmental biodegradability of [14C] single-walled carbon nanotubes by Trametes versicolor and natural microbial cultures found in New Bedford Harbor sediment and aerated wastewater treatment plant sludge. Environ Toxicol Chem. 34:247–251.

Parks AN, Chandler GT, Portis LM, Sullivan JC, Perron MM, Cantwell MG, Burgess RM, Ho KT, Ferguson PL. 2014. Effects of single-walled carbon nanotubes on the bioavailability of PCBs in field-contaminated sediments. Nanotoxicology. 8:111–117.

Part F, Zecha G, Causon T, Sinner E-K, Huber-Humer M. 2015. Current limitations and challenges in nanowaste detection, characterisation and monitoring. Waste Manag. 43:407–420.

PCAST. 2014. Report to the President and Congress on the Fifth Assessment of the National Nanotechnology Initiative. Washington (DC): PsCoAoSa Technology.

Pearson RM, Juettner V, Hong S. 2014. Biomolecular corona on nanoparticles: a survey of recent literature and its implications in targeted drug delivery. Front Chem. 2:108.

Petersen EJ, Diamond SA, Kennedy AJ, Goss GG, Ho K, Lead J, Hanna SK, Hartmann NB, Hund-Rinke K, Mader B, et al. 2015. Adapting OECD aquatic toxicity tests for use with manufactured nanomaterials: key issues and consensus recommendations. Environ Sci Technol. 49:9532–9547.

Petersen EJ, Nelson BC. 2010. Mechanisms and measurements of nanomaterial-induced oxidative damage to DNA. Anal Bioanal Chem. 398:613–650.

Petersen EJ, Zhang L, Mattison NT, O'Carroll DM, Whelton AJ, Uddin N, Nguyen T, Huang Q, Henry TB, Holbrook RD, Chen KL. 2011. Potential release pathways, environmental fate, and ecological risks of carbon nanotubes. Environ Sci Technol. 45:9837–9856.

Pflucker F, Wendel V, Hohenberg H, Gartner E, Will T, Pfeiffer S, Wepf R, Gers-Barlag H. 2001. The human stratum corneum layer: an effective barrier against dermal uptake of different forms of topically applied micronised titanium dioxide. Skin Pharmacol Appl Skin Physiol. 14(Suppl 1):92–97.

Pietroiusti A, Campagnolo L, Fadeel B. 2013. Interactions of engineered nanoparticles with organs protected by internal biological barriers. Small. 9:1557–1572.

Pietroiusti A, Magrini A. 2014. Engineered nanoparticles at the workplace: current knowledge about workers' risk. Occup Med. 64:319–330.

Pietroiusti A, Massimiani M, Fenoglio I, Colonna M, Valentini F, Palleschi G, Camaioni A, Magrini A, Siracusa G, Bergamaschi A, et al. 2011. Low doses of pristine and oxidized single-wall carbon nanotubes affect mammalian embryonic development. ACS Nano. 5:4624–4633.

Pilou M, Vaquero-Moralejo C, Jaen M, Lopez D, Ipina Pena J, Neofytou P, Housiadas C. 2016. Modeling of occupational exposure to accidentally released manufactured nanomaterials in a production facility and calculation of internal doses by inhalation. Int J Occup Environ Health. 22:249–258.

Platten WE III, Sylvest N, Warren C, Arambewela M, Harmon S, Bradham K, Rogers K, Thomas T, Luxton TP. 2016. Estimating dermal transfer of copper particles from the surfaces of pressure-treated lumber and implications for exposure. Sci Total Environ. 548–549:441–449.

Powers CM, Grieger K, Meacham CA, Gooding ML, Gift JS, Lehmann GM, Hendren CO, Davis JM, Burgoon L. 2016. Applying comprehensive environmental assessment to research planning for multiwalled carbon nanotubes: refinements to inform future stakeholder engagement. Integr Environ Assess Manag. 12:96–108.

Praetorius A, Scheringer M, Hungerbühler K. 2012. Development of environmental fate models for engineered nanoparticles—a case study of TiO2 nanoparticles in the Rhine river. Environ Sci Technol. 46:6705–6713.

Prasad RY, Simmons SO, Killius MG, Zucker RM, Kligerman AD, Blackman CF, Fry RC, Demarini DM. 2014. Cellular interactions and biological responses to titanium dioxide nanoparticles in HepG2 and BEAS-2B cells: role of cell culture media. Environ Mol Mutagen. 55:336–342.

Prasad RY, Wallace K, Daniel KM, Tennant AH, Zucker RM, Strickland J, Dreher K, Kligerman AD, Blackman CF, Demarini DM. 2013. Effect of treatment media on the agglomeration of titanium dioxide nanoparticles: impact on genotoxicity, cellular interaction, and cell cycle. ACS Nano. 7:1929–1942.

Priester JH, Ge Y, Mielke RE, Horst AM, Moritz SC, Espinosa K, Gelb J, Walker SL, Nisbet RM, An YJ, et al. 2012. Soybean susceptibility to manufactured nanomaterials with evidence for food quality and soil fertility interruption. Proc Natl Acad Sci U S A. 109:E2451–E2456.

Project on Emerging Nanotechnologies P. 2013. Consumer products inventory. Virginia: Wilson Center, Virginia Tech.

Pu Y, Tang F, Adam PM, Laratte B, Ionescu RE. 2016. Fate and characterization factors of nanoparticles in seventeen subcontinental freshwaters: a case study on copper nanoparticles. Environ. Sci. Technol. 50:9370–9379.

Quadros ME, Marr LC. 2011. Silver nanoparticles and total aerosols emitted by nanotechnology-related consumer spray products. Environ Sci Technol. 45:10713–10719.

Quadros ME, Pierson R, Tulve NS, Willis R, Rogers K, Thomas T, Marr L. 2013. Release of silver from nanotechnology-based consumer products for children. Environ Sci Technol. 47:8894–8901.

Quik JTK, de Klein JJM, Koelmans AA. 2015. Spatially explicit fate modelling of nanomaterials in natural waters. Water Res. 80:200–208.

Radhika RSR, Ganesh KV, Stanley AL, Inbakandan D. 2010. Studies on the toxicological effects of engineered nanoparticles in environment – a review. Int J Appl Bioeng. 4:44–53.

RCC-NI. 2014. Work Element 3: Risk Assessment/Risk Management, Regulatory Cooperation Council Nanotechnology Initiative

Rico CM, Johnson MG, Marcus MA, Andersen CP. 2017. Intergenerational responses of wheat (Triticum aestivum L.) to cerium oxide nanoparticles exposure. Environ Sci: Nano. 4:700–711.

Rico CM, Majumdar S, Duarte-Gardea M, Peralta-Videa JR, Gardea-Torresdey JL. 2011. Interaction of nanoparticles with edible plants and their possible implications in the food chain. J Agric Food Chem. 59:3485–3498.

Ritz S, Schöttler S, Kotman N, Baier G, Musyanovych A, Kuharev J, Landfester K, Schild H, Jahn O, Tenzer S, et al. 2015. Protein corona of nanoparticles: distinct proteins regulate the cellular uptake. Biomacromolecules. 16:1311–1321.

Riviere JE. 2009. Pharmacokinetics of nanomaterials: an overview of carbon nanotubes, fullerenes and quantum dots. WIREs Nanmed Nanobiotechnol. 1:26–34.

Roco MC. 1999. Nanoparticles and nanotechnology research. J Nanopart Res. 1:1–6.

Rodrigues DF, Jaisi DP, Elimelech M. 2013. Toxicity of functionalized single-walled carbon nanotubes on soil microbial communities: implications for nutrient cycling in soil. Environ Sci Technol. 47:625–633.

Rodriguez-Yañez Y, Muñoz B, Albores A. 2013. Mechanisms of toxicity by carbon nanotubes. Toxicol Mech Methods. 23:178–195.

Rogers KR, Bradham K, Tolaymat T, Thomas DJ, Hartmann T, Ma L, Williams A. 2012. Alterations in physical state of silver nanoparticles exposed to synthetic human stomach fluid. Sci Total Environ. 420:334–339.

Rosenbaum R, Bachmann T, Gold L, Huijbregts MJ, Jolliet O, Juraske R, Koehler A, Larsen HF, Macleod M, Margni M, et al. 2008. USEtox: the UNEP-SETAC toxicity model: recommended characterisation factors for human toxicity and freshwater ecotoxicity in life cycle impact assessment. Int J Life Cycle Assess. 13:532–546.

Royce SG, Mukherjee D, Cai T, Xu SS, Alexander JA, Mi Z, Calderon L, Mainelis G, Lee K, Lioy PJ, et al. 2014. Modeling population exposures

to silver nanoparticles present in consumer products. J Nanopart Res. 16:1–25.

Sadeghi L, Yousefi Babadi V, Espanani HR. 2015. Toxic effects of the Fe2O3 nanoparticles on the liver and lung tissue. Bratisl Lek Listy. 116:373–378.

Sakhtianchi R, Minchin RF, Lee K-B, Alkilany AM, Serpooshan V, Mahmoudi M. 2013. Exocytosis of nanoparticles from cells: role in cellular retention and toxicity. Adv Colloid Interface Sci. 201–202:18–29.

Saleh NB, Pfefferle LD, Elimelech M. 2008. Aggregation kinetics of multiwalled carbon nanotubes in aquatic systems: measurements and environmental implications. Environ Sci Technol. 42:7963–7969.

Salminen R, Batista MJ, Bidovec M, Demetriades A, De Vivo B, De Vos W, Duris M, Gilucis A, Gregorauskienė V, Halamic J, et al. 2005. Geochemical Atlas of Europe. Part 1: Background Information, Methodology and Maps. Espoo, Finland: Geological Survey of Finland.

Sanders K, Degn LL, Mundy WR, Zucker RM, Dreher K, Zhao B, Roberts JE, Boyes WK. 2012. *In vitro* phototoxicity and hazard identification of nano-scale titanium dioxide. Toxicol Appl Pharmacol. 258:226–236.

Santiago-Rodríguez L, Griggs JL, Bradham KD, Nelson C, Luxton T, Platten WE, Rogers KR. 2015. Assessment of the bioaccessibility of micronized copper wood in synthetic stomach fluid. Environ Nanotechnol Monit Manag. 4:85–92.

Saunders M. 2009. Transplacental transport of nanomaterials. Wiley Interdiscip Rev Nanomed Nanobiotechnol. 1:671–684.

Sayre LM, Perry G, Smith MA. 2008. Oxidative stress and neurotoxicity. Chem Res Toxicol. 21:172–188.

Schleh C, Semmler-Behnke M, Lipka J, Wenk A, Hirn S, Schäffler M, Schmid G, Simon U, Kreyling WG. 2012. Size and surface charge of gold nanoparticles determine absorption across intestinal barriers and accumulation in secondary target organs after oral administration. Nanotoxicology. 6:36–46.

Schulte PA, Geraci CL, Murashov V, Kuempel ED, Zumwalde RD, Castranova V, Hoover MD, Hodson L, Martinez KF. 2014. Occupational safety and health criteria for responsible development of nanotechnology. J Nanopart Res. 16:2.

Sekine R, Brunetti G, Donner E, Khaksar M, Vasilev K, Jämting ÅK, Scheckel KG, Kappen P, Zhang H, Lombi E. 2015. Speciation and lability of Ag-, AgCl-, and Ag2S-nanoparticles in soil determined by X-ray absorption spectroscopy and diffusive gradients in thin films. Environ Sci Technol. 49:897–905.

Sekine R, Khaksar M, Brunetti G, Donner E, Scheckel KG, Lombi E, Vasilev K. 2013. Surface immobilization of engineered nanomaterials for *in situ* study of their environmental transformations and fate. Environ Sci Technol. 47:9308–9316.

Settimio L, McLaughlin MJ, Kirby JK, Langdon KA. 2014. A method to determine silver partitioning and lability in soils. Environ Chem. 11:63–71.

Shandilya N, Le Bihan O, Bressot C, Morgeneyer M. 2015. Emission of titanium dioxide nanoparticles from building materials to the environment by wear and weather. Environ Sci Technol. 49:2163–2170.

Shannahan JH, Podila R, Aldossari AA, Emerson H, Powell BA, Ke PC, Rao AM, Brown JM. 2015. Formation of a protein corona on silver nanoparticles mediates cellular toxicity via scavenger receptors. Toxicol Sci. 143:136–146.

Shaw BJ, Handy RD. 2011. Physiological effects of nanoparticles on fish: a comparison of nanometals versus metal ions. Environ Int. 37:1083–1097.

Shen C, James SA, de Jonge MD, Turney TW, Wright PF, Feltis BN. 2013. Relating cytotoxicity, zinc ions, and reactive oxygen in ZnO nanoparticle-exposed human immune cells. Toxicol Sci. 120–130.

Shukla RK, Kumar A, Gurbani D, Pandey AK, Singh S, Dhawan A. 2013. TiO(2) nanoparticles induce oxidative DNA damage and apoptosis in human liver cells. Nanotoxicology. 7:48–60.

Shukla RK, Kumar A, Pandey AK, Singh SS, Dhawan A. 2011. Titanium dioxide nanoparticles induce oxidative stress-mediated apoptosis in human keratinocyte cells. J Biomed Nanotechnol. 7:100–101.

Simonin M, Richaume A. 2015. Impact of engineered nanoparticles on the activity, abundance, and diversity of soil microbial communities: a review. Environ Sci Pollut Res Int. 22:13710–13723.

Singh RP, Ramarao P. 2012. Cellular uptake, intracellular trafficking and cytotoxicity of silver nanoparticles. Toxicol Lett. 213:249–259.

Skalska J, Dabrowska-Bouta B, Struzynska L. 2016. Oxidative stress in rat brain but not in liver following oral administration of a low dose of nanoparticulate silver. Food Chem Toxicol. 97:307–315.

Snow SJ, McGee J, Miller DB, Bass V, Schladweiler MC, Thomas RF, Krantz T, King C, Ledbetter AD, Richards J, et al. 2014. Inhaled diesel emissions generated with cerium oxide nanoparticle fuel additive induce adverse pulmonary and systemic effects. Toxicol Sci. 142:403–417.

Soenen SJ, Parak WJ, Rejman J, Manshian B. 2015. (Intra)Cellular stability of inorganic nanoparticles: effects on cytotoxicity, particle functionality, and biomedical applications. Chem Rev. 115:2109–2135.

Som C, Nowack B, Krug HF, Wick P. 2012. Toward the development of decision supporting tools that can be used for safe production and use of nanomaterials. Acc Chem Res. 46:863–872.

Sotiriou GA, Singh D, Zhang F, Chalbot M-CG, Spielman-Sun E, Hoering L, Kavouras IG, Lowry GV, Wohlleben W, Demokritou P. 2016. Thermal decomposition of nano-enabled thermoplastics: possible environmental health and safety implications. J Hazard Mater. 305:87–95.

Stapleton PA, Nurkiewicz TR. 2014. Vascular distribution of nanomaterials. Wiley Interdiscip Rev Nanomed Nanobiotechnol. 6:338–348.

Stevenson FJ, Cole MA. 1999. Cycles of soils: carbon, nitrogen, phosphorus, sulfur, micronutrients. 2nd ed. New York: John Wiley and Sons, Inc.

Stone V, Pozzi-Mucelli S, Tran L, Aschberger K, Sabella S, Vogel U, Poland C, Balharry D, Fernandes T, Gottardo S, et al. 2014. ITS-NANO-prioritising nanosafety research to develop a stakeholder driven intelligent testing strategy. Part Fibre Toxicol. 11:9.

Sun TY, Conroy G, Donner E, Hungerbuhler K, Lombi E, Nowack B. 2015. Probabilistic modelling of engineered nanomaterial emissions to the environment: a spatio-temporal approach. Environ Sci: Nano. 2:340–351.

Sun TY, Gottschalk F, Hungerbühler K, Nowack B. 2014. Comprehensive probabilistic modelling of environmental emissions of engineered nanomaterials. Environ Pollut. 185:69–76.

Suzui M, Futakuchi M, Fukamachi K, Numano T, Abdelgied M, Takahashi S, Ohnishi M, Omori T, Tsuruoka S, Hirose A, et al. 2016. Multiwalled carbon nanotubes intratracheally instilled into the rat lung induce development of pleural malignant mesothelioma and lung tumors. Cancer Sci. 107:924–935.

Takahashi S, Matsuoka O. 1981. Cross placental transfer of ^{198}Au-colloid in near term rats. J Radiat Res. 22:242–249.

Tamai I, Tsuji A. 2000. Transporter-mediated permeation of drugs across the blood-brain barrier. J Pharm Sci. 89:1371–1388.

Tantra R, Oksel C, Puzyn T, Wang J, Robinson KN, Wang XZ, Ma CY, Wilkins T. 2014. Nano(Q)SAR: challenges, pitfalls and perspectives. Nanotoxicology. 9:636–642.

Teeguarden JG, Hinderliter PM, Orr G, Thrall BD, Pounds JG. 2007. Particokinetics *in vitro*: dosimetry considerations for *in vitro* nanoparticle toxicity assessments. Toxicol Sci. 95:300–312.

Thai S-F, Wallace KA, Jones CP, Ren H, Castellon BT, Crooks J, Grulke EA, Kitchin KT. 2015. Differential genomic effects on signaling pathways by two different CeO2 nanoparticles in HepG2 cells. J Nanosci Nanotechnol. 15:9925–9937.

Thalmann B, Voegelin A, Sinnet B, Morgenroth E, Kaegi R. 2014. Sulfidation kinetics of silver nanoparticles reacted with metal sulfides. Environ Sci Technol. 48:4885–4892.

Thomas RS, Philbert MA, Auerbach SS, Wetmore BA, Devito MJ, Cote I, Rowlands JC, Whelan MP, Hays SM, Andersen ME, et al. 2013. Incorporating new technologies into toxicity testing and risk assessment: moving from 21st century vision to a data-driven framework. Toxicol Sci. 136:4–18.

Thomas T, Bahadori T, Savage N, Thomas K. 2009. Moving toward exposure and risk evaluation of nanomaterials: challenges and future directions. Nanomed Nanobiotechnol. 1:426–433.

Thompson D, Chen S-C, Wang J, Pui DY. 2015. Aerosol emission monitoring and assessment of potential exposure to multi-walled carbon nanotubes in the manufacture of polymer nanocomposites. Ann Occup Hyg. 49:1135–1151.

Tkachenko AG, Xie H, Coleman D, Glomm W, Ryan J, Anderson MF, Franzen S, Feldheim DL. 2003. Multifunctional gold nanoparticle–peptide complexes for nuclear targeting. J Am Chem Soc. 125:4700–4701.

Tolaymat T, El Badawy A, Sequeira R, Genaidy A. 2015. A system-of-systems approach as a broad and integrated paradigm for sustainable engineered nanomaterials. Sci Total Environ. 511:595–607.

Tourinho PS, van Gestel CAM, Lofts S, Svendsen C, Soares AMVM, Loureiro S. 2012. Metal-based nanoparticles in soil: fate, behavior, and effects on soil invertebrates. Environ Toxicol Chem. 31:1679–1692.

Treuel L, Brandholt S, Maffre P, Wiegele S, Shang L, Nienhaus GU. 2014. Impact of protein modification on the protein corona on nanoparticles and nanoparticle–cell interactions. ACS Nano. 8:503–513.

Treuel L, Jiang X, Nienhaus GU. 2013. New views on cellular uptake and trafficking of manufactured nanoparticles. J R Soc Interface. 10:20120939.

Trevisan R, Delapedra G, Mello DF, Arl M, Schmidt ÉC, Meder F, Monopoli M, Cargnin-Ferreira E, Bouzon ZL, Fisher AS, et al. 2014. Gills are an initial target of zinc oxide nanoparticles in oysters Crassostrea gigas, leading to mitochondrial disruption and oxidative stress. Aquat Toxicol. 153:27–38.

Tulve NS, Stefaniak AB, Vance ME, Rogers K, Mwilu S, LeBouf RF, Schwegler-Berry D, Willis R, Thomas TA, Marr LC, et al. 2015. Characterization of silver nanoparticles in selected consumer products and its relevance for predicting children's potential exposures. Int J Hyg Environ Health. 218:345–357.

Tumburu L, Andersen CP, Rygiewicz PT, Reichman JR. 2015. Phenotypic and genomic responses to titanium dioxide and cerium oxide nanoparticles in Arabidopsis germinants. Environ Toxicol Chem. 34:70–83.

Tumburu L, Andersen CP, Rygiewicz PT, Reichman JR. 2017. Molecular and physiological responses to titanium dioxide and cerium oxide nanoparticles in Arabidopsis. Environ Toxicol Chem. 36:71–82.

U.S. 1999. PART 503: standards for the use or disposal of sewage sludge. In: Code of Federal Regulations: Title 40. UEP Agency, US Government Publishing Office.

Unfried K, Sydlik U, Bierhals K, Weissenberg A, Abel J. 2008. Carbon nanoparticle-induced lung epithelial cell proliferation is mediated by receptor-dependent Akt activation. Am J Physiol./Lung Cell Mol Physiol. 294:L358–LL67.

Uskokovic V. 2013. Entering the era of nanoscience: time to be so small. J Biomed Nanotechnol. 9:1441–1470.

Vance ME, Kuiken T, Vejerano EP, McGinnis SP, Hochella MF, Rejeski D, Hull MS. 2015. Nanotechnology in the real world: redeveloping the nanomaterial consumer products inventory. Beilstein J Nanotechnol. 6:1769–1780.

Velzeboer I, Quik JTK, van de Meent D, Koelmans AA. 2014. Rapid settling of nanoparticles due to heteroaggregation with suspended sediment. Environ Toxicol Chem. 33:1766–1773.

Verma A, Stellacci F. 2010. Effect of surface properties on nanoparticle–-cell interactions. Small. 6:12–21.

Vietti G, Lison D, van den Brule S. 2016. Mechanisms of lung fibrosis induced by carbon nanotubes: towards an Adverse Outcome Pathway (AOP). Part Fibre Toxicol. 13:11.

Walczak AP, Fokkink R, Peters R, Tromp P, Herrera Rivera ZE, Rietjens IM, Hendriksen PJ, Bouwmeester H. 2013. Behaviour of silver nanoparticles and silver ions in an *in vitro* human gastrointestinal digestion model. Nanotoxicology. 7:1198–1210.

Walczak AP, Kramer E, Hendriksen PJ, Helsdingen R, van der Zande M, Rietjens IM, Bouwmeester H. 2015. *In vitro* gastrointestinal digestion increases the translocation of polystyrene nanoparticles in an *in vitro* intestinal co-culture model. Nanotoxicology. 9:886–894.

Walkey CD, Olsen JB, Guo H, Emili A, Chan WCW. 2012. Nanoparticle size and surface chemistry determine serum protein adsorption and macrophage uptake. J Am Chem Soc. 134:2139–2147.

Walters CR, Pool EJ, Somerset VS. 2014. Ecotoxicity of silver nanomaterials in the aquatic environment: a review of literature and gaps in nanotoxicological research. J Environ Sci Health A Tox Hazard Subst Environ Eng. 49:1588–1601.

Wang H, Burgess RM, Cantwell MG, Portis LM, Perron MM, Wu F, Ho KT. 2014a. Stability and aggregation of silver and titanium dioxide nanoparticles in seawater: role of salinity and dissolved organic carbon. Environ Toxicol Chem. 33:1023–1029.

Wang H, Ho KT, Scheckel KG, Wu F, Cantwell MG, Katz DR, Horowitz DB, Boothman WS, Burgess RM. 2014b. Toxicity, bioaccumulation, and biotransformation of silver nanoparticles in marine organisms. Environ Sci Technol. 48:13711–13717.

Wang J, Zhou G, Chen C, Yu H, Wang T, Ma Y, Jia G, Gao Y, Li B, Sun J, et al. 2007. Acute toxicity and biodistribution of different sized titanium dioxide particles in mice after oral administration. Toxicol Lett. 168:176–185.

Wang Y, Wu Q, Sui K, Chen X-X, Fang J, Hu X, Wu M, Liu Y. 2013. A quantitative study of exocytosis of titanium dioxide nanoparticles from neural stem cells. Nanoscale. 5:4737–4743.

Wehmas LC, Anders C, Chess J, Punnoose A, Pereira CB, Greenwood JA, Tanguay RL. 2015. Comparative metal oxide nanoparticle toxicity using embryonic zebrafish. Toxicol Rep. 2:702–715.

Werlin R, Priester JH, Mielke RE, Kramer S, Jackson S, Stoimenov PK, Stucky GD, Cherr GN, Orias E, Holden PA, et al. 2011. Biomagnification of cadmium selenide quantum dots in a simple experimental microbial food chain. Nat Nanotechnol. 6:65–71.

West GH, Lippy BE, Cooper MR, Marsick D, Burrelli LG, Griffin KN, Segrave AM. 2016. Toward responsible development and effective risk management of nano-enabled products in the U.S. construction industry. J Nanopart Res. 18:49.

WHO-IARC. 2010. Titanium dioxide. In: IARC monographs on the evaluation of carcinogenic risks to humans. Lyon (France): International Agency for Research on Cancer; p. 193–276.

Wiecinski PN, Metz KM, Mangham AN, Jacobson KH, Hamers RJ, Pedersen JA. 2009. Gastrointestinal biodurability of engineered nanoparticles: development of an in vitro assay. Nanotoxicology. 3:202–214.

Wiesner MR, Lowry GV, Casman E, Bertsch PM, Matson CW, Di Giulio RT, Liu J, Hochella MF. 2011. Meditations on the ubiquity and mutability of nano-sized materials in the environment. ACS Nano. 5:8466–8470.

Woodruff RS, Li Y, Yan J, Bishop M, Jones MY, Watanabe F, Biris AS, Rice P, Zhou T, Chen T, et al. 2012. Genotoxicity evaluation of titanium dioxide nanoparticles using the Ames test and Comet assay. J Appl Toxicol. 32:934–943.

Xie H, Mason MM, Wise JP, Sr. 2011. Genotoxicity of metal nanoparticles. Rev Environ Health. 26:251–268.

Xin L, Wang J, Wu Y, Guo S, Tong J. 2015. Increased oxidative stress and activated heat shock proteins in human cell lines by silver nanoparticles. Hum Exp Toxicol. 34:315–323.

Xu J, Alexander DB, Futakuchi M, Numano T, Fukamachi K, Suzui M, Omori T, Kanno J, Hirose A, Tsuda H. 2014. Size-and shape-dependent pleural translocation, deposition, fibrogenesis, and mesothelial proliferation by multiwalled carbon nanotubes. Cancer Sci. 105:763–769.

Yamashita K, Yoshioka Y, Higashisaka K, Mimura K, Morishita Y, Nozaki M, Yoshida T, Ogura T, Nabeshi H, Nagano K, et al. 2011. Silica and titanium dioxide nanoparticles cause pregnancy complications in mice. Nat Nanotechnol. 6:321–328.

Yang F, Hong F, You W, Liu C, Gao F, Wu C, Yang P. 2006. Influences of nano-anatase TiO2 on the nitrogen metabolism of growing spinach. Biol Trace Elem Res. 110:179–190.

Yang F, Liu C, Gao F, Su M, Wu X, Zheng L, Hong F, Yang P. 2007. The improvement of spinach growth by nano-anatase TiO2 treatment is related to nitrogen photoreduction. Biol Trace Elem Res. 119:77–88.

Yang Y, Westerhoff P. 2014. Presence in, and release of, nanomaterials from consumer products in nanomaterial. In: Capco DG, Chen Y, editors. Netherlands: Springer; p. 1–17.

Yang Z, Zhang Y, Yang Y, Sun L, Han D, Li H, Wang C. 2010. Pharmacological and toxicological target organelles and safe use of single-walled carbon nanotubes as drug carriers in treating Alzheimer disease. Nanomedicine. 6:427–441.

Yokel RA, Au TC, MacPhail R, Hardas SS, Butterfield DA, Sultana R, Goodman M, Tseng MT, Dan M, Haghnazar H, et al. 2012. Distribution, elimination, and biopersistence to 90 days of a systemically introduced 30 nm ceria-engineered nanomaterial in rats. Toxicol Sci. 127:256–268.

Zartarian V, Bahadori T, McKone T. 2004. Adoption of an official ISEA glossary. J Expo Anal Environ Epidemiol. 15:1–5.

Zeni O, Sannino A, Romeo S, Micciulla F, Bellucci S, Scarfi MR. 2015. Growth inhibition, cell-cycle alteration and apoptosis in stimulated human peripheral blood lymphocytes by multiwalled carbon nanotube buckypaper. Nanomedicine (Lond). 10:351–360.

Zhang Y, Yan B. 2012. Cell cycle regulation by carboxylated multiwalled carbon nanotubes through p53-independent induction of p21 under the control of the BMP signaling pathway. Chem Resn Toxicol. 25:1212–1221.

Zhao F, Zhao Y, Liu Y, Chang X, Chen C, Zhao Y. 2011. Cellular uptake, intracellular trafficking, and cytotoxicity of nanomaterials. Small. 7:1322–1337.

Zheng L, Hong F, Lu S, Liu C. 2005. Effect of nano-TiO2 on strength of naturally aged seeds and growth of spinach. Biol Trace Elem Res. 104:83–91.

Zhu M, Nie G, Meng H, Xia T, Nel A, Zhao Y. 2012. Physicochemical properties determine nanomaterial cellular uptake, transport, and fate. Acc Chem Res. 46:622–631.

Zhu M, Wang H, Keller AA, Wang T, Li F. 2014. The effect of humic acid on the aggregation of titanium dioxide nanoparticles under different pH and ionic strengths. Sci Total Environ. 487:375–380.

Zhu Z-J, Carboni R, Quercio MJ, Yan B, Miranda OR, et al. 2010. Surface properties dictate uptake, distribution, excretion, and toxicity of nanoparticles in fish. Small. 6:2261–2265.

Zucker RM, Daniel KM, Massaro EJ, Karafas SJ, Degn LL, Boyes WK. 2013. Detection of silver nanoparticles in cells by flow cytometry using light scatter and far-red fluorescence. Cytometry A. 83:962–972.

Zucker RM, Massaro EJ, Sanders KM, Degn LL, Boyes WK. 2010. Detection of TiO2 nanoparticles in cells by flow cytometry. Cytometry A. 77:677–685.

2020 STAA Nomination

Category: Review Articles (RA)

Record of Percentage Agreement

Each author contributed equally to the manuscript. Proportional effort was determined by dividing 100% by the number of authors (18).

Author	Eligible	Total proportion effort (%)
Boyes, W. K	yes	5.5
Thornton, B. L	no	5.5
Al-Abed, S. R	yes	5.5
Andersen, C. P	yes	5.5
Bouchard, D. C.	yes	5.5
Burgess, R. M.	yes	5.5
Cohen Hubal, E. A.	yes	5.5
Ho, K. T.	yes	5.5
Hughes, M. F.	yes	5.5
Kitchin, K. T.	yes	5.5
Reichman, J. R	yes	5.5
Rogers, K. R.	yes	5.5
Ross, J. A.,	yes	5.5
Rygiewicz, P. T.	yes	5.5
Scheckel, K. G.	yes	5.5
Thai, S.-F.	yes	5.5
Zepp, R. G.	yes	5.5
Zucker, R. M	yes	5.5

Nominated Publication:

Boyes, W. K., Thornton, B. L., Al-Abed, S. R., Andersen, C. P., Bouchard, D. C., Burgess, R. M., Cohen Hubal, E. A., Ho, K. T., Hughes, M. F., Kitchin, K. T., Reichman, J. R., Rogers, K. R., Ross, J. A., Rygiewicz, P. T., Scheckel, K. G., Thai, S.-F., Zepp, R. G., Zucker, R. M. Comprehensive framework for evaluating the environmental health and safety implications of engineered nanomaterials. Critical Reviews in Toxicology, Crit Rev Toxicol. 2017 Oct;47(9):767-810. doi: 10.1080/10408444.2017.1328400

Bibliometric Journal Statistics

Journal	Journal Impact Factor	Immediacy Index	Cited Half-Life
Critical Reviews in Toxicology	4.771	1.33	8.6

**Data collected on 24 April 2020 from publisher's website.*

Supplemental Items

none

Justification

1. Citations for each publication nominated

Boyes, W. K., Thornton, B. L., Al-Abed, S. R., Andersen, C. P., Bouchard, D. C., Burgess, R. M., Cohen Hubal, E. A., Ho, K. T., Hughes, M. F., Kitchin, K. T., Reichman, J. R., Rogers, K. R., Ross, J. A., Rygiewicz, P. T., Scheckel, K. G., Thai, S.-F., Zepp, R. G., Zucker, R. M. Comprehensive framework for evaluating the environmental health and safety implications of engineered nanomaterials. Critical Reviews in Toxicology, Crit Rev Toxicol. 2017 Oct;47(9):767-810. doi: 10.1080/10408444.2017.1328400

Engineered nanomaterials (ENM) are a growing aspect of the global economy, and their safe and sustainable development, use, and eventual disposal requires the capability to forecast and avoid potential problems. This review provides a framework to evaluate the health and safety implications of ENM releases into the environment, including purposeful releases such as for antimicrobial sprays or nano-enabled pesticides, and inadvertent releases as a consequence of other intended applications. Considerations encompass product life cycles, environmental media, exposed populations, and possible adverse outcomes. This framework is presented as a series of compartmental flow diagrams that serve as a basis to help derive future quantitative predictive models, guide research, and support development of tools for making risk-based decisions. After use, ENM are not expected to remain in their original form due to reactivity and/or propensity for hetero-agglomeration in environmental media. Therefore, emphasis is placed on characterizing ENM as they occur in environmental or biological matrices. In addition, predicting the activity of ENM in the environment is difficult due to the multiple dynamic interactions between the physical/chemical aspects of ENM and similarly complex environmental conditions. Others have proposed the use of simple predictive functional assays as an intermediate step to address the challenge of using physical/chemical properties to predict environmental fate and behavior of ENM. The nodes and interactions of the framework presented here reflect phase transitions that could be targets for development of such assays to estimate kinetic reaction rates and simplify model predictions. Application, refinement, and demonstration of this framework, along with an associated knowledgebase that includes targeted functional assay data, will allow better de novo predictions of potential exposures and adverse outcomes.

2. If research has been invited for presentation at national/international societies. The following invited presentations resulted from this research:
    - Boyes WK. A Decision Support Framework for Environmental Health and Safety Evaluation of Engineered Nanomaterials. Invited presentation to the American Public Health Association Meeting, Denver, Oct 29- Nov 2, 2016.
    - Boyes, WK. Evaluating the Environmental Health and Safety Implications of Engineered Nanomaterials. Conference Keynote Speaker. Nanosafety 2017. Saarbrucken, Germany. Oct. 10-13, 2017.
    - Boyes, WK . A Framework for Evaluation of Engineered Nanomaterials. Invited presentation to the Genetics and Environmental Mutagenesis Society, Research Triangle Park, NC. May 2. 2018
    - Boyes, WK. A Comprehensive Framework for Evaluation of Engineered Nanomaterials. Invited webinar briefing for EPA Regional Science Liaisons. April 24. 2018
    - Boyes, WK . Overview of EPA Office of Research and Development (ORD) Research Activities Related to Nanomaterials. Webinar presented to the Nanomaterial Environmental Health Implications (NEHI) subcommittee of the National Nanotechnology Initiative (NNI). May 24. 2018
    - Boyes, WK . Evaluating the Environmental Health and Safety Impact of Engineered Nanomaterials. North East Nanomaterials Meeting (NENM2018), Lake Placid NY June 1-3. 2018. http://nny.sites.acs.org/2018nenanomeeting.htm
    - Boyes, WK. Round Table Panel member. Connecting the Pieces: Linking Manufacture and Use of Nanomaterials or Nanotechnology-Enabled Products with Exposure, Outcome, and Risk. QEEN II: 2nd Quantifying Exposure to Engineered Nanomaterials from Manufactured Products Workshop, Washington DC, Oct. 9-10. 2018.
    - Boyes, WK. Chair, Plenary Session. Exposure-Driven Risk Assessment for Nanosafety Research. QEEN II: 2nd Quantifying Exposure to Engineered Nanomaterials from Manufactured Products Workshop, Washington DC, Oct. 9-10. 2018.
    - Sheckel K. Application of X-ray Absorption Spectroscopy for Monitoring Transformation of Nanomaterials. 2nd Quantifying Exposure to Engineered Nanomaterials (QEEN) from Manufactured Products Workshop, Washington, DC, 2018.
    - K. Scheckel, E. Donner, R. Sekine, G. Brunetti, and E. Lombi. Environmental Transformations of Silver and Zinc Oxide Nanoparticles Drive Risk Assessment Understanding. 55th Annual Meeting of the Clay Minerals Society, Urbanna, IL, 2018.
    - Boyes, WK. Nanosafety Research: The US EPA Perspective. Invited presentation to a workshop entitled “Fostering EU-US cooperation in Nanosafety Research” sponsored by the European Union. Harvard University, Boston Mass. March 5-6. 2019
    - Boyes, WK. Invited Moderator, Respiratory Effects of Engineered Nanomaterials in Relation to Physiochemical Properties. NanoEHS Webinar Series, U.S. National Nanotechnology Initiative. September 10, 2019.
    - Boyes, WK. Update on Nanomaterial Research at EPA. Invited seminar. Annual meeting of the Center for Environmental Implications of Nanotechnology (CEINT), Duke Univ., September 13, 2019.

3. Unique source of funding for research

    All funding came from the intramural research budget of the EPA Office of Research and Development

4. Any awards Internal/External to EPA that were received for the research

None to date

5. Number of times the publication has been downloaded/viewed
6. How many times it has been cited (Google Scholar)

Publication	Number of downloads/views	Number of citations (Google Scholar)
Boyes et al., 2017	716	29

7. Letters of Recommendation

Link for multiple publications

na

STAA Nominated publications previous six years

Boyes, (2015) STAA level III. Evaluation of the developmental toxicity of inhaled ethanol as a component of renewable automotive fuels. Boyes, W.K., Degn L., Martin S.A., Lyke D. F., and Herr D.W. Neurophysiological assessment of auditory, peripheral nerve, somatosensory, and visual system functions after developmental exposure to ethanol vapors. Neurotoxicology and Teratology 43(0): 1-10, 2014. (Unrelated to current nomination).

Hughes (2015) STAA Level III. Biogeographical Analysis of Chemical Co-Occurrence Data to Identify Priorities for Mixtures Research Risk Analysis/Peer Reviewed, 32(2):224-236 (2) Environmentally Relevant Mixtures in Cumulative Assessments: an Acute Study of Toxicokinetics and Effects on Motor Activity in Rats Exposed to a Mixture of Pyrethroids Toxicological Sciences/Peer Reviewed, 130(2):309-318 (3) A Pharmacokinetic Model of Cis-and Trans-Permethrin Disposition in Rats and Humans with Aggregate Exposure Application Toxicological Sciences/Peer Reviewed, 130(1):33-47. (Unrelated to current nomination).

Hughes (2016} STAA Level II. Bradham, K.D., Scheckel. K.G., Nelson, C.M., Seales, P.E., Lee, G.E., Hughes, M.F., Miller, B.W., Yeow, A., Gilmore, T., Harper, S., Thomas, D.J. (2011) Relative Bioavailability and Bioaccessibility and Speciation of Arsenic in Contaminated Soils. Environ. Health Perspect. 119(11): 1629–1634. (Unrelated to current nomination).

Citation: For creating a comprehensive framework to consider the environmental effects of engineered nanomaterials.

From: Paul Rygiewicz
To: Andersen, Christian
Cc: Boyes, William
Subject: Re: STAA award Nomination
Date: Monday, April 27, 2020 5:34:07 PM

Contribution sounds good to me.

I am doing well. The sheltering in place has been good in that so many of my never-finished projects are getting done !

Sent from my iPad

> On Apr 27, 2020, at 8:49 AM, Andersen, Christian <Andersen.Christian@epa.gov> wrote:
>
> Hi Paul- Will Boyes is going to submit our "Comprehensive framework…" review article for a possible STAA award. As part of the submission process, he has to list the proportional contribution of each author to the manuscript, and then receive an email indicating that authors agree with the percentage he has listed for them. Will decided to split the contribution evenly, so all authors will be listed as contributing 5.5% to the effort.
>
> If you could reply to this email to both Will and I that you agree with the percentage, that would be great. Hope you are doing well! Chris
>
> **********
>
> "Facts do not cease to exist because they are ignored." - Aldous Huxley
>
> **********
>
> Christian P. Andersen, PhD
> Plant Physiologist
> US Environmental Protection Agency
> Pacific Ecological Systems Division
> Center for Public Health and Environmental Assessment
> 200 SW 35th St.
> Corvallis, OR 97333
> 541-754-4791

From: Andersen, Christian
To: Boyes, William; Reichman, Jay
Subject: RE: STAA nomination for review article
Date: Friday, April 24, 2020 6:08:16 PM

Hi Will- this looks great, thanks for putting it together. Seems like you and Lila did most of the heavy lifting on that paper, I don't think anyone would be upset at a higher percentage for you. Also, Paul Rygiewicz is retired- I can try to get ahold of him, but he is a bit off the grid (he doesn't typically respond quickly). Do you need an email from him even tho he won't be getting any of the award? I will try to contact him if you want. Chris

---

From: Boyes, William <Boyes.William@epa.gov>
Sent: Friday, April 24, 2020 2:41 PM
To: Lila Thornton <lila.thornton@duke.edu>; Al-Abed, Souhail <al-abed.souhail@epa.gov>; Andersen, Christian <Andersen.Christian@epa.gov>; Burgess, Robert <Burgess.Robert@epa.gov>; Hubal, Elaine <Hubal.Elaine@epa.gov>; Ho, Kay <Ho.Kay@epa.gov>; Hughes, MichaelF <Hughes.MichaelF@epa.gov>; Reichman, Jay <Reichman.Jay@epa.gov>; Rogers, Kim <Rogers.Kim@epa.gov>; Scheckel, Kirk <Scheckel.Kirk@epa.gov>; Thai, Sheau-Fung <Thai.Sheau-Fung@epa.gov>; Zepp, Richard <Zepp.Richard@epa.gov>; Zucker, Robert <Zucker.Robert@epa.gov>
Subject: STAA nomination for review article

Hi All,

I thought it would be a good idea to submit our 2017 review article for an STAA award. I have enclosed a draft of the award nomination and the original paper. Only EPA authors are eligible for a cash award (sorry Lila).

1. Please send me any revisions to the nomination form./
2. Please send me an Email that you agree with the proportional division of effort (equal for all authors).

I hope you ae all well and staying safe during these strange times.

If anyone is in contact with the retired EPA authors please either forward this message to them or send me a current E-mail address – Thanks!

Will

William K. Boyes, Ph.D.
Neurological and Endocrine Toxicology Branch
Public Health and Integrated Toxicology Division
Center for Public Health and Environmental Assessment
Office of Research and Development

Mail Code B105-04
Environmental Protection Agency
109 T.W. Alexander Drive
Research Triangle Park, NC 27711

Phone: 919-541-7538
Mobile (alternate worksite contact): 919-417-2105
boyes.william@epa.gov

From: Burgess, Robert
To: Boyes, William
Cc: Burgess, Robert
Subject: RE: STAA nomination for review article
Date: Monday, April 27, 2020 6:30:07 PM

Will,

The nomination looks great and I agree with the proportional division of effort.

Best of luck and thank you for preparing the nomination.

Stay well,

Rob

From: Boyes, William <Boyes.William@epa.gov>
Sent: Friday, April 24, 2020 5:41 PM
To: Lila Thornton <lila.thornton@duke.edu>; Al-Abed, Souhail <al-abed.souhail@epa.gov>; Andersen, Christian <Andersen.Christian@epa.gov>; Burgess, Robert <Burgess.Robert@epa.gov>; Hubal, Elaine <Hubal.Elaine@epa.gov>; Ho, Kay <Ho.Kay@epa.gov>; Hughes, MichaelF <Hughes.MichaelF@epa.gov>; Reichman, Jay <Reichman.Jay@epa.gov>; Rogers, Kim <Rogers.Kim@epa.gov>; Scheckel, Kirk <Scheckel.Kirk@epa.gov>; Thai, Sheau-Fung <Thai.Sheau-Fung@epa.gov>; Zepp, Richard <Zepp.Richard@epa.gov>; Zucker, Robert <Zucker.Robert@epa.gov>
Subject: STAA nomination for review article

Hi All,

I thought it would be a good idea to submit our 2017 review article for an STAA award. I have enclosed a draft of the award nomination and the original paper. Only EPA authors are eligible for a cash award (sorry Lila).

1. Please send me any revisions to the nomination form./
2. Please send me an Email that you agree with the proportional division of effort (equal for all authors).

I hope you ae all well and staying safe during these strange times.

If anyone is in contact with the retired EPA authors please either forward this message to them or send me a current E-mail address – Thanks!

Will

William K. Boyes, Ph.D.
Neurological and Endocrine Toxicology Branch
Public Health and Integrated Toxicology Division

Center for Public Health and Environmental Assessment
Office of Research and Development
Mail Code B105-04
Environmental Protection Agency
109 T.W. Alexander Drive
Research Triangle Park, NC 27711

Phone: 919-541-7538
Mobile (alternate worksite contact): 919-417-2105
boyes.william@epa.gov

From: Hughes, MichaelF
To: Boyes, William
Subject: RE: STAA nomination for review article
Date: Friday, April 24, 2020 6:02:26 PM

Hi Will,

I agree with my level of effort on this paper. Thank you for putting this application together. Hope you and your family are healthy.

Best regards,
Mike

Michael F. Hughes, PhD, DABT
U.S. Environmental Protection Agency
ORD/CCTE/CCED/ETTB
MD B105-03
Research Triangle Park, NC 27711
(T): 919-541-2160; (F): 919-541-4284

From: Boyes, William <Boyes.William@epa.gov>
Sent: Friday, April 24, 2020 5:41 PM
To: Lila Thornton <lila.thornton@duke.edu>; Al-Abed, Souhail <al-abed.souhail@epa.gov>; Andersen, Christian <Andersen.Christian@epa.gov>; Burgess, Robert <Burgess.Robert@epa.gov>; Hubal, Elaine <Hubal.Elaine@epa.gov>; Ho, Kay <Ho.Kay@epa.gov>; Hughes, MichaelF <Hughes.MichaelF@epa.gov>; Reichman, Jay <Reichman.Jay@epa.gov>; Rogers, Kim <Rogers.Kim@epa.gov>; Scheckel, Kirk <Scheckel.Kirk@epa.gov>; Thai, Sheau-Fung <Thai.Sheau-Fung@epa.gov>; Zepp, Richard <Zepp.Richard@epa.gov>; Zucker, Robert <Zucker.Robert@epa.gov>
Subject: STAA nomination for review article

Hi All,

I thought it would be a good idea to submit our 2017 review article for an STAA award. I have enclosed a draft of the award nomination and the original paper. Only EPA authors are eligible for a cash award (sorry Lila).

1. Please send me any revisions to the nomination form./
2. Please send me an Email that you agree with the proportional division of effort (equal for all authors).

I hope you ae all well and staying safe during these strange times.

If anyone is in contact with the retired EPA authors please either forward this message to them or send me a current E-mail address – Thanks!

Will

William K. Boyes, Ph.D.
Neurological and Endocrine Toxicology Branch
Public Health and Integrated Toxicology Division
Center for Public Health and Environmental Assessment
Office of Research and Development
Mail Code B105-04
Environmental Protection Agency
109 T.W. Alexander Drive
Research Triangle Park, NC 27711

Phone: 919-541-7538
Mobile (alternate worksite contact): 919-417-2105
boyes.william@epa.gov

From: Rogers, Kim
To: Boyes, William
Subject: RE: STAA nomination for review article
Date: Monday, April 27, 2020 2:04:04 PM

I agree with the allocation of effort.

Kim Rogers, Ph.D.
MMB/WECD/CEMM
U.S. EPA, RTP, NC
Cell: 702-374-3284
e-mail: rogers.kim@epa.gov

From: Boyes, William <Boyes.William@epa.gov>
Sent: Friday, April 24, 2020 5:41 PM
To: Lila Thornton <lila.thornton@duke.edu>; Al-Abed, Souhail <al-abed.souhail@epa.gov>; Andersen, Christian <Andersen.Christian@epa.gov>; Burgess, Robert <Burgess.Robert@epa.gov>; Hubal, Elaine <Hubal.Elaine@epa.gov>; Ho, Kay <Ho.Kay@epa.gov>; Hughes, MichaelF <Hughes.MichaelF@epa.gov>; Reichman, Jay <Reichman.Jay@epa.gov>; Rogers, Kim <Rogers.Kim@epa.gov>; Scheckel, Kirk <Scheckel.Kirk@epa.gov>; Thai, Sheau-Fung <Thai.Sheau-Fung@epa.gov>; Zepp, Richard <Zepp.Richard@epa.gov>; Zucker, Robert <Zucker.Robert@epa.gov>
Subject: STAA nomination for review article

Hi All,

I thought it would be a good idea to submit our 2017 review article for an STAA award. I have enclosed a draft of the award nomination and the original paper. Only EPA authors are eligible for a cash award (sorry Lila).

1. Please send me any revisions to the nomination form./
2. Please send me an Email that you agree with the proportional division of effort (equal for all authors).

I hope you ae all well and staying safe during these strange times.

If anyone is in contact with the retired EPA authors please either forward this message to them or send me a current E-mail address – Thanks!

Will

William K. Boyes, Ph.D.
Neurological and Endocrine Toxicology Branch
Public Health and Integrated Toxicology Division
Center for Public Health and Environmental Assessment
Office of Research and Development
Mail Code B105-04

Environmental Protection Agency
109 T.W. Alexander Drive
Research Triangle Park, NC 27711

Phone: 919-541-7538
Mobile (alternate worksite contact): 919-417-2105
boyes.william@epa.gov

From: Zucker, Robert
To: Boyes, William
Subject: RE: STAA nomination for review article Zucker
Date: Friday, April 24, 2020 6:12:38 PM

Dear will
I approve of the division of labor on this fantastic submission to STAA
Bob Zucker

From: Boyes, William <Boyes.William@epa.gov>
Sent: Friday, April 24, 2020 5:41 PM
To: Lila Thornton <lila.thornton@duke.edu>; Al-Abed, Souhail <al-abed.souhail@epa.gov>; Andersen, Christian <Andersen.Christian@epa.gov>; Burgess, Robert <Burgess.Robert@epa.gov>; Hubal, Elaine <Hubal.Elaine@epa.gov>; Ho, Kay <Ho.Kay@epa.gov>; Hughes, MichaelF <Hughes.MichaelF@epa.gov>; Reichman, Jay <Reichman.Jay@epa.gov>; Rogers, Kim <Rogers.Kim@epa.gov>; Scheckel, Kirk <Scheckel.Kirk@epa.gov>; Thai, Sheau-Fung <Thai.Sheau-Fung@epa.gov>; Zepp, Richard <Zepp.Richard@epa.gov>; Zucker, Robert <Zucker.Robert@epa.gov>
Subject: STAA nomination for review article

Hi All,

I thought it would be a good idea to submit our 2017 review article for an STAA award. I have enclosed a draft of the award nomination and the original paper. Only EPA authors are eligible for a cash award (sorry Lila).

1. Please send me any revisions to the nomination form./
2. Please send me an Email that you agree with the proportional division of effort (equal for all authors).

I hope you ae all well and staying safe during these strange times.

If anyone is in contact with the retired EPA authors please either forward this message to them or send me a current E-mail address – Thanks!

Will

William K. Boyes, Ph.D.
Neurological and Endocrine Toxicology Branch
Public Health and Integrated Toxicology Division
Center for Public Health and Environmental Assessment
Office of Research and Development
Mail Code B105-04
Environmental Protection Agency
109 T.W. Alexander Drive
Research Triangle Park, NC 27711

Phone: 919-541-7538
Mobile (alternate worksite contact): 919-417-2105
boyes.william@epa.gov

From:	Lila Thornton
To:	Boyes, William
Subject:	Re: STAA nomination for review article
Date:	Friday, April 24, 2020 5:48:45 PM
Attachments:	ATT00001.txt

No worries, an award would still be nice!

Lila

From: "Boyes, William" <Boyes.William@epa.gov>
Date: Friday, April 24, 2020 at 5:46 PM
To: Lila Thornton <lila.thornton@duke.edu>, "Al-Abed, Souhail" <al-abed.souhail@epa.gov>, "Andersen, Christian" <Andersen.Christian@epa.gov>, "Burgess, Robert" <Burgess.Robert@epa.gov>, "Hubal, Elaine" <Hubal.Elaine@epa.gov>, "Ho, Kay" <Ho.Kay@epa.gov>, "Hughes, MichaelF" <Hughes.MichaelF@epa.gov>, "Reichman, Jay" <Reichman.Jay@epa.gov>, "Rogers, Kim" <Rogers.Kim@epa.gov>, "Scheckel, Kirk" <Scheckel.Kirk@epa.gov>, "Thai, Sheau-Fung" <Thai.Sheau-Fung@epa.gov>, "Zepp, Richard" <Zepp.Richard@epa.gov>, "Zucker, Robert" <Zucker.Robert@epa.gov>
Subject: STAA nomination for review article

Hi All,

I thought it would be a good idea to submit our 2017 review article for an STAA award. I have enclosed a draft of the award nomination and the original paper. Only EPA authors are eligible for a cash award (sorry Lila).

1. Please send me any revisions to the nomination form./
2. Please send me an Email that you agree with the proportional division of effort (equal for all authors).

I hope you ae all well and staying safe during these strange times.

If anyone is in contact with the retired EPA authors please either forward this message to them or send me a current E-mail address – Thanks!

Will

William K. Boyes, Ph.D.
Neurological and Endocrine Toxicology Branch
Public Health and Integrated Toxicology Division
Center for Public Health and Environmental Assessment
Office of Research and Development
Mail Code B105-04
Environmental Protection Agency

109 T.W. Alexander Drive
Research Triangle Park, NC 27711

Phone: 919-541-7538
Mobile (alternate worksite contact): 919-417-2105
boyes.william@epa.gov

Critical Reviews in Toxicology

ISSN: 1040-8444 (Print) 1547-6898 (Online) Journal homepage: http://www.tandfonline.com/loi/itxc20

A comprehensive framework for evaluating the environmental health and safety implications of engineered nanomaterials

William K. Boyes , Brittany Lila M. Thornton, Souhail R. Al-Abed , Christian P. Andersen , Dermont C. Bouchard , Robert M. Burgess , Elaine A. Cohen Hubal , Kay T. Ho , Michael F. Hughes , Kirk Kitchin , Jay R. Reichman, Kim R. Rogers, Jeffrey A. Ross , Paul T. Rygiewicz, Kirk G. Scheckel , Sheau-Fung Thai, Richard G. Zepp & Robert M. Zucker

To cite this article: William K. Boyes , Brittany Lila M. Thornton, Souhail R. Al-Abed , Christian P. Andersen , Dermont C. Bouchard , Robert M. Burgess , Elaine A. Cohen Hubal , Kay T. Ho , Michael F. Hughes , Kirk Kitchin , Jay R. Reichman, Kim R. Rogers, Jeffrey A. Ross , Paul T. Rygiewicz, Kirk G. Scheckel , Sheau-Fung Thai, Richard G. Zepp & Robert M. Zucker (2017): A comprehensive framework for evaluating the environmental health and safety implications of engineered nanomaterials, Critical Reviews in Toxicology

To link to this article: http://dx.doi.org/10.1080/10408444.2017.1328400

Published online: 29 Jun 2017.

Submit your article to this journal

View related articles

View Crossmark data

Full Terms & Conditions of access and use can be found at
http://www.tandfonline.com/action/journalInformation?journalCode=itxc20

Download by: [US EPA Library] **Date:** 29 June 2017, At: 10:33

CRITICAL REVIEWS IN TOXICOLOGY, 2017
https://doi.org/10.1080/10408444.2017.1328400

Taylor & Francis
Taylor & Francis Group

REVIEW ARTICLE

Check for updates

A comprehensive framework for evaluating the environmental health and safety implications of engineered nanomaterials

William K. Boyes[a], Brittany Lila M. Thornton[a]*, Souhail R. Al-Abed[b], Christian P. Andersen[c], Dermont C. Bouchard[d], Robert M. Burgess[e], Elaine A. Cohen Hubal[a], Kay T. Ho[e], Michael F. Hughes[a], Kirk Kitchin[a], Jay R. Reichman[c], Kim R. Rogers[f], Jeffrey A. Ross[a], Paul T. Rygiewicz[c], Kirk G. Scheckel[b], Sheau-Fung Thai[a], Richard G. Zepp[d] and Robert M. Zucker[a]†

[a]National Health and Environmental Effects Research Laboratory, Office of Research and Development, U.S. Environmental Protection Agency, Research Triangle Park, NC, USA; [b]National Risk Management Research Laboratory, Office of Research and Development, U.S. Environmental Protection Agency, Cincinnati, OH, USA; [c]National Health and Environmental Effects Research Laboratory, Office of Research and Development, U.S. Environmental Protection Agency, Corvallis, OR, USA; [d]National Exposure Research Laboratory, Office of Research and Development, U.S. Environmental Protection Agency, Athens, GA, USA; [e]National Health and Environmental Effects Research Laboratory, Office of Research and Development, U.S. Environmental Protection Agency, Narragansett, RI, USA; [f]National Exposure Research Laboratory, Office of Research and Development, U.S. Environmental Protection Agency, Research Triangle Park, NC, USA

ABSTRACT

Engineered nanomaterials (ENM) are a growing aspect of the global economy, and their safe and sustainable development, use, and eventual disposal requires the capability to forecast and avoid potential problems. This review provides a framework to evaluate the health and safety implications of ENM releases into the environment, including purposeful releases such as for antimicrobial sprays or nano-enabled pesticides, and inadvertent releases as a consequence of other intended applications. Considerations encompass product life cycles, environmental media, exposed populations, and possible adverse outcomes. This framework is presented as a series of compartmental flow diagrams that serve as a basis to help derive future quantitative predictive models, guide research, and support development of tools for making risk-based decisions. After use, ENM are not expected to remain in their original form due to reactivity and/or propensity for hetero-agglomeration in environmental media. Therefore, emphasis is placed on characterizing ENM as they occur in environmental or biological matrices. In addition, predicting the activity of ENM in the environment is difficult due to the multiple dynamic interactions between the physical/chemical aspects of ENM and similarly complex environmental conditions. Others have proposed the use of simple predictive functional assays as an intermediate step to address the challenge of using physical/chemical properties to predict environmental fate and behavior of ENM. The nodes and interactions of the framework presented here reflect phase transitions that could be targets for development of such assays to estimate kinetic reaction rates and simplify model predictions. Application, refinement, and demonstration of this framework, along with an associated knowledgebase that includes targeted functional assay data, will allow better *de novo* predictions of potential exposures and adverse outcomes.

ARTICLE HISTORY
Received 22 October 2016
Revised 25 April 2017
Accepted 5 May 2017

KEYWORDS
Engineered nanomaterials; nanoparticles; life cycle; environmental fate and transport; transformations; exposure; adverse outcome pathway; oxidative stress; inflammation; nanotoxicity; human health; ecotoxicity

Table of contents

Introduction ... 2
Comprehensive framework structure ... 4
Life cycle ... 5
Manufacture ... 6
Product use ... 7
Disposal ... 11
Landfills ... 11
Wastewater treatment ... 12
Incineration ... 14
Recycling and recovery ... 14
Fate, transport, and transformation ... 14
Air ... 14
Soil ... 15
Aquatic ... 16
Exposure and biodistribution ... 18
Human exposure ... 19
Human biodistribution (dosimetry) ... 20
Absorption: portals of entry ... 20
Distribution ... 21

CONTACT William K. Boyes boyes.william@epa.gov National Health and Environmental Effects Research Laboratory, Office of Research and Development, Mail Code B105-04, U.S. Environmental Protection Agency, 109 T.W. Alexander Drive, Research Triangle Park, NC 27711, USA
*Current address: Department of Civil and Environmental Engineering, Duke University, Durham NC, USA
†After first two, authors are listed alphabetically.

This article has been reviewed in accordance with the policy of the National Health and Environmental Effects Research Laboratory, U.S. Environmental Protection Agency and approved for publication. Approval does not signify that the contents necessarily reflect the views and policies of the Agency, nor does mention of trade names or commercial products constitute endorsement or recommendation for use.

© 2017 US Government author

Metabolism ... 21
Elimination and excretion ... 21
Physiologically based PK modeling ... 22
Extracellular interactions ... 22
Protein corona/opsonization ... 22
Biological barriers (e.g. BBB, placenta) ... 23
Cellular uptake and intracellular fate ... 24
Endocytosis ... 24
Pinocytosis ... 25
Phagocytosis ... 25
Intracellular destination ... 25
Exocytosis ... 25
Terrestrial exposure and biodistribution ... 25
Terrestrial plants and animals ... 26
Aquatic species exposure and biodistribution ... 26
Effects ... 28
MIE/cellular, organ response ... 28
Oxidative stress ... 28
Ion toxicity after dissolution of nanomaterials ... 29
Altered cell physiology: altered cell cycle, growth ... 29
Cytotoxicity ... 29
Genotoxicity ... 29
Inflammation ... 30
Cross-kingdom effects – MIE/cellular responses ... 30
Whole organism terrestrial and aquatic species effects 31
Terrestrial plants ... 32
Discussion ... 32
Conclusions ... 33
Acknowledgements ... 34
Declaration of interest ... 34
ORCID ... 34
References ... 34

Introduction

Engineered nanomaterials (ENM) are particles which are manufactured to have at least one dimension between approximately 1 and 100 nm, and have other desirable novel properties due to their size (Roco 1999). This classification includes materials that were designed and built from the ground up as well as those produced by other process, such as grinding powders to a nanoscale. When particles are in the nanometer size range they can develop a variety of unique properties that make them valuable in a number of commercial, industrial or biomedical applications. The production and use of ENM are anticipated to be substantial components of future global economic activity (PCAST 2014). As nanotechnologies advance and grow, it is essential to ensure that new products do not cause collateral adverse effects on human health or the environment. Responsible development should include an evaluation of the potential for release of ENM across the life cycle of nanomaterial-enabled products, transformations of these reactive materials in environmental media, and both exposures and adverse effects of exposures to humans and ecologically relevant or sensitive species.

Evaluating the effects of novel nanoscale materials and their transformation products in complex environmental matrices and biological media is extremely challenging. There are many non-ENM industrial chemicals with insufficient toxicological information, and the costs of performing traditional toxicological evaluations are too high to address the tens of thousands of materials now employed in commerce (NRC 2007). The increasing number and variety of ENM and ENM-enabled products compounds this issue, as the number and pace of ENM developments exceeds traditional testing capacity. Furthermore, materials are developed at the nanometer scale in order to take advantage of special nanoscale properties such as: elevated rates of reactivity caused by high surface area to mass ratios, high tensile strength and durability, and in some cases, added dispersion and mobility (Uskokovic 2013). These nanoscale properties may convey unique fate, transport, and toxic properties not observed with bulk-sized conventional materials. There is ongoing debate about whether ENM possess special toxicological properties in addition to those of the composite chemicals (Donaldson & Poland 2013; Maynard 2014). It is clear, however, that the biodistribution and enhanced biological activity of nanoparticles on a mass basis can differ from that of their bulk (i.e. micron-sized or larger) counterparts and lead to potential unique target sites and effects (García-Alonso et al. 2014; Wang et al. 2014b). For these reasons, novel approaches are required to determine whether there are concerns for present and future uses of ENM. These approaches must be efficient and predictive, so that applications of ENM with higher probability of exposure or hazard can be quickly identified. Rapid and efficient testing and predictive approaches could be mutually beneficial to many resource-constrained sectors of the nanotechnology community, including regulatory decision makers, industry, and other developers seeking opportunities for innovation and commercialization. Using a tiered approach would allow rapid and efficient screening of many materials to identify a smaller number that are most likely to pose a potential hazard. Those few materials could then be assessed using more traditional and thorough approaches. Data from the more extensive evaluations would then build the basis for risk assessments as described by the National Research Council (NRC 1983), with screening data becoming a component of the traditional Hazard Identification stage of the risk assessment process. The question is: what is the best approach for screening to efficiently consider a myriad of potential environmental effects across the life cycle of uses of diverse and numerous nano-enabled products? To answer this question will require a more comprehensive understanding of ENM across the life cycle of nano-enabled products, ENM movement in the environment, exposures, and effects, and the critical points along these pathways in which the fate and actions of ENM are determined.

Several strategies have been proposed in order to aid the assessment of ENM, such as grouping of materials for "read-across" risk assessment, and prioritization of toxicity testing (Som et al. 2012; Hansen et al. 2013; Arts et al. 2014; Oomen et al. 2014; Stone et al. 2014; Godwin et al. 2015).

Table 1. A list of supplementary models organized by evaluation area.

Model	Description	Reference
Life cycle emissions		
protégé	Models human near-field exposure across the life cycle	Royce et al. (2014)
Fate & transport		
NanoDUFLOW	Links ENM processes to hydrologic model	Quik et al. (2015)
WASP	Mechanistic model being adapted to assess ENM exposure in aquatic media	Knightes (2015)
	Transport of TiO_2 Nanoparticles into Leachate of Municipal Waste Landfills	de Castro et al. (2012)
Exposure		
PRoTEGE	Models human near-field exposure across the life cycle	Royce et al. (2014)
USEtox	Models human far-field and fresh-water ecotoxicity exposure; evaluated for organic chemicals (not ENM)	Rosenbaum et al. (2008)
SHEDS	Stochastic Human Exposure and Dose Simulation (SHEDS) Model	Isaacs et al. (2014)
NanoRiskCat	Decision support tool to estimate exposure and hazard ratings for consumer products containing ENM	Hansen et al. (2013)
Pharmacokinetic/dosimetric		
MPPD	Models particle deposition in the respiratory tract	Asgharian et al. (2001) and Cassee et al. (2002)
PBPK	Physiologically based pharmacokinetic models describe particle absorption, distribution and elimination based on physiological parameters; Models have been published for Ag and TiO_2 ENM, PLGA/mPEG particles	Bachler et al. (2013, 2015) and Li et al. (2012)
ISDD	*In vitro* Sedimentation, Diffusion and Dosimetry model; predicts particle dosimetry for adherent cells in tissue culture systems	Teeguarden et al. (2007), Hinderliter et al. (2010), and Cohen et al. (2014)
Effects		
NanoRiskCat	Decision support tool to estimate exposure and hazard ratings for consumer products containing ENM	Hansen et al. (2013)

For example, NanoRiskCat (Table 1) is a model that categorizes levels of potential risk and hazard in order to help decision makers even where data are lacking (Hansen et al. 2013). Grieger et al. (2012) reviewed and evaluated a number of frameworks for environmental health and safety risk analysis and concluded that most were primarily applicable to occupational settings with minor environmental considerations. In addition, there are differences among frameworks as to their threshold for concern. For example, one scheme considered fibrous ENM with aspect ratios greater than 3:1 as candidates for further testing (RCC-NI 2014), while another set the boundary at 100:1 (Som et al. 2012). Arts et al. (2014) reviewed the concept of grouping ENM as a means of streamlining nanomaterial testing, and concluded that none of the available approaches fully considered the nanomaterial life cycle, material properties and biophysical interactions, types of use, exposure, biokinetics, and early and apical toxicological effects. Thomas et al. (2009) also emphasized the need for evaluating potential exposure to ENM along with hazard in risk assessments. A framework for Comprehensive Environmental Assessment has been proposed that emphasizes a process for input from stakeholders and topical experts to set research priorities for evaluating ENM (Powers et al. 2016).

Environmental transformations or fate and transport of ENM across media are considered by few frameworks. Oomen et al. (2014) and Stone et al. (2014) provided approaches to tiered prioritizations of nanomaterial testing, but their foci were on testing materials and not on developing predictive capability. Cohen et al. (2013b) offered an approach that could become predictive based on high-throughput toxicity data and *in silico* quantitative structure activity relationships (QSAR) analyses. At this time, however, nano-QSAR are limited by the extent of quality data available for modeling (Ivask et al. 2013; Tantra et al. 2014; Oksel et al. 2015). Similarly, case study assessments of ENM risks to human health and the environment have limited data and are associated with high uncertainties (Aschberger et al. 2011). Toxicity testing strategies have been proposed based on *in vitro* systems, including high-throughput systems (Nel et al. 2013) or representing priority target tissues (Farcal et al. 2015) or toxic mechanisms (Costa & Fadeel 2016). Among the challenges of ENM alternative toxicity testing systems are selecting and characterizing ENM for study, preparation of adequate dispersions, determining dose to target cells or tissues, and potential interference of ENM suspensions with optical readouts (Johnston et al. 2013; Cohen et al. 2014). There is additional complexity when considering nanomaterial life cycles within a framework of higher level societal and economic systems (Tolaymat et al. 2015).

A recent review of frameworks and tools for risk assessment of nanomaterials developed eight criteria for evaluating frameworks that included: nano-specific requirements (such as physicochemical properties that may influence kinetics); life cycle thinking (including changes in nanomaterial characteristics across their life cycle); pre-assessment phase (screening to focus assessments); exposure driven approach (to prioritize toxicity testing); transparency of objectives and communication with stakeholders; documented applications; and allowing for grouping or read-across assessments (Hristozov et al. 2016). In their review, Hristozov et al. concluded that none of the nanomaterial risk assessment frameworks currently available satisfied all of these criteria.

The complexity of nanomaterial transformations, life cycles, and environmental interactions further complicates environmental health and safety assessments (Lowry et al. 2012;

Grassian et al. 2016). It is important to understand ENM in complex realistic environments (Murphy et al. 2015). For example, environmental transformations can potentially modulate the toxicity of silver nanoparticles (Ag ENM) by converting them to toxic silver ions, but Ag ENM may also be produced with the reduction of ionic silver by natural organic matter (Hou et al. 2013). TiO_2 in either bulk pigment grade or ENM forms may be coated with a substance such as $AlOH_3$ to improve dispersion and to prevent UV activation and subsequent product degradation (WHO-IARC 2010). When $AlOH_3$-coated TiO_2 ENM, as incorporated into cosmetics or sunscreens, is exposed to swimming pool water, however, the coating can degrade increasing the potential phototoxicity of the transformed ENM (Al-Abed et al. 2016). Thus, consideration of ENM transformations and release from products should play a central role in ascertaining and predicting how ENM propagate through environmental systems to reach important ecological and human receptors and their potential actions at those receptors. In all, we are not aware of any comprehensive frameworks to date that seek to build a quantitative and predictive capability using realistic environmental and biological compartments, and also consider: potential environmental release of ENM across product life cycles; ENM fate, transport, and transformation in environmental media; ENM exposure to receptor populations; and potential effects in susceptible species or humans.

Here we propose a framework for the evaluation which is organized to reflect the potential movement of ENM across realistic environmental or biological systems. We discuss the key phenomena captured in the framework and review the literature related to characterizing these phenomena. Finally, we identify key gaps in this knowledge and where we see potential for methods development to address these gaps. We believe that the consideration of environmental and biological compartments with associated parameters such as transfer rates, affinity coefficients, dissolution rates, and other relevant metrics, where applicable, will benefit the long-term ability to develop and demonstrate relevant, quantitative, predictive models of both ENM exposures and effects across product life cycles. Data to fill such a vision are currently far from complete. The framework will guide future research to design efficient approaches for characterizing potential impacts of ENM and ENM-enabled products and support risk-based decisions.

Comprehensive framework structure

The overall framework is divided into four separate, but linked, stages of assessment (Figure 1). The structure of these stages resembles the topical layout proposed for comprehensive environmental assessment (Powers et al. 2016), but here the emphasis is on understanding and predicting the movement, fate, and behavior of ENM across environmental compartments. The first of these evaluation stages addresses the potential release of ENM across the life cycle of nano-enabled products, including initial production of ENM, incorporation of ENM into products, product use, and final disposal. The second stage considers the movement, transformation, and fate of ENM in environmental media, specifically air, soil, and aquatic compartments. In the third stage, the focus is on exposure to receptor populations, comprising aquatic and terrestrial species, including humans. This includes biokinetic and biotransformation processes. The final stage concerns the development of adverse effects along an adverse outcome pathway (AOP) sequence, as recently suggested by Gerloff et al. (2017). The concept of an AOP begins with a molecular initiating event (MIE) and progresses to the generation of adverse health outcomes in an individual or a population (Ankley et al. 2010). An AOP is an analytical concept that enables linking mechanistic information into a predictive framework (OECD 2016). The concept is independent of the chemical or material that causes the MIE, and thus AOPs developed for toxic chemicals in theory could also be applicable to nanoparticles causing the same MIE (Gerloff et al. 2017). These four evaluation stages are intended to identify pathways of sequential compartments along which a nanomaterial might travel, and the considerations – including ENM physical and chemical properties – that might influence them to take one path or another.

Figure 1. An overview of the four over-arching evaluation areas considered in this evaluation framework for engineered nanomaterial (ENM) safety. Each of these evaluation areas – (1) life cycle emissions, (2) fate and transport, (3) exposure, and (4) effects – is broken down into focus areas that will be described in subsequent detail.

The framework, at present, is qualitative and reflects probable routes of potential concern. We hope to identify a few critical steps along these pathways that are key for predicting the fate and transport of materials. A strategy for nanomaterial assessment has been proposed by Hendren et al. (2015) in which a few functional assays could simplify attempts to use a complex set of physical and chemical ENM parameters to predict similarly complex environmental behaviors. For example, they propose surface affinity and dissolution rate as two examples of functional assays that would serve as critical determinants of the environmental fate of ENM. Similarly, Ivask et al. (2013) identified three factors determining the toxicity of silver, zinc oxide, and copper oxide ENM to relevant environmental test species. These factors were dissolution (in agreement with Hendren et al. 2015), organism-dependent cellular uptake, and induction of oxidative stress and consequent cellular damage. We propose a similar approach to identify a few critical parameters along the four stages of our framework. In this way, we hope that critical parameters measured by standardized functional assays can be identified that will serve as initial screening points for evaluating potential risks of novel materials.

The National Research Council has recommended development of models that link behavior of ENM to their

characteristics and to properties of systems into which they are released (NRC 2012, 2013). It may be possible to associate rate parameters with these transition points (represented by arrows in Figures 1–10), where applicable, so that the models can become more quantitative and predictive. A number of compartmental models for factors such as life cycle emissions, environmental fate and transport, exposure, dosimetry, and particle kinetics have been developed for chemicals or ambient particles that might be applied or adapted for ENM (Table 1). We hope that the conceptual framework proposed here will facilitate identification of needs for further model development to adequately describe important mechanisms unique to ENM so that resulting models can be applied and demonstrated to predict potential for impacts across the ENM life cycle.

With this manuscript, we hope to

- Establish a framework that could eventually be used to screen ENM based on a minimal set of measured information and then prioritize for more in depth testing and evaluation.
- Identify key nodes in the framework that are critical determinants of ENM behavior.
- Identify research needs where further information is necessary to develop the structure of the model and/or parameterize relevant functions.
- Evaluate knowledge gaps regarding nanomaterial environmental health and safety in a context that enables a value of information assessment to better prioritize needs for future research.

Additionally, with this framework, we hope in the future to

- Identify alternative testing methodologies for the key nodes at which development of simple functional predictive assays will be possible.
- Achieve the ability to quantify transitions and rate functions as a basis for development of quantitative predictive models.
- Develop quantitative predictive models for screening-level evaluations of novel ENM.
- Foster a process for demonstration and refinement of the framework and its associated knowledgebase.

The intended users of this framework include

- Regulatory authorities throughout the world who must evaluate submissions for registration of novel ENM or new uses of ENM in a short period of time and with little data.
- Research planners who need to determine where new research is most needed and would most efficiently refine and reduce uncertainties in the framework and its associated models and knowledgebase.
- Developers and engineers who are interested in designing materials likely to be sustainable and not associated with significant environmental impacts.

Life cycle

The potential for release of ENM into the environment should be considered across the successive stages of a product life cycle including manufacture, use, and disposal (Figure 2).

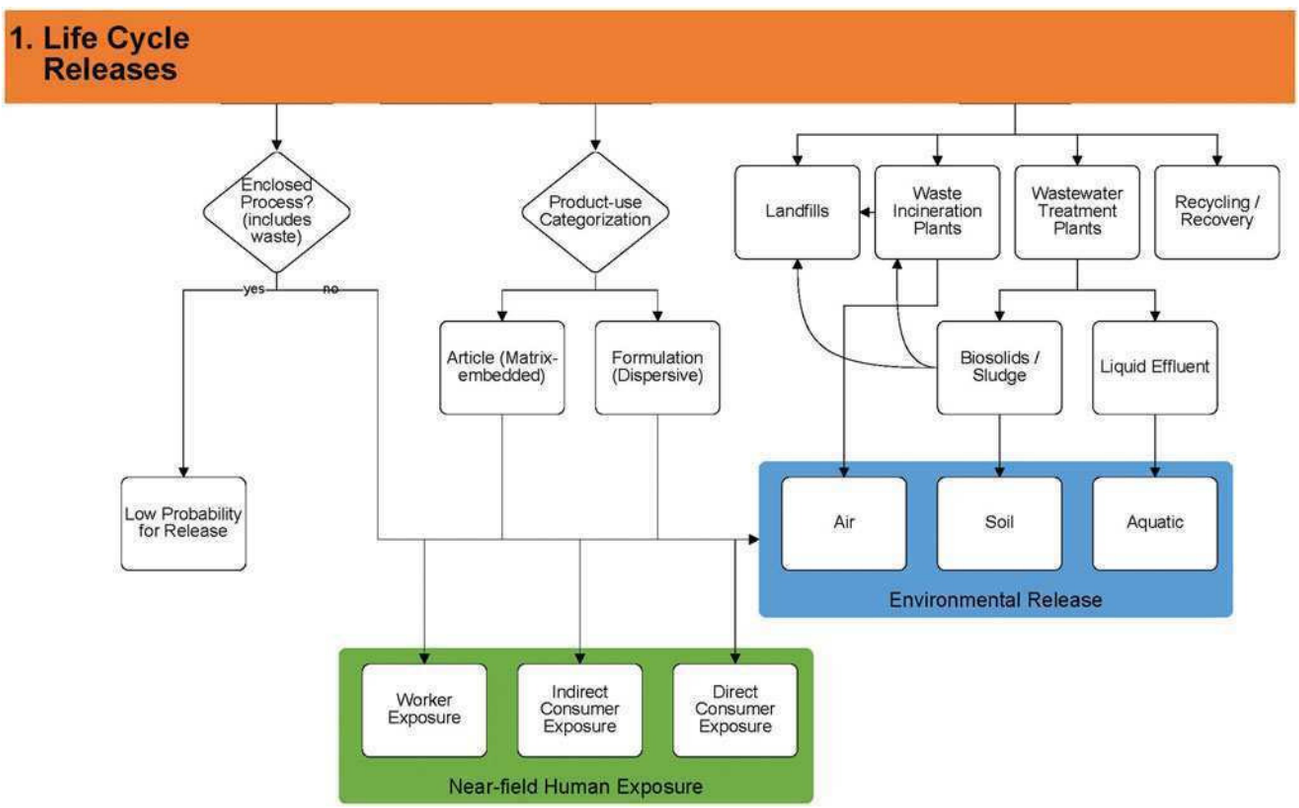

Figure 2. Potential pathways for ENM release across the ENM or product life cycle (manufacture, use, and disposal).

Manufacture

The manufacture of ENM and ENM-enabled products includes a risk of release of ENM into the workplace and exposure to workers and surrounding environment. ENM may be released inadvertently as a byproduct of synthesis, application, recycling, and disposal of nanoparticles or ENM enabled products. Manufacturing processes greatly influence the potential for release of ENM into the environment. Processes that are enclosed have low probability of releasing ENM during routine operations, although materials can be released during transport or handling, or during equipment maintenance or failure. Processes that are not enclosed have a greater potential for releasing materials into the workplace where near-field exposure to workers may occur. In addition, opened manufacturing has the potential to release ENM into air, soil or aquatic environmental media (Figure 2).

In the US, environmental concerns for the use of ENM are regulated primarily through the Toxics Substances Control Act (TSCA), which was recently updated as the Frank R. Lautenberg Chemical Safety for the Twenty-first Century Act, and under the Federal Insecticide, Rodenticide and Fungicide Act (FIFRA). Neither TSCA nor FIFRA has the authority to regulate commercial particles based solely on particle size. Novel chemical structures must be registered under TSCA prior to being manufactured or imported into the US, which applies to ENM such as carbon nanotubes, but not to materials such as TiO_2 in a nanomaterial form, because the chemical structure was previously registered and used as a bulk material. With regard to pesticides, ENM that are included in products for the express purpose of biocidal activity must be registered under FIFRA, but manufacturers who use Ag ENM in products without claiming a biocidal function are not legally required to register the product under FIFRA. Currently, it is unclear the extent to which non-registered ENM are being produced and perhaps released into environmental media. To attain information regarding broader application of ENM in commerce, EPA published a rule in January 2017 under TSCA (8a) that requests manufacturers and formulators to provide EPA with information regarding their use of chemical substances when manufactured or processed as nanoscale materials which were not previously reported to EPA (EPA 2017). The rule did not require companies to acquire data not currently available, and did not have direct implications for controlling the use of ENM in industry or commerce.

Inadvertent releases of registered or non-registered ENM could include accidental releases during manufacturing or plant maintenance, or spills from transportation or shipping accidents. Such inadvertent or accidental releases cannot be anticipated to any level of specificity, and the accuracy of data on the historical frequency of chemical spills is in question (McClure et al. 2013).

Although potential large scale transportation accidents involving ENM has not been addressed in the literature to our knowledge, modeling efforts for possible nanomaterial exposure due to accidental release in a manufacturing facility has been reported (Pilou et al. 2016).

Product use

Advancement in nanoparticle manufacturing, as well as a better understanding of the unique properties that these materials impart to products and processes, has significantly increased the number and scope of ENM-enabled products in recent years. Yet we know little concerning the number of ENM-enabled products (in the US and worldwide) and the amount and composition of ENM in these products. In the US, manufacturers and distributors of consumer products are not required to specify whether product ingredients are nano-sized. We also know little concerning the release of particles, particle–polymer fragments, or dissolved ions during typical use or misuse of ENM-enabled products. The ability to derive quantitative transfer coefficients that reflect release of ENM from products during their consumer usage is limited by the small proportion of products and exposure scenarios evaluated (Caballero-Guzman & Nowack 2016). This lack of information at the product-use stage represents a significant data gap in exposure and risk analyses.

There are a few publicly available international inventories that list consumer products with "nano-claims". These sources (Table 2) include the joint Wilson Center and Virginia Tech "[Nanotechnology] Consumer Products Inventory" (CPI) (Project on Emerging Nanotechnologies 2013); the 2010 and 2012 (nanosilver-only) inventories by the European Consumer Organization (BEUC) and the European Consumer Voice in Standardisation (ANEC) (ANEC & BEUC 2010, 2012); "The Nanodatabase" (Hansen et al. 2016); and the German BUND database (BUND). The CPI and The Nanodatabase are currently curated for the addition of new products and removal of discontinued products that are no longer commercially available. Reviews and analyses of these databases have been

Table 2. Publically available inventories and/or databases of consumer products that claim to contain nanomaterials or nanotechnology.

Inventory/database name	Organization	Scope	Source
Consumer Products Inventory (CPI)	Wilson Center; Virginia Tech	Global market; continuously updated through wiki-style platform	Project on Emerging Nanotechnologies (2013) and Vance et al. (2015)
The Nanodatabase	DTU Environment; Danish Ecological Council; Danish Consumer Council	European market; continuously updated; includes pictorial overviews of potential exposure and hazard	Hansen et al. (2016)
ANEC/BEUC 2010 inventory	European Consumer Voice in Standardisation (ANEC); European Consumer Organization (BEUC)	European market; last updated in 2010	ANEC and BEUC (2010)
ANEC/BEUC 2012 nanosilver inventory	ANEC; BEUC	European market (nanosilver only); last updated in 2010	ANEC and BEUC (2012)
Nanoprodukt-datenbank des BUND	BUND (Friends of the Earth Germany)	German market; "continuously updated and expanded"	BUND

recently published and describe the wide range of ENM-enabled or enhanced products (Yang & Westerhoff 2014; Vance et al. 2015; Hansen et al. 2016).

Although there is evidence for the presence of ENM in many products, most of these products do not advertise the composition or in many cases even the presence of ENM (Vance et al. 2015). Of those products where manufacturers have disclosed the presence of ENM, information other than composition is not often available. Consequently, information concerning particle size, concentration, distribution (within the product), and leaching of ENM during normal use is unavailable except where added by a third party. Analyses of products in the CPI with compositional information have suggested that metal particles (primarily silver and to a lesser extent titanium, zinc, and gold) were present in the greatest number followed by products containing carbon and silicon (Yang & Westerhoff 2014; Vance et al. 2015). The release of ENM from consumer products has not been well described for most common ENM in a wide range of products. In addition, information on the relative penetration of nano-enabled products in the marketplace, that is, what proportion of the products sold in a given category, such as sunscreen, would be those brands containing ENM, is not generally available.

Because there is considerable uncertainty regarding the potential future uses of ENM, one screening level approach to approximate potential release is to consider surrogate chemicals that serve the intended purpose in the product that will be assumed by the ENM. The potential for ENM-release from products might be different than for chemical releases from similar products, but a surrogate approach based on consumer product usage data can at least bound the estimates of the degree of use of ENM-enabled products. In general, consumer product categories can be condensed into (1) formulas, including liquids and sprays, where direct consumer exposure may be possible; and (2) articles, including hard surfaces and textiles such as furniture, where chemicals or nanoparticles might be a component of the product, but are typically less available for direct consumer exposure (Isaacs et al. 2014; Figure 2). For ENM applications in which the particles can be physically separated from their matrix (i.e. a suspension), exposure can be considered in two steps: the first being the release of particles from the product and the second the contact of ENM with the target organism. For ENM-enabled products intended to be ingested or applied to the skin (typically liquid, cream, or gel suspensions), these steps might be combined. Estimates of ENM exposure based on chemical surrogates could be considered as a first pass estimate of the potential levels of ENM usage.

Although there is minimal information concerning the characterization and release of ENM present in consumer products, research results have been reported for a limited number of consumer products. For example, characterization and release of nanosilver from a number of consumer products have been reported (Benn & Westerhoff 2008; Benn et al. 2010; Quadros & Marr 2011; Quadros et al. 2013; Tulve et al. 2015). Population-level exposure to silver nanoparticles present in consumer products was estimated on the basis of the Consumer Product Inventory of the US-based Project on Engineered Nanotechnologies (PEN) and a tiered life cycle analysis and exposure modeling approach referred to as Prioritization/Ranking of Toxic Exposures with GIS (geographic information system) Extension (PRoTEGE) (Royce et al. 2014; Table 1).

One of the subcategories for consumer products is personal care products. Depending on how they are categorized, these nano-enabled consumer products comprise 39% of the 505 health and fitness products listed in the US Nanotechnology Consumer Products Index (CPI) (Vance et al. 2015) or 233 out of 2231 products listed in the European Union Nanodatabase (Hansen et al. 2016). In both cases, nanoscale silver is the most commonly reported ENM. Consumer products typically include toothbrushes, lotions, mouthwashes, as well as hairstyling tools and products (Vance et al. 2015). Depending on the particular product, the most dominant exposure route is dermal followed by ingestion and inhalation (Hansen et al. 2016). Because CPI focuses on ENM-enabled consumer products, ENM-enabled industrial products used to improve construction materials or energy-sector products have not been typically covered by this database, but may be available elsewhere (West et al. 2016). These applications include the use of micronized copper in treated lumber (Santiago-Rodríguez et al. 2015; Platten III et al. 2016) and, for automobiles outside the U.S., nanoscale cerium oxide added to diesel fuel (Cassee et al. 2011; Gantt et al. 2014). The potential for release of carbon nanotubes (CNTs) from composite materials under a variety of usage scenarios has been the focus of a multi-institute research effort (Nowack et al. 2013; Froggett et al. 2014). There are a number of products in which CNTs are embedded in polymers or resins. This project evaluated the potential for CNT release either directly during manufacture or subsequently from the matrix during various usage scenarios, including those with substantial abrasion or other destructive conditions. The potential for release was present during manufacturing; however, this condition was best able to be controlled. For most of the life cycle stages evaluated, the potential for CNT release from a solid product matrix was low. One exception was the use of CNTs in tires where abrasion could result in their release into the environment. In addition, the proposed use of CNTs in textiles could also lead to consumer exposures. Another potential source of CNT release was identified during recycling operations if polymers containing CNTs were mixed for handling with other polymer materials.

Disposal

Landfills, waste incinerators, and wastewater treatment plants (WWTPs) giving rise to biosolids are important routes of disposal at the end of the ENM life cycle. These are, therefore, key intermediaries between the usage phase of nano-enabled products and the environment (Dale et al. 2015). Additional releases of ENMs, may occur during recycling and recovery processes.

Landfills

Landfills are the predominant global disposal option for ENM across all use categories. Based on a market study of global production rates and product life cycles, Keller et al. (2013a, 2013b) estimated that of 260,000–309,000 metric tons of

ENM used in commercial or industrial applications worldwide, 63–91% were eventually disposed of in landfills in 2010. Keller et al. incorporated high and low bound estimates for rates of ENM release into the environment during manufacture, use, and disposal of ENM enabled products. Materials released from ENM-enabled products would likely no longer be in their original nanoscale form, depending on the ENM, the product matrix, and use. Additionally, most of the ENM-containing waste released during manufacturing (up to 80%) ends up in landfills. It is likely that ENM would be affected (e.g. aggregated, dissolved, destabilized, oxidized or reduced, complexed with organic matter) by their interaction with landfill leachate. In particular, the coating could be altered, compromising the particles' stability and reducing the potential to migrate into other media. Several factors have been found to affect the surface charge and aggregation state of Ag nanoparticles: pH, oxygen concentration, organic matter content, chloride concentration, sulfide concentration, and type of coating agent (El Badawy et al. 2010; Gitipour et al. 2013). This is important because if the ENM coating is not affected by the landfill leachate, the particles would be stable in the aqueous phase, potentially endangering the surrounding municipal solid waste aquifers and surface waters. Bolyard et al. (2013) found that ZnO, TiO_2, and Ag ENM exposed to landfill leachate in a stirred reactor (humic acid concentrations from 300 to 6500 mg/L, pH 7.4–7.9) increased Zn, Ti, and Ag concentrations in the aqueous phase, and that released particles tended to agglomerate. Nevertheless, the concentrations of dissolved metals were minimal because of the small concentrations of ENM added onto the reactor and the low solubility of the ENM in water. The authors also concluded that ENM did not significantly change the ability of microorganisms under aerobic or anaerobic conditions tested to break down organic matter present in landfill leachate. Zhu et al. (2014) concluded that at high ionic concentrations, which is expected from landfill leachate, humic acid has a bridging effect and promotes the aggregation and sedimentation of TiO_2 nanoparticles.

More research is required on the interaction of ENM with landfill leachate, including high humic acid concentrations, and how these interactions affect their coating and stability (Bolyard et al. 2013). New and improved analytical techniques are needed to determine ENM fate in landfills because current methods do not allow ENM identification and quantification in complex heterogeneous matrices such as landfill leachate. This is an area of active research, however, and evolving capabilities (Badireddy et al. 2012; Huynh et al. 2016). Less than 1 mg/L of ENMs (ZnO, TiO_2, or Ag) added to leachate at a concentration of approximately 100 mg/L and incubated for 30 d under controlled experimental conditions, was predicted to be in the free ionized metal form (Bolyard et al. 2013). There is a need to standardize the sampling, separation and quantification methods used for ENM. One of the most challenging aspects of ENM determination is how to differentiate naturally occurring particles or those that are incidentally produced (such as in combustion) from purposefully manufactured ENM (Wiesner et al. 2011; Part et al. 2015).

Since many ENM transform during wastewater treatment, assessment of landfill disposal of biosolids or sludge produced during wastewater treatment must consider these transformed phases, which are distinctly different than pristine ENM. Chemical speciation in the aqueous phase of systems containing ENM is currently being modeled in literature using Visual Minteq or similar software (Bolyard et al. 2013; MINTEQ 2013). Since the coating materials used to stabilize ENM are not typically contained in software databases, research could be conducted to determine the equilibrium coefficients for these coating materials at different pH-Eh conditions to improve the accuracy of estimations.

de Castro et al. (2012) modeled the behavior of TiO_2 ENM in landfill leachate in a 5-year period using a Fortran-based code and evaluated the model with experimental data obtained in column experiments. The results showed that TiO_2 ENM were adsorbed onto the soil within the protection barriers of the landfill over the 5-year-simulated period.

Wastewater treatment

An inevitable pathway of ENM in consumer products is from the home to the local WWTP. Several studies have shown that ENM accumulate in biosolids during wastewater treatment; TiO_2 in particular has a high retention in sewage sludge – as high as 99% (Judy et al. 2012; Tourinho et al. 2012). Partitioning of Ag ENM in biosolids is typically greater than 90% and, in many cases, greater than 99% (Kaegi et al. 2011; Impellitteri et al. 2013). The distribution of ENM in WWTP primarily to solids is expected due to surface charges and reactive sites suitable to retain ENM; the small amount of particles that remain suspended during clarification may pass through to the effluent. Research on the impact of ENM in effluent beyond the WWTP is limited, likely due to high retention in biosolids, but the restricted continuation of ENM through WWTP to drinking water distribution systems warrants further research to be protective to drinking water supplies.

Upon entering the WWTP, ENM will encounter a unique chemical and physical environment that includes primary and secondary clarifiers where ENM will partition to other solids in wastewater, followed by anaerobic digestion. If not transformed to other phases by this point, anaerobic digestion likely will act on redox sensitive ENM to form sulfides. Some ENM, such as TiO_2, are resistant to transformation, whereas ENM like Ag, Zn, Cu, and Cd quantum dots are highly sensitive to sulfidation change. After anaerobic digestion, the sewage sludge is further processed by composting or stabilization to hinder microbial activity before being land applied as biosolids for fertilization. Some of the transformed ENM will remain unchanged during composting (i.e. Ag_2S), while others may transform again governed by the environmental conditions of composting and aging (i.e. Zn and Cu) (Table 3). It is important to note that this pathway begins in the home with a consumer product containing ENM traveling through home drains to a network of service lines connected to the WWTP, which means ENM are not added at the end of the process in the fresh or composted biosolids. In fact, convincing research shows that sulfidation reactions occur in the urban wastewater service line network prior to reaching the WWTP (Kaegi et al. 2013; Thalmann et al. 2014). The fact that ENM may be transformed in the sewage service line network

Table 3. Examples of transformations of metallic ENM in biosolids systems.

ENM	Study	Analysis	Transformation products	Citation
Ag	2009 TNSSS Report. Source of Ag in the sample is unknown	TEM-EDX	α-Ag_2S nano-clusters	Kim et al. (2010a)
Ag	Investigation of Ag ENM in a pilot scale WWTP observed	TEM and XAS	∼90% Ag ENM partitioned of to biosolids with transformation to Ag_2S	Kaegi et al. (2011)
Ag	Three Ag ENM (citrate, PVS, and MSA coated) and one AgCl ENM were exposed to a pilot scale WWTP along with a $AgNO_3$ positive control. Samples were evaluated as a function of time within the WWTP system and post-processing simulated composting up to 6 months	XAS	All ENM and $AgNO_3$ were transformed to Ag_2S	Lombi et al. (2013)
Ag	A full scale pilot WWTP consisting of a primary clarifier (PC), aeration basin, and secondary clarifier (SC) connected to a municipal WWTP feed was utilized to examine citrate coated Ag ENM, Ag_2S ENM, and $AgNO_3$ in solids from the PC and SC	XAS	Ag_2S in both the PC and SC.	Impellitteri et al. (2013)
Ag	Plasma polymerization employed to immobilize citrate, polyethylene glycol, and polyethyleneimine capped Ag ENM on a Kapton substrate (nanoparticle in-situ deployment devices – nIDDs) and deployed directly in a municipal WWTP's primary sewage sludge for 24 h	XAS, SEM/EDX	Full conversion to Ag sulfide phases was not observed; 14–60% of Ag was retained as metallic Ag	Sekine et al. (2013)
Ag	This study examines the speciation and lability of Ag in archived, stockpiled, and contemporary biosolids from the UK, USA and Australia, and indicated that biosolids Ag concentrations decreased significantly over recent decades. Reduced-sulfur binding environments was important for Ag speciation in materials ranging from freshly produced sludge to biosolids weathered under ambient environmental conditions for more than 50 years	XAS	Ag in biosolids was predominantly Ag sulfides and had low lability (0.0002–3.4%) upon land application.	Donner et al. (2015)
ZnO	Three ZnO ENM (OECD NM112, OECD NM112 capric/caprylic triglyceride capped, Co-doped ZnO) and $ZnCl_2$ control were exposed to a pilot scale WWTP. Samples were evaluated as a function of time within the WWTP system and post-processing simulated composting up to 6 months	XAS	ENM and $ZnCl_2$ were transformed to ZnS within the WWTP; however, upon composting ZnS was re-transformed to Zn-adsorbed to iron oxides, Zn phosphate, and Zn organic matter complexes	Lombi et al. (2012)
ZnO	Utilizing an established full pilot scale WWTP, ZnO nIDDs or $ZnCl_2$ were added to evaluate Zn transformations. Application of nIDDs permits usage of substrates with immobilized ENM in relevant environmental systems with recovery of the substrate for analytical analysis	XAS, TEM	Over the course of the study ZnO dissolved resulting in ZnS (∼90%) and Zn ligands (cysteine and citrate)	Brunetti et al. (2015)
CuO	There have been no studies of CuO nanoparticles in a pilot scale WWTP to date; however, related studies can provide potential insight. Ma et al. (2014) examined the sulfidation of CuO in sulfidized water. Donner et al. (2011) examined native Cu in fresh and aged (composted) biosolids from 5 WWTPs	XAS, XRD, and TEM	Covelite (CuS) and amorphous Cu_xS_y in sulfidized water Cu speciation in the fresh (direct from secondary treatment) sludge was identified as chalcocite (Cu2S), cubanite (CuFe2S3), and Cu sorbed to organic matter. However, upon aging, Cu was further altered to ∼70% Cu sorbed to organic matter followed by cubanite, covelite, and Cu phosphate	Ma et al. (2014) Donner et al. (2011)
TiO_2	Ti concentrations and Ti phase were examined in effluent samples from several WWTPs	SEM/EDX	Ti particles ranging from 10s nm to >0.7 μm. The particles comprised of primarily Ti and O presuming TiO_2; some larger particles also contained Si with Ti.	Kiser et al. (2009)
TiO_2	Nano and larger TiO_2 phases were identified in biosolids and biosolids amended soils	SEM, TEM	No phase transformations occur within a WWTP for TiO_2	Kim et al. (2012)

Table 4. Relevant concentrations of nano-based constituents in soils and biosolids, and predicted concentrations of ENM in biosolids.

Material	Common range in soil (mg/kg)[a]	Average in soil (mg/kg)[a]	Targeted National Sewage Sludge Survey Report (mg/kg)[b]				Predicted ENM contribution (mg/kg) range in biosolids[c]	Predicted ENM contribution (mg/kg) range in biosolids[d]
			Range	Average	50th Percentile	95th Percentile		
Silver/Ag ENM	0.01–3.15	0.27	1.94–856	31.6	13.6	63.6	10^{-4}–10^{1}	10^{-5}–10^{-1}
Zinc/ZnO ENM	3–2900	52	216–8550	994	784	2068	10^{1}	10^{-1}–10^{1}
Titanium/TiO_2 ENM	210–54500	5720	11.6–4805	286	12.7	915	10^{-2}–10^{4}	10°–10^{2}
Copper/CuO ENM	1–256	14	115–1720	558	463	1248	ND	ND
Cerium/CeO_2 ENM	15–100	50	ND				$10^{-5.5}$	ND
CNT			ND				10^{-1}	10^{-4}–10^{-1}
Fullerenes			ND				10^{-3}–10^{-1}	10^{-4}–10^{-1}

ND: not determined.
[a]Salminen et al. (2005).
[b]TNSSS Report (EPA 2009).
[c]Gottschalk et al. (2013).
[d]Sun et al. (2015).

(within hours) between the home and WWTP to species that are typically less toxic provides some protection during sewer overflow discharge resulting from excessive storm water and groundwater input, that may account for 2–10% of total inflow (Mueller & Nowack 2008).

In the US, 50–60% of biosolids are recycled for land-application and are applied on less than one percent of farmland (Gottschalk et al. 2009; EPA 2012). Land application of biosolids is regulated under Title 40 of the Code of Federal Regulations (US 1999) with the goal to protect human health and the environment from any reasonably anticipated adverse effects of certain pollutants, including metals, which might be present in biosolids. Table 4 shows documented distributions of Ag, Zn, Ti, Cu, Ce, CNT, and fullerenes for ranges and averages naturally in soils, results of the Targeted National Sewage Sludge Survey (TNSSS) Report (EPA 2009), and literature predictions of ENM concentrations in biosolids. Information from the TNSSS report shows the range, average, 50th percentile, and 95th percentile for Ag, Zn, Ti, and Cu in biosolids collected in 2006 and 2007 from 74 randomly selected WWTP. This information can be very helpful in designing experiments. For example, a number of studies of Ag in biosolids or soils have utilized a value close to 1000 mg/kg based on the maximum value of Ag (846 mg/kg; a documented outlier) in the TNSSS report. However, the average Ag concentration in biosolids measured for the report is only about 32 mg/kg and the 50th percentile (median) is approximately 14 mg/kg. Likewise, biosolids are often applied at a rate of 5–10 tonnes/hectare, which upon mixing in the top 15 cm of topsoil results in a dilution factor of 100–50, respectively. For example, while predicted contributions of ZnO ENM to total biosolids concentration may be on the order of 10 mg/kg, the effective increase in soil concentration from ZnO ENM would range from 0.1 to 0.2 mg/kg per application. Quantitation of rate parameters such as these will be essential for eventual quantitative modeling based on this framework. Also worth noting about the TNSSS report in relation to the predicted contribution of ENM to biosolids is the fact that some native metal concentrations in biosolids may be significantly higher than the input from ENM, making the distinction of ENM-associated risk difficult to assess with current procedures. Better methods for detection and characterization of ENM in complex matrices are critically needed.

Incineration

Alternative disposal methods of biosolids include landfill (see discussion above) and incineration. Approximately 20% of sludge from wastewater treatment facilities is incinerated in the US (Holder et al. 2013). Incineration of biosolids impacted by ENM has received little attention (Impellitteri et al. 2013; Meier et al. 2016), but historical research of metal-laden biosolids incineration is plentiful. One study examined the path of Ag ENM through a pilot scale WWTP along with a $AgNO_3$ control (Impellitteri et al. 2013). Samples were collected from the primary clarifier (fresh biosolids) and the secondary clarifier (aged biosolids) and in each case the transformed Ag species was primarily Ag_2S with some Ag sulfhydryl and metallic Ag phases as determined by X-ray absorption spectroscopy (XAS). The fresh and aged samples were then incinerated at 850 °C for 4 h and the residual ash examined by XAS to determine changes in Ag speciation. Incineration impacted Ag speciation by shifting Ag_2S → Ag sulfhydryl → metallic Ag in the fresh and aged biosolids to metallic Ag → Ag sulfhydryl → Ag sulfate in the ash. Scanning electron microscope images show accumulation of Ag clusters (1–3 μm) in the incineration ash; however, the stability of these clusters warrants further research. Since incineration ash is typically landfilled, the caution above related to assessing risk based on the transformed phases rather than the pristine ENM is applicable. Recently, it was shown that Fe_2O_3 nanofiller in thermoplastics altered the shape and composition of residual incinerator ash to be more brittle and have surface-exposed nanofillers when subjected to incinerator-like thermo decomposition, although with CNT-enabled products no carbon nanotubes were found to escape in the aerosol form (Sotiriou et al. 2016). These results illustrate that information on transformation products in the system being assessed is required for sound decision making.

Recycling and recovery

A number of ENM-containing consumer products (electronics, construction materials, batteries, textiles) may become

recycled. Caballero-Guzman et al. (2015) concluded that, during the recycling process in Switzerland, most of the nano-sized TiO_2, ZnO, or Ag was not recovered for returning to product re-manufacturing, but instead was subsequently transferred to be incinerated or landfilled. The only ENM-containing products that were traced back into the productive process were small quantities of ENM that are part of construction waste or plastics. Very small ENM release into wastewater was found in the recycling process. The authors also concluded that more research is needed focusing on occupational exposure, waste incineration, and landfills.

Fate, transport, and transformation

When ENMs are released into environmental media, these are likely to react or heteroaggregate with constituents of the environmental matrix (air, water, or soil), so that eventual exposures to environmental species or humans, for the most part, will not be to the original form of the material but instead to highly diluted ENM transformation or degredation products.

These environmental reactions will not occur under highly constrained laboratory or manufacturing conditions, but instead will be subject to a range of conditions and essentially stochastic forces which will dynamically change across time and location. Therefore, if exposures to environmental transformation products of ENM occur, the exposures will likely be to multiple forms of environmental transformations including a range of particle agglomerates, sizes, and coatings. Life cycle models for estimating chemical exposures from multiple routes and sources have been developed (e.g. USEtox, WASP; Table 1), and are beginning to be adapted to estimate exposures to ENM (Pu et al. 2016).

Air

A large body of literature describes the behavior of ambient air particles in the atmosphere that is largely applicable to ENM (Oberdörster et al. 2005; Bakand et al. 2012). When released into the air, aerosolized particles are subject to abiotic and biotic transformations, including agglomeration and photooxidation, and are transported with wind or air currents (Figure 3). Advective transport involves the movement of ENM by bulk movements of air, including indoor air currents, wind, up currents, down currents, etc. Particles with smaller aerodynamic diameter and lower mass remain suspended for longer periods of time and can lead to far-field inhalation exposures for humans or other breathing terrestrial species. Airborne particles may also become deposited onto soil, water and plant surfaces. It is estimated that only 0.1–1.5% of globally produced ENM mass is released into ambient air (Keller et al. 2013b). One potential source for the release of EMNs into ambient air involves the use of nanoscale CeO_2 as an automotive diesel fuel additive (Cassee et al. 2011). Nanoscale CeO_2 is widely used in both off-road and on-road vehicles in Europe but is currently only licensed for off-road use in the US (Erdakos et al. 2014). The use of CeO_2 as a fuel additive has been shown to increase fuel efficiency and

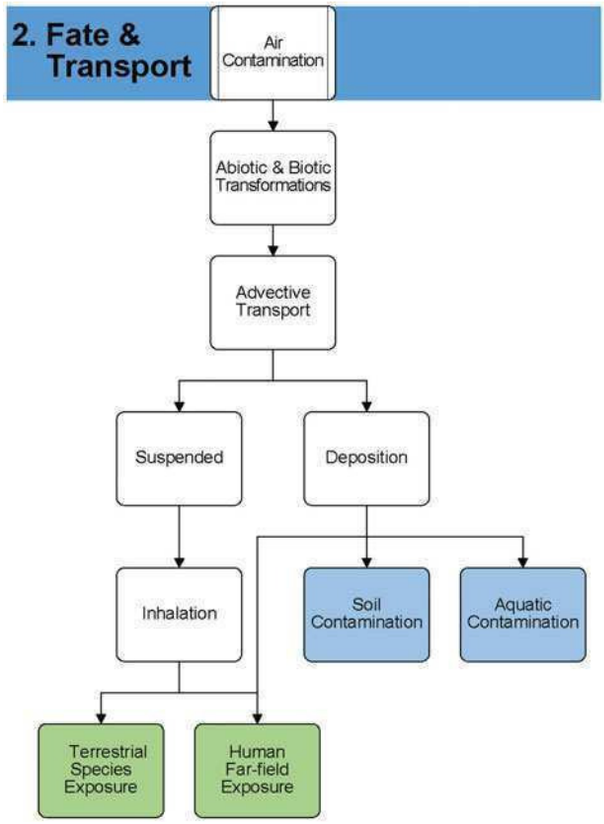

Figure 3. Potential pathways of ENM starting from release into ambient or indoor air. ENM may eventually be transported to another environmental compartment – either media or a human or ecological receptor.

decrease total particulate matter emissions. Despite a lower total mass of particulate emissions, the number of particles in the respirable size range increases, and the particles have greater adverse pulmonary effects in animal models (Snow et al. 2014).

Even though the release into ambient air represents only a small portion of the ENM production volume, there are several exposure scenarios where ENM release into air may pose a potential risk of direct inhalation for humans or local deposition for ecosystem exposure. These include occupational exposure during manufacture, formulation or modification of the ENM-enhanced polymer (through drilling, grinding, sanding, etc.), use of ENM-containing building materials, or formation of aerosols during spray applications (Figure 2). Although engineering control measures have been suggested to lower exposure to airborne EMNs in occupational settings, monitoring worker exposure and health effects remains a challenge (Evans et al. 2010). Exposures to ENMs during manufacture have presented a number of challenges to traditional approaches for protecting worker health. Significant challenges are also involved in relating exposure to risk and include issues such as small and often variable particulate size (within the nano-size range), lung deposition, as well as metrics that are used to measure exposure and effects (e.g. particle mass, surface area or number) (Liao et al. 2014; Eastlake et al. 2016a, 2016b). A battery of pulmonary and cardiovascular disease markers as well as inflammatory and oxidative stress markers, anti-oxidant enzymes, and genotoxicity

markers were compared in nanomaterial-handling and unexposed workers at 14 manufacturing plants in Taiwan (Liao et al. 2014). For this study, the ENM were associated with manufacturing, fabrication or use, and included Ag, TiO_2, SiO_2, Fe_2O_3, and CNT. Significant changes in several biomarkers including antioxidant enzymes (superoxide dismutase, glutathione peroxidase) and cardiovascular markers (vascular cell adhesion molecule, paraoxonase) were associated with exposure at the 6-month follow-up for handlers of carbon nanotubes, TiO_2, SiO_2, and Ag ENM. These results are relevant to the current framework, indicating that oxidative stress and inflammation represent key events along the AOP.

Another area where ENMs might be released into air is through the application and eventual weathering of coatings on building materials, or the remodeling or demolition of those structures (Shandilya et al. 2015). Photocatalytic TiO_2 ENM are released from ceramic building materials or coatings during weathering or abrasion, (Shandilya et al. 2015). West et al. (2016) documented over 450 construction products reported to be nano-enabled. The most frequently reported ENMs included TiO_2, silica, ZnO, and CNT. A case study using TiO_2-coated ENM tiles suggested that local exhaust ventilation during cutting and grinding of tiles significantly reduced Ti-containing respirable dust in the personal breathing zone and local construction areas. Recommendations also suggested better quantification of worker exposure and the effects of transformation and release over the product life cycles (West et al. 2016).

In addition to the aerosol application of coatings involved with building material surfaces, the use of ENM-enabled consumer spray products as coatings or disinfectants also show the potential for near-field human exposures. ENM-enabled products are quite diverse in terms of intended uses as well as the ENM employed. Examples of products that have been described in the literature include; antiperspirants, anti-odor shoe spray, and "plant-strengthening spray" (Lorenz et al. 2011) as well as anti-odor spray for hunters, surface disinfectant and throat spray (Quadros & Marr 2011). These exposures could be assessed according to the outline of Figure 2; Product Use; Dispersive Formulation; leading to Direct Consumer Exposures.

Soil

When ENM enter the soil environment, they are subject to biotic and abiotic transformations as in other environmental media, and they may either become bound and immobilized in the soil matrix, or remain unbound and relatively available for exposures or for transport to other environmental compartments (Figure 4). Assessing the fate and transport of ENM in soils is complex due to highly varying soil physical, chemical, and biological characteristics and processes, all of which can react spatially (angstroms to landscapes), temporally (instantaneous to geologic time steps), and biologically (across scales from prions to ecosystems). The biogeochemistry of a soil at any given locale results from continuous interactions among these characteristics and processes while the soil also reacts to ever changing environmental factors. Soil exposure to ENM may occur through direct deposition,

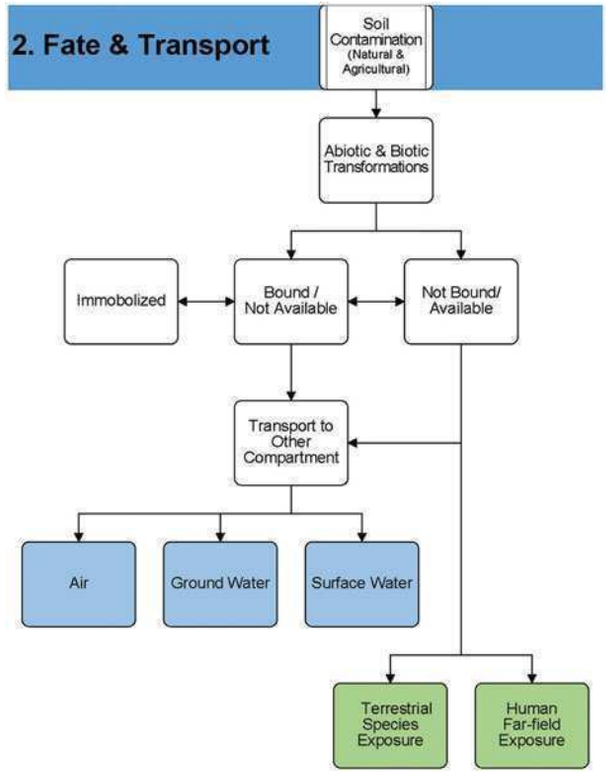

Figure 4. Potential pathways of ENM starting from release into natural or agricultural soil. ENM may eventually be transported to another environmental compartment – either media or a human or ecological receptor.

rainfall removal of excluded (non-bound) ENM from leaves, or from decomposition of vegetation containing ENM. Soils contain significant diversity in forms of organic matter, which may bind and influence aggregation and availability to soil flora and fauna.

Once in the soil, numerous transformations may occur, including physicochemical, macromolecular, or biological (Dwivedi et al. 2015). Other soil characteristics such as water content, pH, mineral content, and bulk density may influence chemical interactions in the soil, including homo- and hetero-aggregation (Dwivedi et al. 2015). In some cases, metal ENM such as Cu and Ag may solubilize and form other complexes. The extent to which an ENM is chemically transformed are constrained by the class and properties of the ENM, e.g. metals, metal oxides, carbon-based, quantum dots, ENM surface coatings, etc., and soil properties; see Dwivedi et al. (2015) for a more thorough discussion of the underlying mechanisms that initiate the abiotic and biotic transformations of ENM. Briefly, an assessment of ENM transformations in soil needs to include the physicochemical processes of aggregation, stability, dissolution, and deposition, and the potential for sunlight to induce photochemical reactions. Soil properties contributing to these processes and reactions include, but are not limited to, the relative and absolute amounts of organic matter of various qualities; soil inorganic particle size distribution; ionic strength; cation exchange capacity; relative soil hydrophobicity/hydrophilicity; type of salts; and the valence of the associated cation, base cation saturation ratio, water content, and pH.

Numerous substances are produced and released into the soil as carbon and nutrient resources (and ENM) that move

along the bidirectional pathway, e.g. ions, organic acids, amino acids, polypeptides, enzymes, and catalysts, all of which will influence the biotic and abiotic transformations of ENM.

Physical processes also contribute to the bound/unavailable and unbound/available status of ENM. Several factors contribute to the fate of ENM on any particular site, such as protocols for soil managment; soil particle size distribution; the absolute and relative quantities of various quality fractions of soil organic matter; and the uptake, translocation, and potential for re-release of ENM by organisms throughout the plant–soil food web. These factors will determine whether ENM remain on-site or will be transported to another environmental compartment. Reviews and more thorough discussions on the roles of soil organic matter, humic, and fulvic acids, and soil colloidal chemistry and physics are available (Hunter 2001; Kleber & Johnson 2010; Essington 2015). Examples of off-site transport include soil removal via actions of wind and water, consumption by mobile consumers [e.g. squirrels eating mushrooms, bird and mammal foraging, uptake of ENM into human food resources (plants and animals), etc.]. The myriad of ways ENM can be transported to another environmental compartment leads to the potential for ENM to be transferred to the atmosphere, ground and surface waters, thereby creating additional pathways of potential exposure to terrestrial species and humans.

The application of biosolids to land is estimated to be the main source of ENM emissions into soil (Tourinho et al. 2012; Gottschalk et al. 2013; Keller et al. 2013a, 2013b; Sun et al. 2014; Figure 4). As discussed earlier, many ENM will be chemically and physically altered during wastewater treatment. Sulfidation of metal and metal oxide ENM is generally the end-product in fresh biosolids, and some of these sulfidation products are further transformed during composting, aging, and stockpiling prior to land application. Pristine ENM are unlikely to enter the soil environment from the consumer → WWTP → soil pathway.

Direct application of ENM as nano-formulated pesticides, or some spray applications such as surface coatings, may result in direct exposure of ENM to soils. Additionally, direct release of ENM as a result of storage or transportation accidents should be considered. Exposure estimates that utilize broad averaging methods to divide nanomaterial potential releases over large geographical areas or environmental compartments may arrive at low estimated exposure concentrations. However, receptors might encounter pockets of higher concentrations of ENM due to latent chronic releases, concentrated intentional distribution, or spills. For these reasons, it is important to be mindful of the implicit assumptions behind exposure scenario descriptions, and assure that they are appropriate reflections of the cases being considered.

Several literature studies have attempted to examine ENM reactions in soils either through the consumer-to-WWTP-to-soil pathway or direct release. Unfortunately, many of these studies employ ENM concentrations that are disproportionately high in relation to probabilistic modeling of ENM release to soil systems, or spike ENM into processed biosolids without taking into account physiochemical reactions that occur in a WWTP (Priester et al. 2012; Colman et al. 2013). Historical research on biosolids application to soil, with particular emphasis on metal risks, highlights the complexity of understanding contaminant chemistry. Metal spiking in soils causes what is called the "salt effect". When metals (or ENM) work their way through a WWTP, the chemical reactions are buffered after the biosolids product has equilibrated for several months before land application. However, spiking a metal salt (i.e. Zn^{2+}) directly into soil or processed biosolids results in forms of Zn that are not similar to Zn phases in the WWTP-reacted, composted biosolid. Further, the spiked Zn^{2+} seeks equilibrium and, through hydrolysis ($Zn^{2+} + 2H_2O \rightarrow Zn(OH)_2 + 2H^+$), causes soil acidification that is not encountered in the equilibrated, composted biosolids. While spiking metal salts or ENM directly into soil would provide the worst case scenario for risk assessment, application, and interpretation of such results is challenging. There are limited examples examining the impact of ENM-influenced biosolids land application as well as realistic direct exposure of ENM in soils.

A case study of Ag salt and Ag ENM spiking directly in soil can be drawn from recent studies (Settimio et al. 2014; Sekine et al. 2015) which examined the lability of Ag_2S ENM represented in biosolids in comparison with labile $AgNO_3$ and metallic Ag ENM. Regardless of soil pH, $AgNO_3$ spiked soils observed more labile Ag than those treated with metallic Ag ENM. The Ag_2S ENM demonstrated virtually no Ag lability. Since the application of biosolids to land is estimated to be the main source of ENM emissions into soil and the primary form of Ag in biosolids is Ag_2S (Kim et al. 2010a; Kaegi et al. 2011; Impellitteri et al. 2013; Lombi et al. 2013), the chemical stability and low Ag lability from Ag_2S should drive the long-term risks of Ag toxicity in the soil environment.

Aquatic

Once an ENM is introduced into the aquatic environment, a series of processes begin that ultimately affect its fate and potential to cause adverse ecological and human health effects (Figure 5). Most fundamentally, and regardless of the source to the aquatic environment (e.g. soil groundwater intrusion, atmospheric deposition, and/or in-flow of surface waters), the ENM will distribute between the surface water and either suspended solids, dissolved organic carbon (DOC) or some other partitioning phase, and ultimately through depositional processes, may be deposited into sediments (Klaine et al. 2008; Praetorius et al. 2012; Dale et al. 2015; Velzeboer et al. 2014, Wang et al. 2014b). However, through competing dynamic processes, including resuspension, an ENM in the sediment may be returned to the surface waters only to be returned again to the sediments when the resuspension event ends. In the surface water or sediment, the ENM will be distributed between the aqueous phase and some form of particulate phase (i.e. heteroaggregation). Heteroaggregation is a process that occurs predominately between colloidal particles. By the time particles reach the microscale, they start to precipitate out in many systems. In the surface waters, this means the ENM will be either suspended in the aqueous phase or associated with suspended

colloids, DOC, or some other phase (Hyung et al. 2007; Klaine et al. 2008; Chang & Bouchard 2016). In the water located between sediment particles, the ENM will remain similarly suspended in the aqueous phase or associated with DOC, colloids, other ligands, and sediment particles.

For ENM in surface waters, transport and transformation will be governed by parameters such as ionic strength, temperature, pH, light intensity, and the concentrations of suspended particle matter (SPM), colloids, and DOC. These parameters affect ENM aggregation state, deposition on surfaces (Hyung et al. 2007; Saleh et al. 2008; Chang & Bouchard 2013), and transformation rates (Lowry et al. 2012; Hou et al. 2013, 2015; Chen & Zepp 2015; Chowdhury et al. 2015a; Mitrano et al. 2015). While the literature is well populated with reports of ENM–ENM interactions (i.e. homoaggregation), there is a growing consensus that heteroaggregation, the interaction of ENM with naturally occurring particles, will be the dominant particle interaction process in most natural systems (Koelmans et al. 2009; Praetorius et al. 2012; Bouchard et al. 2015). The reason for heteroaggregation dominance is that naturally occurring particles will greatly outnumber ENM in most environmental waters (Figure 5).

Relative to transport mechanisms, ENM released into a water body will interact with SPM, colloids and DOC and will then be subject to advective transport with water flow (e.g. stream and riverine flow, tidal motion) and to a lesser degree diffusive transport. Eventually ENM will be deposited to stream, lake or estuary bed with settleable SPM. Once deposited, the SMP-ENM aggregate may be buried in sediments or resuspended in the water column depending on water body

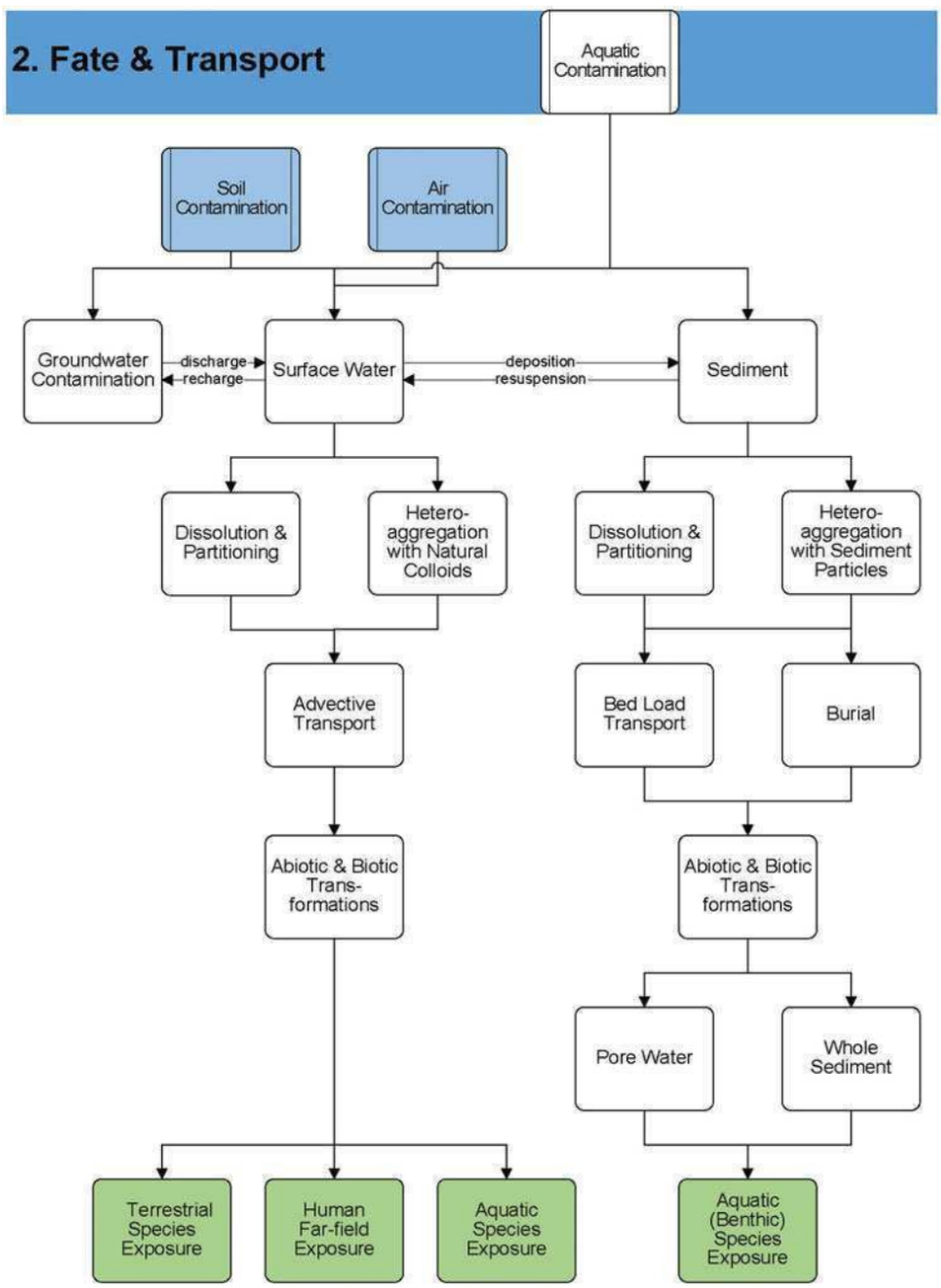

Figure 5. Potential pathways of ENM starting from release into surface water, groundwater, or sediment. ENM are less likely to transport to another form of environmental media. ENM will likely come into contact with an ecological receptor.

hydrodynamics. Within the sediment interstitial water, the aqueous phase ENM may also be transported by diffusive processes which may result in ENM exiting the interstitial water at the sediment water interface and entering the surface water. Along with the physicochemical and transport processes just discussed, there are also abiotic and biotic transformations (e.g. photodegradation, microbial degradation) that may affect ENM. For example, Chowdhury et al. (2013) reported that graphene oxide, a modified form of graphene, was stable and did not precipitate for days in natural and synthetic surface waters.

Given the extensive research and development that have produced the currently available contaminant transport and diffusive models (see Table 1 for examples), novel ENM models should not need to be developed. Rather, existing transport and diffusive parameters may be modified to address processes that differ between traditional dissolved contaminants (solutes) and ENM. One important difference is that most existing contaminant transport models use equilibrium solute partitioning to describe solute interactions with environmental particle surfaces, whereas ENM interactions are classically described using particle attachment kinetics. It is important to consider the complexity and interconnected nature of the various environmental compartments and the biota within them in determining fate (and toxicity) of the ENM. Sediments are the final sink for many anthropogenic contaminants including ENM. In many aquatic systems, particularly marine systems, ENM enter the water column and in a relatively short time frame move to the sediment phase via heteroaggregation and precipitation (Figure 5).

Hendren et al. (2013) have assessed the utility and limitations of existing contaminant transport and fate models for their application to ENM. There is a small but growing literature on ENM transport in surface waters. Streambed-water column exchange of TiO_2 nanoparticles has been modeled using particle–particle interactions and stream bed filtration processes (Boncagni et al. 2009) and ENM-specific processes have been linked to a spatially explicit hydrologic model (Quik et al. 2015). In an application of heteroaggregation attachment efficiencies, TiO_2–SPM interactions and TiO_2 concentrations in the water column and in sediments have been estimated (Praetorius et al. 2012). As these types of modeling approaches progress, data from ENM transformation and biota response studies should be incorporated into simulation models to provide more thorough estimates of the environmental distribution and potential for adverse effects from ENM released to water bodies.

In aquatic systems, as in other complex media, environmental transformations of ENM have important effects on their transport and toxicity (Lowry et al. 2012; Mitrano et al. 2015). Transformations are typically dependent on the chemical and biological conditions surrounding the ENM, so rates and products vary throughout the life cycles. Transformations are likely to be most varied during the use phase of life cycles due to the high variability of environmental conditions that apply during use. Mathematical models are one potentially useful tool for evaluating the variable effects of transformations on human and ecological exposures to ENM. For example, the Water Quality Analysis Simulation Program (WASP) is a mechanistic fate and transport water quality model that includes transformation processes (Table 1). WASP has been widely utilized for modeling the fate of traditional contaminants, but is now being updated to allow simulation of ENM exposures in aquatic environment (Knightes 2015). Process descriptors and data (e.g. for aggregation, deposition and transformations) and data inputs for conditions prevalent in aquatic environments are incorporated into WASP to provide improved understanding of the factors that influence exposure to ENM. Transformed (i.e. aged) ENM or ENM released during product use typically no longer have the same characteristics of their pristine counterparts (Lowry et al. 2012; Froggett et al. 2014; Kingston et al. 2014; Mitrano et al. 2015).

Considerations of carbon ENM illustrate the varied potential impacts of transformations on exposures and toxicity of ENM. These changes can be mediated by aggregation of the ENM. Increases in ionic strength alter the aggregation of CNTs and these changes may alter phototoxicity by increasing photoproduction of toxic singlet oxygen by the CNTs (Chen & Zepp 2015). Environmental transformation of the ENM released from products such as plastic composites can be initiated by sunlight (Froggett et al. 2014; Kingston et al. 2014; Mitrano et al. 2015). Direct and indirect processes are both competitively involved in the environmental phototransformation of ENM. For example, graphene oxide (GO) – a promising precursor to graphene-based materials – strongly absorbs sunlight in the ultraviolet and visible spectral regions, making direct photochemical reactions an important determinant of the persistence of these materials (Hou et al. 2015). Light-induced transformations of GO ENM produce much more hydrophobic, and likely more toxic, polycyclic aromatic hydrocarbons (Chowdhury et al. 2015a, Hou et al. 2015). Transformations can be driven by photochemical reactions, oxidation reactions, and biological processes, all of which affect their environmental transport (Chowdhury et al. 2015a). In the case of GO in natural waters, direct photoreaction likely dominates the initial phototransformation of GO into reduced graphene oxide species, low molecular weight (LMW) species and CO_2; these photoproducts are significantly less photoreactive, however, and persist under direct photolysis conditions. Thus, indirect photolysis initiated by natural organic matter is likely to dominate the secondary phototransformation process, ultimately converting reduced graphene oxide and LMW species into CO_2 (Hou et al. 2015). During this mineralization process, the intermediate species exhibit decreasing size and higher carboxyl group concentrations, and greater stability against aggregation and reduced surface deposition, indicating they would be more mobile than parent GO (Chowdhury et al. 2015a). This information combined with rate data can be used to model the fate of the GO ENM outlined in Figure 5.

Information on transformation processes can be used as inputs to water quality models such as WASP to evaluate the drivers of exposure concentrations in various compartments of aquatic environments such as rivers, ponds, lakes, estuaries, and coastal environments. Transformations can be responsible for evaluating exposure concentration changes in aquatic systems, including changes in the toxicity of ENM.

This information can be useful in designing monitoring and remediation strategies for contaminated systems. Also changes such as potential releases of ENM from plastics and related effects on ENM distribution and biological uptake can be evaluated using this modeling approach. Graphene oxide provides a good example of an ENM that can be evaluated using this modeling approach. Changes caused by photo-transformations can alter the persistence, mobility, and toxicity of graphene oxide residues (Hou et al. 2015, 2016).

CNT's have been shown to be stabilized in water by DOC, which acts like a surfactant to keep the CNT's suspended in the aqueous phase (Hyung et al. 2007; Kennedy et al. 2009). For graphene family materials, GO, with its substantial oxygen content is readily suspendable in water (Chowdhury et al. 2015b). In natural waters, particularly those with high DOC contents, carbon-based ENM can be stable in the water column resulting in organism exposures. Regarding transport and uptake of CNTs in water and soil, these materials are usually incorporated as composites with various matrices such as plastics in many commercial products and these composites have different fate and transport characteristics than pristine (pure) CNTs. It is now recognized that plastics have become widely distributed in aquatic environments and incorporated into food webs. Also, it has been shown that CNTs can be released from the composites by weathering and abrasion.

Some ENM release truly dissolved materials which are readily bioavailable, but arguably are no longer ENM. Nevertheless, because nano-scaled particles have a significantly larger surface area per unit mass and dissolve more rapidly than their micron-scale counterparts, the rapid release of toxic ions at the biological interface is a mechanistic consideration for ENM. A good example in consumer products is copper which is often in the chemical form of copper carbonates ($CuCO_3$) (e.g. pressure treated lumber), and releases the readily bioavailable and toxic Cu^{2+} (Parks et al. 2015). Silver ENM are often used in commercial products as vehicles for controlled release of silver ion at biological interfaces. Very low free Ag ion concentrations might be expected for fresh water or estuary environments that are likely to contain chloride, phosphate, and carbonate ions. Dissolution and transformation of Ag ENM in suspension compared with those interacting with bacteria and other aquatic organisms presents a significant uncertainty. Contact with aquatic organisms may increase the release of silver ions within the organism's local membrane environment (Fabrega et al. 2011). As a consequence, biotic as well as abiotic effects on dissolution and transformation should be considered in assessing risk of ENM to ecosystem targets (Navarro et al. 2008b).

Exposure and biodistribution

The determination of potential risk from ENM-enabled products requires assessments of exposure and hazard. As a simplistic example, a highly hazardous type of ENM may rarely be encountered by a target organism – or by contrast, a target organism may be chronically exposed to an ENM that shows only a moderate acute toxicological response. In any case, risk-based decisions will consider relative potential for exposure and hazard.

Exposure and biodistribution to terrestrial species, including humans, is depicted in Figure 6. Terrestrial fungi and microbes, as well as the roots of terrestrial plants, may become exposed to ENM in the soil. Terrestrial plants may also become exposed through the foliage after aerosol deposition or the application of nano-enabled agricultural products. Following such contact, the ENM may be absorbed, adsorbed, or excluded. Absorbed and adsorbed materials may be translocated to the interior of the organism leading to cellular level exposures, or they may be released or excreted causing a transfer to other environmental compartments. Exposures to terrestrial animals, including humans, through inhalation, oral, or dermal routes can lead to transformations at the point of contact, and perhaps either translocation across the biological barriers to the interior of the organism, or exclusion. Nanoparticles that reach pulmonary fluid, the gut, or the blood plasma typically will be coated with a protein corona, as discussed below. *In vitro* modeling of gastrointestinal digestion for polystyrene nanoparticles influenced the protein corona composition and increased translocation of these particles into Caco-2 and HT29-MTX cells. Variations in the protein corona and translocation rates were dependent on the biochemical surface modification of the polystyrene nanoparticles (Walczak et al. 2015). The composition of the corona may include opsonin or other proteins which can trigger macrophage phagocytosis leading to degredation or excretion. The protein corona also may influence distribution across biological barriers and cellular uptake. Modification of the surface of nanoparticles with polyethylene glycol (PEG) can alter binding of proteins to the nanoparticles, and thus impacts protein corona formation. This modification of the nanoparticles using PEG results in decreased uptake by macrophages and prolonged tissue residence time (Pearson et al. 2014). Such changes in particle coatings could change rate constants for nanoparticle transitions for systemic absorption, distribution, and clearance (Figure 6). Particle aerodynamic diameter influences the region of deposition in the respiratory tract, but the effect of particle size on macrophage uptake may not be a factor. Blank et al. (2013) have shown that there was no difference in murine alveolar macrophage uptake between 20 and 1000 nm sized polystyrene nanoparticles.

Human exposure

The exposure of humans or indicator organisms to ENM or ENM-enabled products may occur at numerous points along the product life cycle. One way to consider human exposure assessment is through analysis of activities along the nanomaterial life cycle that bring these materials into contact with receptors. In addition to estimating these activities, it is important to consider the magnitude, frequency and duration of exposure to an agent, along with the number and characteristics of the exposed population (Zartarian et al. 2004). These factors are part of the exposure assessment for a risk assessment for any chemical or physical agents. Two sources of human exposure to airborne ENM are during manufacturing and use of ENM-enabled construction products (coatings, cements, and concrete). Given the relatively high number

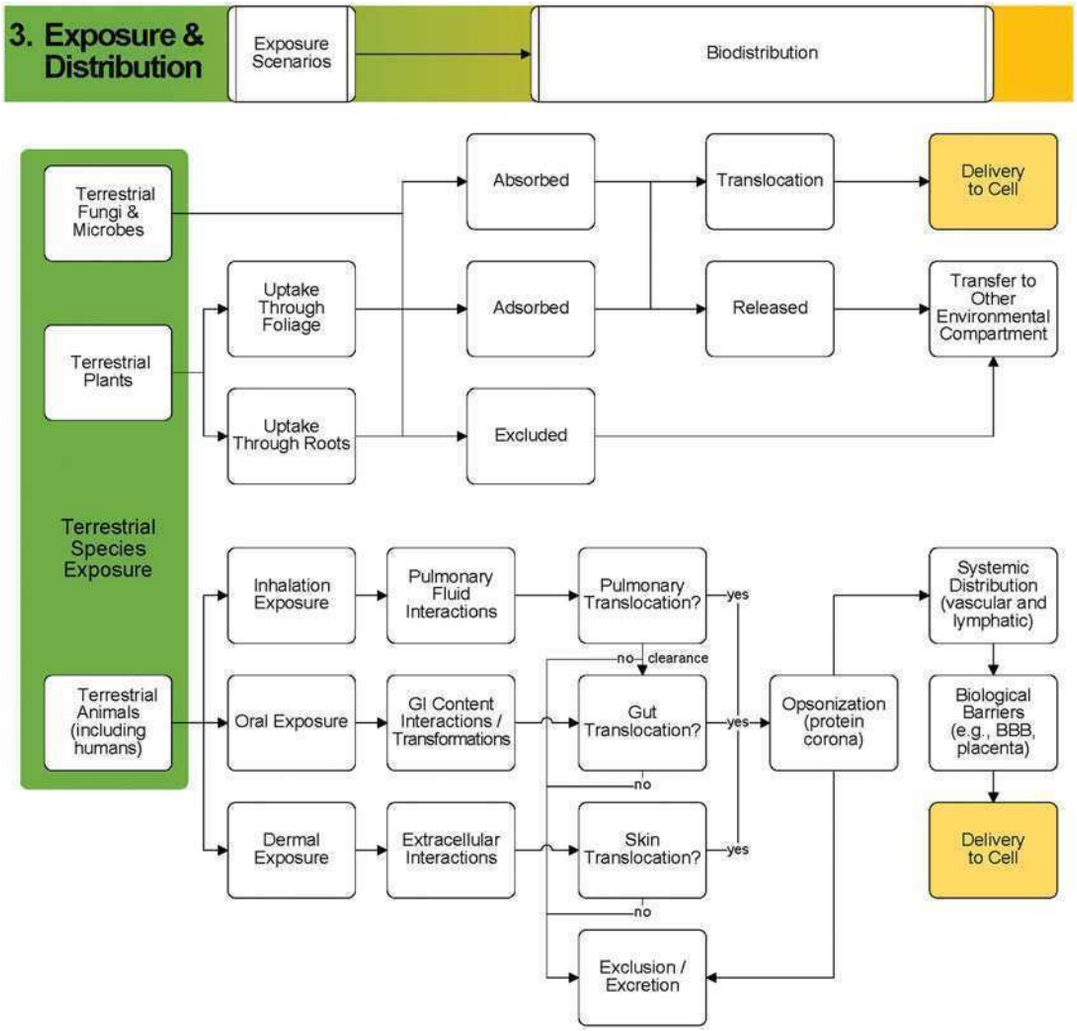

Figure 6. Potential terrestrial species exposure and biouptake pathways, including pharmacokinetic distribution routes that continue up to contact with cells.

(70–80%) of construction workers who are unaware of the presence of nanomaterials in the products that they routinely spray, cut, or sand, the potential use of personal protective equipment or use of engineering controls are likely to be limited (West et al. 2016).

Occupational exposure can occur during the synthesis, application, recycling and disposal of nanoparticles or ENM-enabled products. Workers may be among the first people exposed to new ENM, and may have higher levels of exposure than do other segments of the population (Schulte et al. 2014). Occupational safety and health achieved through limiting worker exposures to ENM is an area of focus for the responsible development and use of nanotechnology. One particular area of focus has been the potential for inhalation exposure to poorly soluble particles and fibers (Kuempel et al. 2012). As the current paper primarily concerns environmentally mediated exposures, interested readers may find detailed considerations of occupational safety issues elsewhere (Pietroiusti & Magrini 2014; Schulte et al. 2014; Thompson et al. 2015; Boonruksa et al. 2016; Brouwer et al. 2016; Larese Filon et al. 2016). Although occupational exposure concentrations may be higher than those of the general public, the number of individuals potentially exposed in the general population is larger than in the workplace, and includes individuals with greater potential susceptibility such as the young, elderly, or those with other compromising health conditions.

The main routes of exposure for particles from ENM-enabled products are shown in Figure 6. Due to the relatively limited total volumes of most manufactured ENM and the limited time that most ENM have been in production (in the absence of a large spill), human exposures from far-field sources (arising from environmental background) are not likely to become a significant contribution to overall exposure in the near future. Consequently, the most significant exposures for humans in a non-occupational setting are expected to be near-field (arising from interaction with ENM-enabled consumer products), as opposed to far-field scenarios. Where nanomaterial composition was identified, analysis of nano-enabled consumer product inventories suggested that the greatest number of currently listed products contain metal-based ENM (Ag or Ti), followed by Si- and carbon-based ENM (Vance et al. 2015; Hansen et al. 2016).

Estimation of an individual's exposure to ENM from the use of ENM-enabled consumer products requires information concerning the product composition (magnitude of

exposure), how often it is likely to be used (frequency of exposure events), the pattern of product use (duration and potential exposure route), and potential for ENM release from the product matrix. Population exposure modeling requires input on market penetration of the product. Modeling of cumulative exposure can be considered for target populations using multiple products containing similar ENM using integrated probabilistic techniques such as the Stochastic Human Exposure and Dose Simulation (SHEDS) Model (Isaacs et al. 2014). Human exposure pathways to ENM include dermal/ocular contact, inhalation, and oral ingestion. The dermal route has the highest probability of exposure to consumer products (Vance et al. 2015). Ingestion and inhalation routes follow, with about half of the number of reported products being metal-ENM, followed by silicon and carbon-based ENM. Inhalation exposure can result from occupational and environmental sources and, of the three pathways, is most likely to occur and poses the greatest risk of adverse outcomes. Oral ingestion could occur from dietary sources or drinking water contaminated with ENM, hand-to-mouth activity following dermal contact of ENM contaminated surfaces, or from swallowing mucous and macrophages containing inhaled ENM that were cleared from the lung by the mucociliary tract lining the conducting airways of this organ. Given the significant changes in matrix conditions that occur along the GI tract including the acidic environment in the stomach and complex intestinal components, transformation is an important consideration for ENM bioavailability (Alger et al. 2014). Silver nanoparticles have been shown to aggregate, react with chloride and sulfide as well as form protein aggregates and coronas (Mwilu et al. 2013; Walczak et al. 2013). In addition, copper carbonate nanoparticles associated with treated lumber have been shown to dissolute into ions in the presence of simulated stomach fluid (Santiago-Rodríguez et al. 2015). Dermal contact may occur through unintentional or intentional exposure – the latter from, for example, applying sunscreen that contains ENM. Although transport of ENM through skin is typically limited, damaged skin may facilitate increased rates of transdermal transport (Baroli 2010).

Human biodistribution (dosimetry)

The pharmacokinetics (PKs) of chemicals including ENM involves aspects of the rate and extent of their absorption, distribution, metabolism, and excretion (ADME) from the body (Figure 6). The role each process has in the disposition of an ENM is dependent on the route of exposure, characteristics of the individual exposed (e.g. age, health status), and properties of the ENM (e.g. size, surface properties, etc.) and exposure medium (e.g. water, soil, etc.). Publications by Elder et al. (2009), Hagens et al. (2007), Landsiedel et al. (2012), Lin et al. (2015), and Riviere (2009) review the PKs of ENM. Overall, exposure of ENM to terrestrial mammalian species can occur by inhalation, ingestion or contact with the skin (Figure 6). The Multiple-Path Particle Dosimetry Model (MPPD; Table 1) calculates deposition in the respiratory tract based on airway geometry and physical/chemical properties of aerosol or particle. Once exposed to the lung, gastrointestinal tract or skin, different extracellular interactions may occur with the ENM between proteins, lipids, and microbiota within the different fluids of each organ. Transformation of nanoparticles in biological fluids depends on the core particle composition, particle coating, and biological fluid. Simulated gastrointestinal exposure to CdSe-core/ZnS-shell quantum dots resulted in solublization of Zn and to a lesser extent Cd (Wiecinski et al. 2009). Similar treatment of Ag ENM resulted in aggregation and formation of a AgCl coating on the particle aggregates (Rogers et al. 2012). The extent of this transformation was dependent on the initial coating used to stabilize the Ag ENM (Mwilu et al. 2013). Biological fluids such as artificial sweat and urine solubilize Ag ions from Ag ENM-enabled fabrics to a greater extent than water or simulated saliva (Quadros et al. 2013).

Translocation of the ENM through each organ may or may not occur (Baroli et al. 2007; George et al. 2014). Translocation is the result of crossing an epithelial barrier and the ENM is absorbed systemically (Larese et al. 2009). The ENM may then interact with proteins and other biomolecules forming a protein corona. The ENM may then distribute to other organs, requiring crossing another barrier eventually being delivered to a cell within an organ (Baroli et al. 2007; George et al. 2014). Systemically absorbed ENM may also be excreted in the urine or bile for eventual fecal elimination.

The commonality of the exposure pathways described above leading to absorption of ENM is that these materials must cross an epithelial barrier. However, the epithelial barriers of the lungs, gastrointestinal (GI) tract and skin (Figure 6) are different in many ways (Elder et al. 2009). Epithelial cell types include columnar, cuboidal, squamous, and others which vary within each organ/system (GI tract consists of several organs) and each cell type has a different function. While the cells that line the lungs and gastrointestinal tract are viable, the outer layer of the skin, the stratum corneum is non-viable. The microenvironment of each organ system differs with respect to hydration, pH, air:surface interface and other factors. Immune cells are integrated differently within each organ system and provide unique means and abilities which may limit absorption of ENM.

Absorption: portals of entry

The outer layer of the skin, the stratum corneum, is non-viable epidermal tissue (Baroli 2010). The stratum corneum consists of keratinocytes filled with the protein keratin surrounded by a lipid membrane. The means of absorption through the skin is passive diffusion. The epidermis contains pores and shunts, which ENM may enter. ENM have been detected in the pores, cracks and hair shafts of skin (Baroli 2010). The results of most dermal absorption studies of ENM indicate that these materials may penetrate to lower levels of the epidermis, which are viable, but rarely penetrate into the dermis, which underlies the epidermis and is the vascularized tissue of the skin. With intact skin, most studies indicate ENM are excluded from entering the body (Pflucker et al. 2001; Monteiro-Riviere et al. 2011). However, if the stratum corneum is damaged from, for example, sunburn, cuts or

abrasions, further penetration of the ENM through the skin may occur with potential systemic absorption (Larese et al. 2009).

Inhalation of ENM can result in their deposition in conducting and respirable airways. The particle size determines the location of deposition in the respiratory tract. Inhaled particles of about 20 nm in size have the highest proportional deposition in the alveolar region (~50%) (Oberdörster et al. 2005; Elder et al. 2009). Conducting airways (bronchi) are lined with mucous and epithelial cells with cilia. Particles that deposit in the mucous are moved up (i.e. cleared) in the respiratory tract by action of the cilia to the trachea, where they are eventually swallowed and translocated to the gastrointestinal tract. ENM that deposit in the respirable region of the lungs can be absorbed through epithelium of the alveoli. The distance between the outer surface of the alveoli and the capillaries ranges from 0.36 to 2.5 μm (Elder et al. 2009). The ENM may enter the vascular or lymphatic system. The size of ENM particles is a determinant for systemic absorption, with particles <55 nm diameter having greater penetration through the alveoli than particles of 200 nm or greater (Elder et al. 2009). If the alveoli/blood vessel interface is inflamed, absorption of the ENM may be potentially increased (Elder et al. 2009). If not absorbed, ENM may be phagocytized by macrophages, which may be cleared by the mucociliary tract and eventually swallowed and translocated to the gastrointestinal tract. Multiwalled carbon nanotubes (MWCNT) that reach the alveoli may eventually translocate to the pleural cavity (Mercer et al. 2013), as has been found with asbestos fibers (Donaldson et al. 2010; Xu et al. 2014). Length and shape of the MWCNT appears to affect its translocation to the pleural cavity (Xu et al. 2014). There is also evidence of absorption of ENM via the olfactory nervous system following inhalation exposure, where particles may enter the brain without crossing the blood–brain barrier (BBB) (Oberdorster et al. 2004; De Lorenzo 2008).

The GI tract is the anatomical organ system exposed to ENM following their ingestion and includes esophagus, stomach, small and large intestine and colon. The cells lining the GI tract, even though epidermal, change in structure, and function as the GI tract progresses from the esophagus to the colon. The pH of the GI tract also changes from acidic conditions in the stomach to slightly basic in the intestine which can affect the physicochemical properties of the ENM (Elder et al. 2009). Surface charge of the ENM can affect GI absorption, as positively charged ENM seem to be absorbed to a greater extent than neutral or negatively charged ENM (Hagens et al. 2007). As for conventional chemicals, most absorption of ENM in the GI tract takes place in the intestine. This is due in part to the large surface area of the intestine, the longer residence time of the ENM within it than in other parts of the gastrointestinal tract, and the epithelial cell type favoring absorption. It appears the most common mechanism of uptake of ENM in intestinal epithelial cells is by endocytosis (Frohlich & Roblegg 2012). Paracellular uptake may also be involved, but may be less than endocytosis because the area available for the former uptake to occur is much less (Hagens et al. 2007). Particle size may affect intestinal absorption, as Desai et al. (Desai et al. 1996, 1997) have reported polylactic polyglycolic acid co-polymer particles of size 100 nm–10 μm show decreased absorption with increased size of particle *in vitro* whether in the rat *in situ* intestinal loop model or in Caco-2 cells (Desai et al. 1997).

Distribution

ENM absorbed into the systemic circulation are distributed to organs within the body (Figure 6) (Almeida et al. 2011; Stapleton & Nurkiewicz 2014). Studies have essentially found that systemically absorbed ENM are distributed to most, if not all, organs, but the levels detected in the organs vary greatly (Hillyer & Albrecht 2001; Oberdorster et al. 2002; Fabian et al. 2008; Landsiedel et al. 2012). Factors that influence the distribution of ENM include route of administration, physicochemical properties of the ENM, physiological environment where the ENM enters the systemic circulation and the morphology of the endothelium (i.e. blood vessel wall) within that organ. Because the physical flow of blood changes with the size of the blood vessel, when the vessel becomes <300 μm, the smaller solutes tend to move towards the vessel wall (Stapleton & Nurkiewicz 2014). Thus, the size of the ENM is an important determinant of its ability to pass through the endothelium of different morphologies. A continuous endothelium is essentially found in lung and muscle capillaries. The endothelium of kidneys is fenestrated, and that of liver and spleen discontinuous (Almeida et al. 2011).

Proteins and other biochemicals in blood may surround ENM to form a corona. The characteristics of the corona are dependent on the physicochemical properties of the ENM (e.g. size, surface properties) and the biochemicals and proteins that interact and bind to the ENM. As ENM are phagocytized by macrophages and monocytes, the blood and organs that possess macrophages such as liver, spleen, lymph nodes, and bone marrow are some of the first organs that sequester ENM (Almeida et al. 2011). ENM may also be absorbed into the lymphatic system and be distributed as well, although little is known about this aspect of ENM distribution. Stapleton and Nurkiewicz (2014) contend that ENM in lymphatics may contribute to inflammation to a greater degree than in the circulatory system. This is because ENM would be in higher concentrations in lymphatics than in blood, their residence time would be longer due to a lower flow rate, and they could interact with neutrophils and propagate inflammatory signals to a greater extent.

Metabolism

Mammalian biological transformations of ENM are not well characterized or known (Hagens et al. 2007). The available information on fullerenes and silica ENM indicates that these materials are not biotransformed (Landsiedel et al. 2012). Metal-based ENM can be in various oxidation states, so there is the potential that these materials could be oxidized or reduced *in situ* based on the pH and oxidation state of the tissue environment. Metal-based ENM taken up by cells via phagocytosis or endocytosis are exposed to enzymes and changes in pH within the endosome/lysosome. These enzymes may degrade corona proteins and the acidic environment of these vesicles may degrade a metal-based ENM

with release of metallic ions (Soenen et al. 2015). Functionalized single-walled carbon nanotubes (SWCNT) *in vitro* are susceptible to degradation by human myeloperoxidase and eosinophil peroxidase (Kagan et al. 2010; Andón et al. 2013). Overall, more studies are needed to understand the metabolism of ENMs.

Elimination and excretion

Systemically absorbed ENM are eliminated via urinary elimination, fecal excretion or both (Landsiedel et al. 2012). The extent of the elimination by these routes is dependent on the physicochemical characteristics such as size, surface chemistry, and charge of the ENM and the route of administration (Lin et al. 2015). Urinary elimination involves filtration of blood plasma through the glomerulus. Although ENM are found in urine, not all ENM are able to pass through the glomerulus. Choi et al. (2007) report that quantum dots (CdSe/ZnS core/shell) with a hydrodynamic diameter less than 5.5 nm, when administered i.v. to mice, are rapidly and efficiently eliminated via the urine. The adsorption of serum proteins to the quantum dots, which could be prevented by zwitterionic or neutral organic coatings on the dots, tended to increase the hydrodynamic diameter and thus retard their urinary elimination. Intravenous administration of Ag ENM (approximately 8 nm size) to rabbits was followed by low urinary excretion (Lee et al. 2012). This suggests that factors in addition to size of ENM can influence elimination of the particle from the body. Functionalized SWCNT and MWCNT have also been detected in urine of laboratory animals administered these carbon-based ENM (Landsiedel et al. 2012). Whether ENM are secreted or absorbed by the renal tubules is not known.

After being absorbed, ENM may be transported via the bile to the gastrointestinal tract and eliminated in the feces. For an ENM to be excreted into the bile, it would have to cross the cell membrane of the hepatocyte, and then be excreted into the biliary tract. Ag ENM were detected in feces of rabbits administered Ag ENM intravenously, suggesting biliary excretion of these particles (Lee et al. 2012). Low levels of polystyrene nanospheres (50 nm diameter) have been detected in rat bile following intravenous administration (Ogawara et al. 1999). The mechanism of the ENM entry into the bile is not known.

Some ENM dissolve to smaller constituents or ions over a time course of days, while other ENM can be strongly persistent. For example, 90 d after i.v. infusion of 30-nm sized CeO_2 in rats, there was little decrease in cerium concentration in any tissue (Yokel et al. 2012).

Physiologically based PK modeling

PK models use mathematical formulas to describe the movement of a chemical or drug in the body. A progression of PK models is the inclusion of physiological, anatomical, biochemical, and other specific aspects in mathematical terms (tissue volumes, flow rates, etc.) to build physiologically based PK (PBPK) models. PBPK models have several advantages over PK models in terms of extrapolating dose, exposure duration, route-to-route and species. A strength of PBPK models is that they can be used for hypothesis testing, to understand mechanisms of toxicity, and to make predictions of movement of a chemical in humans using *in vitro* and *in vivo* PK animal data. PBPK models are extremely useful for regulators because of the information they can gather from this predictive tool. PBPK models have been applied primarily to inorganic and organic compounds, such as drugs, with a MW less than approximately 900 Da. The PKs of small molecules are different from ENM in areas of diffusion, active transport, metabolism, and excretion. The physiological, biochemical, and metabolic processes that the body imposes upon ENM are generally different than those for non-particulate or small molecules (Li et al. 2012). For these reasons, only a few PBPK models have been published for ENM and include those on Ag (Bachler et al. 2013), ZnO (Chen et al. 2015), and TiO_2 (Bachler et al. 2015) (Table 1).

The Ag ENM PBPK model (Bachler et al. 2013) included structures for ionic and nanoparticulate Ag and were based on PK data from intravenous studies in rats. The modeling results, within the confines of particle sizes (15–150 nm) and coatings (polyvinylpyrrolidone and carboxymethyl cellulose), indicate that particle size and coating had minimal impact on the distribution and organ uptake of the Ag ENM; dissolution to Ag ions was not significant; the ENM were stored as insoluble salt particles; and uptake of Ag ENM by macrophages was of minimal significance for relevant human exposure levels. The ZnO PBPK model (Chen et al. 2015) was based on previous PK studies using ZnO ENM (10 and 71 nm) and $ZnNO_2$ (soluble) administered to mice. The modeling efforts showed that the tissue partition coefficients of ZnO ENM were greater than those of soluble zinc; the excretion and elimination rates in liver and gastrointestinal tract of 71 nm ZnO ENM and soluble Zn were important determinants of their PKs; ZnO ENM decomposed to soluble Zn after 1 week in the body. The TiO_2 PBPK model (Bachler et al. 2015) was based on published PK data of mice and rats administered TiO_2 ENM intravenously. The modeling results showed that particle size (15–150 nm) and crystalline structure of nano-TiO_2 had limited impact on the distribution; and the nanoparticles agglomerated at high concentrations and were engulfed by macrophages (Bachler et al. 2015). Extrapolating the results to human oral exposures to nano-TiO_2, Bachler et al. (2015) reported that the organ concentrations of titanium at the 95th percentile level were lower than concentrations in *in vitro* studies that resulted in toxic effects.

There has been a great research effort to understand the biodistribution and dosimetry of ENM over the past 10–15 years. Certainly the physical and chemical properties of the ENM, such as chemical composition, size, coatings, have a tremendous impact on how the body interacts with these particles regarding their absorption, distribution, metabolism, and excretion. But the most critical ENM property affecting biodistribution and dosimetry has not been clearly defined, and represents a significant data gap. With all of the different types of ENM (e.g. metals, metal oxides, SW-, and MWCNT) currently in use and with their transformation/degradation in the environment to a variety of products, it may not be possible delineate a specific property of the ENM that has the greatest impact on its biodistribution and dosimetry within the body.

Testing the potential toxicity of ENM frequently includes *in vitro* assessments as a component of the testing strategy. Understanding dosimetry to cells *in vitro* has become an important consideration (Teeguarden et al. 2007). Typically the cells to be tested are adherent to the bottom of a flash or well and the nanomaterial suspension is added to the media over the cells, with the dose expressed as the mass concentration per unit volume. However, the amount of nanoparticles reaching the cell layer can differ substantially from the added concentration. The behavior of ENM suspended in media is dependent on forces of diffusion, where particles tend to remain in suspension, and sedimentation, where particles tend to settle gravimetrically (Teeguarden et al. 2007; Hinderliter et al. 2010). Computational models (Table 1) have been developed to predict dose delivered over time to the celluar layer, including the *In vitro* Sedimentation, Diffusion and Dosimetry (ISDD) model (Hinderliter et al. 2010). Subsequently, procedures were standardized for preparations of particle suspensions (Cohen et al. 2013a, 2014), and estimating density of particle agglomerates (DeLoid et al. 2014) with corresponding model updates, to better estimate *in vitro* particle dosimetry.

Extracellular interactions

Protein corona/opsonization

Once introduced into a biological fluid such as blood, ENM interact with a variety of cells, proteins and other biochemicals. The interaction of ENM with proteins in blood *in vivo* or serum *in vitro* results in formation of a protein corona (Figure 7) (Nel et al. 2009; Zhu et al. 2012; Fleischer & Payne 2014; Pearson et al. 2014; Treuel et al. 2014). Proteins that have been found in the corona include albumin, immunoglobulins, apolipoproteins, and fibrinogen (Lundqvist et al. 2008). In some circumstances, over 80 proteins have been associated with citrate stabilized Ag ENM (Shannahan et al. 2015). The formation of these complexes is a dynamic process that is dependent on surface characteristics of the ENM, properties of the suspending media (e.g. salts and multivalent ions), the solid-liquid interface (e.g. surface hydration and dehydration) and the ENM–protein interface (e.g. conformational change in protein) (Nel et al. 2009; Ritz et al. 2015). The adsorption of proteins to ENM occurs at various rates because of differing affinities the proteins have towards the surface of the ENM (Ritz et al. 2015). It was proposed that eventually, a "hard" corona is formed with proteins that have a high affinity towards the surface of the ENM and an overlaying "soft" corona, consisting of proteins having a lower affinity to the ENM (Lynch et al. 2007). Others find the protein coronas to be unstable and reversible, similar to other forms of heteroaggregation (Liu et al. 2013). The forces controlling the interactions between ENM and protein include hydrodynamic, electrodynamic, electrostatic, solvent, steric, and polymer bridging (Nel et al. 2009). The formation of the ENM-protein corona complex may alter the physicochemical properties of

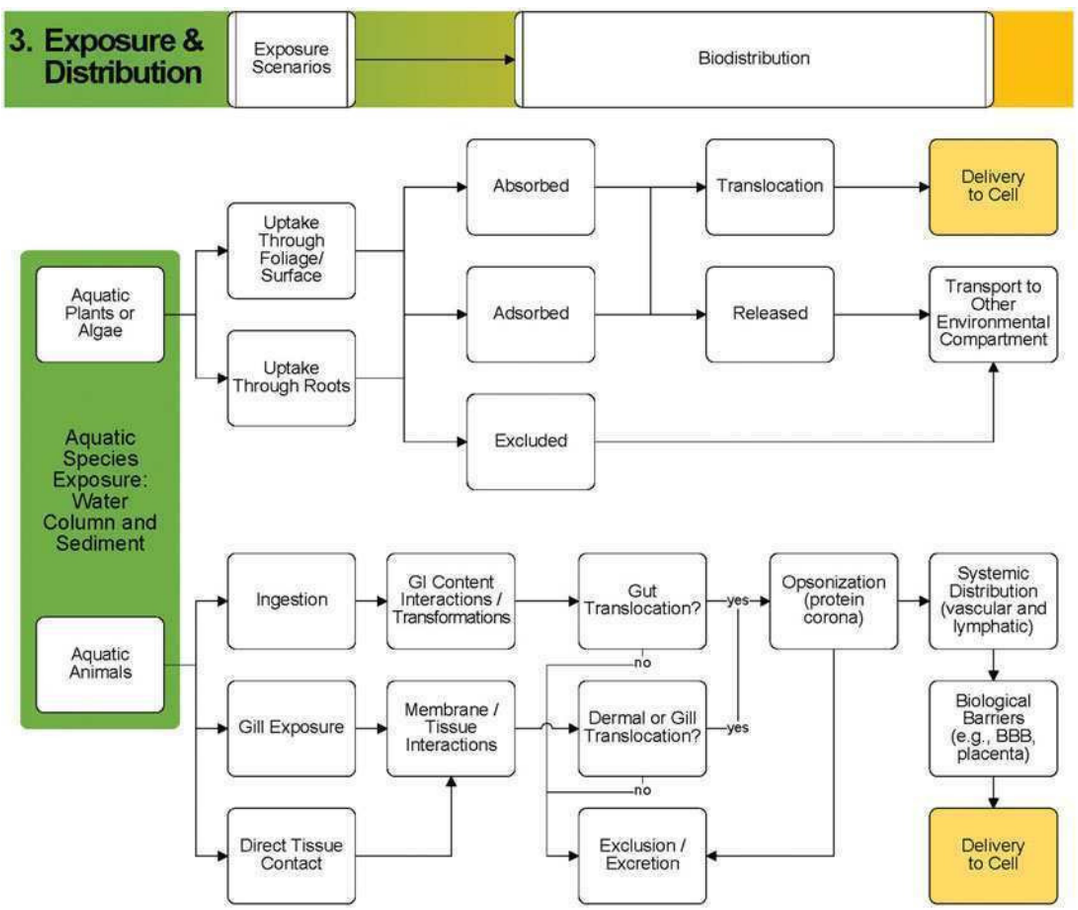

Figure 7. Potential aquatic species exposure and biouptake pathways, including pharmacokinetic distribution routes that continue up to contact with cells.

the ENM such as zeta potential and agglomeration of the ENM (Pearson et al. 2014; Treuel et al. 2014). Conformational changes in the protein as a result of this interaction with an ENM may result in exposure of new epitopes (leading to potential allergenicity), altered function (protein no longer recognized by cellular receptors), and changes in avidity (Nel et al. 2009; Shannahan et al. 2015). Knowledge of the ENM–protein corona complex and how it is formed will enable an understanding how ENM are internalized into cells, as these complexes can bind to specific receptors involved with cellular uptake.

Opsonization is a biological process that promotes, but does not always result in, clearance of ENM from the systemic circulation. Complement proteins adsorbed to the ENM are recognized by receptors on macrophages (Walkey et al. 2012). Macrophages internalize the ENM-protein corona complex via receptor mediated phagocytosis. Remarkably, modifying an ENM with polyethylene glycol (PEG) will reduce uptake of the ENM by macrophages (Pearson et al. 2014). The uptake of gold ENM by murine macrophages is decreased by 75% or more when the density of polyethylene glycol grafted on to the gold nanoparticles reaches 0.32 PEG/nm^2 (Walkey et al. 2012). This effectively increases the systemic circulation time of the ENM. PEGylation of ENM reduces binding of proteins to the ENM. Because of differences in the physicochemical properties of ENM, such as size, the effect of PEGylation on the ENM must be made on a case by case basis.

Biological barriers (e.g. BBB, placenta)

ENM that have reached the systemic circulation following oral, pulmonary, or dermal exposure have translocated through an epithelial barrier. To translocate from the systemic circulation into internal organs, ENM must pass through an endothelial barrier – the wall of the blood vessel. The lining of blood vessels by the endothelium, which varies from organ to organ, is continuous, fenestrated, or discontinuous. Organs such as the liver and spleen have a discontinuous endothelial cell lining and are more "leaky" than other organs. This allows for substances in the blood to be absorbed more easily by these organs. Other organs such as the brain have a continuous endothelium that is more specialized. This distinctive lining limits the absorption of many exogenous chemicals in these organs and provides a level of protection.

The brain is a unique and sensitive target organ for toxicants because of its limited ability to regenerate cells and tissue after toxic insult. The uptake of many exogenous chemicals including ENM from the systemic circulation into the brain may be limited due to its specialized barrier, the BBB (Bhaskar et al. 2010). The endothelial cells of the vasculature within the brain are connected by special protein complexes that form tight junctions between the cells (Pietroiusti et al. 2013). Efflux transporter proteins also line the endothelium that carries xenobiotics out of the brain (Tamai & Tsuji 2000). However, the role of transporters eliminating ENM out of the brain is not well defined. Despite the BBB, chemicals including ENM are still absorbed into this organ following oral administration or intra-tracheal instillation (He et al. 2010; Hu et al. 2010; Kim et al. 2010b; Park et al. 2010; Yang et al. 2010; Schleh et al. 2012). Molecules of low molecular mass (<400–500 Da) and lipophilic compounds may cross the BBB and enter the brain tissue by passive diffusion (Bhaskar et al. 2010). Although not quite clear, ENM may be absorbed into the brain by receptor-mediated endocytosis or pinocytosis (Bhaskar et al. 2010; Zhao et al. 2011). ENM from extravascular sources that enter the body are absorbed to a very limited extent if at all into the brain (<0.03% of the administered dose) (Pietroiusti et al. 2013). However, animal studies have shown damage to brain (e.g. inflammation, altered morphology of neurons, perturbations in neurotransmitter secretion) following administration of ENM such as carbon black, TiO_2, and SWCNT following intra-tracheal instillation, oral administration, and inhalation (Wang et al. 2007; Hu et al. 2010; Jackson et al. 2011; Pietroiusti et al. 2013; Karmakar et al. 2014). ENM are also being developed for intravascular administration targeting the brain for purposes of medical imaging or as a carrier of therapeutic drugs (Bhaskar et al. 2010; Domínguez et al. 2014), indicating that the BBB is not impermeable to ENM.

Male germ cells mature in the seminiferous tubules within the testes. The blood–testis barrier (BTB) protects these germ cells from exposure to potential toxicants. This epithelial barrier consists of Sertoli cells, with specialized proteins (tight junction, desmosome, basal ectoplasmic specialization, and gap junction) between adjacent cells (Cheng et al. 2011; Cheng & Mruk 2012). An anatomical feature that enhances protection to the seminiferous tubules is that they are not infiltrated by blood vessels, lymph vessels, or nerves. Nevertheless, despite this epithelial barrier, animal studies have shown translocation of several ENM (Ag, CeO_2, Fe_2O_3) from the systemic circulation to the testes and damage to this organ as well (carbon black, TiO_2, SiO_2) (Pietroiusti et al. 2013). Relative to the BBB, the BTB appears to be less effective as a long-term barrier to ENM. This may be due to damage to the Sertoli cells, decreased ability to translocate ENM out of the Sertoli cells, or both (Pietroiusti et al. 2013).

The developing fetus is extremely vulnerable and susceptible to toxic insults from a variety of toxicants. Toxicants in the mother's systemic circulation have the ability to distribute to the fetus. ENM that adversely interact with the placenta itself may affect the developing fetus. Knowledge on the ability of ENM to cross the placenta is limited. The placenta is a "short-term" barrier, unlike the BBB and BTB (Saunders 2009). It is present in the mother only for the term of the fetus. Nutrients from the mother are transferred through the placenta for the growth and development of the fetus. The placenta also metabolizes endogenous and exogenous compounds, exchanges gas between mother and fetus, plays a role in immune function and removes waste products from the fetus (Saunders 2009). The barrier is the trophoblast, a continuously fused non-replicating epithelial tissue derived from the fetus. The trophoblast is immersed in the maternal blood, and pores within it are thought to be no greater than 10 nm (Saunders 2009). To reach the fetal circulation, chemicals must traverse the trophoblast (which consists of two layers of cells), basement membrane, connective tissue, and endothelial wall of the fetal blood vessel. The placental barrier changes over time, from a hemodichorial architecture in

the first trimester to a hemomonochorial architecture during the second and third trimesters (Juch et al. 2013). The barrier thus becomes thinner and presumably more permeable as the fetus develops. Translocation of chemicals is thought to be primarily by diffusion, but mechanisms including receptor-mediated endocytosis, phagocytosis, and transporter proteins may also be involved (Saunders 2009). Several studies in which pregnant rodents were administered ENM (e.g. SiO_2, TiO_2, fullernes, Au, SWCNT) reported translocation and/or toxicity to the embryo/fetus/pup (Pietroiusti et al. 2013). These outcomes were dependent on the type of ENM used (metalloid, metal, metal oxide, carbon nanotube), dose administered, route of administration (sc, oral, iv), and day of gestation (single or multiple days) (Takahashi & Matsuoka 1981; Lim et al. 2011; Pietroiusti et al. 2011; Yamashita et al. 2011).

Cellular uptake and intracellular fate

A simple schematic depicting uptake and distribution of ENM at the cellular level is presented in Figure 8. The physical and chemical interactions among the nanoparticle, its protein corona, and the cell membrane surface determine the probability that the particle will enter the cell or be excluded from it (Verma & Stellacci 2010; Zhao et al. 2011; Zhu et al. 2012; Oh & Park 2014).

The uptake of ENM into cells has been an active area of drug development research because ENM may enable drugs to enter cells or cross biological barriers where they otherwise would not. Cellular uptake of ENM is also a key determinant of nanotoxicity (Ivask et al. 2013). Although studies of cellular uptake frequently use electron microscopy (e.g. Chithrani & Chan 2007) uptake of fluorescently labeled ENM has been observed using fluorescent or confocal microscopy (Davda & Labhasetwar 2002; Treuel et al. 2013). Cellular uptake of nanoparticles composed of materials that reflect light, such as Ag or Ti, can be observed with dark-field microscopy and quantified using flow cytometry (Zucker et al. 2010). Plasmonic resonance of Ag ENM in a cellular matrix also presents an opportunity to detect ENM with a larger signal to noise ratio than by using light scattering (Zucker et al. 2013). Much of the nano-pharmaceutical understanding of mechanisms through which cells internalize particles, and the influence of nanoparticle physical and chemical parameters, can be applied to considerations for nanotoxicology. Numerous factors influence cellular uptake pathways including particle size, shape, charge, hydrophobicity, surface modifications, and dissolution.

Mammalian cells have mechanisms for particle uptake, although different types of cells take up particles to different degrees. The uptake mechanisms are distinguished by the size of particles processed, the signaling and enzymatic pathways involved and the destination of the internalized materials. In addition to direct penetration through the membrane, which occurs primarily for very small particles, the following uptake pathways have been described: phagocytosis, through which macrophages and other phagocytic cells engulf foreign materials, including nanoparticles; pinocytosis, through which cells engulf fluids, nutrients and other materials; and endocytosis, membrane receptor-mediated processes involving either clathrin (clathrin-mediated endocytosis), caveolin (caveolin-mediated endocytosis), or neither (clathrin/caveolin-independent endocytosis). Detailed reviews and diagrams of these cellular uptake pathways are available elsewhere (Dobrovolskaia & McNeil 2007; Jin et al. 2009; Zhao et al. 2011; Canton & Battaglia 2012; Zhu et al. 2012; Adjei et al. 2014; Oh & Park 2014).

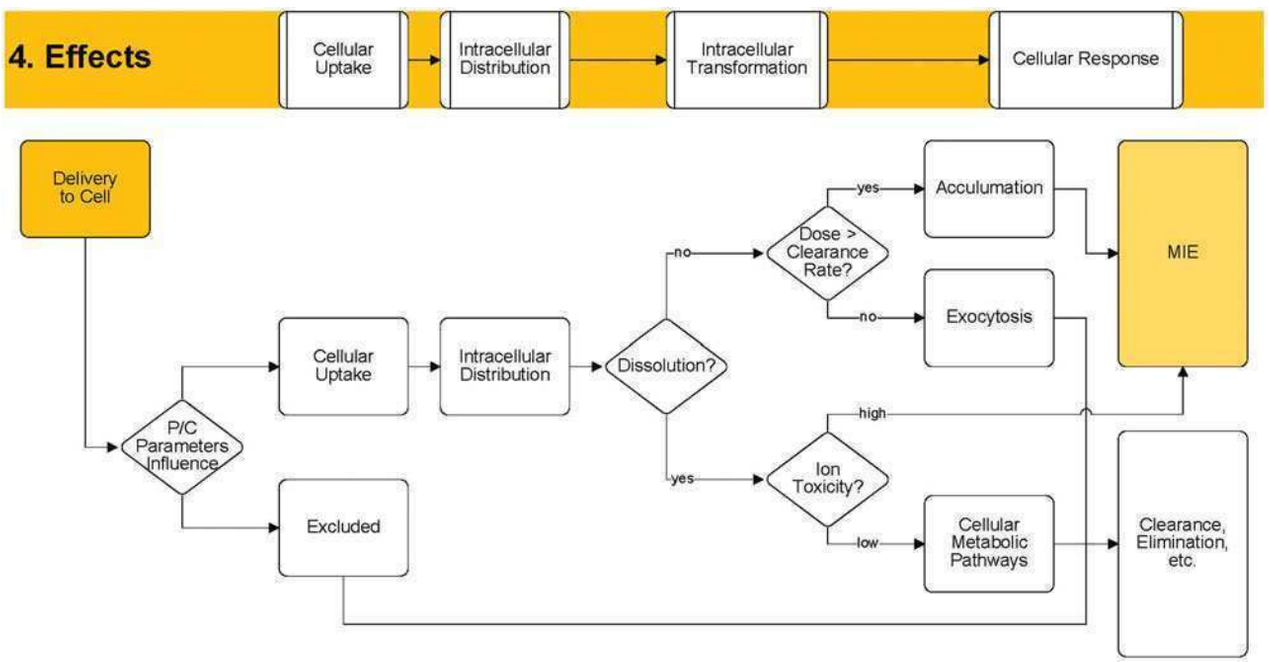

Figure 8. Potential pathways between cellular contact with a biologically transformed ENM and potential molecular perturbations, including molecular initiating events (MIE). Labelled branches indicate directional selectivity based on ENM physicochemical (P/C) properties.

Endocytosis

In clathrin-mediated endocytosis, clathrin is a membrane resident receptor protein that recognizes ligands for absorption, including opsonin-bound particles (Canton & Battaglia 2012; Oh & Park 2014). Caveolin-dependent endocytosis involves invaginations of the cell membrane that enclose primarily sphingolipids bound to cholesterol or the protein caveolin in the membrane (Nabi & Le 2003). The composition of the ENM and its coating influence which endocytic pathway are involved.

In clathrin-mediated endocytosis, biomechanical thermodynamic modeling indicates that ENM of around 55 nm have the fastest membrane wrapping time and are taken up more rapidly and efficiently than bigger or smaller particles (Gao et al. 2005). Gold ENM that were spherical and 50 nm in diameter were taken up to a greater extent than 14 nm spherical particles or rod shaped gold ENM (Chithrani et al. 2006; Chithrani & Chan 2007). Smaller ENM cluster on the cell membrane until there is sufficient thermodynamic energy to overcome membrane elastic resistance and the entropic energy barrier to form vesicles for endocytosis (Chithrani & Chan 2007; Jin et al. 2009). Smaller ENM are taken up by endocytosis more slowly and in batches that are then packaged together in membrane bound vesicles. These vessels fuse together after uptake to contain higher number of particles per vessel. This results in larger particle agglomerates inside of cells than outside.

Pinocytosis

Pinocytosis is a process by which cells intake fluids by extending the cell membrane to surround a portion of the extracellular space and engulf the fluids along with solutes and suspended materials as well including ENM (Buono et al. 2009). Pinocytosis can take up a wide range of particle sizes (up to 10 μm) (Adjei et al. 2014). Pinocytosis may be the primary uptake mechanism for small particles (<25 nm) where, at reasonable exposure concentrations, it is unlikely that sufficient numbers of the particles co-locate on proximate receptors to trigger clathrin-mediated endocytosis (Adjei et al. 2014). Nanoparticles taken up by pinocytosis do not need to interact with cell membrane receptors, but the amount taken up in this way is lower than that through receptor mediated endocytosis pathways.

Phagocytosis

Phagocytosis is a process present primarily in cells with immunological or similar functions to defend against pathogens or to cleanup waste and debris (Zhu et al. 2012). These cells include phagocytes such as macrophages, neutrophils, and monocytes. Particles that are first coated with opsonin, immunoglobulin, complement, or serum proteins are subject to phagocytosis. The opsonized nanoparticles bind to cell surface receptors; the cell membrane forms a cup-shaped extension and internalizes the material into membrane bound phagosomes. The phagosomes are transported internally and fuze with lysosomes, transferring the vesicle contents to the acidic environment of the lysosome that also contains enzymes to digest and destroy the contents. Phagocytosis of ENM by cells in the immune system may trigger production of inflammatory cytokines and inflammatory reactions (Dobrovolskaia & McNeil 2007; Kim & Choi 2012).

Intracellular destination

The intracellular destination of ENM is determined by several factors, as discussed subsequently, one of which is the potential for dissolution. Some metal or metal-oxide ENM are prone for dissolving and releasing metallic ions, where others are relatively insoluble and stable in the intracellular environment. Particles that dissolve can release toxic ions, such as Ag (Singh & Ramarao 2012) or Zn (Shen et al. 2013). Materials that are insoluble can be removed from the cell by exocytosis (Sakhtianchi et al. 2013; Wang et al. 2013; Oh & Park 2014). If the rate of uptake exceeds that of removal, ENM could bioaccumulate inside cells, however, feedback mechanisms may exist to reduce further cellular uptake when ENM accumulate in cells (Gunduz et al. 2017). The release of toxic soluble components, or bioaccumulation of persistent materials, could lead to a MIE which then begins a sequence of key events leading to an adverse outcome (Gerloff et al. 2017).

Nanomaterials packaged in endosomes may merge, leading to agglomeration into larger sized particles. Endosomes may be transferred to the endoplasmic reticulum or Golgi apparatus and the contents can become packaged in lysosomes. Over time nanoparticles accumulate in lysosomes where low pH and proteolytic enzymes digest opsonin coatings and soluble nanomaterial components. Nanoparticles composed of soluble metals, such as silver, iron, or zinc, may dissolve in a lysosomal environment and release ionic forms of the metals. Dissolution rates depend on both cellular and material factors. Cellular compartments vary in terms of pH, ionic strength, and concentration. Materials with core/shell composition dissolve layer by layer. Other factors influencing dissolution include surface area (smaller particles dissolve faster than larger), diffusion coefficient of the material; volume of solution, and thickness of diffusion layer. Nanoparticles composed of relatively insoluble materials, such as TiO_2 or CeO_2, may resist dissolution, even in an acidic lysosomal environment. Depending on rates of uptake and removal, particles may persist in cells for weeks or months and accumulate into large intracellular deposits (Zucker et al. 2010). Small particles may cross the nuclear membrane through the nuclear pore complex which is 20–50 nm in diameter (Tkachenko et al. 2003). ENM absorbed cellularly, if not retained, can be re-packaged for expulsion from the cell by exocytosis (Frohlich 2016).

Exocytosis

In comparison with the large number of studies on endocytosis and other uptake pathways, there has been relatively less research evaluating ENM exocytosis. Removal by exocytosis involves fusion of an exosomal vessel with the cell wall and expulsion of the vessel contents into the extracellular space. For transferrin-coated gold ENM, smaller particles were removed from HeLa cells by exocytosis at a faster rate than

larger particles, as the rate of exocytosis was inversely proportional to particle surface area (Chithrani & Chan 2007). The rate of exocytosis varies substantially across different types of cells (Sakhtianchi et al. 2013). Particle shape and coatings influence the rate of exocytosis; however, the literature is mixed as to the influence of rod shape and aspect ratios relative to spherical particles (Oh & Park 2014). In addition to exocytosis, the ENM content of cells may be reduced by cell death releasing nanomaterials into the extracellular space, cell division where daughter cells may inherit the parent cell ENM content, through dissolution or degredation of the ENM, or via transcytosis where ENM are transferred directly to another cell avoiding the extracellular space (Frohlich 2016).

Terrestrial exposure and biodistribution

ENM exposure to terrestrial ecosystems can occur through air, soil or water (see Figures 3–5 for illustrations of related fate and transport). In all cases, interactions in the soil, and on plant and animal surfaces, can influence the activity and likelihood of uptake into terrestrial organisms. The biological processes and ecology of soil organisms, viewed as a functioning ecosystem, also are complex (Coleman et al. 2004). Generally, soil biota can be organized by functional groups, and for some organisms within groups as guilds, all of which are situated along a multi-level trophic-gradient food web. Carbon produced through photosynthesis is transferred from primary producers (e.g. green plants) to an extensive array of consumers in the food web along a carbon utilization pathway whereby the end products of each sequential consumption step become more resistant to decomposition (Stevenson & Cole 1999). A nutrient utilization pathway processes resources in the opposite direction, i.e. from the soil biogeochemical matrix, along the pathway, to the primary producers. Once consumed, and depending on the niche and life history of the consumer, ENM may be transformed, sequestered, or re-released to the soil environment via internal physiological processes and/or turnover/food web consumption/decomposition processes. At each release of an ENM, it may be become bound again and unavailable (adsorbed/absorbed), or may it be transformed remaining unbound and available for further biological acquisition (Figure 4). It is anticipated that ENMs may be acquired internally (adsorbed and/or absorbed) by any of the innumerable species deployed throughout the food web, similar to other particles, however to our knowledge no studies have yet examined ENM fate and transfer in the soil food web organisms. Although the number of studies is currently limited, there are some examples of ENM being transferred through the food chain. Holbrook et al. (2008) showed quantum dots being transferred from protozoans to rotifers in a simple aquatic food chain. Biomagnification of cadmium selenide quantum dots was observed in an experimental microbial food chain (Werlin et al. 2011). In a terrestrial food chain, Judy et al. (2011) demonstrated the transfer of Au ENM from tobacco plants to the tobacco hornworm. Because of the small number of studies available on the dynamics of ENM in food chains, it is too soon to state definitively whether or not ENM move up food chains.

Release of ENM to soil can lead to exposure of soil microfauna and flora (Figure 6). Free-living fungi, micro- and macroinvertebrates, and bacteria in soil form a unique ecosystem comprised of high structural and functional diversity.

Terrestrial plants and animals

When ENM enter the environment, they may interact directly with plants via deposition to foliage, or to soil, wherein they may be taken up through roots (Dietz & Herth 2011). At the surface of roots, ENM uptake is a complex and poorly understood process, in large part due to the heterogeneity of soils and the complexity of rhizosphere interactions. Several studies have found differential uptake by plant species (Ma et al. 2010; Rico et al. 2011; Judy et al. 2012). Judy et al. (2011) suggested that differential uptake may be related to the types of root exudates present in the rhizosphere, an area where more research is needed. Many of these exudates play important roles in nutrient acquisition and sequestration by plants. For example, Manceau et al. (2008) found that Cu was transformed into metallic nanoparticles in the rhizosphere of wetland plants. They also found that arbuscular mycorrhizal (AM) fungi were involved in the chemical transformation. It is possible that root exudates and symbiotic AM associates have developed these rhizosphere compounds as a means to avoid copper toxicity. Given the range and surface chemistries of the ENM in production, additional research is needed to better elucidate how rhizosphere chemistry influences ENM transformation and exposure at the root surface.

Foliar deposition does not necessarily mean that the ENM will be taken up into the leaves; some particles may tightly bind to cell walls or lipophilic surface cuticles, but not move intracellularly across the plasmalemma (living cell membrane). They also may be actively excluded through various mechanisms. There may be uptake into the substomatal cavity through stomates, leading to direct exposure of internal mesophyll cells (Navarro et al. 2008a). Regardless of site of deposition, particles may be adsorbed, absorbed, or excluded (Figure 6).

If particles are not bound or taken up into cells (i.e. excluded), then they may move to another terrestrial compartment either through wind dispersal or by rainfall removal. They also may be transported to other terrestrial organisms or compartments following consumption by grazers (Figure 6).

Regardless of whether the particle is taken up through roots or through leaves, terrestrial organisms that feed on vegetation may be exposed to ENM. Recent studies have shown that there can be biomagnification of ENM by organisms feeding on plant foliage (Judy et al. 2011). For example, Majumdar et al. (2016) found significant biomagnification of CeO_2 from kidney bean plants to Mexican bean beetles to spined soldier bugs. Overall, however, there has been little research into biomagnification in terrestrial food webs or on the potential entry of ENM into the human food chain through various agricultural products (Rico et al. 2011). Wheat did not take up ENM CeO_2 via the plant roots, but barley did, although it was unclear whether uptake was in the particle or ionic form (Rico et al. 2017).

In addition to ingestion, terrestrial animals also may be exposed to ENM through inhalation and dermal absorption (Figure 6). Many of the studies examining routes of exposure to terrestrial animals have been done using species such as mice and rats as human analogs (Mitchell et al. 2009; Larsen et al. 2016). As a result, there is considerable understanding of ENM effects on mammals (i.e. typical laboratory study species), however information on the extent of exposure of native populations of animals in terrestrial ecosystems is lacking.

Aquatic species exposure and biodistribution

Once an ENM is introduced into the aquatic environment, a series of processes begin that ultimately affect its fate and potential to cause adverse ecological and human health effects (Figure 7). For aquatic and terrestrial species, including humans and plants, exposure to ENM may occur from surface waters directly, the sediment interstitial water, or whole sediment. Uptake may occur through foliage, roots, ingestion, gills, and direct contact with skin or tissues. Each of these processes is described in more detail below. Much of the bioavailability literature indicates that traditional contaminants associated with SPM, colloids, DOC, ligands related to ionic strength, and sediment are not as bioavailable as the aqueous form of the chemical (Di Toro et al. 1991). However, once associated with an environmental particle, an ENM may be more easily taken-up by filter- or deposit-feeding organisms (although not necessarily in a bioavailable form). Learning from existing traditional materials and understanding the differences in the relationships between the transport pathways of specific ENM in aquatic systems and observed ecological effects is critical. Ultimately, all these environmental processes will affect the likelihood of the ENM being exposed to organisms (e.g. aquatic and terrestrial species as well as humans) via the surface waters directly, the sediment interstitial water, or whole sediment.

Although sediments will be a primary route of aquatic exposure to ENM, water column exposure should not be overlooked as organisms can be exposed as ENM pass through the aqueous phase or remain suspended in the water column due to functionalization of the ENM, episodic discharges or pseudo-persistence (when concentrations of degradable or removable chemicals persist in the environment through continual input) (Holden et al. 2016). Such pseudo persistence could be modeled in the Framework as a chronic exposure.

When considering exposures to aquatic organisms, it is helpful to differentiate between carbon-based and metallic ENM. Exposure investigations with carbon-based ENM, specifically SWCNT and MWCNT, so far indicate that little actual exposure to aquatic organisms occurs before the CNTs precipitate from the overlying water and are buried in the sediments in a non-bioavailable form (Petersen et al. 2011; Parks et al. 2014). However, in fresh waters with significant DOC contents, CNTs may be quite stable and remain suspended in the water column. Furthermore, if the carbon-based ENM are ingested by an aquatic organism (e.g. associated with sediment particles), indirect evidence suggests that the carbon-based ENM pass through the organism's digestive tract, which are then deposited into the sediment as pseudo-feces (Parks et al. 2014). Little exposure research in the aquatic environment has been performed on non-functionalized fullerene and graphene carbon-based ENM, although it is likely they will behave in a similar fashion to the SWCNT and MWCNT.

A source of uncertainty regarding the exposure of aquatic organisms to carbon-based ENM is associated with the modified forms of SWCNT, MWCNT, fullerenes, and graphene. While most of the current research has been performed on pristine versions of carbon-based ENM, the materials used in products are often modified, altering their physicochemical behavior to make them more water soluble. This makes ENM less likely to associate with sediment particles and potentially increases exposures and bioavailability. A measure of heteroaggregation in natural water models might help quantify such behavior. Gaps in understanding of this aspect of aquatic organism exposure to carbon-based ENM remain.

In contrast to carbon-based ENM, metallic ENM have been shown to be bioavailable to aquatic organisms. Exposure can occur via skin (dermal), gill, or ingestion of contaminated prey or sediment. For many aquatic organisms, particularly invertebrates, internal organs are bathed directly by overlying water or pore-water. Compared with terrestrial organisms, this blurring of internal and external exposure results in less of a division for aquatic organisms between dermal and non-dermal exposure. For example, in bivalves the pericardial cavity, gonads and ganglion epidermis may be exposed directly to ENM in water that enters the shell. Uptake of ENM in mollusks also may occur through filtration or ingestion of suspended sediments to which ENM are associated. Bivalves can selectively filter particles sizes ranging from 2 to 10 μm (Kraeuter & Castagna 2001), and ENM heteroaggregation in marine waters can increase the size of individual nanoparticles to microparticles within hours of introduction to marine systems (Wang et al. 2014a). This increases the possibility of ENM exposure to bivalves and other invertebrate filter feeders. For fish and other vertebrates, exposure to suspended ENM can occur primarily via gills and ingestion. The occurrence of dermal exposure may be less than in terrestrial organisms as fish are often protected by a mucous layer that is difficult to penetrate (Handy et al. 2008).

In aquatic organisms, the gills are often a targeted tissue for ENM exposure. The gills necessarily have a high exposure to large volumes of water and nanoparticles can be entrapped in gill tissue. For example, exposure to TiO_2 ENM resulted in damage to fish gills including edema, thickening of the lamellae, decreases in Na^+K^+-ATPase activity, and increased levels of thiobarbituric acid reactive substances (TBARS) and glutathione (GSH) (Federici et al. 2007). There is also evidence that metal nanoparticles interact differently than metal ions in gills (Kádár et al. 2010; Gomes et al. 2011), and that gill damage from ENM particles goes beyond solubilization of metals from nano-copper or nano-silver particles (Griffitt et al. 2007, 2009; Shaw & Handy 2011; Trevisan et al. 2014).

Because of the difficulty in detecting ENM within organisms, there are many knowledge gaps in assessing exposure

to and distribution of ENM in aquatic organisms. In fish, the gills, gut, liver, and brain may be target organs, but streamlined methods of detecting ENM within organisms need to be developed. Not surprisingly, the surface properties of ENM affect the movement through the organism (Wang et al. 2014b, Zhu et al. 2010). Metallic ENM move through the walls of the digestive tract and into the body of organisms. Researchers have shown that Au ENM are internalized into the cytoplasm and co-localized with DNA in nuclei (Joubert et al. 2013). Titanium ENM have been found in bivalve hemocytes (Marisa et al. 2015) and Cu, Ag, and Ti ENM have been identified in the lysosomes and lumen of digestive glands (Jimeno-Romero et al. 2012). Overall, in mollusks, the digestive gland or hepatopancreas appears to be a target organ for metallic ENM (Gomes et al. 2012); however, more research is needed on the systemic biodistribution of ENM in aquatic organisms.

Uptake of ENM whether through ingestion or other processes, may increase the availability of ENM transferred through the food web. Researchers have shown that Au ENM can easily pass from the water column into the food web with mollusks taking up the majority of the ENM (Ferry et al. 2009). The bioavailability of ENM will be affected by environmental conditions, like suspended sediments, and will reduce exposures. In contrast, some ENM, depending on their physicochemical characteristics, will be bioavailable. If ENMs do not enter the body, either absorbed through the gut, skin or gills, they could pass through the digestive tract of aquatic organisms where they are also bioprocessed (i.e. repackaged into different sized metallo-organic molecules) (Hull et al. 2011; Pan et al. 2012) that will have varying fate pathways compared to pristine ENM. The fate of bioprocessed ENM is unknown, however, if ENM enter the mollusk body, there is a good chance they would enter the food web as the mollusk flesh is often consumed whole by predators including humans.

Effects

Consideration of adverse effects follows the potential for ENM exposures. A sequence of steps is described between external exposure to the material and the PK and pharmacodynamic steps that lead to the occurrence of a MIE (Figures 5–8). The AOP sequence, then, progresses from a MIE through a sequence of key events (KE) occurring at progressively higher levels of organization including cellular, organ level, and whole organism responses (Figure 9). The AOP sequence can continue to describe effects at the population level if ecosystem effects are of concern (Figure 10). Here we use AOP as a conceptual progression under which to organize information, and are not proposing specific AOP sequences for any particular adverse outcome. This prevents more specific delineation of an AOP pathway. The effects of ENM on organisms have been studied primarily in mammalian systems, with a few notable exceptions such as the relatively extensive testing of zebrafish (Fako & Furgeson 2009; Harper et al. 2011; Muller et al. 2015; Wehmas et al. 2015; Chakraborty et al. 2016), and a some other aquatic species (Petersen et al. 2015). The discussion below considers

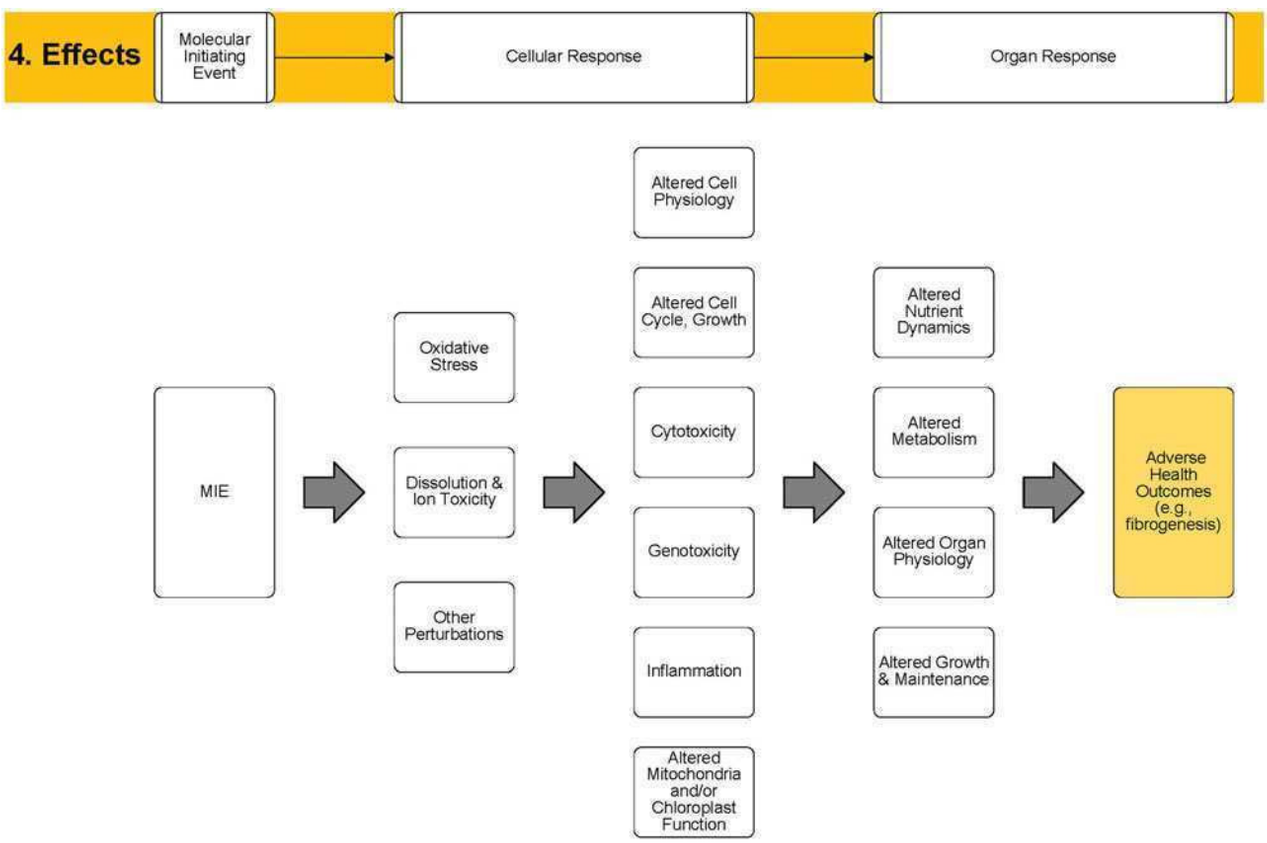

Figure 9. Potential ENM effects on organisms from the molecular initiating event (MIE) to individual adverse health outcomes.

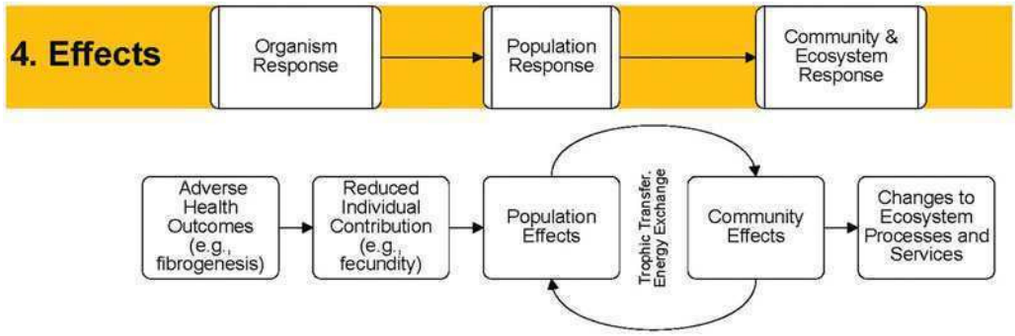

Figure 10. Cascade of potential effects from individual adverse health outcomes to greater potential subsequent effects on relevant populations, communities, and ecosystems.

primarily mammalian species where the majority of the mechanistic-level research has occurred.

MIE/cellular, organ response

A schematic concept of an AOP for the toxic effects of exposure to ENM at the cellular level is depicted in Figure 9. Ankley et al. (2010) produced a conceptual framework of an AOP leading to the production of a toxic or adverse event. The AOP concept is anchored by an MIE that is linked through a series of Key Events to an adverse outcome with significance to risk assessment. Conceptually, AOPs are independent of a specific chemical trigger, so that any potential toxicant causing a MIE would be expected to trigger the sequence of events in the AOP and potentially lead to the adverse outcome. In this way, observations of mechanistic or molecular toxic events can be projected to their potential adversity and aid in the support and interpretation of mechanistic data for risk assessment purposes (Gerloff et al. 2017). Because AOPs theoretically apply to multiple chemicals, it could be argued that development of AOPs for ENM are irrelevant if the ENM induces the same MIE as a toxic chemical. Here we limit the discussion to MIE or KE that have been attributed to ENM and AOP frameworks in which they have been applied.

Recently published studies on CuO ENM and MWCNT have included the concept of AOPs in their toxicological evaluation. Muller et al. (2015) examined the effect of CuO ENM on hatching in zebrafish and reported that CuO ENM elevated the Cu level in the hatchlings (the perivitelline space) at a greater rate relative to Cu salts. The MIE was considered to be inhibition of Zebrafish Hatching Enzyme 1 (ZHE1) by released Cu^{2+} ions.

Labib et al. (2016) applied toxicogenomics to the AOP framework for lung fibrosis in mice exposed to three individual MWCNT. The MWCNT had different physicochemical properties, yet comparable biological pathways were perturbed across dose and time. The transcriptional bench mark dose values for the MWCNT were similar to the values for lung fibrotic lesions induced by these materials. The authors concluded the genomic data in an AOP framework could be used to estimate levels of exposure that would be acceptable in the absence of epidemiological data (Labib et al. 2016). Multiple pathways leading to lung fibrosis were considered by which carbon nanotubes could induce fibrosis, including release of pro-inflammatory or pro-fibrotic mediators, oxidative stress, and direct effects on fibroblasts (Vietti et al. 2016).

In mammalian cells, changes in signaling pathways and microRNAs indicated effects of TiO_2 on a number of pathways including cell-cycle regulation, apoptosis, calcium signaling, Nrf2 responses, IGF1 signaling, RAS signaling, PI3K/AKT signaling, cytoskeleton remodeling, cell adhesion, BMP signaling, and inflammatory responses (Thai et al. 2015). Rat dopaminergic cells exposed to Ag ENM showed genomic response pathways generally indicative of mitochondrial disruption (Chorley et al. 2014). Gerloff et al. (2017) proposed an AOP framework for hepatic toxicity that could be suitable for metal oxide ENM. Gerloff et al. (2017) point out that MIEs for chemicals or ENM can vary widely and may not be completely understood, and, therefore, it may make more sense to use Key Events rather than MIEs as linking factors when trying to map ENMs to chemical-derived AOPs.

Oxidative stress

Nanomaterial exposures in biological systems are strongly linked to generation of reactive oxygen species (ROS) and, to a much lesser extent, reactive nitrogen species (RNS). For ENM exposures, higher degrees of positive association and/or causality are available for ROS species like superoxide, hydrogen peroxide and hydroxyl radical. One way ENM produce ROS is by a direct property of the nanomaterial itself, and another is via an interaction between the ENM and the biological system. Examples include electron donation from the nanomaterial to molecular oxygen to produce superoxide, redox cycling of quinones, semiquinones and other organics, Fenton chemistry, band gap (energy difference between conducting and valence bond electrons), and UV light producing electron hole pairs in ENM (Nel et al. 2006).

For ROS production by ENM, determinants of outcome include ENM chemical composition, surface area, surface reactivity, agglomerated size, and dose to target organ (Kitchin et al. 2011). ENM surface area was associated with depletion of lung cell GSH for four ENM (carbon black, TiO_2, Co, and Ni) as well as for four other larger particles (TiO_2, carbon black, $BaSO_4$, and alpha quartz) (Monteiller et al. 2007). In tissues or organisms with UVA exposure, photoactivation may be a dominant causal factor such as with photoactivatable forms of TiO_2 (Sanders et al. 2012; Ma & Diamond 2013).

There are many commonly used biomarkers for oxidative stress including molecular redox probes, such as 2′,7′-dichlorofluorescein diacetate, Mitosox, isoprostanes, lipid peroxidation markers, membrane damage (e.g. lactic dehydrogenase enzyme leakage), phagocytic oxidative bursts, and decreased antioxidant defenses (GSH concentration, superoxide dismutase, and glutathione peroxidase).

Associations between oxidative stress and adverse outcome have been made in many cases including DNA damage (Xie et al. 2011), mutation (Xie et al. 2011), cancer (Klaunig et al. 2011); and in multiple tissues: skin (Shukla et al. 2011), central nervous system (Sayre et al. 2008; Skalska et al. 2016), lung (Li et al. 2008; Madl et al. 2014), liver (Kim et al. 2009; Shukla et al. 2013), and kidney (Liang et al. 2009; Guan et al. 2012). For SWCNT or MWCNT in lung tissues, oxidative stress may be a mediator of inflammation and fibrosis, with a potential to progress to pleural malignant mesothelioma and lung tumors (Muller et al. 2005; Chou et al. 2008; Kim et al. 2014; Suzui et al. 2016).

Ion toxicity after dissolution of nanomaterials

Metal ions may be released from ENM that are composed of metals, metal oxides, or inorganic carbon containing residual metal catalysts (e.g. MWCNT). If this happens, a relatively high concentration of metal ions could occur near the site where the nanomaterial is located, with the ENM releasing toxic metal ions acting as a "Trojan horse". Enhanced uptake of CuO ENM, followed by local release of Cu^{2+} ions to inhibit Zebrafish Hatching Enzyme, was considered as the mechanism for impaired Zebrafish hatching (Muller et al. 2015). Similarly, adverse effects could result in a number of organ systems, including mammalian lungs and blood vessels (reviewed in Rodriguez-Yañez et al. 2013).

Metal responsive genes that can act as biomarkers of metal ion exposure include heme oxygenase-1, metallothioneins, and catalase. For reasons of specificity and sensitivity, analytical chemistry measures of metals (such as ICP-MS) are often used as measures of exposure.

Altered cell physiology: altered cell cycle, growth

ENM also may impair cell-cycle progression and proliferation, dependent on the chemical composition, particle size, and other physical/chemical properties (Mahmoudi et al. 2011; Marano et al. 2011; Asharani et al. 2012). At low concentrations, increased cell proliferation *in vitro* is dependent on the ENM chemical composition, size, surface reactivity, agglomerated size, dispersion medium, and activation of different signaling pathways. For example, Unfried et al. (2008) reported that carbon ENM (nano-particulate carbon black) and silica ENM (amorphous SiO_2), both with a median diameter of 14 nm, induced proliferation in a rat lung epithelial cell line. Huang et al. (2009) showed that exposure to non-toxic concentrations of TiO_2 ENM enhanced cell proliferation and growth of cultured fibroblast cells (NIH3T3).

When the concentrations of ENM are high enough to induce oxidative stress, they will generally alter many different stress response/metabolic/signaling pathways including inflammation, NRF-2 mediated stress response, and protein and lipid peroxidation. These alterations may in turn lead to changes in cell cycle progression/proliferation, some may even result in cell cycle arrest or cell death. These ENM include metals and metal oxides (Au, Ag, Cu, Zn, Ti, Fe, Pd, Ni, and Ce), SiO_2, and carbon nanotubes (Huang et al. 2010; Mahmoudi et al. 2011; Manke et al. 2013). There are also reports of cell-cycle alteration caused by SWCNT and MWCNT *in vitro* (Zhang & Yan 2012; Chen et al. 2012; Zeni et al. 2015). While both carboxylated and pristine MWCNT caused cell cycle arrest, carboxylated MWCNT seemed to induce less apoptosis (Liu et al. 2015).

Cytotoxicity

Cytotoxicity can be an outcome of ENM exposure either *in vitro* or *in vivo*. Either the necrotic or apoptotic pathways could be dominant depending on the exposure. ENM can exert toxicity either from outside or inside of cells. Generally, the most important factors in determining cytotoxicity are the ENM chemical composition, dose, dose rate, surface reactivity, surface area, and agglomerated size.

There are many approaches to quantifying a response to nanomaterial exposure such as the *in vitro* approaches of dye exclusion (trypan blue), dye uptake (neutral red, propidium iodide, and ethidium bromide), cellular reductive enzymes (calcein-AM, MTT, MTS, or alamar blue), ATP content, and DNA-based stains. Enzymes that are released from membrane damaged or dead cells can be useful indicators of effect such as lactate dehydrogenase, alanine aminotransferase, or aspartate aminotransferase. Cell-based assays that are reliant on fluorescent or luminance quantification may be subject to optical interference from nanoparticles in suspension, and should be used with appropriate controls (Kroll et al. 2009; Guadagnini et al. 2015).

Genotoxicity

Genotoxicity encompasses any change to cellular DNA that has the potential to interfere with the transmission of genetic information, either through impacts on replication or on transcription. Genotoxicity is important to assessing the potential health risks posed by exposure to ENM because it represents an important early molecular event in the induction of cancer, and is strongly associated with other adverse health outcomes such as atherosclerosis (Mercer et al. 2010). The ability to induce genotoxic effects has been well studied for a variety of ENM, and several recent reviews are available (Kumar & Dhawan 2013; Magdolenova et al. 2014; Golbamaki et al. 2015; Guo & Chen 2015). Genotoxicity studies on ENM have generally focused on the induction of DNA damage, the induction of mutations, or on induction of expression of DNA damage response genes or functional alteration of DNA damage response proteins in exposed cells.

The most frequently used approach for the assessment of ENM-induced DNA damage is the single-cell gel electrophoresis, or Comet assay. The assay is capable of detecting a variety of types of DNA damage, including single strand breaks,

double strand breaks, abasic sites, and other alkali-labile types of DNA damage. When the assay is modified by incorporating *in vitro* digestion with DNA-damage specific nucleases or glycosylases, the range of types of damage detectable can be extended. In general, the enzyme enhanced version of the assay yields a higher sensitivity for detecting DNA damage induced by ENM. Additional assays for DNA damage include the observation of chromosome level effects, such as the micronucleus (MN) assay, and the chromosomal aberration (CA) assay. *In vitro*, ENM have been found to induce MN in more cases than CA, while *in vivo* the situation appears to be reversed, although fewer ENM have been evaluated for CA (Guo & Chen 2015). The agglomeration state of ENM and treatment media may influence assays of genotoxicity differently (Prasad et al. 2013, 2014). Other approaches for directly measuring DNA damage, such as ^{32}P-postlabeling and ELISA, have also been used (Foldbjerg et al. 2011).

A recent review found that the most commonly used genotoxicity/mutagenicity tests for ENM were (a) Comet assay (19 studies), (b) micronucleus (14 studies), and the Ames test (6 studies) (Golbamaki et al. 2015). These authors offered seven recommendations for genotoxicity testing of ENM: (a) know what nanomaterial has been tested and in what form, (b) recognize that ENM are not all the same, (c) consider uptake and distribution of ENM, (d) take ENM-specific properties into account, (e) use standardized methods, (f) use *in vivo* studies to correlate *in vitro* results, and (g) learn about the mechanism of ENM genotoxic effects. The key difference between these recommendations for ENM and general recommendations for assessing the genotoxic effects of chemicals lies in the need for rigorous characterization of the physical properties of the ENM being tested in addition to their chemical properties. Relative to the uptake of various nanomaterial in the bacteria *Salmonella typhimurium* (Ames test), bacterial uptake was reported for ENM composed of ZnO and TiO_2 as measured by transmission electron microscopy (TEM), scanning electron microscopy (SEM), and flow cytometry (Kumar et al. 2011). In contrast, uptake of TiO_2 in *Salmonella typhimurium* was not demonstrated by others, who questioned the TEM results of Kumar et al. (2011) regarding mismatch of the reported particle sizes and lack of chemical component analysis (Woodruff et al. 2012). Further, Woodruff et al. argue that ENM cannot enter bacterial cells, probably due to a lack of endocytosis mechanisms, and have a cell wall unlike eukaryotic cells, and, therefore, the Ames assay may be an inappropriate assay for ENM genotoxicity. Subsequently, however, uptake of Au, CeO_2, SWCNT, and MWCNT by *Salmonella typhimurium* was reported, but without showing mutagenicity (Clift et al. 2013).

The inference of DNA damage from monitoring cellular DNA damage response pathways provides useful indirect evidence for the genotoxic potential of ENM. Focal accumulation of phosphorylated γ-H2AX is diagnostic for double strand breaks in DNA and has been documented for a variety of ENM (Petersen & Nelson 2010). Silica ENM have been shown to activate the Chk1-dependent G2/M checkpoint DNA damage response signaling pathway (Duan et al. 2013) and both SWCNT and MWCNT induce the Erk1/2 signaling pathway, which is involved in cell proliferation and is also induced by asbestos exposure (Pacurari et al. 2010).

Inflammation

ENM cause inflammation in many organs, with the lungs being the most studied. The biological purpose of inflammation is to eliminate the cause of cell injury (e.g. bacteria). With biopersistent ENM like CeO_2, there may be no "off" switch to stop the inflammation process and the inflammation would become persistent. Many potential determining factors for ENM-induced inflammation have been studied including dose, surface reactivity, surface area, pulmonary deposition and clearance, agglomerated size, chemical composition, surface charge, dissolution rate (solubility), hydrophobicity, hydrophilicity, shape, primary particle size, purity, and crystal structure (Braakhuis et al. 2014). Cells types mediating the inflammatory response include macrophages, mast cells, eosinophils, neutrophils, and dendritic cells. The infusion of neutrophils into tissues is a common measure of inflammation. Other commonly used inflammatory biomarkers are the cytokines (e.g. interferons, interleukins, TNF-alpha, IL-10, and TGF-beta), chemokines (e.g. IL-8 and MCP-1), NF-kB, and prostaglandins.

In normal aging, chronic inflammation may lead to many diseases, such as atherosclerosis, rheumatoid arthritis, and cancer. ENM exposures have been linked to inflammation in several organs, particularly in the lung, liver, and skin (Murray et al. 2009; Braakhuis et al. 2014; Sadeghi et al. 2015). Various degrees of organ effects have been observed in the central nervous system, lung, liver, gastrointestinal tract, heart, spleen, blood vessels, and skin following carbon nanotube exposures (Rodriguez-Yañez et al. 2013). In lungs, inflammation, granuloma formation, fibrosis, alveolitis, genotoxicity, and cancer have been observed; while in blood vessels, endothelial cell activation, platelet activation, thrombus formation, and changes in blood pressure have been seen (Morimoto et al. 2013; Rodriguez-Yañez et al. 2013; Kasai et al. 2015).

Cross-kingdom effects – MIE/cellular responses

Most of what is currently known about MIEs induced by ENM exposure has been developed through studies on human and animal systems. As described above, plants in a variety of habitats are also likely to be exposed to ENM inadvertently through aerial deposition and water runoff or purposefully by application of wastewater sludge to soils. Now, there is an increasing recognition that altered survival, development, and reproduction of plants may be affected by exposure to ENM. Furthermore, such impacts to plants could have economic, ecological, and health consequences for people as well. An understanding of ENM-induced MIEs in plants is only beginning to emerge and is an area where there is a clear need for more research.

Early studies evaluated changes in plant transcriptomes following exposures to ENM and dose levels required for toxicity (reviewed in Park et al. 2014). These papers, however, generally did not link exposure and gene expression change

MIEs to altered plant physiology/morphology. More recently, some of the first associations between transcriptomic responses and phenotypic development were established in TiO_2 and CeO_2 ENM exposed *Arabidopsis* plants (Tumburu et al. 2015). The authors reported significant EMN-induced regulation of genes that are responsive to abiotic and biotic stress and control DNA metabolism, hormone metabolism, tetrapyrrole synthesis, photosynthesis, and root development. They also demonstrated that the ENM exposures resulted in increased percentages of germinating seeds and early growth of leaves.

Surprising follow-up work showed CeO_2 ENM induction of *Arabidopsis* DREB transcription factor genes (Tumburu et al. 2017). These responses were remarkable because DREBs are known for initiating cascades of gene expression and cellular restructuring that results in cold-acclimation (Liu et al. 2000; Agarwal et al. 2006; Knight & Knight 2012). CeO_2 ENM up-regulation of DREBs was not expected. Within these experiments, development of exposed plants also mimicked cold-acclimatization responses with delayed growth and increased leaf number. Superficially, such changes might not seem like adverse outcomes; however, downstream effects could include reduced fecundity of exposed plants. Transcription of DREB genes is rapidly triggered by a transient increase in cytosolic Ca^{2+} (Knight & Knight 2012; Miura & Furumoto 2013), which suggests that the MIE of CeO_2 EMN exposure in plants affects Ca^{2+} signaling. Whether or not similar responses would be observed under more natural conditions or in more distantly related plant species or animals remains to be determined.

Identification of ENM that are capable of causing MIEs linked to adverse outcomes across large taxonomic groups is of high interest. The greater the conservation of molecular, cellular and structural features among organisms, the higher the likelihood of comparable MIEs and downstream responses. Plant and animal cells appear to have more characteristics in common than those that differentiate them, but the most recent common ancestor of plants and animals was a single celled organism that existed more than 1 billion years ago. It is accepted that multicellularity evolved independently within each lineage. So, there is substantial divergence between the plant and animal membrane-bound receptors and signaling pathways that affect homeostasis, development and reproduction (Alberts et al. 2002). This points to the possibility that ENM which bring about the same generalized MIEs in many species (e.g. photoactivated toxicity beginning with reactive singlet oxygen causing oxidative damage to a wide variety of biological molecules) could very well produce distinct adverse outcomes in plants and animals. Another scenario to consider is that mitochondria are found in both cell types, but chloroplasts are unique to phototrophs. Thus, if an ENM affects a mitochondrial-centric process, there may be a greater likelihood for "broad" cross species fidelity in MIEs. Conversely, if an ENM affects a chloroplast-centric process, at least among phototrophs there may be broad commonalities, but shared MIEs between phototrophs and non-phototrophs may not occur (Figure 9). The range of responses across species may become more important to consider in risk assessments of certain EMNs where there is potential for wide-spread exposure.

Whole organism terrestrial and aquatic species effects

The AOP concept is a sequence of events beginning with a MIE and acting at a cellular level (Figure 9), which continues to build until adverse effects occur at the levels of the organ, individual, population, and community or ecosystem level (Holden et al. 2013; Figure 10). Community-level effects can involve terrestrial or aquatic systems (or both). A search performed in August 2016 in the Web of Science database yielded 473 references when querying for titles, abstracts, and key words with the topical terms "aquatic", "environmental", "organism", "toxicity", and "nanomaterials" in publications released from 1990 to August 2016. This number of references suggests strongly that nanomaterials will cause adverse effects to whole organisms. Among the references were several recent review articles discussing responses to a range of ENM. For example, ENM described in the review articles include Ag (Walters et al. 2014; Xin et al. 2015), TiO_2 (in seawater) (Minetto et al. 2014), CNT (Petersen et al. 2011; Boncel et al. 2015), and nanowires (Kwak & An 2015), as well as all-inclusive reviews of multiple ENM (Nowack & Bucheli 2007; Handy et al. 2008; Klaine et al. 2008; Radhika et al. 2010; Kumar et al. 2015) and Canesi and Corsi's (2016) review of nanomaterial effects on marine invertebrates. In addition, Hou et al. (2013) reviewed the accumulation of ENM by organisms under the assumption that, in general, accumulation of the ENM must first occur before effects will be observed.

In their comprehensive review, Klaine et al. (2008) reported toxicity to bacteria caused by fullerenes, SWCNT, MWCNT, metallic Cu and Ag, and metal oxides including Ti, Ce, Zn, and Si. Specific toxic effects to bacteria were described as antibacterial and bactericidal impacts. Similarly, freshwater and marine plants, invertebrates, and vertebrates demonstrated toxicity from exposure to a range of ENM including fullerenes, SW- and MWCNT, metallic copper and silver, and the metal oxides titanium and zinc, and quantum dots (Handy et al. 2008; Klaine et al. 2008). Toxic effects included some increases in mortality and evidence of reductions in growth and development, as well as a wide range of sub-lethal cellular insults. The highly variable effects on bacteria suggest that their susceptibility needs to be examined in order to fully understand community and ecosystem-level effects (Figure 10). Reviews of the literature performed concurrently to Klaine et al. (2008) and those that were published later, demonstrated similar findings of evidence of toxic effects to a range of organisms resulting from exposure to multiple types of ENM. However, some of these findings have been modified. For example, for carbon nanotubes, most recent data suggest that because of their limited bioavailability, toxic effects are unlikely to occur in the environment except at very high and unrealistic concentrations, such as 1000 mg/kg and 100 mg/L (OECD 2000, 2004) for sediment and water, respectively (Petersen & Nelson 2010).

Relative to the exposure of ENM to aquatic plants and algae, there is a "moderate" amount of literature on algae and less so aquatic plants. Researchers have reported TiO_2 toxicity

of algae ranging from low mg/L to over 100 mg/L (Hund-Rinke & Simon 2006; Aruoja et al. 2009; Hall et al. 2009). Zn and CuO nanoparticles are also noted to elicit toxicity in algae in the low mg/L range (Aruoja et al. 2009). In addition, trophic transfer of Cd-based quantum dots has been observed between algae and *Cerodaphnia dubia* (Bouldin et al. 2008). Much of this work has focused on short-term studies, often with traditional toxicity tests in monoculture. These tests offer little aid in evaluating how ENM affect complex aquatic systems (i.e. food chain, competitive interactions, carbon and nitrogen cycling, etc.). Overall, how ENM affect algae and aquatic plants in an ecological context is not well known.

Terrestrial plants

If ENM are bound on the surface or in the cuticle (e.g. adsorbed), they may not alter cellular properties but they may influence light harvesting properties of leaves through either photoactivity or reflection of specific light wavelengths. Yang et al. (2006, 2007) found that TiO_2 on spinach leaves may interact with N_2 to form reduced nitrogen compounds that can be subsequently taken up and increase plant growth. ENM may also be taken into internal plant organs but remain in the apoplast (non-living) portion of the plant, where additional binding and dissolution may occur. Bound particles also may influence cell wall chemistry and interact with other surface particles to influence uptake of other materials and gasses. Finally, certain particles may alter cuticular waxes, which may affect the hydrodynamics of the leaf.

If ENM are taken up into living cells into the symplast (e.g. absorption), there may be further interactions that alter the characteristics of the particle, such as binding or dissolution. Once in the symplast or living portion of the plant, particles may initiate a cascade of events leading to altered biochemistry, physiology, and growth (Figure 8). There is currently very little information regarding the fate and effects of ENM taken up through foliage (Rico et al. 2011; Chichiriccò & Poma 2015).

Plant studies have shown a variety of responses to ENM including growth reductions, increases, or no effect at all, depending on the nanomaterial and plant species being studied (Ma et al. 2010; Kumar et al. 2013). Klaine et al. (2008) reported toxicity to terrestrial plants (e.g. corn, cucumber, lettuce, radish, mustard rape, radish, and ryegrass) from ENM including fullerenes and MWCNT, metallic aluminum and zinc, aluminum, titanium and zinc oxides. Alternatively, CNTs, Au, CeO_2, and TiO_2 have been found to enhance seed germination and early plant development in some studies (Zheng et al. 2005; Kumar et al. 2013; Tumburu et al. 2015), but not others (López-Moreno et al. 2010). In some cases, the variable responses may be due to the composition of the ENM and whether or not it is soluble: ENM forms of Fe, Cu, and Zn, for example, may enhance growth via improved plant nutrition since they are required plant nutrients. In other cases, the presence of ENM forms of Ag and Cu, for example, may provide some plant protection from pathogens in the root zone, resulting in enhanced growth. Interpreting the conflicting results is often complicated by differences in methodology, poor characterization, or unrealistically high doses of ENM exposure. In order to better understand effects on plant growth and development, there is a need for longer-term studies with ENMs that incorporate natural soil microbial communities (Ge et al. 2016).

Whole-organism effects can also lead to changes in how individuals interact as members of an ecosystem. Disruption of specific structural or functional groups by ENM may lead to changes in community structure and function, altering important ecosystem processes such as nutrient cycling (Dinesh et al. 2012; Rodrigues et al. 2013; Simonin & Richaume 2015). Organisms compete for resources throughout their life cycle, and differential sensitivity to ENM may alter the competitive nature of interspecies interactions. There is currently insufficient information available for most species to be able to predict effects at larger scales.

Discussion

Some general conclusions drawn from the literature that may become starting places for further research are as follows:

1. If ENM are released into environmental media, they will likely react or heteroaggregate with constituents of the environmental matrix (air, water, or soil), and be dispersed into a relatively large receiving compartment, so that eventual exposures to environmental species or humans, for the most part, will not be to the original form of the material but instead to highly diluted ENM transformation or degredation products.
2. These environmental reactions will not occur under highly constrained laboratory or manufacturing conditions, but instead will be subject to a range of conditions and stochastic forces which will dynamically change across time and location. Therefore, if exposures to environmental transformation products of ENM occur, the exposures will likely be to multiple forms of these products including a range of particle agglomerates, sizes and coatings.
3. We currently have insufficient information regarding (i) the uses of ENM in industry and commerce, (ii) the penetration of ENM-enabled products into the marketplace, (iii) the potential for release of ENM from products, or (iv) the form of ENM that may be released. Notably, these limitations are also characteristic of the uses of standard industrial chemicals. Such uncertainties hamper accurate assessments of ENM exposure as they do for conventional materials.
4. For the general population, near-field exposures from consumer use of ENM products, particularly with dispersive applications, will likely be higher than far-field exposures.
5. The predominant destiny of ENM emitted into wastewater systems will likely be biosolids, over half of which may be recycled through land application.
6. The predominant destiny of ENM emitted into solid waste systems will be landfills.
7. The predominant destiny of ENM emitted into aquatic ecosystems will be to become complexed with natural organic matter or other constituents of the aquatic system and subsequent deposition into sediments. An

exception may be polarizable materials such as graphene oxide that may have the ability to remain suspended in the water column for long term transport. In a decision framework, such polarizable suspended materials may be considered a higher risk exposure to organisms in the water column, as opposed to those residing in the sediment.

8. Aquatic organisms residing in the sediments including filter feeding organisms will likely experience higher levels of exposure to ENM than will other aquatic species.
9. Soluble and reactive metal-based ENM, such as those composed of silver, will likely react with constituents such as sulfides in the environment to form less soluble metallic salts. This is particularly relevant in wastewater systems.
10. Rates of uptake of ENM may be low by oral and dermal of exposure, but elimination rates of systemically absorbed ENM may be even lower. By inhalation exposure, ENM deposition in the respiratory tract may cause local oxidative stress and inflammation, and systemic absorption may become significant.
11. In biologic media, ENM will be coated with a protein corona or similar biomolecules that influence the biokinetics of particles and reactions with cellular receptors.
12. Uptake and penetration barriers at the portal of entry and within the body at important organs, such as the brain and placenta, may limit the biodistribution of absorbed ENM. Typically, these barriers are not absolute, and serve to reduce, but not eliminate, diffusion or translocation of materials.
13. Most mammalian cells have the ability to uptake particles through several pathways, although the rates of uptake vary across cell types and are dependent on numerous physical and chemical factors of the particles such as size, coatings, surface charge, and biological transformations.
14. ENM may initiate molecular events associated with adverse outcomes such as induction of reactive oxygen species, dissolution to toxic metal ions, or initiation of inflammation.
15. The greater the conservation of molecular, cellular, and structural features among organisms exposed to EMNs, the higher the likelihood of comparable MIEs and downstream responses.
16. Because there is substantial divergence between the plant and animal membrane-bound receptors and signaling pathways that affect homeostasis, development and reproduction, ENM which bring about the same generalized MIEs in many species could very well produce distinct adverse outcomes in plants and animals.
17. Potential adverse outcomes are not limited to effects within cells or organs. They extend to whole organisms, communities and ecosystems.

Conclusions

Nanotechnology and the production of ENM have the potential to significantly enhance future economic development and to produce advanced capabilities that will benefit many segments of society (PCAST 2014). We are at a time where the informed development and use of these new materials can be done in a way that avoids many of the mishaps of the past such as those associated with the early development of the chemical industry. The ability to forecast and avoid potential environmental problems across the life cycle of material development, including use and disposal, is required if we are to achieve sustainable development of nanotechnology. Here we propose a series of compartmental stages that encompass the full life cycle of ENM, their potential release into environmental media, their fate, transport, and transformation in the environment, potential exposures to sensitive species including humans, and the possibility to cause adverse effects in those species. There are currently large numbers of ENM used in industrial and commercial applications, but there is insufficient information about the potential for those materials to enter the environment. Many potential scenarios involve release of dissolved ions rather than nanoparticles, such as copper ions leaching from pressure treated lumber or silver ions released from children's clothing or other products. Other scenarios of potential release, such as sawing or sanding nano-enabled solid materials, are likely to release ENM that are still attached to parts of the original product matrix rather than release ENM in their originally manufactured form. In other cases, the release of ENM in nanoparticle form is possible, such as for nanoparticles suspended in liquid or cream formulations including spray cleaners, personal care products, or as nano-formulated pesticides. A potential for a large release of ENM into the environment may be from road or rail accidents involving ENM transporting vehicles. In recognition of the difficulty of modeling the complex networks of ENM with novel physical and chemical properties, we propose that critical nodes along these pathways should be considered as the targets to develop simple functional assays that can be used to efficiently determine the likely behavior of ENM in these systems. The diagrams presented here may serve as guidance for targeted assay development. In addition, this compartmental framework will assist in placing the results of specific investigations into context for interpretation of broader environmental implications. These diagrams may also assist in development of quantitative modeling as rates and transformation functions for movement of particles across compartments are developed.

The framework described here currently addresses some, but not all, of the criteria listed by Hristozov et al. (2016). The framework can be said to consider their criteria in that it includes nano-specific requirements, life cycle thinking, an exposure-driven approach, an iterative and adaptive structure, and transparency of objectives. The current framework is not completed, however. At this point, it provides guidance for development of functional assays and models that will eventually lead to a simplification of ENM evaluations, but does not yet identify specific assays or models. Future implementation of the framework also should be amendable to grouping, read across or other simplifying approaches to risk assessment. The development of documented applications should

await the definition of the critical nodes and functional assays.

Although ENMs share a common size range, many of their properties are as unique as the elements from which they are composed. The properties they provide for a wide variety of products vary greatly, as well as their potential release, exposure, and mechanism of effect. Consequently knowledge gaps with respect to release, exposure, and effects are often ENM- and product specific. Never-the-less, there are broad and general gaps of data and predictive modeling which include: incomplete information regarding ENM composition, concentration and potential releases from ENM-enabled products; measuring and predicting affinity of ENM for environmental substrates; dissolution rates of metal-based ENM in environmental and biological media; environmental transformation and degredation products; influence of environmental transformations on biodistribution and toxicity; AOP specifications; as well as species differences in uptake, biodistribution, and susceptibility. Future research addressing these data gaps can be incorporated into the growing exposition of the pathways outlined in the framework presented here.

Acknowledgements

The authors thank Dr. Christine Hendren (Duke University, Center for Environmental Implications of Nanotechnology) and Maureen Gwinn (U.S. EPA Office of Research of Development, National Center for Environmental Assessment) for their extremely helpful reviews of an earlier version of the manuscript. The authors also are very appreciative of the extensive review comments from peer-reviewers selected by the Editor and anonymous to the authors. This input served to greatly strengthen the manuscript.

Declaration of interest

The authors declare that there are no financial conflicts of interest. The author's affiliations are as shown on the cover page. The authors have sole responsibility for the writing and content of the paper. The work was conducted under the EPA Office of Research and Development Chemical Safety for Sustainability Research Program. This article was reviewed in accordance with the policy of the National Health and Environmental Effects Research Laboratory, U.S. Environmental Protection Agency and approved for publication. Approval does not signify that the contents necessarily reflect the views and policies of the Agency, nor does mention of trade names or commercial products constitute endorsement or recommendation for use.

All of the authors, with one exception, were employees of the U.S. Environmental Protection Agency, and development of this document was a portion of their job responsibilities. The exception was Ms. B. L. Thornton, who was an independent student services contractor to the EPA, and preparation of this manuscript was a portion of her assigned work duties (Contract no. EP-13-C-000164).

None of the authors, with one exception, have participated in legal or regulatory proceedings regarding the content of this manuscript within the last 5 years. The exception was Dr. W. K. Boyes, who served on workgroups related to the issuance of a Toxics Substances Control Act (TSCA) Section 8(a) action: "Chemical Substances When Manufactured or Processed as Nanoscale Materials; TSCA Reporting and Recordkeeping Requirements", and in responding to public comments related to this action (40 CFR Part 704; Fed. Reg.82 (8) 3641–3655, 2017).

This work was supported by the U.S. Environmental Protection Agency.

ORCID

William K. Boyes http://orcid.org/0000-0002-3598-0032
Souhail R. Al-Abed http://orcid.org/0000-0002-5595-1300
Christian P. Andersen http://orcid.org/0000-0003-2169-2520
Dermont C. Bouchard http://orcid.org/0000-0002-7467-0248
Robert M. Burgess http://orcid.org/0000-0003-4504-5125
Elaine A. Cohen Hubal http://orcid.org/0000-0002-9650-3483
Kay T. Ho http://orcid.org/0000-0002-6750-4487
Michael F. Hughes http://orcid.org/0000-0002-5571-5447
Kirk Kitchin http://orcid.org/0000-003-0693-8967
Jeffrey A. Ross http://orcid.org/0000-0002-7002-4548
Kirk G. Scheckel http://orcid.org/0000-0001-9326-9241

References

Adjei IM, Sharma B, Labhasetwar V. 2014. Nanoparticles: cellular uptake and cytotoxicity. In: Capco DG, Chen Y, editor. Nanomaterial. Netherlands: Springer; p. 73–91.

Agarwal PK, Agarwal P, Reddy MK, Sopory SK. 2006. Role of DREB transcription factors in abiotic and biotic stress tolerance in plants. Plant Cell Rep. 25:1263–1274.

Al-Abed SR, Virkutyte J, Ortenzio JNR, McCarrick RM, Degn LL, Zucker R, Coates NH, Childs K, Ma H, Diamond S, et al. 2016. Environmental aging alters Al(OH)3 coating of TiO2 nanoparticles enhancing their photocatalytic and phototoxic activities. Environ Sci: Nano. 2016;3:593–601.

Alberts B, Johnson A, Lewis J, Raff M, Roberts K, Walter P. 2002. Molecular biology of the cell. New York: Garland Science.

Alger H, Momcilovic D, Carlander D, Duncan TV. 2014. Methods to evaluate uptake of engineered nanomaterials by the alimentary tract. Compr Rev Food Sci Food Saf. 13:705–729.

Almeida JPM, Chen AL, Foster A, Drezek R. 2011. *In vivo* biodistribution of nanoparticles. Nanomedicine (Lond). 6:815–835.

Andón FT, Kapralov AA, Yanamala N, Feng W, Baygan A, Chambers BJ, Hultenby K, Ye F, Toprak MS, Brandner BD, et al. 2013. Biodegradation of Single-Walled Carbon Nanotubes by Eosinophil Peroxidase. Small. 9:2721–2729.

ANEC, BEUC. 2010. ANEC/BEUC inventory of products claiming to contain nanoparticles available on the EU market. European Consumers Organization and the European Consumer Voice in Standardization.

ANEC, BEUC. 2012. ANEC/BEUC inventory of products claiming to contain nano-silver particles available on the EU market. European Consumers Organization; European Consumer Voice in Standardization.

Ankley GT, Bennett RS, Erickson RJ, Hoff DJ, Hornung MW, Johnson RD, Mount DR, Nichols JW, Russom CL, Schmieder PK, et al. 2010. Adverse outcome pathways: a conceptual framework to support ecotoxicology research and risk assessment. Environ Toxicol Chem. 29:730–741.

Arts JHE, Hadi M, Keene AM, Kreiling R, Lyon D, Maier M, Michel K, Petry T, Sauer UG, Warheit D, et al. 2014. A critical appraisal of existing concepts for the grouping of nanomaterials. Regul Toxicol Pharmacol. 70:492–506.

Aruoja V, Dubourguier H-C, Kasemets K, Kahru A. 2009. Toxicity of nanoparticles of CuO, ZnO and TiO2 to microalgae Pseudokirchneriella subcapitata. Sci Total Environ. 407:1461–1468.

Aschberger K, Micheletti C, Sokull-Klüttgen B, Christensen FM. 2011. Analysis of currently available data for characterising the risk of engineered nanomaterials to the environment and human health—lessons learned from four case studies. Environ Int. 37:1143–1156.

Asgharian B, Hofmann W, Bergmann R. 2001. Particle deposition in a multiple-path model of the human lung. Aerosol Sci Technol. 34:332–339.

Asharani P, Sethu S, Lim HK, Balaji G, Valiyaveettil S, Hande MP. 2012. Differential regulation of intracellular factors mediating cell cycle, DNA

repair and inflammation following exposure to silver nanoparticles in human cells. Genome Integr. 3:2.
Bachler G, von Goetz N, Hungerbuhler K. 2015. Using physiologically based pharmacokinetic (PBPK) modeling for dietary risk assessment of titanium dioxide (TiO2) nanoparticles. Nanotoxicology. 9:373–380.
Bachler G, von Goetz N, Hungerbühler K. 2013. A physiologically based pharmacokinetic model for ionic silver and silver nanoparticles. Int J Nanomedicine. 8:3365–3382.
Badireddy AR, Wiesner MR, Liu J. 2012. Detection, characterization, and abundance of engineered nanoparticles in complex waters by hyperspectral imagery with enhanced darkfield microscopy. Environ Sci Technol. 46:10081–10088.
Bakand S, Hayes A, Dechsakulthorn F. 2012. Nanoparticles: a review of particle toxicology following inhalation exposure. Inhal Toxicol. 24:125–135.
Baroli B. 2010. Penetration of nanoparticles and nanomaterials in the skin: Fiction or reality? J Pharm Sci. 99:21–50.
Baroli B, Ennas MG, Loffredo F, Isola M, Pinna R, Lopez-Quintela MA. 2007. Penetration of metallic nanoparticles in human full-thickness skin. J Invest Dermatol. 127:1701–1712.
Benn T, Cavanagh B, Hristovski K, Posner JD, Westerhoff P. 2010. The release of nanosilver from consumer products used in the home. J Environ Qual. 39:1875–1882.
Benn TM, Westerhoff P. 2008. Nanoparticle silver released into water from commercially available sock fabrics. Environ Sci Technol. 42:4133–4139.
Bhaskar S, Tian F, Stoeger T, Kreyling W, de la Fuente JM, Grazú V, Borm P, Estrada G, Ntziachristos V, Razansky D. 2010. Multifunctional Nanocarriers for diagnostics, drug delivery and targeted treatment across blood–brain barrier: perspectives on tracking and neuroimaging. Part Fibre Toxicol. 7:3–3.
Blank F, Stumbles PA, Seydoux E, Holt PG, Fink A, Rothen-Rutishauser B, Strickland DH, von Garnier C. 2013. Size-dependent uptake of particles by pulmonary antigen-presenting cell populations and trafficking to regional lymph nodes. Am J Respir Cell Mol Biol. 49:67–77.
Bolyard SC, Reinhart DR, Santra S. 2013. Behavior of engineered nanoparticles in landfill leachate. Environ Sci Technol. 47:8114–8122.
Boncagni NT, Otaegui JM, Warner E, Curran T, Ren J, Fidalgo de Cortalezzi MM. 2009. Exchange of TiO2 nanoparticles between streams and streambeds. Environ Sci Technol. 43:7699–7705.
Boncel S, Kyzioł-Komosińska J, Krzyżewska I, Czupioł J. 2015. Interactions of carbon nanotubes with aqueous/aquatic media containing organic/inorganic contaminants and selected organisms of aquatic ecosystems – a review. Chemosphere. 136:211–221.
Boonruksa P, Bello D, Zhang J, Isaacs JA, Mead JL, Woskie SR. 2016. Characterization of potential exposures to nanoparticles and fibers during manufacturing and recycling of carbon nanotube reinforced polypropylene composites. Ann Occup Hyg. 60:40–55.
Bouchard D, Chang X, Chowdhury I. 2015. Heteroaggregation of multiwalled carbon nanotubes with sediments. Environ Nanotechnol Monit Manag. 4:42–50.
Bouldin JL, Ingle TM, Sengupta A, Alexander R, Hannigan RE, Buchanan RA. 2008. Aqueous toxicity and food chain transfer of quantum dots™ in freshwater algae and *Ceriodaphnia dubia*. Environ Toxicol Chem. 27:1958–1963.
Braakhuis HM, Park MV, Gosens I, D, Jong WH, Cassee FR. 2014. Physicochemical characteristics of nanomaterials that affect pulmonary inflammation. Part Fibre Toxicol. 11:1–25.
Brouwer DH, Spaan S, Roff M, Sleeuwenhoek A, Tuinman I, Goede H, van Duuren-Stuurman B, Filon FL, Bello D, Cherrie JW. 2016. Occupational dermal exposure to nanoparticles and nano-enabled products: Part 2, exploration of exposure processes and methods of assessment. Int J Hyg Environ Health. 219:503–512.
Brunetti G, Donner E, Laera G, Sekine R, Scheckel KG, Khaksar M, Vasilev K, De Mastro G, Lombi E. 2015. Fate of zinc and silver engineered nanoparticles in sewerage networks. Water Res. 77:72–84.
BUND. Nanoproduktdatenbank Des BUND. Germany: Der Bund für Umwelt und Naturschutz Deutschland [Friends of the Earth Germany].
Buono C, Anzinger JJ, Amar M, Kruth HS. 2009. Fluorescent pegylated nanoparticles demonstrate fluid-phase pinocytosis by macrophages in mouse atherosclerotic lesions. J Clin Invest. 119:1373–1381.
Caballero-Guzman A, Nowack B. 2016. A critical review of engineered nanomaterial release data: are current data useful for material flow modeling? Environ Pollut. 213:502–517.
Caballero-Guzman A, Sun T, Nowack B. 2015. Flows of engineered nanomaterials through the recycling process in Switzerland. Waste Manag. 36:33–43.
Canesi L, Corsi I. 2016. Effects of nanomaterials on marine invertebrates. Sci Total Environ. 565:933–940.
Canton I, Battaglia G. 2012. Endocytosis at the nanoscale. Chem Soc Rev. 41:2718–2739.
Cassee F, Muijser H, Duistermaat E, Freijer J, Geerse K, Marijnissen JC, Arts JH. 2002. Particle size-dependent total mass deposition in lungs determines inhalation toxicity of cadmium chloride aerosols in rats. Application of a multiple path dosimetry model. Arch Toxicol. 76:277–286.
Cassee FR, van Balen EC, Singh C, Green D, Muijser H, Weinstein J, Dreher K. 2011. Exposure, health- and ecological effects review of engineered nanoscale cerium and cerium oxide associated with its use as a fuel additive. Crit Rev Toxicol. 41:213–229.
Chakraborty C, Sharma AR, Sharma G, Lee S-S. 2016. Zebrafish: a complete animal model to enumerate the nanoparticle toxicity. J Nanobiotechnol. 14:1–13.
Chang X, Bouchard DC. 2013. Multiwalled carbon nanotube deposition on model environmental surfaces. Environ Sci Technol. 47:10372–10380.
Chang X, Bouchard DC. 2016. Surfactant-wrapped multiwalled carbon nanotubes in aquatic systems: surfactant displacement in the presence of humic acid. Environ Sci Technol. 50:9214–9222.
Chen C-Y, Zepp RG. 2015. Probing photosensitization by functionalized carbon nanotubes. Environ Sci Technol. 49:13835–13843.
Chen W-Y, Cheng Y-H, Hsieh N-H, Wu B-C, Chou W-C, Ho CC, Chen JK, Liao CM, Lin P. 2015. Physiologically based pharmacokinetic modeling of zinc oxide nanoparticles and zinc nitrate in mice. Int J Nanomed. 10:6277–6292.
Chen Y, Qu K, Zhao C, Wu L, Ren J, Wang J, Qu X. 2012. Insights into the biomedical effects of carboxylated single-wall carbon nanotubes on telomerase and telomeres. Nat Commun. 3:1074.
Cheng CY, Mruk DD. 2012. The blood–testis barrier and its implications for male contraception. Pharmacol Rev. 64:16–64.
Cheng CY, Wong EWP, Lie PPY, Li MWM, Mruk DD, Yan HH, Mok KW, Mannu J, Mathur PP, Lui WY, et al. 2011. Regulation of blood–testis barrier dynamics by desmosome, gap junction, hemidesmosome and polarity proteins. Spermatogenesis. 1:105–115.
Chichiriccò G, Poma A. 2015. Penetration and toxicity of nanomaterials in higher plants. Nanomaterials (Basel). 5:851.
Chithrani BD, Chan WCW. 2007. Elucidating the mechanism of cellular uptake and removal of protein-coated gold nanoparticles of different sizes and shapes. Nano Lett. 7:1542–1550.
Chithrani BD, Ghazani AA, Chan WCW. 2006. Determining the size and shape dependence of gold nanoparticle uptake into mammalian cells. Nano Lett. 6:662–668.
Choi HS, Liu W, Misra P, Tanaka E, Zimmer JP, Ipe BI, Bawendi M, Frangioni JV. 2007. Renal clearance of quantum dots. Nat Biotechnol. 25:1165–1170.
Chorley B, Ward W, Simmons SO, Vallanat B, Veronesi B. 2014. The cellular and genomic response of rat dopaminergic neurons (N27) to coated nanosilver. NeuroToxicology. 45:12–21.
Chou C-C, Hsiao H-Y, Hong Q-S, Chen C-H, Peng Y-W, Chen HW, Yang PC. 2008. Single-walled carbon nanotubes can induce pulmonary injury in mouse model. Nano Lett. 8:437–445.
Chowdhury I, Duch MC, Mansukhani ND, Hersam MC, Bouchard D. 2013. Colloidal properties and stability of graphene oxide nanomaterials in the aquatic environment. Environ Sci Technol. 47:6288–6296.
Chowdhury I, Hou WC, Goodwin D, Henderson M, Zepp RG, Bouchard D. 2015a. Sunlight affects aggregation and deposition of graphene oxide in the aquatic environment. Water Res. 78:37–46.

Chowdhury I, Mansukhani ND, Guiney LM, Hersam MC, Bouchard D. 2015b. Aggregation and stability of reduced graphene oxide: complex roles of divalent cations, pH, and natural organic matter. Environ Sci Technol. 49:10886–10893.

Clift MJD, Raemy DO, Endes C, Ali Z, Lehmann AD, Brandenberger C, Petri-Fink A, Wick P, Parak WJ, Gehr P, et al. 2013. Can the Ames test provide an insight into nano-object mutagenicity? Investigating the interaction between nano-objects and bacteria. Nanotoxicology. 7:1373–1385.

Cohen J, Deloid G, Pyrgiotakis G, Demokritou P. 2013a. Interactions of engineered nanomaterials in physiological media and implications for *in vitro* dosimetry. Nanotoxicology. 7:417–431.

Cohen JM, Teeguarden JG, Demokritou P. 2014. An integrated approach for the *in vitro* dosimetry of engineered nanomaterials. Part Fibre Toxicol. 11:20–20.

Cohen Y, Rallo R, Liu R, Liu HH. 2013b. In silico analysis of nanomaterials: hazard and risk. Acc Chem Res. 46:802–812.

Coleman DC, Crossley DA, Hendrix PF. 2004. Fundamentals of soil ecology. New York: Elsevier Academic Press.

Colman BP, Arnaout CL, Anciaux S, Gunsch CK, Hochella MF Jr., Kim B, Lowry GV, McGill BM, Reinsch BC, Richardson CJ, et al. 2013. Low concentrations of silver nanoparticles in biosolids cause adverse ecosystem responses under realistic field scenario. PLoS One. 8:e57189.

Costa PM, Fadeel B. 2016. Emerging systems biology approaches in nanotoxicology: towards a mechanism-based understanding of nanomaterial hazard and risk. Toxicol Appl Pharmacol. 299:101–111.

Dale AL, Casman EA, Lowry GV, Lead JR, Viparelli E, Baalousha M. 2015. Modeling nanomaterial environmental fate in aquatic systems. Environ Sci Technol. 49:2587–2593.

Davda J, Labhasetwar V. 2002. Characterization of nanoparticle uptake by endothelial cells. Int J Pharm. 233:51–59.

de Castro JA, Pereira BA, Tassi E, Pini R, Araujo ASF, Valadão ICP. 2012. Modeling the transport phenomena of TiO2 nanoparticles into Leachate of Municipal Waste Landfills. In: Salgado L, Filho FA, editors. Materials science forum. Switzerland: Trans Tech Publications; p. 1695–1700.

De Lorenzo AJD. 2008. The olfactory neuron and the blood-brain barrier. In: Ciba Foundation Symposium: internal secretions of the pancreas (Colloquia on Endocrinology). New York: John Wiley & Sons, Ltd.; p. 151–176.

DeLoid G, Cohen JM, Darrah T, Derk R, Rojanasakul L, Pyrgiotakis G, Wohlleben W, Philip Demokritou P. 2014. Estimating the effective density of engineered nanomaterials for *in vitro* dosimetry. Nat Commun. 5:3514.

Desai MP, Labhasetwar V, Amidon GL, Levy RJ. 1996. Gastrointestinal uptake of biodegradable microparticles: effect of particle size. Pharm Res. 13:1838–1845.

Desai MP, Labhasetwar V, Walter E, Levy RJ, Amidon GL. 1997. The mechanism of uptake of biodegradable microparticles in Caco-2 cells is size dependent. Pharm Res. 14:1568–1573.

Di Toro DM, Zarba CS, Hansen DJ, Berry WJ, Swartz RC, Cowan C, Pavlou S, Allen H. 1991. Technical basis for establishing sediment quality criteria for nonionic organic chemicals using equilibrium partitioning. Environ Toxicol Chem. 10:1541–1583.

Dietz K-J, Herth S. 2011. Plant nanotoxicology. Trends Plant Sci. 16:582–589.

Dinesh R, Anandaraj M, Srinivasan V, Hamza S. 2012. Engineered nanoparticles in the soil and their potential implications to microbial activity. Geoderma. 173:19–27.

Dobrovolskaia MA, McNeil SE. 2007. Immunological properties of engineered nanomaterials. Nat Nanotechnol. 2:469–478.

Domínguez A, Suárez-Merino B, Goñi-de-Cerio F. 2014. Nanoparticles and blood-brain barrier: the key to central nervous system diseases. J Nanosci Nanotechnol. 14:766–779.

Donaldson K, Murphy FA, Duffin R, Poland CA. 2010. Asbestos, carbon nanotubes and the pleural mesothelium: a review of the hypothesis regarding the role of long fibre retention in the parietal pleura, inflammation and mesothelioma. Part Fibre Toxicol. 7:5.

Donaldson K, Poland CA. 2013. Nanotoxicity: challenging the myth of nano-specific toxicity. Curr Opin Biotechnol. 24:724–734.

Donner E, Howard DL, Jonge MDd, Paterson D, Cheah MH, Naidu R, Lombi E. 2011. X-ray absorption and micro X-ray fluorescence spectroscopy investigation of copper and zinc speciation in biosolids. Environ Sci Technol. 45:7249–7257.

Donner E, Scheckel K, Sekine R, Popelka-Filcoff RS, Bennett JW, Brunetti G, Naidu R, McGrath SP, Lombi E. 2015. Non-labile silver species in biosolids remain stable throughout 50 years of weathering and ageing. Environ Pollut. 205:78–86.

Duan J, Yu Y, Li Y, Yu Y, Li Y, Zhou X, Huang P, Sun Z. 2013. Toxic effect of silica nanoparticles on endothelial cells through DNA damage response via Chk1-dependent G2/M checkpoint. PLoS One. 8:e62087.

Dwivedi AD, Dubey SP, Sillanpää M, Kwon Y-N, Lee C, Varma RS. 2015. Fate of engineered nanoparticles: implications in the environment. Coord Chem Rev. 287:64–78.

Eastlake A, Zumwalde R, Geraci C. 2016a. Can control banding be useful for the safe handling of nanomaterials? A systematic review. J Nanopart Res: Interdiscip Forum Nanoscale Sci Technol. 18:169.

Eastlake AC, Beaucham C, Martinez KF, Dahm MM, Sparks C, Hodson LL, Geraci CL. 2016b. Refinement of the nanoparticle emission assessment technique into the Nanomaterial Exposure Assessment Technique (NEAT 2.0). J Occup Environ Hygiene. 13:708–717.

El Badawy AM, Luxton TP, Silva RG, Scheckel KG, Suidan MT, Tolaymat TM. 2010. Impact of environmental conditions (pH, ionic strength, and electrolyte type) on the surface charge and aggregation of silver nanoparticles suspensions. Environ Sci Technol. 44:1260–1266.

Elder A, Vidyasagar S, DeLouise L. 2009. Physicochemical factors that affect metal and metal oxide nanoparticle passage across epithelial barriers. Wiley Interdiscip Rev Nanomed Nanobiotechnol. 1:434–450.

EPA. 2009. *Targeted National Sewage Sludge Survey Sampling and Analysis Technical Report*. Washington (DC): U.S. Environmental Protection Agency, Office of Water.

EPA. 2012. Water: Sewage Sludge (Biosolids): Frequently Asked Questions. U.S. Environmental Protection Agency.

EPA. 2017. Chemical Substances When Manufactured or Processed as Nanoscale Materials; TSCA Reporting and Recordkeeping Requirements ed. OoPPa Toxics. Washington (DC): Federal Register; p. 3641–3655.

Erdakos GB, Bhave PV, Pouliot GA, Simon H, Mathur R. 2014. Predicting the effects of nanoscale cerium additives in diesel fuel on regional-scale air quality. Environ Sci Technol. 48:12775–12782.

Essington ME. 2015. Soil and water chemistry: an integrative approach. 2nd ed. Boca Raton (FL): CRC Press, Taylor and Francis Group.

Evans DE, Ku BK, Birch ME, Dunn KH. 2010. Aerosol monitoring during carbon nanofiber production: mobile direct-reading sampling. Ann Occup Hyg. 54:514–531.

Fabian E, Landsiedel R, Ma-Hock L, Wiench K, Wohlleben W, van Ravenzwaay B. 2008. Tissue distribution and toxicity of intravenously administered titanium dioxide nanoparticles in rats. Arch Toxicol. 82.

Fabrega J, Luoma SN, Tyler CR, Galloway TS, Lead JR. 2011. Silver nanoparticles: behaviour and effects in the aquatic environment. Environ Int. 37:517–531.

Fako VE, Furgeson DY. 2009. Zebrafish as a correlative and predictive model for assessing biomaterial nanotoxicity. Adv Drug Deliv Rev. 61:478–486.

Farcal L, Torres Andón F, Di Cristo L, Rotoli BM, Bussolati O, Bergamaschi E, Mech A, Hartmann NB, Rasmussen K, Riego-Sintes J, et al. 2015. Comprehensive *in vitro* toxicity testing of a panel of representative oxide nanomaterials: first steps towards an intelligent testing strategy. PLoS One. 2015;10:e0127174.

Federici G, Shaw BJ, Handy RD. 2007. Toxicity of titanium dioxide nanoparticles to rainbow trout (*Oncorhynchus mykiss*): gill injury, oxidative stress, and other physiological effects. Aquat Toxicol. 84:415–430.

Ferry JL, Craig P, Hexel C, Sisco P, Frey R, Paul LP, Michael HF, Geoff SI, Alan WD, Shosaku K, et al. 2009. Transfer of gold nanoparticles from the water column to the estuarine food web. Nat Nano. 4:441–444.

Fleischer CC, Payne CK. 2014. Nanoparticle–cell interactions: molecular structure of the protein corona and cellular outcomes. Accounts Chem Res. 47:2651–2659.

Foldbjerg R, Dang DA, Autrup H. 2011. Cytotoxicity and genotoxicity of silver nanoparticles in the human lung cancer cell line, A549. Arch Toxicol. 85:743–750.

Froggett SJ, Clancy SF, Boverhof DR, Canady RA. 2014. A review and perspective of existing research on the release of nanomaterials from solid nanocomposites. Part Fibre Toxicol. 11:1–28.

Frohlich E. 2016. Cellular elimination of nanoparticles. Environ Toxicol Pharmacol. 46:90–94.

Frohlich E, Roblegg E. 2012. Models for oral uptake of nanoparticles in consumer products. Toxicology. 291:10–17.

Gantt B, Hoque S, Willis RD, Fahey KM, Delgado-Saborit JM, Harrison RM, Erdakos GB, Bhave PV, Zhang KM, Kovalcik K, Pye HO. 2014. Near-road modeling and measurement of cerium-containing particles generated by nanoparticle diesel fuel additive use. Environ Sci Technol. 48:10607–10613.

Gao H, Shi W, Freund LB. 2005. Mechanics of receptor-mediated endocytosis. Proc Natl Acad Sci USA. 102:9469–9474.

García-Alonso J, Rodriguez-Sanchez N, Misra SK, Valsami-Jones E, Croteau M-N, Luoma SN, Rainbow PS. 2014. Toxicity and accumulation of silver nanoparticles during development of the marine polychaete *Platynereis dumerilii*. Sci Total Environ. 476–477:688–695.

Ge Y, Priester JH, Mortimer M, Chang CH, Ji Z, Schimel JP, Holden PA. 2016. Long-term effects of multiwalled carbon nanotubes and graphene on microbial communities in dry soil. Environ Sci Technol. 50:3965–3974.

George R, Merten S, Wang TT, Kennedy P, Maitz P. 2014. *In vivo* analysis of dermal and systemic absorption of silver nanoparticles through healthy human skin. Australas J Dermatol. 55:185–190.

Gerloff K, Landesmann B, Worth A, Munn S, Palosaari T, Whelan M. 2017. The adverse outcome pathway approach in nanotoxicology. Comput Toxicol. 1:3–11.

Gitipour A, El Badawy A, Arambewela M, Miller B, Scheckel K, Elk M, Ryu H, Gomez-Alvarez V, Domingo JS, Thiel S, et al. 2013. The impact of silver nanoparticles on the composting of municipal solid waste. Environ Sci Technol. 47:14385–14393.

Godwin H, Nameth C, Avery D, Bergeson LL, Bernard D, Beryt E, Boyes W, Brown S, Clippinger AJ, Cohen Y, et al. 2015. Nanomaterial categorization for assessing risk potential to facilitate regulatory decision-making. ACS Nano. 9:3409–3417.

Golbamaki N, Rasulev B, Cassano A, Marchese Robinson RL, Benfenati E, Leszczynski J, Cronin MT. 2015. Genotoxicity of metal oxide nanomaterials: review of recent data and discussion of possible mechanisms. Nanoscale. 7:2154–2198.

Gomes T, Pereira CG, Cardoso C, Pinheiro JP, Cancio I, Bebianno MJ. 2012. Accumulation and toxicity of copper oxide nanoparticles in the digestive gland of *Mytilus galloprovincialis*. Aquat Toxicol. 118–119:72–79.

Gomes T, Pinheiro JP, Cancio I, Pereira CG, Cardoso C, Bebianno MJ. 2011. Effects of copper nanoparticles exposure in the Mussel *Mytilus galloprovincialis*. Environ Sci Technol. 45:9356–9362.

Gottschalk F, Sonderer T, Scholz RW, Nowack B. 2009. Modeled environmental concentrations of engineered nanomaterials (TiO2, ZnO, Ag, CNT, fullerenes) for different regions. Environ Sci Technol. 43:9216–9222.

Gottschalk F, Sun T, Nowack B. 2013. Environmental concentrations of engineered nanomaterials: review of modeling and analytical studies. Environ Pollut. 181:287–300.

Grassian VH, Haes AJ, Mudunkotuwa IA, Demokritou P, Kane AB, Murphy CJ, Hutchinson JE, Issacs JA, Jun Y-S, Karn B, et al. 2016. NanoEHS: defining fundamental science needs: no easy feat when the simple itself is complex. Environ Sci: Nano. 3:15–27.

Grieger KD, Linkov I, Hansen SF, Baun A. 2012. Environmental risk analysis for nanomaterials: review and evaluation of frameworks. Nanotoxicology. 6:196–212.

Griffitt RJ, Hyndman K, Denslow ND, Barber DS. 2009. Comparison of molecular and histological changes in zebrafish gills exposed to metallic nanoparticles. Toxicol Sci. 107:404–415.

Griffitt RJ, Weil R, Hyndman KA, Denslow ND, Powers K, Taylor D, Barber DS. 2007. Exposure to copper nanoparticles causes gill injury and acute lethality in zebrafish (Danio rerio). Environ Sci Technol. 41:8178–8186.

Guadagnini R, Halamoda Kenzaoui B, Walker L, Pojana G, Magdolenova Z, Bilanicova D, Saunders M, Juillerat-Jeanneret L, Marcomini A, Huk A, et al. 2015. Toxicity screenings of nanomaterials: challenges due to interference with assay processes and components of classic *in vitro* tests. Nanotoxicology. 9:13–24.

Guan R, Kang T, Lu F, Zhang Z, Shen H, Liu M. 2012. Cytotoxicity, oxidative stress, and genotoxicity in human hepatocyte and embryonic kidney cells exposed to ZnO nanoparticles. Nanoscale Res Lett. 7:602.

Gunduz N, Ceylan H, Guler MO, Tekinay AB. 2017. Intracellular accumulation of gold nanoparticles leads to inhibition of macropinocytosis to reduce the endoplasmic reticulum stress. Sci Rep. 7:40493.

Guo X, Chen T. 2015. Chapter 7. Progress in genotoxicity evaluation of engineered nanomaterials. In: Soloneski S, Larramendy ML, editors. Nanomaterials: toxicity and risk assessment. Rijeka: Intech.

Hagens WI, Oomen AG, de Jong WH, Cassee FR, Sips AJ. 2007. What do we (need to) know about the kinetic properties of nanoparticles in the body? Regul Toxicol Pharmacol. 49:217–229.

Hall S, Bradley T, Moore JT, Kuykindall T, Minella L. 2009. Acute and chronic toxicity of nano-scale TiO2 particles to freshwater fish, cladocerans, and green algae, and effects of organic and inorganic substrate on TiO2 toxicity. Nanotoxicology. 3:91–97.

Handy R, Henry T, Scown T, Johnston B, Tyler C. 2008. Manufactured nanoparticles: their uptake and effects on fish – a mechanistic analysis. Ecotoxicology. 17:396–409.

Hansen S, Jensen K, Baun A. 2013. NanoRiskCat: a conceptual tool for categorization and communication of exposure potentials and hazards of nanomaterials in consumer products. J Nanopart Res. 16:1–25.

Hansen SF, Heggelund LR, Revilla Besora P, Mackevica A, Boldrin A, Baun A. 2016. Nanoproducts -what is actually available to European consumers? Environ Sci: Nano. 3:169–180.

Harper SL, Carriere JL, Miller JM, Hutchison JE, Maddux BL, Tanguay RL. 2011. Systematic evaluation of nanomaterial toxicity: utility of standardized materials and rapid assays. ACS Nano. 5.

He X, Zhang H, Ma Y, Bai W, Zhang Z, Lu K, Ding Y, Zhao Y, Chai Z. 2010. Lung deposition and extrapulmonary translocation of nano-ceria after intratracheal instillation. Nanotechnology. 21:285103.

Hendren CO, Lowry GV, Unrine JM, Wiesner MR. 2015. A functional assay-based strategy for nanomaterial risk forecasting. Sci Total Environ. 536:1029–1037.

Hendren CO, Lowry M, Grieger KD, Money ES, Johnston JM, Wiesner MR, Beaulieu SM. 2013. Modeling approaches for characterizing and evaluating environmental exposure to engineered nanomaterials in support of risk-based decision making. Environ Sci Technol. 47:1190–1205.

Hillyer JF, Albrecht RM. 2001. Gastrointestinal persorption and tissue distribution of differently sized colloidal gold nanoparticles. J Pharm Sci. 90:1927–1936.

Hinderliter PM, Minard KR, Orr G, Chrisler WB, Thrall BD, Pounds JG, Teeguarden JG. 2010. ISDD: a computational model of particle sedimentation, diffusion and target cell dosimetry for *in vitro* toxicity studies. Part Fibre Toxicol. 7:36.

Holbrook RD, Murphy KE, Morrow JB, Cole KD. 2008. Trophic transfer of nanoparticles in a simplified invertebrate food web. Nat Nano. 3:352–355.

Holden PA, Gardea-Torresdey JL, Klaessig F, Turco RF, Mortimer M, Hund-Rinke K, Cohen Hubal EA, Avery D, Barceló D, Behra R, et al. 2016. Considerations of environmentally relevant test conditions for improved evaluation of ecological hazards of engineered nanomaterials. Environ Sci Technol. 50:6124–6145.

Holden PA, Nisbet RM, Lenihan HS, Miller RJ, Cherr GN, Schimel JP, Gardea-Torresdey JL. 2013. Ecological nanotoxicology: integrating nanomaterial hazard considerations across the subcellular, population, community, and ecosystems levels. Acc Chem Res. 46:813–822.

Holder AL, Vejerano EP, Zhou X, Marr LC. 2013. Nanomaterial disposal by incineration. Environ Sci Process Impacts. 15:1652–1664.

Hou W-C, Chowdhury I, Goodwin DG, Henderson WM, Fairbrother DH, Bouchard D, Zepp RG. 2015. Photochemical transformation of graphene oxide in sunlight. Environ Sci Technol. 49:3435–3443.

Hou W-C, Henderson WM, Chowdhury I, Goodwin DG Jr., Chang X, Martinf S, Fairbrotherd DH, Boucharde D, Zepp RG. 2016. The contribution of indirect photolysis to the degradation of graphene oxide in sunlight. Carbon. 110:426–437.

Hou WC, Stuart B, Howes R, Zepp RG. 2013. Sunlight-driven reduction of silver ions by natural organic matter: formation and transformation of silver nanoparticles. Environ Sci Technol. 47:7713–7721.

Hristozov D, Gottardo S, Semenzin E, Oomen A, Bos P, Peijnenburg W, van Tongeren M, Nowack B, Hunt N, Brunelli A, et al. 2016. Frameworks and tools for risk assessment of manufactured nanomaterials. Environ Int. 95:36–53.

Hu R, Gong X, Duan Y, Li N, Che Y, Cui Y, Zhou M, Liu C, Wang H, Hong F. 2010. Neurotoxicological effects and the impairment of spatial recognition memory in mice caused by exposure to TiO2 nanoparticles. Biomaterials. 31:8043–8050.

Huang S, Chueh PJ, Lin YW, Shih TS, Chuang SM. 2009. Disturbed mitotic progression and genome segregation are involved in cell transformation mediated by nano-TiO2 long-term exposure. Toxicol Appl Pharmacol. 241:182–194.

Huang YW, Wu C, Aronstam RS. 2010. Toxicity of transition metal oxide nanoparticles: recent insights from *in vitro* studies. Materials. 3:4842–4859.

Hull MS, Chaurand P, Rose J, Auffan M, Bottero J-Y, Jones JC, Schultz IR, Vikesland PJ. 2011. Filter-feeding bivalves store and biodeposit colloidally stable gold nanoparticles. Environ Sci Technol. 45:6592–6599.

Hund-Rinke K, Simon M. 2006. Ecotoxic effect of photocatalytic active nanoparticles (TiO2) on algae and daphnids (8 pp). Environ Sci Pollut Res Int. 13:225–232.

Hunter RJ. 2001. Foundations of colloid science. Oxford (UK): Oxford University Press.

Huynh KA, Siska E, Heithmar E, Tadjiki S, Pergantis SA. 2016. Detection and quantification of silver nanoparticles at environmentally relevant concentrations using asymmetric flow field–flow fractionation online with single particle inductively coupled plasma mass spectrometry. Anal Chem. 88:4909–4916.

Hyung H, Fortner JD, Hughes JB, Kim J-H. 2007. Natural organic matter stabilizes carbon nanotubes in the aqueous phase. Environ Sci Technol. 41:179–184.

Impellitteri CA, Harmon S, Silva RG, Miller BW, Scheckel KG, Luxtona TP, Schuppb D, Panguluri S. 2013. Transformation of silver nanoparticles in fresh, aged, and incinerated biosolids. Water Res. 47:3878–3886.

Isaacs KK, Glen WG, Egeghy P, Goldsmith M-R, Smith L, Vallero D, Brooks R, Grulke CM, Özkaynak H. 2014. SHEDS-HT: an integrated probabilistic exposure model for prioritizing exposures to chemicals with near-field and dietary sources. Environ Sci Technol. 48:12750–12759.

Ivask A, Juganson K, Bondarenko O, Mortimer M, Aruoja V, Kasemets K, Blinova I, Heinlaan M, Slaveykova V, Kahru A. 2013. Mechanisms of toxic action of Ag, ZnO and CuO nanoparticles to selected ecotoxicological test organisms and mammalian cells *in vitro*: a comparative review. Nanotoxicology. 8:57–71.

Jackson P, Vogel U, Wallin H, Hougaard KS. 2011. Prenatal exposure to carbon black (printex 90): effects on sexual development and neurofunction. Basic Clin Pharmacol Toxicol. 109:434–437.

Jimeno-Romero A, Berhanu D, Reip P, Oron M, Gilliland D, Valsami-Jones E, Cajaraville MP, Warley A, Marigómez I, Soto M. 2012. Down the rabbit hole: Subcellular localization and x-ray microanalysis of a set of metallic nanoparticles in mussels. Comp Biochem Physiol A: Mol Integr Physiol. 163:S23–S24.

Jin H, Heller DA, Sharma R, Strano MS. 2009. Size-dependent cellular uptake and expulsion of single-walled carbon nanotubes: single particle tracking and a generic uptake model for nanoparticles. ACS Nano. 3:149–158.

Johnston H, Pojana G, Zuin S, Jacobsen NR, Moller P, Loft S, Semmler-Behnke M, McGuiness C, Balharry D, Marcomini A, et al. 2013. Engineered nanomaterial risk. Lessons learnt from completed nanotoxicology studies: potential solutions to current and future challenges. Crit Rev Toxicol. 43:1–20.

Joubert Y, Pan J-F, Buffet P-E, Pilet P, Gilliland D, Valsami-Jones E, Mouneyrac C, Amiard-Triquet C. 2013. Subcellular localization of gold nanoparticles in the estuarine bivalve *Scrobicularia plana* after exposure through the water. Gold Bull. 46:47–56.

Juch H, Nikitina L, Debbage P, Dohr G, Gauster M. 2013. Nanomaterial interference with early human placenta: sophisticated matter meets sophisticated tissues. Reprod Toxicol. 41:73–79.

Judy JD, Unrine JM, Bertsch PM. 2011. Evidence for biomagnification of gold nanoparticles within a terrestrial food chain. Environ Sci Technol. 45:776–781.

Judy JD, Unrine JM, Rao W, Wirick S, Bertsch PM. 2012. Bioavailability of gold nanomaterials to plants: importance of particle size and surface coating. Environ Sci Technol. 46:8467–8474.

Kádár E, Lowe D, Solé M, Fisher A, Jha A, Readman JW, Hutchinson TH. 2010. Uptake and biological responses to nano-Fe versus soluble FeCl3 in excised mussel gills. Anal Bioanal Chem. 396:657–666.

Kaegi R, Voegelin A, Ort C, Sinnet B, Thalmann B, Krismerb J, Hagendorferc H, Elumelua M, Mueller E. 2013. Fate and transformation of silver nanoparticles in urban wastewater systems. Water Res. 47:3866–3877.

Kaegi R, Voegelin A, Sinnet B, Zuleeg S, Hagendorfer H, Burkhardt M, Siegrist H. 2011. Behavior of metallic silver nanoparticles in a pilot wastewater treatment plant. Environ Sci Technol. 45:3902–3908.

Kagan VE, Konduru NV, Feng W, Allen BL, Conroy J, Volkov Y, Vlasova II, Belikova NA, Yanamala N, Kapralov A, et al. 2010. Carbon nanotubes degraded by neutrophil myeloperoxidase induce less pulmonary inflammation. Nat Nano. 5:354–359.

Karmakar A, Zhang Q, Zhang Y. 2014. Neurotoxicity of nanoscale materials. J Food Drug Anal. 22:147–160.

Kasai T, Umeda Y, Ohnishi M, Mine T, Kondo H, Takeuchi T, Matsumoto M, Fukushima S. 2015. Lung carcinogenicity of inhaled multi-walled carbon nanotube in rats. Part Fibre Toxicol. 13:53.

Keller A, McFerran S, Lazareva A, Suh S. 2013a. Global life cycle releases of engineered nanomaterials. J Nanopart Res. 15:1–17.

Keller AA, McFerran S, Lazareva A, Suh S. 2013b. Global life cycle releases of engineered nanomaterials. J Nanopart Res. 15:1692.

Kennedy AJ, Gunter JC, Chappell MA, Goss JD, Hull MS, Kirgan RA, Steevens JA. 2009. Influence of nanotube preparation in aquatic bioassays. Environ Toxicol Chem. 28:1930–1938.

Kim B, Murayama M, Colman BP, Hochella MF. 2012. Characterization and environmental implications of nano- and larger TiO2 particles in sewage sludge, and soils amended with sewage sludge. J Environ Monit. 14:1128–1136.

Kim B, Park C-S, Murayama M, Hochella MF. 2010a. Discovery and characterization of silver sulfide nanoparticles in final sewage sludge products. Environ Sci Technol. 44:7509–7514.

Kim JS, Sung JH, Choi BG, Ryu HY, Song KS, Shin JH, Lee JS, Hwang JH, Lee JH, Lee GH, et al. 2014. *In vivo* genotoxicity evaluation of lung cells from Fischer 344 rats following 28 days of inhalation exposure to MWCNTs, plus 28 days and 90 days post-exposure. Inhal Toxicol. 26:222–234.

Kim S, Choi I-H. 2012. Phagocytosis and endocytosis of silver nanoparticles induce interleukin-8 production in human macrophages. Yonsei Med J. 53:654–657.

Kim S, Choi JE, Choi J, Chung KH, Park K, Yi J, Ryu DY. 2009. Oxidative stress-dependent toxicity of silver nanoparticles in human hepatoma cells. Toxicol In Vitro. 23:1076–1084.

Kim YS, Song MY, Park JD, Song KS, Ryu HR, Chung YH, Chang HK, Lee JH, Oh KH, Kelman BJ, et al. 2010b. Subchronic oral toxicity of silver nanoparticles. Part Fibre Toxicol. 7:20.

Kingston C, Zepp R, Andrady A, Boverhof D, Fehir R, Hawkins D, Roberts J, Sayre P, Shelton B, Sultan Y, et al. 2014. Release characteristics of selected carbon nanotube polymer composites. Carbon. 68:33–57.

Kiser MA, Westerhoff P, Benn T, Wang Y, Pérez-Rivera J, Hristovski K. 2009. Titanium nanomaterial removal and release from wastewater treatment plants. Environ Sci Technol. 43:6757–6763.

Kitchin KT, Prasad RY, Wallace K. 2011. Oxidative stress studies of six TiO2 and two CeO2 nanomaterials: immuno-spin trapping results with DNA. Nanotoxicology. 5:546–556.

Klaine SJ, Alvarez PJJ, Batley GE, Fernandes TF, Handy RD, Lyon DY, Mahendra S, McLaughlin MJ, Lead JR. 2008. Nanomaterials in the

environment: behavior, fate, bioavailability, and effects. Environ Toxicol Chem. 27:1825–1851.
Klaunig JE, Wang Z, Pu X, Zhou S. 2011. Oxidative stress and oxidative damage in chemical carcinogenesis. Toxicol Appl Pharmacol. 254:86–99.
Kleber M, Johnson MG. 2010. Advances in understanding the molecular structure of soil organic matter: implications for interactions in the environment. Adv Agronomy. 106:77–142.
Knight MR, Knight H. 2012. Low-temperature perception leading to gene expression and cold tolerance in higher plants. New Phytol. 195:737–751.
Knightes C. 2015. Simulating the fate and transport of nanomaterials in surface waters. In: Quantifying exposure to engineered nanomaterials from manufactured products: addressing environmental, health, and safety implications, consumer products safety commission. Washington, DC: National Nanotechnology Initiative.
Koelmans AA, Nowack B, Wiesner MR. 2009. Comparison of manufactured and black carbon nanoparticle concentrations in aquatic sediments. Environ Pollut. 157:1110–1116.
Kraeuter JN, Castagna M. 2001. Biology of the hard clam. Amsterdam: Elsevier.
Kroll A, Pillukat MH, Hahn D, Schnekenburger J. 2009. Current *in vitro* methods in nanoparticle risk assessment: limitations and challenges. Eur J Pharm Biopharm. 72:370–377.
Kuempel ED, Castranova V, Geraci CL, Schulte PA. 2012. Development of risk-based nanomaterial groups for occupational exposure control. J Nanopart Res. 14:1029.
Kumar A, Dhawan A. 2013. Genotoxic and carcinogenic potential of engineered nanoparticles: an update. Arch Toxicol. 87:1883–1900.
Kumar A, Pandey AK, Singh SS, Shanker R, Dhawan A. 2011. Cellular uptake and mutagenic potential of metal oxide nanoparticles in bacterial cells. Chemosphere. 83:1124–1132.
Kumar A, Shanker R, Alok D. 2015. Nanotoxicity: aquatic organisms and ecosystems. In: Reisner D, editor. Aquananotechnology: global prospects. London: CRC Press; p. 97–106.
Kumar V, Guleria P, Kumar V, Yadav SK. 2013. Gold nanoparticle exposure induces growth and yield enhancement in Arabidopsis thaliana. Sci Total Environ. 461–462:462–468.
Kwak JI, An Y-J. 2015. A review of the ecotoxicological effects of nanowires. Int J Environ Sci Technol. 12:1163–1172.
Labib S, Williams A, Yauk CL, Nikota JK, Wallin H, Vogel U, Halappanavar S. 2016. Nano-risk science: application of toxicogenomics in an adverse outcome pathway framework for risk assessment of multi-walled carbon nanotubes. Part Fibre Toxicol. 13:1–17.
Landsiedel R, Fabian E, Ma-Hock L, Wohlleben W, Wiench K, Oesch F. 2012. Toxico-/biokinetics of nanomaterials. Arch Toxicol. 86:1021–1060.
Larese FF, D'Agostin F, Crosera M, Adami G, Renzi N, Bovenzi M, Maina G. 2009. Human skin penetration of silver nanoparticles through intact and damaged skin. Toxicology. 255:33–37.
Larese Filon F, Bello D, Cherrie JW, Sleeuwenhoek A, Spaan S, Brouwer DH. 2016. Occupational dermal exposure to nanoparticles and nano-enabled products: Part I. Factors affecting skin absorption. Int J Hyg Environ Health. 219:536–544.
Larsen ST, Jackson P, Poulsen SS, Levin M, Jensen KA, Wallin H, Nielsen GD, Koponen IK. 2016. Airway irritation, inflammation, and toxicity in mice following inhalation of metal oxide nanoparticles. Nanotoxicology. 10:1254–1262.
Lee Y, Kim P, Yoon J, Lee B, Choi K, Kil KH, Park K. 2012. Serum kinetics, distribution and excretion of silver in rabbits following 28 days after a single intravenous injection of silver nanoparticles. Nanotoxicology. 7:1120–1130.
Li M, Panagi Z, Avgoustakis K, Reineke J. 2012. Physiologically based pharmacokinetic modeling of PLGA nanoparticles with varied mPEG content. Int J Nanomedicine. 7:1345–1356.
Li N, Xia T, Nel AE. 2008. The role of oxidative stress in ambient particulate matter-induced lung diseases and its implications in the toxicity of engineered nanoparticles. Free Radic Biol Med. 44:1689–1699.
Liang G, Pu Y, Yin L, Liu R, Ye B, Su Y, Li Y. 2009. Influence of different sizes of titanium dioxide nanoparticles on hepatic and renal functions in rats with correlation to oxidative stress. J Toxicol Environ Health Part A. 72:740–745.
Liao H-Y, Chung Y-T, Lai C-H, Wang S-L, Chiang H-C, Li LA, Tsou TC, Li WF, Lee HL, Wu WT, et al. 2014. Six-month follow-up study of health markers of nanomaterials among workers handling engineered nanomaterials. Nanotoxicology. 8:100–110.
Lim JH, Kim SH, Shin IS, Park NH, Moon C, Kang SS, Kim SH, Park SC, Kim JC. 2011. Maternal exposure to multi-wall carbon nanotubes does not induce embryo-fetal developmental toxicity in rats. Birth Defects Res Part B Dev Reprod Toxicol. 92:69–76.
Lin Z, Monteiro-Riviere NA, Riviere JE. 2015. Pharmacokinetics of metallic nanoparticles. Wiley Interdiscip Rev Nanomed Nanobiotechnol. 7:189–217.
Liu Q, Zhao N, Yamaguch-Shinozaki K, Shinozaki K. 2000. Regulatory role of DREB transcription factors in plant drought, salt and cold tolerance. Chin Sci Bull. 45:970–975.
Liu W, Rose J, Plantevin S, Auffan M, Bottero J-Y, Vidaud C. 2013. Protein corona formation for nanomaterials and proteins of a similar size: hard or soft corona? Nanoscale. 5:1658–1668.
Liu Z, Liu Y, Peng D. 2015. Carboxylation of multiwalled carbon nanotube attenuated the cytotoxicity by limiting the oxidative stress initiated cell membrane integrity damage, cell cycle arrestment, and death receptor mediated apoptotic pathway. J Biomed Mater Res Part A. 103:2770–2777.
Lombi E, Donner E, Taheri S, Tavakkoli E, Jämting ÅK, McClure S, Naidu R, Miller BW, Scheckel KG, Vasilev K. 2013. Transformation of four silver/silver chloride nanoparticles during anaerobic treatment of wastewater and post-processing of sewage sludge. Environ Pollut. 176:193–197.
Lombi E, Donner E, Tavakkoli E, Turney TW, Naidu R, Miller BW, Scheckel KG. 2012. Fate of zinc oxide nanoparticles during anaerobic digestion of wastewater and post-treatment processing of sewage sludge. Environ Sci Technol. 46:9089–9096.
López-Moreno ML, de la Rosa G, Hernández-Viezcas JA, Peralta-Videa JR, Gardea-Torresdey JL. 2010. X-ray absorption spectroscopy (XAS) corroboration of the uptake and storage of CeO2 nanoparticles and assessment of their differential toxicity in four edible plant species. J Agric Food Chem. 58:3689–3693.
Lorenz C, Hagendorfer H, von Goetz N, Kaegi R, Gehrig R, Ulrich A, Scheringer M, Hungerbühler K. 2011. Nanosized aerosols from consumer sprays: experimental analysis and exposure modeling for four commercial products. J Nanopart Res. 13:3377–3391.
Lowry GV, Gregory KB, Apte SC, Lead JR. 2012. Transformations of nanomaterials in the environment. Environ Sci Technol. 46:6893–6899.
Lundqvist M, Stigler J, Elia G, Lynch I, Cedervall T, Dawson KA. 2008. Nanoparticle size and surface properties determine the protein corona with possible implications for biological impacts. Proc Natl Acad Sci. 105:14265–14270.
Lynch I, Cedervall T, Lundqvist M, Cabaleiro-Lago C, Linse S, Dawson KA. 2007. The nanoparticle–protein complex as a biological entity; a complex fluids and surface science challenge for the 21st century. Adv Colloid Interface Sci. 134–135:167–174.
Ma H, Diamond SA. 2013. Phototoxicity of TiO2 nanoparticles to zebrafish (Danio rerio) is dependent on life stage. Environ Toxicol Chem. 32:2139–2143.
Ma R, Stegemeier J, Levard C, Dale JG, Noack CW, Yang T, Brown G, Lowry GV. 2014. Sulfidation of copper oxide nanoparticles and properties of resulting copper sulfide. Environ Sci: Nano. 1:347–357.
Ma X, Geiser-Lee J, Deng Y, Kolmakov A. 2010. Interactions between engineered nanoparticles (ENPs) and plants: phytotoxicity, uptake and accumulation. Sci Total Environ. 408:3053–3061.
Madl AK, Plummer LE, Carosino C, Pinkerton KE. 2014. Nanoparticles, lung injury, and the role of oxidant stress. Annu Rev Physiol. 76:447–465.
Magdolenova Z, Collins A, Kumar A, Dhawan A, Stone V, Dusinska M. 2014. Mechanisms of genotoxicity. A review of *in vitro* and *in vivo* studies with engineered nanoparticles. Nanotoxicology. 8:233–278.
Mahmoudi M, Azadmanesh K, Shokrgozar MA, Journeay WS, Laurent S. 2011. Effect of nanoparticles on the cell life cycle. Chem Rev. 111:3407–3432.
Majumdar S, Trujillo-Reyes J, Hernandez-Viezcas JA, White JC, Peralta-Videa JR, Gardea-Torresdey JL. 2016. Cerium biomagnification in a

terrestrial food chain: influence of particle size and growth stage. Environ Sci Technol. 50:6782–6792.
Manceau A, Nagy KL, Marcus MA, Lanson M, Geoffroy N, Jacquet T, Kirpichtchikova T. 2008. Formation of metallic copper nanoparticles at the soil–root interface. Environ Sci Technol. 42:1766–1772.
Manke A, Wang L, Rojanasakul Y. 2013. Mechanisms of nanoparticle-induced oxidative stress and toxicity. BioMed Res Int. 2013:942916.
Marano F, Hussain S, Rodrigues-Lima F, Baeza-Squiban A, Boland S. 2011. Nanoparticles: molecular targets and cell signalling. Arch Toxicol. 85:733–741.
Marisa I, Marin MG, Caicci F, Franceschinis E, Martucci A, Matozzo V. 2015. *In vitro* exposure of haemocytes of the clam Ruditapes philippinarum to titanium dioxide (TiO2) nanoparticles: nanoparticle characterisation, effects on phagocytic activity and internalisation of nanoparticles into haemocytes. Mar Environ Res. 103:11–17.
Maynard AD. 2014. Is novelty overrated? Nat Nanotechnol. 9:409–410.
McClure J, Lathrop D, Jacob M. 2013. After West disaster, News study finds U.S. chemical safety data about 90 percent wrong. The Dallas Morning News. Aug 24, 2013.
Meier C, Voegelin A, Pradas del Real A, Sarret G, Mueller CR, Kaegi R. 2016. Transformation of silver nanoparticles in sewage sludge during incineration. Environ Sci Technol. 50:3503–3510.
Mercer JR, Cheng KK, Figg N, Gorenne I, Mahmoudi M, Griffin J, Vidal-Puig A, Logan A, Murphy MP, Bennett M. 2010. DNA damage links mitochondrial dysfunction to atherosclerosis and the metabolic syndrome. Circ Res. 107:1021–1031.
Mercer RR, Scabilloni JF, Hubbs AF, Wang L, Battelli LA, McKinney W, Castranova V, Porter DW. 2013. Extrapulmonary transport of MWCNT following inhalation exposure. Part Fibre Toxicol. 10:38.
Minetto D, Libralato G, Volpi Ghirardini A. 2014. Ecotoxicity of engineered TiO2 nanoparticles to saltwater organisms: an overview. Environ Int. 66:18–27.
MINTEQ V. 2013. [Cited 2017 Feb 15]. Available from: https://vminteq.lwr.kth.se/
Mitchell LA, Lauer FT, Burchiel SW, McDonald JD. 2009. Mechanisms for how inhaled multiwalled carbon nanotubes suppress systemic immune function in mice. Nat Nano. 4:451–456.
Mitrano DM, Motellier S, Clavaguera S, Nowack B. 2015. Review of nanomaterial aging and transformations through the life cycle of nano-enhanced products. Environ Int. 77:132–147.
Miura K, Furumoto T. 2013. Cold signaling and cold response in plants. Int J Mol Sci. 14:5312–5337.
Monteiller C, Tran L, MacNee W, Faux S, Jones A, Miller B, Donaldson K. 2007. The pro-inflammatory effects of low-toxicity low-solubility particles, nanoparticles and fine particles, on epithelial cells *in vitro*: the role of surface area. Occup Environ Med. 64:609–615.
Monteiro-Riviere NA, Wiench K, Landsiedel R, Schulte S, Inman AO, Riviere JE. 2011. Safety evaluation of sunscreen formulations containing titanium dioxide and zinc oxide nanoparticles in UVB sunburned skin: an *in vitro* and *in vivo* study. Toxicol Sci. 123:264–280.
Morimoto Y, Horie M, Kobayashi N, Shinohara N, Shimada M. 2013. Inhalation toxicity assessment of carbon-based nanoparticles. Acc Chem Res. 46:770–781.
Mueller NC, Nowack B. 2008. Exposure modeling of engineered nanoparticles in the environment. Environ Sci Technol. 42:4447–4453.
Muller EB, Lin S, Nisbet RM. 2015. Quantitative adverse outcome pathway analysis of hatching in zebrafish with CuO nanoparticles. Environ Sci Technol. 49:11817–11824.
Muller J, Huaux F, Moreau N, Misson P, Heilier JF, Delos M, Arras M, Fonseca A, Nagy JB, Lison D. 2005. Respiratory toxicity of multi-wall carbon nanotubes. Toxicol Appl Pharmacol. 207:221–231.
Murphy CJ, Vartanian AM, Geiger FM, Hamers RJ, Pedersen J, Cui Q, Haynes CL, Carlson EE, Hernandez R, Klaper RD, et al. 2015. Biological responses to engineered nanomaterials: needs for the next decade. ACS Cent Sci. 1:117–123.
Murray AR, Kisin E, Leonard SS, Young SH, Kommineni C, Kagan VE, Castranova V, Shvedova AA. 2009. Oxidative stress and inflammatory response in dermal toxicity of single-walled carbon nanotubes. Toxicology. 257:161–171.
Mwilu SK, El Badawy AM, Bradham K, Nelson C, Thomas D, Scheckel KG, Tolaymat T, Ma L, Rogers KR. 2013. Changes in silver nanoparticles exposed to human synthetic stomach fluid: effects of particle size and surface chemistry. Sci Total Environ. 447:90–98.
Nabi IR, Le PU. 2003. Caveolae/raft-dependent endocytosis. J Cell Biol. 161:673–677.
Navarro E, Baun A, Behra R, Hartmann NB, Filser J, Miao AJ, Quigg A, Santschi PH, Sigg L. 2008a. Environmental behavior and ecotoxicity of engineered nanoparticles to algae, plants, and fungi. Ecotoxicology. 17:372–386.
Navarro E, Piccapietra F, Wagner B, Marconi F, Kaegi R, Odzak N, Sigg L, Behra R. 2008b. Toxicity of silver nanoparticles to *Chlamydomonas reinhardtii*. Environ Sci Technol. 42:8959–8964.
Nel A, Xia T, Mädler L, Li N. 2006. Toxic potential of materials at the nanolevel. Science. 311:622–627.
Nel A, Xia T, Meng H, Wang X, Lin S, Ji Z, Zhang H. 2013. Nanomaterial toxicity testing in the 21st century: use of a predictive toxicological approach and high throughput screening. Acc Chem Res. 46:607–621.
Nel AE, Madler L, Velegol D, Xia T, Hoek EMV, Somasundaran P, Klaessig F, Castranova V, Thompson M. 2009. Understanding biophysicochemical interactions at the nano-bio interface. Nat Mater. 8:543–557.
Nowack B, Bucheli TD. 2007. Occurrence, behavior and effects of nanoparticles in the environment. Environ Pollut. 150:5–22.
Nowack B, David RM, Fissan H, Morris H, Shatkin JA, Stintzf M, Zeppg R, Brouwer D. 2013. Potential release scenarios for carbon nanotubes used in composites. Environ Int. 59:1–11.
NRC. 1983. Risk assessment in the federal government: managing the process. Washington (DC): The National Academies Press. 191 p.
NRC. 2007. Toxicity testing in the 21st century: a vision and a strategy. Washington, DC: The National Academies Press. 216 p.
NRC. 2012. A research strategy for environmental, health, and safety aspects of engineered nanomaterials. Washington (DC): The National Academies Press. 212 p.
NRC. 2013. Research progress on environmental, health, and safety aspects of engineered nanomaterials. Washington (DC): The National Academies Press. 162 p.
Oberdörster G, Oberdörster E, Oberdörster J. 2005. Nanotoxicology: an emerging discipline evolving from studies of ultrafine particles. Environ Health Perspect. 113:823–839.
Oberdorster G, Sharp Z, Atudorei V, Elder A, Gelein R, Kreyling W, Cox C. 2004. Translocation of inhaled ultrafine particles to the brain. Inhal Toxicol. 16:437–445.
Oberdorster G, Sharp Z, Atudorei V, Elder A, Gelein R, Lunts A, Kreyling W, Cox C. 2002. Extrapulmonary translocation of ultrafine carbon particles following whole-body inhalation exposure of rats. J Toxicol Environ Health Part A. 65:1531–1543.
OECD OfEC-oaD. 2000. Guidance document on aquatic toxicity testing of difficult substances and mixtures. ed. Paris: OfEC-oa Development.
OECD OfEC-oaD. 2004. Test No. 218: sediment water chironomid toxicity using spiked sediment. ed. Paris: OfEC-oa Development.
OECD OfEC-oaD. 2016. Adverse outcome pathways, molecular screening and toxicogenomics. Organisation for Economic Co-operation and Development.
Ogawara K-I, Yoshida M, Furumoto K, Takakura Y, Hashida M, Higaki K, Kimura T. 1999. Uptake by hepatocytes and biliary excretion of intravenously administered polystyrene microspheres in rats. J Drug Target. 7:213–221.
Oh N, Park J-H. 2014. Endocytosis and exocytosis of nanoparticles in mammalian cells. Int J Nanomedicine. 9:51–63.
Oksel C, Ma CY, Wang XZ. 2015. Current situation on the availability of nanostructure – biological activity data. SAR QSAR Environ Res. 26:79–94.
Oomen AG, Bos PMJ, Fernandes TF, Hund-Rinke K, Boraschi D, Byrne HJ, Aschberger K, Gottardo S, von der Kammer F, Kühnel D, et al. 2014. Concern-driven integrated approaches to nanomaterial testing and assessment – report of the NanoSafety Cluster Working Group 10. Nanotoxicology. 8:334–348.
Pacurari M, Castranova V, Vallyathan V. 2010. Single- and multi-wall carbon nanotubes versus asbestos: are the carbon nanotubes a new health risk to humans? J Toxicol Environ Health A. 73:378–395.

Pan J-F, Buffet P-E, Poirier L, Amiard-Triquet C, Gilliland D, Joubert Y, Pilet P, Guibbolini M, Risso de Faverney C, Roméo M, et al. 2012. Size dependent bioaccumulation and ecotoxicity of gold nanoparticles in an endobenthic invertebrate: the Tellinid clam *Scrobicularia plana*. Environ Poll. 168:37–43.

Park EJ, Bae E, Yi J, Kim Y, Choi K, Lee SH, Yoon J, Lee BC, Park K. 2010. Repeated-dose toxicity and inflammatory responses in mice by oral administration of silver nanoparticles. Environ Toxicol Pharmacol. 30:162–168.

Park S, Woodhall J, Ma G, Veinot JGC, Cresser MS, Boxall ABA. 2014. Regulatory ecotoxicity testing of engineered nanoparticles: are the results relevant to the natural environment? Nanotoxicology. 8:583–592.

Parks AN, Chandler GT, Ho KT, Burgess RM, Ferguson PL. 2015. Environmental biodegradability of [14C] single-walled carbon nanotubes by Trametes versicolor and natural microbial cultures found in New Bedford Harbor sediment and aerated wastewater treatment plant sludge. Environ Toxicol Chem. 34:247–251.

Parks AN, Chandler GT, Portis LM, Sullivan JC, Perron MM, Cantwell MG, Burgess RM, Ho KT, Ferguson PL. 2014. Effects of single-walled carbon nanotubes on the bioavailability of PCBs in field-contaminated sediments. Nanotoxicology. 8:111–117.

Part F, Zecha G, Causon T, Sinner E-K, Huber-Humer M. 2015. Current limitations and challenges in nanowaste detection, characterisation and monitoring. Waste Manag. 43:407–420.

PCAST. 2014. Report to the President and Congress on the Fifth Assessment of the National Nanotechnology Initiative. Washington (DC): PsCoAoSa Technology.

Pearson RM, Juettner V, Hong S. 2014. Biomolecular corona on nanoparticles: a survey of recent literature and its implications in targeted drug delivery. Front Chem. 2:108.

Petersen EJ, Diamond SA, Kennedy AJ, Goss GG, Ho K, Lead J, Hanna SK, Hartmann NB, Hund-Rinke K, Mader B, et al. 2015. Adapting OECD aquatic toxicity tests for use with manufactured nanomaterials: key issues and consensus recommendations. Environ Sci Technol. 49:9532–9547.

Petersen EJ, Nelson BC. 2010. Mechanisms and measurements of nanomaterial-induced oxidative damage to DNA. Anal Bioanal Chem. 398:613–650.

Petersen EJ, Zhang L, Mattison NT, O'Carroll DM, Whelton AJ, Uddin N, Nguyen T, Huang Q, Henry TB, Holbrook RD, Chen KL. 2011. Potential release pathways, environmental fate, and ecological risks of carbon nanotubes. Environ Sci Technol. 45:9837–9856.

Pflucker F, Wendel V, Hohenberg H, Gartner E, Will T, Pfeiffer S, Wepf R, Gers-Barlag H. 2001. The human stratum corneum layer: an effective barrier against dermal uptake of different forms of topically applied micronised titanium dioxide. Skin Pharmacol Appl Skin Physiol. 14(Suppl 1):92–97.

Pietroiusti A, Campagnolo L, Fadeel B. 2013. Interactions of engineered nanoparticles with organs protected by internal biological barriers. Small. 9:1557–1572.

Pietroiusti A, Magrini A. 2014. Engineered nanoparticles at the workplace: current knowledge about workers' risk. Occup Med. 64:319–330.

Pietroiusti A, Massimiani M, Fenoglio I, Colonna M, Valentini F, Palleschi G, Camaioni A, Magrini A, Siracusa G, Bergamaschi A, et al. 2011. Low doses of pristine and oxidized single-wall carbon nanotubes affect mammalian embryonic development. ACS Nano. 5:4624–4633.

Pilou M, Vaquero-Moralejo C, Jaen M, Lopez D, Ipina Pena J, Neofytou P, Housiadas C. 2016. Modeling of occupational exposure to accidentally released manufactured nanomaterials in a production facility and calculation of internal doses by inhalation. Int J Occup Environ Health. 22:249–258.

Platten WE III, Sylvest N, Warren C, Arambewela M, Harmon S, Bradham K, Rogers K, Thomas T, Luxton TP. 2016. Estimating dermal transfer of copper particles from the surfaces of pressure-treated lumber and implications for exposure. Sci Total Environ. 548–549:441–449.

Powers CM, Grieger K, Meacham CA, Gooding ML, Gift JS, Lehmann GM, Hendren CO, Davis JM, Burgoon L. 2016. Applying comprehensive environmental assessment to research planning for multiwalled carbon nanotubes: refinements to inform future stakeholder engagement. Integr Environ Assess Manag. 12:96–108.

Praetorius A, Scheringer M, Hungerbühler K. 2012. Development of environmental fate models for engineered nanoparticles—a case study of TiO2 nanoparticles in the Rhine river. Environ Sci Technol. 46:6705–6713.

Prasad RY, Simmons SO, Killius MG, Zucker RM, Kligerman AD, Blackman CF, Fry RC, Demarini DM. 2014. Cellular interactions and biological responses to titanium dioxide nanoparticles in HepG2 and BEAS-2B cells: role of cell culture media. Environ Mol Mutagen. 55:336–342.

Prasad RY, Wallace K, Daniel KM, Tennant AH, Zucker RM, Strickland J, Dreher K, Kligerman AD, Blackman CF, Demarini DM. 2013. Effect of treatment media on the agglomeration of titanium dioxide nanoparticles: impact on genotoxicity, cellular interaction, and cell cycle. ACS Nano. 7:1929–1942.

Priester JH, Ge Y, Mielke RE, Horst AM, Moritz SC, Espinosa K, Gelb J, Walker SL, Nisbet RM, An YJ, et al. 2012. Soybean susceptibility to manufactured nanomaterials with evidence for food quality and soil fertility interruption. Proc Natl Acad Sci U S A. 109:E2451–E2456.

Project on Emerging Nanotechnologies P. 2013. Consumer products inventory. Virginia: Wilson Center, Virginia Tech.

Pu Y, Tang F, Adam PM, Laratte B, Ionescu RE. 2016. Fate and characterization factors of nanoparticles in seventeen subcontinental freshwaters: a case study on copper nanoparticles. Environ. Sci. Technol. 50:9370–9379.

Quadros ME, Marr LC. 2011. Silver nanoparticles and total aerosols emitted by nanotechnology-related consumer spray products. Environ Sci Technol. 45:10713–10719.

Quadros ME, Pierson R, Tulve NS, Willis R, Rogers K, Thomas T, Marr L. 2013. Release of silver from nanotechnology-based consumer products for children. Environ Sci Technol. 47:8894–8901.

Quik JTK, de Klein JJM, Koelmans AA. 2015. Spatially explicit fate modelling of nanomaterials in natural waters. Water Res. 80:200–208.

Radhika RSR, Ganesh KV, Stanley AL, Inbakandan D. 2010. Studies on the toxicological effects of engineered nanoparticles in environment – a review. Int J Appl Bioeng. 4:44–53.

RCC-NI. 2014. Work Element 3: Risk Assessment/Risk Management, Regulatory Cooperation Council Nanotechnology Initiative

Rico CM, Johnson MG, Marcus MA, Andersen CP. 2017. Intergenerational responses of wheat (Triticum aestivum L.) to cerium oxide nanoparticles exposure. Environ Sci: Nano. 4:700–711.

Rico CM, Majumdar S, Duarte-Gardea M, Peralta-Videa JR, Gardea-Torresdey JL. 2011. Interaction of nanoparticles with edible plants and their possible implications in the food chain. J Agric Food Chem. 59:3485–3498.

Ritz S, Schöttler S, Kotman N, Baier G, Musyanovych A, Kuharev J, Landfester K, Schild H, Jahn O, Tenzer S, et al. 2015. Protein corona of nanoparticles: distinct proteins regulate the cellular uptake. Biomacromolecules. 16:1311–1321.

Riviere JE. 2009. Pharmacokinetics of nanomaterials: an overview of carbon nanotubes, fullerenes and quantum dots. WIREs Nanmed Nanobiotechnol. 1:26–34.

Roco MC. 1999. Nanoparticles and nanotechnology research. J Nanopart Res. 1:1–6.

Rodrigues DF, Jaisi DP, Elimelech M. 2013. Toxicity of functionalized single-walled carbon nanotubes on soil microbial communities: implications for nutrient cycling in soil. Environ Sci Technol. 47:625–633.

Rodriguez-Yañez Y, Muñoz B, Albores A. 2013. Mechanisms of toxicity by carbon nanotubes. Toxicol Mech Methods. 23:178–195.

Rogers KR, Bradham K, Tolaymat T, Thomas DJ, Hartmann T, Ma L, Williams A. 2012. Alterations in physical state of silver nanoparticles exposed to synthetic human stomach fluid. Sci Total Environ. 420:334–339.

Rosenbaum R, Bachmann T, Gold L, Huijbregts MJ, Jolliet O, Juraske R, Koehler A, Larsen HF, Macleod M, Margni M, et al. 2008. USEtox: the UNEP-SETAC toxicity model: recommended characterisation factors for human toxicity and freshwater ecotoxicity in life cycle impact assessment. Int J Life Cycle Assess. 13:532–546.

Royce SG, Mukherjee D, Cai T, Xu SS, Alexander JA, Mi Z, Calderon L, Mainelis G, Lee K, Lioy PJ, et al. 2014. Modeling population exposures

to silver nanoparticles present in consumer products. J Nanopart Res. 16:1–25.

Sadeghi L, Yousefi Babadi V, Espanani HR. 2015. Toxic effects of the Fe2O3 nanoparticles on the liver and lung tissue. Bratisl Lek Listy. 116:373–378.

Sakhtianchi R, Minchin RF, Lee K-B, Alkilany AM, Serpooshan V, Mahmoudi M. 2013. Exocytosis of nanoparticles from cells: role in cellular retention and toxicity. Adv Colloid Interface Sci. 201–202:18–29.

Saleh NB, Pfefferle LD, Elimelech M. 2008. Aggregation kinetics of multiwalled carbon nanotubes in aquatic systems: measurements and environmental implications. Environ Sci Technol. 42:7963–7969.

Salminen R, Batista MJ, Bidovec M, Demetriades A, De Vivo B, De Vos W, Duris M, Gilucis A, Gregorauskienė V, Halamic J, et al. 2005. Geochemical Atlas of Europe. Part 1: Background Information, Methodology and Maps. Espoo, Finland: Geological Survey of Finland.

Sanders K, Degn LL, Mundy WR, Zucker RM, Dreher K, Zhao B, Roberts JE, Boyes WK. 2012. *In vitro* phototoxicity and hazard identification of nano-scale titanium dioxide. Toxicol Appl Pharmacol. 258:226–236.

Santiago-Rodríguez L, Griggs JL, Bradham KD, Nelson C, Luxton T, Platten WE, Rogers KR. 2015. Assessment of the bioaccessibility of micronized copper wood in synthetic stomach fluid. Environ Nanotechnol Monit Manag. 4:85–92.

Saunders M. 2009. Transplacental transport of nanomaterials. Wiley Interdiscip Rev Nanomed Nanobiotechnol. 1:671–684.

Sayre LM, Perry G, Smith MA. 2008. Oxidative stress and neurotoxicity. Chem Res Toxicol. 21:172–188.

Schleh C, Semmler-Behnke M, Lipka J, Wenk A, Hirn S, Schäffler M, Schmid G, Simon U, Kreyling WG. 2012. Size and surface charge of gold nanoparticles determine absorption across intestinal barriers and accumulation in secondary target organs after oral administration. Nanotoxicology. 6:36–46.

Schulte PA, Geraci CL, Murashov V, Kuempel ED, Zumwalde RD, Castranova V, Hoover MD, Hodson L, Martinez KF. 2014. Occupational safety and health criteria for responsible development of nanotechnology. J Nanopart Res. 16:2.

Sekine R, Brunetti G, Donner E, Khaksar M, Vasilev K, Jämting ÅK, Scheckel KG, Kappen P, Zhang H, Lombi E. 2015. Speciation and lability of Ag-, AgCl-, and Ag2S-nanoparticles in soil determined by X-ray absorption spectroscopy and diffusive gradients in thin films. Environ Sci Technol. 49:897–905.

Sekine R, Khaksar M, Brunetti G, Donner E, Scheckel KG, Lombi E, Vasilev K. 2013. Surface immobilization of engineered nanomaterials for *in situ* study of their environmental transformations and fate. Environ Sci Technol. 47:9308–9316.

Settimio L, McLaughlin MJ, Kirby JK, Langdon KA. 2014. A method to determine silver partitioning and lability in soils. Environ Chem. 11:63–71.

Shandilya N, Le Bihan O, Bressot C, Morgeneyer M. 2015. Emission of titanium dioxide nanoparticles from building materials to the environment by wear and weather. Environ Sci Technol. 49:2163–2170.

Shannahan JH, Podila R, Aldossari AA, Emerson H, Powell BA, Ke PC, Rao AM, Brown JM. 2015. Formation of a protein corona on silver nanoparticles mediates cellular toxicity via scavenger receptors. Toxicol Sci. 143:136–146.

Shaw BJ, Handy RD. 2011. Physiological effects of nanoparticles on fish: a comparison of nanometals versus metal ions. Environ Int. 37:1083–1097.

Shen C, James SA, de Jonge MD, Turney TW, Wright PF, Feltis BN. 2013. Relating cytotoxicity, zinc ions, and reactive oxygen in ZnO nanoparticle-exposed human immune cells. Toxicol Sci. 120–130.

Shukla RK, Kumar A, Gurbani D, Pandey AK, Singh S, Dhawan A. 2013. TiO(2) nanoparticles induce oxidative DNA damage and apoptosis in human liver cells. Nanotoxicology. 7:48–60.

Shukla RK, Kumar A, Pandey AK, Singh SS, Dhawan A. 2011. Titanium dioxide nanoparticles induce oxidative stress-mediated apoptosis in human keratinocyte cells. J Biomed Nanotechnol. 7:100–101.

Simonin M, Richaume A. 2015. Impact of engineered nanoparticles on the activity, abundance, and diversity of soil microbial communities: a review. Environ Sci Pollut Res Int. 22:13710–13723.

Singh RP, Ramarao P. 2012. Cellular uptake, intracellular trafficking and cytotoxicity of silver nanoparticles. Toxicol Lett. 213:249–259.

Skalska J, Dabrowska-Bouta B, Struzynska L. 2016. Oxidative stress in rat brain but not in liver following oral administration of a low dose of nanoparticulate silver. Food Chem Toxicol. 97:307–315.

Snow SJ, McGee J, Miller DB, Bass V, Schladweiler MC, Thomas RF, Krantz T, King C, Ledbetter AD, Richards J, et al. 2014. Inhaled diesel emissions generated with cerium oxide nanoparticle fuel additive induce adverse pulmonary and systemic effects. Toxicol Sci. 142:403–417.

Soenen SJ, Parak WJ, Rejman J, Manshian B. 2015. (Intra)Cellular stability of inorganic nanoparticles: effects on cytotoxicity, particle functionality, and biomedical applications. Chem Rev. 115:2109–2135.

Som C, Nowack B, Krug HF, Wick P. 2012. Toward the development of decision supporting tools that can be used for safe production and use of nanomaterials. Acc Chem Res. 46:863–872.

Sotiriou GA, Singh D, Zhang F, Chalbot M-CG, Spielman-Sun E, Hoering L, Kavouras IG, Lowry GV, Wohlleben W, Demokritou P. 2016. Thermal decomposition of nano-enabled thermoplastics: possible environmental health and safety implications. J Hazard Mater. 305:87–95.

Stapleton PA, Nurkiewicz TR. 2014. Vascular distribution of nanomaterials. Wiley Interdiscip Rev Nanomed Nanobiotechnol. 6:338–348.

Stevenson FJ, Cole MA. 1999. Cycles of soils: carbon, nitrogen, phosphorus, sulfur, micronutrients. 2nd ed. New York: John Wiley and Sons, Inc.

Stone V, Pozzi-Mucelli S, Tran L, Aschberger K, Sabella S, Vogel U, Poland C, Balharry D, Fernandes T, Gottardo S, et al. 2014. ITS-NANO-prioritising nanosafety research to develop a stakeholder driven intelligent testing strategy. Part Fibre Toxicol. 11:9.

Sun TY, Conroy G, Donner E, Hungerbuhler K, Lombi E, Nowack B. 2015. Probabilistic modelling of engineered nanomaterial emissions to the environment: a spatio-temporal approach. Environ Sci: Nano. 2:340–351.

Sun TY, Gottschalk F, Hungerbühler K, Nowack B. 2014. Comprehensive probabilistic modelling of environmental emissions of engineered nanomaterials. Environ Pollut. 185:69–76.

Suzui M, Futakuchi M, Fukamachi K, Numano T, Abdelgied M, Takahashi S, Ohnishi M, Omori T, Tsuruoka S, Hirose A, et al. 2016. Multiwalled carbon nanotubes intratracheally instilled into the rat lung induce development of pleural malignant mesothelioma and lung tumors. Cancer Sci. 107:924–935.

Takahashi S, Matsuoka O. 1981. Cross placental transfer of ^{198}Au-colloid in near term rats. J Radiat Res. 22:242–249.

Tamai I, Tsuji A. 2000. Transporter-mediated permeation of drugs across the blood-brain barrier. J Pharm Sci. 89:1371–1388.

Tantra R, Oksel C, Puzyn T, Wang J, Robinson KN, Wang XZ, Ma CY, Wilkins T. 2014. Nano(Q)SAR: challenges, pitfalls and perspectives. Nanotoxicology. 9:636–642.

Teeguarden JG, Hinderliter PM, Orr G, Thrall BD, Pounds JG. 2007. Particokinetics *in vitro*: dosimetry considerations for *in vitro* nanoparticle toxicity assessments. Toxicol Sci. 95:300–312.

Thai S-F, Wallace KA, Jones CP, Ren H, Castellon BT, Crooks J, Grulke EA, Kitchin KT. 2015. Differential genomic effects on signaling pathways by two different CeO2 nanoparticles in HepG2 cells. J Nanosci Nanotechnol. 15:9925–9937.

Thalmann B, Voegelin A, Sinnet B, Morgenroth E, Kaegi R. 2014. Sulfidation kinetics of silver nanoparticles reacted with metal sulfides. Environ Sci Technol. 48:4885–4892.

Thomas RS, Philbert MA, Auerbach SS, Wetmore BA, Devito MJ, Cote I, Rowlands JC, Whelan MP, Hays SM, Andersen ME, et al. 2013. Incorporating new technologies into toxicity testing and risk assessment: moving from 21st century vision to a data-driven framework. Toxicol Sci. 136:4–18.

Thomas T, Bahadori T, Savage N, Thomas K. 2009. Moving toward exposure and risk evaluation of nanomaterials: challenges and future directions. Nanomed Nanobiotechnol. 1:426–433.

Thompson D, Chen S-C, Wang J, Pui DY. 2015. Aerosol emission monitoring and assessment of potential exposure to multi-walled carbon nanotubes in the manufacture of polymer nanocomposites. Ann Occup Hyg. 49:1135–1151.

Tkachenko AG, Xie H, Coleman D, Glomm W, Ryan J, Anderson MF, Franzen S, Feldheim DL. 2003. Multifunctional gold nanoparticle–peptide complexes for nuclear targeting. J Am Chem Soc. 125:4700–4701.

Tolaymat T, El Badawy A, Sequeira R, Genaidy A. 2015. A system-of-systems approach as a broad and integrated paradigm for sustainable engineered nanomaterials. Sci Total Environ. 511:595–607.

Tourinho PS, van Gestel CAM, Lofts S, Svendsen C, Soares AMVM, Loureiro S. 2012. Metal-based nanoparticles in soil: fate, behavior, and effects on soil invertebrates. Environ Toxicol Chem. 31:1679–1692.

Treuel L, Brandholt S, Maffre P, Wiegele S, Shang L, Nienhaus GU. 2014. Impact of protein modification on the protein corona on nanoparticles and nanoparticle–cell interactions. ACS Nano. 8:503–513.

Treuel L, Jiang X, Nienhaus GU. 2013. New views on cellular uptake and trafficking of manufactured nanoparticles. J R Soc Interface. 10:20120939.

Trevisan R, Delapedra G, Mello DF, Arl M, Schmidt ÉC, Meder F, Monopoli M, Cargnin-Ferreira E, Bouzon ZL, Fisher AS, et al. 2014. Gills are an initial target of zinc oxide nanoparticles in oysters Crassostrea gigas, leading to mitochondrial disruption and oxidative stress. Aquat Toxicol. 153:27–38.

Tulve NS, Stefaniak AB, Vance ME, Rogers K, Mwilu S, LeBouf RF, Schwegler-Berry D, Willis R, Thomas TA, Marr LC, et al. 2015. Characterization of silver nanoparticles in selected consumer products and its relevance for predicting children's potential exposures. Int J Hyg Environ Health. 218:345–357.

Tumburu L, Andersen CP, Rygiewicz PT, Reichman JR. 2015. Phenotypic and genomic responses to titanium dioxide and cerium oxide nanoparticles in Arabidopsis germinants. Environ Toxicol Chem. 34:70–83.

Tumburu L, Andersen CP, Rygiewicz PT, Reichman JR. 2017. Molecular and physiological responses to titanium dioxide and cerium oxide nanoparticles in Arabidopsis. Environ Toxicol Chem. 36:71–82.

U.S. 1999. PART 503: standards for the use or disposal of sewage sludge. In: Code of Federal Regulations: Title 40. UEP Agency, US Government Publishing Office.

Unfried K, Sydlik U, Bierhals K, Weissenberg A, Abel J. 2008. Carbon nanoparticle-induced lung epithelial cell proliferation is mediated by receptor-dependent Akt activation. Am J Physiol./Lung Cell Mol Physiol. 294:L358–LL67.

Uskokovic V. 2013. Entering the era of nanoscience: time to be so small. J Biomed Nanotechnol. 9:1441–1470.

Vance ME, Kuiken T, Vejerano EP, McGinnis SP, Hochella MF, Rejeski D, Hull MS. 2015. Nanotechnology in the real world: redeveloping the nanomaterial consumer products inventory. Beilstein J Nanotechnol. 6:1769–1780.

Velzeboer I, Quik JTK, van de Meent D, Koelmans AA. 2014. Rapid settling of nanoparticles due to heteroaggregation with suspended sediment. Environ Toxicol Chem. 33:1766–1773.

Verma A, Stellacci F. 2010. Effect of surface properties on nanoparticle–-cell interactions. Small. 6:12–21.

Vietti G, Lison D, van den Brule S. 2016. Mechanisms of lung fibrosis induced by carbon nanotubes: towards an Adverse Outcome Pathway (AOP). Part Fibre Toxicol. 13:11.

Walczak AP, Fokkink R, Peters R, Tromp P, Herrera Rivera ZE, Rietjens IM, Hendriksen PJ, Bouwmeester H. 2013. Behaviour of silver nanoparticles and silver ions in an *in vitro* human gastrointestinal digestion model. Nanotoxicology. 7:1198–1210.

Walczak AP, Kramer E, Hendriksen PJ, Helsdingen R, van der Zande M, Rietjens IM, Bouwmeester H. 2015. *In vitro* gastrointestinal digestion increases the translocation of polystyrene nanoparticles in an *in vitro* intestinal co-culture model. Nanotoxicology. 9:886–894.

Walkey CD, Olsen JB, Guo H, Emili A, Chan WCW. 2012. Nanoparticle size and surface chemistry determine serum protein adsorption and macrophage uptake. J Am Chem Soc. 134:2139–2147.

Walters CR, Pool EJ, Somerset VS. 2014. Ecotoxicity of silver nanomaterials in the aquatic environment: a review of literature and gaps in nanotoxicological research. J Environ Sci Health A Tox Hazard Subst Environ Eng. 49:1588–1601.

Wang H, Burgess RM, Cantwell MG, Portis LM, Perron MM, Wu F, Ho KT. 2014a. Stability and aggregation of silver and titanium dioxide nanoparticles in seawater: role of salinity and dissolved organic carbon. Environ Toxicol Chem. 33:1023–1029.

Wang H, Ho KT, Scheckel KG, Wu F, Cantwell MG, Katz DR, Horowitz DB, Boothman WS, Burgess RM. 2014b. Toxicity, bioaccumulation, and biotransformation of silver nanoparticles in marine organisms. Environ Sci Technol. 48:13711–13717.

Wang J, Zhou G, Chen C, Yu H, Wang T, Ma Y, Jia G, Gao Y, Li B, Sun J, et al. 2007. Acute toxicity and biodistribution of different sized titanium dioxide particles in mice after oral administration. Toxicol Lett. 168:176–185.

Wang Y, Wu Q, Sui K, Chen X-X, Fang J, Hu X, Wu M, Liu Y. 2013. A quantitative study of exocytosis of titanium dioxide nanoparticles from neural stem cells. Nanoscale. 5:4737–4743.

Wehmas LC, Anders C, Chess J, Punnoose A, Pereira CB, Greenwood JA, Tanguay RL. 2015. Comparative metal oxide nanoparticle toxicity using embryonic zebrafish. Toxicol Rep. 2:702–715.

Werlin R, Priester JH, Mielke RE, Kramer S, Jackson S, Stoimenov PK, Stucky GD, Cherr GN, Orias E, Holden PA, et al. 2011. Biomagnification of cadmium selenide quantum dots in a simple experimental microbial food chain. Nat Nanotechnol. 6:65–71.

West GH, Lippy BE, Cooper MR, Marsick D, Burrelli LG, Griffin KN, Segrave AM. 2016. Toward responsible development and effective risk management of nano-enabled products in the U.S. construction industry. J Nanopart Res. 18:49.

WHO-IARC. 2010. Titanium dioxide. In: IARC monographs on the evaluation of carcinogenic risks to humans. Lyon (France): International Agency for Research on Cancer; p. 193–276.

Wiecinski PN, Metz KM, Mangham AN, Jacobson KH, Hamers RJ, Pedersen JA. 2009. Gastrointestinal biodurability of engineered nanoparticles: development of an in vitro assay. Nanotoxicology. 3:202–214.

Wiesner MR, Lowry GV, Casman E, Bertsch PM, Matson CW, Di Giulio RT, Liu J, Hochella MF. 2011. Meditations on the ubiquity and mutability of nano-sized materials in the environment. ACS Nano. 5:8466–8470.

Woodruff RS, Li Y, Yan J, Bishop M, Jones MY, Watanabe F, Biris AS, Rice P, Zhou T, Chen T, et al. 2012. Genotoxicity evaluation of titanium dioxide nanoparticles using the Ames test and Comet assay. J Appl Toxicol. 32:934–943.

Xie H, Mason MM, Wise JP, Sr. 2011. Genotoxicity of metal nanoparticles. Rev Environ Health. 26:251–268.

Xin L, Wang J, Wu Y, Guo S, Tong J. 2015. Increased oxidative stress and activated heat shock proteins in human cell lines by silver nanoparticles. Hum Exp Toxicol. 34:315–323.

Xu J, Alexander DB, Futakuchi M, Numano T, Fukamachi K, Suzui M, Omori T, Kanno J, Hirose A, Tsuda H. 2014. Size-and shape-dependent pleural translocation, deposition, fibrogenesis, and mesothelial proliferation by multiwalled carbon nanotubes. Cancer Sci. 105:763–769.

Yamashita K, Yoshioka Y, Higashisaka K, Mimura K, Morishita Y, Nozaki M, Yoshida T, Ogura T, Nabeshi H, Nagano K, et al. 2011. Silica and titanium dioxide nanoparticles cause pregnancy complications in mice. Nat Nanotechnol. 6:321–328.

Yang F, Hong F, You W, Liu C, Gao F, Wu C, Yang P. 2006. Influences of nano-anatase TiO2 on the nitrogen metabolism of growing spinach. Biol Trace Elem Res. 110:179–190.

Yang F, Liu C, Gao F, Su M, Wu X, Zheng L, Hong F, Yang P. 2007. The improvement of spinach growth by nano-anatase TiO2 treatment is related to nitrogen photoreduction. Biol Trace Elem Res. 119:77–88.

Yang Y, Westerhoff P. 2014. Presence in, and release of, nanomaterials from consumer products in nanomaterial. In: Capco DG, Chen Y, editors. Netherlands: Springer; p. 1–17.

Yang Z, Zhang Y, Yang Y, Sun L, Han D, Li H, Wang C. 2010. Pharmacological and toxicological target organelles and safe use of single-walled carbon nanotubes as drug carriers in treating Alzheimer disease. Nanomedicine. 6:427–441.

Yokel RA, Au TC, MacPhail R, Hardas SS, Butterfield DA, Sultana R, Goodman M, Tseng MT, Dan M, Haghnazar H, et al. 2012. Distribution, elimination, and biopersistence to 90 days of a systemically introduced 30 nm ceria-engineered nanomaterial in rats. Toxicol Sci. 127:256–268.

Zartarian V, Bahadori T, McKone T. 2004. Adoption of an official ISEA glossary. J Expo Anal Environ Epidemiol. 15:1–5.

Zeni O, Sannino A, Romeo S, Micciulla F, Bellucci S, Scarfi MR. 2015. Growth inhibition, cell-cycle alteration and apoptosis in stimulated human peripheral blood lymphocytes by multiwalled carbon nanotube buckypaper. Nanomedicine (Lond). 10:351–360.

Zhang Y, Yan B. 2012. Cell cycle regulation by carboxylated multiwalled carbon nanotubes through p53-independent induction of p21 under the control of the BMP signaling pathway. Chem Resn Toxicol. 25:1212–1221.

Zhao F, Zhao Y, Liu Y, Chang X, Chen C, Zhao Y. 2011. Cellular uptake, intracellular trafficking, and cytotoxicity of nanomaterials. Small. 7:1322–1337.

Zheng L, Hong F, Lu S, Liu C. 2005. Effect of nano-TiO2 on strength of naturally aged seeds and growth of spinach. Biol Trace Elem Res. 104:83–91.

Zhu M, Nie G, Meng H, Xia T, Nel A, Zhao Y. 2012. Physicochemical properties determine nanomaterial cellular uptake, transport, and fate. Acc Chem Res. 46:622–631.

Zhu M, Wang H, Keller AA, Wang T, Li F. 2014. The effect of humic acid on the aggregation of titanium dioxide nanoparticles under different pH and ionic strengths. Sci Total Environ. 487:375–380.

Zhu Z-J, Carboni R, Quercio MJ, Yan B, Miranda OR, et al. 2010. Surface properties dictate uptake, distribution, excretion, and toxicity of nanoparticles in fish. Small. 6:2261–2265.

Zucker RM, Daniel KM, Massaro EJ, Karafas SJ, Degn LL, Boyes WK. 2013. Detection of silver nanoparticles in cells by flow cytometry using light scatter and far-red fluorescence. Cytometry A. 83:962–972.

Zucker RM, Massaro EJ, Sanders KM, Degn LL, Boyes WK. 2010. Detection of TiO2 nanoparticles in cells by flow cytometry. Cytometry A. 77:677–685.

From: Boyes, William
To: Boyes, William
Subject: FW: STAA nomination for review article
Date: Tuesday, April 28, 2020 1:53:45 PM
Attachments: ATP Scan In Progress.msg

I agree with the percentage allocation of resources – equal for all authors

William K Boyes

From: Boyes, William
Sent: Friday, April 24, 2020 5:41 PM
To: Lila Thornton <lila.thornton@duke.edu>; Al-Abed, Souhail <al-abed.souhail@epa.gov>; Andersen, Christian <Andersen.Christian@epa.gov>; Burgess, Robert <Burgess.Robert@epa.gov>; Elaine Cohen-Hubal (hubal.elaine@epa.gov) <hubal.elaine@epa.gov>; Ho, Kay <Ho.Kay@epa.gov>; Hughes, MichaelF <Hughes.MichaelF@epa.gov>; Reichman, Jay <Reichman.Jay@epa.gov>; Rogers, Kim <Rogers.Kim@epa.gov>; Scheckel, Kirk <Scheckel.Kirk@epa.gov>; Thai, Sheau-Fung <Thai.Sheau-Fung@epa.gov>; Zepp, Richard <Zepp.Richard@epa.gov>; Zucker, Robert <Zucker.Robert@epa.gov>
Subject: STAA nomination for review article

Hi All,

I thought it would be a good idea to submit our 2017 review article for an STAA award. I have enclosed a draft of the award nomination and the original paper. Only EPA authors are eligible for a cash award (sorry Lila).

1. Please send me any revisions to the nomination form./
2. Please send me an Email that you agree with the proportional division of effort (equal for all authors).

I hope you ae all well and staying safe during these strange times.

If anyone is in contact with the retired EPA authors please either forward this message to them or send me a current E-mail address – Thanks!

Will

William K. Boyes, Ph.D.
Neurological and Endocrine Toxicology Branch
Public Health and Integrated Toxicology Division
Center for Public Health and Environmental Assessment
Office of Research and Development
Mail Code B105-04
Environmental Protection Agency
109 T.W. Alexander Drive

Research Triangle Park, NC 27711

Phone: 919-541-7538
Mobile (alternate worksite contact): 919-417-2105
boyes.william@epa.gov

From: Ho, Kay
To: Boyes, William
Subject: RE: STAA nomination for review article
Date: Monday, April 27, 2020 9:32:07 AM

I agree with the proportional division of effort (equal for all authors.

Thank you

From: Boyes, William <Boyes.William@epa.gov>
Sent: Friday, April 24, 2020 5:41 PM
To: Lila Thornton <lila.thornton@duke.edu>; Al-Abed, Souhail <al-abed.souhail@epa.gov>; Andersen, Christian <Andersen.Christian@epa.gov>; Burgess, Robert <Burgess.Robert@epa.gov>; Hubal, Elaine <Hubal.Elaine@epa.gov>; Ho, Kay <Ho.Kay@epa.gov>; Hughes, MichaelF <Hughes.MichaelF@epa.gov>; Reichman, Jay <Reichman.Jay@epa.gov>; Rogers, Kim <Rogers.Kim@epa.gov>; Scheckel, Kirk <Scheckel.Kirk@epa.gov>; Thai, Sheau-Fung <Thai.Sheau-Fung@epa.gov>; Zepp, Richard <Zepp.Richard@epa.gov>; Zucker, Robert <Zucker.Robert@epa.gov>
Subject: STAA nomination for review article

Hi All,

I thought it would be a good idea to submit our 2017 review article for an STAA award. I have enclosed a draft of the award nomination and the original paper. Only EPA authors are eligible for a cash award (sorry Lila).

1. Please send me any revisions to the nomination form./
2. Please send me an Email that you agree with the proportional division of effort (equal for all authors).

I hope you ae all well and staying safe during these strange times.

If anyone is in contact with the retired EPA authors please either forward this message to them or send me a current E-mail address – Thanks!

Will

William K. Boyes, Ph.D.
Neurological and Endocrine Toxicology Branch
Public Health and Integrated Toxicology Division
Center for Public Health and Environmental Assessment
Office of Research and Development
Mail Code B105-04
Environmental Protection Agency
109 T.W. Alexander Drive
Research Triangle Park, NC 27711

Phone: 919-541-7538
Mobile (alternate worksite contact): 919-417-2105
boyes.william@epa.gov

From: Scheckel, Kirk
To: Boyes, William
Subject: RE: STAA nomination for review article
Date: Monday, April 27, 2020 10:37:09 AM
Attachments: image002.png

Hi Will,

The write up looks great. If it helps, below are two more recent invited presentations:

Application of X-ray Absorption Spectroscopy for Monitoring Transformation of Nanomaterials. K. Scheckel. 2nd Quantifying Exposure to Engineered Nanomaterials (QEEN) from Manufactured Products Workshop, Washington, DC, 2018.

Environmental Transformations of Silver and Zinc Oxide Nanoparticles Drive Risk Assessment Understanding. K. Scheckel, E. Donner, R. Sekine, G. Brunetti, and E. Lombi. 55th Annual Meeting of the Clay Minerals Society, Urbanna, IL, 2018.

Thank you for taking a lead in this and I agree with the proportional division of effort (equal for all authors).

Regards,
Kirk

Kirk G. Scheckel, Ph.D.
Director, Land Remediation & Technology Division

United States Environmental Protection Agency
Office of Research & Development
Center for Environmental Solutions & Emergency Response
26 West Martin Luther King Drive, Office 191
Cincinnati, OH 45268

Office: (513) 487-2865 Scheckel.Kirk@epa.gov
Cell: (513) 405-5086 www.epa.gov

Celebrating EPA's 50th Anniversary
http://www.epa.gov/50

From: Boyes, William <Boyes.William@epa.gov>
Sent: Friday, April 24, 2020 5:41 PM
To: Lila Thornton <lila.thornton@duke.edu>; Al-Abed, Souhail <al-abed.souhail@epa.gov>; Andersen, Christian <Andersen.Christian@epa.gov>; Burgess, Robert <Burgess.Robert@epa.gov>; Hubal, Elaine <Hubal.Elaine@epa.gov>; Ho, Kay <Ho.Kay@epa.gov>; Hughes, MichaelF <Hughes.MichaelF@epa.gov>; Reichman, Jay <Reichman.Jay@epa.gov>; Rogers, Kim <Rogers.Kim@epa.gov>; Scheckel, Kirk <Scheckel.Kirk@epa.gov>; Thai, Sheau-Fung <Thai.Sheau-Fung@epa.gov>; Zepp, Richard <Zepp.Richard@epa.gov>; Zucker, Robert <Zucker.Robert@epa.gov>
Subject: STAA nomination for review article

Hi All,

I thought it would be a good idea to submit our 2017 review article for an STAA award. I have enclosed a draft of the award nomination and the original paper. Only EPA authors are eligible for a cash award (sorry Lila).

1. Please send me any revisions to the nomination form./
2. Please send me an Email that you agree with the proportional division of effort (equal for all authors).

I hope you ae all well and staying safe during these strange times.

If anyone is in contact with the retired EPA authors please either forward this message to them or send me a current E-mail address – Thanks!

Will

William K. Boyes, Ph.D.
Neurological and Endocrine Toxicology Branch
Public Health and Integrated Toxicology Division
Center for Public Health and Environmental Assessment
Office of Research and Development
Mail Code B105-04
Environmental Protection Agency
109 T.W. Alexander Drive
Research Triangle Park, NC 27711

Phone: 919-541-7538
Mobile (alternate worksite contact): 919-417-2105
boyes.william@epa.gov

From:	Boyes, William
To:	Lila Thornton; Al-Abed, Souhail; Andersen, Christian; Burgess, Robert; Elaine Cohen-Hubal (hubal.elaine@epa.gov); Ho, Kay; Hughes, MichaelF; Reichman, Jay; Rogers, Kim; Scheckel, Kirk; Thai, Sheau-Fung; Zepp, Richard; Zucker, Robert
Subject:	STAA nomination for review article
Date:	Friday, April 24, 2020 5:40:00 PM
Attachments:	2020 STAA Nomination reviews.docx Boyes et al 2017 A comprehensive framework for evaluating....pdf

---

Hi All,

I thought it would be a good idea to submit our 2017 review article for an STAA award. I have enclosed a draft of the award nomination and the original paper. Only EPA authors are eligible for a cash award (sorry Lila).

1. Please send me any revisions to the nomination form./
2. Please send me an Email that you agree with the proportional division of effort (equal for all authors).

I hope you ae all well and staying safe during these strange times.

If anyone is in contact with the retired EPA authors please either forward this message to them or send me a current E-mail address – Thanks!

Will

William K. Boyes, Ph.D.
Neurological and Endocrine Toxicology Branch
Public Health and Integrated Toxicology Division
Center for Public Health and Environmental Assessment
Office of Research and Development
Mail Code B105-04
Environmental Protection Agency
109 T.W. Alexander Drive
Research Triangle Park, NC 27711

Phone: 919-541-7538
Mobile (alternate worksite contact): 919-417-2105
boyes.william@epa.gov

From: Zepp, Richard
To: Boyes, William
Subject: Submission of review for STAA award
Date: Friday, April 24, 2020 5:51:25 PM

Hi Will:

I agree with submission of our review, "A comprehensive framework for evaluating the environmental health and safety implications of engineered nanomaterials" for an STAA award. I agree with the proportional division of effort (equal for all authors). Thank you for your efforts on the paper and putting together the award submission!

Richard G. Zepp
U.S. EPA
ORD/CEMM
960 College Station Rd.
Athens, Georgia 30605
USA
Email: zepp.richard@epa.gov
Tel. (706)- 355-8117
Fax (706)-355-8007

From: Al-Abed, Souhail
To: Boyes, William
Subject: Record of Percentage Agreement – Souhail Al-Abed
Date: Tuesday, April 28, 2020 1:29:49 PM
Attachments: image001.png

Name: Souhail Al-Abed
Organization: ORD/CESER/LRTD/CSSB
Nominee's name: William Boyes
Title: Comprehensive framework for evaluating the environmental health and safety implications of engineered nanomaterials. Critical Reviews in Toxicology, Crit Rev Toxicol. 2017 Oct;47(9):767-810. doi: 10.1080/10408444.2017.1328400

I agree with the following designated percentage of contribution:

Souhail Al-Abed 5.5%

Souhail Al-Abed
Souhail Al-Abed, Ph.D., ACS Fellow
Center for Environmental Solutions and Emergency Response
Office of Research and Development
United States Environmental Protection Agency
26 West Martin Luther King Dr. Cincinnati, Ohio 45268
Phone: 513-569-7849 | **Fax:** 513-569-7879 | **Mobile**: 513-442-9904
Email: al-abed.souhail@epa.gov
Web: http://www.epa.gov/
Shipping Address
USEPA
5995 Center Hill Av.
Cincinnati, Ohio 45224

From: Paul Rygiewicz
To: Andersen, Christian
Cc: Boyes, William
Subject: Re: STAA award Nomination
Date: Monday, April 27, 2020 5:34:07 PM

Contribution sounds good to me.

I am doing well. The sheltering in place has been good in that so many of my never-finished projects are getting done !

Sent from my iPad

> On Apr 27, 2020, at 8:49 AM, Andersen, Christian <Andersen.Christian@epa.gov> wrote:
>
> Hi Paul- Will Boyes is going to submit our "Comprehensive framework…" review article for a possible STAA award. As part of the submission process, he has to list the proportional contribution of each author to the manuscript, and then receive an email indicating that authors agree with the percentage he has listed for them. Will decided to split the contribution evenly, so all authors will be listed as contributing 5.5% to the effort.
>
> If you could reply to this email to both Will and I that you agree with the percentage, that would be great. Hope you are doing well! Chris
>
> **********
>
> "Facts do not cease to exist because they are ignored." - Aldous Huxley
>
> **********
>
> Christian P. Andersen, PhD
> Plant Physiologist
> US Environmental Protection Agency
> Pacific Ecological Systems Division
> Center for Public Health and Environmental Assessment
> 200 SW 35th St.
> Corvallis, OR 97333
> 541-754-4791

From: Andersen, Christian
To: Boyes, William; Reichman, Jay
Subject: RE: STAA nomination for review article
Date: Friday, April 24, 2020 6:08:16 PM

Hi Will- this looks great, thanks for putting it together. Seems like you and Lila did most of the heavy lifting on that paper, I don't think anyone would be upset at a higher percentage for you. Also, Paul Rygiewicz is retired- I can try to get ahold of him, but he is a bit off the grid (he doesn't typically respond quickly). Do you need an email from him even tho he won't be getting any of the award? I will try to contact him if you want. Chris

---

From: Boyes, William <Boyes.William@epa.gov>
Sent: Friday, April 24, 2020 2:41 PM
To: Lila Thornton <lila.thornton@duke.edu>; Al-Abed, Souhail <al-abed.souhail@epa.gov>; Andersen, Christian <Andersen.Christian@epa.gov>; Burgess, Robert <Burgess.Robert@epa.gov>; Hubal, Elaine <Hubal.Elaine@epa.gov>; Ho, Kay <Ho.Kay@epa.gov>; Hughes, MichaelF <Hughes.MichaelF@epa.gov>; Reichman, Jay <Reichman.Jay@epa.gov>; Rogers, Kim <Rogers.Kim@epa.gov>; Scheckel, Kirk <Scheckel.Kirk@epa.gov>; Thai, Sheau-Fung <Thai.Sheau-Fung@epa.gov>; Zepp, Richard <Zepp.Richard@epa.gov>; Zucker, Robert <Zucker.Robert@epa.gov>
Subject: STAA nomination for review article

Hi All,

I thought it would be a good idea to submit our 2017 review article for an STAA award. I have enclosed a draft of the award nomination and the original paper. Only EPA authors are eligible for a cash award (sorry Lila).

1. Please send me any revisions to the nomination form./
2. Please send me an Email that you agree with the proportional division of effort (equal for all authors).

I hope you ae all well and staying safe during these strange times.

If anyone is in contact with the retired EPA authors please either forward this message to them or send me a current E-mail address – Thanks!

Will

William K. Boyes, Ph.D.
Neurological and Endocrine Toxicology Branch
Public Health and Integrated Toxicology Division
Center for Public Health and Environmental Assessment
Office of Research and Development

Mail Code B105-04
Environmental Protection Agency
109 T.W. Alexander Drive
Research Triangle Park, NC 27711

Phone: 919-541-7538
Mobile (alternate worksite contact): 919-417-2105
boyes.william@epa.gov

From: Burgess, Robert
To: Boyes, William
Cc: Burgess, Robert
Subject: RE: STAA nomination for review article
Date: Monday, April 27, 2020 6:30:07 PM

Will,

The nomination looks great and I agree with the proportional division of effort.

Best of luck and thank you for preparing the nomination.

Stay well,

Rob

From: Boyes, William <Boyes.William@epa.gov>
Sent: Friday, April 24, 2020 5:41 PM
To: Lila Thornton <lila.thornton@duke.edu>; Al-Abed, Souhail <al-abed.souhail@epa.gov>; Andersen, Christian <Andersen.Christian@epa.gov>; Burgess, Robert <Burgess.Robert@epa.gov>; Hubal, Elaine <Hubal.Elaine@epa.gov>; Ho, Kay <Ho.Kay@epa.gov>; Hughes, MichaelF <Hughes.MichaelF@epa.gov>; Reichman, Jay <Reichman.Jay@epa.gov>; Rogers, Kim <Rogers.Kim@epa.gov>; Scheckel, Kirk <Scheckel.Kirk@epa.gov>; Thai, Sheau-Fung <Thai.Sheau-Fung@epa.gov>; Zepp, Richard <Zepp.Richard@epa.gov>; Zucker, Robert <Zucker.Robert@epa.gov>
Subject: STAA nomination for review article

Hi All,

I thought it would be a good idea to submit our 2017 review article for an STAA award. I have enclosed a draft of the award nomination and the original paper. Only EPA authors are eligible for a cash award (sorry Lila).

1. Please send me any revisions to the nomination form./
2. Please send me an Email that you agree with the proportional division of effort (equal for all authors).

I hope you ae all well and staying safe during these strange times.

If anyone is in contact with the retired EPA authors please either forward this message to them or send me a current E-mail address – Thanks!

Will

William K. Boyes, Ph.D.
Neurological and Endocrine Toxicology Branch
Public Health and Integrated Toxicology Division

Center for Public Health and Environmental Assessment
Office of Research and Development
Mail Code B105-04
Environmental Protection Agency
109 T.W. Alexander Drive
Research Triangle Park, NC 27711

Phone: 919-541-7538
Mobile (alternate worksite contact): 919-417-2105
boyes.william@epa.gov

From: Hughes, MichaelF
To: Boyes, William
Subject: RE: STAA nomination for review article
Date: Friday, April 24, 2020 6:02:26 PM

Hi Will,

I agree with my level of effort on this paper. Thank you for putting this application together. Hope you and your family are healthy.

Best regards,
Mike

Michael F. Hughes, PhD, DABT
U.S. Environmental Protection Agency
ORD/CCTE/CCED/ETTB
MD B105-03
Research Triangle Park, NC 27711
(T): 919-541-2160; (F): 919-541-4284

From: Boyes, William <Boyes.William@epa.gov>
Sent: Friday, April 24, 2020 5:41 PM
To: Lila Thornton <lila.thornton@duke.edu>; Al-Abed, Souhail <al-abed.souhail@epa.gov>; Andersen, Christian <Andersen.Christian@epa.gov>; Burgess, Robert <Burgess.Robert@epa.gov>; Hubal, Elaine <Hubal.Elaine@epa.gov>; Ho, Kay <Ho.Kay@epa.gov>; Hughes, MichaelF <Hughes.MichaelF@epa.gov>; Reichman, Jay <Reichman.Jay@epa.gov>; Rogers, Kim <Rogers.Kim@epa.gov>; Scheckel, Kirk <Scheckel.Kirk@epa.gov>; Thai, Sheau-Fung <Thai.Sheau-Fung@epa.gov>; Zepp, Richard <Zepp.Richard@epa.gov>; Zucker, Robert <Zucker.Robert@epa.gov>
Subject: STAA nomination for review article

Hi All,

I thought it would be a good idea to submit our 2017 review article for an STAA award. I have enclosed a draft of the award nomination and the original paper. Only EPA authors are eligible for a cash award (sorry Lila).

1. Please send me any revisions to the nomination form./
2. Please send me an Email that you agree with the proportional division of effort (equal for all authors).

I hope you ae all well and staying safe during these strange times.

If anyone is in contact with the retired EPA authors please either forward this message to them or send me a current E-mail address – Thanks!

Will

William K. Boyes, Ph.D.
Neurological and Endocrine Toxicology Branch
Public Health and Integrated Toxicology Division
Center for Public Health and Environmental Assessment
Office of Research and Development
Mail Code B105-04
Environmental Protection Agency
109 T.W. Alexander Drive
Research Triangle Park, NC 27711

Phone: 919-541-7538
Mobile (alternate worksite contact): 919-417-2105
boyes.william@epa.gov

From: Rogers, Kim
To: Boyes, William
Subject: RE: STAA nomination for review article
Date: Monday, April 27, 2020 2:04:04 PM

I agree with the allocation of effort.

Kim Rogers, Ph.D.
MMB/WECD/CEMM
U.S. EPA, RTP, NC
Cell: 702-374-3284
e-mail: rogers.kim@epa.gov

From: Boyes, William <Boyes.William@epa.gov>
Sent: Friday, April 24, 2020 5:41 PM
To: Lila Thornton <lila.thornton@duke.edu>; Al-Abed, Souhail <al-abed.souhail@epa.gov>; Andersen, Christian <Andersen.Christian@epa.gov>; Burgess, Robert <Burgess.Robert@epa.gov>; Hubal, Elaine <Hubal.Elaine@epa.gov>; Ho, Kay <Ho.Kay@epa.gov>; Hughes, MichaelF <Hughes.MichaelF@epa.gov>; Reichman, Jay <Reichman.Jay@epa.gov>; Rogers, Kim <Rogers.Kim@epa.gov>; Scheckel, Kirk <Scheckel.Kirk@epa.gov>; Thai, Sheau-Fung <Thai.Sheau-Fung@epa.gov>; Zepp, Richard <Zepp.Richard@epa.gov>; Zucker, Robert <Zucker.Robert@epa.gov>
Subject: STAA nomination for review article

Hi All,

I thought it would be a good idea to submit our 2017 review article for an STAA award. I have enclosed a draft of the award nomination and the original paper. Only EPA authors are eligible for a cash award (sorry Lila).

1. Please send me any revisions to the nomination form./
2. Please send me an Email that you agree with the proportional division of effort (equal for all authors).

I hope you ae all well and staying safe during these strange times.

If anyone is in contact with the retired EPA authors please either forward this message to them or send me a current E-mail address – Thanks!

Will

William K. Boyes, Ph.D.
Neurological and Endocrine Toxicology Branch
Public Health and Integrated Toxicology Division
Center for Public Health and Environmental Assessment
Office of Research and Development
Mail Code B105-04

Environmental Protection Agency
109 T.W. Alexander Drive
Research Triangle Park, NC 27711

Phone: 919-541-7538
Mobile (alternate worksite contact): 919-417-2105
boyes.william@epa.gov

From: Zucker, Robert
To: Boyes, William
Subject: RE: STAA nomination for review article Zucker
Date: Friday, April 24, 2020 6:12:38 PM

Dear will
I approve of the division of labor on this fantastic submission to STAA
Bob Zucker

From: Boyes, William <Boyes.William@epa.gov>
Sent: Friday, April 24, 2020 5:41 PM
To: Lila Thornton <lila.thornton@duke.edu>; Al-Abed, Souhail <al-abed.souhail@epa.gov>; Andersen, Christian <Andersen.Christian@epa.gov>; Burgess, Robert <Burgess.Robert@epa.gov>; Hubal, Elaine <Hubal.Elaine@epa.gov>; Ho, Kay <Ho.Kay@epa.gov>; Hughes, MichaelF <Hughes.MichaelF@epa.gov>; Reichman, Jay <Reichman.Jay@epa.gov>; Rogers, Kim <Rogers.Kim@epa.gov>; Scheckel, Kirk <Scheckel.Kirk@epa.gov>; Thai, Sheau-Fung <Thai.Sheau-Fung@epa.gov>; Zepp, Richard <Zepp.Richard@epa.gov>; Zucker, Robert <Zucker.Robert@epa.gov>
Subject: STAA nomination for review article

Hi All,

I thought it would be a good idea to submit our 2017 review article for an STAA award. I have enclosed a draft of the award nomination and the original paper. Only EPA authors are eligible for a cash award (sorry Lila).

1. Please send me any revisions to the nomination form./
2. Please send me an Email that you agree with the proportional division of effort (equal for all authors).

I hope you ae all well and staying safe during these strange times.

If anyone is in contact with the retired EPA authors please either forward this message to them or send me a current E-mail address – Thanks!

Will

William K. Boyes, Ph.D.
Neurological and Endocrine Toxicology Branch
Public Health and Integrated Toxicology Division
Center for Public Health and Environmental Assessment
Office of Research and Development
Mail Code B105-04
Environmental Protection Agency
109 T.W. Alexander Drive
Research Triangle Park, NC 27711

Phone: 919-541-7538
Mobile (alternate worksite contact): 919-417-2105
boyes.william@epa.gov

From:	Lila Thornton
To:	Boyes, William
Subject:	Re: STAA nomination for review article
Date:	Friday, April 24, 2020 5:48:45 PM
Attachments:	ATT00001.txt

No worries, an award would still be nice!

Lila

From: "Boyes, William" <Boyes.William@epa.gov>
Date: Friday, April 24, 2020 at 5:46 PM
To: Lila Thornton <lila.thornton@duke.edu>, "Al-Abed, Souhail" <al-abed.souhail@epa.gov>, "Andersen, Christian" <Andersen.Christian@epa.gov>, "Burgess, Robert" <Burgess.Robert@epa.gov>, "Hubal, Elaine" <Hubal.Elaine@epa.gov>, "Ho, Kay" <Ho.Kay@epa.gov>, "Hughes, MichaelF" <Hughes.MichaelF@epa.gov>, "Reichman, Jay" <Reichman.Jay@epa.gov>, "Rogers, Kim" <Rogers.Kim@epa.gov>, "Scheckel, Kirk" <Scheckel.Kirk@epa.gov>, "Thai, Sheau-Fung" <Thai.Sheau-Fung@epa.gov>, "Zepp, Richard" <Zepp.Richard@epa.gov>, "Zucker, Robert" <Zucker.Robert@epa.gov>
Subject: STAA nomination for review article

Hi All,

I thought it would be a good idea to submit our 2017 review article for an STAA award. I have enclosed a draft of the award nomination and the original paper. Only EPA authors are eligible for a cash award (sorry Lila).

1. Please send me any revisions to the nomination form./
2. Please send me an Email that you agree with the proportional division of effort (equal for all authors).

I hope you ae all well and staying safe during these strange times.

If anyone is in contact with the retired EPA authors please either forward this message to them or send me a current E-mail address – Thanks!

Will

William K. Boyes, Ph.D.
Neurological and Endocrine Toxicology Branch
Public Health and Integrated Toxicology Division
Center for Public Health and Environmental Assessment
Office of Research and Development
Mail Code B105-04
Environmental Protection Agency

109 T.W. Alexander Drive
Research Triangle Park, NC 27711

Phone: 919-541-7538
Mobile (alternate worksite contact): 919-417-2105
boyes.william@epa.gov

From: Boyes, William
To: Boyes, William
Subject: FW: STAA nomination for review article
Date: Tuesday, April 28, 2020 1:53:45 PM
Attachments: ATP Scan In Progress.msg

I agree with the percentage allocation of resources – equal for all authors

William K Boyes

From: Boyes, William
Sent: Friday, April 24, 2020 5:41 PM
To: Lila Thornton <lila.thornton@duke.edu>; Al-Abed, Souhail <al-abed.souhail@epa.gov>; Andersen, Christian <Andersen.Christian@epa.gov>; Burgess, Robert <Burgess.Robert@epa.gov>; Elaine Cohen-Hubal (hubal.elaine@epa.gov) <hubal.elaine@epa.gov>; Ho, Kay <Ho.Kay@epa.gov>; Hughes, MichaelF <Hughes.MichaelF@epa.gov>; Reichman, Jay <Reichman.Jay@epa.gov>; Rogers, Kim <Rogers.Kim@epa.gov>; Scheckel, Kirk <Scheckel.Kirk@epa.gov>; Thai, Sheau-Fung <Thai.Sheau-Fung@epa.gov>; Zepp, Richard <Zepp.Richard@epa.gov>; Zucker, Robert <Zucker.Robert@epa.gov>
Subject: STAA nomination for review article

Hi All,

I thought it would be a good idea to submit our 2017 review article for an STAA award. I have enclosed a draft of the award nomination and the original paper. Only EPA authors are eligible for a cash award (sorry Lila).

1. Please send me any revisions to the nomination form./
2. Please send me an Email that you agree with the proportional division of effort (equal for all authors).

I hope you ae all well and staying safe during these strange times.

If anyone is in contact with the retired EPA authors please either forward this message to them or send me a current E-mail address – Thanks!

Will

William K. Boyes, Ph.D.
Neurological and Endocrine Toxicology Branch
Public Health and Integrated Toxicology Division
Center for Public Health and Environmental Assessment
Office of Research and Development
Mail Code B105-04
Environmental Protection Agency
109 T.W. Alexander Drive

Research Triangle Park, NC 27711

Phone: 919-541-7538
Mobile (alternate worksite contact): 919-417-2105
boyes.william@epa.gov

From: Al-Abed, Souhail
To: Boyes, William
Subject: Record of Percentage Agreement – Souhail Al-Abed
Date: Tuesday, April 28, 2020 1:29:49 PM
Attachments: image001.png

Name: Souhail Al-Abed
Organization: ORD/CESER/LRTD/CSSB
Nominee's name: William Boyes
Title: Comprehensive framework for evaluating the environmental health and safety implications of engineered nanomaterials. Critical Reviews in Toxicology, Crit Rev Toxicol. 2017 Oct;47(9):767-810. doi: 10.1080/10408444.2017.1328400

I agree with the following designated percentage of contribution:

Souhail Al-Abed 5.5%

Souhail Al-Abed
Souhail Al-Abed, Ph.D., ACS Fellow
Center for Environmental Solutions and Emergency Response
Office of Research and Development
United States Environmental Protection Agency
26 West Martin Luther King Dr. Cincinnati, Ohio 45268
Phone: 513-569-7849 | **Fax:** 513-569-7879 | **Mobile**: 513-442-9904
Email: al-abed.souhail@epa.gov
Web: http://www.epa.gov/
Shipping Address
USEPA
5995 Center Hill Av.
Cincinnati, Ohio 45224

From:	Boyes, William
To:	Lila Thornton; Al-Abed, Souhail; Andersen, Christian; Burgess, Robert; Elaine Cohen-Hubal (hubal.elaine@epa.gov); Ho, Kay; Hughes, MichaelF; Reichman, Jay; Rogers, Kim; Scheckel, Kirk; Thai, Sheau-Fung; Zepp, Richard; Zucker, Robert
Subject:	STAA nomination for review article
Date:	Friday, April 24, 2020 5:40:00 PM
Attachments:	2020 STAA Nomination reviews.docx Boyes et al 2017 A comprehensive framework for evaluating....pdf

---

Hi All,

I thought it would be a good idea to submit our 2017 review article for an STAA award. I have enclosed a draft of the award nomination and the original paper. Only EPA authors are eligible for a cash award (sorry Lila).

1. Please send me any revisions to the nomination form./
2. Please send me an Email that you agree with the proportional division of effort (equal for all authors).

I hope you ae all well and staying safe during these strange times.

If anyone is in contact with the retired EPA authors please either forward this message to them or send me a current E-mail address – Thanks!

Will

William K. Boyes, Ph.D.
Neurological and Endocrine Toxicology Branch
Public Health and Integrated Toxicology Division
Center for Public Health and Environmental Assessment
Office of Research and Development
Mail Code B105-04
Environmental Protection Agency
109 T.W. Alexander Drive
Research Triangle Park, NC 27711

Phone: 919-541-7538
Mobile (alternate worksite contact): 919-417-2105
boyes.william@epa.gov

From: Scheckel, Kirk
To: Boyes, William
Subject: RE: STAA nomination for review article
Date: Monday, April 27, 2020 10:37:09 AM
Attachments: image002.png

Hi Will,

The write up looks great. If it helps, below are two more recent invited presentations:

Application of X-ray Absorption Spectroscopy for Monitoring Transformation of Nanomaterials. K. Scheckel. 2nd Quantifying Exposure to Engineered Nanomaterials (QEEN) from Manufactured Products Workshop, Washington, DC, 2018.

Environmental Transformations of Silver and Zinc Oxide Nanoparticles Drive Risk Assessment Understanding. K. Scheckel, E. Donner, R. Sekine, G. Brunetti, and E. Lombi. 55th Annual Meeting of the Clay Minerals Society, Urbanna, IL, 2018.

Thank you for taking a lead in this and I agree with the proportional division of effort (equal for all authors).

Regards,
Kirk

Kirk G. Scheckel, Ph.D.
Director, Land Remediation & Technology Division

United States Environmental Protection Agency
Office of Research & Development
Center for Environmental Solutions & Emergency Response
26 West Martin Luther King Drive, Office 191
Cincinnati, OH 45268

Office: (513) 487-2865 Scheckel.Kirk@epa.gov
Cell: (513) 405-5086 www.epa.gov

Celebrating EPA's 50th Anniversary
http://www.epa.gov/50

From: Boyes, William <Boyes.William@epa.gov>
Sent: Friday, April 24, 2020 5:41 PM
To: Lila Thornton <lila.thornton@duke.edu>; Al-Abed, Souhail <al-abed.souhail@epa.gov>; Andersen, Christian <Andersen.Christian@epa.gov>; Burgess, Robert <Burgess.Robert@epa.gov>; Hubal, Elaine <Hubal.Elaine@epa.gov>; Ho, Kay <Ho.Kay@epa.gov>; Hughes, MichaelF <Hughes.MichaelF@epa.gov>; Reichman, Jay <Reichman.Jay@epa.gov>; Rogers, Kim <Rogers.Kim@epa.gov>; Scheckel, Kirk <Scheckel.Kirk@epa.gov>; Thai, Sheau-Fung <Thai.Sheau-Fung@epa.gov>; Zepp, Richard <Zepp.Richard@epa.gov>; Zucker, Robert <Zucker.Robert@epa.gov>
Subject: STAA nomination for review article

Hi All,

I thought it would be a good idea to submit our 2017 review article for an STAA award. I have enclosed a draft of the award nomination and the original paper. Only EPA authors are eligible for a cash award (sorry Lila).

1. Please send me any revisions to the nomination form./
2. Please send me an Email that you agree with the proportional division of effort (equal for all authors).

I hope you ae all well and staying safe during these strange times.

If anyone is in contact with the retired EPA authors please either forward this message to them or send me a current E-mail address – Thanks!

Will

William K. Boyes, Ph.D.
Neurological and Endocrine Toxicology Branch
Public Health and Integrated Toxicology Division
Center for Public Health and Environmental Assessment
Office of Research and Development
Mail Code B105-04
Environmental Protection Agency
109 T.W. Alexander Drive
Research Triangle Park, NC 27711

Phone: 919-541-7538
Mobile (alternate worksite contact): 919-417-2105
boyes.william@epa.gov

From: Zepp, Richard
To: Boyes, William
Subject: Submission of review for STAA award
Date: Friday, April 24, 2020 5:51:25 PM

Hi Will:

I agree with submission of our review, "A comprehensive framework for evaluating the environmental health and safety implications of engineered nanomaterials" for an STAA award. I agree with the proportional division of effort (equal for all authors). Thank you for your efforts on the paper and putting together the award submission!

Richard G. Zepp
U.S. EPA
ORD/CEMM
960 College Station Rd.
Athens, Georgia 30605
USA
Email: zepp.richard@epa.gov
Tel. (706)- 355-8117
Fax (706)-355-8007

From: Ho, Kay
To: Boyes, William
Subject: RE: STAA nomination for review article
Date: Monday, April 27, 2020 9:32:07 AM

I agree with the proportional division of effort (equal for all authors.

Thank you

From: Boyes, William <Boyes.William@epa.gov>
Sent: Friday, April 24, 2020 5:41 PM
To: Lila Thornton <lila.thornton@duke.edu>; Al-Abed, Souhail <al-abed.souhail@epa.gov>; Andersen, Christian <Andersen.Christian@epa.gov>; Burgess, Robert <Burgess.Robert@epa.gov>; Hubal, Elaine <Hubal.Elaine@epa.gov>; Ho, Kay <Ho.Kay@epa.gov>; Hughes, MichaelF <Hughes.MichaelF@epa.gov>; Reichman, Jay <Reichman.Jay@epa.gov>; Rogers, Kim <Rogers.Kim@epa.gov>; Scheckel, Kirk <Scheckel.Kirk@epa.gov>; Thai, Sheau-Fung <Thai.Sheau-Fung@epa.gov>; Zepp, Richard <Zepp.Richard@epa.gov>; Zucker, Robert <Zucker.Robert@epa.gov>
Subject: STAA nomination for review article

Hi All,

I thought it would be a good idea to submit our 2017 review article for an STAA award. I have enclosed a draft of the award nomination and the original paper. Only EPA authors are eligible for a cash award (sorry Lila).

1. Please send me any revisions to the nomination form./
2. Please send me an Email that you agree with the proportional division of effort (equal for all authors).

I hope you ae all well and staying safe during these strange times.

If anyone is in contact with the retired EPA authors please either forward this message to them or send me a current E-mail address – Thanks!

Will

William K. Boyes, Ph.D.
Neurological and Endocrine Toxicology Branch
Public Health and Integrated Toxicology Division
Center for Public Health and Environmental Assessment
Office of Research and Development
Mail Code B105-04
Environmental Protection Agency
109 T.W. Alexander Drive
Research Triangle Park, NC 27711

Phone: 919-541-7538
Mobile (alternate worksite contact): 919-417-2105
boyes.william@epa.gov

2020 STAA Nomination

Category: Review Articles (RA)

Record of Percentage Agreement

Each author contributed equally to the manuscript. Proportional effort was determined by dividing 100% by the number of authors (18).

Author	Eligible	Total proportion effort (%)
Boyes, W. K	yes	5.5
Thornton, B. L	no	5.5
Al-Abed, S. R	yes	5.5
Andersen, C. P	yes	5.5
Bouchard, D. C.	yes	5.5
Burgess, R. M.	yes	5.5
Cohen Hubal, E. A.	yes	5.5
Ho, K. T.	yes	5.5
Hughes, M. F.	yes	5.5
Kitchin, K. T.	yes	5.5
Reichman, J. R	yes	5.5
Rogers, K. R.	yes	5.5
Ross, J. A.,	yes	5.5
Rygiewicz, P. T.	yes	5.5
Scheckel, K. G.	yes	5.5
Thai, S.-F.	yes	5.5
Zepp, R. G.	yes	5.5
Zucker, R. M	yes	5.5

Nominated Publication:

Boyes, W. K., Thornton, B. L., Al-Abed, S. R., Andersen, C. P., Bouchard, D. C., Burgess, R. M., Cohen Hubal, E. A., Ho, K. T., Hughes, M. F., Kitchin, K. T., Reichman, J. R., Rogers, K. R., Ross, J. A., Rygiewicz, P. T., Scheckel, K. G., Thai, S.-F., Zepp, R. G., Zucker, R. M. Comprehensive framework for evaluating the environmental health and safety implications of engineered nanomaterials. Critical Reviews in Toxicology, Crit Rev Toxicol. 2017 Oct;47(9):767-810. doi: 10.1080/10408444.2017.1328400

Bibliometric Journal Statistics

Journal	Journal Impact Factor	Immediacy Index	Cited Half-Life
Critical Reviews in Toxicology	4.771	1.33	8.6

**Data collected on 24 April 2020 from publisher's website.*

Supplemental Items

none

Justification

1. Citations for each publication nominated

Boyes, W. K., Thornton, B. L., Al-Abed, S. R., Andersen, C. P., Bouchard, D. C., Burgess, R. M., Cohen Hubal, E. A., Ho, K. T., Hughes, M. F., Kitchin, K. T., Reichman, J. R., Rogers, K. R., Ross, J. A., Rygiewicz, P. T., Scheckel, K. G., Thai, S.-F., Zepp, R. G., Zucker, R. M. Comprehensive framework for evaluating the environmental health and safety implications of engineered nanomaterials. Critical Reviews in Toxicology, Crit Rev Toxicol. 2017 Oct;47(9):767-810. doi: 10.1080/10408444.2017.1328400

Engineered nanomaterials (ENM) are a growing aspect of the global economy, and their safe and sustainable development, use, and eventual disposal requires the capability to forecast and avoid potential problems. This review provides a framework to evaluate the health and safety implications of ENM releases into the environment, including purposeful releases such as for antimicrobial sprays or nano-enabled pesticides, and inadvertent releases as a consequence of other intended applications. Considerations encompass product life cycles, environmental media, exposed populations, and possible adverse outcomes. This framework is presented as a series of compartmental flow diagrams that serve as a basis to help derive future quantitative predictive models, guide research, and support development of tools for making risk-based decisions. After use, ENM are not expected to remain in their original form due to reactivity and/or propensity for hetero-agglomeration in environmental media. Therefore, emphasis is placed on characterizing ENM as they occur in environmental or biological matrices. In addition, predicting the activity of ENM in the environment is difficult due to the multiple dynamic interactions between the physical/chemical aspects of ENM and similarly complex environmental conditions. Others have proposed the use of simple predictive functional assays as an intermediate step to address the challenge of using physical/chemical properties to predict environmental fate and behavior of ENM. The nodes and interactions of the framework presented here reflect phase transitions that could be targets for development of such assays to estimate kinetic reaction rates and simplify model predictions. Application, refinement, and demonstration of this framework, along with an associated knowledgebase that includes targeted functional assay data, will allow better de novo predictions of potential exposures and adverse outcomes.

2. If research has been invited for presentation at national/international societies. The following invited presentations resulted from this research:
    - Boyes WK. A Decision Support Framework for Environmental Health and Safety Evaluation of Engineered Nanomaterials. Invited presentation to the American Public Health Association Meeting, Denver, Oct 29- Nov 2, 2016.
    - Boyes, WK. Evaluating the Environmental Health and Safety Implications of Engineered Nanomaterials. Conference Keynote Speaker. Nanosafety 2017. Saarbrucken, Germany. Oct. 10-13, 2017.
    - Boyes, WK . A Framework for Evaluation of Engineered Nanomaterials. Invited presentation to the Genetics and Environmental Mutagenesis Society, Research Triangle Park, NC. May 2. 2018
    - Boyes, WK. A Comprehensive Framework for Evaluation of Engineered Nanomaterials. Invited webinar briefing for EPA Regional Science Liaisons. April 24. 2018
    - Boyes, WK . Overview of EPA Office of Research and Development (ORD) Research Activities Related to Nanomaterials. Webinar presented to the Nanomaterial Environmental Health Implications (NEHI) subcommittee of the National Nanotechnology Initiative (NNI). May 24. 2018
    - Boyes, WK . Evaluating the Environmental Health and Safety Impact of Engineered Nanomaterials. North East Nanomaterials Meeting (NENM2018), Lake Placid NY June 1-3. 2018. http://nny.sites.acs.org/2018nenanomeeting.htm
    - Boyes, WK. Round Table Panel member. Connecting the Pieces: Linking Manufacture and Use of Nanomaterials or Nanotechnology-Enabled Products with Exposure, Outcome, and Risk. QEEN II: 2nd Quantifying Exposure to Engineered Nanomaterials from Manufactured Products Workshop, Washington DC, Oct. 9-10. 2018.
    - Boyes, WK. Chair, Plenary Session. Exposure-Driven Risk Assessment for Nanosafety Research. QEEN II: 2nd Quantifying Exposure to Engineered Nanomaterials from Manufactured Products Workshop, Washington DC, Oct. 9-10. 2018.
    - Sheckel K. Application of X-ray Absorption Spectroscopy for Monitoring Transformation of Nanomaterials. 2nd Quantifying Exposure to Engineered Nanomaterials (QEEN) from Manufactured Products Workshop, Washington, DC, 2018.
    - K. Scheckel, E. Donner, R. Sekine, G. Brunetti, and E. Lombi. Environmental Transformations of Silver and Zinc Oxide Nanoparticles Drive Risk Assessment Understanding. 55th Annual Meeting of the Clay Minerals Society, Urbanna, IL, 2018.
    - Boyes, WK. Nanosafety Research: The US EPA Perspective. Invited presentation to a workshop entitled “Fostering EU-US cooperation in Nanosafety Research” sponsored by the European Union. Harvard University, Boston Mass. March 5-6. 2019
    - Boyes, WK. Invited Moderator, Respiratory Effects of Engineered Nanomaterials in Relation to Physiochemical Properties. NanoEHS Webinar Series, U.S. National Nanotechnology Initiative. September 10, 2019.
    - Boyes, WK. Update on Nanomaterial Research at EPA. Invited seminar. Annual meeting of the Center for Environmental Implications of Nanotechnology (CEINT), Duke Univ., September 13, 2019.

3. Unique source of funding for research

    All funding came from the intramural research budget of the EPA Office of Research and Development

4. Any awards Internal/External to EPA that were received for the research

None to date

5. Number of times the publication has been downloaded/viewed
6. How many times it has been cited (Google Scholar)

Publication	Number of downloads/views	Number of citations (Google Scholar)
Boyes et al., 2017	716	29

7. Letters of Recommendation

Link for multiple publications

na

STAA Nominated publications previous six years

Boyes, (2015) STAA level III. Evaluation of the developmental toxicity of inhaled ethanol as a component of renewable automotive fuels. Boyes, W.K., Degn L., Martin S.A., Lyke D. F., and Herr D.W. Neurophysiological assessment of auditory, peripheral nerve, somatosensory, and visual system functions after developmental exposure to ethanol vapors. Neurotoxicology and Teratology 43(0): 1-10, 2014. (Unrelated to current nomination).

Hughes (2015) STAA Level III. Biogeographical Analysis of Chemical Co-Occurrence Data to Identify Priorities for Mixtures Research Risk Analysis/Peer Reviewed, 32(2):224-236 (2) Environmentally Relevant Mixtures in Cumulative Assessments: an Acute Study of Toxicokinetics and Effects on Motor Activity in Rats Exposed to a Mixture of Pyrethroids Toxicological Sciences/Peer Reviewed, 130(2):309-318 (3) A Pharmacokinetic Model of Cis-and Trans-Permethrin Disposition in Rats and Humans with Aggregate Exposure Application Toxicological Sciences/Peer Reviewed, 130(1):33-47. (Unrelated to current nomination).

Hughes (2016} STAA Level II. Bradham, K.D., Scheckel. K.G., Nelson, C.M., Seales, P.E., Lee, G.E., Hughes, M.F., Miller, B.W., Yeow, A., Gilmore, T., Harper, S., Thomas, D.J. (2011) Relative Bioavailability and Bioaccessibility and Speciation of Arsenic in Contaminated Soils. Environ. Health Perspect. 119(11): 1629–1634. (Unrelated to current nomination).

Citation: For creating a comprehensive framework to consider the environmental effects of engineered nanomaterials.

Table of Contents

General_Authors_Publications.....2
LI-266469_berberich_et_al_2019.....26
LI-266473_Beaulieu_et_al_Ecosystems_2017.....49
LI-266476_Beaulieu-2016-Estimates_of_reservo.....69
LI-266477_Beaulieu_et_al_2014__ES&T__CH4_emissions.....83
Percent_Agreement.....92

STAA REPORT FOR THE SCIENTIST NOMINATIONS

General Information:

Nomination ID/App ID:	20-117
Research Category Primary:	Ecological Research (ER)
Research Category Secondary:	Monitoring and Measurement Methods (MM)
Laboratory/Office Name:	ORD
Nomination Entered By:	Jake Beaulieu

Eligibility Checklist:

[Y] The nominated publication(s) has not been submitted to a previous STAA competition.

[Y] The nominated publication(s) was published on or before January 1, 2017 and on or after January 1,2012

[Y] The principal author was an EPA employee or a PHS employee assigned to EPA when the research was performed

[Y] The EPA authors (includes PHS employees assigned to EPA) contributed collectively a minimum of 50% toward the publication(s)

Nominating Official Name:	Kevin Oshima
Nominating Official Title:	BIOLOGIST
Nominating OfficialEmail:	oshima.kevin@epa.gov
STAA Coordinator Name:	Kathleen Wiser
STAA Coordinator Email:	wiser.kathi@epa.gov

Justifications:

Justification 1:

Water reservoirs, created when rivers are dammed, provide many important societal services including flood control, drinking water, low cost transportation networks for commerce, and hydropower. These benefits come along with adverse social and ecological effects, however, including enhanced greenhouse gas (GHG) emissions. Methane (CH_4), a GHG 34 times more powerful than carbon dioxide, is produced in aquatic sediments through natural decomposition processes. These natural processes are greatly enhanced when free flowing rivers are converted to reservoirs. Furthermore, the flooding of dry lands surrounding the original river channel can convert soils from GHG sinks to GHG sources. Cumulatively, these effects lead to a net increase in the GHG footprint of the flooded area. As recently as 2010 the magnitude of reservoir GHG emissions was largely unknown, making it difficult to incorporate these emissions into national GHG inventories or impact assessments for proposed reservoirs. The research described in this nomination paved the way for improved estimates of reservoir GHG emissions and identified novel management actions to mitigate these emissions.

In 2011, when the nominees began working in this research area, the best available data indicated that reservoir GHG emissions decrease exponentially from equatorial regions toward the poles. This was largely attributed to patterns in air and water temperatures across this global latitudinal gradient. At the time, very few measurements had been made in mid-latitude regions, however, with most work having been conducted in boreal and tropical biomes. We hypothesized that mid-latitude reservoirs in the midwestern U.S. supported higher emission rates than predicted from their latitude. This prediction was based on differences in land-use conditions between the largely undeveloped watersheds surrounding the boreal and tropical reservoirs included in previous studies, and the predominantly agricultural watersheds in the midwestern U.S.. Erosion and nutrient runoff from agricultural soils is likely to promote oxygen depletion and algal blooms in reservoirs. These conditions are likely to stimulate CH_4 production because 1) CH_4 is only produced in low oxygen environments and 2) algal derived carbon (C) is readily converted to CH_4 in aquatic ecosystems. To test this hypothesis we measured CH4 emission rates from Harsha Lake, a reservoir draining a watershed managed for soy and corn production in Ohio. We found that Harsha Lake emitted CH4 at rates that were among the highest ever reported in the literature, equivalent to those observed in

tropical systems. We also found a striking spatial pattern in emission rates, with areas near tributary inputs having emission rates that were an order of magnitude greater than elsewhere in the reservoir (see Supporting Materials Beaulieu et al. 2014). These results indicated that 1) mid-latitude reservoirs may play a larger role

in GHG inventories than previously recognized, and 2) accurate emission estimates for individual waterbodies require spatially explicit survey designs that accurately capture emissions from hotspot areas.

Given the important implications of our 2014 paper, we conducted a follow-up study that focused on better quantifying the spatial distribution of emission rates within the reservoir (nominated paper Beaulieu et al. 2016). For this study, we expand the research team to include a spatial ecologist from the National Center for Ecological Assessment (NCEA) and designed a statistical survey that included 115 sampling sites in Harsha Lake, as compared to six sites in the original 2014 paper. The reservoir-scale emission rate estimated from the more thorough spatial sampling was very similar to that reported in the first paper, reinforcing our finding that mid-latitude reservoirs can emit more CH4 than previously recognized. We also confirmed that areas located immediately below tributary inflows supported much higher emission rates than other areas of the reservoir. Although these areas occupy only 12% of the reservoir surface area in Harsha Lake, they emit 41% of the CH4 emanating from the reservoir. This finding demonstrates that it is critically important that investigators account for hot spots in emission rate estimates.

An important contribution of the 2016 paper is that it offered a statistically robust method for measuring GHG emission rates in reservoirs that 1) accounts for the spatial distribution of emission hot spots, 2) allows for rigorous population level estimates of mean and variance, and 3) generates emission rate estimates that can be compared across different waterbodies. Earlier investigations of reservoir GHG emissions often entailed monitoring at one location in the waterbody, usually the deepest location, and used poorly defined methods for upscaling to the entire reservoir surface area. This approach likely resulted in emission estimates that were biased low because emission hot spots were overlooked. Furthermore, inconsistencies in survey designs and upscaling procedures made it difficult to compare emission rates across studies, hindering progress in this area of research. The nominated publication, published in a special issue of Limnology and Oceanography on CH_4 emissions from aquatic ecosystems, has been cited 16 times and has contributed to the rapid improvement in the quality of emission rate estimates more recent literature.

The two studies at Harsha Lake demonstrated that the system has a persistent pattern of elevated emission rates near tributaries, but the reason for the pattern wasn't clear. It also wasn't clear to what extent other reservoirs might exhibit similar patterns. To better understand the mechanisms leading to this spatial pattern, we measured CH4 production rates and a suite of biogeochemical indicators from sediment cores collected at 15 sites within the reservoir (nominated paper Berberich et al. 2019). Stable isotope and molecular indicators revealed that sediments in hot-spot areas have a mix of carbon (C) derived from terrestrial sources (e.g., erosion from agricultural soils) and algal blooms. Terrestrially derived organic matter likely provides a steady background supply of C for CH4 production while higher quality C derived from algae is converted to CH4 more quickly. Both C sources are particularly abundant at the river mouth where sedimentation rates are highest and nutrients from the inflowing river stimulate large algae blooms, leading to the high rates of CH4 production consistently observed in this area. These patterns are likely a common feature of reservoirs draining agricultural watersheds suggesting that CH4 hot spots near river mouths may be a persistent feature of these systems.

The previously discussed papers demonstrate that Harsha Lake supports much higher CH4 emission rates than previously expected. We estimate that if all U.S. reservoirs draining watersheds managed for corn and soybean production emitted CH4 at rates equivalent to that of Harsha Lake, these systems would be the fourth largest anthropogenic CH4 source in the country; equivalent to half of the CH4 emitted from all U.S. landfills. While accurately estimating the magnitude of CH4 emissions from reservoirs is an important research objective, EPA is also committed to providing solutions to environmental problems. In the next phase of the research we partnered with the U.S. Army Corps of Engineers (USACE) to develop mitigation strategies. Specifically, we considered whether water-level management could be used as a tool for CH4 mitigation. An important mechanism for CH4 release from sediments is ebullition, or the release of CH4 rich bubbles. Aquatic sediments, including those in reservoirs, often contain large volumes of stored gas. This is well known to anyone who has stepped into muddy sediments at the edge of a lake or river and saw (or smelled!) bubbles emerging from the water. These bubbles are typically held within sediments by the pressure of the overlying water column (hydrostatic pressure) but can be released during periods of water level decline. To quantify the degree to which CH4 emissions are regulated by water level change, we conducted an experiment at Harsha Lake. We partnered with the dam operators (USACE) and implemented a water level management plan that entailed relatively constant water levels during the summer months, followed

by a 2 foot drop in water levels over a 24 hour period in early Fall. We found that the experimental drop in water levels triggered a 10-fold increase in bubbling rates across the reservoir. While these bubbling rates were extraordinarily high, they were short lived and constituted only a minor component of annual CH4 emissions because the reservoir has quite high bubbling rates even during periods of constant water levels. This is in contrast to reservoirs with cleaner water and much lower algal abundance where bubbling is largely confined to periods of water level decline. Our conclusion is that water-level management can be an effective tool for mitigating CH4 emissions from clear-water reservoirs, but not in systems with poor water quality, large algae blooms and high bubbling rates. It appears that the only way to mitigate emissions from eutrophic systems is to implement watershed-scale nutrient management plans to reduce nutrient loading, algae blooms, and C availability in the reservoir.

Collectively, these papers represent important scientific advancements. First, we have shown that mid-latitude reservoirs play a much larger role in regional/national/global CH4 budgets than previously recognized. This is likely due to land-use conditions that load reservoirs with carbon and nutrients, leading to high rates of CH4 production, particularly near river inflows where these materials first enter reservoirs. Secondly, we demonstrated how tools developed by spatial ecologists can be used to design statistically robust survey designs, allowing for upscaling from point measurements to entire reservoirs, and facilitating comparison among different studies. Finally, our works suggests that these emissions can be mitigated through watershed-scale nutrient management in eutrophic reservoirs, and water-level management in less productive reservoirs.

This work has played a pivot role in advancing EPA/Office of Air and Radiation's (OAR) efforts to include reservoirs as an anthropogenic GHG source in the *U.S. Inventory of Greenhouse Gas Emissions and Sinks*. The inventory is compiled annually by OAR and reported to the Intergovernmental Panel on Climate Change (IPCC) in compliance with the nation's treaty obligations under the United Nations Framework Convention on Climate Change. OAR nominated Jake Beaulieu to serve as a subject matter expert during several meetings of the IPCC, culminating with Dr. Beaulieu serving as a Lead Author on the IPCC methodology for estimating reservoir emissions. Dr. Beaulieu is now working with OAR to measure CH4 emissions from over 100 reservoirs distributed across the US. These data will form the basis of the first national-scale estimate of reservoir CH4 emissions for the US.

This work also led to an invitation to publish in a special issue of Limnology and Oceanography highlighting aquatic CH4 emissions, an invited talk at the 2015 meeting of the Association for the Sciences of Limnology and Oceanography (ASLO), and to co-chair special sessions on aquatic GHG fluxes at the 2019 and 2020 ASLO meetings. Beaulieu has also served on committees for PhD and Masters students working in this area of research.

Justification 2A:

The three nominated publications, and one supporting publication, build off one another, as described in Justification 1. The supporting publication describes our 2012 survey of methane emission rates from Harsha Lake. The survey described in the nominated 2016 publication follows up on the 2012 survey using improved spatial resolution and a more robust statistical survey design. The nominated 2019 publication describes a study where we investigated the mechanisms leading to the spatial patterns observed in the earlier Harsha Lake surveys. Finally, the nominated 2018 paper describes a study of management actions that might be used to mitigate methane emissions from the lake.

Justification 2B:

Beaulieu

2018

Level III for An investigation of the effects of urban stream burial on nitrogen uptake and ecosystem metabolism.

Beaulieu, J. J., H. E. Golden, C. D. Knightes, P. M. Mayer, S. S. Kaushal, M. J. Pennino, C. P. Arango, D. A. Balz, C. M. Elonen, K. M. Fritz, and B. H. Hill. 2015. Urban Stream Burial Increases Watershed-Scale Nitrate Export. PLoS ONE **10**:e0132256.

Pennino, M. J., S. S. Kaushal, J. J. Beaulieu, P. M. Mayer, and C. P. Arango. 2014. Effects of urban stream burial on nitrogen uptake and ecosystem metabolism: implications for watershed nitrogen and carbon fluxes. Biogeochemistry **121**:247-269.

Beaulieu, J. J., P. M. Mayer, S. S. Kaushal, M. J. Pennino, C. P. Arango, D. A. Balz, T. J. Canfield, C. M. Elonen, K. M. Fritz, B. H. Hill, H. Ryu, and J. W. S. Domingo. 2014. Effects of urban stream burial on organic matter dynamics and reach scale nitrate retention. Biogeochemistry **121**:107-126.

2017

Level II for an Investigation of the Role of Reservoirs in Removing Excess Reactive Nitrogen from the Environment

Beaulieu, J. J., R. L. Smolenski, C. T. Nietch, A. Townsend-Small, M. S. Elovitz, and J. P. Schubauer-Berigan. 2014. Denitrification alternates between a source and sink of nitrous oxide in the hypolimnion of a thermally stratified reservoir. Limnology and Oceanography **59**:495-506.

Beaulieu, J. J., C. T. Nietch, and J. L. Young. 2015. Controls on nitrous oxide production and consumption in reservoirs of the Ohio River Basin. Journal of Geophysical Research-Biogeosciences **120**:1995-2010.

2016

Honorable Mention for ‘Continuous Monitoring Reveals Multiple Controls on Ecosystem Metabolism in a Suburban Stream’

Beaulieu, J. J., C. P. Arango, D. A. Balz, and W. D. Shuster. 2013. Continuous monitoring reveals multiple controls on ecosystem metabolism in a suburban stream. Freshwater Biology **58**:918-937.

Hall, R. O., and J. J. Beaulieu. 2013. Estimating autotrophic respiration in streams using daily metabolism data. Freshwater Science:507-516.

2015

Honorable Mention for ‘A Demonstration of Enhanced Methane-Gas Transfer for a Large River’.

Beaulieu, J. J., W. D. Shuster, and J. A. Rebholz. 2012. Controls on gas transfer velocities in a large river. J. Geophys. Res. **117**:G02007.

Balz

2018

Level III for An investigation of the effects of urban stream burial on nitrogen uptake and ecosystem metabolism.

Nominated publications:

Beaulieu, J. J., H. E. Golden, C. D. Knightes, P. M. Mayer, S. S. Kaushal, M. J. Pennino, C. P. Arango, D. A. Balz, C. M. Elonen, K. M. Fritz, and B. H. Hill. 2015. Urban Stream Burial Increases Watershed-Scale Nitrate Export. PLoS ONE **10**:e0132256.

Pennino, M. J., S. S. Kaushal, J. J. Beaulieu, P. M. Mayer, and C. P. Arango. 2014. Effects of urban stream burial on nitrogen uptake and ecosystem metabolism: implications for watershed nitrogen and carbon fluxes. Biogeochemistry **121**:247-269.

Beaulieu, J. J., P. M. Mayer, S. S. Kaushal, M. J. Pennino, C. P. Arango, D. A. Balz, T. J. Canfield, C. M. Elonen, K. M. Fritz, B. H. Hill, H. Ryu, and J. W. S. Domingo. 2014. Effects of urban stream burial on organic matter dynamics and reach scale nitrate retention. Biogeochemistry **121**:107-126.

Berberich

N/A

Birchfield

N/A

Buffam

N/A

Hamilton

N/A

Harrison

N/A

McManus

Nietch

2017

2017 Level III for Comparing Drinking Water Treatment Costs to Source Water Protection

Nominated publication:

Costs Using Time Series Analysis (Heberling, M., C. Nietch, H. Thurston, M. Elovitz, K. Birkenhauer, S. Panguluri, B. Ramakrishnan, E. Heiser, T. Neyer), 2018

2017

Level II for an Investigation of the Role of Reservoirs in Removing Excess Reactive Nitrogen from the Environment

Beaulieu, J. J., R. L. Smolenski, C. T. Nietch, A. Townsend-Small, M. S. Elovitz, and J. P. Schubauer-Berigan. 2014. Denitrification alternates between a source and sink of nitrous oxide in the hypolimnion of a thermally stratified reservoir. Limnology and Oceanography **59**:495-506.

Beaulieu, J. J., C. T. Nietch, and J. L. Young. 2015. Controls on nitrous oxide production and consumption in reservoirs of the Ohio River Basin. Journal of Geophysical Research-Biogeosciences **120**:1995-2010.

2016

Level II for Development and Application of Test Methods Using a More Relevant and Sensitive Mayfly Species for Assessing Toxicity (Weaver, Paul; Struewing, Katherine; Nietch, Christopher; Lazorchak, James; Johnson, Brent; Funk, David; DeCelles, Susanna; Buchwalter, David)

Platz

N/A

Squier

N/A

Waldo

N/A

Walker

2015

Level III, “Linking Agricultural Crop Management and Air-Quality Models for Regional-to-National-Scale Nitrogen Assessments”

Nominated publications:

Walker, J.T., Jones, M.R., Bash, J.O., Myles, L., Meyers, T., Schwede, D., Herrick, J., Nemitz, E., Robarge, W., 2013. Processes of ammonia air-surface exchange in a fertilized *Zea mays* canopy. Biogeosciences, 10, 981-998.

Bash, J.O., Cooter, E.J., Dennis, R.L., Walker, J.T., Pleim, J.E. 2012. Evaluation of a regional air-quality model with bi-directional NH_3 exchange coupled to an agro-ecosystem model. Biogeosciences, 10, 1635-1645

Cooter, E.J., Bash, J.O., Benson, V., Ran, L-M., 2012. Linking Agricultural Management and Air-Quality models for Regional to National-Scale Nitrogen Deposition Assessments. Biogeosciences, 9, 4023-4035.

White

N/A

Young

2017

Level II for an Investigation of the Role of Reservoirs in Removing Excess Reactive Nitrogen from the Environment

Nominated publications:

Beaulieu, J. J., R. L. Smolenski, C. T. Nietch, A. Townsend-Small, M. S. Elovitz, and J. P. Schubauer-Berigan. 2014. Denitrification alternates between a source and sink of nitrous oxide in the hypolimnion of a thermally stratified reservoir. Limnology and Oceanography **59**:495-506.

Beaulieu, J. J., C. T. Nietch, and J. L. Young. 2015. Controls on nitrous oxide production and consumption in reservoirs of the Ohio River Basin. Journal of Geophysical Research-Biogeosciences **120**:1995-2010.

Justification 2C:

The 2017 Level II award for an Investigation of the 'Role of Reservoirs in Removing Excess Reactive Nitrogen from the Environment' also pertains to biogeochemical cycling in reservoirs, but focuses on nitrogen processing, whereas the current nomination focuses on carbon cycling. The nominations represent distinct research efforts resulting in independent publications supports different Agency programmatic needs.

Justification 2D:

n/a

Justification 2E:

n/a

Justification 3A:

This work led to Dr. Jake Beaulieu becoming an internationally recognized subject matter expert. Most prominently, Beaulieu was invited to serve as Lead Author on

the methodology report used by the Intergovernmental Panel on Climate Change (IPCC) to estimate the magnitude of methane emissions from reservoirs. This work also led to an invitation to publish in a special issue of Limnology and Oceanography highlighting aquatic methane emissions, an invited talk at the 2015 meeting of the Association for the Sciences of Limnology and Oceanography (ASLO), and to co-chair special sessions on aquatic GHG fluxes at the 2019 and 2020 ASLO meetings. Beaulieu has also served on committees for PhD and Masters students working in this area of research.

Justification 3B:

The nominated publications were subject to peer review via the journal's peer review process. Each article was reviewed by 2 -3 reviewers and the editor. All reviewer comments were addressed and the revision submitted to the journal. In some cases a second round of revisions were required, while in others the revised manuscript was accepted.

AUTHORS

Principal Author

Author Name:	Jake J. Beaulieu		
Professional Title:		Salutation:	
Email:	beaulieu.jake@epa.gov	Organization:	
Mailing Address:			
Street Line 1:			
City:			
Zip Code:		State:	
At time of research was:	EPA Employee		
Separation Date:			
% of Effort:	16		

Contributing Author

Author Name:	Hamilton	
Professional Title:		Salutation:
Email:	trinityh@umn.edu	Organization:
Mailing Address:		
Street Line 1:		
City:		
Zip Code:		State:
At time of research was:	Non EPA Personnel	
Separation Date:		
% of Effort:	6	

Contributing Author

Author Name:	Waldo	
Professional Title:		Salutation:
Email:	sarahrwaldo@gmail.com	Organization:
Mailing Address:		
Street Line 1:		
City:		
Zip Code:		State:
At time of research was:	Non EPA Personnel	
Separation Date:		
% of Effort:	6	

Contributing Author

Author Name:	Buffam	
Professional Title:		Salutation:
Email:	buffamii@ucmail.uc.edu	Organization:
Mailing Address:		
Street Line 1:		
City:		
Zip Code:		State:
At time of research was:	Non EPA Personnel	
Separation Date:		
% of Effort:	6	

Contributing Author

Author Name:	Harrison	
Professional Title:		Salutation:
Email:	john_harrison@wsu.edu	Organization:
Mailing Address:		
Street Line 1:		
City:		
Zip Code:		State:
At time of research was:	Non EPA Personnel	
Separation Date:		
% of Effort:	6	

Contributing Author

Author Name:	David Balz	
Professional Title:		Salutation:
Email:	balz.adam@epa.gov	Organization:
Mailing Address:		
Street Line 1:		
City:		
Zip Code:		State:
At time of research was:	Non EPA Personnel	
Separation Date:		
% of Effort:	6	

Contributing Author

Author Name:	Berberich	
Professional Title:		Salutation:
Email:	berberichme@gmail.com	Organization:
Mailing Address:		
Street Line 1:		
City:		
Zip Code:		State:
At time of research was:	Non EPA Personnel	
Separation Date:		
% of Effort:	6	

Contributing Author

Author Name:	Birchfield	
Professional Title:		Salutation:
Email:	mkeithbirch@wsu.edu	Organization:
Mailing Address:		
Street Line 1:		
City:		
Zip Code:		State:
At time of research was:	Non EPA Personnel	
Separation Date:		
% of Effort:	6	

Contributing Author

Author Name:	Squier	
Professional Title:		Salutation:
Email:	squier.bill@epa.gov	Organization:
Mailing Address:		
Street Line 1:		
City:		
Zip Code:		State:
At time of research was:	EPA Employee	
Separation Date:		
% of Effort:	6	

Contributing Author

Author Name:	Young	
Professional Title:		Salutation:
Email:	jade.l.young@usace.army.mil	Organization:
Mailing Address:		
Street Line 1:		
City:		
Zip Code:		State:
At time of research was:	Non EPA Personnel	
Separation Date:		
% of Effort:	6	

Contributing Author

Author Name:	Nietch	
Professional Title:		Salutation:
Email:	nietch.christopher@epa.gov	Organization:
Mailing Address:		
Street Line 1:		
City:		
Zip Code:		State:
At time of research was:	EPA Employee	
Separation Date:		
% of Effort:	6	

Contributing Author

Author Name:	Platz	
Professional Title:		Salutation:
Email:	platzmc05@gmail.com	Organization:
Mailing Address:		
Street Line 1:		
City:		
Zip Code:		State:
At time of research was:	Non EPA Personnel	
Separation Date:		
% of Effort:	6	

Contributing Author

Author Name:	McManus	
Professional Title:		Salutation:
Email:	mcmanus.michael@epa.gov	Organization:
Mailing Address:		
Street Line 1:		
City:		
Zip Code:		State:
At time of research was:	EPA Employee	
Separation Date:		
% of Effort:	6	

Contributing Author

Author Name:	Walker	
Professional Title:		Salutation:
Email:	walker.johnt@epa.gov	Organization:
Mailing Address:		
Street Line 1:		
City:		
Zip Code:		State:
At time of research was:	EPA Employee	
Separation Date:		
% of Effort:	6	

Contributing Author

Author Name:	White	
Professional Title:		Salutation:
Email:	white.karenm@epa.gov	Organization:
Mailing Address:		
Street Line 1:		
City:		
Zip Code:		State:
At time of research was:	EPA Employee	
Separation Date:		
% of Effort:	6	

PUBLICATIONS

Publication 1:

Publication Title:	Spatial variability of sediment methane production and methanogen communities within a eutrophic res		
Publication Date:	Wed Dec 04 00:00:00 GMT 2019		
Journal/Publication Method:	online		
All Author(s):			
Volume:	n/a	Number:	n/a
Pages:	23	Immediately Index:	Immediately Index:
Citation ½ Life:	8.4	Impact Factor:	4.325

Publication 2:

Publication Title:	Effects of an Experimental Water-level Drawdown on Methane Emissions from a Eutrophic Reservoir.		
Publication Date:	Tue Sep 05 00:00:00 GMT 2017		
Journal/Publication Method:	online/print		
All Author(s):			
Volume:	21	Number:	n/a
Pages:	657-674	Immediately Index:	Immediately Index:
Citation ½ Life:	10.2	Impact Factor:	4.555

Publication 3:

Publication Title:	Estimates of reservoir methane emissions based on a spatially balanced probabilistic-survey.		
Publication Date:	Tue Apr 05 00:00:00 GMT 2016		
Journal/Publication Method:	online/print		
All Author(s):			
Volume:	61	Number:	n/a
Pages:	27-40	Immediately Index:	Immediately Index:
Citation ½ Life:	8.4	Impact Factor:	4.3254

Publication 4:

Publication Title:	High Methane Emissions from a Midlatitude Reservoir Draining an Agricultural Watershed.		
Publication Date:	Tue Aug 26 00:00:00 GMT 2014		
Journal/Publication Method:	print/online		
All Author(s):			
Volume:	48	Number:	n/a
Pages:	100-108	Immediately Index:	Immediately Index:
Citation ½ Life:	7.1	Impact Factor:	7.149

LIMNOLOGY and OCEANOGRAPHY

ASLO

Limnol. Oceanogr. 9999, 2019, 1–23
© 2019 The Authors. *Limnology and Oceanography* published by Wiley Periodicals, Inc. on behalf of Association for the Sciences of Limnology and Oceanography.
doi: 10.1002/lno.11392

Spatial variability of sediment methane production and methanogen communities within a eutrophic reservoir: Importance of organic matter source and quantity

Megan E. Berberich [1*,a] **Jake J. Beaulieu,** [2] **Trinity L. Hamilton,** [1,b] **Sarah Waldo,** [2,c] **Ishi Buffam** [1]

[1]Department of Biological Sciences, University of Cincinnati, Cincinnati, Ohio
[2]USEPA, Office of Research and Development, Cincinnati, Ohio

Abstract

Freshwater reservoirs are an important source of the greenhouse gas methane (CH_4) to the atmosphere, but global emission estimates are poorly constrained (13.3–52.5 Tg C yr^{-1}), partially due to extreme spatial variability in emission rates within and among reservoirs. Spatial heterogeneity in the availability of organic matter (OM) for biological CH_4 production by methanogenic archaea may be an important contributor to this variation. To investigate this, we measured sediment CH_4 potential production rates, OM source and quantity, and methanogen community composition at 15 sites within a eutrophic reservoir in Ohio, USA. CH_4 production rates were highest in the shallow riverine inlet zone of the reservoir, even when rates were normalized to OM quantity, indicating that OM was more readily utilized by methanogens in the riverine zone than in the transitional or lacustrine zones. Sediment stable isotopes and C:N indicated a greater proportion of terrestrial OM in the particulate sediment of this zone. Methanogens were present at all sites, but the riverine zone contained a higher relative abundance of methanogens capable of acetoclastic and methylotrophic methanogenesis, likely reflecting differences in decomposition processes or OM quality. While we found that methane potential production rates were negatively correlated with autochthonous carbon in particulate sediment OM, rates were positively correlated with indicators of autochthonous carbon in the porewater dissolved OM. It is likely that both dissolved and particulate sediment OM affect CH_4 production rates, and that both terrestrial and aquatic OM sources are important in the riverine methane production hot spot.

Lakes and reservoirs are a globally significant source of methane (CH_4) (Bastviken et al. 2011; Holgerson and Raymond 2016; Stanley et al. 2016; DelSontro et al. 2018), a greenhouse gas (GHG) with 45 times the sustained-flux global warming potential of carbon dioxide (CO_2) over a 100-year timescale (Neubauer and Megonigal 2015). Global CH_4 fluxes from reservoirs remain poorly constrained (13.3–52.2 Tg C yr^{-1}; Deemer et al. 2016), due in part to uncertainty in reported emission rate estimates for individual reservoirs. Methane emissions from reservoirs (impoundments created by damming rivers) are of particular interest due to the increasing number of these systems, their land coverage area, and their high biogeochemical processing rates relative to lakes (Downing et al. 2006; Harrison et al. 2009; Zarfl et al. 2015). For example, compared to natural lakes, reservoirs tend to have a high watershed area-to-surface area ratio that can result in high sediment and nutrient loading from the surrounding catchment (Thornton et al. 1990; Hayes et al. 2017). This can lead to higher production (Hayes et al. 2017) and C burial rates (Knoll et al. 2014), with the potential to increase methane generation in these systems.

Methane is the end-product of organic matter (OM) decomposition in anoxic freshwater sediments in the absence of more favorable electron acceptors such as sulfate. OM availability is therefore an important constraint on the production of CH_4 in freshwater sediments. Sediment OM is a complex mixture of autochthonous material, derived from in situ primary production within the waterbody (OM_{aq}), and allochthonous material, derived from terrestrial watershed sources transported to the waterbody (OM_{terr}), in different stages of decomposition.

*Correspondence: berberme@mail.uc.edu

This is an open access article under the terms of the Creative Commons Attribution License, which permits use, distribution and reproduction in any medium, provided the original work is properly cited.

Additional Supporting Information may be found in the online version of this article.

[a]Present address: International Institute of Tropical Forestry, USDA Forest Service, Luquillo, Puerto Rico
[b]Department of Plant and Microbial Biology and the BioTechnology Institute, University of Minnesota, St. Paul, MN
[c]Puget Sound Clean Air Agency, WA

Throughout the decomposition process, fermenting bacteria and archaea convert complex OM molecules to smaller substrates such as acetate or C1 compounds (methanol, methyl-amines, etc.) that can be utilized by methanogenic archaea (methanogens) in the terminal stages of decomposition to produce CH_4 (see Liu and Whitman 2008).

The chemical composition of OM can be used to infer origin (i.e., OM_{terr} vs. OM_{aq}; e.g., McKnight et al. 2001; Stedmon et al. 2003; Hood et al. 2005; Mladenov et al. 2010) and determines, in part, the bioavailability of the material (e.g., Sun et al. 1997). For example, algae and aquatic microorganisms, components of OM_{aq}, are generally composed primarily of protein, and contain variable amounts of both lipids and carbohydrates (Bianchi and Canuel 2011). Higher plants, a component of OM_{terr}, are composed mainly of cellulose and structural compounds, and contain a lower fraction of proteins (Bianchi and Canuel 2011). During biodegradation, aquatic OM, which is associated with aliphatic and peptide-like compounds (Kellerman et al. 2018), is generally considered to be more labile than terrestrial-derived OM (del Giorgio and Davis 2003) that can be comprised of complex structural polysaccharides and phenolic aromatic compounds such as those found in lignin. Therefore, OM source and OM quality are often discussed in conjunction.

Methanogens and the potential role OM plays in shaping microbial communities in freshwater environments (Fagervold et al. 2014) underlie the relationship between OM source and methane production. Little is known about the response of the methanogenic community's composition and activity to variations in OM source or quantity in freshwater ecosystems, despite the significant role methanogens play in the global carbon cycle. Discrete taxonomic groups of methanogens vary in their ability to use different substrates (Liu and Whitman 2008); thus, variation in substrate availability in freshwater sediment likely affects methanogen community structure and activity, including the pathway utilized by methanogens to generate CH_4.

Reservoirs are ideal ecosystems for investigating the relationship between OM dynamics and CH_4 production due to the predictable patterns of OM input across their length. Reservoirs are comprised of three functional zones—riverine, transitional, and lacustrine—characterized by differences in depth, thermal stratification, sediment composition, primary productivity, and water velocity (Thornton et al. 1990). The quantity of OM in the sediment is expected to vary across reservoir zones, as is the relative contribution of OM_{aq} and OM_{terr} to the sediments. Further, reservoir tributary inlets and depositional zones have been demonstrated to be hot spots for CH_4 emissions across the air-water interface (DelSontro et al. 2011; Grinham et al. 2011; Maeck et al. 2013; Beaulieu et al. 2014*a*; Beaulieu et al. 2016), suggesting these depositional zones may be hot spots for sediment CH_4 production.

OM additions to lake sediments in laboratory experiments have been shown to increase CH_4 production rates (Schwarz et al. 2008; West et al. 2012, 2015*a*; Grasset et al. 2018), but our understanding of the contribution of OM_{terr} and OM_{aq} to CH_4 production rates at an ecosystem scale is not well constrained. Specifically, it is unknown if, at an ecosystem scale, CH_4 hot spots reflect inputs of presumed-labile OM_{aq} or environmental conditions that facilitate the degradation of more complex molecules derived from OM_{terr} into methanogenic substrates. In several lab studies, OM_{aq} stimulated an increase in CH_4 production (Schwarz et al. 2008; West et al. 2012, 2015*a*), including a greater increase in CH_4 production compared to OM_{terr} additions (West et al. 2012). This is consistent with reports that sediment CH_4 production rates across different lakes are positively correlated with lake productivity and sediment OM derived from OM_{aq} (Duc et al. 2010; West et al. 2015*b*), and that reservoir productivity and CH_4 emissions from the air-water interface are positively correlated at a global scale (Deemer et al. 2016; DelSontro et al. 2018). In contrast, other recent studies demonstrate the importance of OM_{terr} and ancient terrestrial OM to carbon cycling in aquatic systems. Grasset et al. (2018) showed that additions of OM_{terr} to lake sediments can stimulate CH_4 production to the same degree as additions of OM_{aq}, and ancient terrestrial OM has been shown to support aquatic respiration and food webs (McCallister and del Giorgio 2012; Guillemette et al. 2017*a*).

Due to the complex nature of OM and OM degradation, the categorization of OM into source is a useful approach to address the major compositional differences expected in aquatic vs. terrestrial derived OM, and to categorize assumed lability. Further, for managed systems such as reservoirs, this grouping provides a framework to assess potential CH_4 mitigation efforts. For example, if CH_4 production is driven primarily by OM_{terr}, efforts aiming to reduce CH_4 emissions should focus on the management of watershed OM inputs such as no-till agricultural practices and stream bank stabilization. On the other hand, if CH_4 production is driven primarily by OM_{aq}, efforts should focus on management of algal and cyanobacterial production, possibly through agricultural best management practices to reduce nutrient loading.

To address the role of carbon source (OM_{terr} vs. OM_{aq}) and quantity on sediment CH_4 production, we investigated methanogenesis rates, sediment OM characteristics, and methanogen communities across 15 sites within Harsha Lake, a eutrophic reservoir located in the midwestern United States, in the late spring of 2016. The objectives of the study were to: (1) establish if the three functional reservoir zones (lacustrine, transitional, and riverine) exhibit predictable patterns in CH_4 production rates, bulk sediment characteristics, sediment OM composition, and sediment methanogen communities, (2) determine the relative influence of OM source, including OM_{terr} vs. OM_{aq}, and OM quantity on sediment CH_4 production rates, and (3) identify the variables that best explain spatial variation in CH_4 production rates from a suite of sediment, water column, and methanogen community measurements. We expected that sediment methanogenesis rates would be highest in the riverine zone, intermediate in the transition zone, and lowest in the lacustrine

zone. Based on direct and indirect evidence of the relationship between aquatic-derived carbon and methanogenesis rates, we hypothesized that the source of OM would best predict methanogenesis rates, with the highest rates associated with high sediment OM_{aq} content due to its presumed greater lability as compared to OM_{terr}. Methanogen abundance was expected to be highest in sites with high CH_4 production rates, and methanogen community composition was expected to vary spatially along the riverine-lacustrine gradient.

METHODS

Site description

William H. Harsha Lake is a reservoir in southwest Ohio that was built on the East Fork of the Little Miami River in 1978. Harsha Lake is located in the ancestral homelands of the Miami, Shawnee, Deleware, and Ojibwe people. The primary functions of this reservoir include flood control, drinking water supply, recreation, and wildlife habitat. It has a surface area of 7.9 km^2, is dimictic, and reaches 32.8 m at its maximum depth. Harsha Lake's watershed is 882 km^2, with agriculture (including corn, soybean and pasture) as the dominant land-use (Beaulieu et al. 2016). Harsha Lake was an ideal system for this study because the surface CH_4 emission rates of this reservoir have been quantified previously, and emission hot spots have been identified (Beaulieu et al. 2014*a*, 2016; Beaulieu et al. 2018). Both CH_4 emissions and summer chlorophyll *a* concentrations are typically highest in the riverine zone near the main tributary of the reservoir (Beaulieu et al. 2016; Beck et al. 2017).

Sample collection

Triplicate sediment cores, water samples, and water column measurements were collected from 15 sites across the reservoir (Fig. 1). Sites were selected to span the length of the reservoir

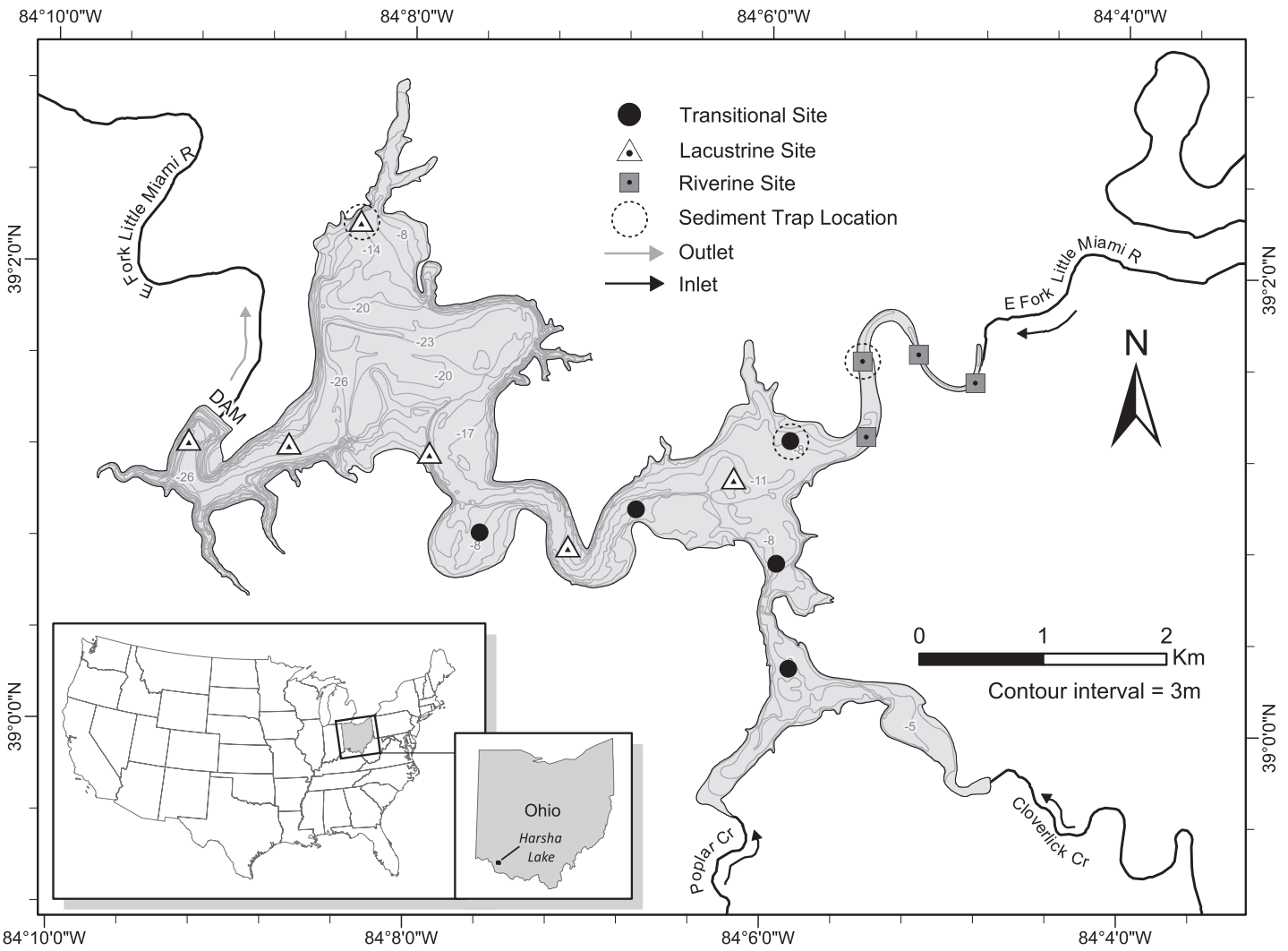

Fig. 1. Harsha Lake sampling sites and site categories. The legend indicates which sites were assigned to the riverine, transitional, and lacustrine zones, and where sediment traps were deployed.

and encompass a range of water depths, temperature, oxygen, productivity, and inputs to the sediment. Sites were categorized into reservoir zones (riverine, transitional, or lacustrine) based on thermal stratification from temperature-depth profiles measured at each site in July 2016, when stratification was expected to be strongest. Thermally stratified sites with a hypolimnion thickness >1 m were defined as lacustrine. Weakly stratified sites with a hypolimnion thickness <1 m were categorized as transitional, and sites that were not stratified were defined as riverine (Saji 2008). Sediment and water sampling was conducted on three separate dates within a 7-day window in late May 2016. On each date, three 5 cm diameter sediment cores were collected from each of five sites distributed across the three reservoir zones using a K-B Corer (Wildco®). Shallow (0.1 m below water surface) and deep (0.5–2 m above sediment) water samples were collected at each site using a Niskin bottle. At each site, depth profiles of water temperature, pH, dissolved oxygen, specific conductivity were measured using a ProDSS multiparameter sonde (YSI), and depth profiles of chromophoric dissolved organic matter (CDOM), in vivo chlorophyll *a*, and turbidity were measured using a C3 Submersible Fluorometer (Turner Designs). Secchi depth and depth profiles of photosynthetically active radiation (PAR) (LiCor LI-250A) were also measured.

Water sample processing

Water samples collected from each site for chlorophyll *a*, total nitrogen (TN) and total phosphorus (TP) analyses were stored at 5°C and analyzed within 24 h, or frozen and analyzed within 28 d. Water samples for dissolved CH_4 were subsampled from the Niskin bottle—collected at both the shallow and deep water depths. Dissolved CH_4 was sampled using the headspace equilibration method, as described by Beaulieu et al. (2018). The spectrophotometric method was used to measure chlorophyll *a* following filtration (0.45 μm pore size) and acetone extraction (APHA 2012). TP was measured following acid persulfate digestion (Boren 2001) and TN was measured following alkaline persulfate digestion (Smith and Bogren 2003) using automated colorimetry (Lachat Instruments QuickChem 8000 Flow Injection Autoanalyzer).

Sediment processing

Sediment cores were sectioned and processed within 24 h of collection. The top 5 cm of each core was extruded, homogenized, and subsampled in a glove box under N_2 atmosphere. Subsamples of sediment were used for CH_4 potential production rate assays, sediment characterization, porewater collection, and nucleic acid extraction. The top sediment section was chosen for our study following similar sediment depths used for CH_4 potential production assays in previous studies (e.g., Schwarz et al. 2008; Duc et al. 2010; Grasset et al. 2018), and after conducting a pilot study to determine sample depth (Supporting Information Table S1). One slurry was prepared from each sediment core, resulting in three slurries per site. Sediment slurries for CH_4 potential production assays were prepared in the glove box by adding 15 mL of sediment and 15 mL of overlying core water to a 120 mL serum bottle using syringes with the tips cut off. Slurries were then capped with a rubber stopper, crimp sealed, and wrapped in aluminum foil. After subsampling for DNA extraction and sediment characterization, sediment was frozen at −80°C (for DNA extraction) or −20°C (for sediment characterization) until further analysis. Samples for porewater collection were stored at 4°C until the porewater was extracted (within 24 h of core subsampling).

Sediment slurries—CH_4 potential production rates

After removing the capped slurries from the glove box, the bottles were shaken vigorously for 2 min and purged with N_2 gas for 5 min to remove the initial dissolved CH_4. All slurries were stored in the dark at room temperature (~23°C) during the 9-day incubation. Eleven milliliter gas samples were taken on days 1, 2, 3, 5, 7, and 9. An equal volume of 11 mL of N_2 gas was returned to the serum bottle after each sampling to maintain pressure during the incubation. Gas samples were analyzed on a gas chromatograph (Bruker 450) equipped with a flame ionization detector (FID). Methane potential production rates for the slurries were calculated by accounting for dilution during sampling, then determining the change in moles of CH_4 over time. Methane potential production rates were expressed either normalized to sediment volume, sediment dry mass, or mass of sediment organic matter per slurry. Mass of sediment OM per slurry was calculated from the dry mass of the slurry multiplied by the percent OM determined from LOI of a sediment subsample taken from the core specifically for that purpose. Details of calculations are available at the Center for Open Science Open Science Framework (OSF) project page (https://osf.io/59hnj/).

$\delta^{13}C$ in CO_2 and CH_4—CH_4 production pathway

Stable isotope ratios of carbon ($\delta^{13}C$) in CO_2 and CH_4 were measured from gas sampled on the last day (day 9) of a subset of the CH_4 production assays to discern between dominant CH_4 production pathways. Analysis was carried out at the UC Davis Stable Isotope Facility. ^{13}C—CO_2 was measured on a ThermoScientific GasBench system interfaced to a ThermoScientific Delta V Plus isotope ratio mass spectrometer (IRMS) (ThermoScientific), and $\delta^{13}C$—CH_4 was measured on a ThermoScientific Precon concentration unit system interfaced to a ThermoScientific Delta V Plus IRMS (ThermoScientific). Precision of the ^{13}C—CO_2 measurement is 0.1‰, and of the ^{13}C—CH_4 measurement is 0.2‰ (stableisotopefacility.ucdavis.edu, accessed 01 September 2019).

The apparent fractionation factor (α_C) of $\delta^{13}C$ in CO_2 and CH_4 was used to estimate the dominant methanogenesis pathway (Whiticar et al. 1986; Conrad 2005) (Eq. 1):

$$\alpha_C = \frac{(\delta CO_2 + 10^3)}{(\delta CH_4 + 10^3)} \quad (1)$$

Apparent fractionation factor values greater than 1.065 indicate that hydrogenotrophic methanogenesis is the dominant pathway, while $\alpha_C < 1.055$ are indicative of acetoclastic methanogenesis (Whiticar et al. 1986; Whiticar 1999; Conrad 2005).

Sediment characterization

Sediment was dried at 60°C for 3 d or until constant weight, and the difference between the wet and dry sediment weight was used to determine water content. Dried sediment was ground with a ceramic mortar and pestle prior to all other analyses. Elemental analysis and stable isotope analysis (^{13}C and ^{15}N) were conducted using an elemental analyzer coupled to an isotope ratio mass spectrometer (EA-IRMS). Sediment was fumigated with hydrochloric acid prior to C and ^{13}C analysis to removed carbonates (Harris et al. 2001). Analysis with EA-IRMS was conducted at the UC Davis Stable Isotope Facility (Elementar Vario EL Cube, Elementar Analysensysteme GmbH interfaced to a PDZ Europa 20–20 isotope ratio mass spectrometer, Sercon Ltd.) or the Stable Isotope Geochemistry Lab in the Department of Geology in the University of Cincinnati (Costech Instruments Elemental Analyzer periphery interfaced to a Thermo Scientific Delta V Advantage Isotope Ratio Mass Spectrometer). An analytical intercomparison between laboratories verified that the different instruments used gave consistent elemental and isotopic results. Precision of the ^{13}C and ^{15}N measurements are 0.2‰ and 0.3‰, respectively (see stableisotopefacility.ucdavis.edu, accessed 01 September 2019). Reference standards USGS-40 and USGS-41 were used to calibrate $\delta^{13}C$ and $\delta^{15}N$ values and checked with previously quantified internal lab standards (glycine and organic wheat). NIST Standard 2710 was used for linearity corrections for both $\delta^{13}C$ and $\delta^{15}N$ at the University of Cincinnati. Density was calculated from the wet weight of a known volume of sediment. OM content was calculated by determining weight loss after ignition (550°C, 4 h). Elemental and isotopic composition of sediment was used to determine the proportion of OM_{aq} and OM_{terr} (see *Mixing model*).

Porewater analyses

Porewater was extracted from a subsample of sediment cores for determination of volatile fatty acids (VFA), dissolved organic carbon (DOC), and for excitation emission matrix (EEMs) fluorescence. Porewater was extracted by centrifuging sediment in 50 mL polypropylene centrifuge tubes at 7800 rpm. The porewater was filtered at 0.45 μm prior to measurement of optical absorbance and fluorescence using a scanning spectrofluorometer (Horiba Aqualog UV-800). The optical data were used to calculate the fluorescence index (FI), biological index (BIX), relative fluorescence efficiency (RFE), humification index (HIX), and the specific ultraviolet absorbance at 254 nm ($SUVA_{254}$), all of which provide information about the composition and source of DOM. FI is calculated as the ratio of emission wavelengths 470 nm/520 nm at excitation 370 (McKnight et al. 2001). BIX is the ratio of emission wavelengths 380 nm/430 nm at excitation 310 nm (Huguet et al. 2009). RFE is the ratio of fluorescence at excitation 370 nm and emission 460 nm to the absorbance at 370 nm (Downing et al. 2009). HIX is defined as the area under the emission spectra between 435 and 480 nm divided by the sum of the peak area at 300–345 nm and 435–480 nm at excitation 254 nm (Ohno 2002). Due to lack of available excitation emission pairs at every wavelength combination, we used a slight modification of the HIX calculation with all values within 2 nm of the published method (Ohno 2002). $SUVA_{254}$ is the absorbance at 254 nm divided by DOC concentration (Weishaar et al. 2003). A summary of these and other optical properties is described by Hansen et al. (2016).

Sediment traps

Sediment traps were deployed at three of the 15 sampling sites (one per reservoir zone, Fig. 1) to determine sedimentation rates and composition of the water column particulates. Sediment traps were deployed for 6 weeks during the summer of 2016, with the initial deployment in early June 2016. Traps were constructed using 5 cm PVC pipe that were capped at the bottom with a height to diameter ratio of 5:1 (following Bloesch and Burns 1980), and were deployed 2 m from the sediment surface for the transitional and lacustrine sites, and 1.5 m above the sediment for the riverine site due to the shallow water depth at this location. Preservatives to prevent degradation of the material in the sediment traps were not used, but traps were sampled weekly to minimize OM decomposition. During trap sampling, samples were stored on ice or at 4°C in the dark until filtered (within 24 h). If necessary, the tubes were scrubbed with a brush before redeployment of the trap. Sedimentation rates were determined by calculating the total solids (TS) per sediment trap area and dividing by the number of days the trap was deployed. OM, chlorophyll *a*, elemental composition (C, N) and stable isotope composition (^{13}C and ^{15}N) for a subset of the samples were measured to evaluate the composition of the sediment trap material, using the methods described earlier.

DNA extraction

DNA was extracted from ~500 mg (wet weight) of sediment from each core using a MoBio PowerSoil® DNA Isolation Kit (MoBio) following the manufacturer's protocol. DNA concentration was determined using a Qubit dsDNA HS Assay kit and a Qubit 3.0 Fluorometer (Invitrogen). DNA was used in *Microbial community analysis* and *qPCR*.

Microbial community analysis

The V4 region of the 16S rRNA gene was amplified and sequenced using the paired-end Illumina MiSeq sequencing platform with the primers 515f and 806rB (Caporaso et al. 2012; Apprill et al. 2015). All sequencing was performed at the Center for Bioinformatics & Functional Genomics at Miami

University. The resulting sequences were subjected to quality control, alignment to the SILVA (v128) database, chimera check, and classification of operational taxonomic units (OTUs) at a sequence identity of 97% using the mothur software (v1.39.5) (Schloss et al. 2009) following the MiSeq SOP protocol from Kozich et al. 2013 (accessed 28 February 2017). All sequences from two sediment cores (one from site T2 and one from site T5) were removed during quality control steps in mothur and were not included in the results. One OTU from an unclassified methanogen order with only one identified sequence was excluded from analysis. Figures for visualizing community data were generated using phyloseq v.1.20.0 (McMurdie and Holmes 2013) and ampvis v.1.27.0. (Albertsen et al. 2015). Raw sequence reads for each sample are available on NCBI Short Read Archive (SRA) under the BioProject number PRJNA532292.

qPCR

Quantitative polymerase chain reactions (qPCR) were performed to determine the abundance of *mcrA* (a biomarker for methanogens), and archaeal 16S rRNA genes on a StepOne Plus ™ Real-Time PCR System. *mcrA* encodes a protein necessary for methanogenesis and has been widely used as a marker for methanogens (Luton et al. 2002). *mcrA* was quantified using the degenerate primers mcrA-F(5′-GGTGGTGTMGGATT CACACARtAYGCWACAGC-3′) and mcrA-R (5′-TTCATTGC RTAGTTWGGRTAGTT-3′) (Luton et al. 2002). Each 20 μL SYBR qPCR reaction contained 2x SYBR Green PCR Universal Master Mix (Applied Biosystems), 2 μL of DNA (prediluted to 2 ng/μL), and 500 nM of the forward and reverse primers using the following cycling conditions: 40 cycles of 15 s at 95°C followed by 60 s at 55°C. A TaqMan probe and primer set developed by Yu et al. (2005) were used to quantify total archaea. TaqMan qPCR assays (20 μL final volume) consisted of 2x TaqMan PCR Universal Master Mix (Applied Biosystems), 500 nM of the forward and reverse primers, 200 nM of the TaqMan probe, and 2 μL of DNA (prediluted to 2 ng/μL) and were performed using the following cycling conditions: 45 cycles of 15 s at 95°C followed by 60 s at 60°C. The standard curve for the SYBR green assay was constructed using an *mcrA* clone (Promega pGEM® -T Easy Vector with JM109 High Efficiency Competent Cells) from environmental DNA. Briefly, *mcrA* was PCR-amplified from a Harsha Lake sediment DNA sample, purified (Wizard® PCR Preps DNA Purification System, Applied Biosystems), inserted into a vector, transformed into JM109 High Efficiency Competent Cells, and then the vector was isolated (Wizard® Plus SV Minipreps DNA Purification System, Applied Biosystems). Manufacturer's instructions were followed for each step. Standard curves for archaeal 16S rRNA genes were constructed from a PCR-amplified 16S rRNA gene from a pure archaeal culture and purified (Wizard® PCR Preps DNA Purification System). The vector and purified PCR product were quantified as described earlier. The copy number of each gene was normalized by the concentration of DNA and the grams of sediment (wet weight) used in the DNA extraction.

Statistical methods and data analysis

All statistical analyses were performed using R version 3.4.0 (R Core Team 2017). Mixed effects (ME) linear models with Satterthwaite approximations for degrees of freedom (Luke 2017) were used to evaluate the effect of reservoir zone on CH_4 potential production and sediment characteristics using the lme4 package (Bates et al. 2015), and differences among least squares means of the zones were compared using the lmerTest package (Kuznetsova et al. 2016). This model structure nests replicate cores within each of the 15 sampling sites, thereby accounting for the likelihood that measurements from replicate cores are more likely to be related to each other than to measurements from cores at other sites.

To evaluate the factors that best explain variation in CH_4 potential production rates, an information-theory approach was used (Anderson 2008). ME linear models with site as a random factor were created using the nlme package (Pinheiro et al. 2017) as described in Zuur et al. (2009). Mixed effects linear models were generated to represent the following working hypotheses: (1) CH_4 production rates are best explained by OM source, (2) CH_4 production rates are best explained by OM quantity, and (3) CH_4 production rates are best explained by the combination of OM source and quantity. All models used CH_4 potential production rates per unit volume of sediment as the response variable. Candidate predictor variables included a large suite of measurements of water column and sediment characteristics at each site, partitioned into variables indicating "OM quantity" or "OM source." All predictors were considered in the "source and quantity model." The full list of variables can be found in Supporting Information Table S2 or at the OSF repository (https://osf.io/59hnj/). Multicollinearity among predictor variables for each model was assessed using variance inflation factor (VIF) scores, and variables with scores higher than 3 were excluded from models (Zuur et al. 2010). Variable selection for each model was conducted using a backward selection approach (Diggle et al. 2002) and all models were compared against the "null" (intercept-only) model. The final model representing each hypothesis was ranked based on AIC score corrected for the number of estimated parameters (AICc). Akaike weights (w_i) representing the relative likelihood of the model, evidence ratios ($E_{i,j}$), and AICc values were calculated as described by Anderson (2008).

In addition, partial least square (PLS) regression analysis was used to investigate which measured parameters best explained variation in CH_4 potential production rates. PLS regression was conducted using the R package "plsdepot" (Sanchez 2012). One response variable, CH_4 potential production rates per unit sediment volume (μmol CH_4 cm^{-3} d^{-1}), was used. Explanatory variables included water column variables (water chemistry, temperature, dissolved oxygen, chlorophyll, etc.), sediment variables (density, OM content, OM source,

etc.), and biological variables (percentage of different methanogen genera). The full list of variables can be found in Supporting Information Table S3 and at the OSF repository (https://osf.io/59hnj/).

Mixing model for determining contribution of OM_{aq} and OM_{terr} to sediment OM

A Bayesian mixing model was used to determine the proportion of OM_{aq} and OM_{terr} found in each sediment sample. The mixing model was generated using the MixSIAR package version 3.1.7 (Stock and Semmens 2013) in R. In this R package, estimation uncertainty of the means and variances for end-members is incorporated into the model (Stock et al. 2018). Uncertainty associated with each of the predicted values (proportion of OM_{aq} for each core) is estimated, and the values presented here are mean proportion estimates. Terrestrial and aquatic end-members were collected, and elemental N:C ratios and $\delta^{15}N$ were analyzed using EA-IRMS (see *sediment characterization*). Terrestrial end-member samples were collected from the surrounding watershed and included stream-bank soil, leaf litter, corn field soil, and corn stalk litter from tributary streams and a field along the perimeter of the reservoir. Aquatic end-members were from shallow water samples from each of the 15 sites collected at the same time of sediment sampling (collected as described earlier). Between 60 and 200 mL of water were filtered through preashed 0.7 μm Whatman GF/F glass fiber filters and dried at 55°C before packing into capsules for elemental and isotopic analysis. Shallow water samples from all sites were included in the determination of N:C ratios and $\delta^{15}N$ values for the aquatic end-member to account for potential compositional variation of algae and cyanobacteria across the reservoir. Chlorophyll *a* (as determined by both in vivo fluorescence and extracted pigment absorbance) was greater than 16.0 $\mu g\ L^{-1}$ at all but one of the sites at the time of sampling, indicating that a substantial fraction of the OM was algal or cyanobacterial biomass.

RESULTS

Site characteristics

The water column depth at the sampling sites ranged from 2.5 to 31 m (Table 1). The depth of the water column averaged 3.6 m in the riverine zone, 9.6 m in the transitional zone, and 20.3 m in the lacustrine zone. All sites were nutrient rich, with surface TN concentrations ranging from 1210 to 2040 $\mu g\ L^{-1}$ and TP concentrations ranging from 166 to 232 $\mu g\ L^{-1}$. The riverine zone had the highest average TN and TP concentrations at the surface (1745 and 210 $\mu g\ L^{-1}$, respectively), and the lacustrine zone had the lowest average concentrations (1380 and 180 $\mu g\ L^{-1}$, respectively). Similarly, average surface chlorophyll *a*, measured by in vivo fluorescence and from extracted pigment absorbance was highest in the riverine zone (4128 RFUB and 47.6 $\mu g\ L^{-1}$, respectively), lowest in the transitional zone (1021 RFUB and 21.8 $\mu g\ L^{-1}$), and intermediate in the lacustrine zone (1877 RFUB and 24.3 $\mu g\ L^{-1}$). Secchi depth increased from the riverine zone (average 0.33 m) to the lacustrine zone (average 0.78 m). The full suite of chemical and physical measurements at each site can be found in the OSF repository.

Methane potential production rates among reservoir zones

Methane potential production rates normalized by sediment volume and by quantity of OM were greater in the riverine zone as compared to the transitional or lacustrine zones ($\mu mol\ CH_4\ cm^{-3}\ d^{-1}$; $F_{2,12} = 12.89$, $p = 0.001$, and $\mu mol\ CH_4\ g\ OM^{-1}\ d^{-1}$; $F_{2,12} = 10.26$, $p = 0.003$) (Fig. 2a,b). Methane potential production rates normalized by dry weight of the sediment slurry were not statistically different among the zones ($F_{2,12} = 2.03$, $p = 0.2$; Fig. 2c). The rate most comparable to CH_4 emissions from the air–water interface, the areal CH_4 potential production rate, was 3.79 $\mu mol\ CH_4\ cm^{-2}\ d^{-1}$ (mean for all cores; range: 0.79–8.56 $\mu mol\ CH_4\ m^{-2}\ d^{-1}$), assuming an active sediment depth of only 5 cm. As the areal CH_4 potential production rate was determined by multiplying the volume-normalized rate by the sampled depth (5 cm for all cores), the spatial variation in areal rate was the same as for the volume-normalized rate, that is, higher in the riverine zone than the other two zones ($F_{2,12} = 12.89$, $p = 0.001$).

Sediment characteristics among reservoir zones

Sediment density was greatest in the riverine zone, intermediate in the transitional zone, and lowest in the lacustrine zone (Table 2), and while the ME model indicated significant differences among zones ($F_{2,12} = 12.3$, $p = 0.001$), the differences between the lacustrine and transitional zone were not statistically significant ($p = 0.24$). Particulate sediment OM trended toward greater abundance in the riverine zone, but the pattern was not significant ($F_{2,12} = 2.02$, $p = 0.18$; Fig. 3a). The concentration of DOC in the sediment porewaters was greatest in the riverine zone ($F_{2,12} = 5.52$, $p = 0.02$; Fig. 3b). Stable isotope and elemental composition data indicated that the source of OM varied significantly among reservoir zones (Fig. 4). The ME linear model indicated that reservoir zone was significant in explaining variation in the proportion of OM_{aq} (calculated from the mixing model) in the bulk sediment ($F_{2,12} = 8.06$, $p = 0.006$). OM_{aq} was lowest in the riverine zone, intermediate in the transitional zone, and highest in the lacustrine zone, though the riverine and transitional zone were not significantly different ($p = 0.13$; Fig. 4).

The ratio of elemental C:N in the bulk sediment can indicate OM source, with higher C:N ratios resulting from terrestrial OM sources due to high C content of structural plant material, and lower C:N ratios resulting from algal and microbial sources. The average C:N ratio of sediment from the riverine zone was 9.6 ± 1.1, while the transitional and lacustrine zones had slightly lower ratios of 7.5 ± 1.0 and 7.4 ± 0.7, respectively (Table 2).

Table 1. Physical and chemical water column properties for each of the sampling sites. Mean values for each zone are shown in bold at the bottom of the table.

Site	Site Depth (m)	Reservoir zone	Secchi depth (m)	Sample depth (m)	Temperature (°C)	Dissolved oxygen (% saturation)	pH	Chlorophyll *a* (μg L^{-1})	Chlorophyll *a* (in vivo) (RFUB*)	CDOM (RFUB*)	TN (μg L^{-1})	TP (μg L^{-1})	Dissolved CH_4 (μM)	SO_4^{2-} (mg L^{-1})
R1	2.5	Riverine	0.22	0.1	27.3	76.1	7.91	-	457	1743	1210	172	7.50	-
				1.5	26.7	58.7	7.56	-	526	1994	1488	210	2.28	16.2
R2	3.0	Riverine	0.38	0.1	22.9	90.3	8.20	4.8	346	2102	2000	232	0.92	-
				2.0	16.3	74.5	7.81	3.2	455	2176	2240	244	1.09	21.7
R3	4.0	Riverine	0.33	0.1	24.1	174.2	8.98	74.2	6958	2036	2040	227	1.33	-
				3.0	19.1	39.3	7.58	1.8	437	2170	2280	287	3.19	18.3
R4	5.0	Riverine	0.40	0.1	22.7	163.5	8.90	63.9	8750	1926	1730	210	1.41	-
				4.0	21.9	133.7	8.47	31.6	8054	2068	1600	185	2.23	17.6
T1	9.0	Transitional	0.52	0.1	27.0	139.5	8.80	-	430	2197	1410	182	1.09	-
				8.0	17.2	3.0	7.45	-	352	2133	1475	216	0.87	16.1
T2	9.0	Transitional	0.68	0.1	26.7	147.3	8.83	-	495	2182	1400	201	0.88	-
				8.0	17.2	3.8	7.35	-	346	2174	1288	203	3.89	15.5
T3	9.0	Transitional	0.73	0.1	22.8	84.0	7.85	18.6	779	1894	1490	220	0.37	-
				8.0	17.1	35.5	7.39	1.7	387	2076	1510	211	0.11	17.7
T4	10.0	Transitional	0.53	0.1	20.4	108.7	8.29	30.4	2333	2184	1490	199	0.47	-
				9.0	16.8	31.7	7.39	5.4	436	2091	1490	216	0.18	17.4
T5	11.0	Transitional	0.80	0.1	19.8	85.5	8.12	16.4	1068	1954	1400	194	0.09	-
				10.0	16.9	31.5	7.36	1.8	286	2140	1520	220	0.00	16.5
L1	12.0	Lacustrine	0.60	0.1	21.4	122.4	8.78	29.2	3620	1983	1380	166	0.28	-
				10.5	16.7	30.4	7.15	0.8	303	2146	1710	B.D.	0.16	21.4
L2	14.0	Lacustrine	0.53	0.1	21.7	143.0	8.56	32.0	3035	1951	1330	167	0.31	-
				12.0	15.6	12.0	7.08	1.9	288	2105	1710	194	0.00	19.7
L3	16.5	Lacustrine	1.04	0.1	27.7	232.7	9.25	-	418	1937	1750	185	0.28	-
				13.5	14.7	1.0	7.28	-	255	1910	1249	215	1.39	13.7
L4	22.5	Lacustrine	0.87	0.1	26.5	198.0	9.25	-	286	1995	1250	188	0.18	-
				19.0	11.0	8.2	7.28	-	237	1968	4575	46	9.23	13.3
L5	26.0	Lacustrine	1.00	0.1	19.5	82.7	7.90	16.0	1078	1881	1320	195	0.23	-
				24.0	10.4	9.5	7.04	0.5	225	1898	1270	248	3.89	13.7
L6	31.0	Lacustrine	0.67	0.1	21.6	133.3	8.57	19.9	2827	1831	1250	177	0.20	-
				24.5	10.3	0.9	6.81	0.5	232	1891	1330	254	0.27	14.4
	3.6	**Riverine**	**0.33**	**Surface**	**24.3**	**126.0**	**8.50**	**47.6**	**4128**	**1952**	**1745**	**210**	**2.79**	-
				Deep	**21.0**	**76.6**	**7.86**	**12.2**	**2368**	**2102**	**1902**	**231**	**2.19**	**18.5**
	9.6	**Transitional**	**0.65**	**Surface**	**23.3**	**113.0**	**8.38**	**21.8**	**1021**	**2082**	**1438**	**199**	**0.58**	-
				Deep	**17.0**	**21.1**	**7.39**	**3.0**	**362**	**2123**	**1457**	**213**	**1.01**	**16.6**
	20.3	**Lacustrine**	**0.78**	**Surface**	**23.1**	**152.0**	**8.72**	**24.3**	**1877**	**1930**	**1380**	**180**	**0.25**	-
				Deep	**13.1**	**10.3**	**7.11**	**0.9**	**257**	**1986**	**1974**	**191**	**2.49**	**16.0**

Cells with no values were not measured for the given parameter. B.D. values were below detection.
*RFUB are blank-subtracted raw fluorescence units from a submersible fluorometer.

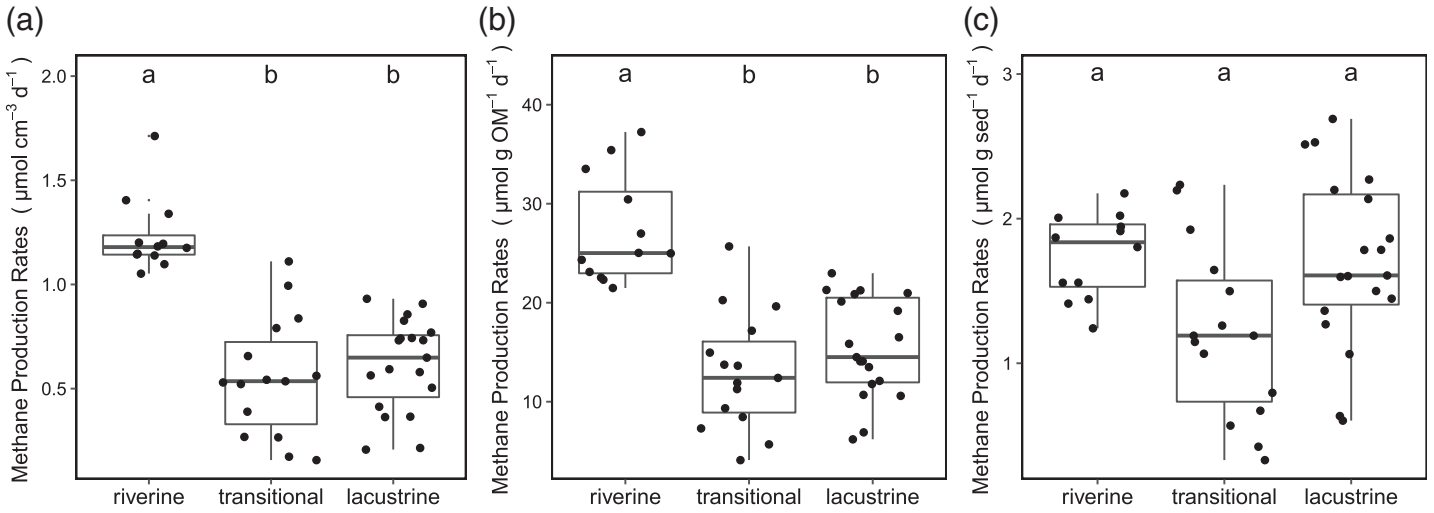

Fig. 2. Methane potential production rates from sediment slurries in each of the reservoir zones, normalized to sediment volume (**a**), sediment organic matter (**b**), and sediment dry mass (**c**). Dots represent the potential CH_4 production rate calculated from each sediment core by a sediment slurry assay. Different lowercase letters indicate significant differences between reservoir zones.

Optical properties of the porewater dissolved OM showed some evidence of differences in DOM source across reservoir zones (Fig. 5; Table 3). Mean site FI values ranged from 1.60 to 1.74, which is on the upper end of the range found in natural waters (1.2–1.8; Hansen et al. 2016), with higher FI values indicating DOM derived from microbial sources (e.g., bacteria and algae) and lower values indicating DOM derived from terrestrial OM (McKnight et al. 2001; Cory et al. 2010). FI values were highest in the riverine zone, indicating a higher proportion of microbial sources as compared to the lacustrine and transitional zones ($F_{2,12.2} = 14.02$, $p = 0.0007$). BIX values, an indicator of autotrophic productivity, did not vary among reservoir zones ($F_{2,12.1} = 1.53$, $p = 0.2$), with site averages ranging from 0.59 to 0.71 (Table 3). A BIX of 0.6–0.7 indicates a low autochthonous component, 0.7–0.8 an intermediate autochthonous component, and higher values indicate increasing contribution of autochthonous sources (Huguet et al. 2009). HIX and $SUVA_{254}$ are both representative of the amount of processing that the DOM has undergone, with higher values representing more humification and higher aromatic content of the OM, respectively (Hansen et al. 2016). The HIX values present in Harsha Lake sediment porewaters were explained by reservoir zone, with averages of 0.72, 0.83, and 0.82 for riverine, transitional, and lacustrine sites ($F_{2,12.2} = 6.51$, $p = 0.01$), respectively. The riverine zone had lower HIX values than the transitional ($p = 0.006$) and lacustrine ($p = 0.009$) zones, while the transitional and lacustrine zones did not differ from each other ($p = 0.73$; Fig. 5). Differences in porewater $SUVA_{254}$ values across all zones were statistically significant ($F_{2,12.9} = 10.74$, $p = 0.002$; Fig. 5). Mean $SUVA_{254}$ was 2.7 L mg-C^{-1} m^{-1} in the riverine zone, 4.2 L mg-C^{-1} m^{-1} in the transitional zone, and 5.5 L mg-C^{-1} m^{-1} in the lacustrine zone.

Sediment deposition rates and deposited sediment composition

Over the 6-week sediment trap deployment period, average sediment deposition rates were highest in the riverine sediment trap site, and lowest in the lacustrine sediment trap site (Table 4). Similar to the benthic sediment, the percent OM of the deposited sediment was lowest in the riverine site (12.3%), intermediate in the transitional site (16.7%), and highest in the lacustrine site (22.5%), but due to the high sedimentation rates, the riverine sediment trap had the highest OM deposition rates. Further, the mean rate of chlorophyll deposition in the riverine sediment trap for the 6-week period exceeded that of the transitional and lacustrine sites (Table 4).

Methanogen communities among reservoir zones

Abundance of the *mcrA* gene and a region of the 16S rRNA gene targeting archaea were determined using qPCR. Copies of *mcrA* ranged from 1.4×10^1 to 3.8×10^4 ng DNA^{-1} g sediment^{-1} (wet weight), with a mean of 3.7×10^3. There were no differences among reservoir zones in copy number for either the *mcrA* gene ($F_{2,12.4} = 0.06$, $p = 0.94$) or the archaeal 16S rRNA gene ($F_{2,12.1} = 1.28$, $p = 0.31$).

From 16S rRNA gene sequencing, 5708 archaeal OTUs were observed across 44 sediment cores. Of the 5708 archaeal OTUs, 939 were assigned to methanogens (16%). Sequences affiliated with four of the six known orders of methanogens were recovered from the Harsha Lake sediments: Methanomicrobiales (606 OTUs), Methanosarcinales (218 OTUs), Methanobacteriales (105 OTUs), and Methanocellales (9 OTUs). On average, methanogens represented 35% of total archaea when calculated from 16S rRNA sequence data, and 34% of total archaea when calculated from qPCR data. Representative OTUs from the order Methanomicrobiales accounted for 53%, 77%, and 76% of total

Table 2. Bulk sediment characteristics for each of the 15 sites. Values are reported as mean ± SD. Mean values for each zone are in bold.

Site	Reservoir zone	CH_4 production rates (μmol cm^{-3} d^{-1})	$\%C_{org}$	$\delta^{13}C_{org}$ (‰)	%N	$\delta^{15}N$ (‰)	C_{org}:N(g:g)	OM (% dry weight)	Density (g mL^{-1})	Proportion autochthonous OM
R1	Riverine	1.10±0.05	1.90±0.11	−26.11±0.42	0.19±0.01	5.35±0.04	10.01±0.79	6.02±0.45	1.66±0.26	0.54±0.00
R2	Riverine	1.36±0.30	2.22±0.18	−26.20±1.10	0.22±0.02	5.25±0.34	10.03±1.76	6.93±0.44	1.36±0.08	0.54±0.01
R3	Riverine	1.31±0.11	1.90±0.26	−25.44±0.28	0.21±0.03	5.68±0.10	8.91±0.76	5.23±0.99	1.45±0.06	0.56±0.00
R4	Riverine	1.16±0.02	2.37±0.15	−25.84±0.52	0.25±0.01	5.68±0.05	9.34±0.79	7.91±0.16	1.35±0.02	0.56±0.00
T1	Transitional	0.97±0.16	2.2±0.22	−25.44±0.47	0.28±0.02	5.75±0.25	8.00±1.00	9.02±0.68	1.2±0.03	0.56±0.01
T2	Transitional	0.55±0.01	2.16±0.24	−25.79±0.51	0.29±0.00	5.86±0.22	7.54±0.92	9.32±0.12	1.2±0.03	0.56±0.01
T3	Transitional	0.36±0.18	1.98±0.40	−25.72±0.26	0.27±0.01	6.01±0.40	7.32±1.30	8.41±0.32	1.27±0.01	0.56±0.01
T4	Transitional	0.67±0.16	2.41±0.28	−25.82±0.41	0.34±0.01	5.73±0.10	7.04±1.06	10.67±0.58	1.21±0.01	0.55±0.01
T5	Transitional	0.23±0.06	1.92±0.23	−26.54±0.38	0.26±0.00	6.23±0.13	7.39±0.95	7.73±0.26	1.26±0.01	0.57±0.01
L1	Lacustrine	0.86±0.1	2.29±0.24	−25.32±0.49	0.29±0.01	6.25±0.18	7.86±0.99	9.34±0.11	1.29±0.01	0.58±0.00
L2	Lacustrine	0.72±0.06	2.51±0.3	−25.38±0.48	0.34±0.01	6.12±0.18	7.49±1.16	10.85±0.21	1.23±0.03	0.57±0.00
L3	Lacustrine	0.26±0.09	2.46±0.03	−26.43±0.46	0.31±0.01	6.38±0.02	7.89±0.24	9.62±0.38	1.08±0.02	0.58±0.00
L4	Lacustrine	0.65±0.14	2.72±0.19	−25.95±0.73	0.37±0.01	6.14±0.34	7.44±0.62	11.49±0.77	1.13±0.03	0.57±0.01
L5	Lacustrine	0.66±0.22	2.90±0.28	−26.17±1.14	0.44±0.02	6.06±0.30	6.63±0.37	11.73±1.12	1.17±0.01	0.56±0.01
L6	Lacustrine	0.54±0.19	3.27±0.11	−26.24±1.13	0.45±0.00	6.24±0.25	7.21±0.20	12.90±0.26	1.05±0.02	0.57±0.01
	Riverine	**1.23±0.18**	**2.1±0.26**	**−25.9±0.64**	**0.22±0.03**	**5.49±0.25**	**9.57±1.07**	**6.52±1.16**	**1.45±0.18**	**0.55±0.01**
	Transitional	**0.56±0.29**	**2.15±0.3**	**−25.86±0.52**	**0.29±0.03**	**5.92±0.28**	**7.46±0.95**	**9.03±1.09**	**1.23±0.03**	**0.56±0.01**
	Lacustrine	**0.62±0.22**	**2.7±0.37**	**−25.91±0.79**	**0.37±0.06**	**6.19±0.24**	**7.42±0.73**	**11.02±1.34**	**1.16±0.09**	**0.57±0.01**

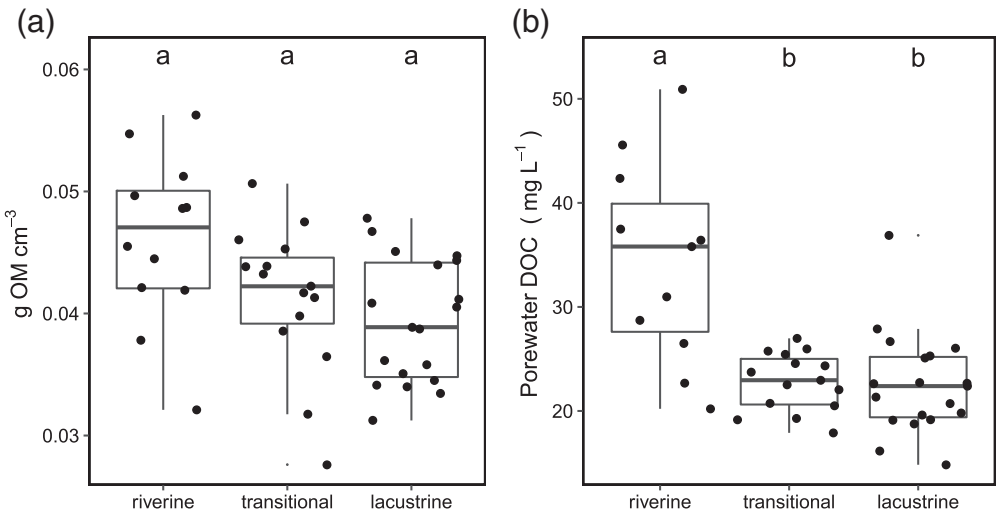

Fig. 3. Comparison of the quantity of OM among reservoir zones. (**a**) The amount of OM found in the bulk sediment, normalized to sediment volume. (**b**) The concentration of the dissolved fraction of OM found in the sediment porewater, measured as dissolved organic carbon (DOC). One riverine value with an exceptionally high DOC concentration (310 mg L^{-1}) was excluded from the plot for readability. Different lowercase letters indicate significant differences between reservoir zones.

methanogen sequences from the riverine, transitional, and lacustrine zones, respectively (Fig. 6). The order Methanosarcinales comprised 34%, 16%, and 17% of riverine, transitional, and lacustrine methanogens, respectively. The two most abundant methanogen genera in all three zones were *Methanoregula* and *Methanosaeta*. *Methanobacterium* was relatively abundant in all three zones, whereas *Methanosarcina* and *Methanospirillum* composed a greater proportion of methanogen genera in the riverine than in other zones.

Methane production pathway

$\delta^{13}C$ of CH_4 ranged from −56.7 to −48.0‰, and values were not explained by reservoir zone ($F_{2,7}$ = 4.52, p = 0.06; Fig. 7a). Apparent fractionation factors (α_C) were consistent with acetoclastic methanogenesis across all zones (range 1.040–1.050). The isotope fractionation trended slightly higher in the lacustrine zone relative to the riverine zone (higher α_C; Fig. 7b), suggesting an increased contribution of hydrogenotrophic methanogenesis in the lacustrine zone compared to the other two zones.

Influence of OM source and quantity on CH_4 potential production rates

The ME model relating CH_4 potential production rates to a combination of OM source and quantity indices was supported more strongly by the data than the models representing the "OM source" only or the "OM quality" only

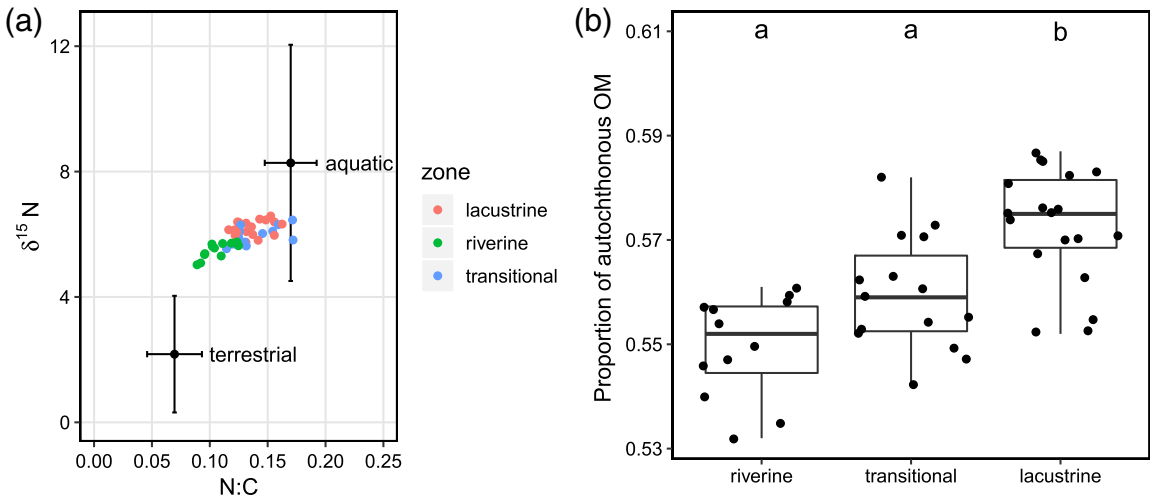

Fig. 4. (**a**) Plot of $\delta^{15}N$ vs. N:C elemental ratios of terrestrial and aquatic OM sources, and the sediment mixtures for each core across the three reservoir zones. The center dots for the two sources represent the mean values (n = 13 for terrestrial sources, n = 16 for aquatic sources), and error bars represent the standard deviation. (**b**) The proportion of autochthonous (aquatic) OM found in each core grouped by reservoir zones, as calculated from the stable isotope mixing model. Different lowercase letters indicate significant differences among reservoir zones.

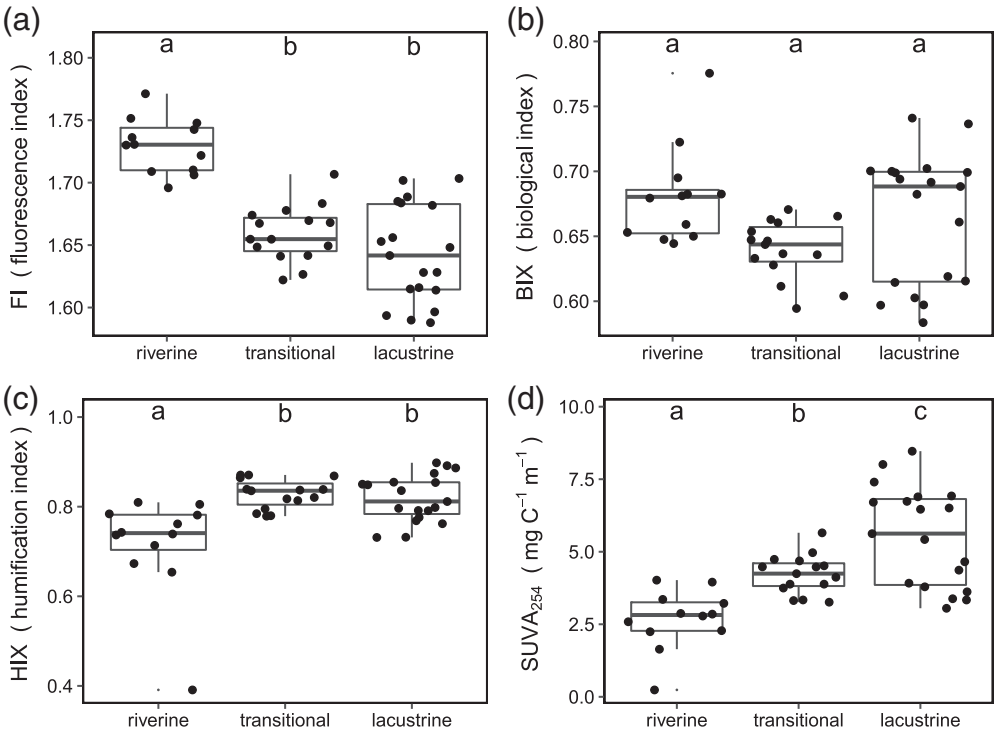

Fig. 5. Optical indices of dissolved organic matter. Higher FI values (**a**) indicate DOM from microbial sources, and higher BIX values (**b**) indicate a stronger OM_{aq} signature. Higher HIX (**c**) and $SUVA_{254}$ (**d**) values represent higher degrees of humification and aromatic content of the OM. Different lowercase letters indicate significant differences between reservoir zones.

hypotheses (model probability of 0.989, marginal R^2 = 0.70, Table 5). The best predictor variables for the "OM source" hypothesis were: (1) the proportion of OM_{aq} in the sediment and (2) BIX (biological index calculated from porewater DOM fluorescence). The best model for the "OM quantity" hypothesis included a single interaction term between the variables:

Table 3. Concentration and optical properties of the porewater DOM for each of the 15 sites. Values are reported as mean ± SD. Mean values for each zone are in bold.

Site	Reservoir zone	DOC (mg L^{-1})	FI	BIX	RFE	HIX	$SUVA_{254}$ (mg C^{-1} m^{-1})
R1	Riverine	28.73±2.24	1.73±0.01	0.65±0.00	1.33±0.06	0.74±0	2.89±0.32
R2	Riverine	134.49±152.23	1.73±0.04	0.69±0.07	1.09±0.18	0.64±0.22	1.59±1.32
R3	Riverine	39.26±5.47	1.72±0.02	0.69±0.02	0.7±0.18	0.68±0.03	3.01±0.86
R4	Riverine	26.79±9.34	1.74±0.02	0.69±0.01	0.9±0.07	0.8±0.01	3.21±0.90
T1	Transitional	23.9±1.47	1.69±0.02	0.65±0.01	1.28±0.13	0.85±0.02	3.31±0.04
T2	Transitional	24.59±2.21	1.66±0.01	0.64±0.01	0.82±0.1	0.84±0.03	3.84±0.08
T3	Transitional	21.45±2.77	1.65±0.03	0.63±0.02	0.89±0.02	0.82±0.04	4.37±0.33
T4	Transitional	24.76±2.04	1.66±0.01	0.67±0.00	0.63±0.06	0.78±0.01	5.04±0.59
T5	Transitional	19.27±1.42	1.64±0.01	0.61±0.02	0.89±0.09	0.84±0.02	4.56±0.11
L1	Lacustrine	22.9±3.56	1.69±0.01	0.70±0.00	0.51±0.26	0.8±0.01	6.08±2.44
L2	Lacustrine	19.23±0.53	1.66±0.04	0.69±0.00	0.57±0.16	0.83±0.03	6.52±1.01
L3	Lacustrine	20.85±1.75	1.60±0.01	0.59±0.01	0.83±0.37	0.87±0.02	5.03±1.67
L4	Lacustrine	26.75±7.04	1.61±0.02	0.61±0.01	1.08±0.08	0.87±0.02	3.49±0.37
L5	Lacustrine	26.09±1.56	1.65±0.01	0.70±0.00	0.38±0.14	0.75±0.03	5.96±1.13
L6	Lacustrine	17.87±4.17	1.66±0.04	0.71±0.05	0.38±0.15	0.77±0.02	6.85±1.46
	Riverine	**57.32±80.16**	**1.73±0.02**	**0.68±0.04**	**1.01±0.27**	**0.72±0.11**	**2.67±1.03**
	Transitional	**22.8±2.8**	**1.66±0.02**	**0.64±0.02**	**0.9±0.23**	**0.83±0.03**	**4.22±0.67**
	Lacustrine	**22.52±4.92**	**1.64±0.04**	**0.66±0.05**	**0.65±0.33**	**0.82±0.05**	**5.54±1.73**

Table 4. Sediment trap data. Sediment traps were deployed during the summer of 2016.

	Sediment deposition rates (g m^{-2} d^{-1})	Chlorophyll a deposition rates (mg m^{-2} d^{-1})	OM deposition rates (g OM m^{-2} d^{-1})	Sediment OM (%)	$\delta^{15}N$	$\delta^{13}C_{org}$	%N	$\%C_{org}$	C_{org}:N (g:g)
Riverine (R1)	473.02	67.77	63.51	12.32	5.87	−27.24	0.57	4.00	6.78
Transitional(T1)	60.34	10.05	9.46	16.70	6.03	−27.81	0.69	4.71	6.71
Lacustrine (L3)	16.33	4.87	3.76	22.52	4.59	−27.15	0.99	6.49	6.71

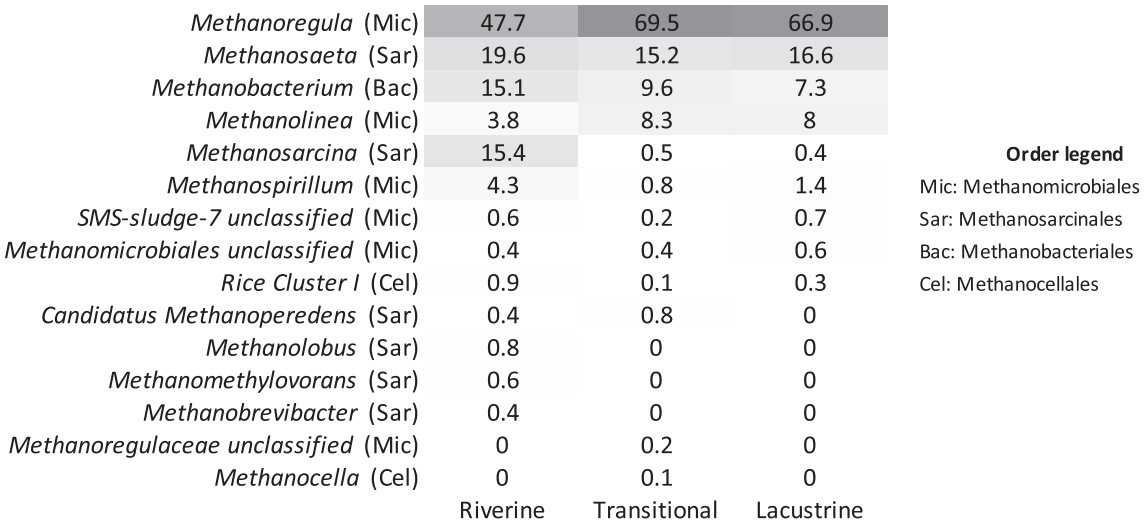

Fig. 6. Heat map showing relative abundance of methanogen genera in sediments, by reservoir zone. Row labels show the genus and order abbreviation in parentheses. Note that values are normalized to total number of sequences of all methanogens (not to total archaea), and that percentages are averages of all samples within a group (within the zone).

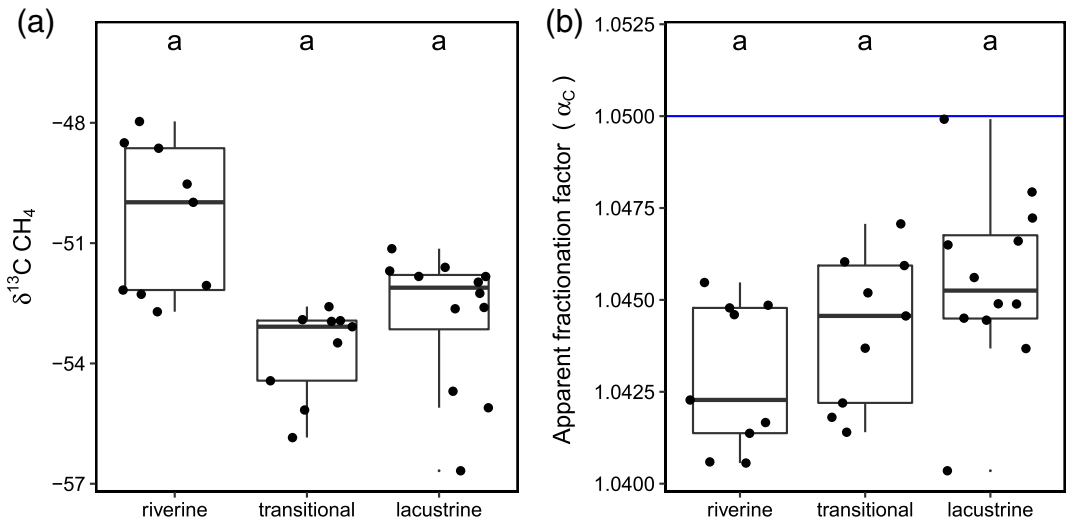

Fig. 7. Carbon isotope signature in CH_4 (**a**) and the apparent fractionation factors (**b**) across reservoir zones. The blue horizontal line in (**c**) indicates the cutoff between hydrogenotrophic (above) and acetoclastic (below) methanogenesis. Methane production pathway was estimated at 10 of the 15 sampling sites (n = 30 sediment cores). Different lowercase letters indicate significant differences between reservoir zones.

Table 5. Results of model hypothesis testing. The response variable was methane production rates (μmol CH4 cm^{-3} d^{-1}). Arrows next to predictor variables indicate a positive (↑) or negative (↓) relationship with the response variable. *K* is the number of estimated parameters, AICc is a second order AIC score used to account for the number of estimated parameters. Δ_i values are AICc differences (compared to the best model). Model probabilities (w_i), otherwise called Akaike weights, are estimates of the probability of the model being the best K-L (Kullback–Leibler) model, given the data and set of competing models (see Anderson 2008). The evidence ratios (Ei,j) measure the strength of evidence of the hypotheses and represent the relative likelihood of hypothesis *i* vs. *j*. In this case they represent the likelihood of the best model (H3) relative to the other models. Marginal R^2 describes the proportion of variance explained by fixed factors alone, and the conditional R^2 describes the proportion of variance explained by both fixed and random effects. Note that ranks, model probabilities, and evidence ratios (Ei,j) are relative to the set of models and dependent on the data used to create the models.

H	Hypothesis	Model	*K*	log(*L*)	AIC	AICc	Rank	Δ_i	Model probability w_i	$E_{i,j}$	Marginal R^2	Conditional R^2
H_1	Source OM	Autochthonous OM (↓)+BIX (↑)	5	13.53	−17.06	−15.56	2	9.6	0.0080	123.8	0.33	0.85
H_2	Quantity OM	log(DOC) (↑) * g OM $slurry^{-1}$ (↑)	6	13.76	−15.52	−13.37	3	11.8	0.0027	370.6	0.48	0.87
H_3	Source OM+ Quantity OM	Autochthonous OM + log(DOC) * g OM $slurry^{-1}$ + BIX	8	22.55	−29.09	−25.20	1	0.0	0.9893		0.70	0.89

(1) porewater DOC concentration and (2) g OM per unit volume of sediment. The best model for the "OM source + quantity" hypothesis included all four of the above variables. In each of the three mixed effects models, all terms were significant. The proportion of OM_{aq} was negatively correlated with CH_4 potential production rates (univariate correlation: R^2 = 0.38, $p < 0.0001$; Supporting Information Fig. S1). All other variables had positive correlations with CH_4 potential production rates, regardless of the model (Supporting Information Fig. S1). Univariate correlations between the predictor variables and CH_4 potential production rates were all significant (BIX: R^2 = 0.31, $p < 0.0001$; DOC: R^2 = 0.25, $p < 0.001$; g OM per sediment volume: R^2 = 0.36, $p < 0.0001$). Despite the "OM quantity" model having a slightly lower model probability and rank than the "OM source" model, the marginal R^2 was higher for the "OM quantity" model, indicating more explained variance (48% for the OM quantity model vs. 33% for the OM quality model).

Contextual parameters that explain spatial variation in CH_4 production rates

PLS analysis confirmed that the three reservoir zones have distinct sediment, water column, and microbial community characteristics, and that the triplicate cores at a given location show tight grouping within their respective zones, with a few exceptions (Fig. 8). The first and second components from PLS regression explained 67.0% and 17.9% of the variance among cores, respectively, and CH_4 production was strongly positively correlated with both of these components, especially axis 1. Axis 1 depicts the main gradient in the data, which shows the transition from terrestrial (riverine) to lacustrine sites across many covarying variables and is reflected in CH_4 potential production rates that increase across the gradient from lacustrine to terrestrial/riverine (Fig. 8b, Supporting Information Table S3). Variables with high positive loadings on axis 1 were indicative of strong terrestrial influence, and included sediment characteristics (high bulk density, OM density, C:N), porewater DOM characteristics (high FI, DOC), and water column characteristics (high turbidity, conductivity, and CDOM from deep water samples). Variables with strong negative loadings on axis 1 were indicative of deeper, lacustrine sites with minimal terrestrial influence, and included bulk sediment characteristics (high OM%, OM_{aq}%, N%, $\delta^{15}N$) as well as site physical and water column characteristics (deep secchi depth and site depth). Two methanogen taxa were also associated with this axis, with *Methanosarcina* associated with the "riverine" sites (positive on axis 1), and *Methanoregula* associated with the "lacustrine/transitional" sites (negative on axis 1). Axis 2 was also positively associated with high CH_4 potential production rates and appeared to represent a secondary gradient of in situ productivity, not associated with the terrestrial-lacustrine gradient. The lacustrine sites were discriminated from the transitional sites on this axis, with lacustrine sites positively associated with axis 2. High values on axis 2 seemed to indicate sites (or cores) with high productivity, as indicated by high positive loadings on this axis of water column chlorophyll concentrations, surface pH, porewater BIX, and bulk sediment $\%C_{org}$. Surface nutrient concentrations (TRP, NH_4^+) were negatively associated with this axis, which could indicate a drawdown of soluble inorganic nutrients at high productivity sites. The methanogen taxa *Methanolinea* was also negatively correlated with axis 2 of the PLS (see Fig. 8b, Supporting Information Table S3).

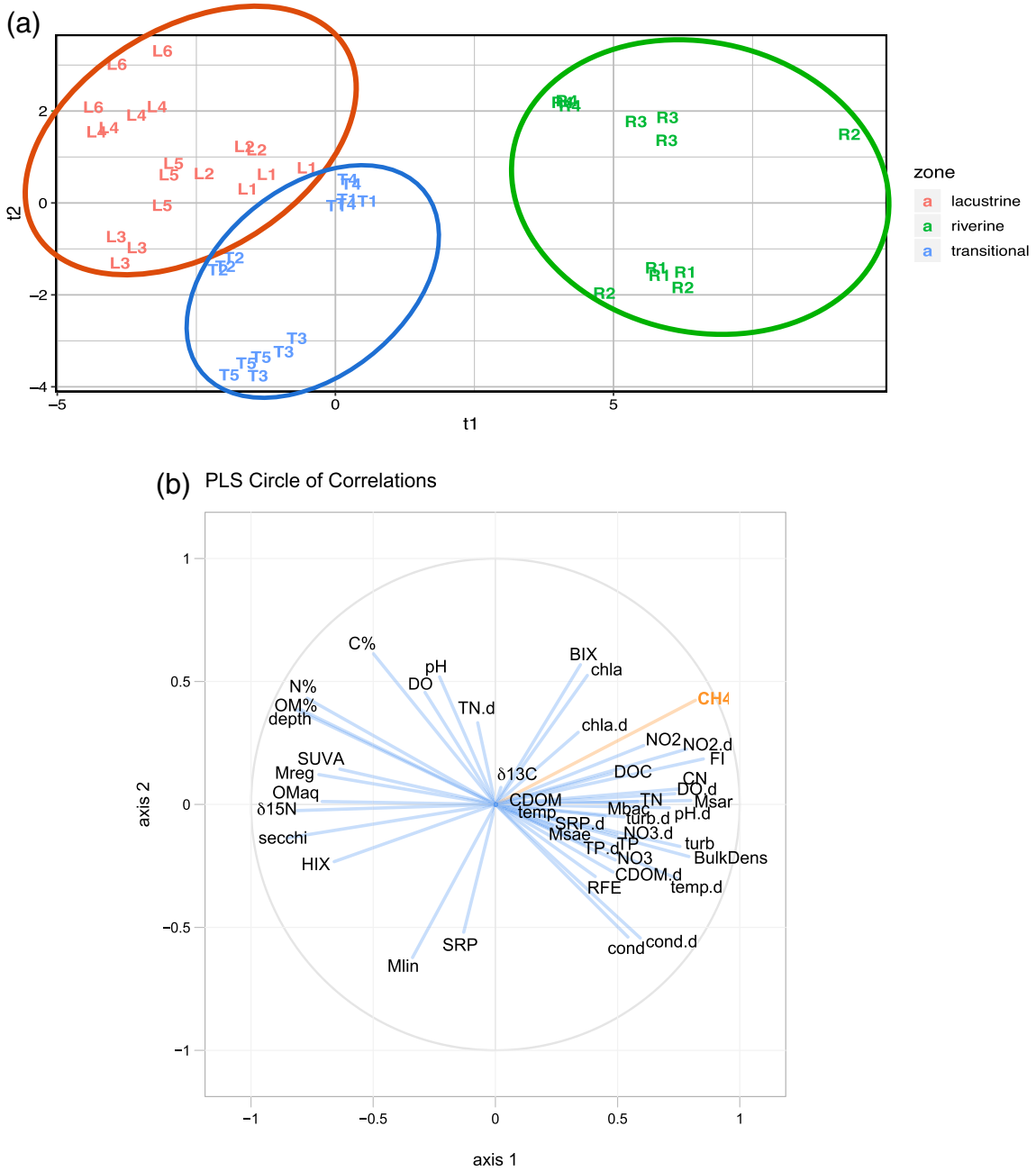

Fig. 8. Multivariate ordination (**a**) of each observation (core) taken in May of 2016 using the first two PLS components (T-components); ovals surrounding the cores for each zone added for visualization purposes. Circle of correlation from partial least square (PLS) analysis (**b**). This illustrates the correlation of predictor variables (blue lines) with methane production rates (orange line). Water column data, sediment composition, and methanogen taxonomic data were included in the PLS analysis. See Supporting Information Table S3 for full list of variables included in the PLS analysis.

Discussion

Spatial variability of sediment measurements across the reservoir

Harsha Lake exhibited strong spatial heterogeneity in sediment characteristics related to longitudinal gradients in reservoir morphology, water velocity, and water residence times (Fig. 8; Supporting Information Table S3). Suspended sediment in the inflowing river rapidly settles out in the riverine zone, resulting in high sedimentation rates, primarily of dense inorganic materials (Table 4), although OM and chlorophyll *a* deposition rates were also much greater than in the transitional or lacustrine zones. Sediments in the riverine zone contained the same amount of OM per unit volume as sediment in downstream portions of the reservoir (Fig. 3a), reflecting

the high rates of inorganic and organic deposition. Porewater DOC was higher in the riverine zone, possibly reflecting high rates of OM deposition in this zone relative to the other zones (Table 4). Sedimentation rates in the transition and lacustrine zones were lower and the deposited material contained a smaller proportion of inorganic material than in the riverine zone (Table 4). This was reflected in lower sediment density and higher sediment %OM in these downstream reservoir zones (Table 2). These differences in OM quantity and quality across the longitudinal gradient coincided with distinct patterns in CH_4 production potential and microbial community composition (Fig. 8). Sediment CH_4 potential production rates, expressed on a volumetric basis, were higher in the riverine than transitional or lacustrine zones (Fig. 2), which is consistent with previous reports of higher CH_4 emission rates in the riverine zone compared to other areas of this reservoir (Beaulieu et al. 2014*a*, 2016; Beaulieu et al. 2018).

The sediment slurry method used to generate CH_4 potential production rates does not represent in situ production rates due to factors including incubation temperature that differs from environmental conditions and the restriction of our assays to the top 5 cm of sediment. Therefore, the data generated from these assays should not be indiscriminately used for upscaling. Acknowledging these limitations, we find it informative to compare results from this study with the published estimates of surface methane emission from the same reservoir, based on thorough spatial and temporal sampling (Beaulieu et al. 2014*a*, 2016, Beaulieu et al. 2018). The following discussion uses volumetric CH_4 potential production rates that were converted to estimated areal rates by assuming an active sediment depth of 5 cm. Previously published areal surface CH_4 emission rates from the Harsha Lake riverine zone (Beaulieu et al. 2016) and the average of our measured riverine zone sediment CH_4 potential production rates from this study were in close agreement; Beaulieu et al. (2016) estimated mean CH_4 emissions from the tributary area to be 33.0 mg CH_4 m^{-2} h^{-1} (95% CI 19.41–46.53 mg CH_4 m^{-2} h^{-1}) while our mean sediment CH_4 potential production was 41.2 mg CH_4 m^{-2} h^{-1} (range 35.2–57.2 mg CH_4 m^{-2} h^{-1}) in the riverine zone. However, CH_4 surface emission rates in the riverine zone in Harsha can be sixfold (Beaulieu et al. 2016) to 2 orders of magnitude (Beaulieu et al. 2014*a*) higher than other areas of the reservoir, while sediment CH_4 potential production rates were only twofold higher in the riverine zone compared to other zones. This difference between CH_4 potential production rates and field-measured emission rates is likely due to methane processing that occurs in the reservoir, such as CH_4 oxidation in the water column, water mixing regimes, and dissolution of ebullitive CH_4 bubbles that increase with water depth (McGinnis et al. 2006). The lacustrine zone, and to a lesser extent the transitional zone, were thermally stratified during the study and most of the CH_4 that diffuses out of the sediment remains in the hypolimnion due to low rates of diffusion and advection across the thermocline (Beaulieu et al. 2014*b*), resulting in limited CH_4 evasion across the air–water interface. Furthermore, in the stratified areas of the reservoir, approximately 25% of the small fraction of hypolimnetic CH_4 that diffuses into the epilimnion is oxidized to CO_2 by methanotrophic bacteria (Beaulieu et al. 2014*a*) rather than evading to the atmosphere (Beaulieu et al. 2014*b*).

Methane potential production rates were consistent with or higher than those reported in other lakes and reservoirs at similar sediment depths. For instance, Eller et al. (2005) found that in the top 6 cm of sediment of a dimictic lake in northern Germany, average CH_4 potential production rates were 0.95 ± 0.10 μmol CH_4 g dry weight^{-1} d^{-1}, and decreased with depth, while values for Harsha Lake averaged 1.56 (range 0.33–2.69) μmol CH_4 g dry weight^{-1} d^{-1} in the top 5 cm of sediment. However, Harsha Lake incubations were conducted at a higher temperature than those reported by Eller et al. (2005). In an oligotrophic and a mesotrophic lake, CH_4 potential production rates were lower than those in our eutrophic lake, producing 0.062 ± 0.018 and 0.054 ± 0.024 μmol CH_4 g dry weight^{-1} d^{-1}, respectively. These incubations were also conducted at lower temperatures (12°C) and evaluated a deeper sediment depth of 15–20 cm, which the authors determined to be more active for methanogenesis in their systems (Fuchs et al. 2016). The average CH_4 potential production rates from the top 5 cm of sediment from 8 northern temperate and boreal lakes was 0.344 μmol CH_4 g dry weight^{-1} d^{-1} (range: 0.012–1.369 μmol CH_4 g dry weight^{-1} d^{-1}) for slurries incubated at 20°C (Duc et al. 2010). These values were still lower than the average found at Harsha Lake, despite having a similar incubation temperature. Few studies evaluate differences in sediment production rates across a reservoir; however, Rodriguez et al. (2018) found that in unamended sediment slurries from the top 10 cm of sediment from Itaparica, a large hydropower reservoir in Brazil, the littoral site had the lowest rates (0.032 μmol CH_4 g dry weight^{-1} d^{-1}; no range or SE available), the intermediate (transitional) site had intermediate rates (0.054 μmol CH_4 g dry weight^{-}1 d^{-}1), and the profundal (lacustrine) site had the largest potential production rates (0.56 μmol CH_4 g dry weight^{-}1 d^{-}1). These data contrast our results where the riverine (most comparable to the littoral site) and lacustrine (most comparable to the profundal site) zones had the highest rates of CH_4 potential production when normalized to sediment dry weight (Fig. 2c). This qualitative difference in CH_4 production in the riverine/littoral zone between studies could be due to the different nature of the "shallow" sites in the two studies. In our study, the shallow riverine sites are specifically in the path of the major tributary entering the reservoir, and thus experience very high sediment (and OM) deposition rates. In contrast, in the study of Itaparica by Rodriguez et al. (2018), the shallow site in the littoral zone may not be subject to the same depositional conditions.

Although volumetric CH_4 potential production rates were higher in the riverine than transitional or lacustrine zones

(Fig. 2a), rates did not differ among reservoir zones when expressed per gram dry mass (Fig. 2c). This illustrates that differences in sediment density contribute to the spatial patterns in volumetric CH_4 potential production rates. Sediment density in the riverine zone was 18–25% greater than in the other reservoir zones and therefore contained more material per unit volume that might enhance CH_4 production. While inorganic fractions of the sediment may provide surface area for microbiota attachment, the organic fraction is the energy source fueling methanogenesis. When normalized to sediment OM, the riverine zone had higher CH_4 potential production rates than the other reservoir zones (Fig. 2c), indicating that OM is more readily converted to CH_4 in the sediments of the riverine zone than in the downstream reservoir zones. This could be due to numerous factors including differences among reservoir zones in the quality of the OM or the composition of microbial communities.

Based on satellite and field measurements indicating greater water column chlorophyll concentration in the riverine than transitional or lacustrine zones in Harsha Lake (Beck et al. 2017), we had predicted that OM in the riverine zone sediment would contain a greater proportion of aquatic derived carbon than elsewhere in the system. However, this prediction was not borne out by the data. In fact, although the riverine zone had the greatest water column chlorophyll *a* during the survey (Table 1) and chlorophyll *a* sedimentation rates were 6–13 times greater than the other reservoir zones (Table 4), the proportion of aquatic derived material in the riverine sediment OM was lower than other portions of the reservoir. This pattern reflects the large input of OM_{terr} that enters the reservoir via the river inflow and is subsequently deposited in the riverine zone, effectively diluting the OM_{aq} carbon signature in the sediment. The OM_{aq} carbon signature in the riverine sediment could also reflect preferential microbial degradation of this labile material. Despite having summer chlorophyll *a* sedimentation rates that are up to an order of magnitude greater than the other reservoir zones, the sediment OM content (g OM cm^{-3}) in the riverine zone sediment cores was no different than the other sites (Fig. 3a).

Characterization of methanogen communities and CH_4 production pathways

Similar to results of other studies in freshwater systems, we found no correlation between methanogen abundance and CH_4 potential production rates (West et al. 2012; Chaudhary et al. 2017). This indicates that CH_4 production rates in Harsha Lake were not limited by methanogen abundance, but instead are linked to other environmental factors such as substrate quantity and/or quality. The variation in substrate availability likely affects methanogen activity, rather than methanogen abundance, and thus determines rates of methanogenesis.

The two methanogen genera with the highest relative abundances across all zones in Harsha Lake, *Methanoregula* and *Methanosaeta*, are the two genera of methanogens that are most frequently encountered in freshwater lakes (Borrel et al. 2011). Combined, sequences from these two genera accounted for 67.3% of total methanogen sequences in the riverine zone, 84.7% in the transitional zone, and 83.5% in the lacustrine zone. The riverine zone had four genera that were each responsible for 10% or more of total methanogen sequences (*Methanoregula*, *Methanosaeta*, *Methanosarcina*, *and Methanobacterium*), while the transitional and lacustrine zone only had two genera (*Methanoregula* and *Methanosaeta*) that were responsible for 10% or more of total methanogen sequences. *Methanoregula* are hydrogenotrophic methanogens, while *Methanosaeta* are acetoclastic methanogens.

The most notable differences in methanogen communities among reservoir zones were the relatively high abundance of *Methanosarcina*, a genus of the Methanosarcinales order capable of both acetoclastic and methylotrophic methanogenesis, and the presence of methylotrophic methanogens *Methanolobus* and *Methanomethylovorans*, in the riverine zone (Fig. 6). *Methanosarcina* comprised an average of 15.4% of methanogens at the riverine sites, but less than 1% of methanogens in the transition and lacustrine zones, possibly reflecting the metabolic diversity of this genera. *Methanosarcina* can generate CH_4 through acetoclastic and methylotrophic pathways, can utilize a diverse range of substrates to produce CH_4, and may be more abundant in the riverine zone due to the diverse mix of terrestrial and aquatic derived material present in this area of the reservoir.

Methanolobus and *Methanomethylovorans* can only utilize methylated compounds. These compounds are derived from the degradation of lignin-containing OM (Penger et al. 2012), as well as degradation of compounds such as pectin (Schink and Zeikus 1982) and cholin (Borrel et al. 2011). Though these compounds were not directly quantified in the sediment samples, lignin is found primarily in terrestrial vascular plants, and our mixing model results indicated a higher proportion of terrestrial derived OM in the riverine sediments. Pectin is a polymer that is found in both plant leaves, as well as cell walls of green algae and cyanobacterial sheaths (Kertesz 1951).

Thus, the high relative abundance of *Methanosarcina* in the riverine zone and the presence of *Methanolobus* and *Methanomethylovorans* could be a result of metabolism of methyl substrates originating from terrestrial plant OM, but could also be indicative of pectin metabolism from both terrestrial and aquatic sources. For example, the riverine zone had high overall OM deposition rates, but also had higher chlorophyll *a* deposition rates compared to the other zones (Table 4). The presence of these genera may indicate a higher functional diversity in terms of methanogenic metabolism in this zone due to the likely presence of a diverse assortment of organic compounds derived from both terrestrial and aquatic sources.

Though our method for estimating the methanogenesis pathway only provides a coarse estimate of the production pathway, our results indicated that acetoclastic methanogenesis was dominant in Harsha Lake, despite the hydrogenotrophic methanogen *Methanoregula* being the most abundant

methanogen in all zones. This is consistent with expectations for freshwater systems (Conrad 1999), but contradicts some reports indicating that hydrogenotrophic methanogenesis may play an important role in freshwater systems (e.g., Murase and Sugimto 2001; Blair et al. 2018).

Combined, the isotope fractionation and methanogen community data indicate that acetoclastic methanogenesis may play a larger role in the riverine zone relative to the rest of the reservoir. This is supported by a higher relative abundance of acetoclastic methanogens (*Methanosaeta* and *Methanosarcina*) and the lower apparent fractionation factor (Fig. 7b) in the riverine zone than in other zones. Concurrent decreases in the contribution of acetoclastic methanogenesis to total methane production and relative abundance of acetoclastic methanogens have been observed with sediment depth, likely as a result of decreased availability of easily degradable OM (Liu et al. 2017). This pattern is observed laterally in Harsha Lake, and could also be a result of spatial variation in OM quality, at that larger scale.

Relationships between sediment characteristics and CH_4 potential production rates

Methane potential production rates were positively correlated with the quantity of particulate sediment OM and dissolved OM (Supporting Information Fig. S1), both of which were greatest in the riverine zone. This relationship likely reflects greater substrate availability for methanogens in organic rich environments; it is consistent with reports of correlation between DOC concentration and diffusive CH_4 fluxes from northern lake and ponds (Wik et al. 2016), and correlation between dissolved CH_4 and DOC concentrations in a eutrophic lake in China (Zhou et al. 2018). Both Duc et al. (2010) and our study found negative correlations between sediment organic carbon (%) and CH_4 production, and water content and CH_4 production; however Duc et al. (2010) report that lower %OM (and high CH_4 production) corresponded with algal C:N sediment signatures, while sediment from Harsha Lake showed the opposite pattern.

The relationship between carbon source and CH_4 potential production rates was different between the solid and dissolved fraction of OM. In the dissolved portion of carbon, potential production rates were positively correlated with BIX, an indicator of OM_{aq}, which is consistent with several reports that algal biomass is a labile carbon source readily utilized by methanogens (Schwarz et al. 2008; Duc et al. 2010; West et al. 2012; Grasset et al. 2018). The CH_4 rates were also negatively correlated with HIX and $SUVA_{254}$, indices that represent humified and aromatic DOM. In the bulk sediment in our study, the estimated proportion of OM_{aq} was negatively correlated to potential production rates. This relationship was driven by the high CH_4 production rates and relatively low proportion of OM_{aq} material in the riverine zone sediment, despite high chlorophyll *a* deposition rates in this zone (Table 4). There are several potential explanations for these results:

1. There are high rates of mineralization in the riverine zone, so OM_{aq} material is more readily and rapidly degraded and less is recovered from the bulk sediment, shifting the sediment OM to a more terrestrial signature. In the riverine zone, the labile OM_{aq} material fuels high CH_4 production rates, while at the same time the high sedimentation rates result in sediments with a higher proportion of terrestrial OM (e.g., Guillemette et al. 2017*b*).
2. The dissolved fraction of OM is what primarily drives CH_4 production; therefore, the relationship that is seen between CH_4 potential production rates and the solid fraction of OM is less relevant. This would suggest that of the total bulk pool of OM in the sediments, the aquatic-derived portion is more readily solubilized and made available for methanogens.
3. Both aquatic and terrestrial derived OM may be important for CH_4 production. OM_{aq} sources may be rapidly degraded while terrestrial OM is degraded over both short and longer time scales (see Guillemette et al. 2017*a*; Grasset et al. 2018). Overall, the riverine zone receives more OM than the other zones, including substantially greater amounts of terrestrial OM. Therefore the high rates of CH_4 potential production can be explained by a slow sustained breakdown of terrestrial OM over time, on top of the higher rates sponsored by OM_{aq}.

While the quantities of OM_{aq} and OM_{terr} (i.e., g OM_{aq} or OM_{terr} cm^{-3}) can be calculated and both exhibit positive relationships with CH_4 potential production rates (correlations not shown), the quantity of OM from a specific source includes measures of both OM source and quantity, and is therefore not as useful for describing source alone relative to the proportion of OM_{aq} or OM_{terr}. Without more direct evidence, we cannot definitively say what the relative influence of each source of OM is in contributing degradation products that fuel methanogenesis with our data set. However, based on our regression analysis, both OM source and quantity are important predictors of CH_4 production rates, much more so than either the source or quantity of OM alone. The predictor variables that were included in the model with source and quantity included the proportion of OM_{aq} in the sediment, BIX of porewater DOM, porewater DOC concentration, and the mass of OM per volume of sediment. The inclusion of DOC concentration and the BIX optical property in the model indicates that the dissolved fraction of OM was important for CH_4 production in terms of both quantity and source. Importantly, all of the models included variables that represented both the particulate and dissolved fractions of OM, suggesting that both pools play a role in CH_4 production.

Our data indicate there may be a link between particulate terrestrial OM and CH_4 production in Harsha Lake. C:N ratios from bulk sediment were positively correlated to CH_4 potential production rates. These results contrast with another study of boreal and northern temperate lake sediments in central

Sweden, which found a negative correlation between CH_4 production rates and C:N ratios (Duc et al. 2010). However, their study was an interlake comparison with a larger range of C:N ratios (8.6–23.4) than the C:N ratios found within Harsha Lake (range 6.6–10.0). Further, Duc et al. (2010) noted that the sediments in their study with the lowest methane production had high C:N ratios and were comprised of peat or flocculated humic matter. The positive correlation between C:N and CH_4 potential production in Harsha Lake aligns with the observation that the highest production rates occurred in the riverine zone, which also receives the highest terrestrial inputs and has the highest proportion of OM_{terr} in the sediments. Thus, the riverine zone is an exceptionally active deposition zone for both OM_{aq} and OM_{terr}, and this material sponsors very high CH_4 production rates relative to other parts of the reservoir.

Summary and conclusion

Sediment methane potential production varied spatially across reservoir zones. Categorizing sites into zones aided in conceptualizing the differences in methane-generating processes across the reservoir. Further, this approach provides a generalizable framework for comparison with other reservoirs. The riverine zone differed from the other areas of the reservoir, and was characterized by high CH_4 potential production rates, high terrestrial carbon inputs, high autotrophic production, dense sediments, and porewater DOM that was less humified, less aromatic, and more aquatic derived relative to other zones. Research on reservoir biogeochemistry should encompass this zone with a goal of understanding gradients and spatial variation across the reservoir continuum. Both source and quantity of OM appeared to be important for CH_4 potential production rates. This has important implications for global carbon cycling, as the amount of sediment OM transported to reservoirs is expected to increase and the number of reservoirs globally are increasing (Downing et al. 2006; Zarfl et al. 2015). In Harsha Lake, relatively recently produced and less aromatic DOM from aquatic and microbial sources appears to fuel CH_4 production in the zone with the highest potential production rates, though compounds derived from terrestrial OM may contribute to these high rates. While OM_{aq} is recognized as a key driver of high methane production rates, the role of the degradation of more complex compounds typically associated with OM_{terr} in contributing to CH_4 production and emission "hot spots" in lacustrine systems warrants further study. These compounds may become bioavailable due to some combination of photodegradation or biological processing that could be occurring in the oxygenated water column.

Although methanogen abundance did not vary specifically among reservoir zones or with CH_4 production rates, methanogen communities did have some variation among zones—largely due to one taxonomic group, *Methanosarcina*; this group added functional diversity to the riverine zone. The methanogen community composition may help explain differences in CH_4 production rates and pathways between the riverine zone and the rest of the reservoir.

Cumulatively, our results indicate that both aquatic and terrestrial sources of OM are important in driving high methane production in the riverine zone of the main reservoir inlet. This has implications for reservoir management, suggesting that both watershed-scale soil erosion control and nutrient reductions may help reduce reservoir methane production. From this study we recognize the potential of terrestrial OM to contribute to "hot spots" of reservoir CH_4 production, particularly in depositional/riverine zones—with many questions remaining to be addressed on the topic. The results presented here contribute to our understanding of environmental factors that may influence spatial variation in CH_4 production and methanogen community composition in freshwater sediments.

Data Availability Statement

Data, code, and supporting documentation for the results found in this publication are available at the Center for Open Science OSF project page: https://osf.io/59hnj/. Raw 16S rRNA gene sequence reads for each sample are also available on NCBI Short Read Archive (SRA) under the BioProject number PRJNA532292.

This document has been reviewed in accordance with U.S. Environmental Protection Agency policy and approved for publication.

References

Albertsen, M., S. M. Karst, A. S. Ziegler, R. H. Kirkegaard, and P. H. Nielsen. 2015. Back to basics - The influence of DNA extraction and primer choice on phylogenetic analysis of activated sludge communities. PLoS ONE **107**: e0132783.

American Public Health Association. 2012. Standard methods for the examination of water and wastewater, v. **22**. Washington, DC: American Public Health Association.

Anderson, D. R. 2008. Model based inference in the life sciences: A primer on evidence. New York, NY: Springer. doi: 10.1016/j.hal.2008.08.017

Apprill, A., S. McNally, R. Parsons, and L. Weber. 2015. Minor revision to V4 region SSU rRNA 806R gene primer greatly increases detection of SAR11 bacterioplankton. Aquat. Microb. Ecol. **75**: 129–137. doi:10.3354/ame01753

Bastviken, D., L. J. Tranvik, J. A. Downing, P. M. Crill, and A. Enrich-Prast. 2011. Freshwater methane emissions offset the continental carbon sink. Science **331**: 50. doi:10.1126/science.1196808

Bates, D., M. Maechler, B. Bolker, and S. Walker. 2015. Fitting linear mixed-effects models using lme4. J. Stat. Softw. **671**: 1–48. doi:10.18637/jss.v067.i01

Beaulieu, J. J., M. G. McManus, and C. T. Nietch. 2016. Estimates of reservoir methane emissions based on a spatially

balanced probabilistic-survey. Limnol. Oceanogr. **61**: S27–S40. doi:10.1002/lno.10284

Beaulieu, J. J., et al. 2018. Effects of an experimental water-level drawdown on methane emissions from a eutrophic reservoir. Ecosystems **21**: 657–674. doi:10.1007/s10021-017-0176-2

Beaulieu, J. J., R. L. Smolenski, C. T. Nietch, A. Townsend-Small, and M. S. Elovitz. 2014*a*. High methane emissions from a midlatitude reservoir draining an agricultural watershed. Environ. Sci. Technol. **48**: 11100–11108. doi:10.1021/es501871g

Beaulieu, J. J., R. L. Smolenski, C. T. Nietch, A. Townsend-Small, M. S. Elovitz, and J. P. Schubauer-Berigan. 2014*b*. Denitrification alternates between a source and sink of nitrous oxide in the hypolimnion of a thermally stratified reservoir. Limnol. Oceanogr. **59**: 495–506. doi:10.4319/lo.2014.59.2.0495

Beck, R., and others. 2017. Comparison of satellite reflectance algorithms for estimating phycocyanin values and cyanobacterial total biovolume in a temperate reservoir using coincident hyperspectral aircraft imagery and dense coincident surface observations. Remote Sens. **96**: 538. doi:10.3390/rs9060538

Bianchi, T. S., and E. A. Canuel. 2011. Chemical biomarkers in aquatic ecosystems. Princeton, NJ: Princeton Univ. Press. doi:10.1900/RDS.2011.8.432

Blair, N. E., and others. 2018. The C-biogeochemistry of a mid-western USA agricultural impoundment in context: Lake Decatur in the intensively managed landscape critical zone observatory. Biogeochemistry **138**: 171–195. doi:10.1007/s10533-018-0439-9

Bloesch, J., and N. M. Burns. 1980. A critical review of sediment trap technique. Schweiz. Z. Hydrol. **42**: 15–55. doi:10.1007/BF02502505

Boren, K. 2001. QuikChem® Method 10-115-01-4-E. Total phosphorus in manual persulfate digests. Latchat Instruments, 5600 Lindburgh Drive, Loveland CO 80539.

Borrel, G., D. Jézéquel, C. Biderre-Petit, N. Morel-Desrosiers, J.-P. Morel, P. Peyret, G. Fonty, and A.-C. Lehours. 2011. Production and consumption of methane in freshwater lake ecosystems. Res. Microbiol. **162**: 832–847. doi:10.1016/j.resmic.2011.06.004

Caporaso, J. G., and others. 2012. Ultra-high-throughput microbial community analysis on the Illumina HiSeq and MiSeq platforms. ISME J. **6**: 1621–1624. doi:10.1038/ismej.2012.8

Chaudhary, P. P., M. Rulík, and M. Blaser. 2017. Is the methanogenic community reflecting the methane emissions of river sediments?-comparison of two study sites. Microbiol. Open **6**: e454. doi:10.1002/mbo3.454

Conrad, R. 1999. Contribution of hydrogen to methane production and control of hydrogen concentrations in methanogenic soils and sediments. FEMS Microbiol. Ecol. **28**: 193–202. doi:10.1111/j.1574-6941.1999.tb00575.x

Conrad, R. 2005. Quantification of methanogenic pathways using stable carbon isotopic signatures: a review and a proposal. Org. Geochem. **36**: 739–752. doi:10.1016/j.orggeochem.2004.09.006

Cory, R. M., K. Mcneill, J. P. Cotner, A. Amado, J. M. Purcell, and A. G. Marshall. 2010. Singlet oxygen in the coupled photochemical and biochemical oxidation of dissolved organic matter. Environ. Sci. Technol. **44**: 3683–3689. doi:10.1021/es902989y

Deemer, B. R., and others. 2016. Greenhouse gas emissions from reservoir water surfaces: a new global synthesis. BioScience **66**: 949–964. doi:10.1093/biosci/biw117

del Giorgio, P. A., and J. Davis. 2003. Patterns in dissolved organic matter lability and consumption across aquatic ecosystems, p. 399–424. *In* S. E. G. Findlay and R. L. Sinsabaugh [eds.], Aquatic ecosystems: Interactivity of dissolved organic matter. Amsterdam: Academic Press.

DelSontro, T., J. J. Beaulieu, and J. A. Downing. 2018. Greenhouse gas emissions from lakes and impoundments: Upscaling in the face of global change. Limnol. Oceanogr. Lett. **3**: 64–75. doi:10.1002/lol2.10073

DelSontro, T., M. J. Kunz, T. Kempter, A. Wüest, B. Wehrli, and D. B. Senn. 2011. Spatial heterogeneity of methane ebullition in a large tropical reservoir. Environ. Sci. Technol. **45**: 9866–9873. doi:10.1021/es2005545

Diggle, P. J., P. Heagerty, K. Y. Liang, and S. L. Zeger. 2002. Analysis of longitudinal data, Second ed. Oxford, England: Oxford Univ. Press. doi:10.1094/PHYTO.2002.92.10.1110

Downing, B. D., E. Boss, B. A. Bergamaschi, J. A. Fleck, M. A. Lionberger, N. K. Ganju, D. H. Schoellhamer, and R. Fujii. 2009. Quantifying fluxes and characterizing compositional changes of dissolved organic matter in aquatic systems in situ using combined acoustic and optical measurements. Limnol. Oceanogr.: Methods **7**: 119–131. doi:10.4319/lom.2009.7.119

Downing, J. A., and others. 2006. The global abundance and size distribution of lakes, ponds, and impoundments. Limnol. Oceanogr. **51**: 2388–2397. doi:10.4319/lo.2006.51.5.2388

Duc, N. T., P. Crill, and D. Bastviken. 2010. Implications of temperature and sediment characteristics on methane formation and oxidation in lake sediments. Biogeochemistry **100**: 185–196. doi:10.1007/s10533-010-9415-8

Eller, G., P. Deines, J. Grey, H. H. Richnow, and M. Krüger. 2005. Methane cycling in lake sediments and its influence on chironomid larval d13C. FEMS Microbiol. Ecol. **54**: 339–350. doi:10.1016/j.femsec.2005.04.006

Fagervold, S. K., S. Bourgeois, A. M. Pruski, F. Charles, P. Kerhervé, G. Vétion, and P. E. Galand. 2014. River organic matter shapes microbial communities in the sediment of the Rhône prodelta. ISME J. **8**: 2327–2338. doi:10.1038/ismej.2014.86

Fuchs, A., E. Lyautey, B. Montuelle, and P. Casper. 2016. Effects of increasing temperatures on methane

concentrations and methanogenesis during experimental incubation of sediments from oligotrophic and mesotrophic lakes. Eur. J. Vasc. Endovasc. Surg. **121**: 1394–1406. doi:10.1002/2016JG003328

Grasset, C., R. Mendonça, G. Villamor Saucedo, D. Bastviken, F. Roland, and S. Sobek. 2018. Large but variable methane production in anoxic freshwater sediment upon addition of allochthonous and autochthonous organic matter. Limnol. Oceanogr. **91**: 1225–1214. doi:10.1002/lno.10786

Grinham, A. M., D. Dunbabin, and J. Udy. 2011. Quantification of ebullitive and diffusive methane release to the atmosphere from a water storage. Atmos. Environ. **459**: 7166–7173. doi:10.1016/j.atmosenv.2011.09.011

Guillemette, F., T. S. Bianchi, and R. G. M. Spencer. 2017*a*. Old before your time: Ancient carbon incorporation in contemporary aquatic foodwebs. Limnol. Oceanogr. **33**: 2–19. doi:10.1002/lno.10525

Guillemette, F., E. von Wachenfeldt, D. N. Kothawala, D. Bastviken, and L. J. Tranvik. 2017*b*. Preferential sequestration of terrestrial organic matter in boreal lake sediments. Eur. J. Vasc. Endovasc. Surg. **122**: 863–874. doi:10.1002/2016JG003735

Hansen, A. M., T. E. C. Kraus, B. A. Pellerin, J. A. Fleck, B. D. Downing, and B. A. Bergamaschi. 2016. Optical properties of dissolved organic matter DOM: Effects of biological and photolytic degradation. Limnol. Oceanogr. **61**: 1015–1032. doi:10.1002/lno.10270

Harris, D., W. R. Horwáth, and C. van Kessel. 2001. Acid fumigation of soils to remove carbonates prior to total organic carbon or carbon-13 isotopic analysis. Soil Sci. Soc. Am. J. **65**: 1853–1856. doi:10.2136/sssaj2001.1853

Harrison, J. A., and others. 2009. The regional and global significance of nitrogen removal in lakes and reservoirs. Biogeochemistry **93**: 143–157. doi:10.1007/s10533-008-9272-x

Hayes, N. M., B. R. Deemer, J. R. Corman, N. R. Razavi, and K. E. Strock. 2017. Key differences between lakes and reservoirs modify climate signals: A case for a new conceptual model. Limnol. Oceanogr. **2**: 47–62. doi:10.1002/lol2.10036

Holgerson, M. A., and P. A. Raymond. 2016. Large contribution to inland water CO_2 and CH_4 emissions from very small ponds. Nat. Geosci. **9**: 222–226. doi:10.1038/ngeo2654

Hood, E., M. W. Williams, and D. M. McKnight. 2005. Sources of dissolved organic matter (DOM) in a rocky mountain stream using chemical fractionation and stable isotopes. Biogeochemistry **74**: 231–255. doi:10.1007/s10533-004-4322-5

Huguet, A. L., S. R. Vacher, S. Saubusse, J. M. Froidefond, and E. Parlanti. 2009. Properties of fluorescent dissolved organic matter in the Gironde Estuary. Org. Geochem. **40**: 706–719. doi:10.1016/j.orggeochem.2009.03.002

Kellerman, A. M., F. Guillemette, D. C. Podgorski, G. R. Aiken, K. D. Butler, and R. G. M. Spencer. 2018. Unifying concepts linking dissolved organic matter composition to persistence in aquatic ecosystems. Environ. Sci. Tech. **52**: 2538–2548. doi:10.1021/acs.est.7b05513

Kertesz, Z. I. 1951. The pectic substances. New York: Interscience Publishers. doi:10.1038/168697a0

Knoll, L. B., M. J. Vanni, W. H. Renwick, and S. Kollie. 2014. Burial rates and stoichiometry of sedimentary carbon, nitrogen and phosphorus in Midwestern US reservoirs. Freshwater Biol. **5911**: 2342–2353. doi:10.1111/fwb.12438

Kozich, J. J., S. L. Westcott, N. T. Baxter, S. K. Highlander, and P. D. Schloss. 2013. Development of a dual-index sequencing strategy and curation pipeline for analyzing amplicon sequence data on the MiSeq Illumina sequencing platform. Appl. Environ. Microbiol. **7917**: 5112–5120. doi:10.1128/AEM.01043-13

Kuznetsova, A., P.B. Brockhoff, and R.H.B Christensen. 2016. lmerTest: Tests in Linear Mixed Effects Models. Rpackage version 2.0–33. https://CRAN.R-project.org/package=lmerTest, DOI: 10.17116/jnevro2016116121126-129

Liu, Y., R. Conrad, T. Yao, G. Gleixner, and P. Claus. 2017. Change of methane production pathway with sediment depth in a lake on the Tibetan plateau. Palaeogeogr. Palaeoclimatol. Palaeoecol. **474**: 279–286. doi:10.1016/j.palaeo.2016.06.021

Liu, Y., and W. B. Whitman. 2008. Metabolic, phylogenetic, and ecological diversity of the methanogenic archaea. Ann. N. Y. Acad. Sci. **1125**: 171–189. doi:10.1196/annals.1419.019

Luke, S. G. 2017. Evaluating significance in linear mixed-effects models in R. Behav. Res. Methods **49**: 1494–1502. doi:10.3758/s13428-016-0809-y

Luton, P. E., J. M. Wayne, R. J. Sharp, and P. W. Riley. 2002. The mcrA gene as an alternative to 16S rRNA in the phylogenetic analysis of methanogen populations in landfill. Microbiology **148**: 3521–3530. doi:10.1099/00221287-148-11-3521

Maeck, A., T. DelSontro, D. F. McGinnis, H. Fischer, S. Flury, M. Schmidt, P. Fietzek, and A. Lorke. 2013. Sediment trapping by dams creates methane emission hot spots. Environ. Sci. Technol. **47**: 8130–8137. doi:10.1021/es4003907

McCallister, S. L., and P. A. del Giorgio. 2012. Evidence for the respiration of ancient terrestrial organic C in northern temperate lakes and streams. Proc. Natl. Acad. Sci. U. S. A. **109**: 16963–16968. doi:10.1073/pnas.1207305109

McGinnis, D. F., J. Greinert, Y. Artemov, S. E. Beaubien, and A. Wüest. 2006. Fate of rising methane bubbles in stratified waters: How much methane reaches the atmosphere? J. Geophys. Res. **111**: C09007. doi:10.1029/2005JC003183

McKnight, D. M., E. W. Boyer, P. K. Westerhoff, P. T. Doran, T. Kulbe, and D. T. Andersen. 2001. Spectrofluorometric characterization of dissolved organic matter for indication of precursor organic material and aromaticity. Limnol. Oceanogr. **46**: 38–48. doi:10.4319/lo.2001.46.1.0038

McMurdie, P. J., and S. Holmes. 2013. phyloseq: An R package for reproducible interactive analysis and graphics of

microbiome census data. PLoS ONE **84**: e61217. doi:10.1371/journal.pone.0061217

Mladenov, N., and others. 2010. Dissolved organic matter sources and consequences for iron and arsenic mobilization in Bangladesh aquifers. Environ. Sci. Technol. **44**: 123–128. doi:10.1021/es901472g

Murase, J., and A. Sugimto. 2001. Spatial distribution of methane in Lake Biwa sediments and its carbon isotopic compositions. Geochem. J. **35**: 257–263. doi:10.2343/geochemj.35.257

Neubauer, S., and J. Megonigal. 2015. Moving beyond global warming potentials to quantify the climatic role of ecosystems. Ecosystems **18**: 1000–1013. doi:https://doi.org/10.1007/s10021-015-9879-4

Ohno, T. 2002. Fluorescence inner-filtering correction for determining the humification index of dissolved organic matter. Environ. Sci. Technol. **36**: 742–746. doi:10.1021/es0155276

Penger, J., R. Conrad, and M. Blaser. 2012. Stable carbon isotope fractionation by methylotrophic methanogenic archaea. Appl. Environ. Microbiol. **78**: 7596–7602. doi:10.1128/AEM.01773-12

Pinheiro, J., D. Bates, S. DebRoy, D. Sarkar, and R Core Team 2017. nlme: Linear and Nonlinear Mixed Effects Models. R package version 3.1-131. Available from https://CRAN.R-project.org/package=nlme, DOI: 10.11646/zootaxa.4365.2.7.

R Core Team. 2017. R: A language and environment for statistical computing. Vienna, Austria: R Foundation for Statistical Computing, Available from https://www.R-project.org/.

Rodriguez, M., T. Gonsiorczyk, and P. Casper. 2018. Methane production increases with warming and carbon additions to incubated sediments from a semiarid reservoir. Inland Waters **8**: 109–121. doi:10.1080/20442041.2018.1429986

Saji, N. 2008. Development of a guide to lake and reservoir zone determination. MS Thesis: Virginia Polytech Institute and State Univ., 284 pages.

Sanchez, G. 2012. plsdepot: Partial Least Squares (PLS) Data Analysis Methods. R package version 0.1.17. https://CRAN.R-project.org/package=plsdepot, DOI: 10.1166/jnn.2012.6776

Schink, B., and J. G. Zeikus. 1982. Microbial ecology of pectin decomposition in anoxic lake sediments. J. Gen. Microbiol. **128**: 393–404. doi:10.1099/00221287-128-2-393

Schloss, P. D., and others. 2009. Introducing mothur: Open-source, platform-independent, community-supported software for describing and comparing microbial communities. Appl. Environ. Microbiol. **75**: 7537–7541. doi:10.1128/AEM.01541-09

Schwarz, J. I. K., W. Eckert, and R. Conrad. 2008. Response of methanogenic microbial community of a profundal lake sediment (Lake Kinneret, Israel) to algal deposition. Limnol. Oceanogr. **53**: 113–121. doi:10.4319/lo.2008.53.1.0113

Smith, P. and K. Bogren. 2003. QuikChem® Method 10-107-04-4-A. Determination of nitrate/nitrite in manual persulfate digestios. Latchat Instruments, Lindburgh Drive, Loveland CO., DOI: 10.3816/SCT.2003.n.004

Stanley, E. H., N. J. Casson, S. T. Christel, J. T. Crawford, L. C. Loken, and S. K. Oliver. 2016. The ecology of methane in streams and rivers: Patterns, controls, and global significance. Ecol. Monogr. **86**: 146–171. doi:10.1890/15-1027

Stedmon, C. A., S. Markager, and R. Bro. 2003. Tracing dissolved organic matter in aquatic environments using a new approach to fluorescence spectroscopy. Mar. Chem. **82**: 239–254. doi:10.1016/S0304-4203(03)00072-0

Stock, B. C., A. L. Jackson, E. J. Ward, A. C. Parnell, D. L. Phillips, and B. X. Simmons. 2018. Analyzing mixing systems using a new generation of Bayesian tracer mixing models. PeerJ **6**: e5096. doi:10.7717/peerj.5096

Stock, B.C. and B.X. Semmens. 2013. MixSIAR GUI User Manual. Version 3.1. https://github.com/brianstock/MixSIAR. doi:10.5281/zenodo.56159.

Sun, L., E. M. Perdue, J. L. Meyer, and J. Weis. 1997. Use of elemental composition to predict bioavailability of dissolved organic matter in a Georgia river. Limnol. Oceanogr. **42**: 714–721. doi:10.4319/lo.1997.42.4.0714

Thornton, K. W., B. L. Kimmel, and F. E. Payne [eds.]. 1990. Reservoir limnology: Ecological perspectives. New York: John Wiley & Sons. doi:10.17226/1486

Weishaar, J. L., G. R. Aiken, B. A. Bergamaschi, M. S. Fram, R. Fujii, and K. Mopper. 2003. Evaluation of specific ultraviolet absorbance as an indicator of the chemical composition and reactivity of dissolved organic carbon. Environ. Sci. Technol. **37**: 4702–4708. doi:10.1021/es030360x

West, W. E., J. J. Coloso, and S. E. Jones. 2012. Effects of algal and terrestrial carbon on methane production rates and methanogen community structure in a temperate lake sediment. Freshwater Biol. **57**: 949–955. doi:10.1111/j.1365-2427.2012.02755.x

West, W. E., K. P. Creamer, and S. E. Jones. 2015*b*. Productivity and depth regulate lake contributions to atmospheric methane. Limnol. Oceanogr. **61**: S51–S61. doi:10.1002/lno.10247

West, W. E., S. M. McCarthy, and S. E. Jones. 2015*a*. Phytoplankton lipid content influences freshwater lake methanogenesis. Freshwater Biol. **60**: 2261–2269. doi:10.1111/fwb.12652

Whiticar, M. J. 1999. Carbon and hydrogen isotope systematics of bacterial formation and oxidation of methane. Chem. Geol. **161**: 291–314. doi:10.1016/S0009-2541(99)00092-3

Whiticar, M. J., E. Faber, and M. Schoell. 1986. Biogenic methane formation in marine and freshwater environments: CO_2 reduction vs. acetate fermentation – Isotope evidence. Geochim. Cosmochim. Acta **50**: 693–709. doi:10.1016/0016-7037(86)90346-7

Wik, M., R. K. Varner, K. W. Anthony, S. MacIntyre, and D. Bastviken. 2016. Climate-sensitive northern lakes and ponds are critical components of methane release. Nat. Geo. **9**: 99–105. doi:10.1038/ngeo2578

Yu, Y., C. Lee, J. Kim, and S. Hwang. 2005. Group-specific primer and probe sets to detect methanogenic communities using quantitative real-time polymerase chain reaction. Biotechnol. Bioeng. **89**: 670–679. doi:10.1002/bit.20347

Zarfl, C., A. Lumsdon, J. Berlekamp, L. Tydecks, and K. Tockner. 2015. A global boom in hydropower dam construction. Aquat. Sci. **77**: 161–170. doi:10.1007/s00027-014-0377-0

Zhou, Y., and others. 2018. Accumulation of terrestrial dissolved organic matter potentially enhances dissolved methane levels in Eutrophic Lake Taihu, China. Environ. Sci. Technol. **52**: 10297–10306. doi:10.1021/acs.est.8b02163

Zuur, A. F., E. N. Ieno, and C. S. Elphick. 2010. A protocol for data exploration to avoid common statistical problems. Methods Ecol. Evol. **1**: 3–14. doi:10.1111/j.2041-210X.2009.00001.x

Zuur, A. F., E. N. Ieno, N. J. Walker, A. A. Saveliev, and G. M. Smith. 2009. Mixed effects modelling for nested data. *In* Mixed effects models and extensions in ecology with R. Statistics for biology and health. New York, NY: Springer.

Acknowledgments

This research was supported in part by a grant from the United States Geological Survey 104(b) program, sub-award #60059469 through the Ohio Water Resources Center. Megan Berberich was supported through the Graduate Research Traineeship program sponsored by the U.S. EPA and administered through the University of Cincinnati, in addition to support from the UC Department of Biological Sciences and the Wieman Wendel Benedict Fund. We thank Joel Allen for support in sediment trap deployment and sampling, Kit Daniels for key assistance with field sample collection, Madison Duke for sediment trap work and field and lab support, Mike Elovitz for advice and insights into DOC EEMs, Jeff Havig for stable isotope and elemental analysis of sediment, Xuan Li for field and laboratory support including EEMs, and Karen White for laboratory assistance; this research was made possible with their help. We are also grateful to Aaron Diefendorf for access to and use of the Stable Isotope Geochemistry Lab in the Department of Geology at the University of Cincinnati.

Conflict of Interest

The authors declare no conflicts of interest.

Submitted 28 April 2019
Revised 07 October 2019
Accepted 09 November 2019

Associate editor: Hans-Peter Grossart

Effects of an Experimental Water-level Drawdown on Methane Emissions from a Eutrophic Reservoir

Jake J. Beaulieu, David A. Balz, M. Keith Birchfield, John A. Harrison, Christopher T. Nietch, Michelle C. Platz, William C. Squier, et al.

Ecosystems

ISSN 1432-9840
Volume 21
Number 4

Ecosystems (2018) 21:657-674
DOI 10.1007/s10021-017-0176-2

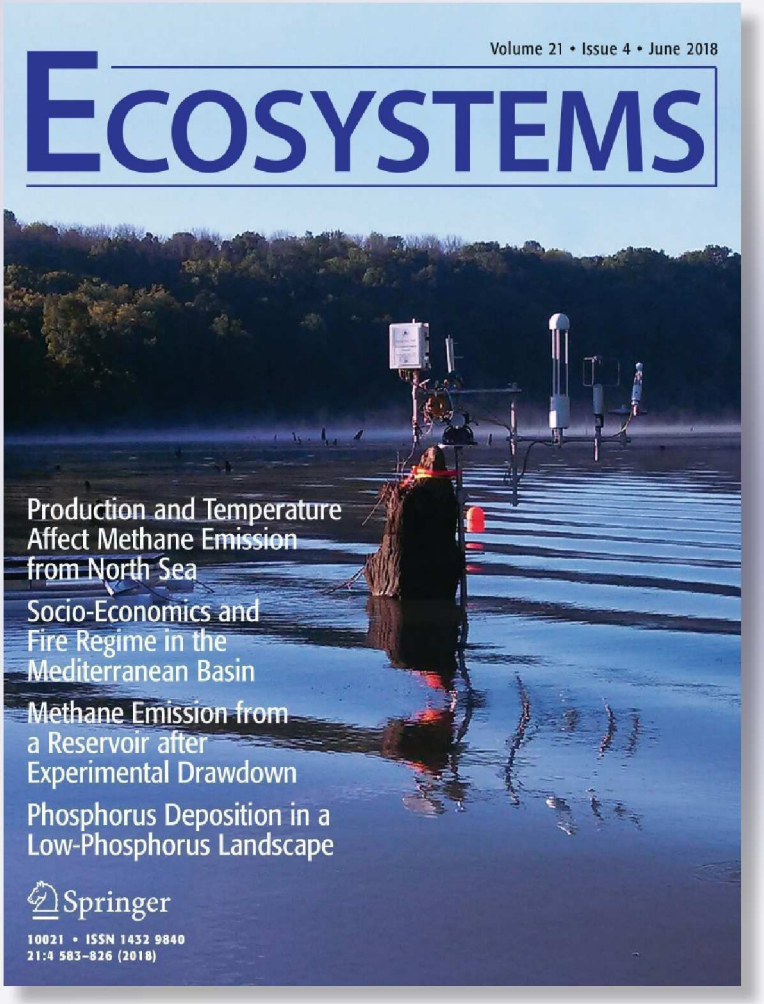

Springer

Your article is published under the Creative Commons Attribution license which allows users to read, copy, distribute and make derivative works, as long as the author of the original work is cited. You may self-archive this article on your own website, an institutional repository or funder's repository and make it publicly available immediately.

Ecosystems (2018) 21: 657–674
DOI: 10.1007/s10021-017-0176-2

© 2017 The Author(s). This article is an open access publication

Effects of an Experimental Water-level Drawdown on Methane Emissions from a Eutrophic Reservoir

Jake J. Beaulieu,[1]* David A. Balz,[2] M. Keith Birchfield,[3] John A. Harrison,[3] Christopher T. Nietch,[1] Michelle C. Platz,[1] William C. Squier,[4] Sarah Waldo,[1] John T. Walker,[5] Karen M. White,[1] and Jade L. Young[6]

[1]*National Risk Management Research Laboratory, United States Environmental Protection Agency, Office of Research and Development, 26 W Martin Luther King Dr, Cincinnati, Ohio 45268, USA;* [2]*Pegasus Technical Services, Cincinnati, Ohio, USA;* [3]*School of the Environment, Washington State University, Vancouver, Washington, USA;* [4]*National Enforcement Investigations Center, United States Environmental Protection Agency, Denver, Colorado, USA;* [5]*National Risk Management Research Laboratory, United States Environmental Protection Agency, Office of Research and Development, Durham, North Carolina, USA;* [6]*United States Army Corps of Engineers, Louisville, Kentucky, USA*

Abstract

Reservoirs are a globally significant source of methane (CH_4) to the atmosphere. However, emission rate estimates may be biased low due to inadequate monitoring during brief periods of elevated emission rates (that is, hot moments). Here we investigate CH_4 bubbling (that is, ebullition) during periods of falling water levels in a eutrophic reservoir in the Midwestern USA. We hypothesized that periods of water-level decline trigger the release of CH_4-rich bubbles from the sediments and that these emissions constitute a substantial fraction of the annual CH_4 flux. We explored this hypothesis by monitoring CH_4 ebullition in a eutrophic reservoir over a 7-month period, which included an experimental water-level drawdown. We found that the ebullitive CH_4 flux rate was among the highest ever reported for a reservoir (mean = 32.3 mg CH_4 m^{-2} h^{-1}). The already high ebullitive flux rates increased by factors of 1.4–77 across the nine monitoring sites during the 24-h experimental water-level drawdown, but these emissions constituted only 3% of the CH_4 flux during the 7-month monitoring period due to the naturally high ebullitive CH_4 flux rates that persist throughout the warm weather season. Although drawdown emissions were found to be a minor component of annual CH_4 emissions in this reservoir, our findings demonstrate a link between water-level change and CH_4 ebullition, suggesting that CH_4 emissions may be mitigated through water-level management in some reservoirs.

Key words: methanogenesis; biogeochemistry; carbon; anthropogenic; management; aquatic.

Received 29 March 2017; accepted 6 July 2017;
published online 5 September 2017

Electronic supplementary material: The online version of this article (doi:10.1007/s10021-017-0176-2) contains supplementary material, which is available to authorized users.

Author contributions JJB, JAH, CTN, and JTW designed the study. JJB, DAB, MP, BS, JTW, KMW, and JLY performed the research. JJB, SW, and JTW analyzed the data. MKB and BS contributed new methods. JJB, SW, and JTW wrote the paper.

*Corresponding author; e-mail: beaulieu.jake@epa.gov

Introduction

Methane (CH_4) is a potent greenhouse gas and the second largest contributor to climate change (IPCC 2013). Reservoirs, which are created when landscapes are flooded behind dams, are a globally significant source of CH_4 to the atmosphere (Barros and others 2011; Bastviken and others 2011; Deemer and others 2016). Reservoirs are extremely numerous, covering more than 30 million ha of the earth's land surface (Downing and others 2006), and the global surface area of reservoirs is expected to increase substantially over the coming decades as developing countries turn to hydropower to meet growing energy demands (Zarfl and others 2015). Methane is created in reservoirs through methanogenesis, a type of microbial metabolism that yields energy from the degradation of organic matter in low oxygen environments. Reservoir sediments are often enriched with organic matter derived from river inflows and internal algal production, among other sources. Relative to lakes, organic matter loading to reservoirs from river inflows can be particularly high due to their characteristically large ratio of catchment area to lake area (Kimmel and others 1990; Knoll and others 2014; Hayes and others 2017). Furthermore, the bottom waters of reservoirs are often anoxic during periods of thermal stratification, providing the mix of high organic matter and low oxygen conditions conducive to CH_4 production.

Efforts to use published data to estimate regional/global scale CH_4 emissions from reservoirs, or to identify large-scale factors driving emission rates (that is, latitude, reservoir age), have been complicated by uncertainty in emission rate measurements (Barros and others 2011; Bastviken and others 2011; Deemer and others 2016). An important source of uncertainty is the degree to which individual studies address high emission rates associated with spatial hot spots and temporal hot moments (McClain and others 2003; Schilder and others 2013; Schilder and others 2016; Wik and others 2016). Methane emission rates can exhibit extreme intra-reservoir spatial heterogeneity. For example, river–reservoir transition zones can be CH_4 emission hot spots due partly to high sedimentation rates which promote the delivery of organic matter to anoxic sediments (DelSontro and others 2011; Beaulieu and others 2014; Beaulieu and others 2016). Grinham and others (2011) reported that 97% of the CH_4 emitted from the surface of a subtropical reservoir was derived from approximately 5% of the reservoir surface area located immediately downstream of the main tributary input. Similarly, low water depths, which promote the transfer of CH_4-rich bubbles from the sediment to the atmosphere, and organic-rich sediments in littoral zones, can also lead to emission hot spots in reservoirs (Juutinen and others 2003; Hofmann 2013). Methane emission rates in reservoirs can also exhibit hot moments where elevated rates occur for brief periods. For example, CH_4 that accumulates under ice in winter, or in the hypolimnion during periods of thermal stratification, can vent to the atmosphere during short windows following spring ice melt and fall turnover, respectively (Michmerhuizen and others 1996; Schubert and others 2012). These lake mixing patterns give rise to brief periods of intense emissions that have been shown to account for up to 45% of annual emissions (Michmerhuizen and others 1996; Bastviken and others 2004). Improving our understanding of spatiotemporal patterns in reservoir-CH_4 emissions is critical to including these systems in greenhouse gas (GHG) inventories (IPCC 2006; Fearnside 2015) and assessing the GHG footprint of hydropower (Hertwich 2013; Scherer and Pfister 2016).

Another process which may give rise to periods of elevated CH_4 emission rates in reservoirs is water-level drawdown. Water-level drawdowns are frequently conducted in reservoirs to increase flood storage capacity, generate hydropower, or to perform dam maintenance, among other reasons (Harrison and others 2017; Hayes and others 2017). Changes in water levels translate to shifts in hydrostatic pressure, which can play an important role in regulating CH_4 emissions. Here we treat hydrostatic pressure as the pressure at the sediment–water interface due to the weight of the overlying column of water and the atmosphere. Under conditions of constant hydrostatic pressure, gases produced via microbial activity dissolve in sediment porewaters until the combined partial pressures of the dissolved gases exceed the hydrostatic pressure, at which point bubbles are formed (Chanton and Whiting 1995). A fraction of these bubbles will grow large enough for their buoyancy to overcome the combined hydrostatic pressure and cohesive strength of the sediment, at which point they will migrate upward through the sediment. Rates of gas production via microbial activity often exceed rates of gas loss via ebullition during warm weather months, however, leading to the accumulation of large volumes of gas in reservoir sediment (Martinez and Anderson 2013; Tyroller and others 2016). When water levels fall, the hydrostatic pressure holding the bubbles in place diminishes, potentially leading to the release of a large fraction of the stored CH_4 to the atmosphere. This phenomenon is well documented in marine systems where tide-driven fluctuations in water le-

vels can trigger the release of CH_4 bubbles from coastal marsh sediments (Chanton and others 1989) and seafloor CH_4 seeps (Boles and others 2001).

Water-level declines have also been shown to trigger ebullition in reservoirs (Eugster and others 2011; Deshmukh and others 2014; Harrison and others 2017). Harrison and others (2017) recently demonstrated that ebullition during drawdown events can constitute more than 90% of annual CH_4 emissions from reservoirs in the Pacific Northwest (PNW) of the USA, suggesting that monitoring emissions during periods of water-level decline may be critical to constructing accurate annual CH_4 budgets.

In this research, we investigated spatial and temporal patterns in CH_4 emission rates from Harsha Lake, a reservoir draining an agricultural watershed in the Midwestern USA. Like the PNW reservoirs, water levels in Harsha Lake are drawn down in the fall to increase winter flood storage capacity. Unlike the PNW reservoirs, however, Harsha Lake supports a very high ebullitive CH_4 flux during the summer months (Beaulieu and others 2014, 2016), when the reservoir is managed for constant water levels. It was unclear whether the already high ebullition rate would be further enhanced by falling water levels in the fall.

We instituted an ecosystem-scale experiment by lowering water levels 27 times faster than normal for the first 24 h of the 3-month drawdown and then reducing the drawdown rate to that prescribed by the management schedule for the balance of the drawdown. Although the experimental drawdown rate (0.46 m day^{-1}) was much higher than that prescribed by the management schedule, it is realistic for this and other reservoirs. For example, the experimental drawdown rate is similar to drawdown rates that occur when flood waters are released from the reservoir following large storms and is comparable to drawdown rates reported for seven PNW reservoirs (0.12–0.66 m day^{-1}) (Harrison and others 2017). We monitored ebullition at nine sites spanning the length of the reservoir allowing us to determine (1) whether ebullition rates are related to rate of water-level decline and (2) whether the ebullitive response to the drawdown varied across the reservoir (that is, shallow vs deep waters).

Methods

Site Description

William H. Harsha Lake is a 7.9-km^2 eutrophic reservoir draining an 882 km^2 watershed in Ohio, USA (Figure 1). The reservoir was constructed in 1978, has a water storage capacity of 1.1×10^8 m^3, a maximum depth of 32.8 m during the summer months, and is monomictic. Large portions of the watershed are managed for agricultural production (63% cultivated crops and pasture), and the reservoir is frequently on the state's advisory list for recreational contact due to the abundance of harmful blue-green algae (http://epa.ohio.gov/habalgae.aspx).

The water-level management plan for the reservoir, known as the guide curve, targets a pool elevation of 223.4 m above mean sea level (m-msl) from May 1 through September 1 (that is, summer pool), at which point the pool is lowered at a constant rate to 221.9 m-msl by Dec. 1 (that is, winter pool), for a total drawdown of 1.5 m over a 3-month period. This period of water-level decline is commonly referred to as the 'fall drawdown.' Winter pool is maintained until April 1, at which point the water level is raised at a constant rate to summer pool by May 1. Low water levels are maintained during the winter, in part, to enhance flood protection.

To test the hypothesis that ebullition rates are dependent on the rate of water-level decline, we imposed an experimental treatment on the guide curve. We delayed the fall drawdown until 9:00 am on September 14, 2015, and then dropped the water level by 0.46 m over 24 h, a drawdown rate 27-fold greater than dictated by the guide curve. After the experimental drawdown, the rate of water-level decline was reduced to that prescribed by the guide curve.

Sampling Strategy

Nine monitoring sites were established across the reservoir (Figure 1). Six of the sites (EOF, EMB, EFL, EEB, ECP, and ENN) were collocated with long-term water quality monitoring sites sampled by the US Environmental Protection Agency and the US Army Corps of Engineers. Two additional sites (EUS2 and EUS3) were located along the river–reservoir transition zone, a known ebullition hot spot (Beaulieu and others 2014, 2016). The ninth site (EEB) was added to better characterize the strong east to west gradient in CH_4 emissions previously documented for the eastern basin.

Routine Sampling Campaign

All sites were sampled every other week from May 1 to July 6 and weekly from July 15, 2015, to December 11, 2015. Continuously recording gas traps (for example, automated traps, see 'Ebullition rate measurement' below) were used to measure volumetric ebullition rates, and discrete gas sam-

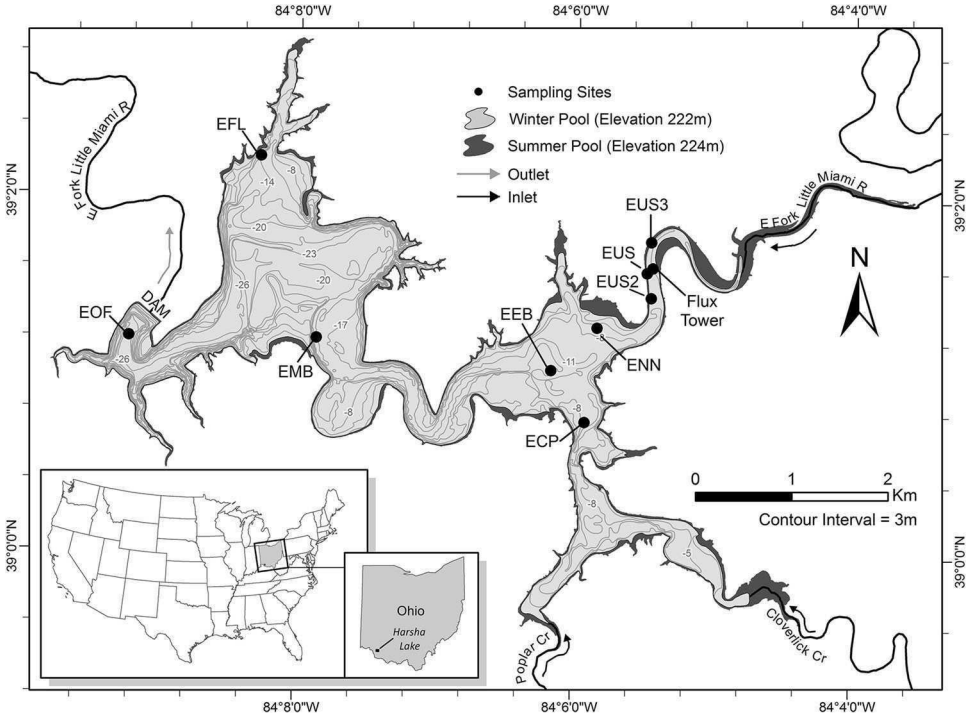

Figure 1. William H. Harsha Lake (Harsha Lake), tributaries, outlet, and sampling sites.

ples were collected from the traps for analysis of gas composition. Dissolved gas samples were collected from near the air–water interface and used to estimate diffusive CH_4 emission.

Drawdown Measurement Campaign

Ebullition rates were measured during the week of the drawdown experiment (September 10–15, 2015) using a version of the gas trap that accommodated higher ebullition rates, but was not equipped for continuous data logging (that is, passive traps, see 'Ebullition rate measurement' below). As with the routine sampling campaign, gas samples were collected from the traps for composition analysis. Emission rates were also measured using an eddy covariance system beginning 2 days before and ending 2 days after the drawdown experiment (September 12–17, 2015). Although diffusive CH_4 emissions were included in the eddy covariance-based estimates of CH_4 flux, dissolved gas concentrations and diffusive emissions were not directly monitored during the drawdown experiment.

Ebullition Rate Measurement

We measured ebullition rates using automated gas traps, with the exception of the week of the drawdown experiment (September 10–15, 2015) when we used passive gas traps. The design of the automated traps is described in Varadharajan and others (2010). Briefly, the automated trap consists of an inverted funnel (0.56 m diameter) suspended from a buoy and connected to a 0.97 m long by 1.25- or 2.5-cm-diameter vertical pipe that serves as a collection chamber. Accumulating gas caused the pressure in the collection chamber to increase, which was recorded every 5 min using a differential pressure sensor (Honeywell) and datalogger (U12–013, Onset Systems, Massachusetts, USA). The automated trap provides continuous measurements of gas volume until the signal from the differential pressure sensor reaches a maximum value, which occurs at a gas column height of 53–80 cm, depending on differences in the condition of individual sensor circuits. The sensors reached their maximum values in hours to days during this study (see Results below). The 1.25 and 2.5 cm collection chambers held up to 250 and 600 ml of gas, respectively, before overflowing into the funnel.

The relationship between the voltage readings from the differential pressure sensor and the height of the gas column in the collection chamber was established for each sensor circuit using laboratory calibrations performed at the beginning and end of the monitoring period. The height of the gas column in the trap (h_g; m) is calculated as:

$$h_g = m(V_{out} - V_{Zero}) \quad (1)$$

where m = sensor-specific laboratory calibration (m V^{-1}), V_{out} = voltage output from the differential pressure sensor, and V_{zero} = voltage output from the differential pressure sensor when there is no

gas in the trap immediately following deployment. The volume of gas (V_g; m^3) in the traps was calculated by multiplying h_g by the cross sectional area of the collection chamber.

During the drawdown experiment, we replaced the gas collection chamber and electronics on the automated traps with a 5-m length of 5.7-cm-diameter tubing. These 'passive' traps, which were not equipped to automatically record gas volumes, were designed to accommodate the high ebullition rates anticipated during the experimental drawdown. The anticipated ebullition rates would have quickly filled the smaller gas collection chambers on the automated traps, thereby greatly reducing the maximum deployment duration. Although we did not conduct a direct comparison of passive and automated gas traps, the systems only differed in the dimensions of the collection chamber (that is, identical funnels, buoys, weights, rope, anchor, etc.), which is unlikely to have affected the measured ebullition rates. The top of the collection chambers on both automated and passive traps was equipped with a rubber septum through which the accumulated gas was sampled with a syringe and needle.

Both automated and passive traps were deployed approximately 0.5 m below an anchored buoy. At each sampling visit, the total volume of gas in the automated or passive trap was measured and up to three 20 ml gas samples were collected in pre-evacuated 12-ml screw-top soda glass vials capped with a silicone-coated Teflon septa stacked on top of a chlorobutyl septa (Labco Ltd., UK). Gas samples were analyzed for CH_4 concentration using a gas chromatograph equipped with an autosampler, 250 µl sample loop, and flame ionization detector (Bruker 450 GC, USA). Mean variability among triplicate field samples was 1.9%.

Ebullitive CH_4 flux (mg CH_4 m^{-2} h^{-1}) is calculated as:

$$\text{Ebullitive } CH_4 \text{ flux} = \frac{V_g[CH_4]}{(T_F - T_I)A_F} \qquad (2)$$

where V_g is the volume of gas in the trap (l), $[CH_4]$ is the CH_4 concentration in the gas (mg CH_4 l^{-1}), T_I is the time the trap was deployed, and A_F is the cross-sectional area of the funnel (m^2). For passive traps, T_F is the time the trap was sampled at the end of a deployment. For automated traps, T_F is either the time the pressure sensor maxed out, or the time the trap was sampled, depending on whether or not the pressure sensor was saturated during the deployment. The calculated ebullition rate therefore represents an integration of the total gas captured between T_I and T_F. The 5-min logging interval was used to accurately determine the date and time that the pressure sensor reached it maximum value (T_F), rather than to calculate ebullition rates at a 5-min frequency.

Root-sum-squared error propagation was used to estimate uncertainty in ebullitive CH_4 flux (equation 2) based on uncertainty in V_g. For the passive traps, V_g was directly measured using syringes and uncertainty was determined by the precision of the syringes, which was 0.5 and 1.0 ml for the 30- and 140-ml syringes, respectively. Uncertainty in V_g for the automated traps was calculated by propagating error in m and electronic noise through equation 1 as described in Varadharajan and others (2010). The automated trap V_g error term also includes a 2-ml dead volume error, which accounts for gas that could be trapped in the fittings at the top of the collection chamber. Error in the other terms in equation 2 was negligible in comparison with the error in V_g.

We used control traps to assess the effect of gas exchange across the air–water interface in the collection chamber on the composition of gas stored in the traps. Control traps consisted of an automated trap (see above) with a 1 m × 1 m plexiglass sheet suspended below the funnel to prevent bubbles from entering the collection chamber. On five separate occasions, we added a mix of 90% CH_4 and 10% CO_2 to the control traps at the beginning of a 5- to 9-day deployment. The mean rate of change of the CH_4 partial pressure in the control traps (-0.28% day^{-1}) during the deployments was not significantly different than 0 (one-sided t test, $p = 0.15$), indicating that the CH_4 content of trapped bubbles was stable for at least 9 days. Harrison and others (2017) report that the CH_4 content of stored gas remained constant for 55 days in similar traps.

Data from deployments where the pressure sensor had not yet reached the maximum value at the time of sampling were used to compare the volume estimates derived from the sensor to those measured manually. The sensor-derived volume estimates were well correlated with manual measurements ($r^2 = 0.98$), and the slope of the regression between the two volume estimates was not statistically different than 1 (0.96 ± 0.059) (Figure S1), indicating that the sensor-derived estimates are precise and accurate.

Eddy Covariance Tower

Eddy covariance (EC) measurements of CH_4 fluxes from the river–reservoir transition zone (39°01′37.08″N, 84°05′26.82″W; Figure 1) started on September 12, 2015, at 8:30 pm, approximately

36 h before the experimental drawdown began and continued through September 17, 2015, at 4:30 pm, for a total of 232 30-min flux measurement periods. The EC system was mounted at 1.22 m above the pre-drawdown water surface by attaching the instrumentation to a large stable tree stump that protruded ~2 m above the water surface. An ultrasonic anemometer was used to measure 3-dimensional wind speed and direction (Model 81000, R. M. Young Company, Traverse City, MI, USA), and an LI-7700 open-path gas analyzer was used for fast measurements of CH_4 partial pressure (LI-COR Inc., Lincoln, NE, USA). Carbon dioxide (CO_2) and H_2O partial pressures were measured with an open-path infrared gas analyzer (LI7500A, LI-COR Inc., Lincoln, NE, USA), and the flux data were logged at 10 Hz using the LI7550 control unit (LI-COR Inc., Lincoln, NE, USA). The gas analyzers were mounted on either side of the ultrasonic anemometer so that the center of the optical paths was at the same height as the center of the ultrasonic anemometer (that is, vertical separation of zero). The horizontal distance between the ultrasonic anemometer and each gas analyzer was 30 cm. The system was powered with solar panels and 12 V batteries.

Data Processing

Fluxes of CH_4, CO_2, sensible heat and latent heat were calculated from the 10 Hz data using the software package EddyPro® (Version 6.1.0, LI-COR Inc., Lincoln, NE) and a flux-averaging interval of 30 min. An optimal averaging interval is as short as possible to characterize temporal patterns in fluxes, but long enough to measure flux contributions from low-frequency eddies. Previous work has shown that low-frequency contributions to turbulent fluxes typically converge at 30 min. Absolute limits were applied to the raw data, which were also de-spiked (Vickers and Mahrt 1997) and detrended using block averaging. Time lags were detected and compensated for via covariance maximization. The Webb, Pearman, Leuning (WPL) correction for density effects was applied for both CH_4 and CO_2 fluxes (Webb and others 1980), and the McDermitt and others (2011) spectroscopic correction for absorption line broadening due to temperature, pressure, and water vapor effects was applied to the LI-7700 CH_4 measurements. Spectral corrections for high- and low-pass filtering were applied (Moncrieff and others 1997, 2004), and flux footprints were estimated using the method of Kormann and Meixner (2001) and Kljun and others (2004). The flux calculations took into account the increase in the sensor height above the water surface as the lake level was drawn down using a dynamic metadata file in EddyPro®.

Several quality assurance criteria were applied to the 30-min CH_4 fluxes. Time periods that did not meet the requirements for stationarity and developed turbulent conditions were filtered (Foken and Wichura 1996; Deshmukh and others 2014). Methane fluxes were also filtered to exclude periods where the received signal strength indicator (RSSI) for the LI-7700 was less than 30% (Podgrajsek and others 2014), and periods where it was determined that greater than 10% of the flux footprint were from outside the lake. The minimum wind speed filter of 1 m s^{-1} used by Podgrajsek and others (2014) was not applicable to this study because of the lower measurement height.

Physicochemical Parameters and Diffusive Emission Rates

Unfiltered water samples were collected from a depth of 0.1 m at six sites (Figure 1; EOF, EFL, EMB, ECP, ENN, and EUS) every 3 weeks and analyzed for total phosphorus (TP), total nitrogen (TN), and chlorophyll *a*. Automated colorimetry (Lachat Instruments QuickChem 8000 Flow Injection Autoanalyzer, Loveland, CO, USA) was used to measure TP (Prokopy 1992) and TN (American Public Health Association 1995, followed by Wendt 1995) following acid persulfate and alkaline persulfate digestion, respectively. Chlorophyll samples were filtered (0.45 µm pore size) and the filtrate extracted with acetone. The absorbance of the extract was measured at 664, 647, and 630 nm with a spectrophotometer, and the chlorophyll *a* concentration was calculated using the trichromatic method (American Public Health Association 2012).

Dissolved oxygen and water temperature were measured at 1.5 m depth intervals at the deepest site (EOF) every two weeks using a data sonde (YSI, Yellow Springs, OH). Dissolved oxygen and water temperature were also measured at a depth 0.1 m below the water surface and 1 m above the sediment–water interface each time a trap was sampled.

A sample for dissolved CH_4 analysis was collected from a depth of 0.1 m during all trap visits from July 1 through December 11, 2015, with the exception of the traps sampled during the week of the experimental drawdown. Dissolved CH_4 samples were also collected at 1 m depth intervals at the deepest site (EOF) on four dates (July 8, August 26, September 30, and December 12, 2015). Dis-

solved CH_4 was sampled via headspace equilibration after collecting a 120-ml water sample using a 140-ml plastic syringe equipped with a 2-way stopcock. Immediately after the sample was collected, 20 ml of ultra-high-purity helium was added to the syringe that was then shaken for 5 min, and the headspace gas transferred to a pre-evacuated 12-ml screw-top soda glass vial capped with a silicone-coated Teflon septa stacked on top of a chlorobutyl septa (Labco Ltd, UK). The CH_4 partial pressure in the gas sample was measured via gas chromatography (see above), and the CH_4 concentration in the water was calculated from a mass balance of the liquid and gas in the syringe following:

$$(CH^0_{4,liq})(V_{liq}) = (CH_{4,liq})(V_{liq}) + (CH_{4,gas})(V_{gas}) \quad (3)$$

where $CH_{4,liq}^0$ is the CH_4 concentration ($\mu mol\ l^{-1}$) in the original water sample, V_{liq} and V_{gas} are the volumes (l) of liquid and gas in the syringe, and $CH_{4,liq}$ and $CH_{4,gas}$ are the CH_4 concentrations ($\mu mol\ l^{-1}$) in the liquid and gas, respectively, after the headspace equilibration. $CH_{4,liq}$ was calculated from $CH_{4,gas}$, the CH_4 Bunsen solubility coefficient for the temperature of the headspace equilibration, and the pressure of the headspace equilibration, which was assumed to be equal to that of the atmosphere. Atmospheric pressure was monitored continuously at the EFL sampling station (Solinst).

The equilibrium-dissolved CH_4 concentration in the reservoir ($CH_{4,eq}$; $\mu mol\ l^{-1}$) at the time of the dissolved gas sampling is calculated as:

$$CH_{4,eq} = (CH_{4,Atm})(\beta_T)(P_{Atm}) \quad (4)$$

where $CH_{4,Atm}$ is the global average CH_4 partial pressure in the atmosphere (1.85 ppm, http://www.esrl.noaa.gov/gmd/ccgg/trends_CH4/), β_T is the Bunsen solubility coefficient for CH_4 at the temperature of the water, and P_{Atm} is the atmospheric pressure (atm).

Diffusive CH_4 flux (mg CH_4 m^{-2} day^{-1}) is calculated according to:

$$\text{Diffusive } CH_4 \text{ flux} = k_{CH_4}(CH^0_{4,liq} - CH_{4,eq})0.16 \quad (5)$$

where k_{CH4} ($cm\ h^{-1}$) is the CH_4 gas transfer velocity (Wanninkhof and others 2009) and 0.16 is a unit conversion constant. k_{CH4} was assumed to be equal to the mean k_{CH4} measured in a survey of 115 sites in Harsha Lake (7.3 ± 0.9 cm h^{-1}) in 2014 (Beaulieu and others 2016).

Total Flux Scaled to Lake

A previous survey of CH_4 fluxes from 115 sites in Harsha Lake demonstrated that the river–reservoir transition zone is the source of 41% of total CH_4 emissions from the reservoir (Beaulieu and others 2016). We used this scaling factor to generate a system-scale estimate of the CH_4 flux rate from the measurements made at the nine monitoring stations following:

$$\text{System scale } CH_4 \text{ flux} = [\text{tributary flux} \times 0.41] + [\text{open water flux} \times 0.59] \quad (6)$$

where the tributary flux is the mean flux measured at EUS, EUS2, and EUS3. Open water flux is the mean flux measured at the remaining sites.

Statistical Analysis

The effect of water-level change on the ebullitive CH_4 flux was determined separately for the experimental drawdown and periods outside of the drawdown. The effect of the experimental drawdown was assessed by comparing the ebullitive CH_4 fluxes immediately prior to the experiment to those measured during the experiment. The effect of changes in water level and barometric pressure outside of the experimental drawdown was assessed using linear models. The dependent variable was the ebullitive CH_4 flux during each deployment at each station ($n = 254$), and the independent variable was the change in water level or barometric pressure during each deployment. The linear models also include 'site' as a main effect and the interaction of site and 'atmospheric pressure change' or 'water-level change.'

The emptying of the pool following large precipitation events in June and July led to several periods when the rate of water-level decline was similar to that during the experimental drawdown (Figure 2B). To determine whether these falling water levels increased the ebullitive CH_4 flux, we compared the ebullitive CH_4 flux during these periods of water-level declines to those measured immediately prior to the decline. All statistical analyses were performed using R (R Development Core Team 2016).

Results

Physical and Biogeochemical Setting

Harsha Lake was thermally stratified from late May, when the first depth profile was collected,

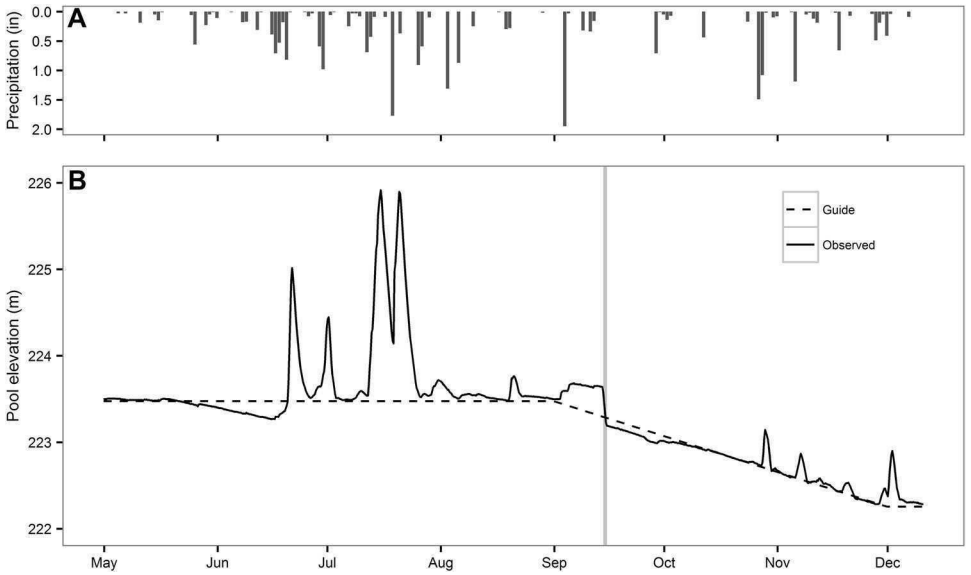

Figure 2. **A** Precipitation and **B** water levels at William H. Harsha Lake from May through December 2015. The *dashed black line* in panel B represents the management target and the *black line* represents the observed water levels. The *vertical gray line* represents the duration of the experimental water-level drawdown (Color figure online).

through mid-October (Figure S2). Dissolved oxygen was less than 0.1 mg l^{-1} in the hypolimnion during the period of stratification and less than 3 mg l^{-1} throughout the lake during fall turnover. Dissolved CH_4 concentration in the hypolimnion progressively increased during the period of thermal stratification, exceeding 1000 µmol l^{-1} by the end of September (Figure S3).

Mean TN and TP at a depth of 0.1 m were 1370 and 144 µg l^{-1}, respectively, across sites and dates (Table 1). Chlorophyll *a* was low in April (mean = 9 µg l^{-1}), high during the warm months (June–September mean = 50.1 µg l^{-1}) and returned to low levels in the fall (October–December mean = 5.9 µg l^{-1}). Dissolved CH_4 was supersaturated in the surface waters at all sites and sampling dates. Dissolved CH_4 at a depth of 0.1 m ranged from 0.03 to 70.2 µmol l^{-1} with an overall mean of 1.51 µmol l^{-1}. On average, the surface waters were supersaturated with CH_4 by a factor of 544 relative to the mean equilibrium concentration of 0.0027 µmol l^{-1}.

Below average precipitation in May and early June (Figure 2A) caused the pool elevation to fall 0.3 m below the management target (Figure 2B), but several large precipitation events in late June and July caused water levels to rise, reaching a maximum value 2.4 m above the management target. The pool elevation largely followed the guide curve in August, but strongly deviated from the guide curve during the experimental treatment in the first half of September. On September 5, 9 days prior to the planned drawdown experiment, the watershed received 1.95 inches of rain causing the pool elevation to rise by 0.17 m. This pool elevation was maintained until 9:00 am on September 14, at which point 0.46 m of water was spilled off the pool in 24 h. After the experimental treatment, the pool elevation fell at a rate closely approximating the guide curve.

Ebullitive and Diffusive Flux

There were 254 individual automated trap deployments during the study with a median deployment duration of 6.97 days. In 69% of the deployments, the differential pressure sensor reached its maximum value and stopped collecting useful data before the trap was sampled. The median period of time over which the pressure sensor collected useful data (that is, integration period) was 14 h for the three traps with a 2.5-cm-diameter collection chamber deployed in the river–reservoir transition zone (EUS, EUS2, and EUS3). The median integration period for all other automated traps was 41 h.

Uncertainty in the circuit calibration and the magnitude of the electronic noise are propagated through equation 2 to estimate uncertainty in the ebullitive CH_4 flux. All circuit calibrations had an r^2 of at least 0.994, and the mean standard deviation among pre- and post-deployment calibrations was 0.0635 cm V^{-1}, equivalent to 2.1% of the mean calibration coefficient (30.41 cm V^{-1}). The mean electronic noise from long-term deployments under constant differential pressure was 0.0005 V. These error terms resulted in an uncertainty in the ebullitive CH_4 flux of 8.2%, on average.

Methane partial pressure in collected bubbles ranged from 15.6 to 91.7% (mean = 64%) and was

Table 1. Monthly Mean (SE) Total Nitrogen (TN; μg N l^{-1}), Total Phosphorus (TP; μg P l^{-1}), Chlorophyll *a* (Chl *a*; μg l^{-1}), Dissolved Methane (CH_4; μmol l^{-1}), and Dissolved Oxygen (DO; mg l^{-1}) at the Monitoring Sites

	April	May	June	July	August	September	October	November	December
EOF									
TN	1385 (35)	998 (41)	1220 (112)	1630	1030	765 (53)	998	1125 (115)	1120
TP	261 (14)	97 (21)	95 (9)	106	82	84 (22)	137	93 (4)	91
Chl *a*	4 (1)	23 (2)	34 (19)	48	33	24 (1)	11	7 (2)	1
CH_4	NA	NA	NA	0.5 (0.3)	0.2 (0)	0.4 (0.1)	0.3 (0.1)	0.1 (0.04)	0.1
DO	NA	NA	NA	15.7 (2.04)	8.48 (0.56)	11.1 (1.1)	4.21 (1.58)	4.46 (0.13)	6.85
EMB									
TN	1686 (227)	1170 (116)	1489 (58)	1467 (133)	1047 (124)	873 (78)	1447 (279)	1300 (223)	1581 (395)
TP	382 (93)	163 (46)	85 (14)	129 (34)	118 (47)	113 (33)	302 (103)	177 (85)	217 (87)
Chl *a*	8 (1)	21 (4)	66 (5)	60 (5)	41 (3)	24 (3)	7 (2)	5 (1)	1 (0)
CH_4	NA	NA	NA	0.6 (0.3)	0.3 (0.1)	0.3 (0.1)	0.4 (0.1)	0.09 (0.03)	0.05
DO	NA	NA	NA	14.97 (1.65)	8.37 (0.92)	8.76 (2.17)	4.62 (0.86)	5.06 (0.27)	6.78 (0.75)
EFL									
TN	2193 (70)	1417 (145)	1591 (74)	1500 (121)	1017 (141)	916 (94)	1810	1923 (33)	1913
TP	587 (14)	222 (67)	124 (23)	126 (34)	122 (59)	139 (52)	480	426 (20)	436
Chl *a*	5 (1)	22 (5)	70 (8)	60 (3)	34 (3)	30 (4)	12	6 (3)	1
CH_4	NA	NA	NA	0.4 (0.1)	0.3 (0)	3.1 (2.8)	0.5 (0.2)	0.14 (0.03)	0.04
DO	NA	NA	NA	14.93 (1.31)	7.31 (0.91)	7.08 (2.65)	4.84 (0.96)	5.81 (0.31)	5.95
EEB									
CH_4	NA	NA	NA	1.1 (0.8)	0.5 (0.1)	0.6 (0.1)	0.4 (0.1)	0.14 (0.05)	0.6 (0.2)
DO	NA	NA	17.61	11.6 (1.43)	9.85 (1.07)	9.88 (2.04)	4.43 (0.85)	5.8 (0.21)	7.18 (0.01)
ECP									
TN	1258 (12)	828 (12)	1873 (315)	1280	1002	781 (85)	957	1139 (26)	1195
TP	249 (14)	69 (6)	163 (28)	170	107	74 (3)	128	93 (7)	98
Chl *a*	8 (7)	13 (1)	34 (10)	118	47	32 (11)	12	6 (1)	1
CH_4	NA	NA	NA	0.4 (0.2)	0.5 (0.1)	0.3 (0)	0.4 (0.2)	0.11 (0.06)	0.4 (0.1)
DO	NA	NA	NA	10.93 (1.18)	9.76 (1.13)	6.96	4.81 (0.68)	5.66 (0.41)	7.01 (0.15)
ENN									
TN	1315 (45)	1035 (46)	1716 (109)	1388 (195)	918 (47)	827 (36)	949	1125 (85)	1220
TP	249 (23)	92 (9)	106 (11)	141 (11)	97 (7)	81 (6)	125	97 (10)	101
Chl *a*	11 (3)	28 (10)	80 (6)	53 (2)	48 (4)	38 (5)	12	6 (2)	1
CH_4	NA	NA	NA	0.6 (0.4)	0.6 (0.2)	0.8 (0.3)	0.4 (0.1)	0.2 (0.1)	0.4 (0.2)
DO	NA	NA	NA	11.02 (0.94)	10.8 (1.29)	9.96 (2.82)	5.29 (0.44)	6.21 (0.26)	7.06 (0.12)
EUS2									
CH_4	NA	NA	NA	3.2 (2.3)	1.5 (0.1)	2.3 (0)	19.4 (16.9)	3.1 (0.5)	3.8 (3.1)
DO	NA	NA	NA	9.85 (1.31)	10.13 (1.05)	4.41 (2.71)	6.5 (0.53)	6.71 (0.56)	9.29 (0.31)
EUS									
TN	1480 (210)	1260 (0)	2837 (490)	1200	1150	1268 (342)	1290	1295 (45)	1490
TP	255 (23)	182 (15)	264 (28)	165	166	199 (67)	192	131 (24)	168
Chl *a*	16 (4)	52 (1)	92 (26)	66	59	62 (38)	29	5 (0)	1
CH_4	NA	NA	NA	2.4 (1.7)	1.3 (0.4)	1.5 (0.2)	1.8 (0.3)	3.1 (0.8)	4.1 (3.3)
DO	NA	NA	NA	8.36 (0.99)	9.43 (0.44)	8.46 (0.12)	6.43 (0.52)	6.66 (0.54)	8.56 (1.1)
EUS3									
CH_4	NA	NA	NA	2.8 (2.3)	1.8 (0.5)	1.6 (0)	2 (0.6)	3.7 (0.9)	3.5 (2.8)
DO	NA	NA	16.09	9.35 (2.19)	9.93 (0.88)	8.87 (0.73)	6.56 (0.75)	6.84 (0.59)	9.65 (0.03)

Samples were collected from a depth of 0.1 m. NA indicates data not available. No standard error provided if only one sample was collected in a month.

greater in the three sites located near the river inlet (EUS, EUS2, EUS3; mean = 72.4%) than the other sites (mean = 58.8%) (Table 2). Mean ebullitive CH_4 fluxes across the study (that is, site means across the 7-month observation period, excluding drawdown experiment) ranged from 4.0 to 109.7 mg CH_4 m^{-2} h^{-1} were highest in the river–reservoir transition zone (EUS, EUS2, ESU3) and

Table 2. Mean (SD) Methane (CH_4) Content of Collected Bubbles During the Study

	EOF	EMB	EFL	EEB	ECP	ENN	EUS	EUS2	EUS3
CH_4 (%)	62.5 (8.2)	60.9 (12.1)	62.9 (11.4)	52.9 (17.3)	54.9 (15.0)	59.2 (18.5)	69.0 (18.5)	75.2 (11.8)	72.9 (11.8)

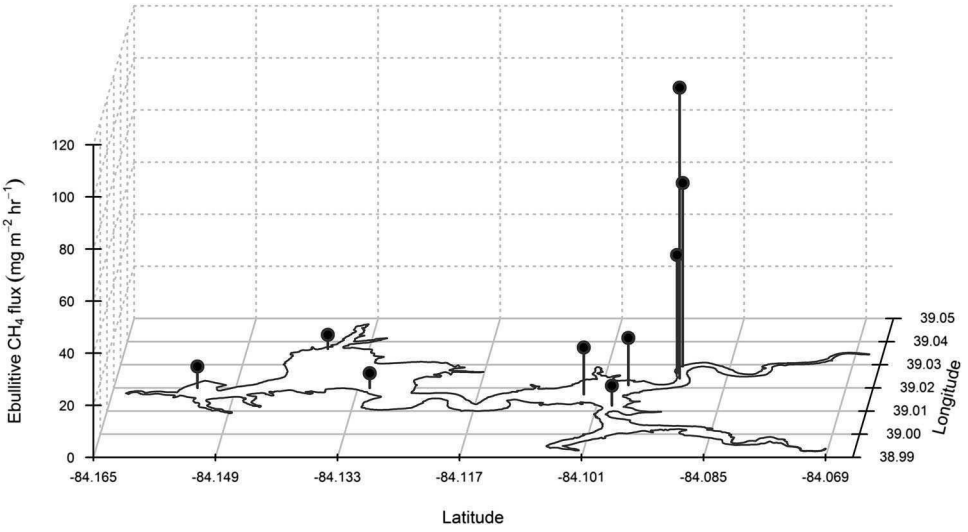

Figure 3. Mean ebullitive methane (CH_4) flux rate measured at the nine monitoring stations during the study. The reservoir perimeter is indicated in *black* on the *xy* plane, and the magnitude of the flux is indicated by the height of the *black line* according the scale on the *z*-axis.

lowest in the deeper waters in the west basin (Figure 3). The mean system-scale ebullitive CH_4 flux during the study, excluding the drawdown experiment, was 32.3 mg CH_4 m^{-2} h^{-1}. The mean diffusive CH_4 flux ranged from 0.39 to 6.75 mg CH_4 m^{-2} h^{-1} across the nine monitoring sites, with the highest rates occurring in the river–reservoir transition zone (Figure 4). At the system scale, diffusive emissions (mean = 2.0 mg CH_4 m^{-2} h^{-1}) comprised 6% of the total mean flux (ebullitive + diffusive; mean = 34.3 mg CH_4 m^{-2} h^{-1}).

Ebullitive CH_4 fluxes increased by a factor of 1.4–77 during the experimental water-level drawdown, but returned to background levels within 1 week (Figure 4). Diffusive emission rates were not measured during the drawdown experiment.

Correlation with Other Forcing Factors

When observations from the drawdown experiment were excluded, ebullitive CH_4 flux was unrelated to changes in barometric pressure ($p = 0.58$), but increased with falling water levels ($p = 0.006$). The effect of water-level change varied by site (significant site*water-level change interaction, $p < 0.001$) was strongest in the three shallowest sites (EUS, EUS2, and EUS3) and had the greatest effect at EUS3 (increase of 71 mg CH_4 m^{-2} h^{-1} per 1 m decline in water level at EUS3).

Eddy Flux Results

The EC measurement footprint is a function of sensor height, atmospheric stability, surface roughness, and wind direction (Kljun and others 2004). Both wind speed and direction displayed a strong diurnal pattern during the drawdown period. Low-speed winds (mean = 0.7 m s^{-1}) from the east by northeast direction were prevalent at night (8:00 pm–8:00 am), whereas moderate-wind speeds (mean = 1.3 m s^{-1}) from the south were prevalent during the day (9:00 am–5:00 pm) (Figure S4A). This resulted in EC measurement footprints that extended an average of 142 m to the south during the day and 45 m to the east by northeast at night (Figure 5A). The EC measurement footprint that captured 90% of the contributing area extended over land in only five of the 232 half-hour CH_4 flux estimates, and these periods were filtered from the final dataset. Applying this filter along with the other quality control checks outlined in the methods resulted in acceptance of 94.8% of the 30-min CH_4 flux data.

This acceptance rate is high relative to studies in terrestrial systems, but similar to the acceptance rates reported in other reservoir studies (Liu and others 2012, 2016). Over land, an important contributor to lower acceptance rates is the filtering of stable nighttime periods that do not pass the test for

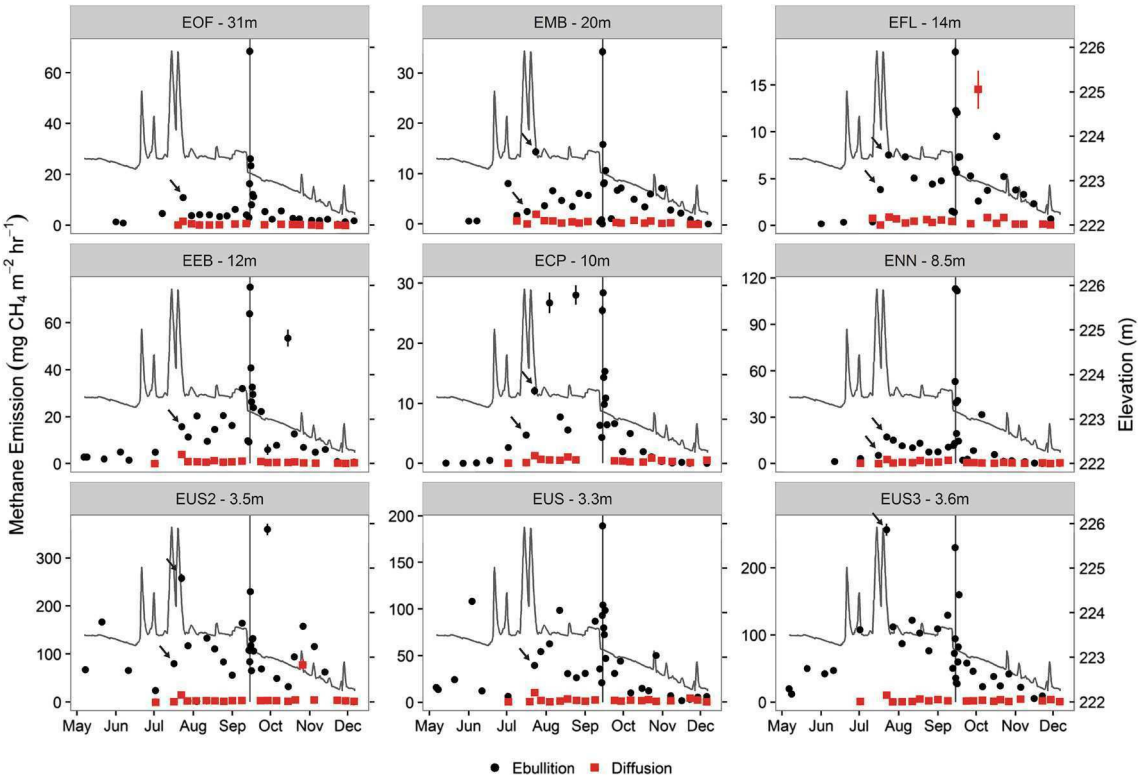

Figure 4. Ebullitive and diffusive methane (CH_4) flux time series at each of the nine monitoring sites. The name and depth of the sampling site are shown in the *gray header* at the *top* of each panel. *Error bars* represent the 95% confidence interval. The *vertical gray line* in each panel represents the duration of the experimental drawdown, and the *dark gray line* indicates the pool elevation. *Arrows* highlight observations made when water levels were falling due to the release of stored storm water.

developed turbulent conditions (Foken and Wichura 1996) or when the friction velocity (u_*) is below a certain threshold (Barr and others 2013). In aquatic systems, heat transfer from the water surface to the overlying air at night leads to convective mixing and unstable atmospheric conditions. Although we did not measure water surface temperature in this study, both the sensible and latent heat fluxes (H and LE, respectively) were positive at night (Figure S4B, C), indicating heat transfer from the water surface to the air. The friction velocity was low at night (u_*, Figure S4D), but since u_* is a measure of mechanically generated turbulence it is not a good indicator of stability regime over water bodies where buoyancy plays a larger role. Therefore, heat loss to the atmosphere at night and resulting buoyancy-generated turbulence lead to the overall high data acceptance rates in this study.

Prior to the drawdown (September 12, 8:30 pm–September 14, 8:30 am), the average (±SE) CH_4 flux was 133 ± 5.4 mg CH_4 m^{-2} h^{-1} (Figure 5B). The average CH_4 flux during the 24-h experimental drawdown (September 14, 9:30 am–September 15, 9:00 am) was 370 ± 20 mg CH_4 m^{-2} h^{-1}, with a maximum emission rate of 646 mg CH_4 m^{-2} h^{-1} observed on September 14 at 6:00 pm. The average CH_4 flux after the experimental drawdown (September 15, 9:30 am–September 17, 4:00 pm) was 212 ± 5.9 mg CH_4 m^{-2} h^{-1}.

Discussion

Methane fluxes from Harsha Lake were approximately tenfold greater in the river–reservoir transition zone (mean = 72.8 mg CH_4 m^{-2} h^{-1}, excluding drawdown) than in the main body of the reservoir (mean = 7.6 mg CH_4 m^{-2} h^{-1}, excluding drawdown) (Figures 3, 6). This is consistent with previous surveys in Harsha Lake, which have shown that the river–reservoir transition zone is a disproportionately important CH_4 source in the system (Beaulieu and others 2014, 2016). This spatial pattern has been documented for a wide variety of reservoirs including subtropical systems in Australia (Grinham and others 2011; Musenze

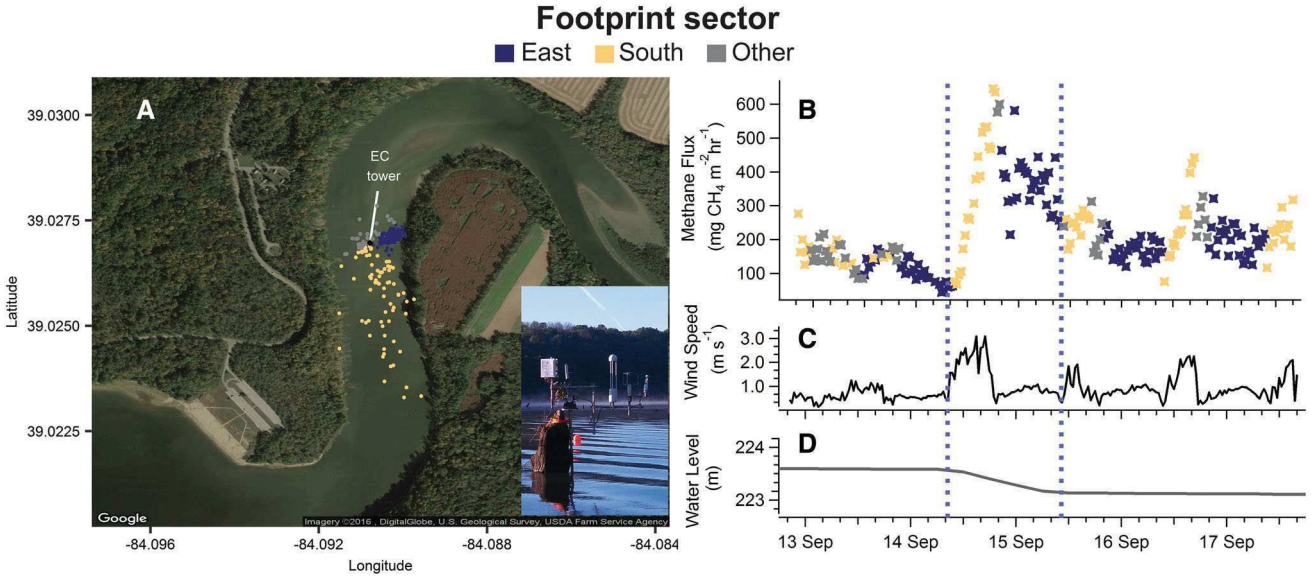

Figure 5. **A** The eddy covariance (EC) measurement footprint that includes 90% of the contributing area for each half-hour averaging period. The distance and angle between a point and the flux tower indicate the maximum extent and orientation, respectively, of the footprint during one half-hour averaging period. EC footprint areas extending to the south, east, and other directions are indicated by *yellow*, *blue*, and *gray dots*, respectively. The *inset* image is the flux tower deployed over the water surface. **B** Methane (CH_4) flux, **C** wind speed, and **D** water-level time series during the EC tower deployment. The *blue dashed lines* indicate the start and end of the experimental drawdown. The *color* of the markers in **B** corresponds to the orientation of the EC footprint area (see panel A) (Color figure online).

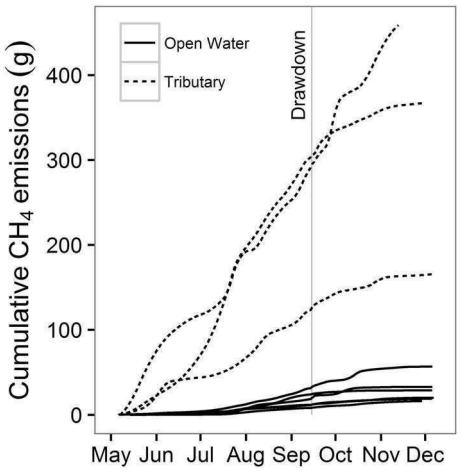

Figure 6. Cumulative methane (CH_4) emissions from the nine monitoring stations from May through December 2015. The *vertical gray line* represents the duration of the 24-h drawdown experiment.

and others 2014; Sturm and others 2014), reservoirs in the Pacific Northwest of the USA (Harrison and others 2017), and a large tropical reservoir (5400 km^2 surface area) in Africa (DelSontro and others 2011). River–reservoir transition zones are characterized by decreasing water velocities and the deposition of suspended sediment (Thornton 1990). When the sedimentation rate exceeds the carbon mineralization rate, labile carbon can be buried into deeper sediments where anoxia and methanogenesis are prevalent, thereby stimulating CH_4 production (Sobek and others 2009; Maeck and others 2013). This mechanism, combined with shallow water depths and low hydrostatic pressure, may account for the persistently high ebullitive CH_4 flux below the tributary inputs.

The mean system-scale total CH_4 flux (ebullition + diffusion) during the study (34.3 mg CH_4 m^{-2} h^{-1}) is higher than previously reported for Harsha Lake during the warm weather months (6.5–8.3 mg CH_4 m^{-2} h^{-1}; Beaulieu and others 2014, 2016), possibly due to methodological differences among studies. The earlier studies measured CH_4 fluxes (ebullitive and diffusive) using short-term (5–12 min) floating chamber deployments, whereas the current work utilized continuous monitoring over hours to days. Short-term monitoring may miss rare, but large, ebullition events, thereby underestimating ebullition rates (Varadharajan and Hemond 2012; Maeck and others 2014). Furthermore, the flux rates measured using the EC tower in the current study are somewhat higher than those measured using inverted funnels at the three monitoring stations located within the EC tower footprint (Figures 5B,

S5), possibly due to discrete hot spots affecting the tower and not the funnels, suggesting that the inverted funnel method is not overestimating the ebullitive CH_4 flux in this study.

The mean system-scale total CH_4 flux (ebullition + diffusion; 34.3 mg CH_4 m^{-2} h^{-1}) observed during this study is the highest yet reported for a reservoir (Figure S6), which contradicts earlier findings that high emission rates are restricted to tropical areas (Barros and others 2011). Our data join a growing body of the literature, indicating that temperate zone reservoirs in Europe and the USA can support CH_4 emission rates as high as those reported for the tropics (DelSontro and others 2010; Gruca-Rokosz and others 2011; Maeck and others 2013; Harrison and others 2017).

The high CH_4 fluxes from Harsha Lake may be linked to the high algal primary productivity of the reservoir. Methane emission rates have been shown to correlate with reservoir productivity at regional (West and others 2016; Harrison and others 2017) and global scales (Deemer and others 2016), suggesting that reservoir productivity may exert a strong control on CH_4 emission rates. Algal productivity could directly enhance CH_4 emissions by providing a source of labile carbon to methanogens. For example, laboratory studies have shown that additions of algal-derived carbon to aquatic sediments can stimulate CH_4 production (West and others 2012). Algal productivity could also indirectly enhance CH_4 emissions by promoting the development of anoxic conditions, which can stimulate methanogenesis and inhibit methanotrophy. Although CH_4 emission rates were not related to dissolved oxygen ($p = 0.17$) in this study, CH_4 concentrations in the anoxic hypolimnion exceeded 1000 μmol l^{-1} by late September (Figure S2), indicating substantial CH_4 production and accumulation in anoxic waters.

Emission Rate Response to Experimental Drawdown

The gas traps indicated that the experimental water-level drawdown at Harsha Lake triggered a synchronous system-wide increase in the ebullitive CH_4 flux (Figure 4). At most sites, ebullitive CH_4 flux during the drawdown was the highest recorded at any time during the 7-month monitoring period and exceeded fluxes observed during the 2–3 days immediately prior to the experiment at all sites. The CH_4 flux rates measured with the EC tower were also higher during the drawdown, increasing by a factor of 5 relative to the average pre-drawdown flux rate. The EC flux data also indicated a strong diurnal cycle, with higher flux rates observed during the day than at night. This diurnal pattern in flux rates coincided with a diurnal pattern in wind speed, wind direction, and turbulent mixing, resulting in a southerly EC footprint during the day and an easterly footprint at night (Figure 5A). The diurnal pattern in flux rates could therefore be partly attributed to higher CH_4 production rates in areas south of the EC tower than areas east of the tower, rather than a temporal pattern in CH_4 flux. Nevertheless, flux rates from both the southerly-daytime and easterly-nighttime footprints were higher during the drawdown compared to the day before the drawdown, indicating that declining water levels triggered ebullition from both footprint areas.

The experiment clearly demonstrated that rapid decreases in water level can trigger ebullition in Harsha Lake, likely due to the release of sediment gas bubbles following the drop in hydrostatic pressure. Although ebullition rates were higher at all sites during the drawdown, the shallow sites responded most strongly (Figure 7). This pattern was also evident when the drawdown data were excluded from the analysis and is consistent with reports from a subtropical reservoir (Nam Theun 2, Southeast Asia) where the effect of water-level change was stronger in shallow than deep sites (Deshmukh and others 2014). This pattern may be partly explained by differences in the proportional change in hydrostatic pressure for a given change in water level among the sites. The 0.46 m drop in

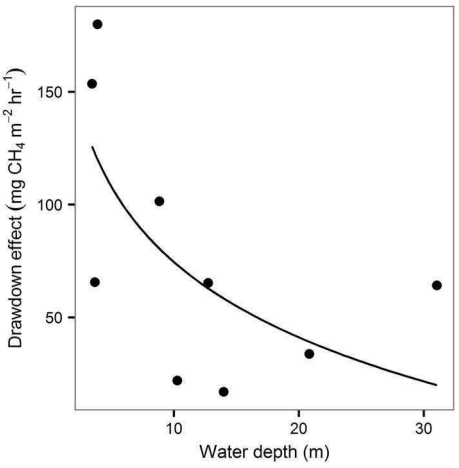

Figure 7. Relationship between the increase in the ebullitive methane (CH_4) flux rate during the 24-h drawdown experiment and water depth. The drawdown effect is calculated as the difference between the maximum ebullitive CH_4 flux during the experimental drawdown and that observed the day prior to the experiment.

water level during the drawdown resulted in less than a 2% decrease in hydrostatic pressure at the sediment surface at the 30-m deep site compared to a 10% decrease at the shallow sites.

Relationship with Water-Level Variation Outside of Drawdown

The rapid emptying of the pool following large precipitation events in June and July led to several periods when the rate of water-level decline was similar to that during the experimental drawdown. Ebullitive CH_4 fluxes during these periods of water-level decline were on average fivefold greater than the preceding week (Figure 4). One potential explanation for this pattern is that the increase in hydrostatic pressure that accompanied the rising water levels allowed additional CH_4 gas to accumulate in the sediments. This gas was subsequently released to the water column when water levels dropped and the system equilibrated to the lessened hydrostatic pressure.

Although rapidly falling water levels following precipitation events triggered elevated ebullitive CH_4 fluxes, at most sites the magnitude of the response was only a fraction of that observed during the experimental drawdown, despite the fact that water levels dropped by as much as 2.4 m following storms, whereas water levels dropped by only 0.46 m during the experimental drawdown. One difference between these periods of water-level decline is the duration that the pool was held at the pre-spill water level. The volume of gas released from sediments during periods of water-level decline will be related to the difference between the amount of gas stored in the sediments prior to the drawdown and the storage capacity of the sediments after the drawdown. While storms caused water levels to rise significantly, the pool was maintained at these high levels for only a brief period, and it is possible that the duration was too short for microbial gas production to substantially increase the volume of gas stored in the sediment. Therefore, the difference between the pre-drawdown gas storage and post-drawdown gas holding capacity may not have been great during the post-storm drawdowns. By contrast, the experimental drawdown dropped the pool to the lowest level in 5 months. The pervasive ebullition observed at all monitoring stations prior to the drawdown indicates that the gas holding capacity of the sediments was fully saturated at this time. Therefore, the difference between the pre-drawdown gas storage and post-drawdown gas holding capacity of the sediment was likely greater during the experimental drawdown than the post-storm drawdowns, possibly explaining why the fall drawdown triggered a much stronger response in the ebullitive CH_4 flux. The drawdown response may have been further enhanced by the 0.17 m rise in pool elevation that occurred nine days before the experiment. This change in pool elevation resulted from water that was stored in response to a 2 in storm event, rather than as a component of the experimental design. Nevertheless, the elevated hydrostatic pressure at the higher pool elevation likely allowed for additional gas to accumulate in the sediments, which was subsequently released to the water column during the drawdown.

Water levels continued to fall after the experimental drawdown, but at the much lower rate prescribed by the guide curve. Interestingly, there is little evidence in the data that the ebullitive CH_4 flux was elevated during this period, possibly because the rate of water-level decline was too low to trigger a detectable increase in ebullition. It is also likely that falling water temperatures during the 2.5-month drawdown caused sediment CH_4 production rates to decrease (Juutinen and others 2009; DelSontro and others 2010; Marotta and others 2014; Rasilo and others 2015), potentially offsetting the stimulatory effect of falling water levels on ebullition.

Cumulative Emissions

Although the ebullitive CH_4 flux increased by as much as an order of magnitude during the experimental drawdown, these elevated emission rates were short lived and constituted only 3.3% of cumulative CH_4 emissions from the sites during the study period (Figure 6). These results contrast markedly with results from Lacamas Lake, a eutrophic reservoir located in the Pacific Northwest USA where CH_4 emissions during an annual water-level drawdown constituted more than 90% of annual CH_4 emissions (Harrison and others 2017). Annual drawdowns in Lacamas Lake were deeper (1.5–2 m) and sustained for longer periods (1–2 weeks) than the experimental drawdown in this study, both factors which may help explain the divergent results between these two studies. Importantly, background ebullitive CH_4 flux rates differ markedly between Harsha and Lacamas lakes. In Lacamas, where ebullition rates were measured at multiple sites including the river–reservoir transition zone, rates outside of the drawdown periods were generally quite low, whereas the background ebullitive CH_4 flux rate at Harsha Lake is among the highest reported for any

reservoir (Figure S6). Given the high ebullitive CH_4 flux rates at Harsha Lake throughout the warm weather season, short-term increases during periods of rapidly falling water levels do not greatly increase annual emissions from the reservoir.

Although the one-time short-term period of rapidly falling water levels did not greatly increase annual CH_4 emissions from Harsha Lake, the effect of multiple periods of rapidly falling water levels should be considered. While this scenario is rare at Harsha Lake, it is the norm at nearby C. J. Brown reservoir where the fall drawdown consists of rapid water-level declines during the weekends to provide recreational flows to a downstream whitewater park (http://www.lrl-wc.usace.army.mil/plots/cbr.htm). Similarly, hydropower reservoirs managed for 'hydropeaking,' a process whereby river flows are increased during the day when energy demand is high and decreased at night when demand is low (Førsund 2007), are subject to regular periods of rapid water-level decline. Additional research is required to assess the impact of multiple drawdown events on annual CH_4 emissions.

Management Implications

Although this study did not test management strategies for reducing reservoir-CH_4 emissions, it adds to the growing body of evidence that water-level drawdowns can stimulate ebullitive CH_4 flux in reservoirs (Deshmukh and others 2014; Harrison and others 2017), thereby establishing a connection between water-level management and CH_4 emissions. Changes to water-level drawdown procedures could reduce annual scale emissions if the changes increase the fraction of CH_4 that is oxidized by methanotrophs (CH_4-oxidizing bacteria) to CO_2, a much less potent greenhouse gas (IPCC 2013). Aerobic CH_4 oxidation at the metalimnion and anaerobic CH_4 oxidation in the hypolimnion can be important CH_4 sinks in stratified lakes and reservoirs (Rudd and Hamilton 1978; Fallon and others 1980; Guérin and Abril 2007; Sturm and others 2016). Methane oxidation can also be a substantial CH_4 sink during fall overturn when oxygen-rich surface waters mix into deeper CH_4-rich waters (Kankaala and others 2006, 2007). Overall, methanotrophs have been shown to oxidize up to 95% of the CH_4 produced during the stratified period, substantially reducing CH_4 emissions to the atmosphere (Rudd and Hamilton 1978; Fallon and others 1980; Guérin and Abril 2007; Bastviken and others 2008). However, the proportion of produced CH_4 that is oxidized to CO_2 can be greatly diminished in systems with active ebullition because rising bubbles rapidly pass through the water column and are largely unaffected by CH_4 oxidation (Bastviken and others 2008), especially in shallow waters (McGinnis and others 2006). Water-level drawdowns that trigger ebullition may therefore increase the fraction of CH_4 that escapes oxidation and is emitted to the atmosphere. In the absence of a drawdown, this CH_4 may dissolve into sediment pore water, diffuse into the water column, and be oxidized to CO_2. This may be particularly relevant in the fall, when water-level drawdowns are frequently conducted, because decreasing water temperature will enhance CH_4 dissolution into porewaters. Furthermore, the temperature sensitivity of methanogens is much greater than that of methanotrophs (Borrel and others 2011) and falling water temperatures may cause the rate of CH_4 oxidation to approach and even exceed the rate of CH_4 production. The combined effects of falling water temperature on CH_4 production, oxidation, and dissolution may cause a growing fraction of sediment CH_4 gas to be oxidized to CO_2 during the fall, assuming that the gas is not stripped from the sediment via drawdown-induced ebullition. Therefore, the management objective should be to retain CH_4 gas within the sediments as long as possible in order to maximize CH_4 oxidation. This might be accomplished by (1) delaying fall drawdowns until after the sediment CH_4 gas load has been exhausted, or (2) conducting the drawdown at a rate of water-level decline that is too low to substantially enhance ebullition. Both of these approaches could be experimentally tested.

Taken together, the reservoir drawdown research conducted in the PNW (Harrison and others 2017) and this study suggest that altered water-level management has the greatest potential to mitigate CH_4 emissions from reservoirs that are subject to frequent drawdown events or have background ebullition rates substantially lower than those in Harsha Lake. Recent work in unproductive reservoirs in the southeastern region of the USA indicates that these systems have low ebullitive CH_4 fluxes during the summer months (0–0.7 mg CH_4 m^{-2} h^{-1}) and undergo water-level drawdown every fall (0.3–16 m) (Bevelhimer and others 2016). These systems meet the criteria for reservoirs where altered water-level management might mitigate emissions, and future research should determine whether emissions during the period of water-level drawdown constitute a disproportionate share of annual CH_4 emissions.

Water-level management represents one approach for mitigating emissions from reservoirs. Another approach that may be effective for reser-

voirs with high background ebullition rates, such as Harsha Lake, is watershed nutrient management. Several studies have shown a correlation between CH_4 emission rates and reservoir productivity (Deemer and others 2016; Harrison and others 2017), suggesting that watershed management strategies aimed at reducing nutrient loading to reservoirs may also reduce CH_4 emissions. A careful consideration of the suite of management options for mitigating CH_4 emissions from reservoirs will help minimize the greenhouse gas footprint of these important ecosystems.

ACKNOWLEDGEMENTS

We thank personnel from the Bob McEwen Water Treatment Plant, East Fork State Park, ODNR-wildlife, and US Army Corps of Engineers for coordinating the water-level drawdown experiment. CSS-Dynamac, Neptune Inc., and SRA International assisted with the preparation of the manuscript figures. Pegasus Technical Services provided field support. Additional laboratory and field support were provided by Megan Berberich, Dana Macke, Maria Mauer, Nick Seiler, Karen White, William Wright, Ryan Daly, and Lee Nanney. The views expressed in this article are those of the authors and do not necessarily reflect the views or policies of the US Environmental Protection Agency.

OPEN ACCESS

This article is distributed under the terms of the Creative Commons Attribution 4.0 International License (http://creativecommons.org/licenses/by/4.0/), which permits unrestricted use, distribution, and reproduction in any medium, provided you give appropriate credit to the original author(s) and the source, provide a link to the Creative Commons license, and indicate if changes were made.

REFERENCES

American Public Health Association. 1995. 4500-Norg D. Persulfate Method (Proposed). Standard Methods for the Examination of Water and Wastewater. Baltimore, MD: United Book Press Inc.

American Public Health Association. 2012. Standard methods for the examination of water and wastewater, Vol. 22Washington DC: American Public Health Association.

Barr AG, Richardson AD, Hollinger DY, Papale D, Arain MA, Black TA, Bohrer G, Dragoni D, Fischer ML, Gu L, Law BE, Margolis HA, McCaughey JH, Munger JW, Oechel W, Schaeffer K. 2013. Use of change-point detection for friction–velocity threshold evaluation in eddy-covariance studies. Agricultural and Forest Meteorology 171–172:31–45.

Barros N, Cole JJ, Tranvik LJ, Prairie YT, Bastviken D, Huszar VLM, del Giorgio P, Roland F. 2011. Carbon emission from hydroelectric reservoirs linked to reservoir age and latitude. Nature Geoscience 4:593–6.

Bastviken D, Cole J, Pace M, Tranvik L. 2004. Methane emissions from lakes: Dependence of lake characteristics, two regional assessments, and a global estimate. Global Biogeochemical Cycles 18:GB4009.

Bastviken D, Cole JJ, Pace M, Van de Bogert MC. 2008. Fates of methane from different lake habitats: Connecting whole-lake budgets and CH_4 emissions. Journal of Geophysical Research-Biogeosciences 113:G02024.

Bastviken D, Tranvik LJ, Downing JA, Crill PM, Enrich-Prast A. 2011. Freshwater Methane Emissions Offset the Continental Carbon Sink. Science 331:50.

Beaulieu JJ, McManus MG, Nietch CT. 2016. Estimates of reservoir methane emissions based on a spatially balanced probabilistic-survey. Limnology and Oceanography 61:S27–40.

Beaulieu JJ, Smolenski RL, Nietch CT, Townsend-Small A, Elovitz MS. 2014. High Methane Emissions from a Midlatitude Reservoir Draining an Agricultural Watershed. Environmental Science & Technology 48:11100–8.

Bevelhimer MS, Stewart AJ, Fortner AM, Phillips JR, Mosher JJ. 2016. CO2 is Dominant Greenhouse Gas Emitted from Six Hydropower Reservoirs in Southeastern United States during Peak Summer Emissions. Water 8:14.

Boles JR, Clark JF, Leifer I, Washburn L. 2001. Temporal variation in natural methane seep rate due to tides, Coal Oil Point area, California. Journal of Geophysical Research-Oceans 106:27077–86.

Borrel G, Jezequel D, Biderre-Petit C, Morel-Desrosiers N, Morel JP, Peyret P, Fonty G, Lehours AC. 2011. Production and consumption of methane in freshwater lake ecosystems. Research in Microbiology 162:832–47.

Chanton JP, Martens CS, Kelley CA. 1989. Gas-transport from methane-saturated, tidal freshwater and wetland sediments. Limnology and Oceanography 34:807–19.

Chanton JP, Whiting GJ. 1995. Trace gas exchange in freshwater and coastal marine environments: ebullition and transport by plants. In: Matson PA, Harriss RC, Eds. Biogenic trace gases: measuring emissions from soil and water. Oxford: Blackwell.

Deemer BR, Harrison JA, Li S, Beaulieu JJ, DelSontro T, Barros N, Bezerra-Neto JF, Powers SM, dos Santos MA, Vonk JA. 2016. Greenhouse Gas Emissions from Reservoir Water Surfaces: A New Global Synthesis. Bioscience 66:949.

DelSontro T, Kunz MJ, Kempter T, Wuest A, Wehrli B, Senn DB. 2011. Spatial Heterogeneity of Methane Ebullition in a Large Tropical Reservoir. Environmental Science & Technology 45:9866–73.

DelSontro T, McGinnis DF, Sobek S, Ostrovsky I, Wehrli B. 2010. Extreme Methane Emissions from a Swiss Hydropower Reservoir: Contribution from Bubbling Sediments. Environmental Science & Technology 44:2419–25.

Deshmukh C, Serça D, Delon C, Tardif R, Demarty M, Jarnot C, Meyerfeld Y, Chanudet V, Guédant P, Rode W, Descloux S, Guérin F. 2014. Physical controls on CH4 emissions from a newly flooded subtropical freshwater hydroelectric reservoir: Nam Theun 2. Biogeosciences 11:4251–69.

Downing JA, Prairie YT, Cole JJ, Duarte CM, Tranvik LJ, Striegl RG, McDowell WH, Kortelainen P, Caraco NF, Melack JM, Middelburg JJ. 2006. The global abundance and size distri-

bution of lakes, ponds, and impoundments. Limnology and Oceanography 51:2388–97.

Eugster W, DelSontro T, Sobek S. 2011. Eddy covariance flux measurements confirm extreme CH_4 emissions from a Swiss hydropower reservoir and resolve their short-term variability. Biogeosciences 8:2815–31.

Fallon RD, Harrits S, Hanson RS, Brock TD. 1980. The Role of Methane in Internal Carbon Cycling in Lake Mendota during Summer Stratification. Limnology and Oceanography 25:357–60.

Fearnside PM. 2015. Emissions from tropical hydropower and the IPCC. Environmental Science & Policy 50:225–39.

Foken T, Wichura B. 1996. Tools for quality assessment of surface-based flux measurements. Agricultural and Forest Meteorology 78:83–105.

Førsund FR. 2007. Hydropower Economics. New York: Springer.

Grinham A, Dunbabin M, Gale D, Udy J. 2011. Quantification of ebullitive and diffusive methane release to atmosphere from a water storage. Atmospheric Environment 45:7166–73.

Gruca-Rokosz R, Czerwieniec E, Tomaszek JA. 2011. Methane Emission from the Nielisz Reservoir. Environment Protection Engineering 37:101–9.

Guérin F, Abril G. 2007. Significance of pelagic aerobic methane oxidation in the methane and carbon budget of a tropical reservoir. Journal of Geophysical Research-Biogeosciences 112:G03006.

Harrison JA, Deemer BR, Birchfield MK, O'Malley MT. 2017. Reservoir Water-Level Drawdowns Accelerate and Amplify Methane Emission. Environmental Science & Technology 51:1267.

Hayes NM, Deemer BR, Corman JR, Razavi NR, Strock KE. 2017. Key differences between lakes and reservoirs modify climate signals: A case for a new conceptual model. Limnology and Oceanography Letters 2:47–62.

Hertwich EG. 2013. Addressing biogenic greenhouse gas emissions from hydropower in LCA. Environmental Science & Technology 47:9604–11.

Hofmann H. 2013. Spatiotemporal distribution patterns of dissolved methane in lakes: How accurate are the current estimations of the diffusive flux path? Geophysical Research Letters 40:2779–84.

IPCC. 2006. Appendix 3: CH4 Emissions from Flooded Land: Basis for Future Methodological Development. In: Eggleston HA, Buendia L, Miwa K, Ngara T, Tanabe K, Eds. IPCC Guidelines for national greenhouse gas inventories, Prepared by the National Greenhouse Gas Inventories Programme. Japan: IGES.

IPCC. 2013. Climate Change 2013: The Physical Science Basis. New York, NY: Cambridge University Press.

Juutinen S, Alm J, Larmola T, Huttunen JT, Morero M, Martikainen PJ, Silvola J. 2003. Major implication of the littoral zone for methane release from boreal lakes. Global Biogeochemical Cycles 17(4):1117. doi:10.1029/2003GB002105.

Juutinen S, Rantakari M, Kortelainen P, Huttunen JT, Larmola T, Alm J, Silvola J, Martikainen PJ. 2009. Methane dynamics in different boreal lake types. Biogeosciences 6:209–23.

Kankaala P, Huotari J, Peltomaa E, Saloranta T, Ojala A. 2006. Methanotrophic activity in relation to methane efflux and total heterotrophic bacterial production in a stratified, humic, boreal lake. Limnology and Oceanography 51:1195–204.

Kankaala PS, Taipale H, Nykanen H, Jones RI. 2007. Oxidation, efflux, and isotopic fractionation of methane during autumnal turnover in a polyhumic, boreal lake. Journal of Geophysical Research-Biogeosciences 112:G02033.

Kimmel BL, Lind OT, Paulson LJ. 1990. Reservoir Primary Production. In: Thornton KW, Kimmel BL, Payne FE, Eds. Reservoir Limnology. New York: Wiley-Interscience.

Kljun N, Calanca P, Rotach MW, Schmid HP. 2004. A simple parameterisation for flux footprint predictions. Boundary-Layer Meteorology 112:503–23.

Knoll LB, Vanni MJ, Renwick WH, Kollie S. 2014. Burial rates and stoichiometry of sedimentary carbon, nitrogen and phosphorus in Midwestern US reservoirs. Freshwater Biology 59:2342–53.

Kormann R, Meixner FX. 2001. An analytical footprint model for non-neutral stratification. Boundary-Layer Meteorology 99:207–24.

Liu HP, Zhang QY, Dowler G. 2012. Environmental Controls on the Surface Energy Budget over a Large Southern Inland Water in the United States: An Analysis of One-Year Eddy Covariance Flux Data. Journal of Hydrometeorology 13:1893–910.

Liu HP, Zhang QY, Katul GG, Cole JJ, Chapin FS, MacIntyre S. 2016. Large CO_2 effluxes at night and during synoptic weather events significantly contribute to CO_2 emissions from a reservoir. Environmental Research Letters 11:064001.

Maeck A, DelSontro T, McGinnis DF, Fischer H, Flury S, Schmidt M, Fietzek P, Lorke A. 2013. Sediment trapping by dams creates methane emission hot spots. Environmental Science & Technology 47:8130–7.

Maeck A, Hofmann H, Lorke A. 2014. Pumping methane out of aquatic sediments - ebullition forcing mechanisms in an impounded river. Biogeosciences 11:2925–38.

Marotta H, Pinho L, Gudasz C, Bastviken D, Tranvik LJ, Enrich-Prast A. 2014. Greenhouse gas production in low-latitude lake sediments responds strongly to warming. Nature Climate Change 4:467–70.

Martinez D, Anderson MA. 2013. Methane production and ebullition in a shallow, artificially aerated, eutrophic temperate lake (Lake Elsinore, CA). Science of the Total Environment 454–455:457–65.

McClain ME, Boyer EW, Dent CL, Gergel SE, Grimm NB, Groffman PM, Hart SC, Harvey JW, Johnston CA, Mayorga E, McDowell WH, Pinay G. 2003. Biogeochemical hot spots and hot moments at the interface of terrestrial and aquatic ecosystems. Ecosystems 6:301–12.

McDermitt D, Burba G, Xu L, Anderson T, Komissarov A, Riensche B, Schedlbauer J, Starr G, Zona D, Oechel W, Oberbauer S, Hastings S. 2011. A new low-power, open-path instrument for measuring methane flux by eddy covariance. Applied Physics B-Lasers and Optics 102:391–405.

McGinnis DF, Greinert J, Artemov Y, Beaubien SE, Wüest A. 2006. Fate of rising methane bubbles in stratified waters: How much methane reaches the atmosphere? Journal of Geophysical Research 111:C09007.

Michmerhuizen CM, Striegl RG, McDonald ME. 1996. Potential methane emission from north-temperate lakes following ice melt. Limnology and Oceanography 41:985–91.

Moncrieff JB, Clement R, Finnigan JJ, Meyers T. 2004. Averaging, detrending, and filtering of eddy covariance time series. In: Lee X, Massman WJ, Law BE, Eds. Handbook of micrometeorology: a guide for surface flux measurements. Dordrecht: Kluwer Academic. p 7–31.

Moncrieff JB, Massheder JM, deBruin H, Elbers J, Friborg T, Heusinkveld B, Kabat P, Scott S, Soegaard H, Verhoef A. 1997.

A system to measure surface fluxes of momentum, sensible heat, water vapour and carbon dioxide. Journal of Hydrology 189:589–611.

Musenze RS, Grinham A, Werner U, Gale D, Sturm K, Udy J, Yuan Z. 2014. Assessing the spatial and temporal variability of diffusive methane and nitrous oxide emissions from subtropical freshwater reservoirs. Environmental Science & Technology 48:14499–507.

Podgrajsek E, Sahlee E, Bastviken D, Holst J, Lindroth A, Tranvik L, Rutgersson A. 2014. Comparison of floating chamber and eddy covariance measurements of lake greenhouse gas fluxes. Biogeosciences 11:4225–33.

Prokopy WR. 1992. Determination of Total Phosphorus by Flow Injection Analysis Colorimetry (Acid Persulfate Digestion Method): Quickchem Method 10-115-01-1-F. Lachat Instruments, Loveland, Colorado.

R Development Core Team. 2016. R: A Language and Environment for Statistical Computing. Vienna: R Foundation for Statistical Computing.

Rasilo T, Prairie YT, Del Giorgio PA. 2015. Large-scale patterns in summer diffusive CH4 fluxes across boreal lakes, and contribution to diffusive C emissions. Global Change Biology 21:1124–39.

Rudd JWM, Hamilton RD. 1978. Methane Cycling in a Eutrophic Shield Lake and its Effects on Whole Lake Metabolism. Limnology and Oceanography 23:337–48.

Scherer L, Pfister S. 2016. Hydropower's Biogenic Carbon Footprint. PLoS ONE 11:e0161947.

Schilder J, Bastviken D, van Hardenbroek M, Heiri O. 2016. Spatiotemporal patterns in methane flux and gas transfer velocity at low wind speeds: Implications for upscaling studies on small lakes. Journal of Geophysical Research: Biogeosciences 121:1456–67.

Schilder J, Bastviken D, van Hardenbroek M, Kankaala P, Rinta P, Stötter T, Heiri O. 2013. Spatial heterogeneity and lake morphology affect diffusive greenhouse gas emission estimates of lakes. Geophysical Research Letters 40:5752. doi:10.1002/2013GL057669.

Schubert CJ, Diem T, Eugster W. 2012. Methane Emissions from a Small Wind Shielded Lake Determined by Eddy Covariance, Flux Chambers, Anchored Funnels, and Boundary Model Calculations: A Comparison. Environmental Science & Technology 46:4515–22.

Sobek S, Durisch-Kaiser E, Zurbrugg R, Wongfun N, Wessels M, Pasche N, Wehrli B. 2009. Organic carbon burial efficiency in lake sediments controlled by oxygen exposure time and sediment source. Limnology and Oceanography 54:2243–54.

Sturm A, Fowle DA, Jones C, Leslie K, Nomosatryo S, Henny C, Canfield DE, Crowe SA. 2016. Rates and pathways of CH4 oxidation in ferruginous Lake Matano. Indonesia. Biogeosciences Discuss. 2016:1–34.

Sturm K, Yuan Z, Gibbes B, Werner U, Grinham A. 2014. Methane and nitrous oxide sources and emissions in a subtropical freshwater reservoir, South East Queensland, Australia. Biogeosciences 11:5245–58.

Thornton KW. 1990. Perspectives on reservoir limnology. In: Thornton KW, Kimmel BL, Payne FE, Eds. Reservoir Limnology: Ecological Perspectives. New York: John Wiley & Sons. p 1–13.

Tyroller L, Tomonaga Y, Brennwald MS, Ndayisaba C, Naeher S, Schubert C, North RP, Kipfer R. 2016. Improved Method for the Quantification of Methane Concentrations in Unconsolidated Lake Sediments. Environmental Science & Technology 50:7047–55.

Varadharajan C, Hemond HF. 2012. Time-series analysis of high-resolution ebullition fluxes from a stratified, freshwater lake. Journal of Geophysical Research-Biogeosciences 117:G02004.

Varadharajan C, Hermosillo R, Hemond HF. 2010. A low-cost automated trap to measure bubbling gas fluxes. Limnology and Oceanography-Methods 8:363–75.

Vickers D, Mahrt L. 1997. Quality control and flux sampling problems for tower and aircraft data. Journal of Atmospheric and Oceanic Technology 14:512–26.

Wanninkhof R, Asher WE, Ho DT, Sweeney C, McGillis WR. 2009. Advances in Quantifying Air-Sea Gas Exchange and Environmental Forcing. Annual Review of Marine Science 1:213–44.

Webb EK, Pearman GI, Leuning R. 1980. Correction of Flux Measurements for Density Effects Due to Heat and Water-Vapor Transfer. Quarterly Journal of the Royal Meteorological Society 106:85–100.

Wendt K. 1995. Determination of nitrate/nitrite in surface and wastewaters by flow injection analysis: Quikchem Method 10-107-04-1-A. Lachat Instruments.

West WE, Coloso JJ, Jones SE. 2012. Effects of algal and terrestrial carbon on methane production rates and methanogen community structure in a temperate lake sediment. Freshwater Biology 57:949–55.

West WE, Creamer KP, Jones SE. 2016. Productivity and depth regulate lake contributions to atmospheric methane. Limnology and Oceanography 61:S51–61.

Wik M, Thornton BF, Bastviken D, Uhlbäck J, Crill PM. 2016. Biased sampling of methane release from northern lakes: A problem for extrapolation. Geophysical Research Letters 43:1256–62.

Zarfl C, Lumsdon AE, Berlekamp J, Tydecks L, Tockner K. 2015. A global boom in hydropower dam construction. Aquatic Sciences 77:161–70.

LIMNOLOGY and OCEANOGRAPHY

ASLO

Limnol. Oceanogr. 00, 2016, 00–00
Published 2016. This article is a U.S. Government work and is in the public domain in the USA. Limnology and Oceanography published by Wiley Periodicals, Inc. on behalf of Association for the Sciences of Limnology and Oceanography
doi: 10.1002/lno.10284

Estimates of reservoir methane emissions based on a spatially balanced probabilistic-survey

Jake J. Beaulieu,*[1] Michael G. McManus,[2] Christopher T. Nietch[1]

[1]US Environmental Protection Agency, National Risk Management Research Laboratory, Water Supply and Water Resources Division, Cincinnati, Ohio

[2]US Environmental Protection Agency, National Center for Environmental Assessment, Biological Assessment Branch, Cincinnati, Ohio

Abstract

Global estimates of methane (CH_4) emissions from reservoirs are poorly constrained, partly due to the challenges of accounting for intra-reservoir spatial variability. Reservoir-scale emission rates are often estimated by extrapolating from measurement made at a few locations; however, error and bias associated with this approach can be large and difficult to quantify. Here, we use a generalized random tessellation survey (GRTS) design to generate unbiased estimates of reservoir-CH_4 emissions rates (±95% CI) for areas below tributary inflows, open-waters, and at the whole-reservoir scale. Total CH_4 emission rates (i.e., sum of ebullition and diffusive emissions) were 4.8 (±2.1), 33.0 (±10.7), and 8.3 (±2.2) mg CH_4 m^{-2} h^{-1} in open-waters, tributary-associated areas, and the whole-reservoir for the period in August 2014 during which 115 sites were sampled across an 7.98 km^2 reservoir in Southwestern, Ohio, U.S.A. Tributary areas occupy 12% of the reservoir surface, but were the source of 41% of total CH_4 emissions, highlighting the importance of riverine-lacustrine transition zones. Ebullition accounted for > 90% of CH_4 emission at all spatial scales. Overall, CH_4 emission rates were high for a temperate zone reservoir, possibly because earlier studies underestimated ebullition or did not include emission hot spots. Confidence interval estimates that incorporated spatial pattern in CH_4 emissions were up to 29% narrower than when spatial independence is assumed among sites. The use of GRTS, or other probabilistic survey designs, can improve the accuracy and precision of reservoir emission rate estimates, which is needed to better constrain uncertainty in global scale emission estimates.

Methane (CH_4) is an important greenhouse gas accounting for approximately 40% of global radiative forcing due to anthropogenic activities (Stocker et al. 2013). Microbial degradation of organic matter in reservoirs is a significant source of CH_4 to the atmosphere, but estimates of the magnitude of this source are poorly constrained, ranging from 20 Tg CH_4 yr^{-1} to 70 Tg CH_4 yr^{-1} (St. Louis et al. 2000; Bastviken et al. 2011), partly due to the large range of CH_4 emission rates reported for reservoirs. Some of the variability in reported emission rates among systems can be attributed to differences in water temperature, reservoir age, and productivity (Barros et al. 2011; West et al. 2012), but another potentially large source of variability among studies is differences in how intra-reservoir spatial patterns in emission rates are assessed and incorporated into system-scale estimates. This source of variability is attributable to methodology, rather than true differences in emission rates, and therefore obscures spatial and temporal patterns in emission rates and adds uncertainty to emission rate estimates.

The factors that govern CH_4 production and emission from aquatic systems can lead to pronounced spatial patterns in CH_4 emission rates. Methane is produced in reservoirs from the degradation of organic matter under anoxic conditions, therefore one factor that governs CH_4 production rates is the quantity and quality of carbon delivered to the sediments (Sobek et al. 2012). Sediment deposition rates in reservoirs are often greatest in the transition zone between tributaries and open waters where water velocities rapidly decrease and suspended solids consequently settle (Thornton 1990). Also,

*Correspondence: Beaulieu.jake@epa.gov

Additional Supporting Information may be found in the online version of this article.

This is an open access article under the terms of the Creative Commons Attribution License, which permits use, distribution and reproduction in any medium, provided the original work is properly cited.

Special Issue: Methane Emissions from Oceans, Wetlands, and Freshwater Habitats: New Perspectives and Feedbacks on Climate
Edited by: Kimberly Wickland and Leila Hamdan.

littoral zone sediments are frequently enriched in organic material from senesced macrophytes (Polunin 1984) and dam forebays can be sites of rapid sediment accumulation in run of the river reservoirs (Maeck et al. 2013), all of which can lead to localized areas of elevated CH_4 production.

An important mechanism for the transport of CH_4 from sediments to the atmosphere is ebullition. Ebullition occurs when biogenic gas production raises the total dissolved gas pressure in sediment pore water above the hydrostatic pressure, leading to the formation of sedimentary gas bubbles. These bubbles can be released from the sediments, typically following a physical perturbation (Joyce and Jewell 2003), and dissolve in the water column as they rise toward the water surface where the residual content of the bubble is released to the atmosphere. The degree of dissolution that occurs is positively related to water depth, therefore a larger fraction of the original bubble mass directly escapes to the atmosphere in shallow compared with deep waters, leading to higher emissions from shallow waters. Additional spatial patterns in CH_4 emission rates within reservoirs can result from large plumes of inflowing river water with low CH_4 content (Hofmann 2013), point source discharges from waste water treatment plants with high organic matter content (DelSontro et al. 2010; Gonzalez-Valencia et al. 2014), and patterns in sediment cohesiveness that partially regulate the release of sedimentary gas bubbles (Joyce and Jewell 2003). Together, these spatial patterns in reservoir CH_4 emissions complicate efforts to generate system-scale estimates.

Estimating system-scale emission rates is problematic for two reasons. First, most investigations of reservoir CH_4 emissions include only 2–8 sampling sites per reservoir (Chen et al. 2011; Beaulieu et al. 2014; Gonzalez-Valencia et al. 2014; Musenze et al. 2014; Sturm et al. 2014), which can lead to large uncertainties in emission rate estimates. Recent advances in hydroacoustics (Ostrovsky et al. 2008; Maeck et al. 2013) and air-side CH_4 sensors (Grinham et al. 2011) can allow for higher sampling densities, but these approaches face several limitations that restrict their application including high detection limits and minimum water-depth requirements. Second, many studies that have detected spatial patterns have used judgment or convenience sampling to locate sites. How representative those samples are of the system is unknown and this can introduce a bias into estimates of reservoir emissions (Lohr 2010; Reynolds 2012).

Generating system-scale estimates of CH_4 emission rates for reservoirs is a problem that can be addressed using statistical survey designs. A key feature of a strong survey design is that the samples (i.e., sample sites) are representative of the population (i.e., whole-reservoir), so that population level estimates can be made with a known degree of accuracy (Lohr 2010). One approach for generating representative samples is probability sampling, in which each unit in the population has a known probability of selection and a randomization procedure is used to choose the specific sample units. A probability sampling approach that has been widely used to assess the status of lakes, estuaries, rivers, and streams in the United States (US Environmental Protection Agency 2009, 2012, 2013) is a generalized random tessellation survey design (GRTS) (Stevens and Olsen 2004; Olsen et al. 2012). An important feature of GRTS designs is that they are spatially balanced, meaning that the samples have a spatial distribution similar to that of the population, whereas random sampling designs can produce clusters of sample sites. GRTS designs can also utilize spatial patterns in the process of interest to generate estimates with less uncertainty than simpler survey designs (Stevens and Olsen 2003).

The focus of this study was William H. Harsha Lake (hereafter called Harsha Lake) located in southwest Ohio, U.S.A. Previous research has shown that total CH_4 emission rates (i.e., sum of ebullition and diffusive emissions) are up to 1000 times greater in areas below the largest tributary inflow than in open-water portions of the reservoir (Beaulieu et al. 2014), but this was based on measurements made at only six sites. The objective of this study was to generate a system-scale estimate of the mean (±95% confidence interval) diffusive, ebullitive, and total (i.e., diffusion + ebullition) CH_4 emission rate for the reservoir. To meet this objective we used a GRTS design. We modified the basic GRTS design to accommodate an "open-water" and "tributary" stratum, which allowed for comparison of emission rates between these areas of the reservoir.

Methods

Site description

The study was conducted at Harsha Lake, a monomictic reservoir located in Ohio, U.S.A. (Fig. 1). Harsha Lake was constructed in 1978 for flood control, water supply, recreation, and wildlife habitat. It has a surface area of 7.9 km^2, water storage capacity of 1.1×10^8 m^3, max depth of 32.8 m, and mean depth of 12.8 m at summer pool elevation. Harsha Lake drains an 882 km^2 watershed managed primarily for agriculture (63% cultivated crops and pasture) and is frequently on the state's advisory list for recreational contact due to the abundance of harmful blue-green algae (http://epa.ohio.gov/habalgae.aspx).

Survey design

The sample frame for a GRTS design is a geographic information system (GIS) layer (Olsen et al. 2012). We used a polygon shapefile of Harsha Lake obtained from the high resolution National Hydrography Dataset (http://nhd.usgs.gov) with an Albers equal area projection. We partitioned the reservoir into "open-water" and "tributary" strata. The tributary stratum contained areas of the reservoir extending from the points where the 13 largest tributaries enter the reservoir out to a depth of 8 m (Fig. 1) and covered 0.97 km^2 of the reservoir surface (Table 1). The boundary between the open-water and tributary strata was based on previous work

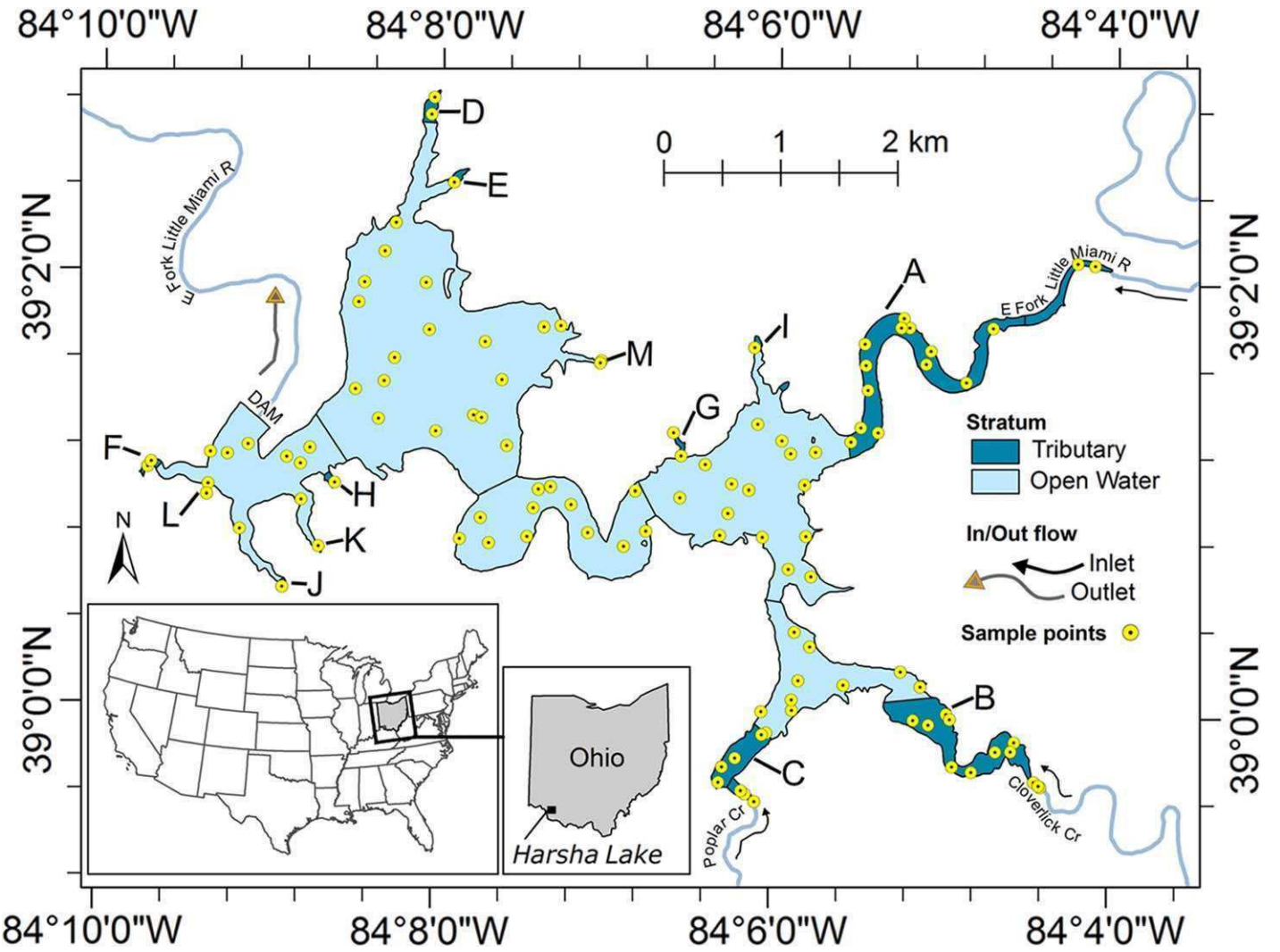

Fig. 1. William H Harsha Lake (Harsha Lake), tributaries, outlet, and sampling sites. Colors differentiate the open-water and tributary strata. Sample sites were allocated to the polygons within each stratum using an unequal probability GRTS survey design. Letters identify the 13 areas below tributary inputs that were sampled.

which indicated that emission rates rapidly decreased at depths > 8 m (Beaulieu et al. 2014). All other portions of the reservoir were included in the open-water stratum which covered 7.01 km^2 of reservoir surface. We allocated sample sites across the sample frame using a GRTS survey design. To ensure that the design included sample points in some of the smaller areas of the reservoir, such as the upstream tips of the tributary-associated areas, the open-water and tributary-associated strata were subdivided into 5 and 20 polygons, respectively. Using an unequal probability GRTS survey design, we specified the number of sample sites to be allocated to each polygon. Previous research indicated that CH_4 emission rates were more spatially variable below tributaries than in open-waters in Harsha Lake (Beaulieu et al. 2014), we therefore adopted a sample density that was 10-fold greater in the tributary than open-water stratum. The multiple constraints we placed on the design (i.e., allocation of sample points to many separate tributary areas, sample points along the length of the largest tributary areas, etc.) resulted in a survey that included 65 and 50 sites in the open-water and tributary strata, respectively (Fig. 1). The GRTS survey was designed using the spsurvey package (Kincaid and Olsen 2015) in the statistical software R (R Development Core Team 2015).

The GRTS algorithm in the spsurvey package imposes a series of nested grids across the sample frame (i.e., reservoir surface area) which are used to map two-dimensional space into one-dimensional space. Sample sites are then allocated to a subset of these grids using a hierarchical randomization process which ensures a spatially well-balanced sample. The probability that a sample will be located in a specific grid cell is proportional to the area of the resource contained

Table 1. Watershed drainage area and reservoir surface area associated with the 13 largest tributaries draining into Harsha Lake. Tributary labels correspond to the site map in Fig. 1.

Tributary	Surface area (km^2)	Drainage area (km^2)
A	0.47	665.0
B	0.30	110.6
C	0.13	65.0
D	0.003	10.0
E	0.010	9.1
F	0.007	5.2
G	0.009	3.5
H	0.024	3.1
I	0.003	2.6
J	0.011	2.6
K	0.002	2.0
L	0.002	2.0
M	0.007	1.0

within the cell. The specific location of a sample point within a cell is determined by selecting random x and y-coordinates while ensuring the coordinates fall within the resource (i.e., within the reservoir). The result is a spatially balanced probabilistic survey design. Consult Olsen et al. (2012), Stevens and Olsen (2004), and Kincaid and Olsen (2015) for a detailed description of the GRTS algorithm.

Methane and CO_2 emission rates, dissolved CO_2, dissolved CH_4, dissolved oxygen, alkalinity, pH, specific conductivity, water temperature, barometric pressure, and air temperature were measured once at each site between 18 August 2014 and 27 August 2014. Chlorophyll *a* (Chl *a*) samples were collected from one tributary and five open-water sites on 12 August 2014 and 02 September 2014.

Water sample collection

Samples for dissolved CH_4 analysis were collected in 160 mL glass infusion bottles. The infusion bottles were prepared in the laboratory by first adding 130 μL of a saturated mercuric chloride solution to the bottles, capping the bottles with gray butyl septa and aluminum crimps, and alternately evacuating to 6.6 Pa and filling with ultra-high purity dinitrogen (UHP N_2) to 101.3 kPa (101.3 kPa = 1 atm). After the third evacuation, 40 mL of UHP N_2 was added to each bottle.

Water samples were collected in the field by suspending the bottle below the water surface, puncturing the septa with a 27 gauge needle and allowing the vacuum in the bottle to draw water through the needle until the headspace pressure in the bottle was equal to the hydrostatic pressure at the needle inlet. The needle was removed underwater and the sample bottle stored in an opaque box during transport to the laboratory.

Within 10 d of collection, the infusion bottles were placed on a shaker table for 1 h to equilibrate the gases between the aqueous and gas phase. Immediately after the headspace equilibration, the septa was punctured with a 27 gauge needle connected to a two-way stopcock and 60 mL syringe. The syringe plunger was withdrawn to 40 mL, the stopcock closed, and the plunger allowed to relax until the pressure in the syringe was equal to that of the lab atmosphere, typically resulting in a 25 mL gas sample at approximately 101.3 kPa (101.3 kPa = 1 atm) pressure. Twenty milliliters of the sample was then transferred to a pre-evacuated (<6.6 Pa) 12 mL glass vial capped with a teflon backed silicon septa stacked on top of a chlorobutyl septa (order code 736W, Labco Ltd, UK) for analysis. Gas samples were analyzed for CH_4 partial pressure (P_{CH_4}) using a gas chromatograph (Bruker 450, Massachusetts, U.S.A.) equipped with an autosampler (PAL LHX-xt, CTC Analytics, Switzerland) and flame ionization detector. The dissolved CH_4 concentration in the original water sample was calculated from the Bunsen solubility coefficient at the temperature of the headspace equilibration and a mass-balance for the headspace equilibration system.

The mercuric chloride preservative depressed the pH of the water sample in the infusion bottles, therefore dissolved CO_2 in the reservoir could not be determined from the headspace equilibration. We calculated dissolved CO_2 from alkalinity, water temperature, pH, and specific conductivity using the seacarb package (Gattuso et al. 2015) in R.

Alkalinity was measured on unfiltered water samples using the titration method and Chl *a* was measured via the spectrophotometric method following acetone extraction (APHA 2012). We measured pH, water temperature, dissolved oxygen, and specific conductivity using a data sonde (YSI 6600, Yellow Springs, Ohio, U.S.A.). Air temperature was measured using an alcohol thermometer and pressure was measured using a barometer (YSI MDS, Yellow Springs, Ohio, U.S.A.).

Emission rate measurements

We measured CO_2 and CH_4 emission rates using 20 L floating acrylic chambers tethered to a drifting boat via a 1 m long boom. The chamber headspace was recirculated through a portable CH_4 and CO_2 analyzer (Ultraportable Greenhouse Gas Analyzer, Los Gatos Research, Los Gatos, Colorado, U.S.A.) carried on-board the boat and powered with a 12 V battery. The analyzer measures CO_2 and CH_4 partial pressures (P_{CO_2} and P_{CH_4}, respectively) at 1 Hz using off-axis integrated cavity output spectroscopy. To minimize analytical noise, we averaged partial pressure measurements made at a frequency of 1 Hz for 20 s before recording a value. The chamber was deployed for 5 min at each site, resulting in 15 recorded partial pressure values per deployment.

We calculated diffusive CO_2 and CH_4 emissions, and when possible, CH_4 ebullition. Methane ebullition was apparent as an abrupt P_{CH_4} increase in the chamber headspace, whereas diffusive emissions caused P_{CH_4} and P_{CO_2} to change at a relatively constant rate (Supporting Information Fig. S1). Diffusive emission rates ($E_{gas,D}$) were calculated from a

minimum of five partial pressure measurements recorded prior to ebullition following:

$$E_{\mathrm{gas},D} = \frac{\mathrm{d}P_{\mathrm{gas}}}{\mathrm{dT}} \left(\frac{V}{A}\right) \left(\frac{P}{RT}\right) \quad (1)$$

where $\frac{\mathrm{d}P_{\mathrm{gas}}}{\mathrm{d}T}$ is the rate of change of $P_{\mathrm{CH_4}}$ or $P_{\mathrm{CO_2}}$ in the chamber headspace, V is the chamber volume, A is the area of the chamber opening, P is the pressure in the chamber headspace, R is the universal gas constant, and T is temperature in the chamber headspace. The rate of change of P_{gas} in the chamber headspace was calculated using simple linear regression and a non-linear model. Linear models underestimate $\frac{\mathrm{d}P_{\mathrm{gas}}}{\mathrm{d}T}$ at $t = 0$ when the rate of change of P_{gas} decreases during the deployment, which can occur in response to the lessening of the concentration gradient between the headspace and the water body during the deployment. The non-linear model took the form:

$$P_{\mathrm{gas},t} = P_{\mathrm{gas,max}} - \left[\left(P_{\mathrm{gas,max}} - P_{\mathrm{gas},0}\right) \exp\left(^{-Kt}\right)\right. \quad (2)$$

where $P_{\mathrm{gas,t}}$ and $P_{\mathrm{gas},0}$ are $P_{\mathrm{CH_4}}$ or $P_{\mathrm{CO_2}}$ at time = t and time = 0, respectively, $P_{\mathrm{gas,max}}$ is the maximum $P_{\mathrm{CH_4}}$ or $P_{\mathrm{CO_2}}$ observed during the deployment, and K is a rate constant (Demello and Hines 1994; Stolk et al. 2009). These terms are regression parameters that were estimated using non-linear curve fitting procedures in the minpack.lm library (Elzhov et al. 2013) in the statistical software R. The regression parameters were used to calculate the rate of change of P_{gas} at $t = 0$ following:

$$\frac{\mathrm{d}P_{\mathrm{gas}}}{\mathrm{d}T} = K\left(P_{\mathrm{gas,max}} - P_{\mathrm{gas},0}\right) \quad (3)$$

Akaike information criterion (AIC) was used to determine whether the linear of non-linear model best described the data and only models with an $r^2 > 0.9$ were retained.

When fewer than five $P_{\mathrm{CH_4}}$ measurements were recorded prior to a CH_4 ebullition event, or the CH_4 model had an $r^2 < 0.9$, $E_{\mathrm{CH_4},D}$ was calculated from the measured dissolved CH_4 concentration and an estimated CH_4 gas transfer velocity ($k_{\mathrm{CH_4}}$):

$$E_{\mathrm{CH_4},D} = k_{\mathrm{CH_4}}\left(C_{\mathrm{CH_4},W} - C_{\mathrm{CH_4,eq}}\right) \quad (4)$$

where $C_{\mathrm{CH_4},W}$ is the measured CH_4 concentration in the water (see below) and $C_{\mathrm{CH_4,eq}}$ is the concentration of CH_4 in the surface water at equilibrium with the atmosphere (Wanninkhof et al. 2009). The equilibrium dissolved CH_4 concentration was calculated from the CH_4 partial pressure in the atmosphere (assuming 100% humidity) and the temperature specific Bunsen solubility coefficient (Colt 2012). The CH_4 gas transfer velocity was calculated one of two ways. In the first approach, $k_{\mathrm{CH_4}}$ was estimated from $k_{\mathrm{CO_2}}$ which was calculated by rearranging Eq. 4 and substituting CO_2 for CH_4. This approach was employed when the chamber data allowed for the calculation of $E_{\mathrm{CO_2},D}$ and the water pH < 8.5. At high pH, $k_{\mathrm{CO_2}}$ is enhanced relative to $k_{\mathrm{CH_4}}$ by the reaction of CO_2 with hydroxide, which maintains a steeper CO_2 concentration profile at the air–water interface (Schindler et al. 1972; Bade and Cole 2006; Wanninkhof et al. 2009). The CH_4 gas transfer velocity was calculated from $k_{\mathrm{CO_2}}$ according to:

$$k_{\mathrm{CH_4}} = k_{\mathrm{CO_2}} \left(\frac{Sc_{\mathrm{CH_4}}}{Sc_{\mathrm{CO_2}}}\right)^{-0.5} \quad (5)$$

where Sc is the Schmidt number for CH_4 ($Sc_{\mathrm{CH_4}}$) and CO_2 ($Sc_{\mathrm{CO_2}}$) (Wanninkhof et al. 2009). Schmidt numbers were calculated following Wanninkhof (1992). If $E_{\mathrm{CO_2},D}$ could not be calculated or the water pH > 8.5, $k_{\mathrm{CH_4}}$ was assumed to be equal to the average of the $k_{\mathrm{CH_4}}$ values measured at the 2–3 closest sites on the same day.

The total CH_4 emission rate ($E_{\mathrm{CH_4},T}$) represents the sum of the ebullitive ($E_{\mathrm{CH_4},E}$) and diffusive ($E_{\mathrm{CH_4},D}$) emission rates. In the instances where no ebullition was observed, $E_{\mathrm{CH_4},T}$ was equal to $E_{\mathrm{CH_4},D}$. When ebullition was observed, however, $E_{\mathrm{CH_4},T}$ was calculated from the difference between the initial and final $P_{\mathrm{CH_4}}$ measurement. The ebullition rate was calculated as the difference between $E_{\mathrm{CH_4},T}$ and $E_{\mathrm{CH_4},D}$.

Data analysis

We calculated population level estimates of the mean $E_{\mathrm{CH_4},T}$, $E_{\mathrm{CH_4},E}$, and $E_{\mathrm{CH_4},D}$ at the stratum (i.e., open-water, tributary) and whole-reservoir scale using an approach based on the Horvitz–Thompson theorem as described in Stevens and Olsen (2003). Population level estimates of variance (i.e., 95% confidence interval) were calculated using the local neighborhood variance estimator (95% $\mathrm{CI_{LN}}$) (Stevens and Olsen 2003) and the Horvitz–Thompson variance estimator, which is based on the assumption of independent random sampling (95% $\mathrm{CI_{IRS}}$). The local neighborhood variance estimator is designed for surveys conducted over space as it can incorporate spatial patterns of the data thereby producing narrower confidence limits than other variance estimators (Stevens and Olsen 2003). Differences in emission rates between the open-water and tributary strata were determined to be statistically significant if the population mean ± 95% $\mathrm{CI_{LN}}$ did not overlap. Population level estimates were made using the spsurvey package (Kincaid and Olsen 2015) in R.

We calculated extent estimates of the proportion of the three spatial areas (e.g., open-water, tributary, and whole-reservoir) that supported ebullition. The analysis was based on whether or not ebullition was observed at each site (i.e., coded as True or False) and was executed using the cat.analysis function in spsurvey package.

To detect spatial patterns in CH_4 ebullition, we created Thiessen polygons around the sample sites, clipped those

polygons to the contour of the lake, and used the polygons to define neighborhoods around the sampling sites based on rook-style contiguity (Bivand et al. 2008). We used a join count statistic to determine if the presence or absence of ebullition in the polygons exhibited spatial autocorrelation (de Smith et al. 2013).

To determine whether differences in CH_4 emission rates between strata could be explained by depth, or whether factors other than depth played a role, we used a generalized least squares model to compare CH_4 emission rates measured at similar depths in the two stratum. We only used observations made at sites with water depths that were represented in both strata, therefore all sites < 1 m (i.e., sites < 1 m deep occurred exclusively in the tributary stratum) and > 4 m (i.e., sites > 4 m deep occurred predominantly in the open-water stratum) in depth were excluded from the analysis. The analysis was done using the nlme package (Pinheiro et al. 2011) in R.

To examine the relationship between sampling effort and population estimates of the total CH_4 emission rate, we calculated the mean and 95% CI_{LN} using subsets of the survey data. Each sample subset was created by selecting the first "n" and "m" points from the list of open-water and tributary sites used in the full survey, respectively. Each sample subset created in this manner represents a spatially balanced probabilistic survey design. Each sample subset had the same ratio of open-water to tributary sites (65: 50) used in the full survey.

Results

Dissolved gases and water chemistry

Dissolved CH_4 was supersaturated at all sites (range; 139–3117% saturation) and concentrations ranged from 0.14–3.1 μM in the open-water stratum and 0.31–2.9 μM in the tributary stratum (Table 2). Carbon dioxide was undersaturated at all open-water sites (range: 8–54% saturation, 0.9–5.8 μM), but was more variable in the tributary-area stratum with concentrations ranging from 0.8 μM to 129 μM (7.5–11,470% saturation; median = 129% saturation). All sites in the open-water stratum had a pH in excess of 8.8 (range: 8.8–9.4), while lower pH values were observed at some sites in the tributary-area stratum (range: 7.5–9.4). Alkalinity ranged from 82 to 144 mg $CaCO_3$ (mean: 96 mg $CaCO_3$), and was very similar among strata. Dissolved oxygen saturation ranged from 51% to 166% (3.4–10.5 mg L^{-1}) across the reservoir and tended to be higher in the open-water (mean: 128%) than tributary-area (mean: 104%) stratum. The mean surface water temperature was 27.3°C and was very similar among strata. Mean Chl *a* was 26 μg L^{-1} and 20 μg L^{-1} on 12 August 2014 and 02 September 2014, respectively.

Emission rates

Linear and non-linear models were fit to the 86 chamber deployments where five or more P_{CH_4} measurements were recorded prior to ebullition. Forty five of these 86 P_{CH_4} profiles were best described by the non-linear model, according to AIC, and the others were best described by the linear model. Only two of the models had an r^2 value < 0.90 (0.80 and 0.89) and the mean r^2 of the best model was 0.98.

In 29 of the 115 chamber deployments, four or fewer P_{CH_4} measurements were recorded prior to rising bubbles emerging into the chamber headspace. Since we required five or more P_{CH_4} measurements to calculate diffusive emissions (see "Emission rate measurements" section) from the chamber deployments, $E_{CH_4,D}$ was calculate using an alternative method. In six of these instances, $E_{CH_4,D}$ was estimated from K_{CO_2} and the dissolved CH_4 concentration. All six chamber P_{CO_2} profiles used to calculate K_{CO_2} had r^2 values > 0.93. In the remaining 23 sites, plus the two sites where the model fit to the P_{CH_4} data had an $r^2 < 0.9$, $E_{CH_4,D}$ was estimated from K_{CH_4} measured at nearby sites.

Diffusive CH_4 emission rates were more variable in the tributary-areas (range (sd): 0.07–6.18 (1.38) mg CH_4 m^2 h^{-1}; Fig. 2A) than open-water areas (range (sd): 0.03–2.18 (0.43) mg CH_4 m^2 h^{-1}). The population mean $E_{CH_4,D}$ (±95% CI_{LN}) was 0.47 (±0.16), 1.61 (±0.95), and 0.60 (±0.25) mg CH_4 m^2 h^{-1} in the open-water, tributary, and whole-reservoir areas, respectively (Table 3). The tributary-areas were the source of 22% of diffusive emissions at the reservoir scale.

There was significant positive spatial autocorrelation in the presence or absence of ebullition across the 115 sites

Table 2. Mean, range, and standard deviation (SD) of dissolved methane (CH_4), dissolved carbon dioxide (CO_2), pH, alkalinity, dissolved oxygen (DO), and water temperature at the study sites.

	Open-water			Tributary-area		
	Mean	Range	SD	Mean	Range	SD
Dissolved CH_4 (μM)	0.39	0.14–3.12	0.38	1.08	0.31–2.94	0.6
Dissolved CO_2 (μM)	2.4	0.9–5.8	1.2	22	0.8–129	25
pH	9.1	8.8–9.4	0.2	8.5	7.5–9.4	0.5
Alkalinity (mg $CaCO_3$ L^{-1})	91	84–98	5	102	82–144	15
DO (mg L^{-1})	8.3	5.8–10.5	1	6.72	3.4–9.9	1.5
Water temperature (°C)	27.2	24.8–30.1	1.1	27.4	25.7–30.8	1.3

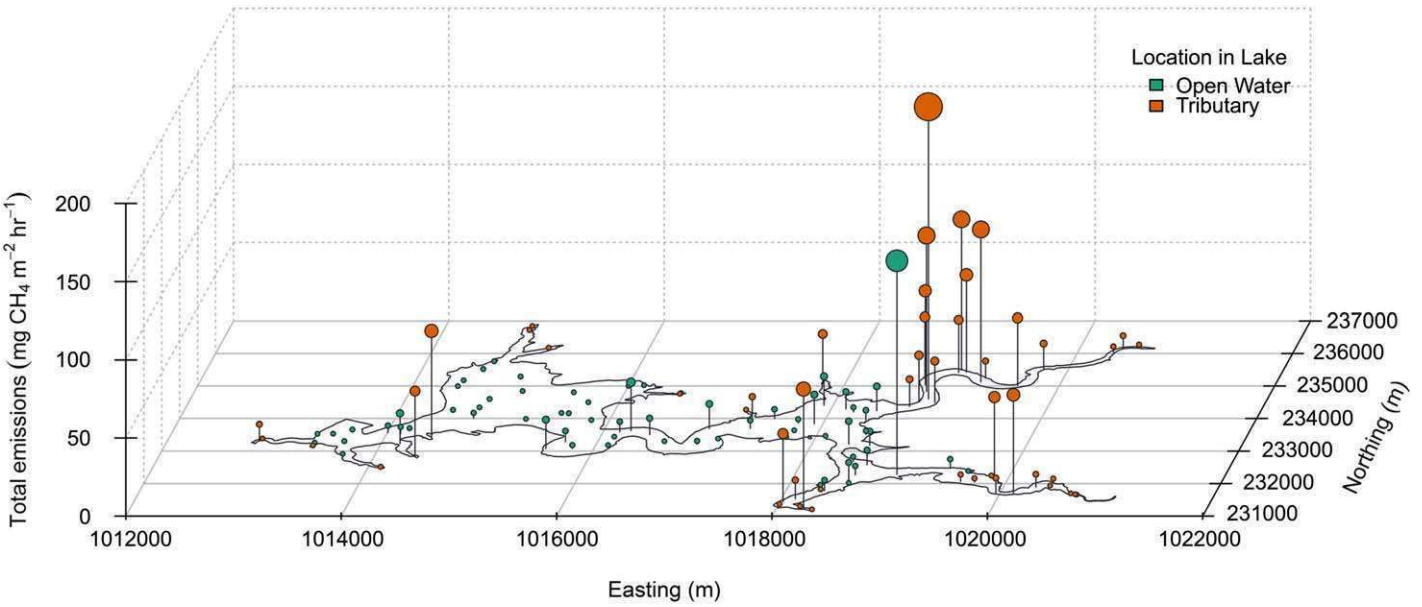

Fig. 2. Total methane emission rates measured at the 115 sample sites across Harsha Lake. The reservoir perimeter is indicated in black on the *xy* plane and the magnitude of the emission rate is indicated by the size of the circle and the height of the black line according the scale on the *z*-axis.

Table 3. Population estimates of the mean and 95% confidence interval (mg CH_4 m^{-2} h^{-1}) methane emission rate for the reservoir, open-water, and tributary stratum. Confidence interval is calculated with the local neighborhood variance estimator (95% CI_{LN}) and the independent random sample estimator (95% CI_{IRS}). Percent reduction is the CI_{LN} estimate compared with the CI_{IRS} estimate.

Stratum	Emission type	Population mean	95% CI_{IRS}	95% CI_{LN}	Percent reduction
Reservoir	Diffusion	0.60	0.48–0.73	0.51–0.7	24
Open-water		0.47	0.36–0.57	0.38–0.55	19
Tributary-area		1.61	1.09–2.13	1.13–2.08	9
Reservoir	Ebullition	7.66	4.54–10.79	5.43–9.9	28
Open-water		4.38	1.84–6.92	2.28–6.48	17
Tributary-area		31.4	17.8–44.93	20.55–42.18	20
Reservoir	Total	8.27	5.11–11.42	6.04–10.5	29
Open-water		4.84	2.3–7.39	2.74–6.94	18
Tributary-area		33.0	19.41–46.53	22.27–43.67	21

(Fig. 3). Sites that had ebullition were more likely to have neighboring sites with ebullition than predicted by chance alone (Join count = 25.1, $p < 0.0001$) and sites without ebullition were more likely to have neighboring sites without ebullition than predicted by chance alone (Join count = 13.6, $p < 0.0001$). The population extent estimate (±95% CI_{LN}) for the occurrence of ebullition was 47% (±10), 84% (±9), and 51% (±9) for the open-water, tributary, and reservoir areas, respectively. Ebullition rates ranged from 0–136.1 mg CH_4 m^2 h^{-1} in the open-water areas and 0–186.1 mg CH_4 m^2 h^{-1} in the tributary-areas. Ebullition rates were highly variable at sites < 10 m deep (range: 0–186.1 mg CH_4 m^2 h^{-1}), although the highest rates (i.e., those in the upper 15th percentile of the distribution) were strictly limited to these shallow waters (Fig. 4A). Overall, ebullition rates were weakly correlated with water depth (Spearman's $\rho = -0.15$). The population mean $E_{CH_4,E}$ (±95% CI_{LN}) was 4.4 (±2.1), 31.4 (±10.8), and 7.7 (±2.2) mg CH_4 m^{-2} h^{-1} in the open-water, tributary areas, and reservoir strata, respectively (Table 3). The tributary-areas were the source of 43% of the ebullitive CH_4 emissions at the reservoir scale.

Total CH_4 emissions reflect the sum of diffusive emissions and ebullition (Fig. 2). The population mean $E_{CH_4,T}$ (±95% CI_{LN}) was 4.8 (±2.1), 33.0 (±10.7), and 8.3 (±2.2) mg CH_4 m^2 h^{-1} in the open-water, tributary, and reservoir areas, respectively (Table 3). The gls model indicated that $E_{CH_4,T}$ at 1–4 m depths was greater in the tributary than open-water stratum ($p = 0.0006$, Fig. 4B). Ebullition represented > 90% of

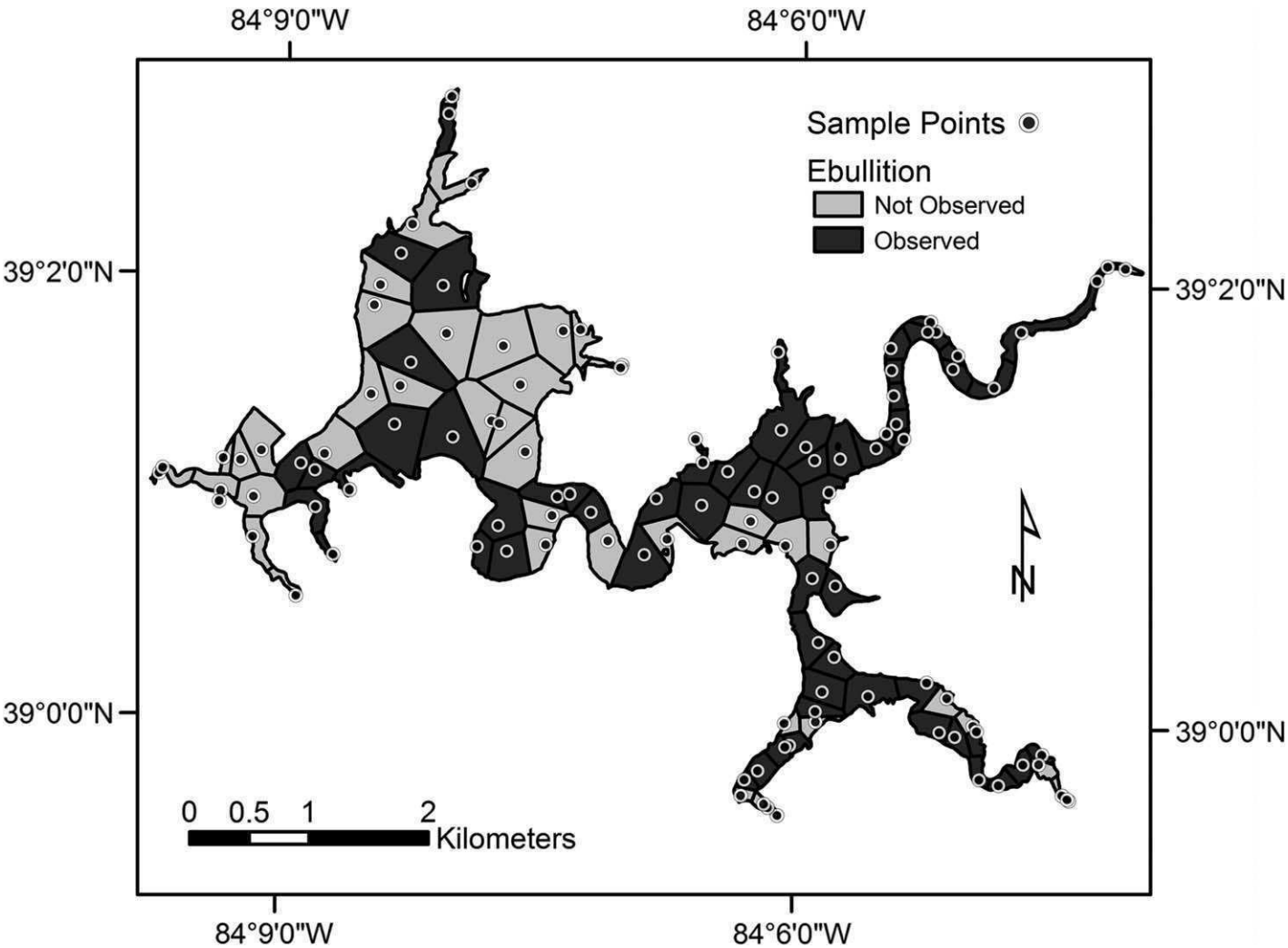

Fig. 3. Thiessen polygons for each sampling point. Polygons are color coded based on whether or not ebullition was observed at the sampling site. Sites where ebullition was observed were more likely to have neighboring sites with ebullition than predicted by chance alone. Similarly, sites where ebullition was absent were more likely to have neighboring sites without ebullition than predicted by chance alone.

total CH_4 emissions from each strata and the tributary stratum was the source of 42% of total CH_4 emissions at the reservoir scale.

All emission pathways (i.e., diffusion, ebullition, and total emissions) exhibited a strong spatial pattern with the highest rates generally occurring in the three large eastern tributary arms and the lowest rates occurring in the western open-water basin (Figs. 2, 3). The local neighborhood variance estimator took advantage of these patterns and produced confidence intervals that were up to 29% lower than those calculated using the IRS procedure (Table 3).

Discussion

In this study, we used a spatially balanced probabilistic survey design to estimate the mean (±95% CI) CH_4 emission rate for a reservoir at multiple spatial scales (e.g., whole-reservoir, tributary stratum, open-water stratum). The results support our hypothesis that reservoir areas below tributary inflows support higher and more variable emission rates than open-water areas, highlighting the importance of including tributary areas in reservoir CH_4 surveys. We also found that ebullition comprised >90% of total CH_4 emissions at all spatial scales, indicating that surveys which only capture diffusive emissions, such as those based on measurement of dissolved CH_4 concentration (Hofmann 2013), may greatly underestimate total CH_4 emissions. Finally, we demonstrate how GRTS, a well-developed and readily accessible statistical survey design, can be used to generate system-scale estimates of CH_4 emissions rates that (1) build on expert knowledge through the incorporation of strata hypothesized to be important in the system and (2) utilize spatial patterns to reduce uncertainty.

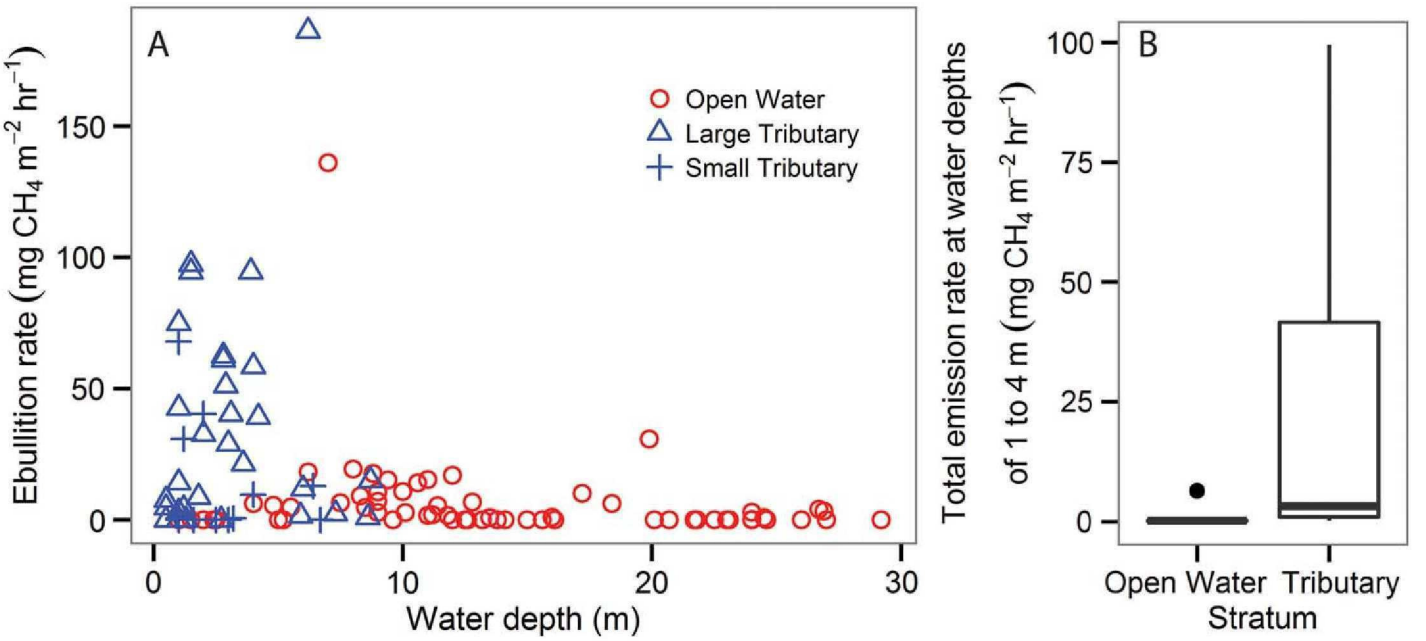

Fig. 4. (A) Methane ebullition rates plotted against water depth. Measurements made within the three largest tributary areas, labeled **(A–C)** in Fig. 1, are represented by blue triangles. Measurements made in the remaining 10 smaller tributary areas are represented by a blue cross. **(B)** Total methane emission rates measured at sites ranging from 1 m to 4 m in depth.

Methane emission rates from tributary and open water areas

The areas of the reservoir associated with tributaries had diffusive, ebullitive, and total CH_4 emission rates that were 3.4, 7.2, and 6.8 times higher than that of the open-water areas, respectively. Overall, the tributary associated areas were the source of 42% of total emissions, despite comprising only 12% of the total reservoir surface area. This finding is consistent with a growing body of evidence indicating that areas below tributary inputs can be hot-spots of CH_4 emissions from reservoirs (DelSontro et al. 2011; Grinham et al. 2011; Musenze et al. 2014; Sturm et al. 2014). This pattern has been shown for subtropical reservoirs in Australia of different sizes and draining different land-use types (0–65% agriculture) (Grinham et al. 2011; Musenze et al. 2014; Sturm et al. 2014), a very large tropical reservoir (5400 km^2 surface area) in Africa (DelSontro et al. 2011), and has been previously reported for Harsha Lake (Beaulieu et al. 2014). One factor which likely contributes to differences in emission rates between open-waters and areas below tributary inflows is depth. Open-water areas are typically deeper than tributary-associated areas (mean depth of 2.6 and 13.4 m in tributary and open-water areas in this study, respectively) resulting in longer rise time and enhanced dissolution and oxidation of CH_4 in bubbles released from sediment (Bastviken et al. 2008). When we restrict the data set to observations made at depths included in both strata (i.e., 1–4 m water), however, total CH_4 emission rates were significantly greater in the tributary strata are than open-waters (Fig. 4B), suggesting that factors other than depth contribute to the difference in emission rates between these strata. Another probable difference between these strata is organic matter loading rates. The tributary areas are a transitional zone between the upstream river and downstream lacustrine zones. This transitional zone is characterized by rapidly decreasing water velocities that cause a large fraction of the river suspended solids, which contains watershed-derived organic matter (i.e., plant residues, eroded soil), to settle out, resulting in high sedimentation rates (Thornton 1990). These higher organic loadings to sediment likely enhance CH_4 production rates (DelSontro et al. 2010; Maeck et al. 2013) relative to the open-water portions of the reservoir.

Methane emission rates below tributary inflows

While the tributary stratum supported higher emission rates than the open-water stratum, emission rates varied considerably within individual tributary areas. Some insight into this variability can be assessed using measurements made within the largest tributary arm (tributary area A in Fig. 1) which had sample sites distributed throughout its length. The data indicate a strong spatial pattern of increasing emission rates with increasing distance from the tributary inflow (Fig. 2), possibly because the extreme upper reaches of the tributary arm are periodically scoured by high flows, thereby limiting sediment accumulation and CH_4 production, whereas locations further downstream are areas of persistent sediment deposition and therefore support high CH_4 production rates. The presence of a strong emission hot spot in the lower reaches of the largest

tributary area suggests that these areas should be well characterized in efforts to generate system-scale estimates.

We also observed variability in CH_4 emission rates among the 13 tributary areas sampled in this survey (Fig. 4A). Nine of the ten highest emission rates observed in the tributary stratum occurred below the three tributaries with the largest drainage areas (Fig. 4A; Table 1), suggesting that watershed area might play a role in regulating CH_4 emission rates from areas below tributary inflows, possibly because the amount of organic matter transported by rivers scales with watershed area (Moeller et al. 1979). Not only did the areas below the three largest tributaries support the highest emission rates observed within the tributary stratum, they also comprise over 90% of the cumulative surface area of the 13 tributary areas (Table 1). This suggests that the vast majority of CH_4 emissions from the tributary stratum emanated from the areas below the three largest tributaries with the remaining 10 tributary areas making a comparatively small contribution. From a survey design perspective, this finding indicates that whether these 10 smaller areas were included in the tributary stratum and allocated sampling points, as was done here, or merged with the open-water stratum and sampled on an equal probability basis, would have little effect on the system-scale emission estimate. Therefore to optimize the trade-off between sampling effort and obtaining a constrained variance estimate in this reservoir, survey designs should include the greatest sampling density below the largest tributaries where emission rates are highest and most variable, while sampling the balance of the reservoir at a lower density.

The ideal survey design will vary among individual reservoirs based on numerous factors, but practitioners should carefully consider whether the system of interest is likely to contain CH_4 emission hot spots. Even relatively small hotspots can be the dominant source of reservoir-scale emissions and should be included in survey designs. In an extreme example of this pattern, Grinham et al. (2011) reported that the 2–7% of the surface area of a reservoir below the main tributary in a subtropical reservoir in Australia was the source of up to 97% of reservoir-scale emissions. Emission hot spots are not always confined to the areas below tributaries, however. Sediment trapping immediately above dams in small reservoirs separated by stretches of flowing waters along rivers can lead to CH_4 emission hot spots (DelSontro et al. 2010; Sobek et al. 2012; Maeck et al. 2013). Others have reported emission hot spots associated with shallow littoral (Keller and Stallard 1994) and draw down (Chen et al. 2009) zones.

Relative importance of ebullition and diffusion

The highest ebullition rates (i.e., >30 mg CH_4 m^{-2} h^{-1}) were restricted to sites with water depths <10 m (Fig. 4A), which is consistent with reports from many other lakes and reservoirs (Ostrovsky et al. 2008; Gunkel 2009; DelSontro et al. 2011). This pattern is generally attributed to lower hydrostatic pressure at shallow depths which allows bubble formation to occur at lower total dissolved gas pressures in sediment porewaters (Bastviken et al. 2004; Ostrovsky et al. 2008; Sturm et al. 2014). Furthermore, CH_4 diffuses from bubbles into the surrounding water as they rise through the water column. The amount of CH_4 that is removed from bubbles during their rise is proportional to the rise height, such that the fraction of the original bubble-CH_4 transported to the water surface is inversely related to water depth (Ostrovsky et al. 2008). While previous studies have used the negative relationship between depth and ebullition rates to upscale ebullition to an entire water body (Bastviken et al. 2004; Martinez and Anderson 2013), we found that the correlation was relatively weak (Spearman's $\rho = -0.15$) in this study, partly due to the extreme variability of ebullition rates in the shallow waters. This suggests that while water depth may exert a strong control on ebullition rates, other factors, such as sedimentation rates, are also important (Joyce and Jewell 2003; DelSontro et al. 2015). An important implication of the high variability of ebullition rates in shallow waters observed in this study is that survey designs should include a high density of sampling sites in these areas to reduce uncertainty in population estimates. This is highlighted by the twofold larger 95% CI for the tributary strata as compared with the open-water strata, despite the tributary strata being sampled at a 10-fold greater density than the open-waters.

The population extent estimates indicate that ebullition was pervasive throughout the tributary stratum (i.e., 84% of the surface area emitting bubbles), which is consistent with reports for tributary associated areas in other reservoirs (DelSontro et al. 2011; Grinham et al. 2011). The proportion of the open-water stratum emitting bubbles (i.e., 47% of surface area) was surprisingly high, however. For example, ebullition was found to be very uncommon in bays (max depth: 20 m depth) not receiving direct river inflows in a tropical reservoir (DelSontro et al. 2011) and at depths greater than 12 m in a subtropical reservoir (Grinham et al. 2011). The relatively high frequency of ebullition in the open water stratum in Harsha Lake may be a result of high algal biomass densities which enrich the sediments with autochthonous carbon that can greatly stimulate CH_4 production (West et al. 2012, 2015). Although ebullition extent and CH_4 flux was much lower in the open-water than tributary stratum, ebullition was the source of 90% of total open-water CH_4 emissions and 93% of whole-reservoir CH_4 emissions. This finding is consistent with reports that ebullitive emissions far exceed diffusive emissions in many temperate, subtropical, and tropical reservoirs (Keller and Stallard 1994; Joyce and Jewell 2003; DelSontro et al. 2010; DelSontro et al. 2011; Grinham et al. 2011; Sobek et al. 2012; Sturm et al. 2014), highlighting the importance of including ebullition in emission surveys. It should be noted, however, that emissions from cold and well oxygenated boreal

reservoirs appear to be dominated by diffusive emissions (Teodoru et al. 2012).

Comparison to other studies

Several literature reviews suggest that total CH_4 emission rates from temperate reservoirs are typically less than 1 mg CH_4 m^{-2} h^{-1} (Barros et al. 2011; Bastviken et al. 2011). The total CH_4 emission rate reported here (8.3 ± 2.2 mg CH_4 m^2 h^{-1}) is well above that value and is in the range more frequently reported for tropical reservoirs. However, recent studies that included hot spots in temperate zone reservoirs have reported emission rates ranging from 4 mg CH_4 m^2 h^{-1} to 13 mg CH_4 m^2 h^{-1} (DelSontro et al. 2010; Maeck et al. 2013; Beaulieu et al. 2014) (excluding CH_4 released during passage through the dam), suggesting that emissions from temperate systems may have been systematically underestimated.

Bias in the selection of sample sites can affect system-scale estimates, possibly contributing to some of the variability among previously published estimates. To explore potential bias in emission estimates for Harsha Lake, we calculated the total CH_4 emission rate following the survey design presented in Beaulieu et al. (2014). In this study, one sampling site was established in the largest tributary area and five sites in open-water areas. Reservoir scale estimates were calculated by weighting the tributary site by 0.05, the proportion of the reservoir surface attributed to the tributary area. Using measurements made at locations nearby these six sites in this study, we calculate total CH_4 emission rates ranging from 4.1 mg CH_4 m^2 h^{-1} to 7.1 mg CH_4 m^2 h^{-1}, depending on which site is used to represent the tributary area [i.e., three sites in this study are located nearby the tributary site used in Beaulieu et al. (2014)]. This range of values reflects the spatial variability in the tributary areas, further highlighting the importance of sampling these areas at a high spatial density. Regardless of which site is used to represent the tributary area, the estimates are biased low compared with the GRTS results (8.3 ± 2.2 mg CH_4 m^2 h^{-1}) and this bias would be even more extreme if the original survey had not included a tributary site (2.1 mg CH_4 m^2 h^{-1}). While this analysis highlights how judgment samples can produce biased estimates, it also demonstrates how judgment samples can be critically important for identifying spatial patterns (i.e., hot spots) that can inform the design of subsequent probabilistic survey designs.

The survey design used in this work included more sample sites and a higher sample density than any previously published investigation using similar measurement methods. One reason for the large sample size is that we placed multiple constraints on the survey design including the requirement that samples be distributed throughout the length of the largest tributary areas and within many separate tributary areas (i.e., 13 areas, Table 1). As discussed above, the inclusion of very small tributary areas likely did not improve system-scale estimates, suggesting that future surveys could

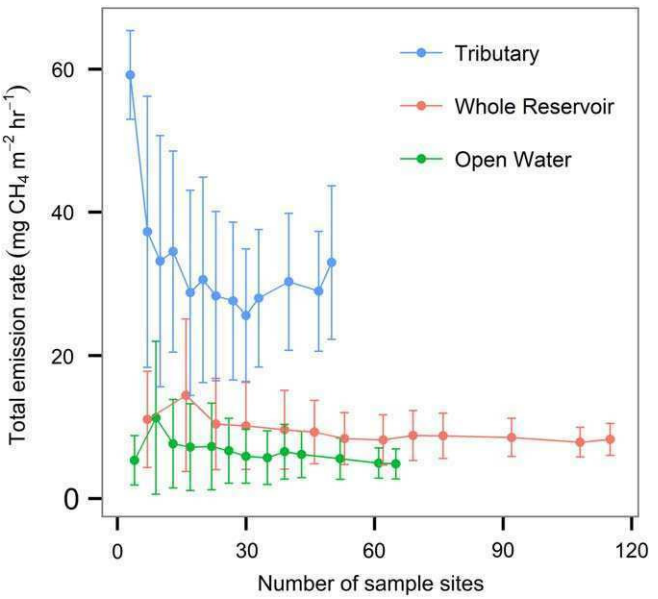

Fig. 5. Population mean (± 95% CI_{LN}) methane emission rate as a function of sample size for the tributary stratum, open-water stratum, and whole-reservoir.

employ fewer samples with minimal loss of information. Given limited resources, investigators must optimize survey designs to meet their data quality needs with the minimum sample size. This consideration becomes even more apparent when designs are expanded to include a temporal element (i.e., detection of seasonal patterns or long-term trends). Our analysis of subsets of the survey data indicate that estimates of the mean total CH_4 emission rate stabilized at sample sizes of ~15 and ~20 in the tributary and open-water stratum, respectively (Fig. 5); however, at this sample size the confidence interval for the system-scale emission rate was a factor of 1.15 greater than the mean (i.e., 9.62 ± 5.53 mg CH_4 m^{-2} h^{-1}). With further increases in sampling effort the 95% CI_{LN} declined to a minimum of 54% of the mean at a sample size of 115. These results suggest that generating well-constrained emission estimates requires a larger sampling effort than is needed to generate accurate estimates, therefore investigators should consider their data quality needs with respect to both accuracy and precision when designing surveys. We recommend conducting preliminary surveys to generate information regarding spatial patterning and variability that can be used to design efficient surveys that meet data quality needs (Reynolds 2012).

Spatial pattern and monitoring

System-scale estimate of CH_4 emission rates convey little information if not accompanied by clearly defined and well-constrained estimates of uncertainty. One feature of GRTS designs is that they allow for uncertainty estimation using a local neighborhood (LN) variance estimator (Stevens and

Olsen 2003) which utilizes spatial pattern to produce better constrained uncertainty estimates than approaches that ignore spatial pattern. This approach has been used to improve uncertainty estimation for a broad range of ecological properties including the biological condition of aquatic ecosystems in the United States (US Environmental Protection Agency 2009), lake evaporation rates (Brooks et al. 2014), and chlorophyll density within a reservoir (Stevens and Olsen 2003). In this study, all emission pathways (i.e., diffusion, ebullition, and total emissions) exhibited a strong spatial pattern with the highest rates generally occurring in the three large eastern tributary arms and the lowest rates occurring in the western open-water basin (Figs. 2, 3). This spatial pattern was reflected in LN uncertainty estimates that were up to 29% more constrained than estimates that ignored spatial pattern (Table 3).

Spatial patterns in CH_4 emission rates within reservoirs may be induced by spatial patterns in the factors that control CH_4 production and evasion (sensu Fortin et al. 2002). For example, spatial patterns in water depth and sediment characteristics (Pearson and Rose 2001) likely conspire to generate spatial patterns in CH_4 emission rates. Spatial patterns in CH_4 emission rates have been reported by numerous investigators and may be quite common. For example, Hofmann (2013) reported a strong offshore-directed gradient in CH_4 emissions between the littoral and open-water areas of a reservoir in Western Europe. Several investigators have reported a gradient in emission rates between river inflows and open-water areas (DelSontro et al. 2011; Grinham et al. 2011; Musenze et al. 2014; Sturm et al. 2014) while others have reported spatial gradients between dams and river segments in run of the river reservoirs (Maeck et al. 2013). In all of these cases, uncertainty estimation could benefit from a computational approach that utilizes spatial patterns.

Conclusions

In this study, we used a spatially balanced probabilistic survey design to estimate the mean (±95% CI) CH_4 emission rate at multiple spatial scales within a reservoir. We found that emission rates from areas below tributary inflows are greater than those in open-water areas and that ebullition was the dominant emission mechanism throughout the reservoir, despite relatively deep waters in portions of the system. The reservoir-scale CH_4 emission rate estimate was relatively high for a temperate zone reservoir, likely because our survey included emission hot-spots, suggesting that previous investigations have underestimated emissions from these systems.

Our survey results are consistent with numerous literature reports indicating that CH_4 emission rates can exhibit strong intra-reservoir variability and highlight the need to account for spatial patterns in reservoir-scale emission estimates. While several approaches are available for designing spatial surveys, we used a GRTS design to generate CH_4 emission rate estimates at multiple spatial scales. GRTS designs produce unbiased estimates and have the added benefit of reducing uncertainty by incorporating spatial pattern into variance estimates. The use of GRTS, or other probabilistic survey designs, can improve the accuracy and precision of reservoir emission rate estimates, which is needed to identify the factors that control reservoir-CH_4 emission rates and to better constrain uncertainty in global scale emission estimates.

References

APHA. 2012. Standard methods for the examination of water and wastewater, 22nd ed. American Public Health Association.

Bade, D. L., and J. J. Cole. 2006. Impact of chemically enhanced diffusion on dissolved inorganic carbon stable isotopes in a fertilized lake. J. Geophys. Res. Oceans **111**: 10. doi:10.1029/2004JC002684

Barros, N., and others. 2011. Carbon emission from hydroelectric reservoirs linked to reservoir age and latitude. Nat. Geosci. **4**: 593–596. doi:10.1038/ngeo1211

Bastviken, D., J. Cole, M. Pace, and L. Tranvik. 2004. Methane emissions from lakes: Dependence of lake characteristics, two regional assessments, and a global estimate. Global Biogeochem. Cycles **18**. doi:10.1029/2004GB002238

Bastviken, D., J. J. Cole, M. L. Pace, and M. C. Van de Bogert. 2008. Fates of methane from different lake habitats: Connecting whole-lake budgets and CH_4 emissions. J. Geophys. Res. Biogeosci. **113**. doi:10.1029/2007JG000608

Bastviken, D., L. J. Tranvik, J. A. Downing, P. M. Crill, and A. Enrich-Prast. 2011. Freshwater methane emissions offset the continental carbon sink. Science **331**: 50. doi:10.1126/science.1196808

Beaulieu, J. J., R. L. Smolenski, C. T. Nietch, A. Townsend-Small, and M. S. Elovitz. 2014. High methane emissions from a midlatitude reservoir draining an agricultural watershed. Environ. Sci. Technol. **48**: 11100–11108. doi:10.1021/es501871g

Bivand, R. S., E. J. Pebesma, and V. Gómez-Rubio. 2008. Applied spatial data analysis with R. Springer.

Brooks, J. R., J. J. Gibson, S. J. Birks, M. H. Weber, K. D. Rodecap, and J. L. Stoddard. 2014. Stable isotope estimates of evaporation: Inflow and water residence time for lakes across the United States as a tool for national lake water quality assessments. Limnol. Oceanogr. **59**: 2150–2165. doi:10.4319/lo.2014.59.6.2150

Chen, H., Y. Y. Wu, X. Z. Yuan, Y. H. Gao, N. Wu, and D. Zhu. 2009. Methane emissions from newly created marshes in the drawdown area of the Three Gorges Reservoir. J. Geophys. Res. Atmos. **114**. doi:10.1029/2009JD012410

Chen, H., and others. 2011. Methane emissions from the surface of the Three Gorges Reservoir. J. Geophys. Res. Atmos. **116**. doi:10.1029/2011JD016244

Colt, J. 2012. Dissolved gas concentration in water. Computation as functions of temperature, salinity and pressure, 2nd ed. Elsevier.

de Smith, M. J., M. F. Goodchild, and P. A. Longley. 2013. Geospatial analysis a comprehensive guide to principles, techniques, and software tools. http://www.spatialanalysisonline.com/.

DelSontro, T., D. F. McGinnis, S. Sobek, I. Ostrovsky, and B. Wehrli. 2010. Extreme methane emissions from a Swiss hydropower reservoir: Contribution from bubbling sediments. Environ. Sci. Technol. **44**: 2419–2425. doi:10.1021/es9031369

DelSontro, T., M. J. Kunz, T. Kempter, A. Wuest, B. Wehrli, and D. B. Senn. 2011. Spatial heterogeneity of methane ebullition in a large tropical reservoir. Environ. Sci. Technol. **45**: 9866–9873. doi:10.1021/es2005545

DelSontro, T., D. F. McGinnis, B. Wehrli, and I. Ostrovsky. 2015. Size does matter: Importance of large bubbles and small-scale hot spots for methane transport. Environ. Sci. Technol. **49**: 1268–1276. doi:10.1021/es5054286

Demello, W. Z., and M. E. Hines. 1994. Application of static and dynamic enclosures for determining dimethyl sulfide and carbonyl sulfide exchange in *Sphagnum* peatlands: Implications for the magnitude and direction of flux. J. Geophys. Res. Atmos. **99**: 14601–14607. doi:10.1029/94JD01025

Elzhov, T. V., K. M. Mullen, A.-N. Spiess, and B. Bolker. 2013. minpack.lm: R interface to the Levenberg-Marquardt nonlinear least-squares algorithm found in MINPACK, plus support for bounds. R package version 1.1-8.

Fortin, M.-J., M. R. T. Dale, and J. ver Hoef. 2002. Spatial analysis in ecology. *In* A. El-Shaarawi and W. W. Piegorsch [eds.], Encyclopedia of environmetrics. John Wiley & Sons, Ltd.

Gattuso, J.-P., J.-M. Epitalon, and H. Lavigne. 2015. seacarb: Seawater carbonate chemistry. R package version 3.0.6.

Gonzalez-Valencia, R., A. Sepulveda-Jauregui, K. Martinez-Cruz, J. Hoyos-Santillan, L. Dendooven, and F. Thalasso. 2014. Methane emissions from Mexican freshwater bodies: Correlations with water pollution. Hydrobiologia **721**: 9–22. doi:10.1007/s10750-013-1632-4

Grinham, A., M. Dunbabin, D. Gale, and J. Udy. 2011. Quantification of ebullitive and diffusive methane release to atmosphere from a water storage. Atmos. Environ. **45**: 7166–7173. doi:10.1016/j.atmosenv.2011.09.011

Gunkel, G. 2009. Hydropower—a green energy? Tropical reservoirs and greenhouse gas emissions. Clean Soil Air Water **37**: 726–734. doi:10.1002/clen.200900062

Hofmann, H. 2013. Spatiotemporal distribution patterns of dissolved methane in lakes: How accurate are the current estimations of the diffusive flux path? Geophys. Res. Lett. **40**: 2779–2784. doi:10.1002/grl.50453

Joyce, J., and P. W. Jewell. 2003. Physical controls on methane ebullition from reservoirs and lakes. Environ. Eng. Geosci. **9**: 167–178. doi:10.2113/9.2.167

Keller, M., and R. F. Stallard. 1994. Methane emission by bubbling from Gatun Lake, Panama. J. Geophys. Res. **99**: 8307–8319. doi:10.1029/92JD02170

Kincaid, T. M., and A. R. Olsen. 2015. spsurvey: Spatial survey design and analysis. R package version 3.0.

Lohr, S. L. 2010. Sampling: Design and analysis, 2nd ed. Brooks/Cole.

Maeck, A., and others. 2013. Sediment trapping by dams creates methane emission hot spots. Environ. Sci. Technol. **47**: 8130–8137. doi:10.1021/es4003907

Martinez, D., and M. A. Anderson. 2013. Methane production and ebullition in a shallow, artificially aerated, eutrophic temperate lake (Lake Elsinore, CA). Sci. Total Environ. **454–455**: 457–465. doi:10.1016/j.scitotenv.2013.03.040

Moeller, J. R., and others. 1979. Transport of dissolved organic carbon in streams of differing physiographic characteristics. Org. Geochem. **1**: 139–150. doi:10.1016/0146-6380(79)90002-0

Musenze, R. S., A. Grinham, U. Werner, D. Gale, K. Sturm, J. Udy, and Z. Yuan. 2014. Assessing the spatial and temporal variability of diffusive methane and nitrous oxide emissions from subtropical freshwater reservoirs. Environ. Sci. Technol. **48**: 14499–14507. doi:10.1021/es505324h

Olsen, A. R., T. M. Kincaid, and Q. Payton. 2012. Spatially balanced survey designs for natural resources, p. 126–150. *In* R. A. Gitzen, J. J. Millspaugh, A. B. Cooper and D. S. Licht [eds.], Design and analysis of long-term ecological monitoring studies. Cambridge Univ. Press.

Ostrovsky, I., D. F. McGinnis, L. Lapidus, and W. Eckert. 2008. Quantifying gas ebullition with echosounder: The role of methane transport by bubbles in a medium-sized lake. Limnol. Oceanogr.: Methods **6**: 105–118. doi:10.4319/lom.2008.6.105

Pearson, S. M., and K. A. Rose. 2001. The effects of sampling design on estimating the magnitude and distribution of contaminated sediments in a large reservoir. Environmetrics **12**: 81–102. doi:10.1002/1099-095x(200102)12:1<81::Aid-Env449>3.0.Co;2-7

Pinheiro, J., D. Bates, S. DebRoy, D. Sarkar, and the R Development Core Team. 2011. nlme: Linear and nonlinear mixed effects models. R package version 3.1-113.

Polunin, N. V. C. 1984. The decomposition of emergent macrophytes in fresh water. Adv. Ecol. Res. **14**: 115–166. doi:10.1016/S0065-2504(08)60170-1

R Development Core Team. 2015. R: A language and environment for statistical computing. R Foundation for Statistical Computing.

Reynolds, J. H. 2012. An overview of statistical consideration in long-term monitoring. *In* R. A. Gitzen, J. J. Millspaugh, A. B. Cooper and D. S. Licht [eds.], Design and analysis of

long-term ecological monitoring studies. Cambridge Univ. Press.

Schindler, D. W., W. S. Broecker, G. J. Brunskil, T. H. Peng, and S. Emerson. 1972. Atmospheric carbon dioxide: Its role in maintaining phytoplankton standing crops. Science **177**: 1192–1194. doi:10.1126/science.177.4055.1192

Sobek, S., T. DelSontro, N. Wongfun, and B. Wehrli. 2012. Extreme organic carbon burial fuels intense methane bubbling in a temperate reservoir. Geophys. Res. Lett. **39**: L01401. doi:10.1029/2011GL050144

St. Louis, V. L., C. A. Kelly, É. Duchemin, J. W. M. Rudd, and D. M. Rosenberg. 2000. Reservoir surfaces as sources of greenhouse gases to the atmosphere: A global estimate. Bioscience **50**: 766–775. doi:10.1641/0006-3568(2000)050[0766:rsasog]2.0.co;2

Stevens, D. L., and A. R. Olsen. 2003. Variance estimation for spatially balanced samples of environmental resources. Environmetrics **14**: 593–610. doi:10.1002/env.606

Stevens, D. L., and A. R. Olsen. 2004. Spatially balanced sampling of natural resources. J. Am. Stat. Assoc. **99**: 262–278. doi:10.1198/016214504000000250

Stocker, T. F., and others [eds.]. 2013. Climate change 2013. The physical science basis. Cambridge Univ. Press.

Stolk, P. C., C. M. J. Jacobs, E. J. Moors, A. Hensen, G. L. Velthof, and P. Kabat. 2009. Significant non-linearity in nitrous oxide chamber data and its effect on calculated annual emissions. Biogeosci. Discuss. **6**: 115–141. doi:10.5194/bgd-6-115-2009

Sturm, K., Z. Yuan, B. Gibbes, U. Werner, and A. Grinham. 2014. Methane and nitrous oxide sources and emissions in a subtropical freshwater reservoir, South East Queensland, Australia. Biogeosciences **11**: 5245–5258. doi:10.5194/bg-11-5245-2014

Teodoru, C. R., and others. 2012. The net carbon footprint of a newly created boreal hydroelectric reservoir. Global Biogeochem. Cycles **26**. doi:10.1029/2011GB004187

Thornton, K. W. 1990. Perspectives on reservoir limnology, p. 1–13. *In* K. W. Thornton, B. L. Kimmel and F. E. Payne [eds.], Reservoir limnology: Ecological perspectives. John Wiley & Sons.

US Environmental Protection Agency. 2009. National lakes assessment: A collabotative survey of the nations's lakes. https://www.epa.gov/sites/production/files/2013-11/documents/nla_newlowres_fullrpt.pdf

US Environmental Protection Agency. 2012. National coastal condition report IV. https://www.epa.gov/sites/production/files/2013-11/documents/nla_newlowres_fullrpt.pdf

US Environmental Protection Agency. 2013. National rivers and streams assessment 2008-2009: A collaborative study. https://www.epa.gov/sites/production/files/2016-03/documents/nrsa_0809_march_2_final.pdf

Wanninkhof, R. 1992. Relationship between wind-speed and gas-exchange over the ocean. J. Geophys. Res. Oceans **97**: 7373–7382. doi:10.1029/92JC00188

Wanninkhof, R., W. E. Asher, D. T. Ho, C. Sweeney, and W. R. McGillis. 2009. Advances in quantifying air-sea gas exchange and environmental forcing. Ann. Rev. Mar. Sci. **1**: 213–244. doi:10.1146/annurev.marine.010908.163742

West, W. E., J. J. Coloso, and S. E. Jones. 2012. Effects of algal and terrestrial carbon on methane production rates and methanogen community structure in a temperate lake sediment. Freshw. Biol. **57**: 949–955. doi:10.1111/j.1365-2427.2012.02755.x

West, W. E., S. M. McCarthy, and S. E. Jones. 2015. Phytoplankton lipid content influences freshwater lake methanogenesis. Freshw. Biol. **60**: 2261–3369. doi:10.1111/fwb.12652

Acknowledgments

We thank Michelle A. Simon, Mark Martin, Cody Schumacher, Dana Macke, Karen White, Don Brown, and William Wright for field and/or laboratory assistance. We thank Tony Olsen for providing survey design and analysis advice. Anna Springsteen and Stephanie Fitchett with Neptune Inc assisted with portions of the R codes used in the analysis. We also thank two anonymous reviewers for insightful comments on the manuscript. The U.S. Environmental Protection Agency, through its Office of Research and Development, funded and managed the research described herein. It has been subjected to the Agency's administrative review and has been approved for external publication. Any opinions expressed in this article are those of the authors and do not necessarily reflect the views of the Agency, therefore, no official endorsement should be inferred. Any mention of trade names or commercial products does not constitute endorsement or recommendation for use.

Submitted 3 September 2015
Revised 17 December 2015
Accepted 13 February 2016

Associate editor: Kimberly Wickland

ACS AuthorChoice

Environmental Science & Technology

Article

pubs.acs.org/est

Terms of Use

High Methane Emissions from a Midlatitude Reservoir Draining an Agricultural Watershed

Jake J. Beaulieu,*[,†] Rebecca L. Smolenski,[†,‡,#] Christopher T. Nietch,[†] Amy Townsend-Small,[‡,§] and Michael S. Elovitz[†]

[†]United States Environmental Protection Agency, Office of Research and Development, National Risk Management Research Laboratory, Cincinnati, Ohio 45268, United States

[‡]Department of Geology, University of Cincinnati, Cincinnati, Ohio 45221, United States

[§]Department of Geography, University of Cincinnati, Cincinnati, Ohio 45221, United States

Supporting Information

ABSTRACT: Reservoirs are a globally significant source of methane (CH_4), although most measurements have been made in tropical and boreal systems draining undeveloped watersheds. To assess the magnitude of CH_4 emissions from reservoirs in midlatitude agricultural regions, we measured CH_4 and carbon dioxide (CO_2) emission rates from William H. Harsha Lake (Ohio, U.S.A.), an agricultural impacted reservoir, over a 13 month period. The reservoir was a strong source of CH_4 throughout the year, emitting on average 176 ± 36 mg C m^{-2} d^{-1}, the highest reservoir CH_4 emissions profile documented in the United States to date. Contrary to our initial hypothesis, the largest CH_4 emissions were during summer stratified conditions, not during fall turnover. The river−reservoir transition zone emitted CH_4 at rates an order of magnitude higher than the rest of the reservoir, and total carbon emissions (i.e., CH_4 + CO_2) were also greater at the transition zone, indicating that the river delta supported greater carbon mineralization rates than elsewhere. Midlatitude agricultural impacted reservoirs may be a larger source of CH_4 to the atmosphere than currently recognized, particularly if river deltas are consistent CH_4 hot spots. We estimate that CH_4 emissions from agricultural reservoirs could be a significant component of anthropogenic CH_4 emissions in the U.S.A.

INTRODUCTION

Methane (CH_4) is a potent greenhouse gas (GHG) with a heat trapping capacity 34 times greater than that of carbon dioxide (CO_2) on a 100 year time scale.[1] Human activities have more than doubled atmospheric CH_4 concentrations since the preindustrial era and current levels are unprecedented in at least the last 650 000 years. Known anthropogenic sources of CH_4 include livestock production, rice agriculture, landfills, and natural gas mining,[2] but current inventories may underestimate CH_4 emissions in the United States,[3] suggesting that additional sources may exist.

An important source of CH_4 is microbial activity in the sediments of aquatic ecosystems. Methane can be transported from sediments via gas bubble ebullition, molecular diffusion, or advection through plant stems.[4] Ebullition and plant stems can be important transport mechanisms in shallow waters and wetlands, but diffusion is typically the dominant evasion pathway in deeper waters. Methane can also be oxidized to CO_2 via methanotrophic bacteria in areas where dissolved CH_4 and oxygen co-occur.[4]

The evasion of CH_4 to the atmosphere from the surfaces of reservoirs constructed for hydropower and other purposes may account for up to 20% of the global anthropogenic budget,[5] but these estimates are largely based on measurements made in undeveloped watersheds in tropical and boreal regions. Relatively little is known about emission rates from midlatitude systems, although ∼30% of all reservoirs are located in this region.[6] Global estimates assume that reservoir CH_4 emissions decrease exponentially from the tropics to boreal regions, a

Received: April 17, 2014
Revised: July 3, 2014
Accepted: August 26, 2014
Published: August 26, 2014

 © 2014 American Chemical Society dx.doi.org/10.1021/es501871g | Environ. Sci. Technol. 2014, 48, 11100−11108

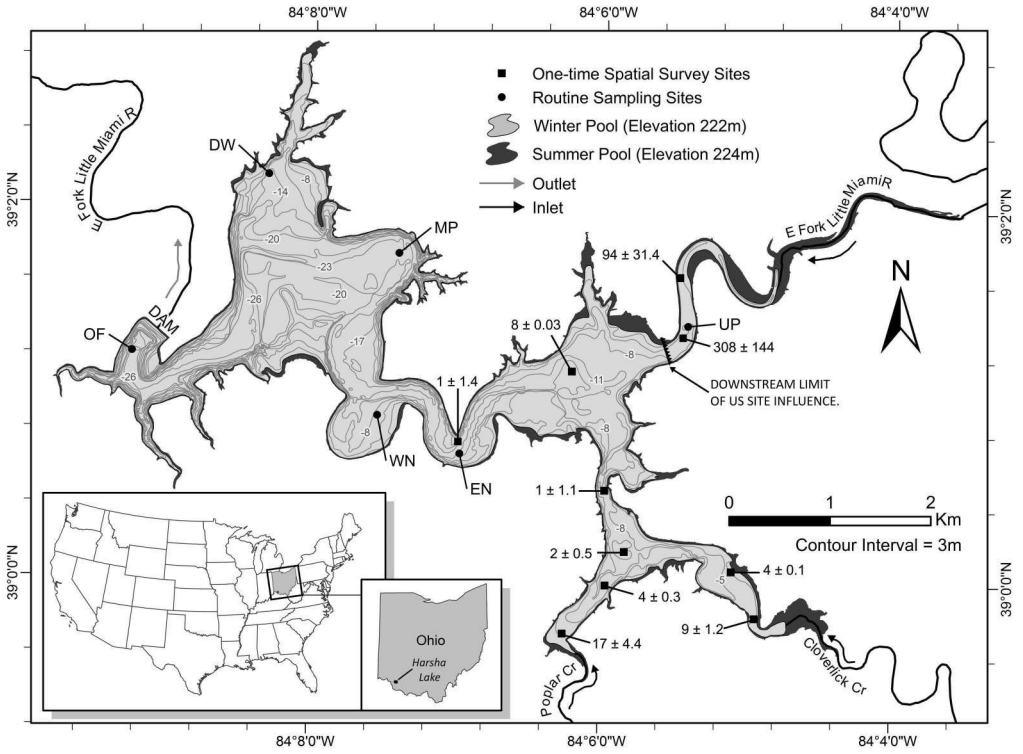

Figure 1. William H. Harsha Lake (Harsha Lake), tributaries, outlet, routine sampling sites, and one-time spatial survey sites. The different pool elevations reflect the change in surface area between the summer and winter pool elevations (224 m and 222 m, respectively). The area upstream of the line labeled 'downstream limit of UP site influence', was used to calculate the portion of the reservoir defined as having a methane (CH_4) emission rate equal to that measured at UP. Results of the CH_4 emission rates (± SE, mg C m^{-2} d^{-1}) measured during the one-time spatial survey, completed on 8 January 2013 in the eastern portion of the reservoir, are reported adjacent to each sampling point as a mean ± SE.

pattern that is largely attributed to differences in temperature.[6] A few studies of midlatitude systems support this pattern;[7] however, local scale characteristics, such as watershed land use or reservoir morphology, may cause CH_4 emissions to deviate from this pattern.

Microbial respiration in oxic sediments mainly produces CO_2, but under anoxic conditions, respiration can also produce CH_4. Impounding river networks promotes sediment anoxia, and this may be particularly true for midlatitude agricultural impacted reservoirs that are subject to high nutrient and sediment loading rates. Watershed soil erosion can stimulate CH_4 production by providing microbial communities with a large source of carbon (C) that can deplete sediment oxygen and fuel CH_4 production. Algal blooms from excessive nutrient loading can further enrich reservoir sediments with labile C.[9] These factors may result in CH_4 emission rates that are much higher than predicted from the generalized relationship between latitude and CH_4 emissions.[6] However, low rates of methanogenesis during winter may balance high CH_4 emission rates during the summer months, complicating efforts to predict the magnitude of CH_4 emissions from midlatitude reservoirs.

To assess the possible importance of agricultural impacted reservoirs in the U.S. anthropogenic CH_4 budget, we constructed an annual CH_4 budget for William H. Harsha Lake, a eutrophic, seasonally stratified reservoir in southwestern Ohio (U.S.A.). Methane and CO_2 emissions were measured approximately monthly in six locations throughout the lake using floating chambers, with increased sampling frequency in fall to assess the importance of CH_4 release during the ventilation of hypolimnetic waters. We combined the measurements with a conservative estimate of the areal extent of agricultural impacted reservoirs in the United States to produce a national scale estimate of CH_4 emissions from agricultural reservoirs.

MATERIALS AND METHODS

Study Site. William H Harsha Lake (hereafter referred to as Harsha Lake) is a 8.74 km^2 flood control reservoir built in 1978 on the East Fork Little Miami River in southwestern Ohio (U.S.A.) (Figure 1). The dam control structure allows for water withdrawal depths ranging from near the sediment−water interface to 3 m below the water surface. The reservoir is located within a state park, where it supports a recreational fishery, swimming beaches, and drinking water withdrawals. This warm monomictic reservoir ranges from ca. 4 m deep at the most upstream portions to 30 m near the dam and has a storage volume of 111 × 10^6 and 101.3 × 10^6 m^3 at the summer and winter pool elevations, respectively. Mean outflows from the reservoir are 78 × 10^3 and 369 × 10^3 m^3 day^{-1} at summer and winter pool elevations, respectively, corresponding to mean water residence times of 1424 and 274 days. The reservoir receives substantial nutrient and sediment loading from the watershed (64% row crop agriculture) and is frequently on the state's advisory list for recreational contact due to excessive blue-green algae (http://epa.ohio.gov/habalgae.aspx).

Six sites (upstream (UP), east narrows (EN), west narrows (WN), midpoint (MP), drinking water intake (DW), and outfall (OF)) were established to characterize spatial patterns in CH_4 and CO_2 dynamics. Sampling began in October 2011 and

continued on a monthly basis until June 2012, when the frequency was increased to every 3 weeks. Sampling frequency was further increased to weekly from October 2012 to November 2012 to better characterize emissions during fall turnover, defined as the period between when thermal stratification begins to degrade and isothermal conditions are achieved.

On 08 January 2013, we measured CH_4 emission rates from two of the routine sampling sites (UP and EN) and an additional 8 sites in the upstream reaches of the reservoir (Figure 1). The objective of this sampling was to determine if bays with tributaries had higher CH_4 emission rates than open water sites.

Water Sample Collection. Water samples were collected for dissolved CH_4 analysis from 0.1 m below the surface and 1 m above the sediment at all sites. During summer stratification (9 May 2012 to 24 Oct 2012) additional samples were collected at 5 m increments throughout the water column at the OF site. At least 10% of the samples were collected in duplicate. Water samples were collected in 125 mL serum bottles and preserved with 1000 μL of saturated mercuric chloride solution. Bottles were capped with gray butyl rubber septa and stored at 5 °C until sample analysis. During the summer of 2013 (24 July, 27 August) seven water samples were collected from throughout the water column at the OF site and analyzed for CH_4 concentration and $\delta^{13}C—CH_4$.

We extracted dissolved gases from the water samples using headspace equilibration.[10] The headspace equilibration was conducted at room temperature by injecting 20 mL of ultra high purity dinitrogen (N_2) into the sample serum vial, while allowing an equivalent volume of water to be displaced from the bottle through a vent needle. The water bottles were then shaken for at least 1 h before the headspace was analyzed. The original dissolved gas concentration was calculated using the measured headspace gas concentration and temperature specific Bunsen solubility coefficients.[11,12] Equilibrium dissolved CH_4 concentrations were calculated for each sampling date using water temperature, barometric pressure, and their average global atmospheric concentration.[13] Dissolved gas saturation ratio was calculated as the ratio of measured to equilibrium dissolved gas concentrations.

We measured water temperature and dissolved oxygen using a data sonde (YSI 600 OMS, Yellow Springs, Ohio, U.S.A.) at each depth where a water sample was collected. Atmospheric pressure was measured using an electronic barometer on each sampling date (YSI 650 MDS, Yellow Springs, OH, U.S.A.). We measured CH_4 and CO_2 using a Shimadzu GC-2014 (Kyoto, Japan) or Bruker 450 (Billerica, MA, U.S.A.) gas chromatograph equipped with a methanizer and flame ionization detector (FID) (additional details in the extended methods section in the SI). Methane $\delta^{13}C—CH_4$ was measured at the University of California Davis Stable Isotope Facility.[14]

CH_4 and CO_2 Emissions. Methane and CO_2 emission rates were measured using the floating chamber technique, as previously described.[15] At each of the six sites, three 20 L acrylic chambers were supported by air filled flotation collars, tethered to the boat, and allowed to drift with the boat. Gas samples (30 mL) were withdrawn from the chamber headspace every 3 min for 12 min and stored in pre-evacuated glass vials. Emission rates were computed from the linear regression of headspace CH_4 or CO_2 partial pressure against time, after accounting for the headspace volume and surface area of the reservoir enclosed by the chamber. Emission rates were only calculated for chambers where the linear regression was significant at the $p < 0.15$ level (see Supporting Information, SI, Methods).

The piston velocity (k; cm hr^{-1}) describes the physical forcing component of air—water gas exchange and can indicate whether rising bubbles or diffusive emissions were captured by the floating chambers. We calculated k from the CH_4 and CO_2 data for each chamber deployment according to the following:

$$k = \text{emission rate}/[C_w - C_{eq}] \quad (1)$$

where C_w (mg C m^{-3}) and C_{eq} (mg C m^{-3}) are the measured and equilibrium dissolved gas concentrations near the water surface (10 cm).[15] If the emissions were purely diffusive, then piston velocities calculated from CH_4 and CO_2 should be identical when normalized to a Schmidt number of 600 (k_{600}). Values of $k_{600\text{-}CH_4}$ that far exceed those of $k_{600\text{-}CO_2}$ can occur when the chambers capture CH_4 rich bubbles and were used as an indicator of ebullition (see SI Extended Methods).

We calculated average reservoir-wide CH_4 emission rates for each sampling date as follows:

$$\text{Reservoir wide emission rate} = \Sigma E_i P_i \quad (2)$$

where E_i and P_i are the measured emission rate and proportion of the reservoir surface area associated with site i, respectively. The reservoir surface area associated with the UP site was defined as extending from the upstream extent of the impounded waters along the East Fork Little Miami River, the main tributary, downstream to the area where the reservoir widens and the depth reaches 8 m (Figure 1). This boundary was selected based on the spatial survey conducted in the fall of 2012. The other five routine sampling sites were weighted equally, because there was no significant difference in emission rates between these sites.

Reservoir-wide CH_4 emissions were estimated for each day of the study by assuming the emission rate on days between sampling events was equal to the emission rate measured on the closest sampling date, and multiplying the reservoir-wide rate by the reservoir surface area. Daily reservoir surface area was calculated from the reported elevation of the water surface and 0.3 m resolution elevation data (0.58 m^2 grid size) using a geographic information system (ESRI, Redlands, California, U.S.A.). An annual reservoir-wide CH_4 emission rate was calculated by summing the daily emissions across the year and normalizing them to the mean annual reservoir surface area.

The standard deviation of the reservoir-wide annual CH_4 emission rate was calculated as the average coefficient of variation (CV) of the replicate emission rate measurements made at each site and date, multiplied by the estimated reservoir-wide annual emission rate (i.e., standard deviation = CV*mean). Standard error was calculated by dividing the standard deviation by the square root of the number of sampling dates.

We estimated the total surface area of agricultural impacted reservoirs in the U.S.A. using data from the National Inventory of Dams[16] and agricultural statistics from the National Agricultural Statistics Service.[17] All reservoirs located in counties with greater than 40 km^2 of corn and soybean were defined as agricultural. This approach does not account for reservoirs affected by other types of agricultural activities, including pastures and confined animal feed lots that could deliver nutrients and sediments to reservoirs.

CH_4 Degassing. We estimated CH_4 degassing as water passed through the dam as the product of daily depth-specific withdrawal rates (provided by the U.S. Army Corps of Engineers) and the dissolved CH_4 concentration at the depth from which

water was being withdrawn. We used measured CH_4 concentrations at the "OF" site which was located ca. 150 m from the withdrawal structure. Linear interpolation was used to extrapolate CH_4 concentration between sampling depths. For dates when dissolved CH_4 was not measured, the CH_4 concentration from the nearest sampling date was used. We assumed that all dissolved CH_4 was emitted (degassed) during transit through the outlet structure or further downstream.

Hypolimnion CH_4 Accumulation, Oxidation, Diffusion, And Production. We estimated the hypolimnion CH_4 production rate (MP_{hypo}) at the OF site during the period of stratification as the sum of hypolimnion CH_4 accumulation (MA_{hypo}), hypolimnion CH_4 oxidation (MOX_{hypo}), and CH_4 diffusion from the hypolimnion into the epilimnion (MD_{hypo}). Detailed descriptions of the calculations can be found in the SI Extended Methods. The hypolimnion CH_4 accumulation rate was calculated from the depth profiles of CH_4 concentration during stratification as previously described.[18] The fraction of CH_4 entering the hypolimnion that was oxidized (f_{ox}) was estimated from the $\delta^{13}C$—CH_4 depth profiles at the OF site using an open-system steady-state model.[19,20] The rate of CH_4 oxidation in the hypolimnion was calculated as follows:

$$MOX_{hypo} = f_{ox} \times MA_{hypo} \quad (3)$$

Methane diffusion across the thermocline from the hypolimnion (MD_{hypo}) was calculated from the vertical diffusion coefficient (K, $m^2\ d^{-1}$) and the CH_4 concentration gradient between the top of the hypolimnion and the epilimnion.[21]

Statistics. We used generalized least-squares (gls) to test for differences in emission rates among sampling sites and to test for a relationship between CH_4 emission rates and water temperature. Heterogeneity in model residuals was reduced by adding variance covariates.[22] We tested for temporal autocorrelation by comparing the Akaike's information criterion (AIC)[23] of models with and without a first-order autoregressive (AR1) temporal correlation structure.[22] The model with the lowest AIC was retained. When emission rates were found to differ by site, pairwise comparisons were made using the Tukey's test. All statistical analysis were conducted using R.[24] The gls models were built with the nlme package[25] and Tukey's tests were conducted using the multcomp package.[26]

RESULTS

Hydrology, Water Temperature, and Dissolved Oxygen. Reservoir water levels were close to the management targets of 222.3 and 223.5 m during the winter and summer, respectively (SI Figure S1). Water levels were dropped to 221 m in April 2012 before the reservoir was filled to the summer management target. Water levels transitioned between the seasonal management targets during fall and were temporarily elevated following precipitation events during the winter and spring. The water column was isothermal from 6 Dec 2011 to 9 May 2012, and some degree of thermal stratification was observed during the balance of the study (SI Figure S2A). The water column was oxygenated until the onset of thermal stratification, when the dissolved oxygen (DO) saturation fell to 0.2−3.8% in the hypolimnion, but remained above 100% in the epilimnion (SI Figure S2B). During fall turnover, DO was approximately 30% saturated throughout the water column.

Piston Velocities. The median gas piston velocities (k_{600} in cm h^{-1}) were 4.2 and 27.2 for CO_2 and CH_4, respectively (Figure 2). In the 97 instances where $k_{600\text{-}CH_4}$ and $k_{600\text{-}CO_2}$ were measured in the same chamber (see the SI Methods for data acceptance criteria), $k_{600\text{-}CH_4}$ was a median factor of 21 times greater than $k_{600\text{-}CO_2}$, suggesting that the chambers intercepted CH_4 rich bubbles rising to the water surface. The difference between the CH_4 and CO_2 k_{600} values was most extreme at the shallowest sites (EN and UP) ($p < 0.005$).

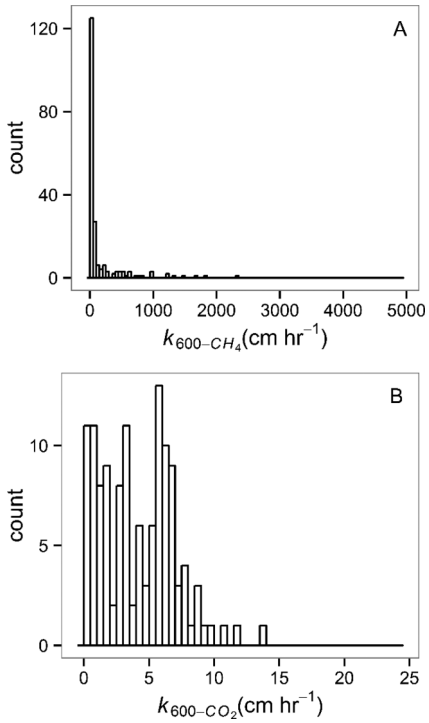

Figure 2. Histogram of (A) piston velocities calculated from dissolved CH_4 concentration and CH_4 emission rates ($k_{600\text{-}CH_4}$), and (B) piston velocities calculated from dissolved CO_2 concentration and CO_2 emission rates ($k_{600\text{-}CO_2}$). Panels A and B have binwidths of 50 and 0.5, respectively.

Methane and Carbon Dioxide. Methane was supersaturated with respect to atmospheric equilibrium throughout the study (SI Table S1). Methane concentration ranged from 0.16 to 250 μg CH_4 L^{-1} in the epilimnion (saturation ratio of 3 to 6800), highest in summer and lowest in the winter (Figure 3). Hypolimnion CH_4 concentration increased exponentially from the thermocline to the sediment−water interface during stratification at the deepest site (OF), reaching a maximum value of 18 500 μg CH_4 L^{-1} (saturation ratio = 374 700) on 24 Oct 2012 (Figure 4). Differences in CH_4 concentration between shallow and deep waters declined with overall site depth and no consistent difference was observed at the shallowest site (UP). See the SI Extended Methods for QA/QC data.

On 24 July and 27 August 2013, $\delta^{13}CH_4$ near the sediment water interface at the OF site ranged from −63.4 to −61.8‰ and increased to −57.5‰ at the top of the hypolimnion (SI Figure S3), equating to f_{ox} values of 0.29 and 0.23, respectively. We therefore assumed an f_{ox} value of 0.25 during the period of thermal stratification in 2012. Hypolimnion CH_4 accumulation (MA_{hypo}) rates at the OF site ranged from 719 to 1531 mg C m^{-2} d^{-1} (median =792) (Table 1). Hypolimnion CH_4 oxidation (MOX_{hypo}), calculated as the product of f_{ox} and MA_{hypo}, ranged from 180−383 mg C m^{-2} d^{-1} (median =198) (Table 1). Rates of CH_4 diffusion across the thermocline (MD_{hypo}) ranged from 6−106 mg C m^{-2} d^{-1} and increased throughout the period of thermal stratification (Table 1; see SI

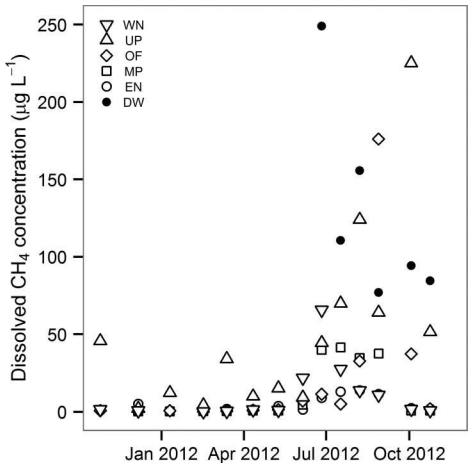

Figure 3. Dissolved methane (CH_4) concentration at ~0.1m depth at the six sampling sites in Harsha Lake from 25 Oct 2011 to 24 Oct 2012.

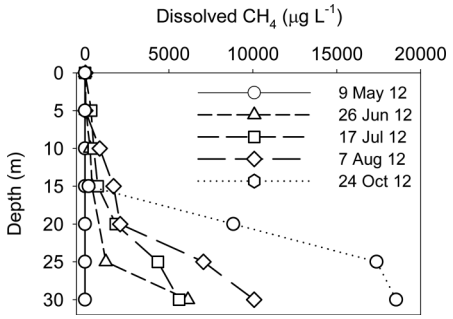

Figure 4. Depth profiles of dissolved methane concentration on given sampling dates at the OF site.

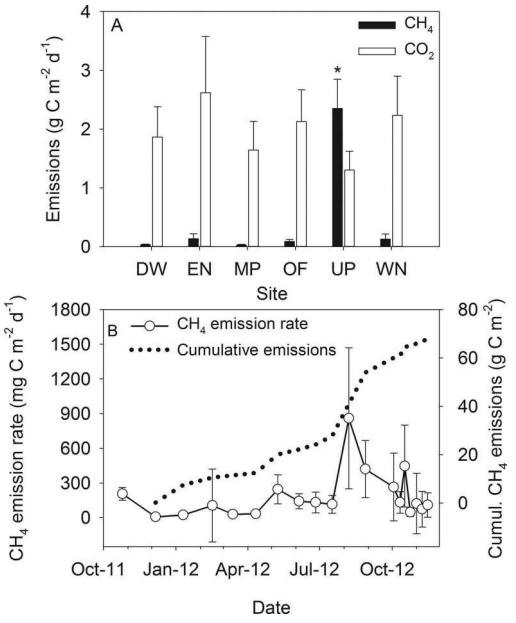

Figure 5. (A) Mean (+SE) methane (CH_4) and carbon dioxide (CO_2) emission rates at the 6 routine sampling sites. The star denotes that CH_4 emission rates at UP were significantly different than the other sites ($p < 0.001$). Methane emission rates did not differ among other sites. (B) Reservoir-wide CH_4 emission rates (±SE) on each sampling date (solid line, open circles, primary y-axis) and cumulative CH_4 emissions from 6 Dec 2011 through 15 Nov 2012 (dashed line, secondary y-axis).

Table S1 for details). Hypolimnion CH_4 production (MP_{hypo}) ranged from 908−1934 mg C m^{-2} d^{-1} (median = 1061) (Table 1).

Of 333 chamber deployments, 49 CH_4 and 30 CO_2 emission rate calculations resulted in regression models with p values greater than 0.15 and were assigned an emission rate of 0. The median coefficient of determination (r^2) for the CH_4 and CO_2 regression models was 0.94 (range: 0.56−0.99) and 0.97 (range: 0.58−0.99), respectively (SI Figure S4). The mean daily CH_4 emission rate (±SE) at the most upstream site (UP) was 2353 ± 495 mg C m^{-2} d^{-1}, was one to 2 orders of magnitude greater than the other sites ($p < 0.001$; Figure 5A, SI Table S2). The CH_4 emission rates observed near the tributaries during the one-time spatial survey on 8 Jan 2013 were on average six times higher than EN, the open water site, but were an order of magnitude lower than at UP (rates reported alongside sampling sites in Figure 1). Methane emission rates increased by 3.5 mg C m^{-2} d^{-1} per degree increase in water temperature ($p < 0.001$, SI Figure S5). A linear model containing site and water temperature explained 47% of the variation in CH_4 emission rates.

The mean annual CO_2 emission rate was lowest at UP (1.3 ± 0.3 g C m^{-2} d^{-1}) and the rates among the other sites did not differ, $p < 0.001$ Figure 5A, SI Table S2). Total carbon emissions (CO_2 + CH_4), an index for total carbon mineralization, were greater at UP (mean ± SE: 3.7 ± 0.6 g C m^{-2} d^{-1}) than all other sites except EN ($p < 0.001$; mean ± SE of all sites excluding UP: 2.2 ± 0.3 g C m^{-2} d^{-1}) (Figure 5A). The proportion of mineralized C emitted as CH_4 was also greater at UP (0.60 ± 0.07) than all other sites ($p < 0.001$, mean ± SE of all sites excluding UP: 0.11 ± 0.05).

Table 1. Hypolimnion Methane (CH_4) Accumulation, Oxidation, Trans-Thermocline Diffusion, And Production Rates Measured at the Deepest Site (OF) during the 2012 Period of Thermal Stratification

period	hypolimnion CH_4 accumulation (mg CH_4−C m^{-2} d^{-1})	hypolimnion CH_4 oxidation[a] (mg CH_4−C m^{-2} d^{-1})	trans-thermocline CH_4 diffusion[b] (mg CH_4−C m^{-2} d^{-1})	hypolimnion CH_4 production[c] (mg CH_4−C m^{-2} d^{-1})
05 Jun to 26 Jun	1409	352	6	1777
26 Jun to 17 Jul	719	180	9	908
17 Jul to 07 Aug	1531	383	21	1934
07 Aug to 28 Aug	792	198	35	1024
28 Aug to 03 Oct	764	190	106	1060

[a]Hypolimnion CH_4 oxidation calculated as the product of f_{ox} and the hypolimnion CH_4 accumulation rate. We assigned a value of 0.25 to f_{ox} based on $\delta^{13}C$—CH_4 data collected during the summer of 2013 (See SI Figure S3). [b]Methane diffusion is reported as the mean of the diffusion rates calculated for the first and last day of the measurement period. Positive values indicate net diffusion from hypolimnion into epilimnion. [c]Hypolimnion CH_4 production is calculated as the sum of hypolimnion CH_4 accumulation, oxidation, and trans-thermocline diffusion.

After accounting for spatial and temporal variability, we estimated the mean annual reservoir-wide CH_4 emission rate as 176 ± 36 mg C m^{-2} d^{-1}. Reservoir wide CH_4 emission rates were relatively low during the winter (mean daily emission rate = 64 mg C m^{-2} d^{-1}, Figure 5B). Rates increased through the spring to a seasonal mean of 117 mg C m^{-2} d^{-1} and reached a maximum of 859 mg C m^{-2} d^{-1} during the warmest months. When the lake was undergoing fall turnover (11 Oct 2012−15 Nov 2012), the daily emission rates varied greatly (47−447 mg C m^{-2} d^{-1}), but had a mean daily emission rate of 157 mg C m^{-2} d^{-1}. Approximately half (51%) of the annual CH_4 emissions occurred during the summer. Spring and fall accounted for 23% and 22% of annual emissions, respectively, while winter accounted for only 6%.

Release of CH_4 to the atmosphere resulting from water passing through the dam control structure was a relatively small part of the annual CH_4 budget. We estimate that an annual average of 10.7 kg CH_4—C d^{-1} was lost as the water degassed during transit through the Harsha Lake dam, equivalent to only 0.8% of the total emissions, or 1.22 mg C m^{-2} d^{-1}.

DISCUSSION

Harsha Lake was a consistent source of atmospheric CH_4 throughout the year. Despite low CH_4 emission rates during the winter months, average annual CH_4 emissions were higher than previously reported for temperate reservoirs in the United States and comparable to those reported for tropical reservoirs.[6] The furthest upstream portions of the reservoir supported CH_4 emissions one to 2 orders of magnitude greater than other portions of the system, highlighting the importance of including river deltas in reservoir CH_4 budgets.

CH_4 Emissions. Seasonal patterns in CH_4 emission rates were characterized by relatively low emissions during the winter months, maximum rates in the summer months, and small peaks superimposed on declining emissions during fall turnover (Figure 5B). Winter emissions were likely limited by low water temperature and greater O_2 availability in bottom waters and sediments, which reduces the metabolic activity of methanogens.[27] The reservoir stratified during the warm summer months and CH_4 progressively accumulated in the hypolimnion, reaching concentrations in excess of 18 000 μg L^{-1} (saturation ratio >300 000; Figure 4). Despite strong thermal stratification that prevented the advective transport of CH_4 from the hypolimnion to the epilimnion, surface emissions also reached a maximum during late summer. Sources of CH_4 to the air−water interface during periods of thermal stratification include diffusion from the hypolimnion,[21] lateral transport from the catchment[28] and littoral zone,[29] microbial CH_4 production in the oxic epilimnion, and ebullition.[30] Rates of CH_4 diffusion from the hypolimnion into the epilimnion were equivalent to a median of 44% (range: 6−481%) of the emission rate at OF during stratification, indicating that diffusion was, at times, an important source of CH_4 to the epilimnion. Presumably lateral transport and oxic CH_4 production accounted for the balance, and ebullition may contribute a significant portion of CH_4 emissions, particularly at shallower sites (see below).

The thermocline progressively sank during fall turnover (SI Table S1, Figure S2A), causing hypolimnetic CH_4 to mix into the epilimnion where it was either oxidized to CO_2 or emitted to the atmosphere. We expected the greatest reservoir-wide emission rates to occur during turnover,[31] but the maximum emission rate during turnover (447 mg C m^{-2} d^{-1}) was only half the highest rate observed during summer (860 mg C m^{-2} d^{-1}), likely because cooler water temperatures during turnover depressed CH_4 production at the shallow sites more than mixing enhanced CH_4 emissions from the deeper sites. Despite the relatively low rates observed during turnover, 22% of annual CH_4 emissions occurred during this time.[32]

Methane emission rates at the sampling site located near the delta at the river−reservoir transition zone (UP site) were consistently one to 2 orders of magnitude greater than the other sampling sites (Figure 5A). This site was typically the shallowest included in the study (mean depth = 4.25 m) and did not stratify during the summer. Shallow waters have been previously identified as CH_4 emission hot spots in lakes and reservoirs[4,29] due partly to low water-column CH_4 oxidation rates. The water residence time of CH_4 in shallow waters is much less than in deeper waters, resulting in reduced methane oxidation efficiencies leading to an "epilimnetic shortcut".[4] This scenario is supported by the high ratio of CH_4 to CO_2 emissions at the upstream site, which suggests that a larger fraction of the sedimentary CH_4 is evading to the atmosphere, rather than being oxidized to CO_2 (Figure 5A).

High rates of CH_4 ebullition likely contributed to enhanced emissions at the UP site. Ebullition rates tend to be highest in shallow areas because short water residence times limit the dissolution of CH_4 rich bubbles released from the sediment.[33] The floating chambers captured both ebullition and diffusive gas emissions and the k values provide insight into the relative importance of these emission mechanisms. Piston velocities calculated from CO_2 ($k_{600\text{-}CO_2}$; median = 4.2 cm hr^{-1}, Figure 2B) were consistent with values previously reported for diffusive emissions,[4,15] suggesting that diffusion was the dominant CO_2 emission pathway and that the floating chambers did not artificially enhance emissions by disturbing the air−water interface.[34] Some CH_4 piston velocities ($k_{600\text{-}CH_4}$; median = 27.2 cm hr^{-1}, Figure 2A) were too large to be attributed strictly to diffusion and were likely enhanced by surfacing CH_4-rich bubbles. The ratio of $k_{600\text{-}CH_4}$ and $k_{600\text{-}CO_2}$ (median = 21) was greatest at the two shallowest sites (UP and EN), suggesting that bubble ebullition was greatest at those sites. The magnitude of the difference between $k_{600\text{-}CH_4}$ and $k_{600\text{-}CO_2}$ was too large to be attributed to surfacing microbubbles, which can enhance CH_4 gas transfer by 5−9 cm hr^{-1},[15,35] and is likely the result of CH_4-rich macrobubbles.

Another explanation for the high CH_4 emissions from the river delta is that sediment CH_4 production at UP was greater than at the other sites. This is consistent with our finding that CH_4 emissions from the UP site were on average ca. 2.7 times greater (median =1.6) than rates of CH_4 production at OF, the most downstream and deepest site, possibly because high loadings and rapid burial of organic matter in river deltas fosters high rates of sediment CH_4 production, as described in the "deltaic zone" hypothesis.[36] This may be particularly important in reservoirs draining agricultural basins which often have high rates of soil erosion and subsequent sediment loading to receiving waters.[37] During an additional survey of CH_4 emissions near tributaries in Harsha Lake (data reported alongside site locations in Figure 1), none of the other delta sites had rates as high as UP, possibly because the other tributaries drained much smaller basins (60−80 km^2) with a lower intensity of agricultural activity. However, the rates were generally 6 times greater than the mid reservoir site (EN), providing additional evidence that river deltas have higher CH_4 emissions than open waters. The UP site also had higher overall respiration rates than the other sites, as

indicated by higher total carbon emissions (CH_4 + CO_2), which is consistent with the notion that the quantity or quality of sediment C was greater at the river delta site.

Comparison to Other Published CH_4 Emission Rates. After accounting for spatial and temporal variability, we estimated an annual reservoir-wide emission rate of 176 ± 36 mg C m^{-2} d^{-1}. This value is within the range of estimates from tropical systems (101−1471 mg C m^{-2} d^{-1}), but up to 3 orders of magnitude higher than most reports from temperate systems (<1−50 mg C m^{-2} d^{-1}).[6] The exceptions to this pattern include a temperate reservoir in Switzerland[38] (117 mg C m^{-2} d^{-1}) and a small river impoundment (0.38 km^2) in Germany[8] (333 mg C m^{-2} d^{-1}), where high emissions were largely attributed to extreme ebullition rates. One reason the rates reported here are relatively high may be that we accounted for emissions from the main river delta, while most of the literature data represent emissions from the surface of deeper areas of reservoirs, which, based on our findings, likely underestimates reservoir-wide emissions.[6] Even when excluding UP from the data set, however, the mean CH_4 emission rate (85 ± 26 mg C m^{-2} d^{-1}) is still higher than estimates from most other midlatitude reservoirs, likely because high nutrient loading, sedimentation, and persistent algae blooms in Harsha Lake have stimulated methanogenesis.[39] It is worth noting that our estimate likely represents a lower bound for the true rate because we did not quantify ebullition hot spots[38] or enhanced night-time emissions that can occur during periods of convective mixing.[32] It is unclear whether our results can be generalized to other midlatitude agricultural impacted reservoirs. Eagle Creek Reservoir (ECR), an agricultural impacted reservoir about 160 km from Harsha Lake, is also subject to high nutrient and sediment loading, yet supports an annual CH_4 emission rate only ∼5% (10 mg C m^{-2} d^{-1})[7] of that at Harsha Lake. The ECR study did not include river deltas, but even after excluding the Harsha Lake river delta site from the comparison, CH_4 emission rates from Harsha were 8.5 times greater than that at ECR (85 vs 10 mg C m^{-2} d^{-1}). Another factor complicating the comparison is that emissions at ECR were estimated using a wind based model while emissions were directly measured at Harsha Lake. Whether Harsha Lake or ECR represents the typical midlatitude agricultural reservoir is unknown, but this question has strong implications for our understanding of the global CH_4 budget. We estimate there are ca. 35 000 km^2 of reservoirs draining corn and soybean croplands, the dominant crops in the Harsha Lake watershed, in the United States. Combining this surface area estimate with the annual emission rate measured at Harsha Lake, results in an estimate of annual CH_4 emissions from agricultural impacted reservoirs in the United States of 2.2 Tg C. This represents potential reservoir CH_4 emissions not accounted for in current inventories and is equivalent to 60% of annual CH_4 emissions from all the landfills in the United States (3.7 Tg CH_4−C yr^{-1}) or about 10% of the nation's annual anthropogenic CH_4 emissions.[40] This estimate should be viewed with caution, however, because it is based on CH_4 emission rate measurements made at only one lake and does not account for numerous variables that could control reservoir CH_4 emissions including the number and size of river deltas in each reservoir.

Greenhouse Gas Emissions Mitigation Strategies. Previous studies have shown that degassing while water is routed through the dam is a major source of CH_4 emissions from reservoirs, comprising up to 33% of total reservoir emissions.[41,42] We estimate that this pathway constitutes only 0.8% of annual CH_4 emissions from Harsha Lake. In Harsha Lake, summer time water withdrawals are largely restricted to shallow depths to protect the dam from corrosive hydrogen sulfide gas and to maintain acceptably high dissolved oxygen in the receiving waters. Consequently, the highly CH_4 supersaturated water in the hypolimnion does not pass through the dam. If water at Harsha Lake were exclusively withdrawn from the hypolimnion, then we estimate that dam degassing would comprise 23−28% of annual CH_4 emissions, assuming that diffusive emissions would be unaffected. Therefore, an important engineering strategy for minimizing CH_4 emissions from reservoirs is to allow for the withdrawal of shallow waters during periods of thermal stratification.

Minimizing the surface area of the river delta through water level management may also reduce overall CH_4 emissions from reservoirs. While the river delta near the UP site comprised a small proportion of the reservoir surface area (i.e., 3−8%, depending on pool elevation), it was the source of 64% of reservoir CH_4 emissions on average (Figure 1, 5A) and should therefore be the focus of CH_4 mitigation actions. Most suggested management actions are long-term and include reducing watershed soil erosion[38] and nutrient exports.[9] While these approaches are the best long-term solution, there is a need for mitigation efforts that have a more immediate effect. We estimate that lowering the target pool elevation during the summer by 2 m would reduce the reservoir surface area by 1.2 km^2, much of which is located in the river delta areas (Figure 1), resulting in up to a 35% reduction in reservoir wide CH_4 emissions, assuming that the newly exposed soils do not emit CH_4. The long-term efficacy of this approach is unclear, however, because the CH_4 emission hot-spot may shift downriver to the site of active sediment deposition established under the lower pool elevation. Another possibility is to periodically dredge river deltas to remove methanogenic sediments and increase water depth, although this process is energy-intensive and will lead to increased anthropogenic CO_2 emissions. While these approaches are untested, they highlight a need for new research that yields actionable mitigation plans that federal and state agencies can use to reduce the greenhouse gas footprint of reservoirs, as encouraged by the White House's 2013 Executive Order.[43]

Future Directions. This study demonstrates that midlatitude agricultural reservoirs have CH_4 emission rates comparable to those observed in the tropics, and intrareservoir variation in emission rates can be extreme. To improve the accuracy of national and global estimates of reservoir CH_4 emissions it is critical that future studies account for emission hotspots within reservoirs. Furthermore, future work should focus on relatively understudied midlatitude agricultural impacted reservoirs, which may comprise a much larger component of the anthropogenic CH_4 budget than currently recognized.

■ ASSOCIATED CONTENT

Supporting Information

An extended methods section, five additional figures, and two tables. This material is available free of charge via the Internet at http://pubs.acs.org/.

■ AUTHOR INFORMATION

Corresponding Author

*beaulieu.jake@epa.gov.

Present Address
[#]URS Corporation, Cincinnati, Ohio 45202.

Notes
The authors declare no competing financial interest.

■ ACKNOWLEDGMENTS

We thank Jade Young and Jim O'Boyle of the U.S. Army Corp of Engineers for logistical support. We also thank Kit Daniels, Dana Macke, Eric Kleiner, and Don Brown for field and lab assistance. The U.S. Environmental Protection Agency, through its Office of Research and Development funded and managed this research. It has been subjected to the Agency's administrative review and has been approved for external publication. Any opinions expressed in this paper are those of the authors and do not necessarily reflect the views of the Agency, therefore, no official endorsement should be inferred. Any mention of trade names or commercial products does not constitute endorsement or recommendation for use.

■ REFERENCES

(1) Myhre, G.; Shindell, D.; Bréon, F.-M.; Collins, W.; Fuglestvedt, J.; Huang, J.; Koch, D.; Lamarque, J.-F.; Lee, D.; Mendoza, B.; Nakajima, T.; Robock, A.; Stephens, G.; Takemura, T.; Zhang, H., Anthropogenic and natural radiative forcing. In *Climate Change 2013: The Physical Science Basis. Contribution of Working Group I to the Fifth Assessment Report of the Intergovernmental Panel on Climate Change*; Stocker, T. F., Qin, D., Plattner, G.-K., Tignor, M., Allen, S. K., Boschung, J., Nauels, A., Bex, V., Midgely, P. M., Eds.; Cambridge University Press: Cambridge, U.K. and New York, U.S.A., 2013.

(2) Townsend-Small, A.; Tyler, S. C.; Pataki, D. E.; Xu, X. M.; Christensen, L. E. Isotopic measurements of atmospheric methane in Los Angeles, influence of "fugitive" fossil fuel emissions, California, U.S.A. *J. Geophys. Res.-Atmos.* **2012**, *117*.

(3) Miller, S. M.; Wofsy, S. C.; Michalak, A. M.; Kort, E. A.; Andrews, A. E.; Biraud, S. C.; Dlugokencky, E. J.; Eluszkiewicz, J.; Fischer, M. L.; Janssens-Maenhout, G.; Miller, B. R.; Miller, J. B.; Montzka, S. A.; Nehrkorn, T.; Sweeney, C. Anthropogenic emissions of methane in the United States. *Proc. Natl. Acad. Sci. U. S. A.*, **2013**.

(4) Bastviken, D.; Cole, J. J.; Pace, M. L.; Van de Bogert, M. C. Fates of methane from different lake habitats: Connecting whole-lake budgets and CH_4 emissions. *J. Geophys. Res.-Biogeosci.* **2008**, *113*, G2.

(5) St. Louis, V. L.; Kelly, C. A.; Duchemin, É.; Rudd, J. W. M.; Rosenberg, D. M. Reservoir surfaces as sources of greenhouse gases to the atmosphere: A global estimate. *Bioscience* **2000**, *50* (9), 766−775.

(6) Barros, N.; Cole, J. J.; Tranvik, L. J.; Prairie, Y. T.; Bastviken, D.; Huszar, V. L. M.; del Giorgio, P.; Roland, F. Carbon emission from hydroelectric reservoirs linked to reservoir age and latitude. *Nat. Geosci.* **2011**, *4* (9), 593−596.

(7) Jacinthe, P. A.; Filippelli, G. M.; Tedesco, L. P.; Raftis, R. Carbon storage and greenhouse gases emission from a fluvial reservoir in an agricultural landscape. *CATENA* **2012**, *94* (0), 53−63.

(8) Maeck, A.; DelSontro, T.; McGinnis, D. F.; Fischer, H.; Flury, S.; Schmidt, M.; Fietzek, P.; Lorke, A. Sediment trapping by dams creates methane emission hot spots. *Environ. Sci. Technol.* **2013**, *47* (15), 8130−8137.

(9) West, W. E.; Coloso, J. J.; Jones, S. E. Effects of algal and terrestrial carbon on methane production rates and methanogen community structure in a temperate lake sediment. *Freshw. Biol.* **2012**, *57* (5), 949−955.

(10) Ioffe, B. V.; Vitenberg, A. G. *Head-Space Analysis and Related Methods in Gas Chromatography*; Wiley: New York, 1984.

(11) Weiss, R. F. Carbon dioxide in water and seawater: the solubility of a non-ideal gas. *Mar. Chem.* **1974**, *2* (3), 203−215.

(12) Yamamoto, S.; Alcauskas, J. B.; Crozier, T. E. Solubility of methane in distilled water and seawater. *J. Chem. Eng. Data* **1976**, *21* (1), 78−80.

(13) Tans, P.; Keeling, R. ESRL/GMD FTP data finder. http://www.esrl.noaa.gov/gmd/dv/data/ (11/05/2013).

(14) Yarnes, C. $\delta^{13}C$ and $\delta^{2}H$ measurement of methane from ecological and geological sources by gas chromatography/combustion/pyrolysis isotope-ratio mass spectrometry. *Rapid Commun. Mass Spectrom.* **2013**, *27* (9), 1036−1044.

(15) Beaulieu, J. J.; Shuster, W. D.; Rebholz, J. A. Controls on gas transfer velocities in a large river. *J. Geophys. Res.* **2012**, *117* (G2), G02007.

(16) United States Army Corps of Engineers National Inventory of Dams. http://geo.usace.army.mil/pgis/f?p=397:1:0.

(17) United States Department of Agriculture Quick Stats 2.0. http://www.nass.usda.gov/Quick_Stats/.

(18) Beaulieu, J. J.; Smolenski, R. L.; Nietch, C. T.; Townsend-Small, A.; Elovitz, M. S.; Schubauer-Berigan, J. P. Denitrification alternates between a source and sink of nitrous oxide in the hypolimnion of a thermally stratified reservoir. *Limnol. Oceanogr.* **2014**, *59* (2), 495−506.

(19) Happell, J. D.; Chanton, J. P.; Showers, W. S. The influence of methane oxidation on the stable isotopic composition of methane emitted from Florida swamp forests. *Geochim. Cosmochim. Acta* **1994**, *58* (20), 4377−4388.

(20) Bastviken, D.; Ejlertsson, J.; Tranvik, L. Measurement of methane oxidation in lakes: A comparison of methods. *Environ. Sci. Technol.* **2002**, *36* (15), 3354−61.

(21) Kankaala, P.; Huotari, J.; Peltomaa, E.; Saloranta, T.; Ojala, A. Methanotrophic activity in relation to methane efflux and total heterotrophic bacterial production in a stratified, humic, boreal lake. *Limnol. Oceanogr.* **2006**, *51* (2), 1195−1204.

(22) Zuur, A. F.; Leno, E. N.; Walker, N. J.; Saveliev, A. A.; Smith, G. M. *Mixed Effects Models and Extensions in Ecology with R*; Springer: New York, NY, 2009.

(23) Sakamoto, Y.; Ishiguro, M.; Kitagawa, G. *Akaike Information Criterion Statistics*; Reidel Publishing Company: Netherlands, 1986.

(24) R Development Core Team. R: A Language and Environment for Statistical Computing. http://www.R-project.org.

(25) Pinheiro, J.; Bates, D.; DebRoy, S.; Sarkar, D. R Development Core Team. nlme: Linear and Nonlinear Mixed Effects Models. R package version 3.1−113. 2011.

(26) Hothorn, T.; Bretz, F.; Westfall, P. Simultaneous inference in general parametric models. *Biomet. J.* **2008**, *50* (3), 346−363.

(27) Kelly, C. A.; Chynoweth, D. P. The contributions of temperature and of the input of organic matter in controlling rates of sediment methanogenesis. *Limnol. Oceanogr.* **1981**, *26* (5), 891−897.

(28) Ojala, A.; Bellido, J. L.; Tulonen, T.; Kankaala, P.; Huotari, J. Carbon gas fluxes from a brown-water and a clear-water lake in the boreal zone during a summer with extreme rain events. *Limnol. Oceanogr.* **2011**, *56* (1), 61−76.

(29) Hofmann, H. Spatiotemporal distribution patterns of dissolved methane in lakes: How accurate are the current estimations of the diffusive flux path? *Geophys. Res. Lett.* **2013**, *40* (11), 2779−2784.

(30) Grossart, H. P.; Frindte, K.; Dziallas, C.; Eckert, W.; Tang, K. W. Microbial methane production in oxygenated water column of an oligotrophic lake. *Proc. Natl. Acad. Sci. U. S. A.* **2011**, *108* (49), 19657−61.

(31) Schubert, C. J.; Diem, T.; Eugster, W. Methane emissions from a small wind shielded lake determined by eddy covariance, flux chambers, anchored funnels, and boundary model calculations: A comparison. *Environ. Sci. Technol.* **2012**, *46* (8), 4515−4522.

(32) Podgrajsek, E.; Sahlee, E.; Rutgersson, A. Diurnal cycle of lake methane flux. *J. Geophys. Res.-Biogeosci.* **2014**, *119* (3), 236−248.

(33) McGinnis, D. F.; Greinert, J.; Artemov, Y.; Beaubien, S. E.; Wüest, A. Fate of rising methane bubbles in stratified waters: How much methane reaches the atmosphere? *J. Geophys. Res.* **2006**, *111* (C9), C09007.

(34) Matthews, C. J. D., St; Louis, V. L.; Hesslein, R. H. Comparison of three techniques used to measure diffusive gas exchange from

sheltered aquatic surfaces. *Environ. Sci. Technol.* **2003**, *37* (4), 772−780.
(35) Prairie, Y. T.; del Giorgio, P. A. A new pathway of freshwater methane emissions and the putative importance of microbubbles. *Inland Waters* **2013**, *3* (3), 311−320.
(36) DelSontro, T.; Kunz, M. J.; Kempter, T.; Wuest, A.; Wehrli, B.; Senn, D. B. Spatial heterogeneity of methane ebullition in a large tropical reservoir. *Environ. Sci. Technol.* **2011**, *45* (23), 9866−9873.
(37) Heathcote, A. J.; Downing, J. A. Impacts of eutrophication on carbon burial in freshwater lakes in an intensively agricultural landscape. *Ecosystems* **2012**, *15* (1), 60−70.
(38) Delsontro, T.; McGinnis, D. F.; Sobek, S.; Ostrovsky, I.; Wehrli, B. Extreme methane emissions from a swiss hydropower reservoir: Contribution from bubbling sediments. *Environ. Sci. Technol.* **2010**, *44* (7), 2419−2425.
(39) Hulthe, G.; Hulth, S.; Hall, P. O. J. Effect of oxygen on degradation rate of refractory and labile organic matter in continental margin sediments. *Geochim. Cosmochim. Acta* **1998**, *62* (8), 1319−1328.
(40) U.S. Environmental Protection Agency. *Inventory of U.S Greenhouse Gas Emissions and Sinks: 1990−2011*, 2013.
(41) Guérin, F.; Abril, G.; Richard, S.; Burban, B.; Reynouard, C.; Seyler, P.; Delmas, R., Methane and carbon dioxide emissions from tropical reservoirs: Significance of downstream rivers. *Geophys. Res. Lett.* **2006**, *33*, (21).
(42) Galy-Lacaux, C.; Delmas, R.; Jambert, C.; Dumestre, J.-F.; Labroue, L.; Richard, S.; Gosse, P. Gaseous emissions and oxygen consumption in hydroelectric dams: A case study in French Guyana. *Global Biogeochem. Cycles* **1997**, *11* (4), 471−483.
(43) Obama, B. *Executive Order—Preparing the United States for the Impacts of Climate Change*. http://www.whitehouse.gov/the-press-office/2013/11/01/executive-order-preparing-united-states-impacts-climate-change (7/3/2014).

Beaulieu, Jake

From: Young, Jade L CIV USARMY CELRL (USA) <Jade.L.Young@usace.army.mil>
Sent: Wednesday, April 29, 2020 12:08 PM
To: Beaulieu, Jake
Subject: Record of Percentage Agreement Jade Young (UNCLASSIFIED)
Attachments: [Non-DoD Source] Nomination for EPA award

CLASSIFICATION: UNCLASSIFIED

Jade L. Young
US Army Corps of Engineers

Beaulieu, J. J., D. A. Balz, M. K. Birchfield, J. A. Harrison, C. T. Nietch, M. C. Platz, W. C. Squier, S. Waldo, J. T. Walker, K. M. White, and J. L. Young. 2018. Effects of an Experimental Water-level Drawdown on Methane Emissions from a Eutrophic Reservoir. Ecosystems 21:657-674.

I agree with the designated percentage of contribution.

Regards,
Jade

Jade L. Young, CLM
Limnologist | Water Quality Team Leader | Contracting Officer's Representative | Facilities Engineer, Level II

US Army Corps of Engineers Louisville District

Alternative phone number during Coronavirus pandemic: 931.248.1226
Phone: 502.315.7439
Fax: 502.315.6309
Email: Jade.L.Young@usace.army.mil
LinkedIn: https://gcc01.safelinks.protection.outlook.com/?url=https%3A%2F%2Fwww.linkedin.com%2Fin%2Fjade-l-young-424252141&data=02%7C01%7CBeaulieu.Jake%40epa.gov%7C38d770adc661434bfc3b08d7ec59f58a%7C88b378b367484867acf976aacbeca6a7%7C0%7C0%7C637237743425612160&sdata=2jfR2bB7%2BpO9cYZ0JiJhYNN0HbD4vxZpqvRc9TltCZc%3D&reserved=0

Louisville District Water Quality Website:
https://gcc01.safelinks.protection.outlook.com/?url=http%3A%2F%2Fwww.lrl.usace.army.mil%2FMissions%2FCivilWorks%2FWaterInformation%2FWaterQuality.aspx&data=02%7C01%7CBeaulieu.Jake%40epa.gov%7C38d770adc661434bfc3b08d7ec59f58a%7C88b378b367484867acf976aacbeca6a7%7C0%7C0%7C637237743425612160&sdata=imIKoXDEgQQjodEx6TEQbJq4zrfZMxFSzM7miGVvWZc%3D&reserved=0

CLASSIFICATION: UNCLASSIFIED

Beaulieu, Jake

From: White, KarenM
Sent: Tuesday, April 28, 2020 5:46 PM
To: Beaulieu, Jake
Subject: Record of Percentage Agreement Karen White

I agree with my designated percentage of the contribution regarding the following publications;

Berberich, M. E., J. J. Beaulieu, T. L. Hamilton, S. Waldo, and I. Buffam. **2019**. Spatial variability of sediment methane production and methanogen communities within a eutrophic reservoir: Importance of organic matter source and quantity. Limnology and Oceanography.

Beaulieu, J. J., D. A. Balz, M. K. Birchfield, J. A. Harrison, C. T. Nietch, M. C. Platz, W. C. Squier, S. Waldo, J. T. Walker, K. M. White, and J. L. Young. **2018**. Effects of an Experimental Water-level Drawdown on Methane Emissions from a Eutrophic Reservoir. Ecosystems **21**:657-674.

Beaulieu, J. J., M. G. McManus, and C. T. Nietch. **2016**. Estimates of reservoir methane emissions based on a spatially balanced probabilistic-survey. Limnology and Oceanography **61**:S27-S40.

Karen M White
Biological Science Technician
Watershed Management Branch
Watershed & Ecosystem Characterization Division
Center for Environmental Measurement and Modeling
Office of Research and Development
U.S. Environmental Protection Agency
26 W. Martin L. King Dr., ms 689
Cincinnati, OH 45268
Phone: 513-569-7248
Fax: 513-487-2850
white.karenm@epa.gov

From: Beaulieu, Jake <Beaulieu.Jake@epa.gov>
Sent: Tuesday, April 28, 2020 9:30 AM
To: berberichme@gmail.com; Trinity Hamilton <trinityh@umn.edu>; sarahrwaldo@gmail.com; Ishi (buffamii) Buffam <buffamii@UCMAIL.UC.EDU>; Balz, Adam <balz.adam@epa.gov>; Birchfield, Keith <mkeithbirch@wsu.edu>; Harrison, John <john_harrison@wsu.edu>; Nietch, Christopher <Nietch.Christopher@epa.gov>; Michelle Platz (platzmc05@gmail.com) <platzmc05@gmail.com>; Squier, Bill <squier.bill@epa.gov>; Walker, JohnT <Walker.Johnt@epa.gov>; White, KarenM <White.Karenm@epa.gov>; Young, Jade L LRL <Jade.L.Young@usace.army.mil>; McManus, Michael <McManus.Michael@epa.gov>
Subject: Nomination for EPA award

Dear colleagues,

Each year the EPA accepts nominations for the Scientific and Technological Achievement Awards (STAA) program. The STAA program promotes and recognizes scientific and technological achievements by EPA employees Agency-wide. ORD provides and manages administrative oversight of the program, while EPA's Science Advisory Board (SAB) provides the scientific and technological evaluation. This year I plan to nominate the three papers listed below. As coauthors, you will all receive a certificate if our nomination is awarded. EPA coauthors will also be eligible for a cash prize. Distribution of the cash award will be based on your percent

Beaulieu, Jake

From: Balz, Adam
Sent: Tuesday, April 28, 2020 2:56 PM
To: Beaulieu, Jake
Subject: Record of Percentage Agreement, Adam Balz

Jake,

I agree with my designated percentage of contribution of 6% on the following papers:

Berberich, M. E., J. J. Beaulieu, T. L. Hamilton, S. Waldo, and I. Buffam. **2019**. Spatial variability of sediment methane production and methanogen communities within a eutrophic reservoir: Importance of organic matter source and quantity. Limnology and Oceanography.

Beaulieu, J. J., D. A. Balz, M. K. Birchfield, J. A. Harrison, C. T. Nietch, M. C. Platz, W. C. Squier, S. Waldo, J. T. Walker, K. M. White, and J. L. Young. **2018**. Effects of an Experimental Water-level Drawdown on Methane Emissions from a Eutrophic Reservoir. Ecosystems **21**:657-674.

Beaulieu, J. J., M. G. McManus, and C. T. Nietch. **2016**. Estimates of reservoir methane emissions based on a spatially balanced probabilistic-survey. Limnology and Oceanography **61**:S27-S40.

Thanks for allowing me to be a member of the team!

Adam Balz

Adam Balz
Environmental Scientist
Pegasus Technical Services, Inc.
On-Site Contractor to U.S. EPA
26 W. Martin Luther King Drive
Cincinnati, OH 45268
Phone: (513) 569 7107
e-mail: balz.adam@epa.gov

From: Beaulieu, Jake <Beaulieu.Jake@epa.gov>
Sent: Tuesday, April 28, 2020 9:30 AM
To: berberichme@gmail.com; Trinity Hamilton <trinityh@umn.edu>; sarahrwaldo@gmail.com; Ishi (buffamii) Buffam <buffamii@UCMAIL.UC.EDU>; Balz, Adam <balz.adam@epa.gov>; Birchfield, Keith <mkeithbirch@wsu.edu>; Harrison, John <john_harrison@wsu.edu>; Nietch, Christopher <Nietch.Christopher@epa.gov>; Michelle Platz (platzmc05@gmail.com) <platzmc05@gmail.com>; Squier, Bill <squier.bill@epa.gov>; Walker, JohnT <Walker.Johnt@epa.gov>; White, KarenM <White.Karenm@epa.gov>; Young, Jade L LRL <Jade.L.Young@usace.army.mil>; McManus, Michael <McManus.Michael@epa.gov>
Subject: Nomination for EPA award

Dear colleagues,

Each year the EPA accepts nominations for the Scientific and Technological Achievement Awards (STAA) program. The STAA program promotes and recognizes scientific and technological achievements by EPA employees Agency-wide. ORD provides and manages administrative oversight of the program, while EPA's Science Advisory Board (SAB) provides the scientific and technological evaluation. This year I plan to nominate the three papers listed below. As coauthors, you

Beaulieu, Jake

From: Megan Berberich <berberichme@gmail.com>
Sent: Tuesday, April 28, 2020 1:05 PM
To: Beaulieu, Jake
Subject: Record of Percentage Agreement - Megan Berberch

Hi Jake,

Great to hear about the nomination for the award - thank you for including our work! I agree with the designated percentage of contribution (6%) for the nominated publications:

- Berberich, M. E., J. J. Beaulieu, T. L. Hamilton, S. Waldo, and I. Buffam. **2019**. Spatial variability of sediment methane production and methanogen communities within a eutrophic reservoir: Importance of organic matter source and quantity. Limnology and Oceanography.
- Beaulieu, J. J., D. A. Balz, M. K. Birchfield, J. A. Harrison, C. T. Nietch, M. C. Platz, W. C. Squier, S. Waldo, J. T. Walker, K. M. White, and J. L. Young. **2018**. Effects of an Experimental Water-level Drawdown on Methane Emissions from a Eutrophic Reservoir. Ecosystems **21**:657-674.
- Beaulieu, J. J., M. G. McManus, and C. T. Nietch. **2016**. Estimates of reservoir methane emissions based on a spatially balanced probabilistic-survey. Limnology and Oceanography **61**:S27-S40.

My name and current organization:

Megan Berberich

International Institute of Tropical Forestry, USDA Forest Service

On-Site Contractor

Luquillo, Puerto Rico

If you need my past organization, please let me know and I can modify.

Thank you,

Megan

Beaulieu, Jake

From: Trinity Hamilton <trinityh@umn.edu>
Sent: Tuesday, April 28, 2020 12:57 PM
To: Beaulieu, Jake
Subject: "Record of Percentage Agreement", Trinity Hamilton

Trinity Hamilton

Berberich, M. E., J. J. Beaulieu, T. L. Hamilton, S. Waldo, and I. Buffam. **2019**. Spatial variability of sediment methane production and methanogen communities within a eutrophic reservoir: Importance of organic matter source and quantity. Limnology and Oceanography.

I agree with my designated percentage of contribution.

Good luck!

Trinity

--
Trinity L Hamilton
Pronouns: She/Her
Assistant Professor
Plant and Microbial Biology
College of Biological Sciences
University of Minnesota
St. Paul, MN 55108
The-Fringe-Lab.com
ResearchGate
Google Scholar

Beaulieu, Jake

From: McManus, Michael
Sent: Tuesday, April 28, 2020 11:13 AM
To: Beaulieu, Jake
Subject: Record of Percentage Agreement, Michael McManus

Michael McManus
US Environmental Protection Agency
Office of Research and Development
Center for Environmental Measurement & Modeling

Nominated Publications
Berberich, M. E., J. J. Beaulieu, T. L. Hamilton, S. Waldo, and I. Buffam. 2019. Spatial variability of sediment methane production and methanogen communities within a eutrophic reservoir: Importance of organic matter source and quantity. Limnology and Oceanography.
Beaulieu, J. J., D. A. Balz, M. K. Birchfield, J. A. Harrison, C. T. Nietch, M. C. Platz, W. C. Squier, S. Waldo, J. T. Walker, K. M. White, and J. L. Young. 2018. Effects of an Experimental Water-level Drawdown on Methane Emissions from a Eutrophic Reservoir. Ecosystems 21:657-674.
Beaulieu, J. J., M. G. McManus, and C. T. Nietch. 2016. Estimates of reservoir methane emissions based on a spatially balanced probabilistic-survey. Limnology and Oceanography 61:S27-S40.

I agree with my designated percentage of contribution.
Mike

Michael McManus
Ecologist, Ph.D.
US Environmental Protection Agency
Office of Research and Development
Center for Environmental Measurement & Modeling
26 W. Martin Luther King Drive (MS-587)
Cincinnati OH 45268
Office: 513.569.7994
Cell: 513.376.3380

Beaulieu, Jake

From: Walker, JohnT
Sent: Tuesday, April 28, 2020 10:42 AM
To: Beaulieu, Jake
Subject: Record of Percentage Agreement - John Walker

Nominated publications for 2020 STAA:

Berberich, M. E., J. J. Beaulieu, T. L. Hamilton, S. Waldo, and I. Buffam. **2019**. Spatial variability of sediment methane production and methanogen communities within a eutrophic reservoir: Importance of organic matter source and quantity. Limnology and Oceanography.

Beaulieu, J. J., D. A. Balz, M. K. Birchfield, J. A. Harrison, C. T. Nietch, M. C. Platz, W. C. Squier, S. Waldo, J. T. Walker, K. M. White, and J. L. Young. **2018**. Effects of an Experimental Water-level Drawdown on Methane Emissions from a Eutrophic Reservoir. Ecosystems **21**:657-674.

Beaulieu, J. J., M. G. McManus, and C. T. Nietch. **2016**. Estimates of reservoir methane emissions based on a spatially balanced probabilistic-survey. Limnology and Oceanography **61**:S27-S40.

I agree with my designated percentage contribution (6%) to this STAA package.

John T. Walker
Center for Environmental Measurement and Modeling
U.S. EPA Office of Research and Development

Beaulieu, Jake

From: Buffam, Ishi (buffamii) <buffamii@UCMAIL.UC.EDU>
Sent: Tuesday, April 28, 2020 9:46 AM
To: Beaulieu, Jake
Subject: Record of Percentage Agreement Ishi Buffam

Name and Affiliation: Ishi Buffam, University of Cincinnati (now at Swedish University of Agricultural Sciences)
Title: Spatial variability of sediment methane production and methanogen communities within a eutrophic reservoir: Importance of organic matter source and quantity
I agree with my designated percentage of contribution.
-Ishi Buffam

From: Beaulieu, Jake <Beaulieu.Jake@epa.gov>
Sent: Tuesday, April 28, 2020 3:29 PM
To: berberichme@gmail.com <berberichme@gmail.com>; Trinity Hamilton <trinityh@umn.edu>; sarahrwaldo@gmail.com <sarahrwaldo@gmail.com>; Buffam, Ishi (buffamii) <buffamii@UCMAIL.UC.EDU>; Balz, Adam <balz.adam@epa.gov>; Birchfield, Keith <mkeithbirch@wsu.edu>; Harrison, John <john_harrison@wsu.edu>; Nietch, Christopher <Nietch.Christopher@epa.gov>; Michelle Platz (platzmc05@gmail.com) <platzmc05@gmail.com>; Squier, Bill <squier.bill@epa.gov>; Walker, JohnT <Walker.Johnt@epa.gov>; White, KarenM <White.Karenm@epa.gov>; Young, Jade L LRL <Jade.L.Young@usace.army.mil>; McManus, Michael <McManus.Michael@epa.gov>
Subject: Nomination for EPA award

Dear colleagues,

Each year the EPA accepts nominations for the Scientific and Technological Achievement Awards (STAA) program. The STAA program promotes and recognizes scientific and technological achievements by EPA employees Agency-wide. ORD provides and manages administrative oversight of the program, while EPA's Science Advisory Board (SAB) provides the scientific and technological evaluation. This year I plan to nominate the three papers listed below. As coauthors, you will all receive a certificate if our nomination is awarded. EPA coauthors will also be eligible for a cash prize. Distribution of the cash award will be based on your percent contribution to the project (see table below). Please note that defining percent contributions among so many coauthors, all of whom made important contributions to the project, is difficult. Rather than getting into the weeds on this, I defaulted to an equal contribution among coauthors.

Per requirements of the award program, please send me an e-mail with "Record of Percentage Agreement" in the subject line, followed by your first and last name. The body of the document should contain your name and organization, the titles of the nominated publications, and a brief statement that you agree with your designated percentage of contribution. Please provide your concurrence today (4/28), if possible.

Thanks for your collaboration over the years. We have been a productive group!

Jake

Nominee	Percent Contribution
Berberich	6
Hamilton	6
Waldo	6
Buffam	6

Beaulieu, Jake

From: Nietch, Christopher
Sent: Tuesday, April 28, 2020 9:42 AM
To: Beaulieu, Jake
Subject: Record of Percentage Agreement - Christopher Nietch

Hello Jake,
I, Christopher Nietch, Research Ecologist, USEPA-ORD-CEMM-WECD-WMB, agree with your designated percentage contribution on the following nominated papers:

Beaulieu, J. J., D. A. Balz, M. K. Birchfield, J. A. Harrison, C. T. Nietch, M. C. Platz, W. C. Squier, S. Waldo, J. T. Walker, K. M. White, and J. L. Young. 2018. Effects of an Experimental Water-level Drawdown on Methane Emissions from a Eutrophic Reservoir. Ecosystems 21:657-674.

Beaulieu, J. J., M. G. McManus, and C. T. Nietch. 2016. Estimates of reservoir methane emissions based on a spatially balanced probabilistic-survey. Limnology and Oceanography 61:S27-S40.

Sincerely,
Chris

==========

Christopher T. Nietch, Ph.D. | Research Ecologist | U.S. EPA | Office of Research and Development
Center for Environmental Measurement and Modelling | Watershed and Ecosystem Characterization Division
Watershed Management Branch | Experimental Stream Facility
26 W. MLK Dr., Cincinnati, OH 45268 | 1003 US HWY 50, Milford, OH 45150
513-569-7460 (Office) | 513-453-5424 (ESF) | 513-317-9394 (Mobile)

From: Harrison, John
To: Beaulieu, Jake
Subject: Record of Percentage Agreement: John Harrison
Date: Thursday, April 30, 2020 7:26:12 PM

Hi Jake,

As requested, I am writing to express my agreement with the designated percentage of agreement for contribution to the following publications:

Berberich, M. E., J. J. Beaulieu, T. L. Hamilton, S. Waldo, and I. Buffam. **2019**. Spatial variability of sediment methane production and methanogen communities within a eutrophic reservoir: Importance of organic matter source and quantity. Limnology and Oceanography.
Beaulieu, J. J., D. A. Balz, M. K. Birchfield, J. A. Harrison, C. T. Nietch, M. C. Platz, W. C. Squier, S. Waldo, J. T. Walker, K. M. White, and J. L. Young. **2018**. Effects of an Experimental Water-level Drawdown on Methane Emissions from a Eutrophic Reservoir. Ecosystems **21**:657-674.
Beaulieu, J. J., M. G. McManus, and C. T. Nietch. **2016**. Estimates of reservoir methane emissions based on a spatially balanced probabilistic-survey. Limnology and Oceanography **61**:S27-S40

Let me know if you need anything else, and good luck with this!

Best,

John

John Harrison
Edward R. Meyer Professor
School of the Environment
Washington State University, Vancouver
14204 NE Salmon Creek Avenue
Vancouver, WA 98686

Phone: 360-546-9210
Email: john_harrison@wsu.edu
Web:http://research.vancouver.wsu.edu/gcwblab

> On Apr 28, 2020, at 6:29 AM, Beaulieu, Jake <Beaulieu.Jake@epa.gov> wrote:
>
> Dear colleagues,
>
> Each year the EPA accepts nominations for the Scientific and Technological Achievement Awards (STAA) program. The STAA program promotes and recognizes scientific and technological achievements by EPA employees Agency-wide. ORD provides and manages administrative oversight of the program, while EPA's Science Advisory Board (SAB) provides the scientific and technological evaluation. This year I plan to nominate the three papers listed below. As coauthors, you will all receive a certificate if our nomination is awarded. EPA coauthors will also be eligible for a cash

From: Sarah W
To: Beaulieu, Jake
Subject: Record of Percentage Agreement, Sarah Waldo
Date: Tuesday, May 5, 2020 7:20:01 PM

Dear Dr. Beaulieu,

It has been a pleasure to collaborate with you on the following peer-reviewed publications:

Berberich, M. E., J. J. Beaulieu, T. L. Hamilton, S. Waldo, and I. Buffam. **2019**. Spatial variability of sediment methane production and methanogen communities within a eutrophic reservoir: Importance of organic matter source and quantity. Limnology and Oceanography.

Beaulieu, J. J., D. A. Balz, M. K. Birchfield, J. A. Harrison, C. T. Nietch, M. C. Platz, W. C. Squier, S. Waldo, J. T. Walker, K. M. White, and J. L. Young. **2018**. Effects of an Experimental Water-level Drawdown on Methane Emissions from a Eutrophic Reservoir. Ecosystems **21**:657-674.

I, Sarah Waldo, agree to the designated percentage contribution of 6%.

At the time of my contribution I was affiliated with EPA ORD as a federal postdoc, but am currently employed with the Puget Sound Clean Air Agency.

Best,

Sarah Waldo, Ph.D.

Air Monitoring Specialist

Puget Sound Clean Air Agency

Table of Contents

General_Authors_Publications.....2
LI-266403_Oliver_etal_2018EMAS_AssessingLandUse.....20
LI-266404_Oliver_etal_2016Developing-a-Multi-Stressor-Gradient-Model.....36
LI-266405_Santavy_etal_2016TheBiologicalConditionGradient.....50
Oliver_etal_2018EMAS_AssessingLandUse.....63
Oliver_etal_2016Developing-a-Multi-Stressor-Gradient-Model.....79
Santavy_etal_2016TheBiologicalConditionGradient.....93
Oliver_STAA_2020_Bundle_-_Journal_Statistics_Supplemental_Information.....106
Oliver_STAA_2020_Bundle_-_percent_contribution_concurrence.....107

United States Environmental Protection Agency
Washington, DC 20460

STAA REPORT FOR THE SCIENTIST NOMINATIONS

General Information:

Nomination ID/App ID:	20-118
Research Category Primary:	Ecological Research (ER)
Research Category Secondary:	Other Environmental Research (OR)
Laboratory/Office Name:	ORD
Nomination Entered By:	Matthew Harwell

Eligibility Checklist:

[Y] The nominated publication(s) has not been submitted to a previous STAA competition.

[Y] The nominated publication(s) was published on or before January 1, 2017 and on or after January 1,2012

[Y] The principal author was an EPA employee or a PHS employee assigned to EPA when the research was performed

[Y] The EPA authors (includes PHS employees assigned to EPA) contributed collectively a minimum of 50% toward the publication(s)

Nominating Official Name:	Susan George
Nominating Official Title:	DIRECTOR, GULF ECOLOGY DIVISION
Nominating OfficialEmail:	george.elizabeth@epa.gov
STAA Coordinator Name:	Kathleen Wiser
STAA Coordinator Email:	wiser.kathi@epa.gov

Justifications:

Justification 1:

The U.S. Clean Water Act (CWA) grants regulatory authority to the EPA to protect the chemical, physical, and biological integrity of the Nation's waters. Protection of biological communities requires both an understanding of what constitutes a "natural" community that is undisturbed by human activities, as well as how communities change in response to human-related (anthropogenic) stress. The manuscripts nominated for STAA contribute to understanding responses of coral reef ecosystems to anthropogenic stress, through development and application of multi- and integrated-stressor models, including the application of a Biological Condition Gradient (BCG). The BCG is a framework to relate biological condition to a gradient of increasing stress that can be applied in the CWA regulatory context. Successful development of a BCG requires biological assessment methods that measure attributes of a community's biological condition, such as species diversity and richness, necessary for natural structure and function of the community. Relevant stressors that are known to negatively impact the biological community must also be quantified using the best available data at a scale corresponding to appropriate regulatory authority. Adoption of a BCG approach by state or territorial jurisdictions supports monitoring of the biological resource so that degradation below a threshold of biological integrity can be detected, and action can then be taken to identify putative stressors and mitigation strategies to restore community integrity. As such, the research presented in this nomination empowers the EPA to meet its regulatory charge under the CWA in a framework that is scalable to regions, states and territorial jurisdictions.

Developing a BCG to support coral reef protection presents challenges not encountered in precedent approaches implemented for protection of streams and aquatic communities of benthic macroinvertebrates. Stream flow is unidirectional, so stress from anthropogenic pollutant discharge can generally be characterized as decreasing with increasing distance downstream from a pollutant source. Coral reefs subject to high levels of anthropogenic stress are usually located near coastal areas with dense human populations. Point and nonpoint pollution sources are often identifiable, and some extent of dilution is assumed with increasing distance. Unlike stream flow, coastal stressor gradients are difficult to quantify due to complex bathymetry, ocean currents, and even wind that influence pollutant transport to coastal biotic communities including coral reefs, mangroves, and seagrass beds. Additionally, a given center of human disturbance (such as a population center)

usually imparts multiple stressors (such as enhanced sedimentation from land conversion to impervious surface), introduction of contaminants, and physical disruption to critical habitat. Approaches developed for stressor characterization

have multiple applications and utilize data sources that, in some cases, are available for the entire planet, creating high potential for transferability both within and outside the U.S.

2016 Santavy et al.: Successful development of a BCG requires not only stressor indicators to be developed, but biocriteria (measurements of components essential to natural structure and function of an ecosystem) must be related to a stressor gradient. Santavy et al. 2016 presented both the transferable methodology for developing stressor gradients (in general) and timely results from deliberations of a coral ecology expert panel charged with developing narrative and draft quantitative attributes of coral reefs ranging from pristine to degraded condition. The expert panel, comprised of scientists and resource managers from academia and multiple environmental regulatory agencies, has worked for years to develop a coral BCG that is defensible and based upon not only on published literature but on the collective experiences of the experts. Dr. Santavy and EPA partners in the OW and Region 2 have been involved in panel member selection, workshop design, and in-person and virtual deliberations from the start of this effort. As described in the manuscript, a series of workshops achieved deep engagement of the experts using structured elicitation of their collective knowledge and systematic distillation of this information with the ultimate goal of developing consensus on components of a healthy coral reef ecosystem and multiple levels of degradation. This process gives maximal credibility to not only coral community biocriteria but to benthic assemblage biocriteria, an outcome generated by deep discussions among coral reef experts described in the Santavy et al. 2016.

ORD has been developing biocriteria for coral reefs using the BCG model framework in collaboration with EPA Office of Water (OW: OST & OWOW) and Region 2's Caribbean Environmental Protection Division (CEPD) and Clean Water Division (CWD). The BCG model rules are used to develop thresholds for coral reef biocriteria, by using biological responses to an anthropogenic stressor gradient. Changes and impacts of anthropogenic stress to coral reef communities can be made by relating water quality parameters with changes in the biological condition of scleractinian coral, fish, algae, and other sessile benthic organisms with increasing distance from the effluent. The BCG approach establishes threshold values for evaluating the biological integrity of a waterbody as a response to increasing levels of anthropogenic stress which can aid in developing permissible levels of different pollutants for regulatory applications intended to be protective of coral reef

environments. Currently, most CWA numeric criteria applied to marine waters have not considered the restrictive oligotrophic conditions required to maintain healthy and functional coral reef communities.

Responsibilities related to coral reef conservation and protection are shared by several federal, state, and territorial and local agencies, with issues related to protection from water quality degradation under the primary purview of EPA OW. Ultimately, the territories are responsible for specific policies and regulations to: (1) establish designated uses for which the quality of the water bodies shall be maintained and protected; (2) promulgate the water quality standards required to sustain the designated uses; (3) identify other rules and regulations applicable to sources of pollution that may affect the quality of the waters; and (4) establish other measures necessary for achieving and maintaining the quality of the waters. The addition of biological criteria, such as those derived based on the results of BCG models (e.g., BCG numeric models for fish and benthic coral reef assemblages), to the chemical and physical numeric criteria that are adopted into the Water Quality Standards Regulations (WQSR) can become a part of regular water quality assessment protocols and will be implemented by various water programs within the Region to comply with reporting requirements by the CWA. Additionally, the BCG is a tool which allows EPA OW and Regions to communicate and estimate the expected change in aquatic and biological conditions resulting from management actions.

Caribbean coral reef ecosystems around the USVI and Puerto Rico are unique to EPA Region 2 and protection of these sensitive ecosystems is important to the Region. Coral reef biocriteria, derived from the numeric coral reef BCG models, are being used by Region 2 to develop water quality thresholds protective for coral reefs and derive corresponding biocriteria applicable for U.S. territories in Caribbean marine waters. EPA Region 2, working with the USVI Department of Planning and Natural Resources (USVI DPNR), the USVI Coastal Zone Management (USVI CZM), the Puerto Rico Environmental Quality Board (PR EQB), and the Puerto Rico Department of Natural and Environmental Resources (PR DNER), whose territorial jurisdiction includes marine coastal waters, are applying model rules for coral reef biocriteria to adopt into USVI and PR Water Quality Standards Regulations (WQSR). They intend to integrate biocriteria into their regular water quality assessment protocols to be implemented by various water programs (WQSR; National Pollutant Discharge Elimination Systems (NPDES)

permits; CWA 305(b)/303(d) assessment/listing and 301(h) waivers (exemptions from secondary treatment requirements for effluent discharged into marine waters); and TMDLs. The information integrated into the biocriteria tool support USEPA OW efforts to estimate the expected change in aquatic condition which result from

different management actions, especially with waste-water treatment effluent and other land-based run off. Results used to derive and implement biocriteria will be transferable to USVI and EPA Regions 2, 4, 6, and 9.

2016 Oliver et al.: This is a companion to complement Santavy et al. 2016 presenting a hybrid approach to stressor indicator development was presented in this manuscript. Spatially explicit data was presented for the near-coastal waters of Puerto Rico for each of three important coral reef stressors individually, and an Integrated Stressor Index was also developed and mapped for the area. Narrative stressor descriptions were developed for three hypothetical levels of anthropogenic disturbance based on the approach used to develop narratives for coral reef condition along a gradient from pristine to severely degraded. This approach includes stressors of concern such as wastewater outflows and associated nutrient pollution for which applicable empirical data was not available.

Three stressors chosen for this manuscript are highly relevant to coral reefs and were determined by years of research experience by the authors, invaluable professional contacts, and discussions by the BCG coral reef expert panel. (1) The dataset employed for temperature stress is available from the NOAA, and presenting it in an integrated stressor estimate represented a novel application of the sea surface temperature anomaly (SSTA) metric which is widely available for the world's oceans. Coral bleaching events are predicted with high certainty by the SSTA. (2) Overfishing is well-studied in coral literature as a deleterious influence on reef health due to reduced grazing of macrophytes that compete with coral for habitat and other ecological interactions disrupted by excess fishing. The fishing pressure estimate applied for Puerto Rico was obtained as a professional courtesy from an academic expert in Puerto Rico and was also a new application of this dataset. (3) Inclusion of the Landscape Development Intensity (LDI) Index is well-founded by previous demonstrations of relationships between increased human activity in watersheds and reduced coral extent and condition (Oliver et al., 2011), and the 2016 manuscript presents watershed LDI values combined with a distance-from-shoreline function, to account for expected dilution of altered landscape effects further from the source. Overall, Oliver et al. 2016 demonstrates a flexible approach to stressor characterization that can be tailored to specific stressors of concern for a given area and emphasizes inclusion of new data to capture changes in land use, mitigation efforts, and regulatory changes such as recreational fishing laws in Puerto Rico.

2018 Oliver et al.: Additional efforts to develop multi- and integrated-stressor models came to fruition in the Oliver et al. 2018 with the application of spatially explicit stressor measurements to coral survey data collected along the south shore of St. Thomas, USVI in 2009. In order to examine coral condition along a gradient of human disturbance, this study was designed around an obvious source of human activity in Charlotte Amalie, St. Thomas, USVI. Stations were selected for coral reef surveys along the south shore of St. Thomas to the East and West of Charlotte Amalie at similar depths, so that depth effects on community composition would be minimized. Survey logistics were implemented that have generated community indicators associated with anthropogenic stressors in previous Caribbean surveys. The spatial indicators of human influence applied presented a distillation of research efforts on the relevance of stressor to specific areas and their predictive relationships with coral condition indicators. The original study design used stressors ranked for each site as 0, 1, 2, or 3 based on observations made during the survey and general knowledge about the area. Analysis presented in the manuscript built on a ranked approach and applied the watershed landscape development intensity (LDI) index, modeled land-based sedimentation threat (WRI and NOAA, 2006), and an impaired water quality (WQ) index based on proximity to impaired water bodies. Water quality impairment data used for the index was reported by the USVI Department of Planning and Natural Resources to the EPA under authority of the CWA and includes impairment from low dissolved oxygen, high enterococci bacteria and elevated nutrient levels, all of which can reduce coral condition. As such, this approach is readily transferrable for it uses data on water quality problems unique to an area. Additionally, an Integrated Stressor Index (a ranking of the summed stressors) was developed to examine the relative power of individual stressors and ISI to be examined for their relative power to predict coral reef condition.

Oliver et al. 2018 builds upon previous work (e.g., Oliver et al. 2011) that demonstrated statistically significant relationships between increased anthropogenic impact and impaired resource condition, and Oliver et al. (2016). Overall, this body of work develops and demonstrates a transferrable approach that can inform a range of applications that require quantification of anthropogenic stress, including the BCG. Publicly available land use/land cover data and EPA data on impaired water bodies are broadly available and this approach demonstrates how these can be applied in a quantitative way to represent human impacts on ecosystems.

Responsible regulation must consider potential impacts on ecosystems and the services they provide within the context of economic reality and ecosystem service prioritization.

The EPA OW and Region 2 is using the science behind the landscape development intensity work from the Oliver et al. 2018 (Research Gate: 140 views and 8 citations) as a proxy for USVI watershed-level impairment to develop nutrient criteria development under the CWA. In one example application resulting from this work, the Office of Water identified the potential utility of fine-scale hydrologic unit code (HUC) LDI calculations for to identify relatively unimpaired and human-influenced areas to steer monitoring efforts. The lead STAA author developed, QA/QC'd, and provided both data and shapefiles for all the USVI islands as part of providing valuable ORD technical support to the OW.

References:

Oliver, Lehrter, J, Fisher. 2011. Relating landscape development intensity to coral reef condition in the watersheds of St. Croix, US Virgin Islands. *Marine Ecology Progress Series*, 427, 293-302.

World Resources Institute, NOAA. 2006. Land-based sources of threat to coral reefs in the U.S. Virgin Islands. Wash. DC.

Justification 2A:

The two 2016 ICRS papers were natural building blocks that led to the 2018 Oliver et al. paper. Analyses of biocriteria, BCG thresholds, and stressor indicators all evolved and developed over time as a result of the researchers ongoing and cumulative investments to ensure the efforts: (a) captured the best science; and (b) worked to advance the state-of-science in coral assessments to most meaningfully inform coral management efforts.

Justification 2B:

Susan Yee; 2015 EPA Scientific and Technological Achievement Award, Honorable Mention; Yee, S.H., J.A. Dittmar, L.M. Oliver. 2014. Comparison of methods for quantifying reef ecosystem services: a case study mapping services for St. Croix, USVI. Ecosystem Services 8:1-15. http://dx.doi.org/10.1016/j.ecoser.2014.01.001

Susan Yee; 2015 EPA Scientific and Technological Achievement Award, Honorable Mention; Yee, S.H., J. Carriger, W.S. Fisher, P. Bradley, B. Dyson. 2015. Developing scientific information to support decisions for sustainable reef ecosystem services. Ecological Economics 115:39-50. http://dx.doi.org/10.1016/j.ecolecon.2014.02.016

Justification 2C:

This nomination advances previously nominated work (Yee et al. 2015 “Developing scientific information to support decisions for sustainable reef ecosystem services” Honorable Mention; and Yee et al. 2015 “Comparison of methods for quantifying reef ecosystem services: a case study mapping services for St. Croix, USVI” Honorable Mention) by continuing to develop a multi- and integrated-stressor model approaches (including BCG) for coral reef assessment to inform coral management. Both Yee et al. 2015 STAA awards focus on development of the connections between ecosystem condition and the benefits of coral ecosystems to people (ecosystem services). This nomination extends the importance of the established connections between coral environments and people by explicitly connecting environmental assessments to tangible environmental decision making efforts.

Justification 2D:

n/a

Justification 2E:

n/a

Justification 3A:

The Oliver et al. (2018) *Environmental Monitoring and Assessment* article has had 140 views and 8 citations (Research Gate). ICRS conference organizers' original plan was that conference presentations would be developed into manuscripts to comprise a dedicated issue of Coral Reefs. These papers were peer-reviewed and formatted to meet Coral Reefs journal standards, but unexpectedly were published in ICRS proceedings instead and as such, citation numbers are not available.

Both Oliver et al. contributions apply datasets that are available on a broad spatial scale in novel ways to inform integrated stressor assessments. The Oliver 2016 ICRS paper used NOAA SST data that is available for the world's oceans and the specific SSTA index mapped for Puerto Rico as a proxy for thermal stress has been associated with coral bleaching events around the world. Continual advances in this dataset are planned that aim to integrate retrospective data from older satellite technology. The Summit to Sea sediment threat model applied in the EMA paper validates this model's application in terms of predictive potential for resource condition.

The larger scientific contribution from this body of work has been demonstrated through acceptance and utilization outside of the original group of researchers, including considerable efforts to reach out to stakeholders, primarily through the use of webinars at numerous forums to inform stakeholders about EPA's role for utilizing the CWA to influence shore-based activities that deleteriously impact coral reef environments. In collaborations between OW, ORD, and Region 2 the following outreach activities have recently been made, after invitations from the sponsors of each venue to present EPAs work on biocriteria and the BCG models for coral reefs:

· Invited presentation to the US Coral Reef Task Force (March 10, 2020) with members from the All Islands Committee (representatives from all US states and territories in Pacific (HA, American Samoa, Guam, U.S. Marshall Islands and other U.S. jurisdictions) and Caribbean (Puerto Rico, USVI, Florida, and Texas). The presentation addressed: indicators and metrics for assessing coral reef condition; setting water quality goals and restoration targets; measuring incremental improvements; informing the development and implementation of biological criteria; and communication to managers and the public. Topics specific to using coral reef BCG to support territorial biological monitoring~~,~~ included assessment and criteria programs~~;~~ and how to develop cross agency standardization, agreement, and endorsement from other federal and territorial representatives.

· Invited presentation to the US EPA Academy of Water Quality Standards (March 31, 2020) training to over 100 class members to present tools used in CWA activities. focusing on development, application, and implementation of the BCG for coral reefs.

· Invited presentation by NOAA Coral Reef Protection Program (April 2020) to present how NOAA's programs and data were used to develop coral reef BCG towards developing better partnerships for design and implementation of their National Coral Reef Monitoring Programs in the future.

· Invited presentation by NOAA National Marine Fisheries Service (NMFS) Southeast Region (SERO) *Acropora* Recovery Implementation Team (May 6, 2020) to brief their team members on the coral reef BCG projects in PR and USVI.

This body of work is being applied to environmental management of corals. US EPA ORD, OW and Region 2 have partnered and provided technical support to both USVI (USVI Department of Planning and Natural Resources (DPNR); USVI Coastal Zone Management (CZM))and Puerto Rico (Puerto Rico Environmental Quality Board (PR EQB), Puerto Rico Department of Natural and Environmental Resources (PR DNER)) whose territorial jurisdiction includes marine coastal waters are applying model rules for coral reef biocriteria to adopt into USVI and PR Water Quality Standards Regulations (WQSR). The USVI DPNR promulgated coral reef biocriteria narrative standards into their WQSR Title 12 in 2010, with Puerto Rico EQB drafting amendments containing both narrative and numeric biocriteria into their revisions that have been postponed due to the natural disaster emergencies from hurricanes and earthquakes. Both territories intend to integrate biocriteria into their regular water quality assessment protocols to be implemented by various water programs (WQSR, National Pollutant Discharge Elimination Systems (NPDES) permits, 305(b)/303(d) assessment/listing, CWA 301(h) waivers (exemptions from secondary treatment requirements for effluent discharged into marine waters) and TMDLs). The information integrated into the biocriteria tool (BCG) support USEPA OW.

The U.S. Virgin Islands (Department of Planning and Natural Resources, Division of Environmental Protection, has applied this research by adopting coral reef "designated uses" into their Water Quality Standards, a step towards applying reef condition standards in regulatory decisions.

Justification 3B:

All manuscripts were reviewed by an external technical reviewer, the Division's Quality Assurance manager, the lead author's first-line supervisor (Branch Chief), and the Division Director according to ORD's scientific and technical information clearance process prior to submission to :(1) *Environmental Monitoring and Assessment*; and (2 & 3) *International Society for Reef Studies*. Each of the manuscripts were further peer reviewed by the journal's corresponding editor and at least one anonymous reviewer as assigned by the editor prior to acceptance and publication.

AUTHORS

Contributing Author

Author Name:	Deborah Santavy		
Professional Title:		Salutation:	
Email:	santavy.debbie@epa.gov	Organization:	
Mailing Address:			
Street Line 1:			
City:			
Zip Code:		State:	
At time of research was:	EPA Employee		
Separation Date:			
% of Effort:	22		

Contributing Author

Author Name:	Patricia Bradley		
Professional Title:		Salutation:	

Email:	patbradley@comcast.net	Organization:
Mailing Address:		
Street Line 1:		
City:		
Zip Code:		State:
At time of research was:	EPA Employee	
Separation Date:	Sat Oct 03 00:00:00 GMT 2015	
% of Effort:	20	

Contributing Author

Author Name:	Leah Oliver	
Professional Title:		Salutation:
Email:	oliver.leah@epa.gov	Organization:
Mailing Address:		
Street Line 1:		
City:		
Zip Code:		State:
At time of research was:	EPA Employee	
Separation Date:		
% of Effort:	33	

Contributing Author

Author Name:	William Fisher	
Professional Title:		Salutation:

Email:	fisher.william@epa.gov	Organization:
Mailing Address:		
Street Line 1:		
City:		
Zip Code:		State:
At time of research was:	EPA Employee	
Separation Date:		
% of Effort:	5	

Contributing Author

Author Name:	Leska Fore	
Professional Title:		Salutation:
Email:	leska.fore@seattle.gov	Organization:
Mailing Address:		
Street Line 1:		
City:		
Zip Code:		State:
At time of research was:	Non EPA Personnel	
Separation Date:		
% of Effort:	5	

Contributing Author

Author Name:	Amelia Smith	
Professional Title:		Salutation:

Email:	amelia.smith4815@gmail.com	Organization:
Mailing Address:		
Street Line 1:		
City:		
Zip Code:		State:
At time of research was:	Non EPA Personnel	
Separation Date:		
% of Effort:	8	

Contributing Author

Author Name:	Jeroen Gerritsen	
Professional Title:		Salutation:
Email:	jeroen.gerritsen@tetratech.com	Organization:
Mailing Address:		
Street Line 1:		
City:		
Zip Code:		State:
At time of research was:	Non EPA Personnel	
Separation Date:		
% of Effort:	7	

PUBLICATIONS

Publication 1:

Assessing land use, sedimentation, and water quality stressors as predictors of

Publication Title:	coral reef condition		
Publication Date:	Tue Mar 13 00:00:00 GMT 2018		
Journal/Publication Method:	Environmental Monitoring and Assessment		
All Author(s):			
Volume:	190	Number:	4
Pages:	213	Immediately Index:	Immediately Index:
Citation ½ Life:	6.7	Impact Factor:	1.959

Publication 2:

Publication Title:	Developing a multi-stressor gradient model for coral reefs of Puerto Rico. 13th ICRS, Honolulu		
Publication Date:	Fri Jun 24 00:00:00 GMT 2016		
Journal/Publication Method:	Published by the International Society for Reef Studies		
All Author(s):			
Volume:	*	Number:	*
Pages:	*	Immediately Index:	Immediately Index:
Citation ½ Life:	see note	Impact Factor:	see note

Publication 3:

Publication Title:	The biological condition gradient, a tool used for describing the condition of US coral reef ecosyst		
Publication Date:	Fri Jun 24 00:00:00 GMT 2016		

Journal/Publication Method:	Published by the International Society for Reef Studies		
All Author(s):			
Volume:	*	Number:	*
Pages:	*	Immediately Index:	Immediately Index:
Citation ½ Life:	see note	Impact Factor:	see note

Environ Monit Assess (2018) 190: 213
https://doi.org/10.1007/s10661-018-6562-1

Assessing land use, sedimentation, and water quality stressors as predictors of coral reef condition in St. Thomas, U.S. Virgin Islands

L. M. Oliver · W. S. Fisher · L. Fore · A. Smith · P. Bradley

Received: 9 June 2017 / Accepted: 19 February 2018 / Published online: 13 March 2018
© This is a U.S. Government work and not under copyright protection in the US; foreign copyright protection may apply 2018

Abstract Coral reef condition on the south shore of St. Thomas, U.S. Virgin Islands, was assessed at various distances from Charlotte Amalie, the most densely populated city on the island. Human influence in the area includes industrial activity, wastewater discharge, cruise ship docks, and impervious surfaces throughout the watershed. Anthropogenic activity was characterized using a landscape development intensity (LDI) index, sedimentation threat (ST) estimates, and water quality (WQ) impairments in the near-coastal zone. Total three-dimensional coral cover, reef rugosity, and coral diversity had significant negative coefficients for LDI index, as did densities of dominant species *Orbicella annularis*, *Orbicella franksi*, *Montastraea cavernosa*, *Orbicella faveolata*, and *Porites porites*. However, overall stony coral colony density was not significantly correlated with stressors. Positive relationships between reef rugosity and ST, between coral diversity and ST, and between coral diversity and WQ were unexpected because these stressors are generally thought to negatively influence coral growth and health. Sponge density was greater with higher disturbance indicators (ST and WQ), consistent with reports of greater resistance by sponges to degraded water quality compared to stony corals. The highest FoRAM (Foraminifera in Reef Assessment and Monitoring) indices indicating good water quality were found offshore from the main island and outside the harbor. Negative associations between stony coral metrics and LDI index have been reported elsewhere in the Caribbean and highlight LDI index potential as a spatial tool to characterize land-based anthropogenic stressor gradients relevant to coral reefs. Fewer relationships were found with an integrated stressor index but with similar trends in response direction.

Keywords Coral reefs · Landscape development intensity · Sedimentation · Impaired water quality

L. M. Oliver (✉) · W. S. Fisher · A. Smith
Office of Research and Development, National Health and Environmental Effects Research Laboratory, Gulf Ecology Division, U.S. Environmental Protection Agency, 1 Sabine Island Drive, Gulf Breeze, FL 32561-5299, USA
e-mail: oliver.leah@epa.gov

L. Fore
Puget Sound Partnership, 326 East D St., Tacoma, WA 98421, USA

P. Bradley
Office of Research and Development, National Health and Environmental Effects Research Laboratory, Atlantic Ecology Division, U.S. Environmental Protection Agency, 24 Tarzwell Drive, Narragansett, RI 02882, USA

Introduction

Coral reefs of the U.S. Virgin Islands (USVI) are heavily impacted by multiple human influences at varying scales (Gardner et al. 2003; Smith et al. 2008; Rogers et al. 2008; Friedlander et al. 2013; Pait et al. 2013a, b; Pittman et al. 2013; Whitall et al. 2014). Global conditions such as elevated ocean temperature have led to coral bleaching and disease, causing stony coral mortality across broad reef areas of the Caribbean Sea. Local resource managers and decision-makers have little

influence over global-scale anthropogenic pressures such as rising ocean temperature, ocean acidification, and elevated ultraviolet light levels. However, they do have some influence over local stressors, such as sediment, contaminants, nutrients, and physical injuries, that can interact with global pressures in additive or synergistic ways (Knowlton and Jackson 2008; Wooldridge and Done 2009; Brown et al. 2013; Ban et al. 2014). Managing stressors that are within local authority can slow the cascade of negative impacts and better sustain reef-derived ecosystem services such as coastal protection from storm surge, habitat provision for commercial and recreational fisheries, and revenue from reef-related tourism (Moberg and Folke 1999; Principe et al. 2012). Effective management requires identifying which stressors are human-generated so that activities can be modified to reduce their adverse effects.

The Clean Water Act (CWA) provides a mechanism to set chemical, physical, and biological criteria for the protection of aquatic ecosystems (Bradley et al. 2009; Fore et al. 2009; Bradley et al. 2010). As part of a process to establish biological water quality standards or biocriteria, the U.S. Virgin Islands government has explicitly identified coral reefs and reef functions as CWA-designated uses and defined biological integrity to lay the foundation for setting condition thresholds (biocriteria) for coral reefs (USVI 2010). This action was spawned in part by the demonstration of stony coral sensitivity to disturbance gradients using various measures of anthropogenic stress. For example, measures of coral reef condition including taxa richness, average colony size, and total and live topographic coral surface area showed significant positive relationships with increasing distance from human disturbance in St. Croix (Fisher et al. 2008). Negative relationships of coral condition with increased watershed land development were demonstrated in St. Croix (Oliver et al. 2011), Hawaii (Rodgers et al. 2012), St. Lucia (Bégin et al. 2016), and Thailand (Golbuu et al. 2008). Because the reefs around St. Thomas, USVI, are located near areas of high human activity (Ennis et al. 2016), they present another opportunity to explore potential links between reef condition and anthropogenic activity.

The USVI economy depends heavily on tourism revenues with an estimated 60–80% of gross domestic product linked to tourism-related activities (Abt Associates 2016). Nearly two million cruise ship tourists visited the USVI annually from 2000 to 2005, and the majority of cruise ships visit St. Thomas (van Beukering et al. 2011). The area of shallow water coral reefs around St. Thomas covers approximately 42 km^2 and comprises mostly linear coral reefs and colonized pavement, with scattered patch reefs farther offshore (Kendall et al. 2001). Stony corals provide important ecosystem services due to the structural reef habitat which supports diverse fish and invertebrate species valued by divers, snorkelers, and recreational and commercial fishers and provides shoreline protection from extreme weather events (van Beukering et al. 2011). Without stony corals, these ecosystem services would be lost or compromised, yet pressure from coastal development, cruise ship and recreational boat activity, and land use change on the 74-km^2 island may threaten the very resource to which visitors are drawn.

Charlotte Amalie on the south shore is the largest city on St. Thomas with a population of approximately 18,481 (2010 US Census). The Charlotte Amalie watershed has 34% impervious surface and nearly no shoreline riparian buffer at either the St. Thomas Harbor or Inner Harbor where two cruise ship ports operate. With a hardened shoreline, presence of power and wastewater treatment plants, and multiple active cruise ship and shipping ports, this area was chosen to represent a center of human disturbance likely to adversely influence adjacent coral reef communities. We hypothesized that coral reef communities near this concentrated human disturbance would be degraded relative to reefs further away, and used two approaches to characterize anthropogenic disturbance. First, we developed three independent measures of potential stress to coral reefs: the watershed landscape development intensity (LDI) index, modeled land-based sedimentation threat (ST), and impaired water quality (WQ) index based on proximity to impaired water bodies. These spatial proxies represent reef stressors that can be managed to some degree, and it would be valuable to discern their relative influence to assist managers in optimizing decisions to invest in the most effective remediation actions. Measures of density, size, and condition of benthic invertebrates including stony corals, gorgonians, sponges, macroinvertebrates, fishes, and foraminifera were assessed for potential responsiveness to these stressors. The reef metrics selected either showed a response to anthropogenic influence in previous studies or are suitable candidates based on their connection to an ecosystem service (e.g., rugosity). Second, stressors were rescaled from 0 to 1 and summed to generate an integrated stressor index (ISI), allowing results from

individual stressors and ISI to be compared for relative power to predict coral reef condition.

Materials and methods

Survey design

Survey sites ($n = 13$) were selected along the south shoreline of St. Thomas and spanned approximately 10 km (Fig. 1a). To control for the effect of natural site differences, we consistently selected sites on or near rocky points of land from Fortuna Bay in the west to Frenchman Bay in the east. All sites were identified as coral reef and colonized hardbottom habitat by Kendall et al. (2001). We also targeted a narrow range of depth from 5.5 to 9.1 m (mean 6.9 m) to minimize habitat differences that could affect coral community composition (Morelock et al. 2001). Based on field observations and knowledge of the area, we assumed Charlotte Amalie Harbor to be the greatest source of intense human disturbance in the area.

Data collection and calculation of reef indicators

Multiple-assemblage surveys were conducted during March 2009 as described by Fisher (2007) and Santavy et al. (2012). All surveys were conducted around a common 25-m transect line stretched along the sea floor. A fish survey was conducted first in a 4 × 25 m transect area (100 m^2 in total), with divers identifying to species, counting and estimating the length of all fish > 5 cm in length (Menza et al. 2006). Macroinvertebrates identified were queen conch, spiny and slipper lobsters, sea urchins (*Diadema* and others), and crabs. These were counted within either 1 or 2 m (due to diver inconsistency) on either side of the transect line for a total area of 50 or 100 m^2. Average reef rugosity index (RI) was calculated from five measurements made at the 0-, 5-, 10-, 15-, and 20-m marks along the transect line using the draped chain method d / l, where d is the linear chain distance when draped over coral reef and l is the constant chain length of 6 m (Risk 1972). Stony coral colonies at least 10 cm in any dimension were counted along one side of the transect line using a 1-m stick placed parallel to the line as a guide. Colonies were measured for height, maximum diameter, and percent live in 10% increments and identified to species (Humann and DeLoach 2002). Sponges and gorgonians were counted in 5 × 1 m^2 quadrants located at 1-, 5-, 10-, 15-, and 20-m transect marks. Each colony was measured for height and diameter, and morphology was recorded as one of nine possible shapes for gorgonians and nine for sponges (Santavy et al. 2012, 2013).

Stony coral three-dimensional (3D) colony surface areas (SAs) were calculated using a modified hemisphere formula $SA = m\pi R^2$, where m is a constant (1–4) based on relative morphological complexity and R is the height-adjusted colony radius calculated as ((diameter / 2) + height) / 2 (Santavy et al. 2012). Regression equations developed for sponges and gorgonians were used to calculate colony SA (Santavy et al. 2013), except SA formula for a circle (πr^2) was used for encrusting sponges and in cases where very small colony measurements result in negative SA using regression equations. Average values for each station from 5 × 1 m^2 quadrats were calculated for SA and abundance of sponges and gorgonians.

Fish lengths were estimated in 5-cm increments. The median value of each increment was assigned to individual fish; for example, 5–10-cm fish were assigned 7.5 cm length except for fish in the smallest size class (< 5 cm) which were assigned 3 cm. Biomass was calculated using the formula $W = \alpha \times L^{\beta}$ with species-specific constants α and β supplied by Froese and Pauly (2013). Invertebrate counts were standardized per square meter. Foraminifera samples were collected in triplicate at each site, and results were averaged to calculate a FoRAM (Foraminifera in Reef Assessment and Monitoring) index based on the methods of Hallock et al. (2003).

Stressor estimates

Land-based anthropogenic activity

A LDI index was calculated as a measure of land-based anthropogenic activity using a 2.4-m resolution land use layer produced for 2007 by NOAA Coastal Change Analysis Program (www.csc.noaa.gov/digitalcoast/data/ccapregional/index.html) and corresponding Emergy coefficients (Brown and Vivas 2005; Oliver et al. 2011). Stations were assigned the LDI value of the adjacent Hydrologic Unit Code (HUC)14 watershed (Islands Resources Foundation et al. 2001), and for stations near a watershed border, the eastward watershed LDI value was used to account for the predominant coastal current (Nemeth and Nowlis 2001). Land use, station locations, and adjacent watershed LDI values along the southern St. Thomas coastline are shown in Fig. 1a, b.

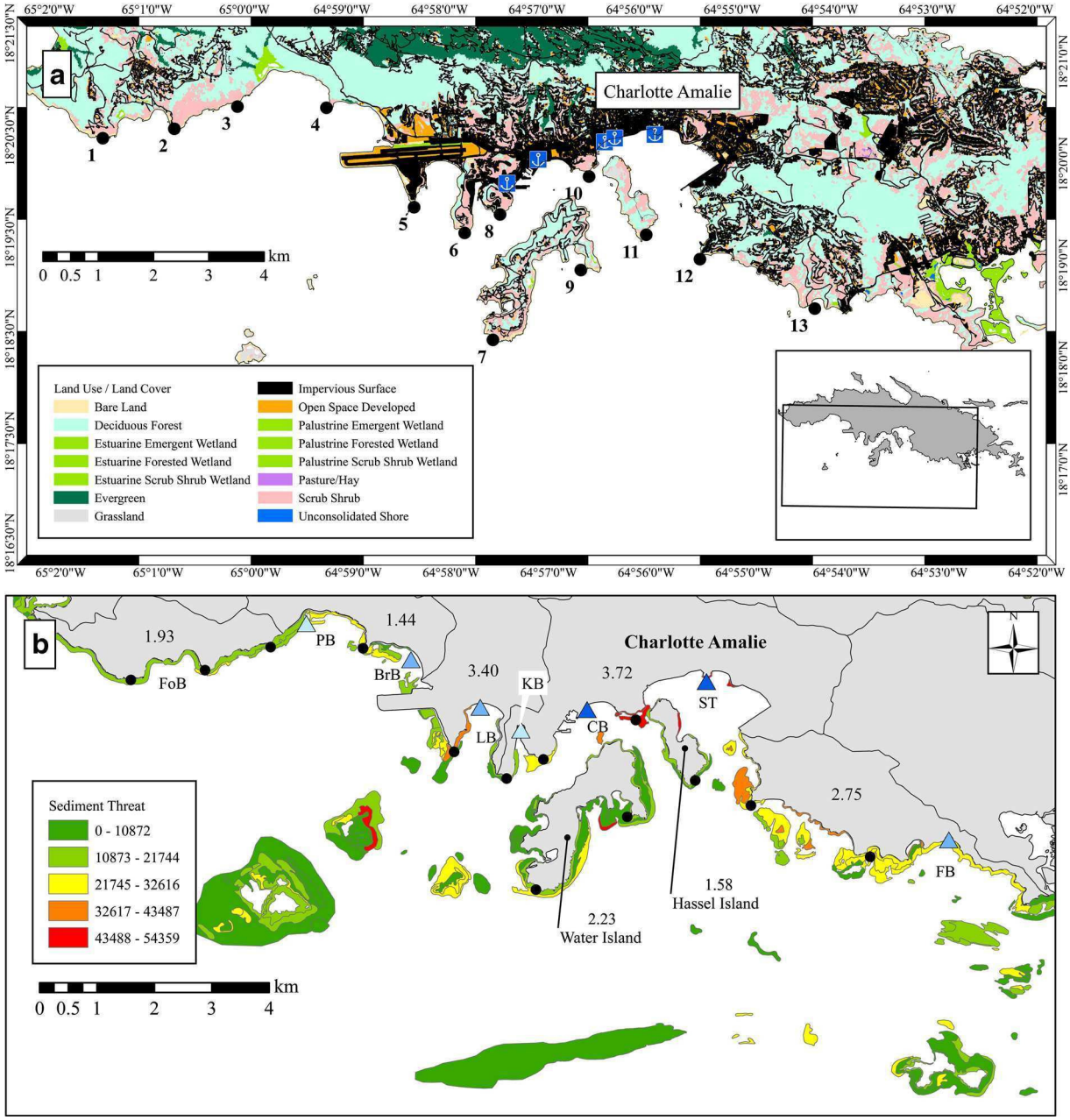

Fig. 1 **a** Land use/land cover (LULC) and coral reef stations sampled in St. Thomas, USVI, around Charlotte Amalie. Numbered black circles indicate sampling stations. Ports are indicated by anchor symbols. **b** HUC14 watersheds are indicated by black lines, and their corresponding LDI values are indicated within watershed polygons. Letters show locations of water bodies which exceeded chemical or physical criteria as reported to USVI DPNR: FoB Fortuna Bay, PB Perseverance Bay, BrB Brewers Bay, LB Lindberg Bay, KB Krum Bay, CB Crowne Bay ST, ST St. Thomas Harbor, FB Frenchman Bay. Triangular symbols grade from light to dark blue, indicating an increasing average number of impaired conditions from 2000 to 2010. Black circles indicate sampling stations

Sedimentation threat

Benthic sediment threat values were obtained from the World Resources Institute and National Oceanic and Atmospheric Administration Summit to Sea model (WRI and NOAA 2006). Summit to Sea is a GIS model that incorporates 30-m resolution land use/land cover data (NASA Geocover-LC 2000), soil type and

associated erodibility factor (US Department of Agriculture/Natural Resources Conservation Service, Soil Service Geographic Database), slope (digital elevation model), and precipitation (NOAA National Climate Data Center, maximum monthly precipitation for the 10-year period (January 1990–January 2001)). Summit to Sea data sources and processing steps are available at https://data.nodc.noaa.gov/coris/data/NOAA/nos/Summit2Sea/USVirginIslands/.

In short, ST was calculated for USVI reef habitats from relative erosion potential for watersheds, adjusted for watershed size, and modeled to correspond with pour points or "guts." Dissipation of sediment into coastal areas employed an ArcView v3.2 Point Density tool with a maximum distance from shore of 5 km.

Water quality

Water quality impairments reported by the USVI Department of Planning and Natural Resources (DPNR 2010) to the U.S. Environmental Protection Agency as required by the Clean Water Act include low dissolved oxygen, high enterococci bacteria, and elevated nutrient concentrations which may all negatively influence coral condition (Villanueva et al. 2006; Kaczmarsky et al. 2005; Voss and Richardson 2006). However, specific loadings and stressor-coral interactions are not understood well enough to weigh the individual stressors for relative importance, hydrologic transport to reefs is unknown, and bays are monitored for water quality exceedances only twice per year. Included in this water quality analysis from west to east were Perseverance Bay (PB), Brewer's Bay (BrB), Lindberg Bay (LB), Krum Bay (KB), St. Thomas Harbor (ST), Inner Harbor (IN), and Frenchman Bay (FB) (Fig. 1b). We assumed that only impaired water bodies east of a station would impact it due to the dominant westward current (Nemeth and Nowlis 2001), that impairment would dissipate with greater distance between station and water body, and that beyond 3 km, no impact would occur. First, the distance between each station and mid-bay shoreline was measured using ArcMap v9.3, and if two bays were within 3 km of a station, distances were summed. Distance values were transformed to (1/distance to bay) so that final WQ value increased with proximity to bays with WQ impairments. This transformation also achieved a nonlinear function assuming that WQ contaminants dissipate rapidly from the source (Fig. 2), although in reality, transport of runoff-borne pollutants to reef habitats is dependent on multiple factors such as precipitation, river density, storms, and wind (Warne et al. 2005).

Data analysis

Reef indicator values for stony corals, gorgonians, sponges, fish, and macroinvertebrates were calculated for each station using SAS© (Cary, North Carolina), except the Shannon-Weiner diversity index which was calculated using PRIMER© (Clark and Gorley 2006). The Spearman nonparametric correlation analysis was used to test for relationships between the three stressors. Distribution of reef indicators was evaluated using the Shapiro-Wilk statistic, and either log10 or rank transformations were applied to correct for deviations from normal distribution. Stepwise regression was employed to discern whether LDI, ST, and WQ were significant predictors of reef indicators with inclusion requirement of $p < 0.25$ and retention requirement of $p < 0.20$.

An ISI was calculated by first rescaling station stressor data values from 0 to 1, then assuming equal effects, the rescaled values were added. The Spearman correlation analysis was conducted with reef metrics and ISI for comparison with stepwise regression results. No correction for multiple comparisons was applied; instead, all results significant at $p < 0.05$ are reported. For all three stressors and ISI, quartile values were assigned for the purpose of comparing relative stressor levels at each station in the gradient.

Results

Station and stressor summary

Stations ranged in depth from 5.5 to 9.1 m and were within 0.1 km from land, with ten stations along the St. Thomas shoreline, two near Water Island and one near Hassel Island (Fig. 1). The lowest LDI values were found in the western portion of the study area with the exception of uninhabited Hassel Island near Charlotte Amalie Harbor, which also had low LDI. The highest LDI values were in the center of the study area near Charlotte Amalie Harbor and the airport where impervious surface covers most of the land and numerous industries are present along the coast. Eastern stations were adjacent to an intermediate-LDI watershed. Some stations had common LDI values because they were adjacent to the same HUC14 watershed (Fig. 1b).

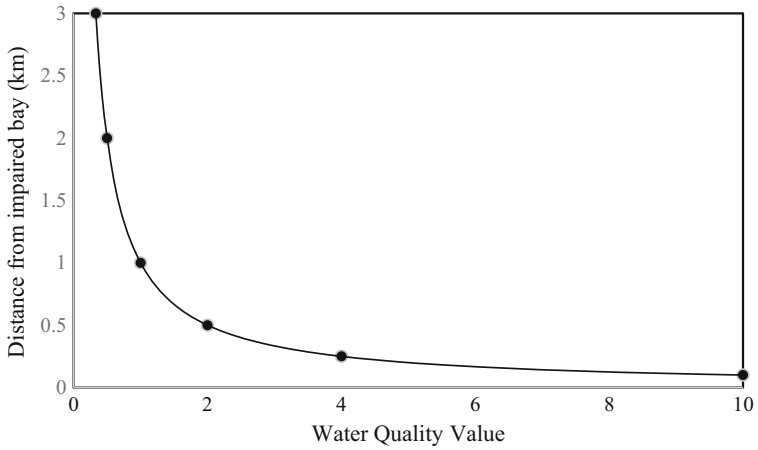

Fig. 2 Water quality (WQ) function used to estimate stress from proximity to St. Thomas bays which are listed as impaired under the Clean Water Act 303(d) program

Sedimentation threat was lowest at station 11 on Hassel Island, and ST was highest at station 10 near Charlotte Amalie Harbor and second highest at station 13 on the eastern edge. A WQ impairment estimate based on distance from impaired bays ranged from 0 at four stations (which exceeded the maximum distance from an impaired bay under our assumptions) to high values at stations 5 and 6 in the center of the study area.

The ISI ranged from 0.40 to 2.37 with an average of 1.23. The lowest values were found at the western edge of the study area and at Hassel Island and the highest values at stations 5, 6, and 10 (Table 1). Station stressor values grouped into quartiles show the most consistent estimates of high human impact were at stations nearest the harbor and at the eastern edge, and most consistent low impact was at western stations and Hassel Island. However, no stations were in the lowest quartile for all stressor estimates. Station values for these three stressors were not significantly correlated with one another.

Stony corals

A total of 1330 stony coral colonies representing 26 taxa were observed and measured. Of these, 52 colonies were not identifiable to species and were eliminated from taxa richness counts and calculation of the Shannon-Weiner diversity index. Most colonies (81.8%) had hemispherical

Table 1 Stressor values and quartiles for landscape development intensity (LDI), sedimentation threat (ST), and impaired water quality (WQ) for 13 stations along the south coast of St. Thomas, USVI

Station	LDI	Quartile	ST	Quartile	WQ	Quartile	ISI	Quartile
1	1.93	2	14,844.3	2	0	1	0.486	1
2	1.93	2	14,844.3	2	0.395	2	0.700	1
3	1.44	1	12,670.0	1	1.193	3	0.882	2
4	1.44	1	21,868.8	3	1.449	4	1.190	3
5	3.40	3	24,166.0	3	1.843	4	2.305	4
6	3.72	4	8055.6	1	1.583	4	2.007	4
7	2.23	2	20,708.1	2	0	1	0.728	2
8	3.72	4	22,381.4	3	1.080	3	1.998	3
9	2.23	2	0.4	1	0	1	0.346	1
10	3.72	4	54,359.0	4	0.685	2	2.371	4
11	1.58	1	2364.3	1	0.538	2	0.397	1
12	2.75	3	27,719.0	4	0	1	1.086	2
13	2.75	3	31,225.6	4	0.813	3	1.591	3

ISI is the sum of individual stressors which were rescaled from 0 to 1

morphology, 15.7% were branching, and 2.5% were flat, and no living *Acropora* colonies were observed. Two colonies (*Orbicella annularis* and *Orbicella faveolata*) were observed at station 13, and one *O. faveolata* colony at station 3 exceeded the average (live + dead) stony coral SA + 3 standard deviations, so these were considered outliers. These colonies were excluded from indicator calculations and subsequent analyses. Eight stony coral species comprised 82% of colony density (Table 2).

Coral density varied from 0.6/m^2 at station 9 near Water Island to 9.1 at stations 1 and 5 (Table 3). Despite low colony density at station 9, those corals present were large with highest CSA_Av and LCSA_Av (see Table 3 for variable names and abbreviations). Coral 3D total cover (3DTC) which includes dead coral ranged from 0.12 to 0.99 m^2 coral/m^2 sea floor, and 3D live cover (3DLC) ranged from 0.05 to 0.59 (Table 3). Due to high correlation ($r^2 = 0.794$, $p < 0.0001$) between 3DTC and 3DLC, only 3DTC was included in regression models and correlation tests with ISI. The total structure of the reef at all five stations west of Charlotte Amalie was largest with higher 3DTC and 3DLC, and stony coral taxa richness (SC_Tx) was also high at these stations relative to most others. Both total and live average colony size varied little except for relatively high values at stations 9 and 3. Average coral LT ranged from lowest values around 55% at stations 3, 8, and 9 to high values over 80% at stations 2, 5, 11, and 13. The CSA_CV of total coral colony size was lowest at stations 8 and 10 and highest at stations 2 and 13.

Increased watershed LDI was negatively related to stony coral reef structure measured by 3DTC and rugosity (Table 4). LDI was also negatively associated with coral diversity (Shannon-Weiner diversity index, SC_H′). Sedimentation threat was significant with reef rugosity and SC_H′ with positive relationships, and WQ had a positive relationship with SC_H′. While not significant for total colony density, LDI was negatively related to colony density of five of eight dominant coral species (Table 5). Water quality had a significant positive relationship with *Porites porites* density (Table 5).

The composite ISI did not correlate with any population-level stony coral metrics. Colony densities of *Orbicella annularis* and *Orbicella franksi* were negatively correlated with ISI with r values = − 0.502 and − 0.49 and $p < 0.08$ and 0.09, respectively.

Gorgonians and sponges

Gorgonians were observed at seven of the 13 stations (Table 6) with a total of 47 colonies exhibiting eight morphologies. The circle SA formula was applied to

Table 2 Stony coral species and density (no./m^2 sea floor) counted at 13 stations along the southern St. Thomas coast (unidentifiable/dead colonies not presented or included in total)

Station:	1	2	3	4	5	6	7	8	9	10	11	12	13
Agaricia agaricites	**0.48**	**0.16**	0.12	0.04	0.04		**0.04**				0.04	0.04	
Agaricia fragilis			0.04		0.04						0.08		
Agaricia lamarcki	**0.04**												
Colpophyllia natans	**0.04**		0.04		0.08								0.04
Dendrogyra cylindrus	**0.04**	**0.04**			0.08		**0.04**						
Dichocoenia stokesi					0.08								
Pseudodiploria labyrinthiformis	**0.56**	**0.48**		0.08	0.32	0.12			**0.04**		0.04		
Diploria strigosa	**1.24**	**0.44**	0.04		0.08		**0.04**			0.08	0.24	0.16	
Eusmilia fastigiata			0.04	0.20				0.16		0.04			
Madracis decactis		**0.04**			0.08			0.04		0.08			
Madracis mirabilis										0.08			
Manicina areolata								0.04					
Meandrina meandrites	**0.04**	**0.04**	0.04	0.20	0.36	0.04	**0.04**			0.16	0.04		0.04
Millepora complanata	**0.20**	**0.12**			0.52		**0.24**		**0.12**			0.04	
Orbicella annularis	**0.44**	**0.48**	0.60	0.36	0.16	0.08	**0.36**		**0.20**	0.04	0.04		0.08
Montastraea cavernosa	**0.24**	**0.32**	0.16	0.28	0.12	0.04	**0.04**	0.08		0.04	0.64	0.28	0.04
Orbicella faveolata	**0.44**	**0.72**	0.36	0.04	0.24	0.04	**0.04**	0.04	**0.04**	0.04	0.16		0.08
Orbicella franksi	**0.48**	**0.20**	0.12	0.16	0.20	0.04	**0.36**	0.08		0.04	0.44		
Porites astreoides	**1.48**	**1.08**	0.52	0.36	2.32	0.68	**0.28**	0.2		1.08	0.12	0.44	0.36
Porites colonensis		**0.12**	0.04								0.04		
Porites divaricata			0.12	0.20		0.04				0.08	0.04		
Porites furcata	**0.04**	**0.04**	0.16	0.12		0.04		0.04		0.20	0.08		
Porites porites	**0.12**	**0.20**	0.24	0.56	0.04	0.20	**0.12**	0.28			0.16	0.04	0.24
Siderastrea siderea	**2.36**	**0.36**	0.52	1.00	3.28	1.04	**0.12**	0.12	**0.12**	0.76	1.08	1.68	0.24
Solenastrea bournoni												0.12	
Stephanocoenia intersepta	**0.32**	**0.16**			0.04			0.04		0.20			0.08
Total Abundance:	**8.56**	**5.00**	3.16	3.60	8.08	2.36	**1.72**	1.12	**0.52**	2.92	3.24	2.80	1.20

Stations in 1st (lowest) LDI quartile have no shading, 2nd LDI quartile in bold font, 3rd LDI quartile shaded light gray, and 4th LDI (highest) quartile shaded dark gray

Table 3 Station depths and mean stony coral indicators: density (SC_Den; no. of colonies/m^2), colony surface area (CSA_Av; m^2 coral), live colony surface area (LCSA_Av; m^2 coral), percent live tissue (LT; %), 3D total cover (3DTC; m^2 coral/m^2 seafloor), 3D live cover (3DLC; m^2 coral/m^2 seafloor), coefficient of variation of colony surface area (CSA_CV), number of taxa (SC_Tx; no. of taxa/m^2), Shannon-Weiner index of diversity (SC_H′), and reef rugosity (RI)

Station	Depth (m)	SC_Den	CSA_Av	LCSA_Av	LT	3DTC	3DLC	CSA_CV	SC_Tx	SC_H′	RI
1	7.62	9.12	0.11	0.06	75.57	0.975	0.557	241.5	0.72	2.24	1.66
2	7.01	8.24	0.09	0.07	82.43	0.757	0.542	321.6	0.68	2.02	1.45
3	9.14	3.32	0.30	0.09	58.43	0.986	0.310	149.1	0.68	2.36	1.66
4	6.71	3.60	0.11	0.05	68.22	0.378	0.186	194.3	0.52	2.22	1.57
5	6.71	9.12	0.10	0.06	81.43	0.869	0.589	198.0	0.76	1.94	1.41
6	7.01	2.44	0.07	0.03	74.92	0.162	0.073	246.7	0.48	1.61	1.35
7	7.62	3.60	0.10	0.05	73.22	0.360	0.182	208.7	0.52	1.94	1.54
8	6.71	1.12	0.11	0.04	54.46	0.121	0.046	124.0	0.44	2.14	1.34
9	6.40	0.64	0.54	0.13	52.50	0.345	0.082	182.8	0.24	1.44	1.28
10	6.40	2.92	0.09	0.07	78.49	0.264	0.199	167.6	0.56	1.93	1.50
11	6.71	4.32	0.09	0.05	81.39	0.373	0.219	287.1	0.60	2.03	1.32
12	5.49	3.52	0.08	0.03	74.20	0.273	0.123	178.7	0.36	1.47	1.45
13	6.10	1.12	0.17	0.07	82.14	0.196	0.074	288.5	0.36	1.89	1.59

two sea plumes < 26 cm in height. Sea rods were dominant, accounting for about 60% of the abundance and 79% of the SA of gorgonians. The highest gorgonian density and SA were found at station 1 (Table 6). Regression analysis detected no significant relationships between any stressors and average gorgonian surface area or gorgonian density. Correlation analysis with ISI revealed no significant relationships with gorgonian metrics.

Sponges were found at all 13 stations (Table 6) with a total of 139 colonies exhibiting seven different morphologies. The most common sponge morphologies were rods (56), mounds (39), and encrusting types (20), with rods contributing 96% of total sponge SA. Three "vase" sponge colonies < 10 cm in height yielded negative SA using regressions, so the formula for a circle was used to estimate SA for these exceptions.

Sedimentation threat and WQ were positively significantly related to sponge colony density (Table 4). Sponge colony density was positively correlated with ISI ($r^2 = 0.395$, $p < 0.02$).

Fish

A total of 1968 fish belonging to 25 families were observed, and eight families comprised 92% of total abundance (highest abundance to lowest): Labridae, Scaridae, Pomacentridae, Acanthuridae, Gobiidae, Haemulidae, Serranidae, and Lutjanidae. These dominant eight families comprised 88% of total biomass (highest biomass to lowest): Scaridae, Serranidae, Acanthuridae, Pomacanthidae, Haemulidae, Pomacentridae, Lutjanidae, and Labridae. From 67 different species, the ten species comprising 70% of total abundance were (from highest to lowest) bluehead, masked/glass goby, striped parrotfish, ocean surgeonfish, blue tang, redband parrotfish, cocoa damselfish, French grunt, and bridled goby. Fish abundance ranged from 45 to 231 in the 100-m^2 survey area. Piscivores were rare and constituted less than 1% of abundance. Zooplanktivores constituted 16%, invertivores 49%, and herbivores 45%.

Station metrics for total fish abundance, total biomass, taxa richness, and Shannon-Weiner diversity index are presented in Table 6. No fish metrics were related to individual stressors, and no significant correlations with ISI were found.

Foraminifera and Macroinvertebrates

The FoRAM index was lowest (2.83) at station 10 near Charlotte Amalie Harbor. Stations 7 and 9 near Water Island had the highest FoRAM values of 6.48 and 4.88, and the remaining station values ranged from 3.06 to 3.84 (Table 6). Sea urchins of various species comprised 98% of macroinvertebrates observed at all stations. Of

Table 4 Results of stepwise regression testing relationships between coral reef indicators and stressors: landscape development intensity (LDI) index, sedimentation threat (ST), and water quality (WQ) with inclusion of $p < 0.25$ and retention of $p < 0.20$. Transformation indicated to meet requirement for normal distribution

Indicator	Transformation	LDI		ST		WQ		Equation
		p value	Partial r^2	*p* value	Partial r^2	*p* value	Partial r^2	
3DTC	log10	0.080	0.252	ns		ns		3DTC = (LDI × − 0.05054)
RI	none	0.012	0.156	0.015	0.392	ns		RI = (LDI × − 0.1088) + (ST × 0.00000659)
SC_H′	none	0.083	0.224	0.187	0.122	0.125	0.185	SC_H′ = (LDI × − 0.24242) + (ST × 0.0000082) + (WQ × 0.21111)
Sp_Den	log10	ns		0.010	0.471	0.194	0.088	Sp_Den = (ST × 0.00001022) + (WQ × 0.09406)

Equation coefficients show direction of relationship

3DTC three-dimensional total cover (live + dead coral), *RI* rugosity index, *SC_H′* Shannon-Weiner diversity index, *Sp_Den* density of sponge colonies

Table 5 Results of stepwise regression testing relationships between colony density of dominant stony coral species and stressors (see Table 4 and text) with inclusion of $p < 0.25$ and retention of $p < 0.20$. Transformation indicated to meet requirement for normal distribution

Stony coral species	Transformation	LDI		ST		WQ		Equation
		p value	Partial r^2	*p* value	Partial r^2	*p* value	Partial r^2	
Orbicella annularis	none	0.0089	0.4773	ns		ns		LDI × − 4.02511
Montastraea cavernosa	none	0.0436	0.3208	ns		ns		LDI × − 2.86174
Orbicella faveolata	log10	0.1469	0.1812	ns		ns		LDI × − 0.18755
Orbicella franksi	none	0.0866	0.2409	ns		ns		LDI × − 2.33885
Porites astreoides	none	ns		ns		ns		ns
Siderastrea siderea	none	ns		ns		ns		ns
Pseudodiploria strigosa	log10	ns		ns		ns		ns
Porites porites	none	0.0415	0.2822	ns		0.0258	0.2016	(LDI × − 2.39872) + (WQ × 3.61828)

Equation coefficients show direction of relationship

ns not significant

all macroinvertebrates, 67% were found at stations 1–5, west of Lindberg Bay (Table 6). Only seven spiny lobsters (five at station 10) were found, and no slipper lobsters, juvenile queen conch, and adult conch were observed at all. Neither the FoRAM index nor invertebrate density showed significant relationships in regressions with individual stressors or in correlation analysis with ISI.

Discussion

Human disturbance on the south shore of St. Thomas was characterized using three independent spatial measures of stressors known to adversely impact coral reefs. The stressors harm coral reefs either directly (Loya 1976; Rogers 1979; Rogers 1990; Fabricius 2005) or synergistically through interaction with other factors

Table 6 Station indicators FoRAM index (FI), invertebrate density (In_Den; no. of invertebrates/m^2 sea floor), gorgonian density (Gorg_Den; no. of gorgonians/m^2), average gorgonian surface area (GSA_Av; m^2 gorgonian SA), sponge density (Sp_Den; no. of sponges/m^2), average sponge surface area (SSA_Av; m^2 sponge SA), fish abundance (F_Abun; no. of fish/transect), fish biomass (F_Biom; total g/transect), F_Tx (number of fish taxa/transect), and Shannon-Weiner index of diversity for fish (F_H′)

Station	FI	In_Den	Gorg_Den	GSA_Av	Sp_Den	SSA_Av	F_Abun	F_Biom	F_Tx	F_H′
1	3.38	0.80	5.4	0.19	0.6	0.03	213	796.1	21	1.87
2	3.15	3.00	0.6	0.20	0.8	0.08	134	2501.8	20	2.14
3	3.22	0.11	0.0	0.0	2.2	5.85	109	316.8	16	2.29
4	3.06	0.37	0.8	0.05	2.0	0.04	231	3046.7	19	1.98
5	3.72	0.31	1.2	0.06	3.4	0.18	151	2810.3	24	2.56
6	3.46	0.16	0	0	1.6	0.01	148	1644.8	21	2.47
7	6.48	0.04	0	0	1.6	0.01	132	1476.8	24	2.53
8	3.84	0.02	0	0	2.0	0.40	156	3509.4	19	2.47
9	4.88	0.09	0	0	0.4	0.10	176	2440.2	25	2.82
10	2.83	0.12	0.2	0.07	7.4	0.69	166	2664.6	22	2.25
11	3.34	0.02	0	0	2.0	0.10	153	5799.7	21	2.52
12	3.69	1.78	0	0	3.0	0.09	45	367.1	14	1.99
13	3.65	0.01	1.2	0.11	0.8	0.06	154	638.0	25	2.31

(Carilli et al. 2009; Vega Thurber et al. 2013). High stressor values at stations closest to Charlotte Amalie Harbor validated selection of the area as an anthropogenic disturbance center where numerous human impacts occur. Our approach included comparing predictive power of individual stressors with a composite stressor index, the latter assuming additive effects as used to model reef stressors on a worldwide scale (Halpern et al. 2008). Land-based human activity represented by watershed LDI (Brown and Vivas 2005) had the most significant relationships with reef rugosity, coral diversity, and coral taxa richness exhibiting consistent negative coefficients in regression models. This supported the hypothesis that increased intensity of human development on land (high LDI) is associated with poor condition of coral reefs adjacent to high-LDI watersheds, as demonstrated in other Caribbean areas (Rogers 1979; Smith et al. 2008; Oliver et al. 2011), Hawaii (Rodgers et al. 2012), and Indonesia (Golbuu et al. 2008). The capability of LDI to predict ecosystem condition in wetlands and nutrient loading in watersheds (Brown and Vivas 2005) extends to predicting characteristics of coral reef condition such as stony coral colony size, species colony density, species diversity, topographic reef complexity, and benthic habitat composition at multiple watershed scales (Pittman et al. 2013). Some of these coral indicators have been related to distance to disturbance or other stress proxies (Fisher et al. 2008; Smith et al. 2008; Rodgers et al. 2012), and our results reinforce their application in stressor-response characterizations.

Stations near high-LDI watersheds had lower stony coral 3D cover and reef rugosity and reduced colony density for five dominant reef-building species (Tables 4 and 5). Total coral colony density and taxa richness were not statistically associated with LDI, but stations adjacent to highest-quartile LDI watersheds tended to have fewer colonies and fewer taxa compared to those near low-quartile LDI watersheds. Also, coral communities at the high-LDI stations were dominated by "weedy" species like *Porites astreoides* and *Siderastrea siderea* (Table 2), which have shown greater resistance to stress in Puerto Rico and other Caribbean areas (Torres and Morelock 2002; Green et al. 2008; Smith et al. 2013), but do not provide the habitat complexity of branching species (e.g., *Acropora*) nor the reef structure of massive corals (e.g., *Orbicella* and *Montastraea*). There were significantly fewer *Orbicella* sp. at stations with higher LDI, a finding that highlights a conclusion similar to Smith et al. (2008) and Ennis et al. (2016), who reported that reduced coral cover near human influence was driven by fewer *O. annularis*, *O. franksi*, and *O. faveolata*. There is particular concern about loss of prime reef-building species (Morelock et al. 2001) and the compromise of multiple ecosystem services that ultimately depend on reef structure (Principe et al. 2012; Alvarez-Filip et al. 2009; Burke and Maidens 2004). *Montastraea cavernosa*, another massive reef-building coral, is thought to be relatively resistant to stress but was also more abundant with lower LDI. These results underscore the importance of species-specific coral monitoring methods to detect community shifts caused by varied tolerance to stressors. Multivariate methods to detect changes across reef assemblages have also been applied to characterizing reef-stressor relationships (Jupiter et al. 2008). Even with well-designed methods, detecting stressor-response relationships requires a broad range of biological conditions possible (Karr and Chu 1997) and locating USVI reefs representative of "reference condition for biological integrity" (or zero human impact) is challenging as most USVI coral reefs are probably affected in some way by human influence (Rothenberger et al. 2008; Friedlander et al. 2013; Pait et al. 2013a, b; Pittman et al. 2013; Whitall et al. 2014; Jackson et al. 2014).

There was a significant, but weak, negative relationship of modeled ST with average stony coral colony size. There were also significant but positive relationships of ST with reef rugosity and coral diversity index, countering a common premise that high sediment loading adversely affects stony coral condition (Rogers 1979; Fabricius 2005). However, all of these results may have little interpretive potential because the range of ST values in this study was relatively small. In addition to testing a wide range of biological responses, the stressor gradient ideally incorporates multiple stressor levels from near-pristine to severe human disturbance levels (Karr and Chu 1997). But here, the highest ST was 54,359 (station 10), which is relatively small compared to the maximum Summit to Sea ST in the region of 251,714. Thresholds of sediment exposure are not well understood (Rogers 1990), and even if they were, the ST model does not convert to actual sediment concentrations. A positive coefficient found for ST and sponge density is consistent with other studies showing some sponge species to be relatively tolerant to stress from excess sediments (Powell et al. 2014). If so, this could indicate a possible phase shift in impacted

environments from coral-dominated habitats to sponge-dominated, and a loss of many ecosystem services (Ward-Paige et al. 2005; Norström et al. 2009).

For coral reefs near Charlotte Amalie, a more relevant source of sediment exposure for corals might be pulsed resuspension of sediments associated with cruise ship traffic in and out of ports in Crowne Bay and Charlotte Amalie Harbor (Kisabeth et al. 2014). Ship traffic creates plumes of resuspended sediment which substantially increase turbidity and total suspended solids compared to undisturbed levels (Kisabeth et al. 2014; Jones et al. 2016). This daily recurring activity is not captured in the ST model, which relies on landscape features, precipitation, and soil erodibility. It may be necessary to adjust sediment delivery models like Summit to Sea to account for factors like ship traffic to improve predictive capabilities. Many other nuances of sediment effects on corals not included in ST are grain size of the sediment, with finer grains generally causing greater harm (Acevedo et al. 1989; Weber et al. 2006), and whether exposure occurs in pulsed or steady sediment regimes (Browne et al. 2015).

As proxy for impaired water quality, a spatial estimate based on distance to disturbance (Fisher et al. 2008) was developed using data reported to the U.S. EPA under the Clean Water Act 305(b) and 303(d) programs (DPNR 2010). Assuming no effect beyond 3 km, three stations were too far away from impaired bays to be affected, and stations 5 and 6 located in the center of the study area had potential impact from three and two bays, respectively, where impaired water quality was reported. Significant positive relationships between WQ and coral diversity index and between WQ and *P. porites* colony density did not indicate that proximity to bays with WQ issues had negative effects on coral reefs. Estimates of WQ stress to benthic organisms could be improved with additional field data to better define potential relationships between specific WQ stressors like turbidity, total suspended solids (TSSs), and low DO on corals. Field measurements such as TSS and nutrients are needed to validate remotely sensed satellite products which can more accurately characterize exposure to WQ conditions over time compared with occasional measurements (Brodie et al. 2010). Fine-scale data on water currents would inform predictions of transport of materials to reef habitats and exposure of coral reefs to WQ stressors. Our distance-based WQ approach detected positive relationship with sponge colony density; more sponge colonies were present closer to bays with WQ impairments. This is similar to results from a study of sponges and land-based nutrient inputs in the Florida Keys (Ward-Paige et al. 2005) and is consistent with the concept of phase shifts from stony corals to sponges with increasing anthropogenic stress.

Modeling environmental stressor gradients is inherently difficult for several reasons. Co-occurrence of stressors in areas of high human disturbance is common, which makes it difficult to discern which stressors are responsible for reduced biological condition. The LDI is one type of composite index that is generated on a watershed basis, integrating inputs of nonrenewable energy to land use parcels (Odum 1996). Watershed management for coral health is not a new concept; for example, many Pacific Island cultures practice "ridge-to-reef" stewardship which assumes a connection between land-based human activities and health of adjacent marine communities (Richmond et al. 2007). Yet, management options may not be obvious using LDI as a predictor unless specific land use types associated with reduced biological condition can be identified. Characterizing all operative stressors regarding a system of interest is likely impossible. Models that incorporate multi-stressor data across broad scales (Halpern et al. 2008; Burke et al. 2011) may provide more comprehensive stressor information, but these scales make the data less useful for small islands like St. Thomas. For some areas of the Caribbean, data about coral reef stressors such as fishing pressure (Shivlani and Koeneke 2010), chemical contaminants (Whitall et al. 2014), and ocean temperature anomalies (Novoa et al. 2012; Liu et al. 2014) could improve forecasting and clarify management options. Development of spatially explicit, comprehensive data on multiple stressors impacting coral reefs and accounting for potential synergistic, additive, or antagonistic effects would best serve reef management needs.

Three westward stations adjacent to sparse human population and undisturbed lands had consistent low stressor estimates below 50% of the mean and among the highest total and live stony coral cover, taxa richness, and colony density. Watersheds adjacent to these stations had high coverage of forest and other natural lands (Fig. 1). Progressing to the east, different patterns were seen depending on the stressor. For example,

station 4 is adjacent to a low-LDI watershed but fits the 4th (highest) quartile for ST due in part to adjacent bare landscape and increased likelihood for runoff. Stressor values for station 13 located farthest east from the center of disturbance indicate greater human influence than might be assumed by its distance from Charlotte Amalie. This station had second-highest LDI and ST values and may combine with another human activity source to the east. Influences such as an unlined landfill located 0.1 km from shore in Bovani Bay (Horsely Witten Group 2013) are not represented in our stressor estimates and could have a large impact. Station 8 with highest LDI values also had the lowest stony coral cover and low percent live tissue. In contrast, station 11 located near uninhabited Hassel Island had low LDI and intermediate coral indicator values. Although uninhabited, Hassel Island is close to the harbor and probably receives resuspended sediment from ship traffic.

Although nonsignificant in regressions and correlations, the FoRAM index was highest (best condition) at stations 7 and 9, located away from the coast and human influences, and lowest at station 10 near Charlotte Amalie Harbor. The FoRAM has shown to be responsive to eutrophication (Hallock et al. 2003) and distance to disturbance (Oliver et al. 2014) and may have a value in reef monitoring protocols. Fish populations may associate with reef structure but are not expected to associate directly with stressors because fish are mobile; a lack of significant findings with stressors is not surprising.

Healthy coral reefs benefit the people and economy of St. Thomas by providing ecosystem services. Although causality cannot be directly determined, a human impact signature was evident from LDI associations with reef condition indicators at 13 stations, showing that reefs around Charlotte Amalie are proportionally affected by human development activities in adjacent watersheds. Management steps to reduce human disturbances can lessen direct impacts on corals, as well as additive or synergistic effects from tropical storms and hurricanes, global-scale ocean temperature anomalies (Hughes and Connell 1999; Maina et al. 2011; Gurney et al. 2013), and ocean acidification (Wooldridge and Done 2009; Ban et al. 2014).

Cost-effective mitigation options to reduce sedimentation for example, have been demonstrated in the USVI (Ramos-Scharrón 2012), and effective spatial mapping of reef stressors can prioritize where such actions are most needed. A balanced approach to coastal management decision-making, which incorporates available scientific research to better characterize stressors and understand their influence, can help protect coral reef ecosystems and the economic, ecological, and esthetic benefits they provide.

Acknowledgements Outstanding field assistance in conducting coral reef surveys was provided by Jed Campbell, Peggy Harris, Becky Hemmer, Robert Quarles, and Sherry Vickery (U.S. EPA Gulf Ecology Division); Charles LoBue and Danny Rodriguez (U.S. EPA Region 2); Mel Parsons (U.S. EPA Region 4); Aaron Hutchins (The Nature Conservancy, St. Croix); Rich Henry (U.S. Fish and Wildlife Service, Environmental Response Team); Alan Humphrey (U.S. EPA, Environmental Response Team); and Jon McBurney and Scott Grossman (Lockheed Martin, Scientific, Engineering, Response and Analytical Services (SERAS) Program). The crew of the OSV *Bold*, Captain Jere Chamberlain, provided excellent support in all aspects of field data collection and logistics. Kent Bernier (U.S. Virgin Islands, Department of Planning and Natural Resources) provided small boat support for the survey teams. The views expressed in this article are those of the authors and do not necessarily reflect the views or policies of the U.S. Environmental Protection Agency.

References

Abt Associates, Inc. (2016). Describing the ocean economies of the U.S. Virgin Islands and Puerto Rico. https://coast.noaa.gov/digitalcoast/training/econ-usvi-pr.html

Acevedo, R. J., Morelock, J., & Olivieri, R. A. (1989). Modification of coral reef zonation by terrigenous sediment stress. *PALAIOS, 4*(1), 92–100.

Alvarez-Filip, L., Dulvy, N. K., Gill, J. A., Côte, I. M., & Watkinson, A. R. (2009). Flattening of Caribbean coral reefs: region-wide declines in architectural complexity. *Proceedings of the Royal Society B, 276*, 3019–3302.

Ban, S. S., Graham, N. A. J., & Connolly, S. (2014). Evidence for multiple stressor interactions and effects on coral reefs. *Global Change Biology, 20*, 681–697.

Bégin, C., Schelten, C. K., Nugues, M. M., Hawkins, J., Roberts, C., & Côté, I. M. (2016). Effects of protection and sediment stress on coral reefs in Saint Lucia. *PLoS One, 11*(2), e0146855. https://doi.org/10.1371/journal.pone.0146855.

Bradley, P., Fisher, W., Bell, H., Davis, W., Chan, V., LoBue, C., & Wiltse, W. (2009). Development and implementation of coral reef biocriteria in U.S. jurisdictions. *Environmental Monitoring & Assessment, 150*, 43–51.

Bradley, P., Fore, L., Fisher, W., & Davis, W. (2010). Coral reef biological criteria: using the Clean Water Act to protect a national treasure. U.S. Environmental Protection Agency, Office of Research and Development, Narragansett, RI. EPA/600/R-10/054, July 2010.

Brodie, J., Schroeder, T., Rohde, K., Faithful, J., Masters, B., Dekker, A., Brando, V., & Maughan, M. (2010). Dispersal of suspended sediments and nutrients in the Great Barrier Reef lagoon during river-discharge events: conclusions from

satellite remote sensing and concurrent flood-plume sampling. *Marine and Freshwater Research, 61*(6), 651–664.

Brown, M. T., & Vivas, M. B. (2005). Landscape development intensity index. *Environmental Monitoring & Assessment, 101*, 289–309.

Brown, C. J., Saunders, M. I., Possingham, H. P., & Richardson, A. J. (2013). Managing for interactions between local and global stressors of ecosystems. *PLoS One, 8*(6), e65765. https://doi.org/10.1371/journal.pone.0065765.

Browne, N. K., Tay, J., & Todd, P. A. (2015). Recreating pulsed turbidity events to determine coral-sediment thresholds for active management. *Journal of Experimental Marine Biology and Ecology, 466*, 98–109.

Burke, L., & Maidens, J. (2004). *Reefs at risk in the Caribbean*. Washington, D.C.: World Resources Institute 81 pp.

Burke, L., Reytar, K., Spalding, M., & Perry, A. (2011). *Reefs at risk revisited*. Washington, D.C.: World Resources Institute.

Carilli, J. E., Norris, R. D., Black, B. A., Walsh, S. M., & McField, M. (2009). Local stressors reduce coral resilience to bleaching. *PLoS One, 4*(7), e6324.

Clark, K.R., & Gorley, R.N. (2006). PRIMER v6: user manual/tutorial, Plymouth, UK.

DPNR, (2010). USVI integrated water quality monitoring & assessment report. Department of Planning and Natural Resources, Division of Environmental Protection Water Quality Management & Planning Program. 165 pp. Retrieved 2018, 10 February from: http://www.horsleywitten.com/stx-east-endwatersheds/pubs/2010IntegratedReport_b.pdf.

Ennis, R. S., Brandt, M. E., Wilson Grimes, K. R., & Smith, T. B. (2016). Coral reef health response to chronic and acute changes in water quality in St. Thomas, United States Virgin Islands. *Marine Pollution Bulletin, 111*, 418–427.

Fabricius, K. (2005). Effects of terrestrial runoff on the ecology of coral reefs: review and synthesis. *Marine Pollution Bulletin, 50*, 125–146.

Fisher, W.S. (2007). Stony coral rapid bioassessment protocol. U.S. Environmental Protection Agency, Office of Research and Development, Gulf Breeze, FL. EPA/600/R-06/167, July 2007.

Fisher, W. S., Fore, L. S., Hutchins, A., Quarles, R. L., Campbell, J. G., LoBue, C., & Davis, W. S. (2008). Evaluation of stony coral indicators for coral reef management. *Marine Pollution Bulletin, 56*, 1737–1745.

Fore, L. S., Karr, J. R., Fisher, W. S., Bradley, P., & Davis, W. S. (2009). Heeding a call to action for US coral reefs: the untapped potential of the Clean Water Act. *Marine Pollution Bulletin, 58*, 1421–1423.

Friedlander, A.M., Jeffrey, C.F.G., Hile, S.D., Pittman, S.J., Monaco, M.E. & Caldow, C., eds. (2013). Coral reef ecosystems of St. John, U.S. Virgin Islands: spatial and temporal patterns in fish and benthic communities (2001-2009). NOAA Technical Memorandum 152. Silver Spring, MD. 150 pp.

Froese, R., & Pauly, D., eds. (2013). FishBase. World Wide Web electronic publication. www.fishbase.org, version (12/2013).

Gardner, T. A., Côte, I. M., Gill, J. A., Grant, A., & Watkinson, A. R. (2003). Long-term region-wide declines in Caribbean reef corals. *Science, 301*, 958–960.

Golbuu, Y., Fabricius, K., Victor, S., & Richmond, R. H. (2008). Gradients in coral reef communities exposed to muddy river discharge in Pohnpei, Micronesia. *Estuarine, Coastal and Shelf Science, 76*, 14–20.

Green, D. H., Edmunds, P. J., & Carpenter, R. C. (2008). Increasing relative abundance of *Porites astreoides* on Caribbean reefs mediated by an overall decline in coral cover. *Marine Ecology Progress Series, 359*, 1–10.

Gurney, G. G., Melbourne-Thomas, J., Geronimo, R. C., Aliño, P. M., & Johnson, C. R. (2013). Modelling coral reef futures to inform management: can reducing local-scale stressors conserve reefs under climate change? *PLoS One, 8*(11), e80137.

Hallock, P., Lidz, B. H., Cockey-Burkhard, E. M., & Donnelly, K. B. (2003). Foraminifera as indicators coral reef assessment and monitoring: the Foram index. *Environmental Modeling & Assessment, 81*, 221–238.

Halpern, B. S., Walbridge, S., Selkoe, K. A., Kappel, C. V., Micheli, F., D'Agrosa, C., Bruno, J. F., Casey, K. S., Ebert, C., Fox, H. E., Fujita, R., Heinemann, D., Lenihan, H. S., Madin, E. M. P., Perry, M. T., Selig, E. R., Spalding, M., Steneck, R., & Watson, R. (2008). A global map of human impact on marine ecosystems. *Science, 319*, 948–952.

Horsely Witten Group, Inc, (2013). St. Thomas East End reserves watershed management plan. Report to NOAA coral Reef Conservation Program, USVI DPNR, and The Nature Conservancy. 73 pp.

Hughes, T. P., & Connell, J. H. (1999). Multiple stressors on coral reefs: a long-term perspective. *Limnology & Oceanography, 44*(3), 932–940.

Humann, P., & DeLoach, N. (2002). *Reef coral identification: Florida Caribbean Bahamas*. Jacksonville: New World.

Islands Resources Foundation, USVI-Conservation Data Center, & U.S. Geological Survey. (2001). Watersheds for St. Thomas and St. John, US Virgin Islands. https://databasin.org/datasets/47140a08e8d340fea9a3f4118f15febe.

Jackson, J. B. C., Donovan, M. K., Cramer, K. L., & Lam, V. V. (Eds.). (2014). *Status and trends of Caribbean coral reefs: 1970-2012*. Gland: Global Coral Reef Monitoring Network, IUCN.

Jones, R., Bessell-Browne, P., Fisher, R., Klonowski, W., & Slivkoff, M. (2016). Assessing the impacts of sediments from dredging on corals. *Marine Pollution Bulletin, 102*(1), 9–29.

Jupiter, S., Roff, G., Marion, G., Henderson, M., Schrameyer, V., McCulloch, M., & Hoegh-Guldberg, O. (2008). Linkages between coral assemblages and coral proxies of terrestrial exposure along a cross-shelf gradient on the southern Great Barrier Reef. *Coral Reefs, 27*(4), 887–903.

Kaczmarsky, L. T., Draud, M., & Williams, E. H. (2005). Is there a relationship between proximity to sewage effluent and the prevalence of coral disease? *Caribbean Journal of Science, 41*(1), 124–137.

Karr, J. R., & Chu, E. W. (1997). *Biological monitoring and assessment: using multimetric indexes effectively*. EPA 235-R97-001. Seattle: University of Washington.

Kendall, M. S., Kruer, C. R., Buja, K. R., Christensen, J. D., Finkbeiner, M., & Monaco, M. E. (2001). *Methods used to map the benthic habitats of Puerto Rico and the U.S. Virgin Islands*. Silver Spring: National Oceanic and Atmospheric Administration, NCCOS Biogeography Program http://biogeo.nos.noaa.gov/projects/mapping/caribbean/startup.htm.

Kisabeth, J. K., Smith, T., Primack, A., & Wilson, K. (2014). *Cruise ship induced sediment resuspension characteristics*

in Charlotte Amalie Harbor and the West Gregerie Channel, St. Thomas, US Virgin Islands. St. Thomas: Doctoral dissertation, University of the Virgin Islands.

Knowlton, N., & Jackson, J. B. C. (2008). Shifting baselines, local impacts, and global change on coral reefs. *PLoS Biology, 6*(2), 215–220.

Liu, G., Heron, S. F., Eakin, C. M., Muller-Karger, F. E., Vega-Rodriguez, M., Guild, L. S., De La Cour, J. L., Geiger, E. F., Skirving, W. J., Burgess, T. F. R., Strong, A. E., Harris, A., Maturi, E., Ignatov, A., Sapper, J., Li, J., & Lynds, S. (2014). Reef-scale thermal stress monitoring of coral ecosystems: new 5-km global products from NOAA Coral Reef Watch. *Remote Sensing, 6*(11), 11579–11606. https://doi.org/10.3390/rs61111579.

Loya, Y. (1976). Effects of water turbidity and sedimentation on the community structure of Puerto Rican corals. *Bulletin of Marine Science, 26*(4), 450–466.

Maina, J., McClanahan, T. R., Venus, V., Ateweberhan, M., & Madin, J. (2011). Global gradients of coral exposure to environmental stresses and implications for local management. *PLoS One, 6*(8), e23064.

Menza, C., Ault, J., Beets, J., Bohnsack, J., Caldow, C., Christensen, J., Friedlander, A., Jeffrey, C., Kendall, M., Luo, J., Monaco, M., Smith, S., & Woody, K., (2006). A guide to monitoring reef fish in the National Parks Service's South Florida/Caribbean Network. NOAA Technical Memorandum NOS NCOOS 39. 169 pp.

Moberg, F., & Folke, C. (1999). Ecological goods and services of coral reef ecosystems. *Ecological Economics, 29*, 215–233.

Morelock, J., Ramirez, W.R., Bruckner, A.W., & Carlo, M. (2001). Status of coral reefs in southwest Puerto Rico. Caribbean Journal Science Special Publication No 4.

Nemeth, R. S., & Nowlis, J. S. (2001). Monitoring the effects of land development on the near-shore reef environment of St. Thomas, USVI. *Bulletin of Marine Science, 69*(2), 759–775.

Norström, A. V., Nyström, M., Lokrantz, J., & Folke, C. (2009). Alternative states on coral reefs: beyond coral-macroalgal phase shifts. *Marine Ecology Progress Series, 376*, 295–306.

Novoa, S., Chust, G., Froidefond, J.M., Petus, C., Franco, J., Orive, E., Seoane, S., & Borja, A. (2012). Water quality monitoring in Basque coastal areas using local chlorophyll-*a* algorithm and MERIS images. Journal of Applied Remote Sensing 6(1), 063519. doi: https://doi.org/10.1117/1.JRS.6.063519.

Odum, H. T. (1996). *Environmental accounting: Emergy and environmental decision making* (p. 370). New York: John Wiley and Sons.

Oliver, L. M., Lehrter, J. C., & Fisher, W. S. (2011). Relating landscape development intensity to coral reef condition in the watersheds of St. Croix, US Virgin Islands. *Marine Ecology Progress Series, 427*, 293–302.

Oliver, L. M., Fisher, W. S., Dittmar, J., Hallock, P., Campbell, J., Quarles, R. L., Harris, P., & LoBue, C. (2014). Contrasting responses of coral reef fauna and foraminiferal assemblages to human influence in La Parguera, Puerto Rico. *Marine Environmental Research, 99*, 95–105.

Pait, A.S., Hartwell, S.I., Mason, A.L., Galdo, F.R. Jr., Warner, R.A., Jeffrey, C.F.G., Hoffman, A.M., Apeti, D.A., & Pittman, S.J. (2013a). An assessment of chemical contaminants detected in passive water samplers deployed in the St. Thomas East End Reserves (STEER). NOAA Technical Memorandum NOS/NCCOS 157. Silver Spring, MD. 22 pp.

Pait, A.S., Hartwell, S.I., Mason, A.L., Warner, R.A., Jeffrey, C.F.G., Hoffman, A.M., Apeti, D.A., Galdo Jr., F.R., & Pittman, S.J. (2013b). An assessment of chemical contaminants, toxicity and benthic infauna in sediments from the St. Thomas East End Reserves (STEER). NOAA Technical Memorandum NOS NCCOS 156.Silver Spring, MD. 70 pp.

Pittman, S.J., Dorfman, D.S., Hile, S.D., Jeffrey, C.F.G., Edwards, M.A. & Caldow, C. (2013). Land-sea characterization of the St. Croix East End Marine Park, U.S. Virgin Islands. NOAA Technical Memorandum NOS NCCOS 170. Silver Spring, MD. 119 pp.

Powell, A., Smith, D. J., Hepburn, L. J., Jones, T., Berman, J., Jompa, J., & Bell, J. J. (2014). Reduced diversity and high sponge abundance on a sedimented Indo-Pacific reef system: implications for future changes in environmental quality. *PLoS One, 9*(1), e85253. https://doi.org/10.1371/journal.pone.0085253.

Principe, P., Bradley, P., Yee, S., Fisher, W., Johnson, E., Allen, P. & Campbell, D. (2012). Quantifying coral reef ecosystem services. U.S. Environmental Protection Agency, Office of Research and Development, Research Triangle Park, NC. EPA/600/R-11/206, January 2012, 147 pp.

Ramos-Scharrón, C. E. (2012). Effectiveness of drainage improvements in reducing sedimenbt production rates from an unpaved road. *Journal of Soil and Water Conservation, 6*(2), 87–100.

Richmond, R. H., Rongo, T., Golbuu, Y., & Victor, S. (2007). Watersheds and coral reefs: conservation science, policy, and implementation. *Bioscience, 57*, 598–607.

Risk, M. (1972). Fish diversity on a coral reef in the Virgin Islands. *Atoll Research Bulletin, 153*, 1–6.

Rodgers, K. S., Kido, M. H., Jokiel, P. L., Edmonds, T., & Brown, E. K. (2012). Use of integrated landscape indicators to evaluate the health of linked watersheds and coral reef environments in the Hawaiian Islands. *Environmental Management, 50*, 21–30.

Rogers, C. S. (1979). The effects of shading on coral-reef structure and function. *Journal of Experimental Marine Biology & Ecology, 41*, 269–288.

Rogers, C. S. (1990). Responses of coral reefs and reef organisms to sedimentation. *Marine Ecology Progress Series, 62*, 185–202.

Rogers, C. S., Miller, J., Muller, E. M., Edmunds, P., Nemeth, R. S., Beets, J. P., Friedlander, A. M., Smith, T. B., Boulon, R., Jeffrey, C. F. G., Menza, C., Caldow, C., Idrisi, N., Kojis, B., Monaco, M. E., Spitzack, A., Gladfelter, E. H., Ogden, J. C., Hillis-Starr, Z., Lundgren, I., Schill, W. B., Kuffner, I. B., Richardson, L. L., Devine, B. E., & Voss, J. D. (2008). Ecology of coral reefs in the US Virgin Islands. In B. Riegl & R. Dodge (Eds.), *Coral reefs of the USA* (Vol. 1, pp. 303–373). Netherlands: Springer.

Rothenberger, P., Blondeau, J., Cox, C., Curtis, S., Fisher, W. S., Garrison, V., Hillis-Starr, Z., Jeffrey, C., Kadison, E., Lundgren, I., Miller, W. J., Muller, E., Nemeth, R., Paterson, S., Rogers, C., Smith, T., Spitzack, A., Taylor, M., Toller, W., Wright, J., Wusinich-Mendea, D., & Waddell, J. (2008). The state of coral reef ecosystems of the U.S. Virgin Islands. In J. E. Wadell & A. M. Clarke (Eds.), *The state of coral reef ecosystems of the United States and*

Pacific Freely Associated States: 2008 (pp. 29–73). Silver Spring: NOAA Center for Coastal Monitoring and Assessment's Biogeography Team.

Santavy, D.L, Fisher, W.S., Campbell, J.G., & Quarles R.L. (2012). Field manual for coral reef assessments. U.S. Environmental Protection Agency, Office of Research and Development, Gulf Ecology Division, Gulf Breeze, FL. EPA/600/R-12/029. April 2012.

Santavy, D. L., Courtney, L. A., Fisher, W. S., Quarles, R. L., & Jordan, S. J. (2013). Estimating the surface area of marine gorgonians and sponges in the field. *Hydrobiologia, 707*, 1–16.

Shivlani, M., & Koeneke, R. (2010). Spatial characterization of artisanal fisheries in Puerto Rico: geographic information systems (GIS) approach for assessing the regional effort and landings. Proceedings 63rd Gulf and Caribbean Fisheries Institute, November 1–5, 2010, San Juan, Puerto Rico.

Smith, T. B., Nemeth, R. S., Blondeau, J., Calnan, J. M., Kadison, E., & Herzlieb, S. (2008). Assessing coral reef health across onshore to offshore stress gradients. *Marine Pollution Bulletin, 56*, 1983–1991.

Smith, T. B., Brandt, M. E., Calnan, J. M., Nemeth, R. S., Blondeau, J., Kadison, E., Taylor, M., & Rothenberger, P. (2013). Convergent mortality responses of Caribbean coral species to seawater warming. *Ecosphere, 4*(7), 87. https://doi.org/10.1890/ES13-00107.1.

Torres, J. T., & Morelock, J. (2002). Effect of terrigenous sediment influx on coral cover and linear extension rates of three Caribbean massive coral species. *Caribbean Journal of Science, 38*(3–4), 222–229.

USVI (U.S. Virgin Islands), (2010). United States Virgin Islands 2010 revisions to: Water Quality Standards Title 12, chapter 7, Government of the Virgin Islands, Department of Planning and Natural Resources, Division of Environmental Protection, 22 pp.

van Beukering, P., Brander, L., Van Zanten, B., Verbrugge, E., Lems, K. (2011). The economic value of the coral reef ecosystems in the United States Virgin Islands. In: Edmunds, P.E.T. (ed.), The economic value of coral reefs, IVM Report number: R-11/06.

Vega Thurber, R. L., Burkepile, D. E., Fuchs, C., Shantz, A. A., McMinds, R., & Zaneveld, J. R. (2013). Chronic nutrient enrichment increases prevalence and severity of coral bleaching. *Global Change Biology*. https://doi.org/10.1111/gcb,12450.

Villanueva, R. D., Yap, H. T., & Montaña, N. E. (2006). Survivorship of coral juveniles in a fish farm environment. *Marine Pollution Bulletin, 51*, 580–589.

Voss, J. D., & Richardson, L. L. (2006). Nutrient enrichment enhances black band disease progression in corals. *Coral Reefs, 25*, 569–576.

Ward-Paige, C. A., Risk, M. J., Sherwood, O. A., & Jaap, W. C. (2005). Clionid sponge surveys on the Florida Reef Tract suggest land-based nutrient inputs. *Marine Pollution Bulletin, 51*, 570–579.

Warne, A. G., Webb, R. M. T., & Larsen, M. C. (2005). Water, sediment, and nutrient discharge characteristics of rivers in Puerto Rico, and their potential influence on coral reefs: U.S. *Geological Survey Scientific Investigations Report, 2005-5206*, 58.

Weber, M., Lott, C., & Fabricius, K. E. (2006). Sedimentation stress in a scleractinian coral exposed to terrestrial and marine sediments with contrasting physical, organic and geochemical properties. *Experimental Marine Biology & Ecology, 336*, 18–32.

Whitall, D., Menza, C., & Hill, R. (2014). A baseline assessment of coral and fish bays (St. John, USVI) in support of ARRA watershed restoration activities. NOAA Technical Memorandum NOS NCCOS 178. Silver Spring, MD. 74 pp.

Wooldridge, S. A., & Done, T. J. (2009). Improved water quality can ameliorate effects of climate change on corals. *Ecological Applications, 19*(6), 1492–1499.

World Resources Institute (WRI), & NOAA (2006). Land-based sources of threat to coral reefs in the U.S. Virgin Islands. Washington, DC.

Session 36

Biodiversity, biogeography and evolution of coral reef organisms

Session chairs:

Danwei Huang, huangdanwei@nus.edu.sg

Francesca Benzoni, francesca.benzoni@unimib.it

Marcelo V. Kitahara. mvkitahara@unifesp.br

James D. Reimer, jreimer@sci.u-ryukyu.ac.jp

Molly Timmers, molly.timmers@noaa.gov

Christopher Meyer, meyerc@si.edu

Forest Rohwer, frohwer@gmail.com

Gustav Paulay, paulay@flmnh.ufl.edu

Peter F. Cowman, peter.cowman@jcu.edu.au

Jennifer Hodge, jhodge@ucdavis.edu

Libby Liggins, l.liggins@massey.ac.nz

Oliver LM, Santavy DL, Bradley P (2016) Developing a multi-stressor gradient model for coral reefs of Puerto Rico. Proceedings of the 13th International Coral Reef Symposium, Honolulu: 245-257

Louis YD, Dyall SD, Bhagooli R (2016) Coast-reef scale physiological responses of *Acropora muricata* harboring *Symbiodinium* clade A. Proceedings of the 13th International Coral Reef Symposium, Honolulu: 258-277

Kaullysing D, Gopeechund A, Mattan-Moorgawa S, Taleb-Hossenkhan N, Kulkarni B, Bhagooli R (2016) Increased density of the corallivore *Drupella cornus* on *Acropora muricata* colonies overgrown by *Padina boryana.* Proceedings of the 13th International Coral Reef Symposium, Honolulu: 278-294

Developing a multi-stressor gradient model for coral reefs of Puerto Rico

Leah M. Oliver, Deborah L. Santavy, Patricia Bradley

Abstract Coral reefs worldwide are threatened by multiple anthropogenic stressors, yet understanding reef responses to multiple stressor gradients is complicated by interactive stressor effects, co-occurrence of some stressors, and inconsistent data availability. Indirect protection of aquatic life under the US Clean Water Act (CWA) may occur through requirements for effluent discharge permits and provisions for setting chemical and physical criteria based on designated waterbody uses for humans. Biological water quality criteria or "biocriteria" established under the CWA offers a direct means to protect corals. Biocriteria are quantitative thresholds or narrative descriptions of coral reef ecosystem attributes needed to maintain biological integrity. Biocriteria development involves defining the biological community associated with a wide range of ecosystem conditions ranging from a pristine, undisturbed state to severe disturbance by human activities. As part of this process for Puerto Rico, Caribbean coral reef ecosystem experts prioritized anthropogenic stressors to coral reef ecosystems as land-based sources of pollution, fishing pressure, and global climate change-related thermal anomalies. Spatial data representing these stressors were mapped, showing some areas where all three stressors were high and also areas where the magnitude of stressors contrasted. In northeast Puerto Rico, urban development around San Juan resulted in the island's highest watershed development index, which co-occurred with high fishing pressure. In contrast, southwest Puerto Rico had high fishing pressure but low watershed development and ocean temperatures compared to other coastal areas. Narrative descriptions were also developed to incorporate stressors for which spatial data is absent or limited. Future expert workshops will refine this model by developing stressor weighting factors and by considering interactive effects. This conceptual framework will contribute to developing a multi-stressor gradient model for the coral reefs of Puerto Rico, identify data needs, stimulate addition of new spatial data, and generate testable hypotheses to calibrate the stressor-response model.

Keywords: coral reefs, land-based pollution, temperature anomalies, fishing pressure, stressor gradient

Leah M. Oliver, Deborah L. Santavy
US EPA, Office of Research & Development, National Health & Environmental Effects Laboratory, Gulf Ecology Division, 1 Sabine Island Drive, Gulf Breeze, FL 32561

Patricia Bradley
Retired, US EPA, Office of Research & Development, National Health & Environmental Effects Laboratory, Atlantic Ecology Division, 27 Tarzwell Drive, Narragansett, RI 02882

Corresponding author: Leah M. Oliver, oliver.leah@epa.gov

Introduction

Coral reefs are often found near coasts where multiple anthropogenic stressors co-occur at areas of high human disturbance. Stressors range in scale of influence and relative manageability from point source discharges and unrestrained coastal development to thermal anomalies and ocean acidification stemming from global climate change (Hughes and Connell 1999; Kleypas et al. 1999; Ban et al. 2014). Understanding which human-induced stressors influence important coral reef attributes is critical to effect management actions that maximize benefits to reefs and the valuable ecosystem services they provide. The US Clean Water Act (CWA) establishes a framework for regulating water quality and directs the EPA to set wastewater standards for industry, issue permits for industrial and municipal discharges, and coordinate with state and territorial governments to adopt water quality criteria to protect against harmful effects of pollutants. Chemical and physical criteria are routinely established, yet the CWA also contains a provision for states and territories to set biocriteria, which are desired states of biological resources linked to designated uses (Bradley et al. 2009). Designated uses are the formally promulgated uses for a given waterbody such as drinking water, fishing and fish consumption, swimming, and supporting aquatic life. The CWA requires that water quality be able to support the designated use(s) for a given waterbody. Based on the designated use(s), desired resource conditions may be customized, for example, biocriteria for lower quality "Class C" waters with heavy human impact may allow for some loss of ecosystem structure and function while those for higher quality "Class A" waters could require full ecosystem integrity on par with an undisturbed, undeveloped, and possibly historic condition indicative of a natural or non-degraded state (US EPA 2016). Although it is not necessary to quantify all stressors which impact biological resources, biocriteria development requires development of relevant indicators for

both stressors and biological condition and a relationship established between reduced resource condition and increasing human disturbance (Karr and Chu 1997; Fore et al. 2009).

Quantitative relationships between anthropogenic stress and coral reef health have been demonstrated in the Caribbean (Fisher et al. 2008; Oliver et al. 2011; Ennis et al. 2016), Hawaii (Rodgers et al. 2012), and Indonesia (Golbuu et al. 2008), employing biological measures of coral size, taxa richness, and coral cover, and stressor estimates such as distance to disturbance and land-use based watershed indices. These studies establish stressor-response relationships for corals and set the stage for integrated stressor approaches. A conceptual model developed for wetland and stream ecosystems relating biological condition to increasing anthropogenic stressors (Fig. 1) was the basis for engaging Caribbean coral reef ecosystem experts to develop a biological condition gradient (BCG), defining attributes of coral reef ecosystems associated with conditions ranging from pristine to severely altered (Davies and Jackson 2006; Bradley et al. 2014; Santavy et al. 2016). During a structured process to assign biological attributes to different levels of the BCG, discussions included which stressors the experts believed were the

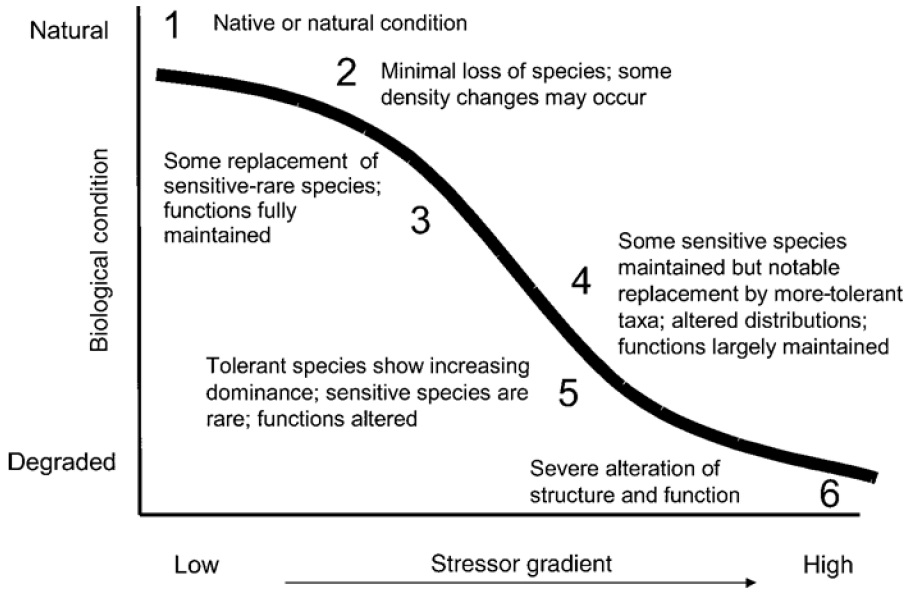

Fig. 1 Conceptual biological condition and stressor gradient model, showing general changes in ecosystem in response to increasing anthropogenic stress. Reprinted from Davies, SP and Jackson SK (2006), The biological condition gradient: a descriptive model for interpreting change in aquatic ecosystems. Ecological Applications, 16: 1251–1266. doi:10.1890/1051-0761(2006)016[1251:TBCGAD]2.0.CO;2, with permission of the Ecological Society of America

most critical for coral reef ecosystems in Puerto Rico and the Caribbean. Experts identified high sea temperatures and land-based pollution as primary stressors for corals, and fishing pressure and land-based pollution for fishes. As part of the BCG development process in which anthropogenic stressor gradients are characterized and associated with different BCG levels, we sought to develop a conceptual framework for an integrated stressor gradient for Puerto Rico's coral reef ecosystems, incorporating both quantitative data and narrative descriptions.

Materials and methods

Land-Based Sources of Pollution (LBSP)

A Landscape Development Intensity Index (LDI) was calculated as a measure of land-based pollution using the method of Brown and Vivas (2005). The LDI method integrates human impact associated with specific land use/land cover (LULC) types, proportional to cumulative inputs of nonrenewable energy (Emergy). In brief, a 30m-resolution LULC dataset (Homer et al. 2007) was reclassified to Emergy coefficients (Odum 1996) blended from Brown and Vivas (2005) and Florida land use cover and classification systems (Janicki 2013) (see Table 2 in Oliver et al. 2011). LDI values were calculated for coastal Hydrologic Unit Code (HUC)-12 watersheds, and weighted for % LULC. Coastal watershed LDI values were extended into adjacent coastal segments or sea-sheds, by drawing cardinal lines from watershed borders in a 10-km offshore buffer using ArcMap v10. To address dilution of pollutants with increased distance from shore, LDI values were assigned unadjusted to coastal segments 0-2 km from shore, reduced by 50% in adjacent coastal segments 2-7 km from shore, and reduced by 70% in segments 7-10 km from shore.

Thermal anomalies

Satellite-derived, sea-surface temperature anomaly (SSTA) data was obtained from NOAA's Coral Reef Watch website (http://www.coralreefwatch.noaa.gov/satellite/bleaching5km/index.php). Annual composite, 5-km resolution SSTA files included all currently available data from 2014 – present day 2016. Files in NetCDF format were downloaded and converted to raster in ArcMap v10.3. Rasters were cropped to the geographic extent of Puerto Rico and a mean SSTA raster was calculated.

SSTA represents positive or negative deviations from average monthly climatology, which is based on historical records of mean monthly night-time SST values (Liu 2014).

Fishing pressure

Geospatial layers of fishing intensity were obtained from Manoj Shivlani (Shivlani and Koeneke 2011), who estimated commercial Puerto Rico fishing effort based on interviews with fishers. Participants were asked to map fishing areas they used, and the number of trips to each. Total fishing effort is the maximum potential number of trips to grid cells of approximate area of 3.3 km^2 for all gears including nets, lines, traps and dive gears (dive gears include spear guns and hand gathering by skin diving or scuba).

Integrated stressor index

Stressor estimates were combined by first converting the LDI and fishing effort polygon layers into rasters. Raster layers for LDI, fishing and SSTA were re-scaled from 0-1 using a linear function with the lowest values corresponding to 0 and the highest values to 1. Rasters were added using the raster calculator tool in ArcMap v10.3, Spatial Analyst toolbox.

Narrative stressor descriptions

Narrative stressor descriptions were developed for undisturbed (pristine), moderately stressed, and severely degraded states of LBSP, thermal anomalies, and fishing pressure. For LBSP these included land use characteristics for low, medium and high LDI watersheds, other conditions which were not represented by LDI such as runoff-related impaired water quality and sediment resuspension, and land conditions which exacerbate pollutant transport such as soil type and slope. Fishing pressure was described in terms of both the fishing activity and also the resulting change in fish populations which is relevant to the health of associated reef-building corals.

Results

Coastal LDI watershed values ranged from 1.2 – 5.7, with the highest values in North East Puerto Rico watersheds including the city of San Juan, the West coast near Mayaguez, and the South coast near Ponce, Santa Isabel, Salinas and Guayama (Fig. 2a). High LDI values in Northern receiving sea-sheds were driven by adjacent land areas containing dense human population and those in Western and Southern sea-sheds were driven by a combination of population and row crop agriculture.

Mean SSTA (2014 – 2016) for Puerto Rico ranged from 0.29 – 0.87ºC, and a pattern of lowest SSTA on the West and South West coasts was observed (Fig. 2b).

Commercial fishing effort was highest on the West coast, Southwest near La Parguera, Cabo Rojo, and Puerto Real; and also around the central North coastal area (Fig. 2c).

Summed, rescaled stressor indices reflected high LDI and fishing pressure near San Juan on the North and South-central coasts, high fishing pressure on Southwest coast and Vieques (Fig. 2d). The West coastal area was intermediate for integrated stressor index but fishing pressure was high in the region.

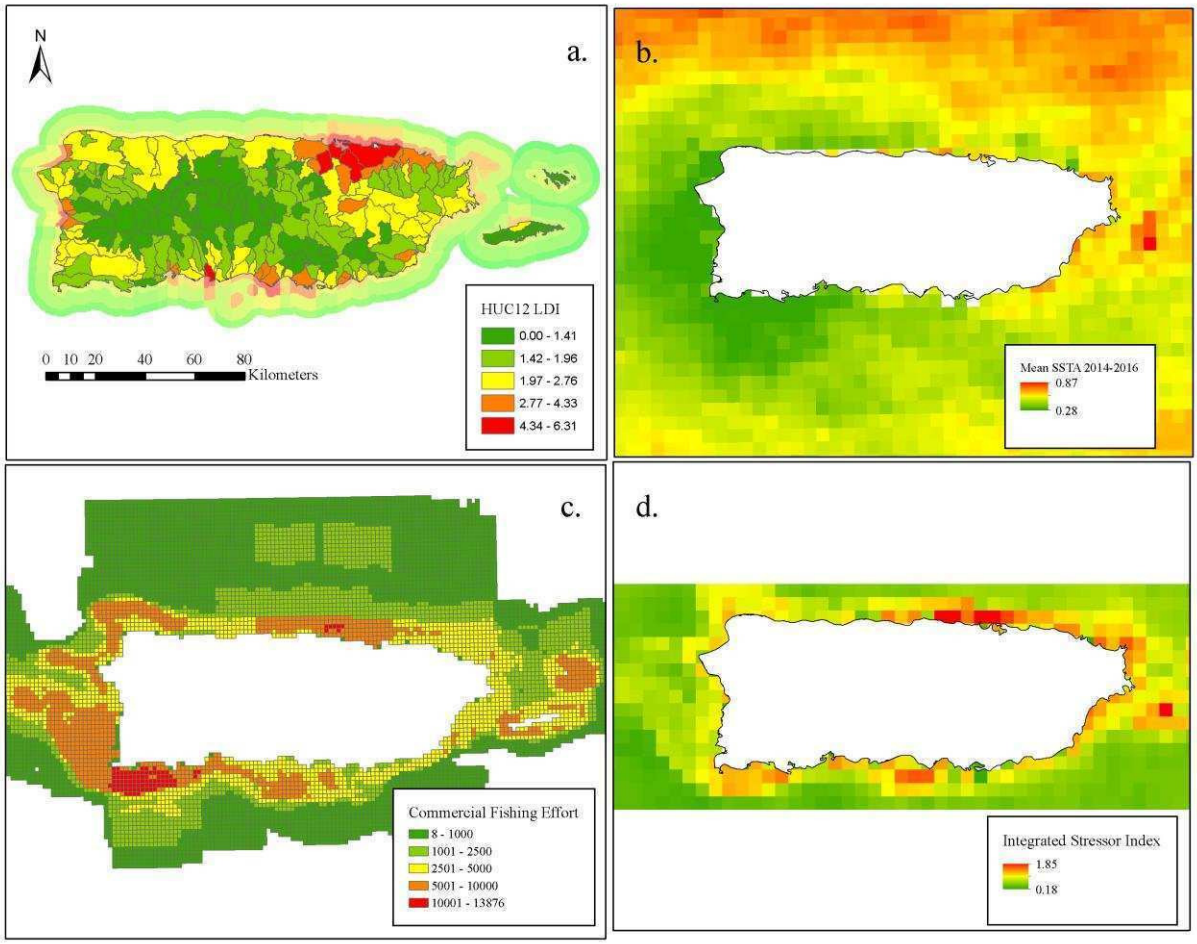

Fig. 2 **a**. Hydrologic Unit Code (HUC12) watersheds of Puerto Rico and associated LDI values. Offshore buffer zones show attenuated LDI value with increased distance from shore. **b**. NOAA Sea Surface Temperature Anomaly (SSTA), mean of monthly composites from 2014-2016. **c**. Total fishing effort modeled as maximum possible trips to each grid cell (Shivlani and Koeneke

Narrative stressor descriptions are presented in Table 1. For LBPS, soil and terrain characteristics which tend to accelerate runoff and increase sediment and pollutant transport to benthic habitats were included. Since the LDI is based on LULC, to avoid redundancy only those additional anthropogenic influences which are not LULC - related were included. Elevated temperature thresholds associated with coral bleaching were derived from literature accounts correlating bleaching with both the magnitude and duration of exposure to elevated sea surface temperature (Eakin et al. 2010; Heron et al., 2016). Fishing pressure was articulated in terms of relative fishing effort which pressures fishery sustainability, and also the resulting fish 2011). **d**. Integrated stressor index was calculated by re-scaling all three stressors (0-1) and summing for a maximum possible value of 3 community expected under varying fishing pressures in order to illustrate the indirect stress to associated corals.

Discussion

Three anthropogenic stressors (land-based sources of pollution, thermal anomalies, and fishing pressure were assembled in a spatially-explicit framework for Puerto Rico coral reef and not fisheries ecosystems, an initial step to support development of biocriteria to protect these unique and important habitats (Fore et al. 2009). Our expectation is that these stressor estimates will be fine-tuned and augmented as additional data becomes available. The LDI index was chosen as a proxy for LBSP, in part due to previous associations with coral condition in St. Croix (Oliver et al. 2011) and with wetland condition in Florida (Brown and Vivas 2005) and Ohio (Mack 2006).

However our narrative description for LBSP highlights land-based stressors which are represented in the LDI. For example, the presence of a wastewater treatment plant or coastal industry is represented in the LDI as a LULC class receiving a high LDI coefficient, but effluents originating from these facilities are not incorporated in LDI. Elevated nutrients are important coral stressors which have been associated with decline of reefs in relatively close proximity to developed coasts (Ennis et al. 2016). The LDI is based on 30-m resolution LULC data circa 2001, but 1-m resolution LULC imagery for Puerto Rico is anticipated in 2016 from the NOAA Coastal Change Analysis Program, allowing finer resolution and more current land cover for new LDI calculations, and possible application of land use changes as an indicator. In the future assumptions regarding the sea-shed transport of land-based pollutants should be refined by adjusting for ocean currents and river flow which affect distance and direction of offshore

Table 1 Narrative descriptions for three stressors representing undisturbed, moderately disturbed and severely disturbed states. For fishing pressure, both fishing activities and resulting fish community are presented. WWTP: Waste water treatment plant, BMP: best management practices

Stressor Level	Land-Based Sources of Pollution	Thermal Anomalies	Fishing Pressure
Undisturbed	Natural landscape conditions present in coastal watersheds. Coastal vegetation such as mangroves and riparian vegetation is intact. Human development absent: no impervious surfaces or facilities such as WWTPs, industries, ports or associated shipping activity. Sediment entry to coastal waters is attenuated by absorbant soil types, presence of coastal vegetation, or both. Area could be Marine Protected Area or Reserve. LDI < 1	Natural temperature regime for the area, no significant departures from normal climatology. DHW remains less than 4°C	Fishing by humans is absent Fish Community: Undisturbed. High diversity in taxa, balanced fish community in terms of size and abundance such that natural trophic interactions are sustained.
Moderately Disturbed	Low to medium density development, coastal industries and/or WWTPs may be present but if so, are compliant with discharge permits, have advanced levels of waste water treatment, and may incorporate biological filtration such as coastal wetlands. Impervious surfaces near the coast are considerable, and along with steep terrain and soils dominated by clays, result in frequent pulses of moderately elevated sediment levels to coastal benthic habitats. Agriculture activity may be broad pasture areas or moderate row crop areas, and BMPs are not universally employed to limit sediment / pollutant transport to marine environment. LDI = 2.01 – 3.0	Departures from normal temperature regime occasionally exceed 4°C-DHW but remain below 8°C-DHW	Fishing activities include a blend of commercial and recreational fishing at levels which are non-threatening to sustainable production. Effective fishing management, enforcement or some combination prevents significant loss of ecosystem functional attributes. Fish Community: Evident changes in structure due to loss of some rare native taxa; shifts in relative abundance of taxa but sensitive-ubiquitous taxa are common and abundant; ecosystem functions are fully maintained through redundant attributes of the system.
Severely Disturbed	Degraded landscape conditions include high percent impervious surface and high-density, near-coastal human development. Near-coastal row crop agriculture lacks BMPs. Sedimentation is severe due to degraded coastal and riparian vegetation and unmitigated land clearing practices, and sediment contains entrained nutrients and other chemical pollutants. Coastal WWTPs lack secondary treatment, and along with industrial discharges, 303(d)[1] listings of impaired water bodies under the CWA are common. Other human influences may include boat traffic in the form of shipping vessels, cruise ships, or recreational vessels which result in sediment resuspension in coastal benthic habitat areas. LDI > 5	Sustained elevated temperature relative to normal, periods exceeding 8°C-DHW	Intense commercial and recreational fishing pressure of reef fish species and pelagic species. Regulations to sustain fishery may be lacking or ignored; enforcement is nonexistent and illegal fishing is common. Gears used include fish traps or others with high bycatch mortality. Fish Community: Low species richness, diversity and abundance compared to other levels. Extremely high densities of tolerant opportunistic species may characterize these systems. Herbivores and apex predators are absent.

[1]Section 303(d) of the US Clean Water Act requires states and territories to submit lists of impaired waters which do not meet water quality standards.

influence, and incorporating shelf bathymetry which affects dispersal of runoff-transported sediment and other pollutants originating on land. Here, we applied simple assumptions of graded influence decay at 2, 7 and 10 km offshore which represent only a coarse estimate.

This analysis used 5-km resolution SSTA data, currently available as annual average composites from 2014 on, pending NOAA's release of additional blended satellite products which will increase retrospective spatial data presented in several ways on NOAA's Coral Reef Watch website. Although SSTA values may be positive or negative, NOAA presents positive deviations or HotSpot values, calculated by subtracting the maximum of monthly mean climatology, and a measure of "Degree Heating Weeks" (DHW) which is the sum of HotSpot values exceeding 1°C for a preceding 12 week period. We demonstrate the potential for SSTA at 5-km resolution to integrate with land-based pollution and fishing data on a reef scale during a time period when thermal-anomaly related coral bleaching was not widespread in Puerto Rico. If the cooler SST values seen in western Puerto Rico (Fig. 2b) persist during a bleaching event, it is possible that corals in those areas might be afforded some degree of protection. Narrative descriptions for thermal anomalies were informed by Eakin et al. (2010) and Heron et al. (2016) who demonstrated threshold DHW values associated with coral bleaching and related mortality, and also the potential for cumulative temperature stress over time to predict coral bleaching susceptibility.

Recreational fishing pressure is thought to be at least as important as commercial landings. We show spatial variation in commercial fishing effort that will be informed by new data when the recreational component of Puerto Rico's fishing law is implemented. In the interim, narrative stressor descriptions were developed for both commercial and recreational fishing activity, including regulatory effectiveness and enforcement capability (Table 1). Indirect effects of fishing pressure on corals were also presented in terms of the associated fish community because with the exception of damage to the reef from fishing gear such as anchors or fishing line, fishing activities do not impact reef corals directly yet lead to ecological dysfunction from overall fishery decline, herbivore reduction and associated algal proliferation on the reef (Hughes et al. 2007). Similarly, model development needs to include indirect effects of climate change-associated anomalies on fish communities, related to bleaching-related coral mortality and loss of reef habitat upon which fish depend for recruitment, refugia, and feeding (Coker et al. 2012; Ainsworth and Mumby 2015).

Simple assumptions (Davies and Jackson 2006) that ecosystem structure and function gradually falter with increased anthropogenic stress represent an accepted general pattern of ecosystem response which can generate testable hypotheses to refine single and cumulative-stressor effects (Hughes and Connell 1999; Ban et al. 2014). An approach to integrate world-scale reef stressors (Halpern et al. 2008; Burke et al. 2011) was used here by summing re-scaled stressor values (Fig. 2d), but future model development needs to consider more complex stressor interactions including weighting, synergistic or antagonistic effects. Observed contrasts in stressor patterns included South West Puerto Rico with low LDI and SSTA, yet high fishing pressure (Fig. 2a, 2b, 2c) A large proportion of Puerto Rico's coral reefs are found in the South West and establishing a no-take reserve has been suggested.

Further development of this multi-stressor model will render it useful to develop biological attributes for BCG levels (US EPA 2016; Santavy et al. in review), inform management decisions, prioritize collection of reef condition data and stressor information, and support stressor-response research studies. Recent guidance for BCG development (US EPA 2016) includes approaches and challenges to defining a generalized multi-stressor axis (x-axis of the BCG, Fig. 1) to represent the cumulative impact of anthropogenic stressors to reef ecosystems ranging from a pristine state to severely disturbed by human activities. Publically available spatial datasets may be employed to represent additional stressors as has been done for the Great Lakes Environmental Indicators project (Danz et al. 2005). Quantitative information on ecosystem condition and anthropogenic stressors for Puerto Rico coral reefs is limited by comparison, but initial steps can be taken. The U.S. Virgin Islands government has identified coral reefs and reef functions as designated uses under the CWA and defined biological integrity in a narrative context (USVI 2010). The foundation exists for Puerto Rico to take similar actions for setting condition thresholds or biocriteria, to protect its valuable coral reefs.

Acknowledgements

We acknowledge Bill Fisher (US EPA Office of Research and Development, Susan Jackson (US EPA Office of Water), Manoj Shivlani (who generously provided Puerto Rico fishing pressure GIS layers), and Amy Smith (US EPA Student Services contractor, for GIS assistance). David Kline (Session No. 36 chair, ICRS 2016) and 2 anonymous reviewers provided suggestions which greatly improved the manuscript.

References

Ainsworth CH, Mumby PJ (2015) Coral-algal phase shifts alter fish communities and reduce fisheries production. Glob Chang Biol 21:165-172

Ban SS, Graham NAJ, Connolly S (2014) Evidence for multiple stressor interactions and effects on coral reefs. Glob Chang Biol 20:681-697

Bradley P, Fisher W, Bell H, Davis W, Chan V, LoBue C, Wiltse W (2009) Development and implementation of coral reef biocriteria in U.S. jurisdictions. Environ Monit Assess 150:43-51

Bradley P, Santavy DL, Gerritsen J (2014) Workshop on Biological Integrity of Coral Reefs, August 21-22, 2012, Caribbean Coral Reef Institute, Isla Magueyes, La Parguera, Puerto Rico. US Environmental Protection Agency, Office of Research and Development, Atlantic Ecology Division, Narragansett, RI. EPA/600/R-13/350

Brown MT, Vivas MB (2005) Landscape development intensity index. Environ Monit Assess 101:289-309

Burke L, Reytar K, Spalding M, Perry A (2011) Reefs at risk revisited. World Resources Institute, Washington, DC

Coker DJ, Graham NAJ, Pratchett MS (2012) Interactive effects of live coral and structural complexity on the recruitment of reef fishes. Coral Reefs 31:919-927

Danz NP, Regal RR, Niemi GJ, Brady VJ, Hollenhorst T, Johnson LB, Host GE, Hanowski JM, Johnston CA, Brown T, Kingston J, Kelly JR (2005) Environmentally stratified sampling design for the development of Great Lakes environmental indicators. Environ Monit Assess 102:41-65

Davies SP, Jackson SK (2006) The biological condition gradient: A descriptive model for interpreting change in aquatic ecosystems. Ecol Appl 16:1251-1266

Eakin CM, Morgan JA, Heron SF, Smith TB, Liu G, Alvarez-Filip L, Baca B, Bartels E, Bastidas C, Bouchon C, Brandt M, Bruckner AW, Bunkley-Williams L, Cameron A, Causey BD, Chiappone M, Christensen TRL, Crabbe MJC, Day O, de la Guardia E, Diaz-Pulido G, DiResta D, Gil-Agudelo DL, Gilliam DS, Ginsburg RN, Gore S, Guzmán HM, Hendee JC, Hernández-Delgado EA, Husain E, Jeffrey CFG, Jones RJ, Jordán-Dahlgren E, Kaufman L, Kline DI, Kramer P, Lang JC, Lirman D, Mallela J, Manfrino C, Maréchal J-P, Marks K, Mihaly J, Miller WJ, Mueller EM, Muller EM, Orozco Toro CA, Oxenford HA, Ponce-Taylor D, Quinn N, Ritchie KB, Rodriguez S, Rodriguez Ramirez A, Romano S, Samhouri JF, Sánchez JA, Schmahl GP, Shank BV, Skirving WJ, Steiner

SCC, Villamizar E, Walsh SM, Walter C, Weil E, Williams EH, Woody Roberson K, Yusuf Y (2010) Caribbean corals in crisis: record thermal stress, bleaching, and mortality in 2005. PLoS ONE 5:e13969 [doi:10.1371/journal.pone.0013969]

Ennis RS, Brandt ME, Wilson KR, Smith TB (2016) Coral reef health response to chronic and acute changes in water quality in St. Thomas, United States Virgin Islands. Mar Pollut Bull 111:418-427

Fisher WS, Fore LS, Hutchins A, Quarles RL, Campbell JG, LoBue C, Davis WS (2008) Evaluation of stony coral indicators for coral reef management. Mar Pollut Bull 56:1737-1745

Fore LS, Karr JR, Fisher WS, Bradley P, Davis WS (2009) Heeding a call to action for US coral reefs: The untapped potential of the Clean Water Act. Mar Pollut Bull 58:1421-1423

Golbuu Y, Fabricius K, Victor S, Richmond RH (2008) Gradients in coral reef communities exposed to muddy river discharge in Pohnpei, Micronesia. Estuar Coast Shelf Sci 76:14-20

Halpern BS, Walbridge S, Selkoe KA, Kappel CV, Micheli F, D'Agrosa C, Bruno JF, Casey KS, Ebert C, Fox HE, Fujita R, Heinemann D, Lenihan HS, Madin EMP, Perry MT, Selig ER, Spalding M, Steneck R, Watson R (2008) A global map of human impact on marine ecosystems. Science 319:948-952

Heron SF, Johnston L, Liu G, Geiger EF, Maynard JA, De La Cour JL, Johnson S, Okano R, Benavente D, Burgess TFR, Iguel J, Perez D, Skirving WJ, Strong AE, Tirak K, Eakin CM (2016) Validation of reef-scale thermal stress satellite products for coral bleaching monitoring. Remote Sens 8(1): 59 [doi: 10.3390/rs8010059]

Homer C, Dewitz J, Fry J, Coan M, Hossain N, Larson C, Herold N, McKerrow A, VanDriel JN, Wickham J (2007) Completion of the 2001 National Land Cover Database for the Conterminous United States. Photogramm Eng Remote Sensing 73:337-341

Hughes TP, Connell JH (1999) Multiple stressors on coral reefs: A long-term perspective, Limnol Oceanogr 44:932-940

Hughes TP, Rodrigues MJ, Bellwood DR, Ceccarelli D, Hoegh-Guldberg O, McCook L, Moltschaniwskyj N, Pratchett MS, Steneck RS, Willis B (2007) Phase shifts, herbivory, and the resilience of coral reefs to climate change. Curr Biol 17:360-365

Janicki T (2013) Land development index (LDI) and cross-walk of Florida land use cover and classification system (FLUCCS) codes to LDI values. Attachment A in: Central Florida Water Initiative's Environmental Measures Team, Development of Environmental Measures for Assessing Effects of Water Level Changes on Lakes and Wetlands in the Central Florida Water Initiative Area, Final Report November 2013

Karr JR, Chu EW (1997) Biological Monitoring and Assessment: Using Multimetric Indexes Effectively. EPA 235-R97-001, University of Washington, Seattle

Kleypas JA, Buddemeier RW, Archer D, Gattuso J-P, Langdon C, Opdyke BN (1999) Geochemical consequences of increased carbon dioxide on coral reefs. Science 284:118-120

Liu G, Heron SF, Eakin CM, Muller-Karger FE, Vega-Rodriguez M, Guild LS, De La Cour JL, Geiger EF, Skirving WJ, Burgess TFR, Strong AE, Harris A, Maturi E, Ignatov A, Sapper J, Li J, Lynds S (2014) Reef-scale thermal stress monitoring of coral ecosystems: new 5-km global products from NOAA coral reef watch. Remote Sens 6:11579-11606, doi:10.3390/rs61111579

Mack JJ (2006) Landscape as a predictor of wetland condition: an evaluation of the Landscape Development Index (LDI) with a large reference wetland dataset from Ohio. Environ Monit Assess 120:221-241

Odum HT (1996) Environmental Accounting: Emergy and Environmental Decision Making. John Wiley and Sons, New York, 370 pp

Oliver LM, Lehrter JC, Fisher WS (2011) Relating landscape development intensity to coral reef condition in the watersheds of St. Croix, US Virgin Islands. Mar Ecol Prog Ser 427: 293-302

Rodgers KS, Kido MH, Jokiel PL, Edmonds T, Brown, EK (2012) Use of integrated landscape indicators to evaluate the health of linked watersheds and coral reef environments in the Hawaiian Islands. Environ Manage 50:21-30

Santavy DL, Bradley P, Gerritsen J, Oliver LM (2016) The biological condition gradient, a tool used for describing the condition of US coral reef ecosystems. Proceedings of the 13th International Coral Reef Symposium, Honolulu: 552-563

Shivlani M, Koeneke R (2011) Spatial characterization of artisanal fisheries in Puerto Rico: Geographic information systems (GIS) approach for assessing the regional effort and landings. Proc of the 63rd Gulf and Caribb Fish Inst., Nov 1-5, 2010

US EPA (2016) A Practitioner's Guide to the Biological Condition Gradient: A Framework to Describe Incremental Change in Aquatic Ecosystems. EPA 842-R-16-001, Washington, DC

USVI (US Virgin Islands) (2010) United States Virgin Islands 2010 Revisions to: Water Quality Standards Title 12, Chapter 7, Government of the Virgin Islands, Department of Planning and Natural Resources, Division of Environmental Protection, 22 pp

Session 75

Prevention, assessment, and mitigation of coral reef impacts resulting from planned and unplanned human activities

Session chairs:

Jocelyn Karazsia, jocelyn.karazsia@noaa.gov

Tom Moore, tom.moore@noaa.gov

Wendy Wiltse, Wiltse.Wendy@epa.gov

Santavy DL, Bradley P, Gerritsen J, Oliver L (2016) The biological condition gradient, a tool used for describing the condition of US coral reef ecosystems. Proceedings of the 13th International Coral Reef Symposium, Honolulu: 548-559

The biological condition gradient, a tool used for describing the condition of US coral reef ecosystems

Deborah L. Santavy, Patricia Bradley, Jeroen Gerritsen, and Leah Oliver

Abstract Understanding the effects of human activity on coral reef ecosystems requires knowing what characteristics constitute a high quality coral reef and identifying measurable criteria. The Biological Condition Gradient (BCG) is a conceptual model that describes how biological attributes of coral reefs change along a gradient of anthropogenic stress. The BCG provides a framework using qualitative and quantitative reef attributes to determine current coral reef conditions. Experts in coral reef assemblages (coral, fish, sponge, gorgonian, and algae) have defined a BCG model for Puerto Rico. The model describes the full range of biological conditions resulting from human disturbance, including community structure, organism condition, ecosystem function and connectivity. Each condition level is defined in terms of biological integrity, which is the biological condition comparable to undisturbed or minimally disturbed conditions caused by human influence. Each level contains a detailed narrative and decision rules for translating the narrative into specific metric scores. Reference condition is a natural fully-functioning coral reef that serves as a non-shifting baseline that is established through expert consensus. Managers can use the BCG model to assess current conditions relative to high quality coral reefs, track changes in condition as responses to management actions, and communicate environmental condition and outcomes to the public. BCG levels can be aligned with designated aquatic life uses specified in water quality standards and used for protection and potential restoration of coral reefs. The BCG model will be broadly applicable to Caribbean reefs, and the process is transferable to other oceanic regions.

Key Words: biological condition gradient, biological criteria, biocriteria, protection coral reefs, Clean Water Act, thresholds

---

Deborah L. Santavy, Leah Oliver
US Environmental Protection Agency, Gulf Ecology Division, ORD, 1 Sabine Island Dr,Gulf Breeze, FL. 32561 USA

Patricia Bradley, Jeroen Gerritsen
Tetra Tech, Inc., Owing Mills, MD., USA

Communicating author: DL Santavy santavy.debbie@epa.gov

Introduction

One of the most influential legal mechanisms available for aquatic resource protection is the U.S. Clean Water Act (CWA) (33 U.S.C. 1251 et seq. 1972), which grants regulatory authorities to the U.S. Environmental Protection Agency (USEPA) to protect the integrity of the Nation's waters (USEPA 2016). The CWA purview includes biological components such as coral reefs that lie within the limit of the territorial seas (Jameson et al. 2001). One authority granted to USEPA is to prevent waterbody degradation or restore habitat quality through the CWA Section 101 (a) (Frey 1977; USEPA 2002). This authority allows decisions to curtail or modify deleterious anthropogenic activities "to restore and maintain the chemical, physical and biological integrity of the nation's waters." Many facets of the CWA are already employed in maintaining high water quality imperative for coral reef persistence (USEPA 2016). However, the broad authority of the CWA is not being used to its full potential for reef protection (Fore et al. 2009; Bradley et al. 2010).

Understanding the effects of human activity on coral reefs requires knowing what attributes constitute high quality coral reefs and identifying measurable criteria. Restoring and maintaining biological integrity is a long-term CWA objective, and like its physical and chemical counterparts, biological criteria can be defined to protect valued biological communities (Davies and Jackson 2006). Biological integrity is the capacity to support and maintain a balanced, integrated, and adaptive community of organisms having a species composition, diversity, and functional organization comparable to the natural habitats within a region (Karr and Dudley 1981). The process includes classifying habitat types, using quantitative measures of species composition, diversity and functional organization; and comparing existing waterbody condition to natural or undisturbed reference conditions (Davis and Simon 2004).

To achieve CWA objectives, the USEPA, States, US Territories, regulated industries, municipalities, and public need comprehensive information about the biological integrity of aquatic environments to complement the physical and chemical integrity. The USEPA has worked with scientists to adapt a conceptual model known as the biological condition gradient (BCG) to protect the biological integrity of tropical Caribbean waters, including marine coastal habitats such as mangroves, seagrasses and coral reefs (Bradley et al. 2014; Bradley and Santavy

2016). The BCG is a conceptual model that describes how biological attributes of coral reefs change along a gradient of anthropogenic stress (Figure 1). The BCG relates the biological responses to increasing levels of anthropogenic stress relative to a baseline anchored in natural condition or minimally disturbed (Karr 1991; Davies and Jackson 2006; USEPA 2016). This framework defines qualitative and quantitative reef attributes to assess the biological condition and ecological state of a coral reef by defining multiple levels of biological responses to increasing anthropogenic stress. BCG level 1 represents the highest condition level or full biological integrity with ideally no anthropogenic stress, and BCG level 6 represents the poorest biological condition impacted by the greatest anthropogenic stress (Fig. 1). Threshold levels can be both numeric values and narrative descriptions dependent on the scientific information available, and they are intended to be protective of the biological integrity of aquatic life inhabiting the waterbody. The BCG model provides guidance to decide whether the biological condition of a coral reef is improving or declining relative to these acceptable threshold levels.

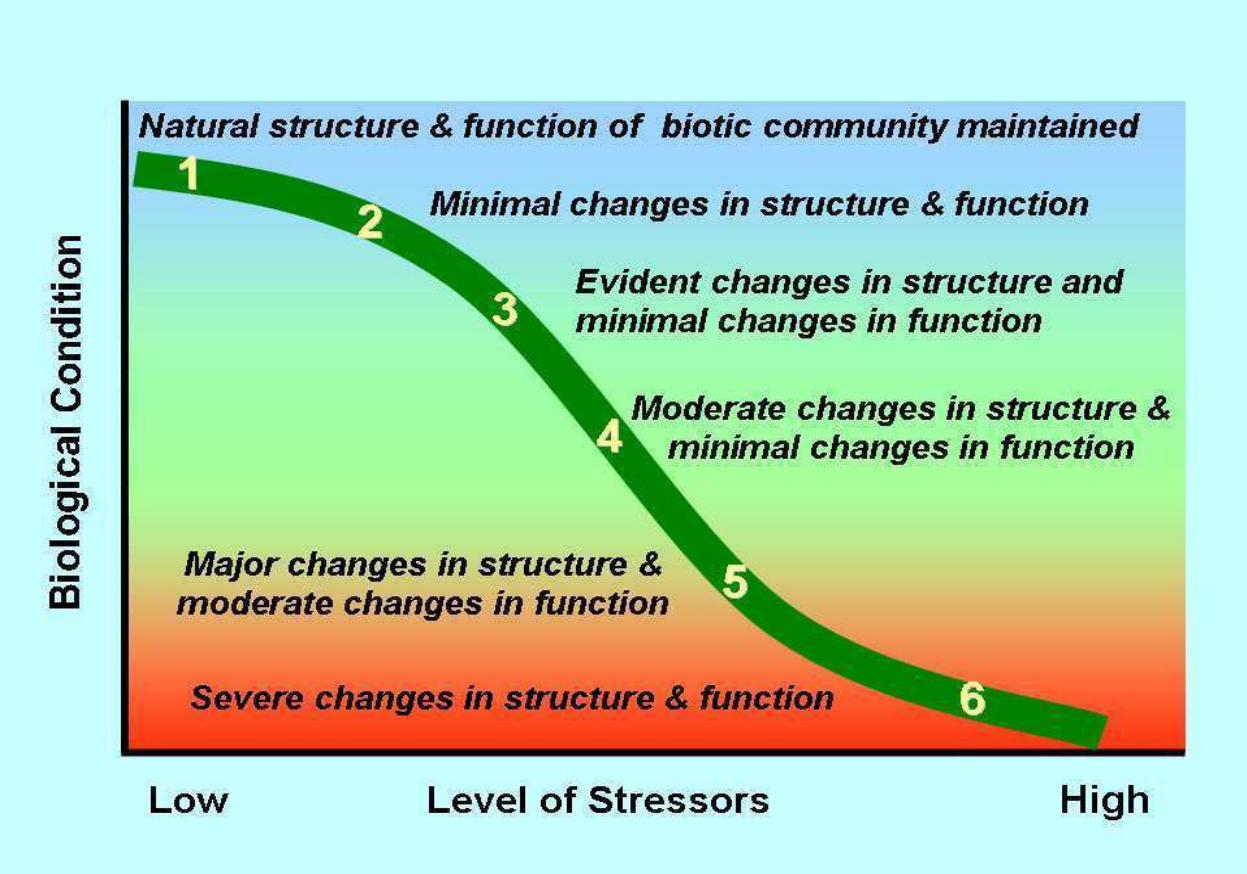

Fig. 1 Conceptual model of the biological condition gradient that describes how biological attributes of coral reefs change along a gradient of anthropogenic stress

The BCG framework allows biological condition to be interpreted independent of assessment methods. Currently, the BCG is used nationally for the management of freshwater ecosystems to communicate to the public and other interested stakeholders the status of aquatic resources and their potential for restoration. To date, almost all applications are in freshwater streams, rivers, and lakes bounded by land. A BCG model is formulated based on expert consensus using best professional judgment. An expert panel works together to define the thresholds at each biological condition level using narrative descriptions. Next, numeric thresholds are developed using bioassessment data to calculate threshold values grounded in the early narrative formulations. Application of the BCG conceptual framework, narrative descriptions developed by experts for qualitative rankings, habitat classifications, and assignment of important reef attributes are presented for fish and coral models.

Materials and methods

USEPA focused on southwestern Puerto Rico to test proof-of-concept, develop, calibrate, and eventually validate the BCG model to support biocriteria development for Caribbean coral reef systems. An expert panel of coral reef scientists participated in three workshops and multiple webinars to elicit best professional judgment to develop narrative and ultimately numeric biocriteria to define multiple BCG condition levels (Bradley et al 2014; Bradley and Santavy 2016). In the first workshop, underwater videos and photographs were viewed by experts to elicit important coral reef attributes to define coral reef condition. This approach allowed experts to draw on their individual and combined knowledge and expertise, without getting mired in CWA and biocriteria concepts and terminology. Linear coral reefs were selected from habitat maps by Kendall et al. 2001. Sites selected for expert review spanned the full range of conditions observed in the data set. Experts rated coral reef condition for 12 stations as either good, fair or poor based on the photos and videos considering all aspects of reef condition and health. They were instructed to document specific characteristics indicative of conditions for corals, sponges, gorgonians, fish, algae, reef rugosity, and topographical heterogeneity. Afterwards, group deliberations used their individual evaluations to focus on identifying common attributes with narrative language to differentiate each level.

During the second and third workshops, two separate BCG models were constructed independently - one for fish communities built by fish experts and the other for scleractinian corals built by coral experts. Each group worked from the narrative descriptive BCG model developed in the first workshop with the ultimate goal of creating a quantitative model with decision rules for threshold levels. Bioassessment data for fish and coral communities were used with sites located along a stressor gradient ranging from low to high land-based stressor levels in similar habitat types for each community (Santavy et al. 2012; Bradley and Santavy 2016). Ideally, data should include the full range of conditions and complement of stressors (e.g., pollution sources, fishing pressure, habitat disturbances, etc.) found at the regional level, such that the full gradient of the responses of the assemblages were included in model development. Since natural, regional, and habitat characteristics affect coral species composition of undisturbed waterbodies, a critical step required habitat classification of natural conditions to the extent they affect structures of fish and benthic communities (USEPA 2016).

The first step for BCG calibration was assigning taxa to BCG attributes I-V (Table 1), based on species sensitivity and tolerances to the most important stressors recommended by the experts. The BCG attribute definitions were those developed for freshwater systems (Table 1). Each taxon was evaluated for: sensitivity and tolerance to anthropogenic stressors, rarity, and endemism (Davies and Jackson; 2006; USEPA 2016). Experts assigned all fish and scleractinian coral taxa present in Puerto Rican bioassessment data from USEPA surveys in 2010 and 2011

Table 1 Ecological attributes used in freshwater BCGs for fish and benthic infauna communities (USEPA 2016)

Attribute	Description
I	Historically documented, sensitive, long-lived or regionally endemic taxa
II	Highly sensitive taxa
III	Intermediate sensitive taxa
IV	Taxa of intermediate tolerance
V	Tolerant taxa
VI	Non-native species
VII	Organism condition
VIII	Ecosystem function
IX	Spatial and temporal extent of detrimental effects
X	Ecosystem connectivity

(Bradley and Santavy 2016). Next, experts assigned BCG biological condition levels (1-6) to each reef site using results from the more complex data-driven analyses and the BCG attribute (I-V) assignments. As more sites were assigned to BCG condition levels, the experts were providing more complex data-driven analyses for improving and informing their judgements to rate additional sites. After condition assignments were made to multiple sites which represented a range of anthropogenic stressors, the experts' rationale for their assignments were carefully documented. This allowed decision rules to emerge for distinguishing different quantitative BCG levels.

Results and Discussion

The first workshop provided proof of concept that the BCG framework could be adapted for coral reef ecosystems (Bradley et al. 2014). During the first workshop, the coral reef experts collectively developed preliminary narratives for defining four BCG condition levels ranging from very good to excellent, good, fair, and poor (Fig. 2) while documenting specific attributes. Using underwater videos, the experts defined eight individual traits into four levels of biological condition. They rated the first level as very good to excellent condition, representing full biological integrity, and it anchored the other condition levels. This condition level was considered by the experts as comparable to levels 1 and 2 of the BCG conceptual model. The second level was considered good condition by the experts as comparable to BCG Level 3. The third level was rated as fair condition and comparable to BCG level 4. The worst condition level was comparable to BCG levels 5 and 6 and considered to be highly degraded.

The experts identified eight narrative attributes used for describing each BCG level. The narrative attributes were: physical structure of the reef which is the topographical heterogeneity, roughness or rugosity of the reef surface; coral characteristics including species, shape, size, and population demographics; sponge and gorgonian characteristics of shape, size and potential for habitat provision; coral condition which is considered the amount of live tissue present and extent of disease, bleaching and tumors; fish abundance, biomass and trophic interactions; the presence of other vertebrates focusing on charismatic megafauna; selected invertebrates including *Diadema antillarum*, conchs, lobsters, and crabs; and finally algae ranging from

calcareous crustose and coralline algae, filamentous microalgae, to fleshy turf algae; and submerged aquatic vegetation.

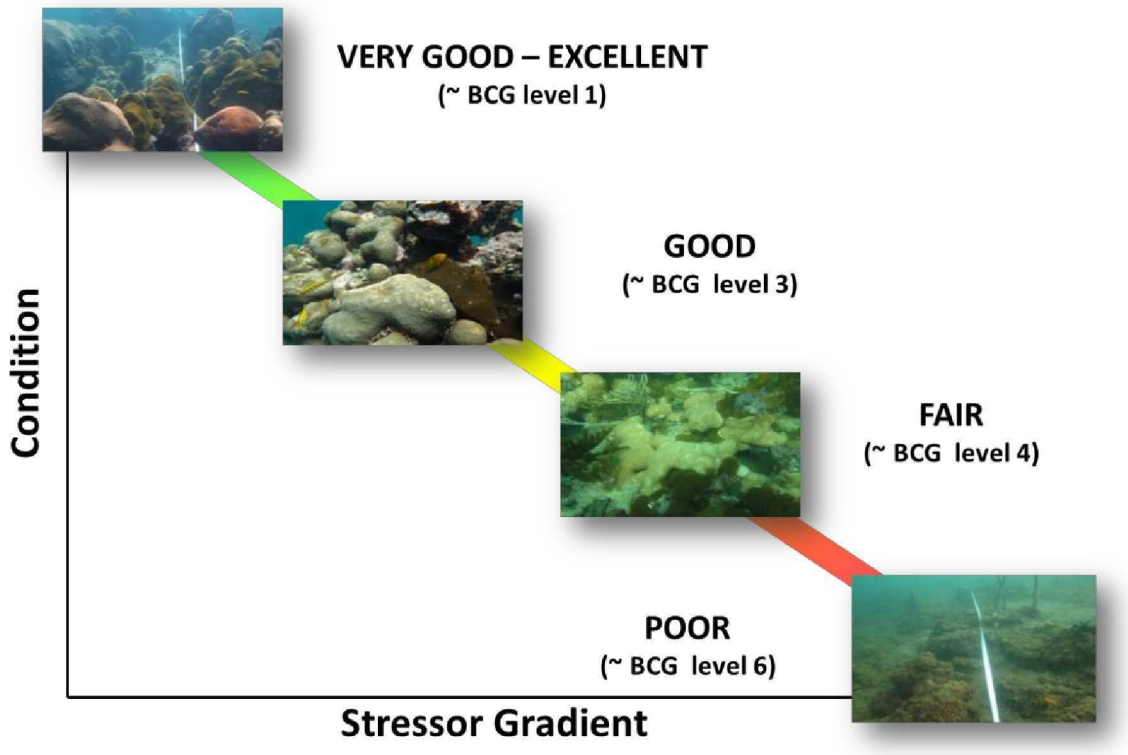

Fig. 2 Conceptual BCG developed during the 1st workshop, using site photos to represent BCG levels in Puerto Rico. Experts agreed natural site equivalent to BCG level 1 is not present in Puerto Rico today

The experts used these eight attributes to describe four coral reef condition levels (Table 2). The best biological condition was grounded in natural, undisturbed condition, represented by high rugosity and species diversity; large colonies of *Orbicella* spp. with high tissue coverage; and balanced population structure that included more corals than gorgonians. The highest quality communities contained large autotrophic and highly sensitive sponge species and low prevalence of disease or tumors in benthic communities. Crustose coralline algae were abundant, and other invertebrates were present (lobster, small crustaceans, and polychaetes), with some large sensitive anemone species. The worst condition had low structure and rugosity, turbid water and sediment films. If coral colonies were present, they were small and highly tolerant species. Heterotrophic, tolerant sponges were buried in sediment. Sediment-dwelling organisms such as

polychaetes and holothurians dominated the substrate with few or no reef invertebrates. If algae were present, it was fleshy macroalgae, with little or no turf or calcareous algae. Crustose coralline algae were absent.

Table 2 Narrative descriptions for eight attributes proposed by coral reef experts to define four BCG condition levels for Puerto Rico linear reefs. (adapted from Davies and Jackson, 2006)

Condition level	Attribute descriptions
Very Good Excellent (approximate BCG Level 1–2)	**Physical structure:** High rugosity or 3D structure; substantial reef built above bedrock; many irregular surfaces provide habitat for fish; very clear water; no sediment, flocs or films
	Corals: High species diversity including rare; large old colonies (*Orbicella*) with high tissue coverage; balanced population structure (old and middle-sized colonies, recruits); *Acropora* thickets present
	Gorgonians: Gorgonians present but subdominant to corals
	Sponges: Large autotrophic and highly sensitive sponges abundant
	Fish: Populations have balanced species abundances, sizes and trophic interactions
	Large vertebrates: Large, long-lived species present and diverse (turtles, eels, sharks)
	Other invertebrates: *Diadema,* lobster, small crustaceans and polychaetes abundant; some large sensitive anemone species present
	Algae: Crustose coralline algae abundant; turf algae present but cropped and grazed by *Diadema* and herbivorous fish; low abundance of fleshy algae
	Condition: Low prevalence of disease and tumors; mostly live tissue on colonies
Good (approximate BCG Level 3)	**Physical structure:** Moderate to high rugosity; moderate reef built above bedrock; some irregular cover for fish habitat; water slightly turbid; low sediment, flocs or films on substrate
	Corals: Moderate coral diversity; large old colonies (*Orbicella*) with some tissue loss; varied population structure (usually old colonies, few middle aged and some recruits); *Acropora* thickets may be present; rare species absent
	Gorgonians: Gorgonians more abundant than Levels 1–2
	Sponges: Autotrophic species present but highly sensitive species missing
	Fish: Decline of large apex predators (e.g., groupers, snappers) noticeable; small reef fishes more abundant
	Large vertebrates: Large, long-lived species locally extirpated (turtles, eels)
	Other invertebrates: *Diadema,* lobster, small crustaceans and polychaetes less abundant than Levels 1–2; large sensitive anemone species absent
	Algae: Crustose coralline algae present but fewer than Levels 1–2; turf algae present and longer, more fleshy algae present than Levels 1–2
	Condition: Disease and tumor presence slightly above background level; more colonies have irregular tissue loss
Fair (approximate	**Physical structure:** Low rugosity; limited reef built above bedrock; erosion of reef structure obvious; water turbid; more sediment accumulation, flocs and films; *Acropora* usually gone or present as rubble for recruitment substrate

BCG Level 4)	**Corals:** Reduced coral diversity; emergence of tolerant species, few or no living large old colonies (*Orbicella*); *Acropora* thickets gone, large remnants mostly dead with long uncropped turf algae
	Gorgonians: Gorgonians more abundant than Levels 1–3, replacing sensitive coral and sponge species
	Sponges: Mostly heterotrophic tolerant species and clionids
	Fish: Absence of small reef fishes (mostly Damselfish remain)
	Large vertebrates: Large, long-lived species locally extirpated (turtles, eels)
	Other invertebrates: *Diadema* absent; *Palythoa* overgrowing corals; crustaceans, polychaetes and sensitive anemones conspicuously absent
	Algae: Some coralline algae present but no crustose algae; turf is uncropped, covered in sediment; abundant fleshy algae (e.g., *Dictyota*) with high diversity
	Condition: High evidence of diseased corals, sponges, gorgonians; evidence high of mortality; usually less tissue than dead portions on colonies
Poor (approximate BCG Level 6)	**Physical structure:** Very low rugosity; no or little reef built above bedrock; no or low relief for fish habitat; very turbid water; thick sediment film and thick floc covering bottom; no substrate for recruits
	Corals: Absence of colonies, those present are small; only highly tolerant species with little or no live tissue
	Gorgonians: Small and sparse colonies; mostly small sea fans; often diseased
	Sponges: Heterotrophic sponges buried deep in sediment; highly tolerant species
	Fish: No large fishes; only a few tolerant species remain; lack of multiple trophic levels
	Large vertebrates: Usually devoid of vertebrates other than fishes
	Other invertebrates: Few or no reef invertebrates; high abundance of sediment dwelling organisms such as polychaetes and holothurians
	Algae: High cover of fleshy algae (*Dictyota)*; complete absence of crustose coralline algae
	Condition: High incidence of disease and low or no tissue coverage on small colonies of corals, sponges and gorgonians, if present

During the second and third workshop, the fish and coral experts worked on two separate BCG models. Development of the coral reef fish BCG model was more adaptable to the freshwater systems framework. Fish experts agreed upon two habitat classifications - sites containing coral reefs and all other hard-bottom habitats. Fish experts considered land-based sedimentation and fishing pressure as the two greatest threats to fish communities in this region, and they assigned 138 fish species to the five BCG attributes. The results from these assignments are too numerous to present here, but they are detailed in Bradley and Santavy 2016. The fish experts will be testing numeric criteria soon to test the fish BCG model for coral reefs to set preliminary model conditions for developing biocriteria for Puerto Rico.

The application of the freshwater BCG tolerance attributes to coral taxa presented a much greater challenge. The coral experts agreed elevated sea temperature and land-based sources of pollution present the most serious threats for Caribbean scleractinian corals. Coral experts had lower confidence in scleractinian coral taxa assignments to BCG attributes I-V and chose to evaluate each taxon for each stressor separately (Bradley and Santavy 2016). During initial attempts to assign species to a BCG attribute, the coral experts contended with reef habitat classification. They held discussions focused on defining expectations of which coral species should be found in different reef zones. Many reef traits were considered because reefs have distinct horizontal and vertical zones created by differences in depth, wave and current energy, temperature, light, and many other habitat characteristics (Zitello et al. 2009). The experts considered several different reef classification systems in an attempt to incorporate most of the critical reef traits discussed (Adey and Burke 1976; Hubbard et al. 2009). They agreed to use the latest edition of NOAA's benthic habitat reef classification as guidance (Zitello et al. 2009), and only use the fore-reef zone for assigning sites to BCG condition levels using the Costa et al. 2013 definition.

The coral experts decided the stressor tolerance attributes (I–V) developed for the freshwater BCGs (Table 1), did not apply very well to coral reef benthic communities. The experts believed tolerances of scleractinian coral species varied based on the individual stressor, and when exposed to multiple stressors the effects could be additive, neutral or synergistic but are largely unknown. The coral experts ultimately recommended focusing on eight narrative attributes developed during the first workshop (Table 2) to assign sites to BCG condition levels. The coral experts all agreed additional benthic assemblages rather than just scleractinian corals should be used. They changed the coral BCG to the benthic BCG model, and recommended inclusion of sponges, gorgonians, algae, organism condition especially disease and coral bleaching, and other reef invertebrates.

Historically water quality management programs and regulatory agencies attempted to protect aquatic life primarily through chemical and physical water criteria alone (USEPA 2002, 2016). Unlike chemical or physical criteria, biocriteria do not require individual threshold values for each and every stressor. The biological response to its environment integrates cumulative impacts of multiple stressors which might be better indicators of ecosystem condition, rather than only relying on established nutrient or physical stressor limits, which might not be protective of

sensitive coral reefs (Bradley et al. 2010; Oliver et al. herein). Coral reef biocriteria are used to benchmark biological conditions required for aquatic life use, and allow bioassessment information to directly link management actions to desired biological goals and endpoints. Often the consequences of management decisions are far-reaching influencing not only inland watersheds but also coastal environments (Bradley et al. 2010).

Acknowledgements

We acknowledge Susan K. Jackson and Kennard Potts (USEPA, Office of Water), William Fisher (USEPA Office of Research and Development), Evelyn Huertas (USEPA Region 2 Caribbean Office) and all the coral reef experts who have contributed their valuable time, expertise, and discussions to develop the coral reef BCG. We thank Jocelyn Karazsia and Wendy Wiltse (session #75 chairs, ICRS 2016) and two anonymous reviewers who provided suggestions which greatly improved the manuscript.

References

Adey W, Burke RB (1976) Holocene bioherms (algal ridges and bank barrier reefs) of the eastern Caribbean. Geol Soc Am Bull 87:95–109

Bradley P, Fore L, Fisher W, Davis W (2010) Coral Reef Biological Criteria: Using the Clean Water Act to Protect a National Treasure. EPA/600/R-10/054. WashDC

Bradley P, Santavy DL (2016) Caribbean Coral Reefs: Benchmarking a Biological Condition Gradient for Puerto Rican Coral Reefs. In: Appendices to: A Practitioner's Guide to the Biological Condition Gradient: A Framework to Describe Incremental Change in Aquatic Ecosystems. EPA 842-R-16-001. pp. B-53 – B-76

Bradley P, Santavy DL, Gerritsen J (2014) Workshop on Biological Integrity of Coral Reefs, August 21–22, 2012, Caribbean Coral Reef Institute, Isla Magueyes, La Parguera, Puerto Rico. EPA/600/R-13/350. WashDC

Costa BM, Kendall MS, Edwards K, Kagesten G, Battista, TA (2013) Benthic Habitats of Fish Bay, Coral Bay, and the St Thomas East End Reserve. NOAA Tech Mem NOS NCCOS 175. Silver Spring, MD

Davies SP, Jackson SK (2006) The Biological Condition Gradient: a descriptive model for interpreting change in aquatic ecosystems. Ecol Appl 16:1251–1266

Davis WS and Simon TP (2004) Biological assessment and criteria: tools for water resource planning and decision making. CRC Press, Inc. Boca Raton, FL

Fore LS, Karr JR, Fisher WS, Bradley P, Davis WS (2009) Heeding a call to action for US coral reefs: The untapped potential of the Clean Water Act. Mar Poll Bull 58:1421-1423

Frey DG (1977) Biological Integrity, a Historical Approach. In The Integrity of Water, Proceedings of a Symposium, ed. RK Ballentine and LJ Guarraia, USEPA, WashDC, March 10–12, 1975, pp. 127–140

Hubbard D, Ramirez W, Cuevas D, Erickson T, Estep A (2009) Holocene reef accretion along the north side of Bahia Enriquillo (western Dominican Republic): Unique insights into patterns of reef development in response to sea-level rise. Proc 11th Int Coral Reef Symp1:43-47

Jameson SC, Erdmann MV, Karr JR, Gibson GR, Potts KW (2001) Charting a course toward diagnostic monitoring: a continuing review of coral reef attributes and a research strategy for creating coral reef indexes of biotic integrity. Bull Mar Sci 69:701- 744

Karr JR (1991) Biological integrity: A long-neglected aspect of water resource management. Ecol Appl 1:66–84

Karr JR, Dudley DN (1981) Ecological perspective on water quality goals. Environ Manag 5:55-68

Kendall MS, Monaco ME, Buja KR, Christensen JD, Kruer CR, Finkbeiner M, Warner RA (2001) Methods used to map the benthic habitats of Puerto Rico. NOAA Technical Memorandum NOS NCCOS CCMA 152

Oliver LM, Santavy DS, Bradley P (2016) Developing a multi-stressor gradient model for coral reefs of Puerto Rico. Proceedings of the 13th International Coral Reef Symposium, Honolulu: 246-261

Santavy DL, Fisher WS, Campbell JG, Quarles RL (2012) Field Manual for Coral Reef Assessments. US Environmental Protection Agency, Office of Research and Development, Gulf Ecology Division, Gulf Breeze, FL. EPA/600/R-12/029. WashDC

USEPA (2002) Biological Assessments and Criteria: Crucial Components of Water Quality Programs. EPA 822-F-02-006. WashDC

USEPA (2016) A Practitioner's Guide to the Biological Condition Gradient: A Framework to Describe Incremental Change in Aquatic Ecosystems. EPA 842-R-16-001. WashDC

Zitello AG, Bauer LJ, Battista TA, Mueller PW, Kendall, MS, Monaco, ME (2009) Shallow-water benthic habitats of St John, USVI. NOAA Tech Mem NOS NCCOS 96. Silver Spring, MD

Environ Monit Assess (2018) 190: 213
https://doi.org/10.1007/s10661-018-6562-1

Assessing land use, sedimentation, and water quality stressors as predictors of coral reef condition in St. Thomas, U.S. Virgin Islands

L. M. Oliver · W. S. Fisher · L. Fore · A. Smith · P. Bradley

Received: 9 June 2017 / Accepted: 19 February 2018 / Published online: 13 March 2018
© This is a U.S. Government work and not under copyright protection in the US; foreign copyright protection may apply 2018

Abstract Coral reef condition on the south shore of St. Thomas, U.S. Virgin Islands, was assessed at various distances from Charlotte Amalie, the most densely populated city on the island. Human influence in the area includes industrial activity, wastewater discharge, cruise ship docks, and impervious surfaces throughout the watershed. Anthropogenic activity was characterized using a landscape development intensity (LDI) index, sedimentation threat (ST) estimates, and water quality (WQ) impairments in the near-coastal zone. Total three-dimensional coral cover, reef rugosity, and coral diversity had significant negative coefficients for LDI index, as did densities of dominant species *Orbicella annularis*, *Orbicella franksi*, *Montastraea cavernosa*, *Orbicella faveolata*, and *Porites porites*. However, overall stony coral colony density was not significantly correlated with stressors. Positive relationships between reef rugosity and ST, between coral diversity and ST, and between coral diversity and WQ were unexpected because these stressors are generally thought to negatively influence coral growth and health. Sponge density was greater with higher disturbance indicators (ST and WQ), consistent with reports of greater resistance by sponges to degraded water quality compared to stony corals. The highest FoRAM (Foraminifera in Reef Assessment and Monitoring) indices indicating good water quality were found offshore from the main island and outside the harbor. Negative associations between stony coral metrics and LDI index have been reported elsewhere in the Caribbean and highlight LDI index potential as a spatial tool to characterize land-based anthropogenic stressor gradients relevant to coral reefs. Fewer relationships were found with an integrated stressor index but with similar trends in response direction.

Keywords Coral reefs · Landscape development intensity · Sedimentation · Impaired water quality

L. M. Oliver (✉) · W. S. Fisher · A. Smith
Office of Research and Development, National Health and Environmental Effects Research Laboratory, Gulf Ecology Division, U.S. Environmental Protection Agency, 1 Sabine Island Drive, Gulf Breeze, FL 32561-5299, USA
e-mail: oliver.leah@epa.gov

L. Fore
Puget Sound Partnership, 326 East D St., Tacoma, WA 98421, USA

P. Bradley
Office of Research and Development, National Health and Environmental Effects Research Laboratory, Atlantic Ecology Division, U.S. Environmental Protection Agency, 24 Tarzwell Drive, Narragansett, RI 02882, USA

Introduction

Coral reefs of the U.S. Virgin Islands (USVI) are heavily impacted by multiple human influences at varying scales (Gardner et al. 2003; Smith et al. 2008; Rogers et al. 2008; Friedlander et al. 2013; Pait et al. 2013a, b; Pittman et al. 2013; Whitall et al. 2014). Global conditions such as elevated ocean temperature have led to coral bleaching and disease, causing stony coral mortality across broad reef areas of the Caribbean Sea. Local resource managers and decision-makers have little

influence over global-scale anthropogenic pressures such as rising ocean temperature, ocean acidification, and elevated ultraviolet light levels. However, they do have some influence over local stressors, such as sediment, contaminants, nutrients, and physical injuries, that can interact with global pressures in additive or synergistic ways (Knowlton and Jackson 2008; Wooldridge and Done 2009; Brown et al. 2013; Ban et al. 2014). Managing stressors that are within local authority can slow the cascade of negative impacts and better sustain reef-derived ecosystem services such as coastal protection from storm surge, habitat provision for commercial and recreational fisheries, and revenue from reef-related tourism (Moberg and Folke 1999; Principe et al. 2012). Effective management requires identifying which stressors are human-generated so that activities can be modified to reduce their adverse effects.

The Clean Water Act (CWA) provides a mechanism to set chemical, physical, and biological criteria for the protection of aquatic ecosystems (Bradley et al. 2009; Fore et al. 2009; Bradley et al. 2010). As part of a process to establish biological water quality standards or biocriteria, the U.S. Virgin Islands government has explicitly identified coral reefs and reef functions as CWA-designated uses and defined biological integrity to lay the foundation for setting condition thresholds (biocriteria) for coral reefs (USVI 2010). This action was spawned in part by the demonstration of stony coral sensitivity to disturbance gradients using various measures of anthropogenic stress. For example, measures of coral reef condition including taxa richness, average colony size, and total and live topographic coral surface area showed significant positive relationships with increasing distance from human disturbance in St. Croix (Fisher et al. 2008). Negative relationships of coral condition with increased watershed land development were demonstrated in St. Croix (Oliver et al. 2011), Hawaii (Rodgers et al. 2012), St. Lucia (Bégin et al. 2016), and Thailand (Golbuu et al. 2008). Because the reefs around St. Thomas, USVI, are located near areas of high human activity (Ennis et al. 2016), they present another opportunity to explore potential links between reef condition and anthropogenic activity.

The USVI economy depends heavily on tourism revenues with an estimated 60–80% of gross domestic product linked to tourism-related activities (Abt Associates 2016). Nearly two million cruise ship tourists visited the USVI annually from 2000 to 2005, and the majority of cruise ships visit St. Thomas (van Beukering et al. 2011). The area of shallow water coral reefs around St. Thomas covers approximately 42 km^2 and comprises mostly linear coral reefs and colonized pavement, with scattered patch reefs farther offshore (Kendall et al. 2001). Stony corals provide important ecosystem services due to the structural reef habitat which supports diverse fish and invertebrate species valued by divers, snorkelers, and recreational and commercial fishers and provides shoreline protection from extreme weather events (van Beukering et al. 2011). Without stony corals, these ecosystem services would be lost or compromised, yet pressure from coastal development, cruise ship and recreational boat activity, and land use change on the 74-km^2 island may threaten the very resource to which visitors are drawn.

Charlotte Amalie on the south shore is the largest city on St. Thomas with a population of approximately 18,481 (2010 US Census). The Charlotte Amalie watershed has 34% impervious surface and nearly no shoreline riparian buffer at either the St. Thomas Harbor or Inner Harbor where two cruise ship ports operate. With a hardened shoreline, presence of power and wastewater treatment plants, and multiple active cruise ship and shipping ports, this area was chosen to represent a center of human disturbance likely to adversely influence adjacent coral reef communities. We hypothesized that coral reef communities near this concentrated human disturbance would be degraded relative to reefs further away, and used two approaches to characterize anthropogenic disturbance. First, we developed three independent measures of potential stress to coral reefs: the watershed landscape development intensity (LDI) index, modeled land-based sedimentation threat (ST), and impaired water quality (WQ) index based on proximity to impaired water bodies. These spatial proxies represent reef stressors that can be managed to some degree, and it would be valuable to discern their relative influence to assist managers in optimizing decisions to invest in the most effective remediation actions. Measures of density, size, and condition of benthic invertebrates including stony corals, gorgonians, sponges, macroinvertebrates, fishes, and foraminifera were assessed for potential responsiveness to these stressors. The reef metrics selected either showed a response to anthropogenic influence in previous studies or are suitable candidates based on their connection to an ecosystem service (e.g., rugosity). Second, stressors were rescaled from 0 to 1 and summed to generate an integrated stressor index (ISI), allowing results from

individual stressors and ISI to be compared for relative power to predict coral reef condition.

Materials and methods

Survey design

Survey sites ($n = 13$) were selected along the south shoreline of St. Thomas and spanned approximately 10 km (Fig. 1a). To control for the effect of natural site differences, we consistently selected sites on or near rocky points of land from Fortuna Bay in the west to Frenchman Bay in the east. All sites were identified as coral reef and colonized hardbottom habitat by Kendall et al. (2001). We also targeted a narrow range of depth from 5.5 to 9.1 m (mean 6.9 m) to minimize habitat differences that could affect coral community composition (Morelock et al. 2001). Based on field observations and knowledge of the area, we assumed Charlotte Amalie Harbor to be the greatest source of intense human disturbance in the area.

Data collection and calculation of reef indicators

Multiple-assemblage surveys were conducted during March 2009 as described by Fisher (2007) and Santavy et al. (2012). All surveys were conducted around a common 25-m transect line stretched along the sea floor. A fish survey was conducted first in a 4 × 25 m transect area (100 m^2 in total), with divers identifying to species, counting and estimating the length of all fish > 5 cm in length (Menza et al. 2006). Macroinvertebrates identified were queen conch, spiny and slipper lobsters, sea urchins (*Diadema* and others), and crabs. These were counted within either 1 or 2 m (due to diver inconsistency) on either side of the transect line for a total area of 50 or 100 m^2. Average reef rugosity index (RI) was calculated from five measurements made at the 0-, 5-, 10-, 15-, and 20-m marks along the transect line using the draped chain method d / l, where d is the linear chain distance when draped over coral reef and l is the constant chain length of 6 m (Risk 1972). Stony coral colonies at least 10 cm in any dimension were counted along one side of the transect line using a 1-m stick placed parallel to the line as a guide. Colonies were measured for height, maximum diameter, and percent live in 10% increments and identified to species (Humann and DeLoach 2002). Sponges and gorgonians were counted in 5 × 1 m^2 quadrants located at 1-, 5-, 10-, 15-, and 20-m transect marks. Each colony was measured for height and diameter, and morphology was recorded as one of nine possible shapes for gorgonians and nine for sponges (Santavy et al. 2012, 2013).

Stony coral three-dimensional (3D) colony surface areas (SAs) were calculated using a modified hemisphere formula $SA = m\pi R^2$, where m is a constant (1–4) based on relative morphological complexity and R is the height-adjusted colony radius calculated as ((diameter / 2) + height) / 2 (Santavy et al. 2012). Regression equations developed for sponges and gorgonians were used to calculate colony SA (Santavy et al. 2013), except SA formula for a circle (πr^2) was used for encrusting sponges and in cases where very small colony measurements result in negative SA using regression equations. Average values for each station from 5 × 1 m^2 quadrats were calculated for SA and abundance of sponges and gorgonians.

Fish lengths were estimated in 5-cm increments. The median value of each increment was assigned to individual fish; for example, 5–10-cm fish were assigned 7.5 cm length except for fish in the smallest size class (< 5 cm) which were assigned 3 cm. Biomass was calculated using the formula $W = \alpha \times L^{\beta}$ with species-specific constants α and β supplied by Froese and Pauly (2013). Invertebrate counts were standardized per square meter. Foraminifera samples were collected in triplicate at each site, and results were averaged to calculate a FoRAM (Foraminifera in Reef Assessment and Monitoring) index based on the methods of Hallock et al. (2003).

Stressor estimates

Land-based anthropogenic activity

A LDI index was calculated as a measure of land-based anthropogenic activity using a 2.4-m resolution land use layer produced for 2007 by NOAA Coastal Change Analysis Program (www.csc.noaa.gov/digitalcoast/data/ccapregional/index.html) and corresponding Emergy coefficients (Brown and Vivas 2005; Oliver et al. 2011). Stations were assigned the LDI value of the adjacent Hydrologic Unit Code (HUC)14 watershed (Islands Resources Foundation et al. 2001), and for stations near a watershed border, the eastward watershed LDI value was used to account for the predominant coastal current (Nemeth and Nowlis 2001). Land use, station locations, and adjacent watershed LDI values along the southern St. Thomas coastline are shown in Fig. 1a, b.

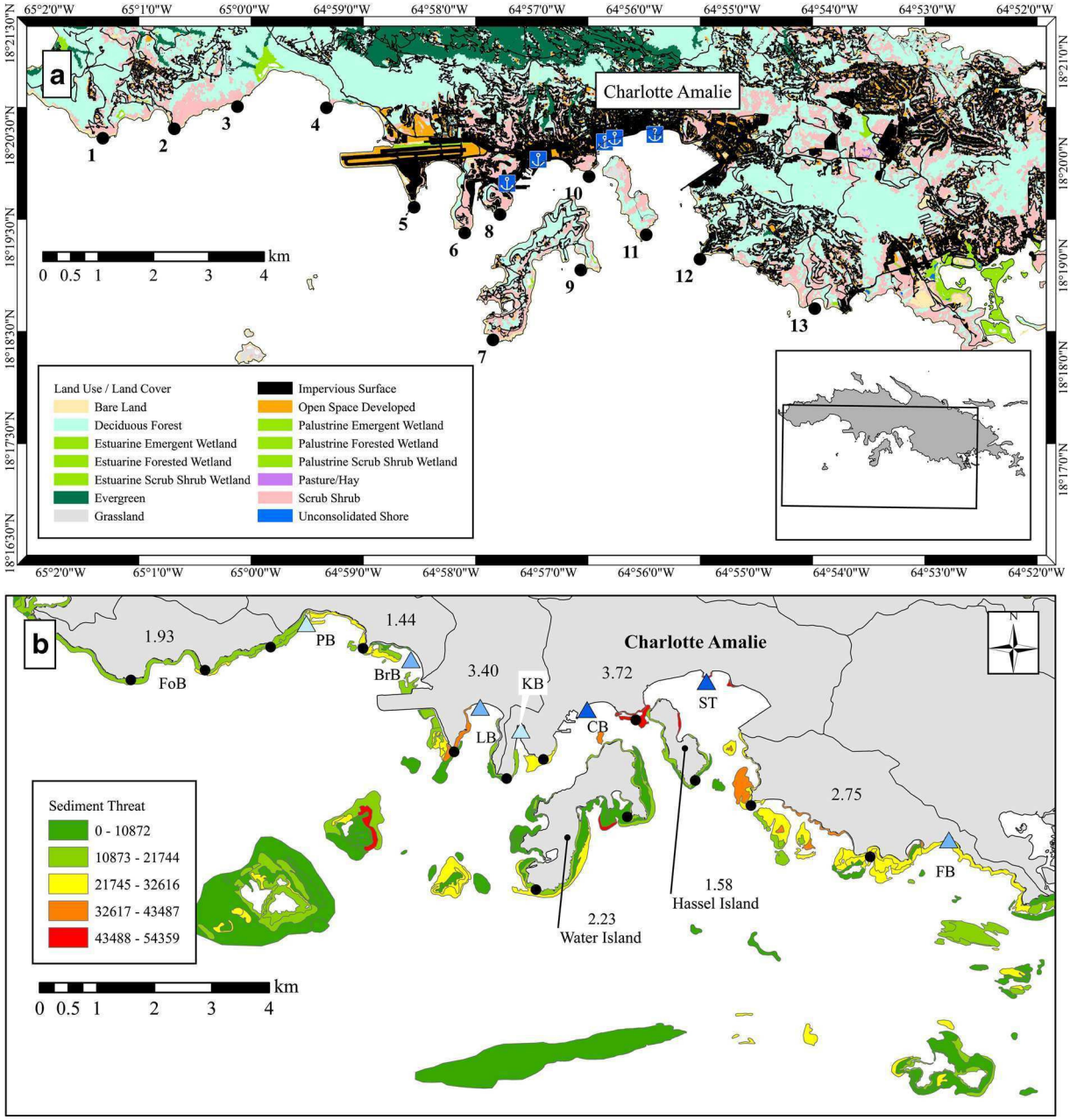

Fig. 1 **a** Land use/land cover (LULC) and coral reef stations sampled in St. Thomas, USVI, around Charlotte Amalie. Numbered black circles indicate sampling stations. Ports are indicated by anchor symbols. **b** HUC14 watersheds are indicated by black lines, and their corresponding LDI values are indicated within watershed polygons. Letters show locations of water bodies which exceeded chemical or physical criteria as reported to USVI DPNR: FoB Fortuna Bay, PB Perseverance Bay, BrB Brewers Bay, LB Lindberg Bay, KB Krum Bay, CB Crowne Bay ST, ST St. Thomas Harbor, FB Frenchman Bay. Triangular symbols grade from light to dark blue, indicating an increasing average number of impaired conditions from 2000 to 2010. Black circles indicate sampling stations

Sedimentation threat

Benthic sediment threat values were obtained from the World Resources Institute and National Oceanic and Atmospheric Administration Summit to Sea model (WRI and NOAA 2006). Summit to Sea is a GIS model that incorporates 30-m resolution land use/land cover data (NASA Geocover-LC 2000), soil type and

associated erodibility factor (US Department of Agriculture/Natural Resources Conservation Service, Soil Service Geographic Database), slope (digital elevation model), and precipitation (NOAA National Climate Data Center, maximum monthly precipitation for the 10-year period (January 1990–January 2001)). Summit to Sea data sources and processing steps are available at https://data.nodc.noaa.gov/coris/data/NOAA/nos/Summit2Sea/USVirginIslands/.

In short, ST was calculated for USVI reef habitats from relative erosion potential for watersheds, adjusted for watershed size, and modeled to correspond with pour points or "guts." Dissipation of sediment into coastal areas employed an ArcView v3.2 Point Density tool with a maximum distance from shore of 5 km.

Water quality

Water quality impairments reported by the USVI Department of Planning and Natural Resources (DPNR 2010) to the U.S. Environmental Protection Agency as required by the Clean Water Act include low dissolved oxygen, high enterococci bacteria, and elevated nutrient concentrations which may all negatively influence coral condition (Villanueva et al. 2006; Kaczmarsky et al. 2005; Voss and Richardson 2006). However, specific loadings and stressor-coral interactions are not understood well enough to weigh the individual stressors for relative importance, hydrologic transport to reefs is unknown, and bays are monitored for water quality exceedances only twice per year. Included in this water quality analysis from west to east were Perseverance Bay (PB), Brewer's Bay (BrB), Lindberg Bay (LB), Krum Bay (KB), St. Thomas Harbor (ST), Inner Harbor (IN), and Frenchman Bay (FB) (Fig. 1b). We assumed that only impaired water bodies east of a station would impact it due to the dominant westward current (Nemeth and Nowlis 2001), that impairment would dissipate with greater distance between station and water body, and that beyond 3 km, no impact would occur. First, the distance between each station and mid-bay shoreline was measured using ArcMap v9.3, and if two bays were within 3 km of a station, distances were summed. Distance values were transformed to (1/distance to bay) so that final WQ value increased with proximity to bays with WQ impairments. This transformation also achieved a nonlinear function assuming that WQ contaminants dissipate rapidly from the source (Fig. 2), although in reality, transport of runoff-borne pollutants to reef habitats is dependent on multiple factors such as precipitation, river density, storms, and wind (Warne et al. 2005).

Data analysis

Reef indicator values for stony corals, gorgonians, sponges, fish, and macroinvertebrates were calculated for each station using SAS© (Cary, North Carolina), except the Shannon-Weiner diversity index which was calculated using PRIMER© (Clark and Gorley 2006). The Spearman nonparametric correlation analysis was used to test for relationships between the three stressors. Distribution of reef indicators was evaluated using the Shapiro-Wilk statistic, and either log10 or rank transformations were applied to correct for deviations from normal distribution. Stepwise regression was employed to discern whether LDI, ST, and WQ were significant predictors of reef indicators with inclusion requirement of $p < 0.25$ and retention requirement of $p < 0.20$.

An ISI was calculated by first rescaling station stressor data values from 0 to 1, then assuming equal effects, the rescaled values were added. The Spearman correlation analysis was conducted with reef metrics and ISI for comparison with stepwise regression results. No correction for multiple comparisons was applied; instead, all results significant at $p < 0.05$ are reported. For all three stressors and ISI, quartile values were assigned for the purpose of comparing relative stressor levels at each station in the gradient.

Results

Station and stressor summary

Stations ranged in depth from 5.5 to 9.1 m and were within 0.1 km from land, with ten stations along the St. Thomas shoreline, two near Water Island and one near Hassel Island (Fig. 1). The lowest LDI values were found in the western portion of the study area with the exception of uninhabited Hassel Island near Charlotte Amalie Harbor, which also had low LDI. The highest LDI values were in the center of the study area near Charlotte Amalie Harbor and the airport where impervious surface covers most of the land and numerous industries are present along the coast. Eastern stations were adjacent to an intermediate-LDI watershed. Some stations had common LDI values because they were adjacent to the same HUC14 watershed (Fig. 1b).

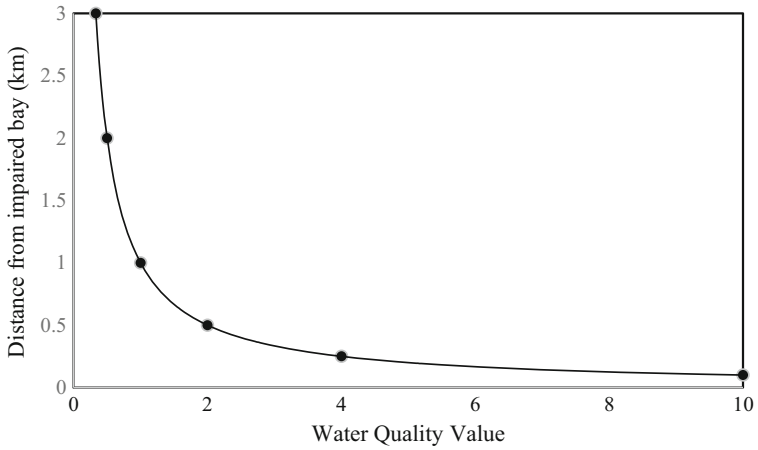

Fig. 2 Water quality (WQ) function used to estimate stress from proximity to St. Thomas bays which are listed as impaired under the Clean Water Act 303(d) program

Sedimentation threat was lowest at station 11 on Hassel Island, and ST was highest at station 10 near Charlotte Amalie Harbor and second highest at station 13 on the eastern edge. A WQ impairment estimate based on distance from impaired bays ranged from 0 at four stations (which exceeded the maximum distance from an impaired bay under our assumptions) to high values at stations 5 and 6 in the center of the study area.

The ISI ranged from 0.40 to 2.37 with an average of 1.23. The lowest values were found at the western edge of the study area and at Hassel Island and the highest values at stations 5, 6, and 10 (Table 1). Station stressor values grouped into quartiles show the most consistent estimates of high human impact were at stations nearest the harbor and at the eastern edge, and most consistent low impact was at western stations and Hassel Island. However, no stations were in the lowest quartile for all stressor estimates. Station values for these three stressors were not significantly correlated with one another.

Stony corals

A total of 1330 stony coral colonies representing 26 taxa were observed and measured. Of these, 52 colonies were not identifiable to species and were eliminated from taxa richness counts and calculation of the Shannon-Weiner diversity index. Most colonies (81.8%) had hemispherical

Table 1 Stressor values and quartiles for landscape development intensity (LDI), sedimentation threat (ST), and impaired water quality (WQ) for 13 stations along the south coast of St. Thomas, USVI

Station	LDI	Quartile	ST	Quartile	WQ	Quartile	ISI	Quartile
1	1.93	2	14,844.3	2	0	1	0.486	1
2	1.93	2	14,844.3	2	0.395	2	0.700	1
3	1.44	1	12,670.0	1	1.193	3	0.882	2
4	1.44	1	21,868.8	3	1.449	4	1.190	3
5	3.40	3	24,166.0	3	1.843	4	2.305	4
6	3.72	4	8055.6	1	1.583	4	2.007	4
7	2.23	2	20,708.1	2	0	1	0.728	2
8	3.72	4	22,381.4	3	1.080	3	1.998	3
9	2.23	2	0.4	1	0	1	0.346	1
10	3.72	4	54,359.0	4	0.685	2	2.371	4
11	1.58	1	2364.3	1	0.538	2	0.397	1
12	2.75	3	27,719.0	4	0	1	1.086	2
13	2.75	3	31,225.6	4	0.813	3	1.591	3

ISI is the sum of individual stressors which were rescaled from 0 to 1

morphology, 15.7% were branching, and 2.5% were flat, and no living *Acropora* colonies were observed. Two colonies (*Orbicella annularis* and *Orbicella faveolata*) were observed at station 13, and one *O. faveolata* colony at station 3 exceeded the average (live + dead) stony coral SA + 3 standard deviations, so these were considered outliers. These colonies were excluded from indicator calculations and subsequent analyses. Eight stony coral species comprised 82% of colony density (Table 2).

Coral density varied from 0.6/m^2 at station 9 near Water Island to 9.1 at stations 1 and 5 (Table 3). Despite low colony density at station 9, those corals present were large with highest CSA_Av and LCSA_Av (see Table 3 for variable names and abbreviations). Coral 3D total cover (3DTC) which includes dead coral ranged from 0.12 to 0.99 m^2 coral/m^2 sea floor, and 3D live cover (3DLC) ranged from 0.05 to 0.59 (Table 3). Due to high correlation ($r^2 = 0.794$, $p < 0.0001$) between 3DTC and 3DLC, only 3DTC was included in regression models and correlation tests with ISI. The total structure of the reef at all five stations west of Charlotte Amalie was largest with higher 3DTC and 3DLC, and stony coral taxa richness (SC_Tx) was also high at these stations relative to most others. Both total and live average colony size varied little except for relatively high values at stations 9 and 3. Average coral LT ranged from lowest values around 55% at stations 3, 8, and 9 to high values over 80% at stations 2, 5, 11, and 13. The CSA_CV of total coral colony size was lowest at stations 8 and 10 and highest at stations 2 and 13.

Increased watershed LDI was negatively related to stony coral reef structure measured by 3DTC and rugosity (Table 4). LDI was also negatively associated with coral diversity (Shannon-Weiner diversity index, SC_H′). Sedimentation threat was significant with reef rugosity and SC_H′ with positive relationships, and WQ had a positive relationship with SC_H′. While not significant for total colony density, LDI was negatively related to colony density of five of eight dominant coral species (Table 5). Water quality had a significant positive relationship with *Porites porites* density (Table 5).

The composite ISI did not correlate with any population-level stony coral metrics. Colony densities of *Orbicella annularis* and *Orbicella franksi* were negatively correlated with ISI with r values = − 0.502 and − 0.49 and $p < 0.08$ and 0.09, respectively.

Gorgonians and sponges

Gorgonians were observed at seven of the 13 stations (Table 6) with a total of 47 colonies exhibiting eight morphologies. The circle SA formula was applied to

Table 2 Stony coral species and density (no./m^2 sea floor) counted at 13 stations along the southern St. Thomas coast (unidentifiable/dead colonies not presented or included in total)

Station:	1	2	3	4	5	6	7	8	9	10	11	12	13
Agaricia agaricites	**0.48**	**0.16**	0.12	0.04	0.04		**0.04**				0.04	0.04	
Agaricia fragilis			0.04		0.04						0.08		
Agaricia lamarcki	**0.04**												
Colpophyllia natans	**0.04**		0.04		0.08								0.04
Dendrogyra cylindrus	**0.04**	**0.04**			0.08		**0.04**						
Dichocoenia stokesi					0.08								
Pseudodiploria labyrinthiformis	**0.56**	**0.48**		0.08	0.32	0.12			**0.04**		0.04		
Diploria strigosa	**1.24**	**0.44**	0.04		0.08		**0.04**			0.08	0.24	0.16	
Eusmilia fastigiata			0.04	0.20				0.16		0.04			
Madracis decactis		**0.04**			0.08			0.04		0.08			
Madracis mirabilis										0.08			
Manicina areolata								0.04					
Meandrina meandrites	**0.04**	**0.04**	0.04	0.20	0.36	0.04	**0.04**			0.16	0.04		0.04
Millepora complanata	**0.20**	**0.12**			0.52		**0.24**		**0.12**			0.04	
Orbicella annularis	**0.44**	**0.48**	0.60	0.36	0.16	0.08	**0.36**		**0.20**	0.04	0.04		0.08
Montastraea cavernosa	**0.24**	**0.32**	0.16	0.28	0.12	0.04	**0.04**	0.08		0.04	0.64	0.28	0.04
Orbicella faveolata	**0.44**	**0.72**	0.36	0.04	0.24	0.04	**0.04**	0.04	**0.04**	0.04	0.16		0.08
Orbicella franksi	**0.48**	**0.20**	0.12	0.16	0.20	0.04	**0.36**	0.08		0.04	0.44		
Porites astreoides	**1.48**	**1.08**	0.52	0.36	2.32	0.68	**0.28**	0.2		1.08	0.12	0.44	0.36
Porites colonensis		**0.12**	0.04								0.04		
Porites divaricata			0.12	0.20		0.04				0.08	0.04		
Porites furcata	**0.04**	**0.04**	0.16	0.12		0.04		0.04		0.20	0.08		
Porites porites	**0.12**	**0.20**	0.24	0.56	0.04	0.20	**0.12**	0.28			0.16	0.04	0.24
Siderastrea siderea	**2.36**	**0.36**	0.52	1.00	3.28	1.04	**0.12**	0.12	**0.12**	0.76	1.08	1.68	0.24
Solenastrea bournoni												0.12	
Stephanocoenia intersepta	**0.32**	**0.16**			0.04			0.04		0.20			0.08
Total Abundance:	**8.56**	**5.00**	3.16	3.60	8.08	2.36	**1.72**	1.12	**0.52**	2.92	3.24	2.80	1.20

Stations in 1st (lowest) LDI quartile have no shading, 2nd LDI quartile in bold font, 3rd LDI quartile shaded light gray, and 4th LDI (highest) quartile shaded dark gray

Table 3 Station depths and mean stony coral indicators: density (SC_Den; no. of colonies/m^2), colony surface area (CSA_Av; m^2 coral), live colony surface area (LCSA_Av; m^2 coral), percent live tissue (LT; %), 3D total cover (3DTC; m^2 coral/m^2 seafloor), 3D live cover (3DLC; m^2 coral/m^2 seafloor), coefficient of variation of colony surface area (CSA_CV), number of taxa (SC_Tx; no. of taxa/m^2), Shannon-Weiner index of diversity (SC_H′), and reef rugosity (RI)

Station	Depth (m)	SC_Den	CSA_Av	LCSA_Av	LT	3DTC	3DLC	CSA_CV	SC_Tx	SC_H′	RI
1	7.62	9.12	0.11	0.06	75.57	0.975	0.557	241.5	0.72	2.24	1.66
2	7.01	8.24	0.09	0.07	82.43	0.757	0.542	321.6	0.68	2.02	1.45
3	9.14	3.32	0.30	0.09	58.43	0.986	0.310	149.1	0.68	2.36	1.66
4	6.71	3.60	0.11	0.05	68.22	0.378	0.186	194.3	0.52	2.22	1.57
5	6.71	9.12	0.10	0.06	81.43	0.869	0.589	198.0	0.76	1.94	1.41
6	7.01	2.44	0.07	0.03	74.92	0.162	0.073	246.7	0.48	1.61	1.35
7	7.62	3.60	0.10	0.05	73.22	0.360	0.182	208.7	0.52	1.94	1.54
8	6.71	1.12	0.11	0.04	54.46	0.121	0.046	124.0	0.44	2.14	1.34
9	6.40	0.64	0.54	0.13	52.50	0.345	0.082	182.8	0.24	1.44	1.28
10	6.40	2.92	0.09	0.07	78.49	0.264	0.199	167.6	0.56	1.93	1.50
11	6.71	4.32	0.09	0.05	81.39	0.373	0.219	287.1	0.60	2.03	1.32
12	5.49	3.52	0.08	0.03	74.20	0.273	0.123	178.7	0.36	1.47	1.45
13	6.10	1.12	0.17	0.07	82.14	0.196	0.074	288.5	0.36	1.89	1.59

two sea plumes < 26 cm in height. Sea rods were dominant, accounting for about 60% of the abundance and 79% of the SA of gorgonians. The highest gorgonian density and SA were found at station 1 (Table 6). Regression analysis detected no significant relationships between any stressors and average gorgonian surface area or gorgonian density. Correlation analysis with ISI revealed no significant relationships with gorgonian metrics.

Sponges were found at all 13 stations (Table 6) with a total of 139 colonies exhibiting seven different morphologies. The most common sponge morphologies were rods (56), mounds (39), and encrusting types (20), with rods contributing 96% of total sponge SA. Three "vase" sponge colonies < 10 cm in height yielded negative SA using regressions, so the formula for a circle was used to estimate SA for these exceptions.

Sedimentation threat and WQ were positively significantly related to sponge colony density (Table 4). Sponge colony density was positively correlated with ISI ($r^2 = 0.395$, $p < 0.02$).

Fish

A total of 1968 fish belonging to 25 families were observed, and eight families comprised 92% of total abundance (highest abundance to lowest): Labridae, Scaridae, Pomacentridae, Acanthuridae, Gobiidae, Haemulidae, Serranidae, and Lutjanidae. These dominant eight families comprised 88% of total biomass (highest biomass to lowest): Scaridae, Serranidae, Acanthuridae, Pomacanthidae, Haemulidae, Pomacentridae, Lutjanidae, and Labridae. From 67 different species, the ten species comprising 70% of total abundance were (from highest to lowest) bluehead, masked/glass goby, striped parrotfish, ocean surgeonfish, blue tang, redband parrotfish, cocoa damselfish, French grunt, and bridled goby. Fish abundance ranged from 45 to 231 in the 100-m^2 survey area. Piscivores were rare and constituted less than 1% of abundance. Zooplanktivores constituted 16%, invertivores 49%, and herbivores 45%.

Station metrics for total fish abundance, total biomass, taxa richness, and Shannon-Weiner diversity index are presented in Table 6. No fish metrics were related to individual stressors, and no significant correlations with ISI were found.

Foraminifera and Macroinvertebrates

The FoRAM index was lowest (2.83) at station 10 near Charlotte Amalie Harbor. Stations 7 and 9 near Water Island had the highest FoRAM values of 6.48 and 4.88, and the remaining station values ranged from 3.06 to 3.84 (Table 6). Sea urchins of various species comprised 98% of macroinvertebrates observed at all stations. Of

Table 4 Results of stepwise regression testing relationships between coral reef indicators and stressors: landscape development intensity (LDI) index, sedimentation threat (ST), and water quality (WQ) with inclusion of $p < 0.25$ and retention of $p < 0.20$. Transformation indicated to meet requirement for normal distribution

Indicator	Transformation	LDI		ST		WQ		Equation
		p value	Partial r^2	*p* value	Partial r^2	*p* value	Partial r^2	
3DTC	log10	0.080	0.252	ns		ns		3DTC = (LDI × − 0.05054)
RI	none	0.012	0.156	0.015	0.392	ns		RI = (LDI × − 0.1088) + (ST × 0.00000659)
SC_H′	none	0.083	0.224	0.187	0.122	0.125	0.185	SC_H′ = (LDI × − 0.24242) + (ST × 0.0000082) + (WQ × 0.21111)
Sp_Den	log10	ns		0.010	0.471	0.194	0.088	Sp_Den = (ST × 0.00001022) + (WQ × 0.09406)

Equation coefficients show direction of relationship

3DTC three-dimensional total cover (live + dead coral), *RI* rugosity index, *SC_H′* Shannon-Weiner diversity index, *Sp_Den* density of sponge colonies

Table 5 Results of stepwise regression testing relationships between colony density of dominant stony coral species and stressors (see Table 4 and text) with inclusion of $p < 0.25$ and retention of $p < 0.20$. Transformation indicated to meet requirement for normal distribution

Stony coral species	Transformation	LDI		ST		WQ		Equation
		p value	Partial r^2	*p* value	Partial r^2	*p* value	Partial r^2	
Orbicella annularis	none	0.0089	0.4773	ns		ns		LDI × − 4.02511
Montastraea cavernosa	none	0.0436	0.3208	ns		ns		LDI × − 2.86174
Orbicella faveolata	log10	0.1469	0.1812	ns		ns		LDI × − 0.18755
Orbicella franksi	none	0.0866	0.2409	ns		ns		LDI × − 2.33885
Porites astreoides	none	ns		ns		ns		ns
Siderastrea siderea	none	ns		ns		ns		ns
Pseudodiploria strigosa	log10	ns		ns		ns		ns
Porites porites	none	0.0415	0.2822	ns		0.0258	0.2016	(LDI × − 2.39872) + (WQ × 3.61828)

Equation coefficients show direction of relationship

ns not significant

all macroinvertebrates, 67% were found at stations 1–5, west of Lindberg Bay (Table 6). Only seven spiny lobsters (five at station 10) were found, and no slipper lobsters, juvenile queen conch, and adult conch were observed at all. Neither the FoRAM index nor invertebrate density showed significant relationships in regressions with individual stressors or in correlation analysis with ISI.

Discussion

Human disturbance on the south shore of St. Thomas was characterized using three independent spatial measures of stressors known to adversely impact coral reefs. The stressors harm coral reefs either directly (Loya 1976; Rogers 1979; Rogers 1990; Fabricius 2005) or synergistically through interaction with other factors

Table 6 Station indicators FoRAM index (FI), invertebrate density (In_Den; no. of invertebrates/m^2 sea floor), gorgonian density (Gorg_Den; no. of gorgonians/m^2), average gorgonian surface area (GSA_Av; m^2 gorgonian SA), sponge density (Sp_Den; no. of sponges/m^2), average sponge surface area (SSA_Av; m^2 sponge SA), fish abundance (F_Abun; no. of fish/transect), fish biomass (F_Biom; total g/transect), F_Tx (number of fish taxa/transect), and Shannon-Weiner index of diversity for fish (F_H′)

Station	FI	In_Den	Gorg_Den	GSA_Av	Sp_Den	SSA_Av	F_Abun	F_Biom	F_Tx	F_H′
1	3.38	0.80	5.4	0.19	0.6	0.03	213	796.1	21	1.87
2	3.15	3.00	0.6	0.20	0.8	0.08	134	2501.8	20	2.14
3	3.22	0.11	0.0	0.0	2.2	5.85	109	316.8	16	2.29
4	3.06	0.37	0.8	0.05	2.0	0.04	231	3046.7	19	1.98
5	3.72	0.31	1.2	0.06	3.4	0.18	151	2810.3	24	2.56
6	3.46	0.16	0	0	1.6	0.01	148	1644.8	21	2.47
7	6.48	0.04	0	0	1.6	0.01	132	1476.8	24	2.53
8	3.84	0.02	0	0	2.0	0.40	156	3509.4	19	2.47
9	4.88	0.09	0	0	0.4	0.10	176	2440.2	25	2.82
10	2.83	0.12	0.2	0.07	7.4	0.69	166	2664.6	22	2.25
11	3.34	0.02	0	0	2.0	0.10	153	5799.7	21	2.52
12	3.69	1.78	0	0	3.0	0.09	45	367.1	14	1.99
13	3.65	0.01	1.2	0.11	0.8	0.06	154	638.0	25	2.31

(Carilli et al. 2009; Vega Thurber et al. 2013). High stressor values at stations closest to Charlotte Amalie Harbor validated selection of the area as an anthropogenic disturbance center where numerous human impacts occur. Our approach included comparing predictive power of individual stressors with a composite stressor index, the latter assuming additive effects as used to model reef stressors on a worldwide scale (Halpern et al. 2008). Land-based human activity represented by watershed LDI (Brown and Vivas 2005) had the most significant relationships with reef rugosity, coral diversity, and coral taxa richness exhibiting consistent negative coefficients in regression models. This supported the hypothesis that increased intensity of human development on land (high LDI) is associated with poor condition of coral reefs adjacent to high-LDI watersheds, as demonstrated in other Caribbean areas (Rogers 1979; Smith et al. 2008; Oliver et al. 2011), Hawaii (Rodgers et al. 2012), and Indonesia (Golbuu et al. 2008). The capability of LDI to predict ecosystem condition in wetlands and nutrient loading in watersheds (Brown and Vivas 2005) extends to predicting characteristics of coral reef condition such as stony coral colony size, species colony density, species diversity, topographic reef complexity, and benthic habitat composition at multiple watershed scales (Pittman et al. 2013). Some of these coral indicators have been related to distance to disturbance or other stress proxies (Fisher et al. 2008; Smith et al. 2008; Rodgers et al. 2012), and our results reinforce their application in stressor-response characterizations.

Stations near high-LDI watersheds had lower stony coral 3D cover and reef rugosity and reduced colony density for five dominant reef-building species (Tables 4 and 5). Total coral colony density and taxa richness were not statistically associated with LDI, but stations adjacent to highest-quartile LDI watersheds tended to have fewer colonies and fewer taxa compared to those near low-quartile LDI watersheds. Also, coral communities at the high-LDI stations were dominated by "weedy" species like *Porites astreoides* and *Siderastrea siderea* (Table 2), which have shown greater resistance to stress in Puerto Rico and other Caribbean areas (Torres and Morelock 2002; Green et al. 2008; Smith et al. 2013), but do not provide the habitat complexity of branching species (e.g., *Acropora*) nor the reef structure of massive corals (e.g., *Orbicella* and *Montastraea*). There were significantly fewer *Orbicella* sp. at stations with higher LDI, a finding that highlights a conclusion similar to Smith et al. (2008) and Ennis et al. (2016), who reported that reduced coral cover near human influence was driven by fewer *O. annularis*, *O. franksi*, and *O. faveolata*. There is particular concern about loss of prime reef-building species (Morelock et al. 2001) and the compromise of multiple ecosystem services that ultimately depend on reef structure (Principe et al. 2012; Alvarez-Filip et al. 2009; Burke and Maidens 2004). *Montastraea cavernosa*, another massive reef-building coral, is thought to be relatively resistant to stress but was also more abundant with lower LDI. These results underscore the importance of species-specific coral monitoring methods to detect community shifts caused by varied tolerance to stressors. Multivariate methods to detect changes across reef assemblages have also been applied to characterizing reef-stressor relationships (Jupiter et al. 2008). Even with well-designed methods, detecting stressor-response relationships requires a broad range of biological conditions possible (Karr and Chu 1997) and locating USVI reefs representative of "reference condition for biological integrity" (or zero human impact) is challenging as most USVI coral reefs are probably affected in some way by human influence (Rothenberger et al. 2008; Friedlander et al. 2013; Pait et al. 2013a, b; Pittman et al. 2013; Whitall et al. 2014; Jackson et al. 2014).

There was a significant, but weak, negative relationship of modeled ST with average stony coral colony size. There were also significant but positive relationships of ST with reef rugosity and coral diversity index, countering a common premise that high sediment loading adversely affects stony coral condition (Rogers 1979; Fabricius 2005). However, all of these results may have little interpretive potential because the range of ST values in this study was relatively small. In addition to testing a wide range of biological responses, the stressor gradient ideally incorporates multiple stressor levels from near-pristine to severe human disturbance levels (Karr and Chu 1997). But here, the highest ST was 54,359 (station 10), which is relatively small compared to the maximum Summit to Sea ST in the region of 251,714. Thresholds of sediment exposure are not well understood (Rogers 1990), and even if they were, the ST model does not convert to actual sediment concentrations. A positive coefficient found for ST and sponge density is consistent with other studies showing some sponge species to be relatively tolerant to stress from excess sediments (Powell et al. 2014). If so, this could indicate a possible phase shift in impacted

environments from coral-dominated habitats to sponge-dominated, and a loss of many ecosystem services (Ward-Paige et al. 2005; Norström et al. 2009).

For coral reefs near Charlotte Amalie, a more relevant source of sediment exposure for corals might be pulsed resuspension of sediments associated with cruise ship traffic in and out of ports in Crowne Bay and Charlotte Amalie Harbor (Kisabeth et al. 2014). Ship traffic creates plumes of resuspended sediment which substantially increase turbidity and total suspended solids compared to undisturbed levels (Kisabeth et al. 2014; Jones et al. 2016). This daily recurring activity is not captured in the ST model, which relies on landscape features, precipitation, and soil erodibility. It may be necessary to adjust sediment delivery models like Summit to Sea to account for factors like ship traffic to improve predictive capabilities. Many other nuances of sediment effects on corals not included in ST are grain size of the sediment, with finer grains generally causing greater harm (Acevedo et al. 1989; Weber et al. 2006), and whether exposure occurs in pulsed or steady sediment regimes (Browne et al. 2015).

As proxy for impaired water quality, a spatial estimate based on distance to disturbance (Fisher et al. 2008) was developed using data reported to the U.S. EPA under the Clean Water Act 305(b) and 303(d) programs (DPNR 2010). Assuming no effect beyond 3 km, three stations were too far away from impaired bays to be affected, and stations 5 and 6 located in the center of the study area had potential impact from three and two bays, respectively, where impaired water quality was reported. Significant positive relationships between WQ and coral diversity index and between WQ and *P. porites* colony density did not indicate that proximity to bays with WQ issues had negative effects on coral reefs. Estimates of WQ stress to benthic organisms could be improved with additional field data to better define potential relationships between specific WQ stressors like turbidity, total suspended solids (TSSs), and low DO on corals. Field measurements such as TSS and nutrients are needed to validate remotely sensed satellite products which can more accurately characterize exposure to WQ conditions over time compared with occasional measurements (Brodie et al. 2010). Fine-scale data on water currents would inform predictions of transport of materials to reef habitats and exposure of coral reefs to WQ stressors. Our distance-based WQ approach detected positive relationship with sponge colony density; more sponge colonies were present closer to bays with WQ impairments. This is similar to results from a study of sponges and land-based nutrient inputs in the Florida Keys (Ward-Paige et al. 2005) and is consistent with the concept of phase shifts from stony corals to sponges with increasing anthropogenic stress.

Modeling environmental stressor gradients is inherently difficult for several reasons. Co-occurrence of stressors in areas of high human disturbance is common, which makes it difficult to discern which stressors are responsible for reduced biological condition. The LDI is one type of composite index that is generated on a watershed basis, integrating inputs of nonrenewable energy to land use parcels (Odum 1996). Watershed management for coral health is not a new concept; for example, many Pacific Island cultures practice "ridge-to-reef" stewardship which assumes a connection between land-based human activities and health of adjacent marine communities (Richmond et al. 2007). Yet, management options may not be obvious using LDI as a predictor unless specific land use types associated with reduced biological condition can be identified. Characterizing all operative stressors regarding a system of interest is likely impossible. Models that incorporate multi-stressor data across broad scales (Halpern et al. 2008; Burke et al. 2011) may provide more comprehensive stressor information, but these scales make the data less useful for small islands like St. Thomas. For some areas of the Caribbean, data about coral reef stressors such as fishing pressure (Shivlani and Koeneke 2010), chemical contaminants (Whitall et al. 2014), and ocean temperature anomalies (Novoa et al. 2012; Liu et al. 2014) could improve forecasting and clarify management options. Development of spatially explicit, comprehensive data on multiple stressors impacting coral reefs and accounting for potential synergistic, additive, or antagonistic effects would best serve reef management needs.

Three westward stations adjacent to sparse human population and undisturbed lands had consistent low stressor estimates below 50% of the mean and among the highest total and live stony coral cover, taxa richness, and colony density. Watersheds adjacent to these stations had high coverage of forest and other natural lands (Fig. 1). Progressing to the east, different patterns were seen depending on the stressor. For example,

station 4 is adjacent to a low-LDI watershed but fits the 4th (highest) quartile for ST due in part to adjacent bare landscape and increased likelihood for runoff. Stressor values for station 13 located farthest east from the center of disturbance indicate greater human influence than might be assumed by its distance from Charlotte Amalie. This station had second-highest LDI and ST values and may combine with another human activity source to the east. Influences such as an unlined landfill located 0.1 km from shore in Bovani Bay (Horsely Witten Group 2013) are not represented in our stressor estimates and could have a large impact. Station 8 with highest LDI values also had the lowest stony coral cover and low percent live tissue. In contrast, station 11 located near uninhabited Hassel Island had low LDI and intermediate coral indicator values. Although uninhabited, Hassel Island is close to the harbor and probably receives resuspended sediment from ship traffic.

Although nonsignificant in regressions and correlations, the FoRAM index was highest (best condition) at stations 7 and 9, located away from the coast and human influences, and lowest at station 10 near Charlotte Amalie Harbor. The FoRAM has shown to be responsive to eutrophication (Hallock et al. 2003) and distance to disturbance (Oliver et al. 2014) and may have a value in reef monitoring protocols. Fish populations may associate with reef structure but are not expected to associate directly with stressors because fish are mobile; a lack of significant findings with stressors is not surprising.

Healthy coral reefs benefit the people and economy of St. Thomas by providing ecosystem services. Although causality cannot be directly determined, a human impact signature was evident from LDI associations with reef condition indicators at 13 stations, showing that reefs around Charlotte Amalie are proportionally affected by human development activities in adjacent watersheds. Management steps to reduce human disturbances can lessen direct impacts on corals, as well as additive or synergistic effects from tropical storms and hurricanes, global-scale ocean temperature anomalies (Hughes and Connell 1999; Maina et al. 2011; Gurney et al. 2013), and ocean acidification (Wooldridge and Done 2009; Ban et al. 2014).

Cost-effective mitigation options to reduce sedimentation for example, have been demonstrated in the USVI (Ramos-Scharrón 2012), and effective spatial mapping of reef stressors can prioritize where such actions are most needed. A balanced approach to coastal management decision-making, which incorporates available scientific research to better characterize stressors and understand their influence, can help protect coral reef ecosystems and the economic, ecological, and esthetic benefits they provide.

Acknowledgements Outstanding field assistance in conducting coral reef surveys was provided by Jed Campbell, Peggy Harris, Becky Hemmer, Robert Quarles, and Sherry Vickery (U.S. EPA Gulf Ecology Division); Charles LoBue and Danny Rodriguez (U.S. EPA Region 2); Mel Parsons (U.S. EPA Region 4); Aaron Hutchins (The Nature Conservancy, St. Croix); Rich Henry (U.S. Fish and Wildlife Service, Environmental Response Team); Alan Humphrey (U.S. EPA, Environmental Response Team); and Jon McBurney and Scott Grossman (Lockheed Martin, Scientific, Engineering, Response and Analytical Services (SERAS) Program). The crew of the OSV *Bold*, Captain Jere Chamberlain, provided excellent support in all aspects of field data collection and logistics. Kent Bernier (U.S. Virgin Islands, Department of Planning and Natural Resources) provided small boat support for the survey teams. The views expressed in this article are those of the authors and do not necessarily reflect the views or policies of the U.S. Environmental Protection Agency.

References

Abt Associates, Inc. (2016). Describing the ocean economies of the U.S. Virgin Islands and Puerto Rico. https://coast.noaa.gov/digitalcoast/training/econ-usvi-pr.html

Acevedo, R. J., Morelock, J., & Olivieri, R. A. (1989). Modification of coral reef zonation by terrigenous sediment stress. *PALAIOS, 4*(1), 92–100.

Alvarez-Filip, L., Dulvy, N. K., Gill, J. A., Côte, I. M., & Watkinson, A. R. (2009). Flattening of Caribbean coral reefs: region-wide declines in architectural complexity. *Proceedings of the Royal Society B, 276*, 3019–3302.

Ban, S. S., Graham, N. A. J., & Connolly, S. (2014). Evidence for multiple stressor interactions and effects on coral reefs. *Global Change Biology, 20*, 681–697.

Bégin, C., Schelten, C. K., Nugues, M. M., Hawkins, J., Roberts, C., & Côté, I. M. (2016). Effects of protection and sediment stress on coral reefs in Saint Lucia. *PLoS One, 11*(2), e0146855. https://doi.org/10.1371/journal.pone.0146855.

Bradley, P., Fisher, W., Bell, H., Davis, W., Chan, V., LoBue, C., & Wiltse, W. (2009). Development and implementation of coral reef biocriteria in U.S. jurisdictions. *Environmental Monitoring & Assessment, 150*, 43–51.

Bradley, P., Fore, L., Fisher, W., & Davis, W. (2010). Coral reef biological criteria: using the Clean Water Act to protect a national treasure. U.S. Environmental Protection Agency, Office of Research and Development, Narragansett, RI. EPA/600/R-10/054, July 2010.

Brodie, J., Schroeder, T., Rohde, K., Faithful, J., Masters, B., Dekker, A., Brando, V., & Maughan, M. (2010). Dispersal of suspended sediments and nutrients in the Great Barrier Reef lagoon during river-discharge events: conclusions from

satellite remote sensing and concurrent flood-plume sampling. *Marine and Freshwater Research, 61*(6), 651–664.

Brown, M. T., & Vivas, M. B. (2005). Landscape development intensity index. *Environmental Monitoring & Assessment, 101*, 289–309.

Brown, C. J., Saunders, M. I., Possingham, H. P., & Richardson, A. J. (2013). Managing for interactions between local and global stressors of ecosystems. *PLoS One, 8*(6), e65765. https://doi.org/10.1371/journal.pone.0065765.

Browne, N. K., Tay, J., & Todd, P. A. (2015). Recreating pulsed turbidity events to determine coral-sediment thresholds for active management. *Journal of Experimental Marine Biology and Ecology, 466*, 98–109.

Burke, L., & Maidens, J. (2004). *Reefs at risk in the Caribbean*. Washington, D.C.: World Resources Institute 81 pp.

Burke, L., Reytar, K., Spalding, M., & Perry, A. (2011). *Reefs at risk revisited*. Washington, D.C.: World Resources Institute.

Carilli, J. E., Norris, R. D., Black, B. A., Walsh, S. M., & McField, M. (2009). Local stressors reduce coral resilience to bleaching. *PLoS One, 4*(7), e6324.

Clark, K.R., & Gorley, R.N. (2006). PRIMER v6: user manual/tutorial, Plymouth, UK.

DPNR, (2010). USVI integrated water quality monitoring & assessment report. Department of Planning and Natural Resources, Division of Environmental Protection Water Quality Management & Planning Program. 165 pp. Retrieved 2018, 10 February from: http://www.horsleywitten.com/stx-east-endwatersheds/pubs/2010IntegratedReport_b.pdf.

Ennis, R. S., Brandt, M. E., Wilson Grimes, K. R., & Smith, T. B. (2016). Coral reef health response to chronic and acute changes in water quality in St. Thomas, United States Virgin Islands. *Marine Pollution Bulletin, 111*, 418–427.

Fabricius, K. (2005). Effects of terrestrial runoff on the ecology of coral reefs: review and synthesis. *Marine Pollution Bulletin, 50*, 125–146.

Fisher, W.S. (2007). Stony coral rapid bioassessment protocol. U.S. Environmental Protection Agency, Office of Research and Development, Gulf Breeze, FL. EPA/600/R-06/167, July 2007.

Fisher, W. S., Fore, L. S., Hutchins, A., Quarles, R. L., Campbell, J. G., LoBue, C., & Davis, W. S. (2008). Evaluation of stony coral indicators for coral reef management. *Marine Pollution Bulletin, 56*, 1737–1745.

Fore, L. S., Karr, J. R., Fisher, W. S., Bradley, P., & Davis, W. S. (2009). Heeding a call to action for US coral reefs: the untapped potential of the Clean Water Act. *Marine Pollution Bulletin, 58*, 1421–1423.

Friedlander, A.M., Jeffrey, C.F.G., Hile, S.D., Pittman, S.J., Monaco, M.E. & Caldow, C., eds. (2013). Coral reef ecosystems of St. John, U.S. Virgin Islands: spatial and temporal patterns in fish and benthic communities (2001-2009). NOAA Technical Memorandum 152. Silver Spring, MD. 150 pp.

Froese, R., & Pauly, D., eds. (2013). FishBase. World Wide Web electronic publication. www.fishbase.org, version (12/2013).

Gardner, T. A., Côte, I. M., Gill, J. A., Grant, A., & Watkinson, A. R. (2003). Long-term region-wide declines in Caribbean reef corals. *Science, 301*, 958–960.

Golbuu, Y., Fabricius, K., Victor, S., & Richmond, R. H. (2008). Gradients in coral reef communities exposed to muddy river discharge in Pohnpei, Micronesia. *Estuarine, Coastal and Shelf Science, 76*, 14–20.

Green, D. H., Edmunds, P. J., & Carpenter, R. C. (2008). Increasing relative abundance of *Porites astreoides* on Caribbean reefs mediated by an overall decline in coral cover. *Marine Ecology Progress Series, 359*, 1–10.

Gurney, G. G., Melbourne-Thomas, J., Geronimo, R. C., Aliño, P. M., & Johnson, C. R. (2013). Modelling coral reef futures to inform management: can reducing local-scale stressors conserve reefs under climate change? *PLoS One, 8*(11), e80137.

Hallock, P., Lidz, B. H., Cockey-Burkhard, E. M., & Donnelly, K. B. (2003). Foraminifera as indicators coral reef assessment and monitoring: the Foram index. *Environmental Modeling & Assessment, 81*, 221–238.

Halpern, B. S., Walbridge, S., Selkoe, K. A., Kappel, C. V., Micheli, F., D'Agrosa, C., Bruno, J. F., Casey, K. S., Ebert, C., Fox, H. E., Fujita, R., Heinemann, D., Lenihan, H. S., Madin, E. M. P., Perry, M. T., Selig, E. R., Spalding, M., Steneck, R., & Watson, R. (2008). A global map of human impact on marine ecosystems. *Science, 319*, 948–952.

Horsely Witten Group, Inc, (2013). St. Thomas East End reserves watershed management plan. Report to NOAA coral Reef Conservation Program, USVI DPNR, and The Nature Conservancy. 73 pp.

Hughes, T. P., & Connell, J. H. (1999). Multiple stressors on coral reefs: a long-term perspective. *Limnology & Oceanography, 44*(3), 932–940.

Humann, P., & DeLoach, N. (2002). *Reef coral identification: Florida Caribbean Bahamas*. Jacksonville: New World.

Islands Resources Foundation, USVI-Conservation Data Center, & U.S. Geological Survey. (2001). Watersheds for St. Thomas and St. John, US Virgin Islands. https://databasin.org/datasets/47140a08e8d340fea9a3f4118f15febe.

Jackson, J. B. C., Donovan, M. K., Cramer, K. L., & Lam, V. V. (Eds.). (2014). *Status and trends of Caribbean coral reefs: 1970-2012*. Gland: Global Coral Reef Monitoring Network, IUCN.

Jones, R., Bessell-Browne, P., Fisher, R., Klonowski, W., & Slivkoff, M. (2016). Assessing the impacts of sediments from dredging on corals. *Marine Pollution Bulletin, 102*(1), 9–29.

Jupiter, S., Roff, G., Marion, G., Henderson, M., Schrameyer, V., McCulloch, M., & Hoegh-Guldberg, O. (2008). Linkages between coral assemblages and coral proxies of terrestrial exposure along a cross-shelf gradient on the southern Great Barrier Reef. *Coral Reefs, 27*(4), 887–903.

Kaczmarsky, L. T., Draud, M., & Williams, E. H. (2005). Is there a relationship between proximity to sewage effluent and the prevalence of coral disease? *Caribbean Journal of Science, 41*(1), 124–137.

Karr, J. R., & Chu, E. W. (1997). *Biological monitoring and assessment: using multimetric indexes effectively*. EPA 235-R97-001. Seattle: University of Washington.

Kendall, M. S., Kruer, C. R., Buja, K. R., Christensen, J. D., Finkbeiner, M., & Monaco, M. E. (2001). *Methods used to map the benthic habitats of Puerto Rico and the U.S. Virgin Islands*. Silver Spring: National Oceanic and Atmospheric Administration, NCCOS Biogeography Program http://biogeo.nos.noaa.gov/projects/mapping/caribbean/startup.htm.

Kisabeth, J. K., Smith, T., Primack, A., & Wilson, K. (2014). *Cruise ship induced sediment resuspension characteristics*

in Charlotte Amalie Harbor and the West Gregerie Channel, St. Thomas, US Virgin Islands. St. Thomas: Doctoral dissertation, University of the Virgin Islands.

Knowlton, N., & Jackson, J. B. C. (2008). Shifting baselines, local impacts, and global change on coral reefs. *PLoS Biology, 6*(2), 215–220.

Liu, G., Heron, S. F., Eakin, C. M., Muller-Karger, F. E., Vega-Rodriguez, M., Guild, L. S., De La Cour, J. L., Geiger, E. F., Skirving, W. J., Burgess, T. F. R., Strong, A. E., Harris, A., Maturi, E., Ignatov, A., Sapper, J., Li, J., & Lynds, S. (2014). Reef-scale thermal stress monitoring of coral ecosystems: new 5-km global products from NOAA Coral Reef Watch. *Remote Sensing, 6*(11), 11579–11606. https://doi.org/10.3390/rs61111579.

Loya, Y. (1976). Effects of water turbidity and sedimentation on the community structure of Puerto Rican corals. *Bulletin of Marine Science, 26*(4), 450–466.

Maina, J., McClanahan, T. R., Venus, V., Ateweberhan, M., & Madin, J. (2011). Global gradients of coral exposure to environmental stresses and implications for local management. *PLoS One, 6*(8), e23064.

Menza, C., Ault, J., Beets, J., Bohnsack, J., Caldow, C., Christensen, J., Friedlander, A., Jeffrey, C., Kendall, M., Luo, J., Monaco, M., Smith, S., & Woody, K., (2006). A guide to monitoring reef fish in the National Parks Service's South Florida/Caribbean Network. NOAA Technical Memorandum NOS NCOOS 39. 169 pp.

Moberg, F., & Folke, C. (1999). Ecological goods and services of coral reef ecosystems. *Ecological Economics, 29*, 215–233.

Morelock, J., Ramirez, W.R., Bruckner, A.W., & Carlo, M. (2001). Status of coral reefs in southwest Puerto Rico. Caribbean Journal Science Special Publication No 4.

Nemeth, R. S., & Nowlis, J. S. (2001). Monitoring the effects of land development on the near-shore reef environment of St. Thomas, USVI. *Bulletin of Marine Science, 69*(2), 759–775.

Norström, A. V., Nyström, M., Lokrantz, J., & Folke, C. (2009). Alternative states on coral reefs: beyond coral-macroalgal phase shifts. *Marine Ecology Progress Series, 376*, 295–306.

Novoa, S., Chust, G., Froidefond, J.M., Petus, C., Franco, J., Orive, E., Seoane, S., & Borja, A. (2012). Water quality monitoring in Basque coastal areas using local chlorophyll-*a* algorithm and MERIS images. Journal of Applied Remote Sensing 6(1), 063519. doi: https://doi.org/10.1117/1.JRS.6.063519.

Odum, H. T. (1996). *Environmental accounting: Emergy and environmental decision making* (p. 370). New York: John Wiley and Sons.

Oliver, L. M., Lehrter, J. C., & Fisher, W. S. (2011). Relating landscape development intensity to coral reef condition in the watersheds of St. Croix, US Virgin Islands. *Marine Ecology Progress Series, 427*, 293–302.

Oliver, L. M., Fisher, W. S., Dittmar, J., Hallock, P., Campbell, J., Quarles, R. L., Harris, P., & LoBue, C. (2014). Contrasting responses of coral reef fauna and foraminiferal assemblages to human influence in La Parguera, Puerto Rico. *Marine Environmental Research, 99*, 95–105.

Pait, A.S., Hartwell, S.I., Mason, A.L., Galdo, F.R. Jr., Warner, R.A., Jeffrey, C.F.G., Hoffman, A.M., Apeti, D.A., & Pittman, S.J. (2013a). An assessment of chemical contaminants detected in passive water samplers deployed in the St. Thomas East End Reserves (STEER). NOAA Technical Memorandum NOS/NCCOS 157. Silver Spring, MD. 22 pp.

Pait, A.S., Hartwell, S.I., Mason, A.L., Warner, R.A., Jeffrey, C.F.G., Hoffman, A.M., Apeti, D.A., Galdo Jr., F.R., & Pittman, S.J. (2013b). An assessment of chemical contaminants, toxicity and benthic infauna in sediments from the St. Thomas East End Reserves (STEER). NOAA Technical Memorandum NOS NCCOS 156.Silver Spring, MD. 70 pp.

Pittman, S.J., Dorfman, D.S., Hile, S.D., Jeffrey, C.F.G., Edwards, M.A. & Caldow, C. (2013). Land-sea characterization of the St. Croix East End Marine Park, U.S. Virgin Islands. NOAA Technical Memorandum NOS NCCOS 170. Silver Spring, MD. 119 pp.

Powell, A., Smith, D. J., Hepburn, L. J., Jones, T., Berman, J., Jompa, J., & Bell, J. J. (2014). Reduced diversity and high sponge abundance on a sedimented Indo-Pacific reef system: implications for future changes in environmental quality. *PLoS One, 9*(1), e85253. https://doi.org/10.1371/journal.pone.0085253.

Principe, P., Bradley, P., Yee, S., Fisher, W., Johnson, E., Allen, P. & Campbell, D. (2012). Quantifying coral reef ecosystem services. U.S. Environmental Protection Agency, Office of Research and Development, Research Triangle Park, NC. EPA/600/R-11/206, January 2012, 147 pp.

Ramos-Scharrón, C. E. (2012). Effectiveness of drainage improvements in reducing sedimenbt production rates from an unpaved road. *Journal of Soil and Water Conservation, 6*(2), 87–100.

Richmond, R. H., Rongo, T., Golbuu, Y., & Victor, S. (2007). Watersheds and coral reefs: conservation science, policy, and implementation. *Bioscience, 57*, 598–607.

Risk, M. (1972). Fish diversity on a coral reef in the Virgin Islands. *Atoll Research Bulletin, 153*, 1–6.

Rodgers, K. S., Kido, M. H., Jokiel, P. L., Edmonds, T., & Brown, E. K. (2012). Use of integrated landscape indicators to evaluate the health of linked watersheds and coral reef environments in the Hawaiian Islands. *Environmental Management, 50*, 21–30.

Rogers, C. S. (1979). The effects of shading on coral-reef structure and function. *Journal of Experimental Marine Biology & Ecology, 41*, 269–288.

Rogers, C. S. (1990). Responses of coral reefs and reef organisms to sedimentation. *Marine Ecology Progress Series, 62*, 185–202.

Rogers, C. S., Miller, J., Muller, E. M., Edmunds, P., Nemeth, R. S., Beets, J. P., Friedlander, A. M., Smith, T. B., Boulon, R., Jeffrey, C. F. G., Menza, C., Caldow, C., Idrisi, N., Kojis, B., Monaco, M. E., Spitzack, A., Gladfelter, E. H., Ogden, J. C., Hillis-Starr, Z., Lundgren, I., Schill, W. B., Kuffner, I. B., Richardson, L. L., Devine, B. E., & Voss, J. D. (2008). Ecology of coral reefs in the US Virgin Islands. In B. Riegl & R. Dodge (Eds.), *Coral reefs of the USA* (Vol. 1, pp. 303–373). Netherlands: Springer.

Rothenberger, P., Blondeau, J., Cox, C., Curtis, S., Fisher, W. S., Garrison, V., Hillis-Starr, Z., Jeffrey, C., Kadison, E., Lundgren, I., Miller, W. J., Muller, E., Nemeth, R., Paterson, S., Rogers, C., Smith, T., Spitzack, A., Taylor, M., Toller, W., Wright, J., Wusinich-Mendea, D., & Waddell, J. (2008). The state of coral reef ecosystems of the U.S. Virgin Islands. In J. E. Wadell & A. M. Clarke (Eds.), *The state of coral reef ecosystems of the United States and*

Pacific Freely Associated States: 2008 (pp. 29–73). Silver Spring: NOAA Center for Coastal Monitoring and Assessment's Biogeography Team.

Santavy, D.L, Fisher, W.S., Campbell, J.G., & Quarles R.L. (2012). Field manual for coral reef assessments. U.S. Environmental Protection Agency, Office of Research and Development, Gulf Ecology Division, Gulf Breeze, FL. EPA/600/R-12/029. April 2012.

Santavy, D. L., Courtney, L. A., Fisher, W. S., Quarles, R. L., & Jordan, S. J. (2013). Estimating the surface area of marine gorgonians and sponges in the field. *Hydrobiologia, 707*, 1–16.

Shivlani, M., & Koeneke, R. (2010). Spatial characterization of artisanal fisheries in Puerto Rico: geographic information systems (GIS) approach for assessing the regional effort and landings. Proceedings 63rd Gulf and Caribbean Fisheries Institute, November 1–5, 2010, San Juan, Puerto Rico.

Smith, T. B., Nemeth, R. S., Blondeau, J., Calnan, J. M., Kadison, E., & Herzlieb, S. (2008). Assessing coral reef health across onshore to offshore stress gradients. *Marine Pollution Bulletin, 56*, 1983–1991.

Smith, T. B., Brandt, M. E., Calnan, J. M., Nemeth, R. S., Blondeau, J., Kadison, E., Taylor, M., & Rothenberger, P. (2013). Convergent mortality responses of Caribbean coral species to seawater warming. *Ecosphere, 4*(7), 87. https://doi.org/10.1890/ES13-00107.1.

Torres, J. T., & Morelock, J. (2002). Effect of terrigenous sediment influx on coral cover and linear extension rates of three Caribbean massive coral species. *Caribbean Journal of Science, 38*(3–4), 222–229.

USVI (U.S. Virgin Islands), (2010). United States Virgin Islands 2010 revisions to: Water Quality Standards Title 12, chapter 7, Government of the Virgin Islands, Department of Planning and Natural Resources, Division of Environmental Protection, 22 pp.

van Beukering, P., Brander, L., Van Zanten, B., Verbrugge, E., Lems, K. (2011). The economic value of the coral reef ecosystems in the United States Virgin Islands. In: Edmunds, P.E.T. (ed.), The economic value of coral reefs, IVM Report number: R-11/06.

Vega Thurber, R. L., Burkepile, D. E., Fuchs, C., Shantz, A. A., McMinds, R., & Zaneveld, J. R. (2013). Chronic nutrient enrichment increases prevalence and severity of coral bleaching. *Global Change Biology*. https://doi.org/10.1111/gcb,12450.

Villanueva, R. D., Yap, H. T., & Montaña, N. E. (2006). Survivorship of coral juveniles in a fish farm environment. *Marine Pollution Bulletin, 51*, 580–589.

Voss, J. D., & Richardson, L. L. (2006). Nutrient enrichment enhances black band disease progression in corals. *Coral Reefs, 25*, 569–576.

Ward-Paige, C. A., Risk, M. J., Sherwood, O. A., & Jaap, W. C. (2005). Clionid sponge surveys on the Florida Reef Tract suggest land-based nutrient inputs. *Marine Pollution Bulletin, 51*, 570–579.

Warne, A. G., Webb, R. M. T., & Larsen, M. C. (2005). Water, sediment, and nutrient discharge characteristics of rivers in Puerto Rico, and their potential influence on coral reefs: U.S. *Geological Survey Scientific Investigations Report, 2005-5206*, 58.

Weber, M., Lott, C., & Fabricius, K. E. (2006). Sedimentation stress in a scleractinian coral exposed to terrestrial and marine sediments with contrasting physical, organic and geochemical properties. *Experimental Marine Biology & Ecology, 336*, 18–32.

Whitall, D., Menza, C., & Hill, R. (2014). A baseline assessment of coral and fish bays (St. John, USVI) in support of ARRA watershed restoration activities. NOAA Technical Memorandum NOS NCCOS 178. Silver Spring, MD. 74 pp.

Wooldridge, S. A., & Done, T. J. (2009). Improved water quality can ameliorate effects of climate change on corals. *Ecological Applications, 19*(6), 1492–1499.

World Resources Institute (WRI), & NOAA (2006). Land-based sources of threat to coral reefs in the U.S. Virgin Islands. Washington, DC.

Session 36

Biodiversity, biogeography and evolution of coral reef organisms

Session chairs:

Danwei Huang, huangdanwei@nus.edu.sg

Francesca Benzoni, francesca.benzoni@unimib.it

Marcelo V. Kitahara. mvkitahara@unifesp.br

James D. Reimer, jreimer@sci.u-ryukyu.ac.jp

Molly Timmers, molly.timmers@noaa.gov

Christopher Meyer, meyerc@si.edu

Forest Rohwer, frohwer@gmail.com

Gustav Paulay, paulay@flmnh.ufl.edu

Peter F. Cowman, peter.cowman@jcu.edu.au

Jennifer Hodge, jhodge@ucdavis.edu

Libby Liggins, l.liggins@massey.ac.nz

Oliver LM, Santavy DL, Bradley P (2016) Developing a multi-stressor gradient model for coral reefs of Puerto Rico. Proceedings of the 13th International Coral Reef Symposium, Honolulu: 245-257

Louis YD, Dyall SD, Bhagooli R (2016) Coast-reef scale physiological responses of *Acropora muricata* harboring *Symbiodinium* clade A. Proceedings of the 13th International Coral Reef Symposium, Honolulu: 258-277

Kaullysing D, Gopeechund A, Mattan-Moorgawa S, Taleb-Hossenkhan N, Kulkarni B, Bhagooli R (2016) Increased density of the corallivore *Drupella cornus* on *Acropora muricata* colonies overgrown by *Padina boryana.* Proceedings of the 13th International Coral Reef Symposium, Honolulu: 278-294

Developing a multi-stressor gradient model for coral reefs of Puerto Rico

Leah M. Oliver, Deborah L. Santavy, Patricia Bradley

Abstract Coral reefs worldwide are threatened by multiple anthropogenic stressors, yet understanding reef responses to multiple stressor gradients is complicated by interactive stressor effects, co-occurrence of some stressors, and inconsistent data availability. Indirect protection of aquatic life under the US Clean Water Act (CWA) may occur through requirements for effluent discharge permits and provisions for setting chemical and physical criteria based on designated waterbody uses for humans. Biological water quality criteria or "biocriteria" established under the CWA offers a direct means to protect corals. Biocriteria are quantitative thresholds or narrative descriptions of coral reef ecosystem attributes needed to maintain biological integrity. Biocriteria development involves defining the biological community associated with a wide range of ecosystem conditions ranging from a pristine, undisturbed state to severe disturbance by human activities. As part of this process for Puerto Rico, Caribbean coral reef ecosystem experts prioritized anthropogenic stressors to coral reef ecosystems as land-based sources of pollution, fishing pressure, and global climate change-related thermal anomalies. Spatial data representing these stressors were mapped, showing some areas where all three stressors were high and also areas where the magnitude of stressors contrasted. In northeast Puerto Rico, urban development around San Juan resulted in the island's highest watershed development index, which co-occurred with high fishing pressure. In contrast, southwest Puerto Rico had high fishing pressure but low watershed development and ocean temperatures compared to other coastal areas. Narrative descriptions were also developed to incorporate stressors for which spatial data is absent or limited. Future expert workshops will refine this model by developing stressor weighting factors and by considering interactive effects. This conceptual framework will contribute to developing a multi-stressor gradient model for the coral reefs of Puerto Rico, identify data needs, stimulate addition of new spatial data, and generate testable hypotheses to calibrate the stressor-response model.

Keywords: coral reefs, land-based pollution, temperature anomalies, fishing pressure, stressor gradient

Leah M. Oliver, Deborah L. Santavy
US EPA, Office of Research & Development, National Health & Environmental Effects Laboratory, Gulf Ecology Division, 1 Sabine Island Drive, Gulf Breeze, FL 32561

Patricia Bradley
Retired, US EPA, Office of Research & Development, National Health & Environmental Effects Laboratory, Atlantic Ecology Division, 27 Tarzwell Drive, Narragansett, RI 02882

Corresponding author: Leah M. Oliver, oliver.leah@epa.gov

Introduction

Coral reefs are often found near coasts where multiple anthropogenic stressors co-occur at areas of high human disturbance. Stressors range in scale of influence and relative manageability from point source discharges and unrestrained coastal development to thermal anomalies and ocean acidification stemming from global climate change (Hughes and Connell 1999; Kleypas et al. 1999; Ban et al. 2014). Understanding which human-induced stressors influence important coral reef attributes is critical to effect management actions that maximize benefits to reefs and the valuable ecosystem services they provide. The US Clean Water Act (CWA) establishes a framework for regulating water quality and directs the EPA to set wastewater standards for industry, issue permits for industrial and municipal discharges, and coordinate with state and territorial governments to adopt water quality criteria to protect against harmful effects of pollutants. Chemical and physical criteria are routinely established, yet the CWA also contains a provision for states and territories to set biocriteria, which are desired states of biological resources linked to designated uses (Bradley et al. 2009). Designated uses are the formally promulgated uses for a given waterbody such as drinking water, fishing and fish consumption, swimming, and supporting aquatic life. The CWA requires that water quality be able to support the designated use(s) for a given waterbody. Based on the designated use(s), desired resource conditions may be customized, for example, biocriteria for lower quality "Class C" waters with heavy human impact may allow for some loss of ecosystem structure and function while those for higher quality "Class A" waters could require full ecosystem integrity on par with an undisturbed, undeveloped, and possibly historic condition indicative of a natural or non-degraded state (US EPA 2016). Although it is not necessary to quantify all stressors which impact biological resources, biocriteria development requires development of relevant indicators for

both stressors and biological condition and a relationship established between reduced resource condition and increasing human disturbance (Karr and Chu 1997; Fore et al. 2009).

Quantitative relationships between anthropogenic stress and coral reef health have been demonstrated in the Caribbean (Fisher et al. 2008; Oliver et al. 2011; Ennis et al. 2016), Hawaii (Rodgers et al. 2012), and Indonesia (Golbuu et al. 2008), employing biological measures of coral size, taxa richness, and coral cover, and stressor estimates such as distance to disturbance and land-use based watershed indices. These studies establish stressor-response relationships for corals and set the stage for integrated stressor approaches. A conceptual model developed for wetland and stream ecosystems relating biological condition to increasing anthropogenic stressors (Fig. 1) was the basis for engaging Caribbean coral reef ecosystem experts to develop a biological condition gradient (BCG), defining attributes of coral reef ecosystems associated with conditions ranging from pristine to severely altered (Davies and Jackson 2006; Bradley et al. 2014; Santavy et al. 2016). During a structured process to assign biological attributes to different levels of the BCG, discussions included which stressors the experts believed were the

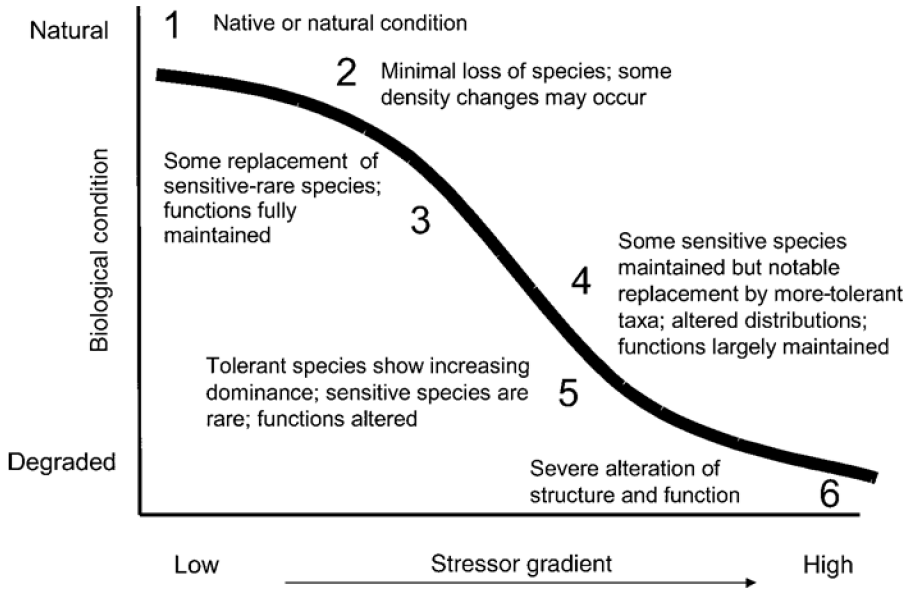

Fig. 1 Conceptual biological condition and stressor gradient model, showing general changes in ecosystem in response to increasing anthropogenic stress. Reprinted from Davies, SP and Jackson SK (2006), The biological condition gradient: a descriptive model for interpreting change in aquatic ecosystems. Ecological Applications, 16: 1251–1266. doi:10.1890/1051-0761(2006)016[1251:TBCGAD]2.0.CO;2, with permission of the Ecological Society of America

most critical for coral reef ecosystems in Puerto Rico and the Caribbean. Experts identified high sea temperatures and land-based pollution as primary stressors for corals, and fishing pressure and land-based pollution for fishes. As part of the BCG development process in which anthropogenic stressor gradients are characterized and associated with different BCG levels, we sought to develop a conceptual framework for an integrated stressor gradient for Puerto Rico's coral reef ecosystems, incorporating both quantitative data and narrative descriptions.

Materials and methods

Land-Based Sources of Pollution (LBSP)

A Landscape Development Intensity Index (LDI) was calculated as a measure of land-based pollution using the method of Brown and Vivas (2005). The LDI method integrates human impact associated with specific land use/land cover (LULC) types, proportional to cumulative inputs of nonrenewable energy (Emergy). In brief, a 30m-resolution LULC dataset (Homer et al. 2007) was reclassified to Emergy coefficients (Odum 1996) blended from Brown and Vivas (2005) and Florida land use cover and classification systems (Janicki 2013) (see Table 2 in Oliver et al. 2011). LDI values were calculated for coastal Hydrologic Unit Code (HUC)-12 watersheds, and weighted for % LULC. Coastal watershed LDI values were extended into adjacent coastal segments or sea-sheds, by drawing cardinal lines from watershed borders in a 10-km offshore buffer using ArcMap v10. To address dilution of pollutants with increased distance from shore, LDI values were assigned unadjusted to coastal segments 0-2 km from shore, reduced by 50% in adjacent coastal segments 2-7 km from shore, and reduced by 70% in segments 7-10 km from shore.

Thermal anomalies

Satellite-derived, sea-surface temperature anomaly (SSTA) data was obtained from NOAA's Coral Reef Watch website (http://www.coralreefwatch.noaa.gov/satellite/bleaching5km/index.php). Annual composite, 5-km resolution SSTA files included all currently available data from 2014 – present day 2016. Files in NetCDF format were downloaded and converted to raster in ArcMap v10.3. Rasters were cropped to the geographic extent of Puerto Rico and a mean SSTA raster was calculated.

SSTA represents positive or negative deviations from average monthly climatology, which is based on historical records of mean monthly night-time SST values (Liu 2014).

Fishing pressure

Geospatial layers of fishing intensity were obtained from Manoj Shivlani (Shivlani and Koeneke 2011), who estimated commercial Puerto Rico fishing effort based on interviews with fishers. Participants were asked to map fishing areas they used, and the number of trips to each. Total fishing effort is the maximum potential number of trips to grid cells of approximate area of 3.3 km^2 for all gears including nets, lines, traps and dive gears (dive gears include spear guns and hand gathering by skin diving or scuba).

Integrated stressor index

Stressor estimates were combined by first converting the LDI and fishing effort polygon layers into rasters. Raster layers for LDI, fishing and SSTA were re-scaled from 0-1 using a linear function with the lowest values corresponding to 0 and the highest values to 1. Rasters were added using the raster calculator tool in ArcMap v10.3, Spatial Analyst toolbox.

Narrative stressor descriptions

Narrative stressor descriptions were developed for undisturbed (pristine), moderately stressed, and severely degraded states of LBSP, thermal anomalies, and fishing pressure. For LBSP these included land use characteristics for low, medium and high LDI watersheds, other conditions which were not represented by LDI such as runoff-related impaired water quality and sediment resuspension, and land conditions which exacerbate pollutant transport such as soil type and slope. Fishing pressure was described in terms of both the fishing activity and also the resulting change in fish populations which is relevant to the health of associated reef-building corals.

Results

Coastal LDI watershed values ranged from 1.2 – 5.7, with the highest values in North East Puerto Rico watersheds including the city of San Juan, the West coast near Mayaguez, and the South coast near Ponce, Santa Isabel, Salinas and Guayama (Fig. 2a). High LDI values in Northern receiving sea-sheds were driven by adjacent land areas containing dense human population and those in Western and Southern sea-sheds were driven by a combination of population and row crop agriculture.

Mean SSTA (2014 – 2016) for Puerto Rico ranged from 0.29 – 0.87ºC, and a pattern of lowest SSTA on the West and South West coasts was observed (Fig. 2b).

Commercial fishing effort was highest on the West coast, Southwest near La Parguera, Cabo Rojo, and Puerto Real; and also around the central North coastal area (Fig. 2c).

Summed, rescaled stressor indices reflected high LDI and fishing pressure near San Juan on the North and South-central coasts, high fishing pressure on Southwest coast and Vieques (Fig. 2d). The West coastal area was intermediate for integrated stressor index but fishing pressure was high in the region.

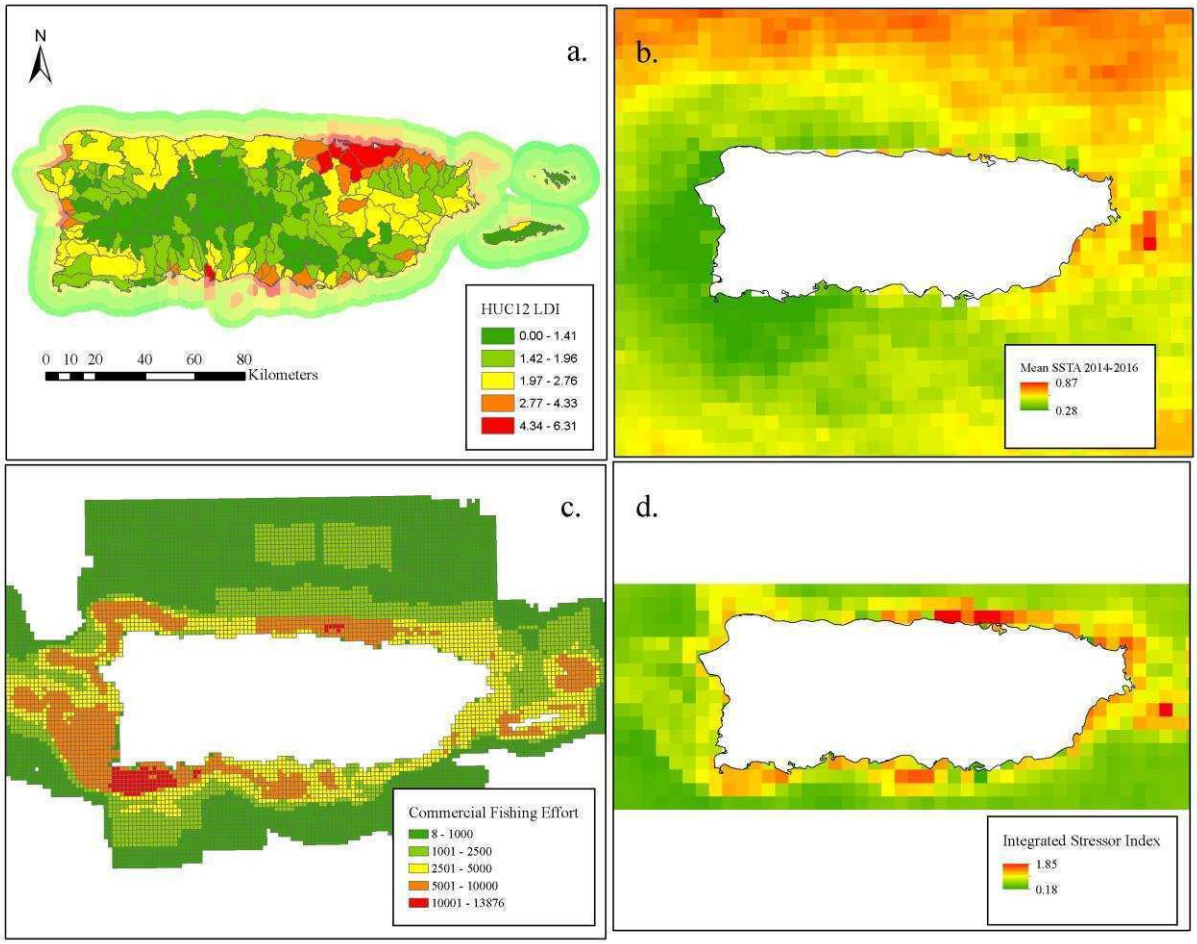

Fig. 2 **a**. Hydrologic Unit Code (HUC12) watersheds of Puerto Rico and associated LDI values. Offshore buffer zones show attenuated LDI value with increased distance from shore. **b**. NOAA Sea Surface Temperature Anomaly (SSTA), mean of monthly composites from 2014-2016. **c**. Total fishing effort modeled as maximum possible trips to each grid cell (Shivlani and Koeneke

Narrative stressor descriptions are presented in Table 1. For LBPS, soil and terrain characteristics which tend to accelerate runoff and increase sediment and pollutant transport to benthic habitats were included. Since the LDI is based on LULC, to avoid redundancy only those additional anthropogenic influences which are not LULC - related were included. Elevated temperature thresholds associated with coral bleaching were derived from literature accounts correlating bleaching with both the magnitude and duration of exposure to elevated sea surface temperature (Eakin et al. 2010; Heron et al., 2016). Fishing pressure was articulated in terms of relative fishing effort which pressures fishery sustainability, and also the resulting fish 2011). **d**. Integrated stressor index was calculated by re-scaling all three stressors (0-1) and summing for a maximum possible value of 3 community expected under varying fishing pressures in order to illustrate the indirect stress to associated corals.

Discussion

Three anthropogenic stressors (land-based sources of pollution, thermal anomalies, and fishing pressure were assembled in a spatially-explicit framework for Puerto Rico coral reef and not fisheries ecosystems, an initial step to support development of biocriteria to protect these unique and important habitats (Fore et al. 2009). Our expectation is that these stressor estimates will be fine-tuned and augmented as additional data becomes available. The LDI index was chosen as a proxy for LBSP, in part due to previous associations with coral condition in St. Croix (Oliver et al. 2011) and with wetland condition in Florida (Brown and Vivas 2005) and Ohio (Mack 2006).

However our narrative description for LBSP highlights land-based stressors which are represented in the LDI. For example, the presence of a wastewater treatment plant or coastal industry is represented in the LDI as a LULC class receiving a high LDI coefficient, but effluents originating from these facilities are not incorporated in LDI. Elevated nutrients are important coral stressors which have been associated with decline of reefs in relatively close proximity to developed coasts (Ennis et al. 2016). The LDI is based on 30-m resolution LULC data circa 2001, but 1-m resolution LULC imagery for Puerto Rico is anticipated in 2016 from the NOAA Coastal Change Analysis Program, allowing finer resolution and more current land cover for new LDI calculations, and possible application of land use changes as an indicator. In the future assumptions regarding the sea-shed transport of land-based pollutants should be refined by adjusting for ocean currents and river flow which affect distance and direction of offshore

Table 1 Narrative descriptions for three stressors representing undisturbed, moderately disturbed and severely disturbed states. For fishing pressure, both fishing activities and resulting fish community are presented. WWTP: Waste water treatment plant, BMP: best management practices

Stressor Level	Land-Based Sources of Pollution	Thermal Anomalies	Fishing Pressure
Undisturbed	Natural landscape conditions present in coastal watersheds. Coastal vegetation such as mangroves and riparian vegetation is intact. Human development absent: no impervious surfaces or facilities such as WWTPs, industries, ports or associated shipping activity. Sediment entry to coastal waters is attenuated by absorbant soil types, presence of coastal vegetation, or both. Area could be Marine Protected Area or Reserve. LDI < 1	Natural temperature regime for the area, no significant departures from normal climatology. DHW remains less than 4°C	Fishing by humans is absent Fish Community: Undisturbed. High diversity in taxa, balanced fish community in terms of size and abundance such that natural trophic interactions are sustained.
Moderately Disturbed	Low to medium density development, coastal industries and/or WWTPs may be present but if so, are compliant with discharge permits, have advanced levels of waste water treatment, and may incorporate biological filtration such as coastal wetlands. Impervious surfaces near the coast are considerable, and along with steep terrain and soils dominated by clays, result in frequent pulses of moderately elevated sediment levels to coastal benthic habitats. Agriculture activity may be broad pasture areas or moderate row crop areas, and BMPs are not universally employed to limit sediment / pollutant transport to marine environment. LDI = 2.01 – 3.0	Departures from normal temperature regime occasionally exceed 4°C-DHW but remain below 8°C-DHW	Fishing activities include a blend of commercial and recreational fishing at levels which are non-threatening to sustainable production. Effective fishing management, enforcement or some combination prevents significant loss of ecosystem functional attributes. Fish Community: Evident changes in structure due to loss of some rare native taxa; shifts in relative abundance of taxa but sensitive-ubiquitous taxa are common and abundant; ecosystem functions are fully maintained through redundant attributes of the system.
Severely Disturbed	Degraded landscape conditions include high percent impervious surface and high-density, near-coastal human development. Near-coastal row crop agriculture lacks BMPs. Sedimentation is severe due to degraded coastal and riparian vegetation and unmitigated land clearing practices, and sediment contains entrained nutrients and other chemical pollutants. Coastal WWTPs lack secondary treatment, and along with industrial discharges, 303(d)[1] listings of impaired water bodies under the CWA are common. Other human influences may include boat traffic in the form of shipping vessels, cruise ships, or recreational vessels which result in sediment resuspension in coastal benthic habitat areas. LDI > 5	Sustained elevated temperature relative to normal, periods exceeding 8°C-DHW	Intense commercial and recreational fishing pressure of reef fish species and pelagic species. Regulations to sustain fishery may be lacking or ignored; enforcement is nonexistent and illegal fishing is common. Gears used include fish traps or others with high bycatch mortality. Fish Community: Low species richness, diversity and abundance compared to other levels. Extremely high densities of tolerant opportunistic species may characterize these systems. Herbivores and apex predators are absent.

[1]Section 303(d) of the US Clean Water Act requires states and territories to submit lists of impaired waters which do not meet water quality standards.

influence, and incorporating shelf bathymetry which affects dispersal of runoff-transported sediment and other pollutants originating on land. Here, we applied simple assumptions of graded influence decay at 2, 7 and 10 km offshore which represent only a coarse estimate.

This analysis used 5-km resolution SSTA data, currently available as annual average composites from 2014 on, pending NOAA's release of additional blended satellite products which will increase retrospective spatial data presented in several ways on NOAA's Coral Reef Watch website. Although SSTA values may be positive or negative, NOAA presents positive deviations or HotSpot values, calculated by subtracting the maximum of monthly mean climatology, and a measure of "Degree Heating Weeks" (DHW) which is the sum of HotSpot values exceeding 1°C for a preceding 12 week period. We demonstrate the potential for SSTA at 5-km resolution to integrate with land-based pollution and fishing data on a reef scale during a time period when thermal-anomaly related coral bleaching was not widespread in Puerto Rico. If the cooler SST values seen in western Puerto Rico (Fig. 2b) persist during a bleaching event, it is possible that corals in those areas might be afforded some degree of protection. Narrative descriptions for thermal anomalies were informed by Eakin et al. (2010) and Heron et al. (2016) who demonstrated threshold DHW values associated with coral bleaching and related mortality, and also the potential for cumulative temperature stress over time to predict coral bleaching susceptibility.

Recreational fishing pressure is thought to be at least as important as commercial landings. We show spatial variation in commercial fishing effort that will be informed by new data when the recreational component of Puerto Rico's fishing law is implemented. In the interim, narrative stressor descriptions were developed for both commercial and recreational fishing activity, including regulatory effectiveness and enforcement capability (Table 1). Indirect effects of fishing pressure on corals were also presented in terms of the associated fish community because with the exception of damage to the reef from fishing gear such as anchors or fishing line, fishing activities do not impact reef corals directly yet lead to ecological dysfunction from overall fishery decline, herbivore reduction and associated algal proliferation on the reef (Hughes et al. 2007). Similarly, model development needs to include indirect effects of climate change-associated anomalies on fish communities, related to bleaching-related coral mortality and loss of reef habitat upon which fish depend for recruitment, refugia, and feeding (Coker et al. 2012; Ainsworth and Mumby 2015).

Simple assumptions (Davies and Jackson 2006) that ecosystem structure and function gradually falter with increased anthropogenic stress represent an accepted general pattern of ecosystem response which can generate testable hypotheses to refine single and cumulative-stressor effects (Hughes and Connell 1999; Ban et al. 2014). An approach to integrate world-scale reef stressors (Halpern et al. 2008; Burke et al. 2011) was used here by summing re-scaled stressor values (Fig. 2d), but future model development needs to consider more complex stressor interactions including weighting, synergistic or antagonistic effects. Observed contrasts in stressor patterns included South West Puerto Rico with low LDI and SSTA, yet high fishing pressure (Fig. 2a, 2b, 2c) A large proportion of Puerto Rico's coral reefs are found in the South West and establishing a no-take reserve has been suggested.

Further development of this multi-stressor model will render it useful to develop biological attributes for BCG levels (US EPA 2016; Santavy et al. in review), inform management decisions, prioritize collection of reef condition data and stressor information, and support stressor-response research studies. Recent guidance for BCG development (US EPA 2016) includes approaches and challenges to defining a generalized multi-stressor axis (x-axis of the BCG, Fig. 1) to represent the cumulative impact of anthropogenic stressors to reef ecosystems ranging from a pristine state to severely disturbed by human activities. Publically available spatial datasets may be employed to represent additional stressors as has been done for the Great Lakes Environmental Indicators project (Danz et al. 2005). Quantitative information on ecosystem condition and anthropogenic stressors for Puerto Rico coral reefs is limited by comparison, but initial steps can be taken. The U.S. Virgin Islands government has identified coral reefs and reef functions as designated uses under the CWA and defined biological integrity in a narrative context (USVI 2010). The foundation exists for Puerto Rico to take similar actions for setting condition thresholds or biocriteria, to protect its valuable coral reefs.

Acknowledgements

We acknowledge Bill Fisher (US EPA Office of Research and Development, Susan Jackson (US EPA Office of Water), Manoj Shivlani (who generously provided Puerto Rico fishing pressure GIS layers), and Amy Smith (US EPA Student Services contractor, for GIS assistance). David Kline (Session No. 36 chair, ICRS 2016) and 2 anonymous reviewers provided suggestions which greatly improved the manuscript.

References

Ainsworth CH, Mumby PJ (2015) Coral-algal phase shifts alter fish communities and reduce fisheries production. Glob Chang Biol 21:165-172

Ban SS, Graham NAJ, Connolly S (2014) Evidence for multiple stressor interactions and effects on coral reefs. Glob Chang Biol 20:681-697

Bradley P, Fisher W, Bell H, Davis W, Chan V, LoBue C, Wiltse W (2009) Development and implementation of coral reef biocriteria in U.S. jurisdictions. Environ Monit Assess 150:43-51

Bradley P, Santavy DL, Gerritsen J (2014) Workshop on Biological Integrity of Coral Reefs, August 21-22, 2012, Caribbean Coral Reef Institute, Isla Magueyes, La Parguera, Puerto Rico. US Environmental Protection Agency, Office of Research and Development, Atlantic Ecology Division, Narragansett, RI. EPA/600/R-13/350

Brown MT, Vivas MB (2005) Landscape development intensity index. Environ Monit Assess 101:289-309

Burke L, Reytar K, Spalding M, Perry A (2011) Reefs at risk revisited. World Resources Institute, Washington, DC

Coker DJ, Graham NAJ, Pratchett MS (2012) Interactive effects of live coral and structural complexity on the recruitment of reef fishes. Coral Reefs 31:919-927

Danz NP, Regal RR, Niemi GJ, Brady VJ, Hollenhorst T, Johnson LB, Host GE, Hanowski JM, Johnston CA, Brown T, Kingston J, Kelly JR (2005) Environmentally stratified sampling design for the development of Great Lakes environmental indicators. Environ Monit Assess 102:41-65

Davies SP, Jackson SK (2006) The biological condition gradient: A descriptive model for interpreting change in aquatic ecosystems. Ecol Appl 16:1251-1266

Eakin CM, Morgan JA, Heron SF, Smith TB, Liu G, Alvarez-Filip L, Baca B, Bartels E, Bastidas C, Bouchon C, Brandt M, Bruckner AW, Bunkley-Williams L, Cameron A, Causey BD, Chiappone M, Christensen TRL, Crabbe MJC, Day O, de la Guardia E, Diaz-Pulido G, DiResta D, Gil-Agudelo DL, Gilliam DS, Ginsburg RN, Gore S, Guzmán HM, Hendee JC, Hernández-Delgado EA, Husain E, Jeffrey CFG, Jones RJ, Jordán-Dahlgren E, Kaufman L, Kline DI, Kramer P, Lang JC, Lirman D, Mallela J, Manfrino C, Maréchal J-P, Marks K, Mihaly J, Miller WJ, Mueller EM, Muller EM, Orozco Toro CA, Oxenford HA, Ponce-Taylor D, Quinn N, Ritchie KB, Rodriguez S, Rodriguez Ramirez A, Romano S, Samhouri JF, Sánchez JA, Schmahl GP, Shank BV, Skirving WJ, Steiner

SCC, Villamizar E, Walsh SM, Walter C, Weil E, Williams EH, Woody Roberson K, Yusuf Y (2010) Caribbean corals in crisis: record thermal stress, bleaching, and mortality in 2005. PLoS ONE 5:e13969 [doi:10.1371/journal.pone.0013969]

Ennis RS, Brandt ME, Wilson KR, Smith TB (2016) Coral reef health response to chronic and acute changes in water quality in St. Thomas, United States Virgin Islands. Mar Pollut Bull 111:418-427

Fisher WS, Fore LS, Hutchins A, Quarles RL, Campbell JG, LoBue C, Davis WS (2008) Evaluation of stony coral indicators for coral reef management. Mar Pollut Bull 56:1737-1745

Fore LS, Karr JR, Fisher WS, Bradley P, Davis WS (2009) Heeding a call to action for US coral reefs: The untapped potential of the Clean Water Act. Mar Pollut Bull 58:1421-1423

Golbuu Y, Fabricius K, Victor S, Richmond RH (2008) Gradients in coral reef communities exposed to muddy river discharge in Pohnpei, Micronesia. Estuar Coast Shelf Sci 76:14-20

Halpern BS, Walbridge S, Selkoe KA, Kappel CV, Micheli F, D'Agrosa C, Bruno JF, Casey KS, Ebert C, Fox HE, Fujita R, Heinemann D, Lenihan HS, Madin EMP, Perry MT, Selig ER, Spalding M, Steneck R, Watson R (2008) A global map of human impact on marine ecosystems. Science 319:948-952

Heron SF, Johnston L, Liu G, Geiger EF, Maynard JA, De La Cour JL, Johnson S, Okano R, Benavente D, Burgess TFR, Iguel J, Perez D, Skirving WJ, Strong AE, Tirak K, Eakin CM (2016) Validation of reef-scale thermal stress satellite products for coral bleaching monitoring. Remote Sens 8(1): 59 [doi: 10.3390/rs8010059]

Homer C, Dewitz J, Fry J, Coan M, Hossain N, Larson C, Herold N, McKerrow A, VanDriel JN, Wickham J (2007) Completion of the 2001 National Land Cover Database for the Conterminous United States. Photogramm Eng Remote Sensing 73:337-341

Hughes TP, Connell JH (1999) Multiple stressors on coral reefs: A long-term perspective, Limnol Oceanogr 44:932-940

Hughes TP, Rodrigues MJ, Bellwood DR, Ceccarelli D, Hoegh-Guldberg O, McCook L, Moltschaniwskyj N, Pratchett MS, Steneck RS, Willis B (2007) Phase shifts, herbivory, and the resilience of coral reefs to climate change. Curr Biol 17:360-365

Janicki T (2013) Land development index (LDI) and cross-walk of Florida land use cover and classification system (FLUCCS) codes to LDI values. Attachment A in: Central Florida Water Initiative's Environmental Measures Team, Development of Environmental Measures for Assessing Effects of Water Level Changes on Lakes and Wetlands in the Central Florida Water Initiative Area, Final Report November 2013

Karr JR, Chu EW (1997) Biological Monitoring and Assessment: Using Multimetric Indexes Effectively. EPA 235-R97-001, University of Washington, Seattle

Kleypas JA, Buddemeier RW, Archer D, Gattuso J-P, Langdon C, Opdyke BN (1999) Geochemical consequences of increased carbon dioxide on coral reefs. Science 284:118-120

Liu G, Heron SF, Eakin CM, Muller-Karger FE, Vega-Rodriguez M, Guild LS, De La Cour JL, Geiger EF, Skirving WJ, Burgess TFR, Strong AE, Harris A, Maturi E, Ignatov A, Sapper J, Li J, Lynds S (2014) Reef-scale thermal stress monitoring of coral ecosystems: new 5-km global products from NOAA coral reef watch. Remote Sens 6:11579-11606, doi:10.3390/rs61111579

Mack JJ (2006) Landscape as a predictor of wetland condition: an evaluation of the Landscape Development Index (LDI) with a large reference wetland dataset from Ohio. Environ Monit Assess 120:221-241

Odum HT (1996) Environmental Accounting: Emergy and Environmental Decision Making. John Wiley and Sons, New York, 370 pp

Oliver LM, Lehrter JC, Fisher WS (2011) Relating landscape development intensity to coral reef condition in the watersheds of St. Croix, US Virgin Islands. Mar Ecol Prog Ser 427: 293-302

Rodgers KS, Kido MH, Jokiel PL, Edmonds T, Brown, EK (2012) Use of integrated landscape indicators to evaluate the health of linked watersheds and coral reef environments in the Hawaiian Islands. Environ Manage 50:21-30

Santavy DL, Bradley P, Gerritsen J, Oliver LM (2016) The biological condition gradient, a tool used for describing the condition of US coral reef ecosystems. Proceedings of the 13th International Coral Reef Symposium, Honolulu: 552-563

Shivlani M, Koeneke R (2011) Spatial characterization of artisanal fisheries in Puerto Rico: Geographic information systems (GIS) approach for assessing the regional effort and landings. Proc of the 63rd Gulf and Caribb Fish Inst., Nov 1-5, 2010

US EPA (2016) A Practitioner's Guide to the Biological Condition Gradient: A Framework to Describe Incremental Change in Aquatic Ecosystems. EPA 842-R-16-001, Washington, DC

USVI (US Virgin Islands) (2010) United States Virgin Islands 2010 Revisions to: Water Quality Standards Title 12, Chapter 7, Government of the Virgin Islands, Department of Planning and Natural Resources, Division of Environmental Protection, 22 pp

Session 75

Prevention, assessment, and mitigation of coral reef impacts resulting from planned and unplanned human activities

Session chairs:

Jocelyn Karazsia, jocelyn.karazsia@noaa.gov

Tom Moore, tom.moore@noaa.gov

Wendy Wiltse, Wiltse.Wendy@epa.gov

Santavy DL, Bradley P, Gerritsen J, Oliver L (2016) The biological condition gradient, a tool used for describing the condition of US coral reef ecosystems. Proceedings of the 13th International Coral Reef Symposium, Honolulu: 548-559

The biological condition gradient, a tool used for describing the condition of US coral reef ecosystems

Deborah L. Santavy, Patricia Bradley, Jeroen Gerritsen, and Leah Oliver

Abstract Understanding the effects of human activity on coral reef ecosystems requires knowing what characteristics constitute a high quality coral reef and identifying measurable criteria. The Biological Condition Gradient (BCG) is a conceptual model that describes how biological attributes of coral reefs change along a gradient of anthropogenic stress. The BCG provides a framework using qualitative and quantitative reef attributes to determine current coral reef conditions. Experts in coral reef assemblages (coral, fish, sponge, gorgonian, and algae) have defined a BCG model for Puerto Rico. The model describes the full range of biological conditions resulting from human disturbance, including community structure, organism condition, ecosystem function and connectivity. Each condition level is defined in terms of biological integrity, which is the biological condition comparable to undisturbed or minimally disturbed conditions caused by human influence. Each level contains a detailed narrative and decision rules for translating the narrative into specific metric scores. Reference condition is a natural fully-functioning coral reef that serves as a non-shifting baseline that is established through expert consensus. Managers can use the BCG model to assess current conditions relative to high quality coral reefs, track changes in condition as responses to management actions, and communicate environmental condition and outcomes to the public. BCG levels can be aligned with designated aquatic life uses specified in water quality standards and used for protection and potential restoration of coral reefs. The BCG model will be broadly applicable to Caribbean reefs, and the process is transferable to other oceanic regions.

Key Words: biological condition gradient, biological criteria, biocriteria, protection coral reefs, Clean Water Act, thresholds

---

Deborah L. Santavy, Leah Oliver
US Environmental Protection Agency, Gulf Ecology Division, ORD, 1 Sabine Island Dr,Gulf Breeze, FL. 32561 USA

Patricia Bradley, Jeroen Gerritsen
Tetra Tech, Inc., Owing Mills, MD., USA

Communicating author: DL Santavy santavy.debbie@epa.gov

Introduction

One of the most influential legal mechanisms available for aquatic resource protection is the U.S. Clean Water Act (CWA) (33 U.S.C. 1251 et seq. 1972), which grants regulatory authorities to the U.S. Environmental Protection Agency (USEPA) to protect the integrity of the Nation's waters (USEPA 2016). The CWA purview includes biological components such as coral reefs that lie within the limit of the territorial seas (Jameson et al. 2001). One authority granted to USEPA is to prevent waterbody degradation or restore habitat quality through the CWA Section 101 (a) (Frey 1977; USEPA 2002). This authority allows decisions to curtail or modify deleterious anthropogenic activities "to restore and maintain the chemical, physical and biological integrity of the nation's waters." Many facets of the CWA are already employed in maintaining high water quality imperative for coral reef persistence (USEPA 2016). However, the broad authority of the CWA is not being used to its full potential for reef protection (Fore et al. 2009; Bradley et al. 2010).

Understanding the effects of human activity on coral reefs requires knowing what attributes constitute high quality coral reefs and identifying measurable criteria. Restoring and maintaining biological integrity is a long-term CWA objective, and like its physical and chemical counterparts, biological criteria can be defined to protect valued biological communities (Davies and Jackson 2006). Biological integrity is the capacity to support and maintain a balanced, integrated, and adaptive community of organisms having a species composition, diversity, and functional organization comparable to the natural habitats within a region (Karr and Dudley 1981). The process includes classifying habitat types, using quantitative measures of species composition, diversity and functional organization; and comparing existing waterbody condition to natural or undisturbed reference conditions (Davis and Simon 2004).

To achieve CWA objectives, the USEPA, States, US Territories, regulated industries, municipalities, and public need comprehensive information about the biological integrity of aquatic environments to complement the physical and chemical integrity. The USEPA has worked with scientists to adapt a conceptual model known as the biological condition gradient (BCG) to protect the biological integrity of tropical Caribbean waters, including marine coastal habitats such as mangroves, seagrasses and coral reefs (Bradley et al. 2014; Bradley and Santavy

2016). The BCG is a conceptual model that describes how biological attributes of coral reefs change along a gradient of anthropogenic stress (Figure 1). The BCG relates the biological responses to increasing levels of anthropogenic stress relative to a baseline anchored in natural condition or minimally disturbed (Karr 1991; Davies and Jackson 2006; USEPA 2016). This framework defines qualitative and quantitative reef attributes to assess the biological condition and ecological state of a coral reef by defining multiple levels of biological responses to increasing anthropogenic stress. BCG level 1 represents the highest condition level or full biological integrity with ideally no anthropogenic stress, and BCG level 6 represents the poorest biological condition impacted by the greatest anthropogenic stress (Fig. 1). Threshold levels can be both numeric values and narrative descriptions dependent on the scientific information available, and they are intended to be protective of the biological integrity of aquatic life inhabiting the waterbody. The BCG model provides guidance to decide whether the biological condition of a coral reef is improving or declining relative to these acceptable threshold levels.

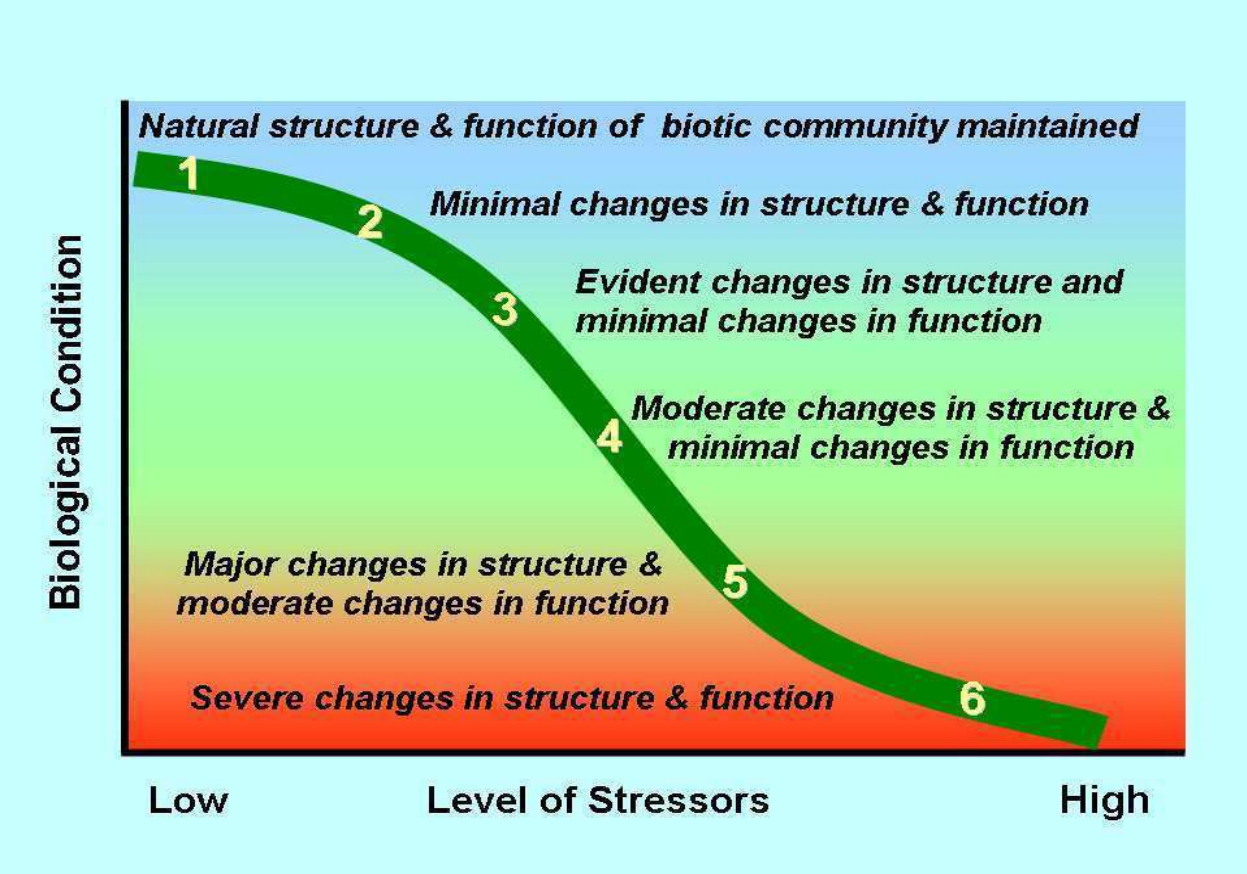

Fig. 1 Conceptual model of the biological condition gradient that describes how biological attributes of coral reefs change along a gradient of anthropogenic stress

The BCG framework allows biological condition to be interpreted independent of assessment methods. Currently, the BCG is used nationally for the management of freshwater ecosystems to communicate to the public and other interested stakeholders the status of aquatic resources and their potential for restoration. To date, almost all applications are in freshwater streams, rivers, and lakes bounded by land. A BCG model is formulated based on expert consensus using best professional judgment. An expert panel works together to define the thresholds at each biological condition level using narrative descriptions. Next, numeric thresholds are developed using bioassessment data to calculate threshold values grounded in the early narrative formulations. Application of the BCG conceptual framework, narrative descriptions developed by experts for qualitative rankings, habitat classifications, and assignment of important reef attributes are presented for fish and coral models.

Materials and methods

USEPA focused on southwestern Puerto Rico to test proof-of-concept, develop, calibrate, and eventually validate the BCG model to support biocriteria development for Caribbean coral reef systems. An expert panel of coral reef scientists participated in three workshops and multiple webinars to elicit best professional judgment to develop narrative and ultimately numeric biocriteria to define multiple BCG condition levels (Bradley et al 2014; Bradley and Santavy 2016). In the first workshop, underwater videos and photographs were viewed by experts to elicit important coral reef attributes to define coral reef condition. This approach allowed experts to draw on their individual and combined knowledge and expertise, without getting mired in CWA and biocriteria concepts and terminology. Linear coral reefs were selected from habitat maps by Kendall et al. 2001. Sites selected for expert review spanned the full range of conditions observed in the data set. Experts rated coral reef condition for 12 stations as either good, fair or poor based on the photos and videos considering all aspects of reef condition and health. They were instructed to document specific characteristics indicative of conditions for corals, sponges, gorgonians, fish, algae, reef rugosity, and topographical heterogeneity. Afterwards, group deliberations used their individual evaluations to focus on identifying common attributes with narrative language to differentiate each level.

During the second and third workshops, two separate BCG models were constructed independently - one for fish communities built by fish experts and the other for scleractinian corals built by coral experts. Each group worked from the narrative descriptive BCG model developed in the first workshop with the ultimate goal of creating a quantitative model with decision rules for threshold levels. Bioassessment data for fish and coral communities were used with sites located along a stressor gradient ranging from low to high land-based stressor levels in similar habitat types for each community (Santavy et al. 2012; Bradley and Santavy 2016). Ideally, data should include the full range of conditions and complement of stressors (e.g., pollution sources, fishing pressure, habitat disturbances, etc.) found at the regional level, such that the full gradient of the responses of the assemblages were included in model development. Since natural, regional, and habitat characteristics affect coral species composition of undisturbed waterbodies, a critical step required habitat classification of natural conditions to the extent they affect structures of fish and benthic communities (USEPA 2016).

The first step for BCG calibration was assigning taxa to BCG attributes I-V (Table 1), based on species sensitivity and tolerances to the most important stressors recommended by the experts. The BCG attribute definitions were those developed for freshwater systems (Table 1). Each taxon was evaluated for: sensitivity and tolerance to anthropogenic stressors, rarity, and endemism (Davies and Jackson; 2006; USEPA 2016). Experts assigned all fish and scleractinian coral taxa present in Puerto Rican bioassessment data from USEPA surveys in 2010 and 2011

Table 1 Ecological attributes used in freshwater BCGs for fish and benthic infauna communities (USEPA 2016)

Attribute	Description
I	Historically documented, sensitive, long-lived or regionally endemic taxa
II	Highly sensitive taxa
III	Intermediate sensitive taxa
IV	Taxa of intermediate tolerance
V	Tolerant taxa
VI	Non-native species
VII	Organism condition
VIII	Ecosystem function
IX	Spatial and temporal extent of detrimental effects
X	Ecosystem connectivity

(Bradley and Santavy 2016). Next, experts assigned BCG biological condition levels (1-6) to each reef site using results from the more complex data-driven analyses and the BCG attribute (I-V) assignments. As more sites were assigned to BCG condition levels, the experts were providing more complex data-driven analyses for improving and informing their judgements to rate additional sites. After condition assignments were made to multiple sites which represented a range of anthropogenic stressors, the experts' rationale for their assignments were carefully documented. This allowed decision rules to emerge for distinguishing different quantitative BCG levels.

Results and Discussion

The first workshop provided proof of concept that the BCG framework could be adapted for coral reef ecosystems (Bradley et al. 2014). During the first workshop, the coral reef experts collectively developed preliminary narratives for defining four BCG condition levels ranging from very good to excellent, good, fair, and poor (Fig. 2) while documenting specific attributes. Using underwater videos, the experts defined eight individual traits into four levels of biological condition. They rated the first level as very good to excellent condition, representing full biological integrity, and it anchored the other condition levels. This condition level was considered by the experts as comparable to levels 1 and 2 of the BCG conceptual model. The second level was considered good condition by the experts as comparable to BCG Level 3. The third level was rated as fair condition and comparable to BCG level 4. The worst condition level was comparable to BCG levels 5 and 6 and considered to be highly degraded.

The experts identified eight narrative attributes used for describing each BCG level. The narrative attributes were: physical structure of the reef which is the topographical heterogeneity, roughness or rugosity of the reef surface; coral characteristics including species, shape, size, and population demographics; sponge and gorgonian characteristics of shape, size and potential for habitat provision; coral condition which is considered the amount of live tissue present and extent of disease, bleaching and tumors; fish abundance, biomass and trophic interactions; the presence of other vertebrates focusing on charismatic megafauna; selected invertebrates including *Diadema antillarum*, conchs, lobsters, and crabs; and finally algae ranging from

calcareous crustose and coralline algae, filamentous microalgae, to fleshy turf algae; and submerged aquatic vegetation.

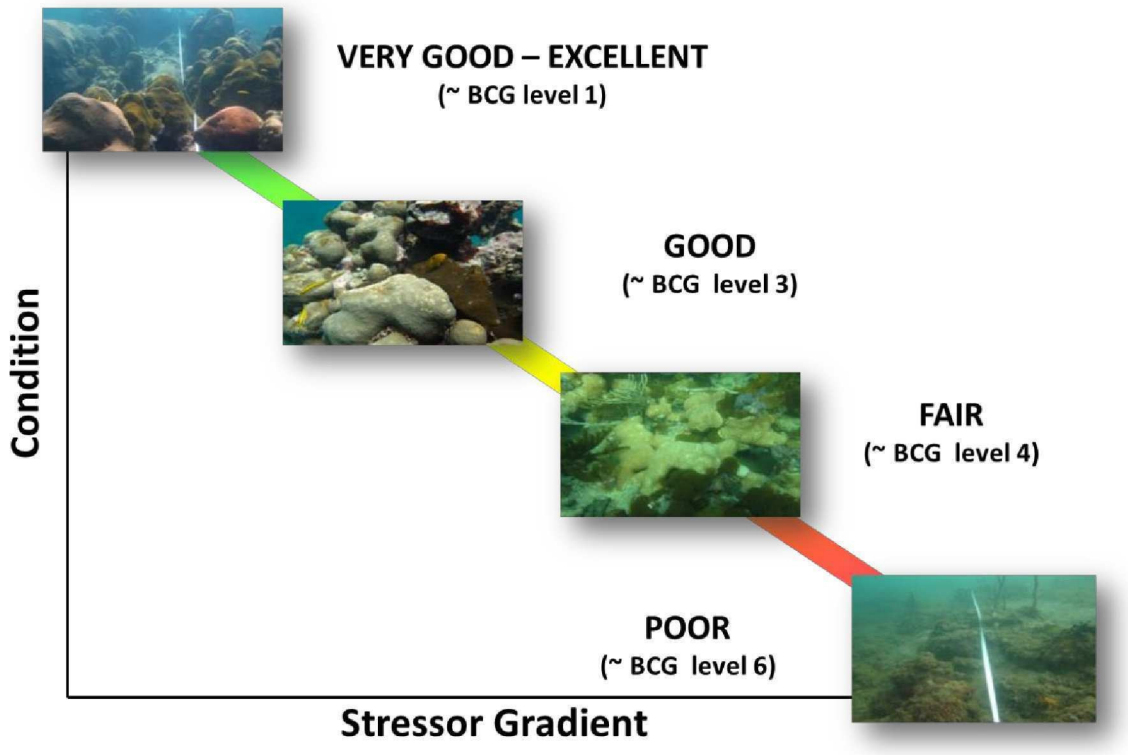

Fig. 2 Conceptual BCG developed during the 1st workshop, using site photos to represent BCG levels in Puerto Rico. Experts agreed natural site equivalent to BCG level 1 is not present in Puerto Rico today

The experts used these eight attributes to describe four coral reef condition levels (Table 2). The best biological condition was grounded in natural, undisturbed condition, represented by high rugosity and species diversity; large colonies of *Orbicella* spp. with high tissue coverage; and balanced population structure that included more corals than gorgonians. The highest quality communities contained large autotrophic and highly sensitive sponge species and low prevalence of disease or tumors in benthic communities. Crustose coralline algae were abundant, and other invertebrates were present (lobster, small crustaceans, and polychaetes), with some large sensitive anemone species. The worst condition had low structure and rugosity, turbid water and sediment films. If coral colonies were present, they were small and highly tolerant species. Heterotrophic, tolerant sponges were buried in sediment. Sediment-dwelling organisms such as

polychaetes and holothurians dominated the substrate with few or no reef invertebrates. If algae were present, it was fleshy macroalgae, with little or no turf or calcareous algae. Crustose coralline algae were absent.

Table 2 Narrative descriptions for eight attributes proposed by coral reef experts to define four BCG condition levels for Puerto Rico linear reefs. (adapted from Davies and Jackson, 2006)

Condition level	Attribute descriptions
Very Good Excellent (approximate BCG Level 1–2)	**Physical structure:** High rugosity or 3D structure; substantial reef built above bedrock; many irregular surfaces provide habitat for fish; very clear water; no sediment, flocs or films
	Corals: High species diversity including rare; large old colonies (*Orbicella*) with high tissue coverage; balanced population structure (old and middle-sized colonies, recruits); *Acropora* thickets present
	Gorgonians: Gorgonians present but subdominant to corals
	Sponges: Large autotrophic and highly sensitive sponges abundant
	Fish: Populations have balanced species abundances, sizes and trophic interactions
	Large vertebrates: Large, long-lived species present and diverse (turtles, eels, sharks)
	Other invertebrates: *Diadema,* lobster, small crustaceans and polychaetes abundant; some large sensitive anemone species present
	Algae: Crustose coralline algae abundant; turf algae present but cropped and grazed by *Diadema* and herbivorous fish; low abundance of fleshy algae
	Condition: Low prevalence of disease and tumors; mostly live tissue on colonies
Good (approximate BCG Level 3)	**Physical structure:** Moderate to high rugosity; moderate reef built above bedrock; some irregular cover for fish habitat; water slightly turbid; low sediment, flocs or films on substrate
	Corals: Moderate coral diversity; large old colonies (*Orbicella*) with some tissue loss; varied population structure (usually old colonies, few middle aged and some recruits); *Acropora* thickets may be present; rare species absent
	Gorgonians: Gorgonians more abundant than Levels 1–2
	Sponges: Autotrophic species present but highly sensitive species missing
	Fish: Decline of large apex predators (e.g., groupers, snappers) noticeable; small reef fishes more abundant
	Large vertebrates: Large, long-lived species locally extirpated (turtles, eels)
	Other invertebrates: *Diadema,* lobster, small crustaceans and polychaetes less abundant than Levels 1–2; large sensitive anemone species absent
	Algae: Crustose coralline algae present but fewer than Levels 1–2; turf algae present and longer, more fleshy algae present than Levels 1–2
	Condition: Disease and tumor presence slightly above background level; more colonies have irregular tissue loss
Fair (approximate	**Physical structure:** Low rugosity; limited reef built above bedrock; erosion of reef structure obvious; water turbid; more sediment accumulation, flocs and films; *Acropora* usually gone or present as rubble for recruitment substrate

BCG Level 4)	**Corals:** Reduced coral diversity; emergence of tolerant species, few or no living large old colonies (*Orbicella*); *Acropora* thickets gone, large remnants mostly dead with long uncropped turf algae
	Gorgonians: Gorgonians more abundant than Levels 1–3, replacing sensitive coral and sponge species
	Sponges: Mostly heterotrophic tolerant species and clionids
	Fish: Absence of small reef fishes (mostly Damselfish remain)
	Large vertebrates: Large, long-lived species locally extirpated (turtles, eels)
	Other invertebrates: *Diadema* absent; *Palythoa* overgrowing corals; crustaceans, polychaetes and sensitive anemones conspicuously absent
	Algae: Some coralline algae present but no crustose algae; turf is uncropped, covered in sediment; abundant fleshy algae (e.g., *Dictyota*) with high diversity
	Condition: High evidence of diseased corals, sponges, gorgonians; evidence high of mortality; usually less tissue than dead portions on colonies
Poor (approximate BCG Level 6)	**Physical structure:** Very low rugosity; no or little reef built above bedrock; no or low relief for fish habitat; very turbid water; thick sediment film and thick floc covering bottom; no substrate for recruits
	Corals: Absence of colonies, those present are small; only highly tolerant species with little or no live tissue
	Gorgonians: Small and sparse colonies; mostly small sea fans; often diseased
	Sponges: Heterotrophic sponges buried deep in sediment; highly tolerant species
	Fish: No large fishes; only a few tolerant species remain; lack of multiple trophic levels
	Large vertebrates: Usually devoid of vertebrates other than fishes
	Other invertebrates: Few or no reef invertebrates; high abundance of sediment dwelling organisms such as polychaetes and holothurians
	Algae: High cover of fleshy algae (*Dictyota)*; complete absence of crustose coralline algae
	Condition: High incidence of disease and low or no tissue coverage on small colonies of corals, sponges and gorgonians, if present

During the second and third workshop, the fish and coral experts worked on two separate BCG models. Development of the coral reef fish BCG model was more adaptable to the freshwater systems framework. Fish experts agreed upon two habitat classifications - sites containing coral reefs and all other hard-bottom habitats. Fish experts considered land-based sedimentation and fishing pressure as the two greatest threats to fish communities in this region, and they assigned 138 fish species to the five BCG attributes. The results from these assignments are too numerous to present here, but they are detailed in Bradley and Santavy 2016. The fish experts will be testing numeric criteria soon to test the fish BCG model for coral reefs to set preliminary model conditions for developing biocriteria for Puerto Rico.

The application of the freshwater BCG tolerance attributes to coral taxa presented a much greater challenge. The coral experts agreed elevated sea temperature and land-based sources of pollution present the most serious threats for Caribbean scleractinian corals. Coral experts had lower confidence in scleractinian coral taxa assignments to BCG attributes I-V and chose to evaluate each taxon for each stressor separately (Bradley and Santavy 2016). During initial attempts to assign species to a BCG attribute, the coral experts contended with reef habitat classification. They held discussions focused on defining expectations of which coral species should be found in different reef zones. Many reef traits were considered because reefs have distinct horizontal and vertical zones created by differences in depth, wave and current energy, temperature, light, and many other habitat characteristics (Zitello et al. 2009). The experts considered several different reef classification systems in an attempt to incorporate most of the critical reef traits discussed (Adey and Burke 1976; Hubbard et al. 2009). They agreed to use the latest edition of NOAA's benthic habitat reef classification as guidance (Zitello et al. 2009), and only use the fore-reef zone for assigning sites to BCG condition levels using the Costa et al. 2013 definition.

The coral experts decided the stressor tolerance attributes (I–V) developed for the freshwater BCGs (Table 1), did not apply very well to coral reef benthic communities. The experts believed tolerances of scleractinian coral species varied based on the individual stressor, and when exposed to multiple stressors the effects could be additive, neutral or synergistic but are largely unknown. The coral experts ultimately recommended focusing on eight narrative attributes developed during the first workshop (Table 2) to assign sites to BCG condition levels. The coral experts all agreed additional benthic assemblages rather than just scleractinian corals should be used. They changed the coral BCG to the benthic BCG model, and recommended inclusion of sponges, gorgonians, algae, organism condition especially disease and coral bleaching, and other reef invertebrates.

Historically water quality management programs and regulatory agencies attempted to protect aquatic life primarily through chemical and physical water criteria alone (USEPA 2002, 2016). Unlike chemical or physical criteria, biocriteria do not require individual threshold values for each and every stressor. The biological response to its environment integrates cumulative impacts of multiple stressors which might be better indicators of ecosystem condition, rather than only relying on established nutrient or physical stressor limits, which might not be protective of

sensitive coral reefs (Bradley et al. 2010; Oliver et al. herein). Coral reef biocriteria are used to benchmark biological conditions required for aquatic life use, and allow bioassessment information to directly link management actions to desired biological goals and endpoints. Often the consequences of management decisions are far-reaching influencing not only inland watersheds but also coastal environments (Bradley et al. 2010).

Acknowledgements

We acknowledge Susan K. Jackson and Kennard Potts (USEPA, Office of Water), William Fisher (USEPA Office of Research and Development), Evelyn Huertas (USEPA Region 2 Caribbean Office) and all the coral reef experts who have contributed their valuable time, expertise, and discussions to develop the coral reef BCG. We thank Jocelyn Karazsia and Wendy Wiltse (session #75 chairs, ICRS 2016) and two anonymous reviewers who provided suggestions which greatly improved the manuscript.

References

Adey W, Burke RB (1976) Holocene bioherms (algal ridges and bank barrier reefs) of the eastern Caribbean. Geol Soc Am Bull 87:95–109

Bradley P, Fore L, Fisher W, Davis W (2010) Coral Reef Biological Criteria: Using the Clean Water Act to Protect a National Treasure. EPA/600/R-10/054. WashDC

Bradley P, Santavy DL (2016) Caribbean Coral Reefs: Benchmarking a Biological Condition Gradient for Puerto Rican Coral Reefs. In: Appendices to: A Practitioner's Guide to the Biological Condition Gradient: A Framework to Describe Incremental Change in Aquatic Ecosystems. EPA 842-R-16-001. pp. B-53 – B-76

Bradley P, Santavy DL, Gerritsen J (2014) Workshop on Biological Integrity of Coral Reefs, August 21–22, 2012, Caribbean Coral Reef Institute, Isla Magueyes, La Parguera, Puerto Rico. EPA/600/R-13/350. WashDC

Costa BM, Kendall MS, Edwards K, Kagesten G, Battista, TA (2013) Benthic Habitats of Fish Bay, Coral Bay, and the St Thomas East End Reserve. NOAA Tech Mem NOS NCCOS 175. Silver Spring, MD

Davies SP, Jackson SK (2006) The Biological Condition Gradient: a descriptive model for interpreting change in aquatic ecosystems. Ecol Appl 16:1251–1266

Davis WS and Simon TP (2004) Biological assessment and criteria: tools for water resource planning and decision making. CRC Press, Inc. Boca Raton, FL

Fore LS, Karr JR, Fisher WS, Bradley P, Davis WS (2009) Heeding a call to action for US coral reefs: The untapped potential of the Clean Water Act. Mar Poll Bull 58:1421-1423

Frey DG (1977) Biological Integrity, a Historical Approach. In The Integrity of Water, Proceedings of a Symposium, ed. RK Ballentine and LJ Guarraia, USEPA, WashDC, March 10–12, 1975, pp. 127–140

Hubbard D, Ramirez W, Cuevas D, Erickson T, Estep A (2009) Holocene reef accretion along the north side of Bahia Enriquillo (western Dominican Republic): Unique insights into patterns of reef development in response to sea-level rise. Proc 11th Int Coral Reef Symp1:43-47

Jameson SC, Erdmann MV, Karr JR, Gibson GR, Potts KW (2001) Charting a course toward diagnostic monitoring: a continuing review of coral reef attributes and a research strategy for creating coral reef indexes of biotic integrity. Bull Mar Sci 69:701- 744

Karr JR (1991) Biological integrity: A long-neglected aspect of water resource management. Ecol Appl 1:66–84

Karr JR, Dudley DN (1981) Ecological perspective on water quality goals. Environ Manag 5:55-68

Kendall MS, Monaco ME, Buja KR, Christensen JD, Kruer CR, Finkbeiner M, Warner RA (2001) Methods used to map the benthic habitats of Puerto Rico. NOAA Technical Memorandum NOS NCCOS CCMA 152

Oliver LM, Santavy DS, Bradley P (2016) Developing a multi-stressor gradient model for coral reefs of Puerto Rico. Proceedings of the 13th International Coral Reef Symposium, Honolulu: 246-261

Santavy DL, Fisher WS, Campbell JG, Quarles RL (2012) Field Manual for Coral Reef Assessments. US Environmental Protection Agency, Office of Research and Development, Gulf Ecology Division, Gulf Breeze, FL. EPA/600/R-12/029. WashDC

USEPA (2002) Biological Assessments and Criteria: Crucial Components of Water Quality Programs. EPA 822-F-02-006. WashDC

USEPA (2016) A Practitioner's Guide to the Biological Condition Gradient: A Framework to Describe Incremental Change in Aquatic Ecosystems. EPA 842-R-16-001. WashDC

Zitello AG, Bauer LJ, Battista TA, Mueller PW, Kendall, MS, Monaco, ME (2009) Shallow-water benthic habitats of St John, USVI. NOAA Tech Mem NOS NCCOS 96. Silver Spring, MD

Supporting Documentation – 2019 STAA Nomination

Oliver et. al "Development of multi- and integrated-stressor models to support coral reef condition assessment and management"

Journal statistics information (Immediacy Index; Citation of Life; Impact Factor) for 2 of the papers in this STAA nomination:

(Paper #2) Oliver, L.M., Santavy, D.L., Bradley, P. (2016) Developing a multi-stressor gradient model for coral reefs of Puerto Rico. 13th ICRS, Honolulu. Published by the *International Society for Reef Studies.* 245 – 257. (Published 6/24/2016). Available at: http://coralreefs.org/publications/icrs-2016-proceedings/

> Statistics (Immediacy Index; Citation of Life; Impact Factor) do not exist for this Conference Proceedings from the *International Society for Reef Studies*. Note: After internal EPA peer review, this paper was externally and anonymously peer-reviewed as per: http://coralreefs.org/publications/icrs-2016-proceedings/. "All contributions have been subject to the normal editorial processes, including refereeing."

(Paper #3) Santavy, D.L., Bradley, P., Gerritsen, J., Oliver, L. (2016) The biological condition gradient, a tool used for describing the condition of US coral reef ecosystems. 13th ICRS, Honolulu. Published by the *International Society for Reef Studies*. 548 – 559. (Published 6/24/2016). Available at: http://coralreefs.org/publications/icrs-2016-proceedings/

> Statistics (Immediacy Index; Citation of Life; Impact Factor) do not exist for this Conference Proceedings from the *International Society for Reef Studies*. Note: After internal EPA peer review, this paper was externally and anonymously peer-reviewed as per: http://coralreefs.org/publications/icrs-2016-proceedings/. "All contributions have been subject to the normal editorial processes, including refereeing."

Concurrence Correspondence: Oliver et al STAA Nomination Package, April 2020

Original Email requesting concurrence from co-authors:

From: Oliver, Leah <Oliver.Leah@epa.gov>
Sent: Tuesday, April 28, 2020 1:45 PM
To: Santavy, Debbie <Santavy.Debbie@epa.gov>; Fisher, Bill <Fisher.William@epa.gov>; Patricia Bradley <patbradley@comcast.net>; Jeroen Gerritsen (jeroen.gerritsen@tetratech.com) <jeroen.gerritsen@tetratech.com>; leska.fore@gmail.com; Amelia Smith <amelia.smith4815@gmail.com>
Subject: STAA 2020 Submission – need reply by Wed night, please!

Dear Colleagues,

I hope you and you families are healthy and not affected by COVID-19.

I am preparing a submission for the 2020 STAA awards for three manuscripts for which each of you contributed. A requirement of the submission is an assessment of the contribution of each author to the publications. My assessment is listed below. If you agree with my assessment please send a return email to me stated that you agree with the assessment. I need to complete all the awards paper by Thursday morning, so please reply by Wednesday night if at all possible. Thanks in advance.

(1) Oliver, L. M., Fisher, W. S., Fore, L., Smith, A., & Bradley, P. (2018). Assessing land use, sedimentation, and water quality stressors as predictors of coral reef condition in St. Thomas, US Virgin Islands. *Environmental Monitoring and Assessment*, 190(4), 213.

Oliver: 30 %
Fisher: 15 %
Fore: 15 %
Smith: 25 %
Bradley: 15 %

(2) Oliver, L.M., Santavy, D.L., Bradley, P. (2016) Developing a multi-stressor gradient model for coral reefs of Puerto Rico. 13th ICRS, Honolulu. Published by the International Society for Reef Studies. 245 – 257. Available at: http://coralreefs.org/publications/icrs-2016-proceedings/

Oliver: 50 %

Santavy: 25 %

Bradley: 25 %

(3) Santavy, D.L., Bradley, P., Gerritsen, J., Oliver, L. (2016) The biological condition gradient, a tool used for describing the condition of US coral reef ecosystems. 13th ICRS, Honolulu. Published by the International Society for Reef Studies. 548 – 559. Available at: http://coralreefs.org/publications/icrs-2016-proceedings/

Santavy: 40 %

Bradley: 20 %
Gerritsen: 20 %

Oliver: 20 %

Leah Oliver

Research Aquatic Biologist

U.S. EPA/ORD/CEMM/GEMMD

1 Sabine Island Dr.

Gulf Breeze, FL 32501

ph. 850 934-2470

fax 850 934-2402

Co-Author Responses:

Santavy: received Tuesday, April 28, 2020 at 1:55 pm

Hi Leah,

I agree to the author assessment for me below. Jeroen Gerritsen has retired a number of years ago and I do not have a current email address, sorry. Pat might be slow to respond she is out with a migraine. Debbie

Bradley: received Tuesday, April 28, 2020 at 2:15 pm

Leah - I concur with percentages.

Pat

Gerritsen: received Tuesday, April 28, 2020 at 3:18 pm

Hi Leah,

Yes, I agree with your estimates of relative contributions.

Please give my regards to Debbie and Bill as well.

Best regards,

Jeroen Gerritsen

Fisher: received Wednesday, April 29, 2020 at 10:30 am

Hi Leah, thanks for the text reminder….of course this is OK with me. Thanks to you and Matt for handling.

All's well here and hope the same for you…

Bill

Fore: received Wednesday, April 29, 2020 at 10:43am

Hi, Leah, yes we are all well here. Nice to hear that you are too.

This breakdown looks fine to me. I respond "OK!"

Thank you for your commitment to bringing all this good science forward.

Best,

Leska

Smith: received Wednesday, April 29, 2020 at 11:51 am

Looks good to me! Thanks, Leah!

~Amy

Oliver: Wednesday, April 29 at 3:15 pm

I concur with the % contributions for all 3 manuscripts in this nomination.

Table of Contents

General_Authors_Publications.....2
JS__STAA_award_nomination_for_the_uranium_paper.....12
MG__STAA_award_nomination_for_the_uranium_paper.....13
Arzuaga_et_al_2010.....15

United States Environmental Protection Agency
Washington, DC 20460

STAA REPORT FOR THE SCIENTIST NOMINATIONS

General Information:

Nomination ID/App ID:	20-121
Research Category Primary:	Health Effects Research and Human Health Risk Assessment (HE)
Research Category Secondary:	Review Articles (RA)
Laboratory/Office Name:	ORD
Nomination Entered By:	Xabier Arzuaga Andino

Eligibility Checklist:

[Y] The nominated publication(s) has not been submitted to a previous STAA competition.

[Y] The nominated publication(s) was published on or before January 1, 2017 and on or after January 1,2012

[Y] The principal author was an EPA employee or a PHS employee assigned to EPA when the research was performed

[Y] The EPA authors (includes PHS employees assigned to EPA) contributed collectively a minimum of 50% toward the publication(s)

Nominating Official Name:	Xabier Arzuaga Andino
Nominating Official Title:	TOXICOLOGIST
Nominating OfficialEmail:	arzuaga.xabier@epa.gov
STAA Coordinator Name:	Kathleen Wiser
STAA Coordinator Email:	wiser.kathi@epa.gov

Justifications:

Justification 1:

The nominated review paper publication provides a case study for the application of the mode of action analysis approach to investigate the potential mechanisms and human relevance of uranium induced non-cancer effects. The mode of action analysis in this paper also helped reveal important data gaps and particularly vulnerable sections of the population. Uranium exposure alters the processes of bone modeling and remodeling; thus, early life stages are susceptible to uranium-induced osteotoxicity. Furthermore, during aging there is a shift in the ratio of bone mineralization versus erosion in bone remodeling, resulting in decreased bone mineralization and increased bone fragility; thus, the elderly may also represent a susceptible population to uranium-induced bone toxicity. Therefore, in addition to assessing the potential nephrotoxic effects of uranium in exposed human populations, epidemiological studies could also consider evaluating indicators of mineral homeostasis and bone health such as Vitamin D, BMD, and serum and urinary levels of biomarkers of bone formation and resorption.

This product furthers the Agency’s core mission to ensure that Americans have clean air, land and water and that national efforts to reduce environmental risks are based on the best available scientific information (https://www.epa.gov/aboutepa/our-mission-and-what-we-do) by advancing improved hazard characterization and risk assessment practices. This publication has been cited in 20 documents including primary research publications investigating uranium-induced developmental and skeletal effects as well as several foreign government guidelines and reports which reviewing the potential human health hazards associated with uranium exposure (see citation list below). The research describe in this publication was funded by the Office of Research and Development/National Center for Environmental Assessment. This publication was not previously nominated for any EPA or external award. According to Google Scholar this review paper has 17 citations, this does not include citations from government agencies outside the US (see complete citation list below).

This work relies on a prior manuscript, published in 2010 and therefore not included in this award application, that reviewed the epidemiological and experimental data on the renal effects of exposure to depleted uranium (see Arzuaga et al 2010 in supporting documents).

1. Banning, A., and M. Benfer. 2017. 'Drinking Water Uranium and Potential Health Effects in the German Federal State of Bavaria', International Journal of Environmental Research and Public Health, 14.

2. Geoscience and Mines Branch. 2018. "A Review and Summary of Activities Related to Uranium in Nova Scotia Well Water." In, edited by Nova Scotia Energy and Mines. Halifax, Nova Scotia, Canada.

3. Gritsaenko, T., V. Pierrefite-Carle, G. Creff, C. Vidaud, G. Carle, and S. Santucci-Darmanin. 2018. 'Methods for Analyzing the Impacts of Natural Uranium on In Vitro Osteoclastogenesis', Jove-Journal of Visualized Experiments.

4. Gritsaenko, T., V. Pierrefite-Carle, T. Lorivel, V. Breuil, G. F. Carle, and S. Santucci-Darmanin. 2017. 'Natural uranium impairs the differentiation and the resorbing function of osteoclasts', Biochimica Et Biophysica Acta-General Subjects, 1861: 715-26.

5. Gueguen, Y., L. Roy, S. Hornhardt, C. Badie, J. Hall, S. Baatout, E. Pernot, L. Tomasek, O. Laurent, T. Ebrahimian, C. Ibanez, S. Grison, S. Kabacik, D. Laurier, and M. Gomolka. 2017. 'Biomarkers for Uranium Risk Assessment for the Development of the CURE (Concerted Uranium Research in Europe) Molecular Epidemiological Protocol', Radiation Research, 187: 107-27.

6. Hall, J., P. A. Jeggo, C. West, M. Gomolka, R. Quintens, C. Badie, O. Laurent, A. Aerts, N. Anastasov, O. Azimzadeh, T. Azizova, S. Baatout, B. Baselet, M. A. Benotmane, E. Blanchardon, Y. Gueguen, S. Haghdoost, M. Harms-Ringhdahl, J. Hess, M. Kreuzer, D. Laurier, E. Macaeva, G. Manning, E. Pernot, J. L. Ravanat, L. Sabatier, K. Tack, S. Tapio, H. Zitzelsberger, and E. Cardis. 2017. 'Ionizing radiation biomarkers in epidemiological studies - An update', Mutation Research-Reviews in Mutation Research, 771: 59-84.

7. Hao, Y. H., R. Gao, B. H. Lu, Y. H. Ran, Z. Y. Yang, J. Liu, and R. Li. 2018. 'Ghrelin protects against depleted uranium-induced bone damage by increasing osteoprotegerin/RANKL ratio', Toxicology and Applied Pharmacology, 343: 62-70.

8. Health Canada. 2017. "Uranium in Drinking Water. Document for Public Consultation." In, edited by Federal-Provincial-Territorial Committee on Drinking Water. Ottawa, Ontario, Canada.

9. Health Canada. 2019. "Guidelines for Canadian Drinking Water Quality. Guideline Technical Document. Uranium." In, edited by Healthy Environments and Consumer Safety Branch. Water and Air Quality Bureau. Ottawa, Ontario, Canada.

10. Hurault, L., G. Creff, A. Hagege, S. Santucci-Darmanin, S. Pagnotta, D. Farlay, C. Den Auwer, V. Pierrefite-Carle, and G. F. Carle. 2019. 'Uranium Effect on Osteocytic Cells In Vitro', Toxicological Sciences, 170: 199-209.

11. Huynh, T. N. S., C. Vidaud, and A. Hagege. 2016. 'Investigation of uranium interactions with calcium phosphate-binding proteins using ICP/MS and CE-ICP/MS', Metallomics, 8: 1185-92.

12. Lan, L., S. Y. Wu, S. D. Yu, J. J. Jiang, H. H. Chen, Y. F. Lou, and G. R. Fan. 2019. 'Fast and direct determination of catechol-3, 6-bis(methyleiminodiacetic acid) prototype in beagle dog plasma using liquid chromatography tandem mass spectrometry: A simplified and high throughput in-vivo method for the metal chelator', Journal of Chromatography A, 1596: 84-95.

13. McDiarmid, M. A., M. Cloeren, J. M. Gaitens, S. Hines, E. Streeten, R. J. Breyer, C. H. Brown, M. Condon, T. Roth, M. Oliver, L. Brown, M. Dux, M. R. Lewin-Smith, F. Strathmann, M. A. Velez-Quinones, and P. Gucer. 2018. 'Surveillance results and bone effects in the Gulf War depleted uranium-exposed cohort', Journal of Toxicology and Environmental Health-Part a-Current Issues, 81: 1083-97.

14. Pierrefite-Carle, V., S. Santucci-Darmanin, V. Breuil, T. Gritsaenko, C. Vidaud, G. Creff, P. L. Solari, S. Pagnotta, R. Al-Sahlanee, C. Den Auwer, and G. F. Carle. 2017. 'Effect of natural uranium on the UMR-106 osteoblastic cell line: impairment of the autophagic process as an underlying mechanism of uranium toxicity', Archives of Toxicology, 91: 1903-14.

15. United Nations Scientific Committee on the Effects of Atomic Radiation. 2016. "Sources, Effects and Risks of Ionizing Radiation: UNSCEAR 2016 Report to the General Assembly, Scientific Annexes A, B, C and D." United Nations. New York, United States of America.

16. Roller, L. K., and L. J. Baumgartner. 2016. 'Metals.' in S. D. Ray (ed.), Side Effects of Drugs Annual: A Worldwide Yearly Survey of New Data in Adverse Drug Reactions, Vol 38.

17. Stojsavljevic, A., S. Borkovic-Mitic, L. Vujotic, D. Grujicic, M. Gavrovic-Jankulovic, and D. Manojlovic. 2019. 'The human biomonitoring study in Serbia: Background levels for arsenic, cadmium, lead, thorium and uranium in the whole blood of adult Serbian population', Ecotoxicology and Environmental Safety, 169: 402-09.

18. Stojsavljevic, A., S. Skrivanj, J. Trifkovic, N. Djokovic, S. R. Trifunovic, S. Borkovic-Mitic, and D. Manojlovic. 2019. 'The content of toxic and essential elements in trabecular and cortical femoral neck: a correlation with whole blood samples', Environmental Science and Pollution Research, 26: 16577-87.

19. Wu, X. M., Q. X. Huang, Y. Mao, X. X. Wang, Y. Y. Wang, Q. H. Hu, H. Q. Wang, and X. K. Wang. 2019. 'Sensors for determination of uranium: A review', Trac-Trends in Analytical Chemistry, 118: 89-111.

Yue, Y. C., M. H. Li, H. B. Wang, B. L. Zhang, and W. He. 2018. 'The toxicological mechanisms and detoxification of depleted uranium exposure', Environmental Health and Preventive Medicine, 23.

Justification 2A:

N/A

Justification 2B:

N/A

Justification 2C:

N/A

Justification 2D:

N/A

Justification 2E:

N/A

Justification 3A:

According to Google Scholar the nominated review paper is has 17 citations, this does not include citations from government agencies outside the US. This publication has been cited in 20 documents including primary research publications investigating uranium-induced developmental and skeletal effects as well as several foreign government guidelines and reports which reviewing the potential human health hazards associated with uranium exposure (see citation list below).

1. Banning, A., and M. Benfer. 2017. 'Drinking Water Uranium and Potential Health Effects in the German Federal State of Bavaria', International Journal of Environmental Research and Public Health, 14.

2. Geoscience and Mines Branch. 2018. "A Review and Summary of Activities Related to Uranium in Nova Scotia Well Water." In, edited by Nova Scotia Energy and Mines. Halifax, Nova Scotia, Canada.

3. Gritsaenko, T., V. Pierrefite-Carle, G. Creff, C. Vidaud, G. Carle, and S. Santucci-Darmanin. 2018. 'Methods for Analyzing the Impacts of Natural Uranium on In Vitro Osteoclastogenesis', Jove-Journal of Visualized Experiments.

4. Gritsaenko, T., V. Pierrefite-Carle, T. Lorivel, V. Breuil, G. F. Carle, and S. Santucci-Darmanin. 2017. 'Natural uranium impairs the differentiation and the resorbing function of osteoclasts', Biochimica Et Biophysica Acta-General Subjects, 1861: 715-26.

5. Gueguen, Y., L. Roy, S. Hornhardt, C. Badie, J. Hall, S. Baatout, E. Pernot, L. Tomasek, O. Laurent, T. Ebrahimian, C. Ibanez, S. Grison, S. Kabacik, D. Laurier, and M. Gomolka. 2017. 'Biomarkers for Uranium Risk Assessment for the Development of the CURE (Concerted Uranium Research in Europe) Molecular Epidemiological Protocol', Radiation Research, 187: 107-27.

6. Hall, J., P. A. Jeggo, C. West, M. Gomolka, R. Quintens, C. Badie, O. Laurent, A. Aerts, N. Anastasov, O. Azimzadeh, T. Azizova, S. Baatout, B. Baselet, M. A. Benotmane, E. Blanchardon, Y. Gueguen, S. Haghdoost, M. Harms-Ringhdahl, J. Hess, M. Kreuzer, D. Laurier, E. Macaeva, G. Manning, E. Pernot, J. L. Ravanat, L. Sabatier, K. Tack, S. Tapio, H. Zitzelsberger, and E. Cardis. 2017. 'Ionizing radiation biomarkers in epidemiological studies - An update', Mutation Research-Reviews in Mutation Research, 771: 59-84.

7. Hao, Y. H., R. Gao, B. H. Lu, Y. H. Ran, Z. Y. Yang, J. Liu, and R. Li. 2018. 'Ghrelin protects against depleted uranium-induced bone damage by increasing osteoprotegerin/RANKL ratio', Toxicology and Applied Pharmacology, 343: 62-70.

8. Health Canada. 2017. "Uranium in Drinking Water. Document for Public Consultation." In, edited by Federal-Provincial-Territorial Committee on Drinking Water. Ottawa, Ontario, Canada.

9. Health Canada. 2019. "Guidelines for Canadian Drinking Water Quality. Guideline Technical Document. Uranium." In, edited by Healthy Environments and Consumer Safety Branch. Water and Air Quality Bureau. Ottawa, Ontario, Canada.

10. Hurault, L., G. Creff, A. Hagege, S. Santucci-Darmanin, S. Pagnotta, D. Farlay, C. Den Auwer, V. Pierrefite-Carle, and G. F. Carle. 2019. 'Uranium Effect on Osteocytic Cells In Vitro', Toxicological Sciences, 170: 199-209.

11. Huynh, T. N. S., C. Vidaud, and A. Hagege. 2016. 'Investigation of uranium interactions with calcium phosphate-binding proteins using ICP/MS and CE-ICP/MS', Metallomics, 8: 1185-92.

12. Lan, L., S. Y. Wu, S. D. Yu, J. J. Jiang, H. H. Chen, Y. F. Lou, and G. R. Fan. 2019. 'Fast and direct determination of catechol-3, 6-bis(methyleiminodiacetic acid) prototype in beagle dog plasma using liquid chromatography tandem mass spectrometry: A simplified and high throughput in-vivo method for the metal chelator', Journal of Chromatography A, 1596: 84-95.

13. McDiarmid, M. A., M. Cloeren, J. M. Gaitens, S. Hines, E. Streeten, R. J. Breyer, C. H. Brown, M. Condon, T. Roth, M. Oliver, L. Brown, M. Dux, M. R. Lewin-Smith, F. Strathmann, M. A. Velez-Quinones, and P. Gucer. 2018. 'Surveillance results and bone effects in the Gulf War depleted uranium-exposed cohort', Journal of Toxicology and Environmental Health-Part a-Current Issues, 81: 1083-97.

14. Pierrefite-Carle, V., S. Santucci-Darmanin, V. Breuil, T. Gritsaenko, C. Vidaud, G. Creff, P. L. Solari, S. Pagnotta, R. Al-Sahlanee, C. Den Auwer, and G. F. Carle. 2017. 'Effect of natural uranium on the UMR-106 osteoblastic cell line: impairment of the autophagic process as an underlying mechanism of uranium toxicity', Archives of Toxicology, 91: 1903-14.

15. United Nations Scientific Committee on the Effects of Atomic Radiation. 2016. "Sources, Effects and Risks of Ionizing Radiation: UNSCEAR 2016 Report to the General Assembly, Scientific Annexes A, B, C and D." United Nations. New York, United States of America.

16. Roller, L. K., and L. J. Baumgartner. 2016. 'Metals.' in S. D. Ray (ed.), Side Effects of Drugs Annual: A Worldwide Yearly Survey of New Data in Adverse Drug Reactions, Vol 38.

17. Stojsavljevic, A., S. Borkovic-Mitic, L. Vujotic, D. Grujicic, M. Gavrovic-Jankulovic, and D. Manojlovic. 2019. 'The human biomonitoring study in Serbia: Background levels for arsenic, cadmium, lead, thorium and uranium in the whole blood of adult Serbian population', Ecotoxicology and Environmental Safety, 169: 402-09.

18. Stojsavljevic, A., S. Skrivanj, J. Trifkovic, N. Djokovic, S. R. Trifunovic, S. Borkovic-Mitic, and D. Manojlovic. 2019. 'The content of toxic and essential elements in trabecular and cortical femoral neck: a correlation with whole blood samples', Environmental Science and Pollution Research, 26: 16577-87.

19. Wu, X. M., Q. X. Huang, Y. Mao, X. X. Wang, Y. Y. Wang, Q. H. Hu, H. Q. Wang, and X. K. Wang. 2019. 'Sensors for determination of uranium: A review', Trac-Trends in Analytical Chemistry, 118: 89-111.

20. Yue, Y. C., M. H. Li, H. B. Wang, B. L. Zhang, and W. He. 2018. 'The toxicological mechanisms and detoxification of depleted uranium exposure', Environmental Health and Preventive Medicine, 23.

Justification 3B:

The nominated paper was submitted to Toxicology Letters (https://www.journals.elsevier.com/toxicology-letters). According to the journal website the “journal operates a single blind review process. All contributions will be initially assessed by the editor for suitability for the journal. Papers deemed suitable are then typically sent to a minimum of two independent expert reviewers to assess the scientific quality of the paper. The Editor is responsible for the final decision regarding acceptance or rejection of articles. The Editor's decision is final.”

AUTHORS

Principal Author

Author Name:	Xabier Arzuaga Andino		
Professional Title:		Salutation:	
Email:	arzuaga.xabier@epa.gov	Organization:	
Mailing Address:			
Street Line 1:			
City:	Washington		
Zip Code:	20460	State:	DC
At time of research was:	EPA Employee		
Separation Date:			

% of Effort:	65		

Contributing Author

Author Name:	Martin Gehlhaus		
Professional Title:		Salutation:	
Email:	gehlhaus.martin@epa.gov	Organization:	
Mailing Address:			
Street Line 1:	USEPA REGION 3 1650 Arch Street Mail Code: 3SD52 Philadelphia, PA 19103-2029		
City:	Philadelphia		
Zip Code:	19103-2029	State:	PA
At time of research was:	EPA Employee		
Separation Date:			
% of Effort:	20		

Contributing Author

Author Name:	Jamie Strong		
Professional Title:		Salutation:	
Email:	strong.jamie@epa.gov	Organization:	
Mailing Address:			
Street Line 1:	USEPA Headquarters William Jefferson Clinton Building 1200 Pennsylvania Avenue, N. W. Mail Code: 4304T Washington, DC 20460		
City:	Washington		

Zip Code:	20460	State:	DC
At time of research was:	EPA Employee		
Separation Date:			
% of Effort:	15		

PUBLICATIONS

Publication 1:

Publication Title:	Modes of action associated with uranium induced adverse effects in bone function and development		
Publication Date:	Mon May 11 00:00:00 GMT 2015		
Journal/Publication Method:	Toxicology Letters		
All Author(s):			
Volume:	236	Number:	2
Pages:	123-130	Immediately Index:	Immediately Index:
Citation ½ Life:	Arzuaga X, et al 2015. Toxicol Lett. 236(2):123-30	Impact Factor:	3.749

From:	Strong, Jamie
To:	Arzuaga, Xabier
Subject:	RE: STAA award nomination for the uranium paper
Date:	Thursday, April 23, 2020 3:37:43 PM

I think that sounds right, hard to remember! I hope you are well and being safe!

From: Arzuaga, Xabier <Arzuaga.Xabier@epa.gov>
Sent: Tuesday, April 21, 2020 1:59 PM
To: Strong, Jamie <Strong.Jamie@epa.gov>
Subject: STAA award nomination for the uranium paper

Hi Jamie,
I hope that you guys are OK and staying healthy. We are doing well at home and have established a routine for the kids. So far its working well. They do their school work during the day and in the afternoons we will do something together. Julian and Sidney are also doing music and karate classes online. I have joined in for the karate and its lots of fun to do with a bunch of 6 year old kids. I am putting together an STAA award nomination for the uranium paper we published in 2015. Please let me know if you are agree with the estimated level of contribution below. Thanks and stay safe!
Xabier

- Jamie Strong; U.S. EPA, Office of Water
- Nominee's name: Xabier Arzuaga
- Publication title: "Modes of action associated with uranium induced adverse effects in bone function
- and development"
- I agree with my designated level of contribution: 15%

Xabier Arzuaga, PhD
Toxicologist
U.S. EPA, Office of Research and Development,
Center for Public Health and Environmental Assessment
1200 Pennsylvania Ave, NW (Mail Code 8601P) | Washington, DC 20460
RRB 71274 | Phone: (202) 564-1361
Email: arzuaga.xabier@epa.gov

From:	Gehlhaus, Martin
To:	Arzuaga, Xabier
Subject:	RE: STAA award nomination for the uranium paper
Date:	Tuesday, April 21, 2020 2:53:28 PM

Xabier!!! Great to hear from you. We're doing well... or as well as can be expected. My wife and I are working throughout the day and the kids have anywhere from 3 to 5 hours of school work... so we tend to fight over the WiFi. Like you and your family, we've settled into a routine to try and make the most of the situation.

I agree with estimated level of contribution.

Take care. Stay well.

Martin Gehlhaus

US Environmental Protection Agency
Region III
Superfund and Emergency Management Division
Risk Assessment Section
3SD52
1650 Arch Street
Philadelphia, PA 19103-2029
215-814-3359

From: Arzuaga, Xabier <Arzuaga.Xabier@epa.gov>
Sent: Tuesday, April 21, 2020 1:53 PM
To: Gehlhaus, Martin <Gehlhaus.Martin@epa.gov>
Subject: STAA award nomination for the uranium paper

Hi Martyn,
I hope that you guys are OK and staying healthy. We are doing well at home and have established a routine for the kids. So far its working well. They do their school work during the day and in the afternoons we will do something together. I am putting together an STAA award nomination for the uranium paper we published in 2015. Please let me know if you are agree with the estimated level of contribution below. Thanks and stay safe!
Xabier

- Martin Gehlhaus; U.S. EPA, Region 3
- Nominee's name: Xabier Arzuaga
- Publication title: "Modes of action associated with uranium induced adverse effects in bone function and
- development"
- I agree with my designated level of contribution: 20%

Xabier Arzuaga, PhD
Toxicologist
U.S. EPA, Office of Research and Development,
Center for Public Health and Environmental Assessment
1200 Pennsylvania Ave, NW (Mail Code 8601P) | Washington, DC 20460
RRB 71274 | Phone: (202) 564-1361
Email: arzuaga.xabier@epa.gov

This article was downloaded by: *[US EPA Environmental Protection Agency]*
On: *22 December 2010*
Access details: *Access Details: [subscription number 789514190]*
Publisher *Taylor & Francis*
Informa Ltd Registered in England and Wales Registered Number: 1072954 Registered office: Mortimer House, 37-41 Mortimer Street, London W1T 3JH, UK

Journal of Toxicology and Environmental Health, Part B
Publication details, including instructions for authors and subscription information:
http://www.informaworld.com/smpp/title~content=t713667286

Renal Effects of Exposure to Natural and Depleted Uranium: A Review of the Epidemiologic and Experimental Data

Xabier Arzuaga[a]; Susan H. Rieth[a]; Ambika Bathija[b]; Glinda S. Cooper[a]
[a] National Center for Environmental Assessment, U.S. Environmental Protection Agency, Washington, DC [b] Health and Ecological Criteria Division, Office of Science & Technology, U.S. Environmental Protection Agency, Washington, DC, USA

Online publication date: 17 December 2010

To cite this Article Arzuaga, Xabier , Rieth, Susan H. , Bathija, Ambika and Cooper, Glinda S.(2010) 'Renal Effects of Exposure to Natural and Depleted Uranium: A Review of the Epidemiologic and Experimental Data', Journal of Toxicology and Environmental Health, Part B, 13: 7, 527 — 545
To link to this Article: DOI: 10.1080/10937404.2010.509015
URL: http://dx.doi.org/10.1080/10937404.2010.509015

PLEASE SCROLL DOWN FOR ARTICLE

Full terms and conditions of use: http://www.informaworld.com/terms-and-conditions-of-access.pdf

This article may be used for research, teaching and private study purposes. Any substantial or systematic reproduction, re-distribution, re-selling, loan or sub-licensing, systematic supply or distribution in any form to anyone is expressly forbidden.

The publisher does not give any warranty express or implied or make any representation that the contents will be complete or accurate or up to date. The accuracy of any instructions, formulae and drug doses should be independently verified with primary sources. The publisher shall not be liable for any loss, actions, claims, proceedings, demand or costs or damages whatsoever or howsoever caused arising directly or indirectly in connection with or arising out of the use of this material.

Journal of Toxicology and Environmental Health, Part B, 13:527–545, 2010
ISSN: 1093-7404 print / 1521-6950 online
DOI: 10.1080/10937404.2010.509015

Taylor & Francis
Taylor & Francis Group

RENAL EFFECTS OF EXPOSURE TO NATURAL AND DEPLETED URANIUM: A REVIEW OF THE EPIDEMIOLOGIC AND EXPERIMENTAL DATA

Xabier Arzuaga[1], Susan H. Rieth[1], Ambika Bathija[2], Glinda S. Cooper[1]

[1]National Center for Environmental Assessment, U.S. Environmental Protection Agency, Washington, DC
[2]Health and Ecological Criteria Division, Office of Science & Technology, U.S. Environmental Protection Agency, Washington, DC, USA

Downloaded By: [US EPA Environmental Protection Agency] At: 17:09 22 December 2010

Elevated levels of naturally occurring uranium in groundwater have been found in small geographic areas throughout the world. Relevant research was reviewed pertaining to natural and depleted uranium (DU) exposure and nephrotoxicity, including epidemiologic community-based and occupational studies, studies of Gulf War veterans exposed to DU, and experimental studies in animals. Occupational cohort studies do not provide evidence of an increased risk of kidney-related mortality among uranium-exposed workers. However, occupational and community-based studies of populations chronically exposed to elevated drinking-water concentrations of uranium provide some evidence of adverse renal effects, as assessed by biomarkers of proximal tubule damage such as urinary levels of glucose, calcium, and various low-molecular-weight proteins. Indications of proximal tubule effects, as evidenced by increased urinary β_2-microglobulin and retinol binding protein levels, were also seen in the most recent follow-up surveillance study of Gulf War veterans exposed to DU. The reported β_2-microglobulin levels in these studies were generally considered to be within normal limits, but the long-term implications of the observed variation in these levels are not established. The kidney was observed to be a target of uranium toxicity following oral and implantation exposure routes in several animal species. The interpretation and importance of the observed changes in biomarkers of proximal tubule function are important questions that indicate the need for additional clinical, epidemiological, and experimental research.

Natural uranium (U) refers to uranium compounds with a naturally occurring composition of radioisotopes uranium-234, uranium-235, and uranium-238. Uranium is found in all soils and rock, with higher concentrations found in phosphate rock, lignite, and monazite sands (ATSDR, 1999). Uranium enrichment processes increase the concentration of U-235 from <1% to 2–4%. Depleted uranium (DU) refers to the less radioactive form of uranium remaining after enrichment. Depleted uranium is approximately 60% less radioactive than naturally occurring U because of decreased levels of U-235 (Bleise et al., 2003), and U has been used by the U.S. Department of Defense (DoD) and Armed Forces for various weapons systems since the late 1970s (Arfsten et al., 2001; Abu-Qare and Abou-Donia, 2002).

Elevated concentrations of U greater than 20 μg/L were detected in various Western groundwater systems and scattered pockets in the groundwaters of North Carolina, Maine, Connecticut, and other Eastern states (Orloff et al., 2004; U.S. EPA, 1985, 2000). Areas of high U concentrations in water are also found in many other countries globally, including Canada, Finland, the United Kingdom, and India (WHO, 2001). According

This article is not subject to U.S. copyright.
The views expressed are those of the authors and do not necessarily reflect the views or policies of the U.S. EPA.
Address correspondence to Glinda S. Cooper, PhD, National Center for Environmental Assessment 8601-P, U.S. Environmental Protection Agency, 1200 Pennsylvania Avenue, NW, Washington, DC 20460, USA. E-mail: cooper.glinda@epa.gov

Downloaded By: [US EPA Environmental Protection Agency] At: 17:09 22 December 2010

to biomonitoring data collected by the Centers for Disease Control (CDC, 2005) as part of the Third National Report on Human Exposure to Environmental Chemicals, the geometric mean concentration of U in urine for the U.S. population (ages 6 yr and older) for survey years 2001–2002 was 0.009 μg/L (95th percentile: 0.046 μg/L).

Craft et al. (2004) summarized data pertaining to a broad range of adverse health effects due to natural U and DU, including neurotoxicity, nephrotoxicity, reproductive effects, cancer, and effects on other systems. Renal effects were the focus of a recent case study of a family in western Connecticut describing the potential for nephrotoxicity from exposure to well water containing elevated levels of naturally occurring U, and the sensitivity of young children resulting from their increased exposure potential and their state of development (Magdo et al., 2007). In this review, research pertaining to U exposure and nephrotoxicity, focusing on the available epidemiologic data including (1) community-based and occupational studies of biomarkers of kidney damage, (2) occupational studies of kidney-related mortality, and (3) studies of soldiers exposed to DU, is presented. The animal nephrotoxicity and mechanism of action data have been reviewed previously (ATSDR, 1999); a summary of this and recent literature is also included later in this article.

STUDIES IN HUMANS

Measures of Renal Function

Kidney disease varies in severity from kidney failure requiring transplantation or dialysis to a subclinical, asymptomatic phase where some level of kidney damage may occur without detectable decreases in renal function. In clinical studies, such as prognostic studies of patients with diabetes or other conditions with a high risk of chronic kidney disease and its related complications, renal function has often been monitored by blood and 24-h urine samples allowing for the measurement of blood urea nitrogen (BUN) levels, total protein in the urine, and calculation of glomerular filtration rate (GFR). In community-based studies, less burdensome data collection techniques are usually required, resulting in the collection of a single urine sample at a study visit (a spot urine sample) or an overnight urine sample (i.e., first morning void). Another difference between clinical and community-based studies is that in the latter, it is more important that the methodology is able to accurately assess variability in the earliest phases of disease, when kidney function is still relatively high (Levey et al., 2009).

In addition to general measures of kidney function, other types of measures address specific types of damage that may occur. Larger molecules, such as albumin, are filtered by the glomeruli and reabsorbed by the proximal tubule through receptor mediated endocytosis (Birn and Christensen, 2006). Most of the albumin reabsorbed by the proximal tubule cells (approximately 95%) is returned to the plasma. The remaining amount is degraded in cell lysosomes and excreted in the urine (Comper et al., 2006). Glomerular and tubular injury may result in increased levels of urinary albumin. Tests of general glomerular function include creatinine clearance or GFR, as well as determination of urinary protein and urinary albumin concentrations, with the latter two measures reflecting the integrity of the glomerulus (i.e., the leakage of molecules through the filter). Damage to the proximal tubule decreases small-molecule reabsorption and results in increased urinary levels of glucose, calcium, and phosphate, and of low-molecular-weight proteins such as β_2-microglobulin, protein human complex forming (HC) [or α-microglobulin]), kappa chains, and retinol binding protein (Emeigh & Kinter, 2005; Seldén et al., 2009). β_2-Microglobulin is an endogenous low-molecular-mass protein (12 kD) that forms part of the class I major histocompatibility complex and is located on the surface of nucleated cells. During cell turnover β_2-microglobulin is released into the extracellular fluid and normally filtered by the glomerulus and reabsorbed in the proximal tubule (Bagshaw et al., 2007; Tolkoff-Rubin et al., 1988). Retinol binding protein (21 kD) is

primarily expressed in the liver and also reabsorbed by the proximal tubule (Bagshaw et al., 2007). Enzyme activity levels have also been used as markers of tissue damage at specific sites, with alkaline phosphatase (AP), *N*-acetyl-β-D-glucosaminidase (NAG), and γ-glutamyl transferase (GGT) reflecting proximal tubular tissue damage and other enzymes, such as lactate dehydrogenase (LDH), more indicative of damage to the distal tubule (Zalups et al., 1988; Emeigh 2005; Zamora et al., 2009; Seldén et al., 2009).

Downloaded By: [US EPA Environmental Protection Agency] At: 17:09 22 December 2010

Community-Based Studies

Several studies of populations chronically exposed to elevated drinking-water concentrations of U were conducted (Kurttio et al., 2002; Kurttio et al., 2006; Mao et al., 1995; Seldén et al., 2009; Zamora et al., 1998; Zamora et al., 2009). Three studies in Canada (in Saskatchewan, Quebec, and Nova Scotia), two in Finland, and one in Sweden evaluated renal function in communities with high concentrations of U in the drinking water supply (Table 1). Mean or median U concentrations in the drinking water of the exposed communities were approximately 7 μg/L in Sweden, 15–20 μg/L in Saskatchewan, 28 μg/L in Finland, 39 μg/L in Quebec (based on the maximum level measured over a 15-yr period), and more than 100 μg/L in Nova Scotia (Figure 1); corresponding values in the comparison nonexposed communities were <1 μg/L. Uranium concentrations in urine also varied considerably among these studies, with a median of 0.03 μg/L in Sweden, 0.078 μg/L in Finland, and 0.14 μg/L in Quebec.

The first of these studies, in Saskatchewan, measured urinary albumin in a first morning urine sample from 60 adults in 2 communities with elevated levels of U in drinking water (means of 14.7 and 19.6 μg/L) and 40 controls from a comparison (control) community (mean drinking water U concentration of 0.71 μg/L) (Mao et al., 1995). Cumulative intake was calculated as the product of concentration of U in water, average number of cups consumed per day, and years at current residence; the mean or range of this measure was not given. A correlation was seen between cumulative intake and urinary albumin, which was of marginal statistical significance when adjusting for age and diabetes history (Table 1).

Subsequent studies used a more extensive array of urinary and serological measures to assess kidney function. The studies from Canada were conducted in Nova Scotia (Zamora et al., 1998) and in a Quebec First Nations community (Zamora et al., 2009), with 30 and 54 exposed participants, respectively (Table 1). The study in Nova Scotia calculated a daily U intake based on the product of concentration of U in water or food and the amount consumed (based on 3-d food and water samples) and ranged from 3 to 570 μg/d in the exposed community and from <1 to 20 μg/d in the control community. Urinary U and glucose, protein, and creatinine concentrations were measured in a 24-h urine sample, and ß$_2$-microglobulin levels were measured in an overnight urine sample. Daily U intake correlated significantly with markers of proximal tubule injury: urinary glucose ($r_s = 0.40$; $p = 0.001$), AP ($r_s = 0.28$; $p = 0.05$), and ß$_2$-microglobulin ($r_s = 0.39$; $p = 0.01$). Weaker or no correlations were seen with urinary NAG activity ($r_s = 0.15$; 0.29), protein ($r_s = 0.17$; 0.23), creatinine ($r_s = 0.11$; 0.45), and LDH activity ($r_s = 0.02$; 0.89) levels, and a negative correlation coefficient was seen with GGT activity ($r_s = -0.22$; 0.12).

In Quebec, the study protocol was similar to that of the Nova Scotia study. Exposure was measured or calculated as the maximum water U concentration in prior 15 yr, cumulative intake in prior 15 yr (median 87 mg), cumulative intake in past 2.8 yr (median 22 mg), and U concentration in urine (median 0.14 μg/L) (Zamora et al., 2009). Adjusting exposure and renal biomarker measures for fluid intake, U concentration in urine was significantly correlated with GGT activity ($r_s = 0.37$) and ß$_2$-microglobulin ($r_s = 0.49$). Weaker correlations were seen with albumin ($r_s = 0.23$), glucose ($r_s = 0.14$), AP activity ($r_s = 0.15$), and NAG activity ($r_s = 0.15$).

Downloaded By: [US EPA Environmental Protection Agency] At: 17:09 22 December 2010

TABLE 1. Community-Based Studies of Markers of Renal Function in Relation to Exposure to Uranium in Drinking Water

Reference(s)	Study location and participants	Exposure measure(s)	Primary positive results
Canada			
Mao et al., 1995	Saskatchewan, Canada ($n = 40$ from one control community, $n = 60$ from two exposed communities). Mean age not reported, range 18 to 84 yr.	Cumulative intake[a] (range not given)	Cumulative intake correlated with urine albumin (per mmol creatinine levels, Beta = 0.13, $p = .03$; per mg/L, Beta = 2.19, $p = .07$), adjusting for age and diabetes history.
Zamora et al., 1998	Nova Scotia, Canada ($n = 30$ from a high exposure eommunity (water uranium concentrations >100 μg/L), $n = 20$ from a low exposure community (water uranium concentrations of <1 μg). Mean age 37, range 13 to 87 yr.	Uranium concentration in drinking water and daily intake[b]	Daily uranium intake correlated with markers of proximal tubule injury: urinary glucose ($r_s = 0.40$, $p = .001$), alkaline phosphatas ($r_s = 0.28$, $p = .05$), and ß$_2$-microglobulin ($r_s = 0.39$, $p = .01$).
Zamora et al., 2009	Quebec First Nations Community (Kitigan Zibi), Canada ($n = 54$). Mean age 38, range 12 to 73 yr.	Maximum water uranium concentration in past 15 yr, cumulative intake in past 15 yr, cumulative intake in past 2.8 yr, urinary uranium	In analyses adjusting exposure and renal biomarker measures for fluid intake, urinary uranium correlated with gamma glutamyl transferase ($r_s = 0.37$, $p = .0064$) and ß$_2$-microglobulin ($r_s = 0.49$, $p = .0047$).
Europe			
Kurttio et al., 2002	Southern Finland ($n = 325$ from areas with high water uranium levels). Mean age 52, range 15 to 82 yr.	Uranium concentration in drinking water, daily intake,[c] cumulative intake,[d] and urinary uranium	All uranium measures correlated with fractional excretion of calcium and increased systolic and diastolic blood pressure; urinary uranium measures also correlated with fractional excretion of phosphate and glucose.
Kurttio et al., 2006	Southern Finland ($n = 193$, subset of Kurttio et al. 2002). Mean age 56, range 18 to 81 yr.	Uranium concentration in drinking water, daily intake,[c] cumulative intake[d]	Glucose excretion associated with cumulative intake measure ($p = .02$); urinary uranium associated with increased systolic ($p = .01$) and diastolic blood pressure ($p = .07$).
Seldén et al., 2009	Arjäng, Sweden ($n = 301$ exposed, $n = 153$ controls). Mean age 51 (exposed) and 55 (controls), range 18 to 74 yr.	Uranium concentration in drinking water, cumulative intake,[d] urinary uranium	Significant correlation between urinary uranium concentrations and β2-microglobulin, protein HC, and kappa chains; in males, cumulative intake was associated with protein HC.

Note. See Figure 1 for more detailed description of water uranium concentrations in exposed communities.
[a]The product of concentration of uranium in the water, average number of cups consumed per day, and years at current residence.
[b]The product of concentration of uranium in the water or food and the amount consumed (based on 3-d food and water samples).
[c]The product of concentration of uranium in the water and volume used per day.
[d]The product of concentration of uranium in the water, volume used, and duration of water consumption.

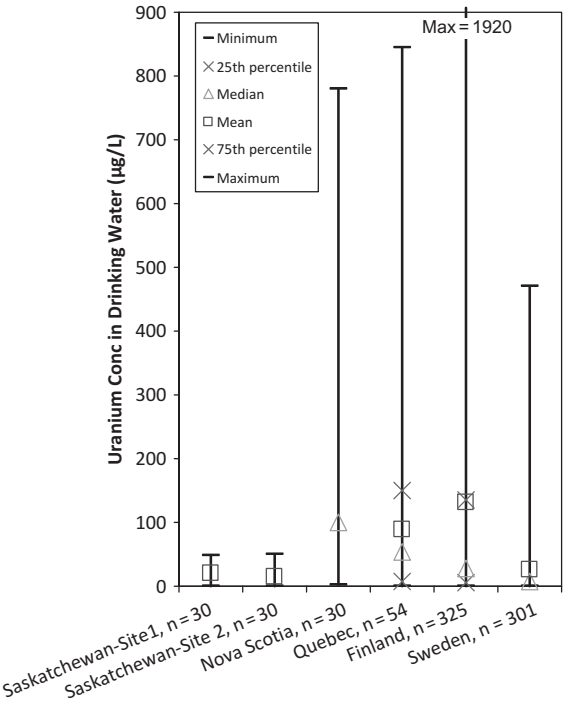

FIGURE 1. Uranium concentrations in drinking (μg/L) water in community studies. Saskatchewan sites 1 and 2, Mao et al. (1985), detection limit = 0.1 μg/L; Nova Scotia, Zamora et al. (1998), detection limit = 0.0006 μg/L; Quebec, Zamora et al. (2009), detection limit = 0.0006 μg/L (concentration values based on table of unadjusted data in Zamora et al., 2009); Finland, Kurttio et al. (2002, 2006), detection limit = 0.0004 μg/L; Sweden, Seldén et al. (2009), detection limit = 0.2 μg/L. Control community drinking water uranium concentrations were <1 μg/L.

Kurttio et al. (2002) conducted a study in 1999 of 325 individuals from areas in Finland with high uranium levels in the drinking water (Table 1). These individuals had used well water for at least 1 yr, and completed a questionnaire that included information on residential history and water consumption, allowing for calculation of measures of daily and cumulative U intake from water. A drinking-water sample (for measurement of U levels), overnight urine sample (for measurement of urinary U, glucose, creatinine, calcium, phosphate, and albumin), spot urine (for β_2-microglobulin measurement), and a nonfasting blood sample were collected. Daily intake ranged from <1 to 4128 μg/d (median 39 μg/d), cumulative intake ranged from <1 to 33,100 mg (median 129 mg), and U concentration in urine ranged from <1 to 5.65 μg/L (median 0.078 μg/L). Urinary U concentrations were correlated with fractional excretion of calcium (beta per 1 unit μg/mmol creatinine increase in urinary uranium = 1.5, 95% CI 0.6–2.3) and phosphate (beta = 13, 95% CI 1.4–25), and more weakly with glucose (beta = 0.7, 95% CI 0.4–1.8); associations with systolic and diastolic blood pressure (age, gender, body mass index, and smoking-adjusted beta = 6.8 and 8.5, respectively) were also seen. Kurttio et al. (2002) did not observe a relationship between U exposure and creatinine clearance, urinary albumin, or β_2-microglobulin. The high proportion (65%) of β_2-microglobulin values below the detection limit in the samples was a limitation of this analysis. In a subsequent study, Kurttio et al. (2006) recontacted the cohort in 2003; 222 (68%) lived in the same house as in 1999 and agreed to participate; 193 of these provided water, an overnight urine, and a blood sample for the follow-up study. β_2-Microglobulin was not measured in this study. Median daily intake of U from drinking water was 36 μg/L, similar to the mean of 39 μg/L in the baseline study reported by Kurttio et al. (2002). In the follow-up study, associations were only seen between urinary U concentrations and systolic and diastolic blood pressure, and between the cumulative intake measure and urinary glucose.

Another relatively large study included 301 participants from western Sweden living in areas with elevated levels of uranium in the drinking water obtained from wells and 151 controls from a nearby city using a city water supply (Seldén et al., 2009) (Table 1). Questionnaire data pertaining to drinking water consumption, smoking history, and other potential exposures were collected, and an overnight urine sample was collected from all participants; the members of the exposed groups and 15 randomly selected members of the control group also provided a water sample. Levels of cadmium (Cd), lead (Pb) and mercury (Hg) in the water samples were low (means ≤ 0.50 μg/L) and similar in both areas. The median U levels in the water were 6.7 and <0.20 μg/L in

Downloaded By: [US EPA Environmental Protection Agency] At: 17:09 22 December 2010

Downloaded By: [US EPA Environmental Protection Agency] At: 17:09 22 December 2010

the exposed and control samples, respectively, and the median U concentrations in urine were 0.03 and 0.0047 μg/L in exposed and controls, respectively. In the regression analyses adjusting for age, gender, and smoking and excluding 23 participants with diabetes, levels of low-molecular-weight proteins (β_2-microglobulin, kappa chains, and protein HC) were increased in relation to a 3-level variable for U concentrations in urine (<0.003, 0.003–0.0149 and ≥0.015 nmol/mmol creatinine). For β_2-microglobulin, the geometric mean was approximately 50% higher (i.e., ratio of geometric mean in the higher compared with lowest group = 1.48, 95% CI 1.03–2.13), and for kappa chains and protein HC, the elevations were 30% (ratio 1.32, 95% CI 1.04–1.68) and 20% (ratio 1.21, 95% CI 1.01–1.44), respectively. An association was also seen between protein HC and cumulative intake in males (ratio 1.40, 95% CI 1.08–1.81 in the middle category and 1.45, 95% CI 1.00–2.08) in the highest category of exposure). This pattern was not seen in females.

Occupational Exposure Studies

An occupational exposure study evaluating renal function in workers in a Colorado U mill also provides evidence of an association between natural U exposure and increased levels of urinary and serum β_2-microglobulin (Thun et al., 1985). In one area of this mill, the yellowcake drying and packaging area, exposure to air concentrations of U dust exceeded occupational standards for several years. Mean U concentrations in workers monitored were 65.2, 18.9, 20.5, and 19.1 μg/L urine in 1975, 1976, 1977, and 1978, respectively; these levels fell to means of 9.1 and 6.2 μg/L urine in 1980 and 1981 after the opening of a new mill in 1979. Workers who had worked at least 1 yr in the yellowcake area ($n = 30$) and workers in the crushing area ($n = 12$) were identified, and 39 of these 42 workers participated in the study. The exposure in the crushing area was to a less soluble form of U. A comparison group, matched by race, gender, and age (within 2 yr), was drawn from workers in a cement production plant in the area; 43 of the identified matches were recruited to the study but 7 of these were subsequently excluded because they had previously worked at the U mill. The final sample included 36 controls and 33 matched pairs. Cadmium levels were similar in the two groups, but blood Pb levels were higher among the controls (mean 0.45 and 0.78 μmol/L in exposed and controls, respectively). Renal function was evaluated through collection of an 8-h urine sample over the course of a workday, and midshift blood samples. Specific measures included serum creatinine and creatinine clearance as markers of glomerular functions and urinary β_2-microglobulin levels as markers of proximal tubular function. The ratio of the β_2-microglobulin clearance to creatinine clearance, denoted the fractional excretion, was calculated to represent the tubular component of β_2-microglobulin excretion. Urinary excretion of β_2-microglobulin was significantly increased in the workers compared with controls: where in the exposed group, mean (± standard deviation, SD) β_2-microglobulin concentration was 0.06 (± 0.38) mg/g creatinine, compared with 0.036 (± 0.031) in controls. Similar patterns were seen with measures expressed as micrograms per liter, micrograms per hour, and clearance (ml/min) (Table 2). Among the workers at the U plant, relative clearance of β_2-microglobulin was markedly correlated with duration of employment in the yellowcake area. In contrast, the tendency shown in the markers of glomerular function such as creatinine clearance was toward improved function in the exposed workers (Table 2).

Several cohort studies of workers at uranium processing facilities have examined mortality risk. Most of the detailed analyses focus on malignant diseases, but some data on mortality due to chronic nephritis (International Classification of Diseases, 9th revision, ICD-9, code 582) or other forms of renal disease are available (Table 3). The standardized mortality ratio of chronic nephritis among 8 cohort studies ranged from 0.67 to 1.88, each with relatively wide confidence intervals, and was approximately evenly distributed

TABLE 2. Renal Function Measures in Uranium Mill Workers and a Comparison Group of Workers From a Cement Plant (Thun et al., 1985)

	Uranium mill, exposed ($n = 39$)			Cement workers ($n = 36$)			
Variable	Mean	SD	Range	Mean	SD	Range	(p value)
β_2-Microglobulin[a]							
Serum (μg/ml)	2.05	0.46	1.28–3.40	1.83	0.26	1.36–2.40	(.01)
Urine (μg/L)	54.9	38.7	4.0–140.0	37.6	39.2	1.0–170.0	(.06)
Urine (μg/h)	4.40	2.99	0.36–13.63	2.50	2.05	0.18–10.01	(.002)
Urine (mg/g creatinine)	0.060	0.38	0.004–0.189	0.036	0.031	0.002–0.164	(.004)
Clearance (ml/min)	0.038	0.27	0.002–0.116	0.023	0.019	0.002–0.087	(.01)
Creatinine[b]							
Serum (mg/100 cm^3)	1.15	0.15	0.92–1.74	1.22	0.11	0.91–1.40	(.02)
Urine (mg/100 cm^3)	102.9	62.6	23.1–285.2	114.6	63.5	11.4–259.6	(.42)
Clearance (ml/min)[c]	95.6	20.6	48.8–172.2	88.4	13.0	39.1–116.6	(.08)
Relative clearance[d]	3.95	2.64	0.23–11.19	2.62	2.17	0.18–10.71	(.02)

[a]1 μg β_2-microglobulin = 1 μmol × 11,600.
[b]1 mg creatinine = 1 mmol × 113.12.
[c]Creatinine standardized to a body surface area of 1.73 m^2.
[d]β_2-Microglobulin clearance × 10^4/creatinine clearance.

Downloaded By: [US EPA Environmental Protection Agency] At: 17:09 22 December 2010

between estimates greater than 1 (Boice et al., 2008; Dupree-Ellis et al., 2000; Pinkerton et al., 2004), around 1 (Frome et al., 1990; McGeoghegan & Binks, 2000a), and less than 1 (Loomis & Wolf, 1996; McGeoghegan & Binks, 2000b; Polednak & Frome, 1981). The highest relative risk (standardized mortality ratio [SMR] = 1.88, based on 6 observed cases) was seen in the study by Dupres-Ellis et al. (2000), but the authors noted that the work environment of 4 of these cases was likely to have included high exposure to silica dust, which has also been linked to chronic kidney disease. None of these studies demonstrated an elevated risk for the broader category of genitourinary disease, and two studies observed a statistically significant decreased mortality risk (McGeoghegan & Binks, 2006; Loomis & Wolf, 1996).

Clinical Studies in Gulf War Veterans

Depleted uranium applications include armor plating for military vehicles, munitions used to penetrate armored targets, helicopter blade rotor tips, and aircraft landing gear. Approximately 10 and 300 tons of DU were expended by the U.S. Armed Forces during the Kosovo air campaign and the Persian Gulf War, respectively (Arfsten et al., 2001). Depleted uranium dusts and vapors, which may be inhaled or ingested, are generated during structure impact and perforation by DU munitions (Arfsten et al., 2001; Parkhurst & Guilmette, 2009). Several clinical studies evaluated the effects of exposure to DU in Gulf War veterans who had been mistakenly fired upon by U.S. forces in incidents that took place in February 1991. Exposure occurred via inhalation and ingestion of DU dust in the immediate aftermath of an incident, and through embedded metal fragments in some individuals who were hit by a high-density, penetrating device. In total, 74 soldiers who had been in or on an Army vehicle during one of these incidents have been followed through the Baltimore Veterans Affairs Depleted Uranium Follow-up program, initiated in 1993. This program has followed the majority of the approximately 90 soldiers involved in these incidents who survived and for whom contact information was available. After the initial study visit in 1994, biennial exams were conducted in 1997, 1999, 2001, and 2003 (reviewed in Squibb and McDiarmid, 2006), 2005, and 2007 (McDiarmid et al., 2007, 2009). The clinical and laboratory evaluations included 24-h urinary uranium concentration, with serum and urinary renal function measures. Examination of the 24-h urinary U concentration data over the 14-yr follow-up period revealed continued elevation of U, with levels ranging from 0.003

Downloaded By: [US EPA Environmental Protection Agency] At: 17:09 22 December 2010

TABLE 3. Studies of Noncancer Renal Disease Mortality Risk in Uranium Mill Workers

Reference(s)[a]	Sample size (*n*), inclusion criteria, follow-up, ICD revision[b]	All genitourinary disease			Chronic nephritis		
		Obs	Exp	SMR (CI)	Obs	Exp	SMR (95% CI)
Oak Ridge facilities							
Checkoway et al., 1988; Loomis and Wolf, 1996	*n* = 8116, Tennessee Eastman Corporation, Y-12 plant, Oak Ridge, TN. Worked ≥30 d between 1947 and 1974, began work after 1947. Follow-up through 1990. ICD-8.	15	NR	0.59 (0.33, 0.97)	5	NR	0.83 (0.27, 1.95)
Frome et al., 1990	*n* = 28,008 white males, Tennessee Eastman Corporation, several plants, Oak Ridge, TN. World War II workers. Worked ≥30 d before 1948 and did not work after January 1, 1948. Follow-up 1950 through 1979. ICD-8.	148	145.3	1.02 (*NR*)	52	52.65	0.99 (*NR*)
Polednak and Frome, 1981	*n* = 18,869 white males, Tennessee Eastman Corporation, Y-12 plant, Oak Ridge, TN. World War II workers. Worked ≥2 d between 1943 and 1947 and did not work after January 1, 1948. Follow-up through 1974. ICD-8.	63	99.04	0.64 (*NR*)	30	39.14	0.77 (*NR*)
Other U.S. facilities							
Boice et al., 2008	*n* = 718, Grants, NM uranium mill workers without mining experience and with likely exposure to uranium. Worked ≥6 mo between 1955 and 2004; 28% worked ≥5 yr. Follow-up through 2005. ICD-9.	NR			3	2.3	1.30 (0.27, 3.79)
Pinkerton et al., 2004; Waxweiler et al., 1983	*n* = 1484, white males, 7 mills, Colorado Plateau. Worked ≥1 year in mill, never worked in uranium mine, worked ≥1 d after 1940. 43% worked <3 yr. Follow-up through 1998. Total person-years = 49,925. ICD-9.	13	13.03	1.00 (0.53, 1.71)	8	5.91	1.35 (0.58, 2.67)
Dupree-Ellis et al., 2000	*n* = 2514, white males, Mallinckrodt Chemical Works, St. Louis, MO. Employed between 1942 and 1966. Average work duration 5.2 yr. Follow-up through 1993. ICD-8.	14	NR	0.95 (0.53, 1.54)	6	NR	1.88 (0.75, 3.81)
Ritz et al., 2000	*n* = 2218, males, Rocketdyne/Atomics International. Worked 1950–1993, monitored for radiation. Follow-up through 1994. Total person-years = 56,610. ICD-8.	5	6.44	0.78 (0.25, 1.81)	NR		
United Kingdom facilities							
McGeoghegan and Binks, 2000b	*n* = 19,454 (*n* = 13,950 radiation workers and *n* = 5489 nonradiation workers), Springfields, Lancashire, United Kingdom. Ever employed before 1996, follow-up through 1995. ICD-8.	Total: 42 67.32 0.62 (NR)[c] Rad: 28 48.94 0.57 (NR)[c] Non-rad: 14 18.38 0.76 (NR)			Total: 15 22.50 0.67 (NR) Rad: 10 16.48 0.61 (NR) Non-rad: 5 6.02 0.83 (NR) (disease category = chronic renal failure)		
McGeoghegan and Binks, 2000a	*n* = 12,544 (*n* = 3244 radiation workers and *n* = 9296 nonradiation workers), Capenhurst, Cheshire, United Kingdom. Ever employed before 1996, follow-up through 1995. ICD-8.	Total: 45 52.14 0.86 (NR) Rad: 7 7.13 0.98 (NR) Non-rad: 38 45.01 0.84 (NR)			Total: 19 17.17 1.1 (NR) Rad: 4 2.20 1.8 (NR) Non-rad:15 14.97 1.0 (NR) (disease category = chronic renal failure)		

Note. Abbreviations: Obs = observed; Exp = expected; CI = confidence interval; ICD = International Classification of Disease; NR = not reported; Rad = radiation workers; Non-rad = nonradiation workers.

[a]When more than one study is available for a cohort, the earlier references are noted but the results from the latest follow-up are provided in the table.

[b]In the studies using ICD-8, all genitourinary disease is based on codes 580–629 and chronic nephritis is based on code 582. In Pinkerton et al. (2004), all genitourinary disease is based on codes 580–629 and chronic nephritis is based on code 582–583 and 585–587. In Boice et al. (2008), the chronic nephritis category is based on code 580–589. McGeoghegan and Binks (2000a, 2000b) do not specify the codes used in their tables of results; all genitourinary disease and the chronic nephritis correspond, respectively, to their categories of genitourinary disease and chronic renal failure.

[c]Significant at $p < .01$.

Downloaded By: [US EPA Environmental Protection Agency] At: 17:09 22 December 2010

to 44.1 μg/g creatinine (Squibb & McDiarmid, 2006). Levels above 0.1 μg/g creatinine (the cut point used to define a high-exposure group) were found in most of the individuals who had retained DU shrapnel. Some indication of renal damage was seen in the 2001 assessment, with increased levels of urinary retinol binding protein (65.68 and 46.13 μg/g creatinine in the high- and low-exposure groups, respectively) and total protein (78.69 and 54.63 mg/g creatinine in the high- and low-exposure groups, respectively) (Table 4). Serum creatinine was quantitatively decreased, however, in the high-exposure group (mean 0.85 and 0.95 mg/dl in the high- and low-exposure groups, respectively). There was little evidence of renal damage in the 2003 and 2005 assessments. In the latest assessment conducted in 2007, however, a trend of elevated urinary retinol binding protein and increased urinary β_2-microglobulin levels was seen in the high-exposure compared with the low-exposure group (McDiarmid et al., 2009).

STUDIES IN ANIMALS

Studies in experimental animals involving different routes and durations of exposure support the conclusion that the kidney is likely to be a sensitive target organ for U toxicity. In addition, data from experimental animals suggest that U compounds of relatively higher solubility are associated with greater kidney damage (Craft et al., 2004; Dygert et al., 1949; Hindin et al., 2005; Maynard et al., 1953). In acute oral exposure studies with uranyl acetate (exposure duration ranging from 1–5 d) changes in kidney function, as evidenced by increases in urinary protein, blood creatinine, and BUN, were reported (Domingo et al., 1987; Ozmen & Yurekli, 1998). Renal damage reported in rabbits, rats, and dogs exposed to uranyl nitrate in the diet for 30 d or less included increased plasma protein plus degenerative changes (particularly of the proximal tubular epithelium and glomeruli) and necrosis (Goel et al., 1980; Maynard & Hodge 1949; Ortega et al., 1989).

The only investigation of chronic oral toxicity of U compounds is the series of experiments performed by Maynard and colleagues in support of the Manhattan Project (Maynard et al., 1953; Maynard & Hodge, 1949). Rats and dogs were exposed to uranyl fluoride, uranyl tetrachloride, uranyl nitrate hexahydrate, uranium dioxide, and uranium tetrafluoride in the diet (or in dogs by capsule if the diet became unpalatable) for 1 yr (dogs) or 2 yr (rats). Exposure protocols are described in Table 5. With the exception of exposure of rats to uranium dioxide, all uranium compounds produced some degee of renal toxicity, which was strongly influenced by compound solubility. For example, administration of 0.5% uranyl nitrate hexahydrate in the diet of rats (approximately 200 mg/kg-d U) produced degeneration of kidney tubules, necrosis, and regeneration. Serial sacrifices revealed that the tubular changes observed after 6 wk of exposure showed no appreciable progression even after 2 yr of exposure (Maynard et al., 1953). More recent subchronic (91-d) drinking-water studies of uranyl nitrate in the rat and rabbit (Gilman et al., 1998a, 1998b, 1998c; McDonald-Taylor et al., 1992, 1997) provide an examination of uranium compound toxicity at lower doses (0.06 to 54 mg/kg-d). See Table 5 for a more detailed summary of renal histopathologic changes reported by these investigators. McDonald-Taylor et al. (1992, 1997) reported histopathologic changes in kidney proximal tubules of rabbits at 1.7 mg/kg-d U, the lowest dose tested. Gilman et al. (1998b, 1998c) similarly reported histopathologic changes of the kidney at the lowest doses tested in rabbits and rats (0.05 and 0.06 mg/kg-d U, respectively). The incidences of renal histopathologic changes (including changes of the renal tubules, glomeruli, and interstitium) reported by Gilman et al. (1998b, 1998c), particular in the rat, were elevated at all dose levels; however, these changes showed a poor dose-response relationship and little if any rise in severity with increasing dose, despite a 600-fold range between the low and high doses used in this study and documentation of a rise in kidney uranium residues with

Downloaded By: [US EPA Environmental Protection Agency] At: 17:09 22 December 2010

TABLE 4. Renal Function Measures in Biennial Evaluations of Gulf War Veterans Exposed to Depleted Uranium in 1991

	Year of evaluation					
				2005		
	1999	2001	2003	Current exposure	Cumulative exposure	2007
n low exposure, *n* high exposure[a]	37, 13	26, 13	19, 13	24, 10	24, 10	25, 10
	p Value and direction of difference[b]					
Renal function measures—urinary						
Creatinine	0.07 H < L	0.29	0.31	0.24	0.08 H < L	0.43
Calcium		0.35	0.79	0.59	0.56	0.14 L < H
Phosphate (PO_4)		0.40	0.44	0.29	0.27	0.57
β_2-Microglobulin	0.27	0.78	0.53	0.22	0.83	0.11 H > L
Intestinal alkaline phosphatase			0.85	0.67	0.52	0.38
N-Acetyl β-glucosaminidase			0.38	0.96	0.90	0.32
Total protein	0.89	0.01 H > L	0.21	0.50	0.25	0.49
Microalbumin			0.85	0.40	0.32	0.17 H > L
Retinol binding protein	0.15 H > L	0.06 H > L	0.54	0.25	0.56	0.07 H > L
Renal function measures—serum						
Creatinine	0.14 H < L	0.03 H < L	0.11 H < L	0.72	0.56	0.11 H < L
Calcium		0.67	0.85	0.24	0.56	0.26
Phosphate (PO_4)		0.63	0.03 H > L	0.70	0.64	0.57
Uric acid	0.12 H < L	0.45	0.32	0.10 H < L	0.03 H < L	0.17 H > L

Note. Sources: McDiarmid et al. (2001), McDiarmid et al. (2004), McDiarmid et al. (2006), McDiarmid et al. (2007), and McDiarmid et al. (2009) for the 1999, 2001, 2003, 2005, and 2007 evaluations, respectively.

[a]Low (L) exposure defined as <0.10 μg uranium/g creatinine and high (H) defined as ≥0.10 μg uranium/g creatinine; *n* for specific assays may vary by 1–2 participants because of sample processing errors.

[b]Direction of difference given for tests in which the *p* value was ≤.20.

Downloaded By: [US EPA Environmental Protection Agency] At: 17:09 22 December 2010

TABLE 5. Summary of Subchronic and Chronic Oral Toxicity Studies of Uranium in Experimental Animals

Reference	Uranium compound	Species, sex, group size	Exposure conditions	Response and LOAEL
Subchronic studies				
McDonald-Taylor et al., 1992, 1997	Uranyl nitrate hexahydrate	Rabbit, New Zealand, M (3/group)	0, 24, 600 mg/L in drinking water (0, 1.7, 42 mg /kg-d U); 91 d. Followed by recovery periods of 0, 45, or 91 d	Kidney histopathology, including increases in glomerular basement membrane thickness and changes in proximal tubule cells seen in lowest dose group.
Gilman et al., 1998c	Uranyl nitrate hexahydrate	Rat, Sprague-Dawley, M & F (15/sex/group)	0, 0.96, 4.8, 24, 120, 600 mg/L in drinking water (M: 0, 0.06, 0.31, 1.52, 7.54, 36.7 mg /kg-d U; F: 0, 0.09, 0.42, 2.01, 9.98, 53.6 mg /kg-d U); 91 d	Histopathologic lesions of the kidney seen in lowest dose group; changes included dilation of tubules, apical displacement, and vesiculation of tubular nuclei and cytoplasmic vacuolation and degranulation in males and capsular sclerosis and reticulin sclerosis of tubular basement membranes and interstitial scarring in females.
Gilman et al., 1998b	Uranyl nitrate hexahydrate	Rabbit, New Zealand, M and F (10/sex/group)	M: 0, 0.96, 4.8, 24, 120, 600 mg/L in drinking water (0, 0.05, 0.20, 0.88, 4.82, 28.7 mg/kg-d U) F: 0, 4.8, 24, 600 mg/L in drinking water (0, 0.49, 1.32, 43.0 mg/kg-d U); 91 d	Histopathologic lesions of the kidney (male) seen in lowest dose group. Lesions included cytoplasmic vacuolation, anisokaryosis, and nuclear vesiculation.
Gilman et al., 1998a	Uranyl nitrate hexahydrate	Rabbit, SPF, M (5–8/group)	0, 24, 600 mg/L in drinking water (0, 1.4, 41.0 mg/kg-d U); 91 d followed by recovery periods of 0, 8, 14, 45, or 91 d	Histopathologic lesions of the kidney seen in 600 mg/L group, no attenuation of effect seen with any recovery period. Observed lesions included cytoplasmic vacuolation, anisokaryosis, nuclear hyperchromicity and vesiculation, tubular dilation, and reticulin sclerosis of the renal interstitial tissue.
Ortega et al., 1989	Uranyl acetate dihydrate	Rat, Sprague-Dawley, M (8/group)	0, 2, 4, 8, or 16 mg uranyl acetate dihydrate/kg-d (0, 1.1, 2.2, 3.4, 4.5, 9.0 mg/kg-d U); 28 d	Increase in total plasma protein seen in lowest dose group; urinary biochemical endpoints were not significantly altered by uranium treatment at any dose.

(Continued)

Downloaded By: [US EPA Environmental Protection Agency] At: 17:09 22 December 2010

TABLE 5. (Continued)

Reference	Uranium compound	Species, sex, group size	Exposure conditions	Response and LOAEL
Guéguen et al., 2007	Uranyl nitrate	Rat, Sprague-Dawley, M (3/group)	0, 40 mg/L in drinking water (0, 3.3 mg/kg-d U); 9 mo	Following single exposure to acetominophen, increased renal proximal tubular cell necrosis, increased gene expression of xenobiotic metabolizing enzymes in kidney relative to animals not exposed to uranium.
Chronic studies				
Maynard et al., 1953	Uranyl fluoride	Rat, Wistar, M and F (15–25/group)	0, 0.01, 0.05, 0.1, 0.15, 0.25, 0.5% in diet; up to 24 mo	Minimal renal changes in 0.15% diet group (~85 mg/kg-d U); marked tubular atrophy with later regeneration seen in 0.5% diet group (~280 mg/kg-d U)
	Uranyl nitrate hexahydrate		0, 0.01, 0.05, 0.1, 0.5, 1, 2% in diet; up to 24 mo	Slight traces of renal injury seen in 0.5% diet group (~200 mg/kg-d U); renal abnormalities (tubular atrophy, and increase in stroma and a narrowing of the cortex in 2% diet group (~700 mg/kg-d U)
	Uranium dioxide		0, 0.5, 2, 20% in diet; up to 24 mo	No effects seen at any dose
	Uranium tetrafluoride		0, 0.5, 2, 20% in diet; up to 24 mo	Mild renal tubular degeneration seen in 20% diet group (~9200 mg/kg-d U)

Downloaded By: [US EPA Environmental Protection Agency] At: 17:09 22 December 2010

dose. McDonald-Taylor et al. (1992, 1997) and Gilman et al. (1998a, 1998b, 1998c) reported a significant increase in ultrastructural and histopathological alterations associated with with tubular cell necrosis (Greaves, 2007; Walling, 1991) in U-exposed animals. These effects included thickening of the glomerular basement membrane. Neither McDonald-Taylor et al. (1992) nor Gilman et al. (1998a) found evidence of reversibility of kidney histopathologic changes after 91-d recovery periods.

The available subchronic and chronic oral toxicity studies on U compounds included limited evaluation of biomarkers of kidney function. Gilman et al. (1998a, 1998b, 1998c) examined urinary parameters in the rabbit, but not rat. In the first rabbit study Gilman et al. (1998b) measured various urinary parameters including levels of urea nitrogen, glucose, creatinine, total protein, and albumin as well as activities of LDH avtivity and NAG. Gilman et al. (1998a, 1998b, 1998c) found no marked effects after exposure to 29 mg U/kg-d for 91 d, but reported urinary parameter effects with the most persistent being increased glucose excretion in a second study in male rabbits exposed to 41 mg U/kg-d for 91 d (Gilman et al., 1998a). A dye clearance test used to assess renal function showed reduced rate of phenolsulfonphthalein excretion in male rabbits exposed to $\geq$ 120 mg/L uranyl nitrate (5 mg U/kg-d) but not in females (Gilman et al., 1998b). Rabbits exposed to lower levels of U in drinking water showed no marked changes in urinary parameters (Gilman et al., 1998a, 1998b).

Two animal studies that explored the renal effects of implanted DU particles in rats provide toxicity information relevant to the hazard associated with exposure of soldiers to embedded fragments of DU (Pellmar et al., 1998, 1999; Zhu et al., 2009). Pellmar et al. (1998, 1999) did not observe significant changes in biochemical or histologic markers of renal damage, while Zhu et al. (2009) reported that DU exposure led to increased renal damage as measured by light and electron microscopy including hypertrophy of epithelial cells, necrosis, fibrosis, increased mitochondria size, glomerulus thickening, and inflammatory-cell infiltration, and biochemical assays as evidenced by increased urinary β_2-microglobulin, albumin, serum creatinine, and BUN. Although both of these studies used similar methodologies for DU pellet implantation within the gastrocnemius muscle in the lower leg of Sprague-Dawley rats, the actual doses of implanted DU can not be compared based upon data provided. Pellmar et al. (1998, 1999) implanted rats with 0, 4, 10, and 20 U pellets (pellet weights not reported). Zhu et al. (2009) implanted rats with 0, 0.1, 0.2, and 0.3 g of DU fragments. After 6 mo of exposure, the highest renal U concentration reported by Pellmar et al. (1999) was 6920 $\pm$ 770 ng/g, while Zhu et al. (2009) reported a renal U concentration of 27,439 $\pm$ 2291 ng/g in the high-dose group. The differences in U-induced renal toxicity observed in these two studies may have been due to differences in U dose, tissue uptake, or diffusion from the implanted pellets.

STUDIES OF MECHANISMS OF RENAL TOXICITY

The cellular, molecular, and biochemical mechanisms for renal U uptake and toxicity have been previously reviewed (ATSDR, 1999). Recent studies using proximal and distal tubule cell lines (MDCK and LLC-PK_1 cells) suggest that U-induced renal toxicity is dependent on the formation of uranyl phosphate complexes, specifically $UO_2(PO_4)^-$ and $UO_2(HPO_4)$, and their uptake by the sodium dependent co-transporter NaPi-II and absorptive endocytosis (Muller et al., 2006, 2008). Furthermore, in vitro studies using isolated human and murine kidney cortex tubules suggest that U exposure inhibits cellular ATP content and gluconeogenesis through enzymatic inhibition of LDH, pyruvate carboxylase, glucose 6-phosphatase, and phoshoenolpyruvate carboxykinase. Toxicogenomic and proteomic studies using human renal HEK293 cells also suggest that U exposure altered expression of genes associated with calcium-dependent cell signaling such as IP3 cascade kinases PI4KII

Downloaded By: [US EPA Environmental Protection Agency] At: 17:09 22 December 2010

and PIK3R1, the intracellular calcium receptor calmodulin, and calmodulin-dependent proteins and cell trafficking pathways such as the potassium channel ABC subunits ATP6V1A1 and ABCC8 (Prat et al., 2005). Both in vivo and in vitro experiments showed that U exposure depleted cellular antioxidants such as glutathione (GSH) and glutathione reductase activity, increased reactive oxygen species (ROS) production and DNA damage, and promoted apoptosis (Banday et al., 2008; Linares et al., 2006; Thiebault et al., 2007). In vivo toxicogenomic studies reported that chronic exposure to U significantly enhanced expression of genes associated with oxidative stress responses such as superoxide dismutase 1 and ion transporters including NaPi-II and Slc34a1 (Taulan et al., 2004).

DISCUSSION

Some evidence of adverse renal effects, particularly with respect to biomarkers of proximal tubule damage, is seen in community-based studies of populations chronically exposed to elevated drinking water concentrations of U. The biomarker for which effects were most consistently seen was urinary levels of β_2-microglobulin (Zamora et al., 1998, 2009; Seldén et al., 2009). The study in Finland (Kurttio et al., 2002) did not demonstrate an association of toxicity to U with β_2-microglobulin levels. Prat et al. (2009) suggested that the calcium-dependent species seen in speciation analyses of the Finnish water samples may result in a low toxicity profile. It should also be noted, however, that 65% of the samples in Kurttio et al. (2002) were below the β_2-microglobulin limit of detection, and in contrast to the other studies, this measure was based on a spot urine rather than an overnight urine sample. β_2-Microglobulin was not included in the measurements used in the follow-up study in Finland (Kurttio et al., 2006). Thun et al. (1985) also reported strong associations between U exposure and β_2-microglobulin measures in urine and serum among workers in a U processing mill. Two of these studies included measures of other metals (Cd and Pb in Seldén et al. [2009] and Cd and Pb in Thun et al. [1985]), and there was no indication that the associations seen with U were the result of confounding by these other exposures. In addition, in the most recent follow-up surveillance study of Gulf War veterans exposed to DU, some indications of proximal tubule effects, as evidenced by increased urinary β_2-microglobulin and retinol binding protein levels, were noted (McDiarmid et al., 2009). Thus, although the subsets of renal tests, sensitivity of assays, and type of exposure measure varied across studies, as a group these studies show considerable consistency with respect to an indicator of proximal tubule damage and either measures of intake or U concentrations in urine. Occupational cohort studies do not provide evidence of an increased risk of kidney-related mortality among U-exposed workers. This outcome would be a relatively insensitive endpoint for the detection of renal damage, however, as it relies on cause of death as reported on death certificates. The reliability of this recording for chronic conditions, such as kidney disease, is much lower than for most cancers and acute events such as accidents and myocardial infarction (Harteloh et al., 2010).

Studies in experimental animals confirm that the kidney is a target of U toxicity following oral and implantation exposure. Both routes of exposure are relevant to human exposure situations. The available animal studies, however, provide an incomplete characterization of the dose-response relationship for kidney effects associated with chronic exposure at low environmental exposure levels. With the exception of early (1940s) studies conducted in support of the Manhattan Project (Dygert et al., 1949; Maynard et al., 1953; Maynard and Hodge, 1949), animal studies are generally limited to exposures of 90 d duration. Further, the majority of subchronic oral toxicity studies (Gilman et al., 1998a, 1998b, 1998c; McDonald-Taylor et al., 1992, 1997) of U compounds failed to identify a no-observed-adverse-effect level, and the kidney effects reported by some investigators (Gilman et al., 1998b, 1998c) did not exhibit a dose response. Investigation of clinical

biomarkers of renal toxicity in experimental animal studies is limited. Mechanistic studies suggest that cell toxicity may result from altered function of cell signaling pathways, increased ROS production, and depletion of endogenous cellular antioxidants.

In summary, various lines of evidence suggest that relatively low levels of U exposure may result in detectable changes in markers of renal damage in humans. The epidemiological studies do not provide evidence of clinically diagnosed kidney disease or renal failure within the exposed populations. Given the limited sample sizes and the potential selection of relatively healthy individuals in these types of community-based and occupational studies, the absence of the observation of this type of kidney disease is not surprising. Rather, these studies are better designed to examine associations within what would be considered the normal range of specific biomarkers of renal function. The question of the interpretation and importance of the observed effects of biomarkers of proximal tubule function is an important question that would benefit from additional clinical, epidemiological, and experimental research.

Downloaded By: [US EPA Environmental Protection Agency] At: 17:09 22 December 2010

REFERENCES

Abu-Qare, A. W., and Abou-Donia, M. B. 2002. Depleted uranium—The growing concern. *J. Appl. Toxicol*. 22:149–152.

Arfsten, D. P., Still, K. R., and Ritchie, G. D. 2001. A review of the effects of uranium and depleted uranium exposure on reproduction and fetal development. *Toxicol. Ind. Health* 17:180–191.

Agency for Toxic Substances and Disease Registry. 1999. *Toxicological profile for uranium*. Atlanta, GA: U.S. Department of Health and Human Services, Agency for Toxic Substances and Disease Registry. http://www.atsdr.cdc.gov/toxprofiles/tp150.pdf

Bagshaw, S. M., Langenberg, C., Haase, M., Wan, L., May, C. N., and Bellomo, R. 2007. Urinary biomarkers in septic acute kidney injury. *Intens. Care Med*. 33:1285–1296.

Banday, A. A., Priyamvada, S., Farooq, N., Yusufi, A. N., and Khan, F. 2008. Effect of uranyl nitrate on enzymes of carbohydrate metabolism and brush border membrane in different kidney tissues. *Food Chem. Toxicol*. 46:2080–2088.

Birn, H., and Christensen, E. I. 2006. Renal albumin absorption in physiology and pathology. *Kidney Int*. 69:440–449.

Bleise, A., Danesi, P. R., and Burkart, W. 2003. Properties, use and health effects of depleted uranium (DU): A general overview. *J. Environ. Radioact*. 64:93–112.

Boice, J. D., Jr., Cohen, S. S., Mumma, M. T., Chadda, B., and Blot, W. J. 2008. A cohort study of uranium millers and miners of Grants, New Mexico, 1979–2005. *J. Radiol. Prot*. 28:303–325.

Centers for Disease Control and Prevention. 2005. *Third national report on human exposure to environmental chemicals*. Atlanta, GA: U.S. Centers for Disease Control and Prevention. http://www.cdc.gov/exposurereport/pdf/thirdreport.pdf

Checkoway, H., Pearce, N., Crawford-Brown, D. J., and Cragle, D. L. 1988. Radiation doses and cause-specific mortality among workers at a nuclear materials fabrication plant. *Am. J. Epidemiol*. 127:255–266.

Comper, W. D., Hilliard, L. M., Nikolic-Paterson, D. J., and Russo, L.M. 2008. Disease-dependent mechanisms of albuminuria. *Am. J. Physiol. Renal Physiol*. 295:F1589–F1600.

Craft, E., Abu-Qare, A., Flaherty, M., Garofolo, M., Rincavage, H., and Abou-Donia, M. 2004. Depleted and natural uranium: Chemistry and toxicological effects. *J. Toxicol. Environ. Health B* 7:297–317.

Domingo, J. L., Llobet, J. M., Tomas, J. M., and Corbella, J. 1987. Acute toxicity of uranium in rats and mice. *Bull. Environ. Contam. Toxicol*. 39:168–174.

Dupree-Ellis, E., Watkins, J., Ingle, J. N., and Phillips, J. 2000. External radiation exposure and mortality in a cohort of uranium processing workers. *Am. J. Epidemiol*. 152:9195.

Dygert, H. P., LaBelle, C. W., Laskin, S., Pozzani, U. C., Roberts, E., Rothermel, J. J., Rothstein, A., Spiegl, C. J., Sprague, G. F., and Strokinger, H. E. 1949. Toxicity following inhalation. In *Pharmacology and Toxicology of Uranium Compounds*, eds. C. Voegtlin and H. C. Hodge, pp. 423–524.New York: McGraw-Hill.

Emeigh, S., and Kinter, L. 2005. Assessing renal effects of toxicants in vitro. In *Toxicology of the kidney*, 3rd ed., ed. J. Tarloff and L. Lash, pp 81–147. Washington, D.C.: CRC Press.

Emeigh Hart, S. 2005. Assessment of renal injury in vivo. *J. Pharmacol. Toxicol. Methods* 52:30–45.

Frome, E. L., Cragle, D. L., and McLain, R. W. 1990. Poisson regression analysis of the mortality among a cohort of World War II nuclear industry workers. *Radiat. Res*. 123:138–152.

Gilman, A. P., Moss, M. A., Villeneuve, D. C., Secours, V. E., Yagminas, A. P., Tracy, B. L., Quinn, J. M., Long, G., and Valli, V. E. 1998a. Uranyl nitrate: 91-Day exposure and recovery studies in the male New Zealand white rabbit. *Toxicol. Sci*. 41:138–151.

Gilman, A. P., Villeneuve, D. C., Secours, V. E., Yagminas, A. P., Tracy, B. L., Quinn, J. M., Valli, V. E., and Moss, M. A. 1998b. Uranyl nitrate: 91-Day toxicity studies in the New Zealand white rabbit. *Toxicol. Sci*. 41:129–137.

Gilman, A. P., Villeneuve, D. C., Secours, V. E., Yagminas, A. P., Tracy, B. L., Quinn, J. M., Valli, V. E., Willes, R. J., and Moss, M. A. 1998c. Uranyl nitrate: 28-day and 91-day toxicity studies in the Sprague-Dawley rat. *Toxicol. Sci*. 41:117–128.

Goel, K. A., Garg, V. K., and Garg, V. 1980. Histopathology of kidney of albino rat poisoned with uranyl nitrate. *Bull. Environ. Contam. Toxicol*. 24:9–12.

Greaves, P. 2007. *Histopathology of preclinical toxicity studies: Interpretation and relevance in drug safety evaluation*, 3rd ed., pp. 570–623. Boston: Academic Press.

Guéguen, Y., L. Grandcolas, C. Baudelin, S. Grison, E. Tissandié, J. R. Jourdain, F. Paquet, P. Voisin, J. Aigueperse, P. Gourmelon, and M. Souidi. 2007. Effect of acetaminophen administration to rats chronically exposed to depleted uranium. *Toxicology* 229:62–72.

Harteloh, P., de Bruin, K., and Kardaun, J. 2010. The reliability of cause-of-death coding in the Netherlands. *Eur. J. Epidemiol*. March 23 [Epub ahead of print].

Hindin, R., Brugge, D., and Panikkar, B. 2005. Teratogenicity of depleted uranium aerosols: A review from an epidemiological perspective. *Environ. Health* 4:17.

Kurttio, P., Auvinen, A., Salonen, L., Saha, H., Pekkanen, J., Makelainen, I., Vaisanen, S. B., Penttila, I. M., and Komulainen, H. 2002. Renal effects of uranium in drinking water. *Environ. Health Perspect*. 110:337–342. Erratum: *Environ. Health Perspect*. 111:632 (2003).

Kurttio, P., Harmoinen, A., Saha, H., Salonen, L., Karpas, Z., Komulainen, H., and Auvinen, A. 2006. Kidney toxicity of ingested uranium from drinking water. *Am. J. Kidney Dis*. 47:972–982.

Levey, A. S., Stevens, L. A., Schmid, C. H., Zhang, Y. L., Castro, A. F. 3rd, Feldman, H. I., Kusek, J. W., Eggers, P., Van Lente, F., Greene, T., and Coresh, J. 2009. A new equation to estimate glomerular filtration rate. *Ann. Intern. Med*. 150:604–612.

Linares, V., Belles, M., Albina, M. L., Sirvent, J. J., Sanchez, D. J., and Domingo, J. L. 2006. Assessment of the pro-oxidant activity of uranium in kidney and testis of rats. *Toxicol. Lett*. 167:152–161.

Loomis, D. P., and Wolf, S. H. 1996. Mortality of workers at a nuclear materials production plant at Oak Ridge, Tennessee, 1947–1990. *Am. J. Ind. Med*. 29:131–141.

Magdo, H. S., Forman, J., Graber, N., Newman, B., Klein, K., Satlin, L., Amler, R. W., Winston, J. A., and Landrigan, P. J. 2007. Grand rounds: Nephrotoxicity in a young child exposed to uranium from contaminated well water. *Environ. Health Perspect*. 115:1237–1241.

Mao, Y., Desmeules, M., Schaubel, D., Berube, D., Dyck, R., Brule, D., and Thomas, B. 1995. Inorganic components of drinking water and microalbuminuria. *Environ. Res*. 71:135–140.

Downloaded By: [US EPA Environmental Protection Agency] At: 17:09 22 December 2010

Downloaded By: [US EPA Environmental Protection Agency] At: 17:09 22 December 2010

Maynard, E. A., and Hodge, H. C. 1949. Study of toxicity of various uranium compounds when fed to experiment animals. In *Pharmacology and toxicology of uranium compounds*, eds. C. Voegtlin and H. C. Hodge, pp. 309–376. New York: McGraw-Hill.

Maynard, E. A., Downs, W. L., and Hodge, H. C. 1953. Oral toxicity of uranium compounds. In *Pharmacology and toxicology of uranium compounds*, eds. C. Voegtlin and H. C. Hodge, pp. 1221–1369. New York: McGraw-Hill.

McDiarmid, M. A., Squibb, K., Engelhardt, S., Oliver, M., Gucer, P., Wilson, P. D., Kane, R., Kabat, M., Kaup, B., Anderson, L., Hoover, D., Brown, L. D., Jacobson-Kram, D., and Depleted Uranium Follow-Up Program. 2001. Surveillance of depleted uranium exposed Gulf War veterans: Health effects observed in an enlarged "friendly fire" cohort. *J. Occup. Environ. Med*. 43:991–1000.

McDiarmid, M. A., Engelhardt, S., Oliver, M., Gucer, P., Wilson, P. D., Kane, R., Kabat, M., Kaup, B., Anderson, L., Hoover, D., Brown, L., Handwerger, B., Albertini, R. J., Jacobson-Kram, D., Thorne, C. D., and Squibb, K. S. 2004. Health effects of depleted uranium on exposed Gulf War veterans: A 10-year follow-up. *J. Toxicol. Environ. Health A* 67:277–296.

McDiarmid, M. A., Engelhardt, S. M., Oliver, M., Gucer, P., Wilson, P. D., Kane, R., Kabat, M., Kaup, B., Anderson, L., Hoover, D., Brown, L., Albertini, R. J., Gudi, R., Jacobson-Kram, D., Thorne, C. D., and Squibb, K. S. 2006. Biological monitoring and surveillance results of Gulf War I veterans exposed to depleted uranium. *Int. Arch. Occup. Environ. Health* 79:11–21.

McDiarmid, M. A., Engelhardt, S. M., Oliver, M., Gucer, P., Wilson, P. D., Kane, R., Cernich, A., Kaup, B., Anderson, L., Hoover, D., Brown, L., Albertini, R., Gudi, R., Jacobson-Kram, D., and Squibb, K. S. 2007. Health surveillance of Gulf War I veterans exposed to depleted uranium: updating the cohort. *Health Phys*. 93:60–73.

McDiarmid, M. A., Engelhardt, S. M., Dorsey, C. D., Oliver, M., Gucer, P., Wilson, P. D., Kane, R., Cernich, A., Kaup, B., Anderson, L., Hoover, D., Brown, L., Albertini, R., Gudi, R., and Squibb, K. S. 2009. Surveillance results of depleted uranium-exposed Gulf War I veterans: Sixteen years of follow-up. *J Toxicol Environ Health A* 72:14–29.

McDonald-Taylor, C. K., Bhatnagar, M. K., Gilman, A., Yagminas, A., and Singh, A. 1992. Uranyl nitrate-induced glomerular basement membrane alterations in rabbits: A quantitative analysis. *Bull. Environ. Contam. Toxicol*. 48:367–373.

McDonald-Taylor, C. K., Singh, A., and Gilman, A. 1997. Uranyl nitrate-induced proximal tubule alterations in rabbits: A quantitative analysis. *Toxicol. Pathol*. 25:381–389.

McGeoghegan, D., and Binks, K. 2000a. The mortality and cancer morbidity experience of workers at the Capenhurst uranium enrichment facility 1946–95. *J. Radiol. Prot*. 20:381–401.

McGeoghegan, D., and Binks, K. 2000b. The mortality and cancer morbidity experience of workers at the Springfields uranium production facility, 1946–95. *J. Radiol. Prot*. 20:111–137.

Muller, D., Houpert, P., Cambar, J., and Henge-Napoli, M. H. 2006. Role of the sodium-dependent phosphate co-transporters and of the phosphate complexes of uranyl in the cytotoxicity of uranium in LLC-PK1 cells. *Toxicol. Appl. Pharmacol*. 214: 166–177.

Muller, D. S., Houpert, P., Cambar, J., and Henge-Napoli, M. H. 2008. Role of the sodium-dependent phosphate cotransporters and absorptive endocytosis in the uptake of low concentrations of uranium and its toxicity at higher concentrations in LLC-PK1 cells. *Toxicol. Sci*. 101: 254–262.

Orloff, K. G., Mistry, K., Charp, P., Metcalf, S., Marino, R., Shelly, T., Melaro, E., Donohoe, A. M., and Jones, R. L. 2004. Human exposure to uranium in groundwater. *Environ. Res*. 94:319–326.

Downloaded By: [US EPA Environmental Protection Agency] At: 17:09 22 December 2010

Ortega, A., Domingo, J. L., Llobet, J. M., Tomas, J. M., and Paternain, J. L. 1989. Evaluation of the oral toxicity of uranium in a 4-week drinking-water study in rats. *Bull. Environ. Contam. Toxicol*. 42:935–941.

Ozmen, M., and Yurekli, M. 1998. Subacute toxicity of uranyl acetate in Swiss-albino mice. *Environ. Toxicol. Pharmacol*. 6:111–115.

Parkhurst, M. A., and Guilmette, R. A. 2009. Overview of the Capstone depleted uranium study of aerosols from impact with armored vehicles: Test setup and aerosol generation, characterization, and application in assessing dose and risk. *Health Phys*. 96:207–220.

Pellmar, T. C., Hogan, J. B., Benson, K. A., and Landauer, M. R. 1998. *Toxicological evaluation of depleted uranium in rats: Six-month evaluation point*. Bethesda, MD: Uniformed Services University of the Health Sciences. ADA410643.

Pellmar, T. C., Fuciarelli, A. F., Ejnik, J. W., Hamilton, M., Hogan, J., Strocko, S., Emond, C., Mottaz, H. M., and Landauer, M. R. 1999. Distribution of uranium in rats implanted with depleted uranium pellets. *Toxicol. Sci*. 49:29–39.

Pinkerton, L. E., Bloom, T. F., Hein, M. J., and Ward, E. M. 2004. Mortality among a cohort of uranium mill workers: An update. *Occup. Environ. Med*. 61:57–64.

Polednak, A. P., and Frome, E. L. 1981. Mortality among men employed between 1943 and 1947 at a uranium-processing plant. *J. Occup. Med*. 23:169–178.

Prat, O., Berenguer, F., Malard, V., Tavan, E., Sage, N., Steinmetz, G., and Quemeneur, E. 2005. Transcriptomic and proteomic responses of human renal HEK293 cells to uranium toxicity. *Proteomics* 5:297–306.

Prat, O., Vercouter, T., Ansoborlo, E., Fichet, P., Perret, P., Kurttio, P., and Salonen, L. 2009. Uranium speciation in drinking water from drilled wells in southern Finland and its potential links to health effects. *Environ. Sci. Technol*. 43:3941–3946.

Renault, S., Faiz, H., Gadet, R., Ferrier, B., Martin, G., Baverel, G., and Conjard-Duplany, A. 2010. Uranyl nitrate inhibits lactate gluconeogenesis in isolated human and mouse renal proximal tubules: A ^{13}C-NMR study. *Toxicol. Appl. Pharmacol*. 242:9–17.

Ritz, B., Morgenstern, H., Crawford-Brown, D., and Young, B. 2000. The effects of internal radiation exposure on cancer mortality in nuclear workers at Rocketdyne/Atomics International. *Environ. Health Perspect*. 108:743–751.

Seldén, A. I., Lundholm, C., Edlund, B., Hogdahl, C., Ek, B. M., Bergstrom, B. E., and Ohlson, C. G. 2009. Nephrotoxicity of uranium in drinking water from private drilled wells. *Environ. Res*. 109:486–494.

Squibb, K. S., and McDiarmid, M. A. 2006. Depleted uranium exposure and health effects in Gulf War veterans. *Philos. Trans. R. Soc. Lond. B Biol. Sci*. 361:639–648.

Taulan, M., Paquet, F., Maubert, C., Delissen, O., Demaille, J., and Romey, M. C. 2004. Renal toxicogenomic response to chronic uranyl nitrate insult in mice. *Environ. Health Perspect*. 112:1628–1635.

Thiebault, C., Carriere, M., Milgram, S., Simon, A., Avoscan, L., and Gouget, B. 2007. Uranium induces apoptosis and is genotoxic to normal rat kidney (NRK-52E) proximal cells. *Toxicol. Sci*. 98:479–487.

Thun, M. J., Baker, D. B., Steenland, K., Smith, A. B., Halperin, W., and Berl, T. 1985. Renal toxicity in uranium mill workers. *Scand. J. Work Environ. Health* 11:83–90.

Tolkoff-Rubin, N. E., Rubin, R. H., and Bonventre, J. V. 1988. Noninvasive renal diagnostic studies. *Clin. Lab. Med*. 8:507–526.

U. S. Environmental Protection Agency. 1985. *Nationwide occurrence of radon and other natural radioactivity in public water supplies*. Montgomery, AL: U. S. Environmental Protection Agency. EPA Number 520585008.

U. S. Environmental Protection Agency. 2000. *Radionuclides notice of data availability technical support document*. Washington, DC: U. S. Environmental Protection Agency.

http://www.epa.gov/OGWDW/radionuclides/pdfs/regulation_radionuclides_rulemaking_techsupportdoc.pdf

Walling, M. A. 1991. Morphologic manifestation of toxic cell injury. In *Handbook of toxicologic pathology*, vol. 2, eds. W. M. Haschek, C. G. Rousseaux, and M. A. Wallig, pp. 39–64. San Diego: Academic Press.

Waxweiler, R. J., Archer, V. E., and Roscoe, R. J. 1983. Mortality patterns among a retrospective cohort of uranium mill workers. In *Epidemiology applied to health physics, Sixteenth midyear topical meeting of the Health Physics Society*, Albuquerque, NM, pp. 428–435.

World Health Organization. 2001. *Depleted uranium sources, Exposure and health effects*. Geneva, Switzerland: World Health Organization. http://whqlibdoc.who.int/hq/2001/WHO_SDE_PHE_01.1.pdf

Zalups, R. K., Gelein, R. M., Morrow, P. E., and Diamond, G. L. 1988. Nephrotoxicity of uranyl fluoride in uninephrectomized and sham-operated rats. *Toxicol. Appl. Pharmacol*. 94:11–22.

Zamora M. L. L., Zielinski, J. M., Moodie, G. B., Falcomer, R. A. F., Hunt, W. C., and Capello, K. 2009. Uranium in drinking water: Renal effects of long-term ingestion by an Aboriginal community. *Arch. Environ. Occup. Health* 64:228–241.

Zamora, M. L., Tracy, B. L., Zielinski, J. M., Meyerhof, D. P., and Moss, M. A. 1998. Chronic ingestion of uranium in drinking water: A study of kidney bioeffects in humans. *Toxicol. Sci*. 43:68–77.

Zhu, G., Xiang, X., Chen, X., Wang, L., Hu, H., and Weng, S. 2009. Renal dysfunction induced by long-term exposure to depleted uranium in rats. *Arch. Toxicol*. 83:37–46.

Downloaded By: [US EPA Environmental Protection Agency] At: 17:09 22 December 2010

Table of Contents

General_Authors_Publications.....2
LI-266492_PLOS_1_Zucker_comparison_nanoparticles.....16
LI-266518_Final__Ortenzio_et_al_2019.....40
LI-266520_Zucker_et_al-Cytometry_Part_A.....50
Jana_No_response.....65
aliceno_response.....67
Boyes_approval.....69
jayna_ortinszio_no_repsonse.....70
kim_approval.....72
Laura_approval.....74
lerner_no_repsonse.....75
McGEE_no_reponse.....77

United States Environmental Protection Agency
Washington, DC 20460

STAA REPORT FOR THE SCIENTIST NOMINATIONS

General Information:

Nomination ID/App ID:	20-122
Research Category Primary:	Health Effects Research and Human Health Risk Assessment (HE)
Research Category Secondary:	Monitoring and Measurement Methods (MM)
Laboratory/Office Name:	ORD
Nomination Entered By:	Robert Zucker

Eligibility Checklist:

[Y] The nominated publication(s) has not been submitted to a previous STAA competition.

[Y] The nominated publication(s) was published on or before January 1, 2017 and on or after January 1,2012

[Y] The principal author was an EPA employee or a PHS employee assigned to EPA when the research was performed

[Y] The EPA authors (includes PHS employees assigned to EPA) contributed collectively a minimum of 50% toward the publication(s)

Nominating Official Name:	David Diazsanchez
Nominating Official Title:	
Nominating OfficialEmail:	diaz-sanchez.david@epa.gov
STAA Coordinator Name:	Robert Zucker
STAA Coordinator Email:	zucker.robert@epa.gov

Justifications:

Justification 1:

Nanotechnology, including the use of engineered nanomaterials (ENM), is a growing part of commerce that is expected to make an ever increasing contribution to global economic development (PCAST, 2014). Nanoparticles are being incorporated into many applications, and although the uses and forms of nanomaterials in many consumer products are unknown, inventories of products suggest that silver nanomaterials (AgNP) are incorporated into more consumer products than nanomaterials of other composition (Hansen et al., 2016; Vance et al., 2015). Among the product categories that may contain silver nanoparticles are personal care products, home and garden products, cosmetics, food and beverage containers, lters, appliances, sporting goods, children's products, electronics, automotive components, and dietary supplements. The variety of engineered materials and their applications is growing at a pace more rapid than can be evaluated for potential hazards in a conventional way. As is true for the large number of conventional chemicals with inadequate toxicity and exposure data (NRC, 2007), alternative approaches for evaluating potential hazards of ENM are necessary if they are to be used in a responsible and sustainable fashion.

EPA has responsibilities for regulation of engineered nanomaterials primarily under the Toxic Substances Control Act (TSCA) and the Federal Insecticide Fungicide and Rodenticide Act (FIFRA). The 2016 reauthorization of TSCA as the Frank R. Lautenberg Chemical Safety for the 21st Century Act, and recent guidance from the EPA Administrator emphasize the development of alternative testing approaches for chemical safety assessment that are not based on traditional whole animal toxicity testing. The need for *in vitro* assessments of potential health effects from exposure to ENM is as pressing as it is for traditional chemicals, and a special need for understanding the dose of nanoparticles that reach cells in *in vitro* test systems has become apparent. One of the primary differences between toxicity of nanoparticles and traditional chemicals is biokinetics, the ability of particles to transition through the body and reach target cells in different local concentrations and over a different time course than do traditional chemicals. The dose reaching cells in vitro cannot be assumed to be proportional to the concentration applied to the culture due to differential dispersion and sedimentation of nanoparticles of different sizes and densities. The ability to measure and cellular dose and observe cellular distribution of ENM In cell culture systems is the common theme linking the three nominated publications. The critical parameter derived from these systems is determining

cellular dose, an essential foundation of dose-response relationships. Accurate determination of cellular dose is required for *in vitro/in vivo* extrapolations to predict potential human health effects.

The first of the nominated manuscripts (Zucker et al., 2016) demonstrated that flow cytometry can be used to determine concentrations and relative sizes of nanoparticles in suspension for *in vitro* test systems and to determine the amount of nanoparticles taken up by cells *in vitro*. The second of the nominated manuscripts (Ortenzio et al, 2019) evaluated different computational models for particle deposition in a fluid media to estimate particle dose delivered to cells, and observed that the size of silver particles was a primary component influencing dose delivered to cells, with as much as 90% of the smaller sized particles remaining in suspension in the cell culture media 24 hours after exposure. The third of the nominated publications (Zucker et al., 2019) demonstrated the role of particle coatings on cellular dose and toxicity, with positively charged coatings providing a higher dose and being more toxic than either neutral or negatively charged surfaces. The conceptual and technological advances provided in these publications will thereby enhance EPA's ability to request and interpret data from alternative test systems when evaluating novel ENM for EPA registration under TSCA or FIFRA.

1. Citations for each publication nominated

a. Zucker RM, Ortenzio JNR, Boyes WK. 2016. Characterization, detection, and counting of metal nanoparticles using flow cytometry. Cytometry Part A 89: 169-83. DOI: 10.1002/cyto.a.22793.

b. Ortenzio J, Degn L, Goldstein-Plesser A, McGee JK, Navratilova, Rogers K, Zucker RM, and Boyes WK. 2019. Determination of silver nanoparticle dose in vitro. NanoImpact, 14: 100156. https://doi.org/10.1016/j.impact.2019.100156

c. Zucker RM, Ortenzio J, Degn LL, Lerner JM, and Boyes WK. 2019. Biophysical Comparison of Four Silver Nanoparticles Coatings using Microscopy, Hyperspectral Imaging and Flow Cytometry. PLOS ONE 14(7): e0219078. https://doi. org/10.1371/journal.pone.0219078

Justification 2A:

The first of the nominated manuscripts (Zucker et al., 2016) demonstrated that flow cytometry can be used to determine concentrations and relative sizes of nanoparticles in suspension for *in vitro* test systems and to determine the amount of nanoparticles taken up by cells *in vitro*. The second of the nominated manuscripts (Ortenzio et al, 2019) evaluated different computational models for particle deposition in a fluid media to estimate particle dose delivered to cells, and observed that the size of silver particles was a primary component influencing dose delivered to cells, with as much as 90% of the smaller sized particles remaining in suspension in the cell culture media 24 hours after exposure. The third of the nominated publications (Zucker et al., 2019) demonstrated the role of particle coatings on cellular dose and toxicity, with positively charged coatings providing a higher dose and being more toxic than either neutral or negatively charged surfaces. The conceptual and technological advances provided in these publications will thereby enhance EPA's ability to request and interpret data from alternative test systems when evaluating novel ENM for EPA registration under TSCA or FIFRA.

Justification 2B:

STAA Nominated publications previous six years

Boyes, 2015 STAA level III. Evaluation of the developmental toxicity of inhaled ethanol as a component of renewable automotive fuels. (Unrelated to current nomination)

Justification 2C:

Zucker-none

Boyes --STAA 2015 not related

Justification 2D:

NA

Justification 2E:

Dr William Boyes has submitted a review paper on the field of nanoparticles. This submission deals with basic research of nanoparticles. They are related.

Justification 3A:

1. If research has been invited for presentation at national/international societies.

The following invited presentations resulted from this research: the

· Zucker, RM. 2016. Guest Editor on the Special Cytometry Issue for the study of nanoparticles submicron particles.: Measurement of Extracellular Vesicles and Other Submicron Size Particles by Flow Cytometry. Joanne Lannigan, John P. Nolan, Robert M. Zucker February 2016 Volume 89, Issue 2 Pages 101–220

· Zucker, RM. Organized workshops at CYTO international flow cytometry meetings (ISAC) on nanoparticles and submicron particles at the following meetings: Vancouver 2019 June 22-26, Prague 2018, June 15-19; Boston 2017, June 10-14; Seattle 2016, June 11-15. Invited to speak at each of these workshop meetings.

· Zucker, RM. Invited to speak at Research Triangle Association meeting on detection of nanoparticles and submicron particles. NIEHS RTP, NC 2016

· Zucker, RM. Invited to contribute 2 review chapters on EPA nanoparticle research to be published in a book entitled “Nanoparticles in Biology and Medicine”. These chapters summarized the last 5 years of our USEPA research,

1. Zucker, R.M. and Boyes W.E. Combination of dark-field and confocal microscopy for the optical detection of Silver and Titanium Nanoparticles in mammalian cells. Nanoparticles in Biology and Medicine. Book edited by Mikhail Soloviev, Methods Mol Biol. 2118:395-414. 2020

2. Zucker, R.M. and Boyes W.E. Detection of silver and TiO_2 Nanoparticles in Cells by Flow Cytometry in Nanoparticles in Biology and Medicine. Book edited by Mikhail Soloviev, Methods Mol Biol 2118, 414-436 2020

· Zucker, RM. Invited to speak at ISAC international meeting in Boston Mass

RM. Zucker, LL Degn, JR Ortenzio and WK. Boyes. CYTO 2017 June 13 Boston Mass Hyperspectral Imaging, Flow Cytometry and Microscopic Morphology of Silver Nanoparticle within Cells: Invited to speak at Cytometry meeting in Seattle 2016

· Invited to speak at ISAC International meeting in Boston Mass

RM Zucker, LL Degn, JNR Ortenzio and WK Boyes. The Cellular Fate and Transport of Silver Nanoparticles: Hyperspectral Imaging, Flow Cytometry and Morphology. CYTO 2016 June 11 Seattle Washington.

RM Zucker: Sub-micron and Nano-particle Characterization, Detection, and Analysis in Flow Cytometry: Problem Focus and Key Questions: Flow Cytometry (FCM) is a key technology that helps to investigate both cell-derived and synthetic. Seattle, Washington, ISAC meeting workshop June 2016

· Zucker, RM. Invited to speak at Southeast flow cytometry meeting in Mobile Alabama March 2016

· Boyes, WK. In vitro dosimetry modeling will be a critical step toward efficient assessment of engineered nanomaterials for environmental health and safety. Invited presentation for workshop entitled: In-vitro dosimetry of engineered nanomaterials: Too complicated to consider too important to ignore. Annual Society of Toxicology Meeting. New Orleans LA, March 2016.

· Boyes, WK . Evaluating the Environmental Health and Safety Impact of Engineered Nanomaterials. North East Nanomaterials Meeting (NENM2018), Lake Placid NY June 1-3. 2018. http://nny.sites.acs.org/2018nenanomeeting.htm

· Boyes, WK. Round Table Panel member. Connecting the Pieces: Linking Manufacture and Use of Nanomaterials or Nanotechnology-Enabled Products with Exposure, Outcome, and Risk. QEEN II: 2nd Quantifying Exposure to Engineered Nanomaterials from Manufactured Products Workshop, Washington DC, Oct. 9-10. 2018.

· Boyes, WK. Chair, Plenary Session. Exposure-Driven Risk Assessment for Nanosafety Research. QEEN II: 2nd Quantifying Exposure to Engineered

Nanomaterials from Manufactured Products Workshop, Washington DC, Oct. 9-10. 2018.

· Boyes, WK. Nanosafety Research: The US EPA Perspective. Invited presentation to a workshop entitled "Fostering EU-US cooperation in Nanosafety Research" sponsored by the European Union. Harvard University, Boston Mass. March 5-6. 2019

· Boyes, WK. Invited Moderator, Respiratory Effects of Engineered Nanomaterials in Relation to Physiochemical Properties. NanoEHS Webinar Series, U.S. National Nanotechnology Initiative. September 10 , 2019.

· Boyes, WK. Update on Nanomaterial Research at EPA. Invited seminar. Annual meeting of the Center for Environmental Implications of Nanotechnology (CEINT), Duke Univ., September 13, 2019.

Justification 3B:

1. Number of times the publication has been downloaded/viewed

2. How many times it has been cited (Google Scholar)

Publication	Number of downloads/views	Number of citations (Google Scholar)
Zucker et al., 2016	Not available	26
Ortenzio et al., 2019	7	1
Zucker et al., 2019		1

1,350 (506 downloads +844 views in 10 months)

AUTHORS

Principal Author

Author Name:	Robert M. Zucker		
Professional Title:		Salutation:	Dr.
Email:	zucker.robert@epa.gov	Organization:	
Mailing Address:			
Street Line 1:	109 TW Alexander Drive		
City:	RTP		
Zip Code:	27711	State:	nc
At time of research was:	EPA Employee		
Separation Date:			
% of Effort:	23		

Contributing Author

Author Name:	William Boyes		
Professional Title:		Salutation:	Dr.
Email:	boyes.william@epa.gov	Organization:	

Mailing Address:			
Street Line 1:	109 TW Alexander Drive		
City:			
Zip Code:	27711	State:	NC
At time of research was:	EPA Employee		
Separation Date:			
% of Effort:	23		

Contributing Author

Author Name:	Alice goldstein-plesser		
Professional Title:		Salutation:	Ms.
Email:	goldstein-plesser.alice@epa.gov	Organization:	
Mailing Address:			
Street Line 1:	109 TW Alexander Drive		
City:	RTP		
Zip Code:	27711	State:	NC
At time of research was:	Non EPA Personnel		
Separation Date:			
% of Effort:	4		

Contributing Author

Author Name:	Kim Rogers		
Professional Title:		Salutation:	Dr.
Email:	rogers.kim@epa.gov	Organization:	

Mailing Address:			
Street Line 1:	109 TW Alexander Drive		
City:	RTP		
Zip Code:	27711	State:	NC
At time of research was:	EPA Employee		
Separation Date:			
% of Effort:	4		

Contributing Author

Author Name:	John McGee		
Professional Title:		Salutation:	Dr.
Email:	mcgee.john@epa.gov	Organization:	
Mailing Address:			
Street Line 1:	109 TW Alexander Drive		
City:	RTP		
Zip Code:	27711	State:	NC
At time of research was:	EPA Employee		
Separation Date:			
% of Effort:	4		

Contributing Author

Author Name:	jayna Ortenzio		
Professional Title:		Salutation:	Ms.
Email:	jayna.ortenzio@gmail.com	Organization:	

Mailing Address:			
Street Line 1:	NA		
City:			
Zip Code:		State:	
At time of research was:	Non EPA Personnel		
Separation Date:	Mon Jul 02 00:00:00 GMT 2018		
% of Effort:	22		

Contributing Author

Author Name:	Laura Degn		
Professional Title:		Salutation:	Dr.
Email:	degn.laura@gmail.com	Organization:	
Mailing Address:			
Street Line 1:	NA		
City:	phoenix		
Zip Code:		State:	arizona
At time of research was:	EPA Employee		
Separation Date:	Tue Oct 31 00:00:00 GMT 2017		
% of Effort:	11		

Contributing Author

Author Name:	Jeremy Lerner		
Professional Title:		Salutation:	Mr.
Email:	jlerner@lightforminc.com	Organization:	

Mailing Address:			
Street Line 1:	Jeremy Lerner LightForm, Inc., 825C Merrimon Ave., Suite 351 Asheville NC 28804		
City:	Asheville		
Zip Code:	28804	State:	nc
At time of research was:	Non EPA Personnel		
Separation Date:			
% of Effort:	5		

Contributing Author

Author Name:	Jana Navaratolova		
Professional Title:		Salutation:	Dr.
Email:	navaratolova.jana@epa.gov	Organization:	
Mailing Address:			
Street Line 1:	109 tw alexander dr		
City:	rtp		
Zip Code:	27711	State:	nc
At time of research was:	Non EPA Personnel		
Separation Date:			
% of Effort:	4		

PUBLICATIONS

Publication 1:

Biophysical comparison of four silver nanoparticles coatings using microscopy,

Publication Title:	hyperspectral imaging		
Publication Date:	Wed Jul 31 00:00:00 GMT 2019		
Journal/Publication Method:	PLOS ONE		
All Author(s):			
Volume:	PLoS ONE 14(7): e0219078.https://doi. org/10.13	Number:	14(7): e02
Pages:	e0219078.	Immediately Index:	Immediately Index:
Citation ½ Life:	4.9	Impact Factor:	2.776

Publication 2:

Publication Title:	Determination of silver nanoparticle dose in vitro		
Publication Date:	Tue Apr 02 00:00:00 GMT 2019		
Journal/Publication Method:	NanoImpact,/online		
All Author(s):			
Volume:	. https://doi.org/10.1016/j.impact.2019.100156	Number:	14
Pages:	1-10	Immediately Index:	Immediately Index:
Citation ½ Life:	NA	Impact Factor:	5.52

Publication 3:

Publication Title:	Characterization, detection, and counting of metal nanoparticles using flow cytometry
Publication Date:	Mon Feb 01 00:00:00 GMT 2016
Journal/Publication Method:	Cytometry Part A \print and online
All Author(s):	

Volume:	89	Number:	2
Pages:	169-183	Immediately Index:	Immediately Index:
Citation ½ Life:	7.2	Impact Factor:	3.433

PLOS ONE

RESEARCH ARTICLE

Biophysical comparison of four silver nanoparticles coatings using microscopy, hyperspectral imaging and flow cytometry

Robert M. Zucker[1]*, Jayna Ortenzio[2], Laura L. Degn[1,3], Jeremy M. Lerner[4], William K. Boyes[1]

1 U.S. Environmental Protection Agency, Office of Research and Development, National Health and Environmental Effects Research Laboratory, Toxicology Assessment Division, Research Triangle Park, NC, United States of America, **2** Oak Ridge Institute for Science and Education (ORISE) appointee at the National Health and Environmental Effects Research Laboratory, USEPA, RTP, NC, United States of America, **3** USEPA, RTP, NC, United States of America, **4** LightForm, Inc, NC, United States of America

* zucker.robert@epa.gov

Check for updates

OPEN ACCESS

Citation: Zucker RM, Ortenzio J, Degn LL, Lerner JM, Boyes WK (2019) Biophysical comparison of four silver nanoparticles coatings using microscopy, hyperspectral imaging and flow cytometry. PLoS ONE 14(7): e0219078. https://doi.org/10.1371/journal.pone.0219078

Editor: Alexander N. Zelikin, Aarhus University, DENMARK

Received: December 21, 2018

Accepted: June 14, 2019

Published: July 31, 2019

Copyright: This is an open access article, free of all copyright, and may be freely reproduced, distributed, transmitted, modified, built upon, or otherwise used by anyone for any lawful purpose. The work is made available under the Creative Commons CC0 public domain dedication.

Data Availability Statement: All relevant data are within the manuscript and its Supporting Information files.

Funding: The information in this document was funded wholly by the U.S. Environmental Protection Agency. It was subjected to review by the National Health and Environmental Effects Research Laboratory and approved for publication. Approval does not signify that the contents reflect the views of the Agency, nor does mention of trade names or commercial products constitute

Abstract

This study compared the relative cellular uptake of 80 nm silver nanoparticles (AgNP) with four different coatings including: branched polyethyleneimine (bPEI), citrate (CIT), polyvinylpyrrolidone (PVP), and polyethylene glycol (PEG). A gold nanoparticle PVP was also compared to the silver nanoparticles. Biophysical parameters of cellular uptake and effects included flow cytometry side scatter (SSC) intensity, nuclear light scatter, cell cycle distributions, surface plasmonic resonance (SPR), fluorescence microscopy of mitochondrial gross structure, and darkfield hyperspectral imaging. The AgNP-bPEI were positively charged and entered cells at a higher rate than the negatively or neutrally charged particles. The AgNP-bPEI were toxic to the cells at lower doses than the other coatings which resulted in mitochondria being transformed from a normal string-like appearance to small round beaded structures. Hyperspectral imaging showed that AgNP-bPEI and AgNP-CIT agglomerated in the cells and on the slides, which was evident by longer spectral wavelengths of scattered light compared to AgNP-PEG and AgNP-PVP particles. In unfixed cells, AgNP-CIT and AgNP-bPEI had higher SPR than either AgNP-PEG or AgNP-PVP particles, presumably due to greater intracellular agglomeration. After 24 hr. incubation with AgNP-bPEI, there was a dose-dependent decrease in the G_1 phase and an increase in the G_2/M and S phases of the cell cycle suggestive of cell cycle inhibition. The nuclei of all the AgNP treated cells showed a dose-dependent increase in nanoparticles following non-ionic detergent treatment in which the nuclei retained extra-nuclear AgNP, suggesting that nanoparticles were attached to the nuclei or cytoplasm and not removed by detergent lysis. In summary, positively charged AgNP-bPEI increased particle cellular uptake. Particles agglomerated in the peri-nuclear region, increased mitochondrial toxicity, disturbed the cell cycle, and caused abnormal adherence of extranuclear material to the nucleus after detergent lysis of cells. These results illustrate the importance of nanoparticle surface coatings and charge in determining potentially toxic cellular interactions.

endorsement or recommendation for use. RMZ, LLD and WKB conducted this research as a component of their regular job assignments at the USEPA. JO was supported by an appointment to the Research Participation Program for the U.S. Environmental Protection Agency, Office of Research and Development, administered by the Oak Ridge Institute for Science and Education through an interagency agreement between the U. S. Department of Energy and EPA. JML is employed by and has a commercial interest in Lightform, Inc., the company that developed and sells the PARISS hyperspectral Imaging system. Lightform, Inc., provided support in the form of salary for author JML, but did not have any additional role in the study design, data collection and analysis, decision to publish, or preparation of the manuscript. The specific role of this author is articulated in the 'author contributions' section.

Competing interests: We have the following interests: JML is employed by and has a commercial interest in Lightform, Inc., the company that developed and sells the PARISS hyperspectral Imaging system. There are no patents, products in development or marketed products to declare. This does not alter our adherence to all the PLOS ONE policies on sharing data and materials. The EPA has no affiliation with a commercial company, Lightform. JML was not paid for his involvement on this study and the EPA received no benefit other than scientific interaction for JL involvement on this study. This interaction does not alter our adherence to PLOS ONE policies on sharing data and materials.

Introduction

Engineered nanomaterials are increasingly used in industry and commerce for a wide range of potentially beneficial and profitable applications. Commercial nanoparticles NP have been designed for use in specific applications by varying their particle composition, size and coatings. The applications of nanoparticles in products, and the particle properties, influence the potential for release of particles from products and, in turn, the potential for inadvertent exposures and toxic reactions [1]. The size and composition of nanoparticles are important factors controlling their uptake into cells and potential for toxicity [2–10]. Because the primary interface between a nanoparticle and a cell occurs at the surface of the nanomaterial, one of the most influential features of nanoparticle bio-distribution and toxicity may be the particle surface coatings. Among other things, the particle surface coatings control surface charge, hydrophilic or hydrophobic nature, reactivity, agglomeration, dispersion stability in suspension media and sedimentation [11–18]. These factors ultimately will determine the potential toxicity of a particle.

The ability to study cellular uptake and distribution of nanoparticles requires the technological capability to detect the location of nanoparticles in the cell and to quantify cellular nanoparticle uptake. Previously, using darkfield microscopy we observed that silver and titanium dioxide nanoparticles readily accumulated with cells in tissue culture [19–25]. To enhance the detection of small nanoparticles we illuminated nanoparticles with a UV and blue wavelength rich Xenon light source in darkfield illumination. Because scatter intensity varies with the inverse 4th power of the wavelength, shorter wavelength illumination will reveal smaller nanoparticles than red rich halogen illumination. By using a Xenon light source objects as small as 20 nm have been detected [21,26]. It was observed under darkfield imaging that TiO_2 or Ag nanoparticles entered the cytoplasm, formed peri-nuclear agglomerations that grew as the exposure concentration increased, and eventually relocated in the lysosomes [18,27].

In addition to observing the location of nanoparticles within cells, it also is important to quantify their uptake. There was a relatively linear relationship between the dose of particles applied to cells and the uptake of particles measured by flow cytometry [22,23]. The relationship between nanoparticle dose and flow cytometry side scatter (SSC) suggests that it was an adequate descriptor of the number of nanoparticles absorbed by cells in culture [28–34].

The present studies evaluated the role of AgNP surface coatings on the nanoparticle's cellular uptake, cellular disposition, and the interactions with cellular constituents. Darkfield microscopy was combined with fluorescent imaging of subcellular organelles to reveal the uptake and disposition/distribution of nanoparticles within the cell. Hyperspectral imaging provided a measure of the configuration of these particles in the cell. Specifically, we studied 80 nm AgNP stabilized with one of four coatings: citrate (CIT), branched polyethyleneimine (bPEI), polyvinylpyrrolidone (PVP), and polyethylene glycol (PEG)(S1 Table).

These particles have different surface charges with unique surfaces. In addition, one 80 nm gold nanoparticle coated with PVP was also evaluated as a comparison to AgNP-PVP. A culture of human-derived retinal pigment epithelial cells APRE-19 was used in these studies [19–23].

It was found that the incubation of both AgNP and AuNP with ARPE-19 cells resulted in a dose-dependent increase in the number of intracellular particles that could be observed by darkfield microscopy and flow cytometry. The flow cytometry intensity in the red fluorescence channels increased after 24-hour incubation with silver nanoparticles. The hyperspectral imaging of NP showed that intracellular nanoparticles had an increased wavelength of light reflected from them compared to extracellular nanoparticles. This observation in conjunction with a change in light scattering properties detected by hyperspectral imaging suggested that

there was a change in the cellular nanoparticles' agglomeration. This NP agglomeration change was accompanied by an increase in SPR [23, 35–37].

Materials and methods

Cell culture

Human-derived retinal pigment epithelial cells ARPE-19 cells ATCC, Manassas, Virginia were grown in T75 culture flasks in a 1:1 mixture of Dulbecco's Modified Eagle's Medium and Ham's F-12 Nutrient Mixture DMEM/F-12 with 10% fetal bovine serum FBS. After reaching confluence, cells were trypsinized 0.05% trypsin, EDTA 0.02%, Sigma, and plated on chambered glass tissue culture slides 1 ml cell suspension per chamber, 2×10^5 cells/ml. Cells were incubated for 24 h 37˚C, 5% CO_2 after plating, and then treated with nanoparticles.

Nanoparticles

Four different coatings of 80 nm silver nanoparticles (AgNP) were compared in these studies: Branched Polyethyleneimine (AgNP-bPEI), citrate, (AgNP-CIT), Polyvinylpyrrolidone AgNP-PVP, and Polyethylene Glycol AgNP-PEG. and 80 nm Gold (AuNP-PVP) was also used as a metallic nanoparticle to compare with the 4 silver nanoparticles. Different suspensions of AgNP were obtained from nanoComposix (San Diego CA). Lot-specific physical/chemical characterization of each nanomaterial was provided by the supplier, including electron micrographic images and particle size distributions. The coated AgNP or the AuNP were obtained as a 1 mg/ml aqueous suspension. The NP were diluted in cell culture media containing FBS. ARPE-19 cells were incubated with the different types of AgNP at concentrations between 0.1 and 30 μg/ml for at 24 hr. prior to observation.

Staining, fixation, and mounting

To identify structures and organelles within the cells, the cells were transfected with the following Invitrogen BacMan 2.0 reagents: Golgi GFP BacMan 2.0 (C10592), lysosome-RFP 2.0 (C10597), mitochondria-GFP 2.0 (C10600) or endoplasmic reticulum ER-GFP 2.0 (C10590) [Invitrogen, Eugene, Oregon]. Prior to fixation, the cells were counterstained with Cell Mask Orange Plasma stain (C10045, Invitrogen) to identify the cellular cytoplasmic area. The cells were washed and fixed with an equal amount of warm 4% paraformaldehyde (PF) in phosphate-buffered saline (PBS). The slides were then mounted with Prolong Gold, containing 10 μg/ml DAPI (P36935, Invitrogen) to stain the nuclei. After the mounting medium dried, the slides were sealed with Permount.

Microscopy

A Nikon Ni upright microscope was used to observe cells in darkfield and fluorescence illumination. Fluorescence excitation cubes were used for DAPI, FITC, TRITC and Cyan GFP. The fifth cube holder space was intentionally left unoccupied to acquire a darkfield image without distortion from filters. The darkfield images were about 100 times brighter than the fluorescence images determined by their relative exposure times. The fluorescent and darkfield images were therefore taken sequentially at different exposure times and the images were combined using Nikon Elements software. Co-localization of the optical system was established with 0.5 μm Tetraspec beads and with 1 μm and 15 μm multi-wavelength fluorescent ring beads (Molecular Probes, Eugene Oregon). The xenon light supply was used with the darkfield images to obtain a bright light source that was optimized for the shorter wavelength excitation

and better detection sensitivity. A GG 420 filter was put in the eyepieces to protect the user's eyes from possible UV damage from the Xenon light source. [21–23].

A 60x Plan Fluor lens with an iris diaphragm to control the numerical aperture NA between 0.55 and 1.25 was used for imaging. Cellular details could be observed with this magnification while the background scatter was controlled by adjusting the diaphragm. The lower NA yielded good depth of field for bright nanoparticles, and the higher NA 1.25 yielded bright fluorescence images of cellular components. By balancing the fluorescence and darkfield signals, a sequential image could be acquired with the same NA setting approximately 0.8 NA. During this study, the darkfield images were obtained with a dry Plan Apo 20x lens (NA 0.75), a 20x multi-immersion (NA 0.75,) and 60x Plan Fluor with iris diaphragm (NA 1.25–0.55).

PARISS hyperspectral imaging system overview

The Prism and Reflector Imaging Spectroscopy System (PARISS) (Lightform, Inc, Asheville, NC, USA) is a "push broom" hyperspectral imaging system that mounts on the video port of a microscope. The system is comprised of a prism-based imaging spectrograph, a CCD camera to record spectra, and a classic imaging camera to record a "visual" image of a field of view (FOV). All wavelengths in each spectrum are acquired and recorded simultaneously [38,39].

A computer-controlled microscope stage translates the sample on a slide, while a microscope objective projects an image of the FOV onto the slit of the imaging spectrograph. Light passes through the slit to the prism for spatially resolved spectral characterization. A typical translation of the FOV takes from a single to thousands of acquisitions, with around 300 being typical. The physical scan is only limited by the extent of objects of interest on the microscope slide. Following data processing, individual acquisitions are combined to form the final hyperspectral image.

Using reference materials, such as nanoparticle inside and outside cells, PARISS records the spectra of all objects that scatter light. The recorded spectra of all objects were classified using either unsupervised or supervised Spectral Waveform Cross Correlation Analysis (SWCCA). Selected classes were put into a "Reference Spectral Library" (RSL). Ubiquitous classes of spectra such as background, or those appearing less than 1% of the time in the FOV, were either deleted or "unchecked" to remove them from the final hyperspectral image.

Creating a hyperspectral image of coated nanoparticles

1) Prepared samples on slides were "push broom" scanned, and all spectra presented by light scattering objects saved to disk. 2) Using SWCCA in either supervised or unsupervised, mode all spectra were classified according to a Minimum Correlation Coefficient (MCC). Limits were set on the number of possible classes by user selection of the MCC. 3) Classified spectra were inserted into an RSL. 4) Each class of spectrum in the RSL was pseudo-colored with a unique color of the operators choosing. Following completion of step 4 the system was ready to characterize unknowns as a function of their correlation with RSL spectra. The MCC was set to provide optimum correlation sensitivity.

Characterizing cells containing nanoparticles. Cells treated with the four coating types of AgNP samples were incubated for 24 hours and then were fixed with paraformaldehyde. Light scattered by AgNP located on the surface of the slide, and those that entered the cell were targets to be characterized with the PARISS system. The microscope was configured with a high NA oil condenser to maximize the photon density and increase the signal intensity. The objective lenses were either a 20x Plan Apo multi-immersion lens NA = 0.75, or a 60x Plan Fluor with a diaphragm iris collar NA 0.5–1.25 to adjust light for darkfield applications. A 75-watt Xenon light was used to illuminate the nanoparticles and act as the scattering light source. Neutral density filters were used to control brightness of the illuminant.

After slide preparation, PARISS physically scanned the slide and stored the spectra presented by all objects across the area of the scan. These spectra were correlated at a user selected MCC with spectra in the RSL. All spectra met the MCC were "painted" with the color of the correlated RSL spectrum onto a hyperspectral image. Spectra that failed to meet the MCC appeared in the hyperspectral image in gray. Clicking on a gray object in the hyperspectral image revealed its spectrum and the option of adding it to the RSL (S1 Fig).

Flow cytometry

A Stratedigm S1000 flow cytometer (San Jose, California) containing 4 lasers 405 nm, 488 nm, 550nm, and 640nm was used. The flow cytometer was set up with a 488-nm excitation using a 50 mw 488 nm laser for scatter and fluorescence measurements and a 405nm 100 mw laser was used for cell cycle DNA measurements. The detection angles for the forward scatter FSC were between 1–8 degrees measured with a pin diode, while the side scatter SSC signal was obtained using a 40x lens with numerical aperture NA of 1.2. This configuration for FSC and SSC used quartz square flow cells like other flow cytometer analyzers. The analyzer instrument electronics necessitated that the first trigger be either forward or side scatter signal derived from the 488-nm laser. The unit contained a new generation of hybrid signal processing technology with a high signal-to-noise ratio, and high data acquisition speed. The doublet discrimination detection electronics helped to remove particles that simultaneously entered the flow cell during analysis.

This Stratedigm flow cytometer analyzer was checked daily for fluidic alignment using either Thermo Scientific 3 μm alignment beads [Cyto-Cal Multifluor plus Violet Intensity Calibrator, FC3MV] or the manufacturer recommended 3 μm Stratedigm QA alignment beads. The system was tested by the manufacturers QA procedures for the following parameters: fluidic flow, laser power, coefficient of variation CV in all the PMTs and the system electronics. The CVs of the test beads were generally between 1 and 3% and did not change greatly between the two flow rates: slow 25μL/min and fast 60μL/min. Both the CVs and mean values of the beads serve as a reference for instrument functionality [40–43].

Measurement of cells and nuclei

The cells were measured with the following parameters. FSC, SSC, and 6 fluorescent parameters. The SPR was measured using the sensitive PMT representing the 690/40 nm channel which is equivalent to the FL3 detector 630 LP on a BD FACSCaliber used previously [23].

The cell cycle assay used mixed non-ionic detergent [NP-40 or Ipgal, Sigma, St. Louis, Mo] with cells to lyse the cytoplasm to obtain nuclei. The nuclei were then stained with Propidium Iodide (PI) 20 μg/ml or DAPI 10 μg/ml. The cells were lysed in 0.5% NP-40 or 0.5% Ipgal in Dulbecco's PBS without Ca/Mg at a dilution of 2 parts lysing buffer to 1-part cells. The sample was put on ice after 20 minutes and then measured on the flow cytometer within a few hours. [43–46]. In addition to measuring PI or DAPI intensity to generate the cell cycle data [G_1, S and G_2/M], the scatter of nuclei was simultaneously obtained after nanoparticle treatment and is compared to control nuclei as illustrated in S2 Fig. The data were quantified using FCS express 6.0 with Multicycle to generate DNA cell cycle populations using the Dean and Jett model [43–46]. The technique is illustrated in S2 Fig that shows a clean nucleus from a control cell and nanoparticles attached to a cell that was treated with nanoparticles. This technique is illustrated with microscopic images from a detergnt lysed nuclei in S3 Fig. The image shows the cell accumulating clumped nanoparticles in the cytoplasm and after treatment with NP40 the image shows the nanoparticles are closely bound or associated with the nuclei.

Concentration of nanoparticles

The concentrations of nanoparticles in samples obtained from the supplier was determined both from the manufacturer's specifications and then checked in the laboratory by a procedure developed to count concentrated nanoparticles in suspension on a flow cytometer [24]. According to the manufacturer there were approximately 10^{12} particles per ml in each sample. The laboratory determination of particle counts involved sequentially dilution of samples with a fixed concentration of 1μm polystyrene beads until a dilute concentration could be counted on a flow cytometer without coincidence. The polystyrene beads were added to the cultures at concentrations between 0.1 μg/ml and 30 μg/ml. The method could then yield the count of NP per ml from the concentrated sample, and thereby allowed our laboratory to confirm the manufacture's specifications of NP concentrations.

All particle samples were diluted to concentrations that ensured yields between 1000 and 6000 counts/sec, as determined by the flow cytometer software event counter. This translated to a concentration in the range of 10^6 and 10^7 counts per ml. If the concentration of particles greatly exceeded 10^7, the observed count rate was reduced by the electronic circuitry of the flow cytometer to eliminate doublet counting, that resulted in the instrument rejecting many of the events that were deemed doublets by the suppression electronic software. The result was an instrument that paradoxically yielded fewer counts/sec in a concentrated sample than in a diluted sample. With this approach, we were able to minimize co-incident counting and obtain an accurate particle concentration measurement.

These diluted 1μm beads were mixed with the unknown AgNP sample that resulted in approximately 1000 counts/sec of beads which served as a reference in determining the proper measurement conditions for Ag nanoparticles. A 1 μm PS bead [Thermo Scientific # 4010A] was diluted to concentration that would yield about 400–500 counts/sec without Ag and Au nanoparticles present. The concentration of the 1 μm bead suspension was determined by mixing it with 2 μm counting beads $5x10^6$ and then comparing the percentages of the two beads in the SSC intensity histograms. With the 1 μm beads, the concentration of the diluent for the metal nanoparticles used in the flow cytometer was approximately $2\text{-}5x10^6$ particles/ml [24]. This was necessary to ensure that we were adding the same number of AgNP to each cell culture. The side scatter intensity data is dependent on the AgNP dose added to each culture.

Results

Four types of Ag nanoparticles with different surface coatings AgNP-bPEI, AgNP-CIT AgNP-PEG and AgNP-PVP having unique properties were added at concentrations between 1 μg/ml and 30 μg/ml to adherent ARPE-19 retinal epithelial cells for 24 hours (S1 Table). Au-PVP, a metallic particle like silver metallic nanoparticles was also measured as a comparison to the 4 silver nanoparticles. After 24 hours, side scatter (SSC), forward scatter (FSC) and far red fluorescence were measured on suspension cells using a flow cytometer. There was a dose dependent increase in SSC for the four AgNP between 1 and 30 μg/ml doses (Figs 1 and 2 and Table 1). Fig 1 shows the dose dependent uptake of AgNP-CIT (Fig 1A) and AgNP-bPEI (Fig 1B).

SSC vs. dose

Cells were treated with four types of AgNP and AuNP-PVP. The AgNP-bPEI had about 3-6-fold more SSC than the other compounds. This observation was presumed to be related to the cellular accumulation of AgNP.

Cells treated with AgNP-bPEI scatter more light at all doses than do cells treated with AgNP-CIT. Cells treated with AgNP-PEG and AgNP-PVP were similar in their SSC dose

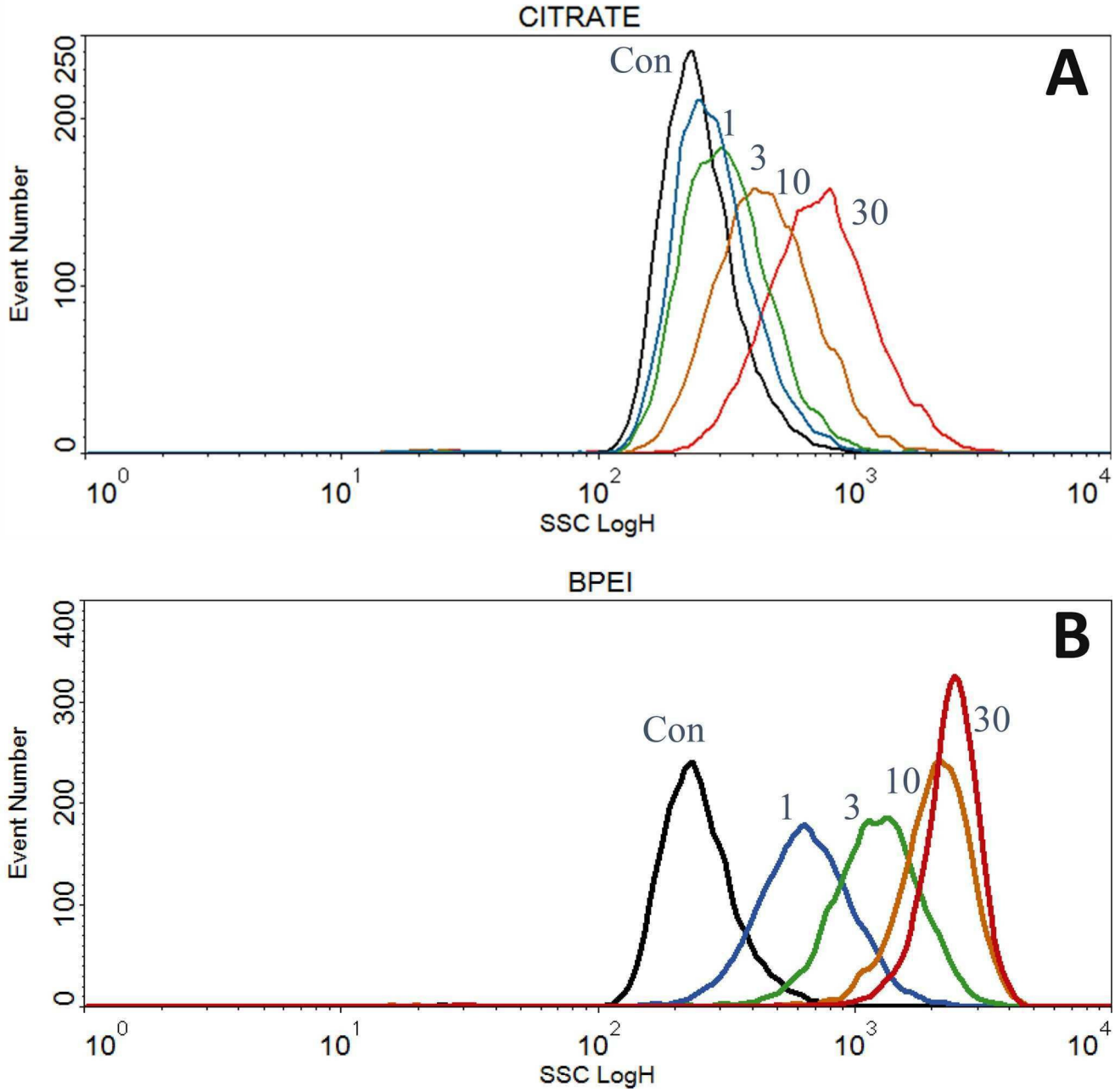

Fig 1. Flow cytometry side scatter ssc measurements of AgNP treated cells. Side scatter SSC measurement of cells were made after treatment with AgNP- CIT and AgNP-bPEI doses between 1μg/ml and 30 μg/ml for 24 hours. AgNP-CIT (Fig 1A, top) and AgNP-bPEI (Fig 1B, bottom).

https://doi.org/10.1371/journal.pone.0219078.g001

response to AgNP-CIT. The forward scatter decreased slightly with each of the four compounds, as was previously reported with TiO_2 and AgNP-PVP [22,23].

The relative SSC data comparing the four AgNP compounds and AuNP-PVP are shown in Table 1. At all the NP dose levels tested, there was an increase in SSC of the AgNP treated cells compared to control cells.

A comparison of the four types of AgNP are shown using doses of 10 μg/ml in Fig 2A and 1 μg/ml in Fig 2B. The AgNP-bPEI had more SSC than the other coatings at all comparable

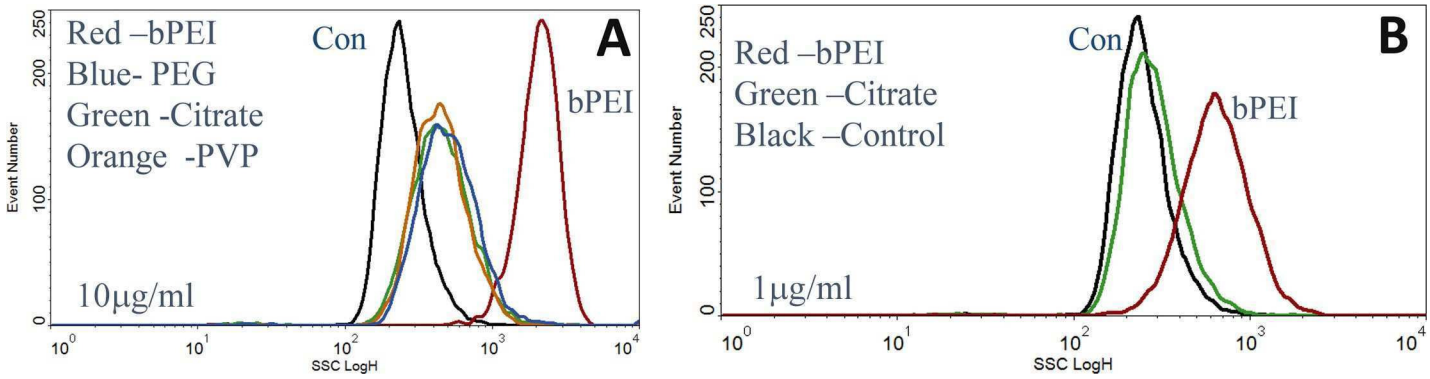

Fig 2. SSC measurements of AgNP-bPEI treated cells compared to other AgNP treated cells. Comparison of SSC of the four AgNP compounds at 10 μg/ml A, left and 1 μg/ml B, right. The AgNP-bPEI showed higher values suggesting greater accumulated than the other compounds at 1μg/ml and 10 μg/ml.

https://doi.org/10.1371/journal.pone.0219078.g002

doses tested (Figs 1 and 2 and Table 1). The SSC derived from AgNP-bPEI was about 3–6 times higher than the other AgNP compounds and about 15 times greater than control cells at 10 μg/ml (Table 1, Fig 1A). Gold nanoparticles (AuNP-PVP) scattered light like AgNP-PVP and AgNP-PEG at equivalent doses.

If the concentration of AgNP-bPEI obtained from the supplier (nanoComposix) was much greater than the other AgNP compounds, it would explain the observed increased SSC with AgNP-bPEI. However, it was found that the concentrations of particles (1 mg/ml) determined by flow cytometry was within the range reported by the manufacturer. The AgNP-bPEI was even about 10% less in concentration than the other AgNP coated particles.

The size of the different 80 nm AgNP in suspension were similar (Fig 3). The 1μm counting beads was measured simultaneous with the AgNP to insure the concentration of the particles were in a measurable range and not generating artifacts from coincidence counting or "Swarming" [47].

In addition to the side scatter measurements, emissions in the far-red channel (690/40 nm) were simultaneously measured using a red sensitive photomultiplier tube (PMT). The far-red fluorescent signal was designated as surface plasmonic resonance (SPR). The AgNP-CIT and AgNP-bPEI displayed greater SPR than the AgNP-PVP or AgNP-PEG. At the 10 μg/ml dose, the amount of SPR in the far-red channel (690/40nm, range 670–710 nm) was approximately 18 times greater for AgNP-CIT while AgNP-bPEI was about 10 times greater than control cells. Cells treated with PVP and PEG had about 2–3 times greater intensity than control cells treated at a dose of 10 μg/ml. Gold coated NP showed no increase in far red fluorescence, resembling control cells SPR fluorescence intensity (Table 2).

Surface Plasmonic Resonance vs. dose

Surface Plasmonic Resonance (SPR) vs. dose of the 4 AgNP compounds and AuNP-PVP at doses between 1 μg/ml and 30 μg/ml. The Ag-CIT had the most SPR followed by AgNP-bPEI,

Table 1. SSC measurements of cells treated with AgNP and AuNP.

Dose μg	bPEI	Citrate	PVP	PEG	AU
1	5.2	2.3	ND	ND	ND
3	9.5	2.6	1.5	1.4	1.4
10	15.5	3.7	2.0	1.8	1.9
30	17.5	6.0	3.1	2.4	2.5

https://doi.org/10.1371/journal.pone.0219078.t001

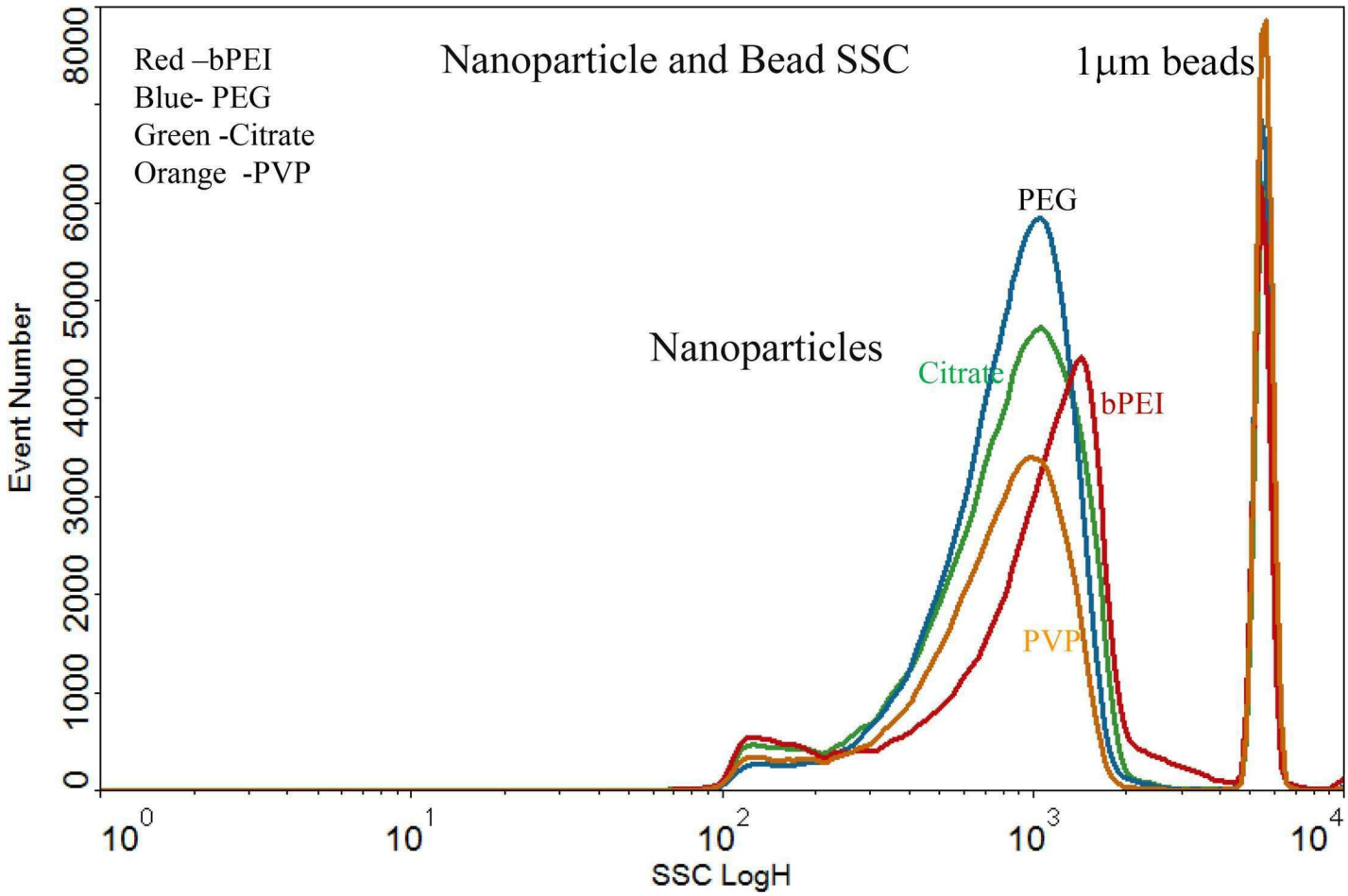

Fig 3. Comparison of nanoparticle SSC intensity of 4 AgNP and 1µm beads. Side scatter comparison of 4 types of 80 nm AgNP particles measured simultaneously with 1µm micron polystyrene beads. The AgNP-bPEI particles had slightly more SSC than the other 3 types of particles. These data were derived by diluting the AgNP with a defined concentration of beads until the AgNP beads were successively diluted to 10^6 counts per ml.

https://doi.org/10.1371/journal.pone.0219078.g003

AgNP-PEG, and AgNP-PVP. AuNP-PVP showed no SPR. The AgNP-CIT treated cells were about 100-fold greater than control cells while the AgNP-bPEI treated cells were about 55-fold greater than control cells at the highest dose used 30 µg/ml.

Microscopic observation of the AgNP inside cells using darkfield microscopy revealed the relative uptake of NP. Fig 4 shows that there was a greater uptake of 3 µg/ml nanoparticles in the AgNP-bPEI treated cells compared to 3 µg/ml AgNP-CIT treated cells. The other AgNP compounds showed similar decreased uptake compared to AgNP-bPEI treated cells (Fig 4).

Non-ionic detergent (NP-40 or Ipgal) was incubated with cells yielding nuclei that were then stained with PI or DAPI generating the cell cycle data (G_1, S and G_2/M) using the flow

Table 2. Surface Plasmonic Resonance (SPR) vs dose.

Dose µg/ml	BEPI	Citrate	PVP	PEG	AU-PVP
1	2.4	1.9	ND	ND	ND
3	3.5	2.8	1.1	1.2	1.1
10	9.5	17.8	3.5	2.8	0.9
30	55.5	104.6	16.3	25.0	.09

https://doi.org/10.1371/journal.pone.0219078.t002

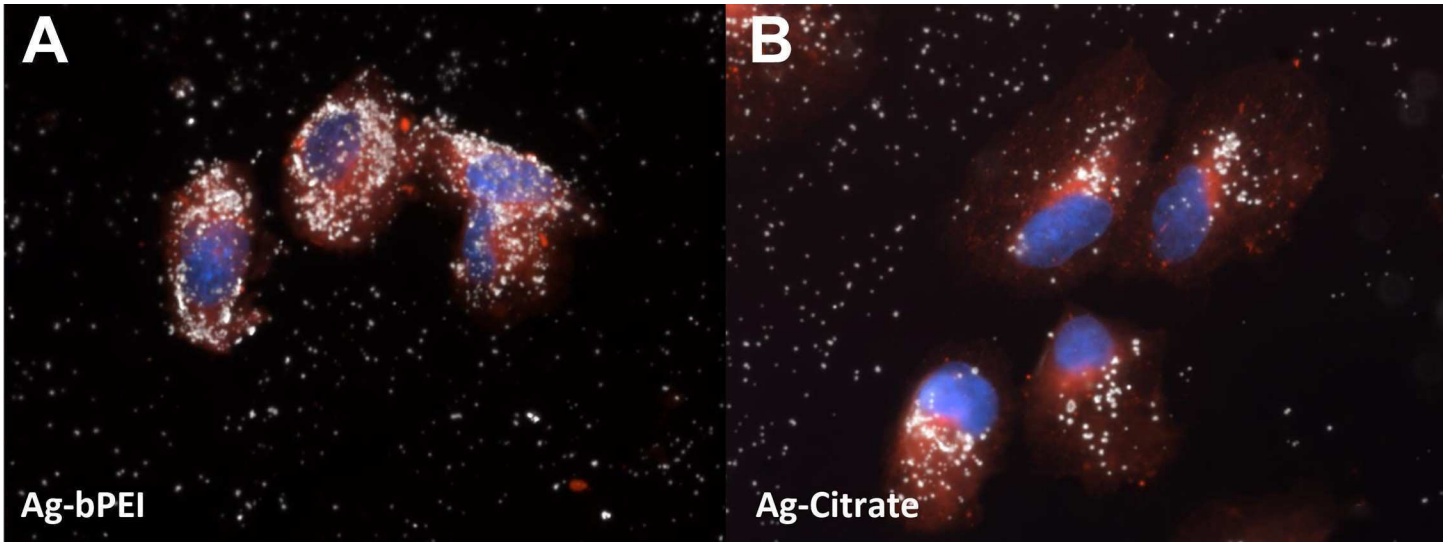

Fig 4. Microscopic observation of bPEI and citrate coated NP. Microscopic images of cells incubated with AgNP-bPEI (Fig 4A) and AgNP-CIT (Fig 4B) for 24 hours. The nuclei were stained with DAPI and the cytoplasm was stained with cell mask orange. The AgNP are represented by the white spots in the darkfield microscopy images. es. Magnification 200x.

https://doi.org/10.1371/journal.pone.0219078.g004

cytometer. The percentages of each phase in the cell cycle was generated using the Dean and Jett model from the Multicycle program contained in the FCS Express 6 software [43]. In addition to measuring DNA intensity with DAPI (10μg/ml) staining, the side scatter of nuclei was simultaneous obtained from the 488 nm laser. The data are displayed in both cytogram (Fig 5) and histogram (Fig 6) formats. Fig 5 shows a sequential increase in scatter as the dose increases from 3 μg/ml to 30 μg/ml for nuclei derived from cells treated with AgNP-bPEI and AgNP-CIT. The Coefficient of variation (CV) of the G_1population increased showing that some nuclei had more scatter than others presumably due to having more nanoparticles attached to the nuclei. Fig 6 shows the relative scatter difference of nuclei derived from cells treated with different types of AgNP compounds. The AgNP-bPEI had greater scatter than the other AgNP compounds. These particles were not observed inside the nucleus of AgNP treated cells under darkfield microscopy suggesting that when the nuclei from treated cells are derived for cell cycle analysis they may have peri-nuclear cytoplasmic tabs containing nanoparticles, which ultimately increases the nuclear scatter.

S2 Fig and S3 Fig show the cells and detergent lysed nuclei with nanoparticles attached the nuclei. The cells have nanoparticles contained in the cytoplasm while the nuclei have the nanoparticles associated closely with the surface of the nuclei either through a direct bond or in cytoplasm remaining attached to nuclei after detergent non-ionic lysis.

The AgNP-bPEI showed the highest increased in nuclei side scatter which was related to the increased particle accumulation shown with cells (Figs 1 and 2 and Table 1). As the dose increased, the percentages of G_1 for the bPEI treated cells decreased while the percentages for S and G_2/M increased. (Table 3). The CV of the G_1 increased as the dose increased indicating reduced accuracy in the DNA cell cycle modeling. It was not possible to acquire cell cycle distribution data from 30 μg/ml AgNP-bPEI. At higher concentrations, the Multicycle program could not generate accurate cell cycle phases due to broadening CV of the G_1 population.

In contrast to AgNP-bPEI the cell cycle phases (G_1 and S and G_2/M) of AgNP-CIT, AgNP-PVP and AgNP-PEG did not vary greatly with the doses used. There was a slight increase in S and G_2/M as the dose increased from 3μg/ml to 30 μg/ml. In summary it appears that the percentages of G_1 decreased while the percentages of S and G_2/M increased suggesting

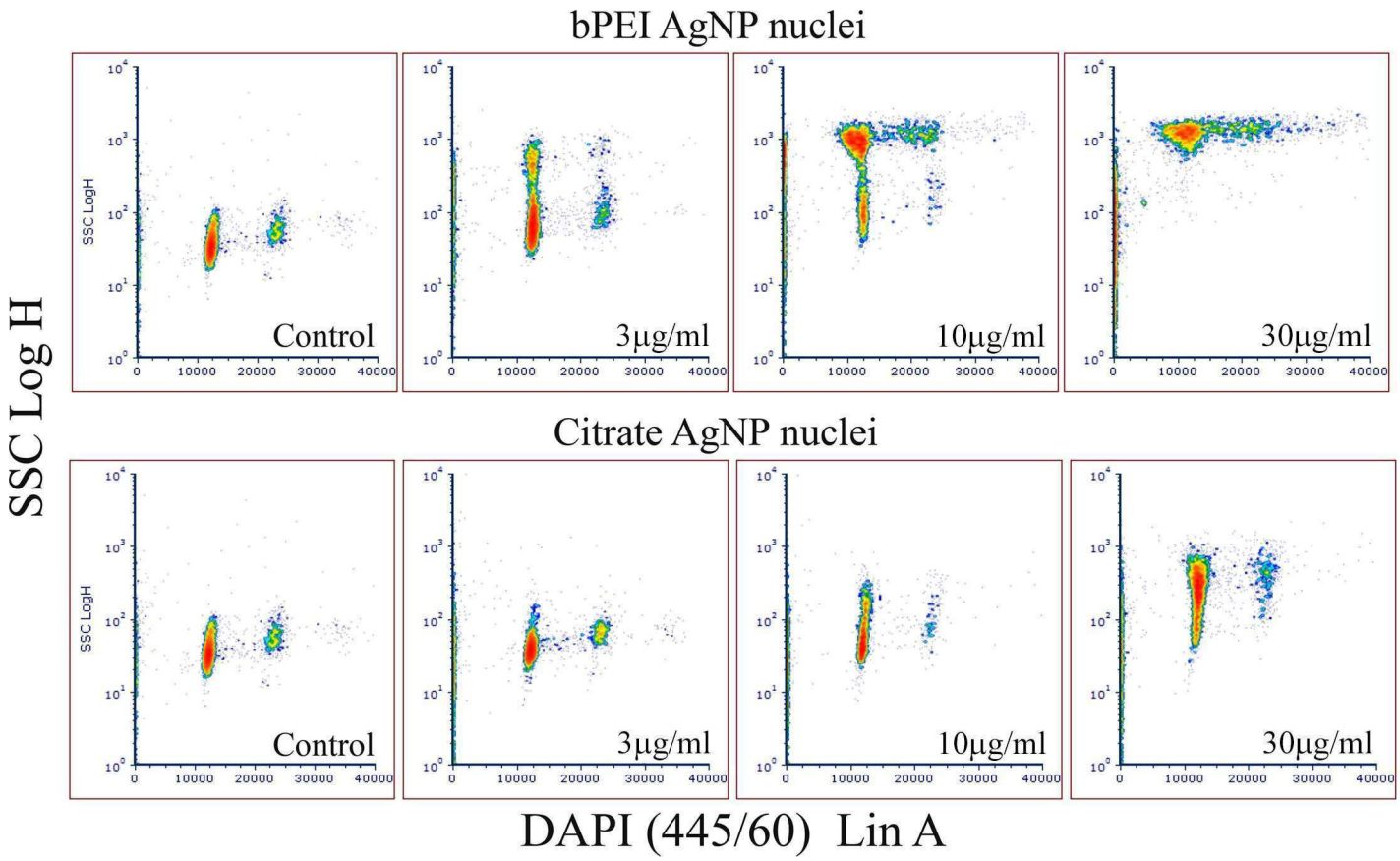

Fig 5. Flow cytometry cytograms of nuclei treated with AgNP-bPEI and AgNP-CIT. Flow cytometry comparison of DAPI stained nuclei derived from cells treated with AgNP-bPEI or AgNP-CIT at doses between 1µg/ml and 30 µg/ml. Each successive higher dose resulted in greater amount of side scatter. This was presumably due to higher uptake of AgNP as shown in the cell scatter data (Figs 1 and 2) and the lack of complete cell lysis at all doses.

https://doi.org/10.1371/journal.pone.0219078.g005

a retardation of the cell cycle progression with a block in the G_2/M phases. The AuNP- PVP had less nuclei scatter than the other compounds.

AgNP-bPEI cell cycle phases

The DNA histograms from AgNP-bPEI treated cells were used to calculate the percentages of cells in each phase of the cell cycle using the Multicycle program located in FCS express 6. The nuclei were derived by detergent lysis with NP40 and stained with DAPI (10µg/ml). There is a decrease in G_1 and an increase in S and G_2/M as the dose increased from 1 to 30µg/ml.

The mitochondria-GFP staining was derived from transfecting the cells for 24 hours with BacMan 2.0 reagents (Thermo-Fisher, Invitrogen). The mitochondria shape was different in the AgNP-bPEI and the AgNP-citrate treated cells (Fig 7). The mitochondria in untreated cells and AgNP-CIT treated cells were thin strands that underwent fusion and fission (Fig 7A). However, after treatment with AgNP-bPEI the mitochondria changed shape and appeared as small beads (Fig 7B). It has been reported that AgNP-bPEI is toxic to cells at high concentrations, and this may be the reason for the observation that the mitochondria changed their shape [48].

The cytoplasm was stained with cell mask orange and the nuclei stained with DAPI. Lysosomes were stained with RFP-BacMan probes. These microscopic images showed higher uptake of nanoparticles in the AgNP-bPEI compared to AgNP-CIT. The nanoparticles appear to be embedded in the region surrounding the nucleus and occupied by the endoplasmic

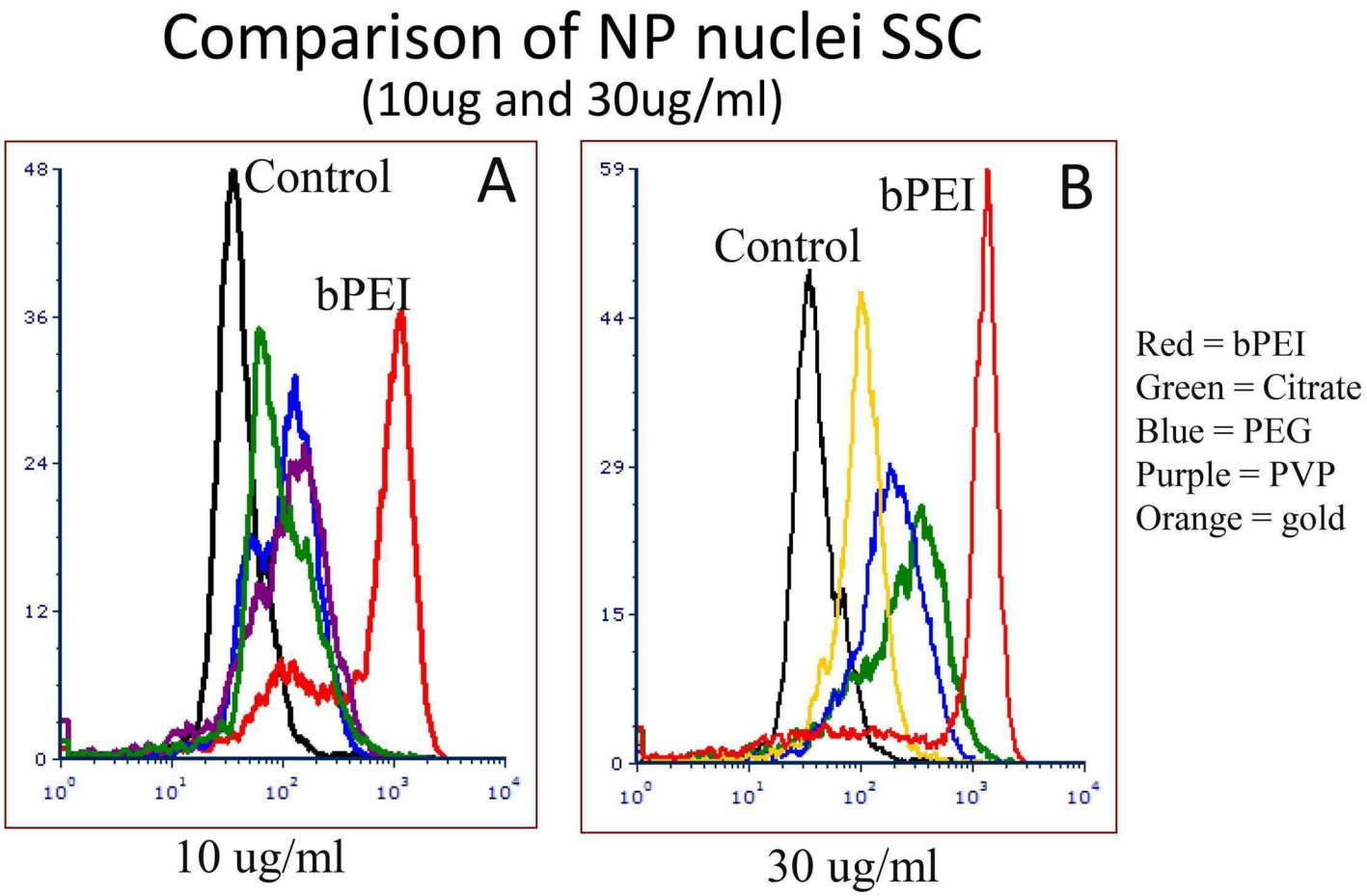

Fig 6. Comparison of nuclei SSC histograms from NP treated cells. Histograms of nuclei derived from cells treated with the 4 types of AgNP at 10 μg/ml (Fig 6A) and 30 μg/ml (Fig 6B). All samples demonstrated an increase of scatter after AgNP incubation for 24 hours at doses between 1 and 30 μg/ml. All the AgNP showed greater SSC than the AuNP.

https://doi.org/10.1371/journal.pone.0219078.g006

reticulum (Figs 7 and 8). The cell mask orange plasma stain was shown to stain membranes which include both interior and exterior cellular membranes. An increased number of particles were observed with darkfield microscopy in Figs 4,7 and 8 as they reflect more light yielding a brighter and more intense signal. This was correlated to increased light scatter intensity measurements observed by flow cytometry with SSC illustrated in Figs 1 and 2.

Hyperspectral imaging

The four different types of nanoparticles were investigated using the PARISS hyperspectral imaging system. To evaluate data derived from the PARISS hyperspectral imaging equipment

Table 3. Cell cycle phases of AgNP-bPEI.

Dose μg/ml	G1	S	G2/M	CV-G1
0	**83.9**	**4.7**	**11.4**	**3.25**
1	**79.7**	**8.0**	**12.4**	**3.67**
3	**81.9**	**5.8**	**12.3**	**3.66**
10	**70**	**16.2**	**13.8**	**8.70**
30	**60**	**ND**	**ND**	**14.7**

https://doi.org/10.1371/journal.pone.0219078.t003

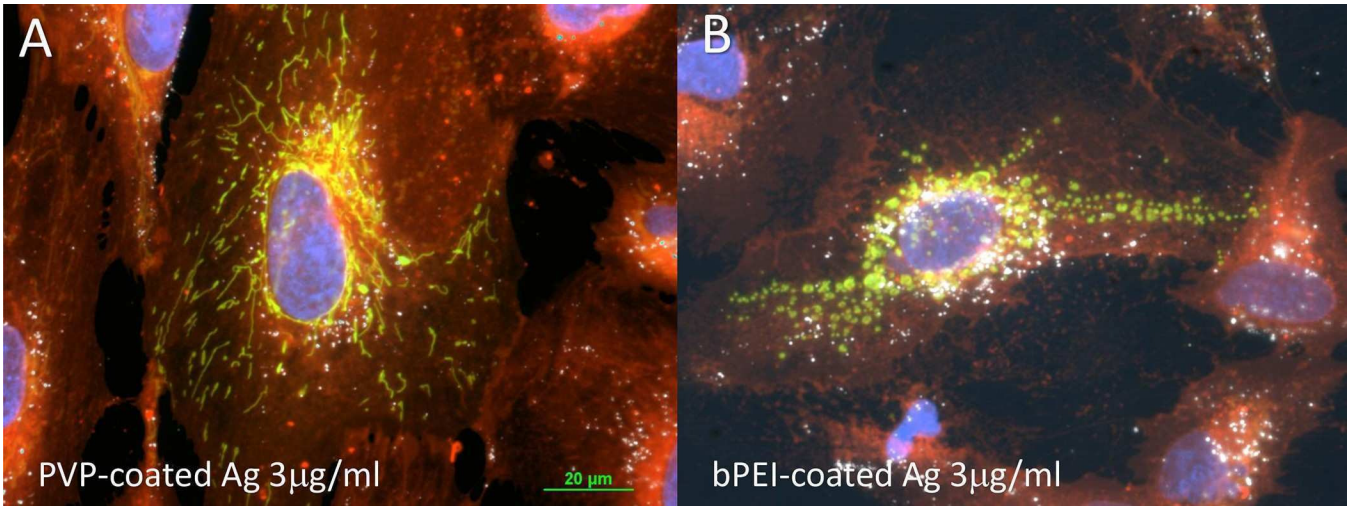

Fig 7. Mitochondria microscopy from AgNP-PVP and AgNP-bPEI treated cells. Comparison of the mitochondria shapes derived from cells treated with 3 μg/ml of AgNP-PVP (Fig 7A) and AgNP-bPEI (Fig 7B). The AgNP-bPEI had beaded shapes while mitochondria derived from the AgNP-PVP treated cells had a linear strand like formation of mitochondria. The cytoplasm is stained with cell mask orange (designated by red), the mitochondria transfected with GFP (designated by green) and the nuclei are stained with DAPI (designated by blue). The NP (designated by white) are accumulated throughout the cytoplasm and around the nuclei with the AgNP-bPEI samples. Magnification 600x.

https://doi.org/10.1371/journal.pone.0219078.g007

the system was set up for darkfield illumination using a 75-watt xenon light source. A library of spectra was derived from light that was scattered by AgNP within the cell and from particles resting on the surface of the slide (Fig 9). The reflectance spectra had relatively shorter wavelengths designated by blue and green pseudo-colors outside of the cell while inside the cell the NP reflectance spectra yielded longer wavelengths designated by orange and yellow pseudo-colors.

A spectrum of the Xenon light source was obtained with no cells present on the slide and this spectrum was divided into the individual spectra of the library to obtain reflectance spectra library (Fig 9A). Observation of the nanoparticles on the slide surface and within the cells are shown in a representative image of AgNP-PVP treated cells. The spectra of AgNP observed outside the cell had shorter wavelengths than spectra derived from AgNP that entered the cell. The dark-field scatter image of a cell is pseudo-colored using the spectral library (Fig 9B). The histogram percentages of each spectra from the cell (Fig 9C) and the region outside of the cell on the slide surface are shown in histograms format (Fig 9D) as percentages of different pixels represented by the colors shown in Fig 9A. The region in the cell's interior contains mostly longer wavelength spectra designated by orange and yellow colors, while the regions outside the cell on the slide surface is represented by blue and green spectra that peaked at shorter wavelengths.

During these studies, many of the cells treated with AgNP had showed a circular structure consisting of concentrated NP on the slides that was not associated with cells (Fig 10). Circles consisting of nanoparticles NP were observed using darkfield illumination on the slides after the ARPE-19 cells were exposed to each of the four compounds at 3 μg/ml NP (top row). These NP circles were pseudo-colored with the spectral reference l library shown in Fig 9A and were represented in the middle row of Fig 10. The percentages of each reference spectrum appearing in these circular structures are shown in the corresponding histograms (bottom row). The AgNP-bPEI and the AgNP-CIT circles had relatively longer wavelengths represented by primarily orange and yellow pseudo-colored spectra while the AgNP-PVP and AgNP-PEG circles had relatively shorter wavelengths represented by primarily blue and green

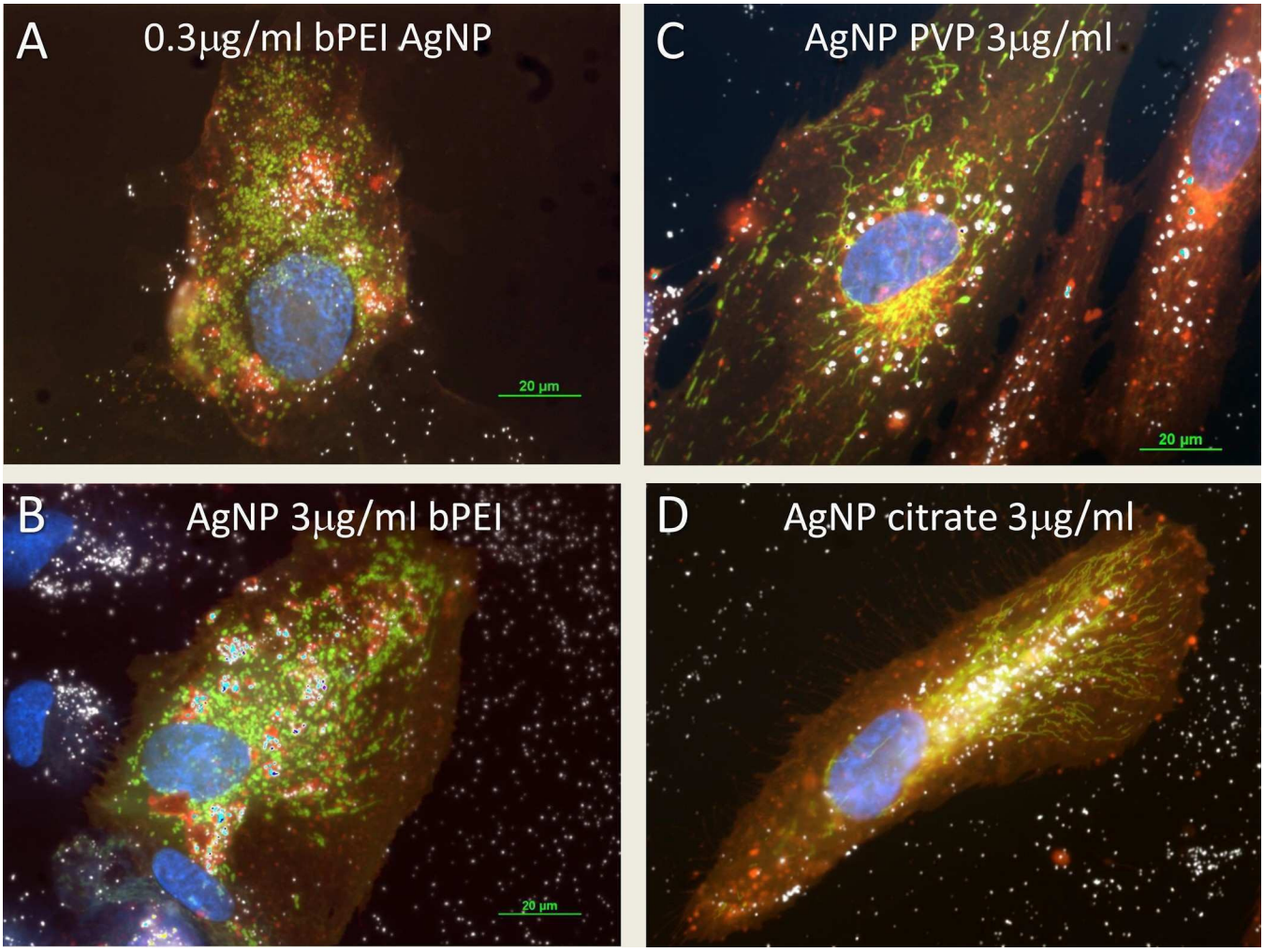

Fig 8. Microscopic comparison between different AgNP. Microscopic comparison of mitochondria after AgNP uptake into cells treated. with AgNP-bPEI, AgNP-PVP or AgNP-CIT for 24 hours. The AgNP-bPEI showed beaded structures of mitochondria at 0.3μg/ml (Fig 8A) and 3μg/ml (Fig 8B) while the AgNP-PVP 3μg/ml, (Fig 8C) and AgNP-CIT 3μg/ml,(Fig 8D) showed an elongated formation of mitochondria (designated by green color). The NP (designated by white color) are accumulated into the lysosomes (designated by red color) with the AgNP-bPEI samples while the NP are accumulated around the nuclei (Fig 8C) or in the ER (Fig 8D) with the other AgNP coated samples. The cytoplasm was stained with cell mask orange (red) and the nuclei are stained with DAPI (blue). Magnification 600x.

https://doi.org/10.1371/journal.pone.0219078.g008

pseudo-colored spectra. This implies that the agglomeration of the particles in the AgNP circles was different with the AgNP-bPEI and AgNP-CIT compared to the AgNP-PVP and Ag-PEG. This agglomeration difference between the different AgNP indicated that the degree and type of agglomeration occurred which could affect the scattering wavelength.

Upon the evaluation of the reflectance of light from these circles, it was found that AgNP-PVP and AgNP-PEG had spectra that peaked in the shorter range while AgNP-CIT and AgNP-bPEI had spectra that tended to peak in the longer range. The nanoparticle circles derived from PVP, PEG, and citrate NP incubations with cells had a hollow core while the branched had a circle the consisted of particles that had equally distributed concentrations without a hollow core center. It is not clear what is generating these circular structures, but it appears from past research in our laboratory that it may be due to adherent proteins that selectively bind nanoparticles during the mitosis process. The positive charge AgNP-bPEI has a

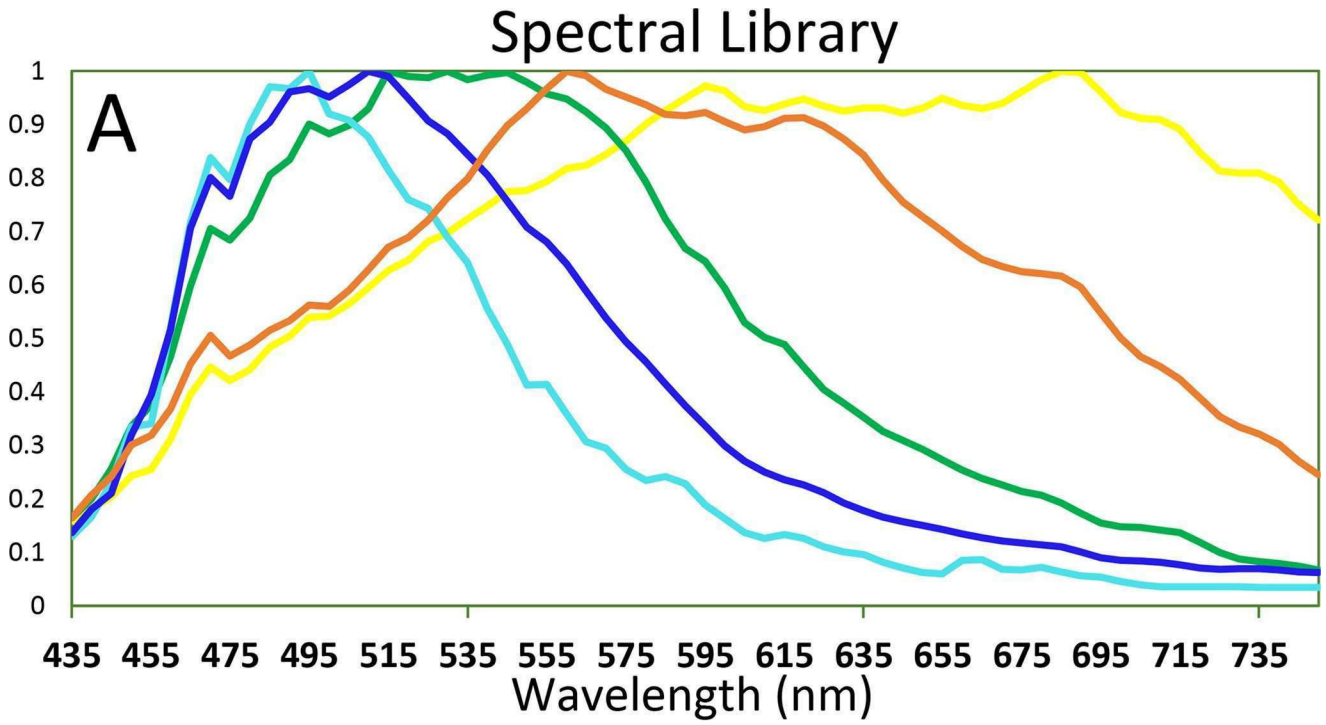
Spectral Library
A
1
0.9
0.8
0.7
0.6
0.5
0.4
0.3
0.2
0.1
0
435 455 475 495 515 535 555 575 595 615 635 655 675 695 715 735
Wavelength (nm)

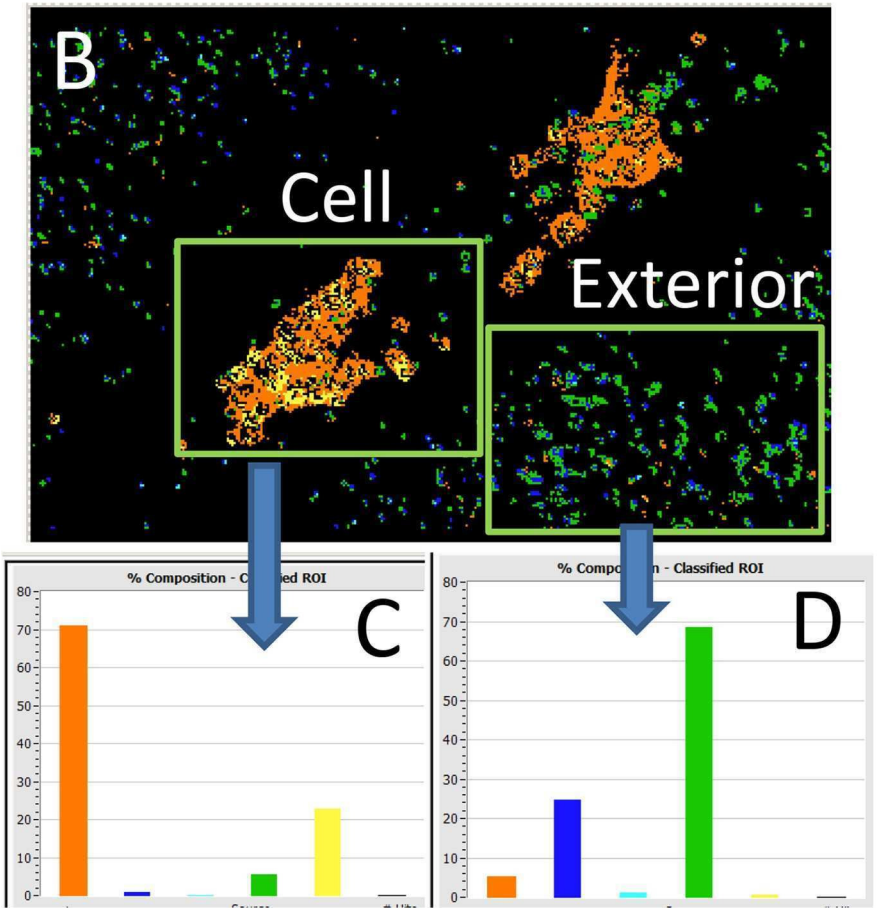
B
Cell
Exterior
% Composition - Classified ROI
C
% Composition - Classified ROI
D

Fig 9. PARISS hyperspectral imaging of cell and exterior. The reference spectral library A was obtained by dividing the internal white xenon spectra with the spectra derived from individual NP or regions of NPs. A region of interest (ROI) was made around in the cell and another ROI was made on the exterior of the cell (Fig 9B) to determine the amount of reference spectra shown in Fig 9A that existed in these two regions that are expressed in a histogram format (Fig 9C and 9D).

https://doi.org/10.1371/journal.pone.0219078.g009

different pattern than the negatively or neutral charged particles and may be responsible for the different patterns that was observed.

Discussion

The primary aim of this paper was to compare the cellular uptake and distribution of AgNP with different capping agents. Four types of 80 nm AgNP were used: Branched Polyethyleneimine (bPEI), citrate (CIT), Polyvinylpyrrolidone (PVP), and Polyethylene Glycol (PEG) (S1 Table). An 80 nm gold NP (AuNP-PVP) was compared to the other AgNP metallic particles.

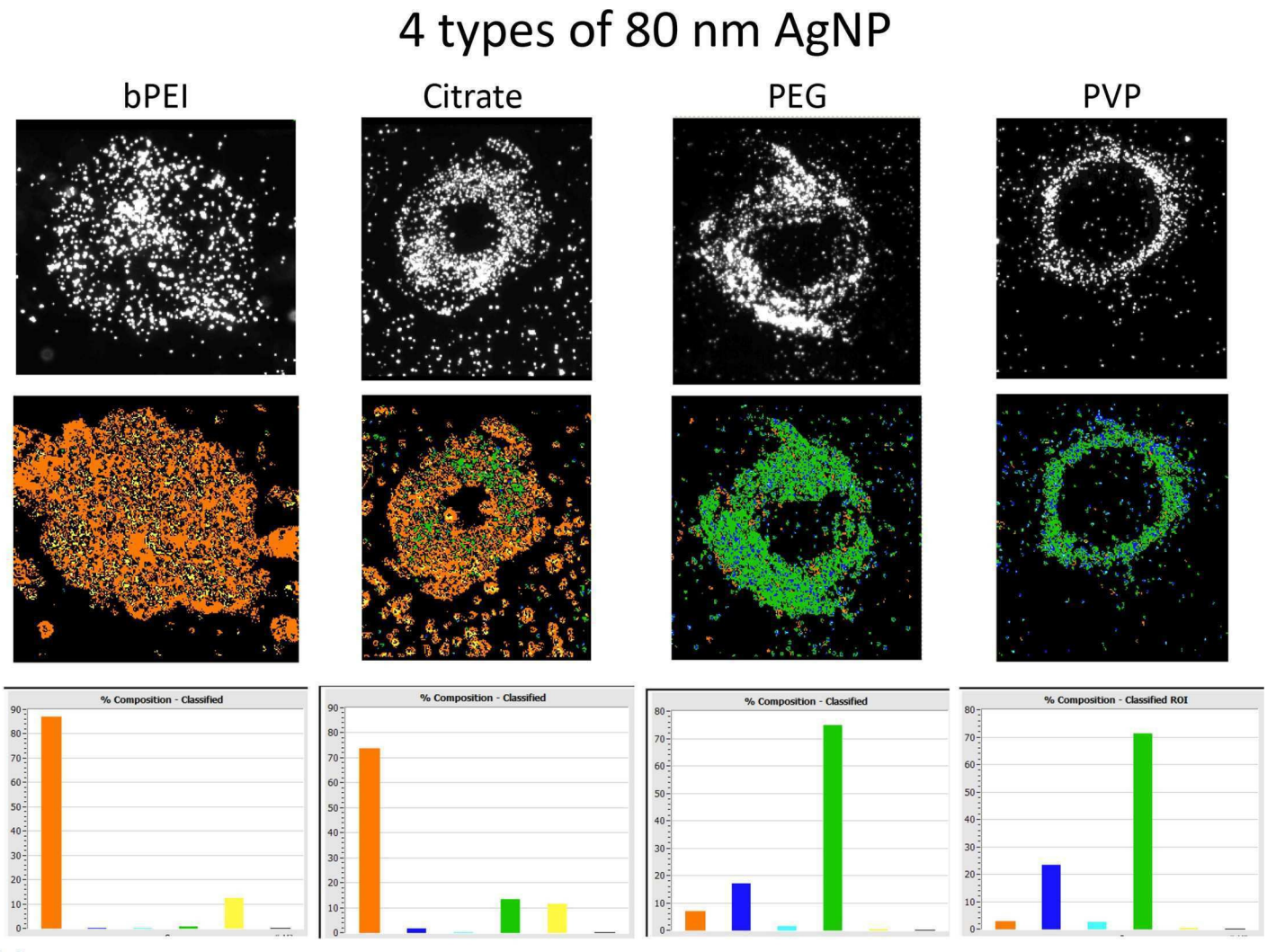

Fig 10. Hyperspectral image comparison of 4 types of AgNP. The top row in Fig 10 consists of scattered images from the PARISS hyperspectral system, while the middle row presents pseudo-colored images using the spectral library shown in Fig 9A. The percentage of each type of spectra is shown in the histograms displayed on the bottom row of Fig 10. The magnification of the images was 600x.

https://doi.org/10.1371/journal.pone.0219078.g010

Measures of NP uptake included flow cytometry, fluorescence, dark field microscopic imaging and PARISS hyperspectral imaging.

The SSC signal was influenced by the type of coating agents i.e. the positively charged AgNP-bPEI accumulated in cells to greater extent compared to the other AgNP studied. All coating types of AgNP entered the cells and were detected by a dose dependent increase in the SSC intensity. The AgNP-CIT and AgNP-bPEI agglomerates, both showed increased emissions in far-red wavelengths indicative of a high surface plasmonic resonance. Silver nanoparticles that settled on the surface of the slides could be observed with darkfield microscopy. These NP on the slide surface reflected relatively shorter wavelengths of light indicating the presence of individual particles or small agglomerates of AgNP. In contrast the silver nanoparticles that entered the cells usually formed larger particles by agglomeration that reflected longer wavelengths of light.

In summary, our research studied the AgNP using the light scatter parameter of the flow cytometer as a measure of cellular uptake [22,23]. The positive charged AgNP-bPEI was accumulated more readily into cells than the other AgNP studied (Figs 1 and 2, Table 1). AgNP-bPEI was associated with changes in mitochondrial shape, high level of nanoparticles binding to the nucleus after non-ionic cell lysis, and interruption of normal cell cycling. Correlated with the AgNP uptake, was the detection of SPR changes using flow cytometry. The degree of agglomeration appeared to affect the SPR intensity detected by flow cytometry with AgNP-bPEI and AgNP-CIT being much greater than AgNP-PEG and AgNP-PVP. Since the doses of nanoparticles used were relatively low, (usually between 1–10μg/ml), there was only limited cytotoxicity observed in 24 hours of cell culture. However, using a fluorescence microscopy, mitochondria transfected with GFP were observed to be converted from long strands into small round balls which is suggestive of toxicity and possibly a loss of function. Additional toxicity of AgNP-bPEI was demonstrated as a decrease in G_1 phase and increase in G_2/M and S phases over a 24-hour period, suggesting an inhibition of the normal cell cycle progression. Thus, the effects of AgNP in a cell culture system could be readily observed and measured, enabling a comparative analysis of the influence of different types of nanoparticle coating materials. A major conclusion from these studies was that the positively charged AgNP-bPEI were accumulated more readily into cells and were generally more toxic to cells than AgNP with other surface coatings.

The different capping agents of Ag nanoparticles contained unique surfaces that were designed to help increase their stability in suspensions and enhance their use in specific applications [13, 14, 17]. For example, PEG coatings deter immunological identification of nanoform drugs and thereby increase their biological half-lives. PVP coatings generally increase stability of nanoparticle suspensions. Positively charged or negatively charged coatings (bPEI and citrate, respectively) provide electrostatic advantages to attach oppositely charged molecules to the nanoparticles, depending on the specific application desired (S1 Table). Thus, biomedical and commercial applications of nanoparticles could involve a large variety of coatings, which profoundly influence the behavior of particles and their potential toxicity. Our data suggests positively charged coatings will be associated with higher potential of accumulating AgNP in cells, which should be a consideration for the AgNP production.

Flow cytometry data

Previously, our laboratory demonstrated that ARPE-19 cells incubated with either TiO_2 or AgNP absorbed particles inside the cells, which was detected as an increase of flow cytometer light side scatter (22, 23). The research in this manuscript compared AgNP with four types of capping agents that provided different surface charges and surface features. The uptake of

AgNP-bPEI by the cell increased the side scatter of both whole cells (Figs 1 and 2) and isolated nuclei (Fig 6). This positively charged AgNP-bPEI had the greatest increase in side scatter, suggesting a high absorption of these particles. The negative and neutral compounds (AgNP-PEG, AgNP-PVP and AgNP-CIT) did not scatter as much light as AgNP-bPEI and were thus assumed not to be less absorbed by the cells compared to AgNP-bPEI.

There is an observation that NP attached to nuclei are increased in a does dependent manner after detergent lysis. One hypothesis to explain the association between the nanoparticles and nuclei is that the NP are imbedded in the ER and this bit of cytoplasm containing NP remains attached to the nuclei after non-ionic treatment. Another hypothesis that may explain the data is that the nuclei becomes extremely sticky binding free floating nanoparticles. There was an increased SSC intensity of the 80nm AgNP-bPEI particles measured on the flow cytometer (Fig 3). This may be due to the surface of the AgNP-bPEI which has rough features as designated by the branched name that suggests these NP will reflect more light than AgNP containing smoother surfaces of the Citrate, PEG and PVP. It is not clear if this roughness parameter effected the absorption or if the positive charge was the primary determinant for absorption.

PARISS hyperspectral imaging

The optical properties of gold and silver nanoparticles are sensitive to particle size, shape, concentration, agglomeration state, and refractive index near the nanoparticle surface, which makes UV/VIS spectroscopy a valuable tool for identifying, characterizing, and studying nanomaterials. Other factors that might affect the wavelength spectra include the microscope configuration, light sources, objectives and mounting media. For many types of nanoparticles, the spectral wavelengths profiles can shift due to changes in the size, shape, coating, or agglomeration state. Blue-shifting refers to an electromagnetic response that is shifted towards shorter wavelengths (higher frequencies, higher energies) while red-shifting refers to shifts towards longer wavelengths. In our studies, AgNP-bPEI and AgNP-CIT appear to clump more inside the cells resulting in a red shift to longer wavelengths. By comparison AgNP-PVP and AgNP-PEG, which do not clump as readily in cells or solution, show a shift toward relatively shorter blue wavelengths. However, particle agglomeration will typically result in a spectral red shift. The surfaces of PVP and PEG are hard and not displaceable, while citrate and bPEI have surfaces which can be modified and exchanged with other molecules making them useful for specific biological applications. These surface features may be partially responsible for the biophysical differences that we observed with flow cytometry and PARISS imaging spectrophotometer instruments.

Surface plasma resonance

The optical properties of silver nanoparticles change when the particles aggregate and the electrons near the surface become delocalized and are then shared among adjacent particles. When this occurs, the surface plasmon shifts to lower energies and the scattering peaks shifts to longer spectra. The SPR occurs when the conduction electrons on the nanoparticle surface undergo a collective oscillation after excitation at specific wavelengths of light [35,36]. This results in a strong absorption of light followed by oscillation of plasmonic nanoparticles and an increase in the scattering of light.

These SPR effects were observed to a greater amount with citrate and bPEI surface AgNP coatings compared with PVP and PEG surface coatings (Table 2). In our studies, AgNP-CIT demonstrated the most SPR fluorescence, followed by AgNP-bPEI, AgNP-PEG, and AgNP-PVP. Cells treated with AuNP-PVP coated showed no SPR in contrast to AgNP-PVP which did show some SPR in the far-red channel on a flow cytometer.

The PARISS hyperspectral imaging data on NP contained in the cells or on the slide showed that AgNP-CIT and AgNP-bPEI shifted the exciting light to longer wavelength spectra suggestive of higher agglomeration. In contrast, AgNP-PVP and AgNP-PEG shifted the light to relatively shorter wavelengths which was suggestive of less agglomeration indicated by the detection of less SPR intensity.

It appears that the PARISS hyperspectral imaging data correlates with the SPR flow cytometer data. The greater agglomeration that was observed with AgNP-bPEI and AgNP-CIT using the PARISS imaging equipment may be related to the flow cytometry data that showed an increased SPR and increased SSC intensity measurements. In summary, both techniques were influenced by the degree of particle agglomeration.

Darkfield microscopy

Dark-field microscopy illumination describes a technique that can be used to enhance contrast in unstained samples. The incident beam is not captured directly by the objective lens, but the light that has been scattered by the sample is captured which results in a bright image with a dark background. Essentially, the scattered light that enters the objective lens will produce an image while the direct light entering the objective is blocked.

Darkfield microscopy has the potential to observe objects below the diffraction limit of the microscope (220 nm) and therefore is useful to observe nanoparticles that are less than 100 nm in size [22,25–27]. However, the major limitation of darkfield microscopy is that the sample has to be strongly illuminated. In the case of nanoparticles, blue biased light from xenon bulbs have higher energy and lower wavelengths making xenon superior to the red biased light derived from halogen bulbs. These halogen bulbs are contained in most microscopes as their primarily bright field light source. Conventional microscopy using differential interference microscopy (DIC) can only measure NP clumps which have physical sizes above the diffraction limits of the microscope (around 220 nm). Darkfield microscopy can observe 20 nm AgNP.

The most observable difference between the four types of AgNP by fluorescence microscopy was that AgNP-bPEI caused mitochondria to change from long strands in control cells or AgNP-PVP treated cells [Fig 7A] to a round shaped mitochondria in cells treated with AgNP-bPEI (Fig 7B). This fluorescence microscopy observation of mitochondrial shape changes may be related to the toxicity data that is present in the literature with AgNP-bPEI [49]. The amount of AgNP uptake by cells was also observed by darkfield microscopy (Figs 4, 7 and 8). There was a greater number of particles absorbed in cells l treated with AgNP-bPEI compared to cells treated with AgNP-CIT at the same 3μg/ml dose (Fig 4). Future expanded studies on mitochondria using TEM may shed more detailed information on the internal configuration of the mitochondria after interaction with positive and negative charged AgNP.

Green chemistry

The coatings on silver particles described in this manuscript were made with chemical and physical synthesis by the supplier, nanoComposix. However, there is the possibility of stabilizing silver molecules by green synthesis with plant extracts and enzymes. These silver nanoparticles synthesized by plant extracts are economical and cost effective and conceivably provide a product that is better and safer and less toxic for humans and the environment. [50,51] The molecules have been reduced and stabilized by a combination of biomolecules. These surfaces on nanoparticles are ecofriendly and may be compatible with biological and pharmaceutical applications.

With these advantages if would be useful to compare the "green synthesized particles" with nanoComposix AgNP in regard to their toxicity, uptake, and flow cytometry light scatter and

their effectiveness in biological applications. This comparison of green chemistry synthesized nanoparticles with nanoComposix produced silver nanoparticles would be a useful endeavor for our future research using the technology described in this manuscript.

Conclusions

NP uptake, intercellular agglomeration, and morphological effects were monitored by microscopy, hyperspectral imaging, flow cytometry and surface plasmonic resonance. Flow cytometry SSC was again shown to be a good dosimeter of the relative uptake of metallic nanoparticles into cells with some coatings of AgNP being accumulated at a greater rate than other AgNP molecules. The flow cytometry measurements of side scatter of cells and nuclei showed that AgNP-bPEI was absorbed more than other compounds at all doses (Table 1 and Fig 1). The positive charged molecules were toxic to mitochondria. The agglomeration characteristics of the particles on the surface of slides and within the cells could be studied by the PARISS hyperspectral imaging system. These methods demonstrated an increase in SPR and a shift to longer wavelengths with increased agglomeration. In future studies, these methods employed in this manuscript may help in to understand how NP interact with cells. Future studies will continue to explore how the different AgNP surfaces effect the potential health risk due to their relative uptake and potential toxicity.

Supporting information

S1 Fig. PARISS imaging spectrophotometer work flow. An imaging spectrograph (PARISS) acquires the spectra presented by a field of view (FOV) as it is translated on a computer-controlled microscope stage. Spectral Waveform Cross Correlation Analysis (SWCCA) classifies all acquired spectra. A reference spectral library of the classified spectra is generated which is then used to classify and pseudo-color a hyperspectral image of the FOV.
(TIF)

S2 Fig. Nuclei detergent lysis method for cell cycle analysis. The cells that were treated with AgNP show nanoparticles bound to the nucleus by microscopy and and increase in scatter by flow cytometry. The flow cytometry data using either PI or DAPI staining shows a dose dependent increase in side scatter in all phases of the cell cycle. The insert shows a cytogram representing the cell cycle stages with the black values being control and red values being the cellular sample that was treated with AgNP. The cell cycle of the nuclei was evaluated with the Multicycle program contained in the FCS express software (De Novo software, Los Angles, Ca).
(TIF)

S3 Fig. Cells (A) were incubated with 10ug/ml TiO2 Degussa. The image on the left (B) shows the nuclei stained with DAPI surrounded by nanoparticles with dispersed nanoparticles in the cytoplasm. After detergent lysis the cytoplasm is largely removed and some of the nanoparticles are attached to the nuclei. Images were acquired sequentially with fluorescence derived from DAPI stained nuclei (blue) and nanoparticles (white) obtained from with darkfield illumination. The two images were combined using Nikon Elements 5.0. About 30 images of the round cells were taken with Nikon widefield imaging software allowing for the generation of a "Z" stack. The images were sharpened using an extended depth focusing algorithm.
(TIF)

S1 Table. Characteristics of Ag coatings of nanoparticles. Derived from the nanoComposix web site https://nanocomposix.com.
(TIF)

Acknowledgments

Thanks, are extended to John Rogers, Chris Lau, Dave Herr, Mike Hughes and Kim Rogers and for their helpful comments and encouragement for many aspects of the paper. We wish to thank Phil Hartig and Mary Cardon for help with the transfection experiments. None of the authors other than JL have any conflict of interest with any of the companies. Jayna Ortenzio was a contractor to the USEPA, awards # EP09D000042 and EP10D000713

Author Contributions

Conceptualization: Robert M. Zucker, Jeremy M. Lerner, William K. Boyes.

Data curation: Robert M. Zucker.

Formal analysis: Robert M. Zucker, Jeremy M. Lerner.

Funding acquisition: Robert M. Zucker, William K. Boyes.

Investigation: Robert M. Zucker, Jayna Ortenzio, Laura L. Degn, William K. Boyes.

Methodology: Robert M. Zucker, Jayna Ortenzio, Laura L. Degn, Jeremy M. Lerner.

Project administration: Robert M. Zucker, William K. Boyes.

Resources: Robert M. Zucker, Laura L. Degn, William K. Boyes.

Software: Robert M. Zucker.

Supervision: Robert M. Zucker, William K. Boyes.

Validation: Robert M. Zucker, Jayna Ortenzio, Jeremy M. Lerner.

Visualization: Robert M. Zucker, Jeremy M. Lerner.

Writing – original draft: Robert M. Zucker.

Writing – review & editing: Robert M. Zucker, Jayna Ortenzio, Laura L. Degn, Jeremy M. Lerner, William K. Boyes.

References

1. Boyes WK, Thornton BL, Al-Abed SR, Andersen CP, Bouchard DC, Burgess RM, et al. A comprehensive framework for evaluating the environmental health and safety implications of engineered nanomaterials. Crit Rev Toxicol. 2017; 47(9):771–814.
2. Wang Z, Li N, Zhao J, White JC, Qu P, Xing B. CuO nanoparticle interaction with human epithelial cells: cellular uptake, location, export, and genotoxicity. Chem Res Toxicol. 2012; 25(7):1512–21. https://doi.org/10.1021/tx3002093 PMID: 22686560
3. Milić M, Leitinger G, Pavičić I, Zebić Avdičević M, Dobrović S, Goessler W, et al. Cellular uptake and toxicity effects of silver nanoparticles in mammalian kidney cells. J Appl Toxicol. 2015; 35(6):581–92. https://doi.org/10.1002/jat.3081 PMID: 25352480
4. Alberola AP, Rädler JO. The defined presentation of nanoparticles to cells and their surface-controlled uptake. Biomaterials. 2009; 30(22):3766–70. https://doi.org/10.1016/j.biomaterials.2009.03.031 PMID: 19375161
5. Singh RP, Ramarao P. Cellular uptake, intracellular trafficking and cytotoxicity of silver nanoparticles. Toxicol Lett. 2012; 213(2):249–59. https://doi.org/10.1016/j.toxlet.2012.07.009 PMID: 22820426
6. Summers HD, Brown MR, Holton MD, Tonkin JA, Hondow N, Brown AP, et al. Quantification of nanoparticle dose and vesicular inheritance in proliferating cells. ACS Nano. 2013; 7(7):6129–37. https://doi.org/10.1021/nn4019619 PMID: 23773085
7. Peuschel H, Ruckelshausen T, Cavelius C, Kraegeloh A. Quantification of internalized silica nanoparticles via STED microscopy. Biomed Res Int. 2015:1–16.

8. Guarnieri D, Sabella S, Muscetti O, Belli V, Malvindi MA, Fusco S, et al. Transport across the cell-membrane dictates nanoparticle fate and toxicity: a new paradigm in nanotoxicology. Nanoscale. 2014; 6 (17):10264–73. https://doi.org/10.1039/c4nr02008a PMID: 25061814
9. dos Santos T, Varela J, Lynch I, Salvati A, Dawson KA. Quantitative assessment of the comparative nanoparticle-uptake efficiency of a range of cell lines. Small. 2011; 7(23):3341–9. https://doi.org/10.1002/smll.201101076 PMID: 22009913
10. Teeguarden JG, Hinderliter PM, Orr G, Thrall BD, Pounds JG. Particokinetics in vitro: dosimetry considerations for in vitro nanoparticle toxicity assessments. Toxicol Sci. 2006; 95(2):300–12. https://doi.org/10.1093/toxsci/kfl165 PMID: 17098817
11. Cohen JM, Teeguarden JG, Demokritou P. An integrated approach for the in vitro dosimetry of engineered nanomaterials. Particle and Fibre Toxicol. 2014; 11(1):20.
12. Hinderliter PM, Minard KR, Orr G, Chrisler WB, Thrall BD, Pounds JG, et al. ISDD: A computational model of particle sedimentation, diffusion and target cell dosimetry for in vitro toxicity studies. Particle and Fibre Toxicol. 2010; 7(1):36.
13. röhlich E. The role of surface charge in cellular uptake and cytotoxicity of medical nanoparticles. Int J Nanomedicine. 2012;5577–91. https://doi.org/10.2147/IJN.S36111 PMID: 23144561
14. Fröhlich E. The role of surface charge in cellular uptake and cytotoxicity of medical nanoparticles. Inorg Chem. 2012:5577.
15. Fröhlich E. Cellular elimination of nanoparticles. Environ Toxicol and Pharmacol.2016; 46:90–4.
16. Yu B, Zhang Y, Zheng W, Fan C, Chen T. Positive Surface Charge Enhances Selective Cellular Uptake and Anticancer Efficacy of Selenium Nanoparticles. Inorg Chem. 2012; 51(16):8956–63. https://doi.org/10.1021/ic301050v PMID: 22873404
17. Hühn D, Kantner K, Geidel C, Brandholt S, De Cock I, Soenen S, et al. Polymer-coated nanoparticles interacting with proteins and cells: focusing on the sign of the net charge. ACS Nano. 2013; 7(4):3253–63. https://doi.org/10.1021/nn3059295 PMID: 23566380
18. Chandran P, Riviere JE, Monteiro-Riviere NA. Surface chemistry of gold nanoparticles determines the biocorona composition impacting cellular uptake, toxicity and gene expression profiles in human endothelial cells. Nanotoxicology. 2017; 11(4):507–19. https://doi.org/10.1080/17435390.2017.1314036 PMID: 28420299
19. Zucker RM, Daniel KM. Detection of TiO2 Nanoparticles in Cells by Flow Cytometry. Nanoparticles in Biology and Medicine: Humana Press; 2012. p. 497–509.
20. Sanders K, Degn LL, Mundy WR, Zucker RM, Dreher K, Zhao B, et al. In vitro phototoxicity and hazard identification of nano-scale titanium dioxide. Toxicol Appl Pharmacol. 2012; 258(2):226–36. https://doi.org/10.1016/j.taap.2011.10.023 PMID: 22115978
21. Zucker RM, Daniel KM. Microscopy Imaging Methods for the Detection of Silver and Titanium Nanoparticles Within Cells. Nanoparticles in Biology and Medicine: Humana Press; 2012. p. 483–96.
22. Zucker RM, Massaro EJ, Sanders KM, Degn LL, Boyes WK. Detection of TiO2 nanoparticles in cells by flow cytometry. Cytometry A. 2010; 77(7):677–85. https://doi.org/10.1002/cyto.a.20927 PMID: 20564539
23. Zucker RM, Daniel KM, Massaro EJ, Karafas SJ, Degn LL, Boyes WK. Detection of silver nanoparticles in cells by flow cytometry using light scatter and far-red fluorescence. Cytometry A. 2013:962–72. https://doi.org/10.1002/cyto.a.22342 PMID: 23943267
24. Zucker RM, Ortenzio JN, Boyes WK. Characterization, detection, and counting of metal nanoparticles using flow cytometry. Cytometry A. 2016; 89(2):169–83. https://doi.org/10.1002/cyto.a.22793 PMID: 26619039
25. Gibbs-Flournoy EA, Bromberg PA, Hofer TPJ, Samet JM, Zucker RM. Darkfield-confocal microscopy detection of nanoscale particle internalization by human lung cells. Part Fibre Toxicol. 2011; 8(1):2. https://doi.org/10.1186/1743-8977-8-2 PMID: 21247485
26. Weinkauf H, Brehm-Stecher BF. Enhanced darkfield microscopy for rapid artifact-free detection of nanoparticle binding to Candida albicans cells and hyphae. Biotechnol J. 2009; 4(6):871–9. https://doi.org/10.1002/biot.200800358 PMID: 19492326
27. Baltazar GC, Guha S, Lu W, Lim J, Boesze-Battaglia K, Laties AM, et al. Acidic nanoparticles are trafficked to lysosomes and restore an acidic lysosomal pH and degradative function to compromised ARPE-19 cells. PLoS ONE. 2012; 7(12): e49635. https://doi.org/10.1371/journal.pone.0049635 PMID: 23272048
28. Suzuki H, Toyooka T, Ibuki Y. Simple and Easy Method to Evaluate Uptake Potential of Nanoparticles in Mammalian Cells Using a Flow Cytometric Light Scatter Analysis. Environ Sci Technol. 2007; 41 (8):3018–24. https://doi.org/10.1021/es0625632 PMID: 17533873

29. Park J, Ha MK, Yang N, Yoon TH. Flow Cytometry-Based Quantification of Cellular Au Nanoparticles. Anal Chem. 2017; 89(4):2449–56. https://doi.org/10.1021/acs.analchem.6b04418 PMID: 28192941

30. Zhao X, Ibuki Y. Evaluating the Toxicity of Silver Nanoparticles by Detecting Phosphorylation of Histone H3 in Combination with Flow Cytometry Side-Scattered Light. Environ Sci Technol. 2015; 49(8):5003–12. https://doi.org/10.1021/acs.est.5b00542 PMID: 25815977

31. Kumar A, Pandey AK, Singh SS, Shanker R, Dhawan A. A flow cytometric method to assess nanoparticle uptake in bacteria. Cytometry A. 2011; 79(9):707–12. https://doi.org/10.1002/cyto.a.21085 PMID: 21638764

32. Toduka Y, Toyooka T, Ibuki Y. Flow cytometric evaluation of nanoparticles using side-scattered light and reactive oxygen species-mediated fluorescence–correlation with genotoxicity. Environ Sci Tech. 2012; 46(14):7629–36.

33. Zhao X, Ibuki Y. Evaluating the Toxicity of Silver Nanoparticles by Detecting Phosphorylation of Histone H3 in Combination with Flow Cytometry Side-Scattered Light. Environ Sci Tech. 2015; 49 (8):5003–12.

34. Mutzke E, Chomyshyn E, Nguyen KC, Blahoianu M, Tayabali AF. Phagocytosis-coupled flow cytometry for detection and size discrimination of anionic polystyrene particles. Anal Biochem. 2015; 483: 40–6. https://doi.org/10.1016/j.ab.2015.04.034 PMID: 25957125

35. Peterson AW, Halter M, Tona A, Bhadriraju K, Plant AL. Surface plasmon resonance imaging of cells and surface-associated fibronectin. BMC Cell Biol. 2009; 10;1–17. https://doi.org/10.1186/1471-2121-10-1

36. Paul S, Vadgama P, Ray AK. Surface plasmon resonance imaging for biosensing. IET Nanobiotechnology. 2009; 3(3):71–80. https://doi.org/10.1049/iet-nbt.2008.0012 PMID: 19640160

37. Hu M, Novo C, Funston A, Wang H, Staleva H, Zou S, et al. Dark-field microscopy studies of single metal nanoparticles: understanding the factors that influence the linewidth of the localized surface plasmon resonance. J Mater Chem. 2008; 18(17):1949–60. https://doi.org/10.1039/b714759g PMID: 18846243

38. Lerner JM. Imaging spectrometer fundamentals for researchers in the biosciences—A tutorial. Cytometry A. 2006; 69(8):712–34. https://doi.org/10.1002/cyto.a.20242 PMID: 16615140

39. Lerner JM, Gat N, Wachman E. Approaches to spectral imaging hardware. Curr Protoc Cytom. 2010; 53(1):12.20–40

40. Zucker RM, Elstein KH, Gershey EL, Massaro EJ. Increasing sensitivity of the Ortho analytical cytofluorograph by modifying the fluid system. Cytometry. 1990; 11(7):848–51. https://doi.org/10.1002/cyto.990110712 PMID: 2272248

41. Zucker RM, Fisher NC. Evaluation and Purchase of an Analytical Flow Cytometer: Some of the Numerous Factors to Consider. Curr Protoc Cytom John. 2013; 63(1):1.28-1–11.

42. Zucker RM. Flow Cytometry Quality Assurance. In: Resch-Genger U, editors. Standardization and Quality Assurance in Fluorescence Measurements II. Springer Series on Fluorescence; 2008. p. 343–70.

43. Zucker RM, Elstein KH, Easterling RE, Massaro EJ. Metal-induced alteration of the cell membrane/cytoplasm complex studied by flow cytometry and detergent lysis. Toxicology. 1988; 53(1):69–78. PMID: 3201476

44. Zucker RM, Elstein KH, Easterling RE, Massaro EJ. Flow cytometric discrimination of mitotic nuclei by right-angle light scatter. Cytometry. 1988; 9(3):226–31. https://doi.org/10.1002/cyto.990090307 PMID: 3132355

45. Zucker RM, Elstein KH, Easterling RE, Massaro EJ. Metal-induced alteration of the cell membrane/cytoplasm complex studied by flow cytometry and detergent lysis. Toxicology. 1988; 53(1):69–78. PMID: 3201476

46. Zucker RM, Elstein KH, Easterling RE, Massaro EJ. Flow cytometric comparison of the effects of trialkyltins on the murine erythroleukemic cell. Toxicology. 1989; 58(2):107–19. PMID: 2799821

47. Van Der Pol E, Van Gemert MJ, Sturk A, Nieuwland R, Van Leeuwen TG. Single vs. swarm detection of microparticles and exosomes by flow cytometry. J Thromb Haemost. 2012; 10(5):919–30. https://doi.org/10.1111/j.1538-7836.2012.04683.x PMID: 22394434

48. Stoehr LC, Gonzalez E, Stampfl A, Casals E, Duschl A, Puntes V, et al. Shape matters: effects of silver nanospheres and wires on human alveolar epithelial cells. Part Fibre Toxicol. 2011; 8(1):36.

49. Pang C, Brunelli A, Zhu C, Hristozov D, Liu Y, Semenzin E, et al. Demonstrating approaches to chemically modify the surface of Ag nanoparticles in order to influence their cytotoxicity and biodistribution after single dose acute intravenous administration. Nanotoxicology. 2016; 10(2):129–39. https://doi.org/10.3109/17435390.2015.1024295 PMID: 25962681

50. Shakeel Ahmed, Mudasir Ahmad,Lal Swami Bubu Ikram, Saiqa. A review on plant extract mediated synthesis of silver nanoparticles for antimicrobial applications: A green expertise. journal of Advanced research 7 17–28 2016 https://doi.org/10.1016/j.jare.2015.02.007

51. Srikar SK, Giri DD, Pal DB, Mishra PK upadhyay SN. Green synthesis of silver nanoparticles: a review Green and Sustainable Chemisty 6 34–56 2016

NanoImpact 14 (2019) 100156

Contents lists available at ScienceDirect

NanoImpact

journal homepage: www.elsevier.com/locate/nanoimpact

Research paper

Determination of silver nanoparticle dose *in vitro*☆

Jayna Ortenzio[b], Laura Degn[a], Alice Goldstein-Plesser[b], John K. McGee[c], Jana Navratilova[d], Kim Rogers[e], Robert M. Zucker[a], William K. Boyes[a,*]

[a] Toxicity Assessment Division, MD B105-04, National Health and Environmental Effects Research Laboratory, Office of Research and Development, USEPA, RTP, NC 27711, United States
[b] Oak Ridge Institute for Science and Education (ORISE) appointee at the National Health and Environmental Effects Research Laboratory, USEPA, RTP, NC 27711, United States
[c] Environmental Public Health Division, MD B105-02 NHEERL, ORD, U.S. E.P.A., Research Triangle Park, NC 27711, United States
[d] National Research Council Fellow at the National Exposure Research Laboratory, USEPA, RTP, NC 27711, United States
[e] Exposure Methods & Measurements Division, National Exposure Research Laboratory, USEPA, RTP, NC 27711, United States

ARTICLE INFO

Keywords:
Silver
Nanoparticles
Flow cytometry
Particle deposition models
ICP-MS

ABSTRACT

An important issue for interpreting *in vitro* nanomaterial testing is quantifying the dose delivered to target cells. Considerations include the concentration added to the culture, the proportion of the applied dose that interacts with the target cells, and the amount that is eventually absorbed by the target cells. Rapid and efficient techniques are needed to determine delivered doses. Previously, we demonstrated that TiO_2 and silver nanoparticles (AgNP) were absorbed by cells in a dose dependent manner between 1 μg/ml and 30 μg/ml and were detected in cells by light scatter using a flow cytometer. Here, we compare four potential indices of the dose of AgNP to cells, including: inductively coupled plasma - mass spectrometry (ICP-MS); flow cytometry side scatter (SSC); and amount of silver deposited to the cell layer as estimated with both an integrated Volumetric Centrifugation Method - *In Vitro* Sedimentation, Diffusion and Dosimetry Model (VCM-ISDD) and a Distorted Grid (DG) model. A retinal pigment epithelial cell line was exposed to 20 nm or 75 nm citrate-coated AgNP for 24 h. The relationships between particle sizes and internalized doses varied according to the dose metric. Twenty-four hours after exposure, the cell layer contained a greater mass of silver when treated with 75 nm AgNP than with 20 nm AgNP. When the dose was expressed as the number of particles or as the total surface area of absorbed particles, however, the reverse was true; the dose to the cells was higher after exposure to 20 than 75 nm AgNP. Flow cytometry SSC increased with dose for both sizes of AgNP, and was correlated with Ag in cells measured by ICP-MS. The rate of SSC increase was greater for 75 than for 20 nm AgNP, suggesting it could be used as an indicator of cellular dose after accounting for particle size and composition. Silver was detected by ICP-MS in re-suspended supernates of the isolated cell layer suggested that not all the silver deposited to the cell layer was absorbed by the cells. Both the VCM-ISDD and DG models estimated the proportion of Ag deposited to the cellular layer, which in both cases was greater than the amount of silver in the cells measured by ICP-MS. Modeled deposition more closely compared to the total Ag deposition by ICP-MS, *i.e.* mass of silver in the cells plus the resuspended, unabsorbed Ag from the cell layer. ICP-MS indicated the mass of silver in cells from AgNP treatment, but not whether the Ag was in the form of particles or dissolved ions. Deposition models predicted the amount of AgNP deposited to the cell layer, but not cellular uptake. Flow cytometry SSC was correlated to cellular uptake of particle-form AgNP and could be calibrated against ICP-MS to indicate mass of cellular uptake. Therefore, a combination of approaches may be required to accurately understand cellular dosimetry of *in vitro* nanotoxicology experiments. In summary, cellular dosimetry is an important consideration for nanotoxicology experiments, and not necessarily related to the applied dose.

☆ The information in this document was funded wholly by the U.S. Environmental Protection Agency. It was subjected to review by the National Health and Environmental Effects Research Laboratory and approved for publication. Approval does not signify that the contents reflect the views of the Agency, nor does mention of trade names or commercial products constitute endorsement or recommendation for use.

* Corresponding author at: 109 T.W. Alexander Drive, B105-04, NHEERL/TAD/NB, U.S. EPA, Research Triangle Park, NC 27711, United States.
E-mail addresses: goldstein-plesser.alice@epa.gov (A. Goldstein-Plesser), Mcgee.john@epa.gov (J.K. McGee), Navratilova.jana@epa.gov (J. Navratilova), Rogers.kim@epa.gov (K. Rogers), Zucker.robert@epa.gov (R.M. Zucker), Boyes.william@epa.gov (W.K. Boyes).

https://doi.org/10.1016/j.impact.2019.100156
Received 22 October 2018; Received in revised form 15 February 2019; Accepted 2 April 2019
Available online 06 April 2019
2452-0748/ © 2019 Published by Elsevier B.V.

1. Introduction

Nanotechnology, including the use of engineered nanomaterials (ENM), is a growing part of commerce that is expected to make an ever increasing contribution to global economic development (PCAST, 2014). Nanoparticles are being incorporated into many applications, and although the uses and forms of nanomaterials in many consumer products are unknown, inventories of products suggest that silver nanomaterials (AgNP) are incorporated into more consumer products than nanomaterials of other composition (Hansen et al., 2016; Vance et al., 2015). Among the product categories that may contain silver nanoparticles are personal care products, home and garden products, cosmetics, food and beverage containers, filters, appliances, sporting goods, children's products, electronics, automotive components, and dietary supplements. The variety of engineered materials and their applications is growing at a pace more rapid than can be evaluated for potential hazards in a conventional way. As is true for the large number of conventional chemicals with inadequate toxicity and exposure data (NRC, 2007), alternative approaches for evaluating potential hazards of ENM are necessary if they are to be used in a responsible and sustainable fashion.

Several alternative testing strategies for ENM are being developed, many of which rely on *in vitro* testing at some phase of a tiered testing sequence (Arts et al., 2015; Arts et al., 2014; Cohen et al., 2013b; Evans et al., 2017; Farcal et al., 2015; Godwin et al., 2015; Hartung and Sabbioni, 2011; Oomen et al., 2014; Som et al., 2013; Stone et al., 2014). With *in vitro* systems, the dose of nanomaterials reaching the cells is an important consideration, and does not necessarily reflect the concentration of materials added to the system (Hinderliter et al., 2010; Schmid and Cassee, 2017; Teeguarden et al., 2007). Typically, *in vitro* test systems involve cells that grow adherently to the bottom of cell culture flasks, or wells of multi-well plates, and nanoparticles are dispersed in a suspension fluid added to the cell culture media above the cell layer. Characteristics of nanoparticle suspensions are dependent on dispersion method and composition of both the dispersed nanomaterial and the dispersing media. In this situation, the dose of particles received by cells is dependent upon processes occurring in the media above the cells such as particle diffusion and sedimentation, which in turn are governed by nanoparticle properties such as size, surface charge, particle agglomeration, agglomerate density, media viscosity, osmolarity and temperature (Cohen et al., 2013a; Cohen et al., 2014; Hinderliter et al., 2010; Teeguarden et al., 2007). In a suspension applied to an *in vitro* system, size and density of nanomaterial agglomerates, along with stability of the suspension over time, affect the cellular dose.

Several successive computational models of particle deposition and dosimetry have been developed to estimate dose of ENM deposited to the cell layer *in vitro* (Cohen et al., 2014; DeLoid et al., 2015; Hinderliter et al., 2010; Thomas et al., 2018). The initial contribution to this area was the *In vitro* Sedimentation, Diffusion and Dosimetry (ISDD) model (Hinderliter et al., 2010) which featured equations for particle diffusion, based on the Stokes-Einstein equation, and gravimetric sedimentation, based on the Stokes Law, while accounting for particle size, particle density, agglomeration state, media viscosity and temperature. A general observation from the ISDD model was that the transport of small particles ($< \sim$10 nm) was governed primarily by diffusion, larger particles ($> \sim$100 nm) primarily by sedimentation, and transport of particles between 10 and 100 nm was governed by a mixture of diffusion and sedimentation. The ISDD model provided reasonable approximations of particle deposition to the cellular layer compared to measured deposition of iron oxide, polystyrene and amorphous silica particles. Deloid, Cohen and co-workers offered a simple volumetric centrifugation method (VCM) to measure agglomerate density, and enhanced the original ISDD model to incorporate the measurements (VCM-ISDD) (Cohen et al., 2014; DeLoid et al., 2014). This was followed by the Distorted Grid (DG) model, which addressed a parameter termed "stickiness" in the VCM-ISDD model. Stickiness refers to the propensity of particles to adhere to the cell layer rather that returning to the media by diffusion. Assuming a sticky lower boundary creates a sink, artificially pulling particles downward due to the concentration gradient. Furthermore, it allowed for multiple agglomerate size populations, considered potential dissolution of particles over time, and modeled particle deposition among layered sections of the media as well as at the cellular layer at the bottom of the well (DeLoid et al., 2015). These models were critically reviewed in 2015 (Cohen et al., 2015), and a recent version of ISDD incorporating potential dissolution (ISD3) has become available (Thomas et al., 2018). Hinderliter and colleagues note that experimental determination of cellular content of nanomaterials is the "gold standard", but that modeling deposition can be a useful adjunct to such measurements (Hinderliter et al., 2010).

Experimental confirmation of cellular dose is not necessarily straightforward. Where nanoparticles are composed of one or more metals, a typical approach to quantitate dose delivered to cells is to measure the concentration of the constituent metals in the cell layer using techniques such as inductively coupled plasma - mass spectrometry (ICP-MS) or inductively coupled plasma - optical emission spectrometry (ICP-OES). These methods can be time- and labor-intensive, are not suitable for higher throughput sampling and cannot be readily applied to carbon-based nanomaterials. Also, it may be difficult to differentiate nanoparticles inside cells from extracellular particles on the cell surface or otherwise deposited among the cell layer. Furthermore, such measurements provide information only about the amount of the ENM constituent elements present in the sample, and not the form; for example, the data do not indicate whether the metal was in a dissolved ionic or particle form.

Previously, a dose-dependent increase of flow cytometry SSC signal was observed when cells were incubated with nanoparticles of TiO_2, silver or other reflective materials (Ha et al., 2018; Sanders et al., 2012; Suzuki et al., 2007; Toduka et al., 2012; Zucker et al., 2013; Zucker et al., 2010). It was apparent that the nanoparticles absorbed into the cells were responsible for the increased reflected light comprising the side-scatter signal, and that flow cytometry was responsive to the presence of nanoparticles rather than ionic components dissolved from the particles. Recently, an international consortium demonstrated good interlaboratory agreement using flow cytometry to measure cellular uptake of fluorescently-labeled polystyrene nanoparticles (Salvati et al., 2018). Flow cytometry was also a more rapid and efficient index of cellular uptake of nanoparticles than ICP-MS. Not all nanoparticles are fluorescent, however, making it necessary to use side scatter measurements to indicate uptake of non-fluorescent particles. The SSC measures the amount of reflected light from a cell and therefore, like fluorescence, is an indirect indicator of particle uptake rather than a direct measure of mass or number of nanoparticles in a cell.

In the current work, cellular dose was evaluated using a human derived retinal pigment epithelial cell line (ARPE-19). The ARPE-19 cells were used primarily to be consistent with previous work (Sanders et al., 2012; Zucker et al., 2013; Zucker et al., 2010). Ocular exposure to nanoparticles might occur either deliberately through application of nano-enabled ophthalmic drugs (Andonova, 2016), or inadvertently through topical or systemic exposure. Nanocarriers for ocular drug delivery are being developed for both topical and systemic routs of delivery (Diebold and Calonge, 2010). Following inadvertent exposure including oral or inhalation exposure and subsequent systemic absorption, posterior portions of the eye could become exposed to nanomaterials *via* blood-borne delivery to the retinal choroid. The retinal choroid features fenestrated arteries and receives 85% to the total ocular blood flow, yielding the highest ratio of blood flow/mass of tissue in the body. The retinal pigment epithelium serves as a diffusion barrier between the retinal choroidal blood flow and the retinal photoreceptor outer segments (Fox and Boyes, 2013). The retinal pigment epithelial cells have a high rate of phagocytosis associated with daily digestion of photoreceptor outer segments. Thus, systemic absorption of

nanomaterials could readily lead to blood-borne RPE exposure. Also important is the slow rate of ocular clearance. Song et al. (Song et al., 2013) showed that 12 weeks after cessation of inhalation exposure to silver nanoparticles, clearance of silver from the eye was slower than from most other tissues except perhaps the brain and, for females, the ovaries. Thus, the high rate of choroidal blood flow, the high rate of RPE phagocytosis and the slow rate of ocular clearance make the posterior segment of the retina and the RPE cell layer a potential target for ENM exposure.

The current experiments evaluated the dose to ARPE-19 cells 24 h after treatment of 20 or 75 nm citrate-coated AgNP. The results of the current experiments demonstrated that particle size was an important factor in cellular dosimetry due to differential partitioning of particles between the culture media and the cell layer. More silver remained in the media 24 h after treatment than was deposited to the cell layer, and more silver remained suspended for 20 than 75 nm AgNP. Conversely, a greater mass of silver was deposited onto the cell layer for 75 than 20 nm AgNP. There were linear relationships between the mass of Ag in cells measured by ICP-MS and flow cytometry SSC, but the relationships differed for different sized AgNP. The VCM-ISDD and DG models estimated a greater mass of silver deposition than was measured by ICP-MS in the cellular layer, a difference reflecting AgNP deposited to the cell layer but not absorbed by the cells. The results indicate that flow cytometry SSC can serve as a rapid index of cellular uptake of light-reflective nanoparticles. Overall, they illustrate the importance of independent confirmation of cellular dose for *in vitro* nanotoxicology research.

2. Materials and methods

2.1. Silver nanoparticles

Biopure AgNP (20 nm and 75 nm) coated with citrate were obtained from NanoComposix (Santa Cruz, CA) as 1 mg/ml suspensions. Each lot of AgNP was characterized by the supplier who provided lot-specific TEM images, particle size distributions, and ultraviolet-visible (UV-Vis) spectroscopy, among other characterization parameters (Supplemental materials, Figs. S1 and S2).

2.2. AgNP suspensions

Dilutions of nanoparticle suspensions were prepared immediately before treating cells and used within 10 min of preparation. The 1 mg/ml stock suspension of AgNP received from the supplier was vortexed (2 5-s bursts), and 1-ml of stock suspension was added to 9 ml of cell culture medium in a 50-ml centrifuge tube. Further dilutions of 3, 10 and 30 μg/ml were made from the resulting 100 μg/ml suspension, and vortexed again immediately prior to cell treatments.

2.3. Characterization of AgNP in cell media

It was important to determine the stability of AgNP in cell culture media over time related to potential dissolution of particles to silver ions, or to formation of agglomerates. The stability of 20 or 75 nm AgNP in assay media over the time of incubation was investigated by dynamic light scattering (DLS), centrifugal ultrafiltration, Nanoparticle Tracking Analysis (NTA), UV − Vis absorption, and by single particle ICP-MS (spICP-MS). A Zetasizer Nano ZS (Malvern Instruments, Ltd., Worcestershire, UK) was used to evaluate hydrodynamic size distributions by DLS, stability and zeta potentials of AgNP in cell culture medium.

Nanoparticle Tracking Analysis (NTA) was performed with a NanoSight NS500 instrument (NanoSight, UK), using procedures described elsewhere (Rogers et al., 2018).

For UV-Vis evaluations, AgNP were dispersed in cell culture media at a concentration of 10 μg/ml and maintained at 37 °C in a heating cabinet. $AgNO_3$ was added to media as a control for total dissolution. At the time points of 0 and 24 h, a 5 ml sub-sample was taken and subsequently filtered through a 10 kDa centrifugation filter (Amicon Ultra-15, 10 K, Millipore, Bedford, MA) at 6000 *g* for 20 min. The total silver concentration in the filtrates was measured by ICP-OES after acid digestion.

The surface plasmon resonance of the AgNP suspensions in deionized water and media was investigated by measuring UV − Vis absorption spectra at the time points 0 and 24 h. UV-Vis spectra were collected over a wavelength range of 200–800 nm. Media blank and AgNP in de-ionized water served as control samples.

The size of the AgNP after 24 h in media was also evaluated by spICP-MS (Degueldre and Favarger, 2003). Prior to the analysis, all samples were diluted to the final silver concentration of 10 ng/L and analyzed in spICP-MS mode. Gold nanoparticle reference material (NIST 8013), with reference value of 60 nm, was diluted to 5 ng/L gold concentration and used for the evaluation of nebulization efficiency.

2.4. Cell culture

A human derived retinal pigment epithelial cell line (ARPE-19 cells; ATCC; Manassas, VA) was selected for comparison with previous work (Al-Abed et al., 2016; Sanders et al., 2012; Zucker et al., 2013; Zucker et al., 2010). The ARPE-19 cells were grown in DMEM/F12 (pH 7.4), without phenol red (Life Technologies, Grand Island, NY), containing 10% FBS, 100 units/ml penicillin, 100 μg/ml streptomycin, and incubated at 37 °C in 95% air and 5% CO_2 (Sanders et al., 2012). The cells were obtained from the supplier at passage 21 and used for experiments at passage 28. Four T-25 cm^2 flasks containing ARPE-19 cells grown to confluence were treated with either 0, 3, 10, or 30 μg/ml of 20 or 75 nm citrate-coated AgNP in cell culture medium. All suspensions of AgNP were thoroughly vortexed prior to application. To treat cells, flasks were gently tipped vertically without disturbing the layer of adherent cells, growth media was removed from the culture flask and replaced with media containing the appropriate concentration of AgNP. After 24 h, samples from flasks with cells were split for analysis by ICP-MS and flow cytometry. Four identical flasks, containing no cells, were also treated with each dose of AgNP and submitted to ICP-MS. A schematic diagram of the experimental design is presented in Supplemental Fig. S3.

2.5. Dosimetry modeling

The deposition of AgNP to the cell layer was estimated through established particle kinetic models. The VCM-ISDD and DG models were used to calculate the fraction of the applied dose deposited to the cell layer as a function of time after treatment (Cohen et al., 2013a; DeLoid et al., 2015; Hinderliter et al., 2010). For the AgNP suspensions, effective density of the agglomerates (ρev) was measured by volumetric centrifugation (MIDSCI; St. Louis, MO) as described by Deloid (DeLoid et al., 2015). In addition to effective density, the model inputs included the hydrodynamic diameter measured by DLS (Table 1), the media volume (5 ml), height within the flask (4 mm), temperature (310 *K*), media density (1.0062 g/cm^3), media viscosity (0.685 cP), and concentration of the initial suspension. For comparison, the VCM-ISDD and DG models were also run with the hydrodynamic diameter values derived from the NTA evaluation.

2.6. Cytotoxicity

Cell viability was assessed with a live/dead assay staining with calcein-AM and propidium iodide (PI) (Invitrogen, Carlsbad, CA) as reported elsewhere (Sanders et al., 2012).

Table 1
Silver nanoparticle agglomerate size determinations by DLS, NTA and spICP-MS.

Nominal size nm	Matrix	Incubation time (hrs)	DLS nm (SD)	PDI	NTA nm (SD)	spICP-MS nm
AgNP 20	DI	NA	53 (4)	0.41	99 (53)	NA
AgNP 20	Cell media	0	244 (14)	0.28	100 (57)	NA
AgNP 20	Cell media	24	251 (18)	0.29	90 (51)	51
AgNP 75	DI	NA	94 (8)	0.19	84 (31)	NA
AgNP 75	Cell media	0	338 (25)	0.18	104 (40)	NA
AgNP 75	Cell media	24	388 (26)	0.18	116 (44)	67

Abbreviations: AgNP - silver nanoparticles; DLS – dynamic light scattering; SD – standard deviation; PDI – poly-dispersion Index; NTA – nanoparticle tracking analysis; spICP-MS – single particle inductively-coupled plasma – mass spectroscopy; DI – distilled deionized water; NA - not available or not applicable.

2.7. Sample collection for ICP-MS and flow cytometry

The uptake of AgNP into cells was measured experimentally. Treatment suspension, original and spent: 100 µl of each original treatment suspension was placed into a pre-weighed tube for ICP-MS analysis. After 24 h, 300 µl of spent treatment suspension was recovered from each flask and placed into a pre-weighed tube for ICP-MS analysis. All flasks were rinsed with 5 ml of Hank's Balanced Salt Solution (HBSS); a 300-µl aliquot of this rinsate was put into pre-weighed tubes for ICP-MS analysis.

Supernatant**:** One ml of trypsin/EDTA (0.05%/0.02%) in HBSS was added to each flask and incubated at 37 °C with 95% air and 5% CO_2 for 7.5 min. Flasks were then washed twice with 5 ml of HBSS. Resuspended washes from each flask were collected in centrifuge tubes and centrifuged at 800 *g* for 7.5 min at room temperature to separate cells from medium. A 300-µl aliquot of each supernatant was added to the corresponding pre-weighed tube for ICP-MS analysis.

Cell Pellet: The remaining supernatant was removed from the centrifuge tubes and discarded. Each cell pellet was resuspended in 500 µl of fresh medium and the resulting cell suspension was divided into two, 250 µl aliquots. One of the aliquots was pipetted into a pre-weighed ICP-MS tube and the other aliquot was saved for analysis by flow cytometry.

2.8. ICP-MS

ICP-MS analysis was performed as described elsewhere (Prasad et al., 2013). Briefly, the samples were digested in an HNO_3:HCl acid mixture (Daskalakis et al., 1997), sonicated, and cooled to room temperature. Following overnight heating in a 60 °C oven, samples were diluted in 0.4% HCl in milli-ultrapure water. Silver content was measured with Inductively Coupled Plasma–Mass Spectrometry (ICP-MS, Model ELAN6000, PerkinElmer, Shelton, CT) according to EPA Method 200.8rev5.4 (US-EPA, 1994).

2.9. Flow cytometry

A flow cytometer (S1000, Stratedigm, San Jose CA) containing a 100 mW 488 nm laser and a 100 mW 405 nm laser was used. The detection of the scatter intensity signals was measured with a forward scatter (FSC) diode detector, and the SSC photomultiplier tube (PMT) detector. Prior to each experiment, the instrument was checked for resolution and sensitivity with Duke 3.0 µm alignment beads (Shapiro, 2001; Zucker, 2008) and with Stratedigm QA beads to insure the machine alignment met specifications. The cytometer was set up to measure FSC and SSC logarithmically using 488 nm trigger laser and 405 nm laser for side scatter detection, as the shorter wavelength provided better resolution. A total of 5000 cells were counted for each sample. The data were analyzed using Stratedigm and FCS Express software. The photomultiplier tube voltage was optimized to use four decades of log amplifiers. Ranges for the maximum SSC signal and minimum FSC signal were set by running the highest dose of nanoparticles first, followed by the control cells. Values for the AgNP-treated cells were normalized to control and expressed as an increase relative to control.

3. Results

3.1. Characterizing nanoparticles and nanoparticle suspensions

The AgNP had a uniform size and spherical shape. Lot-specific TEM images of AgNP obtained from the supplier are presented in Supplemental Figs. S1 and S2.

The dispersions of AgNP in FBS-containing cell culture media were determined at 0 and 24 h after preparation of the suspensions using the Dynamic Light Scattering (DLS), which provided both a measure of hydrodynamic diameter and a poly-dispersion index (PDI), by Nanoparticle Tracking Analysis (NTA) (Table 1). There was little difference between time 0 and 24 h measurements within either DLS or NTA assessments, indicating that the AgNP suspensions in cell culture media were stable over the duration of the experiment. The hydrodymnamic diameters measured by DLS were larger than those measured by NTA, reflecting the different analytic approaches used by the two instruments, as discussed below.

The potential dissolution or agglomeration of AgNP was measured in cell culture media. The filtrates observed from the centrifugal ultrafiltration experiment were analyzed after acid digestion by ICP-OES; however, all data observed from media spiked with AgNP were below the method detection limit for silver (10 µg/L). After filtration of assay media spiked with $AgNO_3$, 91% of silver was recovered in the filtrates. These results suggest that there was little dissolution of AgNP into silver ions. In case of $AgNO_3$ prepared in deionized water, 100% of silver was recovered in the filtrates, suggesting that the presence of proteins altered the filtration process and bound what free silver ions existed, causing incomplete recovery of silver ions in the assay media.

To clarify the agglomeration behavior, AgNP were incubated in media over the experimental time course and analyzed using UV-Vis spectrophotometry. Although no loss in the distinctive yellow color of AgNP was observed in media by the end of the study, UV − Vis absorbance spectra showed changes that were in some cases indicative of particle agglomeration (Fig. 1). In the case of 20 nm AgNP upon addition of cell culture media, an immediate loss in absorbance at 400 nm was observed compared to AgNP in DI water. This change in plasmon resonance absorbance was followed by a slight broadening and less intense peak after 24 h. The loss of absorbance, broadening of the peak, and slight shift toward longer wavelengths were also accompanied by the appearance of an absorbance peak around 550 nm, all of which are indicative of particle agglomeration.

For the 75 nm AgNP in water or media at time zero and 24 h, the AgNP showed little change in the absorbance peak at about 440 nm. Nevertheless, the plasmon resonance absorbance peak shifted slightly toward the red after 24 h incubation in media, indicating only minor agglomeration of the large particles (Fig. 1).

Single particle ICP-MS analyses were performed on both 20 and 75 nm particles incubated in cell suspension media for 24 h. Assuming the spherical shape and knowing the molecular mass of Ag, the equivalent sphere diameter was calculated and compared with the TEM data provided by supplier. The size detection limit of the spICP-MS method for AgNP was determined to be 18 ± 5 nm. The data from the analysis of the 20 nm AgNP in cell media after 24 h incubation were fitted with the log normal function resulting in mean value of 51 nm (compared to the manufacturer TEM analysis, Supplemental Fig. S1, 19 nm) suggesting partial aggregation of the 20 nm nanoparticles after 24 h (Supplemental Fig. S4).

By contrast, the 75 nm AgNP in media for 24 h showed Gaussian

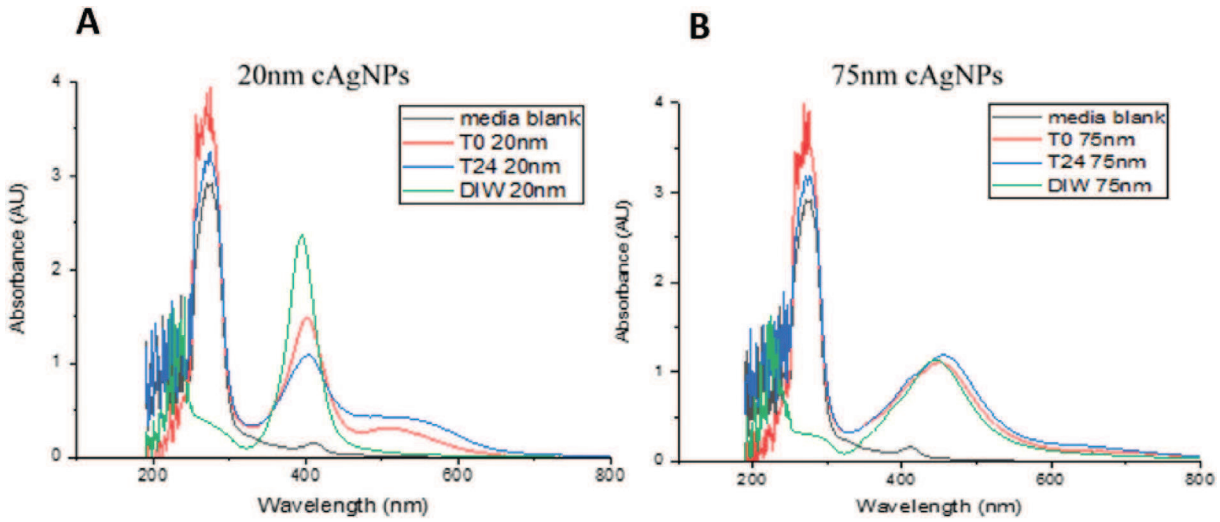

Fig. 1. UV-Vis absorbance of 20 nm (Panel A) or 75 nm (Panel B) AgNP. Data represent readings from the cell culture media blank (black), citrate-AgNP in media at time point 0 h (red) or 24 h (blue), or citrate-AgNP in deionized water at 0 h (green). The 20 nm signal showed a reduction in the 400 nm peak when moving from DI water to media, and between 0 and 24 h in media, indicating a reduction of individual particles in suspension. These was a simultaneous increase in surface plasmon resonance between 500 and 600 nm, which reflects an increase of agglomerated particles. The 75 nm signal, in contrast, was stable across media and over time, indicating a lack of agglomeration of the 75 nm particles. The stability of the 75 nm signal suggests that there was relatively little dissolution to silver ions over the 24 h period. (For interpretation of the references to color in this figure legend, the reader is referred to the web version of this article.)

distribution with a mean value of 67 nm (compared to the manufacturer TEM centered around 75 nm). The results suggested that the 75 nm AgNP showed little agglomeration.

3.2. Modeling AgNP deposition

The VCM-ISDD and DG models were used to predict particle sedimentation over time and estimate dose delivered to the cell layer following treatment with either 20 or 75 nm AgNP. The effective density of the agglomerates (ρev) in cell culture media measured by volumetric centrifugation for 20 nm AgNP was ρev = 2.41 g/cm^3, and for 75 nm AgNP was ρev = 3.45 g/cm^3. The percentage of particle deposition predicted by the VCM-ISDD and DG models for each population of agglomerated silver particles is presented in Fig. 2. Over 24 h, the VCM-ISDD model predicted the total deposition to the cellular layer of 26% of the applied does for 20 nm AgNP and nearly 100% of the applied dose for 75 nm AgNP. The DG model, assuming a non-sticky parameter, estimated 20% fraction deposited for 20 nm AgNP and 59% for 75 nm AgNP.

3.3. Measuring Ag mass deposition and distribution

The mass of silver was measured by ICP-MS in the cell layer, supernatant post trypsinization, cell media and washes of the cell layer 24 h after treatment with either 20 or 75 nm AgNP. Silver content in the media and cell layer are presented in Fig. 3. Silver was present in the spent treatment suspension, the cell pellet, and supernatant, but no silver was detected in the HBSS or media washes. The potential loss of particles to the flask walls was evaluated by calculating % recovery from the ICP-MS samples. Recovery of the applied dose of silver added to the flasks ranged from 94 to 99% for 20 nm AgNP, and 86–93% for 75 nm AgNP. By ICP-MS, the amount of silver in the cell pellet 24 h after treatment averaged 9% of applied dose for 20 nm AgNP and 35% of applied dose for 75 nm AgNP. As the supernatant reflected deposited but not internalized AgNP, the average total fraction deposited was 13% and 40% for 20 nm and 75 nm AgNP, respectively. In both cases, most of silver remained in the media 24 h after treatment, and the percentage of silver in the media was greater following 20 nm (88%) than 75 nm (60%) AgNP.

The fraction of silver deposited to the cell layer, estimated by the

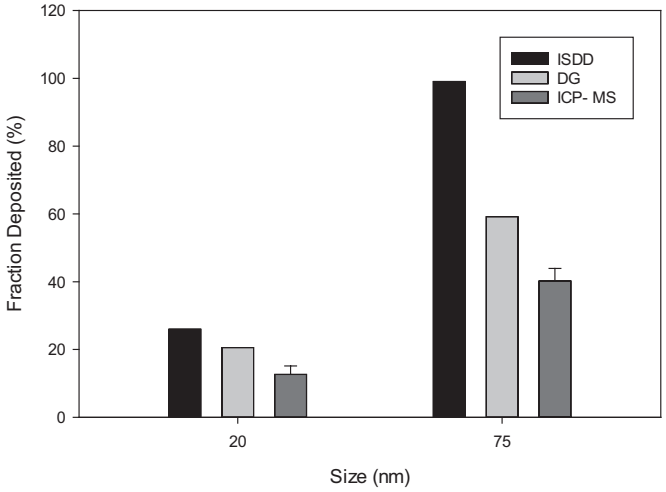

Fig. 2. Fractional deposition of Ag to the cellular layer 24 h after treatment with 20 or 75 nm AgNP. Deposition was measured by ICP-MS and modeled by both the ISDD and DG models. The quantity measured by ICP-MS was a sum of that measured in the cells and that measured in the supernatant from the cell layer sample, which represents Ag deposited to the bottom of the culture plate but not absorbed by the cells. The ICP-MS data reflect the mean (± SEM) of the three applied concentrations tested (3, 10 and 30 μg/ml). The deposition fraction estimated by both models did not vary by added initial concentration. Both models overestimated the proportion of silver deposited, but the DG model was a closer approximation of measured deposition than the ISDD model. Both models provided closer approximations of deposition for 20 than for 75 nm AgNP.

VCM-ISDD and DG models, was compared to the total measured fraction deposited (cell pellet and supernatant) by ICP-MS 24 h after exposure to 20 or 75 nm AgNP (Fig. 2). The fraction of silver deposited in the cell layer estimated by DG was 39% higher than the ICP-MS measured concentration of silver in the ARPE-19 cells for 20 nm AgNP, and estimated by VCM-ISDD was 52% more than the ICP-MS measured amount. For 75 nm AgNP both models overestimated the fraction deposited, by 32% in the case of DG and 59% for VCM-ISDD.

The amount of silver measured in the cell pellet by ICP-MS was used

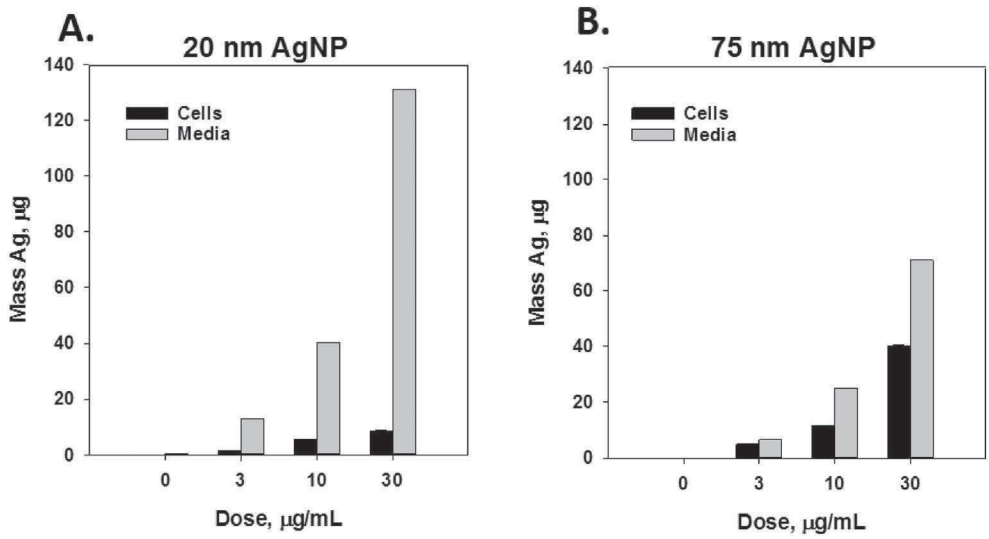

Fig. 3. Ag in cell layer and media measured by ICP-MS as a function of the concentration of either 20 nm (Panel A) or 75 nm AgNP (Panel B) applied to the cells. After 24 h, much of the silver mass remained in the media, and the amount depended on particle size. More of the silver remained in suspended in the media for 20 than 75 nm AgNP, Data are from one T-25 flask per dose. Standard deviation error bars from 6 replicate ICP-MS analyses are smaller than the plotted lines.

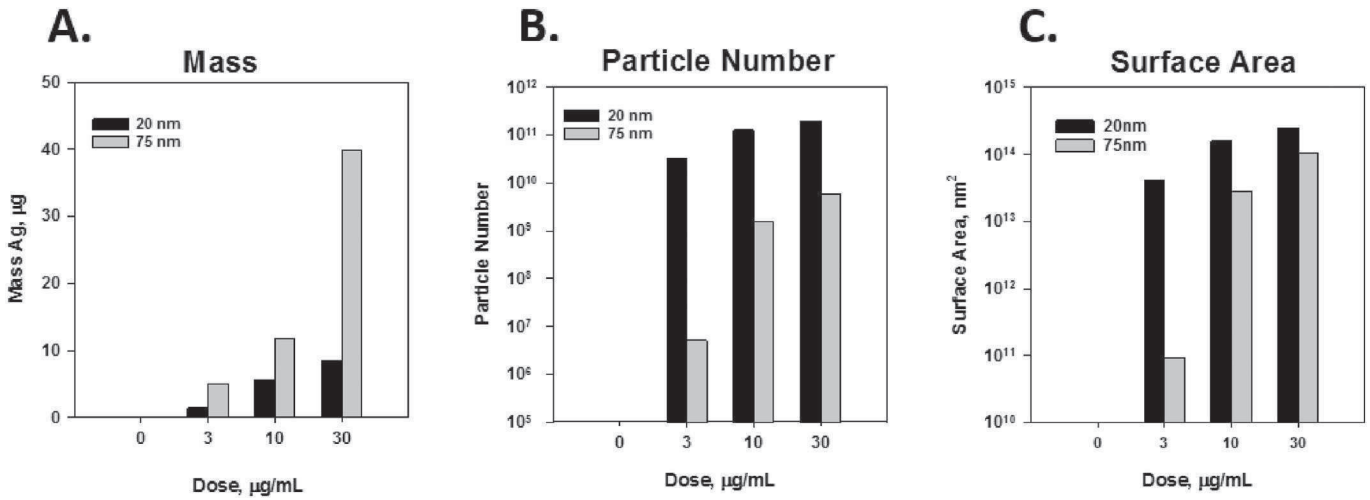

Fig. 4. Dose to the cell layer 24 h after treatment with either AgNP, where dose was expressed as mass (Panel A), particle number (Panel B), or surface area (Panel C). Smaller diameter particles have a higher surface area to mass ratio, and a higher particle number to mass ratio than larger particles. Different measures of dose can lead to opposite conclusions, when expressed as mass, the dose to the cells was higher for 75 and 20 nm AgNP, but the opposite was true for the other two measures of dose.

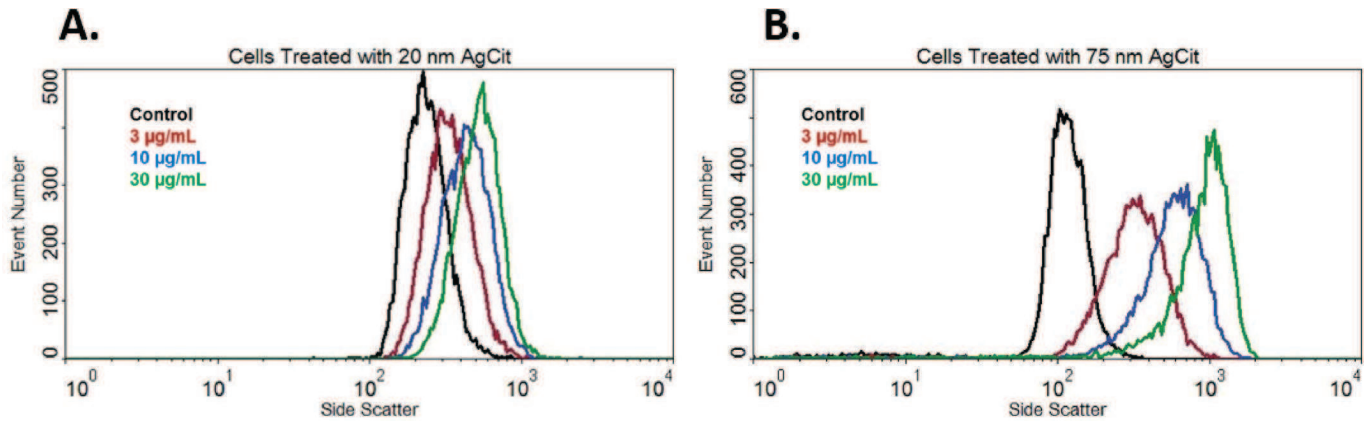

Fig. 5. Flow cytometry side scatter measured 24 h after treatment with either 20 (Panel A) or 75 nm AgNP (Panel B). The cells were counted in a Stratedigm flow cytometer measuring the forward scatter and side scatter cluster. The side scatter intensity signal was approximately proportional to the amount of Ag citrate that was applied to the cell cultures. The 75 nm particles scattered a greater amount of light than the 20 nm particles at all doses.

to calculate three internalized dose measures under the assumption that the particles were of uniform spherical shape and size. The dose measures included: silver mass expressed as μg, number of particles, and total surface area (nm^2) (Fig. 4). Expressing the dose to the cells in these three ways led to different conclusions. When measured as mass, the dose to the cells was higher following treatment with 75 nm than 20 nm AgNP. The reverse was true, however, with the other two measures. The comparable dose to cells was higher following 20 than 75 nm AgNP when expressed as either particle count or surface area.

3.4. Cytotoxicity

The toxicity of AgNP on ARPE-19 cells was studied through a live-dead stain assay (Sanders et al., 2012). There were no decreases in cell viability at dose levels below 55 μg/ml (Supplemental Fig. S5). These data assured that deposition and uptake measurements following dose levels at or below 30 μg/ml were not confounded by cytotoxicity.

3.5. Measuring AgNP cellular uptake

Side scatter (SSC) intensity was measured from ARPE-19 cells 24 h after treatment with 20 or 75 nm AgNP at 0, 3, 10 or 30 μg/ml. For both 20 and 75 nm AgNP, there was a dose-dependent increase in SSC intensity (Fig. 5). Cells treated with 75 nm NPs showed greater relative increase in SSC intensity than cells treated with the same applied dose of 20 nm AgNP.

The relative flow cytometry side scatter values of cells treated with 20 or 75 nm AgNP are plotted against the mass of silver measured by ICP-MS in split samples from the same batches of treated cells (Fig. 6). For both 20 and 75 nm AgNP, there was an approximately linear relationship between the mass of silver in the samples and the amount of side scatter light reflected from the cells in the samples. The slope of the relationships between silver mass and side scatter differed for the different particle sizes, consistent with the fact that larger sized particles reflect more light than smaller sized particles.

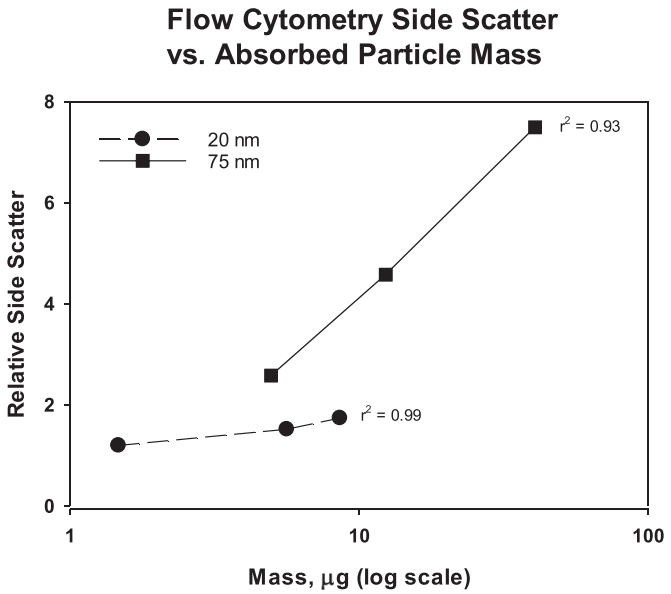

Fig. 6. Comparison of silver concentration in the cell layer as measured by ICP-MS and the relative side scatter signal from flow cytometry. Side scatter signal was linearly related to silver mass concentration in the cell layer, but the functions differed by particle size. Linear regressions equations (y = b[0] + b [1] x) were fit to data for 20 nm (b[0] = 1.04, b[1] = 0.08, r^2 = 0.99), and 75 nm (b[0] = 1.76, b[1] = 0.15, r^2 = 0.93).

4. Discussion

4.1. Major outcomes

The current experiments demonstrated that there was a substantial difference between the dose of nanoparticles added to an *in vitro* test system and the dose delivered to the cells. The results of the ICP-MS assay showed that the amount of silver taken up by the target cells 24 h after treatment differed considerably from the dose applied to the cell culture wells, and varied considerably based on particle size. As much as 87% of the silver applied to the culture as 20 nm AgNP remained suspended in the media 24 h after treatment. The discrepancy between applied and intracellular doses was less extreme for 75 nm AgNP, but still a substantial portion (~60%) of the applied dose remained in suspension at 24 h after treatment. This discrepancy between applied and delivered doses illustrates the peril of using applied concentration as the dose measure in *in vitro* nanotoxicology experiments.

To determine the dose of AgNP delivered to cells, several approaches were evaluated. First it was necessary to determine if the AgNP had dissolved to silver ions or remained in particle form. This was evaluated by filtration, UV-Vis and spICP-MS assays, all of which indicated that little dissolution occurred. Next it was necessary to assess the dispersion and agglomeration state of the particles in suspension using DLS and NTA assays. Both assays indicated formation of larger hydrodynamic structures, with the apparent agglomerate size being larger by DLS than NTA. Values of agglomeration diameter and density were used as input parameters to model deposition of AgNP to the bottom of the cell culture plates using two deposition models VCM-ISDD and DG. Those deposition results were compared to measurements of silver concentrations in the cell layer by ICP-MS. Finally, flow cytometry was used to confirm AgNP uptake in cells and calibrated against ICP-MS measurements of silver content in cells liberated from the cell layer. The deposition model results overestimated ICP-MS mass of intracellular silver but agreed reasonably with the summed intracellular and unadsorbed but deposited silver, revealing the importance of accounting for deposited but unabsorbed AgNP. Finally, flow cytometry SSC was linearly related to intracellular silver mass by ICP-MS and could be useful as an efficient surrogate measure for the absorbed cellular dose of nanoparticles.

4.2. Stability of particles

One possibility to account for the relatively large proportion of silver remaining in the media 24 h after treatment was that the AgNP dissolved into silver ions. Potential dissolution of AgNP over the course of 24 h in cell culture media was evaluated by filtration. Although silver nitrate solution readily passed the filter, no silver was detected in filtrate of AgNP suspensions, suggesting that little particle dissolution occurred. The data from both the UV-Vis and spICP-MS assays were also consistent with the continued presence of silver in the nanoparticle form after 24 h in media.

The state of particle agglomeration in cell culture media was evaluated by UV-Vis absorbance, and spICP-MS. The UV-Vis analysis indicated agglomeration of the 20 nm particles in cell culture media over 24 h but showed little evidence of agglomeration for 75 nm AgNP. The spICP-MS data suggested a primary particle size of 51 nm for the 20 nm AgNP and 67 nm for the 75 nm AgNP, which indicates that the 75 nm particles were primarily un-agglomerated. The spICP-MS results for 20 nm particles suggested agglomeration of the particles by 24 h to form clusters of approximately 50 nm in diameter.

Suspensions of AgNP in cell media that contain proteins typically result in the formation of a 'protein corona' which increases the AgNP hydrodynamic diameter. The DLS and NTA data indicated that both 20 and 75 nm particles in media formed structures with larger hydrodynamic diameters, however, notably different agglomerate sizes were reported by the two methods. The output of the DLS is based on an

intensity weighted distribution, meaning that smaller sized populations of agglomerate have the potential to be overlooked. This is especially the case if the most abundant population is significantly larger than any other. Agglomeration of particles to each other or to nanoscale proteins or micelles can result in poly-dispersed particle collections, especially for small (> 20 nm) particles. DLS provides a polydispersity index (PDI) with every sample. The PDI is a measure of the relative distribution of population sizes within a sample. A smaller PDI indicates a less diversely populated sample. While DLS calculations may overestimate the average particle hydrodynamic diameter in polydisperse suspensions due to the significantly greater scattering signal from larger particles, NTA reflects averages of individual particles in a sample rather than global average and is there for less prone to influence of large agglomerates.

4.3. Comparison of methods to measure dose

Clearly, procedures to determine cellular nanoparticle dose are desirable, but the determination of dose to cells is not straightforward. The dose of particles delivered to cells is affected by competing forces of diffusion and sedimentation, which differentially influence different particles. The rates of diffusion and sedimentation are a function of multiple factors including: particle size, agglomeration, density and charge, and media osmolarity, temperature and viscosity. Because expressing dose in nanotoxicology experiments as the applied concentration is inadequate, we compared experimental and modeling approaches to determine cellular dose.

The experimental approaches included ICP-MS and flow cytometry SSC. There is a dose-related increase in flow cytometry SSC after cells absorb light-reflective nanomaterials (Ha et al., 2018; Ibuki and Toyooka, 2012; Sanders et al., 2012; Suzuki et al., 2007; Toduka et al., 2012; Zucker et al., 2013; Zucker et al., 2010). Here we show that SSC was correlated with measurements of silver mass in the cellular layer determined by ICP-MS. Flow cytometry measures the relative amount of light reflected from cells and their intracellular constituents, the most relevant of which were intracellular particles of silver. Silver nanoparticles reflect light, where dissolved ionic silver does not, meaning that side scatter light is indicative of the particulate form of Ag in the cellular layer. The ICP-MS, in contrast, measured silver mass in cells, and did not distinguish silver ions from particles. Flow cytometry has an additional advantage of providing measurements from individual cells, enabling computation of uptake variation among cells and other population statistics if desired. The slope of the functions between SSC and silver mass was dependent on particle size, being greater for 75 than 20 nm AgNP, since larger sized particles reflect a greater amount of light than smaller particles. The 75 nm AgNP gave a larger signal than the 20 nm AgNP and had a better signal to noise ratio. Because the slopes differ by particle sizes, it would not be possible to compare internal cellular doses across different particle sizes directly using only SSC. Once calibrated for particle composition and size against ICP-MS, however, flow cytometry SSC could be an economical and rapid indicator of the number or mass of light-reflective particles taken up by cells.

Two modeling approaches to estimate dose delivered to cells were also evaluated: the VCM-ISDD and DG models (Cohen et al., 2014; DeLoid et al., 2015; Hinderliter et al., 2010; Teeguarden et al., 2007). These models were used instead of the ISD3 model because there was little evidence of AgNP dissolution in the current conditions, and the ISD3 model introduced complexities that were unnecessary where dissolution was not a significant factor (Thomas et al., 2018). Both the version of VCM-ISDD and the DG models used here featured agglomerate diameter measured by DLS and effective density measured by VCM as input parameters. VCM, while providing a simple, cheap, and accessible method for determining the agglomerate density, has a significant flaw. The method depends on precisely measuring the volume of a small pellet by eye with a sliding fine-scale ruler. A difference of a < 1 mm changed the density by > 5%, which in turn changed estimated deposition the VCM-ISDD model by 9% and the DG by 11% in the case of the 20 nm AgNP. Thus, there was a relatively high sensitivity of the deposition models to small measurement variations of VCM.

Particle deposition modeling should be evaluated against measurements in the system being used. In this case, deposition model results were compared against silver deposition measured by ICP-MS. There is an important distinction between delivered dose and intracellular dose. Silver was measured by ICP-MS in the media aspirated off the dosed cells, and after trypsinizing in the supernatant from the cells, and the cells themselves. The presence of silver in the supernatant fraction revealed that there was silver deposited onto the cell layer that was not taken up by the cells. Overall, both models reasonably predicted silver deposition to the cell layer, which was greater that the cellular dose of silver due to deposited, but unabsorbed, AgNP.

4.4. Dose metrics

Three dose metrics, based on mass, particle count and particle surface area were compared. Note that particle count and surface area were calculated based on ICP-MS measured mass in the cell fraction, the molecular weight of silver, and the volume and surface area of spheres the size of the particles. For simplicity, the calculation did not consider possible agglomeration. Unsurprisingly, the measurement metric of delivered dose was important. Comparing 20 and 75 nm AgNP, the larger particles deposited greater mass on cells, but fewer particles and a smaller surface area. The issue of which measure of dose is most predictive of nanomaterial toxicity has been debated previously, with a common conclusion that surface area is the preferred measure (Oberdörster, 2012). The data presented here (Fig. 4) reinforces how influential the measure of dose can be. Supposing that equivalent toxicity was observed following the same applied doses of 20 and 75 nm AgNP, if the dose was expressed as mass concentration, then the conclusion would be that 20 nm was more potent since the delivered dose was lower to produce the same toxic effect. On the other hand, if dose was expressed as either surface area or particle number, the conclusion would be that 75 nm AgNP was more potent since the number of particles and the surface area in the cells required to produce the effect was less. In most cases, it is observed that smaller particles are more toxic than larger particles when based on an applied dose mass concentration. This can be attributed to higher surface area of the smaller particles in the dose delivered to the cells, as shown in Fig. 4.

4.5. Use of in vitro models in risk assessment

Toxicity testing of newly developed engineered nanoparticles likely will rely on *in vitro* test systems as an early screening step in future tiered testing strategies. For those studies, the dose delivered to the target cells is an important consideration for interpreting the results of toxicity assays. Among the potential uses of *in vitro* nanotoxicity data are: ranking of relative potential hazards of different particles; prioritizing materials for further testing; informing structure activity relationships; performing read-across risk assessments; and facilitating the design of safer nanomaterials (Arts et al., 2015; Arts et al., 2014; Godwin et al., 2015; Oomen et al., 2014; Som et al., 2013; Stone et al., 2014). The goal of *in vitro* testing in all these strategies is to efficiently test potential toxicity. To make such determinations from *in vitro* data, an important consideration is relating any adverse effects observed to the dose of the material, and the dose delivered to the cells differed from the dose added to the system. The reliance on applied concentrations may substantially misrepresent the actual dose to the target cells and could cause misrepresentation of the relative hazards of differently sized materials.

Liu and coworkers compared relative toxicity rankings of seven uncapped metal oxide nanoparticles based on applied *vs.* deposited doses, and concluded that the relative toxicity rankings were not

altered substantially by expressing dose as delivered rather than applied (Liu et al., 2015). However, the seven metal oxide materials selected for analysis in that study deposited readily to the cell layer by the time of testing 24 h after treatment (Zhang et al., 2012). As noted by Liu et al., there was a high correlation between their applied and delivered doses, since almost all the applied material settled to the cellular layer by the time of testing. Therefore, the relative toxicity rankings did not differ greatly when based on two highly correlated measures of applied and delivered dose. The case presented here is different because a considerable portion of the applied silver, especially for the smaller 20 nm AgNP, remained suspended in the media 24 h after treatment. The differential amounts of settling between 20 and 75 nm AgNP led to proportional differences between applied and deposited doses. In a case where a significant portion of the applied dose never reached the target cells, expressing the dose as delivered dose is preferred.

4.6. Summary and conclusions

The accurate determination of dose-response relationships is fundamental to toxicological sciences, however, the dose of nanoparticles delivered to cells for *in vitro* testing can be very uncertain. It is important to independently determine the intracellular dose to target tissues for nanotoxicology experiments conducted *in vitro*, rather than rely on the concentration added to the system. Four alternative approaches to estimate delivered dose were compared for two different sizes of nanoparticles. The mass of silver in cells could be determined by ICP-MS, but not whether the Ag was in the form of particles or dissolved ions. Computational models predicted deposition of AgNP to the cell layer, but not cellular uptake. Light scatter from flow cytometry indicated the cellular uptake of nanoparticles, but not directly the mass. Flow cytometry SSC was correlated to ICP-MS mass, and could be calibrated against ICP-MS to indicate mass of cellular uptake. Flow cytometry was an inexpensive and fast method to determine in the number of particles absorbed. By accounting for deposited but not absorbed particles, and the influence of particle size on light scatter, it was possible to use SSC as an effective index of particles taken up into cells. While none of the examined approaches by itself provided an unambiguous determination of cellular AgNP dose, a combination of approaches could provide a means of establishing the amount and nature of particles absorbed by cells and would be preferred to the expression of nanotoxicology results as a function of applied concentrations.

Supplementary data to this article can be found online at https://doi.org/10.1016/j.impact.2019.100156.

Acknowledgments and declarations

The funding for this research was provided through the intermural research funds of the Office of Research and Development, U.S. Environmental Protection Agency. This research was supported in part by an appointment to the Research Participation Program for the U.S. Environmental Protection Agency, Office of Research and Development, administered by the Oak Ridge Institute for Science and Education through an interagency agreement between the U.S. Department of Energy and U.S. EPA. All of the authors have contributed substantially to the manuscript and consent to publication. The authors declare that they have no competing financial interests. The original data supporting this manuscript are available from the U.S. Environmental Protection Agency.

The authors thank Sarah Karafas for technical contributions. The authors also thank Justin Teeguarden, Philip Demokritou, Glen DeLoid, Joel Cohen, Sandra Pirela for providing code for the particle deposition models, training and consultation on how to use them. In addition, the authors thank Dr. James Harrington of RTI for generously providing access to spICP-MS instrumentation. The authors acknowledge Nanocomposix for providing the particle characterization data presented in Supplemental Figs. S1 and S2. The authors thank Dr. Tim Shafer and Dr. Michael Hughes for comments on a previous version of the manuscript.

References

Al-Abed, S.R., Virkutyte, J., Ortenzio, J.N.R., McCarrick, R.M., Degn, L.L., et al., 2016. Environmental aging alters Al(OH)3 coating of TiO2 nanoparticles enhancing their photocatalytic and phototoxic activities. Environ. Sci.: Nano 3, 593–601.

Andonova, V.Y., 2016. A new direction in ophthalmic development: nanoparticle drug delivery systems. Curr. Pharm. Des. 22, 6313–6329.

Arts JHE, Hadi M, Keene AM, Kreiling R, Lyon D, et al. 2014. A critical appraisal of existing concepts for the grouping of nanomaterials. Regul. Toxicol. Pharmacol. 70: 492–506.

Arts JHE, Hadi M, Irfan M-A, Keene AM, Kreiling R, et al. 2015. A decision-making framework for the grouping and testing of nanomaterials (DF4nanoGrouping). Regul. Toxicol. Pharmacol. 71: S1–S27.

Cohen, J., Deloid, G., Pyrgiotakis, G., Demokritou, P., 2013a. Interactions of engineered nanomaterials in physiological media and implications for in vitro dosimetry. Nanotoxicology 7, 417–431.

Cohen, Y., Rallo, R., Liu, R., Liu, H.H., 2013b. In silico analysis of nanomaterials hazard and risk. Acc. Chem. Res. 46, 802–812.

Cohen, J.M., Teeguarden, J.G., Demokritou, P., 2014. An integrated approach for the in vitro dosimetry of engineered nanomaterials. Part. Fibre Toxicol. 11, 20.

Cohen, J.M., DeLoid, G.M., Demokritou, P., 2015. A critical review of in vitro dosimetry for engineered nanomaterials. Nanomedicine (London) 10, 3015–3032.

Daskalakis, K.D., O'Connor, T.P., Crecelius, E.A., 1997. Evaluation of digestion procedures for determining silver in mussels and oysters. Environ. Sci. Technol. 31, 2303–2306.

Degueldre, C., Favarger, P.Y., 2003. Colloid analysis by single particle inductively coupled plasma-mass spectroscopy: a feasibility study. Colloids Surf. A Physicochem. Eng. Asp. 217, 137–142.

DeLoid, G., Cohen, J.M., Darrah, T., Derk, R., Rojanasakul, L., et al., 2014. Estimating the effective density of engineered nanomaterials for in vitro dosimetry. Nat. Commun. 5, 3514.

DeLoid GM, Cohen JM, Pyrgiotakis G, Pirela SV, Pal A, et al. 2015. Advanced computational modeling for in vitro nanomaterial dosimetry. Part. Fibre Toxicol. 12: 32.

Diebold, Y., Calonge, M., 2010. Applications of nanoparticles in ophthalmology. Prog. Retin. Eye Res. 29, 596–609.

Evans SJ, Clift MJ, Singh N, de Oliveira Mallia J, Burgum M, et al. 2017. Critical review of the current and future challenges associated with advanced in vitro systems towards the study of nanoparticle (secondary) genotoxicity. Mutagenesis 32: 233–41.

Farcal L, Torres Andon F, Di Cristo L, Rotoli BM, Bussolati O, et al. 2015. Comprehensive in vitro toxicity testing of a panel of representative oxide nanomaterials: first steps towards an intelligent testing strategy. PLoS One 10: e0127174.

Fox, D.A., Boyes, W.K., 2013. Toxic responses of the ocular and visual system. In: Klaassen, C.D. (Ed.), Casarett and Doull's Toxicology: The Basic Science of Poisons, Eighth edition. McGraw-Hill Medical Publishing Division, New York, pp. 767–798.

Godwin H, Nameth C, Avery D, Bergeson LL, Bernard D, et al. 2015. Nanomaterial categorization for assessing risk potential to facilitate regulatory decision-making. ACS Nano.

Ha MK, Shim YJ, Yoon TH. 2018. Effects of agglomeration on in vitro dosimetry and cellular association of silver nanoparticles. Environ. Sci.: Nano 5: 446–55.

Hansen, S.F., Heggelund, L.R., Revilla Besora, P., Mackevica, A., Boldrin, A., Baun, A., 2016. Nanoproducts - what is actually available to European consumers? Environ. Sci.: Nano 3, 169–180.

Hartung, T., Sabbioni, E., 2011. Alternative in vitro assays in nanomaterial toxicology. Wiley Interdiscip. Rev. Nanomed. Nanobiotechnol. 3, 545–573.

Hinderliter P, Minard K, Orr G, Chrisler W, Thrall B, et al. 2010. ISDD: a computational model of particle sedimentation, diffusion and target cell dosimetry for in vitro toxicity studies. Part. Fibre Toxicol. 7: 36.

Ibuki, Y., Toyooka, T., 2012. Nanoparticle uptake measured by flow cytometry. Methods Mol. Biol. 926, 157–166.

Liu R, Liu HH, Ji Z, Chang CH, Xia T, et al. 2015. Evaluation of toxicity ranking for metal oxide nanoparticles via an in vitro dosimetry model. ACS Nano 9: 9303–13.

NRC, 2007. Toxicity Testing in the 21st Century: A Vision and a Strategy. vol. 216 The National Academies Press, Washington, DC.

Oberdörster, G., 2012. Nanotoxicology: in vitro-in vivo dosimetry. Environ. Health Perspect. 120.

Oomen AG, Bos PMJ, Fernandes TF, Hund-Rinke K, Boraschi D, et al. 2014. Concern-driven integrated approaches to nanomaterial testing and assessment – report of the NanoSafety cluster working group 10. Nanotoxicology 8: 334–48.

PCAST, 2014. Report to the President and Congress on the Fifth Assessment of the National Nanotechnology Initiative. Ed. PsCoAoSa Technology, Washington, DC.

Prasad RY, McGee JK, Killius MG, Suarez DA, Blackman CF, et al. 2013. Investigating oxidative stress and inflammatory responses elicited by silver nanoparticles using high-throughput reporter genes in HepG2 cells: effect of size, surface coating, and intracellular uptake. Toxicol. in Vitro 27: 2013–21.

Rogers KR, Navratilova J, Stefaniak A, Bowers L, Knepp AK, et al. 2018. Characterization of engineered nanoparticles in commercially available spray disinfectant products advertised to contain colloidal silver. Sci. Total Environ. 619–620: 1375–84.

Salvati A, Nelissen I, Haase A, Åberg C, Moya S, et al. 2018. Quantitative measurement of nanoparticle uptake by flow cytometry illustrated by an interlaboratory comparison of the uptake of labelled polystyrene nanoparticles. NanoImpact 9: 42–50.

Sanders K, Degn LL, Mundy WR, Zucker RM, Dreher K, et al. 2012. In vitro Phototoxicity and Hazard identification of nano-scale titanium dioxide. Toxicol. Appl. Pharmacol.

258: 226–36.
Schmid, O., Cassee, F.R., 2017. On the pivotal role of dose for particle toxicology and risk assessment: exposure is a poor surrogate for delivered dose. Part. Fibre Toxicol. 14, 52.
Shapiro, H.M., 2001. Optical measurements in cytometry: light scattering, extinction, absorption, and fluorescence. Methods Cell Biol. 63, 107–129.
Som, C., Nowack, B., Krug, H.F., Wick, P., 2013. Toward the development of decision supporting tools that can be used for safe production and use of nanomaterials. Acc. Chem. Res. 46, 863–872.
Song KS, Sung JH, Ji JH, Lee JH, Lee JS, et al. 2013. Recovery from silver-nanoparticle-exposure-induced lung inflammation and lung function changes in Sprague Dawley rats. Nanotoxicology 7: 169–80.
Stone V, Pozzi-Mucelli S, Tran L, Aschberger K, Sabella S, et al. 2014. ITS-NANO–prioritising nanosafety research to develop a stakeholder driven intelligent testing strategy. Part. Fibre Toxicol. 11: 9.
Suzuki, H., Toyooka, T., Ibuki, Y., 2007. Simple and easy method to evaluate uptake potential of nanoparticles in mammalian cells using a flow cytometric light scatter analysis. Environ. Sci. Technol. 41, 3018–3024.
Teeguarden, J.G., Hinderliter, P.M., Orr, G., Thrall, B.D., Pounds, J.G., 2007. Particokinetics in vitro: dosimetry considerations for in vitro nanoparticle toxicity assessments. Toxicol. Sci. 95, 300–312.
Thomas, D.G., Smith, J.N., Thrall, B.D., Baer, D.R., Jolley, H., et al., 2018. ISD3: a particokinetic model for predicting the combined effects of particle sedimentation, diffusion and dissolution on cellular dosimetry for in vitro systems. Part. Fibre Toxicol. 15, 6.
Toduka, Y., Toyooka, T., Ibuki, Y., 2012. Flow cytometric evaluation of nanoparticles using side-scattered light and reactive oxygen species-mediated fluorescence–correlation with genotoxicity. Environ. Sci. Technol. 46, 7629–7636.
US-EPA, 1994. Method 200.8 revision 5.4: Determination of metals and trace elements in water and wastes by inductively coupled plasma - mass spectrometry. In: Methods for the Determination of Metals in Environmental Samples, Supplement I, . https://www.nemi.gov/apex/f?p=237:38:2584375861061420::::P38_METHOD_ID:46:EPA/600/R-94/111.
Vance ME, Kuiken T, Vejerano EP, McGinnis SP, Hochella MF, et al. 2015. Nanotechnology in the real world: redeveloping the nanomaterial consumer products inventory. Beilstein J. Nanotechnol. 6: 1769–80.
Zhang H, Ji Z, Xia T, Meng H, Low-Kam C, et al. 2012. Use of metal oxide nanoparticle band gap to develop a predictive paradigm for oxidative stress and acute pulmonary inflammation. ACS Nano 6: 4349–68.
Zucker, R.M., 2008. Flow cytometry quality Assurance in Volume Standardization in Fluorometry: State-of-the-art and future challenges. In: Rench-Genger, U. (Ed.), Methods and Applications of Fluorescence. Springer.
Zucker, R.M., Massaro, E.J., Sanders, K.M., Degn, L.L., Boyes, W.K., 2010. Detection of TiO2 nanoparticles in cells by flow cytometry. Cytometry A 77, 677–685.
Zucker, R.M., Daniel, K.M., Massaro, E.J., Karafas, S.J., Degn, L.L., Boyes, W.K., 2013. Detection of silver nanoparticles in cells by flow cytometry using light scatter and far-red fluorescence. Cytometry A 83, 962–972.

Cytometry
PART A
Journal of the International Society for Advancement of Cytometry

Characterization, Detection, and Counting of Metal Nanoparticles Using Flow Cytometry

Robert M. Zucker,[1]* Jayna N.R. Ortenzio,[2] William K. Boyes[1]

[1]U.S. Environmental Protection Agency, Office of Research and Development, National Health and Environmental Effects Research Laboratory, Toxicology Assessment Division (MD-B105-04), North Carolina 27711

[2]Oak Ridge Institute for Science and Education (ORISE) appointee at the National Health and Environmental Effects Research Laboratory, USEPA, RTP, North Carolina 27711

Received 31 October 2015; Revised 14 July 2015; Accepted 12 October 2015

Additional Supporting Information may be found in the online version of this article.

Correspondence to: Robert. M. Zucker, U.S. Environmental Protection Agency, Office of Research and Development, National Health and Environmental Effects Research Laboratory, Toxicology Assessment Division (MD-B105-04), NC 27711, USA. E-mail: zucker.robert@epa.gov

Published online 00 Month 2015 in Wiley Online Library (wileyonlinelibrary.com)

DOI: 10.1002/cyto.a.22793

© 2015 International Society for Advancement of Cytometry

Abstract

There is a need to accurately detect, characterize, and quantify nanoparticles in suspensions. This study helps to understand the complex interactions between similar types of nanoparticles. Before initiating a study of metal nanoparticles, five submicron PS beads with sizes between 200 nm and 1 μm were used to derive a reference scale that was useful in evaluating the flow cytometer for functionality, sensitivity, resolution, and reproducibility. Side scatter intensity (SSC) from metal nanoparticles was obtained simultaneously from 405 nm and 488 nm lasers. The 405 nm laser generally yielded histogram distributions with smaller CVs, less side scatter intensity, better separation indices between beads and decreased scatter differences between different sized particles compared with the 488 nm laser. Submicron particles must be diluted to 10^6 and 10^7 particles/mL before flow cytometer analysis to avoid coincidence counting artifacts. When particles were too concentrated the following occurred: swarm, electronic overload, coincidence counting, activation of doublet discrimination and rejection circuitry, increase of mean SSC histogram distributions, alterations of SSC and pulse width histogram shape, decrease and fluctuations in counting rate and decrease or elimination of particulate water noise and 1 μm reference bead. To insure that the concentrations were in the proper counting range, the nanoparticle samples were mixed with a known concentration of 1μm counting beads. Sequential dilutions of metal nanoparticles in a 1 μm counting bead suspension helped determine the diluted concentration needed for flow cytometer analysis. It was found that the original concentrated nanoparticle samples had to be diluted, between 1:10,000 and 1:100,000, before characterization by flow cytometry. The concentration of silver or gold nanoparticles in the undiluted sample were determined by comparing them with a known concentration (1.9×10^6 beads/mL) of 1 μm polystyrene reference beads. © 2015 International Society for Advancement of Cytometry

Key terms

flow cytometry; nanoparticles; submicron particles; swarm; silver nanoparticles; gold nanoparticles; gold; silver; TiO2; side scatter; forward scatter; fluorescence

METALLIC nanoparticles may become potential toxicants to animals or humans. Exposure to silver nanoparticles has been associated with inflammatory, oxidative, genotoxic, and cytotoxic consequences in in vivo and in vitro toxicity studies (1). There is concern that nanoparticle exposures may lead to pulmonary disease, cancer, or other human health disorders (2–5). In order to study the impact of nanoparticles on human health, it is important to develop new methods to quantify those particles in biological media, and to devise better laboratory test methods for understanding the dynamics of nanoparticles in suspension and toxicity of nanoparticles to cells (6–27).

Submicron particles are defined as particles with sizes below 1 μm in diameter, while nanoparticles are generally defined as particles that have a diameter between 1 and 100 nm in at least one dimension. Currently, a number of microscopic and biophysical techniques are used to characterize submicron and nanoparticles (21–47). Unfortunately, there is not a universal "gold" standard test that can be used to quantify and characterize submicron and nanoparticles in suspension. Thus, there is a

ISAC
International Society for Advancement of Cytometry

need to develop rapid, sensitive, and economical methods to detect, characterize, and quantify submicron and nanoparticles in suspensions, cells, and tissues (45–49). These new methods could be used initially in laboratory settings where the variables are easier to control

A number of investigators have proposed using flow cytometers for the detection, counting, and characterization of submicron particles derived from blood samples (5–27,46–49). However, there are numerous artifacts that occur in the analysis of these submicron particles that also exist when analyzing suspensions of engineered nanomaterials by flow cytometry. This manuscript incorporates the use of submicron polystyrene beads as standards and 1 μm counting beads as reference particles to study metal nanoparticles. This article investigates some of the problems that can occur in characterizing unknown populations of submicron particles or nanoparticles using a flow cytometer. If the flow cytometer is operated incorrectly it could generate artifacts that would ultimately lead to incorrect conclusions. Some of these factors that influence the data generation have been previously described by Nolan and Stoner (15), Robert and coworkers (6–10), Nolte-t' Hoen and coworkers (24–26), and others in their attempts to bring clarity and reproducibility when counting submicron particles (13–16,23–27,46–49). The generation of potential artifacts is complicated as different flow cytometers have unique configurations of hardware, electronics, and software which effect the data acquisition. The data obtained and the potential artifacts will not necessarily be identical on all machines. With this in mind, the following major items should be considered when using a flow cytometer to study submicron and nanoparticles: 1) detection range of PS particle sizes, 2) reference particles used for calibration, and 3) concentrations of submicron particles measured.

Detection Range of Particle Sizes

At the lower size limits of detection, it is often difficult to determine if the particles under consideration give a real signal or if the signal merely represents the system noise. If possible, it is advantageous to include channels lower than the smallest particle, as this separation of signal from background can serve as a check to ensure that the particle is, in fact, real and not noise. It is important to consider the detection size range, as it is not always possible to count very small particles on the same scale as larger particles due to electronic and log decade scale limitation. If reference beads are needed for counting, it is important to select a size of particle that can be displayed on the scale with the submicron particles that are being measured.

Reference Beads

The use of five PS submicron particles helped determine the optimal trigger and set up conditions. The side scatter intensity measurement is more sensitive than the forward scatter intensity, but the cytogram displays two scatter signals simultaneously serving as a reference pattern for the determination of machine functionality. Having one or two of the reference particles that are fluorescent can be helpful in locating the bead signals and ensuring that all the particles are detected with the trigger parameters that are used.

Concentrations of Submicron Particles Measured

When the concentration of sample particles is too high, coincident counts will occur, which will affect the accurate measurement of individual submicron particles in the sample (15–17,23). Particles that enter the flow cell at too high of a concentration will generate a flow cytometry artifact entitled "swarm" yielding false and misleading data. The nanoparticle sample concentration can be evaluated by making sequential dilutions that will reduce coincident counting. Sequential dilutions reduce the chance that multiple particles simultaneously enter the flow cell and lower particle concentrations permit the system's electronics to operate without activating the internal abort circuitry (15). Our improvement on this sequential dilution protocol was to use a known concentration (2×10^6) of 1 or 2 μm PS counting beads that was used for all sample dilutions. This particle dilution procedure permitted the determination of the original nanoparticle particle concentration and the concentrations of that were diluted into a range in which they could be measured without coincidence counting.

Materials and Methods

Flow Cytometry

A Stratedigm S1000 (San Jose, CA) flow cytometer containing two lasers (405 nm and 488 nm) was used. The flow cytometer was set up with a 488 nm excitation using a 50 mW 488 nm laser and with a 405 nm excitation using a 100 mW laser. A 405/10 nm band pass filter was used in place of the 445/60 to obtain 405 nm side scatter. The channel normally used for DAPI fluorescence (445/60) was fitted with a 405/10 nm band pass filter to obtain 405 nm side scatter). In the case of the Stratedigm instrument, SSC was a more sensitive signal than FSC. This flow cytometer system was operated by having 488 nm side scatter as the primary trigger. The 405 nm scatter measurement was obtained after the particles passed through the 488 nm laser and were detected with a 488 nm scatter trigger. The detection angles for the forward scatter (FSC) were between 1 and 8 degrees measured with a pin diode, while the side scatter (SSC) signal was obtained using a 40× lens with numerical aperture (NA) of 1.2. This configuration for FSC and SSC used quartz square flow cells similar to other flow cytometer analyzers. The analyzer instrument electronics necessitated that the first trigger be forward or side scatter derived from the 488 nm laser. A primary trigger with the 405 nm second laser path was not possible but a secondary trigger with a FSC particle or fluorescent parameter could be used for added gating.

The flow cytometer was configured to enhance the acquisition and counting of submicron particles by improving the sensitivity, detection, and electronics of the system. The unit contained a new generation of hybrid signal processing technology with a high signal-to-noise ratio, and high data acquisition speed. The doublet discrimination detection electronics helped to remove particles that simultaneously entered the flow cell during analysis. The specific architecture of the Stratedigm electronics responsible for the doublet discrimination is not available until the manufacturer receives the associated patents.

Some unique features of the Stratedigm flow cytometer included the following: 1) increased signal-to-noise ratio with doublet discrimination appropriate for small and large particles and 2) true pulse width histogram measurements and counting rates. The result of these electronic features was high sensitivity with low thresholding capabilities which were critical for dim signals and studying submicron particles. The pulse width parameter has not previously been used in many research studies but has been shown to be useful in cell cycle studies for removing G1 doublets from G2/M cells, and in some cases to detect high fluorescence objects located in a cell (50). In the current studies, pulse width was measured directly and not used as a calculated ratio between other signal parameters (i.e. area and height). Although the maximum event rate was approximately 10,000 counts/s with a 2 to 4% rejection rate, the samples in this study were measured at a count rate of approximately 6,000 counts/s to help reduce the possibility of doublets and particle rejection. The parameters of pulse width and counting rates were useful to monitor as the particles were counted. The barrier filters in the Stratedigm 1000 system were the following: 445/60, 530/30, 580/30, 615/30, 690/40, and 740 LP. A stable fluidic stream with either fast (60 μL/mL) and slow (25 μL/mL) flow rates was used with SSC as a primary trigger. The SSC dynamic range could measure 200 nm to 7 μm polystyrene beads with a PMT value of 31%. The ranges useful for smaller nanoparticles was approximately 150 nm to 1.5 μm with a PMT value set to 100%.

Flow Cytometry QA

This analyzer was checked daily for fluidic alignment using either Thermo Scientific 3 μm alignment beads (Cyto-Cal Multifluor plus Violet Intensity Calibrator, FC3MV) or the manufacturer recommended 3 μm Stratedigm QA alignment beads to help reduce the possibility of doublets. The system was extensively tested for the following by the manufactures QA procedures: fluidic flow, laser power, coefficient of variation (CV) in all of the PMTs and the system electronics. The CVs of the test beads were generally between 1 and 3% and did not change greatly between the two flow rates: slow (25 μL/min) and fast (60 μL/min). Both the CVs and mean values of the beads serve as a reference for machine functionality (32,51–55). The sensitivity of the machine was checked by measuring the means and standard deviations (SD) of the two smaller bead peaks (for example, 200 nm and 300 nm) using the following separation index (SI) formula:

$$SI = \frac{Mean_{200} - Mean_{300}}{SD_{200} + SD_{300}}$$

This parameter was similar to the Fisher's Discriminant Ratio (Rd) value measurement, which is a measure of the statistical separation between two populations using their means and standard deviations (51–53). The Rd has been previously described for flow and image cytometers (51–55).

Operation of the Flow Cytometer

In counting nanoparticles or submicron particles, it is critical to have low background and a relatively high particle concentration in order to separate the contribution of particle events from background. If the sheath fluid had too many background counts, it would influence the reference bead signature and the absolute count of beads and nanoparticles. To reduce background, the sheath tank contained 0.1% sodium azide (diluted from 5% (w/v): catalog# 7144.8–16, Ricca Chemical Co, Arlington, TX). Deionized or distilled filtered water (0.1 μm) was used to reduce background particle noise. Before the use of the flow cytometer the sheath was replaced with distilled and deionized water that was freshly filtered (0.1 μm) using a Minntech 0.05 fiber flow filter (cat L1-050-A). The machine was then run for a 1 to 3 h with filtered water to ensure the count rate was below 100 counts/s at a slow flow rate of approximately 25 μL/min. The background count was in the range of 100 events/s at the settings that were used to measure 200 to 1,000 nm PS reference beads.

Establishing a Polystyrene Bead Reference Scale

Before using a flow cytometer for submicron particle counting, the limits of size detection on the lower and upper end of the PMT scale were established. A relative size scale using nonfluorescent polystyrene beads of different submicron sizes was made to characterize the number and size of submicron particles. The following National Institute of Standards and Technology (NIST) beads obtained from Thermo Scientific were used: [200 nm (3200A) 300 nm (3300A), 500 nm (3500A), 800 nm (3800A), and 1 μm (4010A); Thermo Scientific, Richmond, CA]. Approximately 0.25 μL of this cocktail was added to 2 mL of water to yield a count of between 2,000 and 6,000 events/s on the flow cytometer at a slow flow rate (25 μL/min). A fresh dilution of the submicron bead cocktail was prepared daily. Storing the beads as concentrated suspensions limited possible clumping, bacterial growth, and changes in bead characteristics that might result from prolonged storage in a diluted state.

To check the dynamic range of the SSC PMT, beads in the micron range were used. These included the following: 1 μm (4010A), 2 μm (4202A), 3 μm (4203A), 5 μm (4205A), and 7 μm (4207A) beads (Thermo Scientific). After modifications to the machine electronics, the flow cytometer could detect beads that ranged between 200 nm and 7 μm by side scatter on the same PMT scale using approximately 3.5 decades of useful dynamic range. To increase the size detection range, the PMT SSC was increased to maximum (100%) value. This yielded an equivalent bead range from approximately 150 nm to 1.5 μm. It was found that when a FSC PMT was used in place of the FSC diode the system will partially resolve the 200 nm and 300 nm bead populations (personal communication Dr. Mike Mooberry, UNC).

Concentration of Nanoparticles

A combination of different measurable parameters was used to help evaluate the counting process which included: counting rate, pulse width histogram, and SSC height intensity histogram, counting rate, and noise suppression. It was important to determine that the particle suspensions were at the right concentration during measurement. All the particle samples were diluted to concentrations between 1,000 and 6,000 events/s as determined by the event count meter built

into the software. This concentration of particles was in the range between 10^6 and 10^7 counts per mL. If the count exceeded the 10,000 counts per second, the count meter needle was at a maximum value suggesting coincidence counting was occurring. If the concentration of particles greatly exceeded 10^7 particles/mL, the observed count rate was actually reduced due to activation of the electronic circuitry to eliminate doublet counting resulting in the machine spending too much of the time in a noncounting mode and rejecting many of the events that were deemed doublets by the software. The result was a machine that yielded fewer counts/s in a concentrated sample than when counting a diluted sample.

If the count was too low, the system noise and solution noise from the sheath fluid could interfere with counting. Under high particle concentration counting conditions, the particles in the sheath and sample were actually reduced, yielding a cytogram size distribution with minimal noise.

The following three steps were taken to ensure the particles did not saturate the electronics of the flow cytometer: 1) a number of sequential 5 to 10-fold dilutions with water were made, 2) if increasing the side scatter threshold increased the count instead of decreasing the count, it would imply that the sample was too concentrated and should be diluted. Similarly, if reducing the threshold decreased the sample counts/s, it would imply that the sample was too concentrated and the sample should be diluted, 3) an aliquot of 2 μm Thermo Scientific beads (5×10^8 beads/mL, Product #4k-02, lot # 41429) was diluted 1:100 (500 μL in 49.5 mL of filtered H_2O to make a 5×10^6 beads/mL) and this suspension was used as the diluent for the concentrated silver samples. If necessary, a concentrated sample of 1 μm Thermo Scientific beads (Thermo Scientific 4010A) can be mixed with the known diluted 2 μm concentrated sample to derive a known concentration of 1 μm beads that can then be used as the media to dilute the nanoparticles. The ratio of beads to nanoparticles in the display was a quick test to determine if the dilution was in the correct range.

Counting Beads

A mixture of 1 or 2 μm beads was made that resulted in approximately 1,000 counts/s of beads. This solution served as a reference for determining the proper measurement conditions to count Ag nanoparticles. The concentrations of 2 μm counting beads from Thermo scientific were checked using a Stratedigm flow cytometer with an automatic sample handler that monitored the volume of liquid that passed the flow illumination points. It was found that the count was within 2% of the Thermo Scientific bead reported values. The concentration of the 1 or 2 μm PS bead solution used to dilute the metal nanoparticles should be approximately 2 to 5×10^6 beads per mL. If 2 μm sized counting beads were too large to simultaneously observe the nanoparticles and counting beads on the same relative PMT scale, then a smaller 1 μm counting bead was used in place of the 2 μm bead as a reference particle. The 1 μm PS bead (Thermo Scientific 4010A) was diluted to concentration that would also yield about 1,000 counts/s without Ag and Au nanoparticles being present. The concentration of the 1 μm bead suspension was determined by mixing it with 2 μm counting beads (5×10^6) and then comparing the percentages of the two beads in the SSC intensity histograms. The SSC intensity and pulse width histogram showed two district peaks representing beads and nanoparticles. When the nanoparticle sample was at a desired counting concentration, there were approximately equal heights of 1 to 2 μm counting reference beads and unknown nanoparticle samples in the SSC histograms. This resulted in about six to eightfold more nanoparticles than reference beads that were counted. A complete list of the beads and nanoparticles used in these experiments are shown in Supporting Information Tables 2, 7A and 7B.

Metal (Ag and Au) Nanoparticles

BioPure Silver (Ag) Nanoparticles with a polyvinylpyrrolidone (PVP) coating were obtained from NanoComposix (San Diego, CA) in diameters of 50 nm, 60 nm, 75 nm, 80 nm, 100 nm, and 110 nm. Bio Pure Gold (Au) nanoparticles with a PVP coating were obtained from NanoComposix (San Diego, CA) in diameters of 60 nm, 80 nm, and 100 nm polyvinylpyrrolidone is a polymer that binds strongly to the silver nanoparticle surface. Different sizes (40 nm, 60 nm, 80 nm, and 100 nm) and coatings of silver and gold nanoparticles were obtained from another manufacturer, Ted Pella (abbreviated TED; Ted Pella, Redding, CA). Econix (PVP-coated Ag NP) and the Lipoic acid capped Ag nanoparticles were also compared with the BioPure PVP Ag. Silica particles were obtained from Spherotech in sizes of 600 nm and 1.2 μm. The particles used in this study are listed in Supporting Information Table 7A-7B.

TiO_2 Nanoparticles Suspension, and Treatment

Five different types of TiO_2 primary particles (10 nm, 25 nm, 32 nm, 200 nm, and 200–400 nm) were obtained including: 10 nm anatase (catalog # 39953, Alfa Aesar, Wardfill, MA), 25 nm anatase/rutile (Aeroxide® TiO_2 P25, Degussa, Alpharetta, GA), 32 nm anatase (catalog # 4469059 nm), anatase/rutile, 30–40 nm NanoAmor, (catalog # 5485HT, Houston, TX), 200 nm anatase (catalog # 21358; Acros, Morris Plains, NJ), and 200–400 nm rutile (catalog # MKN-TiO_2-R250, Mknano, Mississauga, Ontario, Canada). Nanoparticles were added to water and sonicated for 1 h. After sonication, the particles were analyzed either in water or tissue culture media (3,22). Only the 200 nm and 200 to 400 nm TiO_2 particles yielded distinct scatter populations distinguishable from the water noise of the system.

Results

Establishing a Polystyrene (PS) Bead Reference Scale

A cocktail of five submicron nonfluorescent PS beads diluted to approximately 20% served as a relative reference scale for subsequent nanoparticle measurements and to monitor daily reproducibility of flow cytometry to detect submicron events. Figure 1 shows the SSC intensity histogram and SSC versus FSC cytogram pattern of the five different sized nonfluorescent beads (200 nm, 300 nm, 500 nm, 800 nm, and 1,000 nm beads) that comprised the reference bead cocktail. The data are displayed in both cytogram contour plot (Fig. 1A, FSC vs. SSC) and a SSC intensity histogram (Fig. 1B).

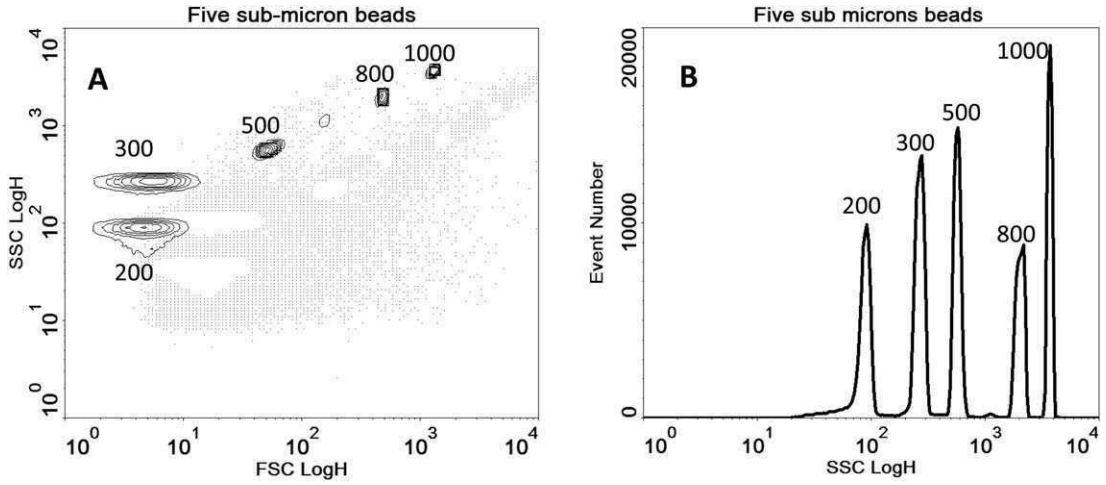

Figure 1. Reference scale of NIST PS submicron beads. A mixture of five different PS beads (sizes: 200, 300, 500, 800, and 1,000 nm) is shown occupying the second, third, and fourth log decades in cytogram (**A**) and histogram (**B**). Beads that are displayed with histograms and cytograms formats generate a useful reference display patterns that helps determine the detection limits of the flow cytometer. The 200 nm and 300 nm beads cannot be resolved by FSC (A) in the cytogram, but can be resolved by SSC (histogram, B). The PS bead means, SI and CV values are shown in Supporting Information Table 1. The concentration of bead particles was approximately 10^7 and the counting rate was <6,000 counts a second at a flow rater of 25 μL/min. The first decade represents dead channels that are used for the SSC trigger and setting the equipment threshold levels.

Both of these display formats were useful to rapidly observe system performance. The SSC intensity histograms show mean positions, percentages of each population, and population CVs, while the cytograms show the position of the bead clusters and the particle noise in the system. Increasing the PMT amplification to maximum (100% value) allowed the 200 nm beads to be placed at channel 84 with the lowest nanoparticle sizes being detected between channels 10 and 80. The amount of side scatter intensity measurements derived from the individual bead populations was nonlinear across the 488 nm log scale (Fig. 1B).

The five bead cocktail was made by mixing the same percentage of five different sized beads together (each approximately 20%) to generate a SSC histogram distribution of the five bead populations with approximately the same peak heights (percentage values shown in Supporting Information Table 1). When each of the five bead populations had approximately the same 20% of the total and were at the same height in the histogram it facilitated evaluating the machine's ability to count small-sized and large-sized beads simultaneously at the chosen specific PMT values. The bead percentages do not always add up to 100% as there was some particle noise counts located between the five peaks.

The Stratedigm flow cytometer measures four decades of data with all the parameters and about three decades if the SSC is used to trigger the events. The Stratedigm machine has a micro particle circuitry that permitted simultaneous evaluation of 200 nm and 5 μm PS beads on the same SSC PMT dynamic scale using a PMT setting of 31% and approximately three decades of log amplification. In order to measure the smallest nanoparticles or submicron particles, the SSC PMT was set at a value of 100% which placed the 1 μm bead in the middle of the fourth decade (Fig. 1, approximately channel 3,500) and the 200 nm in the second decade (mean at channel 89, Supporting Information Table 1). The appearance of some noise events using debris and particles in the sheath and samples that are located below the lowest bead size (200 nm in these studies) helps to determine the lower range of particle sizes that can effectively be detected. The addition of a 140 nm bead to the cocktail of five beads population helped to determine the lower level of detection and system sensitivity. As seen in Supporting Information Figure 2, there is a separation between the 140 nm and 200 nm suggesting the system measured events below the 200 nm bead size range. However, since there did not appear to be any counts below the 140 nm peak with these settings, the limit of detection with this flow cytometry system was approximately 140 nm. There appeared to be some system noise or submicron particle noise mixed in with the 140 nm population (Supporting Information Fig. 2). The separation index between the 140 nm and the 200 nm bead was 4.7 for 488 nm and 3.9 for the 405 nm excitation suggesting that the system was slightly more sensitive using the 488 nm laser line excitation.

Two types of bead relative reference scales were used in these studies. For a large dynamic range scale the PMT was adjusted to 31% that measured PS bead sizes between slightly below 200 nm to 5 μm. Alternatively adjusting the PMT value to 100% allowed the smallest submicron particles to be detected with a range between 140 nm and around 1.5 μm (Figs. 1 and 5 and Supporting Information Fig. 2). When the PMT voltage value was set at 100%, the 200 nm bead population was placed at a channel value of 89 (second decade) and the 1,000 nm bead population had a mean channel value of 3,545 (fourth decade) (Figs. 1 and 5 and Supporting Information Table 1).

405 nm SSC Versus 488 nm SSC

It has been suggested that better resolution for submicron particles will be obtained by using 405 nm SSC intensity instead of using 488 nm SSC intensity. The SSC intensity comparison of the means and CVs of the five bead populations derived with 488 nm (50 mW) and 405 nm (100 mW) excitation are shown in Supporting Information Figure 1 and the corresponding Supporting Information Table 1. The relative channel position of the SCC intensity derived from the beads and the separation of the peaks between different beads were dependent on the excitation wavelength (488 nm vs.405 nm, shown in Supporting Information Fig. 1 and Supporting Information Table 1). The CVs of the PS beads derived from the 405 nm laser were generally smaller compared with those derived from the 488 nm laser (Fig. 1, Supporting Information Fig. 1 and Supporting Information Table 1). However, the mean channel separation between different sized beads was greater with the 488 nm laser compared with that of the 405 nm laser, suggesting that there was more scatter intensity with the 488 nm laser. The separation index (SI) between the 200 nm and 300 nm (a measuring system for sensitivity) was 9.9 for the 405 nm laser and 5.4 for the 488 nm laser suggesting that the 405 nm had better sensitivity (Supporting Information Fig. 1 and Supporting Information Table 1). The SI values between adjacent beads are shown in Supporting Information Table 1. In summary, the histogram SSC intensity distributions showed higher peaks and narrower CVs for the PS beads using the 405 nm laser compared with the 488 nm laser (Supporting Information Fig. 1 and Supporting Information Table 1). Although the 405 nm laser yielded better histogram CVs (less value), the scatter intensity between the micron sized beads was noticeably less with 405 nm compared with the 488 nm laser. This effect is shown with the 500 nm, 800 nm and 1um nanoparticles where the distance between the particles is greater in 488 nm excitation compared with 405 excitation. The effect is more pronounced with 3 and 5 μm particles (data not shown).

Measuring Metal Nanoparticles

The SSC histogram distributions of 60 nm, 80 nm, and 100 nm sized Ag PVP and Au PVP coated nanoparticles and five-peak submicron polystyrene beads are shown in Figure 2. The corresponding histogram distributions from the 405 nm excitation are shown in Supporting Information Figure 3. The SSC intensity of different sized Ag and Au nanoparticles increased as the TEM-designated physical size increased (Fig. 2D). The relationship between Ag, Au, and five different sized PS beads shown in panels A, B, and C are displayed in Figure 2D. As a relative size reference, a submicron PS bead reference scale derived from the mixture of the five beads shown in Figure 1 is displayed as a less intense gray light background for the nanoparticles histograms in Figure 2 (488 nm scatter) and Supporting Information Figure 3 (405 nm scatter). These PS beads represent a relative reference scale that can be used to quickly compare the SSC intensity from different sized metal (Ag and Au) nanoparticles and other particles (i.e. silica) to a relative PS intensity reference. The corresponding mean and CV numerical values from the 405 nm and 488 nm excitation of Ag PVP and Au PVP coated nanoparticles is shown in Supporting Information Table 2.

The silver particles were generally monodispersed with CVs becoming narrower as the nanoparticle size increased (Fig. 2A). In contrast, the gold nanoparticles showed a bimodal distribution for the 80 nm and 100 nm particles, and a monodispersed peak for the 60 nm particle (Fig. 2B). The gold histogram CVs became larger as the population size increased; presumably due to the presence of a bimodal peak which increased in size with the 100 nm nanoparticles compared with 80 nm and 60 nm Au nanoparticles. The monodispersed population of 60 nm gold may suggests that the entire bimodal population was not detected due to their small size, or alternatively that the interaction of the laser beam with the smaller 60 nm particle was different than the larger sized 80 nm and 100 nm gold nanoparticles. A small part of the 60 nm silver histogram distribution and a larger part of the 60 to 80 nm gold NP were located in channels below the mean SSC intensity peak of the 200 nm bead (mean channel 89). From the histogram data displayed in Figure 2 for the metal nanoparticles, it was not clear if the entire population of 60 nm and 80 nm gold particles were captured because the means of the 60 nm and 80 nm gold nanoparticles were below the mean of 200 nm reference PS bead. The lowest detection channels of the 60 nm gold approached the lower SSC detection channels and threshold detection limit of the flow cytometer with the current settings (SSC PMT 100%). When the Stratedigm engineers increased the PMT electronic amplification voltage scale in demo mode, it showed that the 60 nm gold peak was actually a bimodal distribution. The smaller intensity values of 60 nm Au are not being displayed when the PMT is set to 100% in a commercial machine.

In contrast to Au nanoparticles, the relative histogram size changes observed between 60 nm and 100 nm Ag nanoparticles were greater with the 488 nm excitation in Figure 2 (488 nm) compared with 405 nm excitation (Supporting Information Fig. 3; 405 nm). In contrast to Ag, the Au histogram distributions derived from the 405 nm laser were similar in size and shape to those derived from the 488 nm laser. This difference between Au and Ag nanoparticle histograms was presumably due to unique interactions and wavelength absorption between these metal nanoparticles with different excitation laser light wavelengths

Counting Nanoparticles

In order to measure nanoparticles on a flow cytometer two requirements must be met: 1) correct concentration and 2) be large enough in size to scatter a sufficient amount of light for detection. For the flow cytometry system to handle the electronic pulses correctly, the concentration should be in the range of approximately 10^6 and 10^7 particles/mL. To eliminate the potential of fluidic "swarm" effects that can occur with high sample concentrations, the samples were sequentially diluted to a concentration that ranged between 10^6 and 10^7 counts per sec (15–17,23). In addition to using sequential dilutions, different cytometric observations helped to determine the proper

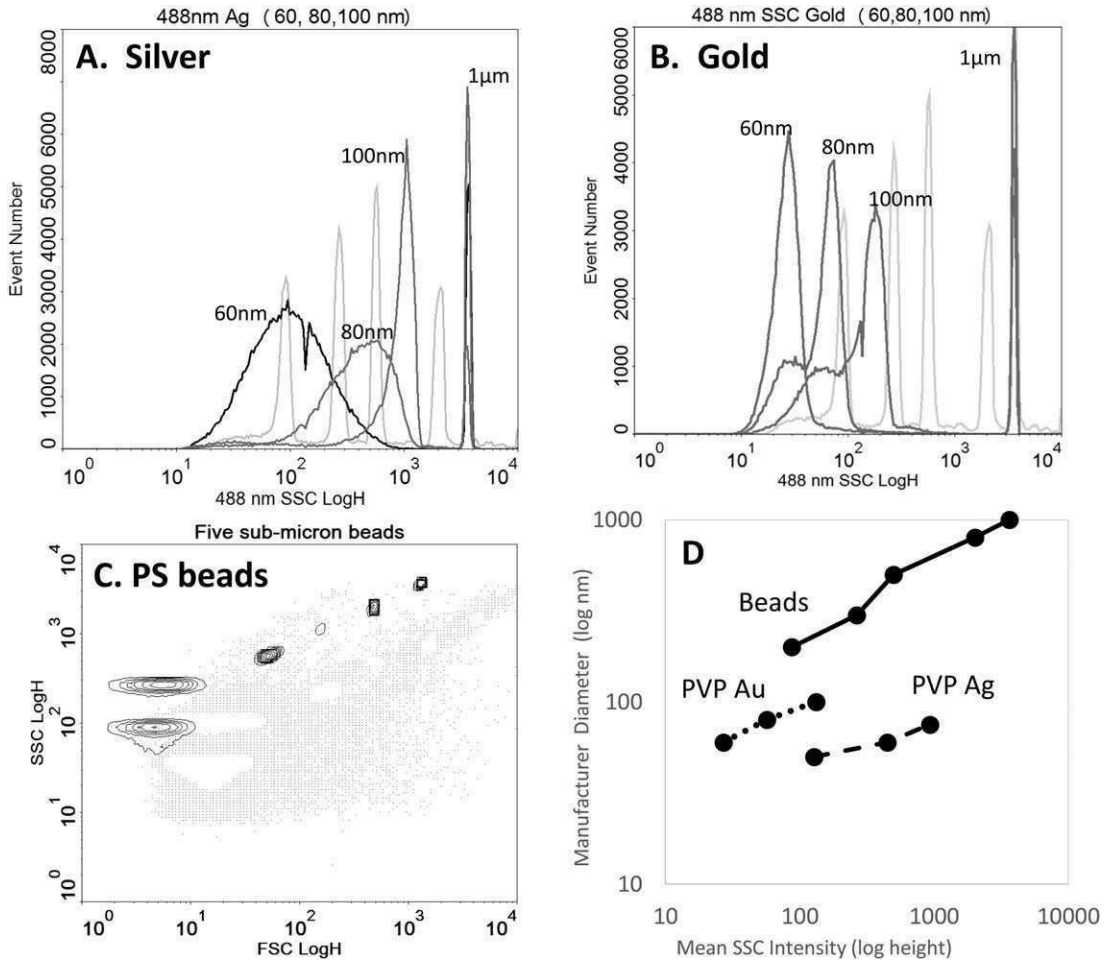

Figure 2. Comparison of SSC from 488 nm excitation of silver and gold nanoparticles (60 nm 80 nm and 100 nm). The 488 nm side scatter of 60 nm, 80 nm, and 100 nm PVP-coated silver (**A**) and PVP-coated gold (**B**) nanoparticles were each measured simultaneously with 1 μm PS counting beads. The five reference beads are displayed in a cytogram of FSC versus SSC, (**C**) and in the background of histograms A and B. The comparison between the observed mean SSC intensity from the Au, Ag and PS beads (*x*-axis) versus the manufactured designated sizes (*y*-axis). (**D**) The mode of 60 nm Ag is located at the same peak channels as the 200 nm bead, while the mode of the 60 nm and 80 nm Au NP are located below the 200 nm bead. The concentration of all nanoparticles particles measured was approximately 10^7 particles per mL. They were calculated to be the following: 60 nm Ag, 13.8×10^6; 80 nm Ag, 25.2×10^6; 100 nm Ag, 7.5×10^6; 60 nm Au, 7.6×10^6; 80 nm Au, 12.2×10^6; 100 nm Au, 14.8×10^6; and PS bead mix, 7.2×10^6.

nanoparticle concentration of the sample. These parameters included the width and SSC shape histogram distributions and SSC mean population size increases. However, the easiest parameter to use to insure the proper sample concentration for analysis was sequential dilutions of the nanoparticles with a known concentration of 1 μm or 2 μm non fluorescent PS counting beads. These beads served as a quick reference to dilute the Ag or Au nanoparticle samples to a suitable concentration without coin incidence artifacts for counting. Data using these 1 μm reference particles is shown throughout this article (Figs. 2–4 and Supporting Information Figs. 3–6 and Supporting Information Tables 3–5). This dilution procedure yielded SSC intensity and width histograms that consisted of beads and nanoparticles at approximately the same peak height when the dilution was approximately 10^7 particles/mL. This ensured that the metal nanoparticles were counted as an individual particles.

Counting and Determining the Concentration of Nanoparticles

Adjustment of the nanoparticles to the correct concentration for analysis was made by sequential dilutions using a suspension of 1 μm PS beads (2×10^6 beads/mL) as the diluent instead of using filtered water (illustrated in Figs. 3 and 4 and Supporting Information Figs. 4–6 and Supporting Information Tables 3–5). By using 1 or 2 μm beads (2 to 5×10^6 beads/mL) as the diluting medium, it ensured that each unknown dilution of the nanoparticles had the same quantity of 1 or 2 μm reference beads. After the nanoparticle samples were sufficiently diluted, the amount of the beads counted would be equivalent to the bead sample without nanoparticles present. If the electronic abort circuitry is activated, or if simultaneous counting of particles occurs, the result would be a reduction in the count of 1–2 μm reference beads, nanoparticles, water debris and system noise that was measured.

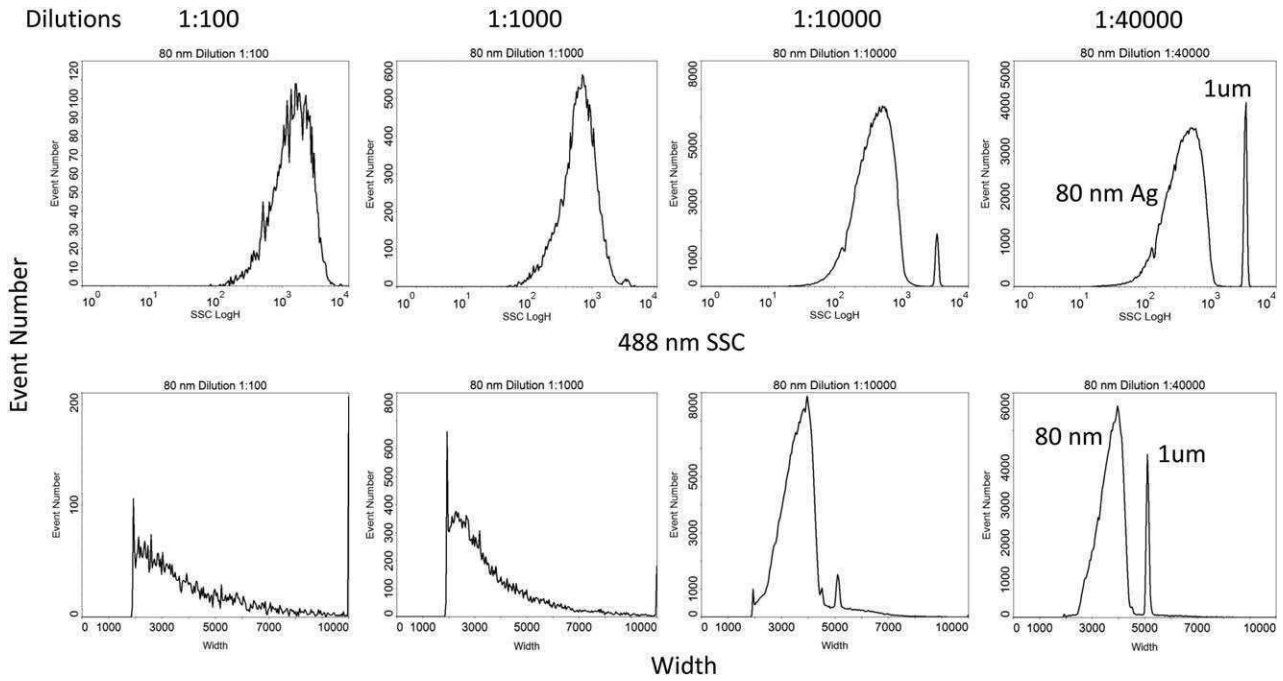

Figure 3. Sequential dilution of 80 nm Ag nanoparticles with 1 μm PS beads. Sequential dilutions of concentrated 80 nm Ag nanoparticles (3.6×10^{11}) were made with a diluent that contained 1 μm beads (1.9×10^6 beads/mL). The dilutions of 1:100, 1:1,000, 1:10,000 and 1:40,000 are displayed in the four horizontal histogram panels representing 488 nm SSC intensity (top) and pulse width (bottom). The histograms representing 10,000 and 40,000 dilutions show the 1 μm PS bead and the 80 nm Ag nanoparticles. The first two panels (1:100 and 1:1,000) show a SSC intensity histogram distribution that has a mean size that is larger than the mean size of populations with dilutions of 10,000 or 40,000. The pulse width histogram distribution does not show a Gaussian histogram of particles or beads below 10,000 counts, but does show the PS beads and a Gaussian distribution for Ag nanoparticles above 10,000 fold dilution. The mixture was counted for 30 s at a slow flow rate (25 μL/min).

These experiments were carried out by initially counting the background, and then counting a 1 or 2 μm bead dilution (2 to 5 $\times 10^6$ beads/sec) for a fixed time period (30 s) with the total number of beads and noise particles recorded. The beads had a count rate of approximately 1,000/s and the particle water noise had a count rate at approximately 100/s. The Ag sample was then sequentially diluted with a 1 μm bead diluent solution. This sequential dilutions resulted in a decrease in the Ag nanoparticles (Figs. 3 and 4, Supporting Information Figs. 4–6, Supporting Information Tables 3–5), and a subsequent increase in the bead count. When the concentration of the beads in the diluted Ag sample was approximately equal to the beads without Ag present, the sample was sufficiently diluted to analyze. This procedure was a key point in determining the proper concentration of nanoparticles that could be counted without coincident artifacts.

As a rapid assessment of the nanoparticle concentration in a tube, it was observed that when the histogram peaks of each population were approximately equal height and the Ag could be counted without coincident counting artifacts (Figs. 3 and 4 and Supporting Information Tables 3–5). Since the CV of the beads was smaller than the CV of Ag nanoparticles, a smaller amount of beads in the solution would yield similar peak heights of Ag particles in the histogram. When there were approximately six to eight times more nanoparticles than beads in the suspension, the modes of the two populations in the histograms were almost equal (Fig. 4; Supporting Information Figs. 4 and 5).

The total count, AgNP count and bead count were measured at different dilutions for 30 s [(Supporting Information Table 3, Ag 60 nm); Supporting Information Table 4 (Ag 80 nm); Supporting Information Table 5 (Ag 100 nm)]. Supporting Information Tables 3 to 5 shows the dilution, the percentage of beads and Ag nanoparticles in each dilution, the bead and Ag count in each dilution and the calculated Ag count. An estimate of the Ag count in the original suspension was be determined by diluting the nanoparticle sample sufficiently so the amount of beads counted in the mixed sample was equivalent to counting beads in diluent cocktail without any silver nanoparticles present. This procedure could determine not only the dilution necessary for counting Ag nanoparticles without major coincidence counting, but also could determine the original Ag nanoparticle concentration. The calculations determined the Ag concentration to be approximately 1,010 to 1,012 particles/mL, which was the same range reported by the NanoComposix, the manufacturer of the Ag particles. Some errors in our data particle calculation may arise from the background counts occurring in the Ag size regions at low Ag concentrations, coincidence counting of the Ag nanoparticle bead mixture at higher dilutions, and possible

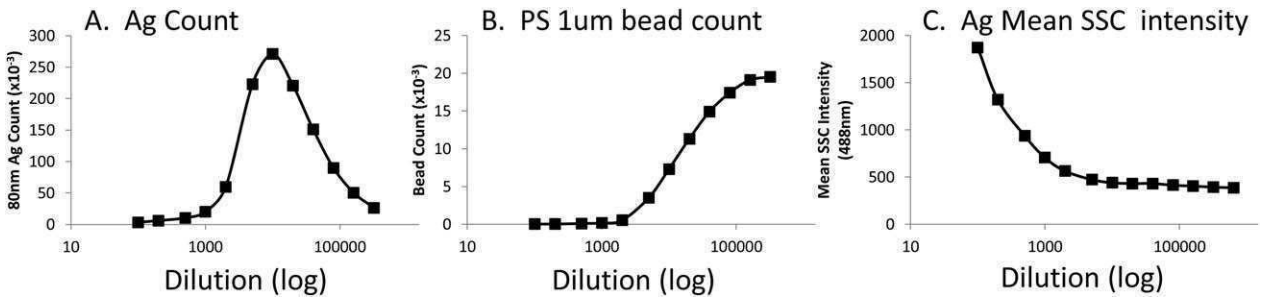

Figure 4. Sequential dilutions of 80 nm nanoparticles with 1 μm PS beads. Concentrated 80 nm Ag nanoparticles (3.6×10^{11}) were sequentially diluted with a mixture of 1.9×10^6 beads per/mL. (**A**) Concentration of silver particles, while (**B**) shows the concentration of PS 1 μm particles counted at each dilution. The normalized Ag count = (Ag count) × (dilution factor). The normalized bead count = (bead count) × (dilution factor). The amount of beads and Ag nanoparticles was determined from their respective regions in the Figure 3 histogram. At high particle concentrations there was a suppression of the nanoparticle and bead counts. By sequentially diluting the nanoparticles with 1 μm beads, the bead count eventually approached the levels of beads without nanoparticles present. The 80 nm Ag original concentration from the NanoComposix web site was 3.86×10^{11}; and the flow cytometry calculation was in the same range with a calculated value of 2.16×10^{11}. A decrease in mean SSC intensity with the dilutions is shown in (**C**). The intensity of the 80 nm particles decreased approximately sixfold. This change in mean intensity can be used as an indicator for the presence of excessive particle concentrations.

human pipetting errors with small samples. The coincidence counting and background counting were not subtracted from the raw data as they vary greatly with Ag concentration.

In the initial experiments with the 100 nm and 110 nm Ag particles, a 2 μm bead was used with the SSC PMT value set at a gain of 31%. However, for the maximum detection of small 60 nm Ag metal nanoparticles, the SSC PMT value was set to 100%, and it was necessary to use a small 1 μm counting bead in place of the 2 μm bead as the relative reference counting bead.

Water Purity

A critical step in measuring submicron particles was to reduce the amount of particles contained in the sheath and the sample suspending medium. If the sheath and suspending water contained submicron particles, their size usually appeared as two clusters: one located under the 200 to 300 nm and one located under the 500 nm SSC peak on the FSC versus SSC cytogram. The position of the clusters suggests that they have the same forward scatter intensity as PS beads but smaller SSC intensity as they are observed as a subpopulation below the 200 to 500 nm bead clusters. Figure 5 shows data from a relatively clean system (<100 counts/s) without many background particles (Fig. 5A), and from a system that had particulate matter and bacterial growth in the sheath (Fig. 5B). If there was a high degree of particle counts in the sheath fluid, the histogram distribution of submicron PS beads or metal nanoparticles was affected as these background submicron particles are displayed in the same channels on the histograms (between 200 and 500 nm on FSC (Fig. 5). In order to reduce the amount of background particle counts to approximately 100–200 counts/s range, the machine was cleaned with a decontamination cycle, a de-bubble cycle and then flushed for a few hours with particle free distilled water before use. It was helpful to purify the water using a 200 nm Pall filter followed by a 50 nm Millitech filter.

Measurement of TiO_2 Submicron Particles

TiO_2 nanoparticle standards in suspension consist of a mixture of different sized particles due to clumping of nanoparticles in suspension (3). It was found that particles in the 200 nm size range could be detected as unique clusters by measuring side and forward scatter. TiO_2 particles in the nanoparticle size range could not be measured due to the diversity of their sizes. The smallest pulses were in the range of the noise. Incubation of TiO_2 particles in serum was used to reduce clumping; however, it also decreased the amount of light scatter generated by TiO_2 particles (data not shown).

Comparison of Different Coatings of Ag and Au Submicron Particles

The coatings of Ag and Au nanoparticles changed the intensity of SSC and the histogram size distribution. A low CV suggests more homogeneity in the scatter. Comparing TED nanoparticles with NanoComposix showed that TED scattered more light, presumably due to the type of coatings on the surface (Supporting Information Fig. 8). Lipoic acid coated particles (100 nm) from NanoComposix had a decrease in mean size and CVs, suggesting that they were more homogenous than their equivalent sized PVP-coated particle. This coating was put on to reduce particle clumping in suspension and in cells. Econix is another version of PVP-coated Ag nanoparticles from NanoComposix that was found to have a lower CVs and scatter more light than the equivalent sized BioPure nanoparticle. However, the same result would be observed if the Econix particle was actually slightly larger than the more expensive BioPure Ag nanoparticle. The 560 nm to 1.2 μm silica particles were much larger in size than the metal nanoparticles. The 1.2 μm silica particle scattered the same amount of light as the 100 nm nanosized silver or 400 nm PS bead due to the difference in the interaction between the particles and light. The CVs from the silica particles were smaller than CVs of silver NP. This suggested that the combination of less variability in the silica scatter signal

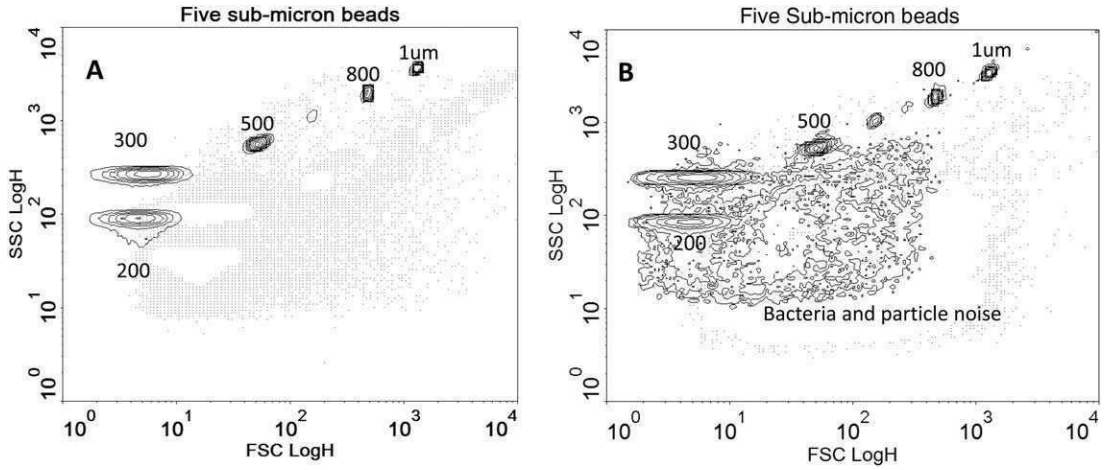

Figure 5. Particles in sheath water. The five PS submicron beads were measured on a machine using sheath filtered (50 nm filter) water with <100 counts/s (**A**) and with a machine that used deionized sheath water that contained numerous particles (**B**). These particles may be bacteria, parts of bacteria, or air bubbles. The particles in the sheath water had less side scatter than the PS beads but interference with the FSC and SSC histograms.

compared with Ag nanoparticles and different RIs between silica and Ag particles may be responsible for the difference (Supporting Information Table 2). It should also be noted that the silver nanoparticles ranged between 60 nm and 100 nm while the silica particles ranged between 560 nm and 1.2 μm. The interaction of light was different between the plasmonic resonator silver and the larger silica particles.

Silver Plasmonic Resonators

A series of NanoXact nonspherical silver nanoplates (1 mg/mL) that were plasmonic resonators (40–43) designed to resonate and emit at 550 nm, 650 nm, 750 nm, 850 nm, and 950 nm were obtained (all from NanoComposix). The particles were discs with an approximate thickness of 10 to 20 nm and length between 45 nm and 150 nm. These particles could not be measured simultaneously in a flow cytometer with 2 μm PS reference beads and then compared with the silver 50 to 200 nm silver spherical particles. These particles present problems for the flow cytometer due to their asymmetrical shape (43,56). The particles going through the flow cell had a high aspect ratio and did not scatter a sufficient amount of light to be detected above the threshold value. Orientation problems exist with these particles which were similar to the effects observed when measuring asymmetrical biological objects like sperm or nucleated chicken RBC (56).

Discussion

This article describes a methodology to detect, characterize, and count nonfluorescent metal nanoparticles and other submicron particles using a flow cytometry side scatter trigger. Before measuring nanoparticles by flow cytometry, there were a number of questions and variables that needed to be addressed. The following factors were considered: 1) type of reference particles, 2) development of a reference scale using multisized micron and submicron PS beads, 3) use of a large SSC range to simultaneously detect small and large size particles, 4) SSC trigger for nonfluorescent particles or a dual trigger for fluorescence particles (SSC + FL), 5) use of clean filtered (0.1 micron) water to reduce background counts, 6) reduction of system noise, 7) comparing resolution and sensitivity of 405 nm SSC and 488 nm SSC excitation for detecting nanoparticles, and 8) a method to determine the proper concentration of nanoparticles by sequential dilutions with either a 1 of 2 μm bead diluent suspensions. A number of these technical issues were addressed during the course of these experiments to ensure that the flow cytometer was correctly configured to count nanoparticles without artifacts occurring.

When these experiments with nanoparticles were initiated, many factors in observing submicron particles involving the use of the equipment were not completely known and a number of methods were proposed to try to achieve increased sensitivity and resolution with the flow cytometer. Some of the factors that needed to be considered included the following: hardware, software, FSC angle, 488 nm SSC, 405 nm SSC, FSC PMT and sample preparation. It was not clear whether the trigger signal should be either a fluorescent parameter, FSC, SSC or an intermediate angle between 0 degrees (FSC) and 90 degrees (SSC). The need for a FSC PMT was also considered to increase submicron resolution and provide extra sensitivity and resolution instead of the less sensitive standard FSC diode that is used with most flow cytometers. Evaluation of the FSC PMT on a similar Stratedigm 1000 machine demonstrated that the FSC PMT did yield slightly better resolution for detecting small particles (200 nm and 300 nm beads), however the benefit of this hardware addition should be carefully evaluated relative to the cost, as it appeared the increase in resolution was small (Dr. Mike Mooberry, personal communication, UNC). The data from this study have confirmed by other laboratories that show that SSC is preferable to use instead of FSC as a trigger parameter when using nonfluorescent particles (11,15,23–26,47).

The suggestion of using a fluorescent trigger has been proposed by Nolan and Stoner to reduce the noise in the system (15,23,46,47). If a fluorescent trigger can be used, it is usually advantageous as it will greatly reduce the background particle counts in the sheath which are generally not fluorescent. However, the studies on nanoparticles reported in this article used a Stratedigm flow cytometer necessitating a SSC light scatter trigger as the primary trigger as the Ag and Au nanoparticles did not contain a fluorescent component that could be used as a primary trigger parameter. Since fluorescence was not available for a primary trigger parameter and nanoparticles were not fluorescent, it was necessary to optimize the equipment for a scatter trigger that reduced the noise in the samples and sheath.

The cytograms and histograms in Figure 1 shows that SSC can differentiate between the 200 and 300 nm particles while the FCS can only differentiate between the 300 nm and 500 nm particles. This is consistent with the general flow cytometry understanding that even though the SSC has less intensity than FSC, it appears to be a more useful signal for detecting small submicron particles as the SSC signal to noise ratio is better than that of FSC signal to noise ratio (31,32).

Another variable that was addressed was whether the SSC derived from the 405 nm versus the 488 nm lasers would yield better resolution and sensitivity. Normally, 405 nm scatter being a shorter wavelength should be superior to 488 nm in detecting SSC and small particles. In these studies the 405 nm excitation usually yielded smaller CVs compared with 488 nm light excitation. However, the scatter intensity of submicron and micron beads was greater with the 488 nm laser than the 405 nm laser excitation. The 405 nm laser excitation actually appeared to yield less resolution between larger sized micron beads due to the specific particle absorption and scattering differences that occur between the 405 nm and 488 nm laser lines. The separation index was greater with the 405 nm than the 488 nm showing there was better resolution and sensitivity with the 405 nm laser exaction.

Counting

When attempting to use a flow cytometer to measure submicron particles, it is important to determine if a sample is at the proper concentration. There are some cytometric parameters that could possibly be used to indicate high sample concentrations. The following changes were observed when a sample was too concentrated: increased SSC mean and mode, reduced noise counts, distorted pulse widths histogram distributions, reduced counting rates, and fluctuations in the counting rate. In this report it was shown that by diluting a concentrated nanoparticle sample the following occurred: a decrease in SSC intensity histogram size (Figs. 4 and 5 and Supporting Information Figs. 4, 5, and 7 and Supporting Information Table 6); reduced pulse spiking during counting (data not shown), increased cell counts after dilution (60 nm Supporting Information Table 3; 80 nm Supporting Information Table 4; 100 nm Supporting Information Table 5); and changes in the Gaussian-shaped pulse width histograms (Fig. 4 and Supporting Information Figs. 4 and 5). As shown in Figure 5, a very high concentration of particles actually decreased the counting rate due to the increased electronic abortion rates, activation of the double discrimination circuitry, and overloading the counting electronics of the flow cytometer (Fig. 4, Supporting Information Figs. 5 and 6 and Supporting Information Tables 3–5). A concentrated submicron particle sample showed occasional spiking and instability of the counting rate instead of a continuous linear counting rate that occurred with a sample diluted into the 10^7 particle/mL range.

In order to determine if the concentration of metal nanoparticles was suitable for counting without measurement artifacts, a procedure was employed that diluted the nanoparticle sample with a known 1 μm bead concentration (approximately 2×10^6 beads/mL). The counting rate of the 1 μm particles was approximately 1,000 counts/s at a slow flow rate (25 μL/min). All of the sequential dilutions were made with a cocktail of these 1 μm beads, which served as an internal reference for this counting procedure. At the proper dilution for analysis, the number of beads counted in a mixed sample for 30 s should have an approximately the same number as beads counted for 30 s without nanoparticles present. Due to the different SSC CVs of the nanoparticles and 1 μm beads, both populations appeared at similar heights in the histograms (Fig. 3; 40,000 dilution). The nanoparticles are about six to eightfold more concentrated than PS beads when they are at the proper dilutions for characterization. This procedure was also effective in diluting different Ag and Au nanoparticle samples to the proper concentration for analysis. It is essential that the nanoparticles are measured at the right concentration, which was found to be between approximately 10^6 and 10^7 particles/mL on the Stratedigm flow cytometer at a slow flow rate of 25 μL/min. If the concentration of nanoparticles is higher than 10^7 particles/mL, coincidence artifacts will occur in the counting procedure.

Particle Concentration and "Swarm" Concept

This research helps to clarify the data in some publications that involve the counting of submicron particles and described the phenomenon entitled "swarm" (15–27,46–48). In our opinion, there have been many articles published that have measured submicron particles at excessively high concentrations which resulted in the measurement of clumps and coincidence counting of multiple particles instead of measuring only individual particles. When too many particles arrive simultaneously in the flow cell, the flow cytometer electronics becomes overworked and unable to process all the pulses generated from the individual particles. A flow cytometer operated with excessively high concentrations of particles introduces many individual particles simultaneously into the flow cell which usually activates of the double discrimination electronic circuitry resulting in a rejection of many doublet counts. However, sometimes an event is counted that contains multiple individual particles in the flow cell that actually bypasses the doublet discrimination circuitry and the software that was devised to reject these multiple particles in the flow cell. Thus, some of these particles that entered the flow cell simultaneously are actually counted as a single larger particle

which results in the mead and mode of the histogram to be increased. In the Stratedigm 1000 flow cytometer system, there is an abort system in the software that senses whether individual or multiple particles arrive almost simultaneously in the flow cell. Other flow cytometry systems may address this problem of concentrated samples in the flow cell in different ways. It was not the scope of this article to try to compare these different systems.

In summary, the physical presence of multiple particles in the flow cell will not only create a "swarm" of particles but it will create problems for the proper functioning of the system electronics and software. These counts have actually been described as a "swarm" of particles measured simultaneously. Nolan and Stoner has stated that much of the data in the field of submicron particle counting may be artificial due to this type of coincidence counting (15). Our research, confirms that of Nolan and his collaborators in demonstrating that the "swarm" phenomenon is an artifact from the coincidence counting of small particles. The data derived from a machine that is counting an excessive high amount of particles simultaneously ("swarm") maybe misinterpreted by investigators to yield flow cytometry data and concepts on submicron particles that are incorrect (5–12,15–21,23,46–48).

Submicron Particles in the Water

One important consideration in measuring submicron particles involves particulate matter impurities contained in the water. These particles become a problem as there is overlap between the metal nanoparticles being measured and the background particle counts in the water. All sheath fluids and samples have some degree of noise due to small particles and perhaps bacteria in the water. The noise can be reduced by using distilled water that is filtered through a 50 to 100 nm filter before use. Even with this procedure, the water may still have around 100 counts/s with the size distribution of these counts usually occurs below the 200 to 300 nm reference beads and sometimes below the 500 nm bead peak, which may be equivalent to the size of bacteria (Fig. 5). The noise in this region may also be due to microbubbles detected by scatter but not fluorescence. One must be aware that systems can show an absence of noise in the lower channels which is not due to clean water but may be due to excessively high counts, which reduces the counting of all particles including background sheath particles. If possible, a fluorescent trigger should be used to eliminate water noise as these water particles are not fluorescent.

Determine a Reference Scale with Submicron Beads

It would be useful to be able to count and size submicron particles and nanoparticles easily, rapidly, and reproducibly with statistical accuracy. In order to accomplish this task, a PS reference bead scale with five different sizes of beads between 200 nm and 1 μm were chosen to create a relative PS bead reference intensity scale (Fig. 1 and Supporting Information Table 1). The unknown submicron particles could then be characterized according to their relative side scatter values compared with the PS bead standards. It should be emphasized that this is a relative PS bead intensity scale moments and not an accurate representation of the nanoparticle size but represents a SSC intensity. These five reference beads can also serve as a QA standard to check system noise and system reproducibility. Since all of the metal nanoparticles used in this study were nonfluorescent, it was important to use QA particles that could be triggered with a SSC trigger.

The use of five PS submicron particles can help determine the suitable trigger and set up conditions to measure these bead sizes and relate them to SSC intensity. Having one or two of the reference particles that are fluorescent can be helpful in finding the particles and ensuring that all the particles are counted. It is also useful to know the relative concentrations of the reference particles as some particles may be discriminated from the count by either system sensitivity or triggering issues (Supporting Information Table 1). By using either similar numbers of particles in each of the five bead populations or similar peak heights in the log distributions of the bead populations, it can be rapidly ascertained if all the bead populations are being measured in the PMT dynamic scale. Knowing the relative amounts of the five bead populations in the reference material is helpful in case there is selective discrimination of either relatively small or large bead sizes. This effect was observed in early configuration of the machine and has since been resolved by the manufacture. To evaluate sensitivity and the ability of the machine to detect the smallest submicron particles, it was beneficial to increase the SSC PMT settings to a maximum value of 100% and then add a bead smaller than the 200 nm to determine the noise and lower levels of relative PS detection. In these experiments, a 140 nm bead was added to the five-bead mix (Supporting Information Fig. 2) and the separation index between the 140 nm and 200 nm bead was determined to yield a value for machine sensitivity and also to determine the lower level of particle size detection.

Relative not Absolute PS Bead Scale

Side scatter derived from a flow cytometer is not an absolute measure of size, but it is only a relative measure of intensity that is based on the unique characteristics of the particles and the interaction of the particles with the specific wavelength of light. The refractive index (RI) of the particles varies as a function of surface composition such that gold, silver, silica and PS beads will each yield different scatter intensity for a similar particle size. Gold and silver metal nanoparticles had unique scatter distributions dependent on the wavelength of light excitation, the size of the particle, and the metallic composition of the particle. It should be emphasized that the scatter, provides a relative measure of intensity based on how the surface composition of the particle interacts with the specific wavelength of light and is not an accurate measure of size determined by electron microscopy, or by particle tracking equipment.

Polystyrene beads between 200 nm and 1 μm can be used to create a relative scale based on the scattering properties of PS beads. Some investigators have compared the PS histogram distribution derived by scatter as a measure of the direct size of particles to be used as a comparison to size other particles.

The PS bead scale is useful to compare relative intensities of particles which roughly relate to the physical size of the particle. To assume that forward scatter is directly related to cell size and side scatter is related to granularity is an oversimplification (31,32). Generally the larger particle of a given material will generally scatter more light than a smaller particle. The scattered light is not a size measurement but it is an intensity measurement based on the physical properties of the particle and its interaction with laser light. The nonlinearity of scale is clearly indicated by comparing the 405 nm and 488 nm excitation of PS beads. Although there are usually better CVs with the 405 nm laser than the 488 nm laser, the intensity of scatter with micron sized particles is not linear and the resolution between larger sized micron particles is much less with the 405 nm laser.

Nanoparticle Light Scatter

Light scatter is a very complex signal and its intensity is based not only on the size of the particle but its composition. Light scatter is an integral part in the operation of a flow cytometer in detecting different types of particles. Since the inception of flow cytometry, investigators have used light scatter to discriminate the different types of blood cells by their relative size and granularity. This article studies the interaction of these specific laser wavelengths (405 nm and 488 nm) with metal nanoparticles and PS submicron beads. The interaction of light with silver is dependent on the size of the particle, the RI of the particle and the excitation wavelength. The amount of light scattered from the interaction between light and nanoparticle is proportional to the inverse fourth power of the wavelength and the sixth power of its size (31,32,38–43).

Metallic Au and Ag nanoparticles absorb and scatter light efficiently by stimulating surface electrons to oscillation. This scattering is also dependent on other factors which include the wavelength of light, nanoparticle diameter, surface coatings, molecules consistency, and unique specific characteristics of the particle. Larger sized nanoparticle will absorb a higher wavelength of light compared with smaller particles which results in more scattered light and a more homogenous distribution (less of the CV). The 405 nm laser light is exciting silver suboptimally and the differences in sizes (resolution) are not as large as that observed with 488 nm excitation. Gold has maximum absorption at 530 nm yielding histogram patterns with both 405 nm and 488 nm excitation that are similar suggesting that the Au sizes are relatively invariant to the excitation wavelength.

Modification on the nanoparticle surface by different coatings will affect the local environment of the particle and thus will affect the amount of light scattered. Different nanomaterials of different sizes and surface coatings will interact with the 405 nm and 488 nm laser light in a unique manner to yield a scatter histogram with different shapes and distributions (Fig. 2 and Supporting Information Fig. 3 and Supporting Information Table 2). These characteristics of light interacting with specific types and sizes of nanoparticles were demonstrated by the gold nanoparticles yielding a bimodal histogram distribution while the silver particles had only a single peak distribution.

Light interacting with small particles is scattered in all directions (Rayleigh scattering) if the particles are small relative to the wavelength (below 250 nm). If the light source is a laser, and thus is monochromatic and coherent, the scattering intensity may fluctuate over time due to the small molecules in solutions undergoing Brownian motion and changing their orientation relative to the laser light. The scattered light can undergo either constructive or destructive interference from the surrounding neighboring particles (38–44). Our data demonstrates a higher CV with smaller Ag nanoparticles suggestive of greater variability of the light with the particle. In contrast to silver nanoparticles, gold nanoparticles (60 nm, 80 nm and 100 nm) show a bimodal distribution resulting from light interacting with particles in a different manner than silver. Generally, different materials of nanoparticles reflect light dependent on their absorption and reflectively. In our studies, Ag was much brighter than Au using either 405 nm or 488 nm excitation laser light.

Small nanoparticles with sizes below the wavelength (488 nm) of excitation light scatter laser light using Raleigh scattering principles while particles larger than the wavelength of light (around 500 nm and larger) scatter light by Mie scattering. Raleigh scattering is strongly affected by the wavelength of light, absorption, refractive index of medium, and the angle of collection. The light scatter from silver nanoparticles, gold nanoparticles and silica particles is dependent not only on the size of the particles but the composition of the particles and how their dipoles interact with different wavelengths of laser light. A comparison of the mean sizes and histogram distribution of similar sized gold and silver nanoparticles shows that the silver scatters more light at both the 488 nm and 405 nm laser beams than gold nanoparticles. Silica has a different RI than the metal particles and does not scatter as much light as the metal nanoparticles for an equivalent physical size. However, the CV of silica particle's distribution is much smaller than the metal nanoparticles illustrating that different materials with different sizes will interact with light in a unique manner and scatter different amounts of light (Supporting Information Table 2). Larger polystyrene beads do not have the dipole moments similar to metal nanoparticles. Thus, larger PS bead sizes are needed to scatter the same amount of light as smaller metal nanoparticles. Silica particles have less RI compared with PS beads and thus larger silica particles are needed to scatter the same amount of light as PS submicron beads. The scattering phenomenon observed with metal nanoparticles on a flow cytometer appears to be due to the unique interaction that metal dipoles moments have with a specific wavelength of light that does not occur with PS beads or silica beads.

It has been shown that silver nanoparticle absorption and scattering properties can be adjusted by controlling the particle size, shape, and the local refractive index near the particle surface as was shown by the production of silver discs. However, in our flow cytometer system there was an insufficient amount of light absorbed and scattered by the particles due to their orientation in the flow cell yielding an insufficient signal to create a unit above background. Other nanoparticles that

are smaller without a metal component will not scatter enough light to be detected by our flow cytometry system. The limits of scatter detection in a commercial Stratedigm 1000 system with the current electronic PMT settings appeared to be about 40 nm for silver and 60 nm for gold about 150 nm for PS beads. Fluorescent triggering of PS beads can reduce the size of PS particle to about 100 nm by eliminating much of the water scatter noise.

Tips and Tricks

Before measuring samples one must be confident that they are actually counting nanoparticles and submicron particles and not clumps or particle coincidence. The following variables should be addressed in any experiment: sample preparation, reference PS beads scale, dynamic PMT range, system electronics, water purity, and trigger signal and particle number/mL.

Some factors to address are the following:

1. Observe a distinct distribution away from the noise of the system.
2. Dilute sample and show that the peaks are still located in the same channels.
3. Use a 1 μm reference bead suspension for serial dilutions of the nanoparticle sample
4. Add a known concentration of 1 to 2 μm counting beads to sample to determine if all the beads and sample particles are counted in a given time unit.
5. Increase the baseline threshold: a rising count indicates that particles are too concentrated and effecting the counting electronics.
6. Decease the baseline threshold: falling count indicates particles are too concentrated and effecting the counting electronics.
7. Be aware of trigger parameter and lower level discriminator.
8. Clean the machine extensively to reduce background particle counts. Use filtered water as sheath that has only 100 to 200 counts/mL at slow flow rates (25 μL/min).

Summary

Submicron sized beads between 140 nm and 1 μm were used as relative reference scale to determine the lower and upper limits of PS particle size detection limits and to determine the dynamic range of the SSC PMTs used for measurement. Silver and gold nanoparticles between 50 nm and 110 nm were detected, characterized, and counted using a flow cytometer with a 488 nm side scatter trigger. It was found that 405 nm excitation usually yielded better CVs and separation indices compared with the 488 nm light excitation, but had less dynamic range in detecting differences between the larger sized particles.

These sequential dilutions of the metal nanoparticles with 1 μm counting beads (2 to 5 $\times$ 10^6) ensured that the machine was in the proper detection range for nanoparticles thus eliminating potential electronic artifacts caused by the high concentrations. This allowed the investigator to detect, count, and measure submicron particles with greater accuracy and minimizing potential counting artifacts. The methodology developed to detect, characterize and count silver and gold nanoparticles could also be applicable to submicron biological particles.

Acknowledgments

Thanks are extended to Nancy Fisher, Nigel Keys, and Micah Mooberry, John Rogers, Chris Lau, Joe Trask, Sam Witherspoon, and Martha Carraway for their helpful comments and encouragement for many aspects of the article. We want to especially thank Shervin Javadi of Stratedigm for helpful discussion and modification of the Stratedigm 1000 to allow them to count accurately and size nanoparticles, submicron and micron sized particles simultaneously. We also thank Keith Tarpley and Chuck Gaul for their excellent graphic support in helping to prepare the figures. We thank Laura Degn, Kaitlyn Daniel, and Dina Abdulhadi for their help in these experiments and for generating some of the preliminary figures and tables and with the preparation of the paper. We wish to greatly thank the following bead companies for generously supplying us with demo samples: Thermo Scientific Beads, Bangs, BD Biosciences, and Spherotech.

This research was supported in part by an appointment to the Research Participation Program for the U.S. Environmental Protection Agency, Office of Research and Development, administered by the Oak Ridge Institute for Science and Education through an interagency agreement between the U.S. Department of Energy and EPA. Research described in this article was supported by the United States Environmental Protection Agency; it has been subjected to Agency review but does not necessarily reflect the views of the Agency. Mention of trade names or commercial products does not constitute endorsement or recommendation for use.

Literature Cited

1. Johnston HJ, Hutchison G, Christensen FM, Peters S, Hankins S, Stone V. A review of the in vivo and in vitro toxicity of silver and gold particulates: Particle attributes and biological mechanisms responsible for the observed toxicity. Crit Rev Toxicol 2010; 40:328–346.
2. Ahamed M, Alsalhi MS, Siddiqui MK. Silver nanoparticle applications and human health. Clin Chim Acta 2010; 411:1841–1848.
3. Sanders K, Degn LL, Mundy WR, Zucker RM, Dreher K, Zhao B, Roberts JE, Boyes WK. In vitro phototoxicity and hazard identification of nano-scale titanium dioxide. Toxicol Appl Pharmacol 2012; 258:226–236.
4. Egger S, Lehmann RP, Height MJ, Loessner MJ, Schuppler M. Antimicrobial properties of a novel silver-silica nanocomposite material. Appl Environ Microbiol 2009; 75:2973–2976.
5. Gliga A, Skoglund S, Wallinder I, Fadeel B, Karlsson H. Size-dependent cytotoxicity of silver nanoparticles in human lung cells: The role of cellular uptake, agglomeration and Ag release. Part Fibre Toxicol 2014; 11: 1743–8977.
6. Robert S, Lacroix R, Poncelet P, Harhouri K, Bouriche T, Judicone C, Wischhusen J, Arnaud L, Dignat-George F. High-sensitivity flow cytometry provides access to standardized measurement of small-size microparticles–brief report. Arterioscler Thromb Vasc Biol 2012; 32:1054–1058.
7. Lacroix R, Robert S, Poncelet P, Dignat-George F. Overcoming limitations of microparticle measurement by flow cytometry. Semin Thromb Hemost 2010; 36:807–818.
8. Robert S, Poncelet P, Lacroix R, Arnaud L, Giraudo L, Hauchard A, Sampol J, Dignat-George F. Standardization of platelet-derived microparticle counting using calibrated beads and a Cytomics FC500 routine flow cytometer: A first step towards multicenter studies? J Thromb Haemost 2009; 7:190–197.
9. Robert S, Poncelet P, Lacroix R, Raoult D, Dignat-George F. More on: Calibration for the measurement of microparticles: Value of calibrated polystyrene beads for flow cytometry-based sizing of biological microparticles. J Thromb Haemost 2011; 9:1676–1678; author reply 1681-1682.
10. Lacroix R, Robert S, Poncelet P, Kasthuri RS, Key NS, Dignat-George F, ISTH SSC Workshop. Standardization of platelet-derived microparticle enumeration by flow cytometry with calibrated beads: Results of the International Society on Thrombosis and Haemostasis SSC Collaborative workshop. J Thromb Haemost 2010; 8: 2571–2574.

11. Lacroix R, Judicone C, Poncelet P, Robert S, Arnaud L, Sampol J, Dignat-George F. Impact of pre-analytical parameters on the measurement of circulating microparticles: Towards standardization of protocol. J Thromb Haemost 2012; 10:437–446.
12. Mullier F, Bailly N, Chatelain C, Dogné JM, Chatelain B. More on: calibration for the measurement of microparticles: Needs, interests, and limitations of calibrated polystyrene beads for flow cytometry-based quantification of biological microparticles. J Thromb Haemost 2011; 9:1679–1681.
13. Orozco AF, Lewis DE. Flow cytometric analysis of circulating microparticles in plasma. Cytometry Part A 2010; 77A:502–514.
14. van der Heyde HC, Gramaglia I, Combes V, George TC, Grau GE. Flow cytometric analysis of microparticles. Methods Mol Biol 2011; 699:337–354.
15. Nolan JP, Stoner SA. A trigger channel threshold artifact in nanoparticle analysis. Cytometry Part A 2013; 83A:301–305.
16. van der Pol E, Hoekstra AG, Sturk A, Otto C, van Leeuwen TG, Nieuwland R. Optical and non-optical methods for detection and characterization of microparticles and exosomes. J Thromb Haemost 2010; 8:2596–2607.
17. van der Pol E, van Gemert MJ, Sturk A, Nieuwland R, van Leeuwen TG. Single vs. swarm detection of microparticles and exosomes by flow cytometry. J Thromb Haemost 2012; 10:919–930.
18. van der Pol E, Coumans F, Varga Z, Krumrey M, Nieuwland R. Innovation in detection of microparticles and exosomes. J Thromb Haemost 2013; 36–45.
19. van der Pol E, Coumans FA, Grootemaat AE, Gardiner C, Sargent IL, Harrison P, Sturk A, van Leeuwen TG, Nieuwland R. Particle size distribution of exosomes and microvesicles determined by transmission electron microscopy, flow cytometry, nanoparticle tracking analysis, and resistive pulse sensing. J Thromb Haemost 2014; 12:1182–1192.
20. Harrison P, Gardiner C. Invisible vesicles swarm within the iceberg. J Thromb Haemost 2012; 10:916–918.
21. Chandler WL, Yeung W, Tait JF. A new microparticle size calibration standard for use in measuring smaller microparticles using a new flow cytometer. J Thromb Haemost 2011; 9:1216–1224.
22. Erdbrügger U, Rudy CK, E Etter M, Dryden KA, Yeager M, Klibanov AL, Lannigan J. Imaging flow cytometry elucidates limitations of microparticle analysis by conventional flow cytometry. Cytometry Part A 2014; 85A:756–770.
23. Kormelink TG, Arkesteijn GJ, Nauwelaers FA, van den Engh G, Nolte-'t Hoen EN, Wauben MH. Prerequisites for the analysis and sorting of extracellular vesicle subpopulations by high-resolution flow cytometry. Cytometry Part A (in press). DOI: 10.1002/cyto.a.22644.
24. van der Vlist EJ, Nolte-'t Hoen EN, Stoorvogel W, Arkesteijn GJ, Wauben MH. Fluorescent labeling of nano-sized vesicles released by cells and subsequent quantitative and qualitative analysis by high-resolution flow cytometry. Nat Protoc 2012; 7: 1311–1326.
25. Nolte-'t Hoen EN, van der Vlist EJ, Aalberts M, Mertens HC, Bosch BJ, Bartelink W, Mastrobattista E, van Gaal EV, Stoorvogel W, Arkesteijn GJ, et al. Quantitative and qualitative flow cytometric analysis of nanosized cell-derived membrane vesicles. Nanomedicine 2012; 8:712–720.
26. Nolte-'t Hoen EN, van der Vlist EJ, de Boer-Brouwer M, Arkesteijn GJ, Stoorvogel W, Wauben MH. Dynamics of dendritic cell-derived vesicles: high-resolution flow cytometric analysis of extracellular vesicle quantity and quality. J Leukoc Biol 2013; 93: 395–402.
27. Varga Z, Yuana Y, Grootemaat A, van der Pol E, Gollwitzer C, Krumrey M, Nieuwland R. Towards traceable size determination of extracellular vesicles. J Extracell Vesicles 2014; 10:3402.
28. Kim JS, Ligler FS. Utilization of microparticles in next-generation assays for microflow cytometers. Anal Bioanal Chem 2010; 398:2373–2382.
29. Xu Y, Nakane N, Maurer-Spurej E. Novel test for microparticles in platelet-rich plasma and platelet concentrates using dynamic light scattering. Transfusion 2011; 51:363–370.
30. Murphy CJ, Gole AM, Stone JW, Sisco PN, Alkilany AM, Goldsmith EC, Baxter SC. Gold nanoparticles in biology: beyond toxicity to cellular imaging. Acc Chem Res 2008; 41:1721–1730.
31. Salzman GC. Light scatter: Detection and usage. Curr Protoc Cytom 2001;Chapter 1:Unit 7.
32. Shapiro HM. Practical Flow Cytometry. New York: Wiley; 2002.
33. Zucker RM, Massaro EJ, Sanders KM, Degn LL, Boyes WK. Detection of TiO_2 nanoparticles in cells by flow cytometry. Cytometry Part A 2010; 77A:677–685.
34. Zucker RM, Daniel KM, Massaro EJ, Karafas SJ, Degn LL, Boyes WK. Detection of silver nanoparticles in cells by flow cytometry using light scatter and far-red fluorescence. Cytometry Part A 2013; 83A:962–972.
35. Zucker RM, Daniel KM. Detection of TiO_2 nanoparticles in cells by flow cytometry. Methods Mol Biol 2012; 906:497–509.
36. Zucker RM, Daniel KM. Microscopy imaging methods for the detection of silver and titanium nanoparticles within cells. In: Soloviev M, editor. Nanoparticles in Biology and Medicine. New York: Springer; 2012. Methods Mol Biol 2012;906:483-496.
37. Qian W, Huang X, Kang B, El-Sayed MA. Dark-field light scattering imaging of living cancer cell component from birth through division using bioconjugated gold nanoprobes. J Biomed Opt 2010; 15:046025.
38. Konokhova AI, Yurkin MA, Moskalensky AE, Chernyshev AV, Tsvetovskaya GA, Chikova ED, Maltsev VP. Light-scattering flow cytometry for identification and characterization of blood microparticles. J Biomed Opt 2012; 17:057006.
39. Lerner JM. Imaging spectrometer fundamentals for researchers in the biosciences–A tutorial. Cytometry Part A 2006; 69A:712–734.
40. Yguerabide J, Yguerabide EE. Light-scattering submicroscopic particles as highly fluorescent analogs and their use as tracer labels in clinical and biological applications. Anal Biochem 1998; 262:157–176.
41. van Dijk MA, Tchebotareva AL, Orrit M, Lippitz M, Berciaud S, Lasne D, Cognet L, Lounis B. Absorption and scattering microscopy of single metal nanoparticles. Phys Chem Chem Phys 2006; 8:3486–3495.
42. van Dijk MA1, Tchebotareva AL, Orrit M, Lippitz M, Berciaud S, Lasne D, Cognet L, Lounis B. Absorption and scattering microscopy of single metal nanoparticles. Adv Drug Deliv Rev 2013; 65:622–648.
43. Jain PK, Lee KS, El-Sayed IH, El-Sayed MA. Calculated absorption and scattering properties of gold nanoparticles of different size, shape, and composition: Applications in biological imaging and biomedicine. J Phys Chem B 2006; 110:7238–7248.
44. Konokhova AI, Chernova DN, Moskalensky AE, Strokotov DI, Yurkin MA, Chernyshev AV, Maltsev VP. Super-resolved calibration-free flow cytometric characterization of platelets and cell-derived microparticles in platelet-rich plasma. Cytometry Part A (in press). DOI: 10.1002/cyto.a.22621.
45. Eustaquio T, Leary JF. Nanobarcoded superparamagnetic iron oxide nanoparticles for nanomedicine: Quantitative studies of cell-nanoparticle interactions by scanning image cytometry. Cytometry Part A (in press). DOI: 10.1002/cyto.a.22699.
46. Arraud N, Gounou C, Turpin D, Brisson AR. Fluorescence triggering: A general strategy for enumerating and phenotyping extracellular vesicles by flow cytometry. Cytometry Part A (in press). DOI: 10.1002/cyto.a.22699
47. Poncelet P, Robert S, Bouriche T, Bez J, Lacroix R, Dignat-George F. Standardized counting of circulating platelet microparticles using currently available flow cytometers and scatter-based triggering: Forward or side scatter? Cytometry Part A (in press). DOI: 10.1002/cyto.a.22685.
48. Inglis HC, Danesh A, Shah A, Lacroix J, Spinella PC, Norris PJ. Techniques to improve detection and analysis of extracellular vesicles using flow cytometry. Cytometry Part A 2015; 87A:1052–1063.
49. Mooberry MJ, Key NS. Microparticle analysis in disorders of hemostasis and thrombosis. Cytometry Part A (in press). DOI: 10.1002/cyto.a.22647.
50. Hoffman RA. Pulse width for particle sizing. Curr Protoc Cytom 2009; Chapter 1: Unit 1.23.
51. Zucker RM, Fisher NC. Evaluation and purchase of an analytical flow cytometer: Some of the numerous factors to consider. Curr Protoc Cytom 2013;Chapter 1:Unit 1.28.
52. Ortyn WE, Perry DJ, Venkatachalam V, Liang L, Hall BE, Frost K, Basiji DA. Extended depth of field imaging for high speed cell analysis. Cytometry Part A 2007; 71A:215–231.
53. Bigos M. Separation index: An easy-to-use metric for evaluation of different configurations on the same flow cytometer. Curr Protoc Cytom 2007;Chapter 1:Unit1.21.
54. Perfetto SP, Chattopadhyay PK, Wood J, Nguyen R, Ambrozak D, Hill JP, Roederer M. Q and B values are critical measurements required for inter-instrument standardization and development of multicolor flow cytometry staining panels. Cytometry Part A 2014; 85A:1037–1048.
55. Wood JC, Hoffman RA. Evaluating fluorescence sensitivity on flow cytometers: An overview. Cytometry 1998; 33: 256–259.
56. Zucker RM, Perreault SD, Elstein KH. Utility of light scatter in the morphological analysis of sperm. Cytometry 1992; 13:39–47.

Zucker, Robert

To: jana Natolovia
Subject: STAA_zucker

No response

From: Boyes, William <Boyes.William@epa.gov>
Sent: Friday, April 24, 2020 5:25 PM
To: Zucker, Robert <Zucker.Robert@epa.gov>; Jayna Ortenzio (jayna.ortenzio@gmail.com) <jayna.ortenzio@gmail.com>; Laura Degn (degn.laura@gmail.com) <degn.laura@gmail.com>; jlerner@lightforminc.com; Goldstein-Plesser, Alice <goldstein-plesser.alice@epa.gov>; McGee, John <Mcgee.John@epa.gov>; Rogers, Kim <Rogers.Kim@epa.gov>
Subject: STAA 2020 nomination

Hi ALL,

Bob and I decided to nominate three of our nanoparticle papers for a Scientific and Technological Award. A draft of the nomination form is attached, along with the three manuscripts. Unfortunately only EPA authors are eligible for award money even though all authors contributed. We were required to split the proportional effort across authors. We split the 100 % effort evenly giving 33% for each paper. Then we split that 33% evenly among all the authors for each paper, and summed the totals across the three papers.

1. Please review the nomination form and send me any corrections or suggestions.
2. Please send me an Email that you agree with the proportional allocation of effort.

I hope you are all well and staying safe during these strange times.

(KIM: can you please forward to Jana? I do not have her current E-mail address).

Will

William K. Boyes, Ph.D.
Neurological and Endocrine Toxicology Branch
Public Health and Integrated Toxicology Division
Center for Public Health and Environmental Assessment
Office of Research and Development
Mail Code B105-04
Environmental Protection Agency
109 T.W. Alexander Drive
Research Triangle Park, NC 27711

Phone: 919-541-7538
Mobile (alternate worksite contact): 919-417-2105
boyes.william@epa.gov

Robert M. Zucker, PhD
Reproductive and Developmental Toxicology Branch
Public Health and Integrated Toxicology Division
Center for Public Health and Environmental Assessment
Office of Research and Development
U.S. Environmental Protection Agency
109 TW Alexander Drive, Mail Drop B105-04
Research Triangle Park, NC 27709, USA
919-541-1585 (office)
zucker.robert@epa.gov

Shipping Address (Fed. Exp., etc.) for Chemicals/Samples
Attn: (Robert Zucker) Chemical Services, Room E-178
Building E Loading Dock, 109 TW Alexander Drive
RTP, NC 27709 USA

Zucker, Robert

To: Goldstein-Plesser, Alice
Subject: FW: STAA 2020 nomination
Attachments: 2020 STAA Nomination.docx; Final_ Ortenzio et al 2019.pdf; PLOS 1 Zucker comparison nanoparticles .pdf; Zucker_et_al-Cytometry_Part_A.pdf

No response

From: Boyes, William <Boyes.William@epa.gov>
Sent: Friday, April 24, 2020 5:25 PM
To: Zucker, Robert <Zucker.Robert@epa.gov>; Jayna Ortenzio (jayna.ortenzio@gmail.com) <jayna.ortenzio@gmail.com>; Laura Degn (degn.laura@gmail.com) <degn.laura@gmail.com>; jlerner@lightforminc.com; Goldstein-Plesser, Alice <goldstein-plesser.alice@epa.gov>; McGee, John <Mcgee.John@epa.gov>; Rogers, Kim <Rogers.Kim@epa.gov>
Subject: STAA 2020 nomination

Hi ALL,

Bob and I decided to nominate three of our nanoparticle papers for a Scientific and Technological Award. A draft of the nomination form is attached, along with the three manuscripts. Unfortunately only EPA authors are eligible for award money even though all authors contributed. We were required to split the proportional effort across authors. We split the 100 % effort evenly giving 33% for each paper. Then we split that 33% evenly among all the authors for each paper, and summed the totals across the three papers.

1. Please review the nomination form and send me any corrections or suggestions.
2. Please send me an Email that you agree with the proportional allocation of effort.

I hope you are all well and staying safe during these strange times.

(KIM: can you please forward to Jana? I do not have her current E-mail address).

Will

William K. Boyes, Ph.D.
Neurological and Endocrine Toxicology Branch
Public Health and Integrated Toxicology Division
Center for Public Health and Environmental Assessment
Office of Research and Development
Mail Code B105-04
Environmental Protection Agency
109 T.W. Alexander Drive
Research Triangle Park, NC 27711

Phone: 919-541-7538
Mobile (alternate worksite contact): 919-417-2105
boyes.william@epa.gov

Zucker, Robert

From: Boyes, William
Sent: Monday, April 27, 2020 10:03 AM
To: Robert Zucker; Zucker, Robert
Subject: RE: STAA

Dear Bob,

I agree with the proportional split in credit for this STAA nomination

Thanks

Will Boyes

From: Robert Zucker <rmzucker61@gmail.com>
Sent: Saturday, April 25, 2020 10:25 AM
To: Zucker, Robert <Zucker.Robert@epa.gov>
Cc: Boyes, William <Boyes.William@epa.gov>
Subject: STAA

will
I added some more items on the invitation
I am trying to get the abstract books as I was involved every year modeling workshops at CYTO meetings.

let me know what you think
I will talk with Kathy Monday afternoon —around 3PM

Zucker, Robert

To: jayna.ortenzio@gmail.com
Subject: FW: STAA 2020 nomination
Attachments: 2020 STAA Nomination.docx; Final_ Ortenzio et al 2019.pdf; PLOS 1 Zucker comparison nanoparticles .pdf; Zucker_et_al-Cytometry_Part_A.pdf

No response

From: Boyes, William <Boyes.William@epa.gov>
Sent: Friday, April 24, 2020 5:25 PM
To: Zucker, Robert <Zucker.Robert@epa.gov>; Jayna Ortenzio (jayna.ortenzio@gmail.com) <jayna.ortenzio@gmail.com>; Laura Degn (degn.laura@gmail.com) <degn.laura@gmail.com>; jlerner@lightforminc.com; Goldstein-Plesser, Alice <goldstein-plesser.alice@epa.gov>; McGee, John <Mcgee.John@epa.gov>; Rogers, Kim <Rogers.Kim@epa.gov>
Subject: STAA 2020 nomination

Hi ALL,

Bob and I decided to nominate three of our nanoparticle papers for a Scientific and Technological Award. A draft of the nomination form is attached, along with the three manuscripts. Unfortunately only EPA authors are eligible for award money even though all authors contributed. We were required to split the proportional effort across authors. We split the 100 % effort evenly giving 33% for each paper. Then we split that 33% evenly among all the authors for each paper, and summed the totals across the three papers.

1. Please review the nomination form and send me any corrections or suggestions.
2. Please send me an Email that you agree with the proportional allocation of effort.

I hope you are all well and staying safe during these strange times.

(KIM: can you please forward to Jana? I do not have her current E-mail address).

Will

William K. Boyes, Ph.D.
Neurological and Endocrine Toxicology Branch
Public Health and Integrated Toxicology Division
Center for Public Health and Environmental Assessment
Office of Research and Development
Mail Code B105-04
Environmental Protection Agency
109 T.W. Alexander Drive
Research Triangle Park, NC 27711

Phone: 919-541-7538
Mobile (alternate worksite contact): 919-417-2105
boyes.william@epa.gov

Zucker, Robert

From: Boyes, William
Sent: Monday, April 27, 2020 2:50 PM
To: Zucker, Robert
Subject: FW: STAA 2020 nomination

Kim's agreement

From: Rogers, Kim <Rogers.Kim@epa.gov>
Sent: Monday, April 27, 2020 2:03 PM
To: Boyes, William <Boyes.William@epa.gov>
Subject: RE: STAA 2020 nomination

I agree with the allocation of effort.

Kim Rogers, Ph.D.
MMB/WECD/CEMM
U.S. EPA, RTP, NC
Cell: 702-374-3284
e-mail: rogers.kim@epa.gov

From: Boyes, William <Boyes.William@epa.gov>
Sent: Friday, April 24, 2020 5:25 PM
To: Zucker, Robert <Zucker.Robert@epa.gov>; Jayna Ortenzio (jayna.ortenzio@gmail.com) <jayna.ortenzio@gmail.com>; Laura Degn (degn.laura@gmail.com) <degn.laura@gmail.com>; jlerner@lightforminc.com; Goldstein-Plesser, Alice <goldstein-plesser.alice@epa.gov>; McGee, John <Mcgee.John@epa.gov>; Rogers, Kim <Rogers.Kim@epa.gov>
Subject: STAA 2020 nomination

Hi ALL,

Bob and I decided to nominate three of our nanoparticle papers for a Scientific and Technological Award. A draft of the nomination form is attached, along with the three manuscripts. Unfortunately only EPA authors are eligible for award money even though all authors contributed. We were required to split the proportional effort across authors. We split the 100 % effort evenly giving 33% for each paper. Then we split that 33% evenly among all the authors for each paper, and summed the totals across the three papers.

1. Please review the nomination form and send me any corrections or suggestions.
2. Please send me an Email that you agree with the proportional allocation of effort.

I hope you are all well and staying safe during these strange times.

(KIM: can you please forward to Jana? I do not have her current E-mail address).

Will

William K. Boyes, Ph.D.
Neurological and Endocrine Toxicology Branch
Public Health and Integrated Toxicology Division

Center for Public Health and Environmental Assessment
Office of Research and Development
Mail Code B105-04
Environmental Protection Agency
109 T.W. Alexander Drive
Research Triangle Park, NC 27711

Phone: 919-541-7538
Mobile (alternate worksite contact): 919-417-2105
boyes.william@epa.gov

Zucker, Robert

From: Laura Degn <degn.laura@gmail.com>
Sent: Monday, April 27, 2020 3:43 PM
To: Boyes, William
Cc: Zucker, Robert
Subject: STAA award

Hi Will,

I have read the STAA award proportional allocation effort and agree that this is correct.

Let me know if you need any additional information.

Thank you,
Laura Degn

Zucker, Robert

To: jlerner@lightforminc.com
Subject: STAA_zucker

No response

From: Boyes, William <Boyes.William@epa.gov>
Sent: Friday, April 24, 2020 5:25 PM
To: Zucker, Robert <Zucker.Robert@epa.gov>; Jayna Ortenzio (jayna.ortenzio@gmail.com) <jayna.ortenzio@gmail.com>; Laura Degn (degn.laura@gmail.com) <degn.laura@gmail.com>; jlerner@lightforminc.com; Goldstein-Plesser, Alice <goldstein-plesser.alice@epa.gov>; McGee, John <Mcgee.John@epa.gov>; Rogers, Kim <Rogers.Kim@epa.gov>
Subject: STAA 2020 nomination

Hi ALL,

Bob and I decided to nominate three of our nanoparticle papers for a Scientific and Technological Award. A draft of the nomination form is attached, along with the three manuscripts. Unfortunately only EPA authors are eligible for award money even though all authors contributed. We were required to split the proportional effort across authors. We split the 100 % effort evenly giving 33% for each paper. Then we split that 33% evenly among all the authors for each paper, and summed the totals across the three papers.

1. Please review the nomination form and send me any corrections or suggestions.
2. Please send me an Email that you agree with the proportional allocation of effort.

I hope you are all well and staying safe during these strange times.

(KIM: can you please forward to Jana? I do not have her current E-mail address).

Will

William K. Boyes, Ph.D.
Neurological and Endocrine Toxicology Branch
Public Health and Integrated Toxicology Division
Center for Public Health and Environmental Assessment
Office of Research and Development
Mail Code B105-04
Environmental Protection Agency
109 T.W. Alexander Drive
Research Triangle Park, NC 27711

Phone: 919-541-7538
Mobile (alternate worksite contact): 919-417-2105
boyes.william@epa.gov

Robert M. Zucker, PhD
Reproductive and Developmental Toxicology Branch
Public Health and Integrated Toxicology Division
Center for Public Health and Environmental Assessment
Office of Research and Development
U.S. Environmental Protection Agency
109 TW Alexander Drive, Mail Drop B105-04
Research Triangle Park, NC 27709, USA
919-541-1585 (office)
zucker.robert@epa.gov

Shipping Address (Fed. Exp., etc.) for Chemicals/Samples
Attn: (Robert Zucker) Chemical Services, Room E-178
Building E Loading Dock, 109 TW Alexander Drive
RTP, NC 27709 USA

Zucker, Robert

To: McGee, John
Subject: STAA_zucker

No response

From: Boyes, William <Boyes.William@epa.gov>
Sent: Friday, April 24, 2020 5:25 PM
To: Zucker, Robert <Zucker.Robert@epa.gov>; Jayna Ortenzio (jayna.ortenzio@gmail.com) <jayna.ortenzio@gmail.com>; Laura Degn (degn.laura@gmail.com) <degn.laura@gmail.com>; jlerner@lightforminc.com; Goldstein-Plesser, Alice <goldstein-plesser.alice@epa.gov>; McGee, John <Mcgee.John@epa.gov>; Rogers, Kim <Rogers.Kim@epa.gov>
Subject: STAA 2020 nomination

Hi ALL,

Bob and I decided to nominate three of our nanoparticle papers for a Scientific and Technological Award. A draft of the nomination form is attached, along with the three manuscripts. Unfortunately only EPA authors are eligible for award money even though all authors contributed. We were required to split the proportional effort across authors. We split the 100 % effort evenly giving 33% for each paper. Then we split that 33% evenly among all the authors for each paper, and summed the totals across the three papers.

1. Please review the nomination form and send me any corrections or suggestions.
2. Please send me an Email that you agree with the proportional allocation of effort.

I hope you are all well and staying safe during these strange times.

(KIM: can you please forward to Jana? I do not have her current E-mail address).

Will

William K. Boyes, Ph.D.
Neurological and Endocrine Toxicology Branch
Public Health and Integrated Toxicology Division
Center for Public Health and Environmental Assessment
Office of Research and Development
Mail Code B105-04
Environmental Protection Agency
109 T.W. Alexander Drive
Research Triangle Park, NC 27711

Phone: 919-541-7538
Mobile (alternate worksite contact): 919-417-2105
boyes.william@epa.gov

Robert M. Zucker, PhD
Reproductive and Developmental Toxicology Branch
Public Health and Integrated Toxicology Division
Center for Public Health and Environmental Assessment
Office of Research and Development
U.S. Environmental Protection Agency
109 TW Alexander Drive, Mail Drop B105-04
Research Triangle Park, NC 27709, USA
919-541-1585 (office)
zucker.robert@epa.gov

Shipping Address (Fed. Exp., etc.) for Chemicals/Samples
Attn: (Robert Zucker) Chemical Services, Room E-178
Building E Loading Dock, 109 TW Alexander Drive
RTP, NC 27709 USA

Table of Contents

General_Authors_Publications.....2
LI-266498_Kotchenruther_2017.....8
Record_of_Percentage_Agreement_Robert_A_Kotchenruther.....18
Robert_Kotchenruther:_supporting_document.....19
Robert_Kotchenruther:_supporting_document_2.....28
Kotchenruther_2017_AE_supplemental_material.....36

United States Environmental Protection Agency
Washington, DC 20460

STAA REPORT FOR THE SCIENTIST NOMINATIONS

General Information:

Nomination ID/App ID:	20-123
Research Category Primary:	Environmental Policy and Decision-Making Studies (EP)
Research Category Secondary:	
Laboratory/Office Name:	OAR
Nomination Entered By:	Margaret Zawacki

Eligibility Checklist:

[Y] The nominated publication(s) has not been submitted to a previous STAA competition.

[Y] The nominated publication(s) was published on or before January 1, 2017 and on or after January 1,2012

[Y] The principal author was an EPA employee or a PHS employee assigned to EPA when the research was performed

[Y] The EPA authors (includes PHS employees assigned to EPA) contributed collectively a minimum of 50% toward the publication(s)

Nominating Official Name:	Linda Anderson-Carnahan
Nominating Official Title:	ASSOCIATE DIRECTOR
Nominating OfficialEmail:	anderson-carnahan.linda@epa.gov
STAA Coordinator Name:	Kathleen Wiser
STAA Coordinator Email:	wiser.kathi@epa.gov

Justifications:

Justification 1:

This study employs an innovative approach which identified source signatures for Category 3 (C3) marine engines before and after the implementation of fuel sulfur limits in order to understand air quality improvements attributable to these fuel limits. Understanding the impacts of regulatory and voluntary programs on air pollution concentrations is critical to evaluating the effectiveness of air pollution control programs. Source apportionment techniques are an important tool for determining how specific sources affect ambient air quality. The fuel limits studied in this analysis are International Convention for the Prevention of Pollution from Ships (MARPOL) Annex VI fuel sulfur limits in the EPA's North American Emissions Control Area (NA ECA) and are a key component of EPA's coordinated strategy to reduce emissions from ocean-going vessels. Beginning in 2015, the sulfur content of the fuel used onboard ships operating in the NA ECA, foreign or domestic, may not exceed 1,000 ppm. This affects the large cargo-carrying ships that operate in U.S. coasts and waters and, if properly implemented, will result in significant particulate emission reductions extending well into the interior of the country.

The author used positive matrix factorization (PMF), a source apportionment methodology, in a novel way to evaluate particulate matter (PM) reductions from the NA ECA fuel change in U.S. coastal waters. Specifically, the author identified chemical signatures from burning residual fuel oil (RFO) and low-sulfur diesel fuel and applied these signatures to analyze chemically speciated monitoring data from EPA's IMPROVE network. Utilizing the change in chemical signatures, which is related to fuel switching to comply with the NA ECA, the author quantified the pre- and post-NA ECA contribution to ambient $PM_{2.5}$ from C3 engines. This scientifically sound and unique application of a source apportionment methodology quantifies the impact of the NA ECA in a way that hasn't been conducted previously. The results of this analysis highlight the significant air quality improvements that result from the NA ECA fuel sulfur limits and the corresponding environmental and public health benefits. This study adds to EPA's understanding of the impacts of our programs and confirms the importance of careful implementation and oversight of such a control program. In addition to the utility of the results, the documentation of the methodology, data handling and analysis, makes it clear that the work is of high quality and rigor, and advances our understanding on how this type of source apportionment can be applied.

Justification 2A:

N/A The nomination is only for one publication.

Justification 2B:

Robert Kotchenruther, "A Regional Assessment of Marine Vessel PM2.5 Impacts in the U.S. Pacific Northwest Using a Receptor-Based Source Apportionment Method" and "The Effects of Marine Vessel Fuel Sulfur Regulations on Ambient PM2.5 Along the West Coast of the U.S.", 2015, Honorable Mention STAA award.

Justification 2C:

This publication includes a time period when the fuel limits, and extent of where the fuel limits applied, changed in all coastal waters of the continental U.S. Earlier papers had focused on only one region, the U.S. west coast, and the level and extent of the fuel limits were smaller. The analysis time frame and domain for this paper allows at least a year of data from each phase of the fuel limit regulation to be included and statistically significant differences in air pollutant contribution to be identified from all coasts of the continental U.S.

Justification 2D:

N/A Previously submitted nominated articles are listed as supplemental information for the current nomination, but previously submitted supplemental information is not listed as supplemental information for the current nomination.

Justification 2E:

N/A The author has not submitted a concurrent nomination to another research category.

Justification 3A:

The author was an invited speaker at the 2016 U.S.-China Green Ports and Vessels Initiative (GPVI) Workshop, held December 5-8, 2016 in Seattle WA. The GPVI is a bi-lateral collaboration between the United States and China, and is led by the Ministry of Environmental Protection, Ministry of Transport and the United States Environmental Protection Agency. The purpose was to share knowledge and expertise on port and vessel emission control policies, green technologies, enforcement, compliance, and emission inventories. Note, at the time of the conference, the paper had been just been accepted by Atmospheric Environment for publication.

The author also presented this paper's findings at the 2017 annual meeting of the Northwest International Air Quality Environmental Science and Technology Consortium (NW-AIRQUEST), June 14-16, 2017, at Washington State University. This is a Pacific Northwest consortium of air quality scientists, including Canadian scientists from British Columbia. The author has also presented this work internally within EPA, both in EPA R10, and for the Office of Transportation and Air Quality (OTAQ).

According to Google Scholar, on April 29, 2020, the paper has been cited 15 times. On April 29, 2020 the Atmospheric Environment website notes that the paper has been captured 44 times.

Justification 3B:

The journal which published this study, Atmospheric Environment, has an established peer review process.

This journal operates a single blind review process. All contributions are initially assessed by the editor for suitability for the journal. Papers deemed suitable are then typically sent to a minimum of two independent expert reviewers to assess the scientific quality of the paper. The Editor is responsible for the final decision regarding acceptance or rejection of articles.

AUTHORS

Principal Author

Author Name:	Robert A Kotchenruther		
Professional Title:		Salutation:	
Email:	kotchenruther.robert@epa.gov	Organization:	
Mailing Address:			
Street Line 1:	1200 6th Avenue Suite 155 (Mailstop 14-D12)		
City:	Seattle		
Zip Code:	98101-3188	State:	WA
At time of research was:	EPA Employee		
Separation Date:			
% of Effort:	100		

PUBLICATIONS

Publication 1:

Publication Title:	The effects of marine vessel fuel sulfur regulations on ambient PM2.5 at coastal and near coastal mo		
Publication Date:	Wed Feb 01 00:00:00 GMT 2017		
Journal/Publication Method:	Atmospheric Environment		
All Author(s):			
Volume:	151	Number:	NA

Pages:	52-61	Immediately Index:	Immediately Index:
Citation ½ Life:	9.3	Impact Factor:	4.012

Atmospheric Environment 151 (2017) 52–61

Contents lists available at ScienceDirect

Atmospheric Environment

journal homepage: www.elsevier.com/locate/atmosenv

The effects of marine vessel fuel sulfur regulations on ambient $PM_{2.5}$ at coastal and near coastal monitoring sites in the U.S.

Robert A. Kotchenruther

U.S. Environmental Protection Agency Region 10, Office of Environmental Review and Assessment, 1200 Sixth Avenue, Mailstop OEA-140, Seattle, WA, 98101, USA

HIGHLIGHTS

- $PM_{2.5}$ source apportionment was performed for 22 sites in U.S. Coastal States.
- $PM_{2.5}$ impacts from marine vessel residual fuel oil combustion were quantified.
- Ambient effects from implementing an emissions control area were determined.
- Reductions in $PM_{2.5}$ from residual fuel oil combustion aligned with regulations.
- Significant reductions in $PM_{2.5}$ from residual fuel oil combustion were found.

ARTICLE INFO

Article history:
Received 5 October 2016
Received in revised form
2 December 2016
Accepted 5 December 2016
Available online 6 December 2016

Keywords:
$PM_{2.5}$
Marine vessel emissions
Positive matrix factorization
Source apportionment
Residual fuel oil
Emissions control area

ABSTRACT

In August of 2012 the U.S. began implementing fuel sulfur limits on certain large commercial marine vessels within 200 nautical miles (nm) of its coasts as part of a North American Emissions Control Area (NA-ECA). The NA-ECA limited fuel sulfur use in these vessels to below 1% in 2012 and to below 0.1% starting in 2015. This work uses ambient $PM_{2.5}$ monitoring data from the U.S. IMPROVE network and Positive Matrix Factorization (PMF) receptor modeling to assess the effectiveness of the NA-ECA at reducing ambient $PM_{2.5}$ from high-sulfur residual fuel oil (RFO) use. RFO combustion emissions of $PM_{2.5}$ are known to have a fairly unique vanadium (V) and nickel (Ni) trace metal signature. To determine if IMPROVE sites were affected by residual fuel oil combustion, V and Ni data from 65 IMPROVE sites in coastal States of the U.S. were analyzed from 2010 to 2011, the two years prior to NA-ECA implementation. 22 of these IMPROVE sites had a V and Ni correlation coefficient (r^2) greater than 0.65 and were selected for further analysis by PMF. The slopes of the correlations between V and Ni at these 22 sites ranged from 2.2 to 4.1, consistent with reported V:Ni emission ratios from RFO combustion. Each of the 22 IMPROVE sites was modeled independently with PMF, using the available $PM_{2.5}$ chemical speciation data from 2010 to 2015. PMF model solutions for the 22 sites contained from 5 to 9 factors, depending on the site. At every site a PMF factor was identified that was associated with RFO combustion, however, 9 sites had PMF factors where RFO combustion was mixed with other aerosol sources. For the remaining 13 sites, $PM_{2.5}$ from RFO combustion was analyzed for three time periods; 2010–2011 representing the time period prior to the NA-ECA implementation (pre-NA-ECA), 2013–2014 representing the time period where fuel sulfur was limited to 1.0% (NA-ECA 1.0% S), and 2015 representing the time period where fuel sulfur was limited to 0.1% (NA-ECA 0.1% S). All 13 sites indicated statistically significant reductions in the contribution of RFO combustion to $PM_{2.5}$ between the pre-NA-ECA period and the two periods of fuel sulfur control. The average decrease in annual average $PM_{2.5}$ from RFO combustion from the pre-NA-ECA to NA-ECA 1% S period was 50.2% (range, 29.0%–65.4%) and from the pre-NA-ECA to NA-ECA 0.1% S period was 74.1% (range, 33.0%–90.4%).

Published by Elsevier Ltd.

1. Introduction

Human exposure to fine particulate matter ($PM_{2.5}$, particles with aerodynamic diameter <2.5 μm) has been linked to cardiovascular and pulmonary disease (Künzli et al., 2005), and lung cancer and

E-mail address: Kotchenruther.Robert@epa.gov.

http://dx.doi.org/10.1016/j.atmosenv.2016.12.012
1352-2310/Published by Elsevier Ltd.

premature mortality (Pope and Dockery, 2006). Anthropogenic emissions of $PM_{2.5}$ also play a role in climate forcing (IPCC, 2014) and deposition of anthropogenic PM can have adverse effects on ecosystem health (Geiser et al., 2010).

Examining air emissions from large commercial marine vessels (CMVs) has been an active area of investigation because these sources typically burn residual fuel oil (RFO), which has a very high sulfur content and high emissions of $PM_{2.5}$, SO_2, and NO_x (Moldanova et al., 2009), and also because CMVs are mobile sources impacting both urban areas and remote coastal areas that have few other direct sources of anthropogenic emissions. RFO is one of several products produced from oil refinery residuum, the residue left over after crude oil distillation. Environmental regulations in developed countries have contributed to a significant decline in onshore applications of RFO as a fuel source. Excluding maritime applications, between 1986 and 2010 the use of RFO as a fuel source in OECD countries has declined by nearly 70% (Ramberg and Van Vactor, 2014). However, until recently, RFO use as a fuel source for CMVs in most areas of the world has been unregulated, and during the same 1986 to 2010 period RFO use as a marine fuel has increased by about 100% (Ramberg and Van Vactor, 2014).

Globally, approximately 60,000 cardiopulmonary and lung cancer deaths annually have been attributed to exposure to marine vessel emissions (Corbett et al., 2007). Regulating marine vessel fuel sulfur content is a typical approach to reducing emissions. Previous studies have shown that significant reductions in $PM_{2.5}$ and SO_2 occur when ocean going vessels switch from high to low sulfur fuels (Kasper et al., 2007; Khan et al., 2012) and Winebrake et al. (2009) have shown that significant reductions in premature mortality from marine vessel emissions can be achieved by regulating fuel sulfur content below the assumed uncontrolled fuel sulfur content of 2.7%.

Concerns over health and ecological effects of marine vessel emissions led the United States (U.S.) and Canadian governments in 2009 to propose to the International Maritime Organization (IMO) the inclusion of North America in an Emissions Control Area (ECA). In March of 2010 the IMO amended the International Convention for the Prevention of Pollution from Ships (MARPOL) to designate specific portions of North American waters as an ECA (U.S. EPA, 2010). Other existing ECAs include the Baltic Sea and North Sea. Beginning in August 2012, the North American ECA (NA-ECA) required marine vessels within 200 nautical miles (nm) of North American coasts, in waters subject to U.S. and Canadian jurisdiction, to use fuels with sulfur content below 10,000 ppm (1%). Starting in 2015 the NA-ECA required a 0.1% fuel sulfur limit in the designated coastal regions. IMO MARPOL regulations have also set a worldwide fuel sulfur limit of 3.5% starting in 2012, and 0.5% starting in 2020.

Regionally within the U.S., in July 2009 the State of California (CA) implemented their Ocean-Going Vessel Clean Fuel Regulation (CA-CFR, http://www.arb.ca.gov/ports/marinevess/ogv.htm). Phase I of the regulation became effective July 1, 2009 and required ocean-going vessels within 24 nm of the CA coast to use distillate fuels with sulfur content at or below 1.5% and after August 1, 2012 to use distillate fuels at or below 1.0%. Starting January 1, 2014, Phase II of the regulation required distillate fuels at or below 0.1% sulfur.

Compliance with the NA-ECA and CA-CFR are expected to come predominantly through fuel switching to lower sulfur liquid fuels. However, utilization of liquefied natural gas or SOx scrubbing may also be means by which vessel operators seek to meet the regulatory requirement. Regardless of the methods used, all are expected to result in significant reductions in $PM_{2.5}$ from marine vessels.

Previous Positive Matrix Factorization (PMF) receptor modeling studies have demonstrated the ability to quantify the contribution of marine vessel RFO combustion to $PM_{2.5}$ (Kotchenruther, 2013, 2015; and references therein) and quantified $PM_{2.5}$ reductions that occurred along the U.S. West Coast as a result of implementing the initial phases of the NA-ECA and CA-CFR (Kotchenruther, 2015). In this work, $PM_{2.5}$ from U.S. monitoring sites along the East, West, and Gulf coasts of the U.S. are analyzed spanning a period from 2010 through 2015, which includes a year or more of data through each phase of the NA-ECA regulation (unregulated, 1.0% sulfur, and 0.1% sulfur limit). PMF receptor modeling is used to quantify the $PM_{2.5}$ contribution from marine vessel RFO combustion, and statistical analysis is used to determine if changes in the contribution of RFO combustion to $PM_{2.5}$, as a result of NA-ECA implementation, are statistically significant.

2. Methods

2.1. Chemically speciated $PM_{2.5}$ data

Chemically speciated $PM_{2.5}$ data were obtained from the Interagency Monitoring of Protected Visual Environments (IMPROVE) Network. IMPROVE samplers collect 24-h integrated $PM_{2.5}$ mass and are operated on a once every third day schedule. Information about the IMPROVE network can be found on the IMPROVE web site (http://vista.cira.colostate.edu/improve/).

Data were analyzed from January 1, 2010 through December 31, 2015. This data record includes three distinct periods with respect to marine vessel fuel sulfur regulations from the NA-ECA; a 31 month period (1/2010 to 7/2012) prior to implementation of the NA-ECA (2.7% world-wide sulfur average), a 29 month period (8/2012 to 12/2014) after implementation of the initial phase of the NA-ECA (1.0% fuel sulfur limit), and a 12 month period (1/2015 to 12/2015) after implementation of the second phase of the NA-ECA (0.1% sulfur limit). These three time periods will be subsequently referred to as the pre-NA-ECA, NA-ECA 1.0% S, and NA-ECA 0.1% S, respectively.

2.2. Monitoring site selection

All IMPROVE sites in U.S. States along the West, East, and Gulf coasts as well as Hawaii were considered for PMF analysis as long as sites had a monitoring record spanning the full study period. The geographic distribution of sites considered within the continental U.S. is shown in Fig. 1, and information about the resulting 65 IMPROVE sites is listed in a table in the Supplemental materials. Of the 65 sites initially considered, site selection for PMF modeling was further narrowed based on vanadium (V) and nickel (Ni) correlation coefficients (r^2). V and Ni are well known trace metals associated with RFO combustion emissions, with V:Ni emission ratios in marine vessel RFO combustion tests typically ranging between 2 and 4.5 (Popovicheva et al., 2012; Agrawal et al., 2008). V and Ni linear r^2 and best fit slopes were computed for the 65 sites based on data from 2010 to 2011, the two years prior to implementation of the NA-ECA. A table listing the V and Ni linear r^2 and best fit slopes for these sites is provided in the Supplemental materials. Sites were selected for PMF analysis if the V:Ni r^2 was greater than 0.65. This resulted in 22 IMPROVE sites, which are listed in Table 1 and identified in Fig. 1. The V:Ni linear best fit slopes for these 22 sites ranged between 2.2 and 4.1, which is consistent with reported V:Ni emissions ratios for marine vessel RFO combustion. For each of the sites listed in Table 1, 48 h back-trajectories were computed for the ten days with highest V + Ni concentrations in 2010 and 2011 using the HYSPLIT model (Stein et al., 2015). These trajectories are provided in the Supplemental materials and demonstrate that air with high V + Ni impacting the sites on these days was overwhelmingly of marine origin, further suggesting a marine vessel origin for the V and Ni.

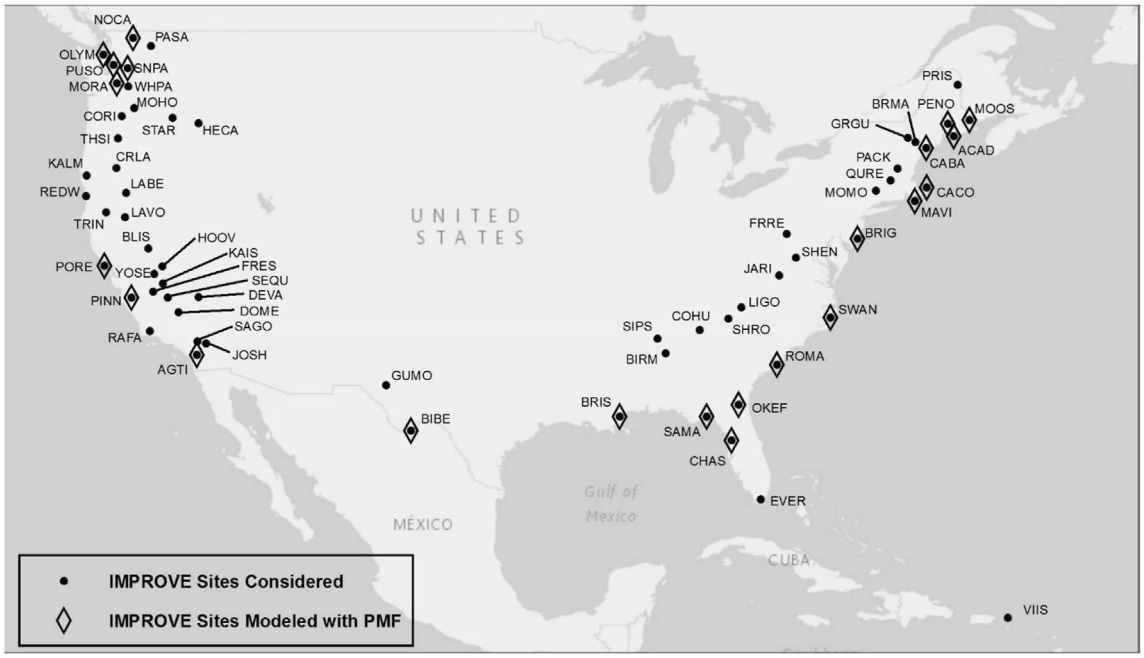

Fig. 1. IMPROVE sites used in this analysis.

2.3. Data preparation and treatment

IMPROVE datasets were processed to correct for missing or negative values, data completeness issues, and species double counting. A detailed discussion of these data preparations is provided in a previous publication by Kotchenruther (2015) and briefly summarized here. Chemical species were omitted in PMF modeling if more than 40% of samples had missing data. For remaining chemical species, missing values were replaced with median concentrations and the uncertainty set to a very high value compared to measured data, typically four times the species median concentration, to minimize the influence of the replaced data on the model solution. Any negative concentrations were reset to zero. The uncertainty of each measurement was estimated based on the measured analytical uncertainty plus 1/3 of the method detection limit. The signal-to-noise (S/N) ratio was also used to evaluate whether chemical species should be included in the PMF modeling, and was used to adjust the data uncertainty. Chemical species were omitted in PMF modeling if the S/N ratio was less than 0.5. For chemical species with S/N between 0.5 and 1.0, data uncertainties were multiplied by a factor of 3 to down-weight the influence of these species in the model solution (Norris et al., 2014). For chlorine, measured in the IMPROVE network by both elemental (Cl) and ion analyses (Cl-), Cl-data was used because of better S/N ratios and Cl not used to avoid double counting. Also, the reported lowest temperature fraction of EC, EC1, is actually the sum of pyrolyzed

Table 1
IMPROVE monitoring sites modeled with PMF in this study.

IMPROVE site name	Abbreviation	State	Latitude	Longitude	Elevation (m)
U.S. West Coast Sites					
North Cascades	NOCA	WA	48.7316	−121.0646	569
Olympic	OLYM	WA	48.0065	−122.9727	600
Puget Sound	PUSO	WA	47.5696	−122.3119	98
Snoqualmie Pass	SNPA	WA	47.4220	−121.4259	1 049
Mount Rainier NP	MORA	WA	46.7583	−122.1244	439
Point Reyes National Seashore	PORE	CA	38.1224	−122.9085	97
Pinnacles NM	PINN	CA	36.4833	−121.1568	302
Agua Tibia	AGTI	CA	33.4636	−116.9706	508
U.S. Gulf Coast Sites					
Big Bend NP	BIBE	TX	29.3027	−103.1780	1 067
Breton Island	BRIS	LA	30.1086	−89.7617	−7
St. Marks	SAMA	FL	30.0926	−84.1614	8
Chassahowitzka NWR	CHAS	FL	28.7484	−82.5549	4
U.S. East Coast Sites					
Moosehorn NWR	MOOS	ME	45.1259	−67.2661	78
Penobscot	PENO	ME	44.9480	−68.6479	45
Acadia NP	ACAD	ME	44.3771	−68.2610	157
Casco Bay	CABA	ME	43.8325	−70.0644	27
Cape Cod	CACO	MA	41.9758	−70.0242	49
Martha's Vineyard	MAVI	MA	41.3309	−70.7846	3
Brigantine NWR	BRIG	NJ	39.4650	−74.4492	5
Swanquarter	SWAN	NC	35.4510	−76.2075	−4
Cape Romain NWR	ROMA	SC	32.9410	−79.6572	5
Okefenokee NWR	OKEF	GA	30.7405	−82.1283	48

organic carbon (OP) and low temperature combusting EC. Hence, EC1 was recalculated as EC1-OP and the measured OP value was used, so as not to double count measured OP.

2.4. Source apportionment

Source apportionment modeling was performed using EPA PMF 5.0 (Norris et al., 2014). A discussion of the mathematical equations underlying EPA PMF can be found in Paatero and Hopke (2003) and Norris et al. (2014). Data from each monitoring site was modeled independently. In each case, the model was run in the robust mode with 20 repeat runs to insure the model least-squares solution represented a global rather than local minimum and the rotational F_{PEAK} variable was held at the default value of 0.0. The model solution with the optimum number of factors was determined somewhat subjectively and was based on inspection of the factors in each solution, the quality of the least-squares fit (analysis of Q_{Robust} and Q_{True} values), and the results from three error estimation methods available in PMF 5.0; bootstrapping (BS), displacement (DISP), and bootstrapping with displacement (BS-DISP) (Norris et al., 2014; Paatero et al., 2014). The scaled residuals for final model solutions were generally normally distributed, falling into the recommended range of +3 to −3.

PMF factors can represent a single source or source category (e.g., RFO combustion, wood burning), a chemical composition (e.g., ammonium nitrate, sea salt), or mixtures of sources and compositions. During PMF modeling of each of the 22 sites in this work, it was sometimes the case that the solution that appeared to present the best delineation of sources and compositions, was in fact shown to have too much solution instability after analysis with DISP, BS, and BS-DISP (e.g., factor swaps; Brown et al., 2015). In cases like this, reducing the number of factors often led to improved solution stability, but also caused some factors to combine and become mixtures of sources, or sources and compositions. Preference in PMF solutions was given to the number of factors with improved solution stability, even if that lead to reduced source delineation. Further information on how the model solution with the optimal number of factors was selected is provided in the Supplemental materials.

3. Results and discussion

3.1. Identified $PM_{2.5}$ sources and compositions

PMF modeling for each of the 22 sites resulted in solutions with from 5 to 9 factors, depending on the site. Table 2 lists the 12 different sources and compositions that were identified at the 22 sites, at how many sites each source or composition was identified, and how often they were identified in a factor by themselves versus in a factor mixed with other sources or compositions. A table in the Supplemental materials lists each site, the number of factors found, and the factor attributions using the source or composition identifiers listed in Table 2. PMF factor mass time series and factor chemical profiles for each site are also provided in the Supplemental materials. The chemical profiles presented in the Supplemental materials are those after the factor chemical composition from each site was normalized. A factor chemical composition was normalized by first assuming an organic mass (OMC) to OC ratio of 1.8 (i.e., multiplying all OC fraction by 1.8). An OMC to OC ratio of 1.8 is a common ratio used for rural and remote monitoring sites and is used to account for the full mass of organic material, not just the carbon portion. Second, in order to fully account for all sulfate and nitrate mass, sulfate and nitrate were assumed to be fully neutralized and present as ammonium sulfate and ammonium nitrate. Ammonium ion is not measured in the IMPROVE network, but given the rural and remote locations of most monitors, full neutralization is a reasonable assumption. Third, to fully account for the mass of fugitive dust, for factors associated with fugitive dust a metal oxide to metal ratio was assumed for aluminum (Al, ratio of 2.2), calcium (Ca, 1.63), iron (Fe, 2.42), titanium (Ti, 1.94), and silicon (Si, 2.49) based on the ratios used in the IMPROVE network (Solomon et al., 2014). Lastly, all of these components and the remaining measured species were summed and each chemical component was divided by the sum to normalize the chemical profile. Presenting the normalized chemical profiles gives a better representation of the importance of each chemical species to the overall profile, and is needed for profile comparisons across multiple sites.

The sources and compositions listed in Table 2 were identified by comparing the chemical composition of PMF factors with chemical profiles in EPA's SPECIATE database of source emissions test data (https://www3.epa.gov/ttnchie1/software/speciate/), comparison with similar PMF factor chemical compositions identified in existing published studies, knowledge of the seasonal emissions patterns of aerosol sources, and composition of aerosols found in the natural environment (e.g., fugitive dust, sea salt). The sections below describe how each source or composition was identified, and for the 7 most commonly found, Fig. 2 depicts the average PMF factor chemical profile from multiple sites. Average profiles were calculated only from those factors that were determined not to be a mixture. The number of individual profiles making up the average profiles in Fig. 2 ranged from 6 to 21, and depended on how well resolved the source or composition was in the modeling results across all sites. Data tables for the average profiles are provided in the Supplemental materials. The average factor profiles were taken after the PMF factor chemical profile

Table 2
Sources and chemical compositions identified by PMF, and the number of sites where appearing as a single PMF factor, or in a factor mixed with other listed sources or chemical compositions.

Source or composition identifier	Identified source or composition	Number of sites where appears	Number of sites where a single factor	Number of sites where in a mixed factor
1	Residual Fuel Oil Combustion	22	13	9
2	Ammonium Sulfate	22	18	4
3	Wood Smoke and Secondary Organic Carbon	22	12	10
4	Fugitive Dust	22	16	6
5	Motor Vehicles	21	6	15
6	Sea Salt	21	21	0
7	Ammonium Nitrate	19	13	6
8	Aged Sea Salt	5	1	4
9	Potassium Rich Ammonium Sulfate	5	2	3
10	Unidentified Organic Aerosol	4	1	3
11	Calcium Rich Fugitive Dust	1	1	0
12	Iron Rich	1	1	0

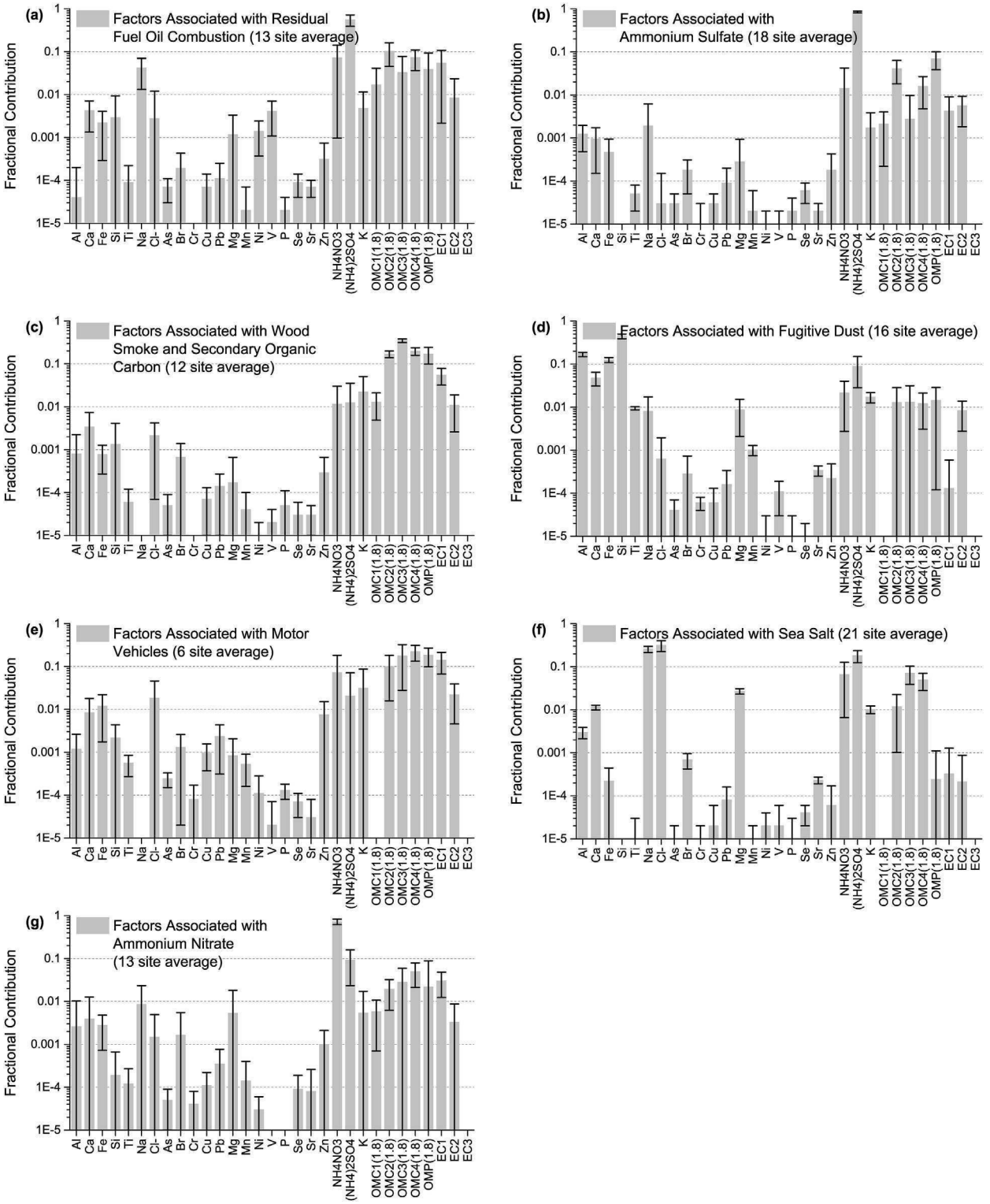

Fig. 2. Average and standard deviation of chemical profiles from PMF factors from multiple sites associated with (a) residual fuel oil combustion, (b) ammonium sulfate, (c) wood smoke and secondary OC, (d) fugitive dust, (e) motor vehicles, (f) sea salt, and (g) ammonium nitrate.

from each site was normalized as described above. Average profiles offer a more robust representation of the chemical composition of an aerosol source than do results from a single PMF solution, and could be useful for comparison to other source apportionment analyses, or even used as source profile inputs in Chemical Mass Balance receptor modeling.

3.1.1. PMF factors associated with residual fuel oil combustion

A PMF factor containing RFO combustion was identified at all 22 sites modeled. This was expected because these sites were chosen based on strong V:Ni correlations and had correlation slopes in the ambient data similar to marine vessel RFO emissions ratios. At 9 sites, inspection of the chemical composition of the factor

associated with RFO combustion resulted in the determination that the factor represented a mixture of other sources in addition to RFO combustion. At the 13 remaining sites, the factor associated with RFO combustion was judged not to be mixed with other sources. At these 13 sites, the V:Ni ratio in the PMF chemical profiles ranged from 2.4 to 3.9 with an average value of 2.9. These V:Ni ratios were similar that from the ambient measurements, which ranged from 2.2 to 3.7 with an average of 3.0 (see Supplemental materials) and are similar to ratios found in Kotchenruther (2015). The average chemical profile from PMF factors at these 13 sites is shown in Fig. 2a.

Other than several categories of stationary sources, no other significant sources of V and Ni have V:Ni emissions ratios above 1.0 in the EPA SPECIATE database. While contributions from stationary sources cannot be completely ruled out, the coastal and remote locations of most sites considered here, along with the marine origin of back-trajectories on high V + Ni monitored days in 2010–2011, suggests RFO combustion from marine vessels is the likely dominant source of V and Ni.

Sulfate is an important component of all PMF factors that were associated with RFO combustion. However, sulfate is a ubiquitous component of ambient $PM_{2.5}$ whenever chemical speciation of $PM_{2.5}$ is performed, and there are often many sources of environmental sulfate. In order to ensure that changes in RFO combustion factor concentrations were not associated with changes in emissions from other sources of environmental sulfate, model results for marine vessel RFO combustion are only used to analyze the effect of the NA-ECA if PMF modeling passed acceptable performance criteria from all three uncertainty estimation methods (BS, DISP, and BS-DISP) recommended in the PMF 5.0 user's guide (Norris et al., 2014) and a separate ammonium sulfate factor was found at that site. A previous publication (Kotchenruther, 2015) demonstrated that when these criteria were met, statistically significant changes in the contribution of RFO combustion to $PM_{2.5}$ only occurred in areas where fuel sulfur was being regulated, even though all sites had shown a statistically significant reduction in ambient sulfate. This gave confidence in the previous published results that changes in the contribution of RFO combustion to $PM_{2.5}$ identified by PMF were not associated with sulfur reduction measures implemented in other source sectors. Adhering to the same performance criteria in this work bolsters a similar confidence.

For 4 of the 9 sites mentioned above where RFO combustion was found to be part of a factor mixed with other sources, this determination was made because no separate factors were identified containing secondary sulfate. In these cases, it was assumed that the sulfate component of the factor associated with RFO combustion represented multiple sources of environmental sulfate, not just from RFO combustion. Hence, these factors were deemed to be from a mixture of sources. At 3 of the 9 sites, RFO combustion was determined to be mixed with other sources of organic aerosol, and at 2 of the 9 sites RFO combustion was determined to be mixed with aged sea salt.

3.1.2. PMF factors associated with ammonium sulfate

The main chemical constituent in this factor was sulfate and was assumed to be fully neutralized by ammonium. This factor typically had a seasonal pattern of higher mass attributions in summer months. The average chemical profile from PMF factors at 18 sites where this source was not mixed with other sources is shown in Fig. 2b.

3.1.3. PMF factors associated with wood smoke and secondary organic carbon

A factor mixing secondary organic aerosol with wood smoke emissions. This factor occurred, unmixed with other sources, at 12 sites and was characterized by a chemical profile dominated by organic carbon (OC), elemental carbon (EC), and potassium and a $PM_{2.5}$ mass time series at most sites having occasional spikes above 5 μg/m3 on top of continuous contributions between 0.5 and 1 μg/m3. The average chemical profile from PMF factors at 12 sites where this source was not mixed with other sources is shown in Fig. 2c.

3.1.4. PMF factors associated with fugitive dust

The principal chemical constituents in this factor were Al, Ca, Fe, and Si. Significant trace constituents were Ti and K. The typical seasonal pattern of mass is higher in late summer and lower in winter and spring and corresponds to the typical seasons with less and more precipitation, respectively. The average chemical profile from PMF factors at 16 sites where this source was not mixed with other sources is shown in Fig. 2d. The fractional contributions of the principal and trace chemical constituents in the average profile are similar to that of numerous soil dust profiles in EPA's SPECIATE database.

3.1.5. PMF factors associated with motor vehicles

The principal chemical constituents in this factor were EC1, OC2, OC3, OC4, and OP. Significant trace constituents were zinc (Zn), lead (Pb), copper (Cu), and Fe. The average chemical profile from PMF factors at 6 sites where this source was not mixed with other sources is shown in Fig. 2e. The dominant chemical constituents are similar to those found for motor vehicles in previous publications (Zhao and Hopke, 2004; Kim and Hopke, 2006; Hwang and Hopke, 2007). The significant trace metal constituents match those commonly found in $PM_{2.5}$ associated with motor vehicles (Song and Gao, 2011; Pant and Harrison, 2013). These factors represent a mixture of vehicle exhaust and non-exhaust (e.g., tire wear) emissions. The near ubiquity of this source at the sites in this study matches the conceptual understanding of motor vehicles as a common source of particulate pollution. Separate factors for gasoline and diesel vehicles were not found in this study, and this factor likely represents a combination of these sources.

3.1.6. PMF factors associated with sea salt

This factor was dominated by Na and Cl. Significant trace constituents were magnesium (Mg) and Ca. Mass impacts for this factor had no discernable seasonal pattern, suggesting these factors are from natural sources rather than winter road salting. The average chemical profile from PMF factors at 21 sites where this source was not mixed with other sources is shown in Fig. 2f.

3.1.7. PMF factors associated with ammonium nitrate

The main chemical constituent in this factor was nitrate and was assumed to be fully neutralized by ammonium. The typical seasonal pattern of mass impacts showed high winter and low summer impacts, which is indicative of secondary formation, and likely from multiple sources of NO_x. The average chemical profile from PMF factors at 13 sites where this source was not mixed with other sources is shown in Fig. 2g.

3.1.8. PMF factors associated with aged sea salt

This factor had the same identifying features as Sea Salt, but with little or no Cl and the addition of a significant contribution from nitrate. The replacement of Cl with nitrate is typical of sea salt after aging (Adachi and Buseck, 2015).

3.1.9. PMF factors associated with potassium rich ammonium sulfate

The main chemical constituent in this factor was sulfate with a significant contribution from potassium. Sulfate was assumed to be fully neutralized by ammonium.

3.1.10. PMF factors associated with unidentified organic aerosol

This classification was given to factors that contained a significant amount of organic mass that could not otherwise be identified. Most factors showed higher concentrations in summer, which could indicate an association with secondary organic aerosol. 4 of the 22 sites had factors like this.

3.1.11. PMF factors associated with calcium rich fugitive dust

This factor was similar to fugitive dust, but with a significantly higher calcium concentration than the typical fugitive dust chemical profile.

3.1.12. PMF factors associated with iron rich

This factor was dominated by Fe, OC2, OC3, OC4, and EC1. Significant trace constituents were chromium, Cu, Zn, and manganese. This factor was only found in Seattle. It is likely this factor is related to metal fabrication or other industrial activity.

3.2. PMF results and NA-ECA effectiveness at reducing RFO combustion from marine vessels

The effectiveness of the NA-ECA at reducing contributions from marine vessel RFO combustion to $PM_{2.5}$ was assessed at the 13 sites where PMF results indicated a well delineated factor associated with RFO combustion (see Section 2.4 above). NA-ECA effectiveness could not be easily assessed at those 9 sites where mixed factors containing RFO combustion were identified. NA-ECA effectiveness was assessed by determining if statistically significant reductions in $PM_{2.5}$ from RFO combustion had occurred. Significance testing was performed using the nonparametric Wilcoxon-Mann-Whitney (WMW) test (ProUCL version 5.0; https://www.epa.gov/land-research/proucl-software).

The distribution of mass impacts for PMF factors associated with RFO combustion was compared between three time periods associated with differing NA-ECA fuel sulfur regulation; 24 months (1/2010 to 12/2011) in the pre-NA-ECA period, 24 months (1/2013 to 12/2014) in the NA-ECA 1.0% S period, and 12 months (1/2015 to 12/2015) in the NA-ECA 0.1% S period. Full annual time periods were compared in the statistical analyses, either 12 or 24 months, because PMF factors associated with RFO combustion at many sites had a pronounced seasonal cycle with higher summer values and lower winter values. This seasonal cycle can be explained by increased stability in the summertime marine boundary layer compared to winter. The heightened stability in the summer marine boundary layer more efficiently traps marine vessel exhaust plumes, and as these plumes transition from over water to over land they undergo coastal fumigation. Because a similar seasonal cycle is observed in the ambient V and Ni measurements, the seasonal cycle is not thought to be significantly related to elevated secondary production of sulfate in summer. However, increased summertime marine vessel activity may contribute to the observed season cycle in some locations, such as locations impacted by seasonal cruise ship activity.

Fig. 3 shows three examples of time series of PMF factors associated with RFO combustion, the $PM_{2.5}$ from RFO combustion at OLYM, BRIS, and CACO IMPROVE monitoring sites. Decreases in $PM_{2.5}$ mass from RFO combustion are apparent in each period of the NA-ECA regulation. Time series of mass impacts for all factors can be found in the Supplemental materials.

Table 3 shows the annualized (the average of 24 or 12 monthly averages) average RFO mass contribution to $PM_{2.5}$ at the 13 IMPROVE sites for the pre-NA-ECA, NA-ECA 1.0% S, and NA-ECA 0.1% S periods. Table 3, Fig. 4, and Fig. 5 show the percent change in annualized average RFO mass from the pre-NA-ECA to NA-ECA 1% S periods and from the pre-NA-ECA to NA-ECA 0.1% S periods. Changes in RFO mass between these periods were all found to be statistically significant at the 99% confidence interval using the WMW test.

To isolate the effect of the NA-ECA regulation from the CA-CFR regulation, results for the 2 sites in CA were excluded. For the remaining 11 sites, the average decrease in $PM_{2.5}$ from RFO combustion was 50.2% from the pre-NA-ECA to NA-ECA 1% S period and 74.1% from the pre-NA-ECA to NA-ECA 0.1% S period.

Decreases in $PM_{2.5}$, from the pre-NA-ECA baseline period of 2010–2011 to the NA-ECA 0.1% S period in 2015, were greater than 77.2% at every site except for the two U.S. Gulf Coast IMPROVE sites of SAMA and CHAS, which only showed reductions of 33.0% and 35.4%, respectively. It is unclear why these two sites did not see similar reductions as the other sites. Potential explanations include that there may be other sources of RFO combustion besides marine vessels that are impacting these sites, that there may be lax compliance with the NA-ECA in this region, or that the ECA zone near the southeastern Florida coast narrows to much less than 200 nm because the ECA cannot be enforced in the territorial waters of other counties. Hence, unregulated emissions outside of that narrowed ECA zone may be impacting these sites. Further study and tracking is recommended.

3.3. Other possible factors influencing the PMF results for changes in annual $PM_{2.5}$ from RFO combustion

In addition to the implementation of marine vessel fuel sulfur regulations, annual changes in marine vessel traffic could affect the amount of marine vessel $PM_{2.5}$ contributing to ambient monitors. To address this concern, data for annual waterborne shipping tonnage in U.S. costal states and annual shipping container traffic volume at major ports were analyzed from 2010 to the latest year of available data, 2014 (US Army Corps of Engineers, 2016). Both data sets showed that annual ship traffic was relatively steady over the 5-year period. Data tables for shipping tonnage and shipping container traffic are provided in the Supplemental data. In regards to passenger vessel traffic such as from cruise ships, annual cruise ship port calls in many ports have also remained relatively constant in the 2010–2015 period covered in this study (e.g., Port of Seattle, 2016; Port Tampa Bay, 2016).

The chemical composition of fuels used by ocean-going vessels can also vary. This study assumes that, in the absence of fuel sulfur regulations, most marine vessels capable of using RFO fuels will do so because of the low cost. However, RFO is a general term for residual fuels that can have varying chemical compositions. While the global average sulfur content of RFO used by marine vessels has been relatively stable between 2.6 and 2.7% in recent years, the sulfur content of RFO on individual ships can vary depending on the fuels' source region (IMO, 2011). The V and Ni concentrations in RFO can span a wide range (Kasper et al., 2007; Khan et al., 2012), however, as noted above the V to Ni ratio in RFO combustion tests typically ranges between 2 and 4.5. While temporal changes in the chemical composition of RFO used along the U.S. coasts could not be determined with available data sources, given that the global average sulfur content has been relatively stable during the time period of this study, it is likely that chemical composition changes implemented to meet the fuel sulfur regulations are significantly larger than the temporal fluctuations in average RFO chemical composition used in the U.S. coastal regions.

Change in meteorology between the years analyzed in this study is also a source of potential variability effecting these results. The most influential meteorological variables are likely precipitation, wind speed, wind direction, and factors effecting coastal fumigation dynamics. However, given the temporal and geographic scope

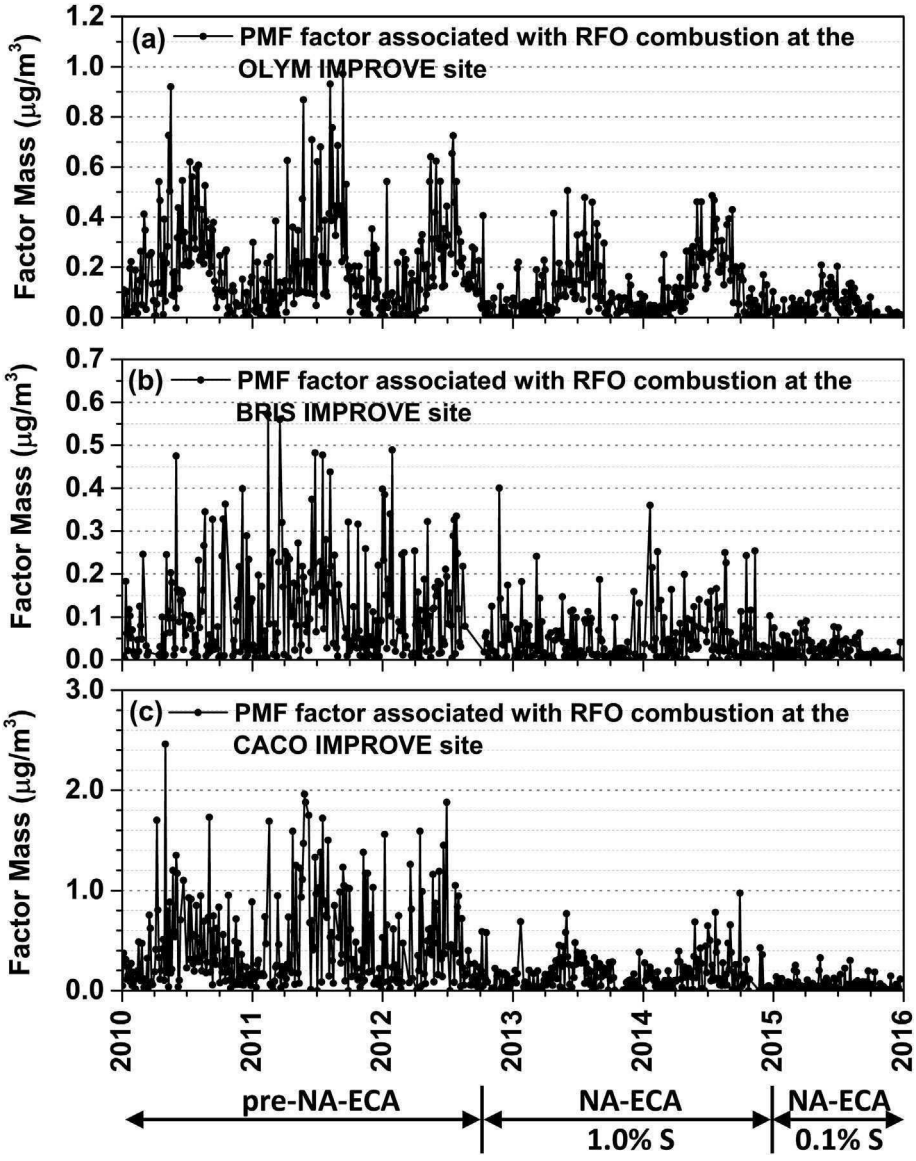

Fig. 3. Time series of PMF factors associated with RFO combustion at the OLYM, BRIS, and CACO IMPROVE monitoring sites.

Table 3
Annualized average RFO combustion emissions contribution to $PM_{2.5}$ for the pre-NA-ECA, NA-ECA 1% S, and NA-ECA 0.1% S periods and percent change in RFO combustion emissions contribution between the annualized average periods.

IMPROVE monitor abbreviation	pre-NA-ECA (2010–2011) RFO mass (μg/m3)	NA-ECA 1% S (2013–2014) RFO mass (μg/m3)	NA-ECA 0.1% S (2015) RFO mass (μg/m3)	pre-NA-ECA to NA-ECA 1% S RFO mass change (%)	pre-NA-ECA to NA-ECA 0.1% S RFO mass change (%)
U.S. West Coast Sites					
OLYM	0.205	0.119	0.039	−41.9	−81.0
PUSO	0.511	0.286	0.104	−44.0	−79.7
PORE	0.005	0.003	0.001	−51.7	−81.6
AGTI	0.235	0.081	0.040	−65.6	−83.0
U.S. Gulf Coast Sites					
BRIS	0.108	0.051	0.021	−53.2	−80.9
SAMA	1.124	0.797	0.753	−29.0	−33.0
CHAS	0.806	0.552	0.521	−31.5	−35.4
U.S. East Coast Sites					
PENO	0.060	0.031	0.009	−48.6	−84.4
ACAD	0.019	0.008	0.002	−57.0	−87.4
CABA	0.735	0.258	0.167	−64.9	−77.3
CACO	0.459	0.159	0.053	−65.4	−88.6
BRIG	0.454	0.169	0.044	−62.7	−90.4
ROMA	0.916	0.425	0.209	−53.6	−77.2

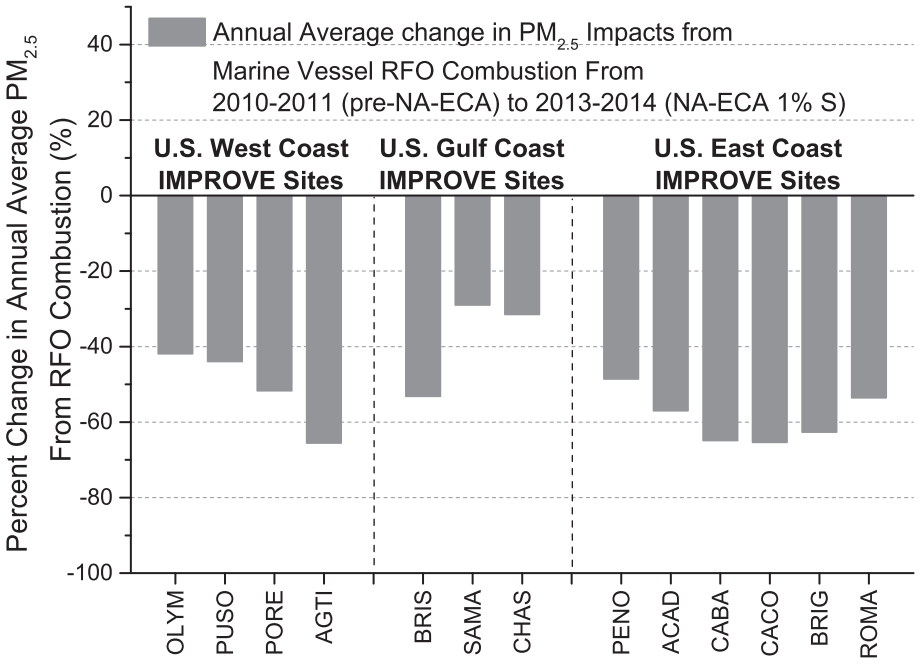

Fig. 4. Percent change in annual average $PM_{2.5}$ from marine vessel RFO combustion from the pre-NA-ECA (2010–2011) to NA-ECA 1% S (2013–2014) periods.

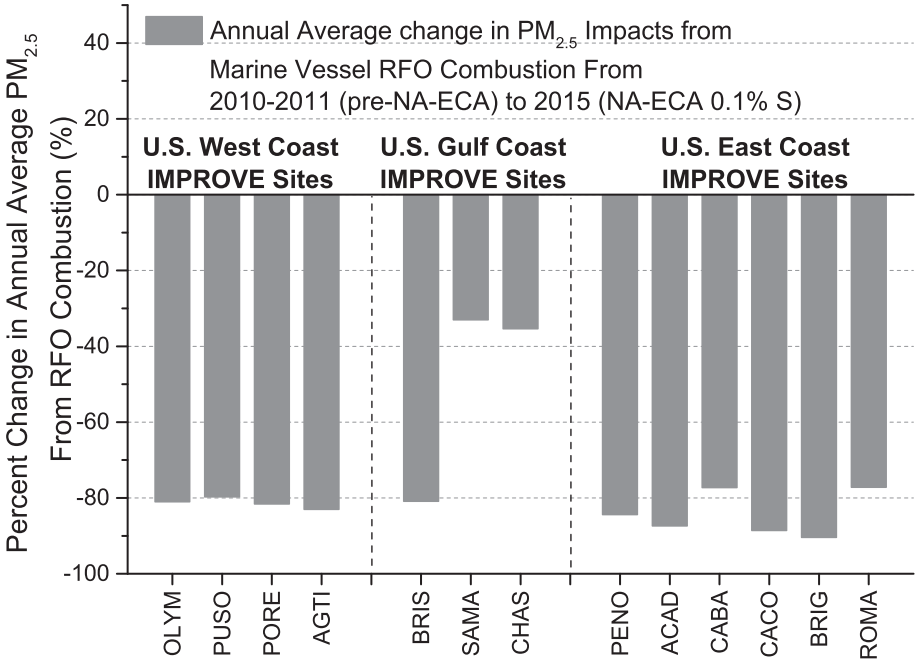

Fig. 5. Percent change in annual average $PM_{2.5}$ from marine vessel RFO combustion from the pre-NA-ECA (2010–2011) to NA-ECA 0.1% S (2015) periods.

of this work, a detailed meteorological analysis for each site is beyond the scope of this study.

4. Conclusions

This work uses ambient $PM_{2.5}$ monitoring data from the U.S. IMPROVE network and PMF receptor modeling to assess the effectiveness of the NA-ECA at reducing ambient $PM_{2.5}$ from marine vessel RFO combustion. V and Ni data from 65 IMPROVE sites in coastal States of the U.S. were analyzed to identify sites with $PM_{2.5}$ contributions from RFO combustion, and 22 of these sites were selected for PMF receptor modeling. Each site was modeled independently with PMF, obtaining from 5 to 9 factors depending on the site. Every site resolved a PMF factor associated with RFO combustion, but these factors at some sites contained RFO combustion mixed with other aerosol sources. 13 sites were deemed to have PMF factors associated with RFO combustion that were not mixed with other sources. For these 13 sites, $PM_{2.5}$ from RFO combustion

was analyzed for three time periods related to various levels of fuel sulfur control under the NA-ECA; pre-NA-ECA, NA-ECA 1.0% S, and NA-ECA 0.1% S. Implementation of the NA-ECA was found to be effective at reducing $PM_{2.5}$ from RFO combustion, with all 13 sites indicating statistically significant reductions in $PM_{2.5}$ from RFO combustion between the pre-NA-ECA period and the two periods of fuel sulfur control. The average decrease in annual average $PM_{2.5}$ from RFO combustion resulting from the NA-ECA implementation was 50.2% from the pre-NA-ECA to NA-ECA 1% S period and 74.1% from the pre-NA-ECA to NA-ECA 0.1% S period.

Appendix A. Supplementary data

Supplementary data related to this article can be found at http://dx.doi.org/10.1016/j.atmosenv.2016.12.012.

References

Adachi, K., Buseck, P.R., 2015. Changes in shape and composition of sea-salt particles upon aging in an urban atmosphere. Atmos. Environ. 100, 1–9.

Agrawal, H., Malloy, Q.G.J., Welch, W.A., Miller, J.W., Cocker III, D.R., 2008. In-use gaseous and particulate matter emissions from a modern ocean going container vessel. Atmos. Environ. 42, 5504–5510.

Brown, S.G., Eberly, S., Paatero, P., Norris, G.A., 2015. Methods for estimating uncertainty in PMF solutions: examples with ambient air and water quality data and guidance on reporting PMF results. Sci. Total Environ. 518–519, 626–635.

Corbett, J.J., Winebrake, J.J., Green, E.H., Kasibhatla, P., Eyring, V., Lauer, A., 2007. Mortality from ship emissions: a global assessment. Environ. Sci. Technol. 41, 8512–8518.

Geiser, L.H., Jovan, S.E., Glavich, D.A., Porter, M.K., 2010. Lichen based critical loads for atmospheric nitrogen deposition in Western Oregon and Washington Forests, USA. Environ. Pollut. 158, 2412–2421.

Hwang, I., Hopke, P.K., 2007. Estimation of source apportionment and potential source locations of $PM_{2.5}$ at a west coastal IMPROVE site. Atmos. Environ. 41, 506–518.

IMO, 2011. Prevention of Air Pollution from Ships: Sulphur Monitoring for 2010. International Maritime Organization Marine Environment Protection Committee. MEPC 62/4.

IPCC, 2014. Climate change 2014: synthesis report. Core Writing Team. In: Pachauri, R.K., Meyer, L.A. (Eds.), Contribution of Working Groups I, II and III to the Fifth Assessment Report of the Intergovernmental Panel on Climate Change. IPCC, Geneva, Switzerland, 151 pp.

Kasper, A., Aufdenblatten, S., Forss, A., Mohr, M., Burtscher, H., 2007. Particulate emissions from a low-speed marine diesel engine. Aerosol Sci. Technol. 41, 24–32.

Khan, M.Y., Giordano, M., Gutierrez, J., Welch, W.A., Asa-Awuku, A., Miller, J.W., Cocker III, D.R., 2012. Benefits of two mitigation strategies for container vessels: cleaner engines and cleaner fuels. Environ. Sci. Technol. 46, 5049–5056.

Kim, E., Hopke, P.K., 2006. Characterization of fine particle sources in the Great Smoky Mountains area. Sci. Total Environ. 368, 781–794.

Kotchenruther, R.A., 2013. A regional assessment of marine vessel $PM_{2.5}$ impacts in the U.S. Pacific Northwest using a receptor-based source apportionment method. Atmos. Environ. 68, 103–111.

Kotchenruther, R.A., 2015. The effects of marine vessel fuel sulfur regulations on ambient $PM_{2.5}$ along the west coast of the U.S. Atmos. Environ. 103, 121–128.

Künzli, N., Jerrett, M., Mack, W.J., Beckerman, B., LaBree, L., Gilliland, F., Thomas, M., Peters, J., Hodis, H.N., 2005. Ambient air pollution and atherosclerosis in Los Angeles. Environ. Health Perspect. 113, 201–206.

Moldanova, J., Fridell, E., Popovicheva, O., Demirdjian, B., Tishkova, V., Faccinetto, A., Focsa, C., 2009. Characterisation of particulate matter and gaseous emissions from a large ship diesel engine. Atmos. Environ. 43, 2632–2641.

Norris, G., Duvall, R., Brown, S., Bai, S., 2014. EPA Positive Matrix Factorization (PMF) 5.0 Fundamentals and User Guide. U.S. Environmental Protection Agency. EPA/600/R-14/108.

Paatero, P., Eberly, S., Brown, S.G., Norris, G.A., 2014. Methods for estimating uncertainty in factor analytic solutions. Atmos. Meas. Tech. 7, 781–797.

Paatero, P., Hopke, P.K., 2003. Discarding or downweighting high-noise variables in factor analytic models. Anal. Chim. Acta 490, 277–289.

Pant, P., Harrison, R.M., 2013. Estimation of the contribution of road traffic emissions to particulate matter concentrations from field measurements: a review. Atmos. Environ. 77, 78–97.

Pope III, C.A., Dockery, D.W., 2006. Health effects of fine particulate air pollution: lines that connect. J. Air & Waste Manag. Assoc. 56, 709–742.

Popovicheva, O., Kireeva, E., Persiantseva, N., Timofeev, M., Bladt, H., Ivleca, N.P., Niessner, R., Moldanova, J., 2012. Microscopic characterization of individual particles from multicomponent ship exhaust. J. Environ. Monit. 14, 3101–3110.

Port of Seattle, 2016. Cruise Seattle 2016 Fact Sheet. https://www.portseattle.org/Cruise/Documents/2016_cruise_factsheet.pdf (accessed 30 November 2016).

Port Tampa Bay, 2016. Port Tampa Bay Fiscal Years 2006-2015 Cargo and Vessel Statistics. https://www.tampaport.com/About-Port-Tampa-Bay/Statistics (accessed 30 November 2016).

Ramberg, D., Van Vactor, S., 2014. Implications of Residual Fuel Oil Phase Out. 37th International Association for Energy Economics (IAEE) International Conference, New York, NY. June 15-18, 2014.

Solomon, P.A., Crumpler, D., Flanagan, J.B., Jayanty, R.K.M., Rickman, E.E., McDade, C.E., 2014. U.S. National $PM_{2.5}$ chemical speciation monitoring networks—CSN and IMPROVE: description of networks. J. Air & Waste Manag. Assoc. 64, 1410–1438.

Song, F., Gao, Y., 2011. Size distributions of trace elements associated with ambient particular matter in the affinity of a major highway in the New Jersey-New York metropolitan area. Atmos. Environ. 45, 6714–6723.

Stein, A.F., Draxler, R.R., Rolph, G.D., Stunder, B.J.B., Cohen, M.D., Ngan, F., 2015. NOAA's HYSPLIT atmospheric transport and dispersion modeling system. Bull. Amer. Meteor. Soc. 96, 2059–2077.

U.S. Environmental Protection Agency, 2010. Designation of North American Emission Control Area to Reduce Emissions from Ships: Regulatory Announcement. EPA-420-F-10–015.

US Army Corps of Engineers, 2016. Waterborne Commerce Statistics Center. http://www.navigationdatacenter.us/wcsc/wcsc.htm (accessed 24 August 2016).

Winebrake, J.J., Corbett, J.J., Green, E.H., Lauer, A., Eyring, V., 2009. Mitigating the health impacts of pollution from oceangoing shipping: an assessment of low-sulfur fuel mandates. Environ. Sci. Technol. 43, 4776–4782.

Zhao, W., Hopke, P.K., 2004. Source apportionment for ambient particles in the San Gorgonio wilderness. Atmos. Environ. 38, 5901–5910.

From: Kotchenruther, Robert
Sent: Thursday, April 23, 2020 5:05 PM
To: Zawacki, Margaret
Cc: Hoyer, Marion
Subject: Record of Percentage Agreement: Robert A. Kotchenruther

Author's Name: Robert A. Kotchenruther; U.S. EPA Region-10; Percentage 100%

Publication: The effects of marine vessel fuel sulfur regulations on ambient PM2.5 at coastal and near
coastal monitoring sites in the U.S. Atmospheric Environment 151 (2017) 52-61.

The author agrees with the total percentage of effort, 100%, listed beside his name entered in the
nomination form.

==========

Robert Kotchenruther, Ph.D.
Environmental Scientist
U.S. EPA Region-10
Laboratory Services & Applied Science Division
Environmental Characterization Branch
1200 6th Avenue
Suite 155 (Mailstop 14-D12)
Seattle, WA 98101-3188
(206) 553-6218
Kotchenruther.Robert@epa.gov

==========

Atmospheric Environment 68 (2013) 103–111

Contents lists available at SciVerse ScienceDirect

Atmospheric Environment

journal homepage: www.elsevier.com/locate/atmosenv

A regional assessment of marine vessel $PM_{2.5}$ impacts in the U.S. Pacific Northwest using a receptor-based source apportionment method

Robert A. Kotchenruther*

U.S. Environmental Protection Agency Region 10, Office of Environmental Assessment, 1200 Sixth Avenue, Suite 900, OEA-095, Seattle, WA 98101, USA

HIGHLIGHTS

- $PM_{2.5}$ source apportionment was performed for 36 sites in the northwest U.S.
- Residual fuel oil factors at 14 locations were linked to marine vessel emissions.
- Monthly average $PM_{2.5}$ impacts from marine vessel emissions are quantified.
- Results are just prior to the start of the North American Emissions Control Area.
- Results set a baseline to measure progress in emissions reductions.

ARTICLE INFO

Article history:
Received 4 September 2012
Received in revised form
26 November 2012
Accepted 30 November 2012

Keywords:
$PM_{2.5}$
Marine vessel emissions
Positive matrix factorization
Source apportionment
Residual fuel oil
Emissions control area

ABSTRACT

This work reports results from a receptor-based source apportionment analysis using the Positive Matrix Factorization (PMF) model on chemically speciated $PM_{2.5}$ data from 36 urban and rural monitoring sites within the U.S. Pacific Northwest. The approach taken is to model each site independently, treats monitor datasets with a common data preparation protocol, and uses a common modeling protocol. Complementary data from two monitoring networks, the urban Chemical Speciation Network (CSN) and rural Interagency Monitoring of Protected Visual Environments (IMPROVE) Network, was modeled for the period of 2007–2011. 15 different factor types were found for CSN sites and 17 for IMPROVE sites, however many factors occurred at only a few locations. Only 3 factor types were common in both networks: sulfate/sulfur rich, nitrate rich, and soil. However, for coastal and near coastal monitoring sites there were three additional factors common in both networks: sea salt, aged sea salt, and residual fuel oil combustion (RFO). This work presents annual average $PM_{2.5}$ mass impacts for all sites and factors found and the results for RFO are explored in greater depth. The association between RFO results and commercial marine vessel emissions is made based on similarities between factor chemical profiles and published emissions profiles, comparisons with emissions inventories, and the similarity in the spatial extent of RFO factor locations to that of the other marine aerosols identified in this study, sea salt and aged sea salt. All 14 monitoring sites with marine vessel RFO factors showed a seasonal cycle of mass impacts, with lower impacts in winter months (monthly average $PM_{2.5}$ between 0.1 $\mu g\ m^{-3}$ and 0.9 $\mu g\ m^{-3}$ in January) and higher impacts in summer months (monthly average $PM_{2.5}$ between 0.3 $\mu g\ m^{-3}$ and 2.7 $\mu g\ m^{-3}$ in August). These results set a baseline to measure progress in emissions reductions that are expected from implementation of the North American Emissions Control Area (ECA) beginning in August 2012.

Published by Elsevier Ltd.

1. Introduction

Human health studies have shown that there is a relationship between exposure to fine particulate matter ($PM_{2.5}$, particles with aerodynamic diameter <2.5 μm) and adverse health effects such as cardiovascular and pulmonary disease (Künzli et al., 2005), and lung cancer and premature mortality (Pope and Dockery, 2006). The preponderance of health studies suggest that there is no PM exposure threshold below which adverse health effects do not occur (Pope and Dockery, 2006), which implies that anthropogenic PM impacts should be of concern even in areas currently meeting national ambient air quality standards. In addition to human health

* Tel.: +1 206 553 6218; fax: +1 206 553 0119.
E-mail address: Kotchenruther.Robert@epa.gov.

1352-2310/$ – see front matter Published by Elsevier Ltd.
http://dx.doi.org/10.1016/j.atmosenv.2012.11.067

effects, deposition of anthropogenic PM has also been linked to adverse effects on ecosystem health (Geiser et al., 2010).

$PM_{2.5}$ emissions from commercial marine vessels has been an active area of investigation because these sources typically burn residual fuel oil (RFO), which has a very high sulfur content, produces large amounts of $PM_{2.5}$, SO_2, and NO_x (Moldanova et al., 2009), and are mobile sources that can impact urban areas as well as remote coastal areas having few other direct sources of anthropogenic emissions. Health studies targeted at seafarers have shown an increased rate of cancer incidence depending on length of time employed (Kaerlev et al., 2005), while globally among the general population marine vessel emissions have been estimated to cause approximately 60,000 cardiopulmonary and lung cancer deaths annually (Corbett et al., 2007). Regulating marine vessel fuel sulfur content is a common approach to reducing emissions. Winebrake et al. (2009) have shown that significant reductions in premature mortality from marine vessel emissions can be achieved by regulating fuel sulfur content at amounts lower than an assumed uncontrolled fuel sulfur content of 2.7%.

Concerns over health and ecological effects of marine vessel emissions led the United States (U.S.) and Canadian governments in 2009 to propose to the International Maritime Organization (IMO) the inclusion of North America in an Emissions Control Area (ECA). In March of 2010 the IMO amended the International Convention for the Prevention of Pollution from Ships (MARPOL) to designate specific portions of North American waters as an ECA (U.S. EPA, 2010). Beginning in August 2012, the ECA requires marine vessels within 200 nautical miles of North American coasts to use fuels with sulfur content no higher than 10,000 ppm (1%) and worldwide no higher than 35,000 ppm (3.5%). Starting in 2015, the ECA will require fuel sulfur content no higher than 1000 ppm (0.1%) within 200 nautical miles of North American coasts.

ECA controls on fuel sulfur content are expected to significantly reduce marine vessel emissions. Analysis of environmental aerosol data in coastal regions using receptor-based source apportionment techniques has often been able to identify impacts from marine vessels burning RFO due to high sulfur and significant Ni and V trace metal content in their emissions (Agrawal et al., 2008). Previous source apportionment studies in the U.S. Pacific Northwest have identified marine vessel RFO impacts at several urban and rural locations (Maykut et al., 2003; Wu et al., 2007; Kim and Hopke, 2008a, 2008b). Recent studies in Los Angeles (Minguillon et al., 2008) and the Netherlands (Mooibroek et al., 2011) used receptor-based techniques to analyze data from multiple monitoring sites and explored the spatial extent and magnitude of marine vessel impacts, however, the number of sites analyzed were relatively few and within the same airshed.

Multi-site receptor-based studies have approached the source apportionment task by either grouping the data into a larger dataset or analyzing data from each site independently. When monitoring sites share a common airshed and are expected to share the same aerosol sources, combining data from multiple sites can be an efficient approach that also increases the sample size, which can be important for receptor models like Positive Matrix Factorization (PMF). However, if there is no expectation of common aerosol sources, then combining data from multiple sites could lead to misidentification of source contributions at sites where they, in reality, do not contribute.

A regional assessment of aerosol source impacts is often addressed using source-oriented methods like photochemical grid modeling that predicts source impacts from emissions inventories, emissions modeling, meteorological simulations, and chemical transport modeling (Wagstrom et al., 2008). While there are clear benefits to source-oriented methods, the results are limited by uncertainties in emissions, errors and biases in meteorological simulations, grid resolution, and uncertainties and simplifications in the representation of atmospheric chemistry.

A regional assessment using receptor-based methods might be assembled from existing published studies. However, while there are many of these studies, most report results for only a few monitoring sites, cover different time periods, and for many monitors there are no published results. Also, when approaching a receptor-based source apportionment analysis there are many decisions that need to be made with regards to data preparation, which model to choose, what modeling protocol to follow, and how to interpret results (Reff et al., 2007). Differences in these choices between researchers can make it difficult to compare results between studies.

In this work a regional receptor-based source apportionment analysis is performed using the PMF model on chemically speciated $PM_{2.5}$ data from 36 sites within the U.S. Pacific Northwest. The approach taken is to model each site independently, to treat data from all sites with a common data preparation protocol, and to use a consistent modeling protocol. The benefits of this approach are that results between sites are as comparable as possible since site-to-site data and modeling have undergone the same treatments. Annual average results are presented for all sites and source factors and the results for RFO from marine vessels are explored in more depth. Marine vessel emissions are well suited to this approach because of their relatively unique chemical signature, they are a large regional source, and are a mobile source with a wide geographic extent. The results presented here for marine vessel impacts are timely because they cover a time period just prior to implementation of the North American ECA, and therefore provide a baseline of source impacts from which 'on the ground' progress in emissions reductions can be assessed.

2. Methods

2.1. $PM_{2.5}$ chemical speciation data

Two monitoring networks in the U.S. Pacific Northwest routinely collect chemically speciated 24-h integrated $PM_{2.5}$ mass: the Chemical Speciation Network (CSN) and the Interagency Monitoring of Protected Visual Environments (IMPROVE) Network. The CSN is one of several urban and suburban monitoring networks funded by the U.S. Environmental Protection Agency (EPA) and operated by state and local agencies. CSN samplers are operated on a daily, every third day, or every sixth day schedule depending on the site. Quality assured CSN data are housed in EPA's Air Quality System (AQS) database. Detailed information about the CSN network and AQS database can be found on the Technology Transfer Network, Ambient Monitoring Technology Information Center section of EPA's web site (http://www.epa.gov/ttn/amtic/). The IMPROVE network is a chemically speciated $PM_{2.5}$ monitoring program associated with the Regional Haze Rule of the U.S. Clean Air Act. IMPROVE samplers are typically sited at remote locations and are operated on a once every third day schedule. Quality assured IMPROVE data are housed in The Visibility Information Exchange Web System (VIEWS). Detailed information about the IMPROVE network and VIEWS can be found on the IMPROVE web site (http://vista.cira.colostate.edu/improve/). While measurement and analytical techniques used to quantify aerosol ionic and elemental concentrations are comparable between the two networks (Chen et al., 2010), elemental and organic carbon (EC and OC, respectively) data have historically been difficult to compare because of differences in carbon sampler design and analytical measurement protocols (Chow et al., 2004). To address this problem and better harmonize the two monitoring networks, EPA replaced all CSN carbon samplers between 2007 and 2009 to match

those of the IMPROVE program and also switched to IMPROVE-based carbon analytical measurement protocols at the same time (U.S. EPA, 2009).

Information about the monitoring sites analyzed in this work is listed in Tables 1 and 2, for CSN and IMPROVE sites, respectively, and also shown in Fig. 1. The start date for data used from the CSN monitors was based on when each site converted to IMPROVE-based carbon sampling methods and the start date for IMPROVE monitors was January 2007. The end date for both networks represents the most recent data available at the time data were extracted. The date range for data from both monitoring networks was chosen to maximize the total amount of available samples from each monitor and to cover the broadest period of temporal overlap after the change in CSN carbon methods.

2.2. Data preparation and treatment

Prior to source apportionment analysis the downloaded datasets were processed to correct for field blanks (CSN only), missing/negative values, data completeness issues, poor signal-to-noise (S/N) ratios, and species double counting. The uncertainty of each reported measurement was also estimated. A detailed discussion of data preparation and treatment is provided in the supplementary materials Section S.1.

2.3. Source apportionment

PMF source apportionment modeling was performed using EPA PMF 3.0 (Norris et al., 2008). A discussion of the mathematical equations underlying EPA PMF can be found in Paatero and Hopke (2003) and Norris et al. (2008). Data from each CSN and IMPROVE monitoring site was modeled independently. In each case, the model was run in the robust mode with 20 repeat runs to insure the model least-squares solution represented a global rather than local minimum and the rotational FPEAK variable was held at the default value of 0.0. The model solution with the optimum number of factors was determined somewhat subjectively based on inspection of the factors in each solution, but also from the quality of the least-squares fit (analysis of Q_{Robust} and Q_{True} values) in the model output. The scaled residuals for final model solutions were generally normally distributed, falling into the recommended range of +3 to −3.

PMF is a receptor model that approaches the task source apportionment through 'factor analysis', that is, the use of mathematical constructs to reduce the overall dataset into a smaller number of 'factors' that can explain the majority of data variability. PMF 'factors' are then related to 'sources' by comparing the chemical composition of factors with chemical profiles from anthropogenic source test data or the natural environment (e.g., soil, sea salt). PMF does not typically provide an exact source apportionment result because factors are often associated with multiple sources. A PMF factor could represent a single source (e.g., industrial point source), multiple sources with similar emissions profiles (e.g., gasoline vehicles), or multiple sources with insufficient variability in the observed dataset or insufficient chemical uniqueness to be separated by the model (e.g., sulfate rich, nitrate rich). PMF factors are also not necessarily mutually exclusive. For example, a factor identified as predominantly ammonium sulfate aerosol is likely from a combination of primary and secondary sources including diesel engines and industrial facilities, even though these sources may also have separately identified PMF factors. Hence, caution should be used in interpreting factor source classifications too literally or with exclusivity.

3. Results and discussion

3.1. Source apportionment results

Tables 3 and 4 list the number of PMF factors determined for each monitoring site for CSN and IMPROVE monitors, respectively, as well as factor names, annual average mass attributions for each factor, and annual average measured $PM_{2.5}$. The annual averages presented in Tables 3 and 4 represent multiyear averages based on the date range of data presented in Tables 1 and 2, respectively. Because some sites had an uneven distribution of samples throughout the annual cycle, monthly average mass attributions were computed and the annual average was calculated from the 12 monthly averages. A description of factors and the rationale for factor names are described in the supplementary materials Sections S.2–S.4.

The uncertainty and robustness of the PMF results were assessed through a bootstrap analysis, where the original data was resampled and the bootstrap PMF results are compared to the original. The number of bootstrap model runs that can be mapped back to the original result is a measure of solution robustness and the variability in bootstrap mass allocations is a measure of uncertainty. The PMF result for each monitoring site was subjected to 200 bootstrap model runs and the factor mapping results for all sites and factor types are provided in the supplementary materials Section S.5. The RFO factor results were found to be generally robust with an average of 96% of bootstrap results mapping back to the original RFO factor. The variability in bootstrap factor mass allocations and percentage of species allocations for RFO factors are provided in the supplementary materials Section S.6. Additionally, because the distribution of sulfur mass between factors will have a significant influence on the amount of mass attributed to RFO, the G-space plots between RFO and sulfur/sulfate rich factors were examined when both factors were identified at a monitoring site. Oblique edges in the G-space plot, if present, suggest that the solution obtained by the given rotation may not be the most

Table 1
CSN monitoring sites modeled in this study.

Site name/city	Date range modeled	Number of samples	State	AQS number	Latitude	Longitude
Boise	5/3/07–9/12/11	532	ID	160010010	43.6003	−116.3479
Klamath Falls	7/6/09–3/28/11	88	OR	410350004	42.1889	−121.7225
Lakeview	10/4/09–3/28/11	83	OR	410370001	42.1889	−120.3519
Oakridge	7/6/09–3/28/11	100	OR	410392013	43.7444	−122.4805
Portland	5/3/07–8/4/11	513	OR	410510080	45.4965	−122.6034
Vancouver	4/1/09–9/6/11	149	WA	530110013	45.6483	−122.5869
Seattle_DW (Duwamish)	11/2/08–9/6/11	174	WA	530330057	47.5632	−122.3405
Seattle_BH (Beacon Hill)	5/3/07–9/12/11	435	WA	530330080	47.5683	−122.3081
Tacoma_SL (South L St.)	5/6/07–9/6/11	260	WA	530530029	47.1864	−122.4517
Tacoma_AL (Alexander Ave.)	11/2/08–9/6/11	174	WA	530530031	47.2656	−122.3858
Marysville	4/7/09–9/6/11	145	WA	530611007	48.0543	−122.1715
Yakima	11/8/07–9/6/11	202	WA	530770009	46.5968	−120.5122

Table 2
IMPROVE network monitoring sites modeled in this study.

Site name	Date range modeled	Number of samples	State	Class 1 area	Latitude	Longitude
CRMO	1/6/07–12/31/10	452	ID	Craters of the Moon	43.4605	−113.5551
SAWT	1/3/07–12/31/10	414	ID	Sawtooth	44.1705	−114.9271
CABI	1/12/07–12/31/10	446	MT	Cabinet Mountains	47.9549	−115.6709
FLAT	1/3/07–12/31/10	451	MT	Flathead	47.7734	−114.2690
GLAC	1/3/07–12/28/10	441	MT	Glacier	48.5105	−113.9966
MONT	1/3/07–12/31/10	443	MT	Monture	47.1222	−113.1544
JARB	1/3/07–12/31/10	453	NV	Jarbidge Wilderness	41.8926	−115.4261
CRLA	1/3/07–12/31/10	432	OR	Crater Lake	42.8958	−122.1361
HECA	1/3/07–12/31/10	420	OR	Hells Canyon	44.9702	−116.8438
KALM	1/3/07–12/31/10	465	OR	Kalmiopsis	42.5520	−124.0589
MOHO	1/3/07–12/31/10	465	OR	Mount Hood	45.2888	−121.7837
STAR	1/6/07–12/31/10	478	OR	Starkey	45.2249	−118.5129
THSI	1/3/07–12/31/10	463	OR	Three Sisters Wilderness	44.2910	−122.0434
LABE	1/3/07–12/31/10	457	CA	Lava Beds	41.7117	−121.5068
REDW	1/3/07–12/31/10	420	CA	Redwood	41.5608	−124.0839
COGO	1/3/07–12/31/10	435	WA	Columbia Gorge	45.5693	−122.2103
CORI	1/3/07–12/31/10	475	WA	Columbia River Gorge	45.6644	−121.0008
MAKA	1/3/07–10/23/10	414	WA	Makah Tribe	48.3719	−124.5950
MORA	1/3/07–12/31/10	458	WA	Mount Rainier	46.7583	−122.1244
NOCA	1/6/07–12/31/10	450	WA	North Cascades	48.7316	−121.0646
OLYM	1/3/07–12/31/10	466	WA	Olympic	48.0065	−122.9727
PASA	1/3/07–12/31/10	453	WA	Pasayten	48.3877	−119.9275
SNPA	1/3/07–12/31/10	473	WA	Snoqualmie Pass	47.4220	−121.4259
WHPA	1/3/07–12/31/10	461	WA	White Pass	46.6243	−121.3881

plausible. Of the 7 sites indicating both RFO and sulfate rich factors, only the OLYM IMPROVE site had an apparent oblique edge in the G-space plot between these two factors (G-space plots for these 7 sites are provided in the supplementary materials Section S.7). This oblique edge was insensitive to variations in rotation using the model FPEAK variable, suggesting the original OLYM site solution has limited rotational freedom.

While the focus of this work is the RFO factor results and the connection to marine vessels, it is worth briefly discussing some of the similarities and differences between PMF results for CSN and IMPROVE sites as a whole as well as comparing these results to those of other published studies. Tables 3 and 4 show that there were 15 different factor types found for CSN sites and 17 different factor types for IMPROVE sites. The larger number of factor types found across IMPROVE sites is understandable given that there are twice as many IMPROVE as CSN sites and the IMPROVE sites represent a wider geographic scope. That said, there were an average of 9 factors found at CSN sites compared to only 6 at IMPROVE sites, which is indicative of urban areas typically having a larger number of $PM_{2.5}$ sources relative to the rural IMPROVE network.

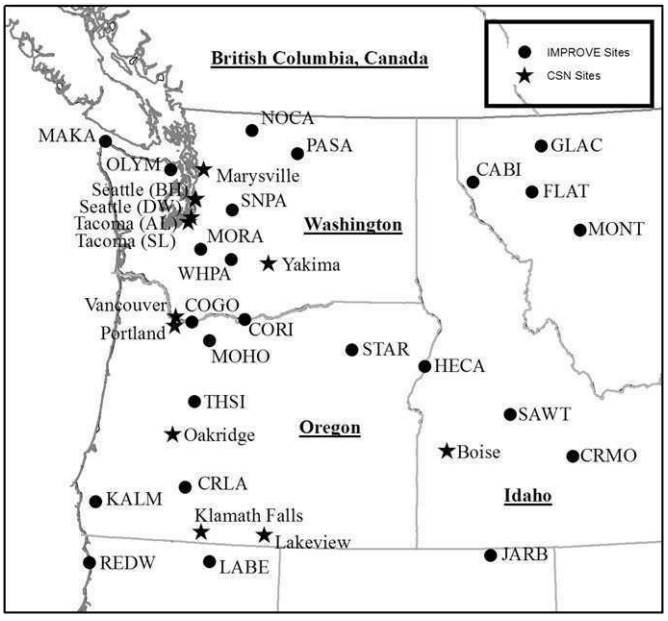

Fig. 1. CSN and IMPROVE $PM_{2.5}$ monitoring sites in the U.S. Pacific Northwest.

Between the two networks, there were nine factor types that had similar enough chemical profiles to be given the same factor names in both the CSN and IMPROVE results (see supplementary materials Sections S.2–S.4). Of these nine factor types, only three were commonly found at both CSN and IMPROVE sites throughout the U.S. Pacific Northwest: sulfate/sulfur rich, nitrate rich, and soil. However, for coastal and near coastal monitoring sites (sites west of the Cascade Mountain range), there were three additional factors common to both CSN and IMPROVE sites: sea salt, aged sea salt, and RFO. RFO appears to be the only factor commonly found at both CSN and IMPROVE monitoring locations in the U.S. Pacific Northwest that can be clearly associated with a particular source of pollution, that is, marine vessels (see Section 3.2).

Previous studies have reported aerosol source apportionment results for some of the monitoring locations also analyzed in this study. Results for Seattle's Beacon Hill monitoring site have been previously reported in a number of published studies. Maykut et al. (2003) reported an 8 factor solution using PMF and found an average RFO contribution of 0.9 μg m^{-3} for data from the period 1997–1999, Kim and Hopke (2008a) reported a 10 factor solution using PMF and found an average RFO contribution of 0.47 μg m^{-3} for data from 2000 to 2005, and Wu et al. (2007) reported a 10 factor solution using ME2 and found an average RFO contribution of 0.78 μg m^{-3} for data from 2000 to 2004. In this work, RFO was found to contribute an average of 1.0 μg m^{-3} at the Beacon Hill site for the period 2007–2011. While the average contribution of RFO for the Seattle Beacon Hill site is higher in this work than in previous studies, marine vessel activity data from the Port of Seattle indicates that the number of annual vessel calls at the Port have increased an average of 39% from the periods of 2002–2005 to 2007–2011 and total tonnage of shipping has increased an average

Table 3
Annual average $PM_{2.5}$ ($\mu g\ m^{-3}$) and source apportionment results for PMF factors found at CSN monitoring sites in the U.S. Pacific Northwest.

Site name	Number of factors found	Measured average $PM_{2.5}$	Calcium rich	Copper rich	Gasoline vehicles	Iron rich	Nitrate rich	Organic pyrolysis (OP) rich	Potassium rich	Sea salt	Aged sea salt	Soil	Sulfur rich	Residual fuel oil	Urban unidentified	Wood smoke	Zinc rich
Boise	8	6.9			0.9		1.3	0.9	0.3			1.0	0.9		0.4	1.2	
Klamath_Falls	5	10.7					0.7	2.1				1.1	0.6			6.4	
Lakeview	7	8.5					0.7	1.4	0.6			0.9	0.4		0.5	4.2	
Oakridge	7	8.0			1.3			1.5		0.3		0.4	0.8			3.8	
Portland	8	8.3			2.5		0.7	0.6		0.4		0.5	1.0		0.8	1.8	
Vancouver	8	7.1			0.1		0.6	1.0		0.3		0.4	1.2		1.6	2.2	
Seattle_DW	11	7.9	0.4		1.6	0.9	0.7	0.3		0.3	0.9	0.5		1.1		1.3	0.2
Seattle_BH	11	6.6		0.0	1.3	0.8	0.6	0.6		0.2	0.9	0.2		1.0	0.4	0.7	
Tacoma_SL	10	9.2			2.0	0.6	0.5	0.8		0.3	0.8	0.3		0.8	0.7	2.8	
Tacoma_AL	9	8.0			1.9	0.3	0.9	0.2		0.5		0.8		1.3	0.5	1.9	
Marysville	9	8.8			1.8		0.9	0.3		0.3	1.0	0.6		0.9	0.4	2.8	
Yakima	10	8.8			1.7	0.4	1.8	0.9		0.3		0.3	0.9		1.0	1.5	0.5

Table 4
Annual average $PM_{2.5}$ ($\mu g\ m^{-3}$) and source apportionment results for PMF factors found at IMPROVE network monitoring sites in the U.S. Pacific Northwest.

Site name	Number of factors found	Measured average $PM_{2.5}$	Iron rich	Mixed, nitrate & sulfate	Mixed, OC, EC & sulfate	Mixed, OC & nitrate	Mixed, OC & soil (Ca rich)	Mixed, sulfate & soil	Mixed, sulfate & soil (Ca rich)	Nitrate rich	Organic pyrolysis (OP) rich	Sea salt	Aged sea salt	Secondary organic aerosol & wood smoke	Soil	Soil (Ca rich)	Sulfate rich	Residual fuel oil	Zinc rich
CRMO	6	2.6								0.2	0.0			1.3	0.6		0.5		0.0
SAWT	6	3.1					0.1				0.1			2.0	0.6		0.3		0.0
CABI	5	2.7								0.1				1.5	0.5		0.6		0.1
FLAT	4	3.0								0.1				1.7	0.4		0.6		
GLAC	5	4.3	0.2							0.2				2.5	0.7		0.8		
MONT	4	3.4				0.2								2.0	0.6		0.6		
JARB	6	2.8								0.1				1.2	0.9	0.4	0.2		0.0
CRLA	4	2.2												1.4	0.3		0.4		0.1
HECA	5	3.6								0.2				2.1	0.3		0.8		0.0
KALM	6	3.1										0.3	0.5	1.5	0.2			0.7	0.0
MOHO	4	2.0		0.4				0.3	0.0					1.2					
STAR	5	3.0								0.2			0.2	1.8	0.3		0.4		
THSI	4	2.8											0.2	1.5	0.6		0.5		
LABE	7	2.8			0.1			0.1		0.1				1.7	0.4		0.4		0.0
REDW	5	3.4	0.1									1.2	0.2	1.2				0.9	
COGO	9	4.3			0.4					0.3		0.2	0.4	1.6	0.4		0.8	0.3	0.0
CORI	7	4.8	0.1							0.6			0.6	1.8	0.9		0.8		0.2
MAKA	7	4.6		0.2								0.7	0.6	1.9	0.2		0.9	0.5	
MORA	7	2.8								0.1			0.2	1.2	0.2		0.6	0.5	0.1
NOCA	5	2.2											0.2	1.1	0.2		0.1	0.7	
OLYM	7	2.7						0.2				0.2	0.4	1.2			0.6	0.2	0.1
PASA	5	2.1								0.0				1.3	0.3		0.5		0.0
SNPA	7	2.5								0.2			0.3	1.1	0.2		0.3	0.4	0.1
WHPA	5	1.8												0.8	0.2		0.4	0.4	0.0

of 29% for the same periods (Port of Seattle, 2012). The reported increase in vessel activity is consistent with the increased RFO contribution found in this work.

Source apportionment results for the Seattle Duwamish monitoring site were reported by Kim and Hopke (2008a) for data covering the period of 2000–2005. They reported 11 PMF factors and found an average RFO contribution of 0.44 μg m^{-3}. In this work, RFO was found to contribute an average of 1.1 μg m^{-3} at the Duwamish site for the period of 2007–2011. The higher RFO contribution reported here, over that of Kim and Hopke, can be partially explained by the increased port activity reported above. Additionally, the slightly higher RFO impacts at the Duwamish site over Beacon Hill reported in this work are consistent with the Duwamish site being both closer to Port of Seattle facilities and sited in the Duwamish valley, nearer the same elevation as the Port, compared to the Beacon Hill site.

Kim and Hopke (2008b) reported PMF source apportionment results for the Olympic IMPROVE monitoring site using data from 2001 to 2004. They report finding 8 factors, with RFO (oil combustion, in that work) contributing an average of 0.50 μg m^{-3} to total $PM_{2.5}$. In this work, RFO was found to contribute an average of 0.2 μg m^{-3} at the Olympic site for the period 2007–2010. The smaller attribution of RFO mass in this work for the more recent period, compared to Kim and Hopke, is inconsistent with the previously discussed marine vessel port call data reported by the Port of Seattle as well as total annual waterborne shipping tonnage data for Washington State (U.S. Corps of Engineers, 2012), which indicates that total tonnage shipped has increased 8.2% in Washington from the periods of 2001–2004 to 2007–2010. The discrepancy in results between this work and Kim and Hopke for the Olympic site is not well understood.

Source apportionment results for the Portland Oregon CSN monitoring site were reported by Kim and Hopke (2008b) for data from 2002 to 2005. They reported 10 PMF factors and, like this work, did not identify a factor related to RFO.

Hwang and Hopke (2007) reported PMF source apportionment results for the Kalmiopsis IMPROVE site in southwestern Oregon. In that work they used data from 2000 to 2004 and found 9 factors, but did not identify a RFO factor. In this work RFO was found to contribute an annual average of 0.7 μg m^{-3} to total $PM_{2.5}$ for the 2007–2010 period. The difference between Hwang and Hopke and this work likely stems from differing interpretations of the source of the high sulfate factor. Hwang and Hopke labeled their high sulfate factor secondary sulfate, but did not attribute that to RFO sources as in this work.

3.2. Results for RFO and linkage to marine vessels

3.2.1. PMF results for RFO and comparison with source test data

Chemically speciated source profiles of primary $PM_{2.5}$ emissions covering a wide range of sources are available through the EPA SPECIATE database Version 4.3 (Hsu and Divita, 2011). The SPECIATE database has two emissions profiles for marine vessels using RFO, profiles 5676 and 5674. The V:Ni ratio in these profiles is 2.6 and 2.3, the weight percent of the sum of V and Ni is 2.5% and 2.2%, the weight percent of sulfate is 44% and 38%, and the weight percent OC is 1.7% and 11.3%, respectively. Additionally, a V:Ni ratio of 4.5 was reported by Agrawal et al. (2008) for marine vessels using RFO. While not reported in the SPECIATE database, marine vessels using RFO also emit volatile organic compounds (VOCs), NO_x, and large amounts of SO_2 due to the very high fuel sulfur content (Agrawal et al., 2008; Moldanova et al., 2009). Downwind of marine vessel emissions, it is expected that the ratio of V:Ni will be maintained but the absolute concentration of sulfate, OC, V, and Ni associated with this source may shift as SO_2, VOCs, and other co-emitted gases undergo photochemistry and gas-to-particle conversion.

Of the 36 sites analyzed in this study, 14 sites had factors that matched the chemical signature of RFO based on high sulfur/sulfate content in the chemical profile, attribution of a significant percentage of measured V and Ni to the factor, and a V:Ni ratio near that reported for RFO. Figs. 2 and 3 show the RFO PMF factor chemical profiles from CSN and IMPROVE sites, respectively. The ratio of V:Ni in these factors ranged from 2.4 to 3.9 for CSN sites and 2.3–5.4 for IMPROVE sites and had an average value of 3.0 and 3.2 for CSN and IMPROVE sites, respectively. A map indicating the location of sites where RFO factors were found is shown in Fig. 4. It should be noted that while all RFO factors have a significant sulfur/sulfate mass attribution, there is large variability in the amount of OC, EC and nitrate attributed to the factors. Some of this variation can be attributed to differences in photochemistry effecting upwind RFO source emissions, but some is also likely associated with factor uncertainty.

3.2.2. Comparison with 2008 emissions inventories

In April of 2012 EPA published Version 2 of its 2008 National Emissions Inventory (NEI). The NEI is a comprehensive and detailed county, state, and nationwide estimate of emissions for a wide range of air pollutants and is prepared every three years by EPA in collaboration with State, Local, and Tribal air agencies (U.S. EPA, 2012a). Of interest for this study is that the 2008 NEI includes

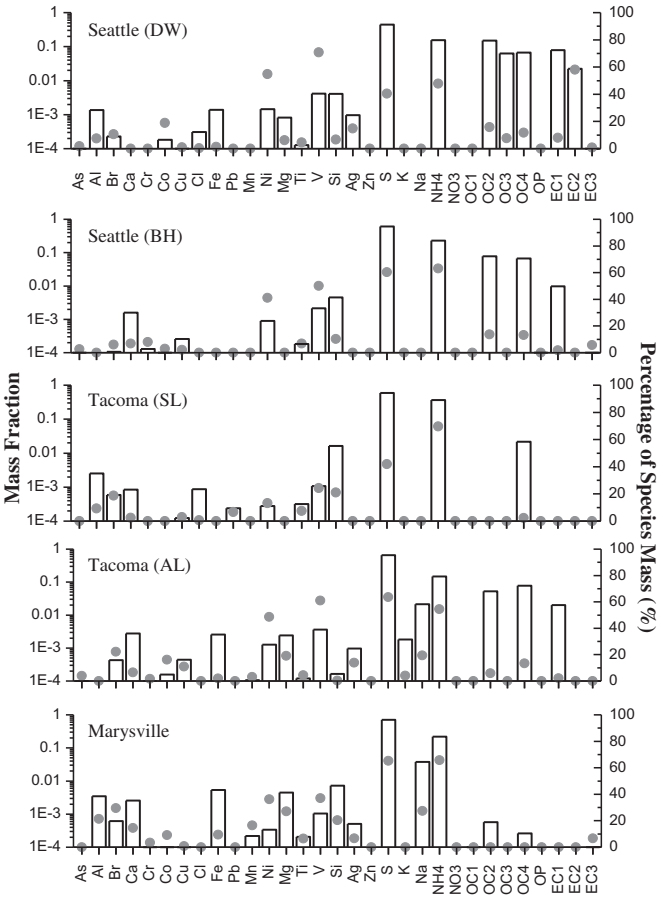

Fig. 2. Residual fuel oil combustion PMF factors for CSN monitoring sites. Vertical bars indicate the fractional contribution (left vertical scale) of chemical species to factor composition, gray dots indicate the percent of chemical species (right vertical scale) observed at each location attributed to residual fuel oil.

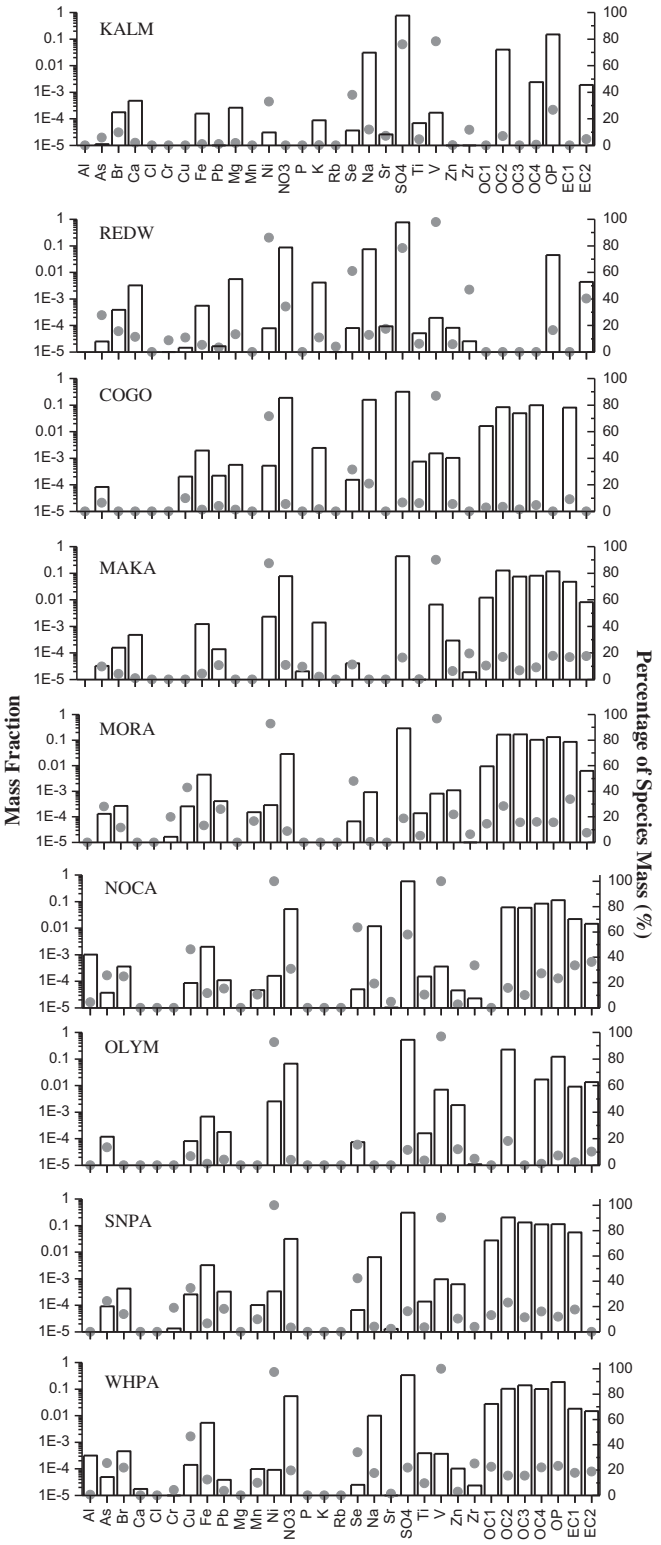

Fig. 3. Residual fuel oil combustion PMF factors for IMPROVE monitoring sites. Vertical bars indicate the fractional contribution (left vertical scale) of chemical species to factor composition, gray dots indicate the percent of chemical species (right vertical scale) observed at each location attributed to residual fuel oil.

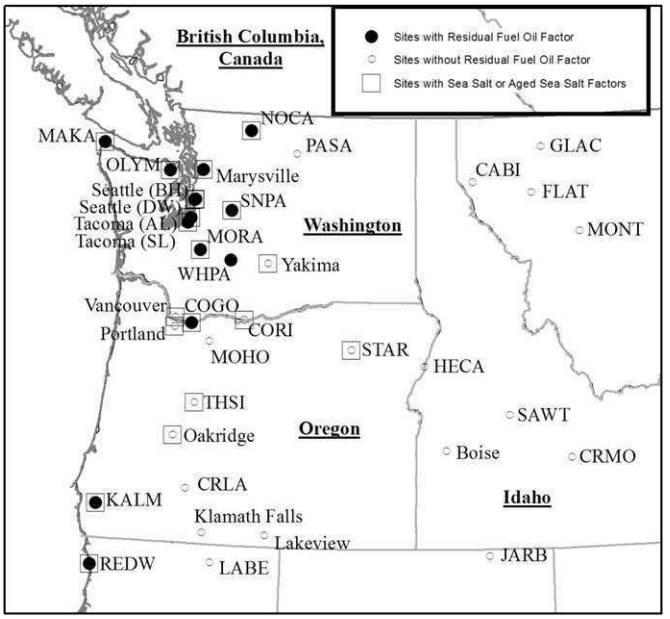

Fig. 4. Monitoring sites where PMF factors for residual fuel oil were found and monitoring sites where PMF factors for either sea salt or aged sea salt were found.

estimates of primary particulate Ni emissions and SO_2 gaseous emissions (primary particulate V and sulfate are not reported). While comparison of county level emissions estimates with PMF results can be informative, it should also be noted that county level emissions represent a broad geographic area whereas the PMF results are specific to a particular monitoring station and the NEI represents emissions from 2008 whereas the PMF results are for 2007–2011. Differences between the two can also be caused by differences in the atmospheric lifetimes of emissions, uncertainties in the emissions estimates, and uncertainties in the PMF results.

For Ni emissions the 2008 NEI indicates that Washington, Oregon and Idaho emitted 30,017 lbs, 5617 lbs, and 1933 lbs, respectively. Of those statewide totals, commercial marine vessels contributed 86% (25,901 lbs), 55% (3107 lbs), and 0% (0 lbs), respectively.

Smaller sources of Ni in the 2008 NEI for Washington State are oil fired industrial boilers (6%, 1806 lbs) and petroleum refinery operations (2%, 546 lbs). The V:Ni ratio in the SPECIATE profiles for of oil fired boilers range from 0.2 to 0.7 and the V:Ni ratio for petroleum refinery operations is 1.6. Given these V:Ni ratios and the relatively small contribution to total Washington State Ni emissions, it is unlikely that these sources significantly contribute to the PMF factors identified as RFO.

Smaller sources of Ni in the 2008 NEI for Oregon are coal fired electrical generation (20%, 1113 lbs) and non-ferrous metal industrial processes (9%, 500 lbs). Oregon had one coal fired power plant in operation from 2007 to 2011, the Portland General Electric plant in Boardman Oregon. The SPECIATE database lists 5 emissions profiles from coal fired power plants using the same emissions control technology as the Boardman plant. The V:Ni emissions ratio in these profiles ranged from 1.6 to 3.6, with an average value of 2.2. While these V:Ni ratios are similar to that of RFO, it is unlikely that the Boardman plant is contributing to the factors identified as RFO because of its location. Boardman Oregon lies along the Columbia river approximately 100 km east of the CORI IMPROVE monitor and 200 km east of the COGO IMPROVE monitor (both CORI and COGO are also along the Columbia river). However, no RFO factor was identified at the closer CORI site whereas RFO was identified at the farther COGO site. Regarding the other smaller source of Ni in Oregon, non-ferrous metal industrial processes, all of these emissions are attributed to one source located outside of Albany OR. While there is no representative emissions profile for this source available in the SPECIATE database, its location also suggests that it is unlikely to be contributing to factors identified as RFO in this

work. This source lies 125 km southwest and 250 km north of the COGO and KALM IMPROVE monitors, respectively, and closer monitors (Portland, MOHO, THSI, Oakridge, and CRLA) show no RFO impacts.

For SO_2 emissions the 2008 NEI indicates that Washington, Oregon and Idaho emitted 36,902 tons, 26,697 tons, and 20,654 tons, respectively. Of those statewide totals, commercial marine vessels contributed 38% (14,094 tons), 6% (1682 tons), and 0% (0 tons), respectively.

Within the 12 Washington State counties bordering Puget Sound and the Strait of Juan de Fuca, commercial marine vessels contributed 49% (12,370 tons) of total SO_2 emissions. Smaller sources of SO_2 in these counties came from industrial point sources including non-ferrous metal facilities in Whatcom County (18%, 4523 tons), petroleum refineries in Whatcom and Skagit Counties (6%, 1552 tons), and industrial oil boilers in Whatcom, Skagit, Clallam and Jefferson Counties (5%, 1389 tons). On-road and non-road mobile sources contributed a combined 8% (1968 tons) of SO_2 emissions in these counties.

In the 5 Oregon and Washington counties bordering the Columbia River near Portland Oregon, commercial marine vessels contributed 39% (2551 tons) of total SO_2 emissions. Smaller sources of SO_2 in these counties came from industrial sources including pulp and paper manufacturing (29%, 1891 tons) and industrial boilers using biomass fuel (7%, 481 tons). On-road and non-road mobile sources contributed a combined 9% (564 tons) of SO_2 emissions in these counties.

For the 3 coastal counties in Oregon and California in the proximity of the KALM and REDW IMPROVE monitoring sites, commercial marine vessels contributed only 6% (114 tons) of total SO_2 emissions. The majority of SO_2 emissions in these counties were attributed to wild and prescribed fires (83%, 1625 tons). While commercial marine vessel SO_2 contributions for these counties is in apparent disagreement with the PMF results at the KALM and REDW sites, it should be noted that the 2008 NEI attributes only near-coastal commercial marine emissions to states and counties (default is emissions within 3 nautical miles, U.S. EPA, 2012b). Hence, the coastal county emissions inventories do not fully account for all commercial marine vessel activity off coastal waters.

The NEI data for both Ni and SO_2 indicate that 2008 commercial marine vessel emissions were approximately an order of magnitude larger in Washington State compared to Oregon, and nonexistent in Idaho. These emissions inventory data indicate that both the relative magnitude and spatial allocation of commercial marine vessel emissions in the 2008 NEI are consistent with the number and location of monitoring sites where PMF factors for RFO were found in Washington and Oregon (Fig. 4).

3.2.3. Spatial extent of residual fuel oil factors

Fig. 4 shows a map indicating the monitoring sites where RFO factors were identified and also shows those sites where either sea salt or aged sea salt factors were identified. Fig. 4 shows that the spatial extent of sites impacted by RFO is very similar to the spatial extent of impacts from sea salt and aged sea salt. The similarity in spatial extent between these three factors is consistent with the hypothesis that the RFO originates from marine sources, namely, marine vessel emissions.

3.2.4. Monthly average contributions from marine vessels using RFO

Based on the evidence presented above, RFO factors identified in this work are attributed to marine vessel emissions. Fig. 5 shows the monthly average $PM_{2.5}$ mass attributed by PMF to RFO emissions from marine vessels for the 14 monitoring sites where this factor was identified. The monthly averages shown in Fig. 5

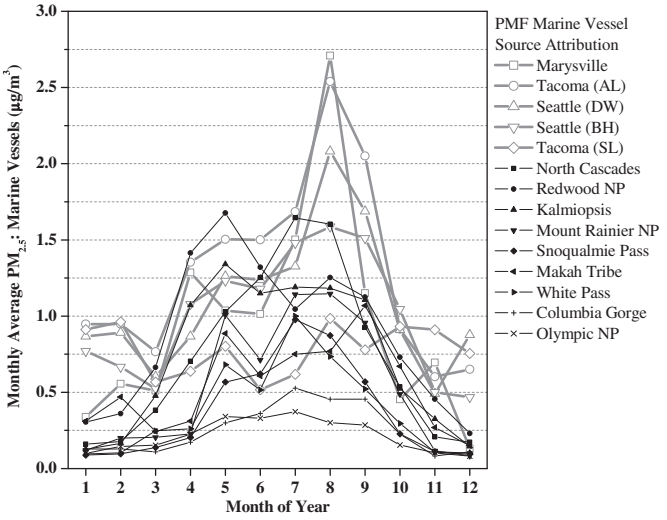

Fig. 5. Monthly average $PM_{2.5}$ ($\mu g\ m^{-3}$) attributed to marine vessels using residual fuel oil for 14 monitoring sites in the U.S. Pacific Northwest.

represent multiyear averages based on the monitoring periods listed in Tables 1 and 2. The bold lines in Fig. 5 represent urban CSN monitors, generally have the highest mass impacts throughout the annual cycle, and are consistent with the majority of these monitors being close to major marine vessel ports where there is a higher density of marine vessel emissions compared to IMPROVE monitors. All monitoring sites show a seasonal cycle in marine vessel impacts, with lower impacts in winter months (monthly average $PM_{2.5}$ between 0.1 $\mu g\ m^{-3}$ and 0.9 $\mu g\ m^{-3}$ in January) and higher impacts in summer months (monthly average $PM_{2.5}$ between 0.3 $\mu g\ m^{-3}$ and 2.7 $\mu g\ m^{-3}$ in August). This seasonal pattern is consistent with more photochemical production of secondary $PM_{2.5}$ from co-emitted gaseous emissions in summer, but also to a smaller extent reflects an average summer increase in cargo traffic of 12% as reported by the Port of Metro Vancouver and the Port of Tacoma (2008–2011 and 2009–2011 data, respectively; Port Metro Vancouver, 2012; Port of Tacoma, 2012) and summertime cruise ship activity. The seasonal pattern may also be influenced by seasonal changes in the prevailing wind patterns. Fig. 6 shows the percent contribution of RFO emissions from marine

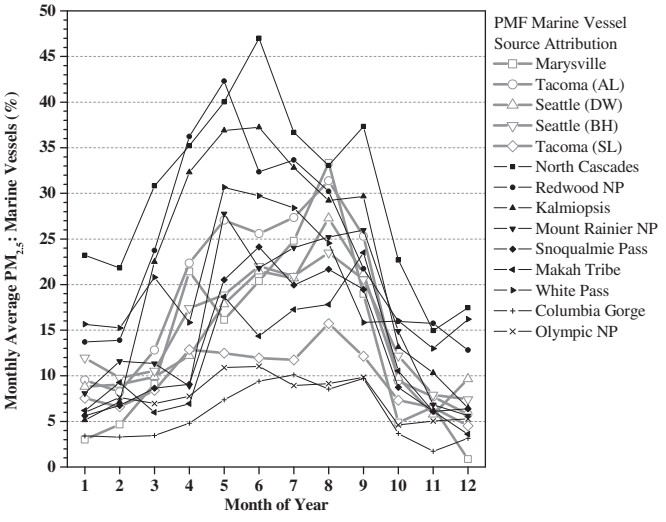

Fig. 6. Monthly average percent of total $PM_{2.5}$ attributed to marine vessels using residual fuel oil for 14 monitoring sites in the U.S. Pacific Northwest.

vessels to total monthly average $PM_{2.5}$ for the 14 monitoring sites where this factor was identified. The seasonal cycle of percent contributions shows smaller contributions from marine vessels in winter (between 3% and 23% of total monthly average $PM_{2.5}$ in January) and larger contributions in summer (between 9% and 47% of total monthly average $PM_{2.5}$ in June). The highest percent impacts from marine vessel emissions throughout the seasonal cycle occur at comparatively clean IMPROVE sites, which is indicative of relatively few anthropogenic sources impacting the remote IMPROVE sites compared to the urban CSN locations.

4. Conclusions

This work presents a regional-scale multi-site source apportionment analysis of $PM_{2.5}$ using PMF on data from 36 urban and rural monitoring sites in the U.S. Pacific Northwest covering the period 2007–2011. Results for 14 of the 36 sites indicated a RFO factor that is associated with marine vessel emissions. Most sites west of the Cascade Mountains indicated some level of impact from marine vessel emissions. The spatial extent of marine vessel emissions impacts was found to be similar to the other marine related aerosols, sea salt and aged sea salt, and consistent with emissions inventories. Monitoring sites indicating marine vessel emissions impacts show a seasonal cycle, with lower impacts in winter months (monthly average $PM_{2.5}$ between 0.1 $\mu g\ m^{-3}$ and 0.9 $\mu g\ m^{-3}$ in January) and higher impacts in summer months (monthly average $PM_{2.5}$ between 0.3 $\mu g\ m^{-3}$ and 2.7 $\mu g\ m^{-3}$ in August). The percent contribution to total monthly average $PM_{2.5}$ from marine vessels had a similar seasonal cycle, with smaller contributions in winter (between 3% and 23% of total monthly average $PM_{2.5}$ in January) and larger contributions in summer (between 9% and 47% of total monthly average $PM_{2.5}$ in June). These results for marine vessels, representing data just prior to the implementation of the North American ECA, provide a baseline assessment of marine vessel emissions impacts from which progress in ECA emissions reductions can be assessed.

Acknowledgments

The author thanks Amy Fowler and Andrew Green at Puget Sound Clean Air Agency for their insights on seasonal marine shipping activity, Brandy Albertson, Phil Allen, Mark Fisher, Miyoung Park and Chris Swab at Oregon DEQ for their help with emission sources in Oregon, Jim Corbett at the University of Delaware for getting me started with information on the health effects of $PM_{2.5}$, and Robert Elleman, Wayne Elson, Mahbubul Islam, and Keith Rose at EPA Region 10 for their helpful insights.

Appendix A. Supplementary data

Supplementary data related to this article can be found at http://dx.doi.org/10.1016/j.atmosenv.2012.11.067.

References

Agrawal, H., Malloy, Q.G.J., Welch, W.A., Miller, J.W., Cocker III, D.R., 2008. In-use gaseous and particulate matter emissions from a modern ocean going container vessel. Atmospheric Environment 42, 5504–5510.

Chen, L.-W.A., Watson, J.G., Chow, J.C., DuBois, D.W., Herschberger, L., 2010. Chemical mass balance source apportionment for combined $PM_{2.5}$ measurements from U.S. non-urban and urban long-term networks. Atmospheric Environment 44, 4908–4918.

Chow, J.C., Watson, J.G., Chen, L.-W.A., Arnott, W.P., Moosmuller, H., 2004. Equivalence of elemental carbon by thermal/optical reflectance and transmittance with different temperature protocols. Environmental Science and Technology 38, 4414–4422.

Corbett, J.J., Winebrake, J.J., Green, E.H., Kasibhatla, P., Eyring, V., Lauer, A., 2007. Mortality from ship emissions: a global assessment. Environmental Science and Technology 41, 8512–8518.

Geiser, L.H., Jovan, S.E., Glavich, D.A., Porter, M.K., 2010. Lichen based critical loads for atmospheric nitrogen deposition in Western Oregon and Washington Forests, USA. Environmental Pollution 158, 2412–2421.

Hsu, Y., Divita, F., 2011. Speciate 4.3: Addendum to Speciate 4.2 Speciation Database Development Documentation. U.S. Environmental Protection Agency. EPA/600/R-11/121.

Hwang, I., Hopke, P.K., 2007. Estimation of source apportionment and potential source locations of $PM_{2.5}$ at a west coastal IMPROVE site. Atmospheric Environment 41, 506–518.

Kaerlev, L., Hansen, J., Hansen, H.L., Nielsen, P.S., 2005. Cancer incidence among Danish seafarers: a population based cohort study. Occupational Environmental Medicine 62, 761–765.

Kim, E., Hopke, P.K., 2008a. Source characterization of ambient fine particles at multiple sites in the Seattle area. Atmospheric Environment 42, 6047–6056.

Kim, E., Hopke, P.K., 2008b. Characterization of ambient fine particles in the Northwestern area and Anchorage, Alaska. Journal of the Air & Waste Management Association 58, 1328–1340.

Künzli, N., Jerrett, M., Mack, W.J., Beckerman, B., LaBree, L., Gilliland, F., Thomas, M., Peters, J., Hodis, H.N., 2005. Ambient air pollution and atherosclerosis in Los Angeles. Environmental Health Perspectives 113, 201–206.

Maykut, N., Lewtas, J., Kim, E., Larson, T., 2003. Source apportionment of PM2.5 at an urban IMPROVE site in Seattle, Washington. Environmental Science and Technology 37, 5135–5142.

Minguillon, M.C., Arhami, M., Schauer, J.J., Sioutas, C., 2008. Seasonal and spatial variations of sources of fine and quasi-ultrafine particulate matter in neighborhoods near the Los Angeles–Long Beach harbor. Atmospheric Environment 42, 7317–7328.

Moldanova, J., Fridell, E., Popovicheva, O., Demirdjian, B., Tishkova, V., Faccinetto, A., Focsa, C., 2009. Characterisation of particulate matter and gaseous emissions from a large ship diesel engine. Atmospheric Environment 43, 2632–2641.

Mooibroek, D., Schaap, M., Weijers, E.P., Hoogerbrugge, R., 2011. Source apportionment and spatial variability of $PM_{2.5}$ using measurements at five sites in the Netherlands. Atmospheric Environment 45, 4180–4191.

Norris, G., Vedantham, R., Wade, K., Brown, S., Prouty, J., Foley, C., 2008. EPA Positive Matrix Factorization (PMF) 3.0: Fundamentals & User Guide. U.S. Environmental Protection Agency. EPA 600/R-08/108.

Paatero, P., Hopke, P.K., 2003. Discarding or downweighting high-noise variables in factor analytic models. Analytica Chimica Acta 490, 277–289.

Pope III, C.A., Dockery, D.W., 2006. Health effects of fine particulate air pollution: lines that connect. Journal of the Air & Waste Management Association 56, 709–742.

Port Metro Vancouver, 2012. Port Metro Vancouver Container Statistics Report 2008–2011. http://www.portmetrovancouver.com/Libraries/ABOUT_Facts_Stats/2008-2011_Container_Statistics_Report.sflb.ashx (accessed 29.08.12.).

Port of Tacoma, 2012. Port of Tacoma Container Volumes 2009–2011. http://www.portoftacoma.com/stats (accessed 29.08.12.).

Port of Seattle, 2012. Seattle Harbor 10 Year History of Cargo Volumes Handled: 2002–2011. http://www.portseattle.org/About/Publications/Statistics/Seaport/Pages/10-Year-History.aspx (accessed 28.08.12.).

Reff, A., Eberly, S.I., Bhave, P.V., 2007. Receptor modeling of ambient particulate matter data using Positive Matrix Factorization: review of existing methods. Journal of the Air & Waste Management Association 57, 146–154.

U.S. Army Corps of Engineers, 2012. Waterborne Commerce Statistics Center. http://www.ndc.iwr.usace.army.mil/wcsc/wcsc.htm (accessed 07.08.12.).

U.S. Environmental Protection Agency, 2009. $PM_{2.5}$ Speciation Network Newsletter, Issue 6, 2009. http://www.epa.gov/ttnamti1/files/ambient/pm25/spec/spnews6.pdf (accessed 02.08.12.).

U.S. Environmental Protection Agency, 2010. Designation of North American Emission Control Area to Reduce Emissions from Ships: Regulatory Announcement. EPA-420-F-10-015.

U.S. Environmental Protection Agency, 2012a. 2008 National Emissions Inventory Version 2.0. http://www.epa.gov/ttnchie1/net/2008inventory.html (accessed 26.07.12.).

U.S. Environmental Protection Agency, 2012b. 2008 NEI Technical Support Document, Draft. http://www.epa.gov/ttn/chief/net/2008neiv2/2008_neiv2_tsd_draft.pdf (accessed 21.11.12.).

Wagstrom, K.M., Pandis, S.N., Yarwood, G., Wilson, G.M., Morris, R.E., 2008. Development and application of a computationally efficient particulate matter apportionment algorithm in a three-dimensional chemical transport model. Atmospheric Environment 42, 5650–5659.

Winebrake, J.J., Corbett, J.J., Green, E.H., Lauer, A., Eyring, V., 2009. Mitigating the health impacts of pollution from oceangoing shipping: an assessment of low-sulfur fuel mandates. Environmental Science and Technology 43, 4776–4782.

Wu, C., Larson, T.V., Wu, S., Williamson, J., Westberg, H.H., Liu, L.-J.S., 2007. Source apportionment of $PM_{2.5}$ and selected hazardous air pollutants in Seattle. Science of the Total Environment 386, 42–52.

Atmospheric Environment 103 (2015) 121–128

Contents lists available at ScienceDirect

Atmospheric Environment

journal homepage: www.elsevier.com/locate/atmosenv

The effects of marine vessel fuel sulfur regulations on ambient $PM_{2.5}$ along the west coast of the U.S.

Robert A. Kotchenruther

U.S. Environmental Protection Agency Region 10, Office of Environmental Assessment, 1200 Sixth Avenue, Mailstop OEA-140, Seattle, WA 98101, USA

HIGHLIGHTS

- Ambient effects from two marine vessel fuel sulfur regulations were investigated.
- Ambient V and Ni data from 31 U.S. west coast sites was analyzed.
- $PM_{2.5}$ source apportionment was performed for 9 sites.
- V + Ni mass and marine vessel $PM_{2.5}$ reductions align with regulated areas.

ARTICLE INFO

Article history:
Received 2 October 2014
Received in revised form
9 December 2014
Accepted 13 December 2014
Available online 17 December 2014

Keywords:
PM2.5
Marine vessel emissions
Positive matrix factorization
Source apportionment
Residual fuel oil
Emissions control area

ABSTRACT

This work uses $PM_{2.5}$ data and Positive Matrix Factorization (PMF) modeling to explore the effects of two marine vessel fuel sulfur regulations along the west coast of the United States (US); California's (CA) Ocean-Going Vessel Clean Fuel Regulation (CA-CFR) implemented in July 2009 and the North American Emissions Control Area (NA-ECA) implemented in August 2012. Data from 31 chemically speciated $PM_{2.5}$ monitors along the US west coast were analyzed and 9 sites with strong linear correlations between vanadium and nickel were selected for PMF modeling. The 9 sites were modeled independently and for 8 sites, 3 in CA and 5 in Washington State (WA), a well-defined factor linked to marine vessel residual fuel oil (RFO) combustion was identified. For these 8 sites, model results were subdivided into three time periods; a three year period prior to implementation of the CA-CFR, a three year period after the CA-CFR but prior to the NA-ECA, and a one year period after implementation of the NA-ECA. Marine vessel $PM_{2.5}$ distributions were compared between the three time periods to determine if statistically significant reductions had occurred. Comparing marine vessel $PM_{2.5}$ for the three years before and after CA-CFR implementation, all CA sites indicated statistically significant reductions, with reductions in annualized average marine vessel $PM_{2.5}$ from 30 to 52% (0.09–0.78 $\mu g/m^3$). Comparing marine vessel $PM_{2.5}$ for the three years before NA-ECA implementation and the 1 year after, 2 of 5 WA sites indicated statistically significant reductions in annualized average impacts (45–50%, 0.12–0.23 $\mu g/m^3$) and 1 of 3 sites in CA (46%, 0.04 $\mu g/m^3$). These results demonstrate that marine vessel fuel sulfur regulations on the west coast of the US have been effective at reducing $PM_{2.5}$ impacts from marine vessel RFO combustion at some locations, with the implementation of the CA-CFR showing more success than the NA-ECA. The greater observed success of the CA-CFR is, to some extent, probably the result of a longer 3-year implementation time compared to only 1 year for the NA-ECA.

Published by Elsevier Ltd.

1. Introduction

Emissions of fine particulate matter ($PM_{2.5}$, particles with aerodynamic diameter <2.5 μm) have been shown to have wide ranging adverse effects. Human exposure to $PM_{2.5}$ has been linked to cardiovascular and pulmonary disease (Künzli et al., 2005), and lung cancer and premature mortality (Pope and Dockery, 2006). Anthropogenic emissions of $PM_{2.5}$ play direct and indirect roles in climate forcing (IPCC, 2013) and deposition of anthropogenic PM can have adverse effects on ecosystem health (Geiser et al., 2010).

$PM_{2.5}$ emissions from commercial marine vessels has been an active area of investigation because these sources typically burn residual fuel oil (RFO), which has a very high sulfur content and

E-mail address: Kotchenruther.Robert@epa.gov.

http://dx.doi.org/10.1016/j.atmosenv.2014.12.040
1352-2310/Published by Elsevier Ltd.

produces large amounts of $PM_{2.5}$, SO_2, and NO_x (Moldanova et al., 2009), and are mobile sources that can impact both urban areas and remote coastal areas having few other direct sources of anthropogenic emissions.

Globally, approximately 60,000 cardiopulmonary and lung cancer deaths annually have been attributed to exposure to marine vessel emissions (Corbett et al., 2007). Regulating marine vessel fuel sulfur content is a common approach to reducing emissions. Winebrake et al. (2009) have shown that significant reductions in premature mortality from marine vessel emissions can be achieved by regulating fuel sulfur content at amounts lower than an assumed uncontrolled fuel sulfur content of 2.7%.

Several fuel sulfur regulations have recently been implemented effecting marine vessels operating along the west coast of the United States (US). In July 2009 California (CA) implemented their Ocean-Going Vessel Clean Fuel Regulation (CA-CFR, http://www.arb.ca.gov/ports/marinevess/ogv.htm). Phase I of the regulation became effective July 1, 2009 and required ocean-going vessels within 24 nautical miles (nm) of the CA coast to use fuels with sulfur content at or below 1.5% and after August 1, 2012 to use fuels at or below 1.0%. Starting January 1, 2014, Phase II of the regulation required fuel sulfur content at or below 0.1%. In a separate regulation, beginning August 1, 2012 the North American Emissions Control Area (NA-ECA; US EPA, 2010) required marine vessels within 200 nm of North American coasts up to 60° latitude to use fuels with sulfur content no higher than 1%. Starting in 2015, the NA-ECA will require fuel sulfur content no higher than 0.1%.

Previous studies have shown that significant reductions in $PM_{2.5}$ and SO_2 occur when ocean going vessels switch from high to low sulfur fuels (Kasper et al., 2007; Khan et al., 2012). However, only a few studies have demonstrated the benefits of implementing fuel sulfur regulations on ambient pollution concentrations. These studies focused on areas near major ports where the largest reductions are expected. Schembari et al. (2012) attributed declines in ambient SO_2 in Mediterranean harbors with implementation of European Union in-port fuel sulfur limits (EC, 2005) and Velders et al. (2011) associated decreases in SO_2 in Rotterdam with the combined effects of a North Sea ECA (MARPOL, 2008) and the European Union in-port fuel sulfur limits. In North America, Tao et al. (2013) associated declines in SO_2 and $PM_{2.5}$ in San Francisco, CA with implementation of the CA-CFR.

Several photochemical modeling studies have estimated regional-scale air quality benefits from implementing marine vessel fuel sulfur regulations (Matthias et al., 2010; Mölders et al., 2013), but no known published studies have demonstrated air quality improvements in remote areas through analysis of ambient measurements.

Previous receptor modeling studies at sites along the US west coast have demonstrated the ability to quantify marine vessel $PM_{2.5}$ impacts (Kotchenruther, 2013 and references therein). In this work $PM_{2.5}$ from select US west coast sites are analyzed in conjunction with Positive Matrix Factorization (PMF) receptor modeling to quantify $PM_{2.5}$ impacts from marine vessel RFO emissions. Marine vessel impacts are compared for three time periods; a three year period prior to the CA-CFR, a three year period after the CA-CFR but prior to the NA-ECA, and a one year period after implementation of the NA-ECA.

2. Methods

2.1. $PM_{2.5}$ data

Chemically speciated $PM_{2.5}$ data were obtained from the Interagency Monitoring of Protected Visual Environments (IMPROVE) Network. IMPROVE samplers collect 24-h integrated $PM_{2.5}$ mass and are operated on a once every third day schedule. Information about the IMPROVE network can be found on the IMPROVE web site (http://vista.cira.colostate.edu/improve/).

2.2. Time period analyzed

Data were analyzed from June 1, 2006 through August 31, 2013. This data record includes three distinct periods with respect to marine vessel fuel sulfur regulations; a 37 month period (6/2006 to 6/2009) prior to implementation of the CA-CFR, a 37 month period (7/2009 to 7/2012) after implementation of the CA-CFR but prior to the implementation of the NA-ECA, and a 13 month period after implementation of the NA-ECA. These three time periods will be subsequently referred to as the pre-regulation (pre-reg), CA-CFR, and NA-ECA periods, respectively.

2.3. Monitoring site selection

All IMPROVE sites in the US west coast states of CA, Oregon (OR), and Washington (WA) were analyzed as long as sites had a monitoring record spanning the full study period. Monitoring sites in states further east were not considered because previous PMF analyses of US Pacific Northwest sites demonstrated that marine vessel $PM_{2.5}$ impacts were detected only in coastal states (Kotchenruther, 2013). The sites considered here are listed north to south in Table 1 and depicted in Fig. 1.

All sites were considered for PMF analysis. Vanadium (V) and nickel (Ni) linear correlation coefficients (r^2) and best fit slopes were computed after outlier removal (see Table 1). Sites were selected for PMF analysis if the V:Ni r^2 was greater than 0.75. The V:Ni linear best fit slopes for the resulting 9 sites ranged between 2.1 and 2.8, which is consistent with reported V:Ni emissions ratios for marine vessel RFO combustion (Agrawal et al., 2008). All nine sites are coastal or near-coastal (see Fig. 1), further suggesting that the V and Ni impacts were from marine vessels.

2.4. Data assessment methods

Two methods were used to determine if significant reductions in ambient impacts from marine vessels had occurred.

First, changes in V, Ni, and sulfate (SO_4) concentrations were assessed. As noted above, V and Ni are established trace metals associated with emissions from marine vessels using RFO and RFO emissions have high concentrations of SO_4. Distillate fuels have much lower V, Ni, and SO_4 emissions compared to RFO (Popovicheva et al., 2012; Tao et al., 2013). Hence, distillate fuels or distillate-RFO blends used to meet marine vessel fuel sulfur requirements can be expected to reduce emissions of V, Ni, and SO_4.

Because emissions of V and Ni are more uniquely associated with marine vessel RFO combustion than SO_4, this first method focuses mainly on changes in V and Ni concentrations. If other sources of environmental V and Ni remain relatively unchanged, then reductions in marine vessel RFO use associated with fuel sulfur regulations should lead to decreases in V and Ni at monitors impacted by primary emissions from marine vessels. However, even if decreases in V and Ni are found, they cannot easily be translated into changes in overall $PM_{2.5}$ impacts.

The second method, PMF modeling, is better suited to address changes in total $PM_{2.5}$ impacts from marine vessels. For sites where PMF identifies a factor linked to marine vessel RFO, then modeled marine vessel $PM_{2.5}$ can be compared for each period associated with varying fuel sulfur regulations to determine if significant reductions have occurred.

Table 1
IMPROVE monitoring sites, V and Ni linear correlation results, annualized average V + Ni and SO_4 concentrations, and Wilcoxon-Mann-Whitney (WMW) p-values testing for significant reductions (bold face, significant at the 99% confidence interval).

Site name	Abbreviation	State	Latitude	Longitude	Number of samples	Sample outliers[a] removed for V:Ni correlation	V:Ni linear correlation coefficient (r^2)	V:Ni linear correlation slope	Pre-reg annualized average V + Ni (ng/m^3)	CA-CFR annualized average V + Ni (ng/m^3)	NA-ECA Annualized average V + Ni (ng/m^3)	Pre-reg to CA-CFR V + Ni WMW p-value	CA-CFR to NA-ECA V + Ni WMW p-value	Pre-reg annualized average SO_4 (μg/m^3)	CA-CFR annualized average SO_4 (μg/m^3)	NA-ECA annualized average SO_4 (μg/m^3)	Pre-reg to CA-CFR SO_4 WMW p-value	CA-CFR to NA-ECA SO_4 WMW p-value
North Cascades	NOCA	WA	48.7316	−121.0646	819	0	0.805	2.342	0.39	0.46	0.28	0.334	0.170	0.46	0.39	0.32	**0.000**	0.115
Pasayten	PASA	WA	48.3877	−119.9275	830	1	0.053	0.334	0.13	0.13	0.11	0.584	0.221	0.35	0.28	0.23	**0.000**	0.049
Olympic	OLYM	WA	48.0065	−122.9727	859	2	0.862	2.733	1.72	1.79	0.94	0.271	**0.000**	0.59	0.50	0.40	**0.000**	**0.000**
Puget Sound	PUSO	WA	47.5696	−122.3119	809	3	0.737	2.104	6.17	6.59	3.44	0.215	**0.000**	0.99	0.80	0.63	**0.000**	**0.003**
Snoqualmie Pass	SNPA	WA	47.422	−121.4259	861	3	0.801	2.415	0.46	0.47	0.31	0.020	0.191	0.44	0.39	0.34	**0.002**	0.075
Mount Rainier	MORA	WA	46.7583	−122.1244	836	2	0.815	2.362	0.62	0.61	0.37	0.271	0.075	0.51	0.44	0.37	**0.002**	0.078
White Pass	WHPA	WA	46.6243	−121.3881	835	1	0.422	1.399	0.15	0.16	0.12	0.449	0.184	0.32	0.24	0.23	**0.000**	0.405
Columbia River Gorge	CORI	WA	45.6644	−121.0008	869	1	0.105	0.818	0.48	0.47	0.31	0.674	**0.001**	0.72	0.55	0.67	**0.000**	0.750
Mount Hood	MOHO	OR	45.2888	−121.7837	855	2	0.232	0.699	0.19	0.20	0.29	0.560	1.000	0.36	0.31	0.26	**0.003**	0.238
Starkey	STAR	OR	45.2249	−118.5129	858	0	0.023	0.352	0.15	0.16	0.12	0.623	0.079	0.42	0.37	0.33	0.024	0.102
Hells Canyon	HECA	OR	44.9702	−116.8438	799	1	0.067	0.329	0.15	0.14	0.11	0.600	0.083	0.45	0.39	0.37	**0.002**	0.283
Three Sisters	THSI	OR	44.291	−122.0434	854	3	0.363	1.369	0.19	0.22	0.19	0.599	0.270	0.39	0.33	0.26	**0.002**	0.028
Crater Lake	CRLA	OR	42.8958	−122.1361	828	3	0.022	0.251	0.12	0.14	0.11	0.801	0.232	0.33	0.27	0.25	**0.001**	0.557
Kalmiopsis	KALM	OR	42.552	−124.0589	850	3	0.488	1.343	0.28	0.22	0.20	0.017	0.700	0.46	0.39	0.35	**0.002**	0.236
Lava Beds	LABE	CA	41.7117	−121.5068	833	1	0.057	0.387	0.15	0.14	0.16	0.178	0.897	0.38	0.32	0.29	**0.003**	0.229
Redwood	REDW	CA	41.5608	−124.0839	811	3	0.579	1.536	0.41	0.26	0.19	**0.000**	0.193	0.59	0.43	0.43	**0.000**	0.496
Trinity	TRIN	CA	40.7864	−122.8046	752	3	0.221	0.753	0.22	0.17	0.16	0.090	0.575	0.44	0.33	0.31	**0.001**	0.406
Lassen Volcanic	LAVO	CA	40.5398	−121.5768	835	1	0.133	0.575	0.21	0.17	0.15	0.011	0.530	0.43	0.33	0.31	**0.000**	0.555
Bliss	BLIS	CA	38.9761	−120.1025	832	1	0.101	0.678	0.18	0.16	0.14	0.031	0.118	0.47	0.38	0.37	**0.005**	0.327
Point Reyes	PORE	CA	38.1224	−122.9085	800	2	0.834	2.298	1.53	0.73	0.40	**0.000**	**0.000**	1.05	0.82	0.68	**0.000**	0.128
Hoover	HOOV	CA	38.0881	−119.1771	788	0	0.004	0.044	0.21	0.25	0.22	0.989	0.263	0.43	0.35	0.37	**0.000**	0.520
Yosemite	YOSE	CA	37.7133	−119.7061	844	1	0.223	0.986	0.29	0.20	0.20	**0.001**	0.342	0.61	0.51	0.55	**0.006**	0.860
Kaiser	KAIS	CA	37.2207	−119.1546	796	3	0.177	0.583	0.23	0.20	0.20	0.054	0.377	0.56	0.48	0.52	0.020	0.629
Fresno	FRES	CA	36.7818	−119.7732	802	2	0.075	1.269	2.47	1.22	0.52	**0.000**	**0.000**	1.39	1.08	0.99	**0.000**	0.383
Sequoia	SEQU	CA	36.4894	−118.8291	860	1	0.247	1.316	0.44	0.32	0.31	**0.000**	0.377	1.14	0.97	0.96	**0.000**	0.562
Pinnacles	PINN	CA	36.4833	−121.1568	852	3	0.769	2.266	0.89	0.51	0.29	**0.000**	**0.000**	0.89	0.67	0.63	**0.000**	0.315
Dome Lands	DOME	CA	35.7278	−118.1377	759	1	0.155	0.942	0.35	0.29	0.28	0.071	0.479	0.92	0.74	0.76	**0.003**	0.656
San Rafael	RAFA	CA	34.7339	−120.0074	801	1	0.778	2.184	0.92	0.46	0.32	**0.000**	**0.001**	0.99	0.70	0.72	**0.000**	0.357
San Gorgonio	SAGO	CA	34.1939	−116.9132	843	1	0.609	2.593	0.85	0.46	0.30	**0.000**	**0.000**	0.84	0.62	0.68	**0.000**	0.794
Joshua Tree	JOSH	CA	34.0695	−116.3889	830	3	0.567	2.768	0.78	0.51	0.39	**0.000**	0.013	0.85	0.66	0.75	**0.000**	0.786
Agua Tibia	AGTI	CA	33.4636	−116.9706	754	1	0.833	2.785	1.95	1.18	0.58	**0.000**	**0.000**	1.56	1.07	1.01	**0.000**	0.405

[a] Outliers were identified as data with studentenized residuals greater than 6 or less than −6.

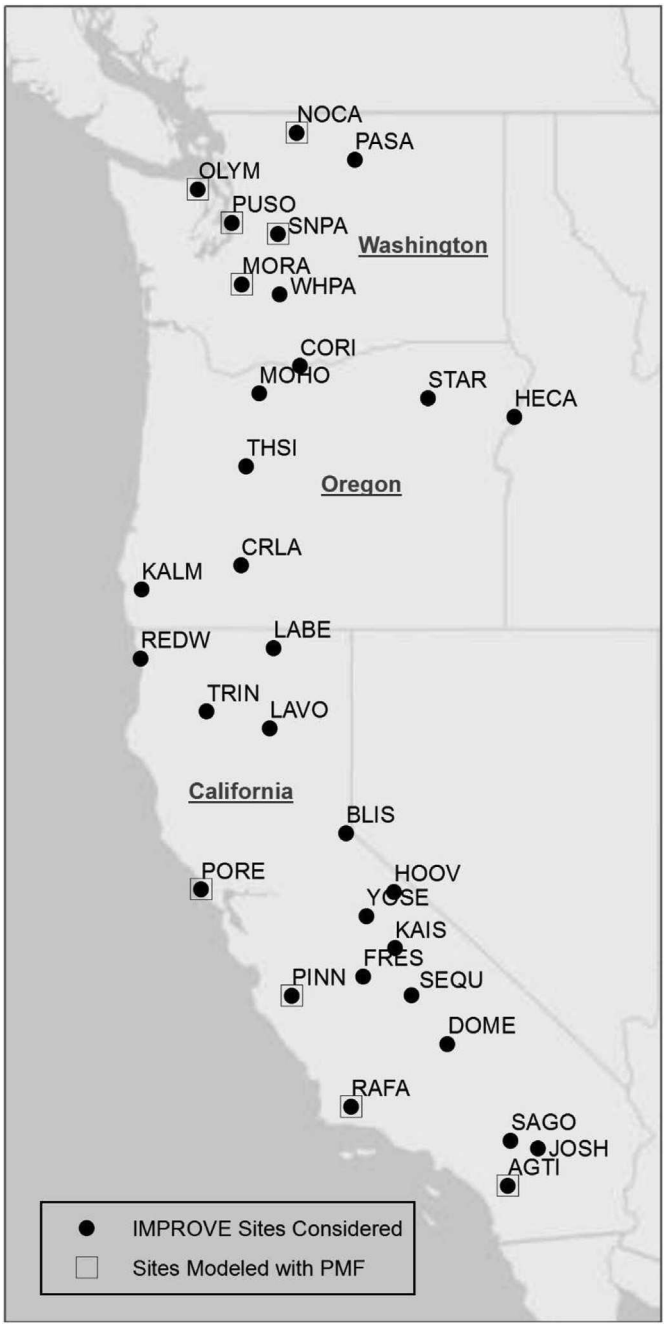

Fig. 1. IMPROVE sites used in this analysis.

2.5. Data preparation for PMF modeling

IMPROVE datasets were processed to correct for missing or negative values, data completeness issues, and species double counting. A detailed discussion of these data preparations is provided in a previous publication by Kotchenruther (2013).

2.6. PMF modeling

PMF source apportionment modeling was performed using EPA PMF 5.0 (http://www.epa.gov/heasd/research/pmf.html). A discussion of the mathematical equations underlying EPA PMF can be found in Paatero and Hopke (2003) and Norris et al. (2014). Data from each monitoring site was modeled independently. In each case, the model was run in the robust mode with 20 repeat runs to insure the model least-squares solution represented a global rather than local minimum and the rotational FPEAK variable was held at the default value of 0.0. The model solution with the optimum number of factors was determined somewhat subjectively and was based on inspection of the factors in each solution, the quality of the least-squares fit (analysis of Q_{Robust} and Q_{True} values), and the results from three error estimation methods available in PMF 5.0 (DISP, BS, and BS-DISP; Norris et al., 2014). The scaled residuals for final model solutions were generally normally distributed, falling into the recommended range of +3 to −3. Observed vs. predicted V and Ni compared well, with an average r^2 of 0.79 for V for the 9 sites (range, 0.58–0.98) and 0.72 for Ni (range, 0.50–0.90). Sites with lower observed vs. predicted r^2 were sites with lower observed concentrations, and therefore higher data scatter.

3. Results and discussion

3.1. Analysis of V, Ni, and SO_4

Data distributions for the pre-reg, CA-CFR, and NA-ECA periods were tested to determine if statistically significant reductions in concentration had occurred. V, Ni, and SO_4 concentrations measured at west coast IMPROVE sites have a strong annual cycle, with higher concentrations in the summer and lower in the winter. Hence, in order not to bias statistical significance testing, the first month of data from each time period was removed so that the analysis was performed on data encompassing one or three annual cycles. The resulting time periods analyzed were the 36 months from July 2006 through June 2009 for the pre-reg period, the 36 months from August 2009 through July 2012 for the CA-CFR period, and the 12 months from September 2012 through August 2013 for the NA-ECA period.

Because V and Ni are trace metals associated with marine vessel RFO combustion, the statistical analysis conducted here was performed on the sum of V + Ni concentrations. Significance tests for reductions in V + Ni concentrations, and separately for SO_4 concentrations, were performed using the nonparametric Wilcoxon-Mann-Whitney (WMW) test (ProUCL version 5.0; http://www.epa.gov/osp/hstl/tsc/software.htm). Table 1 lists the significance test p-values and annualized average V + Ni and SO_4 concentrations for each data set and time period (annualized averages are the average of 12 or 36 monthly averages, depending on the period). P-values less than 0.01, indicating significant reductions at the 99% confidence level (CL), are listed in bold font in Table 1.

Comparing data between the pre-reg and CA-CFR periods, significant reductions in V + Ni were only observed at CA sites. Table 1 shows that significant V + Ni reductions were at CA coastal locations (REDW, PORE, PINN, RAFA, AGTI) or sites in western portions of CA (YOSE, FRES, SEQU, SAGO, JOSH). The absence of significant V + Ni reductions in WA, OR, and sites in the eastern portions of CA is consistent with CA-CFR regulations reducing V + Ni concentrations by reducing the overall amount of RFO combustion from marine vessels. Of the CA sites showing significant V + Ni reductions, the FRES site had high V + Ni concentrations but poor V:Ni correlation, suggesting that V + Ni reductions at the FRES site could be related to emissions reductions from non-RFO sources. In contrast to the V + Ni data, all but two sites showed significant reductions in SO_4 at the 99% CL, and every site at the 95% CL. This is likely a result of nation-wide regulations to reduce sulfur emissions from many source categories.

Comparing data between CA-CFR and NA-ECA periods, significant reductions in V + Ni were observed in multiple states. In WA the PUSO, OLYM, and CORI sites indicated significant V + Ni reductions at the 99% CL. However, the NOCA, SNPA, WHPA, MORA,

and KALM sites identified in a previous publication as impacted by marine vessel RFO (Kotchenruther, 2013), did not indicate significant V + Ni reductions at the 99% or 95% CL. In CA, 6 of the 10 sites that indicated significant V + Ni reductions from the pre-reg to the CA-CFR period also showed significant further reductions (99% CL) in the first year of the NA-ECA. Comparing SO_4 data between CA-CFR and NA-ECA periods, only 2 sites in WA (PUSO and OLYM) indicated significant reductions at the 99% CL.

The more widespread success in CA in reducing V + Ni concentrations from implementation of the CA-CFR may be because the CA-CFR has had 3 years of implementation time compared to only 1 year since the implementation of the NA-ECA. It should also be noted that the Canadian government only authorized Canadian enforcement of the NA-ECA in May 2013 (Canada Gazette, 2013), ten months after taking effect in the US. The delay in Canadian enforcement may have resulted in reduced compliance in Canadian waters during a portion of the NA-ECA period analyzed in this study and therefore may have impacted V + Ni and SO_4 concentrations observed in WA.

3.2. PMF results

Tables 2a–c show PMF results for 9 IMPROVE sites sorted by latitude north to south, and show the annualized average PMF factor $PM_{2.5}$ concentrations for the pre-reg, CA-CFR and NA-ECA periods, respectively. The annualized averages were computed as the average of 12 or 36 monthly averages, as described above.

11 different PMF factor types were identified during PMF modeling of the 9 sites, with between 5 and 9 factors being identified at individual sites. 3 factor types were ubiquitous: fugitive dust, gasoline engines, and sea salt. 4 factors occurred at most sites: secondary organic aerosol plus wood smoke, marine vessel RFO, secondary nitrate (NO_3), and secondary SO_4. 4 remaining factors were less common, occurring at one or only a few sites: marine vessel RFO plus secondary SO_4, metal processing, diesel engines, and secondary SO_4 plus aged sea salt. Section 3.3 describes each factor type and its major identifying features. Detailed PMF results including factor chemical profiles, concentration time series, and error estimation analyses can be found in the supplementary materials Sections S.1–S.9.

3.3. PMF factor identification

11 PMF factor types were identified among the 9 sites analyzed. Factor identification was based on factor chemical profiles, seasonal factor concentration patterns, previous published studies, and comparisons with source profiles in the EPA SPECIATE database (http://www.epa.gov/ttnchie1/software/speciate/).

3.3.1. Secondary organic aerosol plus wood smoke

A factor mixing secondary organic aerosol with primary wood smoke emissions. This factor occurred at 7 sites and was characterized by a chemical profile dominated by organic carbon (OC), elemental carbon (EC), and potassium and a $PM_{2.5}$ mass time series with occasional spikes above 5 $\mu g/m^3$ on top of continuous contributions between 0.5 and 1 $\mu g/m^3$.

3.3.2. Fugitive dust

This factor occurred at all sites and was characterized by a chemical profile dominated by the crustal elements aluminum, calcium, iron, and titanium.

3.3.3. Marine vessel RFO

This factor occurred at 8 sites and was characterized by a chemical profile containing significant SO_4 and trace metal contributions from V and Ni. The chemical profile V:Ni ratio ranged between 2.4 and 3.4 across the 8 sites, which is consistent with previous studies of marine vessel RFO combustion (Popovicheva et al., 2012; Agrawal et al., 2008).

3.3.4. Marine vessel RFO plus secondary SO_4

This factor occurred at only the RAFA site and was identified by a chemical profile with V:Ni ratio of 2.7 typical of marine vessel RFO emissions, a strong SO_4 component, and the absence of a separate PMF factor for secondary SO_4. It is likely this factor results from PMF being unable to separate RFO sources from other SO_4 sources.

3.3.5. Metal processing

This factor occurred at only the PUSO site and was characterized by a chemical profile with SO_4, EC, and significant trace metal contributions from chromium and manganese.

3.3.6. Mobile, diesel dominant

This factor occurred at 4 sites and was characterized by a chemical profile similar to the mobile, gasoline dominant factor but with higher contributions from EC relative to OC and significant trace metal contributions from zinc (Zn) (Mazzei et al., 2008).

3.3.7. Mobile, gasoline dominant

This factor occurred at all sites and was characterized by a chemical profile similar to the mobile, diesel engine dominant factor but with a higher contribution from OC relative to EC and significant trace elemental contributions from Zn, copper, lead, and bromine. These trace elements have been previously associated with mobile source emissions (Mazzei et al., 2008).

3.3.8. Sea salt

This factor occurred at all sites and was characterized by a chemical profile dominated by sodium (Na), chloride ion (Chl), and

Table 2a
PMF factor average mass ($\mu g/m^3$) for the pre-reg period July 2006–June 2009.

Site	Secondary organic aerosol plus wood smoke	Fugitive dust	Marine vessel RFO	Marine vessel RFO plus secondary sulfate	Metal processing	Mobile, diesel dominant	Mobile, gasoline dominant	Sea salt	Secondary nitrate	Secondary sulfate	Secondary sulfate plus aged sea salt	Measured $PM_{2.5}$
NOCA	0.78	0.12	0.47				0.31	0.23		0.32		2.13
OLYM	0.61	0.13	0.23			0.01	0.63	0.22	0.21	0.57	0.23	2.76
PUSO	1.09	0.50	0.50		0.18		1.74	0.43	1.16	0.99		6.67
SNPA	0.92	0.21	0.45			0.08	0.15	0.13	0.18	0.44		2.58
MORA	1.09	0.22	0.74				0.39	0.16		0.42		2.98
PORE		0.30	0.18				0.65	3.12	0.75	1.00		5.86
PINN	1.30	0.35	0.98			0.20	0.28	0.44	0.37		0.82	4.81
RAFA		0.70		1.88			1.43	0.48	0.31			5.09
AGTI	0.49	0.68	1.85			0.06	1.19	0.30	0.62		0.97	6.11

Table 2b
PMF factor average mass (μg/m^3) for the CA-CFR period August 2009–July 2012.

Site	Secondary organic aerosol plus wood smoke	Fugitive dust	Marine vessel RFO	Marine vessel RFO plus secondary sulfate	Metal processing	Mobile, diesel dominant	Mobile, gasoline dominant	Sea salt	Secondary nitrate	Secondary sulfate	Secondary sulfate plus aged sea salt	Measured $PM_{2.5}$
NOCA	0.78	0.11	0.47				0.27	0.21		0.26		2.14
OLYM	0.48	0.10	0.24			0.00	0.52	0.22	0.15	0.45	0.19	2.37
PUSO	0.87	0.35	0.52		0.10		1.59	0.43	0.82	0.79		5.45
SNPA	0.84	0.20	0.41			0.06	0.11	0.15	0.14	0.38		2.24
MORA	0.92	0.19	0.67				0.32	0.16		0.40		2.69
PORE		0.27	0.09				0.49	2.91	0.63	0.75		5.40
PINN	1.03	0.29	0.68			0.13	0.25	0.48	0.25		0.72	3.88
RAFA		0.64		1.28			1.09	0.50	0.23			3.86
AGTI	0.39	0.57	1.07			0.04	1.20	0.28	0.40		0.95	5.02

Table 2c
PMF factor average mass (μg/m^3) for the NA-ECA period September 2012–August 2013.

Site	Secondary organic aerosol plus wood smoke	Fugitive dust	Marine vessel RFO	Marine vessel RFO plus secondary sulfate	Metal processing	Mobile, diesel dominant	Mobile, gasoline dominant	Sea salt	Secondary nitrate	Secondary sulfate	Secondary sulfate plus aged sea salt	Measured $PM_{2.5}$
NOCA	0.83	0.11	0.37				0.22	0.18		0.22		2.08
OLYM	0.41	0.11	0.12			0.00	0.44	0.18	0.16	0.40	0.17	2.09
PUSO	0.79	0.32	0.29		0.10		1.28	0.37	0.90	0.61		4.87
SNPA	1.61	0.20	0.34			0.06	0.10	0.09	0.15	0.33		3.01
MORA	1.02	0.16	0.70				0.33	0.11		0.37		2.90
PORE		0.22	0.05				0.29	3.01	0.27	0.59		5.09
PINN	0.97	0.34	0.65			0.13	0.22	0.44	0.25		0.66	3.78
RAFA		0.61		1.32			0.92	0.52	0.23			3.76
AGTI	0.35	0.56	0.85			0.05	1.09	0.24	0.36		1.03	4.79

magnesium (Mg).

3.3.9. Secondary NO_3

This factor occurred at 7 sites and was characterized by a chemical profile dominated by NO_3. This factor typically had a seasonal pattern of higher mass attributions in winter months.

3.3.10. Secondary SO_4

This factor occurred at 6 sites and was characterized by a chemical profile dominated by SO_4. This factor typically had a seasonal pattern of higher mass attributions in summer months.

3.3.11. Secondary SO_4 plus aged sea salt

This factor occurred at 3 sites and was characterized by a chemical profile dominated by aged sea salt with secondary SO_4. Aged sea salt was identified by the importance of Na, Mg, and NO_3 in the chemical profile, but the absence of Chl. This factor typically had a seasonal pattern of higher mass attributions in summer months.

3.4. Delineation of marine vessel RFO from other sources

A marine vessel RFO combustion factor was identified at 9 sites. This was expected because these sites were chosen based on strong V:Ni correlations and correlation slopes similar to marine vessel RFO emissions ratios. The V:Ni ratio in the 9 PMF profiles for RFO combustion ranged from 2.4 to 3.4 with an average value of 2.7. This ratio was generally higher than that from the ambient measurements, which ranged from 2.1 to 2.8 with an average of 2.4 (Table 1). This difference is likely caused by differing amounts of environmental sources of V compared to Ni, external to RFO.

Other than several categories of stationary sources, no other significant sources of V and Ni have V:Ni emissions ratios above about 1.0 in the EPA SPECIATE database. While impacts from stationary sources cannot be completely ruled out, the coastal and remote locations of most sites considered here makes RFO combustion from marine vessels the likely dominant source of V and Ni.

In addition to a marine vessel RFO factor, PMF modeling also produced a separate factor for secondary sulfate at all but the RAFA site. The PMF version used here has three uncertainty estimation methods, and a summary of the results for each PMF run is provided in supplemental data sections S.1–S.9. All uncertainty estimation results fell within the suggested guidelines (Norris et al., 2014) and provide added confidence that marine vessel RFO factors were well delineated from secondary SO_4 sources, with the exception of the RAFA site. Further evidence of good source separation between marine vessel RFO and secondary SO_4 is provided when comparing the significance testing results for measured SO_4 (Table 1) with the testing results for significant declines in marine vessel RFO impacts (Table 3, further discussed in Section 3.5). While significant declines in SO_4 are virtually ubiquitous from the pre-reg to CA-CFR period, declines in PMF factor marine vessel RFO impacts

Table 3
Change in RFO factor annualized mass between fuel sulfur regulatory periods and significance testing results.

Site name	Pre-reg to CA-CFR, change in annualized average RFO mass (μg/m^3)	CA-CFR to NA-ECA, change in annualized average RFO mass (μg/m^3)	Pre-reg to CA-CFR, change in annualized average RFO mass (%)	CA-CFR to NA-ECA, change in annualized average RFO mass (%)	Pre-reg to CA-CFR RFO mass WMW p-value	CA-CFR to NA-ECA RFO mass WMW p-value
NOCA	0.00	−0.10	−0.4	−22.1	0.055	0.318
OLYM	0.01	−0.12	4.7	−49.6	0.357	**0.000**
PUSO	0.01	−0.23	2.8	−44.7	0.336	**0.000**
SNPA	−0.04	−0.07	−9.0	−16.4	0.134	0.108
MORA	−0.07	0.03	−9.5	4.1	0.363	0.345
PORE	−0.09	−0.04	−51.9	−46.5	**0.000**	**0.000**
PINN	−0.30	−0.03	−30.3	−4.2	**0.000**	0.624
AGTI	−0.78	−0.22	−42.0	−20.9	**0.000**	0.168

only occur in areas where fuel sulfur regulations have been applied.

For the RAFA site, PMF modeling was unable to resolve RFO from other sources of SO_4, so the RAFA sites was excluded from the analyses in Section 3.5.

3.5. Testing for significant reductions in marine vessel RFO impacts

Similar to significance testing described above for V + Ni and SO_4 measurements, marine vessel RFO factor results were tested to determine if there were statistically significant reductions between time periods associated with varying fuel sulfur regulations. Table 3 and Fig. 2 show changes in marine vessel RFO annual average mass and Table 3 lists the WMW p-values, testing for significant mass reductions, with p-values less than 0.01 listed in bold font (significant reductions at the 99% CL).

Similar to results for V + Ni measurements, only sites in CA showed significant reductions in marine vessel RFO between pre-reg and CA-CFR periods. Since CA-CFR regulations were only applicable in CA waters, this provides evidence of the effectiveness of the CA-CFR regulations compared to unregulated waters.

Comparing marine vessel RFO results between CA-CFR and NA-ECA periods, 2 of 5 sites in WA showed significant reductions (OLYM and PUSO) and one site in CA (PORE) showed significant additional reductions beyond those achieved in the transition from pre-reg to CA-CFR. The lack of significant marine vessel RFO mass reductions at the WA sites NOCA, SNPA, and MORA may be due to lower than expected initial compliance rates, as vessel operators adapt to the new regulations, as well as the 10 month delay of enforcement authority in Canadian waters. The lack of significant further observed marine vessel RFO reductions at the PINN and AGTI sites may be a result of the relative similarity in fuel sulfur standards between the CA-CFR and the first phase of the NA-ECA as well as the relatively short implementation time since adoption of the NA-ECA.

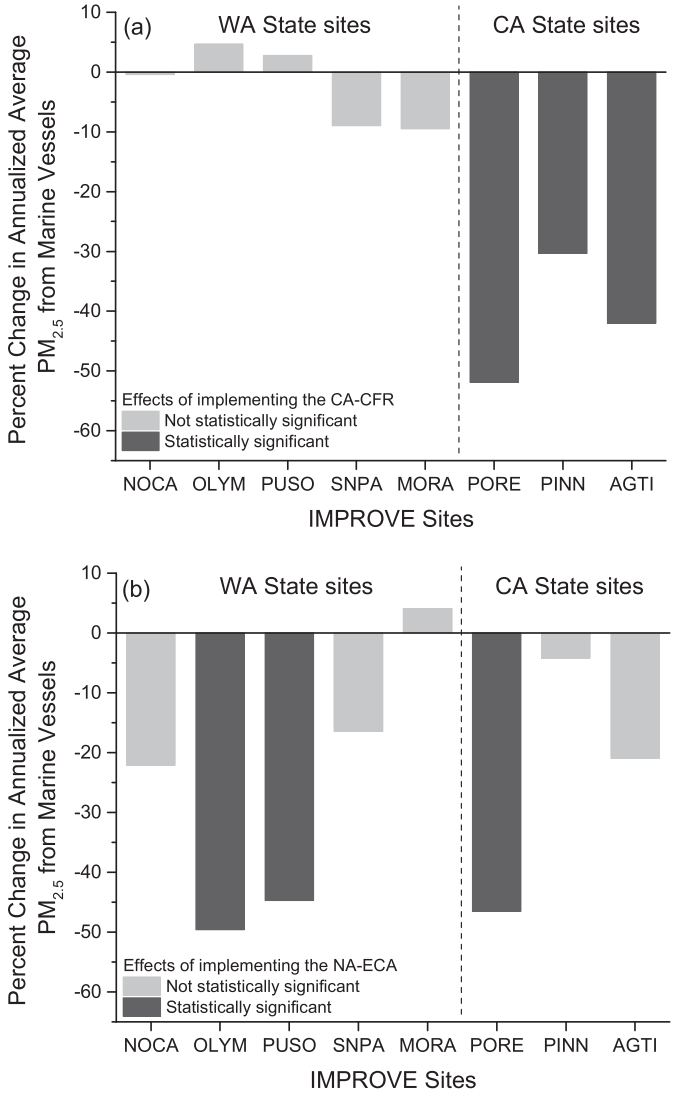

Fig. 2. The percent change in marine vessel $PM_{2.5}$ impacting US west coast IMPROVE sites from before and after implementation of (a) the CA-CFR and (b) the NA-ECA.

3.6. Other factors influencing the V + Ni and PMF results

In addition to the implementation of marine vessel fuel sulfur regulations, annual changes in marine vessel traffic could affect the amount of V + Ni and marine vessel $PM_{2.5}$ impacting ambient monitors. To address this concern, data for annual waterborne shipping tonnage in WA, OR and CA and annual shipping container traffic volume at major ports were analyzed from 2006 to 2012 (US Corps of Engineers, 2014). Both datasets showed that annual ship traffic was relatively steady over the 7-year period except for 2009 when volumes dropped by about 15%. Data tables for shipping tonnage and shipping container traffic are provided in the supplemental data, section S.10.

The chemical composition of fuels used by ocean-going vessels can also vary. This study assumes that, in the absence of fuel sulfur regulations, marine vessels capable of using RFO fuels will do so because of the low cost. However, RFO is a general term for residual fuels that can have varying chemical compositions. While the global average sulfur content of RFO used by marine vessels has been relatively stable between 2.6 and 2.7% in recent years, the sulfur content of RFO on individual ships can vary depending on the fuels' source region (IMO, 2011). The V and Ni concentrations in RFO can span a wide range (Kasper et al., 2007; Khan et al., 2012), however the V to Ni ratio in RFO combustion tests typically ranges between 2 and 4.5 (Popovicheva et al., 2012; Agrawal et al., 2008). While temporal changes in the chemical composition of RFO used along the U.S. west coast could not be determined with available data sources, given that the global average sulfur content has been relatively stable during the time period of this study, it is likely that chemical composition changes implemented to meet the fuel sulfur regulations are significantly larger than the temporal fluctuations in average RFO chemical composition used in the U.S. west coast region.

Change in meteorology is also a source of potential variability effecting these results. The most influential meteorological variables are likely precipitation, wind speed, wind direction, and factors effecting coastal fumigation dynamics. However, given the temporal and geographic scope of this work a detailed meteorological analysis is beyond the scope of this study.

4. Conclusions

This work presents an analysis of ambient $PM_{2.5}$ data and uses PMF modeling to explore the air quality impact from implementation of the CA-CFR and NA-ECA marine vessel fuel sulfur regulations. Data from three time periods were analyzed representing three differing periods of regulatory control over marine fuel sulfur on the US west coast. The locations of statistically significant reductions in V + Ni concentrations and marine vessel RFO impacts were consistent with locations where fuel sulfur regulations were in effect. However, not all sites impacted by marine

vessels showed statistically significant reductions after the regulations went into effect. Implementation of the CA-CFR was found more effective than that of the NA-ECA, but this is likely connected with the longer 3-year implementation time compared to only 1 year for the NA-ECA and also with delayed enforcement of the NA-ECA in Canadian waters. Annualized decreases in marine vessel $PM_{2.5}$ impacts associated with implementation of the CA-CFR were between 30 and 52% (0.09–0.78 μg/m^3) for sites in CA. Annualized decreases in marine vessel $PM_{2.5}$ impacts associated with implementation of the NA-ECA were between 45 and 50% (0.12–0.23 μg/m^3) for 2 of 5 sites in WA and 46% (0.04 μg/m^3) for 1 site in CA, but 3 WA sites and 2 CA sites showed no statistically significant reduction.

Appendix A. Supplementary data

Supplementary data related to this article can be found at http://dx.doi.org/10.1016/j.atmosenv.2014.12.040.

References

Agrawal, H., Malloy, Q.G.J., Welch, W.A., Miller, J.W., Cocker III, D.R., 2008. In-use gaseous and particulate matter emissions from a modern ocean going container vessel. Atmos. Environ. 42, 5504–5510.

Canada Gazette, May 8, 2013. Regulations Amending the Vessel Pollution and Dangerous Chemicals Regulations, vol. 147, No. 10. http://www.gazette.gc.ca/rp-pr/p2/2013/2013-05-08/html/sor-dors68-eng.html (accessed 25.09.14.).

Corbett, J.J., Winebrake, J.J., Green, E.H., Kasibhatla, P., Eyring, V., Lauer, A., 2007. Mortality from ship emissions: a global assessment. Environ. Sci. Technol. 41, 8512–8518.

EC, 2005. Directive 2005/33/EC of the European Parliament and of the Council of 6 July 2005 Amending Directive 1999/32/EC as Regards the Sulphur Content of Marine Fuels. European Commission, Brussels, Belgium.

Geiser, L.H., Jovan, S.E., Glavich, D.A., Porter, M.K., 2010. Lichen based critical loads for atmospheric nitrogen deposition in Western Oregon and Washington Forests, USA. Environ. Pollut. 158, 2412–2421.

IMO, 2011. Prevention of Air Pollution from Ships: Sulphur Monitoring for 2010. International Maritime Organization Marine Environment Protection Committee. MEPC 62/4.

IPCC, 2013. Climate change 2013: the physical science basis. In: Stocker, T.F., Qin, D., Plattner, G.-K., Tignor, M., Allen, S.K., Boschung, J., Nauels, A., Xia, Y., Bex, V., Midgley, P.M. (Eds.), Contribution of Working Group I to the Fifth Assessment Report of the Intergovernmental Panel on Climate Change. Cambridge University Press, Cambridge, United Kingdom and New York, NY, USA, p. 1535.

Kasper, A., Aufdenblatten, S., Forss, A., Mohr, M., Burtscher, H., 2007. Particulate emissions from a low-speed marine diesel engine. Aerosol Sci. Technol. 41, 24–32.

Khan, M.Y., Giordano, M., Gutierrez, J., Welch, W.A., Asa-Awuku, A., Miller, J.W., Cocker III, D.R., 2012. Benefits of two mitigation strategies for container vessels: cleaner engines and cleaner fuels. Environ. Sci. Technol. 46, 5049–5056.

Kotchenruther, R.A., 2013. A regional assessment of marine vessel $PM_{2.5}$ impacts in the U.S. Pacific Northwest using a receptor-based source apportionment method. Atmos. Environ. 68, 103–111.

Künzli, N., Jerrett, M., Mack, W.J., Beckerman, B., LaBree, L., Gilliland, F., Thomas, M., Peters, J., Hodis, H.N., 2005. Ambient air pollution and atherosclerosis in Los Angeles. Environ. Health Perspect. 113, 201–206.

MARPOL, 2008. Amendments to the Annex of the Protocol of 1997 to Amend the International Convention for the Prevention of Pollution from Ships. Annex 13 Resolution MEPC.176(58). International Maritime Organization, London, United Kingdom.

Matthias, V., Bewersdorff, I., Aulinger, A., Quante, M., 2010. The contribution of ship emissions to air pollution in the North Sea regions. Environ. Pollut. 158, 2241–2250.

Mazzei, F., D'Alessandro, A., Lucarelli, F., Nava, S., Prati, P., Valli, G., Vecchi, R., 2008. Characterization of particulate matter sources in an urban environment. Sci. Total Environ. 401, 81–89.

Moldanova, J., Fridell, E., Popovicheva, O., Demirdjian, B., Tishkova, V., Faccinetto, A., Focsa, C., 2009. Characterisation of particulate matter and gaseous emissions from a large ship diesel engine. Atmos. Environ. 43, 2632–2641.

Mölders, N., Gende, S., Pirhalla, M., 2013. Assessment of cruise–ship activity influences on emissions, air quality, and visibility in Glacier Bay National Park. Atmos. Pollut. Res. 4, 435–445.

Norris, G., Duvall, R., Brown, S., Bai, S., 2014. EPA Positive Matrix Factorization (PMF) 5.0 Fundamentals and User Guide. U.S. Environmental Protection Agency. EPA/600/R-14/108.

Paatero, P., Hopke, P.K., 2003. Discarding or downweighting high-noise variables in factor analytic models. Anal. Chim. Acta 490, 277–289.

Pope III, C.A., Dockery, D.W., 2006. Health effects of fine particulate air pollution: lines that connect. J. Air Waste Manag. Assoc. 56, 709–742.

Popovicheva, O., Kireeva, E., Persiantseva, N., Timofeev, M., Bladt, H., Ivleca, N.P., Niessner, R., Moldanova, J., 2012. Microscopic characterization of individual particles from multicomponent ship exhaust. J. Environ. Monit. 14, 3101–3110.

Schembari, C., Cavalli, F., Cuccia, E., Hjorth, J., Calzolai, G., Pérez, N., Pey, J., Prati, P., Raes, F., 2012. Impact of a European directive on ship emissions on air quality in Mediterranean harbours. Atmos. Environ. 61, 661–669.

Tao, L., Fairley, D., Kleeman, M.J., Harley, R.A., 2013. Effects of switching to lower sulfur marine fuel oil on air quality in the San Francisco Bay area. Environ. Sci. Technol. 47, 10171–10178.

U.S. Environmental Protection Agency, 2010. Designation of North American Emission Control Area to Reduce Emissions from Ships: Regulatory Announcement. EPA-420-F-10–015.

US Army Corps of Engineers, 2014. Waterborne Commerce Statistics Center. http://www.navigationdatacenter.us/wcsc/wcsc.htm, (accessed 25.09.14.).

Velders, G.J.M., Snijder, A., Hoogerbrugge, R., 2011. Recent decreases in observed atmospheric concentrations of SO_2 in the Netherlands in line with emission reductions. Atmos. Environ. 45, 5647–5651.

Winebrake, J.J., Corbett, J.J., Green, E.H., Lauer, A., Eyring, V., 2009. Mitigating the health impacts of pollution from Oceangoing shipping: an assessment of low-sulfur fuel mandates. Environ. Sci. Technol. 43, 4776–4782.

Supplemental materials for:

The effects of marine vessel fuel sulfur regulations on ambient $PM_{2.5}$ at coastal and near coastal monitoring sites in the U.S.

Robert A Kotchenruther[a]

[a]U.S. Environmental Protection Agency Region 10, Office of Environmental Review and Assessment, 1200 Sixth Avenue, Mailstop OEA-140, Seattle, Washington, 98101, USA.

Corresponding author: Robert A. Kotchenruther, Kotchenruther.Robert@epa.gov, 206-553-6218

Supplemental Materials Sections:

1. IMPROVE sites considered in this analysis.
2. Method used to determine the optimal number of PMF factors at each site modeled.
3. Number of factors found at each monitoring site, factor compositions, and annualized average mass attributions based on three periods of marine vessel fuel S control under the NA-ECA.
4. Average PMF factor profile data.
5. Annual waterborne shipping tonnage in continental U.S. states and annual shipping container traffic volume at major ports from 2010 – 2014.
6. PMF factor profiles and time series of mass attributions for each monitoring site.
7. HYSPLIT back-trajectories for the top 10 V+Ni days in 2010 – 2011 for each of the 22 IMPROVE sites modeled with PMF in this study.

Supplemental Materials Section 1. IMPROVE sites considered in this analysis.

Table 1.1. MPROVE monitoring sites considered and V and Ni linear correlation results using data from 2010 – 2011.

Site Name	Abbreviation	State	Latitude	Longitude	Elevation (m)	V:Ni linear correlation coefficient* (r^2)	V:Ni linear correlation slope*
North Birmingham	BIRM	AL	33.5531	-86.8148	176	0.016	0.11
Sipsey Wilderness	SIPS	AL	34.3433	-87.3388	286	0.294	1.78
Agua Tibia	AGTI	CA	33.4636	-116.9706	508	0.844	3.61
Bliss SP	BLIS	CA	38.9761	-120.1025	2131	0.055	0.50
Death Valley NP	DEVA	CA	36.5089	-116.8478	130	0.096	0.55
Dome Lands Wilderness	DOME	CA	35.7278	-118.1377	927	0.094	0.59
Fresno	FRES	CA	36.7818	-119.7732	100	0.023	0.48
Hoover	HOOV	CA	38.0881	-119.1771	2561	-0.005	0.00
Joshua Tree NP	JOSH	CA	34.0695	-116.3889	1235	0.423	2.27
Kaiser	KAIS	CA	37.2207	-119.1546	2598	0.030	0.39
Lassen Volcanic NP	LAVO	CA	40.5398	-121.5768	1733	0.085	0.41
Lava Beds NM	LABE	CA	41.7117	-121.5068	1460	0.061	0.44
Pinnacles NM	PINN	CA	36.4833	-121.1568	302	0.726	2.60
Point Reyes National Seashore	PORE	CA	38.1224	-122.9085	97	0.708	2.79
Redwood NP	REDW	CA	41.5608	-124.0839	244	0.409	1.61
San Gorgonio Wilderness	SAGO	CA	34.1939	-116.9132	1726	0.379	1.99
San Rafael	RAFA	CA	34.7339	-120.0074	957	0.550	2.18
Sequoia NP	SEQU	CA	36.4894	-118.8291	519	0.108	0.81
Trinity	TRIN	CA	40.7864	-122.8046	1014	0.287	1.17
Yosemite NP	YOSE	CA	37.7133	-119.7061	1603	0.107	0.83
Mohawk Mt.	MOMO	CT	41.8214	-73.2973	522	0.626	1.65
Chassahowitzka NWR	CHAS	FL	28.7484	-82.5549	4	0.721	3.01
Everglades NP	EVER	FL	25.3910	-80.6806	1	0.596	2.32
St. Marks	SAMA	FL	30.0926	-84.1614	8	0.743	3.07
Cohutta	COHU	GA	34.7852	-84.6265	735	0.110	0.93
Okefenokee NWR	OKEF	GA	30.7405	-82.1283	48	0.654	2.70
Haleakala Crater	HACR	HI	20.7585	-156.2479	2158	0.066	0.43
Hawaii Volcanoes NP	HAVO	HI	19.4309	-155.2579	1259	0.032	0.08
Breton Island	BRIS	LA	30.1086	-89.7617	-7	0.944	3.72
Cape Cod	CACO	MA	41.9758	-70.0242	49	0.698	2.70
Martha's Vineyard	MAVI	MA	41.3309	-70.7846	3	0.879	3.15
Quabbin Summit	QURE	MA	42.2985	-72.3346	318	0.592	1.50

Frostberg Reservoir	FRRE	MD	39.7058	-79.0122	767	0.058	0.38
Acadia NP	ACAD	ME	44.3771	-68.2610	157	0.853	2.81
Bridgton	BRMA	ME	44.1074	-70.7292	234	0.601	1.74
Casco Bay	CABA	ME	43.8325	-70.0644	27	0.783	2.54
Moosehorn NWR	MOOS	ME	45.1259	-67.2661	78	0.677	2.33
Penobscot	PENO	ME	44.9480	-68.6479	45	0.766	2.24
Presque Isle	PRIS	ME	46.6964	-68.0333	166	0.478	0.93
Linville Gorge	LIGO	NC	35.9723	-81.9331	969	0.203	1.07
Shining Rock Wilderness	SHRO	NC	35.3937	-82.7744	1617	0.265	1.39
Swanquarter	SWAN	NC	35.4510	-76.2075	-4	0.692	2.54
Great Gulf Wilderness	GRGU	NH	44.3082	-71.2177	454	0.353	1.14
Pack Monadnock Summit	PACK	NH	42.8619	-71.8786	695	0.585	1.81
Brigantine NWR	BRIG	NJ	39.4650	-74.4492	5	0.822	3.02
Crater Lake NP	CRLA	OR	42.8958	-122.1361	1996	0.028	0.30
Hells Canyon	HECA	OR	44.9702	-116.8438	655	0.011	0.18
Kalmiopsis	KALM	OR	42.5520	-124.0589	80	0.360	1.39
Mount Hood	MOHO	OR	45.2888	-121.7837	1531	0.247	1.17
Starkey	STAR	OR	45.2249	-118.5129	1259	0.033	0.48
Three Sisters Wilderness	THSI	OR	44.2910	-122.0434	885	0.409	1.62
Cape Romain NWR	ROMA	SC	32.9410	-79.6572	5	0.765	2.90
Big Bend NP	BIBE	TX	29.3027	-103.1780	1067	0.684	4.11
Guadalupe Mountains NP	GUMO	TX	31.8330	-104.8094	1672	0.073	0.46
James River Face Wilderness	JARI	VA	37.6266	-79.5125	290	0.271	1.11
Shenandoah NP	SHEN	VA	38.5229	-78.4348	1079	0.168	0.68
Virgin Islands NP	VIIS	VI	18.3363	-64.7962	51	0.610	3.04
Columbia River Gorge	CORI	WA	45.6644	-121.0008	179	0.103	0.81
Mount Rainier NP	MORA	WA	46.7583	-122.1244	439	0.831	2.59
North Cascades	NOCA	WA	48.7316	-121.0646	569	0.777	2.48
Olympic	OLYM	WA	48.0065	-122.9727	600	0.893	3.19
Pasayten	PASA	WA	48.3877	-119.9275	1627	0.011	0.15
Puget Sound	PUSO	WA	47.5696	-122.3119	98	0.874	3.09
Snoqualmie Pass	SNPA	WA	47.4220	-121.4259	1049	0.807	2.82
White Pass	WHPA	WA	46.6243	-121.3881	1827	0.367	1.46

*V:Ni R^2 and slope computed after outlier removal. Outliers were identified as data with studentenized residuals greater than 6 or less than -6.

Supplemental Materials Section 2. Method used to determine the optimal number of PMF factors at each site modeled.

Data from each monitoring site was modeled independently. In each case, the model was run in the robust mode with 20 repeat runs to insure the model least-squares solution represented a global rather than local minimum and the rotational F_{PEAK} variable was held at the default value of 0.0. The model solution with the optimum number of factors was determined somewhat subjectively and was based on inspection of the factors in each solution, the quality of the least-squares fit (analysis of Q_{Robust} and Q_{True} values), and the results from three error estimation methods available in PMF 5.0; bootstrapping (BS), displacement (DISP), and bootstrapping with displacement (BS-DISP).

The typical procedure to find the optimum number of factors for each site was to run PMF multiple times, progressively increasing the number of factors, starting with a 3-factor solution, then a 4-factor solution, then a 5-factor solution, etc., and inspection the solution results each time. Typically, factors in low factor number solutions (e.g., 3-factor and 4-factor solutions) would have some factors representing a mixture of sources or chemical compositions. Increasing the number of factors in PMF (e.g., from a 4-factor solution to a 5-factor solution) usually caused mixed factors in lower factor number solutions to be better resolved (i.e., fewer mixed factors) in the higher factor number solutions. However, there would often come a point when it was clear in the resulting factor chemical profiles that too many factors had been selected in the PMF solution. For example, a 6-factor solution may have a clear fugitive dust factor comprised mainly of Al, Ca, Fe, Si, and Ti. Increasing the number of PMF factors to a 7-factor solution might cause this fugitive dust factor to split into 2 factors, one with elevated Ca, the other with no Ca, but with the other dust components Al, Fe, Si, and Ti. In this example, the progressive increasing of the number of PMF factors would be stopped at the 6-factor solution. This 6-factor solution would then be analyzed by the three error estimation methods available in PMF 5.0; BS, DISP, and BS-DISP. Several publications list statistical guidance criteria for the outputs of BS, DISP, and BS-DISP

(Paatero et al., 2014, Brown et al., 2015). Paatero et al. (2014) and Brown et al. (2015) have demonstrated that the statistical outputs for BS, DISP, and BS-DISP provide valuable information on the quality of the PMF solution. If, in this example, the 6-factor solution passed the statistical guidance criteria for all three methods and the values of Q_{Robust} and Q_{True} were in acceptable ranges as per model guidance, then the 6-factor solution was chosen as the optimal solution. If, on the other hand, the 6-factor solution failed one or more of the statistical guidance criteria for BS, DISP, or BS-DISP, then the number of PMF factors would be reduced by one (reduced to a 5-factor solution in this example) and BS, DISP, and BS-DISP would be rerun and the output statistics analyzed. This process would be repeated and the optimal PMF solution was chosen as the one with the best statistical results for the BS, DISP, and BS-DISP evaluation methods.

Supplemental Materials Section 3. Number of factors found at each monitoring site, factor compositions, and annualized average mass attributions based on three periods of marine vessel fuel S control under the NA-ECA.

Table 3.1. Number of factors found at each monitoring site and factor compositions. For factor composition reference identifiers, see Table 2 in the main text.

IMPROVE monitor abbreviation	Number of PMF factors	Factor 1 composition identifier(s)	Factor 2 composition identifier(s)	Factor 3 composition identifier(s)	Factor 4 composition identifier(s)	Factor 5 composition identifier(s)	Factor 6 composition identifier(s)	Factor 7 composition identifier(s)	Factor 8 composition identifier(s)	Factor 9 composition identifier(s)
AGTI	8	7	4	3	5	1	8	2	6	
PINN	6	6	4	1+2	5	7	3			
PORE	6	6	1	4+2	3+5	7	2			
CHAS	6	3+5	2	4	6	7+2	1			
SAMA	6	2	1	6	4	3+5	7			
OKEF	7	4	2	7+5	6	3	1+8	9		
BRIS	7	4	3	5	7+2	2	1	6		
CACO	7	7	1	6	4+2	2	3	5		
MAVI	5	7+2	1+2	4+8	3+5	6				
ACAD	7	9+5	7	6	3	4+2	1	2		
CABA	6	3+5	2	4	1	6	7+2			
MOOS	6	1+2	3	4+2	9	7	6			
PENO	9	9+5	7	6	4	2	1	3	7+2	3
SWAN	5	6	4	3+5	7+2	1+2				
BRIG	7	7	2	5	1	3	4	6		
ROMA	7	7	2	1	5+2	4	3	6		
BIBE	6	2	4	11	3	9+5	1+8			
MORA	5	2	6	1+10	3+5	4				
NOCA	6	2	1+10	3	4	5	6			
OLYM	6	3+5	4	2	1	6	7			
PUSO	8	2	1	4+8	3+5	6	10	12	7	
SNPA	6	4	6	3+5	7	2	1+10			

Table 3.2. Annualized average* PMF factor $PM_{2.5}$ mass and total annualized average observed $PM_{2.5}$ mass for the pre-NA-ECA period of 2010-2011. For the identification of which sources, compositions, or mixtures are associated with each site factor, see Table 2 in the main text and Table 3.1 in the supplemental materials.

IMPROVE monitor abbreviation	Factor 1 (μg/m^3)	Factor 2 (μg/m^3)	Factor 3 (μg/m^3)	Factor 4 (μg/m^3)	Factor 5 (μg/m^3)	Factor 6 (μg/m^3)	Factor 7 (μg/m^3)	Factor 8 (μg/m^3)	Factor 9 (μg/m^3)	Total $PM_{2.5}$ (μg/m^3)
AGTI	0.36	0.46	0.27	0.98	0.23	1.02	1.13	0.30		4.96
PINN	0.78	0.33	0.87	0.95	0.35	0.52				3.78
PORE	2.86	0.01	0.19	0.60	0.59	0.93				5.28
CHAS	2.08	2.50	0.91	0.61	0.23	0.81				7.32
SAMA	2.92	1.12	0.47	0.74	2.43	0.01				8.02
OKEF	0.79	3.09	0.17	0.36	2.59	0.56	1.07			8.45
BRIS	0.82	0.67	1.74	0.47	4.01	0.11	0.56			8.54
CACO	0.31	0.46	1.08	0.27	1.71	1.51	0.08			5.27
MAVI	0.67	2.43	0.42	1.20	1.57					6.14
ACAD	0.07	0.20	0.35	1.46	0.22	0.02	1.36			3.71
CABA	1.78	1.55	0.23	0.74	0.32	0.28				5.03
MOOS	1.29	1.38	0.19	0.19	0.07	0.38				3.42
PENO	0.03	0.04	0.23	0.21	1.47	0.06	1.57	0.30	0.75	4.78
SWAN	0.76	0.45	1.87	0.20	3.65					7.40
BRIG	0.87	3.19	0.10	0.45	1.99	0.31	0.46			7.65
ROMA	0.20	3.13	0.92	0.35	0.52	2.25	0.72			8.47
BIBE	2.25	0.86	0.62	1.54	0.22	0.27				5.86
MORA	0.53	0.23	0.69	0.97	0.22					2.62
NOCA	0.39	0.34	0.93	0.13	0.02	0.20				2.10
OLYM	0.67	0.13	0.79	0.20	0.36	0.15				2.37
PUSO	1.06	0.51	0.20	1.65	0.44	0.32	0.48	0.71		5.31
SNPA	0.16	0.18	0.67	0.13	0.27	0.78				2.14

*Represents the average of the 24 monthly averages from 2010-2011.

Table 3.3. Annualized average* PMF factor $PM_{2.5}$ mass and total annualized average observed $PM_{2.5}$ mass for the NA-ECA 1% S period of 2013-2014. For the identification of which sources, compositions, or mixtures are associated with each site factor, see Table 2 in the main text and Table 3.1 in the supplemental materials.

IMPROVE monitor abbreviation	Factor 1 ($\mu g/m^3$)	Factor 2 ($\mu g/m^3$)	Factor 3 ($\mu g/m^3$)	Factor 4 ($\mu g/m^3$)	Factor 5 ($\mu g/m^3$)	Factor 6 ($\mu g/m^3$)	Factor 7 ($\mu g/m^3$)	Factor 8 ($\mu g/m^3$)	Factor 9 ($\mu g/m^3$)	Total $PM_{2.5}$ ($\mu g/m^3$)
AGTI	0.36	0.63	0.23	0.90	0.08	1.21	1.00	0.37		4.79
PINN	0.79	0.42	0.74	0.95	0.38	0.53				3.86
PORE	2.66	0.00	0.25	0.74	0.66	0.76				5.76
CHAS	2.13	1.90	0.86	0.66	0.22	0.55				6.54
SAMA	2.13	0.80	0.55	0.88	2.14	0.01				6.71
OKEF	0.84	2.14	0.17	0.56	1.60	0.42	0.93			7.11
BRIS	0.82	0.55	1.40	0.40	2.99	0.05	0.50			7.21
CACO	0.36	0.16	1.03	0.26	1.47	1.39	0.07			4.84
MAVI	0.64	1.72	0.39	1.04	1.50					5.57
ACAD	0.08	0.24	0.44	1.32	0.18	0.01	1.05			3.56
CABA	1.73	1.17	0.18	0.26	0.56	0.43				4.73
MOOS	1.10	1.21	0.16	0.18	0.09	0.50				3.31
PENO	0.03	0.04	0.31	0.24	1.08	0.03	1.32	0.34	0.81	4.34
SWAN	0.93	0.45	1.72	0.22	2.57					5.96
BRIG	0.98	2.47	0.09	0.17	1.79	0.25	0.53			6.71
ROMA	0.18	2.44	0.42	0.36	0.46	2.16	0.61			6.77
BIBE	2.33	1.19	0.51	0.79	0.22	0.29				5.39
MORA	0.49	0.18	0.59	1.16	0.16					2.69
NOCA	0.31	0.25	1.06	0.13	0.03	0.19				2.02
OLYM	0.81	0.14	0.73	0.12	0.33	0.17				2.44
PUSO	1.03	0.29	0.14	1.77	0.43	0.31	0.46	0.90		5.45
SNPA	0.15	0.16	0.80	0.13	0.24	0.70				2.28

*Represents the average of the 24 monthly averages from 2013-2014.

Table 3.4. Annualized average* PMF factor $PM_{2.5}$ mass and total annualized average observed $PM_{2.5}$ mass for the NA-ECA 0.1% S period of 2015. For the identification of which sources, compositions, or mixtures are associated with each site factor, see Table 2 in the main text and Table 3.1 in the supplemental materials.

IMPROVE monitor abbreviation	Factor 1 ($\mu g/m^3$)	Factor 2 ($\mu g/m^3$)	Factor 3 ($\mu g/m^3$)	Factor 4 ($\mu g/m^3$)	Factor 5 ($\mu g/m^3$)	Factor 6 ($\mu g/m^3$)	Factor 7 ($\mu g/m^3$)	Factor 8 ($\mu g/m^3$)	Factor 9 ($\mu g/m^3$)	Total $PM_{2.5}$ ($\mu g/m^3$)
AGTI	0.22	0.55	0.33	0.92	0.04	1.18	0.84	0.27		4.53
PINN	0.83	0.36	0.63	1.05	0.38	0.69				4.16
PORE	2.82	0.00	0.20	0.88	0.46	0.66				6.40
CHAS	1.87	1.56	0.77	0.77	0.20	0.52				6.24
SAMA	1.65	0.75	0.61	0.74	2.11	0.01				6.05
OKEF	0.87	1.61	0.15	0.64	1.44	0.36	0.81			6.05
BRIS	1.10	0.66	1.53	0.37	2.38	0.02	0.52			7.27
CACO	0.34	0.05	0.97	0.32	1.35	1.59	0.07			5.02
MAVI	0.66	1.51	0.48	1.17	1.38					5.96
ACAD	0.08	0.23	0.42	1.59	0.24	0.00	0.94			3.61
CABA	1.89	0.93	0.25	0.17	0.84	0.46				5.26
MOOS	0.94	1.33	0.19	0.19	0.09	0.53				3.39
PENO	0.03	0.06	0.33	0.22	0.99	0.01	1.46	0.35	1.08	4.85
SWAN	1.04	0.74	1.70	0.20	1.87					5.84
BRIG	0.92	1.93	0.08	0.04	2.14	0.34	0.56			6.69
ROMA	0.15	1.84	0.21	0.32	0.69	1.92	1.03			6.34
BIBE	2.23	0.75	0.22	0.88	0.18	0.23				4.69
MORA	0.36	0.23	0.50	1.38	0.19					2.93
NOCA	0.26	0.19	1.38	0.14	0.03	0.21				2.40
OLYM	0.89	0.14	0.56	0.04	0.28	0.19				2.48
PUSO	0.74	0.10	0.15	1.94	0.39	0.33	0.56	0.82		5.38
SNPA	0.18	0.12	1.04	0.14	0.18	0.68				2.60

*Represents the average of the 12 monthly averages from 2015.

Supplemental Materials Section 4. Average PMF factor profile data.

The chemical profiles presented are those after the factor chemical composition from each site was normalized. A factor chemical composition was normalized by assuming an organic mass (OMC) to OC ratio of 1.8 (i.e., multiplying all OC fraction by 1.8), assuming all sulfate and nitrate were fully neutralized and present as ammonium sulfate (AmSO4) and ammonium nitrate (AmNO3), summing all of the measured chemical constituents using the assumed OMC, AmSO4, and AmNO3 instead of OC, SO4 and NO3, respectively, and dividing each chemical component by the summed constituents. Additionally, for factors associated with fugitive dust, a metal oxide to metal ratio was assumed for aluminum (Al, 2.2), calcium (Ca, 1.63), iron (Fe, 2.42), titanium (Ti, 1.94), and silicon (Si, 2.49) based on the ratios used in the IMPROVE network (http://vista.cira.colostate.edu/improve/).

Table 4.1. Average profile for PMF factors associated with residual fuel oil combustion.

Species	Species Average (mass fraction)	Species Standard Deviation (mass fraction)
AL	0.00004	0.00016
CA	0.00422	0.00289
FE	0.00219	0.00190
SI	0.00292	0.00639
TI	0.00009	0.00013
NA	0.04162	0.02849
CL-	0.00278	0.00920
AS	0.00007	0.00004
BR	0.00019	0.00024
CR	0.00000	0.00000
CU	0.00007	0.00007
PB	0.00011	0.00014
MG	0.00116	0.00215
MN	0.00002	0.00005
NI	0.00140	0.00103
V	0.00409	0.00300
P	0.00002	0.00002
SE	0.00009	0.00005
SR	0.00007	0.00003
ZN	0.00031	0.00043
AmNO3	0.07151	0.07055
AmSO4	0.55306	0.16323
K	0.00480	0.00671
OMC1(1.8)	0.01676	0.02425
OMC2(1.8)	0.10272	0.05743
OMC3(1.8)	0.03249	0.04459
OMC4(1.8)	0.07301	0.03635
OMP(1.8)	0.03845	0.05493
EC1	0.05454	0.05239
EC2	0.00832	0.01510
EC3		

Table 4.2. Average profile for PMF factors associated with ammonium sulfate.

Species	Species Average (mass fraction)	Species Standard Deviation (mass fraction)
AL	0.00122	0.00074
CA	0.00094	0.00079
FE	0.00047	0.00047
SI	0.00000	0.00000
TI	0.00005	0.00003
NA	0.00190	0.00432
CL-	0.00003	0.00012
AS	0.00003	0.00002
BR	0.00018	0.00013
CR	0.00001	0.00002
CU	0.00003	0.00002
PB	0.00009	0.00011
MG	0.00028	0.00065
MN	0.00002	0.00004
NI	0.00001	0.00001
V	0.00001	0.00001
P	0.00002	0.00002
SE	0.00006	0.00003
SR	0.00002	0.00001
ZN	0.00018	0.00025
AmNO3	0.01411	0.02800
AmSO4	0.84051	0.04249
K	0.00173	0.00213
OMC1(1.8)	0.00212	0.00190
OMC2(1.8)	0.04085	0.02284
OMC3(1.8)	0.00274	0.00692
OMC4(1.8)	0.01579	0.01102
OMP(1.8)	0.06927	0.03070
EC1	0.00425	0.00475
EC2	0.00558	0.00375
EC3		

Table 4.3. Average profile for PMF factors associated with wood smoke and secondary organic carbon.

Species	Species Average (mass fraction)	Species Standard Deviation (mass fraction)
AL	0.00080	0.00143
CA	0.00339	0.00392
FE	0.00077	0.00050
SI	0.00134	0.00279
TI	0.00006	0.00006
NA	0.00000	0.00000
CL-	0.00213	0.00206
AS	0.00005	0.00004
BR	0.00066	0.00073
CR	0.00000	0.00000
CU	0.00007	0.00006
PB	0.00014	0.00013
MG	0.00017	0.00049
MN	0.00004	0.00006
NI	0.00001	0.00001
V	0.00002	0.00002
P	0.00005	0.00006
SE	0.00003	0.00003
SR	0.00003	0.00002
ZN	0.00029	0.00037
AmNO3	0.01147	0.01872
AmSO4	0.01245	0.02297
K	0.02208	0.02877
OMC1(1.8)	0.01293	0.00807
OMC2(1.8)	0.16970	0.03107
OMC3(1.8)	0.34732	0.03312
OMC4(1.8)	0.19821	0.03935
OMP(1.8)	0.17005	0.07114
EC1	0.05498	0.02314
EC2	0.01078	0.00820
EC3		

Table 4.4. Average profile for PMF factors associated with fugitive dust.

Species	Species Average (mass fraction)	Species Standard Deviation (mass fraction)
AL	0.16742	0.01924
CA	0.04764	0.01663
FE	0.12460	0.01611
SI	0.44302	0.05469
TI	0.00946	0.00081
NA	0.00808	0.00923
CL-	0.00062	0.00131
AS	0.00004	0.00003
BR	0.00028	0.00045
CR	0.00006	0.00002
CU	0.00006	0.00007
PB	0.00016	0.00018
MG	0.00866	0.00659
MN	0.00101	0.00027
NI	0.00001	0.00002
V	0.00011	0.00008
P	0.00001	0.00002
SE	0.00001	0.00001
SR	0.00034	0.00009
ZN	0.00022	0.00026
AmNO3	0.02138	0.01864
AmSO4	0.08872	0.06039
K	0.01715	0.00465
OMC1(1.8)	0.00000	0.00000
OMC2(1.8)	0.01296	0.01553
OMC3(1.8)	0.01315	0.01825
OMC4(1.8)	0.01213	0.00906
OMP(1.8)	0.01435	0.01423
EC1	0.00013	0.00046
EC2	0.00828	0.00551
EC3		

Table 4.5. Average profile for PMF factors associated with motor vehicles.

Species	Species Average (mass fraction)	Species Standard Deviation (mass fraction)
AL	0.00118	0.00146
CA	0.00839	0.00952
FE	0.01188	0.01013
SI	0.00215	0.00221
TI	0.00056	0.00029
NA	0.00000	0.00000
CL-	0.01814	0.02782
AS	0.00024	0.00009
BR	0.00131	0.00129
CR	0.00008	0.00009
CU	0.00096	0.00059
PB	0.00233	0.00202
MG	0.00083	0.00124
MN	0.00053	0.00037
NI	0.00011	0.00017
V	0.00002	0.00005
P	0.00013	0.00005
SE	0.00007	0.00004
SR	0.00003	0.00005
ZN	0.00749	0.00756
AmNO3	0.07211	0.11192
AmSO4	0.02059	0.05043
K	0.03138	0.05577
OMC1(1.8)		
OMC2(1.8)	0.09905	0.08322
OMC3(1.8)	0.17609	0.14823
OMC4(1.8)	0.22161	0.08855
OMP(1.8)	0.18328	0.08593
EC1	0.13981	0.07337
EC2	0.02189	0.01732
EC3		

Table 4.6. Average profile for PMF factors associated with sea salt.

Species	Species Average (mass fraction)	Species Standard Deviation (mass fraction)
AL	0.00299	0.00088
CA	0.01131	0.00142
FE	0.00022	0.00022
SI	0.00000	0.00001
TI	0.00001	0.00002
NA	0.25573	0.04179
CL-	0.31331	0.09002
AS	0.00001	0.00001
BR	0.00069	0.00027
CR	0.00001	0.00001
CU	0.00002	0.00004
PB	0.00008	0.00008
MG	0.02688	0.00398
MN	0.00001	0.00001
NI	0.00002	0.00002
V	0.00002	0.00004
P	0.00001	0.00002
SE	0.00004	0.00002
SR	0.00023	0.00004
ZN	0.00006	0.00011
AmNO3	0.06593	0.05936
AmSO4	0.17975	0.05605
K	0.01011	0.00204
OMC1(1.8)	0.00000	0.00000
OMC2(1.8)	0.01184	0.01082
OMC3(1.8)	0.07085	0.03201
OMC4(1.8)	0.04917	0.02136
OMP(1.8)	0.00024	0.00087
EC1	0.00032	0.00096
EC2	0.00021	0.00067
EC3		

Table 4.7. Average profile for PMF factors associated with ammonium nitrate.

Species	Species Average (mass fraction)	Species Standard Deviation (mass fraction)
AL	0.00259	0.00773
CA	0.00391	0.00874
FE	0.00275	0.00203
SI	0.00019	0.00047
TI	0.00012	0.00015
NA	0.00848	0.01491
CL-	0.00147	0.00348
AS	0.00005	0.00004
BR	0.00164	0.00388
CR	0.00004	0.00004
CU	0.00011	0.00011
PB	0.00035	0.00042
MG	0.00526	0.01292
MN	0.00014	0.00026
NI	0.00003	0.00003
V	0.00000	0.00001
P	0.00000	0.00001
SE	0.00009	0.00010
SR	0.00008	0.00018
ZN	0.00100	0.00110
AmNO3	0.72349	0.10540
AmSO4	0.09114	0.06763
K	0.00535	0.01183
OMC1(1.8)	0.00568	0.00498
OMC2(1.8)	0.01927	0.01306
OMC3(1.8)	0.02826	0.03070
OMC4(1.8)	0.05012	0.02900
OMP(1.8)	0.02169	0.06668
EC1	0.03012	0.01779
EC2	0.00326	0.00546
EC3		

Supplemental Materials Section 5. Annual waterborne shipping tonnage in continental U.S. states and annual shipping container traffic volume at major ports from 2010 – 2014.

Table 5.1. State annual waterborne shipping tonnage from 2010 to 2014.

State	2010 (tons, x1000)	2011 (tons, x1000)	2012 (tons, x1000)	2013 (tons, x1000)	2014 (tons, x1000)
Alabama	72,696	70,560	69,539	69,394	81,579
Arkansas	14,334	14,561	16,430	17,409	18,164
California	212,285	224,088	220,836	226,174	230,228
Connecticut	16,229	12,977	10,645	11,368	13,313
Delaware	8,510	13,232	15,794	13,936	14,384
District of Columbia	108	110	113	128	117
Florida	101,455	96,769	91,501	93,925	98,747
Georgia	37,120	37,511	36,879	35,216	37,613
Guam	435	508	509	444	493
Idaho	654	619	868	825	763
Illinois	108,083	109,663	106,399	92,015	106,517
Indiana	60,805	67,442	68,322	64,922	73,203
Iowa	10,470	9,740	10,327	7,861	8,854
Kansas	239	227	346	391	178
Kentucky	91,357	92,548	94,688	100,232	101,110
Louisiana	483,050	500,885	510,788	501,077	543,774
Maine	20,907	15,411	15,127	14,078	11,964
Maryland	45,277	49,251	45,268	40,669	40,980
Massachusetts	22,661	20,646	17,298	18,866	18,733
Michigan	59,067	61,851	57,547	58,222	60,030
Minnesota	40,408	43,109	42,872	41,466	43,465
Mississippi	54,210	50,763	48,592	48,582	45,487
Missouri	32,953	33,111	34,066	36,979	38,761
Nebraska	46	21	22	9	9
New Hampshire	2,964	3,347	2,419	2,679	2,803
New Jersey	155,130	158,698	152,685	145,991	147,237
New York	50,492	42,923	38,875	38,706	38,415
North Carolina	12,011	11,622	11,028	11,632	9,683
Ohio	98,986	95,518	90,569	93,749	97,402
Oklahoma	5,020	5,349	6,116	6,777	6,248
Oregon	30,198	31,142	30,758	30,259	32,145
Pennsylvania	90,373	82,297	70,431	73,546	64,952
Puerto Rico	21,172	19,444	19,424	18,853	20,723
Rhode Island	8,315	8,378	7,567	9,072	8,754
South Carolina	18,110	18,396	19,539	18,916	20,339

Tennessee	34,314	33,675	34,076	34,755	34,805
Texas	486,658	490,426	485,884	492,659	506,602
Vermont					
Virgin Islands	41,076	34,314	3,730	2,074	3,017
Virginia	69,095	75,945	79,821	83,834	78,777
Washington	112,314	115,780	115,598	112,212	119,249
West Virginia	69,704	69,177	64,984	62,629	63,850
Wisconsin	34,494	32,042	31,634	34,225	33,877

Table 5.2. State major ports annual total TEU container traffic 2010 to 2014.

Port Waterway Name	**State**	**2010 (TEU)**	**2011 (TEU)**	**2012 (TEU)**	**2013 (TEU)**	**2014 (TEU)**
Mobile	AL	80,953	108,551	149,844	165,250	174,731
Long Beach	CA	4,736,900	4,687,728	4,713,965	5,297,562	5,349,776
Los Angeles	CA	5,479,351	5,901,905	5,672,564	5,556,230	5,912,415
Oakland	CA	1,673,857	1,693,993	1,690,612	1,762,202	1,769,048
Port Hueneme	CA	24,566	20,509	51,500	54,093	53,968
San Diego	CA	51,335	49,697	52,080	50,653	55,484
Wilmington	DE	154,698	157,365	179,753	193,266	194,248
Fernandina Beach	FL	15,690	9,482	6,541	4,724	4,564
Fort Pierce	FL	11,338	9,994	7,114		
Jacksonville	FL	725,472	771,203	715,887	752,402	800,630
Miami	FL	678,916	701,815	735,893	709,504	682,386
Palm Beach	FL	108,987	91,046	119,078	144,023	156,366
Panama City	FL	26,872	28,638	33,140	35,825	27,400
Port Everglades	FL	578,950	608,355	638,546	698,673	748,501
Port Manatee	FL	15,923	7,965	11,391	10,487	12,013
Tampa	FL	27,626	24,917	28,835	43,844	38,049
Savannah	GA	2,147,792	2,269,213	2,289,094	2,349,151	2,605,288
Apra Harbor	GU	67,332	62,016	66,387	63,599	65,530
Clearwater River	ID	3,371	2,957	4,908	3,888	1,838
Lake Charles	LA	2,141	1,324			
New Orleans	LA	274,692	306,735	292,301	301,704	329,768
South Louisiana, Port of	LA	1,991				
Boston	MA	130,206	142,965	146,421	161,080	179,705
Baltimore	MD	495,158	505,636	544,018	555,407	574,375
Eastport Harbor	ME		1,133			
Fore River	ME					4,820
Portland	ME		526			

Pacific Islands Under U.S. Trust	MH					383
Saipan	MP					3,265
Gulfport	MS	177,172	182,366	165,869	168,452	149,269
Morehead City	NC		2,054			
Wilmington	NC	199,727	222,240	190,100	222,898	229,565
Camden-Gloucester	NJ	85,548	85,642	92,906	90,976	84,405
Salem River	NJ	3,744	3,597	4,899	4,082	
New York (NY and NJ)	NY	4,216,136	4,431,053	4,406,913	4,208,723	4,368,846
Columbia River, Dalles-McNary	OR	16,953	14,318	21,670	18,070	17,845
Columbia River, Vancouver-Dalles	OR		12,202	17,788	16,001	16
Other Columbia Riv (OR,WA,ID)2	OR	14				
Portland	OR	135,885	156,837	155,396	148,425	132,125
Pacific Islands Under U.S. Trust	OT	5,608		4,487	482	
Chester	PA	80,553	87,546	84,735	87,669	89,300
Philadelphia	PA	166,335	184,414	202,294	264,174	317,789
Mayaguez	PR	10,069	2,528	4,442	2,701	1,395
San Juan	PR	824,964	806,102	720,307	752,254	773,900
Charleston	SC	1,061,326	1,122,392	1,209,812	1,289,066	1,433,720
Cedar Bayou	TX		6,578		10,333	12,157
Freeport	TX	57,331	50,025	55,383	71,869	62,060
Galveston	TX	11,483	13,121	11,309	18,955	19,625
Houston	TX	1,341,897	1,430,907	1,491,920	1,563,060	1,664,448
Elizabeth River	VA					1,999,229
Elizabeth River, South	VA					7,170
Newport News	VA					4,773
Norfolk Harbor	VA	1,472,851	1,527,426	1,727,195	1,872,462	
Richmond	VA	3,447	4,505	9,129	10,867	15,856
Columbia River, Vancouver-Dalles	WA					17,703
Everett	WA	13,792	8,440	11,382	8,204	25,854
Seattle	WA	1,601,842	1,573,558	1,435,402	1,236,727	1,008,263
Tacoma	WA	1,086,347	1,156,017	1,387,552	1,573,954	1,714,089
Vancouver	WA	15,443				1,432

Supplemental Materials Section 6. PMF factor profiles and time series of mass attributions for each monitoring site.

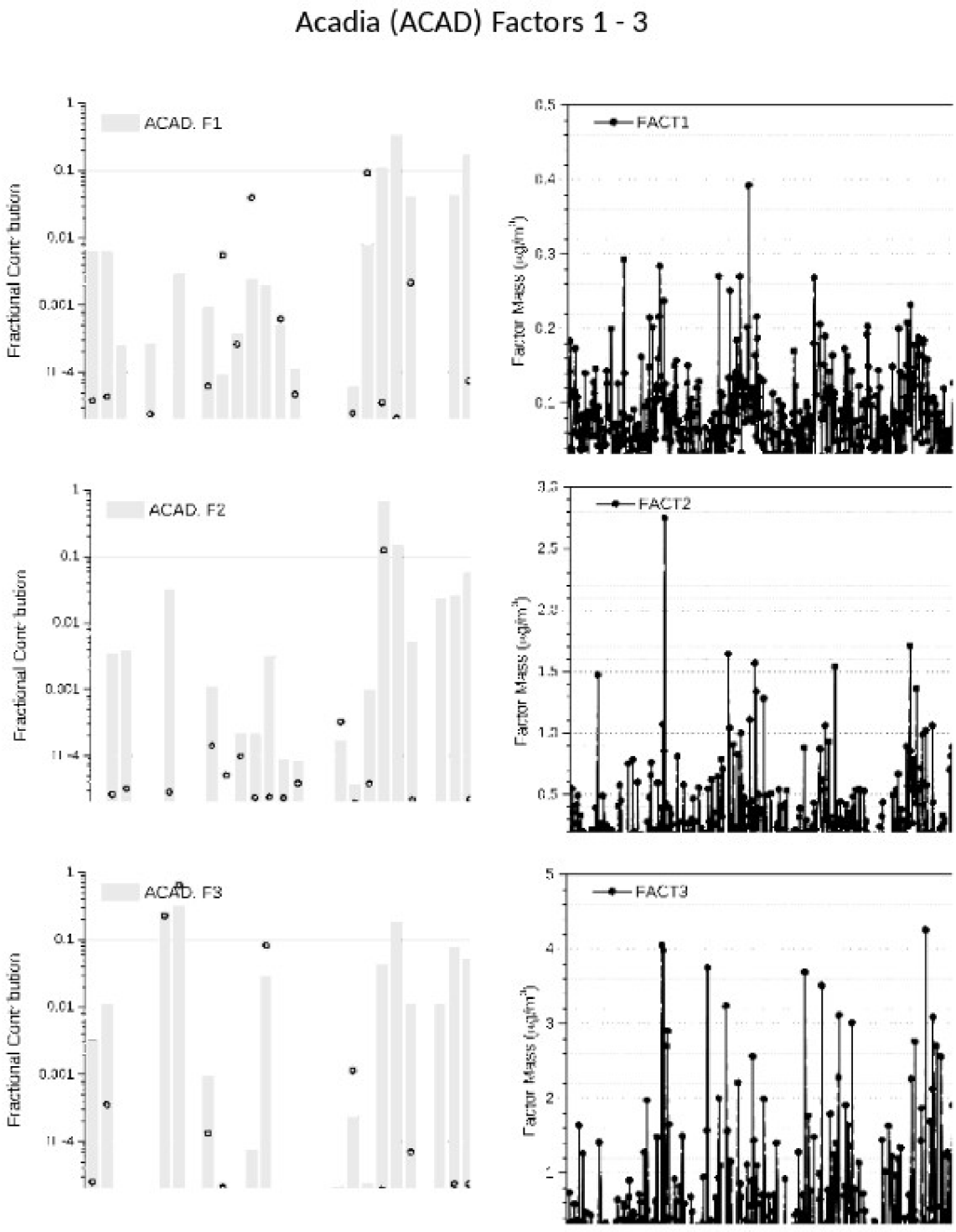

Acadia (ACAD) Factors 4 - 6

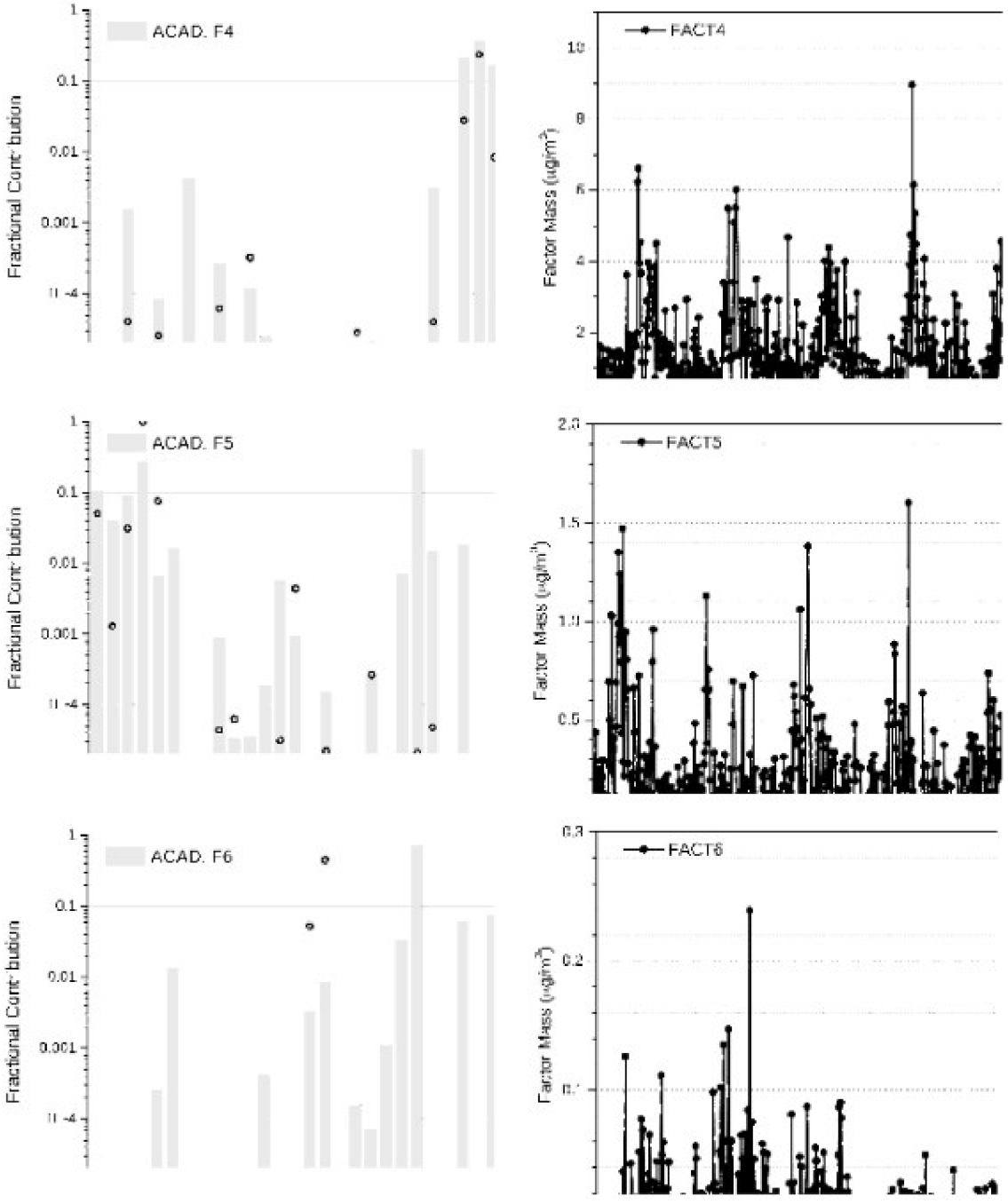

Acadia (ACAD) Factor 7

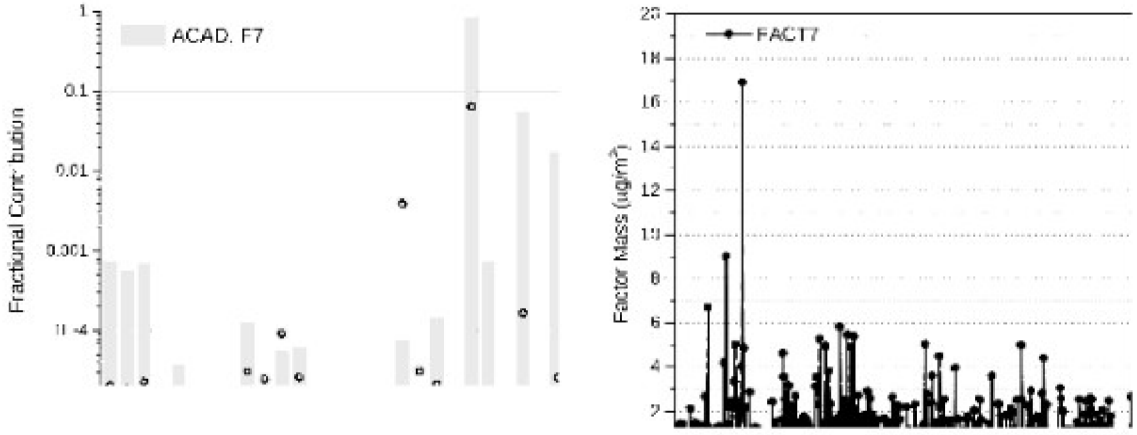

Agua Tibia (AGTI) Factors 1 - 3

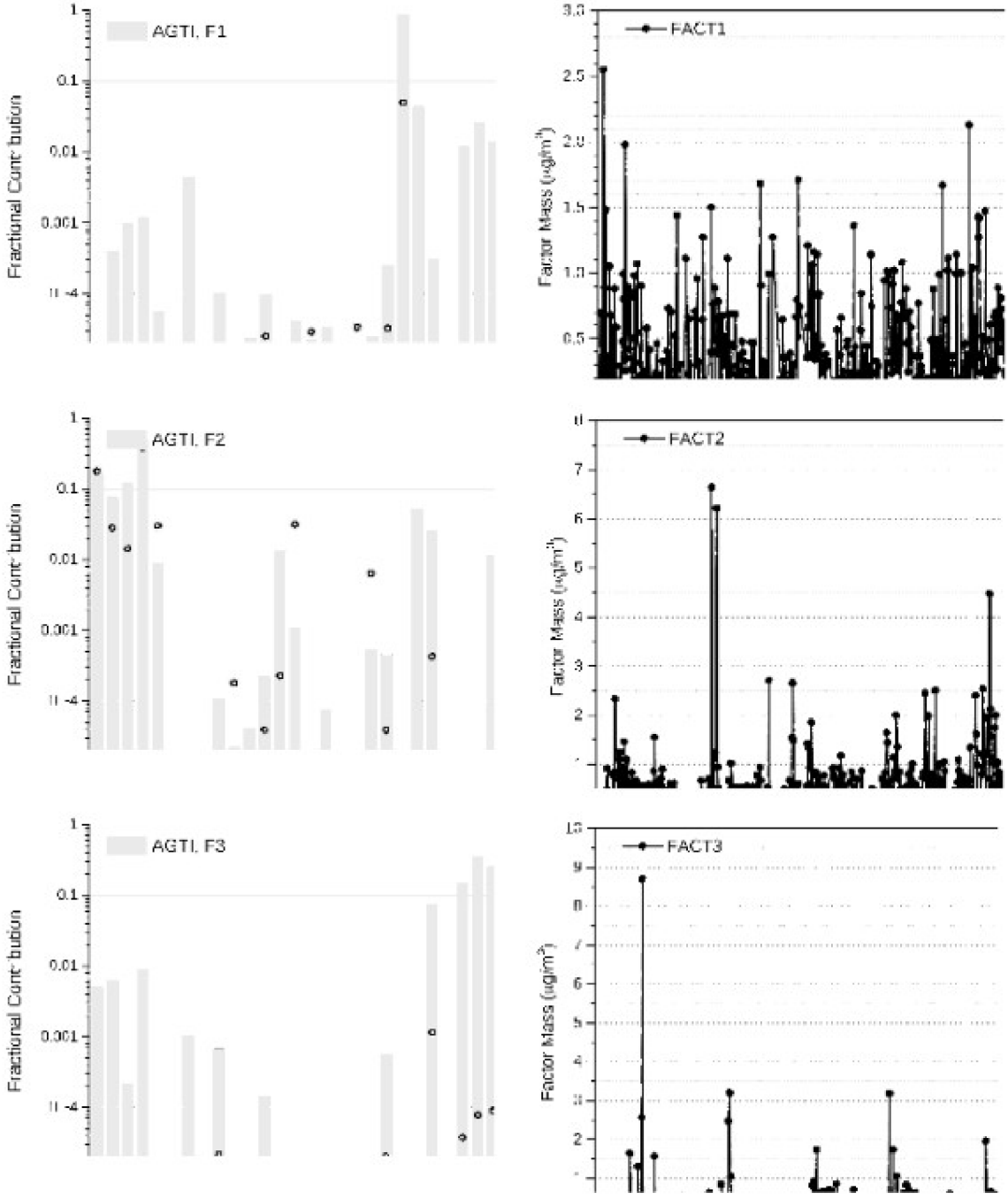

Agua Tibia (AGTI) Factors 4 - 6

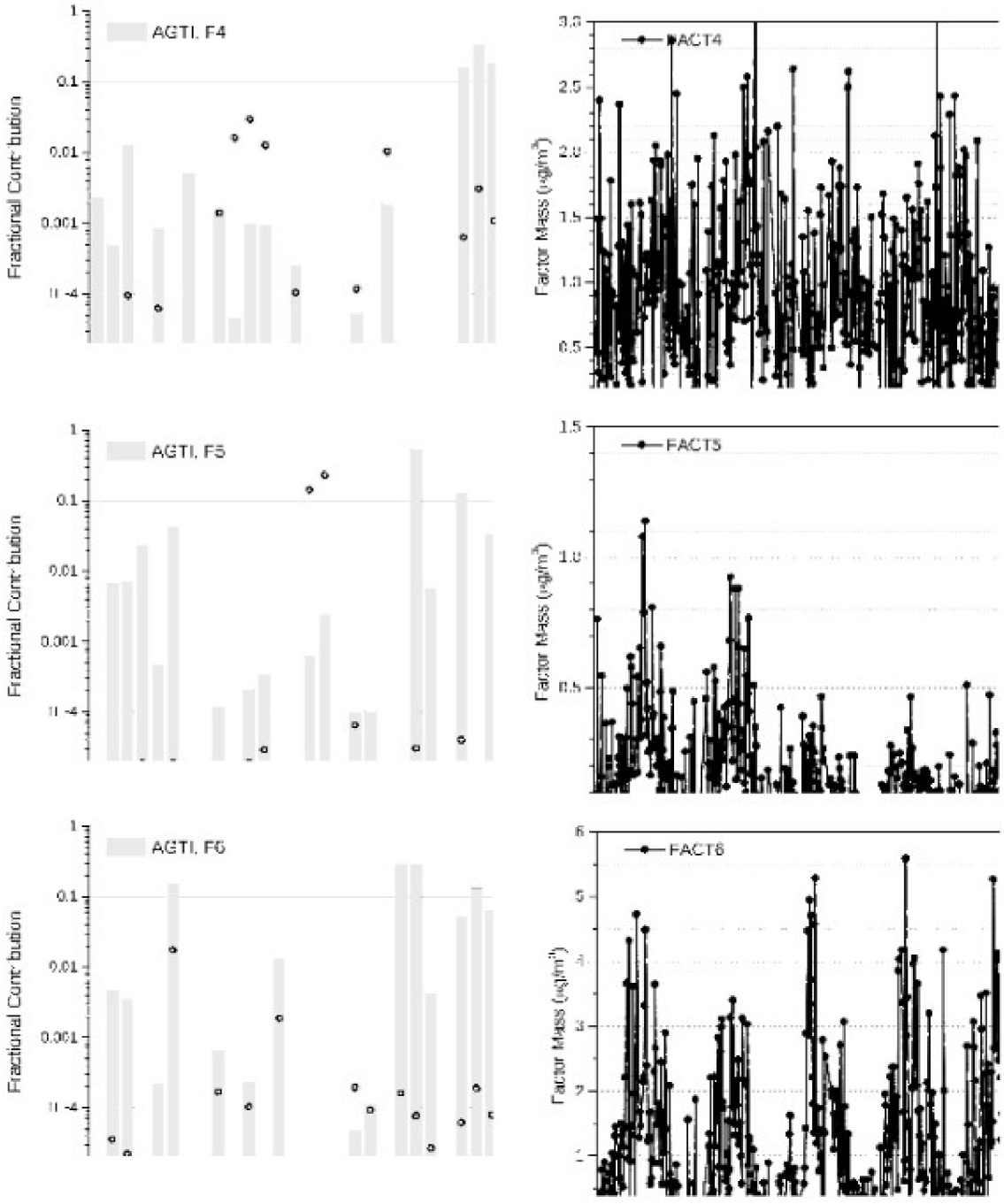

Agua Tibia (AGTI) Factors 7 - 8

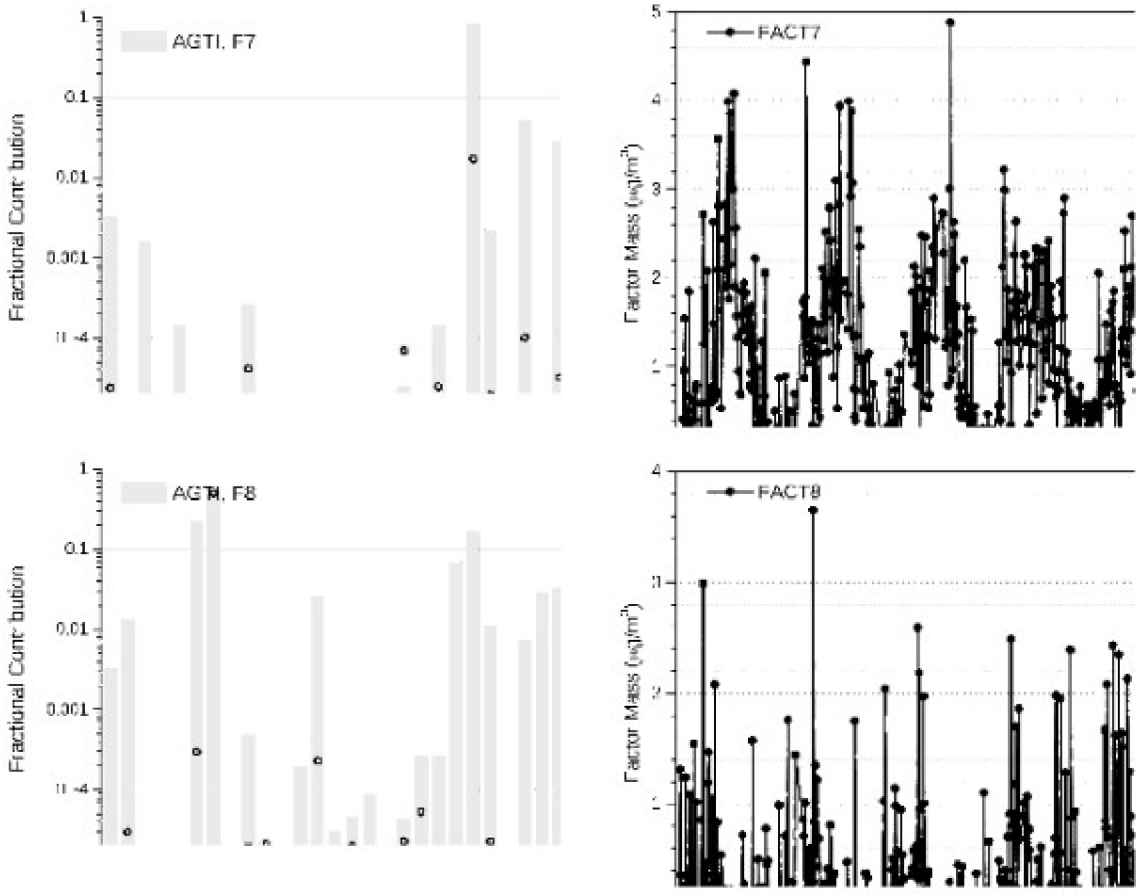

Big Bend (BIBE) Factors 1 - 3

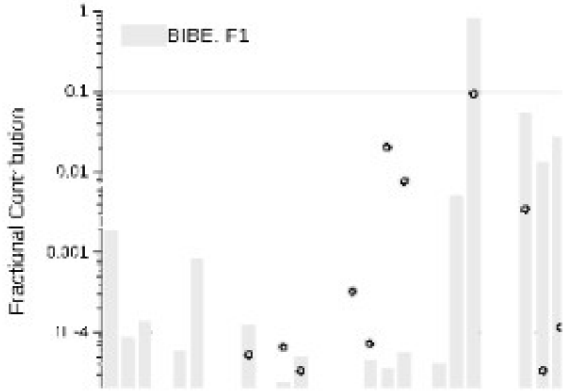

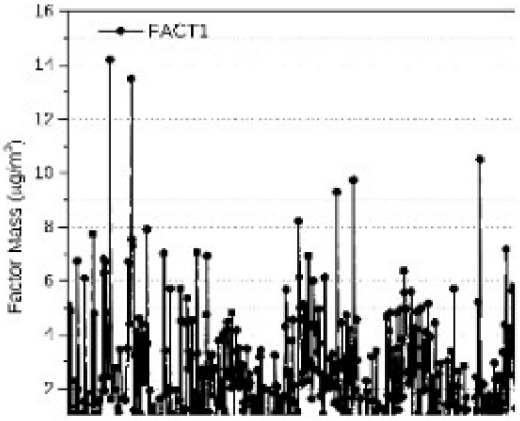

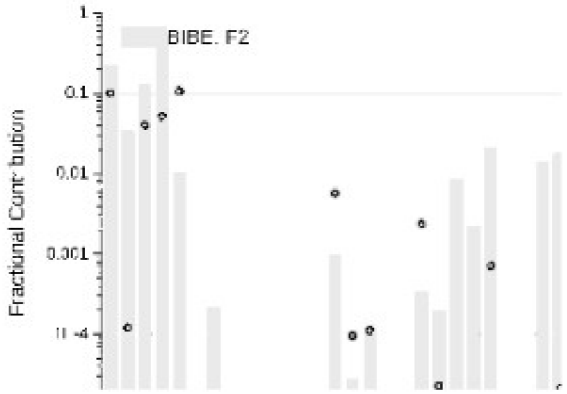

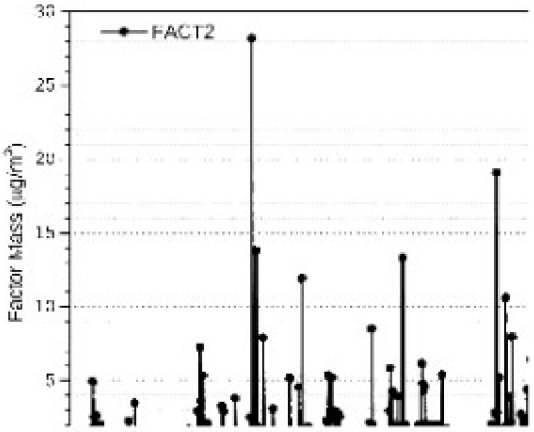

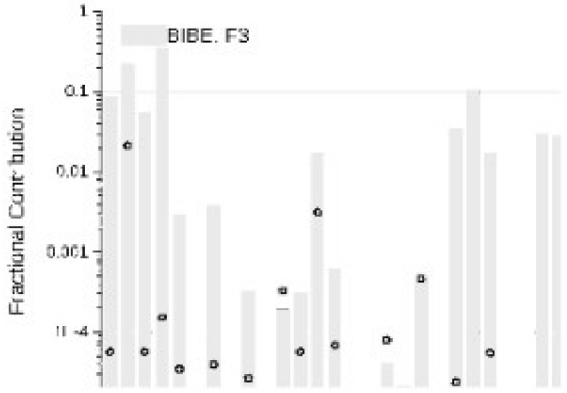

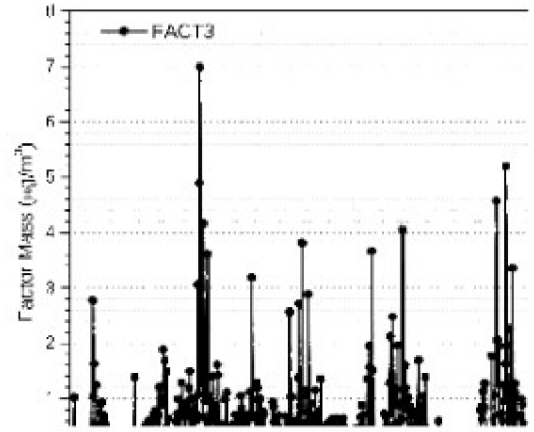

Big Bend (BIBE) Factors 4 - 6

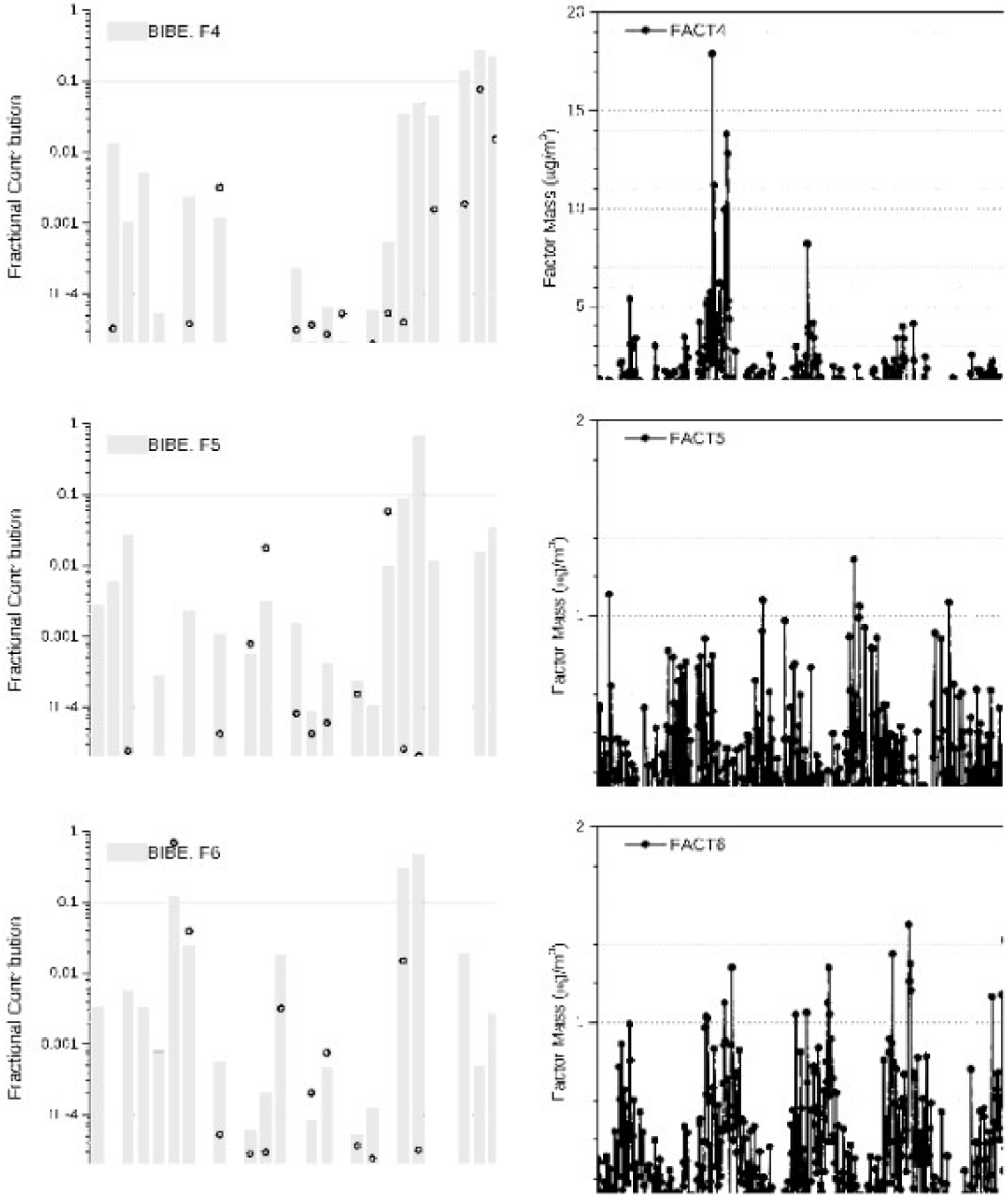

Brigantine (BRIG) Factors 1 - 3

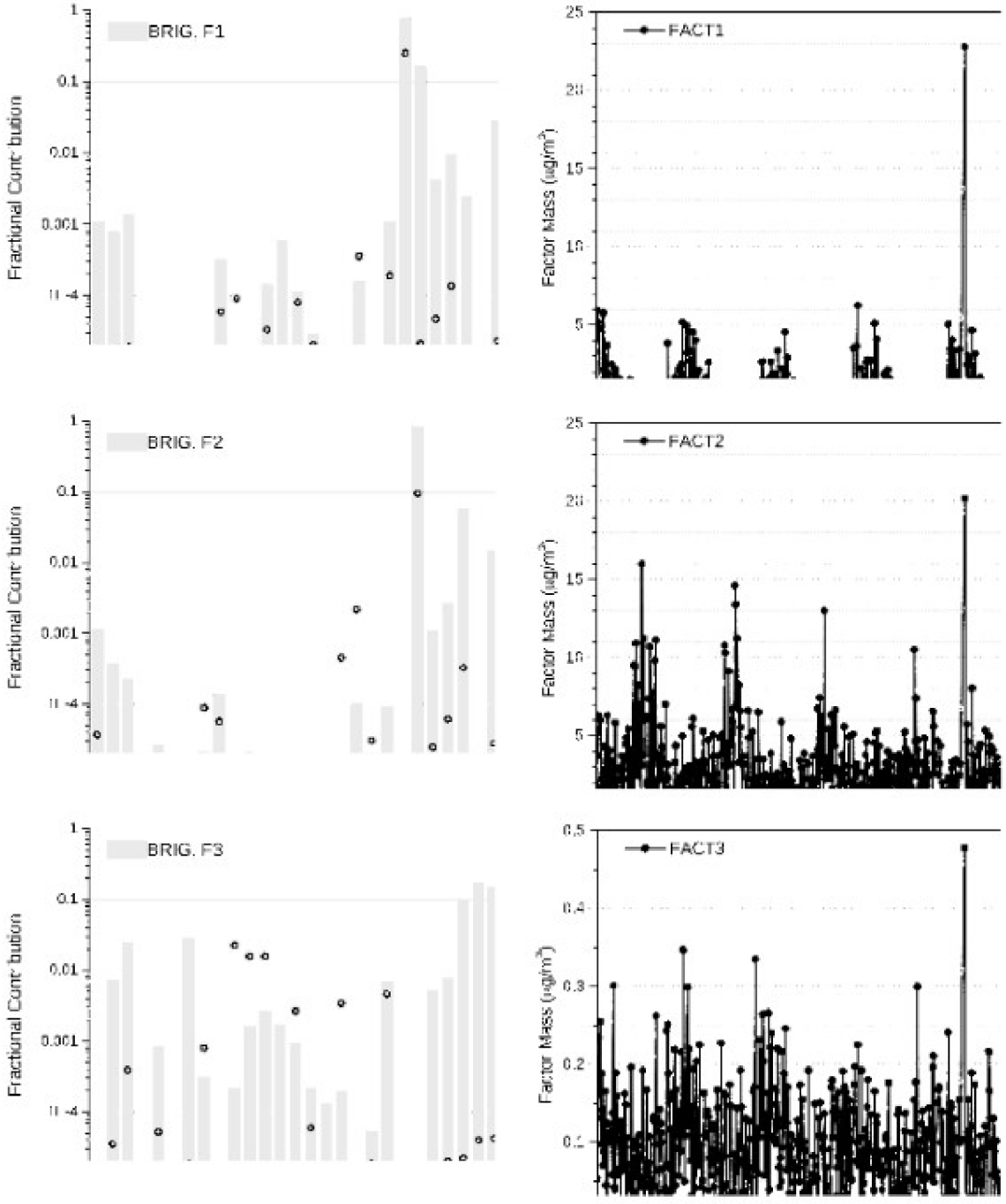

Brigantine (BRIG) Factors 4 - 6

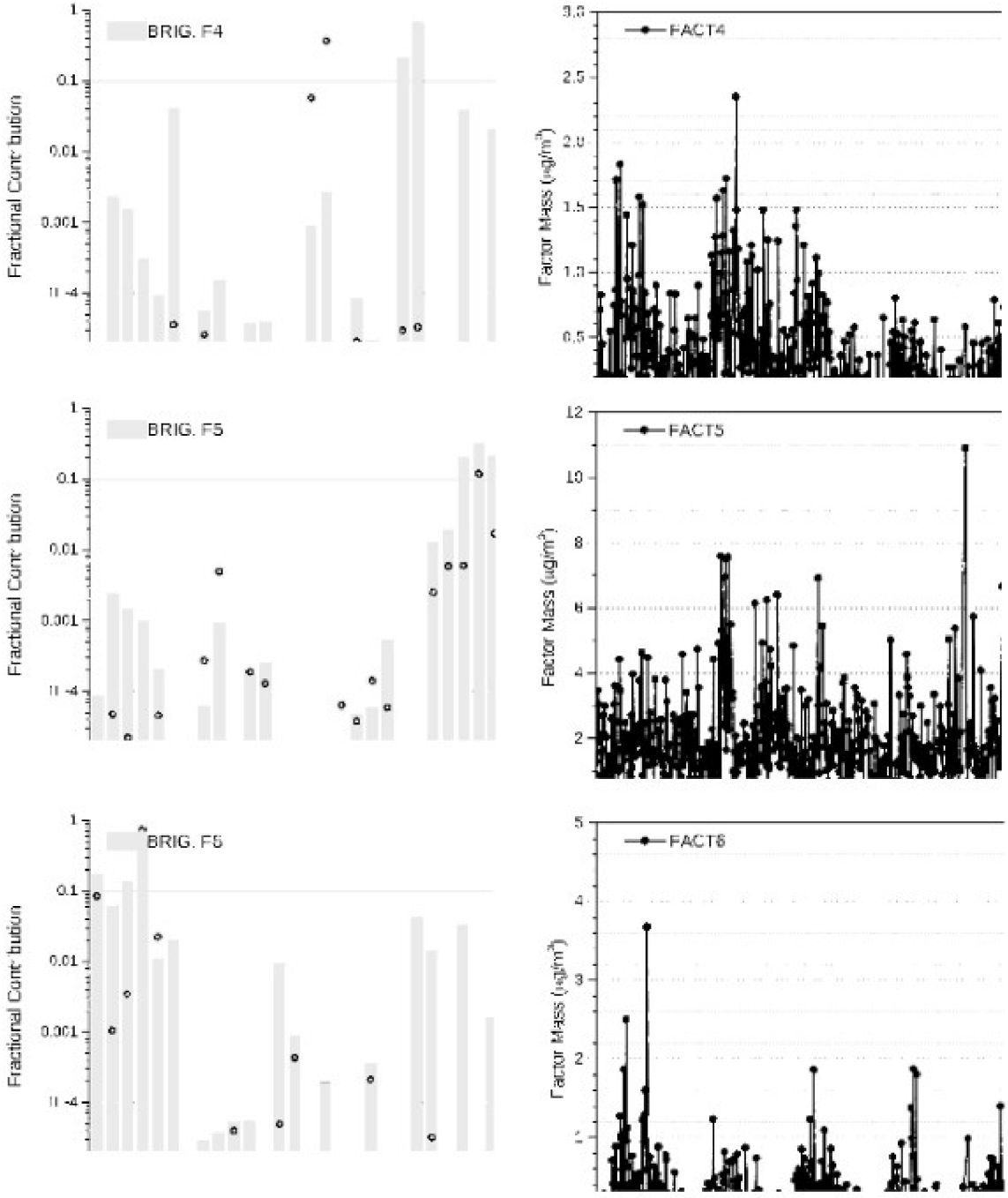

Brigantine (BRIG) Factor 7

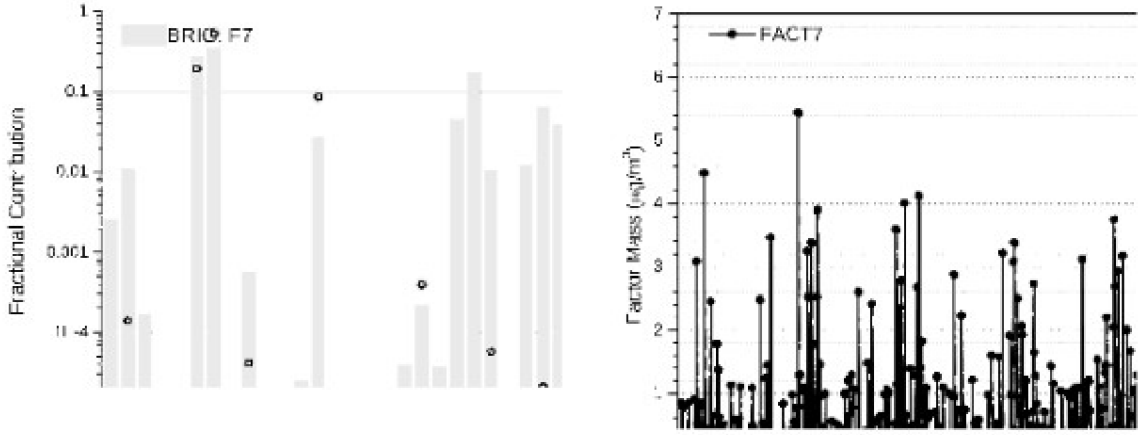

Breton Island (BRIS) Factors 1 - 3

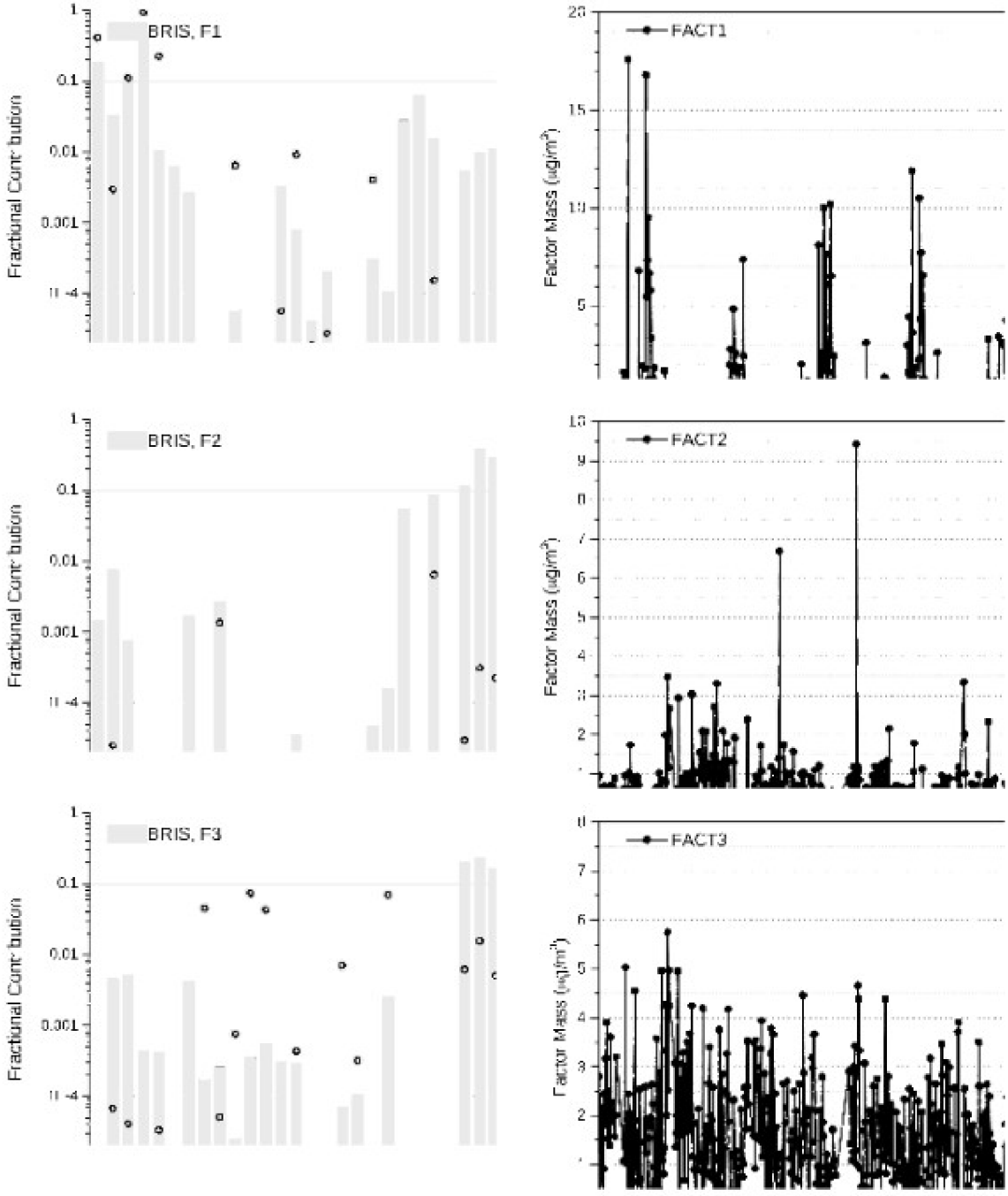

Breton Island (BRIS) Factors 4 - 6

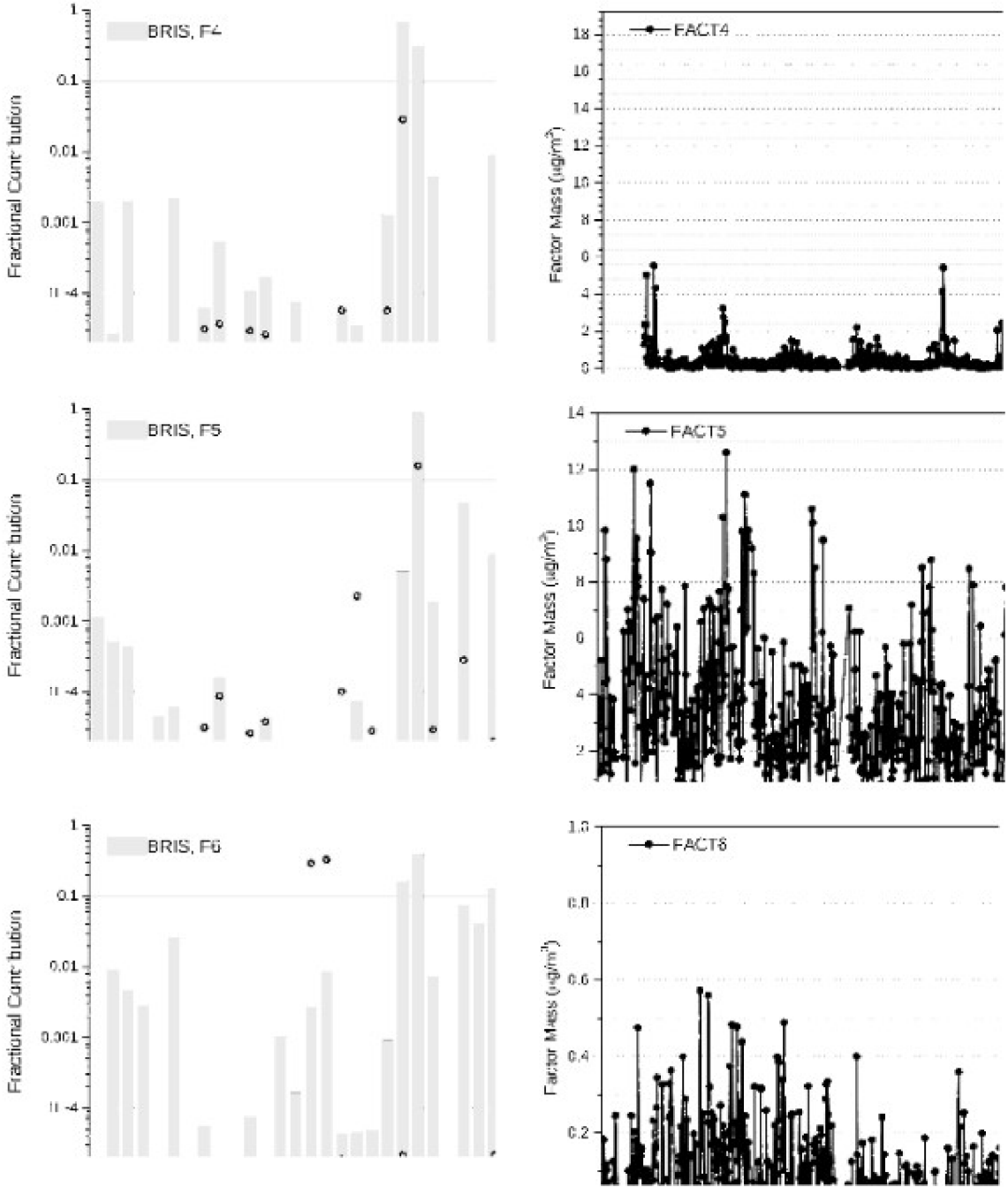

Breton Island (BRIS) Factor 7

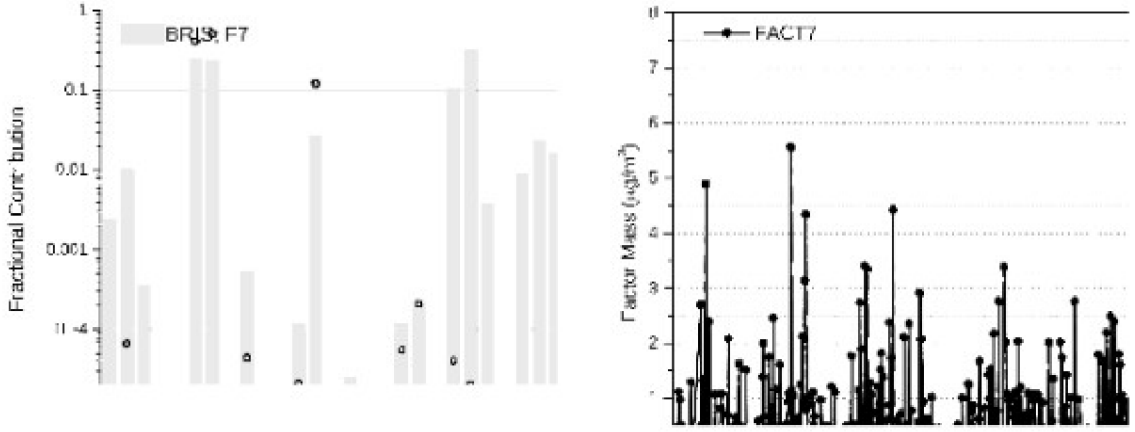

Casco Bay (CABA) Factors 1 - 3

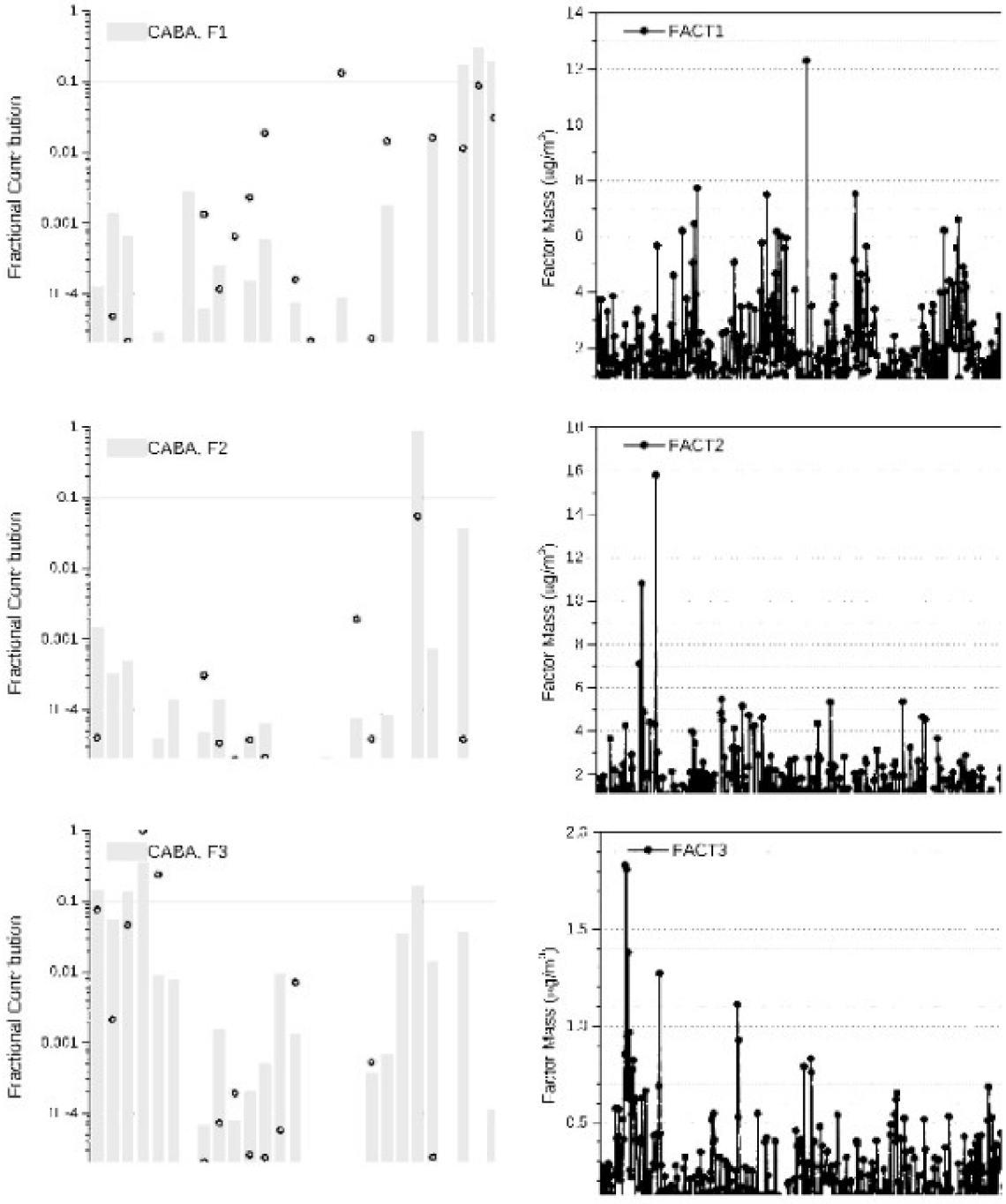

Casco Bay (CABA) Factors 4 - 6

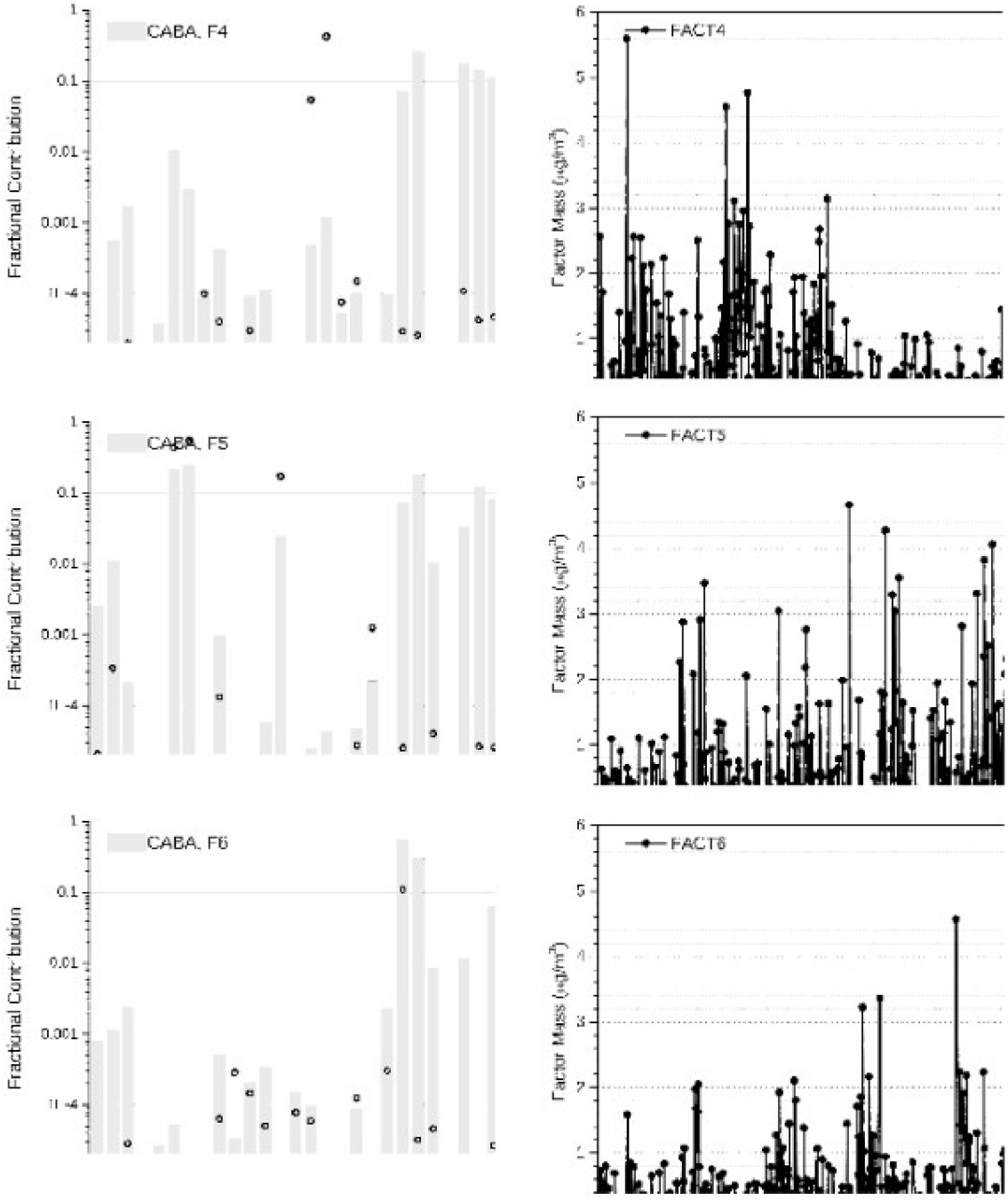

Cape Cod (CACO) Factors 1 - 3

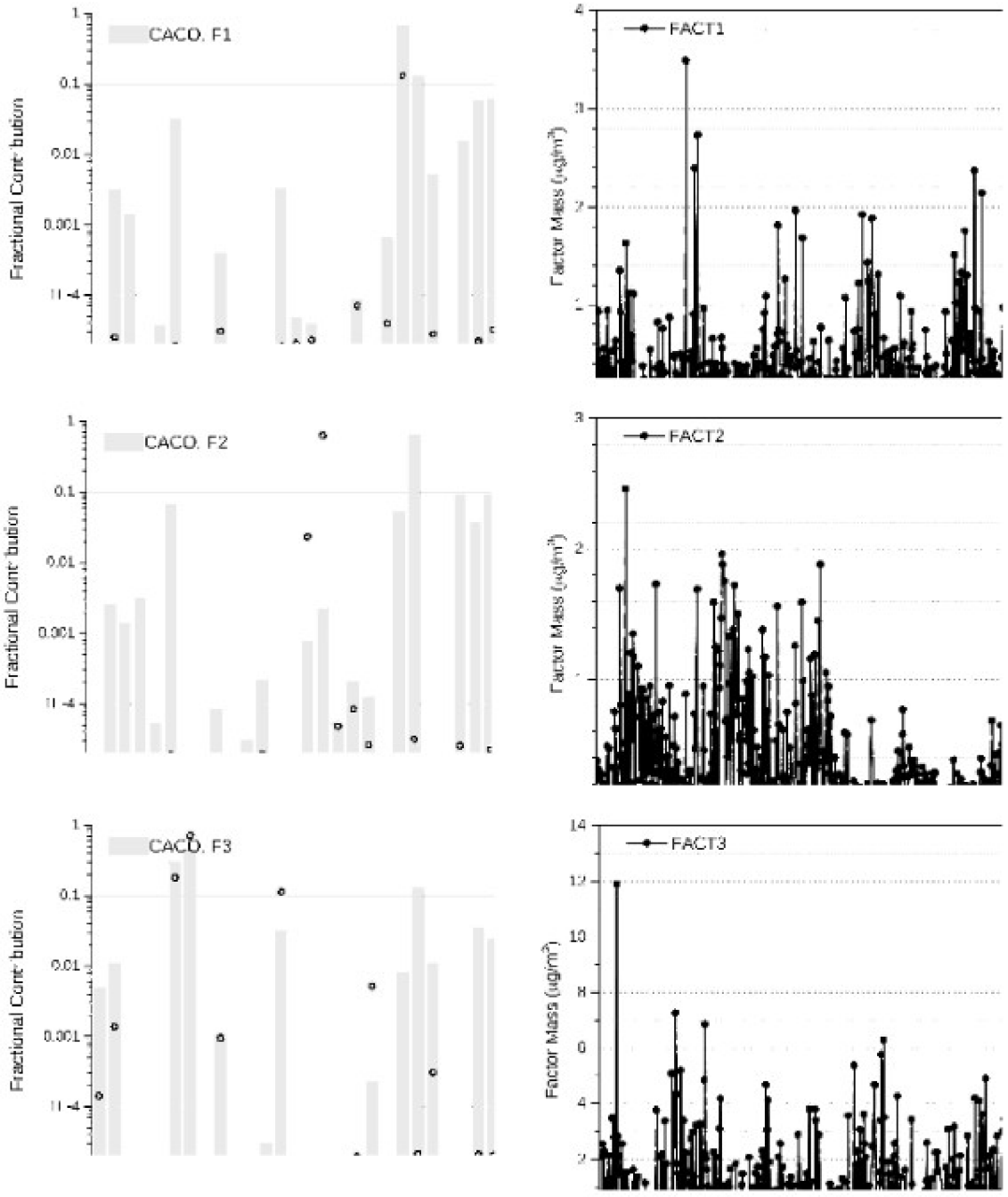

Cape Cod (CACO) Factors 4 - 6

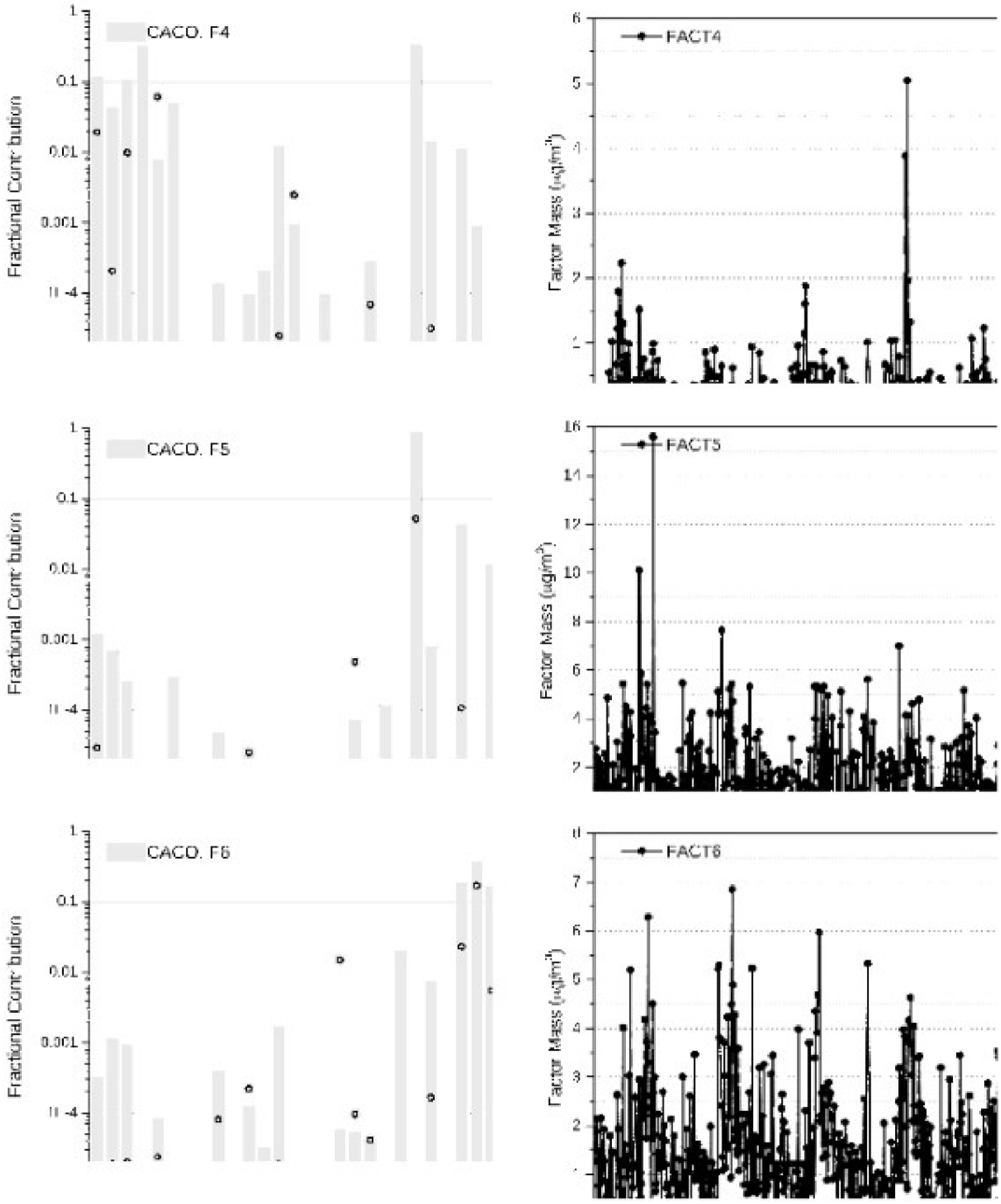

Cape Cod (CACO) Factor 7

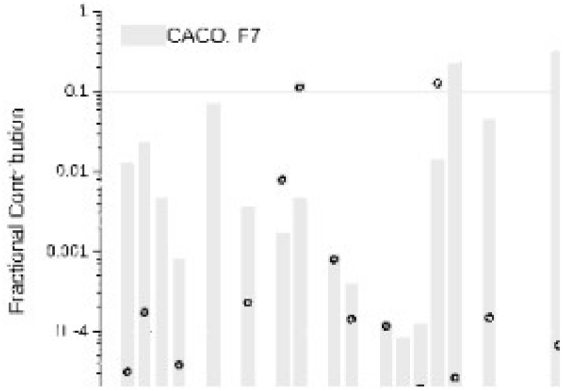

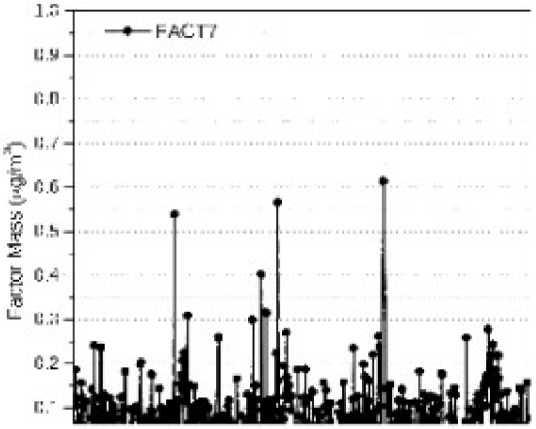

Chassahowitzka (CHAS) Factors 1 - 3

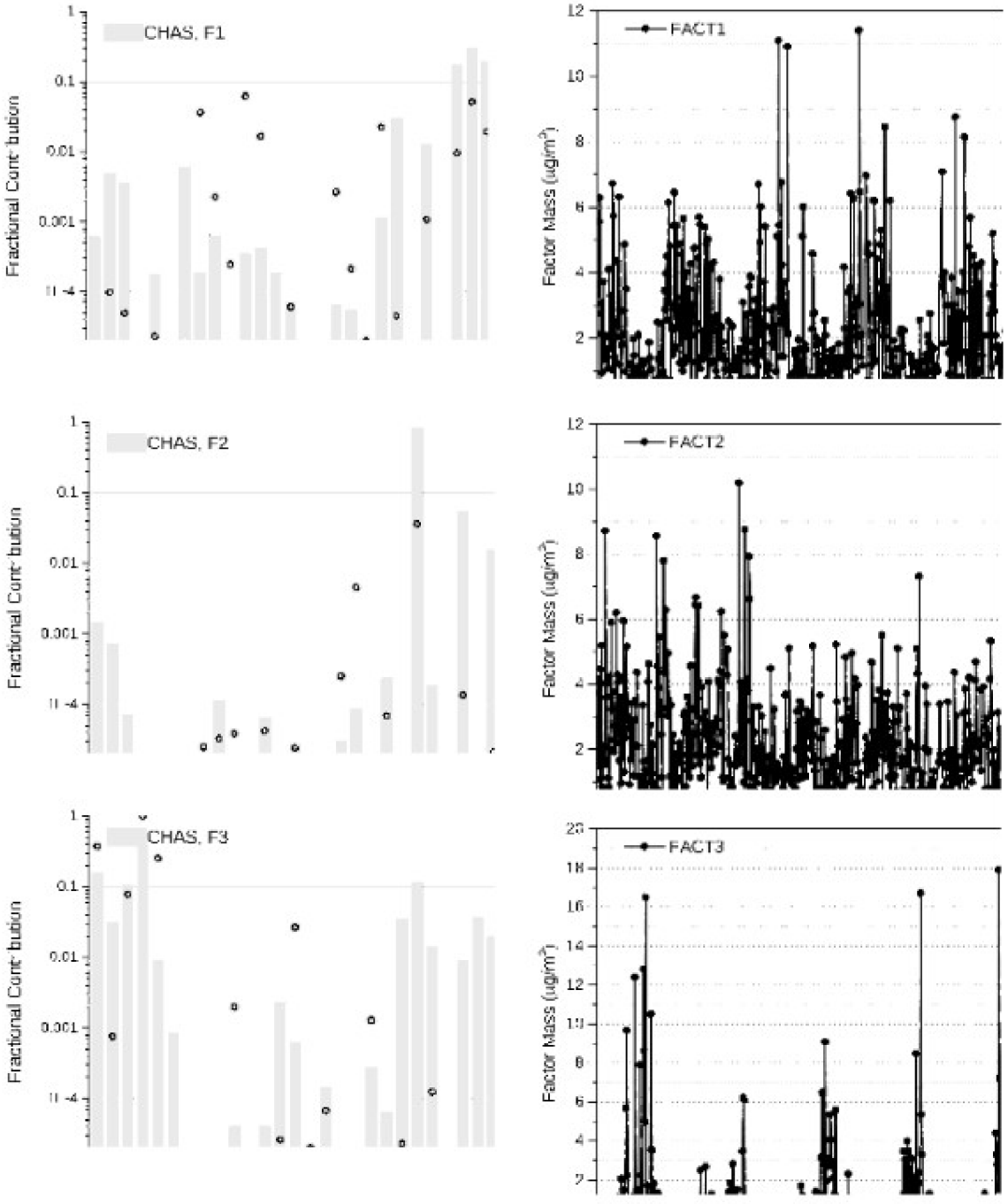

Chassahowitzka (CHAS) Factors 4 - 6

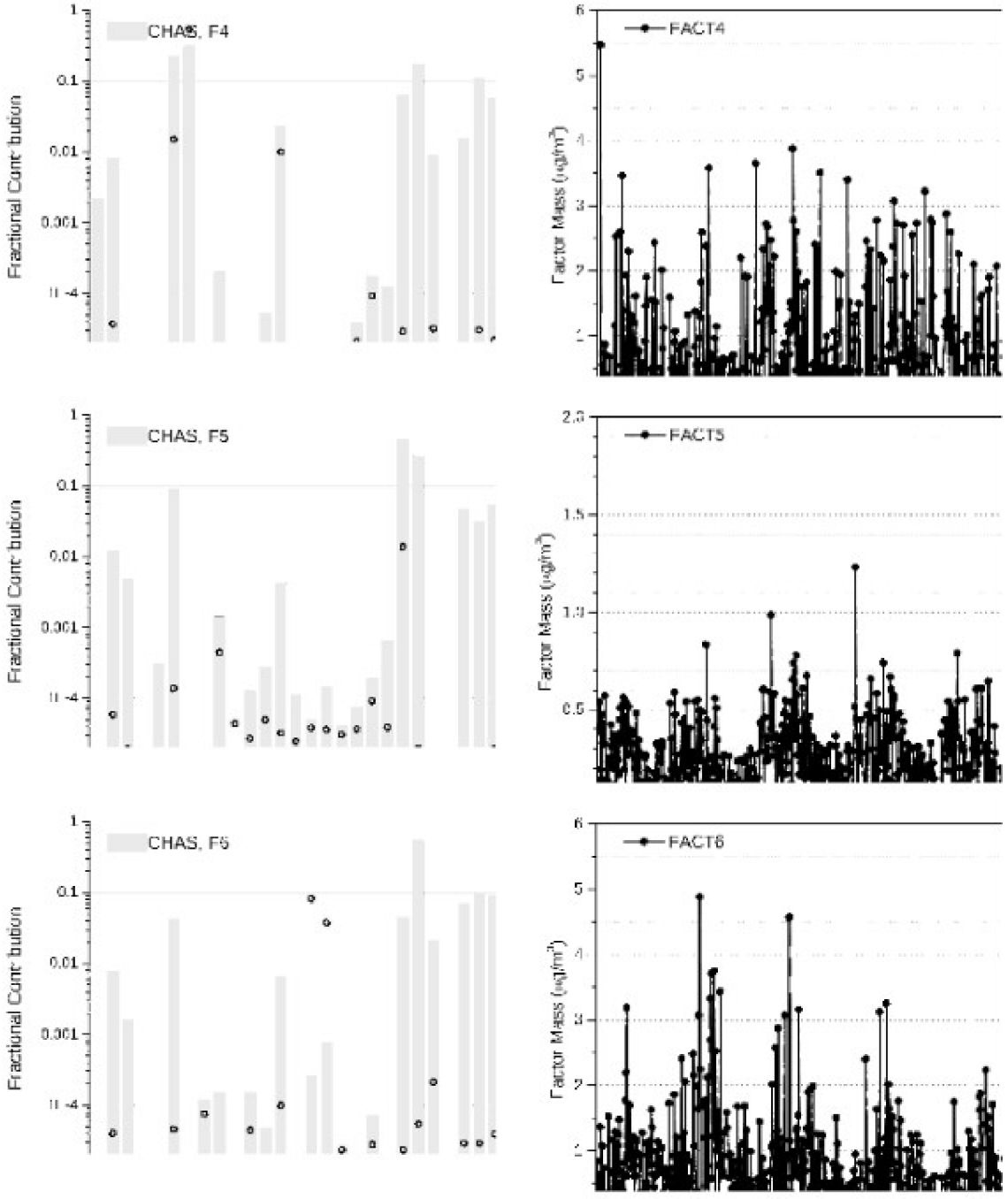

Martha's Vineyard (MAVI) Factors 1 - 3

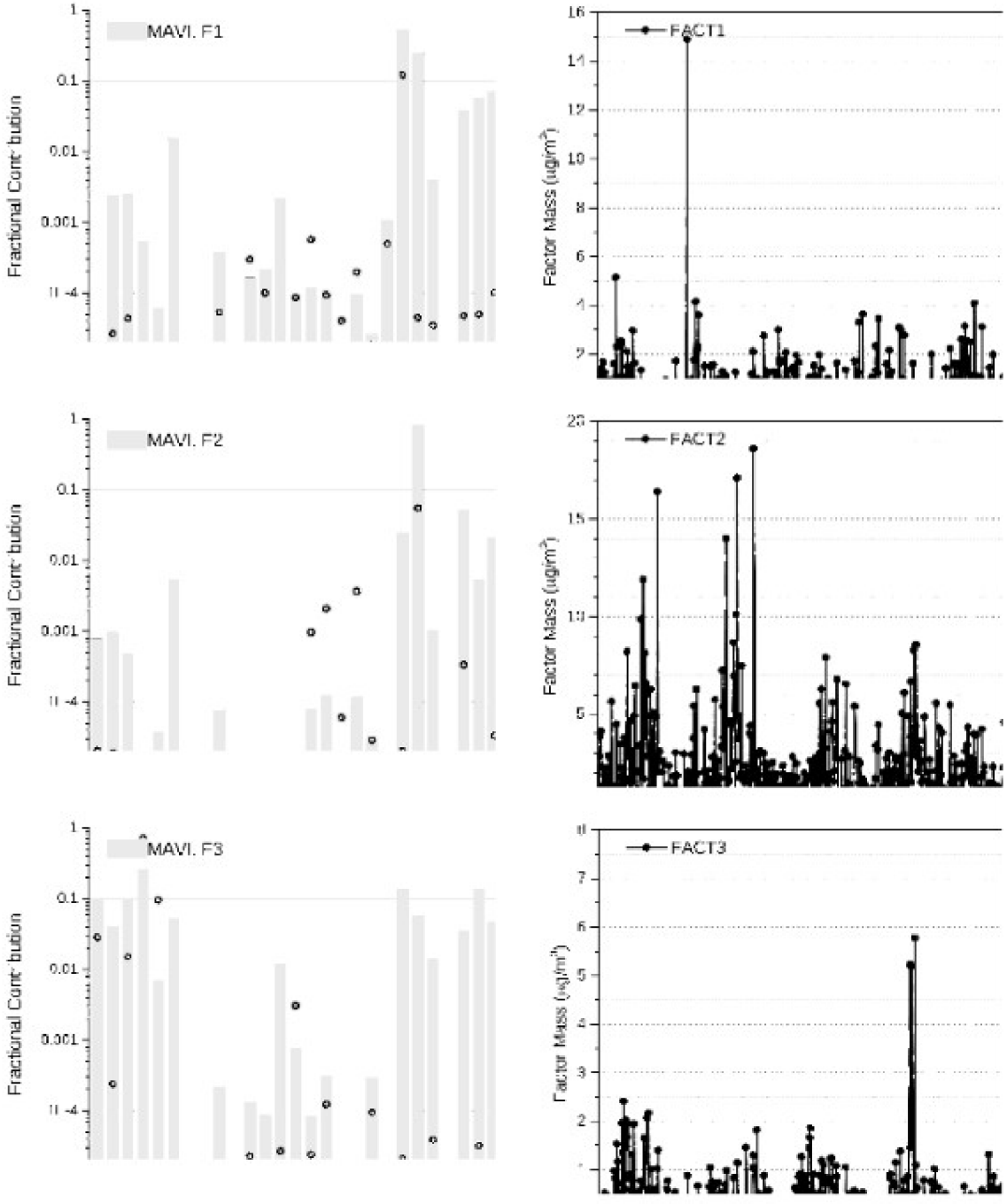

Martha's Vineyard (MAVI) Factors 4 - 5

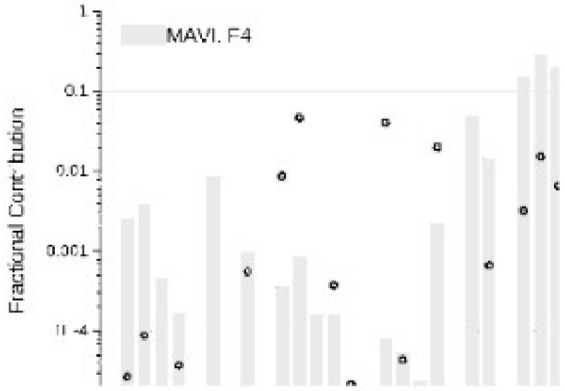

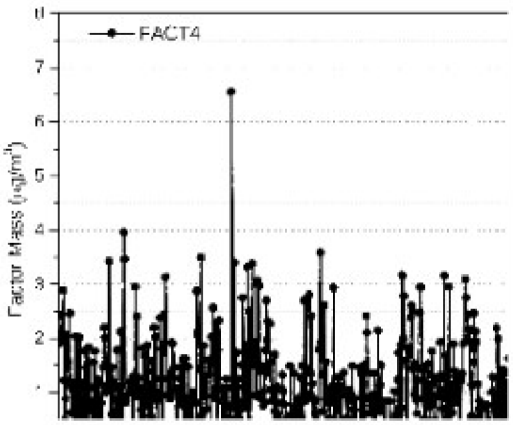

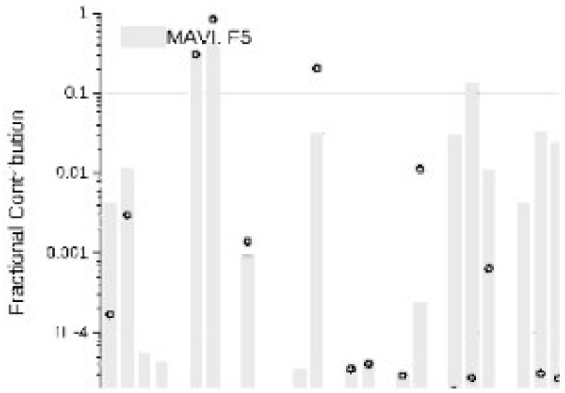

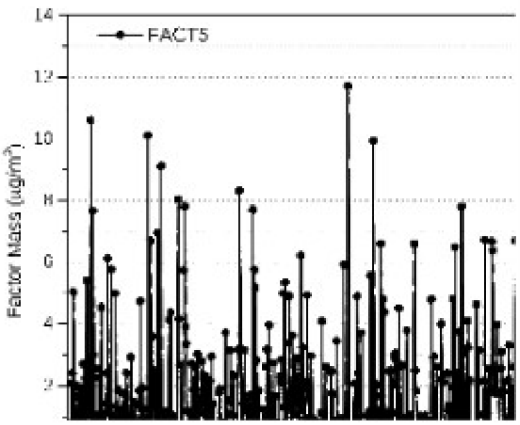

Moosehorn (MOOS) Factors 1 - 3

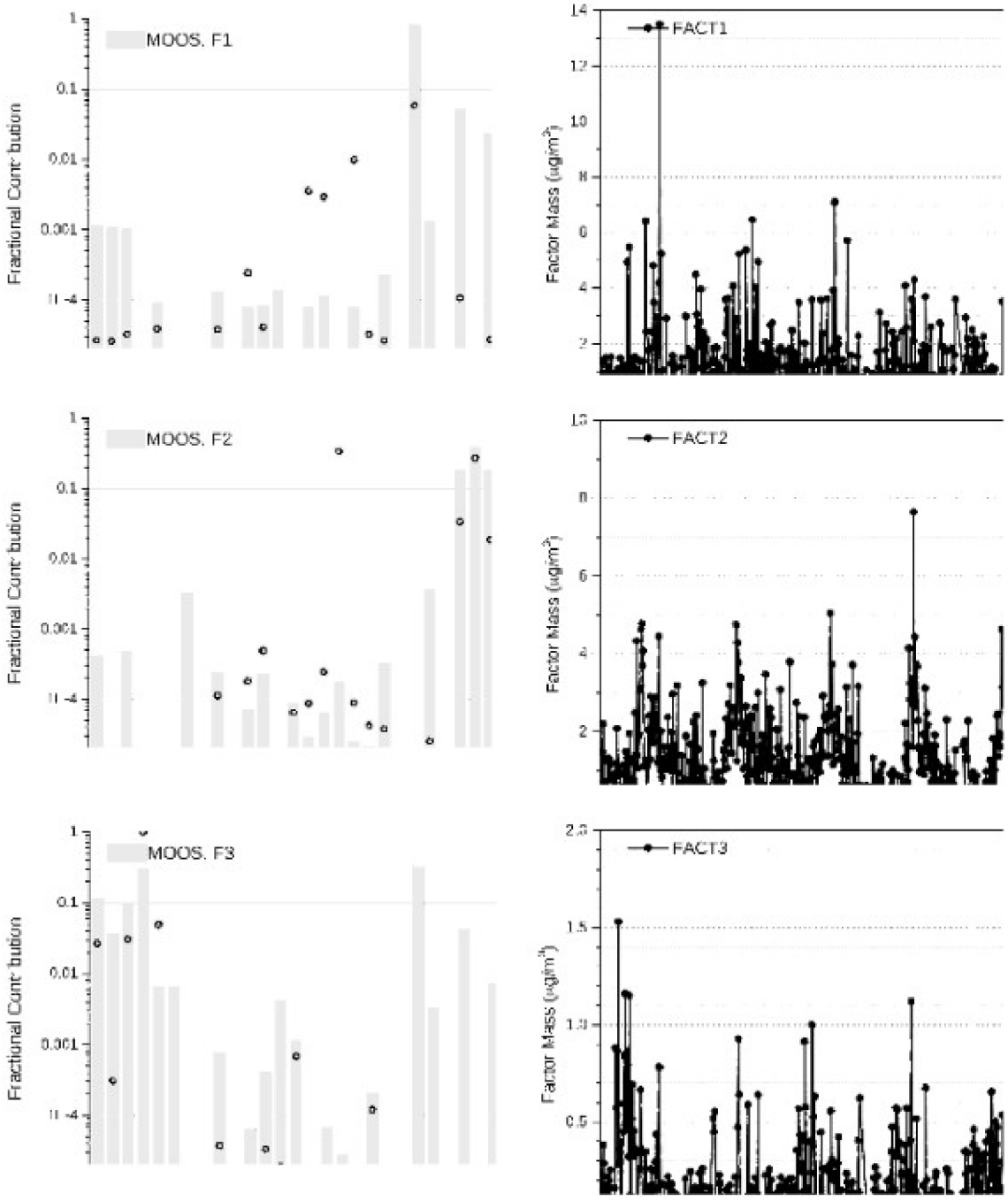

Moosehorn (MOOS) Factors 4 - 6

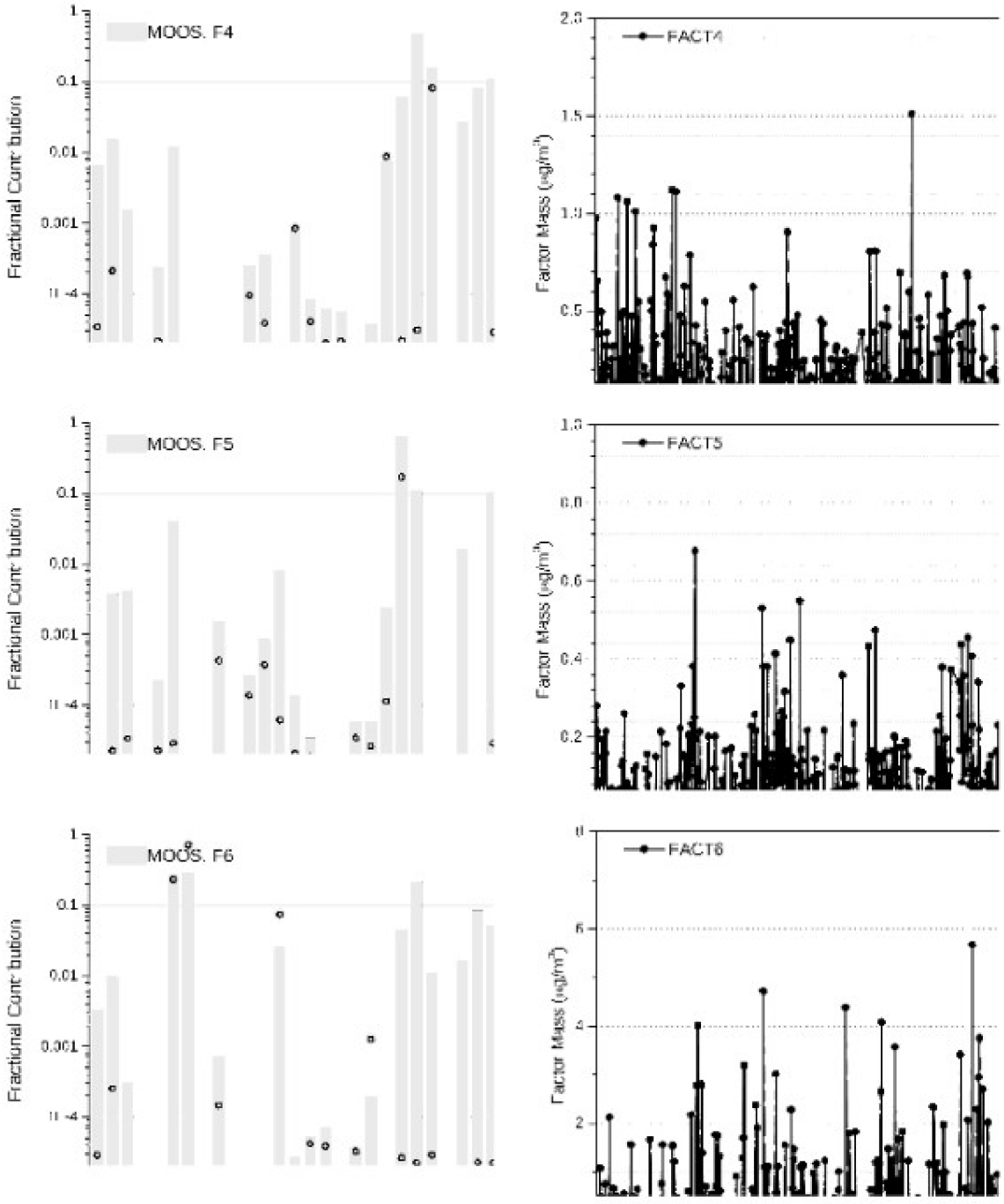

Mount Rainier (MORA) Factors 1 - 3

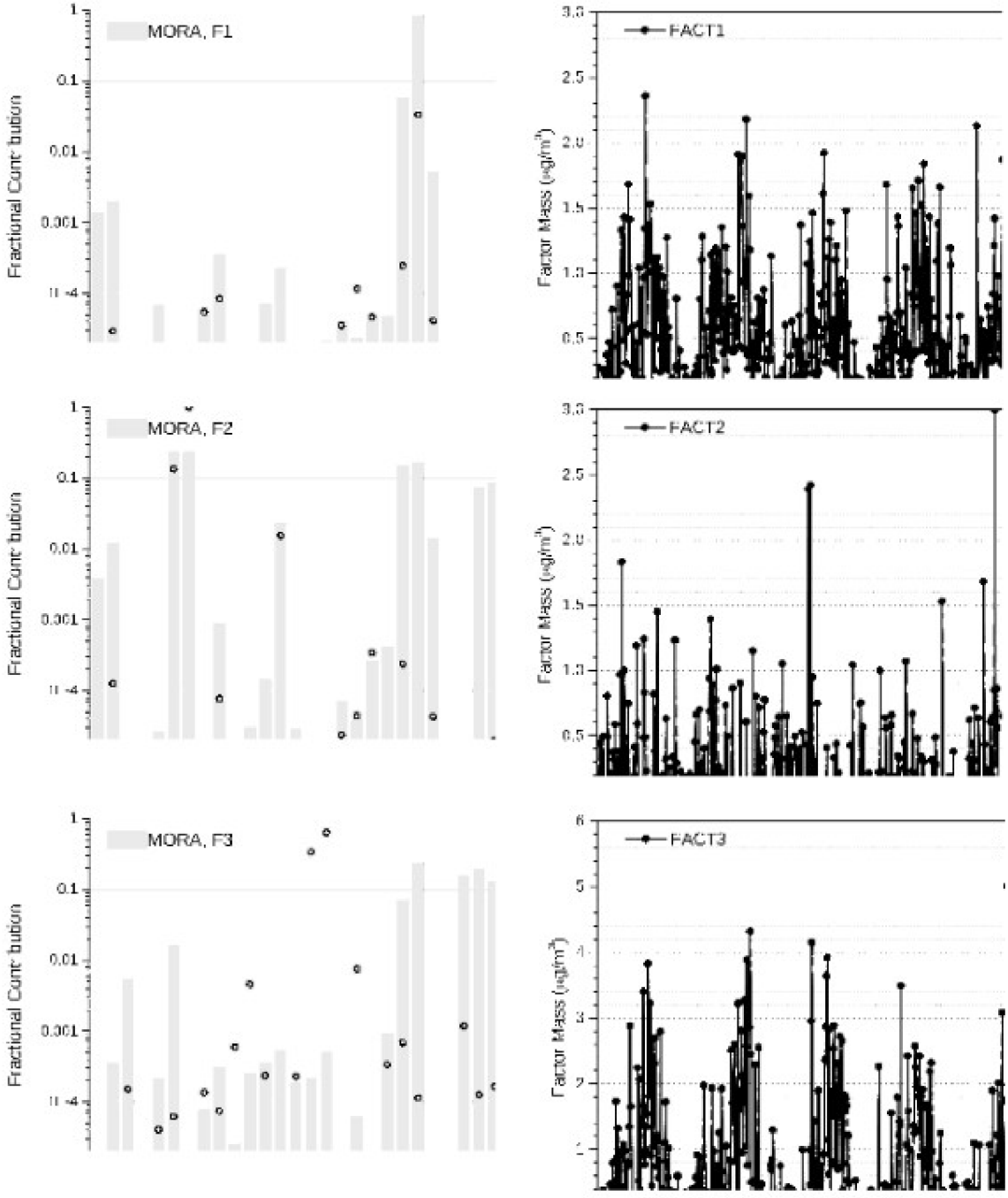

Mount Rainier (MORA) Factors 4 - 5

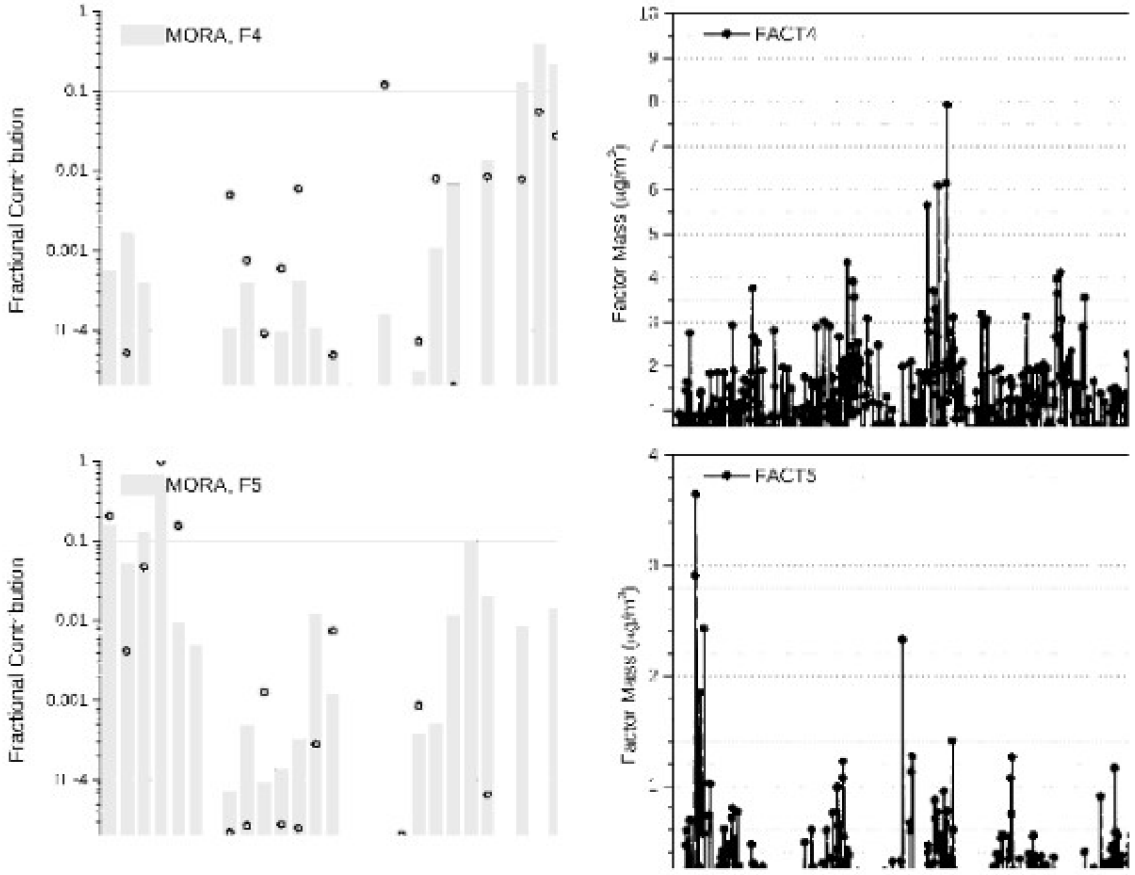

North Cascades (NOCA) Factors 1 - 3

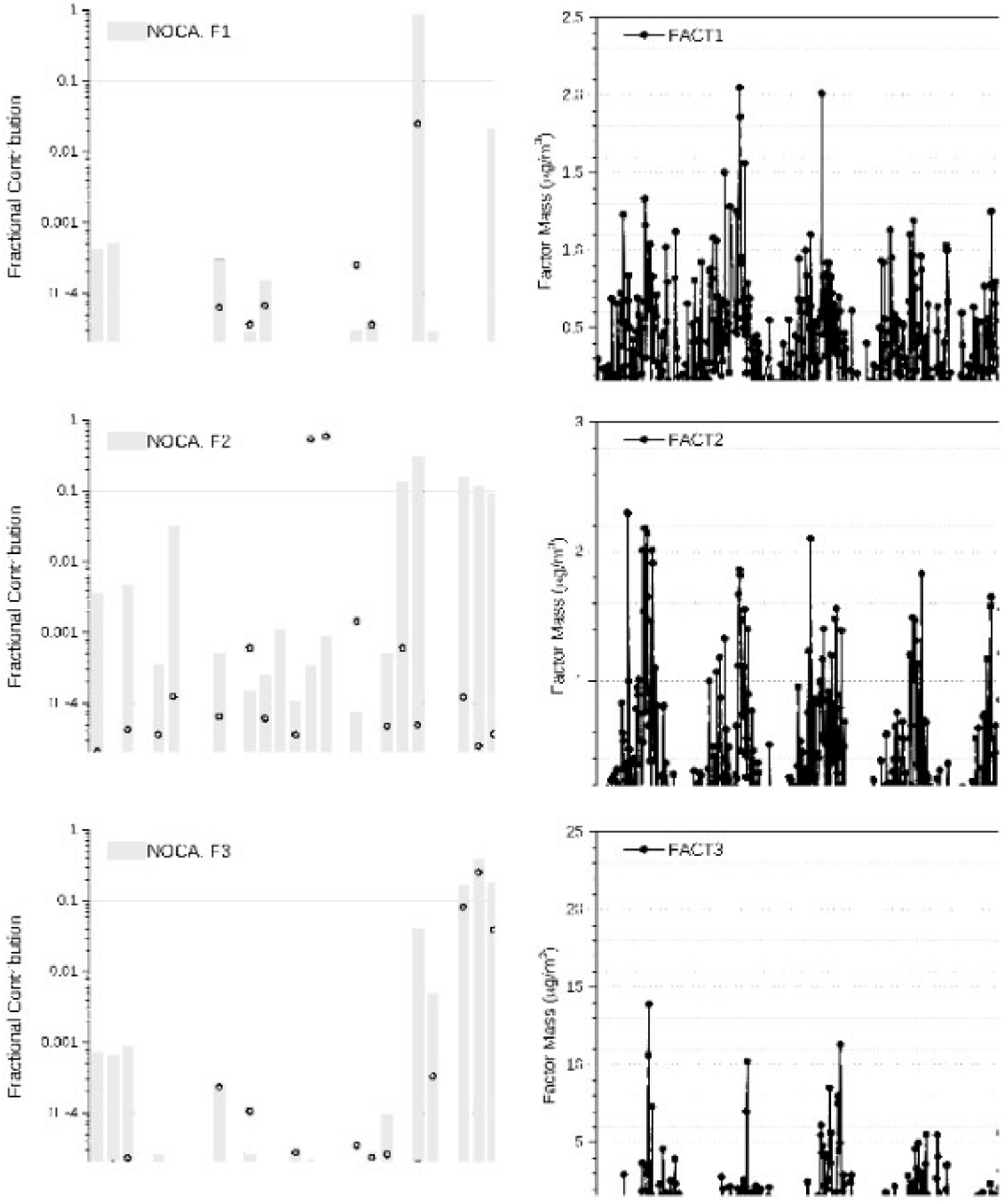

North Cascades (NOCA) Factors 4 - 6

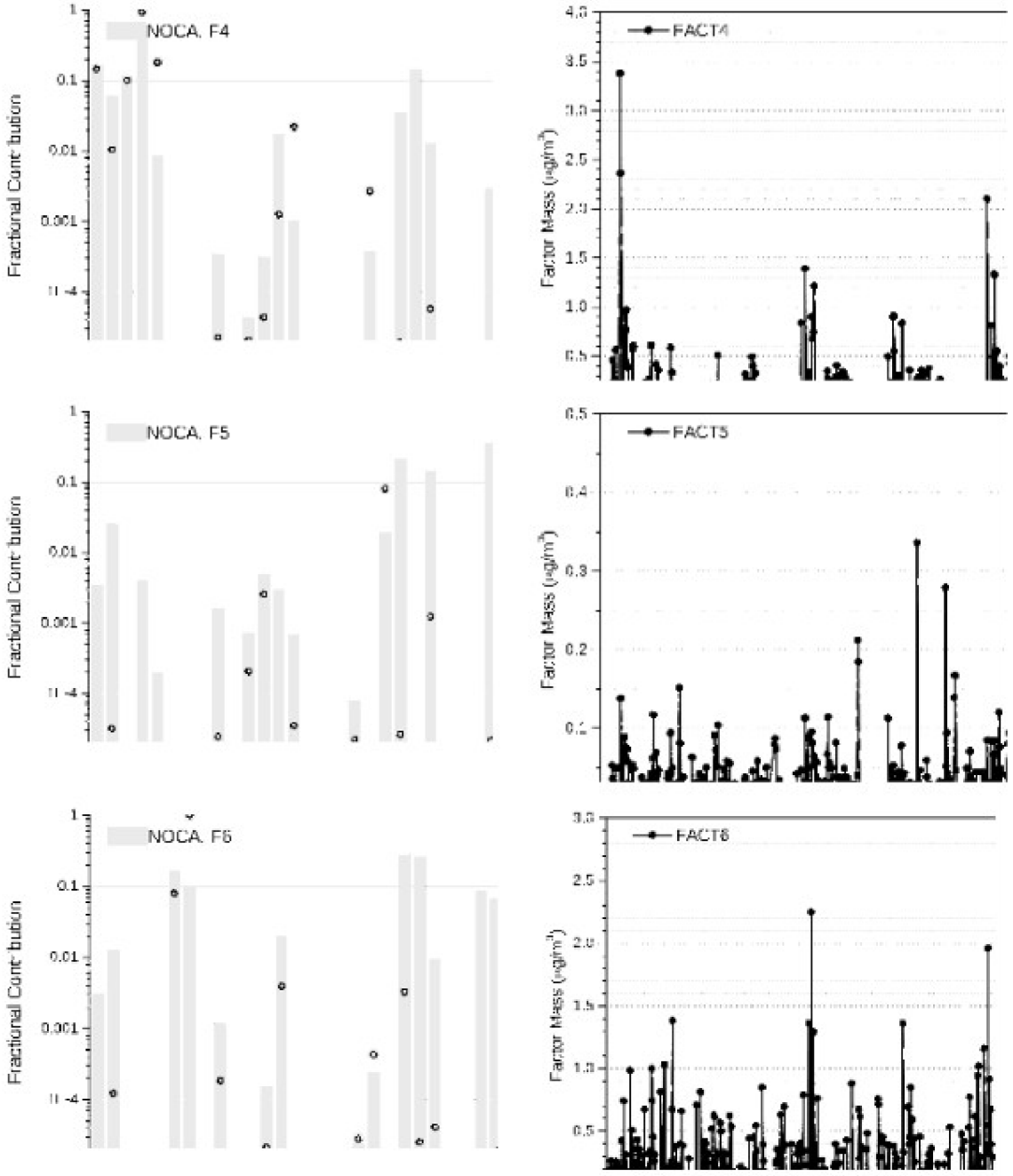

Okefenokee (OKEF) Factors 1 - 3

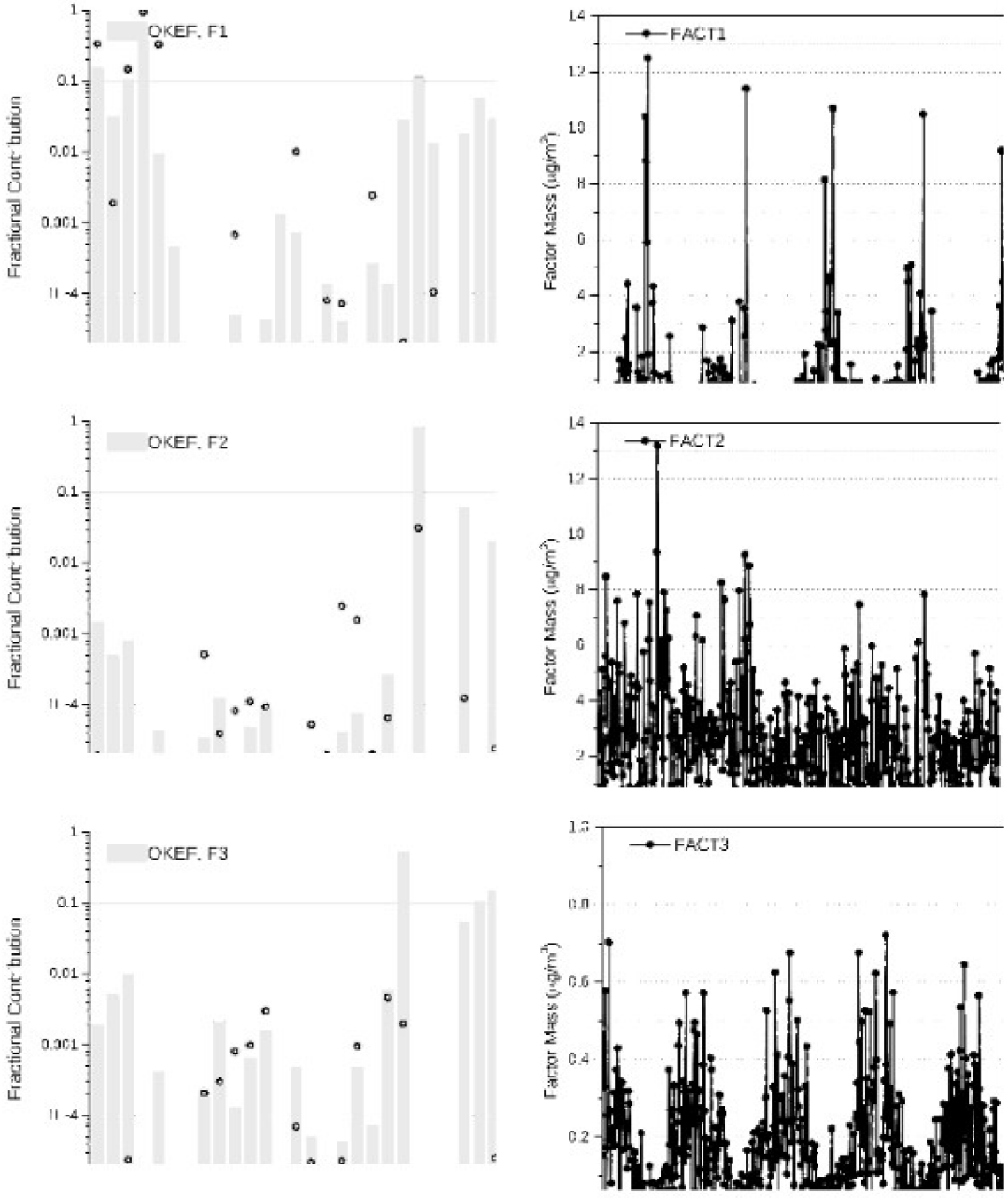

Okefenokee (OKEF) Factors 4 - 6

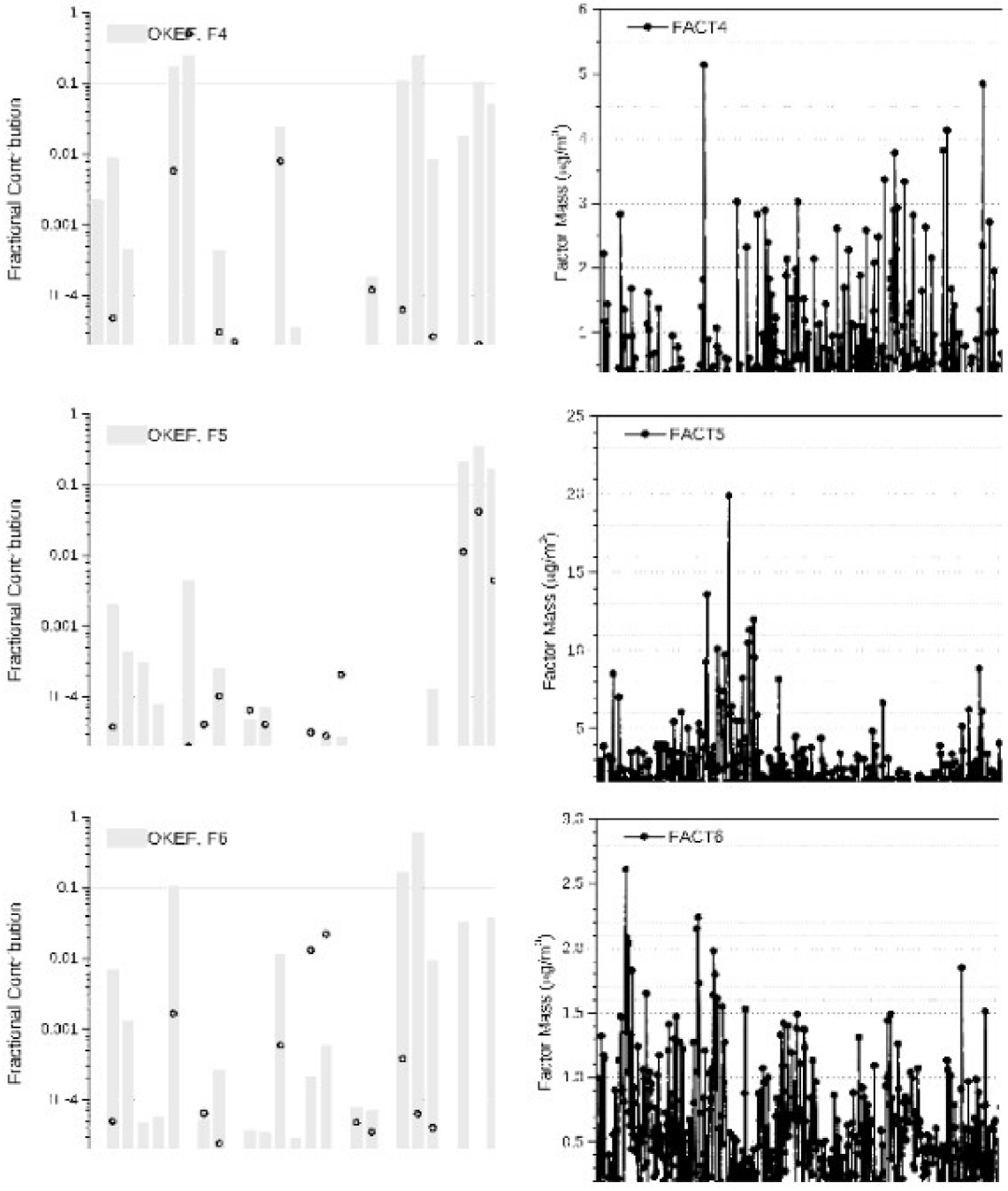

Okefenokee (OKEF) Factor 7

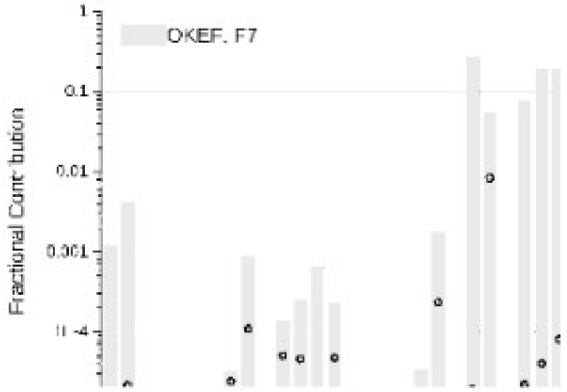

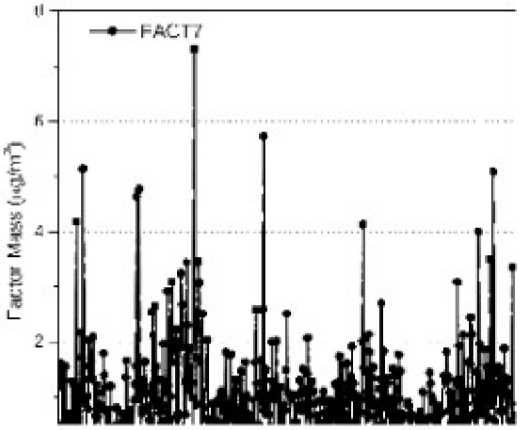

Olympic (OLYM) Factors 1 - 3

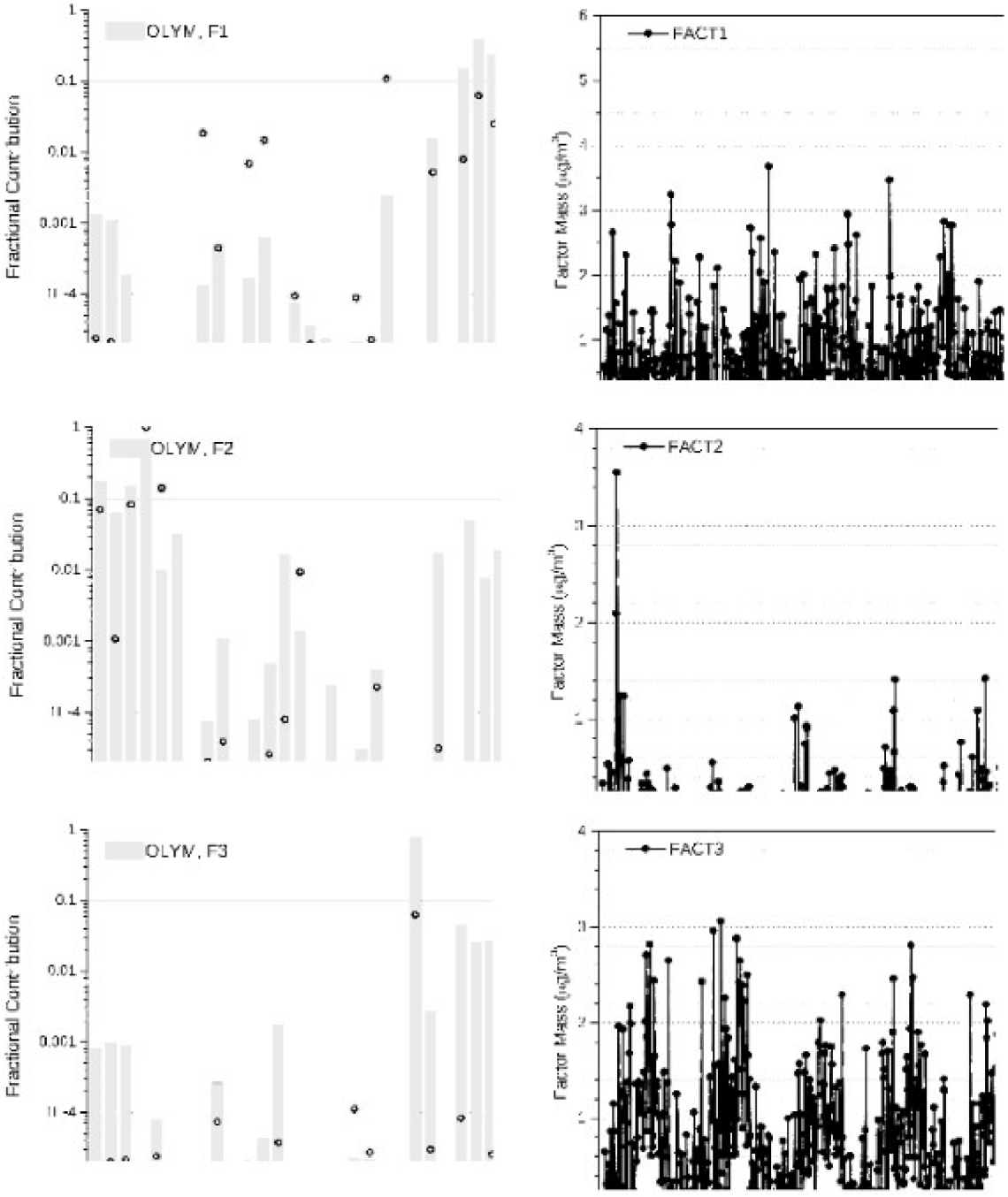

Olympic (OLYM) Factors 4 - 6

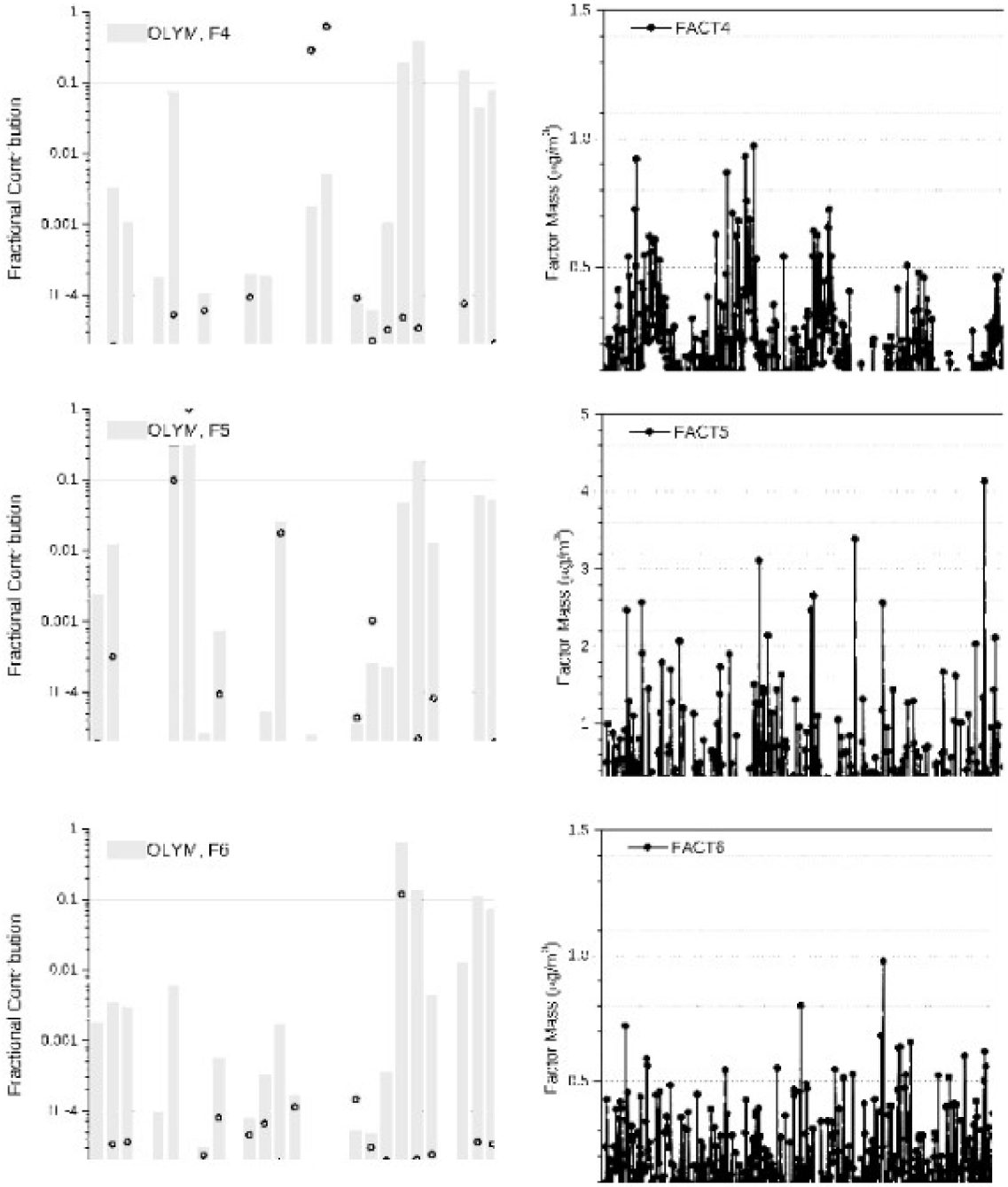

Penobscot (PENO) Factors 1 - 3

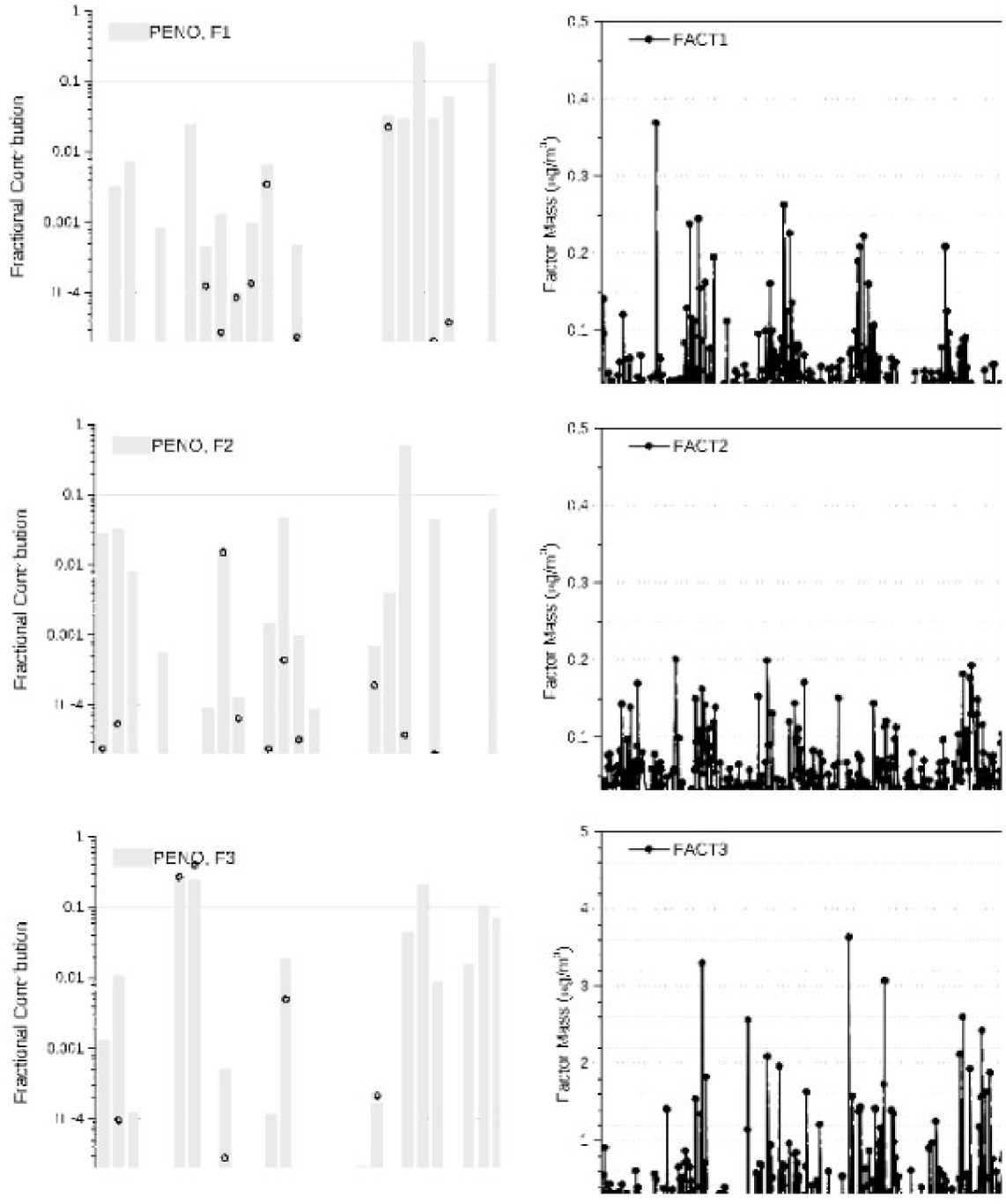

Penobscot (PENO) Factors 4 - 6

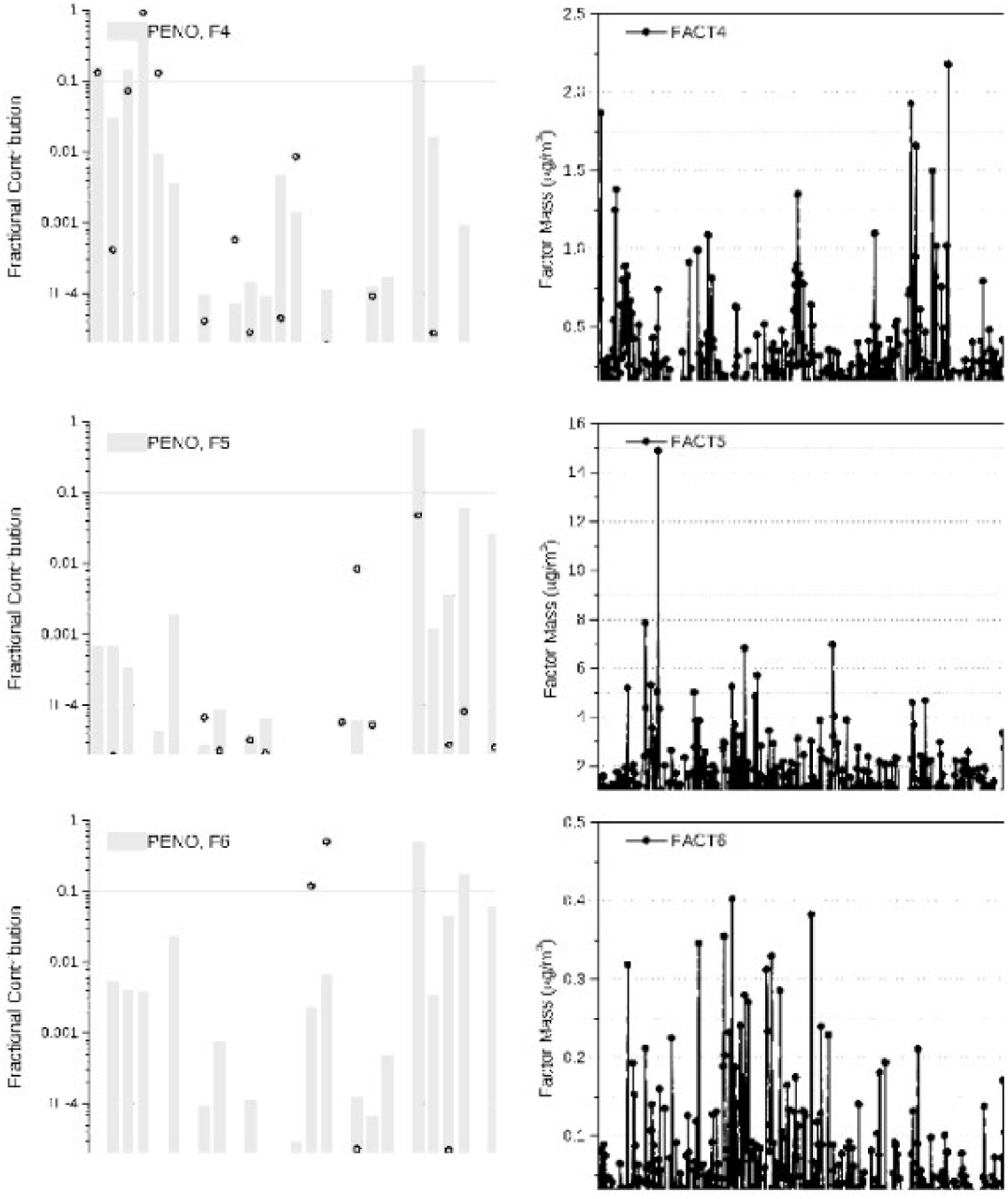

Penobscot (PENO) Factor 7 - 9

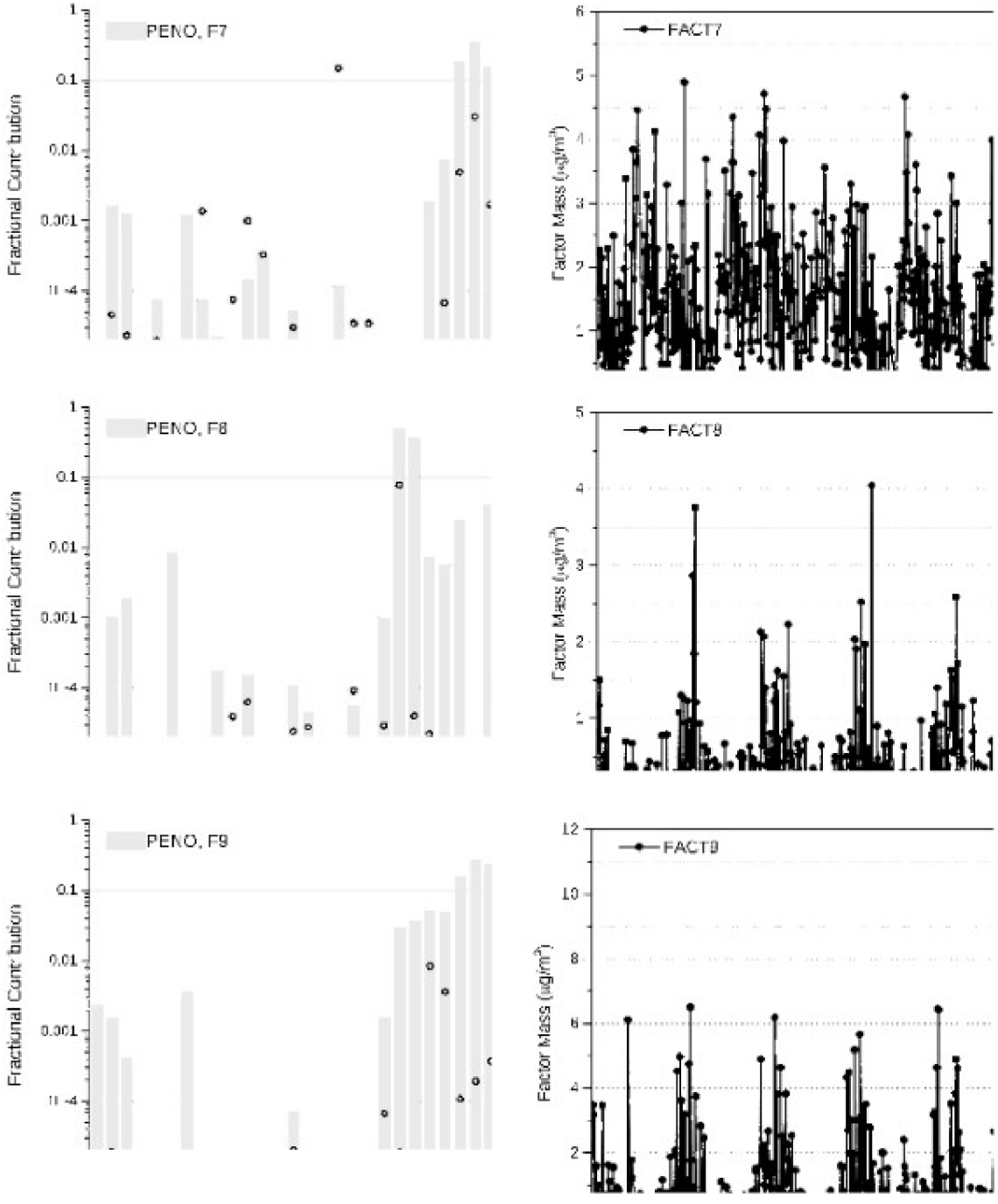

Pinnacles (PINN) Factors 1 - 3

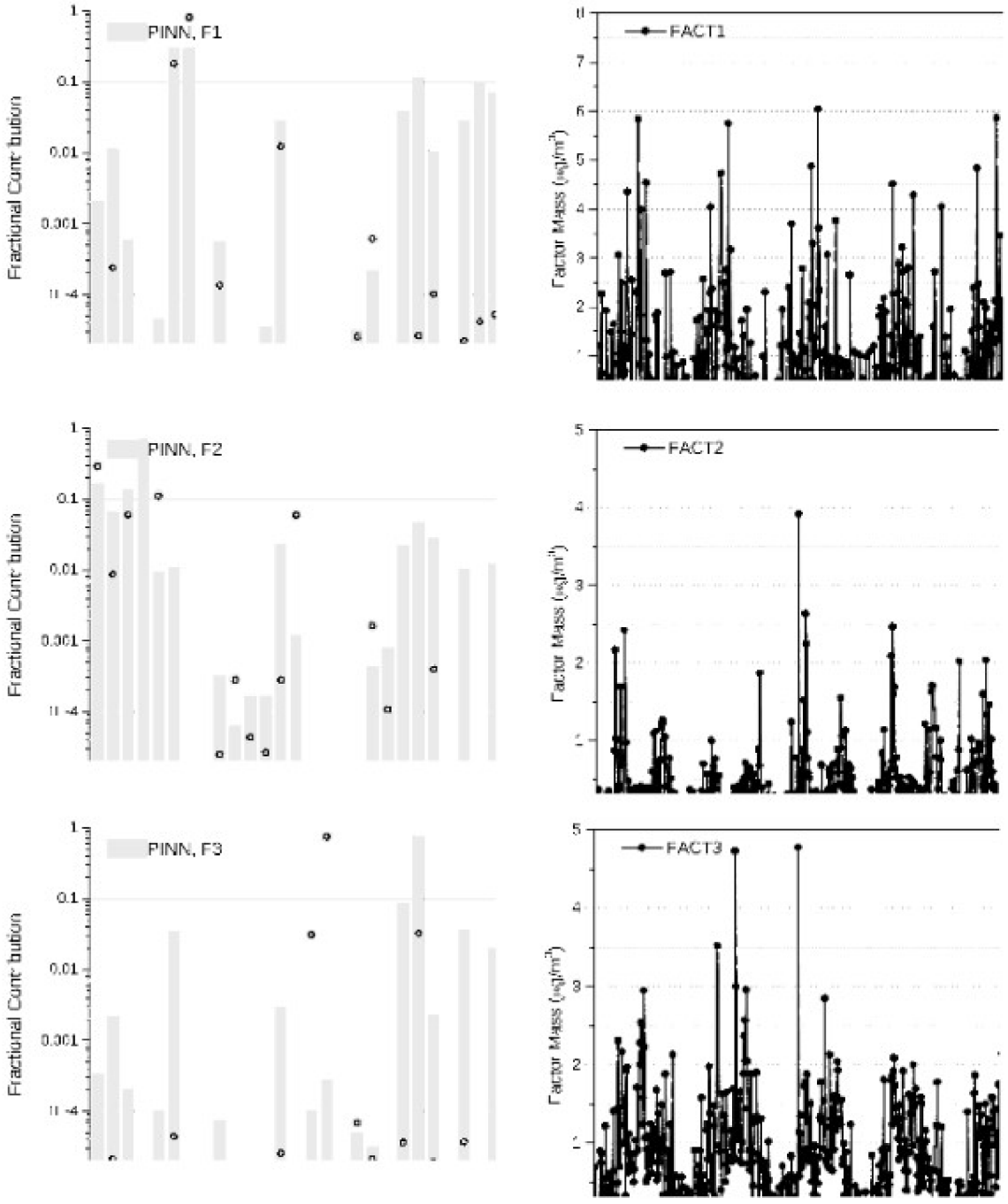

Pinnacles (PINN) Factors 4 - 6

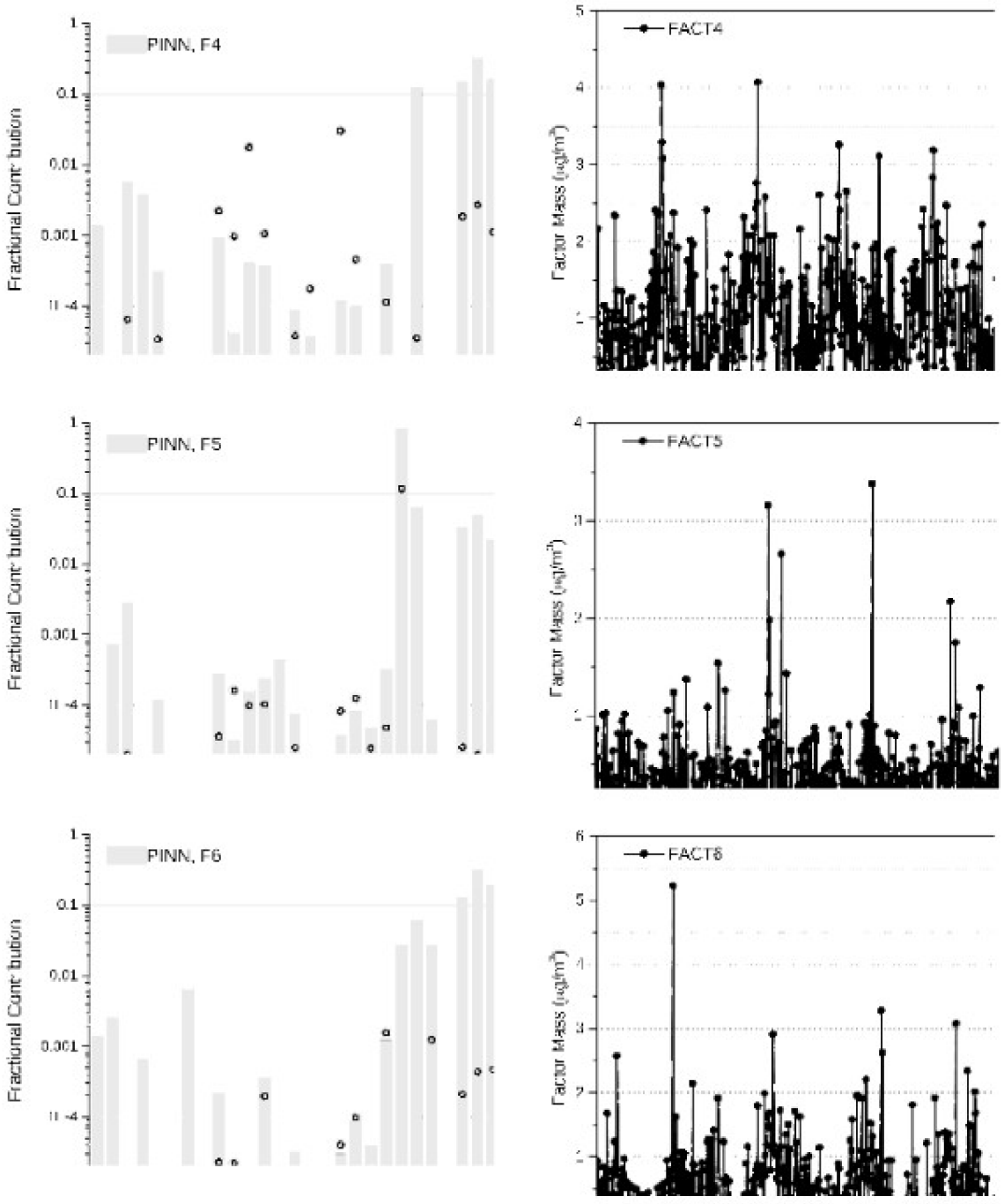

Point Reyes (PORE) Factors 1 - 3

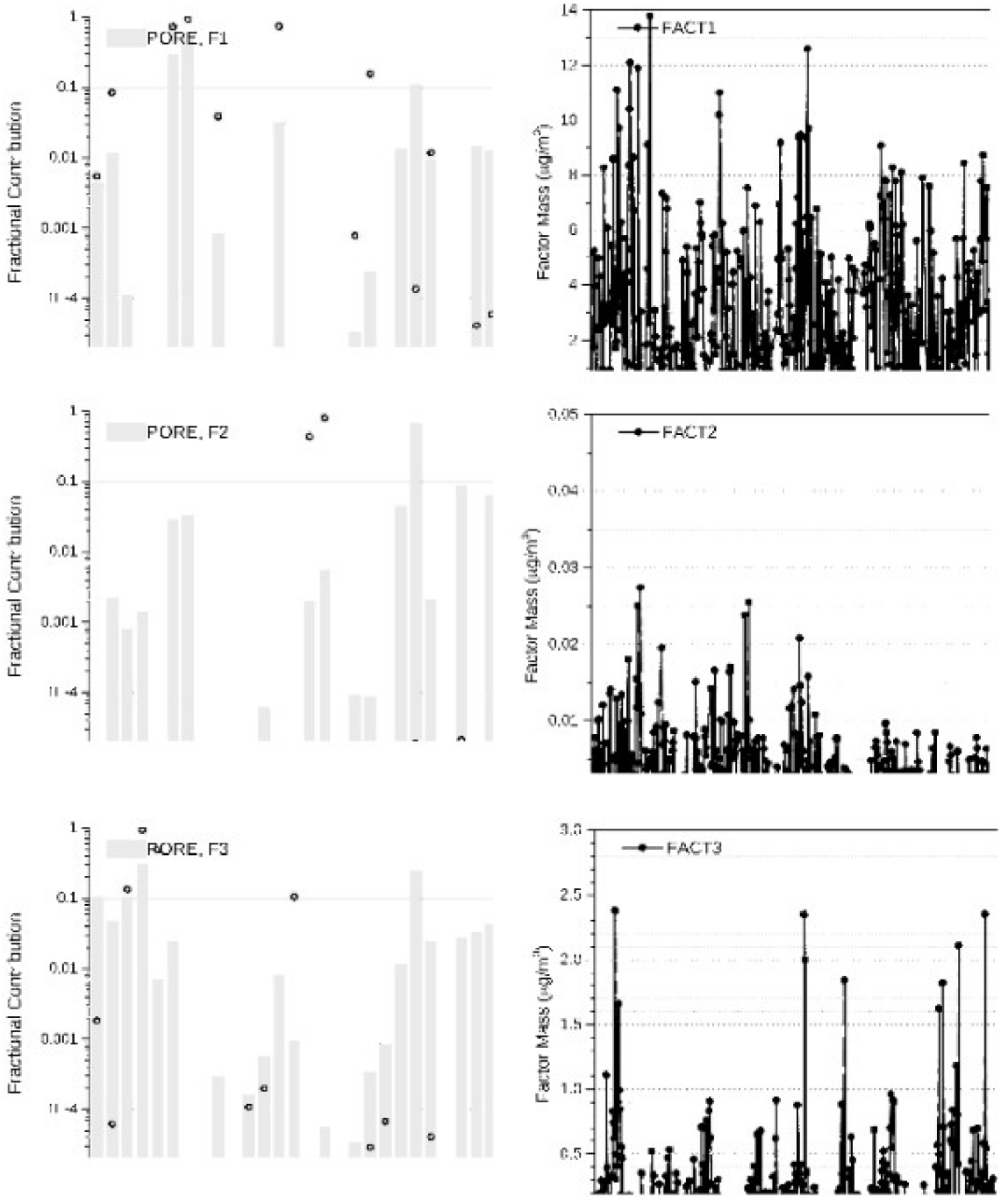

Point Reyes (PORE) Factors 4 - 6

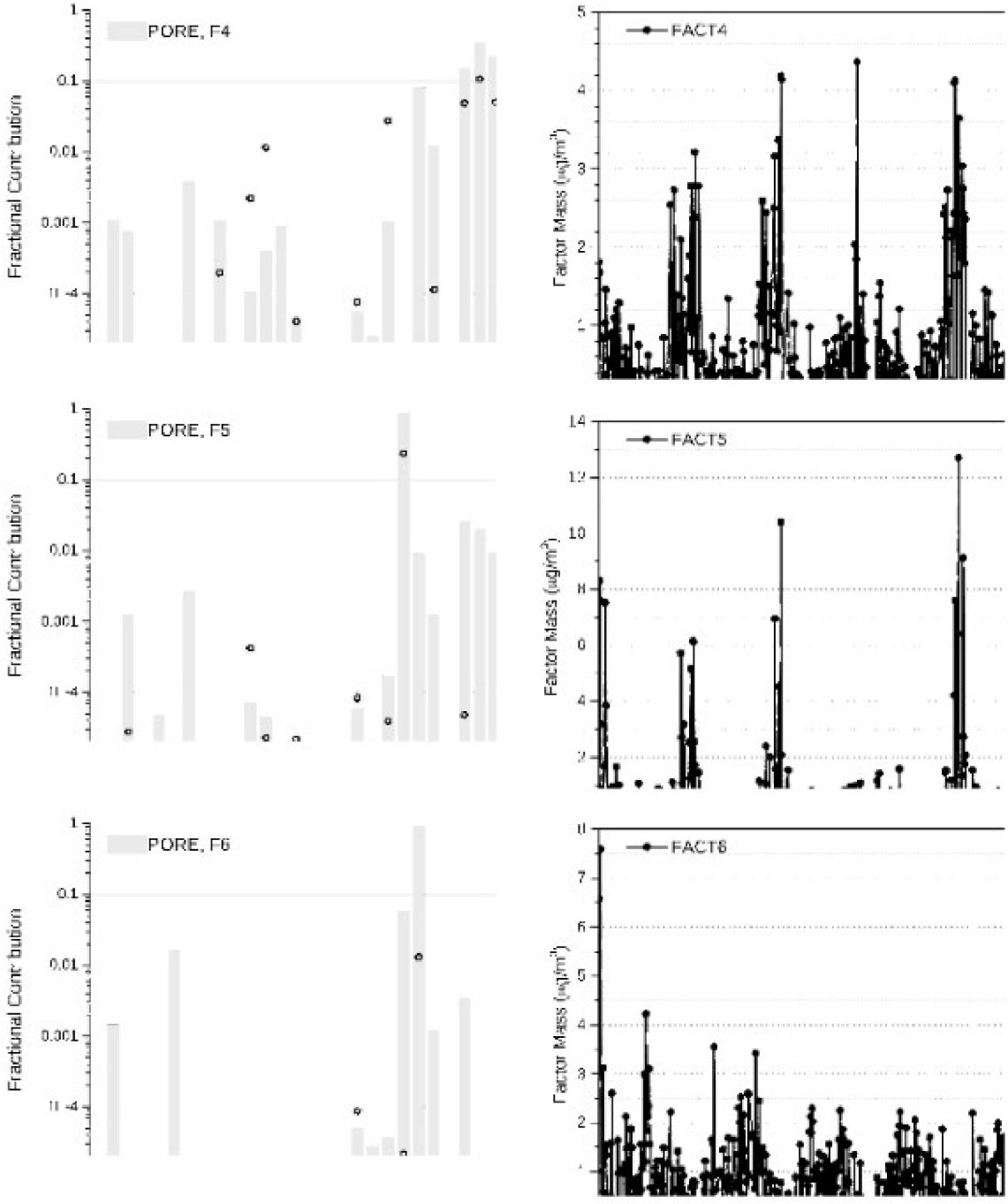

Puget Sound (PUSO) Factors 1 - 3

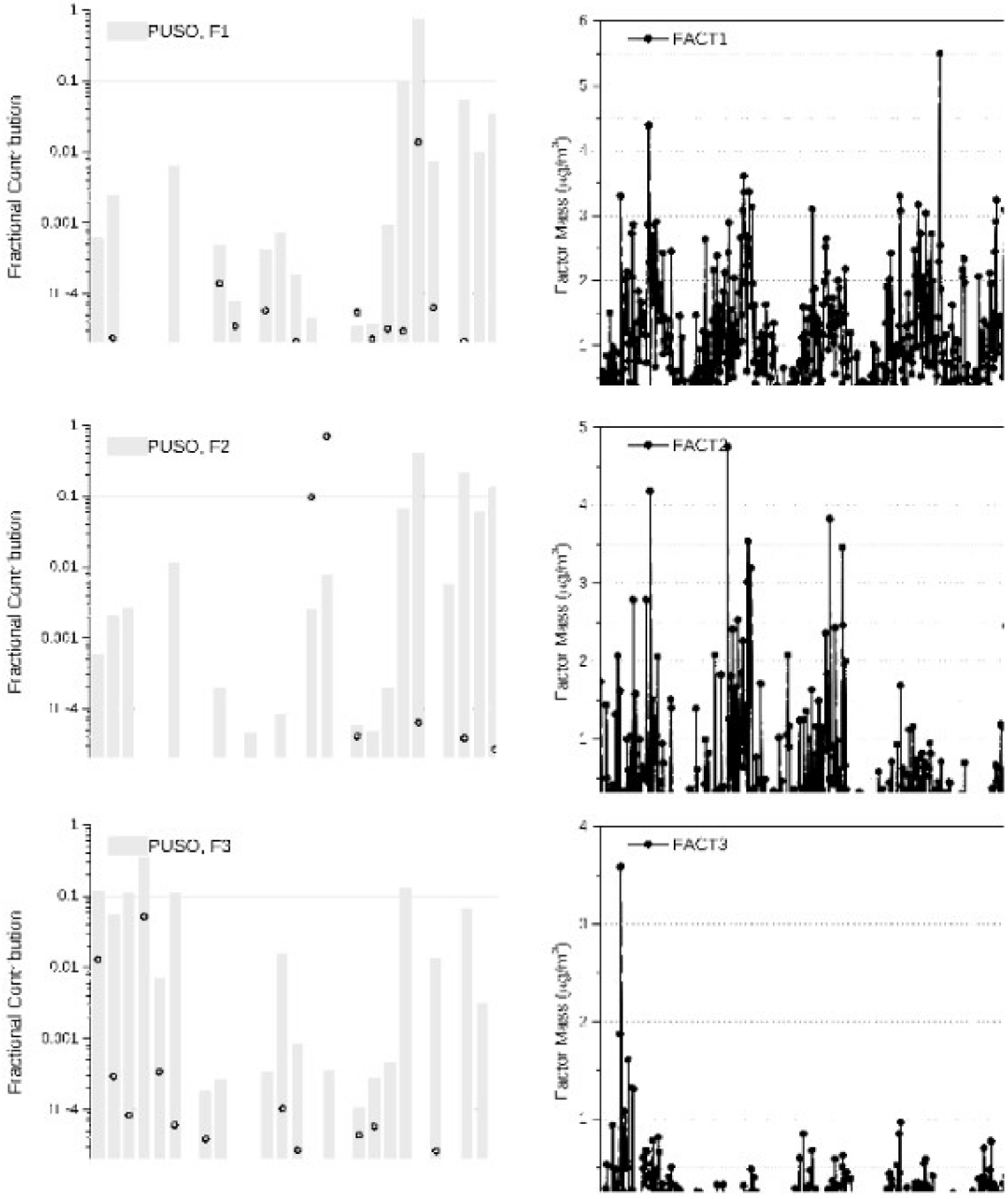

Puget Sound (PUSO) Factors 4 - 6

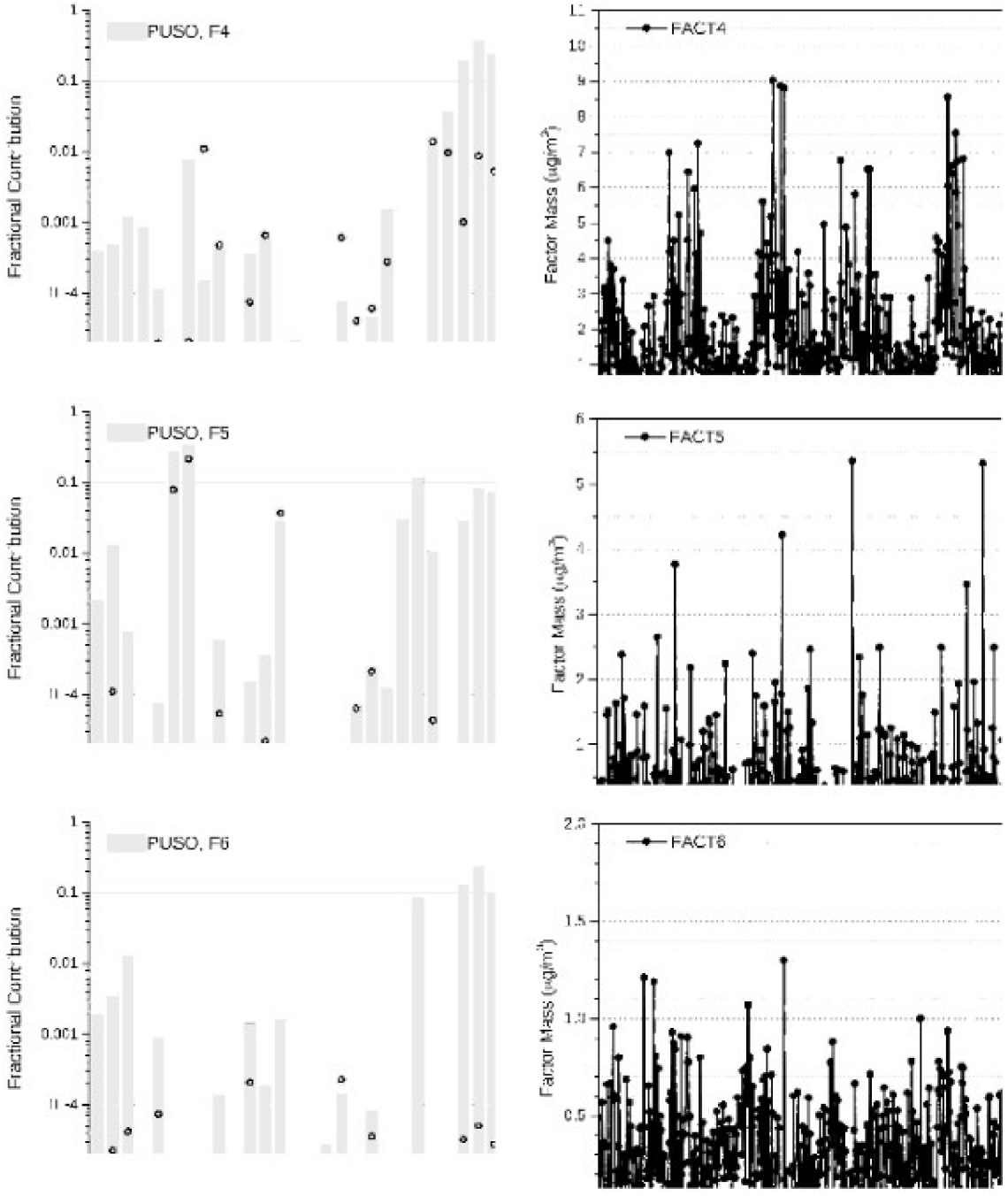

Puget Sound (PUSO) Factor 7 - 8

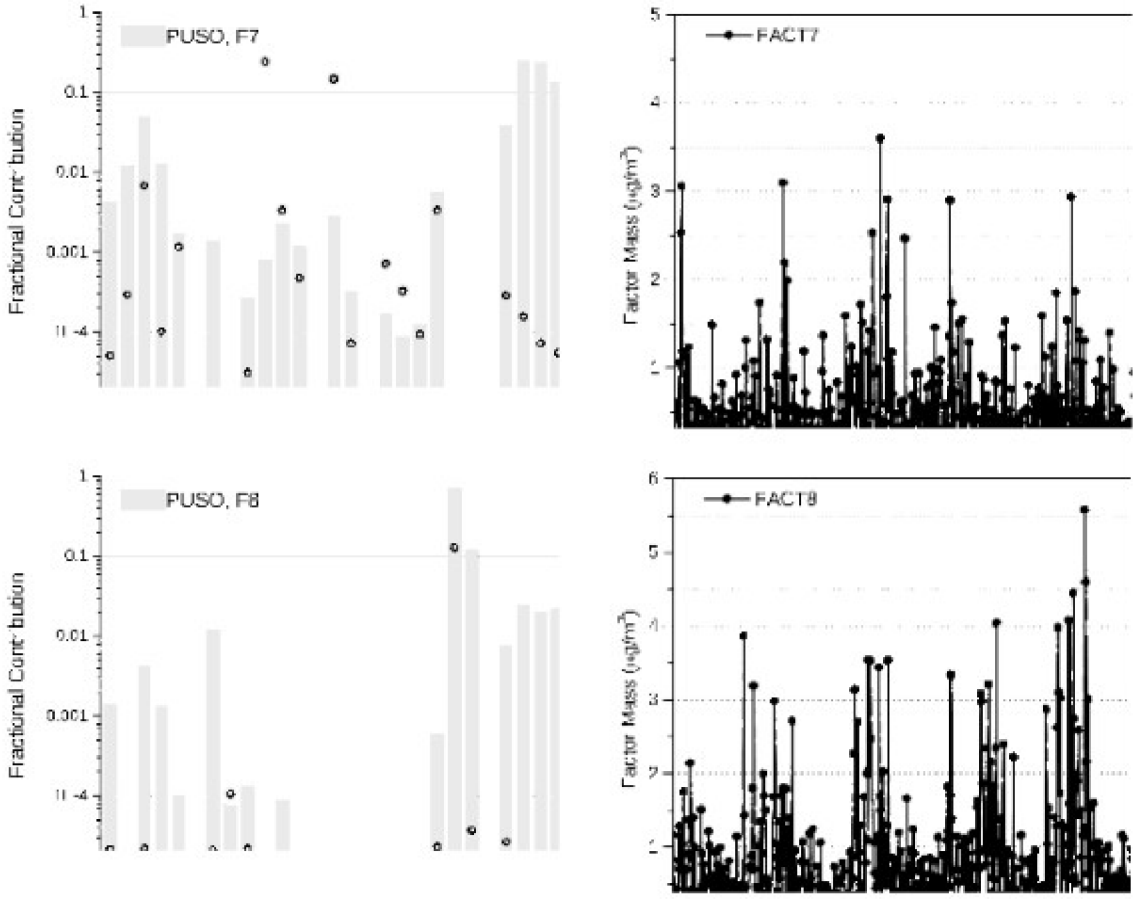

Cape Romain (ROMA) Factors 1 - 3

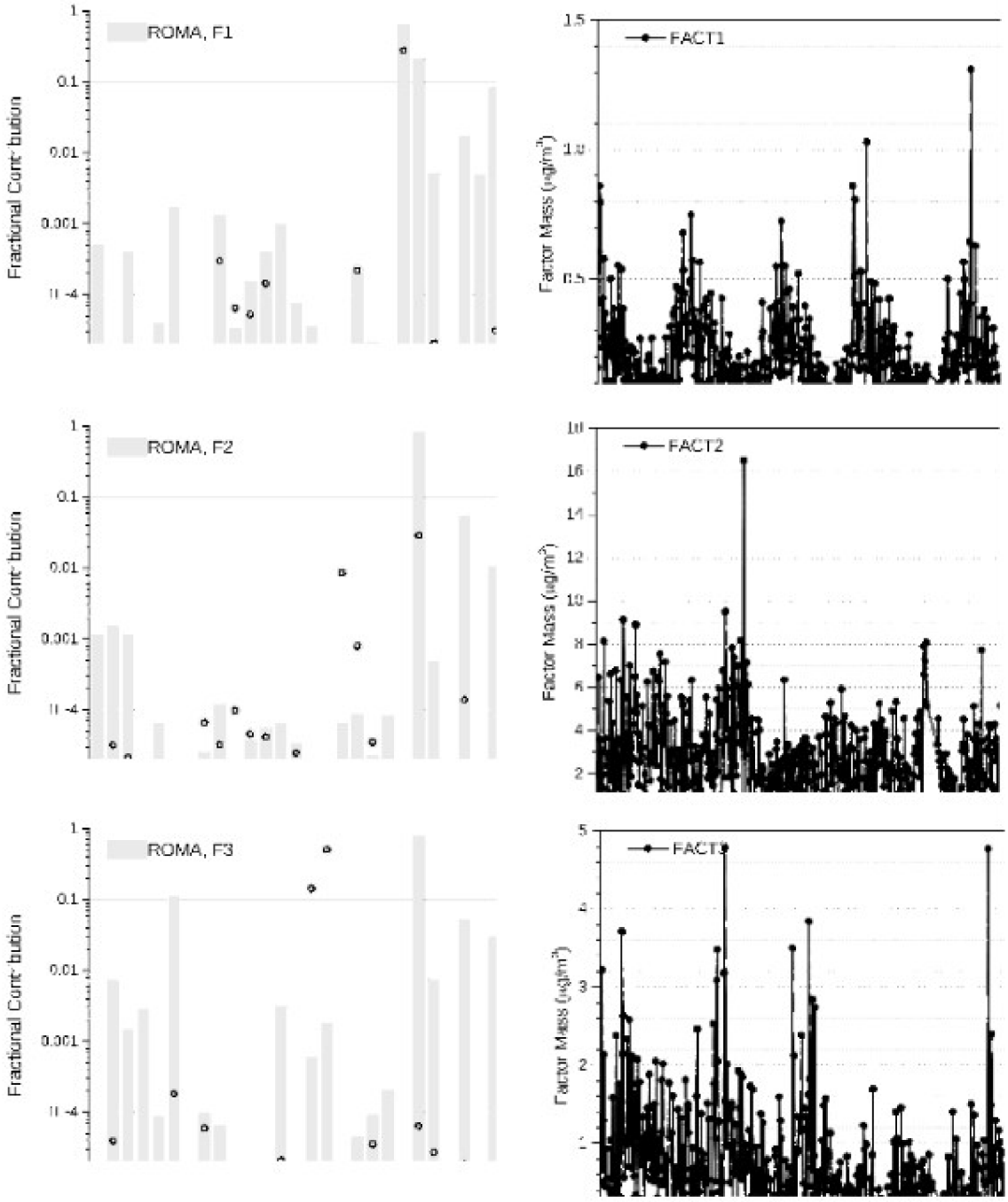

Cape Romain (ROMA) Factors 4 - 6

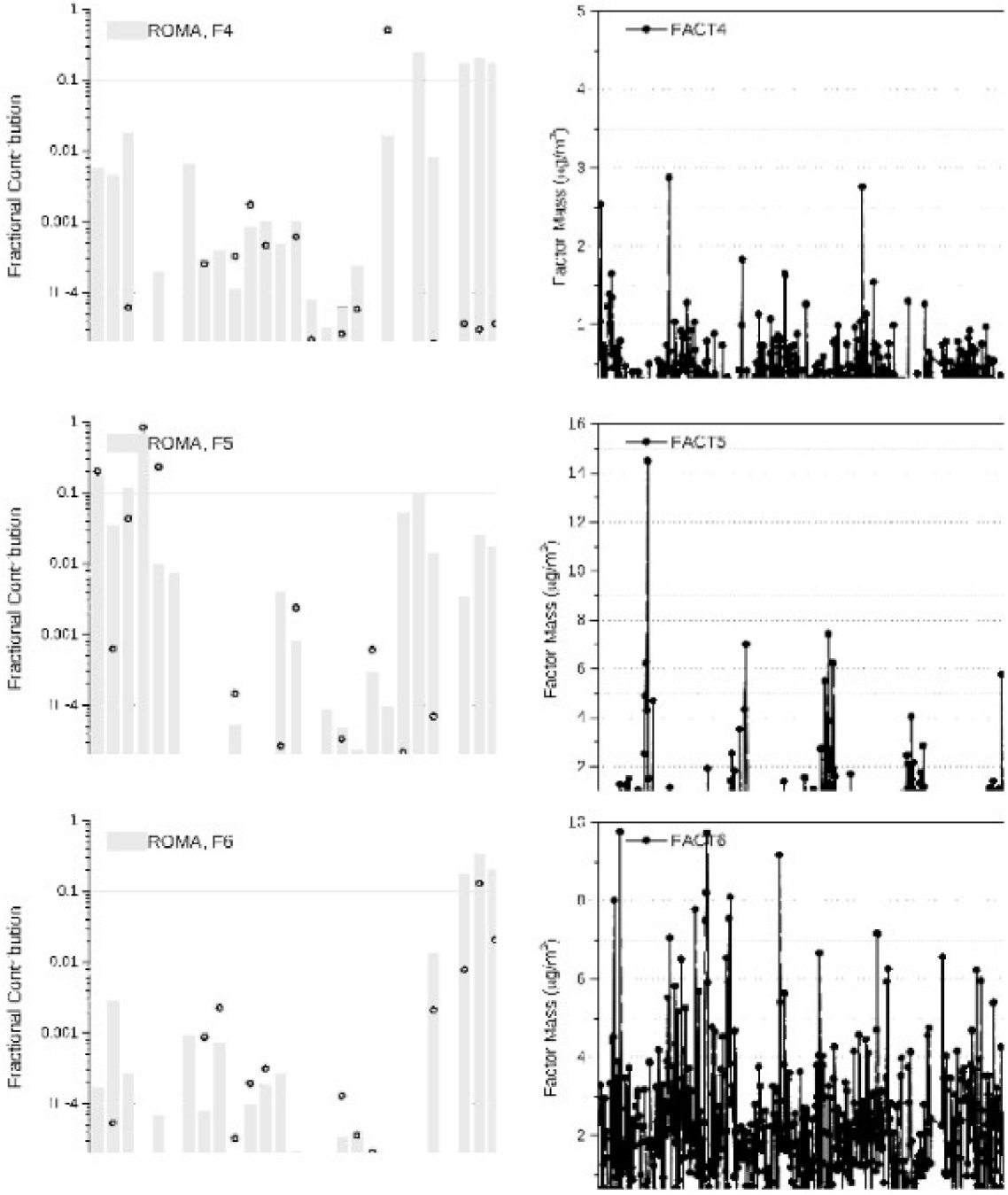

Cape Romain (ROMA) Factor 7

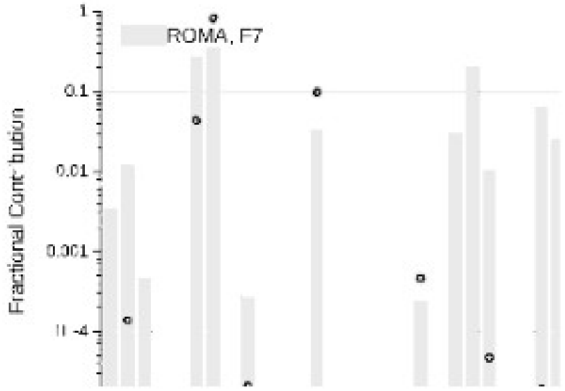

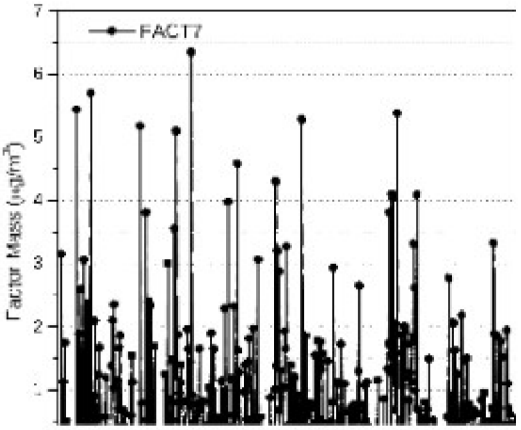

St. Marks (SAMA) Factors 1 - 3

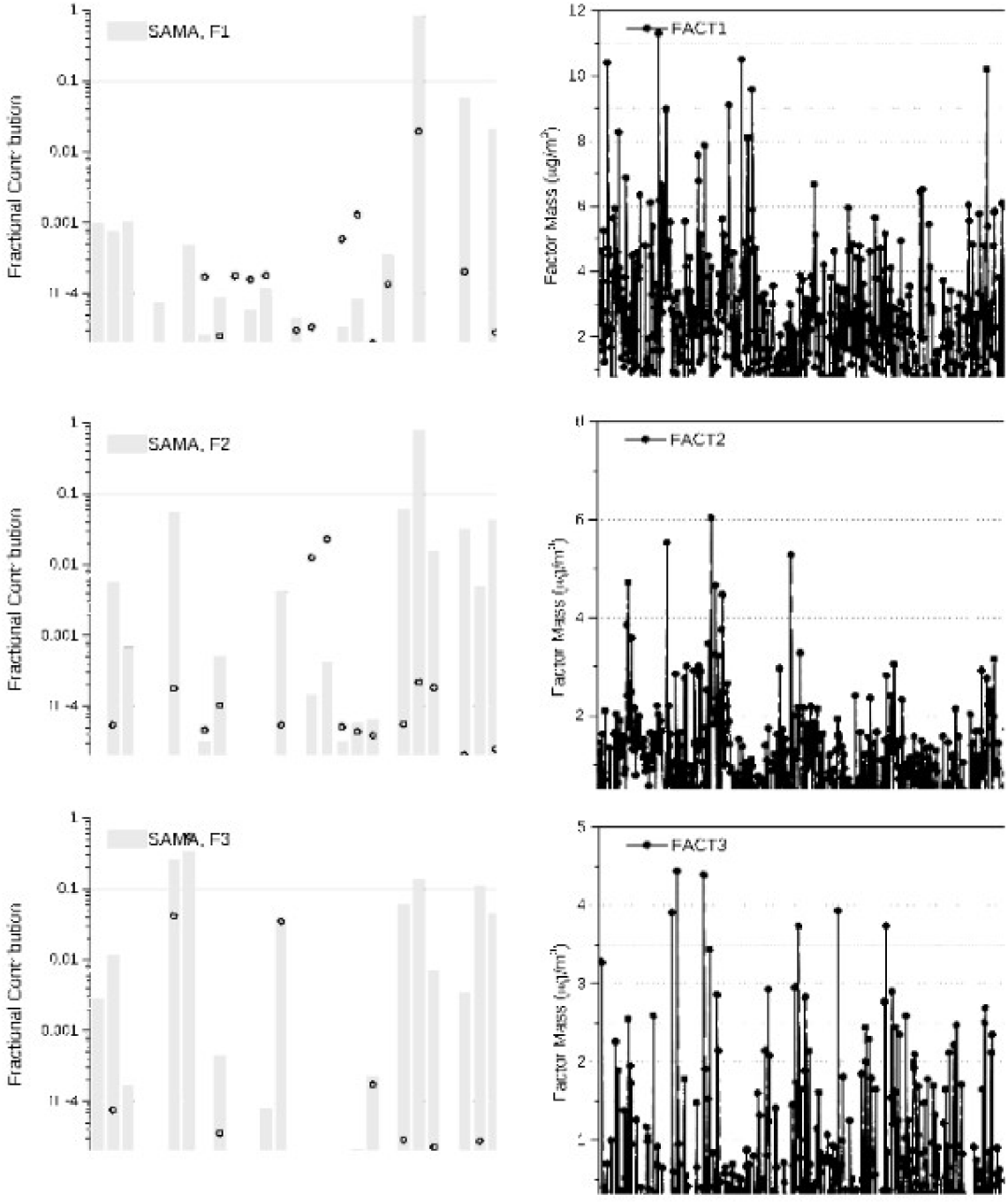

St. Marks (SAMA) Factors 4 - 6

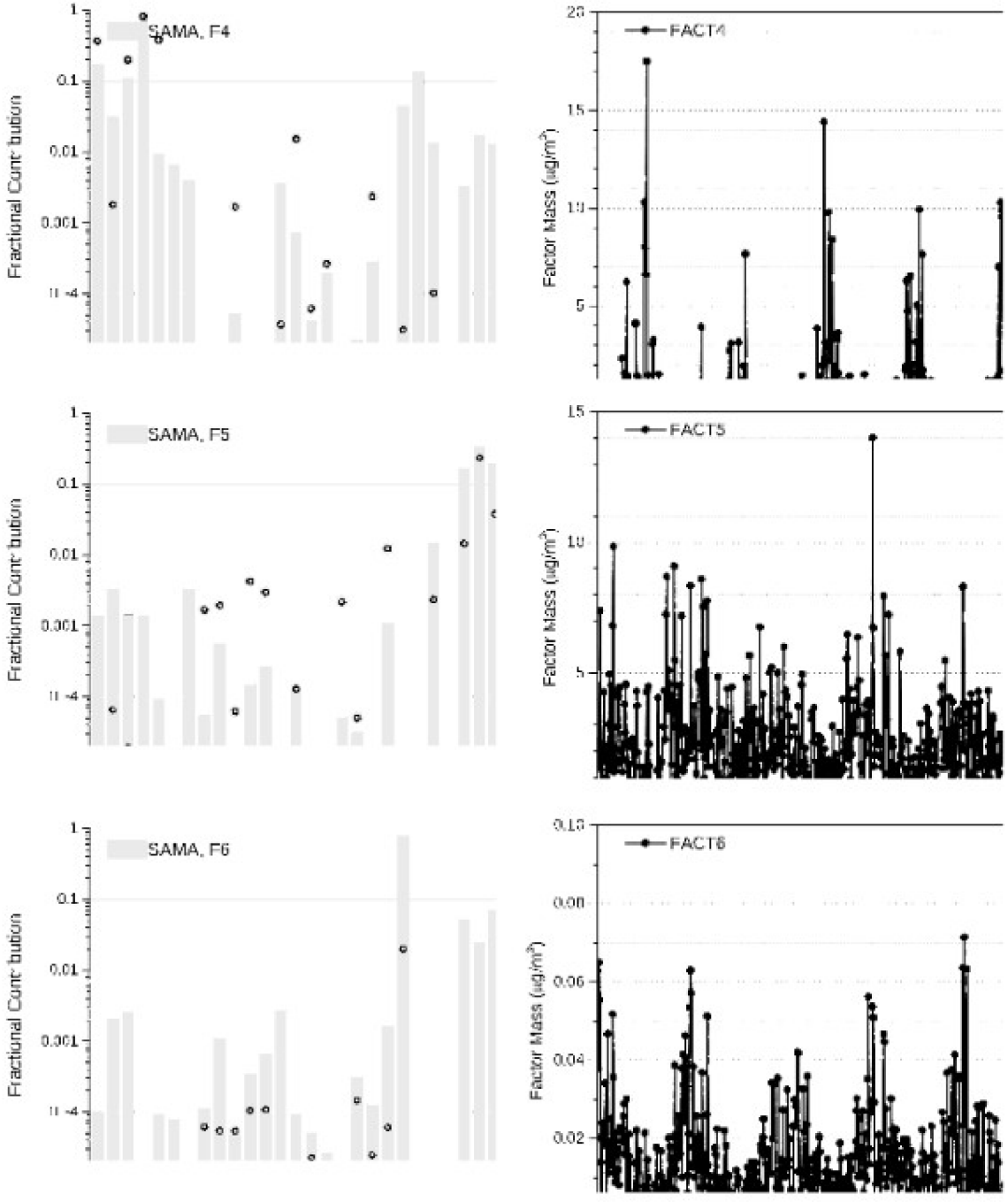

Snoqualmie Pass (SNPA) Factors 1 - 3

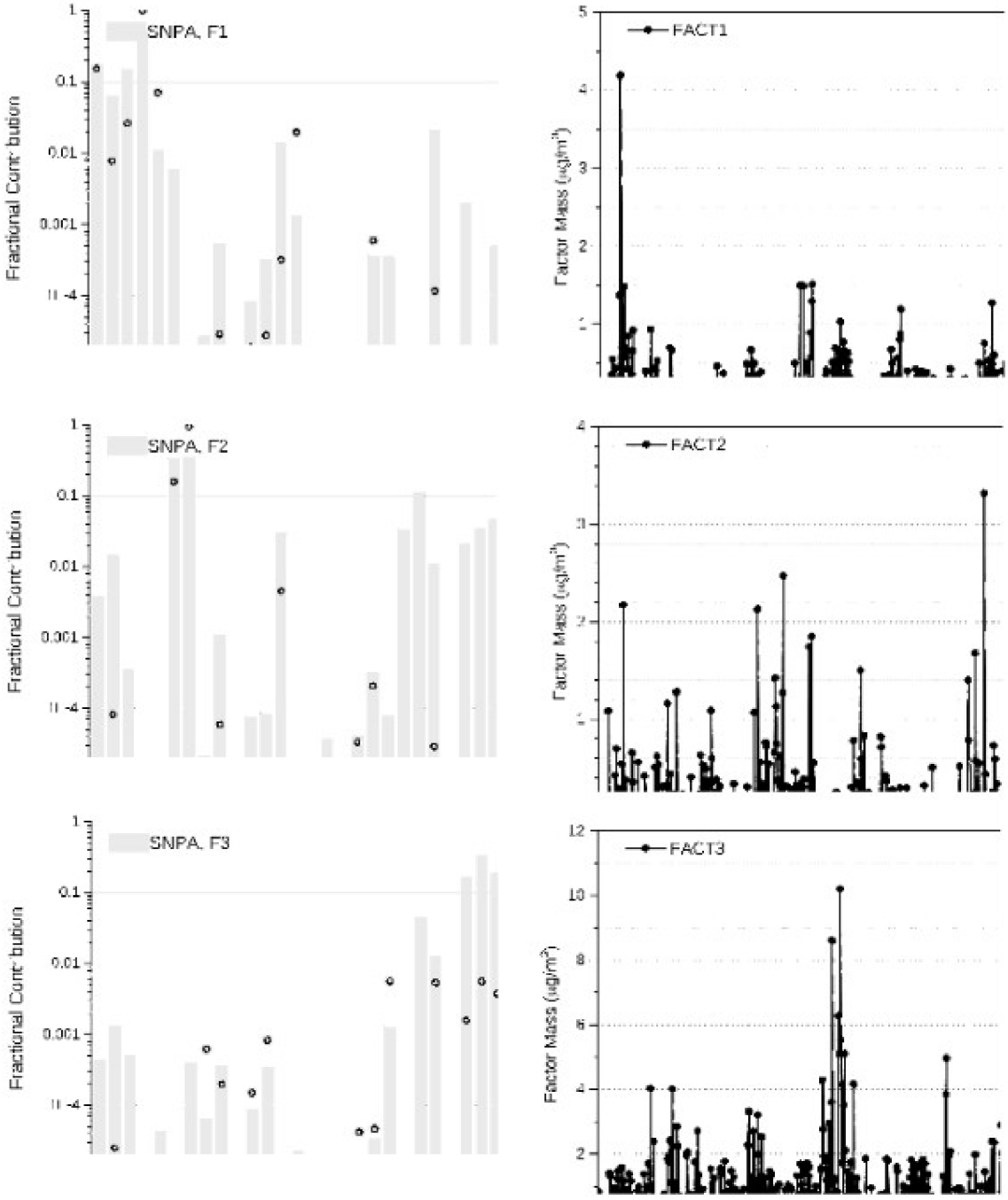

Snoqualmie Pass (SNPA) Factors 4 - 6

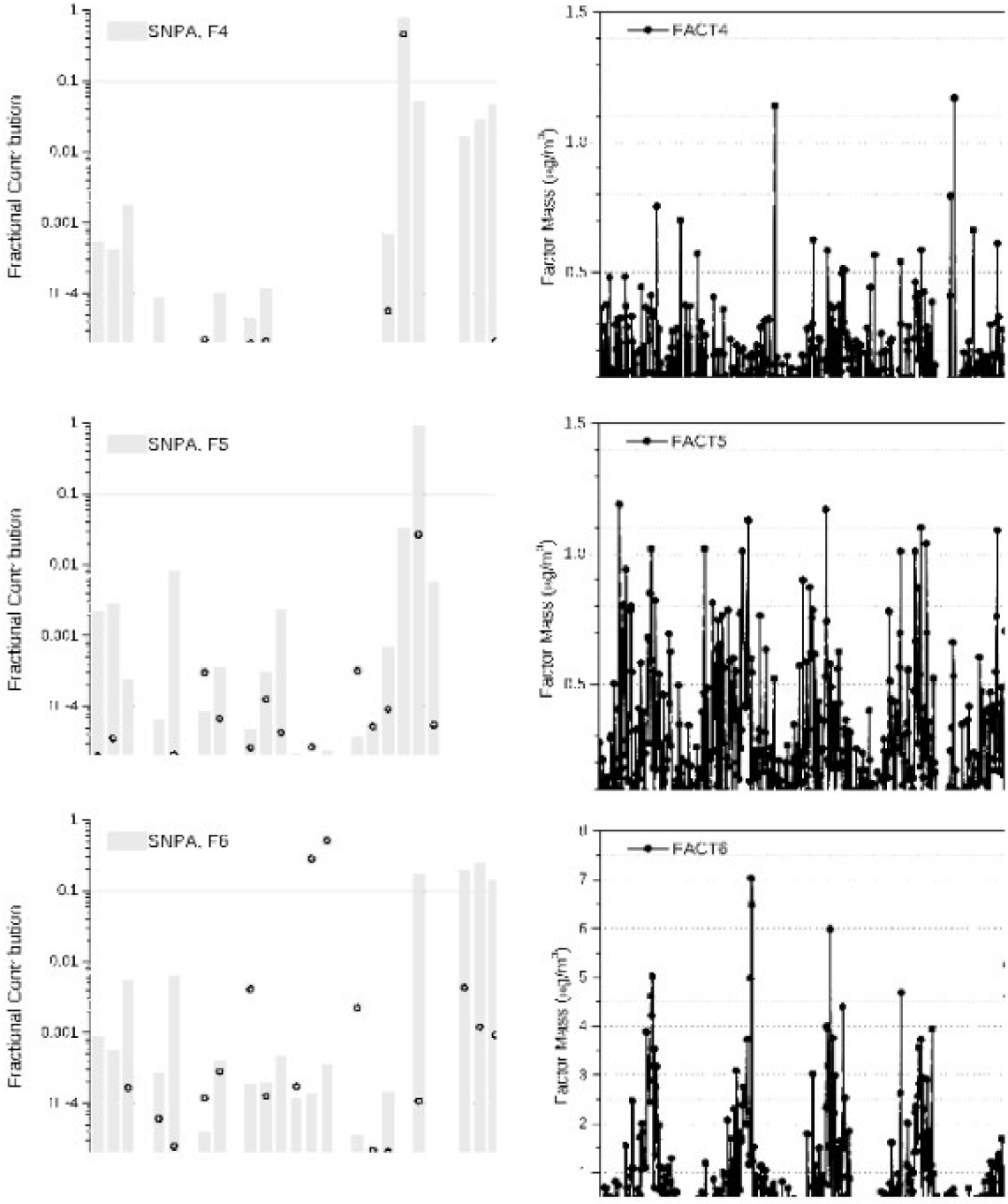

Swanquarter (SWAN) Factors 1 - 3

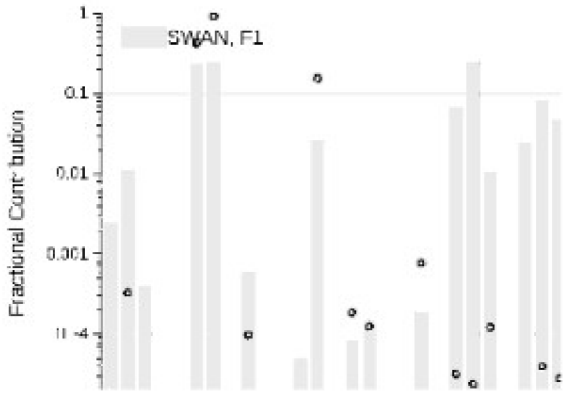

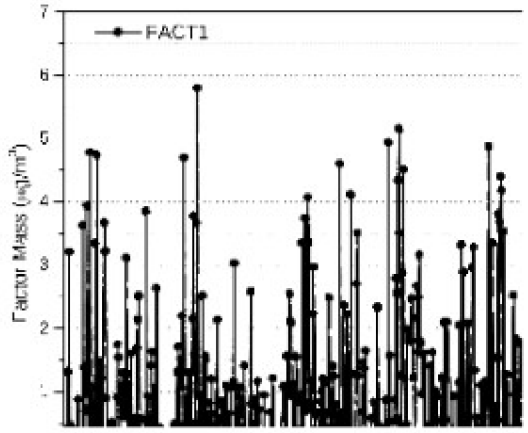

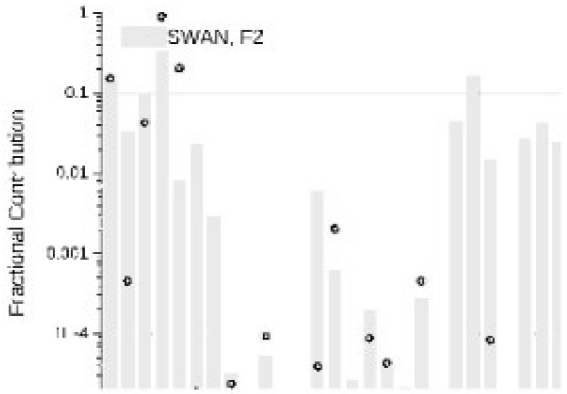

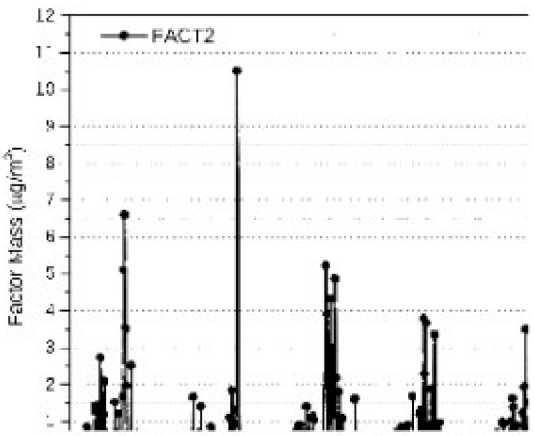

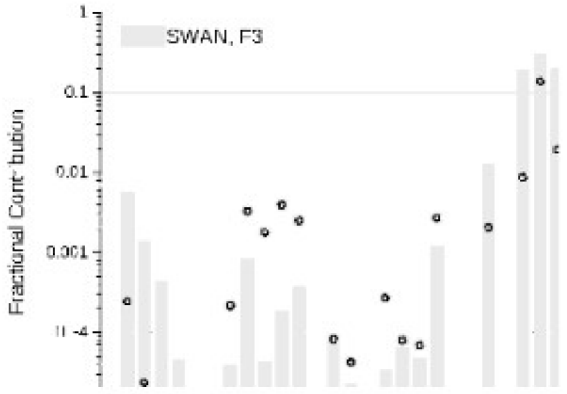

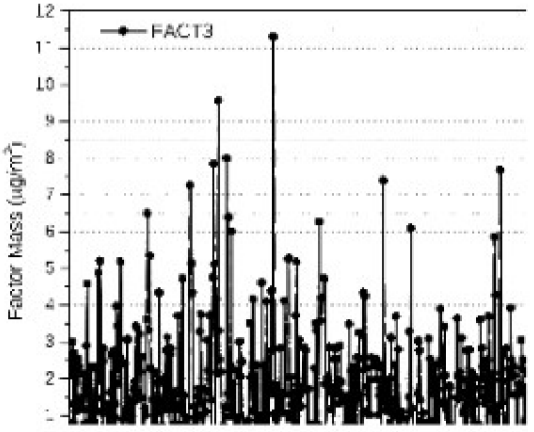

Swanquarter (SWAN) Factors 4 - 5

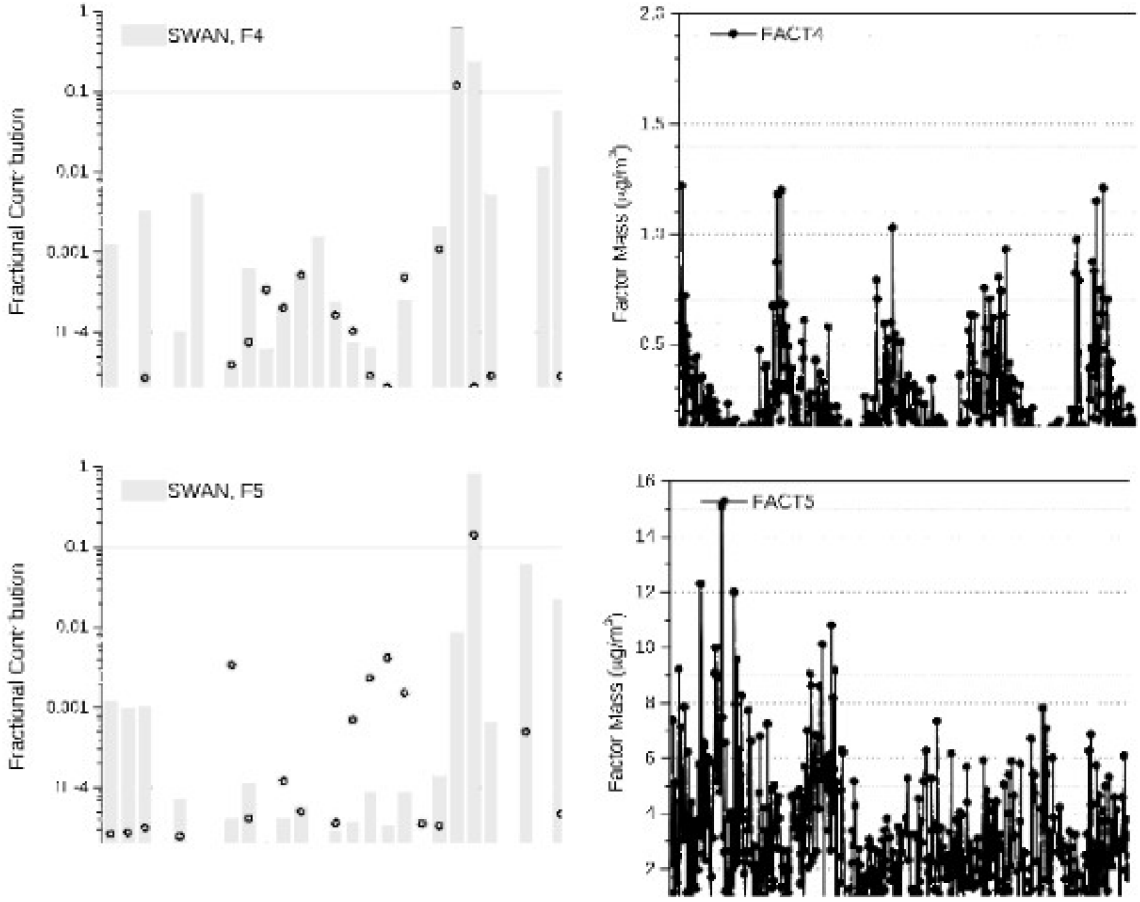

Supplemental Materials Section 7. HYSPLIT back-trajectories for the top 10 V+Ni days in 2010 – 2011 for each of the 22 IMPROVE sites modeled with PMF in this study.

ACAD HYSPLIT back-trajectories

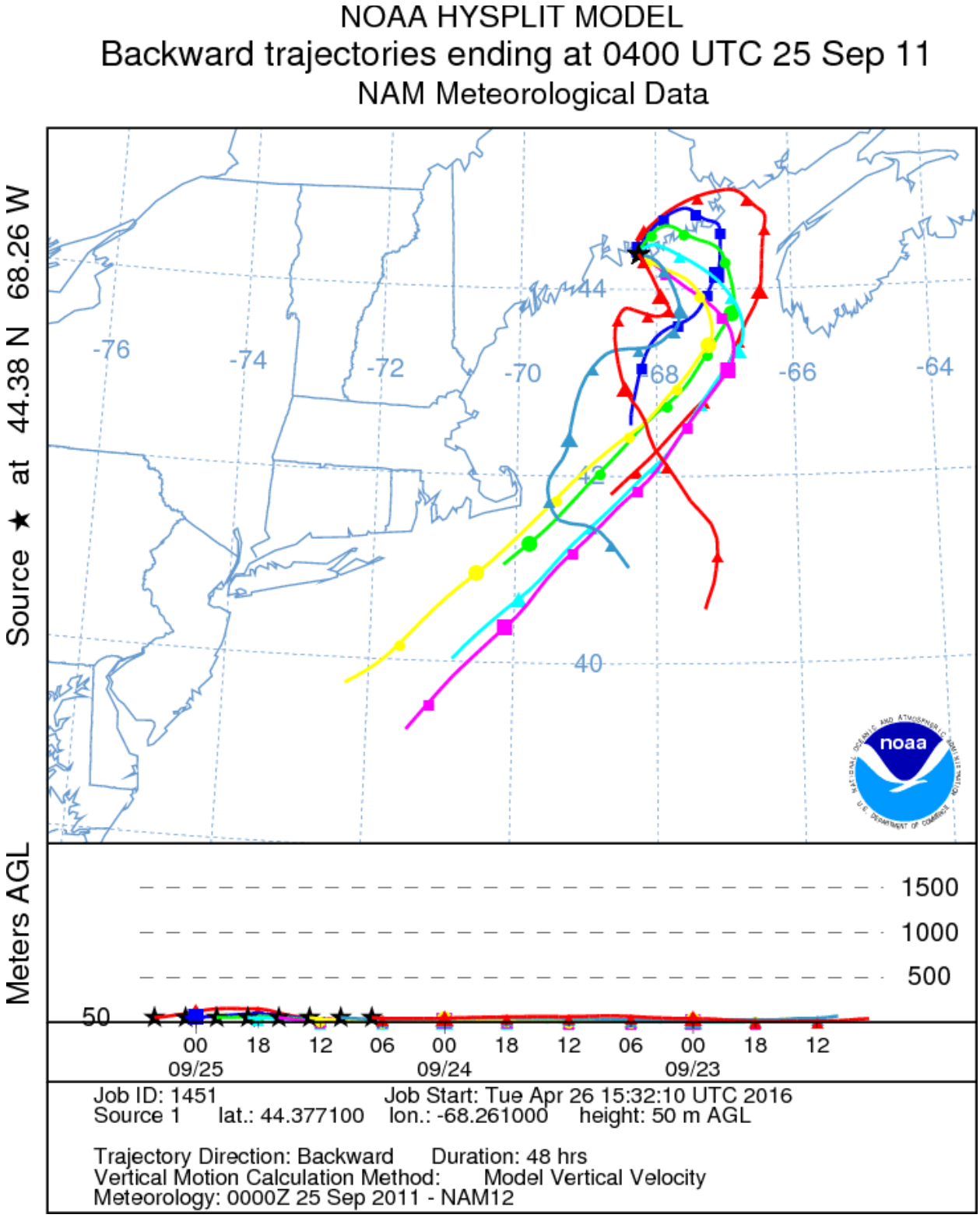
NOAA HYSPLIT MODEL
Backward trajectories ending at 0400 UTC 25 Sep 11
NAM Meteorological Data
Source ★ at 44.38 N 68.26 W
-76
-74
-72
-70
-68
-66
-64
44
42
40
noaa
Meters AGL
1500
1000
500
50
00 18 12 06 00 18 12 06 00 18 12
09/25
09/24
09/23
Job ID: 1451 Job Start: Tue Apr 26 15:32:10 UTC 2016
Source 1 lat.: 44.377100 lon.: -68.261000 height: 50 m AGL
Trajectory Direction: Backward Duration: 48 hrs
Vertical Motion Calculation Method: Model Vertical Velocity
Meteorology: 0000Z 25 Sep 2011 - NAM12

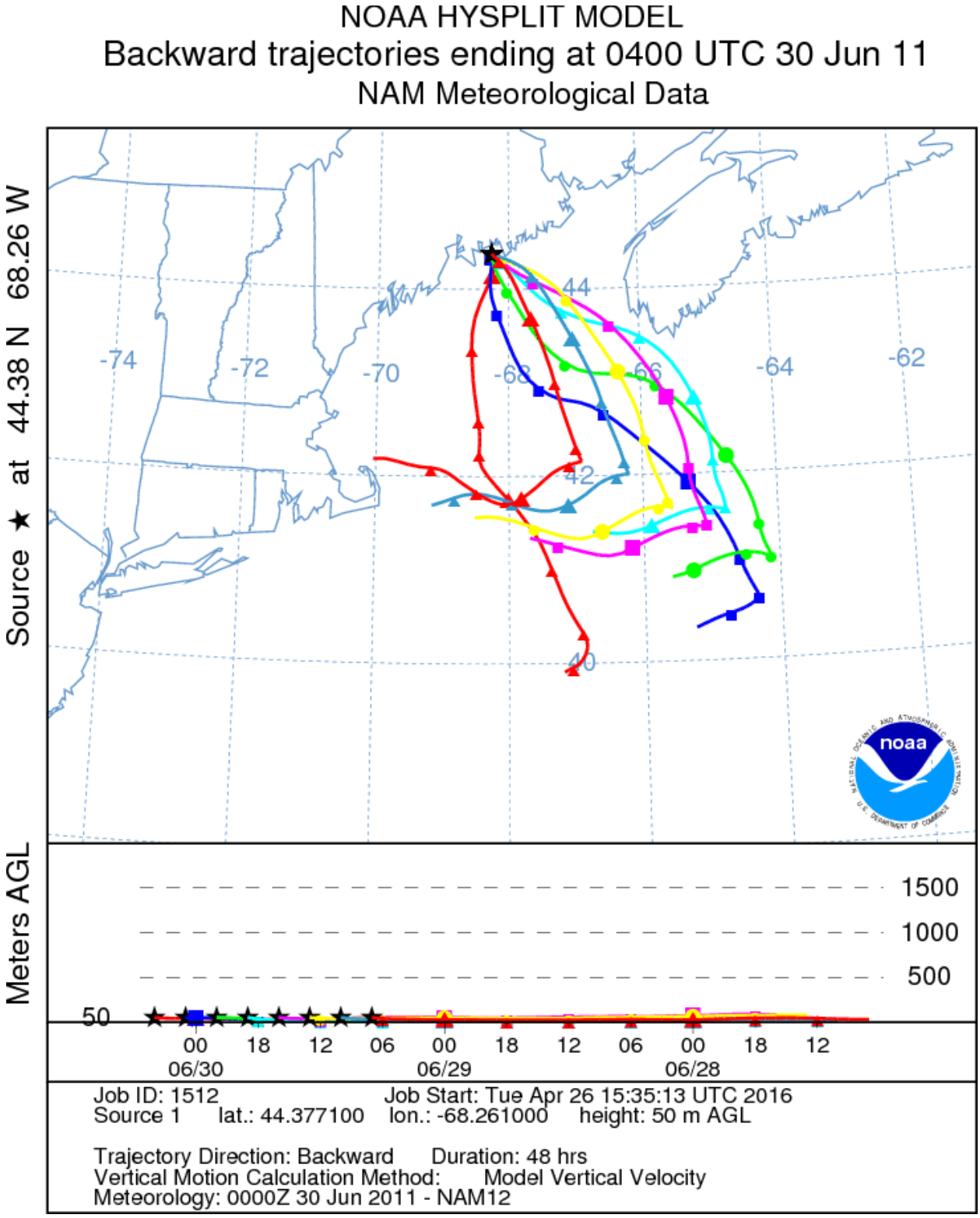
NOAA HYSPLIT MODEL
Backward trajectories ending at 0400 UTC 30 Jun 11
NAM Meteorological Data
Source ★ at 44.38 N 68.26 W
-74
-72
-70
-68
-66
-64
-62
44
42
40
noaa
Meters AGL
1500
1000
500
50
00 18 12 06 00 18 12 06 00 18 12
06/30 06/29 06/28
Job ID: 1512 Job Start: Tue Apr 26 15:35:13 UTC 2016
Source 1 lat.: 44.377100 lon.: -68.261000 height: 50 m AGL
Trajectory Direction: Backward Duration: 48 hrs
Vertical Motion Calculation Method: Model Vertical Velocity
Meteorology: 0000Z 30 Jun 2011 - NAM12

NOAA HYSPLIT MODEL
Backward trajectories ending at 0400 UTC 03 May 10
NAM Meteorological Data

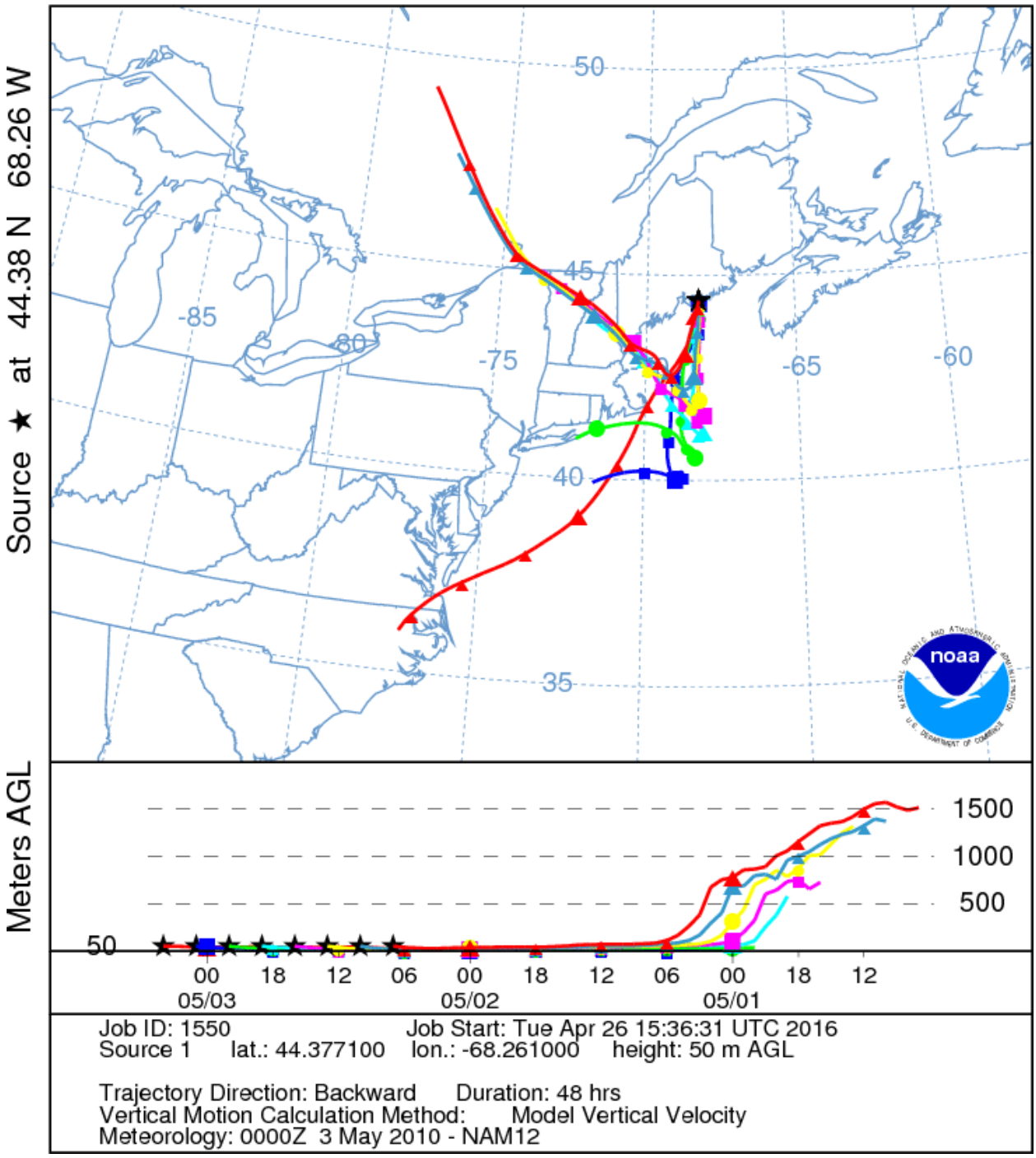

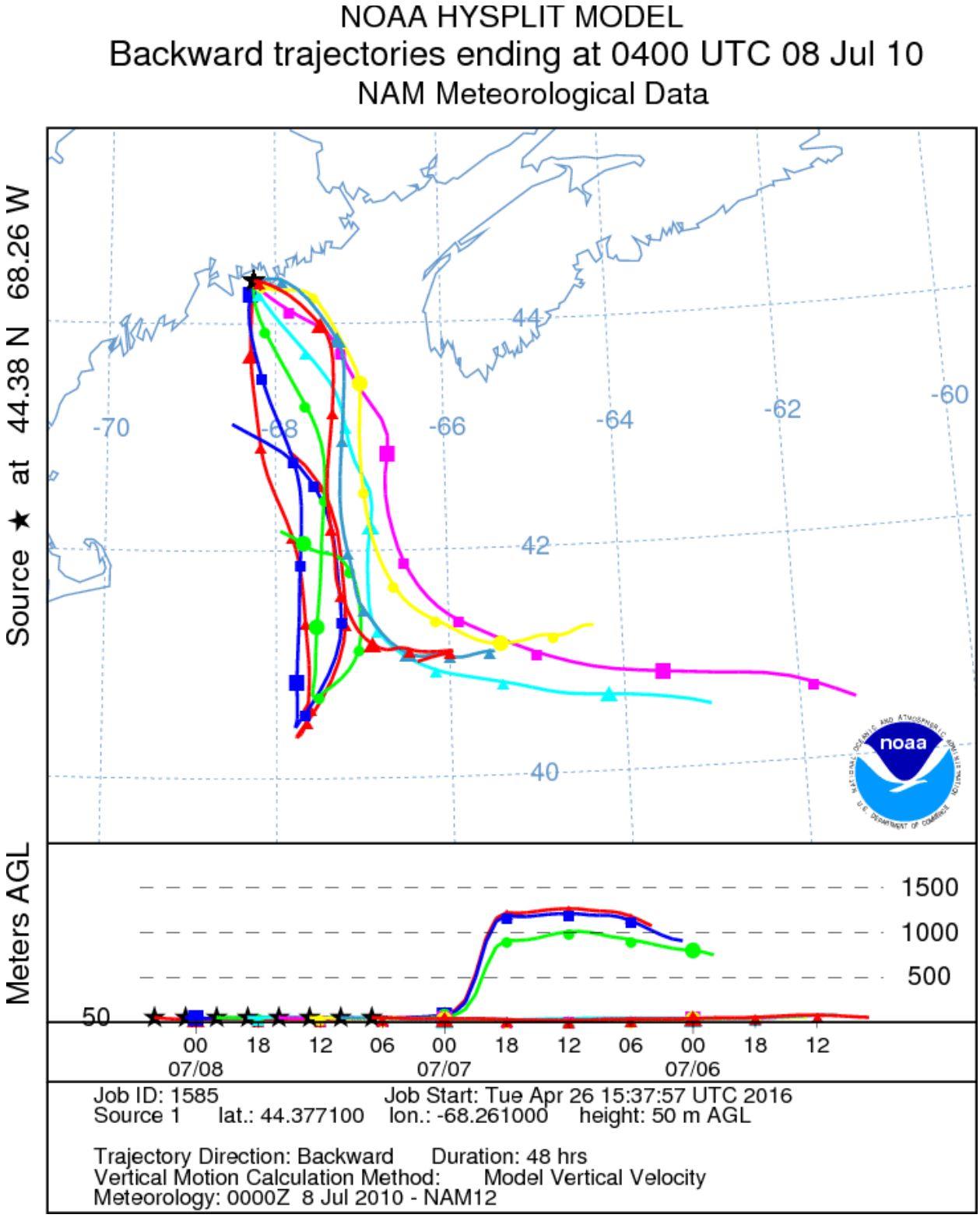
NOAA HYSPLIT MODEL
Backward trajectories ending at 0400 UTC 08 Jul 10
NAM Meteorological Data
Source ★ at 44.38 N 68.26 W
-70
-68
-66
-64
-62
-60
44
42
40
noaa
Meters AGL
1500
1000
500
50
00 18 12 06 00 18 12 06 00 18 12
07/08
07/07
07/06
Job ID: 1585 Job Start: Tue Apr 26 15:37:57 UTC 2016
Source 1 lat.: 44.377100 lon.: -68.261000 height: 50 m AGL
Trajectory Direction: Backward Duration: 48 hrs
Vertical Motion Calculation Method: Model Vertical Velocity
Meteorology: 0000Z 8 Jul 2010 - NAM12

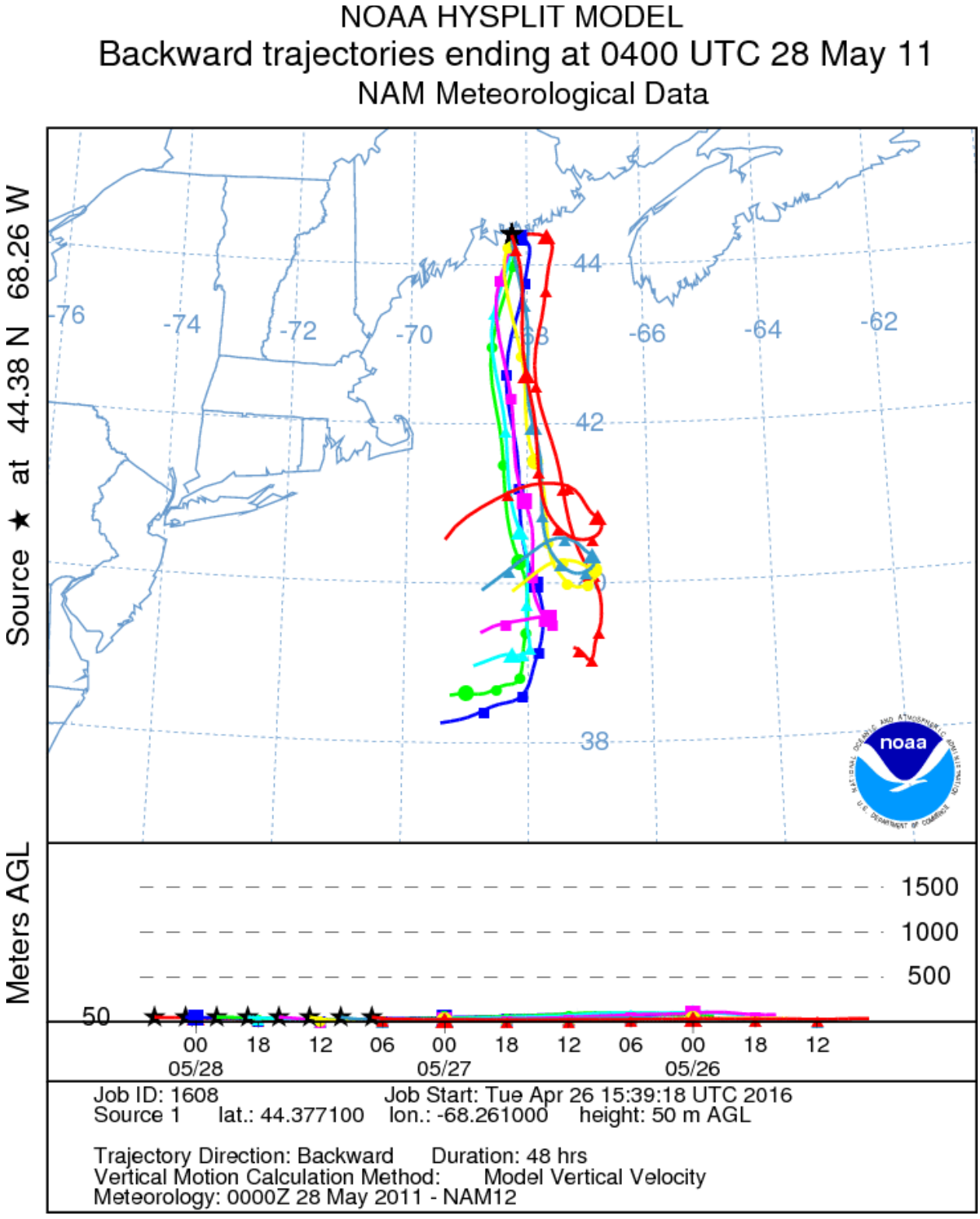
NOAA HYSPLIT MODEL
Backward trajectories ending at 0400 UTC 28 May 11
NAM Meteorological Data
Source ★ at 44.38 N 68.26 W
-76
-74
-72
-70
-66
-64
-62
44
42
38
noaa
Meters AGL
1500
1000
500
50
00 18 12 06 00 18 12 06 00 18 12
05/28
05/27
05/26
Job ID: 1608
Job Start: Tue Apr 26 15:39:18 UTC 2016
Source 1 lat.: 44.377100 lon.: -68.261000 height: 50 m AGL
Trajectory Direction: Backward Duration: 48 hrs
Vertical Motion Calculation Method: Model Vertical Velocity
Meteorology: 0000Z 28 May 2011 - NAM12

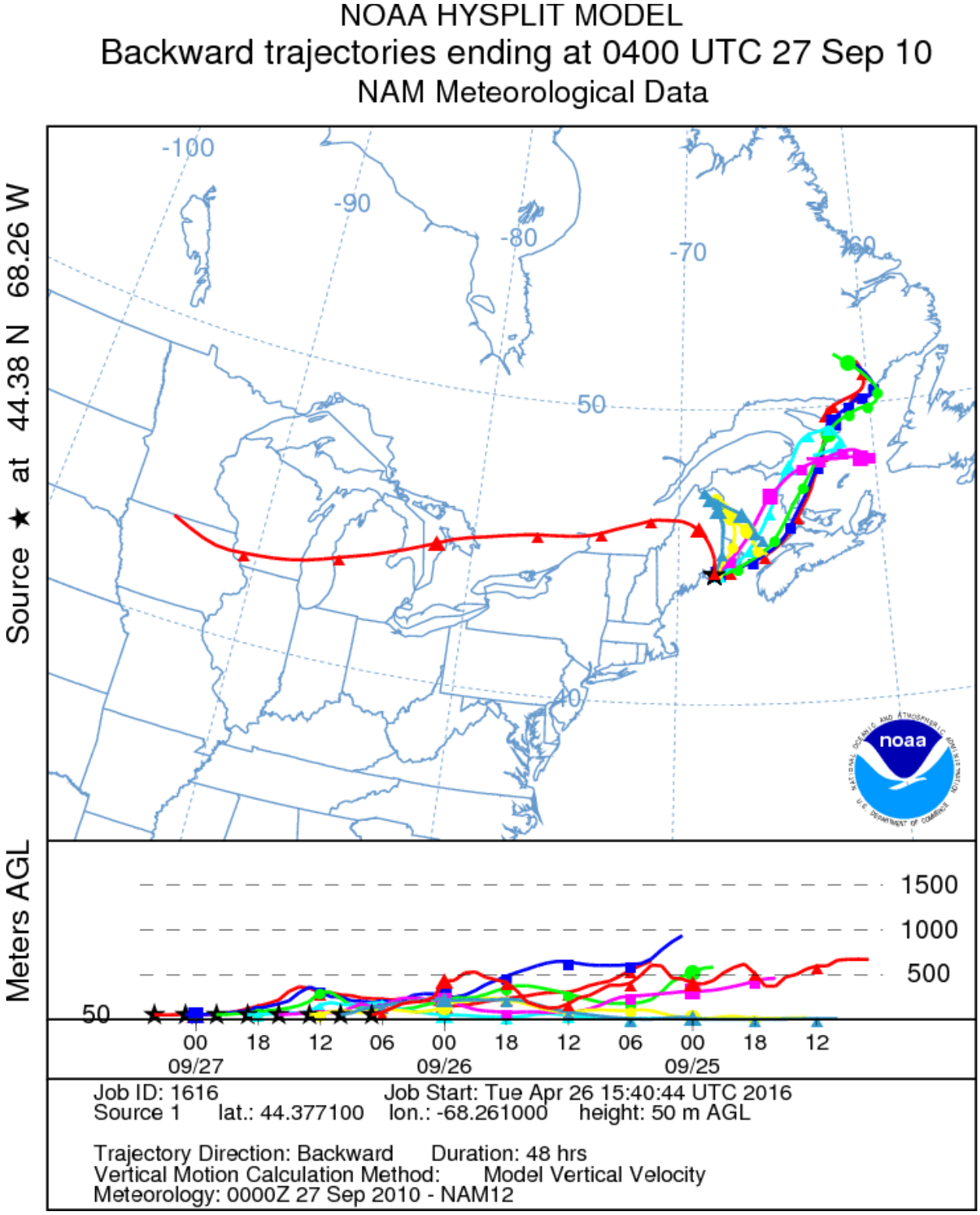
NOAA HYSPLIT MODEL
Backward trajectories ending at 0400 UTC 27 Sep 10
NAM Meteorological Data
Source ★ at 44.38 N 68.26 W
-100
-90
-80
-70
-60
50
40
noaa
Meters AGL
1500
1000
500
50
00 18 12 06 00 18 12 06 00 18 12
09/27 09/26 09/25
Job ID: 1616 Job Start: Tue Apr 26 15:40:44 UTC 2016
Source 1 lat.: 44.377100 lon.: -68.261000 height: 50 m AGL
Trajectory Direction: Backward Duration: 48 hrs
Vertical Motion Calculation Method: Model Vertical Velocity
Meteorology: 0000Z 27 Sep 2010 - NAM12

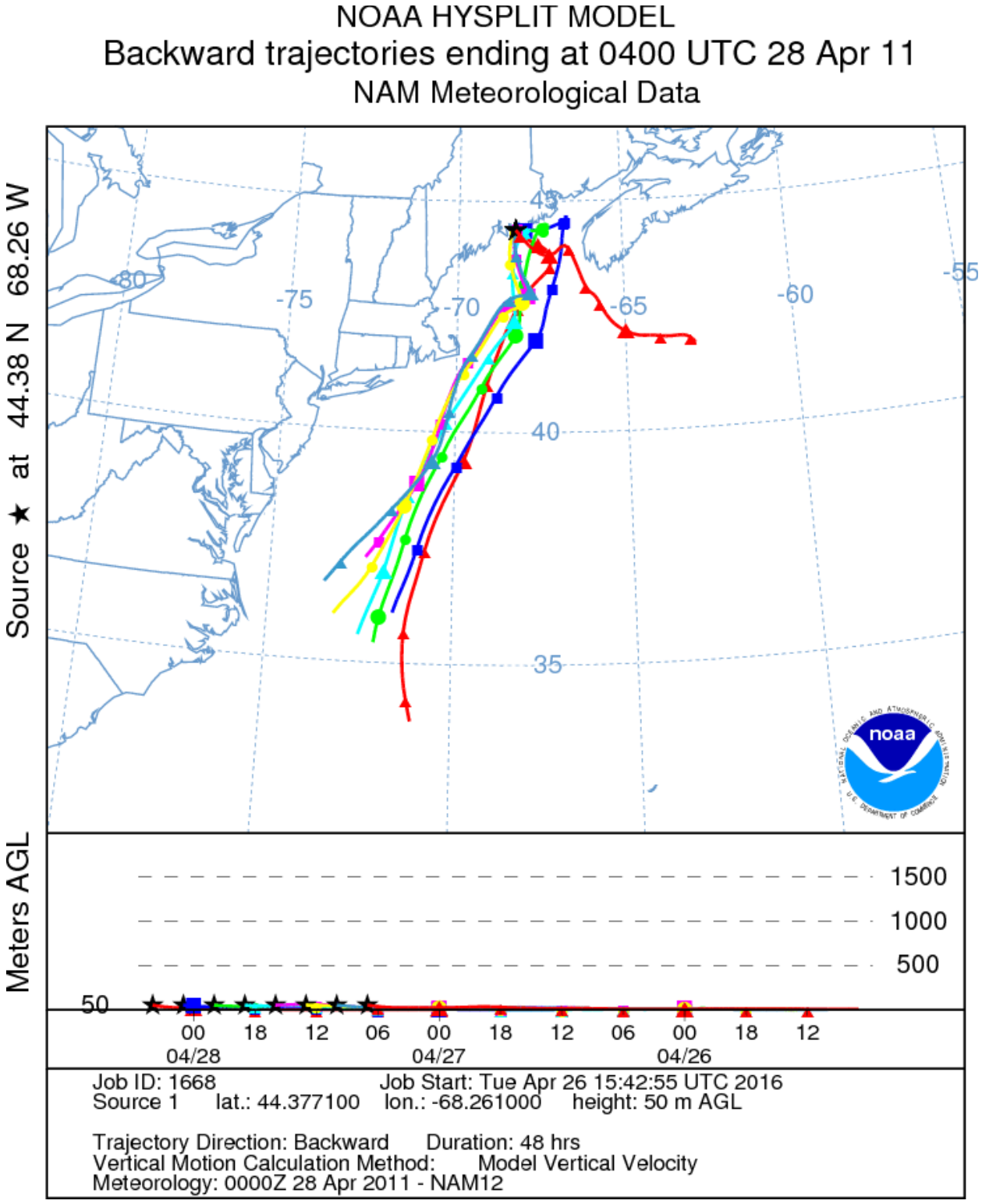
NOAA HYSPLIT MODEL
Backward trajectories ending at 0400 UTC 28 Apr 11
NAM Meteorological Data
Source ★ at 44.38 N 68.26 W
Meters AGL
1500
1000
500
50
00 18 12 06 00 18 12 06 00 18 12
04/28 04/27 04/26
Job ID: 1668 Job Start: Tue Apr 26 15:42:55 UTC 2016
Source 1 lat.: 44.377100 lon.: -68.261000 height: 50 m AGL
Trajectory Direction: Backward Duration: 48 hrs
Vertical Motion Calculation Method: Model Vertical Velocity
Meteorology: 0000Z 28 Apr 2011 - NAM12

NOAA HYSPLIT MODEL
Backward trajectories ending at 0400 UTC 02 Aug 11
NAM Meteorological Data

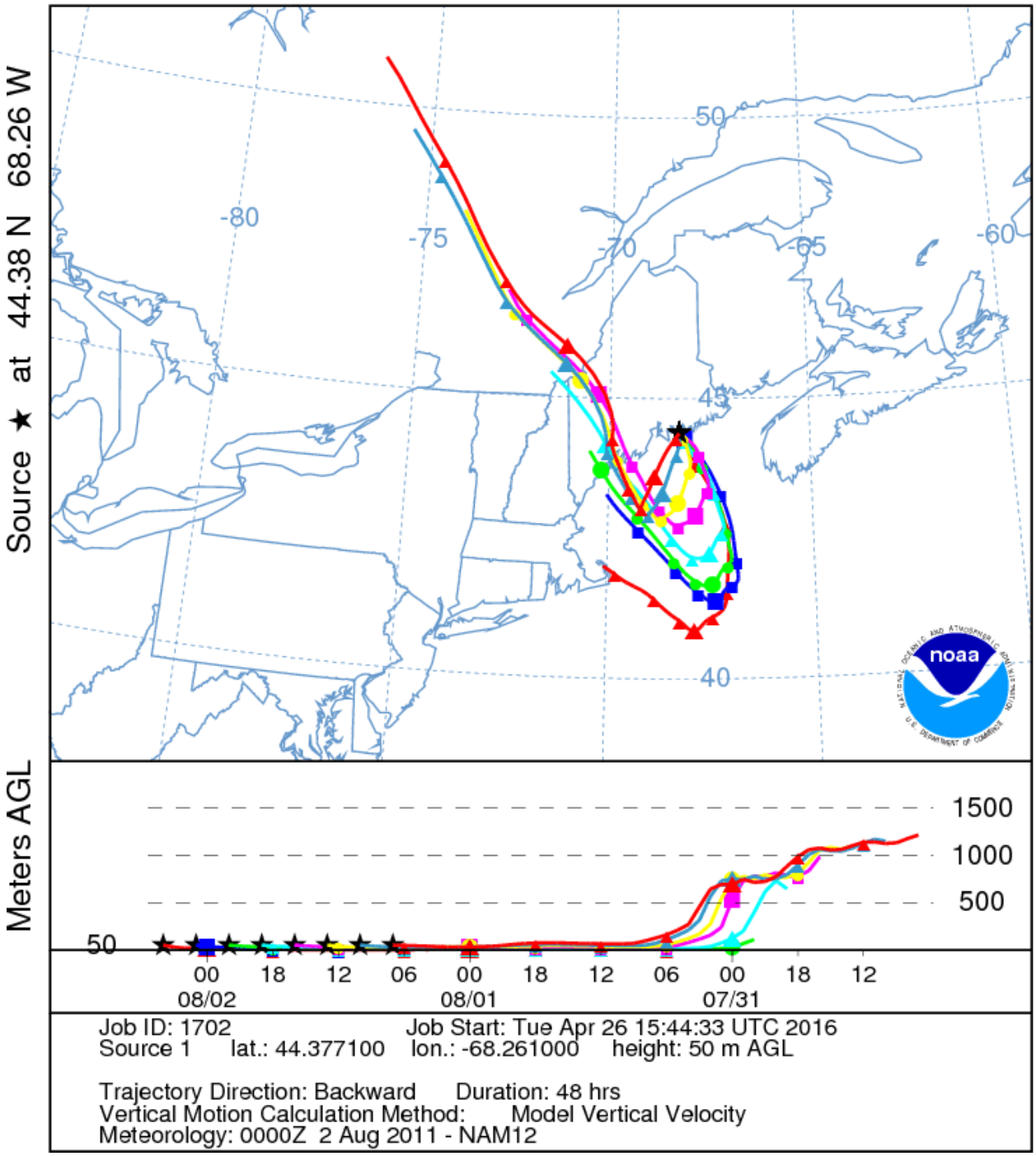

Job ID: 1702 Job Start: Tue Apr 26 15:44:33 UTC 2016
Source 1 lat.: 44.377100 lon.: -68.261000 height: 50 m AGL

Trajectory Direction: Backward Duration: 48 hrs
Vertical Motion Calculation Method: Model Vertical Velocity
Meteorology: 0000Z 2 Aug 2011 - NAM12

NOAA HYSPLIT MODEL
Backward trajectories ending at 0400 UTC 16 Sep 11
NAM Meteorological Data

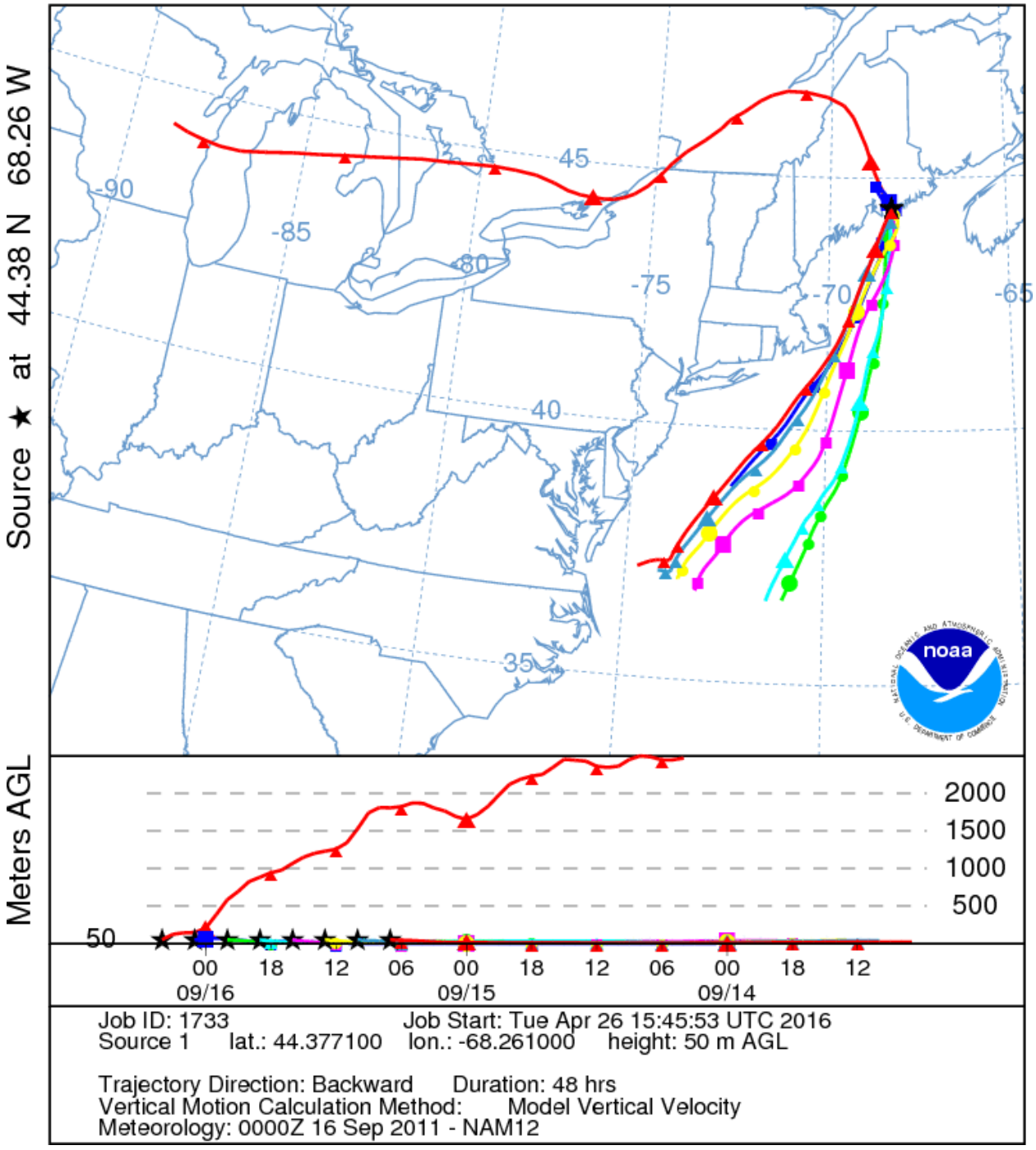

AGTI HYSPLIT back-trajectories

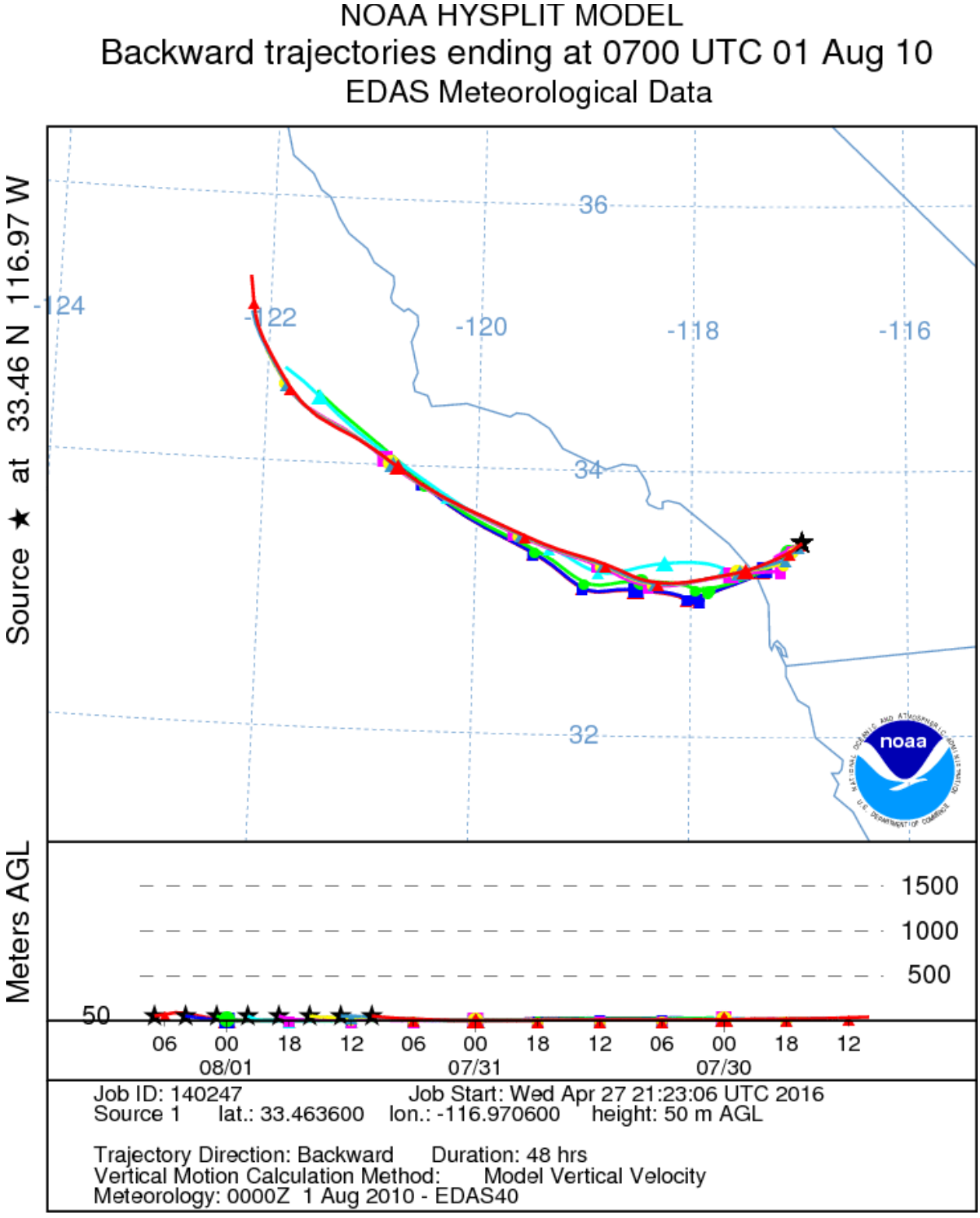
NOAA HYSPLIT MODEL
Backward trajectories ending at 0700 UTC 01 Aug 10
EDAS Meteorological Data
Source ★ at 33.46 N 116.97 W
36
34
32
-124
-122
-120
-118
-116
noaa
Meters AGL
1500
1000
500
50
06 00 18 12 06 00 18 12 06 00 18 12
08/01
07/31
07/30
Job ID: 140247
Job Start: Wed Apr 27 21:23:06 UTC 2016
Source 1 lat.: 33.463600 lon.: -116.970600 height: 50 m AGL
Trajectory Direction: Backward Duration: 48 hrs
Vertical Motion Calculation Method: Model Vertical Velocity
Meteorology: 0000Z 1 Aug 2010 - EDAS40

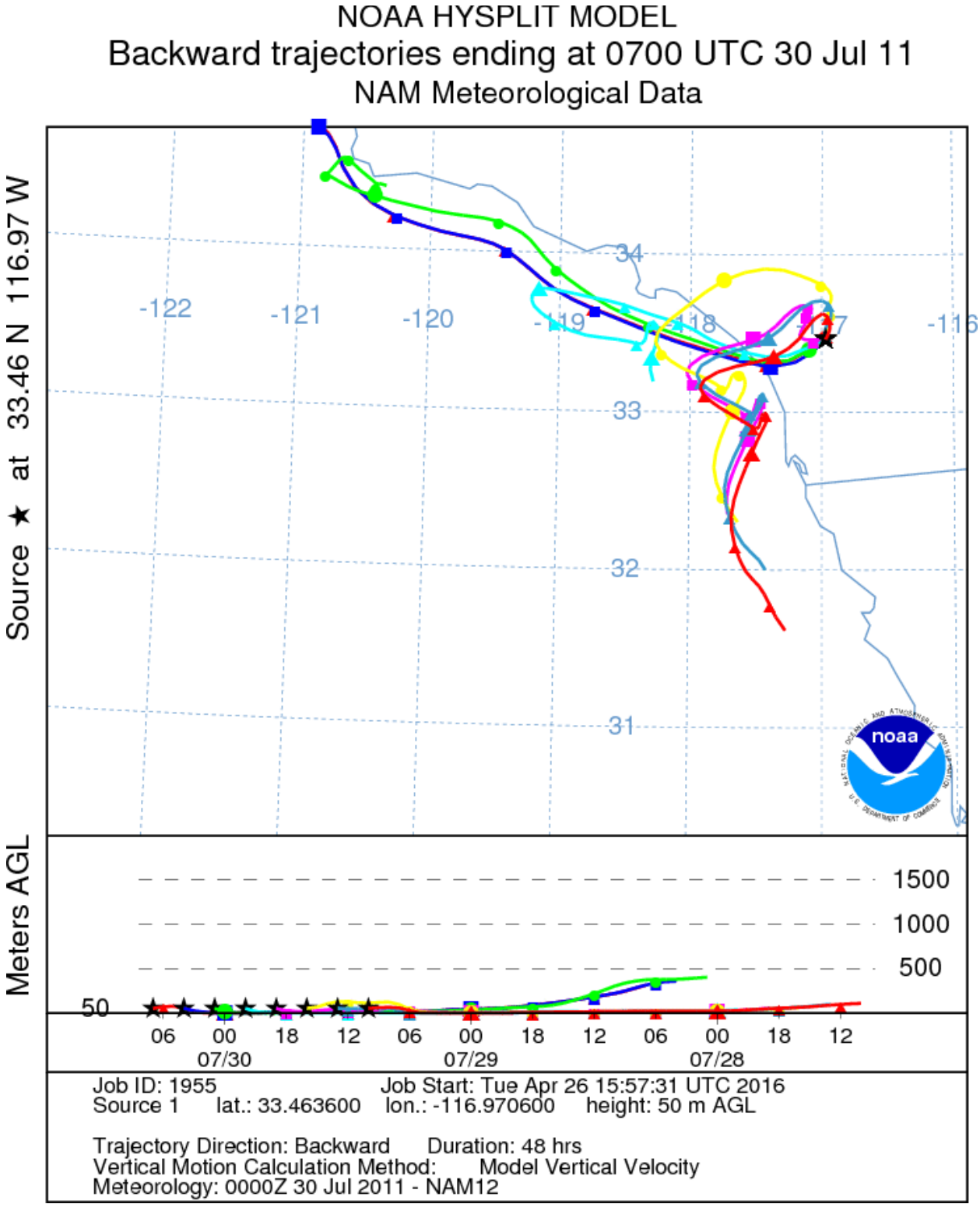
NOAA HYSPLIT MODEL
Backward trajectories ending at 0700 UTC 30 Jul 11
NAM Meteorological Data
Source ★ at 33.46 N 116.97 W
-122
-121
-120
-119
-118
-117
-116
34
33
32
31
noaa
Meters AGL
1500
1000
500
50
06 00 18 12 06 00 18 12 06 00 18 12
07/30
07/29
07/28
Job ID: 1955
Job Start: Tue Apr 26 15:57:31 UTC 2016
Source 1 lat.: 33.463600 lon.: -116.970600 height: 50 m AGL
Trajectory Direction: Backward Duration: 48 hrs
Vertical Motion Calculation Method: Model Vertical Velocity
Meteorology: 0000Z 30 Jul 2011 - NAM12

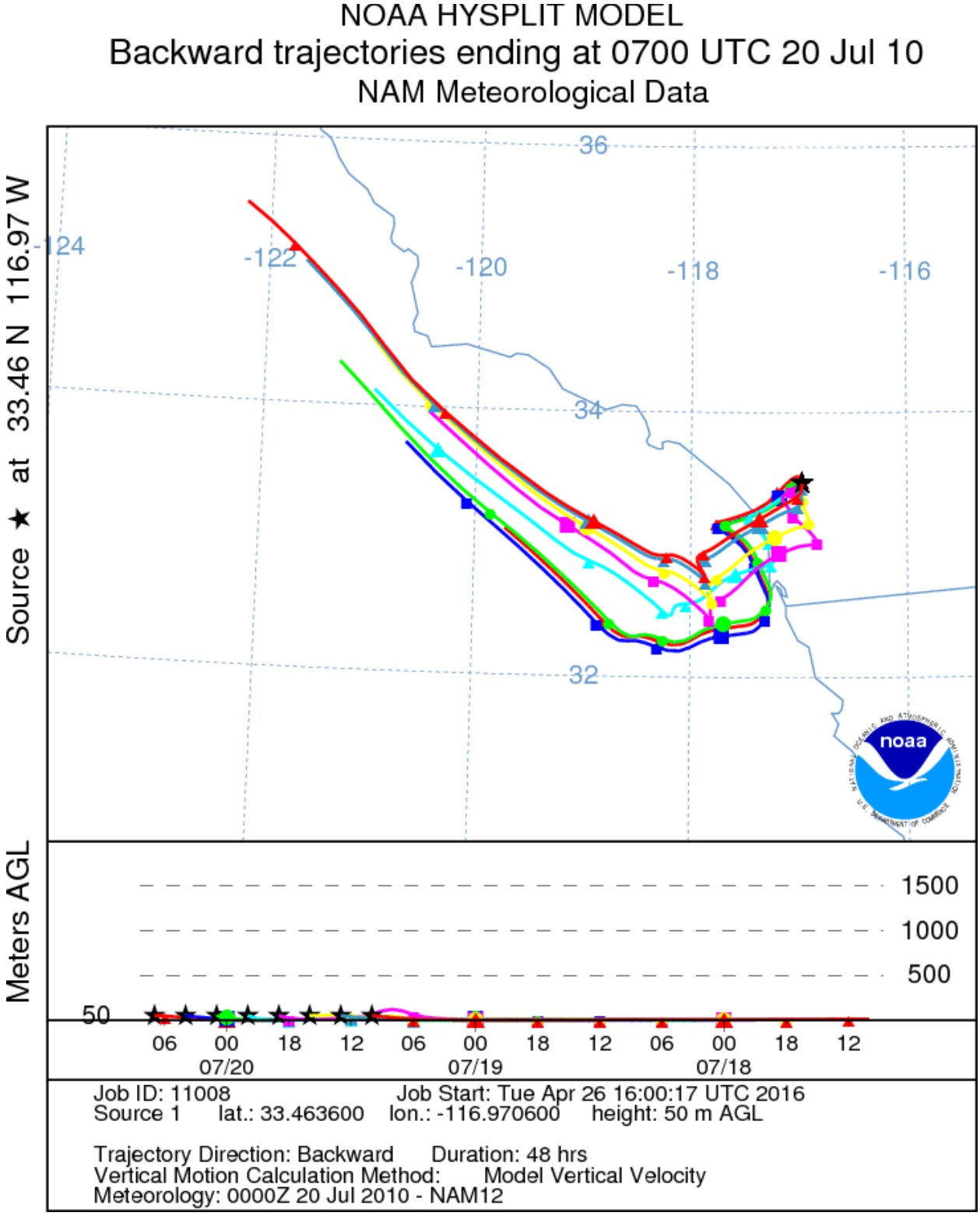
NOAA HYSPLIT MODEL
Backward trajectories ending at 0700 UTC 20 Jul 10
NAM Meteorological Data
Source ★ at 33.46 N 116.97 W
36
34
32
-124
-122
-120
-118
-116
noaa
Meters AGL
1500
1000
500
50
06 00 18 12 06 00 18 12 06 00 18 12
07/20
07/19
07/18
Job ID: 11008 Job Start: Tue Apr 26 16:00:17 UTC 2016
Source 1 lat.: 33.463600 lon.: -116.970600 height: 50 m AGL
Trajectory Direction: Backward Duration: 48 hrs
Vertical Motion Calculation Method: Model Vertical Velocity
Meteorology: 0000Z 20 Jul 2010 - NAM12

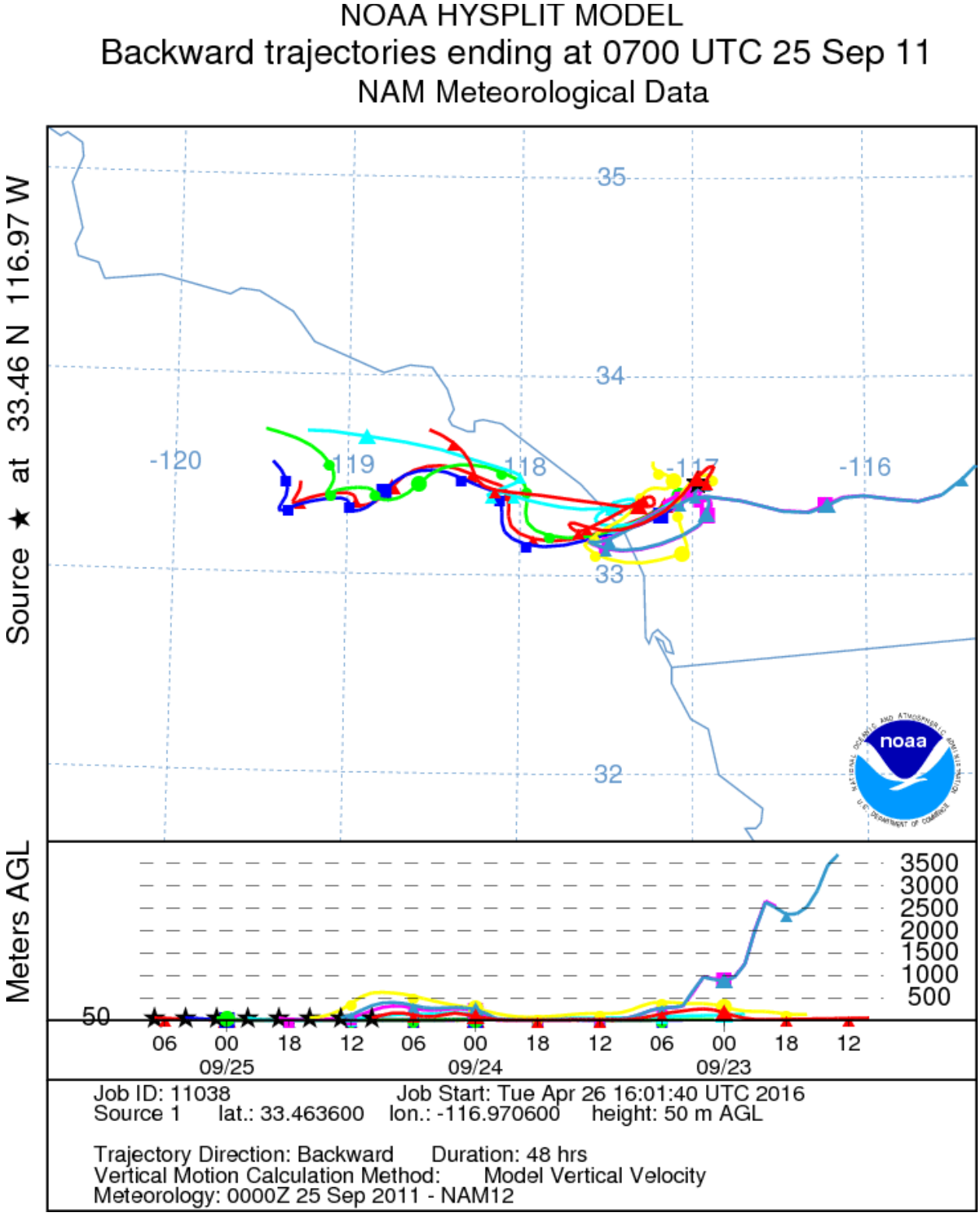
NOAA HYSPLIT MODEL
Backward trajectories ending at 0700 UTC 25 Sep 11
NAM Meteorological Data
Source ★ at 33.46 N 116.97 W
35
34
33
32
-120
-119
-118
-117
-116
noaa
Meters AGL
3500
3000
2500
2000
1500
1000
500
50
06 00 18 12 06 00 18 12 06 00 18 12
09/25
09/24
09/23
Job ID: 11038 Job Start: Tue Apr 26 16:01:40 UTC 2016
Source 1 lat.: 33.463600 lon.: -116.970600 height: 50 m AGL
Trajectory Direction: Backward Duration: 48 hrs
Vertical Motion Calculation Method: Model Vertical Velocity
Meteorology: 0000Z 25 Sep 2011 - NAM12

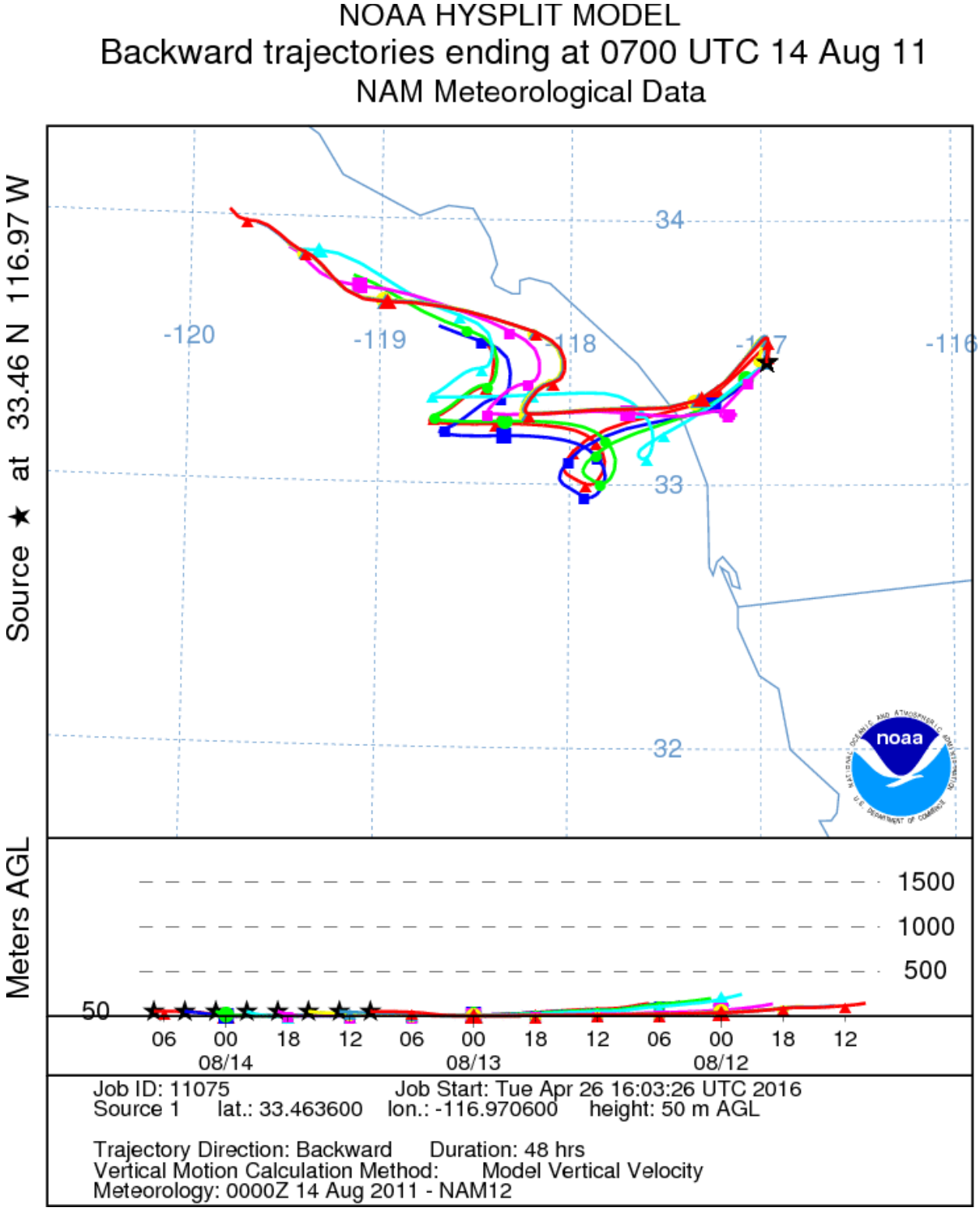
NOAA HYSPLIT MODEL
Backward trajectories ending at 0700 UTC 14 Aug 11
NAM Meteorological Data
Source ★ at 33.46 N 116.97 W
34
33
32
-120
-119
-118
-117
-116
noaa
Meters AGL
1500
1000
500
50
06 00 18 12 06 00 18 12 06 00 18 12
08/14
08/13
08/12
Job ID: 11075 Job Start: Tue Apr 26 16:03:26 UTC 2016
Source 1 lat.: 33.463600 lon.: -116.970600 height: 50 m AGL
Trajectory Direction: Backward Duration: 48 hrs
Vertical Motion Calculation Method: Model Vertical Velocity
Meteorology: 0000Z 14 Aug 2011 - NAM12

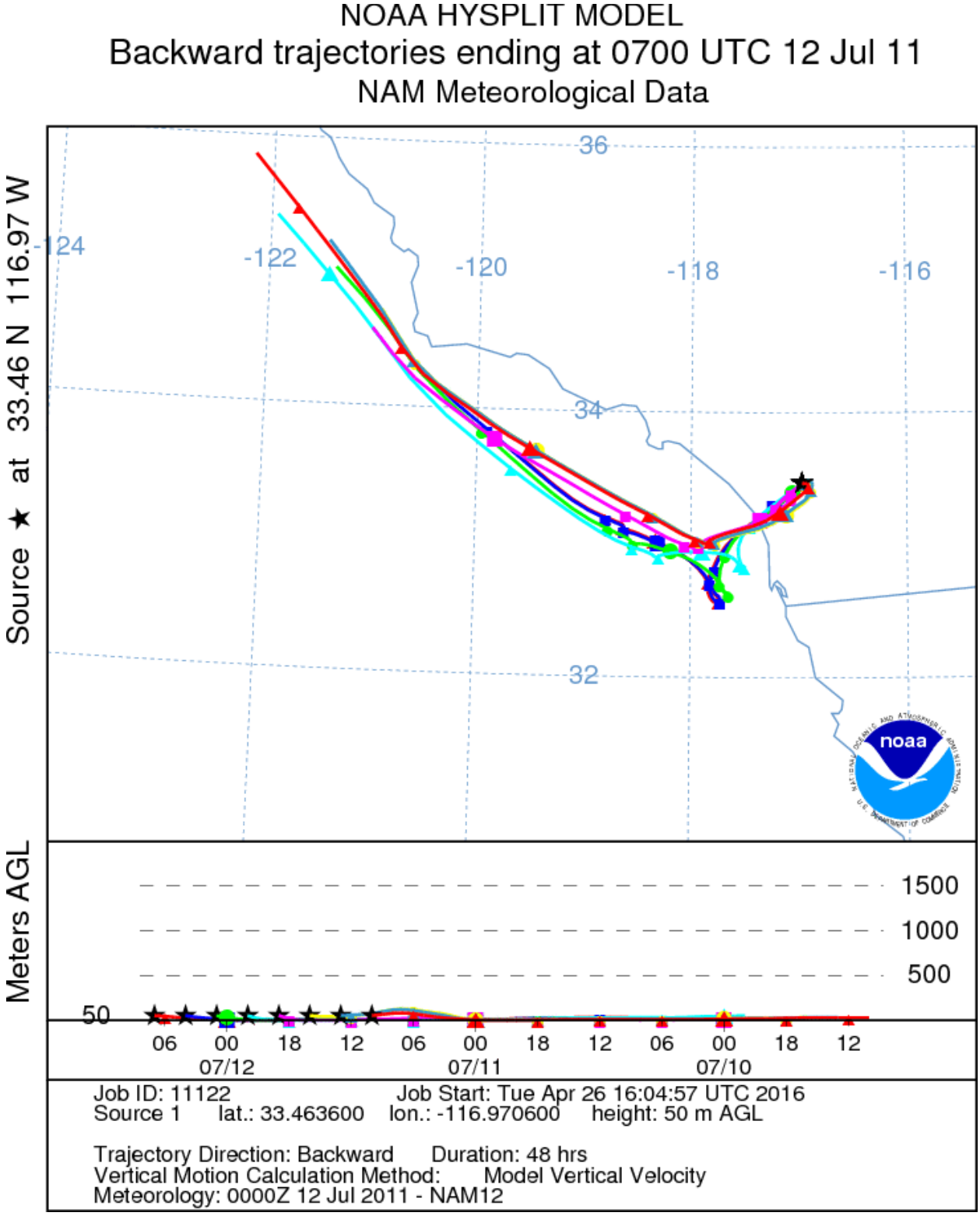
NOAA HYSPLIT MODEL
Backward trajectories ending at 0700 UTC 12 Jul 11
NAM Meteorological Data
Source ★ at 33.46 N 116.97 W
-124
-122
-120
-118
-116
36
34
32
noaa
Meters AGL
1500
1000
500
50
06 00 18 12 06 00 18 12 06 00 18 12
07/12
07/11
07/10
Job ID: 11122 Job Start: Tue Apr 26 16:04:57 UTC 2016
Source 1 lat.: 33.463600 lon.: -116.970600 height: 50 m AGL
Trajectory Direction: Backward Duration: 48 hrs
Vertical Motion Calculation Method: Model Vertical Velocity
Meteorology: 0000Z 12 Jul 2011 - NAM12

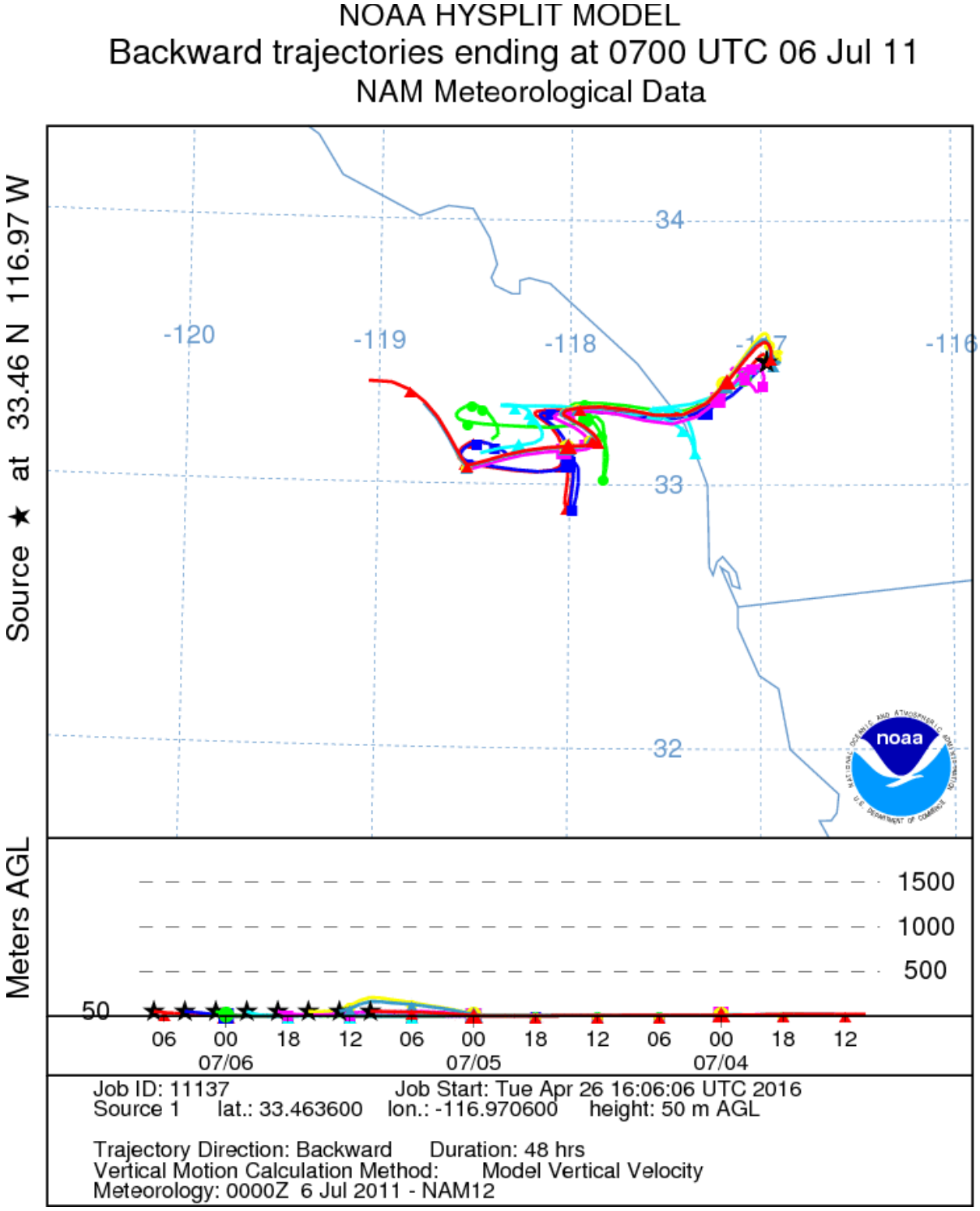
NOAA HYSPLIT MODEL
Backward trajectories ending at 0700 UTC 06 Jul 11
NAM Meteorological Data
Source ★ at 33.46 N 116.97 W
34
33
32
-120
-119
-118
-116
noaa
Meters AGL
1500
1000
500
50
06 00 18 12 06 00 18 12 06 00 18 12
07/06
07/05
07/04
Job ID: 11137 Job Start: Tue Apr 26 16:06:06 UTC 2016
Source 1 lat.: 33.463600 lon.: -116.970600 height: 50 m AGL
Trajectory Direction: Backward Duration: 48 hrs
Vertical Motion Calculation Method: Model Vertical Velocity
Meteorology: 0000Z 6 Jul 2011 - NAM12

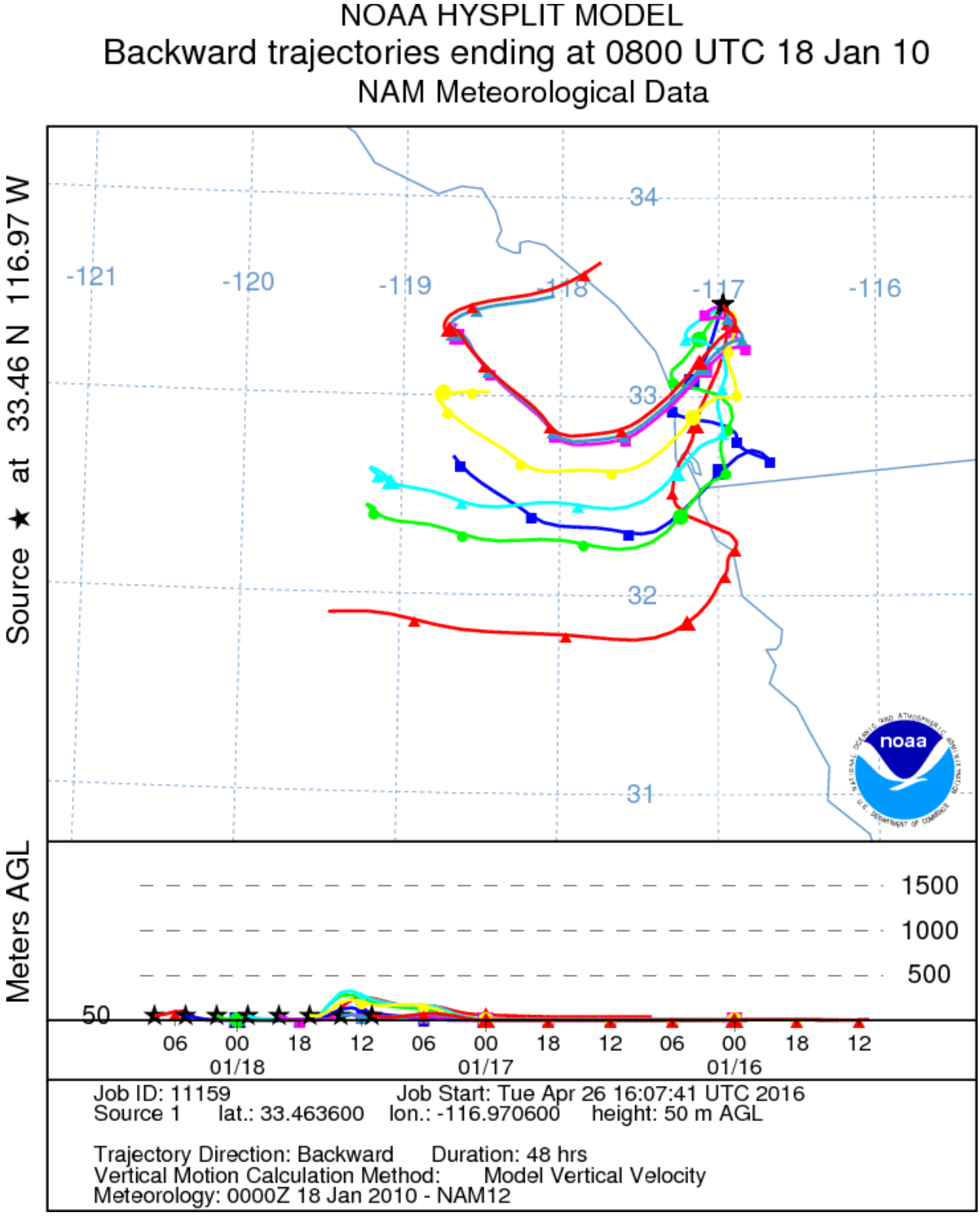
NOAA HYSPLIT MODEL
Backward trajectories ending at 0800 UTC 18 Jan 10
NAM Meteorological Data
Source ★ at 33.46 N 116.97 W
-121
-120
-119
-118
-117
-116
34
33
32
31
noaa
Meters AGL
1500
1000
500
50
06 00 18 12 06 00 18 12 06 00 18 12
01/18
01/17
01/16
Job ID: 11159 Job Start: Tue Apr 26 16:07:41 UTC 2016
Source 1 lat.: 33.463600 lon.: -116.970600 height: 50 m AGL
Trajectory Direction: Backward Duration: 48 hrs
Vertical Motion Calculation Method: Model Vertical Velocity
Meteorology: 0000Z 18 Jan 2010 - NAM12

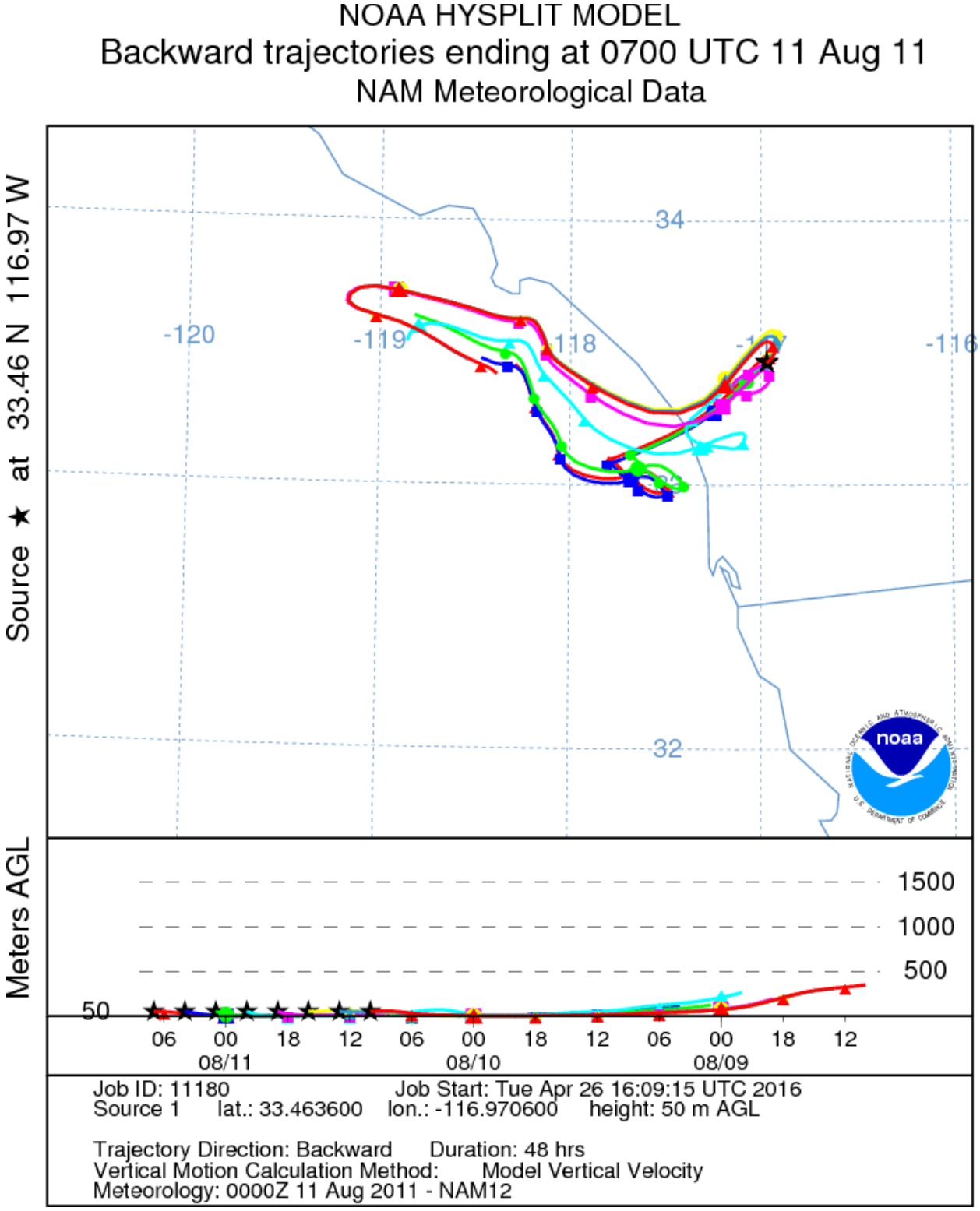
NOAA HYSPLIT MODEL
Backward trajectories ending at 0700 UTC 11 Aug 11
NAM Meteorological Data
Source ★ at 33.46 N 116.97 W
34
32
-120
-119
-118
-116
noaa
Meters AGL
1500
1000
500
50
06 00 18 12 06 00 18 12 06 00 18 12
08/11
08/10
08/09
Job ID: 11180 Job Start: Tue Apr 26 16:09:15 UTC 2016
Source 1 lat.: 33.463600 lon.: -116.970600 height: 50 m AGL
Trajectory Direction: Backward Duration: 48 hrs
Vertical Motion Calculation Method: Model Vertical Velocity
Meteorology: 0000Z 11 Aug 2011 - NAM12

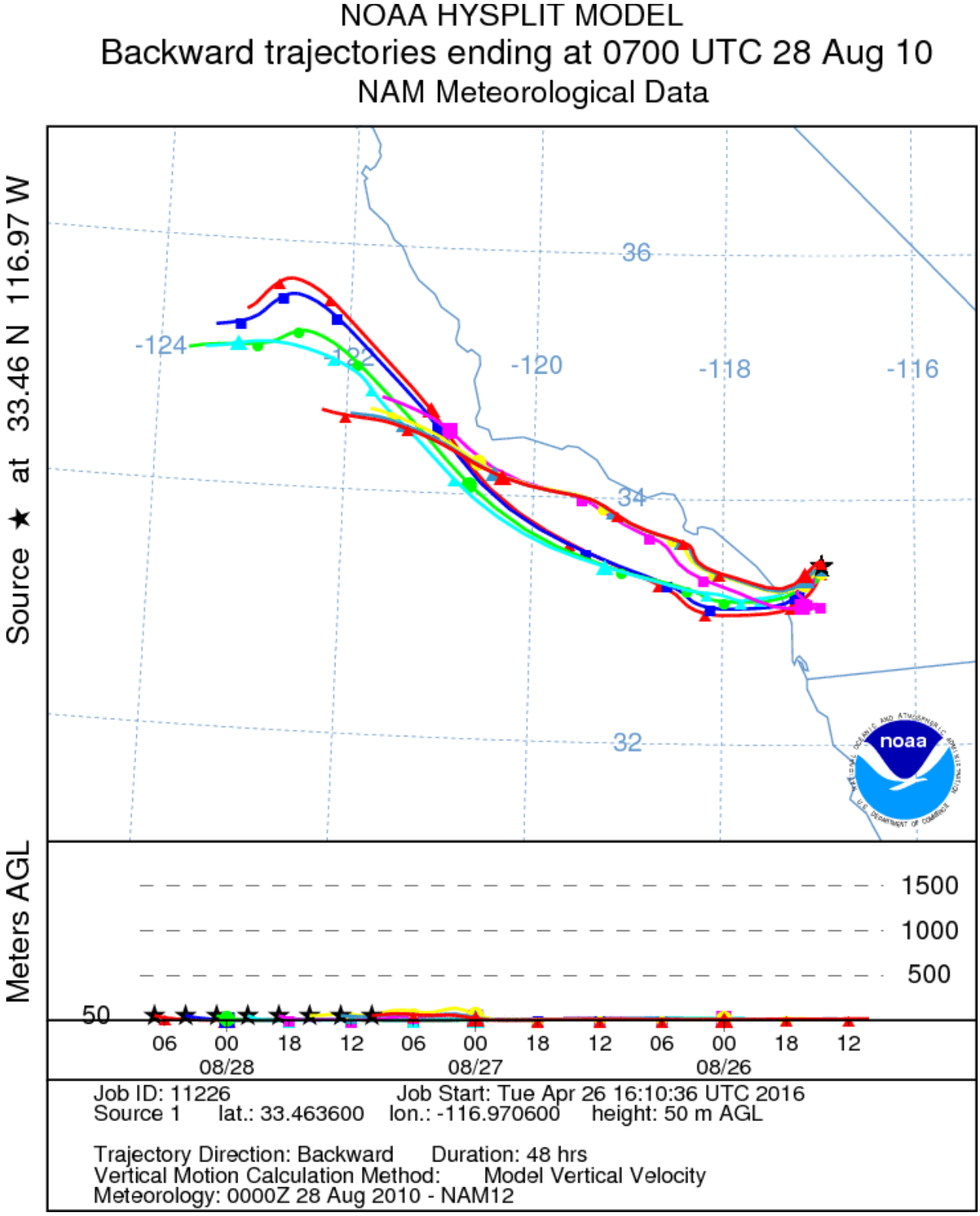
NOAA HYSPLIT MODEL
Backward trajectories ending at 0700 UTC 28 Aug 10
NAM Meteorological Data
Source ★ at 33.46 N 116.97 W
36
-124
-122
-120
-118
-116
34
32
noaa
Meters AGL
1500
1000
500
50
06 00 18 12 06 00 18 12 06 00 18 12
08/28
08/27
08/26
Job ID: 11226 Job Start: Tue Apr 26 16:10:36 UTC 2016
Source 1 lat.: 33.463600 lon.: -116.970600 height: 50 m AGL
Trajectory Direction: Backward Duration: 48 hrs
Vertical Motion Calculation Method: Model Vertical Velocity
Meteorology: 0000Z 28 Aug 2010 - NAM12

BIBE HYSPLIT back-trajectories

NOAA HYSPLIT MODEL
Backward trajectories ending at 0500 UTC 06 Jul 11
NAM Meteorological Data

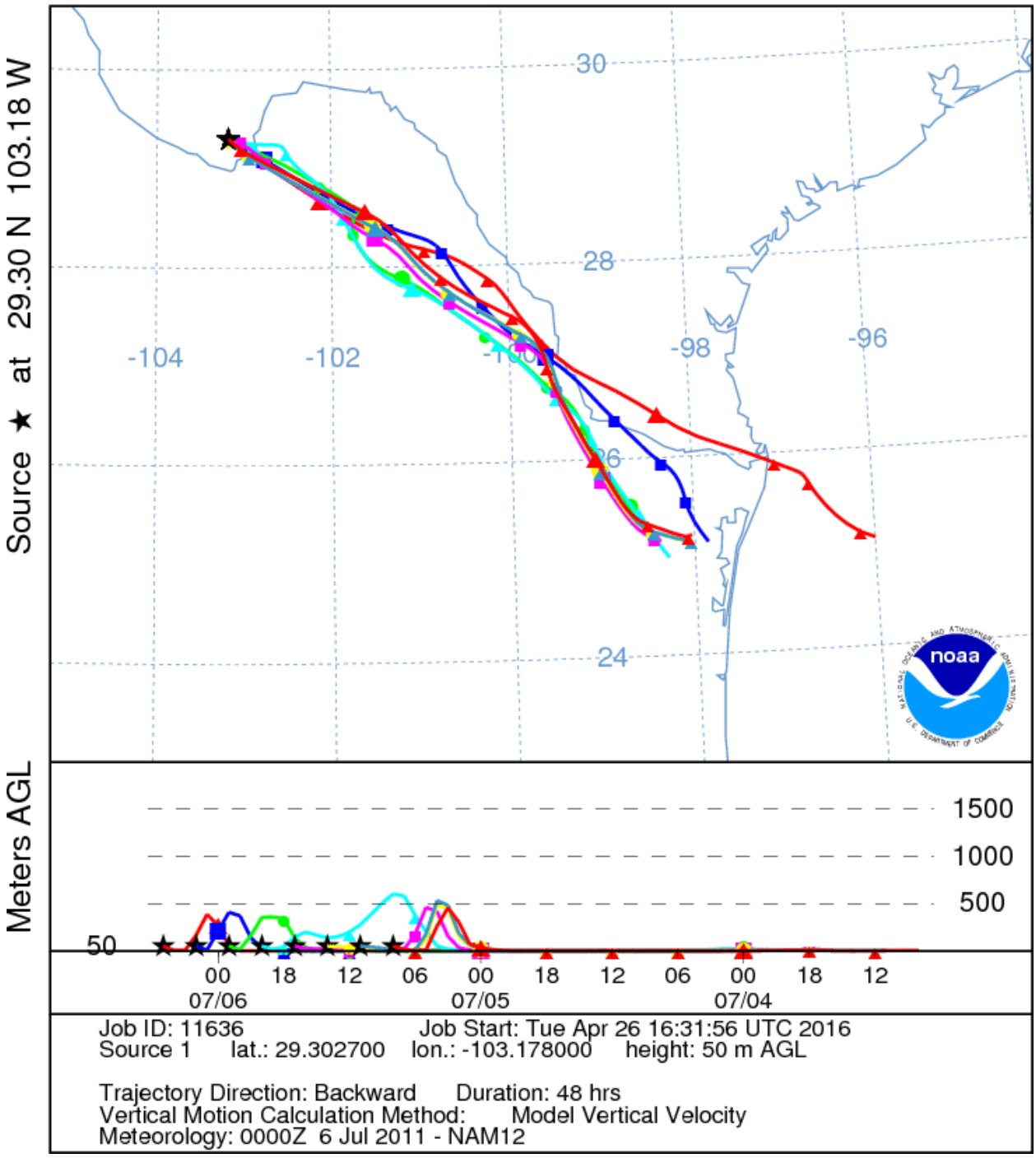

Job ID: 11636 Job Start: Tue Apr 26 16:31:56 UTC 2016
Source 1 lat.: 29.302700 lon.: -103.178000 height: 50 m AGL

Trajectory Direction: Backward Duration: 48 hrs
Vertical Motion Calculation Method: Model Vertical Velocity
Meteorology: 0000Z 6 Jul 2011 - NAM12

NOAA HYSPLIT MODEL
Backward trajectories ending at 0500 UTC 19 Oct 11
NAM Meteorological Data

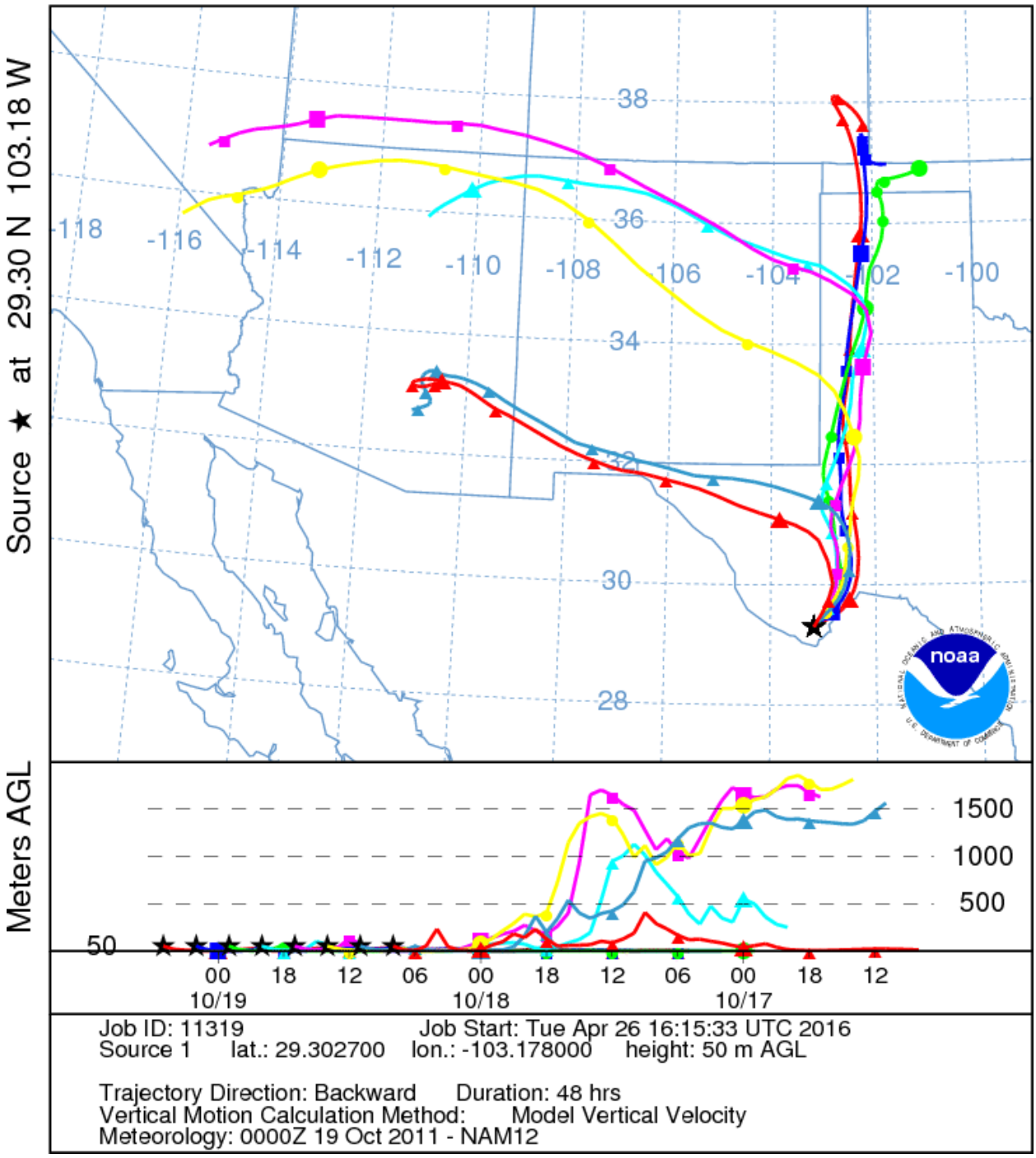

NOAA HYSPLIT MODEL
Backward trajectories ending at 0500 UTC 22 Apr 11
NAM Meteorological Data

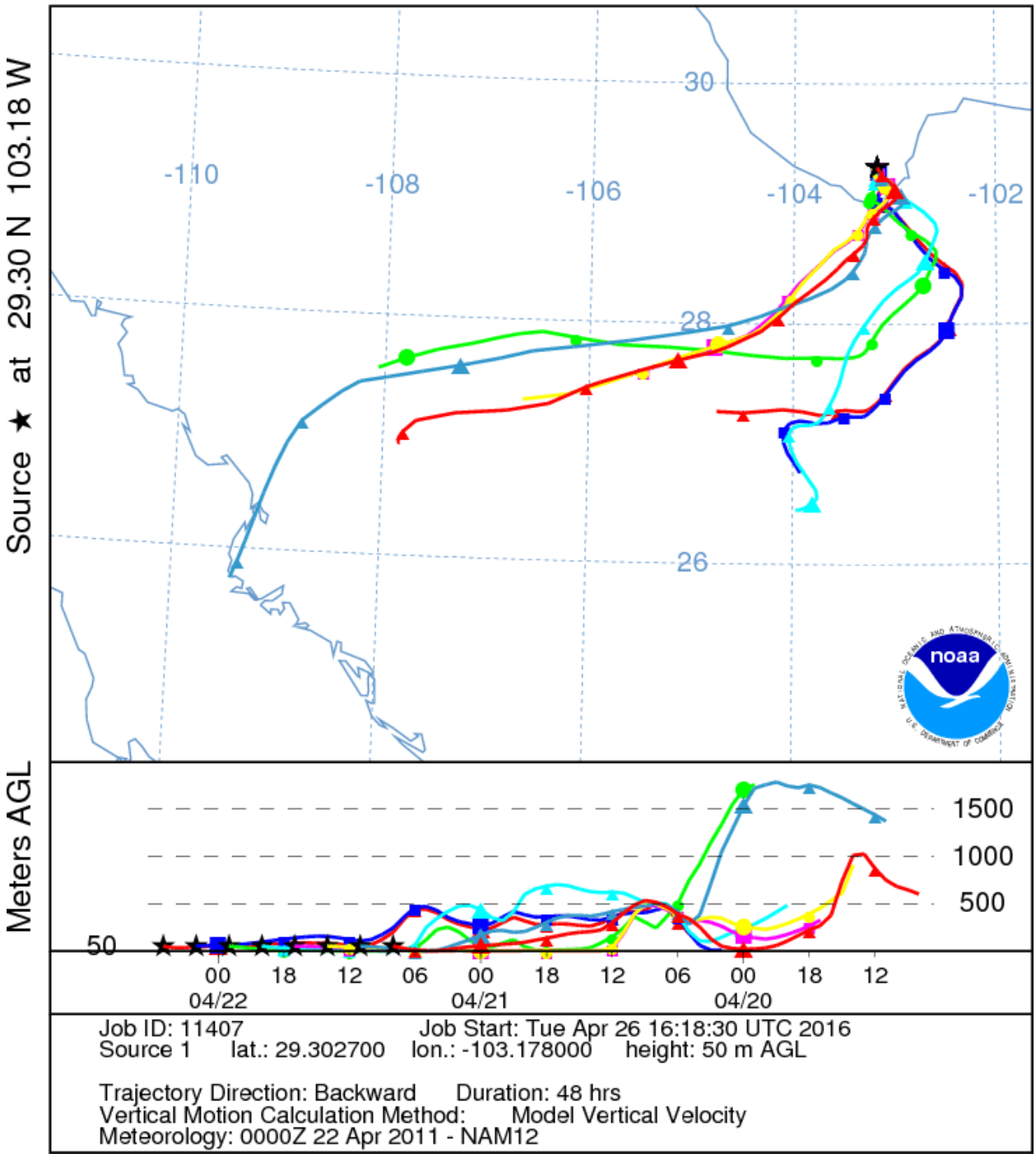

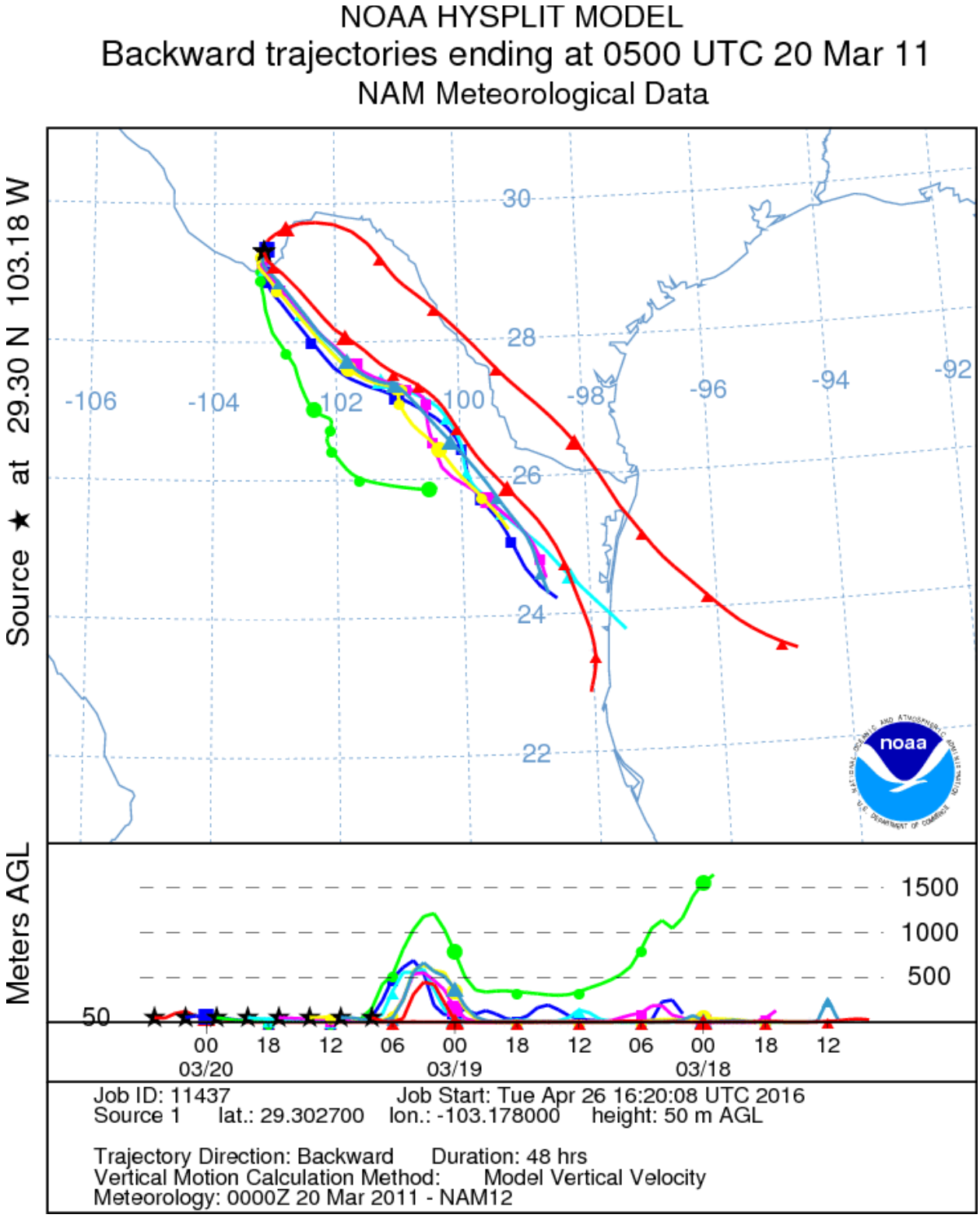
NOAA HYSPLIT MODEL
Backward trajectories ending at 0500 UTC 20 Mar 11
NAM Meteorological Data
Source ★ at 29.30 N 103.18 W
30
28
26
24
22
-106
-104
-102
-100
-98
-96
-94
-92
noaa
Meters AGL
1500
1000
500
50
00 18 12 06 00 18 12 06 00 18 12
03/20 03/19 03/18
Job ID: 11437 Job Start: Tue Apr 26 16:20:08 UTC 2016
Source 1 lat.: 29.302700 lon.: -103.178000 height: 50 m AGL
Trajectory Direction: Backward Duration: 48 hrs
Vertical Motion Calculation Method: Model Vertical Velocity
Meteorology: 0000Z 20 Mar 2011 - NAM12

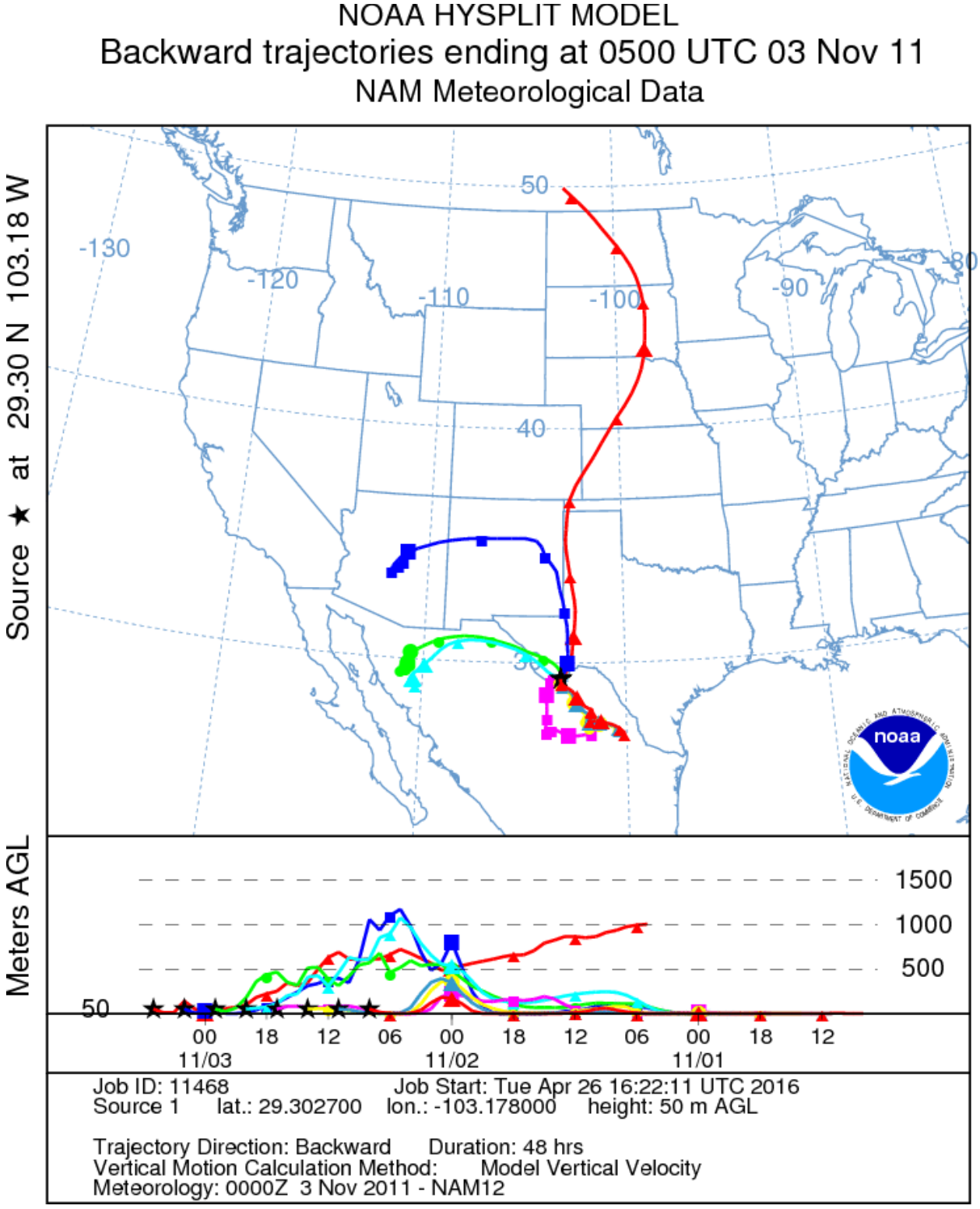
NOAA HYSPLIT MODEL
Backward trajectories ending at 0500 UTC 03 Nov 11
NAM Meteorological Data
Source ★ at 29.30 N 103.18 W
50
40
-130
-120
-110
-100
-90
-80
noaa
Meters AGL
1500
1000
500
50
00 18 12 06 00 18 12 06 00 18 12
11/03
11/02
11/01
Job ID: 11468 Job Start: Tue Apr 26 16:22:11 UTC 2016
Source 1 lat.: 29.302700 lon.: -103.178000 height: 50 m AGL
Trajectory Direction: Backward Duration: 48 hrs
Vertical Motion Calculation Method: Model Vertical Velocity
Meteorology: 0000Z 3 Nov 2011 - NAM12

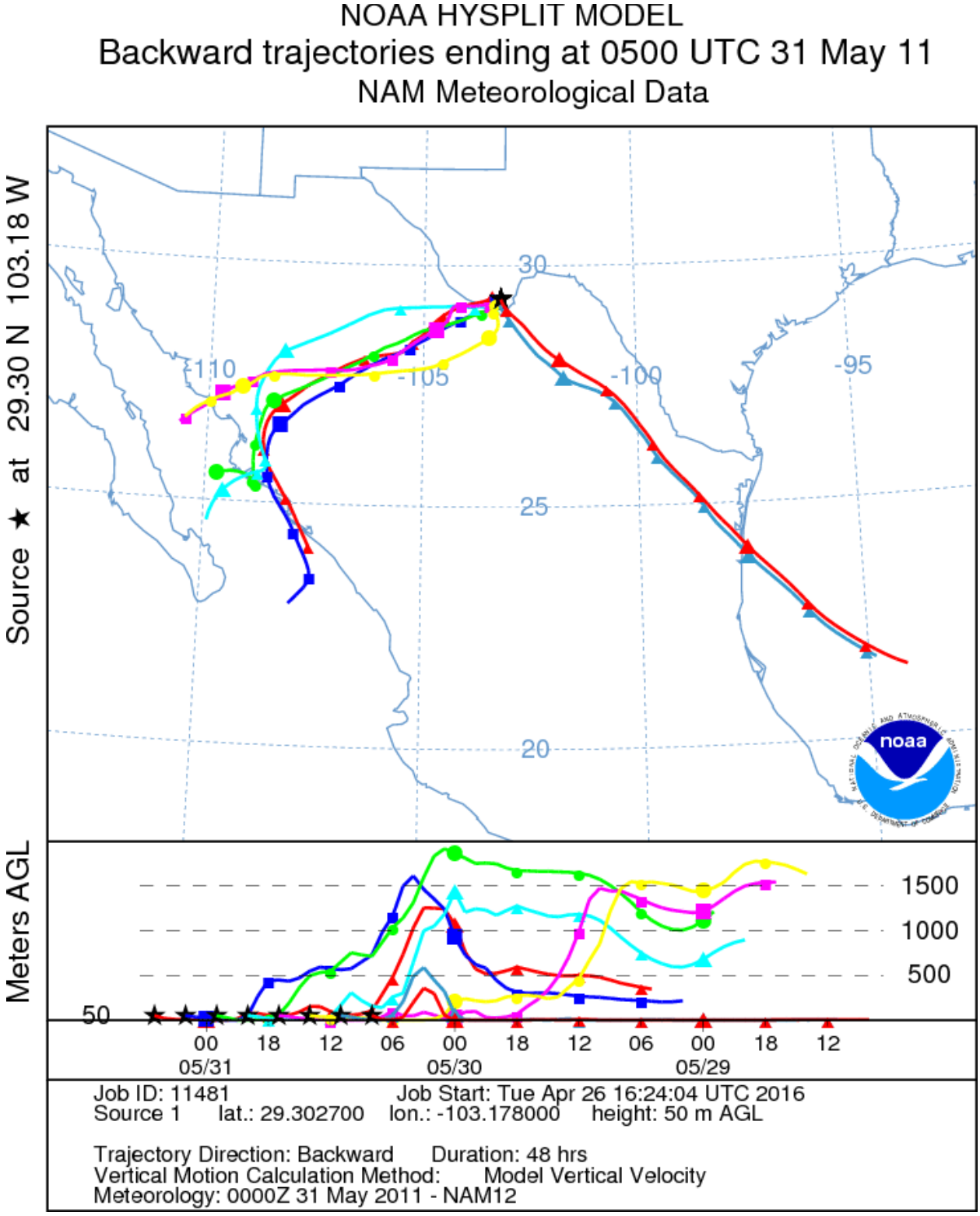
NOAA HYSPLIT MODEL
Backward trajectories ending at 0500 UTC 31 May 11
NAM Meteorological Data
Source ★ at 29.30 N 103.18 W
30
25
20
-110
-105
-100
-95
noaa
Meters AGL
1500
1000
500
50
00 18 12 06 00 18 12 06 00 18 12
05/31
05/30
05/29
Job ID: 11481 Job Start: Tue Apr 26 16:24:04 UTC 2016
Source 1 lat.: 29.302700 lon.: -103.178000 height: 50 m AGL
Trajectory Direction: Backward Duration: 48 hrs
Vertical Motion Calculation Method: Model Vertical Velocity
Meteorology: 0000Z 31 May 2011 - NAM12

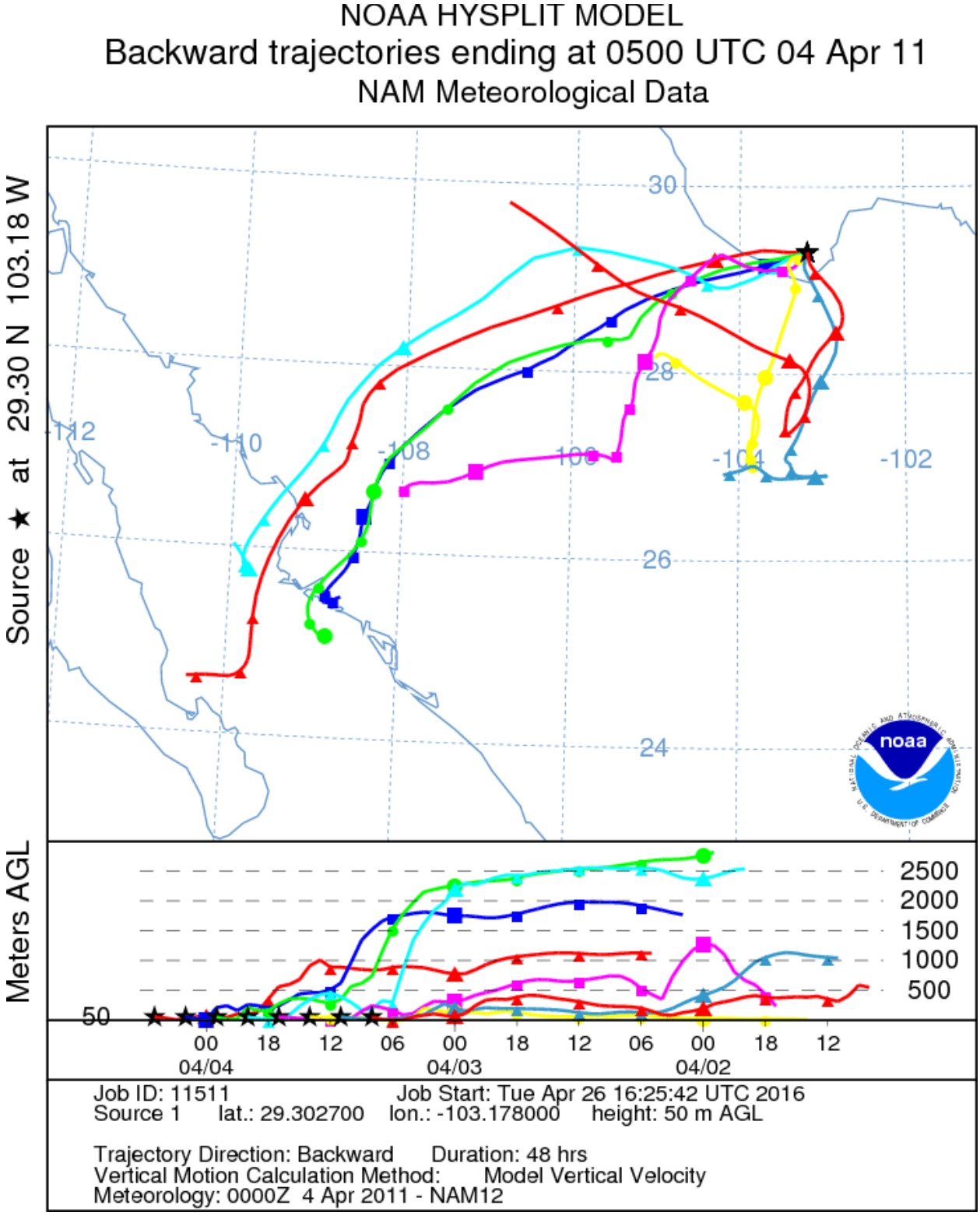
NOAA HYSPLIT MODEL
Backward trajectories ending at 0500 UTC 04 Apr 11
NAM Meteorological Data
Source ★ at 29.30 N 103.18 W
30
28
26
24
-112
-110
-108
-106
-104
-102
noaa
Meters AGL
2500
2000
1500
1000
500
50
00 18 12 06 00 18 12 06 00 18 12
04/04
04/03
04/02
Job ID: 11511
Job Start: Tue Apr 26 16:25:42 UTC 2016
Source 1 lat.: 29.302700 lon.: -103.178000 height: 50 m AGL
Trajectory Direction: Backward Duration: 48 hrs
Vertical Motion Calculation Method: Model Vertical Velocity
Meteorology: 0000Z 4 Apr 2011 - NAM12

NOAA HYSPLIT MODEL
Backward trajectories ending at 0600 UTC 21 Feb 11
NAM Meteorological Data

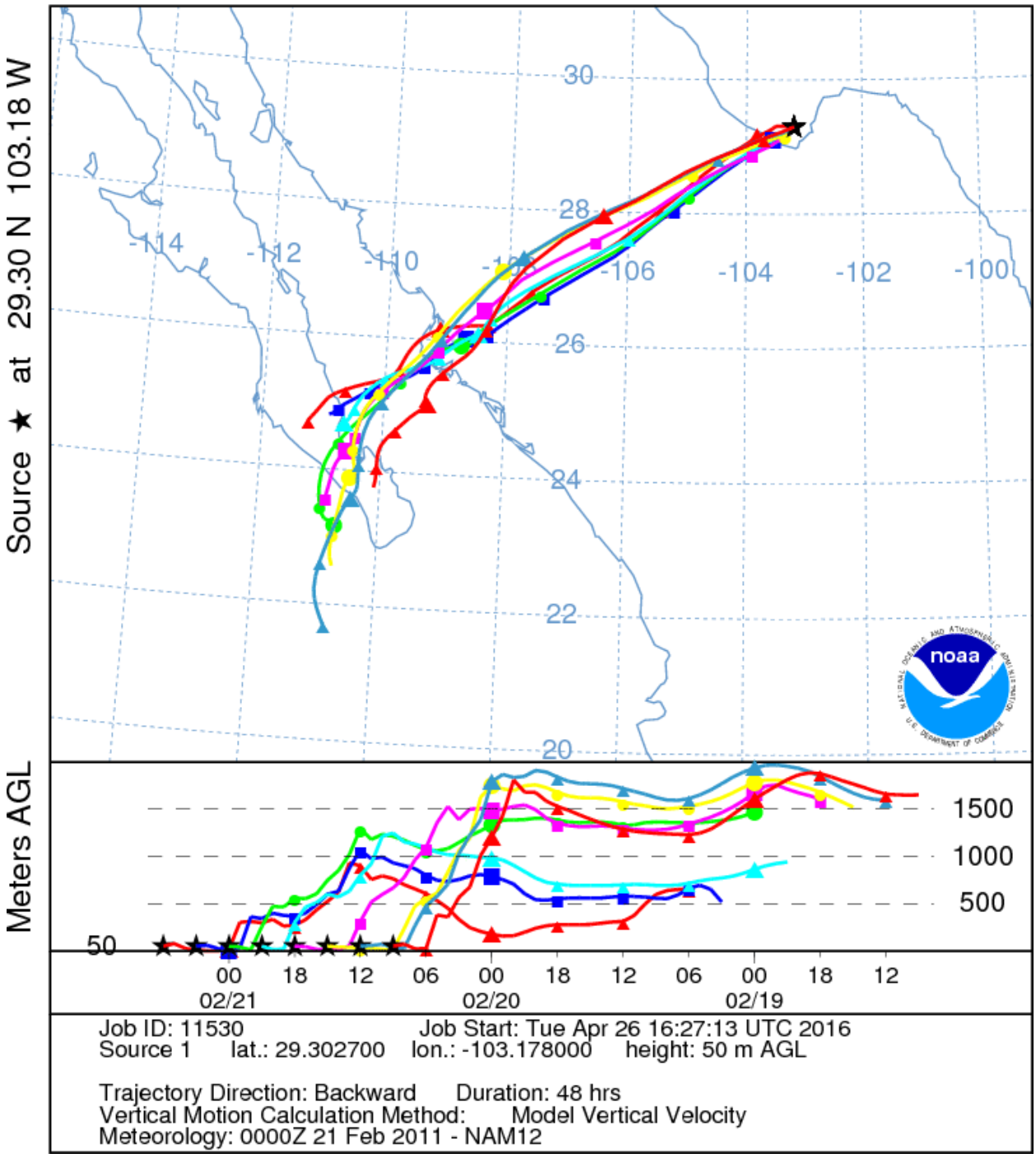

Job ID: 11530 Job Start: Tue Apr 26 16:27:13 UTC 2016
Source 1 lat.: 29.302700 lon.: -103.178000 height: 50 m AGL

Trajectory Direction: Backward Duration: 48 hrs
Vertical Motion Calculation Method: Model Vertical Velocity
Meteorology: 0000Z 21 Feb 2011 - NAM12

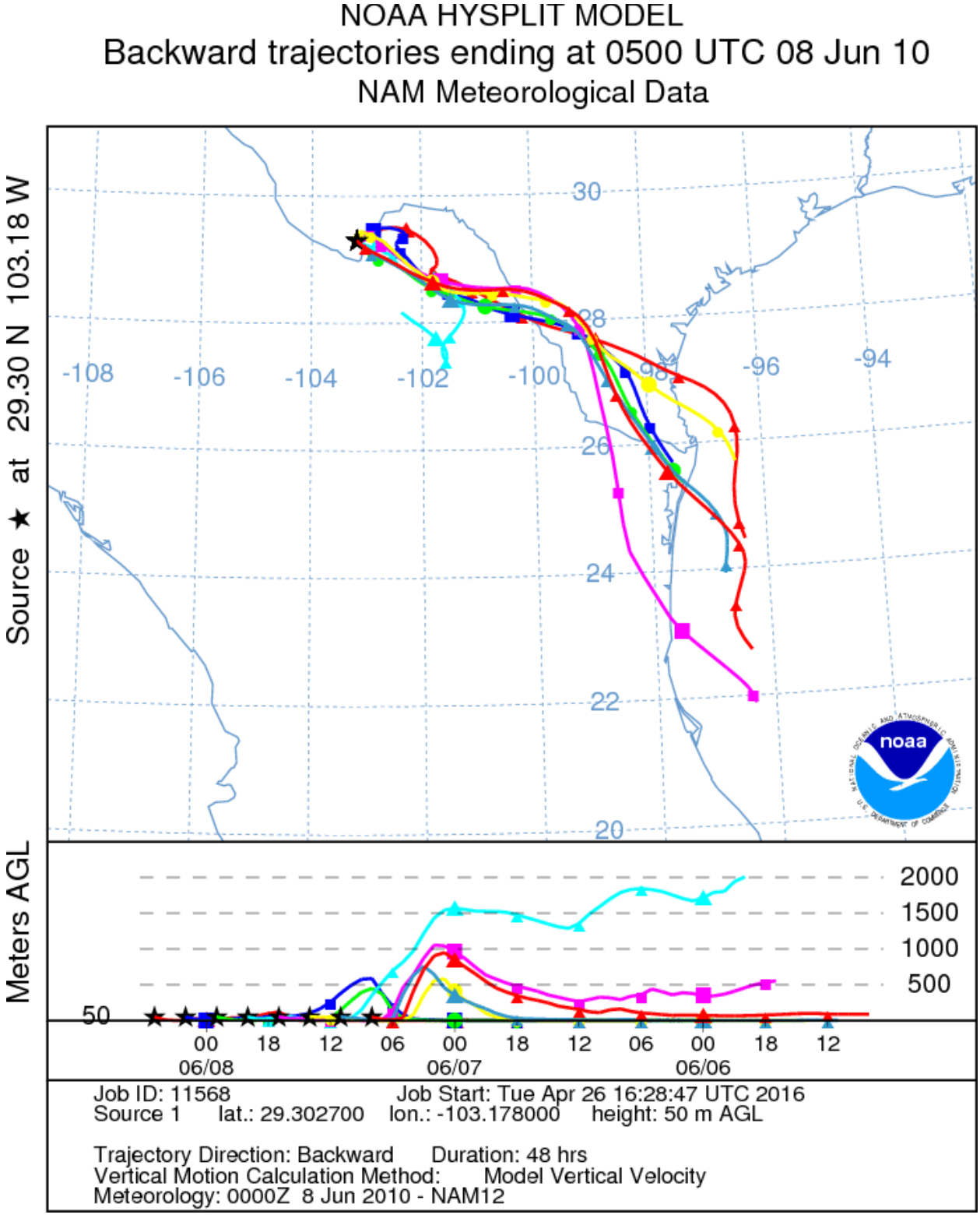
NOAA HYSPLIT MODEL
Backward trajectories ending at 0500 UTC 08 Jun 10
NAM Meteorological Data
Source ★ at 29.30 N 103.18 W
30
28
26
24
22
20
-108
-106
-104
-102
-100
-98
-96
-94
noaa
Meters AGL
2000
1500
1000
500
50
00 18 12 06 00 18 12 06 00 18 12
06/08 06/07 06/06
Job ID: 11568 Job Start: Tue Apr 26 16:28:47 UTC 2016
Source 1 lat.: 29.302700 lon.: -103.178000 height: 50 m AGL
Trajectory Direction: Backward Duration: 48 hrs
Vertical Motion Calculation Method: Model Vertical Velocity
Meteorology: 0000Z 8 Jun 2010 - NAM12

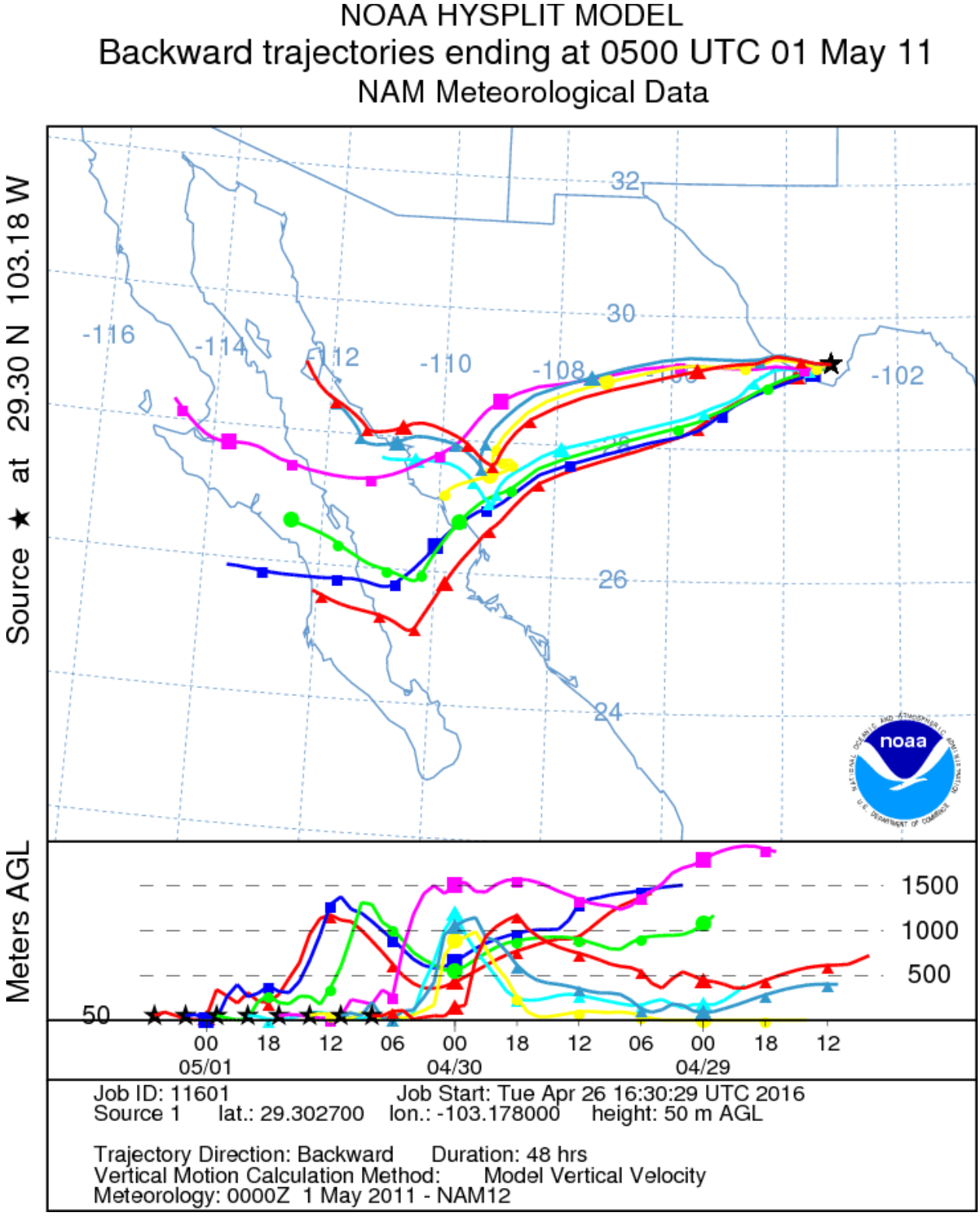
NOAA HYSPLIT MODEL
Backward trajectories ending at 0500 UTC 01 May 11
NAM Meteorological Data
Source ★ at 29.30 N 103.18 W
32
30
26
24
-116
-114
-112
-110
-108
-102
noaa
Meters AGL
1500
1000
500
50
00 18 12 06 00 18 12 06 00 18 12
05/01
04/30
04/29
Job ID: 11601 Job Start: Tue Apr 26 16:30:29 UTC 2016
Source 1 lat.: 29.302700 lon.: -103.178000 height: 50 m AGL
Trajectory Direction: Backward Duration: 48 hrs
Vertical Motion Calculation Method: Model Vertical Velocity
Meteorology: 0000Z 1 May 2011 - NAM12

BRIG HYSPLIT back-trajectories

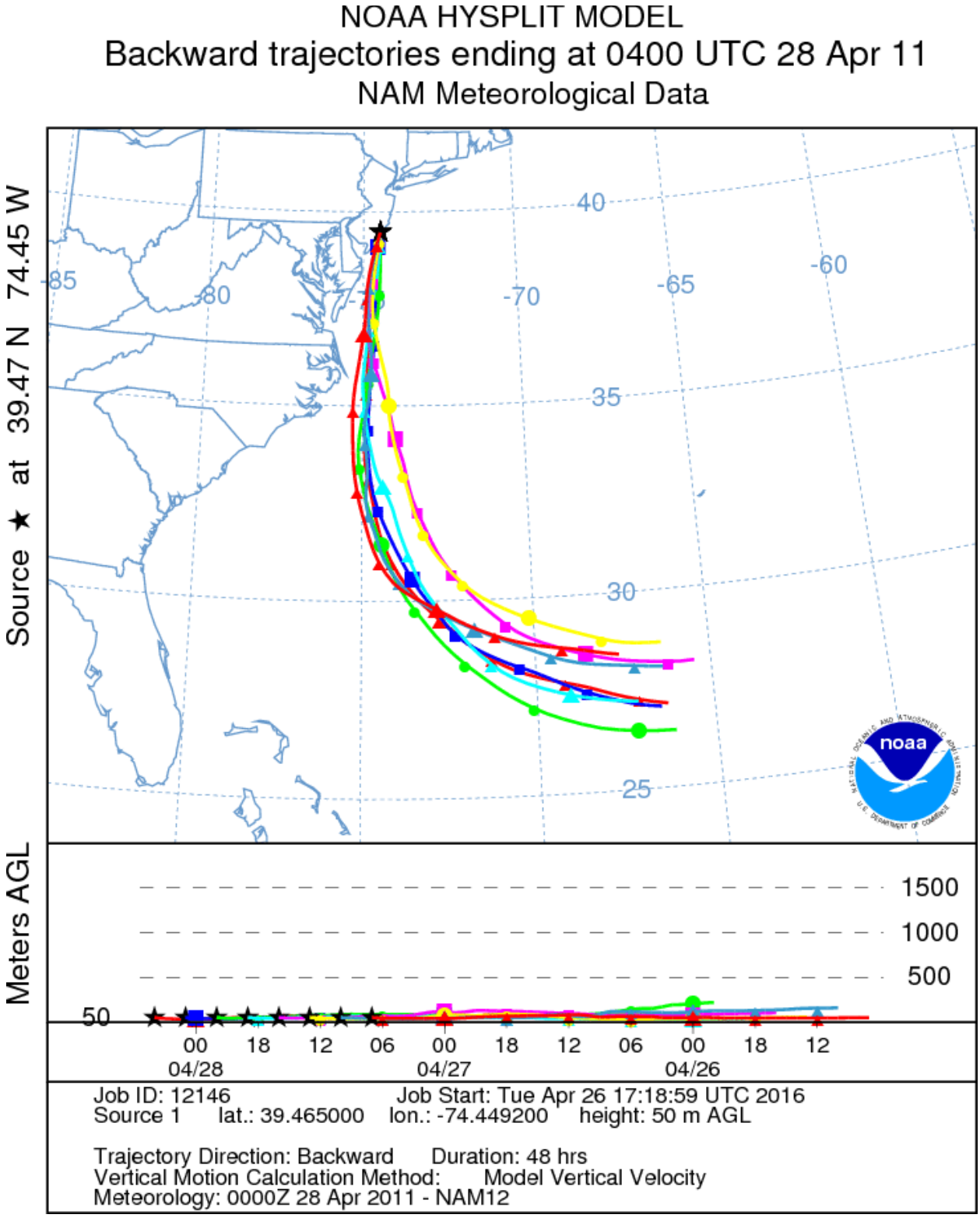
NOAA HYSPLIT MODEL
Backward trajectories ending at 0400 UTC 28 Apr 11
NAM Meteorological Data
Source ★ at 39.47 N 74.45 W
Meters AGL
1500
1000
500
50
00 18 12 06 00 18 12 06 00 18 12
04/28 04/27 04/26
Job ID: 12146 Job Start: Tue Apr 26 17:18:59 UTC 2016
Source 1 lat.: 39.465000 lon.: -74.449200 height: 50 m AGL
Trajectory Direction: Backward Duration: 48 hrs
Vertical Motion Calculation Method: Model Vertical Velocity
Meteorology: 0000Z 28 Apr 2011 - NAM12

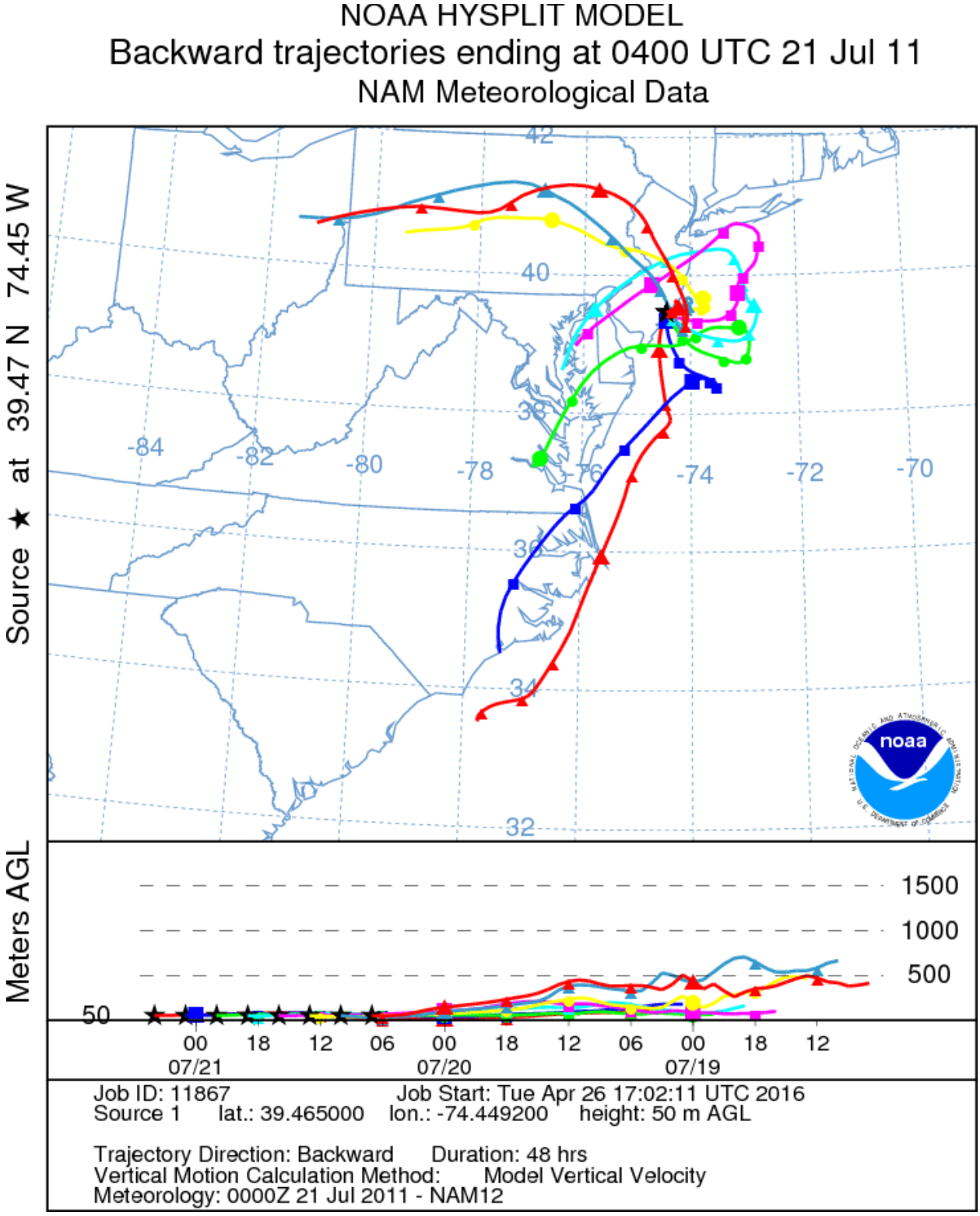
NOAA HYSPLIT MODEL
Backward trajectories ending at 0400 UTC 21 Jul 11
NAM Meteorological Data
Source ★ at 39.47 N 74.45 W
Meters AGL
1500
1000
500
50
00 18 12 06 00 18 12 06 00 18 12
07/21 07/20 07/19
Job ID: 11867 Job Start: Tue Apr 26 17:02:11 UTC 2016
Source 1 lat.: 39.465000 lon.: -74.449200 height: 50 m AGL
Trajectory Direction: Backward Duration: 48 hrs
Vertical Motion Calculation Method: Model Vertical Velocity
Meteorology: 0000Z 21 Jul 2011 - NAM12

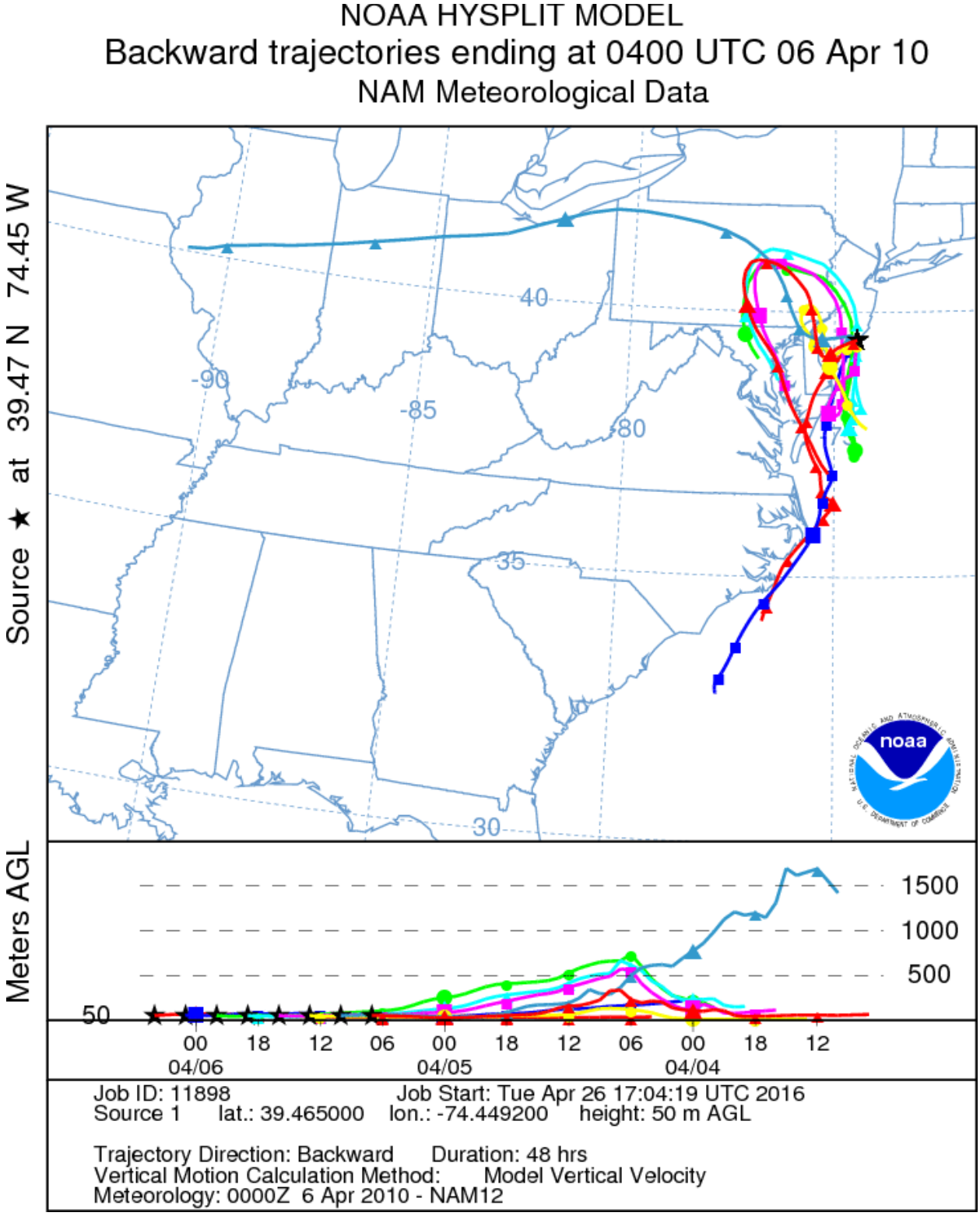
NOAA HYSPLIT MODEL
Backward trajectories ending at 0400 UTC 06 Apr 10
NAM Meteorological Data
Source ★ at 39.47 N 74.45 W
40
-90
-85
-80
35
30
noaa
Meters AGL
1500
1000
500
50
00 18 12 06 00 18 12 06 00 18 12
04/06
04/05
04/04
Job ID: 11898 Job Start: Tue Apr 26 17:04:19 UTC 2016
Source 1 lat.: 39.465000 lon.: -74.449200 height: 50 m AGL
Trajectory Direction: Backward Duration: 48 hrs
Vertical Motion Calculation Method: Model Vertical Velocity
Meteorology: 0000Z 6 Apr 2010 - NAM12

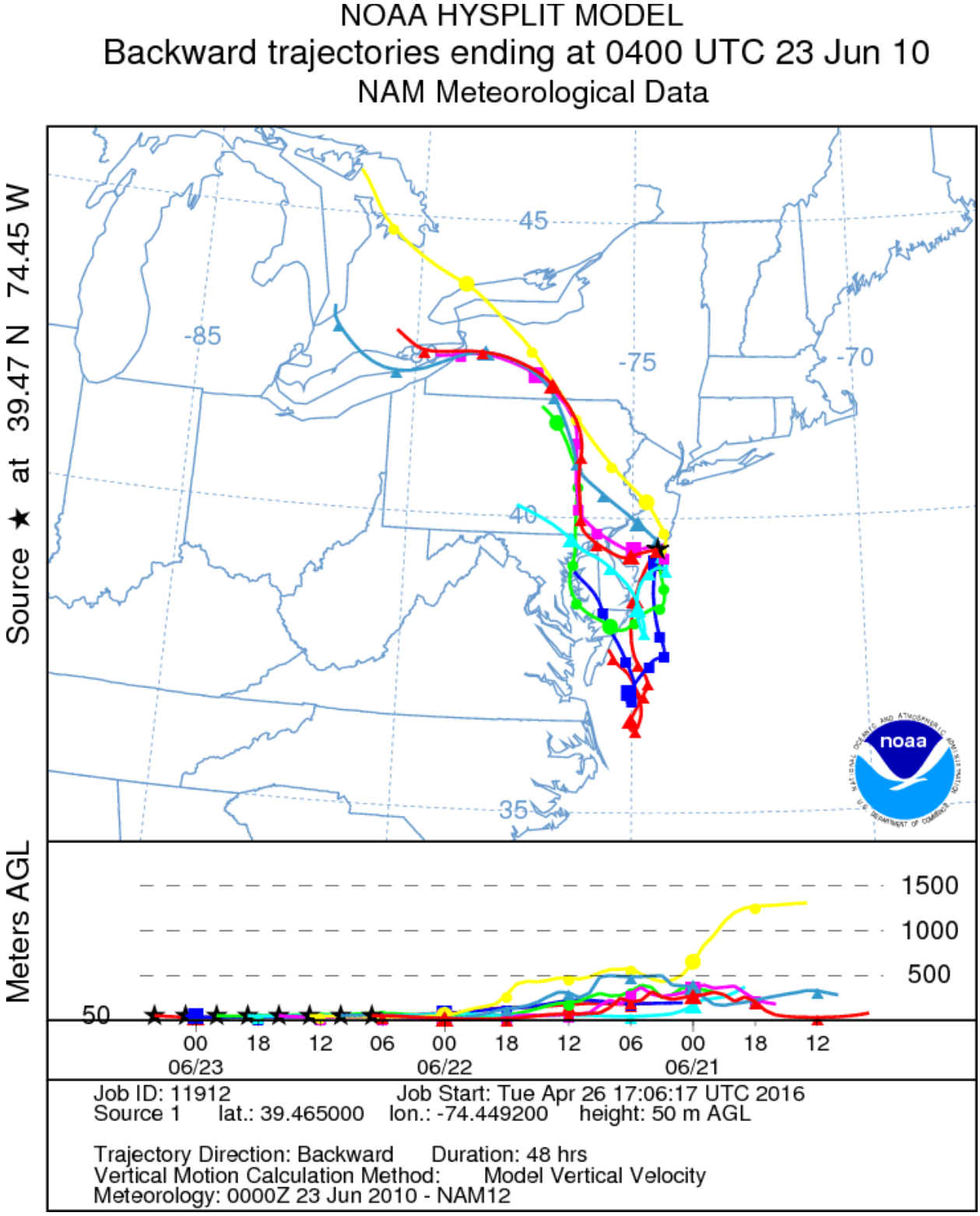
NOAA HYSPLIT MODEL
Backward trajectories ending at 0400 UTC 23 Jun 10
NAM Meteorological Data
Source ★ at 39.47 N 74.45 W
45
-85
-75
-70
40
35
noaa
Meters AGL
1500
1000
500
50
00 18 12 06 00 18 12 06 00 18 12
06/23 06/22 06/21
Job ID: 11912 Job Start: Tue Apr 26 17:06:17 UTC 2016
Source 1 lat.: 39.465000 lon.: -74.449200 height: 50 m AGL
Trajectory Direction: Backward Duration: 48 hrs
Vertical Motion Calculation Method: Model Vertical Velocity
Meteorology: 0000Z 23 Jun 2010 - NAM12

NOAA HYSPLIT MODEL
Backward trajectories ending at 0400 UTC 22 Mar 10
NAM Meteorological Data

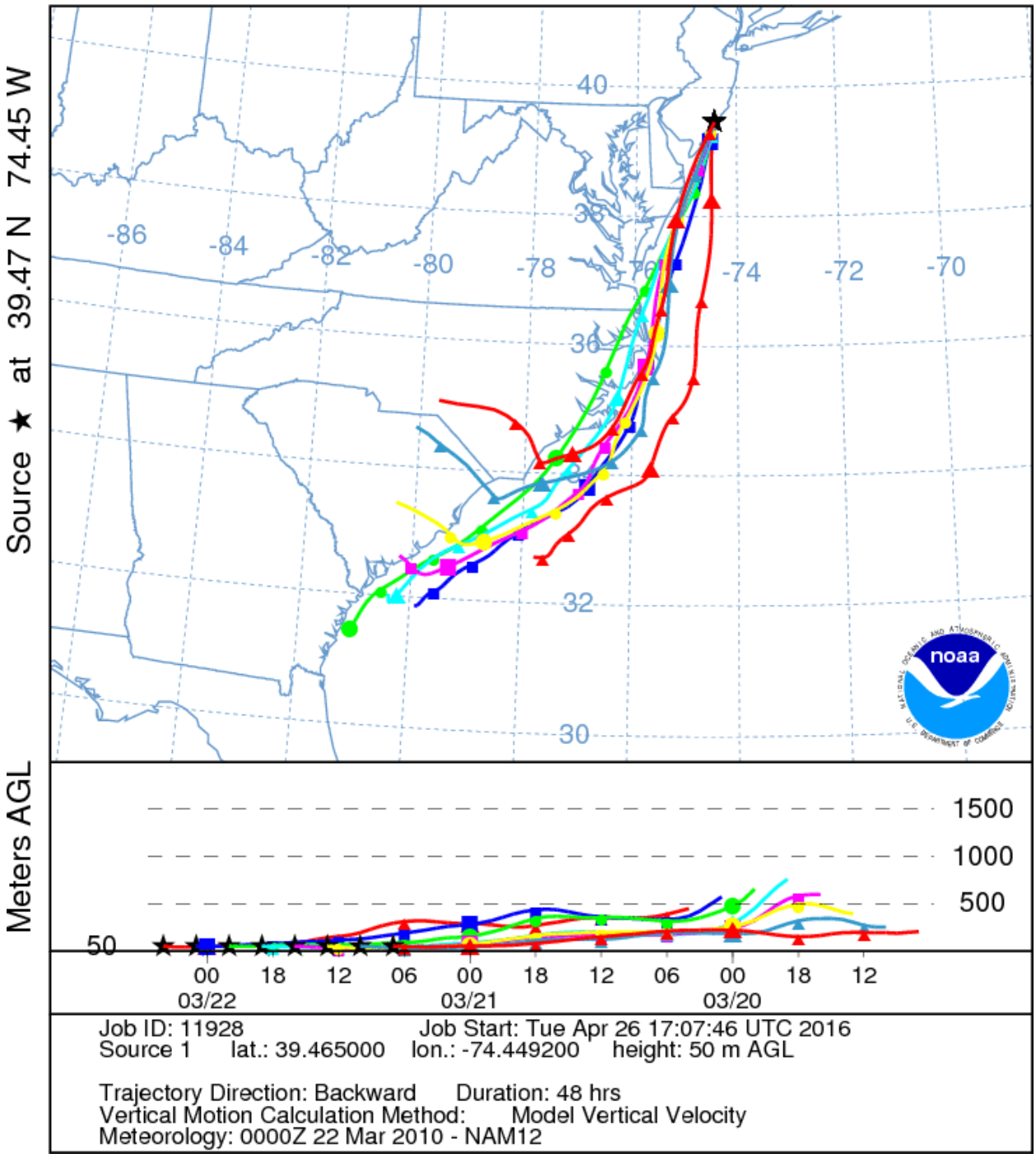

Job ID: 11928 Job Start: Tue Apr 26 17:07:46 UTC 2016
Source 1 lat.: 39.465000 lon.: -74.449200 height: 50 m AGL

Trajectory Direction: Backward Duration: 48 hrs
Vertical Motion Calculation Method: Model Vertical Velocity
Meteorology: 0000Z 22 Mar 2010 - NAM12

NOAA HYSPLIT MODEL
Backward trajectories ending at 0400 UTC 12 Jun 11
NAM Meteorological Data

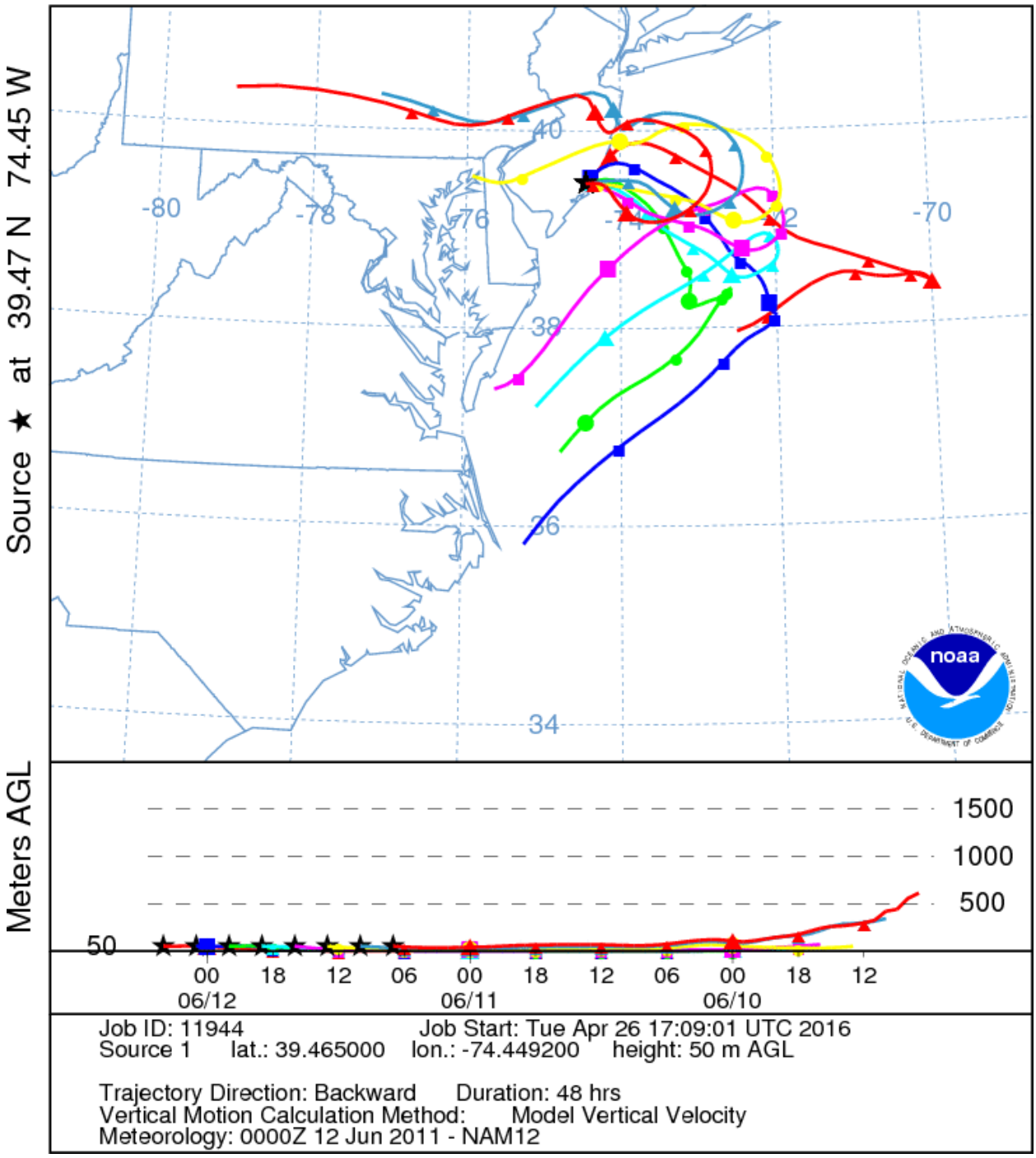

Job ID: 11944 Job Start: Tue Apr 26 17:09:01 UTC 2016
Source 1 lat.: 39.465000 lon.: -74.449200 height: 50 m AGL

Trajectory Direction: Backward Duration: 48 hrs
Vertical Motion Calculation Method: Model Vertical Velocity
Meteorology: 0000Z 12 Jun 2011 - NAM12

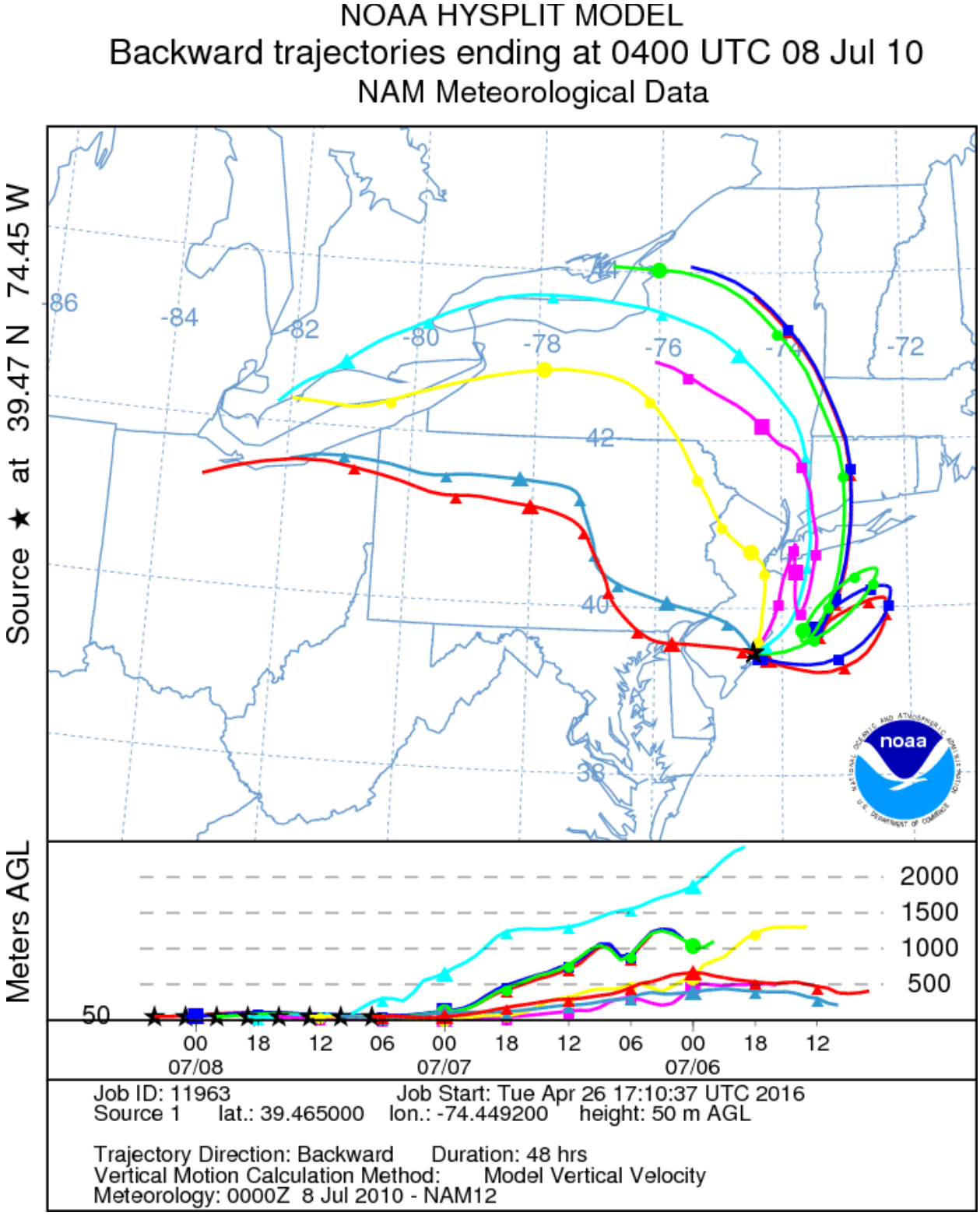
NOAA HYSPLIT MODEL
Backward trajectories ending at 0400 UTC 08 Jul 10
NAM Meteorological Data
Source ★ at 39.47 N 74.45 W
-86
-84
-82
-80
-78
-76
-74
-72
42
40
38
noaa
Meters AGL
2000
1500
1000
500
50
00 18 12 06 00 18 12 06 00 18 12
07/08 07/07 07/06
Job ID: 11963 Job Start: Tue Apr 26 17:10:37 UTC 2016
Source 1 lat.: 39.465000 lon.: -74.449200 height: 50 m AGL
Trajectory Direction: Backward Duration: 48 hrs
Vertical Motion Calculation Method: Model Vertical Velocity
Meteorology: 0000Z 8 Jul 2010 - NAM12

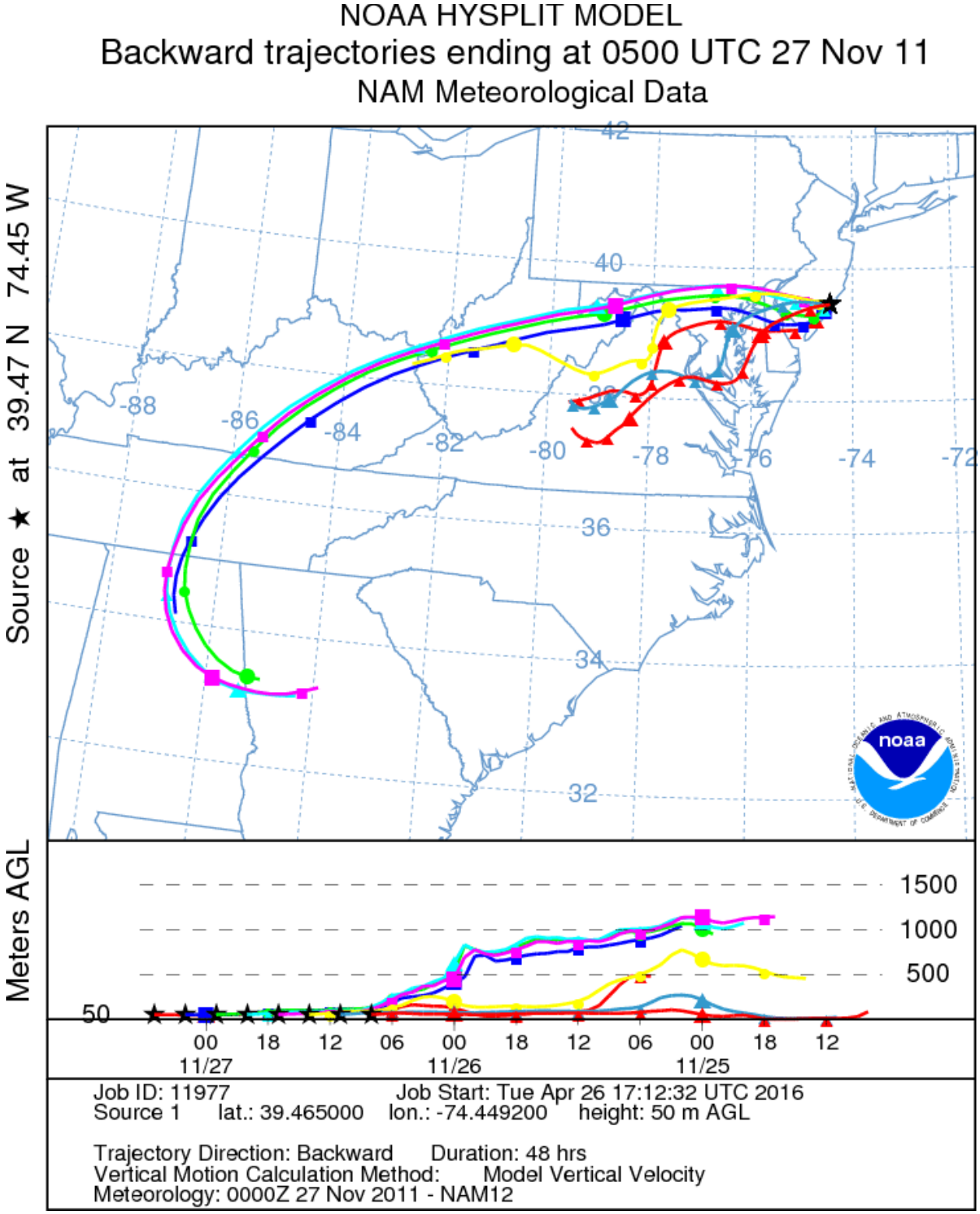
NOAA HYSPLIT MODEL
Backward trajectories ending at 0500 UTC 27 Nov 11
NAM Meteorological Data
Source ★ at 39.47 N 74.45 W
42
40
36
34
32
-88
-86
-84
-82
-80
-78
-76
-74
-72
noaa
Meters AGL
1500
1000
500
50
00 18 12 06 00 18 12 06 00 18 12
11/27
11/26
11/25
Job ID: 11977 Job Start: Tue Apr 26 17:12:32 UTC 2016
Source 1 lat.: 39.465000 lon.: -74.449200 height: 50 m AGL
Trajectory Direction: Backward Duration: 48 hrs
Vertical Motion Calculation Method: Model Vertical Velocity
Meteorology: 0000Z 27 Nov 2011 - NAM12

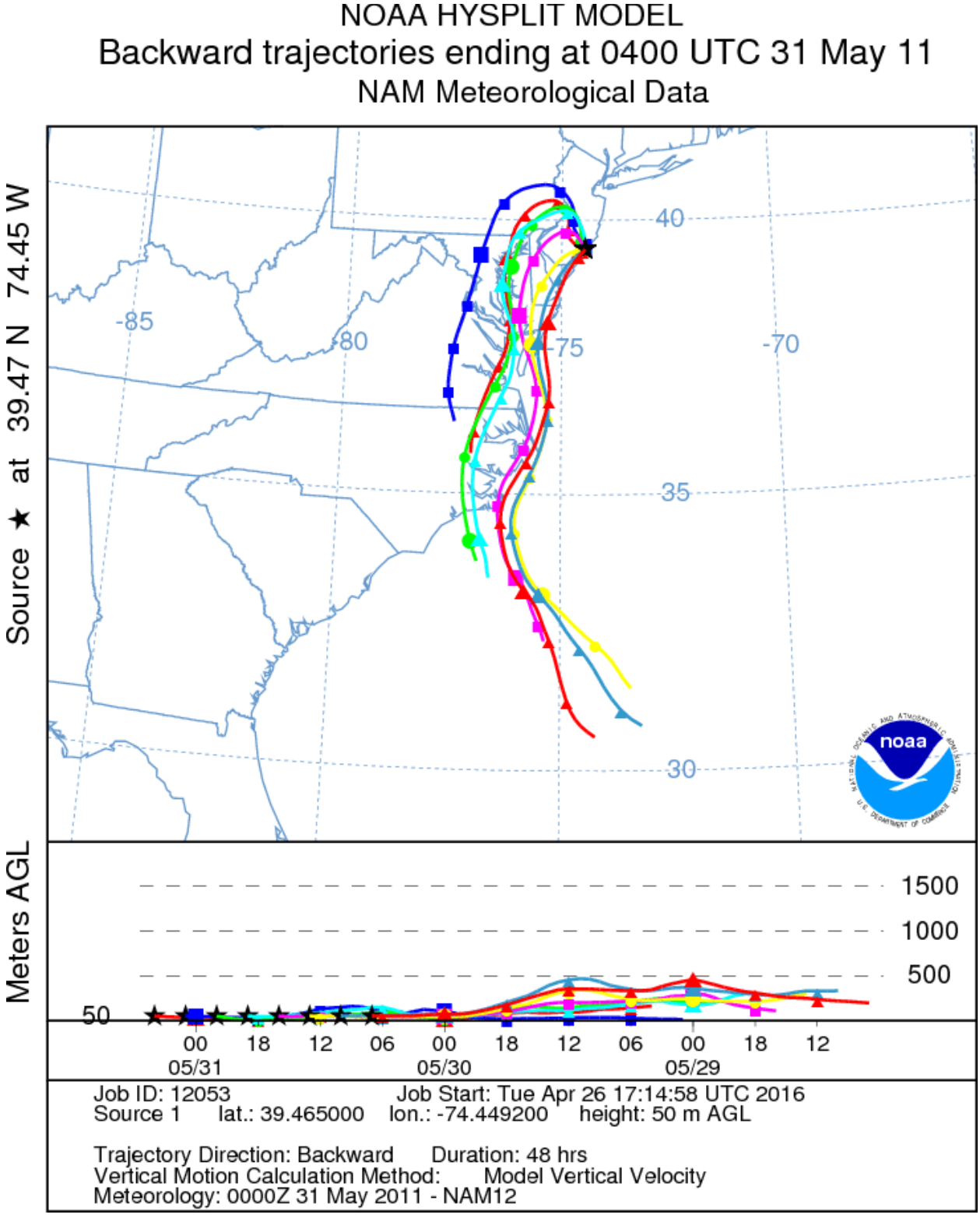
NOAA HYSPLIT MODEL
Backward trajectories ending at 0400 UTC 31 May 11
NAM Meteorological Data
Source ★ at 39.47 N 74.45 W
-85
-80
-75
-70
40
35
30
noaa
Meters AGL
1500
1000
500
50
00 18 12 06 00 18 12 06 00 18 12
05/31
05/30
05/29
Job ID: 12053 Job Start: Tue Apr 26 17:14:58 UTC 2016
Source 1 lat.: 39.465000 lon.: -74.449200 height: 50 m AGL
Trajectory Direction: Backward Duration: 48 hrs
Vertical Motion Calculation Method: Model Vertical Velocity
Meteorology: 0000Z 31 May 2011 - NAM12

NOAA HYSPLIT MODEL
Backward trajectories ending at 0400 UTC 24 Jul 11
NAM Meteorological Data

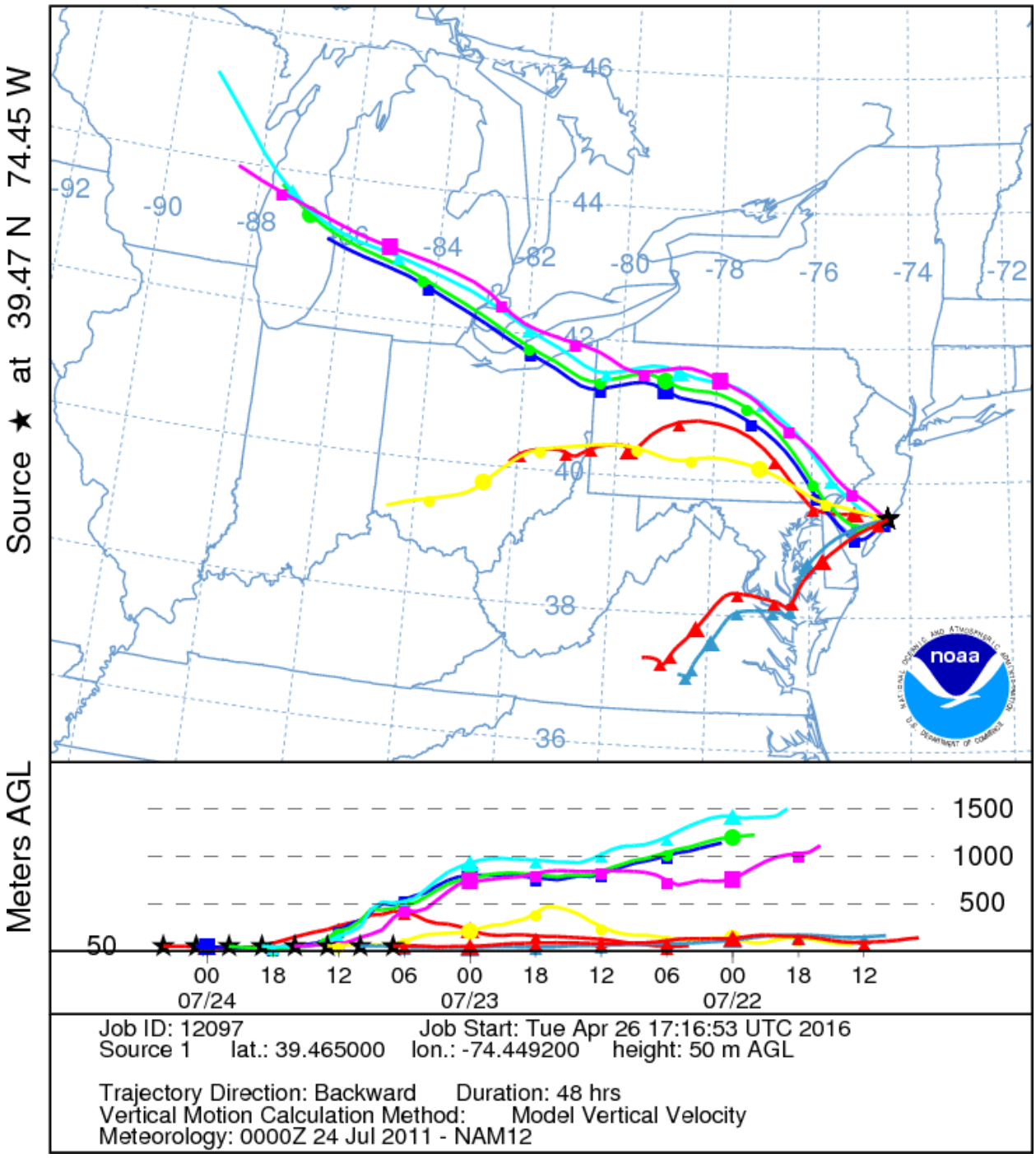

Job ID: 12097 Job Start: Tue Apr 26 17:16:53 UTC 2016
Source 1 lat.: 39.465000 lon.: -74.449200 height: 50 m AGL

Trajectory Direction: Backward Duration: 48 hrs
Vertical Motion Calculation Method: Model Vertical Velocity
Meteorology: 0000Z 24 Jul 2011 - NAM12

BRIS HYSPLIT back-trajectories

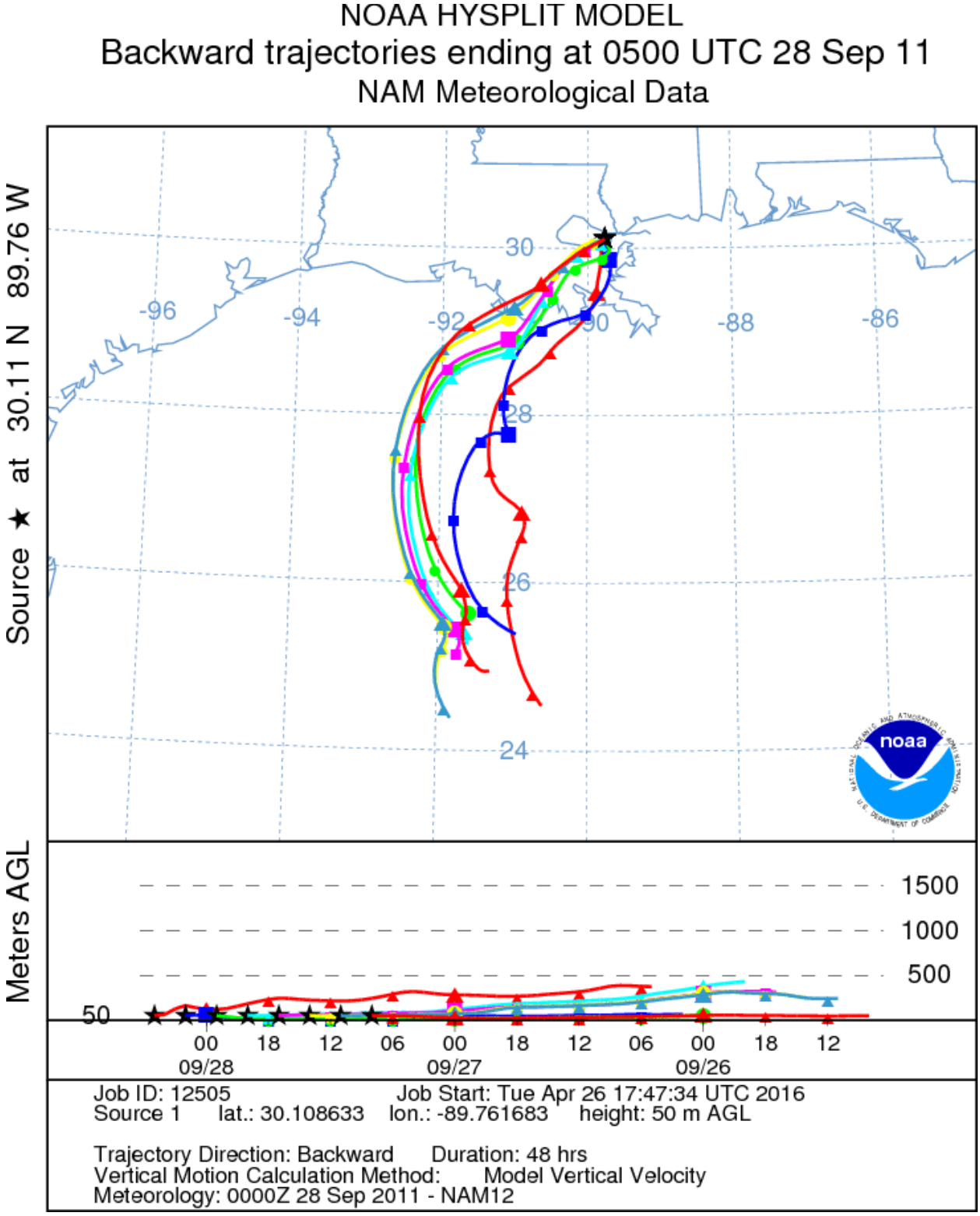
NOAA HYSPLIT MODEL
Backward trajectories ending at 0500 UTC 28 Sep 11
NAM Meteorological Data
Source ★ at 30.11 N 89.76 W
-96
-94
-92
-90
-88
-86
30
28
26
24
noaa
Meters AGL
1500
1000
500
50
00 18 12 06 00 18 12 06 00 18 12
09/28
09/27
09/26
Job ID: 12505 Job Start: Tue Apr 26 17:47:34 UTC 2016
Source 1 lat.: 30.108633 lon.: -89.761683 height: 50 m AGL
Trajectory Direction: Backward Duration: 48 hrs
Vertical Motion Calculation Method: Model Vertical Velocity
Meteorology: 0000Z 28 Sep 2011 - NAM12

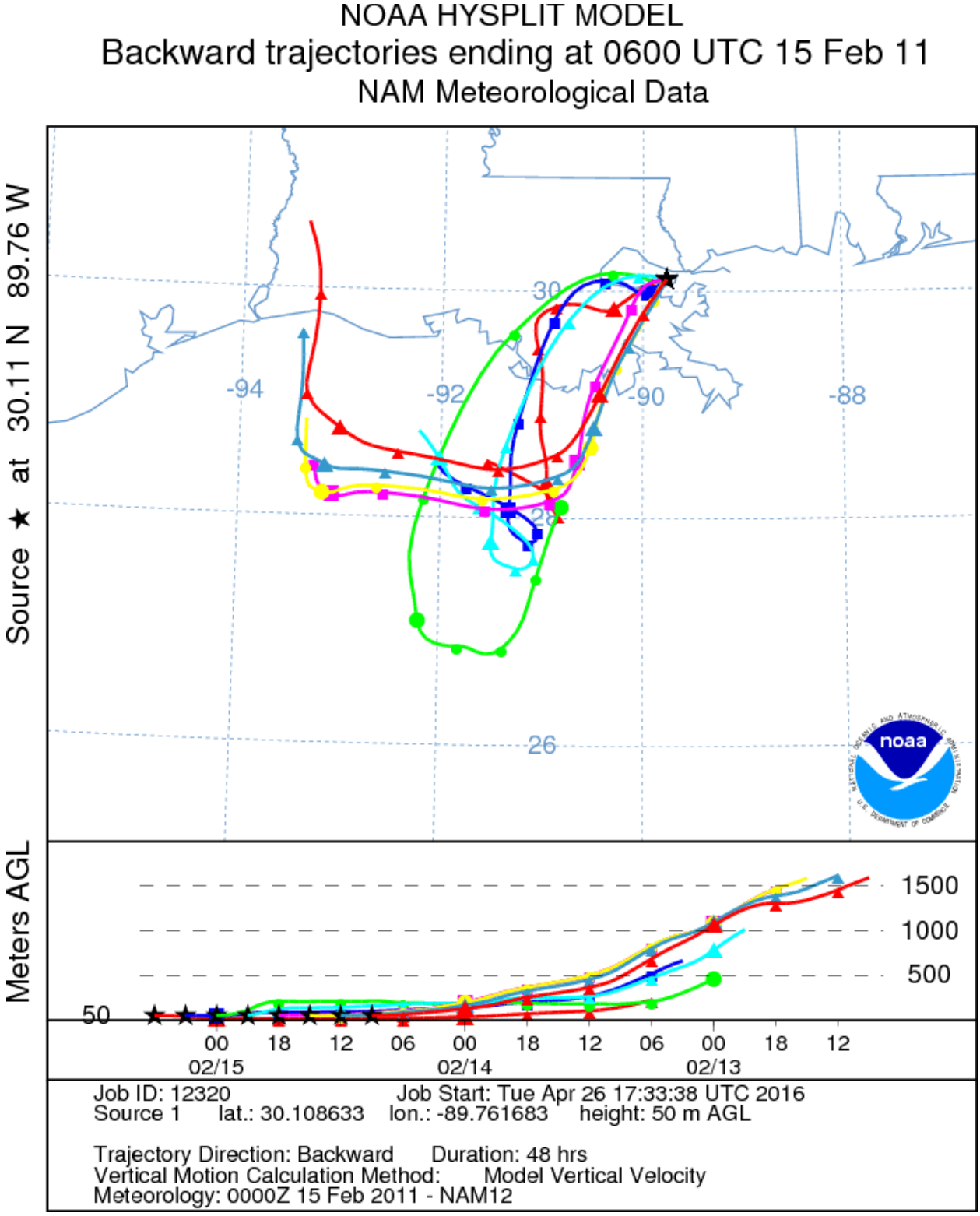
NOAA HYSPLIT MODEL
Backward trajectories ending at 0600 UTC 15 Feb 11
NAM Meteorological Data
Source ★ at 30.11 N 89.76 W
30
28
26
-94
-92
-90
-88
noaa
Meters AGL
1500
1000
500
50
00 18 12 06 00 18 12 06 00 18 12
02/15
02/14
02/13
Job ID: 12320 Job Start: Tue Apr 26 17:33:38 UTC 2016
Source 1 lat.: 30.108633 lon.: -89.761683 height: 50 m AGL
Trajectory Direction: Backward Duration: 48 hrs
Vertical Motion Calculation Method: Model Vertical Velocity
Meteorology: 0000Z 15 Feb 2011 - NAM12

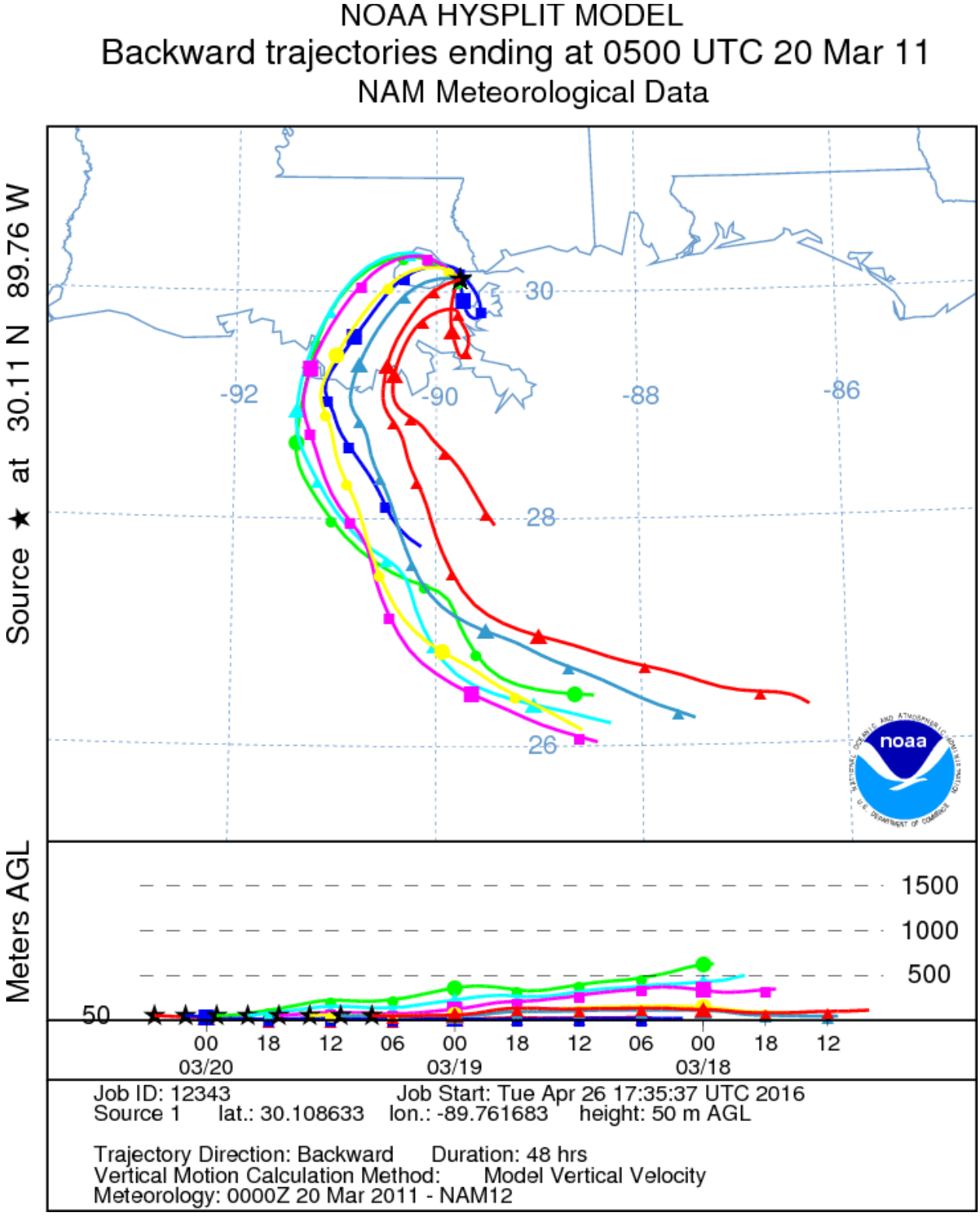
NOAA HYSPLIT MODEL
Backward trajectories ending at 0500 UTC 20 Mar 11
NAM Meteorological Data
Source ★ at 30.11 N 89.76 W
30
28
26
-92
-90
-88
-86
noaa
Meters AGL
1500
1000
500
50
00 18 12 06 00 18 12 06 00 18 12
03/20 03/19 03/18
Job ID: 12343 Job Start: Tue Apr 26 17:35:37 UTC 2016
Source 1 lat.: 30.108633 lon.: -89.761683 height: 50 m AGL
Trajectory Direction: Backward Duration: 48 hrs
Vertical Motion Calculation Method: Model Vertical Velocity
Meteorology: 0000Z 20 Mar 2011 - NAM12

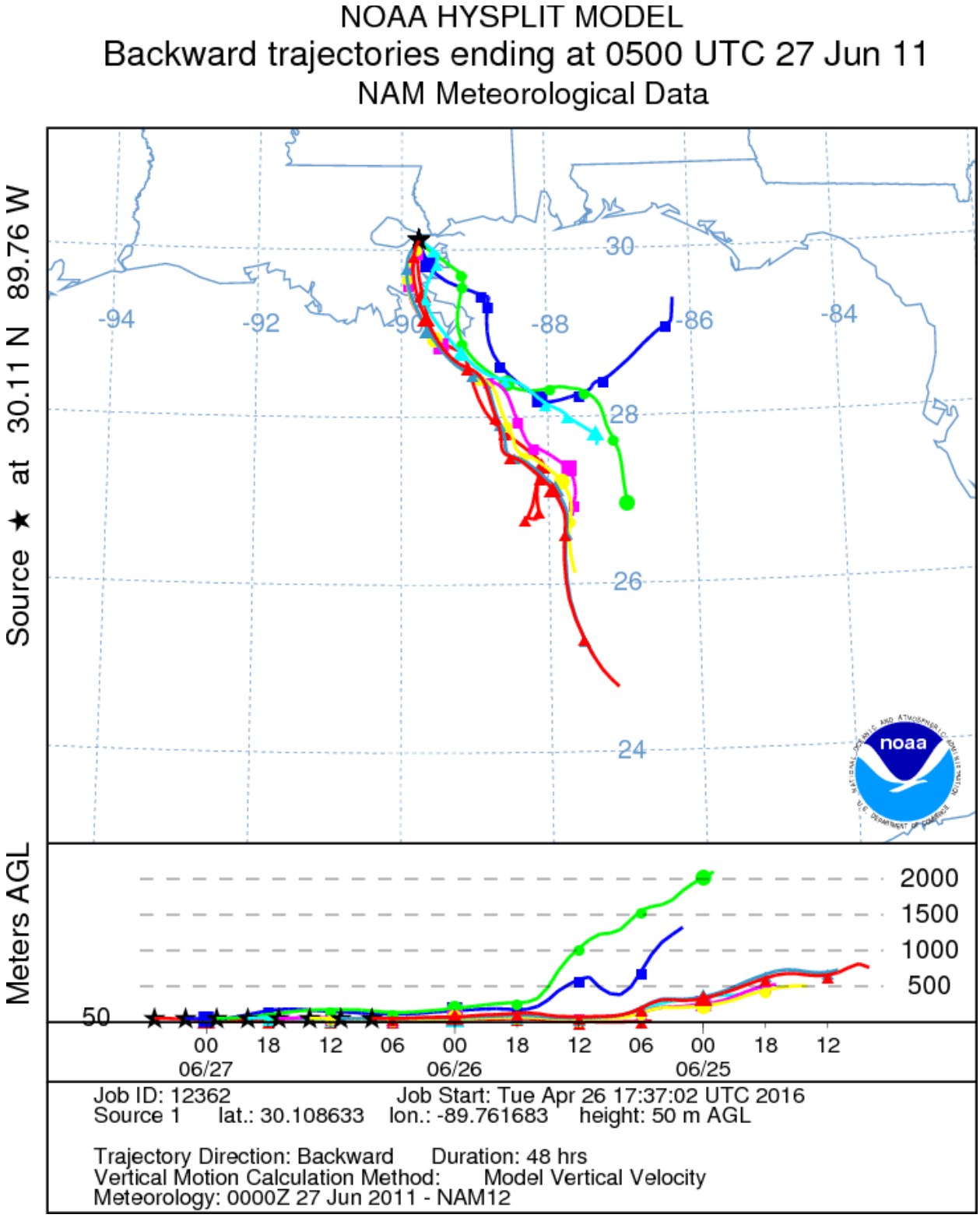
NOAA HYSPLIT MODEL
Backward trajectories ending at 0500 UTC 27 Jun 11
NAM Meteorological Data
Source ★ at 30.11 N 89.76 W
-94
-92
-90
-88
-86
-84
30
28
26
24
noaa
Meters AGL
2000
1500
1000
500
50
00 18 12 06 00 18 12 06 00 18 12
06/27 06/26 06/25
Job ID: 12362 Job Start: Tue Apr 26 17:37:02 UTC 2016
Source 1 lat.: 30.108633 lon.: -89.761683 height: 50 m AGL
Trajectory Direction: Backward Duration: 48 hrs
Vertical Motion Calculation Method: Model Vertical Velocity
Meteorology: 0000Z 27 Jun 2011 - NAM12

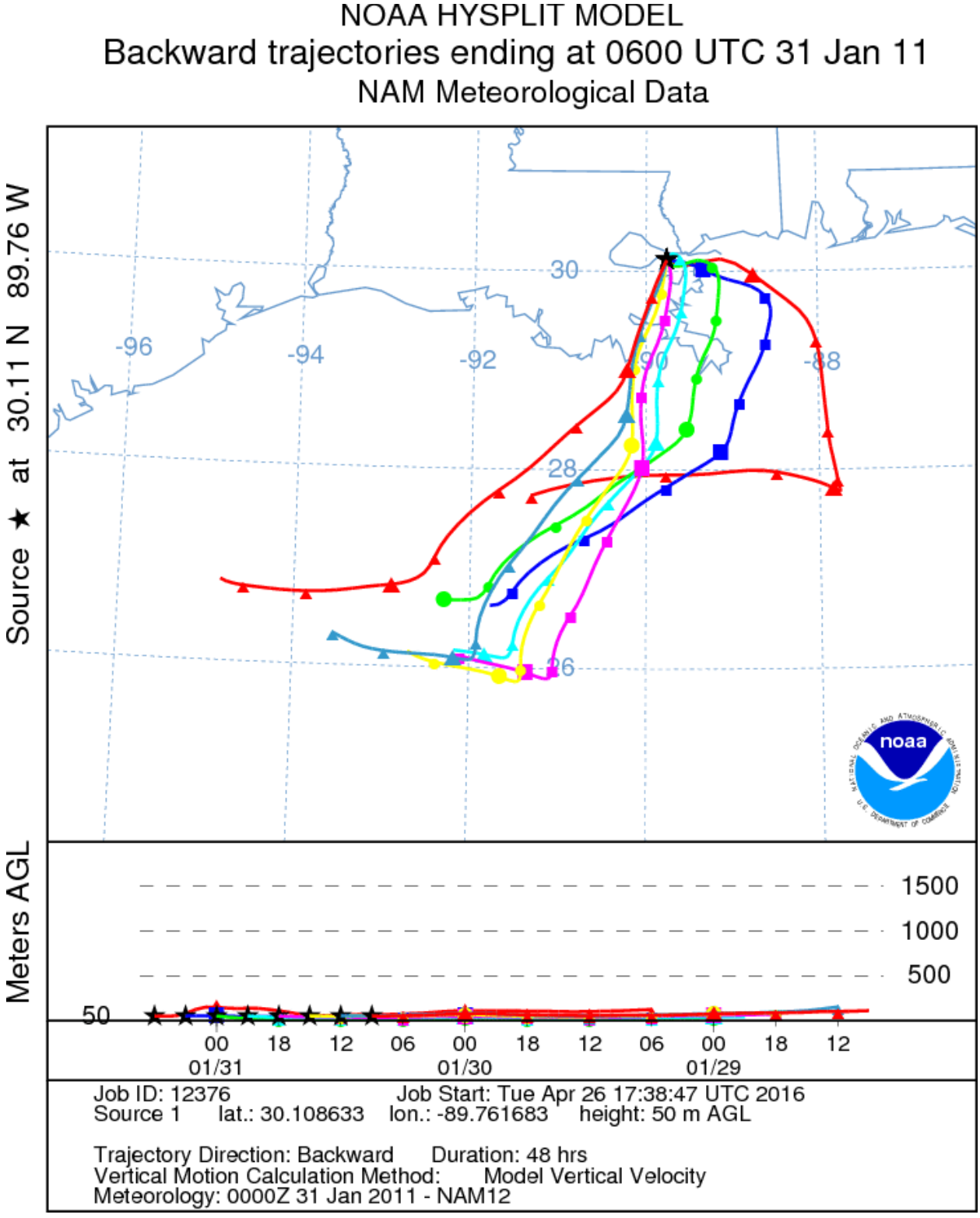
NOAA HYSPLIT MODEL
Backward trajectories ending at 0600 UTC 31 Jan 11
NAM Meteorological Data
Source ★ at 30.11 N 89.76 W
-96
-94
-92
-90
-88
30
28
26
noaa
Meters AGL
1500
1000
500
50
00 18 12 06 00 18 12 06 00 18 12
01/31
01/30
01/29
Job ID: 12376 Job Start: Tue Apr 26 17:38:47 UTC 2016
Source 1 lat.: 30.108633 lon.: -89.761683 height: 50 m AGL
Trajectory Direction: Backward Duration: 48 hrs
Vertical Motion Calculation Method: Model Vertical Velocity
Meteorology: 0000Z 31 Jan 2011 - NAM12

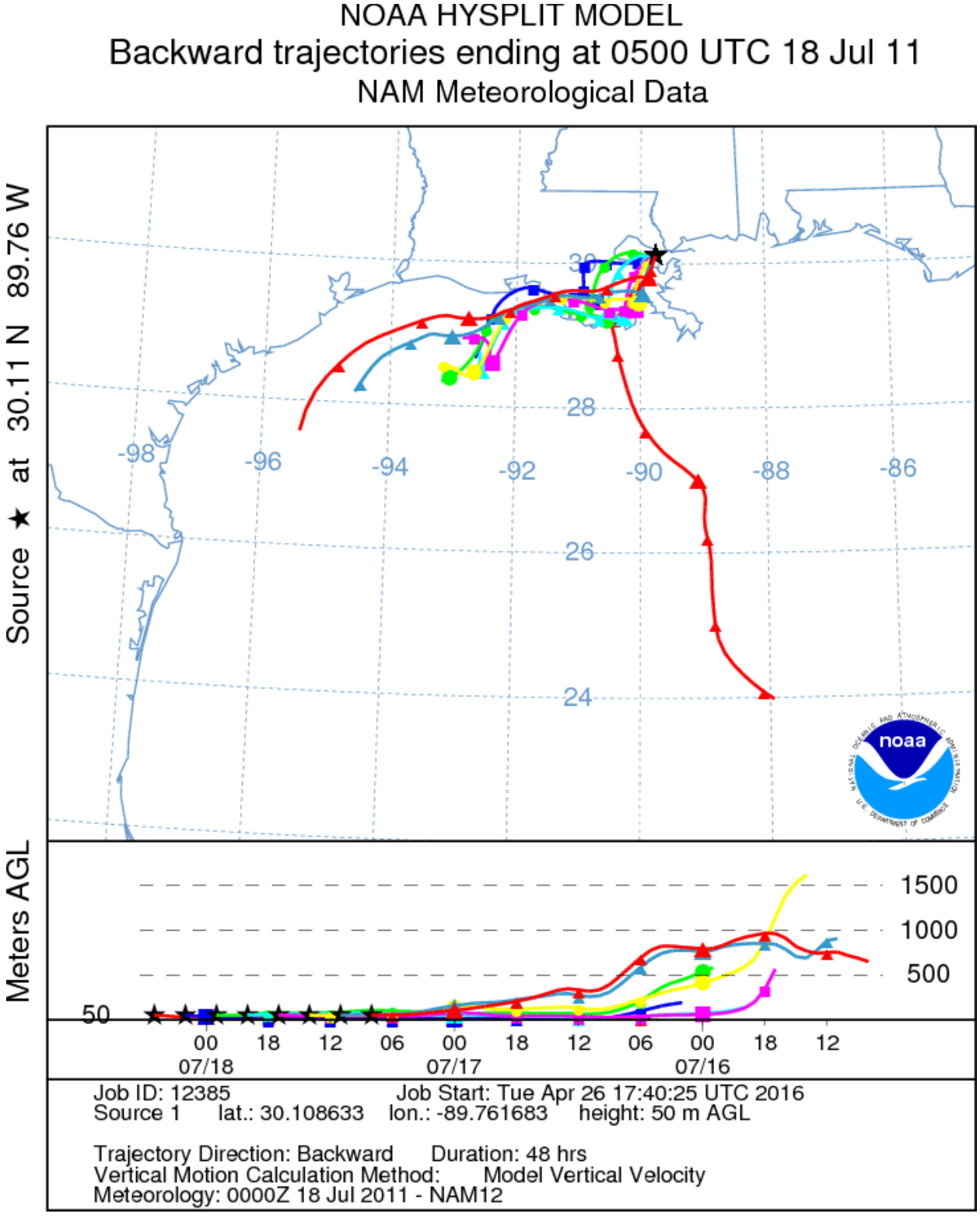
NOAA HYSPLIT MODEL
Backward trajectories ending at 0500 UTC 18 Jul 11
NAM Meteorological Data
Source ★ at 30.11 N 89.76 W
-98
-96
-94
-92
-90
-88
-86
28
26
24
noaa
Meters AGL
1500
1000
500
50
00 18 12 06 00 18 12 06 00 18 12
07/18
07/17
07/16
Job ID: 12385 Job Start: Tue Apr 26 17:40:25 UTC 2016
Source 1 lat.: 30.108633 lon.: -89.761683 height: 50 m AGL
Trajectory Direction: Backward Duration: 48 hrs
Vertical Motion Calculation Method: Model Vertical Velocity
Meteorology: 0000Z 18 Jul 2011 - NAM12

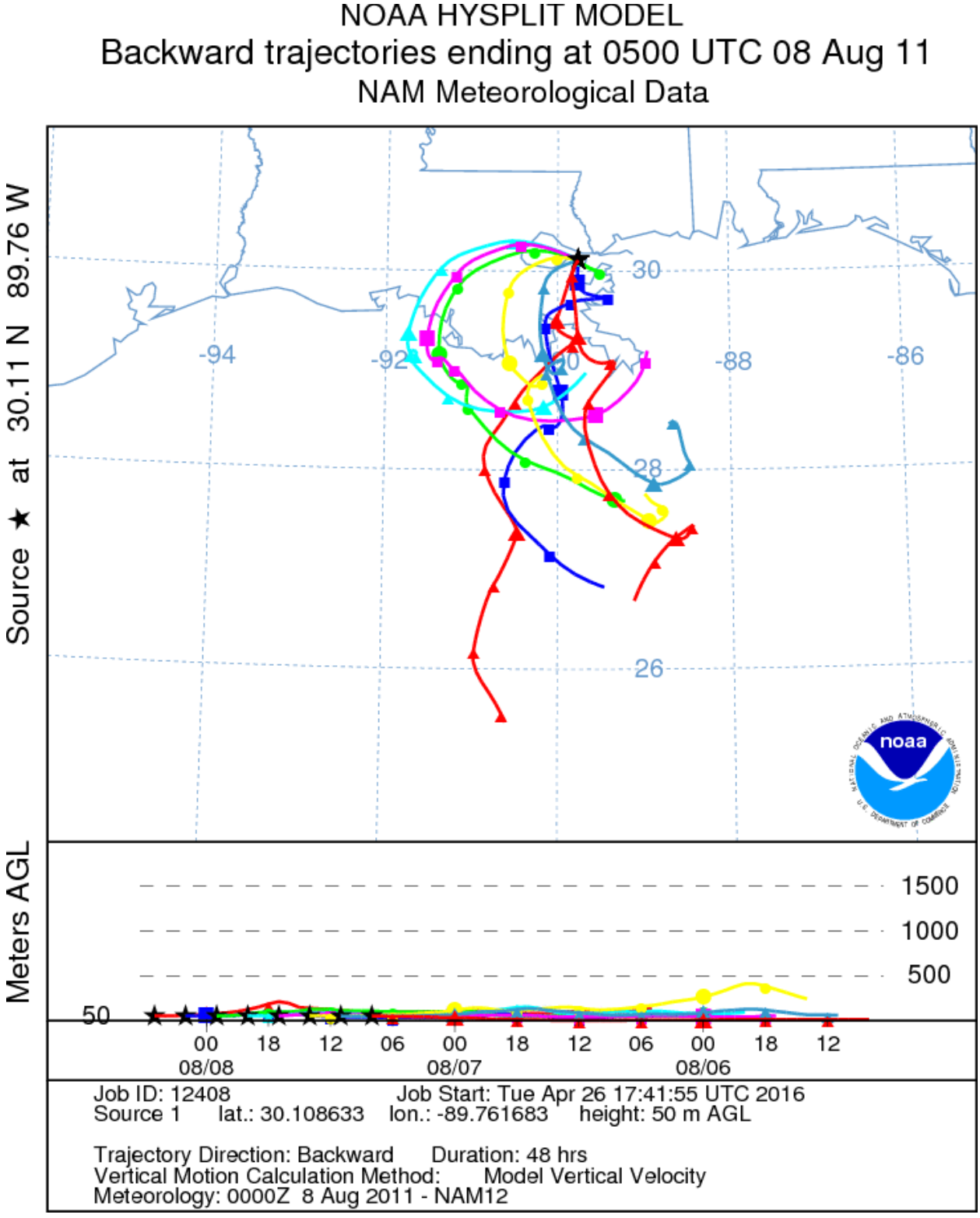
NOAA HYSPLIT MODEL
Backward trajectories ending at 0500 UTC 08 Aug 11
NAM Meteorological Data
Source ★ at 30.11 N 89.76 W
-94
-92
-90
-88
-86
30
28
26
noaa
Meters AGL
1500
1000
500
50
00 18 12 06 00 18 12 06 00 18 12
08/08 08/07 08/06
Job ID: 12408 Job Start: Tue Apr 26 17:41:55 UTC 2016
Source 1 lat.: 30.108633 lon.: -89.761683 height: 50 m AGL
Trajectory Direction: Backward Duration: 48 hrs
Vertical Motion Calculation Method: Model Vertical Velocity
Meteorology: 0000Z 8 Aug 2011 - NAM12

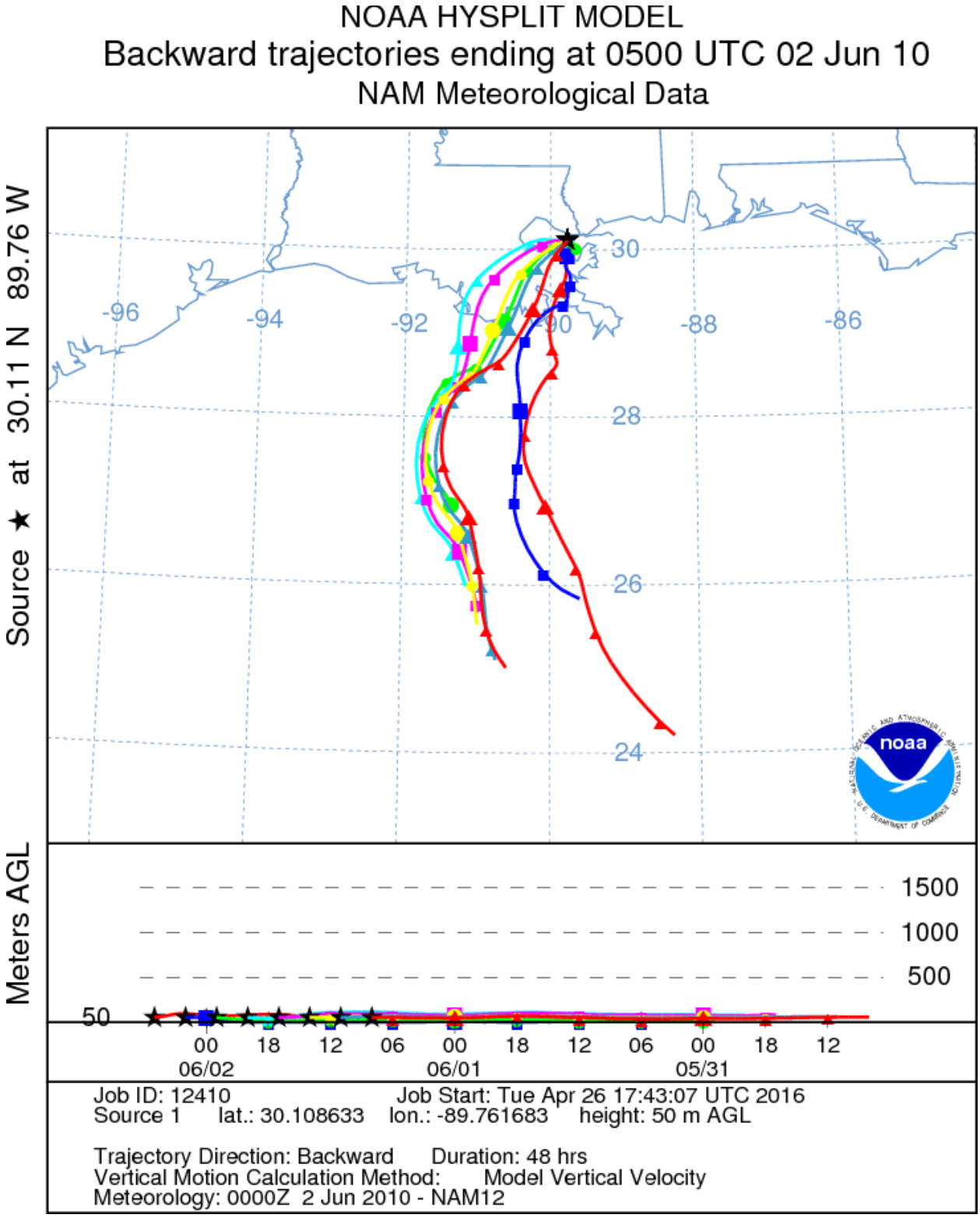
NOAA HYSPLIT MODEL
Backward trajectories ending at 0500 UTC 02 Jun 10
NAM Meteorological Data
Source ★ at 30.11 N 89.76 W
-96
-94
-92
-90
-88
-86
30
28
26
24
noaa
Meters AGL
1500
1000
500
50
00 18 12 06 00 18 12 06 00 18 12
06/02 06/01 05/31
Job ID: 12410 Job Start: Tue Apr 26 17:43:07 UTC 2016
Source 1 lat.: 30.108633 lon.: -89.761683 height: 50 m AGL
Trajectory Direction: Backward Duration: 48 hrs
Vertical Motion Calculation Method: Model Vertical Velocity
Meteorology: 0000Z 2 Jun 2010 - NAM12

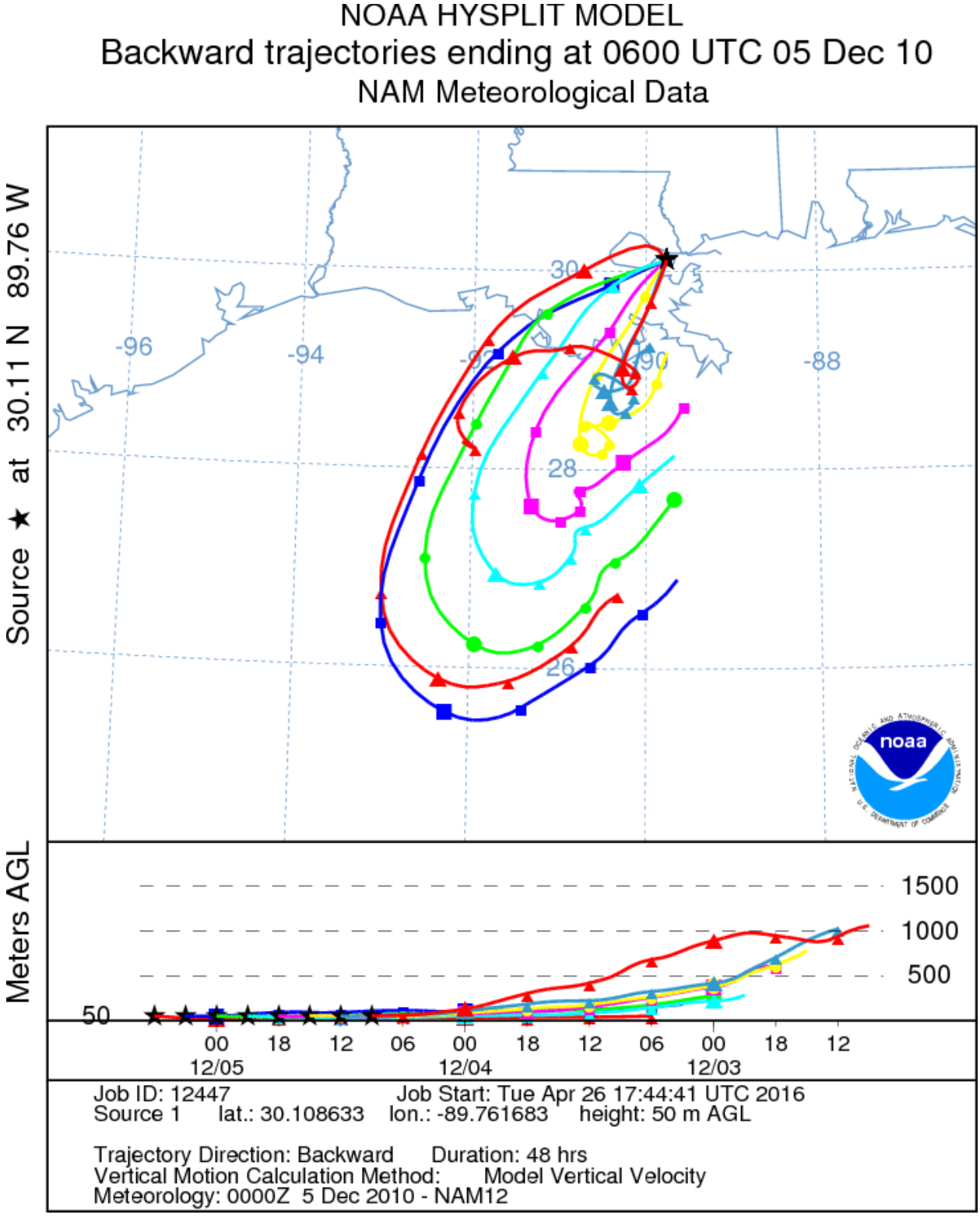
NOAA HYSPLIT MODEL
Backward trajectories ending at 0600 UTC 05 Dec 10
NAM Meteorological Data
Source ★ at 30.11 N 89.76 W
-96
-94
-92
-90
-88
30
28
26
noaa
Meters AGL
1500
1000
500
50
00 18 12 06 00 18 12 06 00 18 12
12/05
12/04
12/03
Job ID: 12447 Job Start: Tue Apr 26 17:44:41 UTC 2016
Source 1 lat.: 30.108633 lon.: -89.761683 height: 50 m AGL
Trajectory Direction: Backward Duration: 48 hrs
Vertical Motion Calculation Method: Model Vertical Velocity
Meteorology: 0000Z 5 Dec 2010 - NAM12

NOAA HYSPLIT MODEL
Backward trajectories ending at 0500 UTC 18 Jun 11
NAM Meteorological Data

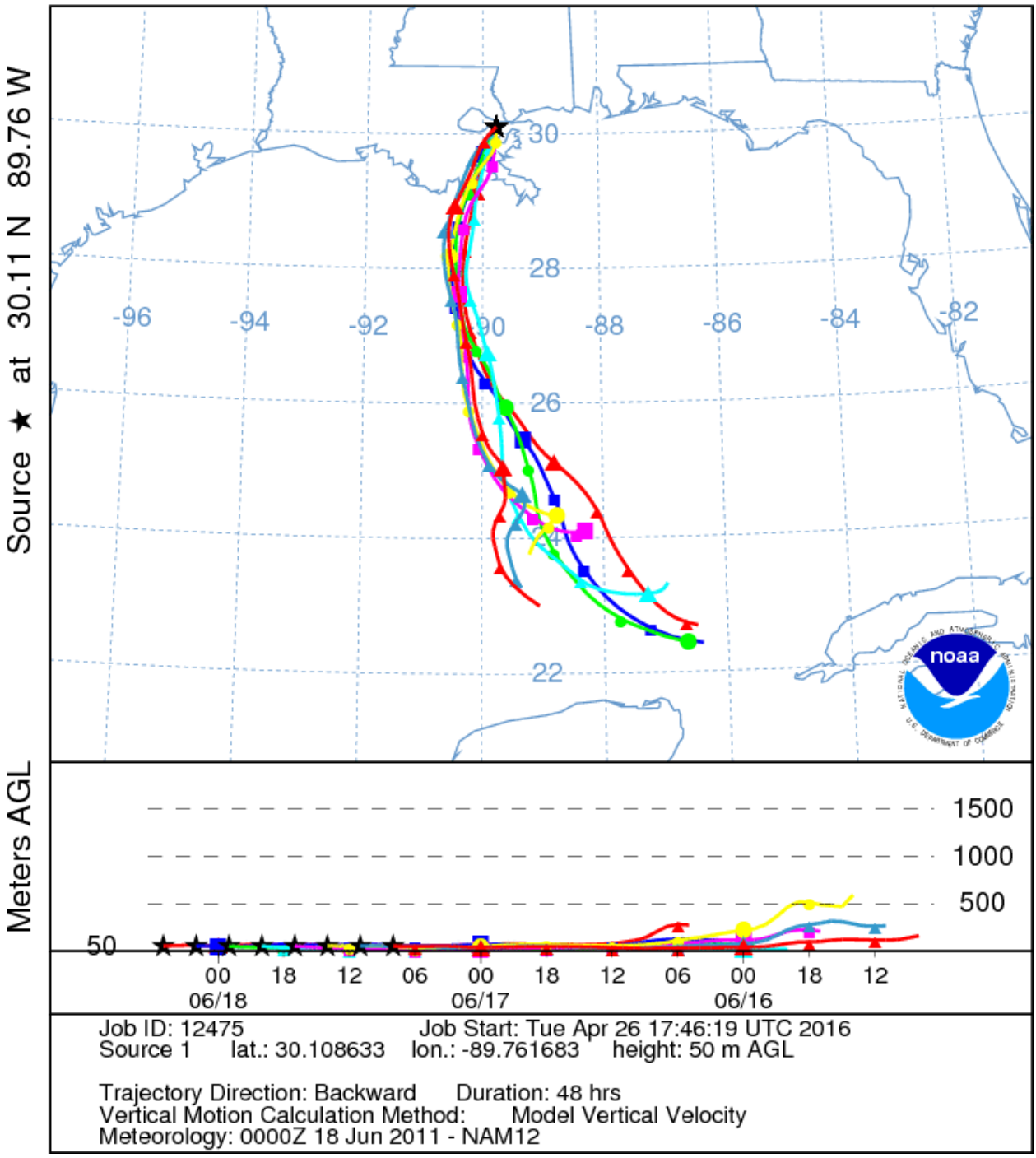

CABA HYSPLIT back-trajectories

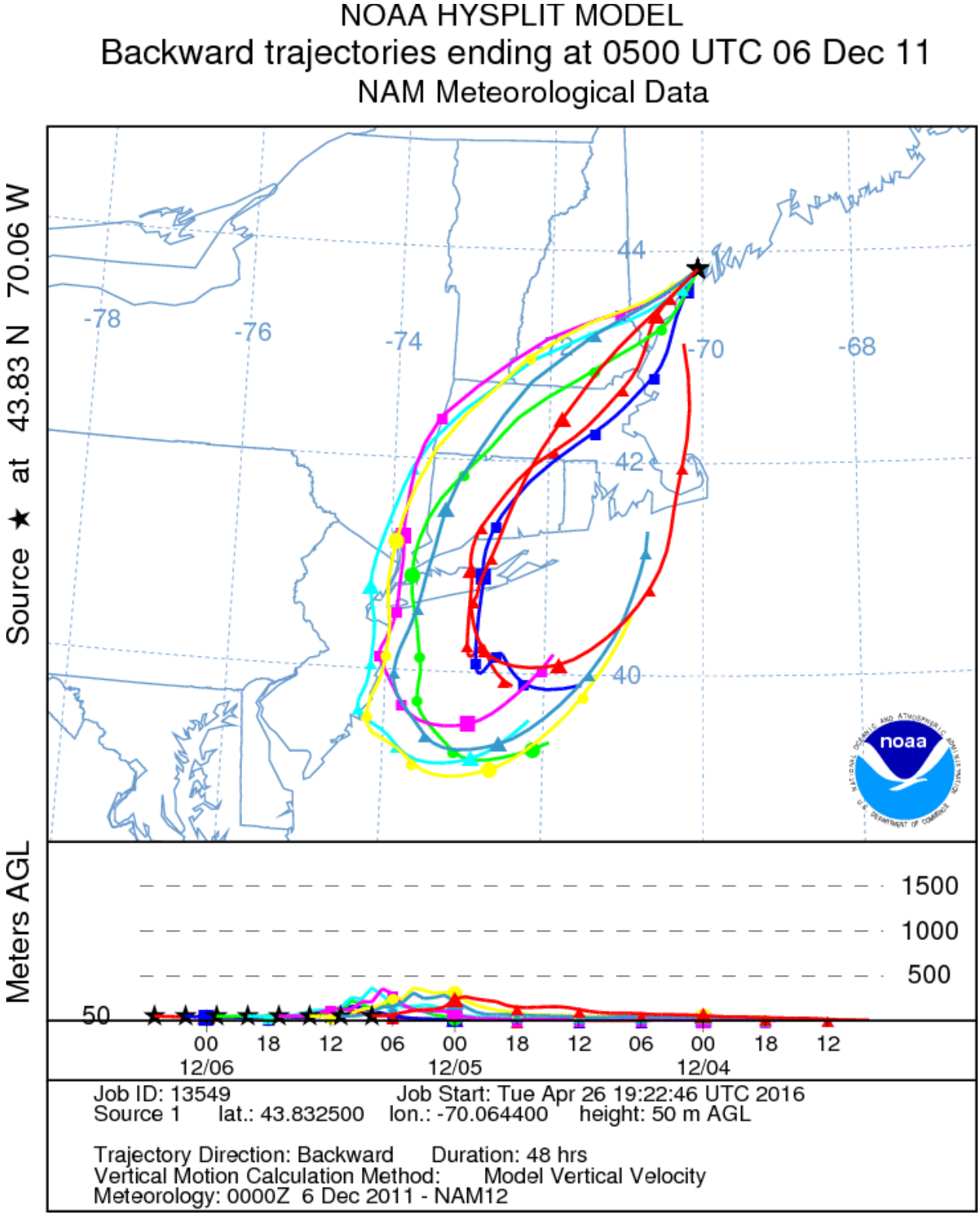
NOAA HYSPLIT MODEL
Backward trajectories ending at 0500 UTC 06 Dec 11
NAM Meteorological Data
Source ★ at 43.83 N 70.06 W
-78
-76
-74
-70
-68
44
42
40
noaa
Meters AGL
1500
1000
500
50
00 18 12 06 00 18 12 06 00 18 12
12/06 12/05 12/04
Job ID: 13549 Job Start: Tue Apr 26 19:22:46 UTC 2016
Source 1 lat.: 43.832500 lon.: -70.064400 height: 50 m AGL
Trajectory Direction: Backward Duration: 48 hrs
Vertical Motion Calculation Method: Model Vertical Velocity
Meteorology: 0000Z 6 Dec 2011 - NAM12

NOAA HYSPLIT MODEL
Backward trajectories ending at 0400 UTC 03 May 10
NAM Meteorological Data

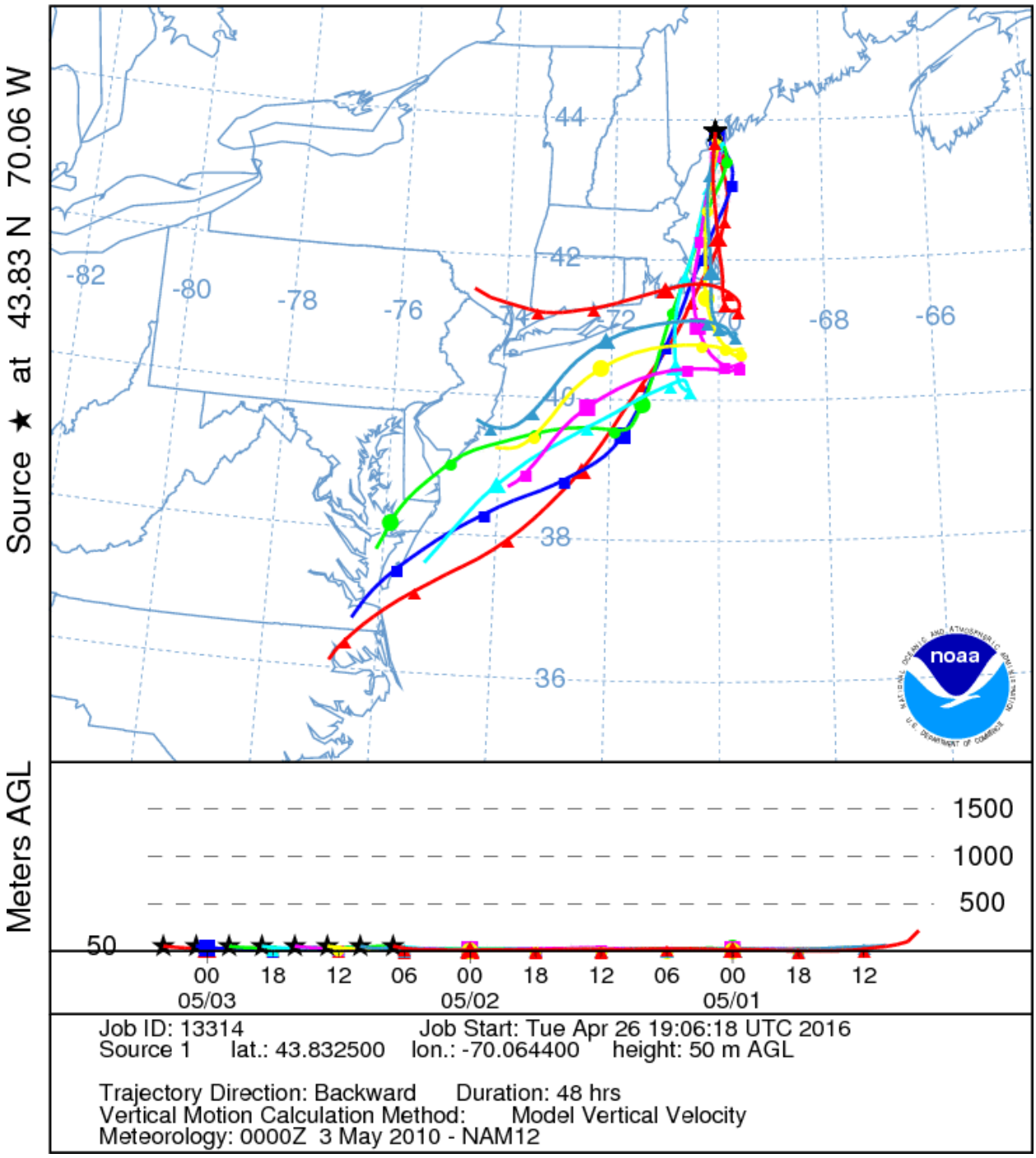

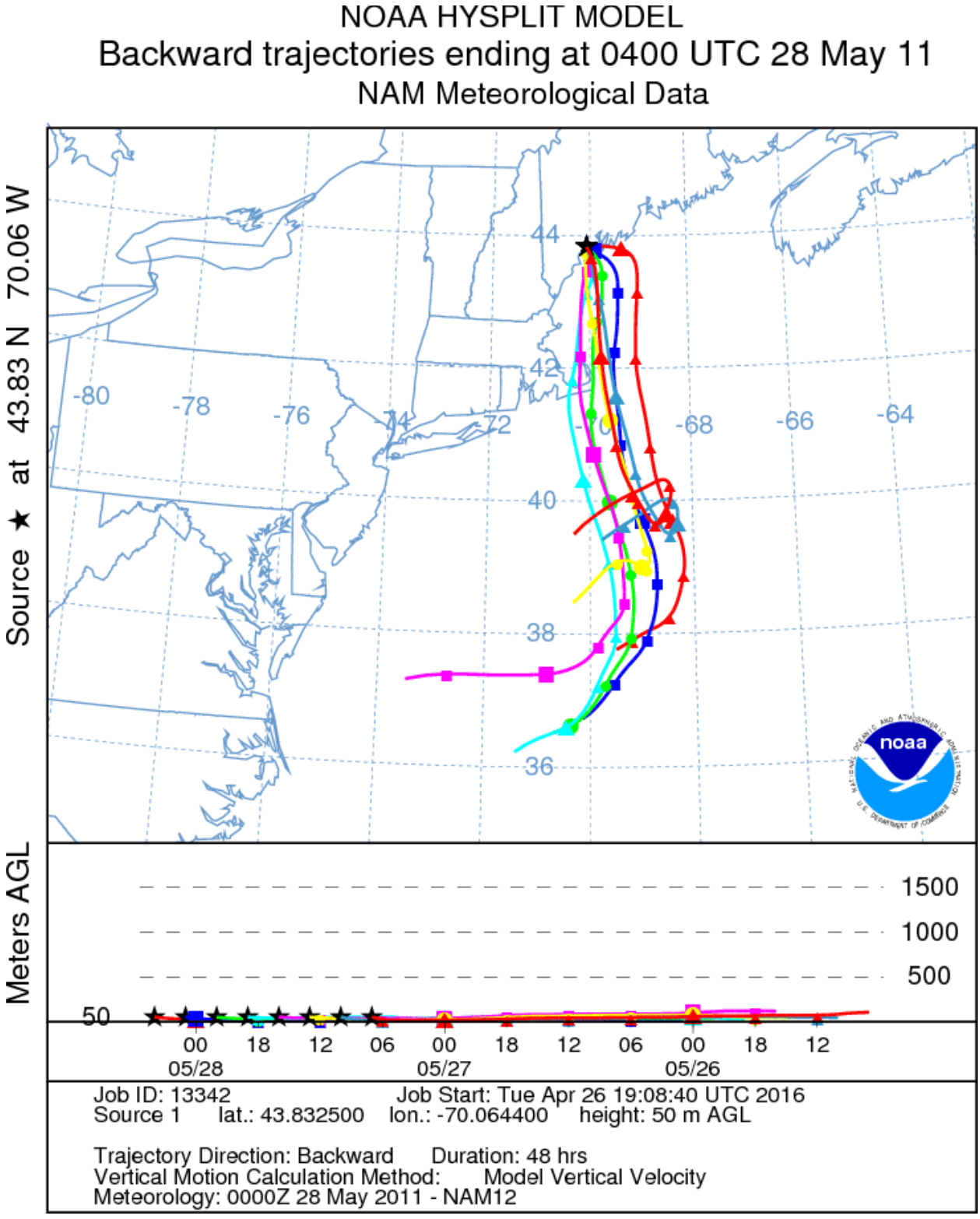
NOAA HYSPLIT MODEL
Backward trajectories ending at 0400 UTC 28 May 11
NAM Meteorological Data
Source ★ at 43.83 N 70.06 W
Meters AGL
1500
1000
500
50
00 18 12 06 00 18 12 06 00 18 12
05/28 05/27 05/26
Job ID: 13342 Job Start: Tue Apr 26 19:08:40 UTC 2016
Source 1 lat.: 43.832500 lon.: -70.064400 height: 50 m AGL
Trajectory Direction: Backward Duration: 48 hrs
Vertical Motion Calculation Method: Model Vertical Velocity
Meteorology: 0000Z 28 May 2011 - NAM12

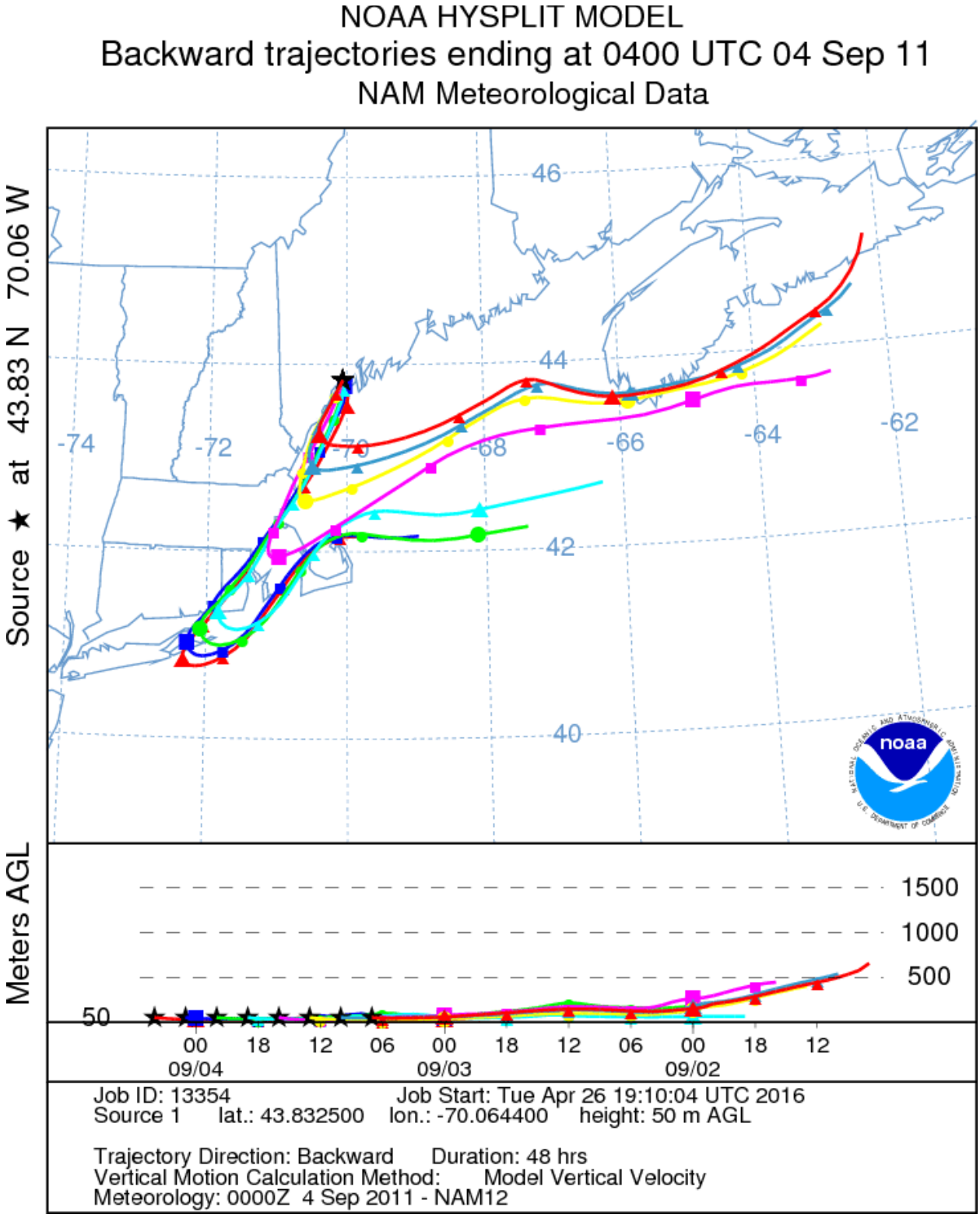
NOAA HYSPLIT MODEL
Backward trajectories ending at 0400 UTC 04 Sep 11
NAM Meteorological Data
Source ★ at 43.83 N 70.06 W
46
44
42
40
-74
-72
-70
-68
-66
-64
-62
noaa
Meters AGL
1500
1000
500
50
00 18 12 06 00 18 12 06 00 18 12
09/04
09/03
09/02
Job ID: 13354 Job Start: Tue Apr 26 19:10:04 UTC 2016
Source 1 lat.: 43.832500 lon.: -70.064400 height: 50 m AGL
Trajectory Direction: Backward Duration: 48 hrs
Vertical Motion Calculation Method: Model Vertical Velocity
Meteorology: 0000Z 4 Sep 2011 - NAM12

NOAA HYSPLIT MODEL
Backward trajectories ending at 0400 UTC 09 Jun 11
NAM Meteorological Data

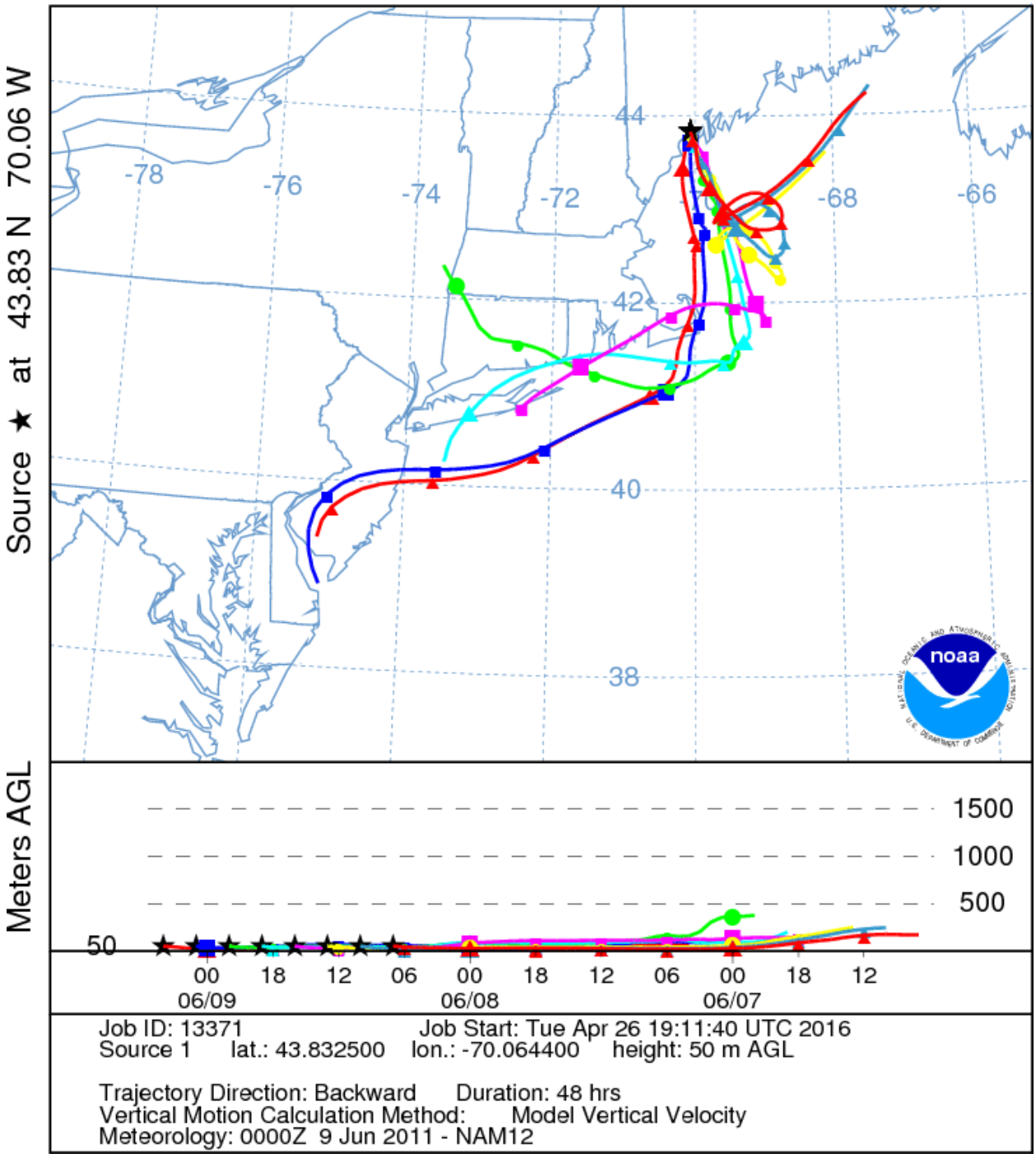

Job ID: 13371 Job Start: Tue Apr 26 19:11:40 UTC 2016
Source 1 lat.: 43.832500 lon.: -70.064400 height: 50 m AGL

Trajectory Direction: Backward Duration: 48 hrs
Vertical Motion Calculation Method: Model Vertical Velocity
Meteorology: 0000Z 9 Jun 2011 - NAM12

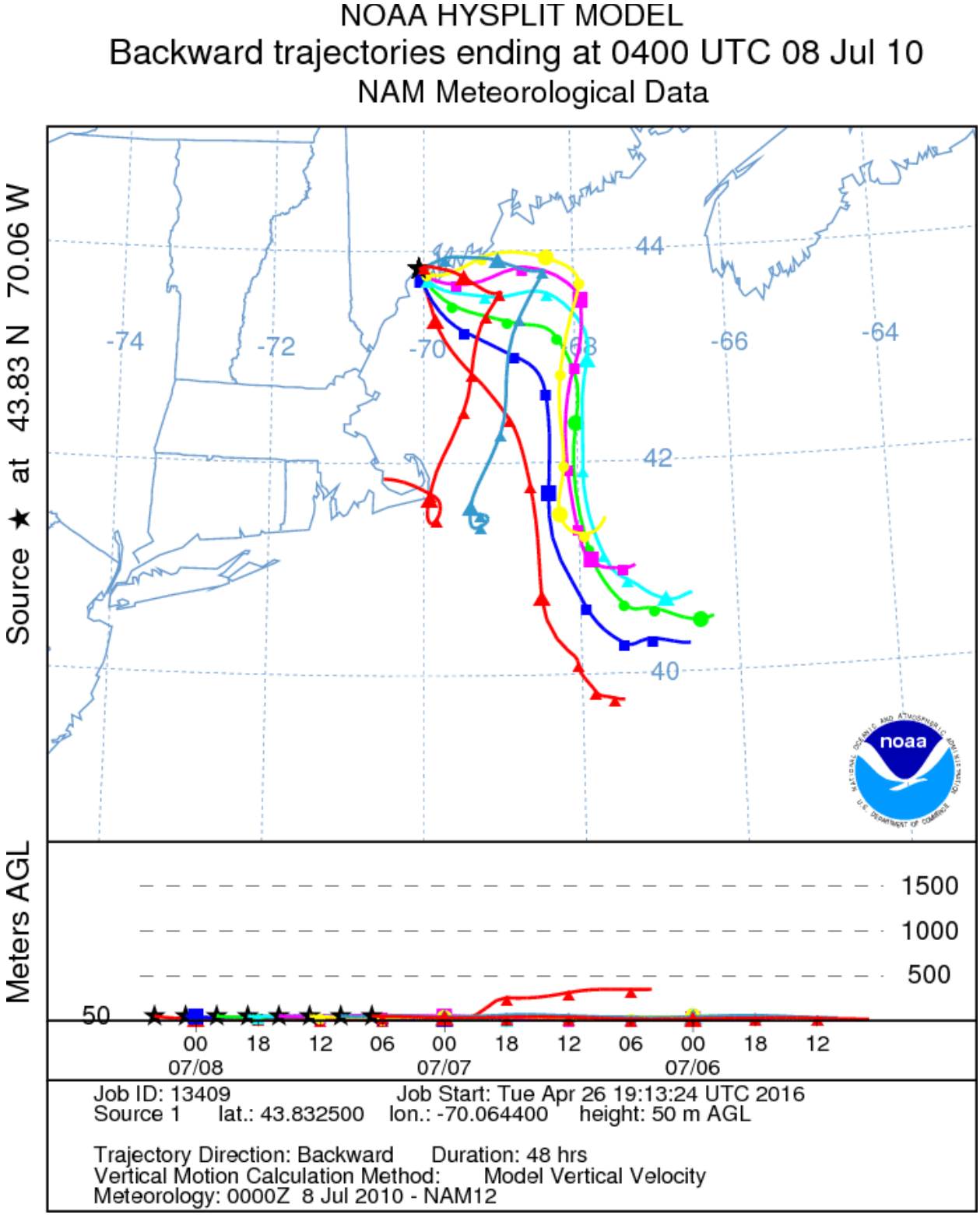
NOAA HYSPLIT MODEL
Backward trajectories ending at 0400 UTC 08 Jul 10
NAM Meteorological Data
Source ★ at 43.83 N 70.06 W
-74
-72
-70
-66
-64
44
42
40
noaa
Meters AGL
1500
1000
500
50
00 18 12 06 00 18 12 06 00 18 12
07/08
07/07
07/06
Job ID: 13409 Job Start: Tue Apr 26 19:13:24 UTC 2016
Source 1 lat.: 43.832500 lon.: -70.064400 height: 50 m AGL
Trajectory Direction: Backward Duration: 48 hrs
Vertical Motion Calculation Method: Model Vertical Velocity
Meteorology: 0000Z 8 Jul 2010 - NAM12

NOAA HYSPLIT MODEL
Backward trajectories ending at 0400 UTC 01 Oct 11
NAM Meteorological Data

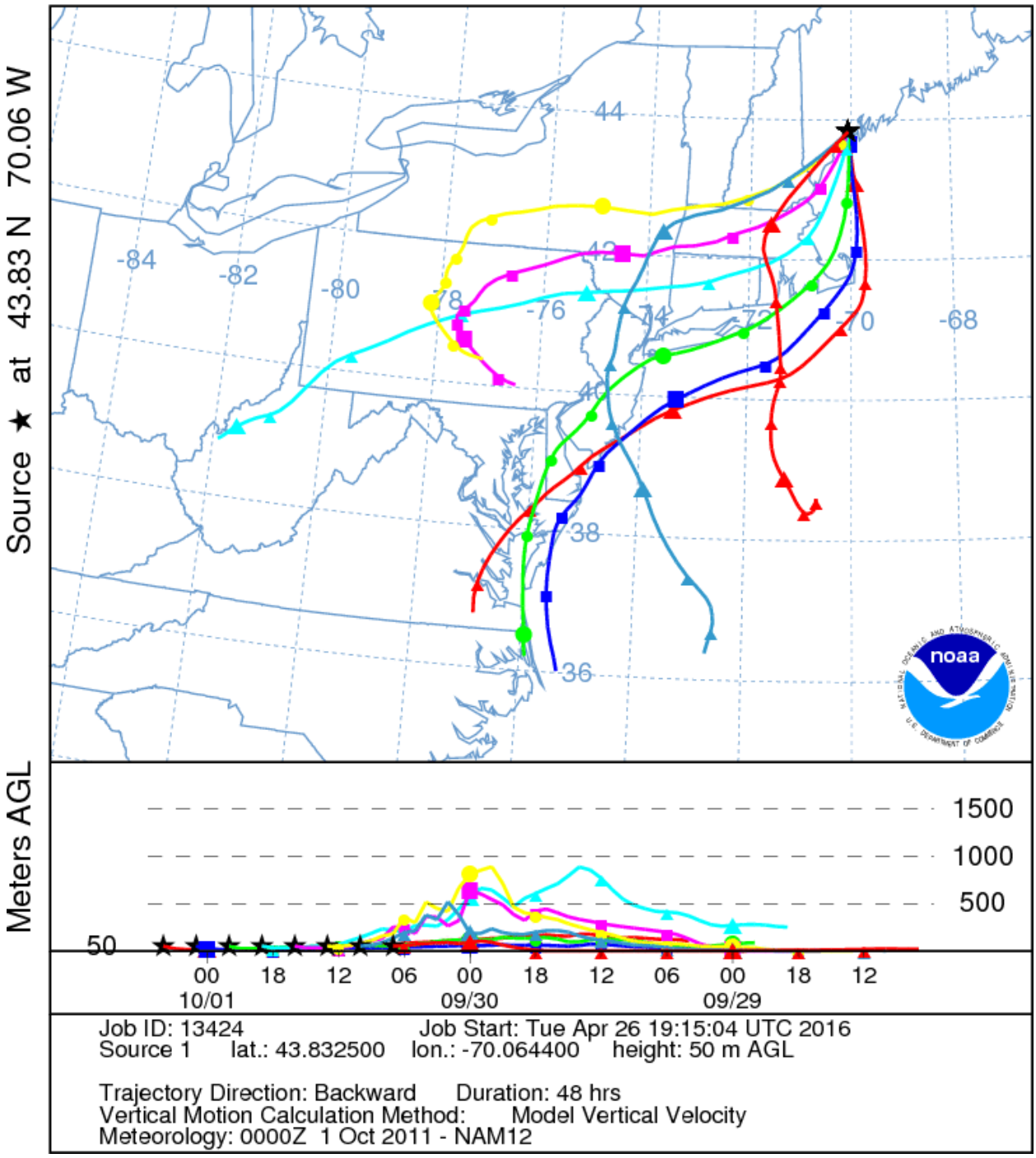

Job ID: 13424 Job Start: Tue Apr 26 19:15:04 UTC 2016
Source 1 lat.: 43.832500 lon.: -70.064400 height: 50 m AGL

Trajectory Direction: Backward Duration: 48 hrs
Vertical Motion Calculation Method: Model Vertical Velocity
Meteorology: 0000Z 1 Oct 2011 - NAM12

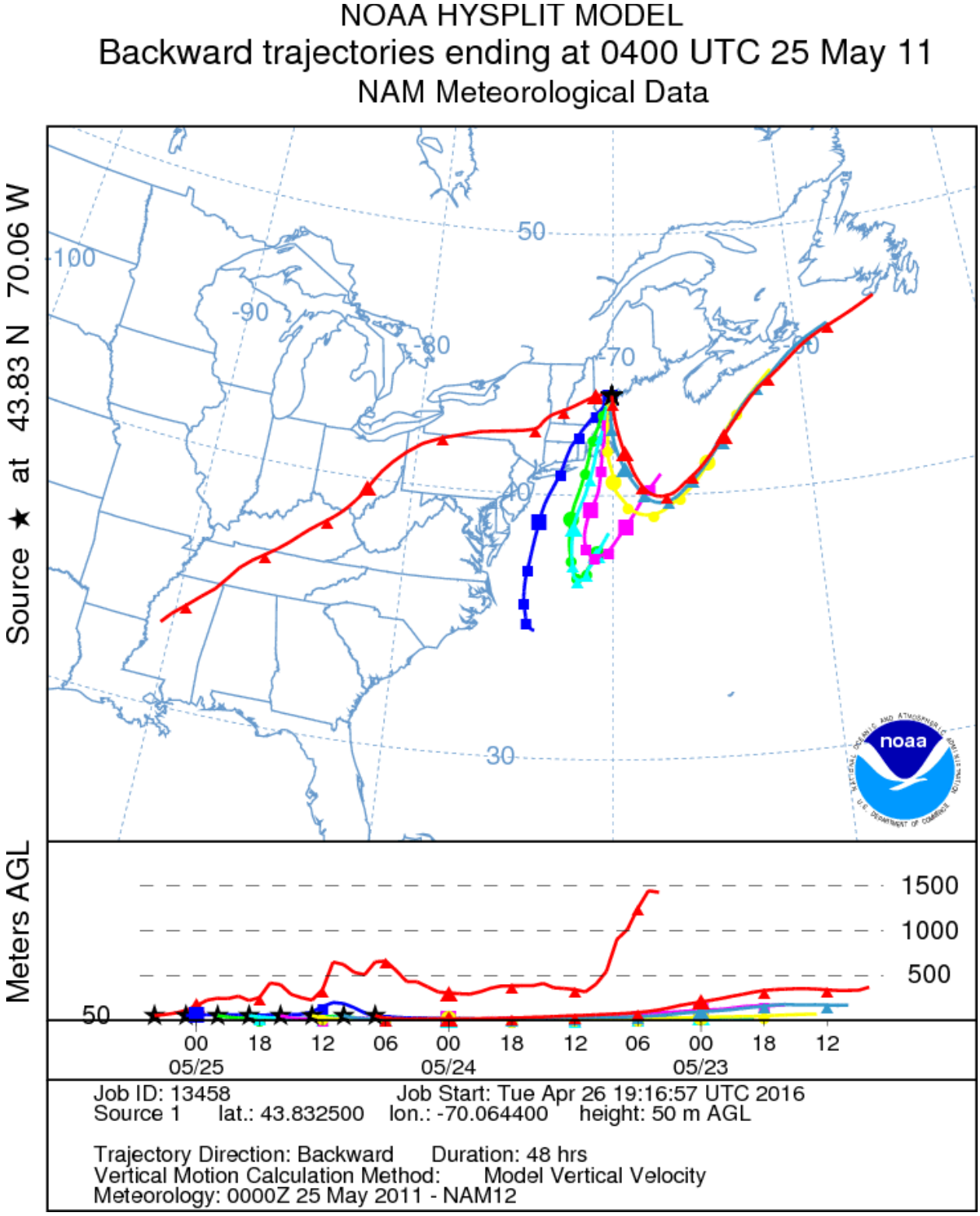
NOAA HYSPLIT MODEL
Backward trajectories ending at 0400 UTC 25 May 11
NAM Meteorological Data
Source ★ at 43.83 N 70.06 W
-100
-90
-80
-70
-60
50
40
30
noaa
Meters AGL
1500
1000
500
50
00 18 12 06 00 18 12 06 00 18 12
05/25 05/24 05/23
Job ID: 13458 Job Start: Tue Apr 26 19:16:57 UTC 2016
Source 1 lat.: 43.832500 lon.: -70.064400 height: 50 m AGL
Trajectory Direction: Backward Duration: 48 hrs
Vertical Motion Calculation Method: Model Vertical Velocity
Meteorology: 0000Z 25 May 2011 - NAM12

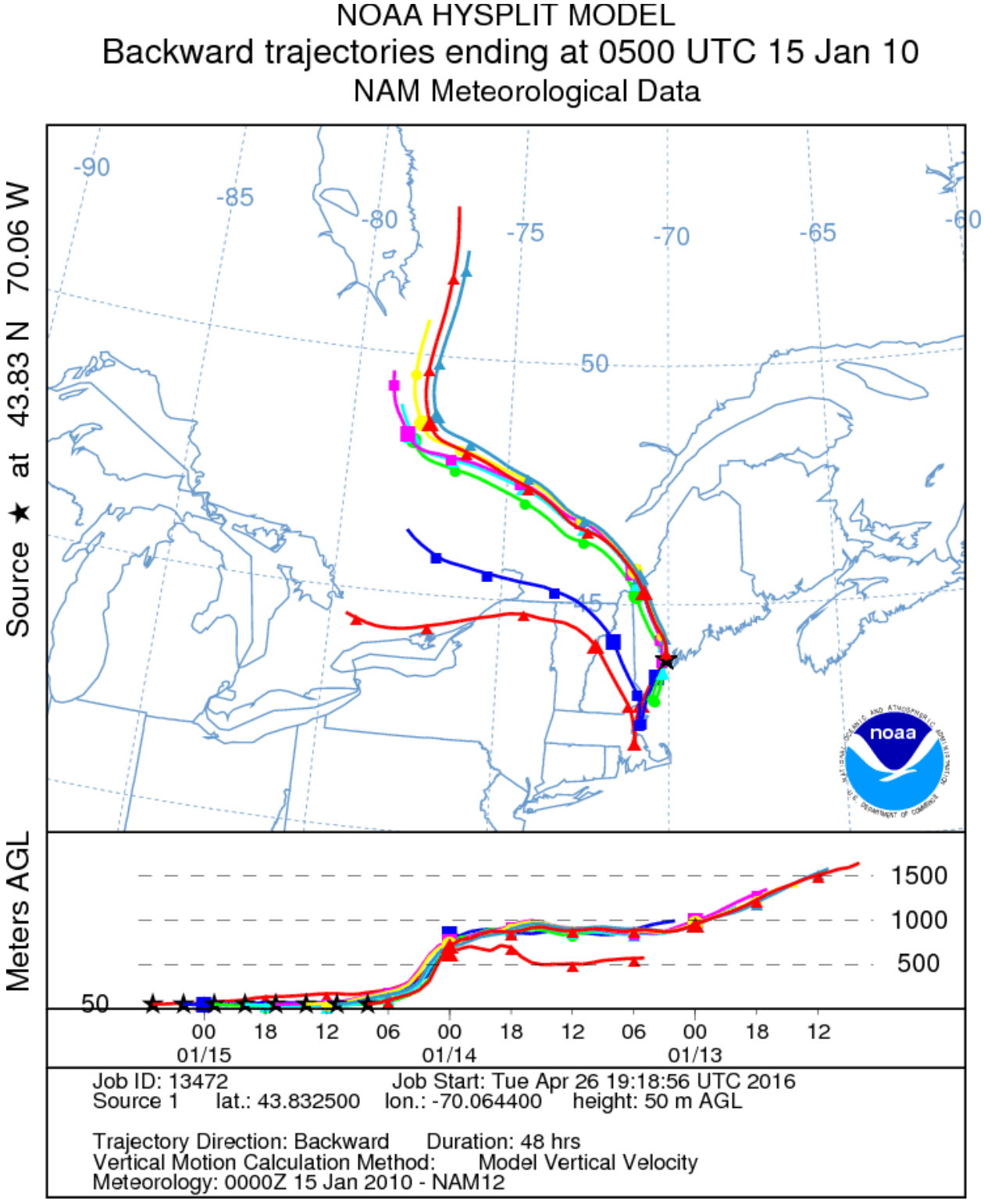
NOAA HYSPLIT MODEL
Backward trajectories ending at 0500 UTC 15 Jan 10
NAM Meteorological Data
Source ★ at 43.83 N 70.06 W
-90
-85
-80
-75
-70
-65
-60
50
45
noaa
Meters AGL
1500
1000
500
50
00 18 12 06 00 18 12 06 00 18 12
01/15
01/14
01/13
Job ID: 13472 Job Start: Tue Apr 26 19:18:56 UTC 2016
Source 1 lat.: 43.832500 lon.: -70.064400 height: 50 m AGL
Trajectory Direction: Backward Duration: 48 hrs
Vertical Motion Calculation Method: Model Vertical Velocity
Meteorology: 0000Z 15 Jan 2010 - NAM12

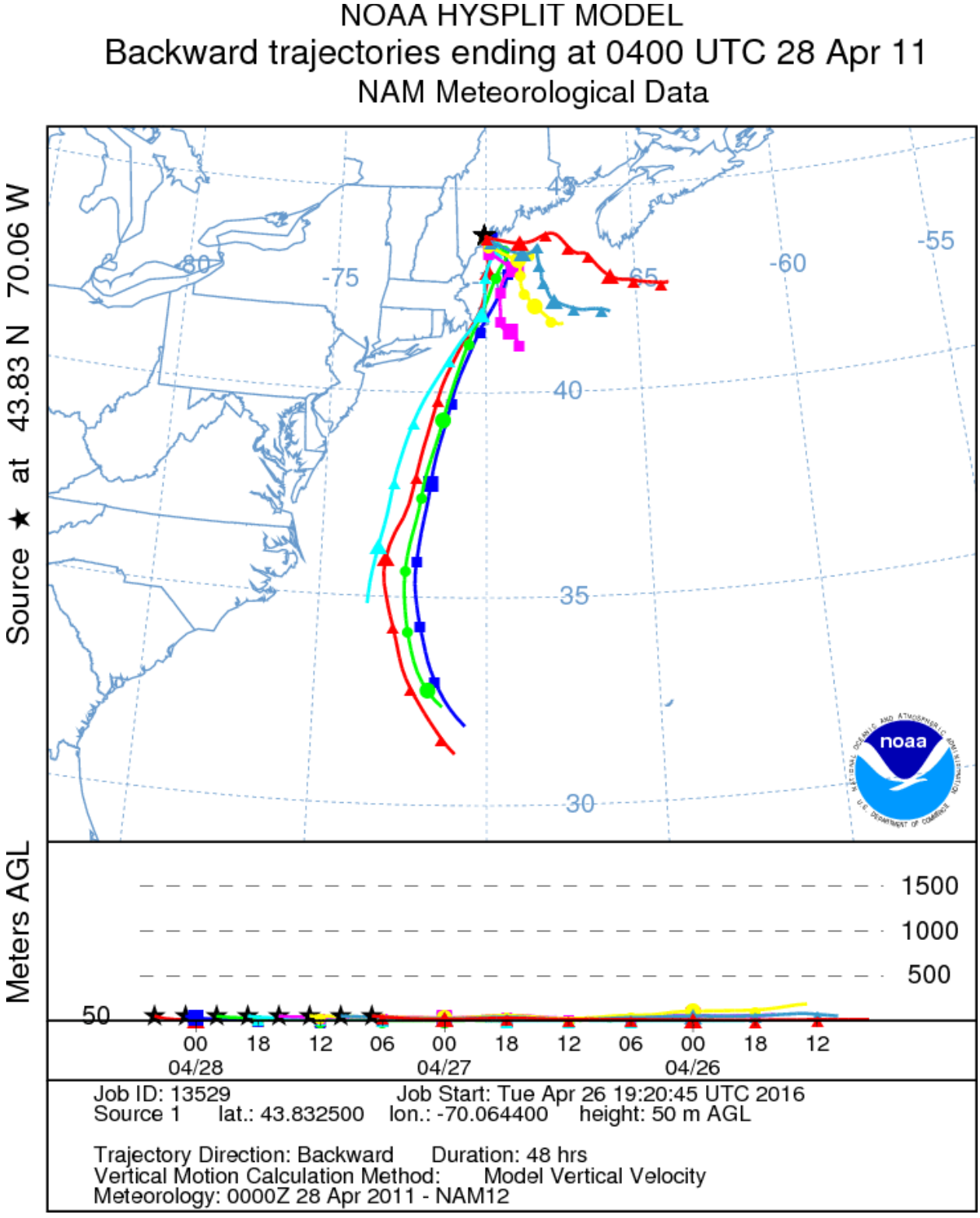
NOAA HYSPLIT MODEL
Backward trajectories ending at 0400 UTC 28 Apr 11
NAM Meteorological Data
Source ★ at 43.83 N 70.06 W
Meters AGL
1500
1000
500
50
00 18 12 06 00 18 12 06 00 18 12
04/28 04/27 04/26
Job ID: 13529 Job Start: Tue Apr 26 19:20:45 UTC 2016
Source 1 lat.: 43.832500 lon.: -70.064400 height: 50 m AGL
Trajectory Direction: Backward Duration: 48 hrs
Vertical Motion Calculation Method: Model Vertical Velocity
Meteorology: 0000Z 28 Apr 2011 - NAM12

CACO HYSPLIT back-trajectories

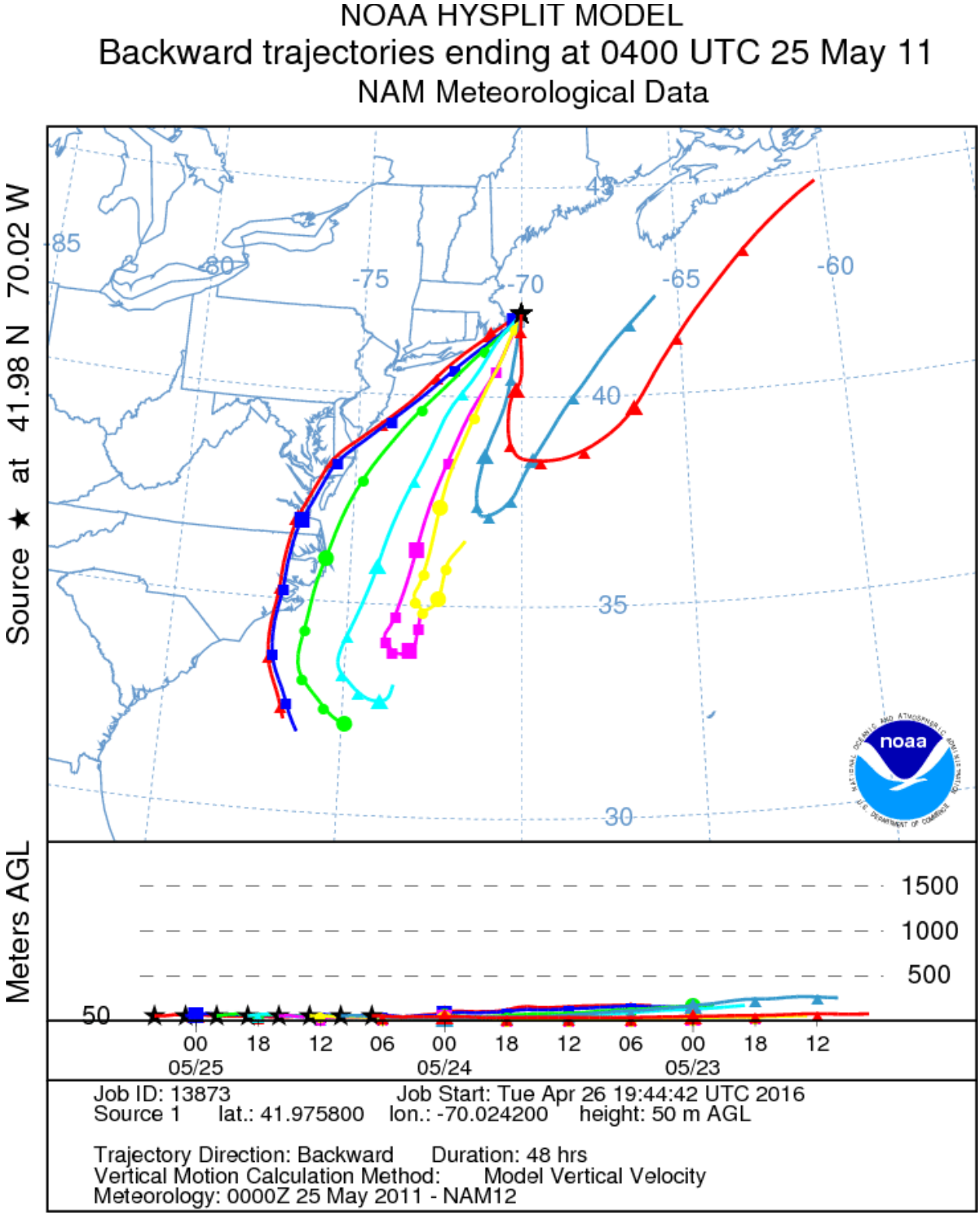
NOAA HYSPLIT MODEL
Backward trajectories ending at 0400 UTC 25 May 11
NAM Meteorological Data
Source ★ at 41.98 N 70.02 W
Meters AGL
1500
1000
500
50
00 18 12 06 00 18 12 06 00 18 12
05/25
05/24
05/23
Job ID: 13873 Job Start: Tue Apr 26 19:44:42 UTC 2016
Source 1 lat.: 41.975800 lon.: -70.024200 height: 50 m AGL
Trajectory Direction: Backward Duration: 48 hrs
Vertical Motion Calculation Method: Model Vertical Velocity
Meteorology: 0000Z 25 May 2011 - NAM12

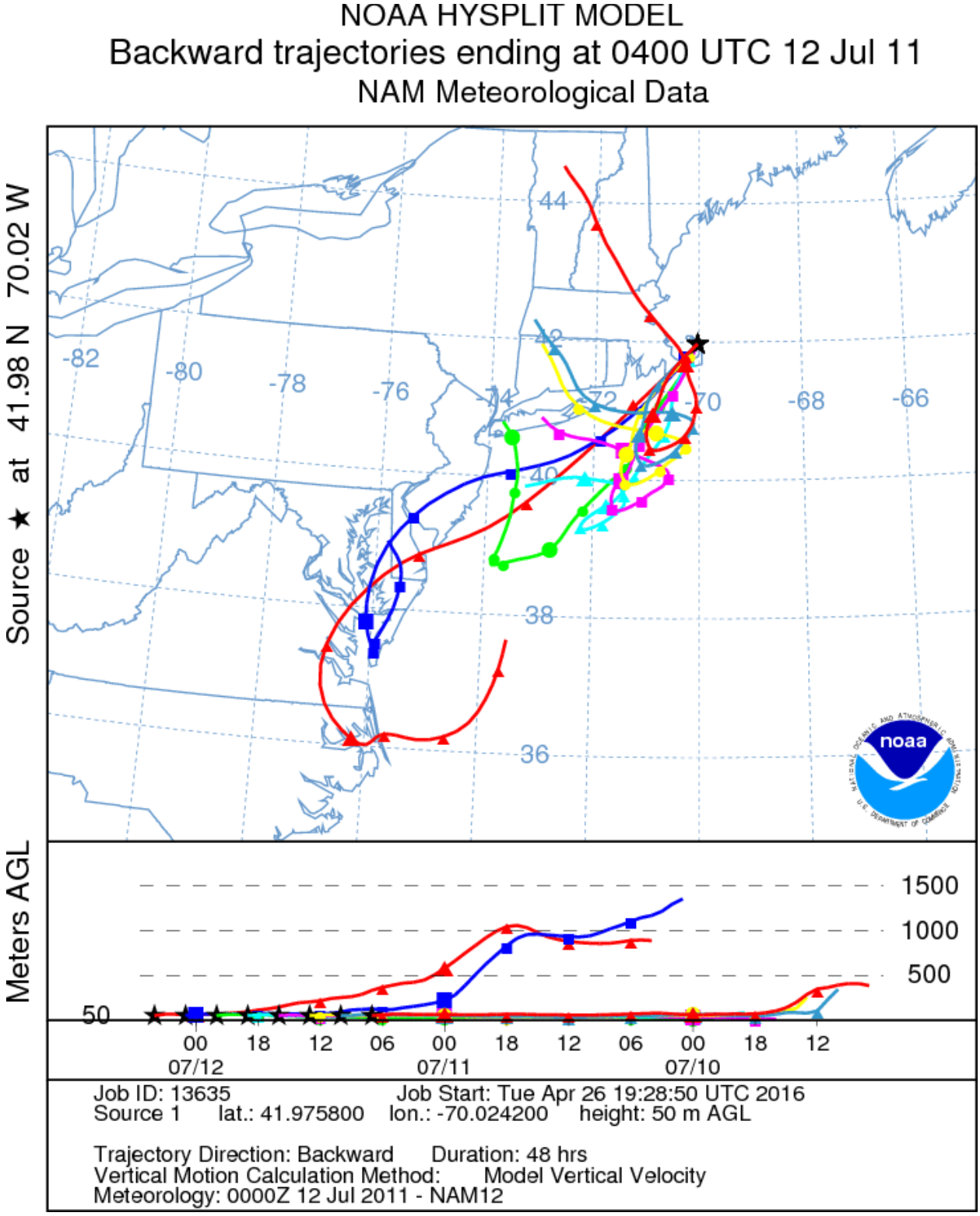
NOAA HYSPLIT MODEL
Backward trajectories ending at 0400 UTC 12 Jul 11
NAM Meteorological Data
Source ★ at 41.98 N 70.02 W
Meters AGL
1500
1000
500
50
00 18 12 06 00 18 12 06 00 18 12
07/12 07/11 07/10
Job ID: 13635 Job Start: Tue Apr 26 19:28:50 UTC 2016
Source 1 lat.: 41.975800 lon.: -70.024200 height: 50 m AGL
Trajectory Direction: Backward Duration: 48 hrs
Vertical Motion Calculation Method: Model Vertical Velocity
Meteorology: 0000Z 12 Jul 2011 - NAM12

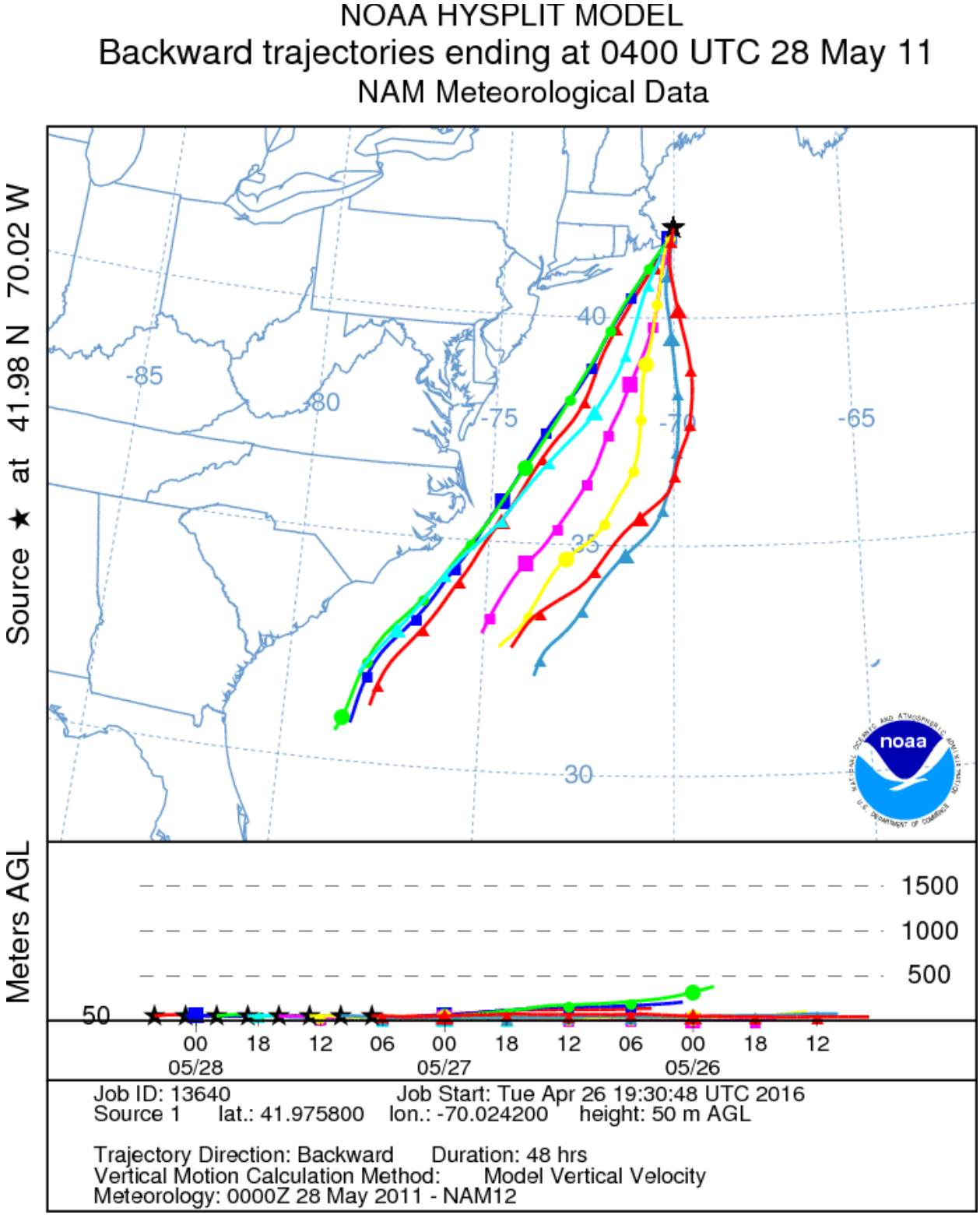
NOAA HYSPLIT MODEL
Backward trajectories ending at 0400 UTC 28 May 11
NAM Meteorological Data
Source ★ at 41.98 N 70.02 W
-85
-80
-75
-70
-65
40
35
30
noaa
Meters AGL
1500
1000
500
50
00 18 12 06 00 18 12 06 00 18 12
05/28 05/27 05/26
Job ID: 13640 Job Start: Tue Apr 26 19:30:48 UTC 2016
Source 1 lat.: 41.975800 lon.: -70.024200 height: 50 m AGL
Trajectory Direction: Backward Duration: 48 hrs
Vertical Motion Calculation Method: Model Vertical Velocity
Meteorology: 0000Z 28 May 2011 - NAM12

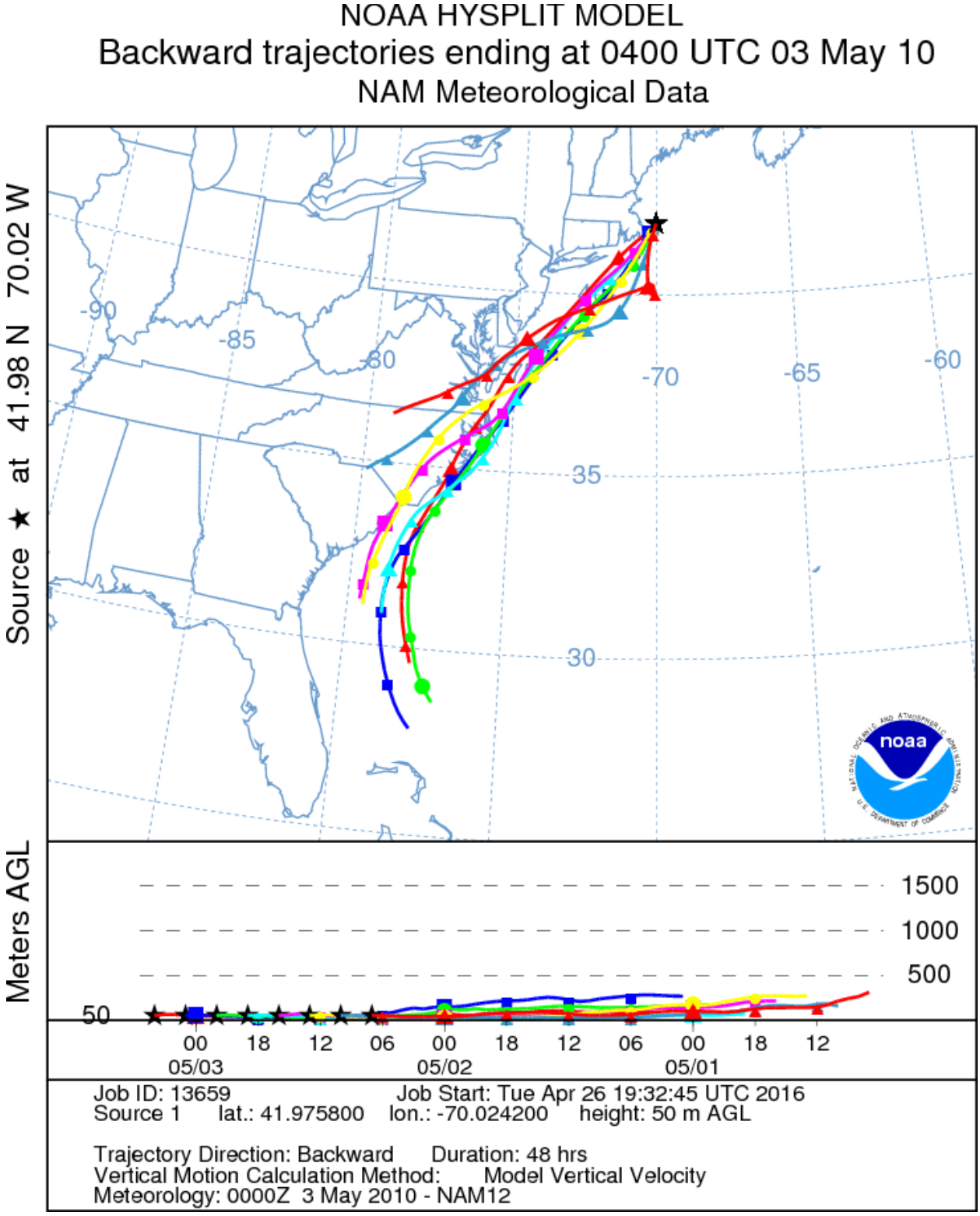
NOAA HYSPLIT MODEL
Backward trajectories ending at 0400 UTC 03 May 10
NAM Meteorological Data
Source ★ at 41.98 N 70.02 W
-90
-85
-80
-70
-65
-60
35
30
noaa
Meters AGL
1500
1000
500
50
00 18 12 06 00 18 12 06 00 18 12
05/03 05/02 05/01
Job ID: 13659 Job Start: Tue Apr 26 19:32:45 UTC 2016
Source 1 lat.: 41.975800 lon.: -70.024200 height: 50 m AGL
Trajectory Direction: Backward Duration: 48 hrs
Vertical Motion Calculation Method: Model Vertical Velocity
Meteorology: 0000Z 3 May 2010 - NAM12

NOAA HYSPLIT MODEL
Backward trajectories ending at 0400 UTC 09 Jun 11
NAM Meteorological Data

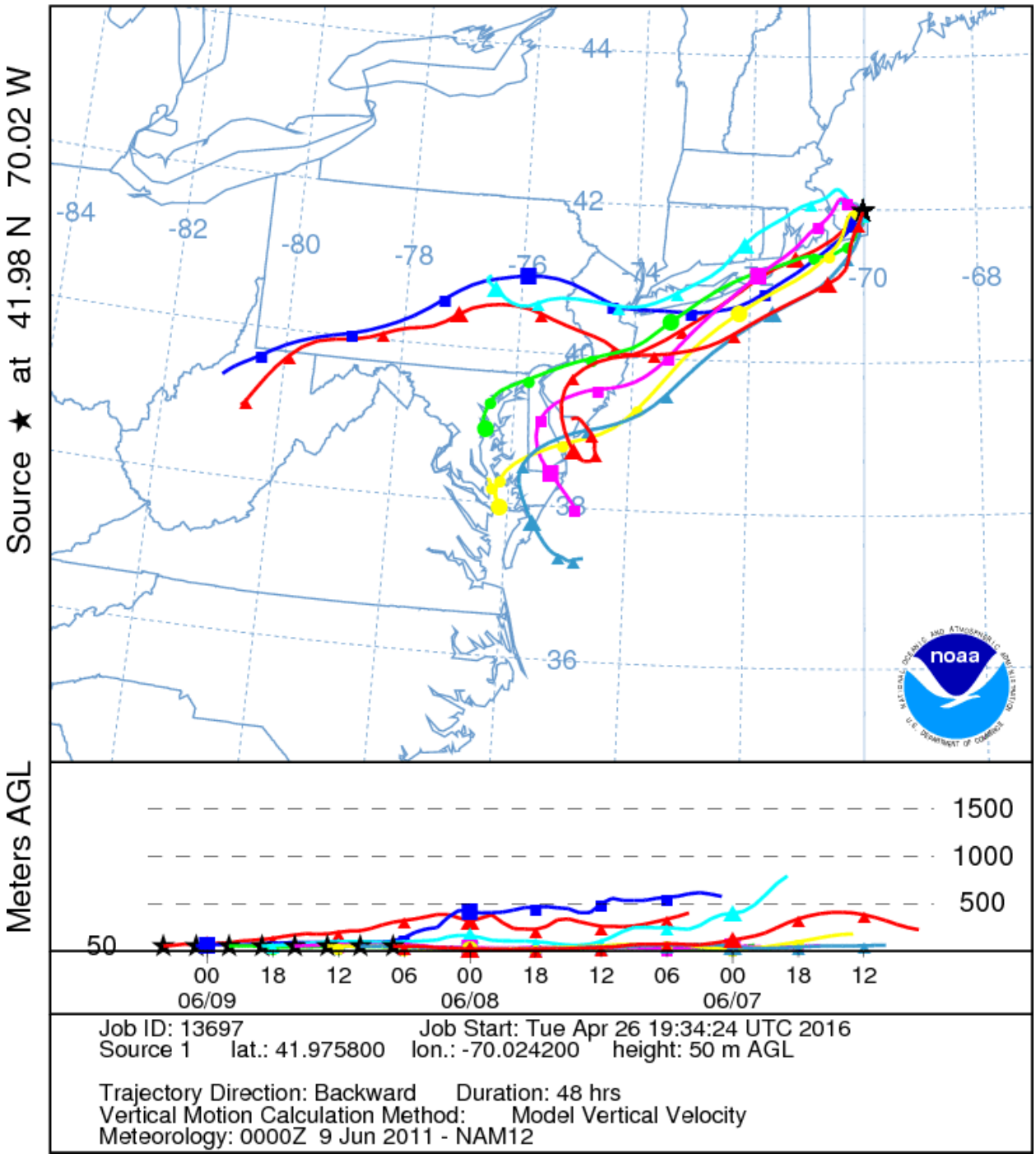

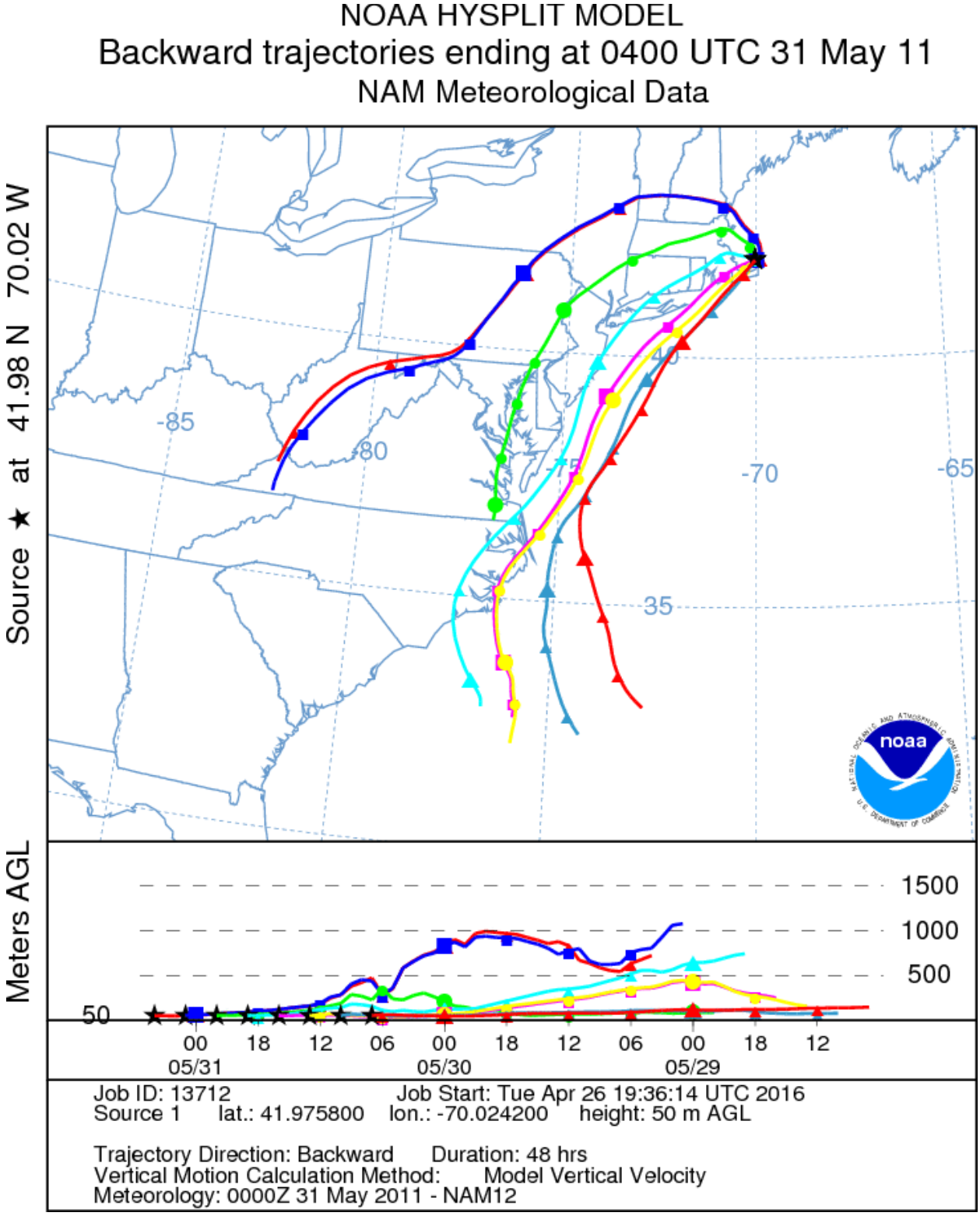
NOAA HYSPLIT MODEL
Backward trajectories ending at 0400 UTC 31 May 11
NAM Meteorological Data
Source ★ at 41.98 N 70.02 W
-85
-80
-75
-70
-65
35
noaa
Meters AGL
1500
1000
500
50
00 18 12 06 00 18 12 06 00 18 12
05/31
05/30
05/29
Job ID: 13712 Job Start: Tue Apr 26 19:36:14 UTC 2016
Source 1 lat.: 41.975800 lon.: -70.024200 height: 50 m AGL
Trajectory Direction: Backward Duration: 48 hrs
Vertical Motion Calculation Method: Model Vertical Velocity
Meteorology: 0000Z 31 May 2011 - NAM12

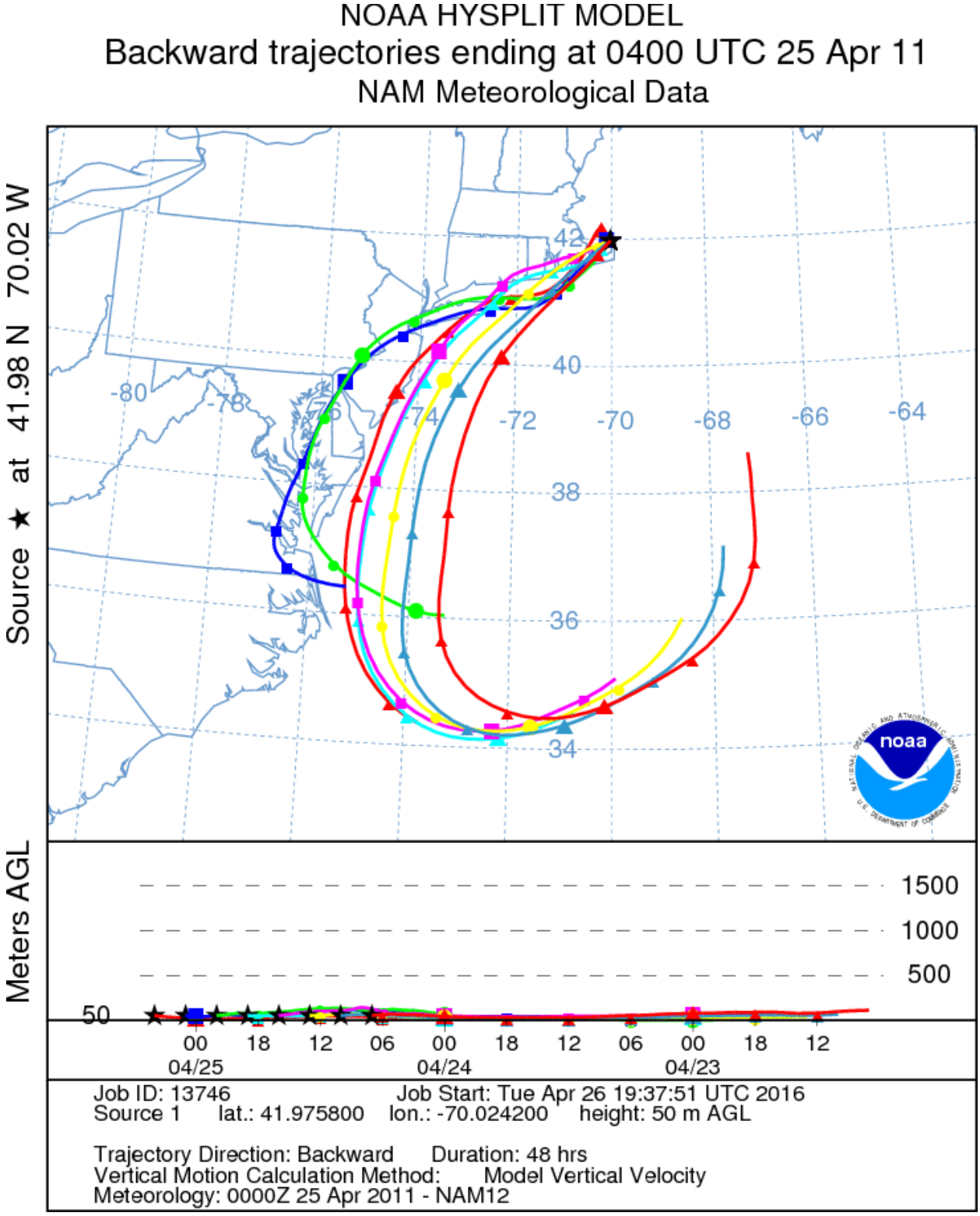
NOAA HYSPLIT MODEL
Backward trajectories ending at 0400 UTC 25 Apr 11
NAM Meteorological Data
Source ★ at 41.98 N 70.02 W
42
40
38
36
34
-80
-78
-74
-72
-70
-68
-66
-64
noaa
Meters AGL
1500
1000
500
50
00 18 12 06 00 18 12 06 00 18 12
04/25
04/24
04/23
Job ID: 13746 Job Start: Tue Apr 26 19:37:51 UTC 2016
Source 1 lat.: 41.975800 lon.: -70.024200 height: 50 m AGL
Trajectory Direction: Backward Duration: 48 hrs
Vertical Motion Calculation Method: Model Vertical Velocity
Meteorology: 0000Z 25 Apr 2011 - NAM12

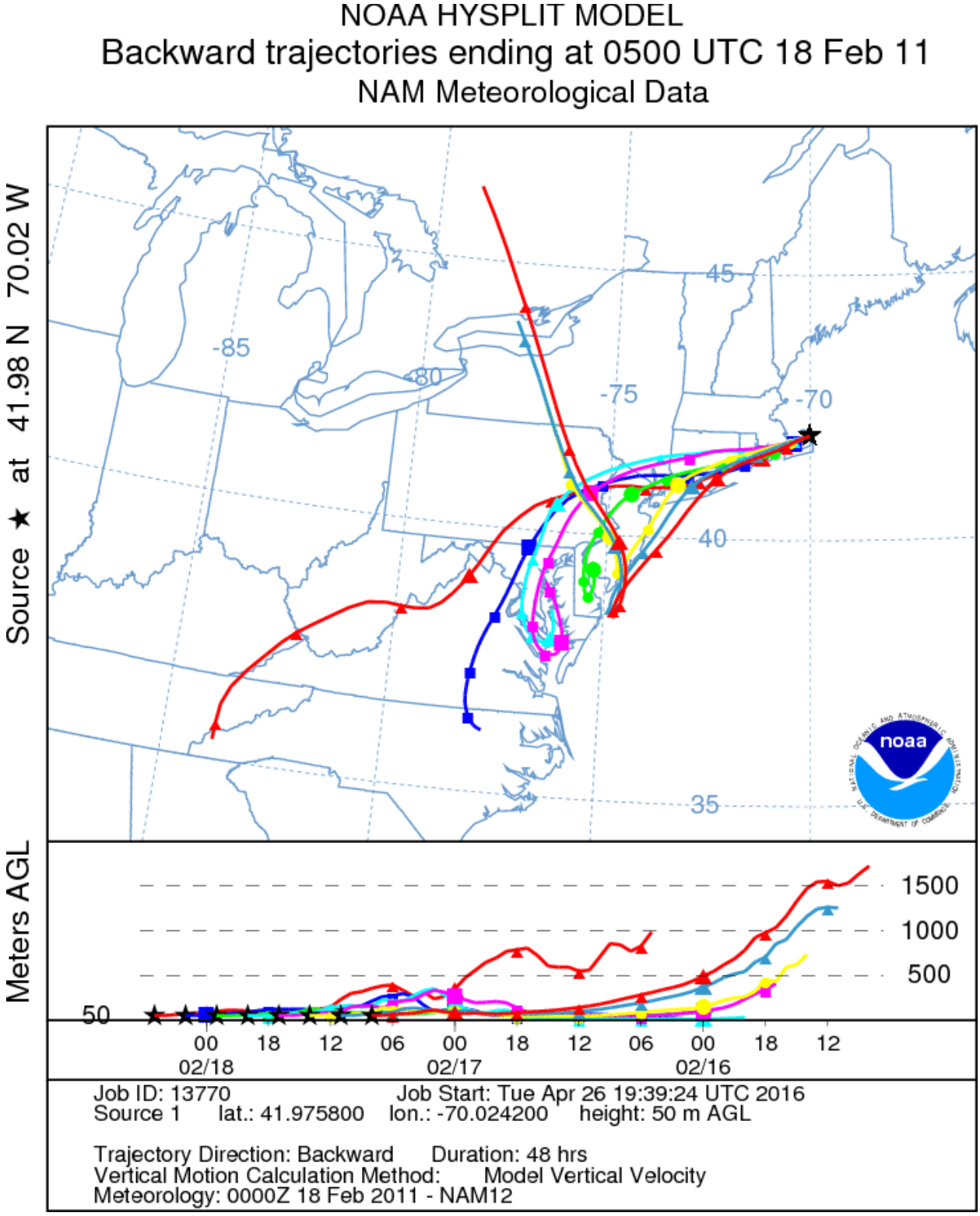
NOAA HYSPLIT MODEL
Backward trajectories ending at 0500 UTC 18 Feb 11
NAM Meteorological Data
Source ★ at 41.98 N 70.02 W
-85
-80
-75
-70
45
40
35
noaa
Meters AGL
1500
1000
500
50
00 18 12 06 00 18 12 06 00 18 12
02/18 02/17 02/16
Job ID: 13770 Job Start: Tue Apr 26 19:39:24 UTC 2016
Source 1 lat.: 41.975800 lon.: -70.024200 height: 50 m AGL
Trajectory Direction: Backward Duration: 48 hrs
Vertical Motion Calculation Method: Model Vertical Velocity
Meteorology: 0000Z 18 Feb 2011 - NAM12

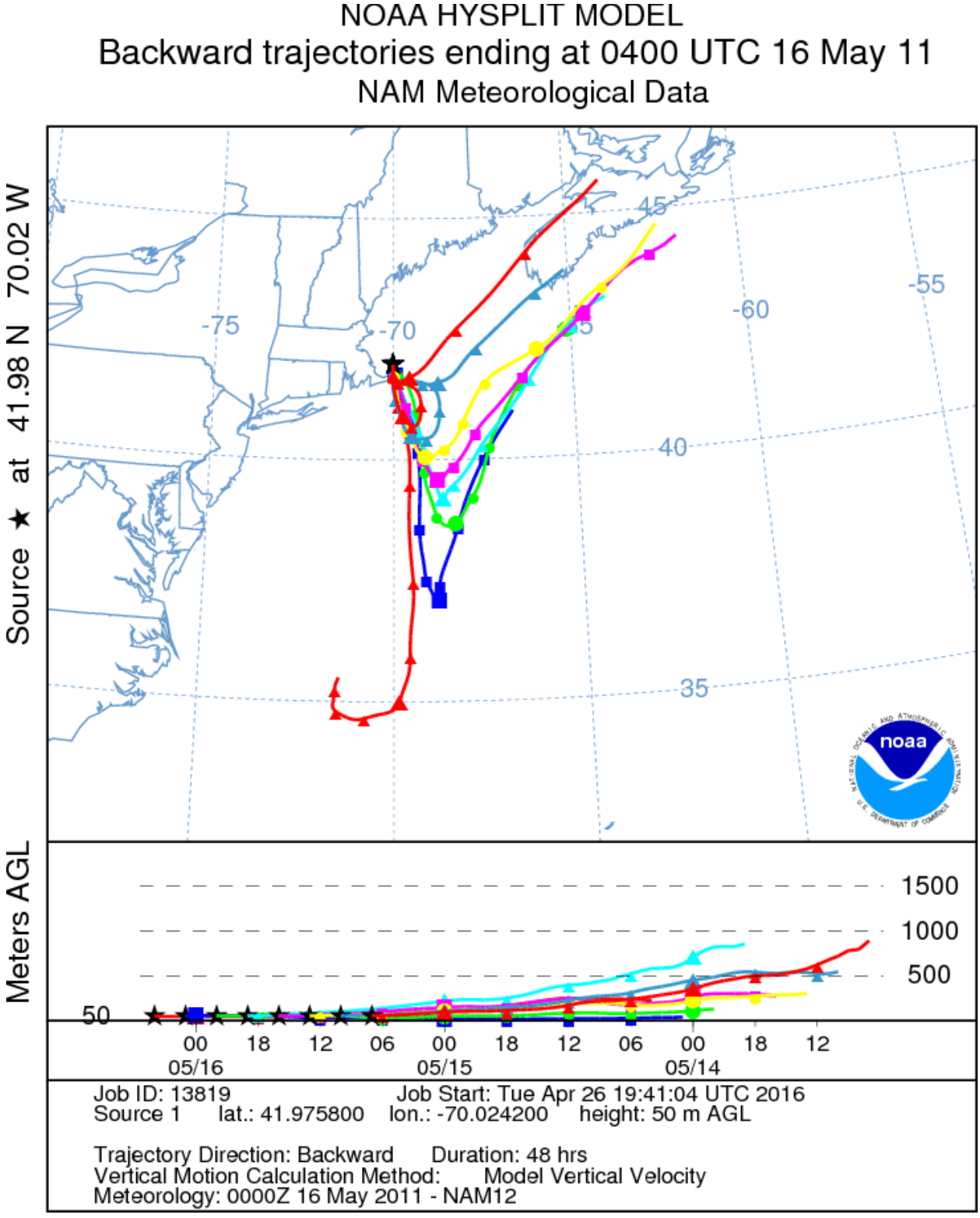
NOAA HYSPLIT MODEL
Backward trajectories ending at 0400 UTC 16 May 11
NAM Meteorological Data
Source ★ at 41.98 N 70.02 W
-75
-70
-60
-55
45
40
35
noaa
Meters AGL
1500
1000
500
50
00 18 12 06 00 18 12 06 00 18 12
05/16 05/15 05/14
Job ID: 13819 Job Start: Tue Apr 26 19:41:04 UTC 2016
Source 1 lat.: 41.975800 lon.: -70.024200 height: 50 m AGL
Trajectory Direction: Backward Duration: 48 hrs
Vertical Motion Calculation Method: Model Vertical Velocity
Meteorology: 0000Z 16 May 2011 - NAM12

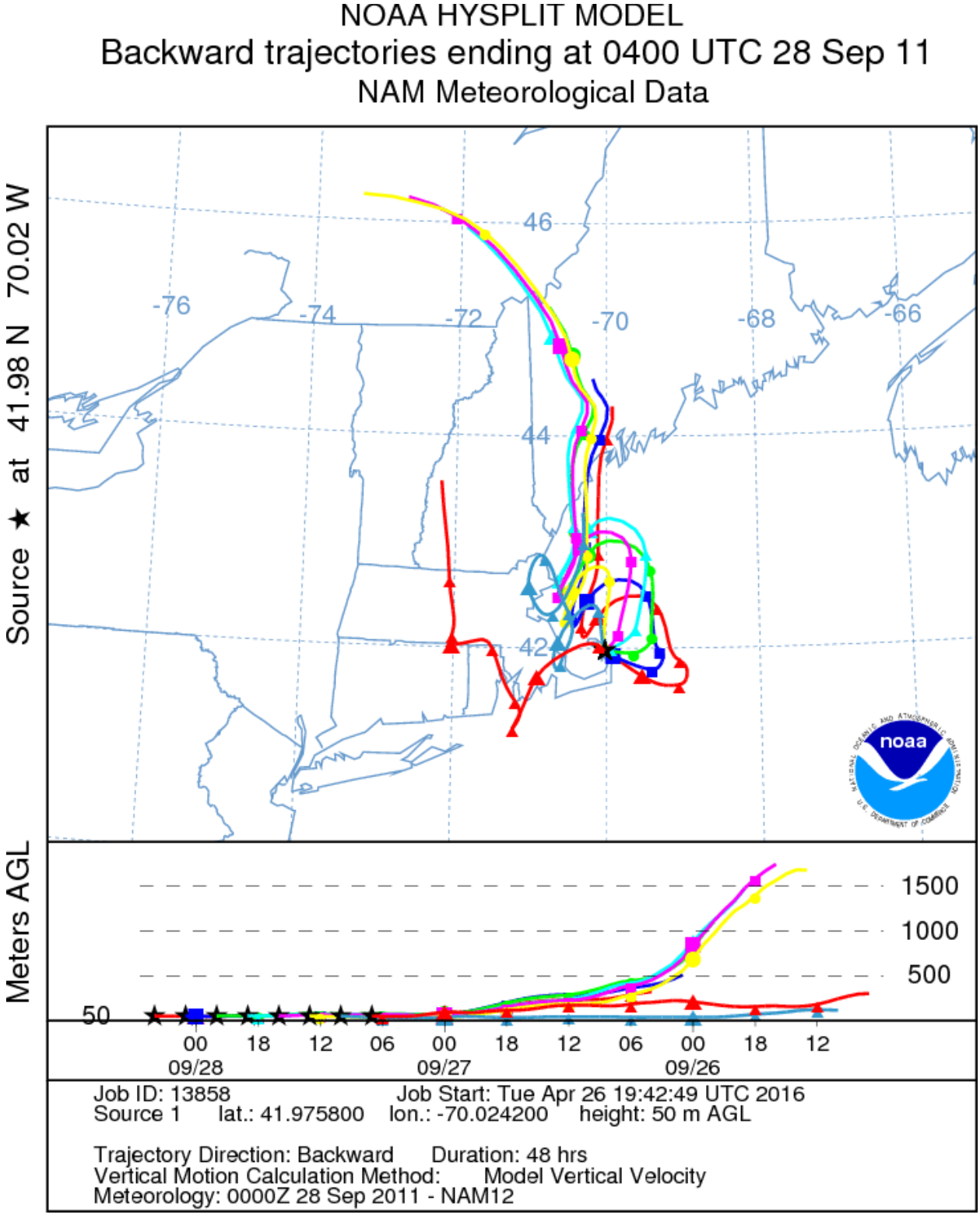
NOAA HYSPLIT MODEL
Backward trajectories ending at 0400 UTC 28 Sep 11
NAM Meteorological Data
Source ★ at 41.98 N 70.02 W
46
44
42
-76
-74
-72
-70
-68
-66
noaa
Meters AGL
1500
1000
500
50
00 18 12 06 00 18 12 06 00 18 12
09/28
09/27
09/26
Job ID: 13858 Job Start: Tue Apr 26 19:42:49 UTC 2016
Source 1 lat.: 41.975800 lon.: -70.024200 height: 50 m AGL
Trajectory Direction: Backward Duration: 48 hrs
Vertical Motion Calculation Method: Model Vertical Velocity
Meteorology: 0000Z 28 Sep 2011 - NAM12

CHAS HYSPLIT back-trajectories

NOAA HYSPLIT MODEL
Backward trajectories ending at 0500 UTC 03 Feb 11
NAM Meteorological Data

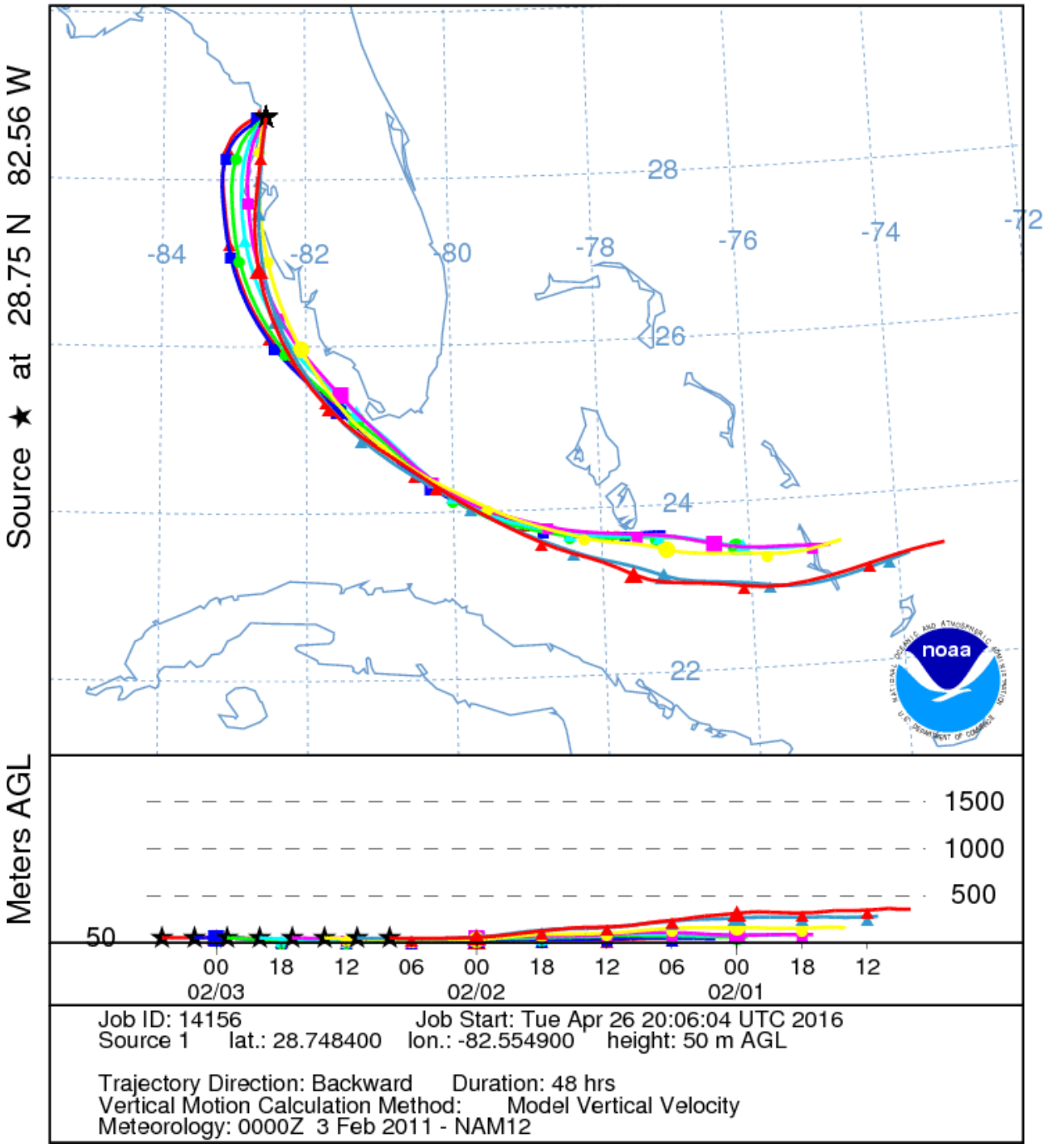

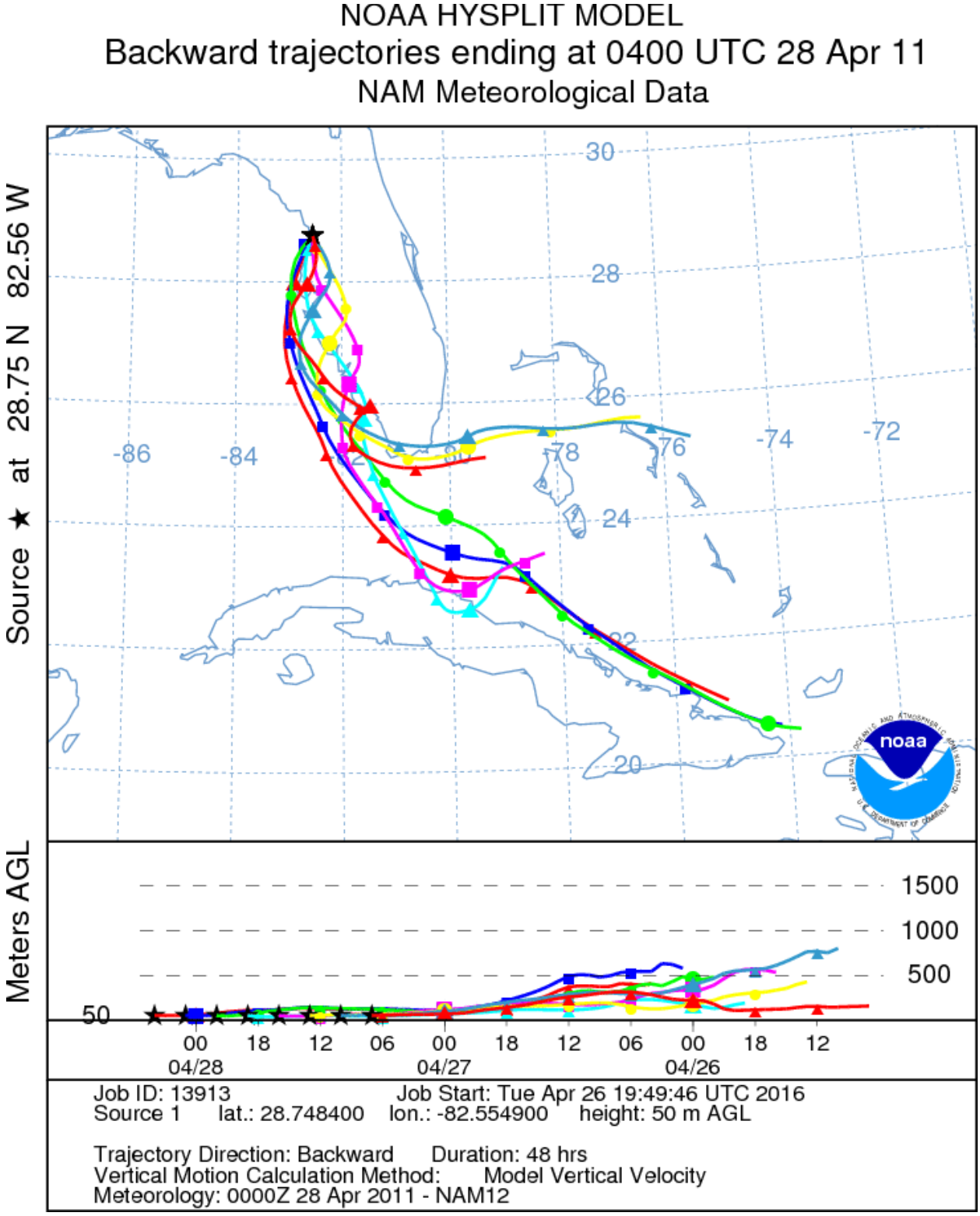
NOAA HYSPLIT MODEL
Backward trajectories ending at 0400 UTC 28 Apr 11
NAM Meteorological Data
Source ★ at 28.75 N 82.56 W
30
28
26
24
22
20
-86
-84
-78
-76
-74
-72
noaa
Meters AGL
1500
1000
500
50
00 18 12 06 00 18 12 06 00 18 12
04/28
04/27
04/26
Job ID: 13913 Job Start: Tue Apr 26 19:49:46 UTC 2016
Source 1 lat.: 28.748400 lon.: -82.554900 height: 50 m AGL
Trajectory Direction: Backward Duration: 48 hrs
Vertical Motion Calculation Method: Model Vertical Velocity
Meteorology: 0000Z 28 Apr 2011 - NAM12

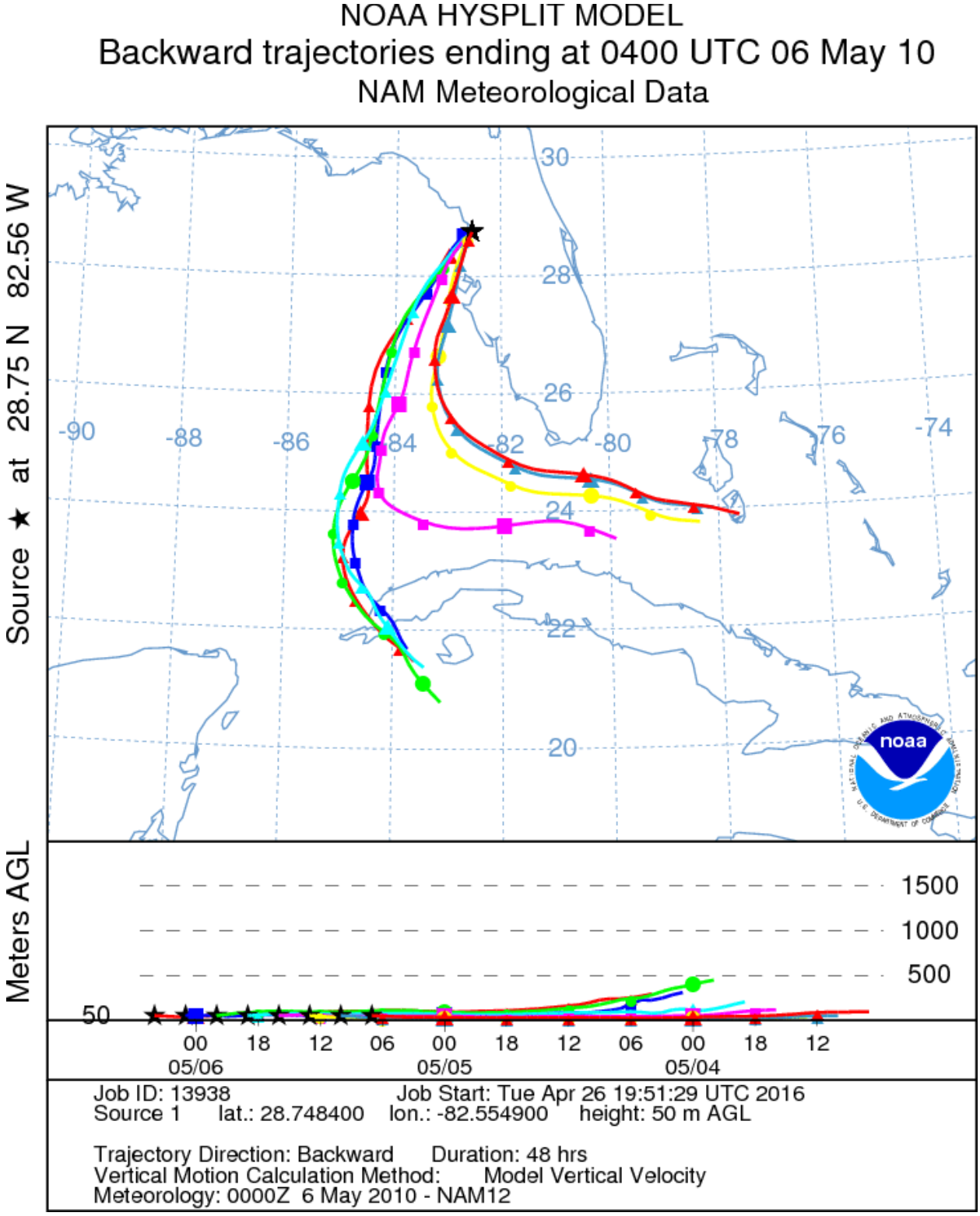
NOAA HYSPLIT MODEL
Backward trajectories ending at 0400 UTC 06 May 10
NAM Meteorological Data
Source ★ at 28.75 N 82.56 W
30
28
26
24
22
20
-90
-88
-86
-84
-82
-80
-78
-76
-74
noaa
Meters AGL
1500
1000
500
50
00 18 12 06 00 18 12 06 00 18 12
05/06 05/05 05/04
Job ID: 13938 Job Start: Tue Apr 26 19:51:29 UTC 2016
Source 1 lat.: 28.748400 lon.: -82.554900 height: 50 m AGL
Trajectory Direction: Backward Duration: 48 hrs
Vertical Motion Calculation Method: Model Vertical Velocity
Meteorology: 0000Z 6 May 2010 - NAM12

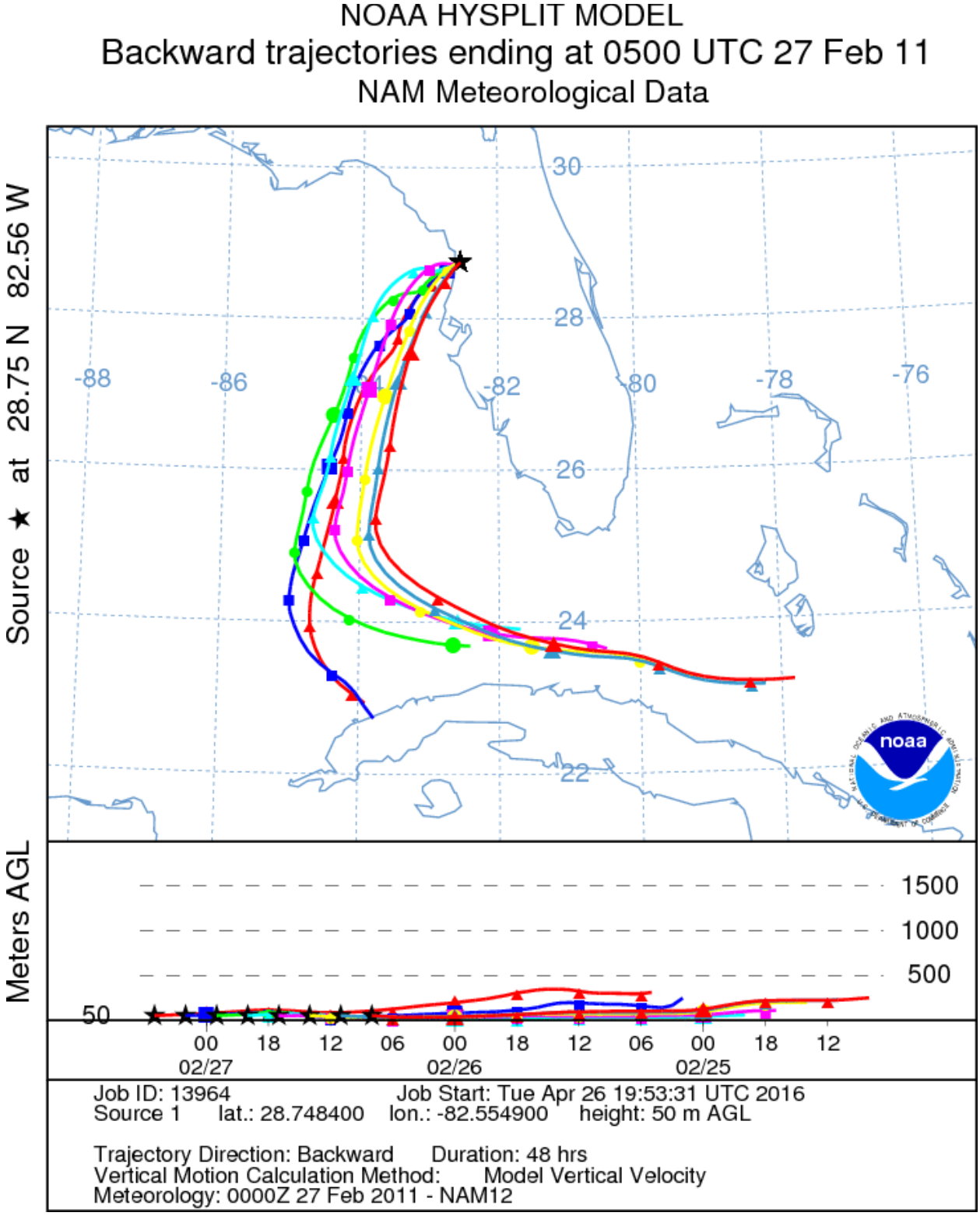
NOAA HYSPLIT MODEL
Backward trajectories ending at 0500 UTC 27 Feb 11
NAM Meteorological Data
Source ★ at 28.75 N 82.56 W
30
28
26
24
22
-88
-86
-82
-80
-78
-76
noaa
Meters AGL
1500
1000
500
50
00 18 12 06 00 18 12 06 00 18 12
02/27
02/26
02/25
Job ID: 13964 Job Start: Tue Apr 26 19:53:31 UTC 2016
Source 1 lat.: 28.748400 lon.: -82.554900 height: 50 m AGL
Trajectory Direction: Backward Duration: 48 hrs
Vertical Motion Calculation Method: Model Vertical Velocity
Meteorology: 0000Z 27 Feb 2011 - NAM12

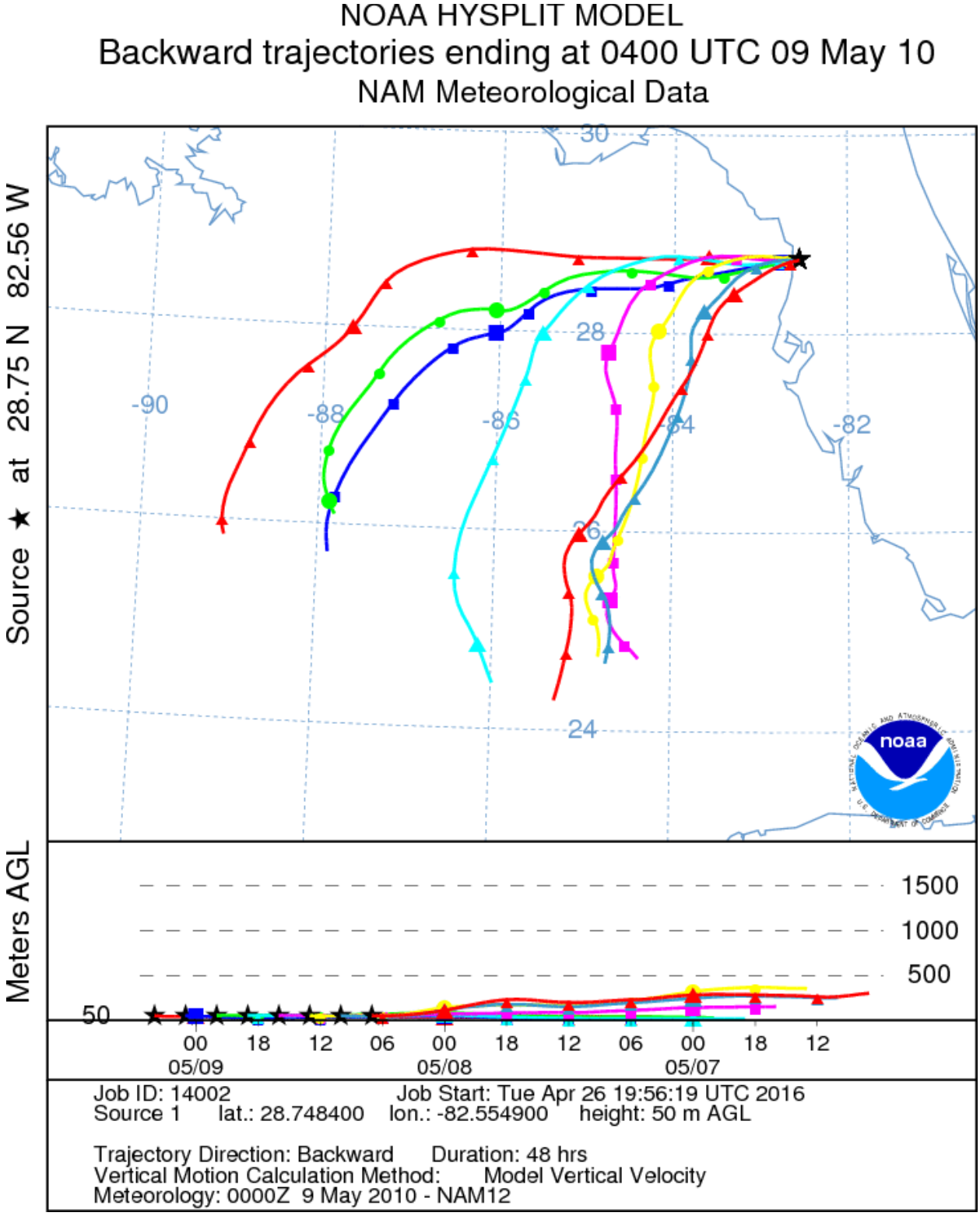
NOAA HYSPLIT MODEL
Backward trajectories ending at 0400 UTC 09 May 10
NAM Meteorological Data
Source ★ at 28.75 N 82.56 W
30
28
26
24
-90
-88
-86
-84
-82
noaa
Meters AGL
1500
1000
500
50
00 18 12 06 00 18 12 06 00 18 12
05/09 05/08 05/07
Job ID: 14002 Job Start: Tue Apr 26 19:56:19 UTC 2016
Source 1 lat.: 28.748400 lon.: -82.554900 height: 50 m AGL
Trajectory Direction: Backward Duration: 48 hrs
Vertical Motion Calculation Method: Model Vertical Velocity
Meteorology: 0000Z 9 May 2010 - NAM12

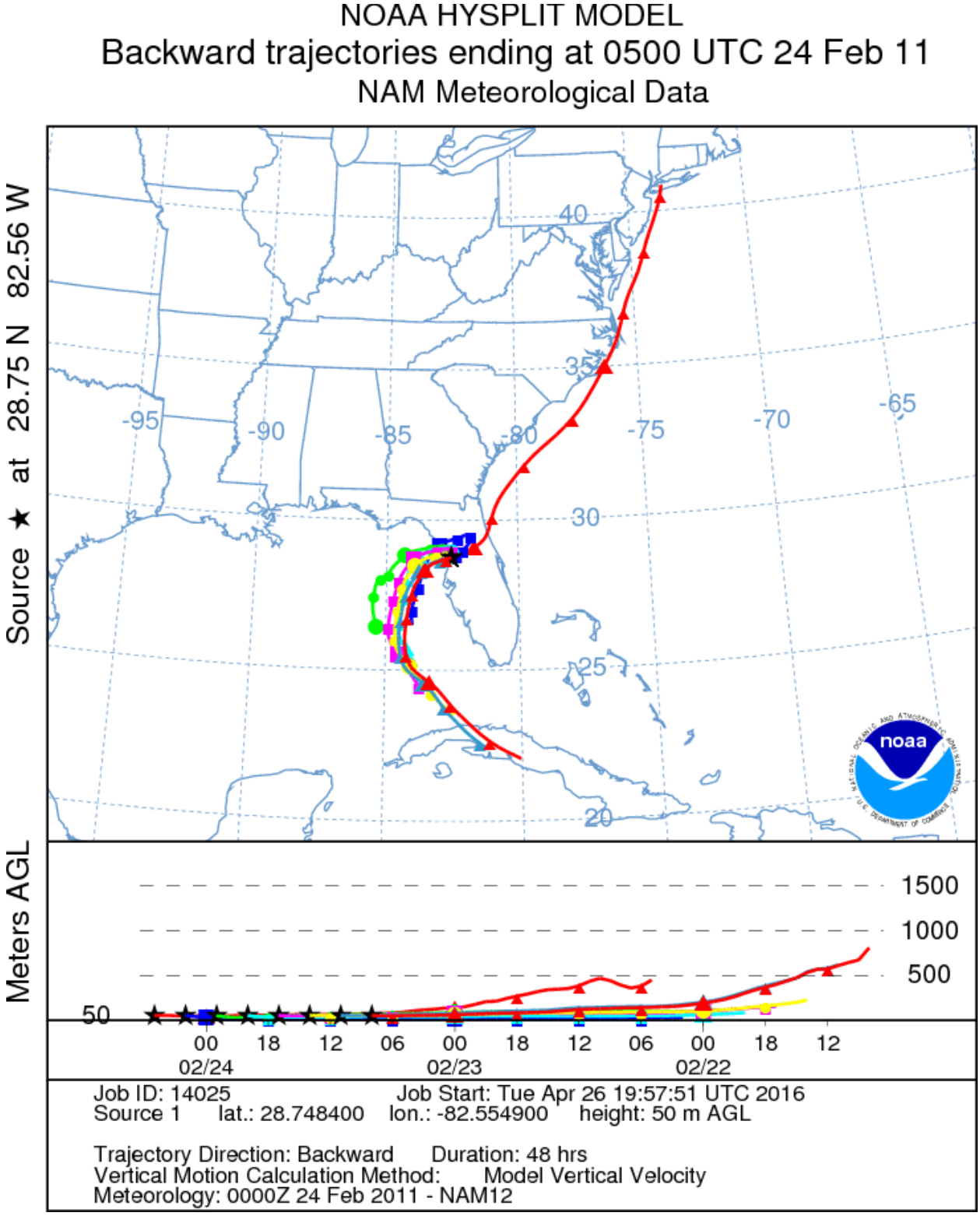
NOAA HYSPLIT MODEL
Backward trajectories ending at 0500 UTC 24 Feb 11
NAM Meteorological Data
Source ★ at 28.75 N 82.56 W
40
35
30
25
20
-95
-90
-85
-80
-75
-70
-65
noaa
Meters AGL
1500
1000
500
50
00 18 12 06 00 18 12 06 00 18 12
02/24
02/23
02/22
Job ID: 14025 Job Start: Tue Apr 26 19:57:51 UTC 2016
Source 1 lat.: 28.748400 lon.: -82.554900 height: 50 m AGL
Trajectory Direction: Backward Duration: 48 hrs
Vertical Motion Calculation Method: Model Vertical Velocity
Meteorology: 0000Z 24 Feb 2011 - NAM12

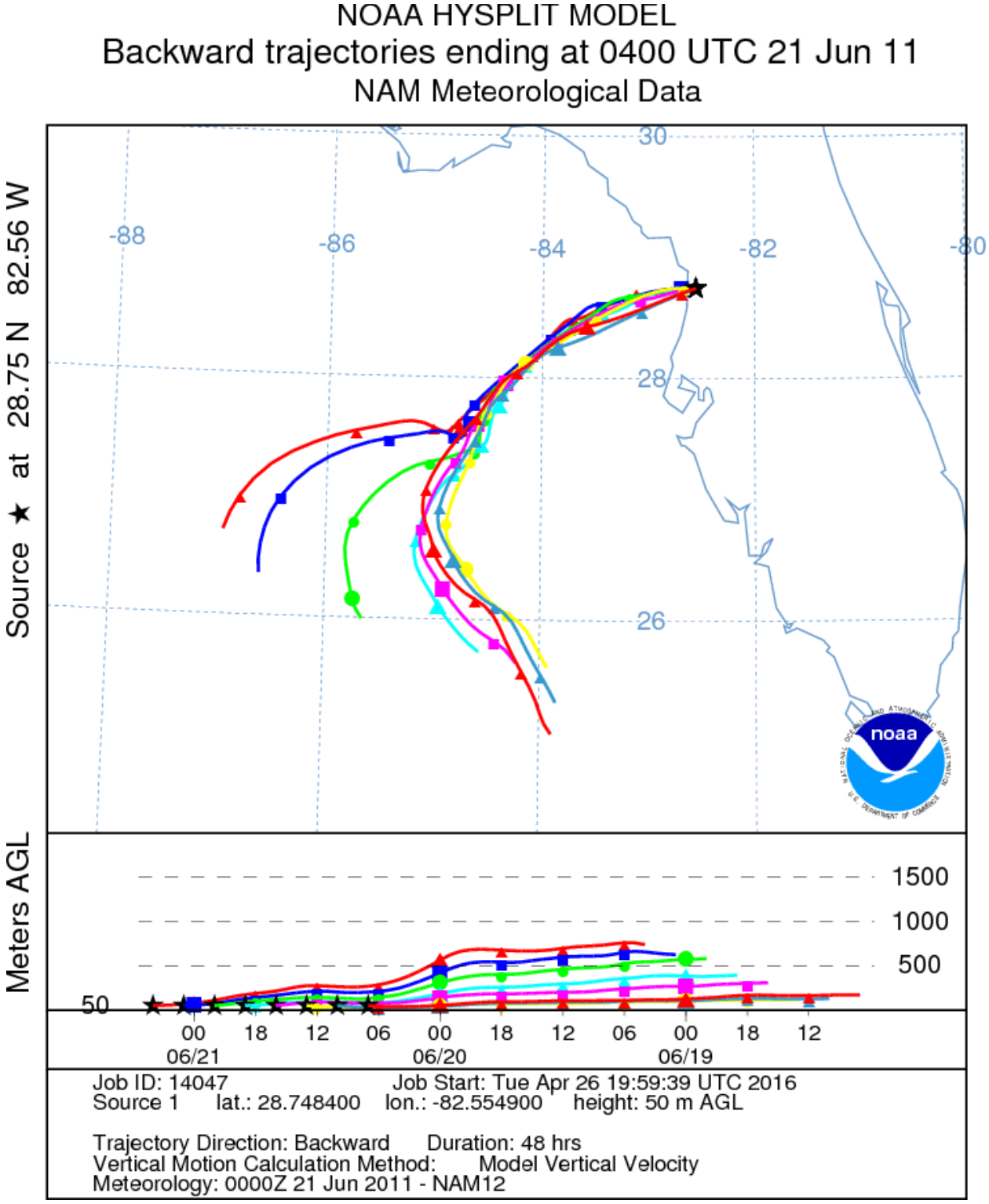
NOAA HYSPLIT MODEL
Backward trajectories ending at 0400 UTC 21 Jun 11
NAM Meteorological Data
Source ★ at 28.75 N 82.56 W
30
28
26
-88
-86
-84
-82
-80
noaa
Meters AGL
1500
1000
500
50
00 18 12 06 00 18 12 06 00 18 12
06/21 06/20 06/19
Job ID: 14047 Job Start: Tue Apr 26 19:59:39 UTC 2016
Source 1 lat.: 28.748400 lon.: -82.554900 height: 50 m AGL
Trajectory Direction: Backward Duration: 48 hrs
Vertical Motion Calculation Method: Model Vertical Velocity
Meteorology: 0000Z 21 Jun 2011 - NAM12

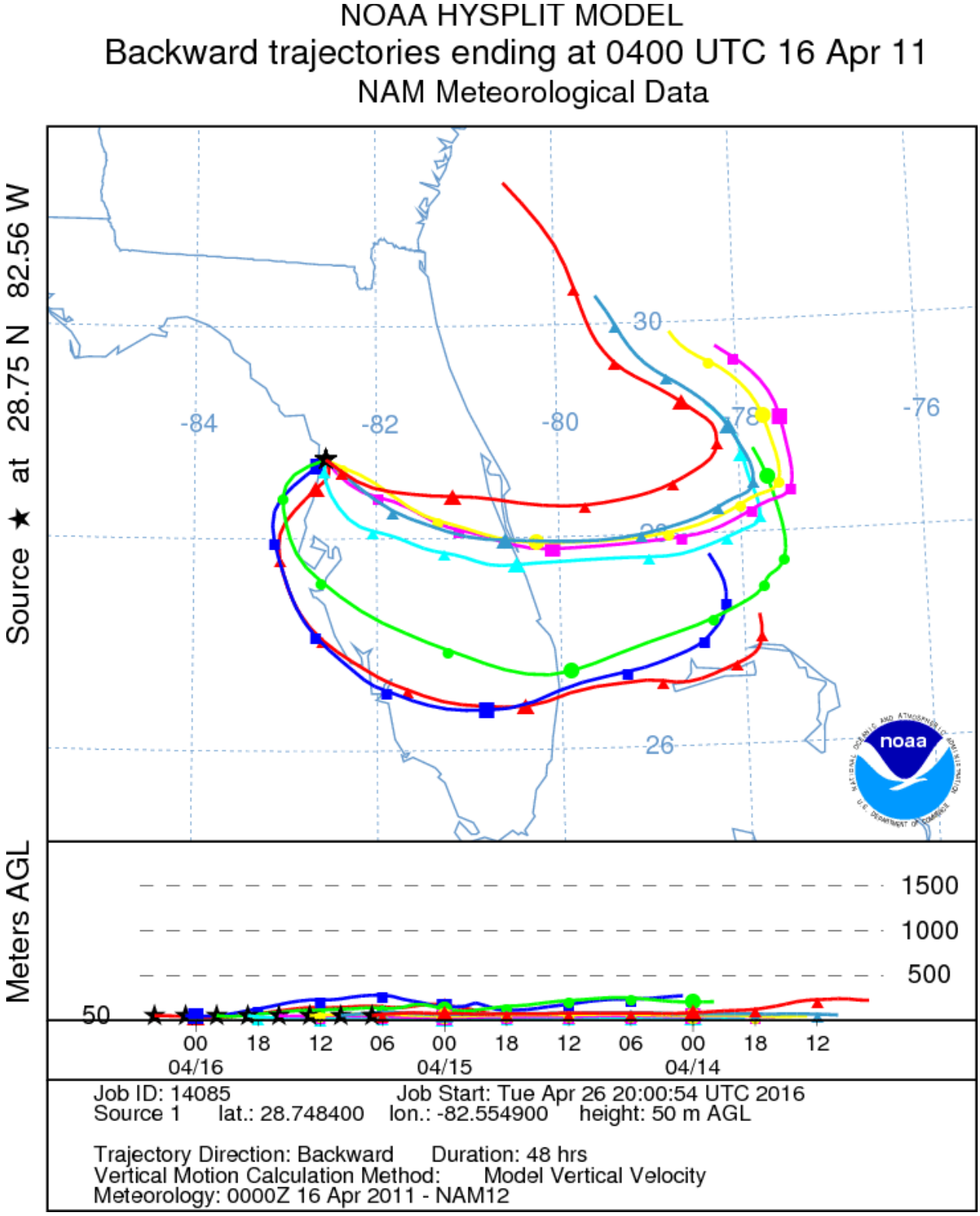
NOAA HYSPLIT MODEL
Backward trajectories ending at 0400 UTC 16 Apr 11
NAM Meteorological Data
Source ★ at 28.75 N 82.56 W
-84
-82
-80
-78
-76
30
26
noaa
Meters AGL
1500
1000
500
50
00 18 12 06 00 18 12 06 00 18 12
04/16
04/15
04/14
Job ID: 14085 Job Start: Tue Apr 26 20:00:54 UTC 2016
Source 1 lat.: 28.748400 lon.: -82.554900 height: 50 m AGL
Trajectory Direction: Backward Duration: 48 hrs
Vertical Motion Calculation Method: Model Vertical Velocity
Meteorology: 0000Z 16 Apr 2011 - NAM12

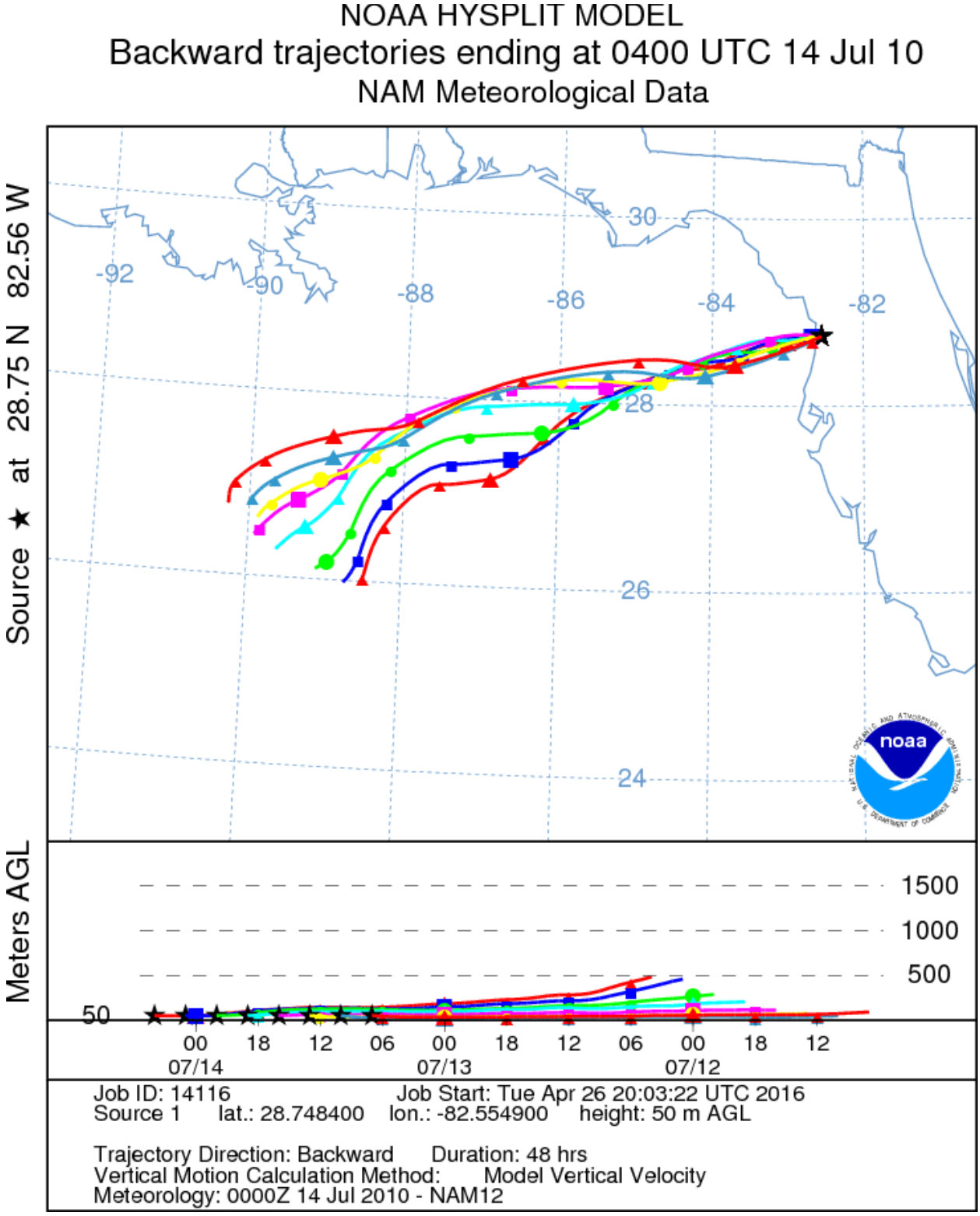
NOAA HYSPLIT MODEL
Backward trajectories ending at 0400 UTC 14 Jul 10
NAM Meteorological Data
Source ★ at 28.75 N 82.56 W
-92
-90
-88
-86
-84
-82
30
28
26
24
noaa
Meters AGL
1500
1000
500
50
00 18 12 06 00 18 12 06 00 18 12
07/14
07/13
07/12
Job ID: 14116 Job Start: Tue Apr 26 20:03:22 UTC 2016
Source 1 lat.: 28.748400 lon.: -82.554900 height: 50 m AGL
Trajectory Direction: Backward Duration: 48 hrs
Vertical Motion Calculation Method: Model Vertical Velocity
Meteorology: 0000Z 14 Jul 2010 - NAM12

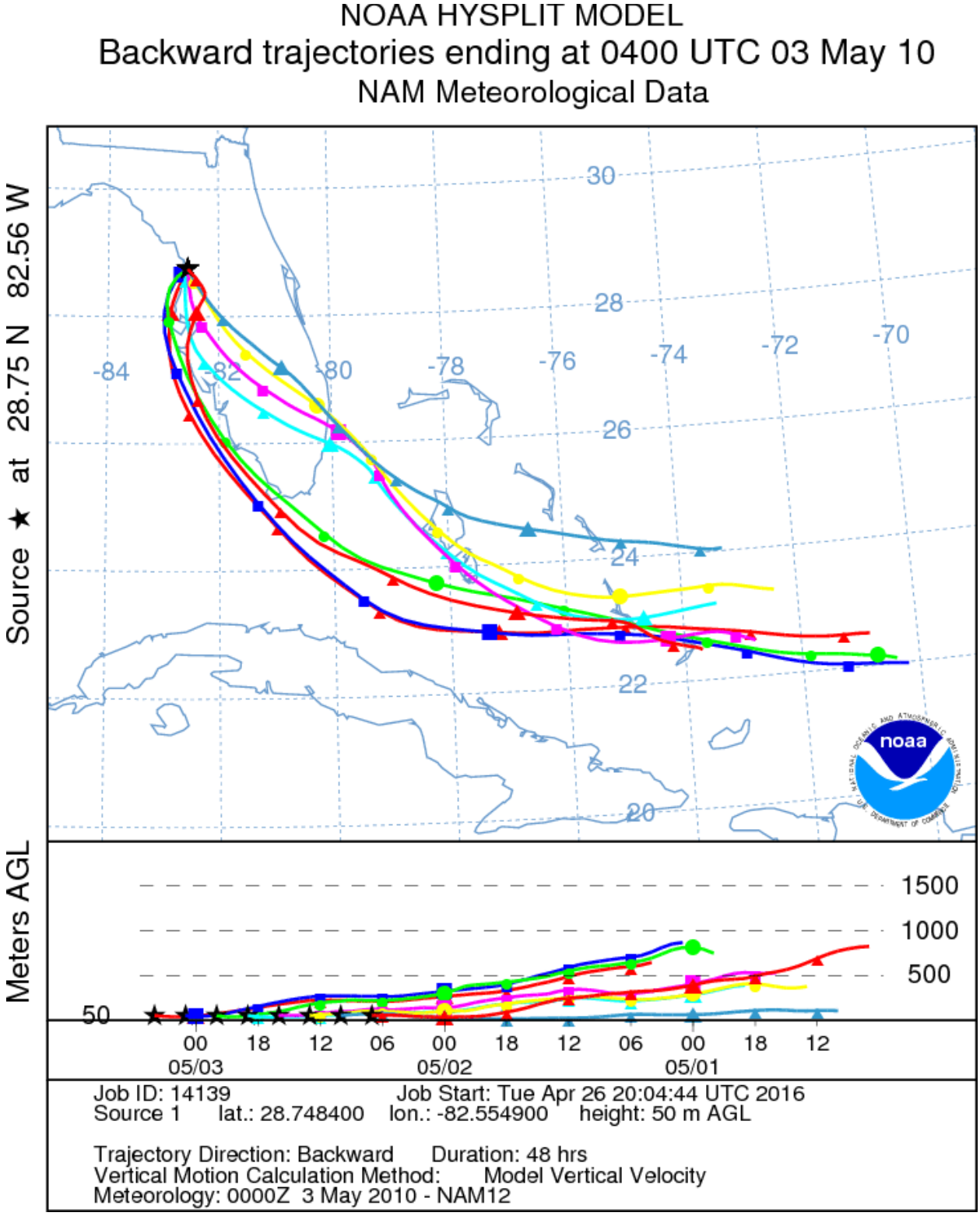
NOAA HYSPLIT MODEL
Backward trajectories ending at 0400 UTC 03 May 10
NAM Meteorological Data
Source ★ at 28.75 N 82.56 W
Meters AGL
1500
1000
500
50
00 18 12 06 00 18 12 06 00 18 12
05/03 05/02 05/01
Job ID: 14139 Job Start: Tue Apr 26 20:04:44 UTC 2016
Source 1 lat.: 28.748400 lon.: -82.554900 height: 50 m AGL
Trajectory Direction: Backward Duration: 48 hrs
Vertical Motion Calculation Method: Model Vertical Velocity
Meteorology: 0000Z 3 May 2010 - NAM12

MAVI HYSPLIT back-trajectories

NOAA HYSPLIT MODEL
Backward trajectories ending at 0400 UTC 24 Jul 11
NAM Meteorological Data

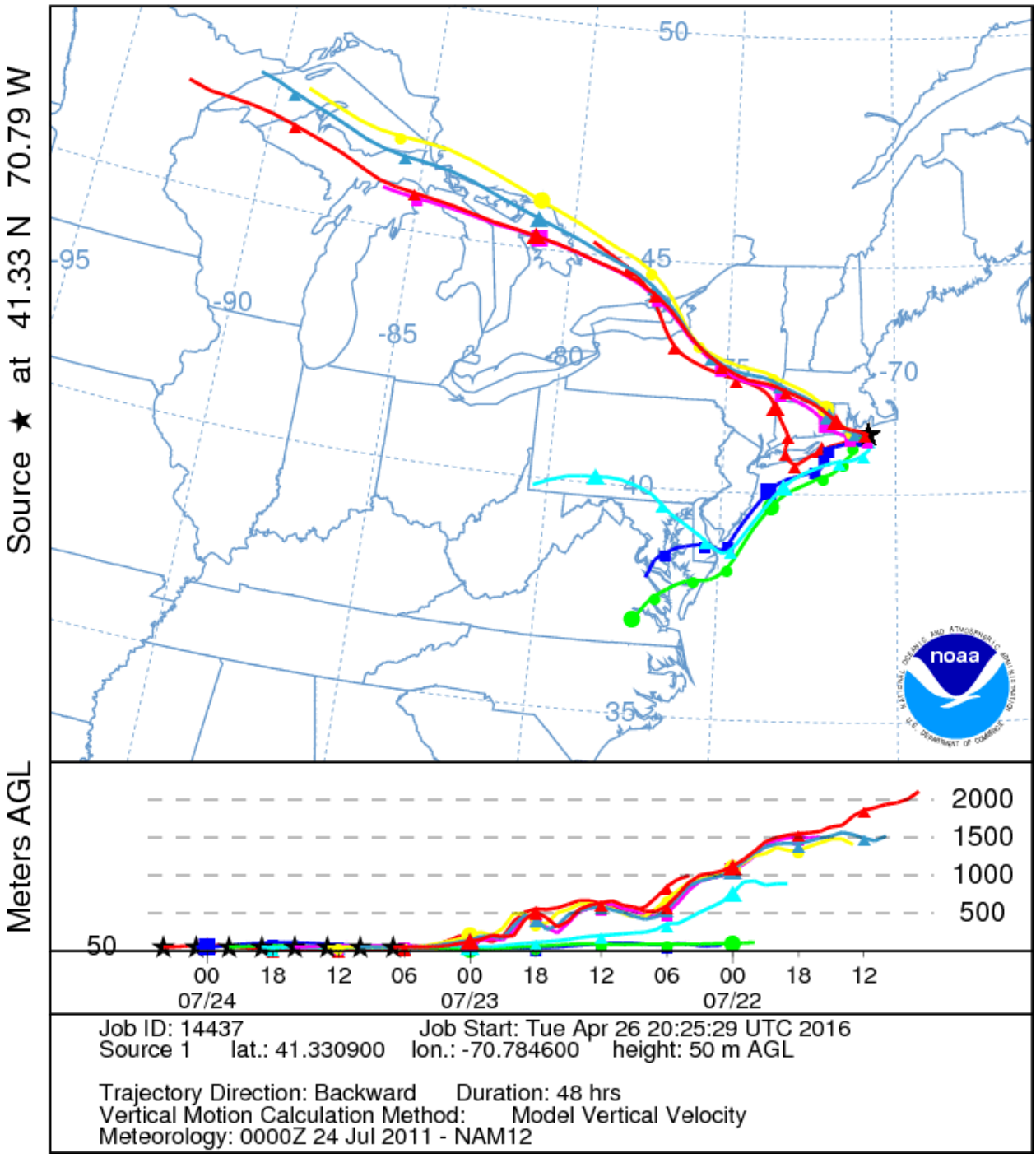

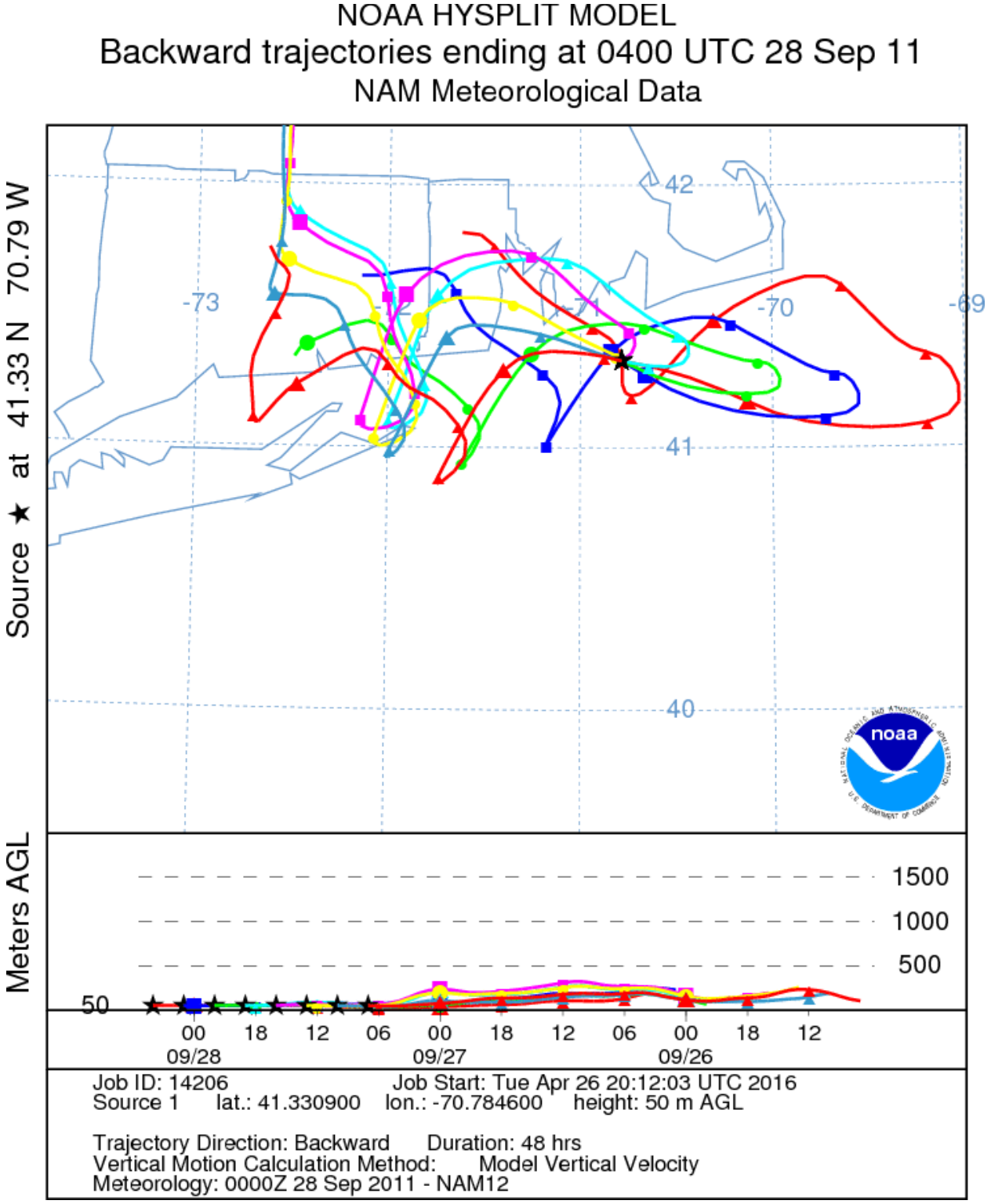
NOAA HYSPLIT MODEL
Backward trajectories ending at 0400 UTC 28 Sep 11
NAM Meteorological Data
Source ★ at 41.33 N 70.79 W
-73
-72
-71
-70
-69
42
41
40
noaa
Meters AGL
1500
1000
500
50
00 18 12 06 00 18 12 06 00 18 12
09/28
09/27
09/26
Job ID: 14206 Job Start: Tue Apr 26 20:12:03 UTC 2016
Source 1 lat.: 41.330900 lon.: -70.784600 height: 50 m AGL
Trajectory Direction: Backward Duration: 48 hrs
Vertical Motion Calculation Method: Model Vertical Velocity
Meteorology: 0000Z 28 Sep 2011 - NAM12

NOAA HYSPLIT MODEL
Backward trajectories ending at 0400 UTC 25 Apr 11
NAM Meteorological Data

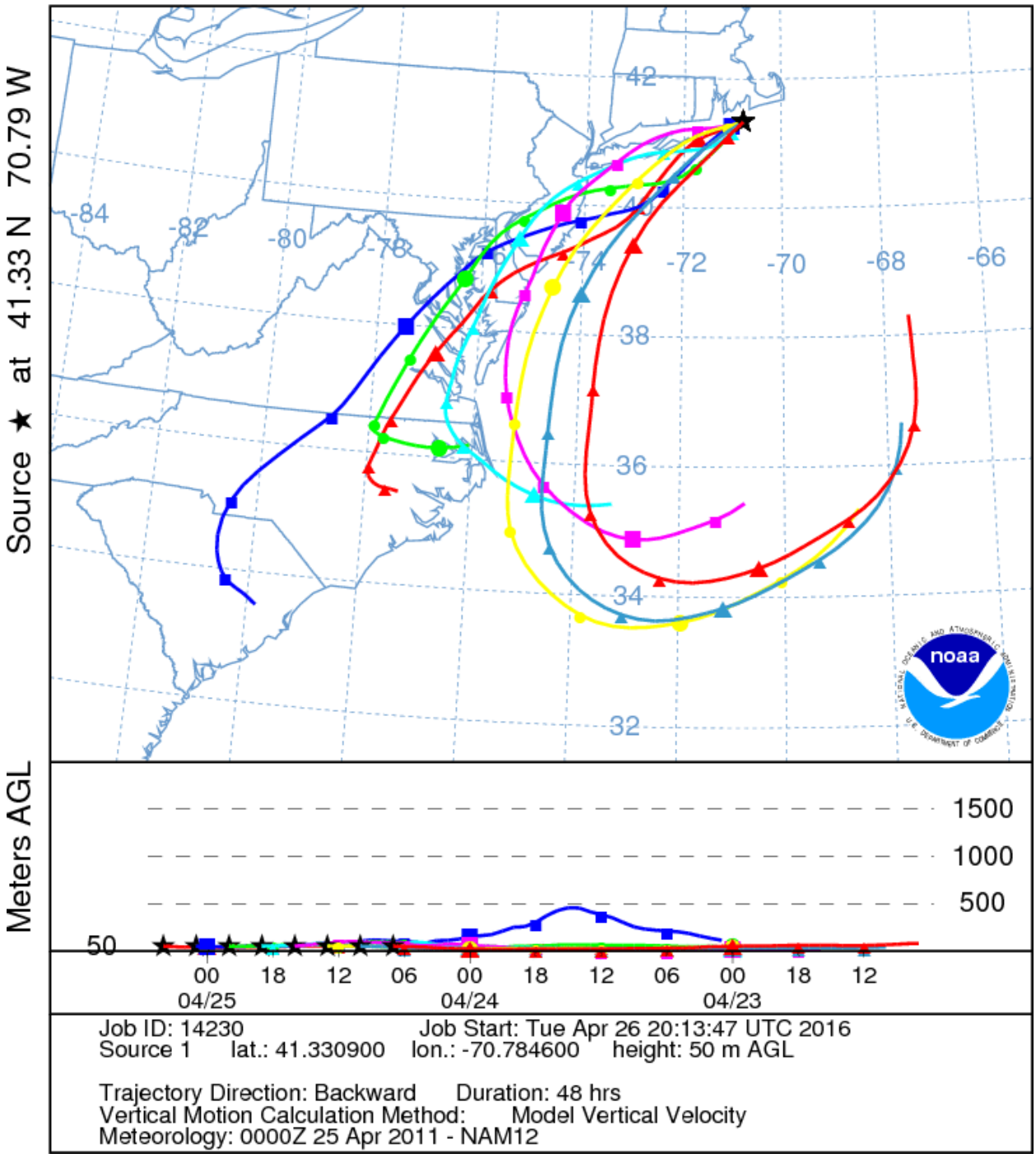

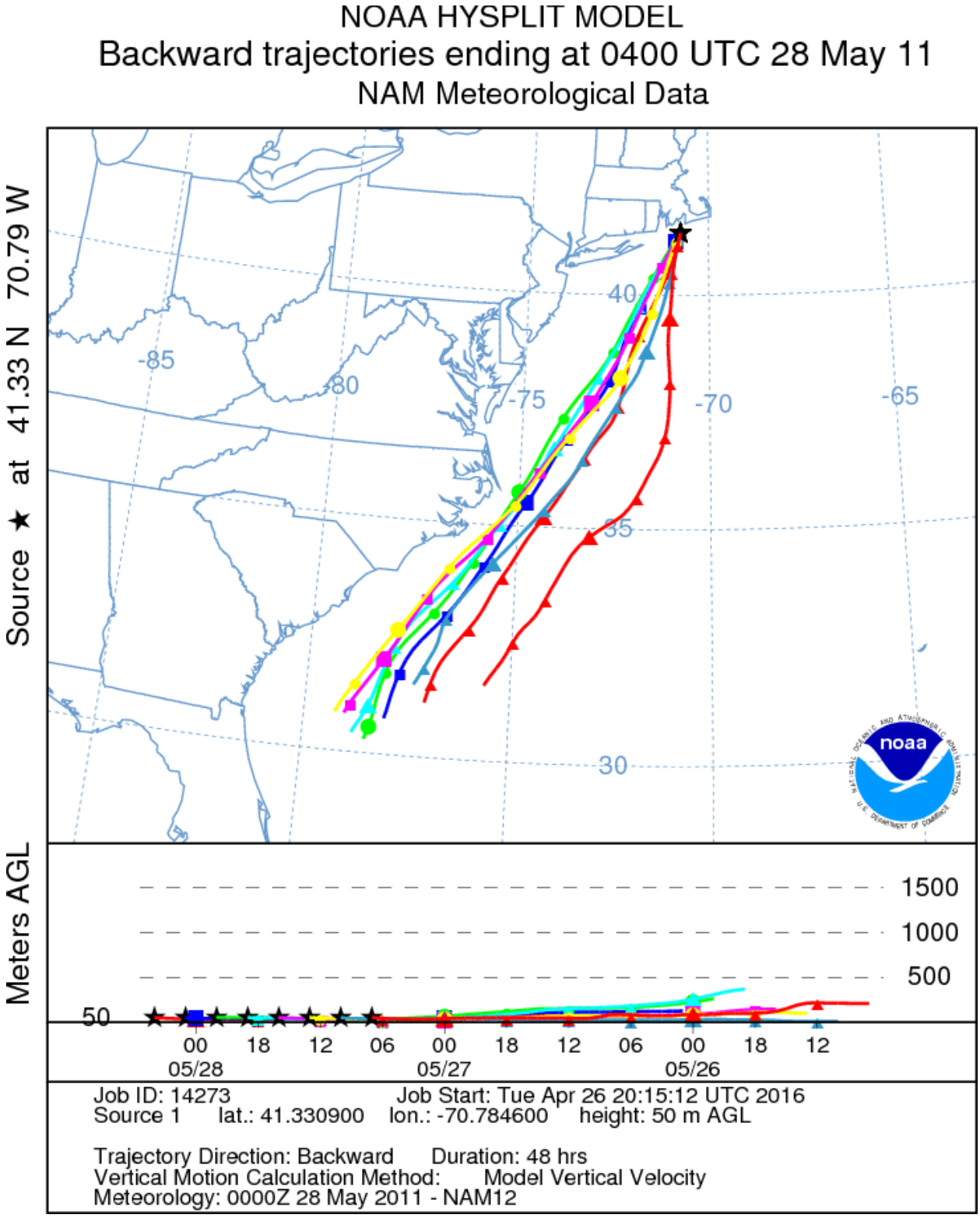
NOAA HYSPLIT MODEL
Backward trajectories ending at 0400 UTC 28 May 11
NAM Meteorological Data
Source ★ at 41.33 N 70.79 W
-85
-80
-75
-70
-65
40
35
30
noaa
Meters AGL
1500
1000
500
50
00 18 12 06 00 18 12 06 00 18 12
05/28
05/27
05/26
Job ID: 14273 Job Start: Tue Apr 26 20:15:12 UTC 2016
Source 1 lat.: 41.330900 lon.: -70.784600 height: 50 m AGL
Trajectory Direction: Backward Duration: 48 hrs
Vertical Motion Calculation Method: Model Vertical Velocity
Meteorology: 0000Z 28 May 2011 - NAM12

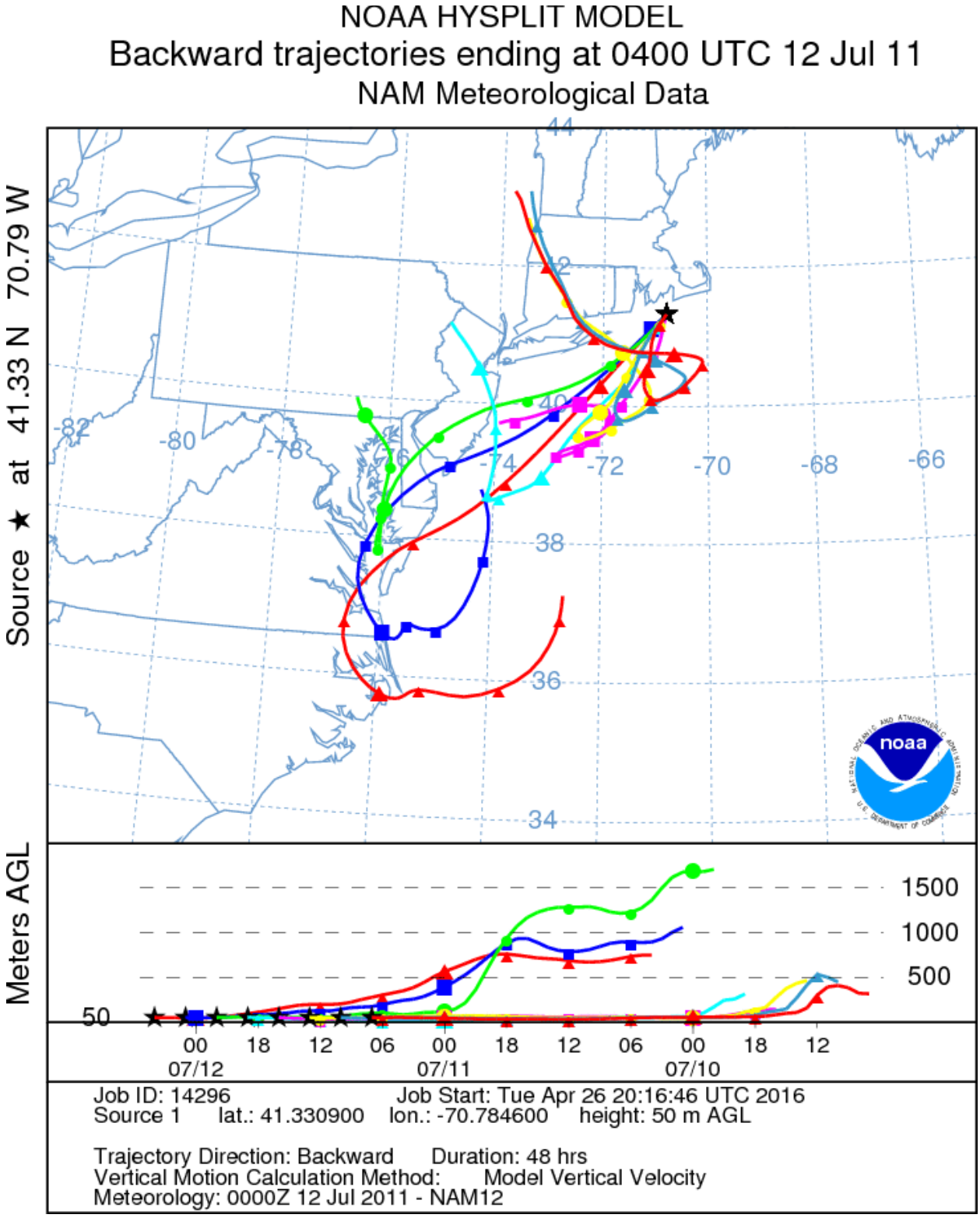
NOAA HYSPLIT MODEL
Backward trajectories ending at 0400 UTC 12 Jul 11
NAM Meteorological Data
Source ★ at 41.33 N 70.79 W
Meters AGL
1500
1000
500
50
00 18 12 06 00 18 12 06 00 18 12
07/12 07/11 07/10
Job ID: 14296 Job Start: Tue Apr 26 20:16:46 UTC 2016
Source 1 lat.: 41.330900 lon.: -70.784600 height: 50 m AGL
Trajectory Direction: Backward Duration: 48 hrs
Vertical Motion Calculation Method: Model Vertical Velocity
Meteorology: 0000Z 12 Jul 2011 - NAM12

NOAA HYSPLIT MODEL
Backward trajectories ending at 0400 UTC 03 Sep 10
NAM Meteorological Data

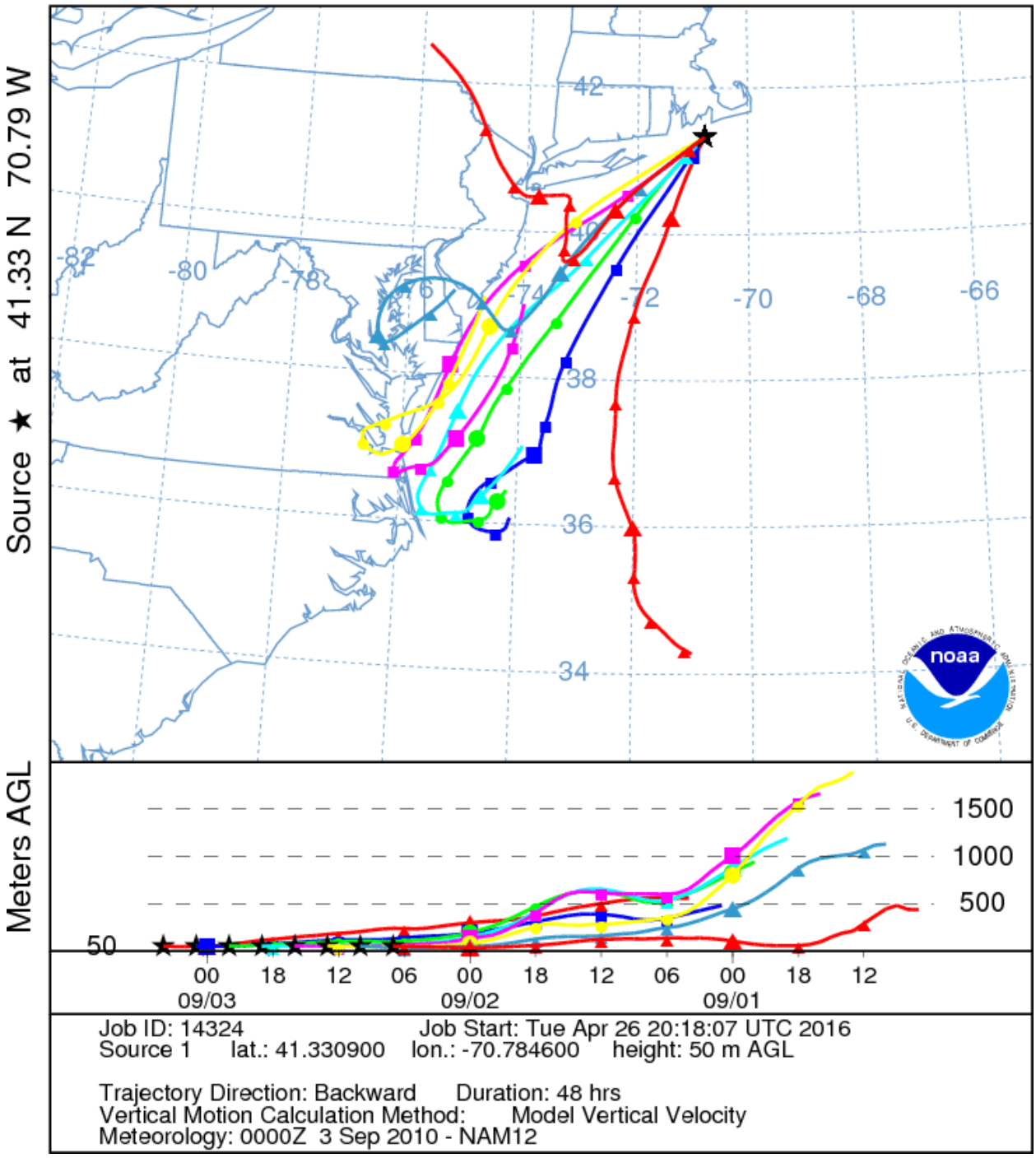

Job ID: 14324 Job Start: Tue Apr 26 20:18:07 UTC 2016
Source 1 lat.: 41.330900 lon.: -70.784600 height: 50 m AGL

Trajectory Direction: Backward Duration: 48 hrs
Vertical Motion Calculation Method: Model Vertical Velocity
Meteorology: 0000Z 3 Sep 2010 - NAM12

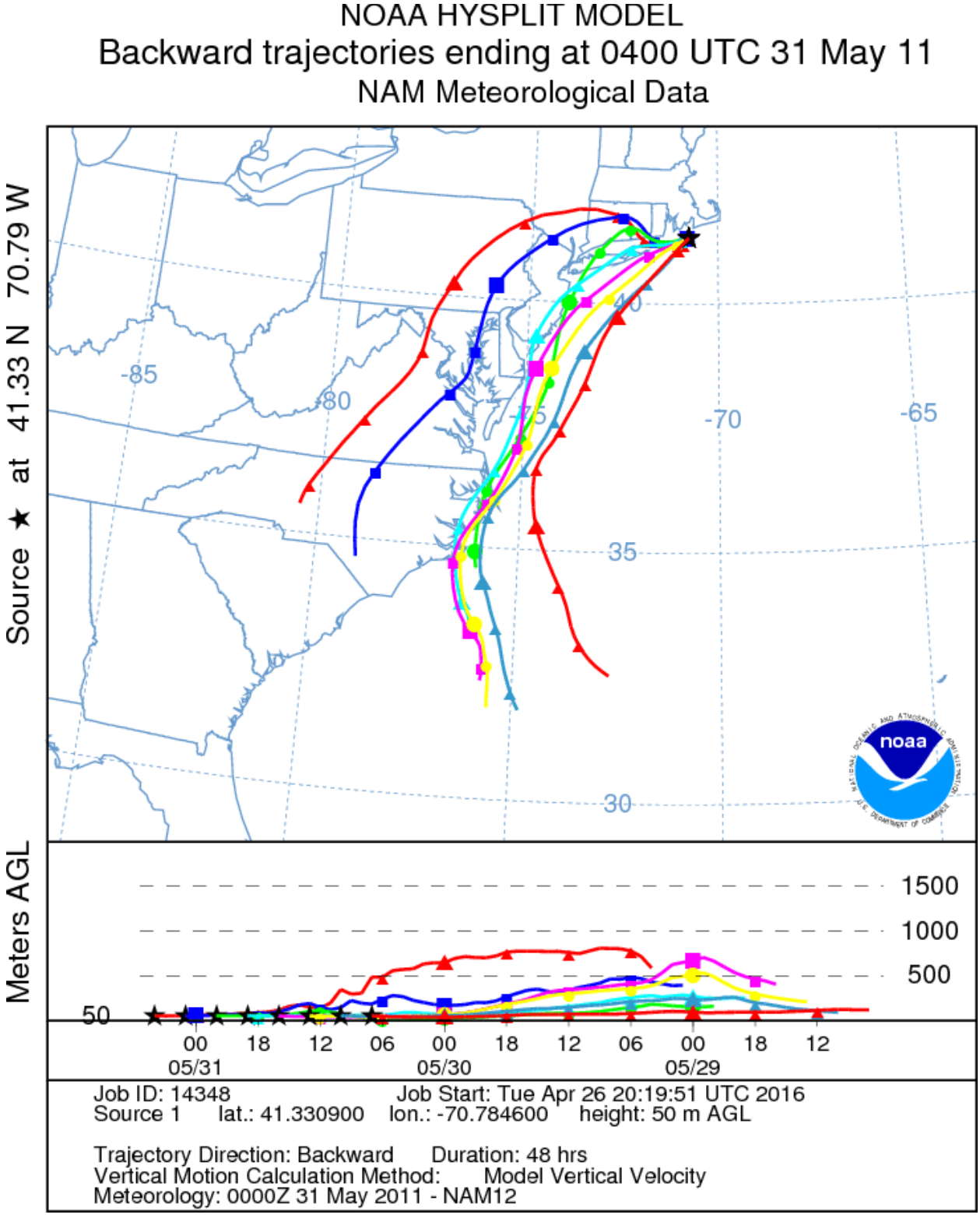
NOAA HYSPLIT MODEL
Backward trajectories ending at 0400 UTC 31 May 11
NAM Meteorological Data
Source ★ at 41.33 N 70.79 W
-85
-80
-75
-70
-65
40
35
30
noaa
Meters AGL
1500
1000
500
50
00 18 12 06 00 18 12 06 00 18 12
05/31
05/30
05/29
Job ID: 14348 Job Start: Tue Apr 26 20:19:51 UTC 2016
Source 1 lat.: 41.330900 lon.: -70.784600 height: 50 m AGL
Trajectory Direction: Backward Duration: 48 hrs
Vertical Motion Calculation Method: Model Vertical Velocity
Meteorology: 0000Z 31 May 2011 - NAM12

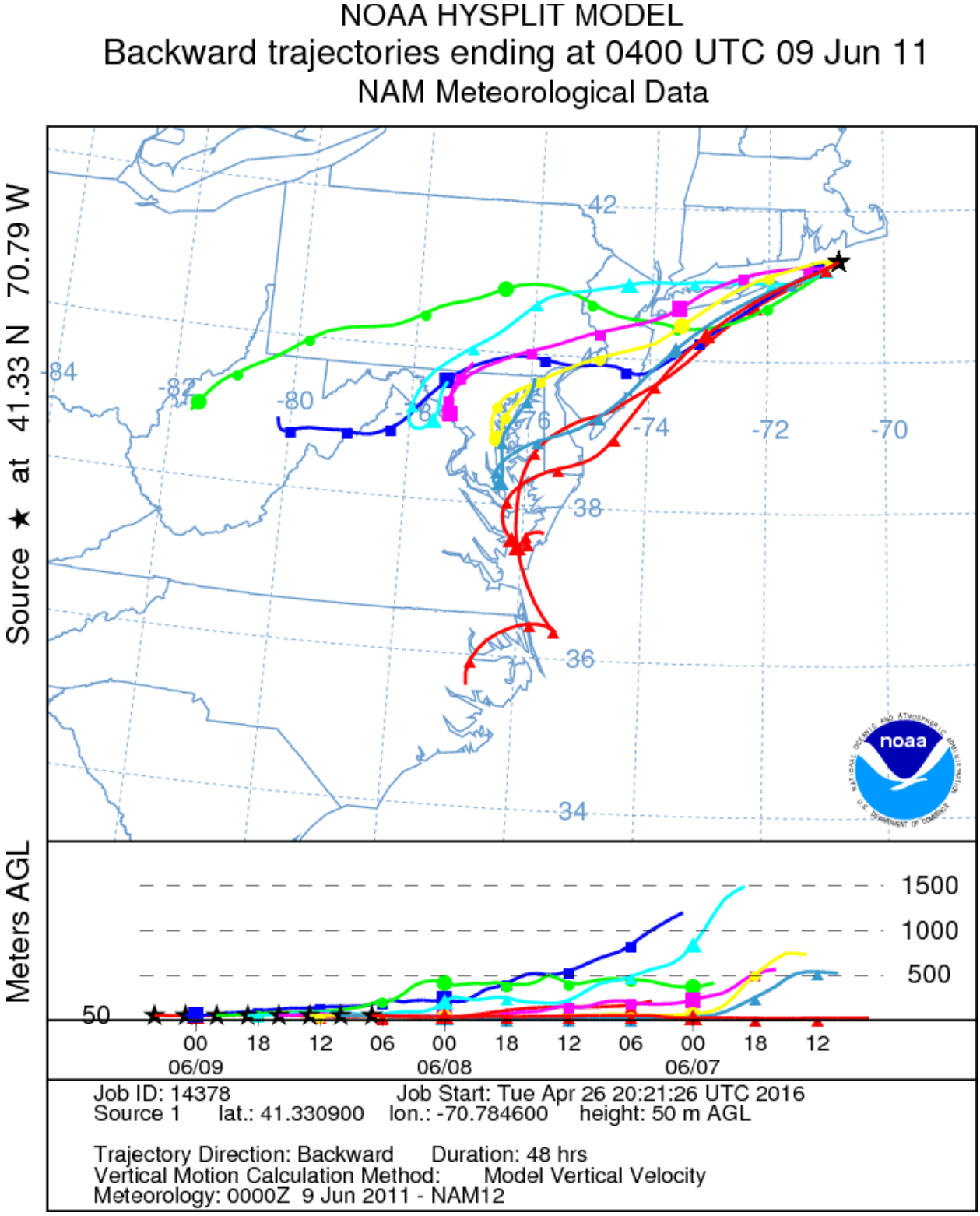
NOAA HYSPLIT MODEL
Backward trajectories ending at 0400 UTC 09 Jun 11
NAM Meteorological Data
Source ★ at 41.33 N 70.79 W
42
-84
-82
-80
-78
-76
-74
-72
-70
38
36
34
noaa
Meters AGL
1500
1000
500
50
00 18 12 06 00 18 12 06 00 18 12
06/09 06/08 06/07
Job ID: 14378 Job Start: Tue Apr 26 20:21:26 UTC 2016
Source 1 lat.: 41.330900 lon.: -70.784600 height: 50 m AGL
Trajectory Direction: Backward Duration: 48 hrs
Vertical Motion Calculation Method: Model Vertical Velocity
Meteorology: 0000Z 9 Jun 2011 - NAM12

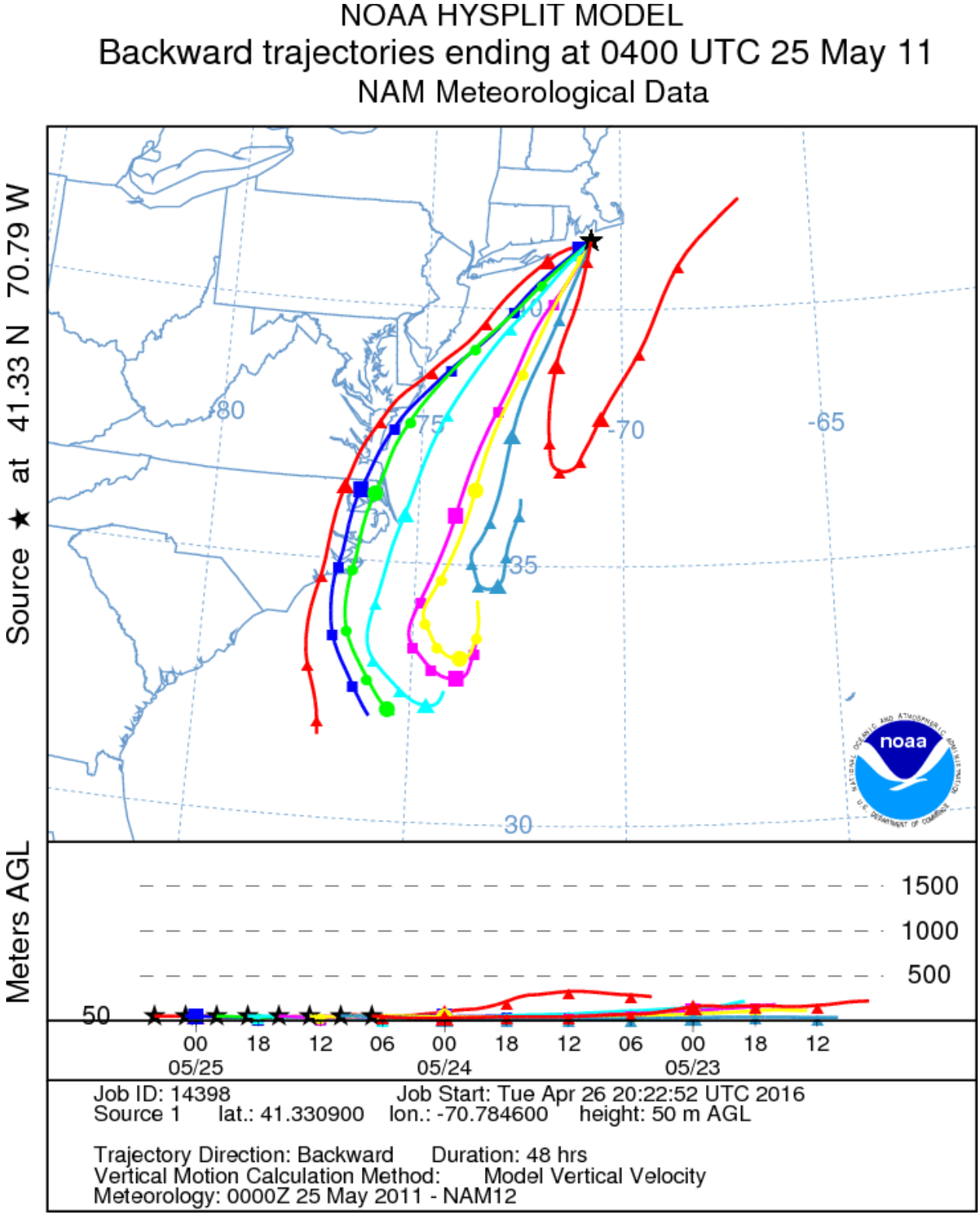
NOAA HYSPLIT MODEL
Backward trajectories ending at 0400 UTC 25 May 11
NAM Meteorological Data
Source ★ at 41.33 N 70.79 W
80
75
70
65
35
30
noaa
Meters AGL
1500
1000
500
50
00 18 12 06 00 18 12 06 00 18 12
05/25
05/24
05/23
Job ID: 14398 Job Start: Tue Apr 26 20:22:52 UTC 2016
Source 1 lat.: 41.330900 lon.: -70.784600 height: 50 m AGL
Trajectory Direction: Backward Duration: 48 hrs
Vertical Motion Calculation Method: Model Vertical Velocity
Meteorology: 0000Z 25 May 2011 - NAM12

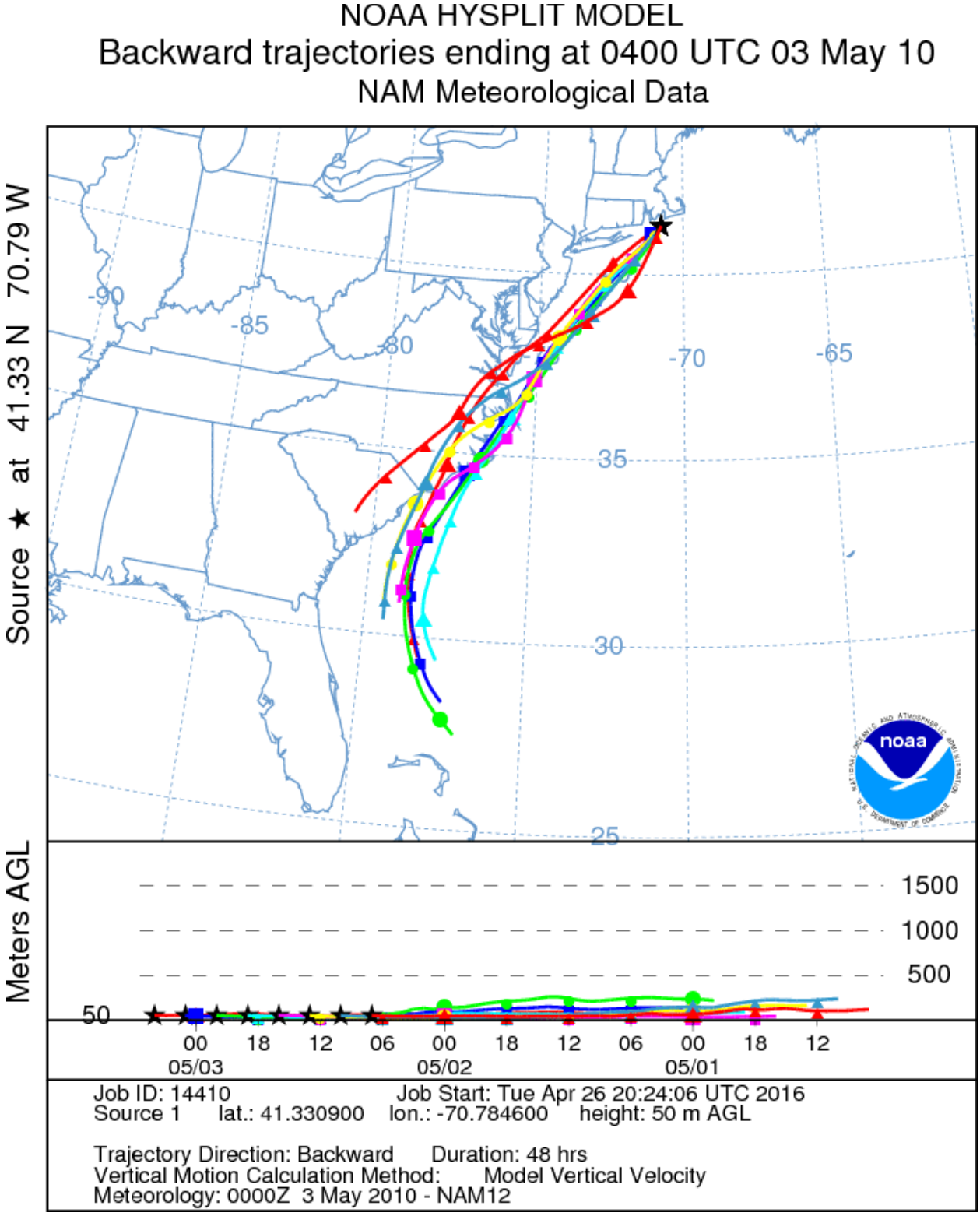
NOAA HYSPLIT MODEL
Backward trajectories ending at 0400 UTC 03 May 10
NAM Meteorological Data
Source ★ at 41.33 N 70.79 W
-90
-85
-80
-70
-65
35
30
25
noaa
Meters AGL
1500
1000
500
50
00 18 12 06 00 18 12 06 00 18 12
05/03 05/02 05/01
Job ID: 14410 Job Start: Tue Apr 26 20:24:06 UTC 2016
Source 1 lat.: 41.330900 lon.: -70.784600 height: 50 m AGL
Trajectory Direction: Backward Duration: 48 hrs
Vertical Motion Calculation Method: Model Vertical Velocity
Meteorology: 0000Z 3 May 2010 - NAM12

MOOS HYSPLIT back-trajectories

NOAA HYSPLIT MODEL
Backward trajectories ending at 0400 UTC 14 Jun 10
NAM Meteorological Data

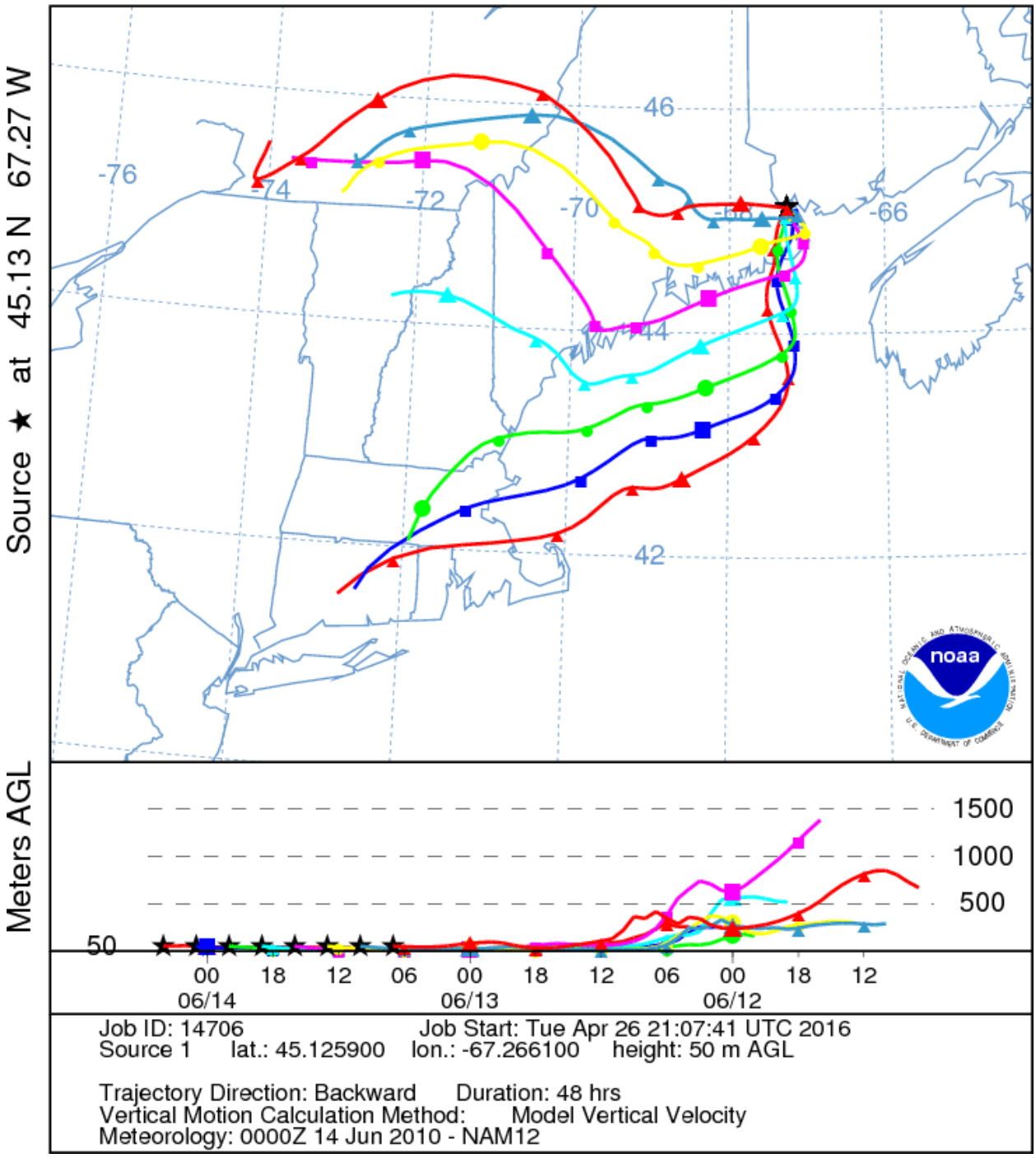

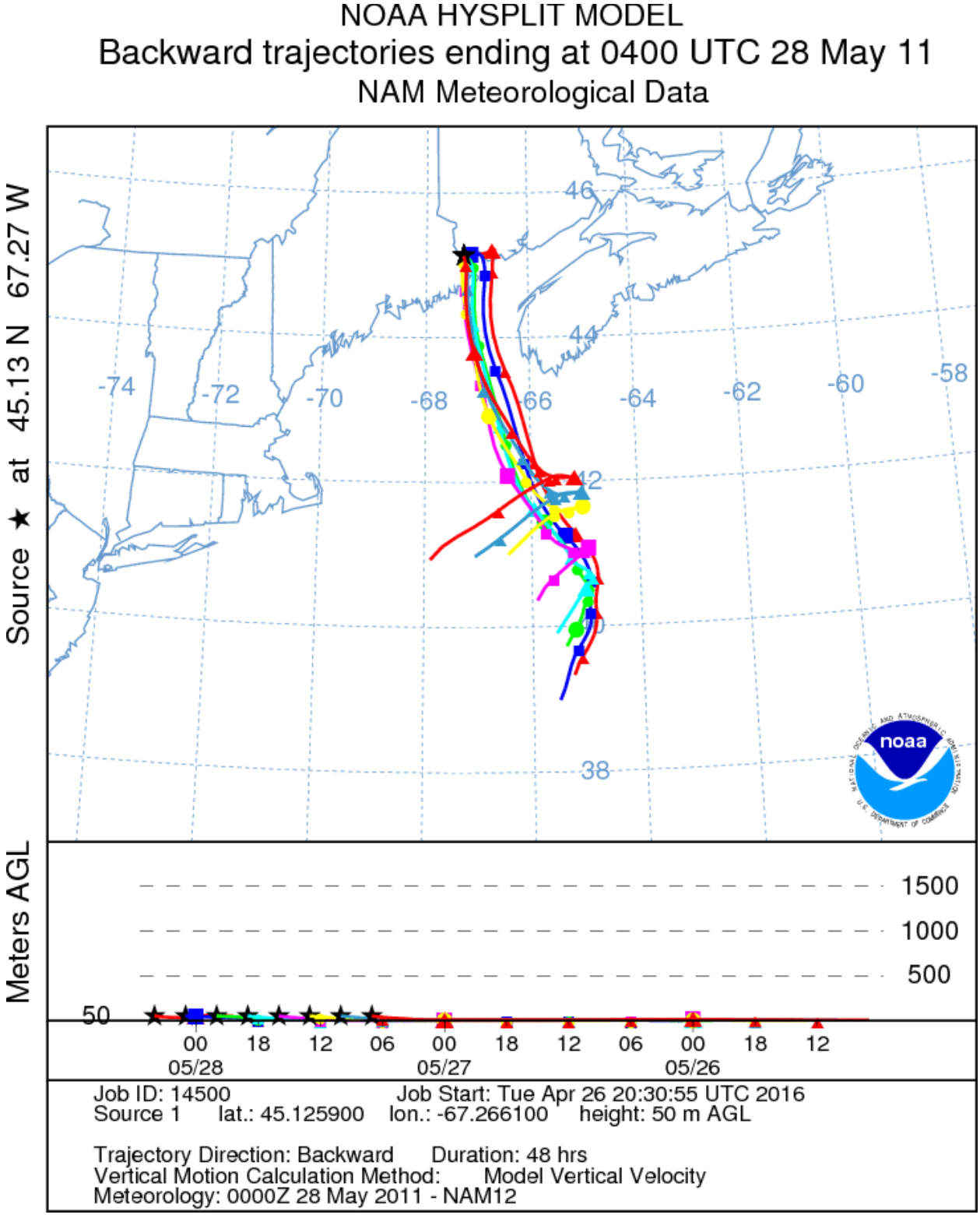
NOAA HYSPLIT MODEL
Backward trajectories ending at 0400 UTC 28 May 11
NAM Meteorological Data
Source ★ at 45.13 N 67.27 W
46
44
42
40
38
-74
-72
-70
-68
66
-64
-62
-60
-58
noaa
Meters AGL
1500
1000
500
50
00 18 12 06 00 18 12 06 00 18 12
05/28
05/27
05/26
Job ID: 14500 Job Start: Tue Apr 26 20:30:55 UTC 2016
Source 1 lat.: 45.125900 lon.: -67.266100 height: 50 m AGL
Trajectory Direction: Backward Duration: 48 hrs
Vertical Motion Calculation Method: Model Vertical Velocity
Meteorology: 0000Z 28 May 2011 - NAM12

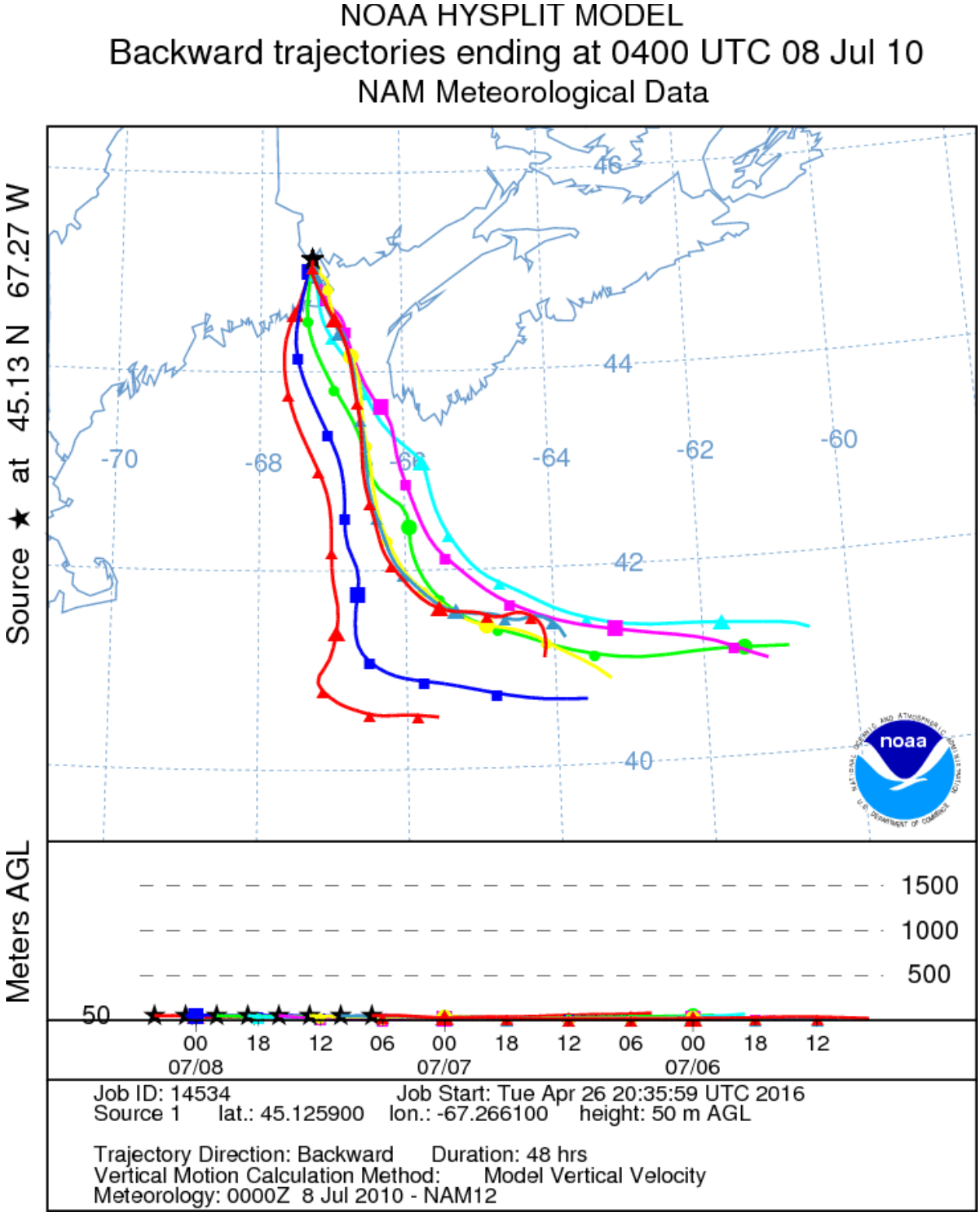
NOAA HYSPLIT MODEL
Backward trajectories ending at 0400 UTC 08 Jul 10
NAM Meteorological Data
Source ★ at 45.13 N 67.27 W
46
44
42
40
-70
-68
-66
-64
-62
-60
noaa
Meters AGL
1500
1000
500
50
00 18 12 06 00 18 12 06 00 18 12
07/08 07/07 07/06
Job ID: 14534 Job Start: Tue Apr 26 20:35:59 UTC 2016
Source 1 lat.: 45.125900 lon.: -67.266100 height: 50 m AGL
Trajectory Direction: Backward Duration: 48 hrs
Vertical Motion Calculation Method: Model Vertical Velocity
Meteorology: 0000Z 8 Jul 2010 - NAM12

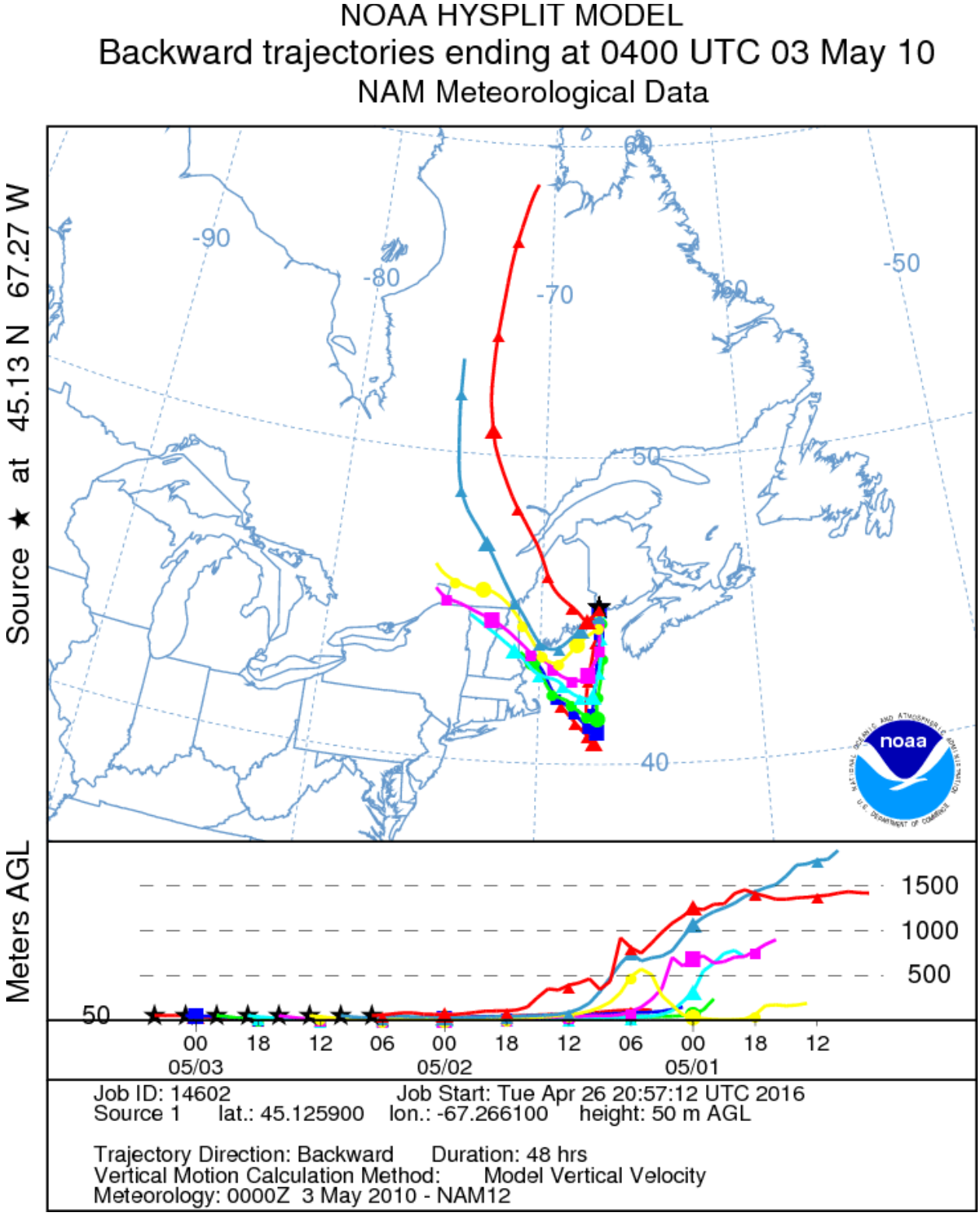
NOAA HYSPLIT MODEL
Backward trajectories ending at 0400 UTC 03 May 10
NAM Meteorological Data
Source ★ at 45.13 N 67.27 W
-90
-80
-70
-60
-50
60
50
40
noaa
Meters AGL
1500
1000
500
50
00 18 12 06 00 18 12 06 00 18 12
05/03 05/02 05/01
Job ID: 14602 Job Start: Tue Apr 26 20:57:12 UTC 2016
Source 1 lat.: 45.125900 lon.: -67.266100 height: 50 m AGL
Trajectory Direction: Backward Duration: 48 hrs
Vertical Motion Calculation Method: Model Vertical Velocity
Meteorology: 0000Z 3 May 2010 - NAM12

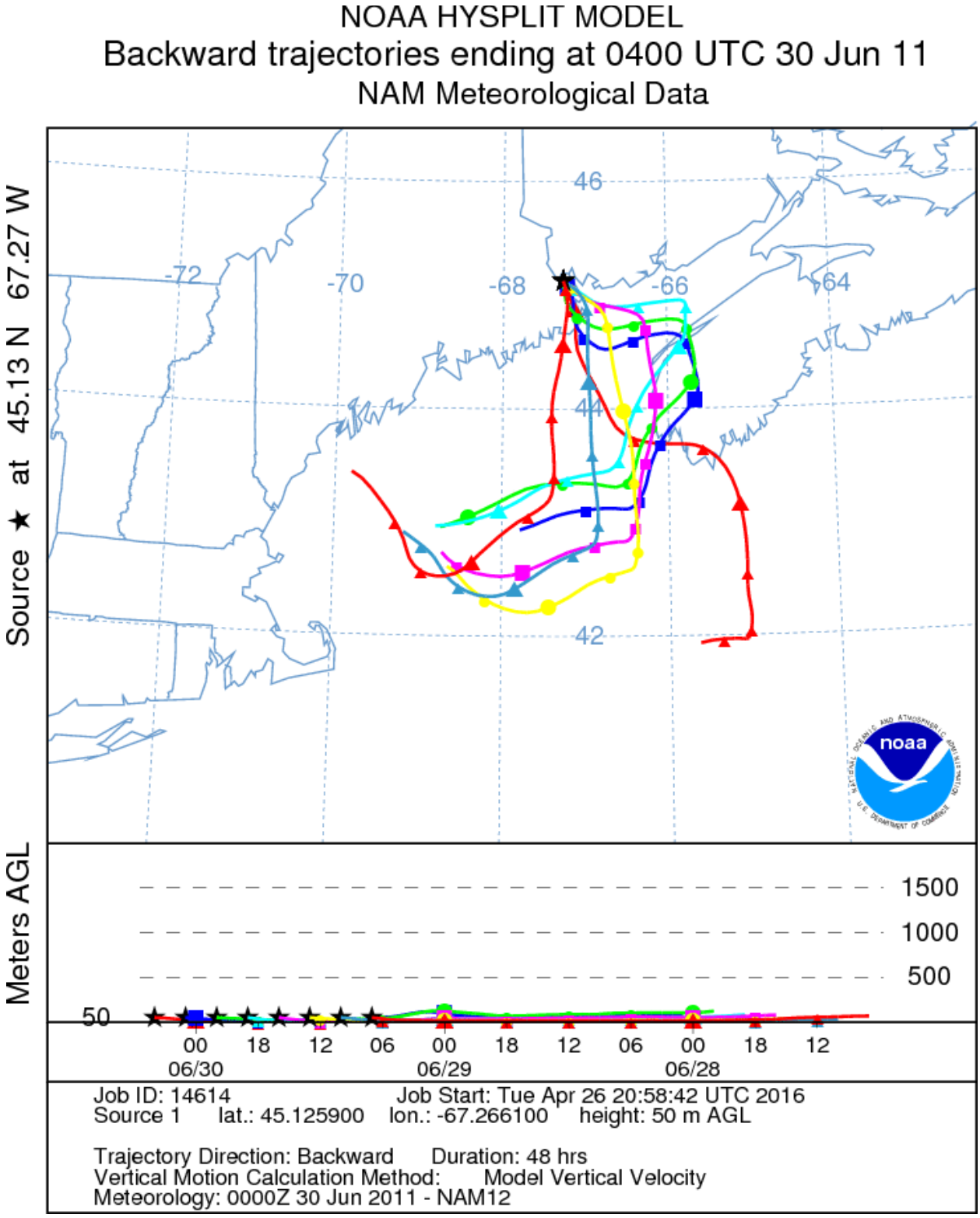
NOAA HYSPLIT MODEL
Backward trajectories ending at 0400 UTC 30 Jun 11
NAM Meteorological Data
Source ★ at 45.13 N 67.27 W
46
44
42
-72
-70
-68
-66
-64
noaa
Meters AGL
1500
1000
500
50
00 18 12 06 00 18 12 06 00 18 12
06/30 06/29 06/28
Job ID: 14614 Job Start: Tue Apr 26 20:58:42 UTC 2016
Source 1 lat.: 45.125900 lon.: -67.266100 height: 50 m AGL
Trajectory Direction: Backward Duration: 48 hrs
Vertical Motion Calculation Method: Model Vertical Velocity
Meteorology: 0000Z 30 Jun 2011 - NAM12

NOAA HYSPLIT MODEL
Backward trajectories ending at 0400 UTC 20 Aug 11
NAM Meteorological Data

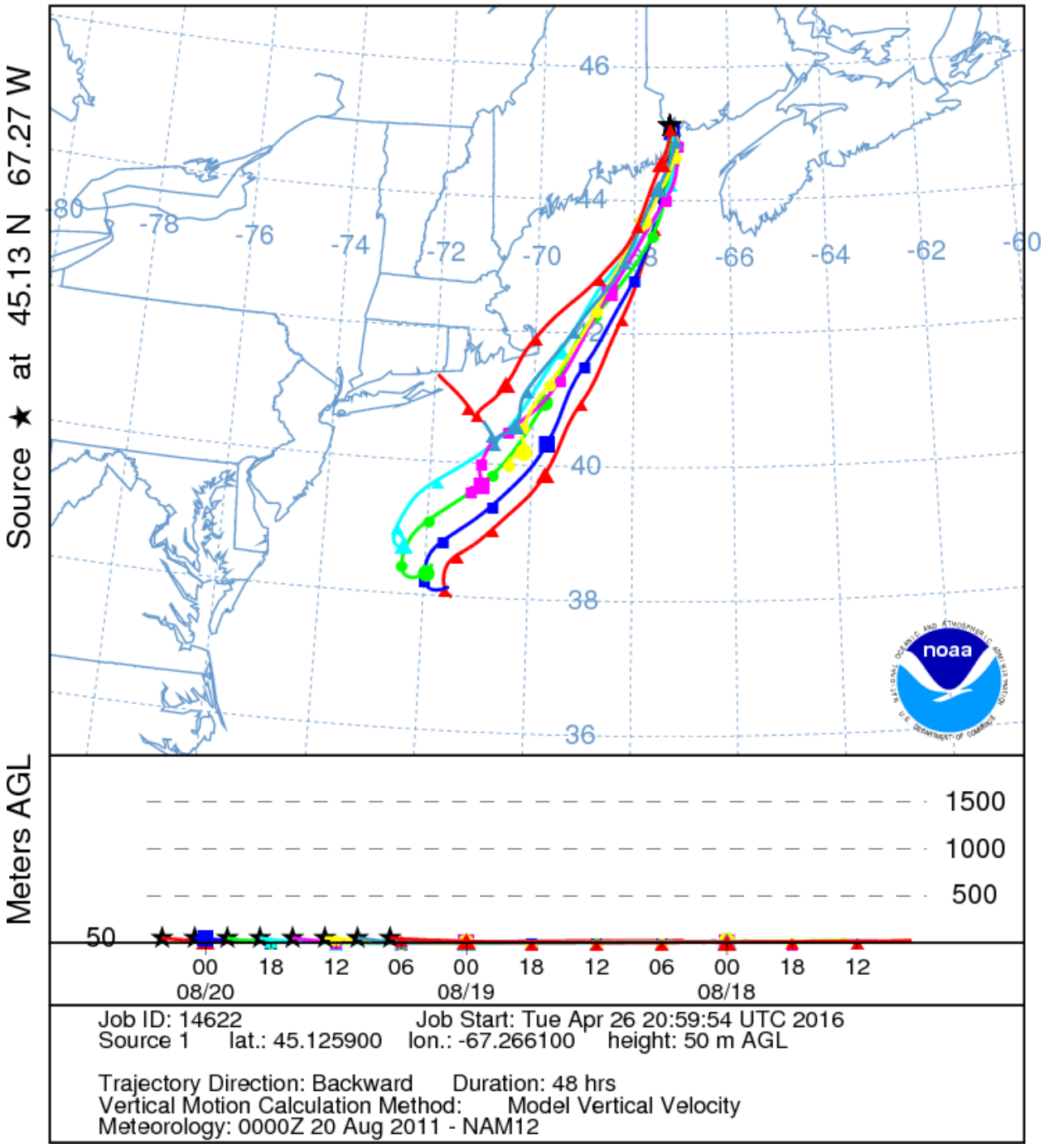

Job ID: 14622 Job Start: Tue Apr 26 20:59:54 UTC 2016
Source 1 lat.: 45.125900 lon.: -67.266100 height: 50 m AGL

Trajectory Direction: Backward Duration: 48 hrs
Vertical Motion Calculation Method: Model Vertical Velocity
Meteorology: 0000Z 20 Aug 2011 - NAM12

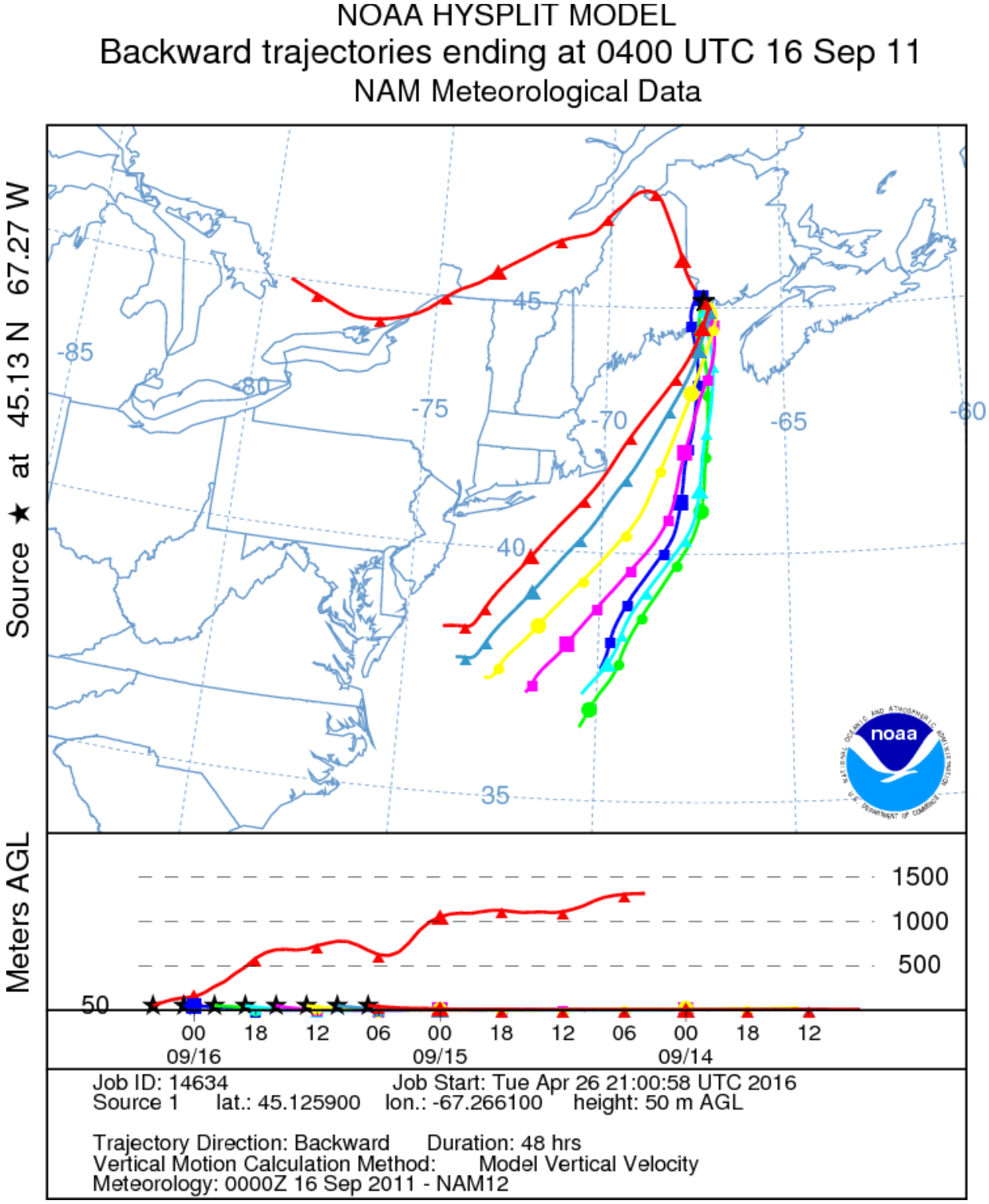
NOAA HYSPLIT MODEL
Backward trajectories ending at 0400 UTC 16 Sep 11
NAM Meteorological Data
Source ★ at 45.13 N 67.27 W
-85
-80
-75
-70
-65
-60
45
40
35
noaa
Meters AGL
1500
1000
500
50
00 18 12 06 00 18 12 06 00 18 12
09/16
09/15
09/14
Job ID: 14634 Job Start: Tue Apr 26 21:00:58 UTC 2016
Source 1 lat.: 45.125900 lon.: -67.266100 height: 50 m AGL
Trajectory Direction: Backward Duration: 48 hrs
Vertical Motion Calculation Method: Model Vertical Velocity
Meteorology: 0000Z 16 Sep 2011 - NAM12

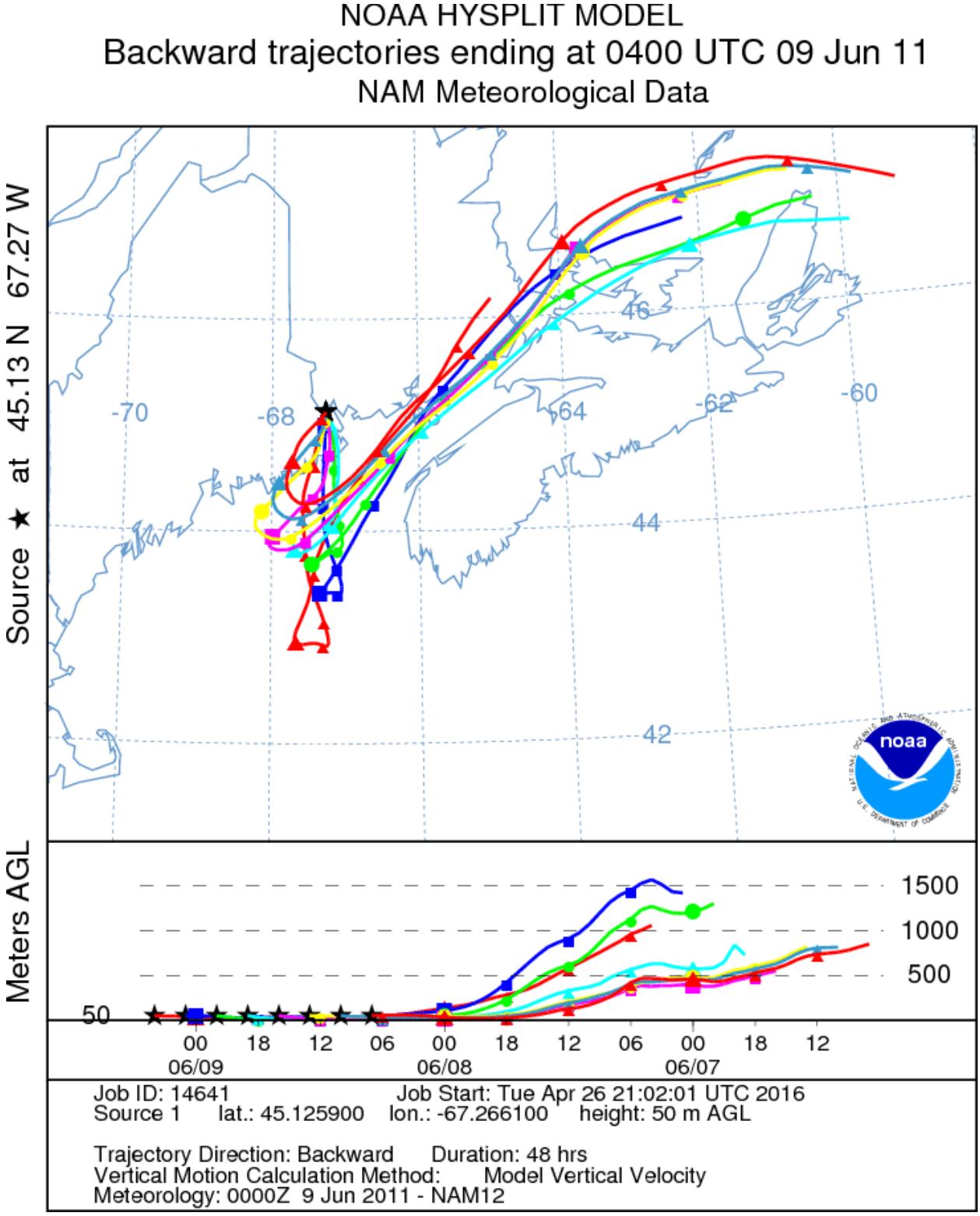
NOAA HYSPLIT MODEL
Backward trajectories ending at 0400 UTC 09 Jun 11
NAM Meteorological Data
Source ★ at 45.13 N 67.27 W
-70
-68
-64
-62
-60
46
44
42
noaa
Meters AGL
1500
1000
500
50
00 18 12 06 00 18 12 06 00 18 12
06/09 06/08 06/07
Job ID: 14641 Job Start: Tue Apr 26 21:02:01 UTC 2016
Source 1 lat.: 45.125900 lon.: -67.266100 height: 50 m AGL
Trajectory Direction: Backward Duration: 48 hrs
Vertical Motion Calculation Method: Model Vertical Velocity
Meteorology: 0000Z 9 Jun 2011 - NAM12

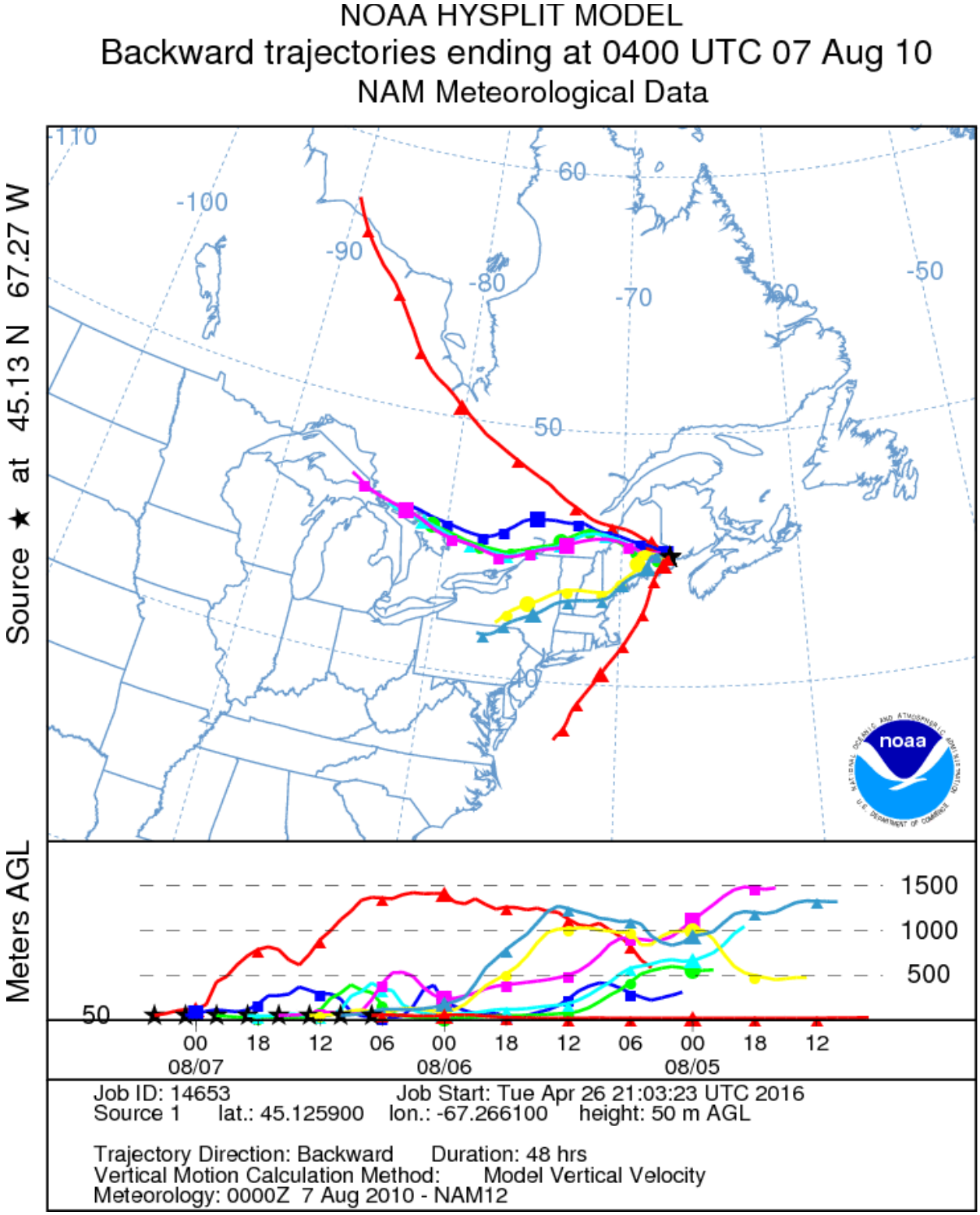
NOAA HYSPLIT MODEL
Backward trajectories ending at 0400 UTC 07 Aug 10
NAM Meteorological Data
Source ★ at 45.13 N 67.27 W
Meters AGL
-110
-100
-90
-80
-70
-60
-50
60
50
40
1500
1000
500
50
00 18 12 06 00 18 12 06 00 18 12
08/07 08/06 08/05
noaa
Job ID: 14653 Job Start: Tue Apr 26 21:03:23 UTC 2016
Source 1 lat.: 45.125900 lon.: -67.266100 height: 50 m AGL
Trajectory Direction: Backward Duration: 48 hrs
Vertical Motion Calculation Method: Model Vertical Velocity
Meteorology: 0000Z 7 Aug 2010 - NAM12

NOAA HYSPLIT MODEL
Backward trajectories ending at 0500 UTC 09 Jan 10
NAM Meteorological Data

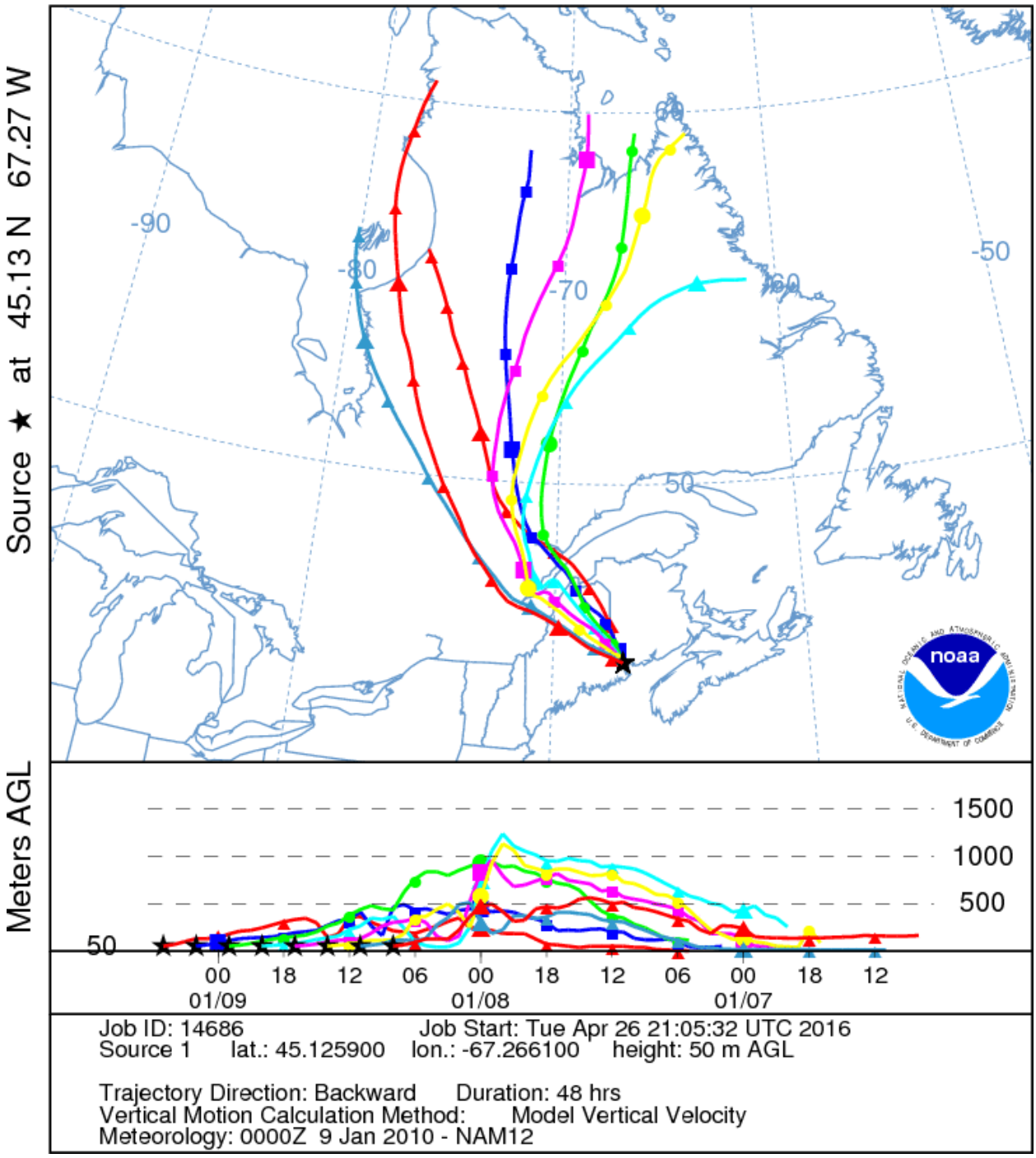

MORA HYSPLIT back-trajectories

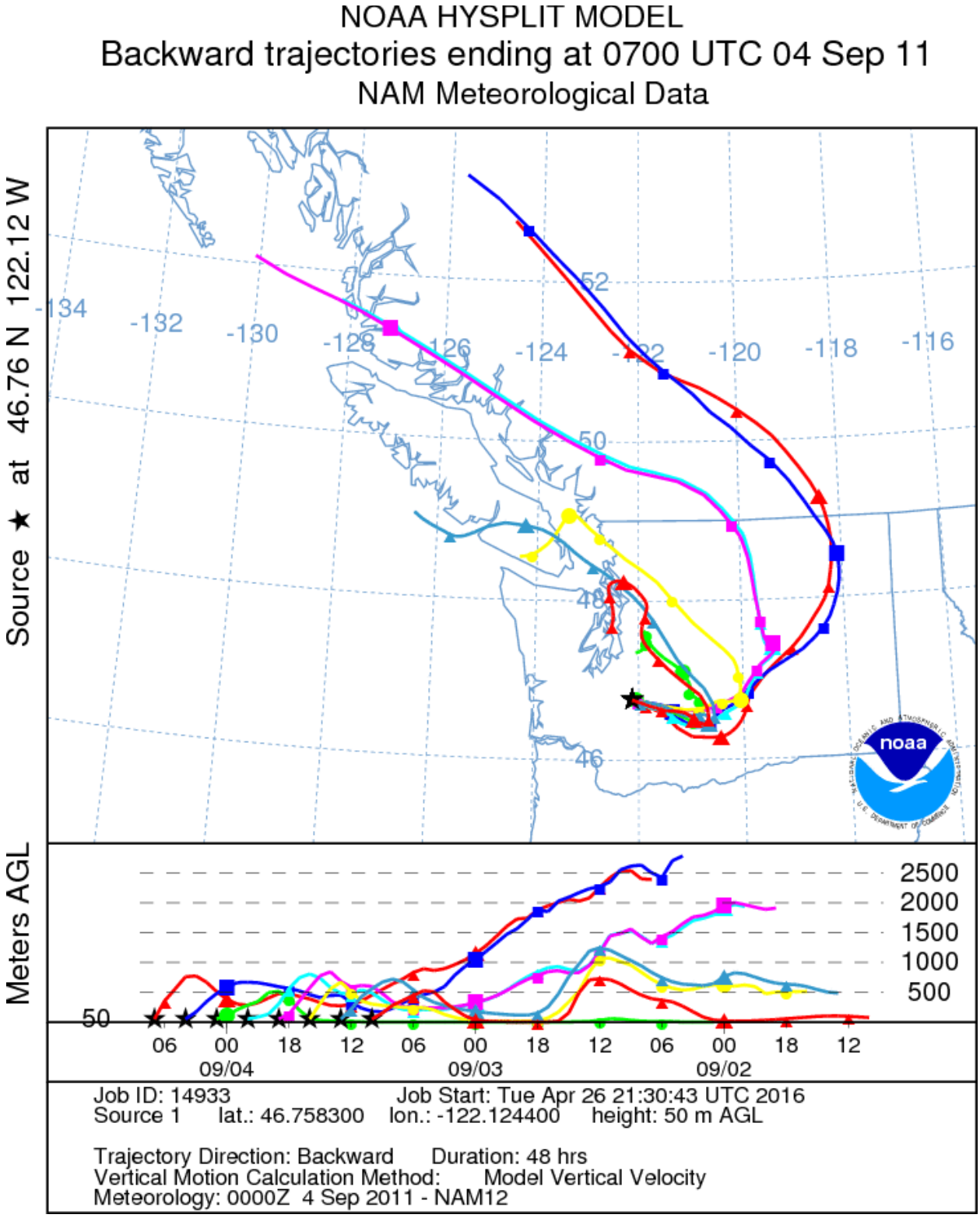
NOAA HYSPLIT MODEL
Backward trajectories ending at 0700 UTC 04 Sep 11
NAM Meteorological Data
Source ★ at 46.76 N 122.12 W
-134
-132
-130
-128
-126
-124
-122
-120
-118
-116
52
50
48
46
noaa
Meters AGL
2500
2000
1500
1000
500
50
06 00 18 12 06 00 18 12 06 00 18 12
09/04
09/03
09/02
Job ID: 14933 Job Start: Tue Apr 26 21:30:43 UTC 2016
Source 1 lat.: 46.758300 lon.: -122.124400 height: 50 m AGL
Trajectory Direction: Backward Duration: 48 hrs
Vertical Motion Calculation Method: Model Vertical Velocity
Meteorology: 0000Z 4 Sep 2011 - NAM12

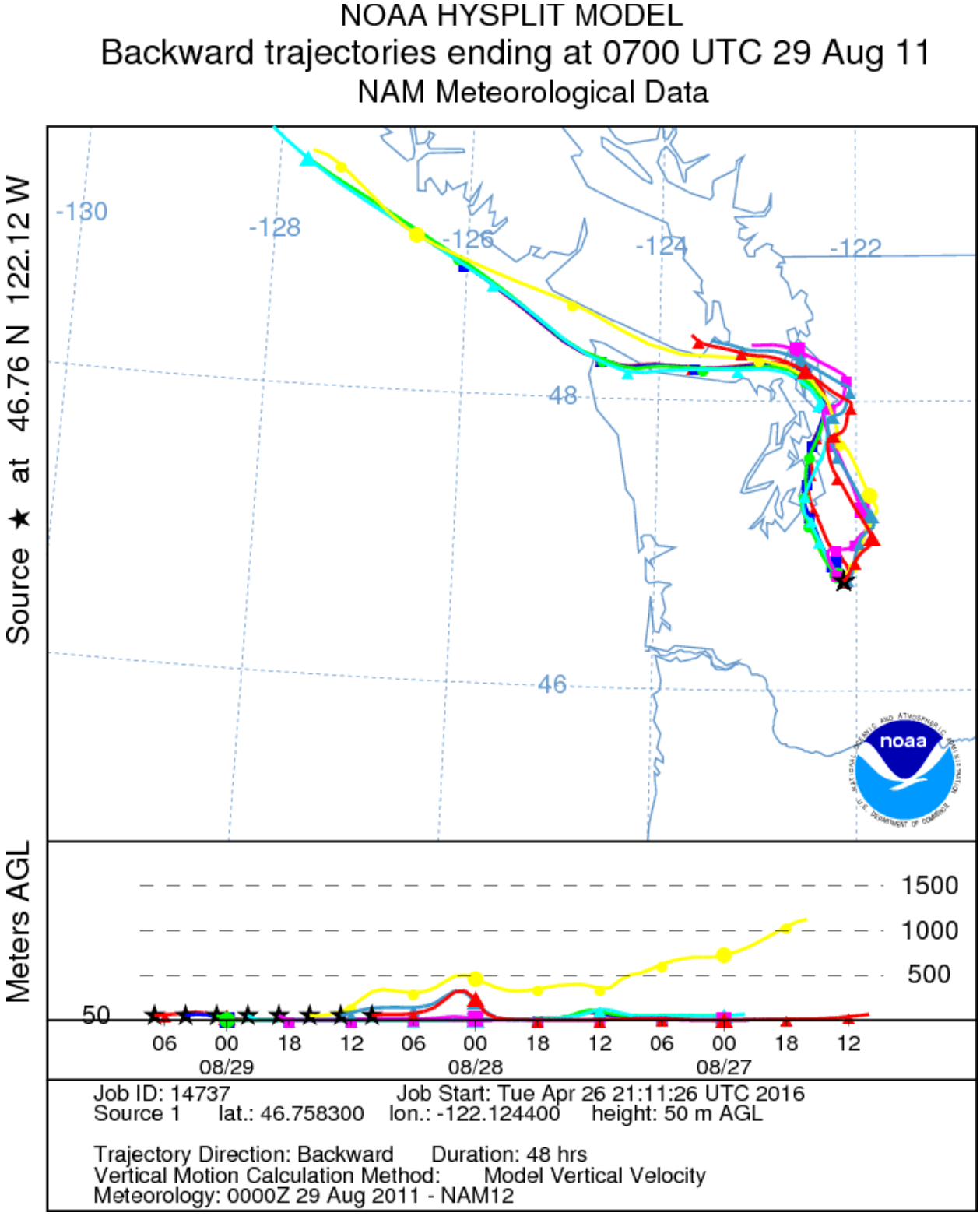
NOAA HYSPLIT MODEL
Backward trajectories ending at 0700 UTC 29 Aug 11
NAM Meteorological Data
Source ★ at 46.76 N 122.12 W
-130
-128
-126
-124
-122
48
46
noaa
Meters AGL
1500
1000
500
50
06 00 18 12 06 00 18 12 06 00 18 12
08/29
08/28
08/27
Job ID: 14737 Job Start: Tue Apr 26 21:11:26 UTC 2016
Source 1 lat.: 46.758300 lon.: -122.124400 height: 50 m AGL
Trajectory Direction: Backward Duration: 48 hrs
Vertical Motion Calculation Method: Model Vertical Velocity
Meteorology: 0000Z 29 Aug 2011 - NAM12

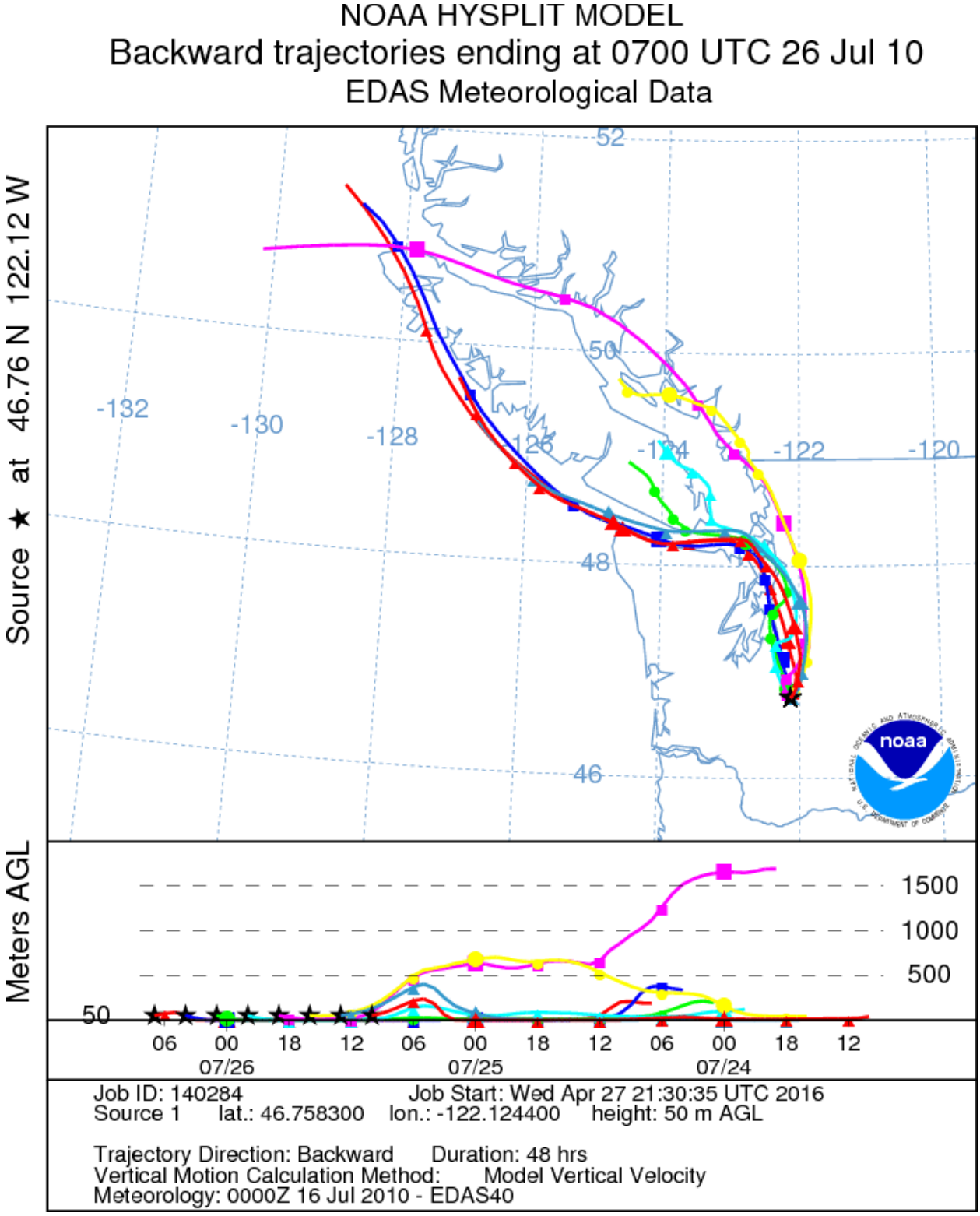
NOAA HYSPLIT MODEL
Backward trajectories ending at 0700 UTC 26 Jul 10
EDAS Meteorological Data
Source ★ at 46.76 N 122.12 W
52
50
48
46
-132
-130
-128
-126
-124
-122
-120
noaa
Meters AGL
1500
1000
500
50
06 00 18 12 06 00 18 12 06 00 18 12
07/26
07/25
07/24
Job ID: 140284 Job Start: Wed Apr 27 21:30:35 UTC 2016
Source 1 lat.: 46.758300 lon.: -122.124400 height: 50 m AGL
Trajectory Direction: Backward Duration: 48 hrs
Vertical Motion Calculation Method: Model Vertical Velocity
Meteorology: 0000Z 16 Jul 2010 - EDAS40

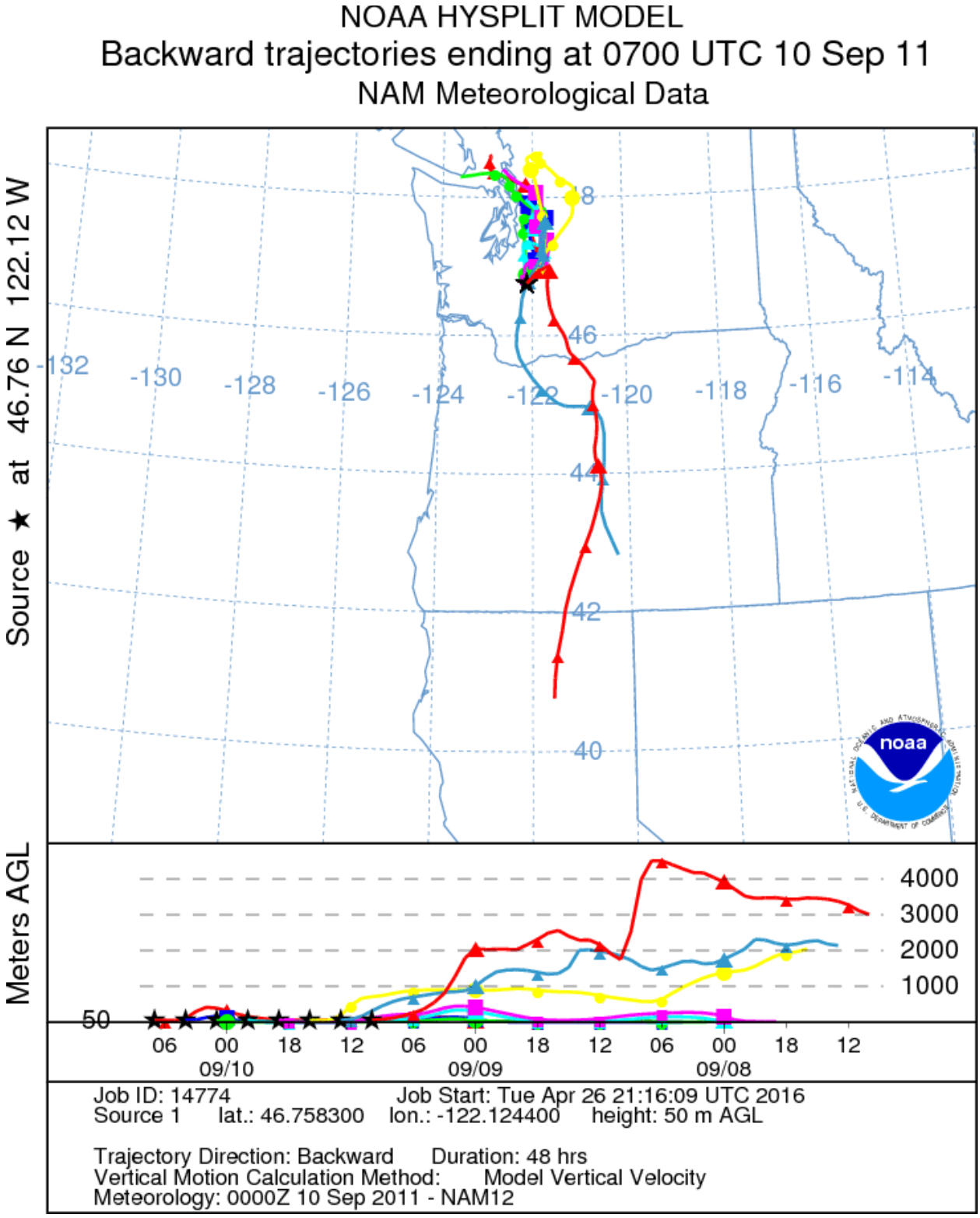
NOAA HYSPLIT MODEL
Backward trajectories ending at 0700 UTC 10 Sep 11
NAM Meteorological Data
Source ★ at 46.76 N 122.12 W
Meters AGL
-132
-130
-128
-126
-124
-122
-120
-118
-116
-114
48
46
44
42
40
noaa
4000
3000
2000
1000
50
06
00
18
12
06
00
18
12
06
00
18
12
09/10
09/09
09/08
Job ID: 14774
Job Start: Tue Apr 26 21:16:09 UTC 2016
Source 1
lat.: 46.758300
lon.: -122.124400
height: 50 m AGL
Trajectory Direction: Backward
Duration: 48 hrs
Vertical Motion Calculation Method:
Model Vertical Velocity
Meteorology: 0000Z 10 Sep 2011 - NAM12

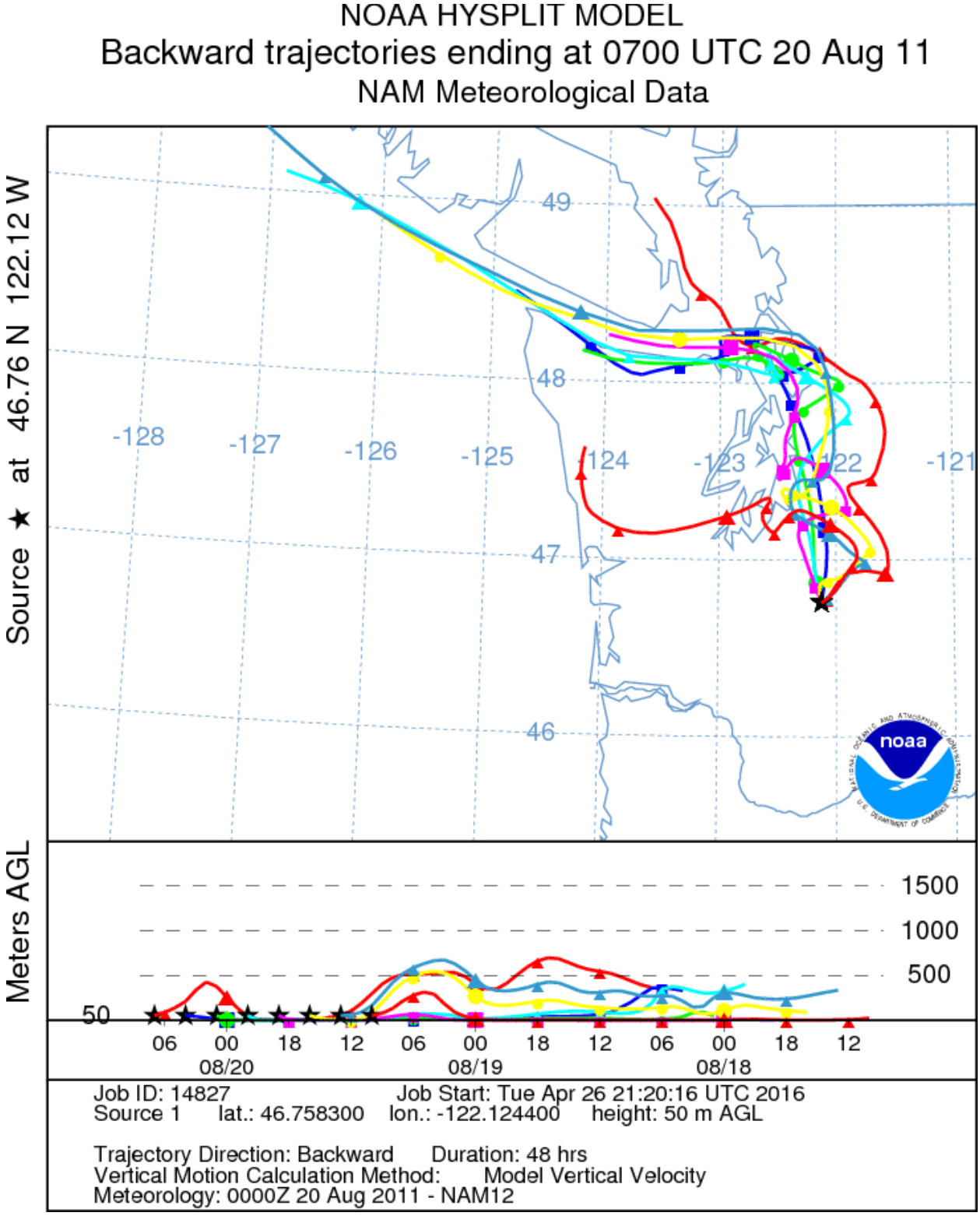
NOAA HYSPLIT MODEL
Backward trajectories ending at 0700 UTC 20 Aug 11
NAM Meteorological Data
Source ★ at 46.76 N 122.12 W
49
48
47
46
-128
-127
-126
-125
-124
-123
-122
-121
noaa
Meters AGL
1500
1000
500
50
06
00
18
12
06
00
18
12
06
00
18
12
08/20
08/19
08/18
Job ID: 14827
Job Start: Tue Apr 26 21:20:16 UTC 2016
Source 1
lat.: 46.758300
lon.: -122.124400
height: 50 m AGL
Trajectory Direction: Backward
Duration: 48 hrs
Vertical Motion Calculation Method:
Model Vertical Velocity
Meteorology: 0000Z 20 Aug 2011 - NAM12

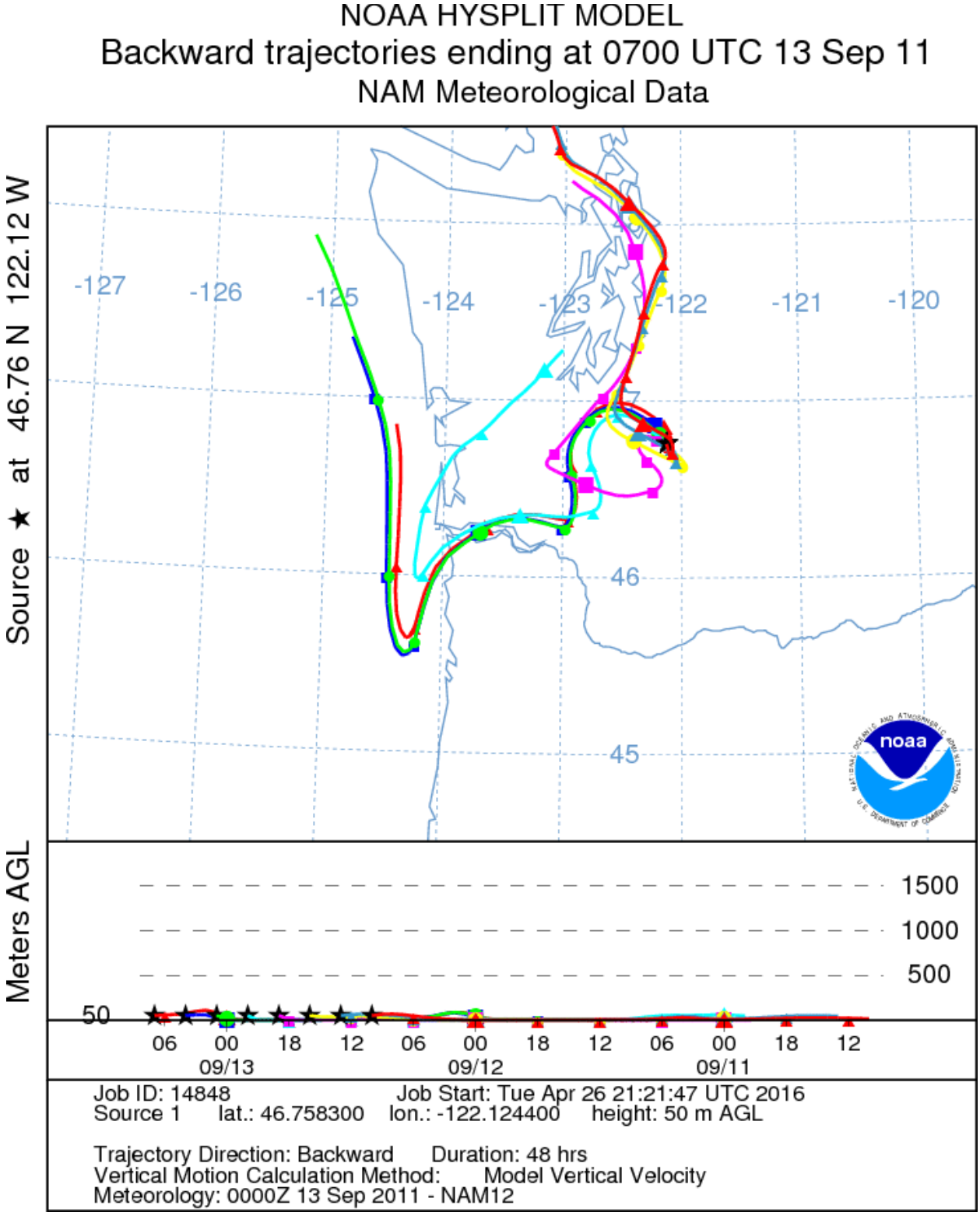
NOAA HYSPLIT MODEL
Backward trajectories ending at 0700 UTC 13 Sep 11
NAM Meteorological Data
Source ★ at 46.76 N 122.12 W
-127
-126
-125
-124
-123
-122
-121
-120
46
45
noaa
Meters AGL
1500
1000
500
50
06 00 18 12 06 00 18 12 06 00 18 12
09/13
09/12
09/11
Job ID: 14848 Job Start: Tue Apr 26 21:21:47 UTC 2016
Source 1 lat.: 46.758300 lon.: -122.124400 height: 50 m AGL
Trajectory Direction: Backward Duration: 48 hrs
Vertical Motion Calculation Method: Model Vertical Velocity
Meteorology: 0000Z 13 Sep 2011 - NAM12

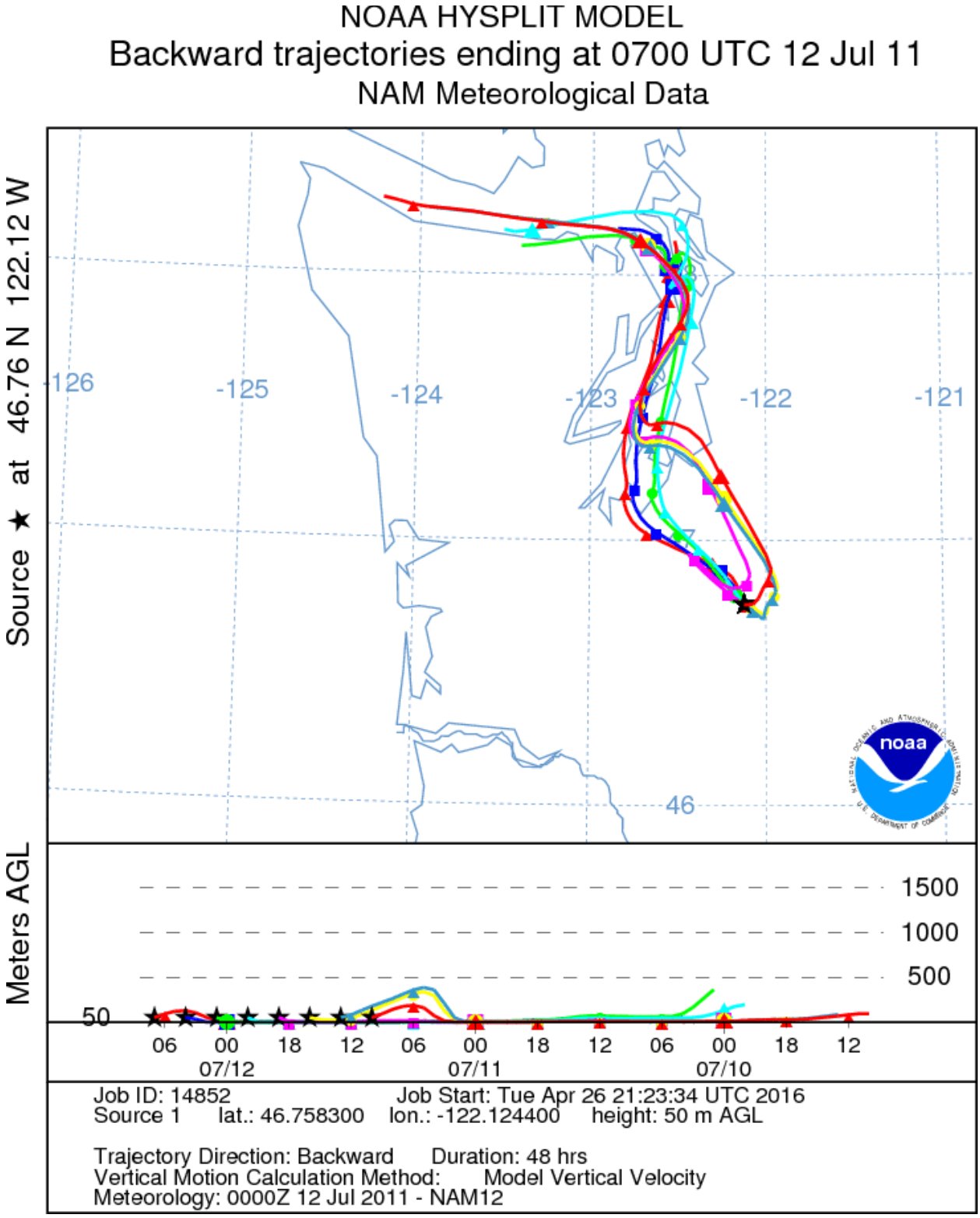
NOAA HYSPLIT MODEL
Backward trajectories ending at 0700 UTC 12 Jul 11
NAM Meteorological Data
Source ★ at 46.76 N 122.12 W
-126
-125
-124
-123
-122
-121
46
noaa
Meters AGL
1500
1000
500
50
06 00 18 12 06 00 18 12 06 00 18 12
07/12
07/11
07/10
Job ID: 14852 Job Start: Tue Apr 26 21:23:34 UTC 2016
Source 1 lat.: 46.758300 lon.: -122.124400 height: 50 m AGL
Trajectory Direction: Backward Duration: 48 hrs
Vertical Motion Calculation Method: Model Vertical Velocity
Meteorology: 0000Z 12 Jul 2011 - NAM12

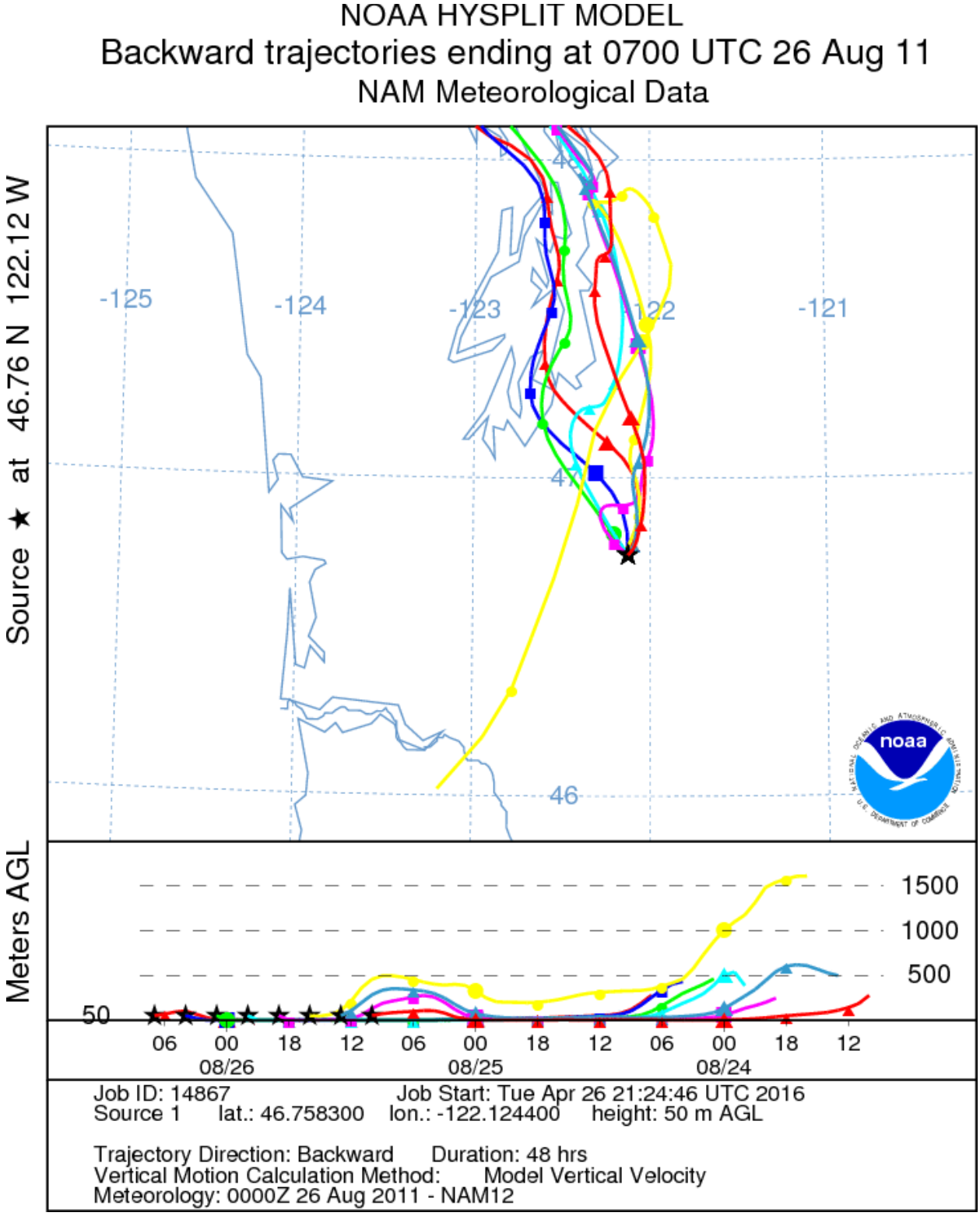
NOAA HYSPLIT MODEL
Backward trajectories ending at 0700 UTC 26 Aug 11
NAM Meteorological Data
Source ★ at 46.76 N 122.12 W
-125
-124
-123
-122
-121
47
46
noaa
Meters AGL
1500
1000
500
50
06 00 18 12 06 00 18 12 06 00 18 12
08/26
08/25
08/24
Job ID: 14867 Job Start: Tue Apr 26 21:24:46 UTC 2016
Source 1 lat.: 46.758300 lon.: -122.124400 height: 50 m AGL
Trajectory Direction: Backward Duration: 48 hrs
Vertical Motion Calculation Method: Model Vertical Velocity
Meteorology: 0000Z 26 Aug 2011 - NAM12

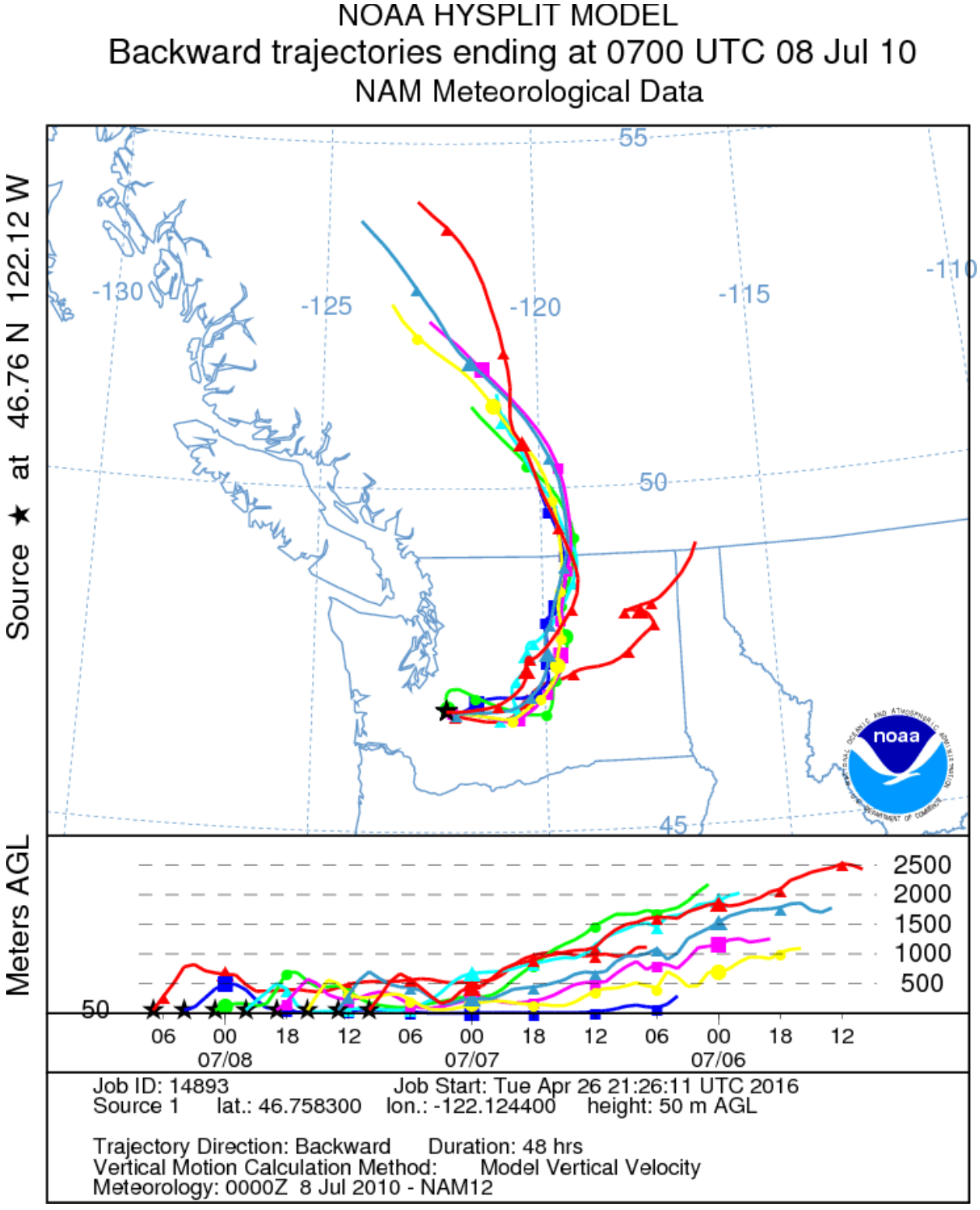
NOAA HYSPLIT MODEL
Backward trajectories ending at 0700 UTC 08 Jul 10
NAM Meteorological Data
Source ★ at 46.76 N 122.12 W
55
50
45
-130
-125
-120
-115
-110
noaa
Meters AGL
2500
2000
1500
1000
500
50
06 00 18 12 06 00 18 12 06 00 18 12
07/08 07/07 07/06
Job ID: 14893 Job Start: Tue Apr 26 21:26:11 UTC 2016
Source 1 lat.: 46.758300 lon.: -122.124400 height: 50 m AGL
Trajectory Direction: Backward Duration: 48 hrs
Vertical Motion Calculation Method: Model Vertical Velocity
Meteorology: 0000Z 8 Jul 2010 - NAM12

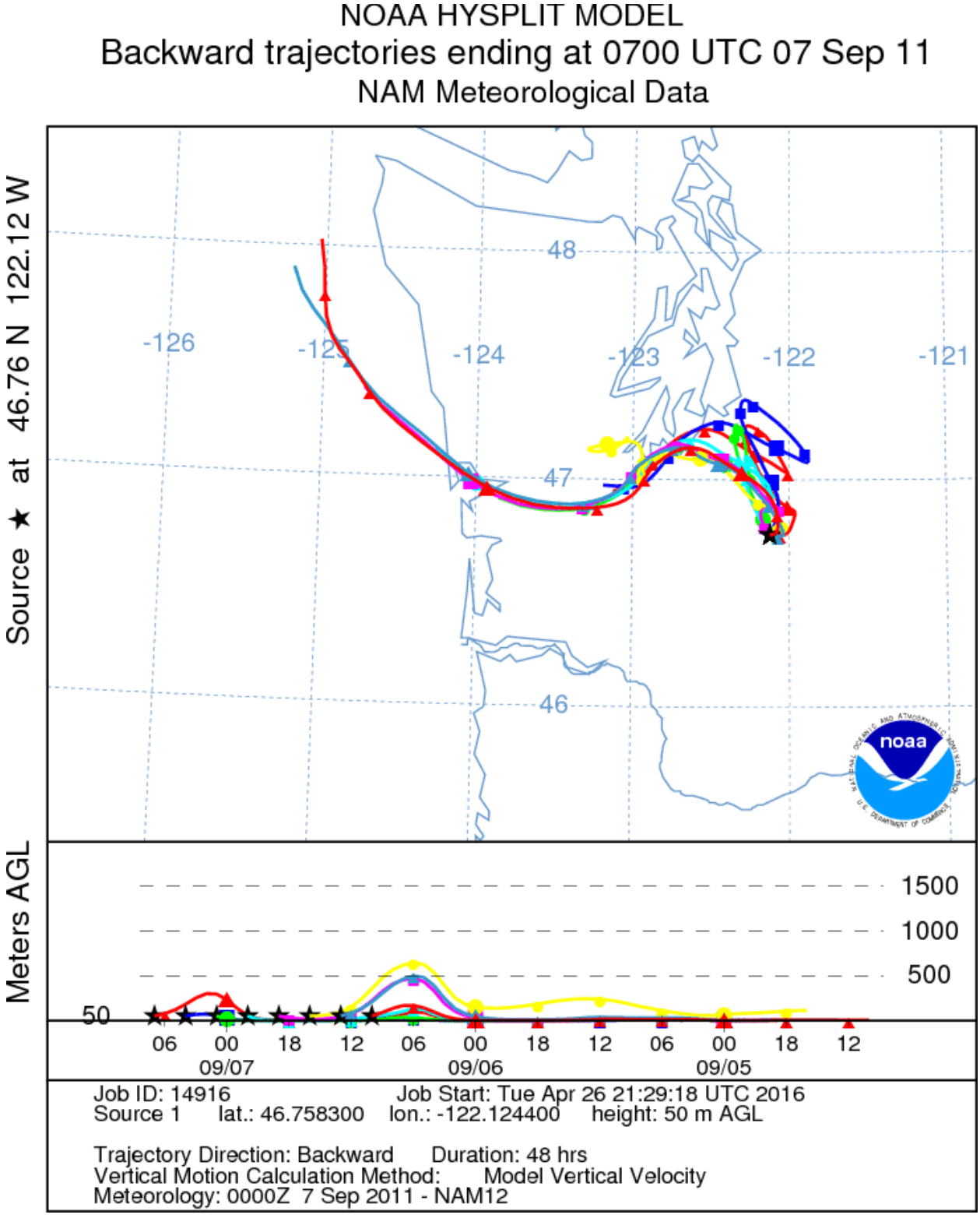
NOAA HYSPLIT MODEL
Backward trajectories ending at 0700 UTC 07 Sep 11
NAM Meteorological Data
Source ★ at 46.76 N 122.12 W
48
47
46
-126
-125
-124
-123
-122
-121
noaa
Meters AGL
1500
1000
500
50
06 00 18 12 06 00 18 12 06 00 18 12
09/07
09/06
09/05
Job ID: 14916 Job Start: Tue Apr 26 21:29:18 UTC 2016
Source 1 lat.: 46.758300 lon.: -122.124400 height: 50 m AGL
Trajectory Direction: Backward Duration: 48 hrs
Vertical Motion Calculation Method: Model Vertical Velocity
Meteorology: 0000Z 7 Sep 2011 - NAM12

NOCA HYSPLIT back-trajectories

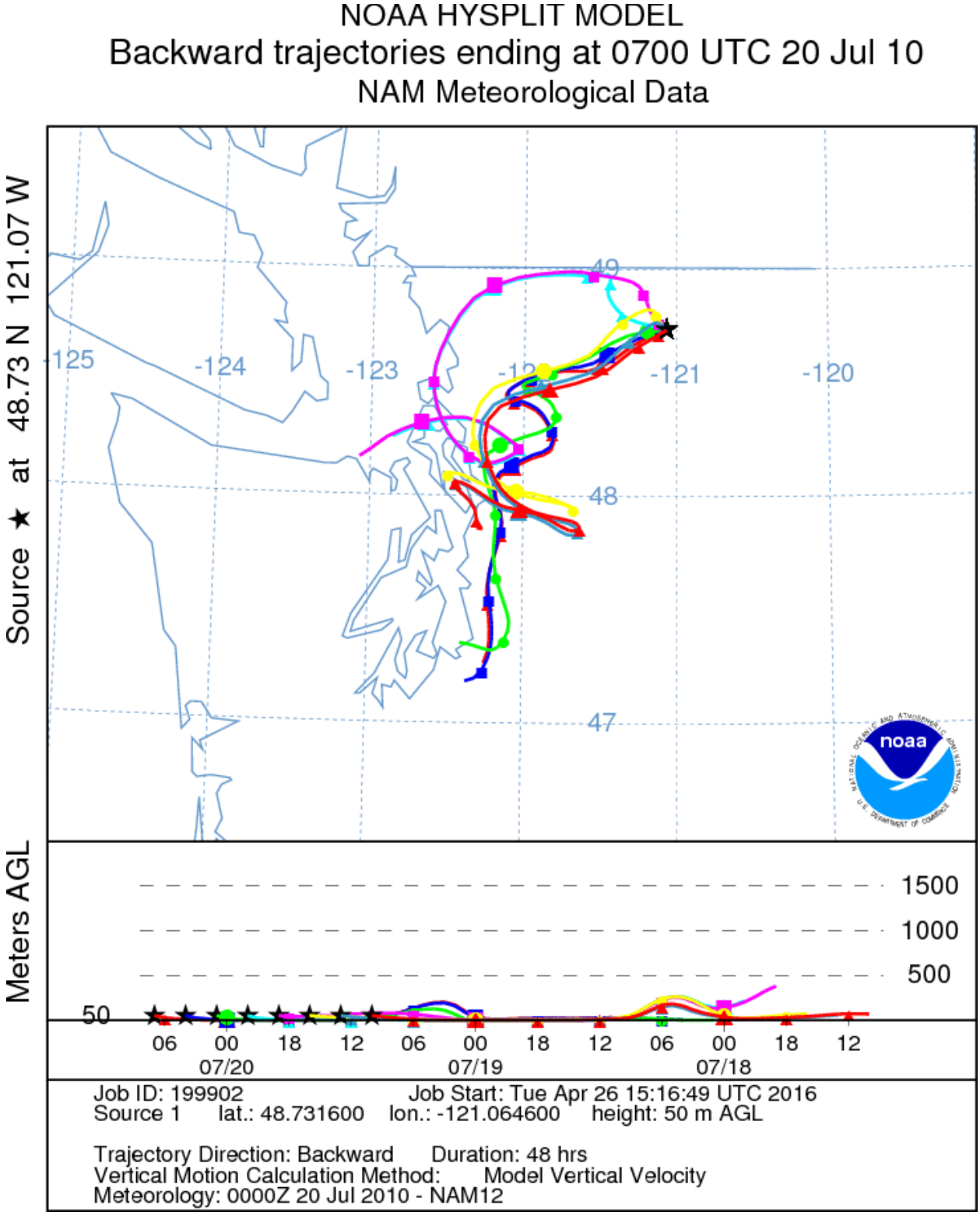
NOAA HYSPLIT MODEL
Backward trajectories ending at 0700 UTC 20 Jul 10
NAM Meteorological Data
Source ★ at 48.73 N 121.07 W
-125
-124
-123
-121
-120
49
48
47
noaa
Meters AGL
1500
1000
500
50
06 00 18 12 06 00 18 12 06 00 18 12
07/20
07/19
07/18
Job ID: 199902 Job Start: Tue Apr 26 15:16:49 UTC 2016
Source 1 lat.: 48.731600 lon.: -121.064600 height: 50 m AGL
Trajectory Direction: Backward Duration: 48 hrs
Vertical Motion Calculation Method: Model Vertical Velocity
Meteorology: 0000Z 20 Jul 2010 - NAM12

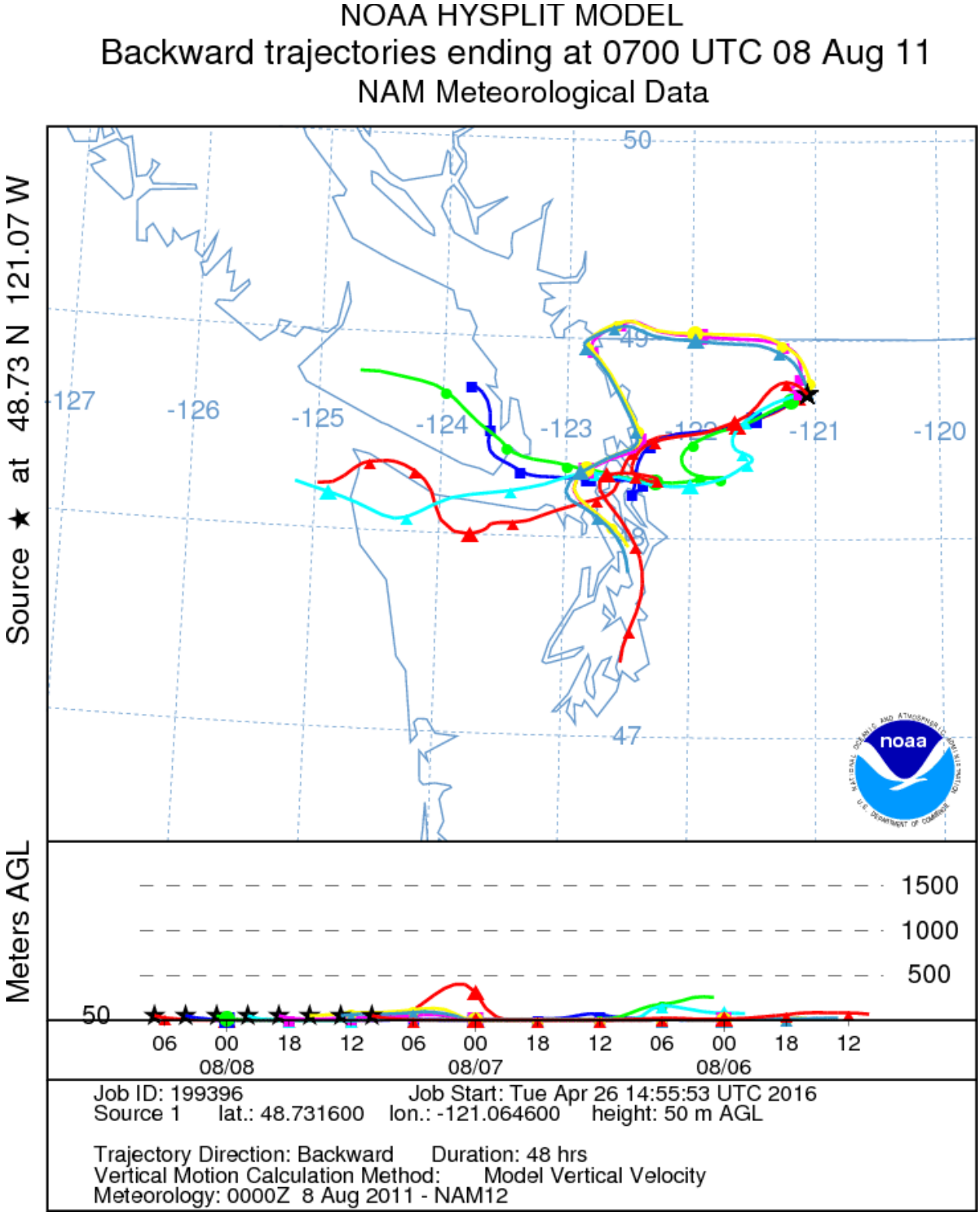
NOAA HYSPLIT MODEL
Backward trajectories ending at 0700 UTC 08 Aug 11
NAM Meteorological Data
Source ★ at 48.73 N 121.07 W
50
49
47
-127
-126
-125
-124
-123
-121
-120
noaa
Meters AGL
1500
1000
500
50
06 00 18 12 06 00 18 12 06 00 18 12
08/08
08/07
08/06
Job ID: 199396 Job Start: Tue Apr 26 14:55:53 UTC 2016
Source 1 lat.: 48.731600 lon.: -121.064600 height: 50 m AGL
Trajectory Direction: Backward Duration: 48 hrs
Vertical Motion Calculation Method: Model Vertical Velocity
Meteorology: 0000Z 8 Aug 2011 - NAM12

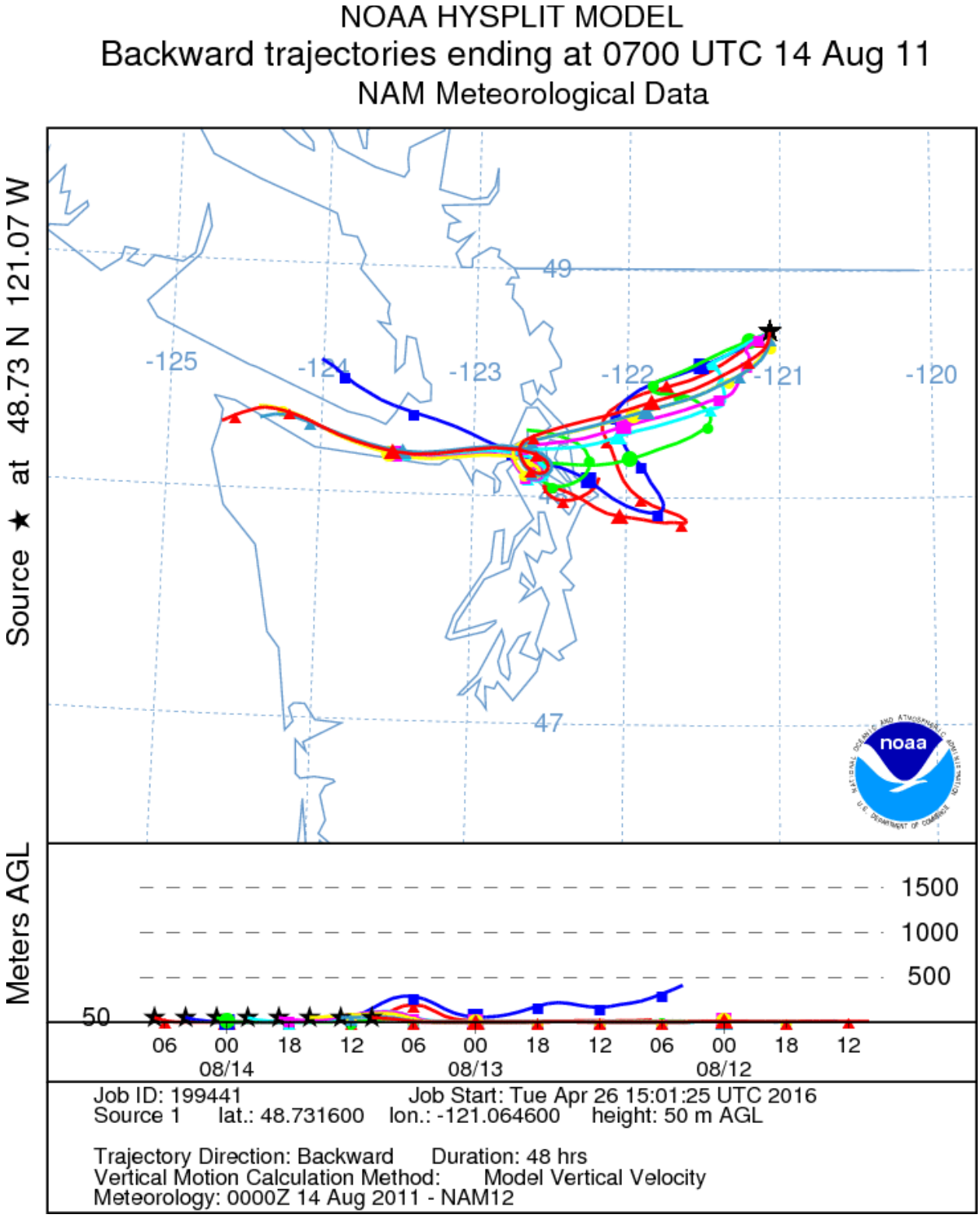
NOAA HYSPLIT MODEL
Backward trajectories ending at 0700 UTC 14 Aug 11
NAM Meteorological Data
Source ★ at 48.73 N 121.07 W
49
47
-125
-124
-123
-122
-121
-120
noaa
Meters AGL
1500
1000
500
50
06 00 18 12 06 00 18 12 06 00 18 12
08/14
08/13
08/12
Job ID: 199441 Job Start: Tue Apr 26 15:01:25 UTC 2016
Source 1 lat.: 48.731600 lon.: -121.064600 height: 50 m AGL
Trajectory Direction: Backward Duration: 48 hrs
Vertical Motion Calculation Method: Model Vertical Velocity
Meteorology: 0000Z 14 Aug 2011 - NAM12

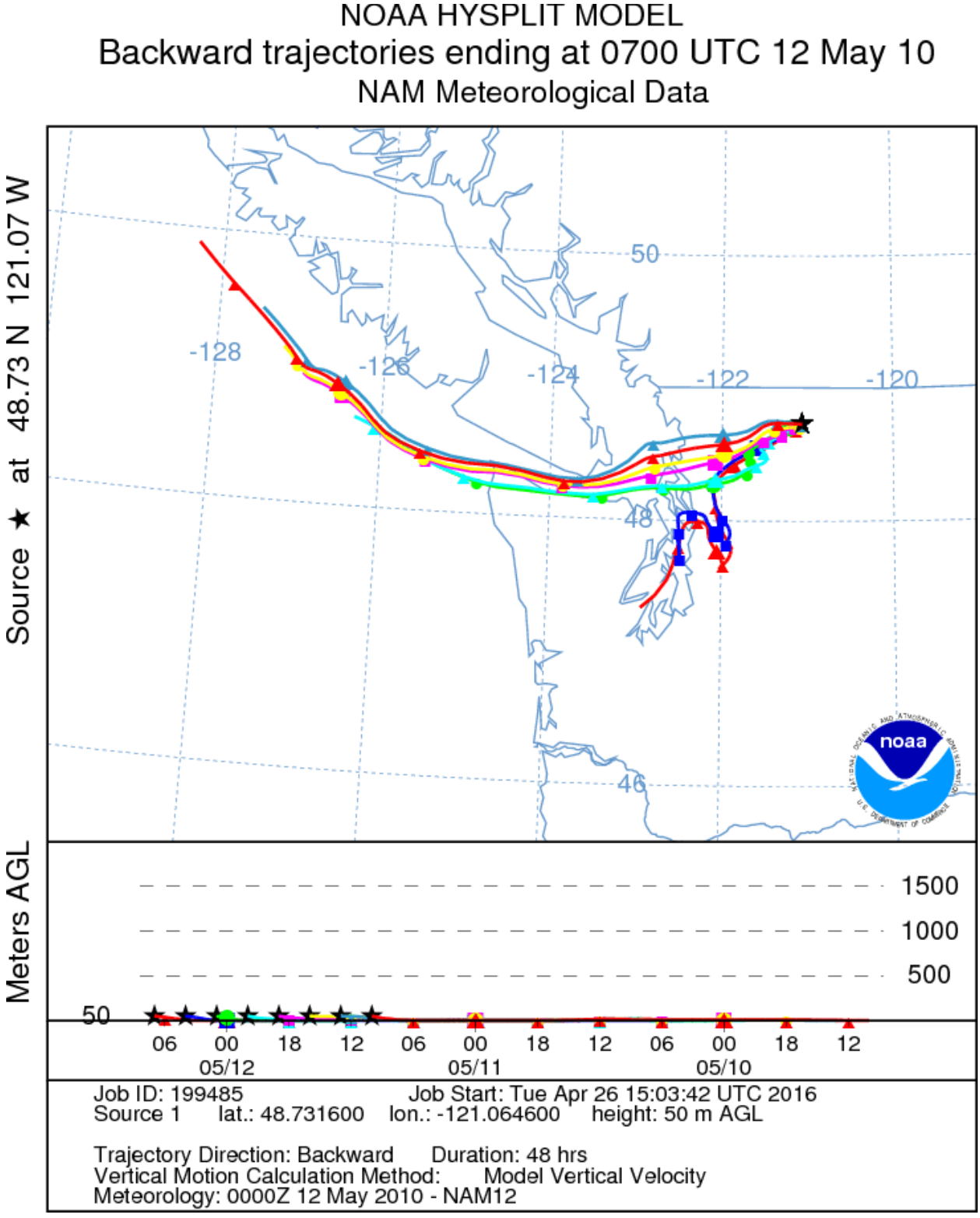
NOAA HYSPLIT MODEL
Backward trajectories ending at 0700 UTC 12 May 10
NAM Meteorological Data
Source ★ at 48.73 N 121.07 W
50
-128
-126
-124
-122
-120
48
46
noaa
Meters AGL
1500
1000
500
50
06 00 18 12 06 00 18 12 06 00 18 12
05/12
05/11
05/10
Job ID: 199485 Job Start: Tue Apr 26 15:03:42 UTC 2016
Source 1 lat.: 48.731600 lon.: -121.064600 height: 50 m AGL
Trajectory Direction: Backward Duration: 48 hrs
Vertical Motion Calculation Method: Model Vertical Velocity
Meteorology: 0000Z 12 May 2010 - NAM12

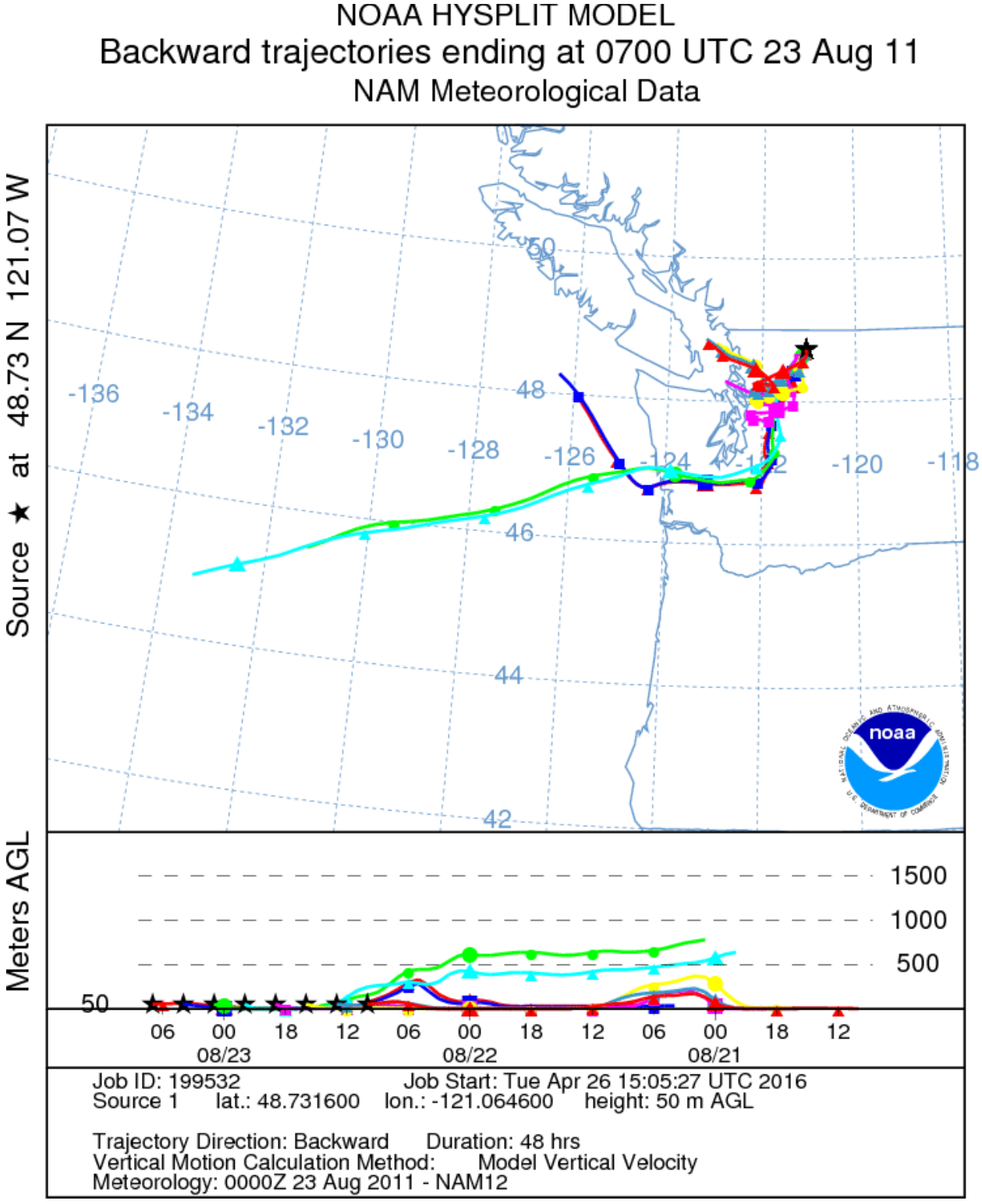
NOAA HYSPLIT MODEL
Backward trajectories ending at 0700 UTC 23 Aug 11
NAM Meteorological Data
Source ★ at 48.73 N 121.07 W
-136
-134
-132
-130
-128
-126
-124
-120
-118
50
48
46
44
42
noaa
Meters AGL
1500
1000
500
50
06 00 18 12 06 00 18 12 06 00 18 12
08/23
08/22
08/21
Job ID: 199532 Job Start: Tue Apr 26 15:05:27 UTC 2016
Source 1 lat.: 48.731600 lon.: -121.064600 height: 50 m AGL
Trajectory Direction: Backward Duration: 48 hrs
Vertical Motion Calculation Method: Model Vertical Velocity
Meteorology: 0000Z 23 Aug 2011 - NAM12

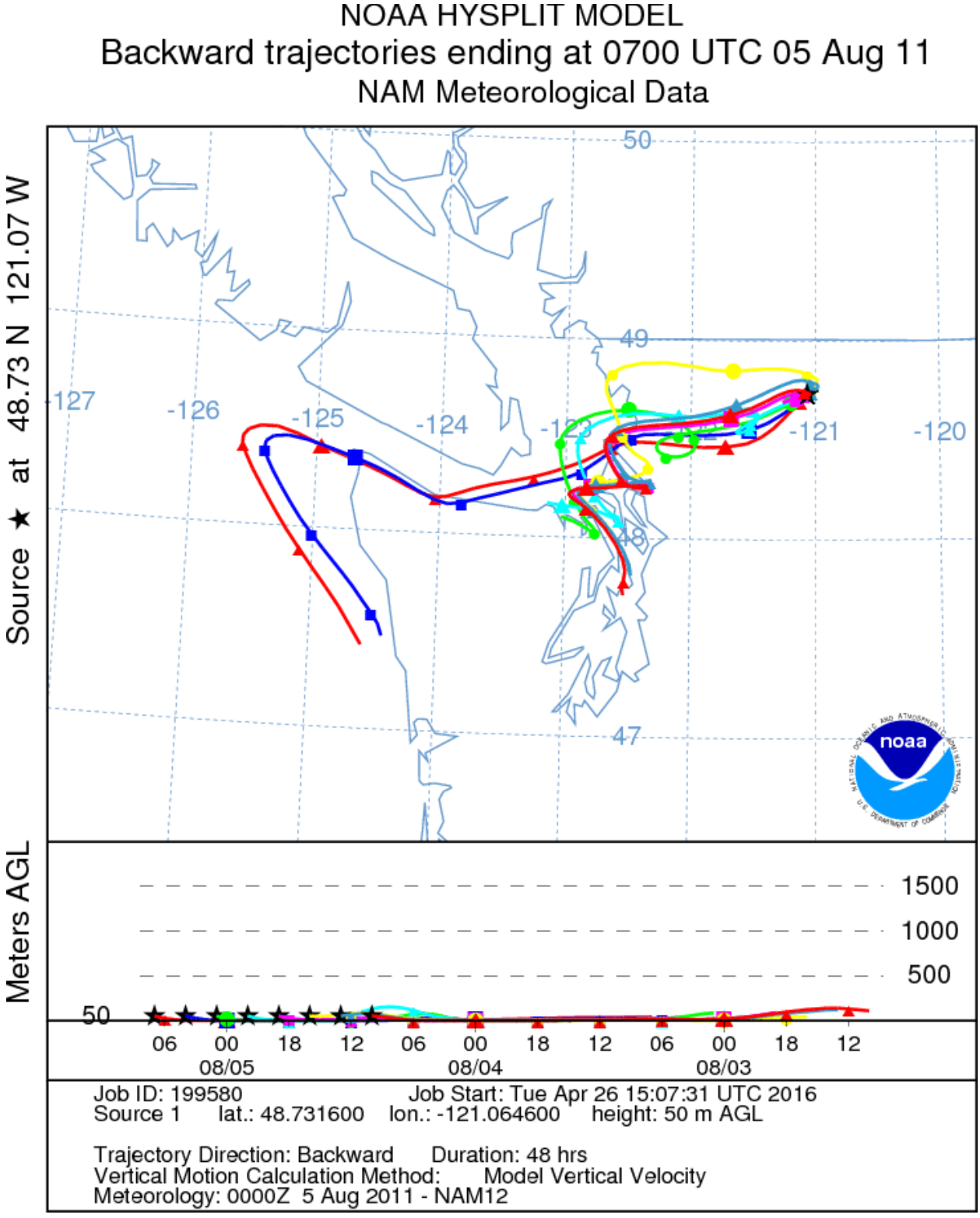
NOAA HYSPLIT MODEL
Backward trajectories ending at 0700 UTC 05 Aug 11
NAM Meteorological Data
Source ★ at 48.73 N 121.07 W
50
49
48
47
-127
-126
-125
-124
-123
-121
-120
noaa
Meters AGL
1500
1000
500
50
06 00 18 12 06 00 18 12 06 00 18 12
08/05
08/04
08/03
Job ID: 199580 Job Start: Tue Apr 26 15:07:31 UTC 2016
Source 1 lat.: 48.731600 lon.: -121.064600 height: 50 m AGL
Trajectory Direction: Backward Duration: 48 hrs
Vertical Motion Calculation Method: Model Vertical Velocity
Meteorology: 0000Z 5 Aug 2011 - NAM12

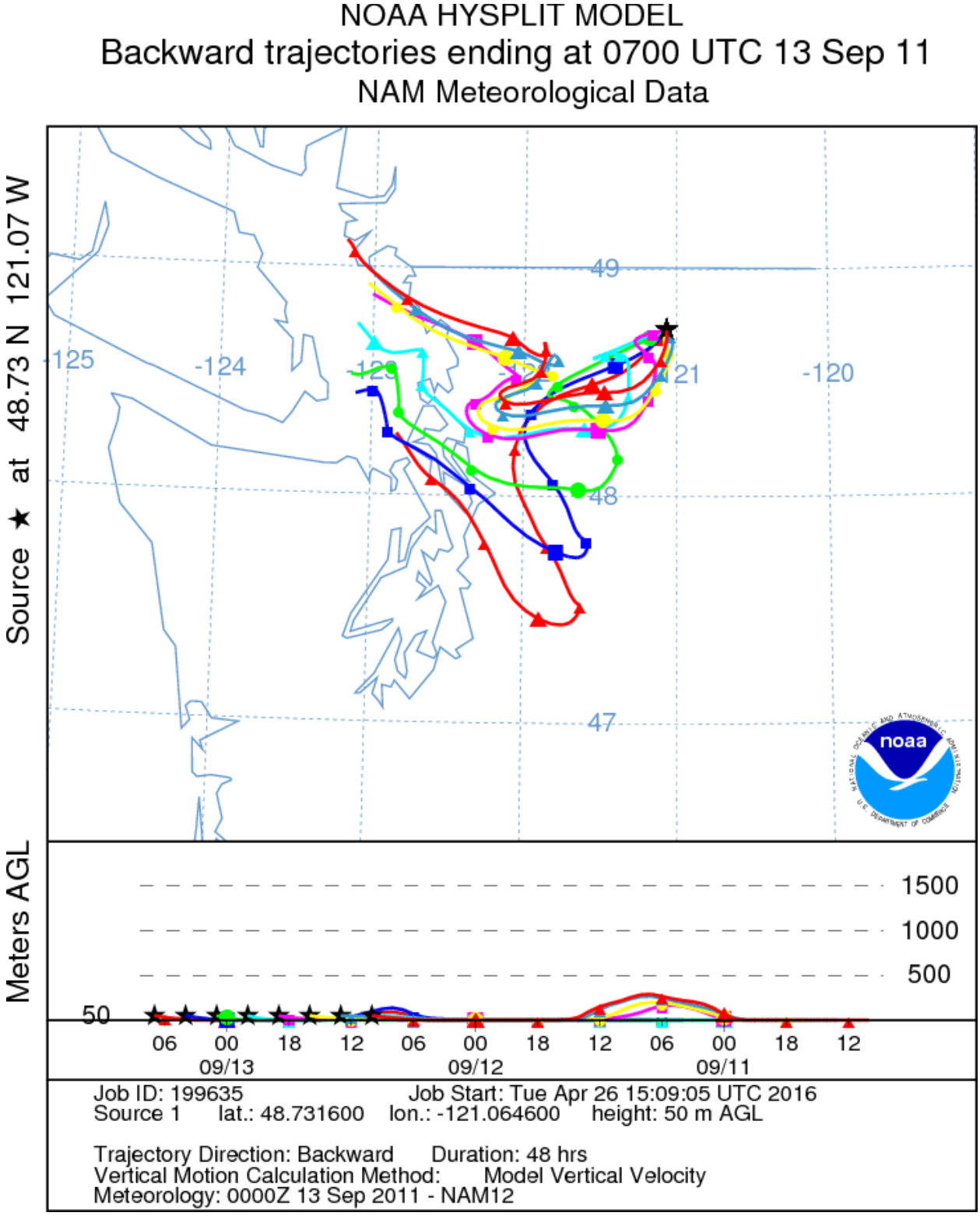
NOAA HYSPLIT MODEL
Backward trajectories ending at 0700 UTC 13 Sep 11
NAM Meteorological Data
Source ★ at 48.73 N 121.07 W
49
48
47
-125
-124
-120
Meters AGL
1500
1000
500
50
06 00 18 12 06 00 18 12 06 00 18 12
09/13
09/12
09/11
Job ID: 199635 Job Start: Tue Apr 26 15:09:05 UTC 2016
Source 1 lat.: 48.731600 lon.: -121.064600 height: 50 m AGL
Trajectory Direction: Backward Duration: 48 hrs
Vertical Motion Calculation Method: Model Vertical Velocity
Meteorology: 0000Z 13 Sep 2011 - NAM12

NOAA HYSPLIT MODEL
Backward trajectories ending at 0700 UTC 11 Jul 10
NAM Meteorological Data

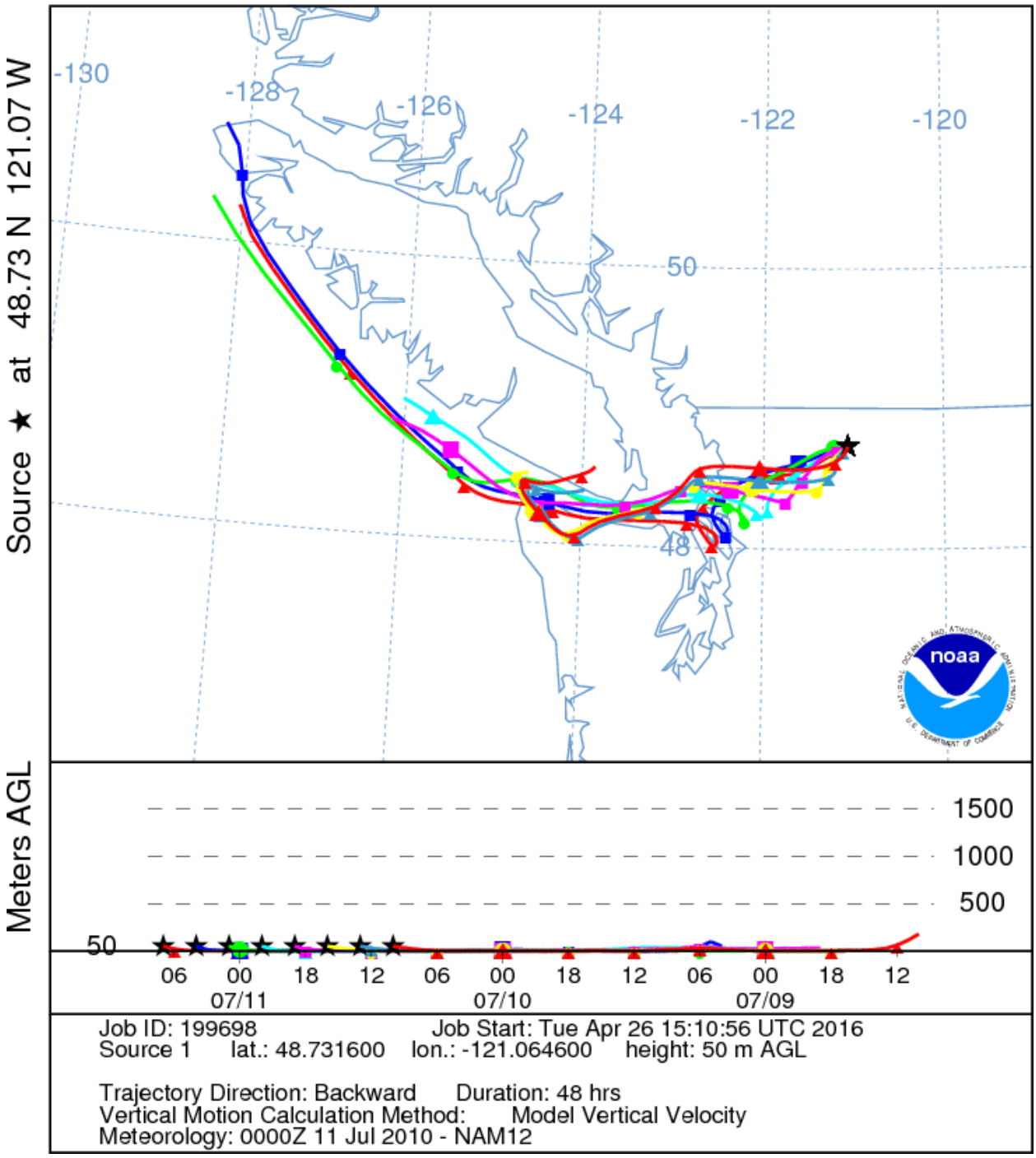

Job ID: 199698 Job Start: Tue Apr 26 15:10:56 UTC 2016
Source 1 lat.: 48.731600 lon.: -121.064600 height: 50 m AGL

Trajectory Direction: Backward Duration: 48 hrs
Vertical Motion Calculation Method: Model Vertical Velocity
Meteorology: 0000Z 11 Jul 2010 - NAM12

NOAA HYSPLIT MODEL
Backward trajectories ending at 0700 UTC 29 Aug 11
NAM Meteorological Data

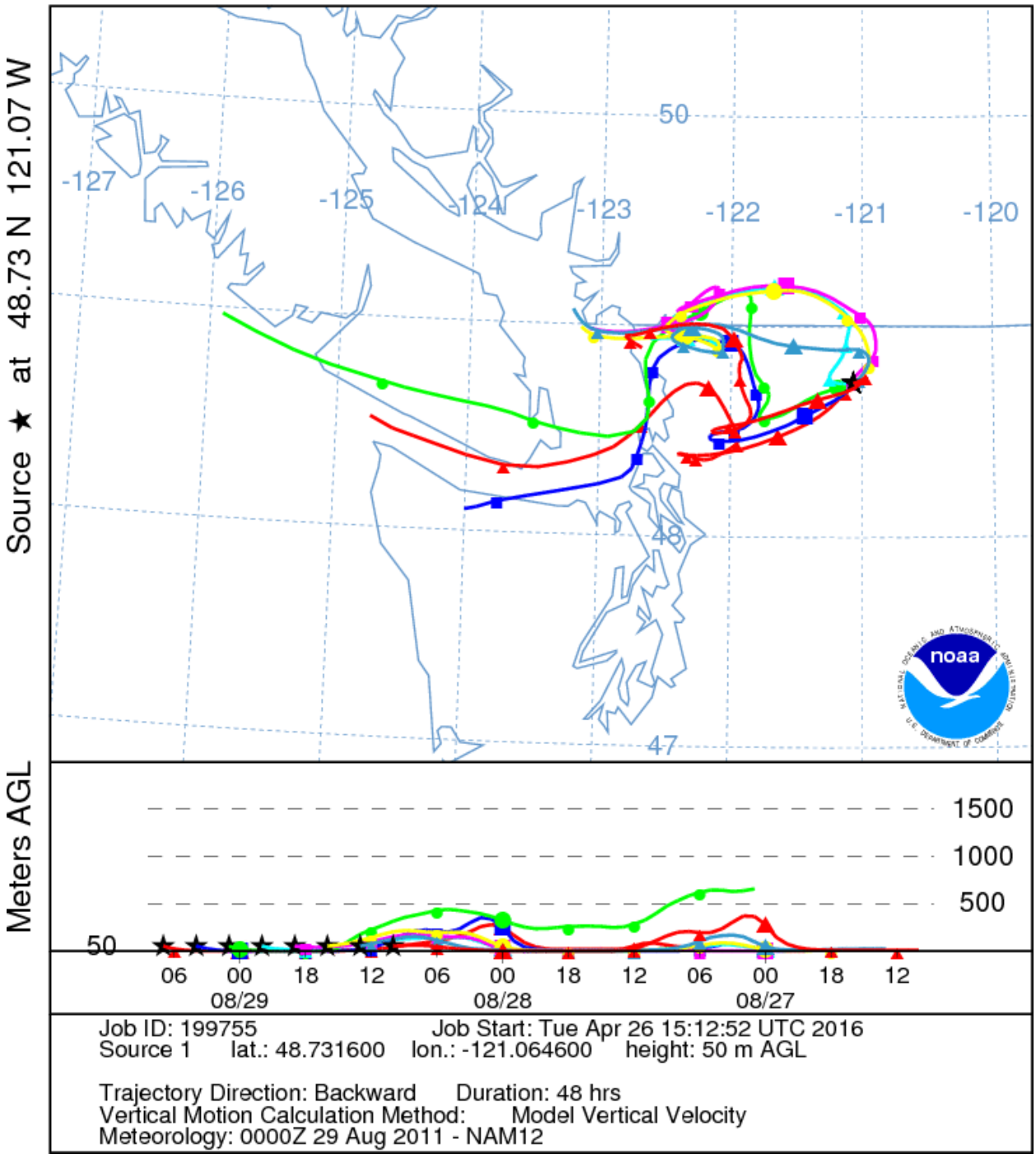

Job ID: 199755 Job Start: Tue Apr 26 15:12:52 UTC 2016
Source 1 lat.: 48.731600 lon.: -121.064600 height: 50 m AGL

Trajectory Direction: Backward Duration: 48 hrs
Vertical Motion Calculation Method: Model Vertical Velocity
Meteorology: 0000Z 29 Aug 2011 - NAM12

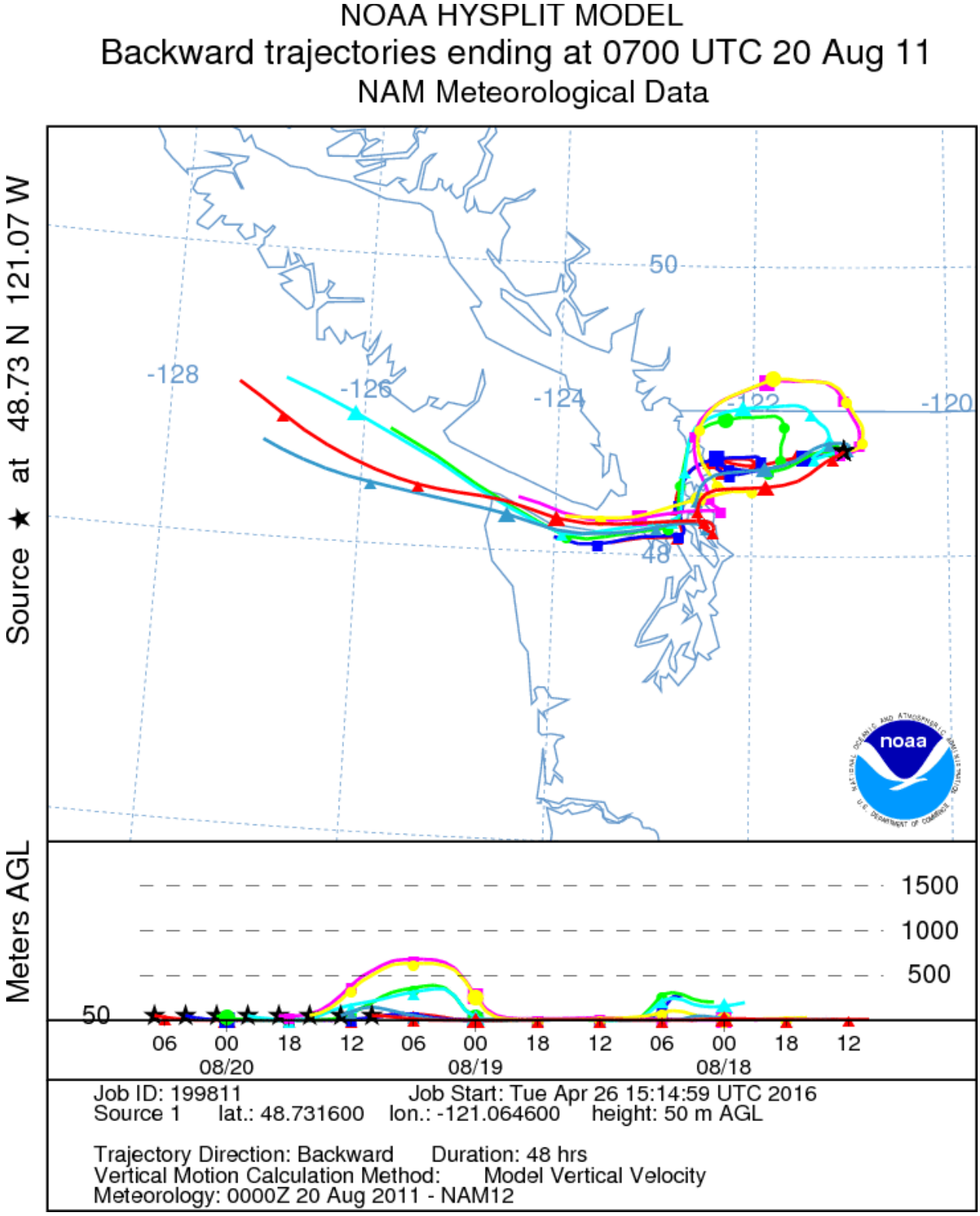
NOAA HYSPLIT MODEL
Backward trajectories ending at 0700 UTC 20 Aug 11
NAM Meteorological Data
Source ★ at 48.73 N 121.07 W
-128
-126
-124
-122
-120
50
48
noaa
Meters AGL
1500
1000
500
50
06 00 18 12 06 00 18 12 06 00 18 12
08/20
08/19
08/18
Job ID: 199811 Job Start: Tue Apr 26 15:14:59 UTC 2016
Source 1 lat.: 48.731600 lon.: -121.064600 height: 50 m AGL
Trajectory Direction: Backward Duration: 48 hrs
Vertical Motion Calculation Method: Model Vertical Velocity
Meteorology: 0000Z 20 Aug 2011 - NAM12

OKEF HYSPLIT back-trajectories

NOAA HYSPLIT MODEL
Backward trajectories ending at 0400 UTC 04 Sep 11
NAM Meteorological Data

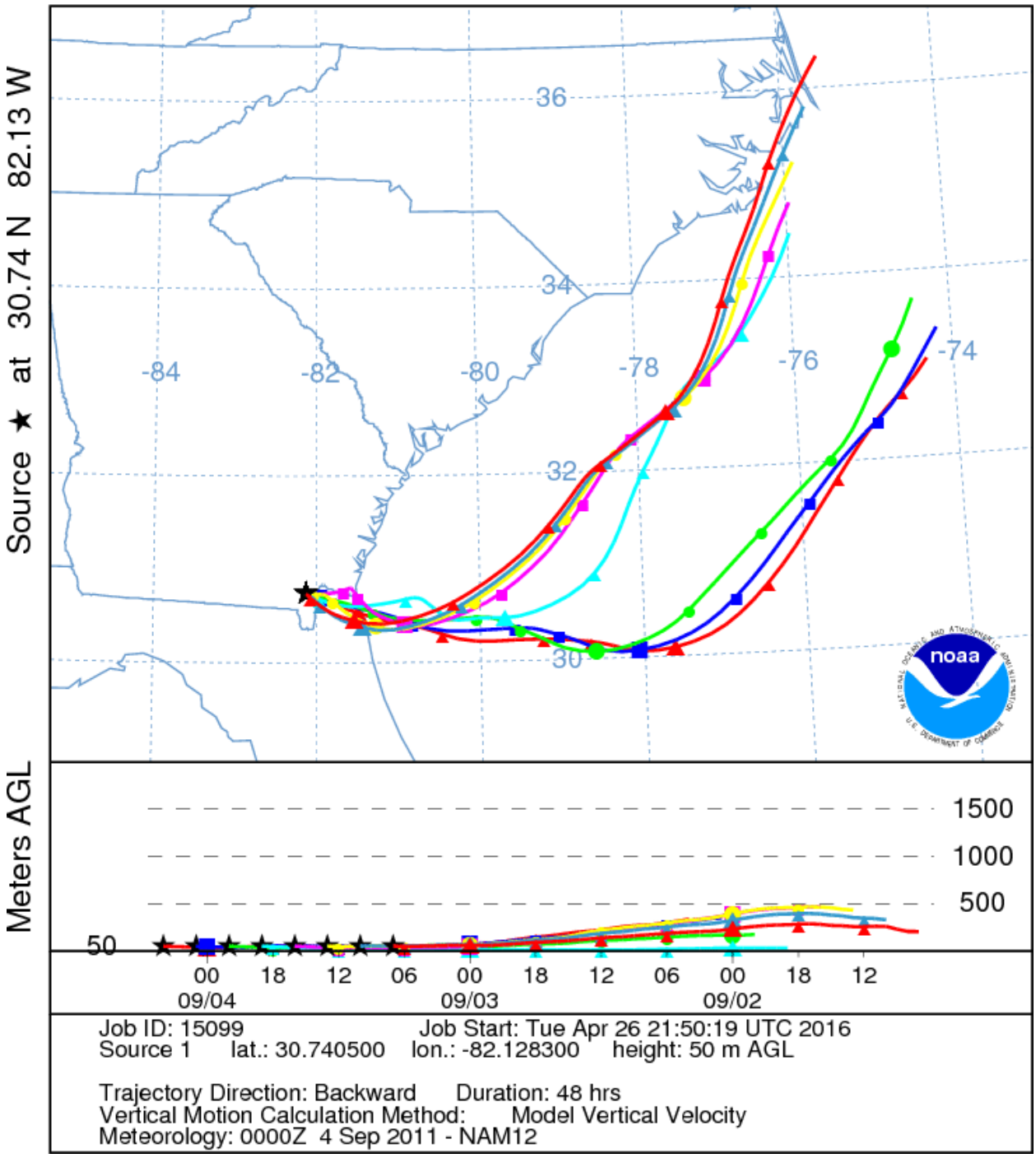

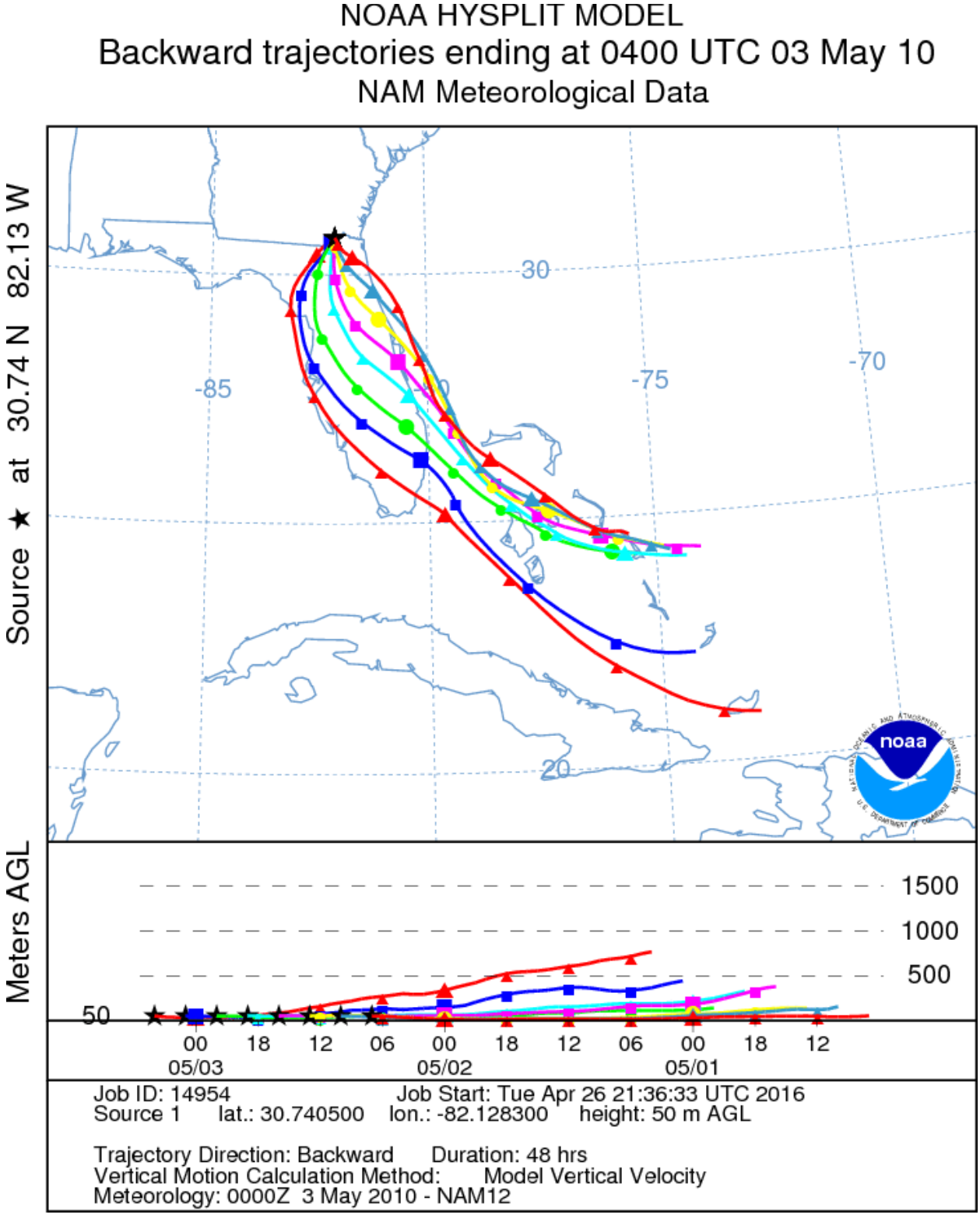
NOAA HYSPLIT MODEL
Backward trajectories ending at 0400 UTC 03 May 10
NAM Meteorological Data
Source ★ at 30.74 N 82.13 W
30
-85
-75
-70
20
noaa
Meters AGL
1500
1000
500
50
00 18 12 06 00 18 12 06 00 18 12
05/03 05/02 05/01
Job ID: 14954 Job Start: Tue Apr 26 21:36:33 UTC 2016
Source 1 lat.: 30.740500 lon.: -82.128300 height: 50 m AGL
Trajectory Direction: Backward Duration: 48 hrs
Vertical Motion Calculation Method: Model Vertical Velocity
Meteorology: 0000Z 3 May 2010 - NAM12

NOAA HYSPLIT MODEL
Backward trajectories ending at 0400 UTC 25 May 11
NAM Meteorological Data

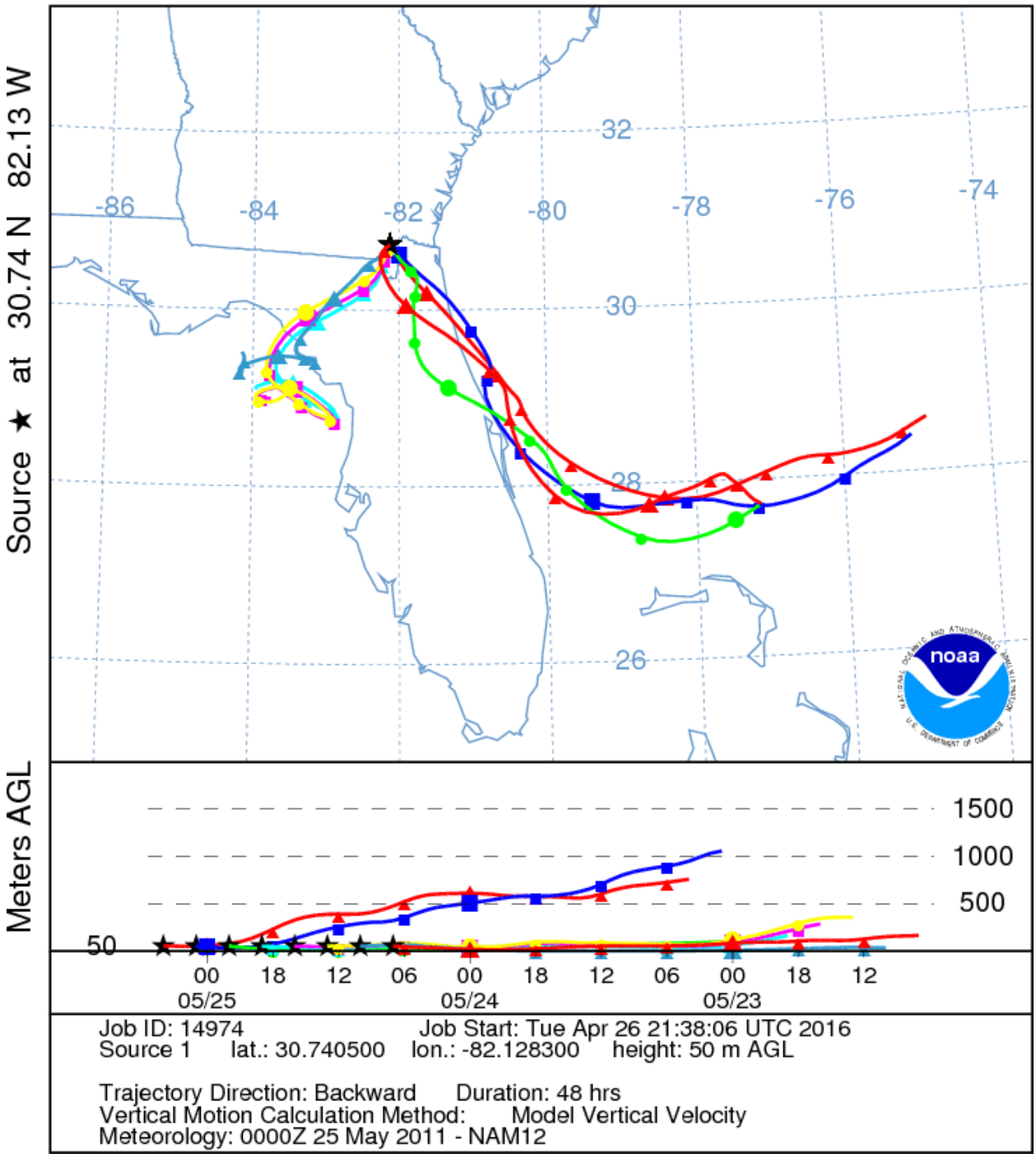

NOAA HYSPLIT MODEL
Backward trajectories ending at 0500 UTC 21 Feb 11
NAM Meteorological Data

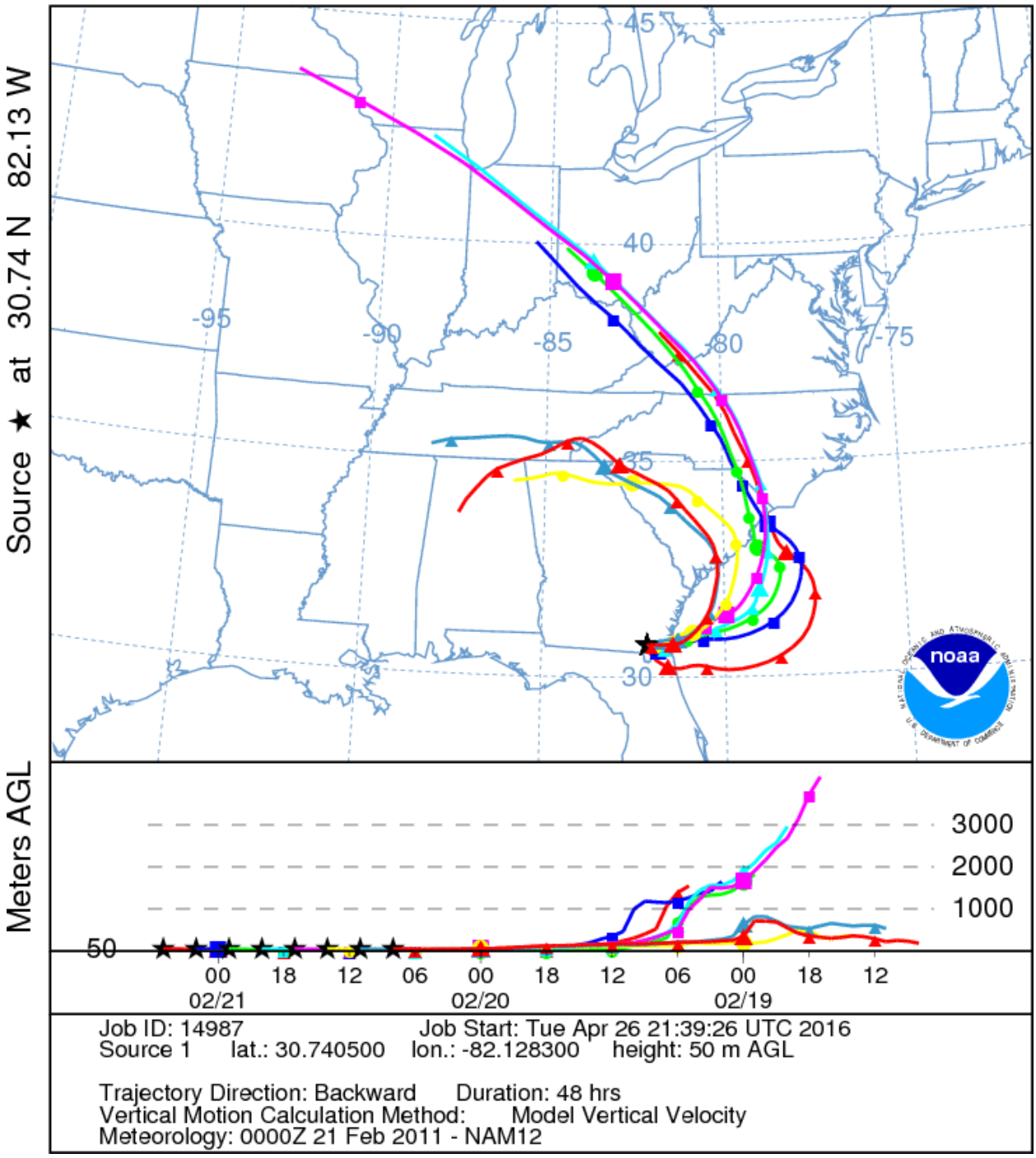

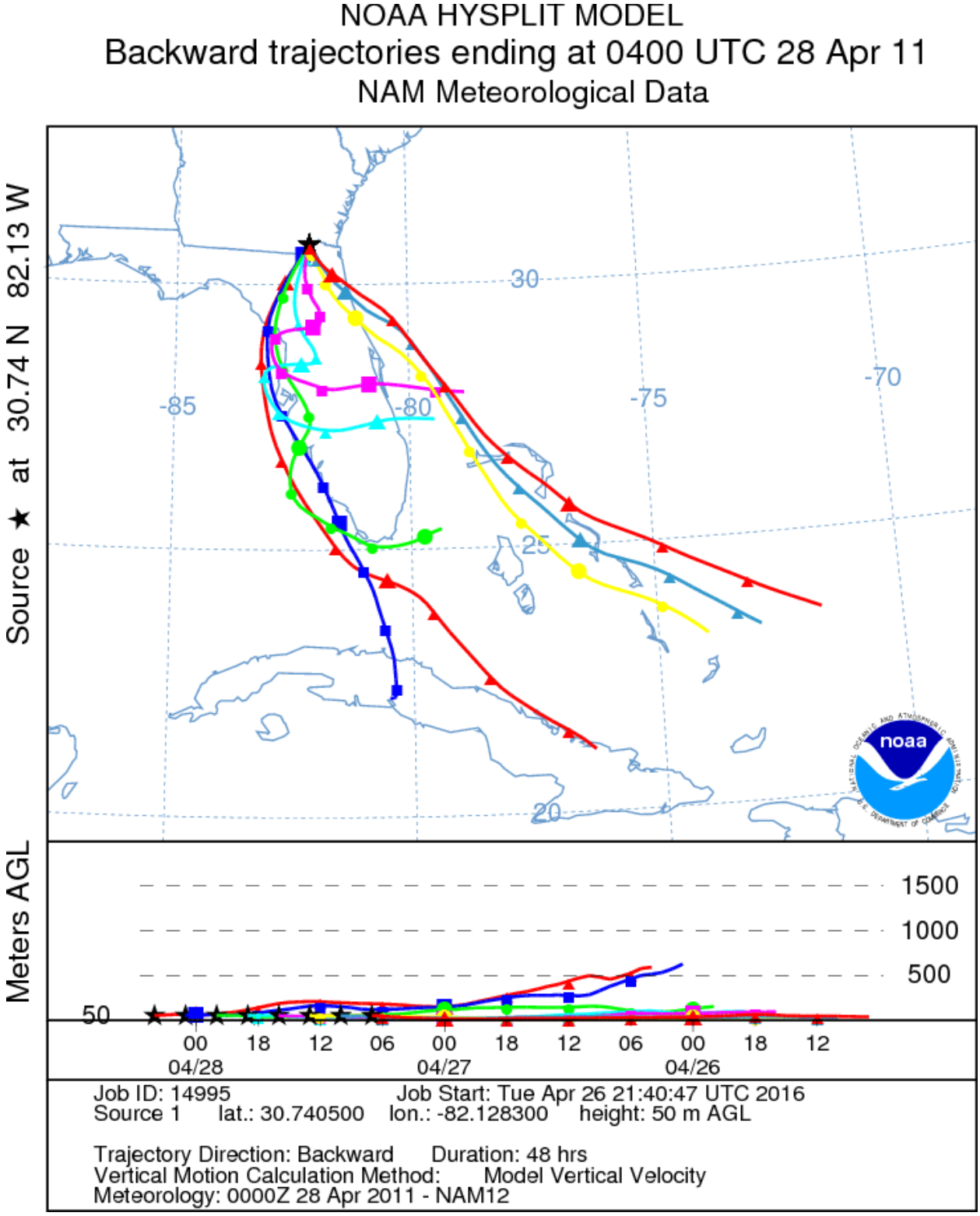
NOAA HYSPLIT MODEL
Backward trajectories ending at 0400 UTC 28 Apr 11
NAM Meteorological Data
Source ★ at 30.74 N 82.13 W
30
-85
-80
-75
-70
25
20
noaa
Meters AGL
1500
1000
500
50
00 18 12 06 00 18 12 06 00 18 12
04/28 04/27 04/26
Job ID: 14995 Job Start: Tue Apr 26 21:40:47 UTC 2016
Source 1 lat.: 30.740500 lon.: -82.128300 height: 50 m AGL
Trajectory Direction: Backward Duration: 48 hrs
Vertical Motion Calculation Method: Model Vertical Velocity
Meteorology: 0000Z 28 Apr 2011 - NAM12

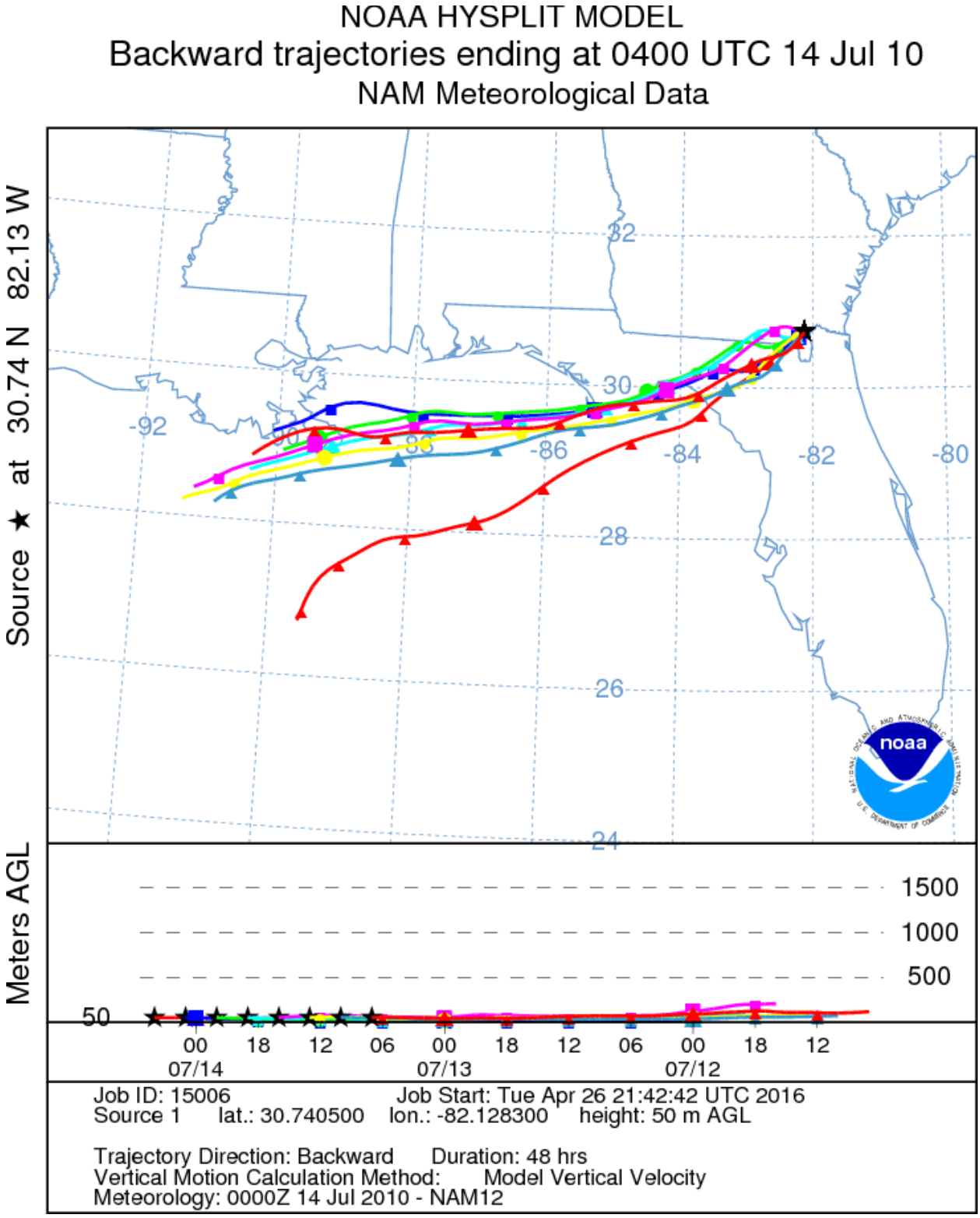
NOAA HYSPLIT MODEL
Backward trajectories ending at 0400 UTC 14 Jul 10
NAM Meteorological Data
Source ★ at 30.74 N 82.13 W
-92
-90
-88
-86
-84
-82
-80
32
30
28
26
24
noaa
Meters AGL
1500
1000
500
50
00 18 12 06 00 18 12 06 00 18 12
07/14
07/13
07/12
Job ID: 15006 Job Start: Tue Apr 26 21:42:42 UTC 2016
Source 1 lat.: 30.740500 lon.: -82.128300 height: 50 m AGL
Trajectory Direction: Backward Duration: 48 hrs
Vertical Motion Calculation Method: Model Vertical Velocity
Meteorology: 0000Z 14 Jul 2010 - NAM12

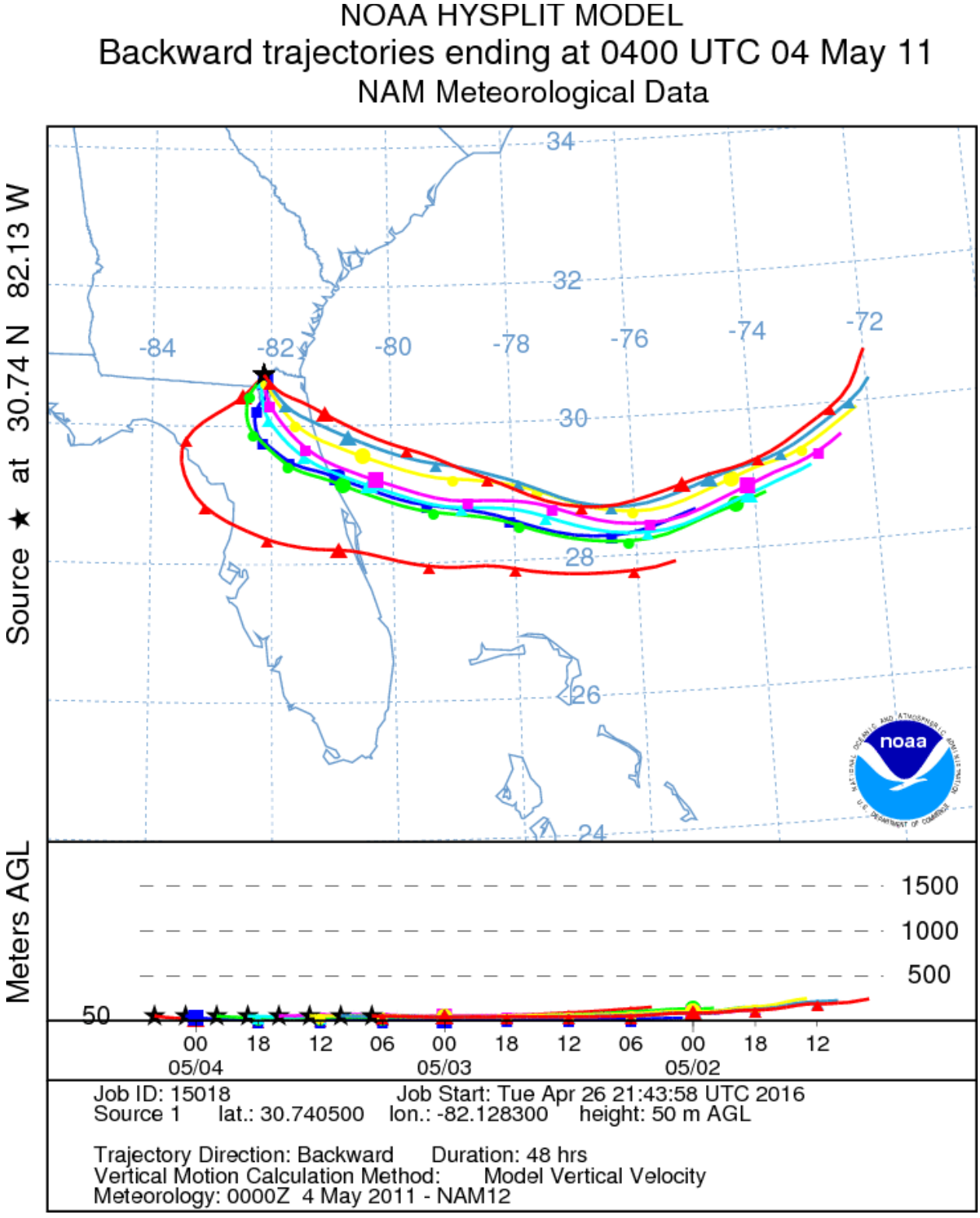
NOAA HYSPLIT MODEL
Backward trajectories ending at 0400 UTC 04 May 11
NAM Meteorological Data
Source ★ at 30.74 N 82.13 W
34
32
30
28
26
24
-84
-82
-80
-78
-76
-74
-72
noaa
Meters AGL
1500
1000
500
50
00 18 12 06 00 18 12 06 00 18 12
05/04
05/03
05/02
Job ID: 15018 Job Start: Tue Apr 26 21:43:58 UTC 2016
Source 1 lat.: 30.740500 lon.: -82.128300 height: 50 m AGL
Trajectory Direction: Backward Duration: 48 hrs
Vertical Motion Calculation Method: Model Vertical Velocity
Meteorology: 0000Z 4 May 2011 - NAM12

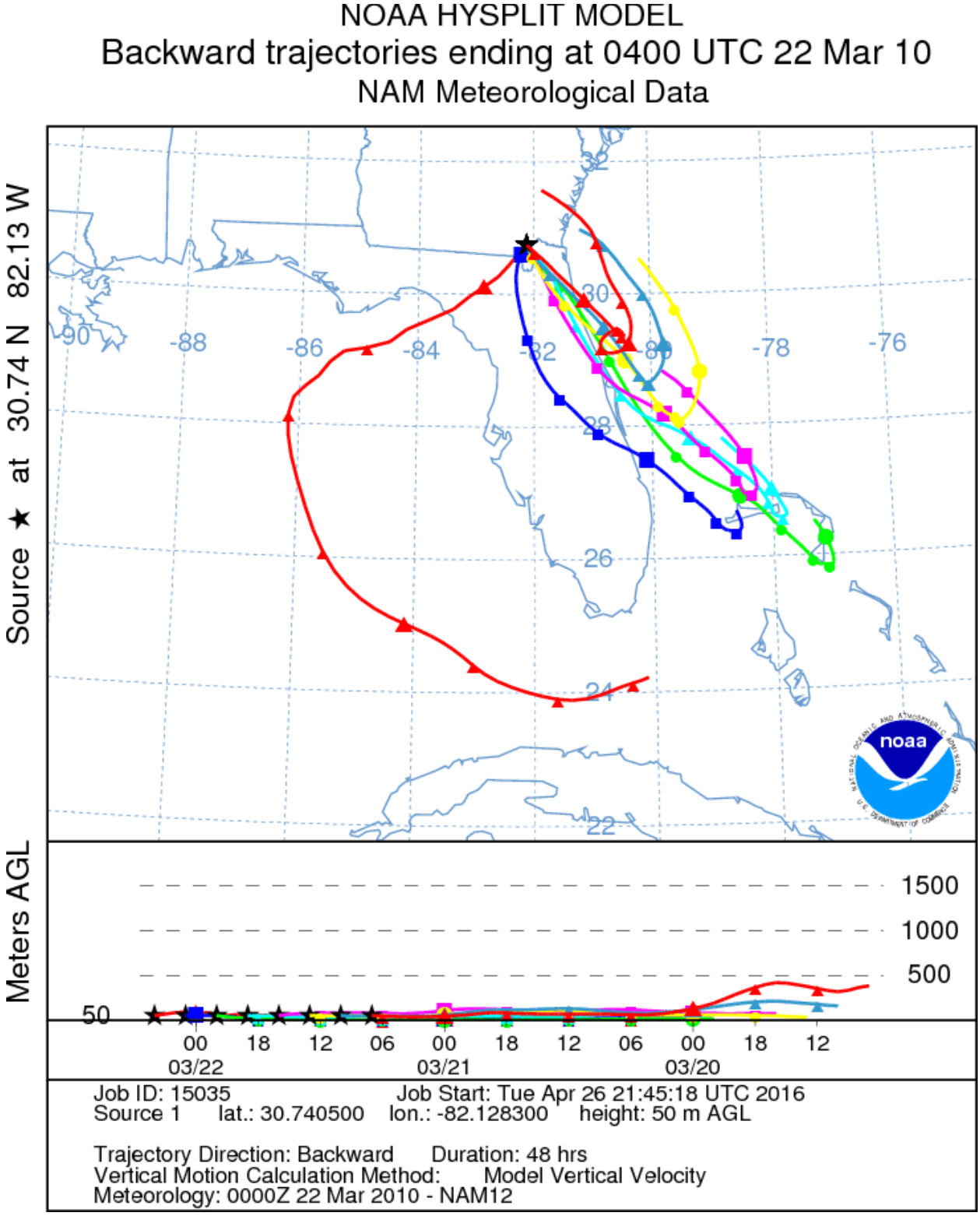
NOAA HYSPLIT MODEL
Backward trajectories ending at 0400 UTC 22 Mar 10
NAM Meteorological Data
Source ★ at 30.74 N 82.13 W
-90
-88
-86
-84
-82
-80
-78
-76
30
28
26
24
22
noaa
Meters AGL
1500
1000
500
50
00 18 12 06 00 18 12 06 00 18 12
03/22
03/21
03/20
Job ID: 15035 Job Start: Tue Apr 26 21:45:18 UTC 2016
Source 1 lat.: 30.740500 lon.: -82.128300 height: 50 m AGL
Trajectory Direction: Backward Duration: 48 hrs
Vertical Motion Calculation Method: Model Vertical Velocity
Meteorology: 0000Z 22 Mar 2010 - NAM12

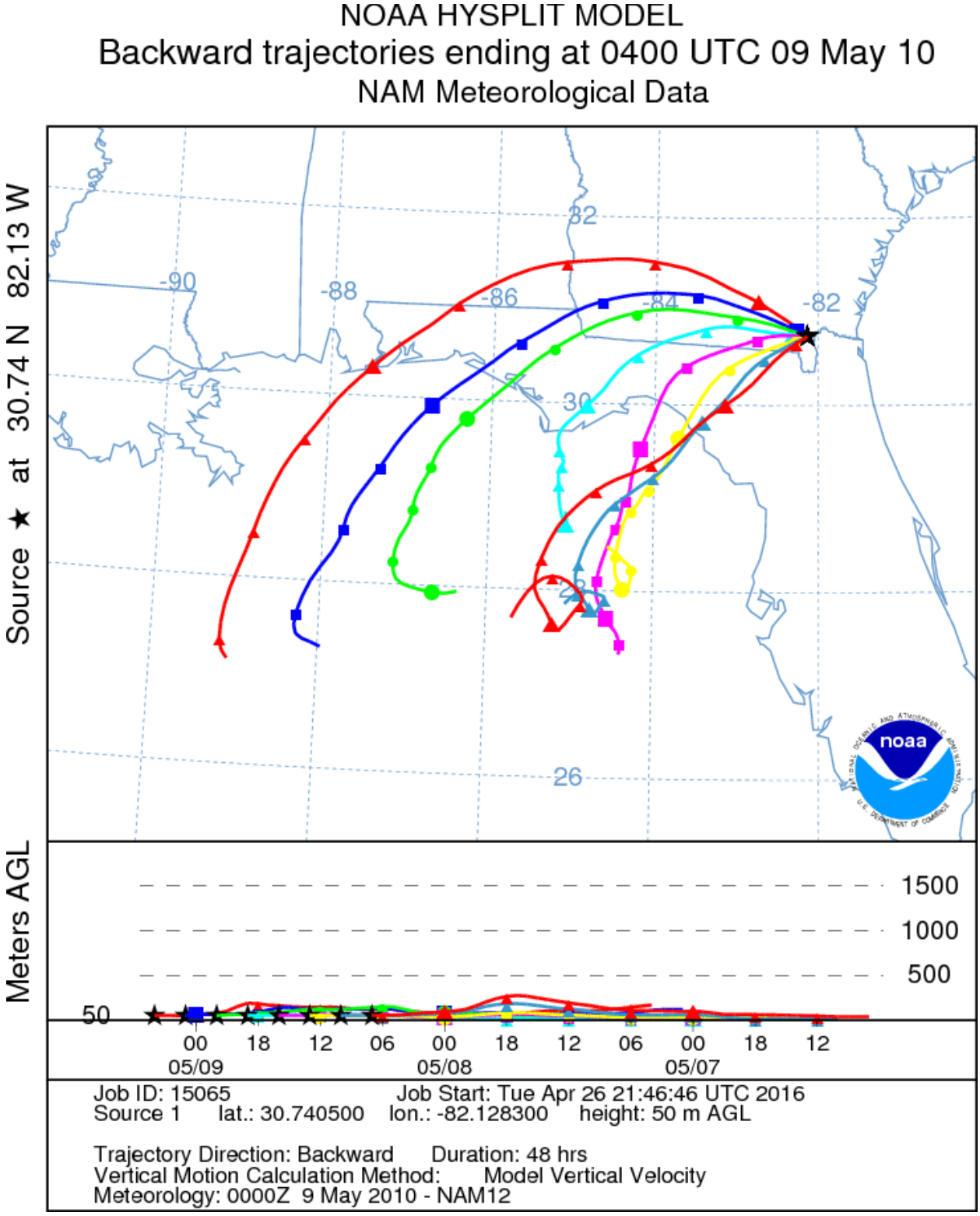
NOAA HYSPLIT MODEL
Backward trajectories ending at 0400 UTC 09 May 10
NAM Meteorological Data
Source ★ at 30.74 N 82.13 W
-90
-88
-86
-84
-82
32
30
28
26
noaa
Meters AGL
1500
1000
500
50
00 18 12 06 00 18 12 06 00 18 12
05/09
05/08
05/07
Job ID: 15065 Job Start: Tue Apr 26 21:46:46 UTC 2016
Source 1 lat.: 30.740500 lon.: -82.128300 height: 50 m AGL
Trajectory Direction: Backward Duration: 48 hrs
Vertical Motion Calculation Method: Model Vertical Velocity
Meteorology: 0000Z 9 May 2010 - NAM12

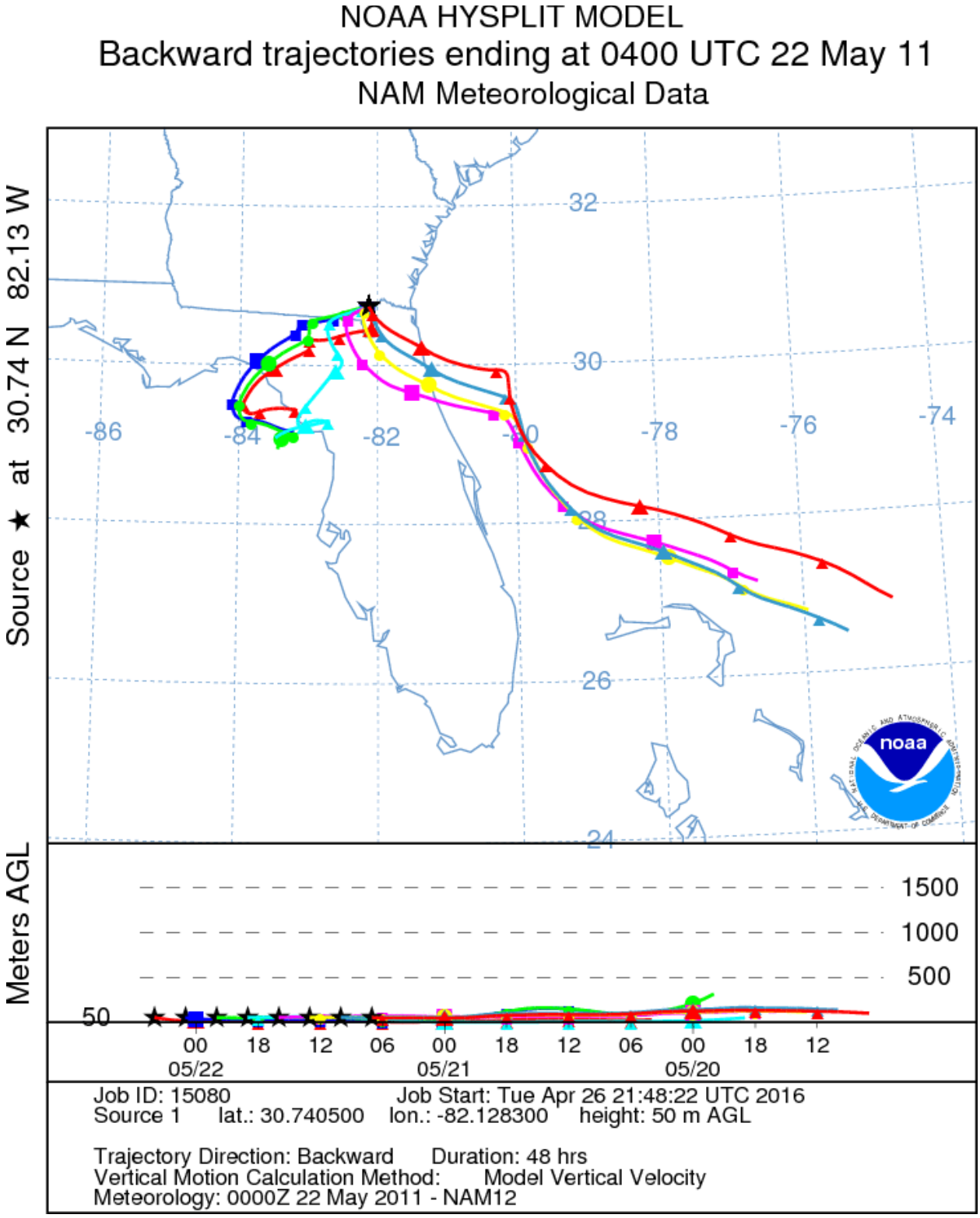
NOAA HYSPLIT MODEL
Backward trajectories ending at 0400 UTC 22 May 11
NAM Meteorological Data
Source ★ at 30.74 N 82.13 W
32
30
28
26
24
-86
-84
-82
-80
-78
-76
-74
noaa
Meters AGL
1500
1000
500
50
00 18 12 06 00 18 12 06 00 18 12
05/22
05/21
05/20
Job ID: 15080 Job Start: Tue Apr 26 21:48:22 UTC 2016
Source 1 lat.: 30.740500 lon.: -82.128300 height: 50 m AGL
Trajectory Direction: Backward Duration: 48 hrs
Vertical Motion Calculation Method: Model Vertical Velocity
Meteorology: 0000Z 22 May 2011 - NAM12

OLYM HYSPLIT back-trajectories

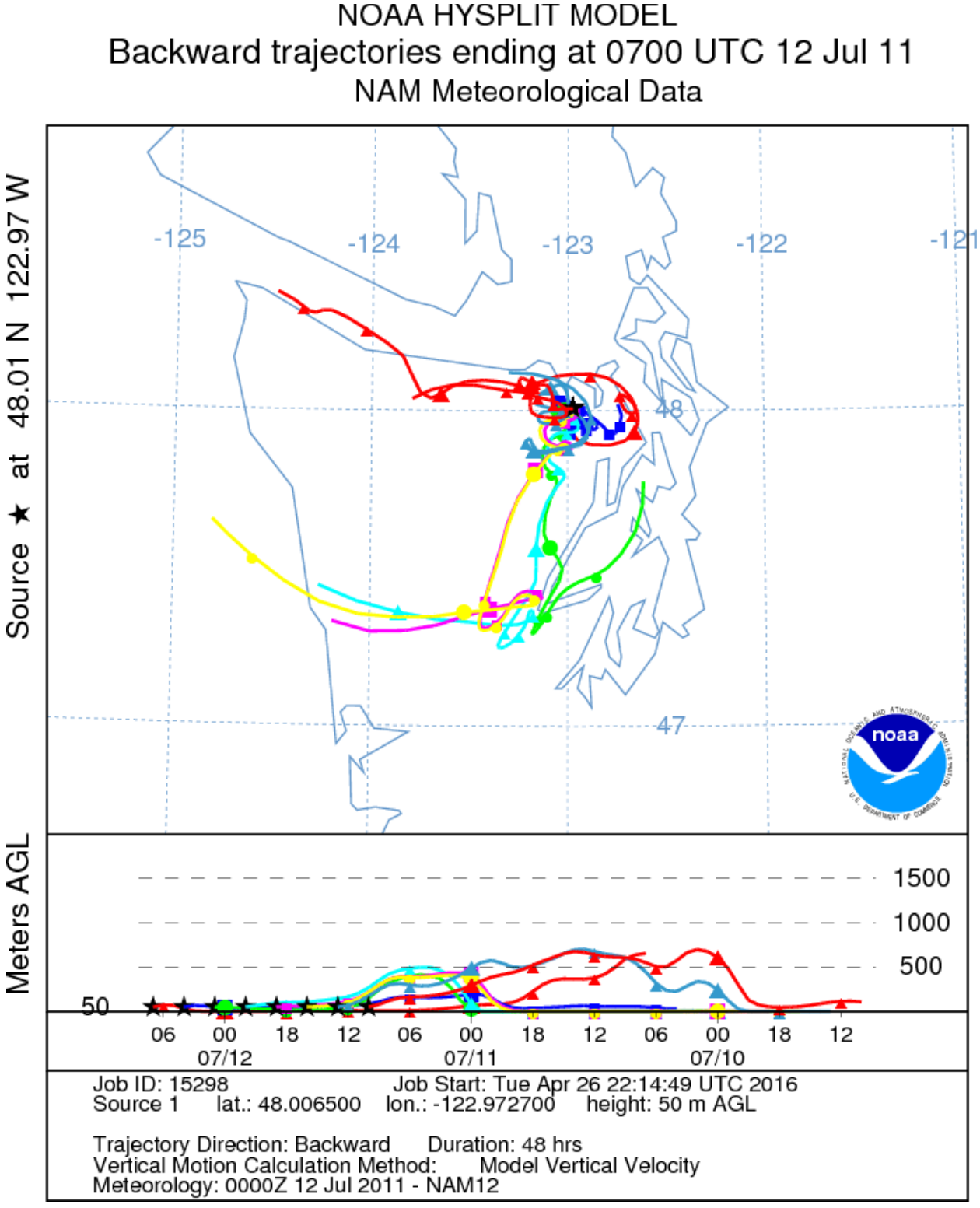
NOAA HYSPLIT MODEL
Backward trajectories ending at 0700 UTC 12 Jul 11
NAM Meteorological Data
Source ★ at 48.01 N 122.97 W
-125
-124
-123
-122
-121
48
47
noaa
Meters AGL
1500
1000
500
50
06
00
18
12
06
00
18
12
06
00
18
12
07/12
07/11
07/10
Job ID: 15298
Job Start: Tue Apr 26 22:14:49 UTC 2016
Source 1 lat.: 48.006500 lon.: -122.972700 height: 50 m AGL
Trajectory Direction: Backward Duration: 48 hrs
Vertical Motion Calculation Method: Model Vertical Velocity
Meteorology: 0000Z 12 Jul 2011 - NAM12

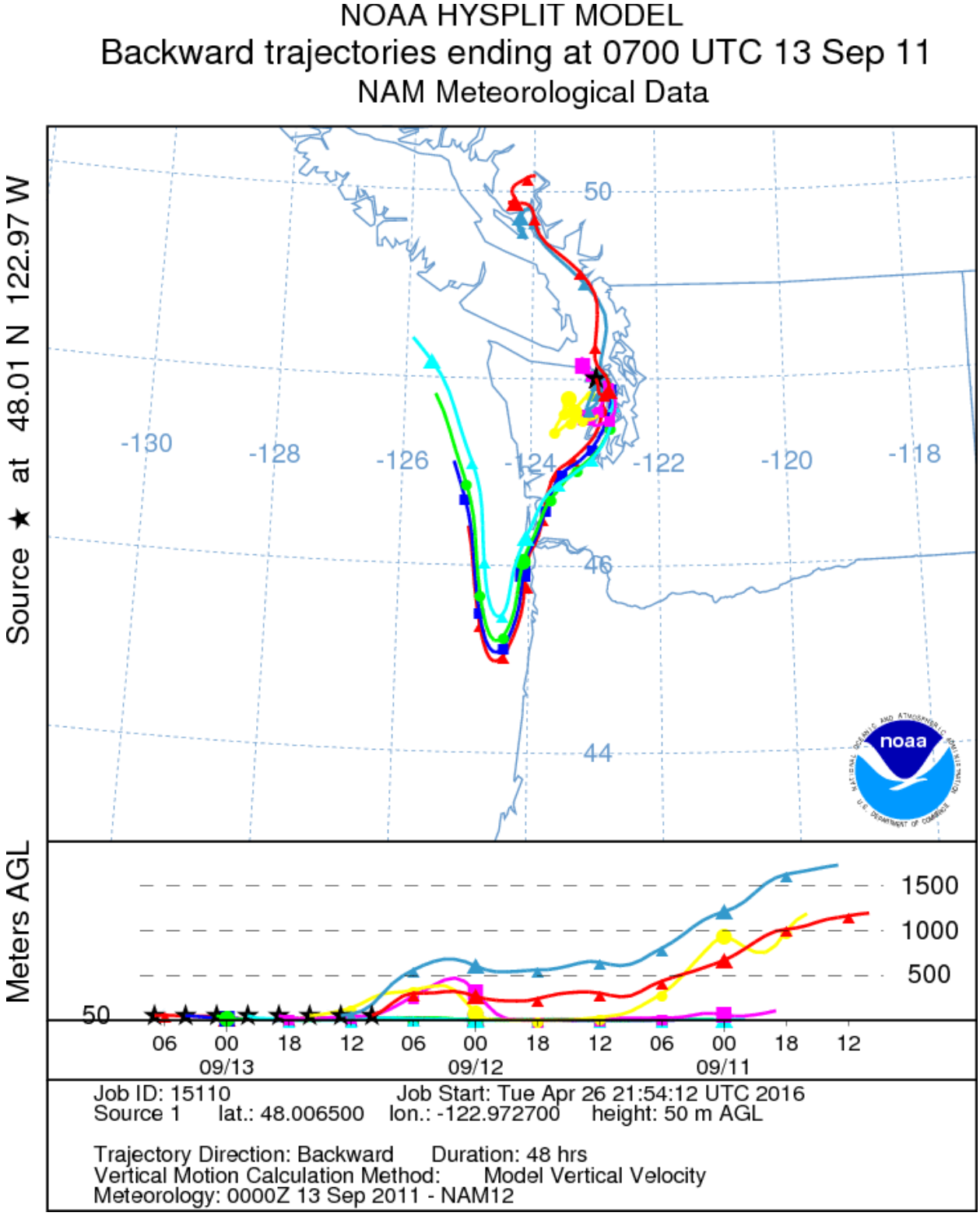
NOAA HYSPLIT MODEL
Backward trajectories ending at 0700 UTC 13 Sep 11
NAM Meteorological Data
Source ★ at 48.01 N 122.97 W
50
46
44
-130
-128
-126
-124
-122
-120
-118
noaa
Meters AGL
1500
1000
500
50
06 00 18 12 06 00 18 12 06 00 18 12
09/13 09/12 09/11
Job ID: 15110 Job Start: Tue Apr 26 21:54:12 UTC 2016
Source 1 lat.: 48.006500 lon.: -122.972700 height: 50 m AGL
Trajectory Direction: Backward Duration: 48 hrs
Vertical Motion Calculation Method: Model Vertical Velocity
Meteorology: 0000Z 13 Sep 2011 - NAM12

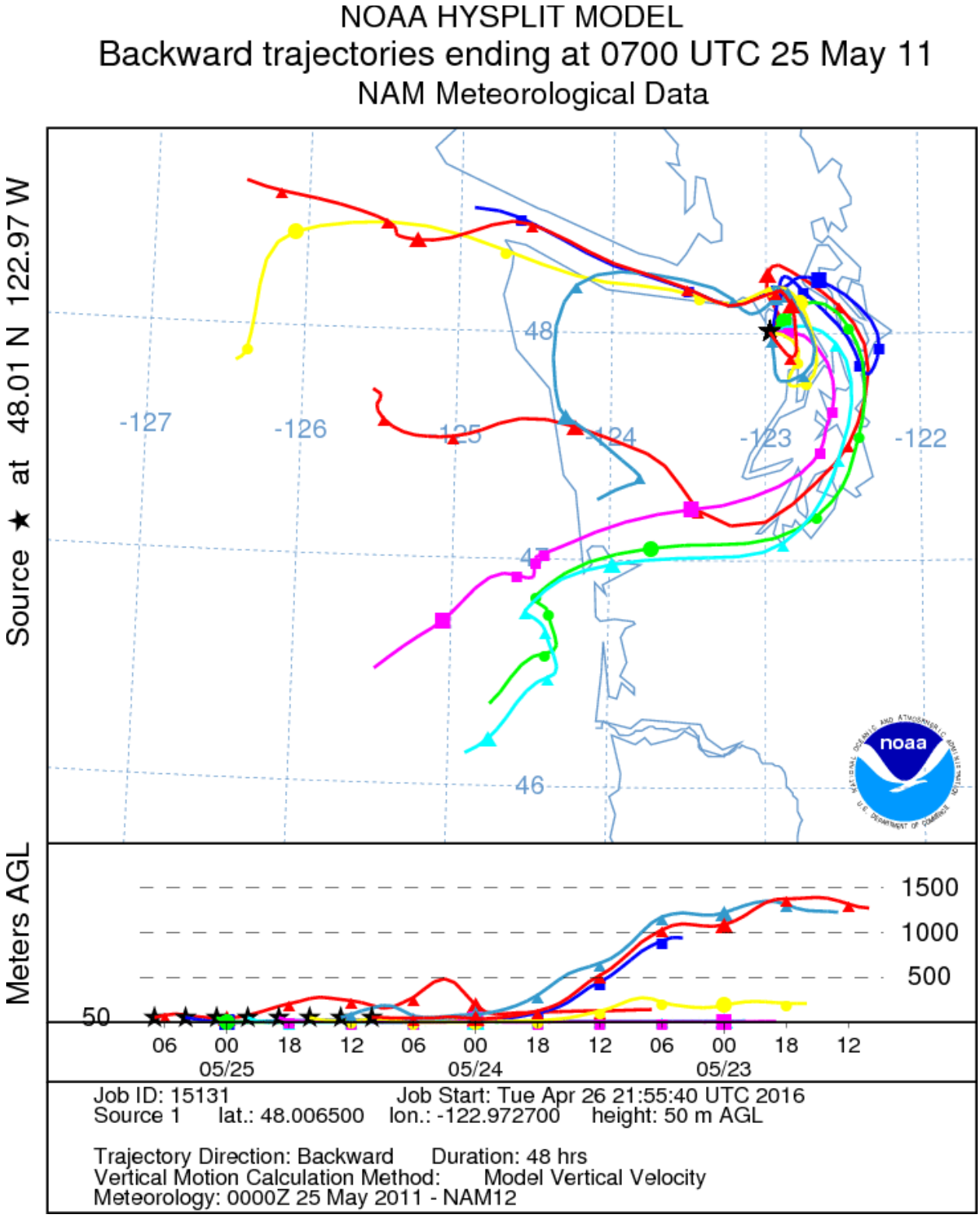
NOAA HYSPLIT MODEL
Backward trajectories ending at 0700 UTC 25 May 11
NAM Meteorological Data
Source ★ at 48.01 N 122.97 W
-127
-126
-123
-122
48
46
noaa
Meters AGL
1500
1000
500
50
06 00 18 12 06 00 18 12 06 00 18 12
05/25
05/24
05/23
Job ID: 15131 Job Start: Tue Apr 26 21:55:40 UTC 2016
Source 1 lat.: 48.006500 lon.: -122.972700 height: 50 m AGL
Trajectory Direction: Backward Duration: 48 hrs
Vertical Motion Calculation Method: Model Vertical Velocity
Meteorology: 0000Z 25 May 2011 - NAM12

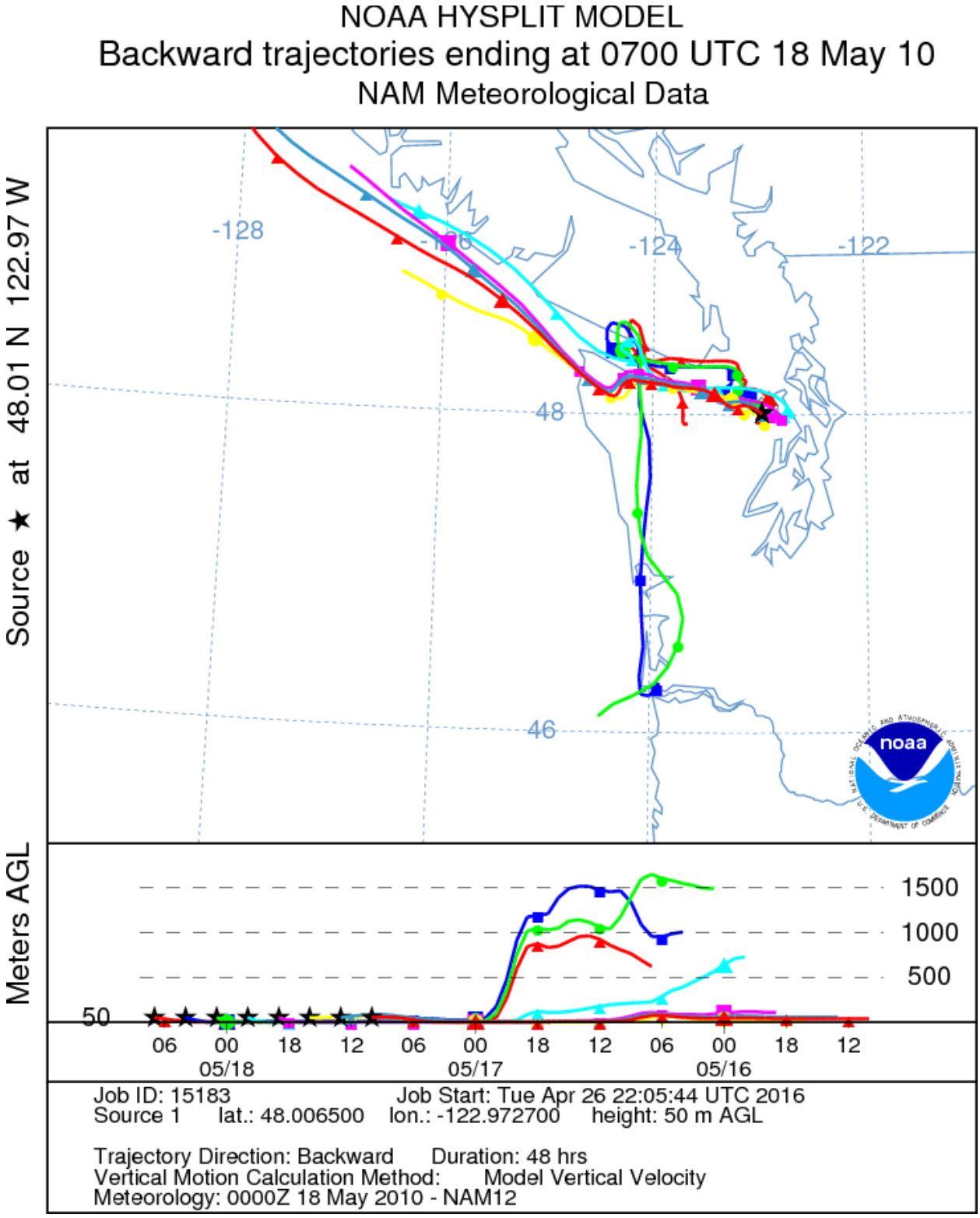
NOAA HYSPLIT MODEL
Backward trajectories ending at 0700 UTC 18 May 10
NAM Meteorological Data
Source ★ at 48.01 N 122.97 W
-128
-126
-124
-122
48
46
noaa
Meters AGL
1500
1000
500
50
06 00 18 12 06 00 18 12 06 00 18 12
05/18
05/17
05/16
Job ID: 15183 Job Start: Tue Apr 26 22:05:44 UTC 2016
Source 1 lat.: 48.006500 lon.: -122.972700 height: 50 m AGL
Trajectory Direction: Backward Duration: 48 hrs
Vertical Motion Calculation Method: Model Vertical Velocity
Meteorology: 0000Z 18 May 2010 - NAM12

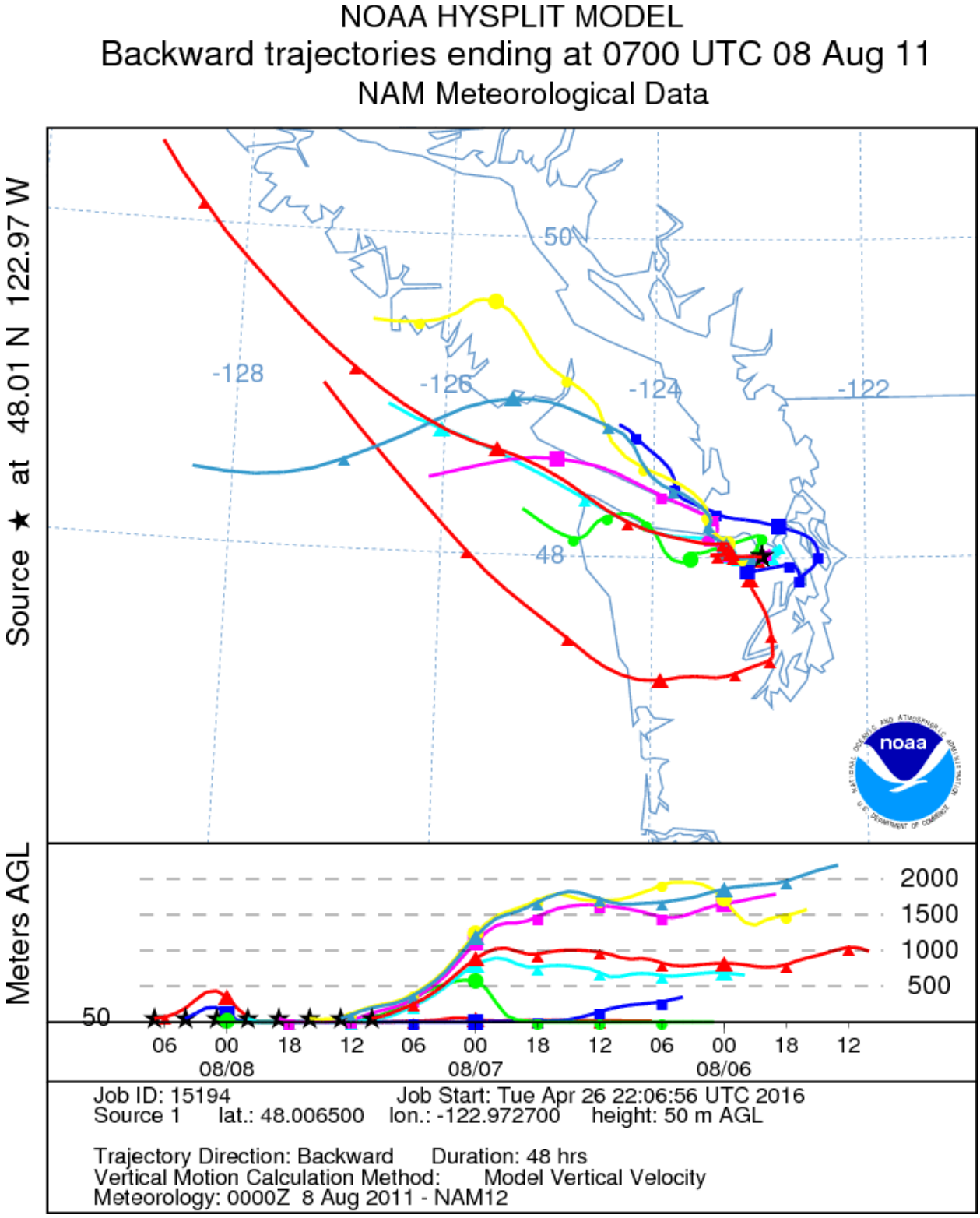
NOAA HYSPLIT MODEL
Backward trajectories ending at 0700 UTC 08 Aug 11
NAM Meteorological Data
Source ★ at 48.01 N 122.97 W
50
48
-128
-126
-124
-122
noaa
Meters AGL
2000
1500
1000
500
50
06 00 18 12 06 00 18 12 06 00 18 12
08/08
08/07
08/06
Job ID: 15194 Job Start: Tue Apr 26 22:06:56 UTC 2016
Source 1 lat.: 48.006500 lon.: -122.972700 height: 50 m AGL
Trajectory Direction: Backward Duration: 48 hrs
Vertical Motion Calculation Method: Model Vertical Velocity
Meteorology: 0000Z 8 Aug 2011 - NAM12

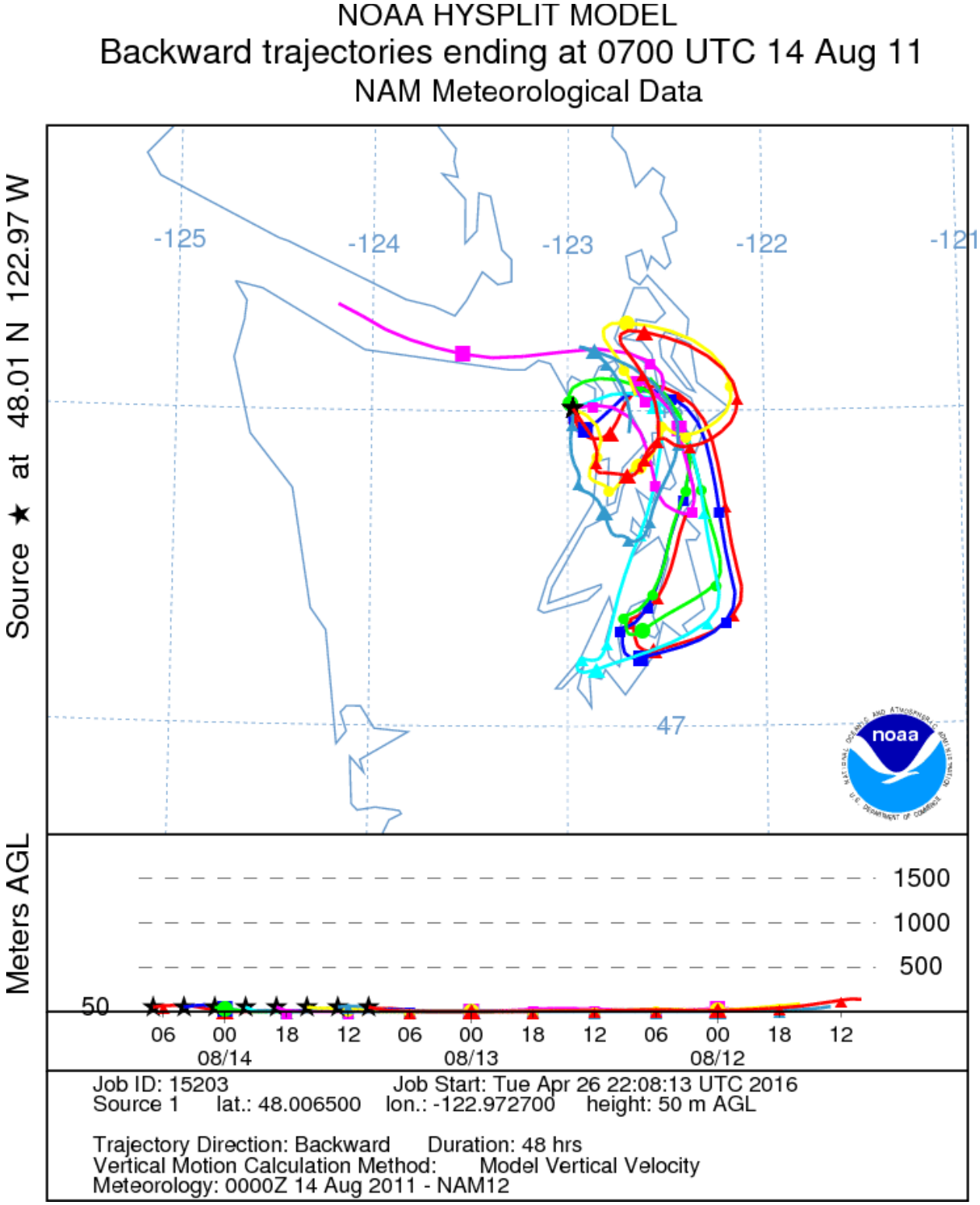
NOAA HYSPLIT MODEL
Backward trajectories ending at 0700 UTC 14 Aug 11
NAM Meteorological Data
Source ★ at 48.01 N 122.97 W
-125
-124
-123
-122
-121
47
noaa
Meters AGL
1500
1000
500
50
06
00
18
12
06
00
18
12
06
00
18
12
08/14
08/13
08/12
Job ID: 15203
Job Start: Tue Apr 26 22:08:13 UTC 2016
Source 1 lat.: 48.006500 lon.: -122.972700 height: 50 m AGL
Trajectory Direction: Backward Duration: 48 hrs
Vertical Motion Calculation Method: Model Vertical Velocity
Meteorology: 0000Z 14 Aug 2011 - NAM12

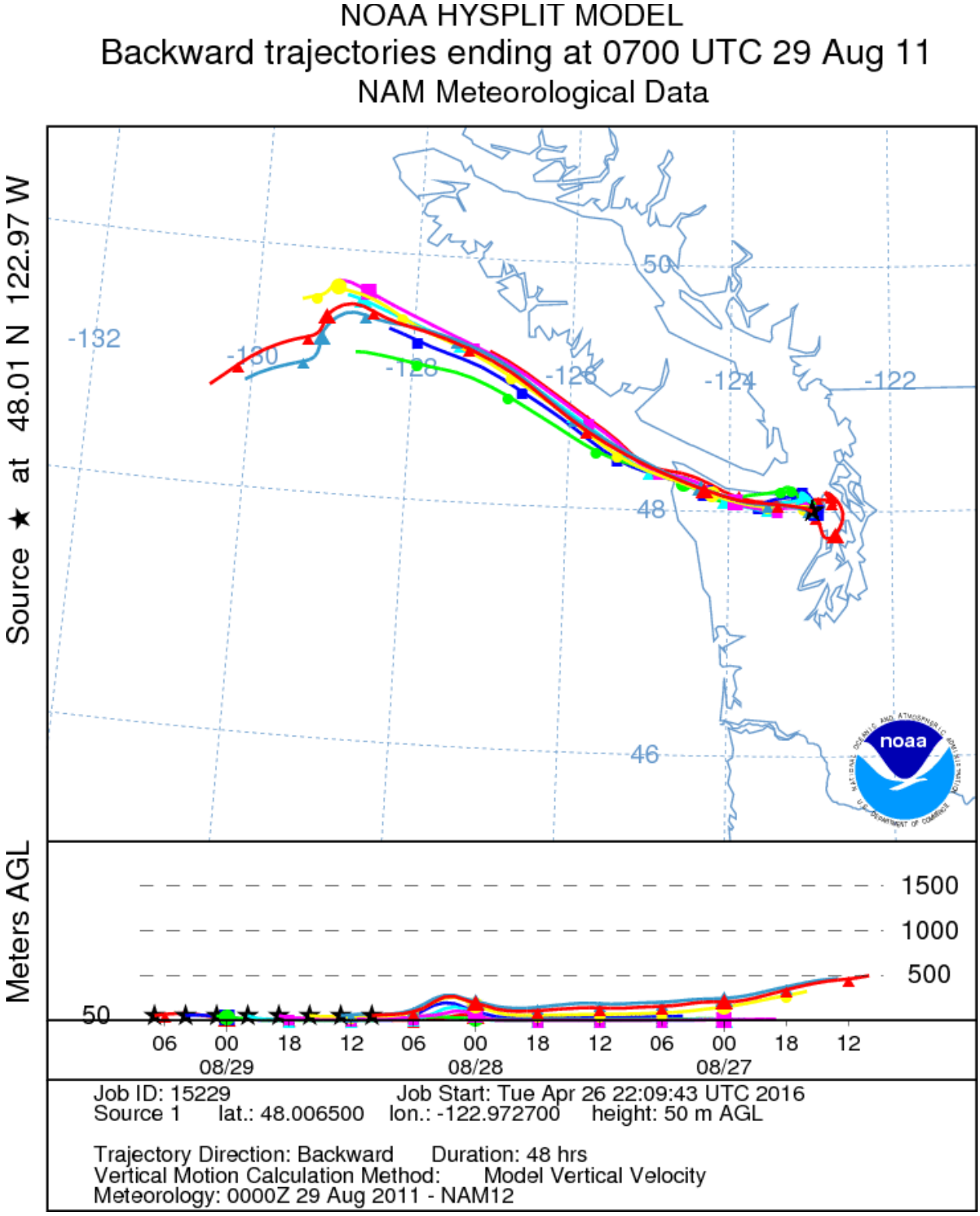
NOAA HYSPLIT MODEL
Backward trajectories ending at 0700 UTC 29 Aug 11
NAM Meteorological Data
Source ★ at 48.01 N 122.97 W
-132
-130
-128
-126
-124
-122
50
48
46
noaa
Meters AGL
1500
1000
500
50
06 00 18 12 06 00 18 12 06 00 18 12
08/29
08/28
08/27
Job ID: 15229 Job Start: Tue Apr 26 22:09:43 UTC 2016
Source 1 lat.: 48.006500 lon.: -122.972700 height: 50 m AGL
Trajectory Direction: Backward Duration: 48 hrs
Vertical Motion Calculation Method: Model Vertical Velocity
Meteorology: 0000Z 29 Aug 2011 - NAM12

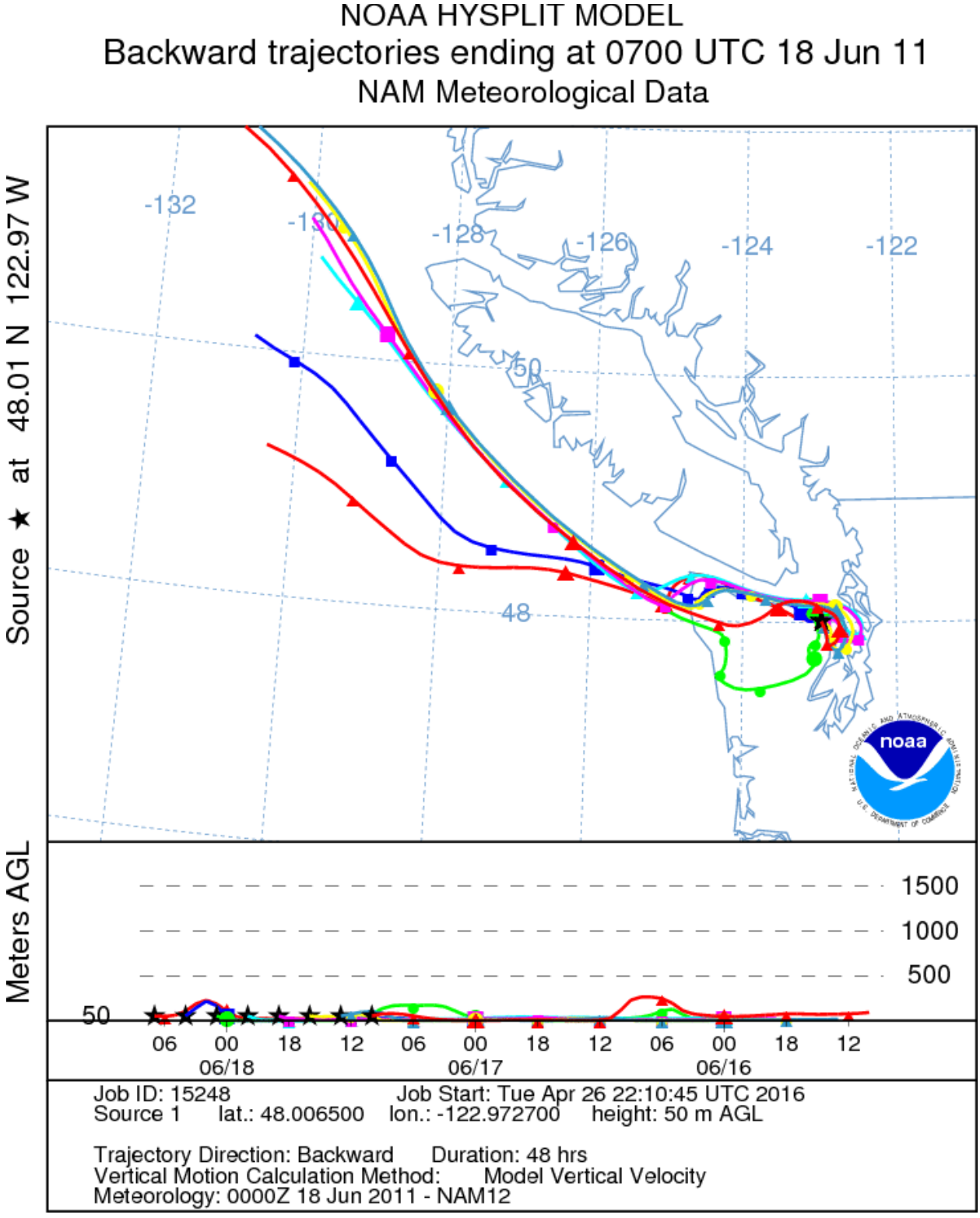
NOAA HYSPLIT MODEL
Backward trajectories ending at 0700 UTC 18 Jun 11
NAM Meteorological Data
Source ★ at 48.01 N 122.97 W
-132
-130
-128
-126
-124
-122
50
48
noaa
Meters AGL
1500
1000
500
50
06 00 18 12 06 00 18 12 06 00 18 12
06/18
06/17
06/16
Job ID: 15248 Job Start: Tue Apr 26 22:10:45 UTC 2016
Source 1 lat.: 48.006500 lon.: -122.972700 height: 50 m AGL
Trajectory Direction: Backward Duration: 48 hrs
Vertical Motion Calculation Method: Model Vertical Velocity
Meteorology: 0000Z 18 Jun 2011 - NAM12

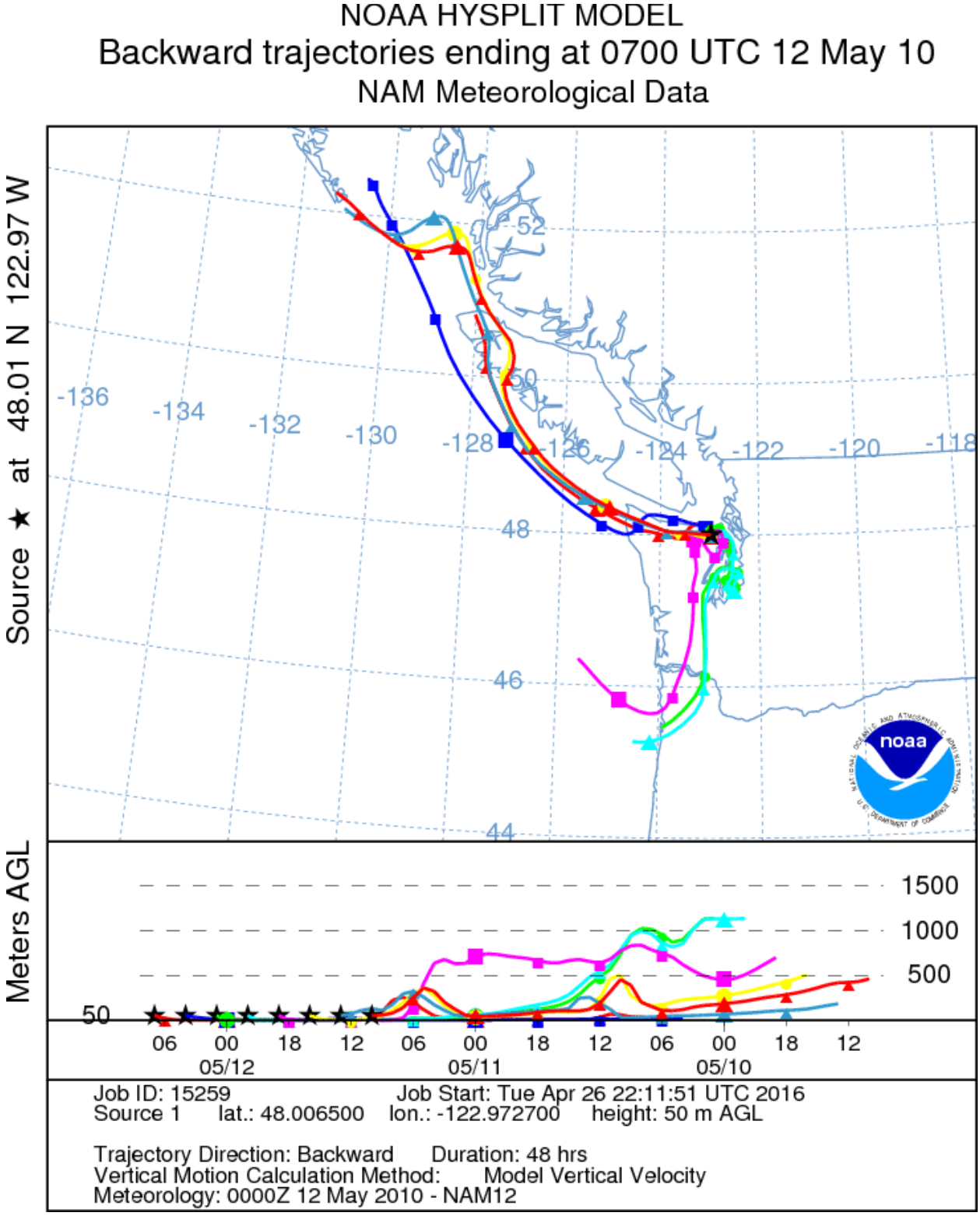
NOAA HYSPLIT MODEL
Backward trajectories ending at 0700 UTC 12 May 10
NAM Meteorological Data
Source ★ at 48.01 N 122.97 W
-136
-134
-132
-130
-128
-126
-124
-122
-120
-118
52
50
48
46
44
noaa
Meters AGL
1500
1000
500
50
06 00 18 12 06 00 18 12 06 00 18 12
05/12
05/11
05/10
Job ID: 15259 Job Start: Tue Apr 26 22:11:51 UTC 2016
Source 1 lat.: 48.006500 lon.: -122.972700 height: 50 m AGL
Trajectory Direction: Backward Duration: 48 hrs
Vertical Motion Calculation Method: Model Vertical Velocity
Meteorology: 0000Z 12 May 2010 - NAM12

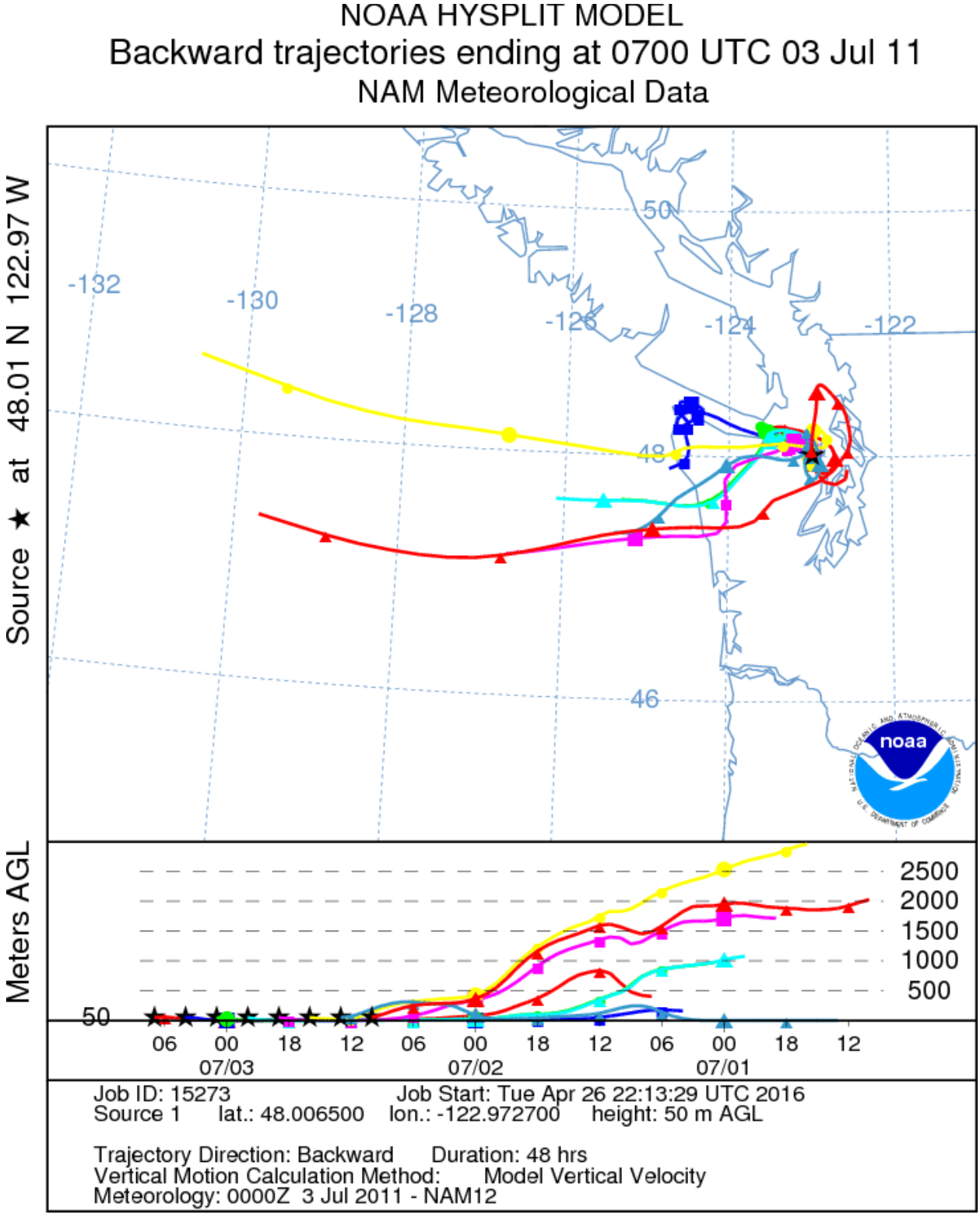
NOAA HYSPLIT MODEL
Backward trajectories ending at 0700 UTC 03 Jul 11
NAM Meteorological Data
Source ★ at 48.01 N 122.97 W
-132
-130
-128
-126
-124
-122
50
48
46
noaa
Meters AGL
2500
2000
1500
1000
500
50
06 00 18 12 06 00 18 12 06 00 18 12
07/03
07/02
07/01
Job ID: 15273 Job Start: Tue Apr 26 22:13:29 UTC 2016
Source 1 lat.: 48.006500 lon.: -122.972700 height: 50 m AGL
Trajectory Direction: Backward Duration: 48 hrs
Vertical Motion Calculation Method: Model Vertical Velocity
Meteorology: 0000Z 3 Jul 2011 - NAM12

PENO HYSPLIT back-trajectories

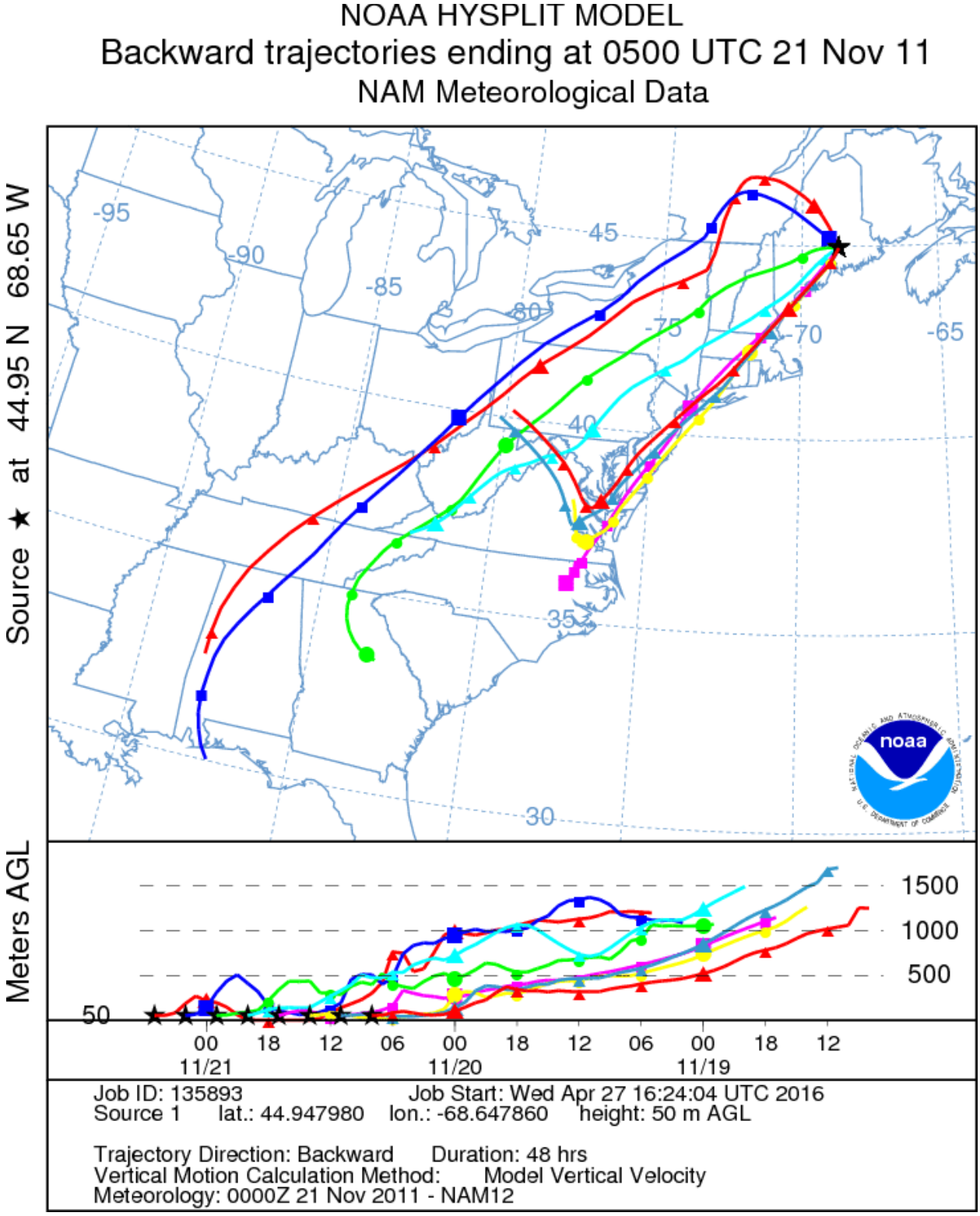
NOAA HYSPLIT MODEL
Backward trajectories ending at 0500 UTC 21 Nov 11
NAM Meteorological Data
Source ★ at 44.95 N 68.65 W
Meters AGL
-95
-90
-85
-80
-75
-70
-65
45
40
35
30
1500
1000
500
50
00 18 12 06 00 18 12 06 00 18 12
11/21 11/20 11/19
noaa
Job ID: 135893 Job Start: Wed Apr 27 16:24:04 UTC 2016
Source 1 lat.: 44.947980 lon.: -68.647860 height: 50 m AGL
Trajectory Direction: Backward Duration: 48 hrs
Vertical Motion Calculation Method: Model Vertical Velocity
Meteorology: 0000Z 21 Nov 2011 - NAM12

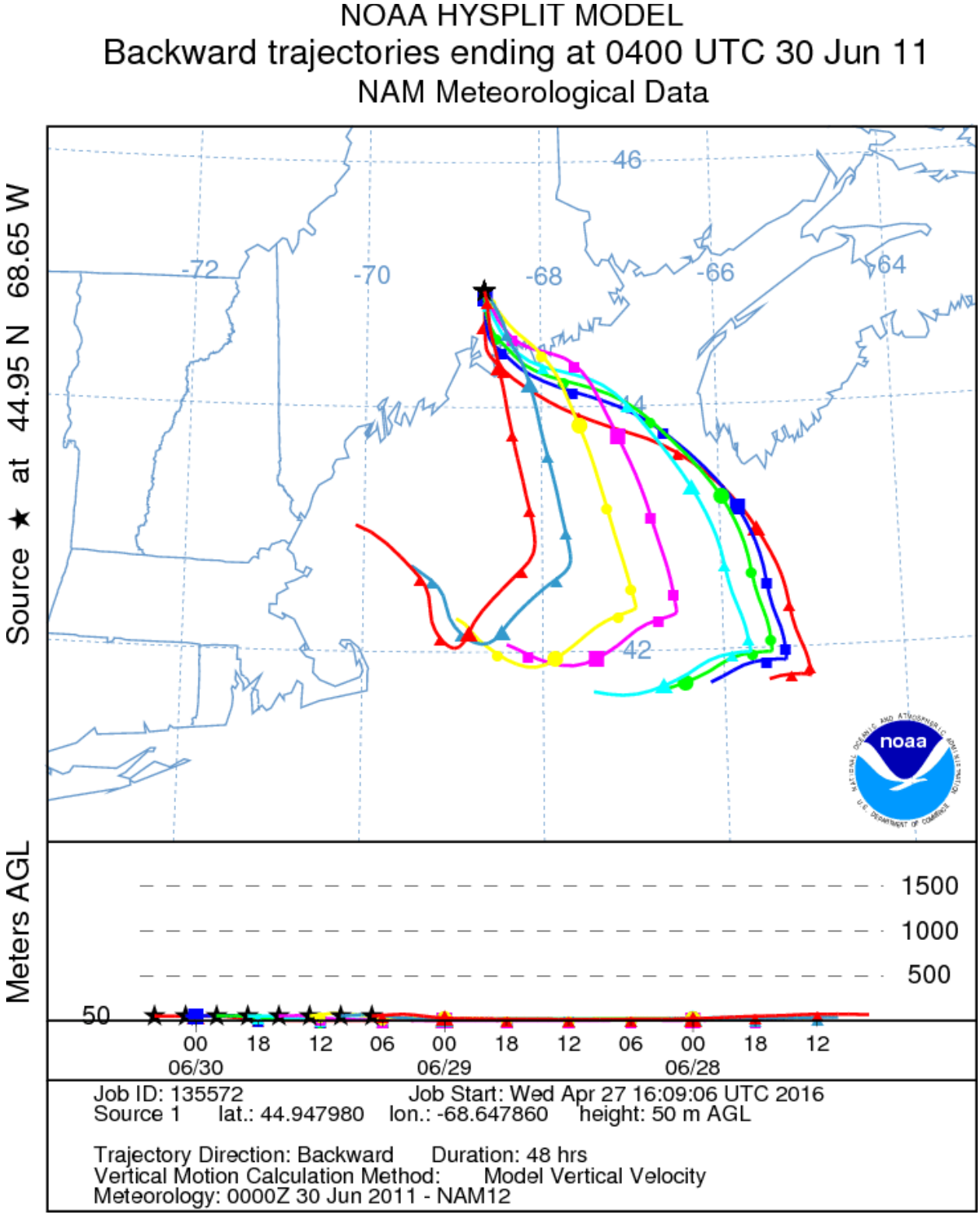
NOAA HYSPLIT MODEL
Backward trajectories ending at 0400 UTC 30 Jun 11
NAM Meteorological Data
Source ★ at 44.95 N 68.65 W
46
-72
-70
-68
-66
-64
-42
noaa
Meters AGL
1500
1000
500
50
00 18 12 06 00 18 12 06 00 18 12
06/30 06/29 06/28
Job ID: 135572 Job Start: Wed Apr 27 16:09:06 UTC 2016
Source 1 lat.: 44.947980 lon.: -68.647860 height: 50 m AGL
Trajectory Direction: Backward Duration: 48 hrs
Vertical Motion Calculation Method: Model Vertical Velocity
Meteorology: 0000Z 30 Jun 2011 - NAM12

NOAA HYSPLIT MODEL
Backward trajectories ending at 0500 UTC 15 Feb 11
NAM Meteorological Data

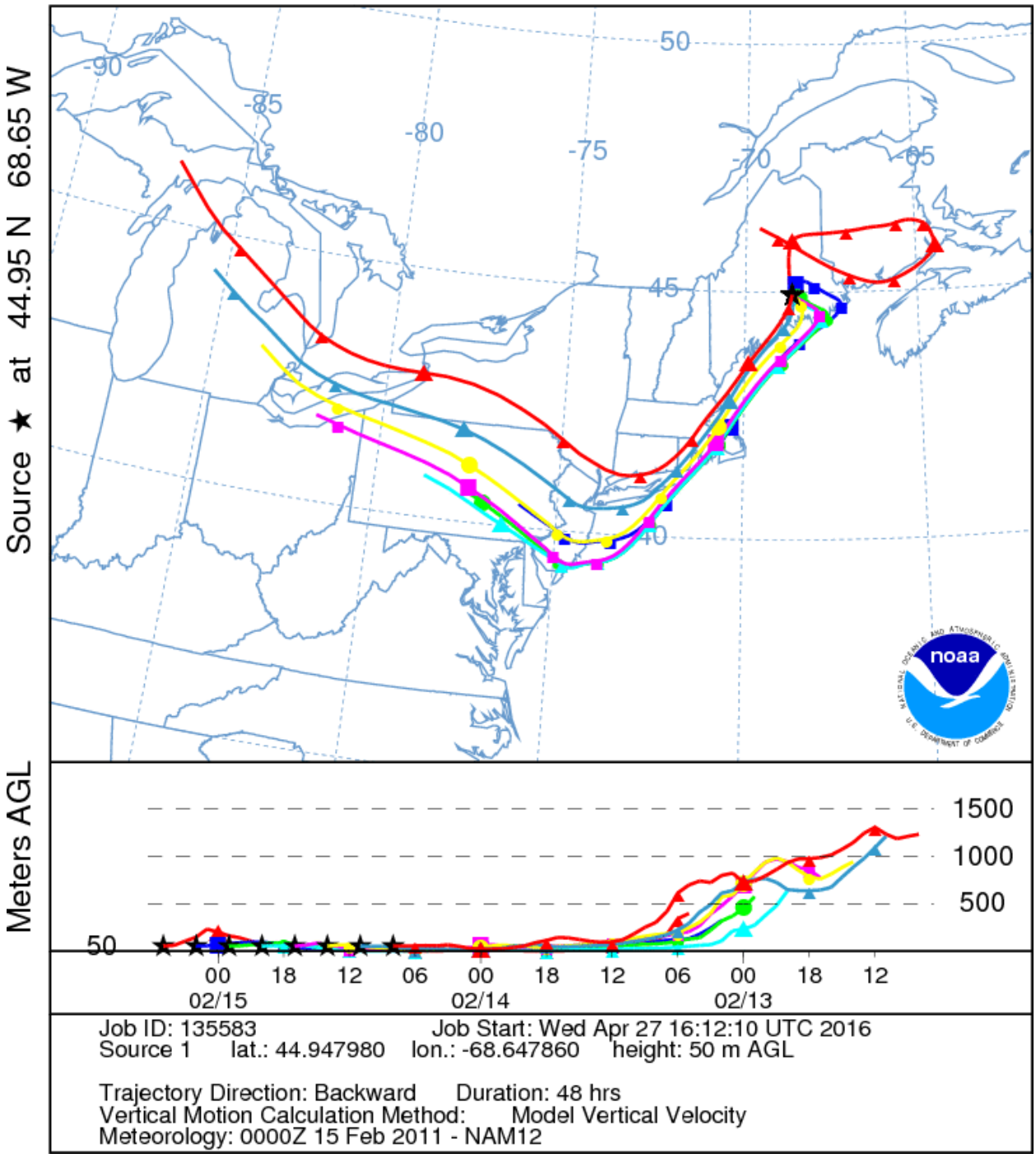

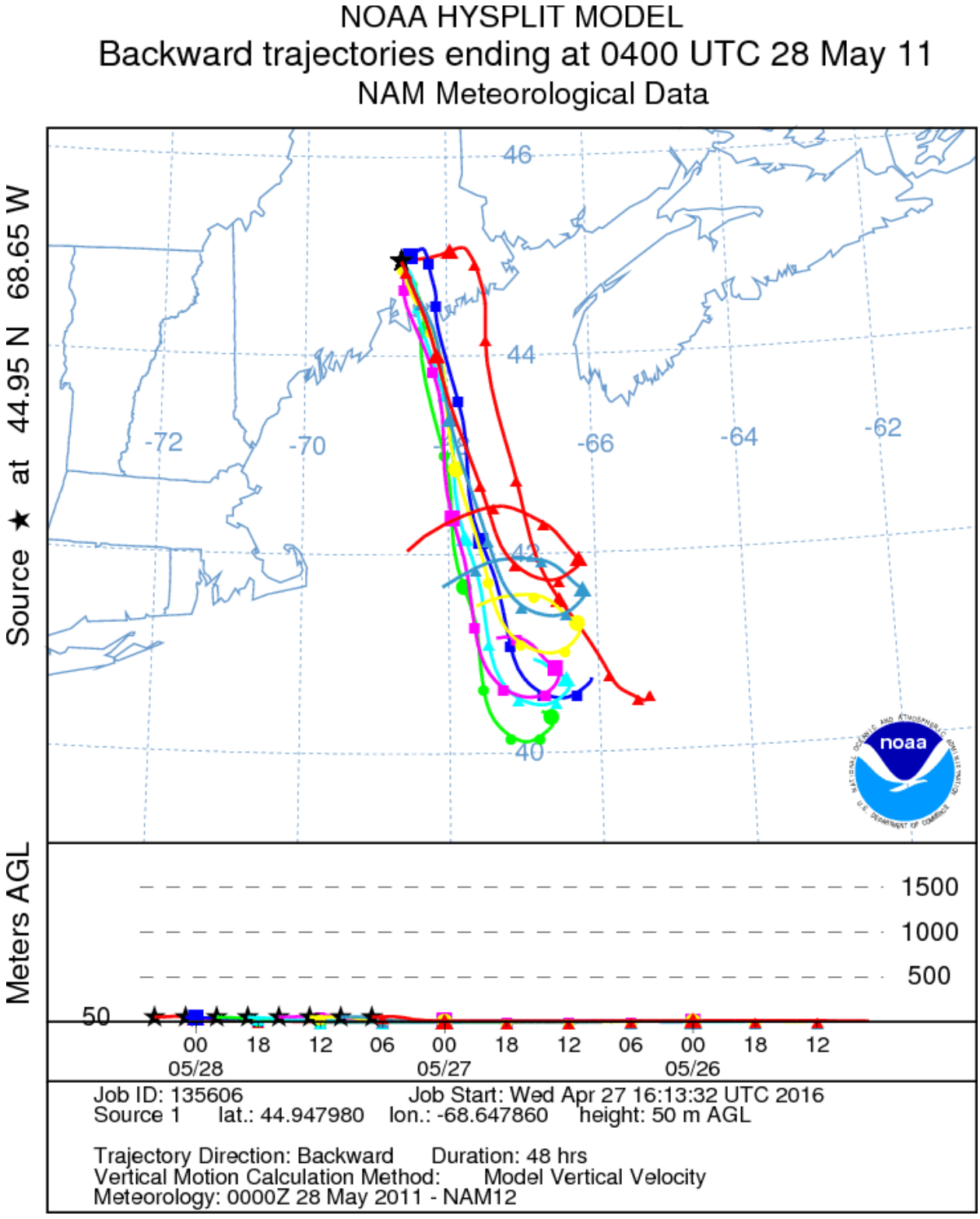
NOAA HYSPLIT MODEL
Backward trajectories ending at 0400 UTC 28 May 11
NAM Meteorological Data
Source ★ at 44.95 N 68.65 W
46
44
42
40
-72
-70
-66
-64
-62
noaa
Meters AGL
1500
1000
500
50
00 18 12 06 00 18 12 06 00 18 12
05/28 05/27 05/26
Job ID: 135606 Job Start: Wed Apr 27 16:13:32 UTC 2016
Source 1 lat.: 44.947980 lon.: -68.647860 height: 50 m AGL
Trajectory Direction: Backward Duration: 48 hrs
Vertical Motion Calculation Method: Model Vertical Velocity
Meteorology: 0000Z 28 May 2011 - NAM12

NOAA HYSPLIT MODEL
Backward trajectories ending at 0500 UTC 06 Dec 11
NAM Meteorological Data

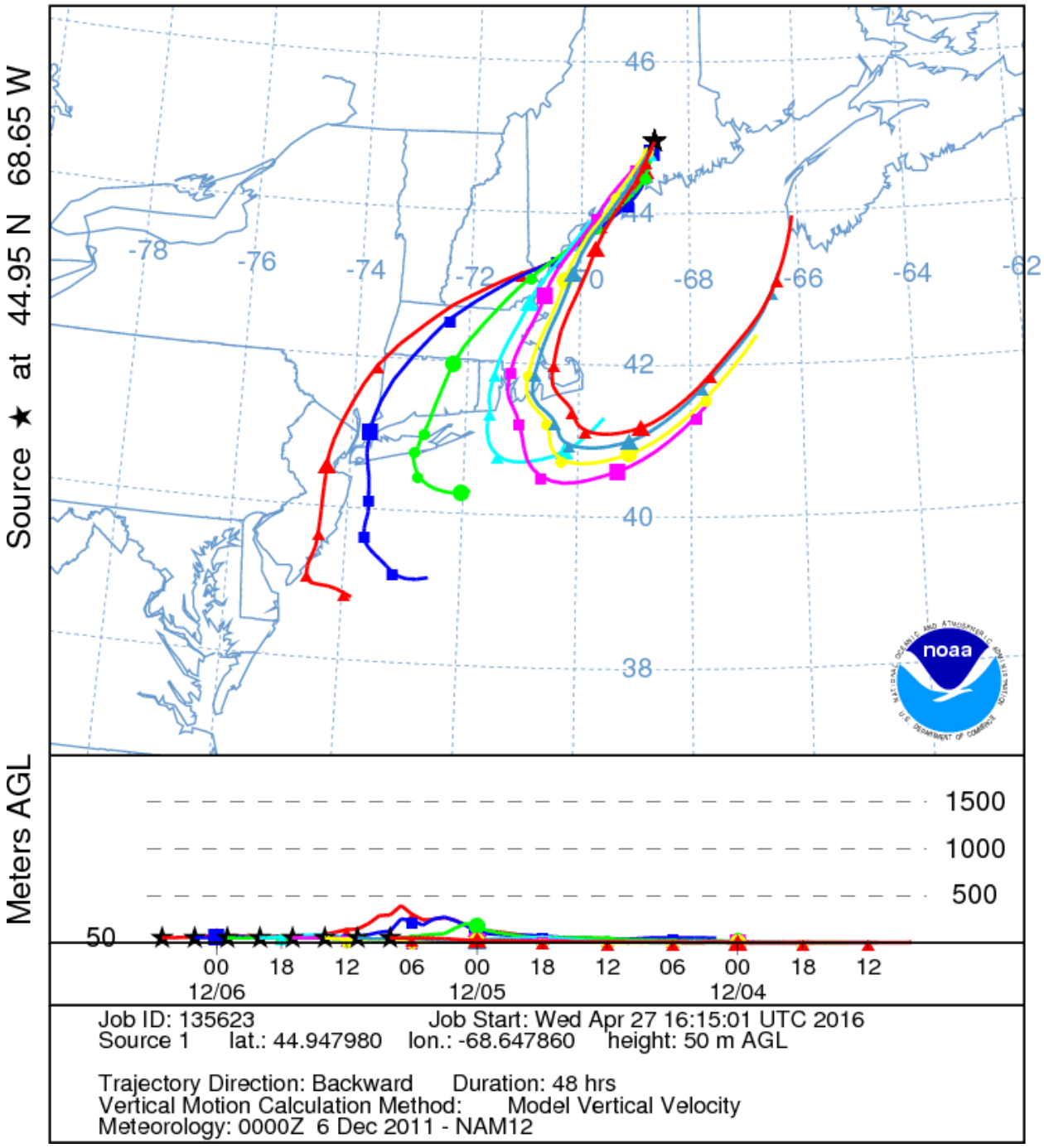

Job ID: 135623 Job Start: Wed Apr 27 16:15:01 UTC 2016
Source 1 lat.: 44.947980 lon.: -68.647860 height: 50 m AGL

Trajectory Direction: Backward Duration: 48 hrs
Vertical Motion Calculation Method: Model Vertical Velocity
Meteorology: 0000Z 6 Dec 2011 - NAM12

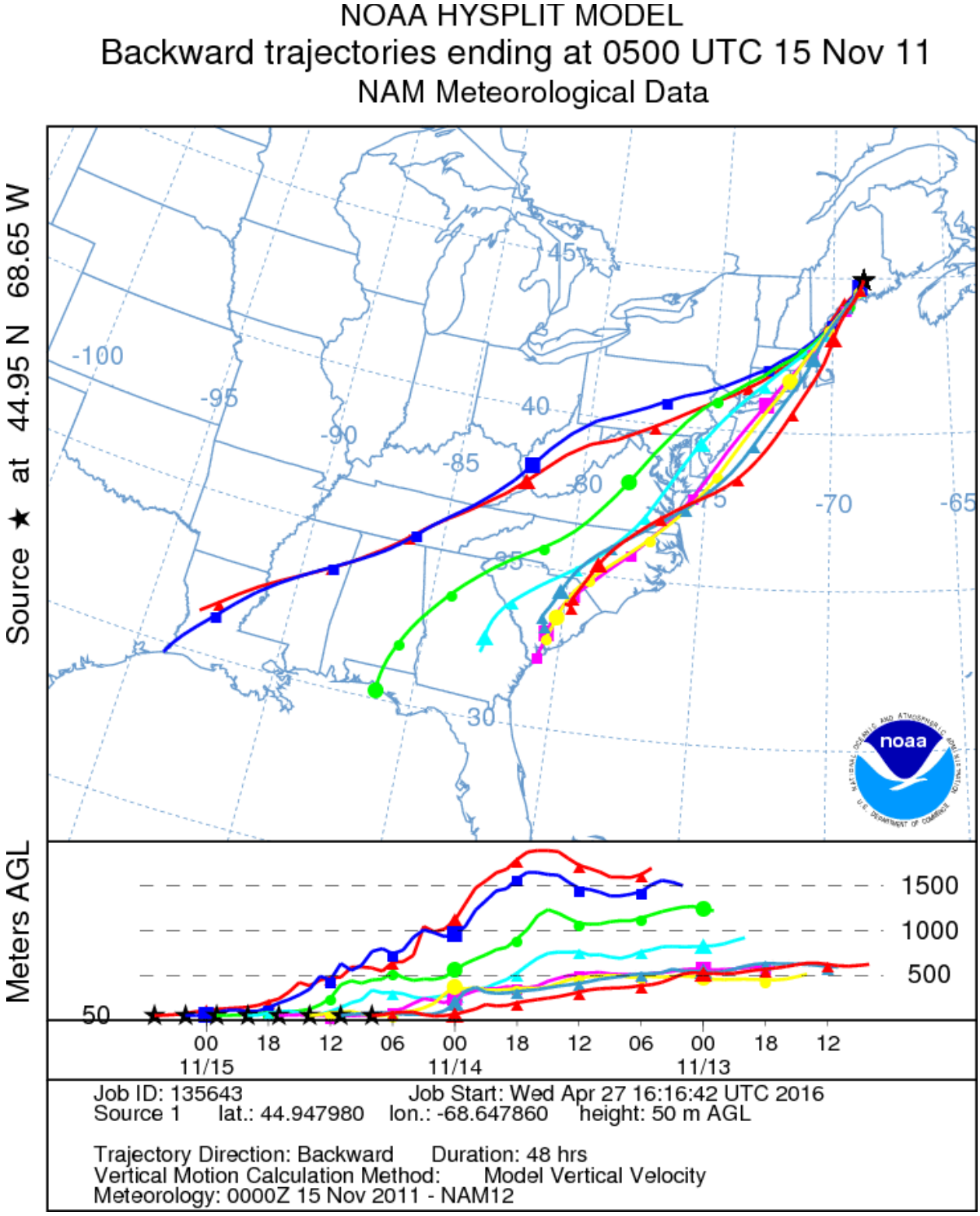
NOAA HYSPLIT MODEL
Backward trajectories ending at 0500 UTC 15 Nov 11
NAM Meteorological Data
Source ★ at 44.95 N 68.65 W
Meters AGL
1500
1000
500
50
00 18 12 06 00 18 12 06 00 18 12
11/15 11/14 11/13
Job ID: 135643 Job Start: Wed Apr 27 16:16:42 UTC 2016
Source 1 lat.: 44.947980 lon.: -68.647860 height: 50 m AGL
Trajectory Direction: Backward Duration: 48 hrs
Vertical Motion Calculation Method: Model Vertical Velocity
Meteorology: 0000Z 15 Nov 2011 - NAM12

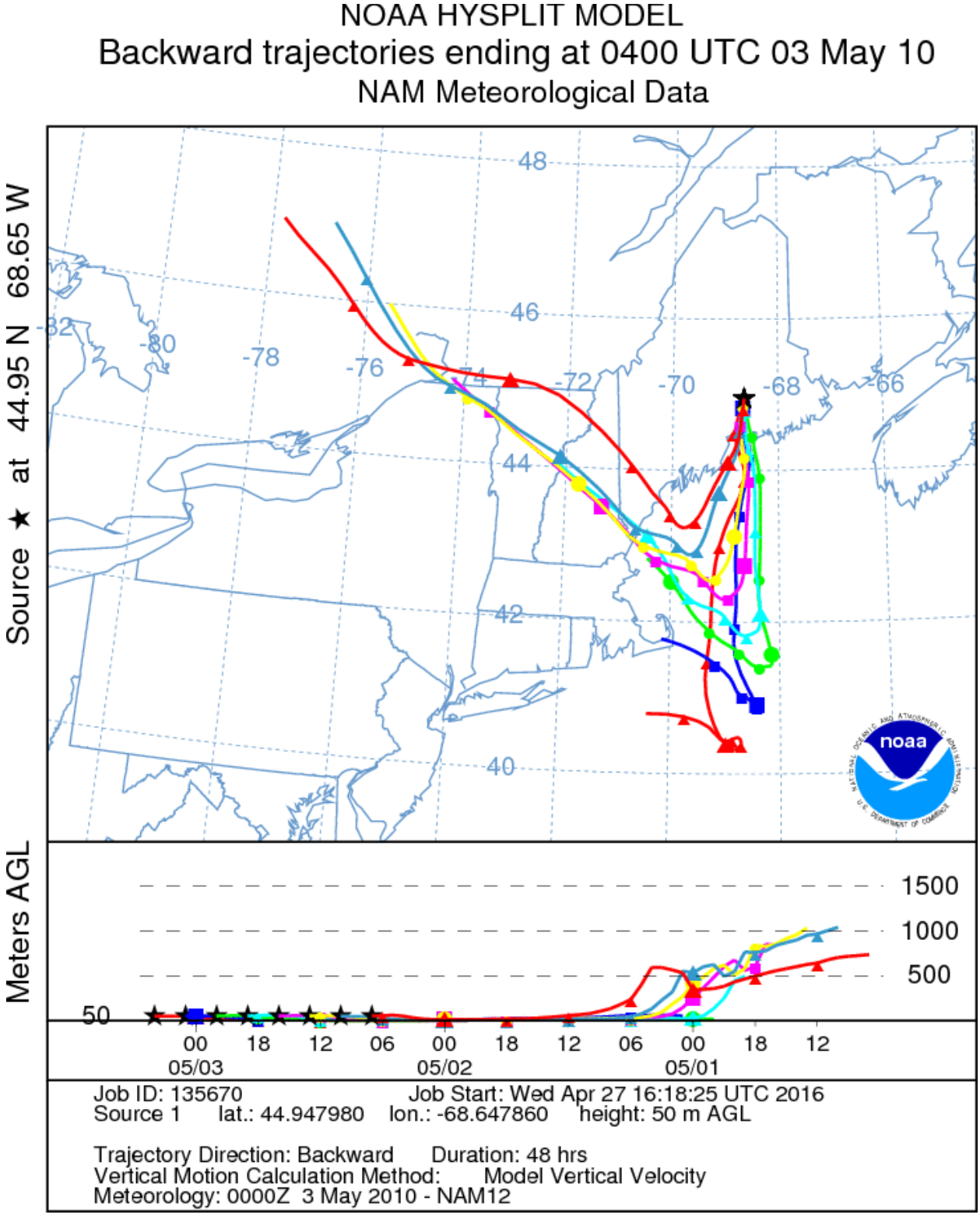
NOAA HYSPLIT MODEL
Backward trajectories ending at 0400 UTC 03 May 10
NAM Meteorological Data
Source ★ at 44.95 N 68.65 W
48
46
44
42
40
-82
-80
-78
-76
-74
-72
-70
-68
-66
noaa
Meters AGL
1500
1000
500
50
00 18 12 06 00 18 12 06 00 18 12
05/03 05/02 05/01
Job ID: 135670 Job Start: Wed Apr 27 16:18:25 UTC 2016
Source 1 lat.: 44.947980 lon.: -68.647860 height: 50 m AGL
Trajectory Direction: Backward Duration: 48 hrs
Vertical Motion Calculation Method: Model Vertical Velocity
Meteorology: 0000Z 3 May 2010 - NAM12

NOAA HYSPLIT MODEL
Backward trajectories ending at 0400 UTC 20 Aug 11
NAM Meteorological Data

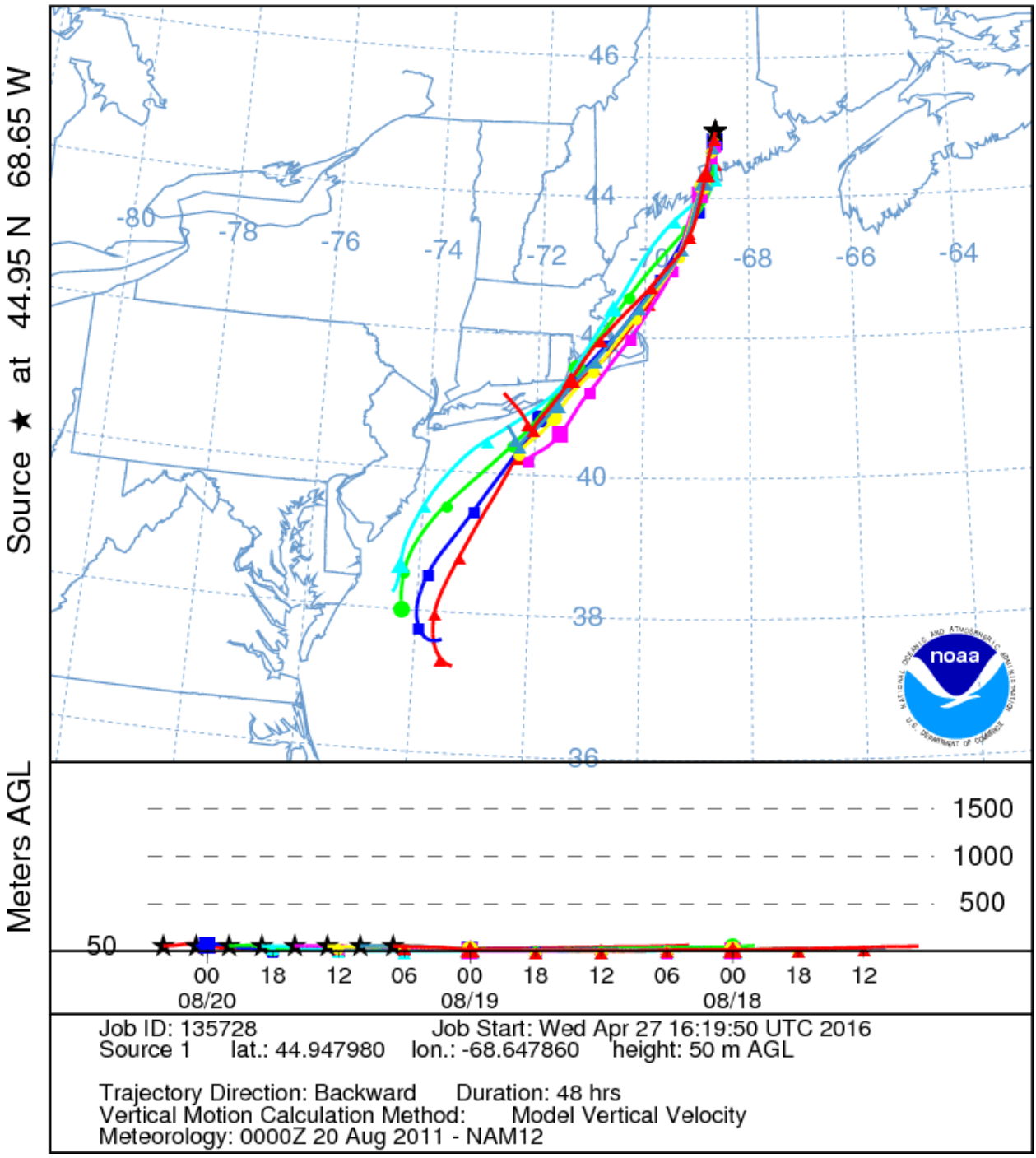

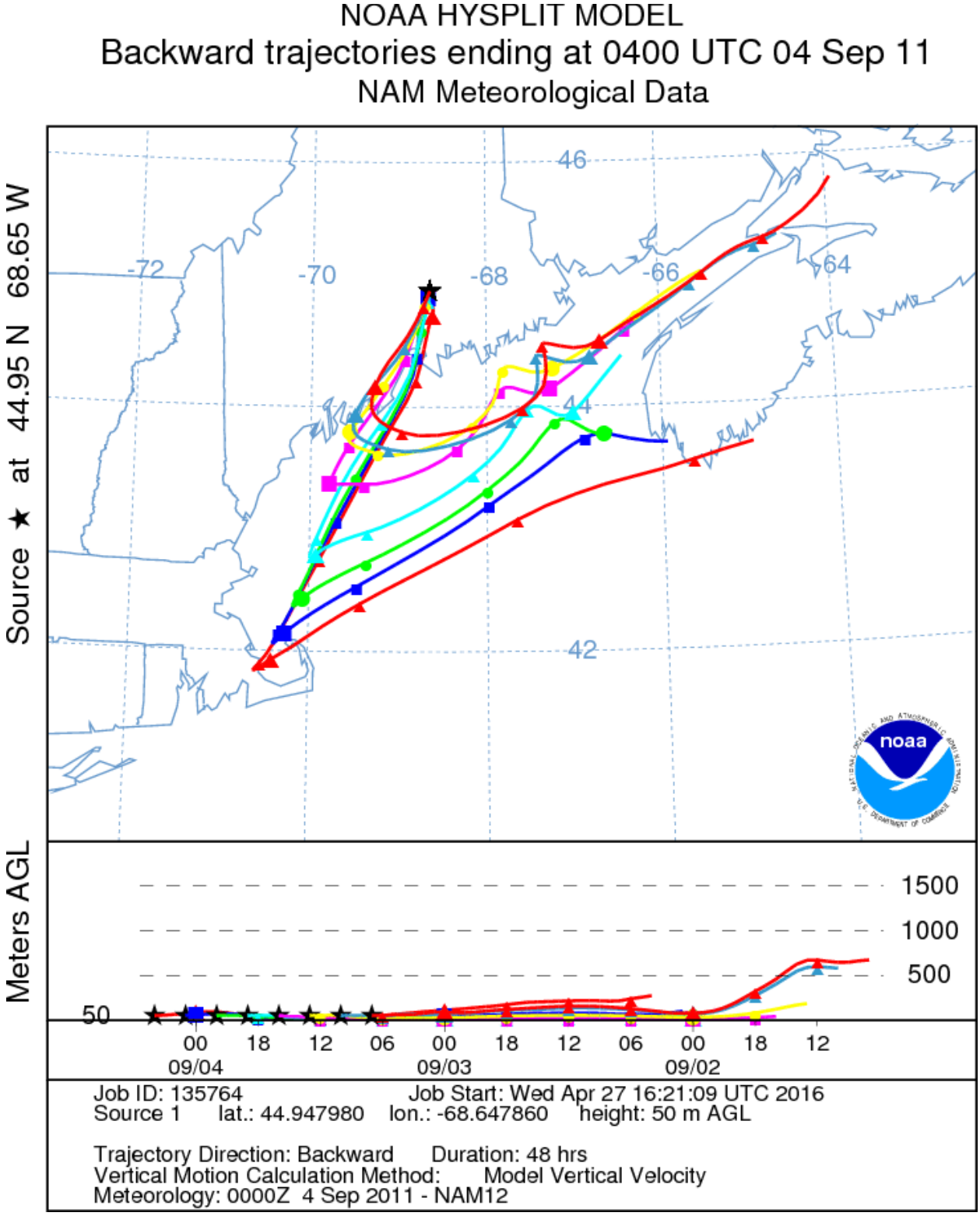
NOAA HYSPLIT MODEL
Backward trajectories ending at 0400 UTC 04 Sep 11
NAM Meteorological Data
Source ★ at 44.95 N 68.65 W
46
44
42
-72
-70
-68
-66
-64
noaa
Meters AGL
1500
1000
500
50
00 18 12 06 00 18 12 06 00 18 12
09/04
09/03
09/02
Job ID: 135764 Job Start: Wed Apr 27 16:21:09 UTC 2016
Source 1 lat.: 44.947980 lon.: -68.647860 height: 50 m AGL
Trajectory Direction: Backward Duration: 48 hrs
Vertical Motion Calculation Method: Model Vertical Velocity
Meteorology: 0000Z 4 Sep 2011 - NAM12

NOAA HYSPLIT MODEL
Backward trajectories ending at 0400 UTC 02 Aug 11
NAM Meteorological Data

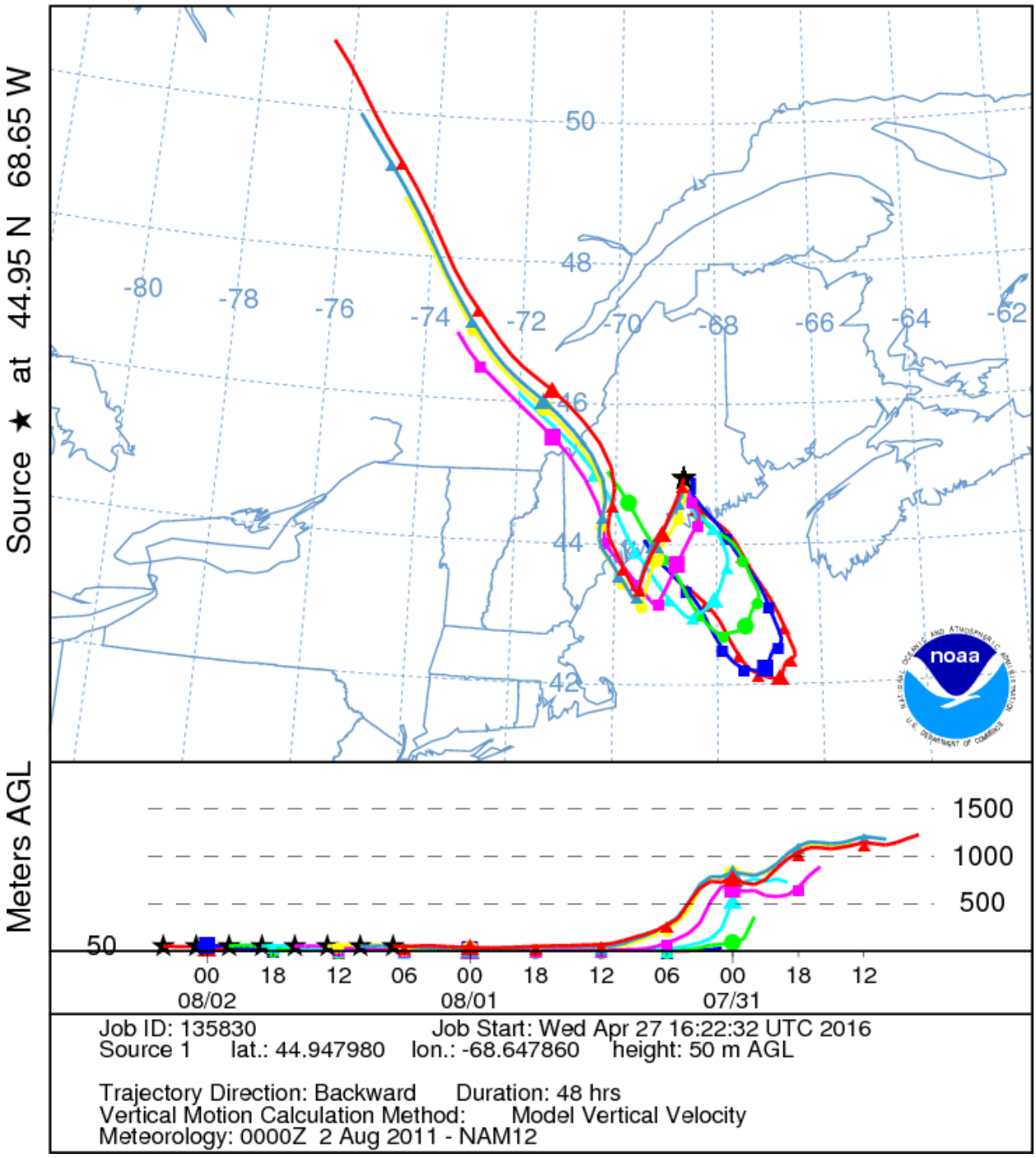

PINN HYSPLIT back-trajectories

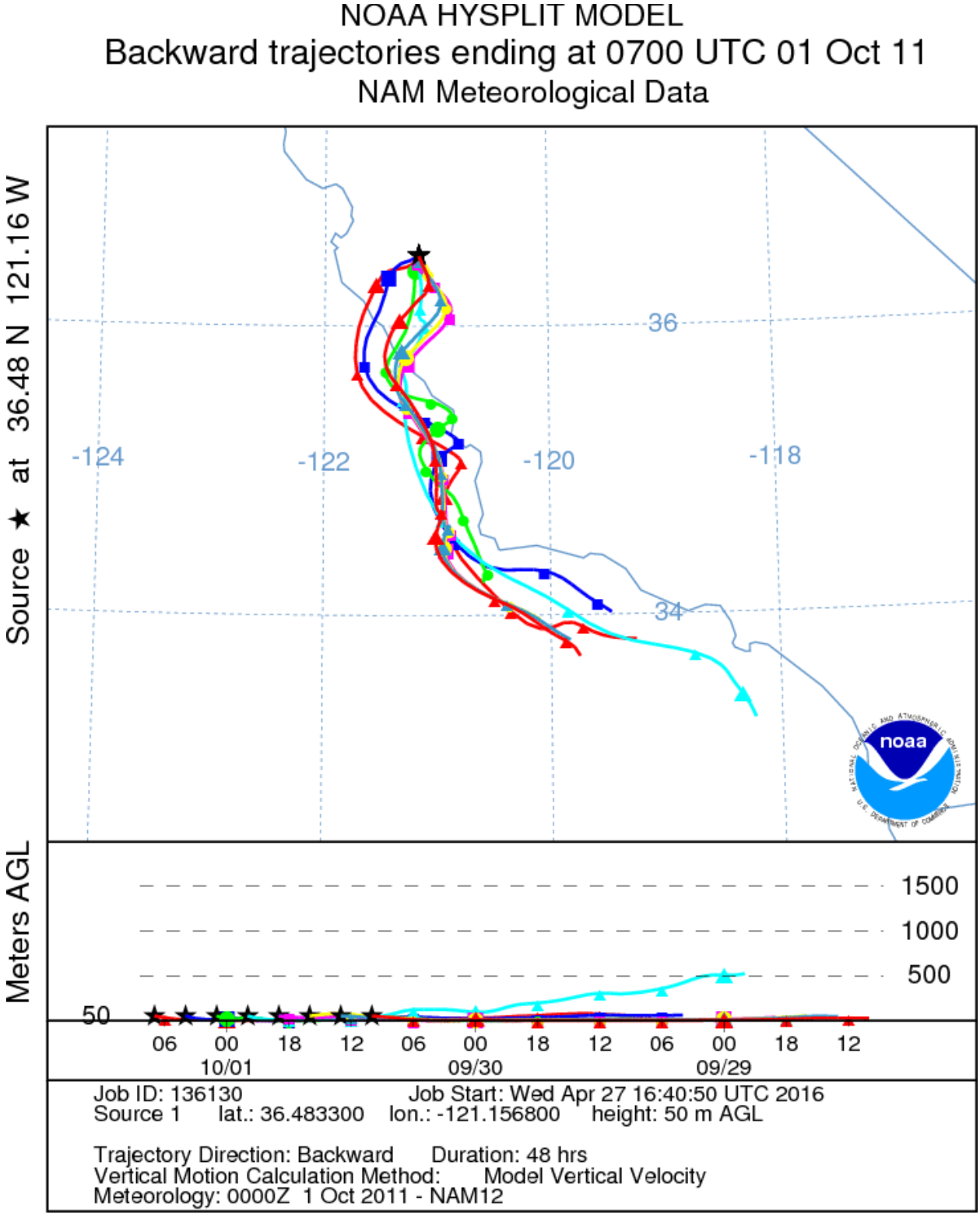
NOAA HYSPLIT MODEL
Backward trajectories ending at 0700 UTC 01 Oct 11
NAM Meteorological Data
Source ★ at 36.48 N 121.16 W
36
34
-124
-122
-120
-118
noaa
Meters AGL
1500
1000
500
50
06 00 18 12 06 00 18 12 06 00 18 12
10/01
09/30
09/29
Job ID: 136130 Job Start: Wed Apr 27 16:40:50 UTC 2016
Source 1 lat.: 36.483300 lon.: -121.156800 height: 50 m AGL
Trajectory Direction: Backward Duration: 48 hrs
Vertical Motion Calculation Method: Model Vertical Velocity
Meteorology: 0000Z 1 Oct 2011 - NAM12

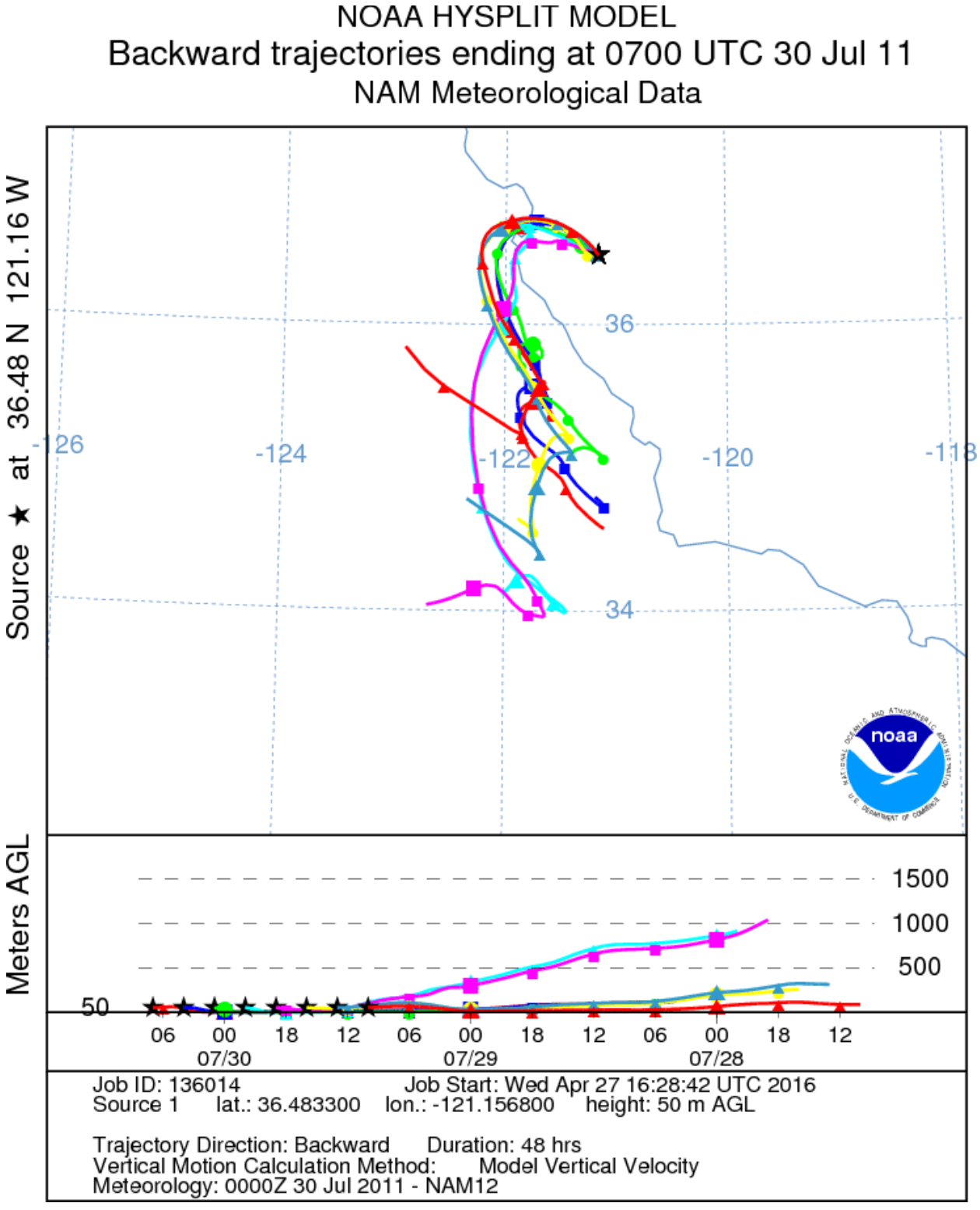
NOAA HYSPLIT MODEL
Backward trajectories ending at 0700 UTC 30 Jul 11
NAM Meteorological Data
Source ★ at 36.48 N 121.16 W
-126
-124
-122
-120
-118
36
34
noaa
Meters AGL
1500
1000
500
50
06 00 18 12 06 00 18 12 06 00 18 12
07/30
07/29
07/28
Job ID: 136014 Job Start: Wed Apr 27 16:28:42 UTC 2016
Source 1 lat.: 36.483300 lon.: -121.156800 height: 50 m AGL
Trajectory Direction: Backward Duration: 48 hrs
Vertical Motion Calculation Method: Model Vertical Velocity
Meteorology: 0000Z 30 Jul 2011 - NAM12

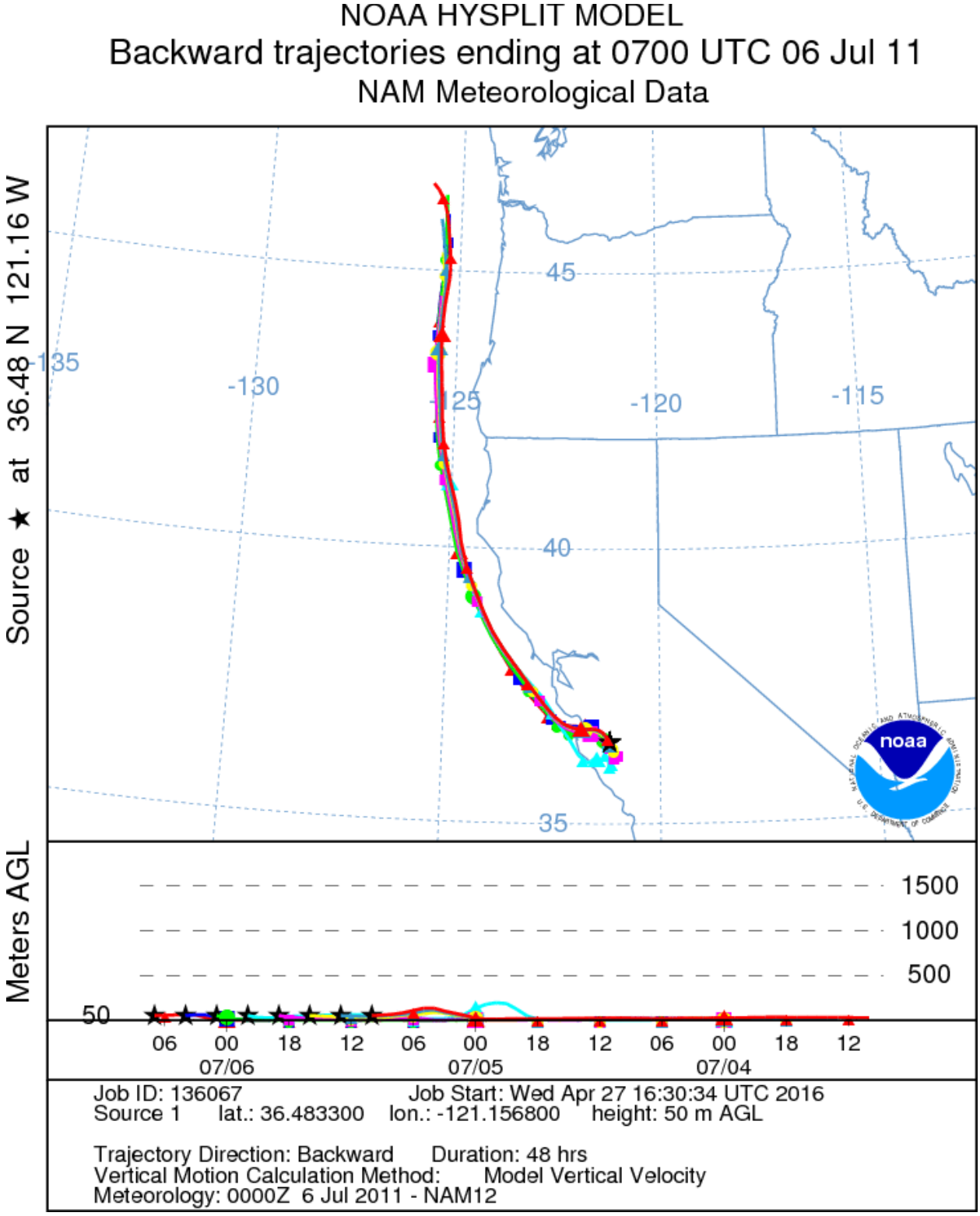
NOAA HYSPLIT MODEL
Backward trajectories ending at 0700 UTC 06 Jul 11
NAM Meteorological Data
Source ★ at 36.48 N 121.16 W
-135
-130
-125
-120
-115
45
40
35
noaa
Meters AGL
1500
1000
500
50
06 00 18 12 06 00 18 12 06 00 18 12
07/06
07/05
07/04
Job ID: 136067 Job Start: Wed Apr 27 16:30:34 UTC 2016
Source 1 lat.: 36.483300 lon.: -121.156800 height: 50 m AGL
Trajectory Direction: Backward Duration: 48 hrs
Vertical Motion Calculation Method: Model Vertical Velocity
Meteorology: 0000Z 6 Jul 2011 - NAM12

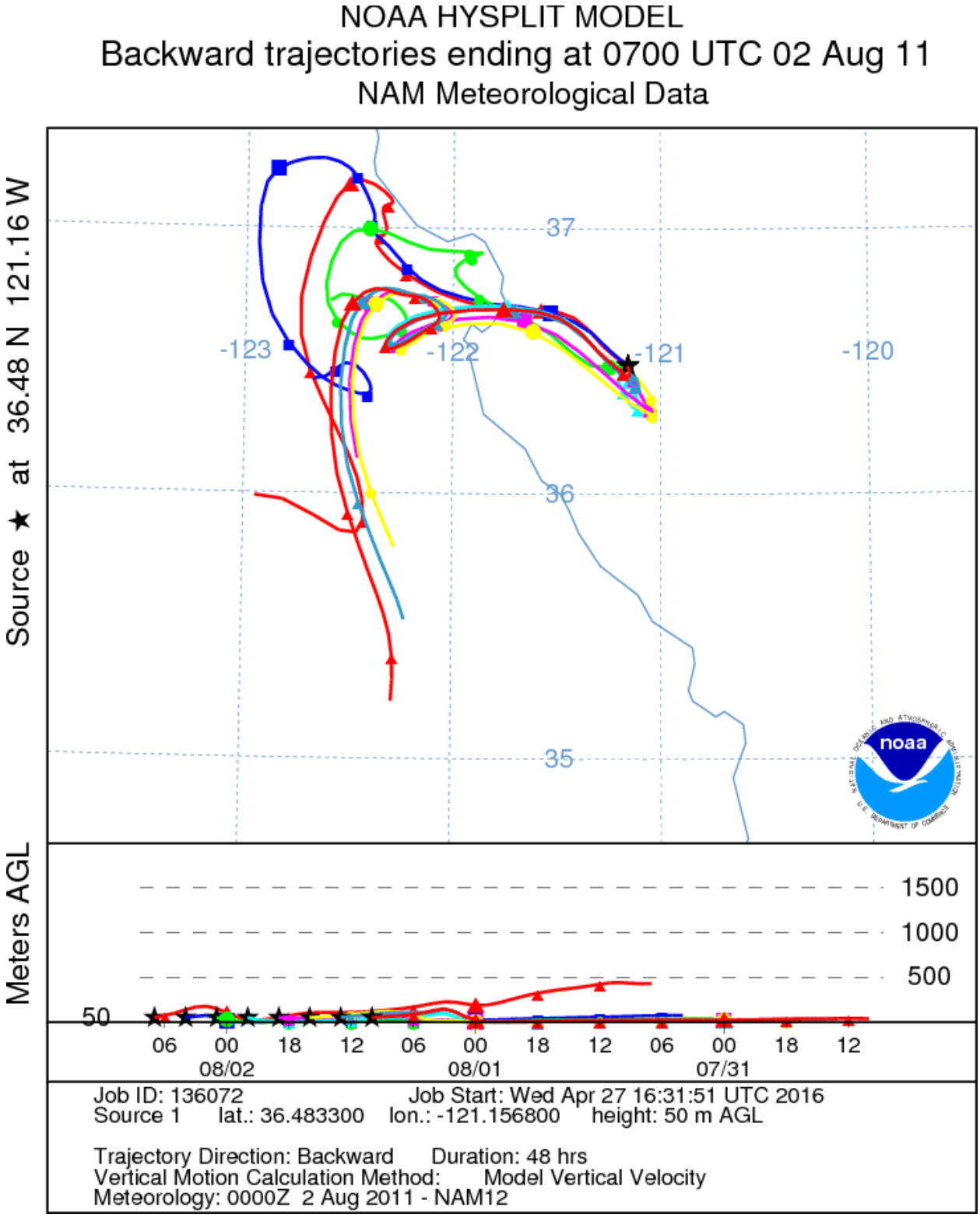
NOAA HYSPLIT MODEL
Backward trajectories ending at 0700 UTC 02 Aug 11
NAM Meteorological Data
Source ★ at 36.48 N 121.16 W
37
36
35
-123
-122
-121
-120
noaa
Meters AGL
1500
1000
500
50
06 00 18 12 06 00 18 12 06 00 18 12
08/02
08/01
07/31
Job ID: 136072 Job Start: Wed Apr 27 16:31:51 UTC 2016
Source 1 lat.: 36.483300 lon.: -121.156800 height: 50 m AGL
Trajectory Direction: Backward Duration: 48 hrs
Vertical Motion Calculation Method: Model Vertical Velocity
Meteorology: 0000Z 2 Aug 2011 - NAM12

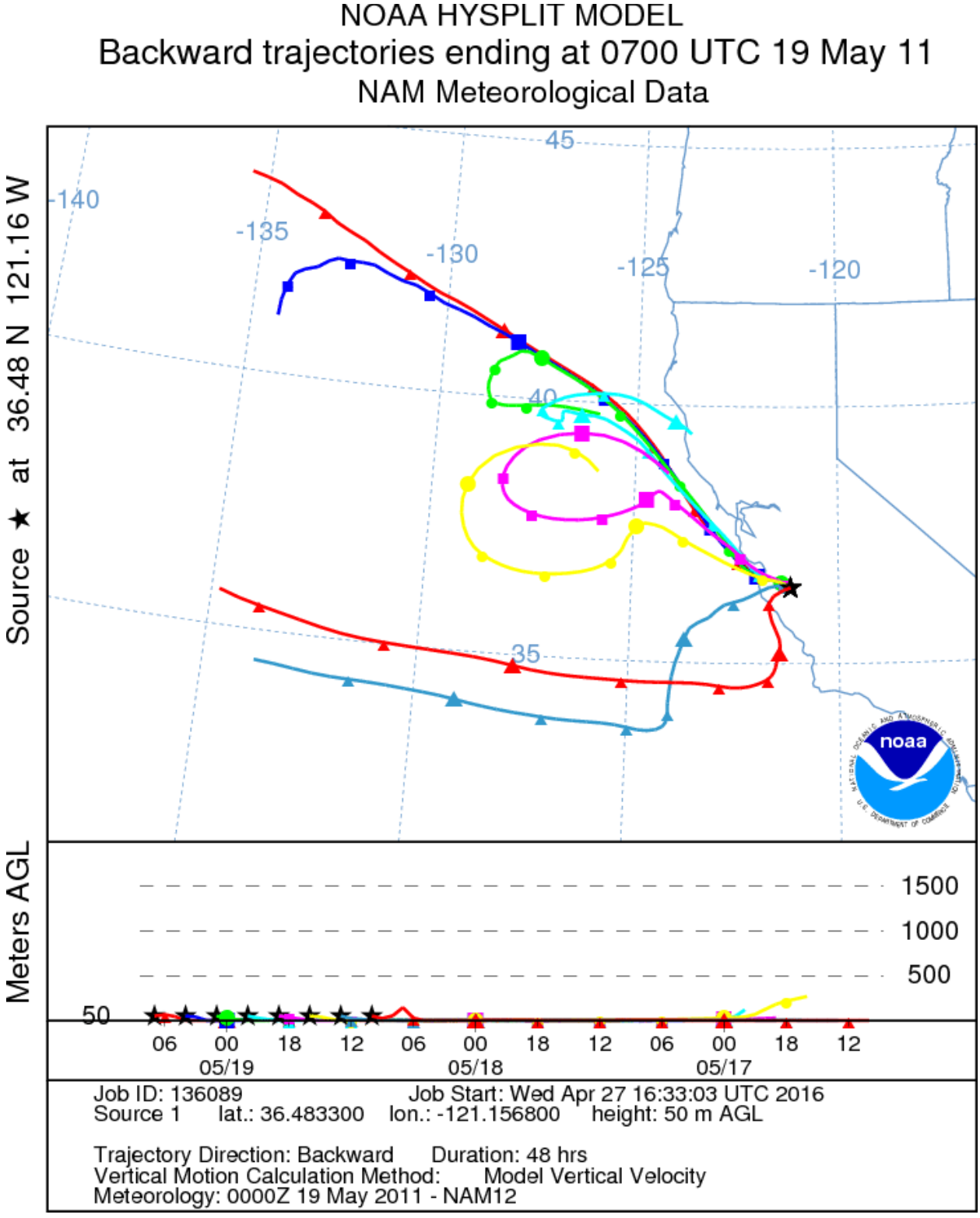
NOAA HYSPLIT MODEL
Backward trajectories ending at 0700 UTC 19 May 11
NAM Meteorological Data
Source ★ at 36.48 N 121.16 W
45
40
35
-140
-135
-130
-125
-120
noaa
Meters AGL
1500
1000
500
50
06 00 18 12 06 00 18 12 06 00 18 12
05/19
05/18
05/17
Job ID: 136089 Job Start: Wed Apr 27 16:33:03 UTC 2016
Source 1 lat.: 36.483300 lon.: -121.156800 height: 50 m AGL
Trajectory Direction: Backward Duration: 48 hrs
Vertical Motion Calculation Method: Model Vertical Velocity
Meteorology: 0000Z 19 May 2011 - NAM12

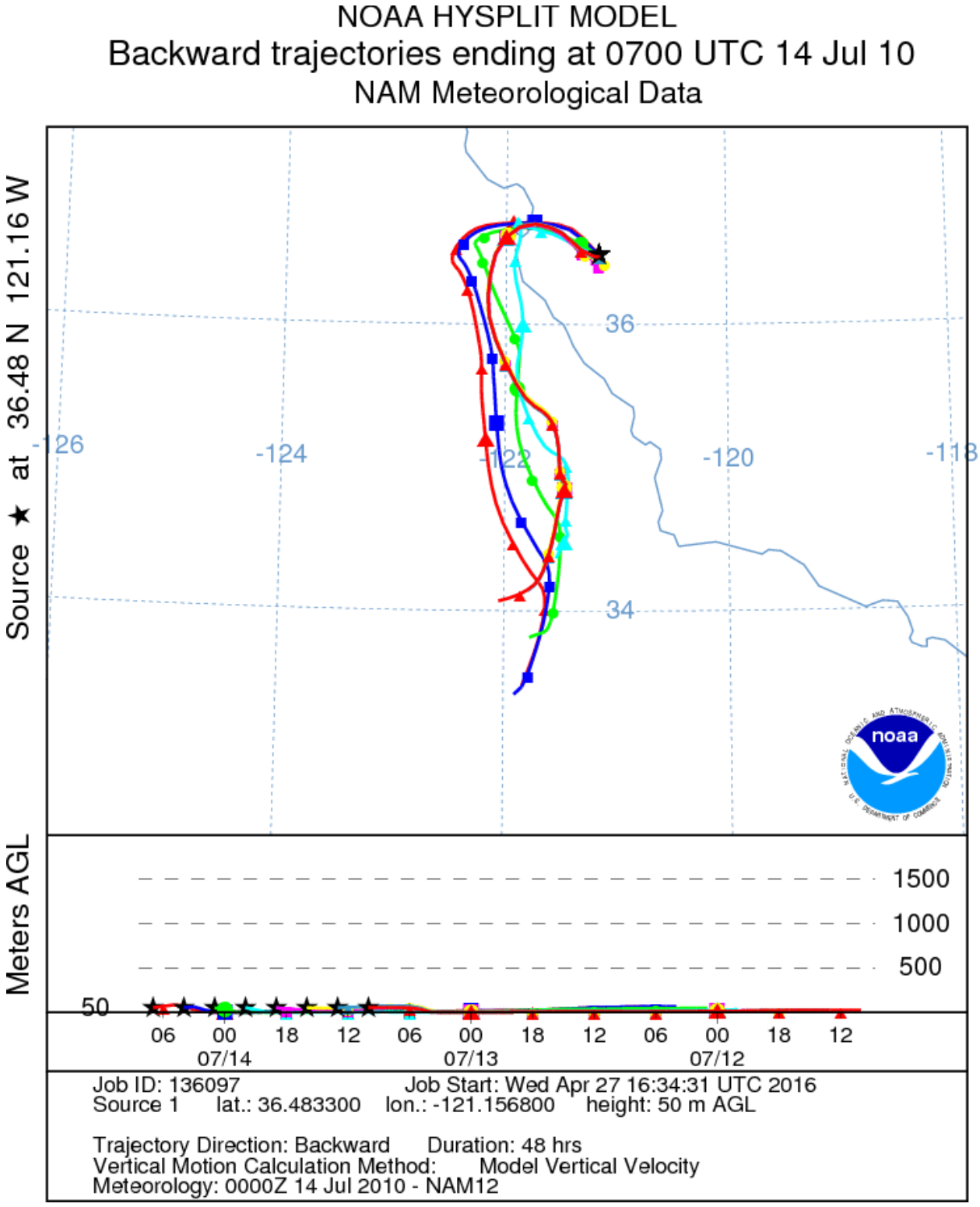
NOAA HYSPLIT MODEL
Backward trajectories ending at 0700 UTC 14 Jul 10
NAM Meteorological Data
Source ★ at 36.48 N 121.16 W
-126
-124
-122
-120
-118
36
34
noaa
Meters AGL
1500
1000
500
50
06 00 18 12 06 00 18 12 06 00 18 12
07/14
07/13
07/12
Job ID: 136097 Job Start: Wed Apr 27 16:34:31 UTC 2016
Source 1 lat.: 36.483300 lon.: -121.156800 height: 50 m AGL
Trajectory Direction: Backward Duration: 48 hrs
Vertical Motion Calculation Method: Model Vertical Velocity
Meteorology: 0000Z 14 Jul 2010 - NAM12

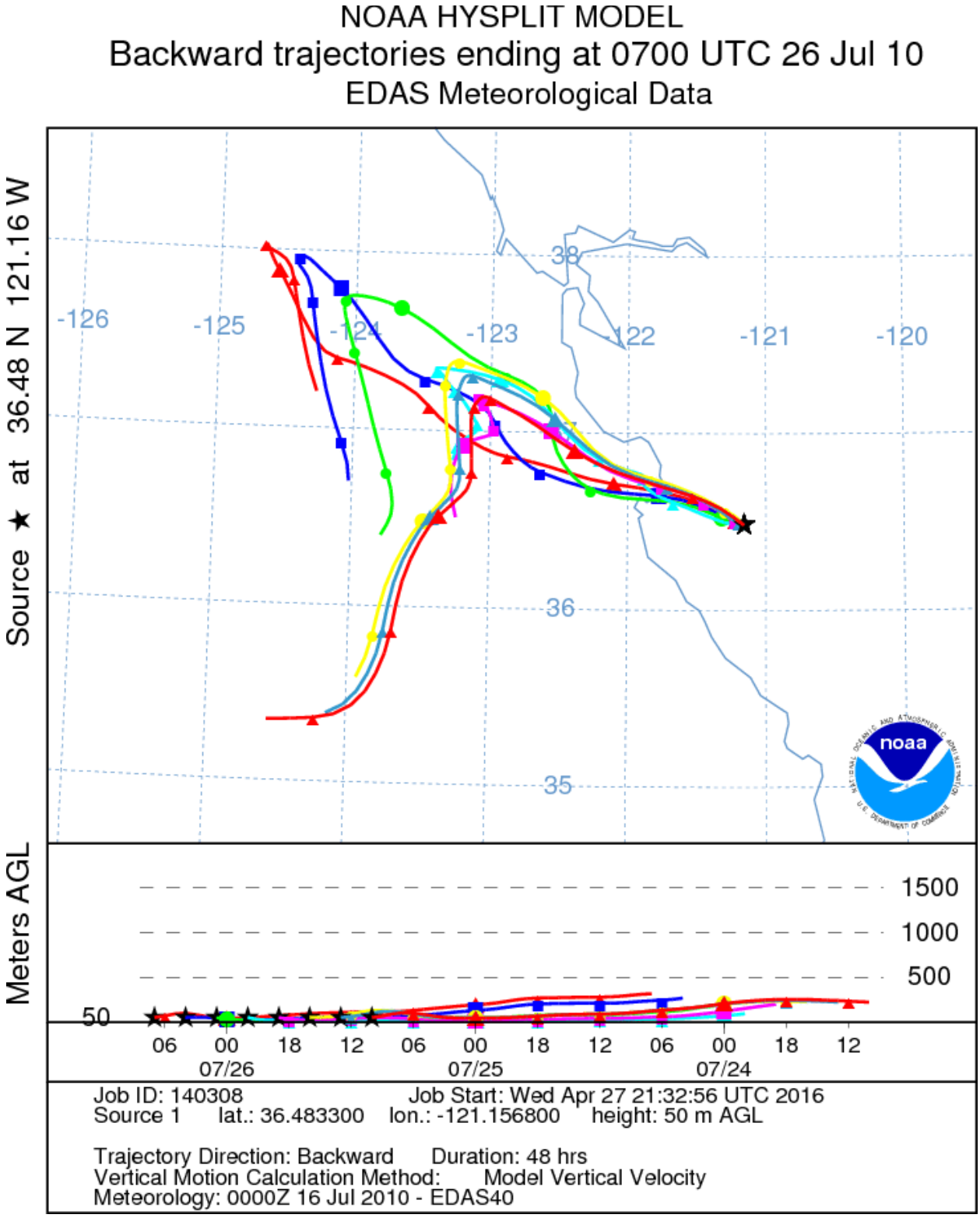
NOAA HYSPLIT MODEL
Backward trajectories ending at 0700 UTC 26 Jul 10
EDAS Meteorological Data
Source ★ at 36.48 N 121.16 W
-126
-125
-124
-123
122
-121
-120
38
36
35
noaa
Meters AGL
1500
1000
500
50
06 00 18 12 06 00 18 12 06 00 18 12
07/26
07/25
07/24
Job ID: 140308 Job Start: Wed Apr 27 21:32:56 UTC 2016
Source 1 lat.: 36.483300 lon.: -121.156800 height: 50 m AGL
Trajectory Direction: Backward Duration: 48 hrs
Vertical Motion Calculation Method: Model Vertical Velocity
Meteorology: 0000Z 16 Jul 2010 - EDAS40

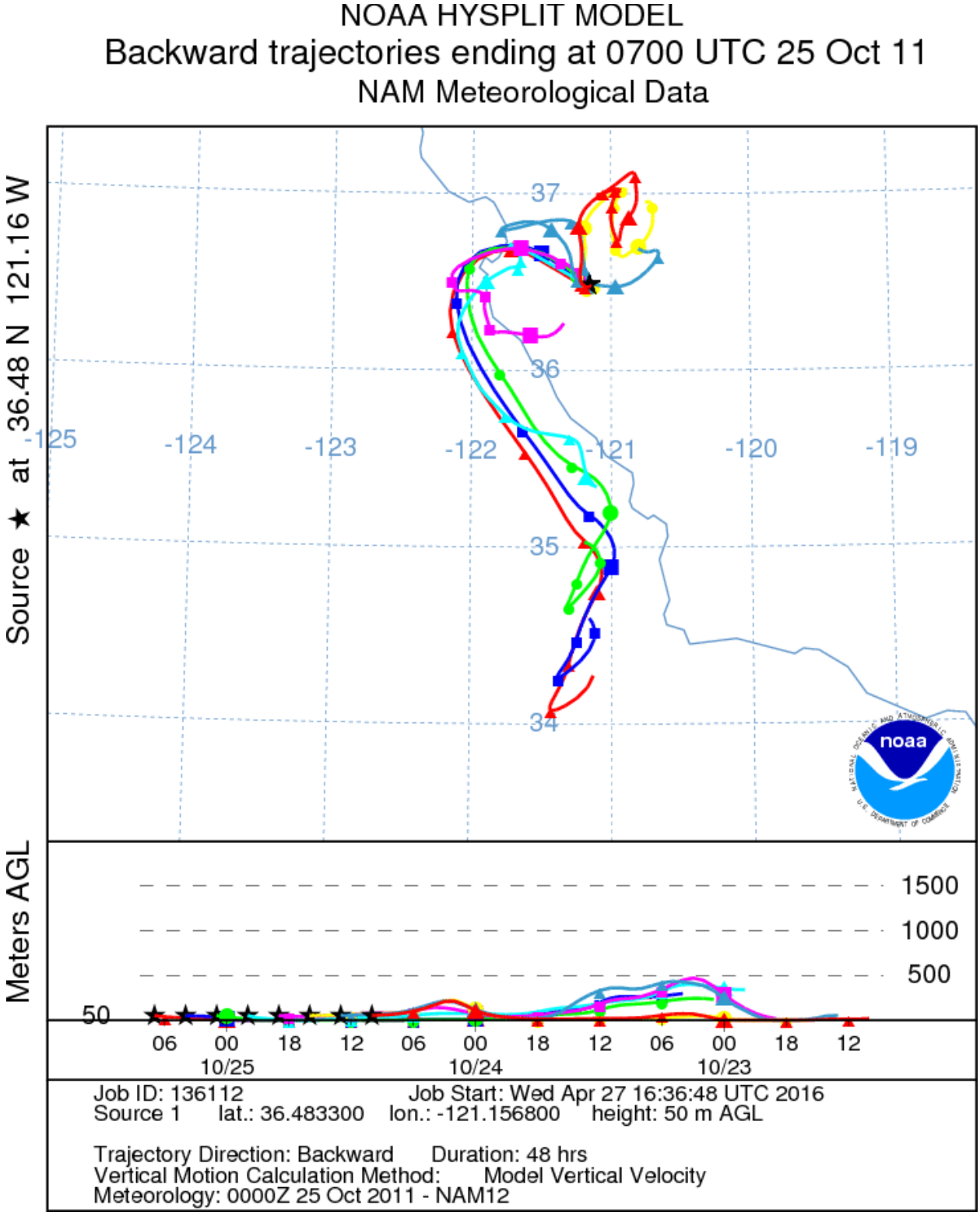
NOAA HYSPLIT MODEL
Backward trajectories ending at 0700 UTC 25 Oct 11
NAM Meteorological Data
Source ★ at 36.48 N 121.16 W
37
36
35
34
-125
-124
-123
-122
-121
-120
-119
noaa
Meters AGL
1500
1000
500
50
06 00 18 12 06 00 18 12 06 00 18 12
10/25
10/24
10/23
Job ID: 136112
Job Start: Wed Apr 27 16:36:48 UTC 2016
Source 1 lat.: 36.483300 lon.: -121.156800 height: 50 m AGL
Trajectory Direction: Backward Duration: 48 hrs
Vertical Motion Calculation Method: Model Vertical Velocity
Meteorology: 0000Z 25 Oct 2011 - NAM12

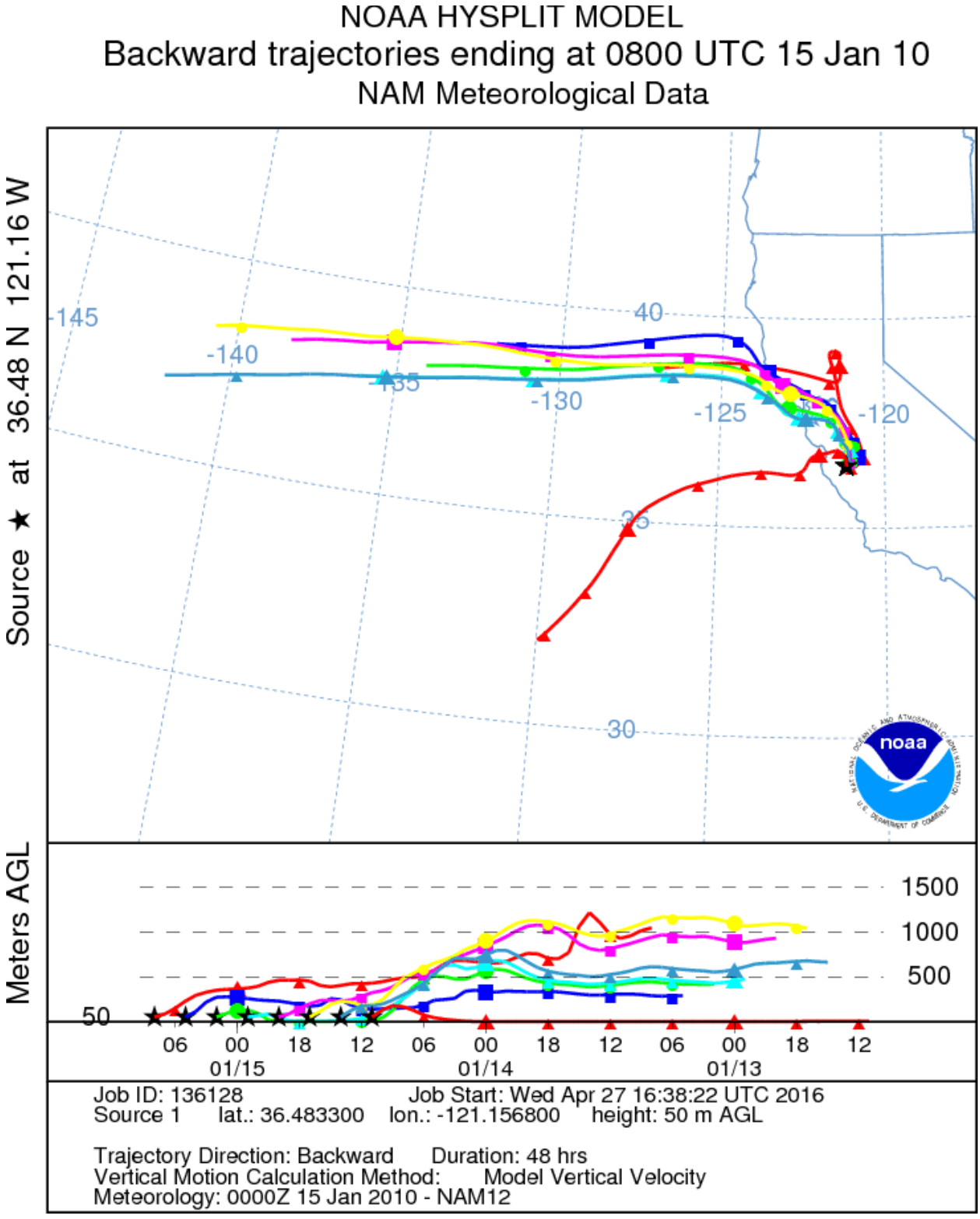
NOAA HYSPLIT MODEL
Backward trajectories ending at 0800 UTC 15 Jan 10
NAM Meteorological Data
Source ★ at 36.48 N 121.16 W
-145
-140
-135
-130
-125
-120
40
35
30
noaa
Meters AGL
1500
1000
500
50
06 00 18 12 06 00 18 12 06 00 18 12
01/15
01/14
01/13
Job ID: 136128
Job Start: Wed Apr 27 16:38:22 UTC 2016
Source 1 lat.: 36.483300 lon.: -121.156800 height: 50 m AGL
Trajectory Direction: Backward Duration: 48 hrs
Vertical Motion Calculation Method: Model Vertical Velocity
Meteorology: 0000Z 15 Jan 2010 - NAM12

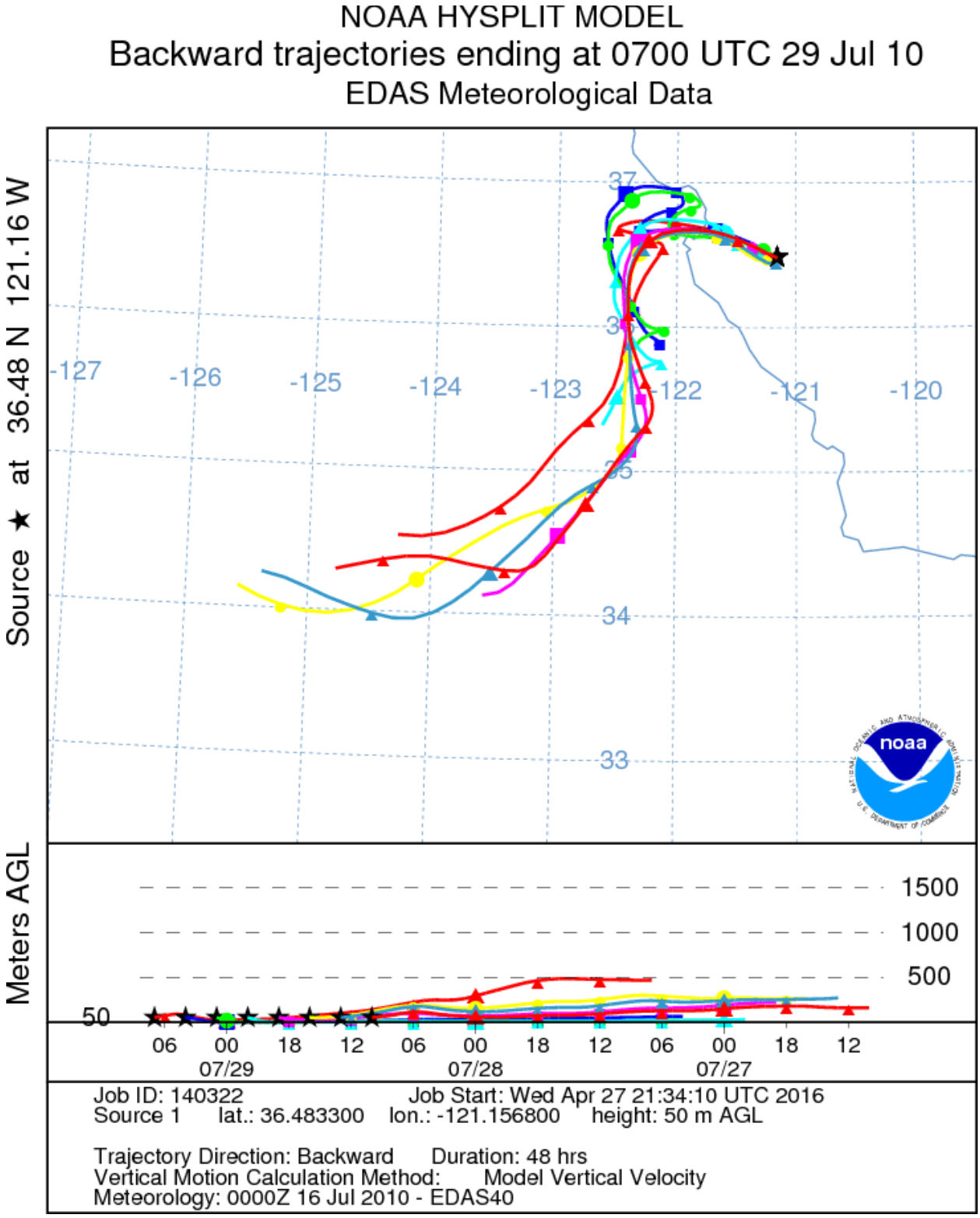
NOAA HYSPLIT MODEL
Backward trajectories ending at 0700 UTC 29 Jul 10
EDAS Meteorological Data
Source ★ at 36.48 N 121.16 W
-127
-126
-125
-124
-123
-122
-121
-120
37
36
35
34
33
noaa
Meters AGL
1500
1000
500
50
06
00
18
12
06
00
18
12
06
00
18
12
07/29
07/28
07/27
Job ID: 140322
Job Start: Wed Apr 27 21:34:10 UTC 2016
Source 1
lat.: 36.483300
lon.: -121.156800
height: 50 m AGL
Trajectory Direction: Backward
Duration: 48 hrs
Vertical Motion Calculation Method:
Model Vertical Velocity
Meteorology: 0000Z 16 Jul 2010 - EDAS40

PORE HYSPLIT back-trajectories

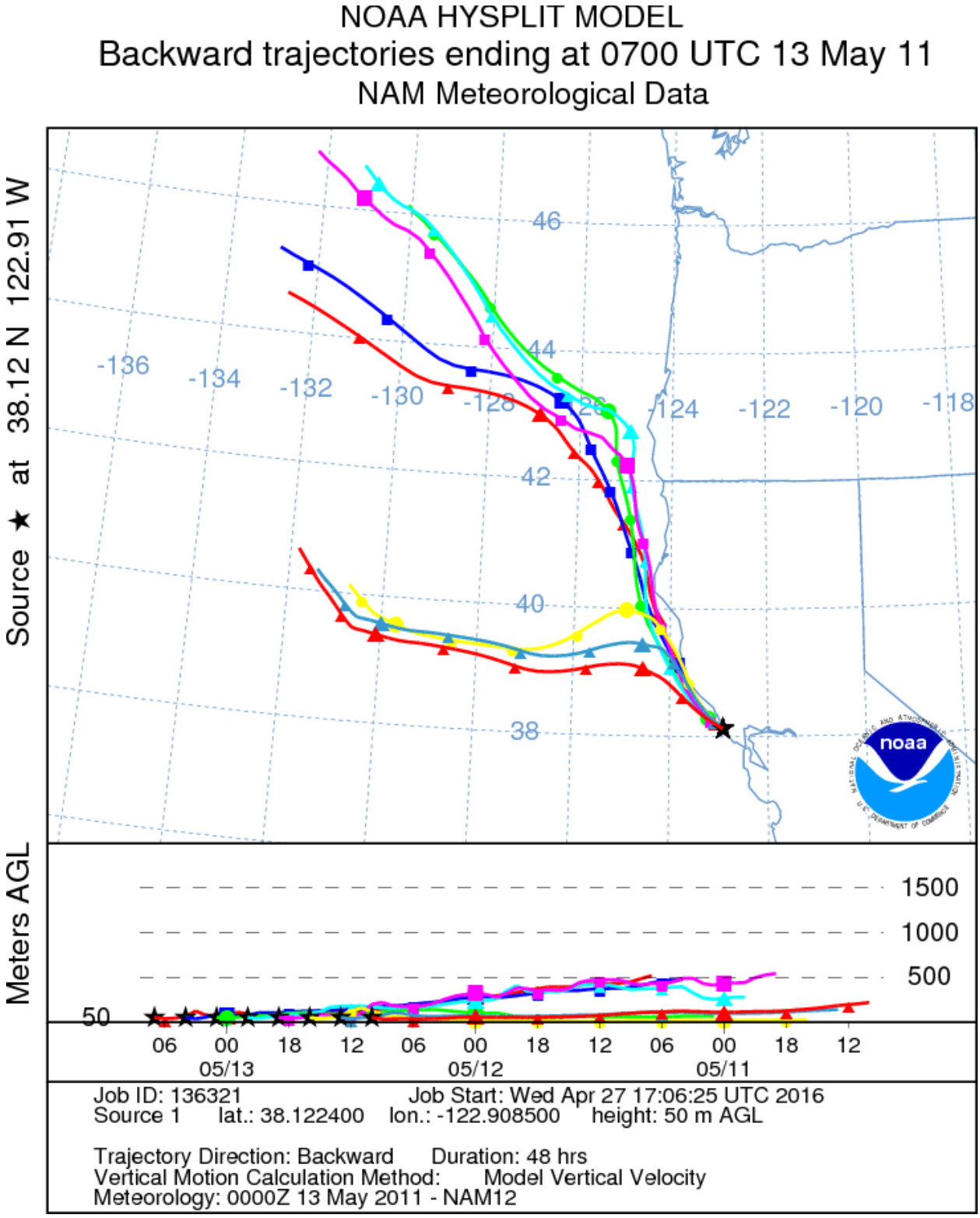
NOAA HYSPLIT MODEL
Backward trajectories ending at 0700 UTC 13 May 11
NAM Meteorological Data
Source ★ at 38.12 N 122.91 W
46
44
42
40
38
-136
-134
-132
-130
-128
-124
-122
-120
-118
noaa
Meters AGL
1500
1000
500
50
06 00 18 12 06 00 18 12 06 00 18 12
05/13
05/12
05/11
Job ID: 136321 Job Start: Wed Apr 27 17:06:25 UTC 2016
Source 1 lat.: 38.122400 lon.: -122.908500 height: 50 m AGL
Trajectory Direction: Backward Duration: 48 hrs
Vertical Motion Calculation Method: Model Vertical Velocity
Meteorology: 0000Z 13 May 2011 - NAM12

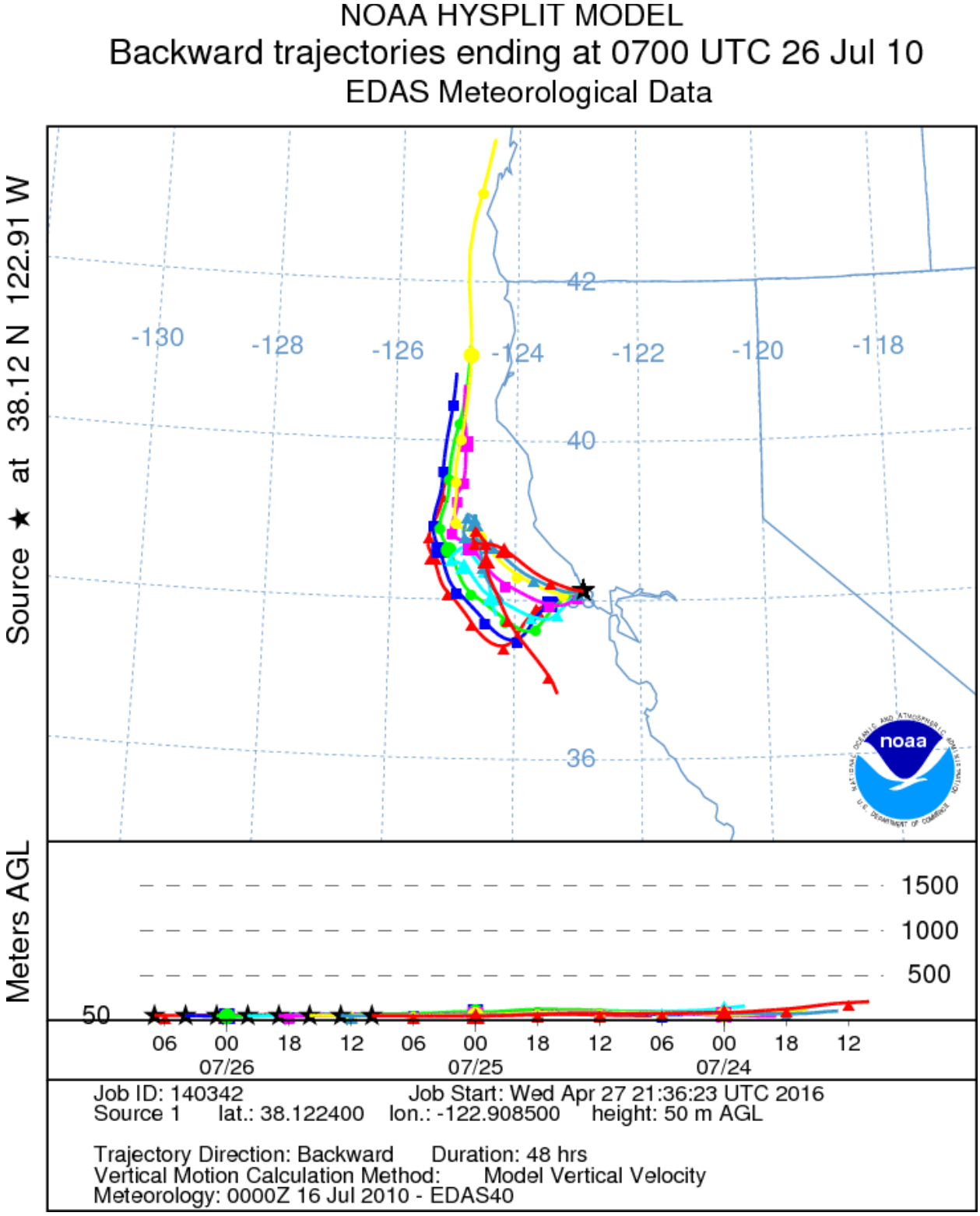
NOAA HYSPLIT MODEL
Backward trajectories ending at 0700 UTC 26 Jul 10
EDAS Meteorological Data
Source ★ at 38.12 N 122.91 W
-130
-128
-126
-124
-122
-120
-118
42
40
36
noaa
Meters AGL
1500
1000
500
50
06 00 18 12 06 00 18 12 06 00 18 12
07/26
07/25
07/24
Job ID: 140342 Job Start: Wed Apr 27 21:36:23 UTC 2016
Source 1 lat.: 38.122400 lon.: -122.908500 height: 50 m AGL
Trajectory Direction: Backward Duration: 48 hrs
Vertical Motion Calculation Method: Model Vertical Velocity
Meteorology: 0000Z 16 Jul 2010 - EDAS40

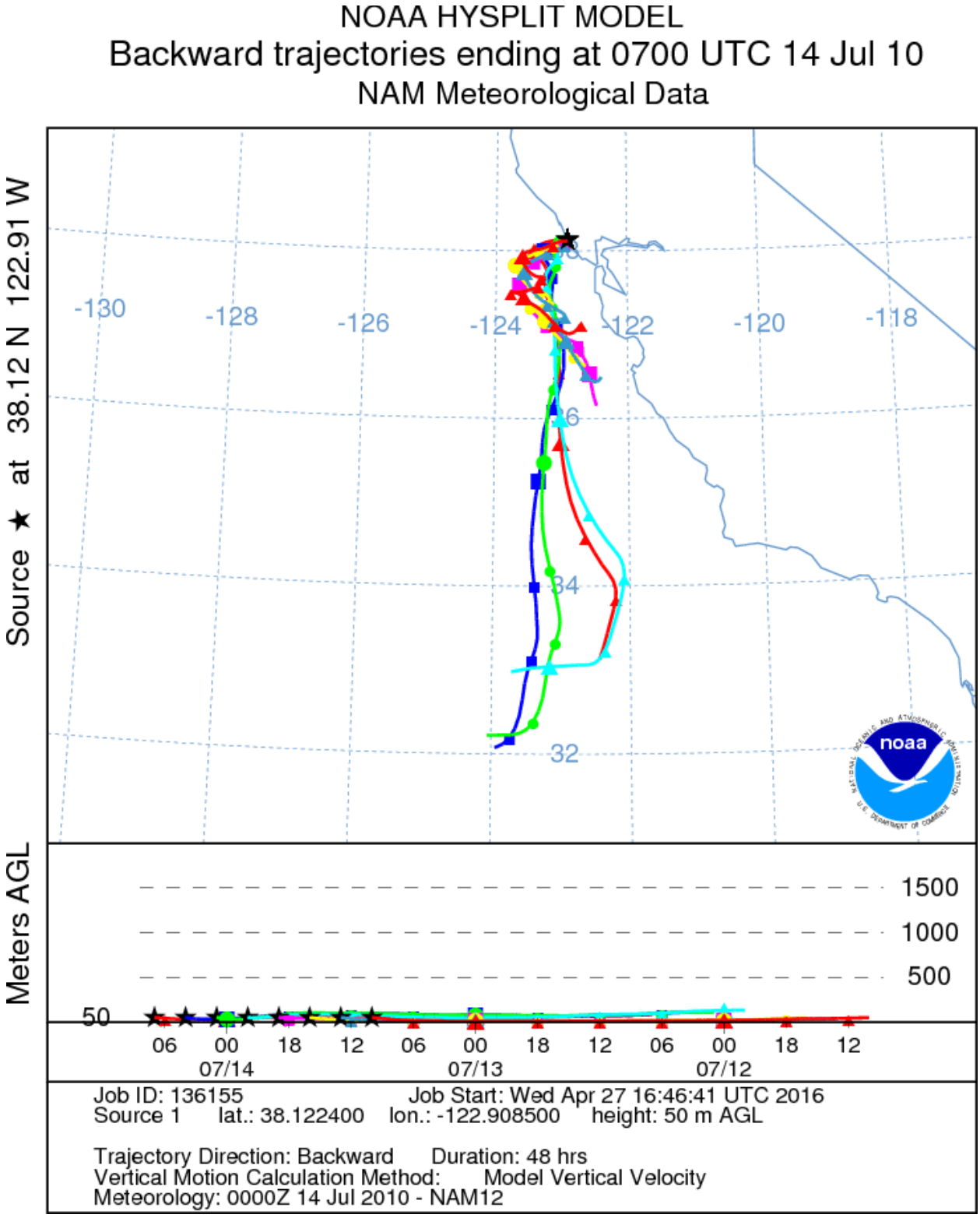
NOAA HYSPLIT MODEL
Backward trajectories ending at 0700 UTC 14 Jul 10
NAM Meteorological Data
Source ★ at 38.12 N 122.91 W
-130
-128
-126
-124
-122
-120
-118
36
34
32
noaa
Meters AGL
1500
1000
500
50
06 00 18 12 06 00 18 12 06 00 18 12
07/14
07/13
07/12
Job ID: 136155 Job Start: Wed Apr 27 16:46:41 UTC 2016
Source 1 lat.: 38.122400 lon.: -122.908500 height: 50 m AGL
Trajectory Direction: Backward Duration: 48 hrs
Vertical Motion Calculation Method: Model Vertical Velocity
Meteorology: 0000Z 14 Jul 2010 - NAM12

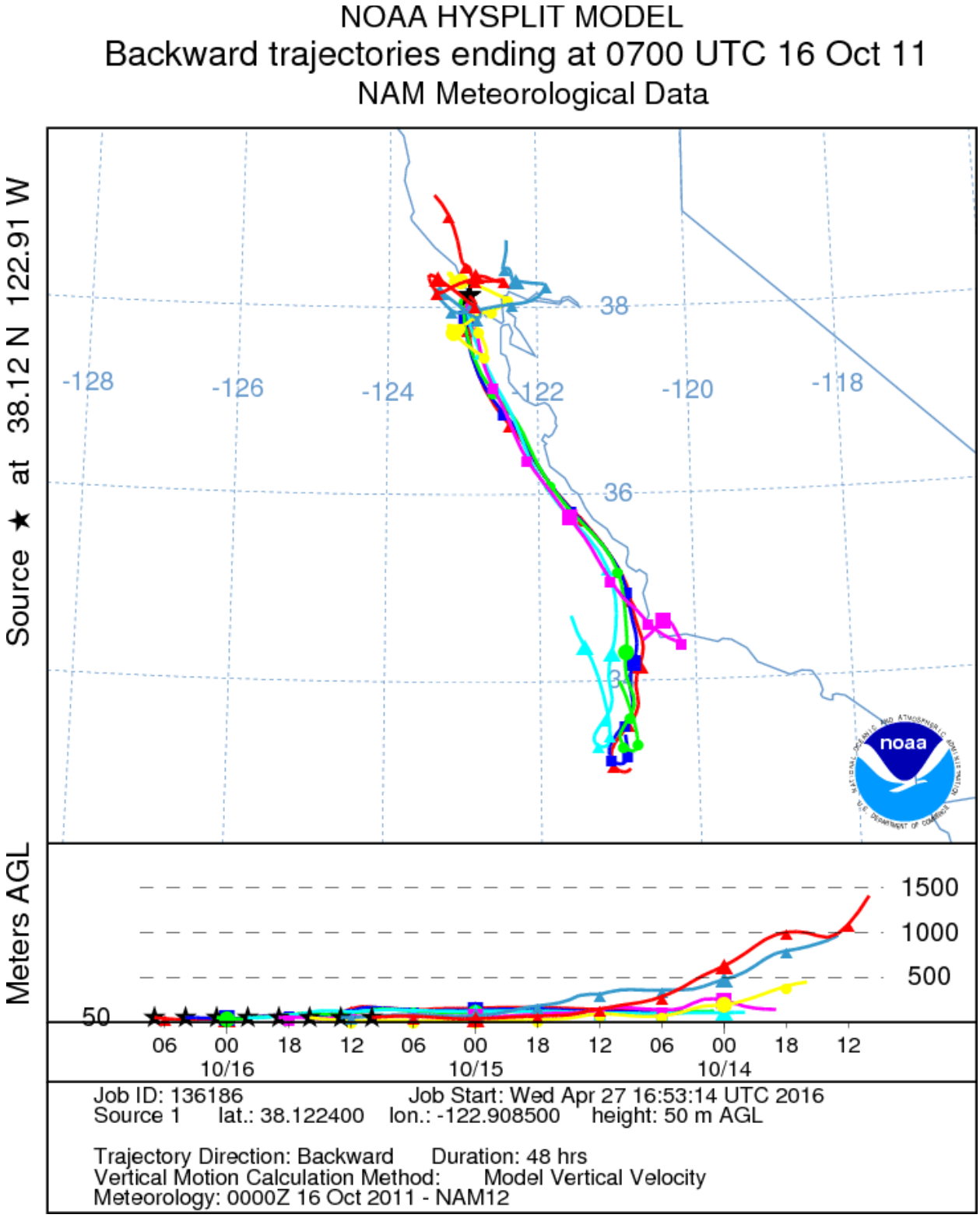
NOAA HYSPLIT MODEL
Backward trajectories ending at 0700 UTC 16 Oct 11
NAM Meteorological Data
Source ★ at 38.12 N 122.91 W
-128
-126
-124
-122
-120
-118
38
36
noaa
Meters AGL
1500
1000
500
50
06 00 18 12 06 00 18 12 06 00 18 12
10/16
10/15
10/14
Job ID: 136186 Job Start: Wed Apr 27 16:53:14 UTC 2016
Source 1 lat.: 38.122400 lon.: -122.908500 height: 50 m AGL
Trajectory Direction: Backward Duration: 48 hrs
Vertical Motion Calculation Method: Model Vertical Velocity
Meteorology: 0000Z 16 Oct 2011 - NAM12

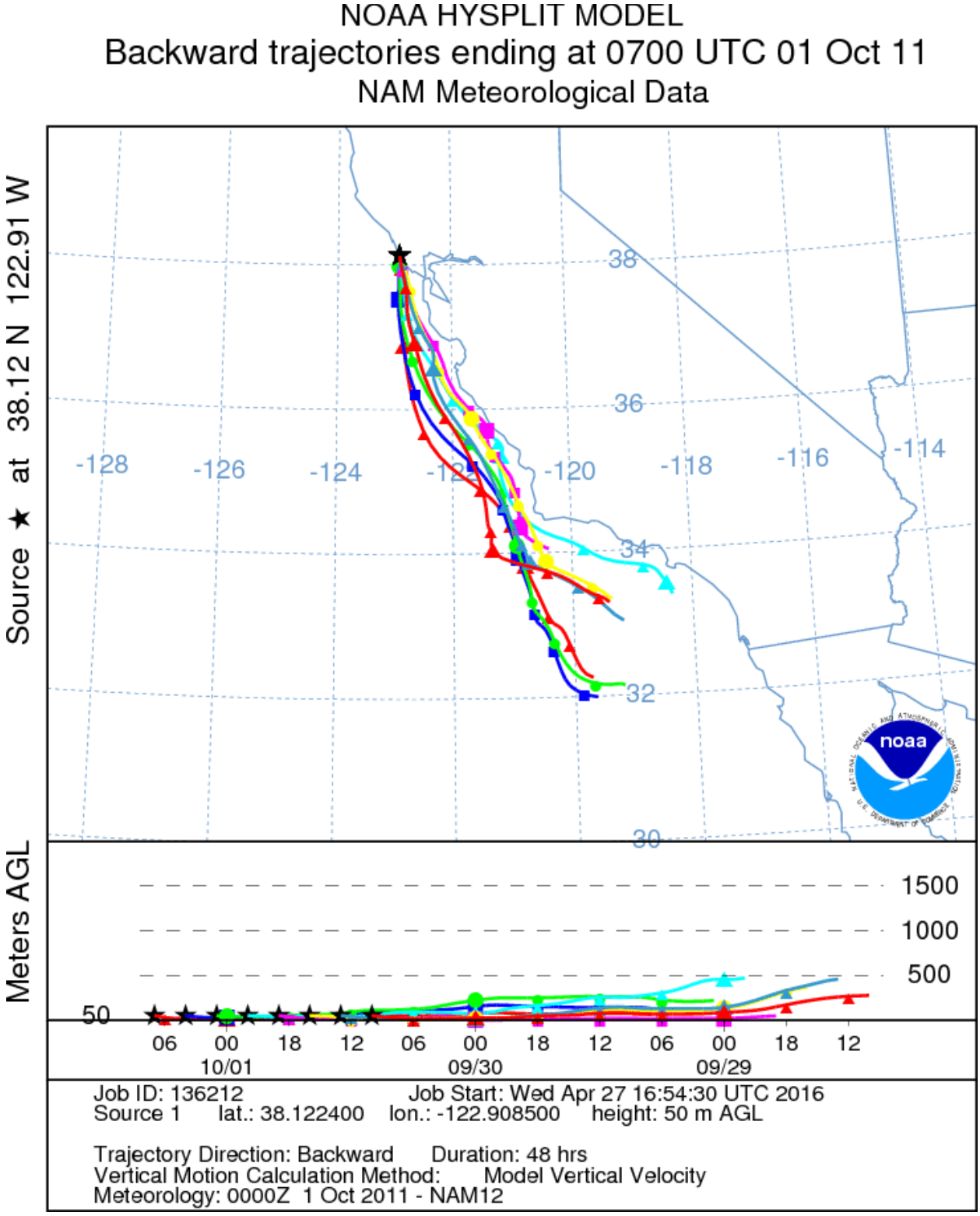
NOAA HYSPLIT MODEL
Backward trajectories ending at 0700 UTC 01 Oct 11
NAM Meteorological Data
Source ★ at 38.12 N 122.91 W
38
36
34
32
30
-128
-126
-124
-120
-118
-116
-114
noaa
Meters AGL
1500
1000
500
50
06 00 18 12 06 00 18 12 06 00 18 12
10/01
09/30
09/29
Job ID: 136212 Job Start: Wed Apr 27 16:54:30 UTC 2016
Source 1 lat.: 38.122400 lon.: -122.908500 height: 50 m AGL
Trajectory Direction: Backward Duration: 48 hrs
Vertical Motion Calculation Method: Model Vertical Velocity
Meteorology: 0000Z 1 Oct 2011 - NAM12

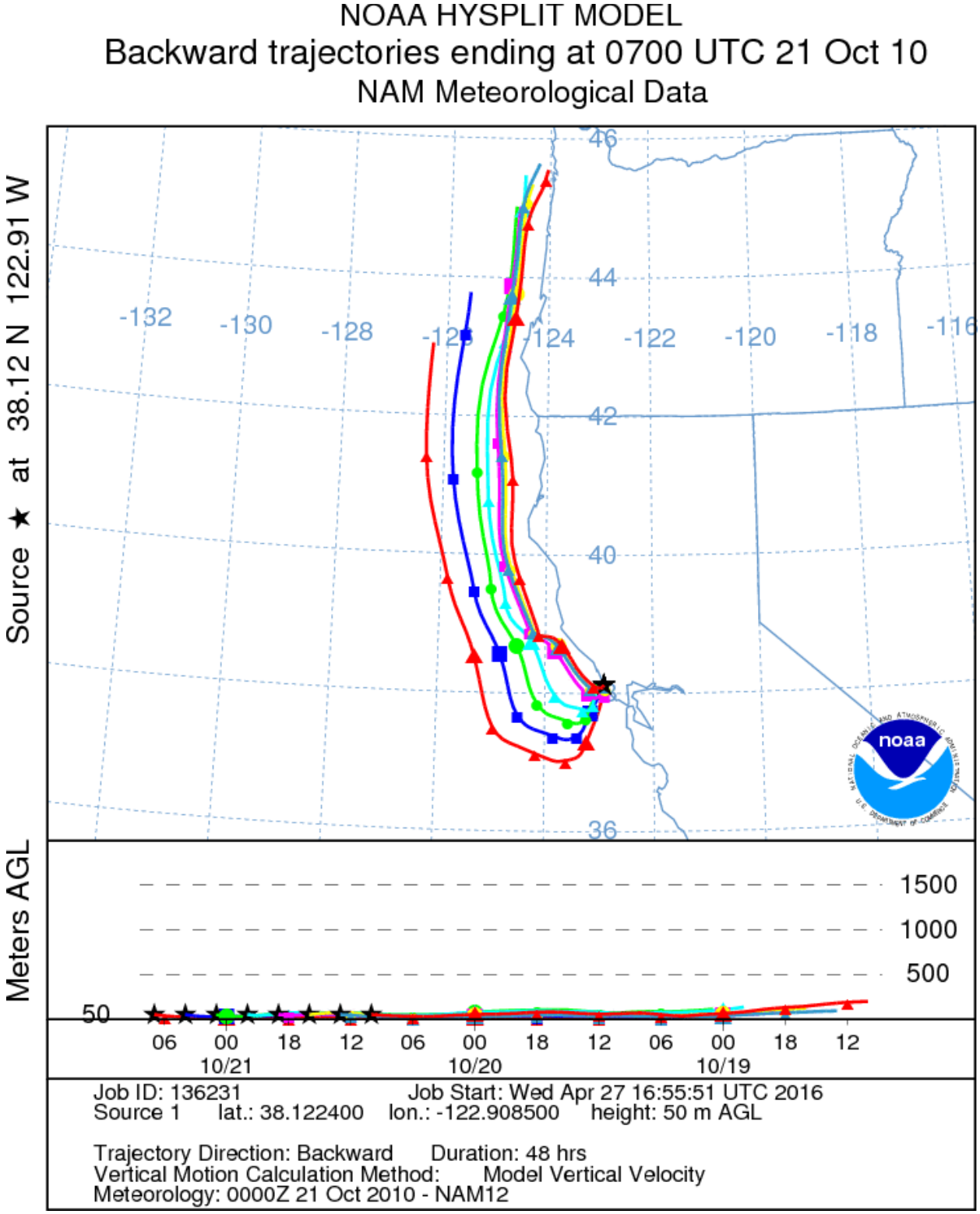
NOAA HYSPLIT MODEL
Backward trajectories ending at 0700 UTC 21 Oct 10
NAM Meteorological Data
Source ★ at 38.12 N 122.91 W
Meters AGL
46
44
42
40
36
-132
-130
-128
-126
-124
-122
-120
-118
-116
1500
1000
500
50
06
00
18
12
06
00
18
12
06
00
18
12
10/21
10/20
10/19
noaa
Job ID: 136231
Job Start: Wed Apr 27 16:55:51 UTC 2016
Source 1
lat.: 38.122400
lon.: -122.908500
height: 50 m AGL
Trajectory Direction: Backward
Duration: 48 hrs
Vertical Motion Calculation Method:
Model Vertical Velocity
Meteorology: 0000Z 21 Oct 2010 - NAM12

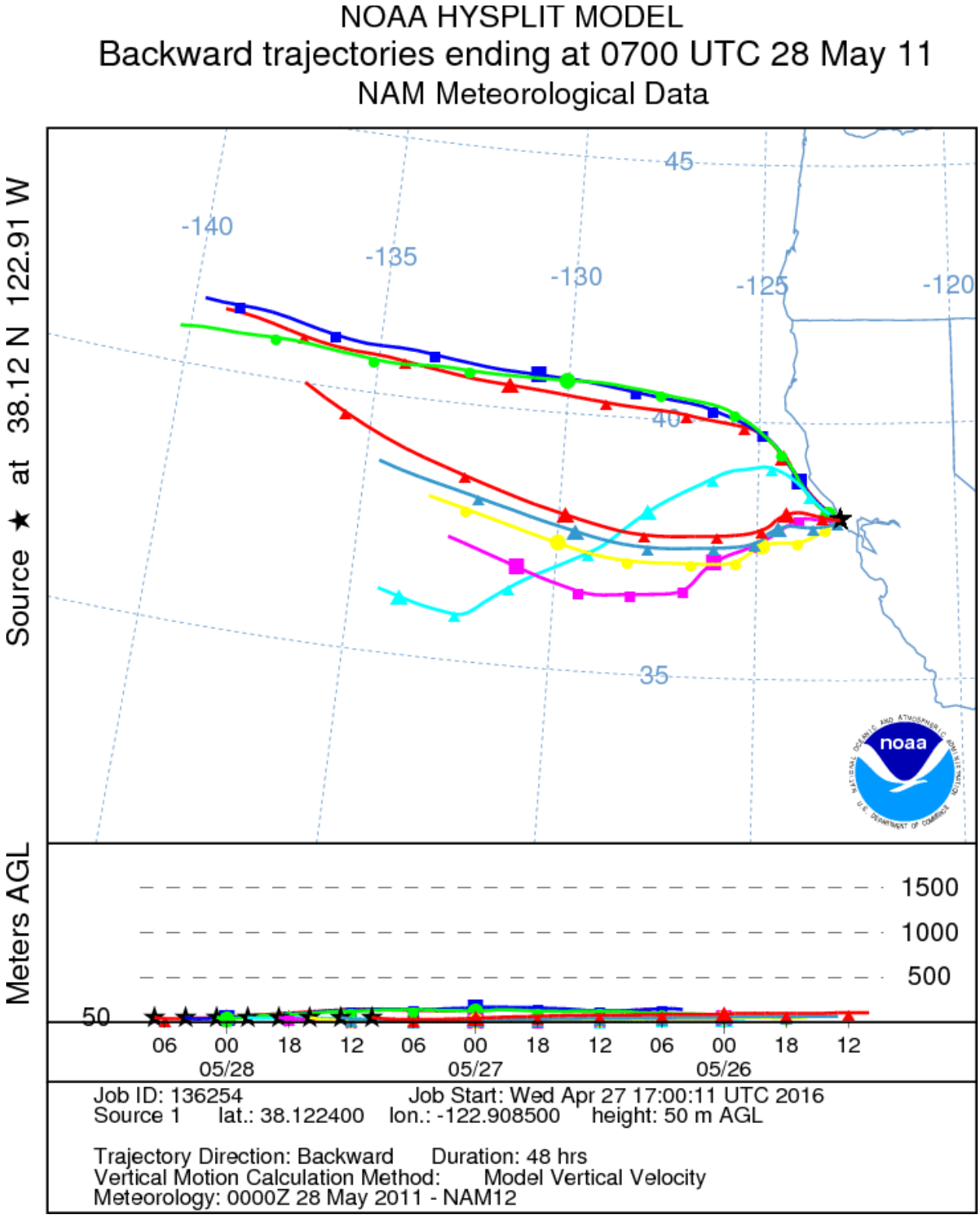
NOAA HYSPLIT MODEL
Backward trajectories ending at 0700 UTC 28 May 11
NAM Meteorological Data
Source ★ at 38.12 N 122.91 W
45
40
35
-140
-135
-130
-125
-120
noaa
Meters AGL
1500
1000
500
50
06 00 18 12 06 00 18 12 06 00 18 12
05/28
05/27
05/26
Job ID: 136254
Job Start: Wed Apr 27 17:00:11 UTC 2016
Source 1 lat.: 38.122400 lon.: -122.908500 height: 50 m AGL
Trajectory Direction: Backward Duration: 48 hrs
Vertical Motion Calculation Method: Model Vertical Velocity
Meteorology: 0000Z 28 May 2011 - NAM12

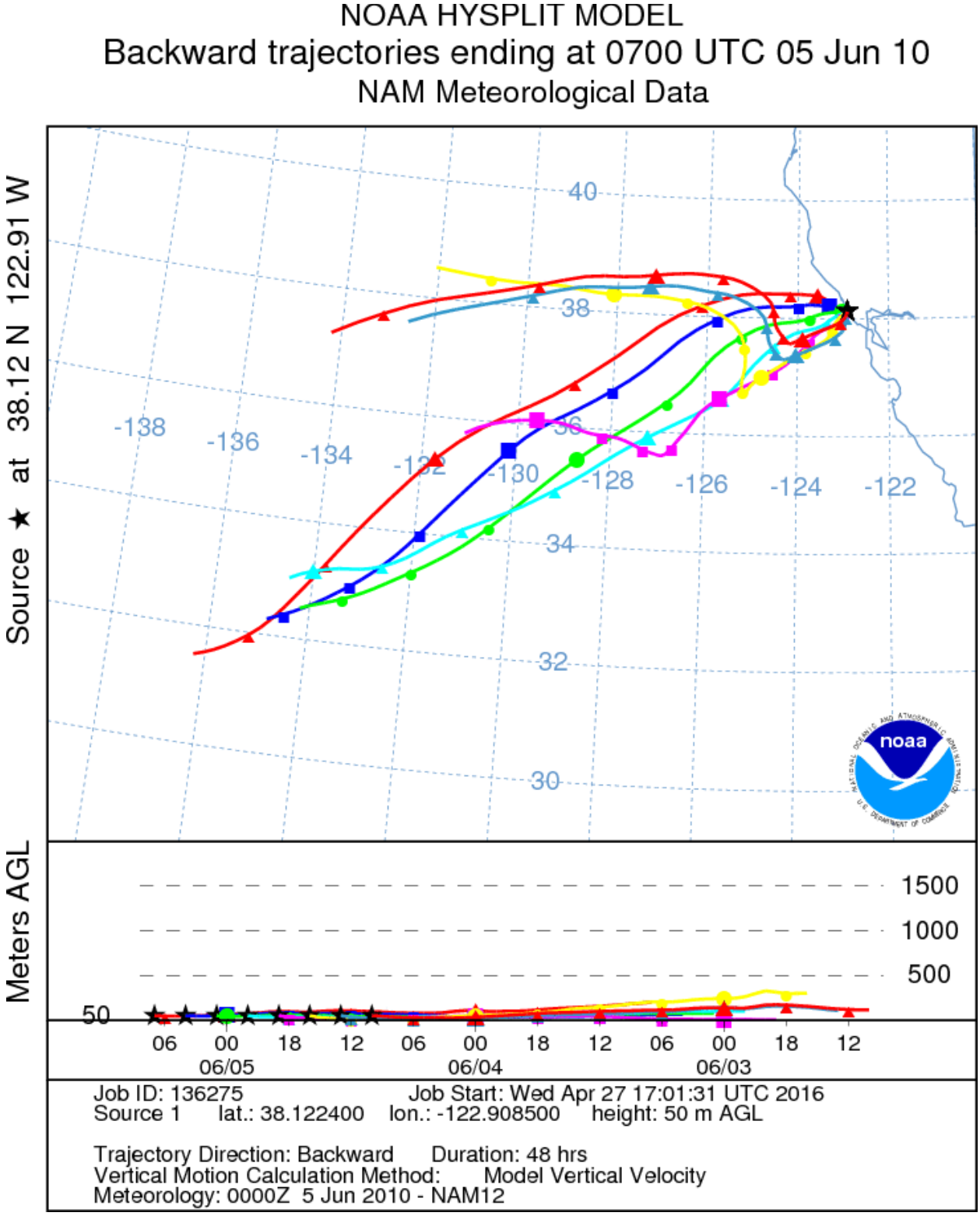
NOAA HYSPLIT MODEL
Backward trajectories ending at 0700 UTC 05 Jun 10
NAM Meteorological Data
Source ★ at 38.12 N 122.91 W
40
38
36
34
32
30
-138
-136
-134
-132
-130
-128
-126
-124
-122
noaa
Meters AGL
1500
1000
500
50
06
00
18
12
06
00
18
12
06
00
18
12
06/05
06/04
06/03
Job ID: 136275
Job Start: Wed Apr 27 17:01:31 UTC 2016
Source 1 lat.: 38.122400 lon.: -122.908500 height: 50 m AGL
Trajectory Direction: Backward Duration: 48 hrs
Vertical Motion Calculation Method: Model Vertical Velocity
Meteorology: 0000Z 5 Jun 2010 - NAM12

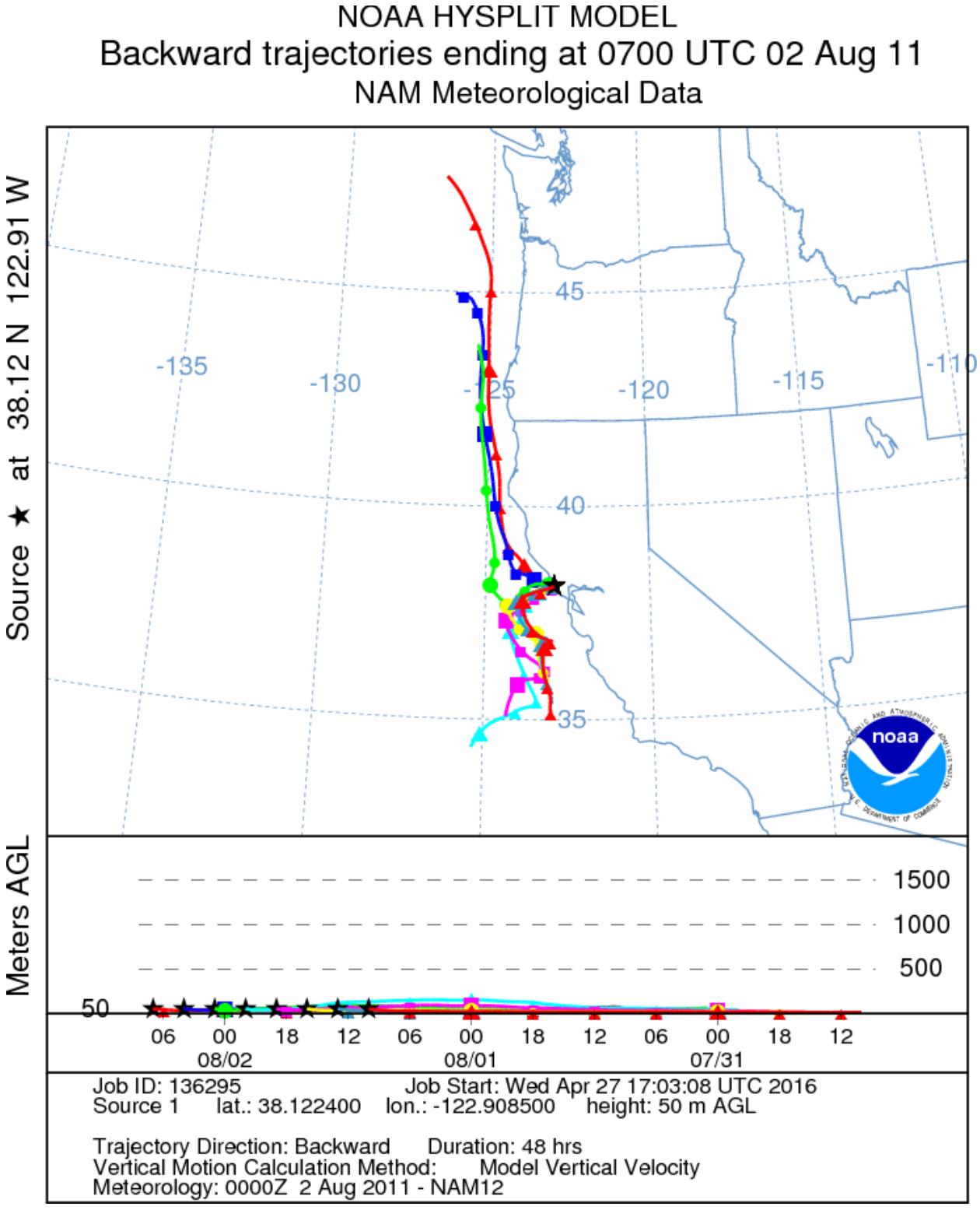
NOAA HYSPLIT MODEL
Backward trajectories ending at 0700 UTC 02 Aug 11
NAM Meteorological Data
Source ★ at 38.12 N 122.91 W
-135
-130
-125
-120
-115
-110
45
40
35
noaa
Meters AGL
1500
1000
500
50
06 00 18 12 06 00 18 12 06 00 18 12
08/02 08/01 07/31
Job ID: 136295 Job Start: Wed Apr 27 17:03:08 UTC 2016
Source 1 lat.: 38.122400 lon.: -122.908500 height: 50 m AGL
Trajectory Direction: Backward Duration: 48 hrs
Vertical Motion Calculation Method: Model Vertical Velocity
Meteorology: 0000Z 2 Aug 2011 - NAM12

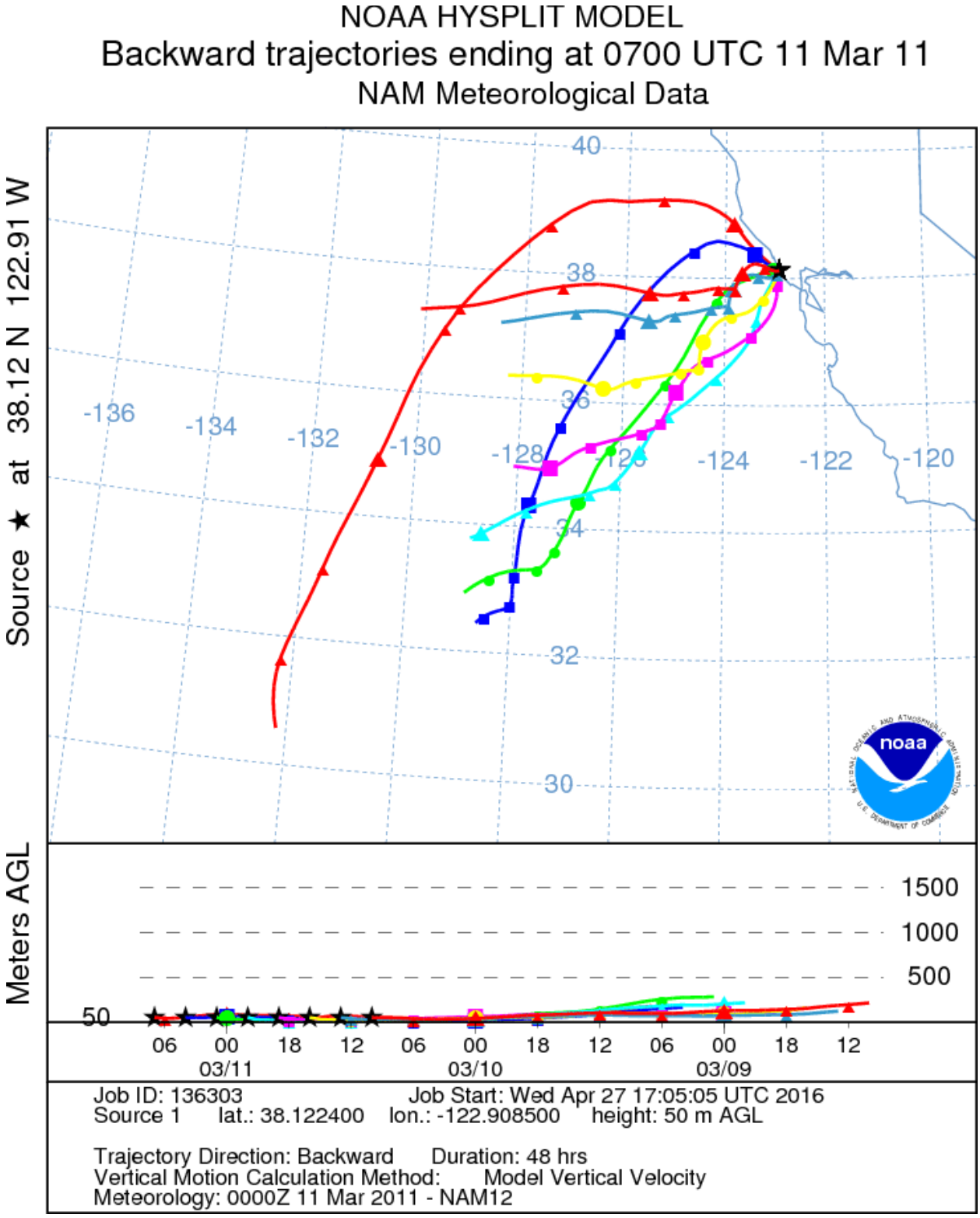
NOAA HYSPLIT MODEL
Backward trajectories ending at 0700 UTC 11 Mar 11
NAM Meteorological Data
Source ★ at 38.12 N 122.91 W
40
38
36
34
32
30
-136
-134
-132
-130
-128
-126
-124
-122
-120
noaa
Meters AGL
1500
1000
500
50
06
00
18
12
06
00
18
12
06
00
18
12
03/11
03/10
03/09
Job ID: 136303
Job Start: Wed Apr 27 17:05:05 UTC 2016
Source 1
lat.: 38.122400
lon.: -122.908500
height: 50 m AGL
Trajectory Direction: Backward
Duration: 48 hrs
Vertical Motion Calculation Method:
Model Vertical Velocity
Meteorology: 0000Z 11 Mar 2011 - NAM12

PUSO HYSPLIT back-trajectories

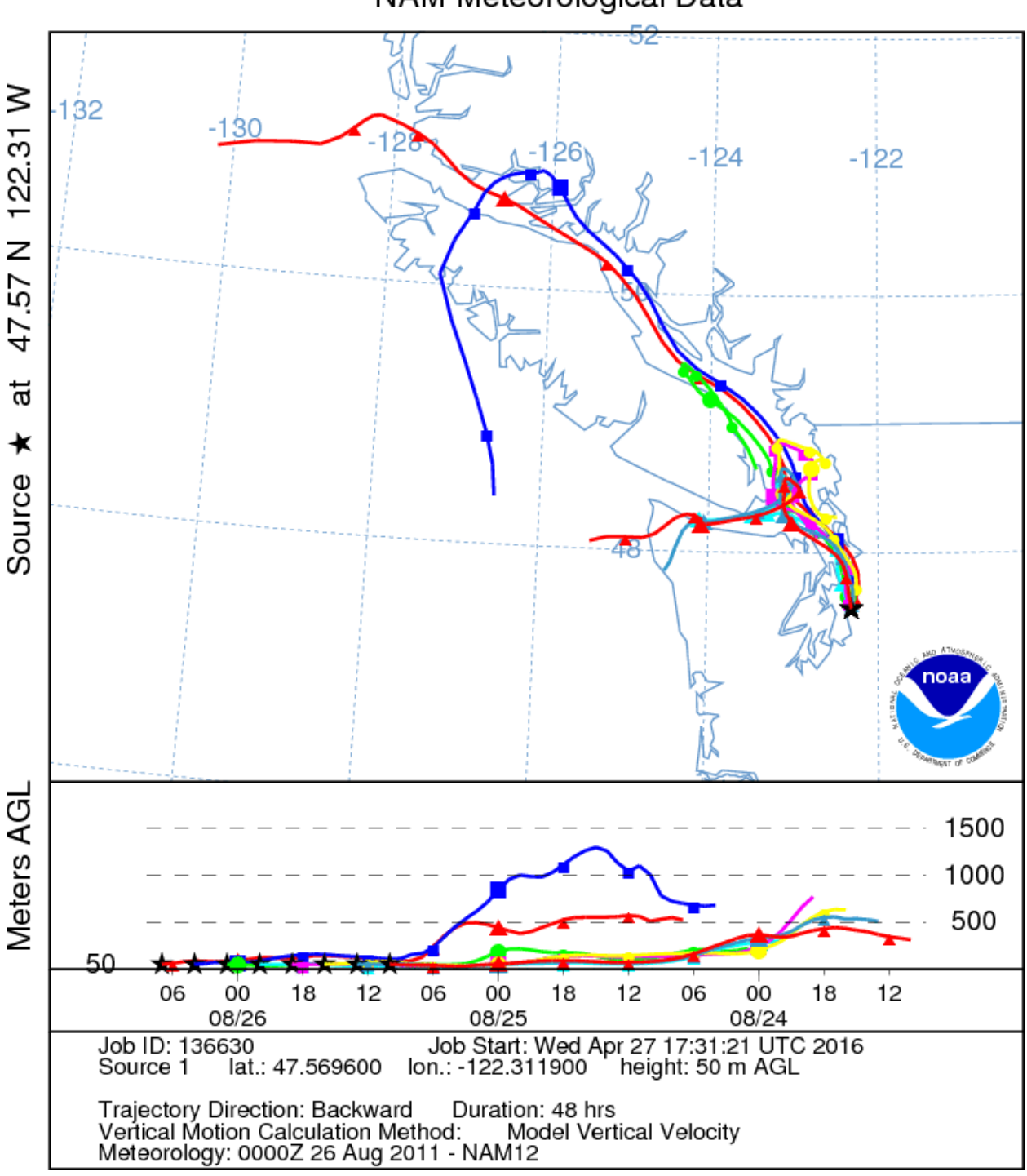
NOAA HYSPLIT MODEL
Backward trajectories ending at 0700 UTC 26 Aug 11
NAM Meteorological Data
Source ★ at 47.57 N 122.31 W
-132
-130
-128
-126
-124
-122
52
50
48
noaa
Meters AGL
1500
1000
500
50
06 00 18 12 06 00 18 12 06 00 18 12
08/26
08/25
08/24
Job ID: 136630
Job Start: Wed Apr 27 17:31:21 UTC 2016
Source 1 lat.: 47.569600 lon.: -122.311900 height: 50 m AGL
Trajectory Direction: Backward Duration: 48 hrs
Vertical Motion Calculation Method: Model Vertical Velocity
Meteorology: 0000Z 26 Aug 2011 - NAM12

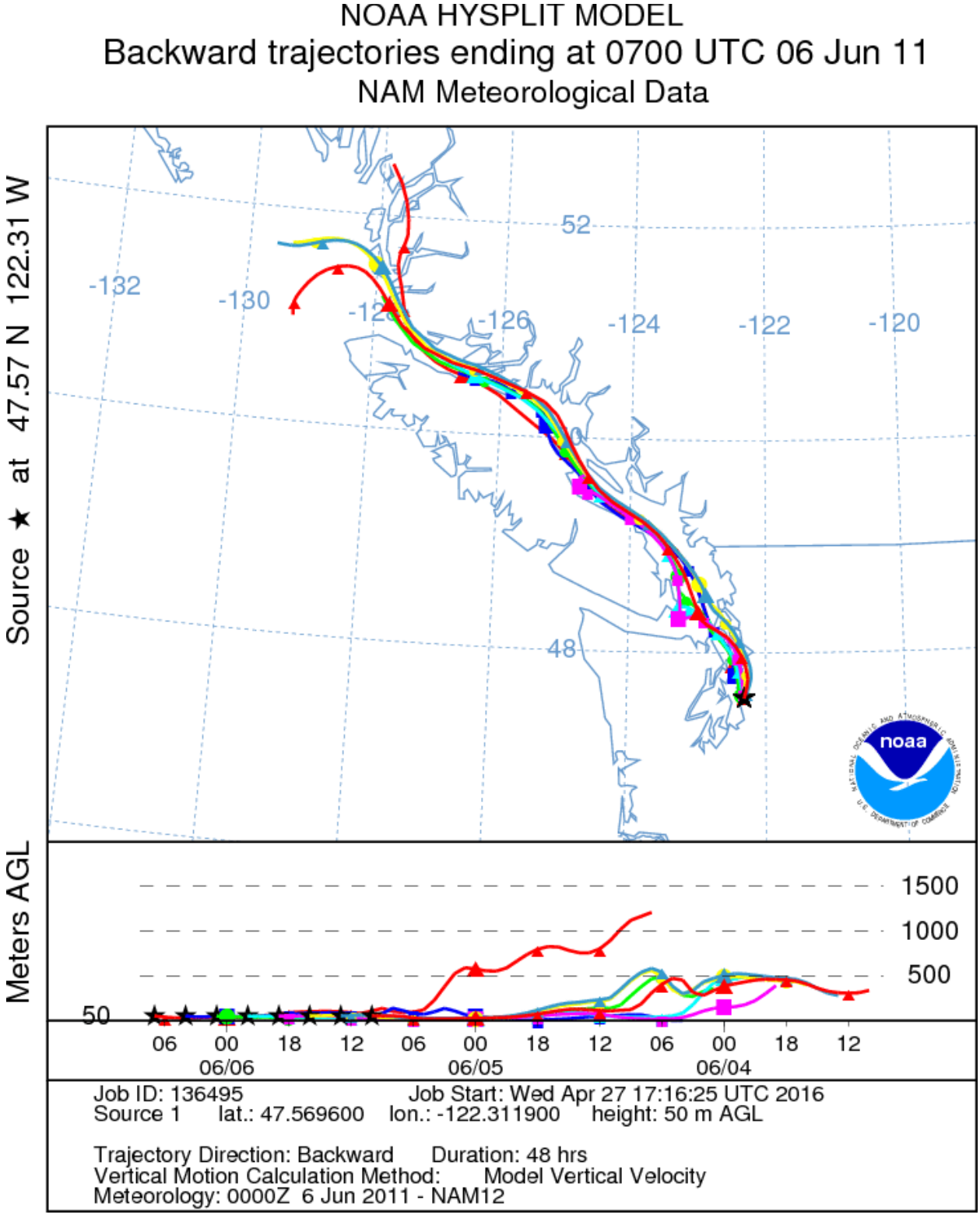
NOAA HYSPLIT MODEL
Backward trajectories ending at 0700 UTC 06 Jun 11
NAM Meteorological Data
Source ★ at 47.57 N 122.31 W
-132
-130
-128
-126
-124
-122
-120
52
48
noaa
Meters AGL
1500
1000
500
50
06 00 18 12 06 00 18 12 06 00 18 12
06/06
06/05
06/04
Job ID: 136495 Job Start: Wed Apr 27 17:16:25 UTC 2016
Source 1 lat.: 47.569600 lon.: -122.311900 height: 50 m AGL
Trajectory Direction: Backward Duration: 48 hrs
Vertical Motion Calculation Method: Model Vertical Velocity
Meteorology: 0000Z 6 Jun 2011 - NAM12

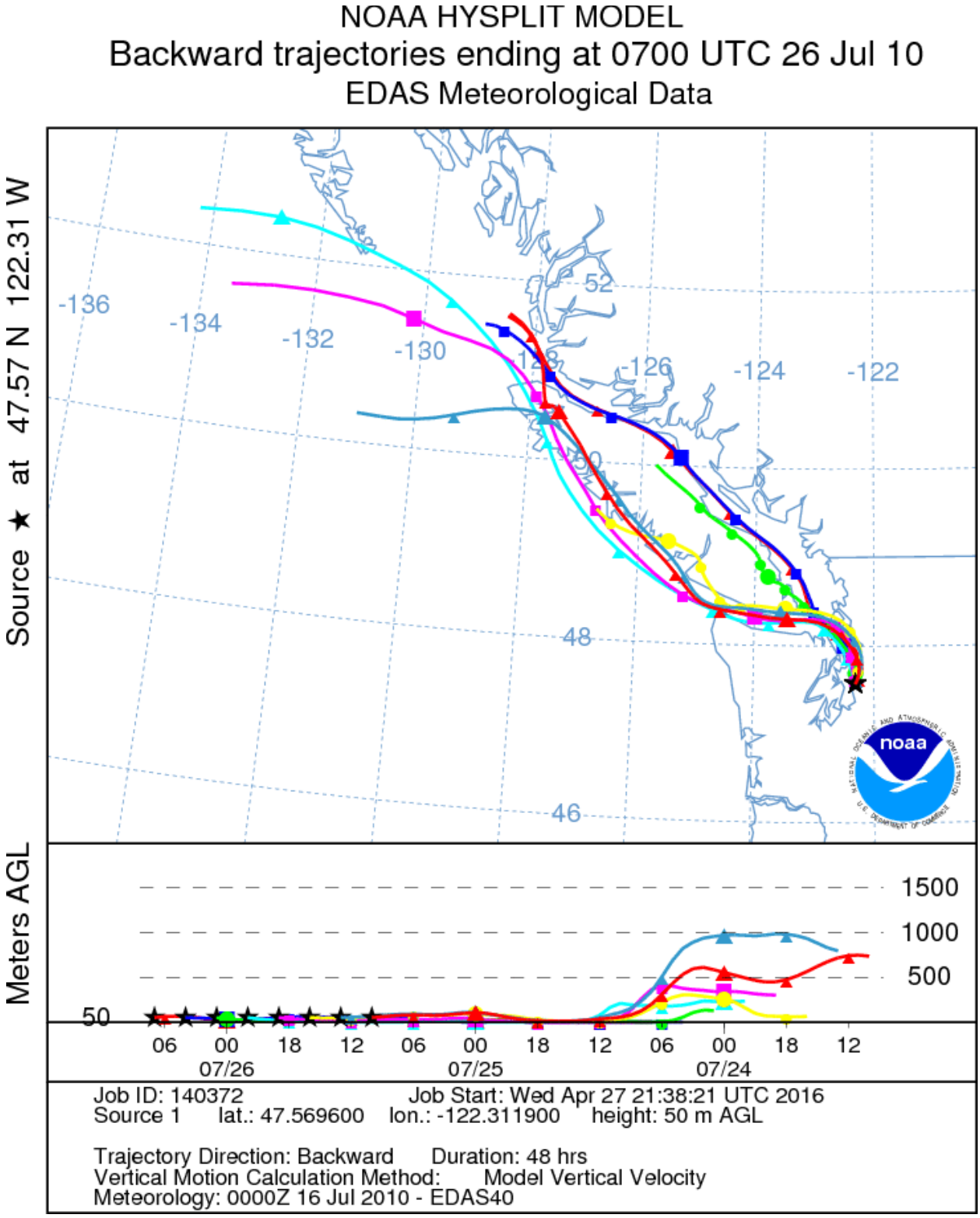
NOAA HYSPLIT MODEL
Backward trajectories ending at 0700 UTC 26 Jul 10
EDAS Meteorological Data
Source ★ at 47.57 N 122.31 W
-136
-134
-132
-130
-126
-124
-122
52
48
46
noaa
Meters AGL
1500
1000
500
50
06 00 18 12 06 00 18 12 06 00 18 12
07/26
07/25
07/24
Job ID: 140372 Job Start: Wed Apr 27 21:38:21 UTC 2016
Source 1 lat.: 47.569600 lon.: -122.311900 height: 50 m AGL
Trajectory Direction: Backward Duration: 48 hrs
Vertical Motion Calculation Method: Model Vertical Velocity
Meteorology: 0000Z 16 Jul 2010 - EDAS40

NOAA HYSPLIT MODEL
Backward trajectories ending at 0700 UTC 03 Oct 10
NAM Meteorological Data

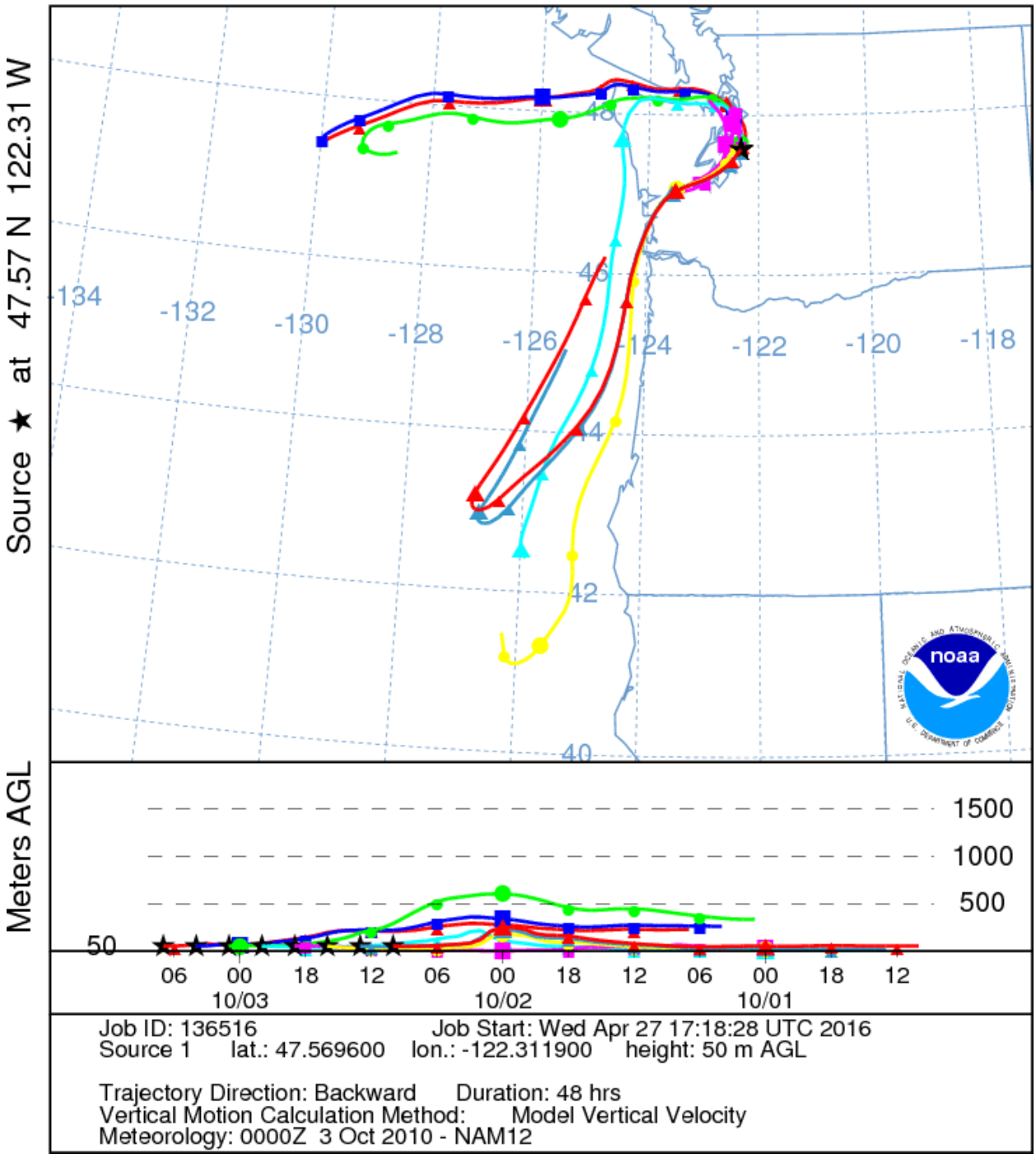

Job ID: 136516 Job Start: Wed Apr 27 17:18:28 UTC 2016
Source 1 lat.: 47.569600 lon.: -122.311900 height: 50 m AGL

Trajectory Direction: Backward Duration: 48 hrs
Vertical Motion Calculation Method: Model Vertical Velocity
Meteorology: 0000Z 3 Oct 2010 - NAM12

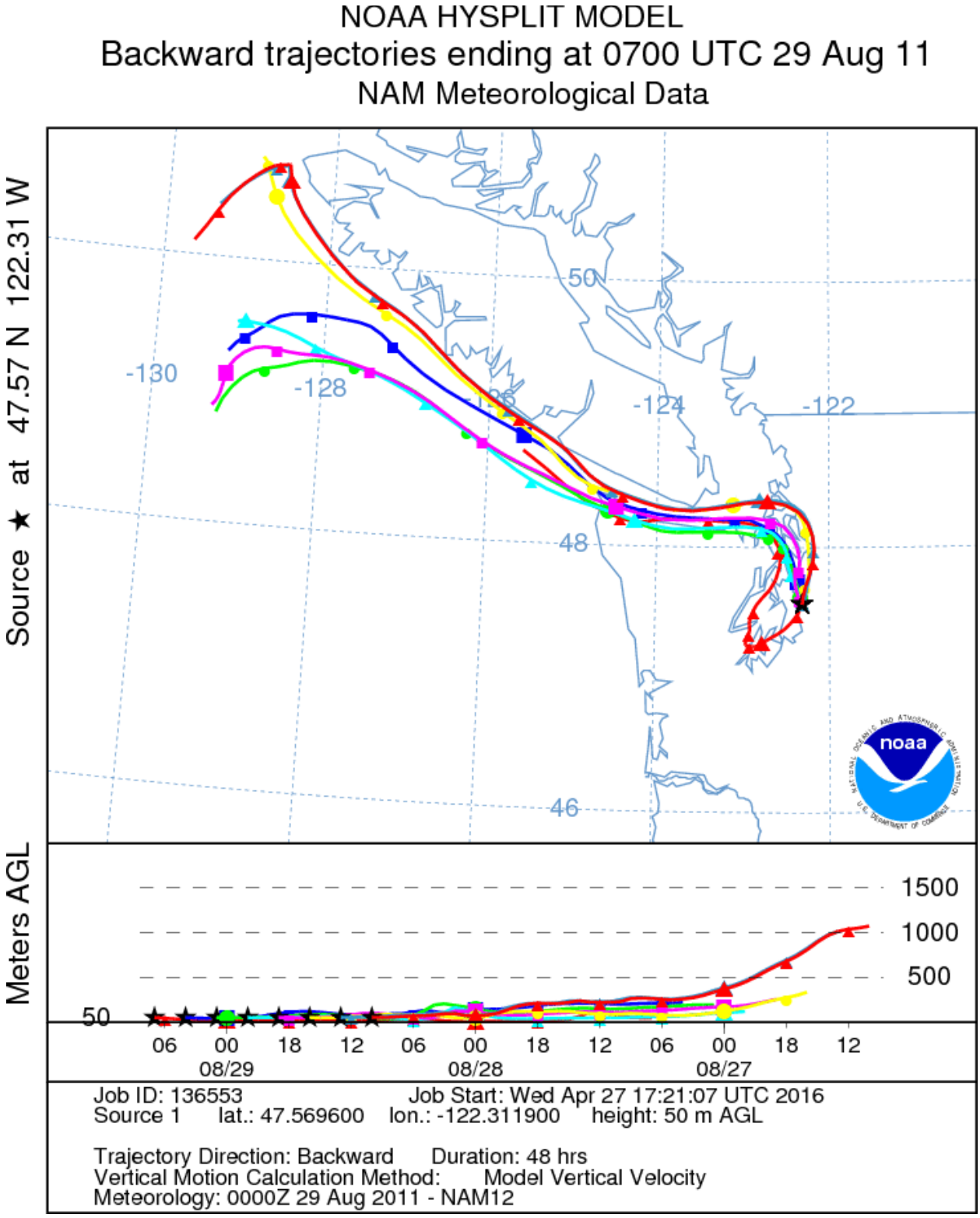
NOAA HYSPLIT MODEL
Backward trajectories ending at 0700 UTC 29 Aug 11
NAM Meteorological Data
Source ★ at 47.57 N 122.31 W
-130
-128
-126
-124
-122
50
48
46
noaa
Meters AGL
1500
1000
500
50
06 00 18 12 06 00 18 12 06 00 18 12
08/29 08/28 08/27
Job ID: 136553 Job Start: Wed Apr 27 17:21:07 UTC 2016
Source 1 lat.: 47.569600 lon.: -122.311900 height: 50 m AGL
Trajectory Direction: Backward Duration: 48 hrs
Vertical Motion Calculation Method: Model Vertical Velocity
Meteorology: 0000Z 29 Aug 2011 - NAM12

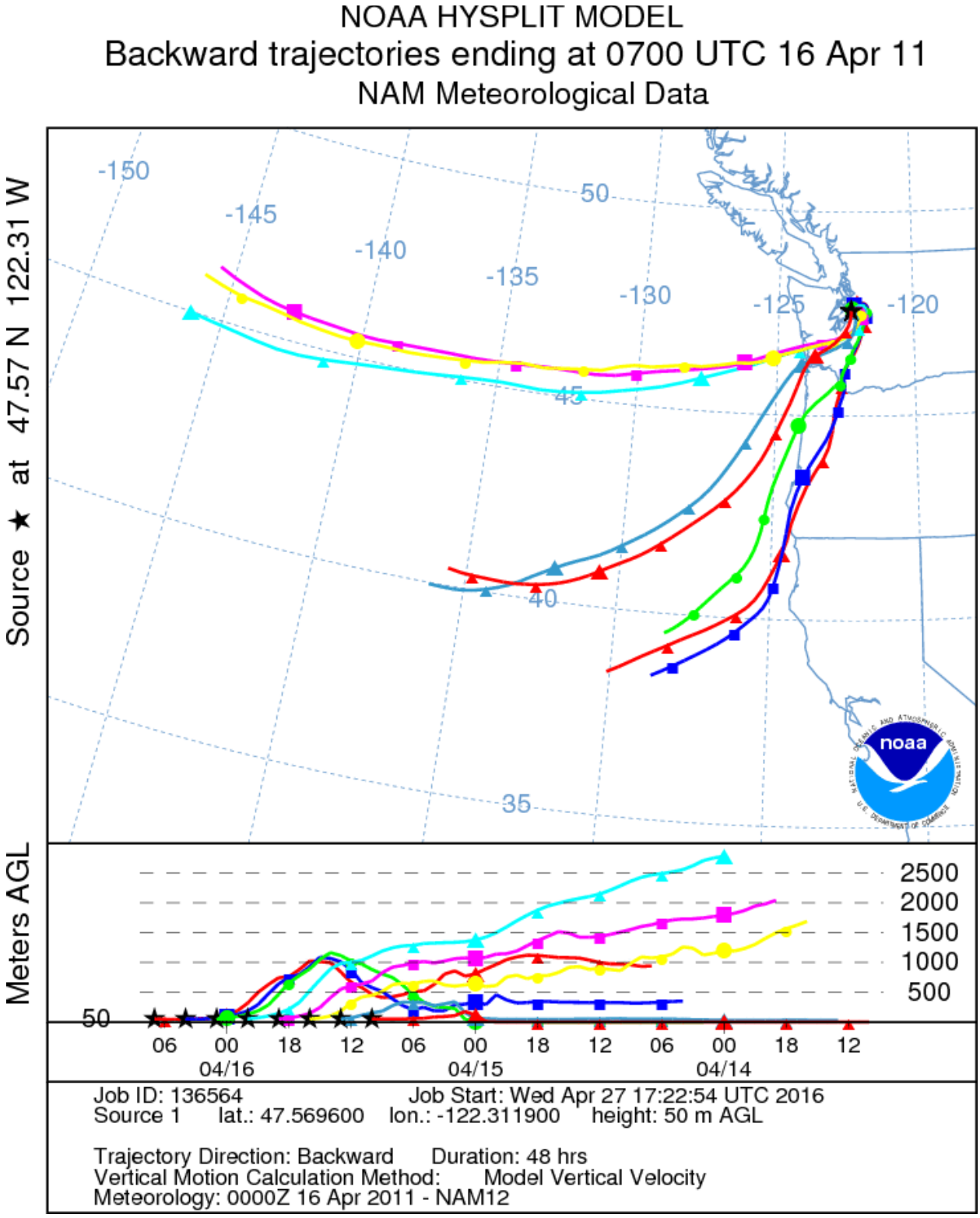
NOAA HYSPLIT MODEL
Backward trajectories ending at 0700 UTC 16 Apr 11
NAM Meteorological Data
Source ★ at 47.57 N 122.31 W
-150
-145
-140
-135
-130
-125
-120
50
45
40
35
noaa
Meters AGL
2500
2000
1500
1000
500
50
06 00 18 12 06 00 18 12 06 00 18 12
04/16
04/15
04/14
Job ID: 136564
Job Start: Wed Apr 27 17:22:54 UTC 2016
Source 1 lat.: 47.569600 lon.: -122.311900 height: 50 m AGL
Trajectory Direction: Backward Duration: 48 hrs
Vertical Motion Calculation Method: Model Vertical Velocity
Meteorology: 0000Z 16 Apr 2011 - NAM12

NOAA HYSPLIT MODEL
Backward trajectories ending at 0700 UTC 18 Jul 11
NAM Meteorological Data

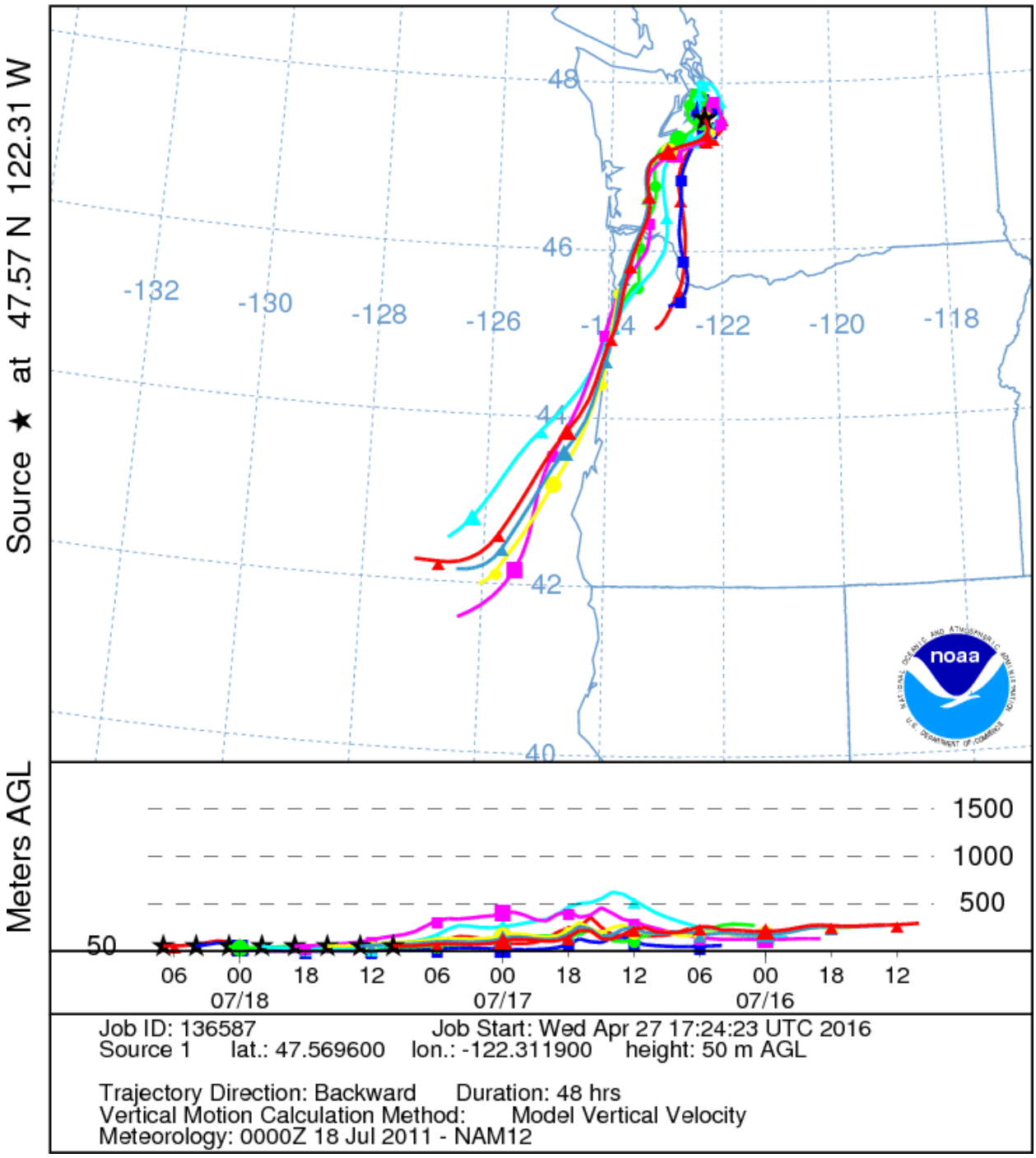

Job ID: 136587 Job Start: Wed Apr 27 17:24:23 UTC 2016
Source 1 lat.: 47.569600 lon.: -122.311900 height: 50 m AGL

Trajectory Direction: Backward Duration: 48 hrs
Vertical Motion Calculation Method: Model Vertical Velocity
Meteorology: 0000Z 18 Jul 2011 - NAM12

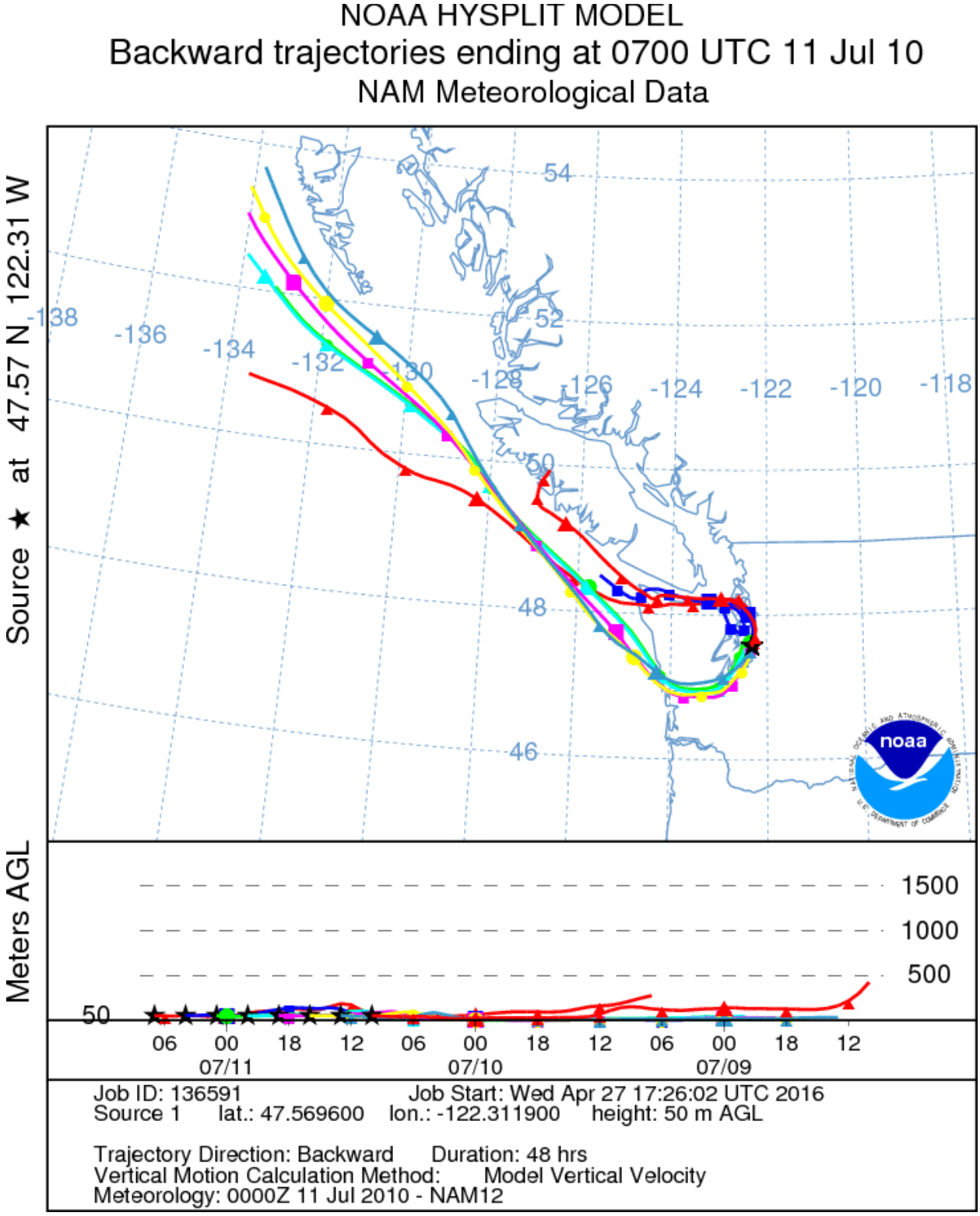
NOAA HYSPLIT MODEL
Backward trajectories ending at 0700 UTC 11 Jul 10
NAM Meteorological Data
Source ★ at 47.57 N 122.31 W
-138
-136
-134
-132
-130
-128
-126
-124
-122
-120
-118
54
52
50
48
46
noaa
Meters AGL
1500
1000
500
50
06 00 18 12 06 00 18 12 06 00 18 12
07/11
07/10
07/09
Job ID: 136591 Job Start: Wed Apr 27 17:26:02 UTC 2016
Source 1 lat.: 47.569600 lon.: -122.311900 height: 50 m AGL
Trajectory Direction: Backward Duration: 48 hrs
Vertical Motion Calculation Method: Model Vertical Velocity
Meteorology: 0000Z 11 Jul 2010 - NAM12

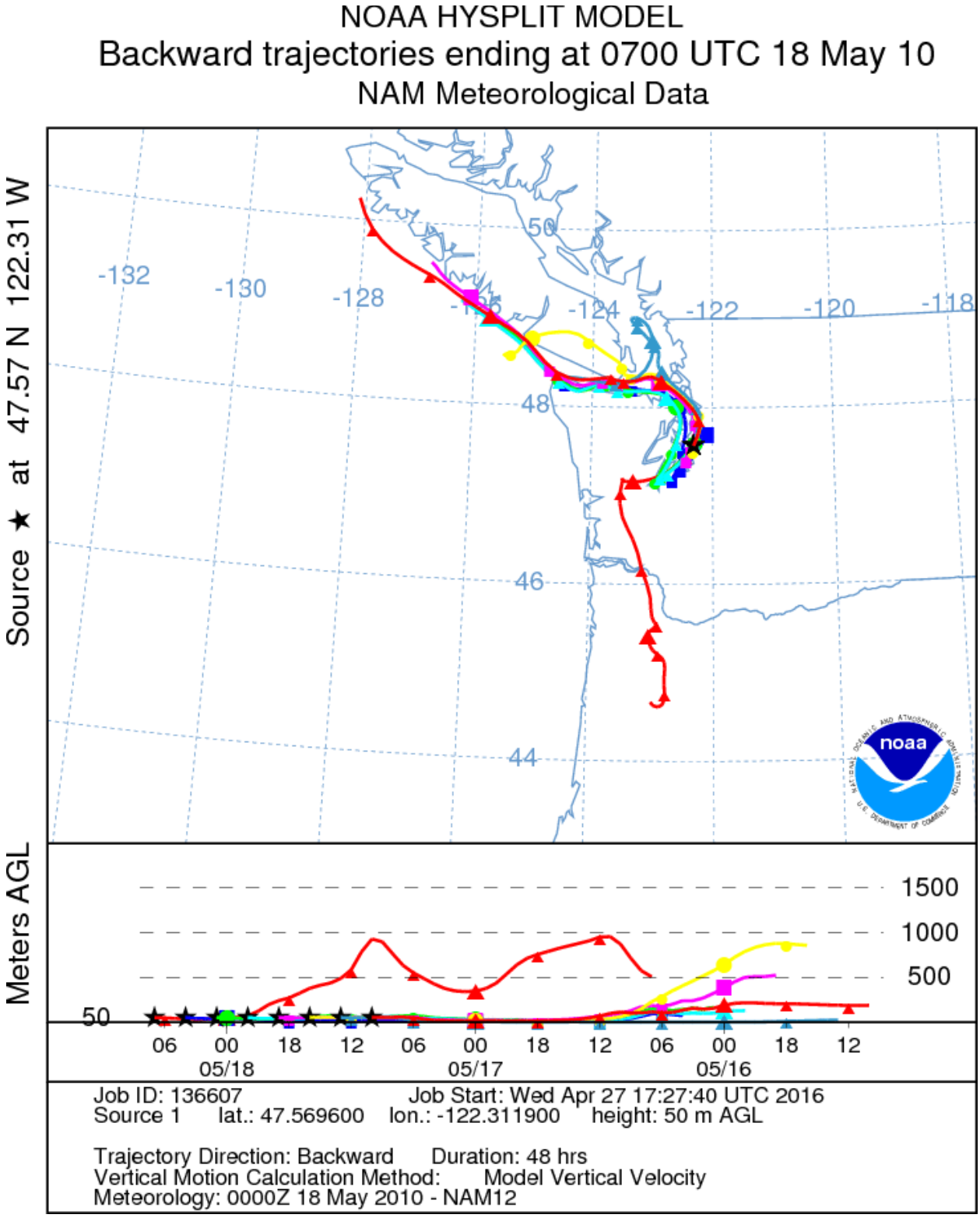
NOAA HYSPLIT MODEL
Backward trajectories ending at 0700 UTC 18 May 10
NAM Meteorological Data
Source ★ at 47.57 N 122.31 W
-132
-130
-128
-126
-124
-122
-120
-118
50
48
46
44
noaa
Meters AGL
1500
1000
500
50
06 00 18 12 06 00 18 12 06 00 18 12
05/18
05/17
05/16
Job ID: 136607 Job Start: Wed Apr 27 17:27:40 UTC 2016
Source 1 lat.: 47.569600 lon.: -122.311900 height: 50 m AGL
Trajectory Direction: Backward Duration: 48 hrs
Vertical Motion Calculation Method: Model Vertical Velocity
Meteorology: 0000Z 18 May 2010 - NAM12

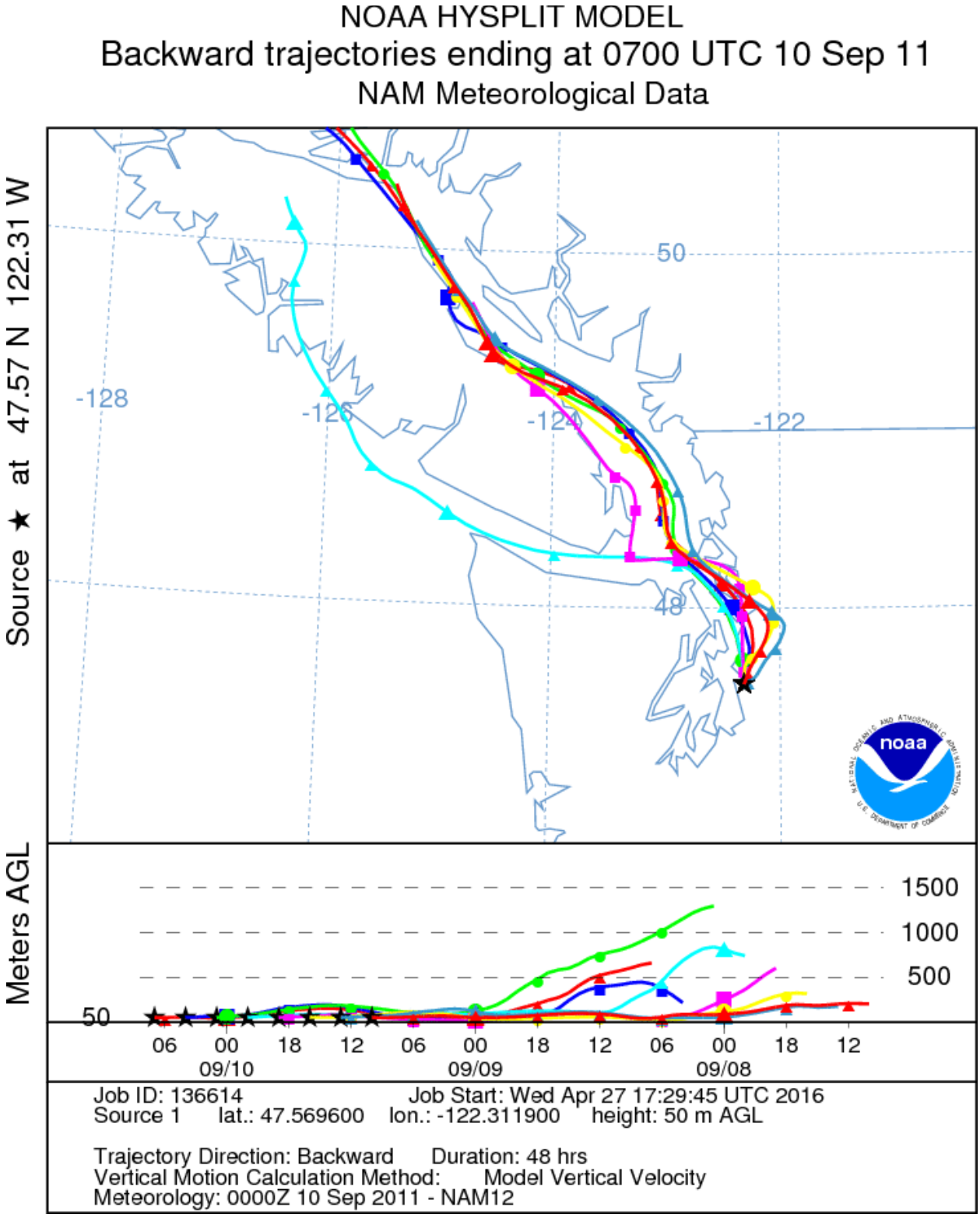
NOAA HYSPLIT MODEL
Backward trajectories ending at 0700 UTC 10 Sep 11
NAM Meteorological Data
Source ★ at 47.57 N 122.31 W
-128
-126
-124
-122
50
48
noaa
Meters AGL
1500
1000
500
50
06 00 18 12 06 00 18 12 06 00 18 12
09/10 09/09 09/08
Job ID: 136614 Job Start: Wed Apr 27 17:29:45 UTC 2016
Source 1 lat.: 47.569600 lon.: -122.311900 height: 50 m AGL
Trajectory Direction: Backward Duration: 48 hrs
Vertical Motion Calculation Method: Model Vertical Velocity
Meteorology: 0000Z 10 Sep 2011 - NAM12

ROMA HYSPLIT back-trajectories

NOAA HYSPLIT MODEL
Backward trajectories ending at 0500 UTC 28 Jan 11
NAM Meteorological Data

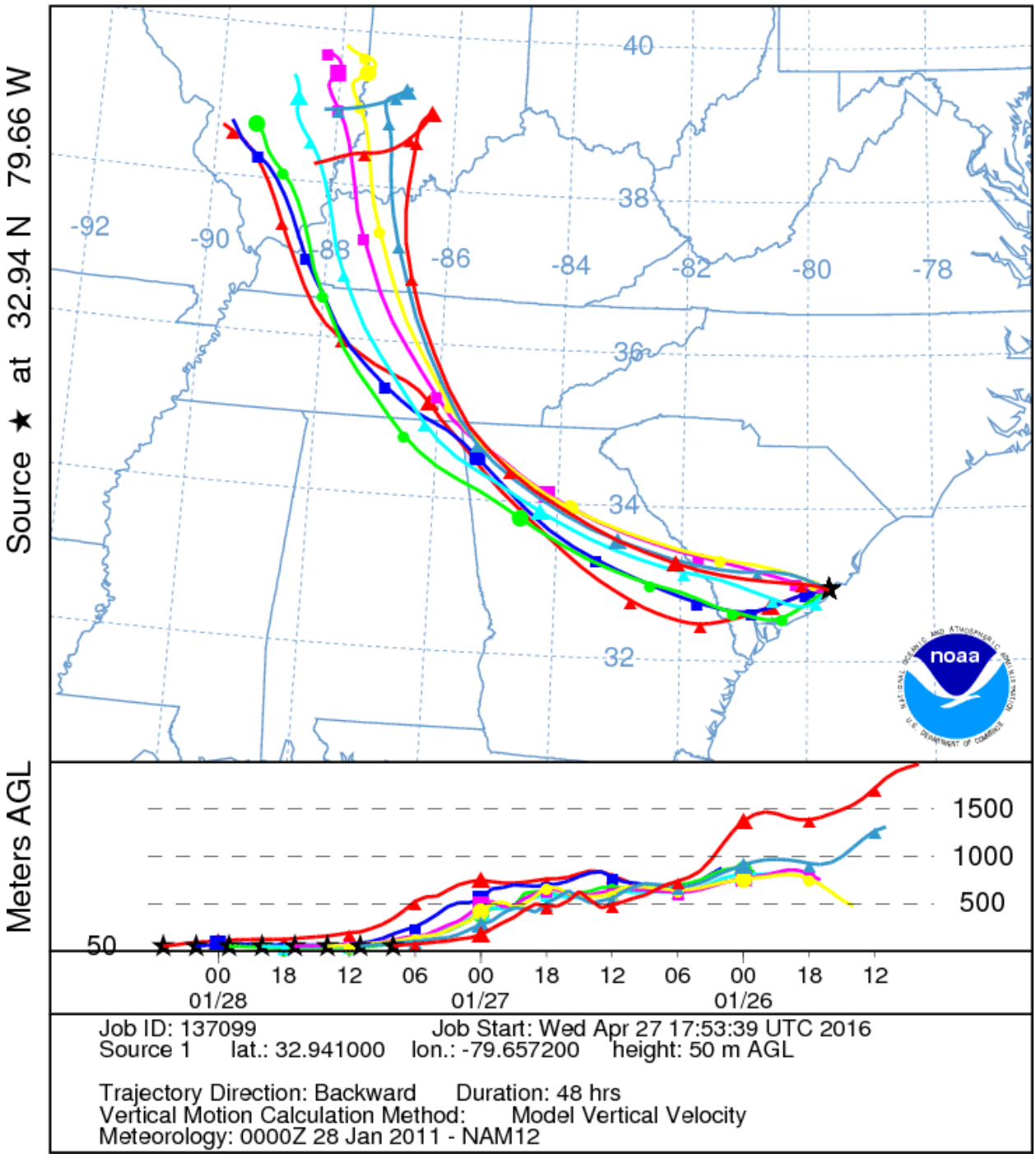

Job ID: 137099 Job Start: Wed Apr 27 17:53:39 UTC 2016
Source 1 lat.: 32.941000 lon.: -79.657200 height: 50 m AGL

Trajectory Direction: Backward Duration: 48 hrs
Vertical Motion Calculation Method: Model Vertical Velocity
Meteorology: 0000Z 28 Jan 2011 - NAM12

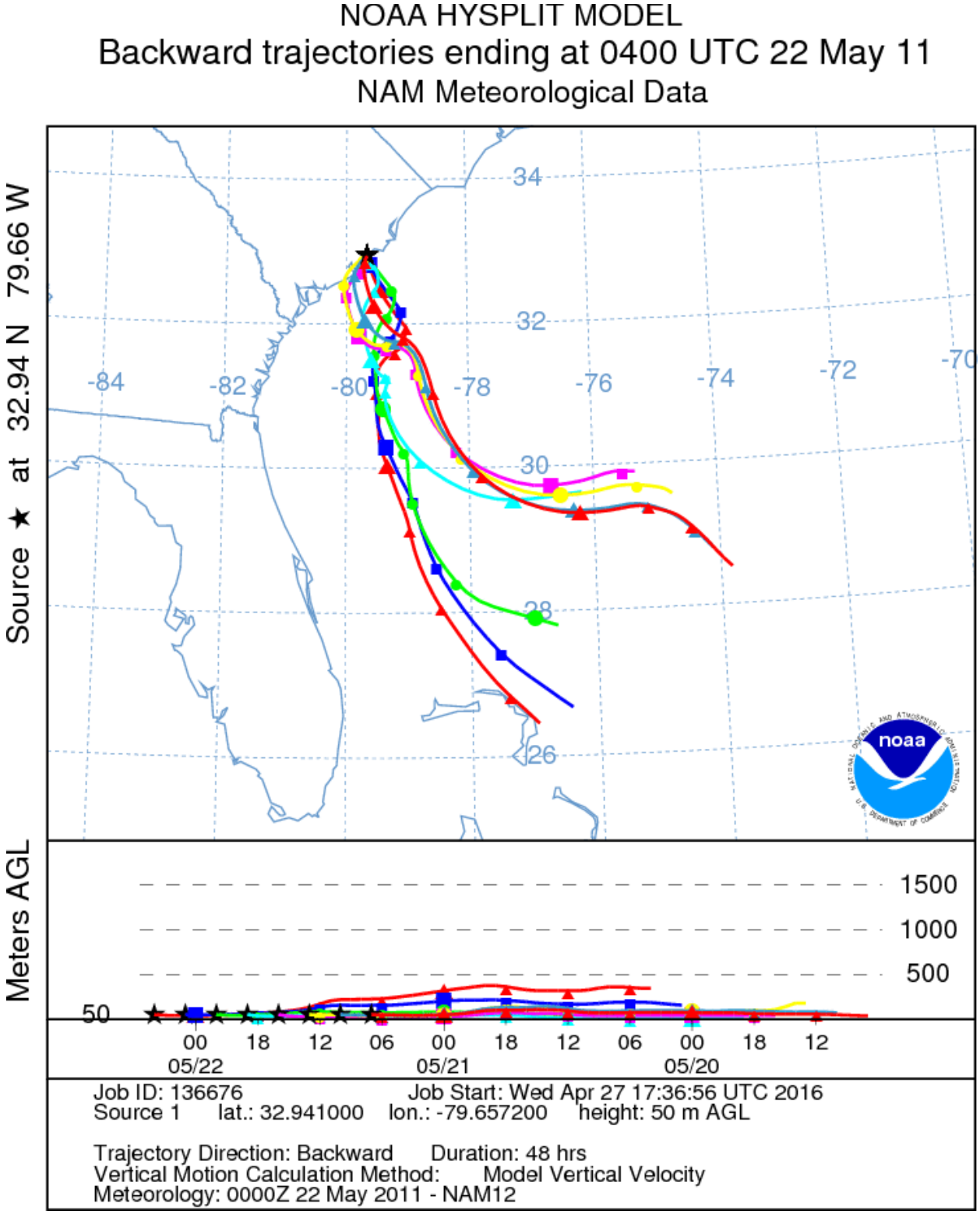
NOAA HYSPLIT MODEL
Backward trajectories ending at 0400 UTC 22 May 11
NAM Meteorological Data
Source ★ at 32.94 N 79.66 W
34
32
30
28
26
-84
-82
-80
-78
-76
-74
-72
-70
noaa
Meters AGL
1500
1000
500
50
00 18 12 06 00 18 12 06 00 18 12
05/22
05/21
05/20
Job ID: 136676 Job Start: Wed Apr 27 17:36:56 UTC 2016
Source 1 lat.: 32.941000 lon.: -79.657200 height: 50 m AGL
Trajectory Direction: Backward Duration: 48 hrs
Vertical Motion Calculation Method: Model Vertical Velocity
Meteorology: 0000Z 22 May 2011 - NAM12

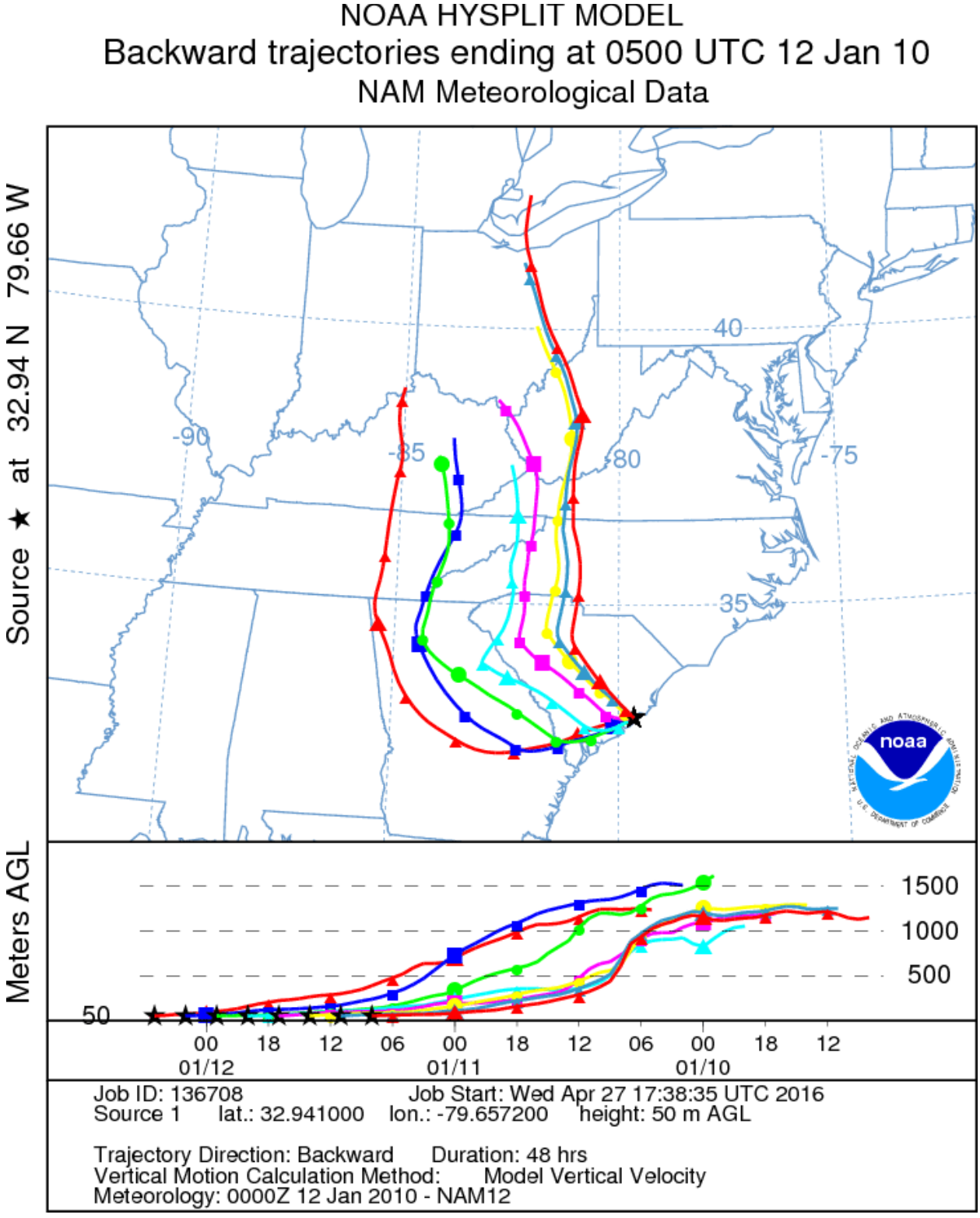
NOAA HYSPLIT MODEL
Backward trajectories ending at 0500 UTC 12 Jan 10
NAM Meteorological Data
Source ★ at 32.94 N 79.66 W
-90
-85
-80
-75
40
35
noaa
Meters AGL
1500
1000
500
50
00 18 12 06 00 18 12 06 00 18 12
01/12 01/11 01/10
Job ID: 136708 Job Start: Wed Apr 27 17:38:35 UTC 2016
Source 1 lat.: 32.941000 lon.: -79.657200 height: 50 m AGL
Trajectory Direction: Backward Duration: 48 hrs
Vertical Motion Calculation Method: Model Vertical Velocity
Meteorology: 0000Z 12 Jan 2010 - NAM12

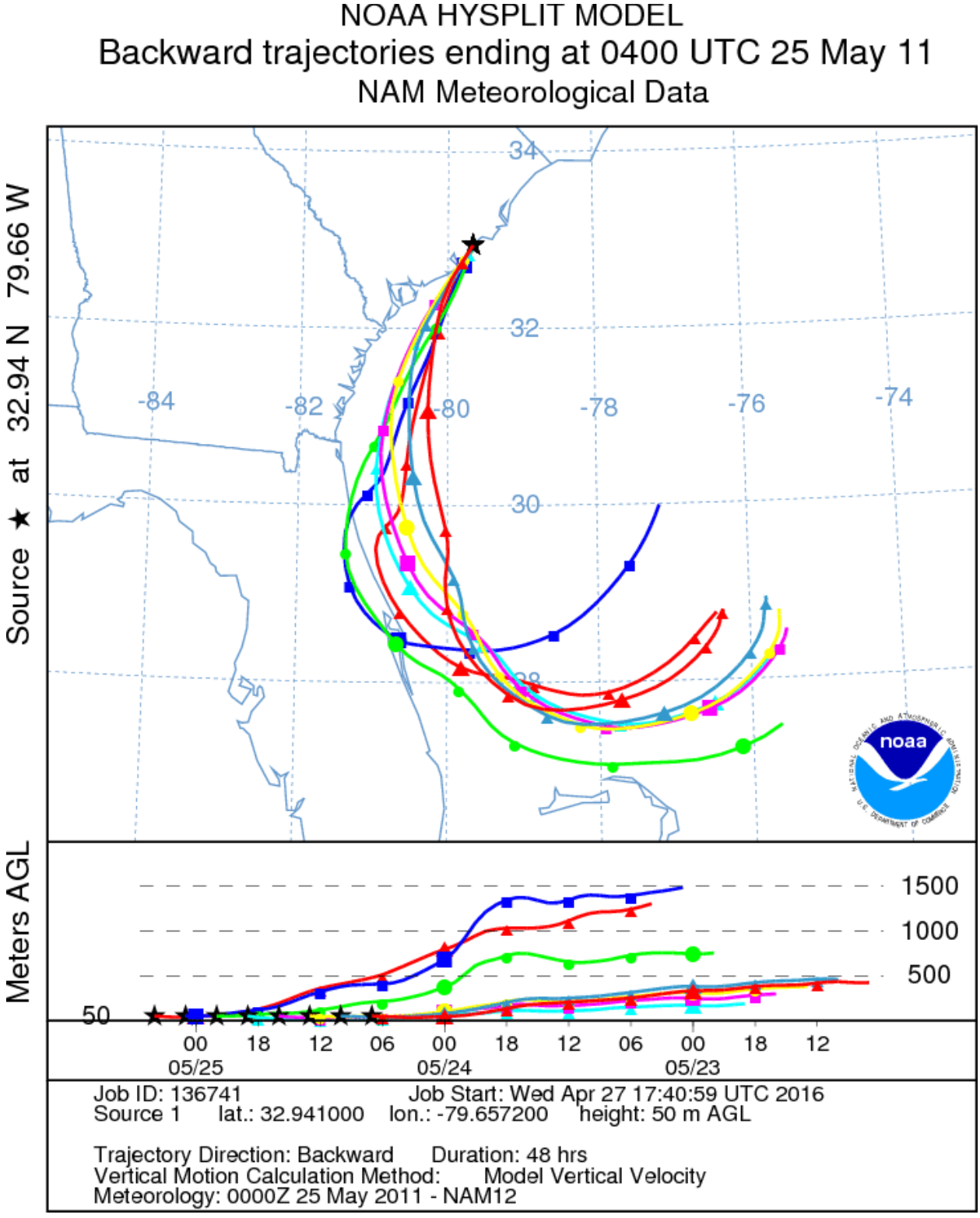
NOAA HYSPLIT MODEL
Backward trajectories ending at 0400 UTC 25 May 11
NAM Meteorological Data
Source ★ at 32.94 N 79.66 W
34
32
30
-84
-82
-80
-78
-76
-74
noaa
Meters AGL
1500
1000
500
50
00 18 12 06 00 18 12 06 00 18 12
05/25
05/24
05/23
Job ID: 136741 Job Start: Wed Apr 27 17:40:59 UTC 2016
Source 1 lat.: 32.941000 lon.: -79.657200 height: 50 m AGL
Trajectory Direction: Backward Duration: 48 hrs
Vertical Motion Calculation Method: Model Vertical Velocity
Meteorology: 0000Z 25 May 2011 - NAM12

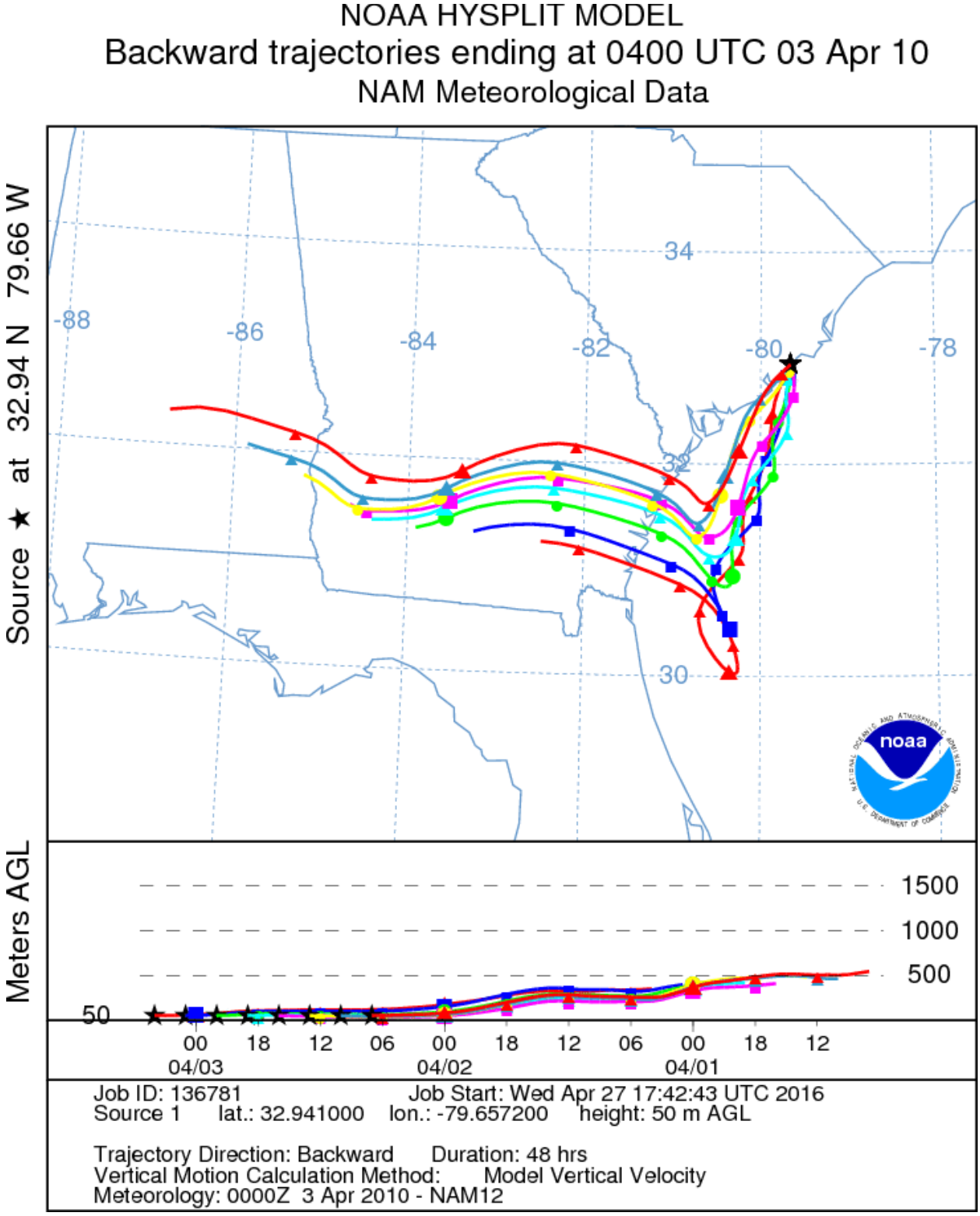
NOAA HYSPLIT MODEL
Backward trajectories ending at 0400 UTC 03 Apr 10
NAM Meteorological Data
Source ★ at 32.94 N 79.66 W
-88
-86
-84
-82
-80
-78
34
32
30
noaa
Meters AGL
1500
1000
500
50
00 18 12 06 00 18 12 06 00 18 12
04/03 04/02 04/01
Job ID: 136781 Job Start: Wed Apr 27 17:42:43 UTC 2016
Source 1 lat.: 32.941000 lon.: -79.657200 height: 50 m AGL
Trajectory Direction: Backward Duration: 48 hrs
Vertical Motion Calculation Method: Model Vertical Velocity
Meteorology: 0000Z 3 Apr 2010 - NAM12

NOAA HYSPLIT MODEL
Backward trajectories ending at 0500 UTC 31 Jan 11
NAM Meteorological Data

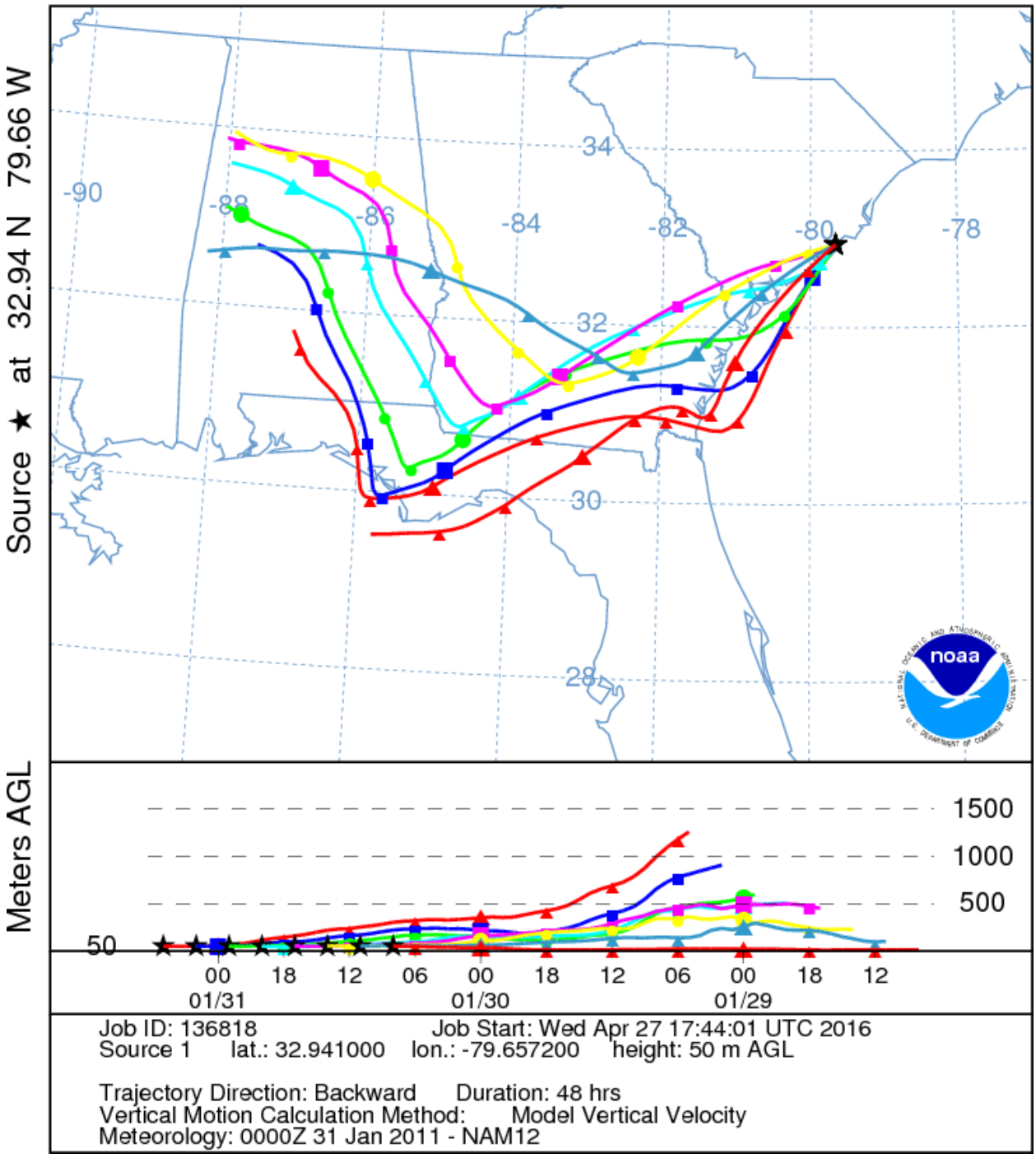

Job ID: 136818 Job Start: Wed Apr 27 17:44:01 UTC 2016
Source 1 lat.: 32.941000 lon.: -79.657200 height: 50 m AGL

Trajectory Direction: Backward Duration: 48 hrs
Vertical Motion Calculation Method: Model Vertical Velocity
Meteorology: 0000Z 31 Jan 2011 - NAM12

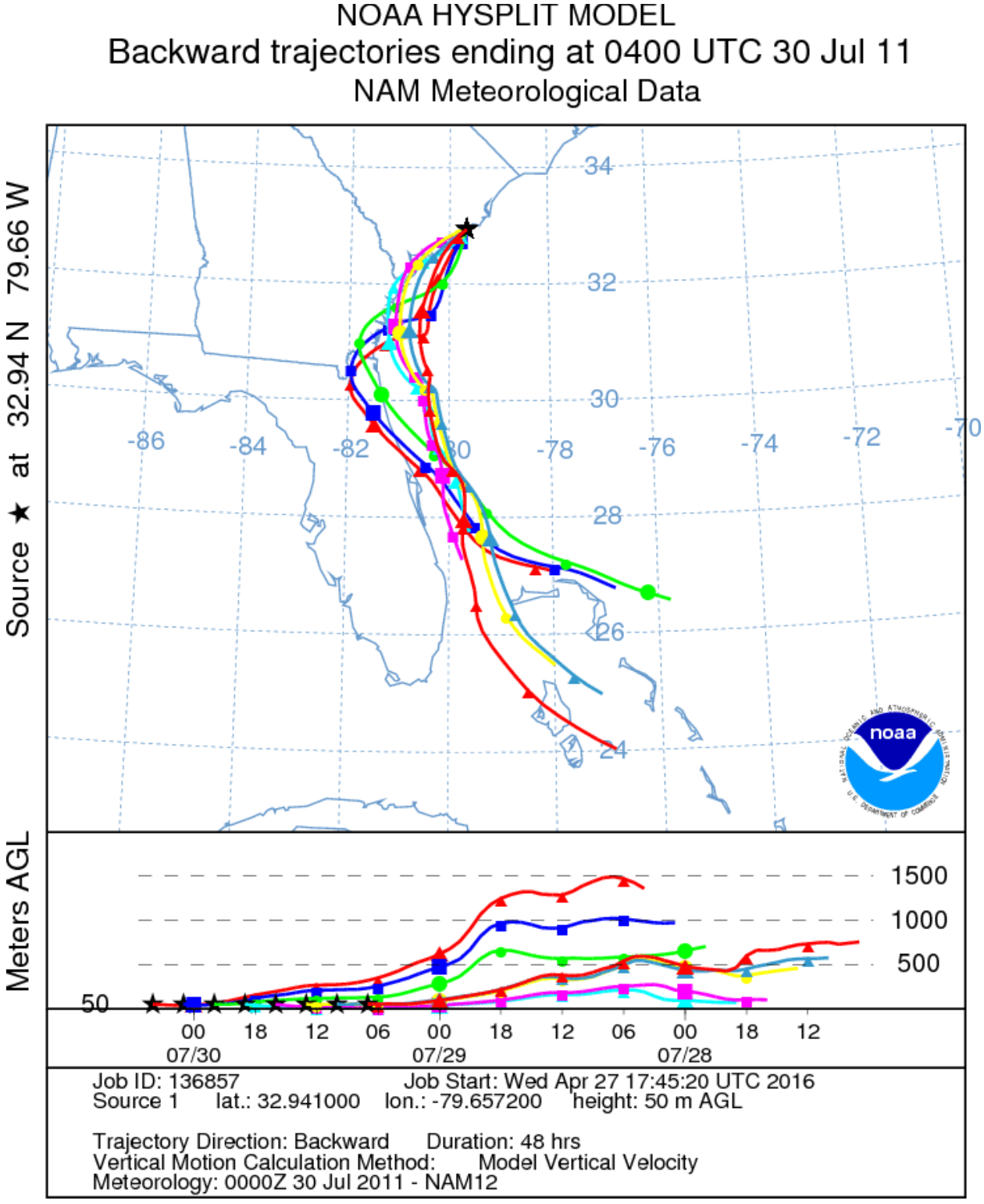
NOAA HYSPLIT MODEL
Backward trajectories ending at 0400 UTC 30 Jul 11
NAM Meteorological Data
Source ★ at 32.94 N 79.66 W
34
32
30
28
26
24
-86
-84
-82
-80
-78
-76
-74
-72
-70
noaa
Meters AGL
1500
1000
500
50
00 18 12 06 00 18 12 06 00 18 12
07/30 07/29 07/28
Job ID: 136857 Job Start: Wed Apr 27 17:45:20 UTC 2016
Source 1 lat.: 32.941000 lon.: -79.657200 height: 50 m AGL
Trajectory Direction: Backward Duration: 48 hrs
Vertical Motion Calculation Method: Model Vertical Velocity
Meteorology: 0000Z 30 Jul 2011 - NAM12

NOAA HYSPLIT MODEL
Backward trajectories ending at 0400 UTC 31 Mar 10
NAM Meteorological Data

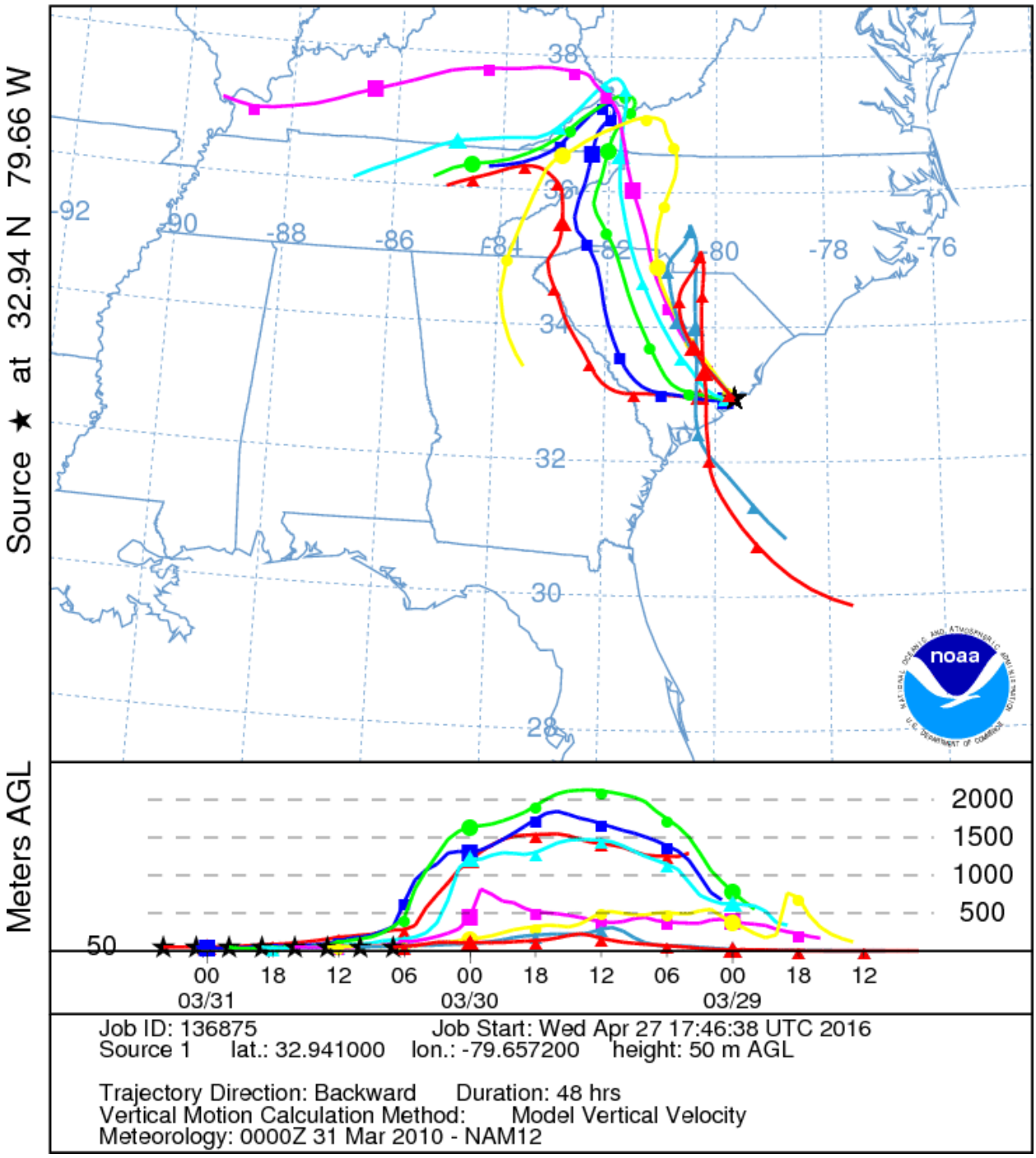

Job ID: 136875 Job Start: Wed Apr 27 17:46:38 UTC 2016
Source 1 lat.: 32.941000 lon.: -79.657200 height: 50 m AGL

Trajectory Direction: Backward Duration: 48 hrs
Vertical Motion Calculation Method: Model Vertical Velocity
Meteorology: 0000Z 31 Mar 2010 - NAM12

NOAA HYSPLIT MODEL
Backward trajectories ending at 0400 UTC 22 Apr 11
NAM Meteorological Data

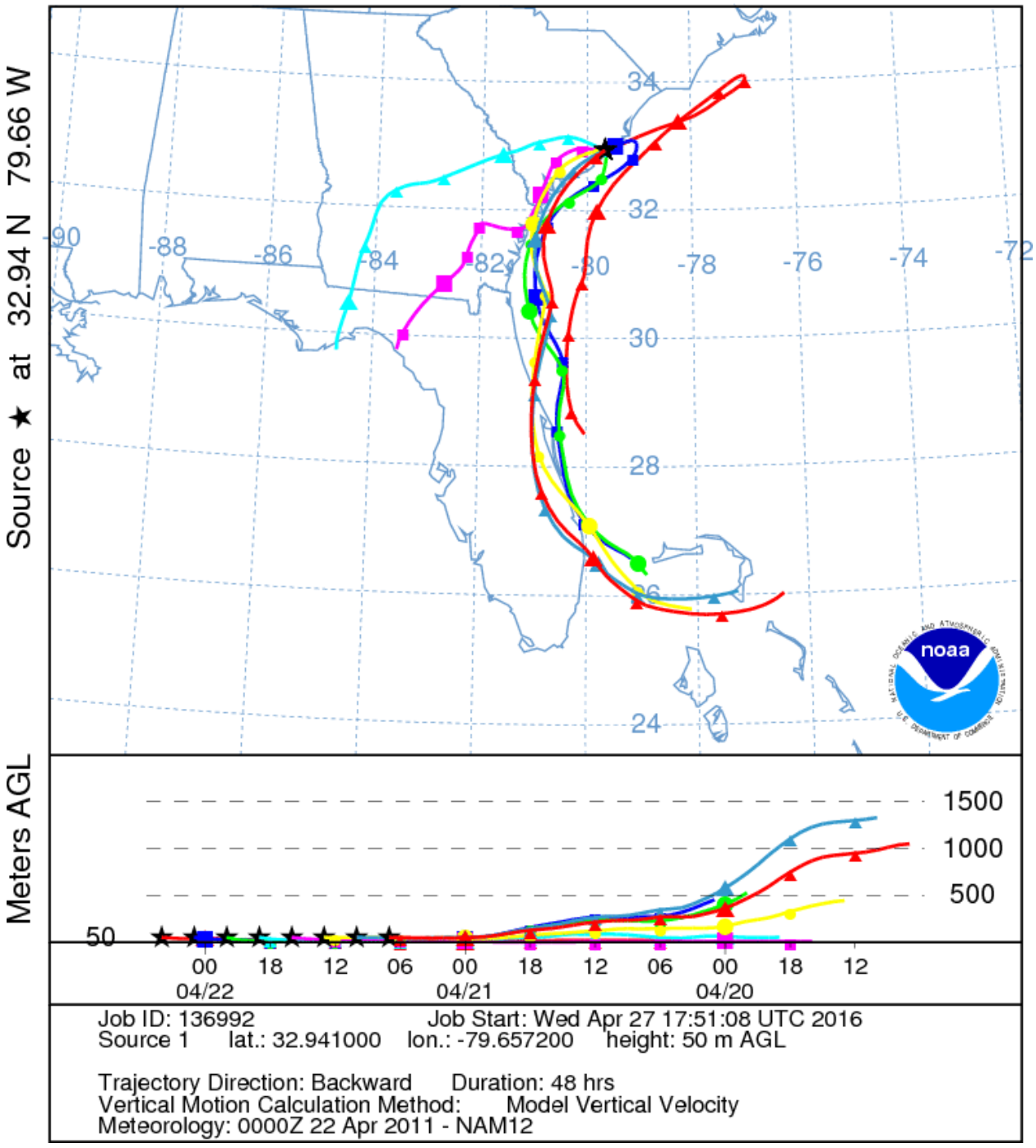

Job ID: 136992 Job Start: Wed Apr 27 17:51:08 UTC 2016
Source 1 lat.: 32.941000 lon.: -79.657200 height: 50 m AGL

Trajectory Direction: Backward Duration: 48 hrs
Vertical Motion Calculation Method: Model Vertical Velocity
Meteorology: 0000Z 22 Apr 2011 - NAM12

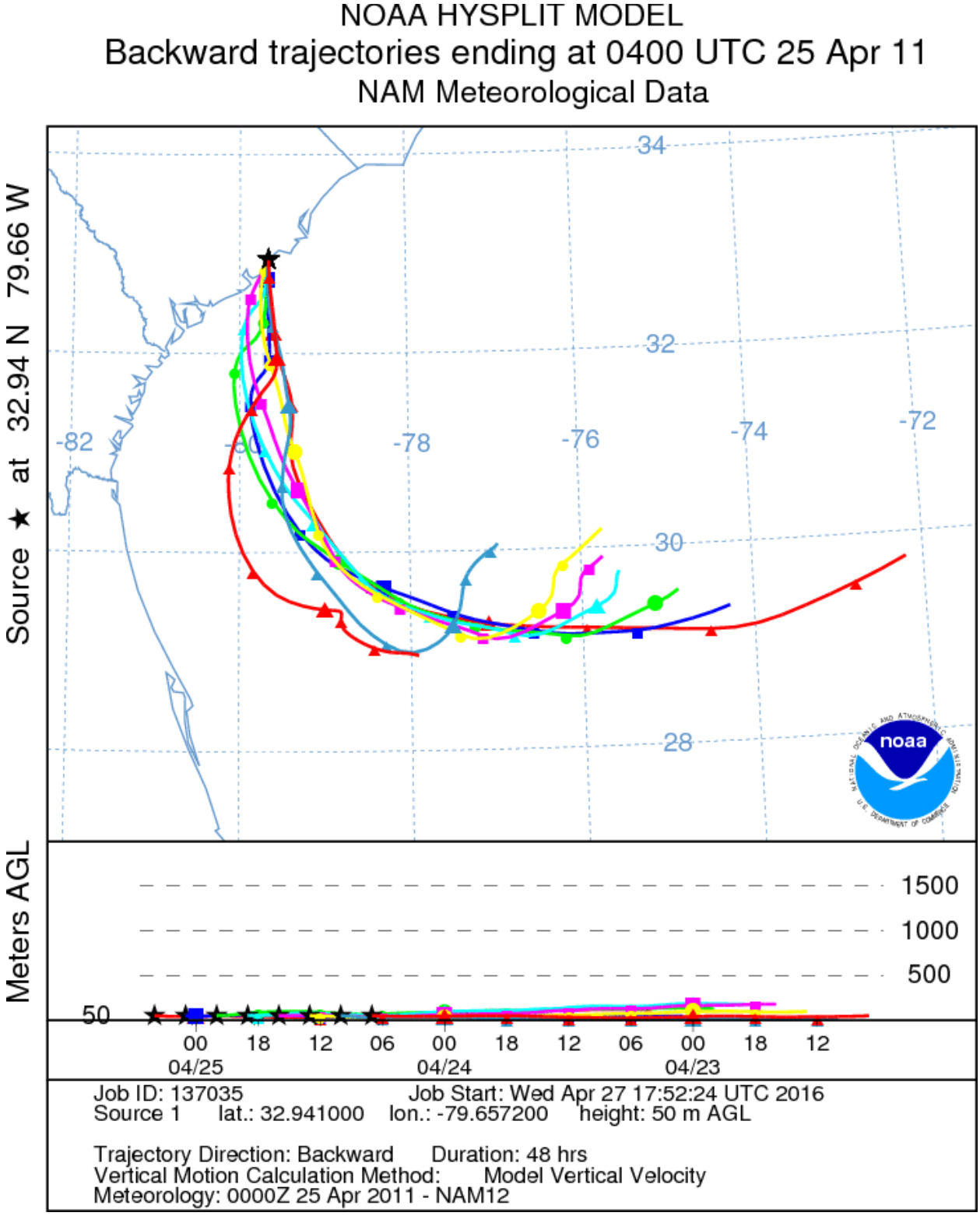
NOAA HYSPLIT MODEL
Backward trajectories ending at 0400 UTC 25 Apr 11
NAM Meteorological Data
Source ★ at 32.94 N 79.66 W
34
32
30
28
-82
-80
-78
-76
-74
-72
noaa
Meters AGL
1500
1000
500
50
00 18 12 06 00 18 12 06 00 18 12
04/25
04/24
04/23
Job ID: 137035 Job Start: Wed Apr 27 17:52:24 UTC 2016
Source 1 lat.: 32.941000 lon.: -79.657200 height: 50 m AGL
Trajectory Direction: Backward Duration: 48 hrs
Vertical Motion Calculation Method: Model Vertical Velocity
Meteorology: 0000Z 25 Apr 2011 - NAM12

SAMA HYSPLIT back-trajectories

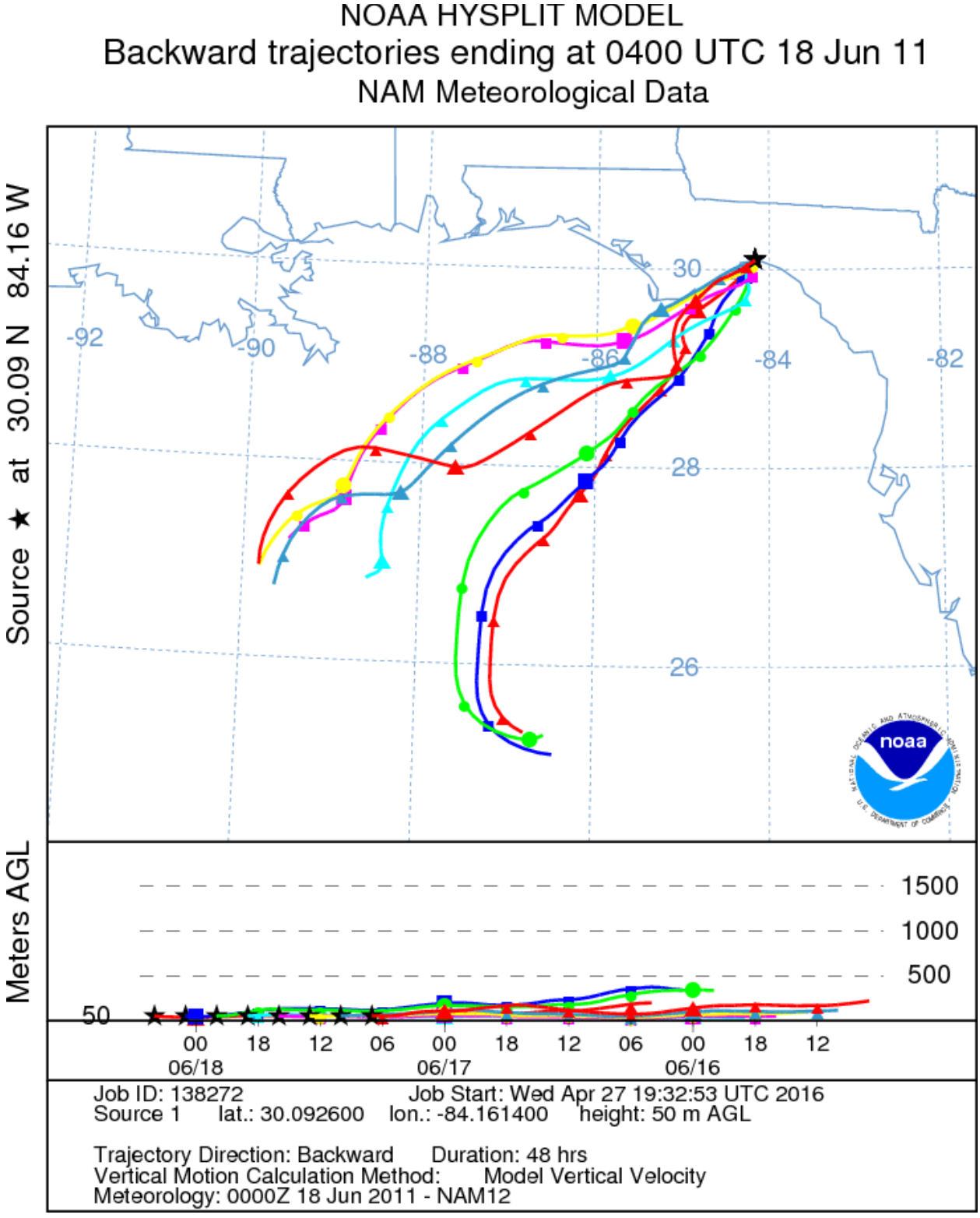
NOAA HYSPLIT MODEL
Backward trajectories ending at 0400 UTC 18 Jun 11
NAM Meteorological Data
Source ★ at 30.09 N 84.16 W
-92
-90
-88
-86
-84
-82
30
28
26
noaa
Meters AGL
1500
1000
500
50
00 18 12 06 00 18 12 06 00 18 12
06/18 06/17 06/16
Job ID: 138272 Job Start: Wed Apr 27 19:32:53 UTC 2016
Source 1 lat.: 30.092600 lon.: -84.161400 height: 50 m AGL
Trajectory Direction: Backward Duration: 48 hrs
Vertical Motion Calculation Method: Model Vertical Velocity
Meteorology: 0000Z 18 Jun 2011 - NAM12

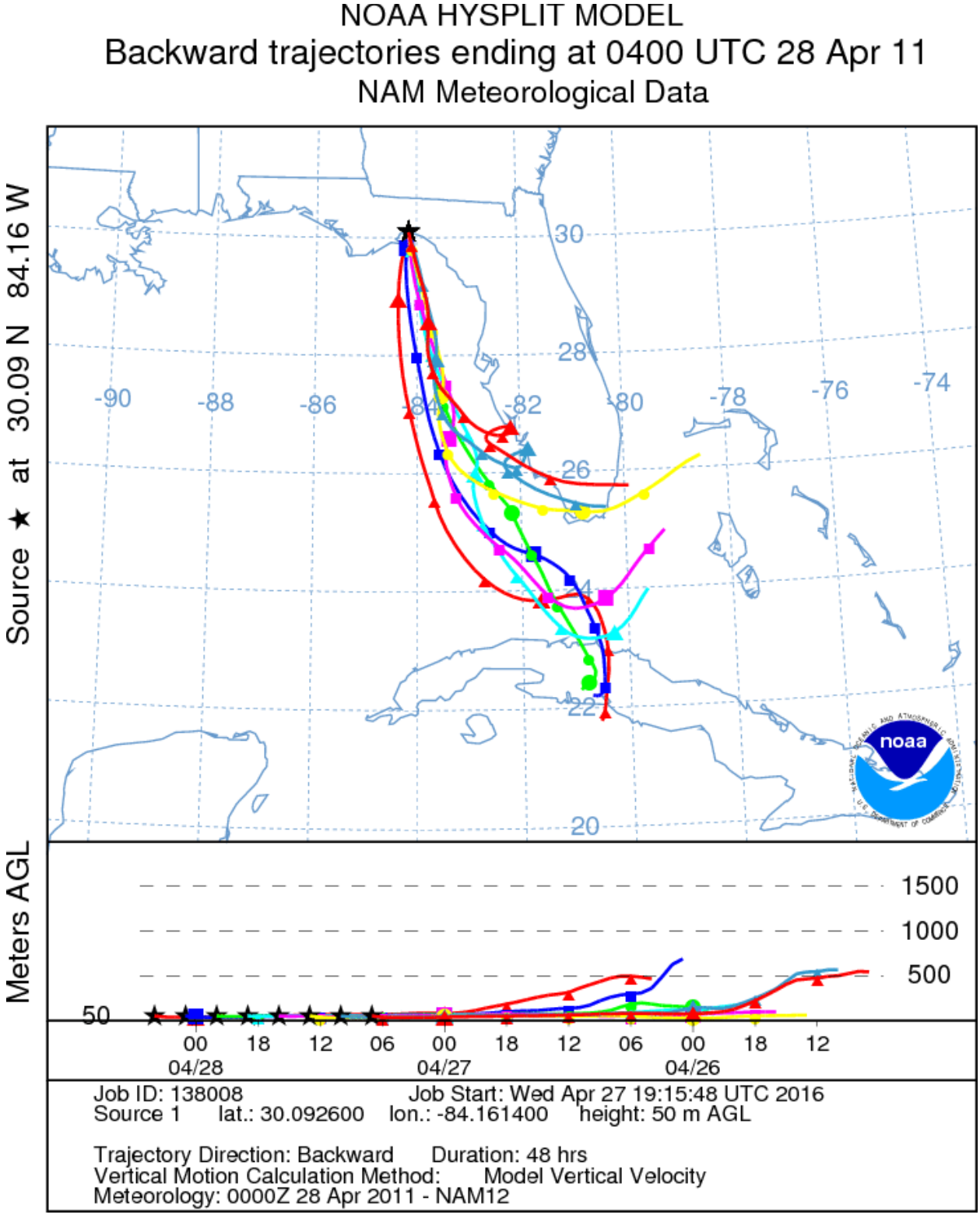
NOAA HYSPLIT MODEL
Backward trajectories ending at 0400 UTC 28 Apr 11
NAM Meteorological Data
Source ★ at 30.09 N 84.16 W
Meters AGL
1500
1000
500
50
00 18 12 06 00 18 12 06 00 18 12
04/28 04/27 04/26
Job ID: 138008 Job Start: Wed Apr 27 19:15:48 UTC 2016
Source 1 lat.: 30.092600 lon.: -84.161400 height: 50 m AGL
Trajectory Direction: Backward Duration: 48 hrs
Vertical Motion Calculation Method: Model Vertical Velocity
Meteorology: 0000Z 28 Apr 2011 - NAM12

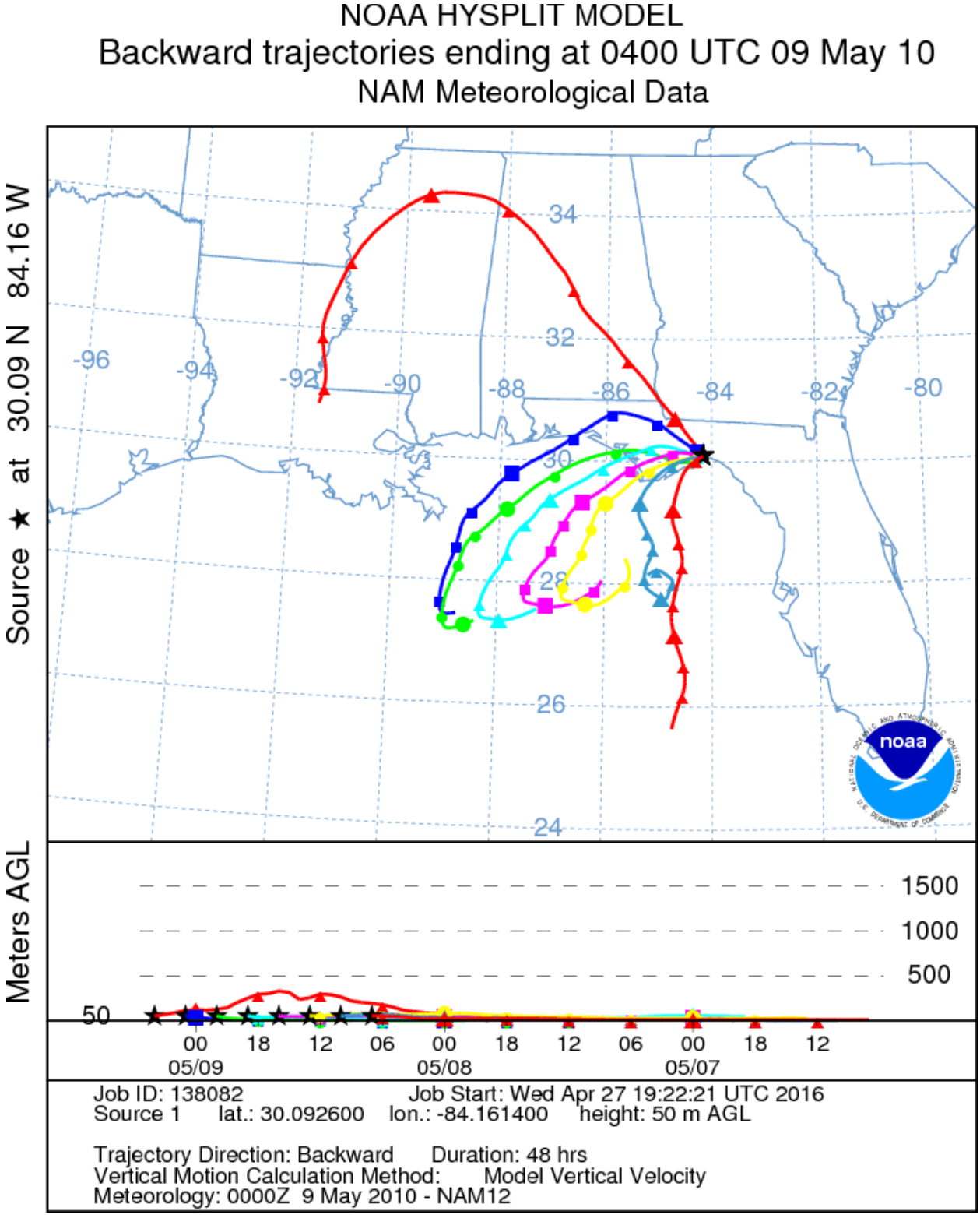
NOAA HYSPLIT MODEL
Backward trajectories ending at 0400 UTC 09 May 10
NAM Meteorological Data
Source ★ at 30.09 N 84.16 W
Meters AGL
1500
1000
500
50
00 18 12 06 00 18 12 06 00 18 12
05/09 05/08 05/07
Job ID: 138082 Job Start: Wed Apr 27 19:22:21 UTC 2016
Source 1 lat.: 30.092600 lon.: -84.161400 height: 50 m AGL
Trajectory Direction: Backward Duration: 48 hrs
Vertical Motion Calculation Method: Model Vertical Velocity
Meteorology: 0000Z 9 May 2010 - NAM12

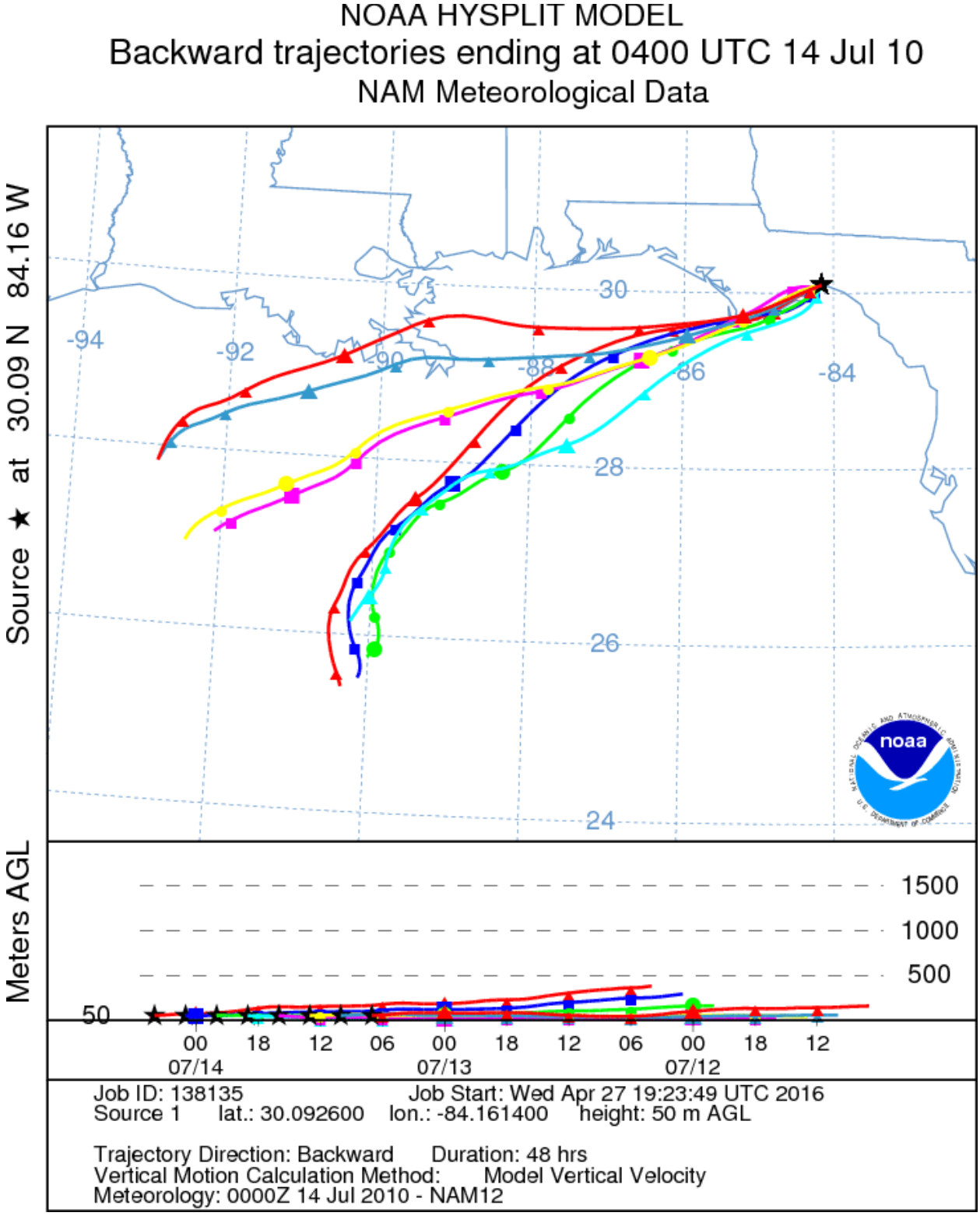
NOAA HYSPLIT MODEL
Backward trajectories ending at 0400 UTC 14 Jul 10
NAM Meteorological Data
Source ★ at 30.09 N 84.16 W
-94
-92
-90
-88
-86
-84
30
28
26
24
noaa
Meters AGL
1500
1000
500
50
00 18 12 06 00 18 12 06 00 18 12
07/14 07/13 07/12
Job ID: 138135 Job Start: Wed Apr 27 19:23:49 UTC 2016
Source 1 lat.: 30.092600 lon.: -84.161400 height: 50 m AGL
Trajectory Direction: Backward Duration: 48 hrs
Vertical Motion Calculation Method: Model Vertical Velocity
Meteorology: 0000Z 14 Jul 2010 - NAM12

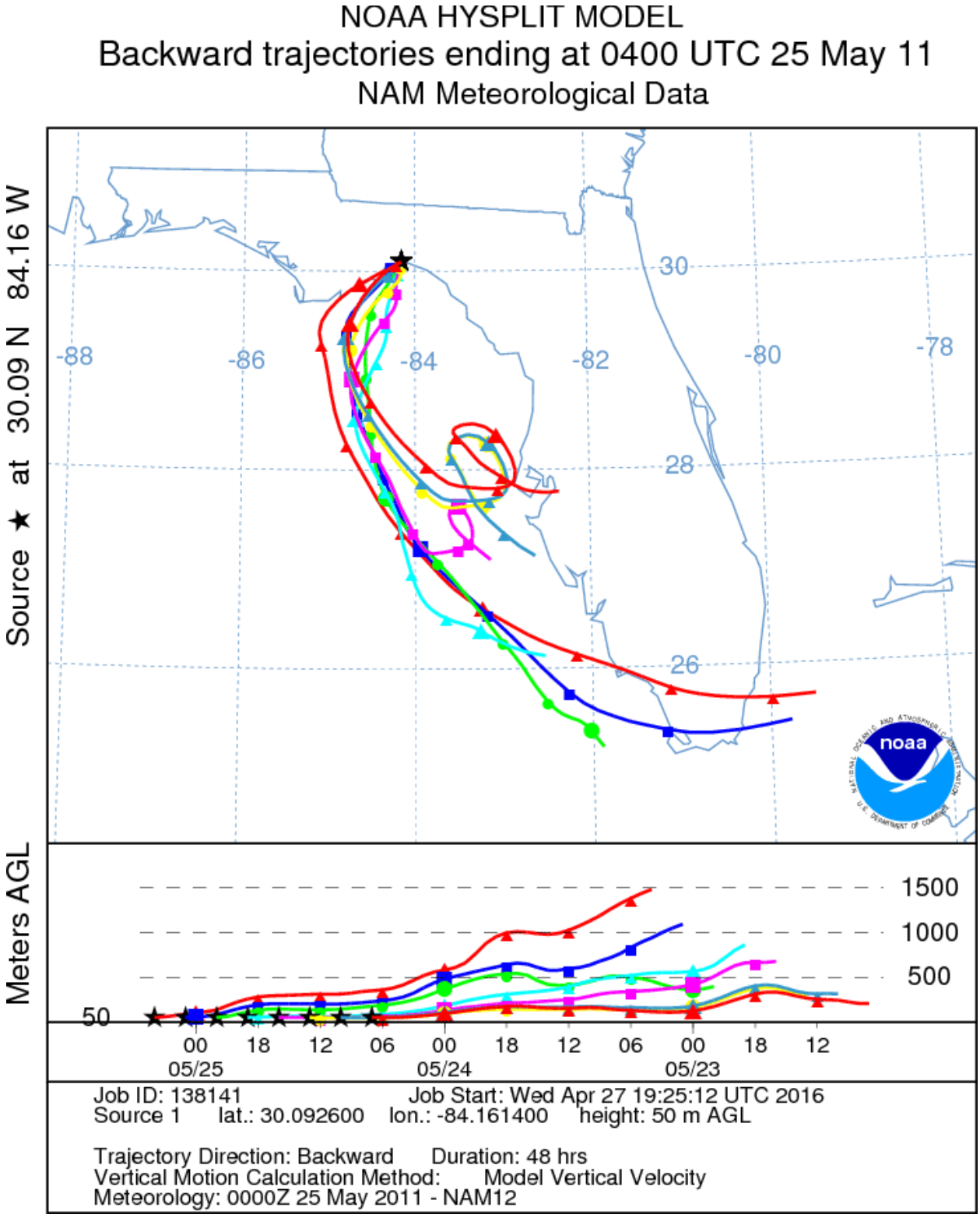
NOAA HYSPLIT MODEL
Backward trajectories ending at 0400 UTC 25 May 11
NAM Meteorological Data
Source ★ at 30.09 N 84.16 W
-88
-86
-84
-82
-80
-78
30
28
26
noaa
Meters AGL
1500
1000
500
50
00 18 12 06 00 18 12 06 00 18 12
05/25
05/24
05/23
Job ID: 138141 Job Start: Wed Apr 27 19:25:12 UTC 2016
Source 1 lat.: 30.092600 lon.: -84.161400 height: 50 m AGL
Trajectory Direction: Backward Duration: 48 hrs
Vertical Motion Calculation Method: Model Vertical Velocity
Meteorology: 0000Z 25 May 2011 - NAM12

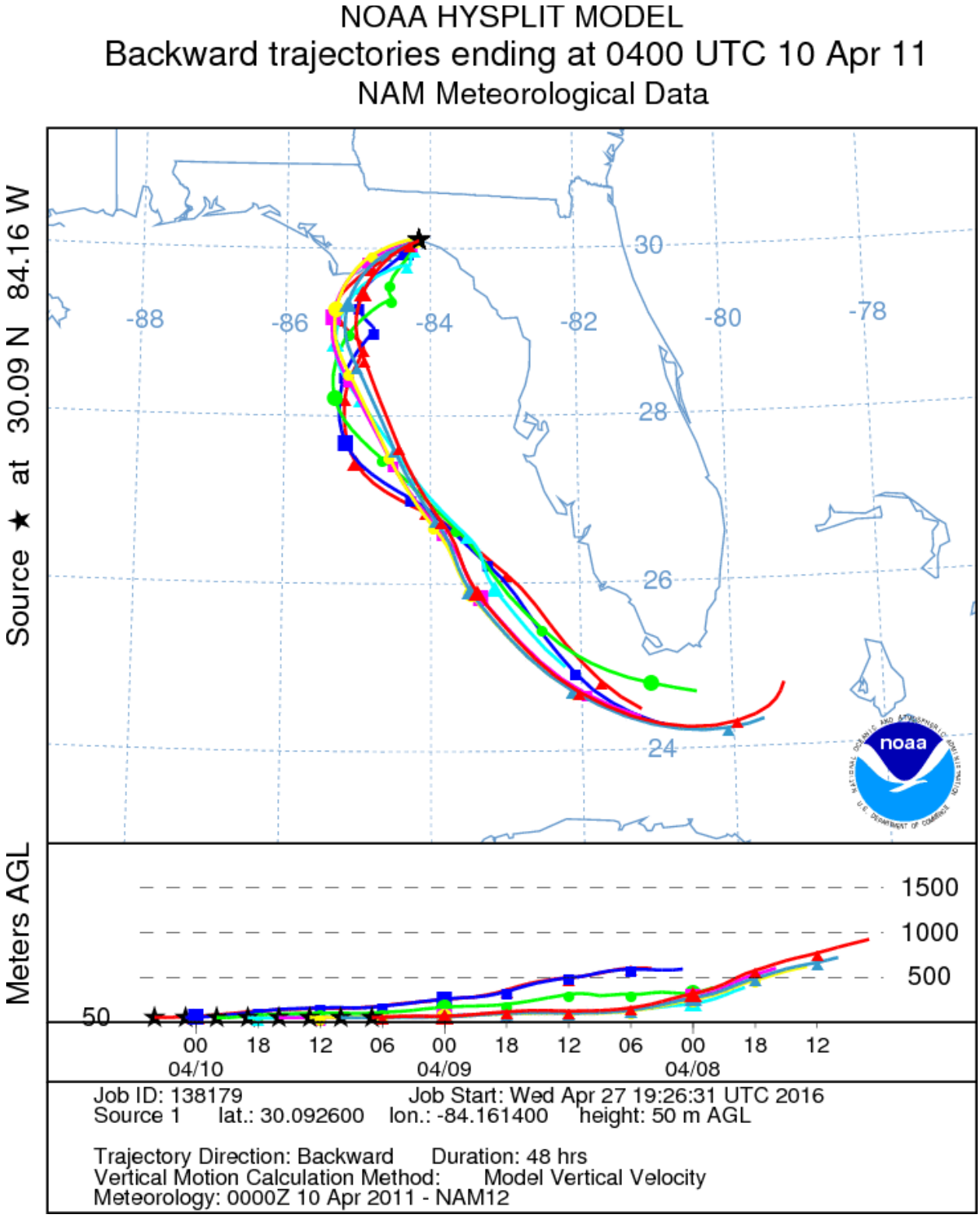
NOAA HYSPLIT MODEL
Backward trajectories ending at 0400 UTC 10 Apr 11
NAM Meteorological Data
Source ★ at 30.09 N 84.16 W
-88
-86
-84
-82
-80
-78
30
28
26
24
noaa
Meters AGL
1500
1000
500
50
00 18 12 06 00 18 12 06 00 18 12
04/10
04/09
04/08
Job ID: 138179 Job Start: Wed Apr 27 19:26:31 UTC 2016
Source 1 lat.: 30.092600 lon.: -84.161400 height: 50 m AGL
Trajectory Direction: Backward Duration: 48 hrs
Vertical Motion Calculation Method: Model Vertical Velocity
Meteorology: 0000Z 10 Apr 2011 - NAM12

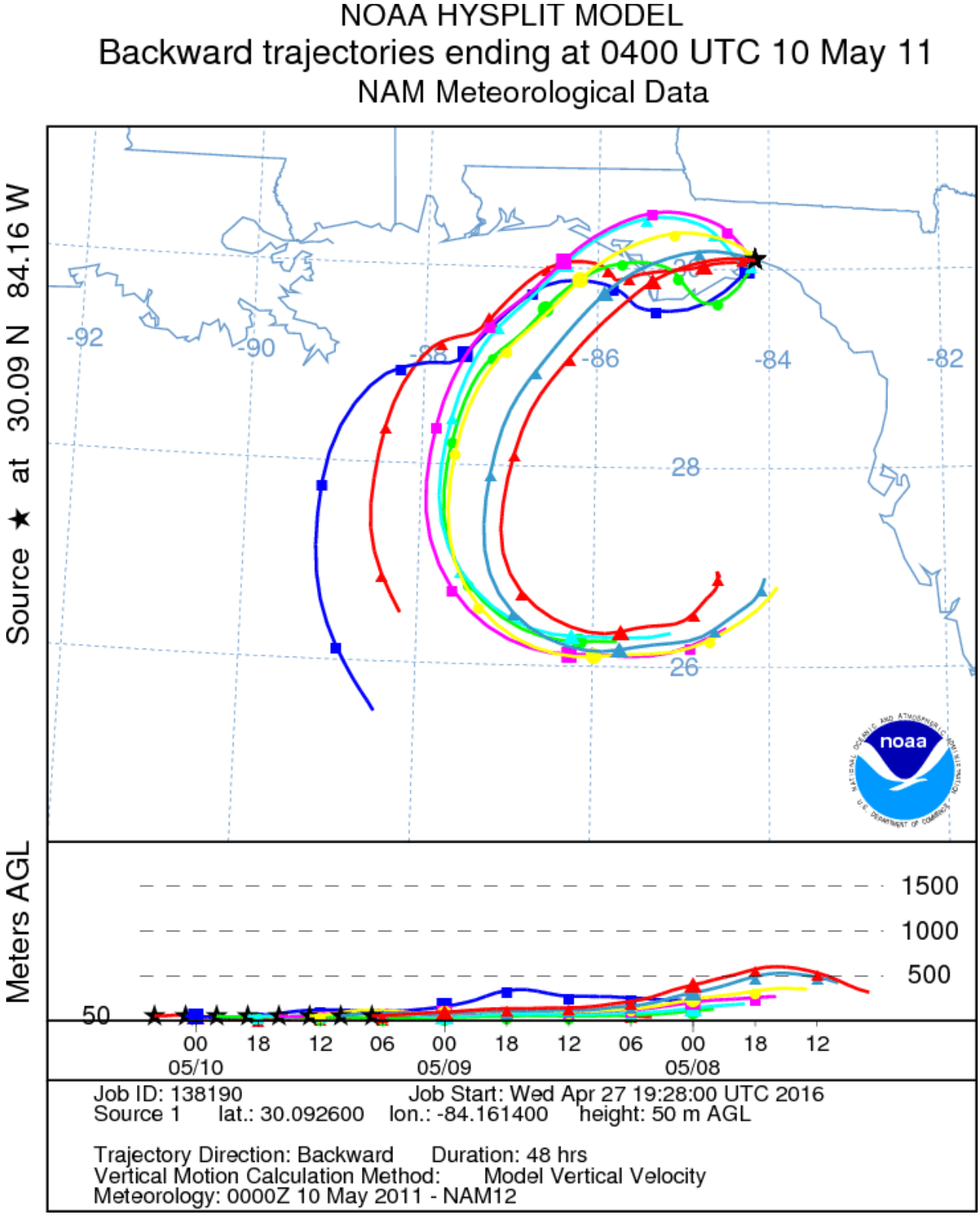
NOAA HYSPLIT MODEL
Backward trajectories ending at 0400 UTC 10 May 11
NAM Meteorological Data
Source ★ at 30.09 N 84.16 W
-92
-90
-86
-84
-82
28
26
noaa
Meters AGL
1500
1000
500
50
00 18 12 06 00 18 12 06 00 18 12
05/10
05/09
05/08
Job ID: 138190 Job Start: Wed Apr 27 19:28:00 UTC 2016
Source 1 lat.: 30.092600 lon.: -84.161400 height: 50 m AGL
Trajectory Direction: Backward Duration: 48 hrs
Vertical Motion Calculation Method: Model Vertical Velocity
Meteorology: 0000Z 10 May 2011 - NAM12

NOAA HYSPLIT MODEL
Backward trajectories ending at 0400 UTC 03 May 10
NAM Meteorological Data

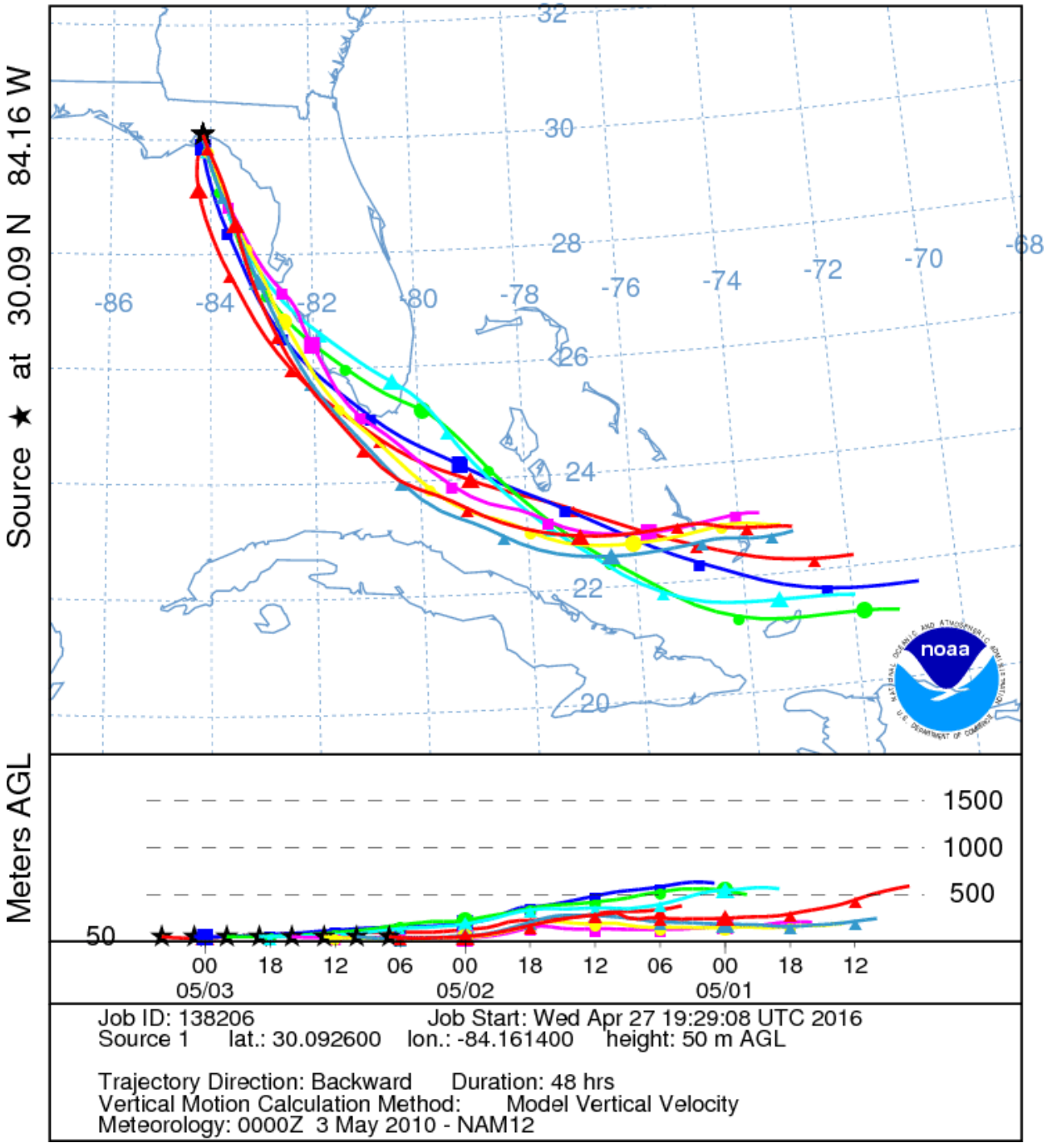

Job ID: 138206 Job Start: Wed Apr 27 19:29:08 UTC 2016
Source 1 lat.: 30.092600 lon.: -84.161400 height: 50 m AGL

Trajectory Direction: Backward Duration: 48 hrs
Vertical Motion Calculation Method: Model Vertical Velocity
Meteorology: 0000Z 3 May 2010 - NAM12

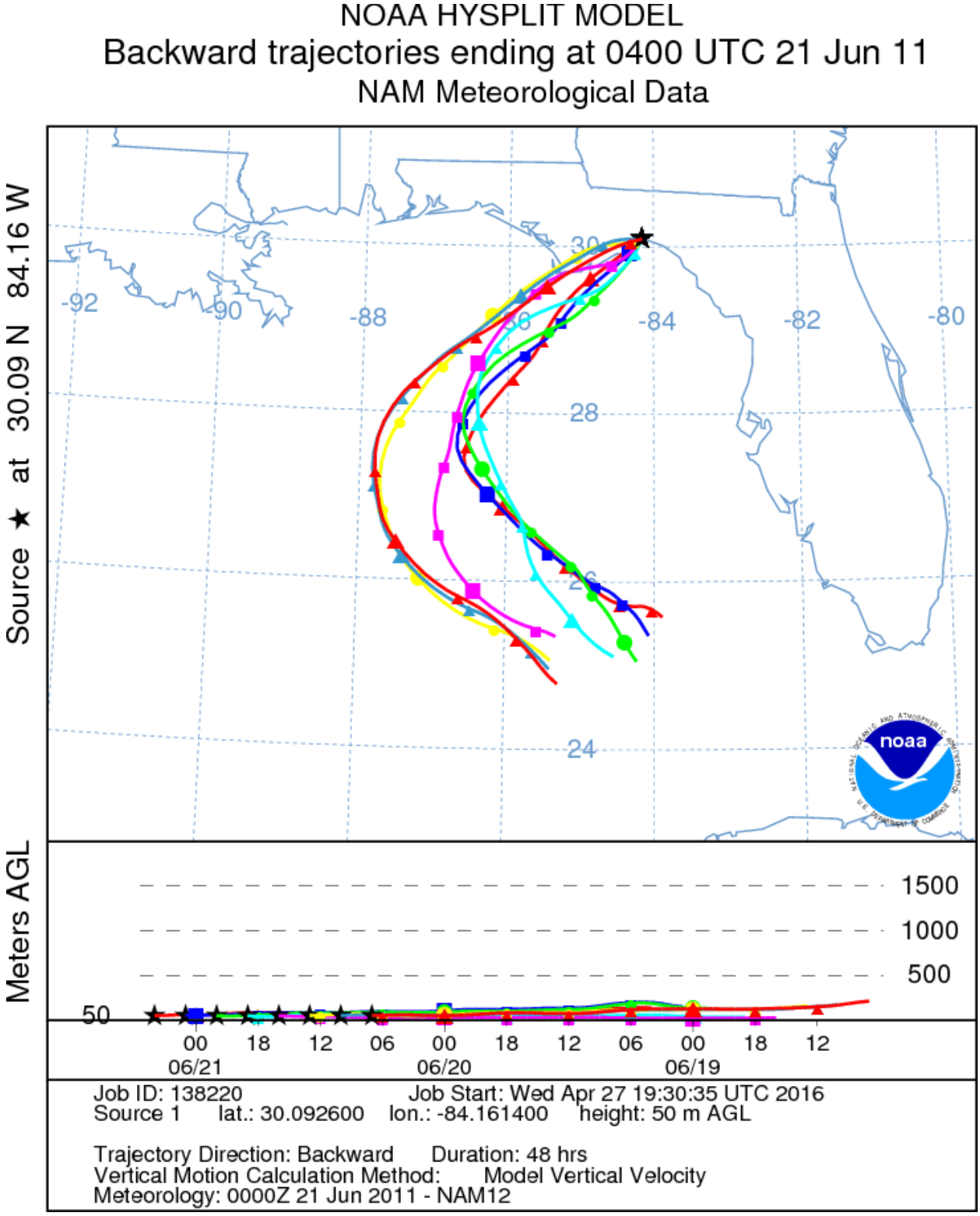
NOAA HYSPLIT MODEL
Backward trajectories ending at 0400 UTC 21 Jun 11
NAM Meteorological Data
Source ★ at 30.09 N 84.16 W
-92
-90
-88
-86
-84
-82
-80
30
28
26
24
noaa
Meters AGL
1500
1000
500
50
00 18 12 06 00 18 12 06 00 18 12
06/21 06/20 06/19
Job ID: 138220 Job Start: Wed Apr 27 19:30:35 UTC 2016
Source 1 lat.: 30.092600 lon.: -84.161400 height: 50 m AGL
Trajectory Direction: Backward Duration: 48 hrs
Vertical Motion Calculation Method: Model Vertical Velocity
Meteorology: 0000Z 21 Jun 2011 - NAM12

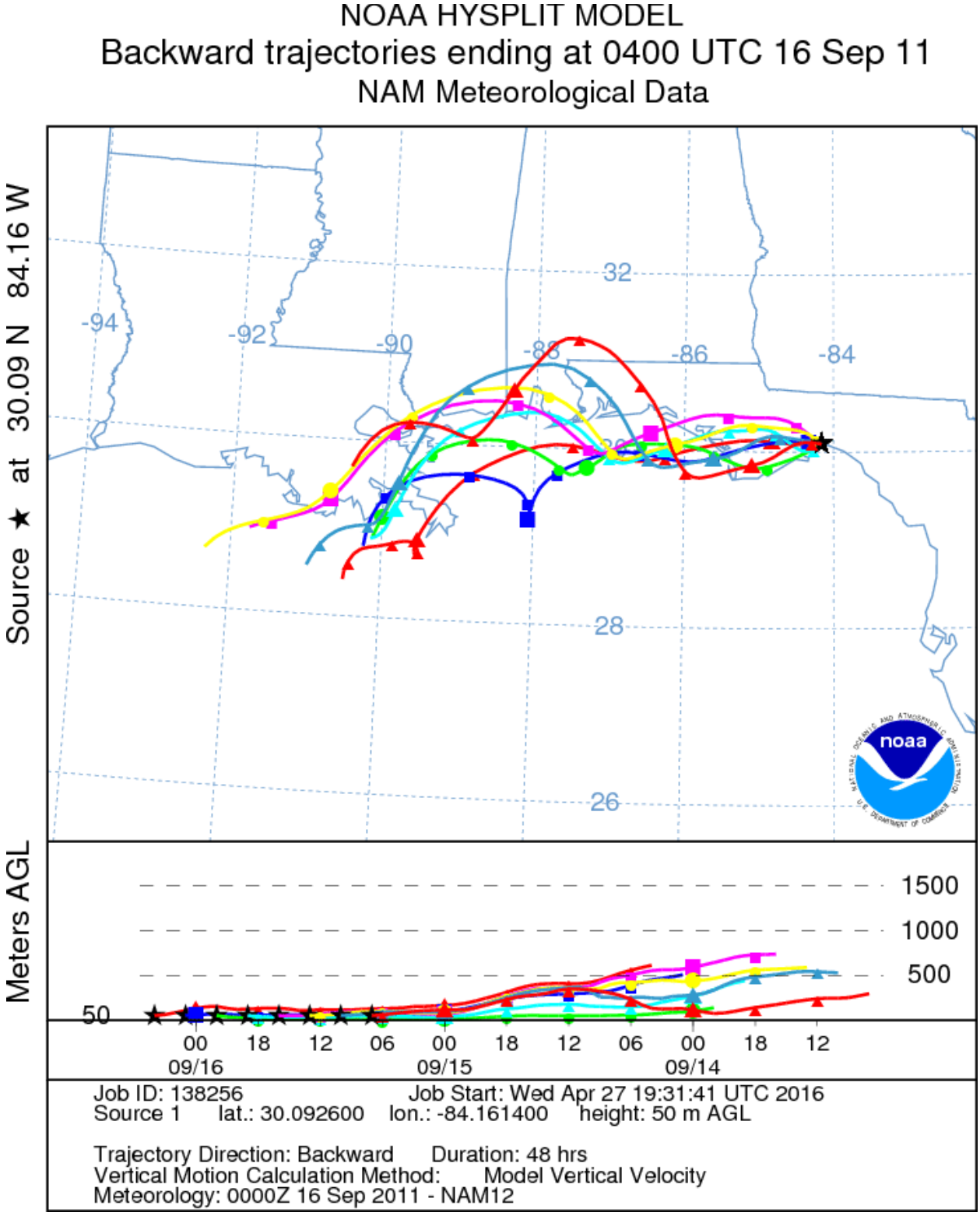
NOAA HYSPLIT MODEL
Backward trajectories ending at 0400 UTC 16 Sep 11
NAM Meteorological Data
Source ★ at 30.09 N 84.16 W
Meters AGL
1500
1000
500
50
00 18 12 06 00 18 12 06 00 18 12
09/16 09/15 09/14
Job ID: 138256 Job Start: Wed Apr 27 19:31:41 UTC 2016
Source 1 lat.: 30.092600 lon.: -84.161400 height: 50 m AGL
Trajectory Direction: Backward Duration: 48 hrs
Vertical Motion Calculation Method: Model Vertical Velocity
Meteorology: 0000Z 16 Sep 2011 - NAM12

SNPA HYSPLIT back-trajectories

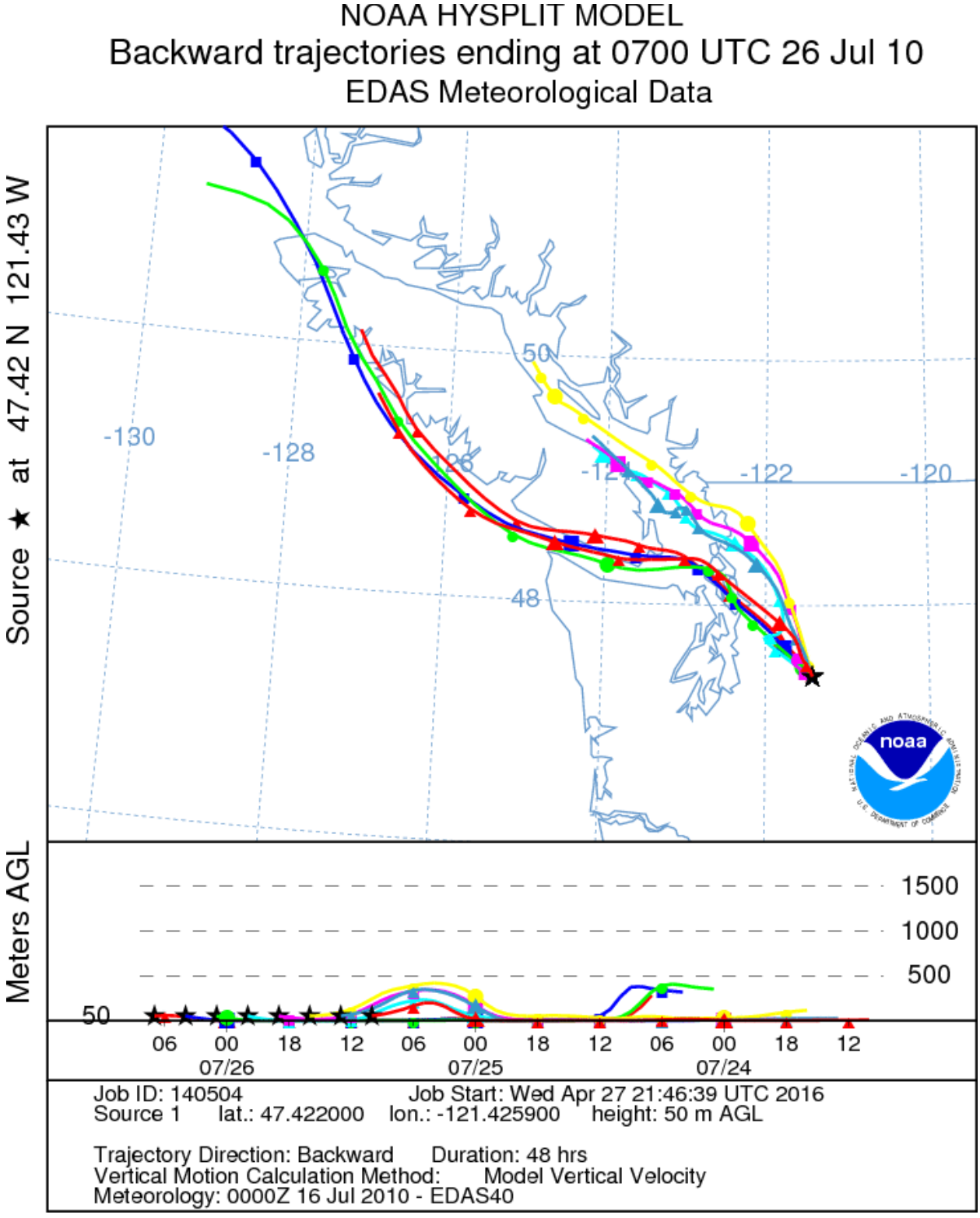
NOAA HYSPLIT MODEL
Backward trajectories ending at 0700 UTC 26 Jul 10
EDAS Meteorological Data
Source ★ at 47.42 N 121.43 W
-130
-128
-126
-124
-122
-120
50
48
noaa
Meters AGL
1500
1000
500
50
06 00 18 12 06 00 18 12 06 00 18 12
07/26
07/25
07/24
Job ID: 140504 Job Start: Wed Apr 27 21:46:39 UTC 2016
Source 1 lat.: 47.422000 lon.: -121.425900 height: 50 m AGL
Trajectory Direction: Backward Duration: 48 hrs
Vertical Motion Calculation Method: Model Vertical Velocity
Meteorology: 0000Z 16 Jul 2010 - EDAS40

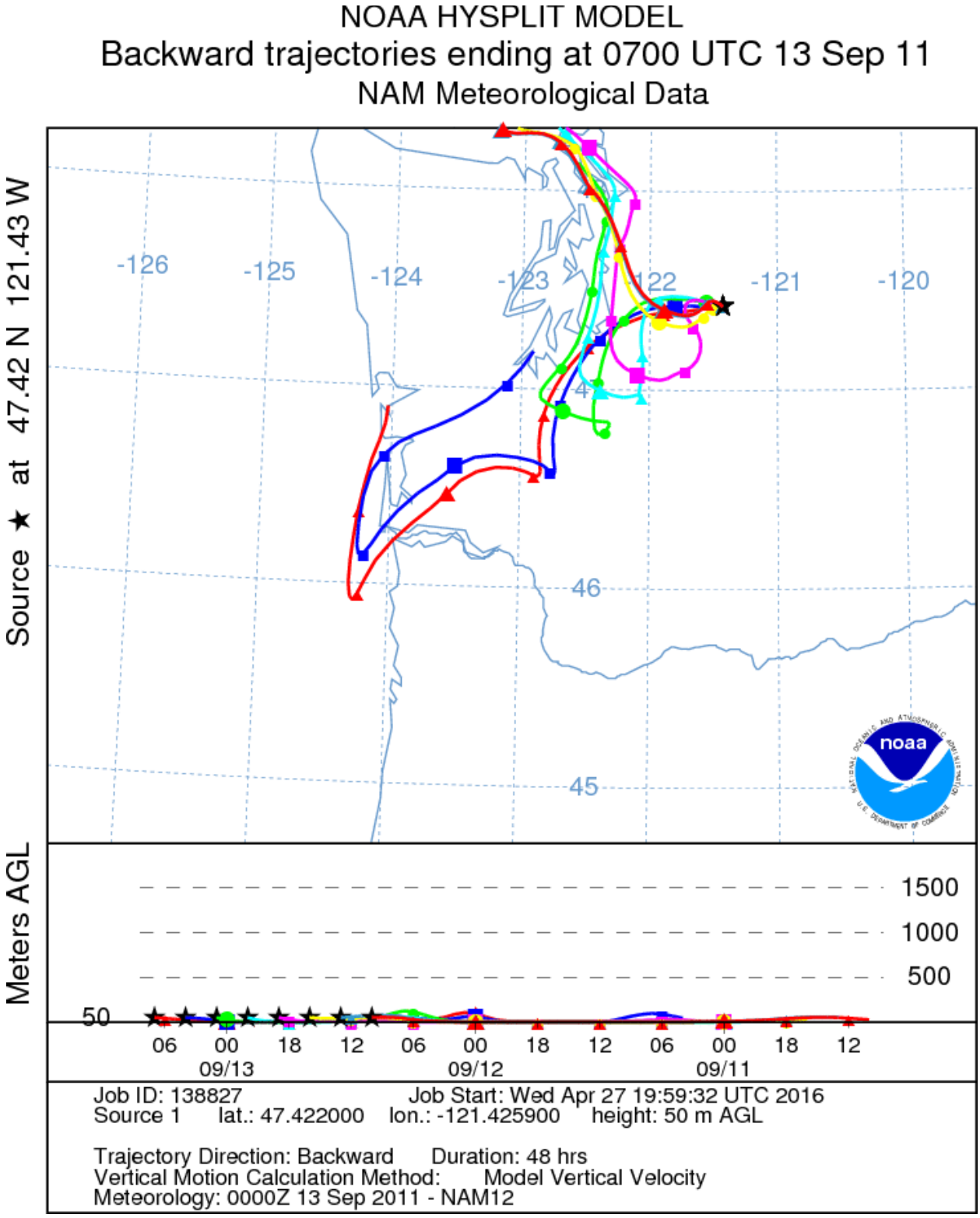
NOAA HYSPLIT MODEL
Backward trajectories ending at 0700 UTC 13 Sep 11
NAM Meteorological Data
Source ★ at 47.42 N 121.43 W
-126
-125
-124
-123
-122
-121
-120
46
45
noaa
Meters AGL
1500
1000
500
50
06 00 18 12 06 00 18 12 06 00 18 12
09/13
09/12
09/11
Job ID: 138827 Job Start: Wed Apr 27 19:59:32 UTC 2016
Source 1 lat.: 47.422000 lon.: -121.425900 height: 50 m AGL
Trajectory Direction: Backward Duration: 48 hrs
Vertical Motion Calculation Method: Model Vertical Velocity
Meteorology: 0000Z 13 Sep 2011 - NAM12

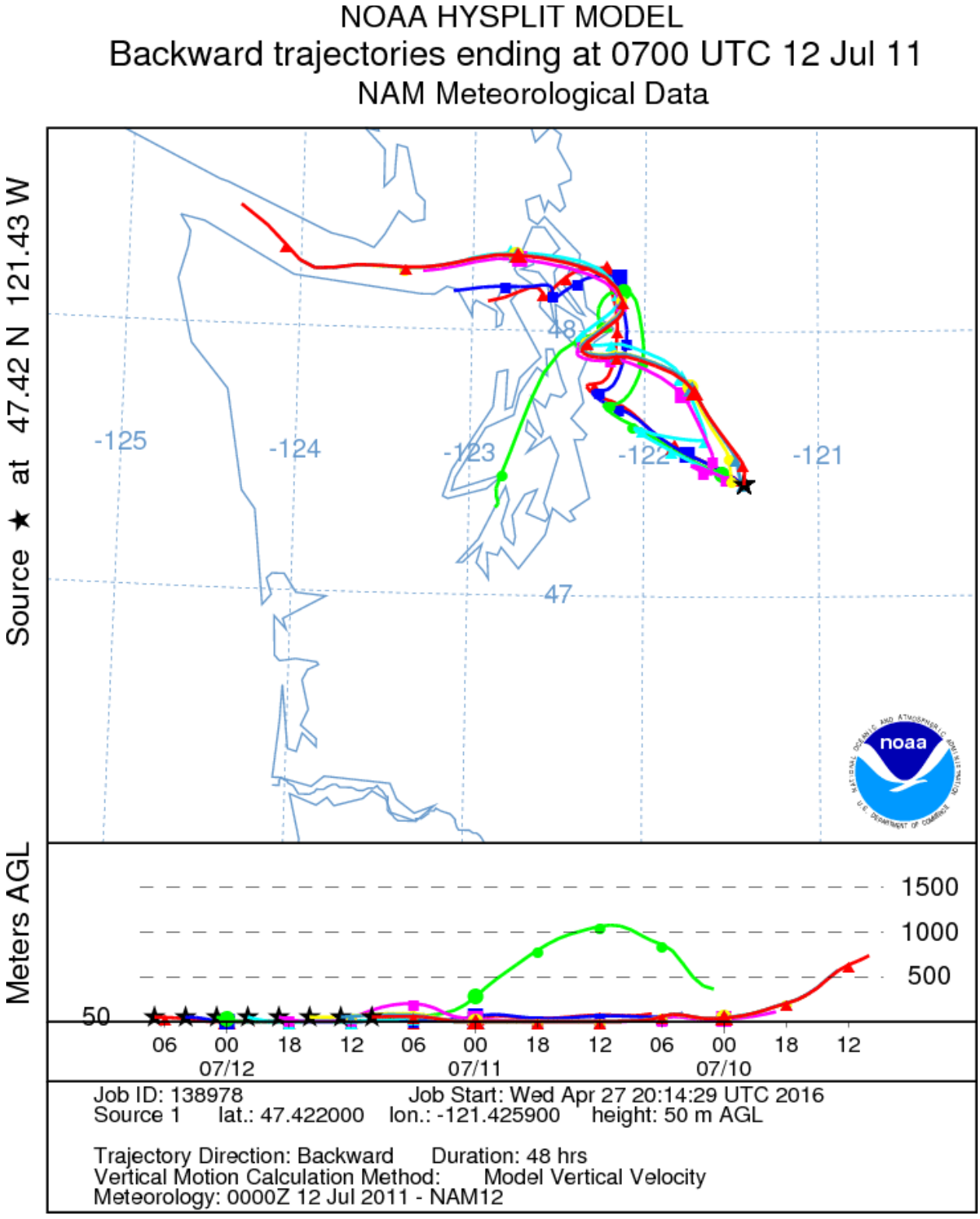
NOAA HYSPLIT MODEL
Backward trajectories ending at 0700 UTC 12 Jul 11
NAM Meteorological Data
Source ★ at 47.42 N 121.43 W
-125
-124
-123
-122
-121
48
47
noaa
Meters AGL
1500
1000
500
50
06 00 18 12 06 00 18 12 06 00 18 12
07/12
07/11
07/10
Job ID: 138978 Job Start: Wed Apr 27 20:14:29 UTC 2016
Source 1 lat.: 47.422000 lon.: -121.425900 height: 50 m AGL
Trajectory Direction: Backward Duration: 48 hrs
Vertical Motion Calculation Method: Model Vertical Velocity
Meteorology: 0000Z 12 Jul 2011 - NAM12

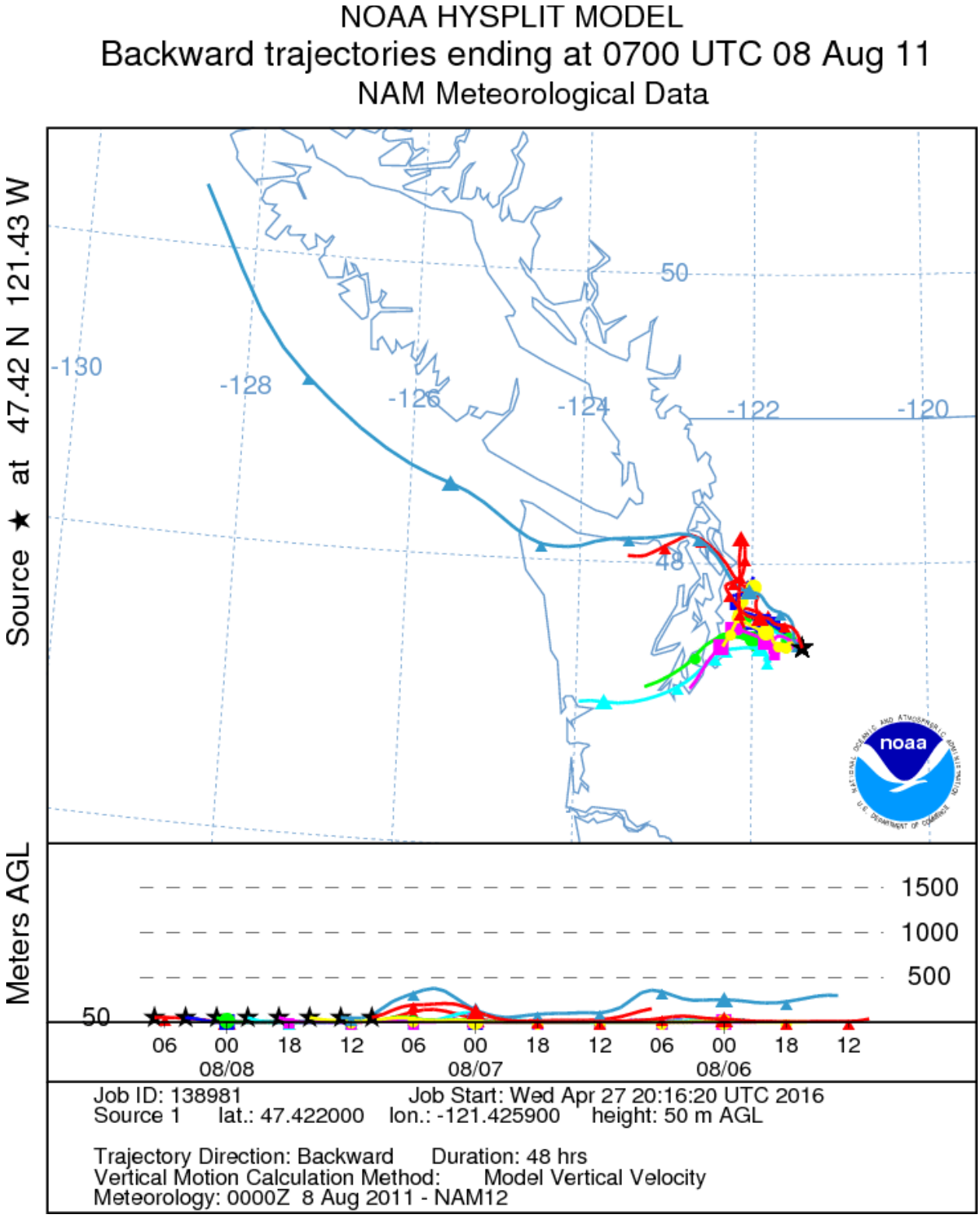
NOAA HYSPLIT MODEL
Backward trajectories ending at 0700 UTC 08 Aug 11
NAM Meteorological Data
Source ★ at 47.42 N 121.43 W
-130
-128
-126
-124
-122
-120
50
48
noaa
Meters AGL
1500
1000
500
50
06 00 18 12 06 00 18 12 06 00 18 12
08/08
08/07
08/06
Job ID: 138981
Job Start: Wed Apr 27 20:16:20 UTC 2016
Source 1 lat.: 47.422000 lon.: -121.425900 height: 50 m AGL
Trajectory Direction: Backward Duration: 48 hrs
Vertical Motion Calculation Method: Model Vertical Velocity
Meteorology: 0000Z 8 Aug 2011 - NAM12

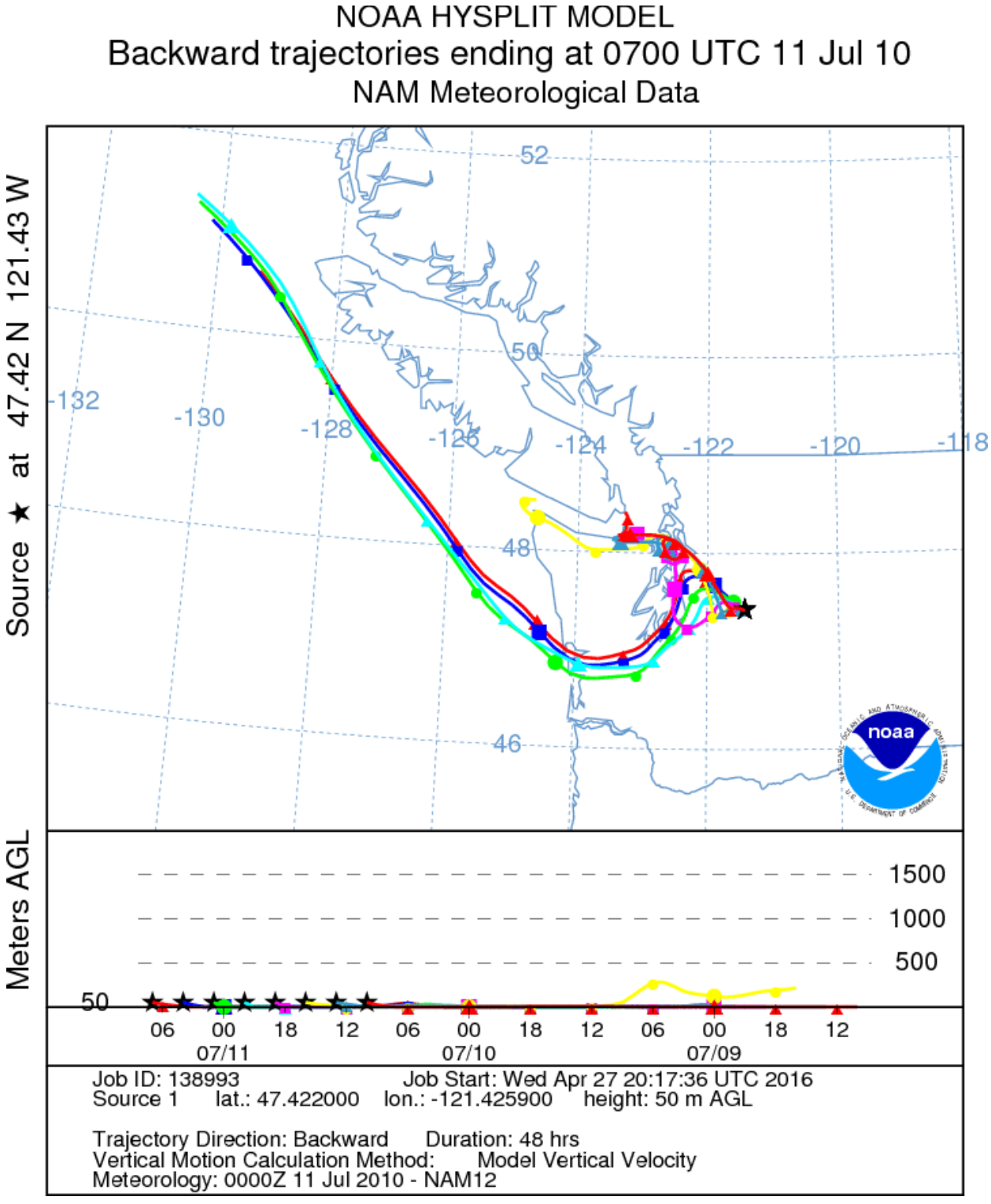
NOAA HYSPLIT MODEL
Backward trajectories ending at 0700 UTC 11 Jul 10
NAM Meteorological Data
Source ★ at 47.42 N 121.43 W
52
50
48
46
-132
-130
-128
-126
-124
-122
-120
-118
noaa
Meters AGL
1500
1000
500
50
06 00 18 12 06 00 18 12 06 00 18 12
07/11
07/10
07/09
Job ID: 138993 Job Start: Wed Apr 27 20:17:36 UTC 2016
Source 1 lat.: 47.422000 lon.: -121.425900 height: 50 m AGL
Trajectory Direction: Backward Duration: 48 hrs
Vertical Motion Calculation Method: Model Vertical Velocity
Meteorology: 0000Z 11 Jul 2010 - NAM12

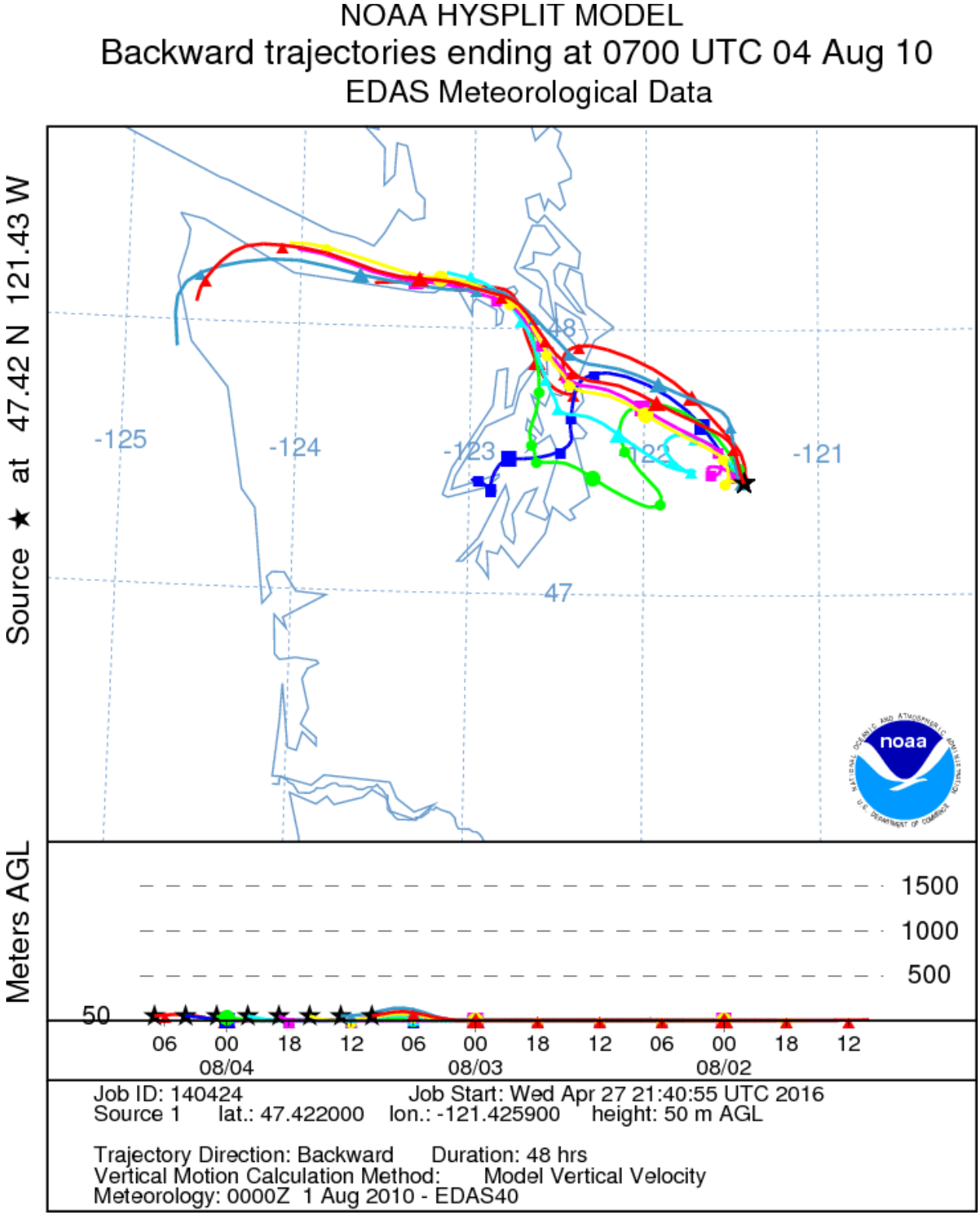
NOAA HYSPLIT MODEL
Backward trajectories ending at 0700 UTC 04 Aug 10
EDAS Meteorological Data
Source ★ at 47.42 N 121.43 W
-125
-124
-123
-122
-121
48
47
noaa
Meters AGL
1500
1000
500
50
06 00 18 12 06 00 18 12 06 00 18 12
08/04
08/03
08/02
Job ID: 140424 Job Start: Wed Apr 27 21:40:55 UTC 2016
Source 1 lat.: 47.422000 lon.: -121.425900 height: 50 m AGL
Trajectory Direction: Backward Duration: 48 hrs
Vertical Motion Calculation Method: Model Vertical Velocity
Meteorology: 0000Z 1 Aug 2010 - EDAS40

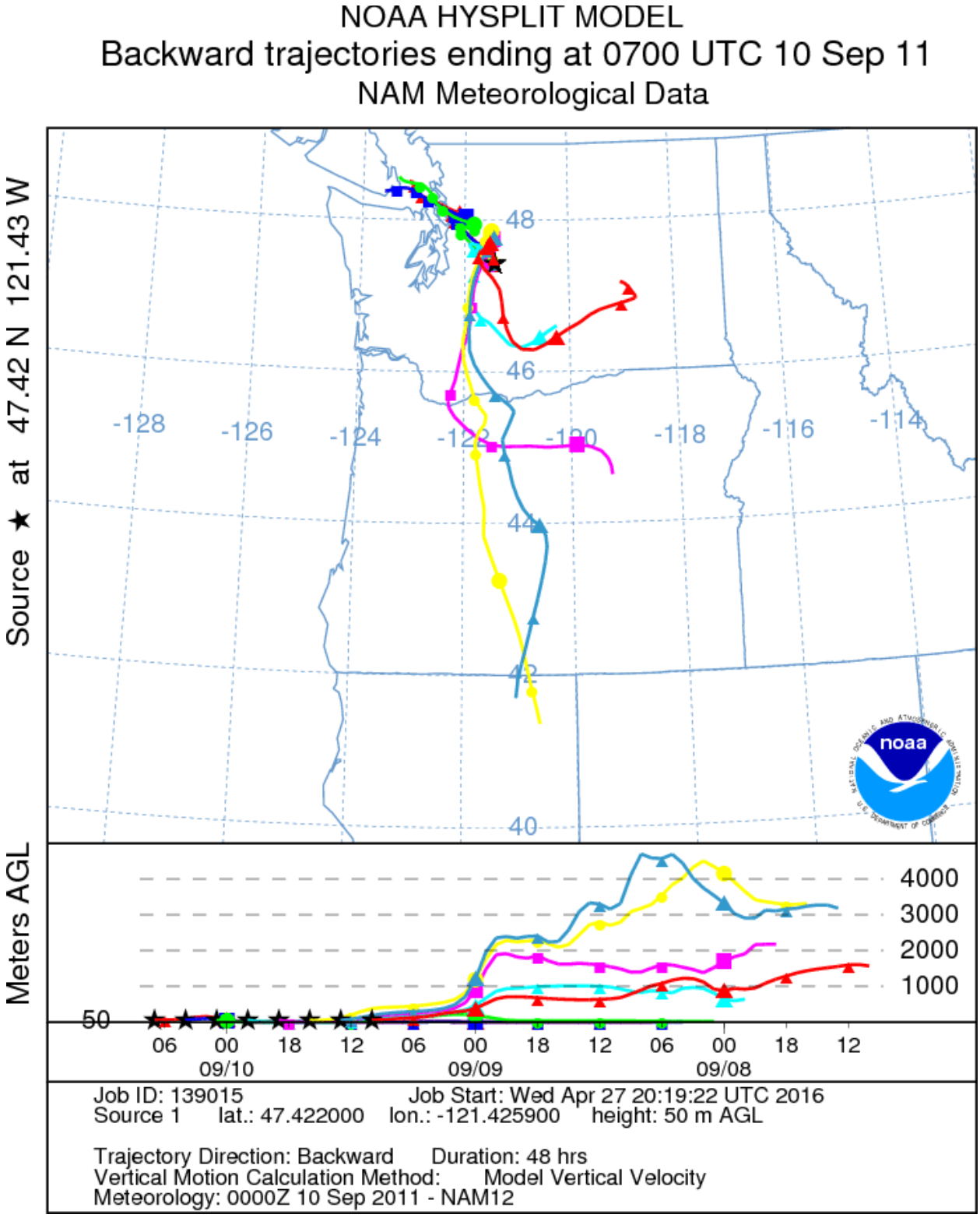
NOAA HYSPLIT MODEL
Backward trajectories ending at 0700 UTC 10 Sep 11
NAM Meteorological Data
Source ★ at 47.42 N 121.43 W
48
46
44
42
40
-128
-126
-124
-122
-120
-118
-116
-114
noaa
Meters AGL
4000
3000
2000
1000
50
06 00 18 12 06 00 18 12 06 00 18 12
09/10 09/09 09/08
Job ID: 139015 Job Start: Wed Apr 27 20:19:22 UTC 2016
Source 1 lat.: 47.422000 lon.: -121.425900 height: 50 m AGL
Trajectory Direction: Backward Duration: 48 hrs
Vertical Motion Calculation Method: Model Vertical Velocity
Meteorology: 0000Z 10 Sep 2011 - NAM12

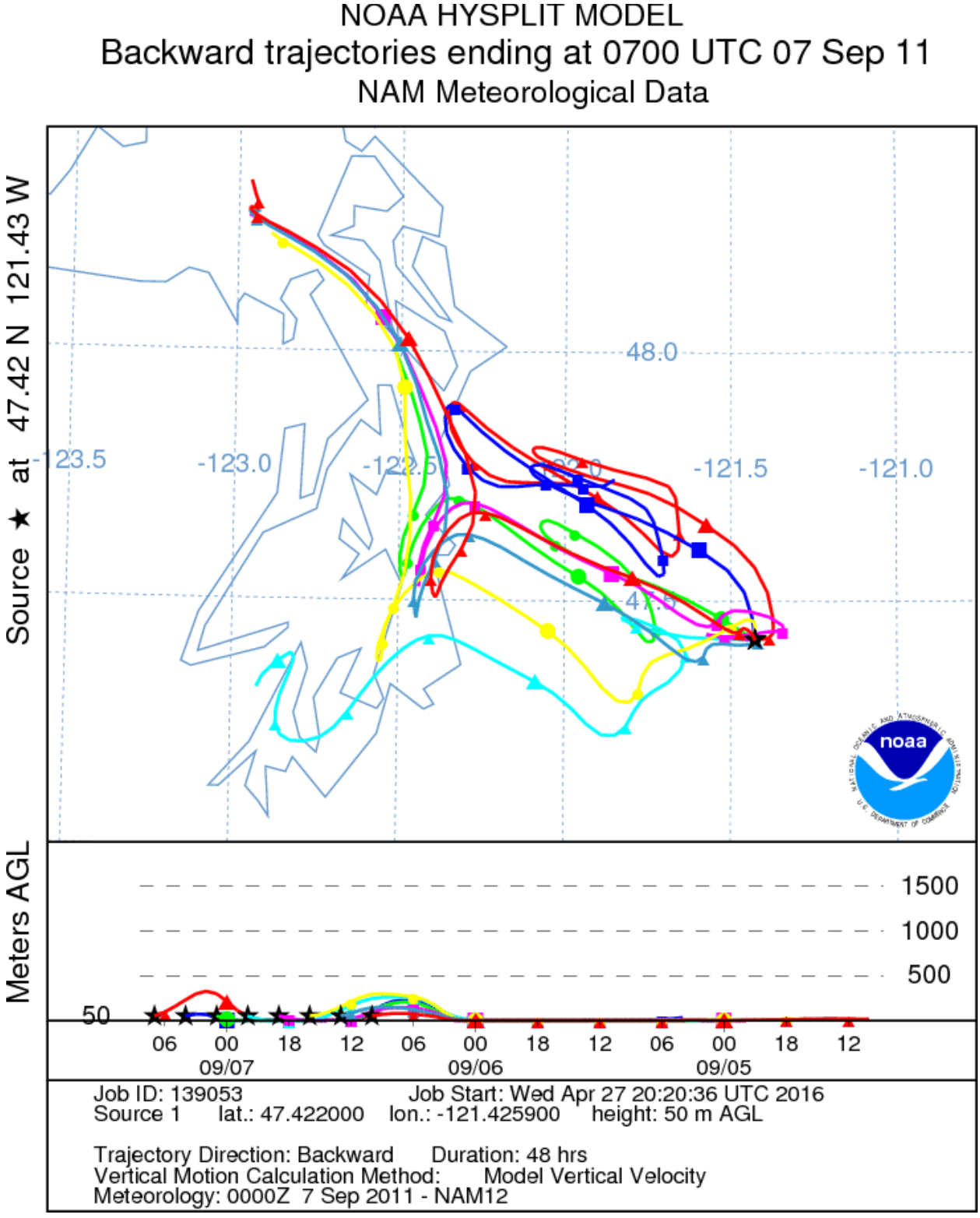
NOAA HYSPLIT MODEL
Backward trajectories ending at 0700 UTC 07 Sep 11
NAM Meteorological Data
Source ★ at 47.42 N 121.43 W
48.0
-123.5
-123.0
-121.5
-121.0
noaa
Meters AGL
1500
1000
500
50
06 00 18 12 06 00 18 12 06 00 18 12
09/07
09/06
09/05
Job ID: 139053 Job Start: Wed Apr 27 20:20:36 UTC 2016
Source 1 lat.: 47.422000 lon.: -121.425900 height: 50 m AGL
Trajectory Direction: Backward Duration: 48 hrs
Vertical Motion Calculation Method: Model Vertical Velocity
Meteorology: 0000Z 7 Sep 2011 - NAM12

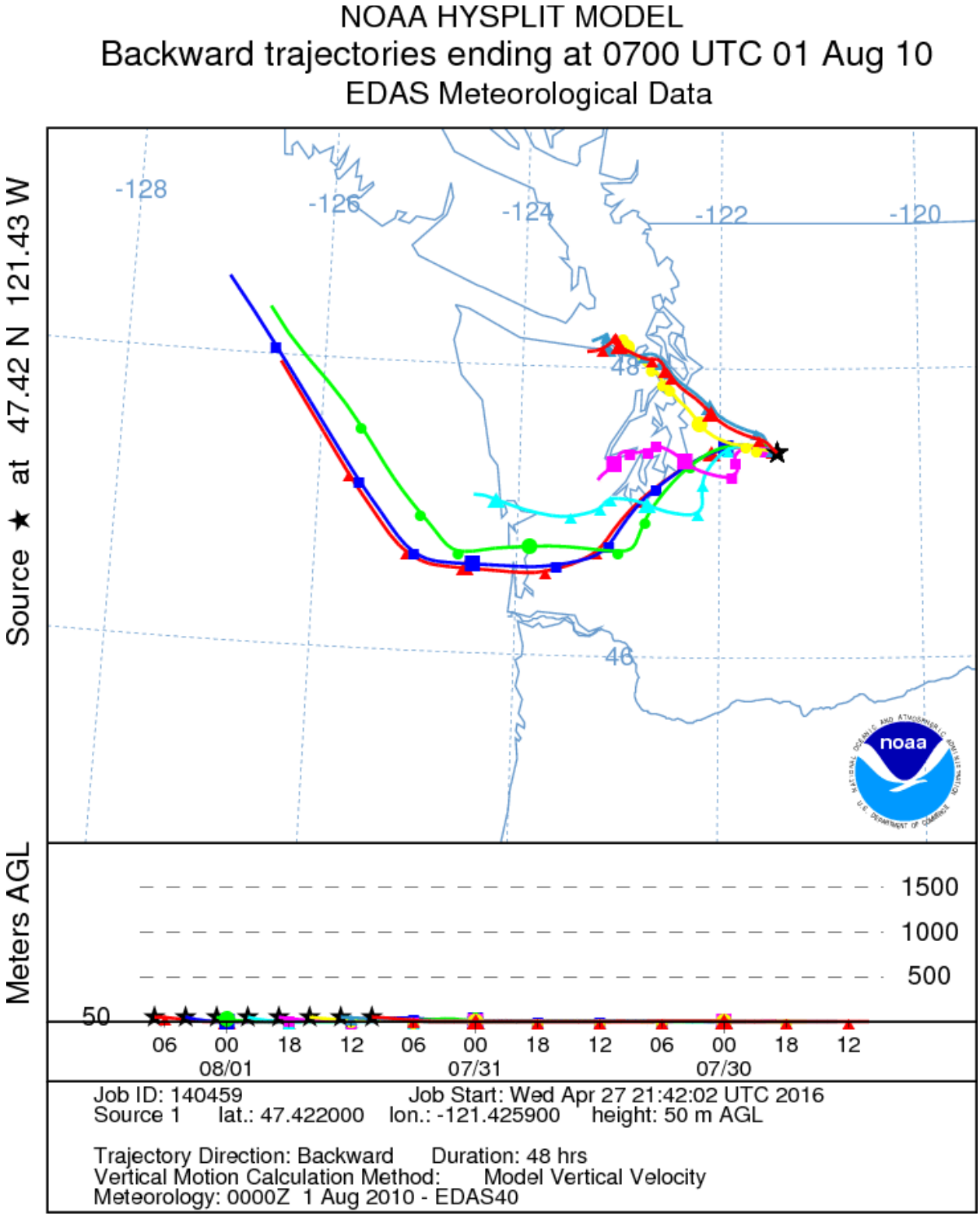
NOAA HYSPLIT MODEL
Backward trajectories ending at 0700 UTC 01 Aug 10
EDAS Meteorological Data
Source ★ at 47.42 N 121.43 W
-128
-126
-124
-122
-120
48
46
noaa
Meters AGL
1500
1000
500
50
06 00 18 12 06 00 18 12 06 00 18 12
08/01
07/31
07/30
Job ID: 140459
Job Start: Wed Apr 27 21:42:02 UTC 2016
Source 1 lat.: 47.422000 lon.: -121.425900 height: 50 m AGL
Trajectory Direction: Backward Duration: 48 hrs
Vertical Motion Calculation Method: Model Vertical Velocity
Meteorology: 0000Z 1 Aug 2010 - EDAS40

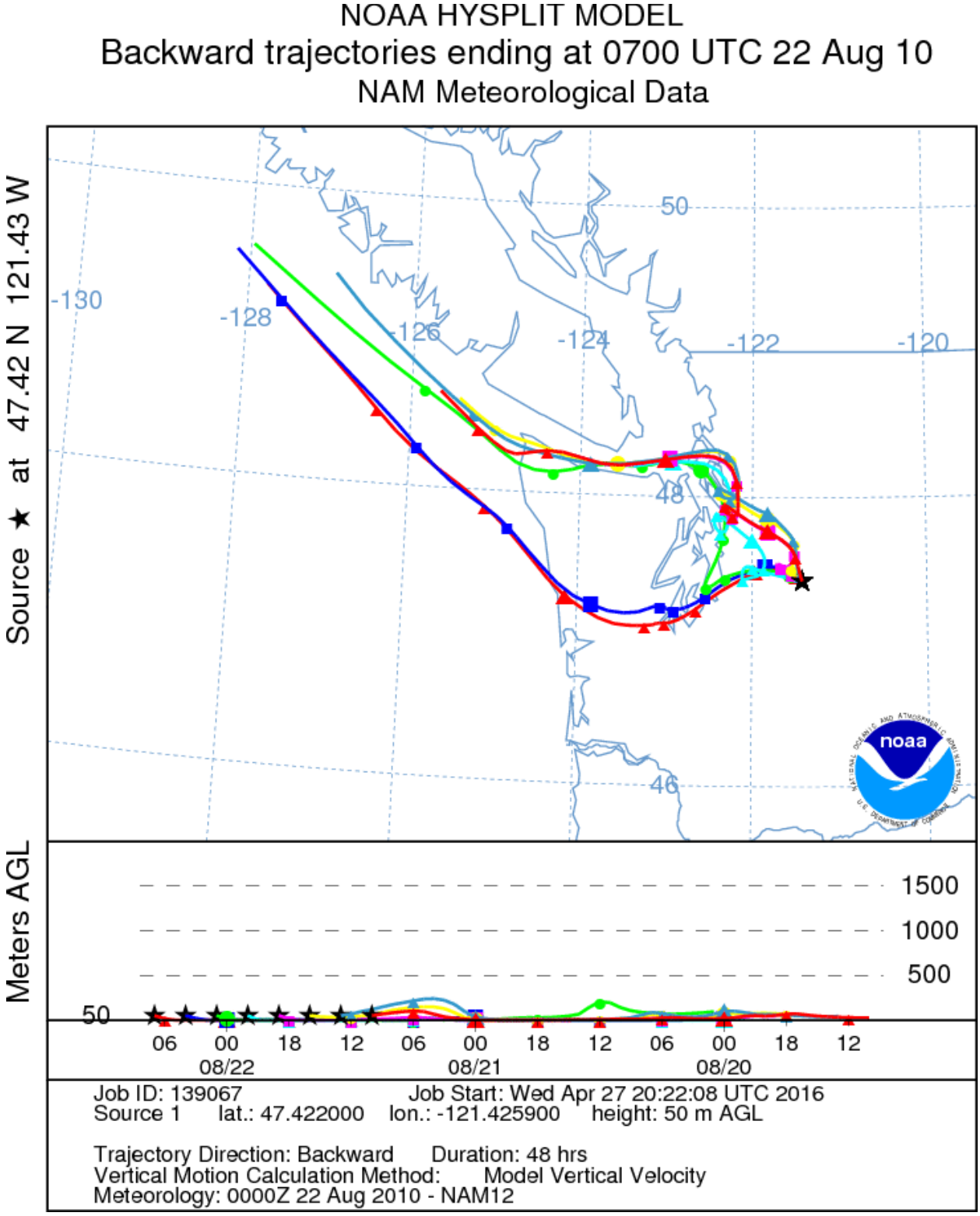
NOAA HYSPLIT MODEL
Backward trajectories ending at 0700 UTC 22 Aug 10
NAM Meteorological Data
Source ★ at 47.42 N 121.43 W
-130
-128
-126
-124
-122
-120
50
48
46
noaa
Meters AGL
1500
1000
500
50
06 00 18 12 06 00 18 12 06 00 18 12
08/22
08/21
08/20
Job ID: 139067
Job Start: Wed Apr 27 20:22:08 UTC 2016
Source 1 lat.: 47.422000 lon.: -121.425900 height: 50 m AGL
Trajectory Direction: Backward Duration: 48 hrs
Vertical Motion Calculation Method: Model Vertical Velocity
Meteorology: 0000Z 22 Aug 2010 - NAM12

SWAN HYSPLIT back-trajectories

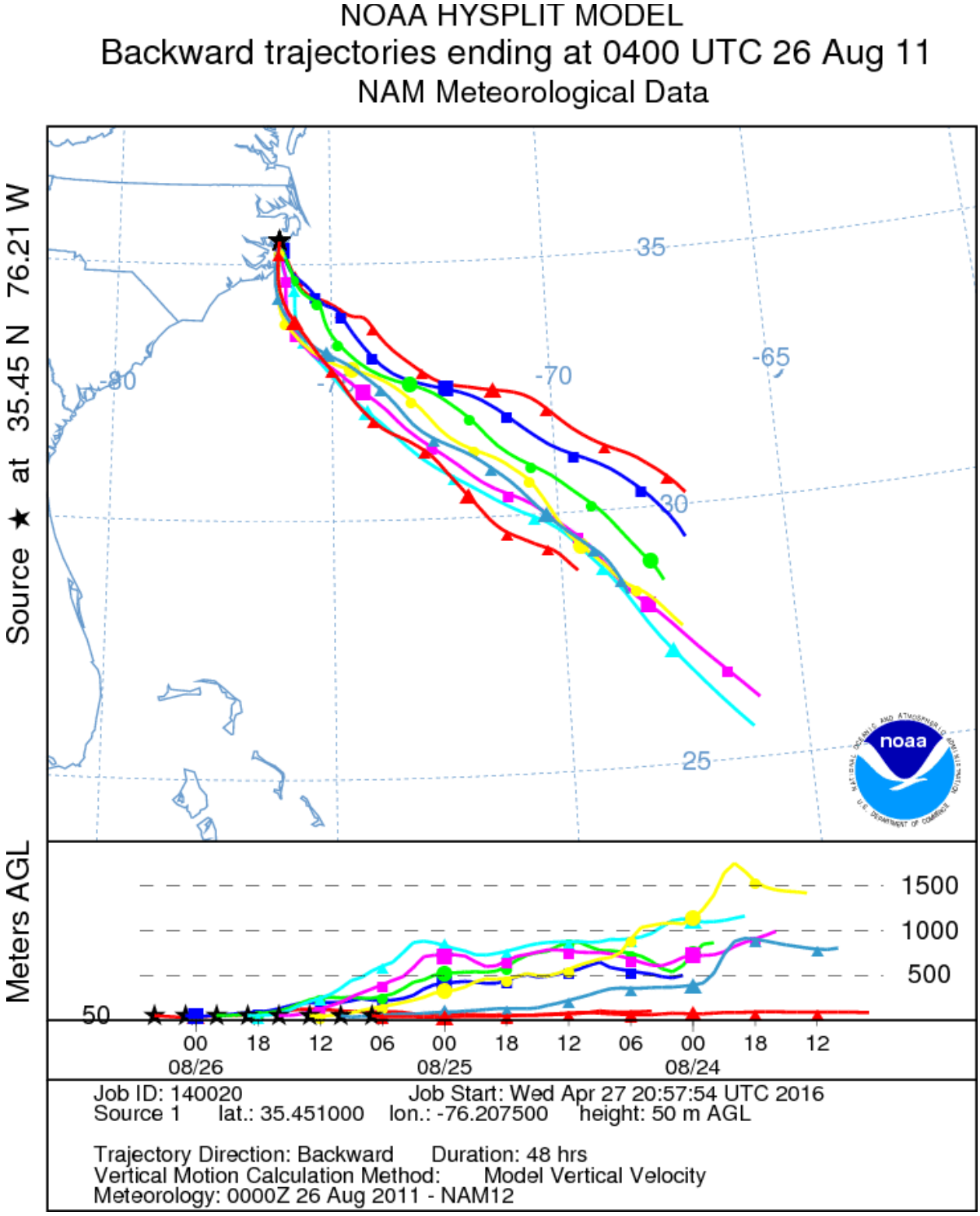
NOAA HYSPLIT MODEL
Backward trajectories ending at 0400 UTC 26 Aug 11
NAM Meteorological Data
Source ★ at 35.45 N 76.21 W
35
-65
-70
30
25
noaa
Meters AGL
1500
1000
500
50
00 18 12 06 00 18 12 06 00 18 12
08/26
08/25
08/24
Job ID: 140020 Job Start: Wed Apr 27 20:57:54 UTC 2016
Source 1 lat.: 35.451000 lon.: -76.207500 height: 50 m AGL
Trajectory Direction: Backward Duration: 48 hrs
Vertical Motion Calculation Method: Model Vertical Velocity
Meteorology: 0000Z 26 Aug 2011 - NAM12

NOAA HYSPLIT MODEL
Backward trajectories ending at 0400 UTC 19 Mar 10
NAM Meteorological Data

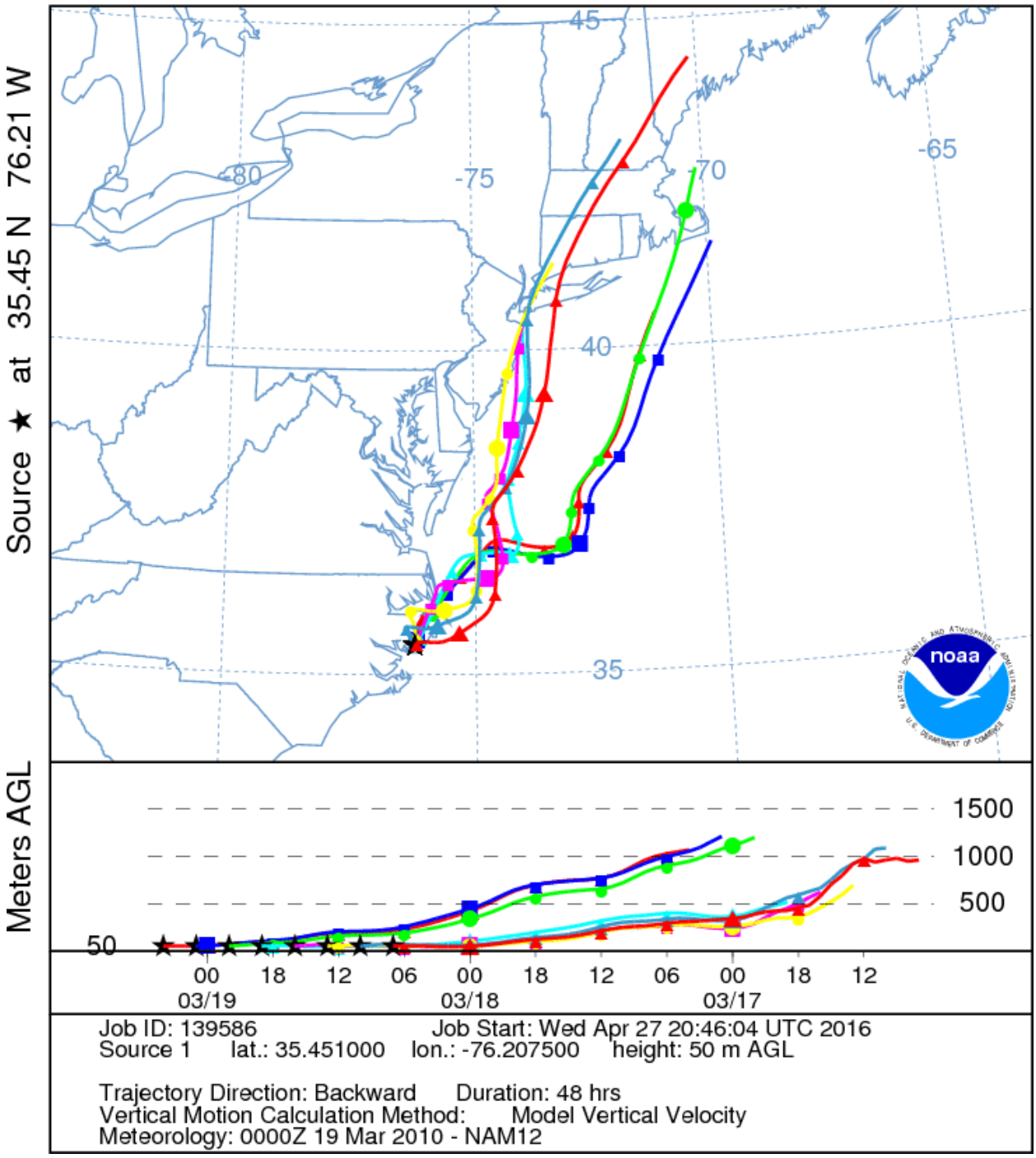

NOAA HYSPLIT MODEL
Backward trajectories ending at 0400 UTC 21 Jul 11
NAM Meteorological Data

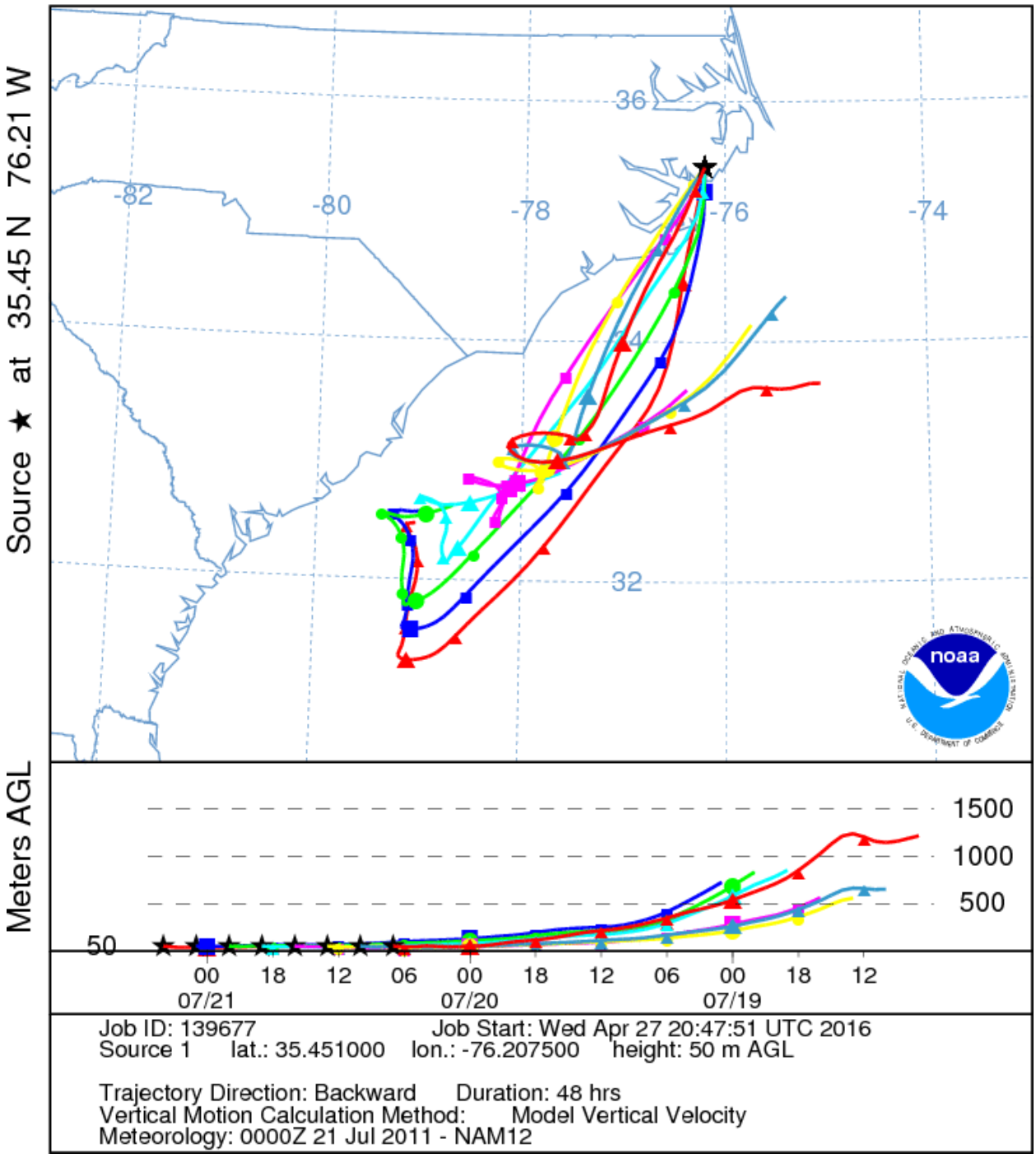

Job ID: 139677 Job Start: Wed Apr 27 20:47:51 UTC 2016
Source 1 lat.: 35.451000 lon.: -76.207500 height: 50 m AGL

Trajectory Direction: Backward Duration: 48 hrs
Vertical Motion Calculation Method: Model Vertical Velocity
Meteorology: 0000Z 21 Jul 2011 - NAM12

NOAA HYSPLIT MODEL
Backward trajectories ending at 0400 UTC 25 May 11
NAM Meteorological Data

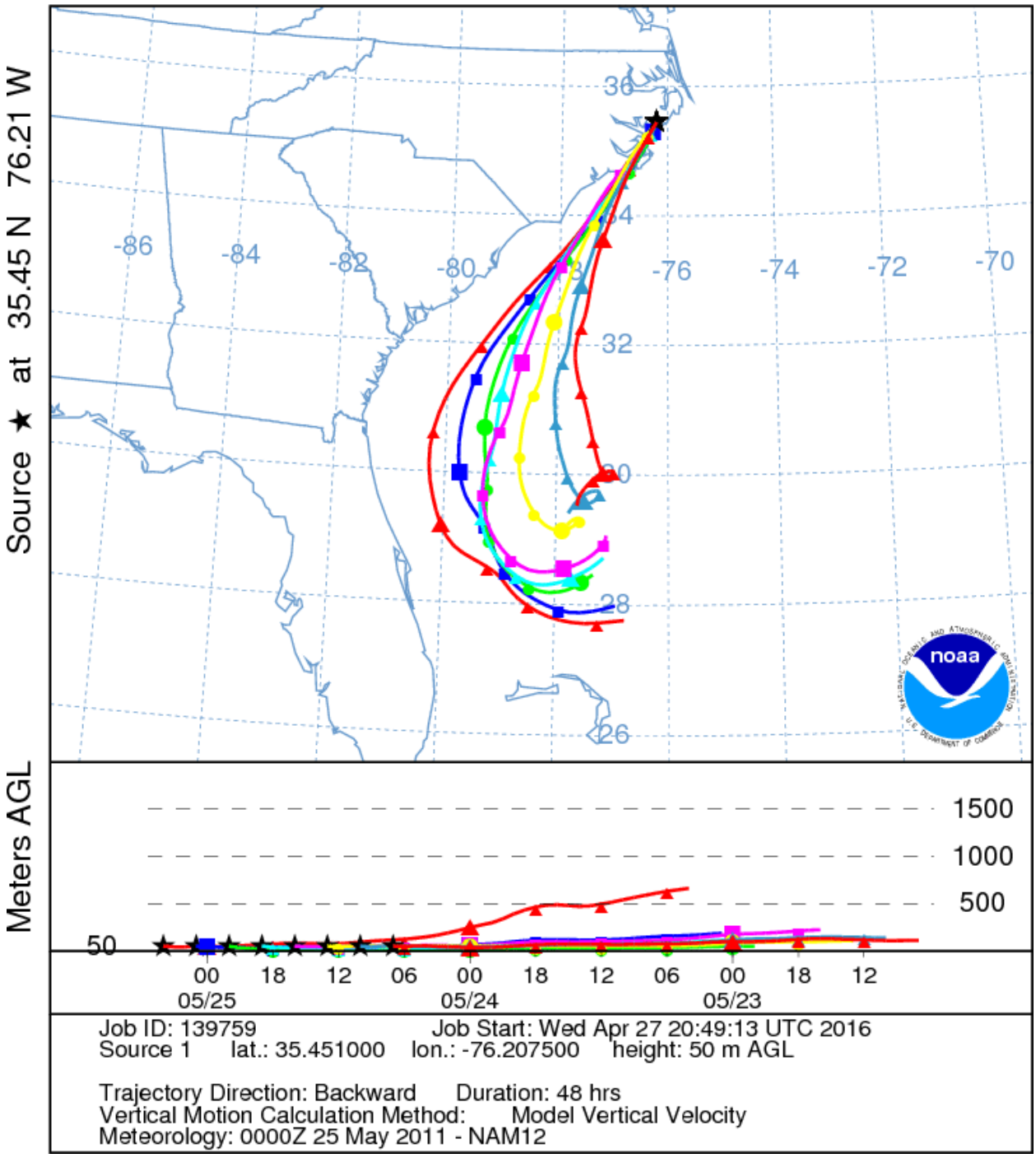

Job ID: 139759 Job Start: Wed Apr 27 20:49:13 UTC 2016
Source 1 lat.: 35.451000 lon.: -76.207500 height: 50 m AGL

Trajectory Direction: Backward Duration: 48 hrs
Vertical Motion Calculation Method: Model Vertical Velocity
Meteorology: 0000Z 25 May 2011 - NAM12

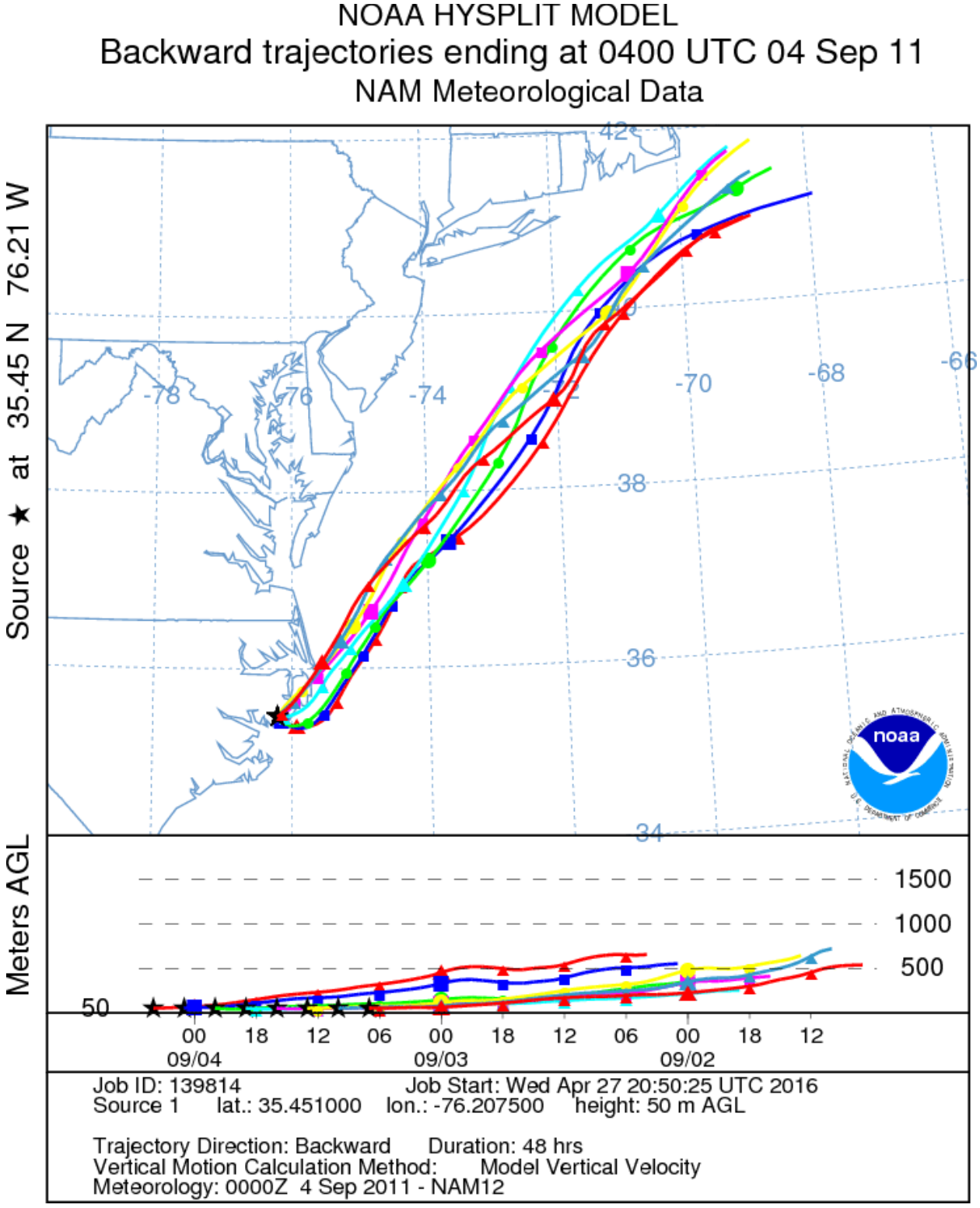
NOAA HYSPLIT MODEL
Backward trajectories ending at 0400 UTC 04 Sep 11
NAM Meteorological Data
Source ★ at 35.45 N 76.21 W
Meters AGL
1500
1000
500
50
00 18 12 06 00 18 12 06 00 18 12
09/04 09/03 09/02
Job ID: 139814 Job Start: Wed Apr 27 20:50:25 UTC 2016
Source 1 lat.: 35.451000 lon.: -76.207500 height: 50 m AGL
Trajectory Direction: Backward Duration: 48 hrs
Vertical Motion Calculation Method: Model Vertical Velocity
Meteorology: 0000Z 4 Sep 2011 - NAM12

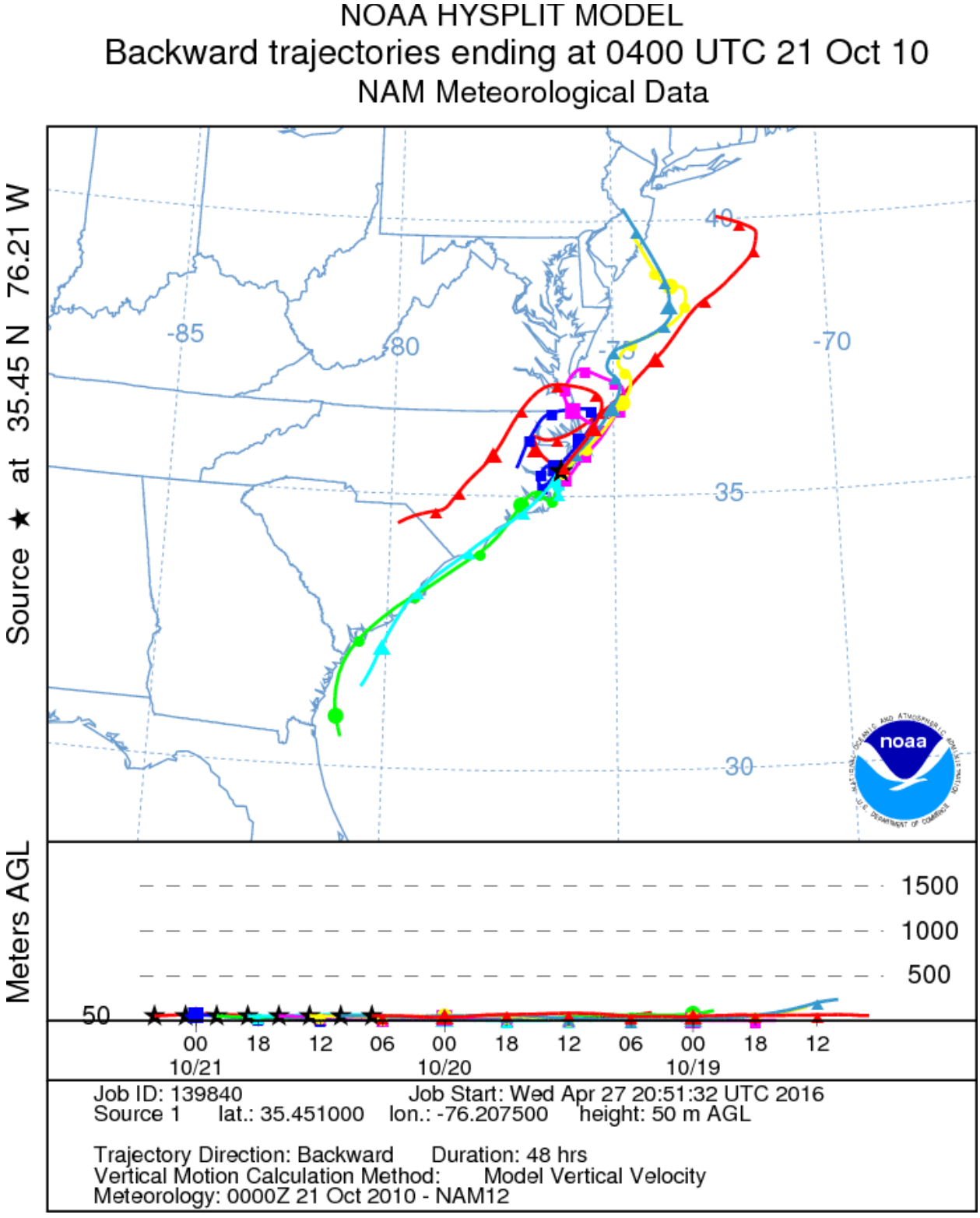
NOAA HYSPLIT MODEL
Backward trajectories ending at 0400 UTC 21 Oct 10
NAM Meteorological Data
Source ★ at 35.45 N 76.21 W
-85
-80
-75
-70
40
35
30
noaa
Meters AGL
1500
1000
500
50
00 18 12 06 00 18 12 06 00 18 12
10/21 10/20 10/19
Job ID: 139840 Job Start: Wed Apr 27 20:51:32 UTC 2016
Source 1 lat.: 35.451000 lon.: -76.207500 height: 50 m AGL
Trajectory Direction: Backward Duration: 48 hrs
Vertical Motion Calculation Method: Model Vertical Velocity
Meteorology: 0000Z 21 Oct 2010 - NAM12

NOAA HYSPLIT MODEL
Backward trajectories ending at 0400 UTC 13 Apr 11
NAM Meteorological Data

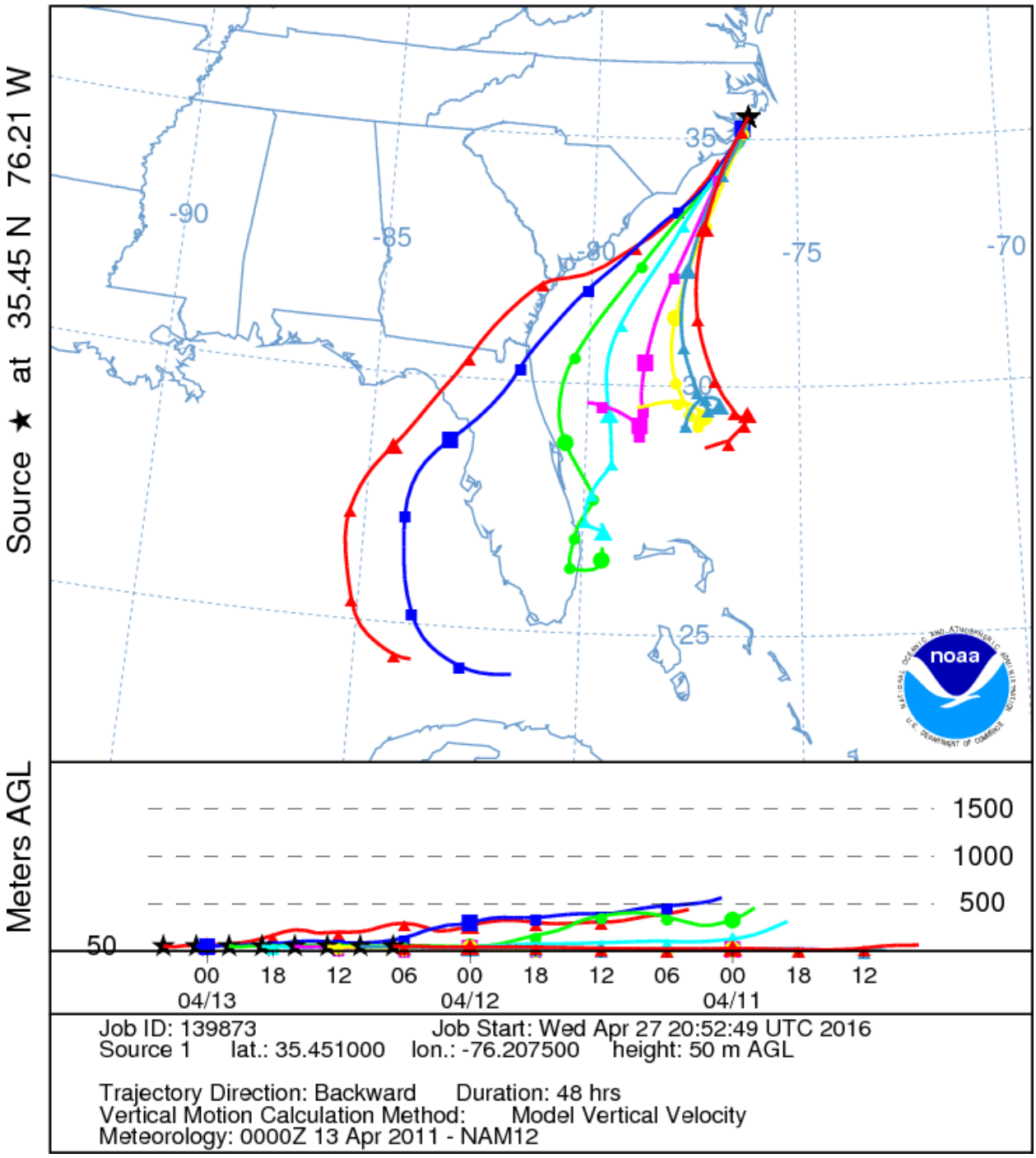

Job ID: 139873 Job Start: Wed Apr 27 20:52:49 UTC 2016
Source 1 lat.: 35.451000 lon.: -76.207500 height: 50 m AGL

Trajectory Direction: Backward Duration: 48 hrs
Vertical Motion Calculation Method: Model Vertical Velocity
Meteorology: 0000Z 13 Apr 2011 - NAM12

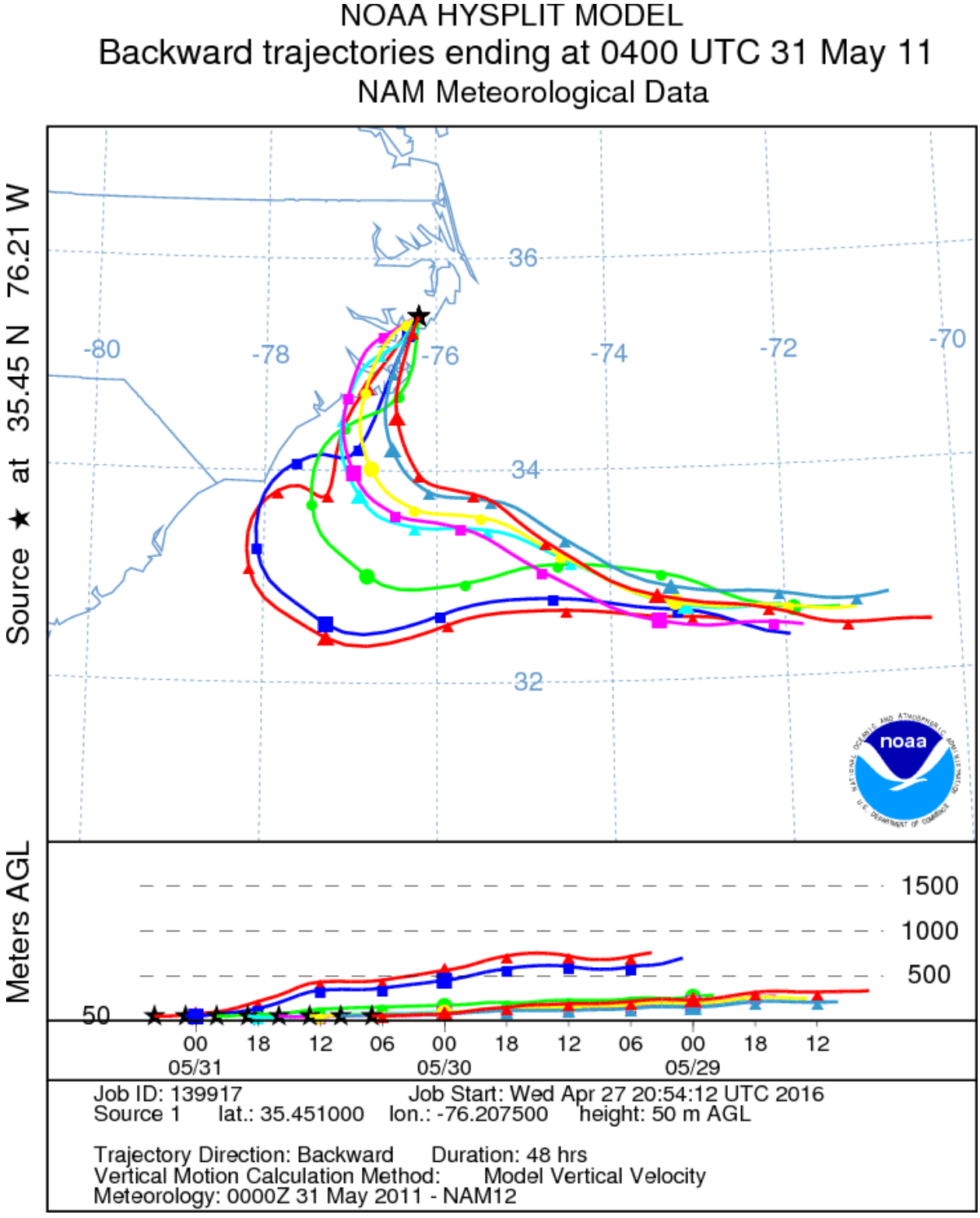
NOAA HYSPLIT MODEL
Backward trajectories ending at 0400 UTC 31 May 11
NAM Meteorological Data
Source ★ at 35.45 N 76.21 W
-80
-78
-76
-74
-72
-70
36
34
32
noaa
Meters AGL
1500
1000
500
50
00 18 12 06 00 18 12 06 00 18 12
05/31
05/30
05/29
Job ID: 139917 Job Start: Wed Apr 27 20:54:12 UTC 2016
Source 1 lat.: 35.451000 lon.: -76.207500 height: 50 m AGL
Trajectory Direction: Backward Duration: 48 hrs
Vertical Motion Calculation Method: Model Vertical Velocity
Meteorology: 0000Z 31 May 2011 - NAM12

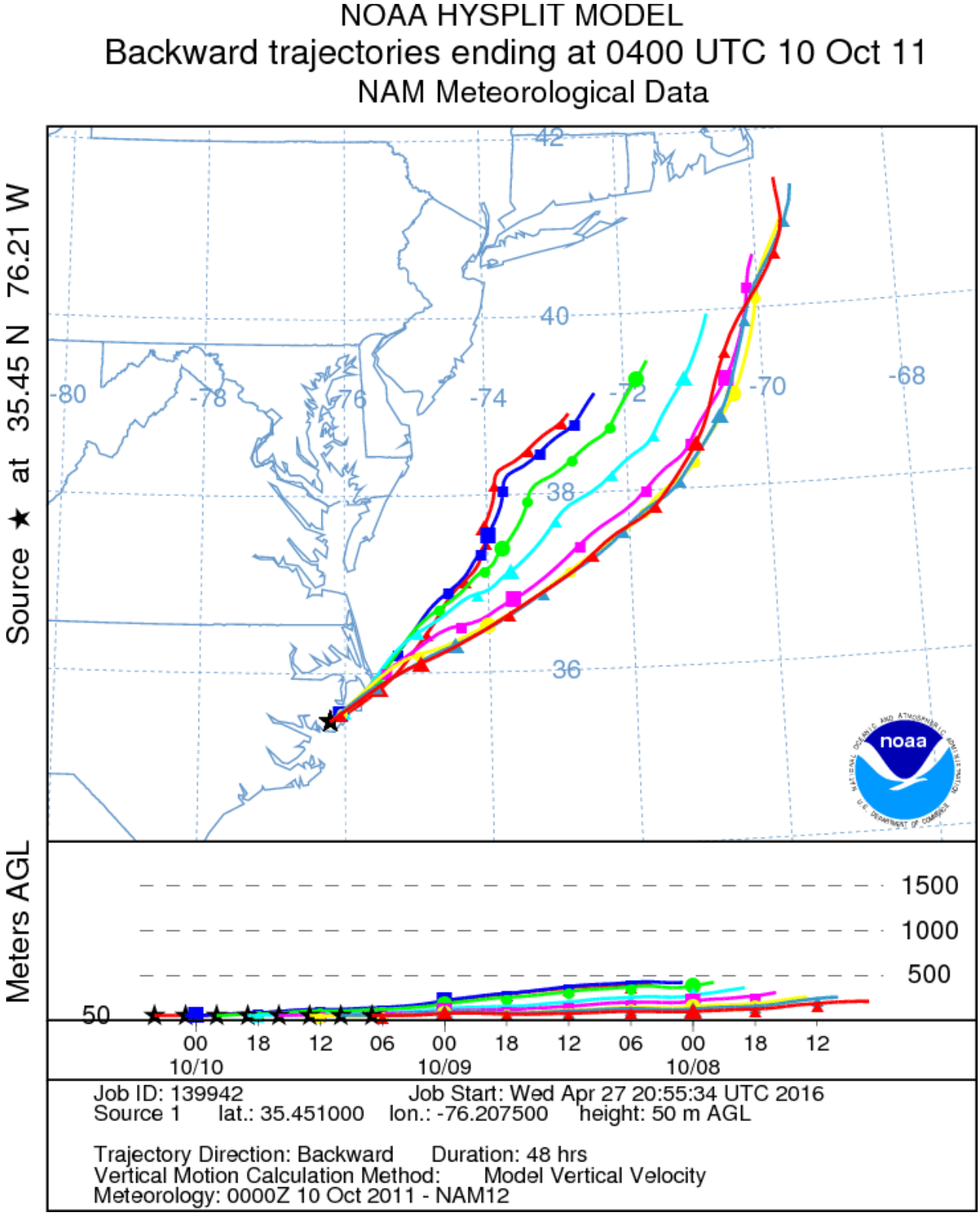
NOAA HYSPLIT MODEL
Backward trajectories ending at 0400 UTC 10 Oct 11
NAM Meteorological Data
Source ★ at 35.45 N 76.21 W
42
40
38
36
-80
-78
-76
-74
-72
-70
-68
noaa
Meters AGL
1500
1000
500
50
00 18 12 06 00 18 12 06 00 18 12
10/10 10/09 10/08
Job ID: 139942 Job Start: Wed Apr 27 20:55:34 UTC 2016
Source 1 lat.: 35.451000 lon.: -76.207500 height: 50 m AGL
Trajectory Direction: Backward Duration: 48 hrs
Vertical Motion Calculation Method: Model Vertical Velocity
Meteorology: 0000Z 10 Oct 2011 - NAM12

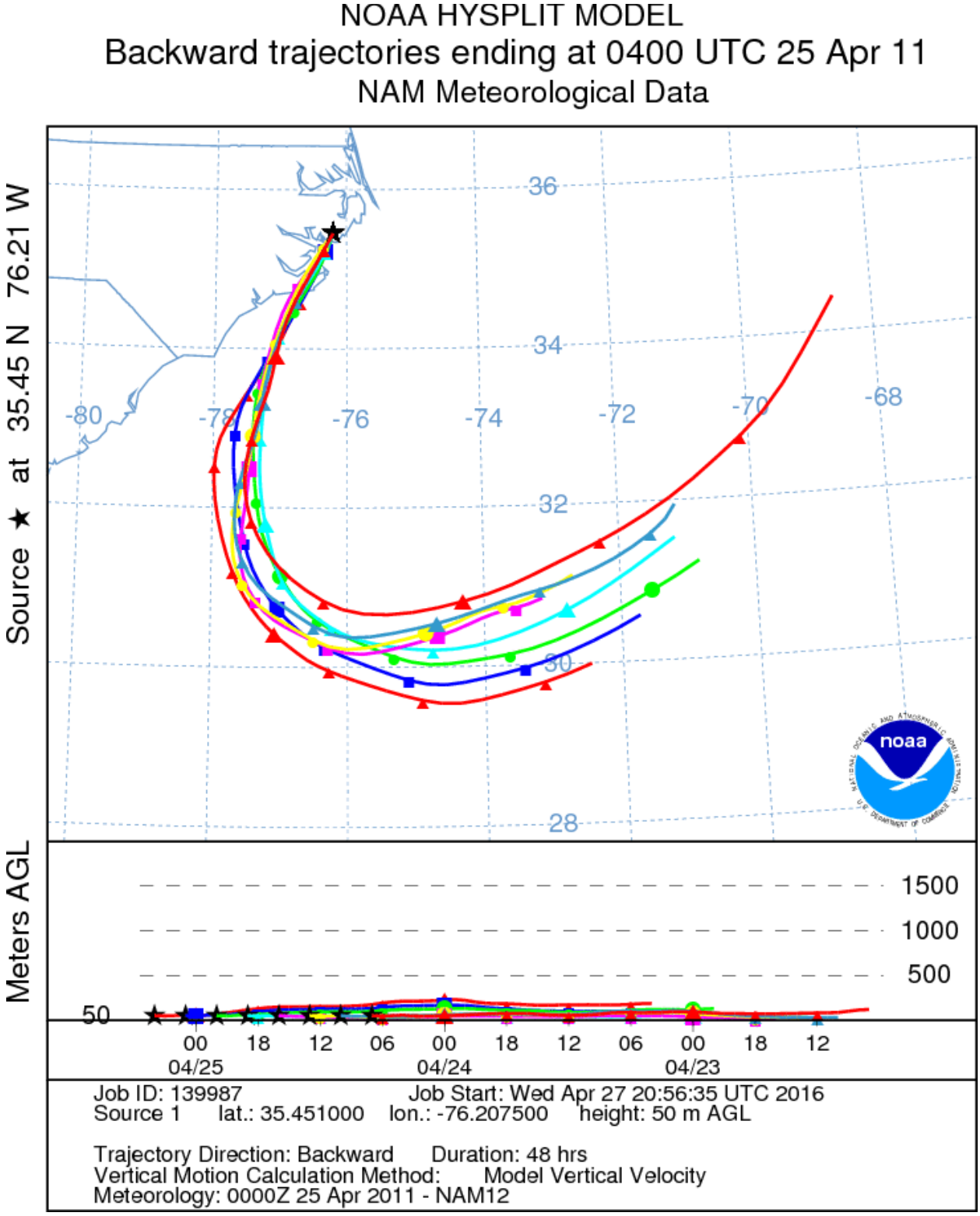
NOAA HYSPLIT MODEL
Backward trajectories ending at 0400 UTC 25 Apr 11
NAM Meteorological Data
Source ★ at 35.45 N 76.21 W
36
34
32
30
28
-80
-78
-76
-74
-72
-70
-68
noaa
Meters AGL
1500
1000
500
50
00 18 12 06 00 18 12 06 00 18 12
04/25
04/24
04/23
Job ID: 139987 Job Start: Wed Apr 27 20:56:35 UTC 2016
Source 1 lat.: 35.451000 lon.: -76.207500 height: 50 m AGL
Trajectory Direction: Backward Duration: 48 hrs
Vertical Motion Calculation Method: Model Vertical Velocity
Meteorology: 0000Z 25 Apr 2011 - NAM12

Table of Contents

General_Authors_Publications.....2
LI-266528_Hines_Rappazzo_Coffman_Systematic_Review_PFAS_Child_Health.....12
LI-266610_Supplemental_material_Systematic_review_child_health_PFAS_ijerph-14-34
STAA_Recognition_Hines_Rappazzo_Coffman.....72
Record_of_Agreement.....77

STAA REPORT FOR THE SCIENTIST NOMINATIONS

General Information:

Nomination ID/App ID:	20-124
Research Category Primary:	Review Articles (RA)
Research Category Secondary:	Health Effects Research and Human Health Risk Assessment (HE)
Laboratory/Office Name:	ORD
Nomination Entered By:	Erin Hines

Eligibility Checklist:

[Y] The nominated publication(s) has not been submitted to a previous STAA competition.

[Y] The nominated publication(s) was published on or before January 1, 2017 and on or after January 1,2012

[Y] The principal author was an EPA employee or a PHS employee assigned to EPA when the research was performed

[Y] The EPA authors (includes PHS employees assigned to EPA) contributed collectively a minimum of 50% toward the publication(s)

Nominating Official Name:	David Diazsanchez
Nominating Official Title:	
Nominating OfficialEmail:	diaz-sanchez.david@epa.gov
STAA Coordinator Name:	Kathleen Wiser
STAA Coordinator Email:	wiser.kathi@epa.gov

Justifications:

Justification 1:

The publication "Exposure to Perfluorinated Alkyl Substances and Health Outcomes in Children: A Systematic Review of the Epid is innovative and important in advancing the scientific knowledge or technology relevant to the EPA's mission to protect human he environment.

A systematic review paradigm is used as a novel tool to explain widespread PFAS exposure in association witl in children by relying on the epidemiologic literature.

The new evidence presented in this publication provides a novel synthesis of which children's health outcomes are ass exposure in the published literature. Six categories of health outcomes emerged in this review article after a thorough e published literature. These categories were: immunity/infection/asthma, cardio-metabolic, neurodevelopmental/attentio and puberty onset. While there are a limited number of studies for any one particular health outcome, this review showe evidence for positive associations between PFAS and dyslipidemia, immunity (including vaccine response), renal functi menarche. Dyslipidemia is also an outcome also associated with PFAS exposure in adults, but many of these outcome children. Our recently published invited review summarizes the strong epidemiologic or human evidence underlying mu findings. This review provides a summary of the health outcomes in the published literature and associated concentrati cohorts with quantified PFAS exposure. Some of the cohorts are from highly exposed populations including children wh point source of PFAS exposure due to industrial exposure but many of these cohorts are from children who receive exp background everyday exposures.

Epidemiologic Evidence of Effects on Children's Health were compiled in a concise review for use by the publi state partners:

States and federal partners often look to vulnerable or at risk groups including children when considering risk assessment determina water standards (i.e. maximum contaminant levels or MCLs) or superfund sites. This review has provided a compilation of childrer streamlined and concise manner that allows for outside stakeholders to readily access outcomes and epidemiologic data. These stud associated data have been cited by multiple states in their regulatory documents and numerous state regulators have thanked us via communication for our efforts in compiling this document for use at the policy level. This publication has been cited in US House I parliament report.

Justification 2A:

This STAA application only includes one highly cited publication. It has been cited 77 times. There are not multiple publications fo

Justification 2B:

Kristen Rappazzo and Evan Coffman have no previous STAA nominations/awards.

Erin Hines

1. STAA 2015, Level III, Providing critical models and information needed for exposure and risk assessment of environmental

(1) Improving Infant Exposure and Health Risk Estimates:

Using Serum Data to Predict Polybrominated Diphenyl Ether

Concentrations in Breast Milk

Environmental Science and Technology, 47:4787-4795

(2) Environmental Chemicals in Breast Milk

Book Chapter in Reference Module in Earth Systems and

Environmental Sciences, Elsevier 2013, :1-13

2. STAA 2016, Honorable Mention, Persistent Environmental Chemicals in Human Milk, (1) Concentrations of Environmental Phe

Milk, Urine and Serum of Lactating North Carolina Women.

Published by Reproductive Toxicology.

(2) Improving the Risk Assessment of Lipophilic Persistent

Environmental Chemicals in Breast Milk. Published by Critical

Reviews in Toxicology.

(3) Environmental Chemicals and Mammary Gland

Development. Book chapter published in Encyclopedia of

Toxicology, published by Elsevier, Inc.

3. STAA 2016, Honorable Mention, NHANES Lead, Blood Pb Air Pb Extrapolations,

(1) The Influence of Declining Air Lead Levels on Blood Lead-Air Lead Slope Factors in Children. Published by Environmental H
(2) A Multi-level Model of Blood Lead as a Function of Air Lead. Published by Science of the Total Environment. (3) Effect Meas
Blood Lead-Air Lead Slope Factors. Published by Journal of Exposure Science and Environmental Epidemiology

Justification 2C:

The previous STAA awards were for

1) NHANES blood lead research.

2) Breast milk and environmental chemicals research, biomonitoring women for background chemical exposure information.

3) Breast milk, environmental chemicals and mathematical modeling to understand risk from exposure to environmental chemicals.

The current research is about an emerging class of chemicals, the per and polyfluorinated chemicals or PFAS, and the associations
children's health outcomes like puberty timing, neurodevelopmental outcomes, cardiometabolic effects, immunization effectiveness
This new STAA nominations is for a disparate body of research that does not overlap with previous awards.

Justification 2D:

N/A

Justification 2E:

N/A

Justification 3A:

The Recognition section is also contained within the application system as an attached form, which provides more visual document STAA application.

This publication has been cited by other publications 77 times. Altmetric lists this publication in the top 5% of his publication has b the Altmetrics citation tool as being in the top 5% of all research outputs it has evaluated.

This submission was recruited to the journal IJERPH for inclusion in the Special Issue on Environmental Chemical Mixtures at Lov Children's Health.

Recognition by Scientific Societies:

1. This publication was recruited for an invited presentation at the 43rd Annual Meeting of the Developmental Neurotoxicology S Conjunction with the 59th Annual Meeting of the Teratology Society. I presented the neurological outcomes from our systematic re entitled, "Developmental Neurotoxicology of PFAS" in San Diego, Ca, June 2019. Presented by Erin Pias Hines.

National Recognition:

1. USA Congressional Briefing: Our publication was cited during a US Congressional briefing before the US House Environment Oversight and Government Reform On Per- and Poly- Fluoroalkyl Substances (PFAS), November 19, 2019. https://www.congress.gov/116/meeting/house/110236/witnesses/HHRG-116-GO28-Wstate-FaberS-20191119.pdf

2. USA Congressional Briefing, Our publication was cited during a Health Subcommittee Meeting of the House Energy and Com On H.R. 2827, PFAS in Food Containers, https://docs.house.gov/meetings/IF/IF14/20200129/110423/HHRG-116-IF14-Bio-Benesl January 29, 2020.

International Recognition: UK Parliament: Our publication was cited in the UK Parliament Briefing notes from July 2018.

State Policy Recognition:

1. The state of NJ recently developed Maximum Contaminant Levels (MCL) for PFOA and PFOS in drinking water. They cited o their "Technical Analysis of New Jersey's Proposed Health-Based Maximum Contaminant Level (MCL)for Perfluorooctane Sulfor was used in support of determinations of the MCLs. https://www.nj.gov/dep/watersupply/pdf/pfos-comment-4b.pdf

2. The State of Pennsylvania's Department of Health recently generated a PFAS Exposure Assessment Technical Toolkit (PEAT in its Final Report (https://www.health.pa.gov/topics/Documents/Environmental%20Health/PEATT%20Pilot%20Project%20Final%20Report%20Apr), it cited our publication.

3. State of Washington cited our work in its recent pilot project: See attached figure

Community Recognition: The National Research Defense Council (NRDC) cited our publication in its fact sheet about PFAS in dri

News: Seven news outlets have cited our publication including CNN, the Intercept and EHP.

Justification 3B:

This paper is published in a top level environmental public health journal in the *International Journal of Environmental Public Health*. This nominated paper followed the manuscript clearance criteria. Upon completion of writing and before journal, papers were internally reviewed by scientists from NHEERL and NCEA. Two scientists reviewed each of these a requirement for internal review. All reviewers commended on the synthesis provided by the systematic review and the compiling children's health outcomes associated with per- and polyfluorinated chemical (PFAS) exposure. Suggestions these reviewers and were addressed prior to submission to the journal for publication. All suggested changes were mad papers prior to submission to *IJERPH*. This submission was recruited to this journal IJERPH for inclusion in the Special Environmental Chemical Mixtures at Low Concentration and Children's Health. Once submitted to the journal, the pape one of the associate editors in the field and then underwent external peer review process for its value and suitability for or three external reviewers that were experts in their respective fields. While all papers were suggested to be revised by each paper, appropriate revisions were made. The review reflected the importance of the study and the value of the fin questions and suggestions were addressed. After submission of the revised manuscripts, the manuscripts were prompt publication in IJERPH. Within days after the acceptance, these papers were published first on-line and then subsequen of the journal.

This publication is in the *International Journal of Environmental Research and Public Health*. *International Journal of E Research and Public Health* (IJERPH) (ISSN1660-4601) is a peer-reviewed scientific journal that publishes original arti reviews, research notes, and short communications in the interdisciplinary area of environmental health sciences and p several scientific disciplines including biology, biochemistry, biotechnology, cellular and molecular biology, chemistry, c ecology, engineering, epidemiology, genetics, immunology, microbiology, oncology, pathology, pharmacology, and toxi integrated fashion, to address critical issues related to environmental quality and public health. Therefore, IJERPH focu publication of scientific and technical information on the impacts of natural phenomena and anthropogenic factors on th environment, the interrelationships between environmental health and the quality of life, as well as the socio-cultural, p and legal considerations related to environmental stewardship, environmental medicine, and public health. As a compre multi-disciplinary journal, IJERPH is comprised of twenty-four major sections including the following: Children's Health, and Health, Digital Health, Ecology and the Environment, Environmental Analysis and Methods, Environmental Chemis Technology, Emerging Contaminants, Environmental Health, Environmental Microbiology, Environmental Remediation Environmental Science and Engineering, Global Health, Health Behavior, Chronic Disease and Health Promotion, Heal and Services, Health Communication, Health Economics, Industrial Ecology

Infectious Disease Epidemiology, Mental Health, Occupational Safety and Health, Public Health Statistics and Risk Assessment, T Health

Journal	Impact Factor	Immediacy Index	Cited Half-life
IJERPH	2.948	0.31	2.81

AUTHORS

Contributing Author

Author Name: Evan Coffman

Professional Title: Salutation:

Email:	coffman.evan@epa.gov	Organization:	
Mailing Address:			
Street Line 1:	US EPA, B105-04, 109 TW Alexander Dr		
City:	RTP		
Zip Code:	27709	State:	North Carc
At time of research was:	EPA Employee		
Separation Date:			
% of Effort:	30		

Principal Author

Author Name:	Erin K. Hines		
Professional Title:		Salutation:	Dr.
Email:	hines.erin@epa.gov	Organization:	
Mailing Address:			
Street Line 1:	US EPA, B105-04, 109 TW Alexander Dr		
City:	RTP		
Zip Code:	27709	State:	North Carc
At time of research was:	EPA Employee		
Separation Date:			
% of Effort:	25		

Contributing Author

Author Name:	Kristen M Rappazzo		
Professional Title:		Salutation:	

Email:	rappazzo.kristen@epa.gov	Organization:	
Mailing Address:			
Street Line 1:	US EPA HS Facility 104 Mason Farm Road		
City:	Chapel Hill		
Zip Code:	27514	State:	NC
At time of research was:	EPA Employee		
Separation Date:			
% of Effort:	45		

PUBLICATIONS

Publication 1:

Publication Title:	Exposure to Perfluorinated Alkyl Substances and Health Outcomes in Children: A Systematic Review of		
Publication Date:	Tue Jun 27 00:00:00 GMT 2017		
Journal/Publication Method:	International Journal of Environmental Research and Public Health		
All Author(s):			
Volume:	14	Number:	
Pages:	1-22	Immediately Index:	
Citation ½ Life:	3.4	Impact Factor:	

Publication 2:

Publication Title:	Supplemental Information, Exposure to Perfluorinated Alkyl Substances and Health Outcomes in Childre		

Publication Date:	Tue Jun 27 00:00:00 GMT 2017		
Journal/Publication Method:	IJERPH		
All Author(s):			
Volume:	14	Number:	
Pages:	S1-S39	Immediately Index:	
Citation ½ Life:	3.4	Impact Factor:	

International Journal of
Environmental Research and Public Health

MDPI

Article

Exposure to Perfluorinated Alkyl Substances and Health Outcomes in Children: A Systematic Review of the Epidemiologic Literature

Kristen M. Rappazzo [1,2], Evan Coffman [1,3] and Erin P. Hines [4,*]

1 Oak Ridge Institute for Science and Education at the U.S. Environmental Protection Agency, National Center for Environmental Assessment, U.S. Environmental Protection Agency, Research Triangle Park, NC 27709, USA; rappazzo.kristen@epa.gov (K.M.R.); coffman.evan@epa.gov (E.C.)
2 National Health and Environmental Effects Research Laboratory, U.S. Environmental Protection Agency, Chapel Hill, NC 27709, USA
3 Office of Air Quality Planning and Standards, Office of Air and Radiation, U.S. Environmental Protection Agency, Research Triangle Park, NC 27709, USA
4 National Center for Environmental Assessment, Office of Research and Development, U.S. Environmental Protection Agency, Research Triangle Park, NC 27709, USA
* Correspondence: Hines.erin@epa.gov; Tel.: +1-(919)-541-4204

Received: 31 March 2017; Accepted: 21 June 2017; Published: 27 June 2017

Abstract: Perfluoroalkyl substances (PFAS), chemicals used to make products stain and stick resistant, have been linked to health effects in adults and adverse birth outcomes. A growing body of literature also addresses health effects in children exposed to PFAS. This review summarizes the epidemiologic evidence for relationships between prenatal and/or childhood exposure to PFAS and health outcomes in children as well as to provide a risk of bias analysis of the literature. A systematic review was performed by searching PubMed for studies on PFAS and child health outcomes. We identified 64 studies for inclusion and performed risk of bias analysis on those studies. We determined that risk of bias across studies was low to moderate. Six categories of health outcomes emerged. These were: immunity/infection/asthma, cardio-metabolic, neurodevelopmental/attention, thyroid, renal, and puberty onset. While there are a limited number of studies for any one particular health outcome, there is evidence for positive associations between PFAS and dyslipidemia, immunity (including vaccine response and asthma), renal function, and age at menarche. One finding of note is that while PFASs are mixtures of multiple compounds few studies examine them as such, therefore the role of these compounds as complex mixtures remains largely unknown.

Keywords: children's health; perfluorooctane sulfonate (PFOS); perfluorooctanoate (PFOA); puberty; immunity

1. Introduction

Perfluoroalkyl substances (PFAS) are highly stable carbon fluorine compounds that have been used since the 1940s as surfactants in products for stain-proof and grease-proof applications. Through biomonitoring the US population, it is known that certain PFAS are ubiquitous in the US population [1]. These compounds include perfluorooctanoate (PFOA), perfluorooctane sulfonate (PFOS), and perfluorononanoic acid (PFNA), among others. Primary exposure routes to PFAS include food and water [2]. Like many other environmental compounds, it has been demonstrated that children have a higher body burden, i.e., elevated serum concentrations of a PFAS, versus adults [1,3]. This is thought to be due to mouthing behaviors, time spent on the floor closer to dust sources, different body size to surface area ratios across ages, exposure through placental transfer, or breastfeeding [4]. The increased burden of PFAS in children has the potential to affect health throughout childhood,

development and potentially later in life. The current and future health of a child can be affected by his/her physical environment, in utero experience, nutrition, socio-economic status, educational level, and the built environment [5–9]. It is increasingly understood that exposure to environmental chemicals during sensitive windows has the potential to permanently alter a child's risk of future morbidity, even at doses that have little effect in adults.

Multiple potential mechanisms of action exist for PFAS. Because PFOA and PFOS have been studied most extensively in laboratory animals, most is known about these PFAS. Of special interest to this review are mechanisms that may affect the developing organism. Potential mechanisms of action include peroxisome proliferation [10], mitochondrial dysfunction and oxidative stress [11,12], effects on reproductive hormones including progesterone [HE1] [13,14], estrogen [14], inhibin [13], and testosterone [15], loss of gap junction intercellular communication [16], and interruption of thyroid function [17]. In the liver, peroxisome proliferation is much stronger in laboratory rodents than in humans [10], likely contributing to inter-species cholesterol differences with PFCs including hypolipidemia or decreased cholesterol in mice and hyperlipidemia in humans. Thus many potential mechanisms could contribute to PFAS-dependent effects on children's health.

Environmental chemicals like PFAS are often studied as individual compounds but in fact exist as complex mixtures in the environment. These mixtures can change over time as older chemistries are phased out and replacement chemistries are introduced. Legacy chemicals with long half-lives can be persistent in the environment and humans long after they are phased out. Many perfluorinated chemicals have been measured in human biological samples, some of which are found ubiquitously in serum of greater than 99% of people sampled in national surveys. Mechanisms of action may be similar or disparate for chemicals within a PFAS mixture, may affect similar signaling pathways or may disrupt developing tissues or metabolic pathways. Many of the PFAS exist in humans and the environment as mixtures, but little is known of the role of these compounds as complex mixtures.

The purpose of this review is to capture and characterize peer-reviewed epidemiologic literature examining associations between PFAS in biological media from children or pregnant women and various health outcomes in children.

2. Methods

A systematic review of the literature was performed by searching PubMed for studies on perfluorinated compounds and child health outcomes; returned references had to include both a PFAS term and a child health outcome term. Search terms included an extensive list of perfluorinated compounds and health/exposure terms ranging from general (e.g., child or children) to specific (e.g., Attention Deficit Hyperactivity Disorder (ADHD)) and were based on authors' knowledge of topic and key terms from known research (see Supplementary Materials Table S1 for search term string). Searches were performed by joining two parenthetical terms with an AND operator. The first term was comprised of PFAS terms linked with OR operators, and the second with health/other terms linked with OR operators. We conducted the search in two forms: (1) "simple" wherein PFAS terms were limited to PFOA, PFOS, PFAS, and PFC and full where all PFAS terms (Table S1) were used. Duplicates were removed from results. Limits applied to the search included human subjects and English language. The initial search returned over 1953 articles that were screened by authors for inclusion first based on title and abstract. Of these, 42 articles were retained for further screening based on the full article, and 38 were included in the final review. The search was updated through June 05, 2017 and 27 new studies were added, and one study was removed due to academic dishonesty concerns (the supervising author Anoop Shankar was discovered in 2012 to have falsified his resume, regarding his degrees and publication history. The removed study was accepted before this occurred and was in an area with few other studies (kidney function). He is also an author on two other papers that we decided to include in this review as they were published in 2014 and in outcomes that had a more substantial body of work (cardiometabolic)), for a total of 64 included studies. For inclusion in this review we required serum, blood, or breast milk concentrations of PFAS that were measured

concomitantly with the health outcome (e.g., serum PFAS and triglyceride concentrations) or early in life and associated with a later health outcome (e.g., PFAS in cord blood and behavioral outcomes in children). Studies were also required to report effect estimates in children under 18 years of age (selected effect estimates are presented in Supplementary Materials Table S1). Because there have been several recent reviews of birth outcomes, specifically of fetal growth, in association with PFAS, birth outcomes were not included as part of this review [18–20].

A risk of bias analysis was performed to evaluate the methodological design and implementation of the studies included in our review (see Supplementary Materials, PFAS Children's Health Risk of Bias Criteria). Risk of bias criteria were derived and adapted from a systematic review of PFOA effects on fetal growth [21], which developed its risk of bias framework from the Cochrane Collaboration's Risk of bias tool and the Agency for Healthcare Research and Quality's criteria [22,23]. Seven criteria for risk of bias were considered: selection bias, exposure assessment, outcome assessment, confounding, missing data, conflict of interest, and "other". The studies included in our review were assigned a risk of bias score for each of the seven categories of interest. Risk of bias scores, determined by a single reviewer (Evan Coffman) according to the set of guidelines for each category, were assigned as "low risk", "probably low risk", "moderate or unclear risk", "probably high risk", or "high risk". The assigned scores and justification of the scores were evaluated by the other two reviewers (Kristen M. Rappazzo and Erin P. Hines), and any disagreements were resolved by selecting the most conservative judgment, as outlined by Johnson, Sutton, Atchley, Koustas, Lam, Sen, Robinson, Axelrad and Woodruff [19].

3. Results

All included studies are summarized in Supplementary Materials Tables S2–S7. Study designs of included articles are primarily cohort or cross-sectional. Study populations tended to be of the general population, including several longitudinal cohort studies such as the Danish National Birth Cohort—a large cohort of pregnant women established to examine exposures during pregnancy and early life, and health outcomes throughout life [24]. Alternatively, study populations also included those with known increased exposure to PFAS, such as the C8 cohort, a population from the mid-Ohio valley with documented elevated body burdens of PFOA due to living near point sources of known PFAS release into the environment [25]. Several population sources are examined repeatedly in the studies included in this review. These include the C8 cohort (n = 8) and the Danish National Birth Cohort (n = 7), as well as the United States National Health and Nutrition Survey (NHANES, n = 8), among others. PFAS concentrations had considerable variability across the study, with mean values ranging from 0.57 to 111 ng/mL across studies for PFOA and PFOS. Measurement of PFAS occurred primarily in serum (including maternal serum) rather than blood, and only a single study used breast milk as a medium. Studies occurred predominantly in the United States (US), Taiwan, or Scandinavian countries, and covered periods from the late 1970s through the early 2010s. Outcomes covered by the included studies include: neurodevelopment and attention (n = 19), cardio-metabolic measures (n = 16), asthma, infection, and immunity (n = 13), pubertal onset indicators (n = 6), thyroid function (n = 7), and renal function (n = 4).

3.1. Neurodevelopment and Attention

The brain and nervous system development is a dynamic process, occurring over various lifestages with important programming and vulnerability at each stage of development [26,27]. Alterations in neurodevelopment have the potential for life-long impact on quality of life. Multiple studies have examined associations between PFAS and neurological outcomes in children, including effects on attention, behavior, motor activity, learning, cognition, and development. Summaries of studies in neurodevelopment and attention are presented in Supplementary Materials Table S2.

Studies that examined childhood developmental milestones or neurodevelopment report primarily null results, though some observed positive associations. In the Danish National Birth Cohort, prenatal PFOA or PFOS concentrations (measured in plasma from maternal blood taken

during the 1st trimester) were not associated with changes in timing to developmental milestones in infants including measures of fine motor control, attention, cognition, and language at 18 months of age [28]. One measure of gross motor control (sitting without support) had inverse hazard ratios with increasing PFOS exposures, and to a lesser degree with PFOA [28]. In an examination of the same cohort at age 7, no associations were found between prenatal PFOS or PFOA and behavioral or motor/coordination problems [29]. In a cohort of newborns, Donauer, et al. [30] observed increased odds ratios (OR) for hypotonicity (low muscle tone, aka "floppy baby syndrome") with log increases in PFOA (maternal serum), though confidence intervals were not reported. Neither PFOA nor PFOS had associations with attention in this cohort [30]. In children from the Taiwan Birth Panel Study, cord blood PFAS were assessed for association with neurodevelopment in 2 year-old children using the Comprehensive Developmental Inventory for Infants and Toddlers, a test with subdomains of cognitive, language, motor, social and self-help; both change in score and odds of poor performance were examined [31]. Chen et al. (2013) [31] observed no association with PFOA and the neurodevelopmental markers examined, but positive ORs of poor performance were observed with increasing PFOS, though linear score changes were less pronounced. In contrast, a Norwegian study that also examined both cognitive and psychomotor development scores and behavioral problems reported generally null associations for PFOA or PFOS with outcomes; though PFAS were measured in breast milk rather than cord blood [32]. Goudarzi, et al. [33] used the Hokkaido Study on Environmental and Children's Health to examine prenatal PFAS in maternal serum and indices of psychomotor or mental development at 6 and 18 months, finding no evidence of associations. They did observe a negative association with PFOA levels and the mental development index in girls at 6 months, but it did not persist at 18 months [33]. In the Ohio Valley C8 cohort, neither PFOA measured in utero or in childhood (serum) was associated with any IQ measure (full, verbal, or performance), academic measure, neuropsychological function score, or attention measure [34]. Likewise, Wang, et al. [35] generally found null results for maternal serum PFAS, including PFOA and PFOS and IQ in the Taiwan Maternal and Infant Cohort Study. In the C8 study, Stein and Savitz [36] found inverse ORs of learning problems with increasing levels of serum PFOS and PFNA, and potentially inverse ORs with PFOA. In another Ohio based cohort, the Health Outcomes and Measures of the Environment (HOME) Study, natural log increases in maternal serum PFOS were associated with increased odds of poorer behavioral regulation, metacognition, and global executive function, while other PFAS were not [37]. In a Danish cohort, Strom, et al. [38] observed no associations between scholastic achievement and maternal serum PFAS.

Nine studies examined either ADHD or related indicators of impulsivity; in general, results for these studies are mixed. In a cross-sectional U.S. study, Gump, et al. [39] found lower response inhibition/impulsivity was associated with increasing PFAS exposures (blood); associations with PFOA were of lower magnitude than associations with other PFAS. One cross-sectional study of NHANES data observed increased odds of parent-reported ADHD with increased serum PFOA, PFOS, and perfluorohexane sulfonate (PFHxS) [40]. Stein and Savitz [36] reported positive associations in the C8 cohort between PFOS and PFHxS, but not PFOA or PFNA, and ADHD after adjusting for medication use. In a cohort across Greenland, the Ukraine, and Poland, Hoyer, et al. [41] observed log-increases in maternal serum PFOA to be associated with increases in both hyperactivity and behavioral problems, and log-increases in maternal PFOS to be associated with hyperactivity. Liew, et al. [42] reported potential positive associations between ADHD and maternal plasma PFOA in the Danish National Birth Cohort, though some associations were only observed when examining quartiles of exposure. In a cohort created by combining data from the Taiwan birth panel study and the Taiwan early-life cohort, Lien, et al. [43] found cord blood PFNA concentrations to be associated with inattention, impulsivity/hyperactivity, and oppositional defiant disorder as measured by the Swanson, Nolan, and Pelham IV scale but not neurobehavioral symptoms measured by the Child Behavior Checklist (CBC) or the Strengths and Difficulties Questionnaire. They also found only null associations between PFOA, PFOS, and PFNA and neurobehavioral symptoms of ADHD [43]. Quaak, et al. [44], using the Dutch Linking Maternal Nutrition to Child Health cohort (PFAS measured in cord blood), found higher

PFOA tertiles associated with potential decreases in externalizing behavior using the CBC, but no associations with the ADHD scale, and no associations with PFOS concentrations; however, they did observe potential negative associations between summed PFAS and both externalizing behavior and ADHD. Other studies have also observed null or negative associations. Ode, et al. [45] reported null ORs between cord serum PFAS and ADHD in a case-control study of Swedish children. In a Danish cohort, Strom, Hansen, Olsen, Haug, Rantakokko, Kiviranta and Halldorsson [38] observed inverse ORs for ADHD with maternal serum PFOA and PFOS, though confidence intervals were large. A study of C8 children examined serum PFOA with mother and teacher reports of executive function, ADHD like behavior, and behavioral problems using standardized score metrics [46]. This study found that associations depended on who was reporting and that associations differed by child's sex. If mothers were reporting, boys had lower scores (indicated fewer behavioral issues) and girls had higher scores with doubling of PFOA concentrations. If teachers were reporting, boys still had lower scores with increasing PFOA, but no associations were observed in girls [46].

One study also examined autism in a case-control study from the Danish National Birth cohort, and found no association with maternal plasma PFOA, PFNA, perfluoroheptanesulfonate (PFHpS), or perfluorodecanoic acid (PFDA) concentrations [42]. PFOS and PFHxS had elevated ORs, although PFOS confidence intervals were wide [42].

Effects for observed neurological outcomes across studies are inconsistent; while some studies observe positive associations for both ADHD and neurodevelopment, there are also several studies that observe negative and null associations. Recent reviews on prenatal exposures to environmental chemicals in association with children's neurodevelopment report similar findings [47,48]. There is some evidence of neurodevelopmental impairments in animals exposed to PFAS. Johansson, et al. [49] demonstrated neurobehavioral deficits in adult mice after neonatal PFOA and PFOS exposure, where spontaneous behavior of adult mice manifested as hyperactivity and inability to habituate. In other toxicological models, fish showed early attainment of habituation with PFOS exposure but elevated spontaneous activity; mechanistic understanding of these changes via pharmaceutical manipulation revealed that multiple neurotransmitter systems including norepinephrine, serotonin, and dopamine were involved in these changes [50]. Also in fish, chronic PFOS-dependent behavioral effects were lifestage specific and spilled over into the next generation [51]. Despite the evidence from animal literature, the mixed nature of findings in humans precludes firm conclusions for the effects of PFAS on neurological outcomes.

3.2. Cardiometabolic

A number of cardiometabolic outcomes, a clustering of conditions that increase the risk for coronary artery disease, stroke, and type 2 diabetes, have been studied in association with PFAS exposure, including overweight or obesity status; factors relating to glucose regulation and metabolic syndrome; and measures of dyslipidemia, abnormal levels of serum total cholesterol, low-density lipoprotein cholesterol (LDL-C), high density lipoprotein-cholesterol (HDL-C), or triglycerides. Overweight or obesity status is itself associated with many poor health outcomes, and puts a child at greater risk for adult morbidity. Disruption of glucose regulation may lead to serious conditions such as Type 2 diabetes. Dyslipidemia in children may lead to earlier development of atherosclerosis and cardiovascular disease [52]. Summaries of studies of cardiometabolic outcomes are presented in Supplemental Materials Table S3.

Nine studies examined anthropometric outcomes, such as weight; of these, eight have done so using prenatal or maternal PFAS concentrations. In studies examining prenatal PFAS concentrations and anthropometric measures of children in the Danish National Birth Cohort (plasma), Andersen, et al. [53] observed null associations between weight, height, or BMI at 5 or 12 months of age with PFOA or PFOS. In a follow up study with the children at 7 years of age, BMI and waist circumference continued to have no associations with PFOA or PFOS [54]. However, overweight status had inverse ORs, with wide CIs, with increasing quartiles of PFOS [54]. In the Ohio based HOME study,

maternal serum PFOA concentrations were associated with higher risk of overweight/obesity at 8 years of age, and with BMI z-score, waist circumference, and body fat percentage; these associations were non-linear, with the 2nd tertile effect estimate being higher than the 3rd [55]. In Bristol England, the Avon Longitudinal Study of Parents and Children (ALSPAC) examination of prenatal PFAS (maternal serum) and weight in girls at 20 months of agefound an increase in weight of 580 g (301, 858 g) when adjusting for birthweight and height at 20 months for the highest tertile ofPFOS compared to the lowest; they observed no associations between PFOA or PFHxS and weight at 20 months in girls, Maisonet, et al. [56]. Alternately, a study examining the children from the Danish Pregnancy Cohort, with a mean age at follow-up of 20 years, observed positive ORs (BMI and waist circumference) with increasing prenatal PFOA exposure (serum) in female offspring but null associations in males and in association with prenatal PFOS [57]. In a cohort from Greenland and the Ukraine, Hoyer, et al. [58] observed only slightly elevated ORs with maternal plasma PFOA and no associations with PFOS for overweight status, but both were associated with increased odds of waist-to-hip ratio >0.5 at five to nine years of age. Height z-score, but not weight, was negatively associated with 3rd trimester maternal serum concentrations of several PFAS (excepting PFOA) for children aged 2 to 11, particularly in girls, in the Taiwan Maternal and Infant Cohort study [59]. In a cross-sectional study, Timmermann, et al. [60] found no associations between serum PFOA or PFOS at age 8 years and anthropometric measures, including BMI. A Danish pregnancy cohort from 1988 to 1989 reported BMI significantly increased across tertile of maternal serum PFOA measured at gestational week 30 in female offspring at age 20, though no effect estimates were reported and interquartile ranges were within normal values [61].

Five cross-sectional studies examined dyslipidemia. In adolescents from NHANES, increases in PFOA, PFOS, or total PFAS serum concentrations were positively associated with high total cholesterol (>170 mg/dL) and high LDL-C; PFAS were not associated with clinically abnormal HDL-C and triglyceride levels [62]. Linear associations were similar, with increases in PFAS associated with increases in total cholesterol and LDL-C, and no associations with triglycerides or HDL-C, though HDL-C levels did show small decreases with increases in plasma PFOA levels [62]. Also in NHANES, Lin et al. [63] found no associations between PFASs and HDL-C or triglyceride levels examined as components of metabolic syndrome in NHANES adolescents. Children and adolescents from the Ohio Valley C8 population had PFOS and PFOA serum concentration associated with increased odds of abnormal total cholesterol and LDL-C; PFOS was also associated with decreased odds of abnormal HDL-C [64]; Linear changes in lipids were also examined, with [64] reporting positive though non-linear trends between PFOS and total cholesterol, LDL-C, and HDL-C. A Danish study found no associations between serum PFOA or PFOS and triglycerides in normal weight children, but did find increases in PFOA or PFOS associated with increases in triglycerides in overweight children [60]. A study in Taiwan found log increases in serum PFOA, PFOS, and PFNA associated with increases in total cholesterol, LDL-C, and triglyceride concentrations [65]. In the ALSPAC cohort examination of lipids in association with maternal serum PFAS, Maisonet, et al. [66] observed positive, though non-linear and non-monotonic, associations with increases in maternal serum PFOA and PFOS and total and LDL-cholesterol.

In a cross-sectional analysis of metabolic syndrome components and indicators among NHANES adolescents (12–17 years), Lin, Chen, Lin and Lin [63] observed a positive association between doubling of serum PFNA concentrations and the glucose component of metabolic syndrome, defined as glucose levels $\geq$5.55 mmol/L or a self-reported use of anti-hyperglycemic medications (OR: 3.15 (1.39–7.12)); however, other metabolic components and overall metabolic syndrome had inverse or null ORs with PFNA. PFNA was also associated with decrements in measures of insulin resistance and B cell function [63]. Other PFAS (PFOA, PFOS, and perfluorohexanesulfonic acid (PFHS) had null or negative associations with metabolic syndrome components and primarily null associations between biomarker measures [63]. In a small Taiwanese cohort, metabolic indicators (insulin, glucose, etc.) were not associated with increasing serum concentrations of PFOA, PFOS, PFNA, or perfluoroundecanoic acid (PFUA) [67]. A cross-sectional study in Denmark observed no associations between serum PFOA or

PFOS and percent change in insulin concentrations in normal weight children, but among overweight children both PFOA and PFOS were associated with increased insulin concentration, higher B-cell activity, and elevated insulin resistance [60]. In the 20 years follow-up of the Danish Pregnancy Cohort, there were positive associations with percent changes of insulin and leptin association and log-unit increases in prenatal serum PFOS [57]. Studies also examined adiponectin, a hormone that plays a role in glucose regulation and fatty acid oxidation, and is important for metabolic homeostasis. In a cohort of hypertensive young people from Taiwan (aged 12–30), higher PFNA serum concentration was associated with elevated serum adiponectin concentration, while PFOA, PFOS, and PFUA were not [67]. Although in this study only the *p*-value for trend and mean response values were reported, rather than comparison effect estimates and the population included adults. In the Danish Pregnancy Cohort, prenatal PFOA exposure (serum) was negatively associated with adiponectin concentrations [57]. Both the study of the Danish Pregnancy Cohort and a cross-sectional study in Denmark observed no associations between PFOS and adiponectin [57,60].

A single study of NHANES examined blood pressure and hypertension in children, finding no associations between blood pressure measurements and increases in serum PFOA or PFOS [52]. Another cross-sectional study examined carotid artery intima-media thickness in a Taiwanese population of which 38% had elevated blood pressure during childhood, finding increased carotid artery intima-media thickness in adolescents aged 12–19 with increasing quartiles of plasma PFOS [68].

Carido-metabolic effects in children were reported in multiple studies. Analyses reported generally higher or abnormal levels of total cholesterol and LDL-C in association with PFAS serum concentration. Some mechanistic analyses have also been performed by Fletcher et al. (2013) [69], who found changes in the expression of genes involved in cholesterol metabolism (transport and mobilization) to be associated with serum PFAS in the C8 population. The evidence for effects on weight or BMI in children across PFAS is mixed with PFOA most frequently associated with overweight status in females but some PFOA studies also show null results. It may be that small positive associations, such as those reported by Maisonet, Terrell, McGeehin, Christensen, Holmes, Calafat and Marcus [56], have cumulative effects over time, which lead to being overweight in adulthood. Rodent models of glycemic control with perinatal exposure to PFAS affected glucose tolerance in adult offspring, including enhanced effects on a high-fat diet [70], and altered signaling pathways like leptin [71]. It is important to note that most of the studies reviewed here are cross-sectional, so temporality cannot be established, and do not account for dietary intake, which can be an import source of PFAS [72] and therefore a potential confounder. Studies of glucose regulation in children have generally reported mixed effects, with limited agreement between studies. A single study of carotid artery intima-media thickness in adolescents found an association with PFOS concentration. The strongest evidence for a relationship between PFAS exposure and cardiometabolic effects in children comes from studies of dyslipidemia.

3.3. Immunity, Allergic Response, Infection, and Asthma

Children are protected from infectious agents by innate and adaptive immunity, which is increasingly understood to be modifiable by our environment. Allergic and immunological responses can also be modulated by exposure to exogenous environmental compounds. Vaccinations substantially reduce disease, disability, death and inequity worldwide [73]. Recent work shows that inoculation with the measles vaccination is associated with an elevated level of protection against other infectious diseases [74]. Because the efficacy of a vaccine depends on the quality of the immune response, it is important to understand if environmental exposures may modulate this response. Summaries of studies in immunity, allergic response, infection, and asthma are presented in Supplementary Materials Table S4.

Three studies examined suppression of vaccine-mediated antibody response in association with PFAS. In a Faroe Islands birth cohort, Grandjean, et al. [75] examined serum PFAS concentrations prenatally and at age 5 in association with tetanus and diphtheria serum antibody titers at age 5

(prior to vaccination booster) and at age 7 (after booster). Antibody concentrations at age 5 were generally not associated with combined PFAS concentrations, except diphtheria where a doubling of prenatal PFAS concentration was associated with a substantial decrease in antibody concentrations [75]. PFAS concentrations at age 5, including when adjusting for prenatal PFAS, have strong negative associations with antibody concentrations for both tetanus and diphtheria at age 7 [75]. For individual PFAS, associations with antibody concentrations at age 7 are congruent with the results for total PFCs [75]. However, prenatal PFOS showed a strong negative association with diphtheria antibody concentration at age 5; prenatal PFNA and PFDA also had negative associations with diphtheria antibody concentrations at age 5. Grandjean, Andersen, Budtz-Jorgensen, Nielsen, Molbak, Weihe and Heilmann [75] also examined odds of antibody levels falling below a clinically protective level (0.1 IU/mL), observing positive ORs for diphtheria and tetanus at age 7 with a two-fold increase in PFOS at age 5; results were similar for PFOA. People from the Faroe Islands have higher persistent organic pollutant (i.e., PCB) and methylmercury serum concentrations than those from the general US population [76]; in this study, PFAS and PCB concentrations were not correlated with each other, and adjustment for PCBs in this model did not appreciably change the results [75]. Granum, et al. [77] also examined antibody concentrations in a subcohort of the Norwegian Mother and Child Cohort Study (MoBa) study. Increases in maternal plasma PFAS concentrations at delivery (PFOA, PFOS, PFNA, PFHxS) were negatively associated with children's anti-rubella antibody titer at three years of age [77]. They also observed potential associations between PFOS and PFOA and measles vaccine antibody concentrations, however these associations were unadjusted for potential confounders [77]. In NHANES (1999–2000 and 2003–2004), Stein et al., (2016) [78] found serum PFOA and PFOS to be associated with decreases in rubella and mumps antibodies in children 12–19 years old. These studies show some effect of PFAS serum concentration on suppression of antibody response to vaccination.

Six recent studies have examined asthma in association with PFAS. In the Taiwanese Genetics and Biomarkers study for Childhood Asthma, Dong, et al. [79] found positive ORs and increasing trends for asthma with serum PFOA, PFOS, PFDA, PFHxS, and PFNA. Perfluorobutanesulfonic acid (PFBS) and perfluorododecanoic acid (PFDoA) had positive ORs for asthma, though without a clear trend or only at the highest exposure levels [79]. In this study, asthmatic children were recruited from hospitals, while non-asthmatic children were recruited from schools. If the school population was not similar to the population that gave rise to the asthmatic population bias may have been introduced [79]. In a subset of the same population, Qin et al., [80] observed decrements in metrics of lung function (forced expiratory volume, forced expiratory flow 25–75%, and forced vital capacity) with doubling of several PFAS concentrations (PFOA, PFOS, PFHxS, PFNA) in children with asthma but not in children without asthma. In a cross-sectional study using adolescent NHANES participants, Humblet, et al. [81] observed a positive OR between self-report of ever having asthma and increasing serum PFOA concentration; PFNA also had a positive OR but a wide CI. Generally null associations were observed for other PFAS (PFOS and PFHxS) and ever asthma, or for any PFAS and current asthma or wheeze [81]. In a subset of that population (NHANES 2005–2006) Stein et al., [78] found similar elevated ORs with wide CIs for PFOA, PFNA and asthma; they also reported elevated ORS with PFOS, but not PFHxS. In another cross-sectional analysis of asthmatic and non-asthmatic children in Taiwan, increasing quartiles of serum PFOA were associated with increasing odds of asthma [82]. PFOS, PFBS, PFDA, PFHxS, and PFNA were also associated with asthma, for some PFAS the associations were divergent by sex (PFOS only associated with asthma in males) or potentially sex divergent (PFBS had stronger effect in males), while the others had similar effects across sexes [82]. In a cohort across Greenland and the Ukraine Smit, et al. [83] reported generally null associations between asthma or wheeze and a factor representing maternal plasma PFAS concentrations.

Five studies looked at allergies or similar outcomes, generally finding null results. In the two analyses of the Hokkaido Study on Environment and Children's Health, no associations with maternal serum PFOA or PFOS and food allergies or eczema, and null to potentially negative associations with total allergies, were observed [84,85]. A cohort in Greenland and the Ukraine reported no association

between a factor representing maternal plasma PFAS concentrations and current or ever eczema in children [83]. Wang et al. (2011) [86] observed no associations with increasing quartiles of cord blood serum PFOA and atopic dermatitis; they did report positive associations with PFOS and PFNA, though both had large confidence limit ratios, indicating low precision, and no trends. In a cross-sectional analysis of NHANES data, Stein et al., [78], observed associations with increased PFOA, PFOS and rhinitis; there was some evidence for associations with allergy as well, but no PFAS were associated with wheeze.

In addition to vaccination antibodies, Granum, Haug, Namork, Stolevik, Thomsen, Aaberge, van Loveren, Lovik and Nygaard [77] also examined allergen-specific IgE antibodies, using a test that distinguishes atopic and non-atopic status, reporting no associations between atopic status and concentrations of any PFAS (plasma) in the Norwegian cohort. Newborn immune function markers were examined in a cohort of 10 Canadian cities and generally null associations were observed between immune function and any maternal serum PFAS [87]. In a Japanese cohort, increasing maternal serum PFOA concentrations were negatively associated with cord blood IgE in 18 months old girls but not boys [85]. In the Taiwan Birth Panel cohort study, IgE levels at 2 years of age were not associated with PFOA, PFOS, or PFNA in cord blood serum [86]. Wang, Hsieh, Chen, Fletcher, Lien, Chiang, Chiang, Wu and Chen [86] also observed positive associations between PFOS and PFOA and IgE levels, both measured in cord blood, but only in boys. Another study in Taiwan examined IgE levels in children with and without asthma, reporting statistically significant p-values for trend with increasing concentrations of serum PFAS (PFOA, PFOS, PFDA, PFDoA, PFNA, and PFTA), though linear changes were not reported [79]. In a cross-sectional analysis of asthmatic boys, Zhu et al. [82] observed higher levels of IgE, and Th1 and TH2 cytokines, which might have contributed to asthma development, with higher levels of serum PFOS, PFOA, and PFDA.

Two studies examined susceptibility to infections or diseases. In the Danish National Birth Cohort, Fei, et al. [88] saw no associations between prenatal exposure to PFOA or PFOS (serum) and risk of hospitalizations for infectious disease in the first year of life. Granum, Haug, Namork, Stolevik, Thomsen, Aaberge, van Loveren, Lovik and Nygaard [77] observed positive associations between maternal plasma PFOA and PFNA and common cold incidence in the first 3 years of life and between PFOA and PFHxS and gastroenteritis. However, these associations were unadjusted for potential confounders [77].

Studies of individual health outcomes are limited in number, therefore conclusions should be made with caution; current evidence potentially suggests that antibody response to vaccination and asthma may be influenced by PFAS. The studies of vaccine response were well done cohort study designs and despite the small number offer compelling evidence. The asthma studies are less consistent and include a broader range of study designs and quality. There is no evidence for relationships between PFAS and IgE levels, allergy, and infection. In the one study that looked across these outcomes, several positive associations were observed and these in combination may indicate that prenatal PFAS exposure is linked to childhood humoral immunomodulation [77], which is supported by animal studies [89].

3.4. Pubertal Onset Indicators

Puberty is the process of sexual maturation, occurring over several years. Early onset or delayed onset puberty can be considered an important indicator of endocrine disruption, and has been associated with altered risk of adult disease: diabetes mellitus, heart disease, bone disease, substance abuse, and asthma [90–93].

Six studies examined pubertal onset indicators (see Supplementary Materials Table S5). Two used data from the ALSPAC cohort; one study focused on menarche before 11.5 years of age while the other examined hormone levels in a subset of girls. The other studies examined both age at menarche and other pubertal parameters, such as hormone levels, using case-control and cross-sectional designs [61,94–96]. Kristensen, Ramlau-Hansen, Ernst, Olsen, Bonde, Vested, Halldorsson, Becher, Haug and Toft [61] examined fetal exposure, through maternal serum at gestational week 30, to PFAS in a longitudinal cohort from Denmark, and observed a one-month delay in menarche per tertile increase of PFOA

(or a 5.3 months delay from highest to lowest tertile of PFOA); no associations were observed with other reproductive parameters examined (e.g., cycle length, follicle stimulating hormone levels, etc.). Fetal PFOS levels were not associated with age at menarche [61]. A cross-sectional analysis of boys and girls in the C8 cohort found delayed menarche associated with both serum PFOA and PFOS concentrations, which held true after adjustment for the other PFAS [95]. Doubling of PFOS was associated with serum testosterone in males and estradiol in females indicating lack of sexual maturation (i.e., inverse odds ratios (OR) for levels above specified cut-offs), while increases in PFOA were not associated with estradiol or testosterone levels [95]. In a further examination of the C8 cohort, [97] found insulin-like growth factor, a marker of pubertal onset, to be negatively associated with serum PFOA (in girls), PFOS and PFNA (both boys and girls). It is important to note that menstrual blood loss is a potential route of PFAS excretion, thus in cross-sectional studies of girls with later pubertal onset may have higher PFAS levels than girls with earlier pubertal onset. Examining age at menarche from a different angle, Christensen, Maisonet, Rubin, Holmes, Calafat, Kato, Flanders, Heron, McGeehin and Marcus [94] used age at menarche before 11.5 years as their outcome in a case-control study of ALSPAC, finding null associations with most PFAS levels measured in maternal serum during pregnancy, but inverse ORs with PFOS. Inverse ORs may indicate the potential for delayed menarche with PFOS, or that girls with higher exposure to PFOS during fetal development were less likely to have early menarche. In a subset of the same population as Christensen, Maisonet, Rubin, Holmes, Calafat, Kato, Flanders, Heron, McGeehin and Marcus [94], higher levels of PFOA, PFOS, and PFHxS were associated with higher levels of total testosterone in girls, while no associations were observed with sex hormone-binding globulin concentrations [96]. A cross-sectional study in Taiwan examined follicle stimulating hormone levels in association with serum PFAS in 12–17 year olds, finding decreased FSH associated with increasing PFOS in boys and PFUA in girls; there was no evidence of associations for PFOA and PFNA [98].

The six studies of pubertal onset indicators have generally mixed results and varied study design. The most consistent evidence is for later age at menarche associated with either PFOA or PFOS exposure or both. This is supported by toxicological evidence from mouse models in which female offspring had delayed mammary gland development [99] and vaginal opening [100] with in utero and peri-pubertal exposure to PFOA, respectively.

3.5. Thyroid Function

Thyroid hormones are essential in regulating growth, development and metabolism and are especially vital for proper brain development early in life, with impairment known to affect neurological endpoints, including intelligence quotient (IQ). Five studies evaluated thyroid function in children in association with PFAS exposure (see Supplementary Materials Table S6).

In a cross-sectional analysis of the Ohio Valley C8 cohort children, Lopez-Espinosa, Mondal, Armstrong, Bloom and Fletcher [17] observed positive associations between clinical hypothyroidism and serum PFOA, while neither PFOS nor PFNA were associated with hypothyroidism. In children with no diagnosed thyroid disease, null associations were observed with PFOA and thyroid stimulating hormone (TSH) and total thyroxine (TT4) levels; TSH and TT4 levels were elevated with the highest concentrations of PFOS, and TT4 levels increased with increasing PFNA concentrations in participants without thyroid disease [17]. Lin, et al. [101] examined thyroid hormones and serum PFAS in a subset of a cohort of adolescents and young adults (12–30 year olds) from Taiwan with abnormal urinalysis (positive tests for any two of: proteinuria, glucosuria, or hematuria). Only PFNA was associated with free T4 levels, though the change was small (0.004 ng/dL (95%CI: 0.001–0.007)) per 1 ng/mL increase in PFNA) and was seen without a concomitant decrease in TSH that would be clinically expected [101]. No other PFAS were associated with thyroid hormone levels in this study. In a study of 52 boys and 31 girls in the Netherlands, increasing T4 levels in girls were associated with increasing cord blood PFOA concentrations [102]. No associations with T4 were observed with PFOS or with PFOA in boys [102]. In a cross-sectional analysis of the Taiwan Birth Panel study, doubling of cord blood plasma PFOS was associated with decreased T4 in boys, and increased TSH in both boys and girls though effects

appeared to be non-linear and magnitude of effects was higher in boys [103]. PFOA, PFNA, PFUnDA were generally not associated with thyroid hormone concentrations [103]. A small South Korean study examined correlations between maternal PFAS during pregnancy and fetal T3, T4 and TSH measured in cord blood [104]. Fetal T3 was negatively correlated with PFOS and perfluorotridecanoic acid (PFTrDA), and had small negative correlations with PFOA and PFHxS [104]. Fetal TSH was positively correlated with PFOS and PFTrDA, while T4 was not substantially correlated with any PFAS [104]. In a Japanese study of 392 mother-infant pairs, maternal cord blood PFOS was positively associated with infant TSH levels, but not free thyroxine, and PFOA was not associated with either [105]. In another small South Korean study, infants with congenital hypothyroidism had higher mean serum levels of PFOA, PFNA, PFDA, PFUnDA, and total PFASs compared to healthy infants [106].

While some associations are observed between thyroid hormones and PFAS, no clear patterns emerge. There is some evidence for hypothyroidism, a finding that has also been observed in an adult NHANES population [107], but not in other studies of PFAS and thyroid function. Given the limited number of studies and the variability in the responses, no conclusions can be reached with certainty.

3.6. Renal Function

The function of the kidneys, or renal function, contributes to the normal homeostatic maintenance of blood pressure, removal of waste products from the body, red blood cell production and electrolyte balance. The long-term health risks of impaired kidney function can be substantial and can be exacerbated in children who are malnourished or those who are overweight or obese.

Four studies have investigated associations between PFAS and renal function in children (see Supplementary Materials Table S7). Two cross-sectional studies in the United States found associations between renal function and PFAS. Watkins, et al. [108] examined estimated glomerular filtration rate (eGFR) in association with serum concentrations of several PFAS, finding decrements in eGFR associated with increases in PFOA and PFOS concentrations and with log-increases in PFNA and PFHxS. Kataria, et al. [109], also using NHANES (2003–2010), found serum PFOA to be associated with eGFR and uric acid concentrations after adjustment for PFOS, while PFOS associations were attenuated after adjustment for PFOA. PFNA and PFHxS were not associated with eGFR or uric acid concentrations, and no PFAS were associated with serum creatinine concentrations [109]. Qin, et al. [110] examined 225 non-asthmatic children in Taiwan, finding serum concentrations of several PFASs associated with increased odds of high uric acid levels, including PFOA, PFOS, PFBS, PFDA, PFHxS, and PFNA. In a side analysis of a cohort of Taiwanese adolescents and young adults who had abnormal urinalysis, serum PFUA concentrations were higher in children with chronic renal failure [101], though only mean levels and p-values were reported, making quantitative interpretation difficult. While all studies of PFAS and kidney function in children to date have been cross-sectional, results from these studies provide evidence for interesting potential associations between PFAS and renal function in children using multiple different markers of kidney function.

3.7. Risk of Bias Analysis

Based on the implementation of our risk of bias criteria, we determined there to be a low to moderate risk of bias in the studies included in our review. While all of the reviewed studies had potential biases relating to at least one of the seven categories of interest (Figure 1), the majority of these instances were classified as "moderate risk" or lower (Figure 2). Of the sources of bias considered, selection bias, exposure assessment, and conflict of interest were most commonly judged to present the highest risks. Participation and non-response bias were the greatest concerns within the selection bias domain. However, studies with high non-participation or non-response rates were determined to comprise lower risk if they had analyses demonstrating minimal differences between participants and non-participants. Although PFAS generally have long half-lives in humans [111], there is uncertainty regarding the use of concurrent PFAS levels as a surrogate for historical PFAS levels during the susceptible time range for the development of the outcome of interest. Due to the abundance of

cross-sectional studies included in our review, many studies were found to have a moderate risk of exposure error, as timing of the exposure could not be ascertained.

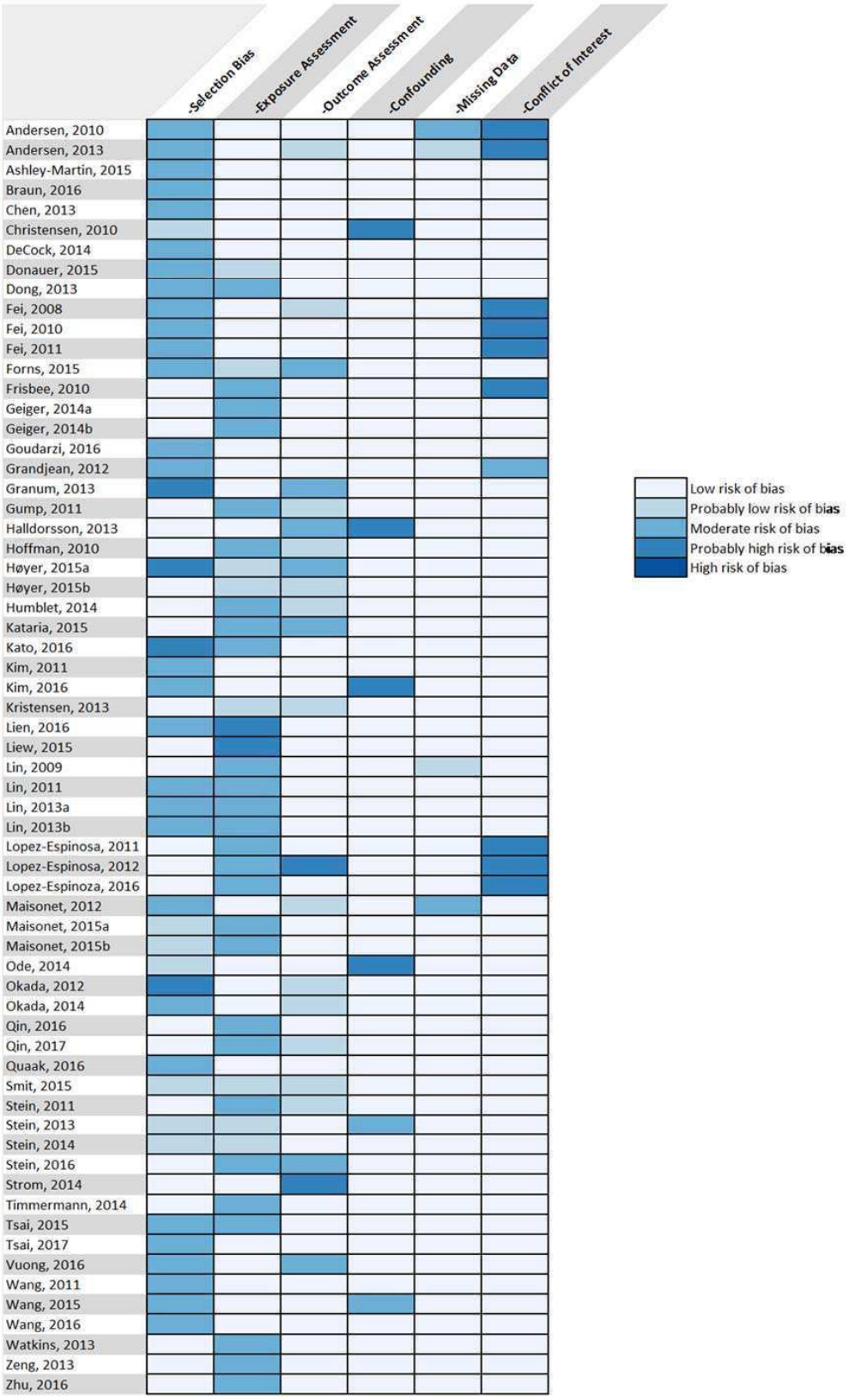

Figure 1. Classification of potential biases within each study.

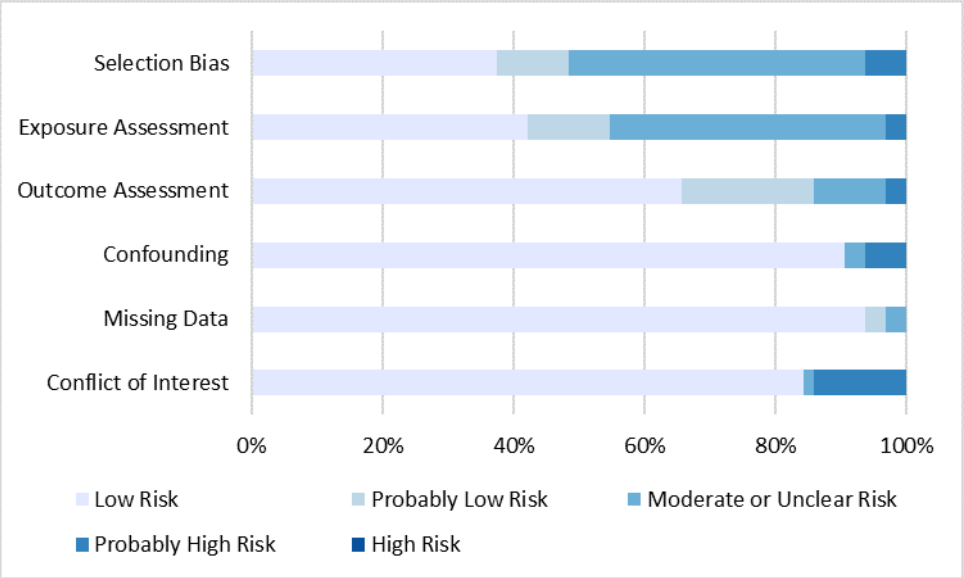

Figure 2. Distribution of potential sources of bias across included studies.

4. Discussion

This systematic review summarizes childhood health outcomes associated with PFAS exposure from peer-reviewed studies that compare associations between measured concentrations in serum, cord blood, or breast milk in early life and a health outcome. Environmental chemicals like PFAS are often studied as individual compounds but exist as complex mixtures in the environment, and the role of these mixtures in children's health is captured herein. The outcomes reported in the published literature with PFAS concentration measurements are diverse and include: cardiometabolic effects, anthropometric measurements, neurological, neurodevelopmental, and attention effects, asthma and immune response, thyroid changes, altered timing of puberty onset, and renal function. Physiological changes in childhood have the potential to alter adult disease risk and contribute to altered risk for adult morbidity and mortality. While there are a limited number of studies for any one particular health outcome, there is evidence for positive associations between PFAS and dyslipidemia, immunity (including vaccine response and asthma), renal function, and age at menarche.

The studies included in this review cover a number of health topics across childhood development. This gives a better, though not complete, picture of the potential for chronic health effects associated with PFAS exposure. These studies also cover both highly exposed populations, such as the C8 cohort, and populations from the general public. These populations may have discordant health outcomes due to differences in exposure or body burden of PFAS, and it is important to examine both types to best inform specific health outcomes. It also appears that some of the health associations observed in these studies show outcomes that differ by sex with only males or females as responders. Thus, it is important to examine effect measure modification on associations by sex when differential responses are suspected or expected. Overall the literature covers a substantial area of research and informs the knowledge of the overall potential impact of serum PFAS concentrations early in life on health outcomes.

Limitations of the studies reviewed here include, in particular, issues of selection bias, exposure assessment, and the potential for conflict of interest. Many studies had non-response issues or loss to follow-up. This is mitigated somewhat in that some studies demonstrate that the non-responders did not differ substantially from the included subjects. However, there are may be underlying, unknown differences leading to the non-response, which may in turn lead to bias in effect estimates if these differences are related to both PFAS exposure and the health outcome of interest. For exposure assessment, the largest concern is the issue of timing of exposure. Many of the findings are obtained

from cross-sectional studies with associations reported between serum PFAS concentration and measured health outcome, which have the potential to be affected by bias due to reverse causality, unlike a longitudinal study with repeated measurements over time. Some of the studies under review are funded by non-governmental sources, leading to concern over conflict of interest. As described by the Institute of Medicine Roundtable on Environmental Health Sciences, Research, and Medicine Institute of Medicine Roundtable on Environmental Health Sciences and Medicine [112], conflicts of interest do not inherently represent an inadequacy of a publication or signal any level of misconduct, but rather describe a set of circumstances under which researchers may rely on the judgment of an outside force, or be influenced by considerations for such parties. The failure to avoid being compromised by these dependencies and influences may lead to a number of biases, including publication bias or selective reporting of outcomes.

More generally for studies of PFAS, their concentrations are likely to be affected by when, and in whom, they are measured, introducing the potential for exposure misclassification. Measures during pregnancy are taken in maternal serum or cord blood. However, not all PFAS are equally transferred across the placenta [113]. Therefore, concentrations of PFAS in maternal serum are likely to differentially represent fetal PFAS, and there will be differential representation based on specific PFAS and placental transfer ability [113]. As well, maternal blood volume expands during pregnancy, leading to the potential for different periods of pregnancy to have different maternal serum concentrations of PFAS due to blood volume changes. Blood samples may also be taken from either fasting or non-fasting participants, which may make between study comparison of cardiovascular and lipid-related makers difficult. These potential sources of exposure misclassification may attenuate health effect estimates, as they are likely non-differential by outcome.

In addition, the potential exists for non-monotonic dose response curves for PFAS, some of which are known endocrine disrupting compounds. It is possible that lower concentrations/exposures may have a more disruptive effect than high concentrations/exposures, in particular with outcomes connected to the endocrine system such as thyroid function or pubertal development.

Relatedly, the toxicological effects of PFASs as a mixture of potentially dozens to hundreds of compounds are generally unknown [114]. Only a handful of studies covered in this review examined PFASs using a mixture method, and this was either a summed value or a factor representing PFAS exposure [44,52,75,83]. While these studies provide some context for effects of PFASs as a mixture, they are limited in number and not performed for all health outcomes. A summed or representative metric of PFAS exposure also cannot inform researchers about potential interactions between individual PFASs. A more through exploration of how PFASs interact with one another, both in a toxicological manner and in effect measure modification, would help the understanding of how these exposures may or may not lead to adverse health outcomes.

With cross-sectional studies, temporality cannot be established. Therefore, it is not possible to determine whether observed health effects are due to PFAS exposure, or if underlying health conditions lead to a buildup of PFAS. Optimal study design to address this challenge would be longitudinal studies with repeated measurements before and after disease onset, which would establish temporality between PFAS exposure and health effects.

Design of studies involving thyroid disease and thyroid hormone concentrations are complicated by disease status and medication use. Those with known thyroid disease should be separated from those who are disease-free for comparison. Patients with thyroid disease are likely monitored and medicated to have thyroid hormone levels in a therapeutic range and comparisons of T4 or TSH with this population's PFAS concentration would not be informative. Autoimmune status and iodine sufficiency are also informative when included in models.

Within the published literature, there is an incomplete assessment of pubertal onset in girls. Epidemiologic publications for pubertal onset in girls across PFAS concentrations look at age at menarche, but lack information on thelarche or the onset of female breast development. Breast development has been shown to be sensitive to PFAS exposure in laboratory animals and the dearth

of information on this endpoint in developing human populations is an area that could be expanded to allow for better cross-species comparison. Existing cohorts of US girls with data on these pubertal endpoints could be mined to understand these associations. The small number of studies for particular health outcomes limits our ability to draw conclusions based on the body of literature. Even general categories of childhood health outcomes (e.g., cardiometabolic) included only a few studies, though the neurodevelopmental literature has grown substantially even in just the past year. In addition, some of the same outcomes were classified or measured differently in different studies, making direct comparisons across studies more difficult. A focus on particular outcomes of import could help define the literature and direct future research in directions of interest and utility, and prompt more direct mechanistic studies.

5. Conclusions

On the basis of our systematic evaluation of PFAS exposure and childhood health outcomes, we observed generally consistent evidence for PFAS' association with dyslipidemia, immunity including vaccine response and asthma, renal function, and age at menarche. Similar to this evaluation, the National Toxicology Program Office of Health Assessment and Translation recently performed a systematic review on the immunotoxicology associated with exposure to PFOA or PFOS and concluded that PFOA or PFOS is "presumed to be an immune hazard to humans" (NTP, 2016). While the body of literature of PFAS and childhood health outcomes continues to develop, there are several areas that could be addressed. One important consideration is the need for more longitudinal studies where timing of exposure versus outcome can be firmly established. Another important factor to consider in future research is the variability in outcome measurement. Cohesive measurement or definition of health outcomes under study would strengthen conclusions based on the whole of the literature. As exposure to certain PFAS is ubiquitous in the US population, it is important to understand the health effects associated with exposure to the mixtures of PFAS, especially in children.

Supplementary Materials: The following are available online at www.mdpi.com/1660-4601/14/7/691/s1, Table S1: Search terms used for systematic review, Table S2: Studies of perfluorinated compounds and neurodevelopmental and attention related outcomes, Table S3: Studies of perfluorinated compounds and cardiometabolic related outcomes, Table S4: Studies of perfluorinated compounds and immunity, infection, and asthma related outcomes, Table S5: Studies of perfluorinated compounds and puberty related outcomes, Table S6: Studies of perfluorinated compounds and thyroid related outcomes, Table S7: Studies of perfluorinated compounds and renal related outcomes.

Acknowledgments: The authors would like to acknowledge Pauline Mendola and Tom Luben for technical review of the manuscript.

Author Contributions: Erin P. Hines conceived the review. Kristen M. Rappazzo performed the literature search and data extraction. Erin P. Hines and Kristen M. Rappazzo reviewed the literature results; Evan Coffman performed risk of bias analysis and wrote those sections and figures. Kristen M. Rappazzo and Erin P. Hines wrote the paper; Kristen M. Rappazzo created the supplemental table; Erin P. Hines and Evan Coffman provided detailed revisions to the paper.

Conflicts of Interest: The authors declare no conflict of interest.

Disclaimer: The views expressed in this manuscript are those of the authors and do not necessarily reflect the views or policies of the U.S. Environmental Protection Agency. Mention of trade names or commercial products does not constitute endorsement or recommendation for use.

References

1. Kato, K.; Wong, L.Y.; Jia, L.T.; Kuklenyik, Z.; Calafat, A.M. Trends in exposure to polyfluoroalkyl chemicals in the U.S. Population: 1999–2008. *Environ. Sci. Technol.* **2011**, *45*, 8037–8045. [CrossRef] [PubMed]
2. Haug, L.S.; Huber, S.; Becher, G.; Thomsen, C. Characterisation of human exposure pathways to perfluorinated compounds—Comparing exposure estimates with biomarkers of exposure. *Environ. Int.* **2011**, *37*, 687–693. [CrossRef] [PubMed]

3. Mondal, D.; Lopez-Espinosa, M.J.; Armstrong, B.; Stein, C.R.; Fletcher, T. Relationships of Perfluorooctanoate and Perfluorooctane Sulfonate Serum Concentrations between Mother-Child Pairs in a Population with Perfluorooctanoate Exposure from Drinking Water. *Environ. Health Perspect.* **2012**, *120*, 752–757. [CrossRef] [PubMed]
4. Wu, X.M.; Bennett, D.H.; Calafat, A.M.; Kato, K.; Strynar, M.; Andersen, E.; Moran, R.E.; Tancredi, D.J.; Tulve, N.S.; Hertz-Picciotto, I. Serum concentrations of perfluorinated compounds (PFC) among selected populations of children and adults in California. *Environ. Res.* **2015**, *136*, 264–273. [CrossRef] [PubMed]
5. Braun, J.M. Early-life exposure to EDCs: Role in childhood obesity and neurodevelopment. *Nat. Rev. Endocrinol.* **2017**, *13*, 161–173. [CrossRef] [PubMed]
6. Calkins, K.; Devaskar, S.U. Fetal origins of adult disease. *Curr. Probl. Pediatr. Adolesc. Health Care* **2011**, *41*, 158–176. [CrossRef] [PubMed]
7. Corkins, M.R.; Daniels, S.R.; de Ferranti, S.D.; Golden, N.H.; Kim, J.H.; Magge, S.N.; Schwarzenberg, S.J. Nutrition in Children and Adolescents. *Med. Clin. N. Am.* **2016**, *100*, 1217–1235. [CrossRef] [PubMed]
8. Gascon, M.; Vrijheid, M.; Nieuwenhuijsen, M.J. The Built Environment and Child Health: An Overview of Current Evidence. *Curr. Environ. Health Rep.* **2016**, *3*, 250–257. [CrossRef] [PubMed]
9. Ruiz, J.D.C.; Quackenboss, J.J.; Tulve, N.S. Contributions of a child's built, natural, and social environments to their general cognitive ability: A systematic scoping review. *PLoS ONE* **2016**, *11*, e0147741. [CrossRef] [PubMed]
10. Palmer, C.N.; Hsu, M.H.; Griffin, K.J.; Raucy, J.L.; Johnson, E.F. Peroxisome proliferator activated receptor-alpha expression in human liver. *Mol. Pharmacol.* **1998**, *53*, 14–22. [PubMed]
11. Chen, Y.; Zhou, L.; Xu, J.; Zhang, L.; Li, M.; Xie, X.; Xie, Y.; Luo, D.; Zhang, D.; Yu, X.; et al. Maternal exposure to perfluorooctanoic acid inhibits luteal function via oxidative stress and apoptosis in pregnant mice. *Reprod. Toxicol.* **2017**, *69*, 159–166. [CrossRef] [PubMed]
12. Mashayekhi, V.; Tehrani, K.H.M.E.; Hashemzaei, M.; Tabrizian, K.; Shahraki, J.; Hosseini, M. Mechanistic approach for the toxic effects of perfluorooctanoic acid on isolated rat liver and brain mitochondria. *Hum. Exp. Toxicol.* **2015**, *34*, 985–996. [CrossRef] [PubMed]
13. Itoh, S.; Araki, A.; Mitsui, T.; Miyashita, C.; Goudarzi, H.; Sasaki, S.; Cho, K.; Nakazawa, H.; Iwasaki, Y.; Shinohara, N.; et al. Association of perfluoroalkyl substances exposure in utero with reproductive hormone levels in cord blood in the Hokkaido Study on Environment and Children's Health. *Environ. Int.* **2016**, *94*, 51–59. [CrossRef] [PubMed]
14. Zhao, Y.; Tan, Y.S.; Strynar, M.J.; Perez, G.; Haslam, S.Z.; Yang, C. Perfluorooctanoic acid effects on ovaries mediate its inhibition of peripubertal mammary gland development in Balb/c and C57Bl/6 mice. *Reprod. Toxicol.* **2012**, *33*, 563–576. [CrossRef] [PubMed]
15. Zhou, Y.; Hu, L.W.; Qian, Z.M.; Chang, J.J.; King, C.; Paul, G.; Lin, S.; Chen, P.C.; Lee, Y.L.; Dong, G.H. Association of perfluoroalkyl substances exposure with reproductive hormone levels in adolescents: By sex status. *Environ. Int.* **2016**, *94*, 189–195. [CrossRef] [PubMed]
16. Upham, B.L.; Park, J.S.; Babica, P.; Sovadinova, I.; Rummel, A.M.; Trosko, J.E.; Hirose, A.; Hasegawa, R.; Kanno, J.; Sai, K. Structure-activity-dependent regulation of cell communication by perfluorinated fatty acids using in vivo and in vitro model systems. *Environ. Health Perspect.* **2009**, *117*, 545–551. [CrossRef] [PubMed]
17. Lopez-Espinosa, M.J.; Mondal, D.; Armstrong, B.; Bloom, M.S.; Fletcher, T. Thyroid function and perfluoroalkyl acids in children living near a chemical plant. *Environ. Health Perspect.* **2012**, *120*, 1036–1041. [CrossRef] [PubMed]
18. Bach, C.C.; Bech, B.H.; Brix, N.; Nohr, E.A.; Bonde, J.P.E.; Henriksen, T.B. Perfluoroalkyl and polyfluoroalkyl substances and human fetal growth: A systematic review. *Crit. Rev. Toxicol.* **2015**, *45*, 53–67. [CrossRef] [PubMed]
19. Johnson, P.I.; Sutton, P.; Atchley, D.S.; Koustas, E.; Lam, J.; Sen, S.; Robinson, K.A.; Axelrad, D.A.; Woodruff, T.J. The Navigation Guide-Evidence-Based Medicine Meets Environmental Health: Systematic Review of Human Evidence for PFOA Effects on Fetal Growth. *Environ. Health Perspect.* **2014**, *122*, 1028–1039. [CrossRef] [PubMed]
20. Olsen, G.W.; Butenhoff, J.L.; Zobel, L.R. Perfluoroalkyl chemicals and human fetal development: An epidemiologic review with clinical and toxicological perspectives. *Reprod. Toxicol.* **2009**, *27*, 212–230. [CrossRef] [PubMed]

21. Johnson, P.I.; Sutton, P.; Atchley, D.; Koustas, E.; Lam, J.; Sen, S.; Robinson, K.; Axelrad, D.; Woodruff, T.J. The Navigation Guide Systematic Review Methodology Proof of Concept: PFOA and Fetal Growth. *Birth Defects Res. A* **2014**, *100*, 395.
22. Higgins, J.; Green, S. *Cochrane Handbook for Systematic Reviews of Interventions*; Version 5.1.0; Wiley-Blackwell: Hoboken, NJ, USA, 2011.
23. Viswanathan, M.; Ansari, M.T.; Berkman, N.D.; Chang, S.; Hartling, L.; McPheeters, M.; Santaguida, P.L.; Shamliyan, T.; Singh, K.; Tsertsvadze, A. Assessing the risk of bias of individual studies in systematic reviews of health care interventions. In *Methods Guide for Effectiveness and Comparative Effectiveness Reviews*; Agency for Healthcare Research and Quality: Rockville, MD, USA, 2012.
24. Olsen, J.; Melbye, M.; Olsen, S.F.; Sorensen, T.I.; Aaby, P.; Andersen, A.M.; Taxbol, D.; Hansen, K.D.; Juhl, M.; Schow, T.B.; et al. The Danish National Birth Cohort—Its background, structure and aim. *Scand. J. Public Health* **2001**, *29*, 300–307. [CrossRef] [PubMed]
25. Frisbee, S.J.; Brooks, A.P., Jr.; Maher, A.; Flensborg, P.; Arnold, S.; Fletcher, T.; Steenland, K.; Shankar, A.; Knox, S.S.; Pollard, C.; et al. The C8 health project: Design, methods, and participants. *Environ. Health Perspect.* **2009**, *117*, 1873–1882. [CrossRef] [PubMed]
26. Hua, J.Y.; Smith, S.J. Neural activity and the dynamics of central nervous system development. *Nat. Neurosci.* **2004**, *7*, 327–332. [CrossRef] [PubMed]
27. Stiles, J.; Jernigan, T.L. The basics of brain development. *Neuropsychol. Rev.* **2010**, *20*, 327–348. [CrossRef] [PubMed]
28. Fei, C.; McLaughlin, J.K.; Lipworth, L.; Olsen, J. Prenatal exposure to perfluorooctanoate (PFOA) and perfluorooctanesulfonate (PFOS) and maternally reported developmental milestones in infancy. *Environ. Health Perspect.* **2008**, *116*, 1391–1395. [CrossRef] [PubMed]
29. Fei, C.; Olsen, J. Prenatal exposure to perfluorinated chemicals and behavioral or coordination problems at age 7 years. *Environ. Health Perspect.* **2011**, *119*, 573–578. [CrossRef] [PubMed]
30. Donauer, S.; Chen, A.; Xu, Y.; Calafat, A.M.; Sjodin, A.; Yolton, K. Prenatal exposure to polybrominated diphenyl ethers and polyfluoroalkyl chemicals and infant neurobehavior. *J. Pediatr.* **2015**, *166*, 736–742. [CrossRef] [PubMed]
31. Chen, M.H.; Ha, E.H.; Liao, H.F.; Jeng, S.F.; Su, Y.N.; Wen, T.W.; Lien, G.W.; Chen, C.Y.; Hsieh, W.S.; Chen, P.C. Perfluorinated compound levels in cord blood and neurodevelopment at 2 years of age. *Epidemiology* **2013**, *24*, 800–808. [CrossRef] [PubMed]
32. Forns, J.; Iszatt, N.; White, R.A.; Mandal, S.; Sabaredzovic, A.; Lamoree, M.; Thomsen, C.; Haug, L.S.; Stigum, H.; Eggesbo, M. Perfluoroalkyl substances measured in breast milk and child neuropsychological development in a Norwegian birth cohort study. *Environ. Int.* **2015**, *83*, 176–182. [CrossRef] [PubMed]
33. Goudarzi, H.; Nakajima, S.; Ikeno, T.; Sasaki, S.; Kobayashi, S.; Miyashita, C.; Ito, S.; Araki, A.; Nakazawa, H.; Kishi, R. Prenatal exposure to perfluorinated chemicals and neurodevelopment in early infancy: The Hokkaido Study. *Sci. Total Environ.* **2016**, *541*, 1002–1010. [CrossRef] [PubMed]
34. Stein, C.R.; Savitz, D.A.; Bellinger, D.C. Perfluorooctanoate and neuropsychological outcomes in children. *Epidemiology* **2013**, *24*, 590–599. [CrossRef] [PubMed]
35. Wang, Y.; Rogan, W.J.; Chen, H.Y.; Chen, P.C.; Su, P.H.; Chen, H.Y.; Wang, S.L. Prenatal exposure to perfluroalkyl substances and children's IQ: The Taiwan maternal and infant cohort study. *Int. J. Hyg. Environ. Health* **2015**, *218*, 639–644. [CrossRef] [PubMed]
36. Stein, C.R.; Savitz, D.A. Serum perfluorinated compound concentration and attention deficit/hyperactivity disorder in children 5–18 years of age. *Environ. Health Perspect.* **2011**, *119*, 1466–1471. [CrossRef] [PubMed]
37. Vuong, A.M.; Yolton, K.; Webster, G.M.; Sjodin, A.; Calafat, A.M.; Braun, J.M.; Dietrich, K.N.; Lanphear, B.P.; Chen, A. Prenatal polybrominated diphenyl ether and perfluoroalkyl substance exposures and executive function in school-age children. *Environ. Res.* **2016**, *147*, 556–564. [CrossRef] [PubMed]
38. Strom, M.; Hansen, S.; Olsen, S.F.; Haug, L.S.; Rantakokko, P.; Kiviranta, H.; Halldorsson, T.I. Persistent organic pollutants measured in maternal serum and offspring neurodevelopmental outcomes—A prospective study with long-term follow-up. *Environ. Int.* **2014**, *68*, 41–48. [CrossRef] [PubMed]
39. Gump, B.B.; Wu, Q.; Dumas, A.K.; Kannan, K. Perfluorochemical (PFC) exposure in children: Associations with impaired response inhibition. *Environ. Sci. Technol.* **2011**, *45*, 8151–8159. [CrossRef] [PubMed]

40. Hoffman, K.; Webster, T.F.; Weisskopf, M.G.; Weinberg, J.; Vieira, V.M. Exposure to polyfluoroalkyl chemicals and attention deficit/hyperactivity disorder in U.S. children 12–15 years of age. *Environ. Health Perspect.* **2010**, *118*, 1762–1767. [CrossRef] [PubMed]
41. Hoyer, B.B.; Ramlau-Hansen, C.H.; Obel, C.; Pedersen, H.S.; Hernik, A.; Ogniev, V.; Jonsson, B.A.; Lindh, C.H.; Rylander, L.; Rignell-Hydbom, A.; et al. Pregnancy serum concentrations of perfluorinated alkyl substances and offspring behaviour and motor development at age 5–9 years—A prospective study. *Environ. Health* **2015**, *14*, 2. [CrossRef] [PubMed]
42. Liew, Z.; Ritz, B.; von Ehrenstein, O.S.; Bech, B.H.; Nohr, E.A.; Fei, C.; Bossi, R.; Henriksen, T.B.; Bonefeld-Jorgensen, E.C.; Olsen, J. Attention deficit/hyperactivity disorder and childhood autism in association with prenatal exposure to perfluoroalkyl substances: A nested case-control study in the Danish National Birth Cohort. *Environ. Health Perspect.* **2015**, *123*, 367–373. [CrossRef] [PubMed]
43. Lien, G.W.; Huang, C.C.; Shiu, J.S.; Chen, M.H.; Hsieh, W.S.; Guo, Y.L.; Chen, P.C. Perfluoroalkyl substances in cord blood and attention deficit/hyperactivity disorder symptoms in seven-year-old children. *Chemosphere* **2016**, *156*, 118–127. [CrossRef] [PubMed]
44. Quaak, I.; de Cock, M.; de Boer, M.; Lamoree, M.; Leonards, P.; van de Bor, M. Prenatal Exposure to Perfluoroalkyl Substances and Behavioral Development in Children. *Int. J. Environ. Res. Public Health* **2016**, *13*, 511. [CrossRef] [PubMed]
45. Ode, A.; Kallen, K.; Gustafsson, P.; Rylander, L.; Jonsson, B.A.; Olofsson, P.; Ivarsson, S.A.; Lindh, C.H.; Rignell-Hydbom, A. Fetal exposure to perfluorinated compounds and attention deficit hyperactivity disorder in childhood. *PLoS ONE* **2014**, *9*, e95891. [CrossRef] [PubMed]
46. Stein, C.R.; Savitz, D.A.; Bellinger, D.C. Perfluorooctanoate exposure in a highly exposed community and parent and teacher reports of behaviour in 6–12-year-old children. *Paediatr. Perinat. Epidemiol.* **2014**, *28*, 146–156. [CrossRef] [PubMed]
47. Bellinger, D.C. Prenatal Exposures to Environmental Chemicals and Children's Neurodevelopment: An Update. *Saf. Health Work* **2013**, *4*, 1–11. [CrossRef] [PubMed]
48. Roth, N.; Wilks, M.F. Neurodevelopmental and neurobehavioural effects of polybrominated and perfluorinated chemicals: A systematic review of the epidemiological literature using a quality assessment scheme. *Toxicol. Lett.* **2014**, *230*, 271–281. [CrossRef] [PubMed]
49. Johansson, N.; Fredriksson, A.; Eriksson, P. Neonatal exposure to perfluorooctane sulfonate (PFOS) and perfluorooctanoic acid (PFOA) causes neurobehavioural defects in adult mice. *Neurotoxicology* **2008**, *29*, 160–169. [CrossRef] [PubMed]
50. Spulber, S.; Kilian, P.; Wan Ibrahim, W.N.; Onishchenko, N.; Ulhaq, M.; Norrgren, L.; Negri, S.; Di Tuccio, M.; Ceccatelli, S. PFOS induces behavioral alterations, including spontaneous hyperactivity that is corrected by dexamfetamine in zebrafish larvae. *PLoS ONE* **2014**, *9*, e94227. [CrossRef] [PubMed]
51. Chen, J.; Das, S.R.; La Du, J.; Corvi, M.M.; Bai, C.; Chen, Y.; Liu, X.; Zhu, G.; Tanguay, R.L.; Dong, Q.; et al. Chronic PFOS exposures induce life stage-specific behavioral deficits in adult zebrafish and produce malformation and behavioral deficits in F1 offspring. *Environ. Toxicol. Chem. SETAC* **2013**, *32*, 201–206. [CrossRef] [PubMed]
52. Geiger, S.D.; Xiao, J.; Shankar, A. No association between perfluoroalkyl chemicals and hypertension in children. *Integr. Blood Press. Control* **2014**, *7*, 1–7. [CrossRef] [PubMed]
53. Andersen, C.S.; Fei, C.; Gamborg, M.; Nohr, E.A.; Sorensen, T.I.; Olsen, J. Prenatal exposures to perfluorinated chemicals and anthropometric measures in infancy. *Am. J. Epidemiol.* **2010**, *172*, 1230–1237. [CrossRef] [PubMed]
54. Andersen, C.S.; Fei, C.; Gamborg, M.; Nohr, E.A.; Sorensen, T.I.; Olsen, J. Prenatal exposures to perfluorinated chemicals and anthropometry at 7 years of age. *Am. J. Epidemiol.* **2013**, *178*, 921–927. [CrossRef] [PubMed]
55. Braun, J.M.; Chen, A.; Romano, M.E.; Calafat, A.M.; Webster, G.M.; Yolton, K.; Lanphear, B.P. Prenatal perfluoroalkyl substance exposure and child adiposity at 8 years of age: The HOME study. *Obesity* **2016**, *24*, 231–237. [CrossRef] [PubMed]
56. Maisonet, M.; Terrell, M.L.; McGeehin, M.A.; Christensen, K.Y.; Holmes, A.; Calafat, A.M.; Marcus, M. Maternal concentrations of polyfluoroalkyl compounds during pregnancy and fetal and postnatal growth in British girls. *Environ. Health Perspect.* **2012**, *120*, 1432–1437. [CrossRef] [PubMed]

57. Halldorsson, T.I.; Rytter, D.; Haug, L.S.; Bech, B.H.; Danielsen, I.; Becher, G.; Henriksen, T.B.; Olsen, S.F. Prenatal exposure to perfluorooctanoate and risk of overweight at 20 years of age: A prospective cohort study. *Environ. Health Perspect.* **2012**, *120*, 668–673. [CrossRef] [PubMed]
58. Hoyer, B.B.; Ramlau-Hansen, C.H.; Vrijheid, M.; Valvi, D.; Pedersen, H.S.; Zviezdai, V.; Jonsson, B.A.; Lindh, C.H.; Bonde, J.P.; Toft, G. Anthropometry in 5- to 9-Year-Old Greenlandic and Ukrainian Children in Relation to Prenatal Exposure to Perfluorinated Alkyl Substances. *Environ. Health Perspect.* **2015**, *123*, 841–846. [CrossRef] [PubMed]
59. Wang, Y.; Adgent, M.; Su, P.H.; Chen, H.Y.; Chen, P.C.; Hsiung, C.A.; Wang, S.L. Prenatal Exposure to Perfluorocarboxylic Acids (PFCAs) and Fetal and Postnatal Growth in the Taiwan Maternal and Infant Cohort Study. *Environ. Health Perspect.* **2016**, *124*, 1794–1800. [CrossRef] [PubMed]
60. Timmermann, C.A.; Rossing, L.I.; Grontved, A.; Ried-Larsen, M.; Dalgard, C.; Andersen, L.B.; Grandjean, P.; Nielsen, F.; Svendsen, K.D.; Scheike, T.; et al. Adiposity and glycemic control in children exposed to perfluorinated compounds. *J. Clin. Endocrinol. Metab.* **2014**, *99*, E608–E614. [CrossRef] [PubMed]
61. Kristensen, S.L.; Ramlau-Hansen, C.H.; Ernst, E.; Olsen, S.F.; Bonde, J.P.; Vested, A.; Halldorsson, T.I.; Becher, G.; Haug, L.S.; Toft, G. Long-term effects of prenatal exposure to perfluoroalkyl substances on female reproduction. *Hum. Reprod.* **2013**, *28*, 3337–3348. [CrossRef] [PubMed]
62. Geiger, S.D.; Xiao, J.; Ducatman, A.; Frisbee, S.; Innes, K.; Shankar, A. The association between PFOA, PFOS and serum lipid levels in adolescents. *Chemosphere* **2014**, *98*, 78–83. [CrossRef] [PubMed]
63. Lin, C.Y.; Chen, P.C.; Lin, Y.C.; Lin, L.Y. Association among serum perfluoroalkyl chemicals, glucose homeostasis, and metabolic syndrome in adolescents and adults. *Diabetes Care* **2009**, *32*, 702–707. [CrossRef] [PubMed]
64. Frisbee, S.J.; Shankar, A.; Knox, S.S.; Steenland, K.; Savitz, D.A.; Fletcher, T.; Ducatman, A.M. Perfluorooctanoic acid, perfluorooctanesulfonate, and serum lipids in children and adolescents: Results from the C8 Health Project. *Arch. Pediatr. Adolesc. Med.* **2010**, *164*, 860–869. [CrossRef] [PubMed]
65. Zeng, X.W.; Qian, Z.; Emo, B.; Vaughn, M.; Bao, J.; Qin, X.D.; Zhu, Y.; Li, J.; Lee, Y.L.; Dong, G.H. Association of polyfluoroalkyl chemical exposure with serum lipids in children. *Sci. Total Environ.* **2015**, *512–513*, 364–370. [CrossRef] [PubMed]
66. Maisonet, M.; Nayha, S.; Lawlor, D.A.; Marcus, M. Prenatal exposures to perfluoroalkyl acids and serum lipids at ages 7 and 15 in females. *Environ. Int.* **2015**, *82*, 49–60. [CrossRef] [PubMed]
67. Lin, C.Y.; Wen, L.L.; Lin, L.Y.; Wen, T.W.; Lien, G.W.; Chen, C.Y.; Hsu, S.H.; Chien, K.L.; Sung, F.C.; Chen, P.C.; et al. Associations between levels of serum perfluorinated chemicals and adiponectin in a young hypertension cohort in Taiwan. *Environ. Sci. Technol.* **2011**, *45*, 10691–10698. [CrossRef] [PubMed]
68. Lin, C.Y.; Lin, L.Y.; Wen, T.W.; Lien, G.W.; Chien, K.L.; Hsu, S.H.; Liao, C.C.; Sung, F.C.; Chen, P.C.; Su, T.C. Association between levels of serum perfluorooctane sulfate and carotid artery intima-media thickness in adolescents and young adults. *Int. J. Cardiol.* **2013**, *168*, 3309–3316. [CrossRef] [PubMed]
69. Fletcher, T.; Galloway, T.S.; Melzer, D.; Holcroft, P.; Cipelli, R.; Pilling, L.C.; Mondal, D.; Luster, M.; Harries, L.W. Associations between PFOA, PFOS and changes in the expression of genes involved in cholesterol metabolism in humans. *Environ. Int.* **2013**, *57–58*, 2–10. [CrossRef] [PubMed]
70. Wan, H.T.; Zhao, Y.G.; Leung, P.Y.; Wong, C.K.C. Perinatal Exposure to Perfluorooctane Sulfonate Affects Glucose Metabolism in Adult Offspring. *PLoS ONE* **2014**, *9*, e87137. [CrossRef] [PubMed]
71. Hines, E.P.; White, S.S.; Stanko, J.P.; Gibbs-Flournoy, E.A.; Lau, C.; Fenton, S.E. Phenotypic dichotomy following developmental exposure to perfluorooctanoic acid (PFOA) in female CD-1 mice: Low doses induce elevated serum leptin and insulin, and overweight in mid-life. *Mol. Cell. Endocrinol.* **2009**, *304*, 97–105. [CrossRef] [PubMed]
72. Tittlemier, S.A.; Pepper, K.; Seymour, C.; Moisey, J.; Bronson, R.; Cao, X.-L.; Dabeka, R.W. Dietary exposure of Canadians to perfluorinated carboxylates and perfluorooctane sulfonate via consumption of meat, fish, fast foods, and food items prepared in their packaging. *J. Agric. Food Chem.* **2007**, *55*, 3203–3210. [CrossRef] [PubMed]
73. Plotkin, S.L.; Plotkin, S.A.; Plotkin, S.A.; Orenstein, W. A short history of vaccination. *Vaccines* **2004**, *5*, 1–16.
74. Mina, M.J.; Metcalf, C.J.; de Swart, R.L.; Osterhaus, A.D.; Grenfell, B.T. Long-term measles-induced immunomodulation increases overall childhood infectious disease mortality. *Science* **2015**, *348*, 694–699. [CrossRef] [PubMed]

75. Grandjean, P.; Andersen, E.W.; Budtz-Jorgensen, E.; Nielsen, F.; Molbak, K.; Weihe, P.; Heilmann, C. Serum vaccine antibody concentrations in children exposed to perfluorinated compounds. *JAMA* **2012**, *307*, 391–397. [CrossRef] [PubMed]
76. Fangstrom, B.; Hovander, L.; Bignert, A.; Athanassiadis, I.; Linderholm, L.; Grandjean, P.; Weihe, P.; Bergman, A. Concentrations of polybrominated diphenyl ethers, polychlonnated biphenyls, and polychlorobiphenylols in serum from pregnant Faroese women and their children 7 years later. *Environ. Sci. Technol.* **2005**, *39*, 9457–9463. [CrossRef] [PubMed]
77. Granum, B.; Haug, L.S.; Namork, E.; Stolevik, S.B.; Thomsen, C.; Aaberge, I.S.; van Loveren, H.; Lovik, M.; Nygaard, U.C. Pre-natal exposure to perfluoroalkyl substances may be associated with altered vaccine antibody levels and immune-related health outcomes in early childhood. *J. Immunotoxicol.* **2013**, *10*, 373–379. [CrossRef] [PubMed]
78. Stein, C.R.; McGovern, K.J.; Pajak, A.M.; Maglione, P.J.; Wolff, M.S. Perfluoroalkyl and polyfluoroalkyl substances and indicators of immune function in children aged 12–19 years: National Health and Nutrition Examination Survey. *Pediatr. Res.* **2016**, *79*, 348–357. [CrossRef] [PubMed]
79. Dong, G.H.; Tung, K.Y.; Tsai, C.H.; Liu, M.M.; Wang, D.; Liu, W.; Jin, Y.H.; Hsieh, W.S.; Lee, Y.L.; Chen, P.C. Serum polyfluoroalkyl concentrations, asthma outcomes, and immunological markers in a case-control study of Taiwanese children. *Environ. Health Perspect.* **2013**, *121*, 507–513. [CrossRef] [PubMed]
80. Qin, X.D.; Qian, Z.M.; Dharmage, S.C.; Perret, J.; Geiger, S.D.; Rigdon, S.E.; Howard, S.; Zeng, X.W.; Hu, L.W.; Yang, B.Y.; et al. Association of perfluoroalkyl substances exposure with impaired lung function in children. *Environ. Res.* **2017**, *155*, 15–21. [CrossRef] [PubMed]
81. Humblet, O.; Diaz-Ramirez, L.G.; Balmes, J.R.; Pinney, S.M.; Hiatt, R.A. Perfluoroalkyl chemicals and asthma among children 12–19 years of age: NHANES (1999–2008). *Environ. Health Perspect.* **2014**, *122*, 1129–1133. [CrossRef] [PubMed]
82. Zhu, Y.; Qin, X.D.; Zeng, X.W.; Paul, G.; Morawska, L.; Su, M.W.; Tsai, C.H.; Wang, S.Q.; Lee, Y.L.; Dong, G.H. Associations of serum perfluoroalkyl acid levels with T-helper cell-specific cytokines in children: By gender and asthma status. *Sci. Total Environ.* **2016**, *559*, 166–173. [CrossRef] [PubMed]
83. Smit, L.A.; Lenters, V.; Høyer, B.B.; Lindh, C.H.; Pedersen, H.S.; Liermontova, I.; Jönsson, B.A.; Piersma, A.H.; Bonde, J.P.; Toft, G. Prenatal exposure to environmental chemical contaminants and asthma and eczema in school-age children. *Allergy* **2015**, *70*, 653–660. [CrossRef] [PubMed]
84. Okada, E.; Sasaki, S.; Kashino, I.; Matsuura, H.; Miyashita, C.; Kobayashi, S.; Itoh, K.; Ikeno, T.; Tamakoshi, A.; Kishi, R. Prenatal exposure to perfluoroalkyl acids and allergic diseases in early childhood. *Environ. Int.* **2014**, *65*, 127–134. [CrossRef] [PubMed]
85. Okada, E.; Sasaki, S.; Saijo, Y.; Washino, N.; Miyashita, C.; Kobayashi, S.; Konishi, K.; Ito, Y.M.; Ito, R.; Nakata, A.; et al. Prenatal exposure to perfluorinated chemicals and relationship with allergies and infectious diseases in infants. *Environ. Res.* **2012**, *112*, 118–125. [CrossRef] [PubMed]
86. Wang, I.-J.; Hsieh, W.-S.; Chen, C.-Y.; Fletcher, T.; Lien, G.-W.; Chiang, H.-L.; Chiang, C.-F.; Wu, T.-N.; Chen, P.-C. The effect of prenatal perfluorinated chemicals exposures on pediatric atopy. *Environ. Res.* **2011**, *111*, 785–791. [CrossRef] [PubMed]
87. Ashley-Martin, J.; Dodds, L.; Levy, A.R.; Platt, R.W.; Marshall, J.S.; Arbuckle, T.E. Prenatal exposure to phthalates, bisphenol A and perfluoroalkyl substances and cord blood levels of IgE, TSLP and IL-33. *Environ. Res.* **2015**, *140*, 360–368. [CrossRef] [PubMed]
88. Fei, C.; McLaughlin, J.K.; Lipworth, L.; Olsen, J. Prenatal exposure to PFOA and PFOS and risk of hospitalization for infectious diseases in early childhood. *Environ. Res.* **2010**, *110*, 773–777. [CrossRef] [PubMed]
89. DeWitt, J.C.; Peden-Adams, M.M.; Keller, J.M.; Germolec, D.R. Immunotoxicity of perfluorinated compounds: Recent developments. *Toxicol. Pathol.* **2012**, *40*, 300–311. [CrossRef] [PubMed]
90. Castellanos-Ryan, N.; Parent, S.; Vitaro, F.; Tremblay, R.E.; Seguin, J.R. Pubertal development, personality, and substance use: A 10-year longitudinal study from childhood to adolescence. *J. Abnorm. Psychol.* **2013**, *122*, 782–796. [CrossRef] [PubMed]
91. Day, F.R.; Elks, C.E.; Murray, A.; Ong, K.K.; Perry, J.R. Puberty timing associated with diabetes, cardiovascular disease and also diverse health outcomes in men and women: The UK Biobank study. *Sci. Rep.* **2015**, *5*, 11208. [CrossRef] [PubMed]

92. Karapanou, O.; Papadimitriou, A. Determinants of menarche. *Reprod. Biol. Endocrinol.* **2010**, *8*, 115. [CrossRef] [PubMed]
93. Wren, T.A.; Kalkwarf, H.J.; Zemel, B.S.; Lappe, J.M.; Oberfield, S.; Shepherd, J.A.; Winer, K.K.; Gilsanz, V. Bone Mineral Density in Childhood Study, G. Longitudinal tracking of dual-energy X-ray absorptiometry bone measures over 6 years in children and adolescents: Persistence of low bone mass to maturity. *J. Pediatr.* **2014**, *164*, 1280–1285. [CrossRef] [PubMed]
94. Christensen, K.Y.; Maisonet, M.; Rubin, C.; Holmes, A.; Calafat, A.M.; Kato, K.; Flanders, W.D.; Heron, J.; McGeehin, M.A.; Marcus, M. Exposure to polyfluoroalkyl chemicals during pregnancy is not associated with offspring age at menarche in a contemporary British cohort. *Environ. Int.* **2011**, *37*, 129–135. [CrossRef] [PubMed]
95. Lopez-Espinosa, M.J.; Fletcher, T.; Armstrong, B.; Genser, B.; Dhatariya, K.; Mondal, D.; Ducatman, A.; Leonardi, G. Association of Perfluorooctanoic Acid (PFOA) and Perfluorooctane Sulfonate (PFOS) with age of puberty among children living near a chemical plant. *Environ. Sci. Technol.* **2011**, *45*, 8160–8166. [CrossRef] [PubMed]
96. Maisonet, M.; Calafat, A.M.; Marcus, M.; Jaakkola, J.J.; Lashen, H. Prenatal Exposure to Perfluoroalkyl Acids and Serum Testosterone Concentrations at 15 Years of Age in Female ALSPAC Study Participants. *Environ. Health Perspect.* **2015**. [CrossRef] [PubMed]
97. Lopez-Espinosa, M.J.; Mondal, D.; Armstrong, B.G.; Eskenazi, B.; Fletcher, T. Perfluoroalkyl Substances, Sex Hormones, and Insulin-like Growth Factor-1 at 6–9 Years of Age: A Cross-Sectional Analysis within the C8 Health Project. *Environ. Health Perspect.* **2016**. [CrossRef] [PubMed]
98. Tsai, M.S.; Lin, C.Y.; Lin, C.C.; Chen, M.H.; Hsu, S.H.; Chien, K.L.; Sung, F.C.; Chen, P.C.; Su, T.C. Association between perfluoroalkyl substances and reproductive hormones in adolescents and young adults. *Int. J. Hyg. Environ. Health* **2015**, *218*, 437–443. [CrossRef] [PubMed]
99. White, S.S.; Stanko, J.P.; Kato, K.; Calafat, A.M.; Hines, E.P.; Fenton, S.E. Gestational and chronic low-dose PFOA exposures and mammary gland growth and differentiation in three generations of CD-1 mice. *Environ. Health Perspect.* **2011**, *119*, 1070–1076. [CrossRef] [PubMed]
100. Yang, C.; Tan, Y.S.; Harkema, J.R.; Haslam, S.Z. Differential effects of peripubertal exposure to perfluorooctanoic acid on mammary gland development in C57Bl/6 and Balb/c mouse strains. *Reprod. Toxicol.* **2009**, *27*, 299–306. [CrossRef] [PubMed]
101. Lin, C.Y.; Wen, L.L.; Lin, L.Y.; Wen, T.W.; Lien, G.W.; Hsu, S.H.; Chien, K.L.; Liao, C.C.; Sung, F.C.; Chen, P.C.; et al. The associations between serum perfluorinated chemicals and thyroid function in adolescents and young adults. *J. Hazard. Mater.* **2013**, *244–245*, 637–644. [CrossRef] [PubMed]
102. De Cock, M.; de Boer, M.R.; Lamoree, M.; Legler, J.; van de Bor, M. Prenatal exposure to endocrine disrupting chemicals in relation to thyroid hormone levels in infants—A Dutch prospective cohort study. *Environ. Health* **2014**, *13*, 106. [CrossRef] [PubMed]
103. Tsai, M.S.; Lin, C.C.; Chen, M.H.; Hsieh, W.S.; Chen, P.C. Perfluoroalkyl substances and thyroid hormones in cord blood. *Environm. Pollut.* **2017**, *222*, 543–548. [CrossRef] [PubMed]
104. Kim, S.; Choi, K.; Ji, K.; Seo, J.; Kho, Y.; Park, J.; Kim, S.; Park, S.; Hwang, I.; Jeon, J.; et al. Trans-placental transfer of thirteen perfluorinated compounds and relations with fetal thyroid hormones. *Environ. Sci. Technol.* **2011**, *45*, 7465–7472. [CrossRef] [PubMed]
105. Kato, S.; Itoh, S.; Yuasa, M.; Baba, T.; Miyashita, C.; Sasaki, S.; Nakajima, S.; Uno, A.; Nakazawa, H.; Iwasaki, Y.; et al. Association of perfluorinated chemical exposure in utero with maternal and infant thyroid hormone levels in the Sapporo cohort of Hokkaido Study on the Environment and Children's Health. *Environ. Health Prev. Med.* **2016**. [CrossRef] [PubMed]
106. Kim, D.H.; Kim, U.J.; Kim, H.Y.; Choi, S.D.; Oh, J.E. Perfluoroalkyl substances in serum from South Korean infants with congenital hypothyroidism and healthy infants—Its relationship with thyroid hormones. *Environ. Res.* **2016**, *147*, 399–404. [CrossRef] [PubMed]
107. Melzer, D.; Rice, N.; Depledge, M.H.; Henley, W.E.; Galloway, T.S. Association between serum perfluorooctanoic acid (PFOA) and thyroid disease in the U.S. National Health and Nutrition Examination Survey. *Environ. Health Perspect.* **2010**, *118*, 686–692. [CrossRef] [PubMed]
108. Watkins, D.J.; Josson, J.; Elston, B.; Bartell, S.M.; Shin, H.M.; Vieira, V.M.; Savitz, D.A.; Fletcher, T.; Wellenius, G.A. Exposure to perfluoroalkyl acids and markers of kidney function among children and adolescents living near a chemical plant. *Environ. Health Perspect.* **2013**, *121*, 625–630. [CrossRef] [PubMed]

109. Kataria, A.; Trachtman, H.; Malaga-Dieguez, L.; Trasande, L. Association between perfluoroalkyl acids and kidney function in a cross-sectional study of adolescents. *Environ. Health* **2015**, *14*, 89. [CrossRef] [PubMed]
110. Qin, X.D.; Qian, Z.; Vaughn, M.G.; Huang, J.; Ward, P.; Zeng, X.W.; Zhou, Y.; Zhu, Y.; Yuan, P.; Li, M.; et al. Positive associations of serum perfluoroalkyl substances with uric acid and hyperuricemia in children from Taiwan. *Environ. Pollut.* **2016**, *212*, 519–524. [CrossRef] [PubMed]
111. Olsen, G.W.; Burris, J.M.; Ehresman, D.J.; Froehlich, J.W.; Seacat, A.M.; Butenhoff, J.L.; Zobel, L.R. Half-life of serum elimination of perfluorooctanesulfonate, perfluorohexanesulfonate, and perfluorooctanoate in retired fluorochemical production workers. *Environ. Health Perspect.* **2007**, *115*, 1298–1305. [CrossRef] [PubMed]
112. IOM (Institute of Medicine). Roundtable on Environmental Health Sciences, Research and Medicine. In *Environmental Health Sciences Decision Making: Risk Management, Evidence, and Ethics-Workshop Summary*; National Academies Press (US): Washington, DC, USA, 2009.
113. Gutzkow, K.B.; Haug, L.S.; Thomsen, C.; Sabaredzovic, A.; Becher, G.; Brunborg, G. Placental transfer of perfluorinated compounds is selective—A Norwegian Mother and Child sub-cohort study. *Int. J. Hyg. Environ. Health* **2012**, *215*, 216–219. [CrossRef] [PubMed]
114. Wang, Z.; DeWitt, J.C.; Higgins, C.P.; Cousins, I.T. *A Never-Ending Story of per and Polyfluoroalkyl Substances (PFASs)?* ACS Publications: Washington, DC, USA, 2017.

© 2017 by the authors. Licensee MDPI, Basel, Switzerland. This article is an open access article distributed under the terms and conditions of the Creative Commons Attribution (CC BY) license (http://creativecommons.org/licenses/by/4.0/).

International Journal of Environmental Research and Public Health

Supplementary Materials: Exposure to Perfluorinated Alkyl Substances and Health Outcomes in Children: A Systematic Review of the Epidemiologic Literature

Kristen M. Rappazzo, Evan Coffman, and Erin P. Hines

Epidemiologic Evidence of Relationships between Perfluorinated Chemical Exposure and Reproductive or Child Health Outcomes

Table S1. Search terms used for systematic review.

Exposure/PFAS Search Terms	Outcome/Other Search Terms
Perfluorinated	Children
perfluorooctane sulfonate	child
perfluorooctanoate	menarche
polyfluoroalkyl compounds	development
Polyfluoroalkyl chemicals	male reproductive health
Perfluorinated chemicals	testosterone
Perfluorooctanoic acid	reproduction
perfluorooctane sulfonic acid	cord blood
perfluorinated acid	Maternal blood
fluorocarbons	Prenatal exposure
Perfluorinated alkyl substances	Fetal exposure
Perfluorohexane sulfonate	Prenatal exposure delayed effects
perfluoroalkyl acids	mental developmental milestones
fluorinated organic compounds	motor developmental milestones
PFOA	neurodevelopment
PFOS	Attention Deficit Hyperactivity Disorder, ADHD
PFAA	offspring obesity
PFNA	overweight
PFC	serum lipids
PFHxS	Adiposity
PFOSA	Glycemic Control
	immunity
	immune
	eGFR
	kidney function
	T4
	Thyroid disease
	Thyroid hormones
	Thyroid stimulating hormone, TSH

Boolean Search examples

Searches were performed by joining two parenthetical terms with an AND operator. The first term was comprised of PFAS terms linked with OR operators, and the second with health/other terms linked with OR operators. Both "simple" (wherein PFAS terms were limited to PFOA, PFOS, and PFAS or PFC) and full (all PFAS terms) were performed.

Simple search with limited exposure terms, initial search was: (PFOA OR PFOS OR PFAS) AND (child

OR children)

(PFOA[All Fields] OR PFOS[All Fields] OR PFAS[All Fields]) AND (("child"[MeSH Terms] OR "child"[All Fields]) OR ("child"[MeSH Terms] OR "child"[All Fields] OR "children"[All Fields])) AND ("humans"[MeSH Terms] AND English[lang])

Full search, all terms included

(Perfluorinated[All Fields] OR ("perfluorooctane sulfonic acid"[Supplementary Concept] OR "perfluorooctane sulfonic acid"[All Fields] OR "perfluorooctane sulfonate"[All Fields]) OR ("perfluorooctanoic acid"[Supplementary Concept] OR "perfluorooctanoic acid"[All Fields] OR "perfluorooctanoate"[All Fields]) OR (polyfluoroalkyl[All Fields] AND compounds[All Fields]) OR (Polyfluoroalkyl[All Fields] AND chemicals[All Fields]) OR (Perfluorinated[All Fields] AND chemicals[All Fields]) OR ("perfluorooctanoic acid"[Supplementary Concept] OR "perfluorooctanoic acid"[All Fields]) OR ("perfluorooctane sulfonic acid"[Supplementary Concept] OR "perfluorooctane sulfonic acid"[All Fields]) OR (perfluorinated[All Fields] AND ("acids"[MeSH Terms] OR "acids"[All Fields] OR "acid"[All Fields]) AND ("fluorocarbons"[MeSH Terms] OR "fluorocarbons"[All Fields])) OR (Perfluorinated[All Fields] AND alkyl[All Fields] AND substances[All Fields]) OR (("perflexane"[Supplementary Concept] OR "perflexane"[All Fields] OR "perfluorohexane"[All Fields]) AND ("alkanesulfonates"[MeSH Terms] OR "alkanesulfonates"[All Fields] OR "sulfonate"[All Fields])) OR (perfluoroalkyl[All Fields] AND ("acids"[MeSH Terms] OR "acids"[All Fields])) OR (fluorinated[All Fields] AND ("organic chemicals"[MeSH Terms] OR ("organic"[All Fields] AND "chemicals"[All Fields]) OR "organic chemicals"[All Fields] OR ("organic"[All Fields] AND "compounds"[All Fields]) OR "organic compounds"[All Fields])) OR PFOA[All Fields] OR PFOS[All Fields] OR PFAA[All Fields] OR PFNA[All Fields] OR PFC[All Fields] OR PFHxS[All Fields] OR ("perfluorooctane sulfonic acid"[Supplementary Concept] OR "perfluorooctane sulfonic acid"[All Fields] OR "pfosa"[All Fields])) AND (eGFR[All Fields] OR (("kidney"[MeSH Terms] OR "kidney"[All Fields]) AND ("physiology"[Subheading] OR "physiology"[All Fields] OR "function"[All Fields] OR "physiology"[MeSH Terms] OR "function"[All Fields])) OR T4[All Fields] OR ("thyroid diseases"[MeSH Terms] OR ("thyroid"[All Fields] AND "diseases"[All Fields]) OR "thyroid diseases"[All Fields] OR ("thyroid"[All Fields] AND "disease"[All Fields]) OR "thyroid disease"[All Fields]) OR ("thyroid hormones"[MeSH Terms] OR ("thyroid"[All Fields] AND "hormones"[All Fields]) OR "thyroid hormones"[All Fields]) OR ("thyrotropin"[MeSH Terms] OR "thyrotropin"[All Fields] OR ("thyroid"[All Fields] AND "stimulating"[All Fields] AND "hormone"[All Fields]) OR "thyroid stimulating hormone"[All Fields]) OR TSH[All Fields] OR ("attention deficit disorder with hyperactivity"[MeSH Terms] OR ("attention"[All Fields] AND "deficit"[All Fields] AND "disorder"[All Fields] AND "hyperactivity"[All Fields]) OR "attention deficit disorder with hyperactivity"[All Fields] OR ("attention"[All Fields] AND "deficit"[All Fields] AND "hyperactivity"[All Fields] AND "disorder"[All Fields]) OR "attention deficit hyperactivity disorder"[All Fields]) OR ("attention deficit disorder with hyperactivity"[MeSH Terms] OR ("attention"[All Fields] AND "deficit"[All Fields] AND "disorder"[All Fields] AND "hyperactivity"[All Fields]) OR "attention deficit disorder with hyperactivity"[All Fields] OR "adhd"[All Fields]) OR (offspring[All Fields] AND ("obesity"[MeSH Terms] OR "obesity"[All Fields])) OR ("overweight"[MeSH Terms] OR "overweight"[All Fields]) OR (("serum"[MeSH Terms] OR "serum"[All Fields]) AND ("lipids"[MeSH Terms] OR "lipids"[All Fields])) OR ("adiposity"[MeSH Terms] OR "adiposity"[All Fields]) OR (Glycemic[All Fields] AND ("prevention and control"[Subheading] OR ("prevention"[All Fields] AND "control"[All Fields]) OR "prevention and control"[All Fields] OR "control"[All Fields] OR "control groups"[MeSH Terms] OR ("control"[All Fields] AND "groups"[All Fields]) OR "control groups"[All Fields])) OR ("immunity"[MeSH Terms] OR "immunity"[All Fields]) OR immune[All Fields] OR ("fetal blood"[MeSH Terms] OR ("fetal"[All Fields] AND "blood"[All Fields]) OR "fetal blood"[All Fields] OR ("cord"[All Fields] AND "blood"[All Fields]) OR "cord blood"[All Fields]) OR (("mothers"[MeSH Terms] OR

"mothers"[All Fields] OR "maternal"[All Fields]) AND ("blood"[Subheading] OR "blood"[All Fields] OR "blood"[MeSH Terms])) OR (("prenatal care"[MeSH Terms] OR ("prenatal"[All Fields] AND "care"[All Fields]) OR "prenatal care"[All Fields] OR "prenatal"[All Fields]) AND exposure[All Fields]) OR (("fetus"[MeSH Terms] OR "fetus"[All Fields] OR "fetal"[All Fields]) AND exposure[All Fields]) OR ("prenatal exposure delayed effects"[MeSH Terms] OR ("prenatal"[All Fields] AND "exposure"[All Fields] AND "delayed"[All Fields] AND "effects"[All Fields]) OR "prenatal exposure delayed effects"[All Fields]) OR (mental[All Fields] AND developmental[All Fields] AND milestones[All Fields]) OR (motor[All Fields] AND developmental[All Fields] AND milestones[All Fields]) OR neurodevelopment[All Fields] OR ("child"[MeSH Terms] OR "child"[All Fields] OR "children"[All Fields]) OR ("child"[MeSH Terms] OR "child"[All Fields]) OR ("menarche"[MeSH Terms] OR "menarche"[All Fields]) OR ("growth and development"[Subheading] OR ("growth"[All Fields] AND "development"[All Fields]) OR "growth and development"[All Fields] OR "development"[All Fields]) OR (("male"[MeSH Terms] OR "male"[All Fields]) AND ("reproductive health"[MeSH Terms] OR ("reproductive"[All Fields] AND "health"[All Fields]) OR "reproductive health"[All Fields])) OR ("testosterone"[MeSH Terms] OR "testosterone"[All Fields]) OR ("reproduction"[MeSH Terms] OR "reproduction"[All Fields])) AND ("humans"[MeSH Terms] AND English[lang])

Guidelines for Making Risk of Bias Determinations in Epidemiologic Studies of Perfluorinated Chemical Exposure and Child Health Outcomes

The following guidelines outline the criteria we used to evaluate the methodological design and implementation of the studies included in our review. The risk of bias criteria in our guidelines were directly adapted from a systematic review of PFOA effects on fetal growth [Johnson et al., 2014], which developed its risk of bias framework from the Cochrane Collaboration's Risk of bias tool and the Agency for Healthcare Research and Quality's criteria [Higgins and Green, 2011; Viswanathan et al., 2012]. The guidelines outline seven potential biases with specific criteria for a low risk of bias determination within each category. Subsequently, there is a general summary of the criteria for higher risks of bias.

1. Selection Bias

   Criteria for a "low risk of bias" judgment:
   - Study participants were recruited/selected from the same population at the same time frame; or:
   - Study participants were not all recruited from the same population, but proportions of participants from each population in each study group are uniform;
     AND:
   - Loss to follow-up in longitudinal studies is minimized and any loss to follow-up is not expected to differ greatly between levels of exposure and/or outcome; and:
   - Other sources of potential selection bias are minimized (e.g., Berkson's bias, nonresponse bias, incidence-prevalence bias, volunteer/self-selection bias)

2. Exposure Assessment

   Criteria for a "low risk of bias" judgment:
   "The reviewers judge that there is low risk of exposure misclassification and any one of the following:
   - There is high confidence in the accuracy of the exposure assessment methods; or:
   - Less-established or less direct exposure measurements are validated against well-established or direct methods"

3. Outcome Assessment

Criteria for a "low risk of bias" judgment:
The reviewers judge that there is low risk of outcome misclassification and any one of the following:

- There is high confidence in the accuracy of the outcome assessment methods (e.g., clinical diagnosis, laboratory testing, sensitive instrument); or:
- Less-established or less direct outcome measurements are validated against well-established or direct methods; or:
- If self- or parental-reported outcomes are being used, there is high confidence in the accuracy of those reports; or:
- If a proxy measure is being used, the outcome being measured provides a reasonable surrogate for the outcome of interest

4. Confounding

Criteria for a "low risk of bias" judgment:
"The study accounted for (i.e., matched, stratified, multivariate analysis or otherwise statistically controlled for) important potential confounders, or reported that potential confounders were evaluated and omitted because inclusion did not substantially affect the results." The determination of specific confounders that should be adjusted for will depend on the details of the individual studies, and evaluation will be subject to the judgment of the reviewer. However, the following is a general list of potentially important confounders:

- Age, Sex, Race, Maternal Age at Delivery, Maternal Education, Family Income, ETS, Maternal Alcohol Use DP, Maternal Smoking DP, and Breast Feeding

5. Missing Data

Criteria for a "low risk of bias" judgment:
"Participants were followed long enough to obtain outcome measurements and any one of the following:

- No missing outcome data; or:
- Reasons for missing outcome data unlikely to be related to true outcome (for survival data, censoring unlikely to be introducing bias); or:
- Missing outcome data balanced in numbers across exposure groups, with similar reasons for missing data across groups; or:
- For dichotomous outcome data, the proportion of missing outcomes compared with observed event risk not enough to have a biologically relevant impact on the intervention effect estimate; or:
- For continuous outcome data, plausible effect size (difference in means or standardized difference in means) among missing outcomes not enough to have a biologically relevant impact on observed effect size; or:
- Missing data have been imputed using appropriate methods"

6. Conflict of Interest

Criteria for a "low risk of bias" judgment:
"The study did not receive support from a company, study author, or other entity having a financial interest in the outcome of the study. Examples include the following:

- Funding source is limited to government, non-profit organizations, or academic grants funded by government, foundations and/or non-profit organizations;

- Chemicals or other treatment used in study were purchased from a supplier;
- Company affiliated staff are not mentioned in the acknowledgements section;
- Authors were not employees of a company with a financial interest in the outcome of the study;
- Company with a financial interest in the outcome of the study was not involved in the design, conduct, analysis, or reporting of the study and authors had complete access to the data;
- Study authors make a claim denying conflicts of interest;
- Study authors are unaffiliated with companies with financial interest, and there is no reason to believe a conflict of interest exists; OR
- All study authors are affiliated with a government agency (are prohibited from involvement in projects for which there is a conflict of interest or an appearance of conflict of interest)."

General Criteria for Subsequent Risk of Bias Judgments

a) Probably low risk of bias:

- A small portion of the "low risk of bias" criteria is violated, and/or there is relevant information or analyses suggesting that the violated criteria are unlikely to introduce bias.

b) Moderate or unclear risk of bias:

- A larger portion of the "low risk of bias" criteria has been violated, but there is evidence that the violated criteria are unlikely to introduce bias; or:
- There is not enough information in the study to determine the risk of bias for a specific category.

c) Probably high risk of bias:

- The "low risk of bias" criteria are violated, but there is some indication that the violated criteria may not introduce substantial bias.

d) High risk of bias:

- The "low risk of bias" criteria are violated and there is no evidence that the violated criteria are unlikely to introduce substantial bias.

Table S2. Studies of perfluorinated compounds and neurodevelopmental and attention related outcomes

Study	Study Characteristics	Exposure Matrix	Exposure Contrast ng/mL (Mean or Median)	Summary of Results	Selected Effect Estimates
Hoffman et al. (2010)	Cross-sectional United States (n=571) 1999-2000, 2003-2004 NHANES	Serum	1 μg/L (PFOA: 4.4)	Positive association with ADHD and PFOA.	PFOA ADHD (OR) 1.12 (1.01, 1.23) Medication use adjusted 1.19 (0.95, 1.49)
			(PFOS: 22.6)	Increases in PFOS associated with increased odds of ADHD.	PFOS ADHD (OR) 1.03 (1.01, 1.05) Adjusted for medication use 1.05 (1.02, 1.08)
Stein and Savitz (2011)	Cross-sectional United States (n=10546) 2005-2006 C8	Serum	PFOA Q1: <13.0 Q2: 13.0 -<28.2 Q3: 28.2 -<65.3 Q4: >65.3	Null or potentially inverse associations with parent-reported ADHD or learning problems and PFOA.	PFOA ADHD (OR) Age 12-15 Q1: ref Q2: 1.18 (0.91, 1.53) Q3: 0.93 (0.71, 1.21) Q4: 0.79 (0.60, 1.04)
			PFOS Q1: < 14.8 Q2: 14.8-20.1 Q3:20.2-27.9 Q4: > 27.9	ADHD associated with PFOS with adjustment for medication use. Inverse ORs for learning problems with increasing PFOS.	ADHD (OR), age 12-15 Q1: ref Q2: 0.91 (0.70, 1.19) Q3: 0.92 (0.71, 1.21) Q4: 0.99 (0.76, 1.30) ADHD + medication use (OR), age 12-15 Q1: ref Q2: 1.40 (0.94, 2.08) Q3: 1.38 (0.92, 2.06) Q4: 1.32 (0.88, 1.99)
			PFHxS Q1: <2.9 Q2: 2.9 - 5.1 Q3: 5.2 - 10.1 Q4: >10.1 PFNA Q1: <1.2 Q2: 1.2 - 1.4	ADHD positively associated with PFHxS. PFNA not associated with ADHD.	PFHxS ADHD (OR), age 12-15 Q1: ref Q2: 1.46 (1.10, 1.93) Q3: 1.45 (1.10, 1.91) Q4: 1.53 (1.15, 2.04) ADHD + medication use (OR), age 12-15 Q1: ref

			Q3: 1.5 – 2.0 Q4: >2.0		Q2: 1.32 (0.87, 1.99) Q3: 1.32 (0.88, 1.97) Q4: 1.42 (0.94, 2.13)
Ode et al. (2014)	Case-control Sweden (n = 206 cases, 206 controls) 1978 - 2005	Cord serum	PFOA: 1 (1.80, 1.83)	No associations between ADHD diagnosis and PFOA.	ADHD (OR) PFOA: 0.98 (0.92, 1.04)
			PFOS: 1 (6.92, 6.77)	No associations between ADHD diagnosis and PFOS.	PFOS: 0.98 (0.94, 1.02)
			PFNA: LOD (0.2)	No associations between ADHD diagnosis and PFNA.	PFNA: <LOD: ref >= LOD: 1.1 (0.75, 1.7)
Donauer et al. (2015)	Cohort United States (n = 327) Mar 2003 – Jan 2006 Health Outcomes and Measures of the Environment Study	Maternal serum	1-log unit (PFOA: 5.49)	No associations between PFOA and neurobehavioral measures. Positive association with hypotonic status and PFOA, CIs not reported.	PFOA Attention (Beta (SE)) 0.01 (0.06) Hypotonicity (Beta (SE)) 0.14 (0.07) Hypotonic status (OR) 3.785
			(PFOS: 13.25)	No associations between PFOS and neurobehavioral measures.	PFOS Attention (Beta (SE)) 0.01 (0.06) Hypotonicity (Beta (SE)) 0.04 (0.07) Hypotonic status (OR) 1.780
Stein et al. (2014)	Cohort United States (n=321) 2005-2006, 2009-2010 C8	Serum	1 Ln-unit (35.1)	Observed effects for ADHD scores depended upon who was reporting. If mothers, boys had improved scores and girls had worse with increasing PFOA. If teachers, sex differences are less pronounced, and potentially improved scores with increasing PFOA are observed.	PFOA BRIEF score (Δ) Mother survey -0.08 (-1.05, 0.89) Boys only -1.76 (-3.23, -0.29) Girls only 1.09 (-0.14, 2.32) Teacher survey -1.32 (-3.10, 0.47) Boys only -2.82 (-4.96, -0.68) Girls only -0.48 (-2.81, 1.85)

Strom et al. (2014)	Cohort Denmark (n=876) 1988-2010 Danish Fetal Origins 1988	Maternal serum	PFOA T1: <=3.13 T2: >3.13–4.39 T3: >4.39	Potential inverse associations between PFOA and ADHD, with wide CI. ORs for depression are positive only for the middle tertile and return to null at the highest exposure. No association scholastic achievement score.	PFOA ADHD (OR) T1: ref T2: 0.48 (0.18, 1.28) T3: 0.74 (0.29, 1.87) Depression (OR) T1: ref T2: 1.37 (0.85, 2.21) T3: 1.03 (0.61, 1.73)
				Potential inverse association between PFOS and ADHD at highest tertile of exposure. ORs for depression are positive only for the middle tertile and return to null at the highest exposure. No association scholastic achievement score.	PFOS ADHD (OR) T1: ref T2: 1.05 (0.43, 2.53) T3: 0.54 (0.19, 1.53) Depression (OR) T1: ref T2: 1.61 (0.99, 2.61) T3: 1.16 (0.69, 1.95)
Hoyer et al. (2015a)	Cohort Greenland, Ukraine, and Poland (n=1106) INUENDO 2002-2004	Maternal serum	1 log-unit (PFOA: 1.4)	Log-increases in PFOA associated with behavioral problems and hyperactivity.	PFOA Behavioral problems (OR) 1.5 (0.9, 2.6) Hyperactivity (OR) 1.6 (0.9, 2.8)
			(PFOS: 10.0)	Log-increases in PFOS associated with increased odds of hyperactivity but not behavioral problems.	PFOS Behavioral problems (OR) 1.1 (0.6, 2.0) Hyperactivity (OR) 1.7 (0.9, 3.2)
Liew et al. (2015)	Case-control Denmark (cases = 220 for each outcome, controls = 550) 1996-2002 Danish National Birth Cohort	Maternal plasma	1 ln-unit (PFOA: 4.00)	Potential positive association between in PFOA and ADHD, for both ln-linear and quartile increases. No association with autism.	PFOA ADHD (OR) 1.21 (0.84, 1.74) Autism (OR) 1.15 (0.68, 1.93)
			(PFOS: 27.40)	Either no or inverse association between PFOS and ADHD, slightly elevated ORs for autism but confidence intervals are very wide.	PFOS ADHD (OR) 1.04 (0.70, 1.56)

					Autism (OR) 1.21 (0.69, 2.13)
				Other PFASs show primarily inverse or null associations. PFHxS has increasing OR for autism with both ln-linear and quartile increases. PFNA shows positive association with ADHD only with quartile increases.	PFHxS ADHD (OR) 1.05 (0.91, 1.20) Autism (OR) 1.26 (1.00, 1.58) PFNA ADHD (OR) 0.99 (0.58, 1.7) Autism(OR) 0.84 (0.48, 1.49)
Fei et al. (2008)	Cohort Denmark (n = 1400) 1996-2002 Danish National Birth Cohort	Plasma from maternal blood during 1st trimester	PFOA Q1: <3.91 Q2: 3.91-5.20 Q3: 5.21 – 6.96 Q4: >6.96	No associations between "developmental milestones" and PFOA. Slight negative association with "sitting without support".	PFOA Walk without support (Hazard ratio (HR)) Q1: ref Q2: 1.10 (0.94, 1.28) Q3: 1.04 (0.88, 1.22) Q4: 0.94 (0.80, 1.12)
			PFOS Q1: <26.1 Q2: 26.1-33.3 Q3: 33.4 – 43.2 Q4: >43.2	Generally null associations or negative associations with large confidence intervals between developmental milestones and PFOS. "Sitting without support" had inverse HRs with PFOS.	PFOS Attention (HR) Q1: ref Q2: 1.13 (0.75, 1.69) Q3: 1.05 (0.69, 1.59) Q4: 0.94 (0.61, 1.44) Sitting w/out support (HR) Q1: ref Q2: 0.93 (0.79–1.08) Q3: 0.85 (0.72–0.99) Q4: 0.86 (0.73–1.01)
Chen et al. (2013)	Cohort Taiwan (n=239) 2004 Taiwan Birth Panel Study	Cord blood	10 (PFOA: 2.6)	No association between neurodevelopmental markers and PFOA.	PFOA Comprehensive Developmental Inventory for Infants and Toddlers Overall (Δ score) -2.4 (-8.9, 4.1) Poor-performance, overall (OR) 0.6 (0.08, 4.8)
			(PFOS: 7.4)	Odds of poor-performance on developmental test measures are increased with PFOS, though the associations for changes in scores are less pronounced.	PFOS Whole test (Δ score) -2.3 (-5.1, 0.4) Whole test (OR poor performance)

					1.3 (0.7, 2.4) Gross-motor skills (Δ score) -4.9 (-8, -1.7) Gross-motor skills (OR poor performance) 2.2 (1.2, 3.9)
Fei and Olsen (2011)	Cohort Denmark (n=1400) 1996-2002, 2005-2010 Danish National Birth Cohort	Plasma from maternal blood during 1st trimester	PFOA Q1: <3.95 Q2: 3.96 – 5.32 Q3: 5.33 – 7.11 Q4: >7.11	Null associations for PFOA with large confidence intervals, there are some inverse associations.	PFOA Strengths and Difficulties Questionnaire/Developmental Coordination Disorder Questionnaire Total Difficulties (OR) Q1: ref Q2: 0.56 (0.27, 1.19) Q3: 0.36 (0.15, 0.82) Q4: 0.91 (0.43, 1.92)
			PFOS Q1: <26.5 Q2: 26.5-34.3 Q3: 34.4-44.3 Q4: >44.3	No association with PFOS and behavioral and motor coordination problems.	Total difficulties (OR) Q1: ref Q2: 0.95 (0.47, 1.91) Q3: 0.56 (0.25, 1.22) Q4: 0.92 (0.45, 1.87)
Lien et al. (2016)	Cohort Taiwan (n=1526) 2004-2005 Taiwan Birth Panel Study and the Taiwan Early-Life Cohort	Cord blood	PFOA 50th percentile: 0.75 75th: 2.09 90th: 3.78	No associations between PFOA and neurobehavioral symptoms related to ADHD measured through the Swanson, Nolan, and Pelham IV scale (SNAP-IV), the Child Behavior Checklist (CBCL), and the Strengths and Difficulties Questionnaire (SDQ) questionnaires.	SNAP-IV Inattention (Δ score) PFOA <50th percentile: ref 50th-74th: -2.29 (-3.09, -1.48) 75th-89th: -1.8 (-3.04, -0.55) >90th: -1.39 (-2.84, 0.07)
			PFOS 50th percentile: 3.7 75th: 5.76 90th: 8.45	No associations between PFOS concentrations and neurobehavioral symptoms.	PFOS <50th percentile: ref 50th-74th: 0.4 (-0.81, 1.6) 75th-89th: -0.51 (-1.95, 0.92) >90th: -0.69 (-2.43, 1.04)
			PFNA 50th percentile: 1.29 75th: 4.69 90th: 14.2 PFUA 50th percentile: 2.86 75th: 11.7	Increasing percentile categories of PFNA were associated with Inattention, hyperactivity/impulsivity, and oppositional defiant disorder measured by SNAP-IV. No associations between PFNA and neurobehavioral symptoms measured by CBCL or SDQ. No associations between PFUA and neurobehavioral symptoms.	PFNA <50th percentile: ref 50th-74th: -0.14 (-1.33, 1.06) 75th-89th: -1.03 (-2.33, 0.26) >90th: -2.11 (-3.99, -0.23) PFUA <50th percentile: ref

			90th: 21.18		50th-74th: -0.52 (-1.56, 0.52) 75th-89th: -1.38 (-2.75, -0.01) >90th: -0.84 (-2.34, 0.66)
Quaak et al. (2016)*	Cohort The Netherlands (n=76) 2011-2013 Linking Maternal Nutrition to Child Health cohort	Cord blood	PFOA 1st tertile: <0.64 2nd: 0.64 – 1.00 3rd: >1.00	Potential associations between externalizing behavior, measured by the Child Behavior Checklist (CBCL) and higher tertiles of PFOA. No associations with ADHD scale.	Externalizing behavior scale (Δ score) PFOA 1st tertile: ref 2nd: -3.33 (-7.65, 0.29) 3rd: -2.3 (-6.88, 1.55)
			PFOS 1st tertile: <1.2 2nd: 1.2 – 1.8 3rd: >1.8	No associations between externalizing behavior or ADHD scales and PFOS	PFOS 1st tertile: ref 2nd: -1.23 (-5.68, 3.85) 3rd: -2.43 (-6.55, 1.93)
			Sum PFAS 1st tertile: <0.64 2nd: 0.64 – 1.00 3rd: >1.00	Potential associations between increasing tertiles of summed PFAS and ADHD scale and CBCL.	ADHD scale (Δ) 1st tertile: ref 2nd: -0.72 (-1.96, 0.59) 3rd: -0.99 (-2.14, 0.18) Externalizing behavior scale (Δ score) 1st tertile: ref 2nd: -1.59 (-5.27, 2.5) 3rd: -3.31 (-6.55, 0.28)
Gump et al. (2011)	Cross-sectional United States (n=83) NR	Blood	1 standard deviation PFOA: 1.30	Potential associations with lower response inhibition and increasing PFOA.	PFOA Inter-response times (Δ) 0-5 min bin -0.03 [-0.24, 0.18] 6-10 min bin -0.11 [-0.34, 0.11] 11-15 min bin -0.20 [-0.41, 0.01] 16-20 min bin -0.17 [-0.39, 0.05]
			PFOS: 6.09	PFOS associated with lower response inhibition.	PFOS Inter-response times (Δ) 0-5 min bin -0.05 [-0.26, 0.16] 6-10 min bin -0.18 [-0.40, 0.04] 11-15 min bin -0.25 [-0.46, -0.04] 16-20 min bin

					-0.20 [-0.42, 0.02]
			PFNA: 0.56 PFDA: 0.13 PFHxS: 8.03 PFOSA: 0.57	PFASs generally associated with lower response inhibition.	PFNA Inter-response times (Δ) 0-5 min bin -0.07 (-0.29, 0.14) 6-10 min bin -0.24 (-0.46, -0.02) 11-15 min bin -0.15 ([-0.38, 0.07) 16-20 min bin -0.05 (-0.28, 0.18)
Stein et al. (2013)	Cohort United States (n=320) 2005-2006, 2009-2010 C8	Serum	1 Ln-unit (15.3)	No associations with PFOA and neuropsychological tests	PFOA IQ (Δ) 0.83 (-0.13, 1.79) Word Reading Score (Δ) 0.5 (-0.4, 1.41)
Forns et al. (2015)	Cohort Norway (n=843-896) 2003-2009 HUMIS	Breast milk, 1 month post delivery	PFOA IQR:37 Median: 40	No associations for abnormal score (AS) in cognitive and psychomotor development with higher PFOA. No associations between behavioral problems and PFOA.	PFOA AS, 6 months (OR) Per IQR: 1.05 (0.77, 1.44) >Median: 1.14 (0.71, 1.80) AS, 24 months (OR) Per IQR: 1.00 (0.78, 1.28) >Median: 1.25 (0.81, 1.95)
			PFOS IQR:77 Median: 110	No associations for abnormal score in cognitive and psychomotor development with higher PFOS. No associations between behavioral problems and PFOS.	PFOS AS, 6 months (OR) Per IQR: 0.96 (076, 1.20) >Median: 0.93 (0.60, 1.44) AS, 24 months (OR) Per IQR: 0.93 (0.74, 1.17) >Median: 0.99 (0.64, 1.52)
Wang et al. (2015)	Cohort Taiwan (n = 120) Dec 2000 – Nov 2001	Maternal serum	1 log-2 unit (PFOA: 2.50)	No association between PFOA and IQ.	Full Scale IQ (Δ score) PFOA 1.2 (-1.0, 3.5)
	Taiwan Maternal and Infant Cohort Study		(PFOS: 13.25)	No association between PFOS and IQ.	PFOS -1.9 (-4.3, 0.5)
			(Ranges from 0.38 to 3.42)	No associations between other PFASs and IQ.	PFNA -0.2 (-2.1, 1.7)

					PFHxS 0.4 (-2.4, 3.1)
Goudarzi et al. (2016)	Cohort Japan (n = 422) July 2002 - Oct 2005 Hokkaido Study on Environment and Children's Health	Maternal serum	1 log-10-unit (PFOA: 1.2)	No association between PFOA and mental development index (MDI) or psychomotor developmental index (PDI) at 6 or 18 months. Small negative association with MDI in girls at 6 months, but does not persist.	MDI at 6 months (Δ score) PFOA Total: −0.045 (−4.33 to 2.56) Boys: 0.110 (−3.31 to 7.14) Girls: −0.296 (−11.96 to −0.682)
			(PFOS: 5.7)	No Association between PFOS and MDI or PDI at 6 or 18 months.	PFOS Total: 0.018 (−4.52 to 5.59) Boys: −0.141 (−11.26 to 3.45) Girls: 0.072 (−5.19 to 9.38)
Vuong et al. (2016)	Cohort United States (n = 256) Mar 2003 – Feb 2006 Health Outcomes and Measures of the Environment Study	Maternal serum	1 ln-unit (PFOA: 5.4)	No association between PFOA and behavioral regulation, metacognition, or global executive function.	Poorer global executive function (OR) PFOA 1.06 (-1.33, 3.45)
			(PFOS: 13.2)	PFOS associated with increased odds of poorer behavioral regulation, metacognition, and global executive function.	PFOS 3.38 (0.86, 5.9)
			(Ranges from 0.1 to 3.6)	No associations between PFHxS, PFNA, or PFDeA and neurodevelopmental outcomes.	PFHxS 1.36 (-0.41, 3.12)

*: Study that examined PFAS as a mixture

Table S3. Studies of perfluorinated compounds and cardiometabolic related outcomes.

Study	Study Characteristics	Exposure matrix	Conc ng/mL	Summary of results	Selected effect estimates
Andersen et al. (2010)	Cohort Denmark (n=1400) 1996-2002 Danish National birth cohort	Maternal blood	1	No meaningful associations between PFOA and weight, height or BMI at 5 or 12 months of age.	PFOA Weight at 5 months (Δg) -9.4 (-28.6, 9.9) Height at 12 months (Δcm) 0.049 (-0.026, 0.124)
				No association between PFOS and weight, height or BMI at 5 or 12 months of age.	PFOS Weight at 5 months (Δg) -0.8 (-4.2, 2.6) Height at 12 months (Δcm) 0.010 (-0.003, 0.023)
Andersen et al. (2013)	Cohort Denmark (n=1400) 1996-2002 Danish National birth cohort	Plasma	1 (PFOA: 5.12, 5.31)	No associations between prenatal PFOA and BMI, waist circumference, or overweight status at age 7.	BMI at age 7 (Δ) PFOA Boys: -0.049 (-0.117, 0.02) Girls: -0.019 (-0.098, 0.058)
			PFOS Q1: <25.5 Q2: 25.6 – 33.5 Q3: 33.6 – 43.4 Q4: >43.4	ORs of overweight potentially inverse in both boys and girls with increasing PFOS. BMI and waist circumference at age 7 not associated with PFOS.	BMI at 7 (Δ) PFOS Boys: -0.008 (-0.016, 0.009) Girls: -0.005 (-0.019, 0.008) Overweight (OR), PFOS, girls Q1: ref Q2: 1.04 (0.45, 2.41) Q3: 0.87 (0.37, 2.02) Q4: 0.60 (0.24, 1.49)
Maisonet et al. (2012)	Cohort England (n=447) 1991-1992 ALSPAC	Maternal serum	T1: <3.1 T2: 3.1-4.4 T3: >4.4	No association between weight at 20 months and maternal PFOA.	PFOA Weight at 20 months (Δg) T1: ref T2: -174.31 (-550.55, 201.94) T3: 9.48 (-405.48, 424.44) Adjusted for birth weight & height at 20 months T1: ref T2: -184.21 (-465.90, 97.48) T3: 128.40 (-180.94, 437.74)
			T1: <16.6 T2: 16.6-23.0 T3: >23.0	Increase in weight at 20 months associated with increasing maternal PFOS.	PFOS Weight at 20 months (Δg) T1: ref T2: 100.93 (-282.81, 484.68) T3: 364.35 (-15.14, 743.83)

					Adjusted for birth weight & height at 20 months T1: ref T2: 310.64 (27.19, 594.08) T3: 579.82 (301.40, 858.25)
			PFHxS T1: <1.3 T2: 1.3-2.0 T3: >2.0	No association between weight at 20 months associated with increasing maternal PFHxS.	PFHxS Weight at 20 months (Δg) T1: ref T2: -31.84 (-416.87, 353.20) T3: 62.86 (-326.68, 452.40) Adjusted for birth weight & height at 20 months T1: ref T2: 12.33 (-275.56, 300.22) T3: 115.4 (-176.69, 407.50)
Wang et al. (2016)	Cohort Taiwan (n = 223) 2000 – 2012 Taiwan Maternal and Infant Cohort Study	Maternal serum, 3rd trimester	1 ln-unit (PFOA: 1.98)	No association between PFOA and weight or height z-score.	Height z-score (Δ score) PFOA Girls: -0.15 (-0.38, 0.08) Boys: 0.01 (-0.24, 0.25)
			(Ranges from 0.28 to 2.89)	PFDeA, PFUnDA, and PFDoDA associated with decreased height z-score in girls. PFNA potentially negatively associated with height in both boys and girls. No associations with weight in boys or girls.	PFNA Girls: -0.21 (-0.42, 0) Boys: -0.15 (-0.37, 0.08) PFDeA Girls: -0.52 (-0.8, -0.24) Boys: -0.05 (-0.34, 0.23)
Braun et al. (2016)	Cohort United States (n = 256) Mar 2003 – Feb 2006 Health Outcomes and Measures of the Environment Study	Maternal serum	PFOA 1st tertile: 0.5-4.2ng/mL 2nd tertile: 4.3-6.4ng/mL 3rd tertile: 6.6-25 ng/mL	Non-linear associations between PFOA and BMI z-score, waist circumference and body fat percentage at 8 years, with middle tertile showing higher odds. Positive ORs for overweight/obesity and PFOA.	PFOA Body fat percent (Δ) 1: ref 2: 3.6 (1.8, 5.5) 3: 1.5 (-0.4, 3.4) Overweight/Obese (RR) 1: ref 2: 1.84 (0.97, 3.5) 3: 1.54 (0.77, 3.07)
			PFOS 1: 0.6 (0.1-0.7) 2: 0.9 (0.8-1.0)	No association between PFOS and child adiposity at age 8.	BMI z-score (Δ score) PFOS 1: ref

			3: 1.3 (1.1-2.9)		2: -0.12 (-0.43, 0.19) 3: -0.05 (-0.36, 0.26)
			PFHxS 1: 0.7 (0.1-0.9) 2: 1.4 (1.0-1.9) 3: 2.9 (2.0-33)	No associations between PFNA or PFHxS and adiposity at age 8.	PFHxS 1: ref 2: 0.22 (-0.10, 0.54) 3: 0.12 (-0.21, 0.45)
Halldorsson et al. (2012)	Cohort Denmark (n = 665) 1988-89, 2008-2009	Serum	PFOA: Q1: <2.8 Q2: 2.8-<3.7 Q3: 3.7-4.8 Q4: >4.8 1 Log-unit	Divergent ORs for males (null) and females (positive) for overweight and waist circumference at highest PFOA quartile exposures. Positive associations with %change insulin and leptin, and negative associations with adiponectin and log-unit increases of PFOA.	Overweight (OR) PFOA: Female: Q1: ref Q2: 1.5 (0.6, 3.5) Q3: 2 (0.9, 4.7) Q4: 3.1 (1.4, 6.9) Male: Q1: ref Q2: 1.2 (0.6, 2.6) Q3: 1.0 (0.4, 2.2) Q4: 1.1 (0.5, 2.6) Leptin (% change) PFOA: Female: 4.8 (0.5, 9.4) Male: 4.5 (-2.6, 12.1)
			PFOS: Q1: <12.4 Q2: 12.4-21.5 Q3: 21.5-30.6 Q4: >30.6	PFOS in gestational not associated with anthropometric measures in 20 year olds	NR
Hoyer et al. (2015b)	Cohort Greenland and Ukraine (n = 1,023) May 2002 to Feb 2004 INEUNDO	Maternal plasma	1 log-unit (PFOA: 1.0 – 1.8)	Potential positive association between PFOA and overweight status at 5-9 years. Log-increases in PFOA associated with increased odds of waist-to-hip ratio >0.5 at 5-9 years of age.	PFOA Overweight (OR) 1.11 (0.88, 1.38) Waist-to-hip ratio >0.5 (OR) 1.30 (0.97, 1.74)
			(PFOS: 5.0 – 20.2)	PFOS not associated with overweight status, but positive ORs observed for waist-to-hip ratio >0.5 at 5-9 years.	PFOS Overweight (OR) 0.97 (0.78, 1.21) Waist-to-hip ratio >0.5 (OR) 1.38 (1.05, 1.82)
Timmermann et al. (2014)	Cross-sectional Denmark (n=590) 1997 EYHS	Serum	10 (PFOA: 9.3)	Positive associations between markers of glycemic control and PFOA observed only in overweight strata, though large confidence intervals. No associations with adiposity.	Insulin (% change) PFOA Normal weight: 0.7 (-3.6, 5.2) Overweight: 16.2 (5.2, 28.3) BMI (% change) PFOA -2.6 (-25.8, 28)

			(PFOS: 41.5)	Increased levels of glycemic control markers associated with PFOS among overweight subjects. No associations between anthropometric measures and PFOS.	Insulin (% change) PFOS Normal weight 0.8 (-3.2, 5) Overweight 16.2 (5.2, 28.3)
Geiger et al. (2014a)*	Cross-sectional United States (n=815) 1999-2008 NHANES	Serum	1 Log-unit (PFOA: 4.2)	Increased LDL-C and total cholesterol, and decreased HDL-C associated with log-unit and increases in PFOA.	PFOA Total cholesterol (Δ): 4.55 (0.90, 8.20) LDL-C: 5.75 (2.16, 9.33) HDL-C: -1.52 (-3.02, -0.03)
			(PFOS: 17.7)	Increased LDL-C associated with log-unit increases in PFOS. No association with HDL-C, or triglycerides.	PFOS Total cholesterol (Δ): 0.06 (0.02, 0.10) LDL-C: 4.28 (1.60, 6.95) Triglycerides: -1.85 (-5.61, 1.91)
				Increased LDL-C, HDL-C total cholesterol, and triglycerides associated with log-unit increases in PFAS.	PFAS LDL-C (Δ) 1.48 (1.15, 1.90) HDL-C: 1.03 (0.70, 1.53) Triglycerides 0.90 (0.56, 1.43)
Lin et al. (2011)	Cohort Taiwan (n = 287) 2006-2008	Serum	PFOA: <50th percentile: 0.75 – 2.37 50-74th: 2.39 – 5.92 75-89th: 6.01 – 9.62 >90th: >9.62	No associations between increasing PFOA and adiponectin, glucose, insulin, HOMA-IR, HDL-C, TG, or CRP concentrations.	NR - Only p for trend reported
				No associations between PFOS and metabolic indicators.	
				Log-increases in serum PFNA associated with log-increases in adiponectin. Other compounds had null associations. No associations between PFUA and metabolic indicators.	
Frisbee et al. (2010)	Cross-sectional United States (n = 12,476) 2005-2006 C8	Serum	Quintile concentrations not reported. Mean (SD) PFOA: 69.2 (111.9)	Associations with abnormal LDL cholesterol and fasting triglycerides (non-linear). No association with HDL cholesterol	Abnormal LDL-C (OR) PFOA Q1: ref Q2: 1.2 (1.0, 1.5) Q3: 1.2 (1.0, 1.4) Q4: 1.2 (1.0, 1.4) Q5: 1.4 (1.2, 1.7)

			PFOS: 22.7 (12.6)	Positive associations for LDL and total cholesterol associated with PFOS. Negative associations for HDL cholesterol, and near null for fasting triglycerides.	HDL-cholesterol (POR) PFOS Q1: ref Q2: 0.9 (0.8, 1.1) Q3: 0.8 (0.7, 1.0) Q4: 0.8 (0.7, 0.9) Q5: 0.7 (0.6, 0.9) LDL-cholesterol (POR) PFOS Q1: ref Q2: 1.2 (1.0, 1.5) Q3: 1.2 (1.0, 1.5) Q4: 1.3 (1.1, 1.6) Q5: 1.6 (1.3, 1.9)
Maisonet et al. (2015b)	Cohort, subset Avon, UK (n = 111, age 7 n = 88, age 15) 1991-1992, recruitment ALSPAC	Maternal serum	NR	Reported positive, though non-linear and non-monotonic, associations with total cholesterol and LDL-cholesterol with PFOA and PFOS. Results were reported from unadjusted models.	Reported as figures. Contrasts not reported.
Lin et al. (2009)	Cross-sectional United States (n=474) 1999-2000 NHANES	Serum	1 Log-unit (log PFOA: 1.51)	No associations between PFOA and glucose homeostasis and indicators of metabolic syndrome. ORs for metabolic syndrome and components were null or negative, with wide confidence intervals.	Glucose (Δ) PFOA -0.03 (-0.13, 0.07) Log-insulin (Δ) PFOA 0.08 (-0.57, 0.21)
			(log PFOS: 3.11)	Log HOMA-IR concentrations positively associated with log-increases in PFOS. Potential positive associations for log insulin and log B-cell concentrations with PFOS. No association for glucose concentration and PFOS. ORs for metabolic syndrome and components were null or negative, with wide confidence intervals.	Glucose (Δ) PFOS -0.03 (-0.1476, 0.0876) Log insulin (Δ) PFOS 0.15 (-0.0068, 0.3068) Log HOMA-IR (Δ) PFOS 0.15 (0.0128, 0.2872) Log B-cell PFOS 0.13 (-0.0464, 0.3064)
			(log PFHS: 0.95) (log PFNA: -0.35)	Negative associations between PFNA and log-insulin, log-HOMA, and log-B-cell	Glucose (Δ) PFNA 0.07 (-0.01, 0.15) Log insulin (Δ) PFNA

				concentrations; no associations with glucose. Positive association between PFHS and log-insulin; null associations otherwise. Log PFNA concentration increases associated with increased ORs for glucose >= 5.55 mmol/l or a self-report of taking antihyperglycemic medications. Other PFNA and PFHS associations null or negative.	-0.10 (-0.20, 0.00) Log HOMA-IR (Δ) PFNA -0.08 (-0.16, 0.00) Log B-cell, PFNA -0.12 (-0.24, 0.00)
Zeng et al. (2015)	Cross-sectional Taiwan (n=225) 2009-2010 Genetic and Biomarkers study for Childhood Asthma (GBCA)	Serum	1 Ln-unit (PFOA: 0.92, 1.1)	Ln-unit increases in PFOA were associated with increases in total cholesterol, LDL-C, and triglyceride concentrations.	PFOA Total-C (Δ) 6.57 (2.72, 10.42) HDL-C (Δ) -1.56 (-3.2, 0.08) LDL-C (Δ) 4.66 (1.67, 7.65) Triglycerides (Δ) 19.63 (14.82, 24.34)
			(PFOS: 32.4, 34.2)	Ln-unit increases in PFOS were associated with increases in total cholesterol, LDL-C, and triglyceride concentrations, though increases were small.	PFOS Total-C (Δ) 0.31 (0.18, 0.45) HDL-C (Δ) -0.01 (-0.07, 0.05) LDL-C (Δ) 0.28 (0.18, 0.38) Triglycerides (Δ) 0.19 (0, 0.38)
			(Ranges from 0.4 to 30.7)	Ln-unit increases in PFNA were associated with increases in total cholesterol, LDL-C, and triglyceride concentrations. Lipid levels were not associated with PFBS, PFDA, PFDoA, PFHxA, PFHxS, or PFTA.	PFNA Total-C (Δ) 12.92 (0.73, 25.1) HDL-C (Δ) -2.35 (-7.49, 2.79) LDL-C (Δ) 9.63 (0.2, 19.06) Triglycerides (Δ) 23.01 (6.49, 39.52) PFDA Total-C (Δ) -1.29 (-9.01, 6.42) HDL-C (Δ)

					-1.12 (-4.4, 2.05) LDL-C (Δ) -0.56 (-6.53, 5.41) Triglycerides (Δ) 0.57 (-9.97, 11.11)
Geiger et al. (2014b)	Cross-sectional United States (n=1655) 1999-2000, 2003-2008 NHANES	Serum	1 Ln-unit (PFOA: 4.4)	No association between changes in systolic (SBP) or diastolic (DBP) blood pressure and PFOA. Odds for hypertension were decreased with increases in PFOA.	PFOA SBP (ΔmmHg): -1.22 (-2.74, 0.31) DBP (ΔmmHg): 0.36 (-0.99, 1.71) Hypertension (OR): 0.76 (0.53, 1.10)
			(PFOS: 18.4)	No association between SBP or DBP and PFOS. Odds for hypertension were decreased with increases in PFOS.	PFOS SBP (ΔmmHg): -0.04 (-1.19, 1.12) DBP (ΔmmHg): 0.47 (-0.81, 1.74) Hypertension (OR): 0.83 (0.58, 1.19)
Lin et al. (2013a)	Cross-sectional Taiwan (n=228) 2006-2008 Young Taiwanese Cohort Study	Plasma	PFOS Q1: ≤5.41 Q2: 5.42 - 8.65 Q3: 8.66 -13.52 Q4: >13.52	Increases in mean carotid artery intima-media thickness with increasing quartiles of PFOS.	Reported as mean (SD) and p for trend.

*: Study that examined PFAS as a mixture

Table S4. Studies of perfluorinated compounds and immunity, infection, and asthma related outcomes.

Study	Study Characteristics	Exposure Matrix	Conc ng/mL	Summary of Results	Selected Effect Estimates
Asthma/allergy/infection					
Dong et al. (2013)	Case-control Taiwan (n = 231 asthmatic, 225 non-asthmatic children) 2009-2010 Genetic and Biomarkers study for Childhood Asthma (GBCA)	Serum	PFOA Median cases: 1.2 Median control: 0.5	Positive associations and increasing trend observed for asthma and increasing PFOA	Asthma (OR) PFOA Q1: ref Q2: 1.58 (0.89, 2.8) Q3: 2.67 (1.49, 4.79) Q4: 4.05 (2.21, 7.42)
			PFOS Median cases: 33.9 Median control: 28.9	Asthma associated with higher concentrations of PFOS.	PFOS Q1: ref Q2: 1.96 (1.11, 3.47) Q3: 1.32 (0.75, 2.32) Q4: 2.63 (1.48, 4.69)
				Asthma positively associated with PFBS, PFDA, PFDoA, PFHxS, and PFNA. Negative association with PFTA.	PFHxS Q1: ref Q2: 1.12 (0.66, 1.91) Q3: 2.63 (1.54, 4.49) Q4: 3.30 (1.92, 5.67)
Humblet et al. (2014)	Cross-sectional United States (n = 1877) 1999-2000, 2003-2008 NHANES	Serum	1 (PFOA: 4.0)	Positive OR between PFOA and ever asthma. No association with current asthma or wheeze.	Ever asthma (OR) PFOA 1.06 (1.00, 1.11)
			(PFOS: 16.8)	No association between ever or current asthma, wheeze and PFOS.	PFOS 0.99 (0.96, 1.02)
			(PFNA: 0.8 PFHxS: 2.0)	Potential positive association between ever asthma and PFNA. No association between PFNA and ever asthma or wheeze. No associations between PFHS and ever or current asthma and wheeze.	PFNA 1.05 (0.89, 1.23) PFHS 0.99 (0.98, 1.01)
Smit et al. (2015)*	Cohort Greenland & Ukraine (n = 1024) 2002-2004 INUENDO	Maternal plasma	1 Standard deviation	No associations between standard deviation increases in factors representing PFASs.	Factor representing PFOA, PFHpA, and PFOS Ever asthma (OR) 0.83 (0.63–1.10)

					Ever eczema (OR) 0.94 (0.77–1.14) Ever wheeze (OR) 0.91 (0.75–1.11) Current wheeze (OR) 1.05 (0.82–1.35) Current eczema (OR) 0.94 (0.73–1.22)
Stein et al. (2016)	Cross-sectional United States (n = 640) 1999-2000, 2003-2004 NHANES	Serum	1 Log(2)-unit (PFOA: 0.97, 1.79)	PFOA increases associated with rhinitis and potentially with asthma and allergy. No association with wheeze.	Asthma (OR) PFOA 1.28 (0.81, 2.04)
			(PFOS: 4.88, 20.6)	PFOS increases potentially associated with rhinitis and asthma, no association with wheeze or allergy.	PFOS 1.20 (0.88, 1.63)
			(PFNA: 0.62, 0.73 PFHxS: 1.53, 2.14)	PFNA increases potentially associated with asthma, allergy, and rhinitis. No evidence for associations between PFHxS increases and odds of asthma, wheeze, allergy, or rhinitis.	PFNA 1.26 (0.79, 2.01) PFHxS 0.98 (0.51, 1.87)
Zhu et al. (2016)	Cross-sectional Taiwan (n = 231 asthmatic children, 225 non-asthmatic children) 2009-2010 Genetic and Biomarkers study for Childhood Asthma (GBCA)	Serum	(PFOA: 1.00)	Increasing quartiles of PFOA were associated with increasing odds of asthma.	Results reported as figures.
			(PFOS: 33.39)	PFOS concentrations were associated with odds of asthma in males, but not in females.	
			(Ranges from 0.48 to 2.10)	PFBS, PFDA, PFHxS, PFNA were all associated with odds of asthma. There is some potential for divergent effects based on sex (e.g., PFBS).	

Qin et al. (2017)	Cross-sectional Taiwan (n=132 asthmatic children, 186 non-asthmatic children) 2009-2010 Genetics and Biomarkers study for Childhood Asthma	Serum	1 ln-unit Medians in case/controls PFOA: 1.02/0.50	Increasing ln-PFOA associated with increasing odds of asthma, forced expiratory volume in 1 s (FEV1) and forced expiratory flow 25–75% (FEF25-75) but not forced vital capacity (FVC) or peak expiratory flow (PEF) in children with asthma. No associations between lung function and PFOA in children without asthma.	PFOA Asthma (OR): 2.76 (1.82, 4.17) FEV1 (ΔL): -0.10 (-0.19, -0.02) FVC (ΔL): -0.07 (-0.17, 0.03)
			PFOS: 31.51/28.83	Increasing ln-PFOS associated with increasing odds of asthma, and decreasing FEV1 and FVC in children with asthma. No association between PEF and FEF25-75 in children with asthma, or lung function metrics in children without asthma.	PFOS Asthma (OR): 1.30 (1.00, 1.69) FEV1 (ΔL): -0.10 (-0.19, -0.02) FVC (ΔL): -0.06 (-0.10, -0.01)
			PFBS: 0.48 PFDA: 1.13/0.93 PFHxA: 0.20/0.18 PFHxS: 2.38/1.07 PFNA: 1.00/0.80 PFTA: 2.65/4.52	Increasing PFHxS and PFNA concentrations were associated with decreases in lung function in asthmatic children. No PFASs were associated with lung function in non-asthmatic children.	FEV1 (ΔL): PFBS: 1.06 (0.93, 1.20) PFDA: 1.24 (0.97, 1.58) PFHxA: 0.99 (0.80, 1.21) PFHxS: 2.14 (1.48, 3.11) PFNA: 1.61 (1.12, 2.31) PFTA: 1.14 (1.06, 1.23) FEV1 (ΔL) PFBS: 0.10 (-0.11, 0.30) PFDA: -0.05 (-0.15, 0.04) PFHxA: -0.03 (-0.10, 0.04) PFHxS: -0.10 (-0.17, -0.04) PFNA: -0.20 (-0.34, -0.06) PFTA: -0.02 (-0.05, 0.01)
Fei et al. (2010)	Cohort Denmark (n=1400) 1996-2002, 2002-2008 Danish National Birth Cohort	Serum	PFOA Q1: <26.1 Q2: 26.1-33.3 Q3: 33.4-43.2 Q4: >43.2	Positive associations with PFOA and hospitalization due to infection in girls and primiparous women, negative associations in boys and multiparous women.	Hospitalization due to infection (IRR) PFOA Girls: 1.21 (1.04, 1.42) Multiparous: 0.87 (0.76, 1.00)

			PFOS Q1: <3.91 Q2: 3.91-5.20 Q3: 5.21-6.96 Q4: >6.96	Positive associations with PFOS and hospitalization due to infection in girls and primiparous women, negative associations in boys and multiparous women.	PFOS Girls: 1.18 (1.03, 1.36) Boys: 0.90 (0.80, 1.02) Primiparous: 1.10 (0.96, 1.27) Multiparous: 0.93 (0.83, 1.05)
Okada et al. (2014)	Cohort Japan (n=2063) 2003-2009 Hokkaido Study on Environment and Children's Health	Serum	PFOA Q1: <1.31 Q2: 1.31-2.01 Q3: 2.01-3.26 Q4: >3.26	Negative associations with higher quartiles of PFOA for allergies and eczema.	PFOA Total allergies Q1: ref Q2: 1.05 (0.81, 1.37) Q3: 0.80 (0.61, 1.06) Q4: 0.79 (0.59, 1.04)
			PFOS Q1: <3.71 Q2: 3.71-5.01 Q3: 5.02-6.82 Q4: >6.82	Potential negative associations with total allergic diseases and eczema with increasing PFOS.	PFOS Total allergic diseases (OR) Q1: ref Q2: 0.97 (0.75, 1.26) Q3: 0.80 (0.61, 1.04) Q4: 0.86 (0.66, 1.13)
Okada et al. (2012)	Cohort Japan (n=268) 2003-2005 Hokkaido Study on Environment and Children's Health	Serum	1 Log(10)-unit cubic (PFOA: 1.4)	Negative associations with IgE levels and PFOA reported for girls, null associations for boys.	Reported as figures.
			(PFOS: 5.6)	No association between PFOS and cord blood IgE levels.	Reported as figures
Wang et al. (2011)	Cohort Taiwan (n = 239) 2004 Taiwan Birth Panel Study	Cord blood	PFOA Q1: <0.085 Q2: 0.085 - 0.57 Q3: 0.57 - 1.085 Q4: >1.085	No associations between PFOA levels and atopic dermatitis or serum IgE at 2 years of age. Positive association with cord blood IgE levels in boys.	PFOA Atopic dermatitis (OR) Q1: ref Q2: 0.84 (0.28, 2.48) Q3: 1.03 (0.42, 2.56) Q4: 0.58 (0.22, 1.58)
			PFOS Q1: <1.25 Q2: 1.25 –1.835 Q3: 1.835-2.775 Q4: >2.775	Potential positive associations with highest quartiles of PFOS and atopic dermatitis or serum IgE at 2 years of age. Positive association with cord blood IgE levels in boys.	PFOS Q1: ref Q2: 0.68 (0.20, 2.30) Q3: 2.34 (0.86, 6.41) Q4: 2.19 (0.78, 6.17)
			PFNA Q1: <0.14	Potential positive associations between PFNA and atopic	PFNA Q1: ref

			Q2: 0.140 - 0.765 Q3: 0.765 - 2.515 Q4: >2.515	dermatitis, though low precision and no trends. No association with serum IgE at 2 years of age.	Q2: 1.46 (0.35, 6.07) Q3: 1.53 (0.59, 3.93) Q4: 0.72 (0.23, 2.21)
Ashley-Martin et al. (2015)	Cohort 10 Canadian cities (n = 1258) 2008-2011 MIREC	Maternal serum	1 log-µg/L (PFOA: 1.7)	No associations between PFOA and newborn immune function markers.	PFOA Elevated (≥80%) IL-33/TSLP (OR) 1.1 (0.6, 1.8) Elevated (≥0.5ku/L) IgE (OR) 1.1 (0.6, 1.9)
			(PFOS: 4.7)	No associations between PFOS and newborn immune function markers.	PFOS IL-33/TSLP 1.1 (0.6, 1.9) IgE 1.1 (0.6, 1.9)
			(PFHxS: 1.0)	No associations between PFHxS and newborn immune function markers.	PFHxS Il-33/TSLP 1.0 (0.7, 1.4) IgE 1.0 (0.7, 1.4)
Granum et al. (2013)	Cohort Norway (n=99, 56) 2007-2011 MoBa	Maternal plasma	1 (PFOA: 1.1)	Associations are unadjusted for potential confounders, positive crude associations found for number of colds and gastroenteritis episodes and PFOA.	PFOA Colds (Δ#) 3rd year of life: 0.42 (0.16, 0.72) Gastroenteritis episodes (Δ#) 1st-3rd years: 0.31 (0.00, 0.61)
			(PFOS: 5.6)	Associations are unadjusted for potential confounders, no associations found for number of colds and gastroenteritis episodes and PFOS.	PFOS Colds (Δ#) 3rd year of life: 0.03 (-0.03, 0.10) Gastroenteritis episodes (Δ#) 1st-3rd years: 0.03 (-0.04, 0.10)
			(PFNA: 0.3, PFHxS: 0.3)	Number of colds positively associated with PFNA and PFHxS. Gastroenteritis episodes positively associated only with PFHxS.	PFNA Colds (Δ#) 3rd year of life: 1.24 (0.08, 2.40) Gastroenteritis episodes (Δ#) 1st-3rd years: -0.10 (-1.36, 1.17)
Vaccination response					
Grandjean et al. (2012)*	Cohort Faroe Islands (n=587) 1997-2000, 2008	Serum, maternal and child at 5 years	1 Log(2) unit (PFOA: 3.20)	Negative associations between tetanus and diphtheria antibody levels at 7 years and PFOA concentration at 5 years,	PFOA Tetanus antibodies (%Δ) Age 7, Maternal serum: 12.3 (−8.6 to 38.1)

				adjusting for antibody levels at 5 years. No associations with maternal PFOA levels.	Age 7, child serum −35.8 (−51.9 to −14.2) Age 7, child serum & adjusted −28.2 (−42.7 to −10.1)
			(PFOS: 27.3)	Maternal PFOS associated with increase in tetanus antibodies concentration at 5 and 7 years, potential negative association with diphtheria antibodies. Child serum PFOS potentially negatively associated with tetanus and diphtheria antibodies.	PFOS Tetanus antibodies (%Δ) Age 7, Maternal serum: 35.3 (−3.9, 90.6) Age 7, child serum -23.8 (-44.3, 4.2) Age 7, child serum & adjusted for age 5 −11.4 (−30.5, 12.8)
			(Ranges from 0.28 – 4.41)	Negative associations with increasing PFHxS, PFNA, and PFDA concentrations and tetanus and diphtheria antibody concentrations, primarily with PFASs measured at age 5, though some associations with maternal concentrations as well.	Tetanus antibodies (%Δ) Age 7, child serum PFHxS -19.7 (-31.6, -5.7) PFNA -17.4 (-34.1, 3.6) PFDA -22.3 (-35.8, -5.8)
				Latent factor representing PFOS, PFOA, and PFHxS was created and doubling of concentration at age 5 (pre-booster) was associated with decreased antibody concentrations for tetanus and diphtheria at age 7 (post-booster). Maternal PFAS negatively associated with diphtheria antibodies at both age 5 and age 7, but not tetanus.	Tetanus antibodies, age 5 pre-booster (%Δ) Maternal : -20.2 (-49.2, 25.2) 5 year old: -20.5 (-44.4, 13.6) 5 year old, adjusted for maternal: -17.2 (-42.1, 18.5) Tetanus antibodies, age 7 post-booster (%Δ) Maternal : 35.1 (-25.4, 144.6) 5 year old: -55.2 (-73.3, -25) 5 year old, adjusted for maternal: -58.8 (-76, -29.3)
Granum et al. (2013)	Cohort Norway (n=99, 56) 2007-2011 MoBa	Maternal plasma	1 (PFOA: 1.1)	Decrease in rubella antibodies associated with increasing PFOA concentration. Potential decrease for measles antibodies, but not adjusted	PFOA Rubella vaccine antibodies (Δ) -0.40 (-0.64, -0.17) Measles vaccine antibodies (Δ) -0.13 (-0.35, 0.09)

				for potential confounders. No association with HiB or tetanus antibodies and PFOA.	
			(PFOS: 5.6)	PFOS negatively associated with rubella and measles antibodies. No association with Hib or tetanus antibodies.	PFOS Rubella vaccine antibodies (Δ) -0.08 (-0.14, -0.02) Measles vaccine antibodies (Δ) -0.05 (-0.10, 0.01)
			(PFNA: 0.3, PFHxS: 0.3)	Rubella antibodies negatively associated with PFNA and PFHxS. Measles Hib and tetanus antibodies not associated with PFNA or PFHxS.	PFNA Rubella vaccine antibodies (Δ) -1.38 (-2.35, -0.40) Measles vaccine antibodies (Δ) -0.55 (-1.51, 0.41)
Stein et al. (2016)	Cross-sectional United States (n = 640) 1999-2000, 2003-2004 NHANES	serum	1 Log(2)-unit (PFOA: 3.59)	No association between doubling of PFOA and measles antibodies. Decreases in rubella antibodies with PFOA doubling were observed in seropositive individuals. PFOA increases were negatively associated with mumps antibodies.	PFOA Mumps vaccine antibodies (Δ) All: -6.0 (-12.4, 0.9) Seropositive: -6.6 (-11.7, -1.5) Measles vaccine antibodies (Δ) All: -0.1 (-13.8, 15.6) Seropositive: -3.4 (-16.7, 11.9)
			(PFOS: 15.0)	Doubling of PFOS was associated with decreases in mumps and rubella antibodies. No associations with measles antibodies.	PFOS Rubella vaccine antibodies (Δ) All: -8.4 (-17.9, 2.1) Seropositive: -13.3 (-19.9, -6.2)
			(PFNA: 0.929, PFHxS: 2.09)	No association between measles, mumps, or rubella antibodies and PFNA. PFHxS was associated with rubella antibodies in seropositive individuals, but measles and mumps were not.	PFNA Mumps vaccine antibodies (Δ) All: -2.7 (-7.2, 2.0) Seropositive: -2.7 (-8.4, 3.4) PFHxS Rubella vaccine antibodies (Δ) All: -50 (-10.8, 1.2) Seropositive: -6.0 (-9.6, -2.2)

*: Study that examined PFAS as a mixture

Table S5. Studies of perfluorinated compounds and puberty related outcomes.

Study	Study Characteristics	Exposure Matrix	Conc (ng/mL)	Summary of Results	Selected Effect Estimates
Christensen et al. (2011)	Case-control United Kingdom (cases = 218, controls = 230) 1991-2004 ALSPAC	Maternal serum	1 log-unit (PFOA: 3.7)	No association for menarche onset before age 11.5 with PFOA.	Menarche before age 11.5 (Odds ratio (OR)) PFOA: 1.01 (0.61, 1.68)
			(PFOS: 19.8)	Negative association between age at menarche before 11.5 years and PFOS.	PFOS: 0.68 (0.40, 1.13)
			(Ranges from 0.2 to 21.7)	No association with PFNA, PFHxS, PROSA, Et-PFOSA-AcOH, sulfonamide esters, or carboxylates. Potential negative associations for Me-PFOSA-AcOH or sulfonates.	PFNA: 0.91 (0.59, 1.4) Sulfonates: 0.66 (0.4, 1.08)
Kristensen et al. (2013)	Cohort Denmark (n = 343) 1988-2008 Danish Pregnancy Cohort	Maternal serum at gestational week 30	PFOA T1: <3.0 T2: 3.0 – 4.3 T3: >4.3	PFOA associated with later age at menarche, no associations with other reproductive parameters examined.	Age at menarche (Δ months) per tertile increase PFOA: 1.01 (0.22, 1.89)
			PFOS T1: <18.0 T2: 18.0 – 23.6 T3: >23.6	No association with age at menarche, menstrual cycle length, follicle number or reproductive hormone concentrations and PFOS.	Age at menarche (Δ months) per tertile increase PFOS: 0.12 (-0.10, 0.34) Cycle length (Δ days), nonusers of hormonal birth control per tertile increase PFOS: 0.001 (-0.007, 0.008)
Lopez-Espinosa et al. (2011)	Cross-sectional United States (n = 3076 boys, 2931 girls) 2005-2006 C8	Serum	1 ln-unit (PFOA: 23)	Later age at menarche and higher concentrations of pubertal indicators associated with PFOA in girls. No associations with pubertal indicators and PFOA in boys.	Menarche status (OR) PFOA: 0.83 (0.73, 0.95) PFOA, adjusted for PFOS: 0.87 (0.75, 1.00)
			(PFOS: 19.4)	Negative associations for hormone concentrations (testosterone and estradiol) and menarche with PFOS.	PFOS: 0.49 (0.36, 0.67) PFOS, adjusted for PFOA: 0.67 (0.48, 0.93)
Maisonet et al. (2015a)	Cohort, subset Avon, UK	Maternal serum	Tertiles PFOA	Higher tertiles of PFOA associated with higher levels of	Total testosterone (Δ nmol/L)

	(n = 72 girls) 1991-1992, recruitment ALSPAC		T1: <2.9 T2: 2.9-4.1 T3: >4.1	total testosterone in girls. No association with serum sex hormone-binding globulin concentrations.	PFOA T1: ref T2: 0.15 (-0.02, 0.32) T3: 0.24 (0.05, 0.43)
			PFOS T1: <15.9 T2: 15.9-22.6 T3: >22.6	Higher tertiles of PFOS associated with higher levels of total testosterone in girls. No association with serum sex hormone-binding globulin concentrations.	PFOS T1: ref T2: 0.1 (-0.07, 0.28) T3: 0.18 (0.01, 0.35)
			PFHxS T1: <1.3 T2: 1.3-1.9 T3: >1.9 PFNA T1: <0.5 T2: 0.5-0.6 T3: >0.6	PFHxS associated with increased testosterone, no association with sex hormone-binding globulin. PFNA not associated with either.	PFHxS T1: ref T2: 0.18 (0.00, 0.37) T3: 0.18 (0.00, 0.35) PFNA T1: ref T2: 0.08 (-0.10, 0.25) T3: 0.05 (-0.14, 0.24)
Lopez-Espinosa et al. (2016)	Cross-sectional United States (n = 2292) 2005-2006 C8	Serum	IQR (median) PFOA Boys: 1.68 (34.8) Girls: 1.70 (30.1)	PFOA concentrations were associated with decreased (log transformed) levels of insulin-like growth factor-1 (IGF-1) in girls. In both sexes, PFOA was potentially associated with decreased total testosterone and increased ln-estradiol.	IGF-1 (% difference) PFOA Boys: -0.4 (-3.4, 2.7) Girls: -3.6 (-6.6, -0.5)
			PFOS Boys: 0.66 (22.4) Girls: 0.65 (20.9)	PFOS was negatively associated with total testosterone, and IGF-1. In boys only PFOS was negatively associated with estradiol.	PFOS Boys: -5.9 (-8.3, -3.3) Girls: -5.6 (-8.2, -2.9)
			PFNA Boys: 0.57 (1.7) Girls: 0.61 (1.7) PFHxS Boys: 1.40 (8.1) Girls: 1.29 (7.0)	PFNA was negatively associated with IGF-1. There was no evidence of associations with PFHxS and sex hormones or IGF-1	PFNA Boys: -3.5 (-6.0, -1.0) Girls: -3.8 (-6.4, -1.2)
Tsai et al. (2015)	Cross-sectional Taiwan (n = 540) 2006-2008	Serum	(PFOA: 2.74)	Increasing PFOA percentile categories were not associated with log transformed follicle stimulating hormone (FSH)	Effects are reported as mean levels and p-value for trend only.

			concentrations among 12-17 year olds.
		(PFOS: 7.78)	PFOS was associated with decreased FSH in 12-17 year old males.
		(PFNA: 1.10 PFUA: 5.84)	PFNA was not associated with FSH, while PFUA was negatively associated with FSH in 12-17 year old females.

Table S6. Studies of perfluorinated compounds and thyroid related outcomes.

Study	Study Characteristics	Exposure matrix	Conc ng/mL	Summary of results	Selected effect estimates
Lopez-Espinosa et al. (2012)	Cross-sectional United States (n = 4713) 2005-2006 C8	Serum	IQR increase PFOA Q1: <13.1 Q2: 13.1 - 29.2 Q3: 29.3 – 67.6 Q4: >67.6	Hyperthyroidism associated with PFOA. No associations between thyroid hormone levels and PFOA.	Hypothyroidism (OR) PFOA: 1.54 (1.00, 2.37) TSH (log- μIU/mL) PFOA: Q1: ref Q2: 1.0 (–1.9, 4.0) Q3: 1.0 (–2.0, 4.1) Q4: 2.4 (–0.6, 5.5)
			PFOS Q1: <14.5 Q2: 14.5-19.9 Q3: 20.0-27.7 Q4: >27.7	Increases in TSH and TT4 at highest PFOS concentrations only.	Hypothyroidism (OR) PFOS: 0.91 (0.63, 1.31) TSH (log- μIU/mL) PFOS: Q1: ref Q2: 0.3 (-2.6, 3.2) Q3: -1.3 (-4.2, 1.7) Q4: 3.1 (0, 6.2)
			PFNA: Q1: <1.2 Q2: 1.2-1.4 Q3: 1.5-1.9 Q4: >1.9	No associations between TSH levels and PFNA. TT4 levels show increases with increasing PFNA.	Hypothyroidism (OR) PFNA: 1.11 (0.77, 1.60) TSH (log- μIU/mL) PFNA: Q1: ref Q2: 0.4 (-2.6, 3.5) Q3: -0.3 (-3.2, 2.6) Q4: 1.5 (-1.6, 4.6)
Lin et al. (2013b)	Cohort Taiwan	Serum	1 (PFOA: 3.64)	No association between levels of free T4 and log-TSH and PFOA	Free T4 (ng/dL) PFOA: 0.001 (-0.002, 0.003)

	(n = 531) 1999-2000 Young Taiwanese Cardiovascular Cohort Study				Log-TSH (m IU/L) PFOA: -0.006 (-0.019, 0.008)
			(PFOS: 5.47)	No association between levels of free T4 and log-TSH and PFOS	Free T4 (ng/dL) PFOS: 0.001 (0.000-0.002) Log-TSH (m IU/L) PFOS: 0.006 (-0.013-0.025)
			(PFUA: 1.50 PFNA: 1.2)	No association between levels of free T4 and log-TSH and PFUA. PFNA has small positive association with free T4 but no association with TSH. Some potential positive ORs for hypothyroidism with both PFNA and PFUA, however case numbers are small and confidence intervals very wide.	Free T4 (ng/dL) PFNA: 0.004 (0.001-0.007) Log-TSH (m IU/L) PFNA: -0.006 (-0.019, 0.008) Free T4 (ng/dL) PFUA: 0.000(0.000-0.001) Log-TSH (m IU/L) PFUA: 0.001 (-0.004-0.007)
de Cock et al. (2014)	Cohort The Netherlands (n = 83) 2011-2013	Cord blood	PFOA Q1: <0.059 Q2: 0.059 – 0.865 Q3: 0.865 – 1.20 Q4: >1.20	Potential positive association between PFOA and T4 levels in girls, but sample size and exposure variability are small.	T4 levels (Δ nmol/L) PFOA, boys Q1: ref Q2: 7.9 (-18.04, 33.92) Q3: -2.1 (-20.94, 16.78) Q4: 6.2 (-16.08, 28.5) PFOA, girls Q1: ref Q2: -5.9 (-26.75, 14.94) Q3: 11.8 (-19.08, 42.72) Q4: 38.6 (13.34, 63.83)
			PFOS Q1: <1.03 Q2: 1.03 – 1.60 Q3: 1.60 – 2.18 Q4: 2.18	No associations between PFOS and T4 levels.	PFOS, boys Q1: ref Q2: -7.9 (-31.56, 15.74) Q3: -16.5 (-40.32, 7.34) Q4: -9.6 (-32.57, 13.31) PFOS, girls Q1: ref Q2: -1.3 (-30.45, 27.94) Q3: 4.5 (-25.95, 34.92) Q4: 15.9 (-10.67, 42.4)
Kim et al. (2011)	Cross-sectional South Korea (n = 44)	Cord blood	Median PFOA: 1.46	Small negative correlations between PFOA and thyroid hormones from cord blood.	Adjusted Pearson correlation Maternal PFOA: Fetal T3: -0.240

	8/2008 – 3/2009				Fetal T4: -0.157 Fetal TSH: 0.089
			PFOS: 2.93	Negative correlations between maternal PFOS and fetal T3 positive correlation with fetal TSH.	Maternal PFOS Fetal T3: -0.414 Fetal T4: -0.071 Fetal TSH: 0.443
			PFNA: 0.44 PFDA: 0.31 PFHxS: 0.55 PFHpS: 0.09 PFUnDA: 0.60 PFTrDA: 0.24	Maternal PFTrDA negatively correlated with fetal T3 and T4. PFHxS small negative correlation with T3.	Maternal PFHxS Fetal T3: -0.261 Fetal T4: 0.030 Fetal TSH: 0.091 Maternal PFTrDA Fetal T3: -0.380 Fetal T4: -0.441 Fetal TSH: 0.288
Kim et al. (2016)	Cross-sectional South Korea (n = 27 cases, 13 controls) July 2009- Feb 2010	Serum	(PFOA: 2.12, 5.398) (PFOS: 4.05, 5.326)	Mean levels of PFOA, PFNA, PFDA, PFUnDA, and total PFASs were higher in infants with congenital hypothyroidism than in health infants.	Reported as figures.
Kato et al. (2016)	Cross-sectional Japan (n = 392 mother-infant pairs) 2002 – 2005 Hokkaido Study on the Environment and Children's Health	Maternal serum	log(10)-unit (PFOA: 1.2)	PFOA was not associated with infant levels of thyroid stimulating hormone (TSH) or free thyroxine (FT4).	PFOA FT4 (Δ log(10) ng/mL): 0.003 (p = 0.960) TSH (Δ log(10) lU/mL): -0.014 (p = 0.801)
			(PFOS: 5.2)	Log(10) increases in PFOS were associated with increases in TSH, but not FT4.	PFOS FT4 (Δ log(10) ng/mL): -0.043 (p = 0.452) TSH (Δ log(10) lU/mL): 0.177 (p = 0.001)
Tsai et al. (2017)	Cross-sectional Taiwan (n = 118 mother-infant pairs) April 2004 – January 2005 Taiwan Birth Panel Study	Cord blood plasma	1 Log-unit (PFOA: 3.14)	No association between concentration of PFOA and T4, TSH, or T3 in either boys or girls.	PFOA T4 (Δ log μg/dL), boys -0.082 (-0.643, 0.48)
			(PFOS: 7.24)	Increasing log-PFOS associated with decreasing log-T4 in boys, but not in girls. Increasing log-PFOS also associated with increasing log-TSH in both boys and girls, but percentile analyses	PFOS T4 (Δ log μg/dL), boys -0.667 (-1.283, -0.05) >90th percentile v. <30th: -2.115 (-3.622, -0.608)

				show non-linear response and stronger magnitude of effects in boys. PFOS not associated with T3 in boys, potential positive association in girls.	T4 (Δ log µg/dL), girls 0.033 (-0.707, 0.773) >90th percentile v. <30th: 0.808 (-0.954, 2.571) TSH (Δ log µIU/mL), Boys: 0.333 (0.012, 0.678) Girls: 0.36 (-0.033, 0.753)
			(PFUnDA: 15.94) (PFNA: 7.55)	No association between concentration of PFUnDA and T4 or T3 in either boys or girls. Potential positive association with TSH in boys only. No association between concentration of PFNA and T4, TSH, or T3 in either boys or girls.	PFUnDA T4 (Δ log µg/dL) Boys: -0.082 (-0.485, 0.321) TSH (Δ log µIU/mL) Boys: 0.142 (-0.062, 0.346)

Table S7. Studies of perfluorinated compounds and renal related outcomes.

Study	Study Characteristics	Exposure matrix	Conc ng/mL	Summary of results	Selected effect estimates
Watkins et al. (2013)	Cross-sectional United States (n = 9660) 2005-2006 C8	Serum	PFOA: 1.63	Increases in PFOA associated with decreased eGFR.	eGFR (Δ rate) PFOA -0.73 (-1.38, -0.08)
			PFOS: 0.64	Increases in PFOS associated with decreased eGFR.	PFOS -1.34 (-1.91, -0.77)
			PFNA: 0.51 PFHxS: 1.27 Ln-unit	Increases in log-concentrations of PFASs negatively associated with eGRF.	PFNA -0.88 (-1.41, -0.36) PFHxS -1.02 (-1.64, -0.40)
Lin et al. (2013b)	Cohort Taiwan (n = 531) 1999-2000 Young Taiwanese Cardiovascular Cohort Study	Serum	(PFOA: 3.64) (PFOS: 5.47) (PFUA: 1.50) (PFNA: 1.2)	PFUA levels higher in children with chronic renal failure.	PFUA, ng/mL geometric mean (SD) No renal failure: 5.68 (2.92) Chronic renal failure: 11.07 (2.64)

Kataria et al. (2015)	Cross-sectional United States (n = 1960) 2003-2010 NHANES	Serum	PFOA Q1: <2.5 ng/mL Q2: 2.5-3.5 Q3: 3.5-4.7 Q4: >=4.7	Increases in PFOA were negatively associated with eGFR and positively associated with uric acid concentrations, this held true after adjusting for PFOS as well. No associations with creatinine.	eGFR (Δ rate) PFOA Q1: ref Q2: −2.81 (−7.16, 1.53) Q3: −5.50 (−11.50, 0.50) Q4: −6.84 (−11.48, −2.19)
			PFOS Q1: <7.9 Q2: 7.9-12.8 Q3: 12.8-19.4 Q4: >=19.4	Increases in PFOS were negatively associated with eGFR and positively associated with uric acid concentrations. This was attenuated after adjustment for PFOA.	PFOS Q1: ref Q2: −5.39 (−9.87, −0.92) Q3: −7.25 (−12.25, −2.25) Q4: −9.69 (−14.78, −4.59)
			PFNA Q1: <0.7 Q2: 0.7-1.0 Q3: 1.0-1.5 Q4: >=1.5	PFNA and PFHxS were not associated with , eGFR, creatinine, or uric acid concentration.	PFNA Q1: ref Q2: 1.25 (−4.30, 6.80) Q3: 2.59 (−1.89, 7.08) Q4: −1.2 (−5.62, 3.22)
Qin et al. (2016)	Cross-sectional Taiwan (n = 225 non-asthmatics) 2009-2010 Genetics and Biomarkers study for Childhood Asthma (GBCA)	Serum	Quartile increase (PFOA: 0.5)	Increasing PFOA was associated with increased odds of high uric acid level (≥6 mg/dL). Potentially higher odds in boys than girls.	High uric acid level (OR) PFOA 2.16 (1.29, 3.61)
			(PFOS: 28.9)	PFOS was potentially associated with high uric acid level.	PFOS 1.35 (0.95, 1.93)
			(Ranges from 0.2 to 5.0)	PFBS, PFDA, PFHxS, and PFNA were potentially associated with high uric acid level. PFDOA, PFHxA, and PFTA were not associated with high uric acid level.	PFNA 1.28 (0.83, 1.96) PFTA 0.97 (0.69, 1.36)

References

Andersen CS, Fei C, Gamborg M, Nohr EA, Sorensen TI, Olsen J. 2010. Prenatal exposures to perfluorinated chemicals and anthropometric measures in infancy. American journal of epidemiology 172:1230-1237.

Andersen CS, Fei C, Gamborg M, Nohr EA, Sorensen TI, Olsen J. 2013. Prenatal exposures to perfluorinated chemicals and anthropometry at 7 years of age. American journal of epidemiology 178:921-927.

Ashley-Martin J, Dodds L, Levy AR, Platt RW, Marshall JS, Arbuckle TE. 2015. Prenatal exposure to phthalates, bisphenol a and perfluoroalkyl substances and cord blood levels of ige, tslp and il-33. Environmental research 140:360-368.

Braun JM, Chen A, Romano ME, Calafat AM, Webster GM, Yolton K, et al. 2016. Prenatal perfluoroalkyl substance exposure and child adiposity at 8 years of age: The home study. Obesity 24:231-237.

Chen MH, Ha EH, Liao HF, Jeng SF, Su YN, Wen TW, et al. 2013. Perfluorinated compound levels in cord blood and neurodevelopment at 2 years of age. Epidemiology (Cambridge, Mass) 24:800-808.

Christensen KY, Maisonet M, Rubin C, Holmes A, Calafat AM, Kato K, et al. 2011. Exposure to polyfluoroalkyl chemicals during pregnancy is not associated with offspring age at menarche in a contemporary british cohort. Environment international 37:129-135.

de Cock M, de Boer MR, Lamoree M, Legler J, van de Bor M. 2014. Prenatal exposure to endocrine disrupting chemicals in relation to thyroid hormone levels in infants - a dutch prospective cohort study. Environmental health : a global access science source 13:106.

Donauer S, Chen A, Xu Y, Calafat AM, Sjodin A, Yolton K. 2015. Prenatal exposure to polybrominated diphenyl ethers and polyfluoroalkyl chemicals and infant neurobehavior. The Journal of pediatrics 166:736-742.

Dong GH, Tung KY, Tsai CH, Liu MM, Wang D, Liu W, et al. 2013. Serum polyfluoroalkyl concentrations, asthma outcomes, and immunological markers in a case-control study of taiwanese children. Environmental health perspectives 121:507-513, 513e501-508.

Fei C, McLaughlin JK, Lipworth L, Olsen J. 2008. Prenatal exposure to perfluorooctanoate (pfoa) and perfluorooctanesulfonate (pfos) and maternally reported developmental milestones in infancy. Environmental health perspectives 116:1391-1395.

Fei C, McLaughlin JK, Lipworth L, Olsen J. 2010. Prenatal exposure to pfoa and pfos and risk of hospitalization for infectious diseases in early childhood. Environmental research 110:773-777.

Fei C, Olsen J. 2011. Prenatal exposure to perfluorinated chemicals and behavioral or coordination problems at age 7 years. Environmental health perspectives 119:573-578.

Forns J, Iszatt N, White RA, Mandal S, Sabaredzovic A, Lamoree M, et al. 2015. Perfluoroalkyl substances measured in breast milk and child neuropsychological development in a norwegian birth cohort study. Environment international 83:176-182.

Frisbee SJ, Shankar A, Knox SS, Steenland K, Savitz DA, Fletcher T, et al. 2010. Perfluorooctanoic acid, perfluorooctanesulfonate, and serum lipids in children and adolescents: Results from the c8 health project. Archives of pediatrics & adolescent medicine 164:860-869.

Geiger SD, Xiao J, Ducatman A, Frisbee S, Innes K, Shankar A. 2014a. The association between pfoa, pfos and serum lipid levels in adolescents. Chemosphere 98:78-83.

Geiger SD, Xiao J, Shankar A. 2014b. No association between perfluoroalkyl chemicals and hypertension in children. Integrated blood pressure control 7:1.

Goudarzi H, Nakajima S, Ikeno T, Sasaki S, Kobayashi S, Miyashita C, et al. 2016. Prenatal exposure to perfluorinated chemicals and neurodevelopment in early infancy: The hokkaido study. The Science of the total environment 541:1002-1010.

Grandjean P, Andersen EW, Budtz-Jorgensen E, Nielsen F, Molbak K, Weihe P, et al. 2012. Serum vaccine antibody concentrations in children exposed to perfluorinated compounds. Jama 307:391-397.

Granum B, Haug LS, Namork E, Stolevik SB, Thomsen C, Aaberge IS, et al. 2013. Pre-natal exposure to perfluoroalkyl substances may be associated with altered vaccine antibody levels and immune-related health outcomes in early childhood. Journal of immunotoxicology 10:373-379.

Gump BB, Wu Q, Dumas AK, Kannan K. 2011. Perfluorochemical (pfc) exposure in children: Associations with impaired response inhibition. Environmental science & technology 45:8151-8159.

Halldorsson TI, Rytter D, Haug LS, Bech BH, Danielsen I, Becher G, et al. 2012. Prenatal exposure to perfluorooctanoate and risk of overweight at 20 years of age: A prospective cohort study. Environmental health perspectives 120:668-673.

Hoffman K, Webster TF, Weisskopf MG, Weinberg J, Vieira VM. 2010. Exposure to polyfluoroalkyl chemicals and attention deficit/hyperactivity disorder in u.S. Children 12-15 years of age. Environmental health perspectives 118:1762-1767.

Hoyer BB, Ramlau-Hansen CH, Obel C, Pedersen HS, Hernik A, Ogniev V, et al. 2015a. Pregnancy serum concentrations of perfluorinated alkyl substances and offspring behaviour and motor development at age 5-9 years--a prospective study. Environmental health : a global access science source 14:2.

Hoyer BB, Ramlau-Hansen CH, Vrijheid M, Valvi D, Pedersen HS, Zviezdai V, et al. 2015b. Anthropometry in 5- to 9-year-old greenlandic and ukrainian children in relation to prenatal exposure to perfluorinated alkyl substances. Environmental health perspectives 123:841-846.

Humblet O, Diaz-Ramirez LG, Balmes JR, Pinney SM, Hiatt RA. 2014. Perfluoroalkyl chemicals and asthma among children 12-19 years of age: Nhanes (1999-2008). Environmental health perspectives 122:1129-1133.

Kataria A, Trachtman H, Malaga-Dieguez L, Trasande L. 2015. Association between perfluoroalkyl acids and kidney function in a cross-sectional study of adolescents. Environmental health : a global access science source 14:89.

Kato S, Itoh S, Yuasa M, Baba T, Miyashita C, Sasaki S, et al. 2016. Association of perfluorinated chemical exposure in utero with maternal and infant thyroid hormone levels in the sapporo cohort of hokkaido study on the environment and children's health. Environmental health and preventive medicine.

Kim DH, Kim UJ, Kim HY, Choi SD, Oh JE. 2016. Perfluoroalkyl substances in serum from south korean infants with congenital hypothyroidism and healthy infants - its relationship with thyroid hormones. Environmental research 147:399-404.

Kim S, Choi K, Ji K, Seo J, Kho Y, Park J, et al. 2011. Trans-placental transfer of thirteen perfluorinated compounds and relations with fetal thyroid hormones. Environmental science & technology 45:7465-7472.

Kristensen SL, Ramlau-Hansen CH, Ernst E, Olsen SF, Bonde JP, Vested A, et al. 2013. Long-term effects of prenatal exposure to perfluoroalkyl substances on female reproduction. Human reproduction (Oxford, England) 28:3337-3348.

Lien GW, Huang CC, Shiu JS, Chen MH, Hsieh WS, Guo YL, et al. 2016. Perfluoroalkyl substances in cord blood and attention deficit/hyperactivity disorder symptoms in seven-year-old children. Chemosphere 156:118-127.

Liew Z, Ritz B, von Ehrenstein OS, Bech BH, Nohr EA, Fei C, et al. 2015. Attention deficit/hyperactivity disorder and childhood autism in association with prenatal exposure to perfluoroalkyl substances: A nested case-control study in the danish national birth cohort. Environmental health perspectives 123:367-373.

Lin CY, Chen PC, Lin YC, Lin LY. 2009. Association among serum perfluoroalkyl chemicals, glucose homeostasis, and metabolic syndrome in adolescents and adults. Diabetes care 32:702-707.

Lin CY, Wen LL, Lin LY, Wen TW, Lien GW, Chen CY, et al. 2011. Associations between levels of serum perfluorinated chemicals and adiponectin in a young hypertension cohort in taiwan. Environmental science & technology 45:10691-10698.

Lin CY, Lin LY, Wen TW, Lien GW, Chien KL, Hsu SH, et al. 2013a. Association between levels of serum perfluorooctane sulfate and carotid artery intima-media thickness in adolescents and young adults. International journal of cardiology 168:3309-3316.

Lin CY, Wen LL, Lin LY, Wen TW, Lien GW, Hsu SH, et al. 2013b. The associations between serum perfluorinated chemicals and thyroid function in adolescents and young adults. Journal of hazardous materials 244-245:637-644.

Lopez-Espinosa MJ, Fletcher T, Armstrong B, Genser B, Dhatariya K, Mondal D, et al. 2011. Association of perfluorooctanoic acid (pfoa) and perfluorooctane sulfonate (pfos) with age of puberty among children living near a chemical plant. Environmental science & technology 45:8160-8166.

Lopez-Espinosa MJ, Mondal D, Armstrong B, Bloom MS, Fletcher T. 2012. Thyroid function and perfluoroalkyl acids in children living near a chemical plant. Environmental health perspectives 120:1036-1041.

Lopez-Espinosa MJ, Mondal D, Armstrong BG, Eskenazi B, Fletcher T. 2016. Perfluoroalkyl substances, sex hormones, and insulin-like growth factor-1 at 6-9 years of age: A cross-sectional analysis within the c8 health project. Environmental health perspectives.

Maisonet M, Terrell ML, McGeehin MA, Christensen KY, Holmes A, Calafat AM, et al. 2012. Maternal concentrations of polyfluoroalkyl compounds during pregnancy and fetal and postnatal growth in british girls. Environmental health perspectives 120:1432-1437.

Maisonet M, Calafat AM, Marcus M, Jaakkola JJ, Lashen H. 2015a. Prenatal exposure to perfluoroalkyl acids and serum testosterone concentrations at 15 years of age in female alspac study participants. Environmental health perspectives.

Maisonet M, Nayha S, Lawlor DA, Marcus M. 2015b. Prenatal exposures to perfluoroalkyl acids and serum lipids at ages 7 and 15 in females. Environment international 82:49-60.

Ode A, Kallen K, Gustafsson P, Rylander L, Jonsson BA, Olofsson P, et al. 2014. Fetal exposure to perfluorinated compounds and attention deficit hyperactivity disorder in childhood. PloS one 9:e95891.

Okada E, Sasaki S, Saijo Y, Washino N, Miyashita C, Kobayashi S, et al. 2012. Prenatal exposure to perfluorinated chemicals and relationship with allergies and infectious diseases in infants. Environmental research 112:118-125.

Okada E, Sasaki S, Kashino I, Matsuura H, Miyashita C, Kobayashi S, et al. 2014. Prenatal exposure to perfluoroalkyl acids and allergic diseases in early childhood. Environment international 65:127-134.

Qin XD, Qian Z, Vaughn MG, Huang J, Ward P, Zeng XW, et al. 2016. Positive associations of serum perfluoroalkyl substances with uric acid and hyperuricemia in children from taiwan. Environmental pollution 212:519-524.

Qin XD, Qian ZM, Dharmage SC, Perret J, Geiger SD, Rigdon SE, et al. 2017. Association of perfluoroalkyl substances exposure with impaired lung function in children. Environmental research 155:15-21.

Quaak I, de Cock M, de Boer M, Lamoree M, Leonards P, van de Bor M. 2016. Prenatal exposure to perfluoroalkyl substances and behavioral development in children. Int J Environ Res Public Health 13.

Smit LA, Lenters V, Hoyer BB, Lindh CH, Pedersen HS, Liermontova I, et al. 2015. Prenatal exposure to environmental chemical contaminants and asthma and eczema in school-age children. Allergy 70:653-660.

Stein CR, Savitz DA. 2011. Serum perfluorinated compound concentration and attention deficit/hyperactivity disorder in children 5-18 years of age. Environmental health perspectives 119:1466-1471.

Stein CR, Savitz DA, Bellinger DC. 2013. Perfluorooctanoate and neuropsychological outcomes in children. Epidemiology (Cambridge, Mass) 24:590-599.

Stein CR, Savitz DA, Bellinger DC. 2014. Perfluorooctanoate exposure in a highly exposed community and parent and teacher reports of behaviour in 6-12-year-old children. Paediatric and perinatal epidemiology 28:146-156.

Stein CR, McGovern KJ, Pajak AM, Maglione PJ, Wolff MS. 2016. Perfluoroalkyl and polyfluoroalkyl substances and indicators of immune function in children aged 12-19 y: National health and nutrition examination survey. Pediatric research 79:348-357.

Strom M, Hansen S, Olsen SF, Haug LS, Rantakokko P, Kiviranta H, et al. 2014. Persistent organic pollutants measured in maternal serum and offspring neurodevelopmental outcomes--a prospective study with long-term follow-up. Environment international 68:41-48.

Timmermann CA, Rossing LI, Grontved A, Ried-Larsen M, Dalgard C, Andersen LB, et al. 2014. Adiposity and glycemic control in children exposed to perfluorinated compounds. The Journal of clinical endocrinology and metabolism 99:E608-614.

Tsai MS, Lin CY, Lin CC, Chen MH, Hsu SH, Chien KL, et al. 2015. Association between perfluoroalkyl substances and reproductive hormones in adolescents and young adults. International journal of hygiene and environmental health 218:437-443.

Tsai MS, Lin CC, Chen MH, Hsieh WS, Chen PC. 2017. Perfluoroalkyl substances and thyroid hormones in cord blood. Environmental pollution 222:543-548.

Vuong AM, Yolton K, Webster GM, Sjodin A, Calafat AM, Braun JM, et al. 2016. Prenatal polybrominated diphenyl ether and perfluoroalkyl substance exposures and executive function in school-age children. Environmental research 147:556-564.

Wang IJ, Hsieh WS, Chen CY, Fletcher T, Lien GW, Chiang HL, et al. 2011. The effect of prenatal perfluorinated chemicals exposures on pediatric atopy. Environmental research 111:785-791.

Wang Y, Rogan WJ, Chen HY, Chen PC, Su PH, Chen HY, et al. 2015. Prenatal exposure to perfluroalkyl substances and children's iq: The taiwan maternal and infant cohort study. International journal of hygiene and environmental health.

Wang Y, Adgent M, Su PH, Chen HY, Chen PC, Hsiung CA, et al. 2016. Prenatal exposure to perfluorocarboxylic acids (pfcas) and fetal and postnatal growth in the taiwan maternal and infant cohort study. Environmental health perspectives.

Watkins DJ, Josson J, Elston B, Bartell SM, Shin HM, Vieira VM, et al. 2013. Exposure to perfluoroalkyl acids and markers of kidney function among children and adolescents living near a chemical plant. Environmental health perspectives 121:625-630.

Zeng XW, Qian Z, Emo B, Vaughn M, Bao J, Qin XD, et al. 2015. Association of polyfluoroalkyl chemical exposure with serum lipids in children. The Science of the total environment 512-513:364-370.

Zhu Y, Qin XD, Zeng XW, Paul G, Morawska L, Su MW, et al. 2016. Associations of serum perfluoroalkyl acid levels with t-helper cell-specific cytokines in children: By gender and asthma status. The Science of the total environment 559:166-173.

RECOGNITION: Exposure to Perfluorinated Alkyl Substances and Health Outcomes in Children: A Systematic Review of the Epidemiologic Literature

Citations	Downloads	Media/News Outlets	International UK Parliament	National US House briefing	Recognition by Scientific Societies	Use by the States
72 times, pubmed 75 times Altmetrics	3823 times	7	1	3	2	3

Citations: Pubmed reports that this publication has been cited 72 times. Similarly, Altmetric shows 75 citations of this publication; see the visual citations below. Altmetrics reports that this publication has been downloaded 3823 times.

www.ncbi.nlm.nih.gov › pubmed

Exposure to Perfluorinated Alkyl Substances and ... - NCBI

Jun 27, 2017 - **Rappazzo** KM(1)(2), Coffman E(3)(4), **Hines EP**(5). ... was performed by searching PubMed for studies on **PFAS** and **child** health outcomes.

by KM Rappazzo - 2017 - Cited by 72 - Related articles

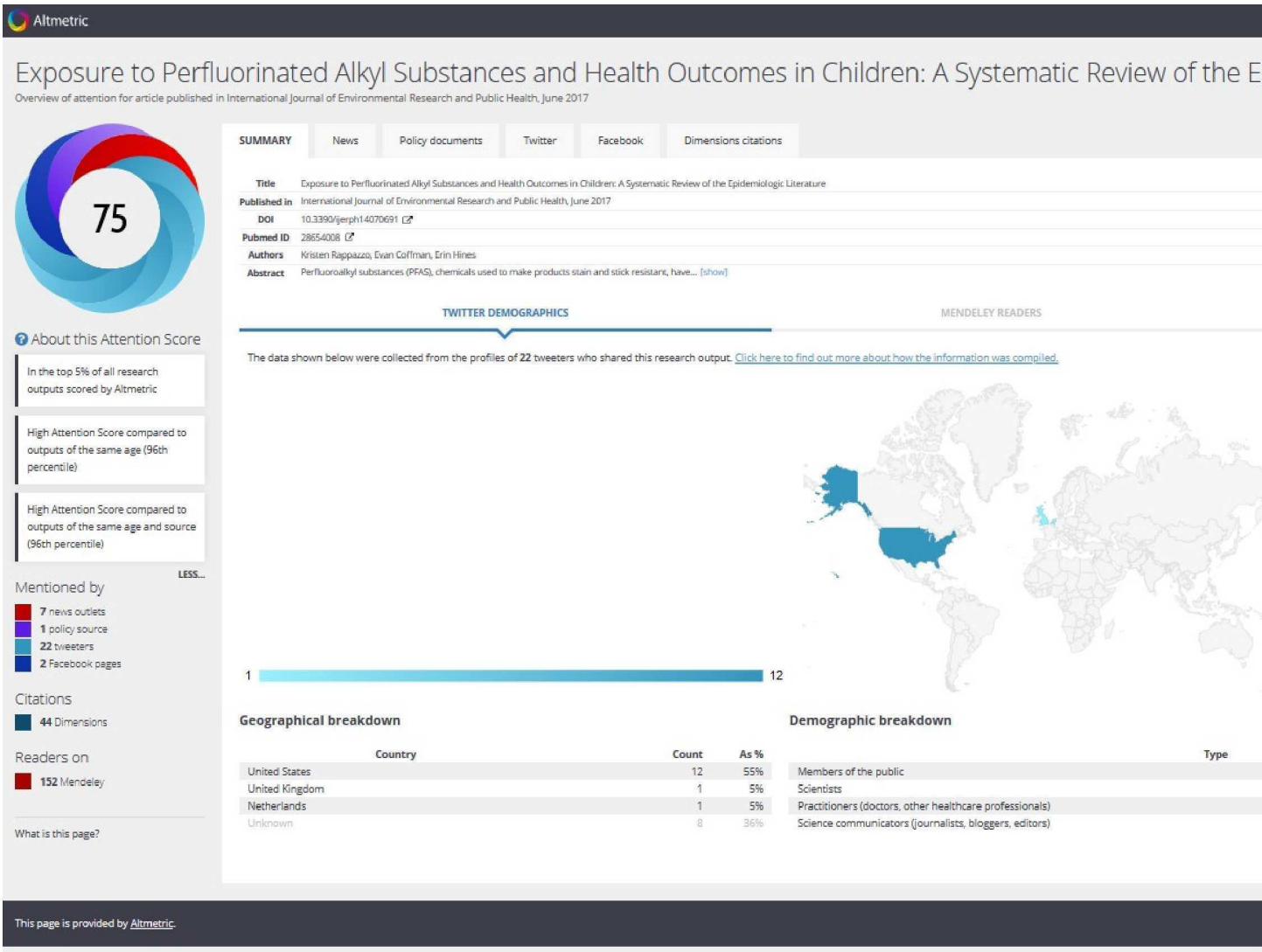

This publication has been recognized by the Altmetrics citation tool as being in the top 5% of all research outputs scored by Altmetrics.
This publication has been cited by other publications 77 times. Altmetric lists this publication in the top 5% of all of the publications it has evaluated.

<u>This submission was recruited to the journal</u> IJERPH for inclusion in the Special Issue on Environmental Chemical Mixtures at Low Concentration and Children's Health.

<u>Recognition by Scientific Societies:</u>

1. This publication was recruited for an invited presentation at the 43rd Annual Meeting of the Developmental Neurotoxicology Society: Held in Conjunction with the 59th Annual Meeting of the Teratology Society. I presented the neurological outcomes from our systematic review in a talk entitled, "Developmental Neurotoxicology of PFAS" in San Diego, Ca, June 2019.
2. EHP also mentioned our article in one of its press releases. See news information at the bottom of this document.

<u>National Recognition:</u>

1. USA Congressional Briefing: Our publication was cited during a US Congressional briefing before the US House Environment Subcommittee on Oversight and Government Reform On Per- and Poly- Fluoroalkyl Substances (PFAS), November 19, 2019. https://www.congress.gov/116/meeting/house/110236/witnesses/HHRG-116-GO28-Wstate-FaberS-20191119.pdf
2. USA Congressional Briefing, Our publication was cited during a Health Subcommittee Meeting of the House Energy and Commerce Committee, On H.R. 2827, PFAS in Food Containers, https://docs.house.gov/meetings/IF/IF14/20200129/110423/HHRG-116-IF14-Bio-BeneshM-20200129.pdf, January 29, 2020.
3. CDC/ATSDR have cited our publication in their PFAS drinking water document: https://www.atsdr.cdc.gov/pfas/docs/nofo/Multi-site-study-protocol-508.pdf

International Recognition: UK Parliament: Our publication was cited in the UK Parliament Briefing notes from July 2018.

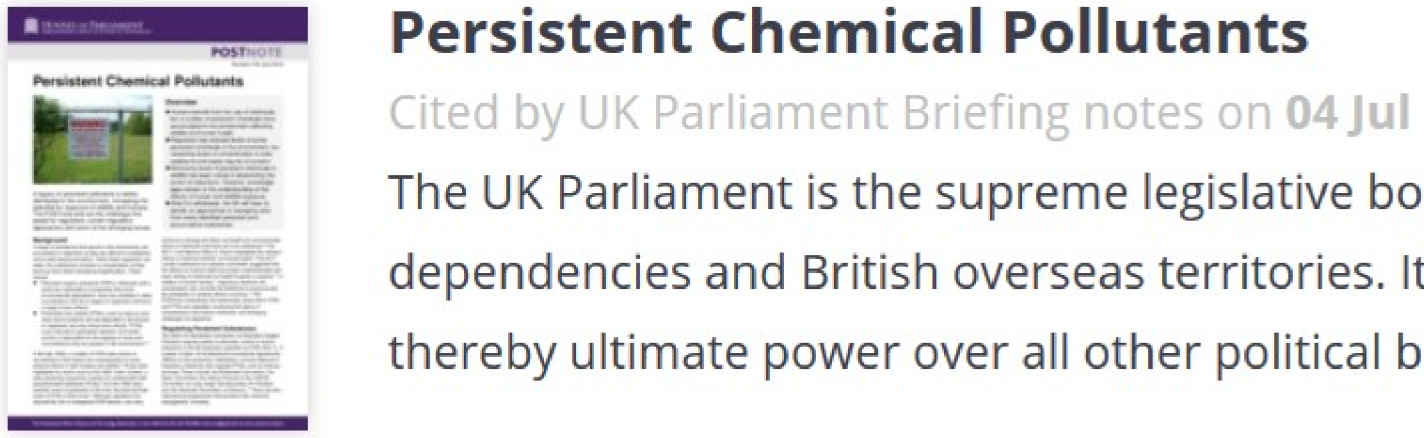

State Recognition:

1. The state of NJ recently developed Maximum Contaminant Levels (MCL) for PFOA and PFOS in drinking water. They cited our publication in their "Technical Analysis of New Jersey's Proposed Health-Based Maximum Contaminant Level (MCL)for Perfluorooctane Sulfonate (PFOS)" that was used in support of determinations of the MCLs. https://www.nj.gov/dep/watersupply/pdf/pfos-comment-4b.pdf
2. The State of Pennsylvania's Department of Health recently generated a PFAS Exposure Assessment Technical Toolkit (PEATT) Pilot Project and in its Final Report (https://www.health.pa.gov/topics/Documents/Environmental%20Health/PEATT%20Pilot%20Project%20Final%20Report%20April%2029%202019.pdf), it cited our publication.
3. State of Washington:

Community Recognition: The National Research Defense Council (NRDC) cited our publication in its fact sheet about PFAS in drinking water.

NRDC

NOVEMBER 2019
FS: 19-10-A

FACT SHEET

TOXIC DRINKING WATER: THE PFAS CONTAMINATION CRISIS[1]

WHAT ARE PFAS CHEMICALS?

Per- and polyfluoroalkyl substances (PFAS) are a large class of approximately 4,700 synthetic chemicals widely used for their oil and water repellency, temperature resistance, and friction reduction.[2,3] Various industries manufacture and use PFAS in items such as cookware, food packaging, firefighting foam, and textiles.

WHY SHOULD I CARE?

PFAS have grown into a global environmental and public health threat. These chemicals tend to share three problematic properties:

- **PFAS are extremely persistent "forever chemicals"** that do not break down easily and can accumulate in the food that we eat and in our own bodies.[4] Due to their widespread use, they are now found in the bodies of virtually all Americans.[5]
- **PFAS are highly mobile** and spread quickly throughout the environment. They are now found in our drinking water, air, food, and homes.[6]
- **PFAS are toxic** and can be harmful at extremely low doses (at the low parts-per-trillion level). PFAS have been linked to serious health effects such as cancer, hormone disruption, kidney and liver damage, developmental and reproductive harm, and immune system toxicity.[7]

WHAT ARE THE HEALTH RISKS?

PFAS have been linked to a variety of serious health effects including kidney and testicular cancer, thyroid disease, decreased fertility, and decreased response to vaccines.[8] PFAS are chemically similar, and it is reported that the health risks associated with one PFAS are expected to occur

for others as well.[9] Because people are often exposed to many of these chemicals at the same time, there is a real concern that different PFAS will target the same biological systems and cause greater effects than any single PFAS on its own.

Some PFAS have been shown to build up in people, even before birth.[10] These can take decades to be eliminated from the human body. Almost all fetuses and young children are exposed to PFAS, through fetal exposure during pregnancy and through contaminated infant formula or breast milk. Fetuses, infants, and children are particularly susceptible to the harmful effects of PFAS due to the rapid growth and complex developmental events they undergo.[11]

For more information, please contact:
Anna Reade
areade@nrdc.org

www.nrdc.org
www.facebook.com/nrdc.org
www.twitter.com/NRDC

News: Seven news outlets have cited our publication including CNN, the Intercept and EHP.

Altmetric

Exposure to Perfluorinated Alkyl Substances and Health Outcomes in Children: A System

Overview of attention for article published in International Journal of Environmental Research and Public Health, June 2017

About this Attention Score

In the top 5% of all research outputs scored by Altmetric

High Attention Score compared to outputs of the same age (96th percentile)

High Attention Score compared to outputs of the same age and source (96th percentile)

LESS...

Mentioned by

- **7** news outlets
- **1** policy source
- **22** tweeters
- **2** Facebook pages

SUMMARY | News | Policy documents | Twitter | Facebook | Dimensions citations

So far, Altmetric has seen **7** news stories from **7** outlets.

PFAS: Your home is full of potentially harmful "forever chemicals" — here's what you need to know
Inverse, 03 Mar 2020
Potentially toxic chemicals called PFAS are found practically everywhere — your home included.

What are toxic 'forever chemicals'
RT Network, 23 Jan 2020
Follow RT on American drinking water is far more contaminated than previously estimated — by carcinogenic 'forever chemicals...

High Levels of Toxic PFAS Chemicals Pollute Breast Milk Around the World
The Intercept, 30 Apr 2019
Decades after DuPont and 3M first discovered that the perfluorinated chemicals making them fortunes could be transmitted from...

不能乾燒又不能刮傷，使用不沾鍋的規矩為什麼這麼多？ - PanSci 泛科學
Pansci, 08 Aug 2018
本文由行政院環境保護署毒物及化學物質局委託，泛科學企劃執行 文 / 陳衍達 給大家 10 秒鐘想一下，以下 2 種物品的關聯性：... 3、2、1，時間到。想到了嗎？ 使用不鏽鋼鍋通常需要先熱鍋熱油，以免得食物黏住鍋面難以清理；那為什麼使用不沾鍋煎蛋時不加油也不須擔...

RECORD of AGREEMENT, Kristen Rappazzo (45%), Evan Coffman (30%), Erin Hines (25%)

Kristen Rappazzo

From: Rappazzo, Kristen <Rappazzo.Kristen@epa.gov>
Sent: Tuesday, April 28, 2020 7:11 PM
To: Hines, Erin <Hines.Erin@epa.gov>; Coffman, Evan <Coffman.Evan@epa.gov>
Subject: RE:

That's fine.

From: Hines, Erin <Hines.Erin@epa.gov>
Sent: Tuesday, April 28, 2020 6:49 PM
To: Rappazzo, Kristen <Rappazzo.Kristen@epa.gov>; Coffman, Evan <Coffman.Evan@epa.gov>
Subject:

How about percent effort of 45% Kristen, 30% Evan, 25% me?

Erin

Evan Coffman

From: Coffman, Evan <Coffman.Evan@epa.gov>
To: Hines, Erin <Hines.Erin@epa.gov>
Subject: RE: STAA and birthday

That's great. Thanks!

Evan

From: Hines, Erin <Hines.Erin@epa.gov>
Sent: Wednesday, April 29, 2020 9:50 PM
To: Coffman, Evan <Coffman.Evan@epa.gov>
Subject: RE: STAA and birthday

Hello Evan-

Happy birthday again. Sorry to keep bugging you. 45% for Kristen, 30 for you and 25% as percent contributions sounds great. Is that ok with you?

Peace

Erin

Table of Contents

General_Authors_Publications.....2
LI-266696_Burgess_et_al_2015.....14
Fernandez_et_al_2012.....28
Fernandez_et_al_2014.....39
Joyce_et_al_2016.....49
Record_of_Agreement.....64

United States Environmental Protection Agency
Washington, DC 20460

STAA REPORT FOR THE SCIENTIST NOMINATIONS

General Information:

Nomination ID/App ID:	20-125
Research Category Primary:	Monitoring and Measurement Methods (MM)
Research Category Secondary:	Ecological Research (ER)
Laboratory/Office Name:	ORD
Nomination Entered By:	Robert Burgess

Eligibility Checklist:

[Y] The nominated publication(s) has not been submitted to a previous STAA competition.

[Y] The nominated publication(s) was published on or before January 1, 2017 and on or after January 1,2012

[Y] The principal author was an EPA employee or a PHS employee assigned to EPA when the research was performed

[Y] The EPA authors (includes PHS employees assigned to EPA) contributed collectively a minimum of 50% toward the publication(s)

Nominating Official Name:	Wayne Munns
Nominating Official Title:	SUPERVISORY ECOLOGIST
Nominating OfficialEmail:	munns.wayne@epa.gov
STAA Coordinator Name:	Kathleen Wiser
STAA Coordinator Email:	wiser.kathi@epa.gov

Justifications:

Justification 1:

This manuscript describes the application of passive sampling at several U.S. EPA Superfund sites. A key tool for assessing the degree of environmental degradation occurring at Superfund sites as a result of the presence of legacy contaminants is the performance of the ecological risk assessment. The risk assessment has two main components: the effects and the exposures. While the effects component is beyond the scope of this nomination, the exposure component is highly relevant. For a risk assessment to be as cost-effective, logistically sound, and scientifically robust as possible, it is critical for the exposure measurement to be highly accurate. For making measurements of the exposure concentrations of legacy contaminants in both water column and sediment matrices, traditionally whole water or sediment measurements would be performed. Over the years, it has become increasingly evident these whole matrix measurements are inaccurate for a variety of reasons including artifacts associated with the measurements themselves and because they do not reliably consider the bioavailability of the contaminants. Both sources of error result in over- or under-estimating the exposure concentrations. Modelling the exposure concentrations of legacy contaminants in the water column and sediment matrices has been extensively investigated but can also suffer from inaccuracies when critical model parameters are not well understood or available (e.g., partition coefficients).

Over the last decade, passive sampling has been increasingly shown to effectively estimate exposure concentrations of legacy contaminants in water column and sediment matrices while limiting the artifacts associated with other monitoring methods and considering the importance of contaminant bioavailability. Scientific consensus is that the best surrogate for capturing the bioavailable concentrations of legacy contaminants in water column and sediment systems is by measuring the freely dissolved concentration (Cfree). During a passive sampler deployment in the environment, it is the Cfree that the passive sampler measures. Consequently, by using passive sampling-based measurements of legacy contaminants, the best surrogate measurements of the bioavailable contaminant is measured. These Cfree values can be used as the exposure concentrations in the ecological risk assessment at a given Superfund site.

This STAA nomination describes the application of passive sampling to measure Cfree at three marine Superfund sites around the United States. The study described in the paper had two main objectives. The first was to compare the performance of several different passive samplers with a range of contaminants to demonstrate the robustness of the passive sampling methods. However, the second, and arguably, more important objective was to illustrate to the reader, and more specifically, the remedial project managers (RPMs) at Superfund sites tasked with managing the site' risk, how effectively passive samplers can be used to measure Cfree and therefore exposure. In this way, the manuscript seeks to inform the RPMs of

the most accurate way to assess the ecological risk at their sites. In separate studies, in the *Supporting Documents* section, we discuss analogous research at another U.S. EPA Superfund site (i.e., Fernandez et al. 2012, 2014). In addition, the manuscript explores the statistical relationship between the bioaccumulation of legacy contaminants and uptake by the passive samplers. In this way, the STAA nomination addresses a second critical question: can the passive sampler polymer be used as a surrogate for the bioaccumulation of target contaminants. This question has real-world relevance under circumstances where insufficient organism mass is available at a contaminated site (e.g., benthic bivalves or polychaetes) to assess bioaccumulation or biomonitoring organisms (e.g., mussels) are not available for deployment at a site to assess remediation effectiveness. In both of these applications, the passive sampler may ultimately be shown to serve as an effective surrogate for organism' bioaccumulation. This is a topic we explored further in one of the papers in the *Supporting Documents* section (i.e., Joyce et al. 2016).

In conclusion, this nomination provides a robust example of the use of passive sampling for measuring Cfree for legacy contaminants to be used in the performance of ecological risk assessments at U.S. EPA Superfund sites. The research addressed by this nomination is also a topic supported in the current Sustainable and Healthy Communities (SHC) Strategic Research Action Plan (specifically *SHC Output 2.1: Methods, Tools, and Guidance on Remediation Options*).

Justification 2A:

n/a

Justification 2B:

U.S. EPA Authors	Publication Title	Nomination Year	STAA Award Level	Comment

	DR Katz, MG Cantwell, MM Perron, RM Burgess, KT Ho, MC Pelletier	Katz DR, MG Cantwell, JC Sullivan, MM Perron, RM Burgess, KT Ho, MA Charpentier. 2013. Factors regulating the accumulation and spatial distribution of the emerging contaminant Triclosan in the sediments of an urbanized estuary: Greenwich Bay, Rhode Island, USA. *Science of the Total Environment*. 443:123-133. Ho KT, A Chariton, LM Portis, D Proestou, MG Cantwell, J Baguley, RM Burgess, SL Simpson, MC Pelletier, MM Perron, C Gunsch, H Bik, A Kamikawa. 2013. Use of a novel sediment exposure to determine the effects of Triclosan on estuarine benthic communities. Environmental Toxicology and Chemistry 32:384-392. Perron, MM, RM Burgess, EM Suuberg, MG Cantwell, KG Pennell. 2013. Performance of passive samplers for monitoring estuarine water column concentrations 2. Emerging contaminants. Environmental Toxicology and Chemistry 32(10): 2190-2196.	2015	No Award	Unrelated to current submission
	RM Burgess, WJ Berry, DR Mount, KT Ho	Burgess RM, WJ Berry, DR Mount, DM Di Toro. 2013. Critical Review: Mechanistic sediment quality guidelines based on contaminant bioavailability:	2016	No Award	Unrelated to current submission

	Equilibrium partitioning Sediment Benchmarks (ESBs). *Environmental Toxicology and Chemistry*. 32:102-114.			
KT Ho, RM Burgess	KT Ho and RM Burgess. 2013. Critical Review: What's causing toxicity in sediments? Results of 20 years of toxicity identification evaluations. Environmental Toxicology and Chemistry 32:2424-2432	2016	Level III Award	Unrelated to current submission
	Burgess RM, KT Ho, W Brack, M Lamoree. 2013. Focus Article: Effects directed analysis (EDA) and toxicity identification evaluation (TIE): complementary but different approaches for diagnosing causes of environmental toxicity. Environmental Toxicology and Chemistry 32:1935-1945			
No Submission	-	2017	-	-
STAA Program Cancelled	-	2018	-	-
No Submission	-	2019	-	-

Justification 2C:

Previous STAA nominations during the last five years involved manuscripts focusing on the aquatic toxicity of the antibacterial chemical triclosan, developing benchmarks for sediment contaminants, and identifying the causes of aquatic toxicity. These topics are very different from the current 2020 STAA nomination. As discussed previously, this nomination addresses measuring the bioavailable concentrations of legacy contaminants at Superfund sites.

Justification 2D:

n/a

Justification 2E:

William Boyes submitted the following paper to this year's STAA in the *Review Article* category:

Boyes W, L Thornton, S Al-Abed, C Andersen, D Bouchard, RM Burgess, E Hubal, K Ho, M Hughes, K Kitchin, J Reichman, K Rogers, J Ross, P Rygiewicz, K Scheckel, S Thai, R Zepp, R Zucker. 2017. Decision-support framework for evaluating the environmental health and safety implications of engineered nanomaterials. *Critical Reviews in Toxicology* 47:767-810.

Robert Burgess is also an author on this submission. This article discusses a framework for assessing the environmental and human health effects of nanomaterials. The topic of this manuscript is very different from the current STAA nomination in terms of topic (i.e., passive sampling versus nanomaterials) and structure (i.e., review article versus research article).

Justification 3A:

Based on Google Scholar, the nominated paper has been cited 28 times in scientific peer-reviewed journals since publication. That level of citation averages to nearly six citations per year since publication in 2015. Unfortunately, the publisher of the journal *Environmental Toxicology and Chemistry* does not provide a summary of the number of downloads or reads for papers published in their journals.

In addition, this publication and its content resulted in two invited presentations, one domestic and the other international:

Burgess RM, Lohmann R, Schubauer-Berigan JP, Reitsma P, Perron MM, Lefkovitz L, Cantwell MG. 2015. Application of passive sampling for measuring dissolved concentrations of organic contaminants in the water column at three U.S. EPA marine Superfund sites. Platform presentation annual meeting of Society of Environmental Toxicology and Chemistry – Europe, Barcelona, Catalonia, Spain.

Burgess RM, Lohmann R, Schubauer-Berigan JP, Reitsma P, Perron MM, Lefkovitz L, Cantwell MG. 2015. Application of passive sampling for measuring dissolved concentrations of organic contaminants in the water column at three U.S. EPA marine Superfund sites. Platform presentation at the annual meeting of the National Environmental Monitoring Conference, Chicago, IL, USA.

as well as a series of in person and web-based presentations sponsored by the U.S. EPA Superfund Program's National Remedial Project Managers (NARPM) organization and the San Francisco Estuary Institute (SFEI):

Burgess RM. 2016. Passive sampling for measuring freely dissolved contaminants in sediments: basics, concepts and principles. Platform presentation at the *Porewater Concentrations and Bioavailability: How You Can Measure Them and Why They Influence Contaminated Sediment Remediation* workshop, U.S. EPA 2016 NARPM meeting, Pittsburgh, PA, USA.

Cantwell MG, RM Burgess. 2016. Passive sampling methods for measuring metals in sediment porewaters. Platform presentation at the *Porewater Concentrations and Bioavailability: How You Can Measure Them and Why*

They Influence Contaminated Sediment Remediation workshop, U.S. EPA 2016 NARPM meeting, Pittsburgh, PA, USA.

Burgess RM. 2017. Passive sampling for measuring freely dissolved contaminant concentrations: An overview. Webinar presentation for the *San Francisco Estuary Institute Regional Monitoring Program for Water Quality in San Francisco Bay: Passive and Alternative Sampling Methods*. San Francisco, CA, USA.

Burgess RM. 2017. Passive sampling for measuring freely dissolved contaminants in sediments: basics, principles & applications. Platform presentation at the *Using Bioavailability to Assess Contaminated Sediment Risk: Passive Sampling and Porewater Remedial Guidelines (PWRGs)* workshop, U.S. EPA 2017 NARPM meeting, Denver, CO, USA.

Burgess RM. 2018. Passive sampling for measuring freely dissolved contaminants in sediments: basics, principles & applications. Part of *NARPM Presents...Using Bioavailability to Assess Contaminated Sediment Risk: Passive Sampling and Porewater Remedial Goals (PWRGs)*. CLUIN Webinar, U.S. EPA, Office of Superfund Remediation and Technology Innovation (OSRTI), Technology Innovation and Field Services Division. Washington, DC, USA.

Justification 3B:

Following the internal review process at our Division, the manuscript was distributed to three external reviewers by the journal's Associate Editor. Following the review, the manuscript was revised by the first author with input from the other five authors and re-submitted to the Associate Editor. Upon receipt, the journal's Associate Editor performed a review to assess the author's responsiveness to the reviewers and accepted the manuscript for publication. Finally, the manuscript underwent review by the Copy Editor before publication.

AUTHORS

Principal Author

Author Name: Robert M. Burgess

Professional Title:		Salutation:	
Email:	burgess.robert@epa.gov	Organization:	
Mailing Address:			
Street Line 1:			
City:			
Zip Code:		State:	
At time of research was:	EPA Employee		
Separation Date:			
% of Effort:	25		

Contributing Author

Author Name:	Rainer Lohmann		
Professional Title:		Salutation:	
Email:	rlohmann@uri.edu	Organization:	
Mailing Address:			
Street Line 1:			
City:			
Zip Code:		State:	
At time of research was:	Non EPA Personnel		
Separation Date:			
% of Effort:	15		

Contributing Author

Author Name:	Joseph Schubauer-Berigan

Professional Title:		Salutation:
Email:	schubajp@uc.edu	Organization:
Mailing Address:		
Street Line 1:		
City:		
Zip Code:		State:
At time of research was:	Non EPA Personnel	
Separation Date:	Mon Apr 30 00:00:00 GMT 2018	
% of Effort:	10	

Contributing Author

Author Name:	Pamela Reitsma	
Professional Title:		Salutation:
Email:	pamelaj34@gmail.com	Organization:
Mailing Address:		
Street Line 1:		
City:		
Zip Code:		State:
At time of research was:	Non EPA Personnel	
Separation Date:		
% of Effort:	10	

Contributing Author

Author Name:	Monique Perron

Professional Title:		Salutation:
Email:	perron.monique@epa.gov	Organization:
Mailing Address:		
Street Line 1:		
City:		
Zip Code:		State:
At time of research was:	EPA Employee	
Separation Date:		
% of Effort:	15	

Contributing Author

Author Name:	Lisa Lefkovitz	
Professional Title:		Salutation:
Email:	lefkovitzl@battelle.org	Organization:
Mailing Address:		
Street Line 1:		
City:		
Zip Code:		State:
At time of research was:	Non EPA Personnel	
Separation Date:		
% of Effort:	10	

Contributing Author

Author Name:	Mark Cantwell

Professional Title:		Salutation:	
Email:	cantwell.mark@epa.gov	Organization:	
Mailing Address:			
Street Line 1:			
City:			
Zip Code:		State:	
At time of research was:	EPA Employee		
Separation Date:			
% of Effort:	15		

PUBLICATIONS

Publication 1:

Publication Title:	Application of passive sampling for measuring dissolved concentrations (Cfree) of organic contaminan		
Publication Date:	Wed Jun 03 00:00:00 GMT 2015		
Journal/Publication Method:	Environmental Toxicology and Chemistry		
All Author(s):			
Volume:	34	Number:	3
Pages:	1720-1733	Immediately Index:	Immediately Index:
Citation ½ Life:	5.1	Impact Factor:	3.421

SETAC PRESS

Environmental Toxicology and Chemistry, Vol. 34, No. 8, pp. 1720–1733, 2015
Published 2015 SETAC
Printed in the USA

APPLICATION OF PASSIVE SAMPLING FOR MEASURING DISSOLVED CONCENTRATIONS OF ORGANIC CONTAMINANTS IN THE WATER COLUMN AT THREE MARINE SUPERFUND SITES

ROBERT M. BURGESS,*† RAINER LOHMANN,‡ JOSEPH P. SCHUBAUER-BERIGAN,§ PAMELA REITSMA,‡‖ MONIQUE M. PERRON,# LISA LEFKOVITZ,†† and MARK G. CANTWELL†

†US Environmental Protection Agency, Office of Research and Development/National Health and Environmental Effects Research Laboratory, Narragansett, Rhode Island, USA
‡Graduate School of Oceanography, University of Rhode Island, Narragansett, Rhode Island, USA
§US Environmental Protection Agency, Office of Research and Development/National Risk Management Research Laboratory, Cincinnati, Ohio, USA
‖Narragansett Bay Commission, Providence, Rhode Island, USA
#US Environmental Protection Agency, Office of Chemical Safety and Pollution Prevention/Office of Pesticide Programs, Washington DC, USA
††Battelle, Duxbury Operations, Duxbury, Massachusetts, USA

(Submitted 2 December 2014; Returned for Revision 15 January 2015; Accepted 15 March 2015)

Abstract: Currently, there is an effort under way to encourage remedial project managers at contaminated sites to use passive sampling to collect freely dissolved concentrations (C_{free}) of hydrophobic organic contaminants to improve site assessments. The objective of the present study was to evaluate the use of passive sampling for measuring water column C_{free} for several hydrophobic organic contaminants at 3 US Environmental Protection Agency Superfund sites. Sites investigated included New Bedford Harbor (New Bedford, MA, USA), Palos Verdes Shelf (Los Angeles, CA, USA), and Naval Station Newport (Newport, RI, USA); and the passive samplers evaluated were polyethylene, polydimethylsiloxane-coated solid-phase microextraction fibers, semipermeable membrane devices, and polyoxymethylene. In general, the different passive samplers demonstrated good agreement, with C_{free} values varying by a factor of 2 to 3. Further, at New Bedford Harbor, where conventional water sample concentrations were also measured (i.e., grab samples), passive sampler–based C_{free} values agreed within a factor of 2. These findings suggest that all of the samplers were experiencing and measuring similar C_{free} during their respective deployments. Also, at New Bedford Harbor, a strong log-linear, correlative, and predictive relationship was found between polyethylene passive sampler accumulation and lipid-normalized blue mussel bioaccumulation of polychlorinated biphenyls ($r^2 = 0.92$, $p < 0.05$). The present study demonstrates the utility of passive sampling for generating scientifically accurate water column C_{free} values, which is critical for making informed environmental management decisions at contaminated sediment sites. *Environ Toxicol Chem* 2015;34:1720–1733. Published 2015 SETAC. This article is a US Government work and is in the public domain in the USA.

Keywords: Passive sampling Bioavailability Freely dissolved concentration Superfund program Dissolved concentration

INTRODUCTION

Studies over the last few decades have demonstrated that many aquatic organisms, including fish and wildlife, are exposed to anthropogenic contaminants present in the water column that originate from contaminated sediments [1,2]. Consequently, to accurately and holistically assess exposures at contaminated sediment sites, including US Environmental Protection Agency (USEPA) Superfund sites, it is critical to measure the water column concentrations directly. Exposure of aquatic organisms to hydrophobic organic chemicals such as polychlorinated biphenyls (PCBs), polycyclic aromatic hydrocarbons (PAHs), polybrominated diphenyl ethers (PBDEs), polychlorinated dibenzo-*p*-dioxins and dibenzofurans, and chlorinated pesticides in the water column is most strongly correlated to the freely dissolved concentration (C_{free}), whereas uptake from environmental sorptive phases such as colloids or suspended particles is often limited [3,4]. Consequently, C_{free} is considered a strong surrogate measurement for the bioavailable concentrations of many hydrophobic organic contaminants. However, measuring the C_{free} in the water column in the field remains technically challenging because of the relatively low concentrations of contaminants, potential for contamination from the sorptive phases, and losses to collection gear. Several recently developed passive sampling methods selectively measure C_{free} for hydrophobic organic contaminants [5] including polyethylene (PE)- and triolein-based semipermeable membrane devices (SPMDs) [6,7], polydimethylsiloxane (PDMS)-based solid-phase microextraction (SPME) [8–10], polyoxymethylene (POM) [11–13], and PE alone [14–21].

All of these passive sampling methods use essentially the same approach for sampling C_{free}. In this approach, contaminants partition between C_{free} (nanograms per liter) in the aqueous phase and some form of passive sampling absorptive carbon-based polymer or liquid phase (C_{PS}; nanograms per liter):

$$C_{free} \leftrightarrow C_{PS} \quad (1)$$

Under equilibrium conditions, the relationship between the passive sampler phase and the dissolved phase can be expressed as a passive sampler–dissolved phase partition coefficient ($K_{PS\text{-}free}$; liters per liter) and used to estimate the C_{free} of a given contaminant:

$$C_{free} = \frac{C_{PS}}{K_{PS-free}} \quad (2)$$

All Supplemental Data may be found in the online version of this article.

* Address correspondence to burgess.robert@epa.gov.

Published online 2 July 2015 in Wiley Online Library (wileyonlinelibrary.com).
DOI: 10.1002/etc.2995

If equilibrium conditions cannot be assumed or demonstrated, Equation 2 can be adjusted to estimate equilibrium concentrations using performance reference compounds similar in physicochemical behavior to the target contaminants [17,22]. Performance reference compounds are introduced to the passive sampler before deployment in the environment and partition into the aqueous phase at a rate comparable to the partitioning of the target contaminants into the polymer. In principle, with these techniques, only the C_{free} contaminants partition into the passive sampler. Therefore, uptake of contaminants into the passive sampler reflects the bioavailable concentration and can be compared with bioaccumulation by water column and sediment deployed biomonitoring organisms (e.g., blue mussels, polychaetes) and/or used to estimate hydrophobic organic contaminants C_{free} exposed to organisms using Equation 2 [12,16,23–25]. This type of exposure information is very important for understanding the direct exposure to water column organisms (e.g., fish) and serves as input information for modeling bioaccumulation and assessing risk to human and ecological health higher in the food chain (e.g., avians, wildlife). Therefore, to successfully predict exposures to water column organisms and model higher-level impacts, it is critical to ensure that measurements of C_{free} are as accurate and scientifically robust as possible.

In recent years, the use of passive sampling for measuring C_{free} at USEPA Superfund sites has been encouraged as a scientifically robust tool for assessing exposure (e.g., USEPA [26,27] and Greenberg et al. [28]), and in a limited number of cases, remedial project managers at Superfund sites have applied passive sampling (e.g., Fernandez et al. [18,19] and Schubauer-Berigan et al. [29]). To this end, the present study evaluates the application of passive samplers at 3 USEPA Superfund sites for measuring water column C_{free} of target contaminants, including PCBs, PAHs, and PBDEs. The Superfund sites investigated included New Bedford Harbor (NBH; New Bedford, MA, USA), the Naval Station Newport (NSN; Newport, RI, USA), and Palos Verdes Shelf (PVS; Los Angeles, CA, USA). Risk at each of these sites is driven by concerns over human consumption of contaminated seafood as well as adverse ecological effects of exposure to dissolved concentrations of bioavailable contaminants (i.e., C_{free}). In general, studies were designed to compare the performance of different types of passive samplers (e.g., SPME, PE, POM, SPMD) to each other and, in some cases, to biomonitoring organisms (e.g., blue mussels, *Mytilus edulis*) under field conditions. The present study also had regulatory objectives, which included establishing baseline water column C_{free} of target contaminants at the sites (e.g., NBH, NSN) and evaluating the feasibility of using passive samplers at a deep-water Superfund site (PVS). At the NBH Superfund site, water column samples were also collected and extracted using conventional techniques (i.e., grab sample with liquid–liquid extraction with organic solvents) and solid-phase extraction for comparison with passive sampling–based findings. The results are intended to encourage remedial project managers at contaminated sediment sites to use passive sampling as an additional tool for making informed environmental management decisions.

MATERIALS AND METHODS

Study designs

New Bedford Harbor Superfund site. To assess baseline water column concentrations of total PCB C_{free}, 2 deployments were performed. Passive samplers were deployed at NBH2 and NBH4, which are 2 long-term USEPA monitoring locations (Table 1; Supplemental Data, Figure S1). In each deployment, passive samplers were deployed 1 m above the sediment bed in 4 temporal intervals: day 0 to day 7, day 0 to day 14, day 0 to day 21, and day 0 to day 28 or day 29. Water samples were also collected 1 m above the sediment bed at the time of passive sampler recovery. In the first study (fall), triplicate PE attached by stainless steel wire to the mooring lines were deployed from 10 October 2007 to 7 November 2007, for a total of 28 d. For comparative purposes, bagged blue mussels (*M. edulis*), also suspended 1 m above the bottom, were exposed for 33 d at stations NBH2 and NBH4 from 19 October 2007 to 21 November 2007. In the second deployment (winter), at each station, SPMD, SPME and PE were deployed on triplicate moorings. On day 0 at each station, a total of 12 SPMD and SPME (in canisters) and wire-attached PE passive samplers were deployed on individual moorings (Supplemental Data, Figure S2A). The monitoring period extended from 19 November 2007 through 18 December 2007, for a total of 29 d. Three SPMD and SPME containing canisters and 3 PE polymer strips were recovered from the moorings on each of the 4 following time periods: 7 d, 14 d, 21 d, and 29 d after

Table 1. Superfund sites, sampling station deployment locations, water depths, and sample types: Polyethylene, solid-phase microextraction, polyoxymethylene, and semipermeable membrane devices

Superfund site	Station	Latitude (NAD 83)	Longitude (NAD 83)	Water depth (m; low tide)	Height above bottom sediment (m)	Deployment duration (d)	Sample types
New Bedford Harbor	NBH2	41.39386	–70.55047	3.4	1.0	28–29	Total water, C_{18} water, PE, SPME, SPMD, mussels
	NBH4	41.37511	–70.54513	2.6	1.0	28–29	Total water, C_{18} water, PE, SPME, SPMD, mussels
Palos Verdes Shelf	PVS1 (B1)	33.7209	–118.344683	19	1.2–1.6	145	PE
	PVS2 (B2)	33.716783	–118.347517	29	3.5–4.0	119	PE
	PVS3 (B3A)	33.709967	–118.354167	55	1.5–1.8	86	PE
	PVS4 (B3B)	33.710967	–118.3563	54	3.8–4.8	86	PE
	PVS5 (B5)	33.6942	–118.329883	65	4.4–5.2	119	PE
	PVS6 (B6A)	33.683833	–118.312717	60	1.4–1.6	120	PE
	PVS7 (B6B)	33.685583	–118.312717	57	4.7	127	PE
Naval Station Newport	NSN1	41.524124	–71.312347	4.3	1.0	21	PE, POM
	NSN2	41.527735	–71.313494	10.1	1.0	21	PE, POM
	NSN3	41.526807	–71.317836	10.7	1.0	21	PE, POM
	NSN4	41.529331	–71.318495	10.4	1.0	21	PE, POM

NAD83 = North American datum 1983; NBH = New Bedford Harbor; NSN = Naval Station Newport; PE = polyethylene; POM = polyoxymethylene; PVS = Palos Verdes Shelf; SPMD = semipermeable membrane device; SPME = solid-phase microextraction.

deployment. As in the fall deployment, water samples were also collected on a weekly basis.

Palos Verdes Shelf Superfund site. For the present study, 3-mo to 5-mo deployments were performed at 7 stations at depths ranging from 19 m to 65 m (Table 1; Supplemental Data, Figure S1), with PCBs as the target contaminant. To assess the effectiveness of passive sampling at this deep-water site, individual PE samplers were deployed, fastened using stainless steel wire to US Geological Survey acoustic Doppler current profilers resting on the sediment surface (Supplemental Data, Figure S2B). Samplers were attached 1.2 m to 5.2 m above the sediment surface, often with multiple samplers on a given profiler (Table 1).

Naval Station Newport Superfund site. At this site, 1 deployment was performed at 4 stations with PCBs, PAHs, and PBDEs as the target contaminants (Table 1; Supplemental Data, Figure S1). Two types of passive samplers, PE and POM, were deployed for 21 d in extended minnow traps (Supplemental Data, Figure S2C) to assess baseline C_{free} in the water column prior to initiation of remediation of portions of the site. All samplers were deployed 1 m above the sediment surface. Additional information about each site is provided in the Supplemental Data.

Passive sampler design, deployment, and recovery

For NBH deployments, SPMDs were composed of 91.4-cm-long, 2.5-cm-wide, flat, hollow, low-density PE ribbons (70–95 μm thick) containing 1 mL pure (99%), high–molecular weight lipid glyceryl trioleate (triolein; Sigma-Aldrich) in a thin film. Prior to deployment, a performance reference compound mixture containing chlorinated biphenyl (CB) 38 and CB50 was prepared in hexane at Battelle and shipped to Environmental Sampling Technologies. At Environmental Sampling Technologies, SPMD PE tubing was triple washed with optima grade hexane, injected with performance reference compound–loaded triolein, and heat-sealed. Triolein had been amended with the performance reference compound mixture for a final concentration of approximately 25 ng/mL triolein in each of CB38 and CB50. The SPMDs were loaded onto stainless steel deployment rigs ("spiders"); packed in airtight, precleaned aluminum containers; and shipped to Battelle. Packages containing the SPMD deployment spiders were stored at –4 °C until the day of deployment. Spiders consisted of a stainless steel plate equipped with a central hole and several Teflon or stainless steel posts. Canisters were deployed in triplicate per deployment period and were constructed from stainless steel–containing ports for ample movement and circulation of the water column through the device.

For NBH deployments, disposable SPMEs consisted of 2.5-cm-long pieces of optical fiber with a 210-μm silica core and a 10-μm PDMS coating (equivalent to 0.000173 mL PDMS; Fiberguide). Prior to deployment, fibers and protective stainless steel pouches (3 cm × 4 cm) were soaked in analytical-grade methanol for at least 10 min, dried at ambient temperatures, and wrapped in aluminum foil. Samplers were then placed in storage containers (e.g., solvent-rinsed glass jars) and shipped to the site. Each SPME replicate consisted of 15 or 30 fibers (total of 0.0026 mL or 0.0052 mL PDMS) per pouch affixed to the top of the SPMD spider inside a canister using stainless steel wire and nylon zip ties. There were 3 replicate SPMEs deployed at each station per deployment period. On recovery, SPMD canisters and SPME pouches were kept on ice, returned to the laboratory, and stored at –4 °C until extraction and chemical analysis.

All PE and POM samplers were precleaned by soaking in acetone or hexane for 24 h and then in dichloromethane for 24 h. For NBH deployments, PEs were prepared from 51-μm-thick, 30.5-cm-long, and 7.62-cm-wide PE film (1.19 mL PE; Carlisle Plastics). Polyethylene was deployed in triplicate approximately 1 m above the sediment surface for each exposure interval using an anchor and flotation buoys. Prior to deployment, these PEs were amended with performance reference compounds in 80:20 methanol and deionized water solution including 2,5-dibromobiphenyl, 2,2′,5,5′-tetrabromobiphenyl, and 2,2′,4,5,6-pentabromobiphenyl at approximately 21 ng/mL, 14 ng/mL, and 9.0 ng/mL PE, respectively, using methods described by Booij et al. [22]. In addition, for a subset of NBH deployments, 2 thicknesses (i.e., 25 μm and 51 μm, 0.58 mL vs 1.19 mL PE) of PE were evaluated for assessing equilibrium. For the PVS deployments, 50-cm-long and 10-cm-wide PE strips (51 μm thick, 2.55 mL; Carlisle Plastics) were fastened using stainless steel wire to the US Geological Survey acoustic Doppler current profilers. Prior to the deployments, as with the NBH deployments, the same 3 dibromophenyls and concentrations were used as performance reference compounds. For NSN deployments, low-density PE (25 μm thickness; Covalence Plastics) and POM (75 μm; CS Hyde) were prepared in 15 cm × 40 cm (1.5 mL PE) and 6 cm × 40 cm (1.8 mL POM) films, respectively. Prior to deployments, PE and POM were amended with stable carbon performance reference compounds including ^{13}C-CB28, ^{13}C-CB52, and ^{13}C-CB138 in 80:20 methanol:water solutions for at least 21 d on an orbital shaker using the methods described in Perron et al. [20]. Films of PE and POM were attached to stainless steel wire (diameter = 0.081 cm; Malin) fastened inside galvanized extended minnow traps (diameter = 22 cm, length = 76.2 cm; Tackle Factory). Inside each trap, 3 strips of PE and POM were arranged to maximize their surface area. Samplers were deployed using an anchor and flotation buoys on a shore-fastened mooring line. On recovery, all PE and POM films were immediately wrapped in precleaned metallic foil or placed in precleaned glass jars, stored on ice or ice packs, and transferred to the laboratory for storage at –4 °C in the dark until extraction and analysis.

Water sample collections

At the NBH stations, discrete water samples (1 L) were collected in triplicate on a weekly basis, following the retrieval or deployment of passive samplers during the fall and winter deployments. Because of logistic issues, samples were not collected on day 14 (3 December 2007) in the winter deployment. Water samples were collected using a 12-volt Teflon diaphragm pump and a length of tygon tubing to reach the sampling depth (1 m above the bottom) of the passive sampling devices and stored in clean glass containers. Following sample collection, the pump and tubing were purged twice with deionized water and 1 rinsate blank was collected. Samples were placed on ice for transport to the laboratory. Once at the laboratory, water samples were filtered through solvent-rinsed glass fiber filters (1 μm effective pore size) within 24 h of collection. As described in the Supplemental Data, water samples were analyzed and reported in 2 ways: as "total" (i.e., dissolved and colloidal) and "C_{18}-based." The C_{18}-based technique is an alternative approach for measuring C_{free}. For discussion, these 2 measurements of PCB concentrations will be referred to jointly as "aqueous" PCB measurements. Prior to extraction and chemical analysis, the samples were stored at 4 °C.

Mussel deployments

For the fall NBH deployment, blue mussels (*M. edulis*) collected from clean sites in coastal Sandwich (MA, USA) were selected by size (~5–7 cm) and placed in mesh plastic bags (~25 mussels/bag). Deployments consisted of 3 to 4 replicate bags exposed at each station positioned 1 m above the bottom. After the 33-d exposure, mussels were recovered, returned to the laboratory in coolers on ice, frozen at –4 °C, and stored in the dark until chemical analysis.

Chemical analyses

Passive samplers, tissues, and water samples were analyzed using gas chromatography/mass spectroscopy for selected PCBs, PAHs, and PBDEs. *Total PCBs* was defined as the sum of measured PCB congeners at each Superfund site: total PCB values at NBH, PVS, and NSN were the sums of 18, 29, and 26 congeners, respectively (Supplemental Data). Water samples from the NBH deployments were also analyzed for dissolved organic carbon (DOC). Preparation, extraction, and instrumental analysis are described in the Supplemental Data.

Calculation of passive sampler–based dissolved concentrations (C_{free})

When assuming equilibrium conditions, C_{free} was calculated using Equation 2. For nonequilibrium conditions, C_{free} values based on PE and POM deployments were calculated using the performance reference compound with the equation

$$C_{free} = \frac{C_{ps}}{(1 - e^{-K_e t})\, K_{ps-free}} \quad (3)$$

where k_e is the performance reference compound transfer coefficient (1/d) and t (days) is the duration of the deployment

$$k_e = \frac{\ln \frac{C_{PRC_i}}{C_{PRC_f}}}{t} \quad (4)$$

and C_{PRCi} and C_{PRCf} are the initial and final concentrations (nanograms per gram) in the polymer, respectively, of the performance reference compounds during the deployment. Performance reference compound percentage equilibration (i.e., $k_e \times 100$) values were regressed against performance reference compound octanol–water partition coefficient (K_{OW}) values to develop correlative relationships for estimating percentage equilibration values for target contaminants. If target contaminant percentage equilibration values were <10%, C_{free} values were not calculated because of insufficient evidence of equilibration of those compounds between the polymer and environmental phases. Sources of partition coefficients for each type of polymer used in the present study are provided in the Supplemental Data.

For calculating C_{free} based on mussel bioaccumulation of PCBs, the lipid–water partition coefficient ($K_{lipid\text{-}free}$) was derived for each PCB congener using the log $K_{lipid\text{-}free}$ to log K_{OW} linear free energy relationship reported by Schwarzenbach et al. [30] (log $K_{lipid\text{-}free} = 0.91 \times \log K_{OW} + 0.5$). The C_{free} based on mussel lipid concentrations was calculated based on Equation 5

$$C_{free} = \frac{C_{lipid}}{K_{lipid-free}} \quad (5)$$

where C_{lipid} is the lipid-normalized PCB concentration measured in the mussel tissues [5].

Statistical analyses

Unless otherwise noted, the mean and 1 standard deviation of 3 replicates are reported for passive sampler, water sample, DOC, and mussel data. Statistical comparisons were performed using analysis of variance followed by protected least significant difference multiple comparison tests (SAS Institute) if more than 2 treatments were being analyzed. Differences between treatments were considered statistically significant using an alpha set at ≤ 0.05.

RESULTS AND DISCUSSION

Comparison of C_{free} measurements

New Bedford Harbor. During the fall deployments, total PCB C_{free} ranged from 25 ng/L to 360 ng/L for NBH4 and NBH2, respectively, based on PE measurements (Figure 1). Aqueous measurements of total PCB concentrations, based on the total water extractions and C_{18}-based measurements, ranged from 21 ng/L to 120 ng/L at the same stations, with total water extractions and C_{18}-based measurements found to be similar (i.e., 5–18%). Further, PE-based C_{free} values at NBH4 were relatively similar to the aqueous measurements—that is, within 20%—whereas PE C_{free} values were 3 times larger than aqueous concentrations at NBH2. Finally, mussel-based estimates of C_{free}, based on Equation 5, at NBH2 were also fairly similar to PE-based C_{free}, 400 ng/L versus 360 ng/L, whereas at station NBH4 mussel-based C_{free}, 58 ng/L, was approximately 2 times greater than PE-based C_{free} (25 ng/L). At NBH2, statistical analysis found that mussel and PE C_{free} values were not significantly different; similarly, water- and C_{18}-based C_{free} values were also not significantly different from each other. However, mussel C_{free} was significantly greater than C_{free} from the other 3 treatments at NBH4. A more detailed comparison of mussel bioaccumulation and PE accumulation of PCBs will be discussed in *Comparing passive sampler uptake and mussel bioaccumulation*.

In the winter deployments, passive sampler–based total PCB C_{free} values ranged from 76 ng/L to 170 ng/L and from 7.7 ng/L to 31 ng/L at stations NBH2 and NBH4, respectively (Figure 1). For comparison, aqueous measurements of total PCBs ranged from 53 ng/L to 97 ng/L and from 16 ng/L to 30 ng/L at NBH2 and NBH4, respectively. Within the passive sampler–based measurements of C_{free}, PE generated the largest C_{free} values compared with SPME and SPMD. For example, at NBH2, PE-based C_{free} was 170 ng/L, whereas SPME and SPMD C_{free} values were 110 ng/L and 76 ng/L, respectively. At NBH4, PE-based C_{free} values were 31 ng/L and SPME and SPMD C_{free} values were 18 ng/L and 7.7 ng/L, respectively. Statistical analysis of the winter deployment data was more complicated to interpret than the fall deployment. At NBH2, C_{free} for PE was significantly different from all other treatments, whereas C_{free} values based on SPME and total water were not different, total water and SPMD C_{free} values were also not different; and, finally, SPMD and C_{18}-based C_{free} values were not different. The NBH4 C_{free} values were not different for PE and total water, SPME and C_{18}-based, and SPMD and C_{18}-based.

Despite the range of C_{free} values, all of the passive sampler–based concentrations were generally within approximately a factor of 2 to 3 of each other, suggesting they were "experiencing" (i.e., exposed to) and measuring similar truly

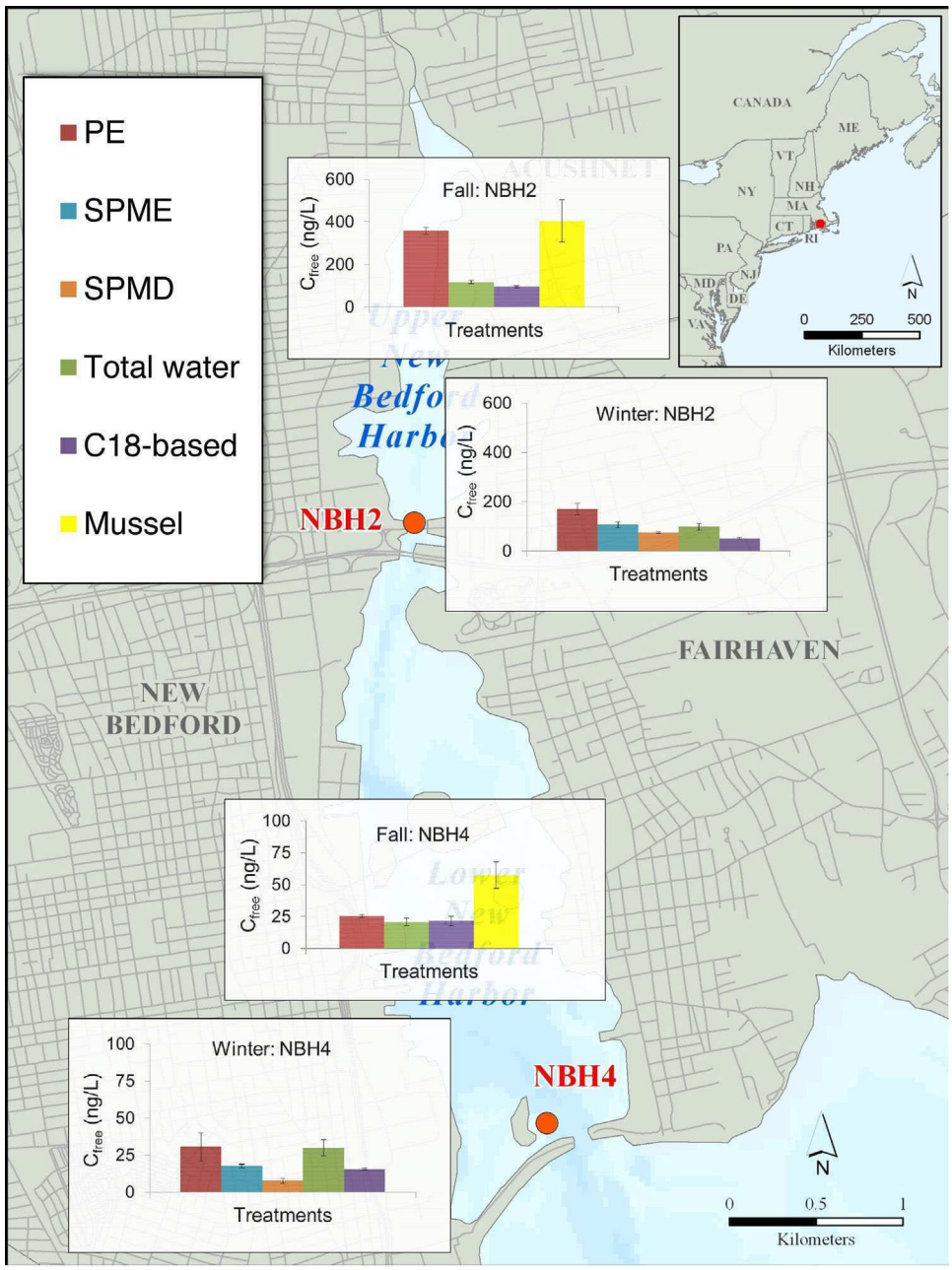

Figure 1. Total polychlorinated biphenyl (PCB) freely dissolved concentrations (C_{fre}) measured in the water column of the New Bedford Harbor Superfund site (NBH; New Bedford, MA, USA) during the fall and winter deployments of polyethylene (PE), solid-phase microextraction (SPME), semipermeable membrane devices (SPMD), the collection of total and C_{18}-based grab water samples, and mussels. Total PCB is equivalent to the sum of measured PCB congeners.

dissolved concentrations of PCBs in the ambient water column of the 2 stations in New Bedford Harbor during their respective deployments. This finding is encouraging and suggests that the samplers will provide comparable C_{free} data for PCBs even though they are deployed and analyzed in different ways using various designs and gear, partition coefficients, and assumptions regarding equilibrium status. For example, as discussed above, for SPME, equilibrium was assumed for the winter deployment, whereas the PE data were adjusted for nonequilibrium conditions based on the performance reference compound concentrations using Equation 3. With the exception of CB206 and CB209, which had <10% equilibrium and for which C_{free} values are not reported, the degree of PE nonequilibration by congener ranged from 20% to 96%, resulting in a relatively minor difference in the unadjusted and equilibrium-adjusted C_{free} for total PCBs after the 29-d winter deployment (i.e., adjusting for nonequilibrium conditions based on the performance reference compounds increased total PCB C_{free} by only 4–8%).

In general, SPMD data would also be adjusted for nonequilibrium conditions based on performance reference compound recovery. As discussed, the performance reference compounds selected for the SPMD in the winter deployment were CB38 and CB50, 2 congeners not usually found in the commercial Aroclor mixtures known to contaminate NBH. Unfortunately, following deployments, analysis of the SPMD extracts detected concentrations of both congeners at levels close to (NBH4) or exceeding (NBH2) their original amendment concentrations. These results indicate that both CB38 and CB50 were present unexpectedly in the NBH water column or

matrix interference with similar molecular weights was present. In either case, the performance reference compound data were not viable, and equilibrium of the SPMD data was assumed for calculation of C_{free}. This demonstrates a weakness in using non-Aroclor PCB congeners as performance reference compounds for target PCBs, especially at very contaminated sites, such as Superfund sites, where there may be unexpected sources of rare congeners. For PE, which used brominated biphenyls as performance reference compounds, there was no evidence of a background presence of these compounds in the NBH water column.

As noted in the *Introduction*, the value of conventionally collected total PCB water concentrations is debatable because of the artifacts that can plague such samples. However, they do serve as a potentially useful point of comparison with passive sampler–inferred C_{free}. Similarities in water concentrations of total PCBs, based on total water extraction or C_{18} solid-phase extraction, and passive sampler C_{free} varied by station and deployment. For example, in the fall deployment at NBH4, PE C_{free} and aqueous measurements were similar, ranging from 21 ng/L to 25 ng/L (Figure 1). Similarly, in the winter deployment at NBH4, PE C_{free} values were fairly comparable to water concentrations, with passive sampler C_{free} values ranging from 7.7 ng/L to 31 ng/L and aqueous concentrations ranging from 16 ng/L to 30 ng/L (Figure 1). In contrast, at NBH2 in the winter deployment, passive sampler C_{free} values ranged more widely, 76 ng/L to 170 ng/L, whereas aqueous concentrations were 53 ng/L to 97 ng/L. As discussed, the SPMD data was not adjusted for nonequilibrium and may represent underestimations of C_{free} (76 ng/L), resulting in the coincidental similarity to the lower trending water concentrations.

Palos Verdes Shelf. Total PCB C_{free} across this site ranged from 45 pg/L to 430 pg/L (Figure 2). Stations closer to shore (PVS1 and PVS2) had the lowest total PCB C_{free} (45–86 pg/L) at the site. Stations PVS3, PVS4, and PVS5, all in the vicinity of the Los Angeles County Sanitation District outfalls, demonstrated the highest C_{free}, with values ranging from 220 pg/L to 430 pg/L. In addition to the general distribution of C_{free} in the water column, the data in Figure 2 indicate, as expected, that PCBs are originating from the sediments of the site and diffusing from the interstitial water into the water column over time. For example, at all stations where PE samplers were deployed at multiple depths on the current profilers, except PVS6, total PCB C_{free} values were observed to increase when approaching the sediment. A second observation is the spatial distribution of total PCB C_{free}. The dominant oceanic current along this section of the Pacific Ocean coastline is the California Current, which follows the California coast 200 km to 300 km offshore with a depth of 300 m moving in a southeastern direction [31]. However, in the area of the California coast where the PVS Superfund site is located (i.e., the Southern California Bight), the Southern California Countercurrent forms the Southern California Eddy, which deflects water in a direction counter to the California Current, that is, in a northwestern direction [32]. As a consequence, the concentrations of water column PCBs and other contaminants associated with sedimentary sources at the site increase in a northwestern direction from the Los Angeles County Sanitation District outfalls. For example, the C_{free} at stations PVS3 and PVS4 reflect these higher values (250–430 pg/L), whereas stations PVS6 and PVS7 (directly to the southeast of the outfalls) show lower C_{free} values (90–180 pg/L). Using passive sampling, Fernandez et al. [18] observed similar depth and spatial distribution trends for dichlorodiphenyltrichloroethane (DDT) and PCBs in the water column at the PVS site.

A principal goal of the present study was to evaluate the deployment of passive samplers in deep water without using elaborate deployment gear. As can be seen in Supplemental Data, Figure S2B, for this deployment, PE samplers were simply attached to the current profilers with stainless steel wire. Of the 21 samplers deployed, all were recovered successfully (although 3 were lost or compromised after recovery), demonstrating the versatility and robustness of the PE and simple deployment system. In another study examining water column concentrations using PE and SPME passive samplers deployed at 11 stations at the PVS Superfund site, Fernandez et al. [18] lost several samplers in the middle and upper water column where the current is the strongest. The losses were attributed to fatigue of the aluminum wire used to secure the samplers to the deployment gear. In the same study, the SPME attached to the gear by stainless steel hose clamps were successfully recovered [18], as were the SPME samplers Zeng et al. [33] deployed, also using stainless steel hose clamps, in another study in the Southern California Bight.

Naval Station Newport. Baseline C_{free} was determined for 3 categories of target contaminants of regulatory concern, including high–molecular weight PAHs, benzo[*a*]pyrene (BaP), and total PCBs (Figure 3). In addition, total PAHs and total PBDEs were investigated (Supplemental Data, Figure S3). The C_{free} of high–molecular weight PAHs ranged from 8.9 ng/L to 16 ng/L and 3.2 ng/L to 6.0 ng/L based on PE and POM, respectively, demonstrating an approximate factor of 2 difference in C_{free} between polymers. Using PE, BaP, a component of the high–molecular weight PAHs, C_{free} values ranged from 100 pg/L to 780 pg/L compared with POM-based C_{free} values, which ranged from 100 pg/L to 220 pg/L. The BaP C_{free} values showed at most a factor of 3 difference between polymers (e.g., NSN2). Total PCB C_{free} values ranged from 110 pg/L to 170 pg/L based on PE, whereas C_{free} values using POM were much lower, ranging across the site from 5.8 pg/L to 11 pg/L. Total PCB C_{free} values were the lowest at this Superfund site compared with the other 2 Superfund sites in the present study. Total PAH and PBDEs C_{free} values ranged from 25 ng/L to 48 ng/L and 130 pg/L to 230 pg/L, respectively, for the PE-based measures. These values are very similar to the POM-based measures of C_{free} across the site: 16 ng/L to 40 ng/L for total PAHs and 160 pg/L to 170 pg/L for total PBDEs (Supplemental Data, Figure S3). Differences in total PCB C_{free} between the PE- and POM-based estimates are the largest we found across this entire investigation. Analysis of POM for PCB congeners found much lower accumulation than in the PE: POM C_{free} were, on average, only 6% of PE C_{free}. In addition, POM accumulated a smaller diversity of PAH molecules compared with PE. Furthermore, performance reference compound data for the POM were problematic when used for adjusting any of the target contaminants for nonequilibrium conditions. Consequently, for POM, C_{free} was calculated using Equation 2, which assumes the target contaminants have attained equilibrium with the polymer. In this case, it is uncertain if that assumption is accurate. It is unclear what caused the problems when working with POM and performance reference compounds in the present study, but the loss of performance reference compounds from the polymer was not found to be linearly correlated with contaminant molecular weight or K_{OW}. In a previous deployment, Perron et al. [20] also reported difficulties working with performance reference compounds and POM when trying to calculate C_{free} for PCBs. Arp et al. [34] recently reported that,

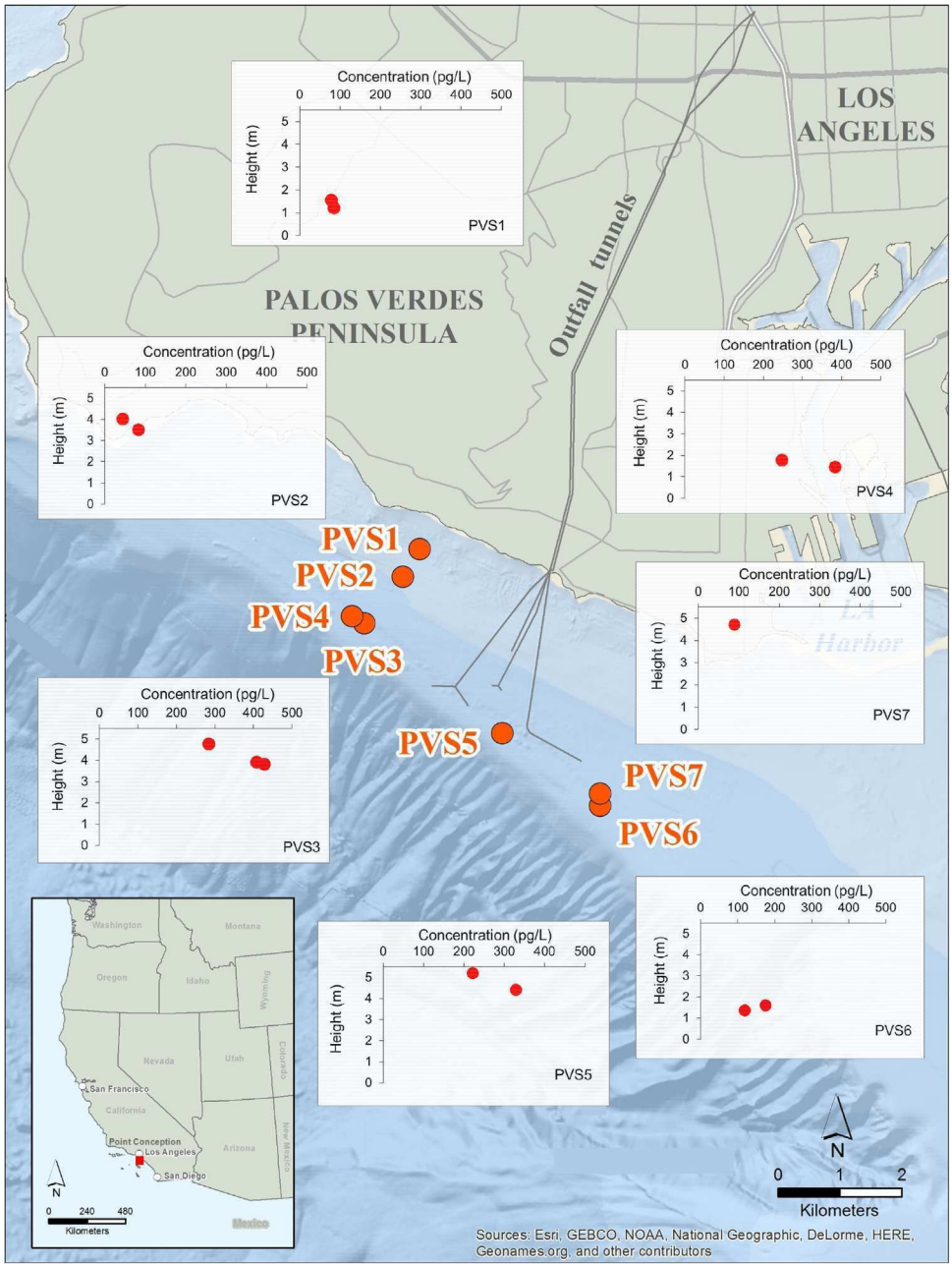

Figure 2. Total polychlorinated biphenyl (PCB) freely dissolved concentrations (C_{free}) measured in the water column of the Palos Verdes Shelf Superfund site (PVS; CA, USA) during polyethylene deployments. Total PCB is equivalent to the sum of measured PCB congeners. Height, on the *y* axis, refers to the distance above sediment surface where the sampler was deployed.

among other variables, incomplete extraction may result in underestimation of target contaminant concentrations in POM. This observation may explain our results for POM and PCBs. In general, as shown in NBH, C_{free} values based on different samplers were relatively similar, lending weight to the conclusion that the samplers experienced and measured similar C_{free} in the water column. Supplemental Data, Table S1 shows the results of statistical analyses comparing C_{free} by passive sampler type and station. Specific trends from the analysis include that total PCB C_{free} values, as well as high–molecular weight PAH C_{free} values, based on PE and POM were always statistically different. Further, PE- and POM-based total PAH C_{free} values were never significantly different. Between these extremes, significant differences in PE and POM C_{free} values occurred at 50% of the stations for BaP and total PBDEs.

Passive sampler equilibrium at the New Bedford Harbor Superfund site

Deployments performed at the NBH Superfund site offer a unique opportunity to assess passive sampler equilibrium status. This is because several different types of samplers were deployed over multiple time periods. As discussed in *Comparison of C_{free} measurements*, *New Bedford Harbor*, equilibrium was assumed for SPMDs and SPMEs, whereas for PE performance reference compounds were used to adjust C_{free} for nonequilibrium conditions. It should be noted that for the SPMDs, because of the polymer thickness on 2 sides (i.e., tube

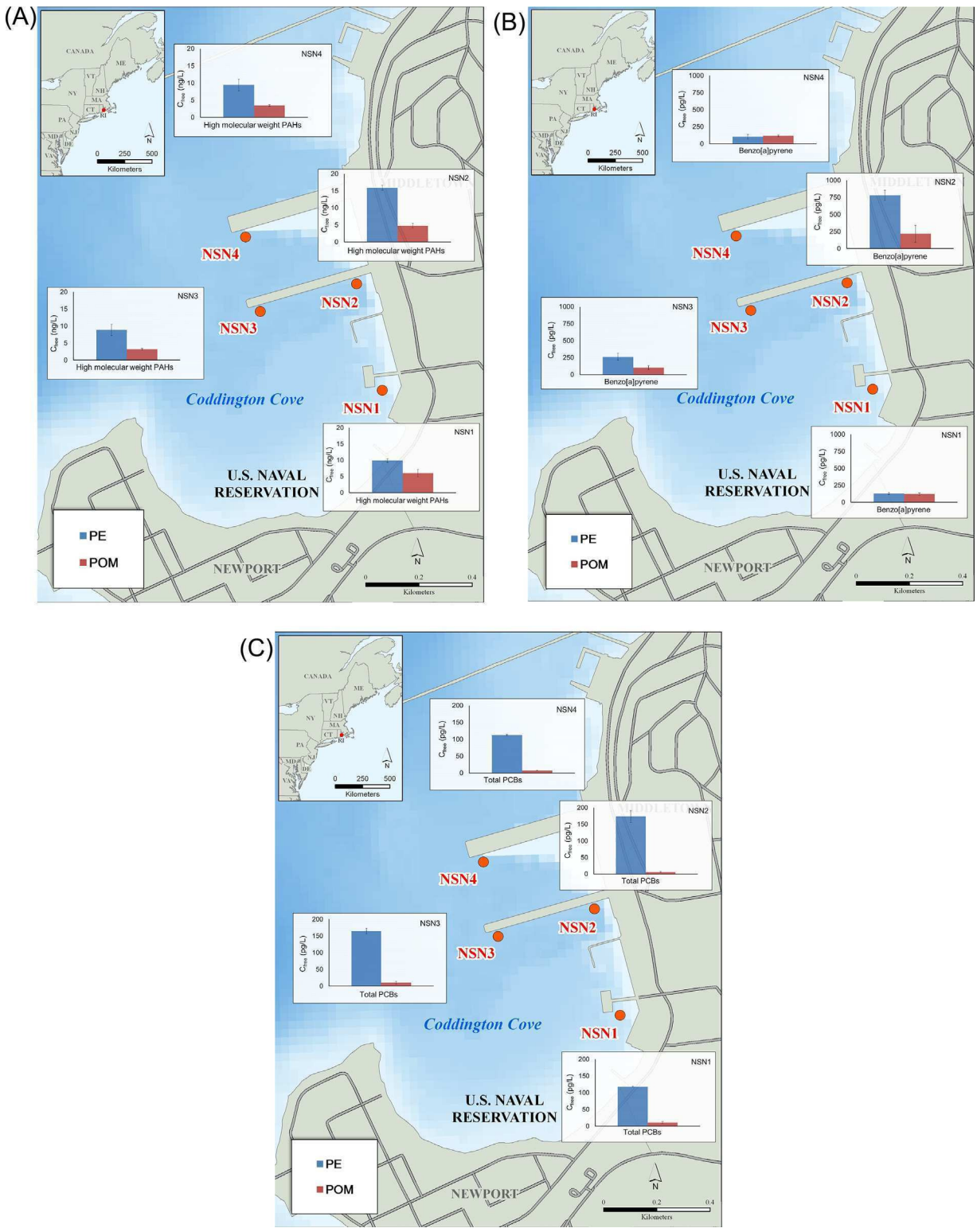

Figure 3. High–molecular weight polycyclic aromatic hydrocarbon (PAH; **A**), benzo[*a*]pyrene (**B**), and total polychlorinated biphenyl (PCB; **C**) freely dissolved concentrations (C_{free}) measured in the water column of the Naval Station Newport Superfund site (NSN; Newport, RI, USA) during the polyethylene (PE) and polyoxymethylene (POM) deployments. High–molecular weight PAH was equivalent to the sum of pyrene, fluoranthene, chrysene, benzo[*a*]pyrene, benz[*a*]anthracene, and dibenz[*a,h*]anthracene. Total PCB is equivalent to the sum of measured PCB congeners. Concentrations of benzo[*a*]pyrene and total PCBs are in picograms per liter and high–molecular weight PAH concentrations are in nanograms per liter.

configuration), this assumption is suspect and the reported concentrations may represent underestimates. Beyond assuming equilibrium or using performance reference compounds, other empirical approaches for assessing the equilibrium status of the passive sampler can be used. One is to perform a temporal series analysis, collecting passive samplers over time to assess when target contaminant concentrations no longer show statistically significant changes in the passive sampler polymer. As discussed, a time series analysis was performed with PE, SPME, and SPMD in the winter deployments at NBH. Figure 4

shows the concentrations of total PCBs over the 29-d deployment at 7-d intervals for each sampler. In general, all 3 samplers showed similar trajectories for total PCB uptake. For example, by day 29, concentrations of total PCBs ranged from 29 000 ng/mL to 39 000 ng/mL polymer and 3200 ng/mL to 7500 ng/mL polymer at stations NBH2 and NBH4, respectively.

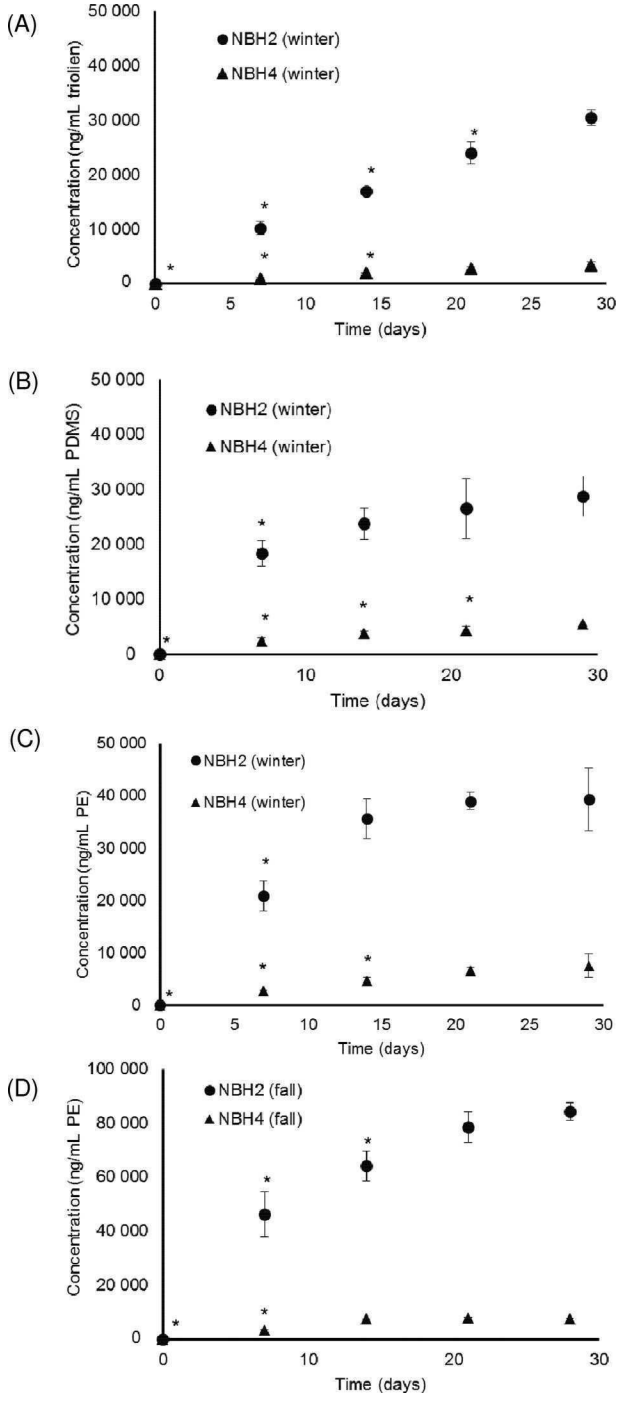

Figure 4. Total polychlorinated biphenyls (PCBs) accumulated by (**A**) semipermeable membrane device, (**B**) solid-phase microextraction, and (**C**) polyethylene during the winter deployment, and (**D**) polyethylene during the fall deployment over multiple sampling periods at the New Bedford Harbor Superfund site (NBH). *Statistically significant differences ($\alpha = 0.05$) between sampler concentrations for the last deployment period (day 28 or day 29) and previous deployment periods. Total PCB is equivalent to the sum of measured PCB congeners. PDMS = polydimethylsiloxane; PE = polyethylene.

Statistical analysis indicated that the SPMD samplers were continuing to accumulate PCBs at NBH2 after 21 d but had achieved equilibrium after day 21 at NBH4 (i.e., no statistically significant difference between polymer and triolein concentrations on day 21 and day 29; Figure 4A). In contrast, after 14 d at NBH2, the SPME samplers were at equilibrium, whereas at NBH4 day 21 and day 29 were significantly different and equilibration had not been achieved (Figure 4B). Finally, analysis of the winter PE samplers suggests equilibrium was achieved after 14 d and 21 d at NBH2 and NBH4, respectively (Figure 4C). This finding agrees with the relatively small performance reference compound–based correction (<10%) applied to the winter PE to adjust for nonequilibrium conditions discussed above in in *Comparison of C_{free} measurements*, *New Bedford Harbor*. A similar analysis is provided in the Supplemental Data section for selected PCB congeners (Supplemental Data, Figures S4 and S5).

For a seasonal comparison, Figure 4D shows the accumulation of total PCBs by the PE in the fall deployment, indicating equilibrium by day 21 and day 14 at NBH2 and NBH4, respectively. At NBH4, the final deployment period (day 28) was similar to the final concentration in the winter deployment (day 29): 7700 ng/mL PE versus 7500 ng/mL PE. However, at NBH2 and unlike NBH4, concentrations of total PCBs were much higher in the fall relative to the winter deployment: 84 000 ng/mL PE versus 39 000 ng/mL PE. Interestingly, the total water and C_{18}-based measures of total PCBs indicated that during the fall deployment NBH2 and NBH4 concentrations were often also elevated compared with the winter deployment (Figure 5A and B).

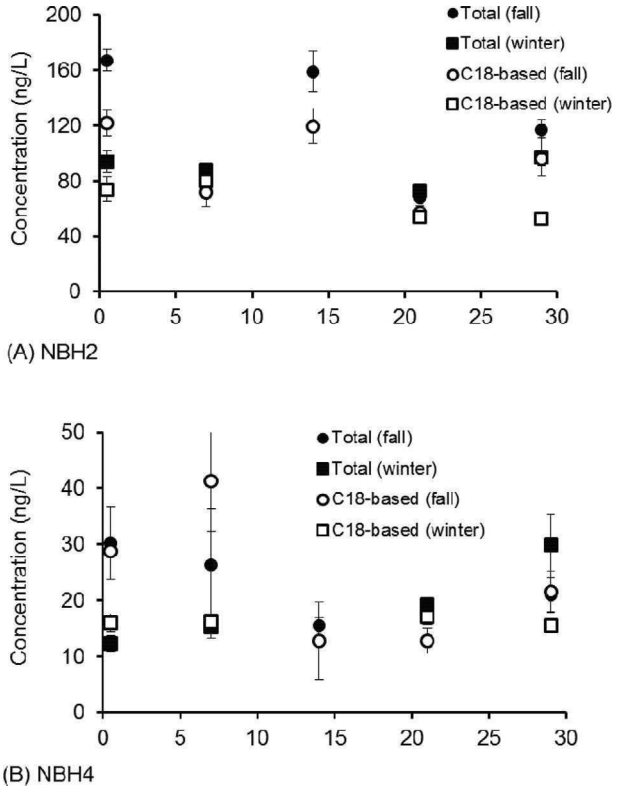

Figure 5. Total polychlorinated biphenyls (PCB) based on total water and C_{18}-based measurements during fall and winter sampling periods at stations (**A**) NBH2 and (**B**) NBH4 of the New Bedford Harbor Superfund site (NBH). Total PCB is equivalent to the sum of measured PCB congeners.

One other approach for assessing equilibrium status is to measure the concentration of target contaminants in polymers of different thicknesses. The premise for this approach is that as target contaminants accumulate, they will partition homogeneously within the polymer. Therefore, when expressed on a mass or volume basis, for 2 different polymer thicknesses, equal concentrations would indicate equilibrium. This type of analysis was performed with 2 PE thicknesses (i.e., 25 μm and 51 μm) in both fall and winter deployments at NBH2 and NBH4. At both stations, after 29 d in the winter, there were no statistical differences between thicknesses, suggesting the PE was at equilibrium (Figure 6A and B). Conversely, at both NBH2 and NBH4, after 28 d in the fall, the 2 thicknesses were statistically different, suggesting equilibrium had not yet been achieved (Figure 6A and B). As noted previously, relatively higher total water concentrations of PCBs in the fall deployment were observed during some of the collections (Figure 5).

Comparing passive sampler uptake and mussel bioaccumulation

Thus far, the focus of the present study has been on examining contaminant C_{free} (i.e., PCBs, PAHs, PBDEs) in the water column at 3 Superfund sites and assessing equilibrium based on the concentration of PCBs in the polymer at the NBH Superfund site. However, another very valuable type of information that passive samplers can provide is an estimate of concentrations of target contaminants that organisms are likely to bioaccumulate. Currently, biomonitoring organisms, such as marine polychaetes and mussels and freshwater and marine fish, are used to determine the amount of bioavailable contaminants in the water column and interstitial waters of Superfund sites [35]. This information has been used for several purposes, including assessing the effectiveness of remediation and the performance of long-term monitoring [35,36]. However, there are limitations to using organisms for measuring bioavailable concentrations. These include field conditions (e.g., high or low water temperatures, low dissolved oxygen, ice formation) adversely affecting biomonitoring organisms, seasonal unavailability of biomonitoring organisms, and logistical challenges and financial costs associated with deploying living organisms [37]. The concept of using passive samplers as surrogates for biomonitoring organisms when such limitations are an issue has a great deal of appeal. Scientific data comparing biomonitoring organisms and passive samplers continue to be collected to evaluate this approach [12,16,23–25,38]. In the present study, mussels were deployed during the fall passive sampler deployment at NBH and provide an opportunity to compare mussel bioaccumulation with passive sampler accumulation of PCBs at 2 stations.

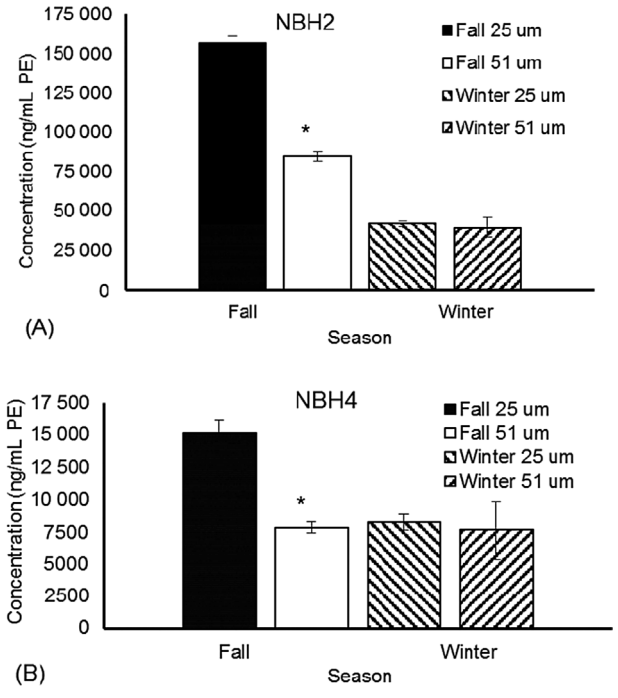

Figure 6. Total polychlorinated biphenyls (PCB) in polyethylene passive samplers of different thicknesses (e.g., 25 μm and 51 μm) at (**A**) NBH2 and (**B**) NBH4 in the fall and winter deployments. *Significant statistical differences ($\alpha = 0.05$) between thicknesses at a given station and season. Total PCB is equivalent to the sum of measured PCB congeners. NBH = New Bedford Harbor; PE = polyethylene.

Mean concentrations of total PCBs in deployed mussels at NBH2 and NBH4 were 350 000 ng/g lipid and 64 000 ng/g lipid, respectively. By comparison, total PCB PE concentrations adjusted for nonequilibrium conditions were 110 000 ng/g PE and 9300 ng/g PE for samplers at NBH2 and NBH4, respectively. This difference results in a mussel bioaccumulation to PE accumulation ratio of 3.2 and 6.9 for NBH2 and NBH4, respectively. In their study at NBH, Hofelt and Shea [38] reported total PCB ratios for mussel bioaccumulation to SPMD accumulation ranging from approximately 1.2 to 4.8. Based on Equation 5, these tissue concentrations, expressed on a mussel lipid basis, are equivalent to mussel-based C_{free} of 404 000 pg/L and 58 000 pg/L at NBH2 and NBH4, respectively. These values compare relatively well to PE-based C_{free} of 360 000 pg/L and 25 000 pg/L at NBH2 and NBH4, respectively. However, to more directly compare mussel bioaccumulation to passive sampler accumulation, Figure 7 shows mussel and PE concentrations of individual PCB congeners at NBH2 and NBH4. There were 27 congeners that had matching accumulation data for both mussels and PE. If mussels and PE accumulated PCB molecules identically, the data points in Figure 7 would fall on the 1:1 line. Instead, a mean offset of approximately 8.6 is observed, indicating that, in general, the mussels accumulated PCBs approximately 9 times more than the PE. In addition, the offset suggests a concentration dependency on the amount of PCB congeners in the overlying water. In other words, at NBH4, where C_{free} is relatively low (Figure 1), the offset ranges from a factor of 2.9 to 22; and at NBH2, where C_{free} is relatively high (Figure 1), the offset range is a factor of 1.5 to 15. Despite the offset, summary statistics demonstrate a strong correlative log-linear relationship between mussel bioaccumulation and PE accumulation:

$$\begin{aligned}&\text{Log PBC bioaccumulation (ng/g lipid)}\\&\quad = 0.74 \times \log \text{PBC accumulation (ng/g PE)} + 1.62 (r^2\\&\quad = 0.92, n = 27, p < 0.05)\end{aligned} \quad (6)$$

Further, the log-linear correlation indicates that the relationship between bioaccumulation and PE accumulation is highly significant, with p values much less than 0.05 (Figure 7). In a similar comparison of PCB passive sampler accumulation versus bioaccumulation, using the marine polychaete *Nereis virens* exposed to NBH sediment, Friedman et al. [24] also reported a strong linear relationship ($r^2 = 0.88$, $n = 48$). In addition, Gschwend et al. [16], using PCB-contaminated sediments from the Hunter's Point Naval Station in San Francisco Bay (CA, USA) exposed to the marine polychaete *Neanthes arenaceodentata*, under 2 exposure regimens (mixed

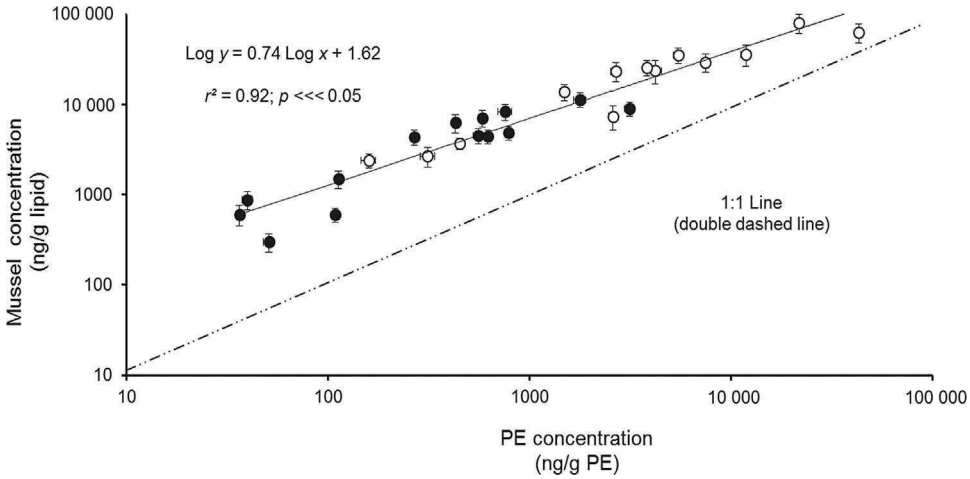

Figure 7. Concentration of polychlorinated biphenyl congeners accumulated by polyethylene (PE) passive samplers versus bioaccumulated by blue mussels (*Mytilus edulis*) during the fall deployment at the New Bedford Harbor Superfund site (NBH). Open and full circles represent stations NBH2 and NBH4, respectively. Polyethylene concentrations have been adjusted for equilibrium conditions.

and passive), reported linear relationships: $r^2 = 0.64$ ($n = 7$) and $r^2 = 0.59$ ($n = 7$), respectively. Interestingly, in the Gschwend et al. [16] comparison of polychaete bioaccumulation to passive sampler accumulation, the authors also included PDMS-coated SPME fibers and POM. In all 4 cases, they found an offset between the 1:1 line between bioaccumulation and accumulation similar in behavior (i.e., linear and favoring bioaccumulation) and scale (i.e., an order of magnitude) to that described in the present study. They attributed the offset to the preferential partitioning of PCBs to lipid compared with the polymers.

This representative selection of measures demonstrates that PE accumulation is correlated with and potentially predictive of organism bioaccumulation, which in turn suggests that PE could be considered a surrogate for biomonitoring organisms (at least at the NBH Superfund site with PCBs). In their evaluation of the relationship between SPMD accumulation and bioaccumulation from a review of 9 studies (including Hofelt and Shea [38]), Booij et al. [39] recommended using passive sampling (in this case SPMDs) for new biomonitoring programs because of the associated advantages relative to the disadvantages of using biomonitoring organisms. These advantages include the facts that $K_{\text{lipid-free}}$ values show greater variability than $K_{\text{PS-free}}$ values; that determining equilibrium status is more difficult with organisms compared with passive samplers; and that the need to use different organisms (to accommodate different habitats) limits the standardization of methods across broad geographic areas, whereas 1 type of passive sampler can be applied everywhere. For existing monitoring studies, Booij et al. [39] acknowledged that switching from biomonitoring organisms to passive samplers is problematic because of the potential loss in data consistency. However, they suggest the performance of multiple comparative studies on a site-specific basis to develop conversion factors between historic bioaccumulation and new passive sampler accumulation data. Similarly, the concept of the systematic global deployment of aquatic passive samplers for monitoring purposes has recently been proposed in the literature [40,41]. Despite the offset observed in this data set and others (e.g., Gschwend et al. [16]), there is growing evidence that passive sampler accumulation of PCBs is linearly correlated with organismal bioaccumulation, suggesting these are predictive relationships that could be useful in instances when the deployment of biomonitoring organisms is not viable.

Comparison of passive sampler–based C_{free} to other studies

Of the 3 Superfund sites investigated, NBH has been the most frequently studied using passive samplers. For example, several studies have used passive samplers to examine the distribution and bioavailability of contaminants in NBH sediments. Specifically, Vinturella et al. [23], Friedman et al. [24], and Lu et al. [25] evaluated PE and SPME as surrogates for measuring the bioaccumulation of PCBs and PAHs by a benthic polychaete (*Nereis virens*) and an oligochaete (*Ilyodrilus templetoni*). Other than the present study, only Hofelt and Shea [38] have used passive sampling to estimate the C_{free} of PCBs in the NBH water column. They performed 30-d SPMD deployments at 5 stations inside and outside of the harbor and detected several organochlorine pesticides and PCBs. Total PCB C_{free} based on SPMDs ranged from 1400 pg/L to 17 000 pg/L (Table 2). By comparison, total PCB C_{free} in the present study was approximately an order of magnitude greater: 25 000 pg/L to 359 000 pg/L based on PE, 18 000 pg/L to 107 000 pg/L based on SPME, and 8000 pg/L to 76 000 pg/L based on SPMD. Although the studies were performed approximately 10 yr apart, they analyzed the same PCB congeners to determine total PCBs. Consequently, it is not clear why such large differences in total PCB C_{free} exist between the investigations.

Three previous studies used passive sampling to investigate the C_{free} of total PCBs and DDTs at the PVS Superfund site. Zeng et al. [33] applied SPME to estimate the C_{free} of total DDTs 2 m above the sediment surface in 30-d deployments, resulting in 4900 pg/L at a station close to the present study's stations (Table 2). In 1 of 2 studies at PVS, Fernandez et al. [18] deployed PE and SPME samplers at 3 depths in the water column at 11 stations. For samplers 5 m above the sediment, C_{free} for total DDTs ranged from 260 pg/L to 1100 pg/L using SPME and 750 pg/L to 2600 pg/L for PE. The differences in the heights of the samplers above the sediments (5 m vs 2 m) may explain the lower C_{free} values in the present study compared with the Zeng et al. [33] measurements. For total PCBs at PVS, the present study found that C_{free} ranged from 45 pg/L to 430 pg/L, whereas Fernandez et al. [18] reported 90 pg/L to

Table 2. Comparison of C_{free} concentrations based on passive sampler measurements for several organic contaminants in the water column of the Superfund sites investigated in the present study[a]

			C_{free} concentration range (pg/L)					
Superfund site	Contaminant	Passive sampler	Present study	Hofelt and Shea [38][b]	Zeng et al. [33][c]	Fernandez et al. [18][d]	Perron et al. [20,21][f]	Fernandez et al. [19][g]
New Bedford Harbor	ΣPCBs (pg/L)	PE	25 300–359 000 (Fall) 35 000–171 000 (Winter)	—	—	—	—	—
		SPME	17 800–107 000	—	—	—	—	
		SPMD	7670–76 000	1400–16 900	—	—	—	
Palos Verdes Shelf	ΣPCBs (pg/L)	PE	45.1–429	—	—	90–316	—	230–460
		POM	—	—	—	—	—	130–450
		SPME	—	—	—	—[e]	—	—[e]
	ΣDDTs (pg/L)	PE	—	—	—	745–2610	—	26 000 –32 000
		POM	—	—	—	—	—	7800–16 000
		SPME	—	—	4870 ± 1510	255–1140	—	1700–4000
Naval Station Newport	ΣPCBs (pg/L)	PE	112–173	—	—	—	119	
	ΣPAHs (ng/L)	PE	25.5–40.3	—	—	—	31.5	
	ΣPBDEs (pg/L)	PE	156–234	—	—	—	39.8	—
	ΣPCBs (pg/L)	POM	5.8–10.7	—	—	—	38.2	—
	ΣPAHs (ng/L)	POM	15.8–39.9	—	—	—	91.4	—
	ΣPBDEs (pg/L)	POM	159–165	—	—	—	90.8	—

[a]Passive samplers included polyethylene, solid phase microextraction, polyoxymethylene, and semipermeable membrane devices. Available C_{free} ranges observed in other studies using passive sampling are also presented.
[b]Concentrations calculated based on data from Hofelt and Shea's [38] Table 2 for 5 stations using triolein-free partition coefficients (see Supplemental Data); stations were 1 m above the bottom for a 30-d deployment; total PCBs were the sum of 16 congeners; 25-μm-thick PE tubing.
[c]One station (6C) 2 m above the bottom for a 30-d deployment; total DDTs were the sum of 4 DDTs (*o,p′*-DDD, *p,p′*-DDD, *o,p′*-DDE, *p,p′*-DDE); PDMS was 100 μm thick.
[d]Nine stations 5 m above the bottom for a 32-d deployment; total PCBs were the sum of up to 27 congeners, and total DDTs were the sum of up to 6 compounds (*o,p′*-DDD, *p,p′*-DDD, *o,p′*-DDE, *p,p′*-DDE, *o,p′*-DDT, *p,p′*-DDT); PE and PDMS were 25 μm and 100 μm thick, respectively.
[e]Deployed but contaminant not detected.
[f]A station in Newport Harbor; samplers deployed for 21 d 1 m above the bottom; total PCBs, PAHs, and PBDEs used the same contaminants as applied in the present study; PE and POM were 25 μm and 76 μm thick, respectively.
[g]For PE and POM, deployments integrated 0–20 cm above the bottom, while SPMEs were 70 cm above the bottom. Deployments were for 43–44 d in duration at 4 stations; total PCBs were the sum of up to 15 congeners, and total DDTs were the sum of up to 7 compounds (*o,p′*-DDD, *p,p′*-DDD, *o,p′*-DDE, *p,p′*-DDE, *o,p′*-DDT, *p,p′*-DDT, *p,p′*-DDMU); PE, PDMS, and POM were 25 μm, 100 μm, and 76 μm thick, respectively.
C_{free} = freely dissolved concentration; DDD = dichlorodiphenyldichlorethane; DDE = dichlorodiphenyldichloroethylene; DDMU = 2,2-bis(chlorophenyl)-1-chloroethylene; DDT = dichlorodiphenyltrichloroethane; PAH = polycyclic aromatic hydrocarbon; PBDE = polybrominated diphenyl ether; PCB = polychlorinated biphenyl; PE = polyethylene; POM = polyoxymethylene; SPMD = semipermeable membrane device; SPME = solid-phase microextraction.

320 pg/L for PE samplers deployed 5 m above the sediment surface. In a second study, Fernandez et al. [19] measured C_{free} of 230 pg/L to 460 pg/L and 130 pg/L to 450 pg/L with PE and POM, respectively, located approximately 20 cm above the sediment surface. For total PCBs, all of these C_{free} values from the different studies are relatively similar despite the use of different types of passive samplers over a 10-yr period; for example, high C_{free} values ranged from 320 pg/L to 460 pg/L. Further, any substantial differences can be explained by the depth at which the samplers were deployed (i.e., higher in the water column resulted in lower target contaminant concentrations), indicating the sediments serve as the primary source of target contaminants at PVS. In addition, Fernandez et al. [19] found total DDT C_{free} in the water column ranging from 26 000 pg/L to 32 000 pg/L and 7800 pg/L to 16 000 pg/L using PE and POM, respectively, in samplers deployed approximately 20 cm above the sediment surface. In the same study, SPME deployed approximately 1 m above the sediments measured C_{free} of 1700 pg/L to 4000 pg/L. Finally, in both Fernandez et al. studies [18,19], SPME was deployed to monitor for total PCB C_{free}; however, unlike the total DDTs, no PCBs were detected analytically. In contrast, both PE and POM were able to detect total PCB C_{free} in the water column at PVS. This difference in the sampler's performance most likely reflects the greater mass of PE and POM that can be deployed compared with SPME. Although SPME achieves equilibrium more rapidly than POM or PE, the smaller mass of PDMS that is generally deployed is sometimes unable to accumulate sufficient target contaminant for detection by analytical instrumentation. However, other configurations of PDMS can be deployed (e.g., Maenpaa et al. [42]) and attain greater detection sensitivity than afforded by SPME.

Finally, no previous studies using passive samplers have investigated C_{free} in the water column at the NSN Superfund site. However, Perron et al. [20,21] reported C_{free} total PCBs, total PAHs, and total PBDEs of 38 pg/L to 120 pg/L, 32 ng/L to 91 ng/L, and 40 pg/L to 91 pg/L, respectively, using PE and POM passive samplers for a station in Newport Harbor approximately 5.5 km south of the Superfund site (Table 2). In general, these concentrations compare relatively well with the C_{free} reported in the present study, where total PCBs, total PAHs, and total PBDEs based on PE were 110 pg/L to 170 pg/L, 26 ng/L to 40 ng/L, and 160 pg/L to 230 pg/L, respectively, and based on POM were 5.8 pg/L to 11 pg/L, 16 ng/L to 40 ng/L, and 160 pg/L to 170 pg/L, respectively. The decades of industrial maritime activity and the resulting sediment contamination at NSN make the higher total PCB C_{free} there compared with Newport Harbor unsurprising. Further, Newport Harbor is an active commercial and recreation harbor; therefore, elevated total PAH C_{free} from boat engines and related sources is not unexpected. However, the elevated C_{free} values for total PBDEs at NSN are of interest. These chemicals are used as flame retardants in some consumer products and are undergoing scrutiny in the United States and Europe because of concerns with mammalian toxicity. The levels at NSN were up to 3 times higher than those seen in Newport Harbor (and anywhere else in Narragansett Bay [21]), suggesting there may be an unknown source in the NSN that requires further investigation.

SUMMARY

In general, the different passive samplers demonstrated good agreement in C_{free} with values varying by a factor of 2 to 3. This level of agreement was clearly demonstrated at the PVS site where C_{free} determined by different passive samplers over several years and deployments varied by less than a factor of 2. Furthermore, in most instances where conventional water samples were collected (i.e., grabs) and compared with passive sampler C_{free} values (i.e., NBH), values were also within a factor of 2 of aqueous measurements. Also, in most cases in NBH, total PCBs were approaching equilibrium in the samplers after nearly 30 d of deployment. These findings suggest that all of the samplers were experiencing and measuring the same C_{free} during their respective deployments and that the remedial project manager's selection of which passive samplers to use at a site can be based on variables such as costs, availability, and logistics rather than which passive sampler is more scientifically accurate. More importantly, passive sampling will enable the remedial project manager to determine both the spatial and the temporal trends of target contaminants, key factors for successfully remediating a contaminated site. At NBH, a strong log-linear, correlative, and predictive relationship was found between passive sampler accumulation and mussel bioaccumulation. Finally, all of the Superfund site investigations discussed here, except for the SPMD deployments, used unsophisticated deployment gear and passive samplers. This evaluation demonstrates the practical utility of passive sampling for generating scientifically accurate water column C_{free}, which is critical for making informed environmental management decisions at contaminated sediment sites.

SUPPLEMENTAL DATA

Table S1.
Figures S1–S6. (10.1 MB DOC).

Acknowledgment—Special acknowledgments go to the remedial project managers at the USEPA Superfund sites investigated: J. Brown (New Bedford Harbor, Region 1, Boston, MA); C. White, S. Lin, and J. Huang (Palos Verdes Shelf, Region 9, San Francisco, CA); and K. Keckler (Naval Station Newport, Region 1, Boston, MA). The authors also thank the following colleagues for their contributions: B.J. Bergen, D. Cobb, D. Katz, W. Nelson, and S. Jarayaraman (USEPA, Narragansett, RI); M.A. Charpentier (Raytheon, Narragansett, RI, USA); Y. Zhang and M.P. McKee (Battelle, Duxbury, MA, USA); R. Lane (University of Kansas, Lawrence, KS, USA); C.L. Friedman (Massachusetts Institute of Technology, Cambridge, MA, USA); M. Noble (US Geological Survey, Menlo Park, CA); K.J. Rosenberger (US Geological Survey, Santa Cruz, CA); C.R. Sherwood (US Geological Survey, Woods Hole, MA); and D. Ward (US Navy, Naval Education and Training Center, Newport, RI). The authors also thank the internal Atlantic Ecology Division reviewers for their insightful comments: B.J. Bergen, A.S. Joyce and J.R. Serbst.

Disclaimer—This is USEPA ORD-009261. Mention of trade names or commercial products does not constitute endorsement or recommendation for use. The present study has been reviewed by the USEPA's Office of Research and Development, National Health and Environmental Effects Research Laboratory, Atlantic Ecology Division, Narragansett, Rhode Island, and approved for publication. Approval does not signify that the contents necessarily reflect the views and policies of the agency.

Data availability—Data, associated metadata, and calculation tools are available on reasonable request from the authors (burgess.robert@epa.gov).

REFERENCES

1. National Research Council. 2001. *A Risk-Management Strategy for PCB-Contaminated Sediments*. National Academy Press, Washington, DC, USA.
2. National Research Council. 2003. *Bioavailability of Contaminants in Soils and Sediments*. National Academy Press, Washington, DC, USA.
3. Di Toro DM, Zarba CS, Hansen DJ, Berry WJ, Swartz RC, Cowan CE, Pavlou SP, Allen HE, Thomas NA, Paquin PR. 1991. Technical basis for the equilibrium partitioning method for establishing sediment quality criteria. *Environ Toxicol Chem* 11:1541–1583.

4. Burgess RM, Mount DR, Berry WJ, Di Toro DM. 2013. Mechanistic sediment quality guidelines based on contaminant bioavailability: Equilibrium partitioning sediment benchmarks. *Environ Toxicol Chem* 32:102–114.
5. Mayer P, Parkerton TF, Adams RG, Cargill JG, Gan J, Gouin T, Gschwend PM, Hawthorne SB, Helm P, Witt G, You J, Escher BI. 2014. Passive sampling methods for contaminated sediments: Scientific rationale supporting use of freely dissolved concentrations. *Integr Environ Assess Manag* 10:197–209.
6. Huckins JN, Manuweera GK, Petty JD, Mackay D, Lebo JA. 1993. Lipid-containing semipermeable membrane devices for monitoring organic contaminants in water. *Environ Sci Technol* 27:2489–2496.
7. Booij K, van Bommel R, van Aken HM, van Haren H, Brummer G-TA, Ridderinkhof H. 2014. Passive sampling of nonpolar contaminants at three deep-ocean sites. *Environ Pollut* 195:101–108.
8. Hawthorne SB, Grabanski CB, Miller DJ, Kreitinger JP. 2005. Solid-phase microextraction measurement of parent and alkyl polycyclic aromatic hydrocarbons in milliliter sediment pore water samples and determination of K_{DOC} values. *Environ Sci Technol* 39:2795–2803.
9. Maruya KA, Zeng EY, Tsukada D, Bay SM. 2009. A passive sampler based on solid-phase microextraction for quantifying hydrophobic organic contaminants in sediment pore water. *Environ Toxicol Chem* 28:733–740.
10. Witt G, Lang S-C, Ullmann D, Schaffrath G, Schulz-Bull D, Mayer P. 2013. Passive equilibrium sampler for in situ measurements of freely dissolved concentrations of hydrophobic organic chemicals in sediments. *Environ Sci Technol* 47:7830–7839.
11. Jonker MTO, Koelmans AA. 2001. Polyoxymethylene solid phase extraction as a partitioning method for hydrophobic organic chemicals in sediment and soot. *Environ Sci Technol* 35:3742–3748.
12. Oen AMP, Janssen EML, Cornelissen G, Breedveld GD, Eek E, Luthy RG. 2011. In situ measurement of PCB pore water concentration profiles in activated carbon-amended sediment using passive samplers. *Environ Sci Technol* 45:4053–4059.
13. Beckingham B, Ghosh U. 2013. Polyoxymethylene passive samplers to monitor changes in bioavailability and flux of PCBs after activated carbon amendment to sediment in the field. *Chemosphere* 91:1401–1407.
14. Lohmann R, Burgess RM, Cantwell MG, Ryba SA, MacFarlane JK, Gschwend PM. 2004. Dependency of polychlorinated biphenyl and polycyclic aromatic hydrocarbon bioaccumulation in *Mya arenaria* on both water column and sediment bed chemical activities. *Environ Toxicol Chem* 23:2551–2562.
15. Adams RG, Lohmann R, Fernandez LA, MacFarlane JK, Gschwend PM. 2007. Polyethylene devices: Passive samplers for measuring dissolved hydrophobic organic compounds in aquatic environments. *Environ Sci Technol* 41:1317–1323.
16. Gschwend PM, MacFarlane JK, Reible DD, Lu X, Hawthorne SB, Nakles DV, Thompson T. 2011. Comparison of polymeric samplers for accurately assessing PCBs in pore waters. *Environ Toxicol Chem* 30:1288–1296.
17. Fernandez LA, MacFarlane JK, Tcaciuc AP, Gschwend PM. 2009. Using performance reference compounds in polyethylene passive samplers to deduce sediment porewater concentrations for numerous target chemicals. *Environ Sci Technol* 43:8888–8894.
18. Fernandez L, Lao W, Maruya K, White C, Burgess RM. 2012. Passive sampling to measure baseline dissolved persistent organic pollutant concentrations in the water column of the Palos Verdes Shelf Superfund site. *Environ Sci Technol* 46:11937–11947.
19. Fernandez LA, Lao W, Maruya K, Burgess RM. 2014. Calculating the diffusive flux of persistent organic pollutants between sediments and the water column on the Palos Verdes Shelf Superfund site using polymeric passive samplers. *Environ Sci Technol* 48:3925–3934.
20. Perron MM, Burgess RM, Suuberg EM, Cantwell MG, Pennell KG. 2013. Performance of passive samplers for monitoring estuarine water column concentrations 1. Contaminants of concern. *Environ Toxicol Chem* 32:2182–2189.
21. Perron MM, Burgess RM, Suuberg EM, Cantwell MG, Pennell KG. 2013. Performance of passive samplers for monitoring estuarine water column concentrations 2. Emerging contaminants. *Environ Toxicol Chem* 32:2190–2196.
22. Booij K, Smedes F, van Weerlee EM. 2002. Spiking of performance reference compounds in low density polyethylene and silicone passive water samplers. *Chemosphere* 46:1157–1161.
23. Vinturella AE, Burgess RM, Coull BA, Thompson KM, Shine JP. 2004. The use of passive samplers to mimic uptake of polycyclic aromatic hydrocarbons by benthic polychaetes. *Environ Sci Technol* 38:1154–1160.
24. Friedman CL, Burgess RM, Cantwell MG, Ho KT, Lohmann R. 2009. Comparing polychaete bioaccumulation and passive sampler uptake to assess the effects of sediment resuspension on PCB bioavailability. *Environ Sci Technol* 43:2865–2870.
25. Lu X, Drake B, Skwarski A, Reible D. 2011. Predicting bioavailability of PAHs and PCBs with pore water concentrations measured by disposable solid-phase micro-extraction fibers. *Environ Toxicol Chem* 30:1109–1116.
26. US Environmental Protection Agency. 2012. Equilibrium partitioning sediment benchmarks (ESBs) for the protection of benthic organisms: Procedures for the determination of the freely dissolved interstitial water concentrations of nonionic organics. EPA 600/R-02/012. Office of Research and Development, Washington, DC.
27. US Environmental Protection Agency. 2012. Guidelines for using passive samplers to monitor organic contaminants at Superfund sediment sites. Sediment Assessment and Monitoring Sheet 3. Office of Research and Development/Office of Superfund Remediation and Technology Innovation, Washington, DC.
28. Greenberg MS, Chapman PM, Allan IJ, Anderson KA, Apitz SE, Beegan C, Bridges TS, Brown SS, Cargill JG IV, McCulloch MC, Menzie CA, Shine JP, Parkerton TF. 2014. Passive sampling methods for contaminated sediments: Risk assessment and management. *Integr Environ Assess Manag* 10:224–236.
29. Schubauer-Berigan JP, Foote EA, Magar VS. 2012. Using SPMDs to assess natural recovery of PCB-contaminated sediments in Lake Hartwell, SC: I. A field test of new in-situ deployment methods. *Soil Sediment Contam* 21:82–100.
30. Schwarzenbach RP, Gschwend PM, Imboden DM. 2003. *Environmental Organic Chemistry*. John Wiley and Sons, Hoboken, NJ, USA.
31. Lynn RJ, Simpson JJ. 1987. The California current system: The seasonal variability of its physical characteristics. *J Geophys Res* 92:12947–12966.
32. Di Lorenzo E. 2003. Seasonal dynamics of the surface circulation in the southern California current system. *Deep-Sea Res Pt II* 50:2371–2388.
33. Zeng E, Tsukada D, Diehl DW. 2004. Development of a solid-phase microextraction-based method for sampling of persistent chlorinated hydrocarbons in an urbanized coastal environment. *Environ Sci Technol* 38:5737–5743.
34. Arp HPH, Hale SE, Krusa ME, Cornelissen G, Grananski CB, Miller DJ, Hawthorne SB. 2015. Review of polyoxymethylene passive sampling methods for quantifying freely dissolved porewater concentrations of hydrophobic organic contaminants. *Environ Toxicol Chem* 34:710–720.
35. US Environmental Protection Agency. 2005. Contaminated sediment remediation guidance for hazardous waste sites. EPA 540/R-05/012. Office of Solid Waste and Emergency Response. Washington, DC.
36. Nelson WG, Bergen BJ. 2012. The New Bedford Harbor Superfund site long-term monitoring program (1993–2009). *Environ Monit Assess* 184:7531–7550.
37. Lohmann R, Booij K, Smedes F, Vrana B. 2012. Use of passive sampling devices for monitoring and compliance checking of POP concentrations in water. *Environ Sci Pollut Res* 19:1885–1895.
38. Hofelt CS, Shea D. 1997. Accumulation of organochlorine pesticides and PCBs by semipermeable membrane devices and *Mytilus edulis* in New Bedford Harbor. *Environ Sci Technol* 31:154–159.
39. Booij K, Smedes F, van Weerlee EM, Honkoop PJC. 2006. Environmental monitoring of hydrophobic organic contaminants: The case of mussels versus semipermeable membrane devices. *Environ Sci Technol* 40:3893–3900.
40. Lohmann R, Muir D. 2010. Global aquatic passive sampling (AQUA-GAPS): Using passive samplers to monitor POPs in the waters of the world. *Environ Sci Technol* 44:860–864.
41. Allan IJ, Harman C. 2011. Global aquatic passive sampling: Maximizing available resources using a novel exposure procedure. *Environ Sci Technol* 45:6233–6234.
42. Maenpaa K, Leppanen MT, Reichenberg F, Figueiredo K, Mayer P. 2011. Equilibrium sampling of persistent and bioaccumulative compounds in soil and sediment: Comparison of two approaches to determine equilibrium partitioning concentrations in lipids. *Environ Sci Technol* 45:1014–1047.

Environmental Science & Technology

Article

pubs.acs.org/est

Passive Sampling to Measure Baseline Dissolved Persistent Organic Pollutant Concentrations in the Water Column of the Palos Verdes Shelf Superfund Site

Loretta A. Fernandez,*[,†] Wenjian Lao,[‡] Keith A. Maruya,[‡] Carmen White,[§] and Robert M. Burgess[†]

[†]U.S. Environmental Protection Agency, Atlantic Ecology Division, Narragansett, Rhode Island 02882, United States

[‡]Southern California Coastal Water Research Project (SCCWRP), Costa Mesa, California 92626, United States

[§]U.S. Environmental Protection Agency, Region 9, San Francisco, California 94109, United States

Supporting Information

ABSTRACT: Passive sampling was used to deduce water concentrations of persistent organic pollutants (POPs) in the vicinity of a marine Superfund site on the Palos Verdes Shelf, California, USA. Precalibrated solid phase microextraction (SPME) fibers and polyethylene (PE) strips that were preloaded with performance reference compounds (PRCs) were codeployed for 32 d along an 11-station gradient at bottom, surface, and midwater depths. Retrieved samplers were analyzed for DDT congeners and their breakdown products (DDE, DDD, DDMU, and DDNU) and 43 PCB congeners using GC-EI- and NCI-MS. PRCs were used to calculate compound-specific fractional equilibration achieved in situ for the PE samplers, using both an exponential approach to equilibrium (EAE) and numerical integration of Fickian diffusion (NI) models. The highest observed concentrations were for *p*,*p*′-DDE, with 2200 and 990 pg/L deduced from PE and SPME, respectively. The difference in these estimates could be largely attributed to uncertainty in equilibrium partition coefficients, unaccounted for disequilibrium between samplers and water, or different time scales over which the samplers average. The concordance between PE and SPME estimated concentrations for DDE was high (R^2 = 0.95). PCBs were only detected in PE samplers, due to their much larger size. Near-bottom waters adjacent to and down current from sediments with the highest bulk concentrations exhibited aqueous concentrations of DDTs and PCBs that exceeded Ambient Water Quality Criteria (AWQC) for human and aquatic health, indicating the need for future monitoring to determine the effectiveness of remedial activities taken to reduce adverse effects of contaminated surface sediments.

INTRODUCTION

Sediments of the Palos Verdes Shelf (PVS) off the coast of California are heavily contaminated with persistent organic pollutants (POPs), specifically, organochlorine pesticides (including dichlorodiphenyltrichloroethane (DDT) and its breakdown products) and polychlorinated biphenyls (PCBs).[1−6] Swartz et al.[7] found the presence of these contaminants likely contributed to elevated whole sediment acute toxicity to marine amphipods exposed to sediments from PVS. These contaminants are primarily the legacy of industrial wastes released to the shelf through the outfall of the Joint Water Pollution Control Plant (JWPCP), a wastewater treatment facility operated by the Los Angeles County Sanitation Districts (LACSD).[8] The prevailing coastal currents and wave activity carry remnants of the discharge in a northwesterly direction from the outfall, located off White Point (Figure 1).[9] As for many contaminated sites, sediments on the shelf continue be a source of chemicals to the water column, and biota living within and above it, long after the most polluted industrial releases have ended.[10−13] To protect human and ecological health, the U.S. Environmental Protection Agency has explored remedial alternatives for the site.[8]

Capping of the most contaminated sediments near the outfall has been selected as the preferred remedial alternative.[8] Monitoring of POP concentrations in the water column before (i.e., baseline conditions), during, and after the capping is necessary to evaluate the effectiveness of the remediation as well as any adverse side effects (e.g., resuspension-caused contaminant release). Measurement of dissolved concentrations ranging from femtograms per liter to tens of nanograms per liter for individual compounds, however, is technically challenging and time-consuming using traditional techniques, requiring pumping and filtering of large volumes of water (hundreds to thousands of liters) in order to collect analytically detectable contaminant masses on sorptive material (e.g., octadecyl resin or polyurethane foam).[12,14,15]

Received: May 31, 2012
Revised: October 4, 2012
Accepted: October 12, 2012
Published: October 12, 2012

 © 2012 American Chemical Society

In situ passive sampling methods, including solid-phase microextraction (SPME) and low-density polyethylene (PE) strips reduce the labor involved in sampling and postcollection processing, while allowing for dissolved POP measurement at very low concentrations. Further, passive sampling avoids many of the artifacts associated with traditional methods that result in over- and under-estimating dissolved concentrations. In general, passive samplers allow dissolved concentrations to be deduced from concentrations in equilibrated polymeric phases using polymer−water partition coefficients (e.g., K_{PEW} and K_f).[16,17]

Zeng et al.[16] applied SPMEs, polydimethylsiloxane (PDMS) coated glass fibers, to measure DDT breakdown products (*p,p′*-DDE, *o,p′*-DDE, and *p,p′*-DDD) dissolved in the water column of the PVS. Concentrations in the range of tens of picograms per liter to nanograms per liter matched those measured using the traditional pumping, filtering, and solid phase extraction of 999 L of seawater. SPME were believed to be equilibrated with the PVS water DDTs after 18 d deployments, as no statistically significant differences in concentration were seen in SPME exposed for 18 and 30 d. Similarly, Adams[18] and Adams et al.[17] used PE strips, exposed for 15 d and assuming sampler/water equilibration, to sample PCB congener #52 in Boston Harbor and lower Hudson River estuary in the range of pictograms per liter. To monitor the effectiveness of remedial efforts on the PVS, water concentrations for individual PCB congeners will have to be detectable to the range of tens of femtograms per liter.

In this work, both SPME and PE passive samplers are used simultaneously to measure selected DDT and PCB concentrations at eleven stations along the PVS and at a background station with historically lower detectable POP concentrations. By using large strips of PE, it is expected that even highly chlorinated PCBs, which have previously been measured in the sediments, but not detectable in the water column due to extremely low solubility, could be measured (expected range of tens to hundreds of femtograms per liter). These data will allow benchmark, time-averaged concentrations to be set for the PVS, to which water column concentrations, measured using similar methods during and after remedial activity at the site, may be compared. Co-deployment of the two types of samplers will allow for a direct comparison of estimated concentrations providing confidence in the techniques where results are consistent, and highlighting necessary adjustments to their methods of use where results are inconsistent. Finally, an alternative method for calibrating the fractional equilibration of membrane samplers is presented and compared with a frequently used, existing method. This alternative method may be used with any sampler material and thickness and may be useful in predicting fractional equilibrations before deployment, helping to improve the design of sampling campaigns.

THEORY

Dissolved concentrations, C_W, may be deduced using data from both types of passive samplers. First, SPME-water partition coefficients, K_f (L_W/L_{PDMS}), may be used to calculate C_W (ng/L) from the mass of analyte sorbed to the fiber, N_f (ng), assuming the fibers and water are fully equilibrated:

$$C_W = N_f/(K_f V_f) \tag{1}$$

where V_f (L_{PDMS}) is the volume of the sorptive coating.

Because equilibrium between PE samplers and water cannot always be assumed for very hydrophobic compounds, such as some DDTs (e.g., DDD, DDE, and DDT) and highly chlorinated PCBs, following short deployments (days to weeks), performance reference compounds (PRCs) are used to correct for nonattainment of equilibrium conditions.[17,19] Similarly to SPME, C_W may be calculated from the concentration of analyte taken up by the PE strips, while accounting for disequilibrium using PRCs that are similar to the analyte in terms of diffusivities and partitioning coefficient:

$$C_W = C^{\infty}{}_{PE}/K_{PEW} \tag{2}$$

$$C^{\infty}{}_{PE} = C_{PE,t}/f_{eq} \tag{3}$$

and

$$f_{eq} = (C^0{}_{PRC} - C_{PRC,t})/C^0{}_{PRC} \tag{4}$$

where $C^{\infty}{}_{PE}$ is the equilibrium analyte concentration in the PE in ng/kg_{PE}, K_{PEW} is the compound-specific polyethylene−water partition coefficient (L_W/kg_{PE}), $C_{PE,t}$ is the concentration in the PE after deployment, $C^0{}_{PRC}$ is the initial concentration of PRC in the sampler, $C_{PRC,t}$ is the concentration of PRC in the sampler after deployment, and f_{eq} is the fractional equilibration of the sampler to the water.

Challenges to using PRCs are encountered when wishing to interpolate between, or extrapolate from, PRCs to compounds that differ in terms of diffusivity and partitioning behavior. Existing methods are based on an exponential approach to equilibrium (EAE) models that were originally developed for semipermeable membrane devices (SPMDs).[20,21] Constant mass transfer coefficients are assumed and uptake/release by polymeric passive samplers is often described as being either polymer-side controlled, or water-side boundary layer controlled, depending on the diffusion rates across each layer. While semiempirical models for specific samplers have been developed to predict the contributions to mass-transfer resistance of the polymer and water-side boundary layers,[22,23] a more generic method, which could be used with any sampler material and thickness, may simplify the application of polymer films as passive samplers.

An alternative to using EAE models may be found in the numerical integration of explicit, finite-difference modeling of Fickian, mass diffusion across both polymer and water layers, while accounting for the no flux boundary at the center of the polymer film (NI method). Using a stagnant film model to describe the water-side boundary layer (BL), one-dimensional Fickian diffusion in a system consisting of a PE sheet, BL, and a well mixed infinite bath is described in the Supporting Information (following Crank[24]). While polymer membrane thicknesses are known, BL thicknesses are unknown for any given deployment, and can change with flow rates and turbulence.[20,21] However, data from multiple PRCs may be used to find the best fit modeled BL. The same model, with a best-fit BL, may then be used to find f_{eq} for compounds which do not have matching PRCs (complete description of model in Supporting Information).[24] For the purposes of this work, BL dependence on a compound's diffusivity in water is neglected.

MATERIALS AND METHODS

Passive Sampler Preparation. PE strips (10 cm ×100 cm) were prepared from low-density polyethylene sheets (25 μm, ACE Hardware Corp., Oak Brook, IL, USA) and solvent

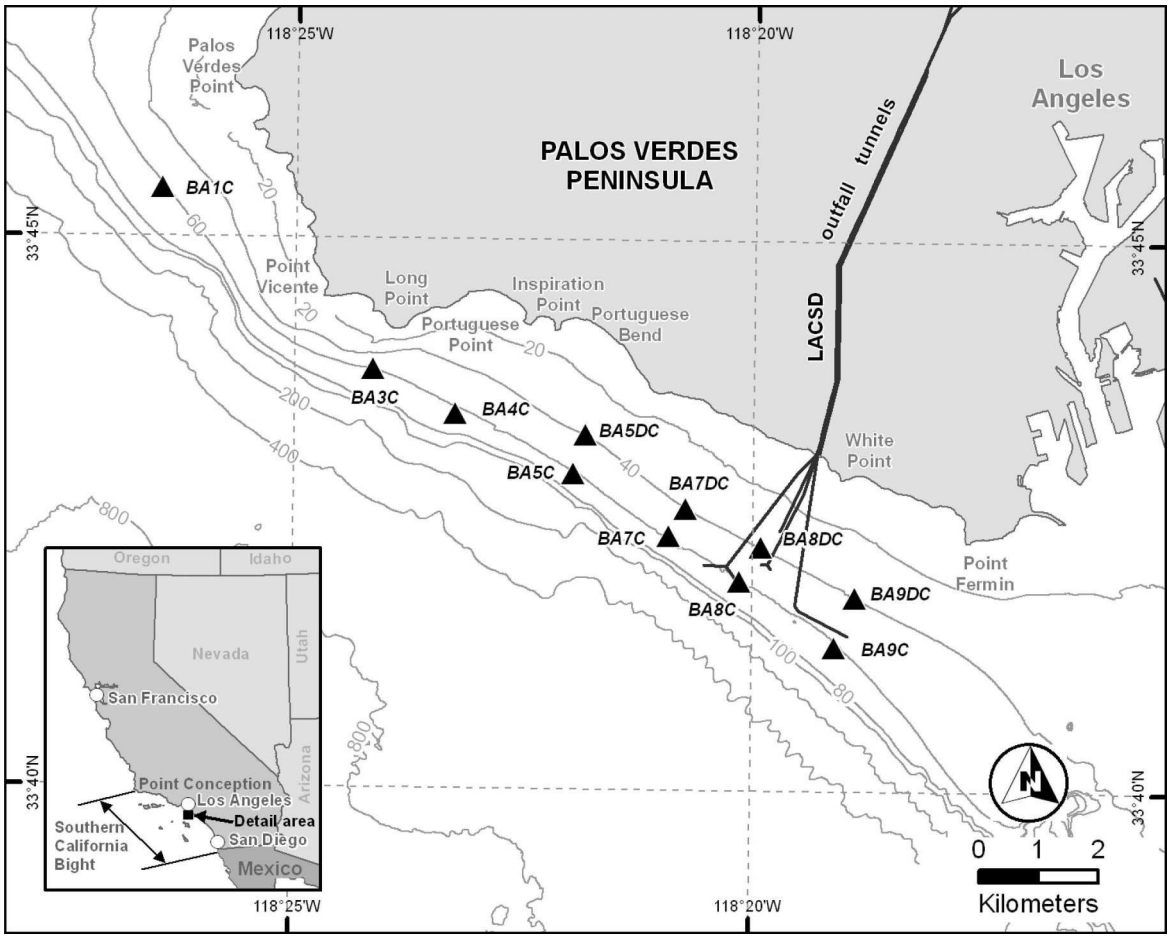

Figure 1. Black triangles indicate sampling stations off Palos Verdes, California (USA). PE and SPME were codeployed at stations BA1C, BA3C, BA4C, BA5C, BA7C, BA7DC, BA8C, BA8DC, BA9C, and T11 (not shown). Only PE samplers were deployed at stations BA5DC and BA9DC.

cleaned as described previously.[25] Each sampler was then soaked in an aqueous PRC solution (^{13}C-labeled *p,p′*-DDT, *p,p′*-DDE, *p,p′*-DDD, PCB#28, PCB#52, PCB#118, and PCB#128 (Cambridge Isotope, Andover, MA, USA)) in a 1-L amber glass jar for at least 20 weeks before deployment. To streamline analysis, target PRC concentrations in PE were approximately ten times the expected concentrations of target chemicals so that all concentrations would fall within the same range, assuming up to 90% loss of PRC during deployment. Finally, samplers were threaded onto solvent-rinsed aluminum wires, wrapped in aluminum foil, and stored at −20 °C or on ice until deployed.

SPME (100-μm PDMS-coated silica fibers, Supelco, Bellefonte, PA, USA) were prepared and handled as described previously.[16] Briefly, newly purchased SPME fibers were preconditioned at 250 °C for 0.5 h prior to assembly into individual perforated copper casings for protection during deployment. Each fiber/casing assembly was kept in a sealed glass vial in a freezer at −20 °C and shipped on ice until deployment.

Field Deployment and Retrieval. In September 2010, PE and SPME samplers, prepared as described above, were codeployed at multiple stations along the 45 and 60 m isobaths of the PVS, from just up current of the JWPCP outfall, to approximately 10 km down current (Figure 1), and at a background station (T11) approximately 24 km SE of the outfall (station labels reflect those used in previous monitoring of PVS sediment and water). Samplers were codeployed at three depths per station: 5 m below the surface ("surface"); 5 m above the bottom ("near bottom"), and 30−35 m below the surface ("mid-depth"). PE samplers were deployed in triplicate at each depth for all 12 stations shown in Figure 1. SPME samplers were deployed in quadruplicate at each depth for 10 of the 12 stations (excluding BA5DC and BA9DC). Both types of samplers were retrieved after 32 days. Because the aluminum wire on which PE were threaded broke for the shallower samplers, only PEs from the near bottom depth were recovered from eight stations, with the addition of the mid-depth samplers at stations BA4C and BA5DC. Copper or stainless steel wire would have been more appropriate for this application. All SPME samplers were recovered. Water temperature and salinity were measured using conductivity, temperature, and depth meter (CTD) casts at time of deployment. Dissolved organic carbon (DOC) was determined on discrete water samples collected at depth using a Niskin bottle. Analyses for DOC were performed on a Shimadzu TOC-VCSH analyzer (Kyoto, Japan). All samplers were returned to the laboratory on ice and remained frozen until analyzed.

Sampler Analysis. PE strips were wiped with laboratory tissues to remove adhering particles and biofilms, cut with clean scissors into small pieces, placed in solvent-rinsed 500-mL amber glass bottles, and spiked with recovery surrogates, dibromooctafluorobiphenyl (DBOFB) and PCB208. PE were then extracted three times by sonicating in 300 mL of

Table 1. SPME-Derived C_W in pg/L for Samplers Deployed at Three Depths (Mean of Two Fibers)

		station									
compound[a]	depth	BA1C	BA3C	BA4C	BA5C	BA7C	BA7DC	BA8C	BA8DC	BA9C	T11
DDNU	5 m below surface	≤12	≤9	≤6	≤3	≤6	<40	<40	<40	<40	<40
	mid-depth	≤14	≤14	≤6	≤9	≤12	<40	<40	<40	≤6	<40
	5 m off bottom	≤17	≤17	≤14	≤12	≤9	<40	<40	<40	≤3	<40
o,p′-DDE	5 m below surface	7	12	8	24	15	24	5	8	5	<1
	mid-depth	21	17	16	44	53	49	33	29	21	<1
	5 m off bottom	37	45	170	120	150	100	49	48	25	<1
DDMU	5 m below surface	15	15	14	41	<4	26	<4	18	<4	<4
	mid-depth	27	35	22	61	69	82	39	58	28	<4
	5 m off bottom	45	120	230	140	180	150	66	70	43	<4
p,p′-DDE	5 m below surface	54	94	68	110	93	140	46	70	36	<9
	mid-depth	170	130	130	300	390	280	280	160	180	<9
	5 m off bottom	330	410	790	810	990	560	420	280	230	<5
o,p′-DDD	5 m below surface	<14	<14	<14	<14	<14	<14	<14	<14	<14	<14
	mid-depth	<14	<14	<14	<14	<14	<14	<14	<14	<14	<14
	5 m off bottom	<14	<14	<14	31	23	<14	<14	<14	<14	<14
o,p′-DDT	5 m below surface	<16	<16	<16	<16	<16	<16	<16	<16	<16	<16
	mid-depth	<14	<16	<16	<16	<16	<16	<16	<16	<16	<16
	5 m off bottom	<16	<16	<16	<16	<16	<16	<16	<16	<16	<16
p,p′-DDD	5 m below surface	<70	<70	<70	<70	<70	<70	<70	<70	<70	<70
	mid-depth	<70	<70	<70	<70	<70	<70	<70	<70	<70	<70
	5 m off bottom	<70	<70	<70	<70	<70	<70	<70	<70	<70	<70
p,p′-DDT	5 m below surface	<30	<30	<30	<30	<30	<30	<30	<30	<30	<30
	mid-depth	<30	<30	<30	<30	<30	<30	<30	<30	<30	<30
	5 m off bottom	<30	<30	<30	<30	<30	<30	<30	<30	<30	<30

[a]DDNU = 1-phenylethenylbenzene; *o,p′*-DDE = *o,p′*-dichlorodiphenyldichloroethylene; DDMU = 1-chloro-4-[2-chloro-1-(4-chlorophenyl)-ethenyl]benzene; *p,p′*-DDE = *p,p′*-dichlorodiphenyldichloroethylene; *o,p′*-DDD = *o,p′*-dichlorodiphenyl dichloroethane; *o,p′*-DDT = *o,p′*-dichlorodiphenyltrichloroethane; *p,p′*-DDD = *p,p′*-dichlorodiphenyl dichloroethane; *p,p′*-DDT = *p,p′*-dichlorodiphenyltrichloroethane.

dichloromethane (DCM) for 15 min. The combined extract was dried with precombusted Na_2SO_4 and concentrated to ∼5 mL using a TurboVap II Concentration Workstation (Caliper Life Sciences, Hopkinton, MA, USA). Extracts were then solvent exchanged into hexane and concentrated to 0.5 mL. After the addition of internal standards, PCB 30 and PCB 205, extracts were analyzed by GC/MSD (see Supporting Information for details). SPME fibers were manually injected on the GC/MSD, and two fibers from each station/depth were analyzed using EI and NCI ionization modes. Target compounds included *p,p′*- and *o,p′*- congeners of DDT, DDE, and DDD, *p,p′*-DDMU, *p,p′*-DDNU, and 43 PCB congeners (Table 2).

Partition Coefficients. The polyethylene−water partition coefficients (K_{PEW}) used in this work were based on laboratory measurements (in seawater) and published values (Supporting Information). For this study, PRCs in PE samplers were assumed to have equivalent K_{PEW} and diffusivities to the non-^{13}C-labeled compounds. Compound-specific SPME−water partition coefficients (K_f) were also measured in seawater, for DDTs and their breakdown products (M. Pirogovsky, unpublished data). Calculation of temperature effects on partition coefficients indicated only small (<20%) differences were expected, thus no site-specific temperature corrections were made in this work.[26]

RESULTS

Dissolved DDT and PCB Concentrations using SPME. The highest dissolved concentrations measured at each station were of *p,p′*-DDE, ranging from 36 pg/L in the surface waters at station 9C, just up-current of the outfall, to 990 pg/L in near bottom water at station BA7C, just down-current of the outfall. At each station, DDE concentrations increased with depth, with the surface water concentrations averaging 16% of the concentrations measured in the bottom waters (Table 1), consistent with the trend observed using SPME water column samplers deployed in 2003−04.[27] Of the remaining compounds, only *o,p′*-DDE and *p,p′*-DDMU were detected frequently, and were 10% (<1 to 170 pg/L) to 30% (<4 to 230 pg/L) of the *p,p′*-DDE concentration at each station and depth, respectively. If detected, a contaminant followed the same depth to concentration trend noted above for *p,p′*-DDE; that is, the highest concentrations were observed at the bottom and decreased toward the surface. The presence of DDE and DDMU reflect the process of sequential reductive dechlorination of DDT in the sediments,[6] and transport of the more water-soluble metabolite DDMU into the water column. Due to the very low concentrations and low polymer mass on SPME, PCB concentrations were all below detection limits (5−200 pg/L depending on the congener). Within the range of DOC detected, 0.2−2.9 mg/L, no corrections for SPME performance were necessary.[16]

Fractional Equilibration of PE Samplers. The fractional equilibration (eq 4) of ^{13}C-labeled PCB28, PCB52, PCB118, PCB128, *p,p′*-DDE, *p,p′*-DDD, and *p,p′*-DDT in each of the samplers was used as the fractional equilibration of the 3, 4, 5, and 6 chlorine PCBs, DDE, DDD, and DDT congeners, respectively. These f_{eq} averaged 85% (±6%), 80% (±7%), 18% (±20%), and 12% (±25%) for PCB28, PCB52, PCB118, and PCB128, respectively, and 31% (±5%), 80% (±4%), and 94% (±6%) for DDE, DDD, and DDT, respectively (uncertainty equal to 1 SD, N = 26). Although only two field blank samplers

Table 2. PE-Derived C_W 5 m above Bottom in pg/L Measured in This Work, and Bulk Sediment Concentrations (μg/kg) of Total PCB and Total DDTs Measured by U.S. EPA in 2009 (Average for Top 6 cm)[a]

	station									
compound	BA1C	BA4C	BA5C	BA5DC	BA7DC	BA8C	BA8DC	BA9C	BA9DC	T11
DDNU	120 ± 20	230 ± 50	190 ± 40	220 ± 50	180 ± 40	140 ± 30	160 ± 30	98 ± 21	120 ± 20	<60
o,p-DDE	130 ± 30	350 ± 70	310 ± 60	230 ± 50	230 ± 50	200 ± 40	160 ± 30	79 ± 16	130 ± 30	4.3 ± 0.9
DDMU	230 ± 50	410 ± 80	410 ± 80	290 ± 60	280 ± 60	310 ± 60	250 ± 50	130 ± 30	180 ± 40	<5
p-p'-DDE	970 ± 170	2200 ± 400	2100 ± 400	1500 ± 300	1600 ± 300	1400 ± 200	1300 ± 200	650 ± 120	950 ± 170	37 ± 7
o,p'-DDD	9.3 ± 2.1	21 ± 5	13 ± 3	11 ± 2	11 ± 2	14 ± 3	11 ± 2	5.4 ± 1.2	7.8 ± 1.8	<2
o,p'-DDT	<7	<7	<7	<7	<7	<7	<7	<7	<7	<7
p,p'-DDD	20 ± 4	42 ± 8	34 ± 7	24 ± 5	27 ± 5	33 ± 6	29 ± 5	11 ± 2	18 ± 3	<6
p,p'-DDT	<8	<8	<8	<8	<8	<8	<8	<8	<8	<8
total PCB[b]	156	316	217	198	174	163	158	90	119	50
PCB8	<17	<17	<17	<17	<17	<17	<17	<17	<17	<17
PCB18	<13	<13	<13	<13	<13	<13	<13	<13	<13	<13
PCB28	<6	<6	<6	<6	<6	<6	<6	<6	<6	<6
PCB52	6.4 ± 1.1	14 ± 3	14 ± 2	16 ± 3	15 ± 3	9.3 ± 1.7	15 ± 3	8.1 ± 1.5	12 ± 2	5.9 ± 1.1
PCB49	7.1 ± 0.9	7.9 ± 1.0	12 ± 2	19 ± 2	15 ± 2	9.7 ± 1.3	8.6 ± 1.1	9.2 ± 1.2	7.8 ± 1.0	<6
PCB44	8.7 ± 1.0	9.7 ± 1.2	14 ± 2	16 ± 2	<4	<4	<4	<4	<4	<4
PCB37	<3	<3	<3	<3	<3	<3	<3	<3	<3	<3
PCB74	4.1 ± 0.7	7.4 ± 1.3	7.2 ± 1.3	5.8 ± 1.0	5.1 ± 1.0	3.9 ± 0.7	4.6 ± 0.8	<1.5	2.3 ± 0.4	<1.5
PCB70	7.0 ± 1.2	16 ± 3	14 ± 3	9.5 ± 1.7	9.1 ± 1.7	11 ± 2	8.5 ± 1.5	3.9 ± 0.7	6.0 ± 1.1	<1.3
PCB66	6.0 ± 3.0	15 ± 8	11 ± 5	8.0 ± 3.9	7.1 ± 3.9	8.0 ± 3.5	6.3 ± 3.0	1.3 ± 1.4	4.9 ± 2.1	<1.8
PCB101	15 ± 4	35 ± 9	22 ± 6	18 ± 5	17 ± 5	17 ± 4	14 ± 4	6.7 ± 1.7	10 ± 3	<2
PCB99	8.1 ± 3.0	18 ± 7	11 ± 4	9.1 ± 3.4	9.3 ± 3.5	8.7 ± 3.2	15 ± 6	3.5 ± 1.3	5.9 ± 2.2	<3
PCB119	1.1 ± 0.4	1.7 ± 0.6	1.1 ± 0.4	<1	<1	<1	<1	<1	<1	<1
PCB87	5.3 ± 1.5	14 ± 4	8.2 ± 2.3	6.4 ± 1.8	6.7 ± 1.9	6.9 ± 1.9	5.6 ± 1.6	0.94 ± 0.26	3.8 ± 1.1	<0.34
PCB110	13 ± 4	32 ± 9	19 ± 6	15 ± 5	15 ± 5	15 ± 5	11 ± 3	5.9 ± 1.8	7.7 ± 2.4	<2
PCB81	<0.2	<0.2	<0.2	<0.2	<0.2	<0.2	<0.2	<0.2	<0.2	<0.2
PCB151	1.3 ± 0.4	2.0 ± 0.5	1.4 ± 0.4	1.2 ± 0.4	1.1 ± 0.4	1.1 ± 0.31	0.88 ± 0.24	0.47 ± 0.15	0.70 ± 0.20	0.13 ± 0.04
PCB77	0.71 ± 0.33	1.2 ± 0.6	1.0 ± 0.5	0.81 ± 0.38	2.5 ± 0.4	0.86 ± 0.41	3.3 ± 1.5	0.15 ± 0.07	0.58 ± 0.27	<0.06
PCB149	1.2 ± 0.4	2.8 ± 1.5	1.4 ± 0.6	1.2 ± 0.4	1.1 ± 0.4	1.2 ± 0.4	0.94 ± 0.32	0.47 ± 0.19	0.68 ± 0.24	0.13 ± 0.05
PCB123	1.9 ± 0.6	6.7 ± 2.1	2.4 ± 0.8	2.0 ± 0.7	2.0 ± 0.7	1.9 ± 0.6	1.6 ± 0.5	0.81 ± 0.26	1.2 ± 0.4	<0.2
PCB118	14 ± 5	53 ± 17	19 ± 6	16 ± 5	15 ± 5	15 ± 5	13 ± 4	6.2 ± 2.0	9.1 ± 2.9	<0.2
PCB114	0.58 ± 0.14	1.1 ± 0.3	0.70 ± 0.17	0.61 ± 0.15	0.58 ± 0.14	0.56 ± 0.13	0.46 ± 0.11	0.22 ± 0.05	0.34 ± 0.08	<0.07
PCB153/168	5.2 ± 1.5	6.8 ± 1.7	5.3 ± 1.7	5.1 ± 1.3	4.2 ± 1.1	4.2 ± 1.3	3.4 ± 1.0	1.9 ± 0.6	2.8 ± 0.8	0.67 ± 0.19
PCB105	5.7 ± 1.5	13 ± 4	7.9 ± 2.1	6.4 ± 1.7	6.2 ± 1.7	6.3 ± 1.7	5.2 ± 1.4	2.4 ± 0.7	3.6 ± 1.0	0.51 ± 0.14
PCB138	4.6 ± 1.3	6.7 ± 1.8	4.8 ± 1.5	4.1 ± 1.1	3.6 ± 0.9	3.6 ± 1.0	2.9 ± 0.8	1.6 ± 0.5	2.2 ± 0.6	0.47 ± 0.14
PCB158	0.59 ± 0.16	0.83 ± 0.21	0.68 ± 0.19	0.54 ± 0.14	0.45 ± 0.12	0.47 ± 0.13	0.36 ± 0.10	0.20 ± 0.06	0.29 ± 0.09	0.056 ± 0.008
PCB187	1.6 ± 0.4	2.0 ± 0.5	1.7 ± 0.4	1.4 ± 0.4	1.1 ± 0.3	1.3 ± 0.3	1.1 ± 0.3	0.77 ± 0.19	0.93 ± 0.23	0.23 ± 0.06
PCB183	0.59 ± 0.14	0.75 ± 0.19	0.64 ± 0.16	0.50 ± 0.13	0.42 ± 0.11	0.45 ± 0.11	0.36 ± 0.09	0.27 ± 0.07	0.31 ± 0.09	0.063 ± 0.015
PCB126	0.16 ± 0.06	0.60 ± 0.24	<0.1	<0.1	<0.1	<0.1	<0.1	<0.1	<0.1	<0.1
PCB128	1.2 ± 0.5	3.4 ± 0.9	1.2 ± 0.4	1.1 ± 0.35	0.93 ± 0.31	0.93 ± 0.34	0.75 ± 0.26	0.43 ± 0.18	0.64 ± 0.23	0.22 ± 0.07
PCB167	0.30 ± 0.08	3.7 ± 0.9	0.26 ± 0.08	0.24 ± 0.07	0.22 ± 0.05	0.21 ± 0.06	0.17 ± 0.05	0.095 ± 0.031	0.14 ± 0.04	<0.03

dx.doi.org/10.1021/es302139y | Environ. Sci. Technol. 2012, 46, 11937−11947

Table 2. continued

compound	station									
	BA1C	BA4C	BA5C	BA5DC	BA7DC	BA8C	BA8DC	BA9C	BA9DC	T11
PCB177	0.64 ± 0.16	2.0 ± 0.5	0.66 ± 0.17	0.51 ± 0.12	0.42 ± 0.11	0.47 ± 0.12	0.38 ± 0.10	0.28 ± 0.07	0.33 ± 0.08	0.074 ± 0.019
PCB200	0.081 ± 0.020	0.18 ± 0.05	0.065 ± 0.016	0.049 ± 0.012	0.048 ± 0.012	0.057 ± 0.014	<0.04	<0.04	<0.04	<0.04
PCB156	0.58 ± 0.18	0.84 ± 0.21	0.57 ± 0.19	0.50 ± 0.14	0.43 ± 0.12	0.46 ± 0.14	0.35 ± 0.10	0.19 ± 0.06	0.27 ± 0.08	0.053 ± 0.015
PCB157	0.21 ± 0.06	0.22 ± 0.06	0.17 ± 0.06	0.13 ± 0.04	0.13 ± 0.04	0.14 ± 0.05	0.11 ± 0.04	0.044 ± 0.011	0.067 ± 0.023	0.062 ± 0.020
PCB180	1.7 ± 0.4	5.8 ± 1.5	2.0 ± 0.5	1.5 ± 0.4	1.3 ± 0.32	1.4 ± 0.4	1.2 ± 0.3	0.83 ± 0.21	0.98 ± 0.25	0.16 ± 0.04
PCB170	0.76 ± 0.19	0.96 ± 0.31	0.82 ± 0.20	0.61 ± 0.15	0.51 ± 0.13	0.58 ± 0.15	0.46 ± 0.12	0.33 ± 0.08	0.39 ± 0.10	0.083 ± 0.021
PCB201	0.56 ± 0.14	0.65 ± 0.15	0.56 ± 0.14	0.42 ± 0.11	0.36 ± 0.09	0.40 ± 0.10	0.32 ± 0.08	0.26 ± 0.07	0.30 ± 0.08	0.11 ± 0.03
PCB169	0.17 ± 0.05	<0.05	<0.05	<0.05	<0.05	<0.05	<0.05	<0.05	<0.05	<0.05
PCB189	0.14 ± 0.04	0.071 ± 0.018	0.063 ± 0.015	0.054 ± 0.014	0.081 ± 0.020	0.063 ± 0.016	0.063 ± 0.016	0.075 ± 0.019	<0.05	<0.05
PCB194	0.39 ± 0.10	0.77 ± 0.19	0.30 ± 0.08	0.20 ± 0.05	0.23 ± 0.06	0.25 ± 0.06	0.17 ± 0.04	0.16 ± 0.04	0.16 ± 0.04	0.099 ± 0.025
PCB206	0.46 ± 0.11	0.33 ± 0.08	0.37 ± 0.09	0.30 ± 0.10	0.34 ± 0.09	0.34 ± 0.09	0.30 ± 0.08	0.29 ± 0.06	0.30 ± 0.08	0.27 ± 0.07
PCB209	<18	<18	<18	<18	<18	<18	<18	<18	<18	<18
bulk sediment concentrations (ug/kg)										
total DDTs[d]	2400	2100	2100	540	330	100 000	2200	1100	710	
total PCBs[c]	100	120	110	35	3.8	2100	52	71	42	

[a]Uncertainty reflects the propagated error of initial and post-deployment PE concentrations (expressed as one standard deviation (1 SD)). [b]Total PCB = sum of congeners reported. One half of the detection limit was included in sum for congeners below detection limit. [c]Total PCBs = sum of PCB8, PCB18, PCB28, PCB44, PCB52, PCB66, PCB77, PCB81, PCB101, PCB105, PCB114, PCB118, PCB123, PCB126, PCB128, PCB138/158, PCB153, PCB157, PCB167, PCB169, PCB170, PCB180, PCB187, PCB189, PCB195, PCB206, and PCB209. [d]Total DDTs = sum of *p,p*-DDT, *o,p′*-DDT, *p,p′*-DDE, *o,p′*-DDE, *p,p′*-DDD, *o,p′*-DDD, *p,p′*-DDMU, and *p,p′*-DDNU.

dx.doi.org/10.1021/es302139y | Environ. Sci. Technol. 2012, 46, 11937−11947

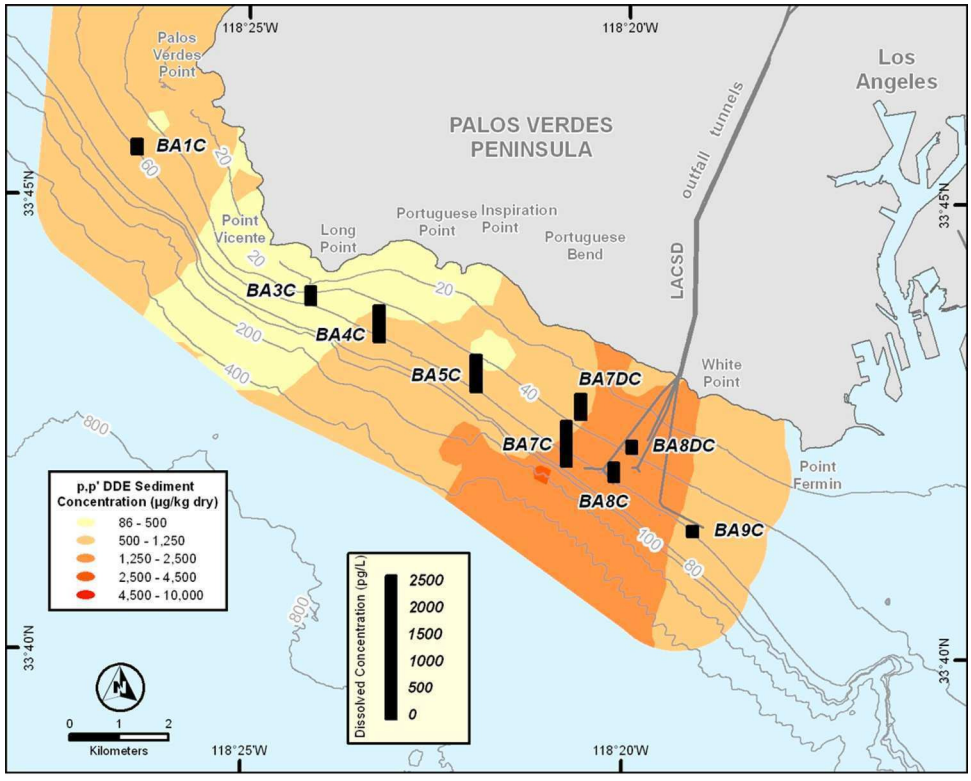

(a)

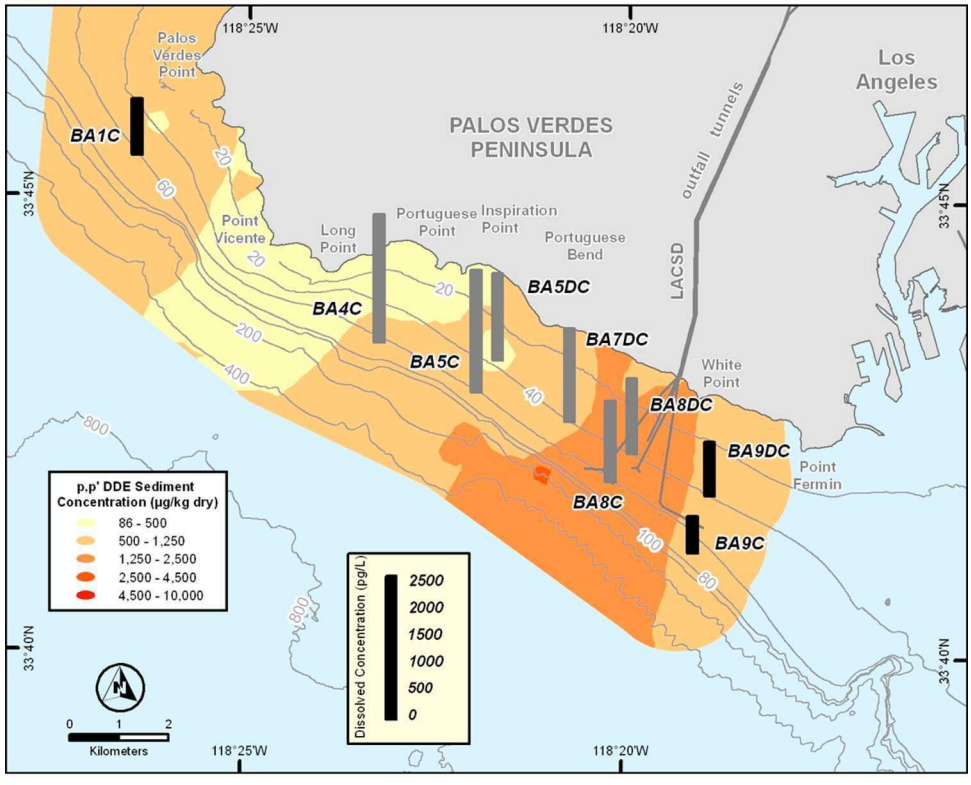

(b)

Figure 2. continued

dx.doi.org/10.1021/es302139y | *Environ. Sci. Technol.* 2012, 46, 11937−11947

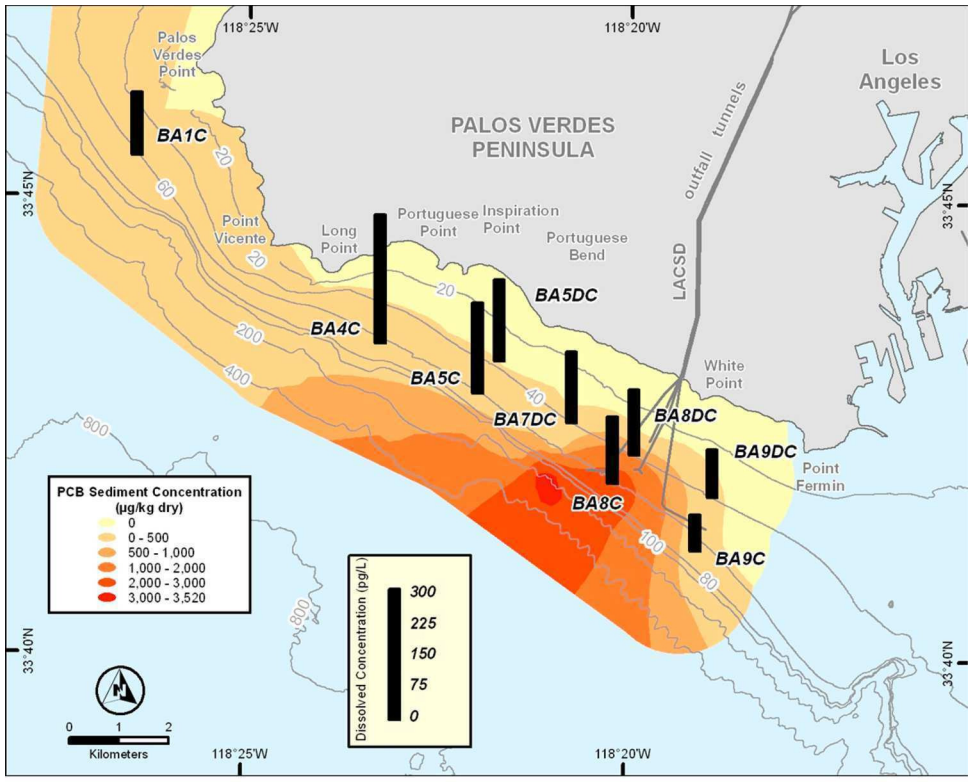

(c)

Figure 2. Dissolved concentrations (pg/L) 5 m above the sediment surface: (a) SPME-based *p,p′*-DDE concentrations; (b) PE-based *p,p′*-DDE concentrations; and (c) PE-based ΣPCB concentrations. Sediment response surface concentrations are based on U.S. EPA unpublished data using a radial basis function. Black columns indicate concentration exceeded the human health ambient water quality criteria (AWQC), and gray columns indicate concentration exceeded both human health and aquatic life AWQC.

were analyzed for initial PRC concentrations, agreement between the two was good. Measurements agreed within 5% for all PRCs except PCB28, which agreed within 16%. For analytes without a matching PRC (i.e., *p,p′*-DDMU, *p,p′*-DDNU, and PCBs with 2, 7, 8, 9, and 10 chlorines), f_{eq} was modeled, using explicit, finite-difference numerical techniques following Crank[24] (NI method) (details and sample Matlab code available in Supporting Information). Diffusivities for DDTs and PCBs in polyethylene were taken from Hale et al.[28] and Rusina et al.,[29] respectively. Diffusivities in water were estimated from their molar volume following Schwarzenbach et al.[30]

As similar PRC losses were measured in the 26 PE samplers, average values were used to model an average BL, which was then used to calculate the fractional equilibration of PE and waters for compounds without a matching PRC. Modeled BL for the six PRCs, excluding ^{13}C-*p,p′*-DDT ranged from 190 to 340 μm. No trend with diffusivity in water was observed. The modeled BL using ^{13}C-*p,p′*-DDT data was only 64 μm, however. The higher than expected, but very consistent loss of most of the ^{13}C-*p,p′*-DDT PRC during deployment (94% on average), suggests that the compound is being transformed during deployment. For this reason, ^{13}C-*p,p′*-DDT was left out when finding an average BL for the samplers. An average modeled BL thickness of 230 μm (SD = 90 μm) was used with the NI model to estimate the fractional equilibration of *p,p′*-DDMU, *p,p′*-DDNU, and PCB congeners with 2, 7, 8, 9, and 10 chlorines.

This mass-transfer modeling indicated that samplers were equilibrated (>99%) with water column for PCBs of low chlorination level (up to 2 Cl), and for DDNU. DDMU were 76% equilibrated with water column, while PCB congeners with seven or more chlorines were less than 4% equilibrated with water column, 3%, 1%, 0.3%, and 0.1% for PCBs with 7, 8, 9, and 10 Cl, respectively.

Dissolved DDT and PCB Concentrations using PE. Due to the much larger polymer mass in the PE samplers as compared to the SPME, detection limits (DL) ranged from 0.01 to 18 pg/L for individual PCBs and 0.4 to 60 pg/L for the individual DDTs (Table 2). As with SPMEs, the compound measured at the highest concentration at every station with PE samplers was *p,p′*-DDE, with a maximum at station BA4C (2200 ± 70 pg/L) (Table 2). Similar to SPME, *o,p′*-DDE concentrations were observed to be 12−16% of the *p,p′*-DDE concentrations at each station (10% on average for SPME), and *p,p′*-DDMU concentrations were 17−24% of the *p,p′*-DDE concentrations (30% on average for SPME). Even with the large polymer mass of PE relative to the SPME, some DDT congeners remained below detection limits (i.e., 7 and 8 pg/L, for *o,p′*-DDT and *p,p′*-DDT, respectively). The reported uncertainties in PE deduced C_W are the propagated uncertainties (1 SD) in the initial and postdeployment PE concentrations.

The PCB congeners measured at the highest concentrations at each station were the pentachlorobiphenyls PCB101, PCB110, and PCB118, with a maximum of 53 pg/L for PCB118 in the bottom waters at station BA4C (Table 2).

Summing the congeners measured in this study (counting one-half of the DL for compounds below the DL), ΣPCBs in the bottom waters ranged from 90 pg/L at station BA9C to 316 pg/L at station BA4C. This station also had the highest *p,p′*-DDE concentration at 2.2 ng/L. At the two stations where mid-depth PE samplers were recovered, ΣPCB concentrations were lower than those observed at the near bottom depth as demonstrated earlier by the SPME results for the detectable DDTs. At the background station, T11 (near bottom), ΣPCB concentrations were 50 pg/L, and the only detectable DDT compounds were *p,p′*- and *o,p′*-DDE, at 37 and 4 pg/L, respectively.

DISCUSSION

Dissolved concentrations measured in this work are similar to those measured in previous studies. For example, Zeng et al.[16] first measured *p,p′*-DDE at 2 m above the sediment−water interface at station BA6C (between stations BA5C and BA7C in this work) in 2003 and reported concentrations of 2.8 to 4.5 ng/L using SPME and 3.2 ng/L using a method of high-volume pumping and solid phase extraction. Dissolved *p,p′*-DDE measured in this work 5 m above the sediment−water interface at station BA5C were 2.1 and 0.81 ng/L using PE and SPME, respectively.

Horizontal Concentration Gradients. Without the influence of horizontal advection, we may expect samplers above the most contaminated sediments to have the highest contaminant concentrations. However, it is interesting to note that with both types of passive samplers DDTs and ΣPCBs were at the highest water concentrations downcurrent of the most contaminated sediments (BA8C) (U.S. EPA, unpublished data): station BA4C for PE and station BA7C for SPME (Table 2) (Figure 2). As demonstrated previously by Zeng et al.,[27] the plume of DDT- and PCB-contaminated waters is carried northwestward by the current, resulting in the highest detected concentrations just downcurrent of the outfall station (i.e., BA8C) and a subsequent decrease with increasing distance away from the Palos Verdes peninsula and into Santa Monica Bay proper.

Relationship of Measured Dissolved Concentrations to Ambient Water Quality Criteria (AWQC). Human and aquatic life AWQC values for DDT are 220 and 1000 pg/L, respectively, and for ΣPCB are 64 and 30 000 pg/L, respectively (http://water.epa.gov/scitech/swguidance/standards/current/index.cfm). To capture the worst case scenario, stations located 5 m above the bottom that exceeded these criteria are shown in Figure 2 (assuming similar toxicity values for *p,p′*-DDE, the predominant compound in ΣDDT at this site). Dissolved concentrations of *p,p′*-DDE based on SPME and PE show that all stations where samplers were deployed, except the background station (T11), exceeded the human health AWQC (Figure 2a,b). Based on the PE, dissolved concentrations of *p,p′*-DDE also exceeded both human health and aquatic life AWQC at several stations (Figure 2b). Further, based on SPME, many stations, exceeded the AWQC for *p,p′*-DDE up into midwater-column depth (Table 1).

PE estimates of dissolved ΣPCB concentrations indicated that all stations, except the background station (T11), exceeded the human health AWQC but none exceeded the aquatic life AWQC (Figure 2c). As noted above, and in agreement with the hypothesis that the sediments serve as the primary source of water column PCBs and DDTs, most AWQC exceedances were associated with samplers close to the sediment−water interface. Future efforts in this project will follow the concentrations of DDTs and PCBs in the water column during and after remediation to assess how effective capping is on decreasing the types of exceedances reported above.

Comparison of Sampler Calibration Methods. With the aim of assessing the performance of numerical integration techniques for interpreting PRC data, both NI and EAE methods were used to predict the average fractional equilibration of the PRCs. In general, both methods predicted the measured f_{eq} well (within a factor of 2 for all PRCs) (Figure SI2, Supporting Information). As mentioned above, the f_{eq} of ^{13}C-*p,p′*-DDT was not included in the analysis due to very high loss of the PRC, suggesting transformation of the compound during deployment. Either EAE or NI method would have yielded similar results in this investigation. However, using a reasonable range of BL values, f_{eq} for the target compounds could have been predicted before deployment began informing the design of the sampling campaign in terms of the thickness of PE used or duration of deployment.

SPME and PE Comparisons. PE-deduced dissolved *o,p′*- and *p,p′*-DDE water concentrations (the compounds for which the most comparable data are available) averaged three times greater than the SPME deduced water concentrations (Figure 3). Part of this difference is likely due to PE data being PRC-corrected (by factors ranging from 2.4 to 4.5) while SPME are assumed to be equilibrated (no correction). Using the NI method to model diffusion of DDE between a PDMS layer (100-μm thickness with no-flux boundary on one side) and water across a 200-μm thick BL for 32 d results in an integrated mass in the PDMS that is 70% of the equilibrium value (assuming D_{PDMS} of $10^{-6.9}$ cm^2/s, extrapolated from PCB diffusivities,[29] and D_W of $10^{-5.3}$ cm^2/s,[30] and ignoring cylindrical geometry of SPME). "Correcting" the SPME-deduced C_W by this fraction has the effect of nudging the PE- and SPME-deduced C_W values closer together. On the other hand, if the fast equilibration assumption for SPME is correct, SPME and PE are time-averaging concentrations over different times. If concentrations of DDE vary with time in the water colmn, then the two methods should give different values for C_W. In addition to kinetic considerations in situ, the

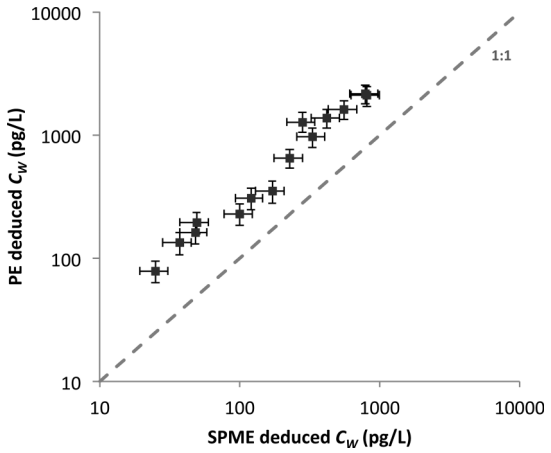

Figure 3. Comparisons of *o,p′*- and *p,p′*-DDE PE deduced, C_W vs SPME (squares), in waters near the bottom at stations BA1C, BA4C, BA5C, BA7DC, BA8C, BA8DC, and BA9C.

difference in concentrations may be due to uncertainties in K_{PEW} and K_f values.

With or without PRC correction, the PE- and SPME-deduced concentrations correlate very well (R^2 = 0.95), indicating that with appropriate corrections, these samplers are capable of converging on in situ dissolved concentrations. Future work should focus on reducing the uncertainties associated with both determination of equilibrium parameters (i.e., K values) and correction factors for nonequilibrium exposure scenarios, including testing the full equilibration assumption for SPME samplers.

■ ASSOCIATED CONTENT

Supporting Information

(1) GC/MSD sample analysis method; (2) polyethylene–water partition coefficients for this work; (3) model describing one-dimensional Fickian mass diffusion in a PE–water system; (4) sample Matlab script for modeling 1-D diffusion from PE, across water-side boundary layer, to well mixed water bath; and (5) modeled vs measured fractional equilibration using EAE and NI methods. This material is available free of charge via the Internet at http://pubs.acs.org.

■ AUTHOR INFORMATION

Corresponding Author

*Phone: 617-513-1441; e-mail: lorettaf@alum.mit.edu.

Notes

The authors declare no competing financial interest.

■ ACKNOWLEDGMENTS

We thank Dario Diehl and David Tsukada of SCCWRP (Costa Mesa, CA, USA) and the crew of the R/V *Early Bird II* for their work deploying and recovering samplers. We also thank Mike Charpentier (Raytheon, Narragansett, RI, USA) for preparing Figures 1 and 2.

■ REFERENCES

(1) Venkatesan, M. I.; Greene, G. E.; Ruth, E.; Chartrand, A. B. DDTs and dumpsite in the Santa Monica Basin, California. *Sci. Total Environ.* **1996**, *179*, 61–71.

(2) Quensen, J. F.; Mueller, S. A.; Jain, M. K.; Tiedje, J. M. Reductive dechlorination of DDE to DDMU in marine sediment microcosms. *Science* **1998**, *280*, 722–724.

(3) Eganhouse, R. P.; Pontolillo, J. Depositional history of organic contaminants on the Palos Verdes Shelf, California. *Mar. Chem.* **2000**, *70*, 317–338.

(4) Eganhouse, R. P.; Pontolillo, J.; Leiker, T. J. Diagenic fate of organic contaminants on the Palos Verdes Shelf, California. *Mar. Chem.* **2000**, *70*, 289–315.

(5) Quensen, J. F.; Tiedje, J. M.; Jain, M. K.; Mueller, S. A. Factors controlling the rate of DDE dechlorination to DDMU in Palos Verdes margin sediments under anaerobic conditions. *Environ. Sci. Technol.* **2001**, *35*, 286–291.

(6) Eganhouse, R. P.; Pontolillo, J. DDE in sediments of the Palos Verdes Shelf, California: In situ transformation rates and geochemical fate. *Environ. Sci. Technol.* **2008**, *42*, 6392–6398.

(7) Swartz, R. C.; Schults, D. W.; Lamberson, J. O.; Ozretich, R. J.; Stull, J. K. Vertical profiles of toxicity, organic carbon, and chemical contaminants in sediment cores from the Palos Verdes Shelf and Santa Monica Bay, California. *Mar. Environ. Res.* **1991**, *31*, 215–225.

(8) U.S.EPA. *EPA Announces Proposed Plan. Palos Verdes Shelf Superfund Site 9 R*; U.S. Environmental Protection Agency: San Francisco, CA, 2009.

(9) Ferre, B.; Sherwood, C. R.; Wiberg, P. L. Sediment transport on the Palos Verdes shelf, California. *Cont. Shelf Res.* **2010**, *30*, 761–780.

(10) Young, D. R.; Heesen, T. C.; McDermott, D. J. An offshore biomonitoring system for chlorinated hydrocarbons. *Mar. Pollut. Bull.* **1976**, *7* (8), 156–159.

(11) Larsson, P. Contaminated sediments of lakes and oceans act as sources of chlorinated hydrocarbons for release to water and atmosphere. *Nature* **1985**, *317*, 347–349.

(12) Zeng, E. Y.; Yu, C. C.; Tran, K. In situ measurements of chlorinated hydrocarbons in the water column off the Palos Verdes Peninsula, California. *Environ. Sci. Technol.* **1999**, *33* (3), 392–398.

(13) Friedman, C. L.; Lohmann, R.; Burgess, R. M.; Perron, M. M.; Cantwell, M. G. Resuspension of PCB-contaminated field sediment: Release to the water column and determination of site-specific K_{DOC}. *Environ. Toxicol. Chem.* **2011**, *30*, 377–384.

(14) Zeng, E. Y.; Peng, J.; Tsukada, D.; Ku, T.-L. In situ measurements of polychlorinated biphenyls in the waters of San Diego Bay, California. *Environ. Sci. Technol.* **2002**, *36*, 4975–4980.

(15) Sobek, A.; Gustafsson, O. Latitudinal fractionation of polychlorinated biphenyls in surface seawater along a 62° N–89° N transect from the southern Norwegian Sea to the North Pole area. *Environ. Sci. Technol.* **2004**, *38* (10), 2746–2751.

(16) Zeng, E. Y.; Tsukada, D.; Diehl, D. W. Development of a solid-phase microextraction-based method for sampling of persistent chlorinated hydrocarbons in an urbanized coastal environment. *Environ. Sci. Technol.* **2004**, *38* (21), 5737–5743.

(17) Adams, R. G.; Lohmann, R.; Fernandez, L. A.; MacFarlane, J. K.; Gschwend, P. M. Polyethylene devices: Passive samplers for measuring dissolved hydrophobic organic compounds in aquatic environments. *Environ. Sci. Technol.* **2007**, *41* (4), 1317–1323.

(18) Adams, R. G. Polyethylene devices and the effects of sediment resuspension on the cycling of PAHs and PCBs in the lower Hudson Estuary. Ph. D. Thesis. Massachusetts Institute of Technology, Cambridge, MA, 2003.

(19) Booij, K.; Smedes, F.; van Weerlee, E. M. Spiking of performance reference compounds in low density polyethylene and silicone passive water samplers. *Chemosphere* **2002**, *46*, 1157–1161.

(20) Booij, K.; Sleiderink, H. M.; Smedes, F. Calibrating the uptake kinetics of semipermeable membrane devices using exposure standards. *Environ. Toxicol. Chem.* **1998**, *17* (7), 1236–1245.

(21) Huckins, J. N.; Petty, J. D.; Lebo, J. A.; Almeida, F. V.; Booij, K.; Alvarez, D. A.; Cranor, W. L.; Clark, R. C.; Mogensen, B. B. Development of the permeability/performance reference compound approach for in situ calibration of semipermeable membrane devices. *Environ. Sci. Technol.* **2002**, *36*, 85–91.

(22) Booij, K.; Hofmans, H. E.; Fischer, C. V.; Weerlee, E. M. Temperature-dependant uptake rates of nonpolar organic compounds by semipermeable membrane devices and low-density polyethylene membranes. *Environ. Sci. Technol.* **2003**, *37*, 361.

(23) Booij, K.; Smedes, F. An improved method for estimating in situ sampling rates of nonpolar passive samplers. *Environ. Sci. Technol.* **2010**, *44*, 6789–6794.

(24) Crank, J. *The Mathematics of Diffusion*, 2nd ed.; Oxford University Press: Oxford, 1975; p 414.

(25) Fernandez, L. A.; MacFarlane, J. K.; Tcaciuc, A. P.; Gschwend, P. M. Measurement of Freely Dissolved PAH Concentrations in Sediment Beds Using Passive Sampling with Low-Density Polyethylene Strips. *Environ. Sci. Technol.* **2009**, *43* (5), 1430–1436.

(26) Lohmann, R. Critical review of low-density polyethylene's partitioning and diffusion coefficients for trace organic contaminants and implications for its use as a passive sampler. *Environ. Sci. Technol.* **2012**, *46*, 606–618.

(27) Zeng, E. Y.; Tsukada, D.; Diehl, D. W.; Peng, J.; Schiff, K.; Noblet, J. A.; Maruya, K. A. Distribution and mass inventory of total dichlorodiphenyldichloroethylene in the water column of the Southern California Bight. *Environ. Sci. Technol.* **2005**, *39*, 8170–8176.

(28) Hale, S. E.; Tomaszewski, J. E.; Luthy, R. G.; Werner, D. Sorption of dichlorodiphenyltrichloroethane (DDT) and its metabolites by activated carbon in clean water and sediment slurries. *Water Res.* **2009**, *43*, 4336–4346.

(29) Rusina, T. P.; Smedes, F.; Klanova, J. Diffusion coefficients of polychlorinated biphenyls and polycyclic aromatic hydrocarbons in polydimethylsiloxane and low-density polyethylene polymers. *J. Appl. Polym. Sci.* **2010**, *116*, 1803−1810.
(30) Schwarzenbach, R.; Gschwend, P.; Imboden, D. *Environmental Organic Chemistry*, 2nd ed.; Wiley: Hoboken, NJ, 2003; p *xiii*, 1313 pp.

Environmental Science & Technology

Article

pubs.acs.org/est

Calculating the Diffusive Flux of Persistent Organic Pollutants between Sediments and the Water Column on the Palos Verdes Shelf Superfund Site Using Polymeric Passive Samplers

Loretta A. Fernandez,*[,‡,†] Wenjian Lao,[§] Keith A. Maruya,[§] and Robert M. Burgess[‡]

[‡]U.S. Environmental Protection Agency, Atlantic Ecology Division, Narragansett, Rhode Island 02882, United States

[§]Southern California Coastal Water Research Project (SCCWRP), Costa Mesa, California 92626, United States

Supporting Information

ABSTRACT: Passive samplers were deployed to the seafloor at a marine Superfund site on the Palos Verdes Shelf, California, USA, and used to determine water concentrations of persistent organic pollutants (POPs) in the surface sediments and near-bottom water. A model of Fickian diffusion across a thin water boundary layer at the sediment-water interface was used to calculate flux of contaminants due to molecular diffusion. Concentrations at four stations were used to calculate the flux of DDE, DDD, DDMU, and selected PCB congeners from sediments to the water column. Three passive sampling materials were compared: PE strips, POM strips, and SPME fibers. Performance reference compounds (PRCs) were used with PE and POM to correct for incomplete equilibration, and the resulting POP concentrations, determined by each material, agreed within 1 order of magnitude. SPME fibers, without PRC corrections, produced values that were generally much lower (1 to 2 orders of magnitude) than those measured using PE and POM, indicating that SPME may not have been fully equilibrated with waters being sampled. In addition, diffusive fluxes measured using PE strips at stations outside of a pilot remedial sand cap area were similar to those measured at a station inside the capped area: 240 to 260 ng cm^{-2} y^{-1} for *p,p′*-DDE. The largest diffusive fluxes of POPs were calculated at station 8C, the site where the highest sediment concentrations have been measured in the past, 1100 ng cm^{-2} y^{-1} for *p,p′*-DDE.

INTRODUCTION

Much of the Palos Verdes Shelf (PVS) Superfund site, off of the coast of California, USA, is under more than 50 m of water. The water column and sediments at the site are contaminated with persistent organic pollutants (POPs), including dichlorodiphenyltrichloroethane (DDT), its breakdown products (e.g., dichlorodiphenyldichloroethylene (DDE), dichlorodiphenyldichloroethane (DDD), and 1-chloro-4-[2-chloro-1-(4-chlorophenyl)benzene (DDMU)), and polychlorinated biphenyls (PCBs).[1−6] These contaminants are the legacy of industrial wastes produced throughout the mid-20th century and released through the wastewater outfall of the Joint Water Pollution Control Plant, operated by the Los Angeles County Sanitation Districts (LACSD).[7] Like other sites where industrial sources of environmental contamination have been controlled or eliminated, the sediments, originally a sink for contaminants, have become a continuing source of contamination to the water column.[8−12]

The flux of POPs between the sediment bed and water column may occur through many different mechanisms.[13] Compounds may desorb from sediment solids to the water column during resuspension events or as benthic organisms pump overlying water through their burrows (i.e., bioirrigation). In areas where groundwater discharges through sediments to the overlying water, contaminants can be carried in the advective flow either dissolved or sorbed to colloids.[14] An additional flux, due to molecular diffusion, occurs at the sediment-water interface, driven by the concentration gradient between sediment porewater and overlying water across a diffusion-controlled boundary layer.[15] Of these mechanisms, only molecular diffusion occurs in every sediment-water system. For this reason, it can be considered a conservative baseline for total flux. In addition, the gradient, which drives diffusive mass-transfer, may also be used to calculate the scale of other flux mechanisms such as bioirrigation and resuspension/desorption.

One remedial alternative that has been explored for the PVS is capping the most contaminated sediments (those near station 8C and the outfall) with a clean layer of sand. It is believed that this would have the effect of reducing contaminant flux during resuspension events as well as reducing flux due to bioirrigation by relocating benthic organisms to a cleaner sediment layer. In 2000, three 45-acre pilot sand caps (covering <0.5% of the contaminated sediment area) were installed on the PVS in

Received: October 7, 2013
Revised: February 20, 2014
Accepted: February 24, 2014
Published: February 24, 2014

 © 2014 American Chemical Society

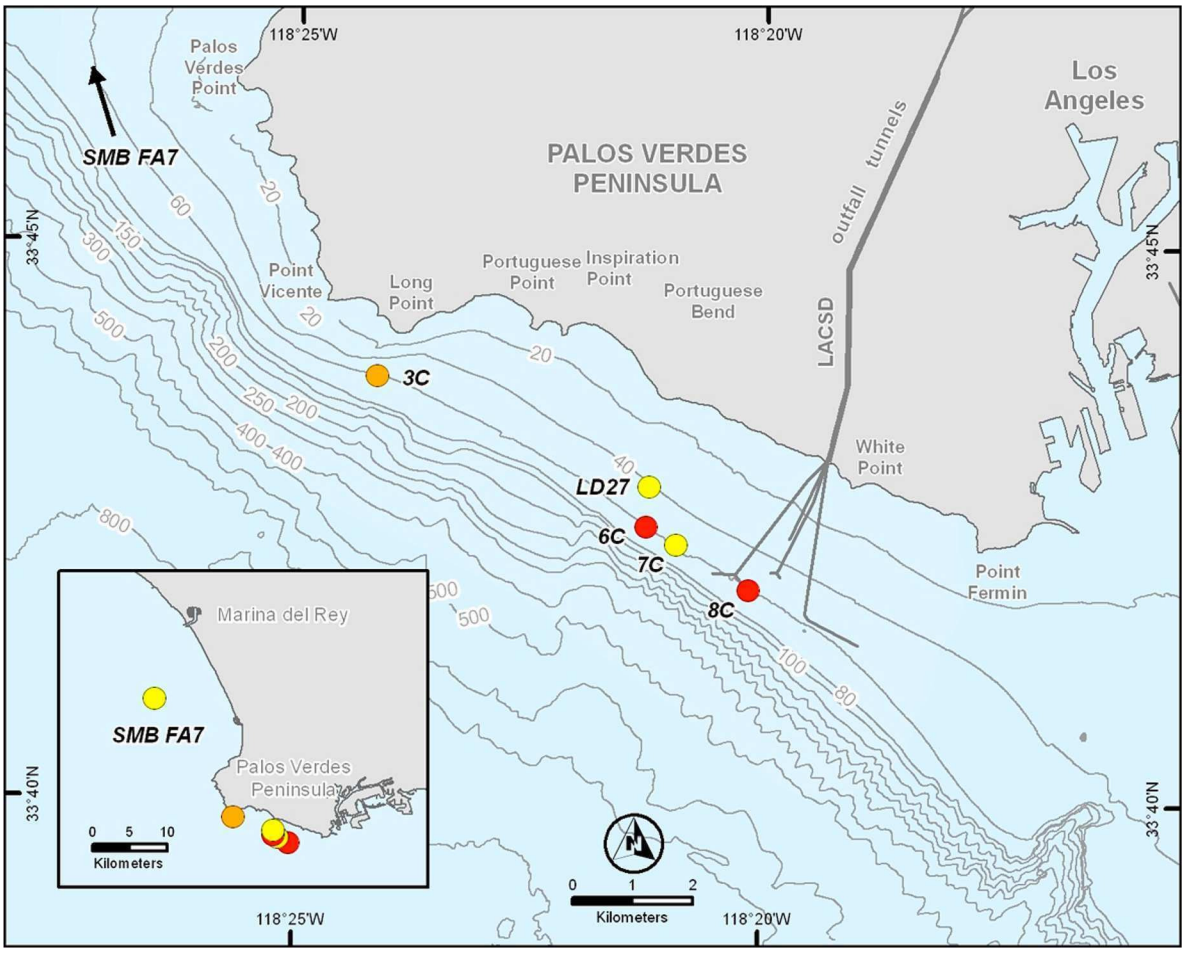

Figure 1. Station locations for sediment sampling and/or passive sampler platform deployments off the coast of Los Angeles, California, USA. Lines indicate depth, with stations 8C, 7C, 6C, and 3C located along the 60 m isobath and station LD27 on the 40 m isobath. The prevailing coastal currents and wave activity carry remnants of the discharge in a northwesterly direction from the outfall, located off White Point. Sediments for laboratory assessment of porewater concentrations were collected from stations 3C, 6C, and 8C (red and orange markers). Passive sampler benthic platforms carrying PE, POM, and SPME were deployed at stations SMB FA7, LD27, 6C, 7C, and 8C (red and yellow markers). Station LD27 is located within an area where a pilot sand cap was placed in 2000. Station SMB FA7 is outside and down-current of the PVS Superfund site. Station names reflect those used in previous monitoring of sediment and water.

order to test cap placement techniques and economic feasibility. Subsequent water sampling found comparable dissolved concentrations of POPs above capped and uncapped areas.[7] Because advection from up-current areas along the shelf is likely, water sampling is insufficient to determine the efficacy of the caps in limiting flux of contaminants from the sediment beds to the water column. Simultaneous measurement of porewater and overlying water concentrations, however, would allow for the assessment of fluxes due to concentration gradients. By comparing measurements made within the pilot cap to those made at uncapped stations nearby, the effectiveness of the sand caps could be assessed.

Flux due to molecular diffusion of contaminants across the sediment-water surface (F) is calculated using Fick's first law of diffusion

$$F = -\frac{D_W}{\delta_{BL}}(C_W - C_{PW}) \quad (1)$$

where D_W is the compound's diffusivity in water, δ_{BL} is the boundary layer thickness, C_W is the concentration in the water column, C_{PW} is the porewater concentration at the surface of the sediment bed, and positive F indicates flux from sediments to water. Using this equation and porewater concentrations estimated from sediment concentrations and an equilibrium partitioning model (EqP), Sherwood et al.[16] calculated diffusive fluxes of *p,p′*-DDE (the most abundant compound in PVS sediments) at PVS station 6C (Figure 1) ranging from 7,000 to 12,000 ng cm^{-2} y^{-1}. The EqP model used to estimate porewater concentration employed a sediment-water partition coefficient that considers partitioning to a single organic carbon pool. Many recent studies have shown, however, that estimating sediment-water partitioning using only organic carbon can be inaccurate, either because organic carbon−water partitioning coefficients can vary over a large range (e.g., over 2 orders of magnitude),[17] or because other sorptive fractions (e.g., black carbon) are included in the organic carbon fraction measurement.[18] Thus, calculations of F based on porewater concentrations estimated using these models could be off by orders of magnitude. In addition, concentrations in the water column have been observed to increase with proximity to the sediment surface.[12] Because flux calculations are based on concentrations on either side of a very thin diffusive boundary layer (tens to hundreds of μm thick[19]), measuring water

dx.doi.org/10.1021/es404475c | Environ. Sci. Technol. 2014, 48, 3925−3934

concentrations as close to the sediment-water interface as possible would improve the accuracy of calculations.

As alternatives to calculating porewater concentrations using EqP models, passive samplers, including polyethylene (PE), polyoxymethylene (POM), and solid-phase microextraction fibers (SPME), have been used to measure both water[12,20−24] and porewater[25−30] concentrations. In a related investigation, Eek et al.[15] used passive sampling techniques to calculate diffusive flux by equilibrating polymers with sediment slurries in the laboratory to find C_{PW}. In the current work, a different approach was taken. By deploying PE and POM strips simultaneously, in situ, across the sediment-water interface,[26] and using performance reference compounds (PRCs) to account for disequilibrium between the sampler and water or porewater,[12,20,25,26] C_W and C_{PW} bounding the diffusive layer were deduced, making flux calculations more accurate. SPME fibers, without PRCs, were also deployed to both sediment beds and overlying water for the purpose of comparing sampler results.

While the primary goal of this work was to investigate the effects of a sand cap on the flux of POPs from the sediment to the water column, the design of the newly developed benthic deployment platform allowed additional objectives to be addressed. These objectives included the following:

(1) observe dissolved POP porewater concentrations as a function of depth at sites with and without a sand cap,

(2) use passive sampler derived concentration gradients to calculate and compare diffusive flux of contaminants between the sediments and water column at stations with and without caps, and

(3) compare the performance of different types of polymeric passive samplers (i.e., PE, POM, SPME) deployed together in situ.

Four stations within the PVS Superfund site were selected (Figure 1). It is expected that the direction of contaminant at these stations would be from the sediment bed to water column. One of these stations (LD27) was within a pilot sand cap area. By comparing fluxes of contaminants at the station within the pilot cap to those at nearby uncapped stations, the effectiveness of the cap in reducing diffusive flux could be assessed. A fifth station (SMB FA7) outside, and down-current, of the PVS Superfund site was included in order to determine the direction of flux at an offsite, less-contaminated station.

MATERIALS AND METHODS

Chemicals. All solvents were Baker Ultraresi-analyzed (Philipsburg, NJ, USA). Laboratory water was treated with an ion-exchange and activated carbon system (Aries Vaponics, Rockland, MA, USA) until 18 MOhm-cm resistance was achieved, followed by UV exposure (TOC reduction unit, Aquafine Corporation, Valencia, CA, USA). DDTs and their breakdown products will be jointly referred to as DDX for the remainder of this work. DDX and PCB standards were purchased from Ultra Scientific (North Kingston, RI, USA) in acetone or methanol. ^{13}C-labeled PRCs and internal standards were purchased from Cambridge Isotope Laboratories, Inc. (Andover, MA, USA) in nonane.

PE, POM, and SPME Samplers. PE strips (10 cm × 50 cm) were prepared from low-density polyethylene sheets (25 μm thick, ACE Hardware Corp., Oak Brook, IL, USA). POM strips (10 cm × 50 cm) were prepared from polyoxymethylene sheets (76 μm thick, CS Hyde Company, Lake Villa, IL, USA). All polymer strips were cleaned and pre-equilibrated with PRCs as described in previous work.[25,26] Briefly, strips were cleaned by soaking twice, for 24 h, in dichloromethane, followed by soaking twice, for 24 h, in methanol, followed by soaking twice for 24 h in water. Samplers were then soaked in water containing seven PRCs (^{13}C labeled- p,p′-DDT, -p,p′-DDE, -p,p′-DDD, -2,4,4′-trichlorobiphenyl (PCB28), -2,2′,5,5′-tetrachlorobiphenyl (PCB52), -2,3′,4,4′,5-pentachlorobiphenyl (PCB118), and -2,2′,3,3′,4,4′-hexachlorobiphenyl (PCB128)) and equilibrated for three months before deployment.

SPME fibers (100-μm PDMS coated silica fiber, Supelco, Bellefonte, PA, USA) were also prepared as previously described.[12,22,29] Briefly, newly purchased SPME fibers were preconditioned at 250 °C for 0.5 h prior to assembly into individual perforated copper casings for protection during deployment. Each fiber/casing assembly was kept in a sealed glass vial in a freezer at −20 °C and shipped on ice until deployment.

Ex Situ PRC Method Testing. While the PRC method to determine fractional equilibration (f_{eq}) of PE samplers in sediments has been tested using deuterium labeled polycyclic aromatic hydrocarbons in the past,[25,26] a preliminary test using ^{13}C-labeled DDX and PCB compounds was conducted in the laboratory. The details of these tests and their results are available in the Supporting Information.

Field Deployment and Retrieval. Deployment platforms were designed and built to carry triplicate PE and POM samplers, and duplicate SPME samplers, to the sediment bed, allowing samplers to penetrate sediments to depths of up to 20 cm (Figures SI1 and SI2). Portions of each PE and POM sampler remained exposed to the water column, and two additional SPME fibers were positioned approximately 70 cm above the sediment-water interface. Platform bases were constructed of stainless steel, while aluminum frames holding PE and POM were secured using PVC spacers, washers, and steel bolts. Platforms were deployed from the sea surface and lowered into position above the seafloor by cable and then released. Each platform carried lead ballast to promote penetration of sampler frames into the sediment bed. Retrieval systems, consisting of a buoy, line, and acoustic release mechanism were attached to the upper portion of each platform. Using these platforms, PE and POM samplers were deployed across the sediment-water interface in triplicate (PE and POM) or duplicate (SPME), at five stations, between July 25 and 27, 2011 (Figure 1). A remotely operated vehicle (ROV), controlled by a team from the LACSD, was used to confirm proper placement of the deployment platform at each station (Figure SI3).

Platforms were retrieved from the sediments following 43 to 44 d deployments, where deployment times were selected based on modeled time required for measurable mass exchange between sampler and sediment, and the availability of the research vessel. Polymer strips were immediately cut from their frames, while marking the location of the sediment water interface (Figure SI4). Copper casings containing the SPME fibers were removed from the platforms, quickly rinsed with seawater, placed into clean capped glass vials, transferred to SCCWRP (Costa Mesa, CA, USA) on ice the same day as the recovery, and stored at −4 °C in the dark until analyzed. Field blanks (PRC loaded, unexposed samplers) were held in the air for approximately 5 min at each station to replicate the time samplers were exposed to air during deployment and recovery. Samplers and field blanks were placed in foil envelopes, stored on ice for overnight shipment to the Gschwend Laboratory

(Massachusetts Institute of Technology, Cambridge, MA, USA), and then stored in a freezer (−4 °C) in the dark until sectioned and extracted.

Sampler Analysis. PE and POM samplers were water rinsed, patted dry using Kim-wipe tissues (Kimberly-Clark Corp., Irving, TX, USA), and sectioned in the laboratory. The top of each sampler, exposed to the water above the sediment bed, was cut into two sections (10 to 18 cm in length, depending on the depth of penetration into the sediment bed). Sediment exposed portions of each sampler were cut in 1 to 2 cm sections using a razor blade and an aluminum sheet as a straight-edge. Internal (surrogate) standards (100 ng each of ^{13}C labeled-*o,p′*-DDE, -2,4′-dichlorobiphenyl (PCB8), -3,3′,4,4′-tetrachlorobiphenyl (PCB77), and -2,2′,4,4′,5,5′-hexachlorobiphenyl (PCB153)) were added to each section before extracting three times in 15 to 200 mL of dichloromethane. Combined extracts were reduced in volume using a rotary evaporator (Buchi Rotavapor-R, Brinkman Instruments, Westbury, NY, USA) and concentrated to a final volume of approximately 1 mL under a gentle stream of ultra pure grade nitrogen (Airgas, Chicago, IL, USA). Injection standard (d_{12}-chrysene) was added to each extract before final analysis.

All extracts were analyzed using gas chromatography−mass spectrometry (GCMS, JEOL GCmate, JEOL Ltd., Tokyo, Japan). On column injections (1 μL) were made onto a 30 m J&W Scientific DB-XLB capillary column (0.32 mm internal diameter with a 0.25 μm film thickness, Agilent Technologies, Santa Clara, CA, USA). The injector port temperature was initially set at 35 °C and then increased with oven temperature at a rate of 25 °C min^{-1} until 200 °C was reached. The temperature was then increased at 4 °C min^{-1} until a temperature of 275 °C was reached and held for 8 min. The MS was operated in selected ion monitoring (SIM) and EI+ modes. Calibration standards containing all target compounds (Table 1), PRCs, and internal and injection standards were run every 4 to 9 sample measurements to monitor instrument stability, determine response factors, and confirm that measurements remained within the linear range for the instrument. Using a thermal desorption extraction system, SPME fibers were manually injected on an Agilent 7890 GC/EI-MS system (Agilent Technologies, Santa Clara, CA, USA). Five-point external standard calibration curves were used to quantify the compounds.[12]

Partition Coefficients. Polyethylene-water partition coefficients, K_{PEW}, were taken from a log K_{OW} vs log K_{PEW} relationship used in previous work[12] and following Lohmann and Muir.[31] Polyoxymethylene-water partition coefficients ($K_{POM\text{-}W}$) were taken from Endo et al.[32] Both were corrected for temperature and salinity following Lohmann[33] (Table 1).

Calculation of Dissolved Concentrations. For equilibrium passive sampling (i.e., field-deployed SPME and PE mixed with sediment slurries in the laboratory (see the SI)), water column and porewater concentrations were calculated from the mass of POP taken up by the sampler. SPME-water partition coefficients, K_f (L_W/L_{PDMS}), were used to calculate C_W (ng L^{-1}) from the mass of analyte sorbed to the fiber, N_f (ng)

$$C_W = \frac{N_f}{(K_f V_f)} \tag{2}$$

where V_f (L_{PDMS}) is the volume of the sorptive polydimethylsiloxane (PDMS) coating.

Table 1. Compounds Measured in This Study with Octanol-Water (K_{OW}) (L/L), Polyethylene-Water (K_{PEW}) (L/kg), and Polyoxymethylene-Water ($K_{POM\text{-}W}$) (L/kg) Partition Coefficients

compound	K_{OW} [a]	log K_{PEW} [b]	T and salinity corrected log K_{PEW} [c]	log $K_{POM\text{-}W}$ [d]	T and salinity corrected log $K_{POM\text{-}W}$ [c]
o,p′-DDE		5.46	5.76	5.16	5.46
p,p′-DDMU	5.5[e]	5.26	5.56	4.96	5.26
p,p′-DDE	5.7[f]	5.46	5.76	5.16	5.46
o,p′-DDD		5.26	5.56	4.96	5.26
o,p′-DDT		5.93	6.23	5.65	5.95
p,p′-DDD	5.5[g]	5.26	5.56	4.96	5.26
p,p′-DDT	6.19[g]	5.93	6.23	5.65	5.95
PCB8	5.07	4.85	5.15	4.52	4.82
PCB18	5.24	5.01	5.31	4.69	4.99
PCB28	5.67	5.43	5.73	5.13	5.43
PCB52	5.84	5.59	5.89	5.30	5.60
PCB44	5.75	5.51	5.81	5.21	5.51
PCB66	6.2	5.94	6.24	5.66	5.96
PCB77	6.36	6.10	6.40	5.82	6.12
PCB101	6.38	6.12	6.42	5.84	6.14
PCB118	6.74	6.46	6.76	6.21	6.51
PCB105	6.65	6.38	6.68	6.12	6.42
PCB126	6.89	6.61	6.91	6.36	6.66
PCB153	6.92	6.64	6.94	6.39	6.69
PCB138	6.83	6.55	6.85	6.30	6.60
PCB128	6.74	6.46	6.76	6.21	6.51
PCB187	7.17	6.88	7.18	6.64	6.94
PCB180	7.36	7.07	7.37	6.83	7.13
PCB170	7.27	6.98	7.28	6.74	7.04
PCB195	7.56	7.26	7.56	7.04	7.34
PCB206	8.09	7.77	8.07	7.57	7.87
PCB209	8.18	7.86	8.16	7.66	7.96

[a]log K_{OW} for PCBs from Hawker and Connell.[35] [b]25 °C, no salt.[12] [c]12 °C, 0.5 M salt. [d]Endo et al.[32] [e]EPISuite estimate.[36] [f]Pontolillo and Eganhouse.[37] [g]Schwarzenbach et al.[38]

For nonequilibrium sampling (i.e., PE inserted to jars in laboratory (see the SI), and PE and POM strips exposed in the field), PRC and target compound concentrations in PE and POM sampler sections were used to calculate dissolved concentrations of target compound in the water column and pore waters[12,25,26]

$$C_W = \frac{C^{\infty}{}_{polymer}}{K_{Polymer\text{-}W}} \tag{3}$$

$$C^{\infty}{}_{polymer} = \frac{C_{polymer,t}}{f_{eq}} \tag{4}$$

and

$$f_{eq} = \frac{(C^0{}_{PRC} - C_{PRC,t})}{C^0{}_{PRC}} \tag{5}$$

where $C^{\infty}{}_{polymer}$ is the equilibrium analyte concentration in the PE or POM in ng kg^{-1}, $K_{Polymer\text{-}W}$ is the compound-specific polymer−water partition coefficient (K_{PEW} or K_{POMW} (L kg^{-1})), $C_{polymer,t}$ is the concentration in the PE or POM after deployment, $C^0{}_{PRC}$ is the initial concentration of PRC in the sampler, $C_{PRC,t}$ is the concentration of PRC in the sampler after

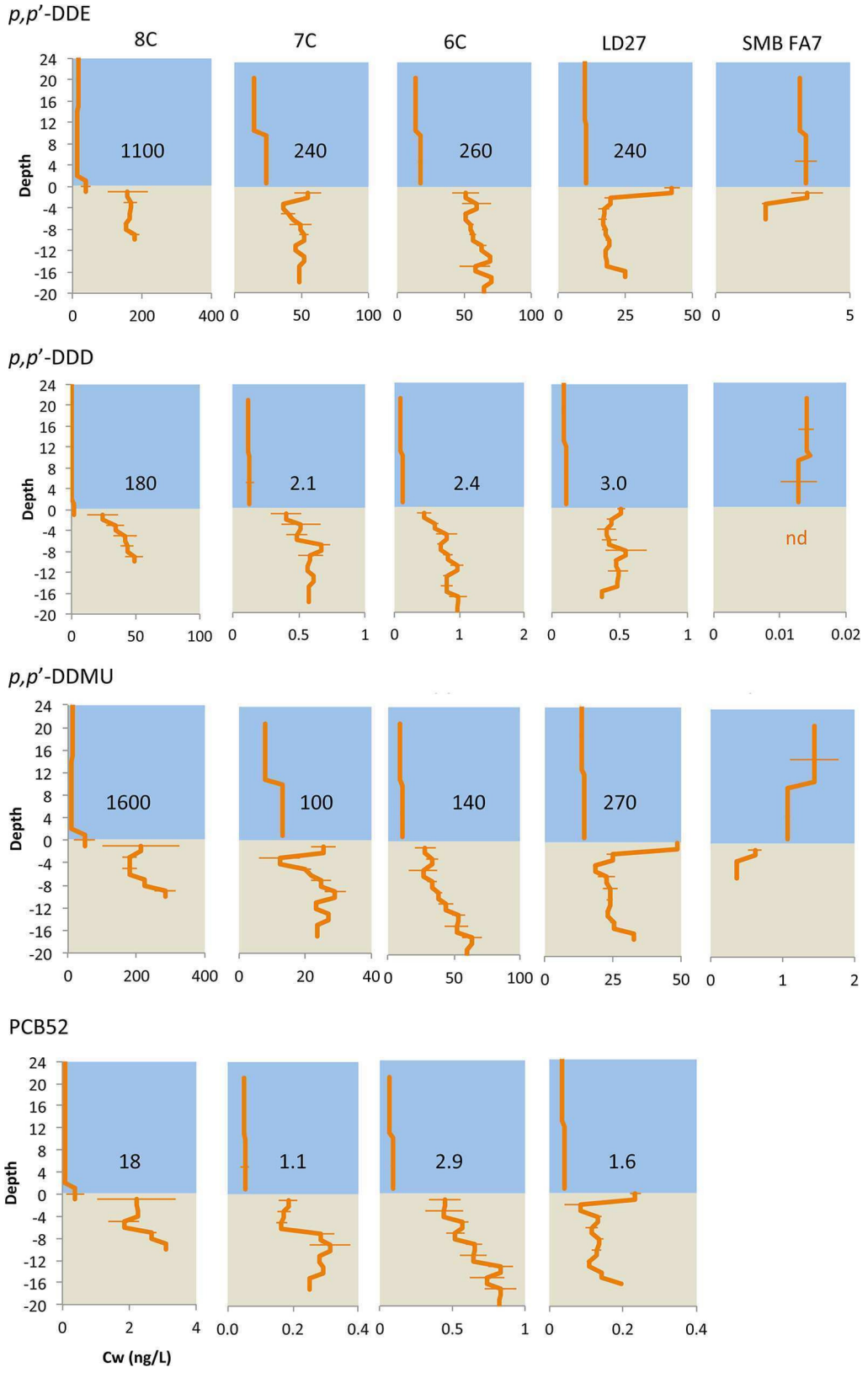

Figure 2. Water column and porewater concentration profiles with depth of *p,p′*-DDE, *p,p′*-DDD, *p,p′*-DDMU, and PCB52 at each station. Values are the average of those generated using three PE passive samplers. Error bars reflect standard error. Values in black are the calculated flux from sediment porewater to the water column in ng cm^{-2} y^{-1}. PCB52 was not detected in the porewaters at the SMB station. Blue background indicates water column matrix and beige background indicates sediment matrix. The *x*-axis scales are different for each station and compound to improve resolution of vertical trends.

dx.doi.org/10.1021/es404475c | *Environ. Sci. Technol.* 2014, 48, 3925−3934

deployment, and f_{eq} is the fractional equilibration of the POPs between the sampler and water. Polymer−water partition coefficients (Table 1) were corrected for the temperature and salinity previously observed in the waters and sediments of PVS[34] following methods described by Lohmann.[33]

The f_{eq} of the ^{13}C-labeled *p,p′*-congeners of DDX compounds were used to determine the fraction equilibration for both *p,p′*- and *o,p′*-forms of the target compounds. The f_{eq}s of ^{13}C-PCB28, ^{13}C-PCB52, ^{13}C-PCB118, and ^{13}C-PCB128 were used as the f_{eq}s for di- and trichlorobiphenyl (PCB8, -18, and -28), tetrachlorobiphenyl (PCB52, -44, and -66), pentachlorobiphenyl (PCB101, -118, and -105), and hexa- and septachlorobiphenyl (PCB153, -138, -128, -187, -180, and -170) target compounds, respectively.

DDX and PCB concentration data from the water column and porewater at the sediment surface of each station were used to calculate diffusive flux for several compounds using eq 1. A boundary layer thicknesses, δ_{BL}, of 0.02 cm was used for all compounds and all stations based on calculations following Sherwood et al.[16] and Chen[19] (kinematic viscosity of 0.013 cm^2 s^{-1} and friction velocity of 0.5 cm s^{-1} were used to calculate δ_{BL}).

RESULTS

Fractional equilibration of PRCs in field exposed samplers varied by compound, sampler type, and environmental matrix (Tables SI1 and SI2). Except for DDT, f_{eq} tended to decrease with increasing polymer−water partition coefficient within each class of compound. ^{13}C-labeled DDT was more depleted in PE exposed to sediments than expected. In most cases, there was better agreement among PE samplers than POM samplers in terms of f_{eq}. Slightly greater f_{eq} were observed in water-side samplers than in sediment side samplers for the more water-soluble compounds, while the trend reversed for the less soluble, penta- and hexachlorobiphenyls.

Water and porewater concentrations were calculated using data from three types of passive samplers for DDXs and PCBs. Water concentrations from PE and POM reflect integrated values over two sections (0 to 10−15 cm above the sediment-water interface, and 10−15 to 20−30 cm above the interface), while SPME sampled water approximately 70 cm above the interface. Porewater concentrations from PE and POM reflect integrations over 1 to 2 cm intervals, to a maximum depth of 20 cm (Tables SI3 and SI4 and Figure 2), while SPME generated porewater concentrations reflect integrations over a 10 cm window at depths between 0 and 20 cm depending on the station. In each set of data, the contaminant observed at the highest concentrations at every station, in either the water column or porewater, was *p,p′*-DDE. Using PE generated concentrations, *p,p′*-DDE averaged 86 (±6)% of the total combined DDX concentrations. The PCBs observed at the highest concentrations were the tri- and tetrachlorobiphenyls, PCB18, -28, -44, and -52, in the range of nanograms per liter in the porewaters at station 8C. Larger PCBs, such as hexa- and septachlorobiphenyls (PCB128, 138, 153, -180 and -187) were calculated to be in the range of 3 to 110 pg L^{-1} in the porewater at the same station but below detection limits (1 to 40 pg L^{-1} for these PCBs) at other stations.

POP concentrations measured just above the sediments at each station were about ten times greater than those measured 5 m above the sediment-water interface a year earlier.[12] This is consistent with observations of increasing dissolved concentrations with depth in the water column. Also, dissolved DDE concentrations just above the sediments are 2 to 5 orders of magnitude greater than background concentrations calculated from measurements in floating PE debris collected from the Northern Pacific Gyre.[39]

Field-Deployed Sampler Comparisons. In general, dissolved POP concentrations determined using PE and POM agreed within 1 order of magnitude. Given uncertainties of 0.2 to 0.5 log units reported for measured and estimated partition coefficients,[20,32,33] agreement within only an order of magnitude is not surprising. More specifically, concentrations of DDXs measured using the two samplers agreed within a factor of 5, with *p,p′*-DDD showing the closest agreement (Figure 3).

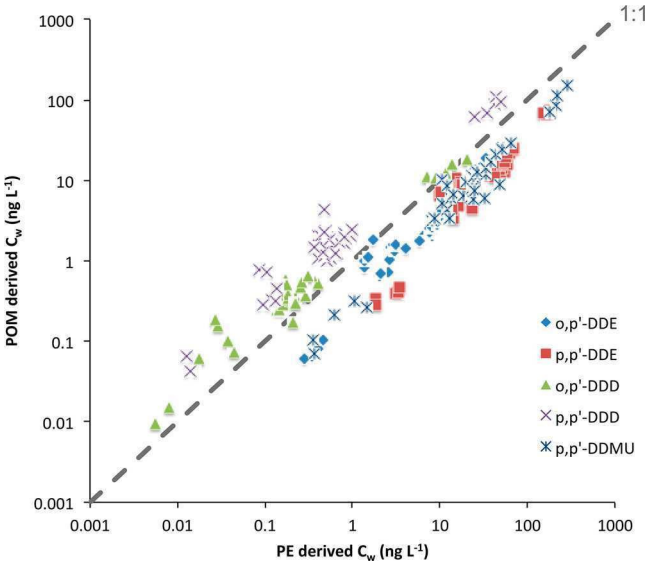

Figure 3. Water column and porewater concentrations generated using field deployed (in situ) POM and PE samplers for DDX compounds. Dashed line indicates 1:1 agreement between values.

Dissolved concentrations of DDEs and DDMU generated from PE measurements were always greater than those generated from POM, while dissolved concentrations of DDDs generated from PE measurement were most often lower than those generated from POM. PE generated PCB concentrations were most often greater than those generated from POM data, with the greatest divergence seen in the septachlorobiphenyl PCB180 (Figure 4). These general trends for differences in calculated water concentrations, for specific compounds, using the two sampler materials, are expected where partition coefficients are uncertain as described above.

Because SPME samplers were exposed to water almost a meter above the sediment water interface, direct comparison of resulting dissolved concentrations to those resulting from PE and POM samplers, exposed within 20 cm of the interface, is not reasonable. In a previous study using PE and SPME samplers in the water column at the PVS Superfund site, concentrations of DDE were observed to increase with depth.[12] SPME derived dissolved concentrations of *p,p′*-DDE measured approximately 70 cm above the sediment-water interface in this work are 2 to 5 times greater at stations 7C and 8C than those measured using SPME suspended 5 m above the sediment water interface in 2010. These measurements would be consistent with a trend of increasing concentrations with approach to sediment bed.

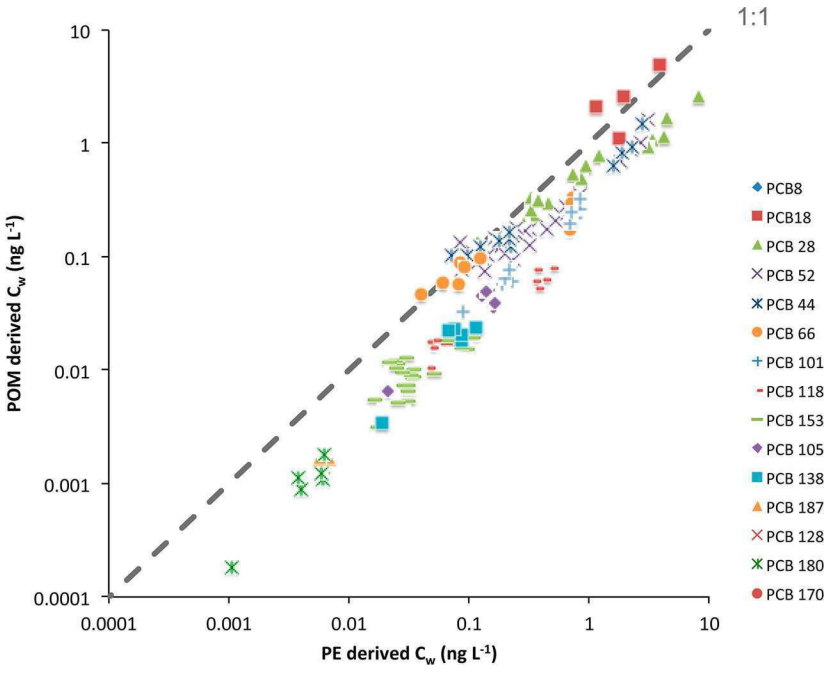

Figure 4. Water column and porewater concentrations generated using field deployed (in situ) POM and PE samplers for selected PCBs. Dashed line indicates 1:1 agreement between values.

PE and SPME derived porewater concentrations, however, were very different. Porewater concentrations determined using PE were up to 230 times larger than those determined using SPME. This large discrepancy may have been due to the way SPME were deployed to the sediment beds. We suspect that attaching SPME copper casings inside of L-shaped steel bars did not allow for sufficient contaminant mass-transfer between porewater and the SPME fibers. As in previous work,[12] another reason calculated dissolved concentrations may differ between the types of samplers deployed is that PE and POM were corrected for nonequilibrium using PRCs, while SPME fibers were assumed to be fully equilibrated. No experiments were conducted, however, that would confirm that SPME deployed in this manner would have reached equilibrium with sediment porewaters within the 43 to 44 d deployment times.

DISCUSSION

Laboratory versus Field Measurements. As previously observed for sediments containing polycyclic aromatic hydrocarbons,[25,26] the experiments conducted in the laboratory using field-collected sediments confirmed that the method of using PRCs to account for disequilibrium between PE and water or porewater is effective (Figures SI5, SI6, and SI7). In addition, laboratory and field exposed PE samplers yielded similar results. Porewater concentrations of *p,p′*-DDE measured using PE (with PRCs) in the laboratory were 170 and 84 ng L^{-1} at stations 8C and 6C, respectively, while porewater concentrations measured in the surface sediments following in situ PE deployment were 160 and 51 ng L^{-1} at stations 8C and 6C, respectively. Similar agreement was seen for *o,p′*-DDE and *p,p′*-DDMU in the same samples.

POP Flux between Sediments and Water Column. While the passive sampling methods used in this work could not resolve the dissolved concentrations at the same scale as the calculated diffusive boundary layer (100 μm scale), the concentrations could be measured much closer to those boundaries than have been attempted in the past (cm scales). Also, because passive samplers are time integrative, temporal variability in water concentrations advecting past each station could not be detected. Concentrations near the sediment-water interface at the PVS stations were assumed to be constant for the calculation of diffusive flux. As expected, the station with the highest previously measured sediment concentrations (8C)[40] was calculated to have the greatest flux of POPs from sediment to water column (Figure 2 and Table 2). Calculated fluxes for DDX were similar at each of the other stations on the PVS (7C, 6C, and LD27). At the off-site station (SMB FA7), fluxes were too small to calculate (concentrations in water and porewater were the same within uncertainty).

The diffusive flux at station 6C calculated using the data collected for this work was more than an order of magnitude

Table 2. Calculated Flux in ng cm^{-2} y^{-1} for DDX and Selected PCB Congeners Calculated from PE Sampler Results[a]

	station			
compound	8C	7C	6C	LD27
o,p′-DDE	190 (±90)	42 (±19)	43 (±22)	33 (±5)
p,p′-DDMU	1600 (±300)	100 (±66)	140 (±90)	270 (±10)
p,p′-DDE	1100 (±300)	240 (±150)	260 (±140)	240 (±40)
o,p′-DDD	52 (±30)	0.71 (±0.46)	1.4 (±0.4)	0.88 (±0.27)
p,p′-DDD	180 (±70)	2.1 (±1.6)	2.4 (±1.5)	3.0 (±0.4)
PCB28	28 (±5)	1.7 (±0.4)		
PCB52	18 (±1)	1.1 (±0.4)	2.9 (±1.6)	1.6 (±0.2)
PCB101	5.9 (±1.1)	0.62 (±0.35)	0.68 (±0.40)	0.78 (±0.18)
PCB153	0.7 (±0.2)		0.14 (±0.05)	0.25 (±0.03)

[a]Positive values indicated flux from sediment porewater to water column. Blank values indicate no flux could be calculated because gradient was within uncertainty. Uncertainty calculated from propagation of error (1 SD, n = 3) of dissolved concentrations in porewater and bottom water.

dx.doi.org/10.1021/es404475c | Environ. Sci. Technol. 2014, 48, 3925−3934

lower than that calculated by Sherwood et al.[16] using porewater concentrations estimated from sediment concentrations and organic carbon fractions. Considering the assumptions of the EqP model used in the Sherwood et al. estimate, this is not surprising. Because the same EqP model was used in their work to calculate desorption during resuspension events, the modeled flux due to resuspension events may also be proportionally off. Even if a field campaign for making in situ measurements as described here is not viable, determining dissolved concentrations using passive samplers exposed to bulk sediment in the laboratory could improve calculations of site-specific sediment-water partition coefficients, K_d, used in the calculation of fluxes due to molecular diffusion and resuspension/desorption.

Sediment Porewater Concentration Gradients. While only the surface sediment porewater concentrations (0−2 cm) were used in calculating diffusive flux of POPs between sediment and water, porewater concentrations profiles with depths were collected (Figure 2). Although the highest sediment concentrations observed in cored samples from stations 8C, 7C, and 6C were found at depths of 20 to 42 cm (U.S. EPA, unpublished data), samplers in this work only reached a maximum depth of 20 cm. Slight gradients with depth may be observed for DDD and DDMU at the uncapped PVS stations, while DDE concentrations appear to be more uniform within the top 20 cm of sediments. The capped site (LD27) shows sharply higher concentrations of DDE, DDMU, and PCB in the top sediment section (0−2 cm depth) similar to those observed at nearby station 6C, while the deeper porewaters had about half the concentration observed at station 6C. While a layer of higher concentration may have formed as sediment, disturbed during the cap placement, resettled, it may also have been generated by sediments from another location settling following resuspension events since cap placement. The second alternative is more consistent with observations made during monitoring of the capped area. While the cap depth at this station is expected to be between 4 and 16 cm,[41] it is not possible to determine if the sampler crossed the sand cap into the original sediment bed.

Effects of the Sand Cap on Flux. Flux calculations based on concentration gradients between the surface sediment layer and the water column above the sediments indicate that the exchange of POPs between sediment and water in the sand capped area due to molecular diffusion is similar to that at nearby stations (Figure 2 and Table 2) (240 ng cm^{-2} y^{-1} at station LD27 vs 260 ng cm^{-2} y^{-1} at station 6C). Assuming that the porewater concentrations at this station are representative of the capped area, the sediments in the capped zone continue to be a source of contamination to the water column in terms of diffusive flux. If the surface layer of sediments with relatively higher porewater concentrations of DDE, DDMU, and PCBs were not present (i.e., surface porewater concentrations were those measured below 2 cm depth in sediments), it could be assumed that the diffusive flux at the station would be reduced by about one-half.

While we did not directly investigate the effects of the sand cap on desorption during resuspension events or on the tissue concentrations of benthic organisms, the porewater concentration data can inform estimates of those effects. Porewater concentrations in the sediment surface layer indicate the maximum concentration the water in contact with resuspended particles would reach. These data can be combined with desorption kinetics models to refine calculations of flux due to resuspension events. Also, tissue concentrations of benthic organisms have been shown to correlate with dissolved porewater concentrations.[42] Depending on the sediment horizon with which benthic organisms in the capped area are most associated, and assuming that sediments below the cap are like those at nearby station 6C, the cap could have the effect of lowering tissue concentrations by half (for organisms associated with sediments below 2 cm thick surface layer, but within capping material) or could have no effect (for organisms associated with sediments in the top 2 cm). Consequently, given these considerations, the cap has the potential to be an effective tool for separating contaminated sediments at PVS from the water column except that the cap itself has been "capped" by contaminated sediments, presumably from another part of the PVS or by sediments disturbed during cap placement. An effective remedy would require the cap to be placed over the most contaminated sediments, using methods that avoid resettling of sediment on cleaner cap material.

Future Work. Although it is expected that the qualities of organic sorbents present in the sediment bed vary across the PVS, the results of this work could contribute to the general accounting of contaminant mass into and out of the water column above the PVS. Porewater concentrations calculated in this work could be combined with bulk sediment concentrations and organic carbon fractions measured previously[40] to produce representative organic carbon−water partition coefficients, $K_{OC,\ PVS}$ for PVS sediments. These partition coefficients combined with organic carbon fractions and POP concentrations in sediments and water column[12] could be used to account for shelf wide contaminant mass transfers. These types of analyses will be the subjects of continued work. In addition, passive samplers and deployment platforms, like those used in this work, could be used to investigate the efficacy of remedial efforts in sediments or to determine the magnitude of sediments as a source or sink for POPs in other aquatic systems.

■ ASSOCIATED CONTENT

Ⓢ Supporting Information

Methods for ex situ PRC method testing. Results of ex situ equilibrium vs nonequilibrium (PRC) method testing. Tables of f_{eq} in PE and POM samplers. Tables of PE, POM, and SPME deduced water column and porewater DDX and PCB concentrations. Images of sampler platform design, deployment, and recovery. Figures comparing results of equilibrium and nonequilibrium sampling of sediment samples in the laboratory to TOC-corrected slurry water concentrations. This material is available free of charge via the Internet at http://pubs.acs.org.

■ AUTHOR INFORMATION

Corresponding Author

*Phone: 617-393-5461. E-mail: l.fernandez@neu.edu.

Present Address

[†]Departments of Civil and Environmental Engineering, and Marine and Environmental Sciences, Northeastern University, 360 Huntington Avenue, 473 Snell Engineering, Boston, MA 02115, USA.

Notes

The authors declare no competing financial interest.

■ ACKNOWLEDGMENTS

The authors thank Fred Stern, Bill Power, Cheryl Brantley, Bill Furlong, Chase McDonald, Chi-Li Tang, and Joe Gully of the Los Angeles County Sanitation Districts, along with Steve Gregson and Robert Harper, of RV *Ocean Sentinel*, for their assistance in the design, assembly, deployment, and recovery of the sampler platforms. We thank Adam Kopacsi of DCT Narragansett for his work in fabricating the sampler platforms. Mike Charpentier (Raytheon, Narragansett, RI, USA) prepared Figure 1. The authors also thank Mark Cantwell, David Katz, Wayne Munns, Ashley Parks, and Brenda Rashleigh for their insightful comments on the draft manuscript. Mention of trade names or commercial products does not constitute endorsement or recommendation for use. This report has been reviewed by the U.S. EPA's Office of Research and Development National Health and Environmental Effects Research Laboratory, Atlantic Ecology Division, Narragansett, RI, and approved for publication. Approval does not signify that the contents necessarily reflect the views and policies of the Agency.This research was performed while the first author held a National Research Council Research Associateship Award at the U.S. EPA, Atlantic Ecology Division, Narragansett, Rhode Island, USA.

■ REFERENCES

(1) Venkatesan, M. I.; Greene, G. E.; Ruth, E.; Chartrand, A. B. DDTs and dumpsite in the Santa Monica Basin, California. *Sci. Total Environ.* **1996**, *179*, 61−71.

(2) Quensen, J. F.; Mueller, S. A.; Jain, M. K.; Tiedje, J. M. Reductive dechlorination of DDE to DDMU in marine sediment microcosms. *Science* **1998**, *280*, 722−724.

(3) Eganhouse, R. P.; Pontolillo, J. Depositional history of organic contaminants on the Palos Verdes Shelf, California. *Mar. Chem.* **2000**, *70*, 317−338.

(4) Eganhouse, R. P.; Pontolillo, J.; Leiker, T. J. Diagenic fate of organic contaminants on the Palos Verdes Shelf, California. *Mar. Chem.* **2000**, *70*, 289−315.

(5) Quensen, J. F.; Tiedje, J. M.; Jain, M. K.; Mueller, S. A. Factors controlling the rate of DDE dechlorination to DDMU in Palos Verdes margin sediments under anaerobic conditions. *Environ. Sci. Technol.* **2001**, *35*, 286−291.

(6) Eganhouse, R. P.; Pontolillo, J. DDE in sediments of the Palos Verdes Shelf, California: *in situ* transformation rates and geochemical fate. *Environ. Sci. Technol.* **2008**, *42*, 6392−6398.

(7) U.S.EPA, EPA Announces Proposed Plan. In *Palos Verdes Shelf Superfund Site* 9, R., Ed.; U.S. Environmental Protection Agency: San Francisco, CA, USA, 2009.

(8) Young, D. R.; Heesen, T. C.; McDermott, D. J. An offshore biomonitoring system for chlorinated hydrocarbons. *Mar. Pollut. Bull.* **1976**, *7* (8), 156−159.

(9) Larsson, P. Contaminated sediments of lakes and oceans act as sources of chlorinated hydrocarbons for release to water and atmosphere. *Nature* **1985**, *317*, 347−349.

(10) Zeng, E. Y.; Yu, C. C.; Tran, K. In situ measurements of chlorinated hydrocarbons in the water column off the Palos Verdes Peninsula, California. *Environ. Sci. Technol.* **1999**, *33* (3), 392−398.

(11) Friedman, C. L.; Lohmann, R.; Burgess, R. M.; Perron, M. M.; Cantwell, M. G. Resuspension of PCB-contaminated field sediment: Release to the water column and determination of site-specific K_{DOC}. *Environ. Toxicol. Chem.* **2011**, *30*, 377−384.

(12) Fernandez, L. A.; Lao, W.; Maruya, K. A.; White, C.; Burgess, R. M. Passive sampling to measure baseline dissolved persistent organic pollutant concentrations in the water column of the Palos Verdes Shelf Superfund site. *Environ. Sci. Technol.* **2012**, *46* (21), 11937−11947.

(13) Lick, W. The sediment-water flux of HOCs due to "diffusion" or Is there a well-mixed layer? If there is, does it matter? *Environ. Sci. Technol.* **2006**, *40*, 5610−5617.

(14) Chadwick, D. B.; Davidson, B.; Hampton, T.; Groves, J.; Guerrero, J.; Stang, P. *Offshore Porewater and Flux Chamber Sampling of San Diego Bay Sediments at Site 9, Naval Air Station, North Island*; SPAWAR Systems Center: San Diego, CA, USA, July 1999, 1999; p 77.

(15) Eek, E.; Cornelissen, G.; Breedveld, G. D. Field measurement of diffusional mass transfer of HOCs at the sediment-water interface. *Environ. Sci. Technol.* **2010**, *44*, 6752−6759.

(16) Sherwood, C. R.; Drake, D. E.; Wiberg, P. L.; Wheatcroft, R. A. Prediction of the fate of *p,p′*-DDE in sediment on the Palos Verdes shelf, California, USA. *Cont. Shelf Res.* **2002**, *22*, 1025−1058.

(17) Hawthorne, S. B.; Grabanski, C. B.; Miller, D. J. Measured partitioning coefficients for parent and alkyl polycyclic aromatic hydrocarbons in 114 historically contaminated sediments: Part 1. Koc values. *Environ. Toxicol. Chem.* **2006**, *25* (11), 2901−2911.

(18) Accardi-Dey, A.; Gschwend, P. Reinterpreting literature sorption data considering both absorption into organic carbon and adsorption onto black carbon. *Environ. Sci. Technol.* **2003**, *37*, 99−106.

(19) Chen, H.-W. *Fluxes of Organic Pollutants from the Sediments in Boston Harbor*. Thesis S.M. - Department of Civil and Environmental Engineering, Massachusetts Institute of Technology, Cambridge, MA, 1993.

(20) Adams, R. G.; Lohmann, R.; Fernandez, L. A.; MacFarlane, J. K.; Gschwend, P. M. Polyethylene devices: Passive samplers for measuring dissolved hydrophobic organic compounds in aquatic environments. *Environ. Sci. Technol.* **2007**, *41* (4), 1317−1323.

(21) Zeng, E. Y.; Peng, J.; Tsukada, D.; Ku, T.-L. In situ measurements of polychlorinated biphenyls in the waters of San Diego Bay, California. *Environ. Sci. Technol.* **2002**, *36*, 4975−4980.

(22) Zeng, E. Y.; Tsukada, D.; Diehl, D. W. Development of a solid-phase microextraction-based method for sampling of persistent chlorinated hydrocarbons in an urbanized coastal environment. *Environ. Sci. Technol.* **2004**, *38* (21), 5737−5743.

(23) Cornelissen, G.; Pettersen, A.; Broman, D.; Mayer, P.; Breedveld, G. Field testing of equilibrium passive samplers to determine freely dissolved native polycyclic aromatic hydrocarbon concentrations. *Environ. Toxicol. Chem.* **2008**, *27*, 499−508.

(24) Perron, M. M.; Burgess, R. M.; Suuberg, E. M.; Cantwell, M. G.; Pennell, K. G. Performance of passive samplers for monitoring estuarine water column concentrations: 2. Emerging contaminants. *Environ. Toxicol. Chem.* **2013**, *32* (10), 2190−2196.

(25) Fernandez, L. A.; Harvey, C. F.; Gschwend, P. M. Using performance reference compounds in polyethylene passive samplers to deduce sediment porewater concentrations for numerous target chemicals. *Environ. Sci. Technol.* **2009**, *43*, 8888−8894.

(26) Fernandez, L. A.; MacFarlane, J. K.; Tcaciuc, A. P.; Gschwend, P. M. Measurement of freely dissolved PAH concentrations in sediment beds using passive sampling with low-density polyethylene strips. *Environ. Sci. Technol.* **2009**, *43* (5), 1430−1436.

(27) Jonker, M. T. O.; Koelmans, A. A. Polyoxymethylene solid phase extraction as a partitioning method for hydrophobic organic chemicals in sediment and soot. *Environ. Sci. Technol.* **2001**, *35* (18), 3742−3748.

(28) Oen, A. M. P.; Janssen, E. M. L.; Cornelissen, G.; Breedveld, G. D.; Eek, E.; Luthy, R. G. In situ measurement of PCB pore water concentration profiles in activated carbon-amended sediment using passive samplers. *Environ. Sci. Technol.* **2011**, *45*, 4053−4059.

(29) Maruya, K. A.; Zeng, E. Y.; Tsukada, D.; Bay, S. M. A Passive sampler based on solid-phase microextraction for quantifying hydrophobic organic contaminants in sediment pore water. *Environ. Toxicol. Chem.* **2009**, *28* (4), 733−740.

(30) Gschwend, P. M.; MacFarlane, J. K.; Reible, D. D.; Lu, X.; Hawthorne, S. B.; Nakles, D. V.; Thompson, T. Comparison of polymeric samplers for accurately assessing PCBs in pore waters. *Environ. Toxicol. Chem.* **2011**, *30* (6), 1288−1296.

(31) Lohmann, R.; Muir, D. C. G. Global aquatic passive sampling (AQUA-GAPS): Using passive samplers to monitor POPs in the Waters of the world. *Environ. Sci. Technol.* **2010**, *44*, 860−864.
(32) Endo, S.; Hale, S. E.; Goss, K.-U.; Arp, H. P. H. Equilibrium partition coefficients of diverse polar and nonpolar organic compounds to polyoxymethylene (POM) passive sampling devices. *Environ. Sci. Technol.* **2011**, *45*, 10124−10132.
(33) Lohmann, R. Critical review of low-density polyethylene's partitioning and diffusion coefficients for trace organic contaminants and implications for its use as a passive sampler. *Environ. Sci. Technol.* **2012**, *46*, 606−618.
(34) Noble, M. A.; Ryan, H. F.; Wiberg, P. L. The dynamics of subtidal poleward flows over a narrow continental shelf, Palos Verdes, CA. *Cont. Shelf Res.* **2002**, *22*, 923−944.
(35) Hawker, D. W.; Connell, D. W. Octanol-water partition coefficients of polychlorinated biphenyl congeners. *Environ. Sci. Technol.* **1988**, *22* (4), 382−387.
(36) U.S.EPA *Estimation Programs Interface Suite for Microsoft Windows*, v. 4.11; United States Environmental Protection Agency: Washington, DC, USA, 2013.
(37) Pontolillo, J.; Eganhouse, R. P. *The Search for reliable aqueous solubility (Sw) and octanol-water partition coefficient (Kow) data for hydrophobic organic compounds: DDT and DDE as a Case Study*; U.S. Geological Survey: 2001.
(38) Schwarzenbach, R.; Gschwend, P.; Imboden, D. *Environmental Organic Chemistry*, 2nd ed.; Wiley: Hoboken, NJ, 2003; p xiii, 1313p.
(39) Rios, L. M.; Jones, P. R.; Moore, C.; Narayan, U. V. Quantitation of persistent organic pollutants adsorbed on plastic debris from the Northern Pacific Gyre's ″eastern garbage patch″. *J. Environ. Monit.* **2010**, *12* (12), 2189−2312.
(40) U.S.EPA *Palos Verdes Shelf Superfund Site Operable Unit 5 of the Montrose Chemical Corp. Superfund Site - Final Feasibility Study*; U.S. Environmental Protection Agency, Region IX: San Francisco, CA, May 2009, 2009; p 239.
(41) (SAIC), S. A. I. C. *Monitoring Results from the March 2002 Post-Cap Survey on the Palos Verdes Shelf - Final Report*; Newport, RI, July 2003, 2003.
(42) DiToro, D. M.; Zarba, C.; Hansen, D. J.; Berry, W.; Swartz, R. C.; Cowan, C.; Pavlou, S.; Allen, H.; Thomas, N.; Paquin, P. Technical basis for establishing sediment quality criteria for nonionic organic-chemicals using equilibrium partitioning. *Environ. Toxicol. Chem.* **1991**, *10*, 1541.

Environmental Science & Technology

Critical Review

pubs.acs.org/est

Evaluating the Relationship between Equilibrium Passive Sampler Uptake and Aquatic Organism Bioaccumulation

Abigail S. Joyce*

U.S. Environmental Protection Agency, ORD/NHEERL Atlantic Ecology Division Narragansett, Rhode Island 02882, United States

Lisa M. Portis

Physical Therapy Department University of Rhode Island Kington, Rhode Island 02881, United States

Ashley N. Parks†

U.S. Environmental Protection Agency, ORD/NHEERL Atlantic Ecology Division Narragansett, Rhode Island 02882, United States

Robert M. Burgess

U.S. Environmental Protection Agency, ORD/NHEERL Atlantic Ecology Division Narragansett, Rhode Island 02882, United States

Supporting Information

ABSTRACT: This Critcal Review evaluates passive sampler uptake of hydrophobic organic contaminants (HOCs) in water column and interstitial water exposures as a surrogate for organism bioaccumulation. Fifty-seven studies were found where both passive sampler uptake and organism bioaccumulation were measured and 19 of these investigations provided direct comparisons relating passive sampler uptake and organism bioaccumulation. Polymers compared included low-density polyethylene (LDPE), polyoxymethylene (POM), and polydimethylsiloxane (PDMS), and organisms ranged from polychaetes and oligochaetes to bivalves, aquatic insects, and gastropods. Regression equations correlating bioaccumulation (C_L) and passive sampler uptake (C_{PS}) were used to assess the strength of observed relationships. Passive sampling based concentrations resulted in log−log predictive relationships, most of which were within one to 2 orders of magnitude of measured bioaccumulation. Mean coefficients of determination (r^2) for LDPE, PDMS, and POM were 0.68, 0.76, and 0.58, respectively. For the available raw, untransformed data, the mean ratio of C_L and C_{PS} was 10.8 ± 18.4 (n = 609). Using passive sampling as a surrogate for organism bioaccumulation is viable when biomonitoring organisms are not available. Passive sampling based estimates of bioaccumulation provide useful information for making informed decisions about the bioavailability of HOCs.

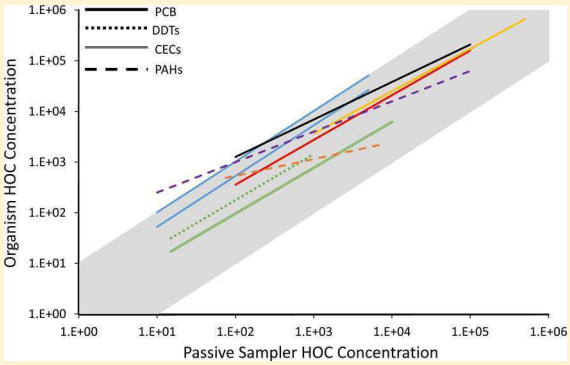

INTRODUCTION

Anthropogenic hydrophobic organic compounds (HOCs), like polychlorinated biphenyls (PCBs), some polycyclic aromatic hydrocarbons (PAHs), chlorinated pesticides, such as dichlorodiphenyltrichloroethane (DDT) and its metabolites, polybrominated diphenyl ethers (PBDEs), and polychlorinated dioxins and furans are found throughout the environment. These types of compounds often bioaccumulate in aquatic organisms, undergo trophic transfer, and, in some cases, biomagnify up the aquatic food chain.[1] In addition, some HOCs at sufficiently elevated concentrations, will cause toxicity to these organisms.[2] Because of their low water solubility and high affinity for organic matter, most HOCs are concentrated in the sediment organic and black carbon reservoirs and in organismal lipid reserves.[2] Over time, sediments can release these legacy HOCs back into the water column via sorption/desorption mechanisms and diffusive and advective processes as well as bioaccumulation-based transfers. Therefore, sediments can serve as a major source of ecosystem and human exposure to HOCs.[3] Continued environmental monitoring of these types of chemicals is essential for identifying historical as well as current HOC sources and evaluating the efficacy of remediation and emission reduction programs.

Received: June 30, 2016
Revised: September 22, 2016
Accepted: September 28, 2016
Published: September 28, 2016

ACS Publications © 2016 American Chemical Society

DOI: 10.1021/acs.est.6b03273
Environ. Sci. Technol. 2016, 50, 11437−11451

Measuring the bioaccumulation of HOCs in aquatic systems (i.e., biomonitoring) provides direct evidence of a chemical's potential for ecological and human health risks by demonstrating the contaminant's bioavailability. That is, HOCs are present in many different environmental phases (e.g., particulate, dissolved, colloidal), bioavailable HOCs are freely dissolved in the aqueous phase and are able to pass through biological membranes for uptake by organisms.[4] Bioavailable contaminants accumulated in an organism's lipids demonstrates those HOCs' large affinity for the lipid phase.[5] The bioaccumulated concentration is often expressed on a lipid basis and is used to calculate partition coefficients, such as the bioaccumulation factor (BAF) (L/g lipid)

$$\mathrm{BAF} = \frac{C_\mathrm{L}}{C_\mathrm{free}} \tag{1}$$

and the biota-sediment accumulation factor (BSAF) (g organic carbon (OC)/g lipid)

$$\mathrm{BSAF} = \frac{C_\mathrm{L}}{C_\mathrm{OC}} \tag{2}$$

where C_L is the lipid-normalized concentration of a given HOC (ng/g lipid) accumulated by an organism, C_free is the freely dissolved water concentration of the HOC (ng/L), and C_OC is the organic carbon normalized concentration of the HOC in the exposure sediment (ng/g OC). Conventionally, bioavailability has been measured through the monitoring of aquatic organism bioaccumulation and several long-term biomonitoring programs have been established using bivalves to track water column HOCs[6−9] and assess the effectiveness of contaminated site remediation.[10,11]

Evaluating the bioavailability of HOCs can also be performed by studying the physicochemical characteristics of the environment since the magnitude of a particular HOC's bioavailability is related to its chemical activity in the system.[12,13] Similar to tissue concentration normalization by lipid content, normalizing the total sediment particle concentration (C_P) (ng/kg sediment dry) of a HOC by the fraction of organic carbon (f_OC) (kg OC/kg sediment dry) has been shown to be effective for predicting the C_free. Specifically, the C_free of a given sediment is calculated by incorporating the HOC's organic carbon normalized-water partitioning coefficient (K_OC) (L/kg OC) as illustrated in eq 3.[2,14] This equilibrium partitioning approach is based on the concept that HOCs strongly bound to sediments (e.g., particulate organic carbon, black carbon) are often not as readily bioavailable and do not directly contribute to the environmental exposure of the contaminant when compared to C_free

$$C_\mathrm{free} = \frac{C_\mathrm{P}}{f_\mathrm{OC} \cdot K_\mathrm{OC}} \tag{3}$$

Another environmental phase affecting the bioavailability of HOCs is sedimentary black carbon. The calculation of C_free in eq 3 can be modified to incorporate the role of black carbon

$$C_\mathrm{free} = \frac{C_\mathrm{P}}{f_\mathrm{OC} \cdot K_\mathrm{OC} + f_\mathrm{BC} \cdot K_\mathrm{BC} \cdot {C_\mathrm{free}}^{n-1}} \tag{4}$$

where f_BC is the fraction of black carbon in the sediment (kg black carbon (BC)/kg sediment dry), K_BC is the black carbon normalized partition coefficient (L/kg BC), and n is the unitless Freundlich exponent, which captures the nonlinear adsorption of HOCs to black carbon.[15] Both approaches for calculating C_free are useful for estimating bioavailability, but for several reasons, including uncertainty associated with the K_OC and K_BC values and confidence in f_BC measurements, eq 3 tends to overestimate C_free, while eq 4 will often underestimate C_free.[16]

Recently, passive sampling has been shown to be a successful tool for a more direct measurement of C_free in comparison to using physicochemical characteristics of the environment.[17,18] Passive sampling provides an integrated measure of HOC C_free by considering contaminant activity across all of the relevant environmental phases (e.g., water, sediments, dissolved organic carbon, colloids, and organisms), often providing a more accurate estimate of bioavailability than sediment-based or lipid-based measurements alone as shown in eqs 3 and 4 for sediments and eqs 1 and 2 for lipids.[19,20] Passive samplers function by concentrating freely dissolved HOCs in the water column or sediment interstitial water into a polymer phase (i.e., the passive sampler) as a result of differences in the HOC's chemical activity among the polymer and different environmental phases. At equilibrium, the HOC concentration ratio between the polymer and the water, expressed by the passive sampler-water partition coefficient (K_PS; $L_\mathrm{water}/kg_\mathrm{polymer}$ or $L_\mathrm{water}/L_\mathrm{polymer}$) is constant. The relationship is

$$K_\mathrm{PS} = \frac{C_\mathrm{PS}}{C_\mathrm{free}} \tag{5}$$

where C_PS (ng/kg polymer or ng/L polymer) is the concentration of the HOC in the polymer phase at equilibrium. The C_free can be estimated by rearranging eq 5 using K_PS (based on literature or empirical values) and measuring C_PS directly.

Passive sampling became popular in the 1990s with the introduction of semipermeable membrane devices (SPMDs)[21] and solid-phase microextraction (SPME).[22] Much research has been dedicated to optimizing and simplifying their use in the water column and sediment interstitial water.[23−27] In North America, three polymers are most popular for sampling HOCs in the water column and sediment interstitial waters: polydimethylsiloxane (PDMS) (used in SPME) and other silicones, low-density polyethylene (LDPE), and polyoxymethylene (POM).[28] Other polymers, including ethylene vinyl acetate (EVA)[29,30] and polyacrylate,[31,32] are also available but are applied to a lesser extent than PDMS, LDPE, and POM.

There are a number of publications describing the development and utility of PDMS,[25] LDPE,[24] and POM[33,34] as passive samplers and comprehensive reviews of their application in water column and sediment deployments have been published.[26,28,35−39] In addition to demonstrating passive sampler dependability and effectiveness in measuring C_free, these reviews also discuss passive sampling's potential value as a surrogate for biomonitoring organisms. The concentration of HOCs accumulated by the polymer (C_PS) allows for the calculation of C_free but C_PS can also be compared to the concentration of HOCs bioaccumulated by organisms (C_L). Recent research has directly compared passive sampler uptake to bioaccumulation by organisms both in situ (i.e., in the field) and ex situ (i.e., in the laboratory). This type of comparison investigates a mechanistic assumption that the passive sampler polymer and the organism lipid have a similar, proportional affinity for a given HOC (i.e., $C_\mathrm{PS} \approx C_\mathrm{L}$). This paradigm stems from the concept that HOCs partition into PDMS, LDPE, and POM in a similar proportionality as they partition into lipids. These similarities are illustrated by the following linear free

DOI: 10.1021/acs.est.6b03273
Environ. Sci. Technol. 2016, 50, 11437−11451

Table 1. Data Used to Compare Tissue Bioaccumulation HOC Concentrations with Passive Sampler HOC Concentrations[a]

ref	target contaminant	passive sampler	equilibrium status	organism	field (F) or laboratory (L) study	equation
Vinturella et al.[78]	PAHs	LDPE	assumed	marine polychaete *Nereis virens*	L	$\log(C_L) = 0.6 \log(C_{PS}) + 1.8$ $r^2 = 0.65$
Gschwend et al.[70]	PCBs	LDPE	adjusted	marine polychaete *Neanthes arenaceodentata*	L	$\log(C_L) = \log(C_{PS}) + 0.722$ $r^2 = 0.59$
Gschwend et al.[70]	PCBs	LDPE	established	marine polychaete *Neanthes arenaceodentata*	L	$\log(C_L) = \log(C_{PS}) + 1.00$ $r^2 = 0.64$
Friedman et al.[71]	PCBs	LDPE	adjusted	marine polychaete *Nereis virens*	L	$\log(C_L) = 0.82 \log(C_{PS}) + 0.79$ $r^2 = 0.94$ $p < 0.0001$
Burgess et al.[72]	PCBs	LDPE	adjusted	marine blue mussel *Mytilus edulis*	F	$\log (C_L) = 0.74 \log(C_{PS}) + 1.62$ $r^2 = 0.92$ $p < 0.0001$
Fernandez and Gschwend[68]	PAHs	LDPE	adjusted	marine soft shell clam *Mya arenaria*	F	$\log (C_L) = 0.33 \log(C_{PS}) + 2.07$ $r^2 = 0.31$
Joyce et al.[74]	DDT	LDPE	adjusted	marine blue mussel *Mytilus californianus*	F	$\log(C_L) = 0.91 \log(C_{PS}) + 0\ 43$ $r^2 = 0.72$ $p < 0.0001$
	PBDEs					$\log (C_L) = 0.91 \log(C_{PS}) + 0\ 17$ $r^2 = 0.54$ $p = 0.0012$
this study	PCBs	LDPE	adjusted	marine polychaete *Nereis virens*	L	$\log(C_L) = 0.84 \log(C_{PS}) + 1.05$ $r^2 = 0.82$ $p < 0.0001$
Smedes[65]	PCBs	silicone-sheeting	adjusted	marine blue mussel *Mytilus edulis*	F	$\log(C_L) = 1.03 \log(C_{PS}) + 0.178$ $r^2 = 0.80$ $p < 0.0001$
Smedes[65]	PAHs	silicone-sheeting	adjusted	marine blue mussel *Mytilus edulis*	F	$\log(C_L) = 0.831 \log(C_{PS}) + 1.09$ $r^2 = 0.78$ $p < 0.0001$
Trimble et al.[69]	PCBs	PDMS-SPME	established	freshwater oligochaete *Lumbriculus variegatu*	L	$\log(C_L) = 1.09 \log(C_{PS}) + 0.51$ $r^2 = 0.86$
Gschwend et al.[70]	PCBs	PDMS-SPME	adjusted	marine polychaete *Neanthes arenaceodentata*	L	$\log(C_L) = \log(C_{PS}) + 1.3$ $r^2 = 0.91$
Harwood et al.[79]	pyrethroid pesticides	PDMS-SPME	assumed	freshwater oligochaete *Lumbriculus variegatus* freshwater burrowing mayfly *Hexagenia sp.*	L	$\log(C_L) = 0.81 \log(C_{PS}) - 0.122$ $r^2 = 0.73$
Muijs and Jonker[77]	PAHs	PDMS-SPME	assumed	freshwater oligochaete *Lumbriculus variegatus*	F	$\log (C_L) = 0.77 \log(C_{PS}) + 2.06$ $r^2 = 0.66$ $p < 0.0001$
Bao et al.[73]	DDTs	PDMS-SPME	adjusted	marine polychaete *Neanthes arenaceodentata*	L	p,p′-DDE: $\log(C_L) = 0.763 \log(C_{PS}) + 0.496$ $r^2 = 0.84$ p,p′-DDD: $\log(C_L) = 0.662 \log(C_{PS}) + 1.09$ $r^2 = 0.83$
Pirogovsky[75]	DDTs	PDMS-SPME	assumed	marine blue mussel *Mytilus californianus*	F	$\log(C_L) = 1.02 \log(C_{PS}) + 1.2$ $r^2 = 0.64$ $p < 0.0001$
Li et al.[80]	PBDE 209 and dechlorane plus	PDMS-SPME	established	freshwater oligochaete *Lumbriculus variegatus*	L	$\log(C_L) = 1.10 \log(C_{PS}) + 1.28$ $r^2 = 0.77$
Maruya et al.[76]	DDTs	PDMS-SPME	assumed	marine clam *Macoma nasuta*	L	$\log(C_L) = 0.61 \log(C_{PS}) + 2.7$ $r^2 = 0.59$ $p = 0.0005$
Cornelissen et al.[18]	PAHs	POM	assumed	marine gastropod *Hinia reticulata*	L	$\log(C_L) = 0.64 \log(C_{PS}) + 1.6$ $r^2 = 0.39$ $p = 0.0002$
				marine polychaete *Nereis diversicolor*		$\log(C_L) = 1.1 \log(C_{PS}) + 0.64$ $r^2 = 0.57$ $p < 0.0001$

DOI: 10.1021/acs.est.6b03273
Environ. Sci. Technol. 2016, 50, 11437−11451

Table 1. continued

ref	target contaminant	passive sampler	equilibrium status	organism	field (F) or laboratory (L) study	equation
Gschwend et al.[70]	PCBs	POM	assumed	marine polychaete *Neanthes arenaceodentata*	L	$\log(C_L) = \log(C_{PS}) + 0.74$ $r^2 = 0.75$
Janssen et al.[67]	PCBs	POM	assumed[b]	marine polychaete *Neanthes arenaceodentata*	F	$\log(C_L) = 0.72 \log(C_{PS}) + 1.07$ $r^2 = 0.44$
Beckingham and Ghosh[3]	PCBs	POM	assumed	freshwater oligochaete *Lumbriculus variegatus*	F	$\log(C_L) = 1.2 \log(C_{PS}) + 2.05$ $r^2 = 0.56$ $p = 0.03$
this study	PCBs	POM	assumed	marine polychaete *Nereis virens*	L	$\log(C_L) = 0.69 \log(C_{PS}) + 2.07$ $r^2 = 0.76$ $p < 0.0001$
Meloche et al.[44]	PCBs	EVA	assumed	marine clam *Macoma balthica*	L	$\log(C_L) = 0.97 \log(C_{PS}) - 0.88$ $r^2 = 0.98$

[a]Equations are reported as presented in the figures. In cases where raw data were available, p values were calculated. [b]PRCs added but not used to correct for disequilibrium conditions.

energy relationships (eqs 6–9) for lipid and each of the polymers discussed using the readily available octanol–water partition coefficient (K_{OW}) as the independent variable (eq 6, ref 40; eqs 7–9, ref 28)

$$\log\left(\frac{C_L}{C_{free}}\right) = 1.01 \log K_{OW} - 0.07, \quad r^2 = 0.89 \tag{6}$$

$$\log\left(\frac{C_{PDMS}}{C_{free}}\right) = 0.947 \log K_{OW} - 0.17, \quad r^2 = 0.89 \tag{7}$$

$$\log\left(\frac{C_{LDPE}}{C_{free}}\right) = 1.18 \log K_{OW} - 1.26, \quad r^2 = 0.95 \tag{8}$$

$$\log\left(\frac{C_{POM}}{C_{free}}\right) = 0.791 \log K_{OW} + 1.02, \quad r^2 = 0.95 \tag{9}$$

where the ratios of C_{PDMS}, C_{LDPE}, and C_{POM} over C_{free} are the polymer–water partition coefficients for PDMS, LDPE, and POM, respectively, and r^2 is the coefficient of determination. Because there can be uncertainties associated with K_{OW} values, whenever possible, it is prudent to use the most measurable data and plot C_L versus C_{PS} directly. Because of the variations in the reported slopes and intercepts in the equations above, C_L and C_{PS} are unlikely to be equivalent but because the slopes and intercepts are of a similar scale, it is reasonable to expect that C_L and C_{PS} will agree within an order of magnitude.

There are several reasons for considering the use of passive samplers as surrogates for biomonitoring organisms. Perhaps most important, passive samplers can be deployed under many environmental conditions unsuitable for living biomonitoring organisms; for example, low dissolved oxygen, high or low water temperatures, and elevated toxicity (especially in sediment studies). Further, biomonitoring organisms are not always readily available from commercial suppliers or clean reference sites (e.g., episodic blue mussel die-offs caused by toxic algal blooms and pathogens limit numbers for biomonitoring). Booij et al. propose that passive samplers are superior monitoring tools because they can be deployed in essentially any aquatic environment and then readily compared to one another.[41] Biomonitoring organisms are limited to specific habitats that do not allow for wider regional or global comparisons.

This review focuses on the use of passive samplers in the water column and sediment interstitial waters as monitoring tools for assessing the bioavailability and bioaccumulation of HOCs. The objectives of this review are to (1) provide a brief overview of the state of the science for passive sampling–focusing on PDMS, LDPE, and POM, and bioaccumulation; (2) critically review the relationship between aquatic organism bioaccumulation and passive sampler uptake of HOCs by conventional biomonitoring organisms (e.g., polychaetes, oligochaetes, bivalves) when codeployed or exposed to the same environmental matrices (e.g., water, sediments); and (3) discuss research data gaps that need to be addressed to successfully implement passive sampling as a surrogate for biomonitoring using organisms.

BACKGROUND AND METHODS

Data Collection and Analysis. A literature search was performed using the ProQuest and American Chemical Society SciFinder systems based on the search terms "bioaccumulation", "biouptake", "biomagnification" and "passive sampling" on peer-reviewed reports published from 1990 to the present. The search provided 57 individual reports where HOCs were quantified in PDMS, LDPE, or POM, as well as within living organisms in the marine or freshwater environment (in situ) or in the laboratory (ex situ). As mentioned SPMDs are another popular passive sampling medium, because SPMDs have a biphasic sampling system (e.g., polyethylene and triolein) C_{PS} is more difficult to define as compared to single phase samplers like PDMS, LDPE, and POM. Further, SPMDs can be difficult to deploy in sediments because of the risk of losing triolein if the polyethylene tubing tears. For these reasons, SPMD will not be discussed in this review. Contaminants included PCBs, PAHs, DDTs, and a selection of contaminants of emerging concern (e.g., pyrethroid pesticides, flame retardants). A summary of these publications and relevant experimental details are given in the Supporting Information (Tables S1a, b). Of these reports, 19 provided a direct comparison of tissue and passive sampler concentrations including regression equations which we used as the primary comparison metric. Unpublished data from a study performed at our laboratory (U.S. EPA, Atlantic Ecology Division, Narragansett, Rhode Island, USA) investigating the uptake of PCBs by LDPE and POM, and the marine polychaete *Nereis virens*, from dilutions of a contaminated sediment, are also included in this data set

DOI: 10.1021/acs.est.6b03273
Environ. Sci. Technol. 2016, 50, 11437–11451

(Table S2a, b). This study used the approach and methods described by Parks et al.[42] To compare the different studies, all regression equations were adjusted to express C_L in ng/g lipid and C_{PS} in ng/g polymer and were correlated in a logarithmic form. A PDMS density of 0.97 g/mL was used to convert volume to mass. A summary of these 19 publications and the equations relating tissue concentrations to passive sampler polymer concentrations is provided in Table 1.

Passive Sampling and Bioaccumulation. *Passive Sampling.* Two sampling configurations predominate when using PDMS, LDPE, and POM: thin film sheeting and thin fiber coatings (SPME). These configurations allow for optimization tailored to a particular application's needs. For instance, if shorter deployment times are necessary, a thin PDMS fiber coating or a relatively thin sheet would perform better, or if very low environmental concentrations are expected, a thicker or a larger sheet along with a longer deployment can result in lower detection limits. Sheets of EVA have been used as a passive sampling polymer but there have been few studies published including the deployment of both EVA and organisms.[29,30,43,44]

Thin sheets or films are commercially available for LDPE, POM, and PDMS (or silicone rubber). LDPE sheets can often be purchased from local hardware stores. They are commercially available in several different thicknesses: the 25 (1 mil), 51 (2 mil), and 76 μm (3 mil) thicknesses are commonly used in the current passive sampling literature. Custom LDPE is available from Brentwood Plastics, Inc. (St. Louis, MO, USA). POM is also commonly deployed as a thin sheet and is commercially available from the CS Hyde and Company (Lake Villa, IL, USA) and is often deployed in 25 and 76 μm thicknesses. Blocks of POM can also be purchased and then sliced to the desired thickness using the appropriate equipment. Manufacturers of silicone or PDMS film sheets are Specialty Silicone Products, Inc. (Ballston Spa, NY, USA), Altec Products Limited (Bude, UK), and Silex Ltd. (Linford, Hampshire, UK). The films that are available commercially range from 20 to 1016 μm in thickness.

SPME, a thin polymer coating usually on a silica fiber, is another common configuration for passive sampling, frequently used with PDMS. The small configuration allows for a relatively simple postrecovery extraction or even direct injection into a gas chromatograph (GC) injection port. Disposable and reuseable SPME fibers are commercially available (e.g., Supelco, St Louis, MO, USA; Fiberguide Industries, Stirling, NJ, USA) in several different polymer thicknesses (~10−100 μm) and types of polymers.

Thin sheet and SPME passive samplers have been deployed in several different environmental settings. Within the context of this review, they are well suited to measure C_{free} in fresh and marine water environments and can be used in sediment interstitial water and water column deployments.[26,28,37] They can also be used to determine the flux of HOCs from the interstitial waters into the water column[45] and from the water column into the atmosphere.[46,47]

The effective use of passive samplers requires that the target contaminant achieves equilibrium between the sampler and other environmental phases or the sampler concentration (C_{PS}) is adjusted for nonequilibrium conditions. However, establishing that the target contaminants have achieved equilibrium between all of the environmental phases (including the passive sampler) is not trivial. There are at least four approaches to addressing the equilibrium status of the target contaminants.[48] First, assume that equilibrium has been established based on previous data. Second, perform a temporal sampling, in which passive samplers are collected over time until a significant change in the concentration of the target contaminant in the passive sampler is not detected between time points. Third, deploy passive samplers of different thicknesses, if the samplers with different thicknesses have the same concentrations for a given target contaminant on a mass or volume polymer basis, equilibrium is assumed to have been achieved for that target contaminant. Each of these approaches has liabilities; for example, different deployments and sites require more or less deployment time, so assuming equilibrium based on past experience can be problematic. Both the second and third approaches require multiple analyses and/or field trips resulting in extra expense and time. A fourth approach, using performance reference compounds (PRCs) avoids these liabilities.[49,50] In this approach, chemicals that behave like the target contaminants are absorbed into the samplers before the deployment. During the deployment, the passive sampler desorbs the PRCs from the polymer into the environment at a rate comparable to the absorbing target contaminants. The equilibrium status of the target contaminants can be calculated and used to adjust for nonequilibrium conditions by measuring the loss of PRCs following the deployment. There are currently at least three approaches recommended for making the nonequilibrium calculations using the raw PRC concentrations including a first order equation,[51−53] a diffusion-based model,[49,54,55] and a sampling rate-based correction.[56] When using PRCs, it is worth noting that for highly hydrophobic contaminants, the passive sampler may accumulate relatively low concentrations while under nonequilibrium conditions making quantification analytically challenging. This sensitivity loss is potentially problematic and makes considering analytical sensitivity an objective when determining deployment duration. For the analysis of passive sampler data reported here, we note in Table 1, if the equilibrium status of the passive sampler has been 'Assumed,' "Established" (i.e., equilibrium between the environmental phases has been demonstrated analytically), or "Adjusted" (i.e., using one of the PRC-based approaches described above).

Bioaccumulation. In general, the studies cited in this report used some combination of established bioaccumulation methods. Studies with whole sediment exposures using polychaetes, oligochaetes and benthic bivalves were often based on American Society for Testing and Materials (ASTM), the Organization of Economic Cooperation and Development (OECD), and U.S. EPA bioaccumulation guidance.[57−59] Similarly, many of the whole sediment studies with freshwater organisms were based on U.S. EPA freshwater bioaccumulation guidance.[60] Finally, mussel bioaccumulation methods have been conducted for decades and continue to be a powerful biomonitoring tool in programs such as "Mussel Watch"[6,61−63] and generally followed methods described in Bergen et al.,[64] Smedes,[65] and ASTM.[66] Studies which did not follow the approaches described above applied methods discussed in each publication.[19,67,68] Bioaccumulation studies with whole sediments were most frequently performed in the laboratory under static-renewal or flow-through conditions, whereas mussel deployments were most often conducted in the water column in the field. Bioaccumulation studies were usually approximately 30 days in duration although, in some cases, the exposures were longer and target contaminants were assumed to have achieved equilibrium with organismal lipids. It is

DOI: 10.1021/acs.est.6b03273
Environ. Sci. Technol. 2016, 50, 11437−11451

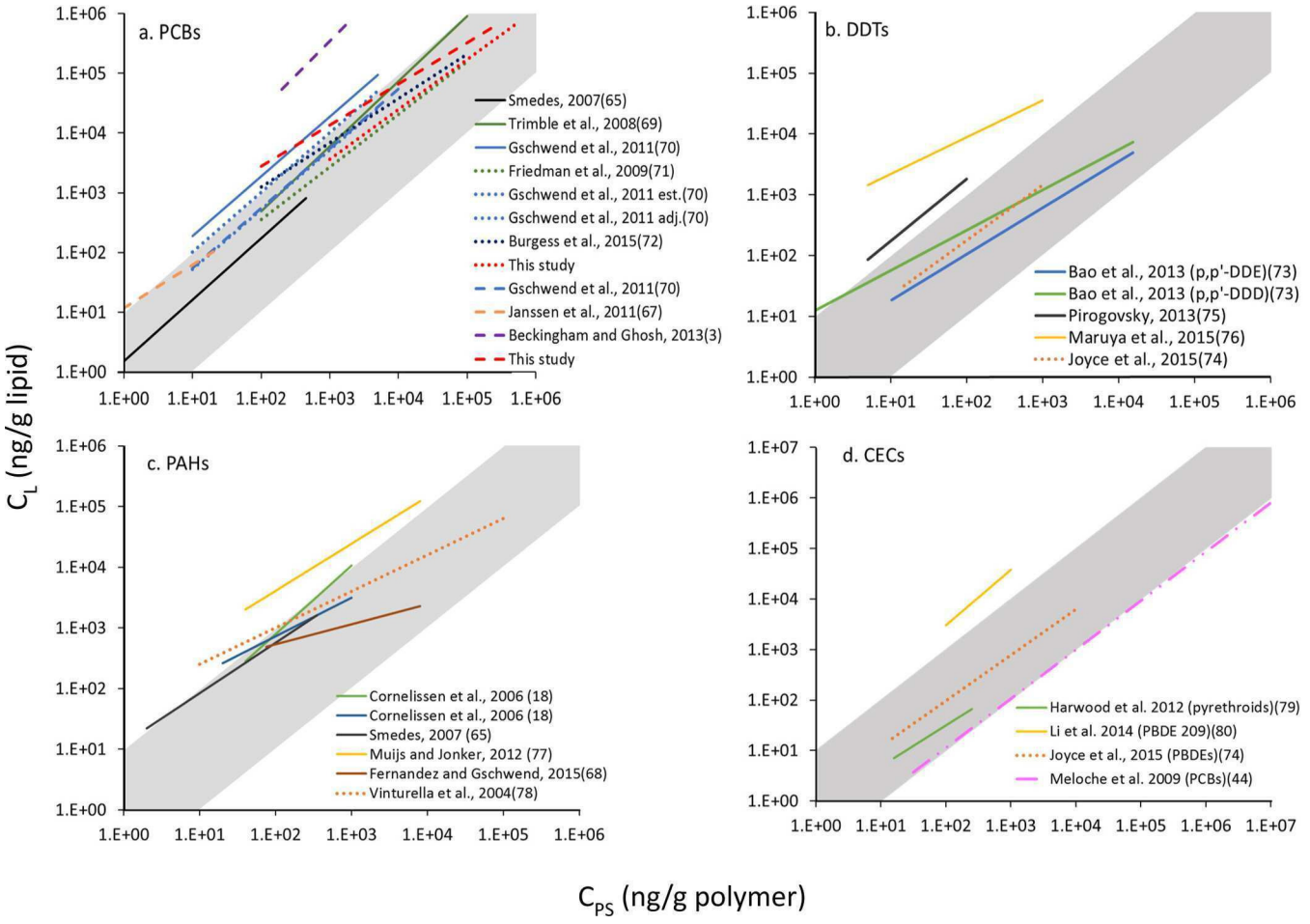

Figure 1. Uptake relationships between lipid-normalized tissue HOC concentrations (C_L) and passive sampler polymer HOC concentrations (C_{PS}). The gray band represents a 1:1 correlation plus or minus a factor of 10. Solid lines, dotted lines, and dashed lines reflect experiments performed using PDMS, LDPE or POM, respectively. Contaminants are plotted by (a) PCBs: two LDPE studies were conducted by Gschwend et al.,[70] one in which C_P was established (est.) by tumbling the LDPE in sediment until the polymers had reached equilibrium ($C_L = 10.2C_{PS}$) and one study in which C_P was adjusted (adj.) using PRCs upon static exposure to sediments ($C_L = 5.28C_{PS}$), (b) DDTs metabolites, (c) PAHs, and (d) contaminants of emerging concern: the dotted-dashed line represents a study using ethylene vinyl acetate (EVA) as a passive sampler. Because of the limited number of publications and correlations using EVA, Meloche et al.[44] was grouped with the contaminants of emerging concern. See Table S1 for more experimental details.

recognized that this assumption may not always be true for higher molecular weight target contaminants.

RESULTS AND DISCUSSION

Passive Sampler: Bioaccumulation Relationships. To reduce the complexity of the data analysis, sampler-organism comparisons were organized by contaminant class: PCBs, DDT and its metabolites, PAHs, and contaminants of emerging concern (CEC) (Figure 1). The regression lines were considered to be the preferable expression of the relationship between organism bioaccumulation and sampler uptake for comparison purposes. In the vast majority of cases, the regression equations were taken from the published papers as reported. Each regression depicted in the figures represents the relationship spanning only the range of data in the source publication. Because some of these studies measured several different HOCs and were performed at or with sediment samples from different sites, the lipid and polymer concentrations measured ranged several orders of magnitude. To visualize all of this data on one plot, the figures are shown using a logarithmic scale.

Along with the sampler-organism regression lines, a gray shaded band representing the 1:1 correlation plus or minus a factor of 10 was superimposed onto the figures as a visual aid to indicate where the data would have occurred if the organism bioaccumulation and passive sampler uptake agreed within an order of magnitude, throughout the discussion this band will be referred to as the "10× band". A regression line falling within the 10× band supports the mechanistic assumption that a passive sampler's affinity for a given HOC is similar to that of an organism's lipids.

PCBs. These contaminants were the most commonly studied class for comparing polymer accumulation with organism lipid bioaccumulation. In total, there were 12 studies with five species of polychaetes and bivalves. The comparisons show that, in general, the lipid concentrations were higher than the polymer concentrations and many of the resulting regressions reported slopes of approximately one (Figure 1a). Several studies illustrate a correlation between C_L and C_{PS} which roughly agree within an order of magnitude (Smedes,[65] Trimble et al.,[69] Gschwend et al.,[70] Friedman et al.,[71] Burgess et al.,[72] Janssen et al.,[67] and the current study (for LDPE)). In

DOI: 10.1021/acs.est.6b03273
Environ. Sci. Technol. 2016, 50, 11437−11451

other studies, the regressions suggest that the relationship between C_L and C_{PS} differed by more than 1 order of magnitude (Beckingham and Ghosh,[3] the current study (POM), and Gschwend et al. (PDMS)[70]). The regressions from Beckingham and Ghosh and the current study fell outside of the 10× band especially as C_{PS} decreased. In the case of Beckingham and Ghosh,[3] the organism lipid percentages were very small compared to the other studies which may contribute substantially to the behavior of the regression line. These low lipid percentages may have resulted from the presence of activated carbon used during the study which does not provide the same amount of organism nutrition as natural sediments not containing the activated carbon. Overall, not one polymer or organism displayed data readily distinguishable or anomalous relative to the others.

DDTs. Four studies were found to correlate DDT and its metabolite's lipid bioaccumulation in mussels, polychaetes, and bivalves with polymer concentrations, resulting in five regression lines (Figure 1b). Of these regression relationships, three fell within the 10× band over the majority of the measured data (Bao et al.[73] and Joyce et al.[74]). These regression equations were comparable to those reported for PCBs in terms of the magnitude for both the slopes and intercepts (Table S3). The other two studies report regression equations with regression lines above the 10× band. In the study by Pirogovsky, several DDT metabolites (e.g., DDE, DDD, DDMU, and DDNU) were measured in PDMS-SPME and mussel tissues, the reported slope (1.02) is in agreement with other studies; however, the intercept (1.2) is slightly larger than reported in the other studies.[75] This discrepancy may be due to the low water column concentrations and relatively high detection limits of the SPMEs used in that study. In the study conducted by Maruya et al.,[76] although the reported slope (0.61) for the regression is similar to other relationships for the DDTs, the intercept was 2.7. In this study, the measured C_L for the data set ranged 3 orders of magnitude, while the C_{PS} ranged over five, resulting in the lower than average slope, the high intercept may be exacerbated due to an outlier with a very low C_{PS} value and a high C_L value (Figure S9c).

PAHs. The literature yielded five studies in which PAH bioaccumulation was compared with polymer uptake. Six different regressions were reported including studies with a gastropod, two using polychaetes, an oligochaete, and two using mussels (Figure 1c). Generally, the slopes demonstrated similar behavior to that observed for the PCBs and DDTs (Table S3). Four of these studies fell within the 10× band (Cornelissen et al.,[18] Smedes,[65] and Fernandez and Gschwend[68]). The study by Muijs and Jonker[77] found the regression between C_L and C_{PS} above the 10× band for the entire data span while the study by Vinturella et al.[78] observed a C_L and C_{PS} relationship greater than ten only at lower concentrations. These elevated relationships are likely due to the elevated sediment contaminant concentrations used in each study and are discussed further in the Highly Contaminated Sediments section.

CECs. Reports were also published comparing passive sampler uptake with other classes of compounds most notably PBDE flame retardants and pyrethroid pesticides (Figure 1d). Two such reports were found in the literature search, one comparing oligochaetes with PDMS-SPME and one comparing mussel bioaccumulation with LDPE. Figure 1d also includes a regression relating bivalve bioaccumulation of PCBs with an EVA passive sampler. This regression is included in Figure 1d because studies with EVA are less prevalent in the literature. The majority of the reported data falls within the 10× band. However, unlike the regression lines for the PCBs, DDTs, and PAHs, the CECs resulted in regression lines that reflected higher polymer concentrations than the corresponding lipid concentrations (Meloche et al.,[44] Harwood et al.[79]). Speculatively, the regression from Harwood et al. may indicate higher concentrations in the polymer due to biotransformations (and thus lower concentrations) in the organisms during the exposures.[79] Because no other regression relationships between lipid bioaccumulation and EVA accumulation were found in the literature, it is difficult to critically compare the data from Meloche et al.[44] to the other PCB regressions (Figure 1a) given that the polymer EVA is more polar than PDMS, LDPE, and POM. However, the expansive linear range of these values and the high r^2 observed (0.98) shows promise for using EVA passive sampling uptake to estimate HOC bioaccumulation (including CECs) and these relationships should be further explored. The regression relationship reported for PBDEs by Joyce et al.[74] fell within the 10× band. Li et al.[80] also reported a correlation for PBDE 209, this regression line lies above the 10× band suggesting C_L values were often more than an order of magnitude higher than measured C_{PS} values. This relatively large discrepancy may, in part, be due to the very lengthy passive sampler equilibrium times required with PBDE 209.

For all classes of HOCs, slopes for the regressions ranged from 0.33 to 1.2 and the intercepts ranged from −0.88 to 2.70 (Table S3). General agreement was observed between all compound classes and polymers studied. Relative to general trends, in many cases studies with a higher intercept (>1) were associated with lower slopes (<0.8). Further, as demonstrated in Figure 1, organism and polymer HOC concentrations correlated in a relatively reproducible fashion between contaminant classes without any outliers that could not be, at least, partially explained (see the Highly Contaminated Sediments section below).

In a second analysis, the data were plotted by polymer type. This approach will be discussed in lesser detail given the same regression lines are examined closely in the first approach described above. Using this approach to sort the data, there were nine PDMS regressions, three for PCBs, two for DDTs, two for PAHs, and two for CECs (Figure S1). Four of the lines were within the 10× band with most relationships above a 1:1 relationship while the remaining five regressions were above the 10× band. For LDPE, there were a total of nine regression lines: five, one, two, and one for PCBs, DDTs, PAHs, and CECs, respectively (Figure S2). Most of the regression lines were within the 10× band and higher than a 1:1 relationship. Finally, POM had six regression lines with four for PCBs and two for PAHs. Three lines were within the 10× band, all above a 1:1 relationship. The other regression lines were either entirely outside of the 10× band or included parts above of the 10× band (Figure S3), suggesting POM may have a lower sorption capacity than lipids and the other samplers reviewed.

In a third analysis, the data were plotted by organism for the two types of organisms with the largest data sets: marine mussels and aquatic worms (Figures S4 and S5, respectively). There were seven studies resulting in nine regressions with bivalve data and 11 studies resulting in 16 regressions for the aquatic worm data. Of the bivalve data, all but three were within the 10× band for the majority of the data measured. Two regressions were above the 10× band, and one below (EVA study). This data set represents PDMS (n = 4), LDPE (4), and

DOI: 10.1021/acs.est.6b03273
Environ. Sci. Technol. 2016, 50, 11437−11451

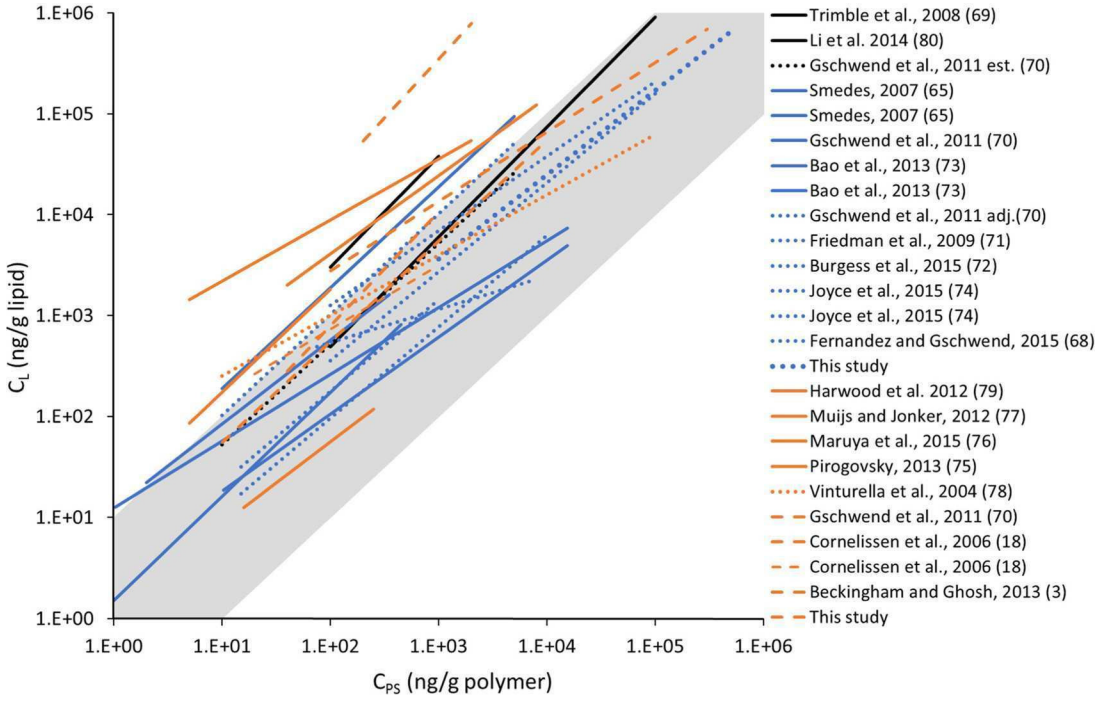

Figure 2. Uptake relationships between lipid-normalized tissue HOC concentrations (C_L) and passive sampler polymer HOC concentrations (C_{PS}) sorted by sampler equilibrium correction method: black lines, equilibrium was established (est.) using temporal sampling; orange lines, equilibrium was assumed based on previous experiments; blue lines, adjusted (adj.) to estimate C_{PS} using modeling (e.g., based on PRCs or other methods). Solid lines, dotted lines, and dashed lines reflect experiments performed using PDMS, LDPE, or POM, respectively. Two LDPE studies were conducted by Gschwend et al.,[70] one in which C_{PS} was established by tumbling the LDPE in sediment until the polymers had reached equilibrium ($C_L = 10.2C_{PS}$) and one study in which C_{PS} was adjusted using PRCs based upon static exposure to sediments ($C_L = 5.28C_{PS}$). See Table S1 for more experimental details.

EVA (1) polymers measuring PCBs (3), PAHs (2), DDTs (3), and CECs (1). A larger fraction of the studies with aquatic worms were above the 10× band. PDMS (6), LPDE (5), and POM (5) were all used to compare uptake with aquatic worms for all the compound classes discussed in this review. About half of the regressions showed all or a substantial portion of the regressions above the 10× band. The larger percentage of aquatic worm studies above the 10× band may be due to the higher concentrations of target contaminants present in the sediments leading to higher reported intercepts as discussed below in the Highly Contaminated Sediments section. Another possible explanation for higher proportions of aquatic worm studies exceeding the 10× band as compared to bivalves is the feeding mechanisms of the animal tested. In a recent study, filter feeders (bivalves) were found to accumulate less PCBs relative to other deposit feeders (aquatic worms) under synonymous exposure conditions.[81] Studies by the same group have shown that species specific traits including: body size, lipid content, diet, digestive process, as well as ingestion and differentiation between sediment and suspended solid particles also play a significant role in bioaccumulation and should be considered when determining the extent of bioaccumulation from the sediment.[81,82] Further, fractions of phospholipids and other sterols that may be present in lipids in different concentrations in different species may also reduce the sorption capacity of some HOCs, and therefore bias some of the observed C_L values.[83]

Highly Contaminated Sediments. Nine of the regressions exhibited data that fell outside of the 10x band. These "outliers" were not explained by the type of contaminant or the kind of polymer as PCBs, DDTs, and PAHs, as well as PDMS and POM all demonstrated high regressions. However, all but two of these studies (Li et al., and Pirogovsky) occurred in sediment exposures in highly contaminated sediments (>600 ng/g dry). This observation suggests that highly contaminated sediments may lead to regressions in which C_L to C_{PS} relationships differ by more than a factor of 10. Four of these studies resulted in unexpectedly high intercepts: the current study (with POM), Muijs and Jonker,[77] Maruya et al.,[76] and Beckingham and Ghosh,[3] where reported intercepts ranging from 2.1 to 2.7 (Table 1). Muijs and Jonker[77] worked with field sediments from an abandoned manufactured gas plant with total PAH concentrations approaching 50,000 mg/kg dry.[84] This point can be further illustrated using data from the current study. PCB contaminated sediments from New Bedford Harbor with total PCBs approaching 400 mg/kg dry[41] were diluted with a clean reference sediment resulting in the following exposures: 25%, 50%, 75%, and 100% contaminated sediments. As the amount of contaminated sediment is diluted to lower PCB concentrations, the regression intercepts for POM decrease from 2.9 to 1.2 and the slopes increase from 0.56 to 0.75 for the 100% and 25% treatments, respectively (Figure S6a). Similar trends were observed in this study when LDPE was used as well (although the intercepts are smaller) (Figure S6b). In both studies the regressions moved toward the center of the 10× band with decreasing sediment contaminant concentrations. Explanations for this behavior are not entirely apparent; however, given biomonitoring is frequently performed at highly contaminated sediment sites, research to better understand the relationship between passive sampler uptake and bioaccumulation is warranted.

DOI: 10.1021/acs.est.6b03273
Environ. Sci. Technol. 2016, 50, 11437−11451

Effects of Equilibrium Status. The results of this review were also analyzed to evaluate how the determination of equilibrium status of the passive samplers affected the estimated C_{PS} values. Each regression relationship was categorized by how equilibrium C_{PS} was determined: established via temporal sampling; corrected or adjusted using PRCs; or equilibrium was assumed (Table 1, Figure 2). Two of the three studies in which equilibrium was established had regression lines within the 10× band over the entire measured data set. Studies in which C_{PS} was adjusted to estimate equilibrium concentrations (n = 12) also generally fell within the 10× band. The 11 regressions in which equilibrium was assumed for C_{PS} resulted in more data trending above the 10× band. This particular method for determining C_{PS} represents studies using all three of the reviewed polymers, as well as each type of organism present within this Critical Review, and encompasses contaminants from each class of HOCs reviewed (e.g., PCBs, DDTs, PAHs, CECs). As such, it is not surprising that studies in which equilibrium was assumed resulted in correlations with the most variable results as well as the highest and the lowest concentrations trends. Regressions in which equilibrium was assumed resulted in lines with the highest C_L concentrations when compared to C_{PS} for PDMS, LDPE, and POM. This finding suggests some target contaminants may not have actually achieved equilibrium with the passive sampling polymer in some of these studies.

The success demonstrated by temporal sampling to confirm equilibrium is noteworthy, but it can also be the most challenging approach for assessing equilibrium status. Considerable variation was also observed for regressions in which C_{PS} was determined using PRCs. This variation may be due to increased uncertainty that is associated with using PRCs to correct for nonequilibrium conditions as well as the differences in the models currently used to adjust passive sampling data based on the PRCs. It should be noted that the study using EVA is not included in Figure 2 as it is unclear if the position of the observed regression line is due to how C_{PS} was determined (e.g., assumed equilibrium, established equilibrium, or adjusted equilibrium concentrations) or because EVA regressions have lower C_L to C_{PS} ratios.[44]

Predictive Power of Organism Lipid−Polymer Relationships. In most cases, strong logarithmic relationships existed between bioaccumulation and polymer uptake which is indicative of a predictive relationship. These relationships were not precisely 1:1 but were very often within a factor of approximately ten (Figure 2); which does not disqualify the relationships from being predictive but means that regressions will need to be considered on a passive sampler, target contaminant, and organism basis, suggesting that a "universal" equation cannot be applied across a range of passive samplers, target contaminants, and organisms to predict bioaccumulation from passive sampler uptake.

The strength of the various relationships in Table 1 and Figures 1 and 2 can be assessed by examining the coefficients of determination (r^2), which express the proportion of variability in the data captured by the modeled log−log regressions. For LDPE, the nine studies had r^2 values ranging from 0.31 to 0.92 with a mean of 0.68 ± 0.20 while the 11 PDMS r^2 values ranged from 0.59 to 0.91 and had a mean of 0.76 ± 0.10 (SI Table S4). The six r^2 values for POM ranged from 0.39 to 0.76 and had a mean of 0.58 ± 0.15. Finally, EVA had one reported r^2 of 0.98. These r^2 values suggest that polymer uptake effectively describes much of the bioaccumulation-uptake variability and should provide confidence that using the modeled relationships has merit for all polymers reviewed in this study. Another useful summary statistic describing these relationships is the "p" value. This value indicates whether the relationship between organism bioaccumulation and passive sampler uptake is statistically significant with values equal to or less than 0.05 generally accepted as indicating a significant relationship. When the raw data was available, p values were calculated, and in each case indicated a significant relationship between C_L and C_{PS} (Table 1) and selected data sets are plotted in SFigure S9a−g.

Organism Lipid−Polymer Relationships versus Target Contaminant Hydrophobicity. The log (C_L/C_{PS}) ratio was calculated for the raw data that was available and plotted versus target contaminant hydrophobicity (expressed as the log K_{OW}). This ratio provided another way of expressing the slope of the relationship between polymer uptake and bioaccumulation and, in principle, should be consistent for all data regardless of the target contaminant or physiochemical properties. A log (C_L/C_{PS}) equal to 0 would indicate that the uptake into the two phases was identical. Overall, the ratio averaged 0.51 ± 0.71 (n = 609). To investigate how this ratio varied with the target contaminants physiochemical properties, ratios were separated by compound class: DDTs and PCBs (combined) and PAHs. The average and standard deviation were calculated for all ratios with a common log K_{OW} and the data was plotted (Figures 3a and b, S7, and S8). For the PCBs and DDTs, the average log (C_L/C_{PS}) for all compounds was 0.52 ± 0.49 (n = 317) (Figure 3a). The individual ratios as well as their standard deviations appear to increase slightly with increasing log K_{OW}. This increase in standard deviation could be due to the contaminants not being at equilibrium with the polymers or increased variation associated with PRC corrections. For PAHs,

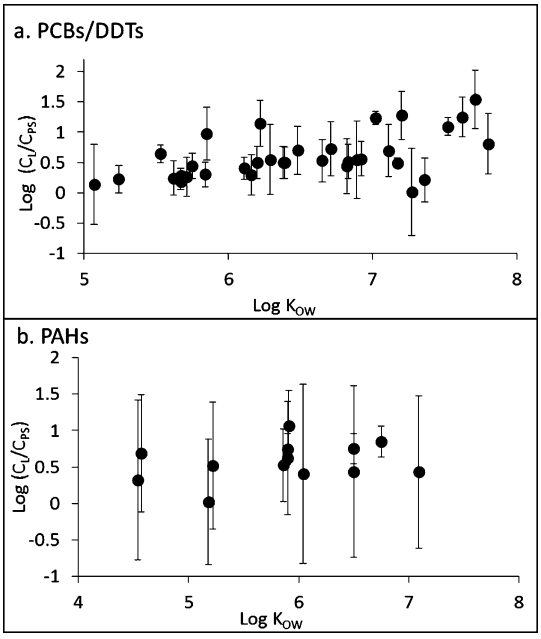

Figure 3. Lipid normalized tissue HOC concentration−passive sampler polymer HOC concentration ratios plotted against log K_{OW} for (a) PCBs and DDTs and (b) PAHs. Ratios plotted are the mean and standard deviation. Log K_{OW} values for PCBs were taken from Hawker and Connell,[110] DDTs were generated from SPARC (http://www.archemcalc.com/sparc.html),[111] and PAHs from Smedes.[65] See Supporting Information for more experimental details.

DOI: 10.1021/acs.est.6b03273
Environ. Sci. Technol. 2016, 50, 11437−11451

the average of all log (C_L/C_{PS}) was 0.50 ± 0.90 (n = 292) (Figure 3b). There is a relatively large ratio and large standard deviations for the lower K_{OW} PAHs like anthracene and phenanthrene. Values for both log (C_L/C_{PS}) and standard deviations then decreased for moderate log K_{OW} (5.5−6) molecules then increased for the higher log K_{OW} PAHs (≥6). The variability observed for the low K_{OW} PAHs is likely due to a combination of organism metabolism of the PAHs and low analytical recoveries of these volatile compounds.[85−87] Causes of the variation observed for the higher K_{OW} PAHs is likely error associated with passive sampler nonequilibrium and PRC corrections.

Basic and Conceptual Data Gaps. Analysis of the relationship between passive sampler uptake and aquatic organism bioaccumulation suggests that passive samplers are promising surrogates for estimating bioaccumulation, though there are basic and conceptual data gaps that require further research and reporting. Addressing these data gaps will improve the future application of passive sampling in the scientific and regulatory arenas.

Basic Data Gaps. An array of target contaminants, organisms, field or laboratory conditions, and equilibrium status approaches were used in the studies discussed in this review and are summarized in Table S5. PDMS, LDPE, and POM have been widely used in comparisons with organism bioaccumulation for a wide range of target contaminants including PCBs, PAHs, and DDTs, as well as pyrethroid pesticides and brominated flame retardants. There is one notable data gap, POM has not been evaluated with DDTs or bivalves. Regarding the organisms used in these comparisons, LDPE and POM have been compared primarily to marine organisms. While there is little reason to conclude that freshwater and marine organisms will differ substantially in C_L under equilibrium conditions, having a balance of representative studies would be beneficial to support the use of passive samplers for predicting bioaccumulation. The types of organisms used in these comparisons range from oligochaetes and polychaetes to bivalves and gastropods to a small number of insects with PDMS demonstrating the greatest diversity of organisms. Relative to field versus laboratory studies, all of the passive samplers had more laboratory studies than field studies. This imbalance is likely due to the logistical, time, and cost challenges associated with conducting in situ field deployments compared to laboratory-based studies. Finally, all of the POM comparisons assumed equilibrium conditions for C_{PS}, while LDPE and PDMS also applied estimates based on temporal sampling and PRC corrections. To address these basic data gaps more studies with LDPE and POM using freshwater organisms including insects and amphipods are needed. In addition, more field studies using PDMS and POM applying temporal sampling should be performed. Another basic data gap is reporting of the types of summary statistics discussed above that assist in assessing the predictive strength of the bioaccumulation-uptake relationships. In the future, researchers should include, at the least, the r^2 and p values for their regressions. Species-specific traits and a more quantitative analysis of the lipid make up should be considered in bioaccumulation studies and may improve observed relationships with passive sampler uptake.[81−83]

Conceptual Data Gaps. It remains unclear how effectively passive sampling captures bioaccumulation resulting from dietary ingestion of contaminated sediments. This particular data gap is part of the ongoing debate of what environmental phases represent the principle sources of exposure to aquatic organisms. In 1991, Di Toro et al. described the equilibrium partitioning (EqP) model for explaining the distribution of HOCs in the aquatic environment.[14] The model describes a system in which at equilibrium the chemical activity of a given HOC is equal across all phases, for example

$$a_{free} = a_{PS} = a_L = a_P \quad (10)$$

where a_{free}, a_{PS}, a_L, and a_P are the respective chemical activities of a given HOC for the C_{free}, C_{PS}, C_L, and the total sediment particle concentration C_P. In this model, if one knows the HOC concentration in any phase and the partition coefficients quantifying the HOC's distribution between phases (e.g., K_{PS}, K_{OC}, K_L), the concentration in any other phase can be determined. Consequently, if one knows the value of C_{free} based on passive sampling measurements then the concentrations in the other phases can be determined including the C_L. This paradigm has served as the basis for the U.S. EPA's Equilibrium Partitioning Sediment Benchmarks (ESBs)[2,88,89] and accurately predicts toxicity and bioaccumulation for several classes of HOCs.[90−92] However, there have been studies suggesting that eq 10 does not accurately describe the chemical activity of some HOCs. For example, Friedman and Lohmann concluded that for higher log K_{OW} HOCs, C_L could not be completely explained by C_{free} and that is was likely there were other contributing factors to the measured C_L.[93] Other studies have reported similar findings that question the universality of the EqP model.[82,94,95] However, if C_{free} is found to not be an effective predictor of C_L for higher K_{OW} HOCs, the utility of passive sampling for predicting the C_L for these same HOCs may be thrown into doubt. This data gap is a fertile area for further research.

Within the passive sampling literature, there is also a lack of consensus on whether field or laboratory studies are more appropriate for comparing passive sampler uptake and organism bioaccumulation. Janssen et al. concluded that laboratory studies are the best way to evaluate equilibrium interstitial water concentrations which, most accurately represent target contaminant bioavailability. However, field studies may be necessary to account for the most relevant "real world" exposure conditions.[67] Ghosh et al. reached a similar conclusion stating that equilibrium between the passive sampler and various environmental phases can be achieved more readily under laboratory conditions, but there is a loss of environmental reality attainable only under field conditions.[28] In addition, comparisons utilizing field conditions can be difficult because target contaminants may take months or longer to reach equilibrium with the passive samplers. As discussed above, lengthy field deployments have been circumvented by using PRCs with passive samplers including LDPE,[49,56,96] POM,[97] and PDMS.[73,98] However, interpolating PRC data is not always straightforward. In addition, PRCs can be expensive and may introduce additional variability to the estimates of target contaminant concentrations that can adversely affect the passive sampler uptake to organism bioaccumulation relationship.[48]

Perhaps the most environmentally significant application, actual passive sampling studies bridging trophic levels are very limited. All of the studies discussed in this review involved organisms that primarily accumulate target contaminants directly from contaminated water or sediment and not via feeding on prey. In this way, the transfer of target contaminants from the relevant environmental phases to the organism's lipids

DOI: 10.1021/acs.est.6b03273
Environ. Sci. Technol. 2016, 50, 11437−11451

is relatively simple (e.g., bivalves filtering contaminated water). To apply the full potential of passive samplers it would be desirable to use C_{PS} data to estimate C_L for higher trophic level organisms (e.g., pelagic fish, wildlife, humans). The most likely route to accomplish this goal would involve using passive sampler C_{PS} data as an input term to bioaccumulation models like those developed by Gobas et al.[5,99,100] The C_{PS} would serve the same role as the lower trophic level organism bioaccumulation C_L data ordinarily collected for inclusion in such models. However, very little of this type of passive sampler C_{PS} data utilization has yet been performed.[101,102] In a related series of studies, investigations have compared measurements of contaminant uptake into silicone (PDMS) coated inside jars. In these experiments, contaminated sediments were tumbled in the PDMS-coated jars and the equilibrium PDMS accumulation compared to the actual bioaccumulation by fish sampled from the areas where the contaminated sediments were collected.[103−107] Results demonstrated strongly predictive linear correlations between the silicone estimates of bioaccumulation and actual fish bioaccumulation. However, the fish bioaccumulation was often less than the silicone-based estimates of bioaccumulation suggesting, that the organisms were not at equilibrium with the sediments in the field. These results may indicate that the fish in the environment are being exposed to contaminants from several other sources along with the contaminated sediments (including contaminated sediments from other locations) and not exposed to contaminants in uncontaminated areas. Alternatively, these findings may simply highlight differences in the sorptive capacities of the lipid versus PDMS. This innovative work highlights one of the challenges associated with using passive samplers with bioaccumulation modeling to predict higher trophic level organism bioaccumulation, higher trophic level organisms are seldom sessile, and they do move around and can be exposed to multiple sources of contamination while passive samplers are generally stationary. This challenge and others will need to be addressed if passive sampling is to be used successfully to predict higher trophic level bioaccumulation.

Implications. This review and analysis of the passive sampler uptake and bioaccumulation data indicates that based on the regression relationships in the majority of the 27 regressions in Table 1, passive samplers accumulated target contaminants within one or two orders of magnitude of the organisms, and, when raw data was available for testing, each of these regressions yielded a statistically significant relationship between C_L and C_{PS} based on the p values. This finding suggests that in many applications, passive samplers can be applied as surrogates for biomonitoring organisms if they are not available or their deployment is problematic (e.g., low dissolved oxygen), with the following caveats. First, in most cases, the C_{PS}, while within an order of magnitude of the C_L, were often lower than the C_L values. In studies, where equilibrium was assumed, this bias becomes more prevalent and may be a reflection of the potential for the target contaminants to not be fully at equilibrium with the polymer. For cases where equilibrium with the polymer was established or adjusted for using PRCs, the results of the regression analyses indicate that the relationship between C_L and C_{PS} were not identical but were predictive. Second, the increase in variability observed between the C_L and C_{PS} ratio with increasing log K_{OW} for PCBs and DDTs (Figure 3a), shows that extra care should be taken when interpreting passive sampler data for the larger, higher K_{OW} target contaminants. This is because the uncertainty associated with the resulting estimated C_L values will be larger than for lower K_{OW} target contaminants. Unfortunately, these larger K_{OW} HOCs, while less bioavailable than smaller contaminants, are often the HOCs of most interest in terms of trophic transfer and toxicity to higher trophic organisms including pelagic fish, wildlife and humans.[108,109] While Figure 3a indicates the variability in the C_L and C_{PS} relationship increases with increasing K_{OW}, it does not necessarily mean that the use of passive samplers as surrogates is flawed, but highlights the challenges with accurately and precisely measuring C_{PS} and C_L for these larger K_{OW} contaminants. By comparison, the level of variability observed in the ratio for PAHs, across molecules (Figure 3b), is likely due to a combination of metabolism and the same issues affecting other high K_{OW} contaminants. This variability occurred despite the relatively good correlations between PAH uptake by passive samplers and bioaccumulation by organisms.

For scientific and regulatory applications, specifically for the classes of HOCs discussed in this review, the use of passive samplers as surrogates for biomonitoring organisms is recommended when necessary (e.g., when biomonitoring organisms are not available). As the relatively high r^2 values reported in this review show, using passive samplers will yield similar spatial trends as well as detect temporal changes in water column and interstitial water concentrations similar to those acquired in a conventional biomonitoring program. The accuracy of this approach will improve if passive sampler equilibrium status is confirmed and the practice is limited to the low and medium log K_{OW} (i.e., 4−7) target HOCs. Passive sampling based concentrations resulted in predictive relationships, most of which were within one to two orders of magnitude of the directly measured bioaccumulation (see Figure 2). Finally, the conclusions reached here will only be strengthened with the performance of more comparisons of passive sampler uptake and organism bioaccumulation.

■ ASSOCIATED CONTENT

Supporting Information

The Supporting Information is available free of charge on the ACS Publications website at DOI: 10.1021/acs.est.6b03273.

Passive sampler uptake and bioaccumulation in published in vivo and in vitro studies, equilibrium polymer concentrations, lipid concentrations, summary of slopes and intercepts for logarithmic equations derived for the data, summary statistics for coefficients of determination, summary of target contaminants, organisms, field, or laboratory conditions and equilibrium status approach, polydimethylsiloxane uptake relationships, low-density polyethylene, polyoxymethylene (POM), bivalve, and aquatic worm uptake relationships between lipid-normalized tissue HOC concentrations and passive sampler polymer HOC concentrations, uptake relationships between lipid-normalized tissue HOC concentrations polyoxymethylene passive sampler polymer HOC concentrations and between lipid-normalized tissue HOC concentrations and low-density polyethylene passive sampler polymer HOC concentrations from exposures to dilutions of a PCB-contaminated sediment, log lipid−polymer concentration ratios sorted by log K_{OW} for PCBs, DDTs, and PAHs, Lipid-normalized tissue and passive sampler-polymer HOC concentration data sets, and additional references (PDF)

DOI: 10.1021/acs.est.6b03273
Environ. Sci. Technol. 2016, 50, 11437−11451

AUTHOR INFORMATION

Corresponding Author

*Phone: (401)782-3096. Fax: (401)782-9670. E-mail: joyce.abbey@epa.gov.

Present Address

†A.N.P.: Southern California Coastal Water Research Project, Costa Mesa, CA

Notes

This is U.S. EPA ORD-015127. Mention of trade names or commercial products does not constitute endorsement or recommendation for use. This report has been reviewed by the U.S. EPA's Office of Research and Development National Health and Environmental Effects Research Laboratory, Atlantic Ecology Division, Narragansett, RI, and approved for publication. Approval does not signify that the contents necessarily reflect the views and policies of the Agency.
The authors declare no competing financial interest.

ACKNOWLEDGMENTS

This research was performed while A. S. Joyce held an NRC Research Associateship award at U.S.Environmental Protection Agency, ORD/NHEERL Atlantic Ecology Division. The authors thank the AED reviewers for their comments: M. Cantwell, J. Li Volsi, R. McKinney, W. Munns, J. Serbst, and G. Thursby. The following colleagues are also thanked for providing their raw data for analysis in this review: L. Fernandez (Northeastern University, Boston, MA, USA); A. M. P Oen (Norwegian Geotechnical Institute (NGI), Norway, Oslo), E. Janssen (ETH, Zurich, Switzerland), G. Cornelissen (NGI) and A. Ruus (Norwegian Institute for Water Research, Oslo, Norway); K. Maruya (Southern California Coastal Water Research Project, Costa Mesa, CA, USA); F. Smedes (Deltares, Utrecht, The Netherlands); and C. Friedman (Corning School of Ocean Studies, Maine Maritime Academy, Castine, ME, USA).

REFERENCES

(1) Gobas, F. A. P. C.; de Wolf, W.; Burkhard, L. P.; Verbruggen, E.; Plotzke, K. Revisiting Bioaccumulation Criteria for POPs and PBT Assessments. *Integr. Environ. Assess. Manage.* **2009**, *5* (4), 624−637.

(2) Burgess, R. M.; Berry, W. J.; Mount, D. R.; Di Toro, D. M. Mechanistic sediment quality guidelines based on contaminant bioavailability: Equilibrium partitioning sediment benchmarks. *Environ. Toxicol. Chem.* **2013**, *32* (1), 102−114.

(3) Beckingham, B.; Ghosh, U. Polyoxymethylene passive samplers to monitor changes in bioavailability and flux of PCBs after activated carbon amendment to sediment in the field. *Chemosphere* **2013**, *91* (10), 1401−1407.

(4) Arnot, J. A.; Gobas, F. A. P. C. A review of bioconcentration factor (BCF) and bioaccumulation factor (BAF) assessments for organic chemicals in aquatic organisms. *Environ. Rev.* **2006**, *14* (4), 257−297.

(5) Gobas, F. A. P. C. A model for predicting the bioaccumulation of hydrophobic organic chemicals in aquatic food-webs: application to Lake Ontario. *Ecol. Modell.* **1993**, *69* (1−2), 1−17.

(6) Goldberg, E. D. The mussel watch — A first step in global marine monitoring. *Mar. Pollut. Bull.* **1975**, *6* (7), 111.

(7) O'Connor, T. P. Concentrations of organic contaminants in mollusks and sediments at NOAA National Status and Trend sites in the coastal and estuarine United States. *Environ. Health Perspect.* **1991**, *90*, 69−73.

(8) O'Connor, T. P. National distribution of chemical concentrations in mussels and oysters in the USA. *Mar. Environ. Res.* **2002**, *53* (2), 117−143.

(9) O'Connor, T. P.; Lauenstein, G. G. Trends in chemical concentrations in mussels and oysters collected along the US coast: Update to 2003. *Mar. Environ. Res.* **2006**, *62* (4), 261−285.

(10) Nelson, W.; Bergen, B. The New Bedford Harbor Superfund site long-term monitoring program (1993−2009). *Environ. Monit. Assess.* **2012**, *184* (12), 7531−7550.

(11) Daskalakis, K. D.; O'Connor, T. P. Distribution of chemical concentrations in US coastal and estuarine sediment. *Mar. Environ. Res.* **1995**, *40* (4), 381−398.

(12) Reichenberg, F.; Mayer, P. Two complementary sides of bioavailability: Accessibility and chemical activity of organic contaminants in sediments and soils. *Environ. Toxicol. Chem.* **2006**, *25* (5), 1239−1245.

(13) Lohmann, R.; Burgess, R. M.; Cantwell, M. G.; Ryba, S. A.; MacFarlane, J. K.; Gschwend, P. M. Dependency of polychlorinated biphenyl and polycyclic aromatic hydrocarbon bioaccumulation in Mya arenaria on both water column and sediment bed chemical activities. *Environ. Toxicol. Chem.* **2004**, *23* (11), 2551−2562.

(14) Di Toro, D. M.; Zarba, C. S.; Hansen, D. J.; Berry, W. J.; Swartz, R. C.; Cowan, C. E.; Pavlou, S. P.; Allen, H. E.; Thomas, N. A.; Paquin, P. R. Technical basis for establishing sediment quality criteria for nonionic organic chemicals using equilibrium partitioning. *Environ. Toxicol. Chem.* **1991**, *10* (12), 1541−1583.

(15) Accardi-Dey, A.; Gschwend, P. M. Assessing the Combined Roles of Natural Organic Matter and Black Carbon as Sorbents in Sediments. *Environ. Sci. Technol.* **2002**, *36* (1), 21−29.

(16) U.S. EPA. *Equilibrium Partitioning Sediment Benchmarks (ESBs) for the Protection of Benthic Organisms: Procedures for the Determination of the Freely Dissolved Insterstitial Water Concentrations of Nonionic Organics*; Office of Research and Development: Washington, DC, 2012.

(17) Oen, A. M. P.; Schaanning, M.; Ruus, A.; Cornelissen, G.; Källqvist, T.; Breedveld, G. D. Predicting low biota to sediment accumulation factors of PAHs by using infinite-sink and equilibrium extraction methods as well as BC-inclusive modeling. *Chemosphere* **2006**, *64* (8), 1412−1420.

(18) Cornelissen, G.; Gustafsson, Ö.; Bucheli, T. D.; Jonker, M. T. O.; Koelmans, A. A.; van Noort, P. C. M. Extensive Sorption of Organic Compounds to Black Carbon, Coal, and Kerogen in Sediments and Soils: Mechanisms and Consequences for Distribution, Bioaccumulation, and Biodegradation. *Environ. Sci. Technol.* **2005**, *39* (18), 6881−6895.

(19) Cornelissen, G.; Breedveld, G. D.; Næs, K.; Oen, A. M. P.; Ruus, A. Bioaccumulation of native polycyclic aromatic hydrocarbons from sediment by a polychaete and a gastropod: Freely dissolved concentrations and activated carbon amendment. *Environ. Toxicol. Chem.* **2006**, *25* (9), 2349−2355.

(20) Hunter, W.; Xu, Y.; Spurlock, F.; Gan, J. Using disposable polydimethylsiloxane fibers to assess the bioavailability of permethrin in sediment. *Environ. Toxicol. Chem.* **2008**, *27* (3), 568−575.

(21) Huckins, J. N.; Tubergen, M. W.; Manuweera, G. K. Semipermeable membrane devices containing model lipid: A new approach to monitoring the bioavaiiability of lipophilic contaminants and estimating their bioconcentration potential. *Chemosphere* **1990**, *20* (5), 533−552.

(22) Arthur, C. L.; Pawliszyn, J. Solid phase microextraction with thermal desorption using fused silica optical fibers. *Anal. Chem.* **1990**, *62* (19), 2145−2148.

(23) Liu, H.-H.; Bao, L.-J.; Feng, W.-H.; Xu, S.-P.; Wu, F.-C.; Zeng, E. Y. A Multisection Passive Sampler for Measuring Sediment Porewater Profile of Dichlorodiphenyltrichloroethane and Its Metabolites. *Anal. Chem.* **2013**, *85* (15), 7117−7124.

(24) Lohmann, R. Critical Review of Low-Density Polyethylene's Partitioning and Diffusion Coefficients for Trace Organic Contaminants and Implications for Its Use As a Passive Sampler. *Environ. Sci. Technol.* **2012**, *46* (2), 606−618.

(25) DiFilippo, E. L.; Eganhouse, R. P. Assessment of PDMS-Water Partition Coefficients: Implications for Passive Environmental

DOI: 10.1021/acs.est.6b03273
Environ. Sci. Technol. 2016, 50, 11437−11451

Sampling of Hydrophobic Organic Compounds. *Environ. Sci. Technol.* **2010**, *44* (18), 6917−6925.
(26) Lydy, M. J.; Landrum, P. F.; Oen, A. M. P.; Allinson, M.; Smedes, F.; Harwood, A. D.; Li, H.; Maruya, K. A.; Liu, J. Passive sampling methods for contaminated sediments: State of the science for organic contaminants. *Integr. Environ. Assess. Manage.* **2014**, *10* (2), 167−178.
(27) Zeng, E. Y.; Tsukada, D.; Diehl, D. W. Development of a Solid-Phase Microextraction-Based Method for Sampling of Persistent Chlorinated Hydrocarbons in an Urbanized Coastal Environment. *Environ. Sci. Technol.* **2004**, *38* (21), 5737−5743.
(28) Ghosh, U.; Kane Driscoll, S.; Burgess, R. M.; Jonker, M. T. O.; Reible, D.; Gobas, F.; Choi, Y.; Apitz, S. E.; Maruya, K. A.; Gala, W. R.; Mortimer, M.; Beegan, C. Passive sampling methods for contaminated sediments: Practical guidance for selection, calibration, and implementation. *Integr. Environ. Assess. Manage.* **2014**, *10* (2), 210−223.
(29) Golding, C. J.; Gobas, F. A. P. C.; Birch, G. F. A fugacity approach for assessing the bioaccumulation of hydrophobic organic compounds from estuarine sediment. *Environ. Toxicol. Chem.* **2008**, *27* (5), 1047−1054.
(30) St. George, T.; Vlahos, P.; Harner, T.; Helm, P.; Wilford, B. A rapidly equilibrating, thin film, passive water sampler for organic contaminants; characterization and field testing. *Environ. Pollut.* **2011**, *159* (2), 481−486.
(31) Leslie, H. A.; Oosthoek, A. J. P.; Busser, F. J. M.; Kraak, M. H. S.; Hermens, J. L. M. Biomimetic solid-phase microextraction to predict body residues and toxicity of chemicals that act by narcosis. *Environ. Toxicol. Chem.* **2002**, *21* (2), 229−234.
(32) Conder, J. M.; La Point, T. W. Solid-phase microextraction for predicting the bioavailability of 2,4,6-trinitrotoluene and its primary transformation products in sediment and water. *Environ. Toxicol. Chem.* **2005**, *24* (5), 1059−1066.
(33) Endo, S.; Hale, S. E.; Goss, K.-U.; Arp, H. P. H. Equilibrium Partition Coefficients of Diverse Polar and Nonpolar Organic Compounds to Polyoxymethylene (POM) Passive Sampling Devices. *Environ. Sci. Technol.* **2011**, *45* (23), 10124−10132.
(34) Arp, H. P. H.; Hale, S. E.; Elmquist Kruså, M.; Cornelissen, G.; Grabanski, C. B.; Miller, D. J.; Hawthorne, S. B. Review of polyoxymethylene passive sampling methods for quantifying freely dissolved porewater concentrations of hydrophobic organic contaminants. *Environ. Toxicol. Chem.* **2015**, *34* (4), 710−720.
(35) Seethapathy, S.; Górecki, T.; Li, X. Passive sampling in environmental analysis. *Journal of Chromatography A* **2008**, *1184* (1−2), 234−253.
(36) Namieśnik, J.; Zabiegała, B.; Kot-Wasik, A.; Partyka, M.; Wasik, A. Passive sampling and/or extraction techniques in environmental analysis: a review. *Anal. Bioanal. Chem.* **2005**, *381* (2), 279−301.
(37) Mayer, P.; Parkerton, T. F.; Adams, R. G.; Cargill, J. G.; Gan, J.; Gouin, T.; Gschwend, P. M.; Hawthorne, S. B.; Helm, P.; Witt, G.; You, J.; Escher, B. I. Passive sampling methods for contaminated sediments: Scientific rationale supporting use of freely dissolved concentrations. *Integr. Environ. Assess. Manage.* **2014**, *10* (2), 197−209.
(38) Vrana, B.; Allan, I. J.; Greenwood, R.; Mills, G. A.; Dominiak, E.; Svensson, K.; Knutsson, J.; Morrison, G. Passive sampling techniques for monitoring pollutants in water. *TrAC, Trends Anal. Chem.* **2005**, *24* (10), 845−868.
(39) Lohmann, R.; Booij, K.; Smedes, F.; Vrana, B. Use of passive sampling devices for monitoring and compliance checking of POP concentrations in water. *Environ. Sci. Pollut. Res.* **2012**, *19* (6), 1885−1895.
(40) Kraaij, R.; Mayer, P.; Busser, F. J. M.; van het Bolscher, M.; Seinen, W.; Tolls, J.; Belfroid, A. C. Measured Pore-Water Concentrations Make Equilibrium Partitioning Work A Data Analysis. *Environ. Sci. Technol.* **2003**, *37* (2), 268−274.
(41) Booij, K.; Smedes, F.; Van Weerlee, E. M.; Honkoop, P. J. C. Environmental Monitoring of Hydrophobic Organic Contaminants: The Case of Mussels versus Semipermeable Membrane Devices. *Environ. Sci. Technol.* **2006**, *40* (12), 3893−3900.
(42) Parks, A. N.; Chandler, G. T.; Portis, L. M.; Sullivan, J. C.; Perron, M. M.; Cantwell, M. G.; Burgess, R. M.; Ho, K. T.; Ferguson, P. L. Effects of single-walled carbon nanotubes on the bioavailability of PCBs in field-contaminated sediments. *Nanotoxicology* **2014**, *8* (sup1), 111−117.
(43) Golding, C. J.; Gobas, F. A. P. C.; Birch, G. F. Characterization of polycyclic aromatic hydrocarbon bioavailability in estuarine sediments using thin-film extraction. *Environ. Toxicol. Chem.* **2007**, *26* (5), 829−836.
(44) Meloche, L. M.; deBruyn, A. M. H.; Otton, S. V.; Ikonomou, M. G.; Gobas, F. A. P. C. Assessing exposure of sediment biota to organic contaminants by thin-film solid phase extraction. *Environ. Toxicol. Chem.* **2009**, *28* (2), 247−253.
(45) Fernandez, L. A.; Lao, W.; Maruya, K. A.; Burgess, R. M. Calculating the Diffusive Flux of Persistent Organic Pollutants between Sediments and the Water Column on the Palos Verdes Shelf Superfund Site Using Polymeric Passive Samplers. *Environ. Sci. Technol.* **2014**, *48* (7), 3925−3934.
(46) Morgan, E. J.; Lohmann, R. Detecting Air−Water and Surface−Deep Water Gradients of PCBs Using Polyethylene Passive Samplers. *Environ. Sci. Technol.* **2008**, *42* (19), 7248−7253.
(47) Friedman, C. L.; Cantwell, M. G.; Lohmann, R. Passive sampling provides evidence for Newark Bay as a source of polychlorinated dibenzo-p-dioxins and furans to the New York/New Jersey, USA, atmosphere. *Environ. Toxicol. Chem.* **2012**, *31* (2), 253−261.
(48) Perron, M. M.; Burgess, R. M.; Cantwell, M. G.; Fernandez, L. A. Evaluating cost when selecting performance reference compounds for the environmental deployment of polyethylene passive samplers. *Integr. Environ. Assess. Manage.* **2015**, *11* (2), 256−265.
(49) Fernandez, L. A.; MacFarlane, J. K.; Tcaciuc, A. P.; Gschwend, P. M. Measurement of Freely Dissolved PAH Concentrations in Sediment Beds Using Passive Sampling with Low-Density Polyethylene Strips. *Environ. Sci. Technol.* **2009**, *43* (5), 1430−1436.
(50) Huckins, J. N.; Petty, J. D.; Lebo, J. A.; Almeida, F. V.; Booij, K.; Alvarez, D. A.; Cranor, W. L.; Clark, R. C.; Mogensen, B. B. Development of the Permeability/Performance Reference Compound Approach for In Situ Calibration of Semipermeable Membrane Devices. *Environ. Sci. Technol.* **2002**, *36* (1), 85−91.
(51) Friedman, C. L.; Lohmann, R.; Burgess, R. M.; Perron, M. M.; Cantwell, M. G. Resuspension of polychlorinated biphenyl-contaminated field sediment: release to the water column and determination of site-specific KDOC. *Environ. Toxicol. Chem.* **2011**, *30* (2), 377−384.
(52) Perron, M. M.; Burgess, R. M.; Suuberg, E. M.; Cantwell, M. G.; Pennell, K. G. Performance of passive samplers for monitoring estuarine water column concentrations: 1. Contaminants of concern. *Environ. Toxicol. Chem.* **2013**, *32* (10), 2182−2189.
(53) Perron, M. M.; Burgess, R. M.; Suuberg, E. M.; Cantwell, M. G.; Pennell, K. G. Performance of passive samplers for monitoring estuarine water column concentrations: 2. Emerging contaminants. *Environ. Toxicol. Chem.* **2013**, *32* (10), 2190−2196.
(54) Thompson, J. M.; Hsieh, C.-H.; Luthy, R. G. Modeling Uptake of Hydrophobic Organic Contaminants into Polyethylene Passive Samplers. *Environ. Sci. Technol.* **2015**, *49* (4), 2270−2277.
(55) Tcaciuc, A. P.; Apell, J. N.; Gschwend, P. M. Modeling the transport of organic chemicals between polyethylene passive samplers and water in finite and infinite bath conditions. *Environ. Toxicol. Chem.* **2015**, *34* (12), 2739−2749.
(56) Booij, K.; Smedes, F. An Improved Method for Estimating in Situ Sampling Rates of Nonpolar Passive Samplers. *Environ. Sci. Technol.* **2010**, *44* (17), 6789−6794.
(57) Organization for Economic Cooperation and Development. Bioaccumulation in Sediment-dwelling Benthic Oligochaetes. In *OECD Guidelines for the Testing of Chemicals*, Section 3; OECD Publishing: Paris, France, 2008.
(58) U.S. EPA. *Guidance Manual: Bedded Sediment Bioaccumulation Tests*, EPA/600/R-93/183; Office of Research and Development: Washington, DC, USA, 1993.

DOI: 10.1021/acs.est.6b03273
Environ. Sci. Technol. 2016, 50, 11437−11451

(59) American Society for Testing Materials. *Standard Guide for Determination of the Bioaccumulation of Sediment-Associated Contaminants by Benthic Invertebrates*, ASTM E1688-10; ASTM International: West Conshohocken, PA, USA, 2010.
(60) U.S. EPA. *Methods for Measuring the Toxicity and Bioaccumulation of Sediment-associated Contaminants with Freshwater Invertebrates*, EPA/600/R-99/064; Office of Research and Development: Duluth, MN, USA, 2000.
(61) Goldberg, E. D.; Bowen, V. T.; Farrington, J. W.; Harvey, G.; Martin, J. H.; Parker, P. L.; Risebrough, R. W.; Robertson, W.; Schneider, E.; Gamble, E. The Mussel Watch. *Environ. Conserv.* **1978**, *5* (02), 101−125.
(62) Maruya, K. A.; Dodder, N. G.; Schaffner, R. A.; Weisberg, S. B.; Gregorio, D.; Klosterhaus, S.; Alvarez, D. A.; Furlong, E. T.; Kimbrough, K. L.; Lauenstein, G. G.; Christensen, J. D. Refocusing Mussel Watch on contaminants of emerging concern (CECs): The California pilot study (2009−10). *Mar. Pollut. Bull.* **2014**, *81* (2), 334−339.
(63) Maruya, K. A.; Dodder, N. G.; Weisberg, S. B.; Gregorio, D.; Bishop, J. S.; Klosterhaus, S.; Alvarez, D. A.; Furlong, E. T.; Bricker, S.; Kimbrough, K. L.; Lauenstein, G. G. The Mussel Watch California pilot study on contaminants of emerging concern (CECs): Synthesis and next steps. *Mar. Pollut. Bull.* **2014**, *81* (2), 355−363.
(64) Bergen, B. J.; Nelson, W. G.; Pruell, R. J. Bioaccumulation of PCB congeners by blue mussels (Mytilus edulis) deployed in New Bedford Harbor, Massachusetts. *Environ. Toxicol. Chem.* **1993**, *12* (9), 1671−1681.
(65) Smedes, F. Monitoring of chlorinated biphenyls and polycyclic aromatic hydrocarbons by passive sampling in concert with deployed mussels. In *Passive Sampling Techniques in Environmental Monitoring*; Greenwood, R., Mills, G. A., Vrana, B., Eds.; Elsevier: Amsterdan, 2007; pp 407−448.
(66) American Society for Testing Materials. *Standard Guide for Conducting In-situ Field Bioassays with Caged Bivalves*, ASTM E2122-13; ASTM International: West Conshohocken, PA, USA, 2013.
(67) Janssen, E. M. L.; Oen, A. M. P.; Luoma, S. N.; Luthy, R. G. Assessment of field-related influences on polychlorinated biphenyl exposures and sorbent amendment using polychaete bioassays and passive sampler measurements. *Environ. Toxicol. Chem.* **2011**, *30* (1), 173−180.
(68) Fernandez, L. A.; Gschwend, P. M. Predicting bioaccumulation of polycyclic aromatic hydrocarbons in soft-shelled clams (Mya arenaria) using field deployments of polyethylene passive samplers. *Environ. Toxicol. Chem.* **2015**, *34* (5), 993−1000.
(69) Trimble, T. A.; You, J.; Lydy, M. J. Bioavailability of PCBs from field-collected sediments: Application of Tenax extraction and matrix-SPME techniques. *Chemosphere* **2008**, *71* (2), 337−344.
(70) Gschwend, P. M.; MacFarlane, J. K.; Reible, D. D.; Lu, X.; Hawthorne, S. B.; Nakles, D. V.; Thompson, T. Comparison of polymeric samplers for accurately assessing PCBs in pore waters. *Environ. Toxicol. Chem.* **2011**, *30* (6), 1288−1296.
(71) Friedman, C. L.; Burgess, R. M.; Perron, M. M.; Cantwell, M. G.; Ho, K. T.; Lohmann, R. Comparing Polychaete and Polyethylene Uptake to Assess Sediment Resuspension Effects on PCB Bioavailability. *Environ. Sci. Technol.* **2009**, *43* (8), 2865−2870.
(72) Burgess, R. M.; Lohmann, R.; Schubauer-Berigan, J. P.; Reitsma, P.; Perron, M. M.; Lefkovitz, L.; Cantwell, M. G. Application of passive sampling for measuring dissolved concentrations of organic contaminants in the water column at three marine superfund sites. *Environ. Toxicol. Chem.* **2015**, *34* (8), 1720−1733.
(73) Bao, L.-J.; Jia, F.; Crago, J.; Zeng, E. Y.; Schlenk, D.; Gan, J. Assessing bioavailability of DDT and metabolites in marine sediments using solid-phase microextraction with performance reference compounds. *Environ. Toxicol. Chem.* **2013**, *32* (9), 1946−1953.
(74) Joyce, A. S.; Pirogovsky, M. S.; Adams, R. G.; Lao, W.; Tsukada, D.; Cash, C. L.; Haw, J. F.; Maruya, K. A. Using performance reference compound-corrected polyethylene passive samplers and caged bivalves to measure hydrophobic contaminants of concern in urban coastal seawaters. *Chemosphere* **2015**, *127* (0), 10−17.
(75) Pirogovsky, M. S. Calibrating solid phase microextraction passive samplers for the in situ measurement of contaminants in Southern California: Comparison to bi-valve bioconcentration. PhD Thesis, University of Southern California, Los Angeles, CA, 2013.
(76) Maruya, K. A.; Lao, W.; Tsukada, D.; Diehl, D. W. A passive sampler based on solid phase microextraction (SPME) for sediment-associated organic pollutants: Comparing freely-dissolved concentration with bioaccumulation. *Chemosphere* **2015**, *137*, 192−197.
(77) Muijs, B.; Jonker, M. T. O. Does Equilibrium Passive Sampling Reflect Actual in Situ Bioaccumulation of PAHs and Petroleum Hydrocarbon Mixtures in Aquatic Worms? *Environ. Sci. Technol.* **2012**, *46* (2), 937−944.
(78) Vinturella, A. E.; Burgess, R. M.; Coull, B. A.; Thompson, K. M.; Shine, J. P. Use of Passive Samplers To Mimic Uptake of Polycyclic Aromatic Hydrocarbons by Benthic Polychaetes. *Environ. Sci. Technol.* **2004**, *38* (4), 1154−1160.
(79) Harwood, A. D.; Landrum, P. F.; Lydy, M. J. Can SPME Fiber and Tenax Methods Predict the Bioavailability of Biotransformed Insecticides? *Environ. Sci. Technol.* **2012**, *46* (4), 2413−2419.
(80) Li, H.; Zhang, B.; Wei, Y.; Wang, F.; Lydy, M. J.; You, J. Bioaccumulation of Highly Hydrophobic Organohalogen Flame Retardants from Sediments: Application of Toxicokinetics and Passive Sampling Techniques. *Environ. Sci. Technol.* **2014**, *48* (12), 6957−6964.
(81) Sidney, L. A.; Diepens, N. J.; Guo, X.; Koelmans, A. A. Trait-based modelling of bioaccumulation by freshwater benthic invertebrates. *Aquat. Toxicol.* **2016**, *176*, 88−96.
(82) Diepens, N. J.; Van den Heuvel-Greve, M. J.; Koelmans, A. A. Modeling of Bioaccumulation in Marine Benthic Invertebrates Using a Multispecies Experimental Approach. *Environ. Sci. Technol.* **2015**, *49* (22), 13575−13585.
(83) Jahnke, A.; Holmbäck, J.; Andersson, R. A.; Kierkegaard, A.; Mayer, P.; MacLeod, M. Differences between Lipids Extracted from Five Species Are Not Sufficient To Explain Biomagnification of Nonpolar Organic Chemicals. *Environ. Sci. Technol. Lett.* **2015**, *2* (7), 193−197.
(84) Hawthorne, S. B.; Poppendieck, D. G.; Grabanski, C. B.; Loehr, R. C. Comparing PAH Availability from Manufactured Gas Plant Soils and Sediments with Chemical and Biological Tests. 1. PAH Release during Water Desorption and Supercritical Carbon Dioxide Extraction. *Environ. Sci. Technol.* **2002**, *36* (22), 4795−4803.
(85) Driscoll, S. K.; McElroy, A. E. Bioaccumulation and metabolism of benzo[A]pyrene in three species of polychaete worms. *Environ. Toxicol. Chem.* **1996**, *15* (8), 1401−1410.
(86) Rust, A. J.; Burgess, R. M.; Brownawell, B. J.; McElroy, A. E. Relationship between metabolism and bioaccumulation of benzo[α]-pyrene in benthic invertebrates. *Environ. Toxicol. Chem.* **2004**, *23* (11), 2587−2593.
(87) Varanasi, U.; Reichert, W. L.; Stein, J. E.; Brown, D. W.; Sanborn, H. R. Bioavailability and biotransformation of aromatic hydrocarbons in benthic organisms exposed to sediment from an urban estuary. *Environ. Sci. Technol.* **1985**, *19* (9), 836−841.
(88) Di Toro, D. M.; McGrath, J. A.; Hansen, D. J. Technical basis for narcotic chemicals and polycyclic aromatic hydrocarbon criteria. I. Water and tissue. *Environ. Toxicol. Chem.* **2000**, *19* (8), 1951−1970.
(89) Di Toro, D. M.; McGrath, J. A. Technical basis for narcotic chemicals and polycyclic aromatic hydrocarbon criteria. II. Mixtures and sediments. *Environ. Toxicol. Chem.* **2000**, *19* (8), 1971−1982.
(90) Swartz, R. C.; Schults, D. W.; Ditsworth, G. R.; Lamberson, J. O.; Dewitt, T. H. Toxicity of fluoranthene in sediment to marine amphipods: A test of the equilibrium partitioning approach to sediment quality criteria. *Environ. Toxicol. Chem.* **1990**, *9* (8), 1071−1080.
(91) Dewitt, T. H.; Jones, J. K. P.; Ozretich, R. J.; Swartz, R. C.; Lamberson, J. O.; Schults, D. W.; Ditsworth, G. R.; Smith, L. M.; Hoselton, L. The influence of organic matter quality on the toxicity and partitioning of sediment-associated fluoranthene. *Environ. Toxicol. Chem.* **1992**, *11* (2), 197−208.

DOI: 10.1021/acs.est.6b03273
Environ. Sci. Technol. 2016, 50, 11437−11451

(92) Hoke, R. A.; Cotter, A. M.; Goldenstein, T.; Kosian, P. A.; van dermeiden, F. M.; Ankley, G. T.; Phipps, G. L. Evaluation of equilibrium partitioning theory for predicting acute toxicity of field-collected sediments contaminated with DDT, DDE and DDD to the amphipod Hyalella azteca. *Environ. Toxicol. Chem.* **1994**, *13* (1), 157−166.
(93) Friedman, C. L.; Lohmann, R. Comparing sediment equilibrium partitioning and passive sampling techniques to estimate benthic biota PCDD/F concentrations in Newark Bay, New Jersey (U.S.A.). *Environ. Pollut.* **2014**, *186* (0), 172−179.
(94) McLeod, P. B.; Luoma, S. N.; Luthy, R. G. Biodynamic Modeling of PCB Uptake by Macoma balthica and Corbicula fluminea from Sediment Amended with Activated Carbon. *Environ. Sci. Technol.* **2008**, *42* (2), 484−490.
(95) McLeod, P. B.; van den Heuvel-Greve, M. J.; Luoma, S. N.; Luthy, R. G. Biological uptake of polychlorinated biphenyls by Macoma balthica from sediment amended with activated carbon. *Environ. Toxicol. Chem.* **2007**, *26* (5), 980−987.
(96) Booij, K.; Smedes, F.; van Weerlee, E. M. Spiking of performance reference compounds in low density polyethylene and silicone passive water samplers. *Chemosphere* **2002**, *46* (8), 1157−1161.
(97) Oen, A. M. P.; Janssen, E. M. L.; Cornelissen, G.; Breedveld, G. D.; Eek, E.; Luthy, R. G. In Situ Measurement of PCB Pore Water Concentration Profiles in Activated Carbon-Amended Sediment Using Passive Samplers. *Environ. Sci. Technol.* **2011**, *45* (9), 4053−4059.
(98) Cui, X.; Bao, L.; Gan, J. Solid-phase Microextraction (SPME) with Stable Isotope Calibration for Measuring Bioavailability of Hydrophobic Organic Contaminants. *Environ. Sci. Technol.* **2013**, *47* (17), 9833−9840.
(99) Morrison, H. A.; Gobas, F. A. P. C.; Lazar, R.; Whittle, D. M.; Haffner, G. D. Development and Verification of a Benthic/Pelagic Food Web Bioaccumulation Model for PCB Congeners in Western Lake Erie. *Environ. Sci. Technol.* **1997**, *31* (11), 3267−3273.
(100) Arnot, J. A.; Gobas, F. A. P. C. A food web bioaccumulation model for organic chemicals in aquatic ecosystems. *Environ. Toxicol. Chem.* **2004**, *23* (10), 2343−2355.
(101) Fadaei, H.; Watson, A.; Place, A.; Connolly, J.; Ghosh, U. Effect of PCB Bioavailability Changes in Sediments on Bioaccumulation in Fish. *Environ. Sci. Technol.* **2015**, *49* (20), 12405−12413.
(102) Khairy, M. A.; Weinstein, M. P.; Lohmann, R. Trophodynamic Behavior of Hydrophobic Organic Contaminants in the Aquatic Food Web of a Tidal River. *Environ. Sci. Technol.* **2014**, *48* (21), 12533−12542.
(103) Jahnke, A.; McLachlan, M. S.; Mayer, P. Equilibrium sampling: Partitioning of organochlorine compounds from lipids into polydimethylsiloxane. *Chemosphere* **2008**, *73* (10), 1575−1581.
(104) Jahnke, A.; Mayer, P.; McLachlan, M. S. Sensitive Equilibrium Sampling To Study Polychlorinated Biphenyl Disposition in Baltic Sea Sediment. *Environ. Sci. Technol.* **2012**, *46* (18), 10114−10122.
(105) Jahnke, A.; MacLeod, M.; Wickström, H.; Mayer, P. Equilibrium Sampling to Determine the Thermodynamic Potential for Bioaccumulation of Persistent Organic Pollutants from Sediment. *Environ. Sci. Technol.* **2014**, *48* (19), 11352−11359.
(106) Jahnke, A.; Mayer, P.; McLachlan, M. S.; Wickstrom, H.; Gilbert, D.; MacLeod, M. Silicone passive equilibrium samplers as 'chemometers' in eels and sediments of a Swedish lake. *Environmental Science: Processes & Impacts* **2014**, *16* (3), 464−472.
(107) Mäenpää, K.; Leppänen, M. T.; Figueiredo, K.; Mayer, P.; Gilbert, D.; Jahnke, A.; Gil-Allué, C.; Akkanen, J.; Nybom, I.; Herve, S. Fate of polychlorinated biphenyls in a contaminated lake ecosystem: Combining equilibrium passive sampling of sediment and water with total concentration measurements of biota. *Environ. Toxicol. Chem.* **2015**, *34* (11), 2463−2474.
(108) The National Research Council. *Risk-Management Strategy for PCB-Contaminated Sediments*. The National Academy Press: Washington, DC, USA, 2001; p 432.
(109) The National Research Council. *Bioavailability of Contaminants in Soils and Sediments: Processes, Tools, and Applications*; In The National Academy Press: Washington, DC, USA, 2003; p 420.
(110) Hawker, D. W.; Connell, D. W. Octanol-water partition coefficients of polychlorinated biphenyl congeners. *Environ. Sci. Technol.* **1988**, *22* (4), 382−387.
(111) Hilal, S. H.; Karickhoff, S. W.; Carreira, L. A. Prediction of the Solubility, Activity Coefficient and Liquid/Liquid Partition Coefficient of Organic Compounds. *QSAR Comb. Sci.* **2004**, *23* (9), 709−720.

DOI: 10.1021/acs.est.6b03273
Environ. Sci. Technol. 2016, 50, 11437−11451

Author	Employer	Percentage Allocation (%)	Status for STAA	E-mail Confirmation of Allocation Agreement (date agreed)
RM Burgess	U.S. EPA	25	Eligible	Yes (27 April 2020)
R Lohman	URI/GSO	15	Ineligible	Yes (28 April 2020)
J Schubauer-Berigan	Former U.S. EPA	10	Retired	Yes (30 April 2020)
P Reitsma	Crooked Cove Sea Farm	10	Ineligible	Yes (28 April 2020)
M Perron	U.S. EPA	15	Eligible	Yes (28 April 2020)
L Lefkovitz	Battelle	10	Ineligible	Yes (28 April 2020)
M Cantwell	U.S. EPA	15	Eligible	Yes (28 April 2020)

Copies of confirmation e-mails:

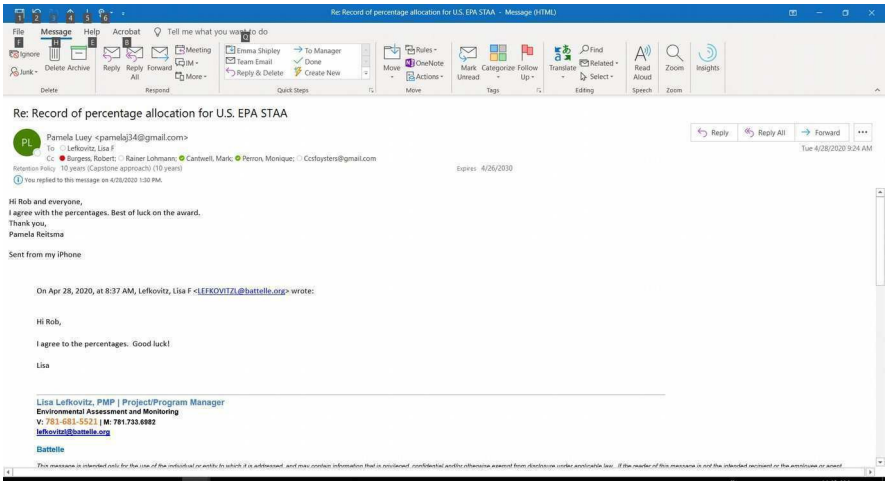

Re: Record of percentage allocation for U.S. EPA STAA

Pamela Luey <pamelaj34@gmail.com>

Hi Rob and everyone,
I agree with the percentages. Best of luck on the award.
Thank you,
Pamela Reitsma

Sent from my iPhone

On Apr 28, 2020, at 8:37 AM, Lefkovitz, Lisa F <LEFKOVITZL@battelle.org> wrote:

Hi Rob,

I agree to the percentages. Good luck!

Lisa

Lisa Lefkovitz, PMP | Project/Program Manager
Environmental Assessment and Monitoring
V: 781-681-5521 | M: 781.733.6982
lefkovitzl@battelle.org

Battelle

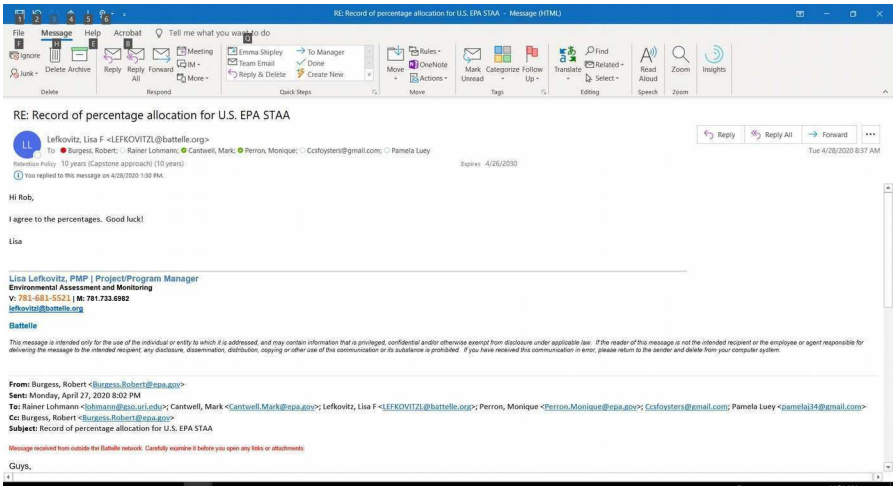

RE: Record of percentage allocation for U.S. EPA STAA

Lefkovitz, Lisa F <LEFKOVITZL@battelle.org>

Hi Rob,

I agree to the percentages. Good luck!

Lisa

Lisa Lefkovitz, PMP | Project/Program Manager
Environmental Assessment and Monitoring
V: 781-681-5521 | M: 781.733.6982
lefkovitzl@battelle.org

Battelle

This message is intended only for the use of the individual or entity to which it is addressed, and may contain information that is privileged, confidential and/or otherwise exempt from disclosure under applicable law. If the reader of this message is not the intended recipient or the employee or agent responsible for delivering the message to the intended recipient, any disclosure, dissemination, distribution, copying or other use of this communication or its substance is prohibited. If you have received this communication in error, please return to the sender and delete from your computer system.

From: Burgess, Robert <Burgess.Robert@epa.gov>
Sent: Monday, April 27, 2020 8:02 PM
To: Rainer Lohmann <lohmann@gso.uri.edu>; Cantwell, Mark <Cantwell.Mark@epa.gov>; Lefkovitz, Lisa F <LEFKOVITZL@battelle.org>; Perron, Monique <Perron.Monique@epa.gov>; Ccsfoysters@gmail.com; Pamela Luey <pamelaj34@gmail.com>
Cc: Burgess, Robert <Burgess.Robert@epa.gov>
Subject: Record of percentage allocation for U.S. EPA STAA

Message received from outside the Battelle network. Carefully examine it before you open any links or attachments.

Guys,

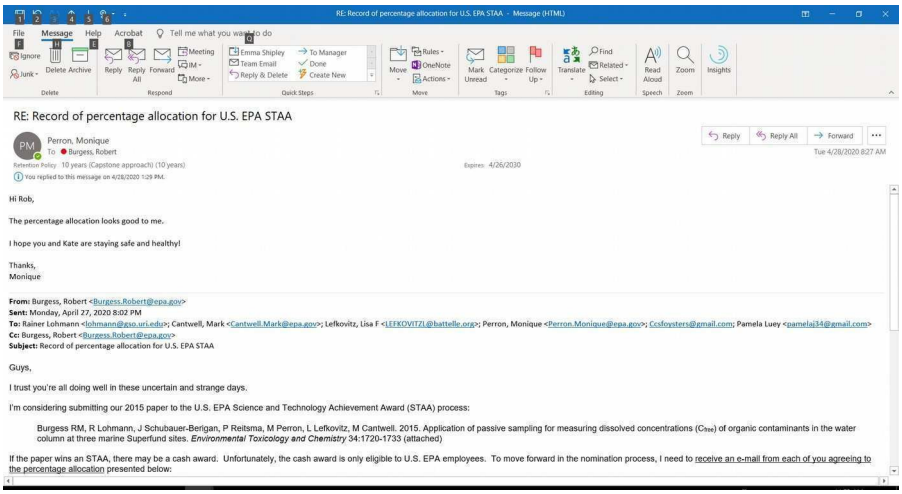

RE: Record of percentage allocation for U.S. EPA STAA - Message (HTML)

File Message Help Acrobat Tell me what you want to do

Ignore Junk Delete Archive | Reply Reply All Forward Meeting IM More | Emma Shipley Team Email Reply & Delete To Manager Done Create New | Move Rules OneNote Actions | Mark Unread Categorize Follow Up | Translate Find Related Select | Read Aloud | Zoom | Insights

Delete Respond Quick Steps Move Tags Editing Speech Zoom

RE: Record of percentage allocation for U.S. EPA STAA

Reply Reply All Forward

PM Perron, Monique
To Burgess, Robert
Tue 4/28/2020 8:27 AM

Retention Policy 10 years (Capstone approach) (10 years) Expires 4/26/2030

You replied to this message on 4/28/2020 1:29 PM.

Hi Rob,

The percentage allocation looks good to me.

I hope you and Kate are staying safe and healthy!

Thanks,
Monique

From: Burgess, Robert <Burgess.Robert@epa.gov>
Sent: Monday, April 27, 2020 8:02 PM
To: Rainer Lohmann <lohmann@gso.uri.edu>; Cantwell, Mark <Cantwell.Mark@epa.gov>; Lefkovitz, Lisa F <LEFKOVITZL@battelle.org>; Perron, Monique <Perron.Monique@epa.gov>; Ccsfoysters@gmail.com; Pamela Luey <pamelaj34@gmail.com>
Cc: Burgess, Robert <Burgess.Robert@epa.gov>
Subject: Record of percentage allocation for U.S. EPA STAA

Guys,

I trust you're all doing well in these uncertain and strange days.

I'm considering submitting our 2015 paper to the U.S. EPA Science and Technology Achievement Award (STAA) process:

> Burgess RM, R Lohmann, J Schubauer-Berigan, P Reitsma, M Perron, L Lefkovitz, M Cantwell. 2015. Application of passive sampling for measuring dissolved concentrations (C_{free}) of organic contaminants in the water column at three marine Superfund sites. *Environmental Toxicology and Chemistry* 34:1720-1733 (attached)

If the paper wins an STAA, there may be a cash award. Unfortunately, the cash award is only eligible to U.S. EPA employees. To move forward in the nomination process, I need to receive an e-mail from each of you agreeing to the percentage allocation presented below:

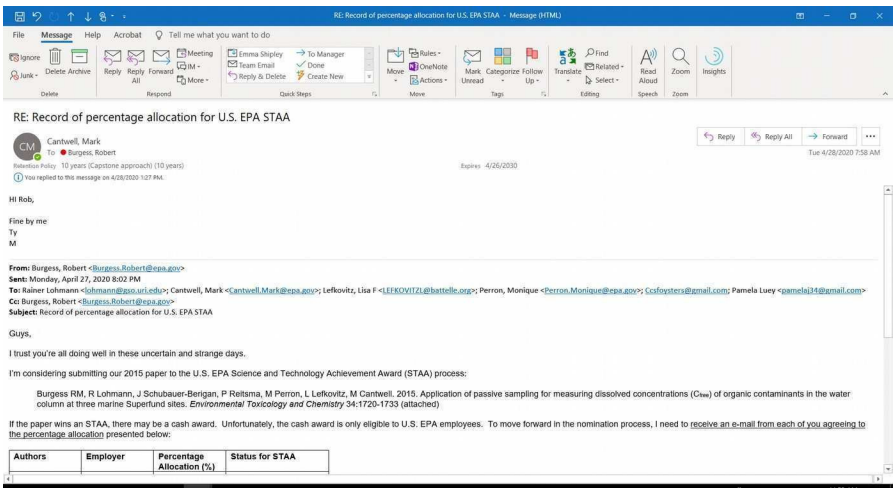

RE: Record of percentage allocation for U.S. EPA STAA - Message (HTML)

File Message Help Acrobat Tell me what you want to do

Ignore Junk Delete Archive | Reply Reply All Forward Meeting IM More | Emma Shipley Team Email Reply & Delete To Manager Done Create New | Move Rules OneNote Actions | Mark Unread Categorize Follow Up | Translate Find Related Select | Read Aloud | Zoom | Insights

Delete Respond Quick Steps Move Tags Editing Speech Zoom

RE: Record of percentage allocation for U.S. EPA STAA

Reply Reply All Forward

CM Cantwell, Mark
To Burgess, Robert
Tue 4/28/2020 7:58 AM

Retention Policy 10 years (Capstone approach) (10 years) Expires 4/26/2030

You replied to this message on 4/28/2020 1:27 PM.

Hi Rob,

Fine by me
Ty
M

From: Burgess, Robert <Burgess.Robert@epa.gov>
Sent: Monday, April 27, 2020 8:02 PM
To: Rainer Lohmann <lohmann@gso.uri.edu>; Cantwell, Mark <Cantwell.Mark@epa.gov>; Lefkovitz, Lisa F <LEFKOVITZL@battelle.org>; Perron, Monique <Perron.Monique@epa.gov>; Ccsfoysters@gmail.com; Pamela Luey <pamelaj34@gmail.com>
Cc: Burgess, Robert <Burgess.Robert@epa.gov>
Subject: Record of percentage allocation for U.S. EPA STAA

Guys,

I trust you're all doing well in these uncertain and strange days.

I'm considering submitting our 2015 paper to the U.S. EPA Science and Technology Achievement Award (STAA) process:

> Burgess RM, R Lohmann, J Schubauer-Berigan, P Reitsma, M Perron, L Lefkovitz, M Cantwell. 2015. Application of passive sampling for measuring dissolved concentrations (C_{free}) of organic contaminants in the water column at three marine Superfund sites. *Environmental Toxicology and Chemistry* 34:1720-1733 (attached)

If the paper wins an STAA, there may be a cash award. Unfortunately, the cash award is only eligible to U.S. EPA employees. To move forward in the nomination process, I need to receive an e-mail from each of you agreeing to the percentage allocation presented below:

Authors	Employer	Percentage Allocation (%)	Status for STAA

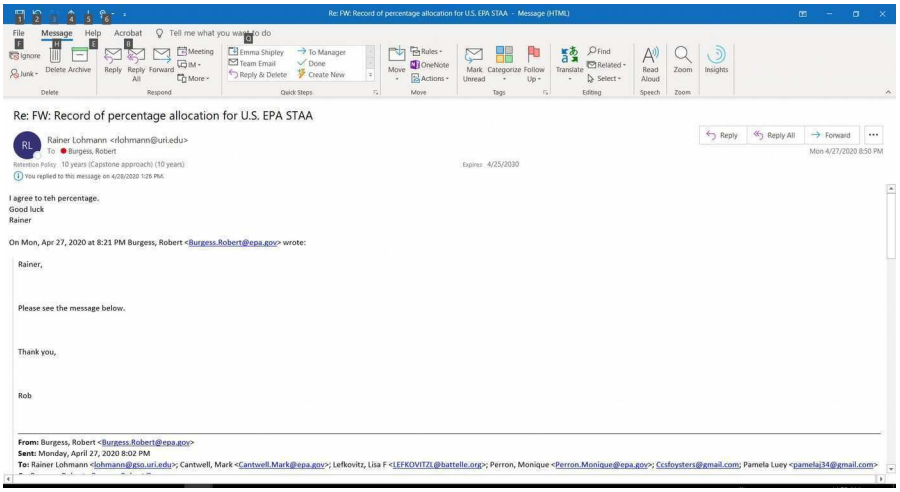

Re: FW: Record of percentage allocation for U.S. EPA STAA - Message (HTML)

File Message Help Acrobat Tell me what you want to do

Ignore Junk Delete Archive | Reply Reply All Forward Meeting IM More | Emma Shipley Team Email Reply & Delete To Manager Done Create New | Move Rules OneNote Actions | Mark Unread Categorize Follow Up | Translate Find Related Select | Read Aloud | Zoom | Insights

Delete Respond Quick Steps Move Tags Editing Speech Zoom

Re: FW: Record of percentage allocation for U.S. EPA STAA

Reply Reply All Forward

RL Rainer Lohmann <rlohmann@uri.edu>
To Burgess, Robert
Mon 4/27/2020 8:50 PM

Retention Policy 10 years (Capstone approach) (10 years) Expires 4/25/2030

You replied to this message on 4/28/2020 1:26 PM.

I agree to teh percentage.
Good luck
Rainer

On Mon, Apr 27, 2020 at 8:21 PM Burgess, Robert <Burgess.Robert@epa.gov> wrote:

> Rainer,
>
> Please see the message below.
>
> Thank you,
>
> Rob
>
> **From:** Burgess, Robert <Burgess.Robert@epa.gov>
> **Sent:** Monday, April 27, 2020 8:02 PM
> **To:** Rainer Lohmann <lohmann@gso.uri.edu>; Cantwell, Mark <Cantwell.Mark@epa.gov>; Lefkovitz, Lisa F <LEFKOVITZL@battelle.org>; Perron, Monique <Perron.Monique@epa.gov>; Ccsfoysters@gmail.com; Pamela Luey <pamelaj34@gmail.com>

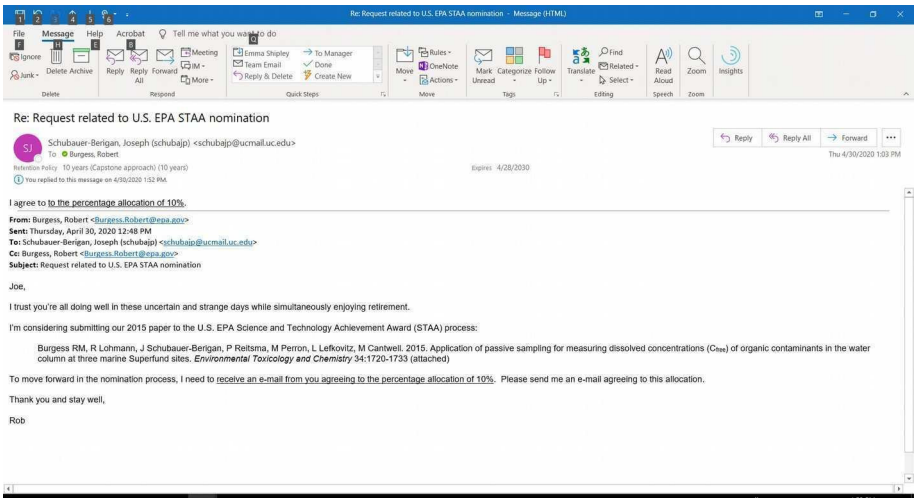
Re: Request related to U.S. EPA STAA nomination - Message (HTML)
File Message Help Acrobat Tell me what you want to do
Ignore Junk Delete Archive Reply Reply All Forward Meeting IM More
Emma Shipley Team Email Reply & Delete To Manager Done Create New
Move Rules OneNote Actions
Mark Unread Categorize Follow Up
Translate Find Related Select
Read Aloud Zoom Insights
Delete Respond Quick Steps Move Tags Editing Speech Zoom
Re: Request related to U.S. EPA STAA nomination
SJ
Schubauer-Berigan, Joseph (schubajp) <schubajp@ucmail.uc.edu>
To Burgess, Robert
Reply Reply All Forward
Thu 4/30/2020 1:03 PM
Retention Policy 10 years (Capstone approach) (10 years)
Expires 4/28/2030
You replied to this message on 4/30/2020 1:52 PM.
I agree to to the percentage allocation of 10%.
From: Burgess, Robert <Burgess.Robert@epa.gov>
Sent: Thursday, April 30, 2020 12:48 PM
To: Schubauer-Berigan, Joseph (schubajp) <schubajp@ucmail.uc.edu>
Cc: Burgess, Robert <Burgess.Robert@epa.gov>
Subject: Request related to U.S. EPA STAA nomination
Joe,
I trust you're all doing well in these uncertain and strange days while simultaneously enjoying retirement.
I'm considering submitting our 2015 paper to the U.S. EPA Science and Technology Achievement Award (STAA) process:
Burgess RM, R Lohmann, J Schubauer-Berigan, P Reitsma, M Perron, L Lefkovitz, M Cantwell. 2015. Application of passive sampling for measuring dissolved concentrations (C_{free}) of organic contaminants in the water column at three marine Superfund sites. Environmental Toxicology and Chemistry 34;1720-1733 (attached)
To move forward in the nomination process, I need to receive an e-mail from you agreeing to the percentage allocation of 10%. Please send me an e-mail agreeing to this allocation.
Thank you and stay well,
Rob

Table of Contents

General_Authors_Publications.....2
LI-266645_Publication_1.....11
LI-266645_Supplemental_along_with_publication_1.....22
LI-266670_Publication_2.....32
LI-266670_Supplemental_along_with_publication_2.....46
Record_of_Percentage_Agreement_(Darren_Lytle).....50
Record_of_Percentage_Agreement_(Ian_Struewing).....52
Record_of_Percentage_Agreement_(Jorge_Santo_Domingo).....54
Record_of_Percentage_Agreement_(Ke_Qin).....56
Record_of_Percentage_Agreement_(Nick_Ashbolt).....58
Record_of_Percentage_Agreement_(Sharon_Yelton).....59
Publication_1.....61
Publication_2.....72
Supplemental_along_with_publication_1.....86
Supplemental_along_with_publication_2.....96
Article_request_for_publication_1.....100
Invitation_for_publication_in_AWWA.....102
Invitation_for_publication_in_Biotechnology.....104

United States Environmental Protection Agency
Washington, DC 20460

STAA REPORT FOR THE SCIENTIST NOMINATIONS

General Information:

Nomination ID/App ID:	20-126
Research Category Primary:	Monitoring and Measurement Methods (MM)
Research Category Secondary:	Homeland Security (HS)
Laboratory/Office Name:	ORD-CEMM
Nomination Entered By:	Jingrang Lu

Eligibility Checklist:

[Y] The nominated publication(s) has not been submitted to a previous STAA competition.

[Y] The nominated publication(s) was published on or before January 1, 2017 and on or after January 1,2012

[Y] The principal author was an EPA employee or a PHS employee assigned to EPA when the research was performed

[Y] The EPA authors (includes PHS employees assigned to EPA) contributed collectively a minimum of 50% toward the publication(s)

Nominating Official Name:	Kevin Oshima
Nominating Official Title:	BIOLOGIST
Nominating OfficialEmail:	oshima.kevin@epa.gov
STAA Coordinator Name:	Kathleen Wiser
STAA Coordinator Email:	wiser.kathi@epa.gov

Justifications:

Justification 1:

Municipal drinking water storage tanks (MDWSTs) are an important component of the distribution system infrastructure. To date, there is limited documentation on pathogen occurrence in MDWSTs, due to complexities and cost associated with sampling of MDWST sediments. Our study on waterborne pathogens in MDWSTs is the original and only survey across the United States. Considering the challenge for collecting sediment samples, we were still able to obtain samples through our established network with storage tank cleaning companies, regional offices, and local health department. This novel method is an early approach of community citizen science.

Considering *Legionella pneumophila* is the species responsible for the majority (>90%) of cases of Legionnaires' disease and more than 58% of outbreaks associated with drinking water, the focus of this study was on the detection of *Legionella* spp. and *L. pneumophila* in MDWSTs. To conduct accurate detection of this pathogen, we designed novel qPCR assays for detecting *Legionella* spp., *L. pneumophila* and *L. pneumophila* sgr.1 (suppl-1). Those new assays were developed with high coverage, specificity, and sensitivity based on the pathogen's virulence factor genes (*sidF, rtxA* and *mipA*). Those assays served not only for this MDWST study, but also were applied in other studies (not described here) on a municipal drinking water distribution system (Lu et al. 2016) and in a shower water system (Lu et al. 2017). The overall success achieved from our study on detecting *Legionella* spp. in drinking water systems, have resulted in the development of protocols for the rapid detection of *L. pneumophila* that were provided to EPA's National Homeland Security Research Center (NHSRC).

The innovative findings are as follows. (1) High occurrence of potential opportunistic pathogens was found to be prevalent within MDWST sediments. They could act as a source of microbial contamination for downstream drinking water users. (2) There was cooccurrence of *Legionella* spp. and potential host *Acanthamoeba* spp. The opportunistic pathogens and microbial communities were associated with some elements derived from corrosion. The organic-matter-rich

sediments contained high opportunistic pathogens. (3) Diverse *Legionella* species were found and some *L. pneumophila*, *L. pneumophila* sg1 and *L. anisa*) were legionellosis-related,

Significance and Impact of the Study are as follows. (1) The information was needed for NHSRC to understand the biological background for assessment of the biological risk in the event of future emergency of biological agent attacks via MDWSTs. Based on this study, we continued our key research collaborations with NHSRC for developing a protocol to detect *Legionella* and *L. pneumophila* within drinking water distribution systems. (2) The occurrence and ecological aspects of opportunistic pathogens provided key scientific support for the Office of Water to develop the *Legionella* guidance document (EPA 810-R-16-001, EPA Office of Water), and now are the one of the key research priorities of US EPA research (SSWR 2019-2022). (3) The outcome of this study provided critical data for *Legionella* to be considered as one of the microbial contaminants for the Contaminant Candidate List (CCL) 5 published by UEPA's Office of Water's Office of Ground Water and Drinking Water. Furthermore, this study can provide basic data for whether there should be guidance or regulation for regular maintenance of tanks and sediment removal.

Justification 2A:

Both publications described the investigations of opportunistic pathogens in MDWST sediments and included the occurrence of opportunistic pathogens detected using qPCR. Publication 1 described the occurrence and quantity of potential opportunistic pathogens across the United States, while the publication 2 were the further continuing investigations including not only the occurrence and densities, but also the microbial community structure, and their associations with sediment elements from smaller scale of sampling sites.

Justification 2B:

1. J. Lu, J. Santo Domingo, J. N. Ashbolt (2014) Impact of drinking water conditions and copper materials on downstream biofilm microbial communities and *Legionella pneumophila* colonization. 2017 EPA STAA (Nominee: Jingrang Lu, Contributing authors: Jorge Santo Domingo, J. N. Ashbolt, etc.)

2. J. Lu, J. N. Ashbolt (2014). Preferential colonization and release of *Legionella pneumophila* from mature drinking water biofilms grown on copper versus Unplasticized polyvinylchloride coupons. 2017 EPA STAA (Nominee: Jingrang Lu, Contributing authors: J. N. Ashbolt etc.)

3. J. Lu, J. N. Ashbolt (2013). *Legionella pneumophila* transcriptional response following exposure to CuO nanoparticles. 2018-2019 EPA STAA (Nominee: Jingrang Lu, Contributing authors: J. N. Ashbolt etc.)

.

Justification 2C:

This nominee's publications described the studies on opportunistic pathogens in MDWSTs and their associations with sediment factors and are significantly different from the previous publications for the studies on the copper impact on *Legionella* and other opportunistic pathogens in drinking water by these authors.

Justification 2D:

The supplemental information for the current nomination doesn't include any previously submitted supplemental information.

Justification 2E:

None of the authors has submitted a concurrent nomination to another Research Category.

Justification 3A:

The manuscripts have received considerable interest and have already been cited 42 and 10 times, respectively, to date, in various academic manuscripts. In addition, the invitations of publications and presentations for this topic have been received (supplemental documents). Finally, the manuscript's authors have given poster presentations describing this work at an ASM conference and WQTC.

Justification 3B:

The manuscript was internally reviewed, in accordance with NERL quality assurance clearance procedure, prior to submission to the journals, “Journal of Applied Microbiology” and “MDPI Pathogens”. A blind review of the manuscript was conducted by the journal editors and external reviewers in accordance with their peer review policy. The manuscripts were then accepted for publication.

AUTHORS

Principal Author

Author Name:	Jingrang Lu		
Professional Title:		Salutation:	
Email:	lu.jingrang@epa.gov	Organization:	
Mailing Address:			
Street Line 1:			
City:			
Zip Code:		State:	
At time of research was:	EPA Employee		
Separation Date:			
% of Effort:	64		

Contributing Author

Author Name:	Ke Qin		
Professional Title:		Salutation:	Dr.
Email:	qinke84@gmail.com	Organization:	
Mailing Address:			

Street Line 1:			
City:			
Zip Code:		State:	
At time of research was:	Non EPA Personnel		
Separation Date:			
% of Effort:	12		

Contributing Author

Author Name:	Nick Ashbolt		
Professional Title:		Salutation:	Dr.
Email:	ashbolt@ualberta.ca	Organization:	
Mailing Address:			
Street Line 1:			
City:			
Zip Code:		State:	
At time of research was:	EPA Employee		
Separation Date:			
% of Effort:	4		

Contributing Author

Author Name:	Ian Struewing		
Professional Title:		Salutation:	Mr.
Email:	struewing.ian@epa.gov	Organization:	
Mailing Address:			

Street Line 1:			
City:			
Zip Code:		State:	
At time of research was:	Non EPA Personnel		
Separation Date:			
% of Effort:	9		

Contributing Author

Author Name:	Darren Lytle		
Professional Title:		Salutation:	Dr.
Email:	lytle.darren@epa.gov	Organization:	
Mailing Address:			
Street Line 1:			
City:			
Zip Code:		State:	
At time of research was:	EPA Employee		
Separation Date:			
% of Effort:	5		

Contributing Author

Author Name:	Sheron Yelton (maiden name)		
Professional Title:		Salutation:	Ms.
Email:	yeltons1@gmail.com	Organization:	
Mailing Address:			

Street Line 1:			
City:			
Zip Code:		State:	
At time of research was:	Non EPA Personnel		
Separation Date:			
% of Effort:	3		

Contributing Author

Author Name:	Jorge Santo Domingo		
Professional Title:		Salutation:	Dr.
Email:	santodomingo.jorge@epa.gov	Organization:	
Mailing Address:			
Street Line 1:			
City:			
Zip Code:		State:	
At time of research was:	EPA Employee		
Separation Date:			
% of Effort:	3		

PUBLICATIONS

Publication 1:

Publication Title:	Molecular survey of occurrence and quantity of Legionella spp., Mycobacterium spp., Pseudomonas aeru
Publication Date:	Fri Apr 10 00:00:00 GMT 2015

Journal/Publication Method:	Journal of applied microbiology		
All Author(s):			
Volume:	119	Number:	1
Pages:	278-288	Immediately Index:	Immediately Index:
Citation ½ Life:	10.2	Impact Factor:	2.683

Publication 2:

Publication Title:	Opportunistic pathogens and microbial communities and their associations with sediment physical para		
Publication Date:	Thu Oct 26 00:00:00 GMT 2017		
Journal/Publication Method:	Pathogens		
All Author(s):			
Volume:	6	Number:	4
Pages:	1-14	Immediately Index:	Immediately Index:
Citation ½ Life:	3.3	Impact Factor:	3.405

Journal of Applied Microbiology

Journal of Applied Microbiology ISSN 1364-5072

ORIGINAL ARTICLE

Molecular survey of occurrence and quantity of *Legionella* spp., *Mycobacterium* spp., *Pseudomonas aeruginosa* and amoeba hosts in municipal drinking water storage tank sediments

J. Lu[1], I. Struewing[2], S. Yelton[2] and N. Ashbolt[3]

1 U.S. EPA National Exposure Research Laboratory, Cincinnati, OH, USA
2 Dynamac Inc., Cincinnati, OH, USA
3 School of Public Health, University of Alberta, Edmonton, AB, Canada

Keywords
drinking water storage tank, free-living amoeba, *Legionella*, nontuberculous mycobacteria, sediment, waterborne pathogens.

Correspondence
Jingrang Lu, 26W Martin Luther King Dr., Cincinnati, OH 45268, USA.
E-mail: lu.jingrang@epa.gov

2014/2560: received 12 December 2014, revised 27 February 2015 and accepted 10 April 2015

doi:10.1111/jam.12831

Abstract

Aims: To examine the occurrence and quantity of potential pathogens and an indicator of microbial contamination in the sediments of municipal drinking water storage tanks (MDWSTs), given the absence of such data across the United States.

Methods and Results: Sediment samples (87 MDWST) from eighteen locations across ten states of the United States were collected and assayed by qPCR for a range of potential enteric and opportunistic microbial pathogens and a sewage-associated *Bacteroides* marker. Potential opportunistic pathogens dominated, with the highest detection of occurrence (per cent positive detection; average cell equivalence (CE)) being *Mycobacterium* spp. (88·9%; $6{\cdot}7 \pm 8{\cdot}5 \times 10^4$ CE g^{-1}), followed by *Legionella* spp. (66·7%; $5{\cdot}2 \pm 5{\cdot}9 \times 10^3$ CE g^{-1}), *Pseudomonas aeruginosa* (22·2%; 250 ± 880 CE g^{-1}) and *Acanthamoeba* spp. (38·9%; 53 ± 70 CE g^{-1}), with no detected *Naegleria fowleri*. Most enteric pathogens (*Campylobacter jejuni*, *Escherichia coli* 0157:H7, *Salmonella enterica*, *Cryptosporidium parvum* and *Giardia duodenalis*) were not detected, except for a trace signal for *Campylobacter* spp. There was significant correlation between the qPCR signals of *Legionella* spp. and *Acanthamoeba* spp. ($R^2 = 0{\cdot}61$, $n = 87$, $P = 0{\cdot}0001$). Diverse *Legionella* spp. including *Leg. pneumophila*, *Leg. pneumophila* sg1 and *Leg. anisa* were identified, each of which might cause legionellosis.

Conclusions: These results imply that potential opportunistic pathogens are common within MDWST sediments and could act as a source of microbial contamination, but need downstream growth to be of potential concern.

Significance and Impact of the Study: The results imply that opportunistic pathogen risks may need to be managed by regular tank cleaning or other management practices.

Introduction

Municipal drinking water storage tanks (MDWSTs) are used for pressure management and to buffer the supply of treated water during periods of high demand such as in firefighting. Little knowledge exists about the potential for the reservoirs to support waterborne pathogens, although MDWSTs may accumulate sediments that allow microbial communities to establish. While ingress of animal excreta into these reservoirs may seed MDWST sediments with enteric pathogens of human health concern, the establishment, growth and continual release of various opportunistic pathogens (such as *Legionella* and nontuberculous mycobacteria (NTM)) (Buse *et al.* 2012) is

more likely. However, due to complexities and cost associated with sampling of MDWST sediments, there is limited documentation of pathogen detection in MDWST across the United States. Historically, public health measures have been directed to enteric pathogens in drinking water systems, including *Shigella* spp., *Salmonella enterica*, *Yersinia enterocolitica*, *Campylobacter jejuni*, *Escherichia coli* O157, *Giardia intestinalis*, *Cryptosporidium* spp. and several viruses (Ashbolt 2015). However, opportunistic pathogens including members within *Pseudomonas aeruginosa*, *Legionella pneumophila*, NTM, *Naegleria fowleri* and some genogroups of *Acanthamoeba* spp. are now generally considered to cause a higher health burden than enteric pathogens via drinking water exposures (Craun *et al.* 2010; Biyela *et al.* 2012; Collier *et al.* 2012). Other free-living amoebae (FLA) of interest: *Vermamoeba* (formerly *Hartmanella*) *vermiformis,* along with various *Acanthamoeba* spp. appear critical to the growth of opportunistic intracellular bacterial pathogens and even virulence increase, such as with *Leg. pneumophila* and various NTM (Thomas and Ashbolt 2011; Valster *et al.* 2011; Biyela *et al.* 2012; Delafont *et al.* 2014).

The detection of potential opportunistic pathogens is complicated partly because of the time consuming methods and labour costs, and partly because of viable but nonculturable forms in drinking water systems (Moore *et al.* 2001; Garduno *et al.* 2002; Giao *et al.* 2009; Wingender and Flemming 2011; Wang *et al.* 2012). Molecular testing, especially qPCR, has many advantages *vs* culture-based approaches, as it provides high throughput, sensitivity, specificity and cost-efficiency, compared to traditional culture-based approaches (Lee *et al.* 2011). Although qPCR is not definitive in differentiating live from dead bacteria (Yáñez *et al.* 2011), which might lead to false positives, qPCR has been used by many research groups as a first screening approach for the range of targets, therefore, it is also considered in the current study. To date, surveys for these opportunistic bacterial pathogens appear to be limited to small in-premise storage containers, such as those in hospitals (Stout *et al.* 1985; Walker *et al.* 1995) and homes (Mathys *et al.* 2008; Lim *et al.* 2011). The objectives of this study were to examine the prevalence and quantity of potential pathogens in MDWST sediments across the United States to evaluate whether there may be a need to reduce microbial risks via tank cleaning or improved management practices.

Materials and methods

Sample collection

A total of 87 samples from 18 MDWSTs (1–5 million gallons in capacity) across ten states were examined with five replicates from each tank except NJ2 ($n = 3$) and NC ($n = 4$), which were collected from April 2012 to May 2014 (Fig. 1 and Table S1). The locations were selected to include five different regions of the United States. (Northeast, East Coast, Midwest, South and West Coast) (Fig. 1). Each sediment sample (approx. 100 ml) from the assigned five replicate subsampling points (East, West, South, North and Centre of the tank base) was collected with a sterile plastic spatula into a 125 ml sterile plastic bottle from completely drained tanks. The samples were placed in a cooler containing ice and immediately shipped overnight to the laboratory at Cincinnati, OH, for further processing. After removing liquid from the top of the sediment, aliquots (10 g) were transferred to separate tubes and processed using PowerMax® Soil DNA Isolation Kit (MO BIO Laboratories, Inc., Carlsbad, CA). Total community DNA was obtained per manufacturer's instructions. General parameters like water temperatures and source of raw water were recorded for each tank (Table S1). In addition, where 8-l sediment samples were available in seven locations (Table S2), other physical and chemical sediment characterization was undertaken (total organic carbon, TOC; total organic matter, TOM; Particle size; pH and total exchange capacity: TEC) using EPA standard or comparable methods (Table S3). Due to the incapability of on-site measurements by cleaning companies, the chlorine concentrations were obtained from local county water quality reports, where the storage tanks were located. Of the 18 locations sampled, all tanks contained chlorinated drinking water meeting US EPA regulated chlorine concentrations (detectable residual disinfectant, maximum level <4 mg l^{-1}), and their sources of water were 61% from ground water and 39% from surface water, while their water temperatures ranged from 2·2– 28·9°C with mean of 15·1 ± 7·0°C (Table S1).

qPCR analysis

A panel of 12 genus- or species-specific qPCR assays was used in order to screen and quantify selected microorganisms. Previously published assays were used except for *Legionella* spp. and *Leg. pneumophila* (in order to cover most of the sequences retrieved from environmental samples in NCBI) (Table S4). The qPCR performances were evaluated with cultures of *Leg. pneumophila* Phi 1 (ATCC 33152), *Mycobacterium avium* (ATCC 25291), *Ps. aeruginosa* (ATCC 10145), *Bacteroides thetaiotaomicron* (ATCC29148), *Camp. jejuni* (ATCC 29428), *Salm. enterica* (ATCC 13076), *E. coli* O157:H7 (ATCC 43895), *Acanthamoeba polyphaga* (ATCC 30461), *Vermamoeba vermiformis* (ATCC 50237), *N. fowleri* (ATCC 30863) and oo/cysts of *Cryptosporidium parvum* and *Giardia duodenalis*, which are representative of six enteric

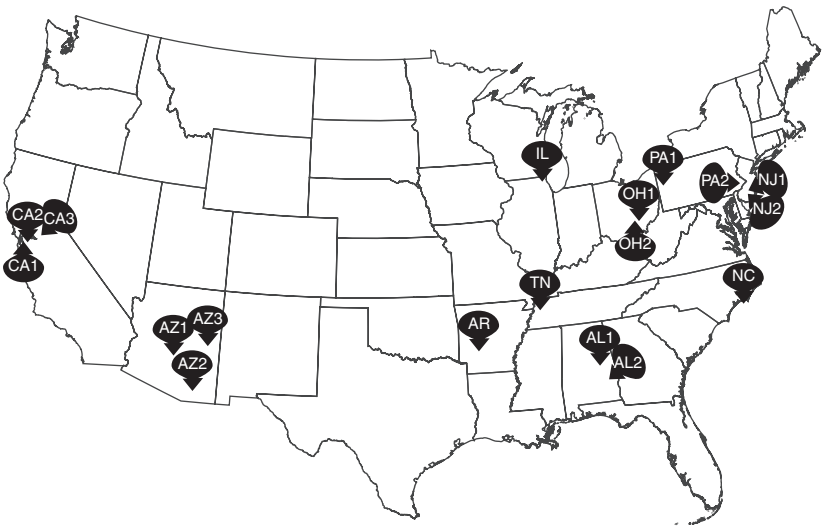

Figure 1 Sampling locations.

and six potential opportunistic pathogens and amoeba hosts. The novel *Legionella* primers and qPCR conditions were tested and optimized by running annealing temperature gradients and using serial dilutions (10–10^7) of *Leg. pneumophila* Phi 1 DNA templates. The primers were tested for host specificity against DNA extracted from the bacteria listed in Tables S5 and S6. The assays for *Ps. aeruginosa* and *E. coli* O157:H7 utilized TaqMan kits (Life Technology, Carlsbad, CA), so the primer sequences are not available (so not listed in Table S4).

Three replicates of serially diluted *Leg. pneumophila* Phi 1 (10^7 CFU ml^{-1}) were spiked into the sediment (250 mg ml^{-1}) previously tested as negative for *Leg. pneumophila,* and filtered and autoclaved Cincinnati tap water, respectively, DNA was isolated independently, qPCR was conducted from each DNA, and standard curves of the assays targeted to the genes of serogroup (sg1) associated with virulence factors: *mipA*, *sidF*, *rtxA*, *cegC1* and LPS cluster (Table S4) were prepared. The assays targeting *sidF*, *rtxA* and *cegC1* were used to confirm the presence of *Leg. pneumophila* Phi 1 for those samples with weak signals, because they are more sensitive than the LPS cluster (data not shown). By comparing the Ct values targeting those *Leg. pneumophila* assays, there was no significant differences in detection limits and the Ct values at each dilution level between spiking *Leg. pneumophila* in sediments and in the water. For other pathogen surrogates, approx. 10^7–10^1 (bacteria) or 10^5–10^1 (eukaryotes) of cultured cells/cysts were spiked and diluted in filtered and autoclaved Cincinnati tap water. All independent DNA extracts were examined in two sets: an original and a 10-fold dilution, both in duplicate, to ascertain inhibition by comparing (i) the difference in Ct values between the original DNA extracts and 10-fold dilutions and (ii) the correlations between Ct values and log numbers of the surrogates spiked. For example, if there was no or low inhibition from the original sample, there was a highly significant correlation between Ct values and log *Leg. pneumophila* concentrations or a slope between 3·58 and 3·10. Target cells in the extracts were reported as numbers of spiked cell/cyst equivalents (CE). If there was no significant inhibition, the data recorded from the experiments were used to generate standard curves, and the qPCR detection limit was estimated (Table S4). This inhibition check protocol has been used for various environmental samples, and inhibition was not commonly found in drinking water and tank sediment samples, so herein factors for correction of inhibition was not described.

All qPCR assays were performed using a 7900 HT Fast Real-Time Sequence Detector (Applied Biosystems, Foster City, CA). Reaction mixtures (20 μl) contained 10 μl 2× qPCR master mix (Applied Biosystems): Power SYBR® Master Mix for qPCR without probe and TaqMan® Environmental Master Mix 2.0 for qPCR with 0·08 μmol l^{-1} TaqMan probe (final concentration), 0·2 μmol l^{-1} primers and 2 μl of template DNA. DNA was treated with Uracil-N-Glycosylase for 2 min at 50°C to prevent carryover contamination. The sample was then held for 10 min at 95°C to denature the template DNA. The following quantification cycling protocol was used: 40 cycles at 95°C for 15 s and various Tm (Table S4) for 30 s with an extension at 72°C for 30 s, and a final hold at 72°C for 5 min. To assay for qPCR inhibitors from the sample DNA, an original and a 10-fold dilution of each DNA extract were assayed. In addition, the TaqMan Exogenous Internal Positive Control Reagents (a VIC-labelled probe) manufactured by ABI™ (Life Technology) was also used as a secondary confirmation. The qPCR for each assay was run on a 96-well plate, which included a serial of

DNA extracts described above for specific target standard curve in the first row of the 96-well plate, and a no-template control for each row of each 96-well plate assayed. Data were analysed with the Sequence Detection Systems software program (ver. 2.3) (Life Technology, Carlsbad, CA). The baseline cycles were set from three to 15 and the threshold value at the point where fluorescence exceeded ten times the standard deviation of the mean baseline emission. According to this standard, a setting of threshold 0·2 were frequently used. Samples in which both the duplicates had a threshold cycle (C_t) value below 40 were regarded as positive. The initial estimates of microbial quantities were produced automatically against a serial of standard DNA, and then the estimates were divided by wet weight (g) of the sediments used for DNA extraction to obtaining the final numbers.

Cloning and sequencing

Amplicons from the samples showing positive signals of *Legionella* spp., *Campylobacter* spp., *Acanthamoeba* spp. and *V. vermiformis* by qPCR screening, genus-specific PCR (Table S4) were cloned into pCR4.1 TOPO (Life Technology) and then individual clones (20 colonies for each library) were sequenced by using BigDye Terminator chemistry (Life Technology), in order to confirm the targets. Raw sequences were edited using Sequencher (Gene Codes Corp., Ann Arbor, MI). Chimeric sequences were identified using UCHIME (Edgar *et al.* 2011) and DECIPHER (Wright *et al.* 2012), and removed from further analyses. Phylogenetic trees were constructed from the alignments of 16S or 18S rRNA gene sequences based on the maximum likelihood method. The software MEGA v5.03 (Tamura *et al.* 2011) was used to build trees using 1000 replicates to develop bootstrap confidence values. Representative *Legionella* 16S rRNA gene sequences from clone libraries were deposited in GenBank with accession numbers: KM624063–KM624177.

Statistical analysis for qPCR data

Microsoft Excel 2003 and sas Systems ver. 9.2 (SAS, Cary, NC) were used for data management and calculations. Correlations used to determine the relationship between *Legionella* spp., *Acanthamoeba* spp. and temperature and correspondence analysis with two dimensions to determine the association between the quantity of *Legionella* spp. and other independent variables (TOC, TOM, Particle size: sand, silt and clay, pH and TEC) along locations were performed. In the correspondence analysis, inertia (variance) is defined as the total Pearson Chi-square for the two-way table divided by the total sum.

Results

The highest frequency of detection was with *Mycobacterium* spp. (88·9%), followed by *Legionella* spp. (66·7%), *Acanthamoeba* spp. (38·9%), *Ps. aeruginosa* (22·2%) and *V. vermiformis* (5·6%). For *Campylobacter* spp. and *V. vermiformis*, some qPCR signals near the detection limit were seen, yet they were later confirmed as true positives. The campylobacters were largely identified as *Camplylobacter lari* (95% of clone sequences), with a few *Camp. jejuni* (5% of clone sequences) present from AR (Fig. 1). Of the *Vermamoeba*, 99% were identical to *V. vermiformis* (from OH1 and AZ3). There was no other positive signal for the other targeted bacteria (human-specific HF183 *Bacteroides*, *Campylobacter* spp., *Salm. enterica*, *E. coli* O157:H7) and protozoan pathogens (*Cryptosporidium* spp. *Giardia* spp. and *N. fowleri*), indicating the absence of enteric pathogens and warm chlorine-free conditions for *N. fowleri*, but potential opportunistic pathogens were generally present in the sediments sampled (Table 1). The quantities of cell equivalence (CE g^{-1}) averaged $6{\cdot}7 \times 10^4$ (SD: $8{\cdot}5 \times 10^4$) for *Mycobacterium* spp., $5{\cdot}2 \times 10^3$ (SD: $5{\cdot}9 \times 10^3$) for *Legionella* spp., 250 (SD: 880) for *Ps. aeruginosa* and 53 (SD: 70) for *Acanthamoeba*. The highest detections for *Legionella* spp., *Acanthamoeba* spp. and *Mycobacterium* spp. occurred in NJ1, yet all three genera were also high at the IL, NJ2, AL1, AZ1, TN and NC sites. There was a significant correlation between *Legionella* and *Acanthamoeba* spp. across all sites ($R^2 = 0{\cdot}61$, $n = 87$, $P = 0{\cdot}0001$, Fig. 2). The correlation was especially demonstrated by the coincidence of the high quantity of both *Legionella* and *Acanthamoeba* spp. at the NJ1, IL, OH2 and NJ2 sites (Table 1, Fig 1). More than 100 CE g^{-1} of *Acanthamoeba* spp. were obtained for all the locations (IL, OH2, NJ1 and NJ2) that contained more than 10^3 CE g^{-1} of *Legionella* spp., although *Acanthamoeba* was not detected at locations, with a low level of *Legionella* spp. To examine potential associations among variables, correspondence analysis was performed using two-dimension Chi-square data analysis and significant differences were observed across site categories (Fig. 3). Over 61 and 35% of the total Chi-square was explained by dimension 1 and 2 (i.e. horizontal and vertical dimensions), respectively. It seemed there were associations between *Legionella* spp. and *Acanthamoeba* spp. and some chemical- and physical-parameters (particle sizes, TOC, TOM, TEC and pH) within the locations. For example, *Legionella* was possibly associated with *Acanthamoeba*, OH2, TN and AL1 along Dimension 1, while *Legionella* and *Acanthamoeba* were associated with clay, silt, TOC, NC and AZ1 along Dimension 2.

Importantly, all sites positive for *Legionella* spp. by the screening qPCR assay were confirmed positive by sequence analysis. It indicated the specificity of both the qPCR and PCR assays designed in this study to target

Table 1 The quantity (cell equivalent, CE wet g^{-1}) of potential opportunistic pathogens in sediments using qPCR in five replicates

Target	*Legionella* spp.		*Acanthamoeba* spp.		*Vermamoeba vermiformis*		*Mycobacterium* spp.		*Pseudomonas aeruginosa*	
Assay	16sF1c/R1c/Leg probe1		AcF1/R1/ taqAcP1		Hv1227F/ 1728R		23SmycoF/R/23SP2		ecfX F/R	
Location*	Mean	SD	Mean	SD	Mean	SD	Mean	SD	Mean	SD
AL1	600	483	0	0	0	0	$2{\cdot}23 \times 10^5$	$3{\cdot}59 \times 10^5$	0	0
AL2	0	0	0	0	0	0	216	194	3670	3720
AR	0	0	0	0	0	0	0	0	0	0
AZ1	304	226	0	0	0	0	$2{\cdot}71 \times 10^4$	$9{\cdot}92 \times 10^3$	0	0
AZ2	22	49	0	0	0	0	$1{\cdot}42 \times 10^4$	$1{\cdot}74 \times 10^4$	6	11
AZ3	51	114	22	50	17	23	$6{\cdot}64 \times 10^4$	$6{\cdot}06 \times 10^4$	0	0
CA1	0	0	25	19	0	0	$7{\cdot}45 \times 10^4$	$5{\cdot}20 \times 10^4$	659	777
CA2	0	0	0	0	0	0	$5{\cdot}58 \times 10^3$	$5{\cdot}87 \times 10^3$	59	92
CA3	30	59	0	0	0	0	$2{\cdot}56 \times 10^3$	$5{\cdot}45 \times 10^3$	0	0
IL	$8{\cdot}66 \times 10^3$	$4{\cdot}59 \times 10^3$	151	82	0	0	0	0	0	0
NC	275	207	10	12	0	0	$6{\cdot}24 \times 10^4$	$1{\cdot}85 \times 10^4$	0	0
OH1	0	0	0	0	0	0	$1{\cdot}92 \times 10^3$	$2{\cdot}04 \times 10^3$	0	0
OH2	$1{\cdot}00 \times 10^3$	519	209	185	0	0	$8{\cdot}30 \times 10^4$	$6{\cdot}39 \times 10^4$	0	0
TN	696	1108	0	0	0	0	156	252	0	0
PA1	0	0	0	0	0	0	39	88	0	0
PA2	113	213	0	0	0	0	$1{\cdot}19 \times 10^4$	$2{\cdot}65 \times 10^4$	67	111
NJ1	$7{\cdot}98 \times 10^4$	$2{\cdot}49 \times 10^4$	391	243	0	0	$6{\cdot}15 \times 10^5$	$1{\cdot}16 \times 10^5$	0	0
NJ2	$1{\cdot}63 \times 10^3$	383	133	68	0	0	$1{\cdot}99 \times 10^4$	$4{\cdot}51 \times 10^3$	0	0

*See Fig. 1 and Table S1.

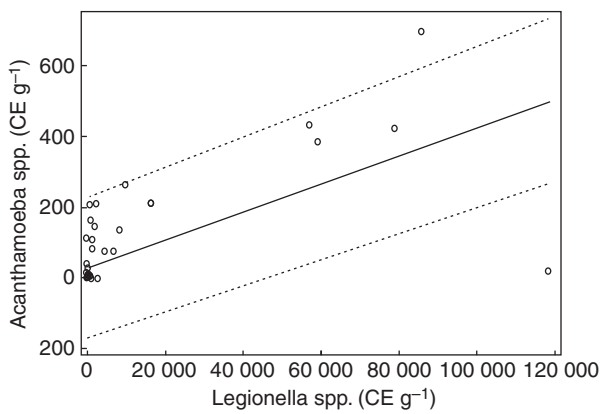

Figure 2 Scatter plot of quantities of *Legionella* spp. (*X*-axis) and *Acanthamoeba* spp. (*Y*-axis) and linear regression analysis (solid line) with 95% confidence interval (dash lines) showing the relationship between *Legionella* spp. and *Acanthamoeba* spp. (R^2 = 0·61, n = 87, P = 0·0001).

Legionella 16S rRNA gene, which covered 99·9% out of 1000 *Legionella*-related sequences in the NCBI database. Furthermore, *Legionella* diversity was high and a total of 115 unique operational taxonomic units (OTU) were identified, of which unknown *Legionella* sequences (38%) dominated in many sites. The dominant sequences were as follows: (10%) similar to *Legionella impletisoli* (identity: 99%) at AL1, AZ1 and OH2, and there were 6 and 5% sequences similar to *Legionella anisa* (identity: 99%) at NJ1, and to *Leg. pneumophila* or even *Leg. pneumophila* sg1 (identity: 99%) at TN and NJ1, respectively, which confirmed the qPCR results described hereafter. The *Legionella* phylogenetic diversities varied across sites. For example, the highest OTUs (n = 36) was in NJ1 and next highest at IL (n = 16) (Table S7, Fig. 4).

The detection of *Leg. pneumophila* (33%) (sites AL1, AZ3, IL, OH2, NJ1, NJ2 and TN) and *Leg. pneumophila* sg1 (28%) across the United States (sites AL1, IL, OH2 and TN) was consistent with several serogroup 1 specific assays (*sidF*, *rtxA*, *cegC1* and P65/66), and confirmed by clone sequencing. For example, one of the positive TN samples was also positive to the panel of assays specific to *Leg. pneumophila* (*mip*) and *Leg. pneumophila* sg1, although the qPCR signals were generally low. Considering the differences in sensitivities for the gene-specific assays developed, the detection and confirmation for *Leg. pneumophila* or *Leg. pneumophila* sg1 was conducted using multiple assays, and the positive samples were recorded, when the qPCR for one or more assays showed strong signals. For example, samples from OH1, OH2 and AL1 were positive by *mipA*, and samples from NC and IL were positive by *sidF* or/and *rtxA* targeted qPCR (Table 2).

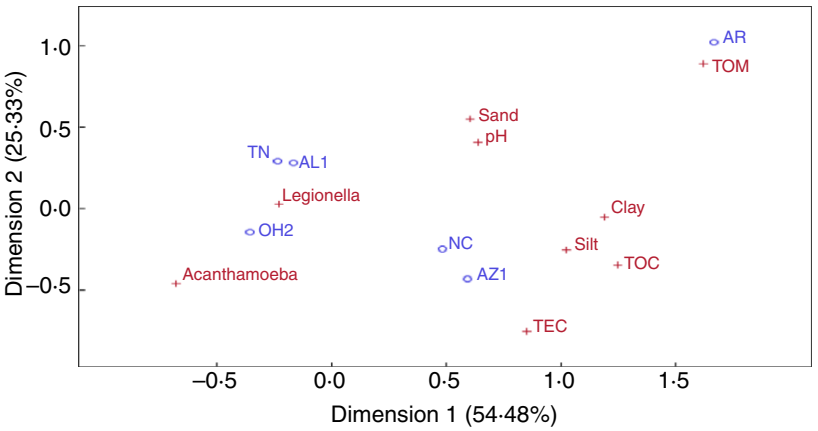

Figure 3 Correspondence analysis showing associations among *Legionella* spp., *Acanthamoeba* spp. and chemical- and physical- parameters (TOC, TOM, TEC, pH and particle sizes: sand, clay and silt) along locations. Possible associations can be seen among those variables, e.g. *Legionella* associated with *Acanthamoeba*, OH2, TN and AL1 along Dimension 1, while *Legionella* and *Acanthamoeba* associated with clay, silt, TOC, NC and AZ1 along Dimension 2.

Acanthamoeba spp. were also confirmed for the IL and OH2 samples in which high densities of *Legionella* spp. co-occurred. They were similar to *Acanthamoeba* sp. (identity: 99%), which was an *Acanthamoeba* isolate from infected corneas of amoebic keratitis patients in Korea (Kim, S.Y., Yu, H.S., Moon, E.K., Kong, H.H., Hahn, T.W. and Chung, D.I. unpublished data at the NCBI Website). More importantly, *Leg. pneumophila* was detected in various locations (AL1, AZ1 and TN), where both *Acanthamoeba* and *V. vermiformis* were undetected and *Legionella* was in low level.

Discussion

This study is the first nationwide survey reported for microbial pathogens associated with MDWST sediments. Based on the results, it would seem that sediments within MDWSTs across the United States may support and allow the growth of *Leg. pneumophila*, other legionellae, NTM, *Ps. aeruginosa* and *Acanthamoeba* spp., all of which potentially contain opportunistic pathogenic members. In contrast, enteric pathogens including *E. coli* O157:H7, *Salmonella* spp., *Giardia intestinalis* and *Cryptosporidium* spp., were undetected, as was the sewage-associated *Bacteroides* marker, but there was a trace detection of *Camp. jejuni* (Table 1). Generally, *Legionella* and NTM species have been considered more of a problem associated with large building plumbing systems and in the use of drinking water supporting cooling towers or humidifiers (Buse *et al.* 2012; Donohue *et al.* 2014), rather than drinking water distribution systems. However, this study and others (Wang *et al.* 2012; van der Wielen and van der Kooij 2013) suggest that nonenteric pathogens may be a concern for water storage tanks and potentially other locations where sediments accumulate within drinking water distribution networks. In addition, pathogenic members are often associated with amoebae (Thomas *et al.* 2010) as was seen in this study. Mounting evidence exists (Thomas and Ashbolt 2011; Biyela *et al.* 2012) that amoebae are critical to intracellular pathogen amplification and even increased virulence of these opportunistic pathogens.

A recent review of microbial disease outbreaks associated with drinking water by the Centers for Disease Control and Prevention (CDC) indicates that *L. pneumophila* is an aetiological agent of major concern (Craun *et al.* 2010), and along with the NTM account for the majority of drinking water associated pathogen hospitalization costs in the United States (Collier *et al.* 2012). Also of concern reported by CDC are increasing *Acanthamoeba*-related eye infections (Yoder *et al.* 2012); noting that in the current study clinically relevant *Acanthomoebae* were identified (Table 1). Other concerns were that *Acanthamoeba* correlated with our finding of high *Legionella* densities compared to most other organisms detected in the sediments (Fig. 2) and that the *Acanthomoebae* may also support replication of various other intracellular pathogens (Greub *et al.* 2004; Thomas *et al.* 2010). Hence, preemptive monitoring of amoebal numbers may provide a useful warning of conditions that could support opportunistic bacterial pathogens (Codony *et al.* 2012).

The diversity of unique OTUs (total of 115) related to *Legionella* spp. from the MDWST sediment samples requires further study to ascertain their clinical relevance. *Legionella* species identified included not only those commonly found in distribution systems, such as *Leg. pneumophila* and non-*Leg. pneumophila* (Yu *et al.* 2002; Lee *et al.* 2010), but also many unique sequences (38%). For *Leg. pneumophila*, the occurrence of sg 1, present in 28% of the locations in which *Legionella* spp. were detected, was higher than the 9% reported from a previous drinking water treatment/distribution system study (Loret and Greub 2010). However, these levels of *Leg. pneumophila* seemed lower than those reported from public buildings.

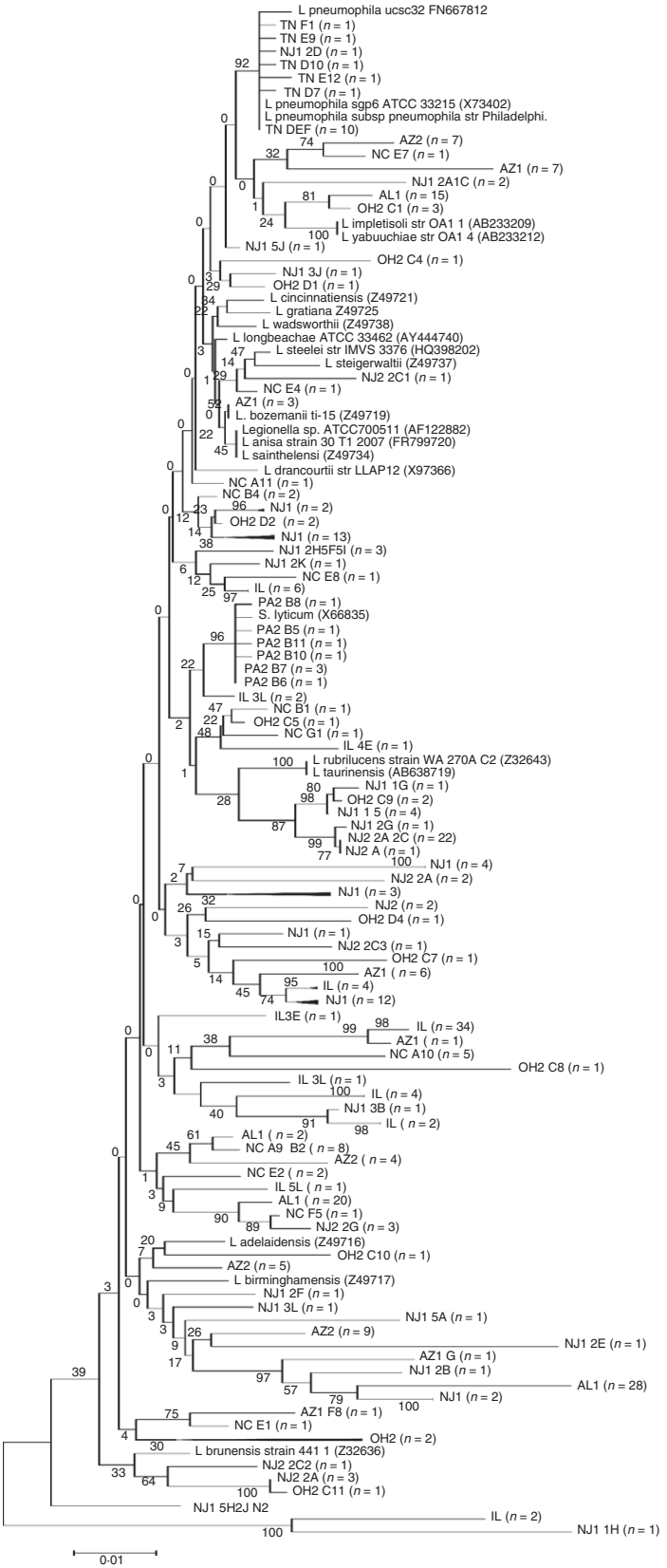

Figure 4 Unrooted neighbour-joining tree of 16S rRNA gene amplified for *Legionella* spp.sequences obtained from clone libraries. Sequences were aligned, and the bootstrap consensus tree was created with MEGA6 (1% divergence).

Table 2 Occurrence, quantification (CE wet g^{-1}) and confirmation with cloning and sequencing of *Legionella pneumophila* and serogroup 1 out of five replicates in each drinking water storage tank sediment

Location	16S	*mipA*	*sidF*	*rtxA*	*cegC1*	P65/66	
	Occurrence and quantity	Occurrence and quantity	Occurrence and quantity	Occurrence and quantity	Occurrence and quantity	Occurrence and quantity	Confirmed by cloning and sequencing
AL1	100% (600 ± 483)	80%[a] (575 ± 1110)[b]	40% (428 ± 908)	60% (244 ± 344)	40% (211 ± 449)	20% (63 ± 140)	Yes. unknown
AZ1	20% (304 ± 226)	0	0	0	0	0	Yes. 6 different OTUs
IL	100% (8660 ± 4590)	60% (80 ± 90)	80% (34 ± 28)	60% (50 ± 64)	20% (7 ± 10)	0	Not available
NC	100% (275 ± 207)	25% (45 ± 64)	25% (30 ± 22)	25% (51 ± 67)	0	0	Yes. 6 different OTUs
OH2	100% (1002 ± 519)	0	20% (30 ± 65)	0	0	20% (10 ± 23)	Yes. 8 different OTUs
PA2	17% (113 ± 213)	20% (10 ± 19)	0	0	0	0	Yes. *Legionella lyticum*
TN	40% (696 ± 1108)	40% (61 ± 103)	0	20% (11 ± 25)	0	20% (50 ± 111)	Yes. *Leg. pneumophila*
AZ3	20% (51 ± 114)	0	0	20% (13 ± 25)	20% (22 ± 38)	0	Not available
NJ1	100% (79 800 ± 24 900)	40% (58 ± 88)	80% (64 ± 38)	60% (63 ± 83)	0	0	Not available
NJ2	100% (1630 ± 383)	40% (23 ± 18)	0	20% (11 ± 25)	0	0	Not available

OTUs, operational taxonomic units.

For example, *Leg. pneumophila* sg1 was detected in nearly half of 68 public and private water taps across the United States using qPCR assays targeted 16S rRNA gene (Donohue *et al.* 2014). For the non-*Leg. pneumophila* identified in the current study, *Leg. anisa* and *Legionella bozemanii* were previously reported to predominate among this category in drinking water (48·1 and 21·0% respectively) (Lee *et al.* 2010). Although it is estimated that some 84% (out of 6868 cases) of legionellosis in the United States are caused by the *Leg. pneumophila* sg1, some non-*Leg. pneumophila* could also cause human health risk, such as Pontiac fever caused by various species including *Leg. anisa* (Fallon and Stack 1990; Fenstersheib *et al.* 1990) or hospital-acquired Legionnaires disease (Bornstein *et al.* 1989). Therefore, the detection of *Leg. anisa* in water samples should be considered an important indication that the water system has been colonized by potentially pathogenic *Legionella* species, including *Leg. pneumophila* (Yu *et al.* 2002; van der Mee-Marquet *et al.* 2006). Understanding the clinical significance of various non-*Leg. pneumophila* strains warrant further investigation for their human health risk.

The results showed high variations in the densities of detected opportunistic pathogens along different geographical locations, indicating their distributions might have been impacted with some physicochemical factors. Current physicochemical data available for this study did not explain the geographical differences observed. Previously, temperature, FLA and biofilm have been noted as key factors for the growth of *Legionella*, in addition to residual disinfectants. In this study, the disinfectant, free chlorine, which was used for all the systems investigated in this study and kept at the level approx. 1 mg l^{-1}, was probably not a major factor influencing the variations observed. Also, *Legionella* is able to survive or/and grow at temperature ranged from 20–50°C in distribution systems (Stout *et al.* 1985; Wadowsky *et al.* 1985). We also found no significant relationship between temperature and *Legionella* quantities of qPCR targets, noting that *Legionella* occurred in locations where temperatures ranged from 2·2–28·9°C with a mean of 15·1 ± 7·0°C, yet those with higher densities (>10^3 CE l^{-1}) were presented in the locations with temperatures >10·6°C. The lack of a possible effect of temperature, may have been influenced by our sampling plan, which did not focus on each season, but rather to address opportunities to sample across geographically diverse locations. It is also reported that the growth of *Legionella* is positively supported by FLA, biofilm and algae (Tison *et al.* 1980; Wadowsky *et al.* 1988; Greub and Raoult 2004), as well as the presence of metal ions (Rakić *et al.* 2011). In distribution system, positive correlations between *V. vermiformis* and total

bacteria, NTM and *V. vermiformis*, and *Legionella* and *V. vermiformis* have been reported (Wang *et al.* 2012; Delafont *et al.* 2014). In addition to our reporting of the co-occurrence between the quantity of *Acanthamoeba* spp. and *Legionella* spp., NTM also co-occurs in MDWST sediments, some of which may be opportunistic pathogens (Falkinham III 2011). For other factors, van der Wielen and van der Kooij reported a positive association between *Leg. pneumophila* and assimilable organic carbon, and further noted that the samples that contained *Leg. pneumophila,* also contained *Ps. aeruginosa* or *Stenotrophomonas maltophilia* (Wadowsky *et al.* 1988; van der Wielen and van der Kooij 2013). In the current study, although limited physical–chemical data were available (Table S2), correspondence analysis indicated that some sediment characteristics, such as TOC, clay and silt, seemed favourable to *Legionella* presence. Collectively, *Legionella* spp. with high species diversity and including potential pathogenic species were detected in more than half of the sediment samples, and other potential pathogens (NTM and *Ps. aeruginosa*) and their potential hosts (*Acanthamoeba* spp.) were also present. Future work needs to focus on possible environmental factors that may influence MDWSTs to support microbial community that harbour opportunistic pathogens and identify ways to manage these potential pathogen issues.

Acknowledgements and disclaimer

This research was supported by EPA ORD's Safe and Sustainable Water Resources Program and EPA's National Homeland Security Research Center (NHSRC). Thanks to Scott Minamyer at NHSRC, Ryan R James at Battelle Memorial Institute, and Darren Lytle at EPA ORD for organizing the project sampling, and Ann Grimm and Gerard Stelma at EPA ORD for their valuable comments. The United States Environmental Protection Agency through its Office of Research and Development funded and managed the research described here. It has been subjected to Agency review and approved for publication. Mention of trade names or commercial products does not constitute endorsement or recommendation for use.

Conflict of Interest

No conflict of interest declared.

References

Ashbolt, N.J. (2015) Microbial contamination of drinking water and human health from community water systems. *Curr Environ Health Rep* **2**, 95–106.

Biyela, P.T., Ryu, H., Brown, A., Alum, A., Abaszadegan, M. and Rittmann, B.E. (2012) Distribution systems as reservoirs of *Naegleria fowleri* and other amoebae. *J Am Water Works Assoc* **104**, E66–E72.

Bornstein, N., Mercatello, A., Marmet, D., Surgot, M., Deveaux, Y. and Fleurette, J. (1989) Pleural infection caused by *Legionella anisa*. *J Clin Microbiol* **27**, 2100–2101.

Buse, H.Y., Schoen, M.E. and Ashbolt, N.J. (2012) Legionellae in engineered systems and use of quantitative microbial risk assessment to predict exposure. *Water Res* **46**, 921–933.

Codony, F., Pérez, L.M., Adrados, B., Agustí, G., Fittipaldi, M. and Morató, J. (2012) Amoeba-related health risk in drinking water systems: could monitoring of amoebae be a complementary approach to current quality control strategies? *Future Microbiol* **7**, 25–31.

Collier, S., Stockman, L., Hicks, L., Garrison, L., Zhou, F. and Beach, M. (2012) Direct healthcare costs of selected diseases primarily or partially transmitted by water. *Epidemiol Infect* **140**, 2003–2013.

Craun, G.F., Brunkard, J.M., Yoder, J.S., Roberts, V.A., Carpenter, J., Wade, T., Calderon, R.L., Roberts, J.M. *et al.* (2010) Causes of outbreaks associated with drinking water in the United States from 1971 to 2006. *Clin Microbiol Rev* **23**, 507–528.

Delafont, V., Mougari, F., Cambau, E., Joyeux, M., Bouchon, D., Héchard, Y. and Moulin, L. (2014) First evidence of amoebae–mycobacteria association in drinking water network. *Environ Sci Technol* **48**, 11872–11882.

Donohue, M.J., O'Connell, K., Vesper, S.J., Mistry, J.H., King, D., Kostich, M. and Pfaller, S. (2014) Widespread molecular detection of *Legionella pneumophila* Serogroup 1 in cold water taps across the United States. *Environ Sci Technol* **48**, 3145–3152.

Edgar, R.C., Haas, B.J., Clemente, J.C., Quince, C. and Knight, R. (2011) UCHIME improves sensitivity and speed of chimera detection. *Bioinformatics* **27**, 2194–2200.

Falkinham, J.O. III (2011) Nontuberculous mycobacteria from household plumbing of patients with nontuberculous mycobacteria disease. *Emerg Infect Dis* **17**, 419.

Fallon, R.J. and Stack, B.H. (1990) Legionnaires' disease due to *Legionella anisa*. *J Infect* **20**, 227–229.

Fenstersheib, M.D., Miller, M., Diggins, C., Liska, S., Detwiler, L., Werner, S.B., Lindquist, D., Thacker, W.L. *et al.* (1990) Outbreak of Pontiac fever due to *Legionella anisa*. *Lancet* **336**, 35–37.

Garduno, R.A., Garduno, E., Hiltz, M. and Hoffman, P.S. (2002) Intracellular growth of *Legionella pneumophila* gives rise to a differentiated form dissimilar to stationary-phase forms. *Infect Immun* **70**, 6273–6283.

Giao, M., Wilks, S., Azevedo, N., Vieira, M. and Keevil, C. (2009) Incorporation of natural uncultivable *Legionella pneumophila* into potable water biofilms provides a

protective niche against chlorination stress. *Biofouling* **25**, 345–351.

Greub, G. and Raoult, D. (2004) Microorganisms resistant to free-living amoebae. *Clin Microbiol Rev* **17**, 413–433.

Greub, G., La Scola, B. and Raoult, D. (2004) Amoebae-resisting bacteria isolated from human nasal swabs by amoebal coculture. *Emerg Infect Dis* **10**, 470–477.

Lee, H.K., Shim, J.I., Kim, H.E., Yu, J.Y. and Kang, Y.H. (2010) Distribution of *Legionella* species from environmental water sources of public facilities and genetic diversity of *L. pneumophila* serogroup 1 in South Korea. *Appl Environ Microbiol* **76**, 6547–6554.

Lee, J., Lai, S., Exner, M., Lenz, J., Gaia, V., Casati, S., Hartemann, P., Lück, C. *et al.* (2011) An international trial of quantitative PCR for monitoring *Legionella* in artificial water systems. *J Appl Microbiol* **110**, 1032–1044.

Lim, Y., Kek, Y.R., Lim, P., Yap, H., Goh, T.V. and Ng, L. (2011) Environmental surveillance and molecular characterization of *Legionella* in tropical Singapore. *Trop Biomed* **28**, 149–159.

Loret, J.F. and Greub, G. (2010) Free-living amoebae: biological by-passes in water treatment. *Int J Hyg Environ Health* **213**, 167–175.

Mathys, W., Stanke, J., Harmuth, M. and Junge-Mathys, E. (2008) Occurrence of *Legionella* in hot water systems of single-family residences in suburbs of two German cities with special reference to solar and district heating. *Int J Hyg Environ Health* **211**, 179–185.

van der Mee-Marquet, N., Domelier, A.S., Arnault, L., Bloc, D., Laudat, P., Hartemann, P. and Quentin, R. (2006) *Legionella anisa*, a possible indicator of water contamination by *Legionella pneumophila*. *J Clin Microbiol* **44**, 56–59.

Moore, J., Caldwell, P. and Millar, B. (2001) Molecular detection of *Campylobacter* spp. in drinking, recreational and environmental water supplies. *Int J Hyg Environ Health* **204**, 185–189.

Rakić, A., Perić, J. and Foglar, L. (2011) Influence of temperature, chlorine residual and heavy metals on the presence of *Legionella pneumophila* in hot water distribution systems. *Ann Agric Environ Med* **19**, 431–436.

Stout, J., Yu, V. and Best, M. (1985) Ecology of *Legionella pneumophila* within water distribution systems. *Appl Environ Microbiol* **49**, 221–228.

Tamura, K., Peterson, D., Peterson, N., Stecher, G., Nei, M. and Kumar, S. (2011) MEGA5: molecular evolutionary genetics analysis using maximum likelihood, evolutionary distance, and maximum parsimony methods. *Mol Biol Evol* **28**, 2731–2739.

Thomas, J.M. and Ashbolt, N.J. (2011) Do free-living amoebae in treated drinking water systems present an emerging health risk? *Environ Sci Technol* **45**, 860–869.

Thomas, V., McDonnell, G., Denyer, S.P. and Maillard, J.Y. (2010) Free-living amoebae and their intracellular pathogenic microorganisms: risks for water quality. *FEMS Microbiol Rev* **34**, 231–259.

Tison, D., Pope, D., Cherry, W. and Fliermans, C. (1980) Growth of *Legionella pneumophila* in association with blue-green algae (cyanobacteria). *Appl Environ Microbiol* **39**, 456–459.

Valster, R.M., Wullings, B.A., van den Berg, R. and van der Kooij, D. (2011) Relationships between free-living protozoa, cultivable *Legionella* spp., and water quality characteristics in three drinking water supplies in the Caribbean. *Appl Environ Microbiol* **77**, 7321–7328.

Wadowsky, R.M., Wolford, R., McNamara, A. and Yee, R.B. (1985) Effect of temperature, pH, and oxygen level on the multiplication of naturally occurring *Legionella pneumophila* in potable water. *Appl Environ Microbiol* **49**, 1197–1205.

Wadowsky, R., Butler, L., Cook, M., Verma, S., Paul, M., Fields, B., Keleti, G., Sykora, J. *et al.* (1988) Growth-supporting activity for *Legionella pneumophila* in tap water cultures and implication of hartmannellid amoebae as growth factors. *Appl Environ Microbiol* **54**, 2677–2682.

Walker, J., Mackerness, C., Mallon, D., Makin, T., Williets, T. and Keevil, C. (1995) Control of *Legionella pneumophila* in a hospital water system by chlorine dioxide. *J Ind Microbiol* **15**, 384–390.

Wang, H., Edwards, M., Falkinham, J.O. 3rd and Pruden, A. (2012) Molecular survey of the occurrence of *Legionella* spp., *Mycobacterium* spp., *Pseudomonas aeruginosa*, and amoeba hosts in two chloraminated drinking water distribution systems. *Appl Environ Microbiol* **78**, 6285–6294.

van der Wielen, P.W. and van der Kooij, D. (2013) Nontuberculous mycobacteria, fungi, and opportunistic pathogens in unchlorinated drinking water in The Netherlands. *Appl Environ Microbiol* **79**, 825–834.

Wingender, J. and Flemming, H.-C. (2011) Biofilms in drinking water and their role as reservoir for pathogens. *Int J Hyg Environ Health* **214**, 417–423.

Wright, E.S., Yilmaz, L.S. and Noguera, D.R. (2012) DECIPHER, a search-based approach to chimera identification for 16S rRNA sequences. *Appl Environ Microbiol* **78**, 717–725.

Yáñez, M.A., Nocker, A., Soria-Soria, E., Múrtula, R., Martínez, L. and Catalán, V. (2011) Quantification of viable *Legionella pneumophila* cells using propidium monoazide combined with quantitative PCR. *J Microbiol Methods* **85**, 124–130.

Yoder, J.S., Verani, J., Heidman, N., Hoppe-Bauer, J., Alfonso, E.C., Miller, D., Jones, D.B., Bruckner, D. *et al.* (2012) Acanthamoeba keratitis: the persistence of cases following a multistate outbreak. *Ophthalmic Epidemiol* **19**, 221–225.

Yu, V.L., Plouffe, J.F., Pastoris, M.C., Stout, J.E., Schousboe, M., Widmer, A., Summersgill, J., File, T. *et al.* (2002) Distribution of *Legionella* species and serogroups isolated by culture in patients with sporadic community-acquired legionellosis: an international collaborative survey. *J Infect Dis* **186**, 127–128.

Supporting Information

Additional Supporting Information may be found in the online version of this article:

Table S1 Locations, dates, water temperatures and water sources of sediment samples.

Table S2 Sediment parameters across seven sampling sites.

Table S3 Screening analyses and methods performed on sediment samples.

Table S4 Oligonucleotide taqMan qPCR primer sequences used to screen pathogens and human-faecal indicator *Bacteroidetes* and PCR primer sequences for clone sequencing.

Table S5 *Legionella* strains used to test PCR coverage.

Table S6 Bacterial strains used to check the specificity of the PCR and qPCR assays **for** *Legionella*.

Table S7 Total clone numbers, unique OTUs and dominant sequences in those sediments showing positive for *Legionella* spp.

Table S1. Locations, dates, water temperatures and water sources of sediment samples

Locations	Date of sampling	Temperature (°C)	Source of water
AL1	6/23/2012	28.9	surface
AL2	6/5/2013	26.7	ground
AR	10/15/2012	17.2	surface
AZ1	11/6/2012	23.9	ground
AZ2	1/14~1/18/2014	12.2	ground
AZ3	1/15/2014	11.7	ground
CA1	3/15/2013	17.8	surface
CA2	3/15/2013	17.8	surface
CA3	1/21/2014	11.1	surface
IL	9/23/2013	15.6	surface
NC	11/9/2012	8.3	ground
NJ1	4/25/2014	15.5	ground
NJ2	4/14/2014	20.2	ground
OH1	9/25/2012	10.6	ground
OH2	9/26/2012	10.6	surface
PA1	6/26/2012	16.1	ground
PA2	1/15/2014	5.6	ground
TN	12/12/2012	2.2	ground

Table S2. Sediment parameters across seven sampling sites

Tank Location	Particle Size			pH	Total Exchange Capacity (ME/100g)	TOC (%)	Organic Matter (%)	Source water
	% Clay	% Silt	% Sand					
TN	0.4	1.06	98.54	8.2	3	0.42	0.43	ground
NC	7.63	23.39	68.98	7.6	110.8	3.11	5.45	ground
OH1	1.36	6.7	91.94	7.1	26.7	0.25	0.89	ground
AL1	2.73	2.33	94.94	7.8	12.2	0.42	0.88	surface
AR	3.91	14.44	81.65	6.7	12.17	2.78	11.45	surface
OH2	1.68	21.67	76.65	6.6	57.34	2.09	5.9	surface
AZ1	7.35	34.34	58.31	6.7	154.14	9.42	4.08	ground

Table S3. Screening analyses and methods performed on sediment samples

Test parameter	Method
Total organic carbon	Automated instrumental analysis of carbon and nitrogen in plant and soil samples (1) (Comparable to EPA Method 9060A) (2).
Total organic matter	Estimation of soil organic matter by weight, loss on ignition (3) (Comparable to EPA Method 160.4 (4).
Particle size analysis (sand, silt, and clay)	ASTM D422 (5) (sieve/hydrometer)
pH	EPA Method 9045C rev 3 (6)
Total exchange capacity	U.S. EPA, EPA Method 9080, Cation Exchange Capacity in Soils, Rev. 0, 1986 (7).

References

1. McGeehan, S.L., and D.V. Naylor. 1988. Automated instrumental analysis of carbon and nitrogen in plant and soil samples. Commun. Soil Sci. Plant Anal. 19:493-505.
2. U.S. EPA, EPA Method 9060A, Total Organic Carbon, Rev. 1, November 2004.
3. Schulte, E.E., and B.G. Hopkins. 1996. Estimation of soil organic matter by weight Loss-On-Ignition. P. 21-32; in: Soil Organic Matter: Analysis and interpretation. (ed.) F.R. Magdoff, M.A. Tabatabai, and E.A. Hanlon, Jr. Special publication No. 46. Soil Sci. Soc. Am. Madison, WI.
4. U.S. EPA, EPA Method 160.4, Volatile Residue, Rev. 1, 1971 in *Methods for Chemical Analysis of Water and Wastes*, EPA/600/4-79/020, March 1983.
5. ASTM Standard D422, 1998, "Standard Test Method for Particle-Size Analysis of Soils," ASTM International, West Conshohocken, PA, www.astm.org.
6. U.S. EPA, EPA Method 9045C, pH in Liquid and Soils, Rev. 1, 2000.
7. U.S. EPA, EPA Method 9080, Cation Exchange Capacity in Soils, Rev. 0, 1986. 8.

Table S4. Oligonucleotide taqMan qPCR primer sequences used to screen pathogens and human-fecal indicator *Bacteroidetes* and PCR primer sequences for clone sequencing

Target	Oligo name	Sequences (5'-3')	Tm (°C)	Detection limit (CE per reaction)	Reference
Human-specific HF183 *Bacteroidales* (qPCR)	HF183F	ATCATGAGTTCACATGTCCG	60	2	Bernhard and Field (2000)
	BthetP1	FAM-CTGAGAGGAAGGTCCCCCACATTGGA-TAMRA			Shanks et al. (2008)
	BthetR1	CGTAGGAGTTTGGACCGTGT			Converse et al. (2009)
Campylobacter spp. (qPCR)	CampF2	CACGTGCTACAATGGCATAT	58	1	Lund et al. 2004
	CampR2	GGCTTCATGCTCTCGAGTT			
	CampP2	FAM-CAGAGAACAATCCGAACTGGGACA-TAMRA			
Campylobacter spp. (PCR)	CampF	GGA TGA CAC TTT TCG GAG C	60	2	Linton, 1996
	CampR	CAT TGT AGC ACG TGT GTC			
Legionella spp. (qPCR)	Leg F1c	TAGTGGAATTTCCGGTGTA	50	2	This study
	Leg R1c	CCAACAGCTAGTTGACATC			
	Leg-probe	6Fam-CGGCTACCTGGCCTAATACTGA-Tamra			
Legionella spp. (PCR)	LegF	GATTAGCCTGCGTCCGATTAG	64	2	This study
	LegR1	GAAATTCCACTACCCTCTCCCA			
	LegR3	AGTGTCAGTATTAGGCCAGGTAGC			
L. pneumophila (qPCR)	mipF1a	AGGATAAGTTGTCTTATAGCA	60	2	This study
	mipR1	TTAAGAACGTCTTTCA TTTG			
	mipProbe	6FAM-TAATCCGGAAGCAATGGCTAA-Tamra			
L. pneumophila (CYBR-Green qPCR)	*rpsL*f	GAAAGCCTCGTGTGGACGTA	64	2	Lu, et al. 2013
	*rpsL*r	CAACCTTACGCATAGC TGAGTTA			
L. pneumophila (CYBR-Green qPCR)	rtxAf	ATTGCGCCTGGCAAACTTTAGGTG	64	2	Lu, et al. 2013
	rtxAr	GGCGCAAATCGTTTCCACCTTGTA			
L. pneumophila (CYBR-Green qPCR)	sidFf	ATTGTTCGCGAGGGTATGAAAGC G	64	2	Lu, et al. 2013
	sidFr	TCTTTCCAAGACAGACTCTCGCGT			
L. pneumophila (CYBR-Green qPCR)	cegC1-F	TGCCTAAACGGTATGACCGCATCA	64	2	Faucher et al. 2011
	cegC1-R	GGCATATGCACCAAAC CACCGAAT			
L. pneumophila (qPCR)	P65f	CAAAGGGCGTTACAGT CAAACC	60	2	Lp-lg1,75bp, 60C, Mérault 2011
	P66r	CAAACACCCCAACCGT AATCA			

	sg1-pb	FAM-TCTTGGGATTGGGTTGGGTTATTTTAACTCCT-BHQ			
Salmonella spp. (qPCR)	invA_176F	CAACGTTTCCTGCGGTACTGT	60	4	Gonzalez-Escalona, N., et al. 2009
	invA-Tx_208	FAM-CTCTTTCGTCTGGCATTATCGATCAGTACCA-TAMRA			
	invA_291R	CCCGAACGTGGCGATAATT			
Mycobacterium spp. (ID)	T-39	GCGAACGGGTGAGTAACACG	50		Talaat et al. (1997).
	T-13	TGCACACAGGCCACAAGGGA			
Mycobacterium spp. (qPCR)	23Smyco F	GGG GTGTGGTGTTTGAG	62	1	Bruijnesteijn van Coppenraet, 2004
	23Smyco R	CTCCCACGTCCTTCATC			
	23Smyco Probe	6-carboxyfluorescein-TGGATAGTGGTTGCGAGCATC-BHQ1			
Acanthamoeba spp. (qPCR)	TaqAcF1	CGACCAGCGATTAGGAGACG	60	2	Riviere et al. 2006
	TaqAcR1	CCGACGCCAAGGACGAC			
	TaqAcP1	FAM-TGAATACAAAACACCACCATCGGCGC-TAMRA			
Vermamoeba vermiformis (qPCR)	Hv1227F	TTA CGA GGT CAG GAC ACT GT	56	2	Kuiper et al. 2006
	Hv1728R	GAC CAT CCG GAG TTC TCG			
Acanthamoeba spp. (PCR)	JDP1	GGCCCAGATCGTTTACCGTGA A	60	2	Schroeder et al. 2001
	JDP2	TCTCACAAGCTGCTAGGGAGTCA			
Cryptosporidium spp. (qPCR)	CRU18Sf	GAG GTA GTG ACA AGA AAT AAC AAT ACA GG	60	2	Hadfield et al 2011
	r	CTG CTT TAA GCA CTC TAA TTT TCT CAA AG			
	P	6FAM-TAC GAG CTT TTT AAC TGC AAC AA-BHQ			
	JVA18S f	ATG ACG GGT AAC GGG GAA T	60	2	Hill et al. 2007
	r	CCA ATT ACA AAA CCA AAA AGT CC			
	p	CGC GCC TGC TGC CTT CCT TAG ATG			
Giardia spp. qPCR	β-Giardin P241 F	CATCCGCGAGGAGGTCAA	60	2	Guy, 2003
	R	GCAGCCATGGTGTCGATCT			
	P	FAM/AAGTCCGCCGACAACATGTACCTAACGA/BHQ-1			
Naegleria fowleri	NaegIF192	GTG CTG AAA CCT AGC TAT TGT AAC TCA GT	63	1	Qvarnstrom et al. 2006
	NaegIR344	CAC TAG AAA AAG CAA ACC TGA AAG G			
	NfowlP	HEX-AT AGC AAT ATA TTC AGG GGA GCT GGG C-BHQ1			

References

Bernhard A.E. and Field, K.G. (2000) A PCR assay to discriminate human and ruminant feces on the basis of host differences in *Bacteroides-Prevotella* genes encoding 16S rRNA. *Appl Environ Microbiol* **66**:4571–4574. http: //dx.doi.org/10.1128/AEM.66.10.4571-4574.2000.

Converse, R.R., Blackwood, A.D., Kirs, M., Griffith, J.F. and Noble, R.T. (2009) Rapid QPCR-based assay for fecal Bacteroides spp. as a tool for assessing fecal contamination in recreational waters. *Water Res* **43**, 4828–4837.

Lu, J., Struewing, I., Buse, H.Y., Kou, J., Shuman, H.A., Faucher, S.P. and Ashbolt, N.J. (2013) *Legionella pneumophila* transcriptional response following exposure to CuO nanoparticles. *Appl Environ Microbiol* **79**: 2713-2720.

Gonzalez-Escalona N., et al. (2009) Detection of live Salmonella sp. cells in produce by a TaqMan-based quantitative reverse transcriptase real-time PCR targeting invA mRNA. *Appl Environ Microbiol* **75**:3714–3720.

Talaat, A.M., Reimschuessel, R. and Trucksis, M. (1997) Identification of mycobacteria infecting fish to the species level using polymerase chain reaction and restriction enzyme analysis. *Vet Microbiol* **58**:229-37.

Bruijnesteijn van Coppenraet, E.S., Lindeboom, J.A., Prins, J.M., Peeters, M.F.,E. Claas, C.J. and Kuijper, E.J. (2004) Real-time PCR assay using fine-needle aspirates and tissue biopsy specimens for rapid diagnosis of mycobacterial lymphadenitis in children. *J Clin Microbiol* **42**:2644

Riviere, D., Szczebara, F.M., Berjeaud, J.M., Frere, J. and Hechard, Y. (2006) Development of a real-time PCR assay for quantification of Acanthamoeba trophozoites and cysts. J *Microbiol Methods* **64**, 78–83.

Schroeder, J.M., Booton, G.C., Hay, J., Niszl, I.A., Seal, D.V., Markus, M.B.,Fuerst, P.A. and Byers, T.J. (2001) Use of subgenic 18S ribosomal DNA PCR and sequencing for genes and genotype identification of acanthamoebae from human with keratitis and sewage sludge. *J Clin Microbiol* **39***:*1903–1911.

Hadfield, S.J., Robinson, G, Elwin, K., Chalmers, R.M. (2011) Detection and differentiation of *Cryptosporidium* spp. in human clinical samples by use of realtime PCR. *J Clin Microbiol* **49**: 918–924.

Hill, V.R., Kahler, A.M., Jothikumar, N., Johnson, T.B., Hahn, D., et al. (2007) Multistate evaluation of an ultrafiltration-based procedure for simultaneous recovery of enteric microbes in 100-liter tap water samples. *Appl Environ Microbiol* **73**: 4218–4225.

Qvarnstrom, Y., Visvesvara, G.S., Sriram, R. and da Silva, A. J. (2006). Multiplex real-time PCR assay for simultaneous detection of *Acanthamoeba* spp., *Balamuthia mandrillaris*, and *Naegleria fowleri*. *J Clin Microbiol* **44**, 3589-3595.

Table S5. *Legionella* strains used to test PCR coverage

Name	ATCC #	Designation	Source	Assay (F2/R1)
Legionella cincinnatiensis	43753	72-OH-0	human lung tissue, Cincinnati, OH	+
Legionella dumoffii	33279	NY23	Cooling tower, New York	+
Legionella feeleii	35849	91-WI-H,	human lung tissue, Wisconsin	+
Legionella gormanii	33297	LS-13 [ALLO3],	soil from creek bank, Atlanta, GA	+
Legionella hackeliae	35250	Lansing 2	human bronchial biopsy, Ann Arbor, MI	+
Legionella jamestowniensis	35298	JA-26-G1-E2	wet soil, Jamestown, NY	+
Legionella longbeacheae	33462	Long Beach 4	human lung	+
Legionella maceachernii	35300	PX-1-G2-E2	water in home evaporator cooler, Phoenix, AZ	+
L. micdadei [*Tatlockia micdadei*]	33218	TATLOCK	blood-human (human blood via yolk sac)	+
Legionella oakridgensis	33761	Oak Ridge 10	industrial cooling tower water, PA	+
Legionella quinlivanii	43830	1442-AUS-E	water in bus air conditioner, Austrailia	+
Legionella rubrilucens	35304	WA-270A-C2	tap water, Los Angeles, CA	+
Legionella sainthelensis	35248	MSH-4	spring water, Mt. St. Helens, WA	+

Legionella wadsworthii	33877	Wadsworth 81-716A	sputum, South Carolina Dept of Health and Environmental Control	+
L. pneumophila strain Lp02		n/a		+
L. pneumophila subsp. *pneumophila* strain Philadelphia-1	33152		human lung	+
L. pneumophila subsp. *pneumophila* strain Bloomington-2	33155		creek water	+
L. pneumophila subsp. *fraseri* strain Dallas 1E	33216		cooling tower	+
L. pneumophila; subsp. *pneumophila* strain Chicago 2	33215		human lung biopsy	+

Table S6 Bacterial strains used to check the specificity of the PCR and qPCR assays for *Legionella*

Strains	Source	Strains	Source
Acinetobacter baumannii	ATCC 19606	*Micrococcus luteus*	ATCC 10240
Aeromonas hydrophila	ATCC 7966T	*Proteus mirabilis*	ATCC 12453
Aeromonas hydrophila	ATCC 7966	*Proteus vulgaris*	ATCC 29905
Aeromonas cavae	ATCC 15468	*Pseudomonas aeruginosa*	ATCC 10145
Bacillus cereus	ATCC 10876	*Salmonella enteriditis*	ATCC 13076
Burkholderia cepacia	ATCC 25416	*Serratia marcescens*	ATCC 14756
Burkholderia cepacia	ATCC 25416	*Serratia marcescens*	ATCC 13880
Campylobacter jejuni	ATCC 29428	*Shewanella putrefaciens*	ATCC 49138
Citrobacter freundii	ATCC 4391	*Shigella sonnei*	ATCC 25931
Citrobacter freundii	ATCC 8090	*Shigella sonnei*	ATCC 9290
Enterobacter aerogenes	ATCC 13048	*Staphylococcus aureus*	ATCC 25923
Enterobacter aerogenes	ATCC 13048	*Staphylococcus aureus*	ATCC 25923
Enterobacter cloacae	ATCC 13047	*Streptococcus pyogenes*	ATCC 19615
Enterococcus faecalis	ATCC 29302	*Yersinia enterocolitica*	ATCC 23715
Enterococcus faecalis	ATCC 19433	*Escherichia coli*	EPA isolate 8
Enterococcus faecium	ATCC 19434	*E. coli*	EPA isolate AD#1
Lactobacillus acidophilus	ATCC 314	*E. coli*	EPA isolate 58
Klebsiella oxytoca	ATCC 13182	*E. coli*	EPA isolate 59
Klebsiella pneumoniae	ATCC 13882	*E. coli*	EPA isolate 62
Klebsiella pneumoniae	ATCC 31488	*Legionella pneumophila* strain Lp02	33152
Listeria monocytogenes	Scott O2	*L. pneumophila* subsp. *pneumophila* strain Philadelphia-1	

Table S7. Total clone numbers, unique OTUs and dominant sequences in those sediments showing positive for *Legionella* spp.

Site	Total clone	OTU#	Dominant	%
AL1	67	6	*L impletisoli* str OA1 1 (AB233209)	22
			unknown	72
AZ1	23	7	*L impletisoli* str OA1 1 (AB233209)	30
			unknown	26
AZ2	24	4	*L impletisoli* str OA1 1 (AB233209)	29
			L adelaidensis (Z49716)	21
			unknown	17
IL	58	16	unknown	93
NC	25	12	unknown	64
NJ1	62	36	*L pneumophila* subsp *pneumophila* str Philadelphi	2
			L anisa strain	31
			L rubrilucens	42
NJ2	36	9	*L rubrilucens*	64
			L brunensis	11
OH2	17	13	*L impletisoli*	18
			L cincinnatiensis	12
			L brunensis	18
PA2	9	6	*S. lyticum*	89
TN	15	6	*L pneumophila* subsp *pneumophila* str Philadelphi	100

pathogens

MDPI

Article

Opportunistic Pathogens and Microbial Communities and Their Associations with Sediment Physical Parameters in Drinking Water Storage Tank Sediments

Ke Qin [1], Ian Struewing [2], Jorge Santo Domingo [3], Darren Lytle [3] and Jingrang Lu [3,*]

1 ORISE, Office of Research and Development, U. S. Environmental Protection Agency, Cincinnati, OH 45268, USA; qin.ke@epa.gov
2 Pegasus Service Inc., Cincinnati, OH 45268, USA; struewing.ian@epa.gov
3 Office of Research and Development, U. S. Environmental Protection Agency, Cincinnati, OH 45268, USA; Santodomingo.Jorge@epa.gov (J.S.D.); lytle.darren@epa.gov (D.L.)
* Correspondence: lu.jingrang@epa.gov

Received: 8 September 2017; Accepted: 10 October 2017; Published: 26 October 2017

Abstract: The occurrence and densities of opportunistic pathogens (OPs), the microbial community structure, and their associations with sediment elements from eight water storage tanks in Ohio, West Virginia, and Texas were investigated. The elemental composition of sediments was measured through X-ray fluorescence (XRF) spectra. The occurrence and densities of OPs and amoeba hosts (i.e., *Legionella* spp. and *L. pneumophila*, *Mycobacterium* spp., *P. aeruginosa*, *V. vermiformis*, *Acanthamoeba* spp.) were determined using genus- or species-specific qPCR assays. Microbial community analysis was performed using next generation sequencing on the Illumina Miseq platform. *Mycobacterium* spp. were most frequently detected in the sediments and water samples (88% and 88%), followed by *Legionella* spp. (50% and 50%), *Acanthamoeba* spp. (63% and 13%), *V. vermiformis* (50% and 25%), and *P. aeruginosa* (0 and 50%) by qPCR method. *Comamonadaceae* (22.8%), *Sphingomonadaceae* (10.3%), and *Oxalobacteraceae* (10.1%) were the most dominant families by sequencing method. Microbial communities in water samples were mostly separated with those in sediment samples, suggesting differences of communities between two matrices even in the same location. There were associations of OPs with microbial communities. Both OPs and microbial community structures were positively associated with some elements (Al and K) in sediments mainly from pipe material corrosions. Opportunistic pathogens presented in both water and sediments, and the latter could act as a reservoir of microbial contamination. There appears to be an association between potential opportunistic pathogens and microbial community structures. These microbial communities may be influenced by constituents within storage tank sediments. The results imply that compositions of microbial community and elements may influence and indicate microbial water quality and pipeline corrosion, and that these constituents may be important for optimal storage tank management within a distribution system.

Keywords: *Legionella*; opportunistic pathogen; storage tank sediment; microbial community; element; corrosion

1. Introduction

Drinking water distribution systems (DWDS) contain complex microbial communities based on both measured by composition [1,2] and genetic network [3]. While drinking water treatment and disinfection considerably reduces risk of exposure, opportunistic pathogens (OP) are often detected in different parts of DWDS. Although most of the attention has been given to the

microbiology of drinking water in premise plumbing and biofilms on pipes, drinking water storage tank sediment has also been shown to harbor OPs [4,5]. Many of these OP, such as *Legionella* spp., *Mycobacterium* spp., *Pseudomonas aeruginosa*, and some of *Acanthamoeba* spp. can pose significant risks to immunocompromised people [6–10]. Free-living amoeba (FLA), such as *Vermamoeba vermiformis*, and some groups of *Acanthamoeba* spp. are also relevant to public health as they are potential hosts to several OPs [7].

Microbial growth within DWDS biofilms has been associated with corrosion of pipes, and the production of various elements in water and sediments in DWDS [11–13]. Teng et al. (2008) found that biofilm can greatly affect element composition and the crystalline phase of corrosion scales. Also, studies have shown that iron-oxidizing bacteria can accelerate corrosion early on, while iron-reducing bacteria (IRB) may inhibit corrosion in later stages, processes that may be influenced by changes in biofilm microbial diversity [12]. DWDS sediments are mainly composed of iron, sulfur, total organic carbon (TOC), calcium, total inorganic carbon (TIC), phosphorous, manganese, magnesium, aluminum, and zinc, and can concentrate trace regulated contaminants such as arsenic and radium [14–16]. The properties distribution system sediment such as elemental composition may impact the composition and structure of their microbial communities. Stein et al. (2001), for example, found that iron- and manganese-enriched sediments also contained two groups related to known metal-oxidizing genera, Leptothrix of the β-Proteobacteria and Hyphomicrobium of the α-Proteobacteria, and a Fe(III)-reducing group related to the Magnetospirillum genus of the α-Proteobacteria [17]. White et al. (2011) reported on the microbiological community structure of sediment and corrosion by-products associated with a DWDS lead pipe using rRNA gene sequencing. They identified bacteria species that have previously reported in heavy-metal-contaminated soils that could potentially impact metal mobility [18].

Elements associated with corrosion by-products can also have an impact in the survival of OPs [19–22]. If elements can protect and promote growth of OPs in storage tank sediments, they may potentially be released into DWDS [23]. Microbial communities could also be impacted by elemental composition of sediments and the redox condition [24–26]. However, relatively little is known on the microbial community in sediments in drinking water storage tanks due to sampling, because samples can only be obtained randomly from tank clean companies [2]. To address this, we examined the occurrence and densities of OPs, the microbial community structure, and their associations with sediment elements. We detected OPs using qPCR [4] and determined the microbial community compositions using next generation sequencing.

2. Materials and Methods

2.1. Sample Collection

Water and sediment samples were collected while industrial storage & water tank cleaning companies were conducting tank cleaning. The samples were collected from eight water storage tanks (16 sediments and water samples) in Ohio (D39-42), West Virginia (D43), and Texas (D50, D53 and D54). For microbial community analysis, an additional sample from Ohio was processed (D84, sediment samples only, collected in triplicate). Sediment and water samples were transferred to sterile containers using aseptic techniques. Collected samples were then placed into ice coolers and shipped overnight to the EPA laboratory (Cincinnati, OH, USA) for different analyses. Water from sediment samples was first removed via centrifugation at 2844× *g* for 3 min using a Swing Bucket Rotor on a Thermo Sorvall® Legend® T Plus centrifuge (Thermo Fisher Scientific., Waltham, MA, USA) and 0.25 g was used to extract DNA using PowerSoil® DNA Isolation Kit (MoBio, Carlsbad, CA, USA) following the manufacturer's instruction. Water samples (1 L) were filtered using EMD Millipore Durapore™ membrane filter (0.40 µm, MilliPore, Foster City, CA, USA). The filtered biomass was lysed using a Beadbeater (BioSpec Products, Inc., Bartlesville, OK, USA) for 1 min. Tubes were centrifuged at 12,000× *g* for 5 min and the supernatant transferred to sterile microcentrifuge tubes.

The DNA extraction was completed using the Master Pure Complete DNA and RNA Purification Kit (Epicentre Technologies Corp., Madison, WI, USA). Extracted DNA was resuspended in 50 µL of molecular grade water. DNA concentrations were measured using Nanodrop 2000 spectrophotometer (NanoDrop Technologies, Inc., Wilmington, DE, USA). Remaining sediment samples were air dried for a period of three days after which elemental composition, and their bulk and particle density were measured with graduated cylinder and mass balance. For the bulk density, about 2 to 3 g of the sample were weighed and the mass was recorded. Then, the sample was placed in a graduated cylinder and the volume was recorded. This volume was the bulk volume because it included the pore spaces between particles. The bulk density was then calculated by dividing the recorded mass by the recorded volume. The procedure was the same for the particle density except the particle volume was determined by the displacement of water.

Porosity was calculated by the following equation:

$$\text{Porosity} = 1 - \frac{bulkdensity}{particledensity}$$

The elemental composition of the sediments was measured through X-ray fluorescence (XRF) of the pressed dried sediments pellets using a Panalytical Axios Instrument (Panalytical, Almelo, The Netherlands).

2.2. qPCR Analysis

The occurrence and densities of OPs and amoeba hosts (i.e., *Legionella* spp. and *L. pneumophila*, *Mycobacterium* spp., *P. aeruginosa*, *V. vermiformis, Acanthamoeba* spp.) were determined using genus- or species-specific qPCR assays, as previously described [2]. Briefly, qPCR assays were performed on a QuantStudio 6 Flex Real-Time PCR System (Applied Biosystems, Foster City, CA, USA) with reaction mixtures. To prevent carryover contamination, an initial incubation at 50 °C for 2 min with uracil-N-glycosylase (UNG) at the onset of the cycling program was conducted before the one cycle of denaturation and enzyme activation at 95 °C for 10 min. The following cycling conditions were used as 40 cycles at 95 °C for 15 s and at the specific Tm (°C) listed in Table S1 for 30 s with an extension at 72 °C for 30 s and a final hold at 72 °C for 5 min, with qPCR reactions for each DNA sample undertaken in duplicate. The standard curves were generated using genomic DNA from each of the targeted groups. Target cells in the extracts are reported as genome copy numbers (GN). The presence of potential qPCR inhibitors was determined using 10-fold dilution of each extract. DNA standards and no-template controls were included on each PCR run.

2.3. Next Generation Sequencing

Sequencing libraries were constructed using water and sediment DNA extracts as PCR templates coupled with barcoded primers targeting the V3–V4 region of the 16S rRNA gene [27]. The reactions used to generate the sequencing libraries were performed in 25 µL volumes using the Ex Taq kit (Takara) with 200 nM for each of the forward and reverse primer and 2 µL of nucleic acid template. Cycling conditions involved an initial 5 min denaturing step at 94 °C, followed by 30 cycles of 45 s at 94 °C, 60 s at 50 °C, and 90 s at 72 °C, and a final elongation step of 10 min at 72 °C. Agarose gel electrophoresis was used to confirm the size of the amplification products. PCR products were then pooled and size selected prior to multiplex sequencing on an Illumina MiSeq benchtop sequencer using paired-end 250 bp kits at the Cincinnati Children's Hospital DNA Core facility. Sequence reads were processed using MOTHUR software [28] as described earlier [3]. Briefly, before analysis, sequence reads with overall low quality scores, or containing homopolymers (>8 nucleotides) and ambiguous base calls (N's), were removed from further analysis [29]. MOTHUR aligned and sorted reads with >97% similarity into operational taxonomic units (OTUs). Chimeric OTUs were screened out by the UCHIME algorithm built within MOTHUR.

2.4. Data Analysis

Statistical analyses were performed using Rstudio (https://www.rstudio.com/). Paired *t*-test was performed to test if there was any significant difference between genome copy number of OP in sediment and water samples. Pearson's linear correlation coefficients were calculated to test the correlation within OP and between OP and environmental physical parameters. For the microbial community analysis, one-way ANOVA was performed to test if there were significant differences between sediment and water samples. Nonmetric multidimensional scaling (NMDS, which acted to visualize the community structure and correlated physicochemical conditions using metaMDS function in the 'vegan' package) was used to cluster microbial communities based on the similarity of OTU distribution. Multiple response permutation procedure (mrpp) analysis was performed to test if there were significant differences in the NMDS plot between water and sediment samples (i.e., if there were two different groups). Correlation coefficients were calculated to check if there was any environmental factor that could explain clustering on the NMDS plot at a statistically significant level.

3. Results

3.1. Opportunistic Pathogens

Mycobacterium spp. were the most frequently detected OPs in the sediments and water samples (88% and 88%, respectively), followed by *Legionella* spp. (50% and 50%), *Acanthamoeba* spp. (63% and 13%), *V. vermiformis* (50% and 25%), and *P. aeruginosa* (0 and 50%). The occurrence of free living amoebae was higher in sediment than in water. *L. pneumophila* was also detected in both sediment (25%) and water (13%) (Table 1). *Mycobacterium* spp., *Legionella* spp., and FLA constituted major OPs, and there were significant correlations between *Legionella* spp. and *Mycobacterium* spp. The major OPs in the sediments presented the highest densities in Texas samples (D53 and D54), followed by Ohio samples (D39 and D40). However, in the water samples, the highest densities of the major OPs occurred in Ohio samples (D39 and D40), followed by the West Virginia sample (D43) and one Texas sample (D50). It should be noted that FLA and *L. pneumophila* occurred more frequently in sediments than in water; *P. aeruginosa* occurred more frequently in water than in sediments (Table 1).

The major elements measured in sediments were Zn (18.7%), Fe (16.0%), Si (7.1%), Mn (3.6%), Al (3.4%), and Ca (3.2%) (Table S2). Element densities were different among samples and locations. For example, particle densities, porosities, Ca, Mg, and Zn were higher in OH samples (D39–42) than in TX samples (D50–54) (Table S3). The Pearson's linear correlation coefficients for each of the OPs studied with the sediment elements measured are listed in Table 2. It showed that OPs were associated with some sediment elements. Specifically, *V. vermiformis*, *Mycobacterium*, *Legionella*, and *L. pneumophila* were positively associated with Al and K. (Table 2).

Table 1. The quantity of opportunistic pathogens in sediments and water of storage tanks using qPCR in two replicates.

Matrix	Location ID	*Acanthamoeba* spp.	*Vermamoeba vermiformis*	*Mycobacterium* spp.	*Pseudomonas aeruginosa*	*Legionella* spp.	*L. pneumophila* (*rtxA*)	*L. pneumophila* (*sidF*)
Sediment (GN G^{-1}: genome copy number per gram sediment)	D39S	5 ± 1	0	$(2.73 \pm 0.68) \times 10^4$	0	335 ± 31	0	0
	D40S	1 ± 1	4	$(8.10 \pm 1.16) \times 10^3$	0	923 ± 34	0	0
	D41S	28 ± 7	0	$(8.00 \pm 1.20) \times 10^1$	0	0	0	0
	D42S	0	0	$(8.47 \pm 10.04) \times 10^3$	0	0	0	0
	D43S	0	0	0	0	0	0	0
	D50S	0	14 ± 22	$(2.00 \pm 4.00) \times 10^1$	0	1 ± 3	0	0
	D53S	7	99 ± 60	$(2.39 \pm 2.24) \times 10^3$	0	282 ± 113	25 ± 51	85 ± 69
	D54S	3	120 ± 43	$(2.57 \pm 0.88) \times 10^5$	0	$(7.20 \pm 3.31) \times 10^4$	300 ± 38	173 ± 87
	Average	6	29	3.79×10^4	0	9.19×10^3	41	32
	Occurrence	63%	50%	88%	0	50%	25%	25%
Water (GN L^{-1}: genome copy number per liter water)	D39w	0	0	$(2.33 \pm 3.28) \times 10^5$	70 ± 91	$(1.24 \pm 1.70) \times 10^4$	0	0
	D40w	0	0	$(5.63 \pm 7.74) \times 10^4$	0	$(6.93 \pm 9.76) \times 10^4$	0	0
	D41w	50	0	6.91×10^3	0	0	0	0
	D42w	0	0	3.37×10^4	0	0	0	0
	D43w	0	0	2.52×10^3	0	1.50×10^3	0	0
	D50w	0	480 ± 670	$(5.07 \pm 0.03) \times 10^3$	2770 ± 14	$(1.84 \pm 1.46) \times 10^4$	82 ± 117	36 ± 52
	D53w	0	0	0	83 ± 117	0	0	0
	D54w	0	98 ± 136	$(2.68 \pm 2.84) \times 10^3$	371 ± 150	0	0	0
	Average	6	613	4.25×10^4	412	1.27×10^4	10	4
	Occurrence	13%	25%	88%	50%	50%	13%	13%

Table 2. Pearson's linear correlation coefficients (R^2) of opportunistic pathogens (OPs) with sediment elements in significant level 95% ($p < 0.05$).

Elements	Pathogens											
	Acanthamoeba		*Vermamoeba vermiformis*		*Mycobacterium*		*Legionella* spp.		*L. pneumophila* (*rtxA*)		*L. pneumophila* (*sidF*)	
	R^2	P	R^2	P	R^2	P	R^2	P	R^2	P	R^2	P
Al					0.93	<0.001	0.93	<0.001	0.92	<0.001	0.80	0.017
K					0.75	<0.031	0.77	<0.025	0.75	<0.031		

3.2. Microbial Community

A total of 25 bacterial families were observed among the OTUs with relative abundance >1% (Figure 1). *Pseudomonadaceae* (19.4%) *Comamonadaceae* (18.5%), *Sinobacteraceae* (15.5%), and *Sphingomonadaceae* (13.0%) were the most dominant, but that of *Mycobacteriaceae* was less than 1%. There were associations of microbial communities between the sediment and water in the same site (Table S4). Many families like *Sphingomonadaceae* presented both in water and sediments in many sites (Table S4). Dominant OTUs varied with samples or locations. For OH samples, *Comamonadaceae* dominated in D39 of both sediments (48.9%) and water samples (90.6%), and water samples in D40 (42.8%) and D41 (38.9%). The dominance of *Comamonadaceae* in water and sediment samples has been previously documented [30,31], probably due to their abilities to restrain other competitors [32]. *Syntrophobacteraceae*, anaerobic sulfur-reducing bacteria [33] prevalent in sediments and soil [34,35], was most abundant in D40 sediments (28.0%). *Oxalobacteraceae*, a ubiquitous family found in drinking water systems [36], dominated in D41 sediment samples (47.5%) and D42 water samples (60.1%), while *Bradyrhizobiaceae* (18.3%) were most abundant in D42 sediment samples. For TX samples, *Pseudomonadaceae* (59.8%) dominated in D53 sediment samples, while *Oxalobacteraceae* (45.12%) represented the majority in water samples. The most abundant families in terms of OTUs percentage in D54 sediment and water samples were *Nitrospiraceae* (57.4%) and *Sphingomonadaceae* (50.2%), respectively.

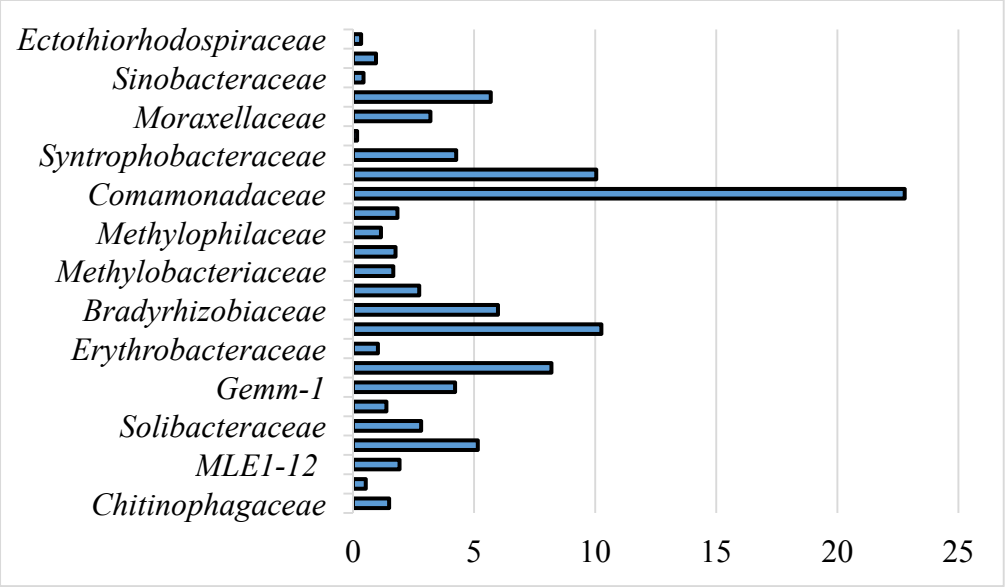

Figure 1. The 25 most abundant families presented in all the samples.

The samples sequenced in both water and sediment were clustered into one major group and several smaller groups according to relative abundance of the 25 families (Figure 2a). The sample type (water and sediment) could be one of the factors explaining microbial community structure. All the sediment samples except for D41 and D42 were in the major group. In sediment samples, the family (*Solibacteraceae*) was significantly higher in sediment than water (6.2% vs. 0.2%, $p = 0.02$, D40, etc.). The location of water system could be another factor, as shown by the two distinct clusters. Two samples from one city (D41 and D42) were clustered together separately from other samples (Figure 2b).

When considering the element's impact on community structure, most microbial communities in water samples (circled with a dash line) were separated from those in sediment samples (with a solid line) (Figure 3a), as inferred from the analysis of NMDS. Only the communities in D39 and D42 water and sediment, which were positioned within the overlap of the two circled areas, were not separated

by the element factor. With the matrices of OTU numbers and relative abundance of each OTU against relative abundance of elements and opportunistic pathogen densities by qPCR in water and sediment samples, it showed significant relationships between the microbial community structures and the densities of *Mycobacterium* spp., and two functional *Legionella pneumophila* genes (i.e., *sidF* and *rtxA*, $p = 0.05$) (Figure 3a). At $p = 0.1$ level, the community composition was also related positively with the densities of *Legionella* (Figure 3b). The vector direction of Zn was in opposite direction of other abiotic parameters including Al, K, Mn and Si, as well as biotic factors including concentrations of *V. vermiformis*, and *sidF,* and *rtxA* genes (Figure 4).

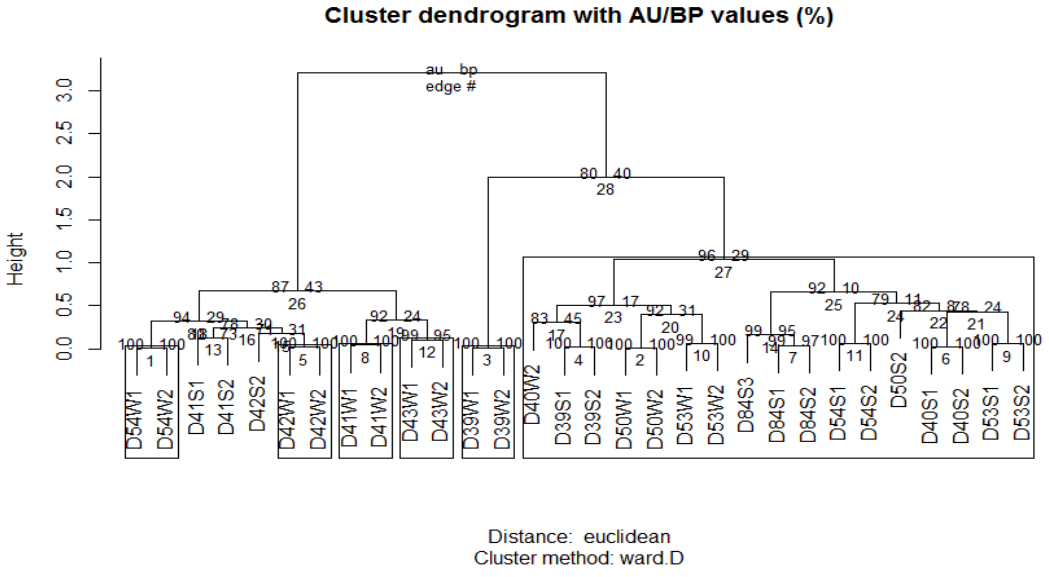

(**a**)

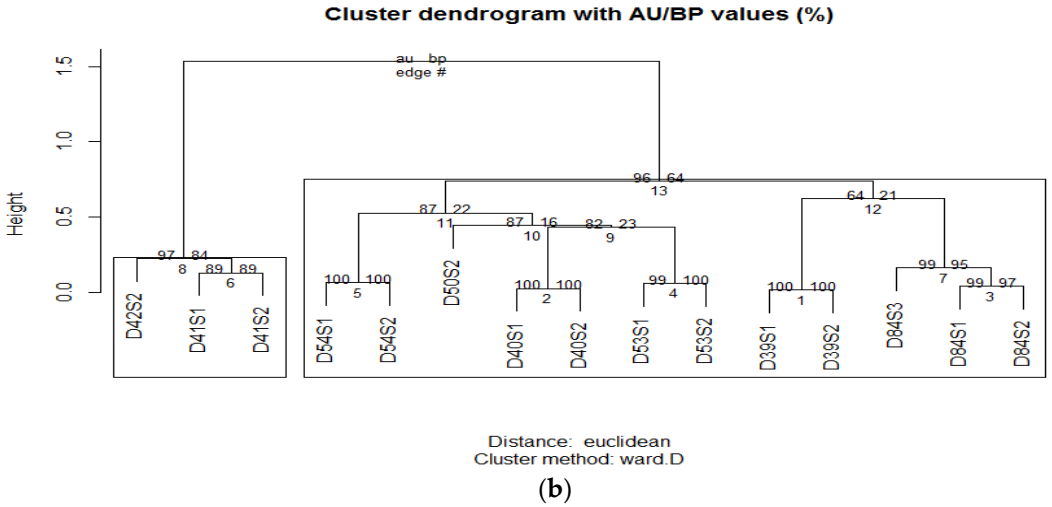

(**b**)

Figure 2. Cluster dendrogram of both sediment and water samples (**a**); and only sediment samples (**b**) based on microbial community structures. Values on the edges of the clustering are *p*-values (%). Top left values are approximately unbiased (AU) *p*-values, and top right values are bootstrap probability (BP) values. Clusters with AU larger than 95% are strongly supported by data.

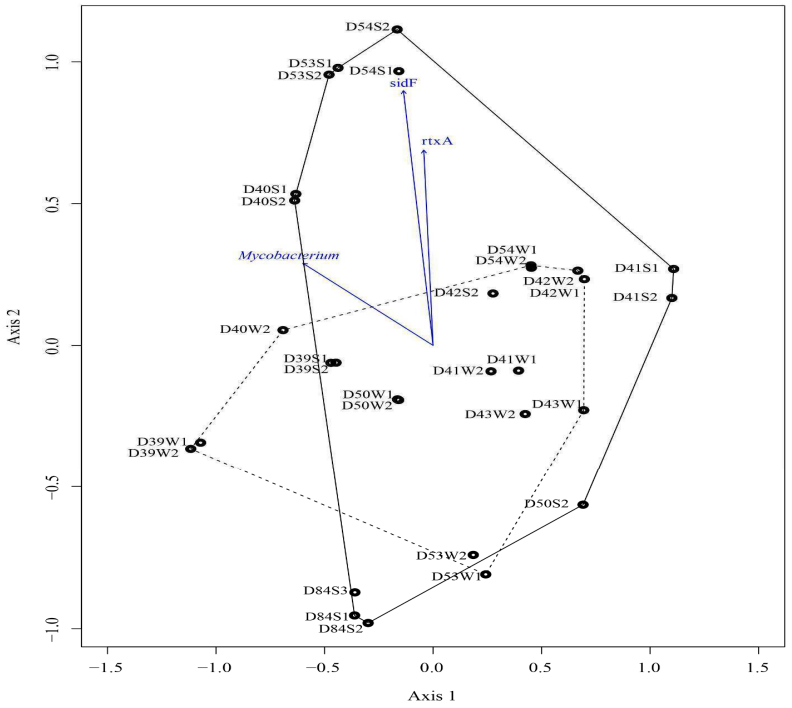

(**a**)

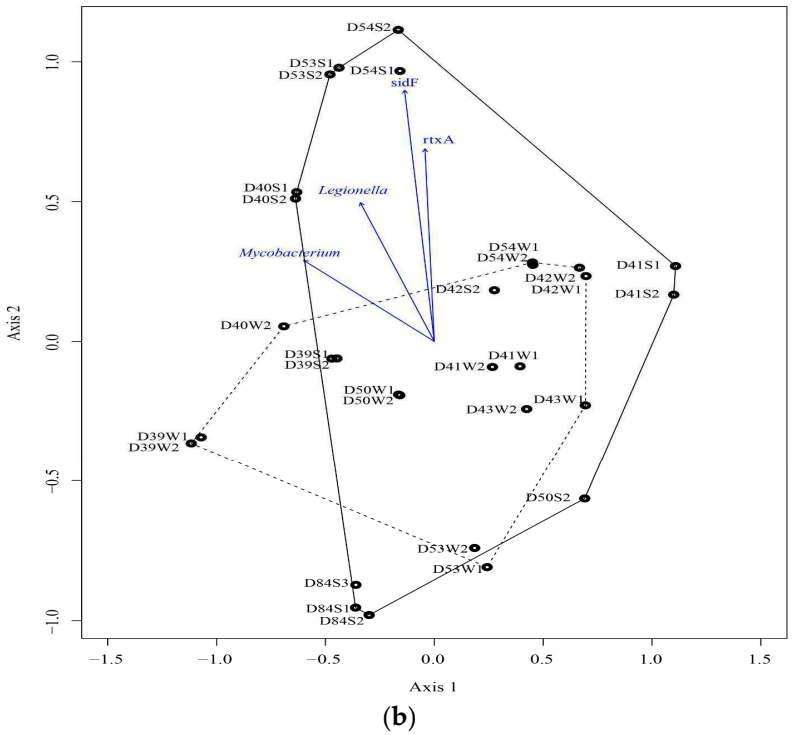

(**b**)

Figure 3. Nonmetric multidimensional scaling (NMDS) of paired water (W) and sediment (S) samples (Ohio: D39-42, West Virginia: D43, and Texas: D50, D53, and D54) based on microbial community structures with operational taxonomic unit (OTU) numbers and relative abundance of each OTU against relative abundance of elements and opportunistic pathogen densities by qPCR at significant level 10% (**a**) and 5% (**b**). The solid circles represent the central tendency of all OTUs detected in each sample from the sediment and water samples, respectively. Symbols that are closer to each other with a dash circle depict samples that contain similar taxa detected by the sequencing. A biplot is overlaid on the ordination to identify environmental parameters that were correlated with the microbial community structure. The length of the line corresponds to the degree of the correlation.

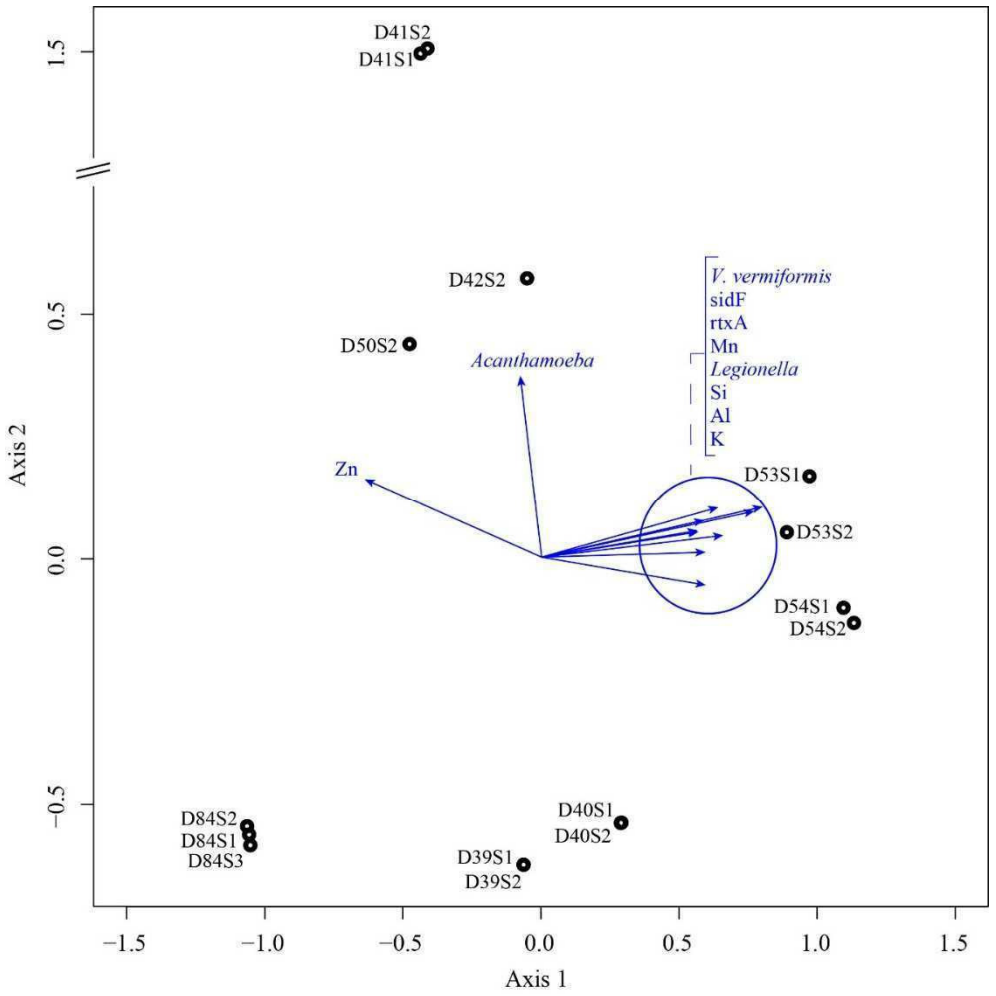

Figure 4. NMDS of sediment (S) samples (Ohio: D39-42, West Virginia: D43, and Texas: D50, D53, and D54) based on microbial community structures with OTU numbers and relative abundance of each OTU against relative abundance of elements and opportunistic pathogen densities by qPCR. The solid circles represent the central tendency of all OTUs detected in each sample from the sediment and water samples, respectively. Symbols that are closer to each other with a dash circle depict samples that contain similar taxa detected by the sequencing. A biplot is overlaid on the ordination to identify environmental parameters that were correlated with the microbial community structure. The length of the line corresponds to the degree of the correlation. Only variables that had a significant correlation ($p < 0.05$) are depicted.

4. Discussion

4.1. OPs in the Samples of Tank Water and Sediments

In this study the occurrences and densities of OPs were investigated and their associations with element concentrations was examined. The occurrences of *Mycobacterium* spp., *Legionella* spp., and *L. pneumophila* detected in this study were comparable to previous studies that investigated storage tank sediments [4] and drinking water distribution system [2]. In addition, higher occurrences of amoebae were also detected in the samples of sediment than those of water detected (Table 1). The free living amoebae may be beneficial to OPs [7]. *Acanthamoeba*, *V. vermiformis*, and other amoebae can serve as hosts for amoeba-resisting bacteria (ARB) like *Legionella* and *Mycobacterium* spp. [37,38]. The higher occurrences of amoebae in sediments than in water for the same storage tank suggest that they are more tightly bound to sediments and could be considered a reservoir of OPs. The targeted two genes

(*rtxA* [39] and *sidF* [40]) encoding toxins can reflect virulence of *L. pneumophila*. Their co-occurrences and similar level of quantities in D50 water and D53 and D54 sediment samples, which belong to a Texas metropolitan area, indicated the presence of *L. pneumophila*. It has been reported that the growth of *Legionella* is positively supported by FLA, biofilm, and algae [41–43]. Positive correlations between *V. vermiformis* and total *Legionella* have been shown for drinking water samples [2]. The co-occurrence of amoebae, *Legionella* spp., and *L. pneumophila* in the sediments, and their relatively higher densities in the sediment samples than in water, suggest that sediments can serve as reservoirs of OPs in storage tank water, and therefore can potentially be released into the distribution system. Taken together, our study reveals the importance of sediments as reservoirs for OPs which should be considered as an important risk factor when developing microbial risk assessment models for various drinking water systems, especially for *Mycobacterium* and *Legionella* spp. The results further stress the importance of maintaining a good disinfectant residual throughout the drinking water distribution system including storage tanks.

4.2. Microbial Communities and Their Relationship with Elements

Dominant OTUs reported in this study shared similarities with other reports focused on DWDS. *Pseudomonadaceae* (mainly *Pseudomonas* spp.) were ubiquitously present in DWDS and proposed as an indicator of potential regrowth [44]. Aerobic heterotrophs *Comamonadaceae* and/or *Sphingomonadaceae* were documented as dominant groups in biofilms [45,46], purified water [47], chlorine treated water [48], and household water tanks [49]. *Sinobacteraceae* (*Nevskia* spp.) were found dominant in biofilms [50]. Nevertheless, the shared microbial compositions between the water and sediment in the same location samples indicated the close associations and interactions between these two different matrices. The bacterial flora attached to sediment could re-enter the water matrix due to normal activity or water flow.

Both the qPCR results of *Mycobacterium* spp. and *Legionella* spp. were significantly associated with the microbial community composition. D39 water samples in OH had the second highest amount of *Mycobacterium* spp. It should be noticed that relative abundance of *Mycobacterium* spp. in microbial community was less than 1%, although it had high prevalence by qPCR. That community had a single dominant family of *Comamonadaceae*, which accounted for 75% of the total OTUs. D39 water samples also had the third highest amount of *Legionella* spp. of all the groups. The highest densities of *Mycobacterium* spp. and *Legionella* spp. were observed in D54 from Texas. The community featured with a couple of dominant families, with *Nitrospiraceae* accounting for 18.6% of total OTUs.

The role that elements play in the microbial community structure of drinking water systems has been poorly documented. In our study we showed that for the sediment samples, elements such as Al, K, Mn and Si (Figure 4), as well as *V. vermiformis* and *L. pneumophila* detected by *sidF* and *rtxA* genes, correlated with the community structures in a similar way, which was the opposite with the heavy metal Zn. That may indirectly suggest which elements could be beneficial or harmful to *Legionella*. Additionally, cluster analysis revealed there was a high association of microbial community structure dominated with *Pseudomonas* spp. (33.5%) and Al and K in D54 (Figure 4), which, in part, is in agreement with previous findings on *Pseudomonas* spp. tolerance to aluminum [51,52]. Interestingly, while Al (III) and S could be reduced simultaneously by *Desulfovibrio* [53], *Desulfovibrio* was very scarce (<0.1%) in total OTUs. The unique community structure dominated by *Geothrix* (belonging to family *Holophagaceae*) (18.0%) and *Sulfuritalea* (17%) significantly associated with the highest iron (III) (50.0%) in D50, which is not surprising as these are known as Fe^{+3} reducing bacteria [54]. Freshwater sediments often contain large quantities of iron and manganese that undergo rapid cycling between reduced and oxidized states [17]. The cycling of these metals is driven by diffusion of soluble Mn^{2+} and Fe^{2+} into oxygenated environments, followed by oxidation and sedimentation of solid Mn^{4+} and Fe^{3+} elements to reducing regions. Microbial communities are thought to play a significant role in both the oxidation and reduction of manganese and iron [55,56].

It was well documented that magnesium had the potential to function as antibiotics to inhibit the growth of *P. aeruginosa* [20] and that iron is a key nutrient for pseudomonads [19]. That may explain the relationships between the qPCR results of *P. aeruginosa* and relative concentrations of magnesium and iron in sediments. On the other hand, since *V. vermiformis* is a potential host of *Legionella* spp. and *Mycobacterium* spp. [2], it is also possible that *P. aeruginosa* was hosted by *V. vermiformis*. Similarly, the associations of element Al with the quantities of *L. pneumophila,* representative of two genes *rtxA* and *sidF* in the sediments, also reflected the impact of metal on them. According to a previous study [57,58], the growth of *L. pneumophila* requires certain amounts of magnesium, cobalt, copper, iron, manganese, molybdenum, vanadium, or zinc to stimulate growth, while higher level of trace metal would inhibit the growth of *L. pneumophila* [59]. However, higher level of trace metal requirement was found for the growth of *P. aeruginosa* and its growth was stimulated by only four metals: calcium, iron, magnesium, and zinc [58].

Supplementary Materials: The following are available online at www.mdpi.com/2076-0817/6/4/54/s1, Table S1: Oligonucleotide taqMan qPCR primer sequences used to screen pathogens and human-fecal indicator *Bacteroidetes* and PCR primer sequences for clone sequencing, Table S2: Element compositions of storage tank sediments, Table S3: Element components in sediments of different locations, Table S4: major bacterial compositions with the relative abundance of OTUs >1% in any samples at 97% similarity level).

Acknowledgments: This research was supported by EPA ORD's Safe and Sustainable Water Resources Program (SSWR 6.01C) and EPA's National Homeland Security Research Center (HS5.02.02). Thanks to Matthew Magnuson at NHSRC for managing funds and Christy Muhlen for arranging sample shipping and receiving. The United States Environmental Protection Agency through its Office of Research and Development funded and managed the research described here. It has been subjected to Agency review and approved for publication. Mention of trade names or commercial products does not constitute endorsement or recommendation for use.

Author Contributions: K.Q. conducted the experiments, analyzed and interpreted data, and participated the manuscript draft. I.S. conducted the experiments. J.S.D. provided the support of the experiments and the critical review of the manuscript. D.L. provided initial experimental design, and critically reviewed and revised the manuscript. J.L. designed the experiment, analyzed data, participated the manuscript draft and revisions.

Conflicts of Interest: The authors declare no conflict of interest.

References

1. Revetta, R.P.; Pemberton, A.; Lamendella, R.; Iker, B.; Santo Domingo, J.W. Identification of bacterial populations in drinking water using 16s rrna-based sequence analyses. *Water Res.* **2010**, *44*, 1353–1360. [CrossRef] [PubMed]
2. Lu, J.; Struewing, I.; Vereen, E.; Kirby, A.E.; Levy, K.; Moe, C.; Ashbolt, N. Molecular detection of *Legionella* spp. And their associations with *Mycobacterium* spp., *Pseudomonas aeruginosa* and amoeba hosts in a drinking water distribution system. *J. Appl. Microbiol.* **2016**, *120*, 509–521. [CrossRef] [PubMed]
3. Gomez-Alvarez, V.; Revetta, R.P.; Santo Domingo, J.W. Metagenomic analyses of drinking water receiving different disinfection treatments. *Appl. Environ. Microbiol.* **2012**, *78*, 6095–6102. [CrossRef] [PubMed]
4. Lu, J.; Struewing, I.; Yelton, S.; Ashbolt, N. Molecular survey of occurrence and quantity of *Legionella* spp., *Mycobacterium* spp., *Pseudomonas aeruginosa* and amoeba hosts in municipal drinking water storage tank sediments. *J. Appl. Microbiol.* **2015**, *119*, 278–288. [CrossRef] [PubMed]
5. Van der Wielen, P.W.; Lut, M.C. Distribution of microbial activity and specific microorganisms across sediment size fractions and pipe wall biofilm in a drinking water distribution system. *Water Sci. Technol.* **2016**, *16*, 896–904. [CrossRef]
6. Buse, H.Y.; Schoen, M.E.; Ashbolt, N.J. *Legionellae* in engineered systems and use of quantitative microbial risk assessment to predict exposure. *Water Res.* **2012**, *46*, 921–933. [CrossRef] [PubMed]
7. Biyela, P.T.; Ryu, H.; Brown, A.; Alum, A.; Abbaszadegan, M.; Rittmann, B.E. Distribution systems as reservoirs of *Naegleria fowleri* and other amoebae. *J. Am. Water Work Assoc.* **2012**, *104*, 49–50. [CrossRef]
8. Craun, G.F.; Brunkard, J.M.; Yoder, J.S.; Roberts, V.A.; Carpenter, J.; Wade, T.; Calderon, R.L.; Roberts, J.M.; Beach, M.J.; Roy, S.L. Causes of outbreaks associated with drinking water in the united states from 1971 to 2006. *Clin. Microbiol. Rev.* **2010**, *23*, 507–528. [CrossRef] [PubMed]

9. Whiley, H.; Keegan, A.; Fallowfield, H.; Bentham, R. Detection of *Legionella*, *L. pneumophila* and mycobacterium avium complex (mac) along potable water distribution pipelines. *Int. J. Environ. Res. Public Health* **2014**, *11*, 7393–7405. [CrossRef] [PubMed]
10. Wang, H.; Edwards, M.; Falkinham, J.O.; Pruden, A. Molecular survey of the occurrence of *Legionella* spp., *Mycobacterium* spp., *Pseudomonas aeruginosa*, and amoeba hosts in two chloraminated drinking water distribution systems. *Appl. Environ. Microbiol.* **2012**, *78*, 6285–6294. [CrossRef] [PubMed]
11. Hallam, N.; West, J.; Forster, C.; Simms, J. The potential for biofilm growth in water distribution systems. *Water Res.* **2001**, *35*, 4063–4071. [CrossRef]
12. Teng, F.; Guan, Y.; Zhu, W. Effect of biofilm on cast iron pipe corrosion in drinking water distribution system: Corrosion scales characterization and microbial community structure investigation. *Corros. Sci.* **2008**, *50*, 2816–2823. [CrossRef]
13. Lytle, D.A.; Gerke, T.L.; Maynard, J.B. Effect of bacterial sulfate reduction on iron-corrosion scales. *Am. Water Works Assoc. J.* **2005**, *97*, 109.
14. Friedman, M.; Hill, A.; Reiber, S.; Valentine, R.; Larsen, G.; Young, A.; Korshin, G.; Peng, C. *Assessment of Inorganics Accumulation in Drinking Water System Scales and Sediments*; Water Research Foundation: Denver, CO, USA, 2010.
15. Lytle, D.A.; Sorg, T.J.; Frietch, C. Accumulation of arsenic in drinking water distribution systems. *Environ. Sci. Technol.* **2004**, *38*, 5365–5372. [CrossRef] [PubMed]
16. Lytle, D.A.; Sorg, T.; Wang, L.; Chen, A. The accumulation of radioactive contaminants in drinking water distribution systems. *Water Res.* **2014**, *50*, 396–407. [CrossRef] [PubMed]
17. Stein, L.Y.; La Duc, M.T.; Grundl, T.J.; Nealson, K.H. Bacterial and archaeal populations associated with freshwater ferromanganous micronodules and sediments. *Environ. Microbiol.* **2001**, *3*, 10–18. [CrossRef] [PubMed]
18. White, C.; Tancos, M.; Lytle, D.A. Microbial community profile of a lead service line removed from a drinking water distribution system. *Appl. Environ. Microbiol.* **2011**, *77*, 5557–5561. [CrossRef] [PubMed]
19. Cornelis, P. Iron uptake and metabolism in pseudomonads. *Appl. Microbiol. Biotechnol.* **2010**, *86*, 1637–1645. [CrossRef] [PubMed]
20. Robinson, D.A.; Griffith, R.W.; Shechtman, D.; Evans, R.B.; Conzemius, M.G. In vitro antibacterial properties of magnesium metal against *Escherichia coli*, *Pseudomonas aeruginosa* and *Staphylococcus aureus*. *Acta Biomater.* **2010**, *6*, 1869–1877. [CrossRef] [PubMed]
21. Serrano-Suarez, A.; Dellunde, J.; Salvado, H.; Cervero-Arago, S.; Mendez, J.; Canals, O.; Blanco, S.; Arcas, A.; Araujo, R. Microbial and physicochemical parameters associated with *Legionella* contamination in hot water recirculation systems. *Environ. Sci. Pollut. Res.* **2013**, *20*, 5534–5544. [CrossRef] [PubMed]
22. Iivanainen, E.; Martikainen, P.; Katila, M.L. Environmental factors affecting the occurrence of mycobacteria in brook sediments. *J. Appl. Microbiol.* **1999**, *86*, 673–681. [CrossRef] [PubMed]
23. Pusch, M.; Fiebig, D.; Brettar, I.; Eisenmann, H.; Ellis, B.K.; Kaplan, L.A.; Lock, M.A.; Naegeli, M.W.; Traunspurger, W. The role of micro-organisms in the ecological connectivity of running waters. *Freshw. Biol.* **1998**, *40*, 453–495. [CrossRef]
24. Li, Y.C.; Yu, S.; Strong, J.; Wang, H.L. Are the biogeochemical cycles of carbon, nitrogen, sulfur, and phosphorus driven by the "fe-iii-fe-ii redox wheel" in dynamic redox environments? *J. Soils Sediments* **2012**, *12*, 683–693. [CrossRef]
25. Borch, T.; Kretzschmar, R.; Kappler, A.; Van Cappellen, P.; Ginder-Vogel, M.; Voegelin, A.; Campbell, K. Biogeochemical redox processes and their impact on contaminant dynamics. *Environ. Sci. Technol.* **2010**, *44*, 15–23. [CrossRef] [PubMed]
26. Lovley, D.R.; Coates, J.D. Bioremediation of metal contamination. *Curr. Opin. Biotechnol.* **1997**, *8*, 285–289. [CrossRef]
27. Caporaso, J.G.; Lauber, C.L.; Walters, W.A.; Berg-Lyons, D.; Huntley, J.; Fierer, N.; Owens, S.M.; Betley, J.; Fraser, L.; Bauer, M. Ultra-high-throughput microbial community analysis on the illumina hiseq and miseq platforms. *ISME J.* **2012**, *6*, 1621. [CrossRef] [PubMed]
28. Schloss, P.D.; Westcott, S.L.; Ryabin, T.; Hall, J.R.; Hartmann, M.; Hollister, E.B.; Lesniewski, R.A.; Oakley, B.B.; Parks, D.H.; Robinson, C.J. Introducing mothur: Open-source, platform-independent, community-supported software for describing and comparing microbial communities. *Appl. Environ. Microbiol.* **2009**, *75*, 7537–7541. [CrossRef] [PubMed]

29. Schloss, P.D.; Gevers, D.; Westcott, S.L. Reducing the effects of pcr amplification and sequencing artifacts on 16s rrna-based studies. *PLoS ONE* **2011**, *6*, e27310. [CrossRef] [PubMed]
30. Lu, S.D.; Sun, Y.J.; Zhao, X.; Wang, L.; Ding, A.Z.; Zhao, X.H. Sequencing insights into microbial communities in the water and sediments of fenghe river, china. *Arch. Environ. Contam. Toxicol.* **2016**, *71*, 122–132. [CrossRef] [PubMed]
31. Chu, L.B.; Wang, J.L. Denitrification performance and biofilm characteristics using biodegradable polymers pcl as carriers and carbon source. *Chemosphere* **2013**, *91*, 1310–1316. [CrossRef] [PubMed]
32. Aguirre-von-Wobeser, E.; Eguiarte, L.E.; Souza, V.; Soberon-Chavez, G. Theoretical analysis of the cost of antagonistic activity for aquatic bacteria in oligotrophic environments. *Front. Microbiol.* **2015**, *6*, 8. [CrossRef] [PubMed]
33. Kuever, J. The family syntrophobacteraceae. In *The Prokaryotes: Deltaproteobacteria and Epsilonproteobacteria*; Rosenberg, E., DeLong, E.F., Lory, S., Stackebrandt, E., Thompson, F., Eds.; Springer: Berlin/Heidelberg, Germany, 2014; pp. 289–299.
34. Bahr, M.; Crump, B.C.; Klepac-Ceraj, V.; Teske, A.; Sogin, M.L.; Hobbie, J.E. Molecular characterization of sulfate-reducing bacteria in a New England salt marsh. *Environ. Microbiol.* **2005**, *7*, 1175–1185. [CrossRef] [PubMed]
35. He, H.; Zhen, Y.; Mi, T.Z.; Xu, B.C.; Wang, G.S.; Zhang, Y.; Yu, Z.G. Community composition and distribution of sulfate- and sulfite-reducing prokaryotes in sediments from the changjiang estuary and adjacent east china sea. *Estuar. Coast. Shelf Sci.* **2015**, *165*, 75–85. [CrossRef]
36. Zhang, Y.; He, Q. Characterization of bacterial diversity in drinking water by pyrosequencing. *Water Sci. Technol.* **2013**, *13*, 358–367. [CrossRef]
37. Berry, D.; Horn, M.; Xi, C.; Raskin, L. Mycobacterium avium infections of *Acanthamoeba* strains: Host strain variability, grazing-acquired infections, and altered dynamics of inactivation with monochloramine. *Appl. Environ. Microbiol.* **2010**, *76*, 6685–6688. [CrossRef] [PubMed]
38. Buse, H.; Ashbolt, N. Differential growth of *Legionella pneumophila* strains within a range of amoebae at various temperatures associated with in-premise plumbing. *Lett. Appl. Microbiol.* **2011**, *53*, 217–224. [CrossRef] [PubMed]
39. Cirillo, S.L.G.; Bermudez, L.E.; El-Etr, S.H.; Duhamel, G.E.; Cirillo, J.D. *Legionella pneumophila* entry gene rtxa is involved in virulence. *Infect. Immun.* **2001**, *69*, 508–517. [CrossRef] [PubMed]
40. Hsu, F.S.; Zhu, W.H.; Brennan, L.; Tao, L.L.; Luo, Z.Q.; Mao, Y.X. Structural basis for substrate recognition by a unique *Legionella phosphoinositide* phosphatase. *Proc. Natl. Acad. Sci. USA* **2012**, *109*, 13567–13572. [CrossRef] [PubMed]
41. Tison, D.; Pope, D.; Cherry, W.; Fliermans, C. Growth of *Legionella pneumophila* in association with blue-green algae (cyanobacteria). *Appl. Environ. Microbiol.* **1980**, *39*, 456–459. [PubMed]
42. Wadowsky, R.; Butler, L.; Cook, M.; Verma, S.; Paul, M.; Fields, B.; Keleti, G.; Sykora, J.; Yee, R. Growth-supporting activity for *Legionella pneumophila* in tap water cultures and implication of hartmannellid amoebae as growth factors. *Appl. Environ. Microbiol.* **1988**, *54*, 2677–2682. [PubMed]
43. Greub, G.; Raoult, D. Morphology of *Legionella pneumophila* according to their location within hartmanella vermiformis. *Res. Microbiol.* **2003**, *154*, 619–621. [CrossRef] [PubMed]
44. Ribas, F.; Perramon, J.; Terradillos, A.; Frias, J.; Lucena, F. The pseudomonas group as an indicator of potential regrowth in water distribution systems. *J. Appl. Microbiol.* **2000**, *88*, 704–710. [CrossRef] [PubMed]
45. Ling, F.Q.; Hwang, C.A.; LeChevallier, M.W.; Andersen, G.L.; Liu, W.T. Core-satellite populations and seasonality of water meter biofilms in a metropolitan drinking water distribution system. *ISME J.* **2016**, *10*, 582–595. [CrossRef] [PubMed]
46. Luhrig, K.; Canback, B.; Paul, C.J.; Johansson, T.; Persson, K.M.; Radstrom, P. Bacterial community analysis of drinking water biofilms in southern sweden. *Microbes Environ.* **2015**, *30*, 99–107. [CrossRef] [PubMed]
47. Proctor, C.R.; Edwards, M.A.; Pruden, A. Microbial composition of purified waters and implications for regrowth control in municipal water systems. *Environ. Sci.* **2015**, *1*, 882–892. [CrossRef]
48. Hwang, C.; Ling, F.Q.; Andersen, G.L.; LeChevallier, M.W.; Liu, W.T. Microbial community dynamics of an urban drinking water distribution system subjected to phases of chloramination and chlorination treatments. *Appl. Environ. Microbiol.* **2012**, *78*, 7856–7865. [CrossRef] [PubMed]
49. Tokajian, S.; Hashwa, F. Microbiological quality and genotypic speciation of heterotrophic bacteria isolated from potable water stored in household tanks. *Water Qual. Res. J. Can.* **2004**, *39*, 64–73.

50. Keinanen-Toivola, M.M.; Revetta, R.P.; Santo Domingo, J.W. Identification of active bacterial communities in a model drinking water biofilm system using 16s rrna-based clone libraries. *FEMS Microbiol. Lett.* **2006**, *257*, 182–188. [CrossRef] [PubMed]
51. Zhao, Y.G.; Ren, N.Q.; Wang, A.J. Contributions of fermentative acidogenic bacteria and sulfate-reducing bacteria to lactate degradation and sulfate reduction. *Chemosphere* **2008**, *72*, 233–242. [CrossRef] [PubMed]
52. Hard, B.C.; Walther, C.; Babel, W. Sorption of aluminum by sulfate-reducing bacteria isolated from uranium mine tailings. *Geomicrobiol. J.* **1999**, *16*, 267–275.
53. Martins, M.; Taborda, R.; Silva, G.; Assuncao, A.; Matos, A.P.; Costa, M.C. Aluminum and sulphate removal by a highly al-resistant dissimilatory sulphate-reducing bacteria community. *Biodegradation* **2012**, *23*, 693–703. [CrossRef] [PubMed]
54. Cardenas, E.; Wu, W.M.; Leigh, M.B.; Carley, J.; Carroll, S.; Gentry, T.; Luo, J.; Watson, D.; Gu, B.; Ginder-Vogel, M.; et al. Microbial communities in contaminated sediments, associated with bioremediation of uranium to submicromolar levels. *Appl. Environ. Microbiol.* **2008**, *74*, 3718–3729. [CrossRef] [PubMed]
55. Ghiorse, W. Biology of iron-and manganese-depositing bacteria. *Annu. Rev. Microbiol.* **1984**, *38*, 515–550. [CrossRef] [PubMed]
56. Nealson, K.H.; Saffarini, D. Iron and manganese in anaerobic respiration: Environmental significance, physiology, and regulation. *Annu. Rev. Microbiol.* **1994**, *48*, 311–343. [CrossRef] [PubMed]
57. Conley, L.; Ceraso, M.; Stephenson, T.; Wolford, R.; Wadowsky, R.; McNamara, A.; Yee, R. Effects of metals on *Legionella pneumophila* growth in drinking water plumbing systems. *Appl. Environ. Microbiol.* **1985**, *50*, 1149–1154.
58. Reeves, M.; Pine, L.; Hutner, S.; George, J.; Harrell, W. Metal requirements of *Legionella pneumophila*. *J. Clin. Microbiol.* **1981**, *13*, 688–695. [PubMed]
59. Rogers, J.; Dowsett, A.; Dennis, P.; Lee, J.; Keevil, C. Influence of plumbing materials on biofilm formation and growth of *Legionella pneumophila* in potable water systems. *Appl. Environ. Microbiol.* **1994**, *60*, 1842–1851. [PubMed]

© 2017 by the authors. Licensee MDPI, Basel, Switzerland. This article is an open access article distributed under the terms and conditions of the Creative Commons Attribution (CC BY) license (http://creativecommons.org/licenses/by/4.0/).

Table S1. Oligonucleotide taqMan qPCR primer sequences used to screen pathogens and human-fecal indicator *Bacteroidetes* and PCR primer sequences for clone sequencing

Target	Oligo name	Sequences (5'-3')	Tm (℃)	Detection limit (CE per reaction)	Reference
Legionella spp. (qPCR)	Leg F1c	TAGTGGAATTTCCGGTGTA	50	2	This study
	Leg R1c	CCAACAGCTAGTTGACATC			
	Leg-probe	6Fam-CGGCTACCTGGCCTAATACTGA-Tamra			
L. pneumophila (qPCR)	mipF1a	AGGATAAGTTGTCTTATAGCA	60	2	This study
	mipR1	TTAAGAACGTCTTTCA TTTG			
	mipProbe	6FAM-TAATCCGGAAGCAATGGCTAA-Tamra			
L. pneumophila (CYBR-Green qPCR)	rtxAf	ATTGCGCCTGGCAAACTTTAGGTG	64	2	Lu, et al. 2013
	rtxAr	GGCGCAAATCGTTTCCACCTTGTA			
L. pneumophila (CYBR-Green qPCR)	sidFf	ATTGTTCGCGAGGGTATGAAAGC G	64	2	Lu, et al. 2013
	sidFr	TCTTTCCAAGACAGACTCTCGCGT			
Mycobacterium spp. (qPCR)	23Smyco F	GGG GTGTGGTGTTTGAG	62	1	Bruijnesteijn van Coppenraet, 2004
	23Smyco R	CTCCCACGTCCTTCATC			
	23Smyco Probe	6-carboxyfluorescein-TGGATAGTGGTTGCGAGCATC-BHQ1			
Acanthamoeba spp. (qPCR)	TaqAcF1	CGACCAGCGATTAGGAGACG	60	2	Riviere et al. 2006
	TaqAcR1	CCGACGCCAAGGACGAC			
	TaqAcP1	FAM-TGAATACAAAACACCACCATCGGC GC-TAMRA			
Vermamoeba vermiformis (qPCR)	Hv1227F	TTA CGA GGT CAG GAC ACT GT	56	2	Kuiper et al. 2006
	Hv1728R	GAC CAT CCG GAG TTC TCG			

Table S2. Element compositions of storage tank sediments

Common Element	Occurrence	Average	Standard Deviation	Minimum Result	Median Result	Maximum Result
Al (wt%)	87.5%	3.35	3.26	0.01	2.00	10.43
Ca (wt%)	87.5%	3.17	2.39	0.59	2.05	6.50
Cl (wt%)	25%	0.96	0.04	0.93	0.96	0.98
Fe (wt%)	100%	15.96	15.52	1.36	13.31	49.98
K (wt%)	25%	0.77	0.16	0.65	0.77	0.88
Mg (wt%)	37.5%	0.61	0.08	0.54	0.65	0.65
Mn (wt%)	37.5%	3.63	1.84	1.62	4.04	5.22
Na (wt%)	62.5%	2.13	1.30	0.96	1.65	4.05
O (wt%)	100%	24.09	4.83	17.72	23.89	33.39
Si (wt%)	100%	7.07	5.94	2.13	5.21	20.60
Zn (wt%)	75%	18.71	14.91	3.01	17.53	41.54

Table S3. Element components in sediments of different locations

Sample	Coefficient of Uniformity	Coefficient of Curvature	Bulk Density	Particle Density	Porosity	Al (wt%)	Ca (wt%)	Cl (wt%)	Fe (wt%)	K (wt%)	Mg (wt%)	Mn (wt%)	Na (wt%)	O (wt%)	Si (wt%)	Zn (wt%)
D39	3.35	0.64	0.54	2.68	0.80	2.26	2.05		19.93					23.47	5.42	19.35
D40	4.33	0.57	0.51	3.58	0.86	2.31	4.33		19.54		0.65			22.86	5	15.71
D41	5.75	0.46	0.75	2.26	0.67	1.17	5.93		1.36					17.72	2.13	41.54
D42	4.37	0.61	0.70	1.39	0.50	1.74	6.5		3.72		0.65		1.65	18.92	3.93	29.03
D43	2.53	0.81				4.12	1.42	0.98	17.53	0.65	0.52	4.04	2.84	24.30	7.94	0.41
D50	5.56	1.33	1.02	1.22	0.17		0.59		49.98				1.13	26.44	2.71	3.62
D53	9.39	0.46	0.45	1.17	0.62	1.45	1.4	0.93	6.56			5.22	4.05	33.39	20.6	3.01
D54	2.93	0.74	0.83	1.24	0.33	10.43			9.08	0.88		1.62	5.96	25.58	8.86	0.03

Table S4. major bacterial compositions with the relative abundance of OTUs > 1% in any samples at 97% similarity level)

Sample Name	1st abundant	Percentage	2nd abundant	Percentage	Correlation (R^2)
D39 Water	Unclassified Comamonadaceae	73.7	Unclassified Sphingomonadaceae	6.3	0.69
D39 Sediment	Unclassified Sphingomonadaceae	23.1	Unclassified Comamonadaceae	20.8	
D40 Water	Unclassified Comamonadaceae	23.7	Reyranella massiliensis	6.4	0.47
D40 Sediment	Unclassified Syntrophobacteraceae	12.2	Unclassified Solibacterales	7.7	
D41 Water	Pseudomonas veronii	34.2	Unclassified Comamonadaceae	16.0	0.88
D41 Sediment	Pseudomonas veronii	49.4	Unclassified Massilia	17.4	
D42 Water	Pseudomonas veronii	46.5	Unclassified Massilia	14.9	0.98
D42 Sediment	Pseudomonas veronii	37.7	Unclassified Massilia	7.7	
D43 Water	Unclassified Pseudomonas	21.5	Unclassified MLE1-12	10.1	n/a
D43 Sediment	n/a				
D50 Water	Unclassified Novosphingobium	26.1	Unclassified Comamonadaceae	6.4	0.38
D50 Sediment	Unclassified Geothrix	18.0	Unclassified Sulfuritalea	17.4	
D51 Water	Unclassified Acinetobacter	49.6	Unclassified Pseudomonadaceae	7.0	
D51 Sediment	Sphingomonas wittichii	38.0	Unclassified Comamonadaceae	18.3	
D53 Water	Blastomonas natatoria	26.5	Unclassified Acinetobacter	11.9	0.11
D53 Sediment	unclassified PK29	9.2	unclassified s-70	8.6	
D54 Water	Unclassified Pseudomonas	48.9	Unclassified Comamonadaceae	6.8	0.07
D54 Sediment	Unclassified Nitrospira	15.7	Unclassified Gemm-1	13.1	
D55 Water	Nevskia ramosa	93.4	Unclassified Sphingomonadaceae	2.0	
D55 Sediment	Unclassified Sphingomonadaceae	42.1	Unclassified Comamonadaceae	24.2	
D56 Water	Unclassfied Enterobacteriaceae	17.2	Unclassified Pseudomonas	6.3	
D56 Sediment	Sphingomonas asaccharolytica	15.8	Dongia mobilis	8.1	
D60 Sediment	Unclassified Novosphingobium	33.0	Peredibacter starrii	19.9	

Lu, Jingrang

From: Lytle, Darren
Sent: Sunday, April 5, 2020 9:16 PM
To: Lu, Jingrang
Subject: RE: Record of Percentage Agreement --Darren Lytle

Hello Jingrang,

I am in agreement with the % contribution you suggested for me. Thank-you, Darren

Darren A. Lytle, Ph.D., P.E.
U.S. Environmental Protection Agency
Drinking Water Management Branch
CESER Water Infrastructure Division
26 West Martin Luther King Dr.
Cincinnati, Ohio 45268
Phone: (513) 569-7432
Cell Phone: (513) 375-8044
Fax: (513) 487-2543
email: lytle.darren@epa.gov

From: Lu, Jingrang <Lu.Jingrang@epa.gov>
Sent: Friday, April 3, 2020 3:33 PM
To: Lytle, Darren <Lytle.Darren@epa.gov>
Subject: Record of Percentage Agreement --Darren Lytle

Dear Dr. Lytle,
We are submitting an application including two manuscripts for consideration for the EPA's Scientific and Technological Achievement Award and one of the requirements is that all authors must agree on the percentage of each author's contribution to the bodies of work. The publications are:

1. Lu, J., Struewing, I., Yelton, S., & Ashbolt, N. (2015). Molecular survey of occurrence and quantity of *Legionella* spp., *Mycobacterium* spp., *Pseudomonas aeruginosa* and amoeba hosts in municipal drinking water storage tank sediments. *Journal of applied microbiology*, *119*(1), 278-288.
2. Qin, K., Struewing, I., Domingo, J. S., Lytle, D., & Lu, J. (2017). Opportunistic pathogens and microbial communities and their associations with sediment physical parameters in drinking water storage tank sediments. *Pathogens,* 6(4), 54.

I have a preliminary breakdown of each author's % contribution according to the calculation using the attached spreadsheet to the manuscripts below.
Please let me know if I have erroneously calculated your level of efforts for this project.
Congratulations to everyone and I'm hoping that everyone's effort will be recognized by the Agency and be awarded for their hard work!
Please help me complete the nomination form.

The deadline for submission to our office is April 30, 2020. We need to complete the application by that time.
Please send an email stating your agreement to the % contribution.
The contribution breakdown:

Jingrang Lu 64.4% USEPA CEMM-WECD_BMB
Ian Struewing 8.3%, Dynamac Inc. during the study (Currently US EPA)
Sheron Yelton 3.1%, Dynamac Inc. during the study
Ke Qin 12.3%, ORISE Postdoctoral Fellow at EPA, Cincinnati, Ohio, USA, during the study
Jorge Santo Domingo 3.1%, USEPA ORD
Nicholas J. Ashbolt 4.2%, School of Public Health, Room 3-57D, South Academic Building, University of Alberta, Edmonton Alberta T6G 2G7, Canada
Darren Lytle 4.5%, USEPA ORD

Best,
Jingrang Lu, Ph.D
Biological Measurements Branch
Watershed & Ecosystem Characterization Division
Center for Environmental Measurement & Modeling
Office of Research and Development, United States Environmental Protection Agency
26 W. Martin Luther King Drive (MS:587) Cincinnati, OH 45268

Lu, Jingrang

From: Struewing, Ian
Sent: Friday, April 3, 2020 2:14 PM
To: Lu, Jingrang
Subject: RE: Record of Percentage Agreement -- Ian Struewing

I agree to the following percentage of contribution.

Ian Struewing

From: Lu, Jingrang <Lu.Jingrang@epa.gov>
Sent: Friday, April 03, 2020 1:42 PM
To: Struewing, Ian <Struewing.Ian@epa.gov>
Subject: Record of Percentage Agreement -- Ian Struewing

Dear Mr. Struewing,
We are submitting an application including two manuscripts for consideration for the EPA's Scientific and Technological Achievement Award and one of the requirements is that all authors must agree on the percentage of each author's contribution to the bodies of work. The publications are:

1. Lu, J., Struewing, I., Yelton, S., & Ashbolt, N. (2015). Molecular survey of occurrence and quantity of *Legionella* spp., *Mycobacterium* spp., *Pseudomonas aeruginosa* and amoeba hosts in municipal drinking water storage tank sediments. *Journal of applied microbiology*, *119*(1), 278-288.
2. Qin, K., Struewing, I., Domingo, J. S., Lytle, D., & Lu, J. (2017). Opportunistic pathogens and microbial communities and their associations with sediment physical parameters in drinking water storage tank sediments. *Pathogens,* 6(4), 54.

I have a preliminary breakdown of each author's % contribution according to the calculation using the attached spreadsheet to the manuscripts below.
Please let me know if I have erroneously calculated your level of efforts for this project.
Congratulations to everyone and I'm hoping that everyone's effort will be recognized by the Agency and be awarded for their hard work!
Please help me complete the nomination form.

The deadline for submission to our office is April 30, 2020. We need to complete the application by that time.
Please send an email stating your agreement to the % contribution.
The contribution breakdown:
Jingrang Lu 64.4% USEPA CEMM-WECD_BMB
Ian Struewing 8.3%, Dynamac Inc. during the study (Currently US EPA)
Sheron Yelton 3.1%, Dynamac Inc. during the study
Ke Qin 12.3%, ORISE Postdoctoral Fellow at EPA, Cincinnati, Ohio, USA, during the study
Jorge Santo Domingo 3.1%, USEPA ORD
Nicholas J. Ashbolt 4.2%, School of Public Health, Room 3-57D, South Academic Building, University of Alberta, Edmonton Alberta T6G 2G7, Canada
Darren Lytle 4.5%, USEPA ORD

Best,
Jingrang Lu, Ph.D
Biological Measurements Branch
Watershed & Ecosystem Characterization Division
Center for Environmental Measurement & Modeling
Office of Research and Development, United States Environmental Protection Agency
26 W. Martin Luther King Drive (MS:587) Cincinnati, OH 45268

Lu, Jingrang

From: SantoDomingo, Jorge
Sent: Wednesday, April 8, 2020 12:59 PM
To: Lu, Jingrang
Subject: Re: Record of Percentage Agreement -- Jorge Santo Domingo

Jingrang,

I agree with my percent contribution.

Thanks,

jorge

From: Lu, Jingrang <Lu.Jingrang@epa.gov>
Sent: Friday, April 3, 2020 3:30 PM
To: SantoDomingo, Jorge <Santodomingo.Jorge@epa.gov>; Jorge Santo Domingo <jorgesd308@gmail.com>
Subject: Record of Percentage Agreement -- Jorge Santo Domingo

Dear Dr. Santo Domingo,
We are submitting an application including two manuscripts for consideration for the EPA's Scientific and Technological Achievement Award and one of the requirements is that all authors must agree on the percentage of each author's contribution to the bodies of work. The publications are:

1. Lu, J., Struewing, I., Yelton, S., & Ashbolt, N. (2015). Molecular survey of occurrence and quantity of *Legionella* spp., *Mycobacterium* spp., *Pseudomonas aeruginosa* and amoeba hosts in municipal drinking water storage tank sediments. *Journal of applied microbiology*, *119*(1), 278-288.
2. Qin, K., Struewing, I., Domingo, J. S., Lytle, D., & Lu, J. (2017). Opportunistic pathogens and microbial communities and their associations with sediment physical parameters in drinking water storage tank sediments. *Pathogens,* 6(4), 54.

I have a preliminary breakdown of each author's % contribution according to the calculation using the attached spreadsheet to the manuscripts below.
Please let me know if I have erroneously calculated your level of efforts for this project.
Congratulations to everyone and I'm hoping that everyone's effort will be recognized by the Agency and be awarded for their hard work!
Please help me complete the nomination form.

The deadline for submission to our office is April 30, 2020. We need to complete the application by that time.
Please send an email stating your agreement to the % contribution.
The contribution breakdown:
Jingrang Lu 64.4% USEPA CEMM-WECD_BMB
Ian Struewing 8.3%, Dynamac Inc. during the study (Currently US EPA)
Sheron Yelton 3.1%, Dynamac Inc. during the study
Ke Qin 12.3%, ORISE Postdoctoral Fellow at EPA, Cincinnati, Ohio, USA, during the study
Jorge Santo Domingo 3.1%, USEPA ORD
Nicholas J. Ashbolt 4.2%, School of Public Health, Room 3-57D, South Academic Building,

University of Alberta, Edmonton Alberta T6G 2G7, Canada
Darren Lytle 4.5%, USEPA ORD

Best,
Jingrang Lu, Ph.D
Biological Measurements Branch
Watershed & Ecosystem Characterization Division
Center for Environmental Measurement & Modeling
Office of Research and Development, United States Environmental Protection Agency
26 W. Martin Luther King Drive (MS:587) Cincinnati, OH 45268

Lu, Jingrang

From: Ke Qin <qinke84@gmail.com>
Sent: Friday, April 3, 2020 3:51 PM
To: Lu, Jingrang
Subject: Re: Record of Percentage Agreement -- Ke Qin

Hi Dr. Lu,

Thank you for sending me the email. I agree on the percentage of contribution. How about the manuscript Chiqian is writing? Do you need any help from me for that manuscript? Thank you.

Best,
Ke

Lu, Jingrang <Lu.Jingrang@epa.gov> 于2020年4月3日周五 下午3:27写道：

> Dear Dr. Qin,
>
> We are submitting an application including two manuscripts for consideration for the EPA's
>
> Scientific and Technological Achievement Award and one of the requirements is that all authors must agree on the percentage of each author's contribution to the bodies of work. The publications are:
>
> 1. Lu, J., Struewing, I., Yelton, S., & Ashbolt, N. (2015). Molecular survey of occurrence and quantity of *Legionella* spp., *Mycobacterium* spp., *Pseudomonas aeruginosa* and amoeba hosts in municipal drinking water storage tank sediments. *Journal of applied microbiology*, *119*(1), 278-288.
>
> 2. Qin, K., Struewing, I., Domingo, J. S., Lytle, D., & Lu, J. (2017). Opportunistic pathogens and microbial communities and their associations with sediment physical parameters in drinking water storage tank sediments. *Pathogens,* 6(4), 54.
>
> I have a preliminary breakdown of each author's % contribution according to the calculation
>
> using the attached spreadsheet to the manuscripts below.
>
> Please let me know if I have erroneously calculated your level of efforts for this project.
>
> Congratulations to everyone and I'm hoping that everyone's effort will be recognized by the Agency and be awarded for their hard work!
>
> **Please help me complete the nomination form**.

The deadline for submission to our office is April 30, 2020. We need to complete the application by that time.

Please send an email stating your agreement to the % contribution.

The contribution breakdown:

Jingrang Lu 64.4% USEPA CEMM-WECD_BMB

Ian Struewing 8.3%, Dynamac Inc. during the study (Currently US EPA)

Sheron Yelton 3.1%, Dynamac Inc. during the study

Ke Qin 12.3%, ORISE Postdoctoral Fellow at EPA, Cincinnati, Ohio, USA, during the study

Jorge Santo Domingo 3.1%, USEPA ORD

Nicholas J. Ashbolt 4.2%, School of Public Health, Room 3-57D, South Academic Building, University of Alberta, Edmonton Alberta T6G 2G7, Canada

Darren Lytle 4.5%, USEPA ORD

Best,

Jingrang Lu, Ph.D

Biological Measurements Branch

Watershed & Ecosystem Characterization Division

Center for Environmental Measurement & Modeling

Office of Research and Development, United States Environmental Protection Agency

26 W. Martin Luther King Drive (MS:587) Cincinnati, OH 45268

Lu, Jingrang

From: Nicholas Ashbolt <ashbolt@ualberta.ca>
Sent: Wednesday, April 8, 2020 12:58 PM
To: Lu, Jingrang
Subject: Re: Record of Percentage Agreement -- Nicholas J. Ashbolt

Dera Jingrang,

Yes I agree with my breakdown allocation of 4.2% for the two papers:
1. Lu, J., Struewing, I., Yelton, S., & Ashbolt, N. (2015). Molecular survey of occurrence and quantity of *Legionella* spp., *Mycobacterium* spp., *Pseudomonas aeruginosa* and amoeba hosts in municipal drinking water storage tank sediments. *Journal of applied microbiology*, *119*(1), 278-288.
2. Qin, K., Struewing, I., Domingo, J. S., Lytle, D., & Lu, J. (2017). Opportunistic pathogens and microbial communities and their associations with sediment physical parameters in drinking water storage tank sediments. *Pathogens,* 6(4), 54.

Kind regards and best wishes,

Nick

Prof. Nicholas J. Ashbolt
Alberta Innovates Translational Health Chair in Water
School of Public Health
Room 3-57D, South Academic Building
University of Alberta
Edmonton Alberta T6G 2G7
Canada

email: ashbolt@ualberta.ca
Tel: +1 780 492 5227
Mobile: +1 587-987-3166

This message and any attached documents are only for the use of the intended recipient(s), are confidential and may contain privileged information. Any unauthorized review, use, retransmission, or other disclosure is strictly prohibited. If you have received this message in error, please notify the sender immediately, and then delete the original message. Thank you.

On Apr 3, 2020, at 1:31 PM, Lu, Jingrang <Lu.Jingrang@epa.gov> wrote:

agreement to the % contribution.
The contribution breakdown:
Jingrang Lu 64.4% USEPA CEMM-WECD_BMB
Ian Struewing 8.3%, Dynamac Inc. during the study (Currently US EPA)
Sheron Yelton 3.1%, Dynamac Inc. during the study
Ke Qin 12.3%, ORISE Postdoctoral Fellow at EPA, Cincinnati, Ohio, USA, during the study
Jorge Santo Domingo 3.1%, USEPA ORD
Nicholas J. Ashbolt 4.2%, School of Public Health, Room 3-57D, South Academic Building, University of Alberta, Edmonton Alberta T6G 2G7, Canada
Darren Lytle 4.5%, USEPA ORD

Lu, Jingrang

From: Sharon Gifford <yeltons1@gmail.com>
Sent: Tuesday, April 7, 2020 10:55 AM
To: Lu, Jingrang
Subject: Re: Record of Percentage Agreement --Sharon Yelton

That's fine, Jingrang. I hope all is well!

Sent from my iPhone

On Apr 7, 2020, at 10:45 AM, Lu, Jingrang <Lu.Jingrang@epa.gov> wrote:

> Dear Ms.Yelton,
> We are submitting an application including two manuscripts for consideration for the EPA's Scientific and Technological Achievement Award and one of the requirements is that all authors must agree on the percentage of each author's contribution to the bodies of work. The publications are:
>
> 1. Lu, J., Struewing, I., Yelton, S., & Ashbolt, N. (2015). Molecular survey of occurrence and quantity of *Legionella* spp., *Mycobacterium* spp., *Pseudomonas aeruginosa* and amoeba hosts in municipal drinking water storage tank sediments. *Journal of applied microbiology*, *119*(1), 278-288.
> 2. Qin, K., Struewing, I., Domingo, J. S., Lytle, D., & Lu, J. (2017). Opportunistic pathogens and microbial communities and their associations with sediment physical parameters in drinking water storage tank sediments. *Pathogens,* 6(4), 54.
>
> I have a preliminary breakdown of each author's % contribution according to the calculation using the attached spreadsheet to the manuscripts below.
> Please let me know if I have erroneously calculated your level of efforts for this project.
> Congratulations to everyone and I'm hoping that everyone's effort will be recognized by the Agency and be awarded for their hard work!
> **Please help me complete the nomination form**.
>
> **The deadline for submission to our office is April 30, 2020. We need to complete the application by that time.**
> Please send an email stating your agreement to the % contribution.
> The contribution breakdown:
> Jingrang Lu 64.4% USEPA CEMM-WECD_BMB
> Ian Struewing 8.3%, Dynamac Inc. during the study (Currently US EPA)
> Sharon Yelton 3.1%, Dynamac Inc. during the study
> Ke Qin 12.3%, ORISE Postdoctoral Fellow at EPA, Cincinnati, Ohio, USA, during the study
> Jorge Santo Domingo 3.1%, USEPA ORD
> Nicholas J. Ashbolt 4.2%, School of Public Health, Room 3-57D, South Academic Building, University of Alberta, Edmonton Alberta T6G 2G7, Canada
> Darren Lytle 4.5%, USEPA ORD
>
> Best,
>
> Jingrang Lu, Ph.D.,

Biological Measurements Branch
Watershed & Ecosystem Characterization Division
Center for Environmental Measurement & Modeling
Office of Research and Development
United States Environmental Protection Agency
26 W. Martin Luther King Drive (MS:587)
Cincinnati, OH 45268
+1 513 569 7177 Office
lu.jingrang@epa.gov

<STAA percentage of individual effort-Lp_detection.xlsx>

Journal of Applied Microbiology

Journal of Applied Microbiology ISSN 1364-5072

ORIGINAL ARTICLE

Molecular survey of occurrence and quantity of *Legionella* spp., *Mycobacterium* spp., *Pseudomonas aeruginosa* and amoeba hosts in municipal drinking water storage tank sediments

J. Lu[1], I. Struewing[2], S. Yelton[2] and N. Ashbolt[3]

1 U.S. EPA National Exposure Research Laboratory, Cincinnati, OH, USA
2 Dynamac Inc., Cincinnati, OH, USA
3 School of Public Health, University of Alberta, Edmonton, AB, Canada

Keywords
drinking water storage tank, free-living amoeba, *Legionella*, nontuberculous mycobacteria, sediment, waterborne pathogens.

Correspondence
Jingrang Lu, 26W Martin Luther King Dr., Cincinnati, OH 45268, USA.
E-mail: lu.jingrang@epa.gov

2014/2560: received 12 December 2014, revised 27 February 2015 and accepted 10 April 2015

doi:10.1111/jam.12831

Abstract

Aims: To examine the occurrence and quantity of potential pathogens and an indicator of microbial contamination in the sediments of municipal drinking water storage tanks (MDWSTs), given the absence of such data across the United States.

Methods and Results: Sediment samples (87 MDWST) from eighteen locations across ten states of the United States were collected and assayed by qPCR for a range of potential enteric and opportunistic microbial pathogens and a sewage-associated *Bacteroides* marker. Potential opportunistic pathogens dominated, with the highest detection of occurrence (per cent positive detection; average cell equivalence (CE)) being *Mycobacterium* spp. (88·9%; $6{\cdot}7 \pm 8{\cdot}5 \times 10^4$ CE g^{-1}), followed by *Legionella* spp. (66·7%; $5{\cdot}2 \pm 5{\cdot}9 \times 10^3$ CE g^{-1}), *Pseudomonas aeruginosa* (22·2%; 250 ± 880 CE g^{-1}) and *Acanthamoeba* spp. (38·9%; 53 ± 70 CE g^{-1}), with no detected *Naegleria fowleri*. Most enteric pathogens (*Campylobacter jejuni*, *Escherichia coli* 0157:H7, *Salmonella enterica*, *Cryptosporidium parvum* and *Giardia duodenalis*) were not detected, except for a trace signal for *Campylobacter* spp. There was significant correlation between the qPCR signals of *Legionella* spp. and *Acanthamoeba* spp. ($R^2 = 0{\cdot}61$, $n = 87$, $P = 0{\cdot}0001$). Diverse *Legionella* spp. including *Leg. pneumophila*, *Leg. pneumophila* sg1 and *Leg. anisa* were identified, each of which might cause legionellosis.

Conclusions: These results imply that potential opportunistic pathogens are common within MDWST sediments and could act as a source of microbial contamination, but need downstream growth to be of potential concern.

Significance and Impact of the Study: The results imply that opportunistic pathogen risks may need to be managed by regular tank cleaning or other management practices.

Introduction

Municipal drinking water storage tanks (MDWSTs) are used for pressure management and to buffer the supply of treated water during periods of high demand such as in firefighting. Little knowledge exists about the potential for the reservoirs to support waterborne pathogens, although MDWSTs may accumulate sediments that allow microbial communities to establish. While ingress of animal excreta into these reservoirs may seed MDWST sediments with enteric pathogens of human health concern, the establishment, growth and continual release of various opportunistic pathogens (such as *Legionella* and nontuberculous mycobacteria (NTM)) (Buse *et al.* 2012) is

more likely. However, due to complexities and cost associated with sampling of MDWST sediments, there is limited documentation of pathogen detection in MDWST across the United States. Historically, public health measures have been directed to enteric pathogens in drinking water systems, including *Shigella* spp., *Salmonella enterica*, *Yersinia enterocolitica*, *Campylobacter jejuni*, *Escherichia coli* O157, *Giardia intestinalis*, *Cryptosporidium* spp. and several viruses (Ashbolt 2015). However, opportunistic pathogens including members within *Pseudomonas aeruginosa*, *Legionella pneumophila*, NTM, *Naegleria fowleri* and some genogroups of *Acanthamoeba* spp. are now generally considered to cause a higher health burden than enteric pathogens via drinking water exposures (Craun *et al.* 2010; Biyela *et al.* 2012; Collier *et al.* 2012). Other free-living amoebae (FLA) of interest: *Vermamoeba* (formerly *Hartmanella*) *vermiformis,* along with various *Acanthamoeba* spp. appear critical to the growth of opportunistic intracellular bacterial pathogens and even virulence increase, such as with *Leg. pneumophila* and various NTM (Thomas and Ashbolt 2011; Valster *et al.* 2011; Biyela *et al.* 2012; Delafont *et al.* 2014).

The detection of potential opportunistic pathogens is complicated partly because of the time consuming methods and labour costs, and partly because of viable but nonculturable forms in drinking water systems (Moore *et al.* 2001; Garduno *et al.* 2002; Giao *et al.* 2009; Wingender and Flemming 2011; Wang *et al.* 2012). Molecular testing, especially qPCR, has many advantages *vs* culture-based approaches, as it provides high throughput, sensitivity, specificity and cost-efficiency, compared to traditional culture-based approaches (Lee *et al.* 2011). Although qPCR is not definitive in differentiating live from dead bacteria (Yáñez *et al.* 2011), which might lead to false positives, qPCR has been used by many research groups as a first screening approach for the range of targets, therefore, it is also considered in the current study. To date, surveys for these opportunistic bacterial pathogens appear to be limited to small in-premise storage containers, such as those in hospitals (Stout *et al.* 1985; Walker *et al.* 1995) and homes (Mathys *et al.* 2008; Lim *et al.* 2011). The objectives of this study were to examine the prevalence and quantity of potential pathogens in MDWST sediments across the United States to evaluate whether there may be a need to reduce microbial risks via tank cleaning or improved management practices.

Materials and methods

Sample collection

A total of 87 samples from 18 MDWSTs (1–5 million gallons in capacity) across ten states were examined with five replicates from each tank except NJ2 ($n = 3$) and NC ($n = 4$), which were collected from April 2012 to May 2014 (Fig. 1 and Table S1). The locations were selected to include five different regions of the United States. (Northeast, East Coast, Midwest, South and West Coast) (Fig. 1). Each sediment sample (approx. 100 ml) from the assigned five replicate subsampling points (East, West, South, North and Centre of the tank base) was collected with a sterile plastic spatula into a 125 ml sterile plastic bottle from completely drained tanks. The samples were placed in a cooler containing ice and immediately shipped overnight to the laboratory at Cincinnati, OH, for further processing. After removing liquid from the top of the sediment, aliquots (10 g) were transferred to separate tubes and processed using PowerMax® Soil DNA Isolation Kit (MO BIO Laboratories, Inc., Carlsbad, CA). Total community DNA was obtained per manufacturer's instructions. General parameters like water temperatures and source of raw water were recorded for each tank (Table S1). In addition, where 8-l sediment samples were available in seven locations (Table S2), other physical and chemical sediment characterization was undertaken (total organic carbon, TOC; total organic matter, TOM; Particle size; pH and total exchange capacity: TEC) using EPA standard or comparable methods (Table S3). Due to the incapability of on-site measurements by cleaning companies, the chlorine concentrations were obtained from local county water quality reports, where the storage tanks were located. Of the 18 locations sampled, all tanks contained chlorinated drinking water meeting US EPA regulated chlorine concentrations (detectable residual disinfectant, maximum level <4 mg l^{-1}), and their sources of water were 61% from ground water and 39% from surface water, while their water temperatures ranged from 2·2– 28·9°C with mean of 15·1 ± 7·0°C (Table S1).

qPCR analysis

A panel of 12 genus- or species-specific qPCR assays was used in order to screen and quantify selected microorganisms. Previously published assays were used except for *Legionella* spp. and *Leg. pneumophila* (in order to cover most of the sequences retrieved from environmental samples in NCBI) (Table S4). The qPCR performances were evaluated with cultures of *Leg. pneumophila* Phi 1 (ATCC 33152), *Mycobacterium avium* (ATCC 25291), *Ps. aeruginosa* (ATCC 10145), *Bacteroides thetaiotaomicron* (ATCC29148), *Camp. jejuni* (ATCC 29428), *Salm. enterica* (ATCC 13076), *E. coli* O157:H7 (ATCC 43895), *Acanthamoeba polyphaga* (ATCC 30461), *Vermamoeba vermiformis* (ATCC 50237), *N. fowleri* (ATCC 30863) and oo/cysts of *Cryptosporidium parvum* and *Giardia duodenalis*, which are representative of six enteric

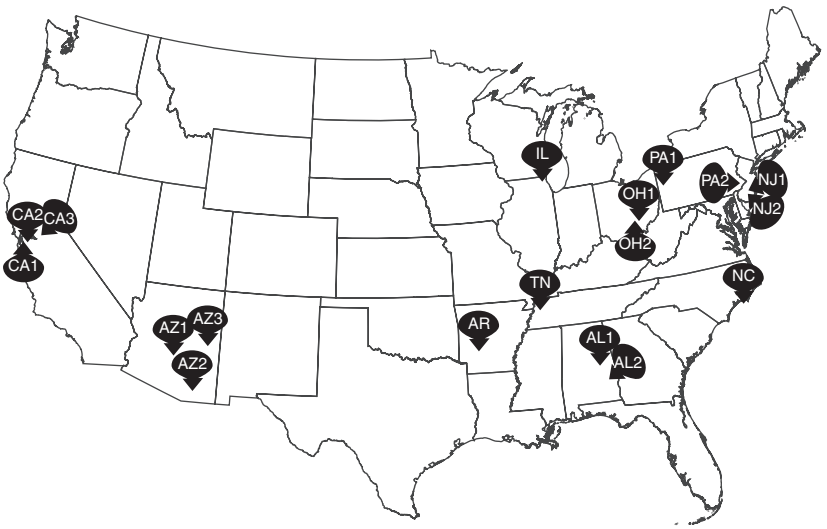

Figure 1 Sampling locations.

and six potential opportunistic pathogens and amoeba hosts. The novel *Legionella* primers and qPCR conditions were tested and optimized by running annealing temperature gradients and using serial dilutions (10–10^7) of *Leg. pneumophila* Phi 1 DNA templates. The primers were tested for host specificity against DNA extracted from the bacteria listed in Tables S5 and S6. The assays for *Ps. aeruginosa* and *E. coli* O157:H7 utilized TaqMan kits (Life Technology, Carlsbad, CA), so the primer sequences are not available (so not listed in Table S4).

Three replicates of serially diluted *Leg. pneumophila* Phi 1 (10^7 CFU ml^{-1}) were spiked into the sediment (250 mg ml^{-1}) previously tested as negative for *Leg. pneumophila,* and filtered and autoclaved Cincinnati tap water, respectively, DNA was isolated independently, qPCR was conducted from each DNA, and standard curves of the assays targeted to the genes of serogroup (sg1) associated with virulence factors: *mipA*, *sidF*, *rtxA*, *cegC1* and LPS cluster (Table S4) were prepared. The assays targeting *sidF*, *rtxA* and *cegC1* were used to confirm the presence of *Leg. pneumophila* Phi 1 for those samples with weak signals, because they are more sensitive than the LPS cluster (data not shown). By comparing the Ct values targeting those *Leg. pneumophila* assays, there was no significant differences in detection limits and the Ct values at each dilution level between spiking *Leg. pneumophila* in sediments and in the water. For other pathogen surrogates, approx. 10^7–10^1 (bacteria) or 10^5–10^1 (eukaryotes) of cultured cells/cysts were spiked and diluted in filtered and autoclaved Cincinnati tap water. All independent DNA extracts were examined in two sets: an original and a 10-fold dilution, both in duplicate, to ascertain inhibition by comparing (i) the difference in Ct values between the original DNA extracts and 10-fold dilutions and (ii) the correlations between Ct values and log numbers of the surrogates spiked. For example, if there was no or low inhibition from the original sample, there was a highly significant correlation between Ct values and log *Leg. pneumophila* concentrations or a slope between 3·58 and 3·10. Target cells in the extracts were reported as numbers of spiked cell/cyst equivalents (CE). If there was no significant inhibition, the data recorded from the experiments were used to generate standard curves, and the qPCR detection limit was estimated (Table S4). This inhibition check protocol has been used for various environmental samples, and inhibition was not commonly found in drinking water and tank sediment samples, so herein factors for correction of inhibition was not described.

All qPCR assays were performed using a 7900 HT Fast Real-Time Sequence Detector (Applied Biosystems, Foster City, CA). Reaction mixtures (20 μl) contained 10 μl 2× qPCR master mix (Applied Biosystems): Power SYBR® Master Mix for qPCR without probe and TaqMan® Environmental Master Mix 2.0 for qPCR with 0·08 μmol l^{-1} TaqMan probe (final concentration), 0·2 μmol l^{-1} primers and 2 μl of template DNA. DNA was treated with Uracil-N-Glycosylase for 2 min at 50°C to prevent carryover contamination. The sample was then held for 10 min at 95°C to denature the template DNA. The following quantification cycling protocol was used: 40 cycles at 95°C for 15 s and various Tm (Table S4) for 30 s with an extension at 72°C for 30 s, and a final hold at 72°C for 5 min. To assay for qPCR inhibitors from the sample DNA, an original and a 10-fold dilution of each DNA extract were assayed. In addition, the TaqMan Exogenous Internal Positive Control Reagents (a VIC-labelled probe) manufactured by ABI™ (Life Technology) was also used as a secondary confirmation. The qPCR for each assay was run on a 96-well plate, which included a serial of

DNA extracts described above for specific target standard curve in the first row of the 96-well plate, and a no-template control for each row of each 96-well plate assayed. Data were analysed with the Sequence Detection Systems software program (ver. 2.3) (Life Technology, Carlsbad, CA). The baseline cycles were set from three to 15 and the threshold value at the point where fluorescence exceeded ten times the standard deviation of the mean baseline emission. According to this standard, a setting of threshold 0·2 were frequently used. Samples in which both the duplicates had a threshold cycle (C_t) value below 40 were regarded as positive. The initial estimates of microbial quantities were produced automatically against a serial of standard DNA, and then the estimates were divided by wet weight (g) of the sediments used for DNA extraction to obtaining the final numbers.

Cloning and sequencing

Amplicons from the samples showing positive signals of *Legionella* spp., *Campylobacter* spp., *Acanthamoeba* spp. and *V. vermiformis* by qPCR screening, genus-specific PCR (Table S4) were cloned into pCR4.1 TOPO (Life Technology) and then individual clones (20 colonies for each library) were sequenced by using BigDye Terminator chemistry (Life Technology), in order to confirm the targets. Raw sequences were edited using Sequencher (Gene Codes Corp., Ann Arbor, MI). Chimeric sequences were identified using UCHIME (Edgar *et al.* 2011) and DECIPHER (Wright *et al.* 2012), and removed from further analyses. Phylogenetic trees were constructed from the alignments of 16S or 18S rRNA gene sequences based on the maximum likelihood method. The software MEGA v5.03 (Tamura *et al.* 2011) was used to build trees using 1000 replicates to develop bootstrap confidence values. Representative *Legionella* 16S rRNA gene sequences from clone libraries were deposited in GenBank with accession numbers: KM624063–KM624177.

Statistical analysis for qPCR data

Microsoft Excel 2003 and sas Systems ver. 9.2 (SAS, Cary, NC) were used for data management and calculations. Correlations used to determine the relationship between *Legionella* spp., *Acanthamoeba* spp. and temperature and correspondence analysis with two dimensions to determine the association between the quantity of *Legionella* spp. and other independent variables (TOC, TOM, Particle size: sand, silt and clay, pH and TEC) along locations were performed. In the correspondence analysis, inertia (variance) is defined as the total Pearson Chi-square for the two-way table divided by the total sum.

Results

The highest frequency of detection was with *Mycobacterium* spp. (88·9%), followed by *Legionella* spp. (66·7%), *Acanthamoeba* spp. (38·9%), *Ps. aeruginosa* (22·2%) and *V. vermiformis* (5·6%). For *Campylobacter* spp. and *V. vermiformis*, some qPCR signals near the detection limit were seen, yet they were later confirmed as true positives. The campylobacters were largely identified as *Camplylobacter lari* (95% of clone sequences), with a few *Camp. jejuni* (5% of clone sequences) present from AR (Fig. 1). Of the *Vermamoeba*, 99% were identical to *V. vermiformis* (from OH1 and AZ3). There was no other positive signal for the other targeted bacteria (human-specific HF183 *Bacteroides*, *Campylobacter* spp., *Salm. enterica*, *E. coli* O157:H7) and protozoan pathogens (*Cryptosporidium* spp. *Giardia* spp. and *N. fowleri*), indicating the absence of enteric pathogens and warm chlorine-free conditions for *N. fowleri*, but potential opportunistic pathogens were generally present in the sediments sampled (Table 1). The quantities of cell equivalence (CE g^{-1}) averaged $6{\cdot}7 \times 10^4$ (SD: $8{\cdot}5 \times 10^4$) for *Mycobacterium* spp., $5{\cdot}2 \times 10^3$ (SD: $5{\cdot}9 \times 10^3$) for *Legionella* spp., 250 (SD: 880) for *Ps. aeruginosa* and 53 (SD: 70) for *Acanthamoeba*. The highest detections for *Legionella* spp., *Acanthamoeba* spp. and *Mycobacterium* spp. occurred in NJ1, yet all three genera were also high at the IL, NJ2, AL1, AZ1, TN and NC sites. There was a significant correlation between *Legionella* and *Acanthamoeba* spp. across all sites ($R^2 = 0{\cdot}61$, $n = 87$, $P = 0{\cdot}0001$, Fig. 2). The correlation was especially demonstrated by the coincidence of the high quantity of both *Legionella* and *Acanthamoeba* spp. at the NJ1, IL, OH2 and NJ2 sites (Table 1, Fig 1). More than 100 CE g^{-1} of *Acanthamoeba* spp. were obtained for all the locations (IL, OH2, NJ1 and NJ2) that contained more than 10^3 CE g^{-1} of *Legionella* spp., although *Acanthamoeba* was not detected at locations, with a low level of *Legionella* spp. To examine potential associations among variables, correspondence analysis was performed using two-dimension Chi-square data analysis and significant differences were observed across site categories (Fig. 3). Over 61 and 35% of the total Chi-square was explained by dimension 1 and 2 (i.e. horizontal and vertical dimensions), respectively. It seemed there were associations between *Legionella* spp. and *Acanthamoeba* spp. and some chemical- and physical-parameters (particle sizes, TOC, TOM, TEC and pH) within the locations. For example, *Legionella* was possibly associated with *Acanthamoeba*, OH2, TN and AL1 along Dimension 1, while *Legionella* and *Acanthamoeba* were associated with clay, silt, TOC, NC and AZ1 along Dimension 2.

Importantly, all sites positive for *Legionella* spp. by the screening qPCR assay were confirmed positive by sequence analysis. It indicated the specificity of both the qPCR and PCR assays designed in this study to target

Table 1 The quantity (cell equivalent, CE wet g^{-1}) of potential opportunistic pathogens in sediments using qPCR in five replicates

Target	*Legionella* spp.		*Acanthamoeba* spp.		*Vermamoeba vermiformis*		*Mycobacterium* spp.		*Pseudomonas aeruginosa*	
Assay	16sF1c/R1c/Leg probe1		AcF1/R1/ taqAcP1		Hv1227F/ 1728R		23SmycoF/R/23SP2		ecfX F/R	
Location*	Mean	SD	Mean	SD	Mean	SD	Mean	SD	Mean	SD
AL1	600	483	0	0	0	0	$2{\cdot}23 \times 10^5$	$3{\cdot}59 \times 10^5$	0	0
AL2	0	0	0	0	0	0	216	194	3670	3720
AR	0	0	0	0	0	0	0	0	0	0
AZ1	304	226	0	0	0	0	$2{\cdot}71 \times 10^4$	$9{\cdot}92 \times 10^3$	0	0
AZ2	22	49	0	0	0	0	$1{\cdot}42 \times 10^4$	$1{\cdot}74 \times 10^4$	6	11
AZ3	51	114	22	50	17	23	$6{\cdot}64 \times 10^4$	$6{\cdot}06 \times 10^4$	0	0
CA1	0	0	25	19	0	0	$7{\cdot}45 \times 10^4$	$5{\cdot}20 \times 10^4$	659	777
CA2	0	0	0	0	0	0	$5{\cdot}58 \times 10^3$	$5{\cdot}87 \times 10^3$	59	92
CA3	30	59	0	0	0	0	$2{\cdot}56 \times 10^3$	$5{\cdot}45 \times 10^3$	0	0
IL	$8{\cdot}66 \times 10^3$	$4{\cdot}59 \times 10^3$	151	82	0	0	0	0	0	0
NC	275	207	10	12	0	0	$6{\cdot}24 \times 10^4$	$1{\cdot}85 \times 10^4$	0	0
OH1	0	0	0	0	0	0	$1{\cdot}92 \times 10^3$	$2{\cdot}04 \times 10^3$	0	0
OH2	$1{\cdot}00 \times 10^3$	519	209	185	0	0	$8{\cdot}30 \times 10^4$	$6{\cdot}39 \times 10^4$	0	0
TN	696	1108	0	0	0	0	156	252	0	0
PA1	0	0	0	0	0	0	39	88	0	0
PA2	113	213	0	0	0	0	$1{\cdot}19 \times 10^4$	$2{\cdot}65 \times 10^4$	67	111
NJ1	$7{\cdot}98 \times 10^4$	$2{\cdot}49 \times 10^4$	391	243	0	0	$6{\cdot}15 \times 10^5$	$1{\cdot}16 \times 10^5$	0	0
NJ2	$1{\cdot}63 \times 10^3$	383	133	68	0	0	$1{\cdot}99 \times 10^4$	$4{\cdot}51 \times 10^3$	0	0

*See Fig. 1 and Table S1.

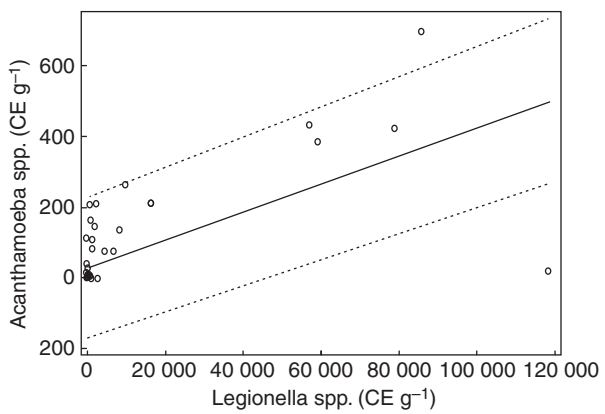

Figure 2 Scatter plot of quantities of *Legionella* spp. (*X*-axis) and *Acanthamoeba* spp. (*Y*-axis) and linear regression analysis (solid line) with 95% confidence interval (dash lines) showing the relationship between *Legionella* spp. and *Acanthamoeba* spp. (R^2 = 0·61, n = 87, P = 0·0001).

Legionella 16S rRNA gene, which covered 99·9% out of 1000 *Legionella*-related sequences in the NCBI database. Furthermore, *Legionella* diversity was high and a total of 115 unique operational taxonomic units (OTU) were identified, of which unknown *Legionella* sequences (38%) dominated in many sites. The dominant sequences were as follows: (10%) similar to *Legionella impletisoli* (identity: 99%) at AL1, AZ1 and OH2, and there were 6 and 5% sequences similar to *Legionella anisa* (identity: 99%) at NJ1, and to *Leg. pneumophila* or even *Leg. pneumophila* sg1 (identity: 99%) at TN and NJ1, respectively, which confirmed the qPCR results described hereafter. The *Legionella* phylogenetic diversities varied across sites. For example, the highest OTUs (n = 36) was in NJ1 and next highest at IL (n = 16) (Table S7, Fig. 4).

The detection of *Leg. pneumophila* (33%) (sites AL1, AZ3, IL, OH2, NJ1, NJ2 and TN) and *Leg. pneumophila* sg1 (28%) across the United States (sites AL1, IL, OH2 and TN) was consistent with several serogroup 1 specific assays (*sidF*, *rtxA*, *cegC1* and P65/66), and confirmed by clone sequencing. For example, one of the positive TN samples was also positive to the panel of assays specific to *Leg. pneumophila* (*mip*) and *Leg. pneumophila* sg1, although the qPCR signals were generally low. Considering the differences in sensitivities for the gene-specific assays developed, the detection and confirmation for *Leg. pneumophila* or *Leg. pneumophila* sg1 was conducted using multiple assays, and the positive samples were recorded, when the qPCR for one or more assays showed strong signals. For example, samples from OH1, OH2 and AL1 were positive by *mipA*, and samples from NC and IL were positive by *sidF* or/and *rtxA* targeted qPCR (Table 2).

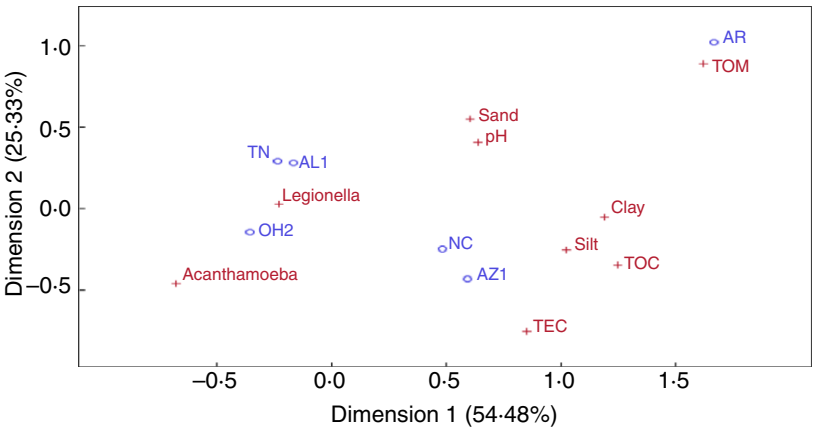

Figure 3 Correspondence analysis showing associations among *Legionella* spp., *Acanthamoeba* spp. and chemical- and physical- parameters (TOC, TOM, TEC, pH and particle sizes: sand, clay and silt) along locations. Possible associations can be seen among those variables, e.g. *Legionella* associated with *Acanthamoeba*, OH2, TN and AL1 along Dimension 1, while *Legionella* and *Acanthamoeba* associated with clay, silt, TOC, NC and AZ1 along Dimension 2.

Acanthamoeba spp. were also confirmed for the IL and OH2 samples in which high densities of *Legionella* spp. co-occurred. They were similar to *Acanthamoeba* sp. (identity: 99%), which was an *Acanthamoeba* isolate from infected corneas of amoebic keratitis patients in Korea (Kim, S.Y., Yu, H.S., Moon, E.K., Kong, H.H., Hahn, T.W. and Chung, D.I. unpublished data at the NCBI Website). More importantly, *Leg. pneumophila* was detected in various locations (AL1, AZ1 and TN), where both *Acanthamoeba* and *V. vermiformis* were undetected and *Legionella* was in low level.

Discussion

This study is the first nationwide survey reported for microbial pathogens associated with MDWST sediments. Based on the results, it would seem that sediments within MDWSTs across the United States may support and allow the growth of *Leg. pneumophila*, other legionellae, NTM, *Ps. aeruginosa* and *Acanthamoeba* spp., all of which potentially contain opportunistic pathogenic members. In contrast, enteric pathogens including *E. coli* O157:H7, *Salmonella* spp., *Giardia intestinalis* and *Cryptosporidium* spp., were undetected, as was the sewage-associated *Bacteroides* marker, but there was a trace detection of *Camp. jejuni* (Table 1). Generally, *Legionella* and NTM species have been considered more of a problem associated with large building plumbing systems and in the use of drinking water supporting cooling towers or humidifiers (Buse *et al.* 2012; Donohue *et al.* 2014), rather than drinking water distribution systems. However, this study and others (Wang *et al.* 2012; van der Wielen and van der Kooij 2013) suggest that nonenteric pathogens may be a concern for water storage tanks and potentially other locations where sediments accumulate within drinking water distribution networks. In addition, pathogenic members are often associated with amoebae (Thomas *et al.* 2010) as was seen in this study. Mounting evidence exists (Thomas and Ashbolt 2011; Biyela *et al.* 2012) that amoebae are critical to intracellular pathogen amplification and even increased virulence of these opportunistic pathogens.

A recent review of microbial disease outbreaks associated with drinking water by the Centers for Disease Control and Prevention (CDC) indicates that *L. pneumophila* is an aetiological agent of major concern (Craun *et al.* 2010), and along with the NTM account for the majority of drinking water associated pathogen hospitalization costs in the United States (Collier *et al.* 2012). Also of concern reported by CDC are increasing *Acanthamoeba*-related eye infections (Yoder *et al.* 2012); noting that in the current study clinically relevant *Acanthomoebae* were identified (Table 1). Other concerns were that *Acanthamoeba* correlated with our finding of high *Legionella* densities compared to most other organisms detected in the sediments (Fig. 2) and that the *Acanthomoebae* may also support replication of various other intracellular pathogens (Greub *et al.* 2004; Thomas *et al.* 2010). Hence, preemptive monitoring of amoebal numbers may provide a useful warning of conditions that could support opportunistic bacterial pathogens (Codony *et al.* 2012).

The diversity of unique OTUs (total of 115) related to *Legionella* spp. from the MDWST sediment samples requires further study to ascertain their clinical relevance. *Legionella* species identified included not only those commonly found in distribution systems, such as *Leg. pneumophila* and non-*Leg. pneumophila* (Yu *et al.* 2002; Lee *et al.* 2010), but also many unique sequences (38%). For *Leg. pneumophila*, the occurrence of sg 1, present in 28% of the locations in which *Legionella* spp. were detected, was higher than the 9% reported from a previous drinking water treatment/distribution system study (Loret and Greub 2010). However, these levels of *Leg. pneumophila* seemed lower than those reported from public buildings.

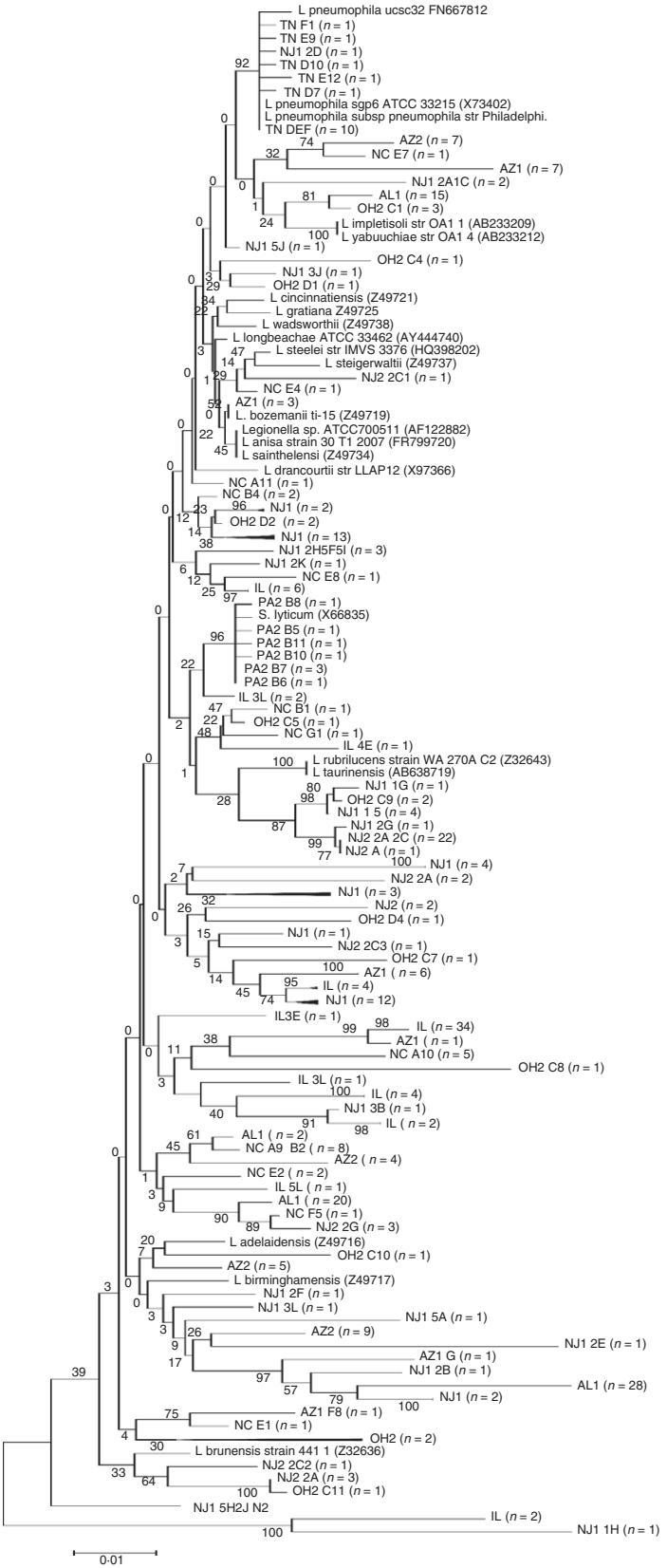

Figure 4 Unrooted neighbour-joining tree of 16S rRNA gene amplified for *Legionella* spp.sequences obtained from clone libraries. Sequences were aligned, and the bootstrap consensus tree was created with MEGA6 (1% divergence).

Table 2 Occurrence, quantification (CE wet g^{-1}) and confirmation with cloning and sequencing of *Legionella pneumophila* and serogroup 1 out of five replicates in each drinking water storage tank sediment

Location	16S	*mipA*	*sidF*	*rtxA*	*cegC1*	P65/66	
	Occurrence and quantity	Occurrence and quantity	Occurrence and quantity	Occurrence and quantity	Occurrence and quantity	Occurrence and quantity	Confirmed by cloning and sequencing
AL1	100% (600 ± 483)	80%[a] (575 ± 1110)[b]	40% (428 ± 908)	60% (244 ± 344)	40% (211 ± 449)	20% (63 ± 140)	Yes. unknown
AZ1	20% (304 ± 226)	0	0	0	0	0	Yes. 6 different OTUs
IL	100% (8660 ± 4590)	60% (80 ± 90)	80% (34 ± 28)	60% (50 ± 64)	20% (7 ± 10)	0	Not available
NC	100% (275 ± 207)	25% (45 ± 64)	25% (30 ± 22)	25% (51 ± 67)	0	0	Yes. 6 different OTUs
OH2	100% (1002 ± 519)	0	20% (30 ± 65)	0	0	20% (10 ± 23)	Yes. 8 different OTUs
PA2	17% (113 ± 213)	20% (10 ± 19)	0	0	0	0	Yes. *Legionella lyticum*
TN	40% (696 ± 1108)	40% (61 ± 103)	0	20% (11 ± 25)	0	20% (50 ± 111)	Yes. *Leg. pneumophila*
AZ3	20% (51 ± 114)	0	0	20% (13 ± 25)	20% (22 ± 38)	0	Not available
NJ1	100% (79 800 ± 24 900)	40% (58 ± 88)	80% (64 ± 38)	60% (63 ± 83)	0	0	Not available
NJ2	100% (1630 ± 383)	40% (23 ± 18)	0	20% (11 ± 25)	0	0	Not available

OTUs, operational taxonomic units.

For example, *Leg. pneumophila* sg1 was detected in nearly half of 68 public and private water taps across the United States using qPCR assays targeted 16S rRNA gene (Donohue *et al.* 2014). For the non-*Leg. pneumophila* identified in the current study, *Leg. anisa* and *Legionella bozemanii* were previously reported to predominate among this category in drinking water (48·1 and 21·0% respectively) (Lee *et al.* 2010). Although it is estimated that some 84% (out of 6868 cases) of legionellosis in the United States are caused by the *Leg. pneumophila* sg1, some non-*Leg. pneumophila* could also cause human health risk, such as Pontiac fever caused by various species including *Leg. anisa* (Fallon and Stack 1990; Fenstersheib *et al.* 1990) or hospital-acquired Legionnaires disease (Bornstein *et al.* 1989). Therefore, the detection of *Leg. anisa* in water samples should be considered an important indication that the water system has been colonized by potentially pathogenic *Legionella* species, including *Leg. pneumophila* (Yu *et al.* 2002; van der Mee-Marquet *et al.* 2006). Understanding the clinical significance of various non-*Leg. pneumophila* strains warrant further investigation for their human health risk.

The results showed high variations in the densities of detected opportunistic pathogens along different geographical locations, indicating their distributions might have been impacted with some physicochemical factors. Current physicochemical data available for this study did not explain the geographical differences observed. Previously, temperature, FLA and biofilm have been noted as key factors for the growth of *Legionella*, in addition to residual disinfectants. In this study, the disinfectant, free chlorine, which was used for all the systems investigated in this study and kept at the level approx. 1 mg l^{-1}, was probably not a major factor influencing the variations observed. Also, *Legionella* is able to survive or/and grow at temperature ranged from 20–50°C in distribution systems (Stout *et al.* 1985; Wadowsky *et al.* 1985). We also found no significant relationship between temperature and *Legionella* quantities of qPCR targets, noting that *Legionella* occurred in locations where temperatures ranged from 2·2–28·9°C with a mean of 15·1 ± 7·0°C, yet those with higher densities (>10^3 CE l^{-1}) were presented in the locations with temperatures >10·6°C. The lack of a possible effect of temperature, may have been influenced by our sampling plan, which did not focus on each season, but rather to address opportunities to sample across geographically diverse locations. It is also reported that the growth of *Legionella* is positively supported by FLA, biofilm and algae (Tison *et al.* 1980; Wadowsky *et al.* 1988; Greub and Raoult 2004), as well as the presence of metal ions (Rakić *et al.* 2011). In distribution system, positive correlations between *V. vermiformis* and total

bacteria, NTM and *V. vermiformis*, and *Legionella* and *V. vermiformis* have been reported (Wang *et al.* 2012; Delafont *et al.* 2014). In addition to our reporting of the co-occurrence between the quantity of *Acanthamoeba* spp. and *Legionella* spp., NTM also co-occurs in MDWST sediments, some of which may be opportunistic pathogens (Falkinham III 2011). For other factors, van der Wielen and van der Kooij reported a positive association between *Leg. pneumophila* and assimilable organic carbon, and further noted that the samples that contained *Leg. pneumophila,* also contained *Ps. aeruginosa* or *Stenotrophomonas maltophilia* (Wadowsky *et al.* 1988; van der Wielen and van der Kooij 2013). In the current study, although limited physical–chemical data were available (Table S2), correspondence analysis indicated that some sediment characteristics, such as TOC, clay and silt, seemed favourable to *Legionella* presence. Collectively, *Legionella* spp. with high species diversity and including potential pathogenic species were detected in more than half of the sediment samples, and other potential pathogens (NTM and *Ps. aeruginosa*) and their potential hosts (*Acanthamoeba* spp.) were also present. Future work needs to focus on possible environmental factors that may influence MDWSTs to support microbial community that harbour opportunistic pathogens and identify ways to manage these potential pathogen issues.

Acknowledgements and disclaimer

This research was supported by EPA ORD's Safe and Sustainable Water Resources Program and EPA's National Homeland Security Research Center (NHSRC). Thanks to Scott Minamyer at NHSRC, Ryan R James at Battelle Memorial Institute, and Darren Lytle at EPA ORD for organizing the project sampling, and Ann Grimm and Gerard Stelma at EPA ORD for their valuable comments. The United States Environmental Protection Agency through its Office of Research and Development funded and managed the research described here. It has been subjected to Agency review and approved for publication. Mention of trade names or commercial products does not constitute endorsement or recommendation for use.

Conflict of Interest

No conflict of interest declared.

References

Ashbolt, N.J. (2015) Microbial contamination of drinking water and human health from community water systems. *Curr Environ Health Rep* **2**, 95–106.

Biyela, P.T., Ryu, H., Brown, A., Alum, A., Abaszadegan, M. and Rittmann, B.E. (2012) Distribution systems as reservoirs of *Naegleria fowleri* and other amoebae. *J Am Water Works Assoc* **104**, E66–E72.

Bornstein, N., Mercatello, A., Marmet, D., Surgot, M., Deveaux, Y. and Fleurette, J. (1989) Pleural infection caused by *Legionella anisa*. *J Clin Microbiol* **27**, 2100–2101.

Buse, H.Y., Schoen, M.E. and Ashbolt, N.J. (2012) Legionellae in engineered systems and use of quantitative microbial risk assessment to predict exposure. *Water Res* **46**, 921–933.

Codony, F., Pérez, L.M., Adrados, B., Agustí, G., Fittipaldi, M. and Morató, J. (2012) Amoeba-related health risk in drinking water systems: could monitoring of amoebae be a complementary approach to current quality control strategies? *Future Microbiol* **7**, 25–31.

Collier, S., Stockman, L., Hicks, L., Garrison, L., Zhou, F. and Beach, M. (2012) Direct healthcare costs of selected diseases primarily or partially transmitted by water. *Epidemiol Infect* **140**, 2003–2013.

Craun, G.F., Brunkard, J.M., Yoder, J.S., Roberts, V.A., Carpenter, J., Wade, T., Calderon, R.L., Roberts, J.M. *et al.* (2010) Causes of outbreaks associated with drinking water in the United States from 1971 to 2006. *Clin Microbiol Rev* **23**, 507–528.

Delafont, V., Mougari, F., Cambau, E., Joyeux, M., Bouchon, D., Héchard, Y. and Moulin, L. (2014) First evidence of amoebae–mycobacteria association in drinking water network. *Environ Sci Technol* **48**, 11872–11882.

Donohue, M.J., O'Connell, K., Vesper, S.J., Mistry, J.H., King, D., Kostich, M. and Pfaller, S. (2014) Widespread molecular detection of *Legionella pneumophila* Serogroup 1 in cold water taps across the United States. *Environ Sci Technol* **48**, 3145–3152.

Edgar, R.C., Haas, B.J., Clemente, J.C., Quince, C. and Knight, R. (2011) UCHIME improves sensitivity and speed of chimera detection. *Bioinformatics* **27**, 2194–2200.

Falkinham, J.O. III (2011) Nontuberculous mycobacteria from household plumbing of patients with nontuberculous mycobacteria disease. *Emerg Infect Dis* **17**, 419.

Fallon, R.J. and Stack, B.H. (1990) Legionnaires' disease due to *Legionella anisa*. *J Infect* **20**, 227–229.

Fenstersheib, M.D., Miller, M., Diggins, C., Liska, S., Detwiler, L., Werner, S.B., Lindquist, D., Thacker, W.L. *et al.* (1990) Outbreak of Pontiac fever due to *Legionella anisa*. *Lancet* **336**, 35–37.

Garduno, R.A., Garduno, E., Hiltz, M. and Hoffman, P.S. (2002) Intracellular growth of *Legionella pneumophila* gives rise to a differentiated form dissimilar to stationary-phase forms. *Infect Immun* **70**, 6273–6283.

Giao, M., Wilks, S., Azevedo, N., Vieira, M. and Keevil, C. (2009) Incorporation of natural uncultivable *Legionella pneumophila* into potable water biofilms provides a

protective niche against chlorination stress. *Biofouling* **25**, 345–351.

Greub, G. and Raoult, D. (2004) Microorganisms resistant to free-living amoebae. *Clin Microbiol Rev* **17**, 413–433.

Greub, G., La Scola, B. and Raoult, D. (2004) Amoebae-resisting bacteria isolated from human nasal swabs by amoebal coculture. *Emerg Infect Dis* **10**, 470–477.

Lee, H.K., Shim, J.I., Kim, H.E., Yu, J.Y. and Kang, Y.H. (2010) Distribution of *Legionella* species from environmental water sources of public facilities and genetic diversity of *L. pneumophila* serogroup 1 in South Korea. *Appl Environ Microbiol* **76**, 6547–6554.

Lee, J., Lai, S., Exner, M., Lenz, J., Gaia, V., Casati, S., Hartemann, P., Lück, C. *et al.* (2011) An international trial of quantitative PCR for monitoring *Legionella* in artificial water systems. *J Appl Microbiol* **110**, 1032–1044.

Lim, Y., Kek, Y.R., Lim, P., Yap, H., Goh, T.V. and Ng, L. (2011) Environmental surveillance and molecular characterization of *Legionella* in tropical Singapore. *Trop Biomed* **28**, 149–159.

Loret, J.F. and Greub, G. (2010) Free-living amoebae: biological by-passes in water treatment. *Int J Hyg Environ Health* **213**, 167–175.

Mathys, W., Stanke, J., Harmuth, M. and Junge-Mathys, E. (2008) Occurrence of *Legionella* in hot water systems of single-family residences in suburbs of two German cities with special reference to solar and district heating. *Int J Hyg Environ Health* **211**, 179–185.

van der Mee-Marquet, N., Domelier, A.S., Arnault, L., Bloc, D., Laudat, P., Hartemann, P. and Quentin, R. (2006) *Legionella anisa*, a possible indicator of water contamination by *Legionella pneumophila*. *J Clin Microbiol* **44**, 56–59.

Moore, J., Caldwell, P. and Millar, B. (2001) Molecular detection of *Campylobacter* spp. in drinking, recreational and environmental water supplies. *Int J Hyg Environ Health* **204**, 185–189.

Rakić, A., Perić, J. and Foglar, L. (2011) Influence of temperature, chlorine residual and heavy metals on the presence of *Legionella pneumophila* in hot water distribution systems. *Ann Agric Environ Med* **19**, 431–436.

Stout, J., Yu, V. and Best, M. (1985) Ecology of *Legionella pneumophila* within water distribution systems. *Appl Environ Microbiol* **49**, 221–228.

Tamura, K., Peterson, D., Peterson, N., Stecher, G., Nei, M. and Kumar, S. (2011) MEGA5: molecular evolutionary genetics analysis using maximum likelihood, evolutionary distance, and maximum parsimony methods. *Mol Biol Evol* **28**, 2731–2739.

Thomas, J.M. and Ashbolt, N.J. (2011) Do free-living amoebae in treated drinking water systems present an emerging health risk? *Environ Sci Technol* **45**, 860–869.

Thomas, V., McDonnell, G., Denyer, S.P. and Maillard, J.Y. (2010) Free-living amoebae and their intracellular pathogenic microorganisms: risks for water quality. *FEMS Microbiol Rev* **34**, 231–259.

Tison, D., Pope, D., Cherry, W. and Fliermans, C. (1980) Growth of *Legionella pneumophila* in association with blue-green algae (cyanobacteria). *Appl Environ Microbiol* **39**, 456–459.

Valster, R.M., Wullings, B.A., van den Berg, R. and van der Kooij, D. (2011) Relationships between free-living protozoa, cultivable *Legionella* spp., and water quality characteristics in three drinking water supplies in the Caribbean. *Appl Environ Microbiol* **77**, 7321–7328.

Wadowsky, R.M., Wolford, R., McNamara, A. and Yee, R.B. (1985) Effect of temperature, pH, and oxygen level on the multiplication of naturally occurring *Legionella pneumophila* in potable water. *Appl Environ Microbiol* **49**, 1197–1205.

Wadowsky, R., Butler, L., Cook, M., Verma, S., Paul, M., Fields, B., Keleti, G., Sykora, J. *et al.* (1988) Growth-supporting activity for *Legionella pneumophila* in tap water cultures and implication of hartmannellid amoebae as growth factors. *Appl Environ Microbiol* **54**, 2677–2682.

Walker, J., Mackerness, C., Mallon, D., Makin, T., Williets, T. and Keevil, C. (1995) Control of *Legionella pneumophila* in a hospital water system by chlorine dioxide. *J Ind Microbiol* **15**, 384–390.

Wang, H., Edwards, M., Falkinham, J.O. 3rd and Pruden, A. (2012) Molecular survey of the occurrence of *Legionella* spp., *Mycobacterium* spp., *Pseudomonas aeruginosa*, and amoeba hosts in two chloraminated drinking water distribution systems. *Appl Environ Microbiol* **78**, 6285–6294.

van der Wielen, P.W. and van der Kooij, D. (2013) Nontuberculous mycobacteria, fungi, and opportunistic pathogens in unchlorinated drinking water in The Netherlands. *Appl Environ Microbiol* **79**, 825–834.

Wingender, J. and Flemming, H.-C. (2011) Biofilms in drinking water and their role as reservoir for pathogens. *Int J Hyg Environ Health* **214**, 417–423.

Wright, E.S., Yilmaz, L.S. and Noguera, D.R. (2012) DECIPHER, a search-based approach to chimera identification for 16S rRNA sequences. *Appl Environ Microbiol* **78**, 717–725.

Yáñez, M.A., Nocker, A., Soria-Soria, E., Múrtula, R., Martínez, L. and Catalán, V. (2011) Quantification of viable *Legionella pneumophila* cells using propidium monoazide combined with quantitative PCR. *J Microbiol Methods* **85**, 124–130.

Yoder, J.S., Verani, J., Heidman, N., Hoppe-Bauer, J., Alfonso, E.C., Miller, D., Jones, D.B., Bruckner, D. *et al.* (2012) Acanthamoeba keratitis: the persistence of cases following a multistate outbreak. *Ophthalmic Epidemiol* **19**, 221–225.

Yu, V.L., Plouffe, J.F., Pastoris, M.C., Stout, J.E., Schousboe, M., Widmer, A., Summersgill, J., File, T. *et al.* (2002) Distribution of *Legionella* species and serogroups isolated by culture in patients with sporadic community-acquired legionellosis: an international collaborative survey. *J Infect Dis* **186**, 127–128.

Supporting Information

Additional Supporting Information may be found in the online version of this article:

Table S1 Locations, dates, water temperatures and water sources of sediment samples.

Table S2 Sediment parameters across seven sampling sites.

Table S3 Screening analyses and methods performed on sediment samples.

Table S4 Oligonucleotide taqMan qPCR primer sequences used to screen pathogens and human-faecal indicator *Bacteroidetes* and PCR primer sequences for clone sequencing.

Table S5 *Legionella* strains used to test PCR coverage.

Table S6 Bacterial strains used to check the specificity of the PCR and qPCR assays **for** *Legionella*.

Table S7 Total clone numbers, unique OTUs and dominant sequences in those sediments showing positive for *Legionella* spp.

pathogens

MDPI

Article

Opportunistic Pathogens and Microbial Communities and Their Associations with Sediment Physical Parameters in Drinking Water Storage Tank Sediments

Ke Qin [1], Ian Struewing [2], Jorge Santo Domingo [3], Darren Lytle [3] and Jingrang Lu [3,*]

1 ORISE, Office of Research and Development, U. S. Environmental Protection Agency, Cincinnati, OH 45268, USA; qin.ke@epa.gov
2 Pegasus Service Inc., Cincinnati, OH 45268, USA; struewing.ian@epa.gov
3 Office of Research and Development, U. S. Environmental Protection Agency, Cincinnati, OH 45268, USA; Santodomingo.Jorge@epa.gov (J.S.D.); lytle.darren@epa.gov (D.L.)
* Correspondence: lu.jingrang@epa.gov

Received: 8 September 2017; Accepted: 10 October 2017; Published: 26 October 2017

Abstract: The occurrence and densities of opportunistic pathogens (OPs), the microbial community structure, and their associations with sediment elements from eight water storage tanks in Ohio, West Virginia, and Texas were investigated. The elemental composition of sediments was measured through X-ray fluorescence (XRF) spectra. The occurrence and densities of OPs and amoeba hosts (i.e., *Legionella* spp. and *L. pneumophila*, *Mycobacterium* spp., *P. aeruginosa*, *V. vermiformis*, *Acanthamoeba* spp.) were determined using genus- or species-specific qPCR assays. Microbial community analysis was performed using next generation sequencing on the Illumina Miseq platform. *Mycobacterium* spp. were most frequently detected in the sediments and water samples (88% and 88%), followed by *Legionella* spp. (50% and 50%), *Acanthamoeba* spp. (63% and 13%), *V. vermiformis* (50% and 25%), and *P. aeruginosa* (0 and 50%) by qPCR method. *Comamonadaceae* (22.8%), *Sphingomonadaceae* (10.3%), and *Oxalobacteraceae* (10.1%) were the most dominant families by sequencing method. Microbial communities in water samples were mostly separated with those in sediment samples, suggesting differences of communities between two matrices even in the same location. There were associations of OPs with microbial communities. Both OPs and microbial community structures were positively associated with some elements (Al and K) in sediments mainly from pipe material corrosions. Opportunistic pathogens presented in both water and sediments, and the latter could act as a reservoir of microbial contamination. There appears to be an association between potential opportunistic pathogens and microbial community structures. These microbial communities may be influenced by constituents within storage tank sediments. The results imply that compositions of microbial community and elements may influence and indicate microbial water quality and pipeline corrosion, and that these constituents may be important for optimal storage tank management within a distribution system.

Keywords: *Legionella*; opportunistic pathogen; storage tank sediment; microbial community; element; corrosion

1. Introduction

Drinking water distribution systems (DWDS) contain complex microbial communities based on both measured by composition [1,2] and genetic network [3]. While drinking water treatment and disinfection considerably reduces risk of exposure, opportunistic pathogens (OP) are often detected in different parts of DWDS. Although most of the attention has been given to the

microbiology of drinking water in premise plumbing and biofilms on pipes, drinking water storage tank sediment has also been shown to harbor OPs [4,5]. Many of these OP, such as *Legionella* spp., *Mycobacterium* spp., *Pseudomonas aeruginosa*, and some of *Acanthamoeba* spp. can pose significant risks to immunocompromised people [6–10]. Free-living amoeba (FLA), such as *Vermamoeba vermiformis*, and some groups of *Acanthamoeba* spp. are also relevant to public health as they are potential hosts to several OPs [7].

Microbial growth within DWDS biofilms has been associated with corrosion of pipes, and the production of various elements in water and sediments in DWDS [11–13]. Teng et al. (2008) found that biofilm can greatly affect element composition and the crystalline phase of corrosion scales. Also, studies have shown that iron-oxidizing bacteria can accelerate corrosion early on, while iron-reducing bacteria (IRB) may inhibit corrosion in later stages, processes that may be influenced by changes in biofilm microbial diversity [12]. DWDS sediments are mainly composed of iron, sulfur, total organic carbon (TOC), calcium, total inorganic carbon (TIC), phosphorous, manganese, magnesium, aluminum, and zinc, and can concentrate trace regulated contaminants such as arsenic and radium [14–16]. The properties distribution system sediment such as elemental composition may impact the composition and structure of their microbial communities. Stein et al. (2001), for example, found that iron- and manganese-enriched sediments also contained two groups related to known metal-oxidizing genera, Leptothrix of the β-Proteobacteria and Hyphomicrobium of the α-Proteobacteria, and a Fe(III)-reducing group related to the Magnetospirillum genus of the α-Proteobacteria [17]. White et al. (2011) reported on the microbiological community structure of sediment and corrosion by-products associated with a DWDS lead pipe using rRNA gene sequencing. They identified bacteria species that have previously reported in heavy-metal-contaminated soils that could potentially impact metal mobility [18].

Elements associated with corrosion by-products can also have an impact in the survival of OPs [19–22]. If elements can protect and promote growth of OPs in storage tank sediments, they may potentially be released into DWDS [23]. Microbial communities could also be impacted by elemental composition of sediments and the redox condition [24–26]. However, relatively little is known on the microbial community in sediments in drinking water storage tanks due to sampling, because samples can only be obtained randomly from tank clean companies [2]. To address this, we examined the occurrence and densities of OPs, the microbial community structure, and their associations with sediment elements. We detected OPs using qPCR [4] and determined the microbial community compositions using next generation sequencing.

2. Materials and Methods

2.1. Sample Collection

Water and sediment samples were collected while industrial storage & water tank cleaning companies were conducting tank cleaning. The samples were collected from eight water storage tanks (16 sediments and water samples) in Ohio (D39-42), West Virginia (D43), and Texas (D50, D53 and D54). For microbial community analysis, an additional sample from Ohio was processed (D84, sediment samples only, collected in triplicate). Sediment and water samples were transferred to sterile containers using aseptic techniques. Collected samples were then placed into ice coolers and shipped overnight to the EPA laboratory (Cincinnati, OH, USA) for different analyses. Water from sediment samples was first removed via centrifugation at 2844× *g* for 3 min using a Swing Bucket Rotor on a Thermo Sorvall® Legend® T Plus centrifuge (Thermo Fisher Scientific., Waltham, MA, USA) and 0.25 g was used to extract DNA using PowerSoil® DNA Isolation Kit (MoBio, Carlsbad, CA, USA) following the manufacturer's instruction. Water samples (1 L) were filtered using EMD Millipore Durapore™ membrane filter (0.40 µm, MilliPore, Foster City, CA, USA). The filtered biomass was lysed using a Beadbeater (BioSpec Products, Inc., Bartlesville, OK, USA) for 1 min. Tubes were centrifuged at 12,000× *g* for 5 min and the supernatant transferred to sterile microcentrifuge tubes.

The DNA extraction was completed using the Master Pure Complete DNA and RNA Purification Kit (Epicentre Technologies Corp., Madison, WI, USA). Extracted DNA was resuspended in 50 µL of molecular grade water. DNA concentrations were measured using Nanodrop 2000 spectrophotometer (NanoDrop Technologies, Inc., Wilmington, DE, USA). Remaining sediment samples were air dried for a period of three days after which elemental composition, and their bulk and particle density were measured with graduated cylinder and mass balance. For the bulk density, about 2 to 3 g of the sample were weighed and the mass was recorded. Then, the sample was placed in a graduated cylinder and the volume was recorded. This volume was the bulk volume because it included the pore spaces between particles. The bulk density was then calculated by dividing the recorded mass by the recorded volume. The procedure was the same for the particle density except the particle volume was determined by the displacement of water.

Porosity was calculated by the following equation:

$$\text{Porosity} = 1 - \frac{bulkdensity}{particledensity}$$

The elemental composition of the sediments was measured through X-ray fluorescence (XRF) of the pressed dried sediments pellets using a Panalytical Axios Instrument (Panalytical, Almelo, The Netherlands).

2.2. qPCR Analysis

The occurrence and densities of OPs and amoeba hosts (i.e., *Legionella* spp. and *L. pneumophila*, *Mycobacterium* spp., *P. aeruginosa*, *V. vermiformis, Acanthamoeba* spp.) were determined using genus- or species-specific qPCR assays, as previously described [2]. Briefly, qPCR assays were performed on a QuantStudio 6 Flex Real-Time PCR System (Applied Biosystems, Foster City, CA, USA) with reaction mixtures. To prevent carryover contamination, an initial incubation at 50 °C for 2 min with uracil-N-glycosylase (UNG) at the onset of the cycling program was conducted before the one cycle of denaturation and enzyme activation at 95 °C for 10 min. The following cycling conditions were used as 40 cycles at 95 °C for 15 s and at the specific Tm (°C) listed in Table S1 for 30 s with an extension at 72 °C for 30 s and a final hold at 72 °C for 5 min, with qPCR reactions for each DNA sample undertaken in duplicate. The standard curves were generated using genomic DNA from each of the targeted groups. Target cells in the extracts are reported as genome copy numbers (GN). The presence of potential qPCR inhibitors was determined using 10-fold dilution of each extract. DNA standards and no-template controls were included on each PCR run.

2.3. Next Generation Sequencing

Sequencing libraries were constructed using water and sediment DNA extracts as PCR templates coupled with barcoded primers targeting the V3–V4 region of the 16S rRNA gene [27]. The reactions used to generate the sequencing libraries were performed in 25 µL volumes using the Ex Taq kit (Takara) with 200 nM for each of the forward and reverse primer and 2 µL of nucleic acid template. Cycling conditions involved an initial 5 min denaturing step at 94 °C, followed by 30 cycles of 45 s at 94 °C, 60 s at 50 °C, and 90 s at 72 °C, and a final elongation step of 10 min at 72 °C. Agarose gel electrophoresis was used to confirm the size of the amplification products. PCR products were then pooled and size selected prior to multiplex sequencing on an Illumina MiSeq benchtop sequencer using paired-end 250 bp kits at the Cincinnati Children's Hospital DNA Core facility. Sequence reads were processed using MOTHUR software [28] as described earlier [3]. Briefly, before analysis, sequence reads with overall low quality scores, or containing homopolymers (>8 nucleotides) and ambiguous base calls (N's), were removed from further analysis [29]. MOTHUR aligned and sorted reads with >97% similarity into operational taxonomic units (OTUs). Chimeric OTUs were screened out by the UCHIME algorithm built within MOTHUR.

2.4. Data Analysis

Statistical analyses were performed using Rstudio (https://www.rstudio.com/). Paired *t*-test was performed to test if there was any significant difference between genome copy number of OP in sediment and water samples. Pearson's linear correlation coefficients were calculated to test the correlation within OP and between OP and environmental physical parameters. For the microbial community analysis, one-way ANOVA was performed to test if there were significant differences between sediment and water samples. Nonmetric multidimensional scaling (NMDS, which acted to visualize the community structure and correlated physicochemical conditions using metaMDS function in the 'vegan' package) was used to cluster microbial communities based on the similarity of OTU distribution. Multiple response permutation procedure (mrpp) analysis was performed to test if there were significant differences in the NMDS plot between water and sediment samples (i.e., if there were two different groups). Correlation coefficients were calculated to check if there was any environmental factor that could explain clustering on the NMDS plot at a statistically significant level.

3. Results

3.1. Opportunistic Pathogens

Mycobacterium spp. were the most frequently detected OPs in the sediments and water samples (88% and 88%, respectively), followed by *Legionella* spp. (50% and 50%), *Acanthamoeba* spp. (63% and 13%), *V. vermiformis* (50% and 25%), and *P. aeruginosa* (0 and 50%). The occurrence of free living amoebae was higher in sediment than in water. *L. pneumophila* was also detected in both sediment (25%) and water (13%) (Table 1). *Mycobacterium* spp., *Legionella* spp., and FLA constituted major OPs, and there were significant correlations between *Legionella* spp. and *Mycobacterium* spp. The major OPs in the sediments presented the highest densities in Texas samples (D53 and D54), followed by Ohio samples (D39 and D40). However, in the water samples, the highest densities of the major OPs occurred in Ohio samples (D39 and D40), followed by the West Virginia sample (D43) and one Texas sample (D50). It should be noted that FLA and *L. pneumophila* occurred more frequently in sediments than in water; *P. aeruginosa* occurred more frequently in water than in sediments (Table 1).

The major elements measured in sediments were Zn (18.7%), Fe (16.0%), Si (7.1%), Mn (3.6%), Al (3.4%), and Ca (3.2%) (Table S2). Element densities were different among samples and locations. For example, particle densities, porosities, Ca, Mg, and Zn were higher in OH samples (D39–42) than in TX samples (D50–54) (Table S3). The Pearson's linear correlation coefficients for each of the OPs studied with the sediment elements measured are listed in Table 2. It showed that OPs were associated with some sediment elements. Specifically, *V. vermiformis*, *Mycobacterium*, *Legionella*, and *L. pneumophila* were positively associated with Al and K. (Table 2).

Table 1. The quantity of opportunistic pathogens in sediments and water of storage tanks using qPCR in two replicates.

Matrix	Location ID	*Acanthamoeba* spp.	*Vermamoeba vermiformis*	*Mycobacterium* spp.	*Pseudomonas aeruginosa*	*Legionella* spp.	*L. pneumophila* (*rtxA*)	*L. pneumophila* (*sidF*)
Sediment (GN G^{-1}: genome copy number per gram sediment)	D39S	5 ± 1	0	$(2.73 \pm 0.68) \times 10^4$	0	335 ± 31	0	0
	D40S	1 ± 1	4	$(8.10 \pm 1.16) \times 10^3$	0	923 ± 34	0	0
	D41S	28 ± 7	0	$(8.00 \pm 1.20) \times 10^1$	0	0	0	0
	D42S	0	0	$(8.47 \pm 10.04) \times 10^3$	0	0	0	0
	D43S	0	0	0	0	0	0	0
	D50S	0	14 ± 22	$(2.00 \pm 4.00) \times 10^1$	0	1 ± 3	0	0
	D53S	7	99 ± 60	$(2.39 \pm 2.24) \times 10^3$	0	282 ± 113	25 ± 51	85 ± 69
	D54S	3	120 ± 43	$(2.57 \pm 0.88) \times 10^5$	0	$(7.20 \pm 3.31) \times 10^4$	300 ± 38	173 ± 87
	Average	6	29	3.79×10^4	0	9.19×10^3	41	32
	Occurrence	63%	50%	88%	0	50%	25%	25%
Water (GN L^{-1}: genome copy number per liter water)	D39w	0	0	$(2.33 \pm 3.28) \times 10^5$	70 ± 91	$(1.24 \pm 1.70) \times 10^4$	0	0
	D40w	0	0	$(5.63 \pm 7.74) \times 10^4$	0	$(6.93 \pm 9.76) \times 10^4$	0	0
	D41w	50	0	6.91×10^3	0	0	0	0
	D42w	0	0	3.37×10^4	0	0	0	0
	D43w	0	0	2.52×10^3	0	1.50×10^3	0	0
	D50w	0	480 ± 670	$(5.07 \pm 0.03) \times 10^3$	2770 ± 14	$(1.84 \pm 1.46) \times 10^4$	82 ± 117	36 ± 52
	D53w	0	0	0	83 ± 117	0	0	0
	D54w	0	98 ± 136	$(2.68 \pm 2.84) \times 10^3$	371 ± 150	0	0	0
	Average	6	613	4.25×10^4	412	1.27×10^4	10	4
	Occurrence	13%	25%	88%	50%	50%	13%	13%

Table 2. Pearson's linear correlation coefficients (R^2) of opportunistic pathogens (OPs) with sediment elements in significant level 95% ($p < 0.05$).

Elements	Pathogens											
	Acanthamoeba		*Vermamoeba vermiformis*		*Mycobacterium*		*Legionella* spp.		*L. pneumophila* (*rtxA*)		*L. pneumophila* (*sidF*)	
	R^2	P	R^2	P	R^2	P	R^2	P	R^2	P	R^2	P
Al					0.93	<0.001	0.93	<0.001	0.92	<0.001	0.80	0.017
K					0.75	<0.031	0.77	<0.025	0.75	<0.031		

3.2. Microbial Community

A total of 25 bacterial families were observed among the OTUs with relative abundance >1% (Figure 1). *Pseudomonadaceae* (19.4%) *Comamonadaceae* (18.5%), *Sinobacteraceae* (15.5%), and *Sphingomonadaceae* (13.0%) were the most dominant, but that of *Mycobacteriaceae* was less than 1%. There were associations of microbial communities between the sediment and water in the same site (Table S4). Many families like *Sphingomonadaceae* presented both in water and sediments in many sites (Table S4). Dominant OTUs varied with samples or locations. For OH samples, *Comamonadaceae* dominated in D39 of both sediments (48.9%) and water samples (90.6%), and water samples in D40 (42.8%) and D41 (38.9%). The dominance of *Comamonadaceae* in water and sediment samples has been previously documented [30,31], probably due to their abilities to restrain other competitors [32]. *Syntrophobacteraceae*, anaerobic sulfur-reducing bacteria [33] prevalent in sediments and soil [34,35], was most abundant in D40 sediments (28.0%). *Oxalobacteraceae*, a ubiquitous family found in drinking water systems [36], dominated in D41 sediment samples (47.5%) and D42 water samples (60.1%), while *Bradyrhizobiaceae* (18.3%) were most abundant in D42 sediment samples. For TX samples, *Pseudomonadaceae* (59.8%) dominated in D53 sediment samples, while *Oxalobacteraceae* (45.12%) represented the majority in water samples. The most abundant families in terms of OTUs percentage in D54 sediment and water samples were *Nitrospiraceae* (57.4%) and *Sphingomonadaceae* (50.2%), respectively.

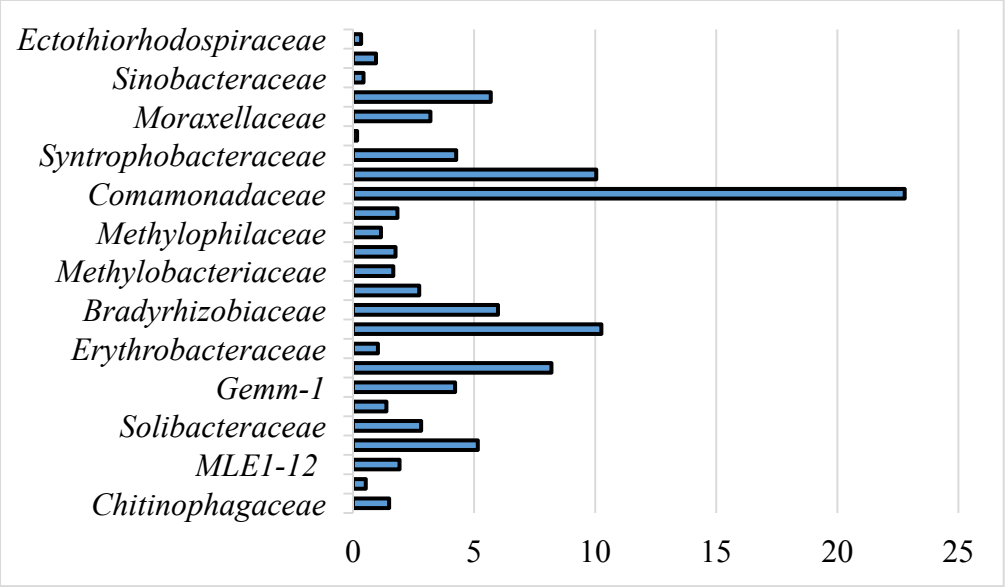

Figure 1. The 25 most abundant families presented in all the samples.

The samples sequenced in both water and sediment were clustered into one major group and several smaller groups according to relative abundance of the 25 families (Figure 2a). The sample type (water and sediment) could be one of the factors explaining microbial community structure. All the sediment samples except for D41 and D42 were in the major group. In sediment samples, the family (*Solibacteraceae*) was significantly higher in sediment than water (6.2% vs. 0.2%, $p = 0.02$, D40, etc.). The location of water system could be another factor, as shown by the two distinct clusters. Two samples from one city (D41 and D42) were clustered together separately from other samples (Figure 2b).

When considering the element's impact on community structure, most microbial communities in water samples (circled with a dash line) were separated from those in sediment samples (with a solid line) (Figure 3a), as inferred from the analysis of NMDS. Only the communities in D39 and D42 water and sediment, which were positioned within the overlap of the two circled areas, were not separated

by the element factor. With the matrices of OTU numbers and relative abundance of each OTU against relative abundance of elements and opportunistic pathogen densities by qPCR in water and sediment samples, it showed significant relationships between the microbial community structures and the densities of *Mycobacterium* spp., and two functional *Legionella pneumophila* genes (i.e., *sidF* and *rtxA*, $p = 0.05$) (Figure 3a). At $p = 0.1$ level, the community composition was also related positively with the densities of *Legionella* (Figure 3b). The vector direction of Zn was in opposite direction of other abiotic parameters including Al, K, Mn and Si, as well as biotic factors including concentrations of *V. vermiformis*, and *sidF,* and *rtxA* genes (Figure 4).

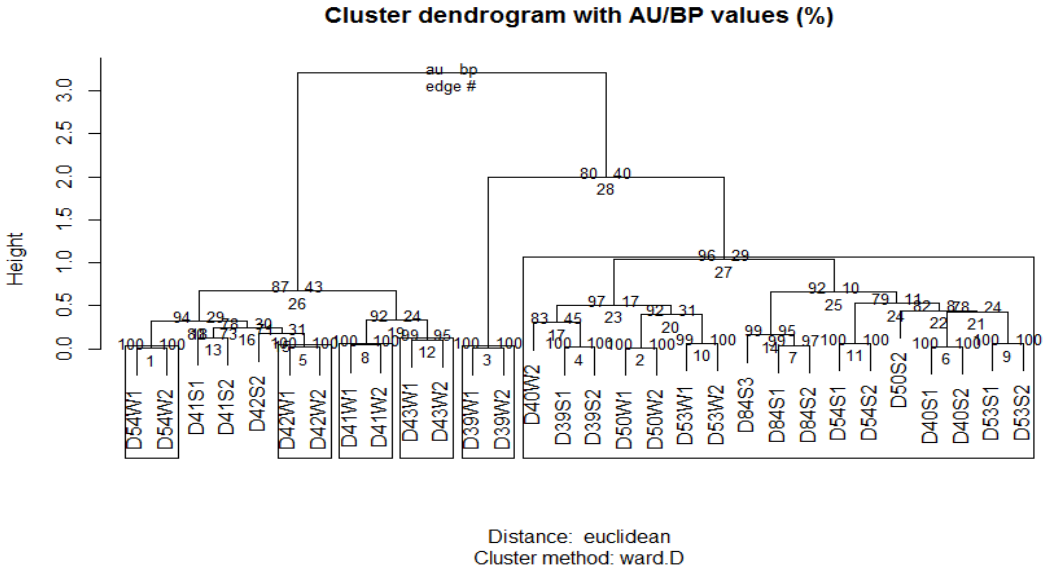

(**a**)

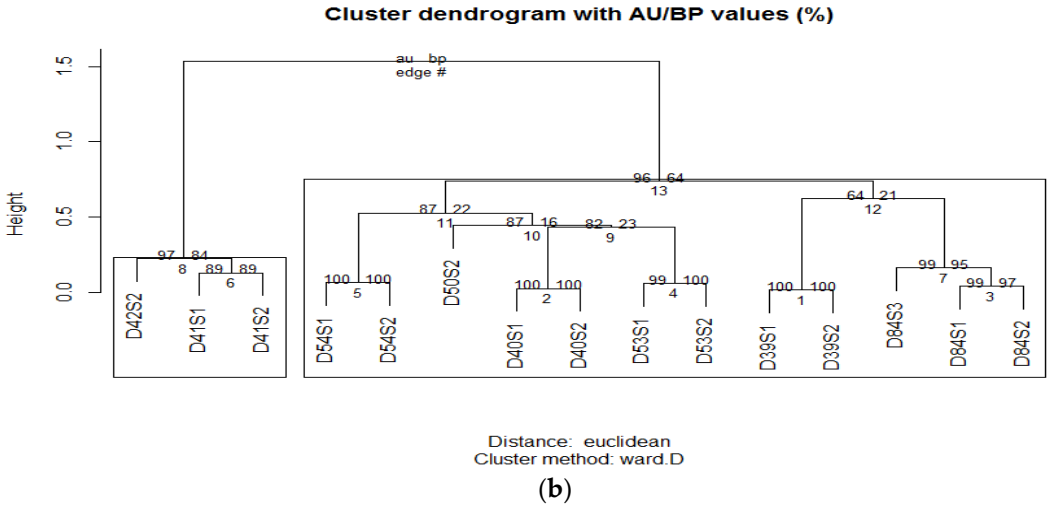

(**b**)

Figure 2. Cluster dendrogram of both sediment and water samples (**a**); and only sediment samples (**b**) based on microbial community structures. Values on the edges of the clustering are *p*-values (%). Top left values are approximately unbiased (AU) *p*-values, and top right values are bootstrap probability (BP) values. Clusters with AU larger than 95% are strongly supported by data.

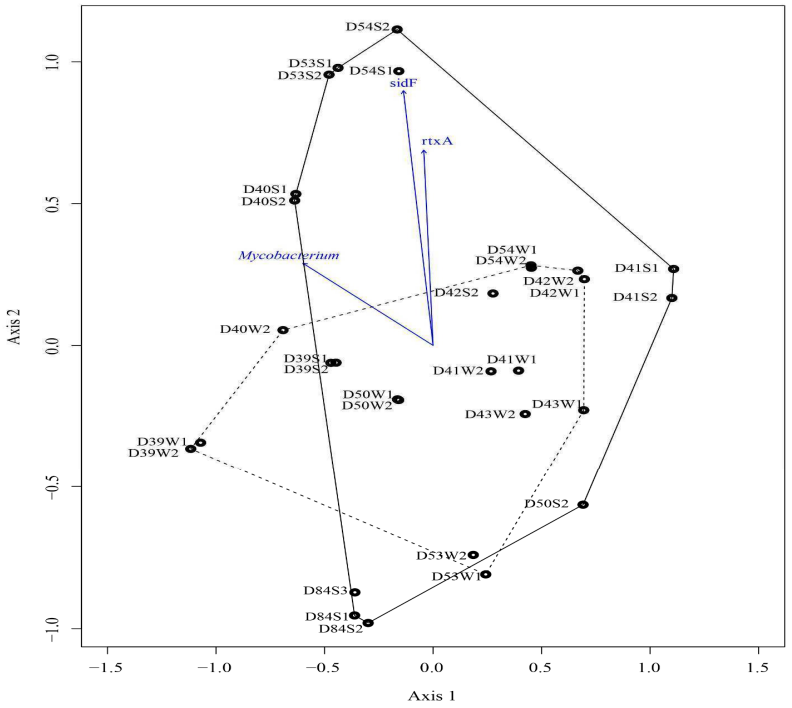

(**a**)

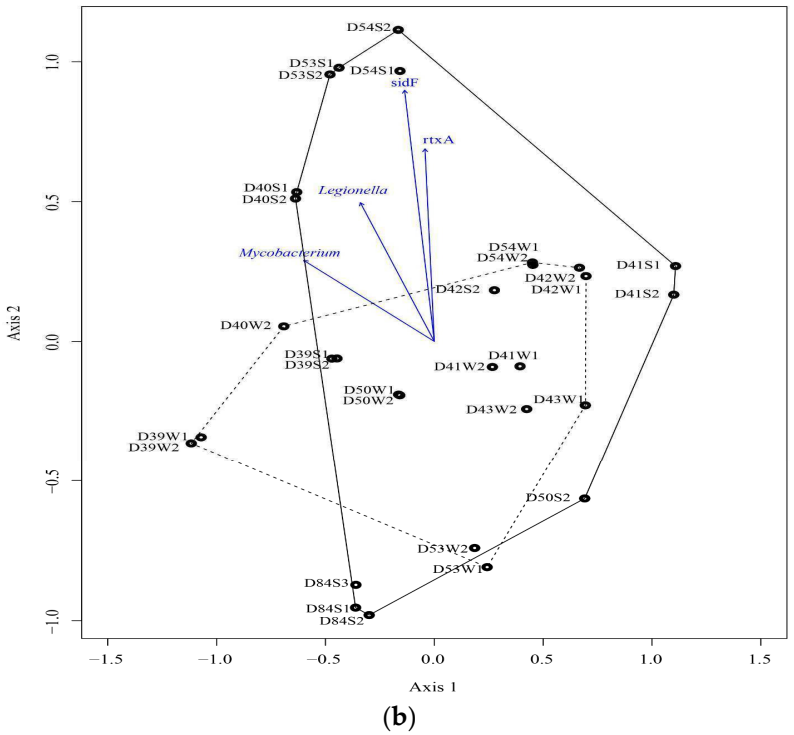

(**b**)

Figure 3. Nonmetric multidimensional scaling (NMDS) of paired water (W) and sediment (S) samples (Ohio: D39-42, West Virginia: D43, and Texas: D50, D53, and D54) based on microbial community structures with operational taxonomic unit (OTU) numbers and relative abundance of each OTU against relative abundance of elements and opportunistic pathogen densities by qPCR at significant level 10% (**a**) and 5% (**b**). The solid circles represent the central tendency of all OTUs detected in each sample from the sediment and water samples, respectively. Symbols that are closer to each other with a dash circle depict samples that contain similar taxa detected by the sequencing. A biplot is overlaid on the ordination to identify environmental parameters that were correlated with the microbial community structure. The length of the line corresponds to the degree of the correlation.

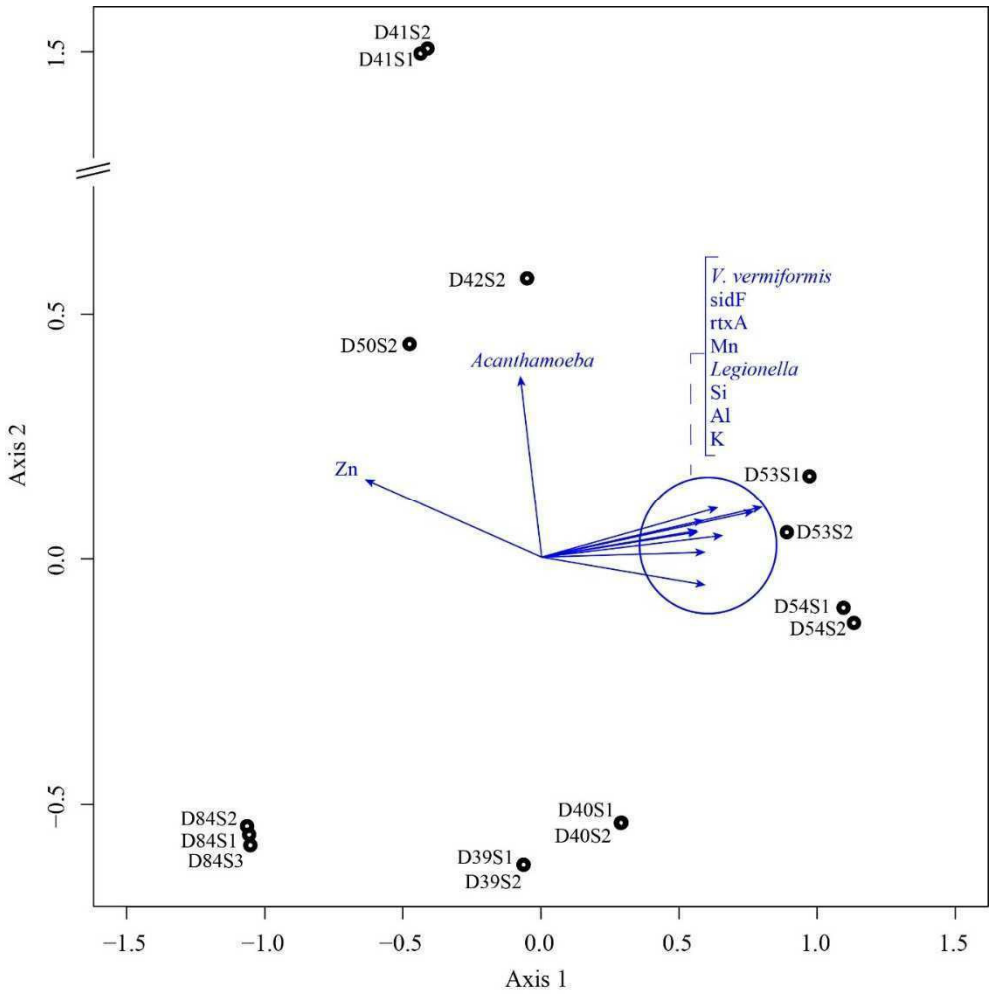

Figure 4. NMDS of sediment (S) samples (Ohio: D39-42, West Virginia: D43, and Texas: D50, D53, and D54) based on microbial community structures with OTU numbers and relative abundance of each OTU against relative abundance of elements and opportunistic pathogen densities by qPCR. The solid circles represent the central tendency of all OTUs detected in each sample from the sediment and water samples, respectively. Symbols that are closer to each other with a dash circle depict samples that contain similar taxa detected by the sequencing. A biplot is overlaid on the ordination to identify environmental parameters that were correlated with the microbial community structure. The length of the line corresponds to the degree of the correlation. Only variables that had a significant correlation ($p < 0.05$) are depicted.

4. Discussion

4.1. OPs in the Samples of Tank Water and Sediments

In this study the occurrences and densities of OPs were investigated and their associations with element concentrations was examined. The occurrences of *Mycobacterium* spp., *Legionella* spp., and *L. pneumophila* detected in this study were comparable to previous studies that investigated storage tank sediments [4] and drinking water distribution system [2]. In addition, higher occurrences of amoebae were also detected in the samples of sediment than those of water detected (Table 1). The free living amoebae may be beneficial to OPs [7]. *Acanthamoeba*, *V. vermiformis*, and other amoebae can serve as hosts for amoeba-resisting bacteria (ARB) like *Legionella* and *Mycobacterium* spp. [37,38]. The higher occurrences of amoebae in sediments than in water for the same storage tank suggest that they are more tightly bound to sediments and could be considered a reservoir of OPs. The targeted two genes

(*rtxA* [39] and *sidF* [40]) encoding toxins can reflect virulence of *L. pneumophila*. Their co-occurrences and similar level of quantities in D50 water and D53 and D54 sediment samples, which belong to a Texas metropolitan area, indicated the presence of *L. pneumophila*. It has been reported that the growth of *Legionella* is positively supported by FLA, biofilm, and algae [41–43]. Positive correlations between *V. vermiformis* and total *Legionella* have been shown for drinking water samples [2]. The co-occurrence of amoebae, *Legionella* spp., and *L. pneumophila* in the sediments, and their relatively higher densities in the sediment samples than in water, suggest that sediments can serve as reservoirs of OPs in storage tank water, and therefore can potentially be released into the distribution system. Taken together, our study reveals the importance of sediments as reservoirs for OPs which should be considered as an important risk factor when developing microbial risk assessment models for various drinking water systems, especially for *Mycobacterium* and *Legionella* spp. The results further stress the importance of maintaining a good disinfectant residual throughout the drinking water distribution system including storage tanks.

4.2. Microbial Communities and Their Relationship with Elements

Dominant OTUs reported in this study shared similarities with other reports focused on DWDS. *Pseudomonadaceae* (mainly *Pseudomonas* spp.) were ubiquitously present in DWDS and proposed as an indicator of potential regrowth [44]. Aerobic heterotrophs *Comamonadaceae* and/or *Sphingomonadaceae* were documented as dominant groups in biofilms [45,46], purified water [47], chlorine treated water [48], and household water tanks [49]. *Sinobacteraceae* (*Nevskia* spp.) were found dominant in biofilms [50]. Nevertheless, the shared microbial compositions between the water and sediment in the same location samples indicated the close associations and interactions between these two different matrices. The bacterial flora attached to sediment could re-enter the water matrix due to normal activity or water flow.

Both the qPCR results of *Mycobacterium* spp. and *Legionella* spp. were significantly associated with the microbial community composition. D39 water samples in OH had the second highest amount of *Mycobacterium* spp. It should be noticed that relative abundance of *Mycobacterium* spp. in microbial community was less than 1%, although it had high prevalence by qPCR. That community had a single dominant family of *Comamonadaceae*, which accounted for 75% of the total OTUs. D39 water samples also had the third highest amount of *Legionella* spp. of all the groups. The highest densities of *Mycobacterium* spp. and *Legionella* spp. were observed in D54 from Texas. The community featured with a couple of dominant families, with *Nitrospiraceae* accounting for 18.6% of total OTUs.

The role that elements play in the microbial community structure of drinking water systems has been poorly documented. In our study we showed that for the sediment samples, elements such as Al, K, Mn and Si (Figure 4), as well as *V. vermiformis* and *L. pneumophila* detected by *sidF* and *rtxA* genes, correlated with the community structures in a similar way, which was the opposite with the heavy metal Zn. That may indirectly suggest which elements could be beneficial or harmful to *Legionella*. Additionally, cluster analysis revealed there was a high association of microbial community structure dominated with *Pseudomonas* spp. (33.5%) and Al and K in D54 (Figure 4), which, in part, is in agreement with previous findings on *Pseudomonas* spp. tolerance to aluminum [51,52]. Interestingly, while Al (III) and S could be reduced simultaneously by *Desulfovibrio* [53], *Desulfovibrio* was very scarce (<0.1%) in total OTUs. The unique community structure dominated by *Geothrix* (belonging to family *Holophagaceae*) (18.0%) and *Sulfuritalea* (17%) significantly associated with the highest iron (III) (50.0%) in D50, which is not surprising as these are known as Fe^{+3} reducing bacteria [54]. Freshwater sediments often contain large quantities of iron and manganese that undergo rapid cycling between reduced and oxidized states [17]. The cycling of these metals is driven by diffusion of soluble Mn^{2+} and Fe^{2+} into oxygenated environments, followed by oxidation and sedimentation of solid Mn^{4+} and Fe^{3+} elements to reducing regions. Microbial communities are thought to play a significant role in both the oxidation and reduction of manganese and iron [55,56].

It was well documented that magnesium had the potential to function as antibiotics to inhibit the growth of *P. aeruginosa* [20] and that iron is a key nutrient for pseudomonads [19]. That may explain the relationships between the qPCR results of *P. aeruginosa* and relative concentrations of magnesium and iron in sediments. On the other hand, since *V. vermiformis* is a potential host of *Legionella* spp. and *Mycobacterium* spp. [2], it is also possible that *P. aeruginosa* was hosted by *V. vermiformis*. Similarly, the associations of element Al with the quantities of *L. pneumophila,* representative of two genes *rtxA* and *sidF* in the sediments, also reflected the impact of metal on them. According to a previous study [57,58], the growth of *L. pneumophila* requires certain amounts of magnesium, cobalt, copper, iron, manganese, molybdenum, vanadium, or zinc to stimulate growth, while higher level of trace metal would inhibit the growth of *L. pneumophila* [59]. However, higher level of trace metal requirement was found for the growth of *P. aeruginosa* and its growth was stimulated by only four metals: calcium, iron, magnesium, and zinc [58].

Supplementary Materials: The following are available online at www.mdpi.com/2076-0817/6/4/54/s1, Table S1: Oligonucleotide taqMan qPCR primer sequences used to screen pathogens and human-fecal indicator *Bacteroidetes* and PCR primer sequences for clone sequencing, Table S2: Element compositions of storage tank sediments, Table S3: Element components in sediments of different locations, Table S4: major bacterial compositions with the relative abundance of OTUs >1% in any samples at 97% similarity level).

Acknowledgments: This research was supported by EPA ORD's Safe and Sustainable Water Resources Program (SSWR 6.01C) and EPA's National Homeland Security Research Center (HS5.02.02). Thanks to Matthew Magnuson at NHSRC for managing funds and Christy Muhlen for arranging sample shipping and receiving. The United States Environmental Protection Agency through its Office of Research and Development funded and managed the research described here. It has been subjected to Agency review and approved for publication. Mention of trade names or commercial products does not constitute endorsement or recommendation for use.

Author Contributions: K.Q. conducted the experiments, analyzed and interpreted data, and participated the manuscript draft. I.S. conducted the experiments. J.S.D. provided the support of the experiments and the critical review of the manuscript. D.L. provided initial experimental design, and critically reviewed and revised the manuscript. J.L. designed the experiment, analyzed data, participated the manuscript draft and revisions.

Conflicts of Interest: The authors declare no conflict of interest.

References

1. Revetta, R.P.; Pemberton, A.; Lamendella, R.; Iker, B.; Santo Domingo, J.W. Identification of bacterial populations in drinking water using 16s rrna-based sequence analyses. *Water Res.* **2010**, *44*, 1353–1360. [CrossRef] [PubMed]
2. Lu, J.; Struewing, I.; Vereen, E.; Kirby, A.E.; Levy, K.; Moe, C.; Ashbolt, N. Molecular detection of *Legionella* spp. And their associations with *Mycobacterium* spp., *Pseudomonas aeruginosa* and amoeba hosts in a drinking water distribution system. *J. Appl. Microbiol.* **2016**, *120*, 509–521. [CrossRef] [PubMed]
3. Gomez-Alvarez, V.; Revetta, R.P.; Santo Domingo, J.W. Metagenomic analyses of drinking water receiving different disinfection treatments. *Appl. Environ. Microbiol.* **2012**, *78*, 6095–6102. [CrossRef] [PubMed]
4. Lu, J.; Struewing, I.; Yelton, S.; Ashbolt, N. Molecular survey of occurrence and quantity of *Legionella* spp., *Mycobacterium* spp., *Pseudomonas aeruginosa* and amoeba hosts in municipal drinking water storage tank sediments. *J. Appl. Microbiol.* **2015**, *119*, 278–288. [CrossRef] [PubMed]
5. Van der Wielen, P.W.; Lut, M.C. Distribution of microbial activity and specific microorganisms across sediment size fractions and pipe wall biofilm in a drinking water distribution system. *Water Sci. Technol.* **2016**, *16*, 896–904. [CrossRef]
6. Buse, H.Y.; Schoen, M.E.; Ashbolt, N.J. *Legionellae* in engineered systems and use of quantitative microbial risk assessment to predict exposure. *Water Res.* **2012**, *46*, 921–933. [CrossRef] [PubMed]
7. Biyela, P.T.; Ryu, H.; Brown, A.; Alum, A.; Abbaszadegan, M.; Rittmann, B.E. Distribution systems as reservoirs of *Naegleria fowleri* and other amoebae. *J. Am. Water Work Assoc.* **2012**, *104*, 49–50. [CrossRef]
8. Craun, G.F.; Brunkard, J.M.; Yoder, J.S.; Roberts, V.A.; Carpenter, J.; Wade, T.; Calderon, R.L.; Roberts, J.M.; Beach, M.J.; Roy, S.L. Causes of outbreaks associated with drinking water in the united states from 1971 to 2006. *Clin. Microbiol. Rev.* **2010**, *23*, 507–528. [CrossRef] [PubMed]

9. Whiley, H.; Keegan, A.; Fallowfield, H.; Bentham, R. Detection of *Legionella*, *L. pneumophila* and mycobacterium avium complex (mac) along potable water distribution pipelines. *Int. J. Environ. Res. Public Health* **2014**, *11*, 7393–7405. [CrossRef] [PubMed]
10. Wang, H.; Edwards, M.; Falkinham, J.O.; Pruden, A. Molecular survey of the occurrence of *Legionella* spp., *Mycobacterium* spp., *Pseudomonas aeruginosa*, and amoeba hosts in two chloraminated drinking water distribution systems. *Appl. Environ. Microbiol.* **2012**, *78*, 6285–6294. [CrossRef] [PubMed]
11. Hallam, N.; West, J.; Forster, C.; Simms, J. The potential for biofilm growth in water distribution systems. *Water Res.* **2001**, *35*, 4063–4071. [CrossRef]
12. Teng, F.; Guan, Y.; Zhu, W. Effect of biofilm on cast iron pipe corrosion in drinking water distribution system: Corrosion scales characterization and microbial community structure investigation. *Corros. Sci.* **2008**, *50*, 2816–2823. [CrossRef]
13. Lytle, D.A.; Gerke, T.L.; Maynard, J.B. Effect of bacterial sulfate reduction on iron-corrosion scales. *Am. Water Works Assoc. J.* **2005**, *97*, 109.
14. Friedman, M.; Hill, A.; Reiber, S.; Valentine, R.; Larsen, G.; Young, A.; Korshin, G.; Peng, C. *Assessment of Inorganics Accumulation in Drinking Water System Scales and Sediments*; Water Research Foundation: Denver, CO, USA, 2010.
15. Lytle, D.A.; Sorg, T.J.; Frietch, C. Accumulation of arsenic in drinking water distribution systems. *Environ. Sci. Technol.* **2004**, *38*, 5365–5372. [CrossRef] [PubMed]
16. Lytle, D.A.; Sorg, T.; Wang, L.; Chen, A. The accumulation of radioactive contaminants in drinking water distribution systems. *Water Res.* **2014**, *50*, 396–407. [CrossRef] [PubMed]
17. Stein, L.Y.; La Duc, M.T.; Grundl, T.J.; Nealson, K.H. Bacterial and archaeal populations associated with freshwater ferromanganous micronodules and sediments. *Environ. Microbiol.* **2001**, *3*, 10–18. [CrossRef] [PubMed]
18. White, C.; Tancos, M.; Lytle, D.A. Microbial community profile of a lead service line removed from a drinking water distribution system. *Appl. Environ. Microbiol.* **2011**, *77*, 5557–5561. [CrossRef] [PubMed]
19. Cornelis, P. Iron uptake and metabolism in pseudomonads. *Appl. Microbiol. Biotechnol.* **2010**, *86*, 1637–1645. [CrossRef] [PubMed]
20. Robinson, D.A.; Griffith, R.W.; Shechtman, D.; Evans, R.B.; Conzemius, M.G. In vitro antibacterial properties of magnesium metal against *Escherichia coli*, *Pseudomonas aeruginosa* and *Staphylococcus aureus*. *Acta Biomater.* **2010**, *6*, 1869–1877. [CrossRef] [PubMed]
21. Serrano-Suarez, A.; Dellunde, J.; Salvado, H.; Cervero-Arago, S.; Mendez, J.; Canals, O.; Blanco, S.; Arcas, A.; Araujo, R. Microbial and physicochemical parameters associated with *Legionella* contamination in hot water recirculation systems. *Environ. Sci. Pollut. Res.* **2013**, *20*, 5534–5544. [CrossRef] [PubMed]
22. Iivanainen, E.; Martikainen, P.; Katila, M.L. Environmental factors affecting the occurrence of mycobacteria in brook sediments. *J. Appl. Microbiol.* **1999**, *86*, 673–681. [CrossRef] [PubMed]
23. Pusch, M.; Fiebig, D.; Brettar, I.; Eisenmann, H.; Ellis, B.K.; Kaplan, L.A.; Lock, M.A.; Naegeli, M.W.; Traunspurger, W. The role of micro-organisms in the ecological connectivity of running waters. *Freshw. Biol.* **1998**, *40*, 453–495. [CrossRef]
24. Li, Y.C.; Yu, S.; Strong, J.; Wang, H.L. Are the biogeochemical cycles of carbon, nitrogen, sulfur, and phosphorus driven by the "fe-iii-fe-ii redox wheel" in dynamic redox environments? *J. Soils Sediments* **2012**, *12*, 683–693. [CrossRef]
25. Borch, T.; Kretzschmar, R.; Kappler, A.; Van Cappellen, P.; Ginder-Vogel, M.; Voegelin, A.; Campbell, K. Biogeochemical redox processes and their impact on contaminant dynamics. *Environ. Sci. Technol.* **2010**, *44*, 15–23. [CrossRef] [PubMed]
26. Lovley, D.R.; Coates, J.D. Bioremediation of metal contamination. *Curr. Opin. Biotechnol.* **1997**, *8*, 285–289. [CrossRef]
27. Caporaso, J.G.; Lauber, C.L.; Walters, W.A.; Berg-Lyons, D.; Huntley, J.; Fierer, N.; Owens, S.M.; Betley, J.; Fraser, L.; Bauer, M. Ultra-high-throughput microbial community analysis on the illumina hiseq and miseq platforms. *ISME J.* **2012**, *6*, 1621. [CrossRef] [PubMed]
28. Schloss, P.D.; Westcott, S.L.; Ryabin, T.; Hall, J.R.; Hartmann, M.; Hollister, E.B.; Lesniewski, R.A.; Oakley, B.B.; Parks, D.H.; Robinson, C.J. Introducing mothur: Open-source, platform-independent, community-supported software for describing and comparing microbial communities. *Appl. Environ. Microbiol.* **2009**, *75*, 7537–7541. [CrossRef] [PubMed]

29. Schloss, P.D.; Gevers, D.; Westcott, S.L. Reducing the effects of pcr amplification and sequencing artifacts on 16s rrna-based studies. *PLoS ONE* **2011**, *6*, e27310. [CrossRef] [PubMed]
30. Lu, S.D.; Sun, Y.J.; Zhao, X.; Wang, L.; Ding, A.Z.; Zhao, X.H. Sequencing insights into microbial communities in the water and sediments of fenghe river, china. *Arch. Environ. Contam. Toxicol.* **2016**, *71*, 122–132. [CrossRef] [PubMed]
31. Chu, L.B.; Wang, J.L. Denitrification performance and biofilm characteristics using biodegradable polymers pcl as carriers and carbon source. *Chemosphere* **2013**, *91*, 1310–1316. [CrossRef] [PubMed]
32. Aguirre-von-Wobeser, E.; Eguiarte, L.E.; Souza, V.; Soberon-Chavez, G. Theoretical analysis of the cost of antagonistic activity for aquatic bacteria in oligotrophic environments. *Front. Microbiol.* **2015**, *6*, 8. [CrossRef] [PubMed]
33. Kuever, J. The family syntrophobacteraceae. In *The Prokaryotes: Deltaproteobacteria and Epsilonproteobacteria*; Rosenberg, E., DeLong, E.F., Lory, S., Stackebrandt, E., Thompson, F., Eds.; Springer: Berlin/Heidelberg, Germany, 2014; pp. 289–299.
34. Bahr, M.; Crump, B.C.; Klepac-Ceraj, V.; Teske, A.; Sogin, M.L.; Hobbie, J.E. Molecular characterization of sulfate-reducing bacteria in a New England salt marsh. *Environ. Microbiol.* **2005**, *7*, 1175–1185. [CrossRef] [PubMed]
35. He, H.; Zhen, Y.; Mi, T.Z.; Xu, B.C.; Wang, G.S.; Zhang, Y.; Yu, Z.G. Community composition and distribution of sulfate- and sulfite-reducing prokaryotes in sediments from the changjiang estuary and adjacent east china sea. *Estuar. Coast. Shelf Sci.* **2015**, *165*, 75–85. [CrossRef]
36. Zhang, Y.; He, Q. Characterization of bacterial diversity in drinking water by pyrosequencing. *Water Sci. Technol.* **2013**, *13*, 358–367. [CrossRef]
37. Berry, D.; Horn, M.; Xi, C.; Raskin, L. Mycobacterium avium infections of *Acanthamoeba* strains: Host strain variability, grazing-acquired infections, and altered dynamics of inactivation with monochloramine. *Appl. Environ. Microbiol.* **2010**, *76*, 6685–6688. [CrossRef] [PubMed]
38. Buse, H.; Ashbolt, N. Differential growth of *Legionella pneumophila* strains within a range of amoebae at various temperatures associated with in-premise plumbing. *Lett. Appl. Microbiol.* **2011**, *53*, 217–224. [CrossRef] [PubMed]
39. Cirillo, S.L.G.; Bermudez, L.E.; El-Etr, S.H.; Duhamel, G.E.; Cirillo, J.D. *Legionella pneumophila* entry gene rtxa is involved in virulence. *Infect. Immun.* **2001**, *69*, 508–517. [CrossRef] [PubMed]
40. Hsu, F.S.; Zhu, W.H.; Brennan, L.; Tao, L.L.; Luo, Z.Q.; Mao, Y.X. Structural basis for substrate recognition by a unique *Legionella phosphoinositide* phosphatase. *Proc. Natl. Acad. Sci. USA* **2012**, *109*, 13567–13572. [CrossRef] [PubMed]
41. Tison, D.; Pope, D.; Cherry, W.; Fliermans, C. Growth of *Legionella pneumophila* in association with blue-green algae (cyanobacteria). *Appl. Environ. Microbiol.* **1980**, *39*, 456–459. [PubMed]
42. Wadowsky, R.; Butler, L.; Cook, M.; Verma, S.; Paul, M.; Fields, B.; Keleti, G.; Sykora, J.; Yee, R. Growth-supporting activity for *Legionella pneumophila* in tap water cultures and implication of hartmannellid amoebae as growth factors. *Appl. Environ. Microbiol.* **1988**, *54*, 2677–2682. [PubMed]
43. Greub, G.; Raoult, D. Morphology of *Legionella pneumophila* according to their location within hartmanella vermiformis. *Res. Microbiol.* **2003**, *154*, 619–621. [CrossRef] [PubMed]
44. Ribas, F.; Perramon, J.; Terradillos, A.; Frias, J.; Lucena, F. The pseudomonas group as an indicator of potential regrowth in water distribution systems. *J. Appl. Microbiol.* **2000**, *88*, 704–710. [CrossRef] [PubMed]
45. Ling, F.Q.; Hwang, C.A.; LeChevallier, M.W.; Andersen, G.L.; Liu, W.T. Core-satellite populations and seasonality of water meter biofilms in a metropolitan drinking water distribution system. *ISME J.* **2016**, *10*, 582–595. [CrossRef] [PubMed]
46. Luhrig, K.; Canback, B.; Paul, C.J.; Johansson, T.; Persson, K.M.; Radstrom, P. Bacterial community analysis of drinking water biofilms in southern sweden. *Microbes Environ.* **2015**, *30*, 99–107. [CrossRef] [PubMed]
47. Proctor, C.R.; Edwards, M.A.; Pruden, A. Microbial composition of purified waters and implications for regrowth control in municipal water systems. *Environ. Sci.* **2015**, *1*, 882–892. [CrossRef]
48. Hwang, C.; Ling, F.Q.; Andersen, G.L.; LeChevallier, M.W.; Liu, W.T. Microbial community dynamics of an urban drinking water distribution system subjected to phases of chloramination and chlorination treatments. *Appl. Environ. Microbiol.* **2012**, *78*, 7856–7865. [CrossRef] [PubMed]
49. Tokajian, S.; Hashwa, F. Microbiological quality and genotypic speciation of heterotrophic bacteria isolated from potable water stored in household tanks. *Water Qual. Res. J. Can.* **2004**, *39*, 64–73.

50. Keinanen-Toivola, M.M.; Revetta, R.P.; Santo Domingo, J.W. Identification of active bacterial communities in a model drinking water biofilm system using 16s rrna-based clone libraries. *FEMS Microbiol. Lett.* **2006**, *257*, 182–188. [CrossRef] [PubMed]
51. Zhao, Y.G.; Ren, N.Q.; Wang, A.J. Contributions of fermentative acidogenic bacteria and sulfate-reducing bacteria to lactate degradation and sulfate reduction. *Chemosphere* **2008**, *72*, 233–242. [CrossRef] [PubMed]
52. Hard, B.C.; Walther, C.; Babel, W. Sorption of aluminum by sulfate-reducing bacteria isolated from uranium mine tailings. *Geomicrobiol. J.* **1999**, *16*, 267–275.
53. Martins, M.; Taborda, R.; Silva, G.; Assuncao, A.; Matos, A.P.; Costa, M.C. Aluminum and sulphate removal by a highly al-resistant dissimilatory sulphate-reducing bacteria community. *Biodegradation* **2012**, *23*, 693–703. [CrossRef] [PubMed]
54. Cardenas, E.; Wu, W.M.; Leigh, M.B.; Carley, J.; Carroll, S.; Gentry, T.; Luo, J.; Watson, D.; Gu, B.; Ginder-Vogel, M.; et al. Microbial communities in contaminated sediments, associated with bioremediation of uranium to submicromolar levels. *Appl. Environ. Microbiol.* **2008**, *74*, 3718–3729. [CrossRef] [PubMed]
55. Ghiorse, W. Biology of iron-and manganese-depositing bacteria. *Annu. Rev. Microbiol.* **1984**, *38*, 515–550. [CrossRef] [PubMed]
56. Nealson, K.H.; Saffarini, D. Iron and manganese in anaerobic respiration: Environmental significance, physiology, and regulation. *Annu. Rev. Microbiol.* **1994**, *48*, 311–343. [CrossRef] [PubMed]
57. Conley, L.; Ceraso, M.; Stephenson, T.; Wolford, R.; Wadowsky, R.; McNamara, A.; Yee, R. Effects of metals on *Legionella pneumophila* growth in drinking water plumbing systems. *Appl. Environ. Microbiol.* **1985**, *50*, 1149–1154.
58. Reeves, M.; Pine, L.; Hutner, S.; George, J.; Harrell, W. Metal requirements of *Legionella pneumophila*. *J. Clin. Microbiol.* **1981**, *13*, 688–695. [PubMed]
59. Rogers, J.; Dowsett, A.; Dennis, P.; Lee, J.; Keevil, C. Influence of plumbing materials on biofilm formation and growth of *Legionella pneumophila* in potable water systems. *Appl. Environ. Microbiol.* **1994**, *60*, 1842–1851. [PubMed]

© 2017 by the authors. Licensee MDPI, Basel, Switzerland. This article is an open access article distributed under the terms and conditions of the Creative Commons Attribution (CC BY) license (http://creativecommons.org/licenses/by/4.0/).

Table S1. Locations, dates, water temperatures and water sources of sediment samples

Locations	Date of sampling	Temperature (°C)	Source of water
AL1	6/23/2012	28.9	surface
AL2	6/5/2013	26.7	ground
AR	10/15/2012	17.2	surface
AZ1	11/6/2012	23.9	ground
AZ2	1/14~1/18/2014	12.2	ground
AZ3	1/15/2014	11.7	ground
CA1	3/15/2013	17.8	surface
CA2	3/15/2013	17.8	surface
CA3	1/21/2014	11.1	surface
IL	9/23/2013	15.6	surface
NC	11/9/2012	8.3	ground
NJ1	4/25/2014	15.5	ground
NJ2	4/14/2014	20.2	ground
OH1	9/25/2012	10.6	ground
OH2	9/26/2012	10.6	surface
PA1	6/26/2012	16.1	ground
PA2	1/15/2014	5.6	ground
TN	12/12/2012	2.2	ground

Table S2. Sediment parameters across seven sampling sites

Tank Location	Particle Size			pH	Total Exchange Capacity (ME/100g)	TOC (%)	Organic Matter (%)	Source water
	% Clay	% Silt	% Sand					
TN	0.4	1.06	98.54	8.2	3	0.42	0.43	ground
NC	7.63	23.39	68.98	7.6	110.8	3.11	5.45	ground
OH1	1.36	6.7	91.94	7.1	26.7	0.25	0.89	ground
AL1	2.73	2.33	94.94	7.8	12.2	0.42	0.88	surface
AR	3.91	14.44	81.65	6.7	12.17	2.78	11.45	surface
OH2	1.68	21.67	76.65	6.6	57.34	2.09	5.9	surface
AZ1	7.35	34.34	58.31	6.7	154.14	9.42	4.08	ground

Table S3. Screening analyses and methods performed on sediment samples

Test parameter	Method
Total organic carbon	Automated instrumental analysis of carbon and nitrogen in plant and soil samples (1) (Comparable to EPA Method 9060A) (2).
Total organic matter	Estimation of soil organic matter by weight, loss on ignition (3) (Comparable to EPA Method 160.4 (4).
Particle size analysis (sand, silt, and clay)	ASTM D422 (5) (sieve/hydrometer)
pH	EPA Method 9045C rev 3 (6)
Total exchange capacity	U.S. EPA, EPA Method 9080, Cation Exchange Capacity in Soils, Rev. 0, 1986 (7).

References

1. McGeehan, S.L., and D.V. Naylor. 1988. Automated instrumental analysis of carbon and nitrogen in plant and soil samples. Commun. Soil Sci. Plant Anal. 19:493-505.
2. U.S. EPA, EPA Method 9060A, Total Organic Carbon, Rev. 1, November 2004.
3. Schulte, E.E., and B.G. Hopkins. 1996. Estimation of soil organic matter by weight Loss-On-Ignition. P. 21-32; in: Soil Organic Matter: Analysis and interpretation. (ed.) F.R. Magdoff, M.A. Tabatabai, and E.A. Hanlon, Jr. Special publication No. 46. Soil Sci. Soc. Am. Madison, WI.
4. U.S. EPA, EPA Method 160.4, Volatile Residue, Rev. 1, 1971 in *Methods for Chemical Analysis of Water and Wastes*, EPA/600/4-79/020, March 1983.
5. ASTM Standard D422, 1998, "Standard Test Method for Particle-Size Analysis of Soils," ASTM International, West Conshohocken, PA, www.astm.org.
6. U.S. EPA, EPA Method 9045C, pH in Liquid and Soils, Rev. 1, 2000.
7. U.S. EPA, EPA Method 9080, Cation Exchange Capacity in Soils, Rev. 0, 1986. 8.

Table S4. Oligonucleotide taqMan qPCR primer sequences used to screen pathogens and human-fecal indicator *Bacteroidetes* and PCR primer sequences for clone sequencing

Target	Oligo name	Sequences (5'-3')	Tm (°C)	Detection limit (CE per reaction)	Reference
Human-specific HF183 *Bacteroidales* (qPCR)	HF183F	ATCATGAGTTCACATGTCCG	60	2	Bernhard and Field (2000)
	BthetP1	FAM-CTGAGAGGAAGGTCCCCCACATTGGA-TAMRA			Shanks et al. (2008)
	BthetR1	CGTAGGAGTTTGGACCGTGT			Converse et al. (2009)
Campylobacter spp. (qPCR)	CampF2	CACGTGCTACAATGGCATAT	58	1	Lund et al. 2004
	CampR2	GGCTTCATGCTCTCGAGTT			
	CampP2	FAM-CAGAGAACAATCCGAACTGGGACA-TAMRA			
Campylobacter spp. (PCR)	CampF	GGA TGA CAC TTT TCG GAG C	60	2	Linton, 1996
	CampR	CAT TGT AGC ACG TGT GTC			
Legionella spp. (qPCR)	Leg F1c	TAGTGGAATTTCCGGTGTA	50	2	This study
	Leg R1c	CCAACAGCTAGTTGACATC			
	Leg-probe	6Fam-CGGCTACCTGGCCTAATACTGA-Tamra			
Legionella spp. (PCR)	LegF	GATTAGCCTGCGTCCGATTAG	64	2	This study
	LegR1	GAAATTCCACTACCCTCTCCCA			
	LegR3	AGTGTCAGTATTAGGCCAGGTAGC			
L. pneumophila (qPCR)	mipF1a	AGGATAAGTTGTCTTATAGCA	60	2	This study
	mipR1	TTAAGAACGTCTTTCA TTTG			
	mipProbe	6FAM-TAATCCGGAAGCAATGGCTAA-Tamra			
L. pneumophila (CYBR-Green qPCR)	*rpsL*f	GAAAGCCTCGTGTGGACGTA	64	2	Lu, et al. 2013
	*rpsL*r	CAACCTTACGCATAGC TGAGTTA			
L. pneumophila (CYBR-Green qPCR)	rtxAf	ATTGCGCCTGGCAAACTTTAGGTG	64	2	Lu, et al. 2013
	rtxAr	GGCGCAAATCGTTTCCACCTTGTA			
L. pneumophila (CYBR-Green qPCR)	sidFf	ATTGTTCGCGAGGGTATGAAAGC G	64	2	Lu, et al. 2013
	sidFr	TCTTTCCAAGACAGACTCTCGCGT			
L. pneumophila (CYBR-Green qPCR)	cegC1-F	TGCCTAAACGGTATGACCGCATCA	64	2	Faucher et al. 2011
	cegC1-R	GGCATATGCACCAAAC CACCGAAT			
L. pneumophila (qPCR)	P65f	CAAAGGGCGTTACAGT CAAACC	60	2	Lp-lg1,75bp, 60C, Mérault 2011
	P66r	CAAACACCCCAACCGT AATCA			

	sg1-pb	FAM-TCTTGGGATTGGGTTGGGTTATTTTAACTCCT-BHQ			
Salmonella spp. (qPCR)	invA_176F	CAACGTTTCCTGCGGTACTGT	60	4	Gonzalez-Escalona, N., et al. 2009
	invA-Tx_208	FAM-CTCTTTCGTCTGGCATTATCGATCAGTACCA-TAMRA			
	invA_291R	CCCGAACGTGGCGATAATT			
Mycobacterium spp. (ID)	T-39	GCGAACGGGTGAGTAACACG	50		Talaat et al. (1997).
	T-13	TGCACACAGGCCACAAGGGA			
Mycobacterium spp. (qPCR)	23Smyco F	GGG GTGTGGTGTTTGAG	62	1	Bruijnesteijn van Coppenraet, 2004
	23Smyco R	CTCCCACGTCCTTCATC			
	23Smyco Probe	6-carboxyfluorescein-TGGATAGTGGTTGCGAGCATC-BHQ1			
Acanthamoeba spp. (qPCR)	TaqAcF1	CGACCAGCGATTAGGAGACG	60	2	Riviere et al. 2006
	TaqAcR1	CCGACGCCAAGGACGAC			
	TaqAcP1	FAM-TGAATACAAAACACCACCATCGGCGC-TAMRA			
Vermamoeba vermiformis (qPCR)	Hv1227F	TTA CGA GGT CAG GAC ACT GT	56	2	Kuiper et al. 2006
	Hv1728R	GAC CAT CCG GAG TTC TCG			
Acanthamoeba spp. (PCR)	JDP1	GGCCCAGATCGTTTACCGTGA A	60	2	Schroeder et al. 2001
	JDP2	TCTCACAAGCTGCTAGGGAGTCA			
Cryptosporidium spp. (qPCR)	CRU18Sf	GAG GTA GTG ACA AGA AAT AAC AAT ACA GG	60	2	Hadfield et al 2011
	r	CTG CTT TAA GCA CTC TAA TTT TCT CAA AG			
	P	6FAM-TAC GAG CTT TTT AAC TGC AAC AA-BHQ			
	JVA18S f	ATG ACG GGT AAC GGG GAA T	60	2	Hill et al. 2007
	r	CCA ATT ACA AAA CCA AAA AGT CC			
	p	CGC GCC TGC TGC CTT CCT TAG ATG			
Giardia spp. qPCR	β-Giardin P241 F	CATCCGCGAGGAGGTCAA	60	2	Guy, 2003
	R	GCAGCCATGGTGTCGATCT			
	P	FAM/AAGTCCGCCGACAACATGTACCTAACGA/BHQ-1			
Naegleria fowleri	NaegIF192	GTG CTG AAA CCT AGC TAT TGT AAC TCA GT	63	1	Qvarnstrom et al. 2006
	NaegIR344	CAC TAG AAA AAG CAA ACC TGA AAG G			
	NfowlP	HEX-AT AGC AAT ATA TTC AGG GGA GCT GGG C-BHQ1			

References

Bernhard A.E. and Field, K.G. (2000) A PCR assay to discriminate human and ruminant feces on the basis of host differences in *Bacteroides-Prevotella* genes encoding 16S rRNA. *Appl Environ Microbiol* **66**:4571–4574. http: //dx.doi.org/10.1128/AEM.66.10.4571-4574.2000.

Converse, R.R., Blackwood, A.D., Kirs, M., Griffith, J.F. and Noble, R.T. (2009) Rapid QPCR-based assay for fecal Bacteroides spp. as a tool for assessing fecal contamination in recreational waters. *Water Res* **43**, 4828–4837.

Lu, J., Struewing, I., Buse, H.Y., Kou, J., Shuman, H.A., Faucher, S.P. and Ashbolt, N.J. (2013) *Legionella pneumophila* transcriptional response following exposure to CuO nanoparticles. *Appl Environ Microbiol* **79**: 2713-2720.

Gonzalez-Escalona N., et al. (2009) Detection of live Salmonella sp. cells in produce by a TaqMan-based quantitative reverse transcriptase real-time PCR targeting invA mRNA. *Appl Environ Microbiol* **75**:3714–3720.

Talaat, A.M., Reimschuessel, R. and Trucksis, M. (1997) Identification of mycobacteria infecting fish to the species level using polymerase chain reaction and restriction enzyme analysis. *Vet Microbiol* **58**:229-37.

Bruijnesteijn van Coppenraet, E.S., Lindeboom, J.A., Prins, J.M., Peeters, M.F.,E. Claas, C.J. and Kuijper, E.J. (2004) Real-time PCR assay using fine-needle aspirates and tissue biopsy specimens for rapid diagnosis of mycobacterial lymphadenitis in children. *J Clin Microbiol* **42**:2644

Riviere, D., Szczebara, F.M., Berjeaud, J.M., Frere, J. and Hechard, Y. (2006) Development of a real-time PCR assay for quantification of Acanthamoeba trophozoites and cysts. J *Microbiol Methods* **64**, 78–83.

Schroeder, J.M., Booton, G.C., Hay, J., Niszl, I.A., Seal, D.V., Markus, M.B.,Fuerst, P.A. and Byers, T.J. (2001) Use of subgenic 18S ribosomal DNA PCR and sequencing for genes and genotype identification of acanthamoebae from human with keratitis and sewage sludge. *J Clin Microbiol* **39***:*1903–1911.

Hadfield, S.J., Robinson, G, Elwin, K., Chalmers, R.M. (2011) Detection and differentiation of *Cryptosporidium* spp. in human clinical samples by use of realtime PCR. *J Clin Microbiol* **49**: 918–924.

Hill, V.R., Kahler, A.M., Jothikumar, N., Johnson, T.B., Hahn, D., et al. (2007) Multistate evaluation of an ultrafiltration-based procedure for simultaneous recovery of enteric microbes in 100-liter tap water samples. *Appl Environ Microbiol* **73**: 4218–4225.

Qvarnstrom, Y., Visvesvara, G.S., Sriram, R. and da Silva, A. J. (2006). Multiplex real-time PCR assay for simultaneous detection of *Acanthamoeba* spp., *Balamuthia mandrillaris*, and *Naegleria fowleri*. *J Clin Microbiol* **44**, 3589-3595.

Table S5. *Legionella* strains used to test PCR coverage

Name	ATCC #	Designation	Source	Assay (F2/R1)
Legionella cincinnatiensis	43753	72-OH-0	human lung tissue, Cincinnati, OH	+
Legionella dumoffii	33279	NY23	Cooling tower, New York	+
Legionella feeleii	35849	91-WI-H,	human lung tissue, Wisconsin	+
Legionella gormanii	33297	LS-13 [ALLO3],	soil from creek bank, Atlanta, GA	+
Legionella hackeliae	35250	Lansing 2	human bronchial biopsy, Ann Arbor, MI	+
Legionella jamestowniensis	35298	JA-26-G1-E2	wet soil, Jamestown, NY	+
Legionella longbeacheae	33462	Long Beach 4	human lung	+
Legionella maceachernii	35300	PX-1-G2-E2	water in home evaporator cooler, Phoenix, AZ	+
L. micdadei [*Tatlockia micdadei*]	33218	TATLOCK	blood-human (human blood via yolk sac)	+
Legionella oakridgensis	33761	Oak Ridge 10	industrial cooling tower water, PA	+
Legionella quinlivanii	43830	1442-AUS-E	water in bus air conditioner, Austrailia	+
Legionella rubrilucens	35304	WA-270A-C2	tap water, Los Angeles, CA	+
Legionella sainthelensis	35248	MSH-4	spring water, Mt. St. Helens, WA	+

Legionella wadsworthii	33877	Wadsworth 81-716A	sputum, South Carolina Dept of Health and Environmental Control	+
L. pneumophila strain Lp02		n/a		+
L. pneumophila subsp. *pneumophila* strain Philadelphia-1	33152		human lung	+
L. pneumophila subsp. *pneumophila* strain Bloomington-2	33155		creek water	+
L. pneumophila subsp. *fraseri* strain Dallas 1E	33216		cooling tower	+
L. pneumophila; subsp. *pneumophila* strain Chicago 2	33215		human lung biopsy	+

Table S6 Bacterial strains used to check the specificity of the PCR and qPCR assays for *Legionella*

Strains	Source	Strains	Source
Acinetobacter baumannii	ATCC 19606	*Micrococcus luteus*	ATCC 10240
Aeromonas hydrophila	ATCC 7966T	*Proteus mirabilis*	ATCC 12453
Aeromonas hydrophila	ATCC 7966	*Proteus vulgaris*	ATCC 29905
Aeromonas cavae	ATCC 15468	*Pseudomonas aeruginosa*	ATCC 10145
Bacillus cereus	ATCC 10876	*Salmonella enteriditis*	ATCC 13076
Burkholderia cepacia	ATCC 25416	*Serratia marcescens*	ATCC 14756
Burkholderia cepacia	ATCC 25416	*Serratia marcescens*	ATCC 13880
Campylobacter jejuni	ATCC 29428	*Shewanella putrefaciens*	ATCC 49138
Citrobacter freundii	ATCC 4391	*Shigella sonnei*	ATCC 25931
Citrobacter freundii	ATCC 8090	*Shigella sonnei*	ATCC 9290
Enterobacter aerogenes	ATCC 13048	*Staphylococcus aureus*	ATCC 25923
Enterobacter aerogenes	ATCC 13048	*Staphylococcus aureus*	ATCC 25923
Enterobacter cloacae	ATCC 13047	*Streptococcus pyogenes*	ATCC 19615
Enterococcus faecalis	ATCC 29302	*Yersinia enterocolitica*	ATCC 23715
Enterococcus faecalis	ATCC 19433	*Escherichia coli*	EPA isolate 8
Enterococcus faecium	ATCC 19434	*E. coli*	EPA isolate AD#1
Lactobacillus acidophilus	ATCC 314	*E. coli*	EPA isolate 58
Klebsiella oxytoca	ATCC 13182	*E. coli*	EPA isolate 59
Klebsiella pneumoniae	ATCC 13882	*E. coli*	EPA isolate 62
Klebsiella pneumoniae	ATCC 31488	*Legionella pneumophila* strain Lp02	33152
Listeria monocytogenes	Scott O2	*L. pneumophila* subsp. *pneumophila* strain Philadelphia-1	

Table S7. Total clone numbers, unique OTUs and dominant sequences in those sediments showing positive for *Legionella* spp.

Site	Total clone	OTU#	Dominant	%
AL1	67	6	*L impletisoli* str OA1 1 (AB233209)	22
			unknown	72
AZ1	23	7	*L impletisoli* str OA1 1 (AB233209)	30
			unknown	26
AZ2	24	4	*L impletisoli* str OA1 1 (AB233209)	29
			L adelaidensis (Z49716)	21
			unknown	17
IL	58	16	unknown	93
NC	25	12	unknown	64
NJ1	62	36	*L pneumophila* subsp *pneumophila* str Philadelphi	2
			L anisa strain	31
			L rubrilucens	42
NJ2	36	9	*L rubrilucens*	64
			L brunensis	11
OH2	17	13	*L impletisoli*	18
			L cincinnatiensis	12
			L brunensis	18
PA2	9	6	*S. lyticum*	89
TN	15	6	*L pneumophila* subsp *pneumophila* str Philadelphi	100

Table S1. Oligonucleotide taqMan qPCR primer sequences used to screen pathogens and human-fecal indicator *Bacteroidetes* and PCR primer sequences for clone sequencing

Target	Oligo name	Sequences (5'-3')	Tm (℃)	Detection limit (CE per reaction)	Reference
Legionella spp. (qPCR)	Leg F1c	TAGTGGAATTTCCGGTGTA	50	2	This study
	Leg R1c	CCAACAGCTAGTTGACATC			
	Leg-probe	6Fam-CGGCTACCTGGCCTAATACTGA-Tamra			
L. pneumophila (qPCR)	mipF1a	AGGATAAGTTGTCTTATAGCA	60	2	This study
	mipR1	TTAAGAACGTCTTTCA TTTG			
	mipProbe	6FAM-TAATCCGGAAGCAATGGCTAA-Tamra			
L. pneumophila (CYBR-Green qPCR)	rtxAf	ATTGCGCCTGGCAAACTTTAGGTG	64	2	Lu, et al. 2013
	rtxAr	GGCGCAAATCGTTTCCACCTTGTA			
L. pneumophila (CYBR-Green qPCR)	sidFf	ATTGTTCGCGAGGGTATGAAAGC G	64	2	Lu, et al. 2013
	sidFr	TCTTTCCAAGACAGACTCTCGCGT			
Mycobacterium spp. (qPCR)	23Smyco F	GGG GTGTGGTGTTTGAG	62	1	Bruijnesteijn van Coppenraet, 2004
	23Smyco R	CTCCCACGTCCTTCATC			
	23Smyco Probe	6-carboxyfluorescein-TGGATAGTGGTTGCGAGCATC-BHQ1			
Acanthamoeba spp. (qPCR)	TaqAcF1	CGACCAGCGATTAGGAGACG	60	2	Riviere et al. 2006
	TaqAcR1	CCGACGCCAAGGACGAC			
	TaqAcP1	FAM-TGAATACAAAACACCACCATCGGC GC-TAMRA			
Vermamoeba vermiformis (qPCR)	Hv1227F	TTA CGA GGT CAG GAC ACT GT	56	2	Kuiper et al. 2006
	Hv1728R	GAC CAT CCG GAG TTC TCG			

Table S2. Element compositions of storage tank sediments

Common Element	Occurrence	Average	Standard Deviation	Minimum Result	Median Result	Maximum Result
Al (wt%)	87.5%	3.35	3.26	0.01	2.00	10.43
Ca (wt%)	87.5%	3.17	2.39	0.59	2.05	6.50
Cl (wt%)	25%	0.96	0.04	0.93	0.96	0.98
Fe (wt%)	100%	15.96	15.52	1.36	13.31	49.98
K (wt%)	25%	0.77	0.16	0.65	0.77	0.88
Mg (wt%)	37.5%	0.61	0.08	0.54	0.65	0.65
Mn (wt%)	37.5%	3.63	1.84	1.62	4.04	5.22
Na (wt%)	62.5%	2.13	1.30	0.96	1.65	4.05
O (wt%)	100%	24.09	4.83	17.72	23.89	33.39
Si (wt%)	100%	7.07	5.94	2.13	5.21	20.60
Zn (wt%)	75%	18.71	14.91	3.01	17.53	41.54

Table S3. Element components in sediments of different locations

Sample	Coefficient of Uniformity	Coefficient of Curvature	Bulk Density	Particle Density	Porosity	Al (wt%)	Ca (wt%)	Cl (wt%)	Fe (wt%)	K (wt%)	Mg (wt%)	Mn (wt%)	Na (wt%)	O (wt%)	Si (wt%)	Zn (wt%)
D39	3.35	0.64	0.54	2.68	0.80	2.26	2.05		19.93					23.47	5.42	19.35
D40	4.33	0.57	0.51	3.58	0.86	2.31	4.33		19.54		0.65			22.86	5	15.71
D41	5.75	0.46	0.75	2.26	0.67	1.17	5.93		1.36					17.72	2.13	41.54
D42	4.37	0.61	0.70	1.39	0.50	1.74	6.5		3.72		0.65		1.65	18.92	3.93	29.03
D43	2.53	0.81				4.12	1.42	0.98	17.53	0.65	0.52	4.04	2.84	24.30	7.94	0.41
D50	5.56	1.33	1.02	1.22	0.17		0.59		49.98				1.13	26.44	2.71	3.62
D53	9.39	0.46	0.45	1.17	0.62	1.45	1.4	0.93	6.56			5.22	4.05	33.39	20.6	3.01
D54	2.93	0.74	0.83	1.24	0.33	10.43			9.08	0.88		1.62	5.96	25.58	8.86	0.03

Table S4. major bacterial compositions with the relative abundance of OTUs > 1% in any samples at 97% similarity level)

Sample Name	1st abundant	Percentage	2nd abundant	Percentage	Correlation (R^2)
D39 Water	Unclassified Comamonadaceae	73.7	Unclassified Sphingomonadaceae	6.3	0.69
D39 Sediment	Unclassified Sphingomonadaceae	23.1	Unclassified Comamonadaceae	20.8	
D40 Water	Unclassified Comamonadaceae	23.7	Reyranella massiliensis	6.4	0.47
D40 Sediment	Unclassified Syntrophobacteraceae	12.2	Unclassified Solibacterales	7.7	
D41 Water	Pseudomonas veronii	34.2	Unclassified Comamonadaceae	16.0	0.88
D41 Sediment	Pseudomonas veronii	49.4	Unclassified Massilia	17.4	
D42 Water	Pseudomonas veronii	46.5	Unclassified Massilia	14.9	0.98
D42 Sediment	Pseudomonas veronii	37.7	Unclassified Massilia	7.7	
D43 Water	Unclassified Pseudomonas	21.5	Unclassified MLE1-12	10.1	n/a
D43 Sediment	n/a				
D50 Water	Unclassified Novosphingobium	26.1	Unclassified Comamonadaceae	6.4	0.38
D50 Sediment	Unclassified Geothrix	18.0	Unclassified Sulfuritalea	17.4	
D51 Water	Unclassified Acinetobacter	49.6	Unclassified Pseudomonadaceae	7.0	
D51 Sediment	Sphingomonas wittichii	38.0	Unclassified Comamonadaceae	18.3	
D53 Water	Blastomonas natatoria	26.5	Unclassified Acinetobacter	11.9	0.11
D53 Sediment	unclassified PK29	9.2	unclassified s-70	8.6	
D54 Water	Unclassified Pseudomonas	48.9	Unclassified Comamonadaceae	6.8	0.07
D54 Sediment	Unclassified Nitrospira	15.7	Unclassified Gemm-1	13.1	
D55 Water	Nevskia ramosa	93.4	Unclassified Sphingomonadaceae	2.0	
D55 Sediment	Unclassified Sphingomonadaceae	42.1	Unclassified Comamonadaceae	24.2	
D56 Water	Unclassfied Enterobacteriaceae	17.2	Unclassified Pseudomonas	6.3	
D56 Sediment	Sphingomonas asaccharolytica	15.8	Dongia mobilis	8.1	
D60 Sediment	Unclassified Novosphingobium	33.0	Peredibacter starrii	19.9	

Lu, Jingrang

From: Ricardo Y. Tsukamoto <bioconsu@uol.com.br>
Sent: Wednesday, January 18, 2017 11:06 AM
To: Lu, Jingrang
Subject: Re: Reprint request to Dr. Lu Jingrang

WOW ! That was fast !

Thank you Dr. Lu for so promptly sending the requested article !

Best regards,
Ricardo

Em 18/01/2017 13:38, Lu, Jingrang escreveu:

> **From:** Ricardo Y. Tsukamoto [mailto:bioconsu@uol.com.br]
> **Sent:** Wednesday, January 18, 2017 10:29 AM
> **To:** Lu, Jingrang <Lu.Jingrang@epa.gov>
> **Subject:** Reprint request to Dr. Lu Jingrang
> **Importance:** High
>
> Dear Dr. Lu Jingrang,
>
> I would greatly appreciate to receive a reprint of your article:
>
> Lu, J.; Struewing, I. & Yelton, S.. 2015.
>
> Molecular survey of occurrence and quantity of *Legionella* spp., *Mycobacterium* spp., *Pseudomonas aeruginosa* and amoeba hosts in municipal drinking water storage tank sediments.
>
> *Journal of Applied Microbiology, 119*(1): 1365-2672.
>
> The reprint could be in any format - digital or in paper.
>
> Thanking for your kind cooperation,
>
> Sincerely Yours,
> Ricardo Y. Tsukamoto, Ph.D.
> Researcher
> Fisheries Institute
>
> Mail Adress:
> Rua Jose Freitas Guimarães, 37
> 01237-010 - Sao Paulo - SP
> BRAZIL

Email: bioconsu@uol.com.br
Phone: +55 11 3864-2536

Lu, Jingrang

From: Ken Mercer <kmercer@awwa.org>
Sent: Thursday, September 19, 2019 1:26 PM
To: Lu, Jingrang
Subject: RE: WQTC18 Presentation to JAWWA Paper? Microbial Community Structures and their Associations with Elements in Storage Tank Sediments

Hello Dr. Lu,

I'm circling back on the potential JAWWA article on storage tank microbial communities we'd discussed earlier this summer. Let me know if this is still on your radar either way, and if you're running into any road blocks, let me know if there's anything I can do to help.

Much obliged and hope this finds you well – Ken

Kenneth Mercer, Ph.D.
Editor-in-Chief, *AWWA Water Science* & *Journal AWWA*
American Water Works Association
kmercer@awwa.org | Direct: 303.347.6191

From: Lu, Jingrang <Lu.Jingrang@epa.gov>
Sent: Friday, June 7, 2019 9:24 AM
To: Ken Mercer <kmercer@awwa.org>
Cc: JAWWA <JAWWA@awwa.org>
Subject: RE: WQTC18 Presentation to JAWWA Paper? Microbial Community Structures and their Associations with Elements in Storage Tank Sediments

Hi Ken,
Thank you for your message. I will get back to you soon, when I get time to work on the manuscript after a travel during July. Jingrang

---

From: Ken Mercer <kmercer@awwa.org>
Sent: Friday, June 07, 2019 11:15 AM
To: Lu, Jingrang <Lu.Jingrang@epa.gov>
Cc: JAWWA <JAWWA@awwa.org>
Subject: WQTC18 Presentation to JAWWA Paper? Microbial Community Structures and their Associations with Elements in Storage Tank Sediments

Hello Dr. Lu,

My name is Ken Mercer and I am the editor-in-Chief of Journal-AWWA. I realize that some time has passed since WQTC18 in Toronto, but I'm following up in the proceedings and was wondering if there is any potential to capture or summarize some of the insights from your presentation (Microbial Community Structures…) into an article for JAWWA. It looks like it was a nice overview of microbial communities in drinking water storage tanks, so if you could write it up as a feature article for Journal, i.e., something readily digestible by a utility manager or manufacturer, I think the whole of the water industry would find it useful and informative.

If you're interested in revising or extending your conference material (and you haven't already published it elsewhere), a good target for word count is ~3,000 words with not much more than 8 tables/figures, where longer is okay as long as

it's a compelling read. On schedule, it typically takes 4-5 months from first submission until publication, but if I got a first draft soon it will be easy to find a place to publish in late 2019. If you're game, you can email me the manuscript directly and we'll go from there; likewise, if you want any feedback on outlines or early drafts, just let me know.

Happy to answer any questions in the meantime, otherwise thanks for your consideration - Ken

Kenneth Mercer, Ph.D.
Editor-in-Chief, *AWWA Water Science* & *Journal AWWA*
American Water Works Association
kmercer@awwa.org | Direct: 303.347.6191

This communication is the property of the American Water Works Association and may contain confidential or privileged information. Unauthorized use of this communication is strictly prohibited and may be unlawful. If you have received this communication in error, please immediately notify the sender by reply email and destroy all copies of the communication and any attachments.

American Water Works Association
Dedicated to the World's Most Important Resource ®

This communication is the property of the American Water Works Association and may contain confidential or privileged information. Unauthorized use of this communication is strictly prohibited and may be unlawful. If you have received this communication in error, please immediately notify the sender by reply email and destroy all copies of the communication and any attachments.

American Water Works Association
Dedicated to the World's Most Important Resource ®

Lu, Jingrang

From: Biotechnology <manager@biocon-conference.com>
Sent: Wednesday, May 08, 2019 7:45 AM
To: Lu, Jingrang
Subject: Opportunistic Pathogens and Microbial Communities and Their Associations with Sediment Physical Parameters in Drinking Water Storage Tank Sediments

Dr. Jingrang Lu:

We are writing this mail with reference to your work on **"Opportunistic Pathogens and Microbial Communities and Their Associations with Sediment Physical Parameters in Drinking Water Storage Tank Sediments"**. The published article of your noteworthy research work brought us to your profile. We would like to know if you are interested to share your recent research with the global audience at "International Congress on Biotechnology" (Biocon-2019) during October 28-30, 2019 | Paris, France

BIOCON-2019: https://biocon-conference.com/

Note: Biocon-2019 provides a chance for registered participants to publish their full length manuscripts in Elsevier Gene Reports Journal (SCImago indexed journal). The submitted papers will be subjected to review by the guest editors.

Thanks in advance; we are always available with any queries whatsoever.

Looking forward to hearing from you.

Regards,
Nilesh Chopra
Conference Secretary
BioCon-2019 Paris, France

If you find this mail unsolicited, please click http://mailto:%20organizer@biocon-conference.com?subject=Remove or Please reply with "Not Interested" as subject line if you do not wish to receive any further emails.

Table of Contents

General_Authors_Publications.....2
LI-266688_Paper_#1_Henriquez_2019-Sci_Reports_-CLENDEX.....20
LI-266691_Paper_#2_Henriquez_et_al_Tox_Sci_Suppl_Materials_2019.....37
LI-266693_Paper_#3_Kodavanti_2019_Tox_Path_Review.....44
Paper_#2_Henriquez_et_al_Tox_Sci_Suppl_Materials_2019.....58
STAA2020-AH-SS-UK_-_Justification.....65
STAA2020-AH-SS-UK_-Justification_2B_and_2C.....69
STAA2020-AH-SS-UK_-_email_confirmation.....74

STAA REPORT FOR THE SCIENTIST NOMINATIONS

General Information:

Nomination ID/App ID:	20-127
Research Category Primary:	Health Effects Research and Human Health Risk Assessment (HE)
Research Category Secondary:	Sustainability and Innovation (SI)
Laboratory/Office Name:	ORD
Nomination Entered By:	Urmila Kodavanti

Eligibility Checklist:

[Y] The nominated publication(s) has not been submitted to a previous STAA competition.

[Y] The nominated publication(s) was published on or before January 1, 2017 and on or after January 1,2012

[Y] The principal author was an EPA employee or a PHS employee assigned to EPA when the research was performed

[Y] The EPA authors (includes PHS employees assigned to EPA) contributed collectively a minimum of 50% toward the publication(s)

Nominating Official Name:	David Diazsanchez
Nominating Official Title:	
Nominating OfficialEmail:	diaz-sanchez.david@epa.gov
STAA Coordinator Name:	Kathleen Wiser
STAA Coordinator Email:	wiser.kathi@epa.gov

Justifications:

Justification 1:

Please see attached file STAA2020-AH-SS-UK-Justification.

Justification 2A:

Relatedness of three nominated papers

These three papers including one review paper involve the role of neuroendocrine system in mediating environmental stressor effects. Two of the the three publications included in the nomination are our original research papers of interventional studies while the third paper – review - details the contribution of of neuroendocrine system in air pollution health effects and how that can be important in contributing to variations in susceptibility to environmental diseases. The first paper addressed the concern that air pollution-induced pulmonary and systemic effects can be modified/exacerbated by widely used therapeutic agents for pulmonary diseases such as asthma and chronic obstructive pulmonary disease. This was hypothesized because our previous studies showed that adrenal-derived stress hormones were necessary to mediate injury and inflammation after ozone exposure. These hormones that are increased after ozone exposure use the same receptors as those occupied by bronchodilators (b2-adrenergic) and corticosteroids (glucocorticoid) prescribed to asthmatics and chronic obstructive pulmonary disease patients. The data show the importance of adrenergic and glucocorticoid receptors and how they synergistically increase ozone-induced injury and inflammation when animals are treated at therapeutically-relevant doses of bronchodilators and steroids. The second paper shows how ozone induces changes in the brain gene expression and how it is linked to secretion of adrenal-derived hormones in the circulation that are involved in neuroendocrine response. When circulating stress hormones, which act on adrenergic and glucocorticoid receptors are removed from circulation using adrenalectomy, all ozone-induced brain effects and hormonal effects are eliminated suggesting the contribution of adrenal-derived hormones and their receptors in mediating ozone neuroendocrine and systemic effects (paper #2). The evidence of the involvement of neuroendocrine system is just emerging in mediating air pollution health effects. Since this very neuroendocrine system is also linked to neurobehavioral disorders and peripheral chronic diseases, the review paper (paper #3) explains the evidence of neuroendocrine system in mediating environmental and non-chemical stressor responses, and how any malfunction of this stress-response system may change

the susceptibility for chronic diseases. Thus, all these three nominated papers are addressing different aspects but based on the involvement of neuroendocrine system.

Justification 2B:

See attached file "STAA2020-AH-SS-UK -Previous STAA Justification 2B and 2C.

Justification 2C:

See attached file "STAA2020-AH-SS-UK -Previous STAA Justification 2B and 2C.

Justification 2D:

No

Justification 2E:

No listed authors have submitted concurrent STAA application.

Justification 3A:

Recognition of the work

(The nature of the external peer review of each of the paper below demonstrates the importance and the quality of research, reflective of recognition)

Specific notable recognitions are also listed below

1) **The first nominated paper is published in Scientific Reports** November 2019 issue, a journal of Nature Publishing group. This is a highly respected 11th most cited journal in the world, with more than 300,000 citations in 2018, and receives widespread attention in policy documents

and the media. Partnering with extensive network of expert peer reviewers, editorial team provides rigorous, objective and constructive peer review. *Scientific Reports* is led by the same ethical and editorial policy guidelines as other Nature Research journals to ensure that all the research is scientifically robust, original, and of the highest quality. As an open access journal, the work is immediately accessible and highly discoverable across a range of channels including nature.com, where the journal receives

approximately 2 million visitors per month. The journal is indexed in Web of Science, PubMed, PubMed Central, Scopus, Dimensions, Google Scholar, DOAJ and SAO/NASA ADS.

Nature of external peer review of the first nominated paper published in this journal:

Although changes in the manuscript were suggested by the external reviewers, it was apparent that the paper was received with great enthusiasm as one reviewer states, "*The results are predictable, but significant for clinical treatments*". Likewise, this is the statement from the second reviewer, "*This study is interesting and data were extensively collected. In addition, this study has focused on a subject that is both scientifically important and clinically relevant. Also, the manuscript represents a large amount of work, which is laudable*".

2) **The second nominated paper is published in *Toxicological Sciences***, the official journal of the Society of Toxicology. The mission of *Toxicological Sciences* is to publish the most influential research in the field of toxicology. *Toxicological Science's* primary focus is on original and hypothesis-driven research articles. The journal also provides expert insight via contemporary reviews, as well as forum articles and editorials that address important topics in the field. The scope of *Toxicological Sciences* is focused on a broad spectrum of impactful toxicological research that will advance the multidisciplinary field of toxicology ranging from basic research to model development and application, and decision making.

Nature of the external peer review of the second nominated paper:

This paper was also well received by three independent external reviewers selected by the journal editor which suggested minor changes. To state some of the comments from reviewers in their own words: Reviewer 1: "*This*

very-well written manuscript describes an experimental study". Second Reviewer: "*These results may have a meaningful impact on better understanding the effects related to long-term exposures to ozone as well as extra-pulmonary effects induced by ozone. Thus, this experimental study adds to the research field of health effects induced by inhaled ozone*." The third reviewer states: "*Interesting publication with minor revisions needed.*

The authors continue their research in this area building from previous, well-received, studies. This study was well-written and adequately constructed and executed."

3) **The third nominated paper is an invited review published in Toxicologic Pathology** in late 2019. Toxicologic Pathology, the official journal of the Society of Toxicologic Pathology, the British Society of Toxicological Pathology and the European Society of Toxicologic Pathology, will publish Original Research Articles, Symposium Articles, Review Articles, Meeting Reports, New Techniques, and Position Papers that are relevant to toxicologic pathology. Relevant topics include reports on safety assessment of pharmaceuticals, chemicals, food additives, pesticides, environmentally relevant chemicals, and medical devices; risk characterization of xenobiotics; investigative studies that contribute to refinement of the safety assessment process; mechanistic studies that provide a basis for interpreting and predicting toxicologic outcome; emerging approaches and methods in toxicologic pathology; spontaneous diseases that may influence toxicology studies, and animal and alternative models relevant to toxicologic pathology.

Nature of the external peer review of the third nominated paper:

This was an invited review and therefore the external peer reviewers were likely friendlier than for the other papers, however some changes were requested prior to acceptance. Here are the remarks of the external peer reviewers of the paper. First reviewer: "*This is an excellent review that covers an important aspect of air pollution and health effects research, namely the elucidation of, and mechanisms underlying, individual susceptibility to inhaled air pollutant(s) exposures. The author has covered the important, state-of-the art research in this area, especially highlighting the work from her research team at the US EPA. This review also nicely represents and extends the information presented by the author at the 2019 STP annual meeting."* The comments from the second reviewer: "*Very nice manuscript. It is clearly written and easily understood."*

Additional awards and recognition for the nominated papers:

- **SOT- Immunotoxicology Specialty Section, Best Paper Award. March 2020:** Exacerbation of ozone-induced pulmonary and systemic effects by $_2$-adrenergic and/or glucocorticoid receptor agonist/s. Sci Rep. 2019 Nov 29;9(1):17925.

Based on the subject matter and the novelty of research results in the second paper in Scientific Reports, The Society of Toxicology, Immunotoxicology Specialty section selected this paper as the best paper. This ward was planned to be presented to authors at the Annual meeting in Anaheim California during March 15-20, 2020 but this was cancelled with a presentation of award with the virtual meeting.

1) **Plenary Lecture, National Society of Toxicologic Pathology, June 9, 2019, Raleigh, NC** The author of the third nominated paper was invited invited to present a lecture on first plenary symposium session during June 2019 meeting. A number of other invited presentations were made by the senior author at different institutions and in the past couple of years emphasizing the role of neuroendocrine system in mediating pulmonary and systemic effects of air pollution.

2) **Presidential Award for Research Competition (PARC), NC SOT, 2018 and associated invited presentation:** The research involving the second nominated paper has led to a number of recognitions, including the PARC award at the 2018, NC SOT meeting, October 2018, Research Triangle Park, NC.

3) **Invitation to contribute to a review paper, STP** The author was also invited to submit a review paper which resulted in the third nominated publication.

Justification 3B:

The manuscript review process

These three papers are published in the three top level journals in the respective fields, Scientific Reports, Toxicological Sciences and Toxicologic Pathology-SAGE Journal. The purpose statements of each journal are explained in the previous section. These nominated papers followed the manuscript clearance criteria. Upon completion of writing and before submission to the journal, papers were internally reviewed by scientists from CPHEA and nearby institutions. Two scientists reviewed each of these papers in detail as a requirement for internal review. All reviewers commented on the new findings, novel data and brand new research previously not considered in the air pollution field. Suggestions were made by these reviewers and were addressed prior to submission to the journals for publication. All suggested changes were made in in all three papers prior to submission to *Scientific Reports* (paper #1), *Toxicological Sciences* (paper #2) and *Toxicologic Pathology* (paper #3, a review paper). Once submitted to the respective journals, each paper was assigned to one of the associate editors in the field and then underwent external peer review process for its value and suitability for publication by two or three external reviewers that were experts in their respective fields. While all papers were suggested to be revised by the reviewers of each paper, appropriate revisions were made. The reviews reflected the importance of the study and the value of the findings. All reviewers' questions and suggestions were addressed. After submission of the revised manuscripts, the manuscripts were promptly accepted for publication in each respective journal. Within few days after the acceptance, these papers were published first on-line and then subsequently in the print form of the journal. All three papers are published in late 2019.

AUTHORS

Contributing Author

Author Name:	Colette N Miller		
Professional Title:		Salutation:	Dr.
Email:	miller.colette@epa.gov	Organization:	
Mailing Address:			
Street Line 1:			
City:			
Zip Code:		State:	
At time of research was:	Non EPA Personnel		
Separation Date:			
% of Effort:	5		

Principal Author

Author Name:	Urmila P. Kodavanti		
Professional Title:		Salutation:	
Email:	kodavanti.urmila@epa.gov	Organization:	
Mailing Address:			
Street Line 1:	109 TW Alexander Drive		
City:	Durham		
Zip Code:	27711	State:	NC
At time of research was:	EPA Employee		
Separation Date:			
% of Effort:	35		

Contributing Author

Author Name:	Mette C Schladweiler		
Professional Title:		Salutation:	Ms.
Email:	schladweiler.mette@epa.gov	Organization:	
Mailing Address:			
Street Line 1:	109 TW Alexander Drive Mail Code: B105-02		
City:	Durham		
Zip Code:	27711	State:	North Carolina
At time of research was:	EPA Employee		
Separation Date:			
% of Effort:	10		

Contributing Author

Author Name:	Andres Henriquez		
Professional Title:		Salutation:	Dr.
Email:	henriquez.andres@epa.gov	Organization:	
Mailing Address:			
Street Line 1:			
City:			
Zip Code:		State:	
At time of research was:	Non EPA Personnel		
Separation Date:			
% of Effort:	10		

Contributing Author

Author Name:	Samantha Snow		
Professional Title:		Salutation:	Dr.
Email:	samanthajsnow@gamil.com	Organization:	
Mailing Address:			
Street Line 1:			
City:			
Zip Code:		State:	
At time of research was:	EPA Employee		
Separation Date:			
% of Effort:	10		

Contributing Author

Author Name:	Prasada Kodavanti		
Professional Title:		Salutation:	Dr.
Email:	kodavanti.prasada@epa.gov	Organization:	
Mailing Address:			
Street Line 1:			
City:			
Zip Code:		State:	
At time of research was:	EPA Employee		
Separation Date:			
% of Effort:	3		

Contributing Author

Author Name:	Janice A Dye		
Professional Title:		Salutation:	Dr.
Email:	dye.janice@epa.gov	Organization:	
Mailing Address:			
Street Line 1:			
City:			
Zip Code:		State:	
At time of research was:	EPA Employee		
Separation Date:			
% of Effort:	5		

Contributing Author

Author Name:	Allen Ledbetter		
Professional Title:		Salutation:	Mr.
Email:	hawbob23@gmail.com	Organization:	
Mailing Address:			
Street Line 1:			
City:			
Zip Code:		State:	
At time of research was:	EPA Employee		
Separation Date:	Sun Sep 30 00:00:00 GMT 2018		
% of Effort:	3		

Contributing Author

Author Name:	Judy Richards		
Professional Title:		Salutation:	Ms.
Email:	jhrichards49@gmail.com	Organization:	
Mailing Address:			
Street Line 1:			
City:			
Zip Code:		State:	
At time of research was:	EPA Employee		
Separation Date:	Mon Sep 30 00:00:00 GMT 2019		
% of Effort:	3		

Contributing Author

Author Name:	Marie McGee		
Professional Title:		Salutation:	Dr.
Email:	mmcgee0913@gmail.com	Organization:	
Mailing Address:			
Street Line 1:			
City:			
Zip Code:		State:	
At time of research was:	Non EPA Personnel		
Separation Date:			
% of Effort:	3		

Contributing Author

Author Name:	Matthew Valdez		
Professional Title:		Salutation:	Dr.
Email:	valdez.matthew@epa.gov	Organization:	
Mailing Address:			
Street Line 1:			
City:			
Zip Code:		State:	
At time of research was:	Non EPA Personnel		
Separation Date:			
% of Effort:	3		

Contributing Author

Author Name:	Anna Fisher		
Professional Title:		Salutation:	Dr.
Email:	fisher.anna@epa.gov	Organization:	
Mailing Address:			
Street Line 1:			
City:			
Zip Code:		State:	
At time of research was:	EPA Employee		
Separation Date:			
% of Effort:	3		

Contributing Author

Author Name:	Hongzu Ren		
Professional Title:		Salutation:	Mr.
Email:	ren.hongzu@epa.gov	Organization:	
Mailing Address:			
Street Line 1:			
City:			
Zip Code:		State:	
At time of research was:	EPA Employee		
Separation Date:			
% of Effort:	3		

Contributing Author

Author Name:	John House		
Professional Title:		Salutation:	Mr.
Email:	john.house@nih.gov	Organization:	
Mailing Address:			
Street Line 1:			
City:			
Zip Code:		State:	
At time of research was:	Non EPA Personnel		
Separation Date:			
% of Effort:	4		

Publication 1:

Publication Title:	Exacerbation of ozone-induced pulmonary and systemic effects by 2-adrenergic and/or glucocorticoid		
Publication Date:	Fri Nov 29 00:00:00 GMT 2019		
Journal/Publication Method:	Scientific Reports		
All Author(s):			
Volume:	9	Number:	1
Pages:	17925	Immediately Index:	Immediately Index:
Citation ½ Life:	2.6	Impact Factor:	4.011

Publication 2:

Publication Title:	Ozone-induced dysregulation of neuroendocrine axes requires adrenal-derived stress hormones		
Publication Date:	Fri Aug 09 00:00:00 GMT 2019		
Journal/Publication Method:	Toxicological Sciences		
All Author(s):			
Volume:	kfz182	Number:	1
Pages:	1-10	Immediately Index:	Immediately Index:
Citation ½ Life:	8.9	Impact Factor:	3.564

Publication 3:

Publication Title:	Susceptibility Variations in Air Pollution Health Effects: Incorporating Neuroendocrine Activation.		
Publication Date:	Sun Dec 01 00:00:00 GMT 2019		
Journal/Publication Method:	Toxicologic Pathology		
All Author(s):			
Volume:	47	Number:	8
Pages:	962-975	Immediately Index:	Immediately Index:
Citation ½ Life:	11.3	Impact Factor:	1.382

SCIENTIFIC REPORTS
nature research

OPEN

Exacerbation of ozone-induced pulmonary and systemic effects by β_2-adrenergic and/or glucocorticoid receptor agonist/s

Andres R. Henriquez[1], Samantha J. Snow[2], Mette C. Schladweiler[3], Colette N. Miller[1], Janice A. Dye[3], Allen D. Ledbetter[3], Marie M. Hargrove[1], Judy E. Richards[3] & Urmila P. Kodavanti[3]*

Agonists of β_2 adrenergic receptors (β_2AR) and glucocorticoid receptors (GR) are prescribed to treat pulmonary diseases. Since ozone effects are mediated through the activation of AR and GR, we hypothesized that the treatment of rats with relevant therapeutic doses of long acting β_2AR agonist (LABA; clenbuterol; CLEN) and/or GR agonist (dexamethasone; DEX) would exacerbate ozone-induced pulmonary and systemic changes. In the first study, male 12-week-old Wistar-Kyoto rats were injected intraperitoneally with vehicle (saline), CLEN (0.004 or 0.02 mg/kg), or DEX (0.02 or 0.1 mg/kg). Since dual therapy is commonly used, in the second study, rats received either saline or combined CLEN + DEX (each at 0.005 or 0.02 mg/kg) one day prior to and on both days of exposure (air or 0.8ppm ozone, 4 hr/day x 2-days). In air-exposed rats CLEN, DEX or CLEN + DEX did not induce lung injury or inflammation, however DEX and CLEN + DEX decreased circulating lymphocytes, spleen and thymus weights, increased free fatty acids (FFA) and produced hyperglycemia and glucose intolerance. Ozone exposure of vehicle-treated rats increased bronchoalveolar lavage fluid protein, albumin, neutrophils, IL-6 and TNF-α. Ozone decreased circulating lymphocytes, increased FFA, and induced hypeerglycemia and glucose intolerance. Drug treatment did not reverse ozone-induced ventillatory changes, however, lung effects (protein and albumin leakage, inflammation, and IL-6 increase) were exacerbated by CLEN and CLEN + DEX pre-treatment in a dose-dependent manner (CLEN > CLEN + DEX). Systemic effects induced by DEX and CLEN + DEX but not CLEN in air-exposed rats were analogous to and more pronounced than those induced by ozone. These data suggest that adverse air pollution effects might be exacerbated in people receiving LABA or LABA plus glucocorticoids.

Recently, we and others have shown that acute exposure to air pollutants, such as ozone, leads to a rapid release of stress hormones (i.e. epinephrine and cortisol/corticosterone) into the circulation through the activation of the neuroendocrine stress axes in rats[1–4] and in humans[5]. We have further shown that systemic and pulmonary injury/inflammation effects of ozone are reduced in adrenalectomized rats with diminished circulating epinephrine and corticosterone[6]. When the receptors for epinephrine (β-adrenergic receptor, βAR) and corticosterone (glucocorticoid receptor, GR) were blocked by propranolol and mifepristone, respectively, ozone-induced systemic and pulmonary effects were inhibited in an antagonist-specific manner[7]. Specifically, ozone-induced vascular leakage was inhibited by each antagonist, but pulmonary neutrophilia was prevented only by βAR antagonist while lymphopenia was prevented by GR antagonist. Furthermore, when βAR and GR were activated by treating rats with high non-therapeutic doses of combined agonists, ozone-induced lung injury and inflammation were exacerbated[8].

Agonists and antagonists of AR and GR are widely used for chronic illnesses involving cardiovascular, pulmonary and inflammatory conditions. Specifically, β_2AR and/or GR agonists are commonly prescribed as singular

[1]Oak Ridge Institute for Science and Education, U.S. Department of Energy, Oak Ridge, Tennessee, United States of America. [2]ICF, Durham, North Carolina, United States of America. [3]Public Health and Integrated Toxicology Division, Center for Public Health and Environmental Assessment, U.S. Environmental Protection Agency, Research Triangle Park, North Carolina, United States of America. *email: kodavanti.urmila@epa.gov

or dual therapies for chronic lung diseases such as asthma and COPD[9]. Activation of β_2AR, one of the many receptors of catecholamines located preferentially in the smooth muscle of the airways, induces relaxation in bronchoconstricted patients[10]. Activation of GR is associated with immunosuppression through downregulation of pro-inflammatory cytokine gene transcription, lymphocyte apoptosis, and migration of cells to/from lymphoid organs[11]. In the Salmeterol Multicenter Asthma Research Trial, death due to respiratory and asthma-related events was increased in patients taking a long acting β_2AR agonist (LABA) monotherapy[12]. However, in a more recent study, LABA monotherapy was not associated with increased asthma-related events, and asthmatic patients taking LABA + inhaled corticosteroids experienced fewer asthma exacerbations than those using corticosteroids only[13].

Given the role of AR and GR activation in acute air pollution-induced lung injury and inflammation[6–8,14], and the use of AR and GR agonists in treatment of chronic asthma and COPD, it is conceivable that patients receiving bronchodilators and/or immunosuppressants might have differential inflammatory processes induced after acute air pollutant exposures[15–18]. For instance, it was found that asthmatic children living in Detroit have worsened responses to ozone and fine particulate matter when compared to those not receiving steroids[19]. Similarly, Gent and colleagues[20] found that asthmatic children using maintenance medication were more vulnerable to ozone-induced pulmonary inflammation when compared to asthmatic children who did not receive medication. In addition, β_2AR agonists were shown to exacerbate particulate matter-induced pulmonary inflammation and injury in mice through increased production of the pro-inflammatory cytokine IL-6[21]. More recently, Ritchie and collaborators[22] demonstrated that β_2AR agonists may promote lung inflammation through activation of the cyclic adenosine monophosphate response element in epithelial cells, while producing bronchodilator effects in smooth muscle cells. These studies suggest that single and/or dual therapies might exacerbate acute pulmonary injury/inflammation induced by air pollutants through activation of AR and GR. Our recent findings indicate that when rats were treated with relatively high non-therapeutic doses of LABA and corticosteroids given together (several folds higher than the therapeutic doses used for humans when adjusted to body weight), ozone-induced lung injury and inflammation were exacerbated in rats[8]. Thus, although we established the role of combined βAR and GR activation using higher (non-therapeutic) doses in ozone-induced pulmonary and systemic effects, the purpose of the current study was to examine if ozone-induced lung injury, inflammation, lymphopenia and metabolic alterations were exacerbated in rats receiving more therapeutically relevant dosages of LABA (clenbuterol; CLEN) or the GR agonist, dexamethasone (DEX), as separate treatments. Moreover, since dual therapy involving LABA and steroids are often recommended over single therapy, and because the dosages of dual drug treatment used in prior study were in a non-therapeutic range[8], in the second study herein, we examined the interactive effects of ozone and the combination therapy of CLEN and DEX at therapeutically relevant doses.

Materials and Methods

Animals. Male Wistar-Kyoto rats (10–11 weeks of age) from Charles River Laboratory (Raleigh, NC) were pair housed in cages containing beta chip bedding in a room under controlled relative humidity (55–65%), temperature (21 °C), and dark/light cycle (12 h each). Rats were provided with water and standard Purina (5001) rat chow (Brentwood, MO) *ad libitum* unless stated. The animal facility is approved by an Association for Assessment and Accreditation of Laboratory Animal Care. Our animal protocols were approved by the U.S. Environmental Protection Agency's Institutional Animal Care and Use Committee and all methods were performed in accordance with the relevant guidelines and regulations (NHEERL LAPR #19-05-002). We previously determined that 5–10% of male Wistar Kyoto rats develop spontaneous cardiac hypertrophy[23] therefore, heart weights were recorded for all animals at necropsy. To avoid the influence of cardiac hypertrophy-related secondary pulmonary changes, those with a heart/body weight ratio above 20% of normal values were excluded from the study as we have reported in previous study[8]. This resulted in n = 6–8 for most endpoints.

Drug treatments. Experimental designs for both studies are detailed in Fig. 1. For each study, rats were randomized by body weight into their respective groups (n = 8/group). In study 1, rats were injected intraperitoneally with sterile saline (1 ml/kg; vehicle), clenbuterol hydrochloride (CLEN, Sigma-Aldrich, St Louis, MO) using a low [0.004 mg/kg] or high [0.02 mg/kg] dose, or dexamethasone sodium phosphate (DEX, Henry Schein, Dublin OH) as a low [0.02 mg/kg] or high [0.1 mg/kg] dose. In study 2, rats were injected intraperitoneally with either saline (1 ml/kg; vehicle), or CLEN followed by DEX (CLEN + DEX; within 5–10 minutes of each other) using a low (both at 0.005 mg/kg) or high (both at 0.02 mg/kg) dose. For each study, daily vehicle/drug treatment began one day before starting air or ozone exposure and continued each day of exposure for a total of 3 daily injections. The treatments occurred in the morning at ~06:30 AM followed by air or 0.8 ppm ozone exposures at ~07:00 AM (4 hr/day for two consecutive days).

Although CLEN is not currently prescribed for humans as a bronchodilator in the U.S., it is used as a performance-enhancing drug and weight loss supplement in humans[24,25]. As we have explained in previous study[8], the recommended bronchodilation dose of CLEN is 0.02–0.06 mg/day for an average 70 kg human, however up to 0.12 mg/day doses (~0.0017 mg/kg body weight) are used for inducing weight loss[26]. DEX is widely prescribed in human and veterinary clinical practices and used in research. The recommended adult dose of DEX ranges from 0.75 to 9 mg which is taken every 6–12 hr for an average 70 kg human. At this level, DEX is anti-inflammatory. However, approximately 0.15 mg/kg/day doses are recommended for adrenal insufficiency[27]. Thus, for these studies, in order to examine potential interaction with ozone, we used these drugs at near therapeutic levels as indicated in Fig. 1, that did not produce lung injury or inflammation in air-exposed animals. However, after determining the influence of the single drug treatment in study 1, we noted that both the low and high doses of DEX resulted in marked lymphopenia (immunosuppressive effect) while CLEN did not influence any of the parameters assessed. Therefore, for the combination treatment in study 2, we further lowered the DEX

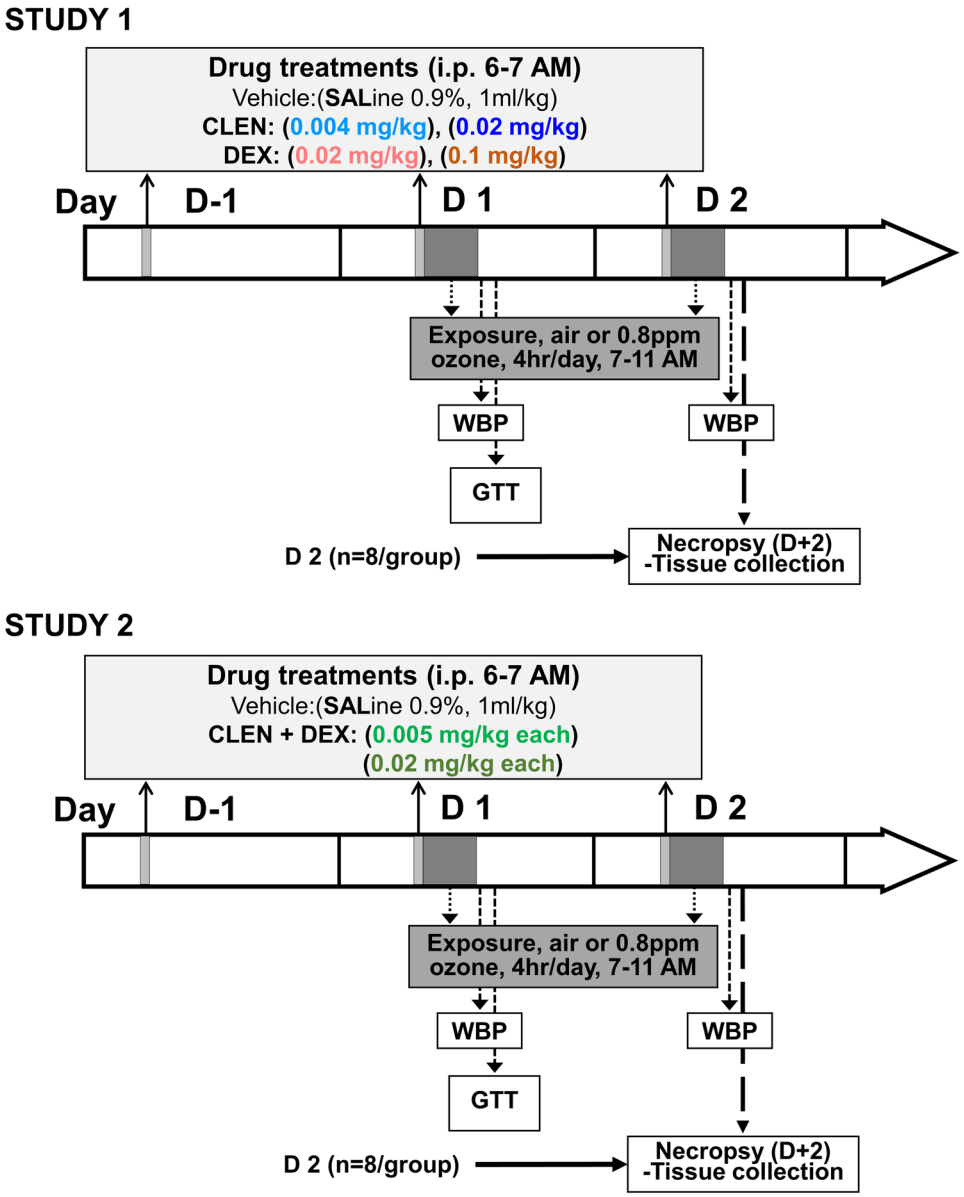

Figure 1. Schema of experimental design for study 1 and 2. The time line of drug treatments, exposures, and necropsies are indicated by arrows. Before air or ozone exposures began, rats were injected with vehicle (Saline, SAL), clenbuterol (CLEN), or dexamethasone (DEX) in study 1 and SAL or CLEN followed by DEX (CLEN + DEX) in study 2 at dose levels indicated. Injections were done in the mornings (~6–7 AM) daily starting one day prior to (D-1) and each day of exposure (D 1 and D 2). For both studies, animals were exposed to air or 0.8 ppm ozone (4 hr/day) for 2 consecutive days. Whole body plethysmography was performed within 30–45 min after each exposure day. Glucose tolerance testing was performed within 0.5–2.5 hr following first day of ozone exposure (D 1) after plethysmography, while necropsy and tissue collection were performed within 0.5–2.5 hr post second day of exposure (D 2) and plethysmography.

doses (Fig. 1). We postulated that this regimen would be appropriate for examining the susceptibility of individuals receiving singular or combinational LABA and corticosteroid therapies to air pollution effects.

Ozone exposures. Rats were exposed whole body to filtered air or 0.8 ppm ozone, 4 hr/day (~7–11 AM) for two consecutive days (Fig. 1)[8]. This concentration of ozone was higher than what may occur environmentally. However, rats have faster lung clearance mechanisms and varied lung deposition patterns compared to humans and thus are likely to require higher doses to achieve the same level of inflammatory insult[28]. Human clinical studies use 0.2 or even 0.3 ppm ozone during intermittent exercise[5]. In resting rats, the deposited ozone dose at 0.8 ppm is comparable to 0.2 ppm ozone in exercising humans[29]. Two-day exposure regimen allowed us to assess glucose tolerance immediately following day 1 exposure; and lung injury and inflammation immediately following day 2 exposure since lung effects are expected to be maximal by the second day[30]. Ozone was generated, delivered

to the chamber and monitored as previously described[8]. For study 1, the ozone chamber concentration was 0.797 ± 0.010 ppm (mean ± SD). RH was 50.1 ± 0.4 and 46.2 ± 0.4%, temperature was 72.2 ± 0.2 and 73.6 ± 0.1 °F, and air flow was 260.5 ± 0.2 and 256 ± 0.1 L/min for filtered air and ozone chambers, respectively. For study 2, ozone concentration was 0.80 ± 0.002 ppm. RH was 48.0 ± 1.1 and 45.7 ± 1%, temperature was 73.0 ± 0.1 and 73.4 ± 0.01 °F, and air flow was 253.5 ± 0.3 and 255.9 ± 0.3 L/min for filtered air and ozone chambers, respectively.

Whole Body Plethysmography. To evaluate possible drug-induced alterations in ventilation that could lead to changes in ozone dosimetry, rats were monitored using whole body plethysmography immediately after air or ozone exposure on D 1 and D 2. Rats were transported to a separate quiet room and placed in plethysmography chambers (n = 8 rats/run). They were allowed a 2 min acclimation period. Data were collected for an additional 5 min similar to our previous study[8]. In brief, spontaneous breathing parameters included (breathing frequency [*f*], tidal volume [TV], minute ventilation [MV], peak inspiratory flow [PIF], peak expiratory flow [PEF], and enhanced pause [Penh]). Penh is a composite parameter computed from the waveform of the box pressure signal during inspiration and expiration with the consideration of early and late expiration timings (Pause), and is generally indicative of labored breathing or bronchoconstriction[31]. All data were collected using EMKA iox 2 software and analyzed (SCIREQ, Montreal, Canada).

Glucose tolerance test. Since glucose intolerance is one of the common systemic responses induced by the activation of neuroendocrine system, glucose tolerance testing was performed in fasted rats immediately after plethysmography as previously described[6].

Necropsy and tissue samples collection. Rats were necropsied within 0.5–2.5 hr after the second exposure (D 2)following euthanesia using Fatal Plus (sodium pentobarbital, Virbac AH, Inc., Fort Worth, TX; >200 mg/kg, intraperitoneal). Blood samples from the abdominal aorta were collected in vacutainer serum separator tubes and EDTA tubes[8]. A complete blood count was performed on a Beckman-Coulter AcT blood analyzer (Beckman-Coulter Inc., Fullerton, California). Thymus and spleens were weighed.

The right lung was lavaged and bronchoalveolar lavage fluid (BALF) total cell counts were performed using Z1 Coulter Counter (Coulter, Inc., Miami, FL)[8]. Cytospin slides were stained and cell differentials were performed (300 cells/slide) as previously described[8]. Total protein, albumin, and *N*-acetyl-β-D-glucosaminidase (NAG) activity were measured in the cell-free BALF using a Konelab Arena 30 clinical analyzer (Thermo Chemical Lab Systems, Espoo, Finland) as described[8].

Plasma and serum analysis. Epinephrine (adrenaline) and corticosterone plasma levels were measured using kits from Rocky Mountain Diagnostics (Colorado Springs, CO) and Arbor Assays (Ann Arbor, MI), respectively. Serum free fatty acids were measured using kits from Cell Biolabs, Inc (San Diego, CA). Free fatty acids (total) protocol was adapted for use on a Konelab Arena 30 clinical analyzer (Thermo Chemical Lab Systems, Espoo, Finland).

Cytokine quantification. The concentrations of BALF cytokines (IL-6 and TNF-α) were determined using a V-plex custom rat cytokine panel (Mesoscale Discovery Inc., Rockville, MD) and following manufacturer's protocol. To increase the sensitivity for detection of cytokines, sample volume per well was increased from the recommended 50 μL to 150 μL. In BALF samples from air control animals, those with levels of TNF-α below the assay detection limit, the values were imputed using the lowest quantified value in the group to avoid issues with the statistical analysis.

Statistics. For all endpoints, each drug treatment (CLEN or DEX, study 1; or CLEN + DEX, study 2) was independently analyzed. Two-way analysis of variance (ANOVA) was used to analyze the effect of drug treatment and/or ozone exposure. The two independent variables for each study were exposure and treatment. For some endpoints, if normal distribution and homoscedasticity were not achieved, data were log transformed using Shapiro-Wilk and Levene's tests, respectively. Area under the curve estimates for glucose tolerance test were calculated using the trapezoidal method. The correction for all multiple comparisons was done using Holm-Sidak *post-hoc* test and when a p-value of ≤0.05 was achieved, the differences were considered significant. The data (mean ± SEM) depicted in graphs and tables represent n = 6–8 animals/group. GraphPad Prism 7 (version 7.04) and Statext 2.7 software were used for statistical analysis and graph generation.

Results

Ozone exposure and drug treatments did not alter body weight but reduced thymic and splenic weights, and induced lymphopenia. In study 1, body weights were not significantly changed by ozone exposure or by treatment with CLEN (Fig. 2A) or DEX (Fig. 2B). Thymic and splenic weights were assessed to characterize any immunosuppressive effects of the drug treatments or of the exposures. Ozone alone did not significantly reduce thymic and splenic weights in SAL-treated rats (Fig. 2C,D). However, the treatment with DEX but not CLEN significantly decreased thymus and spleen weights in a dose-dependent manner in both air and ozone-exposed rats when compared to SAL (Fig. 2C). Spleen weights were significantly decreased in ozone-exposed rats after high dose CLEN (Fig. 2D).

Ozone-induced lymphopenia has been reported in our previous studies[6,7]. In study 1, treatment with CLEN did not alter the number of circulating lymphocytes in air-exposed rats, however treatment with DEX at both dosages significantly depleted circulating lymphocytes in air-exposed rats (Fig. 2E). Ozone exposure also significantly depleted circulating lymphocytes in SAL and CLEN-treated rats, however, and due to the robust dose-dependent DEX effect on lymphocyte depletion, and additional ozone-induced lymphopenia in DEX-treated animals was not detactable (Fig. 2E).

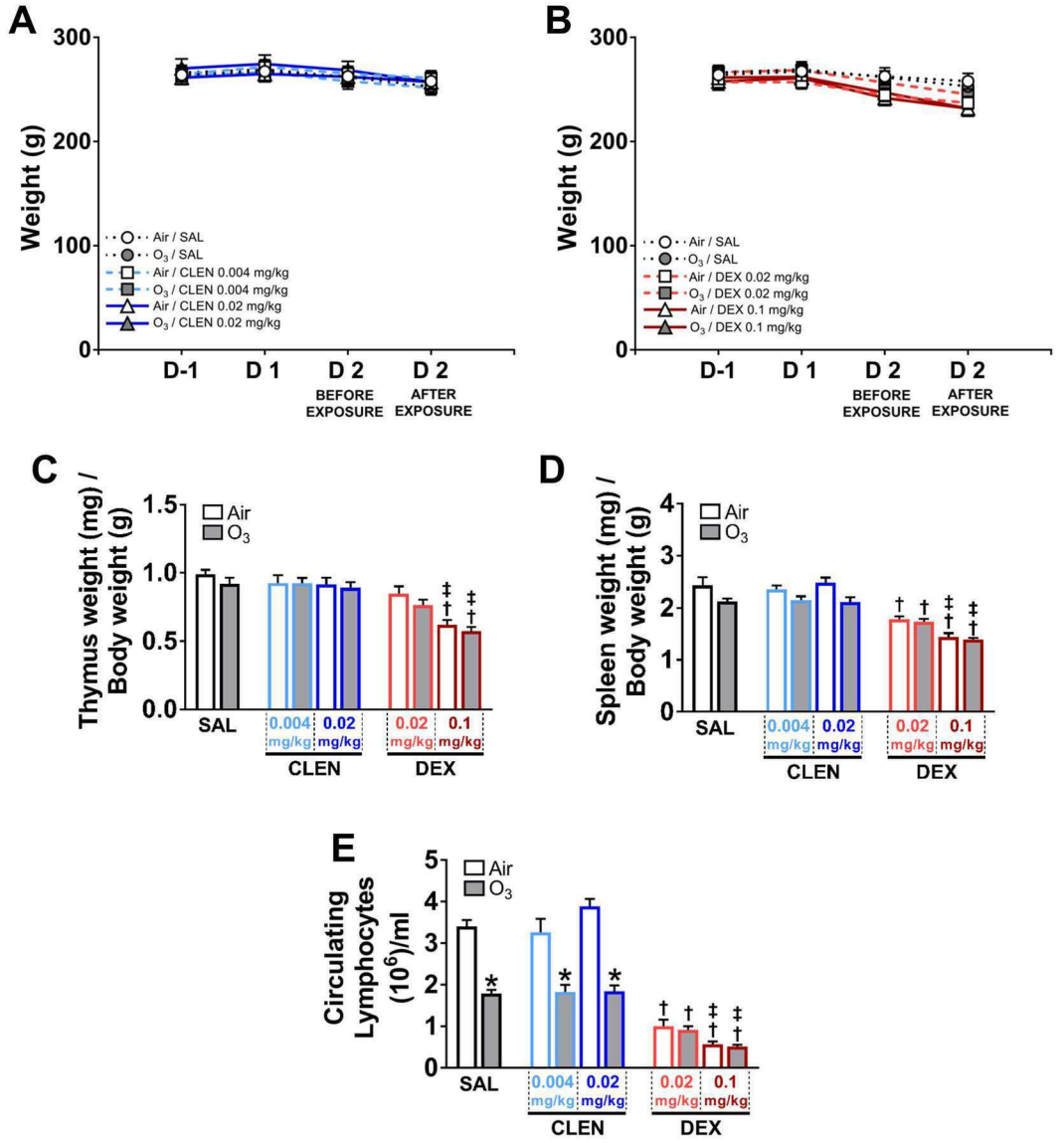

Figure 2. Ozone and/or CLEN or DEX treatments did not alter body weights, however DEX treatment reduced thymic and spleen weights, while both ozone and DEX reduced circulating lymphocytes (study 1). Body weights were assessed in rats at one day prior to (D-1), D 1, D 2 before exposure, and at D 2 immediately after exposure in CLEN (**A**) and DEX treatment groups (**B**). Thymus (**C**) and spleen (**D**) weights, and circulating lymphocytes (**E**) were assessed in rats during necropsy in all groups. Line and bar graphs show mean ± SEM of n = 6–8 animals/group. Significant differences between groups (p value ≤ 0.05) are indicated by * for ozone effect when compared to corresponding air-exposed rats, † for drug effect when compared to corresponding vehicle (SAL; saline)-treated rats, and ‡ for drug dose effect for the same exposure.

In study 2, neither the CLEN + DEX treatment nor ozone exposure significantly affected body weights (Fig. 3A). However, CLEN + DEX did decrease thymus weight in both air and ozone-exposed rats (Fig. 3B) and spleen weights in ozone-exposed rats when compared to saline-treated rats (Fig. 3C).

In study 2, treatment with CLEN + DEX at both dosages significantly depleted circulating lymphocytes in air-exposed rats (Fig. 3D). Ozone-induced depletion of circulating lymphocytes in CLEN + DEX-treated rats was not detectable at high dose due to the robust effect of this drug treatment (Fig. 3D).

Ozone-induced changes in ventilation were not reversed by concurrent drug treatments. To understand the effects of drug treatment on breathing and the potential to influence inhaled ozone dosimetry, whole body plethysmography was performed immediately after each day of air or ozone exposure. No consistent changes were observed in *f* or MV calculated in rats due to drug treatment or exposure conditions in either study (data not shown). In study 1, CLEN or DEX treatment alone did not significantly alter ventilatory parameters in air-exposed rats on D 1 or D 2 (Fig. 4). After ozone exposure, TV was not significantly changed, except for an increase in the high dose CLEN treatment group on D 2 (Fig. 4A,B). In general, ozone exposure

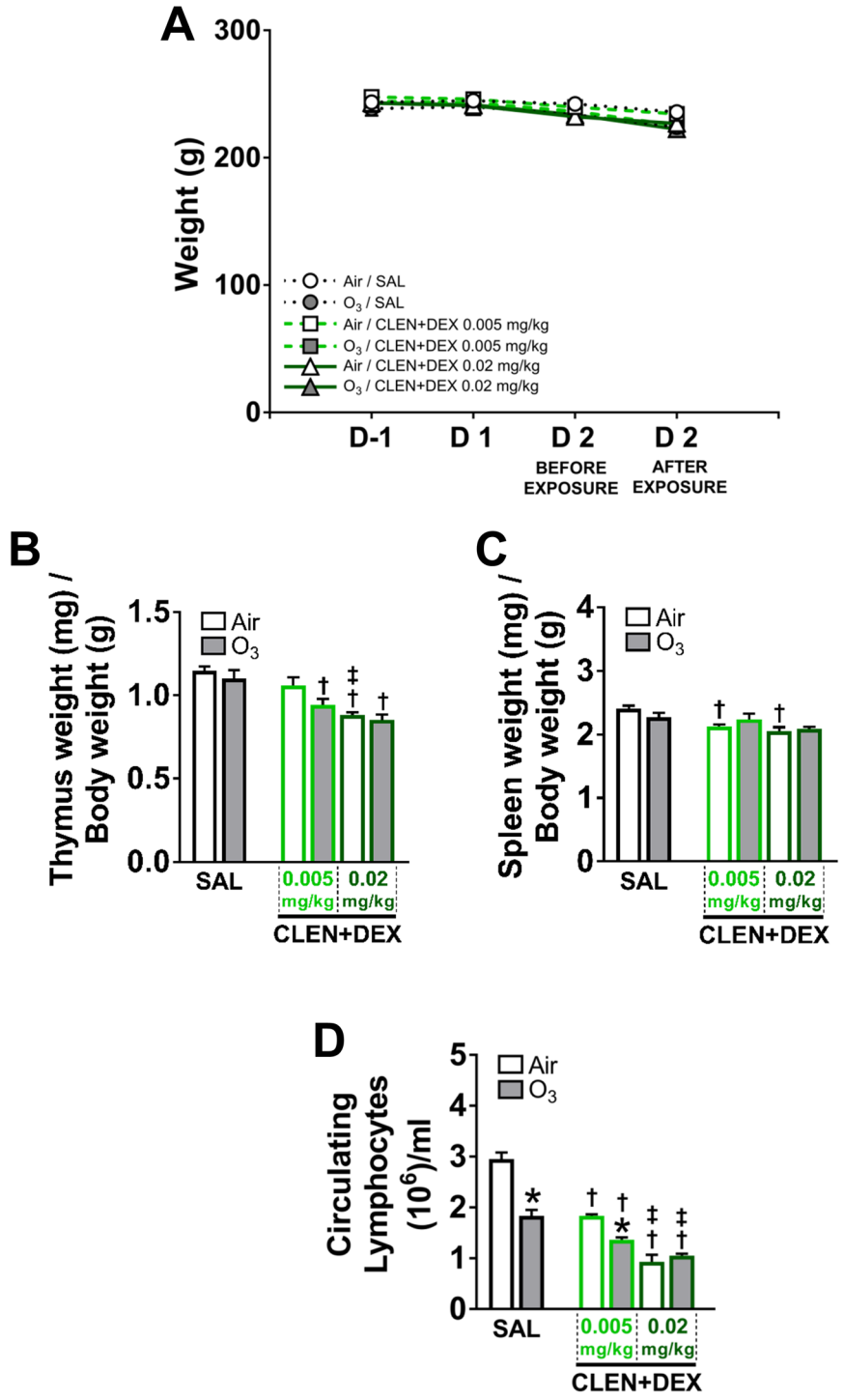

Figure 3. Ozone and/or CLEN + DEX treatments did not alter body weights; CLEN + DEX treatment reduced thymus and spleen weights, while both ozone and CLEN + DEX decreased circulating lymphocytes (study 2). Body weights (**A**) were assessed in rats at one day prior to (D-1), D 1, D 2 before exposure, and at D 2 immediately after exposure. Thymus (**B**) and spleen (**C**) weights, and circulating lymphocytes (**D**) were assessed in rats during necropsy. Bar graphs show mean ± SEM of n = 6–8 animals/group. Significant differences between groups (p value ≤ 0.05) are indicated by * for ozone effect when compared to corresponding air-exposed rats, † for drug effect when compared to corresponding vehicle (SAL; saline)-treated rats, and ‡ for drug dose effect for the same exposure.

was associated with significantly increased PIF (mainly at D 2, Fig. 4C,D), PEF and Penh (on both D 1 and D 2) (Fig. 4E,H). For a comparable breathing frequency, such changes are consistent with increased ventilatory effort. At D 2, rats receiving high dose CLEN treatment had exacerbated ozone-induced increases in both PIF and PEF

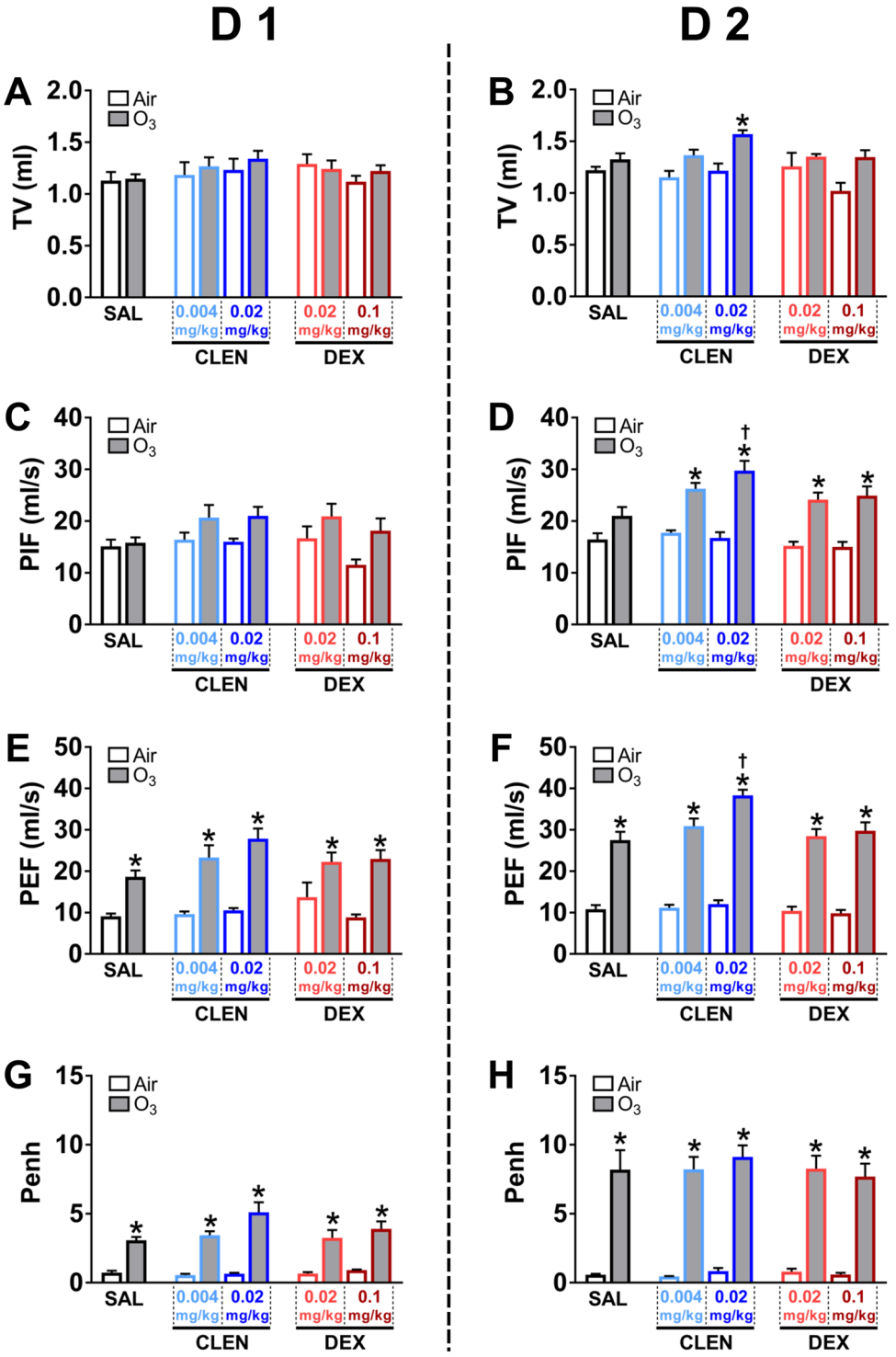

Figure 4. The influence of CLEN or DEX treatments on ozone-induced changes in ventilatory parameters (study 1). Of all ventilatory parameters assessed in rats through whole body plethysmography immediately after each day of air or ozone (0.8 ppm) exposure, the data for tidal volume (TV, **A,B**), peak inspiratory flow (PIF, **C,D**), peak expiratory flow (PEF, **E,F**), and enhanced pause (Penh, **G,H**) are shown. Bar graphs show mean ± SEM of n = 6–8 animals/group. Significant differences between groups (p value ≤ 0.05) are indicated by * for ozone effect when compared to corresponding air-exposed rats, and † for drug effect when compared to corresponding vehicle (SAL; saline)-treated rats.

(Fig. 4D,F). The magnitude of these changes was greater by D 2, consistent with worsening of respiratory distress (i.e., labored breathing and/or bronchoconstriction). The high dose CLEN group had proportionate increases in PIF and PEF which when combined with greater TV, suggests development of both expiratory effort (i.e.

bronchoconstriction) and hyperpnea (i.e., increased TV with no corresponding decrease in breathing frequency). Such changes suggest development of a combination of pulmonary edema and airflow obstruction. For study 2, similar to study 1, CLEN + DEX treatment did not influence breathing parameters in air controls. However, ozone exposure again was associated with increased PIF (on D 2; Fig. 5C,D), PEF and Penh (on both D 1 and D 2) (Fig. 5E–H). Importantly, ozone-induced changes in Penh were not reversed by CLEN + DEX treatment on D 1 or D 2 (Fig. 5G,H).

Ozone-induced lung protein leakage and inflammation were exacerbated by CLEN treatment. BALF protein and albumin were assessed to quantify pulmonary microvascular leakage, while BALF pro-inflammatory cytokines, macrophage and neutrophil count were quantified to assess pulmonary inflammation. In study 1, neither CLEN nor DEX treatment increased BALF protein or albumin leakage in air-exposed rats except for the high dose CLEN which modestly increased albumin levels. Ozone-induced increases in BALF protein and albumin were apparent in SAL-treated rats (Fig. 6A,B). CLEN, but not DEX, at the high dose exacerbated ozone-induced pulmonary protein and albumin leakage (Fig. 6A,B). CLEN or DEX treatment did not change BALF NAG activity (a marker of macrophage activation) in air-exposed rats except for a small increase in animals treated with high dose of CLEN. Ozone exposure was associated with increases in BALF NAG activity in SAL-treated rats. This ozone effect on NAG activity was not significantly affected by CLEN or DEX (Fig. 6C). Pro-inflammatory cytokines IL-6 and TNF-α were quantified in BALF to determine the degree and severity of the pulmonary inflammatory response. In air-exposed rats, only high dose CLEN treatment increased BALF IL-6 (Fig. 6D). IL-6 was increased after ozone exposure in SAL treated rats. CLEN but not DEX markedly exacerbated ozone-induced IL-6 increases in a dose-dependent manner (Fig. 6D). BALF TNF-α levels were not as consistent as IL-6 and high variability was noted in the data. Neither CLEN nor DEX treatments changed BALF TNF-α levels in air-exposed rats. TNF-α levels were slightly increased by ozone in most treatment groups; however, levels were only significantly increased in animals given high dose CLEN or low dose DEX (Fig. 6E). In air-exposed rats, there were no effects of either drug treatment on BALF macrophage numbers. BALF macrophages increased in those treated with high dose CLEN and exposed to ozone when compared to SAL (Fig. 6F). Ozone-induced pulmonary inflammation in rats was characterized by the recruitment of neutrophils to the alveolar space. CLEN or DEX did not increase neutrophils in air-exposed rats, however, ozone induced-neutrophilia was apparent in all rats. CLEN but not DEX treatment exacerbated ozone-induced neutrophilia in a dose-dependent manner (Fig. 6G).

In study 2, CLEN + DEX did not increase BALF protein and albumin leakage in air-exposed rats (Fig. 7A,B). Ozone increased BALF protein and albumin in SAL-treated rats. High dose CLEN + DEX when compared to SAL potentiated ozone-induced vascular protein and albumin leakage (Fig. 7A,B). CLEN + DEX treatments did not change BALF NAG activity in air-exposed rats but ozone exposure increased BALF NAG activity similarly in SAL and CLEN + DEX treated rats (Fig. 7C). CLEN + DEX treatment did not change BALF IL-6 in air-exposed rats (Fig. 7D). BALF IL-6 was increased after ozone exposure in SAL and CLEN + DEX-treated rats. High dose CLEN + DEX exacerbated ozone-induced IL-6 increase when compared with SAL treated-animals (Fig. 7D). BALF TNF-α did not change after CLEN + DEX treatment in air-exposed rats, however there was a small increase after ozone exposure in SAL and high dose CLEN + DEX-treated rats (Fig. 7E). BALF macrophage count was generally unaffected by CLEN + DEX or ozone exposure, except for a small decrease in air-exposed CLEN + DEX treated rats (Fig. 7F). BALF neutrophil numbers did not change by CLEN + DEX treatment in air-exposed rats however, ozone-induced neutrophilia was evident in all groups. Although not significant, the neutrophil count was higher in high dose CLEN + DEX-treated animals exposed to ozone when compared to SAL-treated air-exposed rats (Fig. 7G).

Ozone-induced metabolic changes were exacerbated by DEX and CLEN + DEX treatments. Our prior studies have shown that acute ozone exposure induces neuroendocrine stress-mediated systemic metabolic alterations[1,3], and therefore, we examined the interactive influence of stress hormone receptor agonists CLEN and DEX on ozone-induced changes in glucose metabolism. Glucose tolerance testing was performed in air- and ozone-exposed rats to determine the modifying effects of CLEN (Fig. 8A) or DEX (Fig. 8B) in study 1 and CLEN + DEX (Fig. 9A) in study 2.

In study 1, DEX but not CLEN treatment produced hyperglycemia (baseline glucose levels at 0 min) and glucose intolerance in air-exposed rats (Fig. 8A–D). Ozone exposure also caused hyperglycemia and glucose intolerance in SAL-treated rats where DEX effect was further exacerbated by ozone exposure (both hyperglycemia and glucose intolerance) (Fig. 8A–D). Area under the curve assessment confirmed DEX effect and the exacerbation of the ozone effect on glucose intolerance in DEX-treated rats (Fig. 8D). Acute increase in circulating free fatty acids in response to ozone exposure was indicative of adipose lipolysis likely mediated by glucocorticoids[32]. Treatment with DEX at both doses significantly increased serum free fatty acids in air-exposed rats (Fig. 8E). Ozone tended to increase free fatty acids in SAL-treated rats. This effect of ozone was significant in CLEN-treated rats. Ozone-exposed DEX-treated rats had additive increases in circulating free fatty acids (Fig. 8E).

In study 2, high dose CLEN + DEX treatment produced hyperglycemia to a small degree but not glucose intolerance in air-exposed rats (Fig. 9B,C). Ozone exposure induced hyperglycemia and glucose intolerance in SAL-treated rats (Fig. 9A–C). Ozone-induced hyperglycemia (Fig. 9B) but not glucose intolerance response (Fig. 9C) was more pronounced in rats treated with high dose CLEN + DEX. Treatment with CLEN + DEX at the high dose significantly increased serum free fatty acids in air-exposed rats (Fig. 9D). Ozone exposure also increased free fatty acids levels in SAL and CLEN + DEX-treated rats (Fig. 9D).

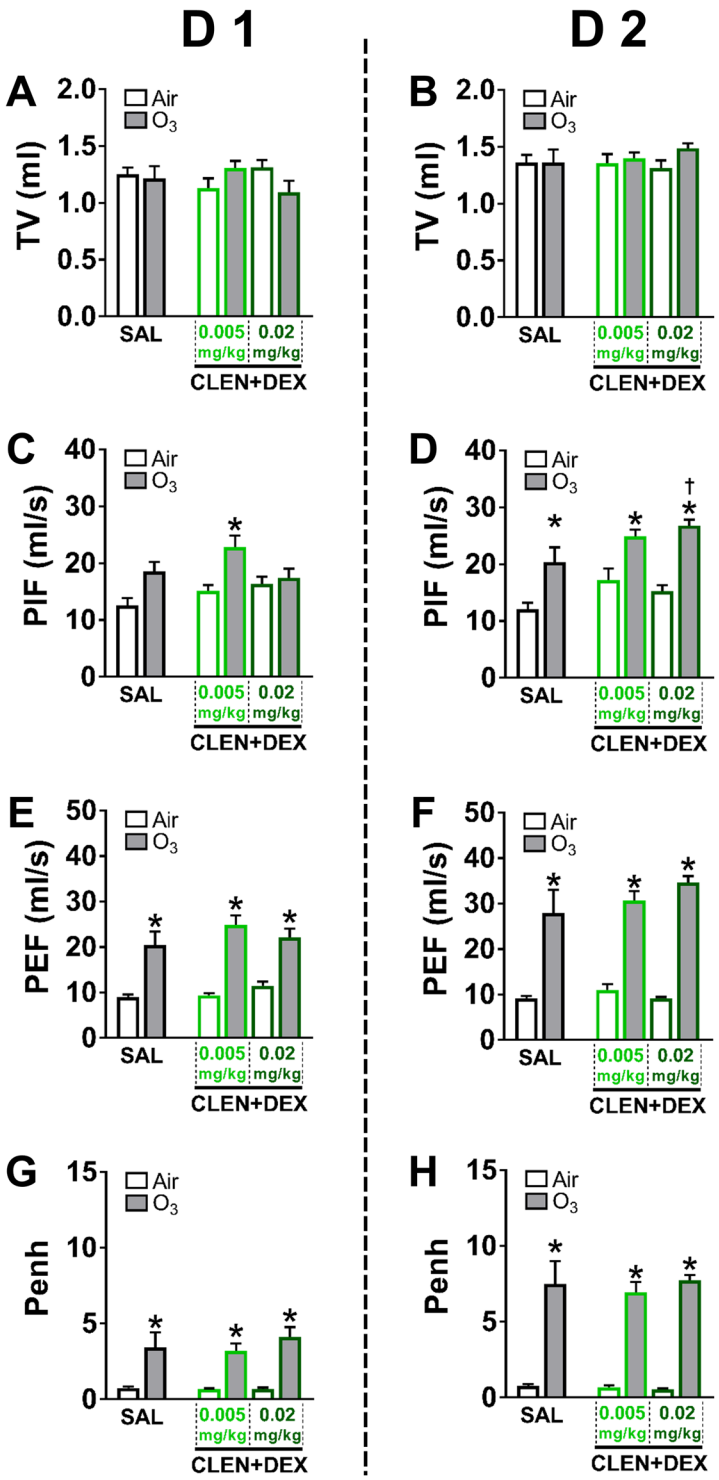

Figure 5. The influence of CLEN + DEX treatments on ozone-induced changes in ventilatory parameters (study 2). Of all ventilatory parameters assessed in rats through whole body plethysmography immediately after each day of air or ozone (0.8 ppm) exposure, the data for tidal volume (TV, **A,B**), peak inspiratory flow (PIF, **C,D**), peak expiratory flow (PEF, **E,F**), and enhanced pause (Penh, **G,H**) are shown. Bar graphs show mean ± SEM of n = 6–8 animals/group. Significant differences between groups (p value ≤ 0.05) are indicated by * for ozone effect when compared to corresponding air-exposed rats, and † for drug effect when compared to corresponding vehicle (SAL; saline)-treated rats.

Stress hormone levels were variably altered by ozone exposure and drug treatment. Although ozone exposure has been shown to increase circulating epinephrine and corticosterone in some of our prior studies[1,3,6], in the present study, the effects were inconsistent. Ozone exposure and drug treatments had mixed

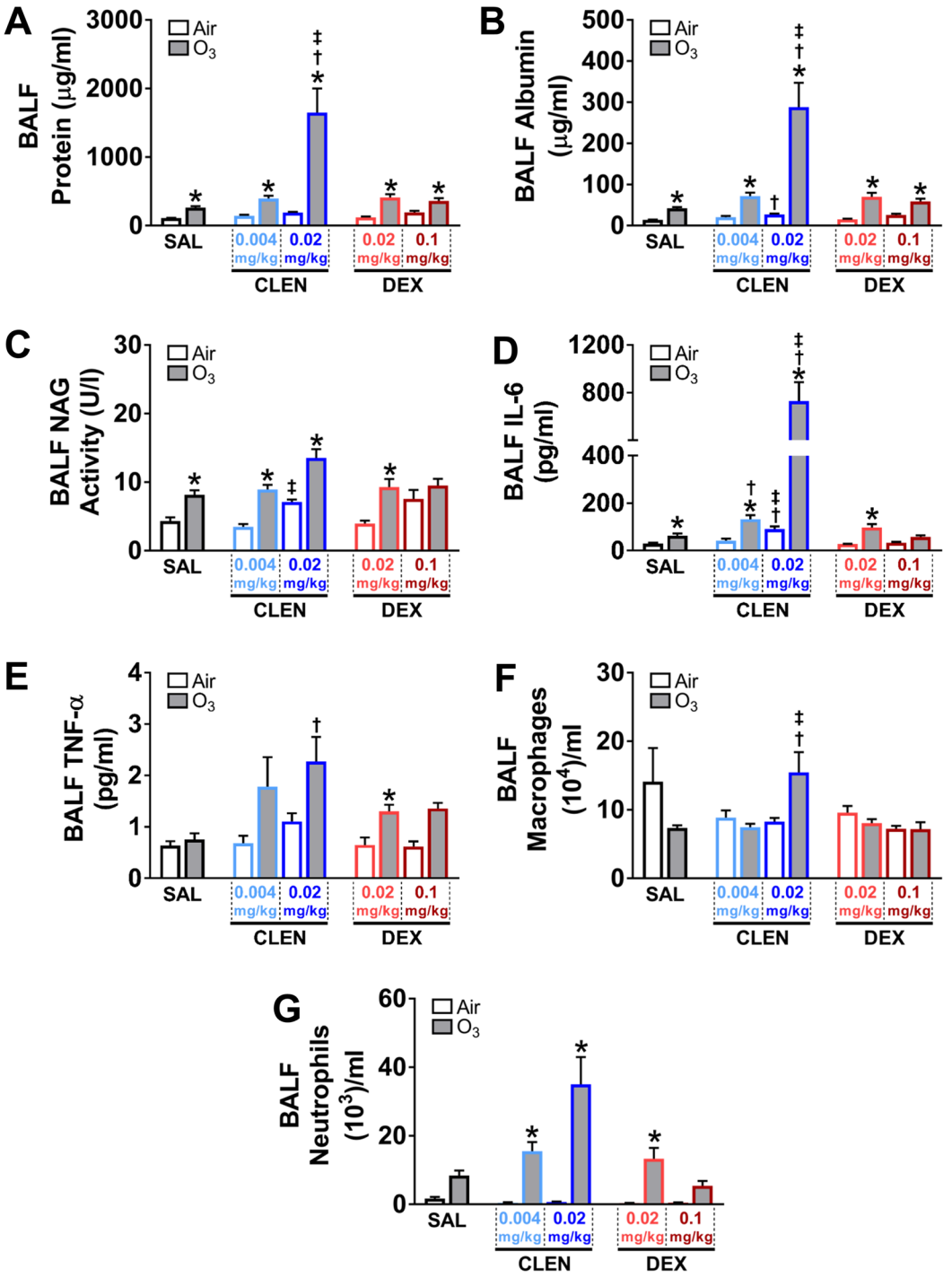

Figure 6. CLEN but not DEX treatment exacerbated ozone-induced lung protein leakage, cytokine changes and neutrophilic inflammation (study 1). BALF protein (**A**), albumin (**B**), NAG activity (**C**), IL-6 (**D**), TNF-α (**E**), macrophage numbers (**F**), and neutrophil numbers (**G**) were assessed in rats after the second day of air or ozone (0.8 ppm) exposure (4 hr/day for 2 consecutive days). Bar graphs show mean ± SEM of n = 6–8 animals/group. Significant differences between groups (p value ≤ 0.05) are indicated by * for ozone effect when compared to corresponding air-exposed rats, † for drug effect when compared to corresponding vehicle (SAL; saline)-treated rats, and ‡ for drug dose effect for the same exposure.

effects on circulating epinephrine and corticosterone. In study 1, the individual CLEN or DEX treatment did not change levels of epinephrine; however, high dose CLEN + DEX in study 2 significantly increased epinephrine in air-exposed rats (Table 1). Ozone exposure tended to increase epinephrine levels in SAL-treated rats. CLEN, DEX or CLEN + DEX had minimal effects on ozone-induced increases. Plasma levels of corticosterone were not

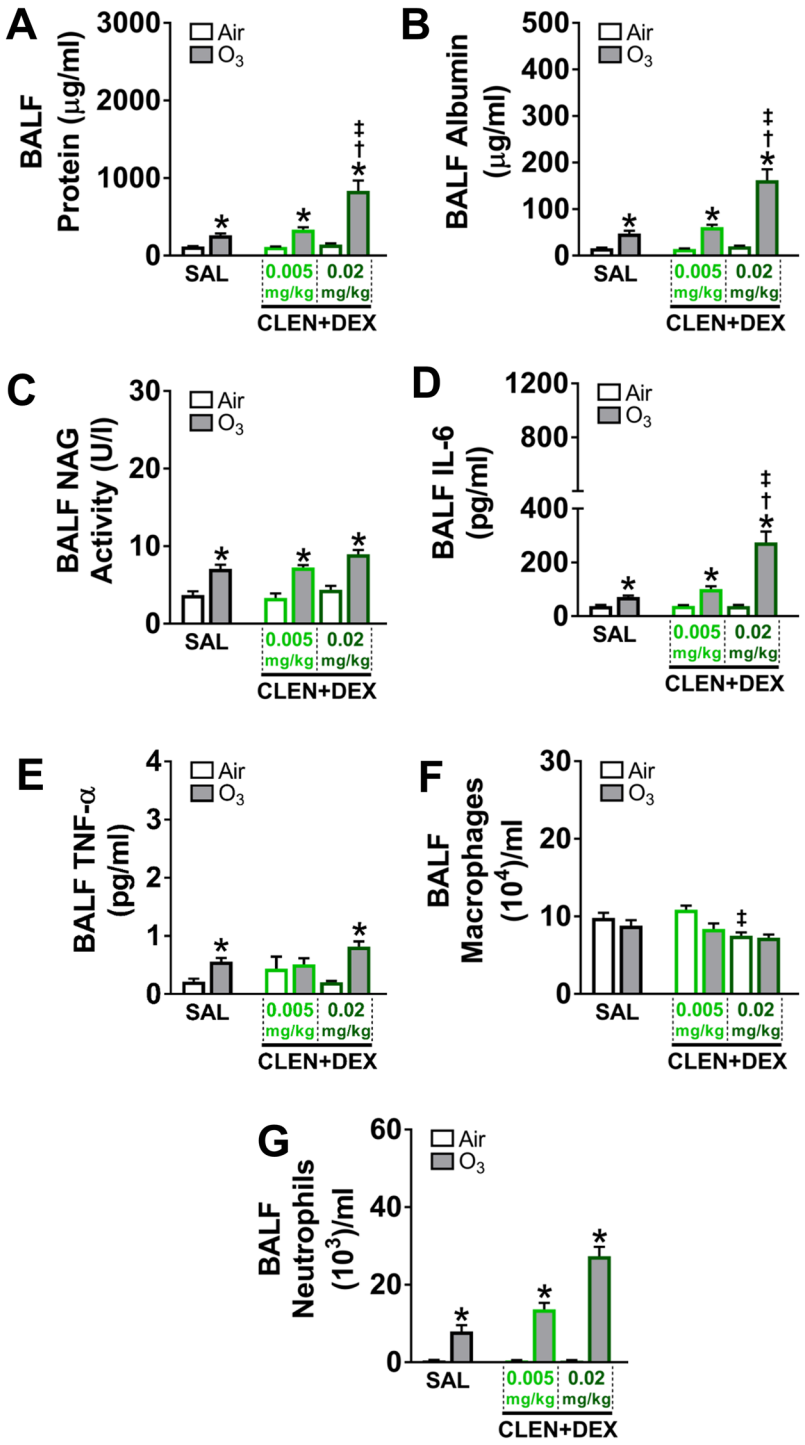

Figure 7. CLEN + DEX treatment exacerbated ozone-induced lung protein leakage, cytokine changes and neutrophilic inflammation (study 2). BALF protein (**A**), albumin (**B**), NAG activity (**C**), IL-6 (**D**), TNF-α (**E**), macrophage numbers (**F**), and neutrophil numbers (**G**) were assessed in rats after the second day of air or ozone (0.8 ppm) exposure (4 hr/day for 2 consecutive days). Bar graphs show mean ± SEM of n = 6–8 animals/group. Significant differences between groups (p value ≤ 0.05) are indicated by * for ozone effect when compared to corresponding air-exposed rats, † for drug effect when compared to corresponding vehicle (SAL; saline)-treated rats, and ‡ for drug dose effect for the same exposure.

affected by CLEN but were significantly decreased in all air and ozone-exposed rats treated with low and high doses of DEX in study 1 and high dose of CLEN + DEX in study 2. Ozone exposure in SAL rats did not significantly change corticosterone levels (Table 1).

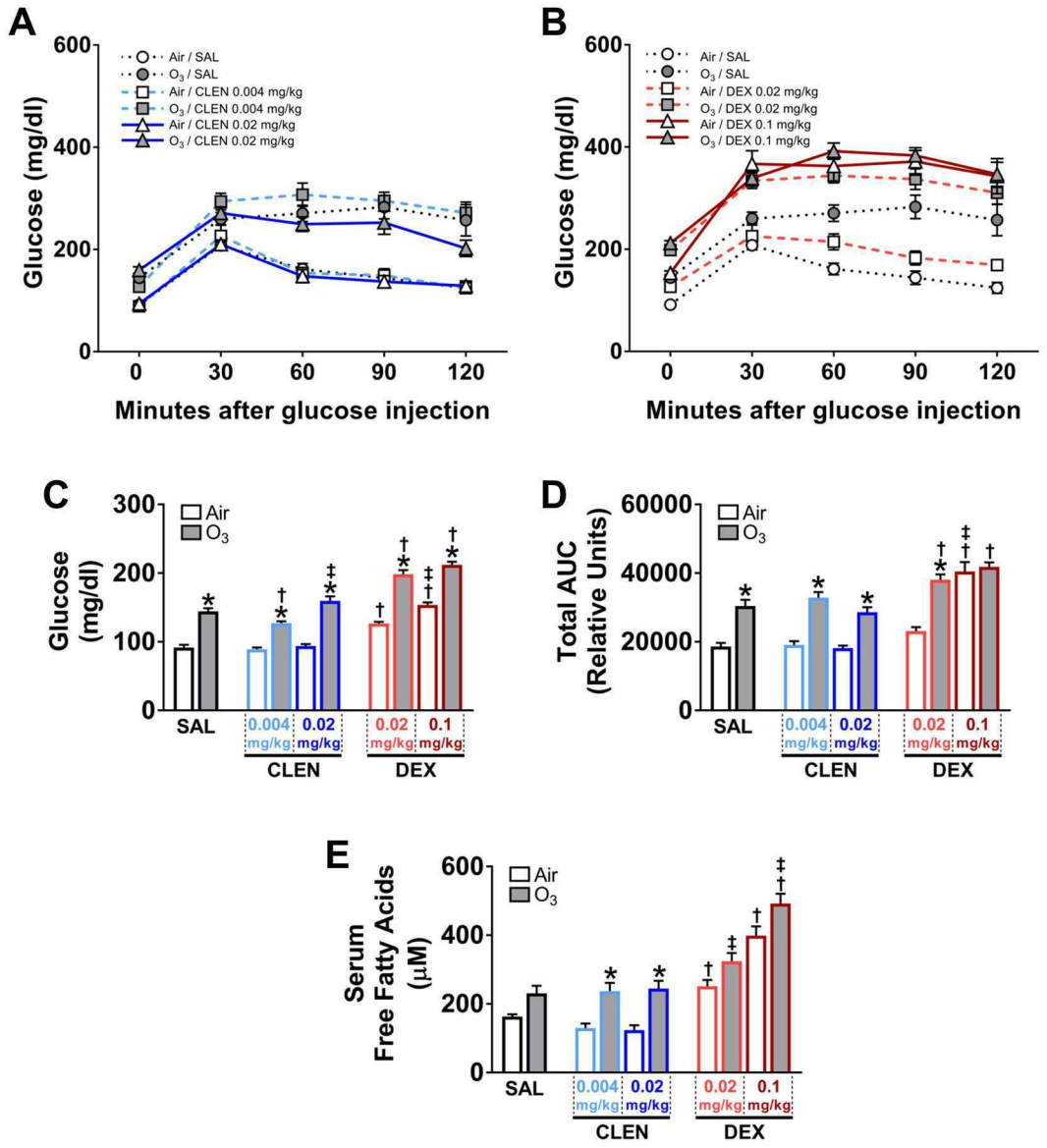

Figure 8. DEX and/or ozone exposure but not CLEN treatment induced hyperglycemia, glucose intolerance, and increased free fatty acids (study 1). Glucose tolerance test for CLEN treatment (**A**) and DEX treatment (**B**), baseline glucose levels before glucose tolerance test (**C**) and area under the curve (AUC) from glucose tolerance test (**D**) were obtained within 0.5–2.5 hr following the first day of air or ozone (0.8 ppm) exposure in rats (4 hr/day). Circulating free fatty acids were analyzed in serum samples collected during necropsy (**E**). Bar graphs show mean ± SEM of n = 6–8 animals/group. Significant differences between groups (p value ≤ 0.05) are indicated by * for ozone effect when compared to corresponding air-exposed rats, † for drug effect when compared to vehicle (SAL; saline)-treated rats, and ‡ for drug dose effect for the same exposure.

Discussion

Asthmatics receiving maintainance medication (such as LABA and/or glucocorticoids) experience exacerbated pulmonary injury and inflammation when exposed to high levels of air pollution[19,20]. We have recently reported that the combination treatment of CLEN + DEX at non-therapeutic high doses (0.2 mg/kg/day and 2 mg/kg/day respectively for 3 days) amplified ozone-induced pulmonary injury and inflammation in sham and adrenalectomized rats[8]. Building upon this, the goal of this study was to determine if β_2AR and/or GR agonists when given at near therapeutic dose range, individually as singular therapy or as combination, (recommended by clinicians for asthma and COPD) would exacerbate acute ozone-induced lung injury/inflammation and also systemic metabolic alterations that were not reported in our previous study[8].

In brief, we previously showed that ozone exposure in vehicle-treated rats caused lung injury, inflammation and BALF cytokine increases[6–8]. Similar to DEX treatment, ozone exposure also induced lymphopenia, decreased spleen weights and produced systemic metabolic alterations including hyperglycemia, glucose intolerance, and the release of free fatty acids into the circulation. Importantly, CLEN, even at the therapeutic concentrations used herein markedly exacerbated ozone-induced lung protein leakage and BALF cytokine release and neutrophilic

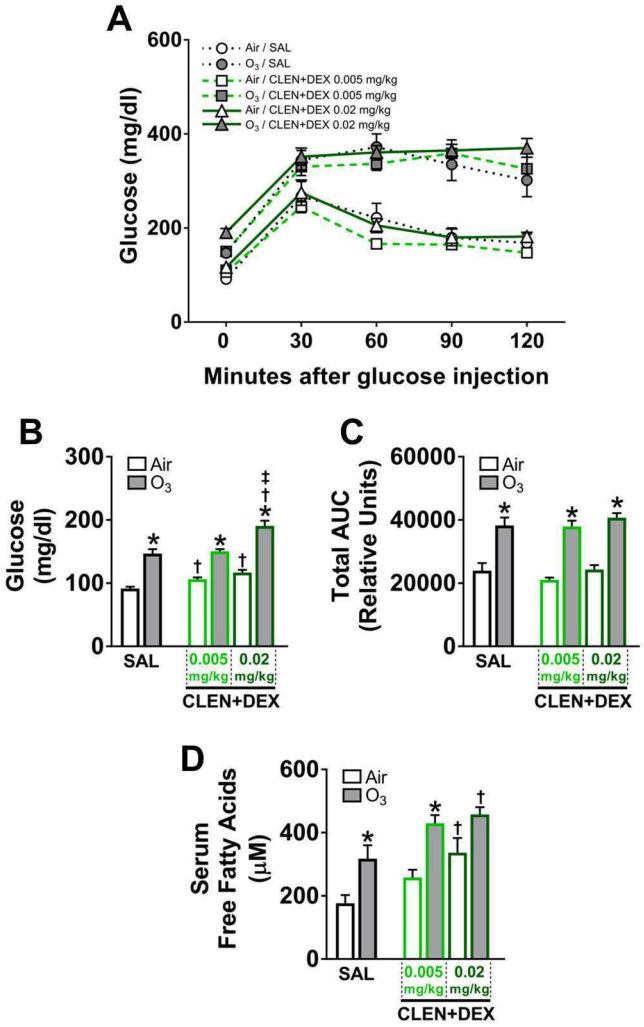

Figure 9. CLEN + DEX treatment alone increased blood glucose and circulating free fatty acids, while ozone exposure induced hyperglycemia glucose intolerance, and increased free fatty acids (study 2). Glucose tolerance test for CLEN + DEX treatment (**A**), baseline glucose levels before glucose tolerance test (**B**) and area under the curve (AUC) from glucose tolerance test (**C**) were obtained within 0.5–2.5 hr following the first day of air or ozone (0.8 ppm) exposure in rats (4 hr/day). Circulating free fatty acids were analyzed in serum samples collected during necropsy (**D**). Bar graphs show mean ± SEM of n = 6–8 animals/group. Significant differences between groups (p value ≤ 0.05) are indicated by * for ozone effect when compared to corresponding air-exposed rats, † for drug effect when compared to vehicle (SAL; saline)-treated rats, and ‡ for drug dose effect for the same exposure.

influx seemingly, without exacerbating systemic effects of ozone. DEX, on the other hand, induced effects such as lymphopenia, hyperglycemia, glucose intolerance and free fatty acid release, that were similar to and more pronounced than those induced by ozone exposure alone. In general, the combination of CLEN + DEX at therapeutic levels showed less remarkable exacerbation of ozone pulmonary and systemic effects relative to CLEN alone. These data demonstrate that ozone-induced pulmonary injury and neutrophilic inflammation are exacerbated in rats receiving singular treatment of LABA (i.e. CLEN) at dose levels used, whereas, systemic immunological and metabolic alterations induced by ozone mimicked those of DEX with both producing additive effects. Thus, the pulmonary and systemic health effects of irritant air pollutants in those using LABA and steroids individually or as combination might be exacerbated because ozone inflammatory and metabolic effects are also mediated through the activation of AR and GR.

Ozone exposure has been shown to induce neuroendocrine-mediated release of adrenal-derived stress hormones, however because of the ultradian fluctuations[33,34] and the influence of other stressors, often the increases in circulating hormones are not evident as we have seen in the present study. However, we have shown that the activation of genes responsive to AR and GR as well as lymphopenia, likely mediated by epinephrine and corticosterone release are readily apparent after ozone exposure[6,8,14]. It is noteworthy that, the treatment with DEX was associated with marked reduction in circulating corticosterone but not epinephrine levels. DEX, has been shown to reduce corticosterone levels due to negative feedback control on the hypothalamus and pituitary to activate CRH-mediated ACTH release[35,36].

	STUDY 1					
		SAL	CLEN LOW	CLEN HIGH	DEX LOW	DEX HIGH
Epinephrine	Air	59.4 ± 14.6	55.6 ± 27.8	35.3 ± 11	44 ± 9.8	46.9 ± 11.8
(pg/ml)	Ozone	87.8 ± 16.1	49.8 ± 7.1	58 ± 12.3	72.2 ± 10.8	84.7 ± 12.7
Corticosterone	Air	375.7 ± 77.2	368 ± 56.3	292.4 ± 80.5	18.8 ± 7.7†	10.2 ± 1†
(ng/ml)	Ozone	462.5 ± 48.6	278.7 ± 24.7	319.1 ± 27.1	134.1 ± 32.6*†	8.8 ± 0.5†‡
		STUDY 2				
		SAL	CLEN + DEX LOW	CLEN + DEX HIGH		
Epinephrine	Air	57 ± 6.3	47.5 ± 5.7	205.6 ± 160.5		
(pg/ml)	Ozone	142.3 ± 13	92.3 ± 13.9	79.7 ± 5.2		
Corticosterone	Air	580.5 ± 93.7	328.4 ± 92.4	36.7 ± 16.4†‡		
(ng/ml)	Ozone	384.4 ± 95.2	166.3 ± 43.7	99.3 ± 41.8†		

Table 1. Plasma stress hormone levels in drug treated animals following acute air or ozone exposure. Values represent mean ± SEM of n = 6–8/group. Significant differences between groups (p value ≤ 0.05) are indicated by *for ozone effect when compared to corresponding air-exposed rats, †for drug effect when compared to corresponding vehicle (SAL)-treated rats, and ‡for drug dose effect for the same exposure. SAL – saline; CLEN – clenbuterol; DEX – dexamethasone.

After ozone exposure, adrenal-derived stress hormones mediate their effects on homeostatic processes through AR and GR activation. In the present study, the exacerbation of ozone-induced pulmonary injury and inflammation in rats receiving therapeutic doses of CLEN or CLEN + DEX could be due to the high affinity of epinephrine for β_2AR which represent ~80% of the total AR subtype in the airways and plays an important role in maintaining lung microvascular permeability, and airway smooth muscle as well as epithelial functions[37]. The activation of β_2AR in airways has been shown to induce inflammatory changes associated with asthma phenotype in a mouse model[38]. We noted that ozone-induced pulmonary neutrophilia and increases in BALF IL-6 were exacerbated by CLEN or CLEN + DEX but not DEX. Although BALF TNF-α seem to show a small increase in CLEN-treated animals exposed to ozone, because of the inconsistency in ozone effects, and low level of this cytokine in BALF, its role in inflammatory response in current experimental setting is unclear. The lack of exacerbation or even slight dampening of ozone-induced neutrophilic inflammation and IL-6 release by DEX might be due to its immunosuppressive effects in the absence of CLEN. Thus, it is plausible that β_2AR agonists use a similar mechanism as the endogenous epinephrine to exacerbate ozone-induced inflammation. The microvascular dilation induced by epinephrine[39] or CLEN could facilitate this process by longer retention of blood in the lung and thus, facilitating neutrophil extravasation to the interstitial spaces in ozone-primed lungs. Immunomodulation of neutrophil release, recruitment and extravasation are dynamically controlled by both glucocorticoids and catecholamines[40,41].

Acute ozone exposure has been shown to induce ventilatory changes in sensitive rat strains such as Wistar Kyoto rats[42] resulting in increased Penh[8], which has been correlated with labored breathing[31]. We previously showed that a non-therapeutic high dose CLEN + DEX treatment resulted in minimal changes in ventilatory parameters when administered to air-exposed rats, however in ozone-exposed rats there were marked increases in pulmonary edema and corresponding ventilatory changes[8]. At the lower dosages of CLEN or CLEN + DEX used in the present study, we also did not observe significant changes in ventilatory parameters in air-treated rats. However, despite using more clinically relevant dosages of CLEN, DEX or the combined treatment, we still were not able to demonstrate improvement in the ozone-induced ventilatory changes. Results suggest that the airflow obstruction and lung injury/pulmonary edema induced by ozone are resistant to glucocorticoid or β_2AR agonists treatment.

Although ozone has been shown to induce pulmonary protein leakage in many studies, the precise contributions of hemodynamic and non-hemodynamic mechanisms are unclear. Our previous study showed that a high dose of CLEN plus DEX even without ozone caused lung protein leakage[8] suggesting the contribution of βAR and circulating epinephrine. This is supported by the evidence that in the presence of therapeutic levels of CLEN, which did not produce edema in air-exposed rats, ozone-induced pulmonary vascular leakage was markedly exacerbated. In the adrenalectomized rats ozone-induced vascular leakage was minimal[5]. Epinephrine-mediated activation of βAR has been implicated in increased lung permeability[43,44]. Since, the predominant response in the lung of β_2AR activation is likely to be vasodilation and bronchodilation, the increases in epinephrine together with CLEN and hemodynamic changes associated with ozone-induced bradycardia might promote fluid filling in the microvasculature[45,46]. When DEX is combined with CLEN (CLEN + DEX) exacerbation of ozone-induced lung protein leakage is less dramatic than that occuring in rats with CLEN-only treatment, suggesting that GR and β_2AR might interactively maintain homeostatic processes to reduce injury induced by a stressor. It may be relevant that, increased risk of asthma-related death by LABA monotherapy is not evident in asthmatic patients taking a combination of LABA plus corticosteroids[12,47].

The neuroendocrine response induced by ozone exposure is associated with the changes in systemic immunological surveillance[48]. Increased numbers of activated macrophages have been found in the lung after ozone exposure[49,50]. Moreover, splenic macrophages have been shown to migrate to the lungs after ozone inhalation[51]. In this study, CLEN-alone treatment increased the number of BALF macrophages in ozone-exposed rats, suggesting

that it likely affected macrophage extravasation. Macrophages express β_2AR and can be activated by LABA treatment[52].

DEX at the concentrations used in both studies induced lymphopenia and reduced thymus and spleen weights, demonstrating the immunosuppressant property. Similar to DEX, ozone exposure has previously shown to induce lymphopenia[6,7,53] and thymic involution[54–56]. In this study, we noted lymphopenia as well as small reductions in thymus and spleen weights after acute ozone exposure; effects that were clear in rats treated with DEX or CLEN + DEX. Concomitantly, GR blockade but not βAR inhibition, prevented ozone-induced lymphopenia[7], suggesting that endogenous GR signaling was required. Both spleen and thymus T lymphocytes were decreased in ozone exposed mice[54]. Collectively, these data suggest that AR and GR, which are therapeutically modulated could affect ozone-induced pulmonary innate immune changes.

In addition to immune surveillance, the stress-induced neuroendocrine activation also orchestrates metabolic energy redistribution and conservation for future needs[57]. Ozone exposure has been shown to induce a shift in metabolites distribution in multiple organs in rats and in humans[1,3,5]. In this study, although the use of β_2AR specific agonist CLEN was targeted to understand its role in the lung tissue, we presumed that CLEN would also have systemic effects, since these receptors are distributed in vascular smooth muscle involved in vasodilation. However, we noted that DEX but not CLEN, independently induced hyperglycemia, glucose intolerance and lipolysis as evident by free fatty acids release. The metabolic changes in CLEN + DEX-treated rats with or without ozone exposure were indicative of the predominant role of glucocorticoids. The understanding of how chronic stimulation of these metabolic processes following long-term pollutant exposure lead to metabolic diseases is critical for causal evidence to support epidemiological associations[58,59].

Some limitations are noted in this study. First, both CLEN and DEX were delivered intraperitoneally to precisely control the dose and to assess pulmonary as well as systemic effects. However, direct lung delivery, which is often used for asthma and COPD treatment, might result in different outcomes. The effectiveness of pulmonary delivery needs to be examined in future studies. Second, the rats are not sensitized or "asthmatic", while people receiving β_2AR agonists are primarily asthmatic individuals. Since asthmatic individuals are more sensitive to ozone-induced inflammation[19,20,60], it is possible that the exacerbation resulting from β_2AR agonist usage during air pollution exposure might be of even greater magnitude. The interactive effect of CLEN, DEX and ozone will need to be examined in an animal model of allergic asthma.

In conclusion, CLEN treatment at therapeutically-relevant dosages, exacerbated ozone-induced pulmonary injury/ inflammation and BALF inflammatory cytokine release through the activation of β_2AR, likely the same mechanism by which ozone also induces vascular leakage and inflammation. The degree of CLEN-related exacerbation of ozone-induced pulmonary effects was reduced when rats were treated with CLEN + DEX combination, while DEX by itself did not influence this pulmonary outcome. However, even at lower than therapeutic dose levels, DEX treatment was associated with systemic metabolic and immunological effects in air-exposed rats that were similar to effects induced by ozone and often additive, suggesting a similar mode of action through the activation of GR. Clinically, the effect of LABA on β_2AR is important as inner-city children, who are more prone to asthma and use bronchodilators, are likely to be exposed to high levels of air pollution[61,62]. These potential drug-air pollution interactions might be critical in those socioeconomically disadvantaged communities with disproportional exposure to elevated levels of air pollution, where high incidence of chronic lung and metabolic diseases coincide with the use of bronchodilators and/or steroids.

Received: 7 August 2019; Accepted: 10 November 2019;
Published online: 29 November 2019

References

1. Bass, V. *et al*. Ozone induces glucose intolerance and systemic metabolic effects in young and aged Brown Norway rats. *Toxicol Appl Pharmacol* **273**(3), 551–60 (2013).
2. Thomson, E. M., Vladisavljevic, D., Mohottalage, S., Kumarathasan, P. & Vincent, R. Mapping acute systemic effects of inhaled particulate matter and ozone: multiorgan gene expression and glucocorticoid activity. *Toxicol Sci* **135**(1), 169–81 (2013).
3. Miller, D. B. *et al*. Inhaled ozone (O3)-induces changes in serum metabolomic and liver transcriptomic profiles in rats. *Toxicol Appl Pharmacol* **286**(2), 65–79 (2015).
4. Kodavanti, U. P. Stretching the stress boundary: Linking air pollution health effects to a neurohormonal stress response. *Biochim Biophys Acta* **1860**(12), 2880–90 (2016).
5. Miller, D. B. *et al*. Ozone Exposure Increases Circulating Stress Hormones and Lipid Metabolites in Humans. *Am J Respir Crit Care Med* **193**(12), 1382–91 (2016).
6. Miller, D. B. *et al*. Acute Ozone-Induced Pulmonary and Systemic Metabolic Effects Are Diminished in Adrenalectomized Rats. *Toxicol Sci* **150**(2), 312–22 (2016).
7. Henriquez, A. R. *et al*. Adrenergic and glucocorticoid receptor antagonists reduce ozone-induced lung injury and inflammation. *Toxicol Appl Pharmacol* **339**, 161–171 (2018).
8. Henriquez, A. R. *et al*. Beta-2 adrenergic and glucocorticoid receptor agonists modulate ozone-induced pulmonary protein leakage and inflammation in healthy and adrenalectomized rats. *Toxicol Sci* **166**(2), 288–305 (2018).
9. Barnes, P. J. Glucocorticosteroids. *Handb Exp Pharmacol* **237**, 93–115 (2017).
10. Billington, C. K., Penn, R. B. & Hall, I. P. β2 Agonists. *Handb Exp Pharmacol* **237**, 23–40 (2017).
11. Newton, R. *et al*. Modulation of Epithelial Cell Function by Glucocorticoids: Anti-Inflammatory and Other Effects in *The Pulmonary Epithelium in Health and* Disease (ed. Proud, D.) Chapter 18 (Wiley, 2008).
12. Nelson, H. S., Weiss, S. T., Bleecker, E. R., Yancey, S. W. & Dorinsky, P. M., SMART Study Group. The Salmeterol Multicenter Asthma Research Trial: a comparison of usual pharmacotherapy for asthma or usual pharmacotherapy plus salmeterol. *Chest* **129**(1), 15–26 (2006).
13. Stempel, D. A. *et al*. Serious Asthma Events with Fluticasone plus Salmeterol versus Fluticasone Alone. *N Engl J Med* **374**(19), 1822–30 (2016).
14. Henriquez, A. *et al*. Adrenal-derived stress hormones modulate ozone-induced lung injury and inflammation. *Toxicol Appl Pharmacol* **329**, 249–258 (2017).

15. Qian, Z. *et al*. Interaction of ambient air pollution with asthma medication on exhaled nitric oxide among asthmatics. *Arch Environ Occup Health* **64**(3), 168–76 (2009).
16. Hernández-Cadena, L. *et al*. Increased levels of outdoor air pollutants are associated with reduced bronchodilation in children with asthma. *Chest* **136**(6), 1529–1536 (2009).
17. McGhan, S. L. *et al*. Factors associated with poor asthma control in children aged five to 13 years. *Can Respir J* **13**(1), 23–9 (2006).
18. von Klot, S. *et al*. Increased asthma medication use in association with ambient fine and ultrafine particles. *Eur Respir J* **20**(3), 691–702 (2002).
19. Lewis, T. C. *et al*. Air pollution and respiratory symptoms among children with asthma: vulnerability by corticosteroid use and residence area. *Sci Total Environ* **448**, 48–55 (2013).
20. Gent, J. F. *et al*. Association of low-level ozone and fine particles with respiratory symptoms in children with asthma. *JAMA* **290**(14), 1859–67 (2003).
21. Chiarella, S. E. *et al*. β_2-Adrenergic agonists augment air pollution-induced IL-6 release and thrombosis. *J Clin Invest* **124**(7), 2935–46 (2014).
22. Ritchie, A. I. *et al*. β2-Agonists Enhance Asthma-Relevant Inflammatory Mediators in Human Airway Epithelial Cells. *Am J Respir Cell Mol Biol* **58**(1), 128–132 (2018).
23. Shannahan, J. H. *et al*. Pulmonary oxidative stress, inflammation, and dysregulated iron homeostasis in rat models of cardiovascular disease. *J Toxicol Environ Health A* **73**(10), 641–56 (2010).
24. Yen, M. & Ewald, M. B. Toxicity of weight loss agents. *J Med Toxicol* **8**(2), 145–52 (2012).
25. Milano, G., Chiappini, S., Mattioli, F., Martelli, A. & Schifano, F. β-2 Agonists as Misusing Drugs? Assessment of both Clenbuterol- and Salbutamol-related European Medicines Agency Pharmacovigilance Database Reports. *Basic Clin Pharmacol Toxicol* **123**(2), 182–187 (2018).
26. Drug Enforcement Administration, 2013. (2017. September 7). Retrieved from https://www.deadiversion.usdoj.gov/drug_chem_info/index.html.
27. Chrousos, G., Pavlaki, A. N. & Magiakou, M. A. Glucocorticoid Therapy and Adrenal Suppression; MDText.com, Inc (2011).
28. Brown, J. S., Wilson, W. E. & Grant, L. D. Dosimetric comparisons of particle deposition and retention in rats and humans. *Inhal Toxicol* **17**(7-8), 355–85 (2005).
29. Hatch, G. E. *et al*. Biomarkers of Dose and Effect of Inhaled Ozone in Resting versus Exercising Human Subjects: Comparison with Resting Rats. *Biomark Insights* **8**, 53–67 (2013).
30. Kodavanti, U. P. *et al*. Variability in ozone-induced pulmonary injury and inflammation in healthy and cardiovascular-compromised rat models. *Inhal Toxicol* **27**(Suppl 1), 39–53 (2015).
31. Hamelmann, E. *et al*. Noninvasive measurement of airway responsiveness in allergic mice using barometric plethysmography. *Am J Respir Crit Care Med* **156**(3 Pt 1), 766–75 (1997).
32. de Kloet, A. D. & Herman, J. P. Fat-brain connections: Adipocyte glucocorticoid control of stress and metabolism. *Front Neuroendocrinol* **48**, 50–57 (2018).
33. Joëls, M., Sarabdjitsingh, R. A. & Karst, H. Unraveling the time domains of corticosteroid hormone influences on brain activity: rapid, slow, and chronic modes. *Pharmacol Rev* **64**(4), 901–38 (2012).
34. Dietl, H., Prast, H. & Philippu, A. Pulsatile release of catecholamines in the hypothalamus of conscious rats. *Naunyn Schmiedebergs Arch Pharmacol* **347**(1), 28–33 (1993).
35. Keller-Wood, M. Hypothalamic-Pituitary–Adrenal Axis-Feedback Control. *Compr Physiol* **5**(3), 1161–82 (2015).
36. Spiga, F., Walker, J. J., Gupta, R., Terry, J. R. & Lightman, S. L. 60 YEARS OF NEUROENDOCRINOLOGY: Glucocorticoid dynamics: insights from mathematical, experimental and clinical studies. *J Endocrinol* **226**(2), T55–66 (2015).
37. Barnes, P. J. Distribution of receptor targets in the lung. *Proc Am Thorac Soc* **1**(4), 345–51 (2004).
38. Nguyen, L. P. *et al*. β2-Adrenoceptor signaling in airway epithelial cells promotes eosinophilic inflammation, mucous metaplasia, and airway contractility. *Proc Natl Acad Sci USA* **114**(43), E9163–E9171 (2017).
39. Chilian, W. M., Layne, S. M., Eastham, C. L. & Marcus, M. L. Effects of epinephrine on coronary microvascular diameters. *Circ Res* **61**(5 Pt 2), II47–53 (1987).
40. Dhabhar, F. S., Malarkey, W. B., Neri, E. & McEwen, B. S. Stress-induced redistribution of immune cells–from barracks to boulevards to battlefields: a tale of three hormones–Curt Richter Award winner. *Psychoneuroendocrinology* **37**(9), 1345–68 (2012).
41. Dhabhar, F. S., Miller, A. H., McEwen, B. S. & Spencer, R. L. Effects of stress on immune cell distribution. Dynamics and hormonal mechanisms. *J Immunol* **154**(10), 5511–27 (1995).
42. Dye, J. A., Ledbetter, A. D., Schladweiler, M. C., Costa, D. L. & Kodavanti, U. P. Whole body plethysmography reveals differential ventilatory responses to ozone in rat models of cardiovascular disease. *Inhal Toxicol* **27**(Suppl 1), 14–25 (2015).
43. Rassler, B. Contribution of α - and β -Adrenergic Mechanisms to the Development of Pulmonary Edema. *Scientifica (Cairo)*, 829504 (2012).
44. Lane, S. M., Maender, K. C., Awender, N. E. & Maron, M. B. Adrenal epinephrine increases alveolar liquid clearance in a canine model of neurogenic pulmonary edema. *Am J Respir Crit Care Med* **158**(3), 760–8 (1998).
45. Gordon, C. J. *et al*. Episodic ozone exposure in adult and senescent Brown Norway rats: acute and delayed effect on heart rate, core temperature and motor activity. *Inhal Toxicol* **26**(7), 380–90 (2014).
46. Wagner, J. G. *et al*. Cardiovascular depression in rats exposed to inhaled particulate matter and ozone: effects of diet-induced metabolic syndrome. *Environ Health Perspect* **122**(1), 27–33 (2014).
47. Currie, G. P., Lee, D. K. & Lipworth, B. J. Long-acting beta2-agonists in asthma: not so SMART? *Drug Saf* **29**(8), 647–56 (2006).
48. Snow, S. J., Henriquez, A. R., Costa, D. L. & Kodavanti, U. P. Neuroendocrine Regulation of Air Pollution Health Effects: Emerging Insights. *Toxicol Sci* **164**(1), 9–20 (2018).
49. Razvi, S. S. *et al*. Resistin deficiency in mice has no effect on pulmonary responses induced by acute ozone exposure. *Am J Physiol Lung Cell Mol Physiol* **309**(10), L1174–85 (2015).
50. Kumarathasan, P. *et al*. Nitrative stress, oxidative stress and plasma endothelin levels after inhalation of particulate matter and ozone. *Part Fibre Toxicol* **12**, 28 (2015).
51. Francis, M. *et al*. Editor's Highlight: Role of Spleen-Derived Macrophages in Ozone-Induced Lung Inflammation and Injury. *Toxicol Sci* **155**(1), 182–195 (2017).
52. Grailer, J. J., Haggadone, M. D., Sarma, J. V., Zetoune, F. S. & Ward, P. A. Induction of M2 regulatory macrophages through the β2-adrenergic receptor with protection during endotoxemia and acute lung injury. *J Innate Immun* **6**(5), 607–18 (2014).
53. Stiegel, M. A., Pleil, J. D., Sobus, J. R. & Madden, M. C. Inflammatory Cytokines and White Blood Cell Counts Response to Environmental Levels of Diesel Exhaust and Ozone Inhalation Exposures. *PLoS One* **11**(4), e0152458 (2016).
54. Li, A. F. & Richters, A. Ambient level ozone effects on subpopulations of thymocytes and spleen T lymphocytes. *Arch Environ Health* **46**(1), 57–63 (1991).
55. Dziedzic, D. & White, H. J. Thymus and pulmonary lymph node response to acute and subchronic ozone inhalation in the mouse. *Environ Res* **41**(2), 598–609 (1986).
56. Jakab, G. J., Spannhake, E. W., Canning, B. J., Kleeberger, S. R. & Gilmour, M. I. The effects of ozone on immune function. *Environ Health Perspect* **103**(Suppl 2), 77–89 (1995).
57. Herman, J. P. *et al*. Regulation of the Hypothalamic-Pituitary-Adrenocortical Stress Response. *Compr Physiol* **6**(2), 603–21 (2016).

58. An, R., Ji, M., Yan, H. & Guan, C. Impact of ambient air pollution on obesity: a systematic review. *Int J Obes (Lond)* **42**(6), 1112–1126 (2018).
59. Rao, X., Montresor-Lopez, J., Puett, R., Rajagopalan, S. & Brook, R. D. Ambient air pollution: an emerging risk factor for diabetes mellitus. *Curr Diab Rep* **15**(6), 603 (2015).
60. Zora, J. E. *et al*. Associations between urban air pollution and pediatric asthma control in El Paso, Texas. *Sci Total Environ* **448**, 56–65 (2013).
61. Shmool, J. L. *et al*. Area-level socioeconomic deprivation, nitrogen dioxide exposure, and term birth weight in New York City. *Environ Res* **142**, 624–32 (2015).
62. Chen, E., Schreier, H. M., Strunk, R. C. & Brauer, M. Chronic traffic-related air pollution and stress interact to predict biologic and clinical outcomes in asthma. *Environ Health Perspect* **116**(7), 970–5 (2008).

Acknowledgements

The authors thank Drs. Aimen Farraj and Ian Gilmour of the US EPA and Rebecca Fry of the University of North Carolina for their critical review of the manuscript. We acknowledge the help of Dr. Mark Higuchi and Mr. Abdul Malek Khan of the US EPA for ozone inhalation exposures. This work was supported in part by Fulbright (Becas Chile, CONICYT; IIE-15120279), the EPA-UNC Center for Environmental Medicine, Asthma and Lung Biology Cooperative Agreement (CR-83515201), ORISE postdoctoral appointee (161550; A.R.H).

Author contributions

A.H., S.J. and U.P. designed the study, graphed, interpreted and analyzed the data; A.H., S.J., M.S., M.H. and U.P. performed the experiments; A.L. and J.D. collected, processed and interpreted ventilatory data; J.R. performed biochemical analyses; and A.H. J.D. and U.P. prepared the manuscript that was read and approved by all authors.

Competing interests

The authors declare no competing interests.

Additional information

Correspondence and requests for materials should be addressed to U.P.K.

Reprints and permissions information is available at www.nature.com/reprints.

Disclaimer: The research described in this article has been reviewed by the Center for Public Health and Environmental Assessment, U.S. Environmental Protection Agency, and approved for publication. Approval does not signify that the contents necessarily reflect the views and policies of the Agency, nor does the mention of trade names of commercial products constitute endorsement or recommendation for use.

Publisher's note Springer Nature remains neutral with regard to jurisdictional claims in published maps and institutional affiliations.

Open Access This article is licensed under a Creative Commons Attribution 4.0 International License, which permits use, sharing, adaptation, distribution and reproduction in any medium or format, as long as you give appropriate credit to the original author(s) and the source, provide a link to the Creative Commons license, and indicate if changes were made. The images or other third party material in this article are included in the article's Creative Commons license, unless indicated otherwise in a credit line to the material. If material is not included in the article's Creative Commons license and your intended use is not permitted by statutory regulation or exceeds the permitted use, you will need to obtain permission directly from the copyright holder. To view a copy of this license, visit http://creativecommons.org/licenses/by/4.0/.

© The Author(s) 2019

Online Data Supplement

Ozone-induced dysregulation of neuroendocrine axes requires adrenal-derived stress hormones

Andres R. Henriquez[1], John S. House[2,3], Samantha J. Snow[4], Colette N. Miller[4], Mette C. Schladweiler[4], Anna Fisher[5], Hongzu Ren[5], Matthew Valdez[1], Prasada R. Kodavanti[6], and Urmila P. Kodavanti[4]**

[1]Oak Ridge Institute for Science and Education, Research Triangle Park, NC, United States; [2]Bioinformatics Research Center, North Carolina State University, Raleigh, NC, United States; [3]Center for Human Health and the Environment, North Carolina State University, Raleigh, NC, United States; [4]Environmental Public Health Division, National Health and Environmental Effects Research Laboratory, U.S. Environmental Protection Agency, Research Triangle Park, NC, United States; [5]Research Cores Unit, National Health and Environmental Effects Research Laboratory, U.S. Environmental Protection Agency, Research Triangle Park, NC, United States; and [6]Toxicity Assessment Division, National Health and Environmental Effects Research Laboratory, U.S. Environmental Protection Agency, Research Triangle Park, NC, United States.

Address correspondence:
**Urmila P. Kodavanti, PhD
MD B105-04, NHEERL, U.S. EPA
Research Triangle Park, NC 27711
kodavanti.urmila@epa.gov
Phone: 919 541-4963; Fax: 919-541-0026

SUPPLEMENTARY METHODS:

Sham and adrenalectomy surgeries in rats

Male 12–13 weeks old rats were anesthetized by injection of ketamine (25–50 mg/kg in saline; i.p.). After confirmation of complete anesthesia, buprenorphine was administered (0.02 mg/kg/ml in saline; s.c.) for analgesia. Animals were placed in sternal recumbency position, prepared for aseptic surgery procedure and given to trained veterinarians from Charles River Laboratories Inc. who performed surgeries under sterile conditions. Surgeries were performed using protocols established at Charles River Laboratories Inc. If needed, additional anesthesia was provided by nose-only inhalation of vaporized isoflurane (3%). Right and left glands were removed for ADREX group while for SH group the same surgical procedures were performed except that adrenals were not removed. Immediately after surgery, the rats were placed on heating pads and closely monitored by observing their movements. Once awake, rats were injected with meloxicam (0.2 mg/kg; s.c.) and for analgesia. Additionally, rats were injected with buprenorphine (0.02 mg/ml/kg, s.c.) for two more times every 8-10 hrs for continued analgesia. After surgery, the animals were pair housed with Enviro Dry enrichment/nesting material. To maintain adequate fluid and electrolyte balance, AD rats were provided with saline (0.9% sodium chloride) while SH rats received normal tap water and both groups were provided with powdered as well as pelleted diets, both ad libitum except during exposure to air or ozone. Based on previous reports (Nicolaides et al., 2013; Sakakibara et al., 2014), rats were given a recovery period of 4–6 days prior to any exposure. There were no signs of evident distress and food and water consumption were similar for SH and AD groups (Miller et al., 2016a).

Brainstem and hypothalamus total RNA isolation and mRNA sequencing

The entire frozen hypothalamic and brainstem regions were processed for RNA extraction (n=4 per group). Total RNA was isolated following manufacturer protocol indicated by Direct-Zol RNA MiniPrep kit from Zymo Research (Irvine, CA, USA) and quantified using Qubit RNA reagent (Invitrogen, Waltham, MA, USA). Using prepX polyA mRNA Isolation Kit (Wafergen Biosystems, Fremont, CA, USA), the mRNA was isolated from total RNA. Samples were run in Apollo324 automated sample processing system for mRNA selection. RNA-Seq library was prepared with Wafergen's PrepX mRNA 48 Protocol. cDNA libraries were amplified by 15 PCR cycles with indexing primers according to Wafergen's protocol. dsDNA from each library was quantified by Qubit dsDNA HS Assay kit (Molecular Probes, Eugene, OR, USA) and the quality was checked by Agilent Bioanalyzer (Agilent Technologies, Santa Clara, CA, USA). Each library was diluted to 4 nM by estimating the average molecular sizes from Bioanalyzer data and the concentration from Qubit measurement. Pooled and indexed libraries were sequenced according to Illumina NextSeq 500 protocols (2.5-3.2 pM + 2% PhiX from Illumina Inc., San Diego, CA, USA). The sequencing data were stored in Illumina's BaseSpace-cloud.

Nextseq data normalization and bioinformatics

Sequenced mRNA reads were mapped to the rat genome (rn6) using ensemble release 83 in the Partek® Flow suite. R version 3.2.3 (2015-12-10). Differential gene expression was assessed in DESeq2 package in R (v. 1.10.1) (Love et al., 2014) rounding the count matrix to the nearest integer and considered different when the

adjusted p value (FDR) was ≤0.1. Pathway heatmaps of normalized counts from DESeq2 were created using the heatmap.2 function of the g-plots package (Warnes et al., 2015). Pathway/set enrichment was performed using the eXploring Genomic Relations (XGR) package in R (http://xgr.r-forge.r-project.org/; Fang et al., 2016). Pathway analyses were conducted using genes identified as differentially expressed at adjusted p value < 0.10. Pathway ontologies were defined by the molecular signature database hallmark gene set (MsigDBH; Liberzon et al., 2015) and the immunologic signature gene sets (MsigDBC7). For each ontology set tested, pathway testing was considered significant at FDR < 0.10 for the enrichment statistic. Upstream analysis tools from Ingenuity Pathways Analysis® (IPA®, QIAGEN Redwood City, www.qiagen.com/ingenuity) software were used to compare our results with previously reported databases. By overlapping genes differentially expressed after ozone exposure with genes differentially expressed by the action of multiple upstream regulators, it is possible to obtain a p-value of the overlap. An activation score predicting an activated state (changes similar to those induced by ozone) or an inhibited state (changes dissimilar to those induced by ozone) is defined by an activation z-score of >2 or <-2, respectively.

Fang H, Knezevic B, Burnham KL, Knight JC. XGR software for enhanced interpretation of genomic summary data, illustrated by application to immunological traits. *Genome Med* 2016;8(1):129.

Liberzon A, Birger C, Thorvaldsdóttir H, Ghandi M, Mesirov JP, Tamayo P. The Molecular Signatures Database (MSigDB) hallmark gene set collection. *Cell Syst* 2015;1(6):417-425.

Love MI, Huber W, Anders S. Moderated estimation of fold change and dispersion for RNA-seq data with DESeq2. *Genome Biol* 2014;15,550

Miller, D.B., Snow, S.J., Schladweiler, M.C., Richards, J.E., Ghio, A.J., Ledbetter, A.D., and Kodavanti, U.P. Acute Ozone-Induced Pulmonary and Systemic Metabolic Effects Are Diminished in Adrenalectomized Rats. *Toxicol Sci* 2016a;150(2):312-22.

Nicolaides, N. C., Chrousos, G. P., and Charmandari, E. (2013). Adrenal Insufficiency. Endotext [Internet]. South Dartmouth (MA): MDText.com, Inc., 2000–2013 Nov 18.

Sakakibara, Y., Katoh, M., Suzuki, M., Kawabe, R., Iwase, K., and Nadai, M. (2014). Effect of adrenalectomy on expression and induction of UDP-glucuronosyltransferase 1A6 and 1A7 in rats. *Biol. Pharm. Bull.* 37, 618–624.

Warnes GR, Bolker B, Bonebakker L, Gentleman R, Huber W, Liaw A, Lumley T, Maechler M, Magnusson A, Moeller S, *et al*. 2015 gplots: Various R Programming Tools for Plotting Data.

Supplementary Figure 1

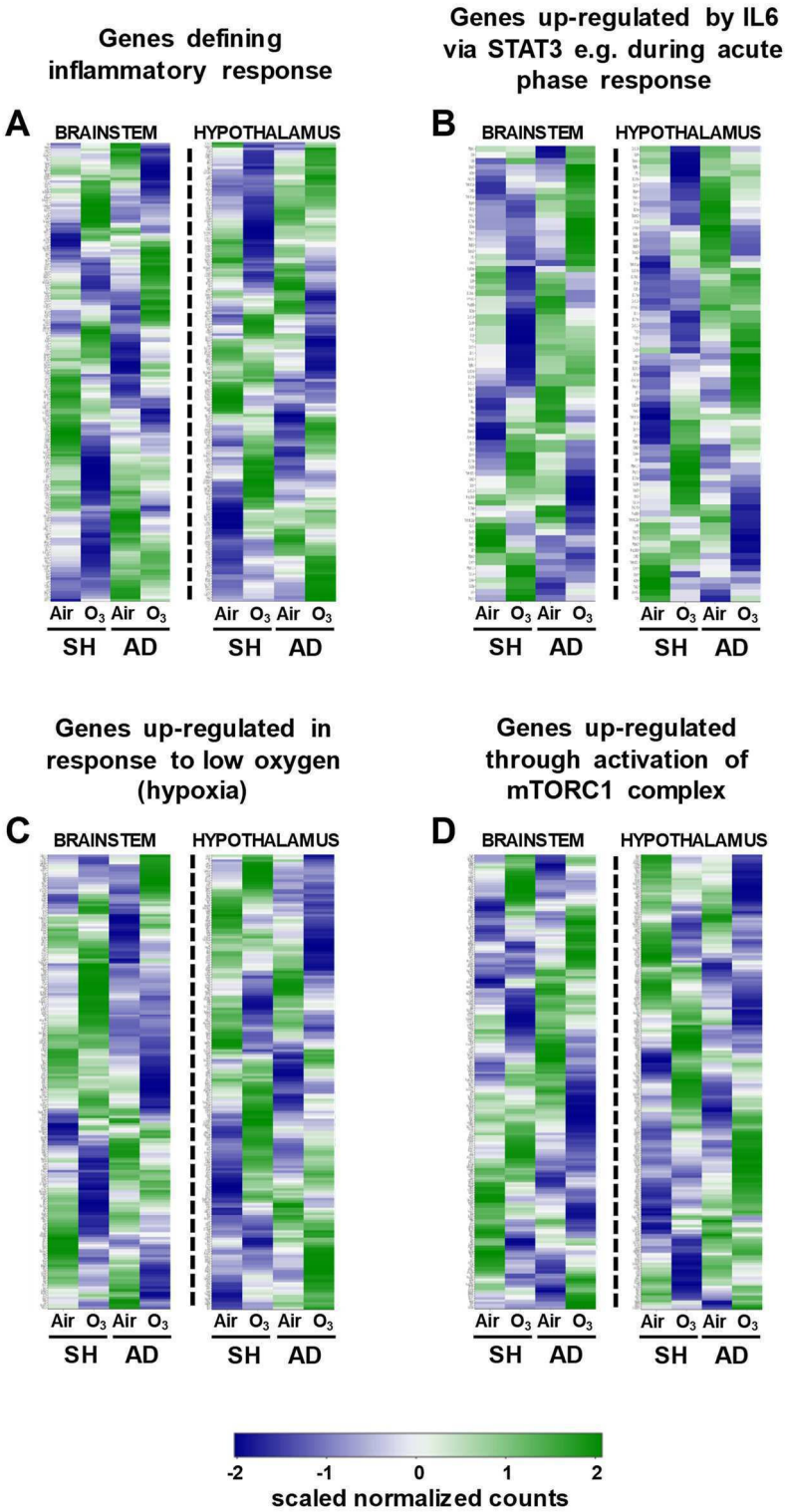

Supplementary Figure 1: Hallmark gene sets significantly enriched after ozone exposure in brainstem and hypothalamus of SHAM rats. Genes for each hallmark gene sets are shown in heatmaps for those defining inflammatory response [200 genes] (A), genes up-regulated by IL6 via STAT3 e.g. during acute phase response [87 genes] (B), genes up-regulated in response to low oxygen (hypoxia) [200 genes] (C), and genes up-regulated through activation of mTORC1 complex [200 genes] (D).

Check for updates

Toxicologic Pathology
1-14
© The Author(s) 2019
Article reuse guidelines:
sagepub.com/journals-permissions
DOI: 10.1177/0192623319878402
journals.sagepub.com/home/tpx
SAGE

Susceptibility Variations in Air Pollution Health Effects: Incorporating Neuroendocrine Activation

Urmila P. Kodavanti[1]

Abstract

Diverse host factors/phenotypes may exacerbate or diminish biological responses induced by air pollutant exposure. We lack an understanding of biological indicators of environmental exposures that culminate in a physiological response versus those that lead to adversity. Variations in response phenotype might arise centrally and/or at the local tissue level. In addition to genetic differences, the current evidence supports the roles of preexisting cardiopulmonary diseases, diabetes, diet, adverse prenatal environments, neurobehavioral disorders, childhood infections, microbiome, sex, and psychosocial stressors in modifying the susceptibility to air pollutant exposures. Animal models of human diseases, obesity, nutritional inadequacies, and neurobehavioral conditions have been compared with healthy controls to understand the causes of variations in susceptibility. Although psychosocial stressors have been associated with increased susceptibility to air pollutant effects, the contribution of neuroendocrine stress pathways in mediating these effects is just emerging. The new findings of neuroendocrine activation leading to systemic metabolic and immunological effects of air pollutants, and the potential contribution to allostatic load, emphasize the consideration of these mechanisms into susceptibility. Variations in susceptibility to air pollution health effects are likely to underlie host genetic and physiological conditions in concert with disrupted neuroendocrine circuitry that alters physiological stability under the influence of stressors.

Keywords

susceptibility variations, air pollution, neuroendocrine, metabolic diseases, allostatic load, animal models

Introduction

The World Health Organization report of May 2018 shows that ambient (outdoor) and household air pollution causes nearly 7 million annual deaths worldwide. Air pollution accounts for nearly 70% of all deaths attributed to environmental causes.[1] However, for decades, we have recognized that not every individual who is exposed to air pollutants or other environmental stressors will die or develop diseases.[2–4] For example, only about 20% of smokers develop chronic obstructive pulmonary disease (COPD).[5] Likewise, variations in susceptibility are likely to predispose some individuals to granulomatous diseases after exposure to silica or asbestos. Individuals from the same genetic background will show relatively similar susceptibility for a given disease.[6,7] When discussing susceptibility variations, one also must keep in mind the impact of longevity and the intensity of environmental exposures. This becomes important as chronic exposures to some pollutants may rarely result in active disease. Understanding the causes of susceptibility variations is critical in developing mitigation strategies and therapeutic interventions. In the context of the current article, "susceptibility" is defined as any unhealthy host condition(s) that modify the biological response to environmental or other stressors. Here, we focus on experimental studies of animal models of selected human susceptibilities and how they modify risk of adverse outcomes caused by air pollution.

Targeted hypothesis-driven research has led us to identify and understand some of the biological pathways and key genetic differences or physiological conditions that make one more susceptible to pollutants.[8–11] In the past 2 decades, the application of a systems approach with high-throughput global gene expression, proteomic, and metabolomic techniques has accelerated the understanding of variations in susceptibilities but has also exposed the complexities of biological networks,

[1] Environmental Public Health Division, National Health and Environmental Effects Research Laboratory, US Environmental Protection Agency, Research Triangle Park, NC, USA

Corresponding Author:
Urmila P. Kodavanti, Environmental Public Health Division, National Health and Environmental Effects Research Laboratory, US Environmental Protection Agency, 109 T.W. Alexander Drive, Room B564, Research Triangle Park, NC 27711, USA.
Email: kodavanti.urmila@epa.gov

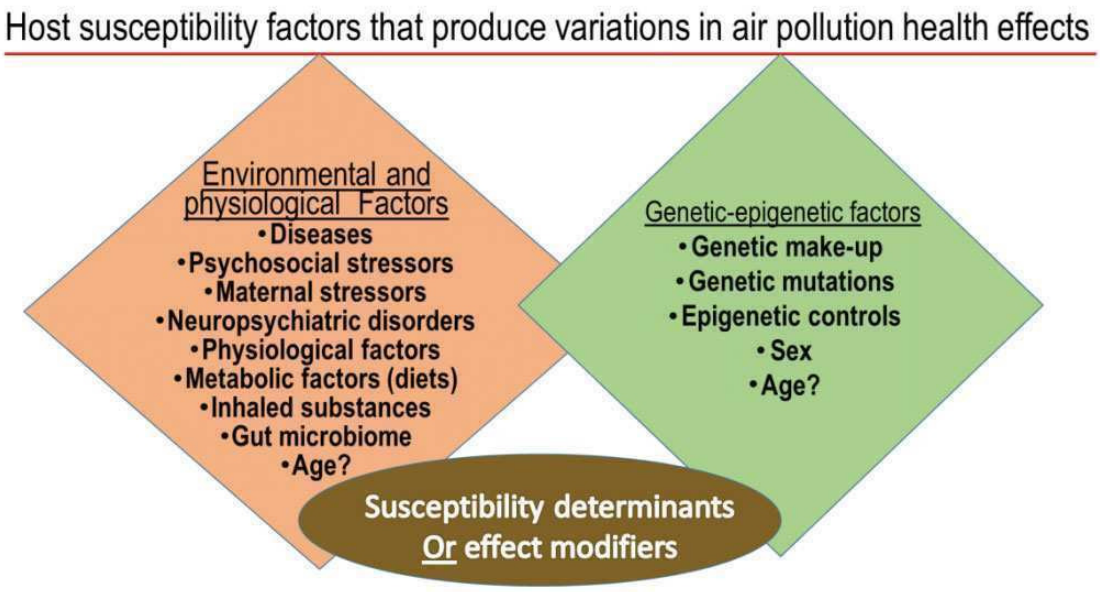

Figure 1. Host susceptibility factors that interactively produce variations in individual response to air pollution health effects.

cross talks between multiple processes within a cell, dynamics of these processes, and the communication between organ systems. At what step in the biological network, and in what organ system the normal homeostatic processes activated by air pollutants are interrupted due to abnormal host conditions, becomes a critical determinant of the type and the degree of variation in response. Perturbation in any one of the homeostatic processes either due to a genetic defect or from chronic or overstimulated responses will likely lead to cumulative or organ-specific impact after exposure to environmental pollutants. In this article, I will first briefly provide a historical perspective on what we have learned using animal models with defined susceptibilities/diseases by giving examples of air pollutant exposures in these models. Recent work[12] on the role of neuroendocrine stress pathways in mediating response to air pollutants will highlight how these new mechanisms will be critical in identifying variations in individual susceptibilities. Based on this body of work, a new mechanistic paradigm is proposed that will be useful when determining causes of variations in susceptibility to air pollutants and the importance of allostatic load. Experimental studies that provide insights into the biological mechanisms of susceptibility variations (noncommunicable; noncancer effects) will be discussed in this article but will not include models of infections, allergies, or developmental stressors.

Historical Perspective on Susceptibility Variations in Air Pollution Research

A variety of host conditions can modify the response to air pollution exposure that can impact health (Figure 1). It is conceivable that one who is susceptible to developing a disease from unknown or known causes is likely to have increased susceptibility to subsequent air pollutant exposure. Likewise, when an individual is exposed chronically to a given air pollutant, he or she will likely develop exposure-related disease over time. However, the mechanisms by which air pollutants may cause disease, or simply exacerbate the preexisting disease condition may depend on each individual's collective and individually tailored response for survival. The understanding of variations in each individual's response is further complicated by the fact that in ambient environmental conditions, individuals are generally exposed to rather low levels of a diverse range of pollutants that produce changes in homeostatic processes through different mechanisms.

Most of the earlier research on air pollution nearly 50 years ago focused on occupational exposures to source-enriched pollutants at rather high concentrations. Because of the lack of exposure controls, workers who were exposed to specific source pollutants developed many types of pulmonary diseases based on the nature of inhalants. Due to the dominance of pulmonary effects, the acute and subtle effects on extrapulmonary organs likely went unnoticed. For example, exposure to silica in miners caused acute and chronic silicosis[13]; coal miners' exposures were associated with coal worker's pneumoconiosis[14]; asbestos mining caused fibrotic lung disease referred to as asbestosis, adenoma, and also pleural diseases with plaques of fibrous tissue, calcification, and mesothelioma[15]; and exposure of farm dust caused hypersensitivity pneumonitis, often referred to as farmer's lung.[16] Some of these pollutants were retained in the lungs with little clearance, and the diseases occurred decades later. For example, mesothelioma occurs in susceptible individuals decades after asbestos exposure.[17] The mechanisms of the delay in expression of disease still puzzle researchers and new insights continue to emerge. It was believed that air pollutants affected primarily the lung while

the knowledge of peripheral effects was limited or these effects were considered nonspecific and therefore of lower significance when examining pulmonary diseases. Thus, the experimental studies mainly included lung pathologies and functional impairment. Likewise, animal models of susceptibility used for research were primarily of those with lung diseases.[18–21]

The October 1948 Donora Pennsylvania smog incident and the December 1952 Great London Smog incident raised the awareness that ambient-level air pollution can cause mortality and morbidity, and influenced the creation of ambient air quality standards for criteria air pollutants.[22] These episodes also prompted epidemiological and toxicological studies to determine what type of pollutants were responsible for adverse health effects and especially who was susceptible. Human mortality and hospital admissions were primarily associated with pulmonary complications of bronchitis and exacerbation of COPD. Based on these observations, and along with the awareness of cigarette smoke-related, allergic, and infectious lung diseases in the population, the emphasis for research was placed on the animal models of bronchitis, COPD, pneumonia, and asthma.[4,23–29] The research experiments included understanding of biological factors/host conditions that may increase pulmonary susceptibility to inflammation and obstructive lung diseases.

Host Genetics as the Contributor to Variations in Air Pollution Health Effects

The contribution of genetic differences to the variations in susceptibility to air pollution health effects continues to be examined experimentally.[20,30–33] Mouse models of different genetic backgrounds have shown differential susceptibilities to pulmonary inflammation after exposure to ozone and other pollutants.[34–37] Linkage analysis studies have provided insights into the contribution of candidate genes within specific chromosomal loci influencing response to air pollutants. For example, in studies involving genetically diverse mouse strains, the DNA sequences on chromosomes 4, 11, and 17 spanning Toll-like receptor 4 and many inflammatory cytokines were linked to increased ozone-induced lung injury and inflammation.[38] The mutations in Toll-like receptor 4 and its contributions to increased allergen-induced lung injury and inflammation were also identified in mouse models as well as in humans.[9] Although these studies provide insights for the gene targets associated with specific pathological conditions, the understanding of collective contribution of gene networks and the causal factors to observed susceptibility differences remains sparse. The limited genetic diversity of laboratory rodents limits the scope of investigations identifying mechanisms of biological variations among genetically diverse humans.

More recent studies have provided insights into the complex interplay of genetic networks that might govern phenotypic expression of disease or adverse health effects in each strain/species of animals.[39,40] The individual strain/species variability in orchestrating transcriptional response will likely be a major contributing factor to producing variability in ultimate disease phenotype. The newer approach of collaborative cross of mouse models to create highly variable genetic backgrounds, which better represent the diversity seen in the human population, will provide some insights. Their systematic assessment using high-throughput platforms of genetic contribution to each disease phenotype has already begun to provide breakthroughs in understanding how individual gene clusters influence the variability in susceptibility not only to air pollutants but also to other types of environmental stressors.[33,41,42]

Use of Animal Models of Human Cardiovascular Diseases in Air Pollution Susceptibility Studies

The robust epidemiological evidence from the 1990s expanding air pollution effects beyond the lung to the cardiovascular system, and how these effects might be important in human mortality and morbidity[43] led to research interest in cardiovascular effects and cardiopulmonary interactions. Likewise, the focus of susceptibility variations expanded from lung disease models to using animal models of cardiovascular diseases for understanding how those with preexisting hypertension or other cardiovascular complications might have exacerbated responses to air pollutants.[4,44–47] Guided by the epidemiological associations between air pollution and cardiovascular diseases, our introduction of the use of a spontaneously hypertensive (SH) rat model in examining their susceptibility to air pollutants has led to the use of these rats in many air pollution studies.[48] These rats are now used worldwide in understanding of the key susceptibility attributes associated with hypertensive disorder in exacerbating pulmonary and cardiovascular effects of air pollutants.[49–54]

We have shown that relative to healthy normotensive rats, SH rats have greater pulmonary injury and inflammation, especially when air pollution exposures occur at high concentrations.[48,49,55] They have compromised ability to increase lung lining antioxidants when exposed to residual oil fly ash particles.[48] Spontaneously hypertensive rats are not able to respond to inhaled combustion source particles by increasing expression of genes involved in inflammation in the lung and the heart as baseline expression of some of these genes is already high in these rats.[48] When global gene expression in the heart of normotensive control Wistar Kyoto (WKY) rats was compared to SH rats following diesel exhaust inhalation, WKY rats showed remarkable changes in gene clusters reflecting cardiovascular disease, and these expression changes mimicked the expression pattern of the same genes at baseline in SH rats.[56] Diesel exhaust inhalation, however, was not able to further exacerbate the transcriptome expression in SH rats, implying that their ability to induce changes in response to pollutant exposure has been compromised due to disease.[56] When hypertensive rats were made normotensive by treating them with hydralazine, diesel exhaust inhalation–induced lung injury, inflammation, and vascular effects were diminished.[10] These data clearly demonstrated the role of hypertension in exacerbating the

effects of inhaled pollutants. However, what brings about hypertension-associated physiological changes becomes an important determinant of the susceptibility of SH rats to pollutant-induced cardiopulmonary effects. These findings led us to understand how susceptibility variations may depend on the phenotypic outcome being selected for in a given genetic background of SH rats and how underlying host conditions might, in a complex and interactive manner, impact the response to air pollution stress. In epidemiological studies, air pollution has been variably linked to increases in blood pressure among healthy and susceptible individuals.[57,58]

Numerous epidemiological studies have linked air pollution to exacerbation of cardiovascular diseases. Since autonomic imbalance can mediate cardiovascular effects of air pollutants,[59,60] the individuals with underlying cardiovascular diseases might be impacted through effects on sensory and central autonomic pathways. Using WKY, SH, and 6 other healthy and cardiovascular and/or metabolically compromised rat models,[46,61] we obtained insights into how underlying host genetics and disease phenotype may influence the response to inhaled ozone. Measures of breathing,[62] injury, and inflammation varied greatly even between healthy strains.[63] Furthermore, alveolar lining levels of antioxidants, namely ascorbate and glutathione, at baseline[64] were correlated with lung physiological changes, protein leakage, and inflammation when the theoretical ozone dose was plotted against levels of ascorbate in the lung lavage fluid.[11] It was apparent that strains with highest levels of ascorbate in the lavage fluid were minimally affected by ozone in terms of injury and inflammation.[63] For example, obese and insulin-resistant James C. Russell (JCR) rats, which have a propensity to develop vascular disease, each having received low ozone effective dose (based on theoretical calculation) and high levels of ascorbate at baseline in the lung lining fluid, were least affected by ozone-induced lung vascular leakage and inflammation. On the contrary, the stroke-prone SH rats, which had the lowest level of lung lining ascorbate and received the highest effective ozone dose, were highly susceptible to lung injury and inflammation from ozone exposure.[11,63] These data collectively demonstrated that ascorbate and glutathione, the first line of defense in the lung lining,[65] are at least one of the critical determinants of susceptibility variation in how ozone may induce lung injury and inflammation. However, the causal mechanisms responsible for achieving differential lung lining antioxidant levels and the connectivity to other cellular physiological processes require further investigations.

When examining the global gene expression patterns of the lung in 5 genetically related strains which included healthy WKY, SH, stroke-prone SH, obese spontaneously hypertensive heart failure (SHHF), and obese insulin resistant JCR rats with vascular impairment,[61] we observed marked strain-related differences in transcriptome at baseline. We noted that the baseline pulmonary expression patterns of genetically closer strains (SH, SH-stroke-prone, and SHHF), which were cardiovascular compromised, were similar and reflected more severe cardiac complications.[40] However, the lung gene expression pattern of JCR rats (genetically somewhat distinct than other strains, derived by crossing LA/N-cp and SH obese rats[46]) was generally the opposite of the other strains, implying a strain-specific variation in the transcriptome. We noted that 2 obese strains due to their leptin receptor mutation (JCR and SHHF) had opposing patterns of expression for most gene clusters in the lung including the genes involved in metabolic processes.[39] When exposed to ozone, these 5 strains shifted their lung expression in the same direction, albeit at different levels.[39] These changes in different rat strains suggest that while inhaled ozone induces similar effects on the lung, there are quantitative differences in expression of specific gene clusters in each strain based on their underlying condition.[39] Ozone effects on genes in the lung were primarily noted in SHR and stoke-prone SHR, but not in severely compromised SHHF and JCR.[39] The whole-transcriptome analysis of WKY and SH after ozone exposure,[39] unlike few inflammatory gene changes examined in these strains after fly ash particle exposure,[48] provided a different picture and insights into greater effects in SH rats of ozone than in WKY rats.

As in the lung, when baseline expression of genes in the heart tissue was determined, it was further apparent that JCR and SHHF had opposing expression profiles, whereas those genetically closer strains SHR, stoke-prone SHR, and SHHF showed similar expression of genes.[40] These data clearly emphasized that the phenotypic expression of disease might be similar in 2 strains of rats; however, the mechanisms that bring about these phenotypes depend on the underlying genetic differences and individual variability in the transcriptional response of regulatory networks. Because of these complexities, the therapeutic interventions targeted for a given disease phenotype might not be similarly effective in all individuals. These studies emphasize that the susceptibility variations are complex, and a systems-based approach with continued use of high-throughput technologies and identification of patterns of changes in gene expression, epigenetic regulators, and phenotypes collectively will provide increased understanding of mechanisms and guide personalized therapeutic interventions that will be effective.

Use of Rodent Models of Metabolic Alterations in Air Pollution Susceptibility Studies

Research on air pollution further expanded to include metabolic diseases as a risk factor for exacerbated air pollution effects, as new epidemiological evidence began to emerge linking air pollution to these diseases (ie,. diabetes, metabolic syndrome, obesity).[66,67] The interest in how diet could modify health effects of pollutants prompted studies that included unhealthy diets as modifiers of air pollution health effects. Since air pollution was linked to a wide array of systemic effects, the quest to identify circulating mediators that produce systemic effects was also apparent.[68–70] Likewise, the choice of animal models used for understanding mechanisms of

susceptibility variations began to include diet-induced predisposition to metabolic diseases, such as obesity and diabetes. A number of studies have been published examining how ozone-induced inflammation may be associated with greater production of interleukin-33 in obese mice and the modulation through interleukin-17A and the influence of gut microbiota in exacerbating ozone-induced airway hyperresponsiveness.[71–73] Although these studies have shown increases in ozone-induced inflammatory response in obese mice, our use of 2 rat models of obesity with genetic predisposition to cardiovascular diseases showed no exacerbation of net ozone–induced injury and inflammation relative to healthy rats.[63] This suggests that multiple host factors including genetic background might be critical in the exacerbation of the inflammatory response in obese models. Moreover, the regulatory mechanisms that control obesity might influence susceptibility to lung injury and inflammation differently in individuals.

Diet supplementations and nutrient deficiencies have been examined as modifying factors of air pollution–induced cardiopulmonary health impairments.[74–77] Feeding of a high-fat diet in healthy rats has been linked to increased metabolic impairment and insulin resistance after repeated particulate matter instillation.[78] In a mouse model, high-fat diet has been shown to increase insulin resistance after repeated exposure to particulate matter, which correlated with increased plasma to tissue ratio of heat shock protein-70 that has been shown to be a biomarker of systemic changes associated with type 2 diabetes.[79] High-fat diet in a mouse model has also been shown to exacerbate changes in blood–brain barrier integrity after traffic-related motor vehicle exhaust exposures as evidenced by increased expression of oxidized low density lipoprotein signaling in the vasculature.[80] High-fat or high-carbohydrate/fructose diets in male and female Brown Norway rats, which are resistant to developing diet-induced obesity, showed increased body fat percentage relative to lean mass in males,[81] but when exposed to ozone, diet did not significantly exacerbate lung injury or inflammation. These studies imply that that diet-induced susceptibility differences are dependent on model selection and biological end point.

Individuals consuming healthy dietary fats might have reduced responsiveness to air pollutants. Based on the health benefits of omega-6 and omega-3 fatty acids in a clinical study showing decreases in particulate air pollution–induced vasoconstriction,[82] we demonstrated that rats fed an omega-3-rich diet, similar to humans, had attenuated vascular contractility response to ozone.[75] However, these rats developed foamy macrophage accumulation in the lung with impaired lipid transporters expression, suggesting inhibition of lipid surfactant clearance.[75] Although it is likely that the type and the concentration of dietary supplements might play a role in this adverse effect, lipid-rich diets with several unsaturated binding sites are likely to have impact on the lung as lipids can accumulate in the form of surfactant. And constant exposure to oxygen and oxidant pollutants also makes the lipids more susceptible to oxidation within the lung. Thus, not only host factors but also the type of intervention can impact the effects of air pollutants.

Air Pollution and Neurobehavioral Impact: Use of Animal Models of Neural Diseases

In the past decade, significant epidemiological and experimental evidence has been accumulated pertaining to the effects of air pollutants on various brain areas and neurobehavioral alterations.[83] In epidemiological studies, exposure to air pollutants has been linked to Alzheimer disease,[84] depression and suicide,[85] cognitive dysfunction,[86] Parkinson disease,[87] autism spectrum disorder,[88] and neurodegenerative diseases.[89] Recently, short-term exposure to air pollution has also been associated with increases in criminal activities.[90] However, to date, only limited experimental studies have used animal models of brain disorders to determine whether and how air pollutants interactively exacerbate the disease phenotype. In one study, exposure to diesel exhaust for 5 to 13 weeks in female 5X familial AD mice prone to Alzheimer disease has been shown to accelerate amyloid-β plaque formation in the brain without having significant systemic inflammation.[91] In a genetic stress-sensitive rat model of depression, the Flinders Sensitive Line rat, repeated ozone exposure is associated with exacerbated behavioral alterations and oxidative stress in the hippocampus and frontal cortex, relative to control animals.[92] These studies are beginning to emphasize the role of neural regulation in health effects of air pollutants and how central mechanisms may contribute to human susceptibility variations.

Evidence of the Role of Neuroendocrine System in Mediating Air Pollutant Health Effects and Its Implications in Susceptibility Variations

It is well-documented that when a stress is encountered, a highly conserved host response will involve the activation of 2 major survival mechanisms, that is (1) mobilization of energy sources from storage sites and channeling of metabolite precursors to organs where they are needed the most and (2) recognizing the location of stress and mobilizing immune cells to the site of injury to fight invading organisms or creating an innate immune response that removes unwanted or damaged tissues/cells to initiate healing process in case of an injury or tissue damage.[93] The degree of host response to a stressor will depend on the underlying physiological condition and genetic variability. The peripheral autonomic sensory nerves recognize stress in the body and relay the information to the brain centers through the activation of stress responsive regions.[94] The sympathetic and parasympathetic arms nervous system are activated. This leads to the activation of neuroendocrine stress response pathways involving sympathetic–adrenal–medullary (SAM) and hypothalamus–pituitary–adrenal (HPA) axes, which release adrenal-derived stress hormones, such as epinephrine and corticosterone/cortisol, respectively.[95,96] These

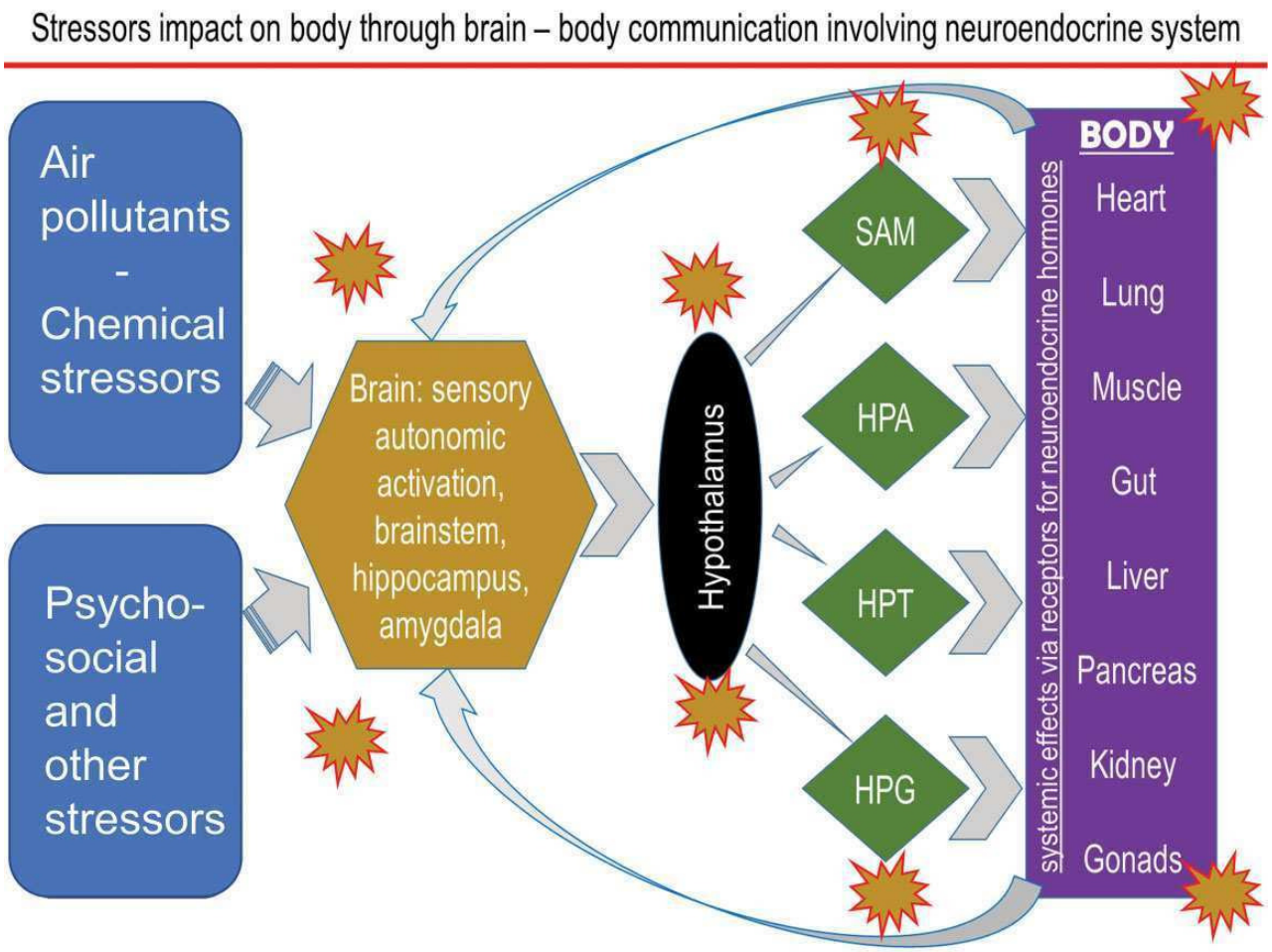

Figure 2. The proposed schematic of the mechanisms by which chemical and nonchemical stressors affect multiple organs through the activation/suppression of neuroendocrine axes. HPA indicates hypothalamic-pituitary-adrenal; HPG, hypothalamus–pituitary–gonadal axes; HPT, hypothalamus–pituitary–thyroid; SAM, sympathetic–adrenal–medullary.

are the hormones, which through their receptors in various tissues, mediate cellular metabolic and immune changes to protect the host from stress. When stress is no longer a threat, these same hormones reverse acute stressor–induced effects through feedback inhibition.[97] Because of selective distribution of the stress hormone receptor subtypes in the brain centers, these hormones also regulate learning and memory that is likely linked to an adaptation/habituation response.[95,98,99] These host survival mechanisms, well characterized for bodily injuries and infections, are tailored to the type of stressor encountered and the location of the injury in the body (Figure 2). Any variations in these mechanisms[100] might impact how individuals differ in their susceptibility to stressors.

Although the neuroendocrine-mediated activation of SAM and HPA stress axes in maintaining homeostatic balance are well characterized, prior air pollution studies neither systematically examined their involvement in peripheral and local health effects nor assessed their potential significance in disease causation or susceptibility variations. In inhalation toxicology studies, these acute reversible physiological changes have been often recognized but not characterized for their systemic and pulmonary consequences.[101] Air pollution effects on autonomic nervous system, and sympathetic and parasympathetic reflex cardiopulmonary changes, however, have been well characterized[102,103] such that air pollution regulations, in part, rely on evidence of autonomically mediated cardiovascular changes in heart rate variability.[104,105]

The research effort for identifying circulating mediators responsible for extrapulmonary effects of air pollutants prompted us to examine a wide array of circulating cytokines, acute phase proteins, and metabolic hormones in our experimental studies. The lack of increases in circulating cytokines, in general, but striking increases in leptin and acute phase proteins in many of our studies[106–108] led us to consider neural effects and subsequent peripheral changes. The Gackière et al[109] paper of 2011 showing the activation of hypothalamic stress responsive regions in rats acutely exposed to ozone served as a catalyst for us to consider neural mechanisms, especially the neuroendocrine stress pathways in examining air pollution health effects and how this may be important in susceptibility variations.

Linking Peripheral Metabolic and Immune Effects of Irritant Air Pollutants to Neuroendocrine Stress Pathways

Our first few studies on neuroendocrine pathways focused on circulating stress hormones and characterization of resultant peripheral effects. We demonstrated that ozone exposure increased circuiting epinephrine, corticosterone/cortisol, and acute phase response proteins.[70,107,108] A single exposure to ozone also resulted in a series of metabolic effects together with depletion of circulating lymphocytes in a reversible manner. These effects were not associated with the release of cytokines from the lung into the circulation as metabolic effects occurred before detectable lung inflammation.[107,108] These effects were characterized by the release of numerous free fatty acids into the circulation, likely through ozone-induced adipose lipolysis, increases in circulating branched-chain amino acids indicating muscle protein catabolism, increased gluconeogenesis, inhibition of lipid synthesis as indicated by downregulated gene expressions in the liver, and inhibition of bile acids release into the circulation with increased cholesterol, indicating inhibition of cholesterol breakdown.[108] Ozone exposure produced hyperglycemia, glucose intolerance, and diminished glucose-mediated insulin secretion from pancreatic β cells.[70,107,108] Subsequently, published epidemiological studies incorporating metabolic homeostasis markers have reported association between air pollution and indices of altered glucose homeostasis.[110,111]

Animal studies involving exposure to another irritant air pollutant, acrolein, which deposits primarily in nasal airways, also exhibited similar peripheral metabolic changes.[112] Acrolein-induced nasal injury/inflammation and also lung inflammation were associated with increases in circulating stress hormones, with diabetic rats being more susceptible to metabolic effects.[112] In a human clinical study where ozone exposure occurred during intermittent exercise, similar increases in a variety of free fatty acids in the circulation and metabolites of membrane lipid breakdown together with increases in cortisol/corticosterone were shown.[113] Virtually, all pathways associated with lipid metabolism were altered as evident by changes in circulating lipid metabolites in humans exposed to ozone.[113] Thus, we demonstrated that this stress response to ozone was coherent between species. There are a few other recent studies that have also examined the activation of the neuroendocrine system, especially the HPA in mediating ozone effects.[114–116] One earlier study examining the effects of concentrated ambient particles in rats with allergic airways disease showed changes in the stress response pathway.[117] All these effects observed in rat models and in humans indicated that SAM and HPA axes were stimulated by ozone and acrolein exposures and caused peripheral effects.[118] This fight-or-flight response, induced by other host stressors or injuries, likely contributes to variations in susceptibility to effects of air pollution. Epidemiological studies have begun examining the biomarkers of HPA activation and subsequent associations with circulating stress hormones as well as metabolic alterations after exposure to increased levels of air pollutants.[119]

The confirmation of the role of circulating stress hormones in mediating systemic and pulmonary effects of ozone was initially made using the intervention of adrenalectomy, since adrenals are the main source of adrenaline and glucocorticoids. As expected, bilateral total adrenalectomy depleted circulating corticosterone and epinephrine nearly completely, but norepinephrine levels did not change as it is produced by nerve terminals and acts locally in a paracrine manner.[120] To our surprise, adrenalectomy resulted in near elimination of all ozone-mediated systemic metabolic, immunological, and pulmonary effects emphasizing the role of circulating adrenal-derived stress hormones in mediating these effects.[120,121] In follow-up studies, we demonstrated that if the receptors of these stress hormones (ie, adrenergic and glucocorticoid) are selectively blocked using pharmacological treatments, ozone-induced lung injury and inflammation were inhibited in an antagonist-specific manner.[122] It was evident that the effect of blocking glucocorticoid receptors was more central and reduced all metabolic effects and systemic immunosuppression effects of ozone (ie, depletion of circulating lymphocytes). On the other hand, as β-adrenergic receptors are densely distributed in the lung and regulate respiratory muscle tone,[123] the blockade of these receptors was associated with reduced local lung vascular leakage and extravasation of neutrophils at the site of stress.[122] These data implied that the tissue distribution for adrenergic and glucocorticoid receptors is a critical determinant of the organ-specific effects of air pollution–induced stress response. The roles of β-adrenergic and glucocorticoid receptors in mediating ozone-induced lung injury/inflammation and systemic effects were further established by a gain-of-function experiment where adrenalectomized rats were treated with β-adrenergic and glucocorticoid receptor agonists and exposed to ozone.[124] Thus, any variations in these receptors distribution in specific organs or the alterations in receptors sensitivity can contribute to variability in host response to environmental stressors in peripheral organs.

The autonomic activation by air pollutants likely involves stimulation of sensory vagus nerves in the lung and brain regions including brain stem and hypothalamus,[109] leading to the activation of SAM and HPA axes. The vagus nerve innervating the lung originates from jugular and nodose ganglion, which receives projections from the nucleus tractus solitarius (NTS) of the brain stem.[125] The neural connection from NTS to hypothalamus involves norepinephrine and glucagon-like peptide-1 neurons.[126] Although ozone has been shown to activate these stress responsive regions, it is still not clear if ozone-induced changes in the lung initiates changes in the brain through vagal sensory nerves or if there are circulating mediators which reach and cross the blood–brain barrier to induce discrete effects on different brain regions including the hypothalamus. The key initiating event for systemic changes is currently being actively investigated in the field of air pollution health effects.[127]

Our recent study has shown that acute ozone exposure induces a wide array of gene expression changes in the brain stem and hypothalamus that are similar to those induced during hypoxia (ie, interferon signaling and the activation of stress pathways).[128] These ozone-induced gene expression changes in rats are associated with increases in adrenaline and corticosterone while depleting prolactin, luteinizing hormone, and also thyroid-stimulating hormone, suggesting the concomitant inhibition of hypothalamus–pituitary–gonadal (HPG) and hypothalamus–pituitary–thyroid (HPT) axes. The activation of SAM and HPA and associated inhibition of HPG and HPT axes have been reported after application of other stressors.[129] These data suggest that air pollutants, especially those that induce lung irritation, impact all neuroendocrine axes leading to suppression of thyroid and reproductive pathways along with the activation of adrenal axes (Figure 2). Importantly, most of the ozone-induced changes in hormones are not evident in adrenalectomized rats, implying the contribution of circulating adrenal-derived stress hormones in regulating brain effects of ozone. Circulating stress hormones are needed to produce lung effects of ozone, and if no lung effects occur due to lack of stress hormones, no changes in brain regions are noted.[128] Glucocorticoids in conjunction with mineralocorticoids and catecholamines have been shown to interactively regulate the process of adaptation and habituation centrally.[99] The regulatory roles of adrenergic and glucocorticoid receptors systems and feedback inhibition need to be further examined in relation to health effects of acute and chronic air pollution exposures and more importantly how neuroendocrine response variations may lead to variations in human susceptibility to air pollution health effects.

The Potential Contribution of Stress Hormones in Adaptation/Plasticity and Susceptibility Variations

Once released into the circulation, stress hormones exert their cellular effects through adrenergic and glucocorticoid receptors.[130,131] Subtypes of adrenergic receptors regulate cardiovascular functionality, smooth muscle tone, and other homeostatic processes.[130] Impaired adrenergic receptor function in the brain has been shown to contribute to chronic stress in the central and peripheral organs.[132–135] Glucocorticoid receptors are important in homeostatic cellular metabolic and immunological response of peripheral organs and also in regulating stress, memory, learning, and habituation centrally.[98,136] Impaired regulation of adrenergic and glucocorticoid receptors in the brain has been linked to chronic stress and a number of neurological disorders including depression and posttraumatic stress disorder. For example, glucocorticoid resistance has been noted in a variety of neuropathies and inflammatory conditions.[131,137] There is evidence that the selective distribution of mineralocorticoid and glucocorticoids receptors in limbic areas, which regulate stress response, is involved in habituation and learning.[99] However, the impacts of air pollutants on these receptor pathways have been poorly examined.

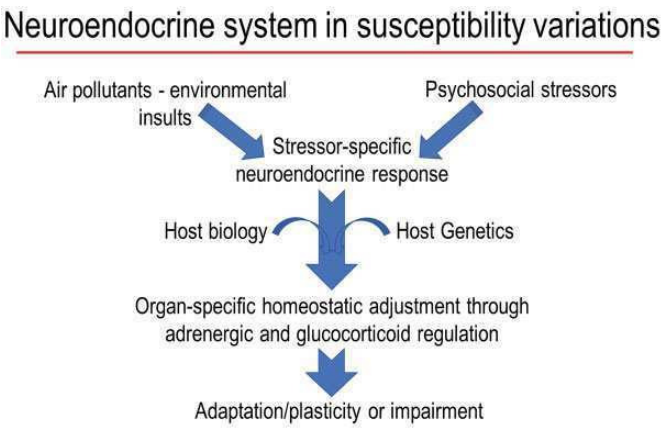

Figure 3. A flowchart of interactive effects of air pollutants and nonchemical stressors. Air pollutant–induced neuroendocrine activation producing a stress response, which when combined with the impact of other stressors and host susceptibilities may still maintain plasticity and lead to adaptation through adrenergic and glucocorticoid receptors or produce an impairment.

Reversibility of air pollution–induced changes and the loss of effects upon repeated daily exposure (often referred to as adaptation, habituation, or tolerance) to some pollutants, specifically ozone, has been the area of research interest with limited understanding of the mechanisms.[138,139] Based on the role of adrenergic and glucocorticoid regulation of habituation, learning, and memory[99,130,131] and the activation of SAM and HPA axes after a single air pollution exposure, it is conceivable that the adaptation that occurs upon repeated exposure to ozone will involve the loss of neuroendocrine activation through adrenergic and glucocorticoid mechanisms. The importance of the presence of catecholamines and glucocorticoids in the peripheral circulation, their increases following stress, and in mediation of systemic, pulmonary, and even brain effects of air pollutants[120,121,124,128] emphasizes their role in regulation of adaptive, homeostatic, and pathological processes.[131,132] It has been shown that after applying psychological stress, the changes in peripheral stress hormones is necessary for inducing inflammatory changes in the brain,[135] implying the regulatory role of peripheral stress hormones in orchestrating brain response. Our recent study showing the lack of ozone effects on brain in adrenalectomized rats corroborates with these findings.[128] Thus, the potential interactions between underlying host neurobehavioral disorders and air pollutant modification of susceptibility through neuroendocrine system are likely (Figure 3). The role of developmental reprogramming of neuroendocrine pathways has been proposed to increase susceptibility of children to allergic respiratory diseases in epidemiological studies.[140,141] The use of animal models with impaired activation of neuroendocrine stress response will prove useful in understanding how loss of adaptation can impact chronic diseases after exposure to air pollutants.

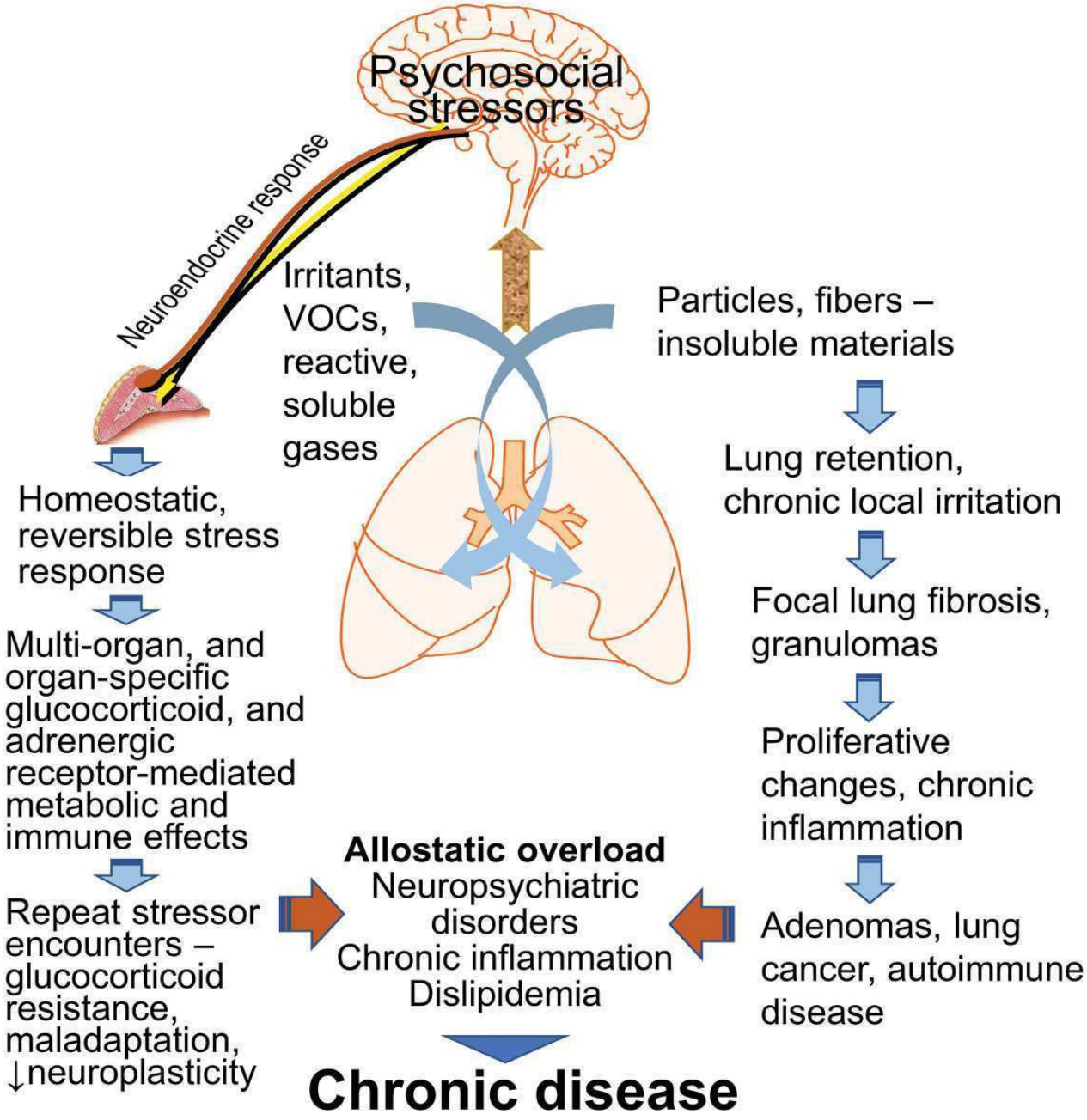

Figure 4. A proposed mechanistic paradigm of how air pollutants with other stressors contribute to individual variations in disease susceptibility. Acute exposure to all air pollutants may produce reversible homeostatic systemic metabolic and immune effects in a stressor-specific manner through neuroendocrine activation. Upon repeated encounter of stressors, however, there is likely a loss of adaptation/plasticity adding to allostatic load which can exacerbate disease. The pollutants that accumulate in the lung over time and produce low chronic irritation in lung epithelial cells additionally can induce local proliferative changes with the loss of adaptive stress response that can ultimately lead to active granuloma/fibrosis and/or lung cancer. This can have added contribution to the allostatic load and contribute to variation in susceptibility. VOCs = volatile organic chemicals.

Neuroendocrine Activation and Allostatic Load in Susceptibility Variations

The concepts of neuroendocrine-mediated allostasis, habituation/adaptation, homeostasis, and allostatic load are not new and have been examined for decades in relation to the plasticity or the lack thereof of neuroendocrine system to accelerate disease.[95,126,142–145] How poor socioeconomic conditions, diets, environmental exposures, and psychosocial stressors together with genetic predisposition can push the homeostatic system to lose plasticity and increase the susceptibility to chronic diseases, including acceleration of aging, has been studied and incorporated in modeling approaches to quantify health burden from stressful life conditions. However, this has

not been done for air pollution as an environmental stressor. The new epidemiological[119,146] and experimental[12] evidence of the involvement of neuroendocrine system in mediating air pollution effects necessitates its incorporation in allostatic load modeling and assessing the contribution to human mortality and morbidity.

Air pollutants are physicochemically diverse, and therefore, their deposition, solubility, and retention can influence the extent to which acute neuroendocrine stress response is produced after inhalation. When exposures occur repeatedly over a long period of time or when chronic exposure leads to retention of inhaled pollutants, local lung irritation can result in induction of fibrotic processes ultimately causing proliferative changes or even cancer with some exposures (Figure 4). The pollutants that activate central stress responsive regions and the neuroendocrine axes will, based on host susceptibilities or the presence of other stressors, induce systemic metabolic and immunological changes to counteract stress. When overwhelmed by repeated encounters of stressors or cumulative impacts, the adrenergic and glucocorticoid functions can be impaired. This can contribute to allostatic load, causing neural dysregulation, chronic inflammation, and peripheral metabolic disorders based on the preexisting conditions (Figure 4). Thus, when examining susceptibility variations from exposure to air pollutants, multiple host conditions, the contribution of neuroendocrine pathways, and chronicity of air pollution exposure should be incorporated into study designs.

Future Perspective

The epidemiological studies have provided associations between air pollution and biological as well as physiological indicators of chronic pulmonary and cardiovascular diseases,[57,58] metabolic diseases (including obesity),[66,67,146] neuropsychiatric disorders, and even low birth weight outcomes,[147] suggesting a mechanistic link. Given the evidence that the air pollutant effects are mediated through changes in endocrine activities, that the impairment of neuroendocrine function is linked to virtually all chronic dieases, and that the neurobehavioral disorders and chronic peripheral diseases coexist, necessitates more focused studies along neuroendocrine axes using systems approach. Epidemiological associations, such as those showing increases in blood glucose[148] and increases in pulmonary inflammation in children who are receiving bronchodilators,[149] can be linked to air pollution–induced activation of neuroendocrine response and release of stress hormones in the circulation.[12,119,146] Thus, the role of neuroendocrine system in air pollution and chronic disease susceptibility is mechanistically plausible; however, clear understanding of stressor-specific outcomes and interactive role of neural regulation in susceptibility variations remains an area needing further research. Although adrenergic and glucocorticoid receptor systems have been widely manipulated for currently used therapeutic interventions to treat chronic diseases,[150,151] further understanding of the role of central neuroendocrine mechanisms in air pollution health effects offers opportunities to identify new mechanistic pathways for therapeutic interventions. Other well-recognized interventions that could improve health of susceptible individuals include access to healthy living conditions, healthy diets, and reduced psychosocial stressors that are linked to health disparities.

Impaired neuroendocrine regulation of homeostasis can contribute to host susceptibility in the presence of other stressors, such as chronic diseases, obesity, psychosocial pressures, poor diets, genetic predisposition, and air pollution. Epidemiological association studies have begun to incorporate the allostatic load concept in air pollution studies.[152,153] The concepts of chemical and nonchemical stressors, external and internal exposomes, and one health have already emerged.[154] Given the role of neuroendocrine system in processing all perceived stress signals centrally and producing stressor-specific metabolic and immune responses through coordination of all organ systems, one can presume that its malfunction can lead to abnormal stress response and increase in host susceptibility. Assessing the biological plausibility for interactive influence of each of these risk factors and identifying the biological indicators or group of indicators of stressor-induced susceptibilities with or without air pollutants will contribute to mechanistic understanding of the overall health outcomes.[145,155,156] As modeling approaches have been applied to assess the risk of cumulative stressors on overall well-being, health, and longevity, more emphasis is needed to understand molecular mechanisms with systems concepts in mind. New insights have also emerged in the biology of developmental processes, and therefore, the research on understanding how early life stresses may predispose one to adulthood diseases has grown[157] (not covered in this article). The incorporation of the neuroendocrine homeostatic mechanisms and dynamicity of response with consideration of all life stressors, host physiology, and genetics, with or without incorporating air pollutant exposure, will be useful in understanding the mechanisms of susceptibility variations.

Authors' Note

The research described in this article has been reviewed by the National Health and Environmental Effects Research Laboratory, US Environmental Protection Agency, and approved for publication. Approval does not signify that the contents necessarily reflect the views and policies of the Agency nor does the mention of trade names of commercial products constitute endorsement or recommendation for use.

Acknowledgments

The authors thank Drs Michael Madden, Colette Miller, and Ian Gilmour of the US EPA for their critical review of the manuscript. Most of the previously published work presented in the second half of the paper is performed at the National Health and Environmental Effects Laboratory of the US Environmental Protection Agency, Research Triangle Park, North Carolina, by my 3 excellent trainees, Drs Andres Henriquez, Samantha Snow, and Desinia Miller.

Declaration of Conflicting Interests

The author(s) declared no potential conflicts of interest with respect to the research, authorship, and/or publication of this article.

Funding

The author(s) disclosed receipt of the following financial support for the research, authorship, and/or publication of this article: The preparation of this review paper was supported by the US Environmental Protection Agency's Intramural Research Program.

ORCID iD

Urmila P. Kodavanti https://orcid.org/0000-0001-6333-1024

References

1. Landrigan PJ, Fuller R, Acosta NJR, et al. The Lancet Commission on pollution and health. *Lancet*. 2018;391(10119):462-512.
2. Brain JD, Valberg PA, Mensah GA. Species differences. In: Brain JD, Beck BD, Warren AJ, Shaikh RA, eds. *Variations in Susceptibility to Inhaled Pollutants. Identification, Mechanisms, and Policy Implications*. Baltimore, MD: The Johns Hopkins University Press; 1988:89-103.
3. Sweeney TD, Brain JD, Godleski JJ. Preexisting disease. In: Brain JD, Beck BD, Warren AJ, Shaikh RA, eds. *Variations in Susceptibility to Inhaled Pollutants. Identification, Mechanisms, and Policy Implications*. Baltimore, MD: The Johns Hopkins University Press; 1988:142-158.
4. Kodavanti UP, Costa DL, Bromberg PA. Rodent models of cardiopulmonary disease: their potential applicability in studies of air pollutant susceptibility. *Environ Health Perspect*. 1998;106(suppl 1):111-130.
5. Siafakas NM, Tzortzaki EG. Few smokers develop COPD. Why? *Respir Med*. 2002;96(8):615-624.
6. Yang IV, Schwartz DA. Epigenetic mechanisms and the development of asthma. *J Allergy Clin Immunol*. 2012;130(6):1243-1255.
7. Yauk CL, Lucas Argueso J, Auerbach SS, et al. Harnessing genomics to identify environmental determinants of heritable disease. *Mutat Res*. 2013; 752(1):6-9.
8. Arbour NC, Lorenz E, Schutte BC, et al. TLR4 mutations are associated with endotoxin hyporesponsiveness in humans. *Nat Genet*. 2000;25(2): 187-191.
9. Hollingsworth JW II, Cook DN, Brass DM, et al. The role of Toll-like receptor 4 in environmental airway injury in mice. *Am J Respir Crit Care Med*. 2004;170(2):126-132.
10. Kodavanti UP, Thomas RF, Ledbetter AD, et al. Diesel exhaust induced pulmonary and cardiovascular impairment: the role of hypertension intervention. *Toxicol Appl Pharmacol*. 2013;268(2):232-240.
11. Dye JA, Costa DL, Kodavanti UP. Executive summary: variation in susceptibility to ozone-induced health effects in rodent models of cardiometabolic disease. *Inhal Toxicol*. 2015;27(suppl 1):105-115.
12. Snow SJ, Henriquez AR, Costa DL, Kodavanti UP. Neuroendocrine regulation of air pollution health effects: emerging insights. *Toxicol Sci*. 2018; 164(1):9-20.
13. Ding M, Chen F, Shi X, Yucesoy B, Mossman B, Vallyathan V. Diseases caused by silica: mechanisms of injury and disease development. *Int Immunopharmacol*. 2002;2(2-3):173-182.
14. Castranova V, Vallyathan V. Silicosis and coal workers' pneumoconiosis. *Environ Health Perspect*. 2000;108(suppl 4):675-684.
15. Huang SX, Jaurand MC, Kamp DW, Whysner J, Hei TK. Role of mutagenicity in asbestos fiber-induced carcinogenicity and other diseases. *J Toxicol Environ Health B Crit Rev*. 2011;14(1-4):179-245.
16. May S, Romberger DJ, Poole JA. Respiratory health effects of large animal farming environments. *J Toxicol Environ Health B Crit Rev*. 2012;15(8): 524-541.
17. Donaldson K, Murphy FA, Duffin R, Poland CA. Asbestos, carbon nanotubes and the pleural mesothelium: a review of the hypothesis regarding the role of long fibre retention in the parietal pleura, inflammation and mesothelioma. *Part Fibre Toxicol*. 2010;7:5. doi:10.1186/1743-8977-7-5.
18. Tryka AF, Sweeney TD, Brain JD, Godleski JJ. Short-term regional clearance of an inhaled submicrometric aerosol in pulmonary fibrosis. *Am Rev Respir Dis*. 1985;132(3):606-611.
19. Adamson IY, Hedgecock C. Patterns of particle deposition and retention after instillation to mouse lung during acute injury and fibrotic repair. *Exp Lung Res*. 1995;21(5):695-709.
20. Kodavanti UP, Jaskot RH, Su WY, Costa DL, Ghio AJ, Dreher KL. Genetic variability in combustion particle-induced chronic lung injury. *Am J Physiol*. 1997;272(3 pt 1):L521-L532.
21. Kodavanti UP, Jackson MC, Ledbetter AD, et al. Lung injury from intratracheal and inhalation exposures to residual oil fly ash in a rat model of monocrotaline-induced pulmonary hypertension. *J Toxicol Environ Health A*. 1999;57(8):543-563.
22. Shy CM. Epidemiologic evidence and the United States air quality standards. *Am J Epidemiol*. 1979;110(6):661-671.
23. Drazen JM, Takebayashi T, Long NC, De Sanctis GT, Shore SA. Animal models of asthma and chronic bronchitis. *Clin Exp Allergy*. 1999;29(suppl 2):37-47.
24. Bice DE, Seagrave J, Green FH. Animal models of asthma: potential usefulness for studying health effects of inhaled particles. *Inhal Toxicol*. 2000;12(9):829-862.
25. Kodavanti UP, Mebane R, Ledbetter A, et al. Variable pulmonary responses from exposure to concentrated ambient air particles in a rat model of bronchitis. *Toxicol Sci*. 2000;54(2):441-451.
26. Kodavanti UP, Schladweiler MC, Ledbetter AD, et al. The spontaneously hypertensive rat: an experimental model of sulfur dioxide-induced airways disease. *Toxicol Sci*. 2006;94(1):193-205.
27. Nikula KJ, Green FH. Animal models of chronic bronchitis and their relevance to studies of particle-induced disease. *Inhal Toxicol*. 2000; 12(suppl 4):123-153.
28. Chapman RW. Canine models of asthma and COPD. *Pulm Pharmacol Ther*. 2008;21(5):731-742.
29. Wright JL, Cosio M, Churg A. Animal models of chronic obstructive pulmonary disease. *Am J Physiol Lung Cell Mol Physiol*. 2008;295(1): L1-L15.
30. Gilmour PS, Schladweiler MC, Richards JH, Ledbetter AD, Kodavanti UP. Hypertensive rats are susceptible to TLR4-mediated signaling following exposure to combustion source particulate matter. *Inhal Toxicol*. 2004; 16(suppl 1):5-18.
31. Romieu I, Moreno-Macias H, London SJ. Gene by environment interaction and ambient air pollution. *Proc Am Thorac Soc*. 2010;7(2):116-122.
32. Scoville DK, Botta D, Galdanes K, et al. Genetic determinants of susceptibility to silver nanoparticle-induced acute lung inflammation in mice. *FASEB J*. 2017;31(10):4600-4611.
33. Saul MC, Philip VM, Reinholdt LG; Center for Systems Neurogenetics of Addiction Chesler EJ. High-diversity mouse populations for complex traits. *Trends Genet*. 2019;35(7):501-514.
34. Savov JD, Whitehead GS, Wang J, et al. Ozone-induced acute pulmonary injury in inbred mouse strains. *Am J Respir Cell Mol Biol*. 2004;31(1): 69-77.
35. Kleeberger SR. Genetic aspects of pulmonary responses to inhaled pollutants. *Exp Toxicol Pathol*. 2005;57(suppl 1):147-153.
36. Bauer AK, Kleeberger SR. Genetic mechanisms of susceptibility to ozone-induced lung disease. *Ann N Y Acad Sci*. 2010;1203:113-119.
37. Gershwin LJ. Comparative immunology of allergic responses. *Annu Rev Anim Biosci*. 2015;3:327-346.
38. Kleeberger SR. Genetic aspects of susceptibility to air pollution. *Eur Respir J Suppl*. 2003;40:52s-56s.
39. Ward WO, Kodavanti UP. Pulmonary transcriptional response to ozone in healthy and cardiovascular compromised rat models. *Inhal Toxicol*. 2015; 27(suppl 1):93-104.
40. Ward WO, Kodavanti UP. Left ventricular gene expression profile of healthy and cardiovascular compromised rat models used in air pollution studies. *Inhal Toxicol*. 2015;27(suppl 1):63-79.
41. Smith CM, Sassetti CM. Modeling diversity: do homogeneous laboratory strains limit discovery? *Trends Microbiol*. 2018;26(11):892-895.

42. Salimova E, Nowak KJ, Estrada AC, et al. Variable outcomes of human heart attack recapitulated in genetically diverse mice. *NPJ Regen Med*. 2019;4:5.
43. Dockery DW, Pope CA III, Xu X, et al. An association between air pollution and mortality in six U.S. cities. *N Engl J Med*. 1993;329(24): 1753-1759.
44. Wallenborn JG, Schladweiler MC, Nyska A, et al. Cardiopulmonary responses of Wistar Kyoto, spontaneously hypertensive, and stroke-prone spontaneously hypertensive rats to particulate matter (PM) exposure. *J Toxicol Environ Health A*. 2007;70(22):1912-1922.
45. Kodavanti UP, Schladweiler MC, Ledbetter AD, et al. Consistent pulmonary and systemic responses from inhalation of fine concentrated ambient particles: roles of rat strains used and physicochemical properties. *Environ Health Perspect*. 2005;113(11):1561-1568.
46. Kodavanti UP, Russell JC, Costa DL. Rat models of cardiometabolic diseases: baseline clinical chemistries, and rationale for their use in examining air pollution health effects. *Inhal Toxicol*. 2015;27(suppl 1):2-13.
47. Costa DL, Kodavanti UP. Toxic responses of the lung to inhaled pollutants: benefits and limitations of lung-disease models. *Toxicol Lett*. 2003; 140-141:195-203.
48. Kodavanti UP, Schladweiler MC, Ledbetter AD, et al. The spontaneously hypertensive rat as a model of human cardiovascular disease: evidence of exacerbated cardiopulmonary injury and oxidative stress from inhaled emission particulate matter. *Toxicol Appl Pharmacol*. 2000;164(3):250-263.
49. Kodavanti UP, Schladweiler MC, Ledbetter AD, et al. Temporal association between pulmonary and systemic effects of particulate matter in healthy and cardiovascular compromised rats. *J Toxicol Environ Health A*. 2002;65(20):1545-1569.
50. Saxena RK, Gilmour MI, Schladweiler MC, McClure M, Hays M, Kodavanti UP. Differential pulmonary retention of diesel exhaust particles in Wistar Kyoto and spontaneously hypertensive rats. *Toxicol Sci*. 2009; 111(2):392-401.
51. Shen YH, Pham AK, Davis B, et al. Sex and strain-based inflammatory response to repeated tobacco smoke exposure in spontaneously hypertensive and Wistar Kyoto rats. *Inhal Toxicol*. 2016;28(14):677-685.
52. Mumaw CL, Surace M, Levesque S, et al. Atypical microglial response to biodiesel exhaust in healthy and hypertensive rats. *Neurotoxicology*. 2017; 59:155-163.
53. Tavera Busso I, Mateos AC, Juncos LI, Canals N, Carreras HA. Kidney damage induced by sub-chronic fine particulate matter exposure. *Environ Int*. 2018;121(pt 1):635-642.
54. Wong EM, Walby WF, Wilson DW, Tablin F, Schelegle ES. Ultrafine particulate matter combined with ozone exacerbates lung injury in mature adult rats with cardiovascular disease. *Toxicol Sci*. 2018;163(1):140-151.
55. Shannahan JH, Nyska A, Cesta M, et al. Subchronic pulmonary pathology, iron overload, and transcriptional activity after Libby amphibole exposure in rat models of cardiovascular disease. *Environ Health Perspect*. 2012; 120(1):85-91.
56. Gottipolu RR, Wallenborn JG, Karoly ED, et al. One-month diesel exhaust inhalation produces hypertensive gene expression pattern in healthy rats. *Environ Health Perspect*. 2009;117(1):38-46.
57. Bind MA, Peters A, Koutrakis P, Coull B, Vokonas P, Schwartz J. Quantile regression analysis of the distributional effects of air pollution on blood pressure, heart rate variability, blood lipids, and biomarkers of inflammation in elderly American men: the Normative Aging Study. *Environ Health Perspect*. 2016; 124(8):1189-1198.
58. Adar SD, Chen YH, D'Souza JC, et al. Longitudinal analysis of long-term air pollution levels and blood pressure: a cautionary tale from the multi-ethnic study of atherosclerosis. *Environ Health Perspect*. 2018; 126(10): 107003.
59. Dabass A, Talbott EO, Rager JR, et al. Systemic inflammatory markers associated with cardiovascular disease and acute and chronic exposure to fine particulate matter air pollution ($PM_{2.5}$) among US NHANES adults with metabolic syndrome. *Environ Res*. 2018;161:485-491.
60. Raza A, Dahlquist M, Lind T, Ljungman PLS. Susceptibility to short-term ozone exposure and cardiovascular and respiratory mortality by previous hospitalizations. *Environ Health*. 2018; 17(1):37.
61. Ramot Y, Kodavanti UP, Kissling GE, Ledbetter AD, Nyska A. Clinical and pathological manifestations of cardiovascular disease in rat models: the influence of acute ozone exposure. *Inhal Toxicol*. 2015;27(suppl 1): 26-38.
62. Dye JA, Ledbetter AD, Schladweiler MC, Costa DL, Kodavanti UP. Whole body plethysmography reveals differential ventilatory responses to ozone in rat models of cardiovascular disease. *Inhal Toxicol*. 2015; 27(suppl 1):14-25.
63. Kodavanti UP, Ledbetter AD, Thomas RF, et al. Variability in ozone-induced pulmonary injury and inflammation in healthy and cardiovascular-compromised rat models. *Inhal Toxicol*. 2015;27(suppl 1):39-53.
64. Hatch GE, Crissman K, Schmid J, et al. Strain differences in antioxidants in rat models of cardiovascular disease exposed to ozone. *Inhal Toxicol*. 2015;27(suppl 1):54-62.
65. Jain A, Mårtensson J, Mehta T, Krauss AN, Auld PA, Meister A. Ascorbic acid prevents oxidative stress in glutathione-deficient mice: effects on lung type 2 cell lamellar bodies, lung surfactant, and skeletal muscle. *Proc Natl Acad Sci U S A*. 1992;89(11):5093-5097.
66. Rajagopalan S, Brook RD. Air pollution and type 2 diabetes: mechanistic insights. *Diabetes*. 2012; 61(12):3037-3045.
67. Thiering E, Heinrich J. Epidemiology of air pollution and diabetes. *Trends Endocrinol Metab*. 2015; 26(7):384-394.
68. Brook RD, Sun Z, Brook JR, et al. Extreme air pollution conditions adversely affect blood pressure and insulin resistance: the air pollution and cardiometabolic disease study. *Hypertension*. 2016;67(1):77-85.
69. Chen Z, Salam MT, Toledo-Corral C, et al. Ambient air pollutants have adverse effects on insulin and glucose homeostasis in Mexican Americans. *Diabetes Care*. 2016;39(4):547-554.
70. Miller DB, Snow SJ, Henriquez A, et al. Systemic metabolic derangement, pulmonary effects, and insulin insufficiency following subchronic ozone exposure in rats. *Toxicol Appl Pharmacol*. 2016;306:47-57.
71. Shore SA. Mechanistic basis for obesity-related increases in ozone-induced airway hyperresponsiveness in mice. *Ann Am Thorac Soc*. 2017;14(suppl 5):S357-S362.
72. Mathews JA, Krishnamoorthy N, Kasahara DI, et al. Augmented responses to ozone in obese mice require IL-17A and gastrin-releasing peptide. *Am J Respir Cell Mol Biol*. 2018;58(3):341-351.
73. Tashiro H, Cho Y, Kasahara DI, et al. Microbiota contribute to obesity-related increases in the pulmonary response to ozone. *Am J Respir Cell Mol Biol*. [published online ahead of print May 30, 2019]. doi:10.1165/rcmb.2019-0144OC.
74. Moon KY, Park MK, Leikauf GD, Park CS, Jang AS. Diesel exhaust particle-induced airway responses are augmented in obese rats. *Int J Toxicol*. 2014;33(1):21-28.
75. Snow SJ, Cheng WY, Henriquez A, et al. Ozone-induced vascular contractility and pulmonary injury are differentially impacted by diets enriched with coconut oil, fish oil, and olive oil. *Toxicol Sci*. 2018;163(1):57-69.
76. Wesselink AK, Hatch EE, Wise LA. Invited commentary: interaction between diet and chemical exposures. *Am J Epidemiol*. 2019;188(9): 1605-1607.
77. Miller CN, Rayalam S. The role of micronutrients in the response to ambient air pollutants: Potential mechanisms and suggestions for research design. *J Toxicol Environ Health B Crit Rev*. 2017; 20(1):38-53.
78. Yan YH, Chou CC, Lee CT, Liu JY, Cheng TJ. Enhanced insulin resistance in diet-induced obese rats exposed to fine particles by instillation. *Inhal Toxicol*. 2011;23(9):507-519.
79. Goettems-Fiorin PB, Grochanke BS, Baldissera FG, et al. Fine particulate matter potentiates type 2 diabetes development in high-fat diet-treated mice: stress response and extracellular to intracellular HSP70 ratio analysis. *J Physiol Biochem*. 2016;72(4):643-656.
80. Suwannasual U, Lucero J, McDonald JD, Lund AK. Exposure to traffic-generated air pollutants mediates alterations in brain microvascular integrity in wildtype mice on a high-fat diet. *Environ Res*. 2018;160:449-461.
81. Gordon CJ, Phillips PM, Johnstone AF, et al. Effect of high-fructose and high-fat diets on pulmonary sensitivity, motor activity, and body

composition of brown Norway rats exposed to ozone. *Inhal Toxicol*. 2016; 28(5):203-215.
82. Brigham EP, Woo H, McCormack M, et al. Omega-3 and omega-6 intake modifies asthma severity and response to indoor air pollution in children. *Am J Respir Crit Care Med*. 2019;199(12):1478-1486.
83. Russ TC, Reis S, van Tongeren M. Air pollution and brain health: defining the research agenda. *Curr Opin Psychiatry*. 2019;32(2):97-104.
84. Calderón-Garcidueñas L, González-Maciel A, Kulesza RJ, et al. Air pollution, combustion and friction derived nanoparticles, and Alzheimer's disease in urban children and young adults [published online ahead of print]. *J Alzheimers Dis*. 2019. doi:10.3233/JAD-190331. PMID: 31256139.
85. Gładka A, Rymaszewska J, Zatoński T. Impact of air pollution on depression and suicide. *Int J Occup Med Environ Health*. 2018;31(6): 711-721.
86. Cipriani G, Danti S, Carlesi C, Borin G.Danger in the air: air pollution and cognitive dysfunction. *Am J Alzheimers Dis Other Demen*. 2018; 33(6):333-341.
87. Palacios N, Fitzgerald KC, Hart JE, et al. Air pollution and risk of Parkinson's disease in a large prospective study of men. *Environ Health Perspect*. 2017;125(8):087011.
88. Lam J, Sutton P, Kalkbrenner A, et al. A systematic review and meta-analysis of multiple airborne pollutants and autism spectrum disorder. *PLoS One*. 2016;11(9):e0161851.
89. Jayaraj RL, Rodriguez EA, Wang Y, Block ML. outdoor ambient air pollution and neurodegenerative diseases: the neuroinflammation hypothesis. *Curr Environ Health Rep*. 2017;4(2):166-179.
90. Berman JD, Burkhardt J, Bayham J, Carter E, Wilson A. Acute air pollution exposure and the risk of violent behavior in the United States [published online ahead of print]. *Epidemiology*. 2019; doi:10.1097/EDE.0000000000001085. PMID: 31430264.
91. Hullmann M, Albrecht C, van Berlo D, et al. Diesel engine exhaust accelerates plaque formation in a mouse model of Alzheimer's disease. *Part Fibre Toxicol*. 2017;14(1):35.
92. Mokoena ML, Harvey BH, Viljoen F, Ellis SM, Brink CB. Ozone exposure of Flinders Sensitive Line rats is a rodent translational model of neurobiological oxidative stress with relevance for depression and antidepressant response. *Psychopharmacology (Berl)*. 2015;232(16): 2921-2938.
93. Russell G, Lightman S. The human stress response [published online ahead of print]. *Nat Rev Endocrinol*. 2019; doi:10.1038/s41574-019-0228-0. Review. PMID: 31249398.
94. Waxenbaum JA, Varacallo M. *Anatomy, Autonomic Nervous System. StatPearls [Internet]*. Treasure Island, FL: StatPearls Publishing; 2019; PMID: 30969667.
95. McEwen BS.From molecules to mind. Stress, individual differences, and the social environment. *Ann N Y Acad Sci*. 2001;935:42-49.
96. Herman JP, McKlveen JM, Ghosal S, et al. Regulation of the hypothalamic-pituitary-adrenocortical stress response. *Compr Physiol*. 2016;6(2):603-621.
97. McEwen BS. In pursuit of resilience: stress, epigenetics, and brain plasticity. *Ann N Y Acad Sci*. 2016;1373(1):56-64.
98. Viho EMG, Buurstede JC, Mahfouz A, et al. Corticosteroid action in the brain: the potential of selective receptor modulation. *Neuroendocrinology*. 2019;109(3):266-276.
99. de Kloet ER, de Kloet SF, de Kloet CS, de Kloet AD. Top-down and bottom-up control of stress-coping. *J Neuroendocrinol*. 2019;31(3): e12675.
100. Levran O, Peles E, Randesi M, et al. Genetic variations in genes of the stress response pathway are associated with prolonged abstinence from heroin. *Pharmacogenomics*. 2018;19(4):333-341.
101. Pauluhn J. Inhalation toxicology: methodological and regulatory challenges. *Exp Toxicol Pathol*. 2008;60(2-3):111-124.
102. Evans JM, Jenkins RA, Ilgner RH, Knapp CF, Zhang Q, Patwardhan AR. Acute cardiovascular autonomic responses to inhaled particulates. *Eur J Appl Physiol*. 2015;115(2):257-268.
103. Perez CM, Hazari MS, Farraj AK. Role of autonomic reflex arcs in cardiovascular responses to air pollution exposure. *Cardiovasc Toxicol*. 2015;15(1):69-78.
104. Park SK, Auchincloss AH, O'Neill MS, et al. Particulate air pollution, metabolic syndrome, and heart rate variability: the Multi-Ethnic Study of Atherosclerosis (MESA). *Environ Health Perspect*. 2010;118(10): 1406-1411.
105. Ljungman PLS, Li W, Rice MB, et al. Long- and short-term air pollution exposure and measures of arterial stiffness in the Framingham Heart Study. *Environ Int*. 2018;121(pt 1):139-147.
106. Shannahan JH, Alzate O, Winnik WM, et al. Acute phase response, inflammation and metabolic syndrome biomarkers of Libby asbestos exposure. *Toxicol Appl Pharmacol*. 2012;260(2):105-114.
107. Bass V, Gordon CJ, Jarema KA, et al. Ozone induces glucose intolerance and systemic metabolic effects in young and aged Brown Norway rats. *Toxicol Appl Pharmacol*. 2013;273(3):551-560.
108. Miller DB, Karoly ED, Jones JC, et al. Inhaled ozone (O3)-induces changes in serum metabolomic and liver transcriptomic profiles in rats. *Toxicol Appl Pharmacol*. 2015;286(2):65-79.
109. Gackière F, Saliba L, Baude A, Bosler O, Strube C. Ozone inhalation activates stress-responsive regions of the CNS. *J Neurochem*. 2011; 117(6):961-972.
110. Li W, Dorans KS, Wilker EH, et al. Ambient air pollution, adipokines, and glucose homeostasis: the Framingham Heart Study. *Environ Int*. 2018; 111:14-22.
111. Yitshak Sade M, Kloog I, Liberty IF, Schwartz J, Novack V. The association between air pollution exposure and glucose and lipids levels. *J Clin Endocrinol Metab*. 2016; 101(6):2460-2467.
112. Snow SJ, McGee MA, Henriquez A, et al. Respiratory effects and systemic stress response following acute acrolein inhalation in *rats* . *Toxicol Sci*. 2017;158(2):454-464.
113. Miller DB, Ghio AJ, Karoly ED, et al. Ozone exposure increases circulating stress hormones and lipid metabolites in humans. *Am J Respir Crit Care Med*. 2016;193(12):1382-1391.
114. Thomson EM, Vladisavljevic D, Mohottalage S, Kumarathasan P, Vincent R. Mapping acute systemic effects of inhaled particulate matter and ozone: multiorgan gene expression and glucocorticoid activity. *Toxicol Sci*. 2013;135(1):169-181.
115. Thomson EM, Pal S, Guénette J, et al. Ozone inhalation provokes glucocorticoid-dependent and -independent effects on inflammatory and metabolic pathways. *Toxicol Sci*. 2016;152(1):17-28.
116. Thomas J, Guénette J, Thomson EM. Stress axis variability is associated with differential ozone-induced lung inflammatory signaling and injury biomarker response. *Environ Res*. 2018;167:751-758.
117. Sirivelu MP, MohanKumar SM, Wagner JG, Harkema JR, MohanKumar PS. Activation of the stress axis and neurochemical alterations in specific brain areas by concentrated ambient particle exposure with concomitant allergic airway disease. *Environ Health Perspect*. 2006.;114(6):870-874.
118. Kodavanti UP.Stretching the stress boundary: linking air pollution health effects to a neurohormonal stress response. *Biochim Biophys Acta*. 2016; 1860(12):2880-2890.
119. Li H, Cai J, Chen R, et al. Particulate matter exposure and stress hormone levels: a randomized, double-blind, crossover trial of air purification. *Circulation*. 2017; 136(7):618-627.
120. Miller DB, Snow SJ, Schladweiler MC, et al. Acute ozone-induced pulmonary and systemic metabolic effects are diminished in adrenalectomized rats. *Toxicol Sci*. 2016;150(2):312-322.
121. Henriquez A, House J, Miller DB, et al. Adrenal-derived stress hormones modulate ozone-induced lung injury and inflammation. *Toxicol Appl Pharmacol*. 2017;329:249-258.
122. Henriquez AR, Snow SJ, Schladweiler MC, et al. Adrenergic and glucocorticoid receptor antagonists reduce ozone-induced lung injury and inflammation. *Toxicol Appl Pharmacol*. 2018;339:161-171.
123. Barnes PJ. Distribution of receptor targets in the lung. *Proc Am Thorac Soc*. 2004;1(4):345-351.
124. Henriquez AR, Snow SJ, Schladweiler MC, et al. Beta-2 adrenergic and glucocorticoid receptor agonists modulate ozone-induced pulmonary

protein leakage and inflammation in healthy and adrenalectomized rats. *Toxicol Sci*. 2018;166(2):288-305.
125. Mazzone SB., Undem BJ. Vagal afferent innervation of the airways in health and disease. *Physiol Rev*. 2016; 96(3): 975-1024.
126. Herman JP. Regulation of hypothalamo-pituitary-adrenocortical responses to stressors by the nucleus of the solitary tract/dorsal vagal complex. *Cell Mol Neurobiol*. 2018;38(1):25-35.
127. Aragon MJ, Topper L, Tyler CR, et al. Serum-borne bioactivity caused by pulmonary multiwalled carbon nanotubes induces neuroinflammation via blood-brain barrier impairment. *Proc Natl Acad Sci U S A*. 2017;114(10): E1968-E1976.
128. Henriquez AR, House JS, Snow SJ, et al. Ozone-induced dysregulation of neuroendocrine axes requires adrenal-derived stress hormones [published online ahead of print]. *Toxicol Sci*. 2019; pii: kfz182. doi:10.1093/toxsci/kfz182. PMID: 31397875.
129. Acevedo-Rodriguez A, Kauffman AS, Cherrington BD, Borges CS, Roepke TA, Laconi M. Emerging insights into hypothalamic-pituitary-gonadal axis regulation and interaction with stress signalling. *J Neuroendocrinol*. 2018;30(10):e12590.
130. Tank AW, Lee Wong D. Peripheral and central effects of circulating catecholamines. *Compr Physiol*. 2015;5(1):1-15.
131. Merkulov VM, Merkulova TI, Bondar NP. Mechanisms of brain glucocorticoid resistance in stress-induced psychopathologies. *Biochemistry (Mosc)*. 2017;82(3):351-365.
132. Mravec B. Role of catecholamine-induced activation of vagal afferent pathways in regulation of sympathoadrenal system activity: negative feedback loop of stress response. *Endocr Regul*. 2011;45(1):37-41.
133. Goldstein DS, Kopin IJ. Linking stress, catecholamine autotoxicity, and allostatic load with neurodegenerative diseases: a focused review in memory of Richard Kvetnansky. *Cell Mol Neurobiol*. 2018;38(1): 13-24.
134. Nakai A, Suzuki K. Adrenergic control of lymphocyte trafficking and adaptive immune responses. *Neurochem Int*. [published online ahead of print October 19, 2018]. doi:10.1016/j.neuint.2018.10.017.
135. Johnson JD, Barnard DF, Kulp AC, Mehta DM. Neuroendocrine regulation of brain cytokines after psychological stress. *J Endocr Soc*. 2019; 3(7):1302-1320.
136. Baker JD, Ozsan I, Rodriguez Ospina S, Gulick D, Blair LJ. Hsp90 heterocomplexes regulate steroid hormone receptors: from stress response to psychiatric disease. *Int J Mol Sci*. 2018;20(1):79.
137. Ingawale DK, Mandlik SK, Patel SS. An emphasis on molecular mechanisms of anti-inflammatory effects and glucocorticoid resistance. *J Complement Integr Med*. 2015;12(1):1-13.
138. Chen CY, Bonham AC, Plopper CG, Joad JP. Neuroplasticity in nucleus tractus solitarius neurons after episodic ozone exposure in infant primates. *J Appl Physiol (1985)*. 2003;94(2):819-827.
139. Jang AS, Choi IS, Lee JH, Park CS, Park CS. Prolonged ozone exposure in an allergic airway disease model: adaptation of airway responsiveness and airway remodeling. *Respir Res*. 2006;7(1):24.
140. Deng Q, Deng L, Lu C, Li Y, Norbäck D. Parental stress and air pollution increase childhood asthma in China. *Environ Res*. 2018;165:23-31.
141. Bandoli G, von Ehrenstein O, Ghosh JK, Ritz B. Synergistic effects of air pollution and psychosocial stressors on adolescent lung function. *J Allergy Clin Immunol*. 2016;138(3):918-920.
142. McEwen BS, Stellar E.Stress and the individual. mechanisms leading to disease. *Arch Intern Med*. 1993;153(18):2093-2101.
143. McEwen BS. Hormones as regulators of brain development: life-long effects related to health and disease. *Acta Paediatr Suppl*. 1997;422: 41-44.
144. Coste SC, Murray SE, Stenzel-Poore MP. Animal models of CRH excess and CRH receptor deficiency display altered adaptations to stress. *Peptides*. 2001;22(5):733-741.
145. Mair CA, Cutchin MP, Kristen Peek M. Allostatic load in an environmental riskscape: the role of stressors and gender. *Health Place*. 2011; 17(4):978-987.
146. Hajat A, Diez Roux AV, Castro-Diehl C, et al. The association between long-term air pollution and urinary catecholamines: evidence from the multi-ethnic study of atherosclerosis. *Environ Health Perspect*. 2019; 127(5):57007.
147. Nobles CJ, Grantz KL, Liu D, et al. Ambient air pollution and fetal growth restriction: physician diagnosis of fetal growth restriction versus population-based small-for-gestational age. *Sci Total Environ*. 2019; 650(Pt 2):2641-2647.
148. Lucht SA, Hennig F, Matthiessen C, et al. Air pollution and glucose metabolism: an analysis in non-diabetic participants of the Heinz Nixdorf Recall Study. *Environ Health Perspect*. 2018; 126(4):047001.
149. Qian Z, Lin HM, Chinchilli VM, et al. Interaction of ambient air pollution with asthma medication on exhaled nitric oxide among asthmatics. *Arch Environ Occup Health*. 2009;64(3):168-176.
150. Dézsi CA, Szentes V. The real role of β-blockers in daily cardiovascular therapy. *Am J Cardiovasc Drugs*. 2017;17(5):361-373.
151. Singh D, Fabbri LM, Vezzoli S, Petruzzelli S, Papi A.Extrafine triple therapy delays COPD clinically important deterioration vs ICS/LABA, LAMA, or LABA/LAMA. *Int J Chron Obstruct Pulmon Dis*. 2019;14:531-546.
152. Egorov AI, Griffin SM, Converse RR, et al. Vegetated land cover near residence is associated with reduced allostatic load and improved biomarkers of neuroendocrine, metabolic and immune functions. *Environ Res*. 2017;158:508-521.
153. Thomson EM. Air Pollution, stress, and allostatic load: linking systemic and central nervous system impacts. *J Alzheimers Dis*. 2019;69(3): 597-614.
154. Burwell-Naney K, Wilson SM, Whitlock ST, Puett R. Hybrid resiliency-stressor conceptual framework for informing decision support tools and addressing environmental injustice and health inequities. *Int J Environ Res Public Health*. 2019;16(8):E1466.
155. Logan AC, Prescott SL, Haahtela T, Katz DL. The importance of the exposome and allostatic load in the planetary health paradigm. *J Physiol Anthropol*. 2018;37(1):15.
156. Crews DE, Kawa NC, Cohen JH, Ulmer GL, Edes AN. Climate change, uncertainty and allostatic load. *Ann Hum Biol*. 2019;46(1):3-16.
157. Morello-Frosch R, Shenassa ED. The environmental "riskscape" and social inequality: implications for explaining maternal and child health disparities. *Environ Health Perspect*. 2006;114(8):1150-1153.

Online Data Supplement

Ozone-induced dysregulation of neuroendocrine axes requires adrenal-derived stress hormones

Andres R. Henriquez[1], John S. House[2,3], Samantha J. Snow[4], Colette N. Miller[4], Mette C. Schladweiler[4], Anna Fisher[5], Hongzu Ren[5], Matthew Valdez[1], Prasada R. Kodavanti[6], and Urmila P. Kodavanti[4]**

[1]Oak Ridge Institute for Science and Education, Research Triangle Park, NC, United States; [2]Bioinformatics Research Center, North Carolina State University, Raleigh, NC, United States; [3]Center for Human Health and the Environment, North Carolina State University, Raleigh, NC, United States; [4]Environmental Public Health Division, National Health and Environmental Effects Research Laboratory, U.S. Environmental Protection Agency, Research Triangle Park, NC, United States; [5]Research Cores Unit, National Health and Environmental Effects Research Laboratory, U.S. Environmental Protection Agency, Research Triangle Park, NC, United States; and [6]Toxicity Assessment Division, National Health and Environmental Effects Research Laboratory, U.S. Environmental Protection Agency, Research Triangle Park, NC, United States.

Address correspondence:
**Urmila P. Kodavanti, PhD
MD B105-04, NHEERL, U.S. EPA
Research Triangle Park, NC 27711
kodavanti.urmila@epa.gov
Phone: 919 541-4963; Fax: 919-541-0026

SUPPLEMENTARY METHODS:

Sham and adrenalectomy surgeries in rats

Male 12–13 weeks old rats were anesthetized by injection of ketamine (25–50 mg/kg in saline; i.p.). After confirmation of complete anesthesia, buprenorphine was administered (0.02 mg/kg/ml in saline; s.c.) for analgesia. Animals were placed in sternal recumbency position, prepared for aseptic surgery procedure and given to trained veterinarians from Charles River Laboratories Inc. who performed surgeries under sterile conditions. Surgeries were performed using protocols established at Charles River Laboratories Inc. If needed, additional anesthesia was provided by nose-only inhalation of vaporized isoflurane (3%). Right and left glands were removed for ADREX group while for SH group the same surgical procedures were performed except that adrenals were not removed. Immediately after surgery, the rats were placed on heating pads and closely monitored by observing their movements. Once awake, rats were injected with meloxicam (0.2 mg/kg; s.c.) and for analgesia. Additionally, rats were injected with buprenorphine (0.02 mg/ml/kg, s.c.) for two more times every 8-10 hrs for continued analgesia. After surgery, the animals were pair housed with Enviro Dry enrichment/nesting material. To maintain adequate fluid and electrolyte balance, AD rats were provided with saline (0.9% sodium chloride) while SH rats received normal tap water and both groups were provided with powdered as well as pelleted diets, both ad libitum except during exposure to air or ozone. Based on previous reports (Nicolaides et al., 2013; Sakakibara et al., 2014), rats were given a recovery period of 4–6 days prior to any exposure. There were no signs of evident distress and food and water consumption were similar for SH and AD groups (Miller et al., 2016a).

Brainstem and hypothalamus total RNA isolation and mRNA sequencing

The entire frozen hypothalamic and brainstem regions were processed for RNA extraction (n=4 per group). Total RNA was isolated following manufacturer protocol indicated by Direct-Zol RNA MiniPrep kit from Zymo Research (Irvine, CA, USA) and quantified using Qubit RNA reagent (Invitrogen, Waltham, MA, USA). Using prepX polyA mRNA Isolation Kit (Wafergen Biosystems, Fremont, CA, USA), the mRNA was isolated from total RNA. Samples were run in Apollo324 automated sample processing system for mRNA selection. RNA-Seq library was prepared with Wafergen's PrepX mRNA 48 Protocol. cDNA libraries were amplified by 15 PCR cycles with indexing primers according to Wafergen's protocol. dsDNA from each library was quantified by Qubit dsDNA HS Assay kit (Molecular Probes, Eugene, OR, USA) and the quality was checked by Agilent Bioanalyzer (Agilent Technologies, Santa Clara, CA, USA). Each library was diluted to 4 nM by estimating the average molecular sizes from Bioanalyzer data and the concentration from Qubit measurement. Pooled and indexed libraries were sequenced according to Illumina NextSeq 500 protocols (2.5-3.2 pM + 2% PhiX from Illumina Inc., San Diego, CA, USA). The sequencing data were stored in Illumina's BaseSpace-cloud.

Nextseq data normalization and bioinformatics

Sequenced mRNA reads were mapped to the rat genome (rn6) using ensemble release 83 in the Partek® Flow suite. R version 3.2.3 (2015-12-10). Differential gene expression was assessed in DESeq2 package in R (v. 1.10.1) (Love et al., 2014) rounding the count matrix to the nearest integer and considered different when the

adjusted p value (FDR) was ≤0.1. Pathway heatmaps of normalized counts from DESeq2 were created using the heatmap.2 function of the g-plots package (Warnes et al., 2015). Pathway/set enrichment was performed using the eXploring Genomic Relations (XGR) package in R (http://xgr.r-forge.r-project.org/; Fang et al., 2016). Pathway analyses were conducted using genes identified as differentially expressed at adjusted p value < 0.10. Pathway ontologies were defined by the molecular signature database hallmark gene set (MsigDBH; Liberzon et al., 2015) and the immunologic signature gene sets (MsigDBC7). For each ontology set tested, pathway testing was considered significant at FDR < 0.10 for the enrichment statistic. Upstream analysis tools from Ingenuity Pathways Analysis® (IPA®, QIAGEN Redwood City, www.qiagen.com/ingenuity) software were used to compare our results with previously reported databases. By overlapping genes differentially expressed after ozone exposure with genes differentially expressed by the action of multiple upstream regulators, it is possible to obtain a p-value of the overlap. An activation score predicting an activated state (changes similar to those induced by ozone) or an inhibited state (changes dissimilar to those induced by ozone) is defined by an activation z-score of >2 or <-2, respectively.

Fang H, Knezevic B, Burnham KL, Knight JC. XGR software for enhanced interpretation of genomic summary data, illustrated by application to immunological traits. *Genome Med* 2016;8(1):129.

Liberzon A, Birger C, Thorvaldsdóttir H, Ghandi M, Mesirov JP, Tamayo P. The Molecular Signatures Database (MSigDB) hallmark gene set collection. *Cell Syst* 2015;1(6):417-425.

Love MI, Huber W, Anders S. Moderated estimation of fold change and dispersion for RNA-seq data with DESeq2. *Genome Biol* 2014;15,550

Miller, D.B., Snow, S.J., Schladweiler, M.C., Richards, J.E., Ghio, A.J., Ledbetter, A.D., and Kodavanti, U.P. Acute Ozone-Induced Pulmonary and Systemic Metabolic Effects Are Diminished in Adrenalectomized Rats. *Toxicol Sci* 2016a;150(2):312-22.

Nicolaides, N. C., Chrousos, G. P., and Charmandari, E. (2013). Adrenal Insufficiency. Endotext [Internet]. South Dartmouth (MA): MDText.com, Inc., 2000–2013 Nov 18.

Sakakibara, Y., Katoh, M., Suzuki, M., Kawabe, R., Iwase, K., and Nadai, M. (2014). Effect of adrenalectomy on expression and induction of UDP-glucuronosyltransferase 1A6 and 1A7 in rats. *Biol. Pharm. Bull.* 37, 618–624.

Warnes GR, Bolker B, Bonebakker L, Gentleman R, Huber W, Liaw A, Lumley T, Maechler M, Magnusson A, Moeller S, *et al*. 2015 gplots: Various R Programming Tools for Plotting Data.

Supplementary Figure 1

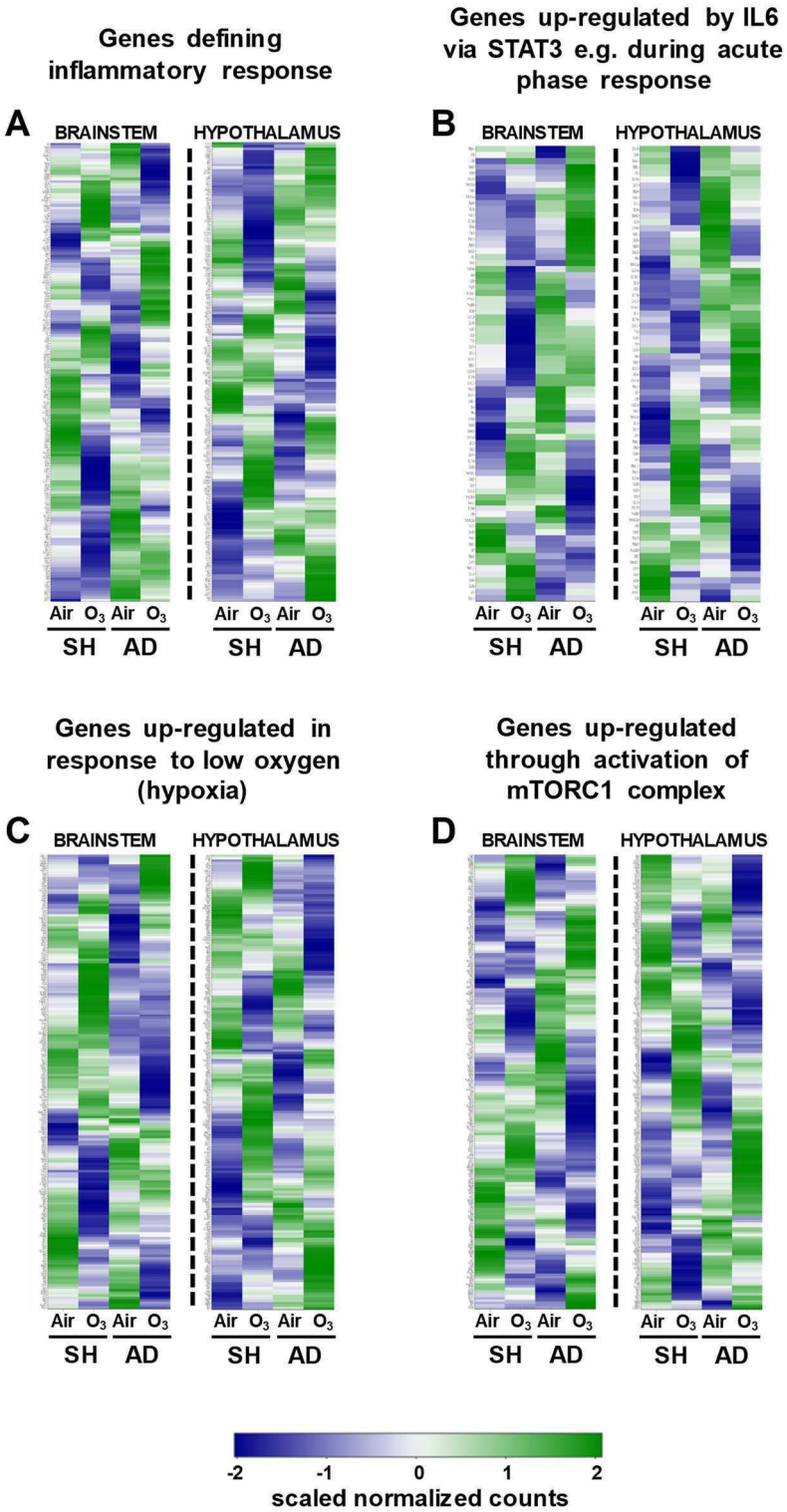

Supplementary Figure 1: Hallmark gene sets significantly enriched after ozone exposure in brainstem and hypothalamus of SHAM rats. Genes for each hallmark gene sets are shown in heatmaps for those defining inflammatory response [200 genes] (A), genes up-regulated by IL6 via STAT3 e.g. during acute phase response [87 genes] (B), genes up-regulated in response to low oxygen (hypoxia) [200 genes] (C), and genes up-regulated through activation of mTORC1 complex [200 genes] (D).

STAA 2020 Nomination:

From: PIHTD, CPHEA, Urmila P Kodavanti

Papers included in the package:

1. Henriquez AR, Snow SJ, Schladweiler MC, Miller CN, Dye JA, Ledbetter AD, Hargrove MM, Richards JE, Kodavanti UP. Exacerbation of ozone-induced pulmonary and systemic effects by β_2-adrenergic and/or glucocorticoid receptor agonist/s. *Sci Rep*. 2019;9(1):17925. Published 2019 Nov 29. doi:10.1038/s41598-019-54269-w

2. Henriquez AR, House JS, Snow SJ, Miller CN, Schladweiler MC, Fisher A, Ren H, Valdez M, Kodavanti PR, Kodavanti UP. Ozone-induced dysregulation of neuroendocrine axes requires adrenal-derived stress hormones [published online ahead of print, 2019 Aug 9]. *Toxicol Sci*. 2019;kfz182. doi:10.1093/toxsci/kfz182

3. Kodavanti UP. Susceptibility Variations in Air Pollution Health Effects: Incorporating Neuroendocrine Activation. *Toxicol Pathol*. 2019;47(8):962–975. doi:10.1177/0192623319878402

Justification

Major therapeutics interact with irritant pollutants to exacerbate lung damage

Bronchodilators, and steroidal anti-inflammatory medications are currently prescribed for major cardiopulmonary and inflammatory as well as autoimmune conditions, or acute allergic reactions. What our study (Henriquez et al., 2019a; paper #1) shows is that at the therapeutically-relevant doses, these drugs can exacerbate pulmonary and systemic effects of irritant air pollutant, such as ozone. Our study is clinically important because of the widespread use of these medications. Because the use of these therapeutics is so common in the entire population that the air pollution health burden for those on mediation can be significant. These observations may lead to new health advisory for those taking mediations to avoid air pollution. Air pollution is the number 5th cause of human mortality and morbidity worldwide.

This exacerbation occurs because irritant air pollutants increase two circulating stress hormones, epinephrine and glucocorticoids, which activate same receptors as those activated by these drugs. In the lung ozone-induced increases in epinephrine and bronchodilators, synergistically activate adrenergic receptors on epithelium which are known to induce innate inflammatory response to air pollutants. Glucocorticoids regulate virtually all biological processes and represent major class of therapeutics. We show that glucocorticoids increased after ozone exposure, bind to same steroidal drug receptors, and exacerbate systemic effects. Most research studies use very high doses of these drugs, but our study used doses in therapeutic range to determine actual clinical relevance. Recent epidemiology shows that asthmatic children taking bronchodilators have exacerbated air pollution response. Our study provides a causal evidence and explains why. Although many studies have been devoted to identifying susceptible subpopulations, the field of therapeutics interactions with environmental chemicals has lagged behind.

Brain is the target organ for air pollutant effects

One may cast doubts about the recent BBC documentary of April 16th, 2019 which is based on epidemiology shows that (http://www.bbc.com/future/story/20190415-how-air-pollution-is-doing-more-than-killing-us) air pollution not only kills humans but makes humans commit crimes. One of our nominated papers makes us believe these findings, and shows causal evidence that how a single irritant pollutant exposure can produce dramatic effects on stress-responsive regions of the brain, the same regions that promote stress-induced psychopathic behaviors (paper #2; Henriquez et al., 2019b). These are the same regions where psychosocial, PTSD, ADHD, depression and other neurological effects are processed. All these conditions are associated with increased circulating stress hormones, the same hormones that are increased after ozone exposure. Hypothalamus is the master processor of stress mediated effects on the body. Using novel and robust high throughput sequencing technology, this paper for the first one to show that the brainstem where the information from lung is relayed to, and the hypothalamus where it is passed, the expression of hundreds of genes changed immediately following a single exposure to ozone. These are the genes that regulate brain processes. We show that these changes in hypothalamus are tied to rapid changes in brain- and pituitary-derived hormones, including one that mediates the release of stress hormones from adrenals. Implementing surgical intervention to remove adrenals, the source of stress hormones, we made even more notable observation that these hormones are absolutely necessary for ozone to affect the brain (Henriquez et al., 2019b). These findings are highly significant because they shed light on how stress responses are generated by air pollutants, why psychosocial stressors might synergistically interact with environmental stressors such as air pollutants, and how they contribute to neuropsychiatric abnormalities. These results also provide insights into potential therapeutic targets and strategies.

Air pollutant induce stress pathways that are also inked to psychosocial stressors

The incidence of neuropsychiatric disorders is increasing at alarming rates in the United states. Because of the current social health crisis, the mental health crises are expected to skyrocket. These include ADHD, PTSD, depression, suicidal and criminal behaviors, schizophrenia, dementia, and Alzheimer's disease. Socioeconomical and environmental factors have been the major contributors. While air pollution accounts for over 70% of all environmental cause aliments, its contribution to mental health can be highly significant and may not be ignored. The ability of brain to sense the injury in lung encountering air pollutant, process the information and relay to the body to promote repair and assure survival is remarkably regulated by the very same circulating stress hormone, cortisol, that tells brain what to do when stress is encountered. We show that removing this hormone from circulation using adrenalectomy in our model abolishes the ability of brain to sense lung injury. Ironically this is the same stress hormone increased in many psychiatric conditions, likely by its altered effectiveness or production. Our recent use of experimental adrenalectomy approach has opened not only our eyes but has influenced the entire field of air pollution and mental health research; as evidenced by new publications incorporating biological endpoints of measuring stress hormones. The use of adrenalectomy in the second nominated paper shows us why adrenal-derived stress hormones are central to sensing the air pollution stress and producing a stress response with its potential connection to mental disorders and also peripheral diseases.

A missing link in susceptibility variations: neuroendocrine stress system

Our non-conventional air pollution studies that link them to neuroendocrine system, mental health, environment and peripheral diseases have been noticed very quickly with enthusiasm

and a sense of cogency by scientific community. Among a number of invited presentations, the most recent being in an inaugural symposium session, attended by over 700 participants at the 2019 Society of Toxicologic Pathology meeting was received with wide interest and compelling desire for discussion. This led to a publication of a review paper, the third nominated paper in the 2019 series published in a special issue of the society journal, Toxicologic Pathology. Critically examining the contribution of neuroendocrine system in exacerbation of air pollution health effects and susceptibility variations was the goal of the review. The mechanistic paradigm is proposed in the paper with incorporation of our research on air pollution health effects and neuroendocrine system, and how those explain a path forward that encompasses holistic systems biology view. This review shows that every cell in our body is directly or indirectly connected to brain through neuroendocrine system and the cell fate decisions are made in the brain through glucocorticoid and adrenergic signaling. Individual variations in susceptibility to disease has been at the center of biomedical research for decades. However, thus far, the roles of central nervous and endocrine systems have not been integrated. The review emphasizes the contribution of the very neuroendocrine stress system, that is involved in the body's survival response to environmental and perceived or internal stressors and how variable degree of impairments in this system can contribute to susceptibility variations to air pollution health effects.

How is this important to EPA?

Inform decision making for A&E and integration in the current StRAP

The first nominated paper identifies a new risk factor for air pollution health effects through experimental evidence: the use of steroidal anti-inflammatory drugs and bronchodilators. These drugs are extensively prescribed to asthmatics and those having chronic obstructive pulmonary disease. The study shows synergistic interaction between β2-adrenergic agonists – bronchodilators and inhaled ozone, exacerbating injury and inflammation response. These drugs use the same receptor systems that are activated by air pollution. The prevalence of use of these medications make it a significant public health issues. These data could be used to develop new patient advisory to avoid high air pollution. The current Strategic Research and Planning process for A&E and CSS Programs includes further assessment of adrenergic and glucocorticoid mechanisms in air pollution health assessment and also for priority chemicals listed by CSS.

We have been able to identify and recognize the involvement of neuroendocrine system as the most important contributor of health effects using ozone, as a prototypic air pollutant. Prior ozone criteria documents did not include the role of neuroendocrine system and resulting systemic response. The current criteria document includes these new studies. We are able to understand the roles of adrenergic and glucocorticoid receptors, the interactive effects of chemical and non-chemical stressors, significant involvement of stress responsive brain regions and the importance of the hormonal system that has not been studied systematically in the field of air pollution and health. Thus, this research has led to a shift in paradigm of air pollution health effects research at EPA and other institutions and has informed the future strategies that involve the contribution of air pollution to mental health.

Support existing AOP and contribution to new AOP development within CSS Program

Based on the research in these publications involving brain and neuroendocrine system effects of ozone, there is an incorporation of new research strategy within CSS StRAP that involves incorporating neuroendocrine mechanisms for methodologically challenging chemicals. Adrenergic and glucocorticoid receptors subtypes for adrenal-derived hormones are distributed

ubiquitously and display diversity that regulate most cellular processes involved in homeostatic metabolic and immune surveillance systemically. The AOP for these receptors has been discussed at various levels for a couple of years now at EPA. This research will incorporate *in vitro* to *in vivo* coherency for the adrenergic and glucocorticoid receptor activities of these methodologically challenging chemicals. These studies will lead to correlating the irritancy of these chemicals and biological impact at neuroendocrine level. Thus, these publications have influenced the research direction for the CSS program and supported new AOP development.

A new research strategy for SHC and A&E programs to incorporate chemical and non-chemical stressors

There is an EPA-wide effort now to systematically examine interactive effects of chemical and non-chemical stressors, and developmental impact of maternal stressors supported by SHC and A&E programs. There is an elaborate planning for green-space living and health benefits research, together with how community stressors may interact with environmental stressors to exacerbate adverse health outcomes. The EPA research on developmental stressors and childhood susceptibility also incorporates the neuroendocrine mechanisms based on our studies. The EPA's epidemiology program now incorporates biomarkers informed from our studies to examine the role of neuroendocrine stress system, mental health and how environmental exposures may be contributing the stress-mediated adverse health outcomes. The impact of our stress research has already been evident by recently published clinically-relevant studies incorporating neuroendocrine stress hormonal assessments in air pollution health at EPA and other institutions.

STAA 2020 Nomination:

From: PIHTD, CPHEA, Urmila P Kodavanti

Papers included in the package:

1. Henriquez AR, Snow SJ, Schladweiler MC, Miller CN, Dye JA, Ledbetter AD, Hargrove MM, Richards JE, Kodavanti UP. Exacerbation of ozone-induced pulmonary and systemic effects by β_2-adrenergic and/or glucocorticoid receptor agonist/s. *Sci Rep*. 2019;9(1):17925. Published 2019 Nov 29. doi:10.1038/s41598-019-54269-w

2. Henriquez AR, House JS, Snow SJ, Miller CN, Schladweiler MC, Fisher A, Ren H, Valdez M, Kodavanti PR, Kodavanti UP. Ozone-induced dysregulation of neuroendocrine axes requires adrenal-derived stress hormones [published online ahead of print, 2019 Aug 9]. *Toxicol Sci*. 2019;kfz182. doi:10.1093/toxsci/kfz182

3. Kodavanti UP. Susceptibility Variations in Air Pollution Health Effects: Incorporating Neuroendocrine Activation. *Toxicol Pathol*. 2019;47(8):962–975. doi:10.1177/0192623319878402

Justification 2B and 2C: Previous 5-years nominated publications of authors:

Kodavanti, Urmila (most authors were also included in these STAAs and therefore, the explanation of relatedness is only given for the first mention of the STAA)

- *2019. Level III, US EPA Scientific and Technological Achievement Award,* New mechanistic paradigm for pulmonary and systemic health effects of oxidant and irritant pollutants (Three published papers).

  The research in this nomination involves the role of circulating stress hormones and their receptors in mediating pulmonary effects of ozone. These papers extend the previous work. The previous nominated papers did not examine the importance of therapeutic use of bronchodilators and glucocorticoids and their potential interaction that are clinically relevant. The previous papers also did not examine brain effects and pituitary hormones after ozone exposure and how adrenalectomy influences brain and secretion of pituitary hormones. The review paper unlike prior nominated paper, addresses neuroendocrine system and susceptibility variations for air pollution health effects.

- *2019.* Honorable Mention, *US EPA Scientific and Technological Achievement Award*. Uterine Artery Flow and Offspring Growth in Long-Evans Rats following Maternal Exposure to Ozone during Implantation. Published in Environmental Health Perspectives.

  This paper addresses maternal stress induced by ozone and intrauterine blood flow changes as well as the fetal growth retardation. This is very different from the currently nominated papers.

- 2018. *Level 2 US EPA Science and Technological Achievement Award* for “Researching the role of neuroendocrine stress axes activation in systemic and pulmonary health effects of air pollutants.”

The research in this nomination involves characterization of peripheral effects of ozone in rodents and humans. The current nominated papers are follow-up papers to determine the role of adrenergic and glucocorticoid receptors and a invited review.

- 2018. Level 3 EPA Scientific and Technological Achievement Award. Evaluating naturally occurring asbestos toxicity to inform risk assessment of contaminated sites.
- 2016. *Honorable Mention for US EPA Science and Technological Achievement Award* for "Executive Summary: Variation in Susceptibility to Ozone Induced Health Effects in Rodent Models of Cardiometabolic Disease Inhalation Toxicology" and other 8 associated publications.

  This paper looked at susceptibility variations in 8 healthy and cardio metabolically compromised animal models.

- 2016. *Honorable Mention for US EPA Science and Technological Achievement Award* for "Ozone induces glucose intolerance and systemic metabolic effects in young and aged Brown Norway rats."

  This nomination pertained to age differences in ozone-induced metabolic effects.

- 2015. *Level 3 US EPA Science and Technological Achievement Award* for "Health effects of inhaled diesel emissions generated with CeO2 nano fuel additive."

  This nomination did not involve ozone and examined diesel exhaust and cerium nano particle effects.

- 2014. *Level 3 US EPA Science and Technological Achievement Award* for "Subchronic Pulmonary Pathology, Iron Overload, and Transcriptional Activity after Libby Amphibole Exposure in Rat Models of Cardiovascular Disease."

  This nomination involved studies of Libby asbestos materials and not ozone

- 2014. *Nomination (no award)* for "Diesel exhaust induced pulmonary and cardiovascular impairment: the role of hypertension intervention."

  This nomination did not involve ozone and examined diesel exhaust particle effects and hypertension intervention.

Ledbetter, Allen

- *2019. Level III, US EPA Scientific and Technological Achievement Award,* New mechanistic paradigm for pulmonary and systemic health effects of oxidant and irritant pollutants (Three published papers).
- *2019.* Honorable Mention, *US EPA Scientific and Technological Achievement Award*. Uterine Artery Flow and Offspring Growth in Long-Evans Rats following Maternal Exposure to Ozone during Implantation. Published in Environmental Health Perspectives.
- 2018. *Level 2 US EPA Science and Technological Achievement Award* for "Researching the role of neuroendocrine stress axes activation in systemic and pulmonary health effects of air pollutants."

- 2016. *Honorable Mention for US EPA Science and Technological Achievement Award* for "Executive Summary: Variation in Susceptibility to Ozone Induced Health Effects in

Rodent Models of Cardiometabolic Disease Inhalation Toxicology" and other 8 associated publications.

- 2016. *Honorable Mention for US EPA Science and Technological Achievement Award* for "Ozone induces glucose intolerance and systemic metabolic effects in young and aged Brown Norway rats."
- 2015. *Level 3 US EPA Science and Technological Achievement Award* for "Health effects of inhaled diesel emissions generated with CeO2 nano fuel additive."
- 2014. *Level 3 US EPA Science and Technological Achievement Award* for "Subchronic Pulmonary Pathology, Iron Overload, and Transcriptional Activity after Libby Amphibole Exposure in Rat Models of Cardiovascular Disease."
- 2014. *Nomination (no award)* for "Diesel exhaust induced pulmonary and cardiovascular impairment: the role of hypertension intervention."

Richards, Judy

- *2019. Level III, US EPA Scientific and Technological Achievement Award,* New mechanistic paradigm for pulmonary and systemic health effects of oxidant and irritant pollutants (Three published papers).
- *2019.* Honorable Mention, *US EPA Scientific and Technological Achievement Award*. Uterine Artery Flow and Offspring Growth in Long-Evans Rats following Maternal Exposure to Ozone during Implantation. Published in Environmental Health Perspectives.
- 2018. *Level 2 US EPA Science and Technological Achievement Award* for "Researching the role of neuroendocrine stress axes activation in systemic and pulmonary health effects of air pollutants."
- 2018. Level 3 EPA Scientific and Technological Achievement Award. Evaluating naturally occurring asbestos toxicity to inform risk assessment of contaminated sites.
- 2016. *Honorable Mention for US EPA Science and Technological Achievement Award* for "Executive Summary: Variation in Susceptibility to Ozone Induced Health Effects in Rodent Models of Cardiometabolic Disease Inhalation Toxicology" and other 8 associated publications.
- 2016. *Honorable Mention for US EPA Science and Technological Achievement Award* for "Ozone induces glucose intolerance and systemic metabolic effects in young and aged Brown Norway rats."
- 2015. *Level 3 US EPA Science and Technological Achievement Award* for "Health effects of inhaled diesel emissions generated with CeO2 nano fuel additive."
- 2014. *Level 3 US EPA Science and Technological Achievement Award* for "Subchronic Pulmonary Pathology, Iron Overload, and Transcriptional Activity after Libby Amphibole Exposure in Rat Models of Cardiovascular Disease."
- 2014. *Nomination (no award)* for "Diesel exhaust induced pulmonary and cardiovascular impairment: the role of hypertension intervention."

Schladweiler, Mette

- *2019. Level III, US EPA Scientific and Technological Achievement Award,* New mechanistic paradigm for pulmonary and systemic health effects of oxidant and irritant pollutants (Three published papers).
- *2019.* Honorable Mention, *US EPA Scientific and Technological Achievement Award*. Uterine Artery Flow and Offspring Growth in Long-Evans Rats following Maternal Exposure to Ozone during Implantation. Published in Environmental Health Perspectives.
- 2018. *Level 2 US EPA Science and Technological Achievement Award* for "Researching the role of neuroendocrine stress axes activation in systemic and pulmonary health effects of air pollutants."
- 2018. Level 3 EPA Scientific and Technological Achievement Award. Evaluating naturally occurring asbestos toxicity to inform risk assessment of contaminated sites.
- 2016. *Honorable Mention for US EPA Science and Technological Achievement Award* for "Executive Summary: Variation in Susceptibility to Ozone Induced Health Effects in Rodent Models of Cardiometabolic Disease Inhalation Toxicology" and other 8 associated publications.
- 2016. *Honorable Mention for US EPA Science and Technological Achievement Award* for "Ozone induces glucose intolerance and systemic metabolic effects in young and aged Brown Norway rats."
- 2015. *Level 3 US EPA Science and Technological Achievement Award* for "Health effects of inhaled diesel emissions generated with CeO2 nano fuel additive."
- 2014. *Level 3 US EPA Science and Technological Achievement Award* for "Subchronic Pulmonary Pathology, Iron Overload, and Transcriptional Activity after Libby Amphibole Exposure in Rat Models of Cardiovascular Disease."
- 2014. *Nomination (no award)* for "Diesel exhaust induced pulmonary and cardiovascular impairment: the role of hypertension intervention."

Snow, Samantha

- *2019. Level III, US EPA Scientific and Technological Achievement Award,* New mechanistic paradigm for pulmonary and systemic health effects of oxidant and irritant pollutants (Three published papers).
- *2019.* Honorable Mention, *US EPA Scientific and Technological Achievement Award*. Uterine Artery Flow and Offspring Growth in Long-Evans Rats following Maternal Exposure to Ozone during Implantation. Published in Environmental Health Perspectives.
- 2017. *Level 2 US EPA Science and Technological Achievement Award* for "Researching the role of neuroendocrine stress axes activation in systemic and pulmonary health effects of air pollutants."
- 2015. *Level 3 US EPA Science and Technological Achievement Award* for "Health effects of inhaled diesel emissions generated with CeO2 nano fuel additive."

Dye, Janice

- *2019. Level III, US EPA Scientific and Technological Achievement Award,* New mechanistic paradigm for pulmonary and systemic health effects of oxidant and irritant pollutants (Three published papers).

- *2019.* Honorable Mention, *US EPA Scientific and Technological Achievement Award*. Uterine Artery Flow and Offspring Growth in Long-Evans Rats following Maternal Exposure to Ozone during Implantation. Published in Environmental Health Perspectives.
- 2017. *Honorable Mention for US EPA Science and Technological Achievement Award* for "Mutagenicity and pollutant emission factors of solid-fuel cookstoves: comparison with other combustion sources."
- 2016. *Honorable Mention for US EPA Science and Technological Achievement Award* for "Toxicity of indoor air emissions resulting from mechanical e-waste recycling operations."
- 2016. *Honorable Mention for US EPA Science and Technological Achievement Award* for "Executive Summary: Variation in Susceptibility to Ozone Induced Health Effects in Rodent Models of Cardiometabolic Disease Inhalation Toxicology" and other 8 associated publications.

  This paper looked at susceptibility variations in 8 healthy and cardio metabolically compromised animal models.

Colette Miller

- *2019. Level III, US EPA Scientific and Technological Achievement Award,* New mechanistic paradigm for pulmonary and systemic health effects of oxidant and irritant pollutants (Three published papers).
- *2019.* Honorable Mention, *US EPA Scientific and Technological Achievement Award*. Uterine Artery Flow and Offspring Growth in Long-Evans Rats following Maternal Exposure to Ozone during Implantation. Published in Environmental Health Perspectives.

STAA 2020 Nomination:

From: PIHTD, CPHEA, Urmila P Kodavanti

Title: The overlooked neuroendocrine system in drug and environmental interactions, mental health and disease susceptibility

Papers included in the package:

1. Henriquez AR, Snow SJ, Schladweiler MC, Miller CN, Dye JA, Ledbetter AD, Hargrove MM, Richards JE, Kodavanti UP. Exacerbation of ozone-induced pulmonary and systemic effects by β_2-adrenergic and/or glucocorticoid receptor agonist/s. *Sci Rep*. 2019;9(1):17925. Published 2019 Nov 29. doi:10.1038/s41598-019-54269-w

2. Henriquez AR, House JS, Snow SJ, Miller CN, Schladweiler MC, Fisher A, Ren H, Valdez M, Kodavanti PR, Kodavanti UP. Ozone-induced dysregulation of neuroendocrine axes requires adrenal-derived stress hormones [published online ahead of print, 2019 Aug 9]. *Toxicol Sci*. 2019;kfz182. doi:10.1093/toxsci/kfz182

3. Kodavanti UP. Susceptibility Variations in Air Pollution Health Effects: Incorporating Neuroendocrine Activation. *Toxicol Pathol*. 2019;47(8):962–975. doi:10.1177/0192623319878402

Authors and contributions (agreement email from each author copied below)

Author	Affiliation when work was done	Email address when work was done	Percent effort	Current affiliation	Current email address
Samantha Snow	EPA	Snow.samantha@epa.gov	10	ICF Inc	samanthajsnow@gamil.com
Andres Henriquez	ORISE	Henriquez.andres@epa.gov	15	ORISE	Henriquez.andres@epa.gov
Urmila Kodavanti	EPA	Kodavanti.urmila@epa.gov	30	EPA	Kodavanti.urmila@epa.gov
Mette Schladweiler	EPA	Schladweiler.mette@epa,gov	10	EPA	Schladweiler.mette@epa,gov
Colette Miller	EPA	Miller.colette@epa.gov	5	ORISE	Miller.colette@epa.gov
Janice Dye	EPA	Dye.janice@epa.gov	5	EPA	Dye.janice@epa.gov
Allen Ledbetter	EPA	Ledbetter.allen@epa.gov	3	Retired	Hawbob23@gmail.com
Judy Richards	EPA	Richards.judy@epa.gov	3	Retired	jhrichards49@gmail.com
Marie McGee	ORISE	Mcgee.marie@epa.gov	3	Syngenta	mmcgee0913@gmail.com

John House	NC State University	jshouse@ncsu.edu	4	NIEHS	john.house@nih.gov
Anna Fisher	EPA	Fisher.anna@epa.gov	3	EPA	Fisher.anna@epa.gov
Hongzu Ren	EPA	Ren.hongzu@epa.gov	3	EPA	Ren.hongzu@epa.gov
Prasada Kodavanti	EPA	Kodavanti.prasada@epa.gov	3	EPA	Kodavanti.prasada@epa.gov
Matthew Valdez	ORISE	Valdez.matthew@epa.gov	3	ORISE	Valdez.matthew@epa.gov

Email confirmation from author's agreeing to % effort

From: Kodavanti, Urmila
Sent: Friday, April 24, 2020 4:57 PM
To: Snow, Samantha <Samantha.Snow@icf.com>; Andres Henriquez <andhencor@gmail.com>; Schladweiler, Mette C. <Schladweiler.Mette@epa.gov>; Miller, Colette <Miller.Colette@epa.gov>; Dye, Janice <Dye.Janice@epa.gov>; Allen Ledbetter <hawbob23@gmail.com>; mmcgee0913@gmail.com; House, John (NIH/NIEHS) [E] <john.house@nih.gov>; Fisher, Anna <Fisher.Anna@epa.gov>; Ren, Hongzu <Ren.Hongzu@epa.gov>; Valdez, Matthew <valdez.matthew@epa.gov>; Kodavanti, Prasada Rao Kodavanti.Prasada@epa.gov; jhrichards49@gmail.com

Subject: Please respond with your agreement for this STAA application.

Dear Authors;
Hope everyone is doing as good as it could be in the midst of Covid-19 crisis.

We are planning to submit a nomination for EPA's 2020 STAA for these three papers (see below) where you have authored one or more papers.

I have estimated your effort level based on your involvement in one or more papers.

The nomination requires agreement from all authors of their level of contribution.

So, please reply to this email stating that you agree with the % effort allocated for you.

If you think you have more contribution, I will be happy to consider that.

So please let me know.

Please stay home safe. Thinking about everyone.

Urmila

Urmila P. Kodavanti, PhD, DABT, Research Biologist
Public Health and Integrated Toxicology Division, Mail Drop - B105-02
Center for Public Health and Environmental Assessment
U.S. Environmental Protection Agency
109 T.W. Alexander Drive, Room B564

Research Triangle Park, NC 27711

Tel: (919) 541-4963
Fax: (919) 541-0026
E-Mail: kodavanti.urmila@epa.gov

From: Andres Henriquez <andhencor@gmail.com>
Sent: Friday, April 24, 2020 6:22 PM
To: Kodavanti, Urmila <Kodavanti.Urmila@epa.gov>
Subject: Re: Please respond with your agreement for this STAA application.

Hi Urmila

I agree with the % effort.
Good luck with the EPA's 2020 STAA application.

Just in case, my current email address should be andhencor@gmail.com

Best

Andres

From: Dye, Janice <Dye.Janice@epa.gov>
Sent: Friday, April 24, 2020 5:02 PM
To: Kodavanti, Urmila <Kodavanti.Urmila@epa.gov>
Subject: RE: Please respond with your agreement for this STAA application.

I agreed with the allocation of 5% effort. Best of luck with this submission. Jan Dye

---

From: Allen Ledbetter <hawbob23@gmail.com>
Sent: Friday, April 24, 2020 5:03 PM
To: Kodavanti, Urmila <Kodavanti.Urmila@epa.gov>
Subject: Re: Please respond with your agreement for this STAA application.

I agree.

Allen Ledbetter

From: House, John (NIH/NIEHS) [E] <john.house@nih.gov>
Sent: Friday, April 24, 2020 5:04 PM
To: Kodavanti, Urmila <Kodavanti.Urmila@epa.gov>
Subject: Re: Please respond with your agreement for this STAA application.

Works for me.
Thanks Urmila.
I hope you and your loved ones are safe.

You are not waiting on analyses from me right?

-Kind Regards,

John

John S. House, PhD
Staff Scientist
NIEHS, Biostatistics & Computational Biology Branch
MSC A3-03, Room A358
111 TW Alexander Dr
RTP, NC 27709
john.house@nih.gov
984-287-3581

From: Kodavanti, Prasada Rao <Kodavanti.Prasada@epa.gov>
Sent: Friday, April 24, 2020 5:05 PM
To: Kodavanti, Urmila <Kodavanti.Urmila@epa.gov>
Subject: RE: Please respond with your agreement for this STAA application.

I AGREE WITH THE PERCENT EFFORT (3%) ALLOCATED TO ME. ALL THE BEST.

PRASADA KODAVANTI

From: Snow, Samantha <Samantha.Snow@icf.com>
Sent: Friday, April 24, 2020 5:06 PM
To: Kodavanti, Urmila <Kodavanti.Urmila@epa.gov>
Subject: RE: Please respond with your agreement for this STAA application.

Hi Urmila,

I'm happy to hear you'll be submitting another STAA application! I agree with the % effort allocation assigned to me.

Thanks and have a great weekend!

Sam

Samantha J. Snow, Ph.D., DABT | Lead Health Scientist | +1 (919) 293-1636 direct
Samantha.Snow@icf.com | icf.com | LinkedIn
ICF | 2635 Meridian Pkwy., Suite 200, Durham, NC 27713 USA

From: Valdez, Matthew <valdez.matthew@epa.gov>
Sent: Friday, April 24, 2020 5:08 PM
To: Kodavanti, Urmila <Kodavanti.Urmila@epa.gov>
Subject: RE: Please respond with your agreement for this STAA application.

Agreed

Matthew Valdez, Ph.D.
ORISE Postdoc

ORD / CPHEA / NETB
U.S. Environmental Protection Agency
Research Triangle Park, NC 27711, USA
Phone: 919.541.0089
Fax: 919.541.4849
E-mail: valdez.matthew@epa.gov

From: Ren, Hongzu <Ren.Hongzu@epa.gov>
Sent: Friday, April 24, 2020 6:01 PM
To: Kodavanti, Urmila <Kodavanti.Urmila@epa.gov>
Subject: RE: Please respond with your agreement for this STAA application.

Thank you, Urmila. I agree with your estimation.

Hongzu

_____

From: Marie McGee Hargrove <mmcgee0913@gmail.com>
Sent: Sunday, April 26, 2020 1:32 PM
To: Kodavanti, Urmila <Kodavanti.Urmila@epa.gov>
Subject: Re: Please respond with your agreement for this STAA application.

Hi Urmila,

I hope all is well with you and your family during this time. Thanks for sending over the STAA application. I agree with the contribution amount.

Good luck with the application! Continue to be safe during this time😊

Sincerely,

Marie

_____

From: Miller, Colette <Miller.Colette@epa.gov>
Sent: Sunday, April 26, 2020 2:30 PM
To: Kodavanti, Urmila <Kodavanti.Urmila@epa.gov>
Subject: RE: Please respond with your agreement for this STAA application.

Urmila,

Thank you for including me in this year's STAA proposal for the exciting work related to the effects of ozone inhalation on neuroendocrine disruption.
I am in agreement with my contribution of 5% effort.

Thank you
Colette

Colette N. Miller, Ph.D., M.S.
Oak Ridge Institute of Science and Education
U.S. Environmental Protection Agency

CPHEA/PHITD/CIB
109 T.W. Alexander Drive
Mail Code: B105-02
Research Triangle Park, NC 27711
(919) 541-3469 [tel]
miller.colette@epa.gov

From: Judy Richards <jhrichards49@gmail.com>
Sent: Sunday, April 26, 2020 4:48 PM
To: Kodavanti, Urmila <Kodavanti.Urmila@epa.gov>
Subject: Re: FW: Please respond with your agreement for this STAA application.

I agree to the 3% effort.

Judy Richards

From: Schladweiler, Mette C. <Schladweiler.Mette@epa.gov>
Sent: Monday, April 27, 2020 8:31 AM
To: Kodavanti, Urmila <Kodavanti.Urmila@epa.gov>
Subject: RE: Please respond with your agreement for this STAA application.

Hey Urmila,
I'm fine with it.
Thanks,
Mette

From: Fisher, Anna <Fisher.Anna@epa.gov>
Sent: Monday, April 27, 2020 6:28 AM
To: Kodavanti, Urmila <Kodavanti.Urmila@epa.gov>
Subject: Re: Please respond with your agreement for this STAA application.

Urmila
Thank you
Yes that's sounds good
Best
Anna

Table of Contents

General_Authors_Publications.....2
LI-266745_Flotemersch_et_al_2016_IWI__RRA.....13
Flotemersch_-_Statement_of_Authorship_Contribution.....31
HIll_-_Statement_of_Authorship_Contribution.....32
Leibowitz_-_Record_of_Percentage_Agreement_for_STAA_Award.....33
Stoddard_-_Statement_of_Authorship_Contribution.....34
Tharme_-_Statement_of_Authorship_Contribution.....35
Thoms_-_Record_of_Percentage_Agreement.....36

United States Environmental Protection Agency
Washington, DC 20460

STAA REPORT FOR THE SCIENTIST NOMINATIONS

General Information:

Nomination ID/App ID:	20-128
Research Category Primary:	Monitoring and Measurement Methods (MM)
Research Category Secondary:	Ecological Research (ER)
Laboratory/Office Name:	ORD
Nomination Entered By:	Joseph Flotemersch

Eligibility Checklist:

[Y] The nominated publication(s) has not been submitted to a previous STAA competition.

[Y] The nominated publication(s) was published on or before January 1, 2017 and on or after January 1,2012

[Y] The principal author was an EPA employee or a PHS employee assigned to EPA when the research was performed

[Y] The EPA authors (includes PHS employees assigned to EPA) contributed collectively a minimum of 50% toward the publication(s)

Nominating Official Name:	Kevin Oshima
Nominating Official Title:	BIOLOGIST
Nominating OfficialEmail:	oshima.kevin@epa.gov
STAA Coordinator Name:	Kathleen Wiser
STAA Coordinator Email:	wiser.kathi@epa.gov

Justifications:

Justification 1:

Watersheds encompass all biotic and abiotic components— including people—within their boundaries and provide a range of services valued by the society. Thus, watersheds are a foundation of our cultural, economic, spiritual and social well-being and, as such, a critical focus of water resource management. Evaluating the integrity of a watershed represents a societal and a scientific challenge, because watersheds are used and managed for a diverse, interrelated range of activities. The concept of watershed integrity is challenging both in terms of defining what it actually is and developing approaches and tools to allow its evaluation. The assessment of watershed integrity also requires approaches that are scale appropriate and enable strategic problem-solving. It has been said that the ultimate challenge for watershed and river science is to integrate and synthesize watershed and river information available from all levels of inquiry into an understanding that is meaningful and can be used by managers and decision-makers. This peer-reviewed publication represents a major step forward in this process in that it provides an agency-reviewed and approved operational definition of the term watershed integrity…and also provides a template for how it can be effectively and efficiently measured.

There are a number of terms related to the aforementioned challenge (e.g. watershed integrity, aquatic condition and watershed health) that have separate meanings. However, these meanings are often blurred because of a lack of standardized definitions. This manuscript, provides distinct definitions for these different terms, which should allow the scientific community to better address the needs of decision-makers. This includes the main focus of this paper, watershed integrity, which was defined as '*as the capacity of a watershed to support and maintain the full range of ecological processes and functions essential to the sustainability of biodiversity and of the watershed resources and services provided to society*'. Beyond defining the term "Watershed Integrity", the paper developed an operational index to evaluate the level of integrity. For this index, a human health analogy was used to identify six key watershed functions (viz. hydrologic regulation, regulation of water chemistry, sediment regulation, hydrologic connectivity, temperature regulation and habitat provision) and the specific risk factors, or stressors, which impact them. Examples of national datasets that can be used to evaluate these risk factors were provided. The authors also derived a mathematical expression that evaluates watershed integrity by combining the

integrity of the six watershed functions, where the integrity of each is based on the relative presence of specific stressors. This expression assumes the quantitative relationships between multiple interacting stressors and the key functions are known. Although such relationships do exist, the availability of this information is limited and represents an ongoing need for additional research. However, the authors also showed how first-order approximations can be used in the absence of such information, given that many of these relationships are as yet unknown. The derived approach can be iteratively applied and improved as these relationships

become known and/or as new national datasets become available. A significant aspect of the developed approach is that it allows users to avoid the use of least degraded sites to describe reference condition.

A characteristic of the developed index is that it can be readily deconstructed in support of strategic adaptive management; that is, the risk factors of the watershed index score can be examined individually to evaluate how each is influencing the overall index score. This affords managers the opportunity to examine how each factor might be managed differently to better achieve overall objectives. For example, if the index score for a given watershed is below an established threshold, the factors bringing the overall index score down can easily be identified. If multiple factors are negatively influencing the overall score, a cost–benefit analysis of available management options then could be conducted to identify the best course of action to achieve desirable management endpoints.

Previous efforts to assess the status of watersheds on larger scales, though limited in number, have been undertaken in the USA and elsewhere. For example, in the USA, the U.S. Fish and Wildlife Service, along with the National Marine Fisheries Service and the Association of Fish and Wildlife Agencies, developed and implemented the National Fish Habitat Action Plan. Its objective was to protect, restore and enhance the nation's fish and aquatic communities through partnerships to foster fish habitat conservation. Similarly, the U.S. Forest Service developed the Watershed Condition Framework, which employed an integrated, systems-based approach for classifying watershed condition based on an evaluation of underlying ecological, hydrological and geomorphic states. These programs focus solely on identifying high-quality aquatic resources and make use of locally collected data (e.g. biota and water quality) that are not available nationally. The author's intent was to develop a watershed integrity index that can be applied nationally. This approach differs because it focuses on the functional attributes of these systems, rather than simply relying on more easily obtainable state components. It also differs technically through its use of appropriately scaled data that identify risk factors that impact these key functions. Beyond informing on the biogeochemical health of the immediate system, a focus on functional attributes provides information that can be used to explain and predict the effects of watershed discharges on downstream riverine and estuarine condition.

Data resulting from the now complete national-scale mapping and assessment of watershed integrity was completed using the StreamCat database. These data are of value to states and watershed organizations initiating healthy watershed and other programs. These programs augment the watershed approach with proactive, holistic aquatic ecosystem conservation and protection designed to conserve critical components of watersheds and, therefore, avoid additional water quality impairments in the future. These national maps are also helping identify watersheds with high integrity as well as those at risk and help to prioritize conservation and restoration. The index of watershed integrity developed is providing high quality information at a broad spatial scale that is allowing ecosystem management to focus on achievable and measurable outcomes underpinned by quality science.

Justification 2A:

n/a

Justification 2B:

n/a

Justification 2C:

n/a

Justification 2D:

n/a

Justification 2E:

n/a

Justification 3A:

The nominated paper has been cited by 45 other scientific papers (Google Scholar). This includes papers authored from the countries of Albania, Australia, Burkina-Faso, Canada, Chili, China, Germany, Ghana, Hungary, Indonesia, Iran, Mexico, Portuguese, Russia, Switzerland, Thailand, and United Kingdom. The application of the developed index was also mentioned in a 2016 United Nations Environmental Program (UNEP) publication titled "International Water Quality Guidelines for Ecosystems" as a tool useful in the desktop screening centered on ecosystem health.

The Index of Watershed Integrity has also been the basis for multiple research efforts at major universities. For example, Kearpack et al. 2020 (Colorado State University; https://www.sciencedirect.com/science/article/abs/pii/S1470160X19310477) used it as the basis for their research towards the develop of an Index of Floodplain Integrity. And at Dartmouth, Jonathon Loos is using data generated by the Index to explore links between biophysical parameters of watershed function to the human systems of governance and institutional factors that impact them.

Researchers working on the IWI project have also been requested to lend their expertise and lead efforts for applying the Index to watersheds of the western Balkans, including rivers in Albania, Bosnia and Herzegovina, Kosovo, North Macedonia, Montenegro, and Serbia (Aho et al. 2020) and the Mat-Su basin in Alaska (Aho et al. 2020). Potential applications to the European Union are of interest (collaborator: Miriam Glendell, The James Hutton Institute) and a separate application for Poland (collaborator: Joanna Zawiejska, Pedagogical University of Krakow, Poland).

Justification 3B:

Given the high-profile nature of this project, this paper was submitted to extensive U.S. EPA review prior to being submitted for external review by the journal. This review process included scientists from within and outside of the Agency. Reviewers from within the Agency, but outside the normal review process included Gary Davis, Thomas Fontaine, Steve Paulsen and Walt Foster (ORD Senior Scientists); Laura Gabanski, Richard Mitchell, Doug Norton, Joseph Tiago and

Karen Metchis (Office of Water); Andy Gillespie (Associate Director for the National Exposure Research Laboratory), and Suzanne van Drunick (National Program Director for ORD's Safe and Sustainable Water Research). Reviewers from outside the agency included Chuck Hawkins (Utah State University), and Murray Scown (University of New England, Australia); both of whom are well recognized in their area of expertise.

After being cleared by U.S.EPA, the manuscript was submitted to River Research and Applications for consideration. Upon the receipt by the journal, the Editor-in-Chief recognized it as a candidate for ARENA designation by the journal. ARENA is a designation reserved for papers of high significance. This designation also means that the manuscript was critically reviewed by then Editor-in-Chief, Dr. Geoffrey Petts, Vice-Chancellor and Rector of the University of Westminister. After review and revision, the paper was indeed published as an ARENA paper.

AUTHORS

Contributing Author

Author Name:	John L Stoddard		
Professional Title:		Salutation:	Dr.
Email:	stoddard.john@epa.gov	Organization:	
Mailing Address:			
Street Line 1:	200 Southwest 35th Street		
City:	Corvallis		
Zip Code:	97333	State:	OR
At time of research was:	EPA Employee		
Separation Date:			
% of Effort:	10		

Principal Author

Author Name:	Joseph E. Flotemersch		
Professional Title:		Salutation:	Dr.
Email:	flotemersch.joseph@epa.gov	Organization:	
Mailing Address:			
Street Line 1:	West Martin Luther King Boulevard		
City:	Cincinnati		
Zip Code:	45268	State:	OH
At time of research was:	EPA Employee		
Separation Date:			
% of Effort:	40		

Contributing Author

Author Name:	Scott G. Leibowitz		
Professional Title:		Salutation:	Dr.
Email:	leibowitz.scott@epa.gov	Organization:	
Mailing Address:			
Street Line 1:	200 Southwest 35th Street		
City:	Corvallis		
Zip Code:	97333	State:	OR
At time of research was:	EPA Employee		
Separation Date:			
% of Effort:	35		

Contributing Author

Author Name:	Ryan A Hill		
Professional Title:		Salutation:	Dr.
Email:	hill.ryan@epa.gov	Organization:	
Mailing Address:			
Street Line 1:	200 Southwest 35th Street		
City:	Corvallis		
Zip Code:	97333	State:	OR
At time of research was:	Non EPA Personnel		
Separation Date:			
% of Effort:	5		

Contributing Author

Author Name:	Rebecca E Tharme		
Professional Title:		Salutation:	Dr.
Email:	rebeccatharme@riverfutures.com	Organization:	
Mailing Address:			
Street Line 1:	48 Middle Row, Cressbrook, Buxton, Derbyshire, UK		
City:	Cressbrook, Buxton		
Zip Code:	SK17 *SX	State:	Derbyshire
At time of research was:	Non EPA Personnel		
Separation Date:			

% of Effort:	5

Contributing Author

Author Name:	Martin C Thoms		
Professional Title:		Salutation:	Dr.
Email:	mthoms2@une.edu.au	Organization:	
Mailing Address:			
Street Line 1:	Riverine Landscapes Research Laboratory, University of New England		
City:	Armidale		
Zip Code:		State:	NSW
At time of research was:	Non EPA Personnel		
Separation Date:			
% of Effort:	5		

PUBLICATIONS

Publication 1:

Publication Title:	A Watershed Integrity Definition and Assessment Approach to Support Strategic Management of Watershe		
Publication Date:	Fri Oct 23 00:00:00 GMT 2015		
Journal/Publication Method:	Journal		
All Author(s):			
Volume:	32	Number:	1
Pages:	1654-1671	Immediately Index:	Immediately Index:

Citation ½ Life: 8.1 Impact Factor: 1.954

RIVER RESEARCH AND APPLICATIONS

River Res. Applic. **32**: 1654–1671 (2016)

Published online 23 October 2015 in Wiley Online Library
(wileyonlinelibrary.com) DOI: 10.1002/rra.2978

ARENA PAPER

A WATERSHED INTEGRITY DEFINITION AND ASSESSMENT APPROACH TO SUPPORT STRATEGIC MANAGEMENT OF WATERSHEDS

J. E. FLOTEMERSCH[a]*, S. G. LEIBOWITZ[b], R. A. HILL[c], J. L. STODDARD[b], M. C. THOMS[d] AND R. E. THARME[e†]

[a] *U.S. Environmental Protection Agency, Office of Research and Development, Cincinnati, Ohio, USA*
[b] *U.S. Environmental Protection Agency, National Health and Environmental Effects Research Laboratory, Corvallis, Oregon, USA*
[c] *ORISE post-doc, c/o USEPA, National Health and Environmental Effects Research Laboratory, Corvallis, Oregon, USA*
[d] *Riverine Landscapes Research Laboratory, University of New England, Armidale, NSW, Australia*
[e] *The Nature Conservancy, Derbyshire, UK*

ABSTRACT

Watersheds are spatially explicit landscape units that contain a range of interacting physical, ecological and social attributes. They are social–ecological systems that provide a range of ecosystem services valued by the society. Their ability to provide these services depends, in part, on the degree to which they are impaired by human-related activity. An array of indicators is used by natural resource managers, both private and government, to assess watersheds and their sub-components. Often these assessments are performed in comparison with a reference condition. However, assessments can be hampered because natural settings of many systems differ from those sites used to characterize reference conditions. Additionally, given the ubiquity of human-related alterations across landscapes (e.g. atmospheric deposition of anthropogenically derived nitrogen), truly unaltered conditions for most, if not all, watersheds cannot be described. Definitions of 'integrity' have been developed for river ecosystems, but mainly at the reach or site scale and usually for particular species, such as fish or macroinvertebrates. These scales are inappropriate for defining integrity at the watershed scale. In addition, current assessments of endpoints do not indicate the source of impairment. Our definition of watershed 'integrity' is the capacity of a watershed to support and maintain the full range of ecological processes and functions essential to the sustainability of biodiversity and of the watershed resources and services provided to society. To operationalize this definition as an assessment tool, we identify key functions of unimpaired watersheds. This approach can then be used to model and map watershed integrity by incorporating risk factors (human-related alterations or stressors) that have been explicitly shown to interfere with and degrade key functions in watersheds. An advantage of this approach is that the index can be readily deconstructed to identify factors influencing index scores, thereby directly supporting the strategic adaptive management of individual components that contribute to watershed integrity. Moreover, the approach can be iteratively applied and improved as new data and information become available. © 2015 The Authors. *River Research and Applications* published by John Wiley & Sons Ltd.

KEY WORDS: index of watershed integrity; IWI; watershed management; scale; sustainability; healthy watersheds

Received 11 May 2015; Revised 27 July 2015; Accepted 21 September 2015

INTRODUCTION

Watersheds provide a range of ecosystem services that are valued by the society (Costanza *et al*., 1997, 2014; TEEB 2010). These include supporting services (e.g. soil formation, nutrients and primary production), provisioning goods and services (e.g. food, water, wood, fibre and fuel), regulating services (e.g. climate regulation, flood regulation and water purification) and cultural services, such as recreation and spiritual activities (de Groot *et al*., 2002; Millennium Ecosystem Assessment, 2005). Many of these services are directly related to the flow and function of water and its constituents within watersheds. Despite the recognition of the importance of these functions, water in many regions is viewed primarily as an exploitable commodity for human use, that is, a provisioning service. As a result, the wider range of benefits of watershed services has had limited recognition outside of scientific circles. The quality and quantity of services generated by watersheds are rapidly declining (Farber *et al*., 2002) because of accelerating rates of land-use change, water consumption and climate change *inter alia*. The deteriorating state of freshwater biodiversity, globally, reflects these impacts (Dudgeon *et al*., 2006; Butchart *et al*., 2010).

Governments recognize the stress that humans can place on the finite natural resources of watersheds and have progressively implemented policies intended to assure greater sustainability of water-dependent services. Early policies

*Correspondence to: J. E. Flotemersch, U.S. Environmental Protection Agency, Office of Research and Development, 26 W. Martin Luther King Dr., Mail Stop 591, Cincinnati, Ohio 45268 USA.
E-mail: flotemersch.joseph@epa.gov
†Present address: Riverfutures Inc., Derbyshire, UK.

© 2015 The Authors. *River Research and Applications* published by John Wiley & Sons Ltd.
This is an open access article under the terms of the Creative Commons Attribution-NonCommercial-NoDerivs License, which permits use and distribution in any medium, provided the original work is properly cited, the use is non-commercial and no modifications or adaptations are made.

focused on specific impacts (e.g. point-source pollutants), the overuse of certain resources, protection or habitat restoration. However, these early efforts often failed to address chronic problems that contribute to longer-term declines in the structure and function of watersheds, such as pollutants associated with non-point run-off from urbanized and agricultural areas (USEPA, 1996). Moreover, the focus on individual resources or habitats usually fails to recognize watersheds as complete, intra-connected systems.

The advent of watershed initiatives in the 1990s brought more holistic and interdisciplinary approaches to watershed management (Mitchell, 1990; Cairns and Crawford, 1991; Noss, 1995; Karr, 1996; Kenney, 1997; Hull *et al*., 2003). This holistic view of watersheds was critical for several reasons. First, watersheds are hierarchical systems that function at different levels of organization and scale (Thoms *et al*., 2007). A feature of hierarchical systems is that changes at large scales have slower rates of behaviour while changes at small scales occur more quickly (O'Neill and King, 1998). In addition, hierarchical systems exhibit emergent properties, whereby properties and behaviours at higher levels cannot be simply deduced from the collective functioning of their parts (Allen and Starr, 1982). Thus, it may be scientifically inappropriate to use information collected at the site or reach scale to assess watershed-scale attributes (Dollar *et al*., 2007). Second, watersheds are social–ecological systems, and their ability to provide a range of services is dependent on each component functioning and interacting properly (Bunch *et al*., 2011; Walker and Salt, 2012). In other words, society depends on ecological systems to provide ecosystem goods and services (hereafter referred to as ecosystem services; Malinga *et al*., 2015 and references therein), and in turn, exploited ecological systems depend on the society to maintain them in a way that ensures their long-term functioning (Berkes, 2007).

Recently, the use of the term 'watershed integrity' to identify and describe desirable watershed management endpoints has increased (USEPA, 1998, 2012c; Novotny, 2004; Van Abs, 2013). However, ambiguity exists as to what this term actually means. At one extreme, watershed integrity has been used as an extension of biological and ecological integrity, thus positioning it as a benchmark free from human influences (Novotny, 2004; USEPA, 2012c). At the other extreme, watershed integrity has been employed to describe systems that support the sustainable flow of ecosystem services to society, such that the term is not divorced from human influence (USEPA, 1998; Van Abs, 2013).

A clear definition of watershed integrity can advance our understanding and discussion of this concept, especially within an interdisciplinary domain such as watershed science (Noss, 1995; Wicklum and Davies, 1995; Karr, 1996; Hull *et al*., 2003; Bennett *et al*., 2009). However, definitions alone do not support the quantification of differences in watershed character between areas, measurement of changes in state over time or specification of the level at which efforts could be made to preserve or restore integrity (Noss, 1995). To do this, we must make the term 'watershed integrity' operational—i.e. capable of being measured. Thus we need to identify the individual features and processes that maintain watershed integrity and identify human-related factors that degrade these features and processes.

With these requirements in mind, we cover three objectives in this paper. First, we provide a definition of watershed integrity. To assist in this definition, we also discuss terms that are closely related to watershed integrity;, including biological integrity, ecological integrity, watershed health, healthy watersheds, aquatic condition, watershed resilience and watershed sustainability. Without such context, watershed integrity may be confused with other terms, creating ambiguity and skepticism as to its value and possibly undermining watershed management strategies (Hull *et al*., 2003). Second, we identify key functions that define unimpaired watersheds. Third, we make watershed integrity operational by identifying risk factors (i.e. human-related stressors) that are known to impact these key functions interfering with and degrading the structure, function and feedbacks of watersheds. Indicators for these stressors are then used to construct an index to assess watershed integrity.

DEFINING WATERSHED INTEGRITY

Watershed integrity is similar to many terms common in the fields of ecology and geomorphology (i.e. sustainability, health, biodiversity and ecological integrity) in that it describes activities at the interface between sub-disciplines of environmental science, policy and management (Hull *et al*., 2003). Successful interdisciplinary research requires the 'explicit joining of two or more areas of understanding into a single conceptual-empirical structure' (Pickett *et al*., 1994), which can then generate common and agreed terms (Dollar *et al*., 2007). Watershed integrity is a compound phrase, and to avoid confusion, misinterpretation or relegation to the status of a buzzword, it requires a comprehensive definition (Wicklum and Davies, 1995). This definition should include a statement of the word's meaning, intended use and how it may be measured or expressed quantitatively or operationalized (Noss, 1990; Hull *et al*., 2003; Lackey, 2003). Herein, the two separate words of watershed integrity are examined independently and then collectively.

Watershed

A watershed is the landscape that contributes surface water to a single location, such as a point on a stream or river, or a single wetland, lake or other waterbody (Langbein and Iseri, 1960; Dingman, 2002; Brutsaert, 2005). A watershed comprises a set of physical, chemical and biological

© 2015 The Authors. *River Research and Applications* published by John Wiley & Sons Ltd.

DOI: 10.1002/rra

elements connected by the flow of water. This definition is analogous to the terms 'catchment' and 'drainage basin'. Watersheds are delimited based on topographic divides; thus, they represent areas that collect precipitation that contribute water to a specific location. Commonly, these surficial watershed boundaries are superimposed on aquifer boundaries, and the two often do not align. Thus, the hydrology of a watershed is not just affected by precipitation and surface water; groundwater also plays a major role. This can be seen by considering what distinguishes ephemeral from perennial and intermittent streams: ephemeral streams respond directly to precipitation, while perennial and intermittent streams receive groundwater inputs for all (perennial) or a portion of (intermittent) the year (Mosley and McKerchar, 1993; Winter *et al*., 1998; Rains and Mount, 2002; Rains *et al*., 2006; Winter, 2007). Reconciling the alignment of surficial and groundwater boundaries, understanding their interaction and assessing how humans influence each are major challenges. In this paper, we focus primarily on surficial watersheds, but inclusion of groundwater/surface water interactions is possible within this framework as consistent, nationwide datasets become available.

Watersheds are hierarchically organized (spatially nested) systems, and their delineation depends on the context of the question being asked and the scale of focus (Thoms *et al*., 2007). For example, a watershed may represent the landscape upstream of a single, first-order tributary or the area could be as large as the Mississippi River, which drains about 42% of the continental USA (Brown *et al*., 2005). While the watershed for a given point on a stream network is dictated by the drainage divide, the question of which point to choose is a matter of objectives. Therefore, any watershed characterization must be scale-dependent, contain a description of how the area was defined and include the questions, management objectives or other factors that led to the watershed delineation.

Integrity

Integrity has two general definitions. First is a *value judgement of human character* (e.g. adherence to moral and ethical principles, soundness of moral character and honesty), and second is a *judgement of condition*. It can also be defined as 'the state of being whole, entire, or undiminished' or 'a sound, unimpaired, or perfect condition' (Merriam-Webster, 1993; Dictionary.com, 2014). Of these definitions, 'judgement of condition' is most consistent with how the word is used with respect to the environment.

Aldo Leopold first used the term 'integrity' in an environmental context, writing that 'a thing is right when it tends to preserve the integrity, stability, and beauty of the biotic community. It is wrong when it tends otherwise' (Leopold 1949; p 224–225). Since Leopold's landmark essay, numerous authors have contributed to the evolving definition of integrity, especially biotic integrity (e.g. Frey, 1975; Karr and Dudley, 1981; Karr *et al*., 1986; Angermeier and Karr, 1994). With these works as a foundation, Karr (1996) defined biological integrity as 'the capacity to support and maintain a balanced, integrated, adaptive biological system having the full range of elements (genes, species, assemblages) and processes (mutation, demography, biotic interactions, nutrient and energy dynamics, and metapopulation processes) expected in the natural habitat of a region'. Karr (1981) explicitly linked the degradation of biological integrity to human-related alterations of aquatic ecosystems. Furthermore, he stated that natural variation, including natural disturbance regimes, in these systems is not considered to alter integrity. For example, streams are inherently dynamic and floods or drought of particular magnitude, frequency and duration may represent natural disturbances, but not stressors (Resh *et al*., 1988, Allan and Castillo, 2007). A similar distinction can be made for systems that are susceptible to other natural disturbance regimes, such as fires (Shinneman *et al*., 2013) or hurricanes (Scatena *et al*., 2012). In addition, biota within these systems exhibits a high degree of adaptation to such disturbances (e.g. Shinneman *et al*., 2013, Bae *et al*., 2014). Here, we likewise distinguish natural disturbances from stressors imposed by human-related activity. However, we recognize and consider human activity that alters natural disturbance regimes to be stressors (e.g. natural flooding disrupted by reservoir management). Similarly, human-induced disturbance that emulates a naturally occurring disturbance would also be considered a stressor (e.g. human-initiated forest fires).

Some uses of the term integrity imply a condition with little or no human-related alteration (Angermeier and Karr, 1994; Callicott *et al*., 1999). In reality, there are few, if any, pristine watersheds (Oliveria and Cortes, 2006), and the probability that altered watersheds could return to pre-industrial conditions with the removal of human influence is low. As such, the society must consider what level of diminished integrity and potential loss of biodiversity is acceptable in exchange for the services provided by watersheds. For some, the question narrows to the following: what level of integrity must be maintained in a system to assure the sustainable flow of services desired by the society?

Here, we define *integrity* in an environmental context as the capacity of a system (and its sub-components) to support and maintain the full range of ecosystem processes and functions essential to the long-term sustainability of its it is diversity and natural resources.

Watershed integrity

Using these separate definitions within an environmental context, we define *watershed integrity* as the capacity of a watershed to support and maintain the full range of

© 2015 The Authors. *River Research and Applications* published by John Wiley & Sons Ltd.

DOI: 10.1002/rra

ecological processes and functions essential to the sustainability of biodiversity and of the watershed resources and services provided to society. This definition positions watershed integrity as a management tool that can be used to address whether or not existing watershed infrastructure is capable of supporting sustainability goals. Note that while this definition focuses on surface water, because of how a watershed is defined, the effects of groundwater in contributing to watershed integrity are acknowledged.

RELATED TERMS

To distinguish *watershed integrity* as a management construct and clarify its role in the larger context of watershed management, a discussion of closely associated watershed conservation terms is warranted.

Biological and ecological integrity

Since Karr's seminal work (Karr 1981), biological integrity has often been used interchangeably with ecological integrity (e.g. Noss, 2004). While similar in concept, biological (or biotic) integrity only refers to the integrity of the biotic components of a system. Ecological integrity expands the domain of focus to include both biological (e.g. species abundance and composition) and physical (e.g. geological, chemical, habitat, water and sediments) components (cf. Barbour *et al*., 2000; Novotny, 2004). Initially, the concept of ecological integrity suffered from a degree of vagueness but was clarified by Woodley (1993) who stated that ecological integrity is optimized for its geographic location. A definition put forth by Schofield and Davies (1996) further clarified ecological integrity as the 'ability of aquatic ecosystems to support and maintain key ecological processes and an adaptive community of organisms having a species composition, diversity, and functional organization comparable to that of natural habitats of the same region'. Ecological integrity has therefore emerged as a concept that encompasses the needs of well-functioning landscapes (Fischman, 2004).

The value that the society places on biological or ecological integrity is evidenced by the appearance of these terms in policy. In the USA, biological or ecological integrity have been stated as policy objectives in several national and bi-national laws and agreements, including the U.S. Water Quality Amendments of 1972. The Clean Water Act has the objective to restore and maintain the chemical, physical and biological integrity of the nation's waters (33 USC § 1251). The term biological integrity also appears in the National Wildlife Refuge System Improvement Act of 1997, which mandates that the U.S. Fish and Wildlife Service 'ensure that the biological integrity, diversity, and environmental health of the System are maintained' (16 USC § 668dd).

Aquatic condition

In environmental management, system condition is normally defined as 'the state of the system when compared to one or more benchmarks and usually includes some form of reference to integrity' (Stoddard *et al*., 2006). Monitoring of the condition of aquatic resources within watersheds can help detect trends over time, identify emerging problems, determine the success of watershed management programmes, help direct efforts for stressor control to areas where they are most needed and track the response of systems to emergencies, such as floods and spills (USEPA, 2013). The actual aquatic resource attributes included as part of a condition assessment depend on the type and scale of the question(s) being addressed by the data collection effort (Thorp *et al*., 2013), as well as the resources available. For example, bioassessment and monitoring data for reporting on the biological condition of fluvial systems are generally collected at the reach scale (Flotemersch *et al*., 2006, 2011, Parsons *et al*., in press).

These data are frequently aggregated up to larger scales to facilitate the reporting of average conditions across larger geographies, such as a watershed, state or nation (e.g. USEPA, 2014; European Commission, 2014). Although these data can be collected across the entire watershed, they are still reach-scale data indicating the aquatic condition of reaches throughout the watershed. This is in contrast to true watershed-scale data, which would result from the kinds of indicators discussed later in this paper.

Watershed resilience

The resilience of a system is defined as 'the amount of change a system can undergo (its capacity to absorb disturbance) and retain the same function, structure, and set of feedbacks' (cf. Holling, 1973; Walker and Meyers, 2004; Walker and Salt, 2012). While this concept has general acceptance within the scientific community, it is often described using different terms. For example, Begon *et al*. (2006) defined the concept using the term 'stability', which encompasses both the 'resistance' of a system (i.e. its ability to 'avoid displacement in the first place') and the 'resilience' of a system (i.e. the ability of a system that is influenced by natural and anthropogenic alterations to recover to its previous state, once the disturbances and stressors are removed). Herein, we have elected to use the term 'resilience'.

Watersheds are influenced by natural and anthropogenic stresses, and their ability to recover and adapt to new conditions is dependent on their resilience (Walker and Salt, 2012). Managing a system to maintain resilience includes protecting sensitive areas and minimizing threats (USEPA, 2012b). It also must include protecting those areas most important to the system homeostasis. For watersheds, this includes ensuring that the system has adaptive attributes

© 2015 The Authors. *River Research and Applications* published by John Wiley & Sons Ltd.

DOI: 10.1002/rra

such as river meander belts, riparian wetlands, floodplains, terraces, groundwater recharge and discharge areas, and material contribution areas, all of which function to increase or maintain its natural resilience (USEPA, 2012b). These adaptive attributes, if present in the appropriate amounts for a given system, help absorb disturbance and stresses and maintain the system in its current state (this is a property of stress-adapted systems). For example, alterations to the watershed may lead to changes in the timing, magnitude or duration of discharge that are outside the natural range of variability and predictability. In a resilient watershed, unless large-scale in character, such perturbations are unlikely to result in a permanent change to the system, because riparian areas and floodplain wetlands would help to partially absorb the disturbance and maintain its state. If the resilience is diminished because of loss of these buffering resources, then the watershed may become vulnerable to such perturbations.

Watershed sustainability

While much has been written on environmental sustainability in general, relatively little has been published in the peer-reviewed literature specifically addressing the topic of watershed sustainability. Recently, Sidle *et al*. (2013) concluded that while sustainability has been defined in many ways, all definitions commonly support 'the harmonization of environmental, economic, and social opportunities for the benefit of present and future generations'. This definition is in line with the goals outlined in the discussion of watershed health later in the text.

Watershed health and healthy watersheds

Watershed health is used as an extension of the concept of ecological or ecosystem health at the watershed scale. Karr and Chu (1999) defined ecosystem health as the preferred state of ecosystems that have been modified by human activity (e.g. farm land, urban environments and managed forests). How this 'preferred state' is derived is unclear, but it is assumed to be a consensus-driven social process and within the limits of the prevailing laws. The watershed health approach is consistent with other discussions of ecosystem health that incorporate human activities and consequences (Rapport *et al*., 1998a; Rapport *et al*., 1998b), including the EU Water Framework Directive (European Commission, 2014), as well as those that consider which societal preferences will take precedence (Lackey, 2003). It is also useful given that most ecosystems have been altered to some degree by human activities (Westra, 1994; Flotemersch *et al*., 2006; Oliveria and Cortes, 2006). A system in good health has the ability to provide a sustainable flow of services (Rapport *et al*., 1998a, 1998b) while maintaining functional and structural components at a level deemed acceptable by stakeholders (Mageau *et al*., 1995; Ross *et al*., 1997). Karr and Chu (1999) added that a healthy system should not degrade the integrity of linked resources. In the context of nested watersheds, a healthy watershed does not negatively impact the larger encompassing watershed and ideally improves its condition. This distinction is important because the definition of watershed health includes societal activities and judgments, that is, it does not imply 'natural'. When considering watershed health, measures of watershed integrity may provide information on a given watershed's ability to maintain the ecological processes and functions essential to the long-term sustainability of the resource. In contrast to watershed health, *healthy watersheds* can refer to specific watershed protection programmes (e.g. Boon, 1991; DEFRA, 2003; USEPA, 2012a). For instance, building on the efforts of many states and other organizations, the USEPA initiated the Healthy Watersheds Program that places an emphasis on helping states and others assess, identify and protect high quality or 'healthy watersheds' (USEPA, 2012a). These 'healthy watershed' initiatives seek to be cost-effective, non-regulatory means of protecting watershed resources in contrast to regulatory actions, such as the Clean Water Act of 1972. An additional objective of these programmes is to protect areas that can serve as biological refugia that support the recolonization of restored and reconnected aquatic resources (USEPA 2012b).

Watershed health is a useful framework for discussing the trade-offs made by the society when implementing ecological policy at the watershed level (Calow, 1992; Lackey, 2003). H. T. Odum's (1996) expositions on environmental accounting established that any change in an environmental system is made at the expense of other aspects of the system. More simply, because everything in the environment was already in use prior to any anthropogenic activities (Campbell, 2013), any changes made to the environment impact these pre-existing uses. In watersheds, the consideration of trade-offs must include water scarcity, conversion of natural lands to human use and ecological consequences of introduced species, among other factors (Shrader-Frechette, 1997). An assessment must be made of how such trade-offs impact the ecological processes and functions essential to the long-term sustainability of the resources (i.e. watershed integrity).

The foregoing discussion illustrates that the literature contains a number of related concepts that range from those that are solely related to ecological benchmarks (e.g. the integrity metrics and aquatic condition) to those that incorporate human values and goals (e.g. watershed sustainability and health). All of these concepts have merit and applicability, but their distinct meanings are often blurred because of a lack of standardized definitions. For the remainder of this paper, we focus on our definition of watershed integrity, specifically how to make it operational so that it can be estimated and applied to decision-making.

© 2015 The Authors. *River Research and Applications* published by John Wiley & Sons Ltd.

DOI: 10.1002/rra

MAKING WATERSHED INTEGRITY OPERATIONAL

An explicit definition of watershed integrity facilitates discussion when comparing assessed areas. However, a definition alone does not support the quantification of differences in watershed characteristics between areas, measurement of changes in state over time or specification of the level at which efforts could be made to preserve or restore integrity (Noss, 1995). To make the definition of watershed integrity operational, we need to identify the key elements and processes that must be present and intact to maintain watershed production of services, determine the availability of data on those elements and processes and then execute the assessment of watershed integrity. Further, any operational definition must not require large resource investment in methods development or construction of major new datasets. This means that an assessment based on such an approach should be able to utilize existing datasets that are broadly available (e.g. nationally). We fully expect this to be an iterative process; that is, initial efforts based on our approach herein will be improved over time as additional data become available and new research provides better information on the critical relationships that are represented.

Given our definition of watershed integrity as the capacity of a watershed to support and maintain the full range of ecological processes and functions, we would like to be able to assess the status of a given watershed relative to the state required in order to fully provide this support. Such assessments require that we know what the full range of processes and functions is, or should be. One way of attaining this information would be to have some standard for comparison, such as a set of watersheds with unaltered (i.e. reference condition) characteristics and functions. This creates a conundrum, because all watersheds are altered to some degree. In the succeeding text, we discuss approaches to defining reference condition, concluding that they do not describe unaltered conditions. We then propose an approach that obviates the need for reference watersheds and allows estimation of expected values that can be used in assessments of watershed integrity.

For individual aquatic entities, such as lakes, wetlands, streams or estuaries, reference condition is typically estimated using systems that are considered to be as close to natural as possible within a region (Hawkins *et al*., 2010). The characteristics of those reference sites (determined through the collection of monitoring data) are then compared against impacted sites within similar settings (Hughes *et al*., 1986). However, practitioners have long recognized that waterbodies in pristine condition rarely exist, and so what is being described as 'reference' condition is actually 'least degraded' (Stoddard *et al*., 2006). In addition, the degree to which a site represents reference condition also varies regionally. For example, agricultural watersheds can be highly altered, resulting in reference sites that are far from reference condition (Kilgour and Stanfield, 2006). However, even sites with only slight alterations might not reflect natural conditions (e.g. Hill *et al*., 2013), depending on how the watershed responds to human-induced landscape alterations (Figure 1). Whereas programmes such as the USEPA's National Aquatic Resource Surveys (http://water.epa.gov/type/watersheds/monitoring/aquaticsurvey_index.cfm) provide field data to describe reference conditions for various waterbodies/aquatic systems, no such programme provides field-based, aquatic monitoring data at the whole-of-watershed scale. Moreover, aggregating information from these surveys to provide an estimate of watershed status may represent a major challenge.

Researchers have focused on improving assessments by selecting reference sites that maximize representativeness of both unaltered conditions (Sánchez-Montoya *et al*., 2009) and the environments of assessed sites (Johnson, 1999); hindcasting of reference condition in heavily altered landscapes (Kilgour and Stanfield, 2006); and refining modelling approaches to more precisely predict both biological (Moss *et al*., 1999) and environmental reference conditions (see review by Hawkins *et al*., 2010). At the same time, our ability to use deviations from biological and environmental reference conditions to map, quantify and link human-related watershed alterations has improved substantially in recent years (e.g. Falcone *et al*., 2010; Vander Laan *et al*., 2013). Despite these improvements, assessments can suffer from the fact that the natural condition of many systems will differ from reference condition. Additionally, given the ubiquity of human-related alterations across

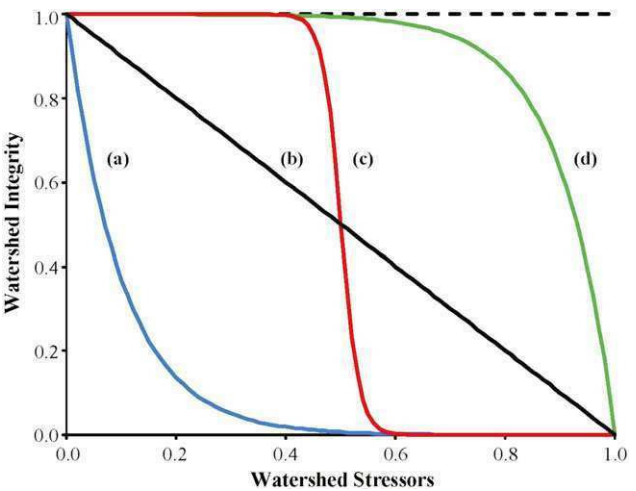

Figure 1. Examples of different responses between watershed integrity and watershed stressors: (a) low resiliency response; (b) negative linear response; (c) threshold (e.g. 'tipping point') response; and (d) high resiliency response. Reference condition is represented by the dashed line. This figure is available in colour online at wileyonlinelibrary.com/journal/rra

© 2015 The Authors. *River Research and Applications* published by John Wiley & Sons Ltd.

DOI: 10.1002/rra

landscapes (e.g. atmospheric deposition of anthropogenically derived nitrogen), we cannot describe truly unaltered conditions for most, if not all, watersheds. Therefore, we need an approach that does not require the use of reference watersheds.

We propose an approach for defining an operational definition of watershed integrity that borrows from the human health field (Van Sickle *et al*., 2006; Van Sickle and Paulsen, 2008). To assess human health, medical practitioners evaluate the condition of different vital systems, for example the circulatory, pulmonary, nervous and endocrine systems. Because the condition of these systems cannot always be directly determined through routine screenings, health practitioners often look for the presence of risk factors as a complementary means of assessment. For example, high cholesterol values, being overweight and inactive, and a history of heart disease are all risk factors related to diseases of the circulatory system. In a similar fashion, we identify key functions that watersheds provide and then identify risk factors (i.e. human-related stressors) that have been explicitly shown to interfere with and degrade these functions. In the succeeding text, we describe both these key watershed features and landscape stressors and then show how they can be used to construct an index of watershed integrity. Note that this approach partitions human stressors (e.g. urban and agricultural land use and density of roads) from natural disturbances (e.g. hurricanes, earthquakes and glaciers). Thus, a watershed that is stressed because of only natural factors could still possess high integrity (Karr, 1981).

Key watershed functions

We have identified six key functions that perform to various degrees in watersheds. A high level of watershed integrity exists when all of these functions are operating at levels that support and maintain the full range of ecological processes and functions essential to the long-term sustainability of biodiversity and ecosystem services. The six key functions are hydrologic regulation, regulation of water chemistry, sediment regulation, hydrologic connectivity, temperature regulation and habitat provision.

Hydrologic regulation (HYD). Water movement is a critical element that defines watersheds. Watersheds function to capture incoming precipitation for varying lengths of time and discharge water as either surface run-off or groundwater (Black, 1997). Below the surface, groundwater and associated constituents move through local, intermediate or regional flowpaths, which can depend on terrain and the specific geologic and hydrologic properties of the underlying soils and aquifers (Winter and LaBaugh, 2003). The details of how these processes operate in a watershed govern the supply, timing and other regime characteristics of water downstream and set the context for the physical, chemical and biological functions of the watershed. Watersheds attenuate the energy of incoming precipitation. Alterations to watershed components and their functions through the construction of impervious surfaces (Shuster *et al*., 2005), agricultural drainage (Naz *et al*., 2009) and irrigation, impoundment (Richter *et al*., 1996), stream channelization and levee construction, wetland and riparian removal (Bruland *et al*., 2003), forest clear cutting, human-caused fires and groundwater pumping all may modify the effectiveness of this attenuation. Such modification results in changes to infiltration, percolation, evapotranspiration, groundwater recharge and surface water export.

Regulation of water chemistry (CHEM). The aquatic chemistry of streams, rivers, lakes and wetlands reflects the processes operating in their watersheds, including physical weathering; plant interception, uptake and release of nutrients; soil formation and transformation; and nutrient retention by wetlands, forests and riparian areas (Grimm *et al*., 1997). The volume, timing and routing of water through a watershed has profound effects on the chemistry of downstream waters (Bormann and Likens, 1979). The retention of nitrogen (Stoddard, 1994; Mayer *et al*., 2007), phosphorus (Richardson, 1985) and ions (i.e. electrical conductivity; USEPA, 2011), in particular, is critical to the downstream water quality and integrity of biota (Minshall and Minshall, 1978). Human activities in the watershed can affect the supply (e.g. fertilizer application and mining), retention (removal of wetlands and/or riparian vegetation and channelization of streams) and processing (sewage and drinking water treatment) of these key chemical elements. In addition, chemical constituents can enter and contaminate groundwater, often with long residence times (Yetiş, 2008).

Sediment regulation (SED). The volume and composition of sediment moving through a watershed depends on a balance between the rates of supply of sediment of various sizes to the stream and the rate at which the flow of water moves them downstream, that is, the stream's sediment transport capacity relative to its sediment supply (Kaufmann *et al*., 2008). The supply rates and sizes of sediment particles delivered to a stream by upslope erosion and mass transport are influenced by basin characteristics, including geology, topography, climate, vegetative cover, run-off characteristics and land disturbances (Buffington *et al*., 2004; Frappier and Eckert, 2007). Changes to sediment regimes following catchment disturbance (either through changed sediment supply, flow modifications or physical barriers) can markedly alter the physical nature of stream channels and consequently their ability to support aquatic organisms (Norris and Thoms, 1999). In addition, fine sediment deposition can smother gravels and disconnect surface water–groundwater interactions within the hyporheic zone of streams (Brunke and Gonser, 1997). Human-related alterations of watersheds can either reduce (e.g. dam building)

© 2015 The Authors. *River Research and Applications* published by John Wiley & Sons Ltd.

DOI: 10.1002/rra

or increase (e.g. agricultural tilling, road building and channelization) sediment transport.

Hydrologic connectivity (CONN). Connectivity is the property that spatially and temporally integrates all of the individual components of a watershed (USEPA 2015). The concept of connectivity builds on classic ideas about how river systems are integrated, such as the river continuum (Vannote *et al*., 1980), serial discontinuity (Ward and Stanford, 1995) and flood pulse (Junk *et al*., 1989) concepts. This integration is achieved through various transport mechanisms that function across multiple spatial and temporal scales to deliver materials and energy between watershed components. Connectivity can be described in terms of the frequency, duration, magnitude, timing and rate of change of energy, water, material and biotic fluxes, which are naturally controlled by climate, geology and terrain. A recent EPA report (USEPA 2015) found that streams and wetlands can have strong influences on the integrity of downstream waters through hydrological, chemical or biological connectivity. However, the degree of those connections varies depending on the environment and human activities (Ward and Stanford, 1995).

Water is the dominant transport mechanism for movement of energy and materials within watersheds. Hydrologic connectivity describes the hydrologically mediated transfer of matter, energy and/or organisms within or between elements of the watershed (Pringle, 2003). Aquatic networks are characterized by a high degree of spatial and temporal heterogeneity with mass, energy and organisms flowing in four dimensions (Nadeau and Rains, 2007): longitudinally (i.e. downstream), laterally (i.e. channel to/from riparian and/or floodplain areas), vertically (i.e. to/from groundwater through the hyporheic zone) and over time. Human uses of the watershed can decrease (e.g. by isolating streams and wetlands from hyporheic zones through arroyo cutting; Wallace *et al*., 1990) or increase (e.g. through ditching or conversion of ephemeral to perennial streams by effluent release) these linkages. Likewise, groundwater pumping directly affects the surface water–groundwater connection (Kirk and Herbert, 2002). Excessive pumping can deplete aquifers and disconnect streams from groundwater sources (Wallace *et al*., 1990). This disconnection can reduce base flow in surface waters (Kirk and Herbert, 2002), thereby increasing vulnerability to disturbances, such as drought (Scanlon *et al*., 2012) and climate change (Hill *et al*., 2014; Leibowitz *et al*., 2014).

Temperature regulation (TEMP). Temperature is a primary control on the structure and function of ecological communities (Brown *et al*., 2004) as well as the chemical composition and transformations within a watershed (Demars *et al*., 2011). The maintenance of coldwater (Epifanio, 2000) and warmwater (Quinn and Kwak, 2003) fisheries, for instance, are both affected by a watershed's ability to regulate water temperature. Watersheds intercept incoming solar radiation and attenuate it through various processes, including riparian shading and evaporative cooling, variations in groundwater infiltration and input, and microclimatic effects (Caissie, 2006). Streamside vegetation removal, dam operations (e.g. hypolimnetic versus epilimnetic flow release), disruption of hydrologic connectivity, effluent release (e.g. from power generation, wastewater or agricultural return flows) and urbanization all have strong influences on water temperature (Poole and Berman, 2001).

Habitat provision (HABT). Natural systems have the ability to convert, transform and organize raw materials and energy into a multitude of habitats that provide for the basic life history requirements of organisms, such as food, shelter and breeding areas. The physical habitat of streams, rivers, wetlands and the near-shore areas of lakes and coastal waters are strongly controlled by watershed structure and function (Allan, 2004). While some aspects of aquatic habitats (e.g. chemical composition and temperature) are included in the previously discussed watershed functions, creating and maintaining the physical structure of habitats are additional critical functions of watersheds. For example, the supply of large woody debris to streams is a key driver of the habitat complexity necessary for native fish species survival (Van Sickle and Gregory, 1990). The presence of dams and reservoirs and impacts to riparian vegetation through roads and urban and agricultural land use are examples of stressors that can affect the habitat provision function.

ASSESSING WATERSHED INTEGRITY: AN OPERATIONAL APPROACH

Given these six functions, we can define an index of watershed integrity as the following:

$$WI = WI_{HYD} \times WI_{CHEM} \times WI_{SED} \times WI_{CONN} \times WI_{TEMP} \times WI_{HABT} \quad (1)$$

where WI represents the overall integrity of the watershed, scaled between 0 and 1 (with higher values indicating greater integrity), and WI_i represents the integrity with respect to the i-th function, with the subscripts referring to the six previously described functions. Note that we take the product of these six values, rather than the sum, because each of these functions is a critical component of watershed integrity and the functions are not substitutable (a complete loss of any one component would cause watershed condition to decline to zero). This is analogous to human health where, for example the circulatory, pulmonary, nervous and endocrine systems are all essential to health, and the failure of

© 2015 The Authors. *River Research and Applications* published by John Wiley & Sons Ltd.

DOI: 10.1002/rra

any one of these systems can cause death. One result of using a product, and the fact that each quotient is scaled from zero to one, is that it is not necessary to include separate weighting factors for each of the six terms in Equation (1).

Because we cannot describe the expected level of each of these six functions for conditions that no longer exist, our approach is to identify and evaluate human-related alterations of watersheds that are known to modify these key functions in ways that degrade watershed integrity (i.e. stressors; Table I). As stressors—such as impervious surface, land use change, wetland loss and stream channelization—are added to a watershed, its integrity declines. The particular shape of the curve (Figure 1) describing the response of watershed condition to a stressor varies, depending on the sensitivity of the watershed to a specific stressor and the mechanism by which each stressor acts on watershed condition (Allan, 2004). For example, Norris and Thoms (1999) cited both linear responses of stream biota (Marchant *et al*., 1997; Karr and Chu, 1999) and non-linear responses of stream sediments (Thoms, 1987) to stressors to develop a conceptual framework of river health that is similar to our concept of watershed integrity (cf. Figure 1 of Norris and Thoms, 1999). In addition, stressors can interact to exacerbate the responses of stream biota to stressor gradients (e.g. Merovich and Petty, 2007; Townsend *et al*., 2008; Piggott *et al*., 2012; Lange *et al*., 2014; Lawrence *et al*., 2014). It is critical to understand how the presence of multiple stressors influences each of the critical watershed functions, because stressors typically do not occur or act in isolation.

In the simplest case, where a watershed is subject to a single stressor j that impacts a single function i, the condition of the watershed with respect to that function is given by

$$WI_i = f_{i,j}\left(\frac{s_{j,obs}}{s_{j,max}}\right) \tag{2}$$

where $s_{j,obs}$ and $s_{j,max}$ are the observed and maximum values of stressor j, respectively, and $f_{i,j}$ is a single-variable mathematical function describing the relationship between function i and stressor j (e.g. the curves in Figure 1). Note that $s_{j,max}$ is used to scale the x-axis in Figure 1 and that $s_{j,obs}/s_{j,max}$ ranges from 0 (unaltered) to 1 (maximum impact). There is a negative relationship between $f_{i,j}$ and $s_{j,obs}/s_{j,max}$; that is, low stressor values correspond to high WI_i values (Figure 1). Stressor values could include the number of dams, length of roads and watershed imperviousness (see Table I for other examples). For stressors such as impervious surface that are based on a proportion, the value for $s_{j,max}$ would be 1. For other stressors, there is no theoretical limit on the upper number that is possible; for example, there could be an arbitrarily large number of roads per unit area. In such cases, $s_{j,max}$ could be the maximum value observed regionally or nationally. Alternatively, a maximum value could be assigned based on what is considered to be the maximum feasible value, dependent on what is physically or socially practical. Note that for any unit where the observed value is equal to the maximum, then watershed condition will be equal to zero, because $s_{j,obs}/s_{j,max}=1$, $WI_i=0$ and therefore $WI=0$ (from Equation (1)).

Although loss of natural infrastructure, such as wetlands, can act as a stressor on the key watershed functions, we do not include these as such, because we do not know the distribution of natural infrastructure under unaltered conditions. While we could use least degraded reference sites to estimate the natural distribution, this would defeat the purpose of our approach, which was to avoid the use of such sites. For stressors that result from losses of natural infrastructure, we instead link these back to the human actions causing those losses. For example, drainage ditches and tile drainage, urbanization and agricultural conversion are stressors causing wetland loss. Presence of built infrastructure can be measured in an absolute sense because it did not exist in the unaltered watershed. For a situation with n multiple stressors, Equation (2) is expanded as follows:

$$WI_i = \sum_{j=1}^{n} g_{i,j}\left(\frac{s_{j,obs}}{s_{j,max}}\right)\Big|s_{k\forall k\neq j} \tag{3}$$

where $g_{i,j}$ is a mathematical function similar to $f_{i,j}$, except that it incorporates the conditional effects of other stressors on the response of WI_i to s_j; and the last terms mean given ('|') the value of s_k for all ('∀') k not equal to j (i.e. for all other stressors besides s_j). As the response of WI_i to s_j is conditioned by these other stressors, it is not necessary to add weighting factors to each sum. Given this, we can combine Equations (1) and (3) into the following:

$$WI = \prod_{i=1}^{6}\left(\sum_{j=1}^{n} g_{i,j}\left(\frac{s_{j,obs}}{s_{j,max}}\right)\Big|s_{k\forall k\neq j}\right) \tag{4}$$

where the product ('$\prod$') is taken over the six watershed functions.

To evaluate WI for watersheds nationally, the major stressors affecting each of the six key functions must be identified, landscape indicators of each stressor must exist from nationally available datasets and the relationship between each function and stressor ($g_{i,j}$) must be known. Table I contains a proposed list of the main stressors affecting each of the six key functions. For each function, stressors are organized by those occurring within and outside of the channel. Included with each stressor is a specific national dataset that could be used to evaluate it. In some cases, no such indicator exists. However, we still include these stressors in Table I, in order to identify missing data layers that need to be developed. Also, explicitly including

© 2015 The Authors. *River Research and Applications* published by John Wiley & Sons Ltd.

DOI: 10.1002/rra

Table I. Key functions that occur in unaltered watersheds and the major stressors affecting these functions

Key function	Description	Major stressors	
		Within channel	Outside channel
Hydrologic regulation (HYD)	Maintenance of the natural timing, pattern, supply and storage of water that flows through the watershed	• Presence and volumes of reservoirs (NID) • Stream channelization and levee construction (NA)	• Percent of the watershed comprising urban and/or agricultural land use (NLCD) • Total length and density of roads (TIGER) • Total length and density of canals/ditches (NHD) • Percent imperviousness of human-related landscapes (NLCD) • Housing unit density (TIGER) • Wetland and riparian removal* (NHD, NLCD) • Boundaries, depths and flows of aquifers (NA) • Groundwater use (GW)
Regulation of water chemistry (CHEM)	Maintenance of the natural timing, supply and storage of the major chemical constituents of freshwaters: nutrients (nitrogen and phosphorus), salinity or conductivity, total dissolved solids, hydrogen ions (pH) and naturally occurring minor constituents (e.g. heavy metals). Human-related alterations can include deviations from naturally occurring concentrations of these constituents or the inclusion of non-naturally occurring constituents, such as pesticides and industrial chemicals.	• Presence and volumes of reservoirs (NID) • Stream channelization and levee construction (NA)	• Atmospheric deposition of anthropogenic sources of nitrogen and acid rain (NADP) • Percent of watershed composed of urban and agricultural land uses (NLCD) • Percent imperviousness of human-related landscapes (NLCD) • Fertilizer application rates (FERT) • Presence and density of wastewater treatment facilities (NPDES), industrial facilities (TRI), superfund sites (SUPERFUND) and mines (MINES) • Cattle density (CATTLE) • Wetland and riparian removal* (NHD, NLCD) • Chemical constituents of groundwater (NA)
Sediment regulation (SED)	Maintenance of the volume and size composition of inorganic particles that are stored or transported through the stream or within lakes, wetlands or estuaries.	• Presence and volumes of reservoirs (NID) • Stream channelization and levee construction (NA)	• Alteration to and spatial arrangement of riparian vegetation (LANDFIRE) • Presence and density of mines (MINES), logging (FOREST) and roads (TIGER) • Agriculture (NLCD) weighted by soil erodibility (STATSGO), landscape slope (NED) and proximity to waterbodies (NHD)
Hydrologic connectivity (CONN)	Presence of hydrologic pathways for the transfer of matter, energy, genes and organisms within watersheds. Systems can vary naturally in their hydrologic isolation (e.g. desert springs) or connectedness (e.g. the Everglades).	• Presence and height of reservoirs (NID) •Stream channelization and levee construction (NA) • Road/stream intersections (TIGER/NHD) weighted by channel slope (NHD)	• Alteration to and spatial arrangement of riparian vegetation (LANDFIRE) • Density of ditches/canals (NHD) • Groundwater use (GW) • Presence and density of wastewater discharge sites (NPDES) • Wetland and riparian removal* (NHD, NLCD)
Temperature regulation (TEMP)	Maintenance of the full range of natural landscape features (both aquatic and terrestrial) required to maintain temperatures that support the aquatic chemistry and biota.	• Presence and volume of reservoirs (NID)	• Alteration to and spatial arrangement of riparian vegetation (LANDFIRE) • Percent of watershed composed of urban and/or agricultural land uses (NLCD) • Percent imperviousness of human-related landscapes (NLCD) • Groundwater use (GW) • Presence and density of wastewater discharge sites (NPDES)

(*Continues*)

© 2015 The Authors. *River Research and Applications* published by John Wiley & Sons Ltd.

DOI: 10.1002/rra

Table I. (Continued)

Key function	Description	Major stressors: Within channel	Major stressors: Outside channel
Habitat provision (HABT)	Presence and maintenance of the full range of natural landscape features (both aquatic and terrestrial) that represent the complete set of conditions that are needed to maintain the natural diversity and abundances of aquatic biota.	• Presence, height and volume of reservoirs (NID)	• Alteration to and spatial arrangement of riparian vegetation (LANDFIRE) • Presence/absence of native vegetation types within riparian zones (LANDFIRE) • Density of human populations and housing unit developments within riparian zones (TIGER) • Percent of watershed composed of urban and agricultural land uses (NLCD) • Density of road/stream intersections (TIGER/NHD) • Density of roads within riparian zones (TIGER)

Data sources that can be used to evaluate the stressors are included parenthetically (see key at succeeding note).
*Indicators for wetland and riparian removal are linked back to the built infrastructure causing those losses, because wetland and riparian distribution under unaltered conditions is generally not known.
CATTLE, USDA National Agriculture Statistics Service (http://www.nass.usda.gov/Charts_and_Maps/Cattle); FERT, County-level estimates of N & P from commercial fertilizer (http://pubs.usgs.gov/sir/2012/5207); FOREST, University of Maryland Global Forest Change map 2000–2012 (http://earthenginepartners.appspot.com/science-2013-global-forest/download.html); GW, Total groundwater usage by US county in yr. 2005 (http://water.usgs.gov/watuse/data/2005); LANDFIRE, USFS and USDOI LANDFIRE Program (http://www.landfire.gov); MINES, USGS Mines Dataset (https://www.sciencebase.gov/catalog/folder/4f4e4767e4b07f02db47e0ad); NA, No nationally available data are available for specified stressor to the best of our knowledge; NAPD, National Atmospheric Deposition Program National Trends Network (http://nadp.sws.uiuc.edu/data/ntn); NED, National Elevation Dataset as distributed with NHD (http://www.horizon-systems.com/NHDPlus/NHDPlusV2_home.php); NHD, National Hydrography Dataset (http://www.horizon-systems.com/NHDPlus/NHDPlusV2_home.php); NID, US Army Corps of Engineers National Inventory of Dams (http://geo.usace.army.mil/pgis/f?p=397:1:0:); NLCD, National Land Cover Dataset (http://www.mrlc.gov/nlcd06_data.php); NPDES, USEPA National Pollutant Discharge Elimination System (http://www.epa.gov/enviro/geo_data.html); STATSGO, USGS State Soil Geographic Data (http://datagateway.nrcs.usda.gov); SUPERFUND, USEPA Superfund Sites (http://www.epa.gov/enviro/geo_data.html); TIGER, US Census Bureau TIGER/Line Program (http://www.census.gov/geo/maps-data/data/pdfs/tiger/tgrshp2013/TGRSHP2013_TechDoc.pdf); TRI, National Toxic Release Inventory (http://www.epa.gov/enviro/geo_data.htm); All websites accessed June 18, 2014.

them allows the effect of these missing stressors to be considered.

The specific relationship between the key functions and each stressor is largely unknown, although we may know $g_{i,j}$ for specific functions and stressors in specific regions. For example, Carlisle *et al*. (2009) found a non-linear response between biological alteration and high-density residential land cover within riparian zones of eastern US highlands: there was a strong effect from 0% to 10% high-density residential areas that reached an asymptote at larger values (Figure 2). Note that, because the relationship in Figure 2 is based on a partial dependence plot, the response takes the conditional effect of other stressors into account (Hastie *et al*., 2009), and so could serve as a g function.

Given the reality that $g_{i,j}$ is largely unknown, we define the following estimator of *WI*:

$$\widehat{WI} = \prod_{i=1}^{6}\left(\sum_{j=1}^{n} 1 - \left(\frac{s_{j,obs}}{s_{j,max}}\right)\right) \quad (5)$$

where $\widehat{WI}$ is our first-order estimate of *WI*, which assumes a negative linear relationship for $g_{i,j}$ and independence among stressors. This estimator provides us with an operational definition of watershed integrity that can be incrementally improved as either specific $g_{i,j}$ relationships are reported or new datasets become available. Because Equation (5) does not include the conditional effects of other stressors, an alternative approach would be to give stressors different weights:

$$\widehat{WI} = \prod_{i=1}^{6}\left(\sum_{j=1}^{n} \alpha_{i,j}\left[1 - \left(\frac{s_{j,obs}}{s_{j,max}}\right)\right]\right) \quad (6)$$

where $\alpha_{i,j}$ is a weighting factor for stressor j with respect to function i.

If $g_{i,j}$ is known for some, but not all stressors, then a hybrid version could be used that combines $g_{i,j}$ with the first-order, weighted estimators. For example,

$$\widehat{WI}_i = \sum_{j=1}^{m} g_{i,j}\left(\frac{s_{j,obs}}{s_{j,max}}\right)\Bigg|_{s_k \forall k \neq j} + \sum_{j=m+1}^{n} \alpha_{i,j}\left[1 - \left(\frac{s_{j,obs}}{s_{j,max}}\right)\right] \quad (7)$$

© 2015 The Authors. *River Research and Applications* published by John Wiley & Sons Ltd.

DOI: 10.1002/rra

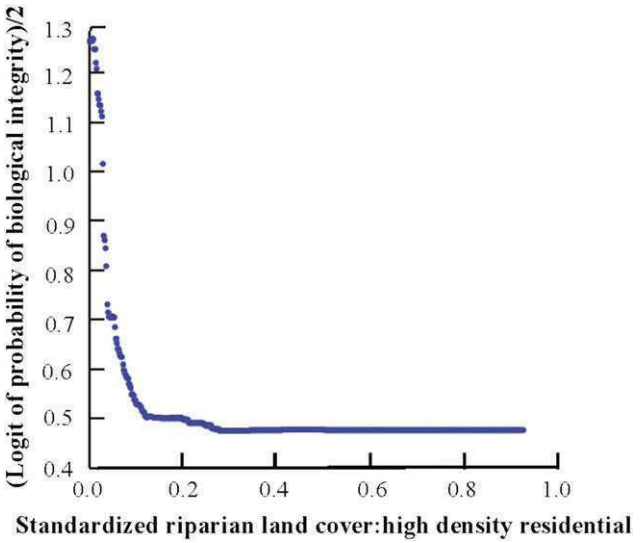

Figure 2. Partial dependence plot showing the relationship between biological integrity and standardized high-density residential land use within riparian zones of the eastern USA. Modified from Carlisle *et al*., 2009. This figure is available in colour online at wileyonlinelibrary.com/journal/rra

where the index m refers to the number of stressors for which $g_{i,j}$ is known.

Finally, we note that there may be instances where the condition of a watershed with respect to a specific key function could be modelled directly. For example, Hill *et al*. (2013) developed a stream temperature model for the USA that, for an individual site, could estimate both the observed temperature and the expected temperature at reference condition. The relationship between these two could then be used as a direct estimate of WI_{TEMP}:

$$WI_{TEMP} = \frac{\left|TEMP_{exp} - TEMP_{obs}\right|}{TEMP_{exp}} \quad (8)$$

where $TEMP_{exp}$ and $TEMP_{obs}$ are the expected (i.e. reference condition) and observed temperatures, respectively. Equation (8) assumes that a positive deviation from the expected value has the same effect as a negative deviation. Other formulations are possible; for example, an equation that has separate responses for $TEMP_{obs}$ greater and less than $TEMP_{exp}$ could be used to give greater weight to warmer temperatures. Equation (8) also assumes that the effects of a given change in temperature are dependent on the expected temperature; for example, a 2 °C change has worse effects at warmer expected temperatures than for cooler expected temperatures. Again, alternative formulations could be used; for example, the expected temperatures could be scaled to one to provide uniform results.

An approach such as Equation (8) is appealing, because it reduces the complexity of dealing with multiple stressors and avoids the problem of having to assume that $g_{i,j}$ is a negative linear relationship. The problem is that this particular modelling approach used reference sites that represent least degraded condition (Hill *et al*., 2013), because unaltered sites did not exist. As previously mentioned, these sites do not fully reflect natural condition, depending on the magnitude of the alteration and the watershed response (Figure 1), which would result in biased WI_{TEMP} estimates. Still, results from a model-based approach (e.g. Equation (8)) could be compared with results using the stressor-based approach (use of Equation (3) with the negative linear assumption) to better understand the strengths and weaknesses of each approach.

As a proof-of-concept study, we are conducting a national assessment of watershed integrity based on this approach and using the StreamCat dataset (Hill *et al*., in press), which was developed, in part, for this purpose. StreamCat contains over 160 landscape variables for all 2.6 million National Hydrography Dataset Plus Version 2 (NHDPlusV2; McKay *et al*., 2012) catchments in the contiguous USA and is being augmented to contain all of the available stressor variables in Table I.

SUMMARY AND CONCLUSIONS

Watersheds encompass all biotic and abiotic components—including people—within their boundaries (*sensu* Likens 1992) and provide a range of services valued by the society. Thus, watersheds are a foundation of our cultural, economic, spiritual and social well-being (Likens *et al*., 2009) and, as such, a critical focus of water resource management. Evaluating the integrity of a watershed represents a societal and a scientific challenge, because watersheds are used and managed for a diverse, interrelated range of activities. The concept of watershed integrity is challenging both in terms of defining what it actually is and developing approaches and tools to allow its evaluation. The assessment of watershed integrity also requires approaches that are scale appropriate (Dollar *et al*., 2007) and enable strategic problem-solving. To paraphrase Likens (1992), the ultimate challenge for watershed and river science is to integrate and synthesize watershed and river information available from all levels of inquiry into an understanding that is meaningful and can be used by managers and decision-makers.

There are a number of terms related to this challenge (e.g. watershed integrity, aquatic condition and watershed health) that have separate meanings. However, these meanings are often blurred because of a lack of standardized definitions. Here, we provide distinct definitions for these different terms, which should allow the scientific community to better address the needs of decision-makers. This includes our main focus, watershed integrity, which we define 'as the capacity of a watershed to support and maintain the full

© 2015 The Authors. *River Research and Applications* published by John Wiley & Sons Ltd.

DOI: 10.1002/rra

range of ecological processes and functions essential to the sustainability of biodiversity and of the watershed resources and services provided to society'. We developed an operational index to evaluate the level of integrity. For this index, we used a human health analogy to identify six key watershed functions (viz. hydrologic regulation, regulation of water chemistry, sediment regulation, hydrologic connectivity, temperature regulation and habitat provision) and the specific risk factors, or stressors, which impact them. Examples of national datasets that can be used to evaluate these risk factors were provided. We derived a mathematical expression (Equation (4)) that evaluates watershed integrity by combining the integrity of the six watershed functions, where the integrity of each is based on the relative presence of specific stressors. This expression assumes the quantitative relationships between multiple interacting stressors and the key functions are known. Although such relationships do exist (e.g. Figure 2), the availability of this information is limited and represents an ongoing need for additional research. However, we also show how first-order approximations can be used in the absence of such information, given that many of these relationships are as yet unknown. The approach can be iteratively applied and improved as these relationships become known and/or as new national datasets become available. For example, the version of the index that uses first-order approximations (Equation (5)) could be replaced as information on weightings (Equation (6)) or conditional effects of other factors (Equations (7)) becomes available. A significant aspect of our approach is that it allows us to avoid the use of least degraded sites to describe reference condition.

A characteristic of our index is that it can be readily deconstructed in support of strategic adaptive management; that is, the risk factors of the watershed index score can be examined individually to evaluate how each is influencing the overall index score. This affords managers the opportunity to examine how each factor might be managed differently to better achieve overall objectives. For example, if the index score for a given watershed is below an established threshold, the factors bringing the overall index score down can easily be identified. If multiple factors are negatively influencing the overall score, a cost–benefit analysis of available management options then could be conducted to identify the best course of action to achieve desirable management endpoints.

Previous efforts to assess the status of watersheds on larger scales, though limited in number, have been undertaken in the USA and elsewhere (e.g. Garrido Pérez *et al*., 2010, for México). For example, in the USA, the U.S. Fish and Wildlife Service, along with the National Marine Fisheries Service and the Association of Fish and Wildlife Agencies, developed and implemented the National Fish Habitat Action Plan (Association of Fish and Wildlife Agencies, 2006). Its objective was to protect, restore and enhance the nation's fish and aquatic communities through partnerships to foster fish habitat conservation. Similarly, the U.S. Forest Service developed the Watershed Condition Framework (USFS, 2011), which employed an integrated, systems-based approach for classifying watershed condition based on an evaluation of underlying ecological, hydrological and geomorphic states. These programmes focus solely on identifying high-quality aquatic resources and make use of locally collected data (e.g. biota and water quality) that are not available nationally. Our intent was to develop a watershed integrity index that can be applied nationally. This approach differs because it focuses on the functional attributes of these systems, rather than simply relying on more easily obtainable state components. It also differs technically through its use of appropriately scaled data that identify risk factors that impact these key functions. Beyond informing on the biogeochemical health of the immediate system, a focus on functional attributes provides information that can be used to explain and predict the effects of watershed discharges on downstream riverine and estuarine condition (Gregory *et al*., 1991).

Data resulting from a national-scale mapping and assessment of watershed integrity should be of value to states and watershed organizations initiating healthy watershed programmes (USEPA, 2012a). These programmes augment the watershed approach with proactive, holistic aquatic ecosystem conservation and protection designed to conserve critical components of watersheds and, therefore, avoid additional water quality impairments in the future. A national evaluation of watershed integrity that uses our approach—which we are currently in the process of conducting, using the StreamCat (Hill *et al.*, submitted) database—would help identify watersheds with high integrity as well as those at risk and help to prioritize conservation and restoration. The index of watershed integrity developed here should provide high-quality information at a broad spatial scale that will help allow ecosystem management to focus on achievable and measureable outcomes underpinned by quality science.

ACKNOWLEDGEMENTS

We thank Tony Olsen and Marc Weber for discussions that helped shape this manuscript. We also thank Mark Bagley, Gary Davis, Thomas Fontaine, Walt Foster, Laura Gabanski, Andy Gillespie, Chuck Hawkins, Karen Metchis, Richard Mitchell, Doug Norton, Steve Paulsen, Justicia Rhodus, Murray Scown, Joseph Tiago, Suzanne van Drunick and two anonymous reviewers for comments on earlier manuscript drafts. M. T. gratefully acknowledges the support of the American Fulbright Senior Scholarship.

The information in this document has been funded entirely by the US Environmental Protection Agency, in part

© 2015 The Authors. *River Research and Applications* published by John Wiley & Sons Ltd.

DOI: 10.1002/rra

by an appointment to the Internship/Research Participation Program at the Office of Research and Development, U.S. Environmental Protection Agency, administered by the Oak Ridge Institute for Science and Education through an interagency agreement between the U.S. Department of Energy and EPA. The views expressed in this journal article are those of the authors and do not necessarily reflect the views or policies of the U.S. Environmental Protection Agency. Mention of trade names or commercial products does not constitute endorsement or recommendation for use.

REFERENCES

Allan JD. 2004. Landscapes and riverscapes: the influence of land use on stream ecosystems. *Annual Review of Ecology, Evolution, and Systematics* **35**: 257–284. DOI:10.1146/annurevecolsys.35.120202.110122.

Allan JD, Castillo MM. 2007. *Stream Ecology: Structure and Function of Running Waters*, 2nd edn. Springer: Dordrecht, The Netherlands.

Allen TFH, Starr TB. 1982. *Hierarchy: Perspectives for Ecological Complexity*. University of Chicago Press: Chicago.

Angermeier PL, Karr JR. 1994. Biological integrity versus biological diversity as policy directives: protecting biotic resources. *BioScience* **44**: 690–697.

Association of Fish and Wildlife Agencies. 2006. *National Fish Habitat Action Plan (NFHAP)*, 1st Edition, April 24, 2006. Association of Fish and Wildlife Agencies: Washington, DC.

Bae M-J, Chon T-S, Park Y-S. 2014. Characterizing differential responses of benthic macroinvertebrate communities to floods and droughts in three different stream types using a Self-Organizing Map. *Ecohydrology* **7**: 115–126.

Barbour MT, Swietlik WF, Jackson SK, Courtemanch DL, Davies SP, Yoder CO. 2000. Measuring the attainment of biological integrity in the USA: a critical element of ecological integrity. *Hydrobiologia* **422** (423): 453–464. DOI:10.1023/A:1017095003609.

Begon M, Townsend CR, Harper JL. 2006. *Ecology: From Individuals to Ecosystems*. Blackwell Publishing Ltd.: Maine.

Bennett EM, Peterson GD, Gordon LJ. 2009. Understanding relationships among multiple ecosystem services. *Ecology Letters* **12**: 1394–1404. DOI:10.1111/j.1461-0248.2009.01387.x.

Berkes F. 2007. Understanding uncertainty and reducing vulnerability: lessons from resilience thinking. *Natural Hazards* **41**: 283–295. DOI:10.1007/s11069-006-9036-7.

Black PE. 1997. Watershed functions. *Journal of the American Water Resources Association* **33**: 1–11. DOI:10.1111/j.1752-1688.1997.tb04077.x.

Boon PJ. 1991. The role of sites of special scientific interest (SSSIs) in the conservation of British rivers. *Freshwater Forum* **1**: 95–108.

Bormann FH, Likens GE. 1979. *Pattern and Process in a Forested Ecosystem*. Springer-Verlag: New York.

Brown AV, Brown KB, Jackson DC, Pierson WK. 2005. Lower Mississippi River and its tributaries. In *Rivers of North America*, Benke AC, Cushing CE (eds). Elsevier, Inc.: Burlington, Massachusetts; 231–281.

Brown JH, Gillooly JF, Allen AP, Savage VM, West GB. 2004. Toward a metabolic theory of ecology. *Ecology* **85**: 1771–1789. DOI:10.1890/03-9000.

Bruland GL, Hanchey MF, Richardson CJ. 2003. Effects of agriculture and wetland restoration on hydrology, soils, and water quality of a Carolina bay complex. *Wetlands Ecology and Management* **11**: 141–156. DOI:10.1023/A:1024244408577.

Brunke M, Gonser T. 1997. The ecological significance of exchange processes between rivers and groundwater. *Freshwater Biology* **37**: 1–33. DOI:10.1046/j.1365-2427.1997.00143.x.

Brutsaert W. 2005. *Hydrology: An Introduction*. Cambridge University Press: New York.

Buffington JM, Montgomery DR, Greenberg HM. 2004. Basin-scale availability of salmonid spawning gravel as influenced by channel type and hydraulic roughness in mountain catchments. *Canadian Journal of Fisheries and Aquatic Sciences* **61**: 2085–2096. DOI:10.1139/f04-141.

Bunch MJ, Morrison KE, Parkes MW, Venema HD. 2011. Promoting health and well-being by managing for social–ecological resilience: the potential of integrating ecohealth and water resources management approaches. *Ecology and Society* **16**: 6. [online] http://www.ecologyandsociety.org/vol16/iss1/art6/; accessed 1 September 2014.

Butchart SHM, Walpole M, Collen B, van Strien A, Scharlemann JPW, Almond REA, Baillie JEM, Bomhard B, Brown C, Bruno J, Carpenter KE, Carr GM, Chanson J, Chenery AAM, Csirke J, Davidson NC, Dentener F, Foster M, Galli A, Galloway JN, Genovesi P, Gregory RD, Hockings M, Kapops V, Lamarque J-F, Leverington F, Loh J, McGeoch MA, McRae L, Minasyan A, Morcillo MH, Oldfield TEE, Pauly D, Quader S, Revenga C, Sauer JR, Skolnik B, Spear D, Stanwell-Smith D, Stuart SN, Symes A, Tiernet M, Tyrrell TD, Vié J-C, Watson R. 2010. Global biodiversity: indicators of recent declines. *Science* **328**: 1164–1168. DOI:10.1126/science; 1187512.

Cairns J Jr, Crawford TV (eds). 1991. *Integrated Environmental Management*. Lewis Publishers, Inc.: Chelsea, Michigan.

Caissie D. 2006. The thermal regime of rivers: a review. *Freshwater Biology* **51**: 1389–1406. DOI:10.1111/j.1365-2427.2006.01597.x.

Callicott JB, Crowder LB, Mumford K. 1999. Current normative concepts in conservation. *Conservation Biology* **13**: 22–35. DOI:10.1046/j.1523-1739.1999.97333.x.

Calow P. 1992. Can ecosystems be healthy? Critical consideration of concepts. *Journal of Aquatic Ecosystem Health* **1**: 1–5. DOI:10.1007/BF00044403.

Campbell DE. 2013. Keeping the books for the environment and society: the unification of emergy and financial accounting methods. *Journal of Environmental Accounting and Management* **1**: 25–41. DOI:10.5890/JEAM.2013.01.003.

Carlisle DM, Falcone J, Meador MR. 2009. Predicting the biological condition of streams: use of geospatial indicators of natural and anthropogenic characteristics of watersheds. *Environmental Monitoring and Assessment* **151**: 143–160. DOI:10.1007/s10661-008-0256-z.

Costanza R, d'Arge R, de Groot R, Farber S, Grasso M, Hannon B, Limburg K, Naeem S, O'Neill RV, Paruelo J, Raskin RG, Sutton P, van den Belt M. 1997. The value of the world's ecosystem services and natural capital. *Nature* **387**: 253–260. DOI:10.1038/387253a0.

Costanza R, de Groot R, Sutton P, van der Ploeg S, Anderson SJ, Kubiszewski I, Farber S, Turner RK. 2014. Changes in the global value of ecosystem services. *Global Environmental Change* **26**: 152–158. DOI:10.1016/j.gloenvcha.2014.04.002.

DEFRA. 2003. *Sites of Special Scientific Interest: Encouraging Positive Partnerships*. Department of Environment, Food and Rural Affairs: London. [online] https://www.gov.uk/government/uploads/system/uploads/attachment_data/file/218711/sssi-code.pdf; accessed 17 August 2014.

de Groot RS, Wilson MA, Boumans RMJ. 2002. A typology for the classification, description and valuation of ecosystem functions, goods and services. *Ecological Economics* **41**: 393–408.

Demars BOL, Manson JR, Ólafsson JS, Gíslason GM, Gudmundsdóttir R, Woodward G, Reiss J, Pichler DE, Rasmussen JJ, Friberg N. 2011. Temperature and the metabolic balance of streams. *Freshwater Biology* **56**: 1106–1121. DOI:10.1111/j.1365-2427.2010.02554.x.

Dictionary.com. "Integrity" in Dictionary.com Unabridged. 2014. http://dictionary.reference.com/browse/integrity. Random House, Inc. [online] http://dictionary.reference.com/; accessed 10 September 2014.

Dingman SL. 2002. *Physical Hydrology*, 2nd edn. Prentice Hall: Upper Saddle River, New Jersey.

© 2015 The Authors. *River Research and Applications* published by John Wiley & Sons Ltd.

Dollar ESJ, James CS, Rogers KH, Thoms MC. 2007. A framework for interdisciplinary understanding of rivers as ecosystems. *Geomorphology* **89**: 147–162. DOI:10.1016/j.geomorph 2006.07.022.

Dudgeon D, Arthington AH, Gessner MO, Kawabata Z-I, Knowler DJ, Lévêque C, Naiman RJ, Prieur-Richard A-H, Soto D, Stiassny MLJ, Sullivan CA. 2006. Freshwater biodiversity: importance, threats, status and conservation challenges. *Biological Reviews* **81**: 163–182. DOI:10.1017/S1464793105006950.

Epifanio J. 2000. The status of coldwater fishery management in the United States: an overview of state programs. *Fisheries* **25**: 13–27. DOI:10.1577/1548-8446(2000)025<0013:TSOCFM>2.0.CO;2.

European Commission. 2014. The EU Water Framework Directive – integrated river basin management for Europe. http://ec.europa.eu/environment/water/water-framework/index_en.html; accessed 01 Sept 2014.

Falcone JA, Carlisle DM, Weber LC. 2010. Quantifying human disturbance in watersheds: variable selection and performance of a GIS-based disturbance index for predicting the biological condition of perennial streams. *Ecological Indicators* **10**: 264–273. DOI:10.1016/j.ecolind.200905.005.

Farber SC, Costanza R, Wilson MA. 2002. Economic and ecological concepts for valuing ecosystem services. *Ecological Economics* **41**: 375–392.

Fischman RL. 2004. The meanings of biological integrity, diversity, and environmental health. *Natural Resources Journal* **44**: 989–1026.

Flotemersch JE, Stribling JB, Hughes RM, Reynolds L, Paul MJ, Wolter C. 2011. Site length for biological assessment of boatable rivers. *River Research and Applications* **27**: 520–535. DOI:10.1002/rra.1367.

Flotemersch JE, Stribling JB, Paul MJ. 2006. *Concepts and Approaches for the Bioassessment of Non-wadeable Streams and Rivers*, EPA/600/R-06/127. U.S. Environmental Protection Agency: Cincinnati, OH.

Frappier B, Eckert RT. 2007. A new index of habitat alteration and a comparison of approaches to predict stream habitat conditions. *Freshwater Biology* **52**: 2009–2020. DOI:10.1111/j.1365-2427.2007.01803.x.

Frey D. 1975. Biological integrity of water: an historical perspective. In *The Integrity of Water: Proceedings of a Symposium, March 10–12, 1975, Washington, D.C*, EPA/832/R-75/103. Environmental Protection Agency: Washington, DC.; 127–140.

Garrido Pérez A, Cuevas ML, Cotler H, González DI, Tharme RE. 2010. Evaluación del grado de alteración ecohidrológica de los ríos y corrientes superficiales de México. *Investigación Ambiental. Ciencia y Política Pública* **2**: 25–46.

Gregory SV, Swanson FJ, McKee WA, Cummins KW. 1991. An ecosystem perspective of riparian zones: focus on links between land and water. *BioScience* **41**: 540–551. DOI:10.2307/1311607.

Grimm NB, Fisher SG, Gregory SV, Marzolf GR, McKnight DM, Triska FJ, Valett HM. 1997. Sustainability of western watersheds: nutrients and productivity. In *Aquatic Ecosystems Symposium: Report to the Western Water Policy Review Advisory Commission*, Minckley WL (ed). National Technical Information Service: Springfield, VA; 33–45.

Hastie T, Tibshirani R, Friedman J. 2009. *The Elements of Statistical Learning: Data Mining, Inference, and Prediction*, Second edn. New York: Springer-Verlag.

Hawkins CP, Olson JR, Hill RA. 2010. The reference condition: predicting benchmarks for ecological and water-quality assessments. *Journal of the North American Benthological Society* **29**: 312–343. DOI:10.1899/09-092.1.

Hill RA, Hawkins CP, Carlisle DM. 2013. Predicting thermal reference conditions for USA streams and rivers. *Freshwater Science* **32**: 39–55. DOI:10.1899/12-009.1.

Hill RA, Hawkins CP, Jin J. 2014. Predicting thermal vulnerability of stream and river ecosystems to climate change. *Climatic Change* **125**: 399–412. DOI:10.1007/s10584-014-1174-4.

Hill RA, Weber MH, Leibowitz SG, Olsen AR, Thornbrugh DJ. in press. The Stream-Catchment (StreamCat) Dataset: a database of watershed metrics for the conterminous USA. *Journal of the American Water Resources Association* (in press).

Holling CS. 1973. Resilience and stability of ecological systems. *Annual Review of Ecology and Systematics* **4**: 1–23. DOI:10.1146/annurev.es.04.110173.000245.

Hughes RM, Larsen DP, Omernik JM. 1986. Regional reference sites: a method for assessing stream potentials. *Environmental Management* **10**: 629–635. DOI:10.1007/BF01866767.

Hull RB, Richert D, Seekamp E, Robertson D, Buhyoff GJ. 2003. Understandings of environmental quality: ambiguities and values held by environmental professionals. *Environmental Management* **31**: 1–13.

Johnson RK. 1999. Regional representativeness of Swedish reference lakes. *Environmental Management* **23**: 115–124. DOI:10.1007/s002679900172.

Junk WJ, Bayley PB, Sparks RE. 1989. The flood pulse concept in river-floodplain systems. Pages 110–127 in Proceedings of the international large river symposium, Canadian Special Publication of Fisheries and Aquatic Sciences 106. D. P. Dodge, editor., Ottawa, Canada.

Karr JR. 1981. Assessment of biotic integrity using fish communities. *Fisheries* **6**: 21–27. DOI:10.1577/1548-8446(1981)006<0021:AOBIUF>2.0.CO;2.

Karr JR. 1996. Ecological integrity and ecological health are not the same thing. In *Engineering Within Ecological Constraints*, Schulze P (ed.). National Academy of Science: Washington, DC; 97–110.

Karr JR, Chu EW. 1999. *Restoring Life in Running Waters: Better Biological Monitoring*. Island Press: Washington, DC.

Karr KR, Dudley DR. 1981. Ecological perspective on water quality goals. *Environmental Management* **5**: 55–68. DOI:10.1007/BF01866609.

Karr JR, Fausch KD, Angermeier PL, Yant PR, Schlosser IJ. 1986. *Assessing Biological Integrity in Running Waters: A Method and Its Rationale*, Special Publication No. 5. Illinois Natural History Survey: Champaign, Illinois.

Kaufmann PR, Faustini JM, Larsen DP, Shirazi MA. 2008. A roughness-corrected index of relative bed stability for regional stream surveys. *Geomorphology* **99**: 150–170. DOI:10.1016/j.geomorph 2007.10.007.

Kenney DS. 1997. *Resource Management at the Watershed Level: An Assessment of the Changing Federal Role in the Emerging Era of Community-based Watershed Management*. Denver, Colorado: Western Water Policy Review Advisory Commission.

Kilgour BW, Stanfield LW. 2006. Hindcasting reference conditions in streams. In *Landscape Influences on Stream Habitats and Biological Assemblages. American Fisheries Society*, Hughes R, Wang L, Seelbach P (eds.), Symposium Volume 48. American Fisheries Society: Bethesda, Maryland; 623–639.

Kirk S, Herbert AW. 2002. Assessing the impact of groundwater abstractions on river flows. In *Sustainable Groundwater Development* Volume 193, Hiscock KM, Rivett MO, Davison RM (eds.). Geological Society: London; 211–233. DOI:10.1144/GSL.SP.2002.193.01.16.

Lackey RT. 2003. Appropriate use of ecosystem health and normative science in ecological policy. In *Managing for Healthy Ecosystems*, Rapport DJ, Lasley WL, Rolston DE, Nielsen NO, Qualset CO, Damania AB (eds.). Taylor and Francis Group, LLC: Boca Raton, Florida; 175–186.

Langbein WB, Iseri KT. 1960. *Manual of Hydrology: Part 1. General Surface-Water Techniques. General Introduction and Hydrologic Definitions*. Geological Survey Water Supply Paper 1541-A. United States Government Printing Office: Washington, DC.

Lange K, Townsend CR, Gabrielsson R, Chanut PCM, Matthaei CD. 2014. Responses of stream fish populations to farming intensity and water abstraction in an agricultural catchment. *Freshwater Biology* **59**: 286–299. DOI:10.1111/fwb.12264.

© 2015 The Authors. *River Research and Applications* published by John Wiley & Sons Ltd.

Lawrence DJ, Stewart-Koster B, Olden JD, Ruesch AS, Torgersen CE, Lawler JJ, Butcher DP, Crown JK. 2014. The interactive effects of climate change, riparian management, and a nonnative predator on stream-rearing salmon. *Ecological Applications* **24**: 895–912.

Leibowitz SG, Comeleo RL, Wigington PJ Jr, Weaver CP, Morefield PE, Sproles EA, Ebersole JL. 2014. Hydrologic landscape classification evaluates streamflow vulnerability to climate change in Oregon, USA. *Hydrology and Earth System Sciences* **18**: 3367–3392. DOI:10.1890/13-0753.1.

Leopold A. 1949. *A Sand County Almanac and Sketches Here and There*. Oxford University Press, Inc.: New York.

Likens GE. 1992. Some applications on the ecosystem approach to environmental problems and resource management. In *Responses of Forest Ecosystems to Environmental Changes*, Teller A, Mathy P, Jeffers JNR (eds.). Elsevier Applied Science: London and New York; 16–30.

Likens GE, Walker KF, Davies PE, Brookes J, Olley J, Young WJ, Thoms MC, Lake PS, Gawne B, Davis J, Arthington AH, Thompson R, Oliver RL. 2009. Ecosystem science: toward a new paradigm for managing Australia's inland aquatic ecosystems. *Marine and Freshwater Research* **60**: 271–279. DOI:10.1071/MF08188.

Mageau MT, Costanza R, Ulanowicz RE. 1995. The development and initial testing of a quantitative assessment of ecosystem health. *Ecosystem Health* **1**: 201–213.

Malinga R, Gordon LJ, Jewitt G, Lindborg R. 2015. Mapping ecosystem services across scales and continents – a review. *Ecosystem Services* **13**: 57–63. [online] 10.1016/j.ecoser.2015.01.006; accessed 1 September 2014.

Marchant R, Hirst A, Norris RH, Butcher R, Metzeling L, Tiller D. 1997. Classification and prediction of macroinvertebrate assemblages from running waters in Victoria, Australia. *Journal of the North American Benthological Society* **16**: 664–681. DOI:10.2307/1468152.

Mayer PM, Reynolds SK Jr, McCutchen MD, Canfield TJ. 2007. Meta-analysis of nitrogen removal in riparian buffers. *Journal of Environmental Quality* **36**: 1172–1180. DOI:10.2134/jeq2006.0462.

McKay, L, Bondelid T, Dewald T, Johnston J, Moore R, Reah A. 2012. NHDPlus Version 2: User Guide. US Environmental Protection Agency. http://www.horizon-systems.com/nhdplus/NHDPlusV2_documentation.php#NHDPlusV2%20User%20Guide.

Merovich GT Jr, Petty JT. 2007. Interactive effects of multiple stressors and restoration priorities in a mined Appalachian watershed. *Hydrobiologia* **575**: 13–31. DOI:10.1007/s10750-006-0277-y.

Merriam-Webster. 1993. Integrity. In *Webster's Third New International Dictionary of the English Language, Unabridged*, Gove PB (ed.). Merriam-Webster: Springfield, Massachusetts.

Millennium Ecosystem Assessment. 2005. *Ecosystems and Human Well-being: Synthesis*. Island Press: Washington, DC.

Minshall GW, Minshall JN. 1978. Further evidence on role of chemical factors in determining distribution of benthic invertebrates in River Duddon. *Archiv für Hydrobiologie* **83**: 324–355.

Mitchell B (ed.). 1990. *Integrated Water Management: International Experiences and Perspectives*. Belhaven Press: London.

Mosley MP, McKerchar AI. 1993. Streamflow. In *Handbook of Hydrology*, Maidment D (ed)(ed.). McGraw-Hill, Inc.: New York; 8.1–8.39.

Moss D, Wright JF, Furse MT, Clarke RT. 1999. A comparison of alternative techniques for prediction of the fauna of running-water sites in Great Britain. *Freshwater Biology* **41**: 167–181. DOI:10.1046/j.1365-2427.1999.00376.x.

Nadeau T-L, Rains MC. 2007. Hydrological connectivity between headwater streams and downstream waters: how science can inform policy. *Journal of the American Water Resources Association* **43**: 118–133. DOI:10.1111/j.1752-1688.2007.00010.x.

Naz BS, Ale S, Bowling LC. 2009. Detecting subsurface drainage systems and estimating drain spacing in intensively managed agricultural landscapes. *Agricultural Water Management* **96**: 627–637. DOI:10.1016/j.agwat.2008.10.002.

Norris RH, Thoms MC. 1999. What is river health? *Freshwater Biology* **41**: 197–209. DOI:10.1046/j.1365-2427.1999.00425.x.

Noss RF. 1990. Indicators for monitoring biodiversity: a hierarchical approach. *Conservation Biology* **4**: 355–364. DOI:10.1111/j.1523-1739.1990.tb00309.x.

Noss RF. 1995. Ecological integrity and sustainability: buzzwords in conflict?. In *Perspectives on Ecological Integrity*, Westra L, Lemons J (eds.). Kluwer Academic Publishers: Dordrecht; 60–76.

Noss RF. 2004. Some suggestions for keeping national wildlife refuges healthy and whole. *Natural Resources Journal* **44**: 1093–1111.

Novotny V. 2004. *Linking Pollution to Water Body Integrity: Literature Review*, Center for Urban Environmental Studies Technical Report 1. Northeastern University: Boston, Massachusetts.

Odum HT. 1996. *Environmental Accounting: Emergy and Environmental Decision Making*. John Wiley & Sons, Inc.: New York.

Oliveria SV, Cortes MV. 2006. Environmental indicators of ecological integrity and their development for running waters in northern Portugal. *Limnetica* **25**: 479–498.

O'Neill RV, King AW. 1998. Homage to St. Michael; or, why are there so many books on scale. In *Ecological Scale*, Peterson DL, Parker VT (eds.). Columbia University Press: New York; 3–16.

Parsons M, Flotemersch JE, Reid M, Thoms M. 2016. Assessing river health: a paradigm shift for the 21st century. In *River Research and Applications: Science and Applications for the 21st Century*, Gilvear D, Greenwood M, Thoms M, Wood P (eds.). Wiley-Blackwell: Hoboken: New Jersey.

Pickett STA, Kolasa J, Jones CG. 1994. *Ecological Understanding: The Nature of Theory and the Theory of Nature*. Academic Press, Inc.: San Diego, California.

Piggott JJ, Lange K, Townsend CR, Matthaei CD. 2012. Multiple stressors in agricultural streams: a mesocosm study of interactions among raised water temperature, sediment addition and nutrient enrichment. *PLoS One* **7**: e49873. DOI:10.1371/journal.pone.0049873.

Poole GC, Berman CH. 2001. An ecological perspective on in-stream temperature: natural heat dynamics and mechanisms of human-caused thermal degradation. *Environmental Management* **27**: 787–802. DOI:10.1007/s002670010188.

Pringle C. 2003. What is hydrologic connectivity and why is it ecologically important? *Hydrological Processes* **17**: 2685–2689. DOI:10.1002/hyp.5145.

Quinn JW, Kwak TJ. 2003. Fish assemblage changes in an Ozark river after impoundment: a long-term perspective. *Transactions of the American Fisheries Society* **132**: 110–119. DOI:10.1577/1548-8659(2003)132<0110:FACIAO>2.0.CO;2.

Rains MC, Fogg GE, Harter T, Dahlgren RA, Williamson RJ. 2006. The role of perched aquifers in hydrological connectivity and biogeochemical processes in vernal pool landscapes, Central Valley, California. *Hydrological Processes* **20**: 1157–1175. DOI:10.1002/hyp.5937.

Rains MC, Mount JF. 2002. Origin of shallow ground water in an alluvial aquifer as determined by isotopic and chemical procedures. *Ground Water* **40**: 552–563. DOI:10.1111/j.1745-6584.2002.tb02540.x.

Rapport DJ, Costanza R, Epstein PR, Gaudet C, Levins R (eds.). 1998a. *Ecosystem Health*. Blackwell Science, Inc.: Malden, Massachusetts and Oxford.

Rapport DJ, Costanza R, McMichael AJ. 1998b. Assessing ecosystem health. *Trends in Ecology & Evolution* **13**: 397–402.

Resh VH, Brown AV, Covich AP, Gurtz ME, Li HW, Minshall GW, Reice SR, Sheldon AL, Wallace JB, Wissmar RC. 1988. The role of disturbance in stream ecology. *Journal of the North American Benthological Society* **7**: 433–455. DOI:10.2307/1467300.

Richardson CJ. 1985. Mechanisms controlling phosphorus retention capacity in freshwater wetlands. *Science* **228**: 1424–1427. DOI:10.1126/science.228.4706.1424.

© 2015 The Authors. *River Research and Applications* published by John Wiley & Sons Ltd.

Richter BD, Baumgartner JV, Powell J, Braun DP. 1996. A method for assessing hydrologic alteration within ecosystems. *Conservation Biology* **10**: 1163–1174. DOI:10.1046/j.1523-1739.1996.10041163.x.

Ross N, Eyles J, Cole D, Iannantuono A. 1997. The ecosystem health metaphor in science and policy. *The Canadian Geographer* **41**: 114–127. DOI:10.1111/j.1541-0064.1997.tb01152.x.

Sánchez-Montoya MM, Vidal-Abarca MR, Puntí T, Poquet JM, Prat N, Rieradevall M, Alba-Tercedor J, Zamora-Muñoz C, Toro M, Robles S, Álvarez M, Suárez ML. 2009. Defining criteria to select reference sites in Mediterranean streams. *Hydrobiologia* **619**: 39–54. DOI:10.1007/s10750-008-9580-0.

Scanlon BR, Faunt CC, Longuevergne L, Reedy RC, Alley WM, McGuire VL, McMahon PB. 2012. Groundwater depletion and sustainability of irrigation in the US High Plains and Central Valley. *Proceedings of the National Academy of Sciences of the United States of America* **109**: 9320–9325. DOI:10.1073/pnas.1200311109.

Scatena FN, Blanco JF, Beard KH, Waide RB, Lugo AE, Brokaw N, Silver WL, Haines BL, Zimmerman JK. 2012. Disturbance regime. In *A Caribbean Forest Tapestry: The Multidimensional Nature of Disturbance and Response*, Brokaw N, Crowl TA, Lugo AE, McDowell WH, Scatena FN, Waide RB, Willig MR (eds.). Oxford University Press: New York; 164–200.

Schofield NJ, Davies PE. 1996. Measuring the health of our rivers. *Water (Australia)* **23**: 39–43.

Shinneman DJ, Baker WL, Rogers PC, Kulakowski D. 2013. Fire regimes of quaking aspen in the Mountain West. *Forest Ecology and Management* **299**: 22–34. DOI:10.1016/j.foreco.2012.11.032.

Shrader-Frechette K. 1997. Ecological risk assessment and ecosystem health: fallacies and solutions. *Ecosystem Health* **3**: 73–81. DOI:10.1111/j.1526-0992.1997.00710.pp.x.

Shuster WD, Bonta J, Thurston H, Warnemuende E, Smith DR. 2005. Impacts of impervious surface on watershed hydrology: a review. *Urban Water Journal* **2**: 263–275. DOI:10.1080/15730620500386529.

Sidle RC, Benson WH, Carriger JF, Kamai T. 2013. Broader perspective on ecosystem sustainability: consequences for decision making. *Proceedings of the National Academy of Sciences of the United States of America* **110**: 9201–9208. DOI:10.1073/pnas.1302328110.

Stoddard JL. 1994. Long-term changes in watershed retention of nitrogen: its causes and aquatic consequences. In *Environmental Chemistry of Lakes and Reservoirs*, Baker LA (ed.), Advances in Chemistry Series, Volume 237. American Chemical Society: Washington, DC; 223–284.

Stoddard JL, Larsen DP, Hawkins CP, Johnson RK, Norris RH. 2006. Setting expectations for the ecological condition of streams: the concept of reference condition. *Ecological Applications* **16**: 1267–1276. DOI:10.1890/1051-0761(2006)016[1267:SEFTEC]2.0.CO;2.

TEEB. 2010. *The Economics of Ecosystems and Biodiversity: Ecological and Economic Foundations*, Kumar P (ed)(ed.). Earthscan: London and Washington, DC.

Thoms MC. 1987. Channel sedimentation within urban gravel-bed rivers. PhD Thesis, Loughborough University, UK. [online] https://dspace.lboro.ac.uk/2134/10844; accessed 1 September 2014.

Thoms MC, Parsons ME, Foster JM. 2007. The use of multivariate statistics to elucidate patterns of floodplain sedimentation at different spatial scales. *Earth Surface Processes and Landforms* **32**: 672–686. DOI:10.1002/esp.1440.

Thorp JH, Flotemersch JE, Williams BS, Gabanski LA. 2013. Critical role for hierarchical geospatial analyses in the design of fluvial research, assessment, and management. *Environmental Monitoring and Assessment* **185**: 7165–7180. DOI:10.1007/s10661-013-3091-9.

Townsend CR, Uhlmann SS, Matthaei CD. 2008. Individual and combined responses of stream ecosystems to multiple stressors. *Journal of Applied Ecology* **45**: 1810–1819. DOI:10.1111/j.1365-2664.2008.01548.x.

USEPA. 1996. *Why Watersheds*? EPA/800/F-96/001. U.S. Environmental Protection Agency: Washington, DC. [online] http://water.epa.gov/type/watersheds/why.cfm; accessed 1 September 2014.

USEPA. 1998. ORD Ecological Research Strategy. In *EPA/600/R-98/086*. U.S. Environmental Protection Agency: Washington, DC.

USEPA. 2011. *A Field-based Aquatic Life Benchmark for Conductivity in Central Appalachian Streams*, EPA/600/R-10/023(Final Report). U.S. Environmental Protection Agency: Washington, D.C.

USEPA. 2012a. *Healthy Watersheds News Issue 1 Winter 2011–2012*. EPA/841/N-12/002. U.S. Environmental Protection Agency: Washington, DC. [online] http://water.epa.gov/polwaste/nps/watershed/upload/hwnews12-1.pdf; accessed 1 September 2014.

USEPA. 2012b. *Identifying and protecting healthy watersheds*: *concepts*, *assessments*, *and management approaches*. In *EPA/841/B-11/002*. U.S. Environmental Protection Agency: Washington, DC.

USEPA. 2012c. *Safe and sustainable water resources*: *strategic research action plan 2012–2016*. In *EPA/601/R-12/004*. U.S. Environmental Protection Agency: Washington, DC.

USEPA. 2013. Monitoring and assessing water quality. http://water.epa.gov/type/watersheds/monitoring/; accessed 1 September 2014.

USEPA. 2014. National rivers and streams assessment. http://water.epa.gov/type/rsl/monitoring/riverssurvey/; accessed 1 September 2014.

USEPA. 2015. *Connectivity of streams and wetlands to downstream waters*: *a review and synthesis of the scientific evidence* (*final report*). In *EPA/600/R-14/475F*. U.S. Environmental Protection Agency: Washington, DC.

USFS. 2011. *Watershed Condition Framework: A Framework for Assessing and Tracking Changes to Watershed Condition*, Publication FS-977. U.S. Department of Agriculture Forest Service: Washington, DC.

Van Abs DJ. 2013. *Water Resources Baseline Assessment Report: Prepared in Support of the Regional Plan for Sustainable Development*. Together North Jersey: New Brunswick, New Jersey.

Vannote RL, Minshall GW, Cummins KW, Sedell JR, Cushing CE. 1980. The river continuum concept. *Canadian Journal of Fisheries and Aquatic Sciences* **37**: 130–137.

Van Sickle J, Gregory SV. 1990. Modeling inputs of large woody debris to streams from falling trees. *Canadian Journal of Forest Research* **20**: 1593–1601. DOI:10.1139/x90-211.

Van Sickle J, Paulsen SG. 2008. Assessing the attributable risks, relative risks, and regional extents of aquatic stressors. *Journal of the North American Benthological Society* **27**: 920–931. DOI:10.1899/07-152.1.

Van Sickle J, Stoddard JL, Paulsen SG, Olsen AR. 2006. Using relative risk to compare the effects of aquatic stressors at a regional scale. *Environmental Management* **38**: 1020–1030. DOI:10.1007/s00267-005-0240-0.

Vander Laan JJ, Hawkins CP, Olson JR, Hill RA. 2013. Linking land use, in-stream stressors, and biological condition to infer causes of regional ecological impairment in streams. *Freshwater Science* **32**: 801–820. DOI:10.1899/12-186.1.

Walker B, Meyers JA. 2004. Thresholds in ecological and socio-ecological systems: a developing database. *Ecology and Society* **9**:3. [online] http://www.ecologyandsociety.org/vol9/iss2/art3/; accessed 1 September 2014.

Walker B, Salt D. 2012. *Resilience Practice: Building Capacity to Absorb Disturbance and Maintain Function*. Island Press: Washington, DC.

Wallace RB, Darama Y, Annable MD. 1990. Stream depletion by cyclic pumping of wells. *Water Resources Research* **26**: 1263–1270. DOI:10.1029/WR026i006p01263.

Ward JV, Stanford JA. 1995. The serial discontinuity concept: extending the model to floodplain rivers. *Regulated Rivers: Research and Management* **10**: 159–168. DOI:10.1002/rrr.3450100211.

© 2015 The Authors. *River Research and Applications* published by John Wiley & Sons Ltd.

Westra L. 1994. *An Environmental Proposal for Ethics: The Principle of Integrity*. Rowman and Littlefield Publishers: Lanham, Maryland.

Wicklum D, Davies RW. 1995. Ecosystem health and integrity? *Canadian Journal of Botany* **73**: 997–1000. DOI:10.1139/b95-108.

Winter TC. 2007. The role of ground water in generating streamflow in headwater areas and in maintaining base flow. *Journal of the American Water Resources Association* **43**: 15–25. DOI:10.1111/j.1752-1688.2007.00003.x.

Winter TC, Harvey JW, Franke OL, Alley WM. 1998. *Ground Water and Surface Water*: *A Single Resource*. U.S. Geological Survey Circular 1139. U.S. Geological Survey: Denver, CO.

Winter TC, LaBaugh JW. 2003. Hydrologic considerations in defining isolated wetlands. *Wetlands* **23**: 532–540. DOI:10.1672/0277-5212(2003)023[0532:HCIDIW]2.0.CO;2.

Woodley S. 1993. Monitoring and measuring ecosystem integrity in Canadian National Parks. In *Ecological Integrity and the Management of Ecosystems*, Woodley S, Kay J, Francis G (eds.). St. Lucie Press: Boca Raton, Florida; 155–176.

Yetiş Ü. 2008. Water quality, pollution and conservation. In *Overexploitation and Contamination of Shared Groundwater Resources*, Darnault CJG (ed.). Springer: Dordrecht, Netherlands; 227–256.

© 2015 The Authors. *River Research and Applications* published by John Wiley & Sons Ltd.

From: Flotemersch, Joseph
To: Flotemersch, Joseph
Subject: Statement of Authorship Contribution
Date: Monday, April 27, 2020 3:24:18 PM

From: Joseph Flotemersch
U.S. Environmental Protection Agency
Office of Research and Development
Cincinnati, OH

Re: Record of Percentage Agreement

This email is to confirm that I was a co-author on the manuscript titled "A Watershed Integrity Definition and Assessment Approach to Support Strategic Management of Watersheds". The authors of this paper were Joseph Flotemersch, Scott Leibowitz, John Stoddard, Ryan Hill, Rebecca Tharme, and Martin Thoms. This paper was published in River Research and Applications in 2016 as an Arena paper. I also agree with the percentage of effort listed beside my name.

It should be noted that at the time of this work, I was an ORISE post-doc with the U.S.EPA National Health and Environmental Effects Research Laboratory in Corvallis, Oregon.

Joseph Flotemersch	40%
Scott Leibowitz	35%
John Stoddard	10%
Ryan Hill	5%
Rebecca Tharme	5%
Martin Thoms	5%

Sincerely, Joseph Flotemersch

****

Joseph E. Flotemersch, Ph.D.
Senior Environmental Scientist
Center for Environmental Measurement and Modeling

Office of Research and Development
U.S. Environmental Protection Agency
flotemersch.joseph@epa.gov | 513-569-7086

26 W. Martin Luther King Dr., Mail Code 587, Cincinnati, OH 45268
****

From: Hill, Ryan A
To: Flotemersch, Joseph
Subject: Statement of Authorship Contribution
Date: Tuesday, April 28, 2020 3:00:10 PM

From: Ryan Hill
U.S. Environmental Protection Agency
Office of Research and Development
Center for Public Health and Environmental Assessment
Pacific Ecological Systems Division
200 SW 35th Street
Corvallis, OR 97333

Re: Record of Percentage Agreement

This email is to confirm that I was a co-author on the manuscript titled "A Watershed Integrity Definition and Assessment Approach to Support Strategic Management of Watersheds". The authors of this paper were Joseph Flotemersch, Scott Leibowitz, John Stoddard, Ryan Hill, Rebecca Tharme, and Martin Thoms. This paper was published in River Research and Applications in 2016 as an Arena paper. I also agree with the percentage of effort listed beside my name.

It should be noted that at the time of this work, I was an ORISE post-doc with the U.S.EPA National Health and Environmental Effects Research Laboratory in Corvallis, Oregon.

Joseph Flotemersch	40%
Scott Leibowitz	35%
John Stoddard	10%
Ryan Hill	5%
Rebecca Tharme	5%
Martin Thoms	5%

Sincerely,
Ryan Hill

From: Leibowitz, Scott
To: Flotemersch, Joseph
Subject: Record of Percentage Agreement for STAA Award
Date: Monday, April 27, 2020 3:07:04 PM

From: Scott Leibowitz
U.S. Environmental Protection Agency
Office of Research and Development
Corvallis, OR

Re: Record of Percentage Agreement for STAA Award

This email is to confirm that I was a co-author on the manuscript titled "A Watershed Integrity Definition and Assessment Approach to Support Strategic Management of Watersheds". The authors of this paper were Joseph Flotemersch, Scott Leibowitz, John Stoddard, Ryan Hill, Rebecca Tharme, and Martin Thoms. This paper was published in River Research and Applications in 2016 as an Arena paper. I also agree with the percentage of effort listed beside my name.

Joseph Flotemersch	40%
Scott Leibowitz	35%
John Stoddard	10%
Ryan Hill	5%
Rebecca Tharme	5%
Martin Thoms	5%

Sincerely, Scott Leibowitz

Scott G. Leibowitz, Ph.D.
Research Ecologist
U.S. Environmental Protection Agency
200 SW 35th St, Corvallis, Oregon 97333
Phone: 541.754.4508
email: leibowitz.scott@epa.gov

From: Stoddard, John
To: Flotemersch, Joseph
Subject: Statement of Authorship Contribution
Date: Monday, April 27, 2020 3:53:24 PM

From: John Stoddard
U.S. Environmental Protection Agency
Office of Research and Development
Corvallis, OR

Re: Record of Percentage Agreement for STAA Award

This email is to confirm that I was a co-author on the manuscript titled "A Watershed Integrity Definition and Assessment Approach to Support Strategic Management of Watersheds". The authors of this paper were Joseph Flotemersch, Scott Leibowitz, John Stoddard, Ryan Hill, Rebecca Tharme, and Martin Thoms. This paper was published in River Research and Applications in 2016 as an Arena paper. I also agree with the percentage of effort listed beside my name.

Joseph Flotemersch	40%
Scott Leibowitz	35%
John Stoddard	10%
Ryan Hill	5%
Rebecca Tharme	5%
Martin Thoms	5%

Sincerely,

John L. Stoddard
U.S. EPA, 200 SW 35th Street
Corvallis, OR 97333
(541) 754-4441

From: rebeccatharme@riverfutures.com
To: Flotemersch, Joseph
Subject: Statement of Authorship Contribution
Date: Monday, April 27, 2020 4:43:53 PM

From: Rebecca Tharme
Director of Riverfutures Ltd.
Derbyshire, UK

Re: Record of Percentage Agreement

This email is to confirm that I was a co-author on the manuscript titled "A Watershed Integrity Definition and Assessment Approach to Support Strategic Management of Watersheds". The authors of this paper were Joseph Flotemersch, Scott Leibowitz, John Stoddard, Ryan Hill, Rebecca Tharme, and Martin Thoms. This paper was published in River Research and Applications in 2016 as an Arena paper. I agree with the percentage of effort listed beside my name.

Joseph Flotemersch	40%
Scott Leibowitz	35%
John Stoddard	10%
Ryan Hill	5%
Rebecca Tharme	5%
Martin Thoms	5%

Sincerely, Rebecca Tharme

LE STUDIUM Loire Valley Institute for Advanced Studies/Marie Skłodowska-Curie Research Fellow
CITERES - Cités, Territoires, Environnement et Sociétés, CNRS/Université de Tours, France

Adjunct Principal Research Fellow
Australian Rivers Institute, Griffith University, Australia

Director
Riverfutures, Peak District National Park, Derbyshire, UK

From: Martin Thoms
To: Flotemersch, Joseph
Subject: Record of Percentage Agreement
Date: Monday, April 27, 2020 5:34:45 PM

US EPA

This email is to confirm that I am a co-author on the manuscript titled “A Watershed Integrity Definition and Assessment Approach to Support Strategic Management of Watersheds”. The full author list of this manuscript are Joseph Flotemersch, Scott Leibowitz, John Stoddard, Ryan Hill, Rebecca Tharme, and Martin Thoms. This paper was published in River Research and Applications in 2016 as an Arena paper. I agree with the following percentage of effort listed beside my name.

Joseph Flotemersch	40%
Scott Leibowitz	35%
John Stoddard	10%
Ryan Hill	5%
Rebecca Tharme	5%
Martin Thoms	5%

Regards

Martin Thoms

STAA REPORT FOR THE SCIENTIST NOMINATIONS

General Information:

Nomination ID/App ID:	20-130
Research Category Primary:	Industry and the Environment (IE)
Research Category Secondary:	Environmental Policy and Decision-Making Studies (EP);Industry and the Environment (IE);Sustainability and Innovation (SI)
Laboratory/Office Name:	ORD
Nomination Entered By:	Mallikarjuna Nadagouda

Eligibility Checklist:

[Y] The nominated publication(s) has not been submitted to a previous STAA competition.

[Y] The nominated publication(s) was published on or before January 1, 2017 and on or after January 1,2012

[Y] The principal author was an EPA employee or a PHS employee assigned to EPA when the research was performed

[Y] The EPA authors (includes PHS employees assigned to EPA) contributed collectively a minimum of 50% toward the publication(s)

Nominating Official Name:	Regan Murray
Nominating Official Title:	SUPERVISORY INTERDISCIPLINARY SCIENTIST
Nominating OfficialEmail:	murray.regan@epa.gov
STAA Coordinator Name:	Kathleen Wiser
STAA Coordinator Email:	wiser.kathi@epa.gov

Justifications:

Justification 1:

The two nominated papers demonstrate the upgrading of biomass and chemical transformation using environmental-friendly processes.

To preserve resources and maintain environmental and economic sustainability, researchers must develop more efficient technologies for the chemical industry. Currently, they have focused on the lack of available non-renewable organic feedstocks to demonstrate the importance of renewable resources. Upgrading biomass and the development of chemical feedstocks from renewable resources are a sustainable method of reducing dependence on petroleum products. Though upgrading and sustainable development hold many advantages for the environment when applied as a petroleum alternative, they also present a significant challenge, since researchers must chemically modify the bio-derived fuels to make them compatible with existing technology. To solve all these challenges, our first nominated paper (Nadagouda, 2019) developed a technology of magnetically separable heterogeneous bimetallic catalysts for the upgrading of lignin-derived guaiacol to cyclohexanol under visible light. The second nominated paper (Nadagouda, 2017) designed a novel method for supporting photoactive heterogeneous catalysis in organic reactions.

Overall, these two papers significantly justify EPA mission, for example, “Sustainable Materials Management (SMM)” as these research articles demonstrate the utilization of sustainable protocols for the upgrading of biomass and chemical transformation. (https://www.epa.gov/sites/production/files/2015-08/documents/sustainable_materials_management_the_road_ahead.pdf). As we know, chemistry is very crucial for daily life and the extent of its application from the development of organic scaffolds to treat various illnesses in the formation of innovative industrial developments. We develop clean, sustainable methods to synthesize industrially relevant products in the prevention of pollution and the elimination of hazardous waste.

Justification 2A:

None of the three nominated or one supporting paper included in this STAA package have been submitted for STAA in the past.

While the STAA guidelines limit a nomination to three publications, the four research articles that are part of this package either as nominees or supporting paper are unavoidably associated as they describe the utilization of different

adsorbents for the same study. As discussed in answer to Question 1, the strength of this study is the breadth of investigations that were conducted in batch as well as column mode on the different cost-effective adsorbents for the treatment of phosphate.

Several efficient adsorbents such modified Bayoxide® E33 adsorbent (Nadagouda et al., 2015) utilized, modified iron oxide-based sorbents (Nadagouda et al., 2016), calcium and magnesium-modified iron-based adsorbents (Nadagouda et al., 2017), cellulose enhanced magnesium carbonate pellets as adsorbent (Nadagouda et al., 2018) were demonstrated for the treatment of phosphate. Working together, these four manuscripts increase the national scale understanding of contaminants of emerging concern in source waters as well as treated wastewater.

Justification 2B:

Response:

Mallikarjuna N. Nadagouda

1. Evaluating Sustainable Pathway to Furanics from Biomass via Heterogeneous Organo-Catalysis Green Chemistry
2. Sustainable Strategy Utilizing Biomass: Visible Light-Mediated Synthesis of g-Valerolactone. Published in ChemCatChem
3. Visible Light Mediated Upgrading of Biomass to Biofuel. Published in Green Chemistry

2017 Honorable Mention STAA

1. The Oxidative C-H activation of amines using protuberant lychee-like goethite. Published in Nature Climate Change
2. Photocatalytic C-H activation and oxidative esterification using Pd@g-C3N4. Published in Catalysis Today

3. Hydroxylation of benzene via C-H activation using bimetallic CuAg@g-C3N4. Published in ACS Sustainable Chemistry and Engineering

2019 Honorable Mention STAA

1. Conversion of spent carbon dioxide into value-added products
2. A sustainable approach to empower the bio-based future: upgrading biomass to value-added products

2019 Level III STTA

Rajender S. Varma

1. Evaluating Sustainable Pathway to Furanics from Biomass via Heterogeneous Organo-Catalysis Green Chemistry
2. Sustainable Strategy Utilizing Biomass: Visible Light-Mediated Synthesis of g-Valerolactone. Published in ChemCatChem
3. Visible Light Mediated Upgrading of Biomass to Biofuel. Published in Green Chemistry

2017 Honorable Mention STAA

1. The Oxidative C-H activation of amines using protuberant lychee-like goethite. Published in Nature Climate Change
2. Photocatalytic C-H activation and oxidative esterification using Pd@g-C3N4. Published in Catalysis Today
3. Hydroxylation of benzene via C-H activation using bimetallic CuAg@g-C3N4. Published in ACS Sustainable Chemistry and Engineering

2019 Honorable Mention STAA

1. Conversion of spent carbon dioxide into value-added products
2. A sustainable approach to empower the bio-based future: upgrading biomass to value-added products

2019 Level III STTA

Justification 2C:

Nadagouda's (2017 Honorable Mention STAA, 2019 Honorable Mention STAA and 2019 Level III STTA) awards are like the currently nominated work, which are directly connected to sustainable chemistry. However, the sustainable process used in the first paper (Nadagouda 2019) utilizes the chitosan derived carbon nitride as catalyst support, and the second paper demonstrates the oxidation of alcohols under visible light. These are new approaches that have been utilized for the environmental upgrading of biomass and sustainable development in organic transformation, respectively.

Varma's (2017 Honorable Mention STAA, 2019 Honorable Mention STAA, and 2019 Level III STTA) awards are like the currently nominated work, which are directly connected to sustainable chemistry. However, the sustainable process used in the first paper (Nadagouda 2019) utilizes the chitosan derived carbon nitride as catalyst support, and the second paper demonstrates the oxidation of alcohols under visible light. These are new approaches that have been utilized for the environmental upgrading of biomass and sustainable development in organic transformation, respectively.

Justification 2D:

None of the supplemental information has been included in previous nominations.

Justification 2E:

There are no concurrent nominations by the authors on this nomination.

Justification 3A:

The first nominated paper (Nadagouda et al., 2019) has selected as a part of the themed collection "Green Biorefinery Technologies based on Waste Biomass" by the Royal Society of Chemistry. It has been published in the prestigious journal "Green Chemistry," which has an Impact Factor of 9.405 and has ranked#3 (h-index: 186) in the "Environmental Science" category. This research work has already been cited in 5 research articles (Google citation

search). Prof. Reina from Department of Chemical and Process Engineering Department, University of Surrey, United Kingdom has adopted our work on the upgrading of biomass in his research article "Jin, W., Pastor-Pérez, L., Yu, J., Odriozola, J.A., Gu, S. and Reina, T.R., 2020. Cost-effective routes for Catalytic Biomass Upgrading. Current Opinion in Green and Sustainable Chemistry". Recently, Prof. Bhoi from Department of Mechanical Engineering, Georgia Southern University, GA, USA has adopted and discussed our research work of AgPd/Fe@CNx catalyst for upgrading of lignin-derived guaiacol to cyclohexanol (98%) under visible light irradiation in his article "Ouedraogo, A.S. and Bhoi, P.R., 2020. Recent progress of metals supported catalysts for hydrodeoxygenation of biomass-derived pyrolysis oil. Journal of Cleaner Production 253, 119957"

The second nominated paper (Nadagouda et al., 2017) has been published in the prestigious journal "Tetrahedron," which has an Impact Factor of 2.645 and has ranked#61 (h-index: 209) in the "Pharmacology, Toxicology and Pharmaceutics" category. This research work has already been cited in 19 research articles (Google citation search) since its publication and highlighted in "**Synfacts**" (Polymer-Supported Synthesis) as **Synfacts, 2017, 13(11), p.1222**.

Recently, prof. Hong from South Korea has cited and highlighted our research work (Nadagouda et al., 2017) on his reaserach article "Hong, K., Sajjadi, M., Suh, J.M., Zhang, K., Nasrollahzadeh, M., Jang, H.W., Varma, R.S. and Shokouhimehr, M., 2020. Palladium Nanoparticles on Assorted Nanostructured Supports: Applications for Suzuki, Heck, and Sonogashira Cross-Coupling Reactions. ACS Applied Nano Materials, 3(3), pp.2070-2103."

Justification 3B:

All of the nominated and supporting manuscript underwent anonymous peer review by the journal to which it was submitted for publication.

AUTHORS

Principal Author

Author Name:	Mallikarjuna N. Nadagouda		
Professional Title:		Salutation:	Dr.
Email:	nadagouda.mallikarjuna@epa.gov	Organization:	
Mailing Address:			
Street Line 1:			
City:			
Zip Code:		State:	
At time of research was:	EPA Employee		
Separation Date:			
% of Effort:	64		

Contributing Author

Author Name:	Jacob Lalley		
Professional Title:		Salutation:	Mr.
Email:	jacobmlalley@gmail.com	Organization:	
Mailing Address:			
Street Line 1:			
City:			
Zip Code:		State:	
At time of research was:	Non EPA Personnel		
Separation Date:			
% of Effort:	10		

Contributing Author

Author Name:	Han Changseok		
Professional Title:		Salutation:	Dr.
Email:	hanck@mail.uc.edu	Organization:	
Mailing Address:			
Street Line 1:			
City:			
Zip Code:		State:	
At time of research was:	Non EPA Personnel		
Separation Date:			
% of Effort:	7		

Contributing Author

Author Name:	Jay Garland		
Professional Title:		Salutation:	Dr.
Email:	garland.jay@epa.gov	Organization:	
Mailing Address:			
Street Line 1:			
City:			
Zip Code:		State:	
At time of research was:	EPA Employee		
Separation Date:			
% of Effort:	3		

Contributing Author

Author Name:	Nidhi Iyanna		
Professional Title:		Salutation:	Ms.
Email:	nii7@pitt.edu	Organization:	
Mailing Address:			
Street Line 1:			
City:			
Zip Code:		State:	
At time of research was:	Non EPA Personnel		
Separation Date:			
% of Effort:	3		

Contributing Author

Author Name:	Thomas Speth		
Professional Title:		Salutation:	Dr.
Email:	speth.thomas@epa.gov	Organization:	
Mailing Address:			
Street Line 1:			
City:			
Zip Code:		State:	
At time of research was:	EPA Employee		
Separation Date:			
% of Effort:	3		

Contributing Author

Author Name:	Dion Dionysiou		
Professional Title:		Salutation:	Dr.
Email:	dionysdd@ucmail.uc.edu	Organization:	
Mailing Address:			
Street Line 1:			
City:			
Zip Code:		State:	
At time of research was:	Non EPA Personnel		
Separation Date:			
% of Effort:	7		

Contributing Author

Author Name:	Gayathri Rammohan		
Professional Title:		Salutation:	Dr.
Email:	gayathri.rammohan@gwinnettcounty.com	Organization:	
Mailing Address:			
Street Line 1:			
City:			
Zip Code:		State:	
At time of research was:	Non EPA Personnel		
Separation Date:			
% of Effort:	3		

PUBLICATIONS

Publication 1:

Publication Title:	Removal of phosphate using calcium and magnesium-modified ironbased		
Publication Date:	Mon May 22 00:00:00 GMT 2017		
Journal/Publication Method:	Materials Chemistry and Physics		
All Author(s):			
Volume:	198	Number:	1
Pages:	115-124	Immediately Index:	Immediately Index:
Citation ½ Life:	6.0	Impact Factor:	2.781

Publication 2:

Publication Title:	Phosphate removal using modified Bayoxide® E33 adsorption media		
Publication Date:	Thu Jan 01 00:00:00 GMT 2015		
Journal/Publication Method:	Environmental Science Water Research & Technology		
All Author(s):			
Volume:	1	Number:	1
Pages:	96-107	Immediately Index:	Immediately Index:
Citation ½ Life:	N/A	Impact Factor:	4.195

Publication 3:

Publication Title:	Phosphate adsorption using modified iron oxide-based sorbents
Publication Date:	Wed Sep 02 00:00:00 GMT 2015

Journal/Publication Method:	Chemical Engineering Journal		
All Author(s):			
Volume:	284	Number:	1
Pages:	1386–1396	Immediately Index:	Immediately Index:
Citation ½ Life:	3.70	Impact Factor:	8.355

Materials Chemistry and Physics 198 (2017) 115–124

Contents lists available at ScienceDirect

Materials Chemistry and Physics

journal homepage: www.elsevier.com/locate/matchemphys

Removal of phosphate using calcium and magnesium-modified iron-based adsorbents

Changseok Han [a, 1], Jacob Lalley [b, 1], Nidhi Iyanna [c], Mallikarjuna N. Nadagouda [d, *]

[a] Oak Ridge Institute for Science and Education (ORISE) Postdoctoral Research Associate, The U.S. Environmental Protection Agency, ORD, NRMRL, STD, CPB, 26 W. Martin Luther King Jr. Drive, Cincinnati, OH, 45268, USA
[b] Pegasus Technical Services Inc., 46 E Hollister St, Cincinnati, OH, 45219, USA
[c] William Mason High School, Mason, 45040, OH, USA
[d] The U.S. Environmental Protection Agency, ORD, NRMRL, WSWD, WQMB, 26 W. Martin Luther King Jr. Drive, Cincinnati, OH, 45268, USA

HIGHLIGHTS

- Magnetic Ca and Mg-modified iron oxide adsorbents were synthesized.
- PVA imparted magnetism to the adsorbents for easy separation.
- Batch adsorption experiments were carried out to gain insights on the adsorption kinetics and equilibrium.
- The adsorbents effectively removed phosphates from water at a capacity of nearly 17 mg g^{-1}.

GRAPHICAL ABSTRACT

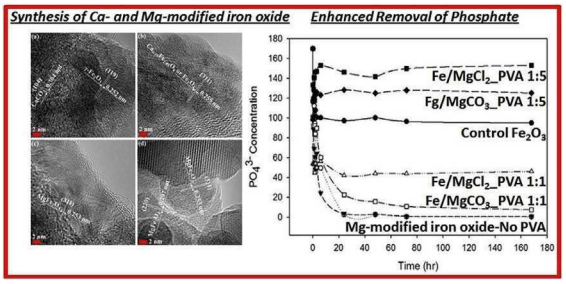

ARTICLE INFO

Article history:
Received 14 June 2016
Received in revised form
22 March 2017
Accepted 21 May 2017
Available online 23 May 2017

Keywords:
Easy separation
Magnetic
Iron oxide
Adsorbent
Phosphate

ABSTRACT

Magnetic calcium (Ca) and magnesium (Mg)-modified iron oxide adsorbents were synthesized using $CaCl_2$, $CaCO_3$, $MgCl_2$, or $MgCO_3$ by a simple combustion method for the remediation of phosphate. Modification with Ca and Mg significantly improved the phosphate adsorption capacity of the magnetic iron oxide adsorbents. Additionally, polyvinyl alcohol (PVA) was incorporated during synthesis to aid in the magnetism of the samples, making the adsorbents easy to separate from solutions. Physicochemical properties of the adsorbents were determined by characterization with X-ray diffraction (XRD), particle analyzer, scanning electron microscopy (SEM), transmission electron microscopy (TEM), and high resolution TEM (HR-TEM). Batch adsorption experiments were carried out to gain insight on the materials' ability to remove phosphate from water supplies. Samples without the addition of PVA had higher phosphate capacities (ranging from 16.92 to 16.97 mg g^{-1}) compared to PVA-containing samples (ranging from 12.39 to 16.74 mg g^{-1}), yet the PVA-containing samples were magnetic and thus, easily separable.

Published by Elsevier B.V.

1. Introduction

Phosphorous (P) is one of the essential elements for all life as it is significantly associated with the DNA/RNA structure, cell membrane formation, energy storage/transfer, as well as enzyme activation or deactivation [1,2]. Phosphorus is commonly found in

* Corresponding author.
E-mail address: Nadagouda.Mallikarjuna@epa.gov (M.N. Nadagouda).
[1] Contributed equally to this work.

http://dx.doi.org/10.1016/j.matchemphys.2017.05.038
0254-0584/Published by Elsevier B.V.

sources of drinking water due to an inflow of urban and industrial wastewater and agricultural run-offs, which contain phosphates [3–7]. Phosphates entering into the nutrient limited aquatic environment are significantly involved in eutrophication, which is associated with the formation of massive algal blooms, excessive growth of microorganisms, and depletion of dissolved oxygen [8–10]. Moreover, massive algal blooms containing cyanobacteria can be a potential hazard to humans and animals because some species of cyanobacteria produce and release toxins, known as cyanotoxins [11–13]. Therefore, it is of great interest to develop reliable technologies for the removal of phosphates from water.

Currently, chemical precipitation [14], biological processes [15], and adsorption [16] have been widely used for removing phosphate from water, yet both chemical precipitation and biological processes have disadvantages. While chemical precipitation has been shown to reduce phosphorus concentrations by 60–95%, depending on many factors including influent water parameters and coagulant dosage [17]; these methods involve high operating costs as well as the production of large amounts of sludge, and the efficiency of this method depends on the types of chemicals used for phosphate removal [18,19]. Biological processes have several drawbacks as well. In order to achieve maximal phosphate removal, operating conditions and water quality parameters must be very specific. For example, the system only functions optimally when phosphate concentrations are $\geq$5–10 mg L^{-1} and when the ratio of BOD to P is at least 35:1 [16]. Therefore, in order to improve the efficiency of phosphate removal by chemical precipitation and biological processes, enhanced biological phosphorus removal (EBPR) has been extensively studied [20–22]. The removal of phosphate was significantly improved by applying EBPR, which employs designed communities of microorganisms (aka, phosphorus accumulating organisms (PAO)). High concentrations of calcium (Ca) and magnesium (Mg) were recommended to achieve high efficiency removal of phosphate in EBPR. The Ca attributes to the formation of hydroxyapatite ($Ca_5(PO_4)_3OH$), which is about 39% of the phosphate precipitation in EBPR and Mg is associated with precipitation of struvite ($MgNH_4PO_4 \cdot 6H_2O$) or newberyite ($MgHPO_4$) [20,23–25]. However, the formation of phosphate precipitates during EBPR operations have caused significant problems including pipe blockage and precipitate accumulation on the surface of equipment such as pumps and centrifuges in the treatment system [26]. Also, ranges of phosphate accumulation vary widely (i.e., from 20 to 80%) based on the PAO used [27]. Therefore, adsorption has attracted much attention for phosphate removal because of its simplicity, inexpensiveness, and low sludge production. Also, adsorption is an appropriate method for removing low concentrations of phosphate [28]. Thus, the use of Ca- and Mg-modified adsorbents were explored as they have been shown effective at improving the EBPR process and can form phosphate precipitates.

2. Materials and methods

Herein, Ca- and Mg-modified ferrites as phosphate adsorbents were synthesized by a simple combustion method using polyvinyl alcohol (PVA). Iron(III) nitrate ($Fe(NO_3)_3 \cdot 9H_2O$, certified ACS, Fisher Scientific), calcium or magnesium precursors, and PVA (MW 89,000–98,000, 99+% hydrolyzed, Sigma-Aldrich) were mixed together using 5 mL of milli-Q grade water. Then, the mixtures were calcined in a muffle furnace (Ney Vulcan, A-550) at 300 °C for 1 h. Calcium carbonate ($CaCO_3$, $\geq$99.0%, Sigma-Aldrich) or calcium chloride ($CaCl_2 \cdot 2H_2O$, 74.27%, Fisher Scientific), and magnesium carbonate ($MgCO_3$, Sigma-Aldrich) or magnesium chloride ($MgCl_2 \cdot 6H_2O$, ACS reagent, J. T. Baker) were used to prepare Ca-ferrite and Mg-ferrite, respectively. Control iron oxide (Fe_2O_3) was synthesized without Ca and Mg precursors or PVA. The detailed information of the ingredients for the synthesis of Ca- and Mg-modified ferrite are summarized in Table 1. Synthesized samples were characterized by X-ray diffraction (XRD, Panalytical X'pert 2-theta diffractometer, obtained from Panalytical, Almelo, Netherlands at a wavelength of 1.54 Å and at 2-theta range 2-90° under CuK_α radiation), porosimetry (using a Tristar 3000 porosimeter analyzer, obtained from Micromeritics), scanning electron microscopy (SEM, model Philips XL 30 ESEM-FEG, at an accelerating voltage of 30 kV), transmission electron microscopy (TEM, a FEI CM20 TEM operated at 200 kV was employed), and high resolution TEM (HR-TEM, model JEM-2010F, obtained from JEOL, was employed with a field gun emission gun at 200 kV). Prior to HR-TEM characterization, the adsorbents were prepared and dispersed by ultrasonication (2510R-DH, Bransonic) in 99.8% pure isopropyl alcohol, obtained from Pharmco-AAPER for 30 min. Then, on a carbon-coated copper grid (LC325-Cu, EMS), a drop of the supernatant was fixed and dried at room temperature. The images obtained from the HR-TEM were analyzed using ImageJ, an image processing software (National Institutes of Health, Maryland, USA). To evaluate the phosphate adsorption capacity of the prepared samples, batch equilibrium experiments at pH 7 were conducted using the buffer 3-(N-morpholino) propanesulfonic acid (MOPS), obtained from Sigma-Aldrich. Variable dose isotherm studies were conducted using different masses of adsorbent (ranging from 0.1 to 1.5 g) in 125 mL Nalgene polypropylene bottles with 100 mL of phosphate solution. The stock phosphate solution was prepared by dissolving 3 g of sodium phosphate monohydrate ($NaH_2PO_4 \cdot H_2O$, Sigma-Aldrich), obtained from Fisher Scientific, in 11 L of deionized water at a target phosphate concentration of 200 mg L^{-1}. The concentrations of phosphate were measured by a standard colorimetry EPA Method 365.1 [29].

3. Results and discussion

3.1. Adsorbent characterization

XRD characterization of the samples are shown in Fig. 1. The XRD patterns of synthesized Ca- and Mg-modified samples were identified with JCPDS 00-036-0398 for magnesioferrite ($MgFe_2O_4$), 00-006-0502 for hematite (α-Fe_2O_3), 00-025-1402 for maghemite (γ-Fe_2O_3), 00-047-1743 for calcite ($CaCO_3$), 00-005-0628 for halite (NaCl), 00-019-0629 for magnetite (Fe_3O_4), and 00-046-0291 for calcium iron oxide ($Ca_{0.15}Fe_{2.85}O_4$). As seen in Fig. 1(c), all peaks corresponding to non-magnetic hematite were detected. This indicates that PVA is necessary to convert non-magnetic iron oxide to magnetic iron oxide (i.e., maghemite, magnetite, and ferrite). Unfortunately, no peaks corresponding to Ca or Mg were found.

Table 1
Ingredients for the synthesis of Ca- and Mg-modified ferrite.

Sample	$Fe(NO_3)_3$ (g)	Ca (g)	Mg (g)	PVA (g)
Control Fe_2O_3	25	0	0	0
Fe/$CaCl_2$-No PVA	40.4	11.0	0	0
Fe/$MgCl_2$-No PVA	40.4	0	9.5	0
Fe/$CaCO_3$-No PVA	64.6	8.0	0	0
Fe/$MgCO_3$-No PVA	64.6	0	6.7	0
Fe/$CaCO_3$_PVA 1:1	40.4	7.4	0	47.8
Fe/$CaCl_2$_PVA 1:1	40.4	11.1	0	51.5
Fe/$CaCO_3$_PVA 1:5	4.04	0.74	0	23.9
Fe/$CaCl_2$_PVA 1:5	4.04	1.11	0	25.8
Fe/$MgCO_3$_PVA 1:1	20.2	0	4.2	24.4
Fe/$MgCl_2$_PVA 1:1	20.2	0	5.1	25.3
Fe/$MgCO_3$_PVA 1:5	4.04	0	0.8	24.2
Fe/$MgCl_2$_PVA 1:5	4.04	0	1.0	25.3

Note: 5 mL of water was used to prepare all samples.

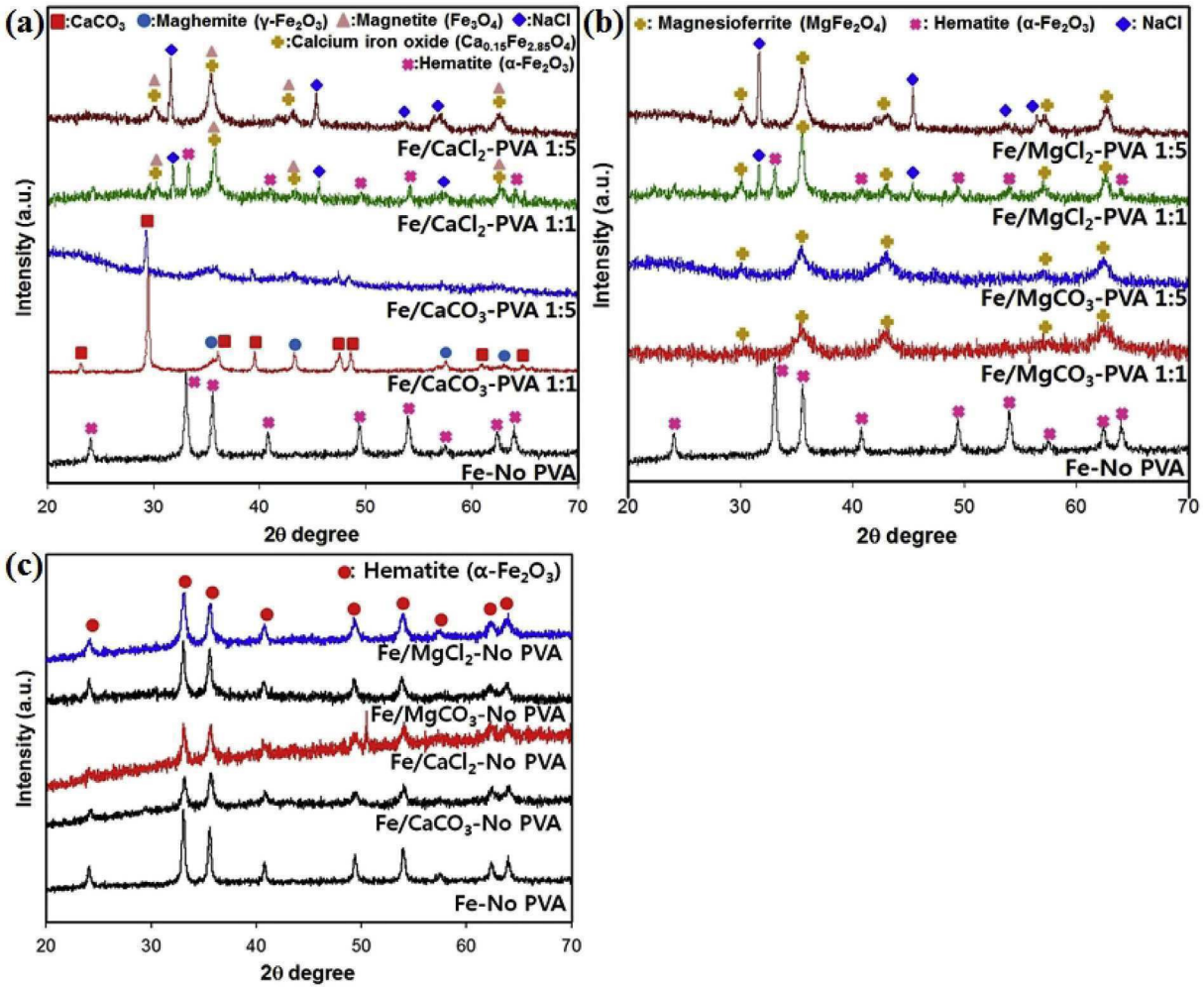

Fig. 1. XRD patterns for Ca- and Mg-modified samples: (a) Ca-modified ferrite with PVA, (b) Mg-modified ferrite with PVA and (c) Ca- and Mg-modified samples without PVA.

However, Ca and Mg were found in the samples with EDS analysis (see Fig. 2). The peaks for Ca and Mg could not be observed from XRD characterization possibly because Ca and Mg exist in an amorphous phase in the synthesized samples.

When PVA was added during synthesis, hematite to maghemite, magnetite, or magnetic ferrite transformations were observed in all samples after the combustion process (see Fig. 1(a) and (b)). However, the formation of calcium iron oxide was not detected in Ca-modified samples with $CaCO_3$. It may result from different ion sizes of Mg (Effective diameter = 0.09 nm), Ca (Effective diameter = 0.14 nm), and Fe (Effective diameter = 0.1 nm) [30]. Since the effective diameter of Mg ions is very similar to that of Fe ions, Mg ions may easily replace Fe ions compared to Ca ions to form Mg-modified ferrite [30]. However, when chlorides (i.e., $CaCl_2$ and $MgCl_2$) were used, calcium iron oxide ($Ca_{0.15}Fe_{2.85}O_4$) and magnesioferrite ($MgFe_2O_4$) formed since chloride salts dissolve well in water compared to carbonates like $CaCO_3$ and $MgCO_3$. However, a small amount of Ca replaced Fe ions due to the large effective diameter of Ca ions and thus, $Ca_{0.15}Fe_{2.85}O_4$ formed instead of $CaFe_2O_4$. Similar phenomena could be found in other studies [12,31]. For example, since the ionic radius of sulfur (S^{2-}) (0.17 nm) is larger than oxygen (O^{2-}) (0.122 nm), sulfur (S^{2-}) could not easily replace oxygen (O^{2-}) and it requires more energy to synthesize sulfur-doped titanium dioxide (TiO_2) [12,31,32]. Moreover, peaks corresponding to non-magnetic hematite observed in the samples of $Fe/CaCl_2$_PVA 1:1 and $Fe/MgCl_2$_PVA 1:1 disappeared. The hematite completely transformed to magnetic ferrite or magnetite by adding more PVA (a ratio of 1:5). This indicates that the combustion method provided enough energy required to synthesize magnetic iron oxides.

SEM characterization of control Fe_2O_3 and the four synthesized Ca- and Mg-modified samples without PVA are shown in Fig. S3. Without Ca and Mg precursors, small spherical iron oxide particles less than 1000 nm formed as shown in Fig. S3(a) and (b). Micro-sized, larger aggregates formed when $CaCl_2$ was used for the modification of Fe_2O_3 as seen in Fig. S3(c). When $CaCO_3$ was used as the Ca precursor, particle sizes decreased to less than 500 nm but they still aggregated (see Fig. S3(d)). Interestingly, similar patterns were observed during the preparation of Mg-modified samples. When a carbonate was used, particle sizes significantly decreased from 950 ± 500 nm to 180 ± 56 nm as seen in Fig. S3(e) and (f). Ca and Mg precursors may affect the aggregation of particles during the synthesis.

Fig. 3 shows the SEM images of Ca-modified samples with PVA. Since $CaCO_3$ has very low solubility in water, the morphology of the control Fe_2O_3 did not change during the combustion process with the ratio of 1:1 (see Fig. S3(b) and Fig. 3(a)). However, it is not easy to find the uniform spherical particles for the samples synthesized with the ratio of 1:5 as shown in Fig. 3(b). The particles appeared to be partially coated, this may be the result of incomplete combustion

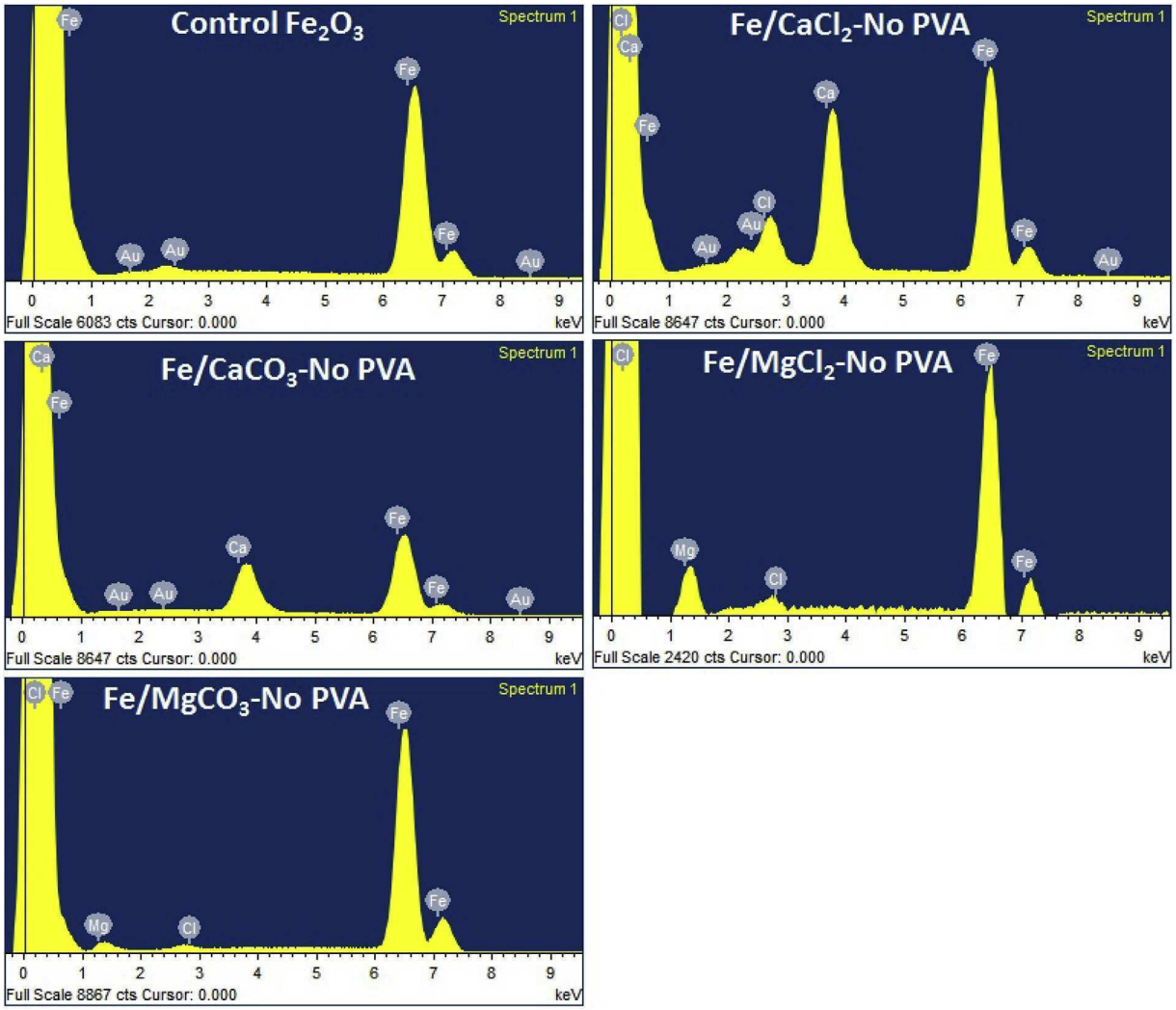

Fig. 2. EDS analysis for Ca- and Mg-modified samples without PVA. It shows the presence of Ca or Mg in the synthesized samples. The presence of gold (Au) was due to the Au coating on the samples during a sputtering process.

of PVA during the synthesis process. However, as shown in Fig. 3(c) and (d), sample size and shape changed by using $CaCl_2$ since $CaCl_2$ dissolves well in water. Larger aggregates formed compared to the $CaCO_3$ modified sample. For the samples prepared with the ratio of 1:5, large aggregates, with sizes ranging from 500 nm to 1 μm, formed. Small nanoparticles ranging from 30 to 80 nm were trapped in the large aggregates. In both cases of $CaCO_3$ and $CaCl_2$ with the ratio of 1:5, carbon content highly increased after the combustion (see the EDS analysis in Table 2). This may indicate PVA was not completely burned out from the synthesized samples and coated nanoparticles to form larger aggregates.

The results of SEM analysis of Mg-modified samples using $MgCO_3$ and $MgCl_2$ are shown in Fig. 4. As shown in Fig. 4(a) and (b), nanoparticles with an average size of 53 ± 12 nm started forming spherical aggregates with an average size of 270 ± 90 nm in the samples prepared with $MgCO_3$. With the ratio of 1:5, slightly larger and more uniform spherical aggregates of 290 ± 37 nm appeared to form. Mg content analyzed by EDS in both large and small aggregates was very similar which indicates Mg was uniformly incorporated into the samples during sample preparation. On the other hand, large aggregates with an average size of 360 ± 55 nm formed in the samples prepared using $MgCl_2$ of 1:1 ratio. With a 1:5 ratio, nanoparticles less than 20 nm formed and did not have a specific structure.

The synthesized samples were also characterized with TEM. As seen in Fig. S4(a), spherical nanoparticles with a diameter ranging from 15 to 120 nm formed in the control Fe_2O_3. This is in good agreement with the SEM analysis showing the formation of nanoparticles (<100 nm). By adding Ca and Mg precursors to modify the control Fe_2O_3, the size and shape of the primary particles changed. Nanoparticles and nanorods with irregular sizes and shapes were synthesized in the Ca- and Mg-modified samples. Additionally, magnetic Ca- and Mg-modified samples were analyzed with TEM (see Figs. 5 and 6). By adding PVA, spherical nanoparticles formed in Ca-modified samples. With excess PVA (i.e., ratio of 1:5), even though small particles with an average diameter of 6.2 ± 1.6 nm for $Fe/CaCO_3$_PVA and 10.6 ± 4.1 nm for $Fe/CaCl_2$_PVA formed, the formed nanoparticles were capped into PVA resulting in a decrease of BET surface area from 8.7 to 0.6 $m^2\ g^{-1}$ for $Fe/CaCO_3$_PVA and from 31.4 to 17.5 $m^2\ g^{-1}$ for $Fe/CaCl_2$_PVA (see Fig. 5). For Mg-modified samples, smaller and uniform particles formed with an average size of 15.0 ± 4.8 nm for $Fe/MgCO_3$_PVA and 19.5 ± 2.4 nm for $Fe/MgCl_2$_PVA in the presence of excess PVA (i.e., ratio of 1:5). In these cases, the BET surface area of the samples decreased from 46.8 to 14.3 $m^2\ g^{-1}$ for $Fe/MgCO_3$_PVA and from 57.9 to 19.5 $m^2\ g^{-1}$ for $Fe/MgCl_2$_PVA at a higher loading of PVA due to an excess of PVA.

Further analysis on the synthesized samples was done using HR-TEM to obtain lattice spacing information as seen in Figs. 7 and 8.

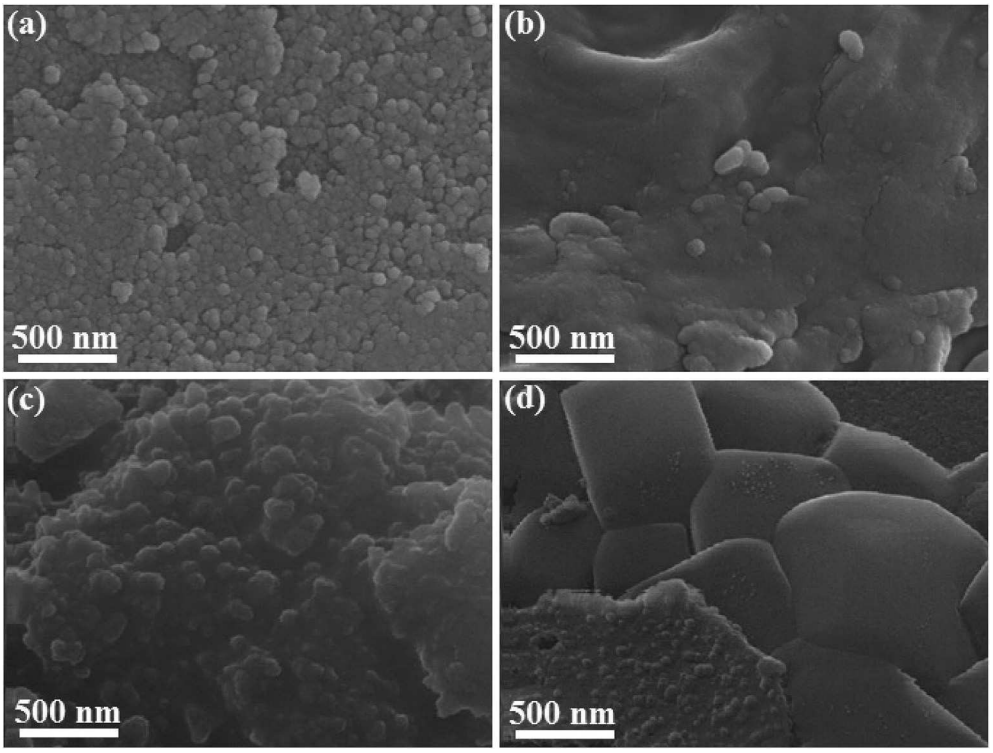

Fig. 3. SEM images of Ca-modified samples with PVA: (a) Fe/$CaCO_3$_PVA 1:1, (b) Fe/$CaCO_3$_PVA 1:5, (c) Fe/$CaCl_2$_PVA 1:1, and (d) Fe/$CaCl_2$_PVA 1:5.

Table 2
EDS analysis for Ca- and Mg-modified samples.

Sample	Carbon (%)	Ca (%)	Mg (%)
Fe/$CaCO_3$_PVA 1:1	18.8	11.9	–
Fe/$CaCO_3$_PVA 1:5	86.5	5.8	–
Fe/$CaCl_2$_PVA 1:1	16.7	8.9	–
Fe/$CaCl_2$_PVA 1:5	66.7	2.4	–
Fe/$MgCO_3$_PVA 1:1	17.0	–	1.2
Fe/$MgCO_3$_PVA 1:5	79.0	–	6.0
Fe/$MgCl_2$_PVA 1:1	31.5	–	5.0
Fe/$MgCl_2$_PVA 1:5	75.1	–	0.8

The measured lattice spacing of the control Fe_2O_3 sample was 0.250 nm, corresponding to (110) plane of α-Fe_2O_3 (see Fig. S1). This confirms the results of XRD analysis reporting the formation of non-magnetic hematite in control Fe_2O_3 samples. In Ca- and Mg-modified samples without PVA, a lattice spacing of 0.250 nm, corresponding to (110) plane for α-Fe_2O_3 was observed, as shown in Fig. 7(a)-(d). In Fig. 8(a) for the Fe/$CaCO_3$_PVA 1:1 sample, the (104) plane of $CaCO_3$ with 0.304 nm was observed along with the measured lattice spacing of 0.252 nm, corresponding to (119) plane of magnetic γ-Fe_2O_3. Since $CaCO_3$ does not dissolve in water, Ca could not be effectively incorporated into the iron oxide during the synthesis but magnetic γ-Fe_2O_3 formed since sufficient energy was provided for phase transformation by PVA incineration. Otherwise, $Ca_{0.15}Fe_{2.85}O_4$ and Fe_3O_4 formed in the sample synthesized with $CaCl_2$. Due to the water solubility of $CaCl_2$, Ca could be incorporated into the iron oxides as seen in Fig. 8(b).

However, as discussed before, a small amount of Ca^{2+} ions could be facilitated to form $Ca_{0.15}Fe_{2.85}O_4$ due to the larger effective size of Ca^{2+} compared to Fe ions. Interestingly, Mg was well incorporated into the iron oxides in both cases using $MgCO_3$ and $MgCl_2$, resulting in the formation of $MgFe_2O_4$ with the PVA assisted-synthesis method (see Fig. 8(c) and (d)). Due to their similar effective diameter (Mg = 0.09 nm and Fe = 0.1 nm) [30], Fe was effectively replaced with Mg. These results are in good agreement with the XRD analysis.

3.2. Adsorption experiments

Adsorption experiments were conducted using the synthesized adsorbents to evaluate their affinity towards phosphate. For the Mg-modified samples, as seen in Fig. 9, the addition of PVA negatively impacted phosphate adsorption. Fe/$MgCO_3$_PVA 1:1 and Fe/$MgCl_2$_PVA 1:1 removed 95.7 and 72.9% of phosphate, respectively. However, Fe/$MgCO_3$_PVA 1:5 and Fe/$MgCl_2$_PVA 1:5 removed 26.3 and 10.0% of phosphate, respectively. Furthermore, the control samples (with no PVA) removed higher percentages of phosphate (99.5 and 99.8% for Fe/$MgCO_3$—No PVA and Fe/$MgCl_2$-No PVA, respectively) yet these samples were not magnetically separable. A similar trend was observed for the Ca-modified samples, where higher ratios of PVA negatively impacted phosphate adsorption. As seen in Fig. 10, Fe/$CaCO_3$_PVA 1:5 and Fe/$CaCl_2$_PVA 1:5 removed 11.2 and 22.3% of phosphate, respectively. The samples with a 1:1 PVA ratio removed 98.5 and 93.0% of phosphate for Fe/$CaCO_3$_PVA 1:1 and Fe/$CaCl_2$_PVA 1:1. Again, with the Ca-modified adsorbents, the samples with no PVA had the highest adsorption percentages. Fe/$CaCO_3$—No PVA removed 99.6% of phosphate and Fe/$CaCl_2$—No PVA removed 99.8% of phosphate. These may result from the positive surface charge of the adsorbent. The added Ca and Mg provide more positive charges on the adsorbents and promote the adsorption of phosphate [33–35]. The use of electrostatic interaction to improve adsorption capacity for the removal of negatively or positively charged contaminants has been extensively reported in many studies [33–37]. Also, phosphate may react with slowly released Ca^{2+} from the adsorbents and then precipitate in the system [38] since iron oxides could dissolve in water at different pHs, resulting in the improvement of phosphate removal.

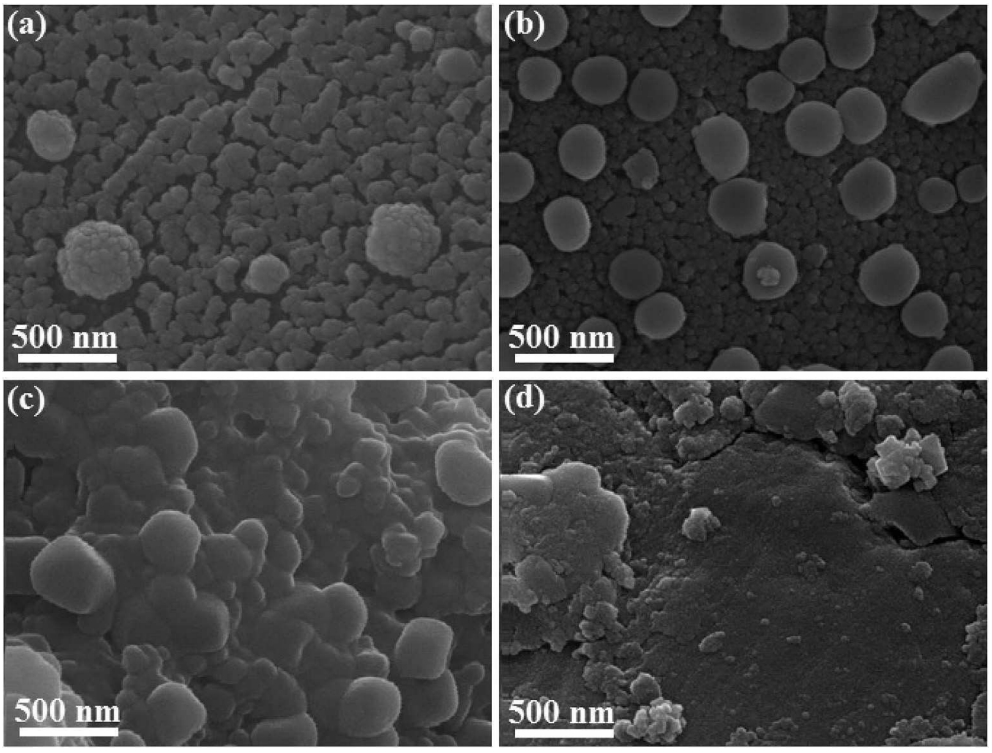

Fig. 4. SEM images of Mg-modified samples with PVA: (a) Fe/$MgCO_3$_PVA 1:1, (b) Fe/$MgCO_3$_PVA 1:5, (c) Fe/$MgCl_2$_PVA 1:1, and (d) Fe/$MgCl_2$_PVA 1:5.

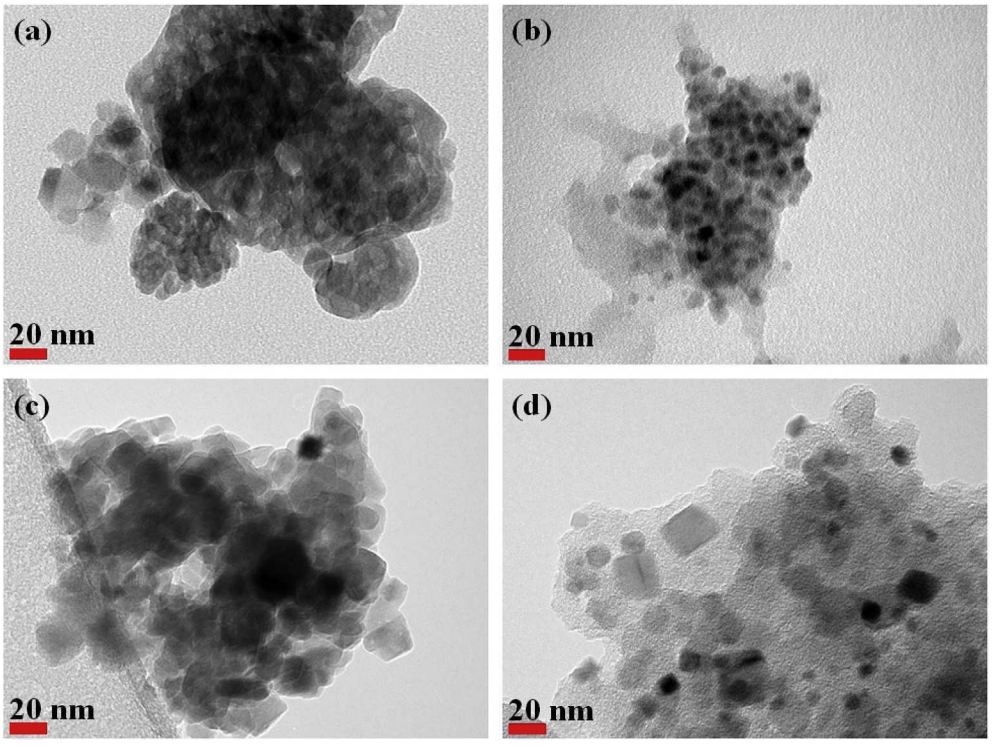

Fig. 5. TEM images of Ca-modified samples with PVA: (a) Fe/$CaCO_3$_PVA 1:1, (b) Fe/$CaCO_3$_PVA 1:5, (c) Fe/$CaCl_2$_PVA 1:1, and (d) Fe/$CaCl_2$_PVA 1:5.

Table 3 summarizes the phosphate adsorption capacity of each adsorbent, clearly indicating the impact PVA had on phosphate adsorption. Apart from the samples without PVA, the best performing samples were the 1:1 ratio carbonate-based adsorbents followed by the chloride-based samples. The best performing sample was Fe/$CaCO_3$_PVA 1:1, followed by Fe/$MgCO_3$_PVA 1:1, Fe/$CaCl_2$_PVA 1:1, and Fe/$MgCl_2$_PVA 1:1, with phosphate adsorption capacities of 16.74, 16.26, 15.81, and 12.39 mg g^{-1}, respectively.

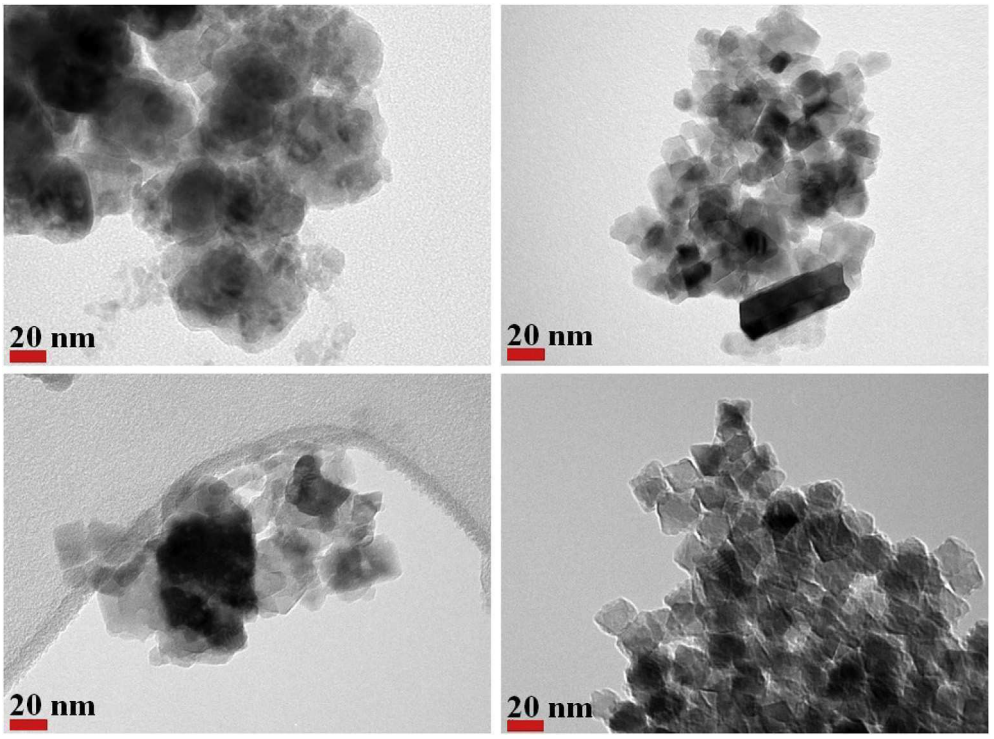

Fig. 6. TEM images of Mg-modified samples with PVA: (a) Fe/$MgCO_3$_PVA 1:1, (b) Fe/$MgCO_3$_PVA 1:5, (c) Fe/$MgCl_2$_PVA 1:1, and (d) Fe/$MgCl_2$_PVA 1:5.

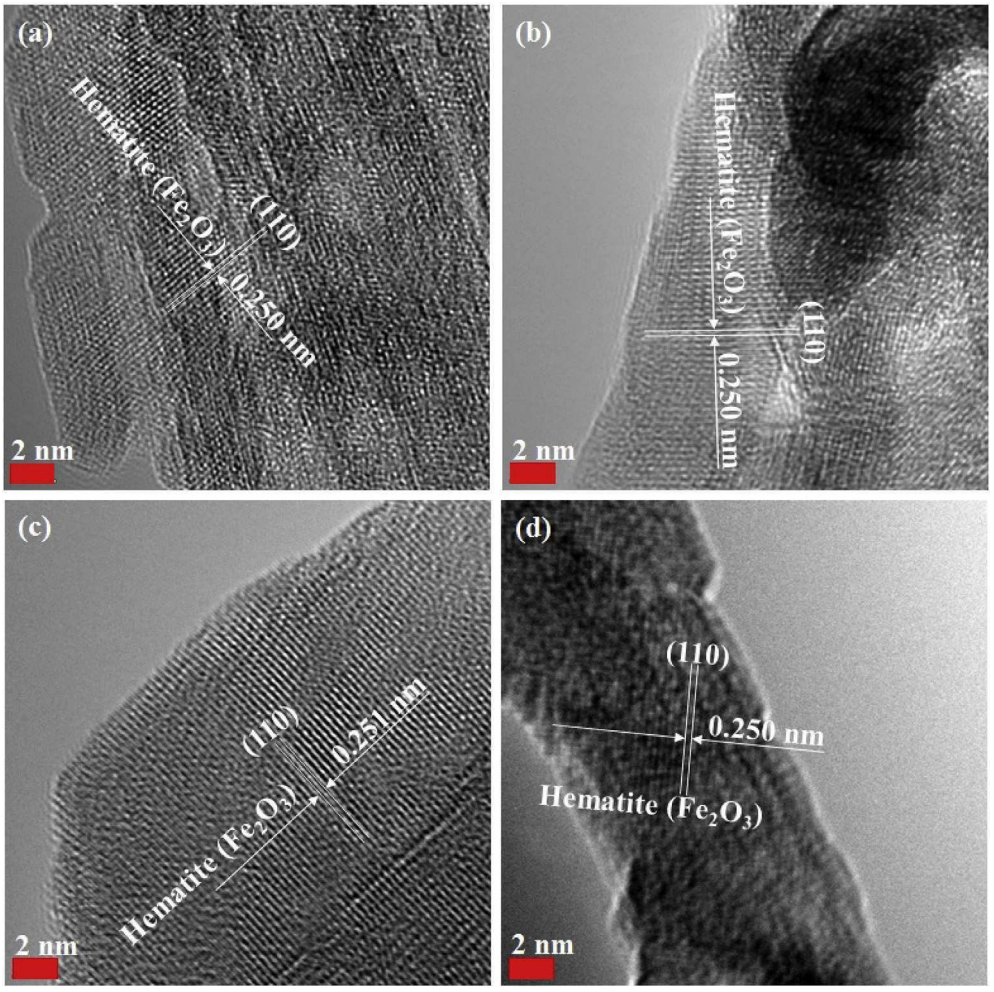

Fig. 7. HR-TEM images of Ca- and Mg-modified samples without PVA: (a) Fe/$CaCl_2$_No PVA, (b) Fe/$CaCO_3$_PVA_No PVA, (c) Fe/$MgCl_2$_No PVA, and (d) Fe/$MgCO_3$_No PVA. Scale bar.

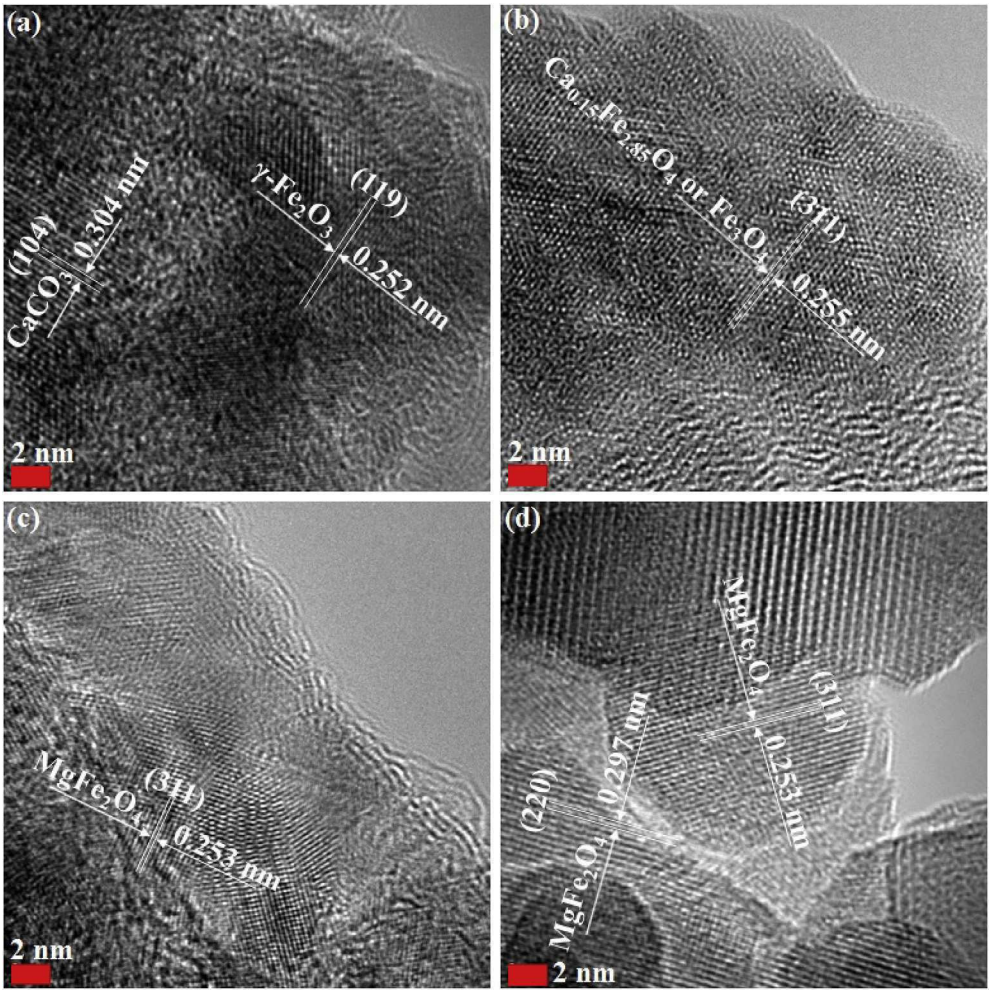

Fig. 8. HR-TEM images of Ca- and Mg-modified, magnetic samples: (a) Fe/$CaCO_3$_PVA 1:1, (b) Fe/$CaCl_2$_PVA 1:1, (c) Fe/$MgCO_3$_PVA 1:1, and (d) Fe/$MgCl_2$_PVA 1:1.

Based on the results for the 1:1 ratio adsorbents, these samples were further investigated by adsorption isotherms.

The adsorption capacities of Ca- and Mg-modified ferrites were compared to other adsorbents found in literature (Table S1). While the Ca- and Mg-modified ferrite adsorbents did not have the highest phosphate adsorption capacity, they performed much better than other commonly used adsorbents including red mud and steel slag.

The samples were evaluated with both the Langmuir [39] and Freundlich [40] isotherm models. The results of the Langmuir

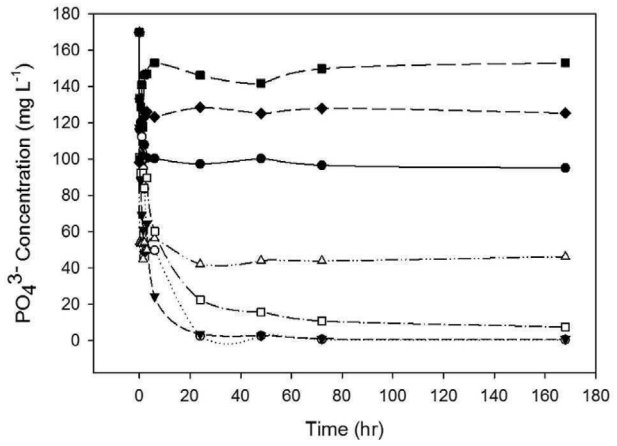

Fig. 9. Adsorption of phosphate with respect to time using Mg-modified adsorbents (●: Control Fe_2O_3, ○: Fe/$MgCl_2$-No PVA, ▼: Fe/$MgCO_3$-No PVA, Δ: Fe/$MgCl_2$_PVA 1:1, ■: Fe/$MgCl_2$_PVA 1:5, □: Fe/$MgCO_3$_PVA 1:1, and ◆: Fg/$MgCO_3$_PVA 1:5).

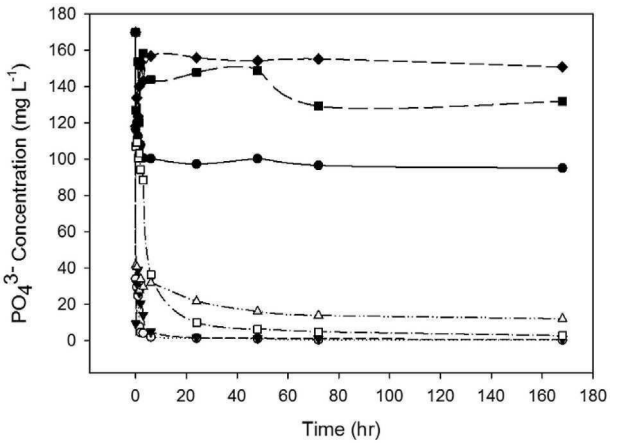

Fig. 10. Adsorption of phosphate with respect to time using Ca-modified adsorbents (●: Control Fe_2O_3, ○: Fe/$CaCl_2$-No PVA, ▼: Fe/$CaCO_3$-No PVA, Δ: Fe/$CaCl_2$_PVA 1:1, ■: Fe/$CaCl_2$_PVA 1:5, □: Fe/$CaCO_3$_PVA 1:1, and ◆: Fg/$CaCO_3$_PVA 1:5).

Table 3
Phosphate adsorption capacity of Ca- and Mg-modified ferrite.

Adsorbent	Phosphate Capacity (mg g^{-1})
Control Fe_2O_3	7.49
Fe/$CaCl_2$-No PVA	16.97
Fe/$MgCl_2$-No PVA	16.96
Fe/$CaCO_3$-No PVA	16.94
Fe/$MgCO_3$-No PVA	16.92
Fe/$CaCO_3$_PVA 1:1	16.74
Fe/$CaCl_2$_PVA 1:1	15.81
Fe/$CaCO_3$_PVA 1:5	1.91
Fe/$CaCl_2$_PVA 1:5	3.79
Fe/$MgCO_3$_PVA 1:1	16.26
Fe/$MgCl_2$_PVA 1:1	12.39
Fe/$MgCO_3$_PVA 1:5	4.46
Fe/$MgCl_2$_PVA 1:5	1.69

Table 4
Adsorption isotherm constants.

Sample	Langmuir isotherm			Freundlich isotherm		
	q_{max}	K_L	R^2	1/n	K_F	R^2
Fe/$CaCO_3$_PVA 1:1	833.3	0.011	0.103	0.958	9.56	0.899
Fe/$CaCl_2$_PVA 1:1	58.14	0.169	0.994	0.330	14.13	0.758
Fe/$MgCO_3$_PVA1:1	22.73	0.649	0.983	0.155	19.41	0.525
Fe/$MgCl_2$_PVA 1:1	33.44	0.024	0.994	0.311	3.79	0.994

isotherm models were found in the supporting information (Fig. S2) and Table 4. Data were evaluated with the Freundlich model by the linearized equation:

$$\log q_e = \log K_F + \frac{1}{n}\log C_e$$

where K_F is the Freundlich constant (mg g^{-1} (L $mg^{-1})^{1/n}$) and 1/n is a dimensionless constant which indicates sorption favourability. The plot of log q_e vs. log C_e, as seen in Fig. 11, provided the isotherm constants as documented in Table 4.

When comparing regression coefficients between the two isotherm models, it is clear that the Langmuir model provides the best fit, with the exception of the Fe/$CaCO_3$_PVA 1:1 sample which had an R^2 of 0.899 using the Freundlich model. However, as previously stated, this could be due to its extremely high capacity for phosphate. Thus, based on adsorption experiments, it could be determined that these materials best followed the Langmuir isotherm, indicating a monolayer adsorption process.

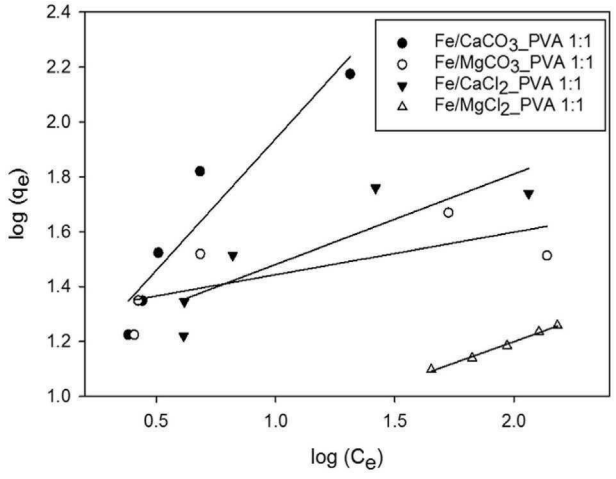

Fig. 11. Linear plot for Freundlich isotherm using samples with a 1:1 ratio of PVA.

4. Conclusions

Ca- and Mg-modified iron oxides using $CaCl_2$, $CaCO_3$, $MgCl_2$, or $MgCO_3$ were successfully synthesized by a simple combustion method. The samples became magnetic by the presence of PVA during the calcination processes. Non-magnetic Ca- and Mg-modified iron oxides demonstrated the highest phosphate adsorption capacity of about 17 mg g^{-1} compared to that of control Fe_2O_3 (7.49 mg g^{-1}) under these experimental conditions. Interestingly, magnetic Ca- and Mg-modified samples also showed a high capacity of phosphate removal, which ranged from 12.4 to 16.74 mg g^{-1}. Even though the values of q_{max} for Ca- and Mg-modified samples without PVA were not calculated, the obtained results indicate successful Ca and Mg modification significantly improves the capacity of phosphate removal from water. Incorporated Ca or Mg into iron oxides may enhance the binding of phosphate on iron oxide, resulting in the improvement of phosphate removal [41]. Moreover, innovative magnetic samples have high potential for easy separation processes to avoid filtration, which requires considerable energy and high costs during water treatment processes.

Notice

The U.S. Environmental Protection Agency, through its Office of Research and Development, funded and managed, or partially funded and collaborated in, the research described herein. It has been subjected to the Agency's administrative review and has been approved for external publication. Any opinions expressed in this paper are those of the author(s) and do not necessarily reflect the views of the Agency, therefore, no official endorsement should be inferred. Any mention of trade names or commercial products does not constitute endorsement or recommendation for use. C. Han was supported by the Postgraduate Research Program at the National Risk Management Research Laboratory administered by the Oak Ridge Institute for Science and Education through an interagency agreement between the U.S. Department of Energy and the U.S. Environmental Protection Agency.

Appendix A. Supplementary data

Supplementary data related to this article can be found at http://dx.doi.org/10.1016/j.matchemphys.2017.05.038.

References

[1] E. Valsami-Jones (Ed.), Phosphorus in Environmental Technologies: Principles and Applications, IWA Publishing, London, UK, 2004.
[2] J. Lalley, C. Han, G.R. Mohan, D.D. Dionysiou, T.F. Speth, J. Garland, M.N. Nadagouda, Environ. Sci. Water Res. Technol. 1 (2015) 96.
[3] H.L. Golterman, Water Res. 7 (1973) 3.
[4] J.J. Schröder, A.L. Smit, D. Cordell, A. Rosemarin, Chemosphere 84 (2011) 822.
[5] A. Sendrowski, T.H. Boyer, Desalination 322 (2013) 104.
[6] Y. Liu, G. Villalba, R.U. Ayres, H. Schroder, J. Ind. Ecol. 12 (2008) 229.
[7] G. Villalba, Y. Liu, H. Schroder, R. U, J. Ind. Ecol. 12 (2008) 557.
[8] M.F. Colmenarejo, E. Sánchez, R. Borja, L. Travieso, S. Cirujano, J.L. Echevarrias, A. Rubio, M.G. González, J. Environ. Sci. Health, Part A 42 (2007) 969.
[9] Z. Liu, W.L. Kingeery, D.H. Huddleston, F. Hossain, N.B. Hashim, J.M. Kieffer, J. Environ. Sci. Health, Part A 43 (2008) 468.
[10] E. Abdallah, A.A. Concalves, G.A. Gangnon, J. Environ. Sci. Health, Part A 44 (2009) 707.
[11] M.G. Antoniou, A.A. de la Cruz, D.D. Dionysiou, D. D, J. Environ. Eng. 131 (2005) 1239.
[12] C. Han, M. Pelaez, V. Likodimos, A.G. Kontos, P. Falaras, K. O'Shea, D.D. Dionysiou, Appl. Catal. B Environ. 107 (2011) 77.
[13] C. Han, A. Doepke, W. Cho, V. Likodimos, A.A. de la Cruz, T. Back, W.R. Heineman, H.B. Halsall, V.N. Shanov, M.J. Schulz, P. Falaras, D.D. Dionysiou, Adv. Funct. Mater. 23 (2013) 1807.

[14] L.E. De-Bashan, Y. Bashan, Water Res. 38 (2004) 4222.
[15] D. Mulkerrins, A.D.W. Dobson, E. Colleran, Environ. Int. 30 (2004) 249.
[16] A. Eskandarpour, K. Sassa, Y. Bando, M. Okido, S. Asai, Mater. Tracsactions 47 (2006) 1832.
[17] D. Rich, Remov. Total Phosphorus Nat. Waters by Precip. (2005).
[18] S. Yeoman, T. Stephenson, J.N. Lester, R. Perry, Environ. Pollut. 49 (1988) 183.
[19] D.W. de Haas, M.C. Wentzel, G.A. Ekama, Water SA 26 (2000) 439.
[20] R. Barat, T. Montoya, A. Seco, J. Ferrer, Water Res. 45 (2011) 3744.
[21] G.R. Mohan, P. Dube, A. MacFar1ene, P. Pullammanappallill, in: G. Wicks, J. Simon, R. Zidan, R. Brigmon, G. Fishman, S. Arepalli, A. Norris, M. McCluer (Eds.), Materials Challenges in Alternative and Renewable Energy II: Ceramic Transactions, vol. 242, John Wiley & Sons, Inc, Hoboken, New Jersey, 2013, pp. 47–58.
[22] J. Hrenovic, M. Rozic, L. Sekovanic, A. Anic-Vucinic, J. Hazard. Mater. 156 (2008) 576.
[23] R. Barat, A. Bouzas, N. Marti, J. Ferrer, A. Seco, J. Environ. Manag. 90 (2009) 850.
[24] G.E. Diwani, S.E. Rafie, N.N.E. Ibiari, H.I.E. Aila, Desalination 214 (2007) 200.
[25] T. Zhang, L. Ding, H. Ren, X. Xiong, Water Res. 43 (2009) 5209.
[26] J.D. Doyle, S.A. Parsons, Water Res. 36 (2002) 3925.
[27] C.M. López-Vázquez, C.M. Hooijmans, D. Brdjanovic, H.J. Gijzen, M.C. van Loosdrecht, Water Res. 42 (2008) 2349.
[28] K. Mohanty, D. Das, M.N. Biswas, Adsorption 12 (2006) 119.
[29] J. Murphy, J.P. Riley, Anal. Chim. Acta 27 (1962) 31.
[30] J. Kielland, J. Am. Chem. Soc. 59 (1937) 1675.
[31] C. Han, J. Andersen, V. Likodimos, P. Falaras, J. Linkugel, D.D. Dionysiou, Catal. Today 224 (2014) 132.
[32] J.C. Yu, W. Ho, J. Yu, H. Yip, P.K. Wong, J. Zhao, Environ. Sci. Technol. 39 (2005) 1175.
[33] C. Fang, T. Zhang, P. Li, R.-f. Jiang, Y.-c. Wang, Int. J. Environ. Res. Public Health 11 (2014) 9217.
[34] F. Xie, F. Wu, G. Liu, Y. Mu, C. Feng, H. Wang, J.P. Giesy, Environ. Sci. Technol. 48 (2014) 582.
[35] Z. Mahmood, S. Nasir, N. Jamil, A. Sheikh, A. Akram, Afr. J. Environ. Sci. Technol. 9 (2015) 274.
[36] L. Wang, C. Han, M.N. Nadagouda, D.D. Dionysiou, J. Hazard. Mater. 313 (2016) 283.
[37] J. Lalley, C. Han, X. Li, D.D. Dionysiou, M.N. Nadagouda, Chem. Eng. J. 284 (2016) 1386.
[38] D. Chen, P. Szostak, Z. Wei, R. Xiao, Sci. Total Environ. 539 (2016) 381.
[39] I. Langmuir, J. Am. Chem. Soc. 40 (1918) 1361.
[40] H. Freundlich, Akad. Verlagsgesellschaft (1922).
[41] L. Weng, W.H. Van Riemsdijk, T. Hiemstra, J. Environ. Qual. 41 (2012) 628.

Environmental Science
Water Research & Technology

PAPER

Cite this: *Environ. Sci.: Water Res. Technol.*, 2015, **1**, 96

Phosphate removal using modified Bayoxide® E33 adsorption media†‡

Jacob Lalley,[ab] Changseok Han,[ac] Gayathri Ram Mohan,[c] Dionysios D. Dionysiou,[b] Thomas F. Speth,[a] Jay Garland[d] and Mallikarjuna N. Nadagouda*[a]

Received 23rd July 2014,
Accepted 19th September 2014

DOI: 10.1039/c4ew00020j

rsc.li/es-water

The adsorption of phosphate onto modified Bayoxide® E33 (E33) and underlying mechanisms were comparatively investigated by batch kinetics, sorption isotherms, rapid small-scale column tests, and material characterization. Synthesis of modified E33 was conducted by the addition of manganese and silver nanoparticles on the surface of the goethite (α-FeOOH)-based E33. Upon successful adsorbent synthesis, the materials were characterized using SEM, TEM, XRD, EDX, HR-TEM, and BET surface area analysis. The adsorption kinetics is described by a fast initial adsorption stage followed by a slow adsorption stage, complying with pseudo second-order kinetics and Elovich kinetics. Sorption isotherms revealed that the equilibrium capacity of one of the modified adsorbents (E33/AgII) exceeded that of unmodified E33 likely due to its increased BET surface area. Column experiments confirmed the results for adsorption kinetics and equilibrium of phosphate sorption onto E33 and modified E33. This suggests that media modification has the potential to improve phosphate removal properties.

Water impact

As a limiting nutrient in the environment, increased loads of phosphates can result in accelerated eutrophication or excessive growth of algae, leading to increased treatment costs and reduced recreational value. Therefore, phosphate removal from wastewater has become an area of emerging concern. In this study, the removal of phosphate using newly surface-modified Bayoxide® E33 was thoroughly examined. Underlying mechanisms were comparatively investigated by batch kinetics, sorption isotherms, rapid small-scale column tests, and material characterization. The adsorption kinetics is well described by a fast initial adsorption stage followed by a slow adsorption stage, complying with pseudo second-order kinetics and Elovich kinetics. The results showed potential for practical applications of the modified material for phosphate removal.

1. Introduction

Phosphates are one of the common mineral nutrients found in wastewaters.[1] Both natural and anthropogenic sources such as agricultural runoffs[2,3] and urban[4] and industrial wastes[5,6] act as major sources of phosphate in surface water bodies. In aquatic systems, phosphates occur in various forms, particulate, organically bound, or dissolved,[7] of which orthophosphates (PO_4^{3-}) are found to be predominant.[8] While it is an essential nutrient, higher concentrations of phosphate in water bodies can be detrimental to aquatic life, human health, and the environment.[9] As a limiting nutrient in the environment, increased loads of phosphates can result in accelerated eutrophication or excessive growth of algae, leading to increased treatment costs and reduced recreational value.[10] Therefore, phosphate removal from wastewaters has become an area of emerging concern.

Conventional methods for phosphate removal include physical, chemical, and biological processes; of which, chemical precipitation[11] and enhanced biological phosphate

[a] *The U.S. Environmental Protection Agency, ORD, NRMRL, WSWRD, WQMB, 26 W. Martin Luther King Jr. Drive, Cincinnati, OH, 45268, USA. E-mail: Nadagouda.mallikarjuna@epa.gov; Fax: +1 (513) 569 7172; Tel: +1 (513) 569 7232*
[b] *Environmental Engineering and Science Program, Department of Biomedical, Chemical and Environmental Engineering (DBCEE), University of Cincinnati, OH, 45221, USA*
[c] *Pegasus Technical Services Inc., 46 E Hollister St, Cincinnati, OH 45219, USA*
[d] *The U.S. Environmental Protection Agency, ORD, NERL, MCEARD, 26 W. Martin Luther King Jr. Drive, Cincinnati, OH, 45268, USA*

† The U.S. Environmental Protection Agency, through its Office of Research and Development, funded and managed, or partially funded and collaborated in, the research described herein. It has been subjected to the Agency's administrative review and has been approved for external publication. Any opinions expressed in this paper are those of the author(s) and do not necessarily reflect the views of the Agency, therefore, no official endorsement should be inferred. Any mention of trade names or commercial products does not constitute endorsement or recommendation for use.

‡ Electronic supplementary information (ESI) available. See DOI: 10.1039/c4ew00020j

This journal is © The Royal Society of Chemistry 2015

removal (EBPR)[12,13] are commonly used. However, due to a number of factors including cost, sludge production, required energy, and issues of reliability and stability,[14,15] other methods are currently being explored. The quickest, easiest, and most economically known method for the removal of phosphate ions is adsorption.[16] To date, a number of different adsorbents have been investigated for phosphate removal including metal oxides,[16–22] red mud,[23–25] steel slag,[26–28] and fly ash.[29,30] Table 1 shows different phosphate adsorbents and their reported adsorption capacity at different parameters. Adsorption also has the benefits of applicability at low concentrations, little to no sludge production, and potential for both batch and continuous processes, and the potential for adsorbent regeneration that could reduce wastes and costs.[31]

One such highly adsorptive material for phosphate removal is the iron oxide goethite (iron(III) oxide-hydroxide).[32–35] The affinity of phosphate adsorption on iron(III) oxide-hydroxide is dependent on phosphate's complexing capacity by ligand exchange as well as electrostatic interactions with the surface.[36] This process involves replacement of a phosphate ion with one or more surface hydroxyl groups, releasing surface structural OH_2 and/or OH^- into the bulk solution,[37] in which stoichiometric changes in the amount of phosphate adsorbed and OH^- released can provide clues on the type of adsorption mechanism.[38] Iron(III) oxide-hydroxide adsorption initially occurs rapidly, followed by a slow stage,[39] attributed to micro/mesopore diffusion[40] or particle aggregation,[41] which is generally dependent on the crystallinity of samples.[42] Phosphate adsorption onto iron oxides involves a ligand exchange mechanism,[43] yet the exact mode of phosphate interaction is not known. IR studies revealed that each adsorbed phosphate ion replaces two, singly coordinated OH surface groups, indicating a bridging, binuclear complex.[44,45] However, other studies have suggested that monodentate surface complexes could exist at low adsorbate concentrations.[46] Using a combination of surface complexes to model adsorption on iron oxides, Geelhoed *et al.*[47] concluded that the bidentate surface complex was most abundant at low to intermediate values of pH.

Goethite (α-FeOOH) is one of the most thermodynamically stable forms of iron oxide and thus is available in abundant quantities.[48] Due to its affinity for ion adsorption, AdEdge Technologies Inc. (USA) has produced Bayoxide® E33 media (E33), a commercially available goethite-based adsorbent for environmental remediation. Although originally designed for arsenic removal,[49,50] E33 has been shown to adsorb a range of ions including phosphates. While several studies have shown that E33 adsorption is an effective technique for phosphate removal,[51–53] surface modifications of E33 can enhance overall adsorption. As adsorption is a surface-based phenomenon dependent on electrostatic interactions and covalent bonding, the addition of di- and tri-valent metals to the surface of E33 should correlate with increased phosphate adsorption.

In this study, the surface of E33 media was modified with manganese and silver. For the removal of phosphate, the adsorptive properties of modified E33 were investigated and then compared to those of the unmodified E33.

2. Experimental

2.1 Materials

The E33 used to study PO_4^{3-} removal was obtained from AdEdge Technologies Inc. (USA). Analytical grade sodium phosphate monohydrate ($NaH_2PO_4{\cdot}(H_2O)$) was obtained from Fisher Scientific and used as a stock solution. A stock phosphate solution at a concentration of ≈80 mg L^{-1} was prepared by dissolving 1 g of $NaH_2PO_4{\cdot}(H_2O)$ in 10 L of Milli-Q water. The pH of the stock phosphate solution was

Table 1 Comparison of phosphate adsorption capacity of different adsorbents

Adsorbent	Capacity (PO_4^{3-} mg g^{-1})	pH	Temperature (°C)	Reference
Metal oxides synthesized from manganese ore tailing	26.3	6.0	25	16
Titanium ion doped ordered mesoporous silica	4.5	7.0	21	17
Magnetic iron oxide nanoparticles	3.7	3.0	15	18
Zinc–aluminum layered double hydroxides	30.0	9.0	20	19
Iron oxide-coated crushed brick	1.8	5.0	20	20
Lithium-intercalated gibbsite	0.3	4.5	25	21
Fe-loaded biomass char	35.4	3.0	25	22
HCl-treated red mud	0.6	5.5	40	23
Red mud granular adsorbents	9.8	9.2	37	24
Red mud	0.5	4.0	25	25
Modified steel slag	11.1	8.0	25	26
Steel slag	5.3	5.5	25	27
Electric arc furnace (EAF) steel slag	2.2	6.0	23	28
Iron oxide/fly ash	27.4	3.0	25	29
Fly ash	18.9	3.0	25	29
Nanshi-modified fly ash	40.7	4.0	21	30
Nanshi-modified zeolite	47.2	4.0	21	30
E33	26.8	7.0	21	This study
E33/Mn	17.8	7.0	21	This study
E33/AgI	19.3	7.0	21	This study
E33/AgII	28.0	7.0	21	This study

maintained constant at 6, 7 and 9, using 2-(*N*-morpholino) ethanesulfonic acid (MES), 3-(*N*-morpholino) propanesulfonic acid (MOPS), and *N*-tris (hydroxymethyl) methyl-3-aminopropanesulfonic acid (TAPS), respectively, all obtained from Sigma Aldrich. Reagent grade silver nitrate ($AgNO_3$), sodium borohydride ($NaBH_4$), and manganese acetate tetrahydrate ($Mn(CH_3COO)_2{\cdot}4H_2O$) were obtained from Sigma Aldrich and used as received.

2.2 Synthesis of modified E33

For the synthesis of silver-modified E33, an initial mixture of 10 g of E33 and 35 mL of Milli-Q water was prepared in a 100 mL conical flask. Then, 2 mL of 0.1 N $AgNO_3$ was added to the flask and shaken by hand for 2 min to ensure thorough mixing. To this initial mixture, two different adsorbents were prepared, one using $NaBH_4$ and the other using tea extract, denoted respectively as (E33/AgI)[50] and (E33/AgII)[50]. For E33/AgI, 10 mL of 0.1 N $NaBH_4$ was added to the initial mixture, hand shaken for 2 min and allowed to react overnight at room temperature. For E33/AgII, 2 g of tea powder (Red Label, India) was boiled in 100 mL of Milli-Q water and the solution was filtered through a 0.20 μm PTFE filter. Then, 20 mL of the tea extract solution was added to the initial mixture, shaken by hand for 2 min, and allowed to react overnight at room temperature. Following the overnight incubation, samples were twice washed with Milli-Q water and air-dried at room temperature prior to characterization and analysis.[50]

For the synthesis of manganese-coated E33 (E33/Mn), 50 g of E33 was mixed with 20 mL of Milli-Q water in a china crucible. Then, 10 g of manganese acetate tetrahydrate ($Mn(CH_3COO)_2{\cdot}4H_2O$, Aldrich product) was added to the crucible and the solution was hand-mixed with a spatula for 5 min to ensure proper mixing. After mixing was complete, the sample was heated at 310 °C for 1 h in a china crucible and then stored for later analysis and characterization.

2.3 Sample characterization

X-ray diffraction (XRD) analysis was performed using a PANalytical (X'pert) 2-theta diffractometer (PANalytical, Almelo, the Netherlands) in the 2-theta range of 2–90° under CuK_α radiation and a wavelength of 1.54 μm in order to determine the adsorbent's crystal structure. An environmental scanning electron microscope (ESEM, model Philips XL 30 ESEM-FEG) at an accelerating voltage of 30 kV was used to characterize the surface morphology of the adsorbents. An energy-dispersive X-ray spectrophotometer (EDX) installed in the ESEM was used to detect the distribution of elemental phosphorus as well as the percent of phosphate adsorbed. For transmission electron microscopy (TEM), a FEI CM20 TEM operated at 200 kV was employed. High-resolution TEM (HR-TEM, JEM-2010F (JEOL)) with a field emission gun at 200 kV was also employed for the characterization of the prepared surface-modified adsorbents. Free software (ImageJ, National Institutes of Health, USA) was used for HR-TEM image analysis. Adsorbent samples were prepared by ultrasonication (2510R-DH Bransonic) for 20 min in isopropyl alcohol (99.8%, Pharmco), and then a drop of the supernatant was fixed on a carbon-coated copper grid (FCF400-Cu, EMS) and dried at room temperature. A Tristar 3000 porosimeter analyzer (Micromeritics) was used to determine the adsorbent's BET surface area, total pore volume, and porosity. Samples were first purged with nitrogen gas at 150 °C for 2 h using Micromeritics FlowPrep 060.

2.4 Adsorption studies

To determine various adsorption parameters of the surface-modified adsorbent, both batch and flow-through column experiments were employed. Batch adsorption kinetic studies were carried out to determine the amount of phosphate adsorbed with respect to time. Experiments were conducted in 250 mL Nalgene polypropylene bottles given the following conditions: (i) temperature: 20–25 °C, (ii) adsorbent amount: 5 g L^{-1}, (iii) pH: 6, 7, and 9, (iv) influent phosphate concentration: ≈80 mg L^{-1}. A constant pH in the batch reactor was maintained using 5 mM MES, MOPS, and TAPS buffer (for pH 6, 7, and 9, respectively) and was continually mixed at a constant speed of 150 rpm (G10 Gyrotary shaker, New Brunswick Scientific Co. Inc., USA). At higher mixing speed, E33 samples started breaking down. Grab samples were collected at various predetermined intervals (*e.g.* after 5, 10, 15, 30, 45 min and 1, 2, 3, 4, 5 h) and filtered using a Whatman 0.45 μm nylon syringe filter. Experiments were conducted in duplicate while each grab sample was a single measurement.

Rapid small scale column tests were performed in Harvel plastic columns 80 cm high and 1.9 cm in diameter. One gram of adsorbent media with a fixed height of 1.27 cm, with sand and gravel above and below, was placed in the columns with a stainless steel sieve at the bottom end of the column to prevent washout. Using a Thermo Scientific™ FH100M Series Peristaltic pump, the phosphate solution was passed through the column at a rate of 2 mL min^{-1} at room temperature. Similar to the kinetic study, solution pH was adjusted initially and buffered to remain constant using 5 mM MES, MOPS, and TAPS. The column effluent samples were collected and analyzed for phosphate concentration at various time periods and run until complete breakthrough (*i.e.* saturation). Flow through experiments were conducted in duplicate while each grab sample was a single measurement.

Variable-dose isotherm adsorption studies were conducted. Different amounts of adsorbent (ranging from 100 to 600 mg) were placed in 250 mL Nalgene polypropylene bottles. One hundred milliliters of the same 80 mg L^{-1} phosphate solution was then added to the bottles. Buffers (5 mM MES, MOPS, and TAPS) were used to maintain constant pH conditions to evaluate adsorption characteristics at varying pH values. The sealed bottles were placed on a tabletop rotating shaker and shaken at a constant 150 rpm at 21 ± 1 °C for 2 weeks, which preliminary test results revealed was sufficient time for

 This journal is © The Royal Society of Chemistry 2015

equilibrium to be reached. The phosphate concentration in all experiments was analyzed by a colorimetric measurement technique in which ammonium molybdate and potassium antimonyl tartrate react in an acidic solution with orthophosphate to form phosphomopydbic acid which can be reduced by ascorbic acid to form an intense blue color.[54] The absorbance due to the blue complex was monitored at 880 nm using UV-Vis spectrophotometry (Hach model number DR 2700). Experiments were conducted once and samples were measured in triplicate and averaged.

3. Results

3.1 Adsorbent characterization

Table 2 summarizes the physical characteristics of E33 and modified E33 samples. The BET surface area of E33 exceeded that of the modified samples except for E33/AgII, which had a slightly higher BET surface area (142.0 m^2 g^{-1} compared to 140.4 m^2 g^{-1}). The manganese-coated E33 had a significantly reduced BET surface area (102.8 m^2 g^{-1}) compared to E33. This suggests that at least a portion of the manganese oxide nanoparticles occupied the pore structure of E33. This table also summarizes structural characteristics of the adsorbent prior to and after phosphate adsorption. Fig. S1 (a) and (b)‡ show N2 adsorption and desorption isotherms for all samples before and after using for phosphate removal. They present typical Type IV adsorption isotherms, indicating the formation of mesoporous materials.[55]

3.1.1 SEM characterization. Fig. 1 illustrates SEM images of E33 and modified E33. Fig. 1(a) and (b) represent unmodified E33 at 12k and 50k magnification, respectively. Based on Fig. 1(b), it could be determined that the particles are spherical and, on average, 75 nm in diameter. Fig. 1(c) and (d) illustrate the surface morphology of E33/Mn at 12k and 50k magnification, respectively. As can be seen in Fig. 1(d), the spherical particles range in size from 50 to 200 nm in diameter. Also, several particle aggregates 500 nm in diameter were present. Fig. 1(e) and (f) illustrate SEM images of E33/AgI. Fig. 1(f) (at 50k magnification) reveals that the average particle size was 75 nm which was similar to the unmodified E33. Fig. 1(e) (at 12k magnification) reveals a smoother surface when compared to the other adsorbents. The surface morphology for E33/AgII is illustrated in Fig. 1(g) and (h), at 12k and 50k magnification, respectively. The average particle size was determined to be 100 nm, and all particles were spherical in shape. The images for EDX mapping show adsorbed phosphate (yellow) on the surface of E33 and E33/AgII. More phosphate was detected on the surface of E33/AgII compared to that of unmodified E33 (please see Fig. S2 in the ESI‡).

3.1.2 XRD analysis. Fig. 2 shows the XRD patterns of all samples used for phosphate removal. The peaks for all samples were defined using reference codes in XRD analysis software corresponding to different materials such as 00-03-0249, 00-001-1053, 00-014-0557, and 00-036-0045 for goethite, hematite, iron manganese oxide hydroxide, and iron phosphate hydroxide, respectively. The XRD patterns of all samples are shown in Fig. S3(a)–(d).‡ The well-defined peaks demonstrated typical XRD patterns of goethite of iron oxides in E33 and Ag-modified E33 in Fig. 2(a), indicating that Ag modification did not affect the phase transformation of goethite. Moreover, the pH of solution for phosphate removal did not affect the goethite phase of iron oxide (see Fig. S3(a), (c), and (d)‡). However, the peaks, which correspond to Ag, were not detected due to low concentration of Ag (see Fig. 2(a)). For Mn-modified E33, the peaks corresponding to hematite of iron oxide were observed, indicating phase transformation from goethite to hematite during the synthesis process. Well-defined peaks corresponding to iron manganese hydroxide were observed, indicating that the surface of E33 was successfully modified with manganese (see Fig. 2(a)). Fig. 2(b) shows XRD patterns of E33 and surface-modified E33 after completion of the phosphate removal studies. The peaks corresponding to iron phosphate hydroxide in E33 and all surface-modified E33 were also observed, which indicates that the media complexed with the dissolved phosphate in the influent water.

3.1.3 TEM and HR-TEM characterization. Fig. 3 represents TEM images at 100k magnification of E33 and the modified adsorbents. The silver-modified adsorbents (E33/AgI and E33/AgII), in Fig. 3(c) and (d), had a rod-like shape, similar to the unmodified E33. These particles were determined to be, on average, 150 nm long and 20 nm across. It seems that the effect of silver modification on the morphological structure of E33 is negligible. On the other hand, the manganese-modified E33 had spherically shaped particles 50 nm in diameter on average. In order to investigate the structure of the crystal in detail, HR-TEM was employed. Fig. 4 shows the images of HR-TEM analysis for unmodified and modified E33 samples. Fig. 4(a) shows that the measured lattice spacing of the sample was 0.42, 0.25, and 0.17 nm, which correspond to the (110), (111), and (221) planes of goethite of iron oxide, respectively.[56] In Fig. 4(b), the lattice fringe with a *d*-spacing of 0.27 nm for the (222) plane of Mn_2O_3 was

Table 2 Structural characteristics of E33 and modified E33 before and after PO_4^{3-} adsorption

	Before adsorption			After adsorption		
Sample	S_{BET} (m^2 g^{-1})	Total pore volume (cm^3 g^{-1})	Porosity (%)	S_{BET} (m^2 g^{-1})	Total pore volume (cm^3 g^{-1})	Porosity (%)
E33	140.4	0.583	16.2	145.0	0.637	15.0
E33/AgI	124.6	0.456	12.6	136.8	0.449	11.1
E33/AgII	142.0	0.553	15.4	143.1	0.618	14.7
E33/Mn	102.8	0.441	12.3	99.5	0.623	14.8

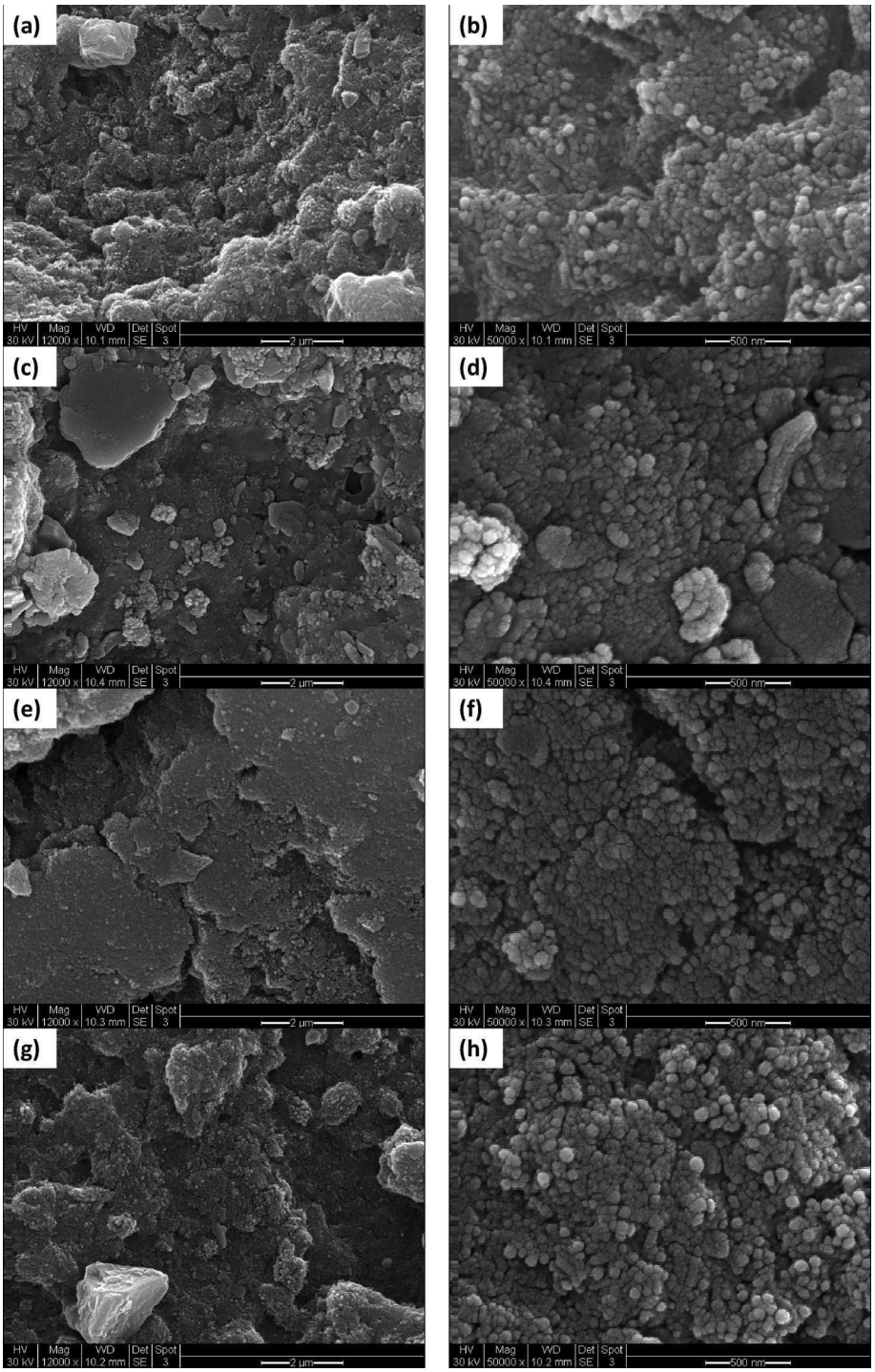

Fig. 1 SEM images of E33 at 12k (a) and at 50k (b), E33/Mn at 12k (c) and at 50k (d), E33/AgI at 12k (e) and at 50k (f), and E33/AgII at 12k (g) and at 50k (h) magnification.

measured, which indicated the formation of Mn_2O_3 during the surface modification of E33 with manganese.[57–59] After the surface modification of E33 with Ag, the presence of Ag was detected with a lattice spacing of 0.24 nm, corresponding to the (111) plane of Ag. The plane of (200) with a measured lattice spacing of 0.20 nm was also observed, indicating that the surface of E33 was successfully modified with Ag,[56,60] although the peaks corresponding to Ag were not detected by XRD analysis due to the low concentration of Ag on the surface of E33.

3.2 Adsorption studies

3.2.1 Effect of contact time. Fig. 5 shows the removal of phosphate as a function of reaction time from 0 up to 220 h.

 This journal is © The Royal Society of Chemistry 2015

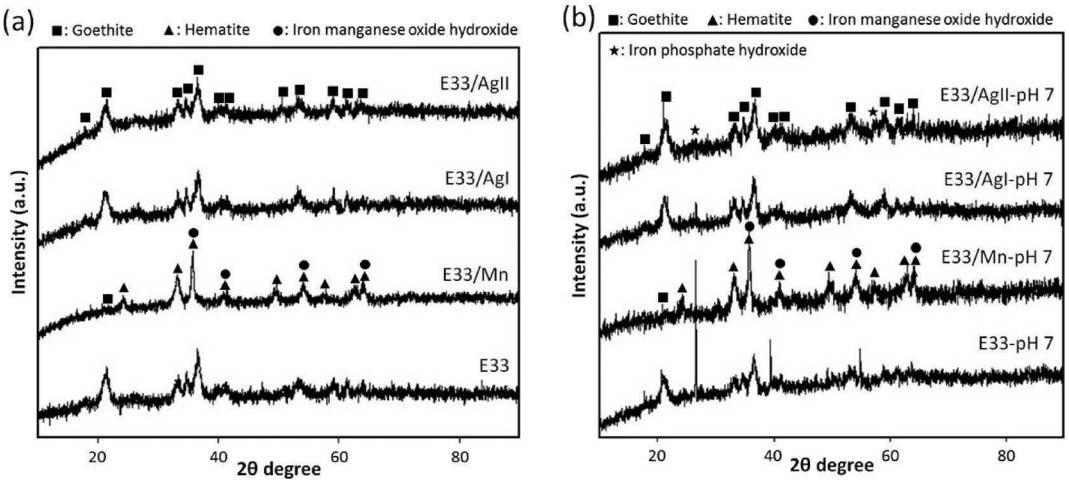

Fig. 2 XRD patterns of E33 and surface-modified E33: (a) before and (b) after using for phosphate removal.

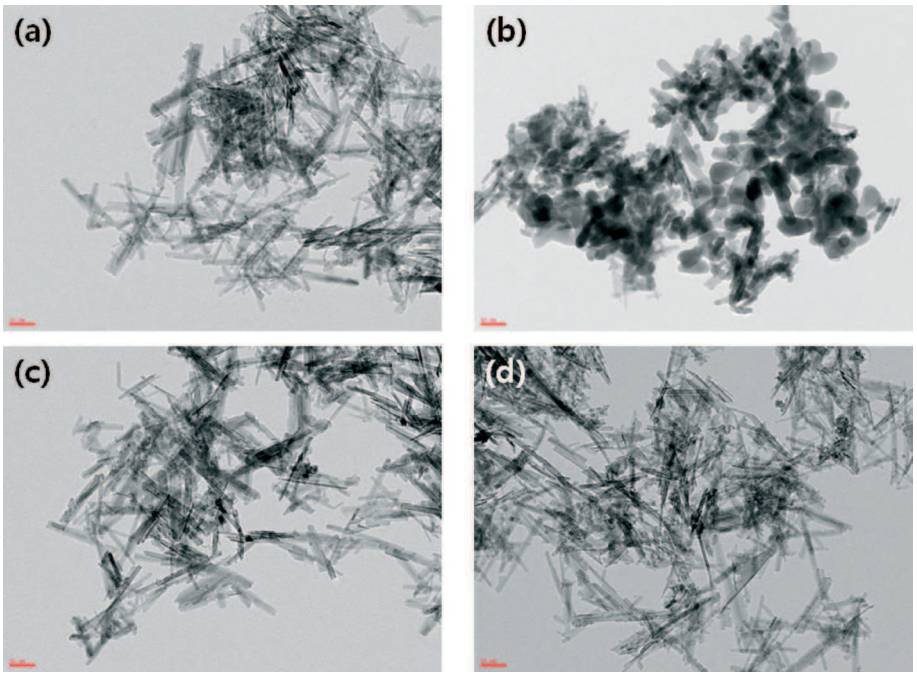

Fig. 3 TEM images at 100k magnification of adsorbent media (a) E33, (b) E33/Mn, (c) E33/AgI, and (d) E33/AgII. (All scale bars: 50 nm.)

The effluent presented a decreasing phosphate concentration with increasing reaction times. While E33/Mn and E33/AgI had lower reductions in phosphate concentration, E33/AgII performed similarly to the unmodified E33. The phosphate adsorption capacity of the different adsorbents correlates to BET surface area (Table 2). The solution pH in the batch reactor noticeably impacted the efficiency of adsorbents for phosphate removal. For example, E33/AgII at pH 7 removed roughly 65% of phosphate after a 3 h reaction time, yet only about 35% at pH 9. Influent pH also impacted overall adsorption. E33/AgII at pH 7 reduced phosphate concentration (initially at 82.66 mg L^{-1}) to 1.71 mg L^{-1}, while with an influent of pH 9, phosphate concentration was reduced to 5.71 mg L^{-1}. These graphs also show that E33/AgII removed 50% of the phosphate in the first hour of adsorption. It then took nearly five more days to reach equilibrium (Fig. 5(b)).

3.2.2 Phosphate adsorption kinetics. The results of kinetic experiments for phosphate adsorption are illustrated in Fig. 6. It can be seen that the adsorption rates of E33 and E33/AgII were slightly higher than those of E33/AgI and E33/Mn. Yet all adsorbents portrayed the typical, two-stage adsorption process, with a rapid initial phase and a slower phase, which likely corresponds to interparticle diffusion. For example, after 2 h of adsorption, the phosphate removal for E33, E33/Mn, E33/AgI, and E33/AgII was 66, 54, 38, and 63%, respectively.

The kinetic data for phosphate adsorption seen in Fig. 6 were fitted to several kinetic models including the pseudo-

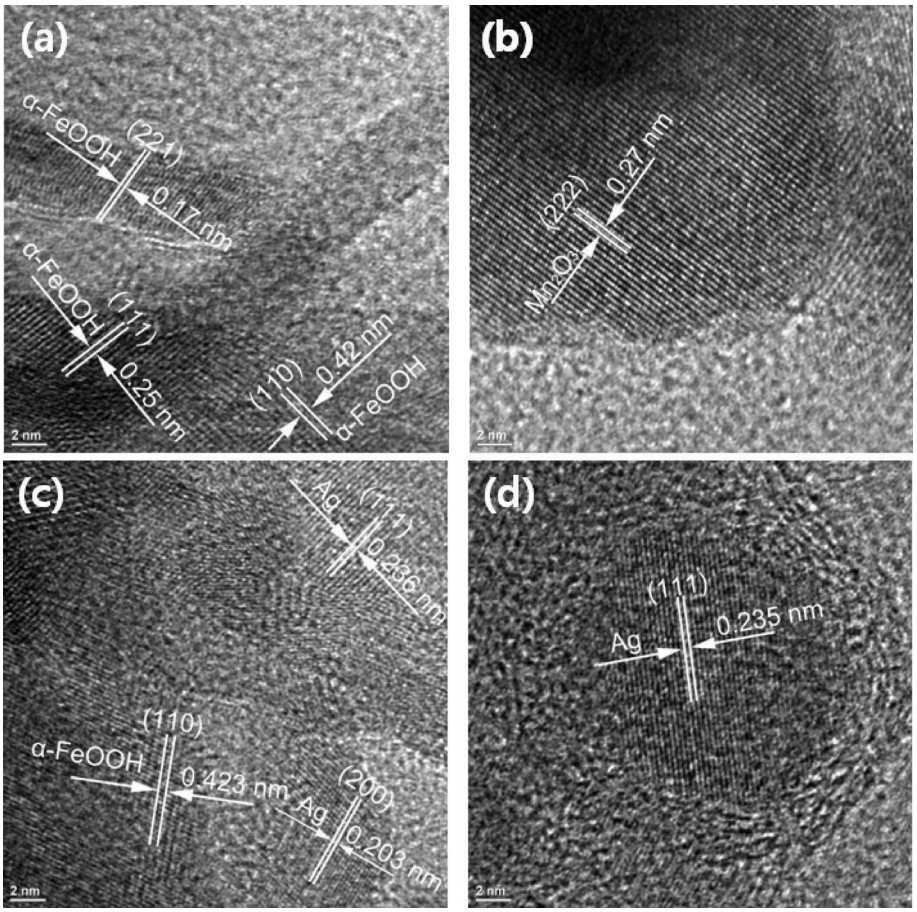

Fig. 4 HR-TEM analysis for unmodified and modified E33 used for phosphate removal: (a) E33, (b) E33/Mn, (c) E33/AgI, and (d) E33/AgII. (All scale bars: 2 nm.)

second-order equation and the simple Elovich equation by non-linear regression using SigmaPlot software. The kinetic equations used and their estimated parameters, with the correlation coefficient R^2, are illustrated in Table 3. Based on the values of R^2, the kinetics of phosphate adsorption on E33 and modified E33 can be satisfactorily described by both the pseudo-second-order equation and the simple Elovich equation; thus, Fig. 6 has both equations plotted also. The apparent applicability of the Elovich equation, which was originally developed to describe chemisorption of gases on heterogeneous solid surfaces,[61] suggests that the sorption sites involved in phosphate sorption are also of a heterogeneous nature. Obtained results were generally in agreement with other results from the literature and can properly explain the kinetics of phosphate adsorption onto commonly found soil minerals such as goethite.[62–64]

3.2.3 Column study. Column experiments were conducted to quantify the mechanism of phosphate adsorption as would be seen in an industrial-scale fixed bed adsorber. The breakthrough curves were constructed by plotting the ratio of PO_4^{3-} concentration at time t to the initial influent concentration (C/C_0) versus time (t). Fig. 7 shows the typical "S" shape of the breakthrough curves indicating the effects of mass transfer parameters as well as internal resistance within the column. Phosphate adsorption was initially high, decreasing with time until fully saturated. The impact of influent pH on phosphate adsorption was also evident where at higher pH (pH 9), breakthrough time (1.5 hr) was longer, while the time to reach saturation was shorter (15 hr), as opposed to the pH 7 where the breakthrough occurred after 1 hr, but took 18 hr to reach full saturation. The cumulative adsorption capacity of the columns was determined. At pH 6, the cumulative column adsorption capacity for E33, E33/Mn, E33/AgI, and E33/AgII was 31.5, 28.5, 29.9, and 40.1 mg g^{-1}, respectively. These results show that the phosphate adsorption capacity of the adsorbents in columns were much higher when compared to batch experiments (e.g. E33/AgII at pH 6 had a capacity of 17.0 mg g^{-1} for batch studies and 40.1 mg g^{-1} for column experiments). However, this is likely due to the volume of solution treated. Batch experiments were conducted using 0.1 L of phosphate solution while the continuous column experiments passed nearly 3 L of phosphate solution through the sorbents. These results indicate that E33/AgII provided a greater capacity for phosphate adsorption when compared to E33 at high (pH 9) and neutral (pH 6) pH values. The adsorption capacities for both batch and column tests are summarized in Table S1.‡

 This journal is © The Royal Society of Chemistry 2015

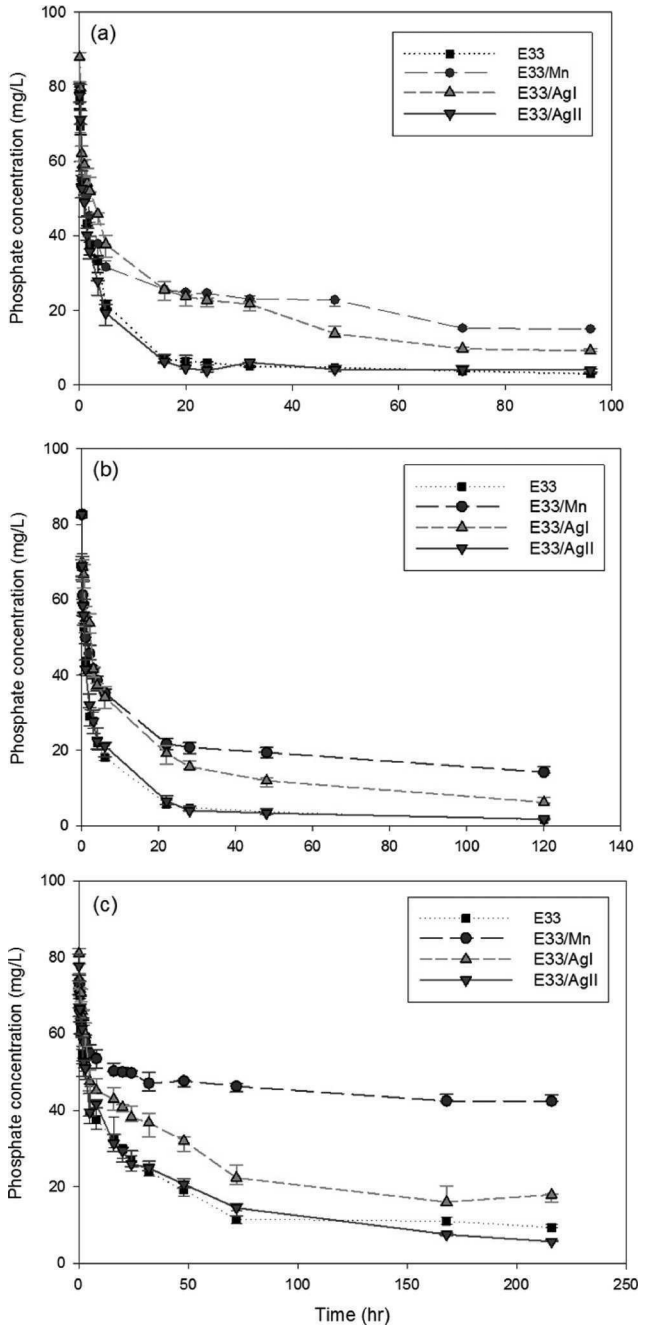

Fig. 5 Rate of E33 and modified E33 adsorption of phosphate at various pH values: (a) pH 6, (b) pH 7, and (c) pH 9.

3.2.4 Adsorption isotherm study. The following equation was used to determine the amount of phosphate anions adsorbed per unit weight of adsorbent (q_e):

$$q_e = \frac{(c_0 - c^*)V}{m}$$

where c_0 is the initial concentration (mg L^{-1}), c^* is the equilibrium concentration (mg L^{-1}), V is the solution volume (L), and m is the adsorbent mass in grams. Table 1 illustrates the phosphate adsorption capacity of a wide range of adsorbents including metal oxides, red mud, steel slag, and fly ash, as well as E33 and modified E33. The most efficient adsorbents were the Nanshi-modified zeolite, the Nanshi-modified fly ash, and Fe-loaded biomass char. However, the stock solution influent pH for these adsorbents was maintained atypically low (pH 3 and 4) to promote enhanced adsorption. At neutral pH, E33/AgII had a phosphate adsorption capacity of 28.0 mg PO_4^{3-} g^{-1}. This was slightly higher than that of the unmodified E33 (26.3 mg PO_4^{3-} g^{-1}), likely due to the increased BET surface area of the E33/AgII sample. The capacities from this study compare favorably with the capacities of other adsorbents as reported in literature.

Adsorption isotherms are used to relate the bulk adsorbate concentration and the amount adsorbed at the surface interface. The isotherm results were analyzed using the Langmuir and Freundlich isotherms. The Langmuir isotherm model, which assumes monolayer saturation with no lateral interaction between adsorbed particles, has previously been

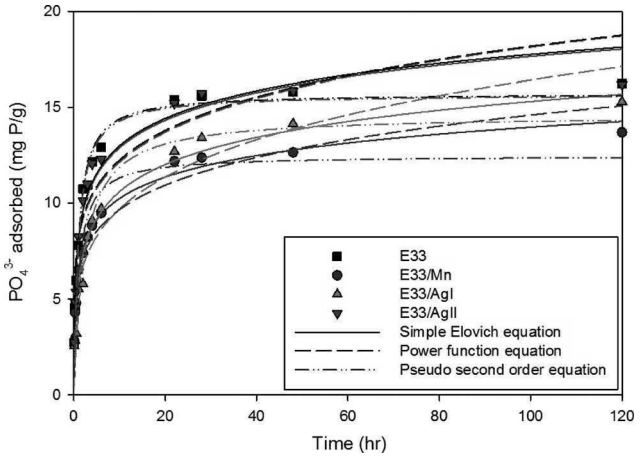

Fig. 6 Phosphate adsorption kinetic data for E33 and modified E33 at 20 °C, pH 7, and an influent concentration of 83 mg P L^{-1}.

Table 3 Estimated parameters for the kinetic model of phosphate adsorption on E33 and modified E33

Power function equation ($q = at^b$)			
	a	b	R^2
E33	8.259	0.1715	0.8718
E33/Mn	6.396	0.1793	0.9464
E33/AgI	5.728	0.2288	0.9343
E33/AgII	8.139	0.1742	0.8817
Simple Elovich equation ($q = a + b \ln t$)			
	a	b	R^2
E33	8.228	2.071	0.9600
E33/Mn	6.513	1.619	0.9894
E33/AgI	5.895	2.045	0.9645
E33/AgII	8.130	2.070	0.9645
Pseudo second-order equation ($q_t = k_2 q_e^2 t/1 + k_2 q_e t$)			
	$q_{e,cal}$	k_2 (g mg^{-1} min^{-1})	R^2
E33	16.34	0.0641	0.9725
E33/Mn	13.74	0.0645	0.9021
E33/AgI	15.46	0.0272	0.9547
E33/AgII	16.31	0.0616	0.9639

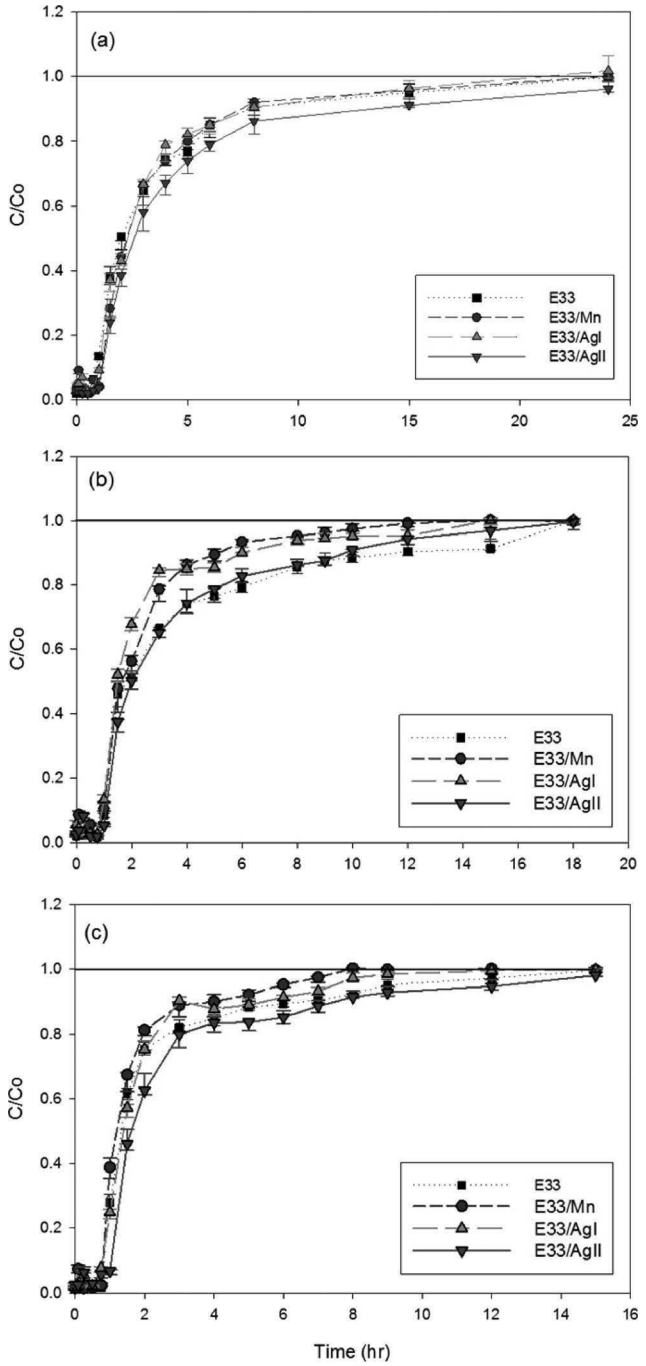

Fig. 7 Column experiments for E33 and modified E33 phosphate adsorption at (a) pH 6, (b) pH 7, and (c) pH 9.

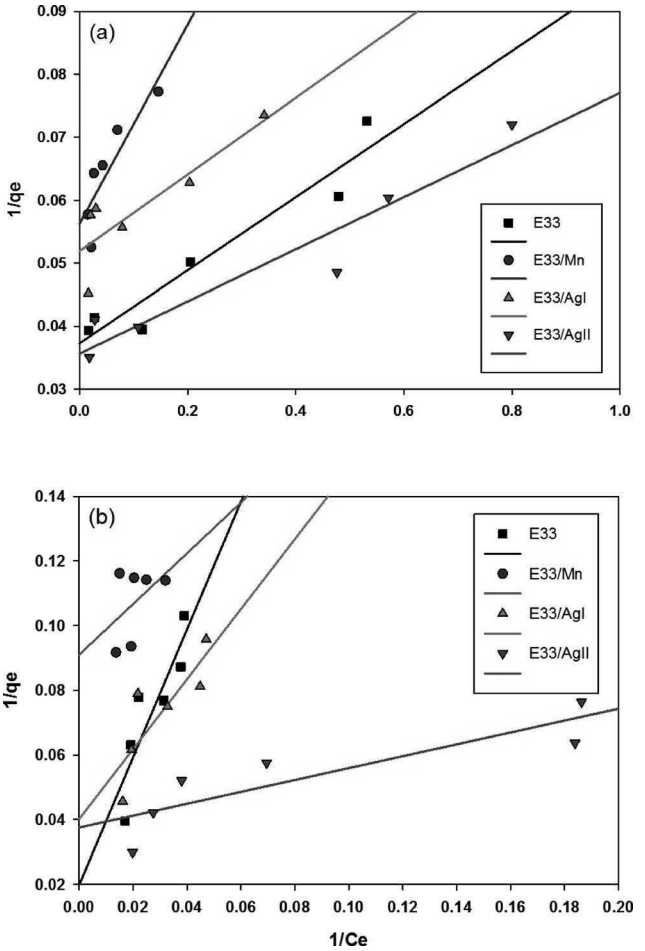

Fig. 8 Langmuir isotherm graphs for (a) pH 7 and (b) pH 9.

Table 4 Isotherm parameters at pH 7

	Langmuir isotherm constants			Freundlich isotherm constants		
Sample	Q_{max} (mg g^{-1})	K_L (dm^3 mg^{-1})	R^2	K_F	$1/n$	R^2
E33	25.71	0.82	0.9999	14.72	0.15	0.7389
E33/Mn	18.73	0.24	0.9836	9.59	0.15	0.8133
E33/AgI	20.58	0.36	0.9642	12.87	0.10	0.6718
E33/AgII	28.01	0.69	0.9917	15.75	0.15	0.7893

employed in similar adsorption experiments.[62–64] The Langmuir adsorption model is mathematically expressed by:

$$q_e = \frac{Q_{max} K_L C_e}{1 + K_L C_e}$$

where q_e (mg g^{-1}) is the amount of adsorbed phosphate per unit mass of adsorbent, C_e (mg L^{-1}) is the unadsorbed phosphate concentration in solution at equilibrium, Q_{max} is the maximum amount of phosphate per unit mass of sorbent to form a complete monolayer on the surface, and K_L (L mg^{-1}) is a constant related to the affinity of the binding sites. The Langmuir adsorption equation can be described by its linearized form:

$$\frac{1}{q_e} = \left(\frac{1}{K_L Q_{max}}\right)\frac{1}{C_e} + \frac{1}{Q_{max}}$$

The linear plot of the above equation (Fig. 8) yields essential specifications of the system. The slope and intercept of the plot were used to determine the Langmuir constants Q_{max} and K_L, which are presented in Table 4.

 This journal is © The Royal Society of Chemistry 2015

Essential characteristics of the Langmuir isotherm model can be expressed in terms of a constant dimensionless separation factor, R_L, given by the equation:

$$R_L = \frac{1}{(1 + K_L C_0)}$$

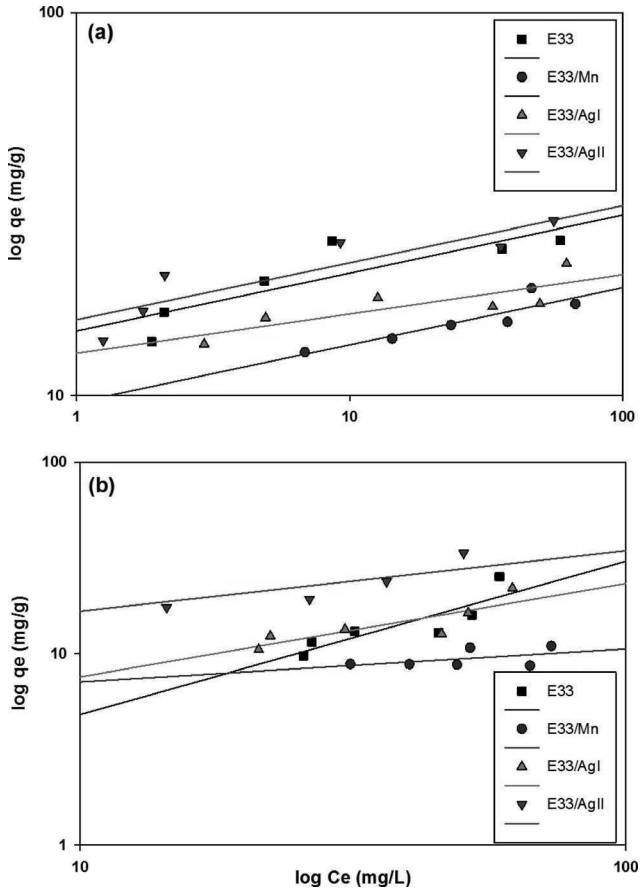

Fig. 9 Freundlich isotherm graphs for influent pH values of (a) 7 and (b) 9.

where C_0 (mg L^{-1}) is the initial adsorbate concentration in solution and K_L (L mg^{-1}) is the Langmuir constant. The value of R_L can indicate if adsorption is unfavorable ($R_L > 1$), linear ($R_L = 1$), irreversible ($R_L = 0$), or favorable ($0 < R_L < 1$). R_L values for E33, E33/Mn, E33/AgI, and E33/AgII were 0.015, 0.050, 0.034, and 0.018, respectively. As all values computed for R_L were less than 1 and greater than 0, adsorption was determined to be favorable.

The Freundlich isotherm is an empirical equation used to explain heterogeneous systems. The Freundlich equation is given by:

$$q_e = K_F (C_e)^{1/n}$$

where K_F ((mg g^{-1}) (L $mg^{-1})^{1/n}$) is the adsorption capacity of the adsorbent and n gives an indication of adsorption favorability, for example, values of $n > 1$ indicate favorable adsorption. Freundlich isotherm constants K_F and n can be determined by the linearization of the Freundlich equation and graphing $\ln(q_e)$ *vs.* $\ln(C_e)$:

$$\ln(q_e) = (K_F) + \frac{1}{n}(\ln(C_e))$$

Values of K_F and n can be determined from the intercept and slope of the plot for the linearized Freundlich equation. The linearized Freundlich isotherm plots for phosphate adsorption onto E33 and modified E33 are presented in Fig. 9. The Freundlich isotherm constants, K_F and $1/n$, were determined by linear regression (Table 4).

Fig. 10 shows phosphate adsorption isotherms for E33 and modified E33 under identical conditions, *i.e.* DI water at pH 7. The results show that E33/AgII had the highest capacity of phosphate adsorption for the modified adsorbents as well as unmodified E33. This is in accordance with BET surface area analysis, which revealed that E33/AgII had the highest specific surface area. Likewise, E33/Mn, which had the lowest phosphate adsorption capacity, also had the lowest BET surface area. Isotherm results were evaluated using both

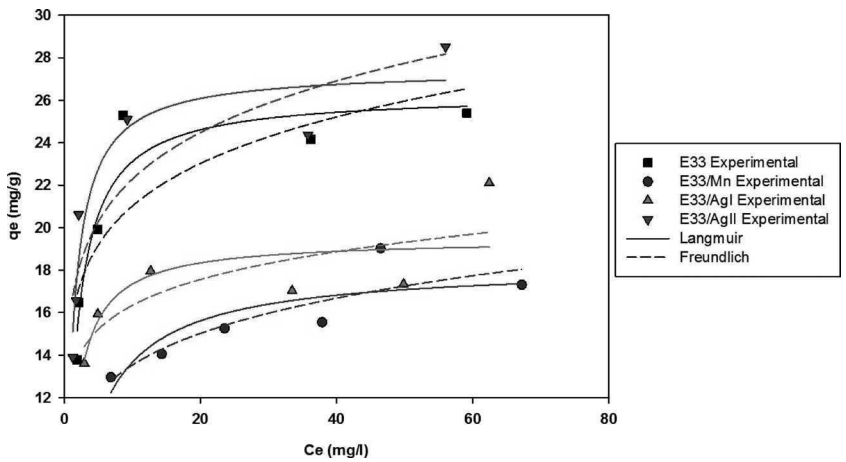

Fig. 10 Isotherm graph for phosphate adsorption at pH 7.

Langmuir and Freundlich isotherm equations. The determined isotherm constants for both models are summarized in Table 4. As can be seen from the coefficients of determination, the Langmuir isotherm appears better suited to explain the adsorption equilibrium data.

4. Conclusion

Three modified adsorbents, based on the commercially available E33 adsorptive medium, were successfully synthesized and characterized using SEM, TEM, XRD, porosimetry analysis and EDX. The adsorption capacity of the synthesized samples was investigated for the removal of phosphate. The results of the characterization of synthesized samples indicated that the surface of E33 was successfully modified with nanostructured Ag and manganese. In particular, for Ag-modified E33, the phase of E33 was not affected by Ag modification while the transformation of goethite to hematite was observed in Mn-modified E33.

Batch and column experiments were conducted to determine the adsorbents' capacity for phosphate adsorption. The phosphate removal was influenced by the pH of solutions. As the solution pH decreased, the amount of phosphate adsorbed increased, presumably because the surface charge of E33 is pH dependent, thus lower pH values correlate to a more positive surface charge on the E33, thus promoting increased PO_4^{3-} adsorption. Of the modified adsorbents synthesized, Ag-modified E33 using tea extract (E33/AgII) had a slightly higher phosphate adsorption capacity compared to unmodified E33. This increase in adsorptive capacity is likely due to an increased BET surface area for E33/AgII. Although Mn-modified E33 (E33/Mn) was believed to promote increased adsorption, a reduction in BET surface area (likely caused by the aggregation of particles resulting in a spherical shape for the E33/Mn particles as revealed by TEM) resulted in a pore blockage and lower phosphate adsorption capacity when compared to unmodified E33. The increased adsorption for E33/AgII suggests the potential for improving the performance of commercially available adsorbents for phosphate removal.

References

1 E. Metcalf, *Wastewater engineering: treatment, disposal and reuse*, McGraw-Hill, New York, 1991.
2 H. L. Golterman, *Water Res.*, 1973, **7**, 3–17.
3 J. J. Schröder, A. L. Smit, D. Cordell and A. Rosemarin, *Chemosphere*, 2011, **84**, 822–831.
4 A. Sendrowski and T. H. Boyer, *Desalination*, 2013, **322**, 104–112.
5 Y. Liu, G. Villalba, R. U. Ayres and H. Schroder, *J. Ind. Ecol.*, 2008, **12**, 229–247.
6 G. Villalba, Y. Liu, H. Schroder and R. U. Ayres, *J. Ind. Ecol.*, 2008, **12**, 557–569.
7 M. Meybeck, *Am. J. Sci.*, 1982, **282**, 401–450.
8 H. Holtan, L. Kamp-Nielsen and A. O. Stuanes, *Hydrobiologia*, 1988, **170**, 19–34.
9 *Phosphorus in environmental technologies: Principles and applications*, ed. E. Valsami-Jones, IWA Publishing, London, UK, 2004.
10 S. Pitois, M. H. Jackson and B. J. Wood, *J. Environ. Health*, 2001, **64**, 25–32.
11 G. R. Mohan, S. Gadekar and P. Pullammanappallil, *Florida Water Resources Journal*, 2011, 17–22.
12 G. R. Mohan, P. Dube, A. MacFarlene and P. Pullammanappallill, in *Materials challenges in alternative and renewable energy II: Ceramic transactions*, ed. G. Wicks, J. Simon, R. Zidan, R. Brigmon, G. Fischman, S. Arepalli, A. Norris and M. McCluer, John Wiley & Sons, Inc., Hoboken, New Jersey, 2013, vol. 242, pp. 47–58.
13 J. Hrenovic, M. Rozic, L. Sekovanic and A. Anic-Vucinic, *J. Hazard. Mater.*, 2008, **156**, 576–582.
14 A. Drews, H. Evenblij and S. Rosenberger, *Environ. Prog.*, 2005, **24**, 426–433.
15 K. Karageorgiou, M. Paschalis and G. N. Anastassakis, *J. Hazard. Mater.*, 2007, **139**, 447–452.
16 T. Liu, K. Wu and L. Zeng, *J. Hazard. Mater.*, 2012, **217**, 29–35.
17 P. Delaney, C. McManamon, J. P. Hanrahan, M. P. Copley, J. D. Holmes and M. A. Morris, *J. Hazard. Mater.*, 2011, **185**, 382–391.
18 S. Y. Yoon, C. G. Lee, J. A. Park, J. H. Kim, S. B. Kim, S. H. Lee and J. W. Choi, *Chem. Eng. J.*, 2014, **236**, 341–347.
19 X. Cheng, X. Huang, X. Wang, B. Zhao, A. Chen and D. Sun, *J. Hazard. Mater.*, 2009, **169**, 958–964.
20 N. Boujelben, J. Bouzid, Z. Elouear, M. Feki, F. Jamoussi and A. Montiel, *J. Hazard. Mater.*, 2008, **151**, 103–110.
21 S. L. Wang, C. Y. Cheng, Y. M. Tzou, R. B. Liaw, T. W. Chang and J. H. Chen, *J. Hazard. Mater.*, 2007, **147**, 205–212.
22 H. Zhou, Z. Jiang and S. Wei, *Journal of Chemistry*, 2013, **2013**, 649868.
23 A. Bhatnagar, V. J. Vilar, C. M. Botelho and R. A. Boaventura, *Environ. Technol.*, 2011, **32**, 231–249.
24 Q. Yue, Y. Zhao, Q. Li, W. Li, B. Gao, S. Han and H. Yu, *J. Hazard. Mater.*, 2010, **176**, 741–748.
25 P. Castaldi, M. Silvetti, G. Garau and S. Deiana, *J. Hazard. Mater.*, 2010, **182**, 266–272.
26 Y. Li, Y. Liu and G. Du, *Proceedings of Bioinformatics and biomedical engineering (iCBBE), 4th International Conference*, Chengdu, 2010.
27 J. Xiong, Z. He, Q. Mahmood, D. Liu, X. Yang and E. Islam, *J. Hazard. Mater.*, 2008, **152**, 211–215.
28 A. Drizo, C. Forget, R. P. Chapuis and Y. Comeau, *Water Res.*, 2006, **40**, 1547–1554.
29 S. Yao, J. Li and Z. Shi, *Adsorpt. Sci. Technol.*, 2009, **27**, 603–614.
30 J. Chen, H. Kong, D. Wu, Z. Hu, Z. Wang and Y. Wang, *J. Colloid Interface Sci.*, 2006, **300**, 491–497.
31 K. Mohanty, D. Das and M. N. Biswas, *Adsorption*, 2006, **12**, 119–132.
32 W. Jiang, J. Lv, L. Luo, K. Yang, Y. Lin, F. Hu and S. Zhang, *J. Hazard. Mater.*, 2013, **262**, 55–63.
33 H. Liu, T. Chen, X. Zou, Q. Xie, C. Qing, D. Chen and R. L. Frost, *Chem. Eng. J.*, 2013, **234**, 80–87.

 This journal is © The Royal Society of Chemistry 2015

34 J. Xi and M. He, *Water Qual. Res. J. Can.*, 2013, **48**, 223–231.
35 S. Aredes, B. Klein and M. Pawlik, *J. Cleaner Prod.*, 2012, **29**, 208–213.
36 W. Stumm, in *Chemistry of the solid-water interface: processes at the mineral-water and particle-water interface in natural systems*, John Wiley & Son Inc., 1992, p. 428.
37 A. Jain, K. P. Raven and R. H. Loeppert, *Environ. Sci. Technol.*, 1999, **33**, 1179–1184.
38 B. Zhong, R. Stanforth, S. Wu and J. P. Chen, *J. Colloid Interface Sci.*, 2007, **308**, 40–48.
39 J. Torrent, V. Barron and U. Schwertmann, *Soil Sci. Soc. Am. J.*, 1990, **54**, 1007–1012.
40 R. Strauss, G. W. Brümmer and N. J. Barrow, *Eur. J. Soil Sci.*, 1997, **48**, 101–114.
41 I. R. Willett, C. J. Chartres and T. T. Nguyen, *J. Soil Sci.*, 1988, **39**, 275–282.
42 R. Strauss, G. W. Brümmer and N. J. Barrow, *Eur. J. Soil Sci.*, 1997, **48**, 87–99.
43 L. Sigg and W. Stumm, *Colloids Surf.*, 1981, **2**, 101–117.
44 R. L. Parfitt, R. J. Atkinson and R. S. C. Smart, *Soil Sci. Soc. Am. J.*, 1975, **39**, 837–841.
45 M. Nanzyo, *Soil Sci. Plant Nutr.*, 1986, **32**, 51–58.
46 T. Hiemstra and W. H. Van Riemsdijk, *J. Colloid Interface Sci.*, 1996, **179**, 488–508.
47 J. S. Geelhoed, T. Hiemstra and W. H. Riemsdijk, *Environ. Sci. Technol.*, 1998, **32**, 2119–2123.
48 J. R. Rustad, A. R. Felmy and B. P. Hay, *Geochim. Cosmochim. Acta*, 1996, **60**, 1563–1576.
49 M. N. Nadagouda and D. A. Lytle, *J. Nanotechnol.*, 2011, **2011**, DOI: 10.1155/2011/972486.
50 M. N. Nadagouda, C. Bennett-Stamper, C. White and D. A. Lytle, *RSC Adv.*, 2012, **2**, 4198–4204.
51 M. Kanematsu, T. M. Young, K. Fukushi, P. G. Green and J. L. Darby, *Environ. Sci. Technol.*, 2010, **44**, 3388–3394.
52 M. Kanematsu, T. M. Young, K. Fukushi, D. A. Sverjensky, P. G. Green and J. L. Darby, *Environ. Sci. Technol.*, 2010, **45**, 561–568.
53 A. Sperlich, *Ph. D. Thesis*, University of Berlin, 2010.
54 J. Murphy and J. P. Riley, *Anal. Chim. Acta*, 1962, **27**, 31–36.
55 C. Han, V. Likodimos, J. A. Khan, M. N. Nadagouda, J. Anderson, P. Falaras, P. Rosales-Lombardi and D. D. Dionysiou, *Environ. Sci. Pollut. Res.*, 2014, **21**, 11781–11793.
56 J. Akai, K. Akai, M. Ito, S. Nakano, Y. Maki and I. Sasagawa, *Am. Mineral.*, 1999, **84**, 171–182.
57 J. N. Park, J. K. Shon, M. Jin, S. H. Hwang, G. O. Park, J. H. Boo, T. H. Han and J. M. Kim, *Chem. Lett.*, 2010, **39**, 93–495.
58 Q. Javed, F. P. Wang, M. Y. Rafique, A. M. Toufiq, Q. S. Li, H. Mahmood and W. Khan, *Nanotechnology*, 2012, **23**, 415603.
59 G. Yang, W. Yan, J. Wang and H. Yang, *CrystEngComm*, 2014, **16**, 6907–6913 (ESI).
60 P. Asanithi, S. Chaiyakun and P. Limsuwan, *J. Nanomater.*, 2012, **2012**, 79.
61 M. J. D. Low, *Chem. Rev.*, 1960, **60**, 267–312.
62 L. Zeng, X. Li and J. Liu, *Water Res.*, 2004, **38**, 1318–1326.
63 X. Wang, F. Liu, W. Tan, W. Li, X. Feng and D. L. Sparks, *Soil Sci.*, 2013, **178**, 1–11.
64 O. K. Borggaard, *J. Soil Sci.*, 1983, **34**, 333–341.

Chemical Engineering Journal 284 (2016) 1386–1396

Contents lists available at ScienceDirect

Chemical Engineering Journal

journal homepage: www.elsevier.com/locate/cej

Phosphate adsorption using modified iron oxide-based sorbents in lake water: Kinetics, equilibrium, and column tests

Jacob Lalley [a,b,1], Changseok Han [a,1], Xuan Li [a], Dionysios D. Dionysiou [b], Mallikarjuna N. Nadagouda [a,*]

[a] The U.S. Environmental Protection Agency, ORD, NRMRL, WSWRD, WQMB, 26 W. Martin Luther King Jr. Drive, Cincinnati, OH 45268, USA
[b] Environmental Engineering and Science Program, Department of Biomedical, Chemical and Environmental Engineering (DBCEE), University of Cincinnati, OH 45221, USA

HIGHLIGHTS

- The adsorbent E33 was successfully modified with silver and manganese nanoparticles.
- One silver modified sorbent had similar PO_4^{3-} adsorption capacity compared to E33.
- Phosphate desorption for its recovery was accomplished by base leaching with NaOH.

GRAPHICAL ABSTRACT

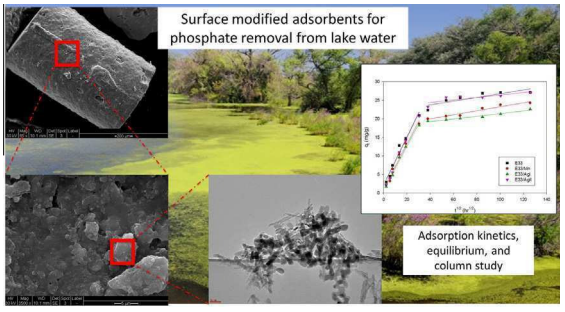

ARTICLE INFO

Article history:
Received 15 June 2015
Received in revised form 24 August 2015
Accepted 26 August 2015
Available online 2 September 2015

Keywords:
Adsorption
Nutrients
Nutrient removal/recovery
Phosphate
Water treatment

ABSTRACT

Adsorption behavior of Bayoxide® E33 (E33) and three E33-modified sorbents for the removal of phosphate from lake water was investigated in this study. E33-modified sorbents were synthesized by coating with manganese (E33/Mn) and silver (E33/AgI and E33/AgII) nanoparticles. Adsorbent characterization was done by X-ray diffraction (XRD), scanning electron microscopy (SEM), energy-dispersive X-ray spectroscopy (EDS), surface area analyzer (BET), transmission electron microscopy (TEM), and high resolution TEM (HR-TEM) analysis. Batch, equilibrium, and column experiments were conducted to determine various adsorption parameters. Equilibrium data were fitted to different adsorption isotherms and the Langmuir isotherm provided the best fit. Based on the Langmuir model, it was found that E33/AgII had a slightly higher maximum monolayer adsorption capacity (38.8 mg g^{-1}) when compared to unmodified E33 (37.7 mg g^{-1}). Data for adsorption kinetics were found to best fit with the pseudo-second-order model, suggesting chemisorption is the mechanism of sorption. Intra-particle diffusion studies indicated that the rate-limiting step for phosphate sorption onto E33 and modified E33 was intra-particle diffusion. Although limited improvements were seen, the results of this study suggest that the surface of E33 can be modified with nanoparticles to enhance the adsorption of phosphate from aqueous solutions and may give other advantages such as limiting biofouling over an extended lifetime of numerous recovery/regeneration steps.

Published by Elsevier B.V.

1. Introduction

Phosphates (PO_4^{3-}), as essential and often limiting nutrients in most aquatic environments, can result in the acceleration of eutrophication; leading to an increase in costs associated with water treatment [1], decreased recreational value of the waterway

* Corresponding author. Tel.: +1 (513) 569 7232; fax: +1 (513) 569 7172.
E-mail address: Nadagouda.mallikarjuna@epa.gov (M.N. Nadagouda).
[1] Contributed equally to this work.

http://dx.doi.org/10.1016/j.cej.2015.08.114
1385-8947/Published by Elsevier B.V.

[2], and the formation of harmful algal blooms (HABs) that may pose a risk to human health from the production of cyanotoxins [3]. Therefore, the remediation of phosphates from aquatic ecosystems is a growing environmental concern. While phosphates are naturally found in surface and waste water, anthropogenic sources from agriculture [4] (fertilizer/animal feed run-off), industry [5] (detergents), and sewage [6] have increased phosphate loads in surface waters, thus accelerating eutrophication.

While conventional treatment techniques like chemical precipitation and biological phosphorus removal exist, problems remain. Chemical precipitation is a costly process, requiring the purchasing, transportation, and storage of chemical precipitants, and produces vast quantities of sludge which must be properly disposed [7]. Biological processes like enhanced biological phosphorus removal (EBPR) are quite sensitive to water parameters including influent carbon source [8] (e.g., acetate, propionate, etc.) and temperature [9], resulting in decreased stability and reliability. Yet, while phosphates act as pollutants at high concentrations, their demand is growing for industrial purposes including fertilizer production and the manufacturing of detergents. As a non-renewable resource with no known alternatives, the need for phosphate recovery and recycling may become necessary. Though experts disagree on when (between 60 and 700 years) [10,11], it is acknowledged that our phosphate reserves will eventually be depleted. Thus, future studies should focus on PO_4^{3-} recovery as well as removal.

One technique that can both remove and recover phosphate is adsorption. Adsorption is a surface-based phenomenon resulting in the adhesion of an adsorbate on the surface of an adsorbent through covalent bonding and electrostatic interactions [12,13]. Unlike chemical precipitation and biological removal processes, adsorption is unique in that it can remove contaminants over a wide pH range and at low concentrations [14]. The iron oxide hydroxide goethite (α-FeOOH) is a highly adsorptive material for phosphate remediation. As the most thermodynamically stable iron oxide in most environmental conditions, goethite is the most frequently encountered iron oxide in nature and occurs in almost every soil type in every climatic region [15].

Iron oxides like goethite typically occur as poorly ordered, minute crystals with large specific surface areas (50–300 $m^2\ g^{-1}$) [16] with hydroxide surface functional groups. These properties substantially contribute to the specific adsorption of anions like PO_4^{3-} as inner sphere complexes. Phosphate adsorption results from the completion of the ligand shell of surface Fe atoms, where the PO_4^{3-} ion reacts with two singly coordinated Fe–OH groups, forming a bridging, binuclear, bidentate complex $(Fe–O)_2–PO_2H$ [17]. Due to goethite's affinity for ion adsorption and relative availability, LANXESS Deutschland GmbH has produced Bayoxide® E33 Adsorption Media (E33), a goethite-based adsorbent which was originally designed for arsenic remediation [18–20], yet studies have shown the ability of E33 to sorb a wide range of ions, including phosphates [21–23].

Previous research has explored phosphate adsorption equilibrium and adsorption kinetics of E33 and three surface modified E33-based adsorbents using a stock phosphate solution [24]. In this study, however, lake water was used to determine the effects of competing species on phosphate removal. The phosphate adsorption capacity and kinetics of E33 and modified E33 were determined, as well as the desorption of phosphate to explore possible reuse.

2. Experimental

2.1. Materials

The E33 adsorbent used to investigate phosphate adsorption was acquired from LANXESS Deutschland GmbH. Lake water, obtained from Winton Lake in Winton Woods (Cincinnati, OH), was spiked with analytical grade sodium phosphate monohydrate ($NaH_2PO_4{\cdot}H_2O$), obtained from Fisher Scientific, at a target concentration of 140 mg L^{-1} and used in all experimentation. The pH of the lake water was maintained constant at pH 7 using propanesulfonic acid (MOPS), obtained from Sigma Aldrich. Modified E33 was synthesized by the deposition of either silver or manganese nanoparticles to the surface of E33. Silver modified E33 was synthesized using reagent grade silver nitrate ($AgNO_3$, obtained from Sigma Aldrich). Either sodium borohydride ($NaBH_4$, Sigma Aldrich) or tea powder (Red Label, India) were used as capping/reducing agents. Manganese modified E33 was synthesized using manganese acetate tetrahydrate ($Mn(CH_3COO)_2{\cdot}4H_2O$) obtained from Sigma Aldrich. The synthesized adsorbents consisted of either manganese or silver coated E33. The procedure for synthesis can be found in our previous study [24].

2.2. Sample characterization

The crystal structure of the adsorbents was determined by X-ray diffraction (XRD) analysis using a Panalytical (Expert) 2-theta diffractometer (Panalytical, Almelo, Netherlands) at a wavelength of 1.54 μm and at 2-theta range 2–90° under CuK_α radiation. The BET surface area, total pore volume, and porosity of the adsorbents were determined using a Tristar 3000 porosimeter analyzer (Micromeritics). Before analysis, the adsorbent samples were purged with nitrogen gas for 2 h and at 150 °C using the Micromeritics FlowPrep 060. For the characterization of the surface morphology of the adsorbents, an environmental scanning electron microscope (ESEM, Philips XL 30 ESEM-FEG), at an accelerating voltage of 30 kV was used. Physical properties of the adsorbent were also studied with transmission electron microscopy (TEM), where a FEI CM20 TEM operated at 200 kV was employed. To further characterize the physical properties of the surface-modified adsorbents, high-resolution TEM (HR-TEM, JEM-2010F, obtained from JEOL) was employed with a field emission gun at 200 kV. Prior to characterization, the adsorbents were prepared and dispersed by ultrasonication (2510R-DH, Bransonic) in 99.8% pure isopropyl alcohol (obtained from Pharmco-AAPER) for 30 min. Then, on a carbon-coated copper grid (LC325-Cu, EMS), a drop of the supernatant was fixed and dried at room temperature. The images obtained from the HR-TEM were analyzed using ImageJ, an image processing software (National Institutes of Health, Maryland, USA). Finally, as adsorption is highly dependent on the adsorbent surface charge, the point of zero charge for the adsorbents was evaluated using a SurPass Surface Electrokinetic Analyzer (Anton Paar, Australia). The zeta potential was measured at different pH values to determine the point of zero charge for the samples. To explore the stability of deposited nanoparticles onto the surface of E33, the concentration of Mn and Ag were determined after adsorption experiments using an Agilent Technologies Inc. (Santa Clara, CA) 7500cs Inductively Coupled Plasma-Mass Spectrometer (ICP-MS). The solutions were first filtered through 0.45 μm Whatman nylon syringe filters and solubilized using nitric acid.

2.3. Adsorption studies

Variable dose isotherm experiments were conducted to determine equilibrium adsorption parameters. Varying masses of adsorbent, ranging from 0.1 to 1.5 g, were placed in 125 mL Nalgene polypropylene bottles with 100 mL of the lake water solution. The solution was prepared by dissolving sodium phosphate monohydrate ($NaH_2PO_4{\cdot}H_2O$) in Winton Lake lake water (at a target concentration of 140 mg $PO_4^{3-}\ L^{-1}$). To this, 15 mM MOPS buffer was added and pH was adjusted to 7.0 with 1 N NaOH. The bottles were placed on a G10 Gyrotary shaker (New Brunswick

Scientific Co. Inc., USA) at 150 rpm for 3 weeks. After adsorbent saturation, samples were analyzed for phosphate concentration remaining in solution.

Adsorption kinetic experiments were conducted to determine various parameters of the adsorbents' kinetics of adsorption. Batch experiments were performed in 125 mL Nalgene polypropylene bottles under the following conditions: (i) adsorbent amount 5 g L^{-1}, (ii) temperature 21 °C, (iii) pH 7.0 ± 0.15, (iv) lake water solution target phosphate concentration 140 mg L^{-1}, and (v) mixing speed 150 rpm. A constant pH was maintained using 15 mM MOPS buffer and bottles were shaken on a G10 Gyrotary shaker for various times. Grab samples were collected at pre-determined times, filtered using a 0.45 μm Whatman nylon syringe filter, and analyzed for phosphate concentration remaining in solution with respect to time.

Fixed bed column tests were conducted in 80 cm high and 1.9 cm diameter Harvel plastic columns. A gram of adsorbent media was placed in the columns with sand and gravel above and below. A stainless steel sieve was placed at the bottom of the column to prevent washout. The lake water solution (at an initial target PO_4^{3-} concentration of 140 mg L^{-1}) was passed through the column at a flow rate of 2 mL min^{-1} and at room temperature using a Thermo Scientific™ FH100M Series Peristaltic pump. Similar to the kinetic and isotherm experiments, the pH of the solution was initially adjusted and buffered to remain constant. The column effluent solutions were collected and analyzed after various time periods for phosphate concentration. All isotherm, kinetic, and column experiments were conducted once and sample measurements were analyzed in triplicate and averaged.

2.4. Desorption studies

To evaluate the potential of phosphate recovery from the E33-based adsorbents, PO_4^{3-} desorption was investigated. As adsorption is strongly dependent on the solution pH, and low pH values promote enhanced adsorption, NaOH was used to increase the solution pH and promote PO_4^{3-} desorption. An initial adsorption isotherm experiment was conducted (same as previous) and the spent sorbents were used for the desorption study. After batch equilibration, the adsorbents were triple washed with DI water to remove any unadsorbed phosphate. The spent adsorbents were then placed in a 125 mL Nalgene bottles and 100 mL of desorption solution was added. Two different desorption solutions were used and compared; a 0.05 M NaOH solution and a 0.10 M NaOH solution. Samples were mixed (at 150 RPM) for the same time as isotherm experiments (3 weeks) at room temperature, and then filtered (0.45 μm PTFE) and analyzed for phosphate concentration in solution using the same colorimetric technique as previously described.

The phosphate concentration for all experiments was determined by a colorimetric measurement technique in which ammonium molybdate and potassium antimonyl tartrate react in an acidic solution with orthophosphate to form phosphomopydbic acid which can be reduced by ascorbic acid to form an intense blue color [25]. The absorbance due to the blue complex was monitored at 880 nm using a UV–Vis spectrophotometry (HACH model number DR 2700).

3. Results

3.1. Adsorbent characterization

3.1.1. Physical characteristics

Physical properties of E33 and modified E33 are summarized in Table 1. The BET surface areas (m^2 g^{-1}) of E33, E33/Mn, E33/AgI, and E33/AgII were found to be 140.4, 102.8, 124.6, and 142.0 m^2 g^{-1}, respectively. For unmodified E33, the company AdEdge Technologies [26] has reported the BET surface area to be from 120 to 200 m^2 g^{-1}, while Naeem et al. [27] and Trotz [28] reported the BET surface area of E33 to be 128.0 and 151.3 m^2 g^{-1}, respectively. The result reported herein for E33 is close to these values. For E33/Mn and E33/AgI, the BET surface area was reduced when compared to unmodified E33. Yet, as can be seen from the reduction in total pore volume (cm^3 g^{-1}) of these adsorbents, it is speculated that Mn and Ag nanoparticles adhered to the E33 surface at these pore sites, thus reducing porosity and total pore volume, as well as overall BET surface area. However, unlike E33/AgI, E33/AgII had a slight increase in BET surface area when compared to unmodified E33. Results from ICP–MS indicated that the concentration of leached Mn and Ag nanoparticles from the E33 surface were minimal and well below the EPA Secondary Drinking Water Regulations MCL (Table S2). This indicates the deposits are highly stable.

3.1.2. SEM characterization

SEM images of E33 and modified E33 are illustrated in Fig. 1. The surface morphology for the different adsorbents were determined to be similar to results previously reported [24]. Table S1 represents the weight percent of iron (Fe), phosphorus (P), manganese (Mn), and silver (Ag) on the adsorbents' surfaces; results were based on EDX analysis. While the adsorption capacity of E33 and E33/AgII were similar (as documented later in this report), the weight percent of phosphorus on the surface differed (see Table S1). This indicates that the PO_4^{3-} adsorption on E33/AgII may be dependent on intra-particle diffusion, in which the adsorbed species migrate into the pores of the adsorbent as opposed to remaining sorbed on the outer surface.

3.1.3. TEM and HR-TEM characterization

Fig. 2 represents TEM images at 220 k magnification of E33 and the modified adsorbents. Results were found to be similar to those previously reported, where E33, E33/AgI, and E33/AgII had rod-like structures and E33/Mn had formed oblong structures [24]. In order to investigate the crystal structure of the adsorbents in detail, HR-TEM was employed.

Fig. 3 shows HR-TEM images of E33 and surface modified E33 samples. The lattice spacing of 0.24 and 0.42 nm corresponding to (1 1 1) and (1 1 0) plane of goethite of iron oxide, respectively, was measured (see Fig. 3(a)) [29]. For the E33/AgI sample, the lattice spacing of 0.22 nm for (2 2 1) plane of goethite and 0.42 nm for (1 1 0) plane of goethite was measured [29]. The measured lattice spacing in the surface-modified samples with Ag was 0.20 and 0.24 nm corresponding to (2 0 0) and (1 1 1) plane of Ag, respectively, indicating the successful surface modification with Ag [30,31] even though no peaks corresponding to Ag were observed by XRD due to the surface-modification with low concentration of Ag (see Section 3.1.4). In the sample modified with Mn, the lattice spacing of 0.27 nm, which corresponds to (2 2 2) plane of Mn_2O_3 was measured [32–34].

3.1.4. XRD analysis

After the phosphate removal in the lake water samples, XRD analysis was conducted. The obtained peaks for all samples, shown in Fig. 4, (i.e., E33, E33/AgI, E33/AgII, and E33/Mn) were consistent with previous experiments which had shown that: (i) for E33, E33/AgI, and E33/AgII, corresponding peaks demonstrated typical XRD patterns for the iron oxide goethite (thus, the incorporation of Ag did not impact the phase transformation of goethite), (ii) peaks corresponding to Ag could not be detected, likely due to the concentration of silver used for modification (0.1 N $AgNO_3$), and (iii) for E33/Mn, peaks corresponding to hematite were detected, indicating a phase transformation [24].

Table 1
Structural characteristics of E33 and modified E33 before and after PO_4^{3-} adsorption.

Sample	Before adsorption			After adsorption		
	S_{BET} ($m^2\ g^{-1}$)	Total pore volume ($cm^3\ g^{-1}$)	Porosity (%)	S_{BET} ($m^2\ g^{-1}$)	Total pore volume ($cm^3\ g^{-1}$)	Porosity (%)
E33	140.4 ± 0.2	0.583	22.6	141.3 ± 0.5	0.582	22.5
E33/Mn	102.8 ± 0.4	0.441	18.1	99.9 ± 0.3	0.447	18.3
E33/AgI	124.6 ± 0.2	0.456	18.6	132.7 ± 0.4	0.552	21.6
E33/AgII	142.0 ± 0.3	0.553	21.7	139.7 ± 0.5	0.673	25.2

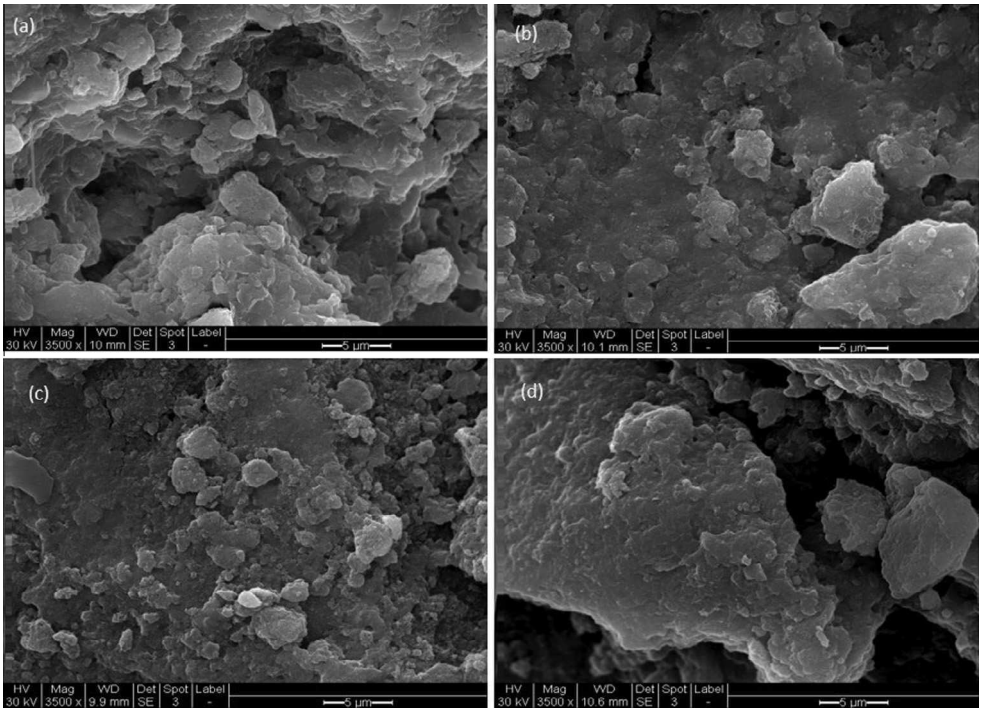

Fig. 1. SEM images of (a) E33, (b) E33/Mn, (c) E33/AgI, and (d) E33/AgII at 3.5 k magnification (all scale bars represent 5 μm).

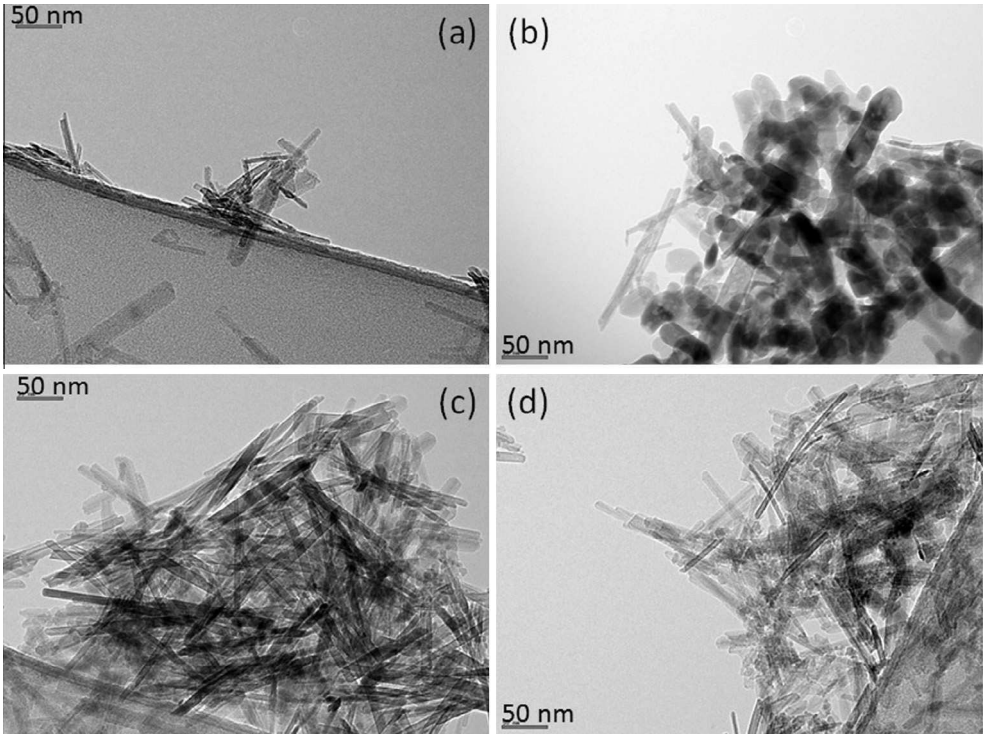

Fig. 2. TEM images of (a) E33, (b) E33/Mn, (c) E33/AgI, and (d) E33/AgII at 220 k magnification (all scale bars represent 50 nm).

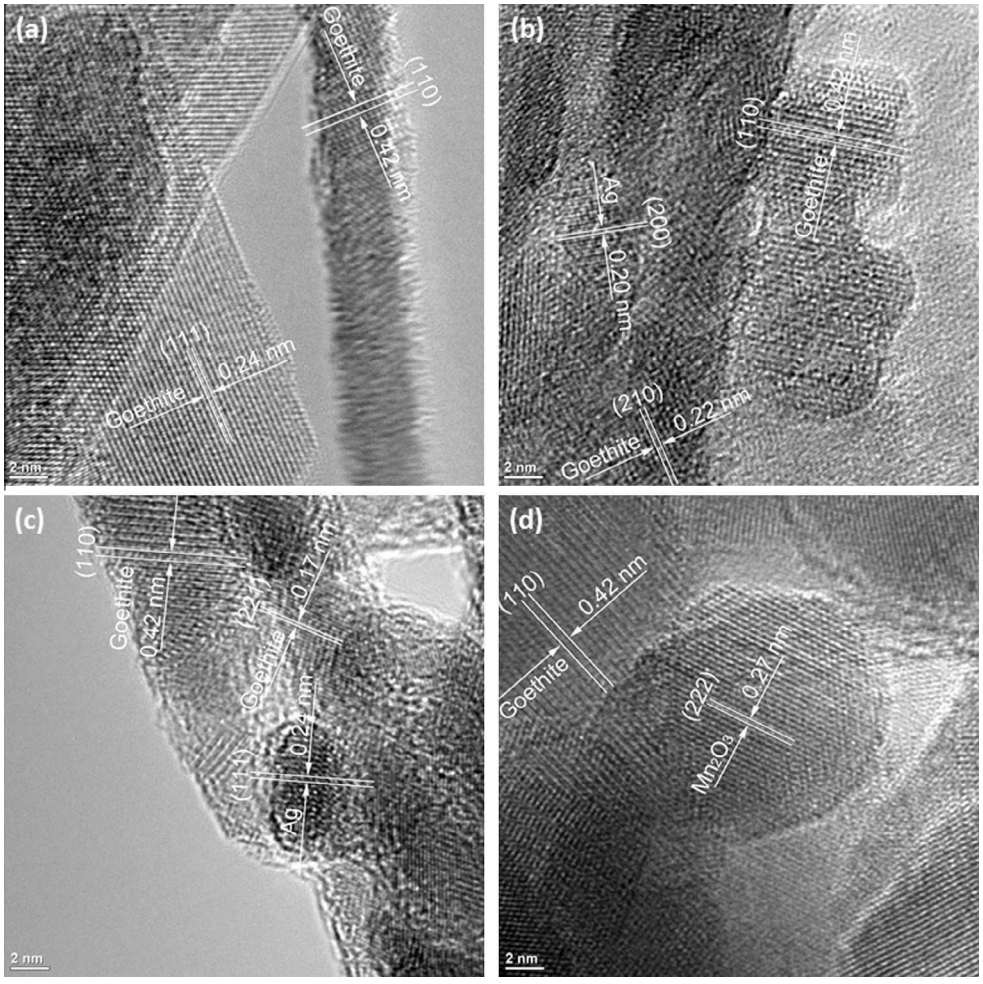

Fig. 3. HR-TEM images of (a) E33, (b) E33/Ag I, (c) E33/Ag II, and (d) E33/Mn used for phosphate removal in real lake water solutions (all scale bars represent 5 μm).

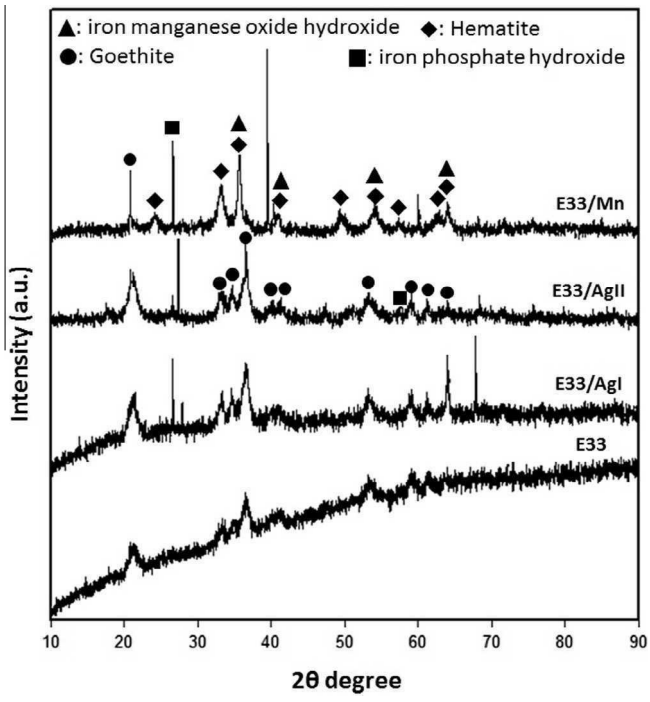

Fig. 4. XRD patterns of unmodified and modified E33 after using for phosphate removal in real lake water solution.

3.1.5. Point of zero charge

The point of zero charge (pH_{ZPC}) of the adsorbent was determined by measuring zeta potential as a function of pH. By interpolating the plot of zeta potential versus pH, results provided an estimate of pH_{ZPC}, which corresponds to the pH at which the zeta potential is equal to zero. The pH_{ZPC} is important in adsorption studies because, given the anionic character of phosphate, surface

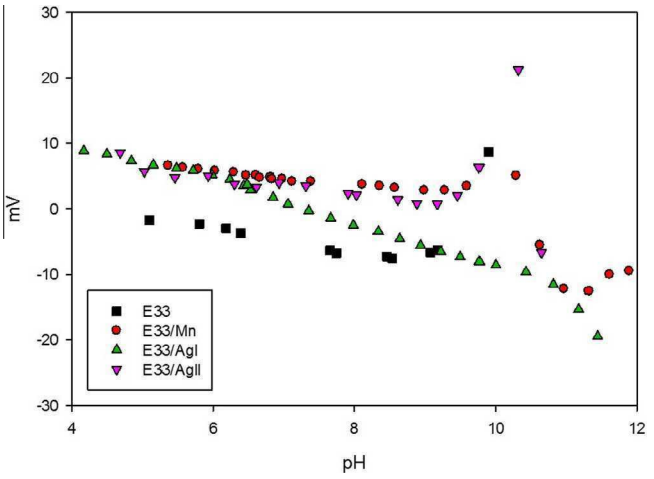

Fig. 5. Zeta potential versus pH of E33 and modified E33.

charge can play a significant role in terms of electrostatic interactions between the adsorbent and adsorbate. When the solution pH is above the pH_{ZPC}, for example, the surface charge on the iron oxide material is negative, thus promoting anion repulsion. However, below the pH_{ZPC}, the adsorbents will have a net positive charge, promoting electrostatic attraction of the negatively charged phosphate ion. Fig. 5 shows the zeta potential changes of unphosphated adsorbents with respect to pH. As pH increases from 4 to 12, the pH_{ZPC} of each adsorbent could be determined. For E33, the pH_{ZPC} was found to be 9.5. Reported pH_{ZPC} values were found to be slightly lower, ranging from 8.3 to 9.0 [26,35,36], yet for goethite (the major constituent of E33) reported pH_{ZPC} values were in the range of 7.2–9.7 [37–39]. The pH_{ZPC} for E33/Mn, E33/AgI, and E33/AgII were determined to be equal to 10.4, 7.3, and 10.5, respectively. These values illustrate the effective pH range for each adsorbent where the sorbent surface is positively charged.

3.2. Adsorption studies

3.2.1. Sorption isotherms

The specific relationship between the equilibrium adsorbate concentration in the bulk and the amount adsorbed at the surface can be revealed by sorption isotherms. The isotherm results for phosphate adsorption onto E33 and modified E33 at a constant temperature of 21 °C were analyzed using three common isotherms, the Langmuir, Freundlich, and Temkin isotherm models. The Langmuir adsorption equation is based on the following assumptions: (i) adsorption is limited to one monolayer, (ii) all surface sites are equivalent (i.e., free of defects), and (iii) adsorption to one site is independent of adjacent sites occupancy condition [40]. The Langmuir isotherm [41] is expressed as:

$$q_e = \frac{q_{max} K_L C_e}{1 + K_L C_e}$$

where q_e is the amount of adsorbate adsorbed per unit mass of adsorbent (mg g^{-1}), C_e is the amount of unadsorbed adsorbate concentration in solution at equilibrium (mg L^{-1}), q_{max} is the maximum amount of adsorbate per unit mass of adsorbent to form a complete monolayer on the surface (mg g^{-1}), and K_L is a constant related to the affinity of the binding sites (L mg^{-1}). In its linear form, the Langmuir equation can be described as:

$$\frac{C_e}{q_e} = \frac{1}{q_{max}} C_e + \frac{1}{K_L q_{max}}$$

A linear plot of specific adsorption against equilibrium concentration ((C_e q_e^{-1}) vs. C_e) as seen in Fig. 6 indicates that phosphate adsorption onto E33 and modified E33 obeys the Langmuir model. The Langmuir constants q_{max} and K_L, determined from the slope and intercept of the plot, are presented in Table 2. The calculated values for q_{max} indicate E33/AgII has a slightly higher capacity for phosphate sorption when compared to unmodified E33. This is consistent with the BET results in Table 1.

The dimensionless constant separation factor R_L [42] can be used to express essential characteristics of the Langmuir isotherm according to the following equation:

$$R_L = \frac{1}{1 + K_L C_0}$$

where C_0 is the initial adsorbate concentration (mg L^{-1}) and K_L is the Langmuir constant (L mg^{-1}). Values of R_L can indicate the favorability of adsorption; that is, for favorable adsorption, $0 < R_L < 1$; for unfavorable adsorption, $R_L > 1$; $R_L = 1$ for linear sorption; and for irreversible adsorption, $R_L = 0$ [42]. Values of R_L, documented in Table 2, were in the range of 0–1, suggesting favorable adsorption of phosphate onto E33 and modified E33.

The Freundlich isotherm [43], applicable for non-ideal adsorption on heterogeneous surfaces with multi-layer sorption, is expressed as:

$$q_e = K_F C_e^{1/n}$$

where K_F is related to the adsorption capacity of the adsorbent (mg g^{-1} (L $mg^{-1})^{1/n}$) and n indicates sorption favorability [44]. The K_F and n constants can be determined by the linearized form of the Freundlich equation:

$$\log q_e = \log K_F + \frac{1}{n} \log C_e$$

The linear plot of the Freundlich isotherm for phosphate adsorption onto E33 and modified E33 is shown in Fig. 7. The Freundlich constants K_F are related to the capacity of the adsorbent at a concentration of 1, depending on units. In this case it is 1 mg/L. The Freundlich constants are documented in Table 2. In this case, the Freundlich K_F is higher for the unmodified E33 as compared to the E33/AgII. However, the capacity of the E33/AgII is higher at other (lower) concentrations.

The effects of some indirect adsorbate/adsorbate interactions on adsorption isotherms was considered by Temkin and Pyzhev [45], who suggested that, due to these interactions, the heat of adsorption of all adsorbates in the layer would decrease linearly with respect to coverage. The Temkin isotherm is typically applied in the form:

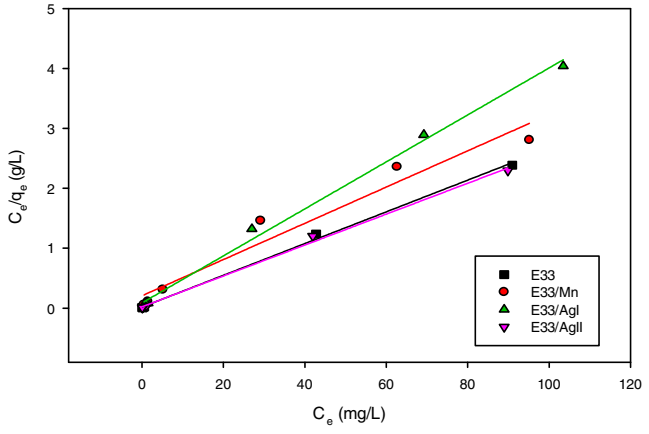

Fig. 6. Linear plot of Langmuir isotherm for phosphate sorption onto E33 and modified E33.

Table 2
Isotherm parameters.

Sorbent	Langmuir isotherm				Freundlich isotherm			Temkin isotherm		
	q_{max} (mg g^{-1})	K_L (L mg^{-1})	R_L	R^2	K_F (mg g^{-1}) (L $mg^{-1})^{1/n}$	$1/n$	R^2	A (mg L^{-1})	B	R^2
E33	37.74	1.359	0.006	0.998	18.92	0.17	0.758	311.7	3.8	0.891
E33/Mn	30.96	0.156	0.047	0.955	10.69	0.23	0.958	12.48	4.1	0.898
E33/AgI	25.52	0.440	0.017	0.996	12.22	0.16	0.846	113.6	2.7	0.920
E33/AgII	38.80	1.112	0.007	0.997	18.58	0.18	0.848	195.7	4.0	0.953

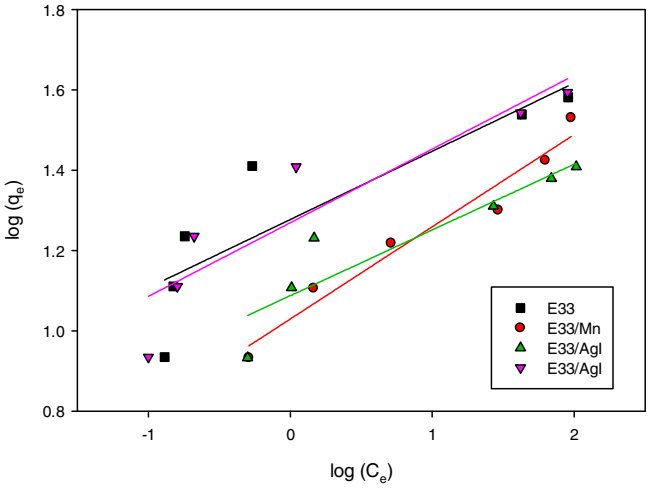

Fig. 7. Linear plot of Freundlich isotherm for phosphate sorption onto E33 and modified E33.

$$q_e = \left(\frac{RT}{b}\right)\ln(AC_e)$$

which can be linearized as:

$$q_e = B\ln A + B\ln C_e$$

where B is equal to $RT\,b^{-1}$, b (J mol^{-1}) is the Temkin constant related to the heat of sorption, A (L/g) is the Temkin isotherm constant, R (8.314 J mol^{-1} K^{-1}) is the universal gas constant, and T is the absolute temperature in Kelvin. Fig. 8 illustrates the linearized plot of the Temkin isotherm for phosphate adsorption onto E33 and modified E33 at constant temperature (21 °C) and the Temkin constants A and B were calculated using the slope and intercept of the plot and are tabulated in Table 2.

Based on the results obtained from isotherm experiments, it was determined that the adsorbents best followed the Langmuir model, which assumes a monolayer adsorption process. According to the model, E33/AgII and E33 had similar values of q_{max} (38.80 and 37.74 mg g^{-1}, respectively) while for E33/AgI and E33/Mn, q_{max} was equal to 25.52 and 30.96 mg g^{-1}, respectively. Previous studies explored the use of these adsorbents in phosphate spiked deionized water where a similar trend of q_{max} was observed [24]. However, in this previous study, a different initial phosphate

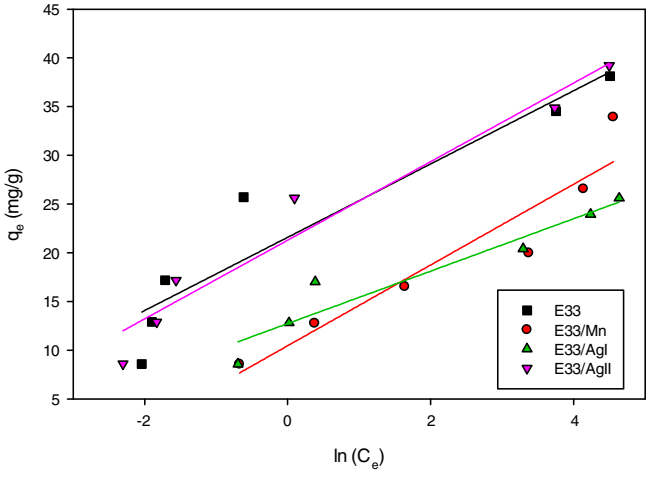

Fig. 8. Linear plot of Temkin isotherm for phosphate sorption onto E33 and modified E33.

Table 3
Effect of coexisting anions.

Concentration of anions (mM)			% PO_4^{3-} removal per adsorbent			
PO_4^{3-}	SO_4^{2-}	NO_3^-	E33	E33/Mn	E33/AgI	E33/AgII
2	0	0	99.93	97.06	99.30	99.93
2	2	0	99.84	95.99	99.08	99.85
2	0	2	97.72	96.84	93.98	99.57

concentration was used (i.e., 80 mg L^{-1}). Yet in comparing the maximum adsorption capacity with respect to initial phosphate concentration (i.e., q_{max}/C_0), the percentage of phosphate adsorbed for each system could be determined. For the DI-spiked solution, E33, E33/Mn, E33/AgI, and E33/AgII removed 31.1%, 22.6%, 24.9%, and 33.9%, respectively while for the lake water solution, removal percentages for the listed adsorbents were 27.0%, 22.1%, 18.2%, and 27.7%, respectively. The decreased phosphate removal percentages was believed to be due to competing species in the lake water. Therefore, the impact of co-existing species was investigated.

Surface and wastewaters generally contain common anions including sulfates (SO_4^{2-}) and nitrates (NO_3^-) in addition to PO_4^{3-}. These anions may interfere in the adsorption of phosphate onto E33 and E33-based adsorbents. Therefore, to evaluate the impact these competing species have on phosphate adsorption, isotherm experiments were conducted using equimolar concentrations of SO_4^{2-} or NO_3^- in the presence of PO_4^{3-}. The results in Table 3 show that no significant change in phosphate adsorption onto E33 after adding equimolar SO_4^{2-} or NO_3^-. This could be credited to specific binding of phosphate onto the adsorbent's specific active sites. Thus, the decreased phosphate adsorption using the lake water solution in comparison to previous studies [24] is believed to be caused by the presence of dissolved organic matter (DOM) in the lake water.

While enhanced phosphate adsorption was not observed for E33/Mn and E33/AgI, these sorbents may have other benefits. Silver-coated E33, for example, has shown to be a bacterial growth inhibitor based on previous experiments. When subjected to a bacterial growth inhibition assay, silver-modified E33 (E33/AgI and E33/AgII) had very high inhibition for *Staphylococcus aureus* and moderate inhibition for *Escherichia coli* [46]. As E33 is commonly used in column systems, issues related to biofouling can negatively impact the overall performance of the column system. Thus, the use of silver-modified E33 could alleviate these issues and result in a better performing system. Furthermore, E33 was originally designed for the remediation of arsenic. The Mn modified sample was found to successfully oxidize the more toxic and mobile As (III) to As(V) and simultaneously remove the As(V) from aqueous solutions [47]. Thus, this adsorbent, while more expensive than unmodified E33, could potentially be used (i.e., if a situation arises where a waterway is contaminated with both As(III) and PO_4^{3-}).

3.2.2. Kinetic studies

Batch experiments were conducted to explore the rate of phosphate adsorption onto E33 and modified E33 at pH 7.0, adsorbent dose of 5 g L^{-1}, and a target initial phosphate concentration of 140 mg L^{-1}. Processing of kinetic adsorption data can be conducted to understand adsorption dynamics in terms of the order of the rate constant. The pseudo-first-order and pseudo-second-order kinetic models were used to represent the kinetics of phosphate adsorption onto goethite-based materials. The pseudo-first-order model and pseudo-second-order model are expressed, respectively, as:

$$\log(q_e - q_t) = \log(q_e) - \frac{k_1 t}{2.303}$$

$$\frac{t}{q_t} = \frac{1}{k_2 q_e^2} + \frac{t}{q_e}$$

where q_t and q_e are the amount of phosphate adsorbed at time t and at equilibrium, respectively, k_1 (min^{-1}) is the rate constant of pseudo-first-order model adsorption, and k_2 ($g\ min^{-1}\ mg^{-1}$) is the rate constant of pseudo-second-order model adsorption. If pseudo-second-order kinetics is applicable, a plot of q_t versus t should provide a linear relationship and if pseudo-first-order kinetics is applicable, a plot of $\log(q_e - q_t)$ versus t should be linear. The calculated regression coefficients for the kinetic models are documented in Table 4. Figs. SI1 and 9 show the plots of the pseudo-first-order model and the pseudo-second-order model, respectively.

The regression coefficients of the pseudo-second-order model ($\geqslant$0.9980 for all adsorbents) revealed to be the best in representing phosphate adsorption onto E33 and modified E33, while the pseudo-first-order model regression coefficients were below 0.9 (except for E33, R^2 = 0.9796), indicating this model is not applicable. The pseudo-second-order model assumes a monolayer adsorption system (which agrees with isotherm results as the Langmuir model also assumes only monolayer adsorption), and that the mechanism of adsorption is determined by chemisorption, as opposed to physisorption. Chemisorption involves valence forces where the adsorbent and adsorbate share or exchange electrons. $k_2 q_e^2$ is considered as the initial adsorption rate ($mg\ g^{-1}\ min^{-1}$), which was determined for E33, E33/Mn, E33/AgI, and E33/AgII and documented in Table 4. Based on these results, while E33/Mn had the lowest adsorption capacity, it had the fastest initial rate of adsorption.

3.2.3. Intra-particle diffusion studies

The process of adsorption contains multiple steps including the transport of molecules from the aqueous phase to the solid surface and then, diffusion of solute molecules into the pores of the adsorbent. This process of pore diffusion is typically slow and thus, is rate determining. The rate q_t for intra-particle diffusion, provided by Webber and Morris [48] is:

$$q_t = k_p t^{1/2} + C$$

where q_t is the amount of phosphate adsorbed per unit mass of adsorbent ($mg\ g^{-1}$) at time t, C is related to the thickness of the boundary layer, and k_p ($mg\ g^{-1}\ min^{1/2}$) is the intra-particle diffusion rate constant. A plot of phosphate adsorbed versus the square root of time (q_t vs. $t^{1/2}$) presents a multi-linearity correlation, as seen in Fig. 10, indicating that two or more steps occurred during the adsorption process. The first phase (i.e. the steeper portion) represents external mass transfer or film diffusion. If the lines pass through the origin in this phase, then intra-particle diffusion is the rate-controlling process. However, values of C (as seen in Table 5) are larger than 0, and are proportional to the thickness of the boundary layer. Thus, it is postulated that a combination of intra-particle diffusion and film diffusion are rate-limiting. The second phase is the equilibrium stage where intra-particle diffusion begins to slow due to: (a) the pores for diffusion become smaller, (b) the electrostatic repulsion of the adsorbent surface was enhanced, and (c) the solute concentration in solution became very low.

It is surmised that E33 and modified E33 rapidly adsorbed phosphate onto its external surface, then phosphate was slowly transported by intra-particle diffusion into the particle and retained in the pores. The intra-particle rate constant, k_p, and C were calculated from the plots in Fig. 10 and the results were reported in Table 5.

While the lines for the plot of q_t vs. $t^{1/2}$ are near the origin, further data analysis can provide more insight into the rate-controlling step by using the following equation:

$$F = 1 - \frac{6}{\pi^2}\exp(-Bt)$$

where F is the fraction of adsorbed solute at different times and Bt is a function of F. F can be expressed by:

$$F = \frac{q_t}{q_e}$$

where q_t and q_e represent the amount of phosphate adsorbed at any time and at equilibrium or infinite time. Substituting the above equations, the expression becomes:

Table 4
Kinetic model parameters.

Adsorbent	Pseudo-second-order model			
	k_2 ($g\ mg^{-1}\ min^{-1}$)	q_e ($mg\ g^{-1}$)	R^2	$k_2 q_e^2$ ($mg\ g^{-1}\ min^{-1}$)
E33	0.0098	27.47	0.999	102.1
E33/Mn	0.0080	24.39	0.999	125.0
E33/AgI	0.0096	22.42	0.998	104.5
E33/AgII	0.0091	27.25	0.999	109.4

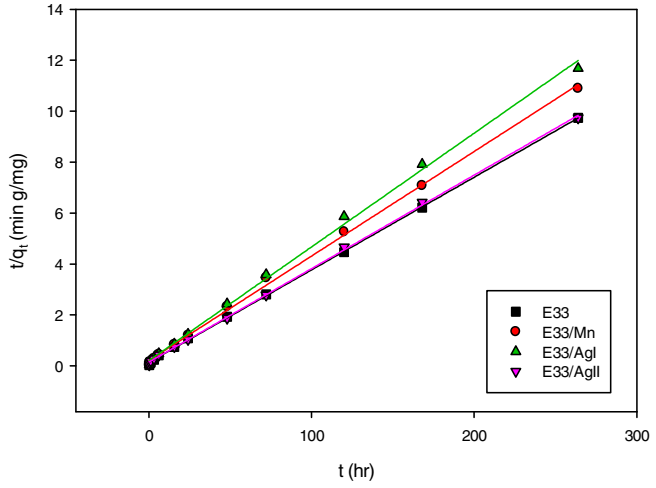

Fig. 9. Pseudo-second-order kinetic model for the adsorption of phosphate by E33 and modified E33.

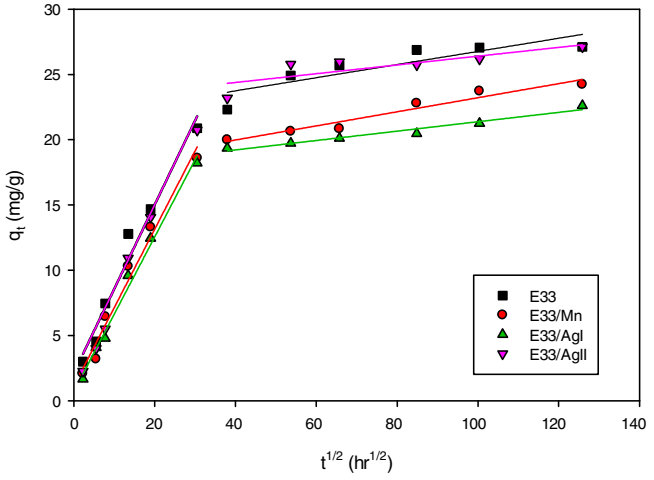

Fig. 10. Intra-particle diffusion kinetics for phosphate adsorption onto E33 and modified E33.

Table 5
Intra-particle diffusion parameters.

Adsorbent	$K_{p,1}$ (mg g^{-1} min$^{-1/2}$)	C (mg g^{-1})	R^2	$K_{p,2}$ (mg g^{-1} min$^{-1/2}$)	C (mg g^{-1})	R^2
E33	0.6441	2.153	0.971	0.0504	21.728	0.760
E33/Mn	0.6001	1.152	0.977	0.0539	17.826	0.948
E33/AgI	0.5906	0.751	0.990	0.0359	17.782	0.956
E33/AgII	0.6726	0.798	0.991	0.0336	23.040	0.680

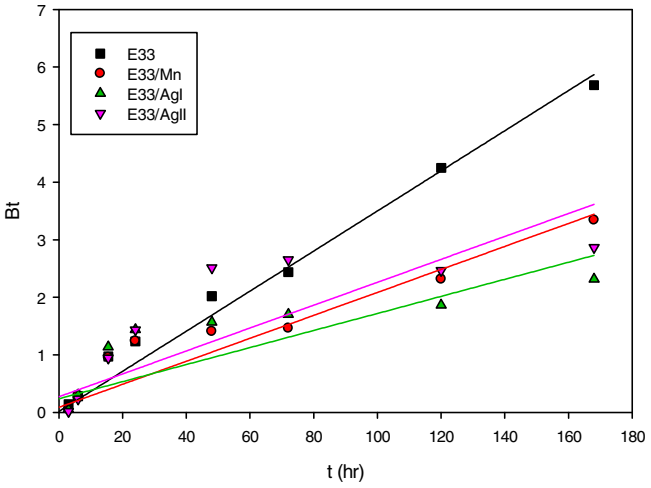

Fig. 11. Correlationship of Bt vs. t for phosphate adsorption onto E33 and modified E33.

$$Bt = -0.4977 - \ln\left(1 - \frac{q_t}{q_e}\right)$$

Therefore, the value of *Bt* can be calculated for each value of *F* and these values were plotted against time as shown in Fig. 11. Fig. 11 provides useful information for distinguishing between film diffusion and intra-particle diffusion rates of adsorption. If *Bt* vs. *t* is a straight line passing though the origin, then adsorption is governed by particle-diffusion. According to Fig. 11, it can be seen that the plots do go through the origin; yet correlation coefficients were low (0.9796, 0.8945, 0.7034, and 0.7145 for E33, E33/Mn, E33/AgI, and E33/AgII, respectively). Thus, a combination of intra-particle diffusion and film diffusion is believed to be the rate-limiting process for all four adsorbents.

3.2.4. Fixed-bed column test

To evaluate the practical application of E33 and modified E33 for the continuous removal of phosphate from solution, fixed bed column tests were conducted. Fig. 12 shows the breakthrough curve for each adsorbent. The breakthrough point for E33, E33/Mn, and E33/AgI were similar and occurred after about 0.75 h, yet for E33/AgII, breakthrough did not occur until about 1.5 h. This indicates that E33/AgII can operate for longer times when compared to the other adsorbents, which will reach saturation faster. E33/Mn had the lowest BET surface area of the investigated adsorbents and was the fastest adsorbent to reach saturation, followed by E33/AgI (which had the second lowest BET surface area) while E33 and E33/AgII reached saturation at nearly the same time. This indicates that the adsorbents' BET surface area plays an important role in breakthrough time of adsorption. It is expected that the anti-microbial aspects of the silver impregnated adsorbent (controlling biofouling) would not affect the results from this experiment because of the short time frame involved.

The process of phosphate adsorption in the columns can be explained by the Yoon–Nelson model, an adsorption model widely applied to single component systems, expressed as:

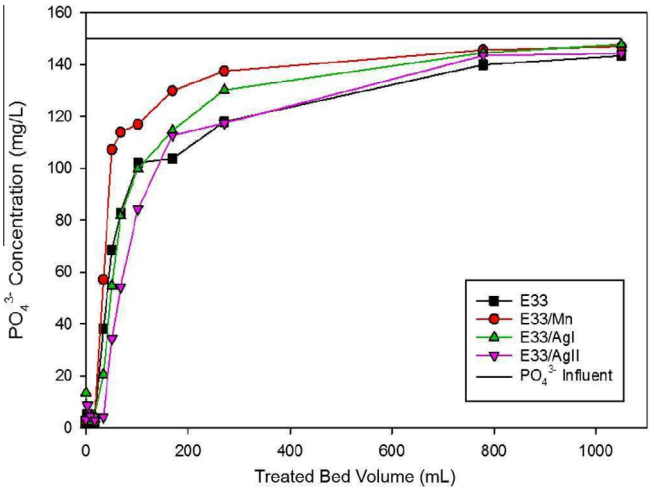

Fig. 12. Breakthrough curve of E33 and modified E33 for phosphate adsorption.

$$\ln\left(C_t/C_i - C_t\right) = K_{YN}(t - \tau)$$

where C_t and C_i are the phosphate concentrations (mg L^{-1}) at time (t) in the effluent and in the influent, respectively, t is the column service time (min), τ is the time required for 50% adsorbate breakthrough (min), and K_{YN} is the proportionality constant (min^{-1}). The Yoon–Nelson model parameters (K_{YN} and τ) were calculated by a plot of $\ln(C_t/C_i - C_t)$ vs. t using linear regression and presented in Table 6. The values of τ obtained from the model, as summarized in Table 6, are in good agreement with those obtained from the column experiment, confirming the applicability of the Yoon–Nelson model to this system.

3.3. Desorption studies

Phosphate desorption tests were conducted using spent adsorbents from isotherm experiments to evaluate the potential for PO_4^{3-} recovery. Desorbability is defined as the ratio of phosphate desorbed over the total phosphate adsorbed by the sorbents. Thus, PO_4^{3-} desorbability can indicate the degree of phosphate desorption from the different adsorbents. The impact of desorption solution was investigated by using two different solutions, a 0.05 M NaOH solution and a 0.10 M NaOH solution. The data in Table 7 show that PO_4^{3-} desorption using 0.05 M NaOH ranged from 30% to 67%, with E33/Mn having the highest desorption percent and E33/AgII the lowest. Also, an increase in the concentration NaOH corresponded to an increase in PO_4^{3-} desorption; where 60–80% of phosphate

Table 6
Yoon–Nelson model parameters obtained from breakthrough curve fitting.

Adsorbent	K_{YN} (min^{-1})	τ (min)	τ_{exp} (min)	R^2
E33	0.044	102.2	99.7	0.878
E33/Mn	0.057	84.6	70.2	0.883
E33/AgI	0.043	107.9	110.4	0.983
E33/AgII	0.033	139.3	158.1	0.840

Table 7
Desorbability of phosphate adsorbed by adsorbents.

Sample	Adsorbed PO_4^{3-} (mg g^{-1})	0.05 M NaOH		0.10 M NaOH	
		Desorbed PO_4^{3-} (mg g^{-1})	Desorption (%)	Desorbed PO_4^{3-} (mg g^{-1})	Desorption (%)
E33	11.02	3.55	32.2	6.68	60.6
E33/Mn	10.97	7.35	67.0	8.67	79.0
E33/AgI	11.01	4.47	43.1	7.10	64.4
E33/AgII	11.02	3.36	30.5	6.48	58.8

desorption was observed using 0.10 M NaOH. Interestingly, the sorbents with the highest PO_4^{3-} adsorption capacity (i.e. E33 and E33/AgII) had lower values of phosphate desorption when compared to the less sorptive samples (E33/Mn and E33/AgI). However, this is most likely due to the types of bonds formed; indicating that E33/Mn and E33/AgI formed weaker bonds with phosphate, making desorption easier for these sorbents.

4. Conclusion

Variable dose isotherm experiments, conducted to determine equilibrium adsorption parameters, indicated the Langmuir isotherm model was most applicable. The maximum adsorption capacity of single monolayer for E33, E33/Mn, E33/AgI, and E33/AgII, based on the Langmuir model, were 37.74, 30.96, 25.52, and 38.80 mg phosphate per gram of adsorbent, respectively. In comparison to previous studies using a DI-based system, results for adsorption capacity herein were reduced. This is likely due to the presence of DOM as neither sulfate nor nitrate proved to impact phosphate adsorption using these adsorbents. Batch experiments revealed the kinetics of adsorption followed the pseudo-second-order model (R^2 for all adsorbents $\geqslant$ 0.998).

Intra-particle diffusion studies indicated that phosphate adsorption onto all studied adsorbents occurred in two different steps; the first (film diffusion) occurred rapidly while the second (intra-particle diffusion) was slow (e.g. for E33/AgII k_{p1} = 0.6726 - mg g^{-1} $min^{-1/2}$ while k_{p2} = 0.0336 mg g^{-1} $min^{-1/2}$). Also, intra-particle diffusion studies showed that, for E33, intra-particle diffusion was the rate-limiting process, while for the three modified sorbents (E33/Mn, E33/AgI, and E33/AgII), the rate-limiting process was a combination of intra-particle diffusion and film diffusion. Finally, column experiments revealed that the time for breakthrough for E33/AgII was twice as long as for the other adsorbents (i.e., 1.5 h compared to 45 min), which implies E33/AgII has a greater phosphate adsorption capacity when compared to unmodified E33. Though isotherm experiments revealed that the maximum adsorption capacity of E33 and E33/AgII were very similar (37.7 vs. 38.8 mg g^{-1}), the multifunctionality of E33/AgII could provide improved adsorption characteristics.

Also, E33/Mn and E33/AgI had higher phosphate desorption as compared to E33 and E33/AgII. Though E33/Mn and E33/AgI had a decreased capacity for phosphate sorption, their desorption percentages were much higher than E33 and E33/AgII indicating their benefits of enhanced desorption for the recovery of phosphate.

Notice

The U.S. Environmental Protection Agency, through its Office of Research and Development, funded and managed, or partially funded and collaborated in, the research described herein. It has been subjected to the Agency's administrative review and has been approved for external publication. Any opinions expressed in this paper are those of the author(s) and do not necessarily reflect the views of the Agency, therefore, no official endorsement should be inferred. Any mention of trade names or commercial products does not constitute endorsement or recommendation for use.

Appendix A. Supplementary data

Supplementary data associated with this article can be found, in the online version, at http://dx.doi.org/10.1016/j.cej.2015.08.114.

References

[1] W.K. Dodds, W.W. Bouska, J.L. Eitzmann, T.J. Pilger, K.L. Pitts, A.J. Riley, J.T. Schloesser, D.J. Thornbrugh, Eutrophication of U.S. freshwaters: analysis of potential economic damages, Environ. Sci. Technol. 43 (2008) 12–19.
[2] T.C. Daniel, A.N. Sharpley, J.L. Lemunyon, Agricultural phosphate and eutrophication: a symposium overview, J. Environ. Qual. 27 (1998) 251–257.
[3] D.M. Anderson, P.M. Glibert, J.M. Burkholder, Harmful algal blooms and eutrophication: nutrient sources, composition, and consequences, Estuaries 25 (2002) 704–726.
[4] J.T. Sims, R.R. Simard, B.C. Joern, Phosphorus loss in agricultural drainage: historical perspective and current research, J. Environ. Qual. 27 (1998) 277–293.
[5] D.G. Devey, N. Harkness, The significance of man-made sources of phosphorus: detergents and sewage, Water Res. 7 (1973) 35–54.
[6] V. Smil, Phosphorus in the environment: natural flows and human interferences, Annu. Rev. Energy Environ. 25 (2000) 53–88.
[7] D.W. De Haas, M.C. Wentzel, G.A. Ekama, The use of simultaneous chemical precipitation in modified activated sludge systems exhibiting biological excess phosphate removal: part 1: literature review, Water SA 26 (2000) 439–452.
[8] A. Oehmen, R.J. Zeng, Z. Yuan, Modeling the aerobic metabolism of polyphosphate-accumulating organisms enriched with propionate as a carbon source, Water Environ. Res. 79 (2007) 2477–2486.
[9] T. Panswad, A. Doungchai, J. Anotai, Temperature effect on microbial community of enhanced biological phosphorus removal system, Water Res. 37 (2003) 409–415.
[10] I. Steen, Phosphorus availability in the 21st century: management of a non-renewable resource, Phosphorus Potassium 217 (1998) 25–31.
[11] R.P. Sheldon, Industrial minerals-with emphasis on phosphate rock, in: D.J. McLaren, B.J. Skinner (Eds.), Resources and World Development, John Wiley & Son Limited, New York, 1987, pp. 347–361.
[12] L. Li, R. Stanforth, Distinguishing adsorption and surface precipitation of phosphate on goethite (α-FeOOH), J. Colloid Interface Sci. 230 (2000) 12–21.
[13] R. Chitrakar, S. Tezuka, A. Sonoda, K. Sakane, K. Ooi, T. Hirotsu, Phosphate adsorption on synthetic goethite and akaganeite, J. Colloid Interface Sci. 298 (2006) 602–608.
[14] J.-Y. Bottero, A. Masion, Adsorbate structure at clay surfaces: surfactants at clay–water interface, in: P. Somasundaran (Ed.), Encyclopedia of Surface and Colloid Science, CRC Press, Boca Raton, Florida, 2006, pp. 140–148.
[15] U. Schwertmann, Solubility and dissolution of iron oxides, Plant Soil 130 (1991) 1–25.
[16] R.M. Cornell, U. Schwertmann, The Iron Oxides: Structure, Properties, Reactions, Occurrences and Uses, second ed., John Wiley & Sons, New York, 2006.
[17] W. Chesworth, Encyclopedia of Soil Science, Springer Science and Business Media, New York, 2008.
[18] M. Badruzzaman, P. Westerhoff, D.R. Knappe, Intraparticle diffusion and adsorption of arsenate onto granular ferric hydroxide (GFH), Water Res. 38 (2004) 4002–4012.
[19] M. Bissen, F.H. Frimmel, Arsenic – a review. Part II: oxidation of arsenic and its removal in water treatment, Acta Hydroch. Hydrob. 31 (2003) 97–107.
[20] T.B. Mlilo, L.R. Brunson, D.A. Sabatini, Arsenic and fluoride removal using simple materials, J. Environ. Eng. 136 (2009) 391–398.
[21] M. Kanematsu, T.M. Young, K. Fukushi, P.G. Green, J.L. Darby, Extended triple layer modeling of arsenate and phosphate adsorption on a goethite-based granular porous adsorbent, Environ. Sci. Technol. 44 (2010) 3388–3394.
[22] M. Kanematsu, T.M. Young, K. Fukushi, D.A. Sverjensky, P.G. Green, J.L. Darby, Quantification of the effects of organic and carbonate buffers on arsenate and phosphate adsorption on a goethite-based granular porous adsorbent, Environ. Sci. Technol. 45 (2011) 561–568.

[23] A. Sperlich, Phosphate adsorption onto granular ferric hydroxide (GFH) for wastewater reuse, Papierflieger (2010) 1–120.
[24] J. Lalley, C. Han, G.R. Mohan, D.D. Dionysiou, T.F. Speth, J. Garland, M.N. Nadagouda, Phosphate removal using modified Bayoxide® E33 adsorption media, Environ. Sci. Water Res. Technol. 1 (2015) 96–107.
[25] J. Murphy, J.P. Riley, A modified single solution method for the determination of phosphate in natural waters, Anal. Chim. Acta 27 (1962) 31–36.
[26] AdEdge Technologies Inc., <http://www.adedgetechnologies.com/index.html>.
[27] A. Naeem, P. Westerhoff, S. Mustafa, Vanadium removal by metal (hydro)oxide adsorbents, Water Res. 41 (2007) 1596–1602.
[28] M.A. Trotz, The feasibility of removing inorganic arsenic from landfill leachate via sorption to mineral oxide surfaces, Florida Center for Solid and Hazardous Waste-report, 2008, pp. 1–62.
[29] J. Akai, K. Akai, M. Ito, S. Nakano, Y. Maki, I. Sasagawa, Biologically induced iron ore at Gunma iron mine, Am. Mineral. 84 (1999) 171–182.
[30] C. Han, V. Likodimos, J.A. Khan, M.N. Nadagouda, J. Anderson, P. Falaras, P. Rosales-Lombardi, D.D. Dionysiou, UV–visible light-activated Ag-decorated, monodisperse TiO_2 aggregates for treatment of the pharmaceutical oxytetracycline, Environ. Sci. Pollut. Res. 21 (2014) 11781–11793.
[31] P. Asanithi, S. Chaiyakun, P. Limsuwan, Growth of silver nanoparticles by DC magnetron sputtering, J. Nanomater. 2012 (2012) 963609.
[32] J.N. Park, J.K. Shon, M. Jin, S.H. Hwang, G.O. Park, J.H. Boo, T.H. Han, J.M. Kim, Highly ordered mesoporous α-Mn_2O_3 for catalytic decomposition of H_2O_2 at low temperature, Chem. Lett. 39 (2010) 493–495.
[33] Q. Javed, F.P. Wang, M.Y. Rafique, A.M. Toufiq, Q.S. Li, H. Mahmood, W. Khan, Diameter-controlled synthesis of α-Mn_2O_3 nanorods and nanowires with enhanced surface morphology and optical properties, Nanotechnology 23 (2012) 415603.
[34] G. Yang, W. Yan, J. Wang, H. Yang, Fabrication and formation mechanism of Mn_2O_3 hollow nanofibers by single-spinneret electrospinning, CrystEngComm 16 (2014) 6907–6913.
[35] G.L. Amy, H.W. Chen, A. Dinzo, P. Brandhuber, Adsorbent Treatment Technologies for Arsenic Removal, American Water Works Association, 2005.
[36] P. Westerhoff, M. De Haan, A. Martindale, M. Badruzzaman, Arsenic adsorptive media technology selection strategies, Water Qual. Res. J. Canada 41 (2006) 171–184.
[37] S. Goldberg, H.S. Forster, C.L. Godfrey, Molybdenum adsorption on oxides, clay minerals, and soils, Soil Sci. Soc. Am. J. 60 (1996) 425–432.
[38] J. Antelo, M. Avena, S. Fiol, R. López, F. Arce, Effects of pH and ionic strength on the adsorption of phosphate and arsenate at the goethite–water interface, J. Colloid Interface Sci. 285 (2005) 476–486.
[39] W.A. Zeltner, M.A. Anderson, Surface charge development at the Goethite/aqueous solution interface: effect of CO_2 adsorption, Langmuir 4 (1988) 469–474.
[40] S.J. Allen, G. McKay, K.Y.H. Khader, Equilibrium adsorption isotherms for basic dyes onto lignite, J. Chem. Technol. Biotechnol. 45 (1989) 291–302.
[41] I. Langmuir, The adsorption of gases on plane surfaces of glass, mica and platinum, J. Am. Chem. Soc. 40 (1918) 1361–1403.
[42] K.R. Hall, L.C. Eagleton, A. Acrivos, T. Vermeulen, Pore- and solid-diffusion kinetics in fixed-bed adsorption under constant-pattern conditions, Ind. Eng. Chem. Fundam. 5 (1966) 212–223.
[43] H.M.F. Freundlich, Über die Adsorption in Lösungen, Z. Phys. Chem. 57 (1906) 385–470.
[44] M.M. Davila-Jimenez, M.P. Elizalde-Gonzalez, A.A. Pelaez-Cid, Adsorption interaction between natural adsorbents and textile dyes in aqueous solution, Colloids Surf. A 254 (2005) 107–114.
[45] M. Temkin, V. Pyzhev, Kinetics of ammonia synthesis on promoted iron catalysts, Acta Physicochim. USSR 12 (1940) 327–356.
[46] M.N. Nadagouda, C. Bennett-Stamper, C. White, D. Lytle, Multifunctional silver coated E-33/iron oxide water filters: Inhibition of biofilm growth and arsenic removal, RSC Adv. 2 (2012) 4198–4204.
[47] M.N. Nadagouda, D.A. Lytle, Microwave-assisted combustion synthesis of nano iron oxide/iron-coated activated carbon, anthracite, cellulose fiber, and silica, with arsenic adsorption studies, Nanotechnology 2011 (2011) 1–8.
[48] W.J. Weber, J.C. Morris, Preliminary appraisal of advanced waste treatment processes, Proc. Int. Conf. Adv. Water Pollut. Res. 2 (1963) 231–241.

Part 1

Phosphorus Treatment and Removal Technologies

Research category: 11. Industry and the Environment (IE)
Or
13. Sustainability and Innovation (SI)

Paper 1

J. Lalley, C. Han, G. R. Mohan, D. D. Dionysiou, T. F. Speth, J. Garland and M. N. Nadagouda "Phosphate removal using modified Bayoxide® E33 adsorption media" *Environmental Science: Water Research & Technology 2015, 1, 96-107* **(IF=4.195; immediacy index= not available; Citation half-life= not available; Citations=33)**

This article is part of the themed collection: Celebrating our 2018 prize and award winners

Paper 2

J. Lalley, C. Han, X. Li, D. D. Dionysiou, M. N. Nadagouda "Phosphate adsorption using modified iron oxide-based sorbents in lake water: kinetics, equilibrium, and column tests" *Chemical Engineering Journal* **2016**, *284*, *1386-1396* **(IF= 8.355; immediacy index=1.05; Citation half-life= 3.70; Citations=194)**

Paper 3

C. Han, J. Lalley, N. Iyanna, M. N. Nadagouda "Removal of phosphate using calcium and magnesium-modified iron-based adsorbents" *Materials Chemistry and Physics* **2017**, *198*, 115-124 **(IF= 2.781; immediacy index=0.42; Citation half-life=6.0; Citations=14)**

SI-1

E. Martin, J. Lalley, W. Wang, M. N. Nadagouda, E. Sahle-Demessie and S. Chae, "Phosphate recovery from water using cellulose enhanced magnesium carbonate pellets: Kinetics, isotherms, and desorption" *Chemical Engineering Journal* **2018**, *352*, 612-624 **(IF= 8.355; immediacy index=1.05; Citation half-life= 3.70; Citations=8)**

Supplemental Items (SI): Supplemental materials provided to journals along with the nominated publications

1. Explain how the nominated paper's represent research that is innovative and important in advancing the scientific knowledge or technology relevant to EPA's mission. It is, important to provide a clear and compelling explanation of the relevance, and impact of the research to EPA's mission (For example, the relevance of the research to one of EPA's strategic goals may be described) (Limit to 16,000 characters including spaces.)

Explanation:

The three nominated and one supporting paper define the results of the most comprehensive collection of contaminants of emerging concern to be eliminated in wastewater treatment. This work summarizes the utilization of cost-effective absorbents for the elimination of phosphate. Adsorption studies were performed to establish adsorption capacity, equilibrium adsorption capacity, and adsorption kinetics.

Phosphorus is an essential element for biological growth. However, its excessive existence as phosphate (PO_4^{3-}) contributes to eutrophication in lakes and rivers and leading to the generation of harmful algal bloom (HAB). Thus, effective treatment technologies for the removal of phosphate in water are essential to prevent deterioration of water quality and health risks to humans. Conventional techniques such as biological treatment, membrane separation, chemical precipitation, and adsorption of phosphorus have been reported. Adsorption using inexpensive materials is the most reasonable method for the treatment of phosphate.

The first nominated paper, Nadagouda et al. (2015), studied the adsorption of phosphate in batch and column mode using modified Bayoxide® E33 (E33) as cost-effective and efficient adsorbent. The adsorption kinetics was described by a fast-initial adsorption stage followed by a slow adsorption stage, complying with pseudo-second-order kinetics and Elovich kinetics. Sorption isotherms revealed that the equilibrium capacity of one of the modified adsorbents (E33/AgII) exceeded that of unmodified E33 likely due to its increased BET surface area. Column experiments confirmed the results for adsorption kinetics and equilibrium of phosphate sorption onto E33 and modified E33. This suggests that media modification has the potential to improve phosphate removal properties. This project was planned to fulfill direct USEPA needs. The research summarized in Nadagouda et al. (2015) is not only treated phosphate efficiently but also provides a platform for large-scale phosphate remediation in wastewater treatment.

In the second nominated paper, Nadagouda et al. (2016), the adsorption behavior of phosphate on Bayoxide ® E33 (E33) and three E33-modified sorbents were studied. E33-modified sorbents were synthesized by coating with manganese (E33/Mn) and silver (E33/AgI and E33/AgII) nanoparticles. This approach takes a complementary approach to eliminate phosphates in wastewater and further support in avoidance of the growth of HAB, which may pose a risk to human health from the production of cyanotoxins.

The third paper included as a nominee is Nadagouda et al. (2017). This paper discusses in detail the adsorption of phosphate using magnetic Calcium (Ca) and magnesium (Mg)-modified iron

oxide as adsorbents. Modification with Ca and Mg significantly improved the phosphate adsorption capacity of the magnetic iron oxide adsorbents. Batch adsorption experiments were carried out to gain insight on the materials' ability to remove phosphate from water supplies.

Non-magnetic Ca- and Mg-modified iron oxides demonstrated the highest phosphate adsorption capacity of about 17mg/g compared to that of control Fe_2O_3 (7.49 mg/g). Interestingly, magnetic Ca- and Mg-modified samples also showed a high capacity for phosphate removal, which ranged from 12.4 to 16.74 mg/g. Incorporated Ca or Mg into iron oxides enhance the binding of phosphate on iron oxide, resulting in the improvement of phosphate removal. Moreover, innovative magnetic samples have a high potential for easy separation processes to avoid filtration, which requires considerable energy and high costs during water treatment processes.

Finally, this work has been performed to fulfill one of the Agency's Core Missions, specifically Goal 1; Objective 1.2 Provide for Clean and Safe Water (U.S. EPA Strategic Plan; https://www.epa.gov/sites/production/files/2018-02/documents/fy18-22-strategic-plan-evidence-and-evaluations.pdf). These three papers and one supporting information on remediation of phosphate and nutrient recovery are providing the foundation and support to the potential future wastewater treatment technologies.

2A. The EPA Guidelines prohibit resubmission of publications nominated for STAA Awards in previous years. If multiple publications are submitted, provide a comprehensive explanation of the relationship and lengths between subject matter among the different nominated publications. For example, the discussion could describe how one publication builds on the results of a second publication. (Limit to 16,000 characters including spaces.) Enter n/a if blank.

Response:

None of the three nominated or one supporting paper included in this STAA package have been submitted for STAA in the past.

While the STAA guidelines limit a nomination to three publications, the four research articles that are part of this package either as nominees or supporting paper are unavoidably associated as they describe the utilization of different adsorbents for the same study. As discussed in answer to Question 1, the strength of this study is the breadth of investigations that were conducted in batch as well as column mode on the different cost-effective adsorbents for the treatment of phosphate.

Several efficient adsorbents such modified Bayoxide® E33 adsorbent (Nadagouda et al., 2015) utilized, modified iron oxide-based sorbents (Nadagouda et al., 2016), calcium and magnesium-modified iron-based adsorbents (Nadagouda et al., 2017), cellulose enhanced magnesium carbonate pellets as adsorbent (Nadagouda et al., 2018) were demonstrated for the treatment of phosphate. Working together, these four manuscripts increase the national scale understanding of contaminants of emerging concern in source waters as well as treated wastewater.

2B. List the previous 5 years of STAA nominations and associated publications for each EPA author. Categorize the list by author and include publication title, year, and award. (For example, John Smith, publication title(s), year(s), award(s).) (Limit to 16,000 characters including spaces.) Enter n/a if blank.

Response:

Mallikarjuna N. Nadagouda

1. Evaluating Sustainable Pathway to Furanics from Biomass via Heterogeneous Organo-Catalysis Green Chemistry
2. Sustainable Strategy Utilizing Biomass: Visible Light-Mediated Synthesis of g-Valerolactone. Published in ChemCatChem
3. Visible Light Mediated Upgrading of Biomass to Biofuel. Published in Green Chemistry

2017 Honorable Mention STAA

1. The Oxidative C-H activation of amines using protuberant lychee-like goethite. Published in Nature Climate Change
2. Photocatalytic C-H activation and oxidative esterification using Pd@g-C3N4. Published in Catalysis Today
3. Hydroxylation of benzene via C-H activation using bimetallic CuAg@g-C3N4. Published in ACS Sustainable Chemistry and Engineering

2019 Honorable Mention STAA

1. Conversion of spent carbon dioxide into value-added products
2. A sustainable approach to empower the bio-based future: upgrading biomass to value-added products

2019 Level III STTA

E. Sahle-Demessie

1. Inhibition of biofilm growth on polymer-MWCNTs composites and metal surfaces
2. Experimental and modeling studies of sorption of ceria nanoparticles on microbial biofilms

2019 Honorable Mention STAA

1. Degradation Studies of Multiwall Carbon Nanotube Reinforced Polypropylene During Environmental Aging
2. Evaluating weathering of food packaging polyethylene-nano- clay composites: Release of nanoparticles and their impacts
3. Effects of source and seasonal variations of natural organic matters on the fate and transport of CeO_2 nanoparticles in the environment

2019 Honorable Mention STAA

2C. Provide a description of how this nomination's publication(s) differ from previous (last 5 years) and current nominations by the author(s). (Limit to 16,000 characters including spaces.) Enter n/a if blank.

Response:
Nadagouda's (2017 Honorable Mention STAA, 2019 Honorable Mention STAA and 2019 Level III STTA) awards are not related to the currently nominated work. The previous works were related to sustainable chemistry and upgrading of biomass/waste. However, the present work is related to the remediation of phosphate using cost-effective and efficient adsorbents in wastewater treatment.

Sahle-Demessie's 2019 Honorable Mention STAA awards are not related to the currently nominated work. The previous works were related to multiwall carbon nanotubes. However, the present work is related to the remediation of phosphate using cost-effective and efficient adsorbents in wastewater treatment.

2D. Indicate whether previously submitted supplemental information is listed as supplemental information for the current nomination. (Limit to 16,000 characters including spaces.) Enter n/a if blank.

Response:

None of the supplemental information has been included in previous nominations.

2E. If any of the authors have submitted a concurrent nomination to another research category, provide sufficient justification to distinguish the difference between nominations. (Limit to 16,000 characters including spaces.) Enter n/a if blank.

Response:

There are no concurrent nominations by the authors on this nomination.

3A. Please provide substantial evidence for each of the following:
Provide evidence of recognition of the contribution from outside. (Limit to 16,000 characters including spaces.)

Response:

The first nominated paper (Nadagouda et al., 2015) has selected in "Themed collection: Celebrating our 2018 prize and award winners" by Royal Society of Chemistry "In celebration of the 2018 Royal Society of Chemistry prizes and awards". It has been published in the prestigious journal "Environmental Science: Water Research & Technology," which has an Impact Factor of

4.195 and has ranked#13 (h-index: 20) in the “Environmental Science” category. This research work has already been cited in 33 research articles (Google citation search).

In 2016, Prof. Zouboulis et al. from Greece has cited and highlighted our work (first paper, Nadagouda et al., 2015) in the main body on phosphate treatment in their research article “Kalaitzidou, K., Mitrakas, M., Raptopoulou, C., Tolkou, A., Palasantza, P.A. and Zouboulis, A., 2016. Pilot-scale phosphate recovery from secondary wastewater effluents. Environmental Processes, 3(1), pp.5-22”. Recently, Dr. Hong et al. from China has discussed and highlighted our adsorbent Bayoxide® E33 (first paper, Nadagouda et al., 2015) in their research article “Hong, X., Zhu, E., Ye, Z., Hui, K.S. and Hui, K.N., 2019. Enhanced phosphate removal under an electric field via multiple mechanisms on MgAl-LDHs/AC composite electrode. Journal of Electroanalytical Chemistry, 836, pp.16-23”

The second nominated paper (Nadagouda et al., 2016) has been published in the prestigious journal “Chemical Engineering Journal," which has an Impact Factor of 8.355 and has ranked#5 (h-index: 172 in the Environmental Science category. This research work has already been cited in 194 research articles (Google citation search).

In 2018, Prof. Kim from Department of Civil and Environmental Engineering, Hanyang University, Republic of Korea had cited and highlighted our work (Nadagouda et al., 2016) in the main body on phosphate in water and wastewater in his research article “Vikrant, K., Kim, K.H., Ok, Y.S., Tsang, D.C., Tsang, Y.F., Giri, B.S. and Singh, R.S., 2018. Engineered/designer biochar for the removal of phosphate in water and wastewater. Science of the total environment, 616, pp.1242-1260”. Dr. Yang et al. from Institute of Agricultural Resources and Environment, Jiangsu Academy of Agricultural Sciences, Nanjing, China has discussed and highlighted the efficiency of our adsorbent such as Fe3O4 NP in phosphate removal (Nadagouda et al., 2016) in their research article “He, S., Zhong, L., Duan, J., Feng, Y., Yang, B. and Yang, L., 2017. Bioremediation of wastewater by iron oxide-biochar nanocomposites loaded with photosynthetic bacteria. Frontiers in microbiology, 8, p.823.”

The third nominated paper (Nadagouda et al., 2017) has been published in the prestigious journal “Materials Chemistry and Physics," which has an Impact Factor of 2.781 and has ranked#121 (h-index: 132 in the Material Science category. This research work has already been cited in 14 research articles (Google citation search).

Recently, Dr. Kumar from Wetsus, European Centre Of Excellence for Sustainable Water Technology, The Netherlands has adopted and highlighted our research (Nadagouda et al., 2017) on phosphate adsorption using calcium ions capability to bind iron oxide surface in his two articles “1) Kumar, P.S., Ejerssa, W.W., Wegener, C.C., Korving, L., Dugulan, A.I., Temmink, H., van Loosdrecht, M.C. and Witkamp, G.J., 2018. Understanding and improving the reusability of phosphate adsorbents for wastewater effluent polishing. Water Research, 145, pp.365-374; 2) Kumar, P.S., Korving, L., van Loosdrecht, M.C. and Witkamp, G.J., 2019. Adsorption as a technology to achieve ultra-low concentrations of phosphate: Research gaps and economic analysis. Water Research 4, p.100029”.

3B Provide an explanation of the external peer review process used to evaluate the scientific merit of the nominated publication(s). (Limit to 16,000 characters including spaces.)

Response

All of the nominated and supporting manuscripts underwent anonymous peer review by the journal to which it was submitted for publication.

Environmental Science
Water Research & Technology

PAPER

Cite this: *Environ. Sci.: Water Res. Technol.*, 2015, **1**, 96

Phosphate removal using modified Bayoxide® E33 adsorption media†‡

Jacob Lalley,[ab] Changseok Han,[ac] Gayathri Ram Mohan,[c] Dionysios D. Dionysiou,[b] Thomas F. Speth,[a] Jay Garland[d] and Mallikarjuna N. Nadagouda*[a]

Received 23rd July 2014,
Accepted 19th September 2014

DOI: 10.1039/c4ew00020j

rsc.li/es-water

The adsorption of phosphate onto modified Bayoxide® E33 (E33) and underlying mechanisms were comparatively investigated by batch kinetics, sorption isotherms, rapid small-scale column tests, and material characterization. Synthesis of modified E33 was conducted by the addition of manganese and silver nanoparticles on the surface of the goethite (α-FeOOH)-based E33. Upon successful adsorbent synthesis, the materials were characterized using SEM, TEM, XRD, EDX, HR-TEM, and BET surface area analysis. The adsorption kinetics is described by a fast initial adsorption stage followed by a slow adsorption stage, complying with pseudo second-order kinetics and Elovich kinetics. Sorption isotherms revealed that the equilibrium capacity of one of the modified adsorbents (E33/AgII) exceeded that of unmodified E33 likely due to its increased BET surface area. Column experiments confirmed the results for adsorption kinetics and equilibrium of phosphate sorption onto E33 and modified E33. This suggests that media modification has the potential to improve phosphate removal properties.

Water impact

As a limiting nutrient in the environment, increased loads of phosphates can result in accelerated eutrophication or excessive growth of algae, leading to increased treatment costs and reduced recreational value. Therefore, phosphate removal from wastewater has become an area of emerging concern. In this study, the removal of phosphate using newly surface-modified Bayoxide® E33 was thoroughly examined. Underlying mechanisms were comparatively investigated by batch kinetics, sorption isotherms, rapid small-scale column tests, and material characterization. The adsorption kinetics is well described by a fast initial adsorption stage followed by a slow adsorption stage, complying with pseudo second-order kinetics and Elovich kinetics. The results showed potential for practical applications of the modified material for phosphate removal.

1. Introduction

Phosphates are one of the common mineral nutrients found in wastewaters.[1] Both natural and anthropogenic sources such as agricultural runoffs[2,3] and urban[4] and industrial wastes[5,6] act as major sources of phosphate in surface water bodies. In aquatic systems, phosphates occur in various forms, particulate, organically bound, or dissolved,[7] of which orthophosphates (PO_4^{3-}) are found to be predominant.[8] While it is an essential nutrient, higher concentrations of phosphate in water bodies can be detrimental to aquatic life, human health, and the environment.[9] As a limiting nutrient in the environment, increased loads of phosphates can result in accelerated eutrophication or excessive growth of algae, leading to increased treatment costs and reduced recreational value.[10] Therefore, phosphate removal from wastewaters has become an area of emerging concern.

Conventional methods for phosphate removal include physical, chemical, and biological processes; of which, chemical precipitation[11] and enhanced biological phosphate

[a] *The U.S. Environmental Protection Agency, ORD, NRMRL, WSWRD, WQMB, 26 W. Martin Luther King Jr. Drive, Cincinnati, OH, 45268, USA. E-mail: Nadagouda.mallikarjuna@epa.gov; Fax: +1 (513) 569 7172; Tel: +1 (513) 569 7232*
[b] *Environmental Engineering and Science Program, Department of Biomedical, Chemical and Environmental Engineering (DBCEE), University of Cincinnati, OH, 45221, USA*
[c] *Pegasus Technical Services Inc., 46 E Hollister St, Cincinnati, OH 45219, USA*
[d] *The U.S. Environmental Protection Agency, ORD, NERL, MCEARD, 26 W. Martin Luther King Jr. Drive, Cincinnati, OH, 45268, USA*

† The U.S. Environmental Protection Agency, through its Office of Research and Development, funded and managed, or partially funded and collaborated in, the research described herein. It has been subjected to the Agency's administrative review and has been approved for external publication. Any opinions expressed in this paper are those of the author(s) and do not necessarily reflect the views of the Agency, therefore, no official endorsement should be inferred. Any mention of trade names or commercial products does not constitute endorsement or recommendation for use.

‡ Electronic supplementary information (ESI) available. See DOI: 10.1039/c4ew00020j

This journal is © The Royal Society of Chemistry 2015

removal (EBPR)[12,13] are commonly used. However, due to a number of factors including cost, sludge production, required energy, and issues of reliability and stability,[14,15] other methods are currently being explored. The quickest, easiest, and most economically known method for the removal of phosphate ions is adsorption.[16] To date, a number of different adsorbents have been investigated for phosphate removal including metal oxides,[16–22] red mud,[23–25] steel slag,[26–28] and fly ash.[29,30] Table 1 shows different phosphate adsorbents and their reported adsorption capacity at different parameters. Adsorption also has the benefits of applicability at low concentrations, little to no sludge production, and potential for both batch and continuous processes, and the potential for adsorbent regeneration that could reduce wastes and costs.[31]

One such highly adsorptive material for phosphate removal is the iron oxide goethite (iron(III) oxide-hydroxide).[32–35] The affinity of phosphate adsorption on iron(III) oxide-hydroxide is dependent on phosphate's complexing capacity by ligand exchange as well as electrostatic interactions with the surface.[36] This process involves replacement of a phosphate ion with one or more surface hydroxyl groups, releasing surface structural OH_2 and/or OH^- into the bulk solution,[37] in which stoichiometric changes in the amount of phosphate adsorbed and OH^- released can provide clues on the type of adsorption mechanism.[38] Iron(III) oxide-hydroxide adsorption initially occurs rapidly, followed by a slow stage,[39] attributed to micro/mesopore diffusion[40] or particle aggregation,[41] which is generally dependent on the crystallinity of samples.[42] Phosphate adsorption onto iron oxides involves a ligand exchange mechanism,[43] yet the exact mode of phosphate interaction is not known. IR studies revealed that each adsorbed phosphate ion replaces two, singly coordinated OH surface groups, indicating a bridging, binuclear complex.[44,45] However, other studies have suggested that monodentate surface complexes could exist at low adsorbate concentrations.[46] Using a combination of surface complexes to model adsorption on iron oxides, Geelhoed *et al.*[47] concluded that the bidentate surface complex was most abundant at low to intermediate values of pH.

Goethite (α-FeOOH) is one of the most thermodynamically stable forms of iron oxide and thus is available in abundant quantities.[48] Due to its affinity for ion adsorption, AdEdge Technologies Inc. (USA) has produced Bayoxide® E33 media (E33), a commercially available goethite-based adsorbent for environmental remediation. Although originally designed for arsenic removal,[49,50] E33 has been shown to adsorb a range of ions including phosphates. While several studies have shown that E33 adsorption is an effective technique for phosphate removal,[51–53] surface modifications of E33 can enhance overall adsorption. As adsorption is a surface-based phenomenon dependent on electrostatic interactions and covalent bonding, the addition of di- and tri-valent metals to the surface of E33 should correlate with increased phosphate adsorption.

In this study, the surface of E33 media was modified with manganese and silver. For the removal of phosphate, the adsorptive properties of modified E33 were investigated and then compared to those of the unmodified E33.

2. Experimental

2.1 Materials

The E33 used to study PO_4^{3-} removal was obtained from AdEdge Technologies Inc. (USA). Analytical grade sodium phosphate monohydrate ($NaH_2PO_4{\cdot}(H_2O)$) was obtained from Fisher Scientific and used as a stock solution. A stock phosphate solution at a concentration of ≈80 mg L^{-1} was prepared by dissolving 1 g of $NaH_2PO_4{\cdot}(H_2O)$ in 10 L of Milli-Q water. The pH of the stock phosphate solution was

Table 1 Comparison of phosphate adsorption capacity of different adsorbents

Adsorbent	Capacity (PO_4^{3-} mg g^{-1})	pH	Temperature (°C)	Reference
Metal oxides synthesized from manganese ore tailing	26.3	6.0	25	16
Titanium ion doped ordered mesoporous silica	4.5	7.0	21	17
Magnetic iron oxide nanoparticles	3.7	3.0	15	18
Zinc–aluminum layered double hydroxides	30.0	9.0	20	19
Iron oxide-coated crushed brick	1.8	5.0	20	20
Lithium-intercalated gibbsite	0.3	4.5	25	21
Fe-loaded biomass char	35.4	3.0	25	22
HCl-treated red mud	0.6	5.5	40	23
Red mud granular adsorbents	9.8	9.2	37	24
Red mud	0.5	4.0	25	25
Modified steel slag	11.1	8.0	25	26
Steel slag	5.3	5.5	25	27
Electric arc furnace (EAF) steel slag	2.2	6.0	23	28
Iron oxide/fly ash	27.4	3.0	25	29
Fly ash	18.9	3.0	25	29
Nanshi-modified fly ash	40.7	4.0	21	30
Nanshi-modified zeolite	47.2	4.0	21	30
E33	26.8	7.0	21	This study
E33/Mn	17.8	7.0	21	This study
E33/AgI	19.3	7.0	21	This study
E33/AgII	28.0	7.0	21	This study

maintained constant at 6, 7 and 9, using 2-(*N*-morpholino) ethanesulfonic acid (MES), 3-(*N*-morpholino) propanesulfonic acid (MOPS), and *N*-tris (hydroxymethyl) methyl-3-aminopropanesulfonic acid (TAPS), respectively, all obtained from Sigma Aldrich. Reagent grade silver nitrate ($AgNO_3$), sodium borohydride ($NaBH_4$), and manganese acetate tetrahydrate ($Mn(CH_3COO)_2{\cdot}4H_2O$) were obtained from Sigma Aldrich and used as received.

2.2 Synthesis of modified E33

For the synthesis of silver-modified E33, an initial mixture of 10 g of E33 and 35 mL of Milli-Q water was prepared in a 100 mL conical flask. Then, 2 mL of 0.1 N $AgNO_3$ was added to the flask and shaken by hand for 2 min to ensure thorough mixing. To this initial mixture, two different adsorbents were prepared, one using $NaBH_4$ and the other using tea extract, denoted respectively as (E33/AgI)[50] and (E33/AgII)[50]. For E33/AgI, 10 mL of 0.1 N $NaBH_4$ was added to the initial mixture, hand shaken for 2 min and allowed to react overnight at room temperature. For E33/AgII, 2 g of tea powder (Red Label, India) was boiled in 100 mL of Milli-Q water and the solution was filtered through a 0.20 μm PTFE filter. Then, 20 mL of the tea extract solution was added to the initial mixture, shaken by hand for 2 min, and allowed to react overnight at room temperature. Following the overnight incubation, samples were twice washed with Milli-Q water and air-dried at room temperature prior to characterization and analysis.[50]

For the synthesis of manganese-coated E33 (E33/Mn), 50 g of E33 was mixed with 20 mL of Milli-Q water in a china crucible. Then, 10 g of manganese acetate tetrahydrate ($Mn(CH_3COO)_2{\cdot}4H_2O$, Aldrich product) was added to the crucible and the solution was hand-mixed with a spatula for 5 min to ensure proper mixing. After mixing was complete, the sample was heated at 310 °C for 1 h in a china crucible and then stored for later analysis and characterization.

2.3 Sample characterization

X-ray diffraction (XRD) analysis was performed using a PANalytical (X'pert) 2-theta diffractometer (PANalytical, Almelo, the Netherlands) in the 2-theta range of 2–90° under CuK_α radiation and a wavelength of 1.54 μm in order to determine the adsorbent's crystal structure. An environmental scanning electron microscope (ESEM, model Philips XL 30 ESEM-FEG) at an accelerating voltage of 30 kV was used to characterize the surface morphology of the adsorbents. An energy-dispersive X-ray spectrophotometer (EDX) installed in the ESEM was used to detect the distribution of elemental phosphorus as well as the percent of phosphate adsorbed. For transmission electron microscopy (TEM), a FEI CM20 TEM operated at 200 kV was employed. High-resolution TEM (HR-TEM, JEM-2010F (JEOL)) with a field emission gun at 200 kV was also employed for the characterization of the prepared surface-modified adsorbents. Free software (ImageJ, National Institutes of Health, USA) was used for HR-TEM image analysis. Adsorbent samples were prepared by ultrasonication (2510R-DH Bransonic) for 20 min in isopropyl alcohol (99.8%, Pharmco), and then a drop of the supernatant was fixed on a carbon-coated copper grid (FCF400-Cu, EMS) and dried at room temperature. A Tristar 3000 porosimeter analyzer (Micromeritics) was used to determine the adsorbent's BET surface area, total pore volume, and porosity. Samples were first purged with nitrogen gas at 150 °C for 2 h using Micromeritics FlowPrep 060.

2.4 Adsorption studies

To determine various adsorption parameters of the surface-modified adsorbent, both batch and flow-through column experiments were employed. Batch adsorption kinetic studies were carried out to determine the amount of phosphate adsorbed with respect to time. Experiments were conducted in 250 mL Nalgene polypropylene bottles given the following conditions: (i) temperature: 20–25 °C, (ii) adsorbent amount: 5 g L^{-1}, (iii) pH: 6, 7, and 9, (iv) influent phosphate concentration: ≈80 mg L^{-1}. A constant pH in the batch reactor was maintained using 5 mM MES, MOPS, and TAPS buffer (for pH 6, 7, and 9, respectively) and was continually mixed at a constant speed of 150 rpm (G10 Gyrotary shaker, New Brunswick Scientific Co. Inc., USA). At higher mixing speed, E33 samples started breaking down. Grab samples were collected at various predetermined intervals (*e.g.* after 5, 10, 15, 30, 45 min and 1, 2, 3, 4, 5 h) and filtered using a Whatman 0.45 μm nylon syringe filter. Experiments were conducted in duplicate while each grab sample was a single measurement.

Rapid small scale column tests were performed in Harvel plastic columns 80 cm high and 1.9 cm in diameter. One gram of adsorbent media with a fixed height of 1.27 cm, with sand and gravel above and below, was placed in the columns with a stainless steel sieve at the bottom end of the column to prevent washout. Using a Thermo Scientific™ FH100M Series Peristaltic pump, the phosphate solution was passed through the column at a rate of 2 mL min^{-1} at room temperature. Similar to the kinetic study, solution pH was adjusted initially and buffered to remain constant using 5 mM MES, MOPS, and TAPS. The column effluent samples were collected and analyzed for phosphate concentration at various time periods and run until complete breakthrough (*i.e.* saturation). Flow through experiments were conducted in duplicate while each grab sample was a single measurement.

Variable-dose isotherm adsorption studies were conducted. Different amounts of adsorbent (ranging from 100 to 600 mg) were placed in 250 mL Nalgene polypropylene bottles. One hundred milliliters of the same 80 mg L^{-1} phosphate solution was then added to the bottles. Buffers (5 mM MES, MOPS, and TAPS) were used to maintain constant pH conditions to evaluate adsorption characteristics at varying pH values. The sealed bottles were placed on a tabletop rotating shaker and shaken at a constant 150 rpm at 21 ± 1 °C for 2 weeks, which preliminary test results revealed was sufficient time for

 This journal is © The Royal Society of Chemistry 2015

equilibrium to be reached. The phosphate concentration in all experiments was analyzed by a colorimetric measurement technique in which ammonium molybdate and potassium antimonyl tartrate react in an acidic solution with orthophosphate to form phosphomopydbic acid which can be reduced by ascorbic acid to form an intense blue color.[54] The absorbance due to the blue complex was monitored at 880 nm using UV-Vis spectrophotometry (Hach model number DR 2700). Experiments were conducted once and samples were measured in triplicate and averaged.

3. Results

3.1 Adsorbent characterization

Table 2 summarizes the physical characteristics of E33 and modified E33 samples. The BET surface area of E33 exceeded that of the modified samples except for E33/AgII, which had a slightly higher BET surface area (142.0 m^2 g^{-1} compared to 140.4 m^2 g^{-1}). The manganese-coated E33 had a significantly reduced BET surface area (102.8 m^2 g^{-1}) compared to E33. This suggests that at least a portion of the manganese oxide nanoparticles occupied the pore structure of E33. This table also summarizes structural characteristics of the adsorbent prior to and after phosphate adsorption. Fig. S1 (a) and (b)‡ show N2 adsorption and desorption isotherms for all samples before and after using for phosphate removal. They present typical Type IV adsorption isotherms, indicating the formation of mesoporous materials.[55]

3.1.1 SEM characterization. Fig. 1 illustrates SEM images of E33 and modified E33. Fig. 1(a) and (b) represent unmodified E33 at 12k and 50k magnification, respectively. Based on Fig. 1(b), it could be determined that the particles are spherical and, on average, 75 nm in diameter. Fig. 1(c) and (d) illustrate the surface morphology of E33/Mn at 12k and 50k magnification, respectively. As can be seen in Fig. 1(d), the spherical particles range in size from 50 to 200 nm in diameter. Also, several particle aggregates 500 nm in diameter were present. Fig. 1(e) and (f) illustrate SEM images of E33/AgI. Fig. 1(f) (at 50k magnification) reveals that the average particle size was 75 nm which was similar to the unmodified E33. Fig. 1(e) (at 12k magnification) reveals a smoother surface when compared to the other adsorbents. The surface morphology for E33/AgII is illustrated in Fig. 1(g) and (h), at 12k and 50k magnification, respectively. The average particle size was determined to be 100 nm, and all particles were spherical in shape. The images for EDX mapping show adsorbed phosphate (yellow) on the surface of E33 and E33/AgII. More phosphate was detected on the surface of E33/AgII compared to that of unmodified E33 (please see Fig. S2 in the ESI‡).

3.1.2 XRD analysis. Fig. 2 shows the XRD patterns of all samples used for phosphate removal. The peaks for all samples were defined using reference codes in XRD analysis software corresponding to different materials such as 00-03-0249, 00-001-1053, 00-014-0557, and 00-036-0045 for goethite, hematite, iron manganese oxide hydroxide, and iron phosphate hydroxide, respectively. The XRD patterns of all samples are shown in Fig. S3(a)–(d).‡ The well-defined peaks demonstrated typical XRD patterns of goethite of iron oxides in E33 and Ag-modified E33 in Fig. 2(a), indicating that Ag modification did not affect the phase transformation of goethite. Moreover, the pH of solution for phosphate removal did not affect the goethite phase of iron oxide (see Fig. S3(a), (c), and (d)‡). However, the peaks, which correspond to Ag, were not detected due to low concentration of Ag (see Fig. 2(a)). For Mn-modified E33, the peaks corresponding to hematite of iron oxide were observed, indicating phase transformation from goethite to hematite during the synthesis process. Well-defined peaks corresponding to iron manganese hydroxide were observed, indicating that the surface of E33 was successfully modified with manganese (see Fig. 2(a)). Fig. 2(b) shows XRD patterns of E33 and surface-modified E33 after completion of the phosphate removal studies. The peaks corresponding to iron phosphate hydroxide in E33 and all surface-modified E33 were also observed, which indicates that the media complexed with the dissolved phosphate in the influent water.

3.1.3 TEM and HR-TEM characterization. Fig. 3 represents TEM images at 100k magnification of E33 and the modified adsorbents. The silver-modified adsorbents (E33/AgI and E33/AgII), in Fig. 3(c) and (d), had a rod-like shape, similar to the unmodified E33. These particles were determined to be, on average, 150 nm long and 20 nm across. It seems that the effect of silver modification on the morphological structure of E33 is negligible. On the other hand, the manganese-modified E33 had spherically shaped particles 50 nm in diameter on average. In order to investigate the structure of the crystal in detail, HR-TEM was employed. Fig. 4 shows the images of HR-TEM analysis for unmodified and modified E33 samples. Fig. 4(a) shows that the measured lattice spacing of the sample was 0.42, 0.25, and 0.17 nm, which correspond to the (110), (111), and (221) planes of goethite of iron oxide, respectively.[56] In Fig. 4(b), the lattice fringe with a *d*-spacing of 0.27 nm for the (222) plane of Mn_2O_3 was

Table 2 Structural characteristics of E33 and modified E33 before and after PO_4^{3-} adsorption

	Before adsorption			After adsorption		
Sample	S_{BET} (m^2 g^{-1})	Total pore volume (cm^3 g^{-1})	Porosity (%)	S_{BET} (m^2 g^{-1})	Total pore volume (cm^3 g^{-1})	Porosity (%)
E33	140.4	0.583	16.2	145.0	0.637	15.0
E33/AgI	124.6	0.456	12.6	136.8	0.449	11.1
E33/AgII	142.0	0.553	15.4	143.1	0.618	14.7
E33/Mn	102.8	0.441	12.3	99.5	0.623	14.8

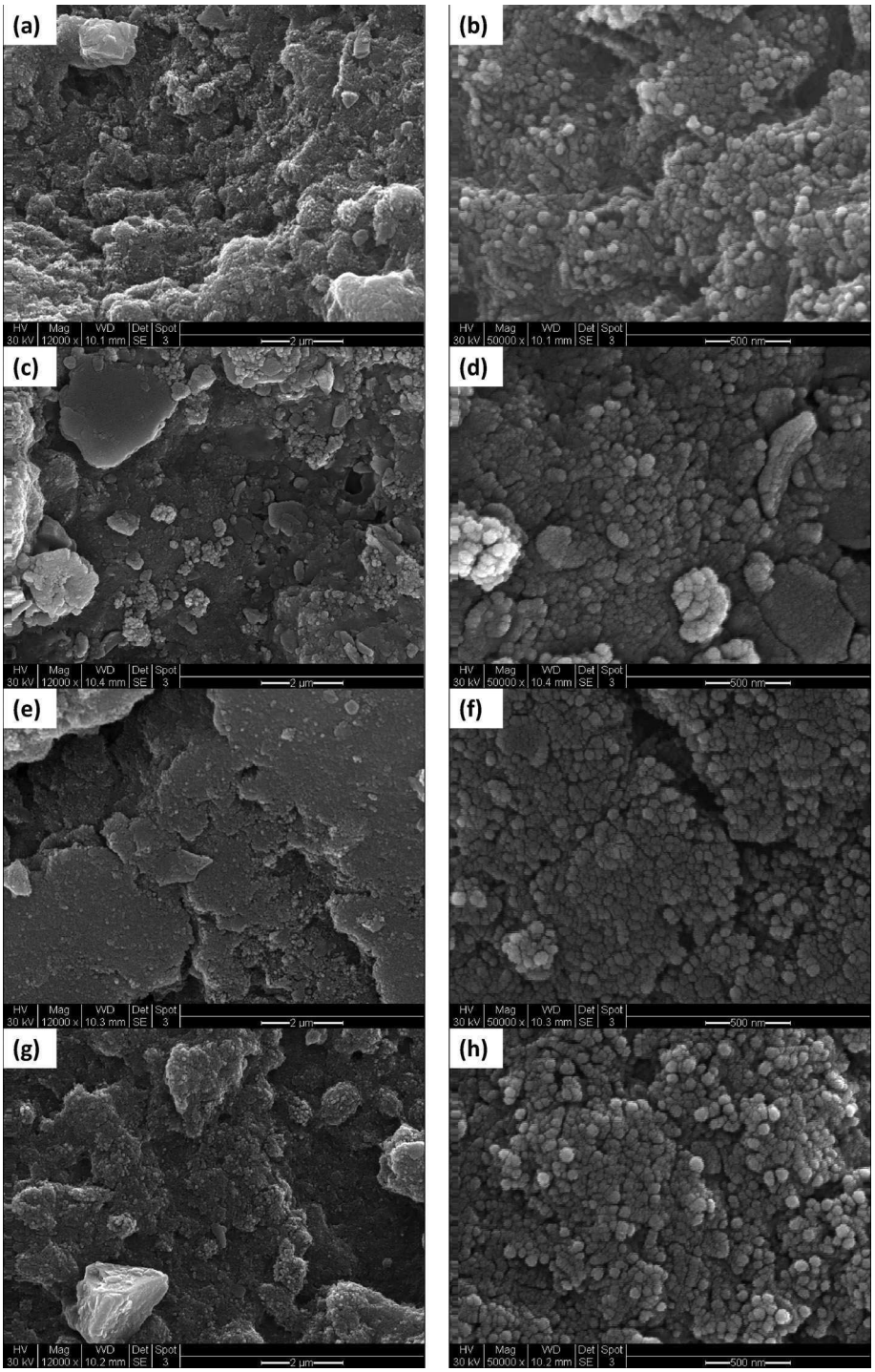

Fig. 1 SEM images of E33 at 12k (a) and at 50k (b), E33/Mn at 12k (c) and at 50k (d), E33/AgI at 12k (e) and at 50k (f), and E33/AgII at 12k (g) and at 50k (h) magnification.

measured, which indicated the formation of Mn_2O_3 during the surface modification of E33 with manganese.[57–59] After the surface modification of E33 with Ag, the presence of Ag was detected with a lattice spacing of 0.24 nm, corresponding to the (111) plane of Ag. The plane of (200) with a measured lattice spacing of 0.20 nm was also observed, indicating that the surface of E33 was successfully modified with Ag,[56,60] although the peaks corresponding to Ag were not detected by XRD analysis due to the low concentration of Ag on the surface of E33.

3.2 Adsorption studies

3.2.1 Effect of contact time. Fig. 5 shows the removal of phosphate as a function of reaction time from 0 up to 220 h.

 This journal is © The Royal Society of Chemistry 2015

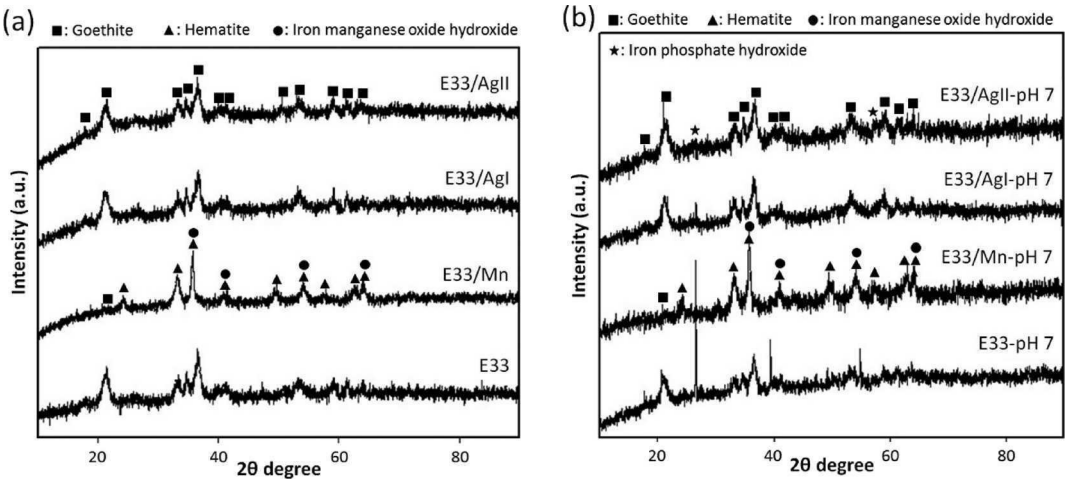

Fig. 2 XRD patterns of E33 and surface-modified E33: (a) before and (b) after using for phosphate removal.

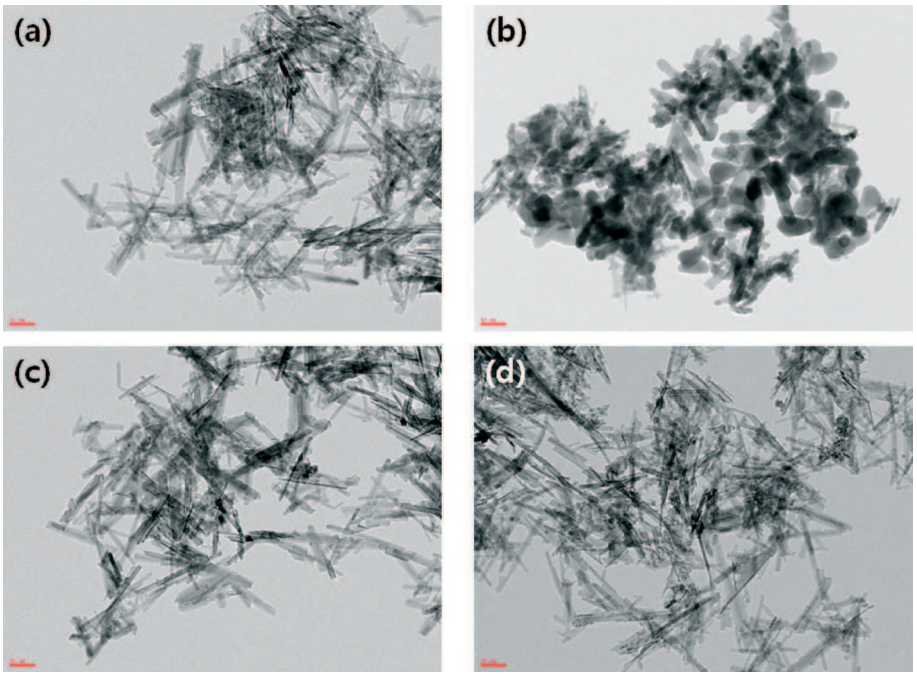

Fig. 3 TEM images at 100k magnification of adsorbent media (a) E33, (b) E33/Mn, (c) E33/AgI, and (d) E33/AgII. (All scale bars: 50 nm.)

The effluent presented a decreasing phosphate concentration with increasing reaction times. While E33/Mn and E33/AgI had lower reductions in phosphate concentration, E33/AgII performed similarly to the unmodified E33. The phosphate adsorption capacity of the different adsorbents correlates to BET surface area (Table 2). The solution pH in the batch reactor noticeably impacted the efficiency of adsorbents for phosphate removal. For example, E33/AgII at pH 7 removed roughly 65% of phosphate after a 3 h reaction time, yet only about 35% at pH 9. Influent pH also impacted overall adsorption. E33/AgII at pH 7 reduced phosphate concentration (initially at 82.66 mg L^{-1}) to 1.71 mg L^{-1}, while with an influent of pH 9, phosphate concentration was reduced to 5.71 mg L^{-1}. These graphs also show that E33/AgII removed 50% of the phosphate in the first hour of adsorption. It then took nearly five more days to reach equilibrium (Fig. 5(b)).

3.2.2 Phosphate adsorption kinetics. The results of kinetic experiments for phosphate adsorption are illustrated in Fig. 6. It can be seen that the adsorption rates of E33 and E33/AgII were slightly higher than those of E33/AgI and E33/Mn. Yet all adsorbents portrayed the typical, two-stage adsorption process, with a rapid initial phase and a slower phase, which likely corresponds to interparticle diffusion. For example, after 2 h of adsorption, the phosphate removal for E33, E33/Mn, E33/AgI, and E33/AgII was 66, 54, 38, and 63%, respectively.

The kinetic data for phosphate adsorption seen in Fig. 6 were fitted to several kinetic models including the pseudo-

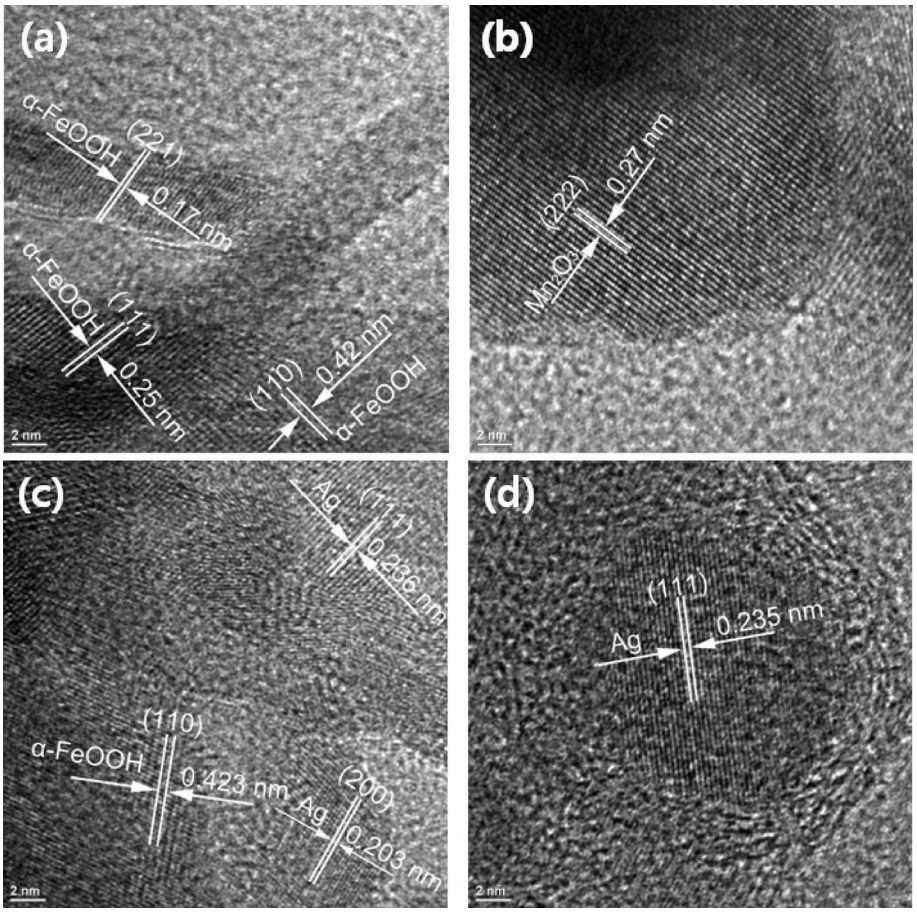

Fig. 4 HR-TEM analysis for unmodified and modified E33 used for phosphate removal: (a) E33, (b) E33/Mn, (c) E33/AgI, and (d) E33/AgII. (All scale bars: 2 nm.)

second-order equation and the simple Elovich equation by non-linear regression using SigmaPlot software. The kinetic equations used and their estimated parameters, with the correlation coefficient R^2, are illustrated in Table 3. Based on the values of R^2, the kinetics of phosphate adsorption on E33 and modified E33 can be satisfactorily described by both the pseudo-second-order equation and the simple Elovich equation; thus, Fig. 6 has both equations plotted also. The apparent applicability of the Elovich equation, which was originally developed to describe chemisorption of gases on heterogeneous solid surfaces,[61] suggests that the sorption sites involved in phosphate sorption are also of a heterogeneous nature. Obtained results were generally in agreement with other results from the literature and can properly explain the kinetics of phosphate adsorption onto commonly found soil minerals such as goethite.[62–64]

3.2.3 Column study. Column experiments were conducted to quantify the mechanism of phosphate adsorption as would be seen in an industrial-scale fixed bed adsorber. The breakthrough curves were constructed by plotting the ratio of PO_4^{3-} concentration at time t to the initial influent concentration (C/C_0) versus time (t). Fig. 7 shows the typical "S" shape of the breakthrough curves indicating the effects of mass transfer parameters as well as internal resistance within the column. Phosphate adsorption was initially high, decreasing with time until fully saturated. The impact of influent pH on phosphate adsorption was also evident where at higher pH (pH 9), breakthrough time (1.5 hr) was longer, while the time to reach saturation was shorter (15 hr), as opposed to the pH 7 where the breakthrough occurred after 1 hr, but took 18 hr to reach full saturation. The cumulative adsorption capacity of the columns was determined. At pH 6, the cumulative column adsorption capacity for E33, E33/Mn, E33/AgI, and E33/AgII was 31.5, 28.5, 29.9, and 40.1 mg g^{-1}, respectively. These results show that the phosphate adsorption capacity of the adsorbents in columns were much higher when compared to batch experiments (e.g. E33/AgII at pH 6 had a capacity of 17.0 mg g^{-1} for batch studies and 40.1 mg g^{-1} for column experiments). However, this is likely due to the volume of solution treated. Batch experiments were conducted using 0.1 L of phosphate solution while the continuous column experiments passed nearly 3 L of phosphate solution through the sorbents. These results indicate that E33/AgII provided a greater capacity for phosphate adsorption when compared to E33 at high (pH 9) and neutral (pH 6) pH values. The adsorption capacities for both batch and column tests are summarized in Table S1.‡

 This journal is © The Royal Society of Chemistry 2015

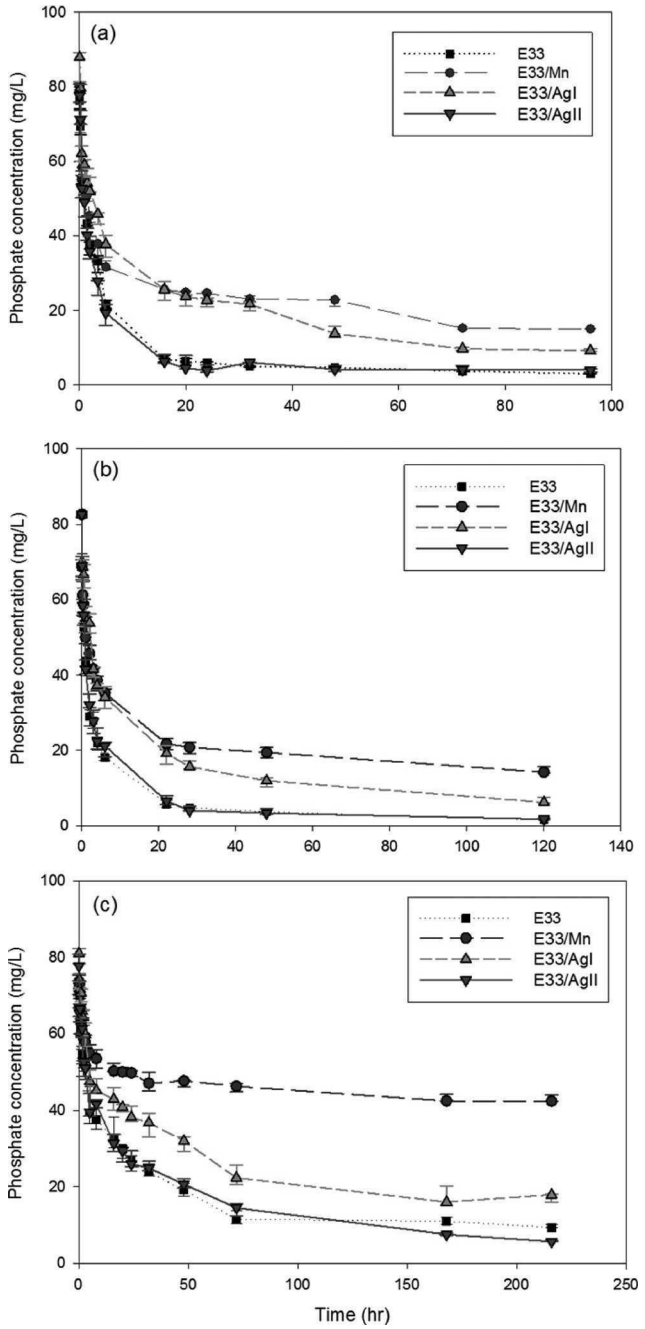

Fig. 5 Rate of E33 and modified E33 adsorption of phosphate at various pH values: (a) pH 6, (b) pH 7, and (c) pH 9.

3.2.4 Adsorption isotherm study. The following equation was used to determine the amount of phosphate anions adsorbed per unit weight of adsorbent (q_e):

$$q_e = \frac{(c_0 - c^*)V}{m}$$

where c_0 is the initial concentration (mg L^{-1}), c^* is the equilibrium concentration (mg L^{-1}), V is the solution volume (L), and m is the adsorbent mass in grams. Table 1 illustrates the phosphate adsorption capacity of a wide range of adsorbents including metal oxides, red mud, steel slag, and fly ash, as well as E33 and modified E33. The most efficient adsorbents were the Nanshi-modified zeolite, the Nanshi-modified fly ash, and Fe-loaded biomass char. However, the stock solution influent pH for these adsorbents was maintained atypically low (pH 3 and 4) to promote enhanced adsorption. At neutral pH, E33/AgII had a phosphate adsorption capacity of 28.0 mg PO_4^{3-} g^{-1}. This was slightly higher than that of the unmodified E33 (26.3 mg PO_4^{3-} g^{-1}), likely due to the increased BET surface area of the E33/AgII sample. The capacities from this study compare favorably with the capacities of other adsorbents as reported in literature.

Adsorption isotherms are used to relate the bulk adsorbate concentration and the amount adsorbed at the surface interface. The isotherm results were analyzed using the Langmuir and Freundlich isotherms. The Langmuir isotherm model, which assumes monolayer saturation with no lateral interaction between adsorbed particles, has previously been

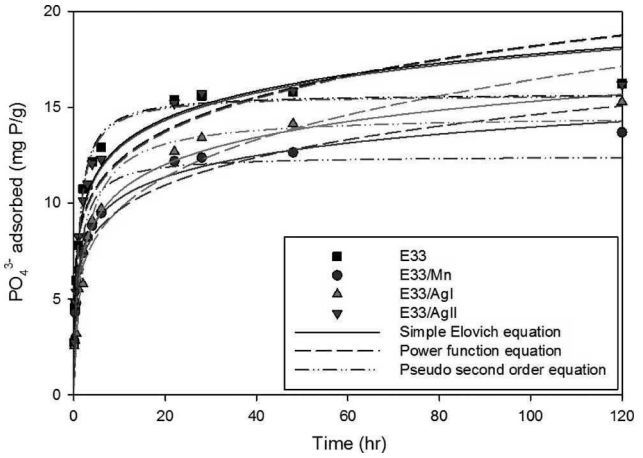

Fig. 6 Phosphate adsorption kinetic data for E33 and modified E33 at 20 °C, pH 7, and an influent concentration of 83 mg P L^{-1}.

Table 3 Estimated parameters for the kinetic model of phosphate adsorption on E33 and modified E33

Power function equation ($q = at^b$)			
	a	b	R^2
E33	8.259	0.1715	0.8718
E33/Mn	6.396	0.1793	0.9464
E33/AgI	5.728	0.2288	0.9343
E33/AgII	8.139	0.1742	0.8817
Simple Elovich equation ($q = a + b \ln t$)			
	a	b	R^2
E33	8.228	2.071	0.9600
E33/Mn	6.513	1.619	0.9894
E33/AgI	5.895	2.045	0.9645
E33/AgII	8.130	2.070	0.9645
Pseudo second-order equation ($q_t = k_2 q_e^2 t/1 + k_2 q_e t$)			
	$q_{e,cal}$	k_2 (g mg^{-1} min^{-1})	R^2
E33	16.34	0.0641	0.9725
E33/Mn	13.74	0.0645	0.9021
E33/AgI	15.46	0.0272	0.9547
E33/AgII	16.31	0.0616	0.9639

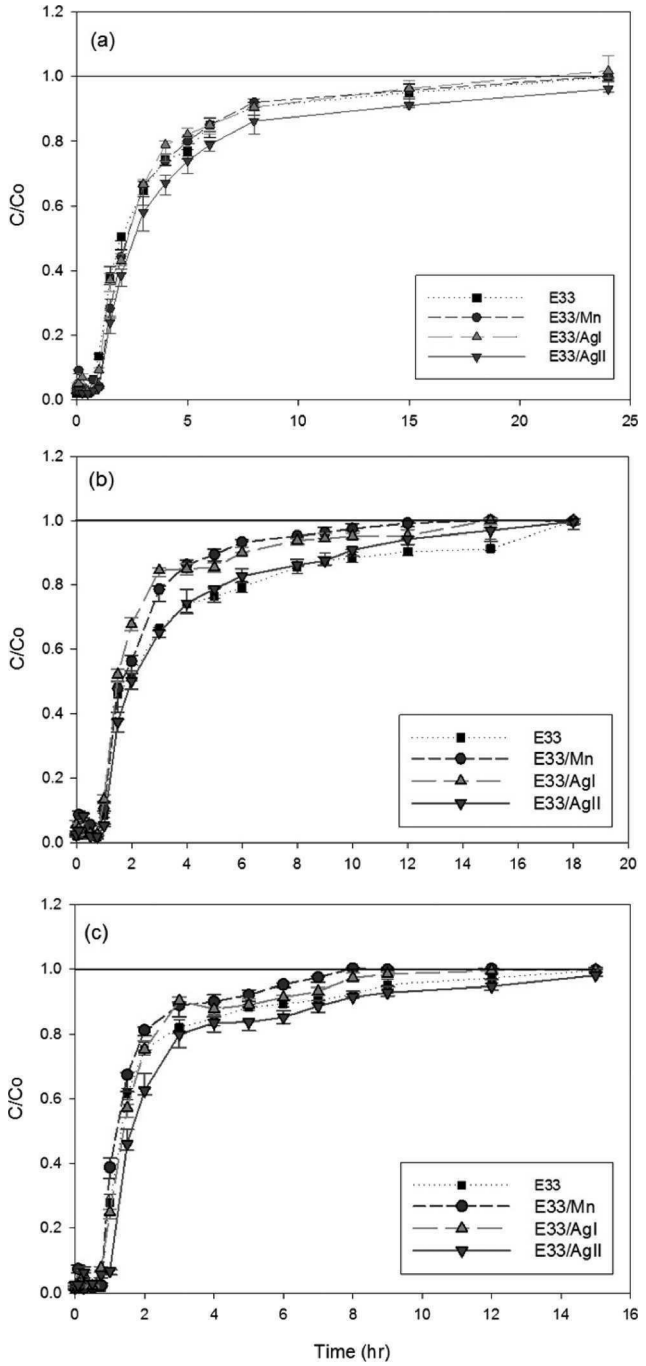

Fig. 7 Column experiments for E33 and modified E33 phosphate adsorption at (a) pH 6, (b) pH 7, and (c) pH 9.

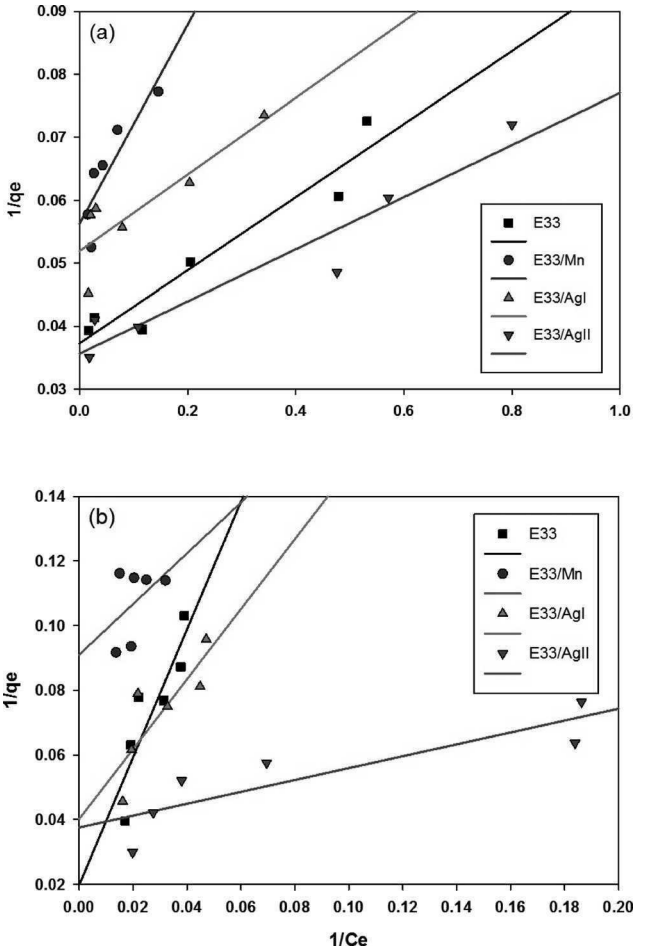

Fig. 8 Langmuir isotherm graphs for (a) pH 7 and (b) pH 9.

Table 4 Isotherm parameters at pH 7

	Langmuir isotherm constants			Freundlich isotherm constants		
Sample	Q_{max} (mg g^{-1})	K_L (dm^3 mg^{-1})	R^2	K_F	$1/n$	R^2
E33	25.71	0.82	0.9999	14.72	0.15	0.7389
E33/Mn	18.73	0.24	0.9836	9.59	0.15	0.8133
E33/AgI	20.58	0.36	0.9642	12.87	0.10	0.6718
E33/AgII	28.01	0.69	0.9917	15.75	0.15	0.7893

employed in similar adsorption experiments.[62–64] The Langmuir adsorption model is mathematically expressed by:

$$q_e = \frac{Q_{max} K_L C_e}{1 + K_L C_e}$$

where q_e (mg g^{-1}) is the amount of adsorbed phosphate per unit mass of adsorbent, C_e (mg L^{-1}) is the unadsorbed phosphate concentration in solution at equilibrium, Q_{max} is the maximum amount of phosphate per unit mass of sorbent to form a complete monolayer on the surface, and K_L (L mg^{-1}) is a constant related to the affinity of the binding sites. The Langmuir adsorption equation can be described by its linearized form:

$$\frac{1}{q_e} = \left(\frac{1}{K_L Q_{max}}\right)\frac{1}{C_e} + \frac{1}{Q_{max}}$$

The linear plot of the above equation (Fig. 8) yields essential specifications of the system. The slope and intercept of the plot were used to determine the Langmuir constants Q_{max} and K_L, which are presented in Table 4.

 This journal is © The Royal Society of Chemistry 2015

Essential characteristics of the Langmuir isotherm model can be expressed in terms of a constant dimensionless separation factor, R_L, given by the equation:

$$R_L = \frac{1}{(1 + K_L C_0)}$$

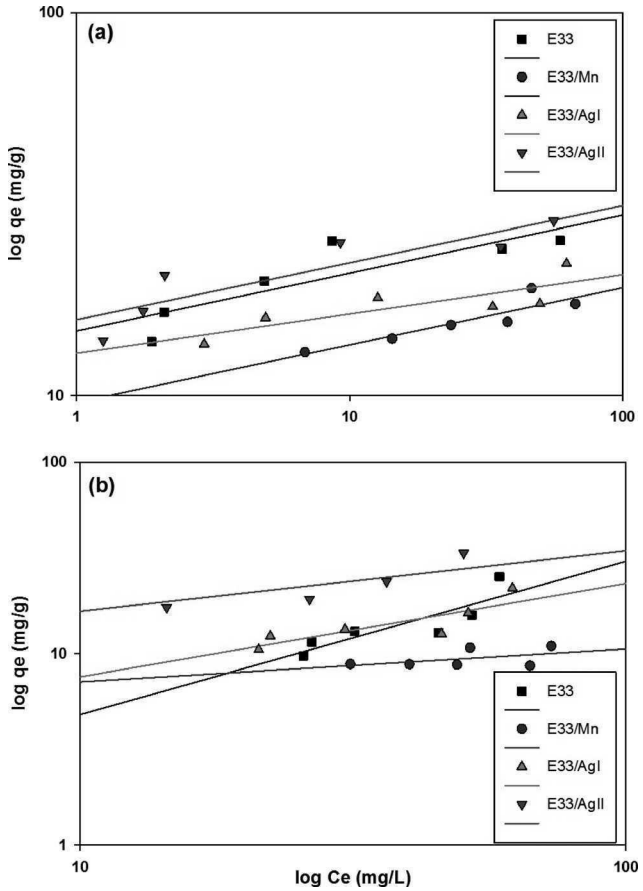

Fig. 9 Freundlich isotherm graphs for influent pH values of (a) 7 and (b) 9.

where C_0 (mg L^{-1}) is the initial adsorbate concentration in solution and K_L (L mg^{-1}) is the Langmuir constant. The value of R_L can indicate if adsorption is unfavorable ($R_L > 1$), linear ($R_L = 1$), irreversible ($R_L = 0$), or favorable ($0 < R_L < 1$). R_L values for E33, E33/Mn, E33/AgI, and E33/AgII were 0.015, 0.050, 0.034, and 0.018, respectively. As all values computed for R_L were less than 1 and greater than 0, adsorption was determined to be favorable.

The Freundlich isotherm is an empirical equation used to explain heterogeneous systems. The Freundlich equation is given by:

$$q_e = K_F (C_e)^{1/n}$$

where K_F ((mg g^{-1}) (L $mg^{-1})^{1/n}$) is the adsorption capacity of the adsorbent and n gives an indication of adsorption favorability, for example, values of $n > 1$ indicate favorable adsorption. Freundlich isotherm constants K_F and n can be determined by the linearization of the Freundlich equation and graphing $\ln(q_e)$ *vs.* $\ln(C_e)$:

$$\ln(q_e) = (K_F) + \frac{1}{n}(\ln(C_e))$$

Values of K_F and n can be determined from the intercept and slope of the plot for the linearized Freundlich equation. The linearized Freundlich isotherm plots for phosphate adsorption onto E33 and modified E33 are presented in Fig. 9. The Freundlich isotherm constants, K_F and $1/n$, were determined by linear regression (Table 4).

Fig. 10 shows phosphate adsorption isotherms for E33 and modified E33 under identical conditions, *i.e.* DI water at pH 7. The results show that E33/AgII had the highest capacity of phosphate adsorption for the modified adsorbents as well as unmodified E33. This is in accordance with BET surface area analysis, which revealed that E33/AgII had the highest specific surface area. Likewise, E33/Mn, which had the lowest phosphate adsorption capacity, also had the lowest BET surface area. Isotherm results were evaluated using both

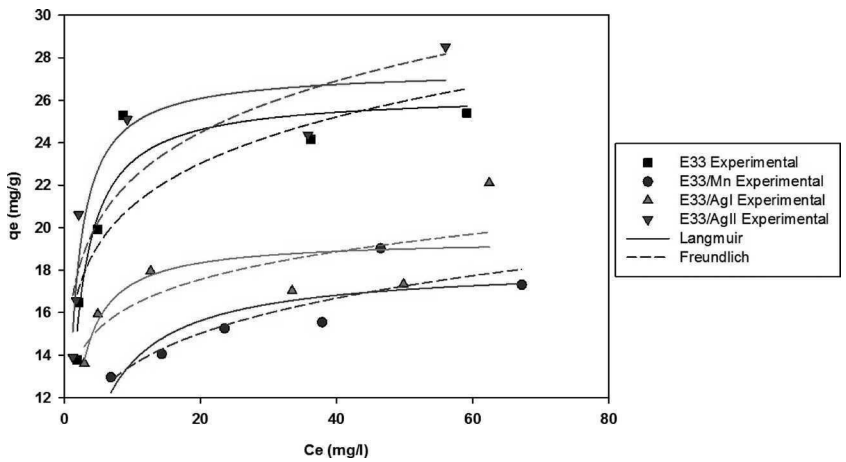

Fig. 10 Isotherm graph for phosphate adsorption at pH 7.

Langmuir and Freundlich isotherm equations. The determined isotherm constants for both models are summarized in Table 4. As can be seen from the coefficients of determination, the Langmuir isotherm appears better suited to explain the adsorption equilibrium data.

4. Conclusion

Three modified adsorbents, based on the commercially available E33 adsorptive medium, were successfully synthesized and characterized using SEM, TEM, XRD, porosimetry analysis and EDX. The adsorption capacity of the synthesized samples was investigated for the removal of phosphate. The results of the characterization of synthesized samples indicated that the surface of E33 was successfully modified with nanostructured Ag and manganese. In particular, for Ag-modified E33, the phase of E33 was not affected by Ag modification while the transformation of goethite to hematite was observed in Mn-modified E33.

Batch and column experiments were conducted to determine the adsorbents' capacity for phosphate adsorption. The phosphate removal was influenced by the pH of solutions. As the solution pH decreased, the amount of phosphate adsorbed increased, presumably because the surface charge of E33 is pH dependent, thus lower pH values correlate to a more positive surface charge on the E33, thus promoting increased PO_4^{3-} adsorption. Of the modified adsorbents synthesized, Ag-modified E33 using tea extract (E33/AgII) had a slightly higher phosphate adsorption capacity compared to unmodified E33. This increase in adsorptive capacity is likely due to an increased BET surface area for E33/AgII. Although Mn-modified E33 (E33/Mn) was believed to promote increased adsorption, a reduction in BET surface area (likely caused by the aggregation of particles resulting in a spherical shape for the E33/Mn particles as revealed by TEM) resulted in a pore blockage and lower phosphate adsorption capacity when compared to unmodified E33. The increased adsorption for E33/AgII suggests the potential for improving the performance of commercially available adsorbents for phosphate removal.

References

1 E. Metcalf, *Wastewater engineering: treatment, disposal and reuse*, McGraw-Hill, New York, 1991.
2 H. L. Golterman, *Water Res.*, 1973, **7**, 3–17.
3 J. J. Schröder, A. L. Smit, D. Cordell and A. Rosemarin, *Chemosphere*, 2011, **84**, 822–831.
4 A. Sendrowski and T. H. Boyer, *Desalination*, 2013, **322**, 104–112.
5 Y. Liu, G. Villalba, R. U. Ayres and H. Schroder, *J. Ind. Ecol.*, 2008, **12**, 229–247.
6 G. Villalba, Y. Liu, H. Schroder and R. U. Ayres, *J. Ind. Ecol.*, 2008, **12**, 557–569.
7 M. Meybeck, *Am. J. Sci.*, 1982, **282**, 401–450.
8 H. Holtan, L. Kamp-Nielsen and A. O. Stuanes, *Hydrobiologia*, 1988, **170**, 19–34.
9 *Phosphorus in environmental technologies: Principles and applications*, ed. E. Valsami-Jones, IWA Publishing, London, UK, 2004.
10 S. Pitois, M. H. Jackson and B. J. Wood, *J. Environ. Health*, 2001, **64**, 25–32.
11 G. R. Mohan, S. Gadekar and P. Pullammanappallil, *Florida Water Resources Journal*, 2011, 17–22.
12 G. R. Mohan, P. Dube, A. MacFarlene and P. Pullammanappallill, in *Materials challenges in alternative and renewable energy II: Ceramic transactions*, ed. G. Wicks, J. Simon, R. Zidan, R. Brigmon, G. Fischman, S. Arepalli, A. Norris and M. McCluer, John Wiley & Sons, Inc., Hoboken, New Jersey, 2013, vol. 242, pp. 47–58.
13 J. Hrenovic, M. Rozic, L. Sekovanic and A. Anic-Vucinic, *J. Hazard. Mater.*, 2008, **156**, 576–582.
14 A. Drews, H. Evenblij and S. Rosenberger, *Environ. Prog.*, 2005, **24**, 426–433.
15 K. Karageorgiou, M. Paschalis and G. N. Anastassakis, *J. Hazard. Mater.*, 2007, **139**, 447–452.
16 T. Liu, K. Wu and L. Zeng, *J. Hazard. Mater.*, 2012, **217**, 29–35.
17 P. Delaney, C. McManamon, J. P. Hanrahan, M. P. Copley, J. D. Holmes and M. A. Morris, *J. Hazard. Mater.*, 2011, **185**, 382–391.
18 S. Y. Yoon, C. G. Lee, J. A. Park, J. H. Kim, S. B. Kim, S. H. Lee and J. W. Choi, *Chem. Eng. J.*, 2014, **236**, 341–347.
19 X. Cheng, X. Huang, X. Wang, B. Zhao, A. Chen and D. Sun, *J. Hazard. Mater.*, 2009, **169**, 958–964.
20 N. Boujelben, J. Bouzid, Z. Elouear, M. Feki, F. Jamoussi and A. Montiel, *J. Hazard. Mater.*, 2008, **151**, 103–110.
21 S. L. Wang, C. Y. Cheng, Y. M. Tzou, R. B. Liaw, T. W. Chang and J. H. Chen, *J. Hazard. Mater.*, 2007, **147**, 205–212.
22 H. Zhou, Z. Jiang and S. Wei, *Journal of Chemistry*, 2013, **2013**, 649868.
23 A. Bhatnagar, V. J. Vilar, C. M. Botelho and R. A. Boaventura, *Environ. Technol.*, 2011, **32**, 231–249.
24 Q. Yue, Y. Zhao, Q. Li, W. Li, B. Gao, S. Han and H. Yu, *J. Hazard. Mater.*, 2010, **176**, 741–748.
25 P. Castaldi, M. Silvetti, G. Garau and S. Deiana, *J. Hazard. Mater.*, 2010, **182**, 266–272.
26 Y. Li, Y. Liu and G. Du, *Proceedings of Bioinformatics and biomedical engineering (iCBBE), 4th International Conference*, Chengdu, 2010.
27 J. Xiong, Z. He, Q. Mahmood, D. Liu, X. Yang and E. Islam, *J. Hazard. Mater.*, 2008, **152**, 211–215.
28 A. Drizo, C. Forget, R. P. Chapuis and Y. Comeau, *Water Res.*, 2006, **40**, 1547–1554.
29 S. Yao, J. Li and Z. Shi, *Adsorpt. Sci. Technol.*, 2009, **27**, 603–614.
30 J. Chen, H. Kong, D. Wu, Z. Hu, Z. Wang and Y. Wang, *J. Colloid Interface Sci.*, 2006, **300**, 491–497.
31 K. Mohanty, D. Das and M. N. Biswas, *Adsorption*, 2006, **12**, 119–132.
32 W. Jiang, J. Lv, L. Luo, K. Yang, Y. Lin, F. Hu and S. Zhang, *J. Hazard. Mater.*, 2013, **262**, 55–63.
33 H. Liu, T. Chen, X. Zou, Q. Xie, C. Qing, D. Chen and R. L. Frost, *Chem. Eng. J.*, 2013, **234**, 80–87.

 This journal is © The Royal Society of Chemistry 2015

34 J. Xi and M. He, *Water Qual. Res. J. Can.*, 2013, **48**, 223–231.
35 S. Aredes, B. Klein and M. Pawlik, *J. Cleaner Prod.*, 2012, **29**, 208–213.
36 W. Stumm, in *Chemistry of the solid-water interface: processes at the mineral-water and particle-water interface in natural systems*, John Wiley & Son Inc., 1992, p. 428.
37 A. Jain, K. P. Raven and R. H. Loeppert, *Environ. Sci. Technol.*, 1999, **33**, 1179–1184.
38 B. Zhong, R. Stanforth, S. Wu and J. P. Chen, *J. Colloid Interface Sci.*, 2007, **308**, 40–48.
39 J. Torrent, V. Barron and U. Schwertmann, *Soil Sci. Soc. Am. J.*, 1990, **54**, 1007–1012.
40 R. Strauss, G. W. Brümmer and N. J. Barrow, *Eur. J. Soil Sci.*, 1997, **48**, 101–114.
41 I. R. Willett, C. J. Chartres and T. T. Nguyen, *J. Soil Sci.*, 1988, **39**, 275–282.
42 R. Strauss, G. W. Brümmer and N. J. Barrow, *Eur. J. Soil Sci.*, 1997, **48**, 87–99.
43 L. Sigg and W. Stumm, *Colloids Surf.*, 1981, **2**, 101–117.
44 R. L. Parfitt, R. J. Atkinson and R. S. C. Smart, *Soil Sci. Soc. Am. J.*, 1975, **39**, 837–841.
45 M. Nanzyo, *Soil Sci. Plant Nutr.*, 1986, **32**, 51–58.
46 T. Hiemstra and W. H. Van Riemsdijk, *J. Colloid Interface Sci.*, 1996, **179**, 488–508.
47 J. S. Geelhoed, T. Hiemstra and W. H. Riemsdijk, *Environ. Sci. Technol.*, 1998, **32**, 2119–2123.
48 J. R. Rustad, A. R. Felmy and B. P. Hay, *Geochim. Cosmochim. Acta*, 1996, **60**, 1563–1576.
49 M. N. Nadagouda and D. A. Lytle, *J. Nanotechnol.*, 2011, **2011**, DOI: 10.1155/2011/972486.
50 M. N. Nadagouda, C. Bennett-Stamper, C. White and D. A. Lytle, *RSC Adv.*, 2012, **2**, 4198–4204.
51 M. Kanematsu, T. M. Young, K. Fukushi, P. G. Green and J. L. Darby, *Environ. Sci. Technol.*, 2010, **44**, 3388–3394.
52 M. Kanematsu, T. M. Young, K. Fukushi, D. A. Sverjensky, P. G. Green and J. L. Darby, *Environ. Sci. Technol.*, 2010, **45**, 561–568.
53 A. Sperlich, *Ph. D. Thesis*, University of Berlin, 2010.
54 J. Murphy and J. P. Riley, *Anal. Chim. Acta*, 1962, **27**, 31–36.
55 C. Han, V. Likodimos, J. A. Khan, M. N. Nadagouda, J. Anderson, P. Falaras, P. Rosales-Lombardi and D. D. Dionysiou, *Environ. Sci. Pollut. Res.*, 2014, **21**, 11781–11793.
56 J. Akai, K. Akai, M. Ito, S. Nakano, Y. Maki and I. Sasagawa, *Am. Mineral.*, 1999, **84**, 171–182.
57 J. N. Park, J. K. Shon, M. Jin, S. H. Hwang, G. O. Park, J. H. Boo, T. H. Han and J. M. Kim, *Chem. Lett.*, 2010, **39**, 93–495.
58 Q. Javed, F. P. Wang, M. Y. Rafique, A. M. Toufiq, Q. S. Li, H. Mahmood and W. Khan, *Nanotechnology*, 2012, **23**, 415603.
59 G. Yang, W. Yan, J. Wang and H. Yang, *CrystEngComm*, 2014, **16**, 6907–6913 (ESI).
60 P. Asanithi, S. Chaiyakun and P. Limsuwan, *J. Nanomater.*, 2012, **2012**, 79.
61 M. J. D. Low, *Chem. Rev.*, 1960, **60**, 267–312.
62 L. Zeng, X. Li and J. Liu, *Water Res.*, 2004, **38**, 1318–1326.
63 X. Wang, F. Liu, W. Tan, W. Li, X. Feng and D. L. Sparks, *Soil Sci.*, 2013, **178**, 1–11.
64 O. K. Borggaard, *J. Soil Sci.*, 1983, **34**, 333–341.

Chemical Engineering Journal 284 (2016) 1386–1396

Contents lists available at ScienceDirect

Chemical Engineering Journal

journal homepage: www.elsevier.com/locate/cej

Phosphate adsorption using modified iron oxide-based sorbents in lake water: Kinetics, equilibrium, and column tests

Jacob Lalley [a,b,1], Changseok Han [a,1], Xuan Li [a], Dionysios D. Dionysiou [b], Mallikarjuna N. Nadagouda [a,*]

[a] The U.S. Environmental Protection Agency, ORD, NRMRL, WSWRD, WQMB, 26 W. Martin Luther King Jr. Drive, Cincinnati, OH 45268, USA
[b] Environmental Engineering and Science Program, Department of Biomedical, Chemical and Environmental Engineering (DBCEE), University of Cincinnati, OH 45221, USA

HIGHLIGHTS

- The adsorbent E33 was successfully modified with silver and manganese nanoparticles.
- One silver modified sorbent had similar PO_4^{3-} adsorption capacity compared to E33.
- Phosphate desorption for its recovery was accomplished by base leaching with NaOH.

GRAPHICAL ABSTRACT

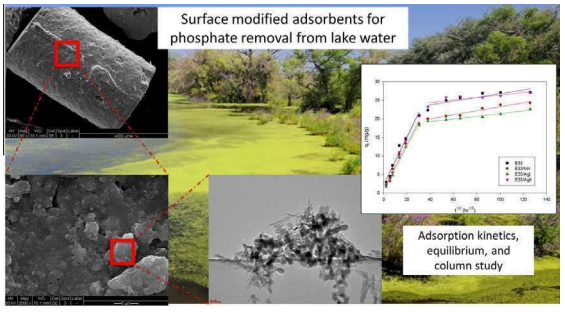

ARTICLE INFO

Article history:
Received 15 June 2015
Received in revised form 24 August 2015
Accepted 26 August 2015
Available online 2 September 2015

Keywords:
Adsorption
Nutrients
Nutrient removal/recovery
Phosphate
Water treatment

ABSTRACT

Adsorption behavior of Bayoxide® E33 (E33) and three E33-modified sorbents for the removal of phosphate from lake water was investigated in this study. E33-modified sorbents were synthesized by coating with manganese (E33/Mn) and silver (E33/AgI and E33/AgII) nanoparticles. Adsorbent characterization was done by X-ray diffraction (XRD), scanning electron microscopy (SEM), energy-dispersive X-ray spectroscopy (EDS), surface area analyzer (BET), transmission electron microscopy (TEM), and high resolution TEM (HR-TEM) analysis. Batch, equilibrium, and column experiments were conducted to determine various adsorption parameters. Equilibrium data were fitted to different adsorption isotherms and the Langmuir isotherm provided the best fit. Based on the Langmuir model, it was found that E33/AgII had a slightly higher maximum monolayer adsorption capacity (38.8 mg g^{-1}) when compared to unmodified E33 (37.7 mg g^{-1}). Data for adsorption kinetics were found to best fit with the pseudo-second-order model, suggesting chemisorption is the mechanism of sorption. Intra-particle diffusion studies indicated that the rate-limiting step for phosphate sorption onto E33 and modified E33 was intra-particle diffusion. Although limited improvements were seen, the results of this study suggest that the surface of E33 can be modified with nanoparticles to enhance the adsorption of phosphate from aqueous solutions and may give other advantages such as limiting biofouling over an extended lifetime of numerous recovery/regeneration steps.

Published by Elsevier B.V.

1. Introduction

Phosphates (PO_4^{3-}), as essential and often limiting nutrients in most aquatic environments, can result in the acceleration of eutrophication; leading to an increase in costs associated with water treatment [1], decreased recreational value of the waterway

* Corresponding author. Tel.: +1 (513) 569 7232; fax: +1 (513) 569 7172.
E-mail address: Nadagouda.mallikarjuna@epa.gov (M.N. Nadagouda).
[1] Contributed equally to this work.

http://dx.doi.org/10.1016/j.cej.2015.08.114
1385-8947/Published by Elsevier B.V.

[2], and the formation of harmful algal blooms (HABs) that may pose a risk to human health from the production of cyanotoxins [3]. Therefore, the remediation of phosphates from aquatic ecosystems is a growing environmental concern. While phosphates are naturally found in surface and waste water, anthropogenic sources from agriculture [4] (fertilizer/animal feed run-off), industry [5] (detergents), and sewage [6] have increased phosphate loads in surface waters, thus accelerating eutrophication.

While conventional treatment techniques like chemical precipitation and biological phosphorus removal exist, problems remain. Chemical precipitation is a costly process, requiring the purchasing, transportation, and storage of chemical precipitants, and produces vast quantities of sludge which must be properly disposed [7]. Biological processes like enhanced biological phosphorus removal (EBPR) are quite sensitive to water parameters including influent carbon source [8] (e.g., acetate, propionate, etc.) and temperature [9], resulting in decreased stability and reliability. Yet, while phosphates act as pollutants at high concentrations, their demand is growing for industrial purposes including fertilizer production and the manufacturing of detergents. As a non-renewable resource with no known alternatives, the need for phosphate recovery and recycling may become necessary. Though experts disagree on when (between 60 and 700 years) [10,11], it is acknowledged that our phosphate reserves will eventually be depleted. Thus, future studies should focus on PO_4^{3-} recovery as well as removal.

One technique that can both remove and recover phosphate is adsorption. Adsorption is a surface-based phenomenon resulting in the adhesion of an adsorbate on the surface of an adsorbent through covalent bonding and electrostatic interactions [12,13]. Unlike chemical precipitation and biological removal processes, adsorption is unique in that it can remove contaminants over a wide pH range and at low concentrations [14]. The iron oxide hydroxide goethite (α-FeOOH) is a highly adsorptive material for phosphate remediation. As the most thermodynamically stable iron oxide in most environmental conditions, goethite is the most frequently encountered iron oxide in nature and occurs in almost every soil type in every climatic region [15].

Iron oxides like goethite typically occur as poorly ordered, minute crystals with large specific surface areas (50–300 $m^2\ g^{-1}$) [16] with hydroxide surface functional groups. These properties substantially contribute to the specific adsorption of anions like PO_4^{3-} as inner sphere complexes. Phosphate adsorption results from the completion of the ligand shell of surface Fe atoms, where the PO_4^{3-} ion reacts with two singly coordinated Fe–OH groups, forming a bridging, binuclear, bidentate complex $(Fe–O)_2–PO_2H$ [17]. Due to goethite's affinity for ion adsorption and relative availability, LANXESS Deutschland GmbH has produced Bayoxide® E33 Adsorption Media (E33), a goethite-based adsorbent which was originally designed for arsenic remediation [18–20], yet studies have shown the ability of E33 to sorb a wide range of ions, including phosphates [21–23].

Previous research has explored phosphate adsorption equilibrium and adsorption kinetics of E33 and three surface modified E33-based adsorbents using a stock phosphate solution [24]. In this study, however, lake water was used to determine the effects of competing species on phosphate removal. The phosphate adsorption capacity and kinetics of E33 and modified E33 were determined, as well as the desorption of phosphate to explore possible reuse.

2. Experimental

2.1. Materials

The E33 adsorbent used to investigate phosphate adsorption was acquired from LANXESS Deutschland GmbH. Lake water, obtained from Winton Lake in Winton Woods (Cincinnati, OH), was spiked with analytical grade sodium phosphate monohydrate ($NaH_2PO_4{\cdot}H_2O$), obtained from Fisher Scientific, at a target concentration of 140 mg L^{-1} and used in all experimentation. The pH of the lake water was maintained constant at pH 7 using propanesulfonic acid (MOPS), obtained from Sigma Aldrich. Modified E33 was synthesized by the deposition of either silver or manganese nanoparticles to the surface of E33. Silver modified E33 was synthesized using reagent grade silver nitrate ($AgNO_3$, obtained from Sigma Aldrich). Either sodium borohydride ($NaBH_4$, Sigma Aldrich) or tea powder (Red Label, India) were used as capping/reducing agents. Manganese modified E33 was synthesized using manganese acetate tetrahydrate ($Mn(CH_3COO)_2{\cdot}4H_2O$) obtained from Sigma Aldrich. The synthesized adsorbents consisted of either manganese or silver coated E33. The procedure for synthesis can be found in our previous study [24].

2.2. Sample characterization

The crystal structure of the adsorbents was determined by X-ray diffraction (XRD) analysis using a Panalytical (Expert) 2-theta diffractometer (Panalytical, Almelo, Netherlands) at a wavelength of 1.54 μm and at 2-theta range 2–90° under CuK_α radiation. The BET surface area, total pore volume, and porosity of the adsorbents were determined using a Tristar 3000 porosimeter analyzer (Micromeritics). Before analysis, the adsorbent samples were purged with nitrogen gas for 2 h and at 150 °C using the Micromeritics FlowPrep 060. For the characterization of the surface morphology of the adsorbents, an environmental scanning electron microscope (ESEM, Philips XL 30 ESEM-FEG), at an accelerating voltage of 30 kV was used. Physical properties of the adsorbent were also studied with transmission electron microscopy (TEM), where a FEI CM20 TEM operated at 200 kV was employed. To further characterize the physical properties of the surface-modified adsorbents, high-resolution TEM (HR-TEM, JEM-2010F, obtained from JEOL) was employed with a field emission gun at 200 kV. Prior to characterization, the adsorbents were prepared and dispersed by ultrasonication (2510R-DH, Bransonic) in 99.8% pure isopropyl alcohol (obtained from Pharmco-AAPER) for 30 min. Then, on a carbon-coated copper grid (LC325-Cu, EMS), a drop of the supernatant was fixed and dried at room temperature. The images obtained from the HR-TEM were analyzed using ImageJ, an image processing software (National Institutes of Health, Maryland, USA). Finally, as adsorption is highly dependent on the adsorbent surface charge, the point of zero charge for the adsorbents was evaluated using a SurPass Surface Electrokinetic Analyzer (Anton Paar, Australia). The zeta potential was measured at different pH values to determine the point of zero charge for the samples. To explore the stability of deposited nanoparticles onto the surface of E33, the concentration of Mn and Ag were determined after adsorption experiments using an Agilent Technologies Inc. (Santa Clara, CA) 7500cs Inductively Coupled Plasma-Mass Spectrometer (ICP-MS). The solutions were first filtered through 0.45 μm Whatman nylon syringe filters and solubilized using nitric acid.

2.3. Adsorption studies

Variable dose isotherm experiments were conducted to determine equilibrium adsorption parameters. Varying masses of adsorbent, ranging from 0.1 to 1.5 g, were placed in 125 mL Nalgene polypropylene bottles with 100 mL of the lake water solution. The solution was prepared by dissolving sodium phosphate monohydrate ($NaH_2PO_4{\cdot}H_2O$) in Winton Lake lake water (at a target concentration of 140 mg $PO_4^{3-}\ L^{-1}$). To this, 15 mM MOPS buffer was added and pH was adjusted to 7.0 with 1 N NaOH. The bottles were placed on a G10 Gyrotary shaker (New Brunswick

Scientific Co. Inc., USA) at 150 rpm for 3 weeks. After adsorbent saturation, samples were analyzed for phosphate concentration remaining in solution.

Adsorption kinetic experiments were conducted to determine various parameters of the adsorbents' kinetics of adsorption. Batch experiments were performed in 125 mL Nalgene polypropylene bottles under the following conditions: (i) adsorbent amount 5 g L^{-1}, (ii) temperature 21 °C, (iii) pH 7.0 ± 0.15, (iv) lake water solution target phosphate concentration 140 mg L^{-1}, and (v) mixing speed 150 rpm. A constant pH was maintained using 15 mM MOPS buffer and bottles were shaken on a G10 Gyrotary shaker for various times. Grab samples were collected at pre-determined times, filtered using a 0.45 μm Whatman nylon syringe filter, and analyzed for phosphate concentration remaining in solution with respect to time.

Fixed bed column tests were conducted in 80 cm high and 1.9 cm diameter Harvel plastic columns. A gram of adsorbent media was placed in the columns with sand and gravel above and below. A stainless steel sieve was placed at the bottom of the column to prevent washout. The lake water solution (at an initial target PO_4^{3-} concentration of 140 mg L^{-1}) was passed through the column at a flow rate of 2 mL min^{-1} and at room temperature using a Thermo Scientific™ FH100M Series Peristaltic pump. Similar to the kinetic and isotherm experiments, the pH of the solution was initially adjusted and buffered to remain constant. The column effluent solutions were collected and analyzed after various time periods for phosphate concentration. All isotherm, kinetic, and column experiments were conducted once and sample measurements were analyzed in triplicate and averaged.

2.4. Desorption studies

To evaluate the potential of phosphate recovery from the E33-based adsorbents, PO_4^{3-} desorption was investigated. As adsorption is strongly dependent on the solution pH, and low pH values promote enhanced adsorption, NaOH was used to increase the solution pH and promote PO_4^{3-} desorption. An initial adsorption isotherm experiment was conducted (same as previous) and the spent sorbents were used for the desorption study. After batch equilibration, the adsorbents were triple washed with DI water to remove any unadsorbed phosphate. The spent adsorbents were then placed in a 125 mL Nalgene bottles and 100 mL of desorption solution was added. Two different desorption solutions were used and compared; a 0.05 M NaOH solution and a 0.10 M NaOH solution. Samples were mixed (at 150 RPM) for the same time as isotherm experiments (3 weeks) at room temperature, and then filtered (0.45 μm PTFE) and analyzed for phosphate concentration in solution using the same colorimetric technique as previously described.

The phosphate concentration for all experiments was determined by a colorimetric measurement technique in which ammonium molybdate and potassium antimonyl tartrate react in an acidic solution with orthophosphate to form phosphomopydbic acid which can be reduced by ascorbic acid to form an intense blue color [25]. The absorbance due to the blue complex was monitored at 880 nm using a UV–Vis spectrophotometry (HACH model number DR 2700).

3. Results

3.1. Adsorbent characterization

3.1.1. Physical characteristics

Physical properties of E33 and modified E33 are summarized in Table 1. The BET surface areas (m^2 g^{-1}) of E33, E33/Mn, E33/AgI, and E33/AgII were found to be 140.4, 102.8, 124.6, and 142.0 m^2 g^{-1}, respectively. For unmodified E33, the company AdEdge Technologies [26] has reported the BET surface area to be from 120 to 200 m^2 g^{-1}, while Naeem et al. [27] and Trotz [28] reported the BET surface area of E33 to be 128.0 and 151.3 m^2 g^{-1}, respectively. The result reported herein for E33 is close to these values. For E33/Mn and E33/AgI, the BET surface area was reduced when compared to unmodified E33. Yet, as can be seen from the reduction in total pore volume (cm^3 g^{-1}) of these adsorbents, it is speculated that Mn and Ag nanoparticles adhered to the E33 surface at these pore sites, thus reducing porosity and total pore volume, as well as overall BET surface area. However, unlike E33/AgI, E33/AgII had a slight increase in BET surface area when compared to unmodified E33. Results from ICP–MS indicated that the concentration of leached Mn and Ag nanoparticles from the E33 surface were minimal and well below the EPA Secondary Drinking Water Regulations MCL (Table S2). This indicates the deposits are highly stable.

3.1.2. SEM characterization

SEM images of E33 and modified E33 are illustrated in Fig. 1. The surface morphology for the different adsorbents were determined to be similar to results previously reported [24]. Table S1 represents the weight percent of iron (Fe), phosphorus (P), manganese (Mn), and silver (Ag) on the adsorbents' surfaces; results were based on EDX analysis. While the adsorption capacity of E33 and E33/AgII were similar (as documented later in this report), the weight percent of phosphorus on the surface differed (see Table S1). This indicates that the PO_4^{3-} adsorption on E33/AgII may be dependent on intra-particle diffusion, in which the adsorbed species migrate into the pores of the adsorbent as opposed to remaining sorbed on the outer surface.

3.1.3. TEM and HR-TEM characterization

Fig. 2 represents TEM images at 220 k magnification of E33 and the modified adsorbents. Results were found to be similar to those previously reported, where E33, E33/AgI, and E33/AgII had rod-like structures and E33/Mn had formed oblong structures [24]. In order to investigate the crystal structure of the adsorbents in detail, HR-TEM was employed.

Fig. 3 shows HR-TEM images of E33 and surface modified E33 samples. The lattice spacing of 0.24 and 0.42 nm corresponding to (1 1 1) and (1 1 0) plane of goethite of iron oxide, respectively, was measured (see Fig. 3(a)) [29]. For the E33/AgI sample, the lattice spacing of 0.22 nm for (2 2 1) plane of goethite and 0.42 nm for (1 1 0) plane of goethite was measured [29]. The measured lattice spacing in the surface-modified samples with Ag was 0.20 and 0.24 nm corresponding to (2 0 0) and (1 1 1) plane of Ag, respectively, indicating the successful surface modification with Ag [30,31] even though no peaks corresponding to Ag were observed by XRD due to the surface-modification with low concentration of Ag (see Section 3.1.4). In the sample modified with Mn, the lattice spacing of 0.27 nm, which corresponds to (2 2 2) plane of Mn_2O_3 was measured [32–34].

3.1.4. XRD analysis

After the phosphate removal in the lake water samples, XRD analysis was conducted. The obtained peaks for all samples, shown in Fig. 4, (i.e., E33, E33/AgI, E33/AgII, and E33/Mn) were consistent with previous experiments which had shown that: (i) for E33, E33/AgI, and E33/AgII, corresponding peaks demonstrated typical XRD patterns for the iron oxide goethite (thus, the incorporation of Ag did not impact the phase transformation of goethite), (ii) peaks corresponding to Ag could not be detected, likely due to the concentration of silver used for modification (0.1 N $AgNO_3$), and (iii) for E33/Mn, peaks corresponding to hematite were detected, indicating a phase transformation [24].

Table 1
Structural characteristics of E33 and modified E33 before and after PO_4^{3-} adsorption.

Sample	Before adsorption			After adsorption		
	S_{BET} ($m^2\ g^{-1}$)	Total pore volume ($cm^3\ g^{-1}$)	Porosity (%)	S_{BET} ($m^2\ g^{-1}$)	Total pore volume ($cm^3\ g^{-1}$)	Porosity (%)
E33	140.4 ± 0.2	0.583	22.6	141.3 ± 0.5	0.582	22.5
E33/Mn	102.8 ± 0.4	0.441	18.1	99.9 ± 0.3	0.447	18.3
E33/AgI	124.6 ± 0.2	0.456	18.6	132.7 ± 0.4	0.552	21.6
E33/AgII	142.0 ± 0.3	0.553	21.7	139.7 ± 0.5	0.673	25.2

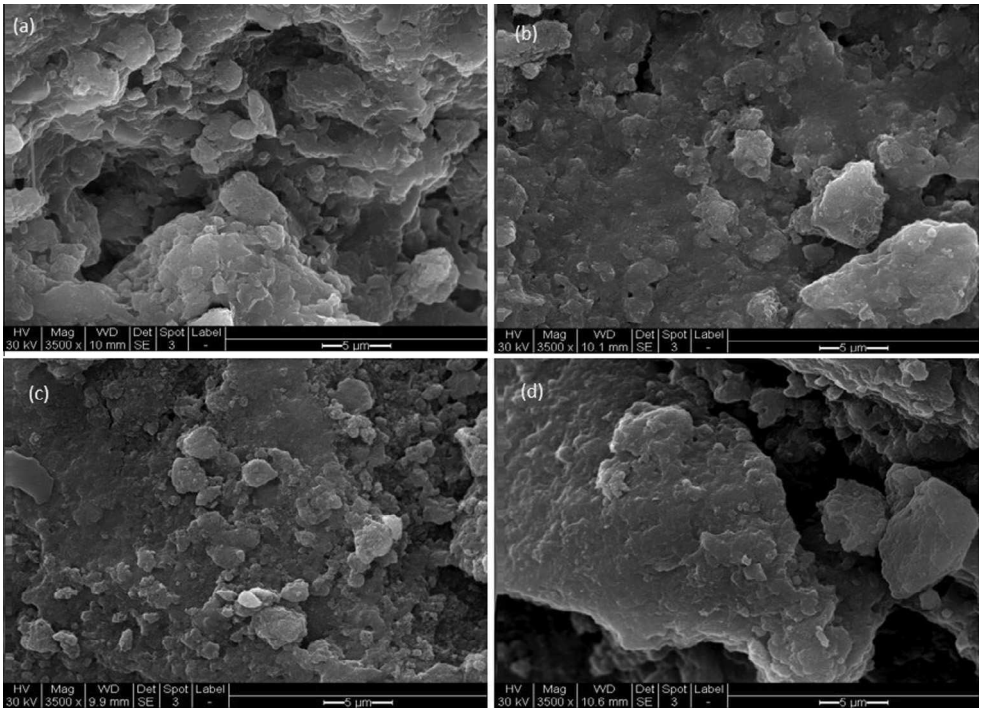

Fig. 1. SEM images of (a) E33, (b) E33/Mn, (c) E33/AgI, and (d) E33/AgII at 3.5 k magnification (all scale bars represent 5 μm).

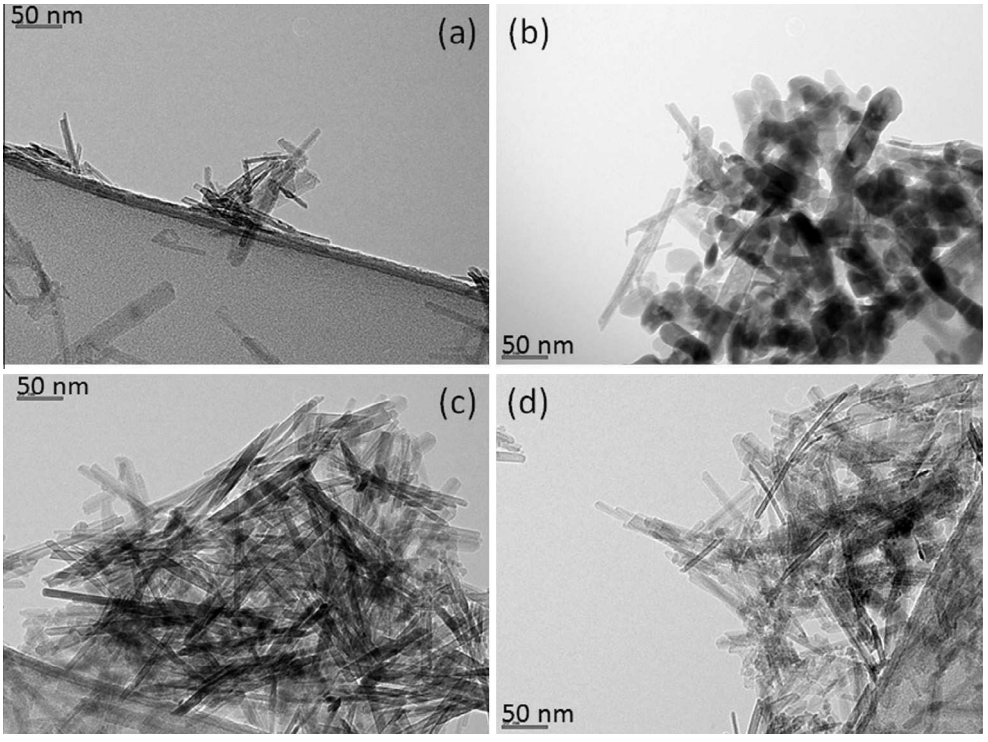

Fig. 2. TEM images of (a) E33, (b) E33/Mn, (c) E33/AgI, and (d) E33/AgII at 220 k magnification (all scale bars represent 50 nm).

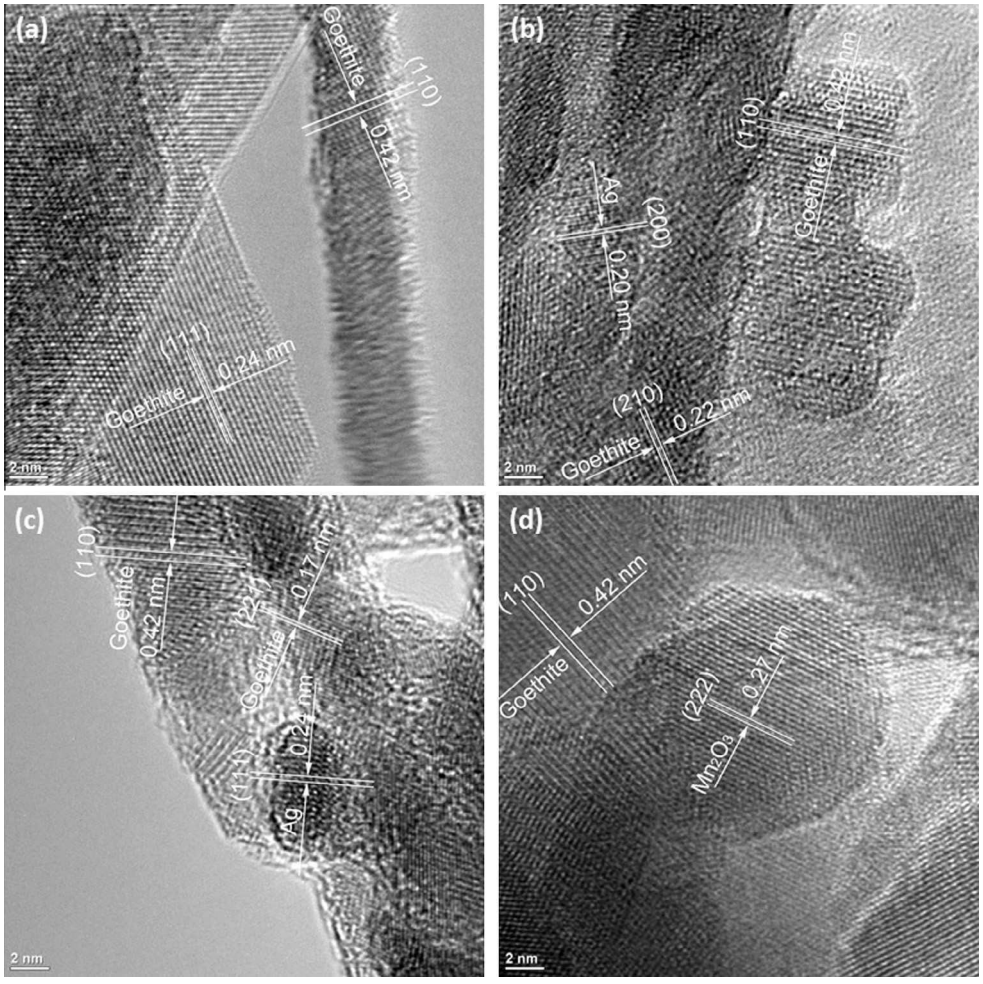

Fig. 3. HR-TEM images of (a) E33, (b) E33/Ag I, (c) E33/Ag II, and (d) E33/Mn used for phosphate removal in real lake water solutions (all scale bars represent 5 μm).

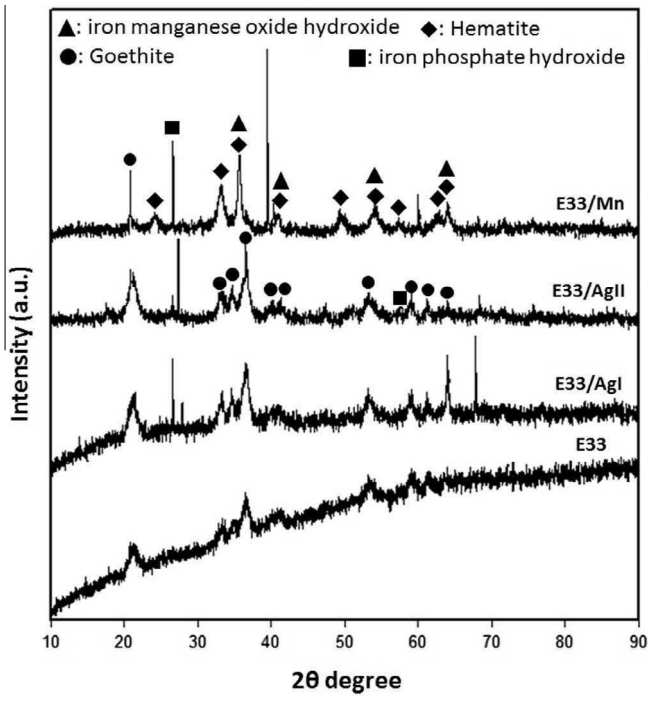

Fig. 4. XRD patterns of unmodified and modified E33 after using for phosphate removal in real lake water solution.

3.1.5. Point of zero charge

The point of zero charge (pH_{ZPC}) of the adsorbent was determined by measuring zeta potential as a function of pH. By interpolating the plot of zeta potential versus pH, results provided an estimate of pH_{ZPC}, which corresponds to the pH at which the zeta potential is equal to zero. The pH_{ZPC} is important in adsorption studies because, given the anionic character of phosphate, surface

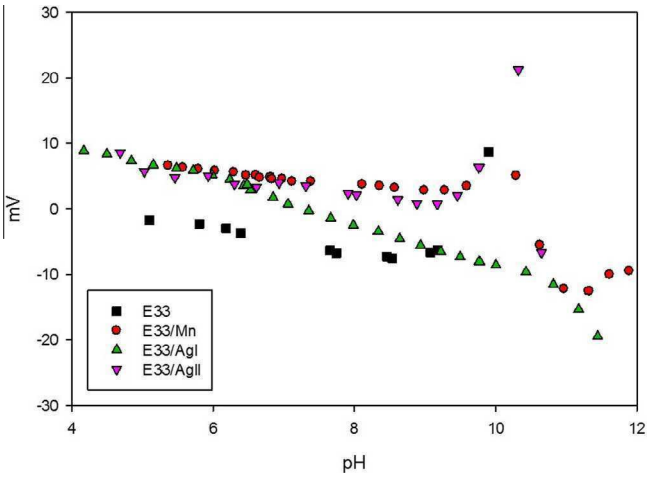

Fig. 5. Zeta potential versus pH of E33 and modified E33.

charge can play a significant role in terms of electrostatic interactions between the adsorbent and adsorbate. When the solution pH is above the pH_{ZPC}, for example, the surface charge on the iron oxide material is negative, thus promoting anion repulsion. However, below the pH_{ZPC}, the adsorbents will have a net positive charge, promoting electrostatic attraction of the negatively charged phosphate ion. Fig. 5 shows the zeta potential changes of unphosphated adsorbents with respect to pH. As pH increases from 4 to 12, the pH_{ZPC} of each adsorbent could be determined. For E33, the pH_{ZPC} was found to be 9.5. Reported pH_{ZPC} values were found to be slightly lower, ranging from 8.3 to 9.0 [26,35,36], yet for goethite (the major constituent of E33) reported pH_{ZPC} values were in the range of 7.2–9.7 [37–39]. The pH_{ZPC} for E33/Mn, E33/AgI, and E33/AgII were determined to be equal to 10.4, 7.3, and 10.5, respectively. These values illustrate the effective pH range for each adsorbent where the sorbent surface is positively charged.

3.2. Adsorption studies

3.2.1. Sorption isotherms

The specific relationship between the equilibrium adsorbate concentration in the bulk and the amount adsorbed at the surface can be revealed by sorption isotherms. The isotherm results for phosphate adsorption onto E33 and modified E33 at a constant temperature of 21 °C were analyzed using three common isotherms, the Langmuir, Freundlich, and Temkin isotherm models. The Langmuir adsorption equation is based on the following assumptions: (i) adsorption is limited to one monolayer, (ii) all surface sites are equivalent (i.e., free of defects), and (iii) adsorption to one site is independent of adjacent sites occupancy condition [40]. The Langmuir isotherm [41] is expressed as:

$$q_e = \frac{q_{max} K_L C_e}{1 + K_L C_e}$$

where q_e is the amount of adsorbate adsorbed per unit mass of adsorbent (mg g^{-1}), C_e is the amount of unadsorbed adsorbate concentration in solution at equilibrium (mg L^{-1}), q_{max} is the maximum amount of adsorbate per unit mass of adsorbent to form a complete monolayer on the surface (mg g^{-1}), and K_L is a constant related to the affinity of the binding sites (L mg^{-1}). In its linear form, the Langmuir equation can be described as:

$$\frac{C_e}{q_e} = \frac{1}{q_{max}} C_e + \frac{1}{K_L q_{max}}$$

A linear plot of specific adsorption against equilibrium concentration ((C_e q_e^{-1}) vs. C_e) as seen in Fig. 6 indicates that phosphate adsorption onto E33 and modified E33 obeys the Langmuir model. The Langmuir constants q_{max} and K_L, determined from the slope and intercept of the plot, are presented in Table 2. The calculated values for q_{max} indicate E33/AgII has a slightly higher capacity for phosphate sorption when compared to unmodified E33. This is consistent with the BET results in Table 1.

The dimensionless constant separation factor R_L [42] can be used to express essential characteristics of the Langmuir isotherm according to the following equation:

$$R_L = \frac{1}{1 + K_L C_0}$$

where C_0 is the initial adsorbate concentration (mg L^{-1}) and K_L is the Langmuir constant (L mg^{-1}). Values of R_L can indicate the favorability of adsorption; that is, for favorable adsorption, $0 < R_L < 1$; for unfavorable adsorption, $R_L > 1$; $R_L = 1$ for linear sorption; and for irreversible adsorption, $R_L = 0$ [42]. Values of R_L, documented in Table 2, were in the range of 0–1, suggesting favorable adsorption of phosphate onto E33 and modified E33.

The Freundlich isotherm [43], applicable for non-ideal adsorption on heterogeneous surfaces with multi-layer sorption, is expressed as:

$$q_e = K_F C_e^{1/n}$$

where K_F is related to the adsorption capacity of the adsorbent (mg g^{-1} (L $mg^{-1})^{1/n}$) and n indicates sorption favorability [44]. The K_F and n constants can be determined by the linearized form of the Freundlich equation:

$$\log q_e = \log K_F + \frac{1}{n} \log C_e$$

The linear plot of the Freundlich isotherm for phosphate adsorption onto E33 and modified E33 is shown in Fig. 7. The Freundlich constants K_F are related to the capacity of the adsorbent at a concentration of 1, depending on units. In this case it is 1 mg/L. The Freundlich constants are documented in Table 2. In this case, the Freundlich K_F is higher for the unmodified E33 as compared to the E33/AgII. However, the capacity of the E33/AgII is higher at other (lower) concentrations.

The effects of some indirect adsorbate/adsorbate interactions on adsorption isotherms was considered by Temkin and Pyzhev [45], who suggested that, due to these interactions, the heat of adsorption of all adsorbates in the layer would decrease linearly with respect to coverage. The Temkin isotherm is typically applied in the form:

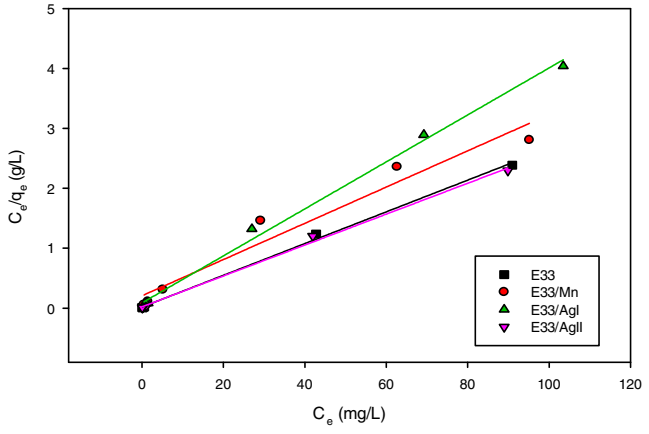

Fig. 6. Linear plot of Langmuir isotherm for phosphate sorption onto E33 and modified E33.

Table 2
Isotherm parameters.

Sorbent	Langmuir isotherm				Freundlich isotherm			Temkin isotherm		
	q_{max} (mg g^{-1})	K_L (L mg^{-1})	R_L	R^2	K_F (mg g^{-1}) (L $mg^{-1})^{1/n}$	$1/n$	R^2	A (mg L^{-1})	B	R^2
E33	37.74	1.359	0.006	0.998	18.92	0.17	0.758	311.7	3.8	0.891
E33/Mn	30.96	0.156	0.047	0.955	10.69	0.23	0.958	12.48	4.1	0.898
E33/AgI	25.52	0.440	0.017	0.996	12.22	0.16	0.846	113.6	2.7	0.920
E33/AgII	38.80	1.112	0.007	0.997	18.58	0.18	0.848	195.7	4.0	0.953

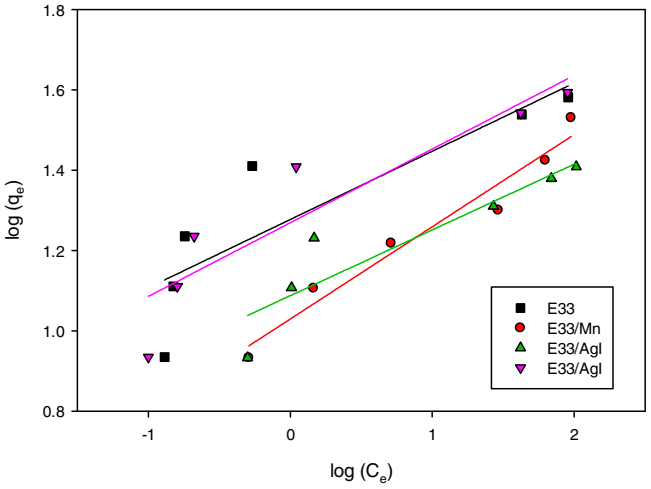

Fig. 7. Linear plot of Freundlich isotherm for phosphate sorption onto E33 and modified E33.

$$q_e = \left(\frac{RT}{b}\right)\ln(AC_e)$$

which can be linearized as:

$$q_e = B\ln A + B\ln C_e$$

where B is equal to $RT\,b^{-1}$, b (J mol^{-1}) is the Temkin constant related to the heat of sorption, A (L/g) is the Temkin isotherm constant, R (8.314 J mol^{-1} K^{-1}) is the universal gas constant, and T is the absolute temperature in Kelvin. Fig. 8 illustrates the linearized plot of the Temkin isotherm for phosphate adsorption onto E33 and modified E33 at constant temperature (21 °C) and the Temkin constants A and B were calculated using the slope and intercept of the plot and are tabulated in Table 2.

Based on the results obtained from isotherm experiments, it was determined that the adsorbents best followed the Langmuir model, which assumes a monolayer adsorption process. According to the model, E33/AgII and E33 had similar values of q_{max} (38.80 and 37.74 mg g^{-1}, respectively) while for E33/AgI and E33/Mn, q_{max} was equal to 25.52 and 30.96 mg g^{-1}, respectively. Previous studies explored the use of these adsorbents in phosphate spiked deionized water where a similar trend of q_{max} was observed [24]. However, in this previous study, a different initial phosphate

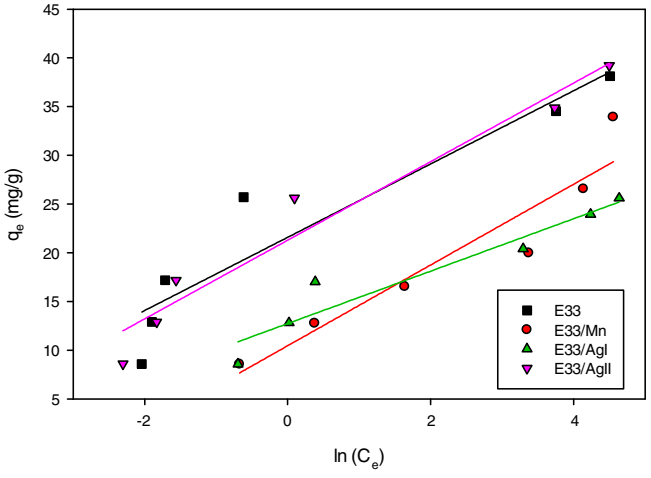

Fig. 8. Linear plot of Temkin isotherm for phosphate sorption onto E33 and modified E33.

Table 3
Effect of coexisting anions.

Concentration of anions (mM)			% PO_4^{3-} removal per adsorbent			
PO_4^{3-}	SO_4^{2-}	NO_3^-	E33	E33/Mn	E33/AgI	E33/AgII
2	0	0	99.93	97.06	99.30	99.93
2	2	0	99.84	95.99	99.08	99.85
2	0	2	97.72	96.84	93.98	99.57

concentration was used (i.e., 80 mg L^{-1}). Yet in comparing the maximum adsorption capacity with respect to initial phosphate concentration (i.e., q_{max}/C_0), the percentage of phosphate adsorbed for each system could be determined. For the DI-spiked solution, E33, E33/Mn, E33/AgI, and E33/AgII removed 31.1%, 22.6%, 24.9%, and 33.9%, respectively while for the lake water solution, removal percentages for the listed adsorbents were 27.0%, 22.1%, 18.2%, and 27.7%, respectively. The decreased phosphate removal percentages was believed to be due to competing species in the lake water. Therefore, the impact of co-existing species was investigated.

Surface and wastewaters generally contain common anions including sulfates (SO_4^{2-}) and nitrates (NO_3^-) in addition to PO_4^{3-}. These anions may interfere in the adsorption of phosphate onto E33 and E33-based adsorbents. Therefore, to evaluate the impact these competing species have on phosphate adsorption, isotherm experiments were conducted using equimolar concentrations of SO_4^{2-} or NO_3^- in the presence of PO_4^{3-}. The results in Table 3 show that no significant change in phosphate adsorption onto E33 after adding equimolar SO_4^{2-} or NO_3^-. This could be credited to specific binding of phosphate onto the adsorbent's specific active sites. Thus, the decreased phosphate adsorption using the lake water solution in comparison to previous studies [24] is believed to be caused by the presence of dissolved organic matter (DOM) in the lake water.

While enhanced phosphate adsorption was not observed for E33/Mn and E33/AgI, these sorbents may have other benefits. Silver-coated E33, for example, has shown to be a bacterial growth inhibitor based on previous experiments. When subjected to a bacterial growth inhibition assay, silver-modified E33 (E33/AgI and E33/AgII) had very high inhibition for *Staphylococcus aureus* and moderate inhibition for *Escherichia coli* [46]. As E33 is commonly used in column systems, issues related to biofouling can negatively impact the overall performance of the column system. Thus, the use of silver-modified E33 could alleviate these issues and result in a better performing system. Furthermore, E33 was originally designed for the remediation of arsenic. The Mn modified sample was found to successfully oxidize the more toxic and mobile As (III) to As(V) and simultaneously remove the As(V) from aqueous solutions [47]. Thus, this adsorbent, while more expensive than unmodified E33, could potentially be used (i.e., if a situation arises where a waterway is contaminated with both As(III) and PO_4^{3-}).

3.2.2. Kinetic studies

Batch experiments were conducted to explore the rate of phosphate adsorption onto E33 and modified E33 at pH 7.0, adsorbent dose of 5 g L^{-1}, and a target initial phosphate concentration of 140 mg L^{-1}. Processing of kinetic adsorption data can be conducted to understand adsorption dynamics in terms of the order of the rate constant. The pseudo-first-order and pseudo-second-order kinetic models were used to represent the kinetics of phosphate adsorption onto goethite-based materials. The pseudo-first-order model and pseudo-second-order model are expressed, respectively, as:

$$\log(q_e - q_t) = \log(q_e) - \frac{k_1 t}{2.303}$$

$$\frac{t}{q_t} = \frac{1}{k_2 q_e^2} + \frac{t}{q_e}$$

where q_t and q_e are the amount of phosphate adsorbed at time t and at equilibrium, respectively, k_1 (min^{-1}) is the rate constant of pseudo-first-order model adsorption, and k_2 ($g\ min^{-1}\ mg^{-1}$) is the rate constant of pseudo-second-order model adsorption. If pseudo-second-order kinetics is applicable, a plot of q_t versus t should provide a linear relationship and if pseudo-first-order kinetics is applicable, a plot of $\log(q_e - q_t)$ versus t should be linear. The calculated regression coefficients for the kinetic models are documented in Table 4. Figs. SI1 and 9 show the plots of the pseudo-first-order model and the pseudo-second-order model, respectively.

The regression coefficients of the pseudo-second-order model ($\geqslant$0.9980 for all adsorbents) revealed to be the best in representing phosphate adsorption onto E33 and modified E33, while the pseudo-first-order model regression coefficients were below 0.9 (except for E33, R^2 = 0.9796), indicating this model is not applicable. The pseudo-second-order model assumes a monolayer adsorption system (which agrees with isotherm results as the Langmuir model also assumes only monolayer adsorption), and that the mechanism of adsorption is determined by chemisorption, as opposed to physisorption. Chemisorption involves valence forces where the adsorbent and adsorbate share or exchange electrons. $k_2 q_e^2$ is considered as the initial adsorption rate ($mg\ g^{-1}\ min^{-1}$), which was determined for E33, E33/Mn, E33/AgI, and E33/AgII and documented in Table 4. Based on these results, while E33/Mn had the lowest adsorption capacity, it had the fastest initial rate of adsorption.

3.2.3. Intra-particle diffusion studies

The process of adsorption contains multiple steps including the transport of molecules from the aqueous phase to the solid surface and then, diffusion of solute molecules into the pores of the adsorbent. This process of pore diffusion is typically slow and thus, is rate determining. The rate q_t for intra-particle diffusion, provided by Webber and Morris [48] is:

$$q_t = k_p t^{1/2} + C$$

where q_t is the amount of phosphate adsorbed per unit mass of adsorbent ($mg\ g^{-1}$) at time t, C is related to the thickness of the boundary layer, and k_p ($mg\ g^{-1}\ min^{1/2}$) is the intra-particle diffusion rate constant. A plot of phosphate adsorbed versus the square root of time (q_t vs. $t^{1/2}$) presents a multi-linearity correlation, as seen in Fig. 10, indicating that two or more steps occurred during the adsorption process. The first phase (i.e. the steeper portion) represents external mass transfer or film diffusion. If the lines pass through the origin in this phase, then intra-particle diffusion is the rate-controlling process. However, values of C (as seen in Table 5) are larger than 0, and are proportional to the thickness of the boundary layer. Thus, it is postulated that a combination of intra-particle diffusion and film diffusion are rate-limiting. The second phase is the equilibrium stage where intra-particle diffusion begins to slow due to: (a) the pores for diffusion become smaller, (b) the electrostatic repulsion of the adsorbent surface was enhanced, and (c) the solute concentration in solution became very low.

It is surmised that E33 and modified E33 rapidly adsorbed phosphate onto its external surface, then phosphate was slowly transported by intra-particle diffusion into the particle and retained in the pores. The intra-particle rate constant, k_p, and C were calculated from the plots in Fig. 10 and the results were reported in Table 5.

While the lines for the plot of q_t vs. $t^{1/2}$ are near the origin, further data analysis can provide more insight into the rate-controlling step by using the following equation:

$$F = 1 - \frac{6}{\pi^2}\exp(-Bt)$$

where F is the fraction of adsorbed solute at different times and Bt is a function of F. F can be expressed by:

$$F = \frac{q_t}{q_e}$$

where q_t and q_e represent the amount of phosphate adsorbed at any time and at equilibrium or infinite time. Substituting the above equations, the expression becomes:

Table 4
Kinetic model parameters.

Adsorbent	Pseudo-second-order model			
	k_2 ($g\ mg^{-1}\ min^{-1}$)	q_e ($mg\ g^{-1}$)	R^2	$k_2 q_e^2$ ($mg\ g^{-1}\ min^{-1}$)
E33	0.0098	27.47	0.999	102.1
E33/Mn	0.0080	24.39	0.999	125.0
E33/AgI	0.0096	22.42	0.998	104.5
E33/AgII	0.0091	27.25	0.999	109.4

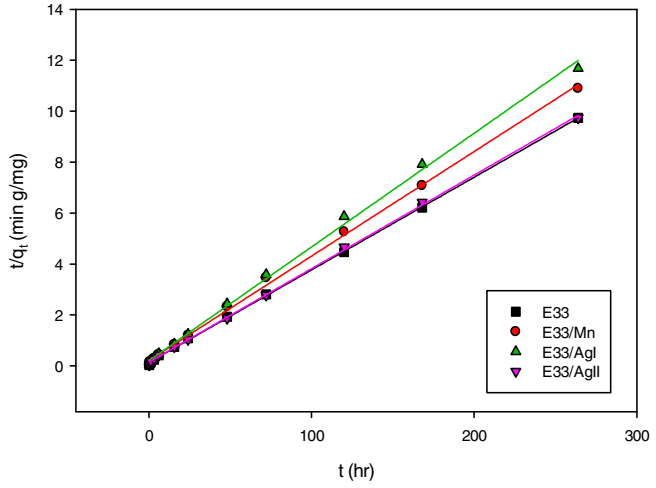

Fig. 9. Pseudo-second-order kinetic model for the adsorption of phosphate by E33 and modified E33.

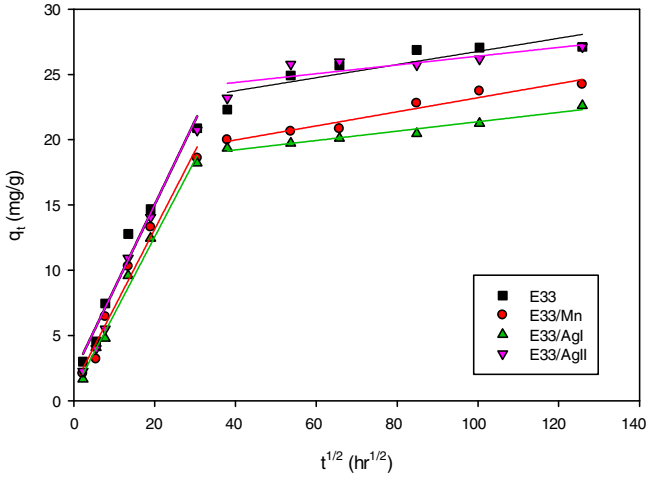

Fig. 10. Intra-particle diffusion kinetics for phosphate adsorption onto E33 and modified E33.

Table 5
Intra-particle diffusion parameters.

Adsorbent	$K_{p,1}$ (mg g^{-1} min$^{-1/2}$)	C (mg g^{-1})	R^2	$K_{p,2}$ (mg g^{-1} min$^{-1/2}$)	C (mg g^{-1})	R^2
E33	0.6441	2.153	0.971	0.0504	21.728	0.760
E33/Mn	0.6001	1.152	0.977	0.0539	17.826	0.948
E33/AgI	0.5906	0.751	0.990	0.0359	17.782	0.956
E33/AgII	0.6726	0.798	0.991	0.0336	23.040	0.680

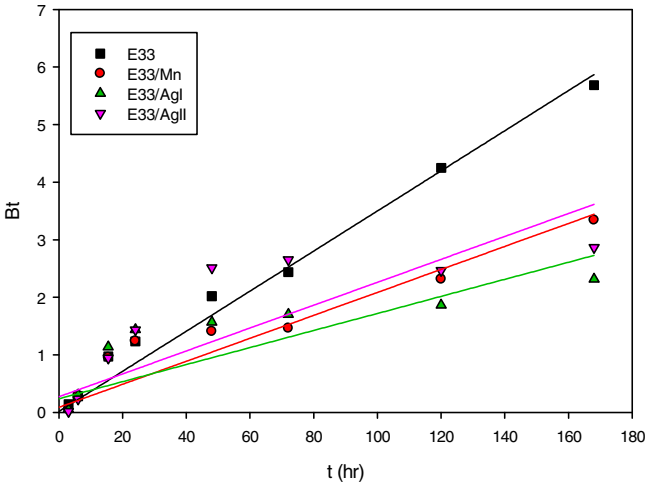

Fig. 11. Correlationship of Bt vs. t for phosphate adsorption onto E33 and modified E33.

$$Bt = -0.4977 - \ln\left(1 - \frac{q_t}{q_e}\right)$$

Therefore, the value of *Bt* can be calculated for each value of *F* and these values were plotted against time as shown in Fig. 11. Fig. 11 provides useful information for distinguishing between film diffusion and intra-particle diffusion rates of adsorption. If *Bt* vs. *t* is a straight line passing though the origin, then adsorption is governed by particle-diffusion. According to Fig. 11, it can be seen that the plots do go through the origin; yet correlation coefficients were low (0.9796, 0.8945, 0.7034, and 0.7145 for E33, E33/Mn, E33/AgI, and E33/AgII, respectively). Thus, a combination of intra-particle diffusion and film diffusion is believed to be the rate-limiting process for all four adsorbents.

3.2.4. Fixed-bed column test

To evaluate the practical application of E33 and modified E33 for the continuous removal of phosphate from solution, fixed bed column tests were conducted. Fig. 12 shows the breakthrough curve for each adsorbent. The breakthrough point for E33, E33/Mn, and E33/AgI were similar and occurred after about 0.75 h, yet for E33/AgII, breakthrough did not occur until about 1.5 h. This indicates that E33/AgII can operate for longer times when compared to the other adsorbents, which will reach saturation faster. E33/Mn had the lowest BET surface area of the investigated adsorbents and was the fastest adsorbent to reach saturation, followed by E33/AgI (which had the second lowest BET surface area) while E33 and E33/AgII reached saturation at nearly the same time. This indicates that the adsorbents' BET surface area plays an important role in breakthrough time of adsorption. It is expected that the anti-microbial aspects of the silver impregnated adsorbent (controlling biofouling) would not affect the results from this experiment because of the short time frame involved.

The process of phosphate adsorption in the columns can be explained by the Yoon–Nelson model, an adsorption model widely applied to single component systems, expressed as:

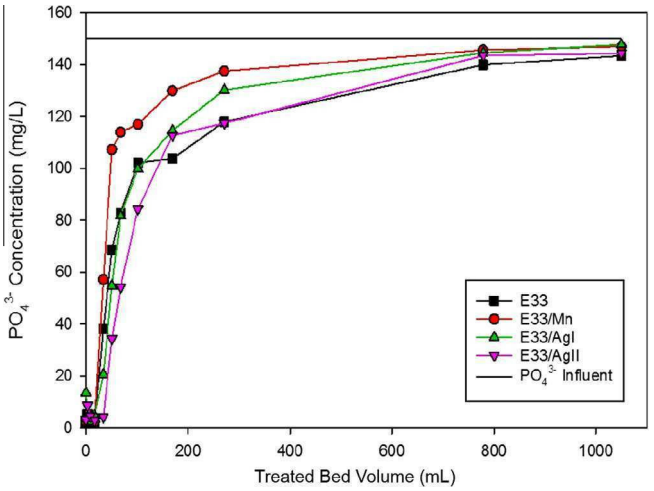

Fig. 12. Breakthrough curve of E33 and modified E33 for phosphate adsorption.

$$\ln\left(C_t/C_i - C_t\right) = K_{YN}(t - \tau)$$

where C_t and C_i are the phosphate concentrations (mg L^{-1}) at time (t) in the effluent and in the influent, respectively, t is the column service time (min), τ is the time required for 50% adsorbate breakthrough (min), and K_{YN} is the proportionality constant (min^{-1}). The Yoon–Nelson model parameters (K_{YN} and τ) were calculated by a plot of $\ln(C_t/C_i - C_t)$ vs. t using linear regression and presented in Table 6. The values of τ obtained from the model, as summarized in Table 6, are in good agreement with those obtained from the column experiment, confirming the applicability of the Yoon–Nelson model to this system.

3.3. Desorption studies

Phosphate desorption tests were conducted using spent adsorbents from isotherm experiments to evaluate the potential for PO_4^{3-} recovery. Desorbability is defined as the ratio of phosphate desorbed over the total phosphate adsorbed by the sorbents. Thus, PO_4^{3-} desorbability can indicate the degree of phosphate desorption from the different adsorbents. The impact of desorption solution was investigated by using two different solutions, a 0.05 M NaOH solution and a 0.10 M NaOH solution. The data in Table 7 show that PO_4^{3-} desorption using 0.05 M NaOH ranged from 30% to 67%, with E33/Mn having the highest desorption percent and E33/AgII the lowest. Also, an increase in the concentration NaOH corresponded to an increase in PO_4^{3-} desorption; where 60–80% of phosphate

Table 6
Yoon–Nelson model parameters obtained from breakthrough curve fitting.

Adsorbent	K_{YN} (min^{-1})	τ (min)	τ_{exp} (min)	R^2
E33	0.044	102.2	99.7	0.878
E33/Mn	0.057	84.6	70.2	0.883
E33/AgI	0.043	107.9	110.4	0.983
E33/AgII	0.033	139.3	158.1	0.840

Table 7
Desorbability of phosphate adsorbed by adsorbents.

Sample	Adsorbed PO_4^{3-} (mg g^{-1})	0.05 M NaOH		0.10 M NaOH	
		Desorbed PO_4^{3-} (mg g^{-1})	Desorption (%)	Desorbed PO_4^{3-} (mg g^{-1})	Desorption (%)
E33	11.02	3.55	32.2	6.68	60.6
E33/Mn	10.97	7.35	67.0	8.67	79.0
E33/AgI	11.01	4.47	43.1	7.10	64.4
E33/AgII	11.02	3.36	30.5	6.48	58.8

desorption was observed using 0.10 M NaOH. Interestingly, the sorbents with the highest PO_4^{3-} adsorption capacity (i.e. E33 and E33/AgII) had lower values of phosphate desorption when compared to the less sorptive samples (E33/Mn and E33/AgI). However, this is most likely due to the types of bonds formed; indicating that E33/Mn and E33/AgI formed weaker bonds with phosphate, making desorption easier for these sorbents.

4. Conclusion

Variable dose isotherm experiments, conducted to determine equilibrium adsorption parameters, indicated the Langmuir isotherm model was most applicable. The maximum adsorption capacity of single monolayer for E33, E33/Mn, E33/AgI, and E33/AgII, based on the Langmuir model, were 37.74, 30.96, 25.52, and 38.80 mg phosphate per gram of adsorbent, respectively. In comparison to previous studies using a DI-based system, results for adsorption capacity herein were reduced. This is likely due to the presence of DOM as neither sulfate nor nitrate proved to impact phosphate adsorption using these adsorbents. Batch experiments revealed the kinetics of adsorption followed the pseudo-second-order model (R^2 for all adsorbents $\geqslant$ 0.998).

Intra-particle diffusion studies indicated that phosphate adsorption onto all studied adsorbents occurred in two different steps; the first (film diffusion) occurred rapidly while the second (intra-particle diffusion) was slow (e.g. for E33/AgII k_{p1} = 0.6726 - mg g^{-1} $min^{-1/2}$ while k_{p2} = 0.0336 mg g^{-1} $min^{-1/2}$). Also, intra-particle diffusion studies showed that, for E33, intra-particle diffusion was the rate-limiting process, while for the three modified sorbents (E33/Mn, E33/AgI, and E33/AgII), the rate-limiting process was a combination of intra-particle diffusion and film diffusion. Finally, column experiments revealed that the time for breakthrough for E33/AgII was twice as long as for the other adsorbents (i.e., 1.5 h compared to 45 min), which implies E33/AgII has a greater phosphate adsorption capacity when compared to unmodified E33. Though isotherm experiments revealed that the maximum adsorption capacity of E33 and E33/AgII were very similar (37.7 vs. 38.8 mg g^{-1}), the multifunctionality of E33/AgII could provide improved adsorption characteristics.

Also, E33/Mn and E33/AgI had higher phosphate desorption as compared to E33 and E33/AgII. Though E33/Mn and E33/AgI had a decreased capacity for phosphate sorption, their desorption percentages were much higher than E33 and E33/AgII indicating their benefits of enhanced desorption for the recovery of phosphate.

Notice

The U.S. Environmental Protection Agency, through its Office of Research and Development, funded and managed, or partially funded and collaborated in, the research described herein. It has been subjected to the Agency's administrative review and has been approved for external publication. Any opinions expressed in this paper are those of the author(s) and do not necessarily reflect the views of the Agency, therefore, no official endorsement should be inferred. Any mention of trade names or commercial products does not constitute endorsement or recommendation for use.

Appendix A. Supplementary data

Supplementary data associated with this article can be found, in the online version, at http://dx.doi.org/10.1016/j.cej.2015.08.114.

References

[1] W.K. Dodds, W.W. Bouska, J.L. Eitzmann, T.J. Pilger, K.L. Pitts, A.J. Riley, J.T. Schloesser, D.J. Thornbrugh, Eutrophication of U.S. freshwaters: analysis of potential economic damages, Environ. Sci. Technol. 43 (2008) 12–19.
[2] T.C. Daniel, A.N. Sharpley, J.L. Lemunyon, Agricultural phosphate and eutrophication: a symposium overview, J. Environ. Qual. 27 (1998) 251–257.
[3] D.M. Anderson, P.M. Glibert, J.M. Burkholder, Harmful algal blooms and eutrophication: nutrient sources, composition, and consequences, Estuaries 25 (2002) 704–726.
[4] J.T. Sims, R.R. Simard, B.C. Joern, Phosphorus loss in agricultural drainage: historical perspective and current research, J. Environ. Qual. 27 (1998) 277–293.
[5] D.G. Devey, N. Harkness, The significance of man-made sources of phosphorus: detergents and sewage, Water Res. 7 (1973) 35–54.
[6] V. Smil, Phosphorus in the environment: natural flows and human interferences, Annu. Rev. Energy Environ. 25 (2000) 53–88.
[7] D.W. De Haas, M.C. Wentzel, G.A. Ekama, The use of simultaneous chemical precipitation in modified activated sludge systems exhibiting biological excess phosphate removal: part 1: literature review, Water SA 26 (2000) 439–452.
[8] A. Oehmen, R.J. Zeng, Z. Yuan, Modeling the aerobic metabolism of polyphosphate-accumulating organisms enriched with propionate as a carbon source, Water Environ. Res. 79 (2007) 2477–2486.
[9] T. Panswad, A. Doungchai, J. Anotai, Temperature effect on microbial community of enhanced biological phosphorus removal system, Water Res. 37 (2003) 409–415.
[10] I. Steen, Phosphorus availability in the 21st century: management of a non-renewable resource, Phosphorus Potassium 217 (1998) 25–31.
[11] R.P. Sheldon, Industrial minerals-with emphasis on phosphate rock, in: D.J. McLaren, B.J. Skinner (Eds.), Resources and World Development, John Wiley & Son Limited, New York, 1987, pp. 347–361.
[12] L. Li, R. Stanforth, Distinguishing adsorption and surface precipitation of phosphate on goethite (α-FeOOH), J. Colloid Interface Sci. 230 (2000) 12–21.
[13] R. Chitrakar, S. Tezuka, A. Sonoda, K. Sakane, K. Ooi, T. Hirotsu, Phosphate adsorption on synthetic goethite and akaganeite, J. Colloid Interface Sci. 298 (2006) 602–608.
[14] J.-Y. Bottero, A. Masion, Adsorbate structure at clay surfaces: surfactants at clay–water interface, in: P. Somasundaran (Ed.), Encyclopedia of Surface and Colloid Science, CRC Press, Boca Raton, Florida, 2006, pp. 140–148.
[15] U. Schwertmann, Solubility and dissolution of iron oxides, Plant Soil 130 (1991) 1–25.
[16] R.M. Cornell, U. Schwertmann, The Iron Oxides: Structure, Properties, Reactions, Occurrences and Uses, second ed., John Wiley & Sons, New York, 2006.
[17] W. Chesworth, Encyclopedia of Soil Science, Springer Science and Business Media, New York, 2008.
[18] M. Badruzzaman, P. Westerhoff, D.R. Knappe, Intraparticle diffusion and adsorption of arsenate onto granular ferric hydroxide (GFH), Water Res. 38 (2004) 4002–4012.
[19] M. Bissen, F.H. Frimmel, Arsenic – a review. Part II: oxidation of arsenic and its removal in water treatment, Acta Hydroch. Hydrob. 31 (2003) 97–107.
[20] T.B. Mlilo, L.R. Brunson, D.A. Sabatini, Arsenic and fluoride removal using simple materials, J. Environ. Eng. 136 (2009) 391–398.
[21] M. Kanematsu, T.M. Young, K. Fukushi, P.G. Green, J.L. Darby, Extended triple layer modeling of arsenate and phosphate adsorption on a goethite-based granular porous adsorbent, Environ. Sci. Technol. 44 (2010) 3388–3394.
[22] M. Kanematsu, T.M. Young, K. Fukushi, D.A. Sverjensky, P.G. Green, J.L. Darby, Quantification of the effects of organic and carbonate buffers on arsenate and phosphate adsorption on a goethite-based granular porous adsorbent, Environ. Sci. Technol. 45 (2011) 561–568.

[23] A. Sperlich, Phosphate adsorption onto granular ferric hydroxide (GFH) for wastewater reuse, Papierflieger (2010) 1–120.
[24] J. Lalley, C. Han, G.R. Mohan, D.D. Dionysiou, T.F. Speth, J. Garland, M.N. Nadagouda, Phosphate removal using modified Bayoxide® E33 adsorption media, Environ. Sci. Water Res. Technol. 1 (2015) 96–107.
[25] J. Murphy, J.P. Riley, A modified single solution method for the determination of phosphate in natural waters, Anal. Chim. Acta 27 (1962) 31–36.
[26] AdEdge Technologies Inc., <http://www.adedgetechnologies.com/index.html>.
[27] A. Naeem, P. Westerhoff, S. Mustafa, Vanadium removal by metal (hydro)oxide adsorbents, Water Res. 41 (2007) 1596–1602.
[28] M.A. Trotz, The feasibility of removing inorganic arsenic from landfill leachate via sorption to mineral oxide surfaces, Florida Center for Solid and Hazardous Waste-report, 2008, pp. 1–62.
[29] J. Akai, K. Akai, M. Ito, S. Nakano, Y. Maki, I. Sasagawa, Biologically induced iron ore at Gunma iron mine, Am. Mineral. 84 (1999) 171–182.
[30] C. Han, V. Likodimos, J.A. Khan, M.N. Nadagouda, J. Anderson, P. Falaras, P. Rosales-Lombardi, D.D. Dionysiou, UV–visible light-activated Ag-decorated, monodisperse TiO_2 aggregates for treatment of the pharmaceutical oxytetracycline, Environ. Sci. Pollut. Res. 21 (2014) 11781–11793.
[31] P. Asanithi, S. Chaiyakun, P. Limsuwan, Growth of silver nanoparticles by DC magnetron sputtering, J. Nanomater. 2012 (2012) 963609.
[32] J.N. Park, J.K. Shon, M. Jin, S.H. Hwang, G.O. Park, J.H. Boo, T.H. Han, J.M. Kim, Highly ordered mesoporous α-Mn_2O_3 for catalytic decomposition of H_2O_2 at low temperature, Chem. Lett. 39 (2010) 493–495.
[33] Q. Javed, F.P. Wang, M.Y. Rafique, A.M. Toufiq, Q.S. Li, H. Mahmood, W. Khan, Diameter-controlled synthesis of α-Mn_2O_3 nanorods and nanowires with enhanced surface morphology and optical properties, Nanotechnology 23 (2012) 415603.
[34] G. Yang, W. Yan, J. Wang, H. Yang, Fabrication and formation mechanism of Mn_2O_3 hollow nanofibers by single-spinneret electrospinning, CrystEngComm 16 (2014) 6907–6913.
[35] G.L. Amy, H.W. Chen, A. Dinzo, P. Brandhuber, Adsorbent Treatment Technologies for Arsenic Removal, American Water Works Association, 2005.
[36] P. Westerhoff, M. De Haan, A. Martindale, M. Badruzzaman, Arsenic adsorptive media technology selection strategies, Water Qual. Res. J. Canada 41 (2006) 171–184.
[37] S. Goldberg, H.S. Forster, C.L. Godfrey, Molybdenum adsorption on oxides, clay minerals, and soils, Soil Sci. Soc. Am. J. 60 (1996) 425–432.
[38] J. Antelo, M. Avena, S. Fiol, R. López, F. Arce, Effects of pH and ionic strength on the adsorption of phosphate and arsenate at the goethite–water interface, J. Colloid Interface Sci. 285 (2005) 476–486.
[39] W.A. Zeltner, M.A. Anderson, Surface charge development at the Goethite/aqueous solution interface: effect of CO_2 adsorption, Langmuir 4 (1988) 469–474.
[40] S.J. Allen, G. McKay, K.Y.H. Khader, Equilibrium adsorption isotherms for basic dyes onto lignite, J. Chem. Technol. Biotechnol. 45 (1989) 291–302.
[41] I. Langmuir, The adsorption of gases on plane surfaces of glass, mica and platinum, J. Am. Chem. Soc. 40 (1918) 1361–1403.
[42] K.R. Hall, L.C. Eagleton, A. Acrivos, T. Vermeulen, Pore- and solid-diffusion kinetics in fixed-bed adsorption under constant-pattern conditions, Ind. Eng. Chem. Fundam. 5 (1966) 212–223.
[43] H.M.F. Freundlich, Über die Adsorption in Lösungen, Z. Phys. Chem. 57 (1906) 385–470.
[44] M.M. Davila-Jimenez, M.P. Elizalde-Gonzalez, A.A. Pelaez-Cid, Adsorption interaction between natural adsorbents and textile dyes in aqueous solution, Colloids Surf. A 254 (2005) 107–114.
[45] M. Temkin, V. Pyzhev, Kinetics of ammonia synthesis on promoted iron catalysts, Acta Physicochim. USSR 12 (1940) 327–356.
[46] M.N. Nadagouda, C. Bennett-Stamper, C. White, D. Lytle, Multifunctional silver coated E-33/iron oxide water filters: Inhibition of biofilm growth and arsenic removal, RSC Adv. 2 (2012) 4198–4204.
[47] M.N. Nadagouda, D.A. Lytle, Microwave-assisted combustion synthesis of nano iron oxide/iron-coated activated carbon, anthracite, cellulose fiber, and silica, with arsenic adsorption studies, Nanotechnology 2011 (2011) 1–8.
[48] W.J. Weber, J.C. Morris, Preliminary appraisal of advanced waste treatment processes, Proc. Int. Conf. Adv. Water Pollut. Res. 2 (1963) 231–241.

Materials Chemistry and Physics 198 (2017) 115–124

Contents lists available at ScienceDirect

Materials Chemistry and Physics

journal homepage: www.elsevier.com/locate/matchemphys

Removal of phosphate using calcium and magnesium-modified iron-based adsorbents

Changseok Han [a, 1], Jacob Lalley [b, 1], Nidhi Iyanna [c], Mallikarjuna N. Nadagouda [d, *]

[a] Oak Ridge Institute for Science and Education (ORISE) Postdoctoral Research Associate, The U.S. Environmental Protection Agency, ORD, NRMRL, STD, CPB, 26 W. Martin Luther King Jr. Drive, Cincinnati, OH, 45268, USA
[b] Pegasus Technical Services Inc., 46 E Hollister St, Cincinnati, OH, 45219, USA
[c] William Mason High School, Mason, 45040, OH, USA
[d] The U.S. Environmental Protection Agency, ORD, NRMRL, WSWD, WQMB, 26 W. Martin Luther King Jr. Drive, Cincinnati, OH, 45268, USA

HIGHLIGHTS

- Magnetic Ca and Mg-modified iron oxide adsorbents were synthesized.
- PVA imparted magnetism to the adsorbents for easy separation.
- Batch adsorption experiments were carried out to gain insights on the adsorption kinetics and equilibrium.
- The adsorbents effectively removed phosphates from water at a capacity of nearly 17 mg g^{-1}.

GRAPHICAL ABSTRACT

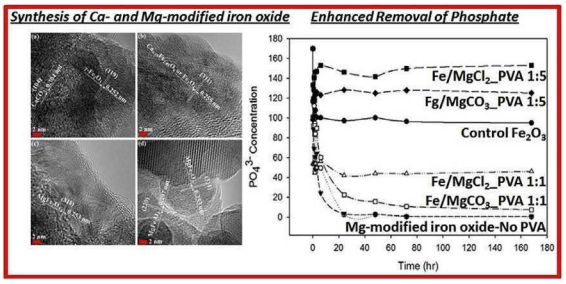

ARTICLE INFO

Article history:
Received 14 June 2016
Received in revised form
22 March 2017
Accepted 21 May 2017
Available online 23 May 2017

Keywords:
Easy separation
Magnetic
Iron oxide
Adsorbent
Phosphate

ABSTRACT

Magnetic calcium (Ca) and magnesium (Mg)-modified iron oxide adsorbents were synthesized using $CaCl_2$, $CaCO_3$, $MgCl_2$, or $MgCO_3$ by a simple combustion method for the remediation of phosphate. Modification with Ca and Mg significantly improved the phosphate adsorption capacity of the magnetic iron oxide adsorbents. Additionally, polyvinyl alcohol (PVA) was incorporated during synthesis to aid in the magnetism of the samples, making the adsorbents easy to separate from solutions. Physicochemical properties of the adsorbents were determined by characterization with X-ray diffraction (XRD), particle analyzer, scanning electron microscopy (SEM), transmission electron microscopy (TEM), and high resolution TEM (HR-TEM). Batch adsorption experiments were carried out to gain insight on the materials' ability to remove phosphate from water supplies. Samples without the addition of PVA had higher phosphate capacities (ranging from 16.92 to 16.97 mg g^{-1}) compared to PVA-containing samples (ranging from 12.39 to 16.74 mg g^{-1}), yet the PVA-containing samples were magnetic and thus, easily separable.

Published by Elsevier B.V.

1. Introduction

Phosphorous (P) is one of the essential elements for all life as it is significantly associated with the DNA/RNA structure, cell membrane formation, energy storage/transfer, as well as enzyme activation or deactivation [1,2]. Phosphorus is commonly found in

* Corresponding author.
E-mail address: Nadagouda.Mallikarjuna@epa.gov (M.N. Nadagouda).
[1] Contributed equally to this work.

http://dx.doi.org/10.1016/j.matchemphys.2017.05.038
0254-0584/Published by Elsevier B.V.

sources of drinking water due to an inflow of urban and industrial wastewater and agricultural run-offs, which contain phosphates [3–7]. Phosphates entering into the nutrient limited aquatic environment are significantly involved in eutrophication, which is associated with the formation of massive algal blooms, excessive growth of microorganisms, and depletion of dissolved oxygen [8–10]. Moreover, massive algal blooms containing cyanobacteria can be a potential hazard to humans and animals because some species of cyanobacteria produce and release toxins, known as cyanotoxins [11–13]. Therefore, it is of great interest to develop reliable technologies for the removal of phosphates from water.

Currently, chemical precipitation [14], biological processes [15], and adsorption [16] have been widely used for removing phosphate from water, yet both chemical precipitation and biological processes have disadvantages. While chemical precipitation has been shown to reduce phosphorus concentrations by 60–95%, depending on many factors including influent water parameters and coagulant dosage [17]; these methods involve high operating costs as well as the production of large amounts of sludge, and the efficiency of this method depends on the types of chemicals used for phosphate removal [18,19]. Biological processes have several drawbacks as well. In order to achieve maximal phosphate removal, operating conditions and water quality parameters must be very specific. For example, the system only functions optimally when phosphate concentrations are $\geq$5–10 mg L^{-1} and when the ratio of BOD to P is at least 35:1 [16]. Therefore, in order to improve the efficiency of phosphate removal by chemical precipitation and biological processes, enhanced biological phosphorus removal (EBPR) has been extensively studied [20–22]. The removal of phosphate was significantly improved by applying EBPR, which employs designed communities of microorganisms (aka, phosphorus accumulating organisms (PAO)). High concentrations of calcium (Ca) and magnesium (Mg) were recommended to achieve high efficiency removal of phosphate in EBPR. The Ca attributes to the formation of hydroxyapatite ($Ca_5(PO_4)_3OH$), which is about 39% of the phosphate precipitation in EBPR and Mg is associated with precipitation of struvite ($MgNH_4PO_4 \cdot 6H_2O$) or newberyite ($MgHPO_4$) [20,23–25]. However, the formation of phosphate precipitates during EBPR operations have caused significant problems including pipe blockage and precipitate accumulation on the surface of equipment such as pumps and centrifuges in the treatment system [26]. Also, ranges of phosphate accumulation vary widely (i.e., from 20 to 80%) based on the PAO used [27]. Therefore, adsorption has attracted much attention for phosphate removal because of its simplicity, inexpensiveness, and low sludge production. Also, adsorption is an appropriate method for removing low concentrations of phosphate [28]. Thus, the use of Ca- and Mg-modified adsorbents were explored as they have been shown effective at improving the EBPR process and can form phosphate precipitates.

2. Materials and methods

Herein, Ca- and Mg-modified ferrites as phosphate adsorbents were synthesized by a simple combustion method using polyvinyl alcohol (PVA). Iron(III) nitrate ($Fe(NO_3)_3 \cdot 9H_2O$, certified ACS, Fisher Scientific), calcium or magnesium precursors, and PVA (MW 89,000–98,000, 99+% hydrolyzed, Sigma-Aldrich) were mixed together using 5 mL of milli-Q grade water. Then, the mixtures were calcined in a muffle furnace (Ney Vulcan, A-550) at 300 °C for 1 h. Calcium carbonate ($CaCO_3$, $\geq$99.0%, Sigma-Aldrich) or calcium chloride ($CaCl_2 \cdot 2H_2O$, 74.27%, Fisher Scientific), and magnesium carbonate ($MgCO_3$, Sigma-Aldrich) or magnesium chloride ($MgCl_2 \cdot 6H_2O$, ACS reagent, J. T. Baker) were used to prepare Ca-ferrite and Mg-ferrite, respectively. Control iron oxide (Fe_2O_3) was synthesized without Ca and Mg precursors or PVA. The detailed information of the ingredients for the synthesis of Ca- and Mg-modified ferrite are summarized in Table 1. Synthesized samples were characterized by X-ray diffraction (XRD, Panalytical X'pert 2-theta diffractometer, obtained from Panalytical, Almelo, Netherlands at a wavelength of 1.54 Å and at 2-theta range 2-90° under CuK_α radiation), porosimetry (using a Tristar 3000 porosimeter analyzer, obtained from Micromeritics), scanning electron microscopy (SEM, model Philips XL 30 ESEM-FEG, at an accelerating voltage of 30 kV), transmission electron microscopy (TEM, a FEI CM20 TEM operated at 200 kV was employed), and high resolution TEM (HR-TEM, model JEM-2010F, obtained from JEOL, was employed with a field gun emission gun at 200 kV). Prior to HR-TEM characterization, the adsorbents were prepared and dispersed by ultrasonication (2510R-DH, Bransonic) in 99.8% pure isopropyl alcohol, obtained from Pharmco-AAPER for 30 min. Then, on a carbon-coated copper grid (LC325-Cu, EMS), a drop of the supernatant was fixed and dried at room temperature. The images obtained from the HR-TEM were analyzed using ImageJ, an image processing software (National Institutes of Health, Maryland, USA). To evaluate the phosphate adsorption capacity of the prepared samples, batch equilibrium experiments at pH 7 were conducted using the buffer 3-(N-morpholino) propanesulfonic acid (MOPS), obtained from Sigma-Aldrich. Variable dose isotherm studies were conducted using different masses of adsorbent (ranging from 0.1 to 1.5 g) in 125 mL Nalgene polypropylene bottles with 100 mL of phosphate solution. The stock phosphate solution was prepared by dissolving 3 g of sodium phosphate monohydrate ($NaH_2PO_4 \cdot H_2O$, Sigma-Aldrich), obtained from Fisher Scientific, in 11 L of deionized water at a target phosphate concentration of 200 mg L^{-1}. The concentrations of phosphate were measured by a standard colorimetry EPA Method 365.1 [29].

3. Results and discussion

3.1. Adsorbent characterization

XRD characterization of the samples are shown in Fig. 1. The XRD patterns of synthesized Ca- and Mg-modified samples were identified with JCPDS 00-036-0398 for magnesioferrite ($MgFe_2O_4$), 00-006-0502 for hematite (α-Fe_2O_3), 00-025-1402 for maghemite (γ-Fe_2O_3), 00-047-1743 for calcite ($CaCO_3$), 00-005-0628 for halite (NaCl), 00-019-0629 for magnetite (Fe_3O_4), and 00-046-0291 for calcium iron oxide ($Ca_{0.15}Fe_{2.85}O_4$). As seen in Fig. 1(c), all peaks corresponding to non-magnetic hematite were detected. This indicates that PVA is necessary to convert non-magnetic iron oxide to magnetic iron oxide (i.e., maghemite, magnetite, and ferrite). Unfortunately, no peaks corresponding to Ca or Mg were found.

Table 1
Ingredients for the synthesis of Ca- and Mg-modified ferrite.

Sample	$Fe(NO_3)_3$ (g)	Ca (g)	Mg (g)	PVA (g)
Control Fe_2O_3	25	0	0	0
Fe/$CaCl_2$-No PVA	40.4	11.0	0	0
Fe/$MgCl_2$-No PVA	40.4	0	9.5	0
Fe/$CaCO_3$-No PVA	64.6	8.0	0	0
Fe/$MgCO_3$-No PVA	64.6	0	6.7	0
Fe/$CaCO_3$_PVA 1:1	40.4	7.4	0	47.8
Fe/$CaCl_2$_PVA 1:1	40.4	11.1	0	51.5
Fe/$CaCO_3$_PVA 1:5	4.04	0.74	0	23.9
Fe/$CaCl_2$_PVA 1:5	4.04	1.11	0	25.8
Fe/$MgCO_3$_PVA 1:1	20.2	0	4.2	24.4
Fe/$MgCl_2$_PVA 1:1	20.2	0	5.1	25.3
Fe/$MgCO_3$_PVA 1:5	4.04	0	0.8	24.2
Fe/$MgCl_2$_PVA 1:5	4.04	0	1.0	25.3

Note: 5 mL of water was used to prepare all samples.

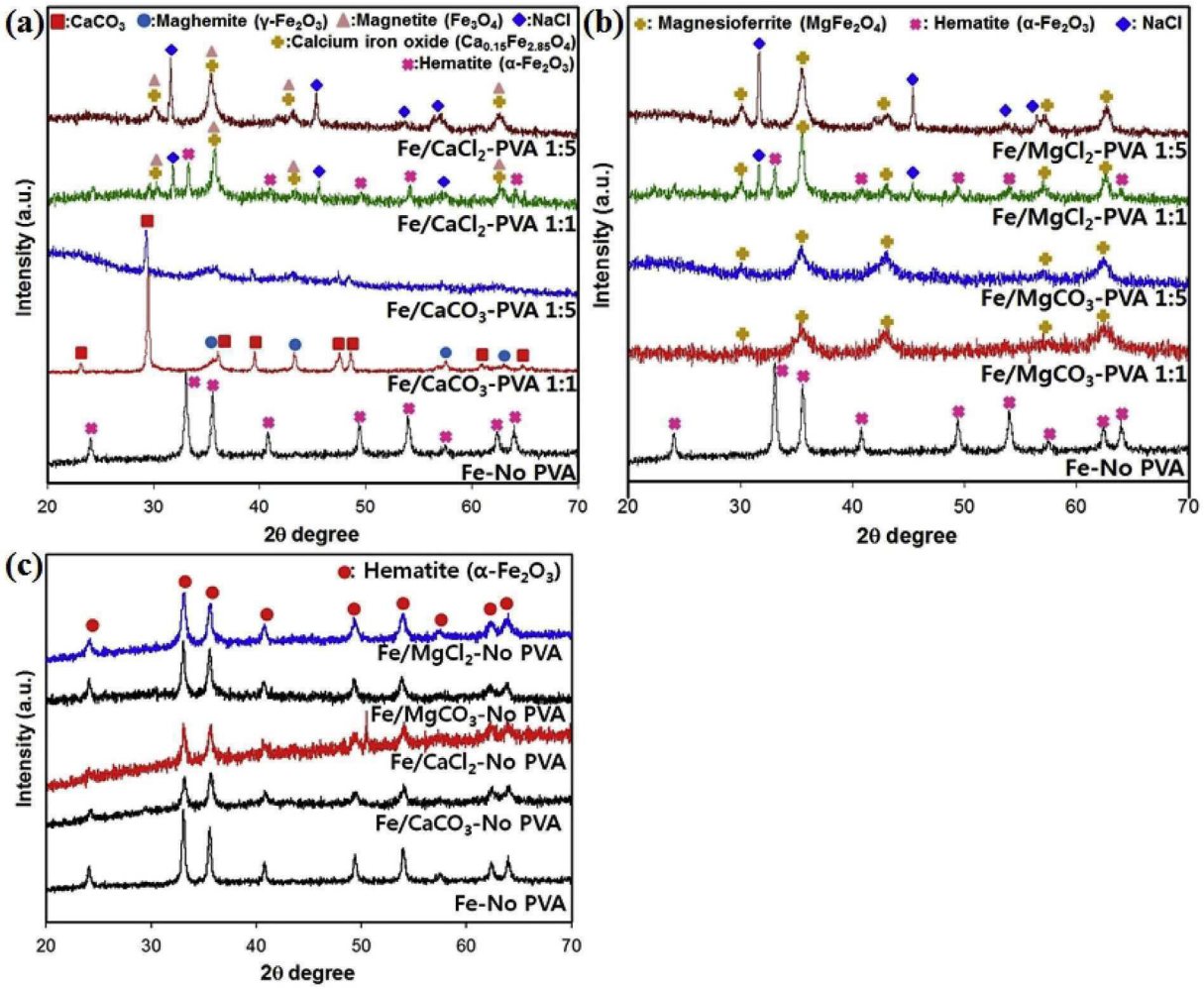

Fig. 1. XRD patterns for Ca- and Mg-modified samples: (a) Ca-modified ferrite with PVA, (b) Mg-modified ferrite with PVA and (c) Ca- and Mg-modified samples without PVA.

However, Ca and Mg were found in the samples with EDS analysis (see Fig. 2). The peaks for Ca and Mg could not be observed from XRD characterization possibly because Ca and Mg exist in an amorphous phase in the synthesized samples.

When PVA was added during synthesis, hematite to maghemite, magnetite, or magnetic ferrite transformations were observed in all samples after the combustion process (see Fig. 1(a) and (b)). However, the formation of calcium iron oxide was not detected in Ca-modified samples with $CaCO_3$. It may result from different ion sizes of Mg (Effective diameter = 0.09 nm), Ca (Effective diameter = 0.14 nm), and Fe (Effective diameter = 0.1 nm) [30]. Since the effective diameter of Mg ions is very similar to that of Fe ions, Mg ions may easily replace Fe ions compared to Ca ions to form Mg-modified ferrite [30]. However, when chlorides (i.e., $CaCl_2$ and $MgCl_2$) were used, calcium iron oxide ($Ca_{0.15}Fe_{2.85}O_4$) and magnesioferrite ($MgFe_2O_4$) formed since chloride salts dissolve well in water compared to carbonates like $CaCO_3$ and $MgCO_3$. However, a small amount of Ca replaced Fe ions due to the large effective diameter of Ca ions and thus, $Ca_{0.15}Fe_{2.85}O_4$ formed instead of $CaFe_2O_4$. Similar phenomena could be found in other studies [12,31]. For example, since the ionic radius of sulfur (S^{2-}) (0.17 nm) is larger than oxygen (O^{2-}) (0.122 nm), sulfur (S^{2-}) could not easily replace oxygen (O^{2-}) and it requires more energy to synthesize sulfur-doped titanium dioxide (TiO_2) [12,31,32]. Moreover, peaks corresponding to non-magnetic hematite observed in the samples of $Fe/CaCl_2$_PVA 1:1 and $Fe/MgCl_2$_PVA 1:1 disappeared. The hematite completely transformed to magnetic ferrite or magnetite by adding more PVA (a ratio of 1:5). This indicates that the combustion method provided enough energy required to synthesize magnetic iron oxides.

SEM characterization of control Fe_2O_3 and the four synthesized Ca- and Mg-modified samples without PVA are shown in Fig. S3. Without Ca and Mg precursors, small spherical iron oxide particles less than 1000 nm formed as shown in Fig. S3(a) and (b). Micro-sized, larger aggregates formed when $CaCl_2$ was used for the modification of Fe_2O_3 as seen in Fig. S3(c). When $CaCO_3$ was used as the Ca precursor, particle sizes decreased to less than 500 nm but they still aggregated (see Fig. S3(d)). Interestingly, similar patterns were observed during the preparation of Mg-modified samples. When a carbonate was used, particle sizes significantly decreased from 950 ± 500 nm to 180 ± 56 nm as seen in Fig. S3(e) and (f). Ca and Mg precursors may affect the aggregation of particles during the synthesis.

Fig. 3 shows the SEM images of Ca-modified samples with PVA. Since $CaCO_3$ has very low solubility in water, the morphology of the control Fe_2O_3 did not change during the combustion process with the ratio of 1:1 (see Fig. S3(b) and Fig. 3(a)). However, it is not easy to find the uniform spherical particles for the samples synthesized with the ratio of 1:5 as shown in Fig. 3(b). The particles appeared to be partially coated, this may be the result of incomplete combustion

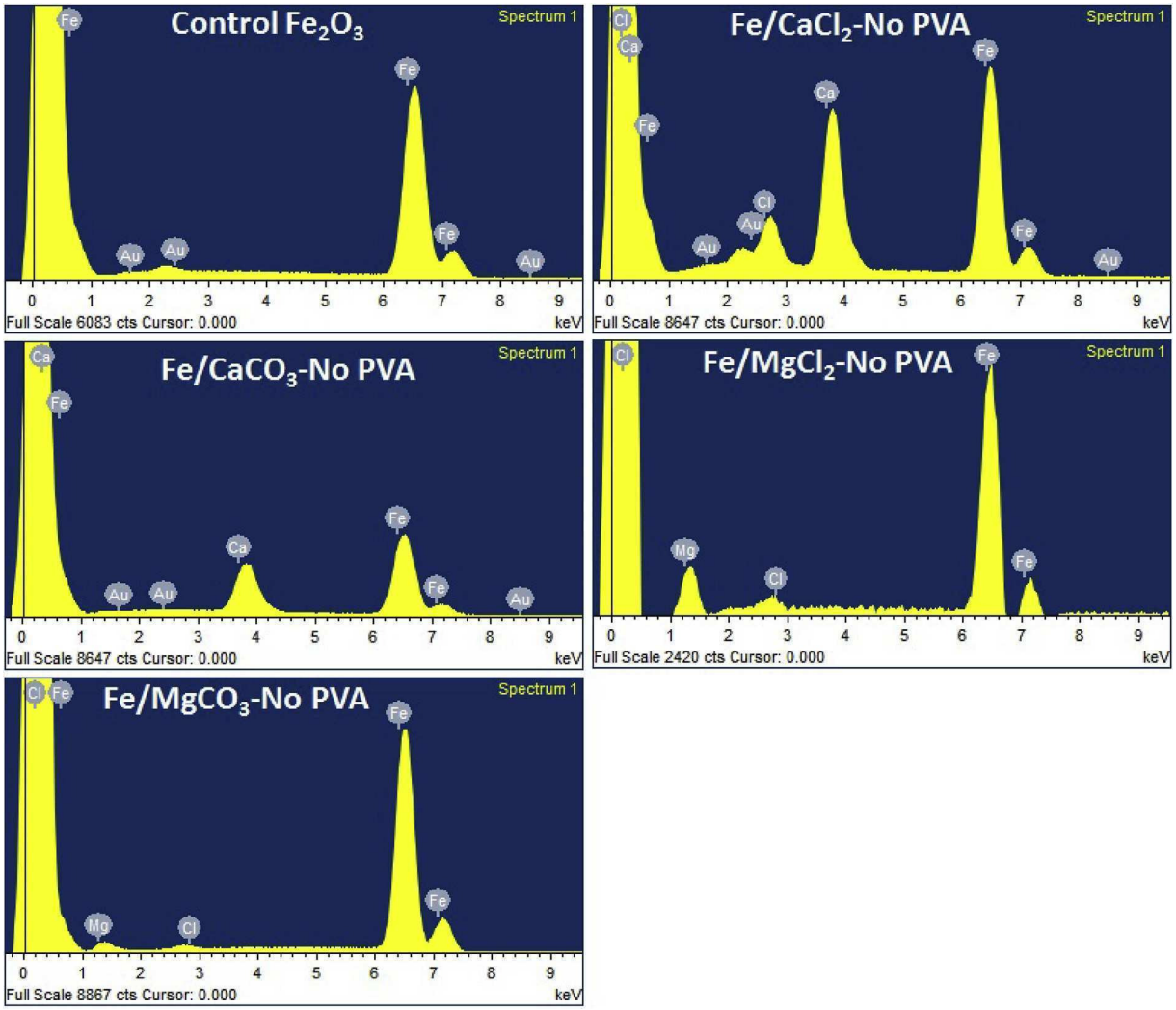

Fig. 2. EDS analysis for Ca- and Mg-modified samples without PVA. It shows the presence of Ca or Mg in the synthesized samples. The presence of gold (Au) was due to the Au coating on the samples during a sputtering process.

of PVA during the synthesis process. However, as shown in Fig. 3(c) and (d), sample size and shape changed by using $CaCl_2$ since $CaCl_2$ dissolves well in water. Larger aggregates formed compared to the $CaCO_3$ modified sample. For the samples prepared with the ratio of 1:5, large aggregates, with sizes ranging from 500 nm to 1 μm, formed. Small nanoparticles ranging from 30 to 80 nm were trapped in the large aggregates. In both cases of $CaCO_3$ and $CaCl_2$ with the ratio of 1:5, carbon content highly increased after the combustion (see the EDS analysis in Table 2). This may indicate PVA was not completely burned out from the synthesized samples and coated nanoparticles to form larger aggregates.

The results of SEM analysis of Mg-modified samples using $MgCO_3$ and $MgCl_2$ are shown in Fig. 4. As shown in Fig. 4(a) and (b), nanoparticles with an average size of 53 ± 12 nm started forming spherical aggregates with an average size of 270 ± 90 nm in the samples prepared with $MgCO_3$. With the ratio of 1:5, slightly larger and more uniform spherical aggregates of 290 ± 37 nm appeared to form. Mg content analyzed by EDS in both large and small aggregates was very similar which indicates Mg was uniformly incorporated into the samples during sample preparation. On the other hand, large aggregates with an average size of 360 ± 55 nm formed in the samples prepared using $MgCl_2$ of 1:1 ratio. With a 1:5 ratio, nanoparticles less than 20 nm formed and did not have a specific structure.

The synthesized samples were also characterized with TEM. As seen in Fig. S4(a), spherical nanoparticles with a diameter ranging from 15 to 120 nm formed in the control Fe_2O_3. This is in good agreement with the SEM analysis showing the formation of nanoparticles (<100 nm). By adding Ca and Mg precursors to modify the control Fe_2O_3, the size and shape of the primary particles changed. Nanoparticles and nanorods with irregular sizes and shapes were synthesized in the Ca- and Mg-modified samples. Additionally, magnetic Ca- and Mg-modified samples were analyzed with TEM (see Figs. 5 and 6). By adding PVA, spherical nanoparticles formed in Ca-modified samples. With excess PVA (i.e., ratio of 1:5), even though small particles with an average diameter of 6.2 ± 1.6 nm for $Fe/CaCO_3$_PVA and 10.6 ± 4.1 nm for $Fe/CaCl_2$_PVA formed, the formed nanoparticles were capped into PVA resulting in a decrease of BET surface area from 8.7 to 0.6 $m^2\ g^{-1}$ for $Fe/CaCO_3$_PVA and from 31.4 to 17.5 $m^2\ g^{-1}$ for $Fe/CaCl_2$_PVA (see Fig. 5). For Mg-modified samples, smaller and uniform particles formed with an average size of 15.0 ± 4.8 nm for $Fe/MgCO_3$_PVA and 19.5 ± 2.4 nm for $Fe/MgCl_2$_PVA in the presence of excess PVA (i.e., ratio of 1:5). In these cases, the BET surface area of the samples decreased from 46.8 to 14.3 $m^2\ g^{-1}$ for $Fe/MgCO_3$_PVA and from 57.9 to 19.5 $m^2\ g^{-1}$ for $Fe/MgCl_2$_PVA at a higher loading of PVA due to an excess of PVA.

Further analysis on the synthesized samples was done using HR-TEM to obtain lattice spacing information as seen in Figs. 7 and 8.

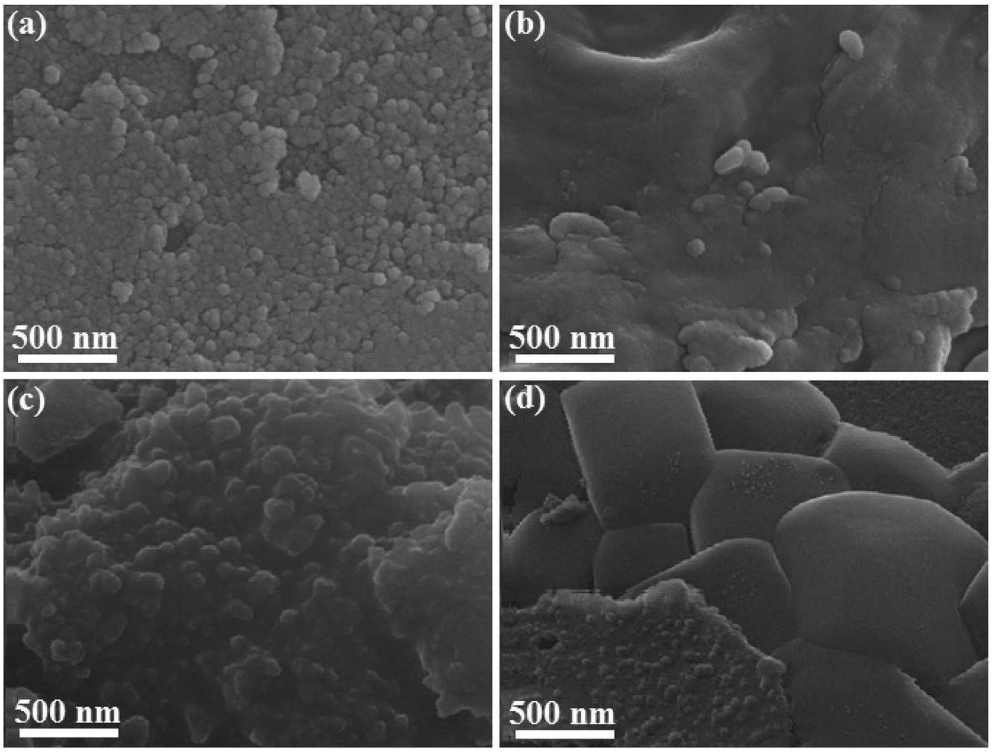

Fig. 3. SEM images of Ca-modified samples with PVA: (a) Fe/$CaCO_3$_PVA 1:1, (b) Fe/$CaCO_3$_PVA 1:5, (c) Fe/$CaCl_2$_PVA 1:1, and (d) Fe/$CaCl_2$_PVA 1:5.

Table 2
EDS analysis for Ca- and Mg-modified samples.

Sample	Carbon (%)	Ca (%)	Mg (%)
Fe/$CaCO_3$_PVA 1:1	18.8	11.9	–
Fe/$CaCO_3$_PVA 1:5	86.5	5.8	–
Fe/$CaCl_2$_PVA 1:1	16.7	8.9	–
Fe/$CaCl_2$_PVA 1:5	66.7	2.4	–
Fe/$MgCO_3$_PVA 1:1	17.0	–	1.2
Fe/$MgCO_3$_PVA 1:5	79.0	–	6.0
Fe/$MgCl_2$_PVA 1:1	31.5	–	5.0
Fe/$MgCl_2$_PVA 1:5	75.1	–	0.8

The measured lattice spacing of the control Fe_2O_3 sample was 0.250 nm, corresponding to (110) plane of α-Fe_2O_3 (see Fig. S1). This confirms the results of XRD analysis reporting the formation of non-magnetic hematite in control Fe_2O_3 samples. In Ca- and Mg-modified samples without PVA, a lattice spacing of 0.250 nm, corresponding to (110) plane for α-Fe_2O_3 was observed, as shown in Fig. 7(a)-(d). In Fig. 8(a) for the Fe/$CaCO_3$_PVA 1:1 sample, the (104) plane of $CaCO_3$ with 0.304 nm was observed along with the measured lattice spacing of 0.252 nm, corresponding to (119) plane of magnetic γ-Fe_2O_3. Since $CaCO_3$ does not dissolve in water, Ca could not be effectively incorporated into the iron oxide during the synthesis but magnetic γ-Fe_2O_3 formed since sufficient energy was provided for phase transformation by PVA incineration. Otherwise, $Ca_{0.15}Fe_{2.85}O_4$ and Fe_3O_4 formed in the sample synthesized with $CaCl_2$. Due to the water solubility of $CaCl_2$, Ca could be incorporated into the iron oxides as seen in Fig. 8(b).

However, as discussed before, a small amount of Ca^{2+} ions could be facilitated to form $Ca_{0.15}Fe_{2.85}O_4$ due to the larger effective size of Ca^{2+} compared to Fe ions. Interestingly, Mg was well incorporated into the iron oxides in both cases using $MgCO_3$ and $MgCl_2$, resulting in the formation of $MgFe_2O_4$ with the PVA assisted-synthesis method (see Fig. 8(c) and (d)). Due to their similar effective diameter (Mg = 0.09 nm and Fe = 0.1 nm) [30], Fe was effectively replaced with Mg. These results are in good agreement with the XRD analysis.

3.2. Adsorption experiments

Adsorption experiments were conducted using the synthesized adsorbents to evaluate their affinity towards phosphate. For the Mg-modified samples, as seen in Fig. 9, the addition of PVA negatively impacted phosphate adsorption. Fe/$MgCO_3$_PVA 1:1 and Fe/$MgCl_2$_PVA 1:1 removed 95.7 and 72.9% of phosphate, respectively. However, Fe/$MgCO_3$_PVA 1:5 and Fe/$MgCl_2$_PVA 1:5 removed 26.3 and 10.0% of phosphate, respectively. Furthermore, the control samples (with no PVA) removed higher percentages of phosphate (99.5 and 99.8% for Fe/$MgCO_3$—No PVA and Fe/$MgCl_2$-No PVA, respectively) yet these samples were not magnetically separable. A similar trend was observed for the Ca-modified samples, where higher ratios of PVA negatively impacted phosphate adsorption. As seen in Fig. 10, Fe/$CaCO_3$_PVA 1:5 and Fe/$CaCl_2$_PVA 1:5 removed 11.2 and 22.3% of phosphate, respectively. The samples with a 1:1 PVA ratio removed 98.5 and 93.0% of phosphate for Fe/$CaCO_3$_PVA 1:1 and Fe/$CaCl_2$_PVA 1:1. Again, with the Ca-modified adsorbents, the samples with no PVA had the highest adsorption percentages. Fe/$CaCO_3$—No PVA removed 99.6% of phosphate and Fe/$CaCl_2$—No PVA removed 99.8% of phosphate. These may result from the positive surface charge of the adsorbent. The added Ca and Mg provide more positive charges on the adsorbents and promote the adsorption of phosphate [33–35]. The use of electrostatic interaction to improve adsorption capacity for the removal of negatively or positively charged contaminants has been extensively reported in many studies [33–37]. Also, phosphate may react with slowly released Ca^{2+} from the adsorbents and then precipitate in the system [38] since iron oxides could dissolve in water at different pHs, resulting in the improvement of phosphate removal.

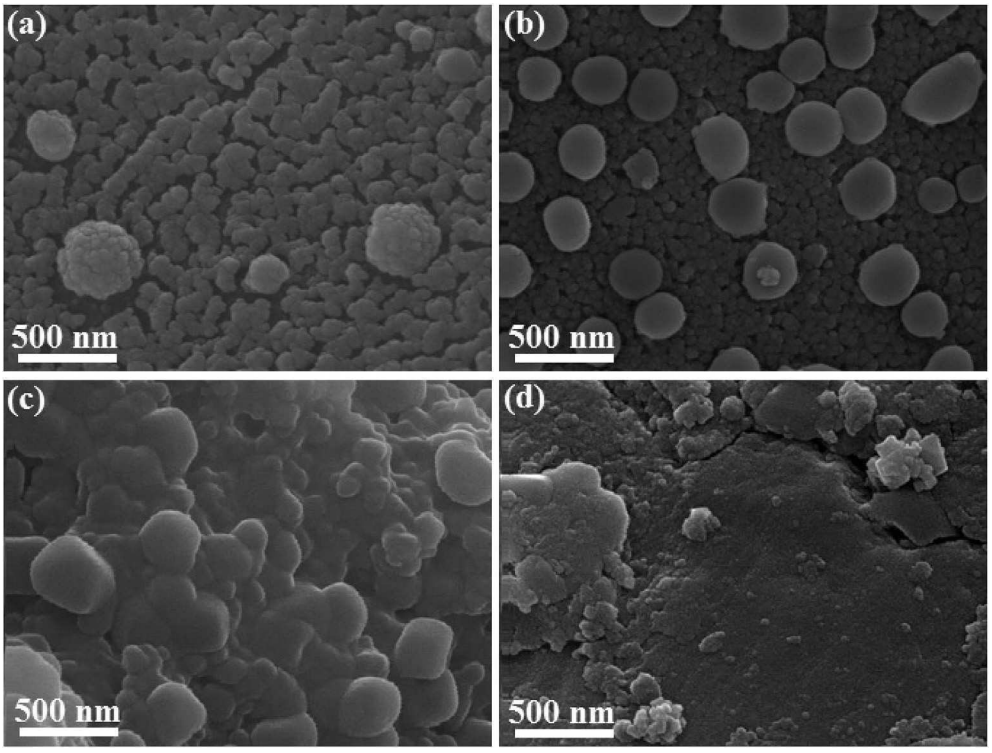

Fig. 4. SEM images of Mg-modified samples with PVA: (a) Fe/$MgCO_3$_PVA 1:1, (b) Fe/$MgCO_3$_PVA 1:5, (c) Fe/$MgCl_2$_PVA 1:1, and (d) Fe/$MgCl_2$_PVA 1:5.

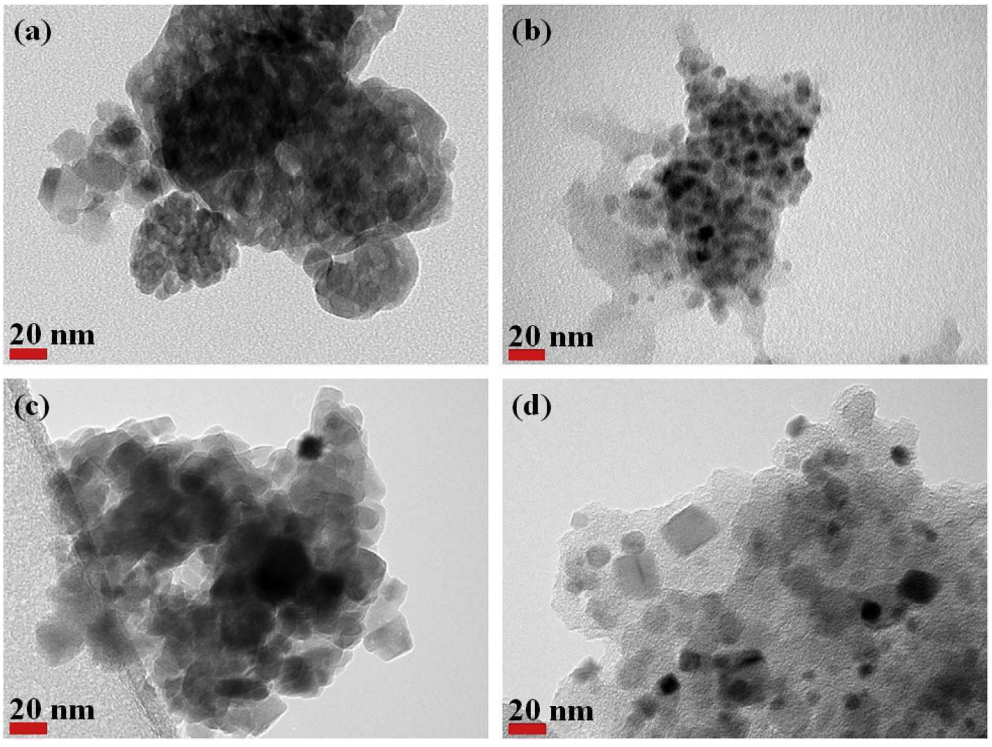

Fig. 5. TEM images of Ca-modified samples with PVA: (a) Fe/$CaCO_3$_PVA 1:1, (b) Fe/$CaCO_3$_PVA 1:5, (c) Fe/$CaCl_2$_PVA 1:1, and (d) Fe/$CaCl_2$_PVA 1:5.

Table 3 summarizes the phosphate adsorption capacity of each adsorbent, clearly indicating the impact PVA had on phosphate adsorption. Apart from the samples without PVA, the best performing samples were the 1:1 ratio carbonate-based adsorbents followed by the chloride-based samples. The best performing sample was Fe/$CaCO_3$_PVA 1:1, followed by Fe/$MgCO_3$_PVA 1:1, Fe/$CaCl_2$_PVA 1:1, and Fe/$MgCl_2$_PVA 1:1, with phosphate adsorption capacities of 16.74, 16.26, 15.81, and 12.39 mg g^{-1}, respectively.

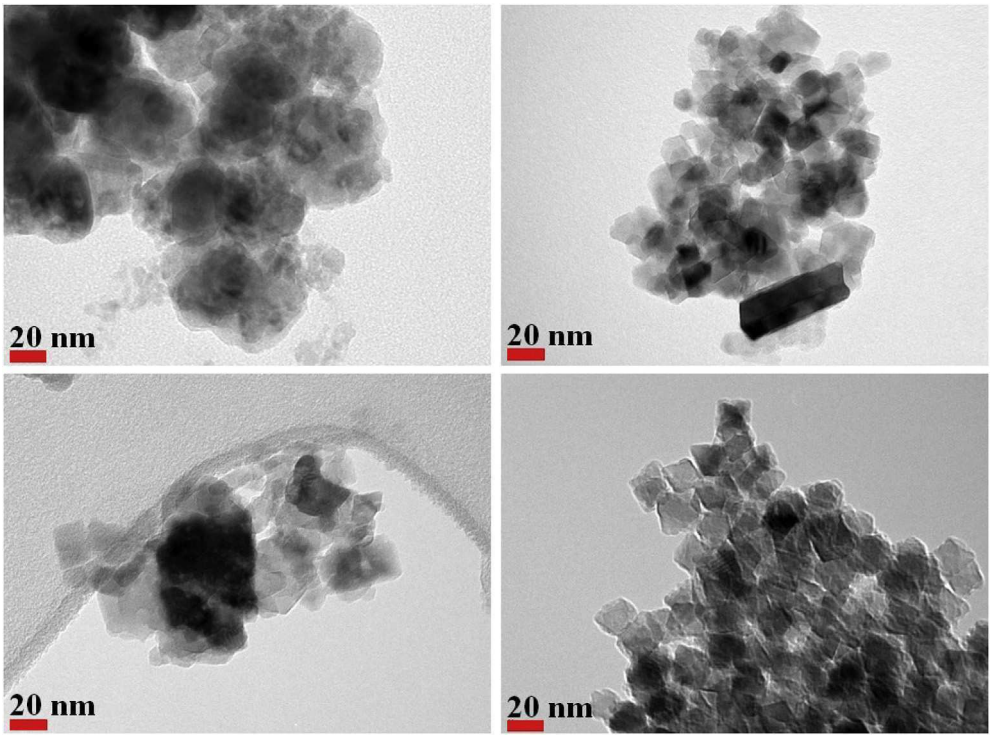

Fig. 6. TEM images of Mg-modified samples with PVA: (a) Fe/$MgCO_3$_PVA 1:1, (b) Fe/$MgCO_3$_PVA 1:5, (c) Fe/$MgCl_2$_PVA 1:1, and (d) Fe/$MgCl_2$_PVA 1:5.

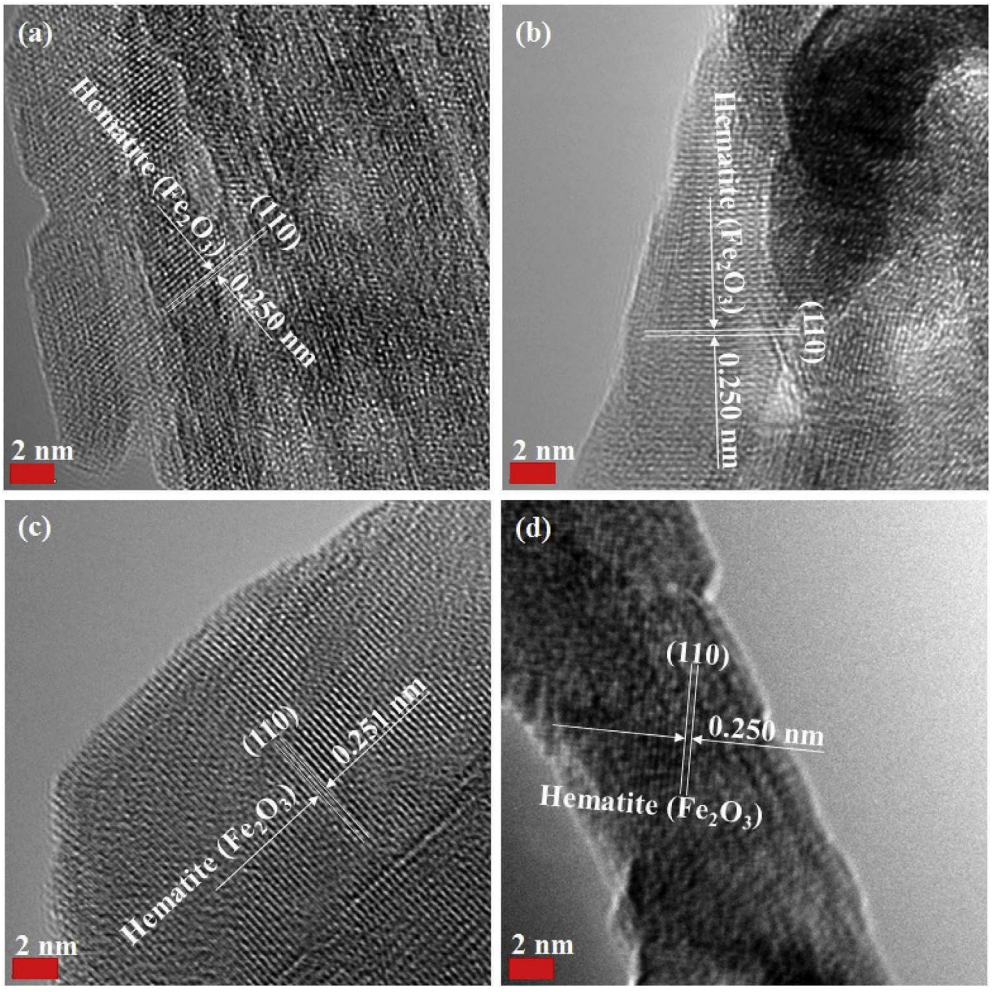

Fig. 7. HR-TEM images of Ca- and Mg-modified samples without PVA: (a) Fe/$CaCl_2$_No PVA, (b) Fe/$CaCO_3$_PVA_No PVA, (c) Fe/$MgCl_2$_No PVA, and (d) Fe/$MgCO_3$_No PVA. Scale bar.

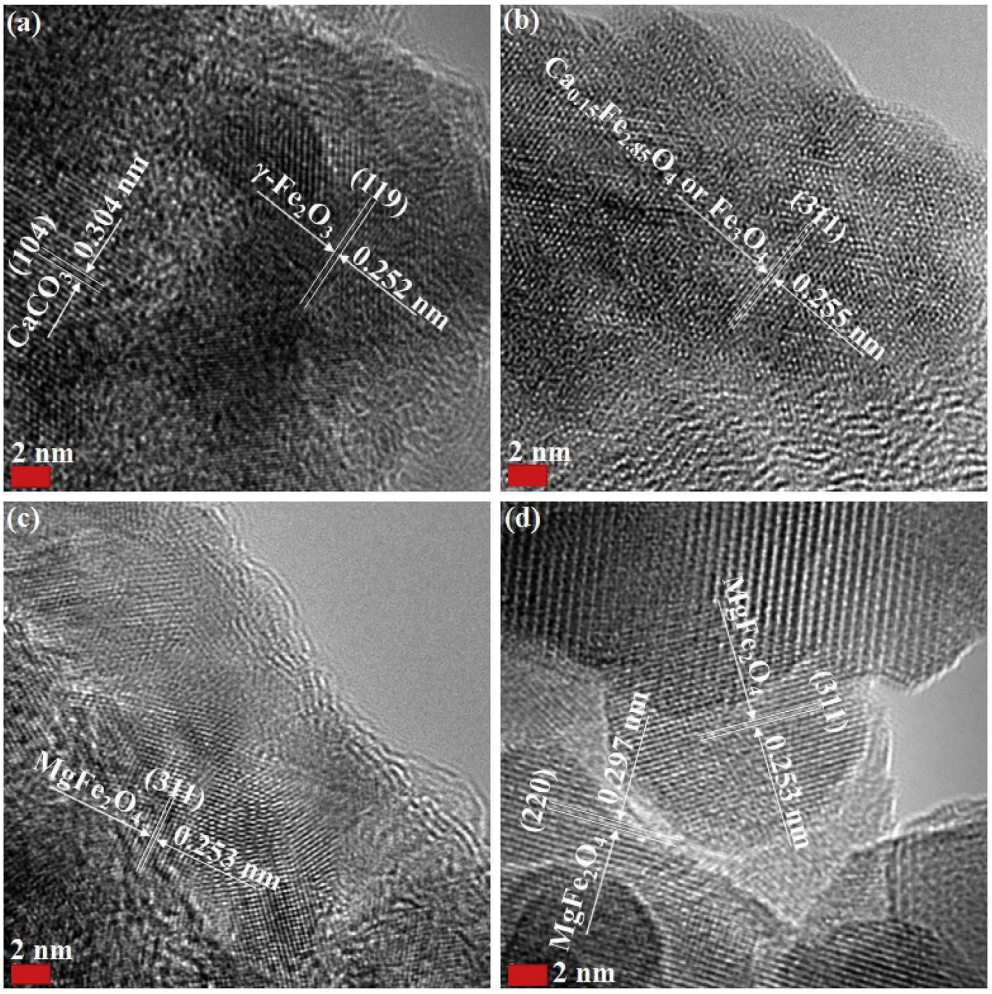

Fig. 8. HR-TEM images of Ca- and Mg-modified, magnetic samples: (a) Fe/$CaCO_3$_PVA 1:1, (b) Fe/$CaCl_2$_PVA 1:1, (c) Fe/$MgCO_3$_PVA 1:1, and (d) Fe/$MgCl_2$_PVA 1:1.

Based on the results for the 1:1 ratio adsorbents, these samples were further investigated by adsorption isotherms.

The adsorption capacities of Ca- and Mg-modified ferrites were compared to other adsorbents found in literature (Table S1). While the Ca- and Mg-modified ferrite adsorbents did not have the highest phosphate adsorption capacity, they performed much better than other commonly used adsorbents including red mud and steel slag.

The samples were evaluated with both the Langmuir [39] and Freundlich [40] isotherm models. The results of the Langmuir

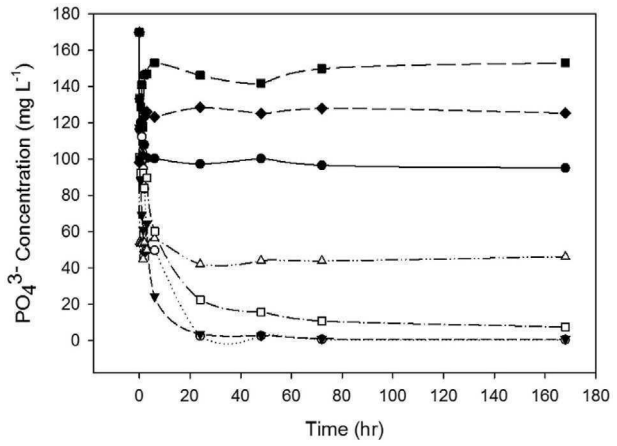

Fig. 9. Adsorption of phosphate with respect to time using Mg-modified adsorbents (●: Control Fe_2O_3, ○: Fe/$MgCl_2$-No PVA, ▼: Fe/$MgCO_3$-No PVA, Δ: Fe/$MgCl_2$_PVA 1:1, ■: Fe/$MgCl_2$_PVA 1:5, □: Fe/$MgCO_3$_PVA 1:1, and ◆: Fg/$MgCO_3$_PVA 1:5).

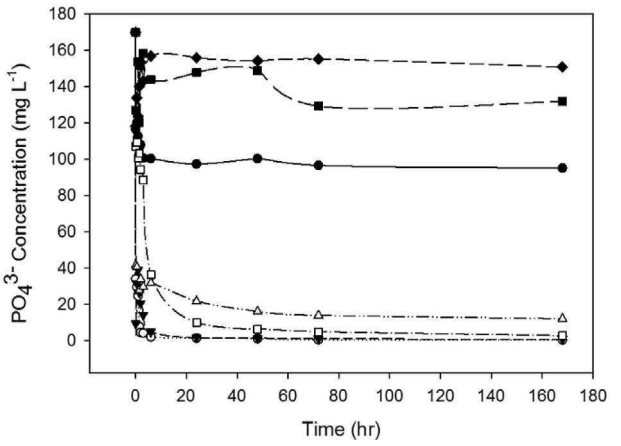

Fig. 10. Adsorption of phosphate with respect to time using Ca-modified adsorbents (●: Control Fe_2O_3, ○: Fe/$CaCl_2$-No PVA, ▼: Fe/$CaCO_3$-No PVA, Δ: Fe/$CaCl_2$_PVA 1:1, ■: Fe/$CaCl_2$_PVA 1:5, □: Fe/$CaCO_3$_PVA 1:1, and ◆: Fg/$CaCO_3$_PVA 1:5).

Table 3
Phosphate adsorption capacity of Ca- and Mg-modified ferrite.

Adsorbent	Phosphate Capacity (mg g^{-1})
Control Fe_2O_3	7.49
Fe/$CaCl_2$-No PVA	16.97
Fe/$MgCl_2$-No PVA	16.96
Fe/$CaCO_3$-No PVA	16.94
Fe/$MgCO_3$-No PVA	16.92
Fe/$CaCO_3$_PVA 1:1	16.74
Fe/$CaCl_2$_PVA 1:1	15.81
Fe/$CaCO_3$_PVA 1:5	1.91
Fe/$CaCl_2$_PVA 1:5	3.79
Fe/$MgCO_3$_PVA 1:1	16.26
Fe/$MgCl_2$_PVA 1:1	12.39
Fe/$MgCO_3$_PVA 1:5	4.46
Fe/$MgCl_2$_PVA 1:5	1.69

Table 4
Adsorption isotherm constants.

Sample	Langmuir isotherm			Freundlich isotherm		
	q_{max}	K_L	R^2	1/n	K_F	R^2
Fe/$CaCO_3$_PVA 1:1	833.3	0.011	0.103	0.958	9.56	0.899
Fe/$CaCl_2$_PVA 1:1	58.14	0.169	0.994	0.330	14.13	0.758
Fe/$MgCO_3$_PVA1:1	22.73	0.649	0.983	0.155	19.41	0.525
Fe/$MgCl_2$_PVA 1:1	33.44	0.024	0.994	0.311	3.79	0.994

isotherm models were found in the supporting information (Fig. S2) and Table 4. Data were evaluated with the Freundlich model by the linearized equation:

$$\log q_e = \log K_F + \frac{1}{n}\log C_e$$

where K_F is the Freundlich constant (mg g^{-1} (L $mg^{-1})^{1/n}$) and 1/n is a dimensionless constant which indicates sorption favourability. The plot of log q_e vs. log C_e, as seen in Fig. 11, provided the isotherm constants as documented in Table 4.

When comparing regression coefficients between the two isotherm models, it is clear that the Langmuir model provides the best fit, with the exception of the Fe/$CaCO_3$_PVA 1:1 sample which had an R^2 of 0.899 using the Freundlich model. However, as previously stated, this could be due to its extremely high capacity for phosphate. Thus, based on adsorption experiments, it could be determined that these materials best followed the Langmuir isotherm, indicating a monolayer adsorption process.

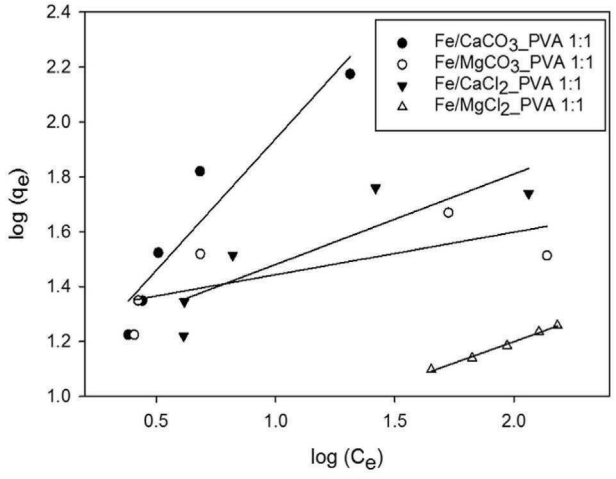

Fig. 11. Linear plot for Freundlich isotherm using samples with a 1:1 ratio of PVA.

4. Conclusions

Ca- and Mg-modified iron oxides using $CaCl_2$, $CaCO_3$, $MgCl_2$, or $MgCO_3$ were successfully synthesized by a simple combustion method. The samples became magnetic by the presence of PVA during the calcination processes. Non-magnetic Ca- and Mg-modified iron oxides demonstrated the highest phosphate adsorption capacity of about 17 mg g^{-1} compared to that of control Fe_2O_3 (7.49 mg g^{-1}) under these experimental conditions. Interestingly, magnetic Ca- and Mg-modified samples also showed a high capacity of phosphate removal, which ranged from 12.4 to 16.74 mg g^{-1}. Even though the values of q_{max} for Ca- and Mg-modified samples without PVA were not calculated, the obtained results indicate successful Ca and Mg modification significantly improves the capacity of phosphate removal from water. Incorporated Ca or Mg into iron oxides may enhance the binding of phosphate on iron oxide, resulting in the improvement of phosphate removal [41]. Moreover, innovative magnetic samples have high potential for easy separation processes to avoid filtration, which requires considerable energy and high costs during water treatment processes.

Notice

The U.S. Environmental Protection Agency, through its Office of Research and Development, funded and managed, or partially funded and collaborated in, the research described herein. It has been subjected to the Agency's administrative review and has been approved for external publication. Any opinions expressed in this paper are those of the author(s) and do not necessarily reflect the views of the Agency, therefore, no official endorsement should be inferred. Any mention of trade names or commercial products does not constitute endorsement or recommendation for use. C. Han was supported by the Postgraduate Research Program at the National Risk Management Research Laboratory administered by the Oak Ridge Institute for Science and Education through an interagency agreement between the U.S. Department of Energy and the U.S. Environmental Protection Agency.

Appendix A. Supplementary data

Supplementary data related to this article can be found at http://dx.doi.org/10.1016/j.matchemphys.2017.05.038.

References

[1] E. Valsami-Jones (Ed.), Phosphorus in Environmental Technologies: Principles and Applications, IWA Publishing, London, UK, 2004.
[2] J. Lalley, C. Han, G.R. Mohan, D.D. Dionysiou, T.F. Speth, J. Garland, M.N. Nadagouda, Environ. Sci. Water Res. Technol. 1 (2015) 96.
[3] H.L. Golterman, Water Res. 7 (1973) 3.
[4] J.J. Schröder, A.L. Smit, D. Cordell, A. Rosemarin, Chemosphere 84 (2011) 822.
[5] A. Sendrowski, T.H. Boyer, Desalination 322 (2013) 104.
[6] Y. Liu, G. Villalba, R.U. Ayres, H. Schroder, J. Ind. Ecol. 12 (2008) 229.
[7] G. Villalba, Y. Liu, H. Schroder, R. U, J. Ind. Ecol. 12 (2008) 557.
[8] M.F. Colmenarejo, E. Sánchez, R. Borja, L. Travieso, S. Cirujano, J.L. Echevarrias, A. Rubio, M.G. González, J. Environ. Sci. Health, Part A 42 (2007) 969.
[9] Z. Liu, W.L. Kingeery, D.H. Huddleston, F. Hossain, N.B. Hashim, J.M. Kieffer, J. Environ. Sci. Health, Part A 43 (2008) 468.
[10] E. Abdallah, A.A. Concalves, G.A. Gangnon, J. Environ. Sci. Health, Part A 44 (2009) 707.
[11] M.G. Antoniou, A.A. de la Cruz, D.D. Dionysiou, D. D, J. Environ. Eng. 131 (2005) 1239.
[12] C. Han, M. Pelaez, V. Likodimos, A.G. Kontos, P. Falaras, K. O'Shea, D.D. Dionysiou, Appl. Catal. B Environ. 107 (2011) 77.
[13] C. Han, A. Doepke, W. Cho, V. Likodimos, A.A. de la Cruz, T. Back, W.R. Heineman, H.B. Halsall, V.N. Shanov, M.J. Schulz, P. Falaras, D.D. Dionysiou, Adv. Funct. Mater. 23 (2013) 1807.

[14] L.E. De-Bashan, Y. Bashan, Water Res. 38 (2004) 4222.
[15] D. Mulkerrins, A.D.W. Dobson, E. Colleran, Environ. Int. 30 (2004) 249.
[16] A. Eskandarpour, K. Sassa, Y. Bando, M. Okido, S. Asai, Mater. Tracsactions 47 (2006) 1832.
[17] D. Rich, Remov. Total Phosphorus Nat. Waters by Precip. (2005).
[18] S. Yeoman, T. Stephenson, J.N. Lester, R. Perry, Environ. Pollut. 49 (1988) 183.
[19] D.W. de Haas, M.C. Wentzel, G.A. Ekama, Water SA 26 (2000) 439.
[20] R. Barat, T. Montoya, A. Seco, J. Ferrer, Water Res. 45 (2011) 3744.
[21] G.R. Mohan, P. Dube, A. MacFar1ene, P. Pullammanappallill, in: G. Wicks, J. Simon, R. Zidan, R. Brigmon, G. Fishman, S. Arepalli, A. Norris, M. McCluer (Eds.), Materials Challenges in Alternative and Renewable Energy II: Ceramic Transactions, vol. 242, John Wiley & Sons, Inc, Hoboken, New Jersey, 2013, pp. 47–58.
[22] J. Hrenovic, M. Rozic, L. Sekovanic, A. Anic-Vucinic, J. Hazard. Mater. 156 (2008) 576.
[23] R. Barat, A. Bouzas, N. Marti, J. Ferrer, A. Seco, J. Environ. Manag. 90 (2009) 850.
[24] G.E. Diwani, S.E. Rafie, N.N.E. Ibiari, H.I.E. Aila, Desalination 214 (2007) 200.
[25] T. Zhang, L. Ding, H. Ren, X. Xiong, Water Res. 43 (2009) 5209.
[26] J.D. Doyle, S.A. Parsons, Water Res. 36 (2002) 3925.
[27] C.M. López-Vázquez, C.M. Hooijmans, D. Brdjanovic, H.J. Gijzen, M.C. van Loosdrecht, Water Res. 42 (2008) 2349.
[28] K. Mohanty, D. Das, M.N. Biswas, Adsorption 12 (2006) 119.
[29] J. Murphy, J.P. Riley, Anal. Chim. Acta 27 (1962) 31.
[30] J. Kielland, J. Am. Chem. Soc. 59 (1937) 1675.
[31] C. Han, J. Andersen, V. Likodimos, P. Falaras, J. Linkugel, D.D. Dionysiou, Catal. Today 224 (2014) 132.
[32] J.C. Yu, W. Ho, J. Yu, H. Yip, P.K. Wong, J. Zhao, Environ. Sci. Technol. 39 (2005) 1175.
[33] C. Fang, T. Zhang, P. Li, R.-f. Jiang, Y.-c. Wang, Int. J. Environ. Res. Public Health 11 (2014) 9217.
[34] F. Xie, F. Wu, G. Liu, Y. Mu, C. Feng, H. Wang, J.P. Giesy, Environ. Sci. Technol. 48 (2014) 582.
[35] Z. Mahmood, S. Nasir, N. Jamil, A. Sheikh, A. Akram, Afr. J. Environ. Sci. Technol. 9 (2015) 274.
[36] L. Wang, C. Han, M.N. Nadagouda, D.D. Dionysiou, J. Hazard. Mater. 313 (2016) 283.
[37] J. Lalley, C. Han, X. Li, D.D. Dionysiou, M.N. Nadagouda, Chem. Eng. J. 284 (2016) 1386.
[38] D. Chen, P. Szostak, Z. Wei, R. Xiao, Sci. Total Environ. 539 (2016) 381.
[39] I. Langmuir, J. Am. Chem. Soc. 40 (1918) 1361.
[40] H. Freundlich, Akad. Verlagsgesellschaft (1922).
[41] L. Weng, W.H. Van Riemsdijk, T. Hiemstra, J. Environ. Qual. 41 (2012) 628.

Chemical Engineering Journal 352 (2018) 612–624

Contents lists available at ScienceDirect

Chemical Engineering Journal

journal homepage: www.elsevier.com/locate/cej

Phosphate recovery from water using cellulose enhanced magnesium carbonate pellets: Kinetics, isotherms, and desorption

Elisabeth Martin[a], Jacob Lalley[b], Wenhu Wang[c], Mallikarjuna N. Nadagouda[d,*], Endalkachew Sahle-Demessie[e], So-Ryong Chae[f,*]

[a] Department of Biomedical, Chemical, and Environmental Engineering, University of Cincinnati, Cincinnati, OH 45221, USA
[b] Pegasus Technical Services Inc., 46 E Hollister St, Cincinnati, OH 45219, USA
[c] Department of Mechanical and Materials Engineering, Wright State University, Dayton, OH 45435, USA
[d] The U.S. Environmental Protection Agency, ORD, NRMRL, WSD, WRRB, 26 W. Martin Luther King Drive, Cincinnati, OH, 45268, USA
[e] The U.S. Environmental Protection Agency, ORD, NRMRL, STD, CPB, 26 W. Martin Luther King Drive, Cincinnati, OH 45268, USA
[f] Department of Chemical and Environmental Engineering, University of Cincinnati, Cincinnati, OH 45221, USA

HIGHLIGHTS

- Magnesium carbonate with cellulose pellets were optimized for phosphate adsorption.
- Adsorption best described by *pseudo*-second-order kinetics and Langmuir isotherm.
- Pellet with 15% cellulose showed best result for phosphate removal across studies.

GRAPHICAL ABSTRACT

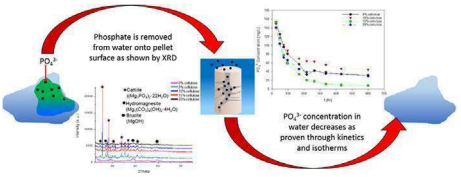

ARTICLE INFO

Keywords:
Phosphorus
Magnesium carbonate
Cellulose
Adsorption
Kinetics and sorption isotherms
Recovery of phosphate from water

ABSTRACT

Phosphorus is an essential and limited nutrient that is supplied by a depleting resource, mineral phosphate rock. Eutrophication is occurring in many water bodies which provides an opportunity to recover this nutrient from the water. One method of recovery is through adsorption; this study focused on fabricating a porous and granular adsorptive material for the removal and recovery of phosphate. Magnesium carbonate was combined with cellulose in varying weight ratios (0, 5, 10, 15, 20%) to synthesize pellets, which were then calcined to increase internal surface area. Physiochemical properties such as surface area, surface morphology, elemental composition, and crystal structure of the materials were characterized using Brunauer, Emmett, and Teller (BET) surface area analysis, X-ray diffraction (XRD), scanning electron microscopy (SEM) and energy-dispersive X-ray spectroscopy (EDS). The pellet proved to be uniform in composition and an increase in BET surface area correlated with an increase in cellulose content until pellet stability was lost. Phosphate adsorption using the pellets was studied via batch kinetics and sorption isotherms. The *pseudo*-second-order kinetics model fits best suggesting that the adsorption occurring was chemisorption. The isotherm model that fit best was the Langmuir isotherm, which showed that the maximum equilibrium adsorption capacity increased with an increase in cellulose content between 10% and 20%. The average adsorption capacity achieved in the triplicate isotherm study was 96.4 mg g^{-1} for pellets synthesized with 15% cellulose. Overall, using cellulose and subsequent calcination created an additional internal surface area for adsorption of phosphate and suggested that granular materials can be modified for efficient removal and recovery of phosphate from water.

* Corresponding authors.
E-mail addresses: Nadagouda.mallikarjuna@epa.gov (M.N. Nadagouda), chaesg@mail.uc.edu (S.-R. Chae).

https://doi.org/10.1016/j.cej.2018.06.183
Received 27 April 2018; Received in revised form 27 June 2018; Accepted 28 June 2018
Available online 30 June 2018
1385-8947/ © 2018 Published by Elsevier B.V.

1. Introduction

As the limiting nutrient in most waterways, increased loads of phosphorus (P) can cause eutrophication, which leads to hypoxia and the proliferation of harmful algal blooms [1–5]. Additionally, while viewed as a pollutant at excessive concentrations (i.e., > 20 μg L^{-1}) [6], phosphate (PO_4^{3-}), the main species of phosphorus in the environment, is necessary for a range of industrial purposes including the production of agricultural fertilizers, animal feeds, and chemical pesticides [7]. Environmental Protection Agency (EPA) limit for acceptable phosphorus levels is only 0.1 mg/L or lower. Phosphate reserves are quickly declining [8], making a recovery and reuse of PO_4^{3-} an essential component of phosphate remediation. Adsorption is a technique which can both remove and recover PO_4^{3-} from aqueous suspensions and has been extensively studied. Adsorbents ranging from modified iron oxide [9,10] to calcined waste eggshells [11], to magnesium modified corn biochar [12] have been investigated for phosphate adsorption. However, adsorption suffers from the problem of

Fig. 1. Pellets were synthesized with magnesium carbonate and cellulose for phosphate adsorption (photo by E. Martin).

Table 1
Physical characteristics of the 5 various pellet recipes (n = 100).

General Characteristics		
Diameter		6.0 mm ± 0.05
Length		17.0 mm ± 2.13
Surface area		377.0 mm^2 ± 40.63
Volume		480.8 mm^3 ± 61.56
Weight		0.4 g ± 0.05
Pellet specific characteristics	**Weight change from calcination (%)**	**BET Surface Area ($m^2 g^{-1}$)**
0%17	−64 ± 2	27.5
5%1	−49 ± 2	33.2
10%2	−46 ± 2	36.9
15%1	−51 ± 2	43.1
20%2	−59 ± 4	37.6

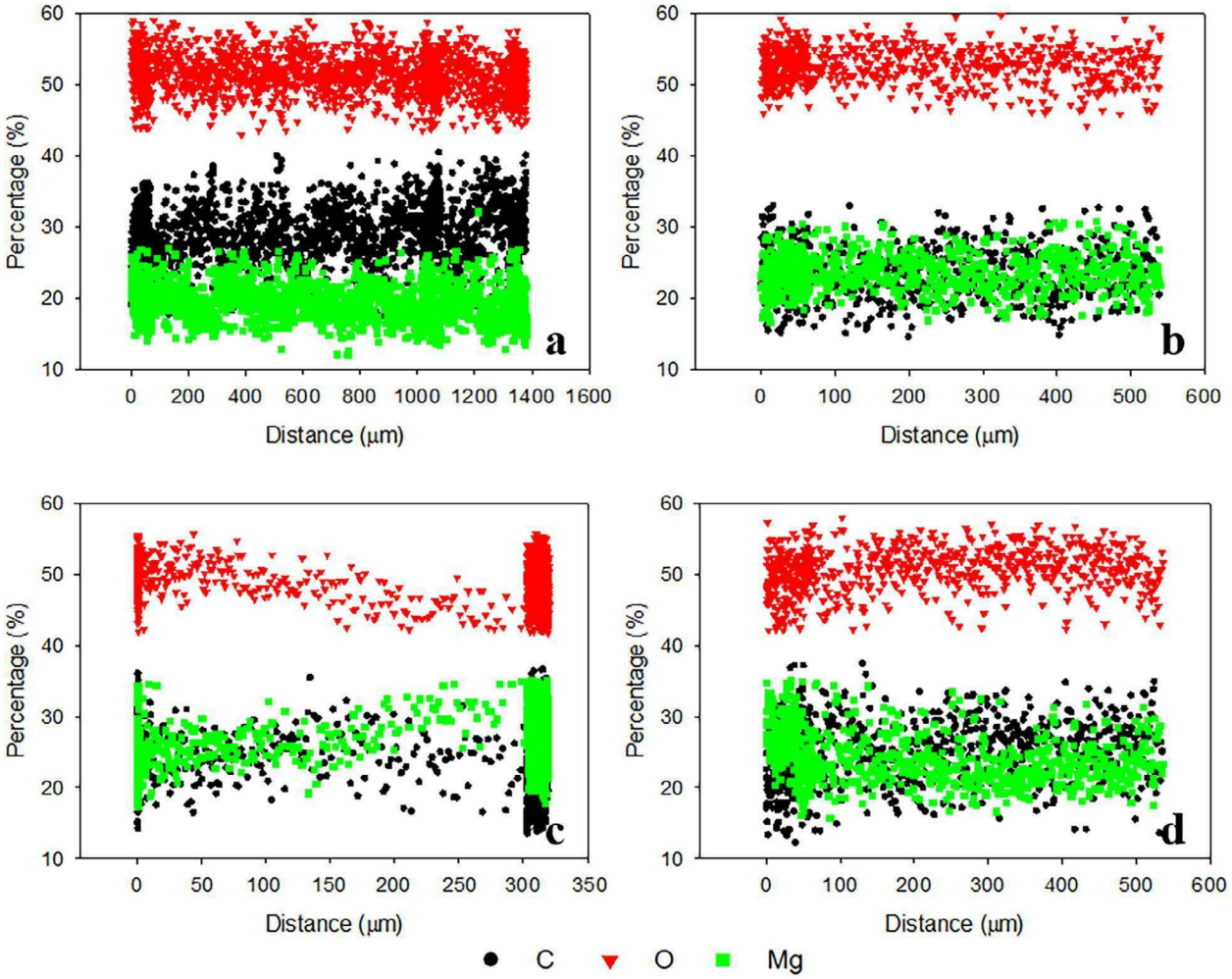

Fig. 2. Line scan and cross-section scans of two 15% cellulose samples for carbon, oxygen, and magnesium; (a) line scan of sample 1, (b) cross-section scan of sample 1, (c) line scan of sample 2, (d) cross-section scan of sample 2.

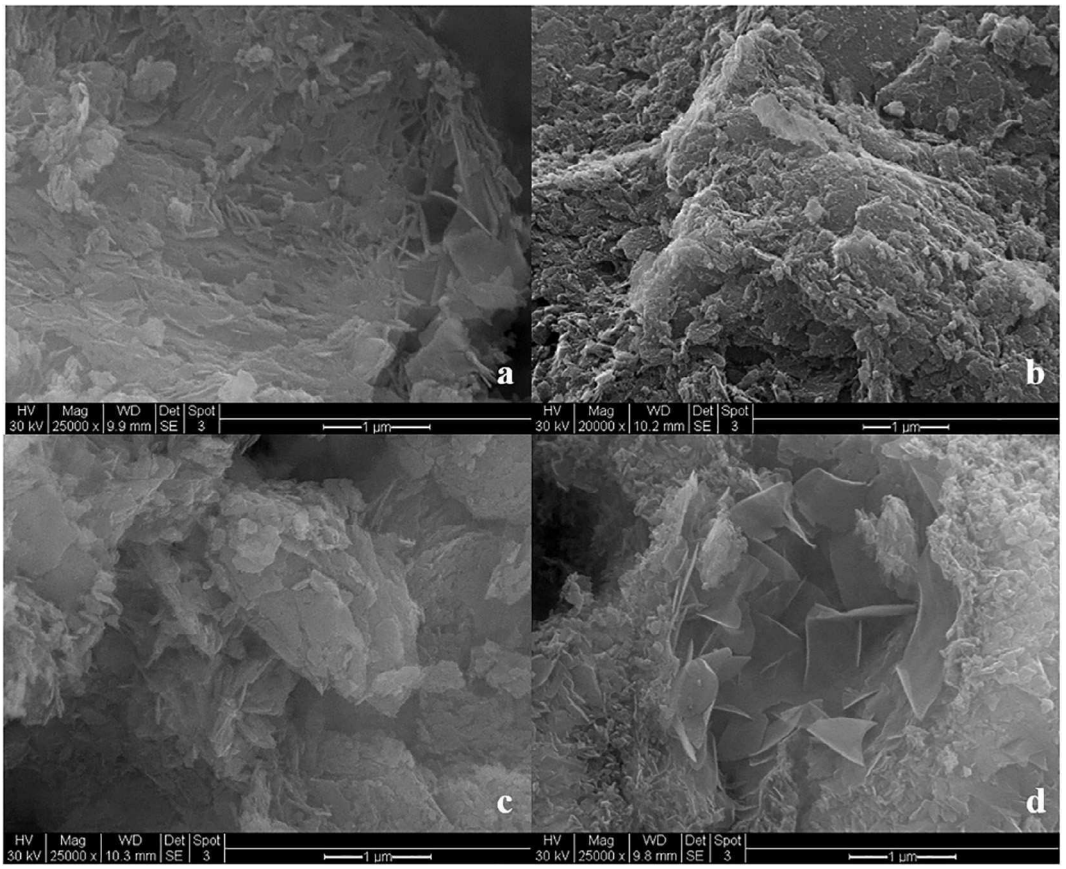

Fig. 3. SEM images of (a) 0%17 pellet before adsorption, (b) 0%17 pellet after adsorption, (c) 10%2 pellet before adsorption and (d) 10%2 pellet after adsorption (all scale bars represent 1 µm).

bottle-necking (i.e., after saturation, the adsorbent will no longer be applicable) [13]. While the use of highly adsorptive fine powders, which can desorb phosphate after remediation, is a growing area of study [14], their removal from the solution after adsorption is difficult. Therefore, the synthesis of highly adsorptive, inexpensive, and granular sized sorbents, which can recycle PO_4^{3-} would be extremely beneficial to the problem of nutrient pollution.

Magnesium (Mg) has been widely used in the medical field as a phosphate binder in dialysis patients as Mg can effectively bind PO_4^{3-} without the adverse health effects demonstrated by aluminum and calcium [15–20]. Additionally, Mg salts have been used for environmental applications in drinking and wastewater [21,22]. For example, Mg has effectively been employed in enhanced biological phosphate removal (EBPR) processes, which allow phosphorus accumulating organisms (PAOs) to release P under anaerobic conditions and then excessively uptake P under aerobic conditions. The addition of Mg salts in EBPR processes under anaerobic conditions resulted in the formation of phosphate precipitates including newberyite ($MgHPO_4$) and struvite ($MgNH_4PO_4{\cdot}6H_2O$) [23–25]. Newberyite and struvite can be used as slow-release fertilizers making their formation during phosphate remediation processes ideal for recycling PO_4^{3-} [21,26–28].

For the above PO_4^{3-} remediation processes, powdered, water-soluble Mg salts (e.g., magnesium chloride) were used [21,27]. Here, magnesium carbonate ($MgCO_3$) was selected to prepare pellets (i.e., 6 mm × 17 mm) as phosphate adsorbents due to its very low water solubility (i.e., 0.11 g L^{-1} at 25 °C) [29]. Mechanically stable pellets were prepared by blending different ratios of $MgCO_3$ and cellulose, which acted as a binder. The cellulose binder was burned off to create porosity in the pellet. After pellet stability in water was ensured, phosphate adsorption was evaluated.

2. Experimental

2.1. Materials

Analytical grade $MgCO_3$ powder (Fisher Scientific) was made into pellets, 6 mm in diameter and 17 mm in length on average, using the MZL Flat Die Pellet Mill (Xuzhou Orient Industry) as seen in Fig. 1. Varying amounts of a cellulose binder, with average particle size of 20 µm (Sigma Aldrich), was used to optimize the pellet design. Pellets were made with a constant moisture content of 45% water to $MgCO_3$ weight ratio. Cellulose was added in varying weight ratios from 0 to 20%. Conditions for the use of the pellet mill were kept as consistent as possible, but the instrument did allow for variation as related to the length of pellets made. After synthesis, the pellets were calcined at 300 °C to remove cellulose for additional porosity without complete decomposition of the magnesium carbonate. Five specific pellet conditions were selected for further study with regard to cellulose ratio and calcination time: 0% cellulose calcined for 17 h (0%17), 5% cellulose calcined for 1 h (5%1), 10% cellulose calcined for 2 h (10%2), 15% cellulose calcined for 1 h (15%1) and 20% cellulose calcined for 2 h (20%2). The calcination temperature was varied based upon the stability test conducted after each trial of pellet production. It is hard to control the pellet uniformity such as how much pressure it can experience, water ratio inside and outside the pellet, cellulose distribution, etc. Due to these effects, the pellets were calcined at different temperatures. The phosphate stock solution was created using analytical grade sodium phosphate monobasic dihydrate ($NaH_2PO_4{\cdot}2H_2O$) (Fisher Scientific).

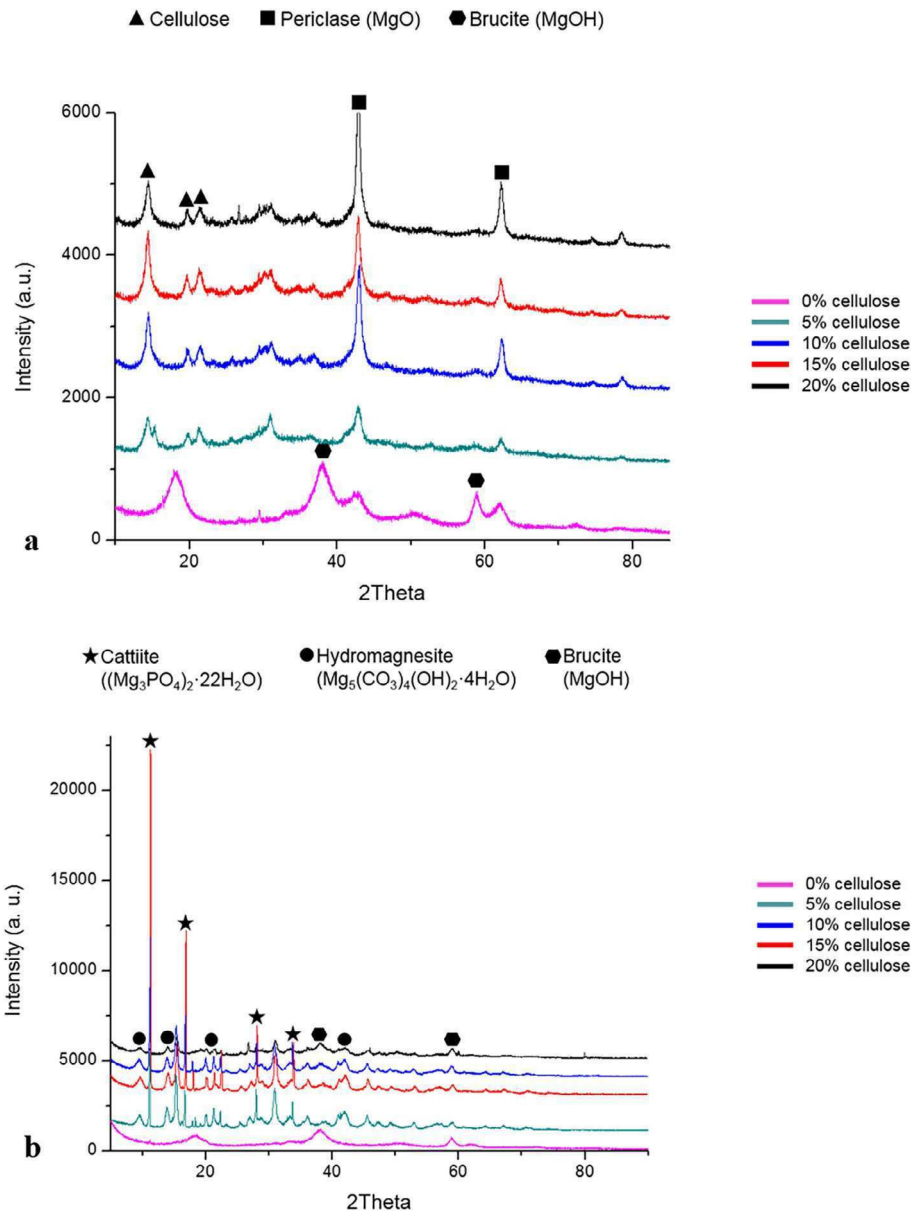

Fig. 4. XRD patterns of the various pellets (a) before and (b) after adsorption isotherms were conducted.

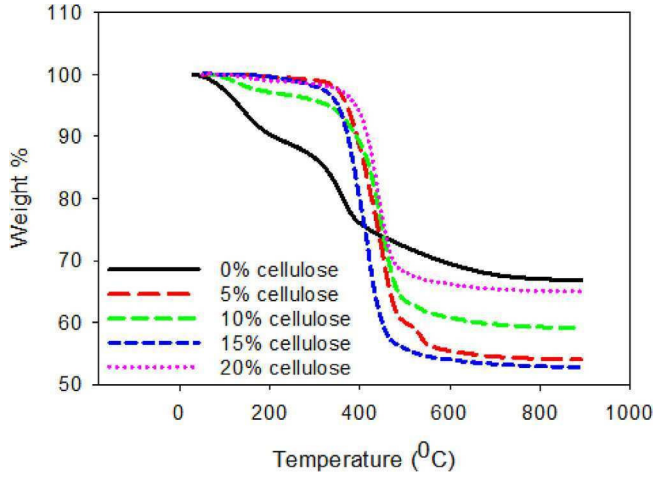

Fig. 5. Fig. 5 presents the loss in weight as the samples were exposed to higher temperatures under oxidative conditions.

2.2. Sample characterization

Pellet composition was examined using SEM-EDS (EDAX JEOL 7401) performing both a line scan and cross-section scan of the pellet from each batch. The uniformity was determined by comparing the percentage of carbon (C), oxygen (O) and Mg present across each scan. The BET surface area was determined using the NOVA 2000e Surface Area & Pore Size Analyzer (Quantachrome). Samples were first purged with nitrogen gas at 150 °C overnight before analysis. The surface morphology of the $MgCO_3$ pellets was observed using SEM (Philips XL 30 ESEM-FEG), at an accelerating voltage of 30 kV. The crystal structure was determined using XRD (PANalytical X'Pert) with the 2-theta diffractometer under CuK_α radiation, and a wavelength of 1.54 μm and the XRD patterns were analyzed using JADE software (MDI, Inc., Livermore, CA).

2.3. Adsorption studies

2.3.1. Kinetic studies

Kinetic experiments were conducted to understand the adsorption

Table 2
Phosphate adsorption capacity, surface area, pH, and temperature for various adsorbents.

Adsorbent	Capacity (mg/g)	Surface area (m^2/g)	pH	Temperature (°C)
Kaolinite in Iran	0.32	3.66	2–10	25
Bentonite in Iran	0.28	84.98	2–10	25
Tunisian kaolinite	38.46	68.5	3–9	25
Tunisian smectite	42.19	106.2	3–9	25
Kanuma clay with corn starch and CaO tablet	4.39	15.401	2–12	288.15, 298.15, 308.15 K
Kanuma clay with corn starch, Fe powder, white cement and CaO tablet	3.61	15.59	2–12	288.15, 298.15, 308.15 K
Electrochemically modified Kanuma clay tablet	5.36	16.12	2–12	288.15, 298.15, 308.15 K
La modified bentonite	0.93	N/A	3–11	25
LaAl/Al pillared montmorillonite	13.022/10.307	N/A	3–8	25,30,35
Phoslock®	10.54	39.3	5–9	10,23,35,40
Zenith/Fe bentonite	11.15	N/A	5–9	15,25,35
Calcined Mg-Al-CO_3 LDHs	187.1*	82.5–143	3–11	25
Calcined hydrotalcite at 500C	244.58	250–300	9	25,45,65
Calcined hydrotalcite at 400C	192.9	250–300	9	25,45,65
Calcined Zn-Al LDH	41.26	81.2	N/A	25
Calcined MgMn LDH in seawater	7.5	68	3–10	10,25,40
Mg LDH	61	202	3–12	25
Dolomite LDH	36	80	3–12	25
Synthetic hydrotalcite	47.3	N/A	7.8	25
Mg-Al LDH	26.4*	64.4	7	10,25,50
Hydrotalcite	60	44	9	25,45,65
Zeolite in Iran	0.37	13.83	2–10	25
Hydrated aluminum oxide modified natural zeolite	7	17.8	2–11	21
Zeolite/lanthanum hydroxide	71.94	55.69	2.5–10.5	25
Synthetic zeolite	52.91	74.5–174.4	3–9	25
La/Al modified zeolite	2.429	N/A	2–12	10,20,30
HUD synthetic zeolite	79.4	500	2.5–10	298 K
Al modified HUD zeolite	75.8	642	2.5–10	298 K
Zeolites from fly ash	11.79–47.17	29–91.49	1.58–12.11	25
Lanthanum hydroxide-doped carbon fiber	16.1	N/A	2–12	25
Commercial/synthesized lanthanum hydroxide	55.56/107.53	31.1/153.3	1.5–13	25
La doped silicate	26.7	763.2	2–12	25,35,45
La doped vesuvianite	6.7	N/A	3–13	5–35
$La(OH)_3$ modified vermiculites	79.6	39.1	3–11	25,30,35,45
La loaded granular ceramic	0.9015	26.83	2–12	20,30,40
Monohydrocalcite	1.67–3.63*	16.4	8–9	15,25,35
Calcite in Iran	1.82	0.98	2–10	25
Calcined waste eggshell	23.02	19.32	2–10	25,35,45
Freshwater mussel shells	6.95	N/A	1.5–9.5	25
Wasted scallop shell	23	N/A	2–10	15,25,35,45
Recycled crab shells	108.9	N/A	2–10	15–45
Calcite/aragonite in seawater	0.4/1*	N/A	7.2–9	5–45
Gas concrete	17.32	22	2,5,11.5	20,55
MgOH in situ from diatomite	52.08	72.53	5–10	288, 298, 308, 318 K
MgO microspheres made in water	3.17	1.82	5	30
MgO microspheres made in PSS	75.13	72.10	5	30
Natural palygorskite	3.73	206	4–9	25
Acid treated palygorskite	6.64	342	4–9	25
Acid/thermal treated palygorskite	8.31	287	4–9	25
Thermally treated palygorskite	42	47	3–9	25
Magnesium modified corn biochar	200–239	382–494	6–10	288,303,318 K
Magnesium amorphous calcium carbonate	199.44*	70.45	6–10	25
Ca-Mg loaded biochar made at 600C	326.63	487.49	4–10	288, 303, 318 K
Natural calcium-rich attapulgite	3.32	N/A	4,7,10	25
Half-burned dolomite	10	N/A	7.5–8.5	25
Dolomite	48	0.14	1–11	20,40,60
E33	37.74	140.4	7	21
E33 coated with Mn	30.96	102.8	7	21
E33 coated with Ag I/II	25.52/38.80	124.6/142.0	7	21
FeO tailings	8.21	47.9	3–10	5,20,35
FeO anion exchange resin	48	N/A	7.2–7.6	24
Goethite	144	316	5,6.7	25,45,65
Zr coated magnetite nanoparticles	42.19	152.46	3–10	N/A
Magnetic Fe-Zr binary oxide	13.65	106.2	3–11	25
Iron sludge	18.7	113	7.6	N/A
Mesoporous ZrO_2	29.71	232	3–11	25
Calcite and Fe-rich calcareous soils	26	0.6	5–8	25
LaO on Fe_3O_4@SiO_2 magnetic nanoparticles	27.8	47.73	2–12	25
2 sedimentary apatites	0.31/1.09	0.72/0.57	8	22
3 igneous apatites	0.41/0.37/0.28	0.53/0.48/0.58	8	22
Aluminumoxid S	34.57	200	6	25,45,65
Activated alumina/2 Al-impregnated silicates	53.7/81.9/58.8*	155/343/328	6.4–7.2	25
Dewatered alum sludge	3.5	N/A	4.3–9	20
Hydrothermally synthesized silicate nanoparticles	93.46	N/A	7	303–323 K

(*continued on next page*)

Table 2 (*continued*)

Adsorbent	Capacity (mg/g)	Surface area (m^2/g)	pH	Temperature (°C)
Alkaline residue (AR)	134.8	28.7	10.83	25
AR treated with NaOH	211.9	14.1	11.58	25
AR treated with HCl	2.2	100.6	3.96	25
AR calcined at 800C	139	29.31	2.5–11.5	25
Chitosan modified with zirconium ions	61.7	7.39	2–10	4,15,23
Drinking water treatment residuals	4.17–8.20	21–74	5,7,9	N/A
Calcined paper sludge	~113.96*	N/A	2–12	10,40,60
Fly ash	32	1.42	3,5,7,9,11	25,40,50,60
Slag	60	1.29	3,5,7,9,11	25,40,50,60
Portland cement	83	1.38	3,5,7,9,11	25,40,50,60

*Converted from original units.
http://rave.ohiolink.edu/etdc/view?acc_num=ucin1490351099058308.

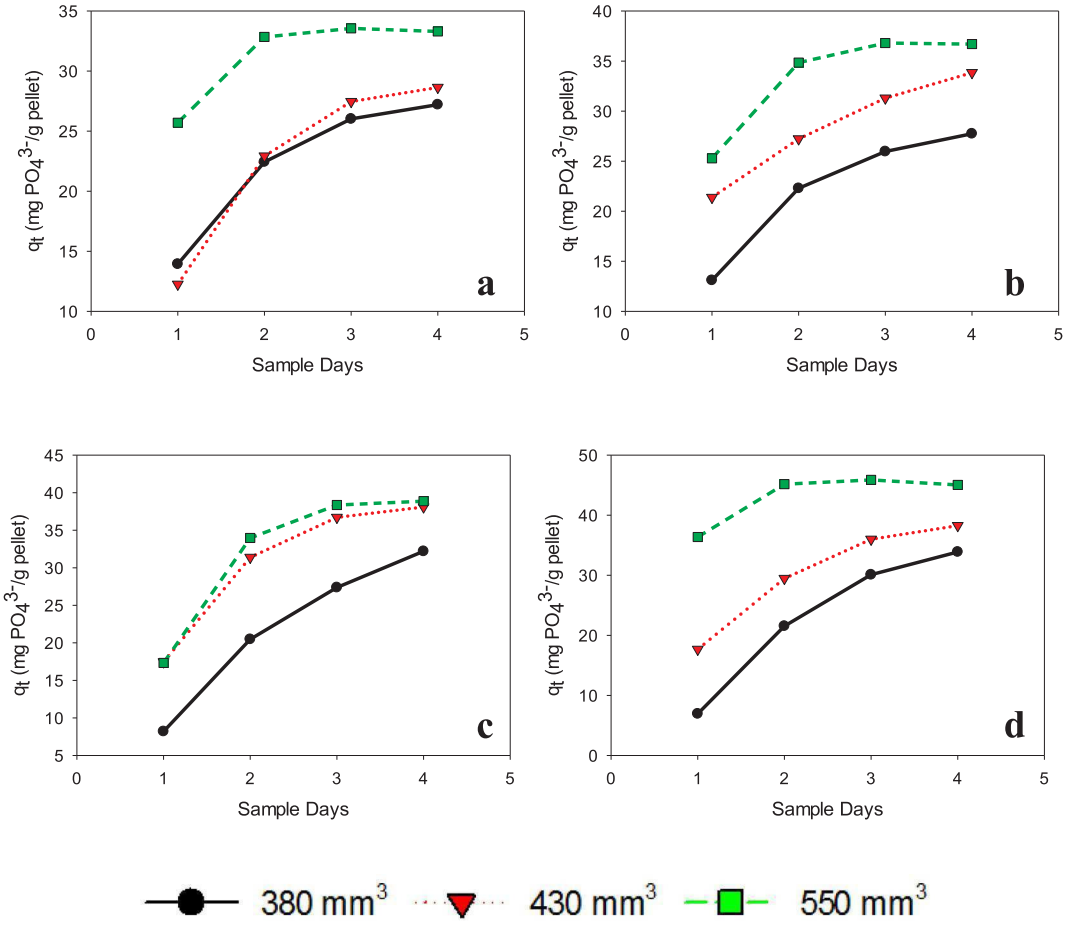

Fig. 6. Adsorptive capacity for the three different surface area conditions for (a) 5%1, (b) 10%2, (c) 15%1 and (d) 20%2.

reaction rates between adsorbate and adsorbent phosphate concentration. The initial conditions for the kinetic study were: (i) adsorbent amount: one pellet (~0.4 g), (ii) temperature: 22.7 °C ± 0.5, (iii) pH: 7.0 ± 0.1, (iv) target phosphate concentration: 160 mg L^{-1}, and (v) mixing speed: 150 rpm. The study was conducted with 125 mL of the sodium phosphate monobasic dihydrate stock solution mixed with the five different $MgCO_3$ pellet compositions in 125 mL Nalgene polypropylene bottles and placed on a G10 Gyratory shaker (New Brunswick Scientific Co., Inc., USA). Samples were taken at various times (1, 2, 3, 4, 7, 9, 11, 14, 18 and 25 days) to analyze for phosphate concentration remaining in the solution. The samples were filtered using a 0.45 µm nylon syringe filter (Whatman) and analyzed for phosphate using a UV–Vis spectrophotometer (DR 2700, HACH) via the US EPA PhosVer 3® (Ascorbic Acid) method at 880 nm. The experiment was conducted once, and the phosphate samples were analyzed in duplicate and averaged.

2.3.2. Sorption studies

Next, an isotherm experiment was completed with varying sorbent masses, from 1 (~0.4 g) to 6 (~2.4 g) pellets, to find the maximum equilibrium adsorption capacity of each material. The phosphate concentration in the stock solution was raised to 330 mg L^{-1} but, otherwise, the conditions were the same as for the kinetics studies. The various 125 mL Nalgene bottles were left on the shaker for 25 days to reach equilibration and then analyzed for phosphate concentration remaining in solution using the US EPA PhosVer 3® method. The isotherm with all five pellet compositions was conducted once. An additional isotherm experiment for the 15%1 pellet was conducted in triplicate.

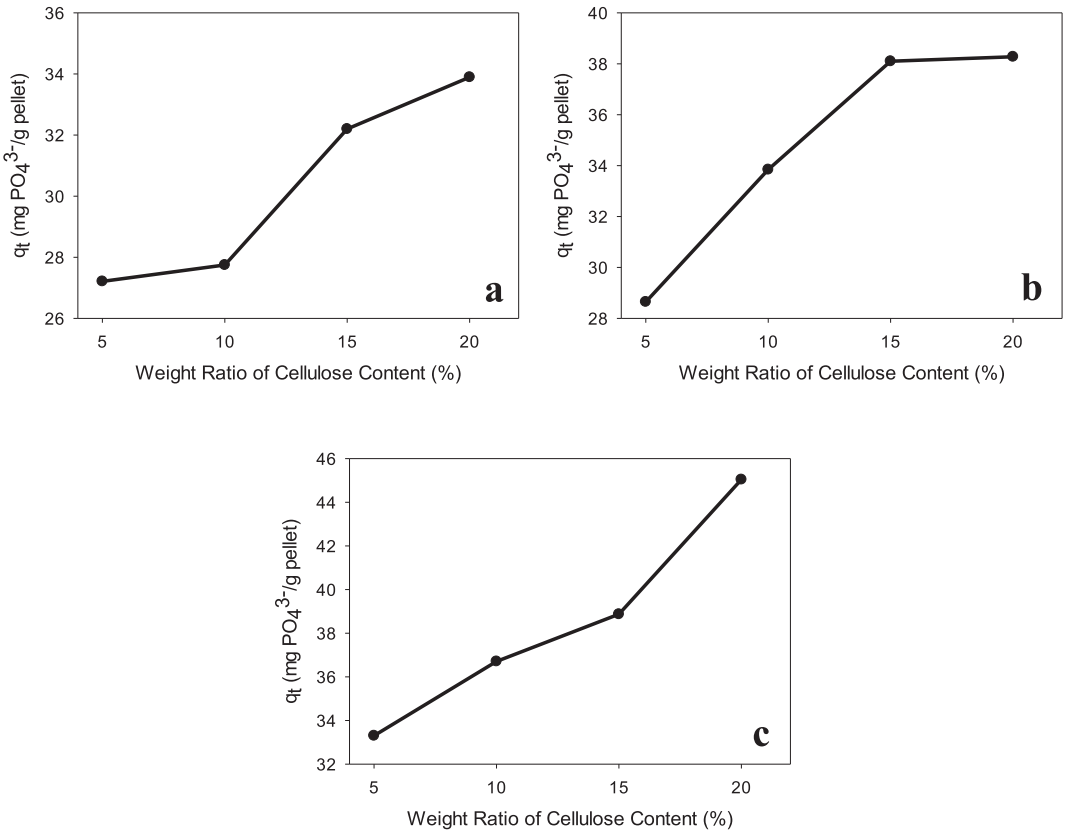

Fig. 7. Adsorptive capacity for the three different surface area conditions for (a) 380 mm^3, (b) 430 mm^3, (c) 550 mm^3.

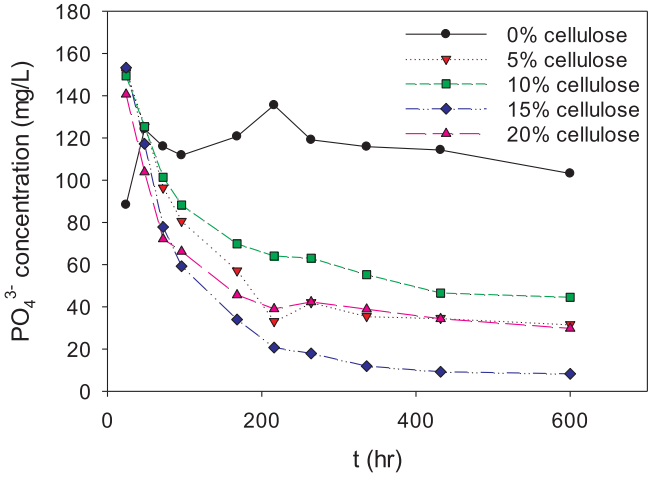

Fig. 8. Phosphate concentration remaining in solution over time as the various pellet recipes reached adsorption capacity.

All of the phosphate analysis was conducted in duplicate and averaged.

2.4. Desorption experiment

The desorption experiments were conducted using 4–6 pellets from the isotherm adsorption experiment in various solutions to analyze the recovery of phosphate. Two solutions varied pH in an attempt to achieve desorption: 0.1 M HCl and 0.1 M NaOH. Pellets were also placed into the deionized water just to measure leaching without changing pH. The spent adsorbents were placed in 125 mL Nalgene bottles with 125 mL of each various solution and left on the shaker at a mixing speed of 150 rpm for 25 days, as with the isotherm experiments. The concentration of phosphate that returned to the solution was measured using the US EPA PhosVer 3® Method mentioned in Section 2.3, and the desorption percentage of phosphate was calculated. This experiment provided insight into the ability of the pellets to release phosphate as a potential slow release fertilizer.

3. Results and discussion

3.1. Sample characterization

3.1.1. Physical characteristics

The first step for pellet characterization was to ensure that the pellets had uniform composition. This was accomplished by investigating two separate batches of a pellet from the same recipe, namely the 15%1 pellet. One pellet from each batch was analyzed using SEM via a line scan as well as a cross-section scan. The elemental composition of these pellets prior to adsorption was determined using EDS for Mg, O, and C. Fig. 2 shows the percentage range of each element across the particular scan of the pellet.

The two cross-section scans have the same distance scanned because the diameters of the pellets were limited to the diameter of the die hole on the pelletizer, which was about 6 mm. The line scans show the variety in length of the two pellets. Overall, the range of percentages of each element was consistent for the two pellets in both the line scan and the cross-section scan. The carbon and magnesium percentages ranged from 15 to 35% and the oxygen ranged from 45 to 55%. This showed uniform composition between the two batches and demonstrated the random distribution of each element within the pellet.

Physical properties of the pellets are summarized in Table 1. The BET surface areas for the 0%17, 5%1, 10%2, 15%1, and 20%2 pellets were 27.5, 33.2, 36.9, 43.1, and 37.6 $m^2 g^{-1}$, respectively. As the ratio of cellulose increased, the BET surface area increased until the 20%2 sample. At this point, the stability of the pellet began to be lost which could account for the decrease in surface area. The 20%2 sample had

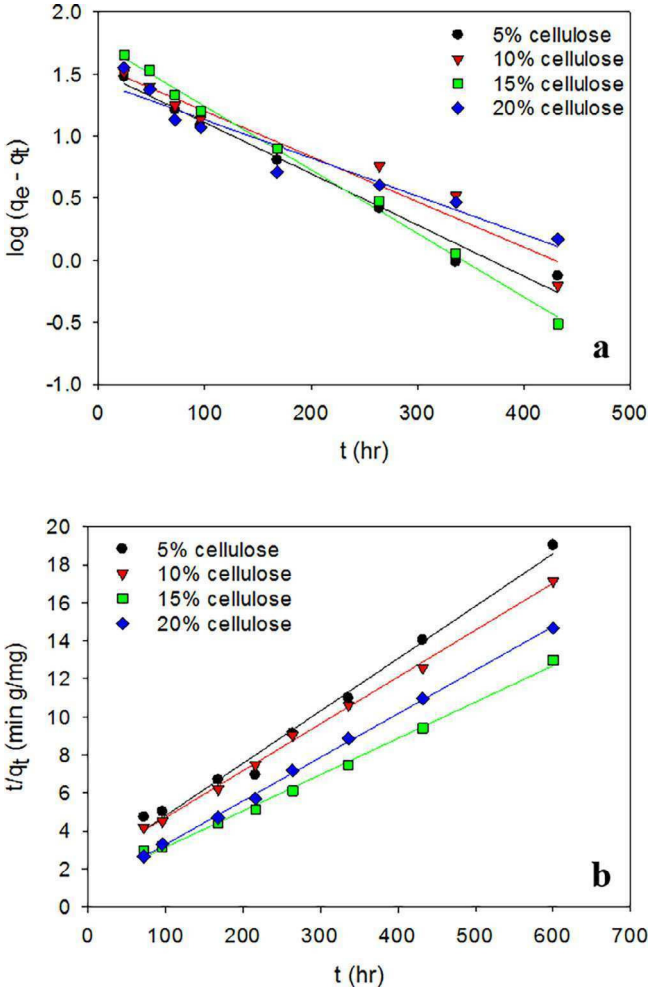

Fig. 9. Linearized (a) *pseudo* first-order kinetics model and (b) *pseudo*-second-order model applied to the four various pellet recipes.

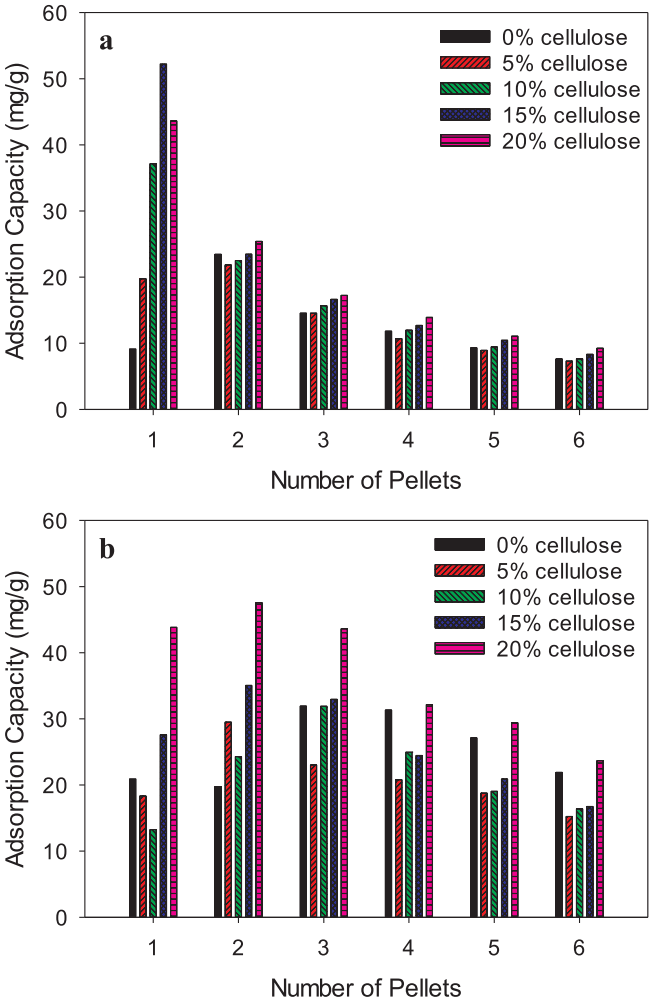

Fig. 10. Adsorption capacity comparison with 5 pellet recipes in two isotherm experiments with initial concentration (a) 160 mg L^{-1} and (b) 330 mg L^{-1}.

more visual char that was clogging the pores and decreasing the surface area. As expected, the addition of cellulose provided additional internal surface area.

3.1.2. Surface morphology of the pellets

Fig. 3 shows SEM images of the surface of the 0% cellulose baseline pellet and the 10% cellulose pellet before and after phosphate adsorption. Many particulate aggregates were observed on the surface of the $MgCO_3$ pellets before phosphate exposure. To confirm phosphate adsorption on the surface of the pellet, the elemental composition was checked with EDS. A clear peak was seen for phosphorus on the 10%2 pellet while the 0%17 pellet did not have such a clear peak. This illustrated that increased cellulose content resulted in an increase in phosphate adsorption, as expected.

3.1.3. XRD analysis

Various magnesium phosphates can form depending upon the pH and molar concentration and are listed below.

- Monomagnesium phosphate ($Mg(H_2PO_4)_2$)
- Dimagnesium phosphate ($MgHPO_4$)
- Magnesium phosphate tribasic ($Mg_3(PO_4)_2$)

Amorphous magnesium phosphate.

The XRD patterns for each sample before and after an adsorption isotherm showed that cellulose, periclase (MgO) and brucite (MgOH) were present for the pellets before adsorption. As shown in Fig. 4a, the pellets had both variations of magnesium present due to mixing magnesium carbonate with water and then calcining the pellets. After

Table 3
Adsorption kinetic models, the corresponding linear forms and parameters of $MgCO_3$ pellets with various amounts of cellulose for 4 different synthesis conditions (percent cellulose and calcination time) with initial pH 7 at 23 °C.

Sorbent	*Pseudo*-first-order $\log(q_e-q_t) = \log(q_e)-k_1 t/2.303$			*Pseudo*-second-order $t/q_t = 1/k_2 q_e^2 + t/q_e$		
	q_e (mg g^{-1})	k_1 (h^{-1})	R^2	q_e (mg g^{-1})	k_2 (g mg^{-1} h^{-1})	R^2
5%1	33.34	0.0095	0.9824	36.22	0.0004	0.9880
10%2	36.91	0.0084	0.9497	40.50	0.0003	0.9979
15%1	56.49	0.0118	0.9959	52.25	0.0003	0.9959
20%2	27.48	0.0071	0.9312	43.54	0.0005	0.9988

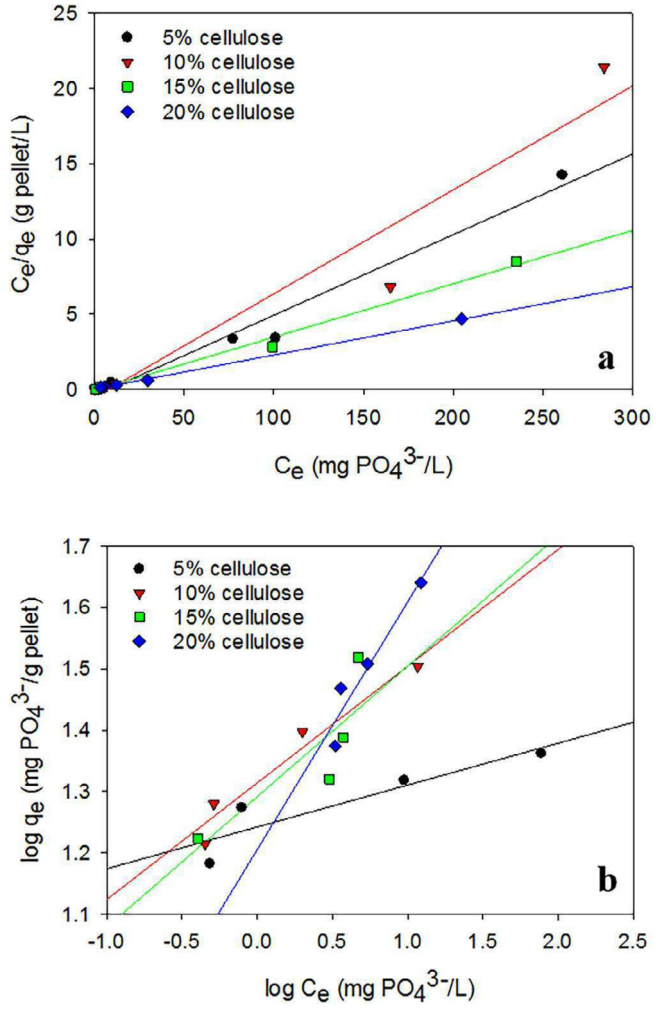

Fig. 11. Linearized (a) Langmuir model and (b) Freundlich model applied to the four various pellet recipes.

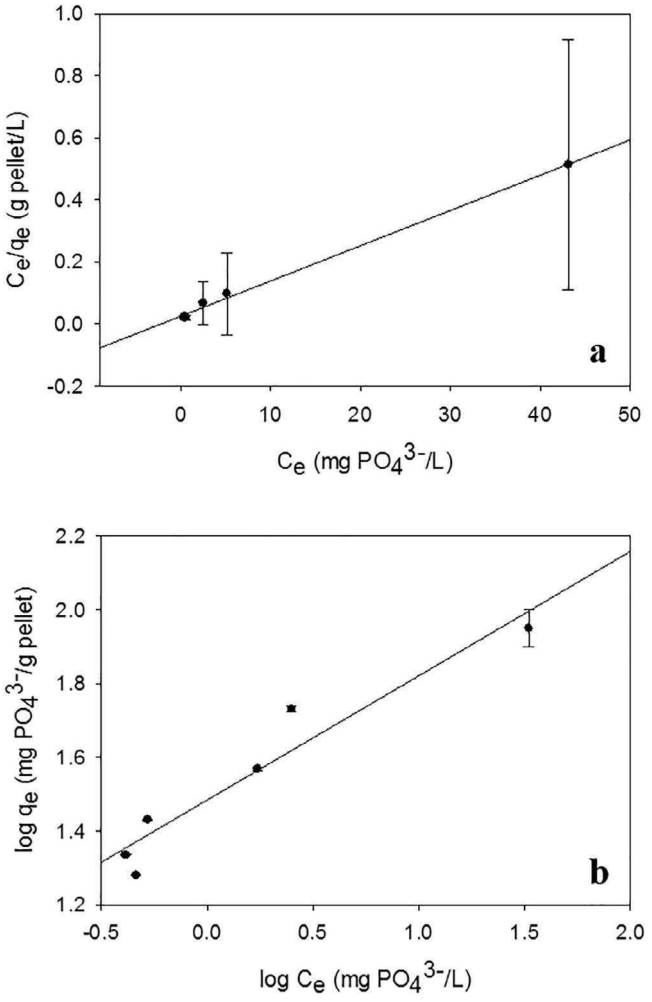

Fig. 12. Linearized (a) Langmuir model and (b) Freundlich model applied on the triplicate isotherm experiment with 15%1 pellets.

adsorption experiments were conducted, magnesium variations were detected mostly as hydromagnesite ($Mg_5(CO_3)_4(OH)_2{\cdot}4H_2O$) with some remaining brucite and magnesium phosphate (as cattiite) as shown in Fig. 4b. The pellet with the most phosphate present was the 15%1 pellet as seen with the highest peak of cattiite. Finding magnesium phosphate after the adsorption experiments further confirmed that adsorption occurred and that the increased surface area from cellulose addition was providing additional adsorption capacity.

3.1.4. Thermal stability of the pellets

The thermal stability of the pellets was investigated using thermogravimetric analysis to determine the pellets made from different proportions of cellulose-water-magnesium carbonate mixture affects the decomposition temperature. The 0%17 pellet provided a good control group to determine if adding cellulose alone affected the thermal stability. Fig. 5 presents the loss in weight as the sample was exposed to higher temperatures.

The 0%17 pellet had a peak for onset degradation temperature at 319 °C as the baseline. The pellets with cellulose showed improvement in onset decomposition temperature. The onset decomposition temperatures for the 5%1, 10%2, 15%1, and 20%2 pellets were 384, 399, 364 and 403 °C, respectively. Cellulose provided binding and increased the thermal stability up until the 15%1 pellet where porosity took control and slightly decreased the stability. The 15%1 pellet still had a higher temperature than the 0%17 pellet. The 20%2 pellet increase thermal stability again because this pellet had more char present on the surface and in the pores which added to thermal stability.

Table 4
Adsorption isotherm models, the corresponding linear forms and parameters of $MgCO_3$ pellets with various amounts of cellulose for 4 different synthesis conditions with initial pH 7 at 23 °C.

Sorbent	Langmuir isotherm $C_e/q_e = 1/q_{max}C_e + 1/K_L q_{max}$			Freundlich isotherm $\log q_e = \log K_F + 1/n \log C_e$		
	q_{max} (mg g^{-1})	K_L (L mg^{-1})	R^2	K_F (mg g^{-1} (L mg^{-1})$^{1/n}$)	n^{-1}	R^2
5%1	18.69	−0.1264	0.9761	17.47	0.0683	0.8257
10%2	14.47	−0.1247	0.9381	20.61	0.1900	0.9513
15%1	28.17	−0.4517	0.9917	19.57	0.2126	0.7094
20%2	44.25	0.9741	0.9995	16.06	0.4031	0.9124

Table 5
Adsorption isotherm models, the corresponding linear forms and parameters of $MgCO_3$ pellets with 15% cellulose with initial pH 7 at 23 °C. Data from triplicate experimental runs.

Sorbent	Langmuir isotherm $C_e/q_e = 1/q_{max}C_e + 1/K_L q_{max}$			Freundlich isotherm $\log q_e = \log K_F + 1/n \log C_e$		
	q_{max} (mg g^{-1})	K_L (L mg^{-1})	R^2	K_F (mg g^{-1} (L mg^{-1})$^{1/n}$)	n^{-1}	R^2
15%1	91.74	0.3586	0.9657	28.95	0.2825	0.9457
15%1	116.28	0.5478	0.9785	36.46	0.4531	0.7824
15%1	81.30	0.4786	0.9944	29.89	0.2333	0.7358
Average	96.44 ± 18.0	0.46 ± 0.1		31.76 ± 4.1	0.32 ± 0.1	

Table 6
Desorption of adsorbed phosphate using three different solutions.

Sorbent	0.1 M HCl			0.1 M NaOH			DI Water		
	Adsorbed PO_4^{3-} (mg g^{-1})	Desorbed PO_4^{3-} (mg g^{-1})	Desorption Percentage	Adsorbed PO_4^{3-} (mg g^{-1})	Desorbed PO_4^{3-} (mg g^{-1})	Desorption Percentage	Adsorbed PO_4^{3-} (mg g^{-1})	Desorbed PO_4^{3-} (mg g^{-1})	Desorption Percentage
5%1	7.29	0.26	3.6%	10.69	0.14	1.3%	8.93	0.01	0.1%
10%2	7.65	0.06	0.7%	11.98	0.23	1.9%	9.43	0.01	0.1%
15%1	8.32	0.08	1.0%	12.69	0.56	**4.4%**	10.44	0.01	0.1%
20%2	9.25	0.07	0.8%	13.91	0.35	2.5%	11.07	0.01	0.1%

3.2. Adsorption studies

Table 2 represents various adsorptive materials used for recovering phosphate from water categorized by the main element or base material modified to create the adsorbents. The range of adsorption capacity is from 0.28 to 326.63 mg of phosphate adsorbed per gram of adsorbent.

3.2.1. Optimum surface area

To study the best dimensions for the physical size of the pellet, pellets were studied with the varying surface area of 380 mm^3, 430 mm^3, and 550 mm^3 via cutting the pellets. Although the pellets were cut, the overall mass used was kept consistent. The adsorption experiment was run over just four days to investigate the change in adsorption capacity of the three conditions, including the full pellet as a reference baseline. Fig. 6 shows the change in adsorption capacity over the four days for each surface area condition for the four pellet recipes.

Overall, each pellet recipe had a higher adsorption capacity with the decrease in pellet length. This is expected since cutting the pellet exposed another surface for adsorption and illustrated that adsorption is occurring on the surface of the pellets. Fig. 7 illustrates that each variation in the surface area still has the same overall trend in adsorption capacity, namely that the capacity increases with the increase in cellulose content.

3.2.2. Kinetic studies

An adsorption experiment was conducted to determine the equilibrium time for the phosphate concentration remaining in the solution after pellets had reached adsorption capacity. Fig. 8 shows how the phosphate concentration in solution changed with respect to time and suggested an apparent equilibrium time of 600 h or 25 days. Each recipe removed a different overall percentage of phosphate; 0%17 removed 34%, 5%1 removed 80%, 10%2 removed 72%, 15%1 removed 95% and 20%2 removed 81%.

Batch experiments, with one pellet in 125 mL of a solution with target phosphate concentration of 160 mg L^{-1}, were conducted to determine the rate of phosphate adsorption, specifically to find the order of the rate constant. The kinetics of each of the five pellet recipes were studied and compared with the *pseudo*-first-order (Fig. 9a) and *pseudo*-second-order (Fig. 9b) kinetics models to find the best fit using linear regression analysis.

The *pseudo*-first-order model and *pseudo*-second-order model are, respectively, as follows:

$$\log(q_e - q_t) = \log(q_e) - k_1 t/2.303 \quad (1)$$

$$t/q_t = 1/k_2 q_e^2 + t/q_e \quad (2)$$

where q_e is the amount of adsorbate adsorbed per unit mass of adsorbent (mg g^{-1}) at equilibrium, q_t is the amount of adsorbate adsorbed per unit mass of adsorbent (mg g^{-1}) at time t, k_1 (h^{-1}) and k_2 (g mg^{-1} h^{-1}) are the rate constants for the *pseudo*-first-order model and *pseudo*-second-order model, respectively. The linear forms of the models, the parameters, and how the parameters correlate with each model (R^2) are listed in Table 3. The pellet recipe without cellulose is not included since it is the baseline.

Overall the best fit model was the *pseudo*-second-order model with $R^2 > 0.98$ for all pellet recipes, but the *pseudo*-first-order model fit all recipes with $R^2 > 0.93$, so both models had a strong correlation, which has been found in other phosphate adsorption experiments [12,30–36]. The *pseudo*-second-order model indicates that the adsorption that occurred was chemisorption, which assumes monolayer adsorption. The highest model adsorption capacity for both models occurred for the 15%1 pellet; q_e was 56.49 mg g^{-1} for *pseudo*-first-order and 52.25 mg g^{-1} for *pseudo*-second-order. In the *pseudo*-second-order model, $k_2 q_e^2$ represents the initial adsorption rate. The rate for the 5%1, 10%2, 15%1 and 20%2 pellets were as follows: 0.492, 0.449, 0.823 and 1.021 mg g^{-1} h^{-1}, respectively. This means that although the 15%1 pellet has the highest adsorption capacity, the 20%2 recipes had the fastest initial adsorption rate of 15%1 as a close second.

3.2.3. Sorption isotherms

Sorption isotherms describe the relationship between the equilibrium adsorbate concentration in the solution and the amount of phosphate adsorbed on the adsorbent. Batch experiments, with one to six pellets in 125 mL of a solution with target phosphate concentration of 330 mg L^{-1}, were conducted to determine the maximum adsorption capacity of the pellets.

The two studies were compared for overall adsorption capacity of phosphate concentration from solution as the adsorbent mass was increased. Fig. 10a and 10b represent the two isotherms for overall adsorption capacity on a number of pellets basis.

The lower concentration was more easily removed using multiple pellets than the higher concentration but the adsorption capacities were higher overall in the solution with higher phosphate concentration

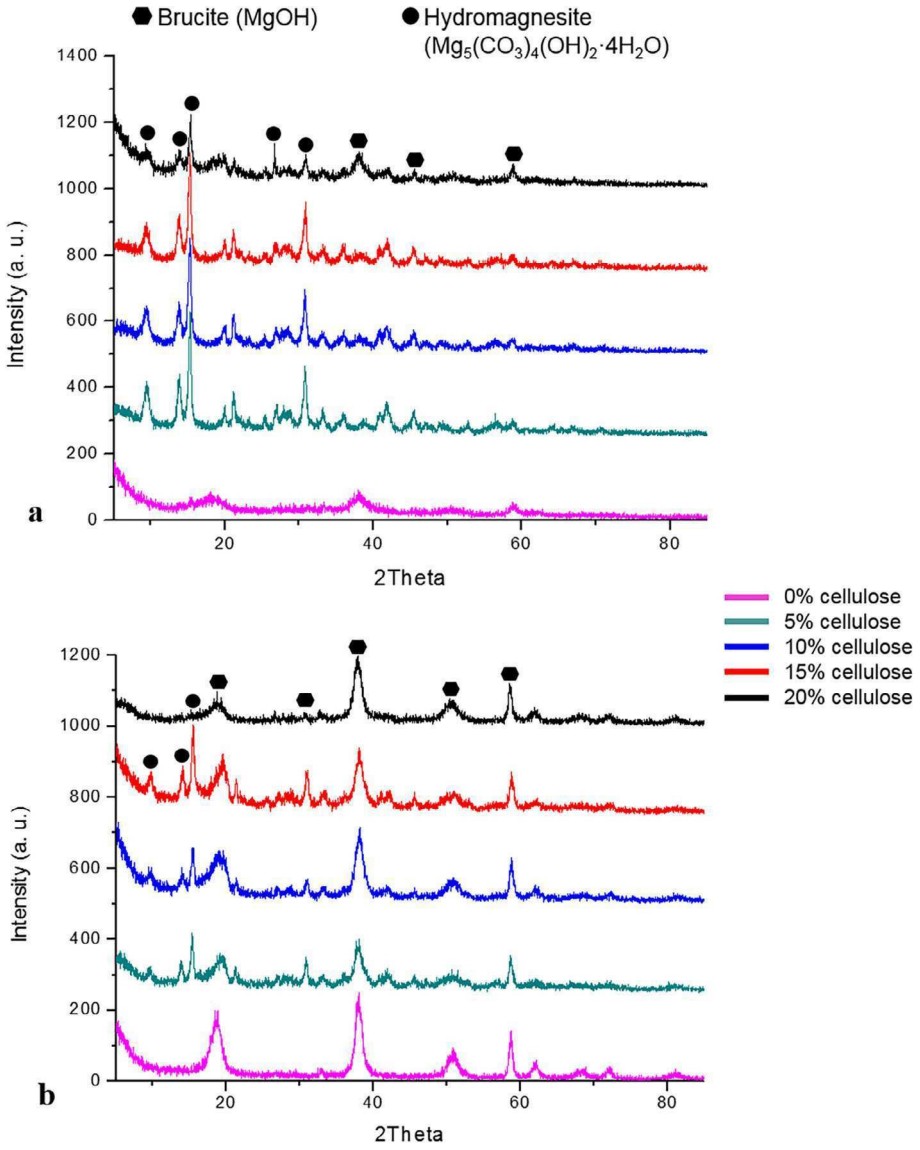

Fig. 13. XRD patterns of the various pellets after (a) 0.1 M HCl solution and (b) 0.1 M NaOH solution desorption experiments were conducted.

originally. Since the only option with the pellets was to increase the mass used for the isotherm, the original concentration used in kinetics for one pellet was not high enough to show a removal trend for multiple pellets.

Isotherm data was fitted to both the Langmuir and Freundlich models (see Figs. S1 and S2) to determine the best fit using regression analysis as shown in Fig. 11a and b, respectively.

The linearized Langmuir equation is as follows:

$$C_e/q_e = 1/q_{max}C_e + 1/K_L q_{max} \quad (3)$$

where q_e is the amount of adsorbate adsorbed per unit mass of adsorbent ($mg\,g^{-1}$), C_e is the amount of unadsorbed adsorbate concentration in solution at equilibrium ($mg\,L^{-1}$), q_{max} is the maximum amount of adsorbate per unit mass of adsorbent to form a complete monolayer on the surface ($mg\,g^{-1}$), and K_L is a constant related to the affinity of the binding sites ($L\,mg^{-1}$). Similarly, the linearized Freundlich equation is as follows:

$$\log q_e = \log K_F + 1/n \log C_e \quad (4)$$

where K_F is the adsorption capacity of the adsorbent ($mg\,g^{-1}$ $(L\,mg^{-1})^{1/n}$) and n indicates sorption favorability. The parameters found via plotting these linearized equations are shown in Table 4, excluding the 0% cellulose baseline pellet.

Based on this analysis, the best fit for the isotherm studies was the Langmuir model revealing that the adsorption occurred in a monolayer fashion. This confirms the findings that the *pseudo*-second-order kinetics model fits best, which also assumes monolayer adsorption. The maximum theoretical adsorption capacities found using the Langmuir model were: 18.7, 14.5, 28.2, and 44.3 $mg\,g^{-1}$ for 5%1, 10%2, 15%1 and 20%1 pellets, respectively. Here the 20%2 pellet had the highest capacity, but this is the least stable pellet.

The final isotherm conducted was completed for the 15%1 pellet in triplicate with the 330 $mg\,L^{-1}$ solution to find the reproducibility of the adsorption capacity. The results were modeled with the linearized Langmuir and Freundlich models as shown in Fig. 12a and b, respectively. The parameters determined from these models are listed in Table 5 (See Fig S3 for SEM and EDS data).

The triplicate analysis of the 15%1 pellet resulted in an average q_{max} of 96.4 $mg\,g^{-1}$ with a standard deviation of 18 $mg\,g^{-1}$ and relative standard deviation of 18.6% for the experiments. The variation in predicted adsorption capacity from the kinetics and isotherm experiments can be explained by the variation in diffusion and surface area of pellets exposed to the solution. The bottles in the kinetics experiment were moved from the shaker for each sample throughout the

experiment whereas the bottles in the isotherm experiment were kept on the table until the full 25 days had passed. During the movement for the kinetics experiment, the pellet may have shifted in the solution and exposed the additional surface area for adsorption.

3.3. Desorption experiment

Since the adsorption of phosphate was proven reasonably successful, pellets from the isotherm were studied for the ability to recover phosphate through desorption. Three different solutions were used to try to achieve this: deionized water (pH ~ 6.6), 0.1 M HCl (pH < 2) and 0.1 M NaOH (pH ~ 12.4). Table 6 shows the percentage of desorption seen after 25 days. This desorbability parameter is defined by the ratio of phosphate desorbed over phosphate adsorbed and provides an indicator for phosphate recovery potential.

Based on the results, leaching into the water without a desorption aid was negligible. Even with the change in pH, only as much as 4% of phosphate was desorbing. To further investigate what was occurring on the surface of the pellet, XRD analysis was conducted on each pellet after desorption in the acidic and basic solutions (Fig. 13a and b, respectively).

From the figure, magnesium phosphate was no longer detected on the pellets after the desorption period (25 days). On closer inspection of the experiment with the acidic solution, phosphorus was detected via EDS but may have been amorphous and not detectable by XRD. For the basic solution desorption experiment, the XRD pattern was shifted slightly such that the phosphate compound and hydromagnesite peaks were not differentiable.

4. Conclusions

$MgCO_3$ pellets prepared with varying amounts of cellulose were found to be effective adsorbents for removing phosphate from aqueous suspensions. The calcination of the pellets with higher cellulose ratios proved to result in increased BET surface area until the pellet with 20% cellulose. The highest surface area achieved was 43.1 $m^2 g^{-1}$ for the 15%1 pellet. The increased surface area corresponded to an increased adsorption capacity as seen through the Langmuir models. Although the highest theoretical adsorption capacity was 44.3 mg g^{-1} for the 20%2 pellet from the isotherm, the 15%1 pellet showed the most promise from kinetics experiments and surface area analysis. The 20%2 pellet was the least stable after calcination so the 15%1 pellet would provide adsorption without the stability being lost. From the isotherm experiments conducted for the 15%1 pellet, the adsorption capacity had an average of 96.4 mg g^{-1}. The surface of the pellets changed as phosphate was adsorbed as shown by the SEM and XRD analysis. While enhanced P availability might occur when exposed to the real world, the simple dissolution/desorption experiment suggested quite a minimal release. It, of course, says nothing about the very slow release.

Disclaimer

The U.S. Environmental Protection Agency, through its Office of Research and Development, funded and managed, or partially funded and collaborated in, the research described herein. It has been subjected to the Agency's administrative review and has been approved for external publication. Any opinions expressed in this paper are those of the author(s) and do not necessarily reflect the views of the Agency. Therefore, no official endorsement should be inferred. Any mention of trade names or commercial products does not constitute endorsement or recommendation for use.

Acknowledgments

Funding: This work was supported by, in part for Elisabeth Martin, a graduate research traineeship through Cooperative Agreement Grant CR 83558601 from the US Environmental Protection Agency to the University of Cincinnati.

Appendix A. Supplementary data

Supplementary data associated with this article can be found, in the online version, at https://doi.org/10.1016/j.cej.2018.06.183.

References

[1] J. Heisler, P.M. Glibert, J.M. Burkholder, D.M. Anderson, W. Cochlan, W.C. Dennison, Q. Dortch, C.J. Gobler, C.A. Heil, E. Humphries, A. Lewitus, R. Magnien, H.G. Marshall, K. Sellner, D.A. Stockwell, D.K. Stoecker, M. Suddleson, Eutrophication and harmful algal blooms: a scientific consensus, Harmful Algae 8 (2008) 3–13, https://doi.org/10.1016/j.hal.2008.08.006.
[2] H.W. Paerl, T.G. Otten, Harmful cyanobacterial blooms: causes, consequences, and controls, Microb. Ecol. 65 (2013) 995–1010, https://doi.org/10.1007/s00248-012-0159-y.
[3] D.J. Conley, H.W. Paerl, R.W. Howarth, D.F. Boesch, S.P. Seitzinger, K.E. Havens, C. Lancelot, G.E. Likens, Controlling eutrophication: nitrogen and phosphorus, Science 323 (2009) 1014–1015.
[4] Joshua T. Bunce, Edmond Ndam, Irina D. Ofiteru, Andrew Moore, David W. Graham, A review of phosphorus removal technologies and their applicability to small-scale domestic wastewater treatment systems, Front. Environ. Sci. 22 (2018), https://doi.org/10.3389/fenvs.2018.00008.
[5] D.W. Schindler, Recent advances in the understanding and management of eutrophication, Limnol. Oceanogr. 51 (2006) 356–363.
[6] D.L. Correll, The role of phosphorus in the eutrophication of receiving waters: a review, J. Environ. Qual. 27 (1998) 261–266.
[7] K. Ashley, D. Cordell, D. Mavinic, A brief history of phosphorus: from the philosopher's stone to nutrient recovery and reuse, Chemosphere 84 (2011) 737–746, https://doi.org/10.1016/j.chemosphere.2011.03.001.
[8] J. Cooper, R. Lombardi, D. Boardman, C. Carliell-Marquet, The future distribution and production of global phosphate rock reserves, Resour. Conserv. Recycl. 57 (2011) 78–86, https://doi.org/10.1016/j.resconrec.2011.09.009.
[9] J. Lalley, C. Han, X. Li, D.D. Dionysiou, M.N. Nadagouda, Phosphate adsorption using modified iron oxide-based sorbents in lake water: kinetics, equilibrium, and column tests, Chem. Eng. J. 284 (2016) 1386–1396, https://doi.org/10.1016/j.cej.2015.08.114.
[10] J. Lalley, C. Han, G.R. Mohan, D.D. Dionysiou, T.F. Speth, J. Garland, M.N. Nadagouda, Phosphate removal using modified Bayoxide® E33 adsorption media, Environ. Sci. Water Res. Technol. 1 (2015) 96–107, https://doi.org/10.1039/C4EW00020J.
[11] T.E. Köse, B. Kıvanç, Adsorption of phosphate from aqueous solutions using calcined waste eggshell, Chem. Eng. J. 178 (2011) 34–39, https://doi.org/10.1016/j.cej.2011.09.129.
[12] C. Fang, T. Zhang, P. Li, R. Jiang, Y. Wang, Application of magnesium modified corn biochar for phosphorus removal and recovery from swine wastewater, Int. J. Environ. Res. Public Health 11 (2014) 9217–9237, https://doi.org/10.3390/ijerph110909217.
[13] L. Lai, Q. Xie, L. Chi, W. Gu, D. Wu, Adsorption of phosphate from water by easily separable Fe3O4@SiO2 core/shell magnetic nanoparticles functionalized with hydrous lanthanum oxide, J. Colloid Interface Sci. 465 (2016) 76–82, https://doi.org/10.1016/j.jcis.2015.11.043.
[14] F. Rouquerol, J. Rouquerol, K.S.W. Sing, G. Maurin, P. Llewellyn, Introduction, in: Adsorpt. Powders Porous Solids, Elsevier, 2014: pp. 1–24. http://linkinghub.elsevier.com/retrieve/pii/B9780080970356000012 (accessed October 14, 2016).
[15] I.P. Tzanakis, A.N. Papadaki, M. Wei, S. Kagia, V.V. Spadidakis, N.E. Kallivretakis, D.G. Oreopoulos, Magnesium carbonate for phosphate control in patients on hemodialysis. A randomized controlled trial, Int. Urol. Nephrol. 40 (2008) 193–201, https://doi.org/10.1007/s11255-007-9300-0.
[16] A.J. Hutchison, M. Wilkie, Use of magnesium as a drug in chronic kidney disease, Clin. Kidney J. 5 (2012) i62–i70, https://doi.org/10.1093/ndtplus/sfr168.
[17] Á.L. de Francisco, L. Belmar, C. Piñera, M. Kislikova, M. Seras, M. Serrano, Z. Albines, C. Sango, M. Arias, Effect of calcium acetate/magnesium carbonate in the treatment of hyperphosphataemia in dialysis patients in real clinical practice. One year follow up, Nefrologia 34 (2014) 617–627.
[18] D.M. Spiegel, Phosphorus metabolism and management in chronic kidney disease: the role of magnesium binders in chronic kidney disease: role of magnesium binders in chronic kidney disease, Semin. Dial. 20 (2007) 333–336, https://doi.org/10.1111/j.1525-139X.2007.00307.x.
[19] D.M. Spiegel, B. Farmer, G. Smits, M. Chonchol, Magnesium carbonate is an effective phosphate binder for chronic hemodialysis patients: a pilot study, J. Ren. Nutr. 17 (2007) 416–422, https://doi.org/10.1053/j.jrn.2007.08.005.
[20] C. Meyer, K. Cameron, New agent to treat elevated phosphate levels: Magnesium carbonate/calcium carbonate tablets, CANNT J. 22 (2012).
[21] G. El Diwani, S. El Rafie, N.N. El Ibiari, H.I. El-Aila, Recovery of ammonia nitrogen from industrial wastewater treatment as struvite slow releasing fertilizer, Desalination 214 (2007) 200–214, https://doi.org/10.1016/j.desal.2006.08.019.
[22] T. Zhang, L. Ding, H. Ren, X. Xiong, Ammonium nitrogen removal from coking wastewater by chemical precipitation recycle technology, Water Res. 43 (2009) 5209–5215, https://doi.org/10.1016/j.watres.2009.08.054.
[23] Y. Liu, S. Kumar, J.-H. Kwag, C. Ra, Magnesium ammonium phosphate formation,

recovery and its application as valuable resources: a review, J. Chem. Technol. Biotechnol. 88 (2013) 181–189.
[24] S. Kataki, H. West, M. Clarke, D.C. Baruah, Phosphorus recovery as struvite: recent concerns for use of seed, alternative Mg source, nitrogen conservation and fertilizer potential, Resour. Conserv. Recycl. 107 (2016) 142–156, https://doi.org/10.1016/j.resconrec.2015.12.009.
[25] K.S. Le Corre, E. Valsami-Jones, P. Hobbs, S.A. Parsons, Kinetics of struvite precipitation: effect of the magnesium dose on induction times and precipitation rates, Environ. Technol. 28 (2007) 1317–1324, https://doi.org/10.1080/09593332808618891.
[26] P.J. Talboys, J. Heppell, T. Roose, J.R. Healey, D.L. Jones, P.J.A. Withers, Struvite: a slow-release fertiliser for sustainable phosphorus management? Plant Soil. 401 (2016) 109–123, https://doi.org/10.1007/s11104-015-2747-3.
[27] M.M. Rahman, M.A.M. Salleh, U. Rashid, A. Ahsan, M.M. Hossain, C.S. Ra, Production of slow release crystal fertilizer from wastewaters through struvite crystallization – a review, Arab. J. Chem. 7 (2014) 139–155, https://doi.org/10.1016/j.arabjc.2013.10.007.
[28] A.E.* Johnston, I.R. Richards, Effectiveness of different precipitated phosphates as phosphorus sources for plants, Soil Use Manage. 19 (2003) 45–49, https://doi.org/10.1079/SUM2002162.
[29] W.M. Haynes (Ed.), CRC Handbook of Chemistry and Physics, 97th ed., CRC Press, 2016.
[30] A. Halajnia, S. Oustan, N. Najafi, A.R. Khataee, A. Lakzian, Adsorption–desorption characteristics of nitrate, phosphate and sulfate on Mg–Al layered double hydroxide, Appl. Clay Sci. 80–81 (2013) 305–312, https://doi.org/10.1016/j.clay.2013.05.002.
[31] D. Guaya, C. Valderrama, A. Farran, C. Armijos, J.L. Cortina, Simultaneous phosphate and ammonium removal from aqueous solution by a hydrated aluminum oxide modified natural zeolite, Chem. Eng. J. 271 (2015) 204–213, https://doi.org/10.1016/j.cej.2015.03.003.
[32] X. Cheng, X. Huang, X. Wang, D. Sun, Influence of calcination on the adsorptive removal of phosphate by Zn–Al layered double hydroxides from excess sludge liquor, J. Hazard. Mater. 177 (2010) 516–523, https://doi.org/10.1016/j.jhazmat.2009.12.063.
[33] F. Gan, J. Zhou, H. Wang, C. Du, X. Chen, Removal of phosphate from aqueous solution by thermally treated natural palygorskite, Water Res. 43 (2009) 2907–2915, https://doi.org/10.1016/j.watres.2009.03.051.
[34] L. Dai, B. Wu, F. Tan, M. He, W. Wang, H. Qin, X. Tang, Q. Zhu, K. Pan, Q. Hu, Engineered hydrochar composites for phosphorus removal/recovery: lanthanum doped hydrochar prepared by hydrothermal carbonization of lanthanum pretreated rice straw, Bioresour. Technol. 161 (2014) 327–332, https://doi.org/10.1016/j.biortech.2014.03.086.
[35] N. Chen, C. Feng, Z. Zhang, R. Liu, Y. Gao, M. Li, N. Sugiura, Preparation and characterization of lanthanum(III) loaded granular ceramic for phosphorus adsorption from aqueous solution, J. Taiwan Inst. Chem. Eng. 43 (2012) 783–789, https://doi.org/10.1016/j.jtice.2012.04.003.
[36] P. Cai, H. Zheng, C. Wang, H. Ma, J. Hu, Y. Pu, P. Liang, Competitive adsorption characteristics of fluoride and phosphate on calcined Mg–Al–CO3 layered double hydroxides, J. Hazard. Mater. 213–214 (2012) 100–108, https://doi.org/10.1016/j.jhazmat.2012.01.069.

From: Gayathri.RamMohan@gwinnettcounty.com
To: Nadagouda, Mallikarjuna
Subject: Co-Author contribution
Date: Wednesday, April 29, 2020 9:09:55 PM
Attachments: image001.png

Dear Dr. Nadagouda- I would like to acknowledge that I have contributed approximately 10% as a co-author to the article entitled "Phosphate removal using modified Bayoxide® E33 adsorption media" published in the Environmental Science: Water Research and Technology journal.

Thanks,
Gaya

Gayathri Ram Mohan, Ph.D., P.E. | Research Scientist V | Dept. of Water Resources, Gwinnett County Government
678-376-6753 (O) I 770-742-5235 (C) | 684 Winder Hwy, Lawrenceville, GA 30045 I www.gwinnettcounty.com

From:	Han, Changseok (hanck)
To:	Nadagouda, Mallikarjuna
Cc:	nnmalli@yahoo.com
Subject:	Contribution to the papers
Date:	Wednesday, April 29, 2020 6:19:28 PM

Dr. Mallik,

My contribution of the works titled "Removal of phosphate using calcium and magnesium-modified iron-based adsorbents", "Phosphate removal using modified Bayoxide E33 adsorption media" and "Phosphate adsorption using modified iron oxide-based sorbents in lake water: Kinetics, equilibrium, and column tests" is 10 %

Thank you.

Best regards,

Changseok Han, Ph.D.

Assistant Professor
Department of Environmental Engineering
College of Engineering
INHA University
100 Inharo, Michuhol-gu Incheon 22212, KOREA
Email: hanck@inha.ac.kr (or changseok.han94@gmail.com)
Office: +82-32-860-7505
Cell Phone: +82-10-3288-1672
https://sites.google.com/site/advancedwatertreatmentlab/
https://sites.google.com/site/changseokhan79/
https://scholar.google.co.in/citations?user=32QMAAEAAAAJ&hl=en
https://www.researchgate.net/profile/Changseok_Han

From: Jacob Lalley
To: Nadagouda, Mallikarjuna
Subject: Fwd:
Date: Thursday, April 30, 2020 9:37:25 AM
Attachments: Part 1_Paper_3.pdf
Part 1_Paper_1.pdf
Part 1_Paper_2.pdf

Hello Dr. Nadagouda,

My contribution to the attached papers was 10%
Removal of phosphate using calcium and magnesium-modified iron-based adsorbents.
Phosphate removal using modified Bayoxide E33 adsorption media.
Phosphate Adsorption using Modified Iron Oxide-based Sorbents in Lake Water: Kinetics, Equilibrium, and Column Tests.

Thank you,

Jacob Lalley
Research Environmental Engineer

Environmental Laboratory
US Army Engineer Research and Development Center
3909 Halls Ferry Road
Vicksburg, MS 39180-6199
601-634-7480

From: Garland, Jay
To: Nadagouda, Mallikarjuna
Subject: RE:
Date: Wednesday, April 29, 2020 4:57:14 PM

This email confirms that my contribution to the publication titled, “Phosphate removal using modified Bayoxide® E33 adsorption media” was 10% of the overall effort.

Jay L. Garland, Ph.D.
Research Scientist, Center for Environmental Solutions and Emergency Response
Office of Research & Development, US EPA
Office (513) 569-7334
Cell (513) 680-9264
Email: garland.jay@epa.gov

From: Nadagouda, Mallikarjuna <nadagouda.mallikarjuna@epa.gov>
Sent: Wednesday, April 29, 2020 3:10 PM
To: Speth, Thomas <Speth.Thomas@epa.gov>; Garland, Jay <Garland.Jay@epa.gov>
Subject:

Hi Tom and Jay,

Can you state your contribution towards the below paper is 10% in a separate e-mail?

Thanks,

Mallikarjuna N. Nadagouda Ph.D.
U. S. Environmental Protection Agency
ORD, Center for Environmental Solutions and Emergency Response
Water Infrastructure Division/ Chemical Methods and Treatment Branch
26 West, Martin Luther King Drive, MS 689, Cincinnati, OH 45268 USA
E-mail: Nadagouda.mallikarjuna@epa.gov
Ph: (513)569-7232

From: Speth, Thomas
To: Nadagouda, Mallikarjuna
Subject: Paper input
Date: Wednesday, April 29, 2020 3:58:48 PM
Attachments: image002.png

Mallik,

My input for the paper “Phosphate removal using modified Bayoxide E33 adsorption media” was 10% of the effort.

Tom

Thomas F. Speth, Ph.D., P.E. (Ohio)
Associate Director
Center for Environmental Solutions and Emergency Response
U.S. Environmental Protection Agency
26 West Martin Luther King Dr.
Cincinnati, OH 45268
(513) 569-7208 Office
(513) 658-1056 Cell
(513) 487-2543 Fax
Speth.Thomas@epa.gov

From: Dionysiou, Dionysios (dionysdd)
To: Nadagouda, Mallikarjuna
Subject: Contribution on articles
Date: Wednesday, April 29, 2020 5:26:11 PM
Attachments: Lalley et al-Environmental Science Water Research & Technology-Vol. 1-pp. 96-107-2015.pdf
Lalley et al-CEJ-Vol. 284-pp. 1386-1396-2016.pdf

Dear Dr. Nadagouda,

This is to indicate my contribution to these two papers attached and listed below is 10%. Please let me know if you need any further information.

Jacob Lalley, Changseok Han, Gayathri Ram Mohan, Dionysios D. Dionysiou, Thomas F. Speth, Jay Garland, and Mallikarjuna N. Nadagouda, Phosphate Removal using Modified Bayoxide® E33 Adsorption Media, Environmental Science: Water Research & Technology 1 (2015) 96-107.

Jacob Lalley, Changseok Han, Xuan Li, Dionysios D. Dionysiou, and Mallikarjuna N. Nadagouda, Phosphate Adsorption using Modified Iron Oxide-based Sorbents in Lake Water: Kinetics, Equilibrium, and Column Tests, Chemical Engineering Journal 284 (2016) 1386-1396.

Best Regards,

Dionysios (Dion) D. Dionysiou, Ph.D.
F. EurASc, F. AEESP, F. ACS, F. IWA, F. RSC, F. CSP, BCEEM
UNESCO Co-Chair Professor of "Water Access and Sustainability"
and Professor of Environmental Engineering
Sustainable Solutions Laboratories (SSLs)
Center of Sustainable Urban Engineering
Drinking Water, Water Supply, Quality, and Treatment, and
Environmental Nanotechnology Laboratories
Environmental Engineering and Science Program
Department of Chemical and Environmental Engineering (ChEE)
705 Engineering Research Center
University of Cincinnati
Cincinnati, OH 45221-0012
Phone (513) 556-0724
Fax (513) 556-4162
Office Number: ERC 780
Email: dionysios.d.dionysiou@uc.edu
Web Page 1: https://dion-lab.weebly.com/
Web Page 2: https://www.ceas3.uc.edu/profiles/dionysdd
Web Page 3: http://ceas.uc.edu/chemical-environmental-engineering/Dr_Dionysios_Dionysiou.html
News and Overview: (1) https://www.uc.edu/news/articles/legacy/enews/2018/05/e26440.html
(2) https://www.uc.edu/news/articles/legacy/enews/2018/02/e26131.html
(3) https://www.uc.edu/news/articles/2019/01/n2059172.html

From:	Han, Changseok (hanck)
To:	Nadagouda, Mallikarjuna
Cc:	nnmalli@yahoo.com
Subject:	Contribution to the papers
Date:	Wednesday, April 29, 2020 6:19:28 PM

Dr. Mallik,

My contribution of the works titled "Removal of phosphate using calcium and magnesium-modified iron-based adsorbents", "Phosphate removal using modified Bayoxide E33 adsorption media" and "Phosphate adsorption using modified iron oxide-based sorbents in lake water: Kinetics, equilibrium, and column tests" is 10 %

Thank you.

Best regards,

Changseok Han, Ph.D.

Assistant Professor
Department of Environmental Engineering
College of Engineering
INHA University
100 Inharo, Michuhol-gu Incheon 22212, KOREA
Email: hanck@inha.ac.kr (or changseok.han94@gmail.com)
Office: +82-32-860-7505
Cell Phone: +82-10-3288-1672
https://sites.google.com/site/advancedwatertreatmentlab/
https://sites.google.com/site/changseokhan79/
https://scholar.google.co.in/citations?user=32QMAAEAAAAJ&hl=en
https://www.researchgate.net/profile/Changseok_Han

From: Nadagouda, Mallikarjuna
To: Nadagouda, Mallikarjuna
Date: Thursday, April 30, 2020 12:58:07 PM

My contribution to the below papers is 64%

Removal of phosphate using calcium and magnesium-modified iron-based adsorbents.
Phosphate removal using modified Bayoxide E33 adsorption media.
Phosphate Adsorption using Modified Iron Oxide-based Sorbents in Lake Water: Kinetics, Equilibrium, and Column Tests.

Thanks,

Mallikarjuna N. Nadagouda Ph.D.
U. S. Environmental Protection Agency
ORD, Center for Environmental Solutions and Emergency Response
Water Infrastructure Division/ Chemical Methods and Treatment Branch
26 West, Martin Luther King Drive, MS 689, Cincinnati, OH 45268 USA
E-mail: Nadagouda.mallikarjuna@epa.gov
Ph: (513)569-7232

From: Iyanna, Nidhi
To: Nadagouda, Mallikarjuna
Subject: Contribution towards paper
Date: Thursday, April 30, 2020 12:25:27 PM

Hello Dr. Nadagouda,

My contribution towards the paper "Removal of phosphate using calcium and magnesium-modified iron-based adsorbents" is less than 10%. It was a pleasure working under your guidance.

Thank You,
Nidhi Iyanna

Table of Contents

General_Authors_Publications.....2
LI-266746_Wright-Disinfection_By-Product_Exposures_and_the_Risk_of_Specific_Ca14
LI-266746_Wright-Disinfection_By-Product_Exposures_and_the_Risk_of_Specific_Ca23
Ohanian-2020_STAA_LOR_Wright.....34
Wright-Disinfection_By-Product_Exposures_and_the_Risk_of_Specific_Cardiac_Birt36
Wright-Disinfection_By-Product_Exposures_and_the_Risk_of_Specific_Cardiac_Birt45

United States Environmental Protection Agency
Washington, DC 20460

STAA REPORT FOR THE SCIENTIST NOMINATIONS

General Information:

Nomination ID/App ID:	20-131
Research Category Primary:	Health Effects Research and Human Health Risk Assessment (HE)
Research Category Secondary:	Other Environmental Research (OR)
Laboratory/Office Name:	ORD
Nomination Entered By:	John Wright

Eligibility Checklist:

[N] The nominated publication(s) has not been submitted to a previous STAA competition.

[N] The nominated publication(s) was published on or before January 1, 2017 and on or after January 1,2012

[N] The principal author was an EPA employee or a PHS employee assigned to EPA when the research was performed

[N] The EPA authors (includes PHS employees assigned to EPA) contributed collectively a minimum of 50% toward the publication(s)

Nominating Official Name:	Kristina Chialton
Nominating Official Title:	SUPERVISORY BIOLOGIST
Nominating OfficialEmail:	thayer.kris@epa.gov
STAA Coordinator Name:	Kathleen Wiser
STAA Coordinator Email:	wiser.kathi@epa.gov

Justifications:

Justification 1:

Although disinfection of drinking water controls water-borne pathogens, the formation of, and exposure to hundreds of disinfection byproducts (DBPs) has raised concerns for other adverse health consequences. The risks for adverse reproductive and developmental effects in relation to DBP exposures remains nebulous, posing an ongoing challenge for US EPA's Stage 2 Rule 6-year Review efforts over the years. The evidence for teratogenicity of some DBPs has been demonstrated in test animals but evidence in humans for specific types of birth defects has been limited. Epidemiological assessment of birth defects related to DBPs has not been sufficiently studied because of many inherent study challenges (e.g., rare outcomes and complex and temporally variable DBP mixture exposures). Previous epidemiological studies had poor exposure assessment and only examined surrogate measures of trihalomethanes (THMs) or were based solely on even more indirect measures such as the type of disinfected water consumed. Many of these studies have therefore been limited in scope and statistical power and have also primarily focused on groups of combined endpoints which may not be etiologically warranted (e.g., All Birth Defects; All Cardiac Defects). These limitations can lead to decreased study sensitivity to detect associations that are present, which can be compounded by important sources of bias such as outcome and exposure misclassification.

In this manuscript entitled "Disinfection By-Product Exposures and the Risk of Specific Cardiac Birth Defects", Dr. Wright and colleagues examine an understudied area and help characterize the potential cardiac defect risk and specificity to particular DBPs (e.g., bromoform, dibromochloromethane, and monobromoacetic acid) as well as for different DBP surrogates such at THM4 (i.e., four regulated THMs). In this analysis, the increased risk of cardiac defects associated with THM4 that was detected is remarkably consistent in magnitude with two other studies, and other brominated DBP (e.g., monobromoacetic acid) results have some coherence with animal toxicological data. The very consistent findings for ventricular septal defects (VSDs) are rare in epidemiological examinations of heterogenous populations based on different exposure metrics. The concordance of this epidemiological evidence with some toxicological data also adds credence to these findings, suggesting that these are biologically plausible associations and not just statistical artifacts. Although no individual epidemiological study by itself implies causality, this study adds to the existing weight of evidence for DBP exposures and cardiac defects. Furthermore, this study represents the first epidemiological study of birth defects and DBPs to examine several individual cardiac defects, different surrogate mixtures [THM4, brominated THMs, regulated haloacetic acids (HAA5), and DBP9 (THM4+HAA5)], and various individual DBP species. This is only the second birth defect study to evaluate exposure to brominated DBPs, which adds some specificity to the potential risks that have been previously noted for THM4. Importantly, it lends additional evidence regarding both consistency and coherence to the literature base, two key considerations when addressing causality in risk assessment based on epidemiologic data.

The nominated manuscript was accepted for publication by what is widely considered the top environmental health journal, *Environmental Health Perspectives* (current Impact Factor of 8.05). This publication has been cited in 31 different research papers as noted by Google Scholar and downloaded 352 times (as of 4-29-20). According to *Environmental Health Perspectives* citation statistics*:* "compared to other publications in the same field, this publication is extremely

highly cited and has received approximately 10 times more citations than average". The citations underscore the national and international importance of this study and included prominent researchers from a variety of countries (e.g., China, Cyprus, England, Canada, Sweden, Portugal, Australia, Germany, Spain, among others) interested in quantifying potential

risks of exposure to DBPs. It has also been cited in recent reviews and weight of evidence evaluations from Canada and the U.S. Given the challenges of characterizing risk to complex mixtures of DBPs, this research will be of increasing importance for various entities engaged in or affected by DBP regulatory determination efforts.

The program areas developed by the nominee's research has focused on quantifying risk and reducing uncertainty related to DBP exposures. The primary impetus for Dr. Wright's DBP exposure assessment and epidemiological research over the years has been the demonstrated research gaps identified by US EPA's Office of Water and others, who have evaluated the reproductive and developmental evidence related to DBPs. As such, this epidemiological study was specifically designed to address some of these limitations and elucidate the risk of individual cardiac defects to specific DBP exposures. Dr. Wright has provided epidemiological and exposure assessment consultations to the Office of Water since 2002 in support of the development of the Stage 2 Disinfection By-product Rule as well as subsequent iterations of their Six-Year reviews. These have been influential in environmental decision-making. As part of this effort, Dr. Wright helped characterize the potential health risk of fetal mortality that was associated with DBP regulations for a cost-benefit analyses. These consultations as well as Dr. Wright's research planning contributions were critical to developing research programs and strategic goals in support of EPA's Office of Water and Regional EPA office needs. The current research has been responsive to Agency needs and provides an example of successful multidisciplinary research to support EPA's mission.

The research described here has been repeatedly vetted through the national and international scientific communities, as well as accepted by a prestigious journal, has helped assure the highest quality scientific support to protect human health and keep the nation's drinking water safe. Drs. Wright and Narotsky continued leadership in the DBP field for over 20 and 25 years, respectively, is acknowledged by being invited participants to the biannual Gordon Research Conference on DBPs since its inception in 2006. This has led to invitations to disseminate the findings from this important work at that meeting in both 2015 and 2019. For this particular study, Dr. Wright and his co-authors have been asked to give numerous oral presentations at other national and international fora. Additional invited talks were given by him at different annual societal meetings including the Society for Risk Analysis and by another co-author (John Kaufman) who delivered an oral presentation of these results at the International Society of Environmental Epidemiology in 2014. Dr. Wright was also invited to present these important research findings to the Australia's New South Wales Ministry of Health in 2014. Most recently, Dr. Wright has included results from this study in briefings to the Office of Water as well as the Federal-State Toxicology and Risk Analysis Committee in 2019. These invitations related to this cardiac defect study shown here are a testament to the importance of this work.

This work led by Drs. Wright and Narotsky have helped target more specific teratogenic DBPs in epidemiological studies and other advances have helped increased the sensitivity of epidemiological studies to allow for effective detection of associations and better integration of epidemiological data in weight of evidence considerations for risk assessment. These efforts should provide valuable information to the Office of Water as part of the next iteration of the 6-year regulatory review of the DBP Stage 2 Rule. Regulators and policy makers at various federal agencies and regulatory bodies inside and outside of the EPA have relied extensively upon Dr. Wright's exposure assessment and

epidemiological research supporting this program area. His previous epidemiological studies have been cited by Canada, the World Health Organization, California EPA's Office of Environmental Health Hazard Assessment as well as the US EPA's Drinking Water Criteria Document and the aforementioned DBP Stage 2 Rule. It is anticipated that this research will have similar if not larger impact on these regulatory determinations. This study also directly supports laws, such as the Safe Drinking Water Act Amendments of 1996 and the Food Quality Protection Act of 1996, which mandate consideration of complex mixtures in risk assessment. In the 2009 Science and Decisions: Advancing Risk assessment (i.e., the "Silver Book") report, the NAS's Committee on Improving Risk Analysis encouraged integration of epidemiological data and further methodological development to advance cumulative risk assessment efforts. This nominated manuscript was the first epidemiological study of birth defects to examine a summary measure of 9 regulated DBPs (i.e. DBP9) and represents the most extensive considerations of different DBP mixture measures considered in an epidemiological study to date.

In summary, this publication has been influential in quantifying risks for distinct birth defects in relation to both individual DBPs and different surrogate measures of DBP mixtures. The success of this paper and the leadership of the ORD scientists to facilitate a successful multi-disciplinary epidemiological study is a model of cross-cutting research to tackle a very challenging problem and demonstrated risk assessment need. This represents a culmination of a unique collaboration between different epidemiological and toxicological research groups at the EPA's Office of Research and Development; the likes of which, while often highlighted as a demonstrated Agency need to integrate research interests, rarely come to fruition with successful products that have considerable regulatory impact. The sustained leadership of the co-authors in the DBP epidemiological and toxicological fields recognized within and outside of the agency exemplifies ORD at its finest. This research will continue to have potential important public health ramifications especially given the ubiquitous nature of DBPs in treated drinking water worldwide.

Justification 2A:

N/A

Justification 2B:

Dr. Wright-N/A

Dr. Narotsky- Awarded Level III STAA in 2016 for a submission of 2 manuscripts:

- Comprehensive Assessment of a Chlorinated Drinking Water Concentrate in a Rat Multigenerational Reproductive Toxicity Study. *Environmental Science and Technology*. 2013.

- Reproductive Toxicity of a Mixture of Regulated Drinking-Water Disinfection By-Products in a Multigenerational Rat Bioassay. *Environmental Health Perspectives*. 2015.

Justification 2C:

The 2016 Level III STAA publications awarded to Dr. Narotsky both report the reproductive and developmental toxicity of mixtures of DBPs in rodents. The current nominated manuscript is also concerned with the developmental effects of DBPs, but it dramatically since it examines humans rather than animals. This nominated paper is an epidemiological study of cardiac birth defects that was conducted based on primary data in Massachusetts.

Justification 2D:

N/A

Justification 2E:

Dr. Wright is included in a nomination submitted under #9 Environmental Policy and Decision-Making Studies. This manuscript entitled "Estimating Potential Increased Bladder Cancer Risk Due to Increased Bromide Concentrations in Sources of Disinfected Drinking Waters published in Environmental Science & Technology in 2015 (49(22): 13094-13102 (2015). Based on secondary data, this other nominated manuscript addresses potential increased weight-of-evidence for bladder cancer being associated with exposure from DBPs, particularly brominated THM species, that occur as a result of drinking water chlorination practices. It specifically addresses risk estimation effort to characterize the public health implications of bromide discharges from industrial sources in the nation’s source drinking waters.

Justification 3A:

Citations:

To date, according to Google Scholar, the paper has been cited 31 times. According to Environmental Health Perspectives, compared to other publications in the same field, this publication is extremely highly cited and has received approximately 10 times more citations than average.

Downloads and Journal Statistics:

Environmental Health Perspectives

Impact Factor: 8.05

5-Year Impact Factor: 9.99

Article Downloads: 352 (as of 4-29-20)

Article Immediacy index: 2.12

Article Cited half-life: 8.60

Invited Presentations

These research findings have been of great interest to those in the field; as such, we have taken great care to vet our study results to many scientific bodies early in the process. For example, preliminary results based on this study were first presented in a poster by Dr. Rivera-Nunez at the International Society of Environmental Epidemiology in 2012. Similar presentations occurred for the cardiac defect analysis in 2014 and 2015 by Dr. Wright and John Kaufman. These individuals have also given numerous invited talks about these important findings as detailed below.

Invited Oral Presentations

Wright JM. The Effect of Disinfection By-Product Exposure on the Risk of Congenital Anomalies and Fetal Growth Restriction. October 15, 2019. Briefing for the US EPA's Office of Water.

Wright JM. The Effect of Disinfection By-Product Exposure on the Risk of Congenital Anomalies and Fetal Growth Restriction: New Epidemiological Study Findings. August 31, 2019. South Hadley, MA. Gordon Research Conference on DBPs.

Kaufman JA, Wright JM. Associations between Disinfection Byproduct Exposures and the Risk of Cardiac and Musculoskeletal Birth Defects. October 2016. Utrecht, Netherlands. International Society for Exposure Science Conference.

Wright JM. The Effect of Disinfection By-product Exposures on Risk of Birth Defects. August 11, 2015. South Hadley, MA. Gordon Research Conference on DBPs.

Wright JM. Developmental Effects of Disinfection Byproducts: Preliminary Epidemiological Results from Massachusetts. December 15, 2014. Sydney, Australia. Environmental Health Branch. New South Wales Ministry of Health.

Wright JM. The Effect of Disinfection By-product Exposures on Risk of Birth Defects. December 7, 2014. Denver, CO. Society for Risk Analysis Conference.

In addition to the presentations of this research at national/international societies, the Gordon Research Conference on DBPs noted above represent especially prestigious invitations. The Gordon Research Conferences are a small, highly selective group of scientists and the subject matter of each invited talk is selected to represent the latest research and to address cutting edge issues and challenges. These meetings are by

invitation only and there are a limited number of presentations provided at each conference. The research briefings provided to the Office of Water and other committees noted above is also considerable recognition of the impact of the work.

Letter of Recommendation

Dr. Ed Ohanian, the Associate Director for Science at EPA's Office of Water has provided a letter of recommendation in support of this nomination (see attachment).

Justification 3B:

Environmental Health Perspective is considered the preeminent peer-reviewed research journal on environmental health and epidemiology. The journal is known in the field for a low acceptance rate and a very rigorous peer-review process. As such, all manuscripts that are deemed acceptable by an initial screening of an associate editor are sent for thorough external peer-review to experts in the field. Manuscripts are typically evaluated by three or more experts and may include multiple rounds of review. Based on the expertise of three peer-reviewers and the editor, this manuscript was considered acceptable after one round of revisions. The timeliness and importance of this work was recognized by the journal editors, as they offered to fast-track this publication into their online systems following acceptance of the revised manuscript including skipping the final substantive journal review (that Environmental Health Perspectives does internally).

AUTHORS

Principal Author

Author Name:	John M. (Michael) Wright		
Professional Title:		Salutation:	Dr.
Email:	wright.michael@epa.gov	Organization:	

Mailing Address:			
Street Line 1:			
City:			
Zip Code:		State:	
At time of research was:	EPA Employee		
Separation Date:			
% of Effort:	60		

Contributing Author

Author Name:	Amanda Evans		
Professional Title:		Salutation:	Mr.
Email:	amanda.evans@stelizabeth.com	Organization:	
Mailing Address:			
Street Line 1:			
City:			
Zip Code:		State:	
At time of research was:	Non EPA Personnel		
Separation Date:			
% of Effort:	10		

Contributing Author

Author Name:	John Kaufman		
Professional Title:		Salutation:	
Email:	kaufman.john.a@gmail.com	Organization:	

Mailing Address:			
Street Line 1:			
City:			
Zip Code:		State:	
At time of research was:	Non EPA Personnel		
Separation Date:			
% of Effort:	10		

Contributing Author

Author Name:	Michael Narotsky		
Professional Title:		Salutation:	Dr.
Email:	narotsky.michael@epa.gov	Organization:	
Mailing Address:			
Street Line 1:			
City:			
Zip Code:		State:	
At time of research was:	EPA Employee		
Separation Date:			
% of Effort:	10		

Contributing Author

Author Name:	Zorimar Rivera-Nunez		
Professional Title:		Salutation:	Dr.
Email:	zr69@eohsi.rutgers	Organization:	

Mailing Address:		
Street Line 1:		
City:		
Zip Code:		State:
At time of research was:	Non EPA Personnel	
Separation Date:		
% of Effort:	10	

PUBLICATIONS

A Section 508–conformant HTML version of this article is available at http://dx.doi.org/10.1289/EHP103.

Disinfection By-Product Exposures and the Risk of Specific Cardiac Birth Defects

J. Michael Wright,[1] Amanda Evans,[2] John A. Kaufman,[3] Zorimar Rivera-Núñez,[4] and Michael G. Narotsky[5]

[1]National Center for Environmental Assessment (NCEA), Office of Research and Development (ORD), U.S. Environmental Protection Agency (EPA), Cincinnati, Ohio, USA; [2]School of Osteopathic Medicine, Campbell University, Lillington, North Carolina, USA; [3]ASPPH/EPA Environmental Health Fellowship Program, hosted by NCEA, ORD, U.S. EPA, Cincinnati, Ohio, USA; [4]Radiation Oncology, Rutgers Cancer Institute of New Jersey, New Brunswick, New Jersey, USA; [5]National Health and Environmental Effects Research Laboratory, ORD, U.S. EPA, Research Triangle Park, North Carolina, USA

Background: Epidemiological studies suggest that women exposed to disinfection by-products (DBPs) have an increased risk of delivering babies with cardiovascular defects (CVDs).

Objective: We examined nine CVDs in relation to categorical DBP exposures including bromoform, chloroform, dibromochloromethane (DBCM), bromodichloromethane (BDCM), monobromoacetic acid (MBAA), dichloroacetic acid (DCAA), trichloroacetic acid (TCAA), and summary DBP measures (HAA5, THMBr, THM4, and DBP9).

Methods: We calculated adjusted odds ratios (aORs) in a case–control study of birth defects in Massachusetts with complete quarterly 1999–2004 trihalomethane (THM) and haloacetic acid (HAA) data. We randomly matched 10 controls each to 904 CVD cases based on week of conception. Weight-averaged aggregate first-trimester DBP exposures were assigned to individuals based on residence at birth.

Results: We detected associations for tetralogy of Fallot and the upper exposure categories for TCAA, DCAA, and HAA5 (aOR range, 3.34–6.51) including positive exposure–response relationships for DCAA and HAA5. aORs consistent in magnitude were detected between atrial septal defects and bromoform (aOR = 1.56; 95% CI: 1.01, 2.43), as well as DBCM, chloroform, and THM4 (aOR range, 1.26–1.67). Ventricular septal defects (VSDs) were associated with the highest bromoform (aOR = 1.85; 95% CI: 1.20, 2.83), MBAA (aOR = 1.81; 95% CI: 0.85, 3.84), and DBCM (aOR = 1.54; 95% CI: 1.00, 2.37) exposure categories.

Conclusions: To our knowledge, this is the first birth defect study to develop multi-DBP adjusted regression models as well as the first CVD study to evaluate HAA exposures and the second to evaluate bromoform exposures. Our findings, therefore, inform exposure specificity for the consistent associations previously reported between THM4 and CVDs including VSDs.

Citation: Wright JM, Evans A, Kaufman JA, Rivera-Núñez Z, Narotsky MG. 2017. Disinfection by-product exposures and the risk of specific cardiac birth defects. Environ Health Perspect 125:269–277; http://dx.doi.org/10.1289/EHP103

Introduction

Cardiovascular defects (CVDs) are the most common type of birth defect, with an estimated incidence in the United States of 8 in 1,000 births (Go et al. 2013). CVDs can lead to a higher infant mortality rate among newborns, and their etiology is often unknown (Kurinczuk et al. 2010; Lee et al. 2001). Some environmental hazards are known teratogens, such as methylmercury and radiation, but the existing evidence for associations between drinking-water contaminants and birth defects is mixed (Brent and Beckman 1990; Nieuwenhuijsen et al. 2009). Although the risk of CVDs in relation to specific disinfection by-products (DBPs) remains unclear, there is some evidence for associations between CVDs and a summary measure of trihalomethanes (THMs) called THM4 [i.e., sum of chloroform, bromoform, bromodichloromethane (BDCM), and dibromochloromethane (DBCM)]. Nieuwenhuijsen et al. (2009) conducted a meta-analysis of 5 case–control studies and 10 retrospective cohort studies using THM concentration data or less direct exposure measures (e.g., treatment type/source water). The authors reported a small but not statistically significant odds ratio of 1.16 [95% confidence interval (CI): 0.98, 1.37] for major CVDs among those with high DBP exposures. A prospective cohort study from Lithuania based on first-trimester internal DBP dose estimates showed elevated odds ratios for CVDs, with exposure–response relationships detected for THM4, BDCM, and chloroform tertiles (Grazuleviciene et al. 2013). Slightly elevated odds ratios were noted in a study from England of major CVDs and the sum of three brominated THMs (i.e., THMBr) ≥ 20 versus < 10 μg/L [adjusted odds ratio (aOR) = 1.13; 95% CI: 0.93, 1.37] and between bromoform ≥ 4 versus < 2 μg/L (aOR = 1.18; 95% CI: 1.00, 1.39) and a restricted group of major CVDs (Nieuwenhuijsen et al. 2008). Stronger associations (aOR = 1.62; 95% CI: 1.04, 2.51) have also been reported for CVDs and THM4 ≥ 130 versus < 60 μg/L in an Australian population using heavily brominated water (Chisholm et al. 2008). Studies with rats exposed to brominated THMs were negative for CVDs (Christian et al. 2001; Ruddick et al. 1983); however, one study examining monobromoacetic acid (MBAA) exposure reported increased incidence of CVDs (Randall et al. 1991). Another study in rats reported CVDs [e.g., ventricular septal defect (VSD), levocardia, right-sided aortic arch, and ductus arteriosus] following exposure to bromochloroacetonitrile (Christ et al. 1995).

The strongest and most consistent associations reported in epidemiological studies of birth defects and DBPs have been for VSDs. Similar to an earlier meta-analysis by Hwang et al. (2008), Nieuwenhuijsen et al. (2009) found a consistent excess risk for VSDs (OR = 1.59; 95% CI: 1.21, 2.07) in three studies using various THM and chlorinated water exposure measures (OR range:

Address correspondence to J.M. Wright, U.S. EPA, National Center for Environmental Assessment, 26 W. Martin Luther King Dr. (MS-A110), Cincinnati, OH 45268 USA. Telephone: (513) 569-7922. E-mail: wright.michael@epa.gov

Supplemental Material is available online (http://dx.doi.org/10.1289/EHP103).

We thank the Massachusetts Department of Environmental Protection, the Massachusetts Department of Public Health, the Massachusetts Water Resource Authority, and other public water utilities for their assistance with the data collection efforts. We also acknowledge the data management efforts of A. Meyer as well as the Technical Support Services staff assistance provided by Highlight Technologies.

A.E. was supported through the Oak Ridge Institute of Science and Education Research Participation Program (agreement no. DW8992376701) sponsored by the U.S. EPA. J.A.K. was supported by cooperative agreement no. X3-83555301 from the U.S. EPA and the Association of Schools and Programs of Public Health (ASPPH). Z.R.-N. was supported through The National Academies, Research Associateship Programs sponsored by the U.S. EPA.

The views expressed in this manuscript are those of the authors and do not necessarily reflect the views or policies of the U.S. EPA or the ASPPH.

The authors declare they have no actual or potential competing financial interests.

Received: 11 March 2016; Revised: 2 June 2016; Accepted: 14 July 2016; Published: 12 August 2016.

Note to readers with disabilities: *EHP* strives to ensure that all journal content is accessible to all readers. However, some figures and Supplemental Material published in *EHP* articles may not conform to 508 standards due to the complexity of the information being presented. If you need assistance accessing journal content, please contact ehponline@niehs.nih.gov. Our staff will work with you to assess and meet your accessibility needs within 3 working days.

1.43–1.81). An earlier study, not included in the published meta-analyses, did not report associations between THM exposure and VSD (Bove et al. 1995). A more recent Italian study also did not show an increased risk of VSD for chlorine dioxide DBPs, including chlorite and chlorate (Righi et al. 2012).

Exposure assessment limitations in epidemiological studies remain a critical challenge in evaluating causality in reported associations between DBPs and various reproductive outcomes given limited spatial and temporal resolution of monitoring data and the lack of direct exposure measures. Previous epidemiological studies of CVDs have not examined exposures beyond THMs and chlorine dioxide DBPs. This remains a key limitation given that animal developmental toxicity studies of THMs are generally negative for teratogenicity (Graves et al. 2001) and that the THMs may be poor surrogates for complex DBP mixtures in chlorinated drinking-water systems. Furthermore, although haloacetic acids (HAAs) have not been examined in epidemiological studies of CVDs and DBPs to date, toxicological studies in rats have shown increased incidence of VSDs and conotruncal defects following exposure to dichloroacetic acid (DCAA) and trichloroacetic acid (TCAA) (Epstein et al. 1992; Johnson et al. 1998; Smith et al. 1989, 1992). Most epidemiological studies of DBPs also have limited exposure contrasts and insufficient statistical power to detect rare outcomes like CVDs. This may preclude the ability to detect statistically significant associations that are small in magnitude and to examine exposure–response relationships for individual CVDs and specific DBP species. To address some of these exposure assessment limitations and expand the scope of the birth defect and DBP combinations that have been previously examined, we assessed the risk of CVDs in relation to weighted first-trimester exposure estimates for nine individual DBPs and four DBP mixture surrogates.

Methods

Study Population

We conducted a case–control study of CVD cases in 68 Massachusetts towns with populations > 500 with complete THM4, HAA5 [i.e., sum of monochloroacetic acid (MCAA), DCAA, TCAA, MBAA, and dibromoacetic acid (DBAA)], water source and disinfection data from 1999 to 2004. We restricted the analysis to nonchromosomal congenital anomalies of the heart and circulatory system (n = 904 cases) and individually matched 10 controls per each case randomly selected (without replacement) from all live births in Massachusetts based on week of conception, for a total study population of 9,944.

Outcome Data

Birth records from 2000 through 2004 were provided by the Massachusetts Department of Public Health and the Massachusetts Birth Defects Monitoring Program. The Massachusetts birth defect registry system collects data from 53 birthing hospitals, 1 tertiary care and 1 specialty hospital in Massachusetts, and 1 Rhode Island birth hospital and 1 Rhode Island tertiary care hospital near the border of these two states. The registry system uses various data sources to ascertain and verify cases including birth certificates, fetal and infant death certificates, hospital discharge reports, hospital nurseries and neonatal units, and hospital surgical and pathology departments. This research was based on birth records data that did not contain personal identifiable information; therefore, institutional review board approval was not obtained nor was informed consent necessary because potential risk was considered to be minimal and no direct contact with study subjects occurred.

Birth defect cases were diagnosed up to age 1 year. Both cases and controls were singleton live births who weighed at least 350 g and were between 22 and 44 gestational weeks. Cases were identified based on the *International Classification of Diseases, 9th Revision* (ICD-9). These included atrial septal defect (ASD; ICD-9 code 745.5), VSD (745.4), pulmonary stenosis (746.02), tetralogy of Fallot (TOF; 745.2), and transposition of the great arteries (TGA; 745.10, 745.11, 745.12, 745.19). We also examined birth defect group combinations including all congenital anomalies of the heart and circulatory system (All CVD; 745–747), and conotruncal heart defects (745.0, 745.10, 745.11, 745.12, 745.2). Gestational age was derived from clinical estimates according to birth records and was subtracted from date of birth to determine week of conception for matching purposes.

Exposure Assessment

We linked town-level drinking-water source, disinfection treatment, and DBP data based on quarterly sampling (1999–2004) to birth records by town of residence and month of birth. The exposure data were supplied by the Massachusetts Department of Environmental Protection and individual public water utilities. Exposures were estimated for specific DBPs as well as summary measures of DBP mixtures including THM4, HAA5, DBP9 (i.e., sum of THM4 and HAA5), and THMBr. We categorized maternal DBP exposure levels for the summary and individual DBP measures into tertiles, quartiles, or quintiles based on the distribution of the available data. Due to a paucity of occurrence data, MCAA was dichotomized at the 97.5th percentile (0.04 µg/L), and bromoform (0.26 µg/L), DBCM (0.47 µg/L), and DBAA (1.53 µg/L) were dichotomized at the upper decile. Births in the lowest DBP exposure category served as the referent for comparison with the upper categories. This categorical approach allowed for evaluation of nonlinear relationships and potential effect measure modification using stratified analyses.

We averaged first-trimester DBP exposures across all sample locations within a public drinking-water system based on quarterly monitoring data assigned to maternal ZIP codes for place of residence at birth. The first-trimester DBP exposure scores were derived from the month of birth of the study participants and the timing of quarterly DBP samples with weighted averages calculated proportionally for multiple quarters that overlapped the first trimester. For example, an infant of 38 gestational weeks born in January of 2000 would have 2 first-trimester weeks that occurred in quarter 1 of 1999 and the remaining 11 weeks occurring in quarter 2 of 1999. Thus, their corresponding exposure score would be as follows: (0.15 times the DBP concentration for quarter 1 of 1999) + (0.85 times the DBP concentration for quarter 2 of 1999). In addition, residents relying on untreated groundwater (e.g., private wells) were assigned DBP concentrations of zero.

Statistical Analysis

SAS (version 9.4; SAS Institute, Inc., Cary, NC) was used for the statistical analysis. We used Spearman correlation coefficients to compare the summary and individual DBP measures. Statistical significance was based on $\alpha \leq 0.05$. We used conditional logistic regression to estimate aORs and 95% CIs for each of the DBP exposure categories. Given the extensive amount of available covariate data, we used a change-in-estimate approach (> 10% change) to identify confounding variables. These covariates included type of water source and treatment, infant sex, infant birth weight, maternal weight gain, maternal race, maternal age, maternal education, marital status (not married vs. married, including within 300 days before birth), maternal smoking (cigarettes/day during pregnancy), parity, number of previous terminations, prenatal care source payment type, income, and various clinical factors (e.g., abruptio placenta, anemia, cardiac disease, chronic or gestational diabetes, chronic or gestational hypertension, eclampsia, hemoglobinopathy, hepatitis, hydramnios/oligohydramnios, incompetent cervix, labor/delivery complication, labor induction, lung disease, lupus, other maternal reproductive risk factors, pharmaceutical inhibition of labor, previous infant > 4,000 g, previous infant with birth defect,

previous premature or small-for-gestational-age infant, premature or prolonged rupture of membrane, renal disease, Rh sensitization, rubella infection, seizure disorder, sickle cell anemia, uterine bleeding). We examined a categorical health index (values ranging from 0 to 5) that included presence of hydramnios/oligohydramnios, chronic hypertension, gestational hypertension, gestational diabetes, and nongestational diabetes. We also evaluated adequacy of prenatal care by the Kotelchuck Index (Kotelchuck 1994), which integrates information on the timing (i.e., first trimester vs. later during pregnancy) of initiation of prenatal care and the number of prenatal visits (< 9, 9–11, 12, 13–15, > 15) from when prenatal care began until delivery. These two individual prenatal covariate constituents were examined separately as confounders, as well as part of the Kotelchuck Index.

All of the covariates were based on the individual-level data obtained from birth records except for income and DBP data, as well as the information on type of water source and type of water treatment. Median household income for maternal residence at birth were obtained from the 2000 U.S. Census (Geolytics, Inc., East Brunswick, NJ). Aggregate-level income covariates were examined at three spatial scales: town, ZIP code, and census tract. We created a socioeconomic status index based on ZIP code–level income data combined with mother's highest education level and prenatal care source of payment. The results presented here are also based on multi-pollutant models by adjusting for THM4 in all of the HAA models and adjusting for HAA5 in the THM models. Effect measure modification by infant sex was examined by stratification for the outcome and DBPs with most consistent and largest aORs (i.e., TOF and VSDs). We conducted a sensitivity analysis of the impact of multiple birth defects, as well as an analysis of the All CVD category excluding patent ductus arteriosus.

Results

Among all reported births from 2000 to 2004 in Massachusetts, there were 904 (45% of the total birth defects) CVDs. The most common CVDs were ASDs (41%) and VSDs (37%). Forty-three percent (n = 390) of the birth defects examined here were isolated CVDs, whereas 57% (n = 514) of the cases had multiple defects. Among the 514 cases with multiple defects, 377 (73%) of them were CVDs only. As shown in Table 1, cases and controls were similar across most study characteristics, with minor exceptions noted for health index scores and the Kotelchuck Index for adequacy of prenatal care. Controls were more likely to be born to healthier mothers based on our health index score.

As shown in Table 2, median and interquartile ranges (μg/L) for the nine predominant DBP metrics were as follows: DBP9 (69.6; 44.1–92.1), THM4 (44.5; 29.3–61.4), chloroform (36.1; 17.4–51.0), THMBr (6.8; 4.8–10.2), BDCM (6.1; 4.5–8.4), DBCM (0.6; 0–1.6), HAA5 (22.4; 11.3–31.2), TCAA (11.0; 5.4–16.3), and DCAA (10.4; 5.3–13.7). We observed Spearman correlation coefficients ≥ 0.9 for the following: DBP9 with THM4, HAA5, and chloroform; HAA5 with TCAA and DCAA; THM4 with chloroform; and THMBr with BDCM (see Table S1). We observed correlations between 0.7 and 0.9 for the following: DBP9 with TCAA and DCAA; HAA5 with THM4 and chloroform; THM4 with TCAA and CCAA; DBCM with BDCM and THMBr; chloroform with TCAA and DCAA; and TCAA with DCAA. The strongest correlations among the individual brominated species were found between DBCM and BDCM

Table 1. Study characteristics of cardiovascular defect (CVD) cases and controls [n (%)].

Characteristic	Study population	Cases	Controls
Total births	9,944 (100)	904 (100)	9,040 (100)
Infant sex			
Male	5,119 (51.5)	468 (51.8)	4,651 (51.4)
Female	4,825 (48.5)	436 (48.2)	4,389 (48.6)
Maternal age (years)			
≤ 20	907 (9.1)	82 (9.1)	825 (9.1)
> 20–25	1,733 (17.4)	169 (18.7)	1,564 (17.3)
> 25–30	2,648 (26.6)	223 (24.7)	2,425 (26.8)
> 30–35	3,008 (30.3)	273 (30.2)	2,735 (30.3)
> 35–40	1,384 (13.9)	122 (13.5)	1,262 (14.0)
> 40	264 (2.7)	35 (3.9)	229 (2.5)
Maternal race			
White	6,614 (66.6)	589 (65.2)	6,025 (66.6)
African American	995 (10.0)	114 (12.6)	881 (9.7)
Asian	747 (7.5)	53 (5.9)	694 (7.7)
American Indian	22 (0.2)	5 (0.6)	17 (0.2)
Other	1,561 (15.7)	143 (15.8)	1,418 (15.7)
Maternal education			
Below high school graduate/GED	1,166 (11.7)	119 (13.2)	1,047 (11.6)
High school graduate/GED	2,689 (27.0)	244 (27.0)	2,445 (27.0)
Some college or associates/technical degree	2,076 (20.9)	184 (20.4)	1,892 (20.9)
College or higher	4,013 (40.4)	357 (39.5)	3,656 (40.4)
Marital status			
Married	6,886 (69.3)	602 (66.6)	6,284 (69.5)
Unmarried	3,041 (30.6)	300 (33.2)	2,741 (30.3)
Missing	17 (0.2)	2 (0.2)	15 (0.2)
Number of previous births			
0	4,508 (45.4)	413 (45.7)	4,095 (45.3)
1	3,269 (32.9)	287 (31.7)	2,982 (33.0)
≥ 2	2,154 (21.7)	204 (22.6)	1,950 (21.6)
Maternal weight gain during pregnancy (lb)			
< 0	112 (1.1)	14 (1.5)	98 (1.1)
0–25	3,867 (39.1)	365 (40.4)	3,502 (38.7)
25–50	5,557 (56.2)	489 (54.1)	5,068 (56.1)
> 50	354 (3.6)	30 (3.3)	324 (3.6)
Maternal smoking during pregnancy (no. of cigarettes/day during pregnancy)			
0	9,165 (92.2)	830 (91.8)	8,335 (92.2)
1–5	327 (3.3)	22 (2.4)	305 (3.4)
6–10	289 (2.9)	34 (3.8)	255 (2.8)
> 10	163 (1.6)	18 (2.0)	145 (1.6)
Prenatal care adequacy (Kotelchuck Index)			
No prenatal care	48 (0.5)	6 (0.7)	42 (0.5)
Inadequate	886 (8.9)	92 (10.2)	794 (8.8)
Intermediate	713 (7.2)	41 (4.5)	672 (7.4)
Adequate	4,583 (46.1)	386 (42.7)	4,197 (46.4)
Adequate plus	3,714 (37.4)	379 (41.9)	3,335 (36.9)
Prenatal care source of payment			
Public	2,611 (26.3)	277 (30.6)	2,334 (25.8)
Private	6,556 (65.9)	566 (62.6)	5,990 (66.3)
Other	777 (7.8)	61 (6.7)	716 (7.9)
Median household income (based on ZIP code from 2000)			
$12,307–36,836	2,492 (25.1)	249 (27.5)	2,243 (24.8)
> $36,836–45,654	2,303 (23.2)	215 (23.8)	2,088 (23.1)
> $45,654–57,815	2,524 (25.4)	219 (24.2)	2,305 (25.5)
> $57,815–153,918	2,625 (26.4)	221 (24.4)	2,404 (26.6)

Note: GED, General Educational Development.

(r = 0.6) and DBAA (r = 0.4), as well as between bromoform and DBCM (r = 0.5) and DBAA (r = 0.3).

We did not detect an increased risk for the overall CVD group (i.e., All CVD) and first-trimester THM4 exposures, but there was a statistically significant association for dichotomized bromoform exposures (aOR = 1.43; 95% CI: 1.10, 1.86) and increased risks in the upper two DCAA quartiles (aOR range, 1.21–1.23) and upper three HAA5 quintiles (aOR range, 1.18–1.42) (Table 3). We saw consistent evidence of associations for conotruncal defects in the upper three HAA quintiles (aOR range, 1.77–3.76) and the upper three TCAA quartiles (aOR range, 1.95–2.13). We detected stronger associations for TOF and the upper exposure categories for TCAA, DCAA, and HAA5 (aOR range, 3.34–6.51) including positive exposure–response relationships for DCAA and HAA5. We detected statistically significant associations for TGA and bromoform exposure (aOR = 2.42; 95% CI: 1.12, 5.23) and for the two intermediate HAA5 quintiles (aOR range, 4.26–4.54); the upper quintile was limited by a small number of cases (n = 9). Inverse associations among the upper exposure categories were detected between TGA and DBP9 and between TOF and chloroform, BDCM, THMBr, and THM4.

Increased aORs were detected for pulmonary stenosis and bromoform exposures (aOR = 2.66; 95% CI: 1.30, 5.43), the upper two DCAA quartiles (aOR range, 1.65–2.02), as well as a positive exposure–response relationship for TCAA (aOR range, 1.47–3.45) (Table 4). aORs consistent in magnitude were detected for ASDs and bromoform (aOR = 1.56; 95% CI: 1.01, 2.43), DBCM (aOR = 1.26; 95% CI: 0.81, 1.97), and for each THM4 (aOR range, 1.28–1.59) and chloroform quintile (aOR range, 1.38–1.67).

Consistent elevated aORs were detected for VSDs and every DBP metric except chloroform, TCAA, and HAA5 (Table 4). aORs were comparable between VSDs and each THM4 (aOR range, 1.39–1.77) and DBP9 (aOR range, 1.33–1.70) quintile. Although not statistically significant, aORs smaller in magnitude were noted between VSDs and the highest BDCM tertile (aOR = 1.21; 95% CI: 0.79, 1.85), the upper THMBr quintile (aOR = 1.34; 95% CI: 0.73, 2.46), and the upper DCAA quartiles (aOR = 1.18; 95% CI: 0.65, 2.14). The strongest associations for VSDs and brominated DBPs were found for bromoform (aOR = 1.85; 95% CI: 1.20, 2.83), MBAA (aOR = 1.81; 95% CI: 0.85, 3.84), and DBCM (aOR = 1.54; 95% CI: 1.00, 2.37).

When we examined the most consistent associations (i.e., TOF and VSDs) for potential effect measure modification by infant sex, no discernible patterns were seen between HAA5 quintiles and TOF. Larger aORs were detected among females for TOF and DCAA, whereas males had higher aORs for TCAA exposures (see Table S2). The aORs for MBAA and VSDs were three times higher among males, with smaller increases detected among males for bromoform, DBCM, and MCAA (see Table S3). aORs for the remaining DBP measures (DBP9, THM4, THMBr, BDCM, and chloroform) were considerably larger among females, including some relationships that were largely null for VSDs in the main analysis (e.g., BDCM and chloroform).

Discussion

Unlike a recent study and meta-analysis, we did not see any evidence for associations between first-trimester THM4 exposures and the All CVD group (Grazuleviciene et al. 2013; Nieuwenhuijsen et al. 2009). The strongest association that we detected for individual DBPs and All CVD was for dichotomized bromoform exposures > 0.26 μg/L (aOR = 1.43; 95% CI: 1.10, 1.86). This is higher than that of the only other study published to date to examine bromoform by Nieuwenhuijsen et al. (2008), who found an aOR of 1.18 (95% CI: 1.00, 1.39) for a subset of etiologically similar cardiac defects and bromoform levels ≥ 4 μg/L (vs. < 2 μg/L). Given that CVDs are a heterogeneous group of outcomes with different underlying mechanisms and etiologies, our primary focus was to examine individual CVDs and etiologically relevant groups in relation to DBPs.

We detected positive exposure–response relationships between TCAA exposure and pulmonary stenosis. The strongest associations that we detected were for the conotruncal defects including TGA and TOF, although the only statistically significant association for TGA was detected for bromoform exposures (aOR = 2.42; 95% CI: 1.12, 5.23). Stronger associations were detected between TOF and the upper exposure categories for TCAA, DCAA, and HAA5 (aOR range, 3.34–6.51) including exposure–response relationships for DCAA and HAA5. These findings are consistent with animal data showing CVDs following TCAA and DCAA exposures (Epstein et al. 1992; Johnson et al. 1998; Smith et al. 1989, 1992). The only epidemiological study of DBPs to examine conotruncal defects as a group saw some suggestion of increased risk only for THM4 exposures (aOR = 1.5; 95% CI: 0.67, 3.50 for 50–74 vs. 0 μg/L), although they did not have sufficient data to examine bromoform or HAA exposures (Shaw et al. 2003). A study in Norway examined TOF and THM4, but their data were hampered by very small cell sizes and a limited exposure contrast (Hwang et al. 2008). We also detected elevated aORs for ASDs and bromoform exposures (aOR = 1.56; 95% CI: 1.01, 2.43) and across every chloroform quintile (aOR range, 1.38–1.67). The magnitude of these associations are consistent with the only other study to examine ASDs, although that study was based on very small sample sizes across THM4 quartiles (Hwang et al. 2008).

Similar to a meta-analysis (OR = 1.59, 95% CI: 1.21, 2.07) by Nieuwenhuijsen et al. (2009), we found consistently elevated aORs (aOR range, 1.39–1.77) for VSD across all exposure THM4 quintiles (beginning at concentrations of 23.05 μg/L) with an aOR of 1.57 (95% CI: 0.70, 3.53) for high THM4 exposures (> 65.27 vs. ≤ 23.05 μg/L). In concordance with two previous VSD studies that evaluated THM4 exposures in the United Kingdom (aOR = 1.43; 95% CI: 1.0, 2.04 for > 60 vs. < 30 μg/L) and Norway (aOR = 1.81; 0.98–3.35 for > 20 vs. ≤ 4 μg/L), our studies add to the consistency reported in epidemiological studies of THMs and VSDs published to date (Hwang et al. 2008; Nieuwenhuijsen et al. 2008). We also saw consistent evidence of associations between VSD and various

Table 2. First-trimester disinfection by-product (DBP) (μg/L) exposure levels for the study population.

DBP metric	Mean ± SD	25th %	50th %	75th %	90th %	95th %	Maximum
DBP9	65.07 ± 36.49	44.14	69.57	92.14	107.8	117.03	181.59
THM4	42.67 ± 24.05	29.26	44.53	61.37	72.71	76.63	125.32
THMBr	8.28 ± 6.51	4.75	6.75	10.17	17.87	21.20	42.48
Chloroform	34.39 ± 21.56	17.38	36.07	51.03	62.65	67.15	98.99
BDCM	6.85 ± 5.05	4.47	6.12	8.36	13.04	16.35	37.38
DBCM	1.32 ± 2.01	0.00	0.56	1.57	3.97	5.98	14.53
Bromoform	0.12 ± 0.46	0.00	0.00	0.00	0.26	0.86	7.06
HAA5	22.40 ± 14.89	11.34	22.38	31.18	42.52	47.49	100.00
TCAA	11.53 ± 8.42	5.40	11.01	16.30	22.16	26.37	73.39
DCAA	9.90 ± 6.61	5.30	10.38	13.67	18.61	21.29	38.89
MCAA	0.83 ± 3.05	0.00	0.05	0.84	1.53	2.13	62.39
DBAA	0.17 ± 0.70	0.00	0.00	0.00	0.47	1.06	21.78
MBAA	0.02 ± 0.26	0.00	0.00	0.00	0.00	0.00	10.63

Note: %, percentile; DBP9, sum of chloroform, bromodichloromethane (BDCM), dibromochloromethane (DBCM), bromoform, monochloroacetic acid (MCAA), dichloroacetic acid (DCAA), trichloroacetic acid (TCAA), monobromoacetic acid (MBAA), and dibromoacetic acid (DBAA); HAA5, sum of MCAA, DCAA, TCAA, MBAA, and DBAA; THM4, sum of chloroform, BDCM, DBCM, and bromoform; THMBr, sum of BDCM, DBCM, and bromoform.

brominated DBP exposure metrics, with the strongest associations noted for bromoform, MBAA, and DBCM (aOR range; 1.54–1.85). The bromoform (aOR = 1.85; 95% CI: 1.20, 2.83) and VSD associations are stronger than those of the only study to examine bromoform exposures (aOR = 1.27; 95% CI: 0.89, 1.82) in relation to isolated VSDs (Nieuwenhuijsen et al. 2008). In our study, bromoform was consistently associated with elevated aORs for all the individual and group CVDs examined. These findings help inform the specificity of reported associations with DBPs and may explain some of the consistent results noted in previous studies for THM4 exposures.

A key study strength was our ability to evaluate numerous individual and summary

Table 3. Adjusted odds ratios (aORs) between disinfection by-product (DBP) exposures and congenital anomalies of the heart and circulatory system (All CVD), conotruncal heart defects, transposition of the great arteries (TGA), and tetralogy of Fallot (TOF).

	All CVD[c]		Conotruncal[d]		TGA[e]		TOF[f]	
DBP metrics (μg/L)[a]	Cases[b] (*n*)	aOR (95% CI)	Cases[b] (*n*)	aOR (95% CI)	Cases[b] (*n*)	aOR (95% CI)	Cases[b] (*n*)	aOR (95% CI)
THM4[g]								
> 23.05–38.05	184	1.04 (0.72, 1.51)	37	0.96 (0.43, 2.14)	21	1.70 (0.58, 4.95)	17	0.32 (0.10, 1.05)
> 38.05–50.41	188	1.02 (0.67, 1.54)	45	1.19 (0.50, 2.82)	26	1.87 (0.57, 6.08)	19	0.51 (0.15, 1.74)
> 50.41–65.27	192	1.04 (0.67, 1.62)	32	0.68 (0.27, 1.74)	13	1.02 (0.28, 3.82)	19	0.31 (0.08, 1.21)
> 65.27–125.32	167	0.81 (0.51, 1.31)	31	0.50 (0.17, 1.48)	15	0.81 (0.17, 3.84)	16	0.19 (0.04, 0.88)
THMBr[g]								
> 4.17–6.04	173	0.99 (0.65, 1.51)	39	0.72 (0.32, 1.60)	14	0.45 (0.13, 1.61)	25	1.00 (0.34, 2.98)
> 6.04–7.80	195	1.05 (0.71, 1.55)	39	0.60 (0.27, 1.30)	26	0.98 (0.35, 2.74)	12	0.23 (0.06, 0.91)
> 7.80–11.51	176	0.97 (0.66, 1.42)	32	0.47 (0.21, 1.02)	14	0.49 (0.16, 1.49)	18	0.45 (0.14, 1.39)
> 11.51–42.48	188	1.02 (0.71, 1.46)	34	0.39 (0.19, 0.80)	19	0.55 (0.20, 1.51)	16	0.26 (0.09, 0.76)
Chloroform[g]								
> 12.07–29.99	181	1.05 (0.73, 1.50)	33	1.22 (0.56, 2.65)	19	1.49 (0.53, 4.24)	14	0.50 (0.16, 1.53)
> 29.99–42.17	197	1.03 (0.68, 1.55)	46	1.46 (0.62, 3.47)	25	1.69 (0.52, 5.50)	21	0.76 (0.22, 2.69)
> 42.17–55.41	184	0.94 (0.60, 1.47)	37	1.42 (0.53, 3.79)	15	1.28 (0.33, 4.95)	22	0.81 (0.20, 3.29)
> 55.41–98.99	167	0.77 (0.47, 1.25)	29	0.63 (0.21, 1.93)	15	0.55 (0.11, 2.83)	14	0.33 (0.07, 1.64)
Bromodichloromethane (BDCM)[g]								
> 4.95–7.55	325	0.97 (0.73, 1.28)	61	0.73 (0.40, 1.34)	36	0.83 (0.37, 1.86)	24	0.49 (0.19, 1.24)
> 7.55–37.38	286	0.93 (0.72, 1.19)	51	0.49 (0.29, 0.82)	24	0.57 (0.27, 1.22)	28	0.38 (0.17, 0.82)
Dibromochloromethane (DBCM)[g]								
> 3.93–14.53	87	1.01 (0.77, 1.33)	16	0.68 (0.36, 1.29)	10	1.01 (0.43, 2.39)	7	0.54 (0.20, 1.41)
Bromoform[g]								
> 0.26–7.06	109	1.43 (1.10, 1.86)	25	1.30 (0.72, 2.33)	16	2.42 (1.12, 5.23)	10	1.14 (0.45, 2.87)
HAA5[h]								
> 8.17–19.33	160	0.99 (0.69, 1.42)	38	1.18 (0.53, 2.66)	17	0.86 (0.28, 2.64)	21	2.13 (0.53, 8.65)
> 19.33–25.79	219	1.42 (0.95, 2.12)	49	3.19 (1.29, 7.89)	29	4.54 (1.26, 16.41)	21	4.98 (1.02, 24.35)
> 25.79–33.97	172	1.35 (0.87, 2.10)	37	3.76 (1.38, 10.24)	19	4.26 (1.02, 17.87)	17	5.88 (1.06, 32.57)
> 33.97–100.00	174	1.18 (0.75, 1.86)	24	1.77 (0.63, 4.97)	9	1.10 (0.23, 5.37)	16	6.51 (1.23, 34.59)
Trichloroacetic acid (TCAA)[h]								
> 5.23–11.09	234	1.17 (0.86, 1.60)	59	2.09 (1.02, 4.29)	30	1.38 (0.53, 3.56)	28	2.72 (0.91, 8.13)
> 11.09–16.38	237	1.11 (0.76, 1.62)	44	2.13 (0.89, 5.14)	22	1.39 (0.40, 4.80)	22	4.30 (1.09, 16.88)
> 16.38–73.39	208	1.03 (0.69, 1.55)	36	1.95 (0.77, 4.92)	18	1.07 (0.29, 3.86)	19	3.89 (0.97, 15.66)
Dichloroacetic acid (DCAA)[h]								
> 5.18–10.44	219	1.04 (0.78, 1.40)	48	1.07 (0.57, 2.04)	27	0.96 (0.41, 2.23)	22	1.39 (0.50, 3.88)
> 10.44–13.85	241	1.21 (0.86, 1.70)	52	1.60 (0.76, 3.36)	28	1.21 (0.43, 3.41)	24	3.08 (0.92, 10.34)
> 13.85–38.89	220	1.23 (0.85, 1.78)	34	1.16 (0.50, 2.70)	12	0.50 (0.14, 1.77)	21	3.34 (0.90, 12.43)
Monochloroacetic acid (MCAA)[h]								
> 1.53–62.39	84	1.06 (0.80, 1.40)	9	0.85 (0.41, 1.77)	6	1.10 (0.43, 2.77)	4	0.83 (0.27, 2.54)
Monobromoacetic acid (MBAA)[h]								
> 0.04–10.63	24	1.17 (0.66, 2.07)	4	0.77 (0.17, 3.48)	1	0.47 (0.06, 3.97)	3	0.80 (0.08, 7.48)
Dibromoacetic acid (DBAA)[h]								
> 0.47–21.78	73	0.81 (0.61, 1.08)	19	0.72 (0.39, 1.33)	11	0.96 (0.41, 2.26)	7	0.59 (0.23, 1.54)
DBP9								
> 33.07–59.95	187	1.37 (0.95, 1.97)	37	1.11 (0.52, 2.37)	21	1.22 (0.45, 3.31)	17	0.80 (0.24, 2.63)
> 59.95–79.13	196	1.30 (0.87, 1.92)	49	1.12 (0.51, 2.49)	24	0.87 (0.29, 2.61)	24	1.15 (0.32, 4.08)
> 79.13–97.67	194	1.37 (0.92, 2.05)	36	1.23 (0.54, 2.78)	19	1.02 (0.34, 3.11)	18	1.39 (0.39, 5.01)
> 97.67–181.59	160	0.96 (0.63, 1.46)	24	0.36 (0.14, 0.95)	10	0.08 (0.01, 0.46)	14	0.94 (0.23, 3.79)

Note: CI, confidence interval; DBP9, sum of chloroform, BDCM, DBCM, bromoform, MCAA, DCAA, TCAA, MBAA, and DBAA; HAA5, sum of MCAA, DCAA, TCAA, MBAA, and DBAA; THM4, sum of chloroform, BDCM, DBCM, and bromoform; THMBr, sum of BDCM, DBCM, and bromoform.

[a]For each DBP metric, the referent for each model includes exposure scores of zero up to the lower bound of the lowest exposure category.

[b]The numbers represent the case distribution across exposure groups before modeling.

[c]Models adjusted for the type of water source and treatment, infant birth weight, town-level income quartile, number of prenatal care visits (< 9, 9–11, 12, 13–15, > 15), health index (gestational diabetes, non-gestational diabetes, chronic hypertension, gestational hypertension, and hydramnios/oligohydramnios), and other maternal reproductive risk factors.

[d]Models adjusted for the type of water source and treatment, health index (gestational diabetes, non-gestational diabetes, chronic hypertension, gestational hypertension, and hydramnios/oligohydramnios), and other maternal reproductive risk factors.

[e]Models adjusted for the type of water source and treatment, number of prenatal care visits (< 9, 9–11, 12, 13–15, > 15), ZIP code–level income quartile, trimester prenatal care began (first, after first), health index (gestational diabetes, nongestational diabetes, chronic hypertension, gestational hypertension, and hydramnios/oligohydramnios), and other maternal reproductive risk factors.

[f]Models adjusted for the type of water source and treatment, infant birth weight, ZIP code–level income quartile, trimester prenatal care began (first, after first), health index (gestational diabetes, nongestational diabetes, chronic hypertension, gestational hypertension, and hydramnios/oligohydramnios), and other maternal reproductive risk factors.

[g]Models also include adjustment for HAA5 concentrations.

[h]Models also include adjustment for THM4 concentrations.

DBP exposure metrics, because the limitation of examining THM4 and other surrogates is well established. This is the first study of CVDs to assess alternative DBP mixture surrogates including HAA5 and DBP9. The large sample size and sufficient DBP exposure gradients also enabled examination of individual birth defects in relation to low-exposure referents for various DBP metrics. Statistical power was limited for some less prevalent DBP metrics (e.g., MCAA and MBAA) and the rarest CVDs such as TGA and TOF; this may have precluded detection of statistically significant associations small in magnitude as well as exposure–response relationships. Although we acknowledge that some of the results for different CVD and DBP combinations that were examined may be due to chance, our study does help address specificity of causal associations that have been identified in the toxicological literature.

Based on the extensive number of available covariates, we adjusted for various confounders including strong maternal risk factors for CVDs as well as other exposures related to DBPs, such as water source and disinfection type. This is also the first birth defect study to develop multi-pollutant models to examine potential confounding by other DBP exposures. We used a matched case–control study design to increase statistical efficiency and to control for time-varying confounding. An additional strength of our population-based case–control study is the low risk of selection bias, because the cases and controls were both drawn from the same study base of all underlying births in Massachusetts. We also saw no evidence to suggest that the CVD cases that were not included due to missing data or other exclusion factors were disproportionately exposed to higher or lower DBP concentrations in drinking water.

One of the main limitations in many epidemiological studies of DBPs is the lack of individual-level exposure data which may better reflect internal dose. We relied on routinely monitored data that were collected at least quarterly for all water systems. Given the known seasonality detected for some DBPs such as the THMs, quarterly measures may not fully capture the extent of temporal variability that may influence exposure estimates. For example, the critical *in utero* exposure period for many of the CVDs is during the 3rd through 8th weeks of gestation, but we did not have samples that corresponded exactly with that time period. Thus, our use of first-trimester average DBP exposure may result in exposure misclassification, which we would expect to be nondifferential in nature. Residential mobility may also lead to exposure misclassification if the address reported at birth differed from the first-trimester residence. A review of 14 environmental epidemiological studies of pregnancy outcomes showed that most moves occurred during the second trimester among the 9–32% of pregnant women who reported moving residence (Bell and Belanger 2012). Previous research has shown that these moves are often short in distance, with only 8% of

Table 4. Adjusted odds ratios (aORs) between disinfection by-product (DBP) exposures and atrial septal defects (ASDs), ventricular septal defects (VSDs), and pulmonary stenosis (PS).

	ASD[c]		VSD[d]		PS[e]	
DBP metrics (μg/L)[a]	Cases[b] (*n*)	aOR (95% CI)	Cases[b] (*n*)	aOR (95% CI)	Cases[b] (*n*)	aOR (95% CI)
THM4[f]						
> 23.05–38.05	78	1.31 (0.70, 2.46)	61	1.39 (0.72, 2.69)	24	0.61 (0.23, 1.61)
> 38.05–50.41	72	1.34 (0.67, 2.66)	80	1.77 (0.87, 3.59)	26	0.70 (0.24, 2.04)
> 50.41–65.27	86	1.59 (0.77, 3.26)	73	1.70 (0.80, 3.63)	18	0.35 (0.11, 1.19)
> 65.27–125.32	67	1.28 (0.58, 2.84)	58	1.57 (0.70, 3.53)	24	0.49 (0.14, 1.75)
THMBr[f]						
> 4.17–6.04	78	0.73 (0.35, 1.52)	56	0.81 (0.39, 1.68)	21	0.84 (0.27, 2.63)
> 6.04–7.80	83	1.10 (0.58, 2.09)	73	0.79 (0.41, 1.55)	25	0.65 (0.24, 1.77)
> 7.80–11.51	67	0.99 (0.53, 1.88)	55	0.89 (0.47, 1.69)	24	0.46 (0.16, 1.29)
> 11.51–42.48	76	1.14 (0.63, 2.06)	82	1.34 (0.73, 2.46)	25	0.91 (0.36, 2.29)
Chloroform[f]						
> 12.07–29.99	75	1.38 (0.73, 2.60)	61	1.05 (0.58, 1.90)	27	0.74 (0.29, 1.89)
> 29.99–42.17	86	1.67 (0.83, 3.38)	74	0.86 (0.43, 1.72)	28	0.73 (0.24, 2.27)
> 42.17–55.41	76	1.50 (0.69, 3.26)	75	1.00 (0.47, 2.12)	19	0.40 (0.12, 1.40)
> 55.41–98.99	68	1.42 (0.61, 3.27)	57	0.79 (0.35, 1.80)	20	0.37 (0.10, 1.44)
Bromodichloromethane (BDCM)[f]						
> 4.95–7.55	139	1.19 (0.75, 1.90)	112	0.81 (0.50, 1.31)	39	0.59 (0.29, 1.23)
> 7.55–37.38	111	1.13 (0.74, 1.72)	116	1.21 (0.79, 1.85)	37	0.69 (0.35, 1.37)
Dibromochloromethane (DBCM)[f]						
> 3.93–14.53	36	1.26 (0.81, 1.97)	40	1.54 (1.00, 2.37)	10	0.96 (0.41, 2.25)
Bromoform[f]						
> 0.26–7.06	46	1.56 (1.01, 2.43)	43	1.85 (1.20, 2.83)	20	2.66 (1.30, 5.43)
HAA5[g]						
> 8.17–19.33	61	0.50 (0.28, 0.90)	50	0.66 (0.37, 1.20)	20	0.72 (0.26, 1.98)
> 19.33–25.79	103	0.91 (0.48, 1.74)	74	1.00 (0.51, 1.94)	29	1.34 (0.42, 4.26)
> 25.79–33.97	65	0.63 (0.31, 1.29)	63	1.01 (0.49, 2.08)	24	1.48 (0.41, 5.36)
> 33.97–100.00	65	0.41 (0.19, 0.86)	78	1.02 (0.49, 2.12)	21	1.06 (0.28, 4.06)
Trichloroacetic acid (TCAA)[g]						
> 5.23–11.09	100	0.69 (0.42, 1.15)	81	0.90 (0.55, 1.50)	29	1.47 (0.57, 3.74)
> 11.09–16.38	97	0.58 (0.31, 1.09)	83	0.81 (0.44, 1.51)	32	2.48 (0.82, 7.46)
> 16.38–73.39	79	0.36 (0.18, 0.70)	86	0.79 (0.41, 1.50)	29	3.45 (1.04, 11.39)
Dichloroacetic acid (DCAA)[g]						
> 5.18–10.44	85	0.78 (0.48, 1.28)	72	0.84 (0.51, 1.39)	23	0.93 (0.38, 2.26)
> 10.44–13.85	103	0.88 (0.50, 1.54)	92	1.28 (0.72, 2.25)	40	2.02 (0.74, 5.50)
> 13.85–38.89	89	0.75 (0.41, 1.37)	88	1.18 (0.65, 2.14)	27	1.65 (0.52, 5.22)
Monochloroacetic acid (MCAA)[g]						
> 1.53–62.39	31	1.08 (0.67, 1.73)	35	1.27 (0.81, 1.97)	7	0.49 (0.20, 1.19)
Monobromoacetic acid (MBAA)[g]						
> 0.04–10.63	8	1.17 (0.49, 2.77)	13	1.81 (0.85, 3.84)	1	0.66 (0.08, 5.13)
Dibromoacetic acid (DBAA)[g]						
> 0.47–21.78	27	0.81 (0.50, 1.32)	28	1.00 (0.63, 1.61)	7	0.38 (0.14, 1.02)
DBP9						
> 33.07–59.95	76	1.12 (0.61, 2.08)	58	1.33 (0.71, 2.48)	26	1.12 (0.42, 2.99)
> 59.95–79.13	87	1.46 (0.77, 2.77)	79	1.70 (0.88, 3.26)	26	1.02 (0.35, 2.96)
> 79.13–97.67	84	1.37 (0.71, 2.64)	71	1.64 (0.83, 3.26)	19	0.63 (0.21, 1.93)
> 97.67–181.59	58	0.67 (0.33, 1.35)	63	1.48 (0.73, 2.98)	24	0.79 (0.25, 2.49)

Note: CI, confidence interval; DBP9, sum of chloroform, BDCM, DBCM, bromoform, MCAA, DCAA, TCAA, MBAA, and DBAA; HAA5, sum of MCAA, DCAA, TCAA, MBAA, and DBAA; THM4, sum of chloroform, BDCM, DBCM, and bromoform; THMBr, sum of BDCM, DBCM, and bromoform.

[a]For each DBP metric, the referent for each model includes exposure scores of zero up to the lower bound of the lowest exposure category.

[b]The numbers represent the case distribution across exposure groups before modeling.

[c]Models adjusted for the type of water source and treatment, infant birth weight, health index (gestational diabetes, nongestational diabetes, chronic hypertension, gestational hypertension, and hydramnios/oligohydramnios), and other maternal reproductive risk factors.

[d]Models adjusted for the type of water source and treatment, maternal marital status (married, including within 300 days before birth; not married), maternal education category, maternal race category, health index (gestational diabetes, non-gestational diabetes, chronic hypertension, gestational hypertension, and hydramnios/oligohydramnios), and other maternal reproductive risk factors.

[e]Models adjusted for the type of water source and treatment, ZIP code–level income quartile, trimester prenatal care began (first, after first), category of prenatal care source payment, health index (gestational diabetes, nongestational diabetes, chronic hypertension, gestational hypertension, and hydramnios/oligohydramnios), and other maternal reproductive risk factors.

[f]Models also include adjustment for HAA5 concentrations.

[g]Models also include adjustment for THM4 concentrations.

cases moving to a different county during the pregnancy (Bell and Belanger 2012; Khoury et al. 1988). This suggests that most moves during pregnancy often occur to residences that rely on the same water system. The impact of mobility on our study results is difficult to determine, but a previous study of DBPs and neural-tube defects reported stronger associations among mothers with confirmed residences at conception compared with the overall population of confirmed and unconfirmed residences (Klotz and Pyrch 1999).

In addition to uncaptured temporal variability, measurement error may result in exposure misclassification from the use of town-average DBP estimates to estimate individual exposures, because they do not include information on inter- and intraindividual variability in water use patterns. Town-average DBP concentrations from different sampling locations in water systems with considerable spatial variability may also not fully reflect residential values, although we are confident that our exposure assessment should largely capture relative categorical rankings of overall DBP exposures via drinking water. Nonetheless, we recognize that these potential sources of measurement error can lead to exposure misclassification, which may bias our results and distort any exposure–response relationships that may exist.

Massachusetts maintains an active statewide, population-based birth defect registry system to track birth defects in the 1st year following pregnancy. Therefore, we would expect minimal case underascertainment to have occurred for CVDs that occur up to 1 year, but are less certain about defects that are detected predominantly beyond the first year. There is some potential for outcome misclassification due to measurement error from the use of the ICD-9 codes (Cronk et al. 2003; Holmes and Westgate 2012; Strickland et al. 2008). Inaccuracies attendant with the use of ICD-9 codes can vary substantially by birth defect subtype and can lead to false positives and false negatives. ICD-9 codes have been shown to be good at classifying certain heart defects, such as TOF (100%), coarctation of the aorta (100%), and VSD (84%), whereas others such as ASDs (50%) and patent ductus arteriosus (22%) are less accurate (Frohnert et al. 2005). Other studies have also reported variability in false positive rates from 2% for TOF to 49% for TGA (Strickland et al. 2008). Some less severe cardiac defects, such as small holes in the heart (e.g., ASDs or VSDs), may spontaneously close or repair themselves during pregnancy or shortly after birth. Such defects may in fact go undetected, so our study population may be capturing fewer minor defects in general. We conducted a sensitivity analysis of the All CVD category excluding patent ductus arteriosus which, as noted above, is prone to misclassification. Following this restriction, comparable results were detected for bromoform and DCAA, with larger aORs found for the highest HAA5 exposure category (1.53 vs. 1.18) (see Table S4).

As with other epidemiological studies based on birth records, we cannot gauge the extent to which elective pregnancy terminations may be related to the prevalence of birth defects among aborted fetuses. Although elective terminations can result in underascertainment of cases detected at birth based on vital records data, CVDs are not often the medical reason why abortions are pursued. For example, the reported elective termination rate when detected prenatally is < 5% for ASDs, VSDs, TGA, and TOF (Boldt et al. 2002; Ethen and Canfield 2002; Papp et al. 1995; Stoll et al. 1993; Wren et al. 2000). Because our study population comprises only live births, we may not be capturing all birth defect cases in this population, including those that resulted in miscarriages. However, many CVDs, such as ASDs, often occur among live births (Botto et al. 2001; Forrester and Merz 2004; Garne et al. 2001).

CVDs are often idiopathic and likely involve multiple etiological factors including genetics, lifestyle factors, and other environmental determinants. We minimized the potential for false-positive associations between DBPs and CVDs through exclusion of chromosomal abnormalities which resulted in a more homogenous study population. We also minimized the influence of known cardiac birth defects risk factors such as rubella by use of statistical adjustment in the confounding analysis. CVDs also represent a wide range of types of malformations, some of which are simple or complex in nature. Complex CVDs, such as TOF, include a combination of CVDs diagnosed together. Because they may obscure some of the relationships that were examined for individual defects, we also conducted a sensitivity analysis to examine the impact of multiple birth defects. The sensitivity analysis was limited to CVDs with the strongest and most consistent associations. The aORs for isolated VSDs were slightly lower for the individual DBPs such as bromoform (1.42 vs. 1.85) and MBA (1.41 vs. 1.81), but were larger for the DBP mixture surrogates THM4 (2.74 vs. 1.57) and DBP9 (2.14 vs. 1.48) (see Table S5). In contrast to the main analysis, a positive exposure–response relationship for VSDs was detected for THM4 with consistent associations in the upper three quintiles (aOR range, 2.41–2.74). The associations for TOF were even stronger in magnitude for isolated TOF cases, where the aORs were from two to three times larger for the highest DCAA quartile (11.11 vs. 3.34), TCAA quartile (9.17 vs 3.89), and the HAA5 quintile (12.37 vs. 6.51) (see Table S6).

As noted earlier, we were able to evaluate numerous risk factors for birth defects from the comprehensive information available from the birth records. The reliance on birth record data, however, may limit the ability to fully consider some potential confounders such as vitamin use, body mass index (BMI), alcohol use, passive smoking, and other socioeconomic indicators. Alcohol consumption, for example, is an important risk factor for some birth defects, but the Massachusetts Department of Public Health had advised that the birth data on maternal alcohol consumption are considered of poor quality and of questionable validity. Thus, we did not include maternal alcohol use in the analyses. This is in contrast to reported smoking during pregnancy, which we have much more confidence in given that we previously demonstrated strong relationships between maternal cigarette use during pregnancy and different fetal growth measures (Rivera-Núñez and Wright 2013; Wright et al. 2004). Previous research also indicates good agreement with cotinine levels and self-reported maternal cigarette use during pregnancy (Searles Nielsen et al. 2014). Although we did not have reliable data for some potential CVD risk factors such as maternal alcohol use and prepregnancy BMI, we do not expect these to be strongly associated with DBP exposures in our study. If present at all, any bias would likely result in negative confounding if DBP exposures and alcohol consumption are inversely associated. Therefore, we would expect any residual confounding from this and other inversely associated covariates, such as obesity and BMI, to attenuate observed associations toward the null if they are not adjusted for or addressed in the study design phase. In addition, we did have data on maternal weight gain during pregnancy, which is likely related to obesity, BMI, and healthful behaviors during pregnancy. Thus, statistical adjustment for weight gain may indirectly control for some of the potential confounding from maternal BMI.

We adjusted for income in most of the logistic regression models, because we saw fairly consistent evidence of confounding by aggregate income levels based on census data for towns, census tracts, or ZIP codes. Because individual-level income data was not available, we recognize that residual confounding is possible if the aggregate measures resulted in misclassification. However, we saw little evidence of confounding by a socioeconomic index that combined aggregate and individual-level data, and our previous study found little evidence that aggregate socioeconomic indices

were associated with DBP concentrations in Massachusetts public drinking water systems (Evans et al. 2013). Given this and our extensive confounding analysis including adjustment for other individual-level correlates of socioeconomic status (e.g., education, marital status, prenatal care source of payment), we would suspect that any potential residual confounding by income would have minimal impact on our results.

Although many of our results were null, we found consistent results for bromoform and every cardiac birth defect that was examined as well as increased risks for VSDs and different DBPs. Toxicological evidence lends credence to our study findings given that dose-dependent VSDs and conotruncal defects have been shown in rats following DCAA and TCAA exposures (Epstein et al. 1992; Johnson et al. 1998; Smith et al. 1989, 1992). Bromochloroacetonitrile has also been reported to cause CVDs in rats (Christ et al. 1995), but the haloacetonitriles have yet to be examined in an epidemiological study. This may be important given that bromochloroacetonitrile was shown to be highly correlated with some DBPs such as haloacetamides and the trihaloacetic acids (e.g., TCAA) in a study from the United Kingdom (Bond et al. 2015). Despite some findings that appear concordant with existing epidemiological and toxicological studies, more research is needed to further elucidate which DBPs or DBP mixtures may be responsible for the epidemiological associations reported to date.

Conclusions

This is the first epidemiological study of birth defects and DBPs to examine several individual CVDs, different exposure surrogate mixtures (THM4, THMBr, HAA5, and DBP9), and various individual DBP species. Future analyses of CVDs and DBPs should expand upon this research and focus efforts to reduce exposure misclassification due to spatial and temporal variability including evaluation of smaller critical exposure windows and peak exposures. This may require more frequent distribution system sampling or temporal modeling/interpolation approaches using existing data. Residential-level sampling or more spatially representative exposure estimates (e.g., geographic information system–based approaches) would also help address spatial variability concerns.

There are fairly consistent results from epidemiological and toxicological studies for associations between DBP exposures and increased risk of some CVDs, especially VSDs. Because our study is only the second one to evaluate exposure to brominated DBPs, it adds some specificity to the potential risks that have been previously noted for THM4. However, further clarity on which of the co-occurring DBP species (or mixture combinations) to sample for and analyze is still needed and may benefit from additional toxicological studies and exposure assessment research. Given the ubiquitous nature of DBPs in treated drinking water, our findings have potential important public health ramifications. Thus, further delineation of the potential impact of *in utero* exposure to environmental teratogens would help inform intervention efforts to reduce exposures during critical windows of pregnancy.

References

Bell ML, Belanger K. 2012. Review of research on residential mobility during pregnancy: consequences for assessment of prenatal environmental exposures. J Expo Sci Environ Epidemiol 22(5):429–438.

Boldt T, Andersson S, Eronen M. 2002. Outcome of structural heart disease diagnosed in utero. Scand Cardiovasc J 36(2):73–79.

Bond T, Templeton MR, Mokhtar Kamal NH, Graham N, Kanda R. 2015. Nitrogenous disinfection byproducts in English drinking water supply systems: occurrence, bromine substitution and correlation analysis. Water Res 85:85–94.

Botto LD, Correa A, Erickson JD. 2001. Racial and temporal variations in the prevalence of heart defects. Pediatrics 107(3):E32.

Bove FJ, Fulcomer MC, Klotz JB, Esmart J, Dufficy EM, Savrin JE. 1995. Public drinking water contamination and birth outcomes. Am J Epidemiol 141(9):850–862.

Brent RL, Beckman DA. 1990. Environmental teratogens. Bull N Y Acad Med 66(2):123–163.

Chisholm K, Cook A, Bower C, Weinstein P. 2008. Risk of birth defects in Australian communities with high levels of brominated disinfection by-products. Environ Health Perspect 116:1267–1273, doi: 10.1289/ehp.10980.

Christ SA, Read EJ, Stober JA, Smith MK. 1995. The developmental toxicity of bromochloroacetonitrile in pregnant Long–Evans rats. Int J Environ Health Res 5(2):175–188.

Christian MS, York RG, Hoberman AM, Diener RM, Fisher LC. 2001. Oral (drinking water) developmental toxicity studies of bromodichloromethane (BDCM) in rats and rabbits. Int J Toxicol 20(4):225–237.

Cronk CE, Malloy ME, Pelech AN, Miller RE, Meyer SA, Cowell M, et al. 2003. Completeness of state administrative databases for surveillance of congenital heart disease. Birth Defects Res A Clin Mol Teratol 67(9):597–603.

Epstein DL, Nolen GA, Randall JL, Christ SA, Read EJ, Stober JA, et al. 1992. Cardiopathic effects of dichloroacetate in the fetal Long-Evans rat. Teratology 46(3):225–235.

Ethen MK, Canfield MA. 2002. Impact of including elective pregnancy terminations before 20 weeks gestation on birth defect rates. Teratology 66(suppl 1):S32–S35.

Evans AM, Wright JM, Meyer A, Rivera-Núñez Z. 2013. Spatial variation of disinfection by-product concentrations: exposure assessment implications. Water Res 47(16):6130–6140.

Forrester MB, Merz RD. 2004. Descriptive epidemiology of selected congenital heart defects, Hawaii, 1986–1999. Paediatr Perinat Epidemiol 18(6):415–424.

Frohnert BK, Lussky RC, Alms MA, Mendelsohn NJ, Symonik DM, Falken MC. 2005. Validity of hospital discharge data for identifying infants with cardiac defects. J Perinatol 25(11):737–742.

Garne E, Stoll C, Clementi M, Euroscan Group. 2001. Evaluation of prenatal diagnosis of congenital heart diseases by ultrasound: experience from 20 European registries. Ultrasound Obstet Gynecol 17(5):386–391.

Go AS, Mozaffarian D, Roger VL, Benjamin EJ, Berry JD, Borden WB, et al. 2013. Heart disease and stroke statistics—2013 update: a report from the American Heart Association. Circulation 127:143–152.

Graves CG, Matanoski GM, Tardiff RG. 2001. Weight of evidence for an association between adverse reproductive and developmental effects and exposure to disinfection by-products: a critical review. Regul Toxicol Pharmacol 34(2):103–124.

Grazuleviciene R, Kapustinskiene V, Vencloviene J, Buinauskiene J, Nieuwenhuijsen MJ. 2013. Risk of congenital anomalies in relation to the uptake of trihalomethane from drinking water during pregnancy. Occup Environ Med 70(4):274–282.

Holmes LB, Westgate MN. 2012. Using ICD-9 codes to establish prevalence of malformations in newborn infants. Birth Defects Res A Clin Mol Teratol 94(4):208–214.

Hwang BF, Jaakkola JJ, Guo HR. 2008. Water disinfection by-products and the risk of specific birth defects: a population-based cross-sectional study in Taiwan. Environ Health 7:23, doi: 10.1186/1476-069X-7-23.

Johnson PD, Dawson BV, Goldberg SJ. 1998. Cardiac teratogenicity of trichloroethylene metabolites. J Am Coll Cardiol 32(2):540–545.

Khoury MJ, Stewart W, Weinstein A, Panny S, Lindsay P, Eisenberg M. 1988. Residential mobility during pregnancy: implications for environmental teratogenesis. J Clin Epidemiol 41(1):15–20.

Klotz JB, Pyrch LA. 1999. Neural tube defects and drinking water disinfection by-products. Epidemiology 10(4):383–390.

Kotelchuck M. 1994. An evaluation of the Kessner Adequacy of Prenatal Care Index and a proposed Adequacy of Prenatal Care Utilization Index. Am J Public Health 84(9):1414–1420.

Kurinczuk JJ, Hollowell J, Boyd PA, Oakley L, Brocklehurst P, Gray R. 2010. The contribution of congenital anomalies to infant mortality. Inequalities in Infant Mortality Project Briefing Paper 4. Oxford, UK:University of Oxford, National Perinatal Epidemiology Unit. https://www.npeu.ox.ac.uk/downloads/files/infant-mortality/Infant-Mortality-Briefing-Paper-4.pdf [accessed 1 March 2016].

Lee K, Khoshnood B, Chen L, Wall SN, Cromie WJ, Mittendorf RL. 2001. Infant mortality from congenital malformations in the United States, 1970–1997. Obstet Gynecol 98(4):620–627.

Nieuwenhuijsen MJ, Martinez D, Grellier J, Bennett J, Best N, Iszatt N, et al. 2009. Chlorination disinfection by-products in drinking water and congenital anomalies: review and meta-analyses. Environ Health Perspect 117:1486–1493, doi: 10.1289/ehp.0900677.

Nieuwenhuijsen MJ, Toledano MB, Bennett J, Best N, Hambly P, de Hoogh C, et al. 2008. Chlorination disinfection by-products and risk of congenital anomalies in England and Wales. Environ Health Perspect 116:216–222, doi: 10.1289/ehp.10636.

Papp Z, Tóth-Pál E, Papp C, Tóth Z, Szabó M, Veress L, et al. 1995. Impact of prenatal mid-trimester screening on the prevalence of fetal structural anomalies: a prospective epidemiological study. Ultrasound Obstet Gynecol 6(5):320–326.

Randall JL, Christ SA, Horton-Perez P, Nolen GA, Read EJ, Smith MK. 1991. Developmental effects of 2-bromoacetic acid in the Long-Evans rat [Abstract P122]. Teratology 43(5):454.

Righi E, Bechtold P, Tortorici D, Lauriola P, Calzolari E,

Astolfi G, et al. 2012. Trihalomethanes, chlorite, chlorate in drinking water and risk of congenital anomalies: a population-based case-control study in Northern Italy. Environ Res 116:66–73.

Rivera-Núñez Z, Wright JM. 2013. Association of brominated trihalomethane and haloacetic acid exposure with fetal growth and preterm delivery in Massachusetts. J Occup Environ Med 55(10):1125–1134.

Ruddick JA, Villeneuve DC, Chu I, Valli VE. 1983. A teratological assessment of four trihalomethanes in the rat. J Environ Sci Health B 18(3):333–349.

Searles Nielsen S, Dills RL, Glass M, Mueller BA. 2014. Accuracy of prenatal smoking data from Washington State birth certificates in a population-based sample with cotinine measurements. Ann Epidemiol 24(3):236–239.

Shaw GM, Ranatunga D, Quach T, Neri E, Correa A, Neutra RR. 2003. Trihalomethane exposures from municipal water supplies and selected congenital malformations. Epidemiology 14:191–199.

Smith MK, Randall JL, Read EJ, Stober JA. 1989. Teratogenic activity of trichloroacetic acid in the rat. Teratology 40(5):445–451.

Smith MK, Randall JL, Read EJ, Stober JA. 1992. Developmental toxicity of dichloroacetate in the rat. Teratology 46(3):217–223.

Stoll C, Alembik Y, Dott B, Roth PM, De Geeter B. 1993. Evaluation of prenatal diagnosis of congenital heart disease. Prenat Diagn 13(6):453–461.

Strickland MJ, Riehle-Colarusso TJ, Jacobs JP, Reller MD, Mahle WT, Botto LD, et al. 2008. The importance of nomenclature for congenital cardiac disease: implications for research and evaluation. Cardiol Young 18(suppl 2):92–100.

Wren C, Richmond S, Donaldson L. 2000. Temporal variability in birth prevalence of cardiovascular malformations. Heart 83(4):414–419.

Wright JM, Schwartz J, Dockery DW. 2004. The effect of disinfection by-products and mutagenic activity on birth weight and gestational duration. Environ Health Perspect 112:920–925, doi: 10.1289/ehp.6779.

Environ Health Perspect
DOI: 10.1289/EHP103

Note to readers with disabilities: *EHP* strives to ensure that all journal content is accessible to all readers. However, some figures and Supplemental Material published in *EHP* articles may not conform to 508 standards due to the complexity of the information being presented. If you need assistance accessing journal content, please contact ehp508@niehs.nih.gov. Our staff will work with you to assess and meet your accessibility needs within 3 working days.

Supplemental Material

Disinfection By-Product Exposures and the Risk of Specific Cardiac Birth Defects

J. Michael Wright, Amanda Evans, John A. Kaufman, Zorimar Rivera-Núñez, and Michael G. Narotsky

Table of Contents

Table S1. Spearman Correlation Coefficients for Disinfection By-Product Metrics

Table S2. Adjusted Odds Ratios (aORs) between Disinfection By-Product (DBP) Exposures and Tetralogy of Fallot Stratified by Sex

Table S3. Adjusted Odds Ratios (aORs) between Disinfection By-Product (DBP) Exposures and Ventricular Septal Defects Stratified by Sex

Table S4. Adjusted Odds Ratios (aORs) between Disinfection By-Product (DBP) Exposures and All Cardiovascular Defects Excluding Patent Ductus Arteriosus

Table S5. Adjusted Odds Ratios (aORs) between Disinfection By-Product (DBP) Exposures and Isolated Ventricular Septal Defect Cases

Table S6. Adjusted Odds Ratios (aORs) between Disinfection By-Product (DBP) Exposures and Isolated Tetralogy of Fallot Cases

Table S1. Spearman Correlation Coefficients for Disinfection By-Product Metrics

	DBP9	HAA5	THM4	THMBr	BDCM	DBCM	TCM	TCAA	DCAA	TBM	MBAA	MCAA	DBAA
DBP9	1.00												
HAA5	0.90	1.00											
THM4	0.95	0.74	1.00										
THMBr	0.40	0.25	0.50	1.00									
BDCM	0.54	0.37	0.63	0.96	1.00								
DBCM	0.05	-0.05	0.13	0.85	0.72	1.00							
TCM	0.94	0.76	0.97	0.33	0.47	-0.02	1.00						
TCAA	0.89	0.96	0.77	0.24	0.37	-0.08	0.79	1.00					
DCAA	0.84	0.93	0.70	0.23	0.34	-0.06	0.74	0.85	1.00				
TBM	-0.25	-0.28	-0.20	0.39	0.20	0.57	-0.30	-0.32	-0.28	1.00			
MBAA	0.03	0.04	0.02	0.03	0.03	0.04	0.02	0.04	0.02	0.03	1.00		
MCAA	0.50	0.57	0.42	0.26	0.30	0.07	0.42	0.46	0.55	-0.13	0.04	1.00	
DBAA	-0.12	-0.09	-0.11	0.31	0.19	0.41	-0.18	-0.17	-0.07	0.54	0.15	0.01	1.00

Note: DBP9 = sum of chloroform (TCM), bromodichloromethane (BDCM), dibromochloromethane (DBCM), bromoform (TBM), monochloroacetic acid (MCAA), dichloroacetic acid (DCAA), trichloroacetic acid (TCAA), bromoacetic acid (MBAA), and dibromoacetic acid (DBAA); HAA5 = sum of MCAA, DCAA, TCAA, MBAA, and DBAA; THM4 = sum of TCM, BDCM, DBCM, and TBM; THMBr = sum of BDCM, DBCM, and TBM

Table S2. Adjusted Odds Ratios (aORs) between Disinfection By-Product (DBP) Exposures and Tetralogy of Fallot Stratified by Sex

DBP Metrics (µg/L)	Cases (*n*)[a]	Total Population aOR (95% CI)[b]	Male aOR (95% CI)[b]	Female aOR (95% CI)[b]
THM4[c]				
≤23.05	15	REF	REF	REF
>23.05–38.05	17	0.32 (0.10, 1.05)	1.52 (0.17, 13.13)	0.15 (0.01, 1.64)
>38.05–50.41	19	0.51 (0.15, 1.74)	3.02 (0.30, 30.43)	0.16 (0.02, 1.47)
>50.41–65.27	19	0.31 (0.08, 1.21)	1.53 (0.14, 16.62)	0.22 (0.02, 2.12)
>65.27–125.32	16	0.19 (0.04, 0.88)	1.06 (0.09, 12.09)	0.05 (0.00, 0.72)
THMBr[c]				
≤4.17	15	REF	REF	REF
>4.17–6.04	25	1.00 (0.34, 2.98)	0.29 (0.04, 2.10)	5.21 (0.58, 46.62)
>6.04–7.80	12	0.23 (0.06, 0.91)	0.19 (0.02, 1.81)	0.45 (0.03, 7.88)
>7.80–11.51	18	0.45 (0.14, 1.39)	0.17 (0.02, 1.32)	1.64 (0.22, 12.36)
>11.51–42.48	16	0.26 (0.09, 0.76)	0.27 (0.04, 1.83)	0.28 (0.03, 2.70)
Chloroform[c]				
≤12.07	15	REF	REF	REF
>12.07–29.99	14	0.50 (0.16, 1.53)	1.06 (0.12, 9.48)	0.19 (0.02, 2.24)
>29.99–42.17	21	0.76 (0.22, 2.69)	1.67 (0.17, 15.96)	0.23 (0.02, 3.32)
>42.17–55.41	22	0.81 (0.20, 3.29)	1.91 (0.14, 26.80)	0.29 (0.02, 3.98)
>55.41–98.99	14	0.33 (0.07, 1.64)	0.50 (0.03, 7.73)	0.06 (0.00, 1.46)
Bromodichloromethane (BDCM)[c]				
≤4.95	34	REF	REF	REF
>4.95–7.55	24	0.49 (0.19, 1.24)	0.73 (0.17, 3.09)	0.53 (0.10, 2.72)
>7.55–37.38	28	0.38 (0.17, 0.82)	0.76 (0.24, 2.44)	0.30 (0.06, 1.40)
Dibromochloromethane (DBCM)[c]				
≤3.93	79	REF	REF	REF
>3.93–14.53	7	0.54 (0.20, 1.41)	0.34 (0.07, 1.55)	0.36 (0.05, 2.79)
Bromoform[c]				
≤0.26	76	REF	REF	REF
>0.26–7.06	10	1.14 (0.45, 2.87)	0.59 (0.15, 2.33)	3.00 (0.34, 26.50)

Table S2. Adjusted Odds Ratios (aORs) between Disinfection By-Product (DBP) Exposures and Tetralogy of Fallot Stratified by Sex (continued)

DBP Metrics (µg/L)	Cases (*n*)[a]	Total Population aOR (95% CI)[b]	Male aOR (95% CI)[b]	Female aOR (95% CI)[b]
HAA5[d]				
≤8.17	11	REF	REF	REF
>8.17–19.33	21	2.13 (0.53, 8.65)	2.59 (0.13, 50.10)	1.36 (0.11, 16.16)
>19.33–25.79	21	4.98 (1.02, 24.35)	8.27 (0.25, 276.35)	6.14 (0.32, 118.72)
>25.79–33.97	17	5.88 (1.06, 32.57)	2.95 (0.08, 114.41)	7.57 (0.30, 192.35)
>33.97–100.00	16	6.51 (1.23, 34.59)	4.79 (0.16, 142.97)	2.97 (0.14, 62.87)
Trichloroacetic acid (TCAA)[d]				
≤5.23	15	REF	REF	REF
>5.23–11.09	28	2.72 (0.91, 8.13)	5.79 (0.60, 55.49)	3.35 (0.35, 32.18)
>11.09–16.38	22	4.30 (1.09, 16.88)	6.82 (0.55, 83.94)	2.97 (0.20, 44.62)
>16.38–73.39	19	3.89 (0.97, 15.66)	5.92 (0.51, 68.40)	2.25 (0.13, 39.31)
Dichloroacetic acid (DCAA)[d]				
≤5.18	17	REF	REF	REF
>5.18–10.44	22	1.39 (0.50, 3.88)	4.09 (0.52, 31.94)	0.87 (0.07, 11.29)
>10.44–13.85	24	3.08 (0.92, 10.34)	2.31 (0.27, 19.90)	7.45 (0.34, 164.24)
>13.85–38.89	21	3.34 (0.90, 12.43)	1.54 (0.11, 20.85)	26.35 (0.94, 737.88)
Monochloroacetic acid (MCAA)[d]				
≤1.53	80	REF	REF	REF
>1.53–62.39	4	0.83 (0.27, 2.54)	0.59 (0.09, 3.78)	0.47 (0.05, 4.67)
Monobromoacetic acid (MBAA)[d]				
≤0.04	81	REF	REF	REF
>0.04–10.63	3	0.80 (0.08, 7.48)	0.53 (0.01, 20.59)	N/E
Dibromoacetic acid (DBAA)[d]				
≤0.47	77	REF	REF	REF
>0.47–21.78	7	0.59 (0.23, 1.54)	0.64 (0.12, 3.38)	0.24 (0.03, 2.22)

Table S2. Adjusted Odds Ratios (aORs) between Disinfection By-Product (DBP) Exposures and Tetralogy of Fallot Stratified by Sex (continued)

DBP Metrics (µg/L)	Cases (*n*)[a]	Total Population aOR (95% CI)[b]	Male aOR (95% CI)[b]	Female aOR (95% CI)[b]
DBP9				
≤33.07	13	REF	REF	REF
>33.07–59.95	17	0.80 (0.24, 2.63)	1.70 (0.19, 14.97)	0.97 (0.09, 10.84)
>59.95–79.13	24	1.15 (0.32, 4.08)	2.62 (0.31, 22.08)	2.95 (0.20, 42.62)
>79.13–97.67	18	1.39 (0.39, 5.01)	4.25 (0.43, 42.28)	0.26 (0.02, 4.49)
>97.67–181.59	14	0.94 (0.23, 3.79)	0.74 (0.07, 7.34)	0.55 (0.03, 9.92)

Note: *n* = sample size; aOR = adjusted odds ratios; CI = confidence interval; REF = referent; THM4 = sum of chloroform, BDCM, DBCM, and bromoform; THMBr = sum of BDCM, DBCM, and bromoform; N/E = not estimable; HAA5 = sum of MCAA, DCAA, TCAA, MBAA, and DBAA; DBP9 = sum of chloroform, BDCM, DBCM, bromoform, MCAA, DCAA, TCAA, MBAA, and DBAA.

[a]The numbers represent the TOF case distribution across exposure groups prior to modeling and stratification.

[b]Models adjusted for the type of water source and treatment, infant birth weight, ZIP code-level income quartile, trimester prenatal care began (first, after first), health index (gestational diabetes, non-gestational diabetes, chronic hypertension, gestational hypertension, and hydramnios/oligohydramnios), and other maternal reproductive risk factors.

[c]Models also include adjustment for HAA5 concentrations.

[d]Models also include adjustment for THM4 concentrations.

Table S3. Adjusted Odds Ratios (aORs) between Disinfection By-Product (DBP) Exposures and Ventricular Septal Defects Stratified by Sex

DBP Metrics (µg/L)	Cases (*n*)[a]	Total Population aOR (95% CI)[b]	Male aOR (95% CI)[b]	Female aOR (95% CI)[b]
THM4[c]				
≤23.05	62	REF	REF	REF
>23.05–38.05	61	1.39 (0.72, 2.69)	1.85 (0.49, 6.93)	1.15 (0.49, 2.71)
>38.05–50.41	80	1.77 (0.87, 3.59)	2.47 (0.60, 10.11)	1.69 (0.66, 4.34)
>50.41–65.27	73	1.70 (0.80, 3.63)	1.93 (0.43, 8.62)	1.60 (0.59, 4.29)
>65.27–125.32	58	1.57 (0.70, 3.53)	1.35 (0.29, 6.37)	2.08 (0.71, 6.12)
THMBr[c]				
≤4.17	67	REF	REF	REF
>4.17–6.04	56	0.81 (0.39, 1.68)	0.39 (0.12, 1.26)	1.70 (0.57, 5.04)
>6.04–7.80	73	0.79 (0.41, 1.55)	0.48 (0.17, 1.38)	1.72 (0.63, 4.69)
>7.80–11.51	55	0.89 (0.47, 1.69)	0.54 (0.20, 1.45)	1.96 (0.73, 5.23)
>11.51–42.48	82	1.34 (0.73, 2.46)	0.96 (0.37, 2.46)	2.52 (0.99, 6.42)
Chloroform[c]				
≤12.07	66	REF	REF	REF
>12.07–29.99	61	1.05 (0.58, 1.90)	1.18 (0.38, 3.69)	1.06 (0.48, 2.34)
>29.99–42.17	74	0.86 (0.43, 1.72)	0.79 (0.22, 2.88)	0.90 (0.34, 2.35)
>42.17–55.41	75	1.00 (0.47, 2.12)	0.75 (0.18, 3.09)	1.04 (0.38, 2.84)
>55.41–98.99	57	0.79 (0.35, 1.80)	0.32 (0.07, 1.43)	1.43 (0.48, 4.22)
Bromodichloromethane (BDCM)[c]				
≤4.95	105	REF	REF	REF
>4.95–7.55	112	0.81 (0.50, 1.31)	0.76 (0.34, 1.71)	1.01 (0.51, 2.01)
>7.55–37.38	116	1.21 (0.79, 1.85)	1.07 (0.53, 2.17)	1.51 (0.84, 2.70)
Dibromochloromethane (DBCM)[c]				
≤3.93	293	REF	REF	REF
>3.93–14.53	40	1.54 (1.00, 2.37)	2.17 (1.06, 4.46)	1.61 (0.87, 2.96)
Bromoform[c]				
≤0.26	290	REF	REF	REF
>0.26–7.06	43	1.85 (1.20, 2.83)	2.23 (1.10, 4.52)	1.88 (1.01, 3.52)

Table S3. Adjusted Odds Ratios (aORs) between Disinfection By-Product (DBP) Exposures and Ventricular Septal Defects Stratified by Sex (continued)

DBP Metrics (µg/L)	Cases (*n*)[a]	Total Population aOR (95% CI)[b]	Male aOR (95% CI)[b]	Female aOR (95% CI)[b]
HAA5[d]				
≤8.17	69	REF	REF	REF
>8.17–19.33	50	0.66 (0.37, 1.20)	0.75 (0.26, 2.16)	0.49 (0.21, 1.12)
>19.33–25.79	74	1.00 (0.51, 1.94)	0.74 (0.22, 2.52)	0.85 (0.34, 2.13)
>25.79–33.97	63	1.01 (0.49, 2.08)	1.65 (0.47, 5.79)	0.39 (0.13, 1.12)
>33.97–100.00	78	1.02 (0.49, 2.12)	1.23 (0.33, 4.64)	0.62 (0.22, 1.75)
Trichloroacetic acid (TCAA)[d]				
≤5.23	80	REF	REF	REF
>5.23–11.09	81	0.90 (0.55, 1.50)	1.18 (0.47, 2.91)	0.63 (0.31, 1.27)
>11.09–16.38	83	0.81 (0.44, 1.51)	1.01 (0.34, 3.00)	0.46 (0.19, 1.10)
>16.38–73.39	86	0.79 (0.41, 1.50)	1.08 (0.34, 3.46)	0.43 (0.18, 1.08)
Dichloroacetic acid (DCAA)[d]				
≤5.18	78	REF	REF	REF
>5.18–10.44	72	0.84 (0.51, 1.39)	0.51 (0.21, 1.19)	0.79 (0.39, 1.59)
>10.44–13.85	92	1.28 (0.72, 2.25)	1.02 (0.41, 2.53)	1.19 (0.52, 2.73)
>13.85–38.89	88	1.18 (0.65, 2.14)	1.14 (0.45, 2.91)	0.83 (0.35, 1.95)
Monochloroacetic acid (MCAA)[d]				
≤1.53	295	REF	REF	REF
>1.53–62.39	35	1.27 (0.81, 1.97)	1.47 (0.72, 2.99)	1.06 (0.55, 2.04)
Monobromoacetic acid (MBAA)[d]				
≤0.04	317	REF	REF	REF
>0.04–10.63	13	1.81 (0.85, 3.84)	6.56 (1.60, 26.83)	1.92 (0.60, 6.16)
Dibromoacetic acid (DBAA)[d]				
≤0.47	302	REF	REF	REF
>0.47–21.78	28	1.00 (0.63, 1.61)	1.09 (0.52, 2.28)	1.08 (0.56, 2.10)

Table S3. Adjusted Odds Ratios (aORs) between Disinfection By-Product (DBP) Exposures and Ventricular Septal Defects Stratified by Sex (continued)

DBP Metrics (µg/L)	Cases (*n*)[a]	Total Population aOR (95% CI)[b]	Male aOR (95% CI)[b]	Female aOR (95% CI)[b]
DBP9				
≤33.07	63	REF	REF	REF
>33.07–59.95	58	1.33 (0.71, 2.48)	1.13 (0.36, 3.48)	1.29 (0.57, 2.91)
>59.95–79.13	79	1.70 (0.88, 3.26)	2.23 (0.68, 7.32)	1.64 (0.69, 3.91)
>79.13–97.67	71	1.64 (0.83, 3.26)	1.45 (0.43, 4.91)	1.37 (0.55, 3.40)
>97.67–181.59	63	1.48 (0.73, 2.98)	1.07 (0.32, 3.62)	1.49 (0.56, 3.94)

Note: *n* = sample size; aOR = adjusted odds ratio; CI = confidence interval; REF = referent; THM4 = sum of chloroform, BDCM, DBCM, and bromoform; THMBr = sum of BDCM, DBCM, and bromoform; HAA5 = sum of MCAA, DCAA, TCAA, MBAA, and DBAA; DBP9 = sum of chloroform, BDCM, DBCM, bromoform, MCAA, DCAA, TCAA, MBAA, and DBAA.

[a]The numbers represent the case distribution across exposure groups prior to modeling and stratification.

[b]Models adjusted for the type of water source and treatment, maternal marital status (married, including within 300 days prior to birth; not married), maternal education category, maternal race category, health index (gestational diabetes, non-gestational diabetes, chronic hypertension, gestational hypertension, and hydramnios/oligohydramnios), and other maternal reproductive risk factors.

[c]Models also include adjustment for HAA5 concentrations.

[d]Models also include adjustment for THM4 concentrations.

Table S4. Adjusted Odds Ratios (aORs) between Disinfection By-Product (DBP) Exposures and All Cardiovascular Defects Excluding Patent Ductus Arteriosus

DBP Metrics (µg/L)	Cases (*n*)[a]	aOR (95% CI)[b]
Bromoform[c]		
≤0.26	532	REF
>0.26–7.06	79	1.50 (1.10, 2.04)
HAA5[d]		
≤8.17	118	REF
>8.17–19.33	111	1.09 (0.71, 1.68)
>19.33–25.79	153	1.57 (0.97, 2.55)
>25.79–33.97	111	1.24 (0.72, 2.12)
>33.97–100.00	119	1.53 (0.90, 2.61)
Dichloroacetic acid (DCAA)[d]		
≤5.18	142	REF
>5.18–10.44	150	1.08 (0.76, 1.53)
>10.44–13.85	169	1.26 (0.83, 1.89)
>13.85–38.89	141	1.29 (0.84, 1.99)

Note: *n* = sample size; aOR = adjusted odds ratio; CI = confidence interval; REF = referent; HAA5 = sum of monochloroacetic acid, DCAA, trichloroacetic acid, monobromoacetic acid, and dibromoacetic acid.

[a]The numbers represent the case distribution across exposure groups prior to modeling.

[b]Models adjusted for the type of water source and treatment, health index (gestational diabetes, non-gestational diabetes, chronic hypertension, gestational hypertension, and hydramnios/oligohydramnios), and other maternal reproductive risk factors.

[c]Model also includes adjustment for HAA5 concentrations.

[d]Models also include adjustment for THM4 (sum of chloroform, bromodichloromethane, dibromochloromethane, and bromoform) concentrations.

Table S5. Adjusted Odds Ratios (aORs) between Disinfection By-Product (DBP) Exposures and Isolated Ventricular Septal Defect Cases

DBP Metrics (µg/L)	Cases (*n*)[a]	aOR (95% CI)[b]
THM4[c]		
≤23.05	22	REF
>23.05–38.05	12	1.17 (0.39, 3.57)
>38.05–50.41	21	2.41 (0.74, 7.82)
>50.41–65.27	23	2.46 (0.66, 9.21)
>65.27–125.32	23	2.74 (0.67, 11.22)
Dibromochloromethane (DBCM)[c]		
≤3.93	89	REF
>3.93–14.53	12	1.07 (0.48, 2.36)
Bromoform[c]		
≤0.26	87	REF
>0.26–7.06	14	1.42 (0.68, 2.98)
Monobromoacetic acid (MBAA)[d]		
≤0.04	97	REF
>0.04–10.63	3	1.41 (0.16, 12.43)
DBP9		
≤33.07	22	REF
>33.07–59.95	14	1.32 (0.46, 3.75)
>59.95–79.13	21	2.08 (0.68, 6.42)
>79.13–97.67	19	1.37 (0.41, 4.63)
>97.67–181.59	25	2.14 (0.66, 6.98)

Note: *n* = sample size; aOR = adjusted odds ratio; CI = confidence interval; REF = referent; THM4 = sum of chloroform, BDCM, DBCM, and bromoform; DBP9 = sum of chloroform, bromodichloromethane (BDCM), DBCM, bromoform, monochloroacetic acid, dichloroacetic acid, trichloroacetic acid, MBAA, and dibromoacetic acid.

[a]The numbers represent the case distribution across exposure groups prior to modeling.

[b]Models adjusted for water source and treatment type, maternal education category, maternal marital status (married, including within 300 days prior to birth; not married), maternal race category, health index (gestational diabetes, non-gestational diabetes, chronic hypertension, gestational hypertension, and hydramnios/oligohydramnios), and other maternal reproductive risk factors.

[c]Models also include adjustment for HAA5 (sum of MCAA, DCAA, TCAA, MBAA, and DBAA) concentrations.

[d]Model also includes adjustment for THM4 concentrations.

Table S6. Adjusted Odds Ratios (aORs) between Disinfection By-Product (DBP) Exposures and Isolated Tetralogy of Fallot Cases

DBP Metrics (µg/L)	Cases (*n*)[a]	aOR (95% CI)[b]
HAA5		
≤8.17	4	REF
>8.17–19.33	6	2.64 (0.26, 26.86)
>19.33–25.79	9	4.90 (0.40, 60.50)
>25.79–33.97	6	3.61 (0.21, 63.15)
>33.97–100.00	7	12.37 (0.75, 204.11)
Dichloroacetic acid (DCAA)		
≤5.18	6	REF
>5.18–10.44	6	1.44 (0.27, 7.54)
>10.44–13.85	7	2.77 (0.34, 22.70)
>13.85–38.89	11	11.11 (1.17, 105.86)
Trichloroacetic acid (TCAA)		
≤5.23	5	REF
>5.23– 11.09	8	6.30 (0.85, 46.84)
>11.09–16.38	10	12.07 (1.02, 143.10)
>16.38–73.39	7	9.17 (0.65, 129.15)

Note: *n* = sample size; aOR = adjusted odds ratio; CI = confidence interval; REF = referent; HAA5 = sum of monochloroacetic acid, DCAA, TCAA, monobromoacetic acid, and dibromoacetic acid.

[a]The numbers represent the case distribution across exposure groups prior to modeling.

[b]Models adjusted for water source and treatment type, trimester prenatal care began (first, after first), birth weight, zip code level income, other maternal reproductive risk factors, health index (gestational diabetes, non-gestational diabetes, chronic hypertension, gestational hypertension, and hydramnios/oligohydramnios), and THM4 (sum of chloroform, bromodichloromethane, dibromochloromethane, and bromoform) concentrations.

April 24, 2020

To Whom it May Concern:

I am delighted to offer my full support to Dr. J. Michael Wright nomination for a well-deserved STAA award. I have known Mike for over 19 years, having first met him when I served as Acting Division Director of US EPA's National Center for Environmental Assessment Office in Cincinnati, Ohio in April 2001. After returning to my permanent position in US EPA's Office of Water, I have kept up on Mike's disinfection byproduct (DBP) important exposure assessment and epidemiological research efforts supporting the National Water Program's requirements. Through various research updates and leadership briefings over the years, Mike has performed an outstanding job keeping the program office apprised of his epidemiological research on DBPs impacting risk assessment basis for drinking water regulations.

Mike has been an invited participant to the biannual Gordon Research Conference on DBPs since it's inception in 2006. As part of this and other presentations at national and internal settings, he has been asked to provide numerous oral presentations as discussant leader and session chair on multiple occassions.

Part of the impetus for his work was the limited reproductive and developmental evidence identified in previous rounds of Stage 2 DBP Rule, since the regulations have been predominately based on epidemiological cancer findings. Since then, Mike was proactive in obtaining exposure and birth outcome data to meet these needs addressing birth defects in relation to DBPs. He has regularly published in the field and his publications have made important impact on advancing the science and helping characterize potential risk to DBPs.

Some of his previous epidemiological studies have been considered as part of Safe Drinking Water Act's Stage 2 DBP Rule review deliberations and this work continues to this day including this nominated manuscript. This paper in question of cardiac birth defects and DBPs published in the top environmental health journal, *Environmental Health Perspectives*, may be his most important work to date. Specifically, it represented the first epidemiological study of birth defects and DBPs to examine several individual cardiac defects, as well as different DBPs and DBP mixtures. Furthermore, it clearly demonstrated an increased risk for a ventricular septal defect (VSD), a type of cardiac defect, for THM4 exposures as well as other brominated trihalomethanes and haloacetic acids.

Ultimately, this nominated manuscript may be the one to move the risk assessment needle on reproductive and developmental effects as it demonstrates a very consistent increased risk of a VSD and THM4 exposures. This observation has been confirmed through two other epidemiological publications as well a meta-analysis. This type of consistency in epidemiological research is rare and especially challenging given the heterogenous populations and DBP mixture scenarios examined across studies. As noted in the manuscript, there is some coherence with toxicological research related to risk of some CVDs, especially ventricular septal defects. The difference between his work and others is that, given his inside knowledge of risk assessment, his previous research has addressed efforts to reduce the potential for

exposure misclassification and other types of biases and allow for the increased use of epidemiological studies in risk assessments.

In sum, I have no doubt that Mike will continue to make important contribution to the field and strongly feel that his recognition of an STAA award is very timely fitting for a well-deserving manuscript (and career) that advances the field forward.

Sincerely,

Edward V. Ohanian, Ph.D.
Associate Director for Science
Office of Water (MC: 4301T)
US EPA

A Section 508–conformant HTML version of this article is available at http://dx.doi.org/10.1289/EHP103.

Disinfection By-Product Exposures and the Risk of Specific Cardiac Birth Defects

J. Michael Wright,[1] Amanda Evans,[2] John A. Kaufman,[3] Zorimar Rivera-Núñez,[4] and Michael G. Narotsky[5]

[1]National Center for Environmental Assessment (NCEA), Office of Research and Development (ORD), U.S. Environmental Protection Agency (EPA), Cincinnati, Ohio, USA; [2]School of Osteopathic Medicine, Campbell University, Lillington, North Carolina, USA; [3]ASPPH/EPA Environmental Health Fellowship Program, hosted by NCEA, ORD, U.S. EPA, Cincinnati, Ohio, USA; [4]Radiation Oncology, Rutgers Cancer Institute of New Jersey, New Brunswick, New Jersey, USA; [5]National Health and Environmental Effects Research Laboratory, ORD, U.S. EPA, Research Triangle Park, North Carolina, USA

Background: Epidemiological studies suggest that women exposed to disinfection by-products (DBPs) have an increased risk of delivering babies with cardiovascular defects (CVDs).

Objective: We examined nine CVDs in relation to categorical DBP exposures including bromoform, chloroform, dibromochloromethane (DBCM), bromodichloromethane (BDCM), monobromoacetic acid (MBAA), dichloroacetic acid (DCAA), trichloroacetic acid (TCAA), and summary DBP measures (HAA5, THMBr, THM4, and DBP9).

Methods: We calculated adjusted odds ratios (aORs) in a case–control study of birth defects in Massachusetts with complete quarterly 1999–2004 trihalomethane (THM) and haloacetic acid (HAA) data. We randomly matched 10 controls each to 904 CVD cases based on week of conception. Weight-averaged aggregate first-trimester DBP exposures were assigned to individuals based on residence at birth.

Results: We detected associations for tetralogy of Fallot and the upper exposure categories for TCAA, DCAA, and HAA5 (aOR range, 3.34–6.51) including positive exposure–response relationships for DCAA and HAA5. aORs consistent in magnitude were detected between atrial septal defects and bromoform (aOR = 1.56; 95% CI: 1.01, 2.43), as well as DBCM, chloroform, and THM4 (aOR range, 1.26–1.67). Ventricular septal defects (VSDs) were associated with the highest bromoform (aOR = 1.85; 95% CI: 1.20, 2.83), MBAA (aOR = 1.81; 95% CI: 0.85, 3.84), and DBCM (aOR = 1.54; 95% CI: 1.00, 2.37) exposure categories.

Conclusions: To our knowledge, this is the first birth defect study to develop multi-DBP adjusted regression models as well as the first CVD study to evaluate HAA exposures and the second to evaluate bromoform exposures. Our findings, therefore, inform exposure specificity for the consistent associations previously reported between THM4 and CVDs including VSDs.

Citation: Wright JM, Evans A, Kaufman JA, Rivera-Núñez Z, Narotsky MG. 2017. Disinfection by-product exposures and the risk of specific cardiac birth defects. Environ Health Perspect 125:269–277; http://dx.doi.org/10.1289/EHP103

Introduction

Cardiovascular defects (CVDs) are the most common type of birth defect, with an estimated incidence in the United States of 8 in 1,000 births (Go et al. 2013). CVDs can lead to a higher infant mortality rate among newborns, and their etiology is often unknown (Kurinczuk et al. 2010; Lee et al. 2001). Some environmental hazards are known teratogens, such as methylmercury and radiation, but the existing evidence for associations between drinking-water contaminants and birth defects is mixed (Brent and Beckman 1990; Nieuwenhuijsen et al. 2009). Although the risk of CVDs in relation to specific disinfection by-products (DBPs) remains unclear, there is some evidence for associations between CVDs and a summary measure of trihalomethanes (THMs) called THM4 [i.e., sum of chloroform, bromoform, bromodichloromethane (BDCM), and dibromochloromethane (DBCM)]. Nieuwenhuijsen et al. (2009) conducted a meta-analysis of 5 case–control studies and 10 retrospective cohort studies using THM concentration data or less direct exposure measures (e.g., treatment type/source water). The authors reported a small but not statistically significant odds ratio of 1.16 [95% confidence interval (CI): 0.98, 1.37] for major CVDs among those with high DBP exposures. A prospective cohort study from Lithuania based on first-trimester internal DBP dose estimates showed elevated odds ratios for CVDs, with exposure–response relationships detected for THM4, BDCM, and chloroform tertiles (Grazuleviciene et al. 2013). Slightly elevated odds ratios were noted in a study from England of major CVDs and the sum of three brominated THMs (i.e., THMBr) ≥ 20 versus < 10 μg/L [adjusted odds ratio (aOR) = 1.13; 95% CI: 0.93, 1.37] and between bromoform ≥ 4 versus < 2 μg/L (aOR = 1.18; 95% CI: 1.00, 1.39) and a restricted group of major CVDs (Nieuwenhuijsen et al. 2008). Stronger associations (aOR = 1.62; 95% CI: 1.04, 2.51) have also been reported for CVDs and THM4 ≥ 130 versus < 60 μg/L in an Australian population using heavily brominated water (Chisholm et al. 2008). Studies with rats exposed to brominated THMs were negative for CVDs (Christian et al. 2001; Ruddick et al. 1983); however, one study examining monobromoacetic acid (MBAA) exposure reported increased incidence of CVDs (Randall et al. 1991). Another study in rats reported CVDs [e.g., ventricular septal defect (VSD), levocardia, right-sided aortic arch, and ductus arteriosus] following exposure to bromochloroacetonitrile (Christ et al. 1995).

The strongest and most consistent associations reported in epidemiological studies of birth defects and DBPs have been for VSDs. Similar to an earlier meta-analysis by Hwang et al. (2008), Nieuwenhuijsen et al. (2009) found a consistent excess risk for VSDs (OR = 1.59; 95% CI: 1.21, 2.07) in three studies using various THM and chlorinated water exposure measures (OR range:

Address correspondence to J.M. Wright, U.S. EPA, National Center for Environmental Assessment, 26 W. Martin Luther King Dr. (MS-A110), Cincinnati, OH 45268 USA. Telephone: (513) 569-7922. E-mail: wright.michael@epa.gov

Supplemental Material is available online (http://dx.doi.org/10.1289/EHP103).

We thank the Massachusetts Department of Environmental Protection, the Massachusetts Department of Public Health, the Massachusetts Water Resource Authority, and other public water utilities for their assistance with the data collection efforts. We also acknowledge the data management efforts of A. Meyer as well as the Technical Support Services staff assistance provided by Highlight Technologies.

A.E. was supported through the Oak Ridge Institute of Science and Education Research Participation Program (agreement no. DW8992376701) sponsored by the U.S. EPA. J.A.K. was supported by cooperative agreement no. X3-83555301 from the U.S. EPA and the Association of Schools and Programs of Public Health (ASPPH). Z.R.-N. was supported through The National Academies, Research Associateship Programs sponsored by the U.S. EPA.

The views expressed in this manuscript are those of the authors and do not necessarily reflect the views or policies of the U.S. EPA or the ASPPH.

The authors declare they have no actual or potential competing financial interests.

Received: 11 March 2016; Revised: 2 June 2016; Accepted: 14 July 2016; Published: 12 August 2016.

Note to readers with disabilities: *EHP* strives to ensure that all journal content is accessible to all readers. However, some figures and Supplemental Material published in *EHP* articles may not conform to 508 standards due to the complexity of the information being presented. If you need assistance accessing journal content, please contact ehponline@niehs.nih.gov. Our staff will work with you to assess and meet your accessibility needs within 3 working days.

1.43–1.81). An earlier study, not included in the published meta-analyses, did not report associations between THM exposure and VSD (Bove et al. 1995). A more recent Italian study also did not show an increased risk of VSD for chlorine dioxide DBPs, including chlorite and chlorate (Righi et al. 2012).

Exposure assessment limitations in epidemiological studies remain a critical challenge in evaluating causality in reported associations between DBPs and various reproductive outcomes given limited spatial and temporal resolution of monitoring data and the lack of direct exposure measures. Previous epidemiological studies of CVDs have not examined exposures beyond THMs and chlorine dioxide DBPs. This remains a key limitation given that animal developmental toxicity studies of THMs are generally negative for teratogenicity (Graves et al. 2001) and that the THMs may be poor surrogates for complex DBP mixtures in chlorinated drinking-water systems. Furthermore, although haloacetic acids (HAAs) have not been examined in epidemiological studies of CVDs and DBPs to date, toxicological studies in rats have shown increased incidence of VSDs and conotruncal defects following exposure to dichloroacetic acid (DCAA) and trichloroacetic acid (TCAA) (Epstein et al. 1992; Johnson et al. 1998; Smith et al. 1989, 1992). Most epidemiological studies of DBPs also have limited exposure contrasts and insufficient statistical power to detect rare outcomes like CVDs. This may preclude the ability to detect statistically significant associations that are small in magnitude and to examine exposure–response relationships for individual CVDs and specific DBP species. To address some of these exposure assessment limitations and expand the scope of the birth defect and DBP combinations that have been previously examined, we assessed the risk of CVDs in relation to weighted first-trimester exposure estimates for nine individual DBPs and four DBP mixture surrogates.

Methods

Study Population

We conducted a case–control study of CVD cases in 68 Massachusetts towns with populations > 500 with complete THM4, HAA5 [i.e., sum of monochloroacetic acid (MCAA), DCAA, TCAA, MBAA, and dibromoacetic acid (DBAA)], water source and disinfection data from 1999 to 2004. We restricted the analysis to nonchromosomal congenital anomalies of the heart and circulatory system (n = 904 cases) and individually matched 10 controls per each case randomly selected (without replacement) from all live births in Massachusetts based on week of conception, for a total study population of 9,944.

Outcome Data

Birth records from 2000 through 2004 were provided by the Massachusetts Department of Public Health and the Massachusetts Birth Defects Monitoring Program. The Massachusetts birth defect registry system collects data from 53 birthing hospitals, 1 tertiary care and 1 specialty hospital in Massachusetts, and 1 Rhode Island birth hospital and 1 Rhode Island tertiary care hospital near the border of these two states. The registry system uses various data sources to ascertain and verify cases including birth certificates, fetal and infant death certificates, hospital discharge reports, hospital nurseries and neonatal units, and hospital surgical and pathology departments. This research was based on birth records data that did not contain personal identifiable information; therefore, institutional review board approval was not obtained nor was informed consent necessary because potential risk was considered to be minimal and no direct contact with study subjects occurred.

Birth defect cases were diagnosed up to age 1 year. Both cases and controls were singleton live births who weighed at least 350 g and were between 22 and 44 gestational weeks. Cases were identified based on the *International Classification of Diseases, 9th Revision* (ICD-9). These included atrial septal defect (ASD; ICD-9 code 745.5), VSD (745.4), pulmonary stenosis (746.02), tetralogy of Fallot (TOF; 745.2), and transposition of the great arteries (TGA; 745.10, 745.11, 745.12, 745.19). We also examined birth defect group combinations including all congenital anomalies of the heart and circulatory system (All CVD; 745–747), and conotruncal heart defects (745.0, 745.10, 745.11, 745.12, 745.2). Gestational age was derived from clinical estimates according to birth records and was subtracted from date of birth to determine week of conception for matching purposes.

Exposure Assessment

We linked town-level drinking-water source, disinfection treatment, and DBP data based on quarterly sampling (1999–2004) to birth records by town of residence and month of birth. The exposure data were supplied by the Massachusetts Department of Environmental Protection and individual public water utilities. Exposures were estimated for specific DBPs as well as summary measures of DBP mixtures including THM4, HAA5, DBP9 (i.e., sum of THM4 and HAA5), and THMBr. We categorized maternal DBP exposure levels for the summary and individual DBP measures into tertiles, quartiles, or quintiles based on the distribution of the available data. Due to a paucity of occurrence data, MCAA was dichotomized at the 97.5th percentile (0.04 µg/L), and bromoform (0.26 µg/L), DBCM (0.47 µg/L), and DBAA (1.53 µg/L) were dichotomized at the upper decile. Births in the lowest DBP exposure category served as the referent for comparison with the upper categories. This categorical approach allowed for evaluation of nonlinear relationships and potential effect measure modification using stratified analyses.

We averaged first-trimester DBP exposures across all sample locations within a public drinking-water system based on quarterly monitoring data assigned to maternal ZIP codes for place of residence at birth. The first-trimester DBP exposure scores were derived from the month of birth of the study participants and the timing of quarterly DBP samples with weighted averages calculated proportionally for multiple quarters that overlapped the first trimester. For example, an infant of 38 gestational weeks born in January of 2000 would have 2 first-trimester weeks that occurred in quarter 1 of 1999 and the remaining 11 weeks occurring in quarter 2 of 1999. Thus, their corresponding exposure score would be as follows: (0.15 times the DBP concentration for quarter 1 of 1999) + (0.85 times the DBP concentration for quarter 2 of 1999). In addition, residents relying on untreated groundwater (e.g., private wells) were assigned DBP concentrations of zero.

Statistical Analysis

SAS (version 9.4; SAS Institute, Inc., Cary, NC) was used for the statistical analysis. We used Spearman correlation coefficients to compare the summary and individual DBP measures. Statistical significance was based on $\alpha \leq 0.05$. We used conditional logistic regression to estimate aORs and 95% CIs for each of the DBP exposure categories. Given the extensive amount of available covariate data, we used a change-in-estimate approach (> 10% change) to identify confounding variables. These covariates included type of water source and treatment, infant sex, infant birth weight, maternal weight gain, maternal race, maternal age, maternal education, marital status (not married vs. married, including within 300 days before birth), maternal smoking (cigarettes/day during pregnancy), parity, number of previous terminations, prenatal care source payment type, income, and various clinical factors (e.g., abruptio placenta, anemia, cardiac disease, chronic or gestational diabetes, chronic or gestational hypertension, eclampsia, hemoglobinopathy, hepatitis, hydramnios/oligohydramnios, incompetent cervix, labor/delivery complication, labor induction, lung disease, lupus, other maternal reproductive risk factors, pharmaceutical inhibition of labor, previous infant > 4,000 g, previous infant with birth defect,

previous premature or small-for-gestational-age infant, premature or prolonged rupture of membrane, renal disease, Rh sensitization, rubella infection, seizure disorder, sickle cell anemia, uterine bleeding). We examined a categorical health index (values ranging from 0 to 5) that included presence of hydramnios/oligohydramnios, chronic hypertension, gestational hypertension, gestational diabetes, and nongestational diabetes. We also evaluated adequacy of prenatal care by the Kotelchuck Index (Kotelchuck 1994), which integrates information on the timing (i.e., first trimester vs. later during pregnancy) of initiation of prenatal care and the number of prenatal visits (< 9, 9–11, 12, 13–15, > 15) from when prenatal care began until delivery. These two individual prenatal covariate constituents were examined separately as confounders, as well as part of the Kotelchuck Index.

All of the covariates were based on the individual-level data obtained from birth records except for income and DBP data, as well as the information on type of water source and type of water treatment. Median household income for maternal residence at birth were obtained from the 2000 U.S. Census (Geolytics, Inc., East Brunswick, NJ). Aggregate-level income covariates were examined at three spatial scales: town, ZIP code, and census tract. We created a socioeconomic status index based on ZIP code–level income data combined with mother's highest education level and prenatal care source of payment. The results presented here are also based on multi-pollutant models by adjusting for THM4 in all of the HAA models and adjusting for HAA5 in the THM models. Effect measure modification by infant sex was examined by stratification for the outcome and DBPs with most consistent and largest aORs (i.e., TOF and VSDs). We conducted a sensitivity analysis of the impact of multiple birth defects, as well as an analysis of the All CVD category excluding patent ductus arteriosus.

Results

Among all reported births from 2000 to 2004 in Massachusetts, there were 904 (45% of the total birth defects) CVDs. The most common CVDs were ASDs (41%) and VSDs (37%). Forty-three percent (n = 390) of the birth defects examined here were isolated CVDs, whereas 57% (n = 514) of the cases had multiple defects. Among the 514 cases with multiple defects, 377 (73%) of them were CVDs only. As shown in Table 1, cases and controls were similar across most study characteristics, with minor exceptions noted for health index scores and the Kotelchuck Index for adequacy of prenatal care. Controls were more likely to be born to healthier mothers based on our health index score.

As shown in Table 2, median and interquartile ranges (μg/L) for the nine predominant DBP metrics were as follows: DBP9 (69.6; 44.1–92.1), THM4 (44.5; 29.3–61.4), chloroform (36.1; 17.4–51.0), THMBr (6.8; 4.8–10.2), BDCM (6.1; 4.5–8.4), DBCM (0.6; 0–1.6), HAA5 (22.4; 11.3–31.2), TCAA (11.0; 5.4–16.3), and DCAA (10.4; 5.3–13.7). We observed Spearman correlation coefficients ≥ 0.9 for the following: DBP9 with THM4, HAA5, and chloroform; HAA5 with TCAA and DCAA; THM4 with chloroform; and THMBr with BDCM (see Table S1). We observed correlations between 0.7 and 0.9 for the following: DBP9 with TCAA and DCAA; HAA5 with THM4 and chloroform; THM4 with TCAA and CCAA; DBCM with BDCM and THMBr; chloroform with TCAA and DCAA; and TCAA with DCAA. The strongest correlations among the individual brominated species were found between DBCM and BDCM

Table 1. Study characteristics of cardiovascular defect (CVD) cases and controls [n (%)].

Characteristic	Study population	Cases	Controls
Total births	9,944 (100)	904 (100)	9,040 (100)
Infant sex			
Male	5,119 (51.5)	468 (51.8)	4,651 (51.4)
Female	4,825 (48.5)	436 (48.2)	4,389 (48.6)
Maternal age (years)			
≤ 20	907 (9.1)	82 (9.1)	825 (9.1)
> 20–25	1,733 (17.4)	169 (18.7)	1,564 (17.3)
> 25–30	2,648 (26.6)	223 (24.7)	2,425 (26.8)
> 30–35	3,008 (30.3)	273 (30.2)	2,735 (30.3)
> 35–40	1,384 (13.9)	122 (13.5)	1,262 (14.0)
> 40	264 (2.7)	35 (3.9)	229 (2.5)
Maternal race			
White	6,614 (66.6)	589 (65.2)	6,025 (66.6)
African American	995 (10.0)	114 (12.6)	881 (9.7)
Asian	747 (7.5)	53 (5.9)	694 (7.7)
American Indian	22 (0.2)	5 (0.6)	17 (0.2)
Other	1,561 (15.7)	143 (15.8)	1,418 (15.7)
Maternal education			
Below high school graduate/GED	1,166 (11.7)	119 (13.2)	1,047 (11.6)
High school graduate/GED	2,689 (27.0)	244 (27.0)	2,445 (27.0)
Some college or associates/technical degree	2,076 (20.9)	184 (20.4)	1,892 (20.9)
College or higher	4,013 (40.4)	357 (39.5)	3,656 (40.4)
Marital status			
Married	6,886 (69.3)	602 (66.6)	6,284 (69.5)
Unmarried	3,041 (30.6)	300 (33.2)	2,741 (30.3)
Missing	17 (0.2)	2 (0.2)	15 (0.2)
Number of previous births			
0	4,508 (45.4)	413 (45.7)	4,095 (45.3)
1	3,269 (32.9)	287 (31.7)	2,982 (33.0)
≥ 2	2,154 (21.7)	204 (22.6)	1,950 (21.6)
Maternal weight gain during pregnancy (lb)			
< 0	112 (1.1)	14 (1.5)	98 (1.1)
0–25	3,867 (39.1)	365 (40.4)	3,502 (38.7)
25–50	5,557 (56.2)	489 (54.1)	5,068 (56.1)
> 50	354 (3.6)	30 (3.3)	324 (3.6)
Maternal smoking during pregnancy (no. of cigarettes/day during pregnancy)			
0	9,165 (92.2)	830 (91.8)	8,335 (92.2)
1–5	327 (3.3)	22 (2.4)	305 (3.4)
6–10	289 (2.9)	34 (3.8)	255 (2.8)
> 10	163 (1.6)	18 (2.0)	145 (1.6)
Prenatal care adequacy (Kotelchuck Index)			
No prenatal care	48 (0.5)	6 (0.7)	42 (0.5)
Inadequate	886 (8.9)	92 (10.2)	794 (8.8)
Intermediate	713 (7.2)	41 (4.5)	672 (7.4)
Adequate	4,583 (46.1)	386 (42.7)	4,197 (46.4)
Adequate plus	3,714 (37.4)	379 (41.9)	3,335 (36.9)
Prenatal care source of payment			
Public	2,611 (26.3)	277 (30.6)	2,334 (25.8)
Private	6,556 (65.9)	566 (62.6)	5,990 (66.3)
Other	777 (7.8)	61 (6.7)	716 (7.9)
Median household income (based on ZIP code from 2000)			
$12,307–36,836	2,492 (25.1)	249 (27.5)	2,243 (24.8)
> $36,836–45,654	2,303 (23.2)	215 (23.8)	2,088 (23.1)
> $45,654–57,815	2,524 (25.4)	219 (24.2)	2,305 (25.5)
> $57,815–153,918	2,625 (26.4)	221 (24.4)	2,404 (26.6)

Note: GED, General Educational Development.

(r = 0.6) and DBAA (r = 0.4), as well as between bromoform and DBCM (r = 0.5) and DBAA (r = 0.3).

We did not detect an increased risk for the overall CVD group (i.e., All CVD) and first-trimester THM4 exposures, but there was a statistically significant association for dichotomized bromoform exposures (aOR = 1.43; 95% CI: 1.10, 1.86) and increased risks in the upper two DCAA quartiles (aOR range, 1.21–1.23) and upper three HAA5 quintiles (aOR range, 1.18–1.42) (Table 3). We saw consistent evidence of associations for conotruncal defects in the upper three HAA quintiles (aOR range, 1.77–3.76) and the upper three TCAA quartiles (aOR range, 1.95–2.13). We detected stronger associations for TOF and the upper exposure categories for TCAA, DCAA, and HAA5 (aOR range, 3.34–6.51) including positive exposure–response relationships for DCAA and HAA5. We detected statistically significant associations for TGA and bromoform exposure (aOR = 2.42; 95% CI: 1.12, 5.23) and for the two intermediate HAA5 quintiles (aOR range, 4.26–4.54); the upper quintile was limited by a small number of cases (n = 9). Inverse associations among the upper exposure categories were detected between TGA and DBP9 and between TOF and chloroform, BDCM, THMBr, and THM4.

Increased aORs were detected for pulmonary stenosis and bromoform exposures (aOR = 2.66; 95% CI: 1.30, 5.43), the upper two DCAA quartiles (aOR range, 1.65–2.02), as well as a positive exposure–response relationship for TCAA (aOR range, 1.47–3.45) (Table 4). aORs consistent in magnitude were detected for ASDs and bromoform (aOR = 1.56; 95% CI: 1.01, 2.43), DBCM (aOR = 1.26; 95% CI: 0.81, 1.97), and for each THM4 (aOR range, 1.28–1.59) and chloroform quintile (aOR range, 1.38–1.67).

Consistent elevated aORs were detected for VSDs and every DBP metric except chloroform, TCAA, and HAA5 (Table 4). aORs were comparable between VSDs and each THM4 (aOR range, 1.39–1.77) and DBP9 (aOR range, 1.33–1.70) quintile. Although not statistically significant, aORs smaller in magnitude were noted between VSDs and the highest BDCM tertile (aOR = 1.21; 95% CI: 0.79, 1.85), the upper THMBr quintile (aOR = 1.34; 95% CI: 0.73, 2.46), and the upper DCAA quartiles (aOR = 1.18; 95% CI: 0.65, 2.14). The strongest associations for VSDs and brominated DBPs were found for bromoform (aOR = 1.85; 95% CI: 1.20, 2.83), MBAA (aOR = 1.81; 95% CI: 0.85, 3.84), and DBCM (aOR = 1.54; 95% CI: 1.00, 2.37).

When we examined the most consistent associations (i.e., TOF and VSDs) for potential effect measure modification by infant sex, no discernible patterns were seen between HAA5 quintiles and TOF. Larger aORs were detected among females for TOF and DCAA, whereas males had higher aORs for TCAA exposures (see Table S2). The aORs for MBAA and VSDs were three times higher among males, with smaller increases detected among males for bromoform, DBCM, and MCAA (see Table S3). aORs for the remaining DBP measures (DBP9, THM4, THMBr, BDCM, and chloroform) were considerably larger among females, including some relationships that were largely null for VSDs in the main analysis (e.g., BDCM and chloroform).

Discussion

Unlike a recent study and meta-analysis, we did not see any evidence for associations between first-trimester THM4 exposures and the All CVD group (Grazuleviciene et al. 2013; Nieuwenhuijsen et al. 2009). The strongest association that we detected for individual DBPs and All CVD was for dichotomized bromoform exposures > 0.26 μg/L (aOR = 1.43; 95% CI: 1.10, 1.86). This is higher than that of the only other study published to date to examine bromoform by Nieuwenhuijsen et al. (2008), who found an aOR of 1.18 (95% CI: 1.00, 1.39) for a subset of etiologically similar cardiac defects and bromoform levels ≥ 4 μg/L (vs. < 2 μg/L). Given that CVDs are a heterogeneous group of outcomes with different underlying mechanisms and etiologies, our primary focus was to examine individual CVDs and etiologically relevant groups in relation to DBPs.

We detected positive exposure–response relationships between TCAA exposure and pulmonary stenosis. The strongest associations that we detected were for the conotruncal defects including TGA and TOF, although the only statistically significant association for TGA was detected for bromoform exposures (aOR = 2.42; 95% CI: 1.12, 5.23). Stronger associations were detected between TOF and the upper exposure categories for TCAA, DCAA, and HAA5 (aOR range, 3.34–6.51) including exposure–response relationships for DCAA and HAA5. These findings are consistent with animal data showing CVDs following TCAA and DCAA exposures (Epstein et al. 1992; Johnson et al. 1998; Smith et al. 1989, 1992). The only epidemiological study of DBPs to examine conotruncal defects as a group saw some suggestion of increased risk only for THM4 exposures (aOR = 1.5; 95% CI: 0.67, 3.50 for 50–74 vs. 0 μg/L), although they did not have sufficient data to examine bromoform or HAA exposures (Shaw et al. 2003). A study in Norway examined TOF and THM4, but their data were hampered by very small cell sizes and a limited exposure contrast (Hwang et al. 2008). We also detected elevated aORs for ASDs and bromoform exposures (aOR = 1.56; 95% CI: 1.01, 2.43) and across every chloroform quintile (aOR range, 1.38–1.67). The magnitude of these associations are consistent with the only other study to examine ASDs, although that study was based on very small sample sizes across THM4 quartiles (Hwang et al. 2008).

Similar to a meta-analysis (OR = 1.59, 95% CI: 1.21, 2.07) by Nieuwenhuijsen et al. (2009), we found consistently elevated aORs (aOR range, 1.39–1.77) for VSD across all exposure THM4 quintiles (beginning at concentrations of 23.05 μg/L) with an aOR of 1.57 (95% CI: 0.70, 3.53) for high THM4 exposures (> 65.27 vs. ≤ 23.05 μg/L). In concordance with two previous VSD studies that evaluated THM4 exposures in the United Kingdom (aOR = 1.43; 95% CI: 1.0, 2.04 for > 60 vs. < 30 μg/L) and Norway (aOR = 1.81; 0.98–3.35 for > 20 vs. ≤ 4 μg/L), our studies add to the consistency reported in epidemiological studies of THMs and VSDs published to date (Hwang et al. 2008; Nieuwenhuijsen et al. 2008). We also saw consistent evidence of associations between VSD and various

Table 2. First-trimester disinfection by-product (DBP) (μg/L) exposure levels for the study population.

DBP metric	Mean ± SD	25th %	50th %	75th %	90th %	95th %	Maximum
DBP9	65.07 ± 36.49	44.14	69.57	92.14	107.8	117.03	181.59
THM4	42.67 ± 24.05	29.26	44.53	61.37	72.71	76.63	125.32
THMBr	8.28 ± 6.51	4.75	6.75	10.17	17.87	21.20	42.48
Chloroform	34.39 ± 21.56	17.38	36.07	51.03	62.65	67.15	98.99
BDCM	6.85 ± 5.05	4.47	6.12	8.36	13.04	16.35	37.38
DBCM	1.32 ± 2.01	0.00	0.56	1.57	3.97	5.98	14.53
Bromoform	0.12 ± 0.46	0.00	0.00	0.00	0.26	0.86	7.06
HAA5	22.40 ± 14.89	11.34	22.38	31.18	42.52	47.49	100.00
TCAA	11.53 ± 8.42	5.40	11.01	16.30	22.16	26.37	73.39
DCAA	9.90 ± 6.61	5.30	10.38	13.67	18.61	21.29	38.89
MCAA	0.83 ± 3.05	0.00	0.05	0.84	1.53	2.13	62.39
DBAA	0.17 ± 0.70	0.00	0.00	0.00	0.47	1.06	21.78
MBAA	0.02 ± 0.26	0.00	0.00	0.00	0.00	0.00	10.63

Note: %, percentile; DBP9, sum of chloroform, bromodichloromethane (BDCM), dibromochloromethane (DBCM), bromoform, monochloroacetic acid (MCAA), dichloroacetic acid (DCAA), trichloroacetic acid (TCAA), monobromoacetic acid (MBAA), and dibromoacetic acid (DBAA); HAA5, sum of MCAA, DCAA, TCAA, MBAA, and DBAA; THM4, sum of chloroform, BDCM, DBCM, and bromoform; THMBr, sum of BDCM, DBCM, and bromoform.

brominated DBP exposure metrics, with the strongest associations noted for bromoform, MBAA, and DBCM (aOR range; 1.54–1.85). The bromoform (aOR = 1.85; 95% CI: 1.20, 2.83) and VSD associations are stronger than those of the only study to examine bromoform exposures (aOR = 1.27; 95% CI: 0.89, 1.82) in relation to isolated VSDs (Nieuwenhuijsen et al. 2008). In our study, bromoform was consistently associated with elevated aORs for all the individual and group CVDs examined. These findings help inform the specificity of reported associations with DBPs and may explain some of the consistent results noted in previous studies for THM4 exposures.

A key study strength was our ability to evaluate numerous individual and summary

Table 3. Adjusted odds ratios (aORs) between disinfection by-product (DBP) exposures and congenital anomalies of the heart and circulatory system (All CVD), conotruncal heart defects, transposition of the great arteries (TGA), and tetralogy of Fallot (TOF).

	All CVD[c]		Conotruncal[d]		TGA[e]		TOF[f]	
DBP metrics (μg/L)[a]	Cases[b] (*n*)	aOR (95% CI)	Cases[b] (*n*)	aOR (95% CI)	Cases[b] (*n*)	aOR (95% CI)	Cases[b] (*n*)	aOR (95% CI)
THM4[g]								
> 23.05–38.05	184	1.04 (0.72, 1.51)	37	0.96 (0.43, 2.14)	21	1.70 (0.58, 4.95)	17	0.32 (0.10, 1.05)
> 38.05–50.41	188	1.02 (0.67, 1.54)	45	1.19 (0.50, 2.82)	26	1.87 (0.57, 6.08)	19	0.51 (0.15, 1.74)
> 50.41–65.27	192	1.04 (0.67, 1.62)	32	0.68 (0.27, 1.74)	13	1.02 (0.28, 3.82)	19	0.31 (0.08, 1.21)
> 65.27–125.32	167	0.81 (0.51, 1.31)	31	0.50 (0.17, 1.48)	15	0.81 (0.17, 3.84)	16	0.19 (0.04, 0.88)
THMBr[g]								
> 4.17–6.04	173	0.99 (0.65, 1.51)	39	0.72 (0.32, 1.60)	14	0.45 (0.13, 1.61)	25	1.00 (0.34, 2.98)
> 6.04–7.80	195	1.05 (0.71, 1.55)	39	0.60 (0.27, 1.30)	26	0.98 (0.35, 2.74)	12	0.23 (0.06, 0.91)
> 7.80–11.51	176	0.97 (0.66, 1.42)	32	0.47 (0.21, 1.02)	14	0.49 (0.16, 1.49)	18	0.45 (0.14, 1.39)
> 11.51–42.48	188	1.02 (0.71, 1.46)	34	0.39 (0.19, 0.80)	19	0.55 (0.20, 1.51)	16	0.26 (0.09, 0.76)
Chloroform[g]								
> 12.07–29.99	181	1.05 (0.73, 1.50)	33	1.22 (0.56, 2.65)	19	1.49 (0.53, 4.24)	14	0.50 (0.16, 1.53)
> 29.99–42.17	197	1.03 (0.68, 1.55)	46	1.46 (0.62, 3.47)	25	1.69 (0.52, 5.50)	21	0.76 (0.22, 2.69)
> 42.17–55.41	184	0.94 (0.60, 1.47)	37	1.42 (0.53, 3.79)	15	1.28 (0.33, 4.95)	22	0.81 (0.20, 3.29)
> 55.41–98.99	167	0.77 (0.47, 1.25)	29	0.63 (0.21, 1.93)	15	0.55 (0.11, 2.83)	14	0.33 (0.07, 1.64)
Bromodichloromethane (BDCM)[g]								
> 4.95–7.55	325	0.97 (0.73, 1.28)	61	0.73 (0.40, 1.34)	36	0.83 (0.37, 1.86)	24	0.49 (0.19, 1.24)
> 7.55–37.38	286	0.93 (0.72, 1.19)	51	0.49 (0.29, 0.82)	24	0.57 (0.27, 1.22)	28	0.38 (0.17, 0.82)
Dibromochloromethane (DBCM)[g]								
> 3.93–14.53	87	1.01 (0.77, 1.33)	16	0.68 (0.36, 1.29)	10	1.01 (0.43, 2.39)	7	0.54 (0.20, 1.41)
Bromoform[g]								
> 0.26–7.06	109	1.43 (1.10, 1.86)	25	1.30 (0.72, 2.33)	16	2.42 (1.12, 5.23)	10	1.14 (0.45, 2.87)
HAA5[h]								
> 8.17–19.33	160	0.99 (0.69, 1.42)	38	1.18 (0.53, 2.66)	17	0.86 (0.28, 2.64)	21	2.13 (0.53, 8.65)
> 19.33–25.79	219	1.42 (0.95, 2.12)	49	3.19 (1.29, 7.89)	29	4.54 (1.26, 16.41)	21	4.98 (1.02, 24.35)
> 25.79–33.97	172	1.35 (0.87, 2.10)	37	3.76 (1.38, 10.24)	19	4.26 (1.02, 17.87)	17	5.88 (1.06, 32.57)
> 33.97–100.00	174	1.18 (0.75, 1.86)	24	1.77 (0.63, 4.97)	9	1.10 (0.23, 5.37)	16	6.51 (1.23, 34.59)
Trichloroacetic acid (TCAA)[h]								
> 5.23–11.09	234	1.17 (0.86, 1.60)	59	2.09 (1.02, 4.29)	30	1.38 (0.53, 3.56)	28	2.72 (0.91, 8.13)
> 11.09–16.38	237	1.11 (0.76, 1.62)	44	2.13 (0.89, 5.14)	22	1.39 (0.40, 4.80)	22	4.30 (1.09, 16.88)
> 16.38–73.39	208	1.03 (0.69, 1.55)	36	1.95 (0.77, 4.92)	18	1.07 (0.29, 3.86)	19	3.89 (0.97, 15.66)
Dichloroacetic acid (DCAA)[h]								
> 5.18–10.44	219	1.04 (0.78, 1.40)	48	1.07 (0.57, 2.04)	27	0.96 (0.41, 2.23)	22	1.39 (0.50, 3.88)
> 10.44–13.85	241	1.21 (0.86, 1.70)	52	1.60 (0.76, 3.36)	28	1.21 (0.43, 3.41)	24	3.08 (0.92, 10.34)
> 13.85–38.89	220	1.23 (0.85, 1.78)	34	1.16 (0.50, 2.70)	12	0.50 (0.14, 1.77)	21	3.34 (0.90, 12.43)
Monochloroacetic acid (MCAA)[h]								
> 1.53–62.39	84	1.06 (0.80, 1.40)	9	0.85 (0.41, 1.77)	6	1.10 (0.43, 2.77)	4	0.83 (0.27, 2.54)
Monobromoacetic acid (MBAA)[h]								
> 0.04–10.63	24	1.17 (0.66, 2.07)	4	0.77 (0.17, 3.48)	1	0.47 (0.06, 3.97)	3	0.80 (0.08, 7.48)
Dibromoacetic acid (DBAA)[h]								
> 0.47–21.78	73	0.81 (0.61, 1.08)	19	0.72 (0.39, 1.33)	11	0.96 (0.41, 2.26)	7	0.59 (0.23, 1.54)
DBP9								
> 33.07–59.95	187	1.37 (0.95, 1.97)	37	1.11 (0.52, 2.37)	21	1.22 (0.45, 3.31)	17	0.80 (0.24, 2.63)
> 59.95–79.13	196	1.30 (0.87, 1.92)	49	1.12 (0.51, 2.49)	24	0.87 (0.29, 2.61)	24	1.15 (0.32, 4.08)
> 79.13–97.67	194	1.37 (0.92, 2.05)	36	1.23 (0.54, 2.78)	19	1.02 (0.34, 3.11)	18	1.39 (0.39, 5.01)
> 97.67–181.59	160	0.96 (0.63, 1.46)	24	0.36 (0.14, 0.95)	10	0.08 (0.01, 0.46)	14	0.94 (0.23, 3.79)

Note: CI, confidence interval; DBP9, sum of chloroform, BDCM, DBCM, bromoform, MCAA, DCAA, TCAA, MBAA, and DBAA; HAA5, sum of MCAA, DCAA, TCAA, MBAA, and DBAA; THM4, sum of chloroform, BDCM, DBCM, and bromoform; THMBr, sum of BDCM, DBCM, and bromoform.

[a]For each DBP metric, the referent for each model includes exposure scores of zero up to the lower bound of the lowest exposure category.

[b]The numbers represent the case distribution across exposure groups before modeling.

[c]Models adjusted for the type of water source and treatment, infant birth weight, town-level income quartile, number of prenatal care visits (< 9, 9–11, 12, 13–15, > 15), health index (gestational diabetes, non-gestational diabetes, chronic hypertension, gestational hypertension, and hydramnios/oligohydramnios), and other maternal reproductive risk factors.

[d]Models adjusted for the type of water source and treatment, health index (gestational diabetes, non-gestational diabetes, chronic hypertension, gestational hypertension, and hydramnios/oligohydramnios), and other maternal reproductive risk factors.

[e]Models adjusted for the type of water source and treatment, number of prenatal care visits (< 9, 9–11, 12, 13–15, > 15), ZIP code–level income quartile, trimester prenatal care began (first, after first), health index (gestational diabetes, nongestational diabetes, chronic hypertension, gestational hypertension, and hydramnios/oligohydramnios), and other maternal reproductive risk factors.

[f]Models adjusted for the type of water source and treatment, infant birth weight, ZIP code–level income quartile, trimester prenatal care began (first, after first), health index (gestational diabetes, nongestational diabetes, chronic hypertension, gestational hypertension, and hydramnios/oligohydramnios), and other maternal reproductive risk factors.

[g]Models also include adjustment for HAA5 concentrations.

[h]Models also include adjustment for THM4 concentrations.

DBP exposure metrics, because the limitation of examining THM4 and other surrogates is well established. This is the first study of CVDs to assess alternative DBP mixture surrogates including HAA5 and DBP9. The large sample size and sufficient DBP exposure gradients also enabled examination of individual birth defects in relation to low-exposure referents for various DBP metrics. Statistical power was limited for some less prevalent DBP metrics (e.g., MCAA and MBAA) and the rarest CVDs such as TGA and TOF; this may have precluded detection of statistically significant associations small in magnitude as well as exposure–response relationships. Although we acknowledge that some of the results for different CVD and DBP combinations that were examined may be due to chance, our study does help address specificity of causal associations that have been identified in the toxicological literature.

Based on the extensive number of available covariates, we adjusted for various confounders including strong maternal risk factors for CVDs as well as other exposures related to DBPs, such as water source and disinfection type. This is also the first birth defect study to develop multi-pollutant models to examine potential confounding by other DBP exposures. We used a matched case–control study design to increase statistical efficiency and to control for time-varying confounding. An additional strength of our population-based case–control study is the low risk of selection bias, because the cases and controls were both drawn from the same study base of all underlying births in Massachusetts. We also saw no evidence to suggest that the CVD cases that were not included due to missing data or other exclusion factors were disproportionately exposed to higher or lower DBP concentrations in drinking water.

One of the main limitations in many epidemiological studies of DBPs is the lack of individual-level exposure data which may better reflect internal dose. We relied on routinely monitored data that were collected at least quarterly for all water systems. Given the known seasonality detected for some DBPs such as the THMs, quarterly measures may not fully capture the extent of temporal variability that may influence exposure estimates. For example, the critical *in utero* exposure period for many of the CVDs is during the 3rd through 8th weeks of gestation, but we did not have samples that corresponded exactly with that time period. Thus, our use of first-trimester average DBP exposure may result in exposure misclassification, which we would expect to be nondifferential in nature. Residential mobility may also lead to exposure misclassification if the address reported at birth differed from the first-trimester residence. A review of 14 environmental epidemiological studies of pregnancy outcomes showed that most moves occurred during the second trimester among the 9–32% of pregnant women who reported moving residence (Bell and Belanger 2012). Previous research has shown that these moves are often short in distance, with only 8% of

Table 4. Adjusted odds ratios (aORs) between disinfection by-product (DBP) exposures and atrial septal defects (ASDs), ventricular septal defects (VSDs), and pulmonary stenosis (PS).

	ASD[c]		VSD[d]		PS[e]	
DBP metrics (μg/L)[a]	Cases[b] (*n*)	aOR (95% CI)	Cases[b] (*n*)	aOR (95% CI)	Cases[b] (*n*)	aOR (95% CI)
THM4[f]						
> 23.05–38.05	78	1.31 (0.70, 2.46)	61	1.39 (0.72, 2.69)	24	0.61 (0.23, 1.61)
> 38.05–50.41	72	1.34 (0.67, 2.66)	80	1.77 (0.87, 3.59)	26	0.70 (0.24, 2.04)
> 50.41–65.27	86	1.59 (0.77, 3.26)	73	1.70 (0.80, 3.63)	18	0.35 (0.11, 1.19)
> 65.27–125.32	67	1.28 (0.58, 2.84)	58	1.57 (0.70, 3.53)	24	0.49 (0.14, 1.75)
THMBr[f]						
> 4.17–6.04	78	0.73 (0.35, 1.52)	56	0.81 (0.39, 1.68)	21	0.84 (0.27, 2.63)
> 6.04–7.80	83	1.10 (0.58, 2.09)	73	0.79 (0.41, 1.55)	25	0.65 (0.24, 1.77)
> 7.80–11.51	67	0.99 (0.53, 1.88)	55	0.89 (0.47, 1.69)	24	0.46 (0.16, 1.29)
> 11.51–42.48	76	1.14 (0.63, 2.06)	82	1.34 (0.73, 2.46)	25	0.91 (0.36, 2.29)
Chloroform[f]						
> 12.07–29.99	75	1.38 (0.73, 2.60)	61	1.05 (0.58, 1.90)	27	0.74 (0.29, 1.89)
> 29.99–42.17	86	1.67 (0.83, 3.38)	74	0.86 (0.43, 1.72)	28	0.73 (0.24, 2.27)
> 42.17–55.41	76	1.50 (0.69, 3.26)	75	1.00 (0.47, 2.12)	19	0.40 (0.12, 1.40)
> 55.41–98.99	68	1.42 (0.61, 3.27)	57	0.79 (0.35, 1.80)	20	0.37 (0.10, 1.44)
Bromodichloromethane (BDCM)[f]						
> 4.95–7.55	139	1.19 (0.75, 1.90)	112	0.81 (0.50, 1.31)	39	0.59 (0.29, 1.23)
> 7.55–37.38	111	1.13 (0.74, 1.72)	116	1.21 (0.79, 1.85)	37	0.69 (0.35, 1.37)
Dibromochloromethane (DBCM)[f]						
> 3.93–14.53	36	1.26 (0.81, 1.97)	40	1.54 (1.00, 2.37)	10	0.96 (0.41, 2.25)
Bromoform[f]						
> 0.26–7.06	46	1.56 (1.01, 2.43)	43	1.85 (1.20, 2.83)	20	2.66 (1.30, 5.43)
HAA5[g]						
> 8.17–19.33	61	0.50 (0.28, 0.90)	50	0.66 (0.37, 1.20)	20	0.72 (0.26, 1.98)
> 19.33–25.79	103	0.91 (0.48, 1.74)	74	1.00 (0.51, 1.94)	29	1.34 (0.42, 4.26)
> 25.79–33.97	65	0.63 (0.31, 1.29)	63	1.01 (0.49, 2.08)	24	1.48 (0.41, 5.36)
> 33.97–100.00	65	0.41 (0.19, 0.86)	78	1.02 (0.49, 2.12)	21	1.06 (0.28, 4.06)
Trichloroacetic acid (TCAA)[g]						
> 5.23–11.09	100	0.69 (0.42, 1.15)	81	0.90 (0.55, 1.50)	29	1.47 (0.57, 3.74)
> 11.09–16.38	97	0.58 (0.31, 1.09)	83	0.81 (0.44, 1.51)	32	2.48 (0.82, 7.46)
> 16.38–73.39	79	0.36 (0.18, 0.70)	86	0.79 (0.41, 1.50)	29	3.45 (1.04, 11.39)
Dichloroacetic acid (DCAA)[g]						
> 5.18–10.44	85	0.78 (0.48, 1.28)	72	0.84 (0.51, 1.39)	23	0.93 (0.38, 2.26)
> 10.44–13.85	103	0.88 (0.50, 1.54)	92	1.28 (0.72, 2.25)	40	2.02 (0.74, 5.50)
> 13.85–38.89	89	0.75 (0.41, 1.37)	88	1.18 (0.65, 2.14)	27	1.65 (0.52, 5.22)
Monochloroacetic acid (MCAA)[g]						
> 1.53–62.39	31	1.08 (0.67, 1.73)	35	1.27 (0.81, 1.97)	7	0.49 (0.20, 1.19)
Monobromoacetic acid (MBAA)[g]						
> 0.04–10.63	8	1.17 (0.49, 2.77)	13	1.81 (0.85, 3.84)	1	0.66 (0.08, 5.13)
Dibromoacetic acid (DBAA)[g]						
> 0.47–21.78	27	0.81 (0.50, 1.32)	28	1.00 (0.63, 1.61)	7	0.38 (0.14, 1.02)
DBP9						
> 33.07–59.95	76	1.12 (0.61, 2.08)	58	1.33 (0.71, 2.48)	26	1.12 (0.42, 2.99)
> 59.95–79.13	87	1.46 (0.77, 2.77)	79	1.70 (0.88, 3.26)	26	1.02 (0.35, 2.96)
> 79.13–97.67	84	1.37 (0.71, 2.64)	71	1.64 (0.83, 3.26)	19	0.63 (0.21, 1.93)
> 97.67–181.59	58	0.67 (0.33, 1.35)	63	1.48 (0.73, 2.98)	24	0.79 (0.25, 2.49)

Note: CI, confidence interval; DBP9, sum of chloroform, BDCM, DBCM, bromoform, MCAA, DCAA, TCAA, MBAA, and DBAA; HAA5, sum of MCAA, DCAA, TCAA, MBAA, and DBAA; THM4, sum of chloroform, BDCM, DBCM, and bromoform; THMBr, sum of BDCM, DBCM, and bromoform.

[a]For each DBP metric, the referent for each model includes exposure scores of zero up to the lower bound of the lowest exposure category.

[b]The numbers represent the case distribution across exposure groups before modeling.

[c]Models adjusted for the type of water source and treatment, infant birth weight, health index (gestational diabetes, nongestational diabetes, chronic hypertension, gestational hypertension, and hydramnios/oligohydramnios), and other maternal reproductive risk factors.

[d]Models adjusted for the type of water source and treatment, maternal marital status (married, including within 300 days before birth; not married), maternal education category, maternal race category, health index (gestational diabetes, non-gestational diabetes, chronic hypertension, gestational hypertension, and hydramnios/oligohydramnios), and other maternal reproductive risk factors.

[e]Models adjusted for the type of water source and treatment, ZIP code–level income quartile, trimester prenatal care began (first, after first), category of prenatal care source payment, health index (gestational diabetes, nongestational diabetes, chronic hypertension, gestational hypertension, and hydramnios/oligohydramnios), and other maternal reproductive risk factors.

[f]Models also include adjustment for HAA5 concentrations.

[g]Models also include adjustment for THM4 concentrations.

cases moving to a different county during the pregnancy (Bell and Belanger 2012; Khoury et al. 1988). This suggests that most moves during pregnancy often occur to residences that rely on the same water system. The impact of mobility on our study results is difficult to determine, but a previous study of DBPs and neural-tube defects reported stronger associations among mothers with confirmed residences at conception compared with the overall population of confirmed and unconfirmed residences (Klotz and Pyrch 1999).

In addition to uncaptured temporal variability, measurement error may result in exposure misclassification from the use of town-average DBP estimates to estimate individual exposures, because they do not include information on inter- and intraindividual variability in water use patterns. Town-average DBP concentrations from different sampling locations in water systems with considerable spatial variability may also not fully reflect residential values, although we are confident that our exposure assessment should largely capture relative categorical rankings of overall DBP exposures via drinking water. Nonetheless, we recognize that these potential sources of measurement error can lead to exposure misclassification, which may bias our results and distort any exposure–response relationships that may exist.

Massachusetts maintains an active statewide, population-based birth defect registry system to track birth defects in the 1st year following pregnancy. Therefore, we would expect minimal case underascertainment to have occurred for CVDs that occur up to 1 year, but are less certain about defects that are detected predominantly beyond the first year. There is some potential for outcome misclassification due to measurement error from the use of the ICD-9 codes (Cronk et al. 2003; Holmes and Westgate 2012; Strickland et al. 2008). Inaccuracies attendant with the use of ICD-9 codes can vary substantially by birth defect subtype and can lead to false positives and false negatives. ICD-9 codes have been shown to be good at classifying certain heart defects, such as TOF (100%), coarctation of the aorta (100%), and VSD (84%), whereas others such as ASDs (50%) and patent ductus arteriosus (22%) are less accurate (Frohnert et al. 2005). Other studies have also reported variability in false positive rates from 2% for TOF to 49% for TGA (Strickland et al. 2008). Some less severe cardiac defects, such as small holes in the heart (e.g., ASDs or VSDs), may spontaneously close or repair themselves during pregnancy or shortly after birth. Such defects may in fact go undetected, so our study population may be capturing fewer minor defects in general. We conducted a sensitivity analysis of the All CVD category excluding patent ductus arteriosus which, as noted above, is prone to misclassification. Following this restriction, comparable results were detected for bromoform and DCAA, with larger aORs found for the highest HAA5 exposure category (1.53 vs. 1.18) (see Table S4).

As with other epidemiological studies based on birth records, we cannot gauge the extent to which elective pregnancy terminations may be related to the prevalence of birth defects among aborted fetuses. Although elective terminations can result in underascertainment of cases detected at birth based on vital records data, CVDs are not often the medical reason why abortions are pursued. For example, the reported elective termination rate when detected prenatally is < 5% for ASDs, VSDs, TGA, and TOF (Boldt et al. 2002; Ethen and Canfield 2002; Papp et al. 1995; Stoll et al. 1993; Wren et al. 2000). Because our study population comprises only live births, we may not be capturing all birth defect cases in this population, including those that resulted in miscarriages. However, many CVDs, such as ASDs, often occur among live births (Botto et al. 2001; Forrester and Merz 2004; Garne et al. 2001).

CVDs are often idiopathic and likely involve multiple etiological factors including genetics, lifestyle factors, and other environmental determinants. We minimized the potential for false-positive associations between DBPs and CVDs through exclusion of chromosomal abnormalities which resulted in a more homogenous study population. We also minimized the influence of known cardiac birth defects risk factors such as rubella by use of statistical adjustment in the confounding analysis. CVDs also represent a wide range of types of malformations, some of which are simple or complex in nature. Complex CVDs, such as TOF, include a combination of CVDs diagnosed together. Because they may obscure some of the relationships that were examined for individual defects, we also conducted a sensitivity analysis to examine the impact of multiple birth defects. The sensitivity analysis was limited to CVDs with the strongest and most consistent associations. The aORs for isolated VSDs were slightly lower for the individual DBPs such as bromoform (1.42 vs. 1.85) and MBA (1.41 vs. 1.81), but were larger for the DBP mixture surrogates THM4 (2.74 vs. 1.57) and DBP9 (2.14 vs. 1.48) (see Table S5). In contrast to the main analysis, a positive exposure–response relationship for VSDs was detected for THM4 with consistent associations in the upper three quintiles (aOR range, 2.41–2.74). The associations for TOF were even stronger in magnitude for isolated TOF cases, where the aORs were from two to three times larger for the highest DCAA quartile (11.11 vs. 3.34), TCAA quartile (9.17 vs 3.89), and the HAA5 quintile (12.37 vs. 6.51) (see Table S6).

As noted earlier, we were able to evaluate numerous risk factors for birth defects from the comprehensive information available from the birth records. The reliance on birth record data, however, may limit the ability to fully consider some potential confounders such as vitamin use, body mass index (BMI), alcohol use, passive smoking, and other socioeconomic indicators. Alcohol consumption, for example, is an important risk factor for some birth defects, but the Massachusetts Department of Public Health had advised that the birth data on maternal alcohol consumption are considered of poor quality and of questionable validity. Thus, we did not include maternal alcohol use in the analyses. This is in contrast to reported smoking during pregnancy, which we have much more confidence in given that we previously demonstrated strong relationships between maternal cigarette use during pregnancy and different fetal growth measures (Rivera-Núñez and Wright 2013; Wright et al. 2004). Previous research also indicates good agreement with cotinine levels and self-reported maternal cigarette use during pregnancy (Searles Nielsen et al. 2014). Although we did not have reliable data for some potential CVD risk factors such as maternal alcohol use and prepregnancy BMI, we do not expect these to be strongly associated with DBP exposures in our study. If present at all, any bias would likely result in negative confounding if DBP exposures and alcohol consumption are inversely associated. Therefore, we would expect any residual confounding from this and other inversely associated covariates, such as obesity and BMI, to attenuate observed associations toward the null if they are not adjusted for or addressed in the study design phase. In addition, we did have data on maternal weight gain during pregnancy, which is likely related to obesity, BMI, and healthful behaviors during pregnancy. Thus, statistical adjustment for weight gain may indirectly control for some of the potential confounding from maternal BMI.

We adjusted for income in most of the logistic regression models, because we saw fairly consistent evidence of confounding by aggregate income levels based on census data for towns, census tracts, or ZIP codes. Because individual-level income data was not available, we recognize that residual confounding is possible if the aggregate measures resulted in misclassification. However, we saw little evidence of confounding by a socioeconomic index that combined aggregate and individual-level data, and our previous study found little evidence that aggregate socioeconomic indices

were associated with DBP concentrations in Massachusetts public drinking water systems (Evans et al. 2013). Given this and our extensive confounding analysis including adjustment for other individual-level correlates of socioeconomic status (e.g., education, marital status, prenatal care source of payment), we would suspect that any potential residual confounding by income would have minimal impact on our results.

Although many of our results were null, we found consistent results for bromoform and every cardiac birth defect that was examined as well as increased risks for VSDs and different DBPs. Toxicological evidence lends credence to our study findings given that dose-dependent VSDs and conotruncal defects have been shown in rats following DCAA and TCAA exposures (Epstein et al. 1992; Johnson et al. 1998; Smith et al. 1989, 1992). Bromochloroacetonitrile has also been reported to cause CVDs in rats (Christ et al. 1995), but the haloacetonitriles have yet to be examined in an epidemiological study. This may be important given that bromochloroacetonitrile was shown to be highly correlated with some DBPs such as haloacetamides and the trihaloacetic acids (e.g., TCAA) in a study from the United Kingdom (Bond et al. 2015). Despite some findings that appear concordant with existing epidemiological and toxicological studies, more research is needed to further elucidate which DBPs or DBP mixtures may be responsible for the epidemiological associations reported to date.

Conclusions

This is the first epidemiological study of birth defects and DBPs to examine several individual CVDs, different exposure surrogate mixtures (THM4, THMBr, HAA5, and DBP9), and various individual DBP species. Future analyses of CVDs and DBPs should expand upon this research and focus efforts to reduce exposure misclassification due to spatial and temporal variability including evaluation of smaller critical exposure windows and peak exposures. This may require more frequent distribution system sampling or temporal modeling/interpolation approaches using existing data. Residential-level sampling or more spatially representative exposure estimates (e.g., geographic information system–based approaches) would also help address spatial variability concerns.

There are fairly consistent results from epidemiological and toxicological studies for associations between DBP exposures and increased risk of some CVDs, especially VSDs. Because our study is only the second one to evaluate exposure to brominated DBPs, it adds some specificity to the potential risks that have been previously noted for THM4. However, further clarity on which of the co-occurring DBP species (or mixture combinations) to sample for and analyze is still needed and may benefit from additional toxicological studies and exposure assessment research. Given the ubiquitous nature of DBPs in treated drinking water, our findings have potential important public health ramifications. Thus, further delineation of the potential impact of *in utero* exposure to environmental teratogens would help inform intervention efforts to reduce exposures during critical windows of pregnancy.

References

Bell ML, Belanger K. 2012. Review of research on residential mobility during pregnancy: consequences for assessment of prenatal environmental exposures. J Expo Sci Environ Epidemiol 22(5):429–438.

Boldt T, Andersson S, Eronen M. 2002. Outcome of structural heart disease diagnosed in utero. Scand Cardiovasc J 36(2):73–79.

Bond T, Templeton MR, Mokhtar Kamal NH, Graham N, Kanda R. 2015. Nitrogenous disinfection byproducts in English drinking water supply systems: occurrence, bromine substitution and correlation analysis. Water Res 85:85–94.

Botto LD, Correa A, Erickson JD. 2001. Racial and temporal variations in the prevalence of heart defects. Pediatrics 107(3):E32.

Bove FJ, Fulcomer MC, Klotz JB, Esmart J, Dufficy EM, Savrin JE. 1995. Public drinking water contamination and birth outcomes. Am J Epidemiol 141(9):850–862.

Brent RL, Beckman DA. 1990. Environmental teratogens. Bull N Y Acad Med 66(2):123–163.

Chisholm K, Cook A, Bower C, Weinstein P. 2008. Risk of birth defects in Australian communities with high levels of brominated disinfection by-products. Environ Health Perspect 116:1267–1273, doi: 10.1289/ehp.10980.

Christ SA, Read EJ, Stober JA, Smith MK. 1995. The developmental toxicity of bromochloroacetonitrile in pregnant Long–Evans rats. Int J Environ Health Res 5(2):175–188.

Christian MS, York RG, Hoberman AM, Diener RM, Fisher LC. 2001. Oral (drinking water) developmental toxicity studies of bromodichloromethane (BDCM) in rats and rabbits. Int J Toxicol 20(4):225–237.

Cronk CE, Malloy ME, Pelech AN, Miller RE, Meyer SA, Cowell M, et al. 2003. Completeness of state administrative databases for surveillance of congenital heart disease. Birth Defects Res A Clin Mol Teratol 67(9):597–603.

Epstein DL, Nolen GA, Randall JL, Christ SA, Read EJ, Stober JA, et al. 1992. Cardiopathic effects of dichloroacetate in the fetal Long-Evans rat. Teratology 46(3):225–235.

Ethen MK, Canfield MA. 2002. Impact of including elective pregnancy terminations before 20 weeks gestation on birth defect rates. Teratology 66(suppl 1):S32–S35.

Evans AM, Wright JM, Meyer A, Rivera-Núñez Z. 2013. Spatial variation of disinfection by-product concentrations: exposure assessment implications. Water Res 47(16):6130–6140.

Forrester MB, Merz RD. 2004. Descriptive epidemiology of selected congenital heart defects, Hawaii, 1986–1999. Paediatr Perinat Epidemiol 18(6):415–424.

Frohnert BK, Lussky RC, Alms MA, Mendelsohn NJ, Symonik DM, Falken MC. 2005. Validity of hospital discharge data for identifying infants with cardiac defects. J Perinatol 25(11):737–742.

Garne E, Stoll C, Clementi M, Euroscan Group. 2001. Evaluation of prenatal diagnosis of congenital heart diseases by ultrasound: experience from 20 European registries. Ultrasound Obstet Gynecol 17(5):386–391.

Go AS, Mozaffarian D, Roger VL, Benjamin EJ, Berry JD, Borden WB, et al. 2013. Heart disease and stroke statistics—2013 update: a report from the American Heart Association. Circulation 127:143–152.

Graves CG, Matanoski GM, Tardiff RG. 2001. Weight of evidence for an association between adverse reproductive and developmental effects and exposure to disinfection by-products: a critical review. Regul Toxicol Pharmacol 34(2):103–124.

Grazuleviciene R, Kapustinskiene V, Vencloviene J, Buinauskiene J, Nieuwenhuijsen MJ. 2013. Risk of congenital anomalies in relation to the uptake of trihalomethane from drinking water during pregnancy. Occup Environ Med 70(4):274–282.

Holmes LB, Westgate MN. 2012. Using ICD-9 codes to establish prevalence of malformations in newborn infants. Birth Defects Res A Clin Mol Teratol 94(4):208–214.

Hwang BF, Jaakkola JJ, Guo HR. 2008. Water disinfection by-products and the risk of specific birth defects: a population-based cross-sectional study in Taiwan. Environ Health 7:23, doi: 10.1186/1476-069X-7-23.

Johnson PD, Dawson BV, Goldberg SJ. 1998. Cardiac teratogenicity of trichloroethylene metabolites. J Am Coll Cardiol 32(2):540–545.

Khoury MJ, Stewart W, Weinstein A, Panny S, Lindsay P, Eisenberg M. 1988. Residential mobility during pregnancy: implications for environmental teratogenesis. J Clin Epidemiol 41(1):15–20.

Klotz JB, Pyrch LA. 1999. Neural tube defects and drinking water disinfection by-products. Epidemiology 10(4):383–390.

Kotelchuck M. 1994. An evaluation of the Kessner Adequacy of Prenatal Care Index and a proposed Adequacy of Prenatal Care Utilization Index. Am J Public Health 84(9):1414–1420.

Kurinczuk JJ, Hollowell J, Boyd PA, Oakley L, Brocklehurst P, Gray R. 2010. The contribution of congenital anomalies to infant mortality. Inequalities in Infant Mortality Project Briefing Paper 4. Oxford, UK:University of Oxford, National Perinatal Epidemiology Unit. https://www.npeu.ox.ac.uk/downloads/files/infant-mortality/Infant-Mortality-Briefing-Paper-4.pdf [accessed 1 March 2016].

Lee K, Khoshnood B, Chen L, Wall SN, Cromie WJ, Mittendorf RL. 2001. Infant mortality from congenital malformations in the United States, 1970–1997. Obstet Gynecol 98(4):620–627.

Nieuwenhuijsen MJ, Martinez D, Grellier J, Bennett J, Best N, Iszatt N, et al. 2009. Chlorination disinfection by-products in drinking water and congenital anomalies: review and meta-analyses. Environ Health Perspect 117:1486–1493, doi: 10.1289/ehp.0900677.

Nieuwenhuijsen MJ, Toledano MB, Bennett J, Best N, Hambly P, de Hoogh C, et al. 2008. Chlorination disinfection by-products and risk of congenital anomalies in England and Wales. Environ Health Perspect 116:216–222, doi: 10.1289/ehp.10636.

Papp Z, Tóth-Pál E, Papp C, Tóth Z, Szabó M, Veress L, et al. 1995. Impact of prenatal mid-trimester screening on the prevalence of fetal structural anomalies: a prospective epidemiological study. Ultrasound Obstet Gynecol 6(5):320–326.

Randall JL, Christ SA, Horton-Perez P, Nolen GA, Read EJ, Smith MK. 1991. Developmental effects of 2-bromoacetic acid in the Long-Evans rat [Abstract P122]. Teratology 43(5):454.

Righi E, Bechtold P, Tortorici D, Lauriola P, Calzolari E,

Astolfi G, et al. 2012. Trihalomethanes, chlorite, chlorate in drinking water and risk of congenital anomalies: a population-based case-control study in Northern Italy. Environ Res 116:66–73.

Rivera-Núñez Z, Wright JM. 2013. Association of brominated trihalomethane and haloacetic acid exposure with fetal growth and preterm delivery in Massachusetts. J Occup Environ Med 55(10):1125–1134.

Ruddick JA, Villeneuve DC, Chu I, Valli VE. 1983. A teratological assessment of four trihalomethanes in the rat. J Environ Sci Health B 18(3):333–349.

Searles Nielsen S, Dills RL, Glass M, Mueller BA. 2014. Accuracy of prenatal smoking data from Washington State birth certificates in a population-based sample with cotinine measurements. Ann Epidemiol 24(3):236–239.

Shaw GM, Ranatunga D, Quach T, Neri E, Correa A, Neutra RR. 2003. Trihalomethane exposures from municipal water supplies and selected congenital malformations. Epidemiology 14:191–199.

Smith MK, Randall JL, Read EJ, Stober JA. 1989. Teratogenic activity of trichloroacetic acid in the rat. Teratology 40(5):445–451.

Smith MK, Randall JL, Read EJ, Stober JA. 1992. Developmental toxicity of dichloroacetate in the rat. Teratology 46(3):217–223.

Stoll C, Alembik Y, Dott B, Roth PM, De Geeter B. 1993. Evaluation of prenatal diagnosis of congenital heart disease. Prenat Diagn 13(6):453–461.

Strickland MJ, Riehle-Colarusso TJ, Jacobs JP, Reller MD, Mahle WT, Botto LD, et al. 2008. The importance of nomenclature for congenital cardiac disease: implications for research and evaluation. Cardiol Young 18(suppl 2):92–100.

Wren C, Richmond S, Donaldson L. 2000. Temporal variability in birth prevalence of cardiovascular malformations. Heart 83(4):414–419.

Wright JM, Schwartz J, Dockery DW. 2004. The effect of disinfection by-products and mutagenic activity on birth weight and gestational duration. Environ Health Perspect 112:920–925, doi: 10.1289/ehp.6779.

Environ Health Perspect
DOI: 10.1289/EHP103

Note to readers with disabilities: *EHP* strives to ensure that all journal content is accessible to all readers. However, some figures and Supplemental Material published in *EHP* articles may not conform to 508 standards due to the complexity of the information being presented. If you need assistance accessing journal content, please contact ehp508@niehs.nih.gov. Our staff will work with you to assess and meet your accessibility needs within 3 working days.

Supplemental Material

Disinfection By-Product Exposures and the Risk of Specific Cardiac Birth Defects

J. Michael Wright, Amanda Evans, John A. Kaufman, Zorimar Rivera-Núñez, and Michael G. Narotsky

Table of Contents

Table S1. Spearman Correlation Coefficients for Disinfection By-Product Metrics

Table S2. Adjusted Odds Ratios (aORs) between Disinfection By-Product (DBP) Exposures and Tetralogy of Fallot Stratified by Sex

Table S3. Adjusted Odds Ratios (aORs) between Disinfection By-Product (DBP) Exposures and Ventricular Septal Defects Stratified by Sex

Table S4. Adjusted Odds Ratios (aORs) between Disinfection By-Product (DBP) Exposures and All Cardiovascular Defects Excluding Patent Ductus Arteriosus

Table S5. Adjusted Odds Ratios (aORs) between Disinfection By-Product (DBP) Exposures and Isolated Ventricular Septal Defect Cases

Table S6. Adjusted Odds Ratios (aORs) between Disinfection By-Product (DBP) Exposures and Isolated Tetralogy of Fallot Cases

Table S1. Spearman Correlation Coefficients for Disinfection By-Product Metrics

	DBP9	HAA5	THM4	THMBr	BDCM	DBCM	TCM	TCAA	DCAA	TBM	MBAA	MCAA	DBAA
DBP9	1.00												
HAA5	0.90	1.00											
THM4	0.95	0.74	1.00										
THMBr	0.40	0.25	0.50	1.00									
BDCM	0.54	0.37	0.63	0.96	1.00								
DBCM	0.05	-0.05	0.13	0.85	0.72	1.00							
TCM	0.94	0.76	0.97	0.33	0.47	-0.02	1.00						
TCAA	0.89	0.96	0.77	0.24	0.37	-0.08	0.79	1.00					
DCAA	0.84	0.93	0.70	0.23	0.34	-0.06	0.74	0.85	1.00				
TBM	-0.25	-0.28	-0.20	0.39	0.20	0.57	-0.30	-0.32	-0.28	1.00			
MBAA	0.03	0.04	0.02	0.03	0.03	0.04	0.02	0.04	0.02	0.03	1.00		
MCAA	0.50	0.57	0.42	0.26	0.30	0.07	0.42	0.46	0.55	-0.13	0.04	1.00	
DBAA	-0.12	-0.09	-0.11	0.31	0.19	0.41	-0.18	-0.17	-0.07	0.54	0.15	0.01	1.00

Note: DBP9 = sum of chloroform (TCM), bromodichloromethane (BDCM), dibromochloromethane (DBCM), bromoform (TBM), monochloroacetic acid (MCAA), dichloroacetic acid (DCAA), trichloroacetic acid (TCAA), bromoacetic acid (MBAA), and dibromoacetic acid (DBAA); HAA5 = sum of MCAA, DCAA, TCAA, MBAA, and DBAA; THM4 = sum of TCM, BDCM, DBCM, and TBM; THMBr = sum of BDCM, DBCM, and TBM

Table S2. Adjusted Odds Ratios (aORs) between Disinfection By-Product (DBP) Exposures and Tetralogy of Fallot Stratified by Sex

DBP Metrics (µg/L)	Cases (*n*)[a]	Total Population aOR (95% CI)[b]	Male aOR (95% CI)[b]	Female aOR (95% CI)[b]
THM4[c]				
≤23.05	15	REF	REF	REF
>23.05–38.05	17	0.32 (0.10, 1.05)	1.52 (0.17, 13.13)	0.15 (0.01, 1.64)
>38.05–50.41	19	0.51 (0.15, 1.74)	3.02 (0.30, 30.43)	0.16 (0.02, 1.47)
>50.41–65.27	19	0.31 (0.08, 1.21)	1.53 (0.14, 16.62)	0.22 (0.02, 2.12)
>65.27–125.32	16	0.19 (0.04, 0.88)	1.06 (0.09, 12.09)	0.05 (0.00, 0.72)
THMBr[c]				
≤4.17	15	REF	REF	REF
>4.17–6.04	25	1.00 (0.34, 2.98)	0.29 (0.04, 2.10)	5.21 (0.58, 46.62)
>6.04–7.80	12	0.23 (0.06, 0.91)	0.19 (0.02, 1.81)	0.45 (0.03, 7.88)
>7.80–11.51	18	0.45 (0.14, 1.39)	0.17 (0.02, 1.32)	1.64 (0.22, 12.36)
>11.51–42.48	16	0.26 (0.09, 0.76)	0.27 (0.04, 1.83)	0.28 (0.03, 2.70)
Chloroform[c]				
≤12.07	15	REF	REF	REF
>12.07–29.99	14	0.50 (0.16, 1.53)	1.06 (0.12, 9.48)	0.19 (0.02, 2.24)
>29.99–42.17	21	0.76 (0.22, 2.69)	1.67 (0.17, 15.96)	0.23 (0.02, 3.32)
>42.17–55.41	22	0.81 (0.20, 3.29)	1.91 (0.14, 26.80)	0.29 (0.02, 3.98)
>55.41–98.99	14	0.33 (0.07, 1.64)	0.50 (0.03, 7.73)	0.06 (0.00, 1.46)
Bromodichloromethane (BDCM)[c]				
≤4.95	34	REF	REF	REF
>4.95–7.55	24	0.49 (0.19, 1.24)	0.73 (0.17, 3.09)	0.53 (0.10, 2.72)
>7.55–37.38	28	0.38 (0.17, 0.82)	0.76 (0.24, 2.44)	0.30 (0.06, 1.40)
Dibromochloromethane (DBCM)[c]				
≤3.93	79	REF	REF	REF
>3.93–14.53	7	0.54 (0.20, 1.41)	0.34 (0.07, 1.55)	0.36 (0.05, 2.79)
Bromoform[c]				
≤0.26	76	REF	REF	REF
>0.26–7.06	10	1.14 (0.45, 2.87)	0.59 (0.15, 2.33)	3.00 (0.34, 26.50)

Table S2. Adjusted Odds Ratios (aORs) between Disinfection By-Product (DBP) Exposures and Tetralogy of Fallot Stratified by Sex (continued)

DBP Metrics (µg/L)	Cases (*n*)[a]	Total Population aOR (95% CI)[b]	Male aOR (95% CI)[b]	Female aOR (95% CI)[b]
HAA5[d]				
≤8.17	11	REF	REF	REF
>8.17–19.33	21	2.13 (0.53, 8.65)	2.59 (0.13, 50.10)	1.36 (0.11, 16.16)
>19.33–25.79	21	4.98 (1.02, 24.35)	8.27 (0.25, 276.35)	6.14 (0.32, 118.72)
>25.79–33.97	17	5.88 (1.06, 32.57)	2.95 (0.08, 114.41)	7.57 (0.30, 192.35)
>33.97–100.00	16	6.51 (1.23, 34.59)	4.79 (0.16, 142.97)	2.97 (0.14, 62.87)
Trichloroacetic acid (TCAA)[d]				
≤5.23	15	REF	REF	REF
>5.23–11.09	28	2.72 (0.91, 8.13)	5.79 (0.60, 55.49)	3.35 (0.35, 32.18)
>11.09–16.38	22	4.30 (1.09, 16.88)	6.82 (0.55, 83.94)	2.97 (0.20, 44.62)
>16.38–73.39	19	3.89 (0.97, 15.66)	5.92 (0.51, 68.40)	2.25 (0.13, 39.31)
Dichloroacetic acid (DCAA)[d]				
≤5.18	17	REF	REF	REF
>5.18–10.44	22	1.39 (0.50, 3.88)	4.09 (0.52, 31.94)	0.87 (0.07, 11.29)
>10.44–13.85	24	3.08 (0.92, 10.34)	2.31 (0.27, 19.90)	7.45 (0.34, 164.24)
>13.85–38.89	21	3.34 (0.90, 12.43)	1.54 (0.11, 20.85)	26.35 (0.94, 737.88)
Monochloroacetic acid (MCAA)[d]				
≤1.53	80	REF	REF	REF
>1.53–62.39	4	0.83 (0.27, 2.54)	0.59 (0.09, 3.78)	0.47 (0.05, 4.67)
Monobromoacetic acid (MBAA)[d]				
≤0.04	81	REF	REF	REF
>0.04–10.63	3	0.80 (0.08, 7.48)	0.53 (0.01, 20.59)	N/E
Dibromoacetic acid (DBAA)[d]				
≤0.47	77	REF	REF	REF
>0.47–21.78	7	0.59 (0.23, 1.54)	0.64 (0.12, 3.38)	0.24 (0.03, 2.22)

Table S2. Adjusted Odds Ratios (aORs) between Disinfection By-Product (DBP) Exposures and Tetralogy of Fallot Stratified by Sex (continued)

DBP Metrics (µg/L)	Cases (*n*)[a]	Total Population aOR (95% CI)[b]	Male aOR (95% CI)[b]	Female aOR (95% CI)[b]
DBP9				
≤33.07	13	REF	REF	REF
>33.07–59.95	17	0.80 (0.24, 2.63)	1.70 (0.19, 14.97)	0.97 (0.09, 10.84)
>59.95–79.13	24	1.15 (0.32, 4.08)	2.62 (0.31, 22.08)	2.95 (0.20, 42.62)
>79.13–97.67	18	1.39 (0.39, 5.01)	4.25 (0.43, 42.28)	0.26 (0.02, 4.49)
>97.67–181.59	14	0.94 (0.23, 3.79)	0.74 (0.07, 7.34)	0.55 (0.03, 9.92)

Note: *n* = sample size; aOR = adjusted odds ratios; CI = confidence interval; REF = referent; THM4 = sum of chloroform, BDCM, DBCM, and bromoform; THMBr = sum of BDCM, DBCM, and bromoform; N/E = not estimable; HAA5 = sum of MCAA, DCAA, TCAA, MBAA, and DBAA; DBP9 = sum of chloroform, BDCM, DBCM, bromoform, MCAA, DCAA, TCAA, MBAA, and DBAA.

[a]The numbers represent the TOF case distribution across exposure groups prior to modeling and stratification.

[b]Models adjusted for the type of water source and treatment, infant birth weight, ZIP code-level income quartile, trimester prenatal care began (first, after first), health index (gestational diabetes, non-gestational diabetes, chronic hypertension, gestational hypertension, and hydramnios/oligohydramnios), and other maternal reproductive risk factors.

[c]Models also include adjustment for HAA5 concentrations.

[d]Models also include adjustment for THM4 concentrations.

Table S3. Adjusted Odds Ratios (aORs) between Disinfection By-Product (DBP) Exposures and Ventricular Septal Defects Stratified by Sex

DBP Metrics (µg/L)	Cases (*n*)[a]	Total Population aOR (95% CI)[b]	Male aOR (95% CI)[b]	Female aOR (95% CI)[b]
THM4[c]				
≤23.05	62	REF	REF	REF
>23.05–38.05	61	1.39 (0.72, 2.69)	1.85 (0.49, 6.93)	1.15 (0.49, 2.71)
>38.05–50.41	80	1.77 (0.87, 3.59)	2.47 (0.60, 10.11)	1.69 (0.66, 4.34)
>50.41–65.27	73	1.70 (0.80, 3.63)	1.93 (0.43, 8.62)	1.60 (0.59, 4.29)
>65.27–125.32	58	1.57 (0.70, 3.53)	1.35 (0.29, 6.37)	2.08 (0.71, 6.12)
THMBr[c]				
≤4.17	67	REF	REF	REF
>4.17–6.04	56	0.81 (0.39, 1.68)	0.39 (0.12, 1.26)	1.70 (0.57, 5.04)
>6.04–7.80	73	0.79 (0.41, 1.55)	0.48 (0.17, 1.38)	1.72 (0.63, 4.69)
>7.80–11.51	55	0.89 (0.47, 1.69)	0.54 (0.20, 1.45)	1.96 (0.73, 5.23)
>11.51–42.48	82	1.34 (0.73, 2.46)	0.96 (0.37, 2.46)	2.52 (0.99, 6.42)
Chloroform[c]				
≤12.07	66	REF	REF	REF
>12.07–29.99	61	1.05 (0.58, 1.90)	1.18 (0.38, 3.69)	1.06 (0.48, 2.34)
>29.99–42.17	74	0.86 (0.43, 1.72)	0.79 (0.22, 2.88)	0.90 (0.34, 2.35)
>42.17–55.41	75	1.00 (0.47, 2.12)	0.75 (0.18, 3.09)	1.04 (0.38, 2.84)
>55.41–98.99	57	0.79 (0.35, 1.80)	0.32 (0.07, 1.43)	1.43 (0.48, 4.22)
Bromodichloromethane (BDCM)[c]				
≤4.95	105	REF	REF	REF
>4.95–7.55	112	0.81 (0.50, 1.31)	0.76 (0.34, 1.71)	1.01 (0.51, 2.01)
>7.55–37.38	116	1.21 (0.79, 1.85)	1.07 (0.53, 2.17)	1.51 (0.84, 2.70)
Dibromochloromethane (DBCM)[c]				
≤3.93	293	REF	REF	REF
>3.93–14.53	40	1.54 (1.00, 2.37)	2.17 (1.06, 4.46)	1.61 (0.87, 2.96)
Bromoform[c]				
≤0.26	290	REF	REF	REF
>0.26–7.06	43	1.85 (1.20, 2.83)	2.23 (1.10, 4.52)	1.88 (1.01, 3.52)

Table S3. Adjusted Odds Ratios (aORs) between Disinfection By-Product (DBP) Exposures and Ventricular Septal Defects Stratified by Sex (continued)

DBP Metrics (µg/L)	Cases (*n*)[a]	Total Population aOR (95% CI)[b]	Male aOR (95% CI)[b]	Female aOR (95% CI)[b]
HAA5[d]				
≤8.17	69	REF	REF	REF
>8.17–19.33	50	0.66 (0.37, 1.20)	0.75 (0.26, 2.16)	0.49 (0.21, 1.12)
>19.33–25.79	74	1.00 (0.51, 1.94)	0.74 (0.22, 2.52)	0.85 (0.34, 2.13)
>25.79–33.97	63	1.01 (0.49, 2.08)	1.65 (0.47, 5.79)	0.39 (0.13, 1.12)
>33.97–100.00	78	1.02 (0.49, 2.12)	1.23 (0.33, 4.64)	0.62 (0.22, 1.75)
Trichloroacetic acid (TCAA)[d]				
≤5.23	80	REF	REF	REF
>5.23–11.09	81	0.90 (0.55, 1.50)	1.18 (0.47, 2.91)	0.63 (0.31, 1.27)
>11.09–16.38	83	0.81 (0.44, 1.51)	1.01 (0.34, 3.00)	0.46 (0.19, 1.10)
>16.38–73.39	86	0.79 (0.41, 1.50)	1.08 (0.34, 3.46)	0.43 (0.18, 1.08)
Dichloroacetic acid (DCAA)[d]				
≤5.18	78	REF	REF	REF
>5.18–10.44	72	0.84 (0.51, 1.39)	0.51 (0.21, 1.19)	0.79 (0.39, 1.59)
>10.44–13.85	92	1.28 (0.72, 2.25)	1.02 (0.41, 2.53)	1.19 (0.52, 2.73)
>13.85–38.89	88	1.18 (0.65, 2.14)	1.14 (0.45, 2.91)	0.83 (0.35, 1.95)
Monochloroacetic acid (MCAA)[d]				
≤1.53	295	REF	REF	REF
>1.53–62.39	35	1.27 (0.81, 1.97)	1.47 (0.72, 2.99)	1.06 (0.55, 2.04)
Monobromoacetic acid (MBAA)[d]				
≤0.04	317	REF	REF	REF
>0.04–10.63	13	1.81 (0.85, 3.84)	6.56 (1.60, 26.83)	1.92 (0.60, 6.16)
Dibromoacetic acid (DBAA)[d]				
≤0.47	302	REF	REF	REF
>0.47–21.78	28	1.00 (0.63, 1.61)	1.09 (0.52, 2.28)	1.08 (0.56, 2.10)

Table S3. Adjusted Odds Ratios (aORs) between Disinfection By-Product (DBP) Exposures and Ventricular Septal Defects Stratified by Sex (continued)

DBP Metrics (µg/L)	Cases (*n*)[a]	Total Population aOR (95% CI)[b]	Male aOR (95% CI)[b]	Female aOR (95% CI)[b]
DBP9				
≤33.07	63	REF	REF	REF
>33.07–59.95	58	1.33 (0.71, 2.48)	1.13 (0.36, 3.48)	1.29 (0.57, 2.91)
>59.95–79.13	79	1.70 (0.88, 3.26)	2.23 (0.68, 7.32)	1.64 (0.69, 3.91)
>79.13–97.67	71	1.64 (0.83, 3.26)	1.45 (0.43, 4.91)	1.37 (0.55, 3.40)
>97.67–181.59	63	1.48 (0.73, 2.98)	1.07 (0.32, 3.62)	1.49 (0.56, 3.94)

Note: *n* = sample size; aOR = adjusted odds ratio; CI = confidence interval; REF = referent; THM4 = sum of chloroform, BDCM, DBCM, and bromoform; THMBr = sum of BDCM, DBCM, and bromoform; HAA5 = sum of MCAA, DCAA, TCAA, MBAA, and DBAA; DBP9 = sum of chloroform, BDCM, DBCM, bromoform, MCAA, DCAA, TCAA, MBAA, and DBAA.

[a]The numbers represent the case distribution across exposure groups prior to modeling and stratification.

[b]Models adjusted for the type of water source and treatment, maternal marital status (married, including within 300 days prior to birth; not married), maternal education category, maternal race category, health index (gestational diabetes, non-gestational diabetes, chronic hypertension, gestational hypertension, and hydramnios/oligohydramnios), and other maternal reproductive risk factors.

[c]Models also include adjustment for HAA5 concentrations.

[d]Models also include adjustment for THM4 concentrations.

Table S4. Adjusted Odds Ratios (aORs) between Disinfection By-Product (DBP) Exposures and All Cardiovascular Defects Excluding Patent Ductus Arteriosus

DBP Metrics (µg/L)	Cases (*n*)[a]	aOR (95% CI)[b]
Bromoform[c]		
≤0.26	532	REF
>0.26–7.06	79	1.50 (1.10, 2.04)
HAA5[d]		
≤8.17	118	REF
>8.17–19.33	111	1.09 (0.71, 1.68)
>19.33–25.79	153	1.57 (0.97, 2.55)
>25.79–33.97	111	1.24 (0.72, 2.12)
>33.97–100.00	119	1.53 (0.90, 2.61)
Dichloroacetic acid (DCAA)[d]		
≤5.18	142	REF
>5.18–10.44	150	1.08 (0.76, 1.53)
>10.44–13.85	169	1.26 (0.83, 1.89)
>13.85–38.89	141	1.29 (0.84, 1.99)

Note: *n* = sample size; aOR = adjusted odds ratio; CI = confidence interval; REF = referent; HAA5 = sum of monochloroacetic acid, DCAA, trichloroacetic acid, monobromoacetic acid, and dibromoacetic acid.

[a]The numbers represent the case distribution across exposure groups prior to modeling.

[b]Models adjusted for the type of water source and treatment, health index (gestational diabetes, non-gestational diabetes, chronic hypertension, gestational hypertension, and hydramnios/oligohydramnios), and other maternal reproductive risk factors.

[c]Model also includes adjustment for HAA5 concentrations.

[d]Models also include adjustment for THM4 (sum of chloroform, bromodichloromethane, dibromochloromethane, and bromoform) concentrations.

Table S5. Adjusted Odds Ratios (aORs) between Disinfection By-Product (DBP) Exposures and Isolated Ventricular Septal Defect Cases

DBP Metrics (µg/L)	Cases (*n*)[a]	aOR (95% CI)[b]
THM4[c]		
≤23.05	22	REF
>23.05–38.05	12	1.17 (0.39, 3.57)
>38.05–50.41	21	2.41 (0.74, 7.82)
>50.41–65.27	23	2.46 (0.66, 9.21)
>65.27–125.32	23	2.74 (0.67, 11.22)
Dibromochloromethane (DBCM)[c]		
≤3.93	89	REF
>3.93–14.53	12	1.07 (0.48, 2.36)
Bromoform[c]		
≤0.26	87	REF
>0.26–7.06	14	1.42 (0.68, 2.98)
Monobromoacetic acid (MBAA)[d]		
≤0.04	97	REF
>0.04–10.63	3	1.41 (0.16, 12.43)
DBP9		
≤33.07	22	REF
>33.07–59.95	14	1.32 (0.46, 3.75)
>59.95–79.13	21	2.08 (0.68, 6.42)
>79.13–97.67	19	1.37 (0.41, 4.63)
>97.67–181.59	25	2.14 (0.66, 6.98)

Note: *n* = sample size; aOR = adjusted odds ratio; CI = confidence interval; REF = referent; THM4 = sum of chloroform, BDCM, DBCM, and bromoform; DBP9 = sum of chloroform, bromodichloromethane (BDCM), DBCM, bromoform, monochloroacetic acid, dichloroacetic acid, trichloroacetic acid, MBAA, and dibromoacetic acid.

[a]The numbers represent the case distribution across exposure groups prior to modeling.

[b]Models adjusted for water source and treatment type, maternal education category, maternal marital status (married, including within 300 days prior to birth; not married), maternal race category, health index (gestational diabetes, non-gestational diabetes, chronic hypertension, gestational hypertension, and hydramnios/oligohydramnios), and other maternal reproductive risk factors.

[c]Models also include adjustment for HAA5 (sum of MCAA, DCAA, TCAA, MBAA, and DBAA) concentrations.

[d]Model also includes adjustment for THM4 concentrations.

Table S6. Adjusted Odds Ratios (aORs) between Disinfection By-Product (DBP) Exposures and Isolated Tetralogy of Fallot Cases

DBP Metrics (µg/L)	Cases (*n*)[a]	aOR (95% CI)[b]
HAA5		
≤8.17	4	REF
>8.17–19.33	6	2.64 (0.26, 26.86)
>19.33–25.79	9	4.90 (0.40, 60.50)
>25.79–33.97	6	3.61 (0.21, 63.15)
>33.97–100.00	7	12.37 (0.75, 204.11)
Dichloroacetic acid (DCAA)		
≤5.18	6	REF
>5.18–10.44	6	1.44 (0.27, 7.54)
>10.44–13.85	7	2.77 (0.34, 22.70)
>13.85–38.89	11	11.11 (1.17, 105.86)
Trichloroacetic acid (TCAA)		
≤5.23	5	REF
>5.23– 11.09	8	6.30 (0.85, 46.84)
>11.09–16.38	10	12.07 (1.02, 143.10)
>16.38–73.39	7	9.17 (0.65, 129.15)

Note: *n* = sample size; aOR = adjusted odds ratio; CI = confidence interval; REF = referent; HAA5 = sum of monochloroacetic acid, DCAA, TCAA, monobromoacetic acid, and dibromoacetic acid.

[a]The numbers represent the case distribution across exposure groups prior to modeling.

[b]Models adjusted for water source and treatment type, trimester prenatal care began (first, after first), birth weight, zip code level income, other maternal reproductive risk factors, health index (gestational diabetes, non-gestational diabetes, chronic hypertension, gestational hypertension, and hydramnios/oligohydramnios), and THM4 (sum of chloroform, bromodichloromethane, dibromochloromethane, and bromoform) concentrations.

Table of Contents

General_Authors_Publications.....2
LI-266749_Manuscript_SOCArXiv_f.....8
Manuscript_SOCArXiv_f.....37

United States Environmental Protection Agency
Washington, DC 20460

STAA REPORT FOR THE SCIENTIST NOMINATIONS

General Information:

Nomination ID/App ID:	20-132
Research Category Primary:	Sustainability and Innovation (SI)
Research Category Secondary:	Environmental Policy and Decision-Making Studies (EP)
Laboratory/Office Name:	ORD/ACESD
Nomination Entered By:	Nathaniel Merrill

Eligibility Checklist:

[Y] The nominated publication(s) has not been submitted to a previous STAA competition.

[Y] The nominated publication(s) was published on or before January 1, 2017 and on or after January 1,2012

[Y] The principal author was an EPA employee or a PHS employee assigned to EPA when the research was performed

[Y] The EPA authors (includes PHS employees assigned to EPA) contributed collectively a minimum of 50% toward the publication(s)

Nominating Official Name:	Wayne Munns
Nominating Official Title:	SUPERVISORY ECOLOGIST
Nominating OfficialEmail:	munns.wayne@epa.gov
STAA Coordinator Name:	Kathleen Wiser
STAA Coordinator Email:	wiser.kathi@epa.gov

Justifications:

Justification 1:

This work validates the use of commercially-available human mobility datasets based on cell phone locations to estimate visitation to natural areas. By combining this data with on-the-ground observations of visitation to water recreation areas in New England, we fit a model to estimate daily visitation for four months to more than 500 sites.The results show the potential for this new big data source of human mobility to overcome limitations in traditional methods of estimating visitation and to provide consistent information at policy-relevant scales. The high-resolution information in both space and time provided by cell phone location-derived data creates opportunities for developing next-generation models of human interactions with the natural environment. This is a new data source for EPA and a novel use in the greater literature for understanding people behavior around natural resources. This work will support EPA's mission to support human health and well-being through providing a new tool to estimate the effect of changes in environmental quality. This work was directly out of an effort with Office of Water to estimate the benefits of improving coastal waters in terms of nutrient pollution and bacteria.

Justification 2A:

single publication

Justification 2B:

The authors have not submitted to STAA before.

Justification 2C:

NA

Justification 2D:

NA

Justification 2E:

They have not.

Justification 3A:

This idea of using this source of data for this purpose was novel to our field of environmental economics. It has influenced work in the field directly through collaborations with universities and E:PA STAR grant recipients around the effort to estimate the benefits of improved water quality. A master's student, Ravi Chitilla and his advisor Roger Van Haefen have collaborated on Ravi's masters thesis using the data and process we created for travel demand modeling. The effort is directly contributing to EPA Region 1's Southern New England Program (SNEP) by providing inputs to the effort to create indicators and quantify ecosystem services supported by SNEP's grant efforts.

Justification 3B:

PLOS ONE is an online, open-access journal. The paper is assigned to a topic editor, who selects reviewers from the related field. It went through 2 round of peer review before acceptance.

AUTHORS

Principal Author

Author Name:	Nathaniel H. Merrill		
Professional Title:		Salutation:	
Email:	merrill.nathaniel@epa.gov	Organization:	
Mailing Address:			
Street Line 1:			
City:			
Zip Code:		State:	

At time of research was:	EPA Employee		
Separation Date:			
% of Effort:	20		

Contributing Author

Author Name:	Sarina F Atkinson		
Professional Title:		Salutation:	
Email:		Organization:	
Mailing Address:			
Street Line 1:			
City:			
Zip Code:		State:	
At time of research was:	Non EPA Personnel		
Separation Date:			
% of Effort:	20		

Contributing Author

Author Name:	Kate K Mulvaney		
Professional Title:		Salutation:	
Email:	mulvaney.kate@epa.gov	Organization:	
Mailing Address:			
Street Line 1:			
City:			
Zip Code:		State:	

At time of research was:	EPA Employee		
Separation Date:			
% of Effort:	20		

Contributing Author

Author Name:	Justin Bousquin		
Professional Title:		Salutation:	
Email:	bousquin.justin@epa.gov	Organization:	
Mailing Address:			
Street Line 1:			
City:			
Zip Code:		State:	
At time of research was:	EPA Employee		
Separation Date:			
% of Effort:	20		

Contributing Author

Author Name:	Marisa J. Mazzotta		
Professional Title:		Salutation:	
Email:	mazzotta.marisa@epa.gov	Organization:	
Mailing Address:			
Street Line 1:			
City:			
Zip Code:		State:	

At time of research was:	EPA Employee
Separation Date:	
% of Effort:	20

PUBLICATIONS

Publication 1:

Publication Title:	Using Data Derived from Cellular Phone Locations to Estimate Visitation to Natural Areas: An Applica		
Publication Date:	Thu Apr 30 00:00:00 GMT 2020		
Journal/Publication Method:	PLOS ONE		
All Author(s):			
Volume:	14	Number:	5
Pages:	e	Immediately Index:	Immediately Index:
Citation ½ Life:	4.9	Impact Factor:	2.776

Title: Using Data Derived from Cellular Phone Locations to Estimate Visitation to Natural Areas: An Application to Water Recreation in New England, USA.

Authors: Nathaniel H. Merrill[1]*, Sarina F. Atkinson[2], Kate K. Mulvaney[1], Marisa J. Mazzotta[1], Justin Bousquin[3]

[1] U.S. Environmental Protection Agency, Office of Research and Development, Center for Environmental Measurement and Modeling, Atlantic Coastal Environmental Sciences Division, Narragansett, Rhode Island, USA

[2] Cooperative Institute for Marine & Atmospheric Studies, Rosenstiel School of Marine & Atmospheric Science, University of Miami, Miami, Florida, USA

[3] U.S. Environmental Protection Agency, Office of Research and Development, Center for Environmental Measurement and Modeling, Gulf Ecosystem Measurement and Modeling Division, Gulf Breeze, Florida, USA

* Corresponding author, U.S. EPA, Office of Research and Development, Center for Environmental Measurement and Modeling, Atlantic Coastal Environmental Sciences Division, 27 Tarzwell Drive, Narragansett, RI 02882, merrill.nathaniel@epa.gov

Author Contribution

N.H.M, S.F.A, K.K.M., M.J.M. designed the study. N.H.M, S.F.A, J.B. performed the analysis. N.H.M, S.F.A, K.K.M., M.J.M., J.B. wrote the manuscript.

Abstract

We introduce and validate the use of commercially-available human mobility datasets based on cell phone locations to estimate visitation to natural areas. By combining this data with on-the-ground observations of visitation to water recreation areas in New England, we fit a model to estimate daily visitation for four months to more than 500 sites. The results show the potential for this new big data source of human mobility to overcome limitations in traditional methods of estimating visitation and to provide consistent information at policy-relevant scales. However, the data providers' opaque and rapidly developing methods for processing locational information required a calibration and validation against data collected by traditional means to confidently reproduce the desired estimates of visitation. We found that with this calibration, the high-resolution information in both space and time provided by cell phone location-derived data creates opportunities for developing next-generation models of human interactions with the natural environment.

Introduction

People visit natural areas to view the scenery and wildlife or to engage in any number of recreational activities they enjoy. These areas are important to society, as shown through the sheer number of people who visit parks, beaches, walking trails, and other natural spaces and their significant contribution to the economy [1]. However, it is difficult to quantify the use of natural areas across the many, diverse locations and the timing of those visits. Observational counts are time consuming and expensive to conduct and traditional survey approaches have their own sampling complications for estimating visitation. Therefore, it is often unknown how many and what types of people visit natural areas -- critical information for managers or researchers to apply in natural resource damage assessments, park and urban planning, economic valuation studies, tourism studies, as well as to inform many other management decisions [2-3].

This paper demonstrates the use of commercially available anonymized and aggregated data on cellular device locations to estimate visitation to natural areas. For brevity, we refer to these cellular device location-based datasets generally as "cell data" in this paper. We investigated how cell data performs in providing the types of visitation

information needed in policy applications, information on the temporal and spatial distribution of visits to natural areas. Specifically, we compared the cell data with on-the-ground daily visitation counts that we collected, along with other federal, state and town records for water recreation areas. We found that the cell data contained useful information for estimating visitor use, but it required a correction (calibration) to match the scale of the observations and to be confident with its wider application. We then built and applied a statistical model to estimate daily visitation with cell data to more than 500 water recreation areas in the northeastern United States for the primary four months of recreational use (June-September) of 2017.

Our application demonstrates the potential for this emerging source of big data to provide comprehensive visitation information across many places and time windows, a feat that would be impractical with traditional methods. The high-resolution information in space and time provided by cell data expands opportunities for developing next-generation models of human interactions with the natural environment. In addition, cell data provides the ability to know not just how many people are visiting specific locations, but also where visitors are coming from within aggregated geographies. This information allows for basic calculations of distance traveled to a location and a deeper understanding of the community composition of visitors. While these new data sources may potentially help overcome many logistical barriers to obtaining behavioral information at scale, our work highlights the ongoing need for traditional methods of collection for calibration and validation for these new data sources to be useful in common applications.

Background

Existing visitation information for natural areas is limited and currently comes from many different, often inconsistent, sources. There are visitation estimates derived from entrance fees, parking fees, lifeguard counts, car or people electronic counters, aerial surveys, remote sensing, or tailored observational sampling plans [4-14]. Each data source comes with its own nuances in terms of sampling issues and geographical and temporal coverage. Most ongoing visitation collection efforts only capture paying customers during the hours of fee collections, thereby providing only a subset of daily use. There are also detailed collections that coincide with a specific project or event, such as an oil spill, but the knowledge is often not generalizable past a particular region or time-period. Often, the

need to obtain visitation information arises after an event has occurred, making the before and after comparison difficult [3]. These event-based data collections are also resource intensive [2].

Efforts to overcome these barriers using other types of digital records include estimates derived from photo-sharing or other types of social media posts [15-21]. These techniques have been useful in estimating visitation to large parks, attractions, and natural areas around the world over long periods of time by providing monthly, seasonal, or yearly visitation estimates. However, these data sources represent only the small fraction of the public that opt to use those specific social media outlets, and they lack adequate temporal and spatial resolution. These factors limit the ability of social-media based methods to inform broader policies or localized environmental management. Use of cellular devices is much more common and the resolution of the information provided is much finer in both time and space.

Cell data come from the digital traces of people's cell phone use and location. In the past, this was based on the location of the tower a device was communicating with or a triangulation from the device to various cellphone towers. This data provided information based on many people, but with locational and temporal accuracy issues related to connectivity to the cellphone tower network and peoples' active use of the phone [22]. With the addition of GPS instrumentation and the growing ubiquity of smartphone-style cellular telephones, these digital traces have become more accurate, more frequent and represent an increasing proportion of the population [23-28]. The device-level, raw data are collected by cellular telephone providers, GPS enabled devices and increasingly by smartphone applications. Several third-party providers on the commercial market combine this information and sell processed data in a variety of formats [28].

Cell data in various forms have been used most widely in the transportation and urban planning fields to understand use of public infrastructure and commuting [23-26] and to assist in land use classifications [27]. This data has also been used to understand economic trends [29], restaurant choice [30] and in epidemiology and population research in developing countries [31-34]. Despite its promise, there are limited environmental applications of the data to date, with notable applications concerning natural disasters [32] and air quality [35-36].

There are a few recent applications of cell data to understand behavior in and around natural areas [37-39]. Kubo et al. [37] used cell data to calculate the economic value of coastal tourism across Japan, but provided no ground truth to the visitation information. For an island park in Korea [38], Kim et al. applied cell data to analyze tradeoffs

between visitation and biodiversity and showed decent correlations between the cell data and monthly estimates of visitation to several specific locations on the island. A study of parks in California, USA, is the closest to the work presented in this paper [39]. The study used a similarly processed cell data product from a third-party vendor to estimate daily park visitation. They calibrated the cell data with just one set of data, vehicle counts on a major nearby road, finding a unit-value correction factor. They then validated their estimates against a single park's gate traffic and parking information. They found good agreement with their corrected cell data model and daily vehicle counts. From there, they used park-specific vehicle-to-people ratios to extrapolate to the number of visitors to the other twenty-one parks of interest. Our study differs by incorporating multiple visitation records representing counts of people to a wider set of locations: eighteen different water recreation areas. We find similar potential for this data source to provide useful, policy-relevant visitor use information at daily and site-level scales for water recreation areas.

Data description

We identified and purchased a dataset of visitation derived from cell phone locations for a set of geographies and time to understand the extent, temporal distribution, and value of water recreation for Cape Cod, Barnstable County, Massachusetts and New England, USA in general. The set of water recreation areas comprises a comprehensive list of all the public beaches and public access points to water (fresh and saltwater beaches, public access points, parks, ways to water, and boat ramps) for Barnstable County, Massachusetts, compiled from federal, state, county, and town GIS information (n=464), and an additional set of beaches across greater New England (n=113). The data we used consists of estimates of visitation to these water recreation areas over the summer months of 2017 (June through September).

We purchased data products processed by a third-party provider, Airsage, Inc. This provider creates population-level estimates of human mobility derived from a panel of over 120 million devices using location information from smartphone applications (see Supporting information). The data provider processes this device-specific locational information. Before we receive it, the data is anonymized and aggregated to contain no personally identifiable information. We do not obtain any device-level information, nor raw device GPS locations, but instead, we obtain

aggregated summaries of visitation by recreation site and estimates of the visitors' origin census block-group geographies. The data provider translates their sample to population-level estimates using weights based on the share of the population their sample represents by census-tract geographies. The cellular device sample we purchased data from includes about 30% of the U.S. population but varies by tract and month.

To obtain the cell data for the sample geographies of interest, we spatially buffered (added area) around the water-access sites which were designated as line or point features in the original spatial databases. In consultation with the data provider and after attempting a range of spatial buffers, a 100-meter buffer was chosen to balance specificity in capturing water recreation visits (i.e., not capturing ancillary points of interest in geographies, like restaurants or stores, for example) with the accuracy of the locational information. We sent the defined water recreation areas to the data provider as a set of geographic extents, or polygons (see Fig 1 for examples of area definitions), and they returned the aggregated and anonymized processed data in tabular form. We include a sample of the dataset below (Table 1) and include the entirety of this dataset available with the code package associated with this work at https://github.com/USEPA/Recreation_Benefits.git.

Table 1: Sample of dataset derived from cell phone locations

POI	DATE	HH00	HH01	HH02	HH03	HH04	HH05	…	HH20	HH21	HH22	HH23	DEVICE_TOTAL
1	20170601	251	96	47	0	171	488	…	668	848	812	222	21895
1	20170602	245	202	133	148	112	646	…	594	604	1157	468	21526
1	20170603	299	148	196	243	340	135	…	922	1283	1100	759	19449
1	20170604	658	332	117	372	414	395	…	1071	186	404	286	19415
2	20170601	0	0	0	0	0	0	…	86	0	0	0	1103
2	20170602	114	0	0	0	0	50	…	138	312	0	48	2746
2	20170603	0	0	0	0	0	0	…	238	226	122	66	2247
2	20170604	66	66	66	66	0	0	…	156	33	0	54	2046

Note: POI indexes the water access locations and each column represents estimated visitation in hourly windows, with HH00 being 12AM-1AM. DEVICE_TOTAL refers to the estimate of unique devices seen in any of the 24 hours at that water access location.

The locational accuracy of the device locations underpinning the data range depending on the source device and the smartphone application. The accuracy of reported locations from applications varies with ranges of 1-10 meters

(GPS), 20-200 meters (Wi-Fi), and 100-2000 meters (cell tower-based) based on the method(s) each application uses to locate each device. We were not able to obtain an average locational accuracy for devices seen in our geographies in our specific dataset since the smartphone applications do not report the exact location methods to the data provider and we do not receive device-specific locational information. Given the potential range in location accuracy, visits attributed to a water recreation area could have actually been to a nearby attraction, or vice-versa. We chose a relatively small buffer around the recreation areas to be conservative in defining the area attributed to use of the site and to minimize any mis-located visits. Given this and other limitations, we relied on the calibration and validation to on-the-ground visitation counts to assess the usefulness and accuracy of the cell data for our application and the choice of spatial definitions and buffers around sites.

Fig 1. Example Definition of Water Recreation Areas. Dowses Beach, Barnstable, Massachusetts, USA and nearby water access areas. Point and line features representing water recreation access were buffered by 100 meters to capture use at the sites. These geographic areas correspond to the sample of visitation estimates from the cell data.

In total, the cell dataset includes visitation estimates for 51,511 days across 577 sites. A complete set would be 70,394 days (577 sites x 122 days), but some of the days for some sites are missing due to low visitation and detection limits. A visit was defined as a device location history implying a stay estimated to be longer than five minutes at a geography that was not the home or work location of the device based on the behavior of that device over the month. Home was defined as the census block group where the device is most often seen over the month between 9PM-6AM (see Supporting Information).

In addition to estimates of visits, the cell data for each area also includes the home location of those visitors, either at the census block-group level or categorized as international if the origin was outside of the United States. For example, the data may show 100 people visited beach x during a time period, with 30 of those people come from census block y, 20 from census block z, and so on. The monthly visitor origin-destination data contains 642,915 data points representing monthly trip totals (577 sites x origin census block groups, which vary by site and month). This total is not inclusive of the data representing zero trips to destinations originating from block groups implied by the full origin-destination matrix. Because of the geographic and temporal scope, collecting this same information with traditional methods would be prohibitively expensive, time consuming, and inconsistent.

Methods

To investigate the cell data's ability to reproduce daily visitation counts, we compared the cell data to a series of observational counts collected from three different, commonly recorded sources for beach and park visitations. We then calibrated a model to translate the cell data into consistent estimates of visitation across many sites in the region of interest and across many days. We purposely designed the calibration to cover a wide range of access location sizes and visitation totals to test the transferability of the cell data and models built from it. No visitation dataset alone was perfect for use in calibration across a wide range of locations due to differences in counting methods, which is a common limitation to visitation records to natural spaces, generally. Capturing visitation to natural areas is very challenging, and existing approaches all have their own limitations for capturing daily visitation [39]. The observational data that overlaps with the cell data consists of: 1) onsite counts of small access points to an estuary,

2) a town's visitation estimates for their managed beaches, and 3) entrance fees collected by a town to a major beach.

Visitation observation methods also vary because the context for taking them differ. Although the objective may be the same, observing visitation at a major beach requires different methods than those used for a set of small access points around an estuary [41]. By comparing and calibrating our data to a combined set representing the variety of recreational visitation count methods that exist in the real world, we show the ability of cell data to both replicate the types of data that are traditionally used and to bridge the various observational visitation records common around natural resources. Each source of observational data is briefly described below.

- **Small:** We quantified use of the Three Bays estuary system on Cape Cod, Massachusetts through observational sampling for eleven public access points within the estuary. The counts were taken as a combination of periodic people and car counts and sunrise-to-sunset counts of visitors and cars. The public access points include beaches, docks, boat ramps, and landings. Observational data from this study include visitation estimates for 11 public access points for seven days from June to August, 2017 [41]. (N=72)

- **Medium:** The diverse set of beaches for Barnstable, Massachusetts, on Cape Cod includes saltwater and freshwater beaches accessible to either the public or to town residents only. The dataset provided by the Town of Barnstable's Recreation Division includes daily visitation estimates from lifeguard counts for seven of their beaches from Memorial Day (May 29) to Labor Day (September 4), 2017. (N=234)

- **Large:** Narragansett Town Beach in Rhode Island is a popular destination for tourists and residents. Access to this beach is divided into resident only and public entrances. The public entrance requires an entrance fee for each person providing an accurate dataset of daily visitation to the beach. However, these entrance fees are only collected for the public part of the beach. By missing those visitors with resident permits, the data provided by the town of Narragansett underestimates visitation to the whole beach. Therefore, based on a .85/1 ratio between public and resident use obtained through parking lot counts conducted in the public and resident parking lots, the data were adjusted to represent daily use for the whole beach (see Supporting

Information for details). Daily visitation numbers are provided from Memorial Day to Labor Day, 2017. (N=86)

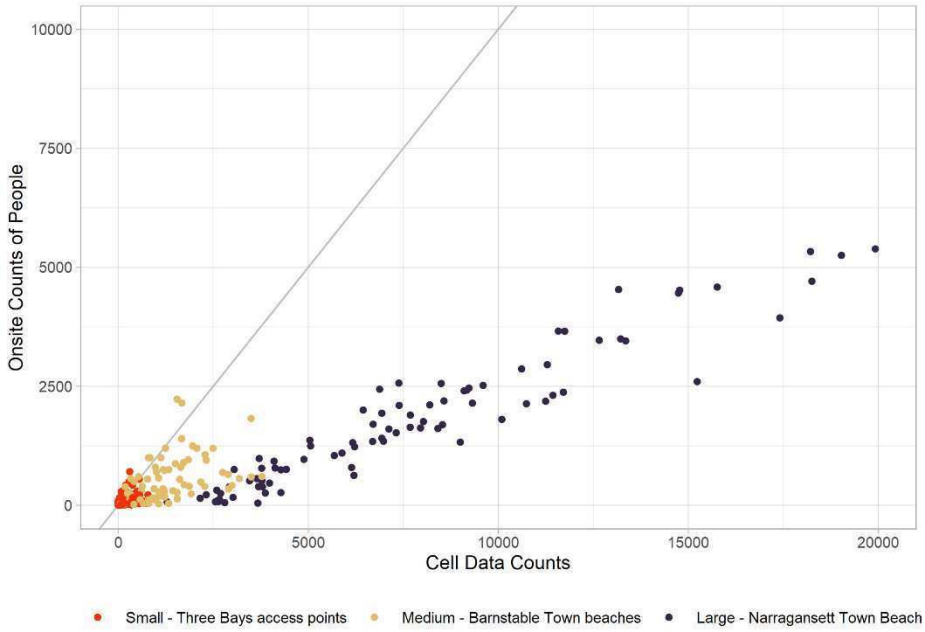

Fig 2. Observational Counts Compared Against Cell Data. Observations of visitation (9AM-4PM) plotted against uncalibrated visitation estimated from the cell data for the same hours.

Fig 2 shows how the cell data-derived counts and observational counts compare. The cell data-derived estimates correspond well, but overestimate the observed visitor counts by about four times. This overestimation is likely due to several confounding assumptions. These assumptions start with choices in how the data provider processes the raw cellular device level information to associate records with geographies in certain time windows and to extrapolate the sample of cellular devices to population level estimates through their estimates of market penetration (see Supporting Information).

The cell data product did not provide counts for the block of time that corresponded to our visitation counts (9AM-4PM), but rather by individual hours. Therefore, we had to translate these hourly counts to our time window by making assumptions on the length of stay of visitors, since the same device would be counted multiple times if it were to stay at the site for multiple hours. Following the data provider's advice to match the cell data-derived

information to visitation observations, we used an assumption of a three-hour average stay to match the time-window of our observations. We could have picked data on one hour in the window to be representative of the whole three hours, the end hour for instance, but this would discard information in the other hours. Instead, we calculated a moving average (three-hour window) of visitation for each hourly visitation estimate from the cell data for each site. We then summed the moving average of only the central hour of three-hour blocks from 8AM-4PM (9AM, 12PM, 3PM) (see Supporting Information for more details). This reduces the cell data counts due to multiple sightings, since we summed only one of the three hours in each window, but maintains the information in the hourly distribution of use through the day.

An assumption of a shorter length of stay would have increased the cell data counts and vice-versa. For example, if we assumed a two-hour average length of stay, we would have used two-hour instead of three-hour windows in the daily sums, increasing the daily total. While three hours may be a long average length of stay for recreational visits to all the water access sites, the data reflecting this assumption were inputs to the calibration models. We sought to correct any bias and inaccuracies introduced by this assumption by using the calibration models fit to on-the-ground counts below. Similarly, there is a difference in the relationship across the three sizes of access points that can also be seen in Fig 2. The differences by group are likely due to differences in the observational counting methods and possibly how well cell data performs based on the size of the area. We control for both possible effects in the statistical models used to calibrate the data.

Models and prediction

Our objective was to develop a model that predicts visitation to a range of water recreation areas using the cell data and other explanatory variables that are easily compiled across many places. These covariates include weather (temperature and precipitation), the month, day of the week, and size of the water access. The model controls for the different counting methods in the observational data. We estimated a varied set of candidate regression models including several functional forms where we defined linear and log-linear relationships between the visitor counts and the cell data and other regressors in R [42]. Since we did not have any preconceived notion of the functional forms of the relationships between the covariates and the dependent variable, we also estimated a more general

random forest model. A random forest model is a type of non-parametric model commonly used in the data science and machine learning fields. They have been shown to reproduce many functional forms and have superior predictive performance over standard multivariate regression models for many applications [43-44].

The candidate model specifications were as follows:

- Linear

$$Y_{it} = \propto + \beta_1 C_{it} + \boldsymbol{\beta_2 D_t} + \boldsymbol{\beta_3 W_t} + \boldsymbol{\beta_4 S_i} + \beta_5 A_i + e_{it} \quad (1)$$

- Log-Linear

$$\log(Y_{it}) = \propto + \beta_1 C_{it} + \boldsymbol{\beta_2 D_t} + \boldsymbol{\beta_3 W_t} + \boldsymbol{\beta_4 S_i} + \beta_5 A_i + e_{it} \quad (2)$$

- Random Forest

$$Y_{it} = f(C_{it}, \boldsymbol{D_t}, \boldsymbol{W_t}, \boldsymbol{S_i}, A_i) \quad (3)$$

Where,

Y_{it} – Observed visits to site, i, on day, t

C_{it} – cell data-derived estimate of visitation to site i on day t

$\boldsymbol{D_t}$ – Matrix of dummy variables for the month, day of the week, weekend, holiday

$\boldsymbol{W_t}$ – Matrix of weather variables (precipitation, temperature, windspeed) for day t from Barnstable Municipal Airport weather station.

$\boldsymbol{S_i}$ – Dummy variables for the source of observed visitation data (Narragansett Beach, Barnstable Town, Three Bays)

A_i – Area of site i

$\propto$ - intercept

e_{it} – error term

We compared the candidate models based on their predictive performance. To avoid selecting an overfit model and therefore being overconfident in its out-of-sample model performance, we conducted a cross validation by splitting the data into training (in-sample) and test (out-of-sample) sets. We fit the candidate models to the training sets of data, predicted the test sets, and calculated fit statistics on the out-of-sample observations. We did this for 10 random splits of the data using a k-fold cross validation and present the average model performances across the 10 test sets in Table 1 [45-46]. Using this cross-validation technique is a statistical check and a data science best practice. Given the predictive purposes of these classes of models, we suggest that, in the future, a similar cross-validation process should be performed when using proxy-types of data for predicting visitation. Additional regression and random forest outputs, goodness-of-fit metrics, and details can be found in the Supporting Information as well as in the code package (https://github.com/USEPA/Recreation_Benefits.git).

Ethics statement

This work was reviewed and deemed exempt by the Institutional Review Board (Study #17-3334) from the University of North Carolina at Chapel Hill.

Results

Using the cell data product from the data provider resulted in about a four-times overestimation of the type of recreational visitation we were looking to estimate when compared against observations. Despite the scale difference, we found the information contained in the cell data to be valuable to predict visitation across a diverse set of sites after calibration. From our models, there are a few ways to show that it is the information in the cell data that is providing most of the explanatory power as compared to the covariates (weather, area, source of the observational counts). Table 1 shows the regression results using just cell data (columns 1-2), then with additional covariates (columns 3-4). Just using cell data produces a decent model in linear form. The additional value of the covariates can be seen in the improved stats between column 1 and 3 and 2 and 4. In the random forest model, the

cell data was by far the most useful in modeling visitation as seen by metrics of variable importance (see Supporting Information)

Table 1: Regression results

	Visits (1)	Log(Visits) (2)	Visits (3)	Log(Visits) (4)
Cell data	0.245***	0.0003***	0.296***	0.0002***
	(0.005)	(0.0000)	(0.007)	(0.0000)
Area (m^2)			0.00003	0.000006***
			(0.0002)	(0.0000006)
Narragansett			-646.796***	0.182
			(72.136)	(0.225)
Town of Barnstable			-60.612	-0.409***
			(42.119)	(0.131)
Temperature (°F)			10.398***	0.066***
			(2.567)	(0.008)
Precipitation (inches)			-26.180	-0.447***
			(47.250)	(0.147)
Constant	33.128*	4.320***	-334.114	0.539
	(19.496)	(0.064)	(206.779)	(0.644)
Observations	392	392	392	392
R^2	0.86	NA	.89	NA
ME	.27	-430.96	.43	-74.35
RMSE	318.08	3161.23	272.47	1030.21
MAE	186.69	791.33	174.68	345.93

* p<0.10** p<0.05p***p<0.01

Note: Dummy variables are included for month and day of the week in columns 3 and 4. Columns 2 and 4 are in log-linear form. See code and Supporting Information for additional details and candidate

models. Goodness of fit statistics are from out-of-sample sets from a 10-fold cross validation. Log-linear model predictions were converted to people terms for goodness of fit statistics. ME= mean error, RMSE = root mean squared error, MAE = mean absolute error.

Table 2: Performance statistics for candidate models

	ME	RMSE	MAE	R-Squared
Linear model	0.43	272.47	174.68	.89
Log-linear model	-74.35	1030.21	345.93	NA
Random forest	-3.78	262.48	154.84	.91

Note: ME= mean error, RMSE = root mean squared error, MAE = mean absolute error. See Supporting Information for complete set of model output and performance statistics.

Of the candidate models, we chose the random forest as the preferred model, given its predictive performance indicated by the lowest RMSE, MAE, and low bias (ME) during cross validation (see Table 2). To create the final comprehensive visitation dataset, we used the preferred random forest model to predict daily visitation to all 577 water-access areas in our sample for the four summer months (June-September) of 2017. Fig 3 plots predicted visitation using the random forest model against observational counts, showing a tight overall in-sample fit. Our calibrated model produced daily visitation estimates with an out-of-sample mean absolute error of 155 people (Table 2) based on the cross-validation.

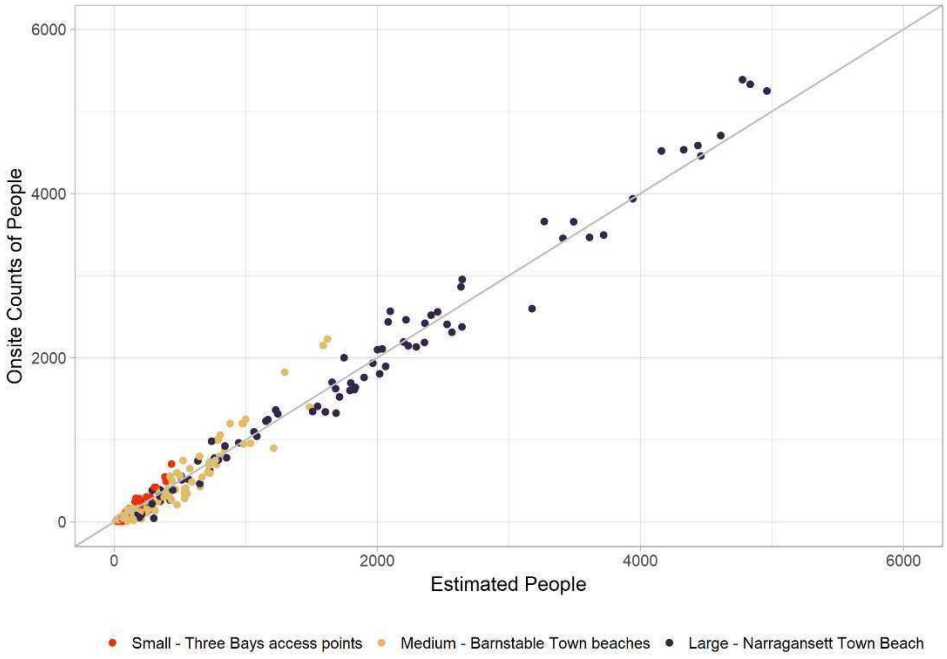

Fig 3. Cell Data Modeled Visitation Compared Against Observations. Predicted daily (9AM-4PM) visits from the cell data model compared to observed visitation at three sizes of water recreation areas in New England, USA.

This model produced comprehensive visitation estimates across the region, but also at each individual site across days. The result of this work, a calibrated dataset of visitation including the code and data for producing the results in this paper can be found at https://github.com/USEPA/Recreation_Benefits.git. As examples of the usefulness of the broad geographical scope of the model and resulting database, Fig 4 shows daily visitation estimates to all public water-access points on Cape Cod for the summer months of 2017. Along with these types of landscape-scale results, the data and model provide focused site-specific information. Fig 5 shows daily visitation to a single beach across the season, information available for all sites and days across the four summer months.

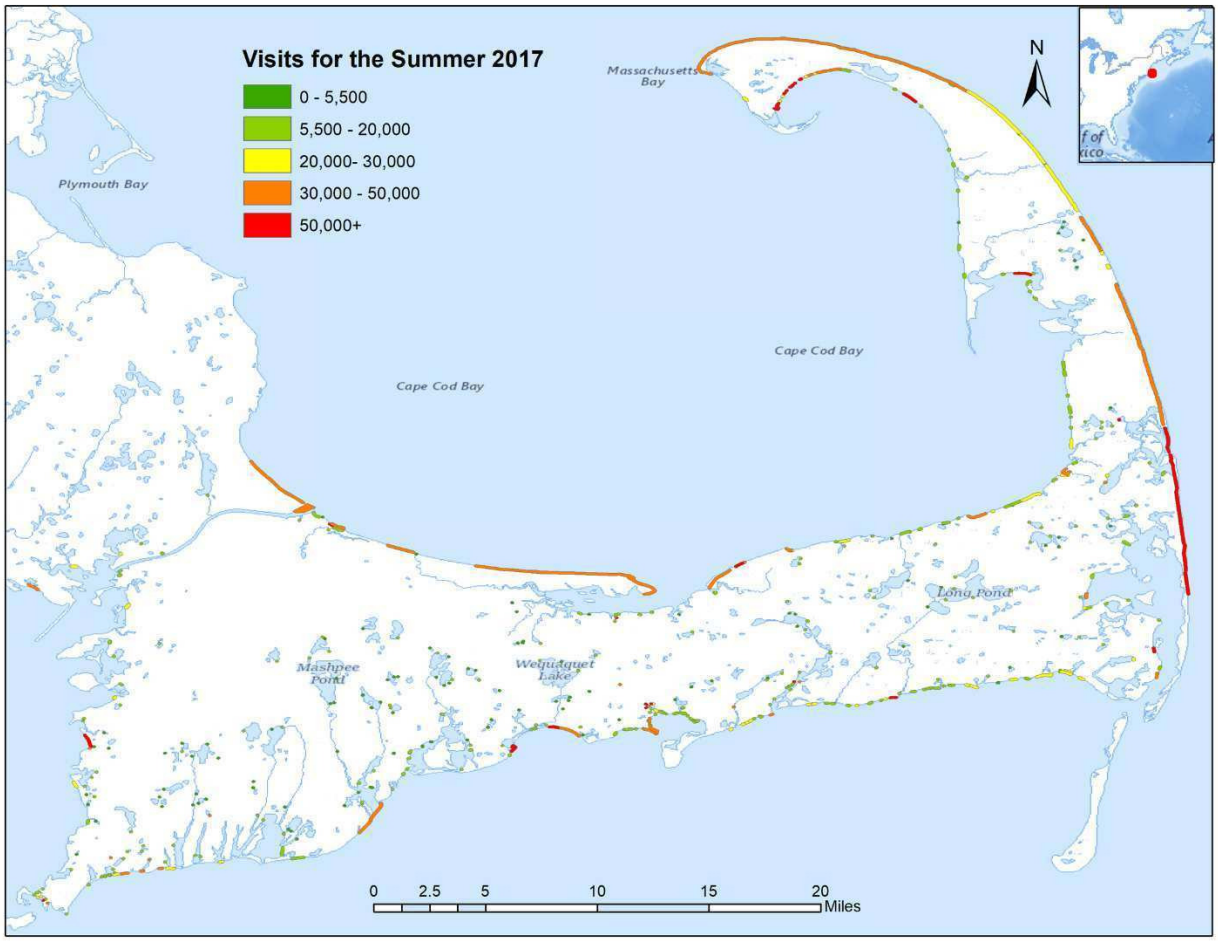

Fig 4. Visitation for Cape Cod, MA, USA for the Summer of 2017. Total predicted visits (9AM-4PM) to water recreation areas for the summer of 2017 (June, July, August, September) for Cape Cod (Barnstable County, MA, USA), using the cell data model.

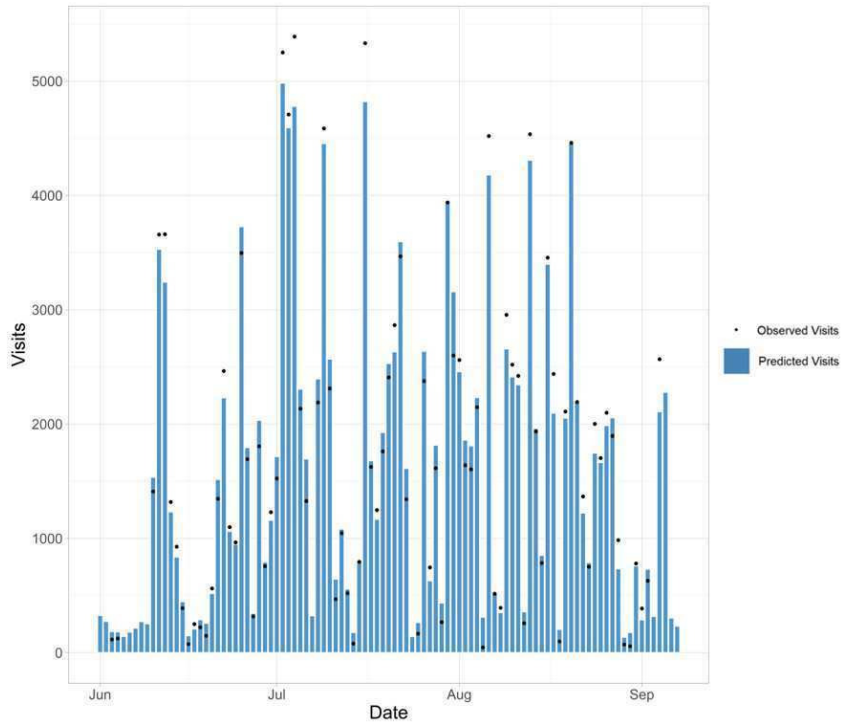

Fig 5. Narragansett Beach, RI, USA, Daily Visitation. Predicted daily (9AM-4PM) visits to Narragansett Town Beach (Narragansett, RI, USA) for the summer of 2017 using the cell data model. These daily predictions are compared to observed visits based on on-the-ground counts.

Since we combined three different sources of visitation data to fit the model, we also ran candidate models on each visitation observation data source separately and the relationships between the cell data and each visitation dataset remained similar (see Supporting Information). The in-sample fit of those models varied, with the smaller access point dataset, Three Bays, the least well fit (R^2 = .36), to better fits with the larger access point of Narragansett Beach (R^2 = .96). The number of observations vary with the sources, as do specifics of how those observations were collected, but we suspect the cell data may be better at predicting visitation to larger areas, with more daily visitation. There are more cellular devices in a sample of a day at the more popular places to estimate visitation from, likely reducing noise in the estimate.

We chose to use the most accurate and unbiased of the candidate statistical models for prediction. However, there are several sources of potential inaccuracies and biases in estimating visitation in this way that are not incorporated

in the metrics of model goodness-of-fit. The observational visitation counts contain their own uncertainties and potential biases based on their sampling design and counting methods. By calibrating and validating to those counts, we may be carrying over those issues to our estimates of visitation. In addition, the cellular data contains uncertainties resulting from the geospatial accuracy of the device locations, our geographic definition of the sites, and the methods of expansion from the device sample to population level estimates. More applications using cell datasets are needed to understand these limitations combined with additional and more consistent collections of visitation observations are crucial to addressing these issues.

The models we fit may also be susceptible to spatial autocorrelation issues resulting from the cell dataset if there are variations in how the data represents visitation geographically. Spatial autocorrelation in models potentially inflates goodness-of-fit estimates, can bias parameters and reduces predictive performance. We have controls in the models for each group of sites, which are geographically clustered. This may alleviate some of the potential issue. Similarly, collinearity in the covariates could potentially cause poor predictions, attributing predictive information to the wrong covariate, for example. We checked for this issue in a few ways, building up the model covariates sequentially starting with cell data alone and adding covariates. This led to little change in the relationships between observations and cell data counts (see Supporting Information for more model details and variations). We also consistently found good out-of-sample goodness-of-fit metrics in a cross validation, giving us more confidence that spatial autocorrelation and collinearity were likely not an issue in the models' predictive performance.

Discussion

We contend that the use of cell data provides a valuable method to quantify visitation across large numbers of areas and over time. When calibrated, the cell data provided an accurate and consistent way to estimate visitation to natural areas. It allowed us to produce a previously unavailable dataset of water visitation at a policy-relevant resolution, spatial extent, and consistency. The information provides visitation details for specific locations at a regional or sub-regional scale, the scale at which most decisions and policies regarding public natural areas are made. Understanding the scale and timing of visitor use of an area allows managers to determine and provide appropriate facilities and safety precautions and researchers to predict impacts of environmental change, measure

effects of natural disasters, and conduct research on social and economic value of public access to natural areas. To date, no other methods for quantifying use have the same capacity for providing location-specific data across broad geographic areas at such a high temporal resolution.

The data can inform landscape-level analyses of behavior to understand, at a broader scale, the impacts of changes in environmental quality across time as well as across access geography. The origin data can be used to better understand who visits an access point based on where they come from. This provides informative profiles regarding the characteristics of people and communities that are, or could be, affected by environmental degradation or improvements or other policy and management decisions. Taking advantage of variations in behavior and environmental quality across time, cell data's fine temporal resolution opens avenues for longitudinal studies. For instance, it provides the ability to quantify the number of visitors affected and economic impacts incurred from beach closures, algal blooms, oil spills, or other events that typically are not captured consistently with current methods or lack baseline data for measuring impacts.

Given our results, we suggest caution in using visitation estimates out-of-the-box from data providers without calibration. There is useful information in the datasets, but we found that calibration was necessary to confidently use the data for our purposes. In its delivered form, the data overestimated use of the type we were interested in quantifying, recreational visits to water-access areas. We hypothesized the need for this correction based on a few practical factors discussed below.

We were only able to define recreation visitation by limiting the area of the requested geographies (the GIS information for the sites we requested from the data providers) where recreation would likely be the primary purpose for visiting the area and during time-windows of interest. Inherently, the on-the-ground visitation observations were more restrictive in capturing visits for recreation and not capturing ancillary or non-recreational visits to the geographies, like walking by the site on a nearby road. It is also reasonable to assume some observational counts may be conservative and under-report recreation visitation due to sampling constraints.

Additionally, there is a cascade of statistical modeling assumptions that are made by the third-party providers to take raw device locational information to the anonymized and aggregated form delivered to the customers (see Supporting Information for the publicly available description of Airsage's process). The exact details of each private provider's data processing workflows are their intellectual property and protected as such. This opaqueness

motivates the use of methods to judge performance critically and the construction of additional models based on common cell data products for popular environmental applications, such as the one described in this paper. Because the methods used by the data providers are constantly in development, estimating performance on common observational datasets and with common methods would provide more clarity and confidence (statistical and otherwise) for cell data's use in policy and management applications. In some cases, lack of cellular connectivity in some natural areas may also limit its usefulness, although GPS-based and application derived locational methods have overcome some of this limitation by passing along information when the device is reconnected to a network. It is in a user's best interest to calibrate the product for their application, when possible, or consider the uncalibrated information as a relative metric. We demonstrated a simple method to do a calibration in this paper and provide the data and code for others to work from and improve as more users apply these types of data products.

While cell data-derived information is an exciting development for researchers and managers, counterintuitively, we found attempting to use it for a practical application only further motivated the need to take more accurate, consistent and unbiased observations of visitation using traditional methods. Modeling methods are hindered by the lack of availability of training datasets and would be greatly improved by larger and more uniformly collected observations. This is especially true regarding machine-learning algorithms [47]. For example, with small and practical tweaks in the way visitation records are collected at water-access areas, such as collecting periodic counts of cars and people at specific times, visitation records could become more harmonized and useful [12,41]. From there, visitation proxies like cell data or social media-based models can provide a platform for spatial and temporal extrapolation across broad geographies, as we demonstrate here. The need for such models is not confined to water-access visitation, as it is relevant to many other similar policy contexts, for example, at national parks or urban green-spaces. The differences in how well our models fit depending on the visitation data source, with larger more popular locations fit better than small, should be cautionary to approaches applying the cell data-derived visitation estimates to settings where there is no similar observational data for comparison.

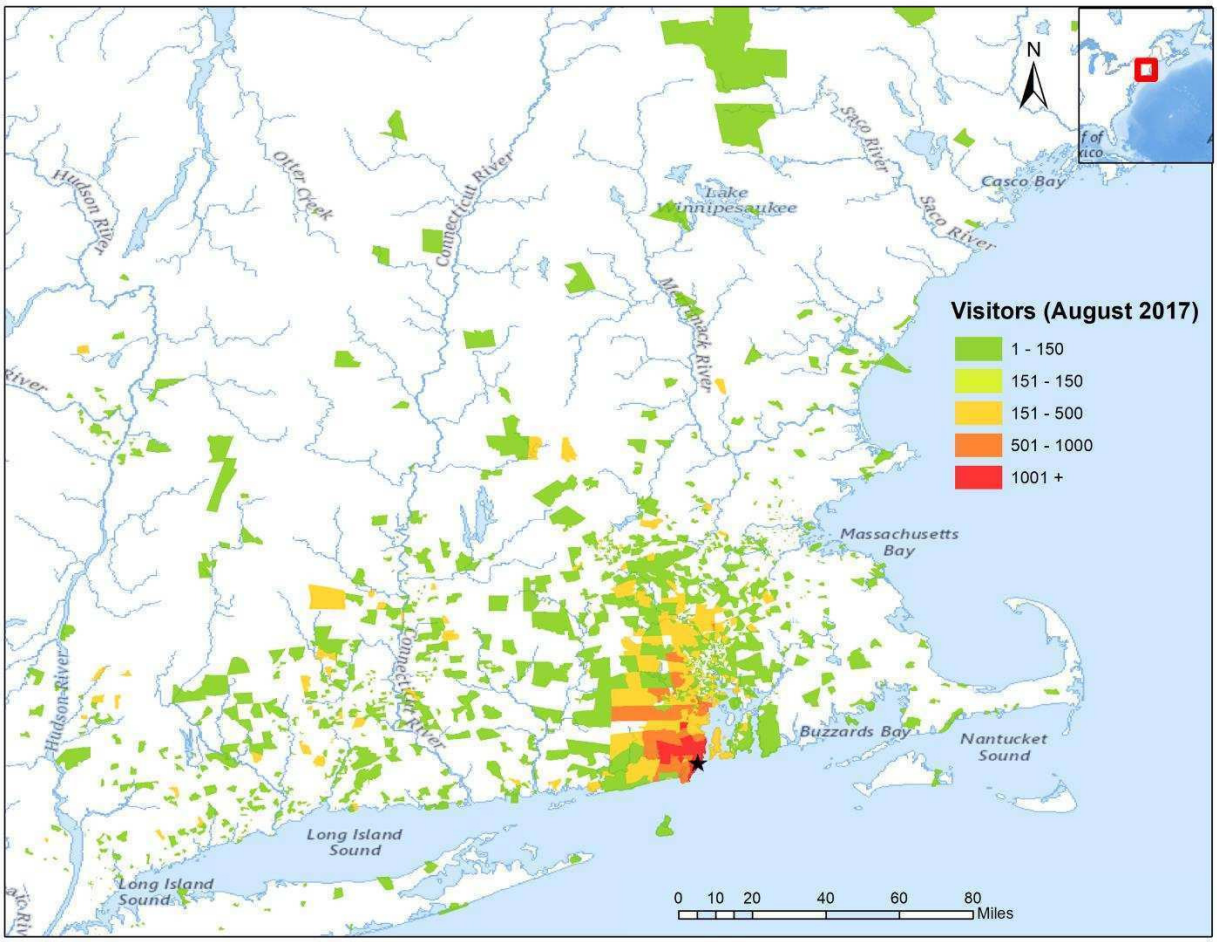

Fig 6. Visitor Origins for Narragansett Beach, RI, USA. Count of visitors by census block group origins for visitors to Narragansett Town Beach, Narragansett RI, USA, (black star on the map) in August 2017. This monthly origin information exists for each of the 577 access points in our sample.

In this paper we explored only a few dimensions of the information in the cell data-derived dataset, focusing on estimating visitation. The origin information provided about the visitors to the water-access sites--monthly visitation by site and census block groups in our case--provides the type of data needed for a myriad of travel-demand models for recreation [48]. Previous social media-based work [18] pointed out this potential opportunity, but travel-demand models typically require more spatially and temporally resolved information than what can be found currently in data derived from social media. Fig 6 displays origin-destination data for one site, Narragansett Beach, Rhode Island, for August 2017. Our dataset includes this information for all sites and months. More work is needed to

calibrate and validate the origin-destination information provided by cell data products for environmental applications and more generally [49]. Validating the origin data and fitting travel-demand models is beyond the scope of this paper and is left for future work. We include the origin-destination data in the data package associated with this paper for any other users that wish to tackle this natural next step. As with the visitation estimates, the possibility of using new sources of data for origin-destination travel-demand models encourages implementation of more commonly-worded and formatted general population and visitor intercept surveys to provide the necessary corroborating and calibrating datasets.

The visitation dataset resulting from the work in this paper is useful for federal, state and town managers and agencies in the region for any number of applications requiring visitor use information. For example, state managers may use this information to determine the allocation of beach monitoring resources, a town shellfish warden may use it to identify the most actively fished sites, or a tourism board could use it to understand the profile of visitors to popular natural attractions. Of broader interest in natural resource management and research, these types of models using cell data and a similar calibration process could be developed for other areas or for other purposes such as understanding the scale of ecosystem services, human-wildlife conflict, water consumption demand, or emergency response, for example.

Acknowledgments

The views expressed in this article are those of the authors and do not necessarily represent the views or policies of the U.S. Environmental Protection Agency. This contribution is identified by tracking number ORD-028692 of the U.S. Environmental Protection Agency, Office of Research and Development, Center for Environmental Measurement and Modeling, Atlantic Coastal Environmental Sciences Division. We would like to thank Anne Neale, Bryan Milstead and Ryan Furey for their thoughtful reviews.

Product Disclaimer

Mention of trade names or manufacturers does not imply U.S. Government endorsement of commercial products.

Competing Interests

The author(s) declare no competing interests.

Data Availability

The code and datasets used and generated during the current study are available in the USEPA Recreation Benefits repository, https://github.com/USEPA/Recreation_Benefits.git. Supporting Information accompanies this paper.

References

1. Leeworthy VR, Wiley PC. Current participation patterns in marine recreation. National Oceanic and Atmospheric Administration. 2001 Nov.
2. Tourangeau R, English E, McConnell KE, Chapman D, Cervantes IF, Horsch E, Meade N, Domanski A, Welsh M. The Gulf recreation study: Assessing lost recreational trips from the 2010 Gulf Oil Spill. Journal of Survey Statistics and Methodology. 2017 Jul 6;5(3):281-309.
3. Horsch E, Welsh M, Price J, Domanski A, Meade NF, Murray J. Best practices for collecting onsite data to assess recreational use impacts from an oil spill. 2017 Available from: ftp://ftp.library.noaa.gov/noaa_documents.lib/NOS/ORR/TM_NOS_ORR/TM_NOS-ORR_54.pdf
4. Deacon RT, Kolstad CD. Valuing beach recreation lost in environmental accidents. Journal of Water Resources Planning and Management. 2000 Dec;126(6):374-81.
5. Da Silva CP. Beach carrying capacity assessment: how important is it? Journal of Coastal Research. 2002 Mar;36(sp1):190-8.
6. Dwight RH, Brinks MV, SharavanaKumar G, Semenza JC. Beach attendance and bathing rates for Southern California beaches. Ocean & Coastal Management. 2007 Jan 1;50(10):847-58.

7. Harada SY, Goto RS, Nathanson AT. Analysis of lifeguard-recorded data at Hanauma Bay, Hawaii. Wilderness & Environmental Medicine. 2011 Mar 1;22(1):72-6.
8. King P, McGregor A. Who's counting: An analysis of beach attendance estimates and methodologies in southern California. Ocean & Coastal Management. 2012 Mar 1;58:17-25.
9. Garcia A, Smith JR. Factors influencing human visitation of southern California rocky intertidal ecosystems. Ocean & Coastal Management. 2013 Mar 1;73:44-53.
10. Kreitler J, Papenfus M, Byrd K, Labiosa W. Interacting coastal based ecosystem services: recreation and water quality in Puget Sound, WA. PloS One. 2013 Feb 22;8(2):e56670.
11. Morgan D. Development of a method to estimate and predict beach visitation. Tourism in Marine Environments. 2016 Dec 12;12(1):69-77.
12. Leggett CG. Sampling strategies for on-site recreation counts. Journal of Survey Statistics and Methodology. 2017 Sep 1;5(3):326-49.
13. Lyon SF, Merrill NH, Mulvaney KK, Mazzotta MJ. Valuing coastal beaches and closures using benefit transfer: An Application to Barnstable, Massachusetts. Journal of ocean and coastal economics. 2018 May;5(1):1-.
14. English DB. Forest Service national visitor use monitoring process: research method documentation. US Forest Service, Southern Research Station; 2002.
15. Fisher DM, Wood SA, White EM, Blahna DJ, Lange S, Weinberg A, Tomco M, Lia E. Recreational use in dispersed public lands measured using social media data and on-site counts. Journal of Environmental Management. 2018 Sep 15;222:465-74.
16. Van Berkel DB, Tabrizian P, Dorning MA, Smart L, Newcomb D, Mehaffey M, Neale A, Meentemeyer RK. Quantifying the visual-sensory landscape qualities that contribute to cultural ecosystem services using social media and LiDAR. Ecosystem Services. 2018 Jun 1;31:326-35.
17. Keeler BL, Wood SA, Polasky S, Kling C, Filstrup CT, Downing JA. Recreational demand for clean water: evidence from geotagged photographs by visitors to lakes. Frontiers in Ecology and the Environment. 2015 Mar;13(2):76-81.
18. Wood SA, Guerry AD, Silver JM, Lacayo M. Using social media to quantify nature-based tourism and recreation. Scientific Reports. 2013 Oct 17;3:2976.

19. Hamstead ZA, Fisher D, Ilieva RT, Wood SA, McPhearson T, Kremer P. Geolocated social media as a rapid indicator of park visitation and equitable park access. Computers, Environment and Urban Systems. 2018 Nov 1;72:38-50.
20. Tenkanen H, Di Minin E, Heikinheimo V, Hausmann A, Herbst M, Kajala L, Toivonen T. Instagram, Flickr, or Twitter: Assessing the usability of social media data for visitor monitoring in protected areas. Scientific Reports. 2017 Dec 14;7(1):17615.
21. Sonter LJ, Watson KB, Wood SA, Ricketts TH. Spatial and temporal dynamics and value of nature-based recreation, estimated via social media. PLoS One. 2016 Sep 9;11(9):e0162372.
22. Solmaz G, Turgut D. A survey of human mobility models. IEEE Access. 2019 Sep 3;7:125711-31.
23. Toole JL, Colak S, Sturt B, Alexander LP, Evsukoff A, González MC. The path most traveled: Travel demand estimation using big data resources. Transportation Research Part C: Emerging Technologies. 2015 Sep 1;58:162-77.
24. Blondel VD, Decuyper A, Krings G. A survey of results on mobile phone datasets analysis. EPJ Data Science. 2015 Dec 1;4(1):10.
25. Calabrese F, Ferrari L, Blondel VD. Urban sensing using mobile phone network data: a survey of research. Acm Computing Surveys (csur). 2014 Nov 12;47(2):1-20.
26. Çolak S, Alexander LP, Alvim BG, Mehndiratta SR, González MC. Analyzing cell phone location data for urban travel: current methods, limitations, and opportunities. Transportation Research Record. 2015 Jan;2526(1):126-35.
27. Toole JL, Ulm M, González MC, Bauer D. Inferring land use from mobile phone activity. In Proceedings of the ACM SIGKDD International Workshop on Urban Computing 2012 Aug 12 (pp. 1-8). ACM.
28. Toch E, Lerner B, Ben-Zion E, Ben-Gal I. Analyzing large-scale human mobility data: a survey of machine learning methods and applications. Knowledge and Information Systems. 2019 Mar 5;58(3):501-23.
29. Frias-Martinez V, Soguero-Ruiz C, Frias-Martinez E, Josephidou M. Forecasting socioeconomic trends with cell phone records. In Proceedings of the 3rd ACM Symposium on Computing for Development 2013 Jan 11 (pp. 1-10).

30. Athey S, Blei D, Donnelly R, Ruiz F, Schmidt T. Estimating heterogeneous consumer preferences for restaurants and travel time using mobile location data. In AEA Papers and Proceedings 2018 May (Vol. 108, pp. 64-67).
31. Kung KS, Greco K, Sobolevsky S, Ratti C. Exploring universal patterns in human home-work commuting from mobile phone data. PloS One. 2014 Jun 16;9(6):e96180.
32. Lu X, Bengtsson L, Holme P. Predictability of population displacement after the 2010 Haiti earthquake. Proceedings of the National Academy of Sciences. 2012 Jul 17;109(29):11576-81.
33. Wesolowski A, Eagle N, Tatem AJ, Smith DL, Noor AM, Snow RW, Buckee CO. Quantifying the impact of human mobility on malaria. Science. 2012 Oct 12;338(6104):267-70.
34. Kraemer MU, Golding N, Bisanzio D, Bhatt S, Pigott DM, Ray SE, Brady OJ, Brownstein JS, Faria NR, Cummings DA, Pybus OG. Utilizing general human movement models to predict the spread of emerging infectious diseases in resource poor settings. Scientific Reports. 2019 Mar 26;9(1):5151.
35. Yu H, Russell A, Mulholland J, Huang Z. Using cell phone location to assess misclassification errors in air pollution exposure estimation. Environmental Pollution. 2018 Feb 1;233:261-6.
36. Li M, Gao S, Lu F, Tong H, Zhang H. Dynamic estimation of individual exposure levels to air pollution using trajectories reconstructed from mobile phone data. International Journal of Environmental Research and Public Health. 2019 Jan;16(22):4522.
37. Kubo T, Uryu S, Yamano H, Tsuge T, Yamakita T, Shirayama Y. Mobile phone network data reveal nationwide economic value of coastal tourism under climate change. Tourism Management. 2020 Apr 1;77:104010.
38. Kim YJ, Lee DK, Kim CK. Spatial tradeoff between biodiversity and nature-based tourism: Considering mobile phone-driven visitation pattern. Global Ecology and Conservation. 2020 Mar 1;21:e00899.
39. Monz C, Mitrovich M, D'Antonio A, Sisneros-Kidd A. Using mobile device data to estimate visitation in parks and protected areas: an example from the nature reserve of orange county, California. Journal of Park and Recreation Administration. 2019;37(4).
40. Wallmo K. Assessment of techniques for estimating beach attendance. Beach Sampling Report of NOAA. 2003 Apr;10.

41. Mulvaney KK, Atkinson SF, Merrill NH, Twichell JH, Mazzotta MJ. Quantifying recreational use of an estuary: a case study of Three Bays, Cape Cod, USA. Estuaries and Coasts. 2020 Jan 1;43(1):7-22.
42. RCore T.E.A.M. R: A language and environment for statistical computing. R Foundation for Statistical Computing, Vienna, Austria. URL http://www. R-project. org. 2016.
43. Ziegler A, König IR. Mining data with random forests: current options for real-world applications. Wiley Interdisciplinary Reviews: Data Mining and Knowledge Discovery. 2014 Jan;4(1):55-63.
44. Wright MN, Ziegler A. ranger: A fast implementation of random forests for high dimensional data in C++ and R. arXiv preprint arXiv:1508.04409. 2015 Aug 18.
45. Kohavi R. A study of cross-validation and bootstrap for accuracy estimation and model selection. In Ijcai 1995 Aug 20 (Vol. 14, No. 2, pp. 1137-1145).
46. Rodriguez JD, Perez A, Lozano JA. Sensitivity analysis of k-fold cross validation in prediction error estimation. IEEE Transactions on Pattern Analysis and Machine Intelligence. 2009 Dec 1;32(3):569-75.
47. Witten IH, Frank E, Hall MA, Pal CJ. Data Mining: Practical machine learning tools and techniques. Morgan Kaufmann; 2016 Oct 1.
48. Phaneuf DJ, Smith VK. Recreation demand models. Handbook of Environmental Economics. 2005 Jan 1;2:671-761.
49. Vanhoof M, Reis F, Ploetz T, Smoreda Z. Assessing the quality of home detection from mobile phone data for official statistics. Journal of Official Statistics. 2018 Dec 1;34(4):935-60.

Supporting Information

Supplementary Table S1. Performance statistics for candidate models. Car counts of resident and public parking lots were used to find the ratio of resident and public use of the beach. This ratio was applied to daily counts from ticket receipts (public only) to estimate total daily visitation.

Supplementary Table S2. Candidate regressions. Dummy variables are included for month and day of the week in each regression. Columns 2 and 4 are in log-linear form. See code for additional details and candidate models.

Supplementary Table S3. Out-of-sample performance statistics for each candidate model. Each candidate model is presented with varying explanatory variables and functional form. ME= mean error, RMSE = root mean squared error, MAE = mean absolute error, MAPE = mean absolute percent error, R-squared= % of out-of-sample variance explained.

Supplementary Table S4: Linear regression results on each observational count source. Each column contains observations from each source of visitation observation information. Dummy variables are included in all regressions for month and day of the week. R-squared= % of in-sample variance explained.

Supplementary Figure S1. Mean squared errors when considering a different number of candidate prediction variables at each split in a tree.

Supplementary Figure S2. Variable importance plot using the 'impurity' method in R package Ranger.

Title: Using Data Derived from Cellular Phone Locations to Estimate Visitation to Natural Areas: An Application to Water Recreation in New England, USA.

Authors: Nathaniel H. Merrill[1]*, Sarina F. Atkinson[2], Kate K. Mulvaney[1], Marisa J. Mazzotta[1], Justin Bousquin[3]

[1] U.S. Environmental Protection Agency, Office of Research and Development, Center for Environmental Measurement and Modeling, Atlantic Coastal Environmental Sciences Division, Narragansett, Rhode Island, USA

[2] Cooperative Institute for Marine & Atmospheric Studies, Rosenstiel School of Marine & Atmospheric Science, University of Miami, Miami, Florida, USA

[3] U.S. Environmental Protection Agency, Office of Research and Development, Center for Environmental Measurement and Modeling, Gulf Ecosystem Measurement and Modeling Division, Gulf Breeze, Florida, USA

* Corresponding author, U.S. EPA, Office of Research and Development, Center for Environmental Measurement and Modeling, Atlantic Coastal Environmental Sciences Division, 27 Tarzwell Drive, Narragansett, RI 02882, merrill.nathaniel@epa.gov

Author Contribution

N.H.M, S.F.A, K.K.M., M.J.M. designed the study. N.H.M, S.F.A, J.B. performed the analysis. N.H.M, S.F.A, K.K.M., M.J.M., J.B. wrote the manuscript.

Abstract

We introduce and validate the use of commercially-available human mobility datasets based on cell phone locations to estimate visitation to natural areas. By combining this data with on-the-ground observations of visitation to water recreation areas in New England, we fit a model to estimate daily visitation for four months to more than 500 sites. The results show the potential for this new big data source of human mobility to overcome limitations in traditional methods of estimating visitation and to provide consistent information at policy-relevant scales. However, the data providers' opaque and rapidly developing methods for processing locational information required a calibration and validation against data collected by traditional means to confidently reproduce the desired estimates of visitation. We found that with this calibration, the high-resolution information in both space and time provided by cell phone location-derived data creates opportunities for developing next-generation models of human interactions with the natural environment.

Introduction

People visit natural areas to view the scenery and wildlife or to engage in any number of recreational activities they enjoy. These areas are important to society, as shown through the sheer number of people who visit parks, beaches, walking trails, and other natural spaces and their significant contribution to the economy [1]. However, it is difficult to quantify the use of natural areas across the many, diverse locations and the timing of those visits. Observational counts are time consuming and expensive to conduct and traditional survey approaches have their own sampling complications for estimating visitation. Therefore, it is often unknown how many and what types of people visit natural areas -- critical information for managers or researchers to apply in natural resource damage assessments, park and urban planning, economic valuation studies, tourism studies, as well as to inform many other management decisions [2-3].

This paper demonstrates the use of commercially available anonymized and aggregated data on cellular device locations to estimate visitation to natural areas. For brevity, we refer to these cellular device location-based datasets generally as "cell data" in this paper. We investigated how cell data performs in providing the types of visitation

information needed in policy applications, information on the temporal and spatial distribution of visits to natural areas. Specifically, we compared the cell data with on-the-ground daily visitation counts that we collected, along with other federal, state and town records for water recreation areas. We found that the cell data contained useful information for estimating visitor use, but it required a correction (calibration) to match the scale of the observations and to be confident with its wider application. We then built and applied a statistical model to estimate daily visitation with cell data to more than 500 water recreation areas in the northeastern United States for the primary four months of recreational use (June-September) of 2017.

Our application demonstrates the potential for this emerging source of big data to provide comprehensive visitation information across many places and time windows, a feat that would be impractical with traditional methods. The high-resolution information in space and time provided by cell data expands opportunities for developing next-generation models of human interactions with the natural environment. In addition, cell data provides the ability to know not just how many people are visiting specific locations, but also where visitors are coming from within aggregated geographies. This information allows for basic calculations of distance traveled to a location and a deeper understanding of the community composition of visitors. While these new data sources may potentially help overcome many logistical barriers to obtaining behavioral information at scale, our work highlights the ongoing need for traditional methods of collection for calibration and validation for these new data sources to be useful in common applications.

Background

Existing visitation information for natural areas is limited and currently comes from many different, often inconsistent, sources. There are visitation estimates derived from entrance fees, parking fees, lifeguard counts, car or people electronic counters, aerial surveys, remote sensing, or tailored observational sampling plans [4-14]. Each data source comes with its own nuances in terms of sampling issues and geographical and temporal coverage. Most ongoing visitation collection efforts only capture paying customers during the hours of fee collections, thereby providing only a subset of daily use. There are also detailed collections that coincide with a specific project or event, such as an oil spill, but the knowledge is often not generalizable past a particular region or time-period. Often, the

need to obtain visitation information arises after an event has occurred, making the before and after comparison difficult [3]. These event-based data collections are also resource intensive [2].

Efforts to overcome these barriers using other types of digital records include estimates derived from photo-sharing or other types of social media posts [15-21]. These techniques have been useful in estimating visitation to large parks, attractions, and natural areas around the world over long periods of time by providing monthly, seasonal, or yearly visitation estimates. However, these data sources represent only the small fraction of the public that opt to use those specific social media outlets, and they lack adequate temporal and spatial resolution. These factors limit the ability of social-media based methods to inform broader policies or localized environmental management. Use of cellular devices is much more common and the resolution of the information provided is much finer in both time and space.

Cell data come from the digital traces of people's cell phone use and location. In the past, this was based on the location of the tower a device was communicating with or a triangulation from the device to various cellphone towers. This data provided information based on many people, but with locational and temporal accuracy issues related to connectivity to the cellphone tower network and peoples' active use of the phone [22]. With the addition of GPS instrumentation and the growing ubiquity of smartphone-style cellular telephones, these digital traces have become more accurate, more frequent and represent an increasing proportion of the population [23-28]. The device-level, raw data are collected by cellular telephone providers, GPS enabled devices and increasingly by smartphone applications. Several third-party providers on the commercial market combine this information and sell processed data in a variety of formats [28].

Cell data in various forms have been used most widely in the transportation and urban planning fields to understand use of public infrastructure and commuting [23-26] and to assist in land use classifications [27]. This data has also been used to understand economic trends [29], restaurant choice [30] and in epidemiology and population research in developing countries [31-34]. Despite its promise, there are limited environmental applications of the data to date, with notable applications concerning natural disasters [32] and air quality [35-36].

There are a few recent applications of cell data to understand behavior in and around natural areas [37-39]. Kubo et al. [37] used cell data to calculate the economic value of coastal tourism across Japan, but provided no ground truth to the visitation information. For an island park in Korea [38], Kim et al. applied cell data to analyze tradeoffs

between visitation and biodiversity and showed decent correlations between the cell data and monthly estimates of visitation to several specific locations on the island. A study of parks in California, USA, is the closest to the work presented in this paper [39]. The study used a similarly processed cell data product from a third-party vendor to estimate daily park visitation. They calibrated the cell data with just one set of data, vehicle counts on a major nearby road, finding a unit-value correction factor. They then validated their estimates against a single park's gate traffic and parking information. They found good agreement with their corrected cell data model and daily vehicle counts. From there, they used park-specific vehicle-to-people ratios to extrapolate to the number of visitors to the other twenty-one parks of interest. Our study differs by incorporating multiple visitation records representing counts of people to a wider set of locations: eighteen different water recreation areas. We find similar potential for this data source to provide useful, policy-relevant visitor use information at daily and site-level scales for water recreation areas.

Data description

We identified and purchased a dataset of visitation derived from cell phone locations for a set of geographies and time to understand the extent, temporal distribution, and value of water recreation for Cape Cod, Barnstable County, Massachusetts and New England, USA in general. The set of water recreation areas comprises a comprehensive list of all the public beaches and public access points to water (fresh and saltwater beaches, public access points, parks, ways to water, and boat ramps) for Barnstable County, Massachusetts, compiled from federal, state, county, and town GIS information (n=464), and an additional set of beaches across greater New England (n=113). The data we used consists of estimates of visitation to these water recreation areas over the summer months of 2017 (June through September).

We purchased data products processed by a third-party provider, Airsage, Inc. This provider creates population-level estimates of human mobility derived from a panel of over 120 million devices using location information from smartphone applications (see Supporting information). The data provider processes this device-specific locational information. Before we receive it, the data is anonymized and aggregated to contain no personally identifiable information. We do not obtain any device-level information, nor raw device GPS locations, but instead, we obtain

aggregated summaries of visitation by recreation site and estimates of the visitors' origin census block-group geographies. The data provider translates their sample to population-level estimates using weights based on the share of the population their sample represents by census-tract geographies. The cellular device sample we purchased data from includes about 30% of the U.S. population but varies by tract and month.

To obtain the cell data for the sample geographies of interest, we spatially buffered (added area) around the water-access sites which were designated as line or point features in the original spatial databases. In consultation with the data provider and after attempting a range of spatial buffers, a 100-meter buffer was chosen to balance specificity in capturing water recreation visits (i.e., not capturing ancillary points of interest in geographies, like restaurants or stores, for example) with the accuracy of the locational information. We sent the defined water recreation areas to the data provider as a set of geographic extents, or polygons (see Fig 1 for examples of area definitions), and they returned the aggregated and anonymized processed data in tabular form. We include a sample of the dataset below (Table 1) and include the entirety of this dataset available with the code package associated with this work at https://github.com/USEPA/Recreation_Benefits.git.

Table 1: Sample of dataset derived from cell phone locations

POI	DATE	HH00	HH01	HH02	HH03	HH04	HH05	…	HH20	HH21	HH22	HH23	DEVICE_TOTAL
1	20170601	251	96	47	0	171	488	…	668	848	812	222	21895
1	20170602	245	202	133	148	112	646	…	594	604	1157	468	21526
1	20170603	299	148	196	243	340	135	…	922	1283	1100	759	19449
1	20170604	658	332	117	372	414	395	…	1071	186	404	286	19415
2	20170601	0	0	0	0	0	0	…	86	0	0	0	1103
2	20170602	114	0	0	0	0	50	…	138	312	0	48	2746
2	20170603	0	0	0	0	0	0	…	238	226	122	66	2247
2	20170604	66	66	66	66	0	0	…	156	33	0	54	2046

Note: POI indexes the water access locations and each column represents estimated visitation in hourly windows, with HH00 being 12AM-1AM. DEVICE_TOTAL refers to the estimate of unique devices seen in any of the 24 hours at that water access location.

The locational accuracy of the device locations underpinning the data range depending on the source device and the smartphone application. The accuracy of reported locations from applications varies with ranges of 1-10 meters

(GPS), 20-200 meters (Wi-Fi), and 100-2000 meters (cell tower-based) based on the method(s) each application uses to locate each device. We were not able to obtain an average locational accuracy for devices seen in our geographies in our specific dataset since the smartphone applications do not report the exact location methods to the data provider and we do not receive device-specific locational information. Given the potential range in location accuracy, visits attributed to a water recreation area could have actually been to a nearby attraction, or vice-versa. We chose a relatively small buffer around the recreation areas to be conservative in defining the area attributed to use of the site and to minimize any mis-located visits. Given this and other limitations, we relied on the calibration and validation to on-the-ground visitation counts to assess the usefulness and accuracy of the cell data for our application and the choice of spatial definitions and buffers around sites.

Fig 1. Example Definition of Water Recreation Areas. Dowses Beach, Barnstable, Massachusetts, USA and nearby water access areas. Point and line features representing water recreation access were buffered by 100 meters to capture use at the sites. These geographic areas correspond to the sample of visitation estimates from the cell data.

In total, the cell dataset includes visitation estimates for 51,511 days across 577 sites. A complete set would be 70,394 days (577 sites x 122 days), but some of the days for some sites are missing due to low visitation and detection limits. A visit was defined as a device location history implying a stay estimated to be longer than five minutes at a geography that was not the home or work location of the device based on the behavior of that device over the month. Home was defined as the census block group where the device is most often seen over the month between 9PM-6AM (see Supporting Information).

In addition to estimates of visits, the cell data for each area also includes the home location of those visitors, either at the census block-group level or categorized as international if the origin was outside of the United States. For example, the data may show 100 people visited beach x during a time period, with 30 of those people come from census block y, 20 from census block z, and so on. The monthly visitor origin-destination data contains 642,915 data points representing monthly trip totals (577 sites x origin census block groups, which vary by site and month). This total is not inclusive of the data representing zero trips to destinations originating from block groups implied by the full origin-destination matrix. Because of the geographic and temporal scope, collecting this same information with traditional methods would be prohibitively expensive, time consuming, and inconsistent.

Methods

To investigate the cell data's ability to reproduce daily visitation counts, we compared the cell data to a series of observational counts collected from three different, commonly recorded sources for beach and park visitations. We then calibrated a model to translate the cell data into consistent estimates of visitation across many sites in the region of interest and across many days. We purposely designed the calibration to cover a wide range of access location sizes and visitation totals to test the transferability of the cell data and models built from it. No visitation dataset alone was perfect for use in calibration across a wide range of locations due to differences in counting methods, which is a common limitation to visitation records to natural spaces, generally. Capturing visitation to natural areas is very challenging, and existing approaches all have their own limitations for capturing daily visitation [39]. The observational data that overlaps with the cell data consists of: 1) onsite counts of small access points to an estuary,

2) a town's visitation estimates for their managed beaches, and 3) entrance fees collected by a town to a major beach.

Visitation observation methods also vary because the context for taking them differ. Although the objective may be the same, observing visitation at a major beach requires different methods than those used for a set of small access points around an estuary [41]. By comparing and calibrating our data to a combined set representing the variety of recreational visitation count methods that exist in the real world, we show the ability of cell data to both replicate the types of data that are traditionally used and to bridge the various observational visitation records common around natural resources. Each source of observational data is briefly described below.

- **Small:** We quantified use of the Three Bays estuary system on Cape Cod, Massachusetts through observational sampling for eleven public access points within the estuary. The counts were taken as a combination of periodic people and car counts and sunrise-to-sunset counts of visitors and cars. The public access points include beaches, docks, boat ramps, and landings. Observational data from this study include visitation estimates for 11 public access points for seven days from June to August, 2017 [41]. (N=72)

- **Medium:** The diverse set of beaches for Barnstable, Massachusetts, on Cape Cod includes saltwater and freshwater beaches accessible to either the public or to town residents only. The dataset provided by the Town of Barnstable's Recreation Division includes daily visitation estimates from lifeguard counts for seven of their beaches from Memorial Day (May 29) to Labor Day (September 4), 2017. (N=234)

- **Large:** Narragansett Town Beach in Rhode Island is a popular destination for tourists and residents. Access to this beach is divided into resident only and public entrances. The public entrance requires an entrance fee for each person providing an accurate dataset of daily visitation to the beach. However, these entrance fees are only collected for the public part of the beach. By missing those visitors with resident permits, the data provided by the town of Narragansett underestimates visitation to the whole beach. Therefore, based on a .85/1 ratio between public and resident use obtained through parking lot counts conducted in the public and resident parking lots, the data were adjusted to represent daily use for the whole beach (see Supporting

Information for details). Daily visitation numbers are provided from Memorial Day to Labor Day, 2017. (N=86)

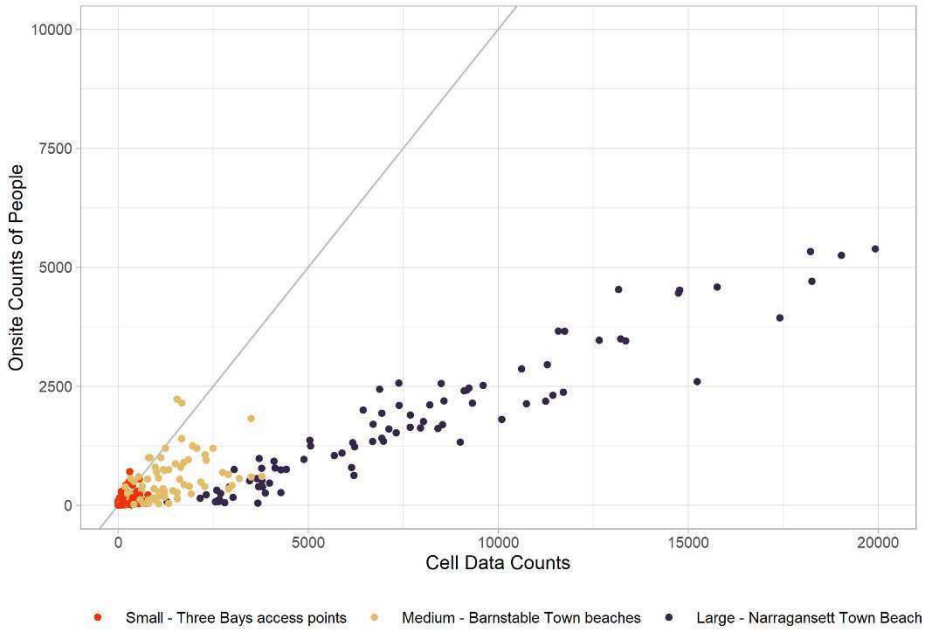

Fig 2. Observational Counts Compared Against Cell Data. Observations of visitation (9AM-4PM) plotted against uncalibrated visitation estimated from the cell data for the same hours.

Fig 2 shows how the cell data-derived counts and observational counts compare. The cell data-derived estimates correspond well, but overestimate the observed visitor counts by about four times. This overestimation is likely due to several confounding assumptions. These assumptions start with choices in how the data provider processes the raw cellular device level information to associate records with geographies in certain time windows and to extrapolate the sample of cellular devices to population level estimates through their estimates of market penetration (see Supporting Information).

The cell data product did not provide counts for the block of time that corresponded to our visitation counts (9AM-4PM), but rather by individual hours. Therefore, we had to translate these hourly counts to our time window by making assumptions on the length of stay of visitors, since the same device would be counted multiple times if it were to stay at the site for multiple hours. Following the data provider's advice to match the cell data-derived

information to visitation observations, we used an assumption of a three-hour average stay to match the time-window of our observations. We could have picked data on one hour in the window to be representative of the whole three hours, the end hour for instance, but this would discard information in the other hours. Instead, we calculated a moving average (three-hour window) of visitation for each hourly visitation estimate from the cell data for each site. We then summed the moving average of only the central hour of three-hour blocks from 8AM-4PM (9AM, 12PM, 3PM) (see Supporting Information for more details). This reduces the cell data counts due to multiple sightings, since we summed only one of the three hours in each window, but maintains the information in the hourly distribution of use through the day.

An assumption of a shorter length of stay would have increased the cell data counts and vice-versa. For example, if we assumed a two-hour average length of stay, we would have used two-hour instead of three-hour windows in the daily sums, increasing the daily total. While three hours may be a long average length of stay for recreational visits to all the water access sites, the data reflecting this assumption were inputs to the calibration models. We sought to correct any bias and inaccuracies introduced by this assumption by using the calibration models fit to on-the-ground counts below. Similarly, there is a difference in the relationship across the three sizes of access points that can also be seen in Fig 2. The differences by group are likely due to differences in the observational counting methods and possibly how well cell data performs based on the size of the area. We control for both possible effects in the statistical models used to calibrate the data.

Models and prediction

Our objective was to develop a model that predicts visitation to a range of water recreation areas using the cell data and other explanatory variables that are easily compiled across many places. These covariates include weather (temperature and precipitation), the month, day of the week, and size of the water access. The model controls for the different counting methods in the observational data. We estimated a varied set of candidate regression models including several functional forms where we defined linear and log-linear relationships between the visitor counts and the cell data and other regressors in R [42]. Since we did not have any preconceived notion of the functional forms of the relationships between the covariates and the dependent variable, we also estimated a more general

random forest model. A random forest model is a type of non-parametric model commonly used in the data science and machine learning fields. They have been shown to reproduce many functional forms and have superior predictive performance over standard multivariate regression models for many applications [43-44].

The candidate model specifications were as follows:

- Linear

$$Y_{it} = \propto + \beta_1 C_{it} + \boldsymbol{\beta_2 D_t} + \boldsymbol{\beta_3 W_t} + \boldsymbol{\beta_4 S_i} + \beta_5 A_i + e_{it} \quad (1)$$

- Log-Linear

$$\log(Y_{it}) = \propto + \beta_1 C_{it} + \boldsymbol{\beta_2 D_t} + \boldsymbol{\beta_3 W_t} + \boldsymbol{\beta_4 S_i} + \beta_5 A_i + e_{it} \quad (2)$$

- Random Forest

$$Y_{it} = f(C_{it}, \boldsymbol{D_t}, \boldsymbol{W_t}, \boldsymbol{S_i}, A_i) \quad (3)$$

Where,

Y_{it} – Observed visits to site, i, on day, t

C_{it} – cell data-derived estimate of visitation to site i on day t

$\boldsymbol{D_t}$ – Matrix of dummy variables for the month, day of the week, weekend, holiday

$\boldsymbol{W_t}$ – Matrix of weather variables (precipitation, temperature, windspeed) for day t from Barnstable Municipal Airport weather station.

$\boldsymbol{S_i}$ – Dummy variables for the source of observed visitation data (Narragansett Beach, Barnstable Town, Three Bays)

A_i – Area of site i

$\propto$ - intercept

e_{it} – error term

We compared the candidate models based on their predictive performance. To avoid selecting an overfit model and therefore being overconfident in its out-of-sample model performance, we conducted a cross validation by splitting the data into training (in-sample) and test (out-of-sample) sets. We fit the candidate models to the training sets of data, predicted the test sets, and calculated fit statistics on the out-of-sample observations. We did this for 10 random splits of the data using a k-fold cross validation and present the average model performances across the 10 test sets in Table 1 [45-46]. Using this cross-validation technique is a statistical check and a data science best practice. Given the predictive purposes of these classes of models, we suggest that, in the future, a similar cross-validation process should be performed when using proxy-types of data for predicting visitation. Additional regression and random forest outputs, goodness-of-fit metrics, and details can be found in the Supporting Information as well as in the code package (https://github.com/USEPA/Recreation_Benefits.git).

Ethics statement

This work was reviewed and deemed exempt by the Institutional Review Board (Study #17-3334) from the University of North Carolina at Chapel Hill.

Results

Using the cell data product from the data provider resulted in about a four-times overestimation of the type of recreational visitation we were looking to estimate when compared against observations. Despite the scale difference, we found the information contained in the cell data to be valuable to predict visitation across a diverse set of sites after calibration. From our models, there are a few ways to show that it is the information in the cell data that is providing most of the explanatory power as compared to the covariates (weather, area, source of the observational counts). Table 1 shows the regression results using just cell data (columns 1-2), then with additional covariates (columns 3-4). Just using cell data produces a decent model in linear form. The additional value of the covariates can be seen in the improved stats between column 1 and 3 and 2 and 4. In the random forest model, the

cell data was by far the most useful in modeling visitation as seen by metrics of variable importance (see Supporting Information)

Table 1: Regression results

	Visits (1)	Log(Visits) (2)	Visits (3)	Log(Visits) (4)
Cell data	0.245***	0.0003***	0.296***	0.0002***
	(0.005)	(0.0000)	(0.007)	(0.0000)
Area (m^2)			0.00003	0.000006***
			(0.0002)	(0.0000006)
Narragansett			-646.796***	0.182
			(72.136)	(0.225)
Town of Barnstable			-60.612	-0.409***
			(42.119)	(0.131)
Temperature (°F)			10.398***	0.066***
			(2.567)	(0.008)
Precipitation (inches)			-26.180	-0.447***
			(47.250)	(0.147)
Constant	33.128*	4.320***	-334.114	0.539
	(19.496)	(0.064)	(206.779)	(0.644)
Observations	392	392	392	392
R^2	0.86	NA	.89	NA
ME	.27	-430.96	.43	-74.35
RMSE	318.08	3161.23	272.47	1030.21
MAE	186.69	791.33	174.68	345.93

* p<0.10** p<0.05p***p<0.01

Note: Dummy variables are included for month and day of the week in columns 3 and 4. Columns 2 and 4 are in log-linear form. See code and Supporting Information for additional details and candidate

models. Goodness of fit statistics are from out-of-sample sets from a 10-fold cross validation. Log-linear model predictions were converted to people terms for goodness of fit statistics. ME= mean error, RMSE = root mean squared error, MAE = mean absolute error.

Table 2: Performance statistics for candidate models

	ME	RMSE	MAE	R-Squared
Linear model	0.43	272.47	174.68	.89
Log-linear model	-74.35	1030.21	345.93	NA
Random forest	-3.78	262.48	154.84	.91

Note: ME= mean error, RMSE = root mean squared error, MAE = mean absolute error. See Supporting Information for complete set of model output and performance statistics.

Of the candidate models, we chose the random forest as the preferred model, given its predictive performance indicated by the lowest RMSE, MAE, and low bias (ME) during cross validation (see Table 2). To create the final comprehensive visitation dataset, we used the preferred random forest model to predict daily visitation to all 577 water-access areas in our sample for the four summer months (June-September) of 2017. Fig 3 plots predicted visitation using the random forest model against observational counts, showing a tight overall in-sample fit. Our calibrated model produced daily visitation estimates with an out-of-sample mean absolute error of 155 people (Table 2) based on the cross-validation.

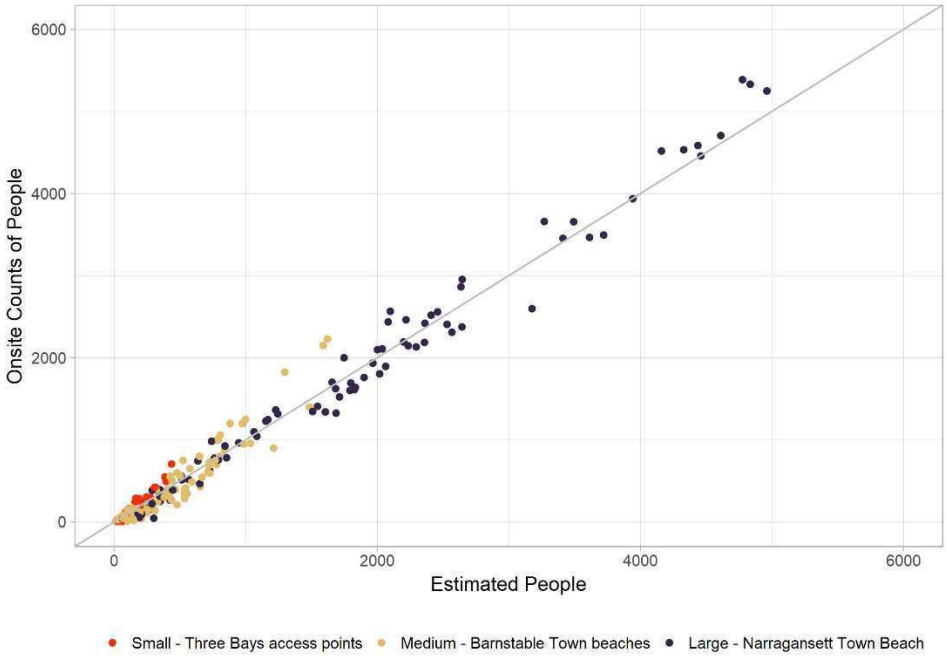

Fig 3. Cell Data Modeled Visitation Compared Against Observations. Predicted daily (9AM-4PM) visits from the cell data model compared to observed visitation at three sizes of water recreation areas in New England, USA.

This model produced comprehensive visitation estimates across the region, but also at each individual site across days. The result of this work, a calibrated dataset of visitation including the code and data for producing the results in this paper can be found at https://github.com/USEPA/Recreation_Benefits.git. As examples of the usefulness of the broad geographical scope of the model and resulting database, Fig 4 shows daily visitation estimates to all public water-access points on Cape Cod for the summer months of 2017. Along with these types of landscape-scale results, the data and model provide focused site-specific information. Fig 5 shows daily visitation to a single beach across the season, information available for all sites and days across the four summer months.

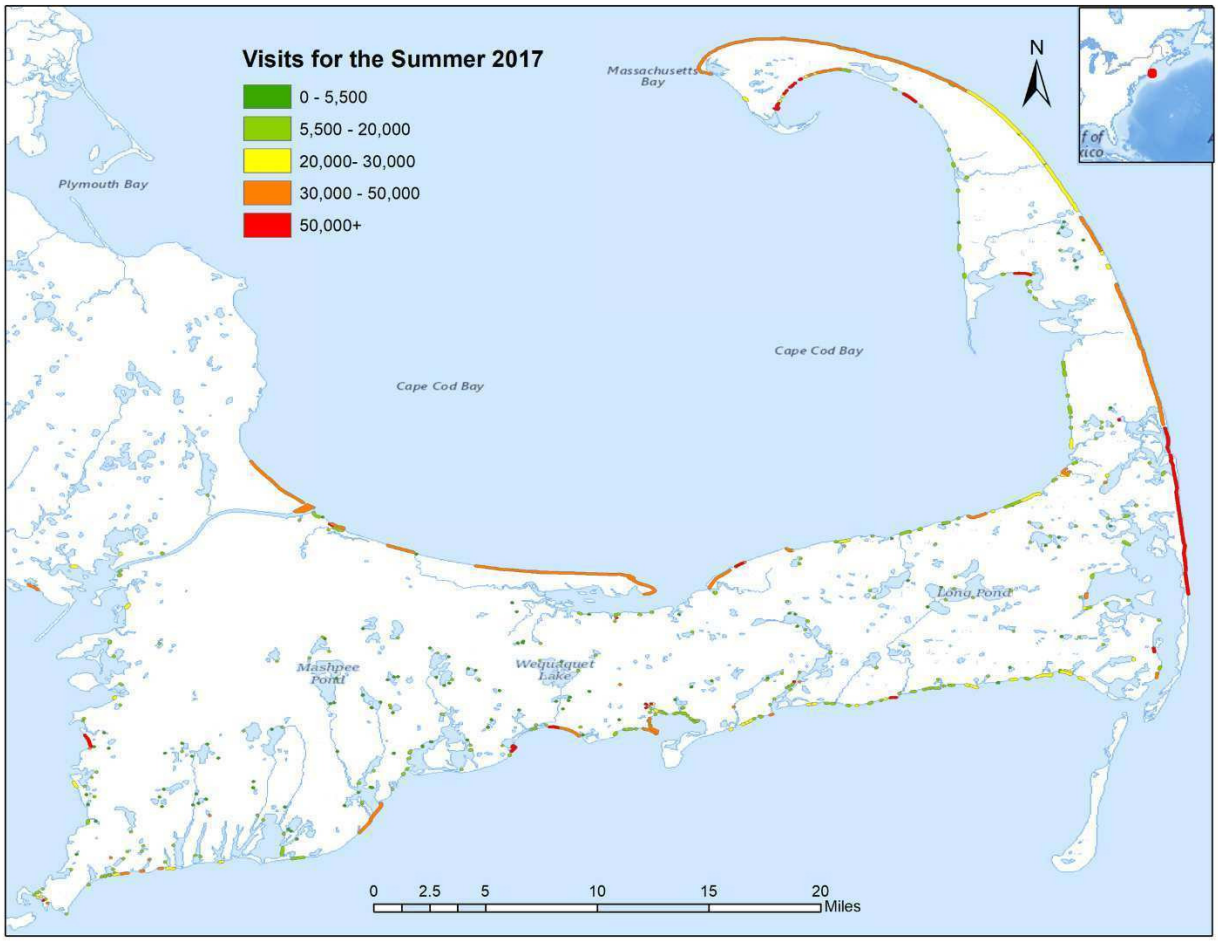

Fig 4. Visitation for Cape Cod, MA, USA for the Summer of 2017. Total predicted visits (9AM-4PM) to water recreation areas for the summer of 2017 (June, July, August, September) for Cape Cod (Barnstable County, MA, USA), using the cell data model.

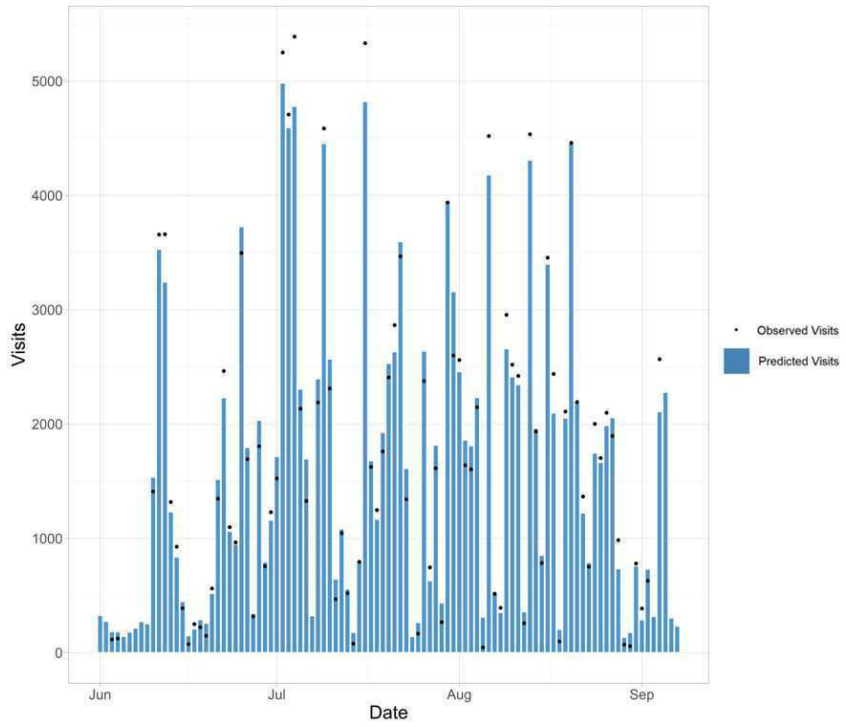

Fig 5. Narragansett Beach, RI, USA, Daily Visitation. Predicted daily (9AM-4PM) visits to Narragansett Town Beach (Narragansett, RI, USA) for the summer of 2017 using the cell data model. These daily predictions are compared to observed visits based on on-the-ground counts.

Since we combined three different sources of visitation data to fit the model, we also ran candidate models on each visitation observation data source separately and the relationships between the cell data and each visitation dataset remained similar (see Supporting Information). The in-sample fit of those models varied, with the smaller access point dataset, Three Bays, the least well fit (R^2 = .36), to better fits with the larger access point of Narragansett Beach (R^2 = .96). The number of observations vary with the sources, as do specifics of how those observations were collected, but we suspect the cell data may be better at predicting visitation to larger areas, with more daily visitation. There are more cellular devices in a sample of a day at the more popular places to estimate visitation from, likely reducing noise in the estimate.

We chose to use the most accurate and unbiased of the candidate statistical models for prediction. However, there are several sources of potential inaccuracies and biases in estimating visitation in this way that are not incorporated

in the metrics of model goodness-of-fit. The observational visitation counts contain their own uncertainties and potential biases based on their sampling design and counting methods. By calibrating and validating to those counts, we may be carrying over those issues to our estimates of visitation. In addition, the cellular data contains uncertainties resulting from the geospatial accuracy of the device locations, our geographic definition of the sites, and the methods of expansion from the device sample to population level estimates. More applications using cell datasets are needed to understand these limitations combined with additional and more consistent collections of visitation observations are crucial to addressing these issues.

The models we fit may also be susceptible to spatial autocorrelation issues resulting from the cell dataset if there are variations in how the data represents visitation geographically. Spatial autocorrelation in models potentially inflates goodness-of-fit estimates, can bias parameters and reduces predictive performance. We have controls in the models for each group of sites, which are geographically clustered. This may alleviate some of the potential issue. Similarly, collinearity in the covariates could potentially cause poor predictions, attributing predictive information to the wrong covariate, for example. We checked for this issue in a few ways, building up the model covariates sequentially starting with cell data alone and adding covariates. This led to little change in the relationships between observations and cell data counts (see Supporting Information for more model details and variations). We also consistently found good out-of-sample goodness-of-fit metrics in a cross validation, giving us more confidence that spatial autocorrelation and collinearity were likely not an issue in the models' predictive performance.

Discussion

We contend that the use of cell data provides a valuable method to quantify visitation across large numbers of areas and over time. When calibrated, the cell data provided an accurate and consistent way to estimate visitation to natural areas. It allowed us to produce a previously unavailable dataset of water visitation at a policy-relevant resolution, spatial extent, and consistency. The information provides visitation details for specific locations at a regional or sub-regional scale, the scale at which most decisions and policies regarding public natural areas are made. Understanding the scale and timing of visitor use of an area allows managers to determine and provide appropriate facilities and safety precautions and researchers to predict impacts of environmental change, measure

effects of natural disasters, and conduct research on social and economic value of public access to natural areas. To date, no other methods for quantifying use have the same capacity for providing location-specific data across broad geographic areas at such a high temporal resolution.

The data can inform landscape-level analyses of behavior to understand, at a broader scale, the impacts of changes in environmental quality across time as well as across access geography. The origin data can be used to better understand who visits an access point based on where they come from. This provides informative profiles regarding the characteristics of people and communities that are, or could be, affected by environmental degradation or improvements or other policy and management decisions. Taking advantage of variations in behavior and environmental quality across time, cell data's fine temporal resolution opens avenues for longitudinal studies. For instance, it provides the ability to quantify the number of visitors affected and economic impacts incurred from beach closures, algal blooms, oil spills, or other events that typically are not captured consistently with current methods or lack baseline data for measuring impacts.

Given our results, we suggest caution in using visitation estimates out-of-the-box from data providers without calibration. There is useful information in the datasets, but we found that calibration was necessary to confidently use the data for our purposes. In its delivered form, the data overestimated use of the type we were interested in quantifying, recreational visits to water-access areas. We hypothesized the need for this correction based on a few practical factors discussed below.

We were only able to define recreation visitation by limiting the area of the requested geographies (the GIS information for the sites we requested from the data providers) where recreation would likely be the primary purpose for visiting the area and during time-windows of interest. Inherently, the on-the-ground visitation observations were more restrictive in capturing visits for recreation and not capturing ancillary or non-recreational visits to the geographies, like walking by the site on a nearby road. It is also reasonable to assume some observational counts may be conservative and under-report recreation visitation due to sampling constraints.

Additionally, there is a cascade of statistical modeling assumptions that are made by the third-party providers to take raw device locational information to the anonymized and aggregated form delivered to the customers (see Supporting Information for the publicly available description of Airsage's process). The exact details of each private provider's data processing workflows are their intellectual property and protected as such. This opaqueness

motivates the use of methods to judge performance critically and the construction of additional models based on common cell data products for popular environmental applications, such as the one described in this paper. Because the methods used by the data providers are constantly in development, estimating performance on common observational datasets and with common methods would provide more clarity and confidence (statistical and otherwise) for cell data's use in policy and management applications. In some cases, lack of cellular connectivity in some natural areas may also limit its usefulness, although GPS-based and application derived locational methods have overcome some of this limitation by passing along information when the device is reconnected to a network. It is in a user's best interest to calibrate the product for their application, when possible, or consider the uncalibrated information as a relative metric. We demonstrated a simple method to do a calibration in this paper and provide the data and code for others to work from and improve as more users apply these types of data products.

While cell data-derived information is an exciting development for researchers and managers, counterintuitively, we found attempting to use it for a practical application only further motivated the need to take more accurate, consistent and unbiased observations of visitation using traditional methods. Modeling methods are hindered by the lack of availability of training datasets and would be greatly improved by larger and more uniformly collected observations. This is especially true regarding machine-learning algorithms [47]. For example, with small and practical tweaks in the way visitation records are collected at water-access areas, such as collecting periodic counts of cars and people at specific times, visitation records could become more harmonized and useful [12,41]. From there, visitation proxies like cell data or social media-based models can provide a platform for spatial and temporal extrapolation across broad geographies, as we demonstrate here. The need for such models is not confined to water-access visitation, as it is relevant to many other similar policy contexts, for example, at national parks or urban green-spaces. The differences in how well our models fit depending on the visitation data source, with larger more popular locations fit better than small, should be cautionary to approaches applying the cell data-derived visitation estimates to settings where there is no similar observational data for comparison.

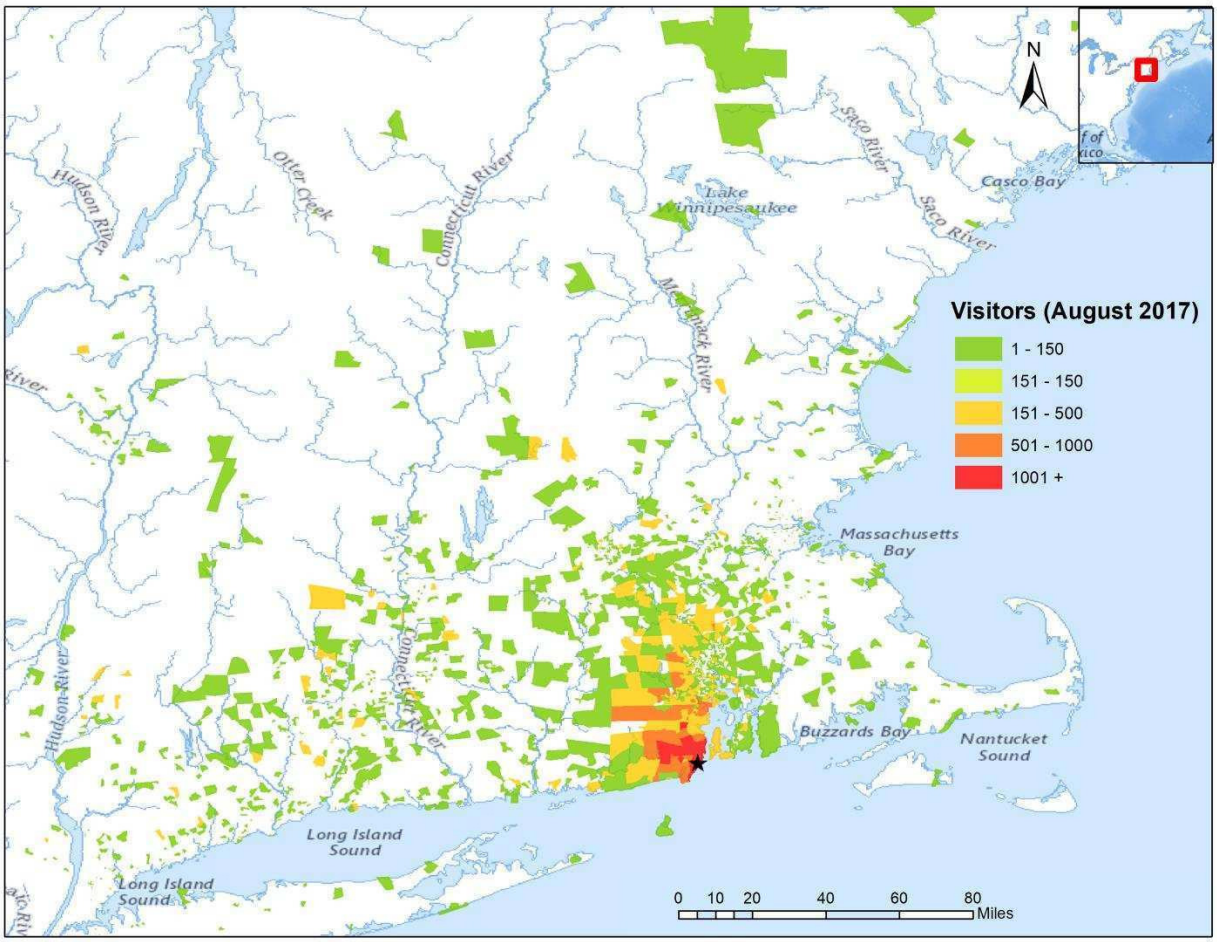

Fig 6. Visitor Origins for Narragansett Beach, RI, USA. Count of visitors by census block group origins for visitors to Narragansett Town Beach, Narragansett RI, USA, (black star on the map) in August 2017. This monthly origin information exists for each of the 577 access points in our sample.

In this paper we explored only a few dimensions of the information in the cell data-derived dataset, focusing on estimating visitation. The origin information provided about the visitors to the water-access sites--monthly visitation by site and census block groups in our case--provides the type of data needed for a myriad of travel-demand models for recreation [48]. Previous social media-based work [18] pointed out this potential opportunity, but travel-demand models typically require more spatially and temporally resolved information than what can be found currently in data derived from social media. Fig 6 displays origin-destination data for one site, Narragansett Beach, Rhode Island, for August 2017. Our dataset includes this information for all sites and months. More work is needed to

calibrate and validate the origin-destination information provided by cell data products for environmental applications and more generally [49]. Validating the origin data and fitting travel-demand models is beyond the scope of this paper and is left for future work. We include the origin-destination data in the data package associated with this paper for any other users that wish to tackle this natural next step. As with the visitation estimates, the possibility of using new sources of data for origin-destination travel-demand models encourages implementation of more commonly-worded and formatted general population and visitor intercept surveys to provide the necessary corroborating and calibrating datasets.

The visitation dataset resulting from the work in this paper is useful for federal, state and town managers and agencies in the region for any number of applications requiring visitor use information. For example, state managers may use this information to determine the allocation of beach monitoring resources, a town shellfish warden may use it to identify the most actively fished sites, or a tourism board could use it to understand the profile of visitors to popular natural attractions. Of broader interest in natural resource management and research, these types of models using cell data and a similar calibration process could be developed for other areas or for other purposes such as understanding the scale of ecosystem services, human-wildlife conflict, water consumption demand, or emergency response, for example.

Acknowledgments

The views expressed in this article are those of the authors and do not necessarily represent the views or policies of the U.S. Environmental Protection Agency. This contribution is identified by tracking number ORD-028692 of the U.S. Environmental Protection Agency, Office of Research and Development, Center for Environmental Measurement and Modeling, Atlantic Coastal Environmental Sciences Division. We would like to thank Anne Neale, Bryan Milstead and Ryan Furey for their thoughtful reviews.

Product Disclaimer

Mention of trade names or manufacturers does not imply U.S. Government endorsement of commercial products.

Competing Interests

The author(s) declare no competing interests.

Data Availability

The code and datasets used and generated during the current study are available in the USEPA Recreation Benefits repository, https://github.com/USEPA/Recreation_Benefits.git. Supporting Information accompanies this paper.

References

1. Leeworthy VR, Wiley PC. Current participation patterns in marine recreation. National Oceanic and Atmospheric Administration. 2001 Nov.
2. Tourangeau R, English E, McConnell KE, Chapman D, Cervantes IF, Horsch E, Meade N, Domanski A, Welsh M. The Gulf recreation study: Assessing lost recreational trips from the 2010 Gulf Oil Spill. Journal of Survey Statistics and Methodology. 2017 Jul 6;5(3):281-309.
3. Horsch E, Welsh M, Price J, Domanski A, Meade NF, Murray J. Best practices for collecting onsite data to assess recreational use impacts from an oil spill. 2017 Available from: ftp://ftp.library.noaa.gov/noaa_documents.lib/NOS/ORR/TM_NOS_ORR/TM_NOS-ORR_54.pdf
4. Deacon RT, Kolstad CD. Valuing beach recreation lost in environmental accidents. Journal of Water Resources Planning and Management. 2000 Dec;126(6):374-81.
5. Da Silva CP. Beach carrying capacity assessment: how important is it? Journal of Coastal Research. 2002 Mar;36(sp1):190-8.
6. Dwight RH, Brinks MV, SharavanaKumar G, Semenza JC. Beach attendance and bathing rates for Southern California beaches. Ocean & Coastal Management. 2007 Jan 1;50(10):847-58.

7. Harada SY, Goto RS, Nathanson AT. Analysis of lifeguard-recorded data at Hanauma Bay, Hawaii. Wilderness & Environmental Medicine. 2011 Mar 1;22(1):72-6.
8. King P, McGregor A. Who's counting: An analysis of beach attendance estimates and methodologies in southern California. Ocean & Coastal Management. 2012 Mar 1;58:17-25.
9. Garcia A, Smith JR. Factors influencing human visitation of southern California rocky intertidal ecosystems. Ocean & Coastal Management. 2013 Mar 1;73:44-53.
10. Kreitler J, Papenfus M, Byrd K, Labiosa W. Interacting coastal based ecosystem services: recreation and water quality in Puget Sound, WA. PloS One. 2013 Feb 22;8(2):e56670.
11. Morgan D. Development of a method to estimate and predict beach visitation. Tourism in Marine Environments. 2016 Dec 12;12(1):69-77.
12. Leggett CG. Sampling strategies for on-site recreation counts. Journal of Survey Statistics and Methodology. 2017 Sep 1;5(3):326-49.
13. Lyon SF, Merrill NH, Mulvaney KK, Mazzotta MJ. Valuing coastal beaches and closures using benefit transfer: An Application to Barnstable, Massachusetts. Journal of ocean and coastal economics. 2018 May;5(1):1-.
14. English DB. Forest Service national visitor use monitoring process: research method documentation. US Forest Service, Southern Research Station; 2002.
15. Fisher DM, Wood SA, White EM, Blahna DJ, Lange S, Weinberg A, Tomco M, Lia E. Recreational use in dispersed public lands measured using social media data and on-site counts. Journal of Environmental Management. 2018 Sep 15;222:465-74.
16. Van Berkel DB, Tabrizian P, Dorning MA, Smart L, Newcomb D, Mehaffey M, Neale A, Meentemeyer RK. Quantifying the visual-sensory landscape qualities that contribute to cultural ecosystem services using social media and LiDAR. Ecosystem Services. 2018 Jun 1;31:326-35.
17. Keeler BL, Wood SA, Polasky S, Kling C, Filstrup CT, Downing JA. Recreational demand for clean water: evidence from geotagged photographs by visitors to lakes. Frontiers in Ecology and the Environment. 2015 Mar;13(2):76-81.
18. Wood SA, Guerry AD, Silver JM, Lacayo M. Using social media to quantify nature-based tourism and recreation. Scientific Reports. 2013 Oct 17;3:2976.

19. Hamstead ZA, Fisher D, Ilieva RT, Wood SA, McPhearson T, Kremer P. Geolocated social media as a rapid indicator of park visitation and equitable park access. Computers, Environment and Urban Systems. 2018 Nov 1;72:38-50.
20. Tenkanen H, Di Minin E, Heikinheimo V, Hausmann A, Herbst M, Kajala L, Toivonen T. Instagram, Flickr, or Twitter: Assessing the usability of social media data for visitor monitoring in protected areas. Scientific Reports. 2017 Dec 14;7(1):17615.
21. Sonter LJ, Watson KB, Wood SA, Ricketts TH. Spatial and temporal dynamics and value of nature-based recreation, estimated via social media. PLoS One. 2016 Sep 9;11(9):e0162372.
22. Solmaz G, Turgut D. A survey of human mobility models. IEEE Access. 2019 Sep 3;7:125711-31.
23. Toole JL, Colak S, Sturt B, Alexander LP, Evsukoff A, González MC. The path most traveled: Travel demand estimation using big data resources. Transportation Research Part C: Emerging Technologies. 2015 Sep 1;58:162-77.
24. Blondel VD, Decuyper A, Krings G. A survey of results on mobile phone datasets analysis. EPJ Data Science. 2015 Dec 1;4(1):10.
25. Calabrese F, Ferrari L, Blondel VD. Urban sensing using mobile phone network data: a survey of research. Acm Computing Surveys (csur). 2014 Nov 12;47(2):1-20.
26. Çolak S, Alexander LP, Alvim BG, Mehndiratta SR, González MC. Analyzing cell phone location data for urban travel: current methods, limitations, and opportunities. Transportation Research Record. 2015 Jan;2526(1):126-35.
27. Toole JL, Ulm M, González MC, Bauer D. Inferring land use from mobile phone activity. In Proceedings of the ACM SIGKDD International Workshop on Urban Computing 2012 Aug 12 (pp. 1-8). ACM.
28. Toch E, Lerner B, Ben-Zion E, Ben-Gal I. Analyzing large-scale human mobility data: a survey of machine learning methods and applications. Knowledge and Information Systems. 2019 Mar 5;58(3):501-23.
29. Frias-Martinez V, Soguero-Ruiz C, Frias-Martinez E, Josephidou M. Forecasting socioeconomic trends with cell phone records. In Proceedings of the 3rd ACM Symposium on Computing for Development 2013 Jan 11 (pp. 1-10).

30. Athey S, Blei D, Donnelly R, Ruiz F, Schmidt T. Estimating heterogeneous consumer preferences for restaurants and travel time using mobile location data. In AEA Papers and Proceedings 2018 May (Vol. 108, pp. 64-67).
31. Kung KS, Greco K, Sobolevsky S, Ratti C. Exploring universal patterns in human home-work commuting from mobile phone data. PloS One. 2014 Jun 16;9(6):e96180.
32. Lu X, Bengtsson L, Holme P. Predictability of population displacement after the 2010 Haiti earthquake. Proceedings of the National Academy of Sciences. 2012 Jul 17;109(29):11576-81.
33. Wesolowski A, Eagle N, Tatem AJ, Smith DL, Noor AM, Snow RW, Buckee CO. Quantifying the impact of human mobility on malaria. Science. 2012 Oct 12;338(6104):267-70.
34. Kraemer MU, Golding N, Bisanzio D, Bhatt S, Pigott DM, Ray SE, Brady OJ, Brownstein JS, Faria NR, Cummings DA, Pybus OG. Utilizing general human movement models to predict the spread of emerging infectious diseases in resource poor settings. Scientific Reports. 2019 Mar 26;9(1):5151.
35. Yu H, Russell A, Mulholland J, Huang Z. Using cell phone location to assess misclassification errors in air pollution exposure estimation. Environmental Pollution. 2018 Feb 1;233:261-6.
36. Li M, Gao S, Lu F, Tong H, Zhang H. Dynamic estimation of individual exposure levels to air pollution using trajectories reconstructed from mobile phone data. International Journal of Environmental Research and Public Health. 2019 Jan;16(22):4522.
37. Kubo T, Uryu S, Yamano H, Tsuge T, Yamakita T, Shirayama Y. Mobile phone network data reveal nationwide economic value of coastal tourism under climate change. Tourism Management. 2020 Apr 1;77:104010.
38. Kim YJ, Lee DK, Kim CK. Spatial tradeoff between biodiversity and nature-based tourism: Considering mobile phone-driven visitation pattern. Global Ecology and Conservation. 2020 Mar 1;21:e00899.
39. Monz C, Mitrovich M, D'Antonio A, Sisneros-Kidd A. Using mobile device data to estimate visitation in parks and protected areas: an example from the nature reserve of orange county, California. Journal of Park and Recreation Administration. 2019;37(4).
40. Wallmo K. Assessment of techniques for estimating beach attendance. Beach Sampling Report of NOAA. 2003 Apr;10.

41. Mulvaney KK, Atkinson SF, Merrill NH, Twichell JH, Mazzotta MJ. Quantifying recreational use of an estuary: a case study of Three Bays, Cape Cod, USA. Estuaries and Coasts. 2020 Jan 1;43(1):7-22.
42. RCore T.E.A.M. R: A language and environment for statistical computing. R Foundation for Statistical Computing, Vienna, Austria. URL http://www. R-project. org. 2016.
43. Ziegler A, König IR. Mining data with random forests: current options for real-world applications. Wiley Interdisciplinary Reviews: Data Mining and Knowledge Discovery. 2014 Jan;4(1):55-63.
44. Wright MN, Ziegler A. ranger: A fast implementation of random forests for high dimensional data in C++ and R. arXiv preprint arXiv:1508.04409. 2015 Aug 18.
45. Kohavi R. A study of cross-validation and bootstrap for accuracy estimation and model selection. In Ijcai 1995 Aug 20 (Vol. 14, No. 2, pp. 1137-1145).
46. Rodriguez JD, Perez A, Lozano JA. Sensitivity analysis of k-fold cross validation in prediction error estimation. IEEE Transactions on Pattern Analysis and Machine Intelligence. 2009 Dec 1;32(3):569-75.
47. Witten IH, Frank E, Hall MA, Pal CJ. Data Mining: Practical machine learning tools and techniques. Morgan Kaufmann; 2016 Oct 1.
48. Phaneuf DJ, Smith VK. Recreation demand models. Handbook of Environmental Economics. 2005 Jan 1;2:671-761.
49. Vanhoof M, Reis F, Ploetz T, Smoreda Z. Assessing the quality of home detection from mobile phone data for official statistics. Journal of Official Statistics. 2018 Dec 1;34(4):935-60.

Supporting Information

Supplementary Table S1. Performance statistics for candidate models. Car counts of resident and public parking lots were used to find the ratio of resident and public use of the beach. This ratio was applied to daily counts from ticket receipts (public only) to estimate total daily visitation.

Supplementary Table S2. Candidate regressions. Dummy variables are included for month and day of the week in each regression. Columns 2 and 4 are in log-linear form. See code for additional details and candidate models.

Supplementary Table S3. Out-of-sample performance statistics for each candidate model. Each candidate model is presented with varying explanatory variables and functional form. ME= mean error, RMSE = root mean squared error, MAE = mean absolute error, MAPE = mean absolute percent error, R-squared= % of out-of-sample variance explained.

Supplementary Table S4: Linear regression results on each observational count source. Each column contains observations from each source of visitation observation information. Dummy variables are included in all regressions for month and day of the week. R-squared= % of in-sample variance explained.

Supplementary Figure S1. Mean squared errors when considering a different number of candidate prediction variables at each split in a tree.

Supplementary Figure S2. Variable importance plot using the 'impurity' method in R package Ranger.

Table of Contents

General_Authors_Publications.....2
LI-266758_Arzuaga_et_al_2015.....12
JS__STAA_award_nomination_for_the_uranium_paper.....20
MG__STAA_award_nomination_for_the_uranium_paper.....21
Arzuaga_et_al_2010.....23

United States Environmental Protection Agency
Washington, DC 20460

STAA REPORT FOR THE SCIENTIST NOMINATIONS

General Information:

Nomination ID/App ID:	20-133
Research Category Primary:	Health Effects Research and Human Health Risk Assessment (HE)
Research Category Secondary:	Review Articles (RA)
Laboratory/Office Name:	ORD
Nomination Entered By:	Xabier Arzuaga Andino

Eligibility Checklist:

[Y] The nominated publication(s) has not been submitted to a previous STAA competition.

[Y] The nominated publication(s) was published on or before January 1, 2017 and on or after January 1,2012

[Y] The principal author was an EPA employee or a PHS employee assigned to EPA when the research was performed

[Y] The EPA authors (includes PHS employees assigned to EPA) contributed collectively a minimum of 50% toward the publication(s)

Nominating Official Name:	Kristina Chialton
Nominating Official Title:	SUPERVISORY BIOLOGIST
Nominating OfficialEmail:	thayer.kris@epa.gov
STAA Coordinator Name:	Kathleen Wiser
STAA Coordinator Email:	wiser.kathi@epa.gov

Justifications:

Justification 1:

The nominated review paper publication provides a case study for the application of the mode of action analysis approach to investigate the potential mechanisms and human relevance of uranium induced non-cancer effects. The mode of action analysis in this paper also helped reveal important data gaps and particularly vulnerable sections of the population. Uranium exposure alters the processes of bone modeling and remodeling; thus, early life stages are susceptible to uranium-induced osteotoxicity. Furthermore, during aging there is a shift in the ratio of bone mineralization versus erosion in bone remodeling, resulting in decreased bone mineralization and increased bone fragility; thus, the elderly may also represent a susceptible population to uranium-induced bone toxicity. Therefore, in addition to assessing the potential nephrotoxic effects of uranium in exposed human populations, epidemiological studies could also consider evaluating indicators of mineral homeostasis and bone health such as Vitamin D, BMD, and serum and urinary levels of biomarkers of bone formation and resorption.

This product furthers the Agency's core mission to ensure that Americans have clean air, land and water and that national efforts to reduce environmental risks are based on the best available scientific information (https://www.epa.gov/aboutepa/our-mission-and-what-we-do) by advancing improved hazard characterization and risk assessment practices. This publication has been cited in 20 documents including primary research publications investigating uranium-induced developmental and skeletal effects as well as several foreign government guidelines and reports which reviewing the potential human health hazards associated with uranium exposure (see citation list below). The research describe in this publication was funded by the Office of Research and Development/National Center for Environmental Assessment. This publication was not previously nominated for any EPA or external award. According to Google Scholar this review paper has 17 citations, this does not include citations from government agencies outside the US (see complete citation list below).

This work relies on a prior manuscript, published in 2010 and therefore not included in this award application, that reviewed the epidemiological and experimental data on the renal effects of exposure to depleted uranium (see Arzuaga et al 2010 in supporting documents).

1. Banning, A., and M. Benfer. 2017. 'Drinking Water Uranium and Potential Health Effects in the German Federal State of Bavaria', International Journal of Environmental Research and Public Health, 14.

2. Geoscience and Mines Branch. 2018. "A Review and Summary of Activities Related to Uranium in Nova Scotia Well Water." In, edited by Nova Scotia Energy and Mines. Halifax, Nova Scotia, Canada.

3. Gritsaenko, T., V. Pierrefite-Carle, G. Creff, C. Vidaud, G. Carle, and S. Santucci-Darmanin. 2018. 'Methods for Analyzing the Impacts of Natural Uranium on In Vitro Osteoclastogenesis', Jove-Journal of Visualized Experiments.

4. Gritsaenko, T., V. Pierrefite-Carle, T. Lorivel, V. Breuil, G. F. Carle, and S. Santucci-Darmanin. 2017. 'Natural uranium impairs the differentiation and the resorbing function of osteoclasts', Biochimica Et Biophysica Acta-General Subjects, 1861: 715-26.

5. Gueguen, Y., L. Roy, S. Hornhardt, C. Badie, J. Hall, S. Baatout, E. Pernot, L. Tomasek, O. Laurent, T. Ebrahimian, C. Ibanez, S. Grison, S. Kabacik, D. Laurier, and M. Gomolka. 2017. 'Biomarkers for Uranium Risk Assessment for the Development of the CURE (Concerted Uranium Research in Europe) Molecular Epidemiological Protocol', Radiation Research, 187: 107-27.

6. Hall, J., P. A. Jeggo, C. West, M. Gomolka, R. Quintens, C. Badie, O. Laurent, A. Aerts, N. Anastasov, O. Azimzadeh, T. Azizova, S. Baatout, B. Baselet, M. A. Benotmane, E. Blanchardon, Y. Gueguen, S. Haghdoost, M. Harms-Ringhdahl, J. Hess, M. Kreuzer, D. Laurier, E. Macaeva, G. Manning, E. Pernot, J. L. Ravanat, L. Sabatier, K. Tack, S. Tapio, H. Zitzelsberger, and E. Cardis. 2017. 'Ionizing radiation biomarkers in epidemiological studies - An update', Mutation Research-Reviews in Mutation Research, 771: 59-84.

7. Hao, Y. H., R. Gao, B. H. Lu, Y. H. Ran, Z. Y. Yang, J. Liu, and R. Li. 2018. 'Ghrelin protects against depleted uranium-induced bone damage by increasing osteoprotegerin/RANKL ratio', Toxicology and Applied Pharmacology, 343: 62-70.

8. Health Canada. 2017. "Uranium in Drinking Water. Document for Public Consultation." In, edited by Federal-Provincial-Territorial Committee on Drinking Water. Ottawa, Ontario, Canada.

9. Health Canada. 2019. "Guidelines for Canadian Drinking Water Quality. Guideline Technical Document. Uranium." In, edited by Healthy Environments and Consumer Safety Branch. Water and Air Quality Bureau. Ottawa, Ontario, Canada.

10. Hurault, L., G. Creff, A. Hagege, S. Santucci-Darmanin, S. Pagnotta, D. Farlay, C. Den Auwer, V. Pierrefite-Carle, and G. F. Carle. 2019. 'Uranium Effect on Osteocytic Cells In Vitro', Toxicological Sciences, 170: 199-209.

11. Huynh, T. N. S., C. Vidaud, and A. Hagege. 2016. 'Investigation of uranium interactions with calcium phosphate-binding proteins using ICP/MS and CE-ICP/MS', Metallomics, 8: 1185-92.

12. Lan, L., S. Y. Wu, S. D. Yu, J. J. Jiang, H. H. Chen, Y. F. Lou, and G. R. Fan. 2019. 'Fast and direct determination of catechol-3, 6-bis(methyleiminodiacetic acid) prototype in beagle dog plasma using liquid chromatography tandem mass spectrometry: A simplified and high throughput in-vivo method for the metal chelator', Journal of Chromatography A, 1596: 84-95.

13. McDiarmid, M. A., M. Cloeren, J. M. Gaitens, S. Hines, E. Streeten, R. J. Breyer, C. H. Brown, M. Condon, T. Roth, M. Oliver, L. Brown, M. Dux, M. R. Lewin-Smith, F. Strathmann, M. A. Velez-Quinones, and P. Gucer. 2018. 'Surveillance results and bone effects in the Gulf War depleted uranium-exposed cohort', Journal of Toxicology and Environmental Health-Part a-Current Issues, 81: 1083-97.

14. Pierrefite-Carle, V., S. Santucci-Darmanin, V. Breuil, T. Gritsaenko, C. Vidaud, G. Creff, P. L. Solari, S. Pagnotta, R. Al-Sahlanee, C. Den Auwer, and G. F. Carle. 2017. 'Effect of natural uranium on the UMR-106 osteoblastic cell line: impairment of the autophagic process as an underlying mechanism of uranium toxicity', Archives of Toxicology, 91: 1903-14.

15. United Nations Scientific Committee on the Effects of Atomic Radiation. 2016. "Sources, Effects and Risks of Ionizing Radiation: UNSCEAR 2016 Report to the General Assembly, Scientific Annexes A, B, C and D." United Nations. New York, United States of America.

16. Roller, L. K., and L. J. Baumgartner. 2016. 'Metals.' in S. D. Ray (ed.), Side Effects of Drugs Annual: A Worldwide Yearly Survey of New Data in Adverse Drug Reactions, Vol 38.

17. Stojsavljevic, A., S. Borkovic-Mitic, L. Vujotic, D. Grujicic, M. Gavrovic-Jankulovic, and D. Manojlovic. 2019. 'The human biomonitoring study in Serbia: Background levels for arsenic, cadmium, lead, thorium and uranium in the whole blood of adult Serbian population', Ecotoxicology and Environmental Safety, 169: 402-09.

18. Stojsavljevic, A., S. Skrivanj, J. Trifkovic, N. Djokovic, S. R. Trifunovic, S. Borkovic-Mitic, and D. Manojlovic. 2019. 'The content of toxic and essential elements in trabecular and cortical femoral neck: a correlation with whole blood samples', Environmental Science and Pollution Research, 26: 16577-87.

19. Wu, X. M., Q. X. Huang, Y. Mao, X. X. Wang, Y. Y. Wang, Q. H. Hu, H. Q. Wang, and X. K. Wang. 2019. 'Sensors for determination of uranium: A review', Trac-Trends in Analytical Chemistry, 118: 89-111.

Yue, Y. C., M. H. Li, H. B. Wang, B. L. Zhang, and W. He. 2018. 'The toxicological mechanisms and detoxification of depleted uranium exposure', Environmental Health and Preventive Medicine, 23.

Justification 2A:

n/a

Justification 2B:

n/a

Justification 2C:

n/a

Justification 2D:

n/a

Justification 2E:

n/a

Justification 3A:

According to Google Scholar the nominated review paper is has 17 citations, this does not include citations from government agencies outside the US. This publication has been cited in 20 documents including primary research publications investigating uranium-induced developmental and skeletal effects as well as several foreign government guidelines and reports which reviewing the potential human health hazards associated with uranium exposure (see citation list below).

1. Banning, A., and M. Benfer. 2017. 'Drinking Water Uranium and Potential Health Effects in the German Federal State of Bavaria', International Journal of Environmental Research and Public Health, 14.

2. Geoscience and Mines Branch. 2018. "A Review and Summary of Activities Related to Uranium in Nova Scotia Well Water." In, edited by Nova Scotia Energy and Mines. Halifax, Nova Scotia, Canada.

3. Gritsaenko, T., V. Pierrefite-Carle, G. Creff, C. Vidaud, G. Carle, and S. Santucci-Darmanin. 2018. 'Methods for Analyzing the Impacts of Natural Uranium on In Vitro Osteoclastogenesis', Jove-Journal of Visualized Experiments.

4. Gritsaenko, T., V. Pierrefite-Carle, T. Lorivel, V. Breuil, G. F. Carle, and S. Santucci-Darmanin. 2017. 'Natural uranium impairs the differentiation and the resorbing function of osteoclasts', Biochimica Et Biophysica Acta-General Subjects, 1861: 715-26.

5. Gueguen, Y., L. Roy, S. Hornhardt, C. Badie, J. Hall, S. Baatout, E. Pernot, L. Tomasek, O. Laurent, T. Ebrahimian, C. Ibanez, S. Grison, S. Kabacik, D. Laurier, and M. Gomolka. 2017. 'Biomarkers for Uranium Risk Assessment for the Development of the CURE (Concerted Uranium Research in Europe) Molecular Epidemiological Protocol', Radiation Research, 187: 107-27.

6. Hall, J., P. A. Jeggo, C. West, M. Gomolka, R. Quintens, C. Badie, O. Laurent, A. Aerts, N. Anastasov, O. Azimzadeh, T. Azizova, S. Baatout, B. Baselet, M. A. Benotmane, E. Blanchardon, Y. Gueguen, S. Haghdoost, M. Harms-Ringhdahl, J. Hess, M. Kreuzer, D. Laurier, E. Macaeva, G. Manning, E. Pernot, J. L. Ravanat, L. Sabatier, K. Tack, S. Tapio, H. Zitzelsberger, and E. Cardis. 2017. 'Ionizing radiation biomarkers in epidemiological studies - An update', Mutation Research-Reviews in Mutation Research, 771: 59-84.

7. Hao, Y. H., R. Gao, B. H. Lu, Y. H. Ran, Z. Y. Yang, J. Liu, and R. Li. 2018. 'Ghrelin protects against depleted uranium-induced bone damage by increasing osteoprotegerin/RANKL ratio', Toxicology and Applied Pharmacology, 343: 62-70.

8. Health Canada. 2017. "Uranium in Drinking Water. Document for Public Consultation." In, edited by Federal-Provincial-Territorial Committee on Drinking Water. Ottawa, Ontario, Canada.

9. Health Canada. 2019. "Guidelines for Canadian Drinking Water Quality. Guideline Technical Document. Uranium." In, edited by Healthy Environments and Consumer Safety Branch. Water and Air Quality Bureau. Ottawa, Ontario, Canada.

10. Hurault, L., G. Creff, A. Hagege, S. Santucci-Darmanin, S. Pagnotta, D. Farlay, C. Den Auwer, V. Pierrefite-Carle, and G. F. Carle. 2019. 'Uranium Effect on Osteocytic Cells In Vitro', Toxicological Sciences, 170: 199-209.

11. Huynh, T. N. S., C. Vidaud, and A. Hagege. 2016. 'Investigation of uranium interactions with calcium phosphate-binding proteins using ICP/MS and CE-ICP/MS', Metallomics, 8: 1185-92.

12. Lan, L., S. Y. Wu, S. D. Yu, J. J. Jiang, H. H. Chen, Y. F. Lou, and G. R. Fan. 2019. 'Fast and direct determination of catechol-3, 6-bis(methyleiminodiacetic acid) prototype in beagle dog plasma using liquid chromatography tandem mass spectrometry: A simplified and high throughput in-vivo method for the metal chelator', Journal of Chromatography A, 1596: 84-95.

13. McDiarmid, M. A., M. Cloeren, J. M. Gaitens, S. Hines, E. Streeten, R. J. Breyer, C. H. Brown, M. Condon, T. Roth, M. Oliver, L. Brown, M. Dux, M. R. Lewin-Smith, F. Strathmann, M. A. Velez-Quinones, and P. Gucer. 2018. 'Surveillance results and bone effects in the Gulf War depleted uranium-exposed cohort', Journal of Toxicology and Environmental Health-Part a-Current Issues, 81: 1083-97.

14. Pierrefite-Carle, V., S. Santucci-Darmanin, V. Breuil, T. Gritsaenko, C. Vidaud, G. Creff, P. L. Solari, S. Pagnotta, R. Al-Sahlanee, C. Den Auwer, and G. F. Carle. 2017. 'Effect of natural uranium on the UMR-106 osteoblastic cell line: impairment of the autophagic process as an underlying mechanism of uranium toxicity', Archives of Toxicology, 91: 1903-14.

15. United Nations Scientific Committee on the Effects of Atomic Radiation. 2016. "Sources, Effects and Risks of Ionizing Radiation: UNSCEAR 2016 Report to the General Assembly, Scientific Annexes A, B, C and D." United Nations. New York, United States of America.

16. Roller, L. K., and L. J. Baumgartner. 2016. 'Metals.' in S. D. Ray (ed.), Side Effects of Drugs Annual: A Worldwide Yearly Survey of New Data in Adverse Drug Reactions, Vol 38.

17. Stojsavljevic, A., S. Borkovic-Mitic, L. Vujotic, D. Grujicic, M. Gavrovic-Jankulovic, and D. Manojlovic. 2019. 'The human biomonitoring study in Serbia: Background levels for arsenic, cadmium, lead, thorium and uranium in the whole blood of adult Serbian population', Ecotoxicology and Environmental Safety, 169: 402-09.

18. Stojsavljevic, A., S. Skrivanj, J. Trifkovic, N. Djokovic, S. R. Trifunovic, S. Borkovic-Mitic, and D. Manojlovic. 2019. 'The content of toxic and essential elements in trabecular and cortical femoral neck: a correlation with whole blood samples', Environmental Science and Pollution Research, 26: 16577-87.

19. Wu, X. M., Q. X. Huang, Y. Mao, X. X. Wang, Y. Y. Wang, Q. H. Hu, H. Q. Wang, and X. K. Wang. 2019. 'Sensors for determination of uranium: A review', Trac-Trends in Analytical Chemistry, 118: 89-111.

20. Yue, Y. C., M. H. Li, H. B. Wang, B. L. Zhang, and W. He. 2018. 'The toxicological mechanisms and detoxification of depleted uranium exposure', Environmental Health and Preventive Medicine, 23.

Justification 3B:

The nominated paper was submitted to Toxicology Letters (https://www.journals.elsevier.com/toxicology-letters). According to the journal website the "journal operates a single blind review process. All contributions will be initially assessed by the editor for suitability for the journal. Papers deemed suitable are then typically sent to a minimum of two independent expert reviewers to assess the scientific quality of the paper. The Editor is responsible for the final decision regarding acceptance or rejection of articles. The Editor's decision is final."

AUTHORS

Principal Author

Author Name:	Xabier Arzuaga Andino		
Professional Title:		Salutation:	
Email:	arzuaga.xabier@epa.gov	Organization:	
Mailing Address:			
Street Line 1:	1200 Pennsylvania Ave, NW Washington, DC 20460		
City:	Washington		
Zip Code:	20460	State:	DC
At time of research was:	EPA Employee		
Separation Date:			
% of Effort:	65		

Contributing Author

Author Name:	Martin Gehlhaus		
Professional Title:		Salutation:	

Email:	gehlhaus.martin@epa.gov	Organization:	
Mailing Address:			
Street Line 1:	USEPA REGION 3 1650 Arch Street Mail Code: 3SD52 Philadelphia, PA 19103-2029		
City:	Philadelphia		
Zip Code:	19103-2029	State:	PA
At time of research was:	EPA Employee		
Separation Date:			
% of Effort:	20		

Contributing Author

Author Name:	Jamie Strong		
Professional Title:		Salutation:	
Email:	strong.jamie@epa.gov	Organization:	
Mailing Address:			
Street Line 1:	USEPA Headquarters William Jefferson Clinton Building 1200 Pennsylvania Avenue, N. W. Mail Code: 4304T Washington, DC 20460		
City:	Washington		
Zip Code:	20460	State:	DC
At time of research was:	EPA Employee		
Separation Date:			
% of Effort:	15		

PUBLICATIONS

Publication 1:

Publication Title:	Modes of action associated with uranium induced adverse effects in bone function and development		
Publication Date:	Mon May 11 00:00:00 GMT 2015		
Journal/Publication Method:	Toxicology Letters		
All Author(s):			
Volume:	236	Number:	2
Pages:	123-130	Immediately Index:	Immediately Index:
Citation ½ Life:	Arzuaga X, et al 2015. Toxicol Lett. 236(2):123-30	Impact Factor:	3.749

Toxicology Letters 236 (2015) 123–130

Contents lists available at ScienceDirect

Toxicology Letters

journal homepage: www.elsevier.com/locate/toxlet

Mini review

Modes of action associated with uranium induced adverse effects in bone function and development

Xabier Arzuaga, Martin Gehlhaus, Jamie Strong *

National Center for Environmental Assessment, U.S. Environmental Protection Agency, WA, DC 20460, USA

ARTICLE INFO

Article history:
Received 10 April 2015
Accepted 7 May 2015
Available online 11 May 2015

Keywords:
Uranium
Bone development
Osteotoxicity
Vitamin D

ABSTRACT

Uranium, a naturally occurring element used in military and industrial applications, accumulates in the skeletal system of animals and humans. Evidence from animal and in-vitro studies demonstrates that uranium exposure is associated with alterations in normal bone functions. The available studies suggest that upon absorption uranium directly affects bone development and maintenance by inhibiting osteoblast differentiation and normal functions, and indirectly by disrupting renal production of Vitamin D. Animal studies also provide evidence for increased susceptibility to uranium-induced bone toxicity during early life stages. The objective of this review is to provide a summary of uranium-induced bone toxicity and the potential mechanisms by which uranium can interfere with bone development and promote fragility. Since normal Vitamin D production and osteoblast functions are essential for bone growth and maintenance, young individuals and the elderly may represent potentially susceptible populations to uranium-induced bone damage.

Published by Elsevier Ireland Ltd.

Contents

1. Introduction . . . 123
2. Approach for literature search on uranium and bone toxicity . . . 124
3. Bone formation and maintenance overview . . . 124
4. Uranium-induced bone toxicity . . . 125
5. Potential mechanisms of uranium-induced toxicity in bone . . . 126
6. Discussion . . . 127
Acknowledgements . . . 128
References . . . 128

1. Introduction

Uranium (U) is a naturally occurring alpha-emitting radioactive metal that is present in soil at a concentration of 2–3 ppm (ATSDR, 2013; Bleise et al., 2003; Craft et al., 2004). Naturally occurring uranium is a mixture of three isotopes, U-234, U-235, and U-238, all of which undergo radioactive decay by emitting alpha particles accompanied by very small amounts of beta particles and gamma emissions (ATSDR, 2013; IAEA, 2008). Uranium is present in all geologic materials and, consequently, in soil, water, plants, animals, food, and ambient air (ATSDR, 2013; NRC, 2008).

The primary source of exposure for naturally occurring uranium is through food and water consumption. However, due to its ubiquitous presence in the environment individuals may be exposed to uranium by multiple routes, including ingestion, inhalation, and/or dermal contact (ATSDR, 2013; Keith et al., 2007; Lariviere et al., 2013). Uranium uptake is low for all exposure routes, but once absorbed it undergoes oxidation and forms soluble complexes with bicarbonate plasma proteins (primarily transferrin) and citrate (Bleise et al., 2003; Craft et al., 2004; Keith et al., 2007). From the bloodstream, the dissolved uranium is rapidly

* Corresponding author at: U.S. Environmental Protection Agency, 1200 Pennsylvania Ave N.W., Washington, DC 20460, USA. Tel.: +1 202 566 0056.
E-mail address: Strong.Jamie@epa.gov (J. Strong).

distributed to target tissues, principally the kidney and bone, or excreted in urine (Eidson, 1994).

Animal and human studies have demonstrated that uranium accumulates in renal and osseous tissues (Adams and Spoor, 1974; Durbin and Wrenn, 1975; Fisenne and Welford, 1986). In humans and animals, uranium deposits in the skeleton in a dose- and time-dependent fashion (Arruda-Neto et al., 2004; Lariviere et al., 2013; Pellmar et al., 1999; Prado et al., 2008) and uranium accumulation in bones occurs at a higher rate in young individuals (Lariviere et al., 2007; Rodrigues et al., 2013). Thus, bone is considered to be the most significant, long term deposit of uranium.

Once deposited in bone, uranium may be retained for long periods of time (Brugge and Buchner, 2011; Zhu et al., 2009), with half lives in bone ranging from 70 to 200 days (ATSDR, 2013). Within the osseous tissue, uranium accumulates in areas of active bone formation, specifically the calcifying zones of skeletal cartilage, where it can mimic and replace calcium (Ca^{2+}) (ATSDR, 2013; Rodrigues et al., 2013).

As described below, various studies using mammalian and cell culture models report that uranium exposure interferes with normal bone functions. Furthermore, a human study reported an association between uranium exposure and biochemical indicators of bone turnover (Kurttio et al., 2005). This review evaluates the current evidence of uranium induced bone toxicity and the potential modes of action by which uranium exposure leads to adverse skeletal health.

2. Approach for literature search on uranium and bone toxicity

Medline, Web of Science and Toxline were searched for epidemiological and animal studies informative to the potential effects of uranium exposure in bones. The search terms used were: uranium and bone or bone growth or bone formation or bone toxicity or bone resorption or bone volume or bone remodeling or bone density or bone mineralization or osteotixicity or osteoblasts or Vitamin D or alkaline phosphatase. Titles and abstracts of retrieved publications were reviewed for relevance to uranium and bone health. The citation list of publications considered informative were evaluated to identify studies not captured in the scientific databases mentioned above.

3. Bone formation and maintenance overview

A brief review of the biological processes of bone formation and maintenance, which have been shown to be affected by exposure to uranium and other osteotoxic heavy metals, is presented below. This section is not meant to be an exhaustive review on bone biology and development of the skeletal system. More in depth reviews are cited herein.

The bones that comprise the skeletal system are rigid organs whose function is to maintain systematic mineral homeostasis, and to provide support, protection and mobility (Teti, 2011; Yang, 2009). The formation and growth of the skeletal system takes place during embryonic development and childhood (Karsenty, 1999). The process of bone formation and mineralization can be categorized into two types:

1. Endochondral ossification, in which the mesenchymal cells differentiate into chondrocytes which form the cartilage template for future bone, and are then replaced by osteoblasts (Karsenty, 1999; Teti, 2011).
2. Intramembranous ossification, in which bone formation occurs directly within the membranous tissue without the formation of a cartilage template (Franz-Odendaal, 2011; Mackie, 2003; Yang, 2009).

During early developmental stages, bones such as the skull, the mandible, and the pectoral girdle are formed via intramembranous ossification, while long bones are formed through endochondral ossification (Franz-Odendaal, 2011; Teti, 2011). The process of intramembranous ossification consists of three major stages: (a) cell induction to the skeletogenic lineage in which mesenchymal and epithelial cells interact and establish the eventual pattern of the skeleton, (b) condensation formation, in which mesenchymal cells aggregate until a critical size is reached, and (c) cell differentiation of osteoblasts which secrete bone matrix and promote bone mineralization (Franz-Odendaal, 2011; Olsen et al., 2000).

In both endochondral and intramembranous ossification, osteoblasts secrete bone matrix and the osteoblasts which become entrapped in the bone matrix are called osteocytes (Franz-Odendaal, 2011; Teti, 2011). Osteocytes form a network through the mineralized bone and their function is to maintain bone structure and metabolism by transducing stress signals from bending and stretching of bone as well as microdamage (Clarke, 2008; Teti, 2011).

Endochondral ossification consists of chondrocyte differentiation, proliferation and hypertrophy, followed by bone matrix secretion and mineralization. Enlarged chondrocytes secrete the matrix and form the bone cartilage model (Mackie et al., 2008). The hypertrophic chondrocytes then undergo apoptosis and are replaced by osteoblasts. The osteoblasts secrete osteoid, the unmineralized organic component of bone matrix, while osteoclasts remove the cartilage model (Karsenty, 1999; Mackie et al., 2008). Finally, the cartilage model is replaced by mineralized bone (Mackie et al., 2008).

Endochondral ossification also occurs during recovery from bone fractures (Shapiro, 2008). The histological appearance and molecular mechanisms involved in the process of fracture recovery are similar to the ones that regulate fetal and childhood skeletal development (Ferguson et al., 1999; Vortkamp et al., 1998). The process of endochondral bone repair also involves chondrocyte differentiation and hypertrophy, secretion of the cartilage bone model, osteoblast recruitment, and bone mineralization (Gerstenfeld et al., 2003; Shapiro, 2008). Endochondral bone repair is considered to recapitulate bone development during early life stages (Gerstenfeld et al., 2003) and, although fracture repair studies are carried out in a postnatal setting, they may be informative to the understanding of the effects of osteotoxic agents on early developmental bone growth.

Bone modeling and remodeling are two lifelong processes which allow growth and maintenance of the skeleton and damage removal (Clarke, 2008; Seeman, 2009). Bone modeling refers to the biological process by which bones change their shape and mineral content in response to physiologic and/or mechanical stimulus. Bone remodeling removes bone microdamage, maintains mineral homeostasis, and manages the extracellular levels of Ca^{2+}, and is governed by bone resorbing osteoclasts and bone re-synthesizing osteoblasts (Clarke, 2008; Seeman, 2009). During bone remodeling osteoblasts activate osteoclast differentiation through increased secretion of the cell membrane bound protein receptor activator of nuclear factor kappa (RANKL) (Karsenty, 1999; Komori, 2014). Upon erosion of the bone matrix by osteoclasts, the osteoblasts then re-mineralize the bone matrix (Anderson et al., 2011; Turner et al., 2012). Thus, osteoclasts remove the damaged portions of the bone, while osteoblasts secrete the bone matrix which is subsequently mineralized to form the new bone (Clarke, 2008; Teti, 2011). Bone remodeling replaces bone without altering its bone mineral content, with the exception of disease states such as osteoporosis where bone resorption occurs at a higher rate than deposition (Teti, 2011). Alterations in the rates of bone formation

versus resorption may lead to increased susceptibility to bone fractures (Clarke, 2008; Seeman, 2009).

Mineral homeostasis of the skeleton and blood calcium concentration are hormonally regulated by Vitamin D and parathyroid hormone (PTH) (Dusso et al., 2005; Norman, 2008). Vitamin D is obtained through the diet and the action of sunlight on the skin. The bioactive form of Vitamin D is produced by sequential enzymatic reactions in the liver and kidney, which are carried out by cytochrome P450 (CYP) enzymes (Dusso et al., 2005; Haussler et al., 2013). Bone cells such as osteoblasts, osteocytes, and osteoclasts have also been shown to metabolize Vitamin D to its bioactive metabolite (Turner et al., 2012). In the liver, cholecalciferol (Vitamin D_3) is hydroxylated to 25 hydroxyVitamin D_3 [25 $(OH)D_3$], which is then converted to the hormonally active Vitamin D metabolite 1,25-dihydroxyVitamin D_3 (1,25-$(OH)_2D_3$) in the renal proximal tubule and/or bone cells (Anderson et al., 2013; Clarke, 2008). Through activation of the Vitamin D receptor (VDR), 1,25-$(OH)_2D_3$ stimulates intestinal absorption of calcium and phosphorous, renal calcium reabsorption, bone modeling and remodeling, growth plate development of long bones, osteoblast differentiation, and osteoclast proliferation and differentiation (Anderson et al., 2013; Dusso et al., 2005; Haussler et al., 2013). Alterations in Vitamin D metabolism and/or inadequate expression of the VRD have been shown to be associated with skeletal disorders such as Rickets disease in children and osteoporosis in the elderly (Bacchetta et al., 2012; Haussler et al., 2013; Lanske and Razzaque, 2007).

4. Uranium-induced bone toxicity

The majority of the available evidence of uranium-induced adverse effects in osseous tissue has been generated from animal bioassays, and various studies demonstrate that early life stages–during which endochondral ossification and bone growth is most active–are susceptible to uranium induced alterations in normal bone functions and development. Wade-Gueye et al. (2012) reported higher susceptibility to uranium induced bone toxicity after exposure during early life stages (Wade-Gueye et al., 2012). Uranium exposure can also decrease tooth eruption and development in pre-pubertal Wistar rats, an effect which is indicative of damage to cementoblasts and odontoblasts (Pujadas Bigi et al., 2003; Pujadas Bigi and Ubios, 2007).

Uranium exposure can significantly alter the process of endochondral ossification (Table 1). In Wistar rats, uranium exposure reduced bone growth, volume, and mineralization of the tibial metaphysis (Diaz Sylvester et al., 2002; Fukuda et al., 2006; Guglielmotti et al., 1984; Ubios et al., 1994) and decreased mandibular bone growth (Diaz Sylvester et al., 2002; Pujadas Bigi and Ubios, 2007; Ubios et al., 1994). Similar effects have been reported in the femoral metaphysis of Balb/c mice and the tibial metaphysis of Wistar rats, in which uranium exposure was associated with decreased growth cartilage, bone volume, bone formation surfaces and mineralization (Bozal et al., 2005; Fukuda et al., 2006; Guglielmotti et al., 1984) (see Supplementary Table S1).

Cabrini et al. (1984), Guglielmotti et al. (1984, 1985, 1987), and Ubios et al. (1991) observed that acute uranium exposure resulted in decreased osteoblast activity and intramembranous ossification in Wistar rats (Table 1) (Cabrini et al., 1984; Guglielmotti et al., 1985, 1984; Ubios et al., 1990). A rat model was used to investigate intramembranous bone formation. It consisted of alveolar bone healing after tooth extraction (Jahangiri et al., 1998; Ubios et al., 1990). Uranium induced delays in intramembranous ossification and bone formation in the healing sockets of alveolar bones from Wistar rats were characterized by decreased bone volume, bone density, and bone formation (Cabrini et al., 1984; Guglielmotti et al., 1985, 1987, 1984; Ubios et al., 1990) and by increased bone resorption (Guglielmotti et al., 1987).

The processes of bone modeling and remodeling have also been shown to be altered by uranium exposure (Table 1). Studies using Wistar rats report that uranium exposure inhibited bone modeling and remodeling in the alveolar and mandibular bones (Diaz Sylvester et al., 2002; Pujadas Bigi et al., 2003; Pujadas Bigi and Ubios, 2007; Ubios et al., 1991, 1994). Exposure to uranium decreased bone formation in the lingual and vestibular (buccal) side of the mandible, two sites where modeling and remodeling take place, respectively (Pujadas Bigi et al., 2003; Ubios et al., 1991). In young animals, uranium exposure also decreased mandibular growth, a process dependent on adequate bone modeling and remodeling, and endochondral ossification (Pujadas Bigi et al., 2003; Pujadas Bigi and Ubios, 2007).

Animal studies have also reported that uranium can increase bone resorption. In Wistar rats, Guglielmotti et al. (1987) and Ubios et al. (1991) reported that bone resorption in the metaphysis of the tibial bone was significantly increased at 60 days post-exposure to a single uranium dose (Guglielmotti et al., 1987; Ubios et al., 1991). Fukuda et al. (2006) reported similar findings in Wistar rats where bone resorption measured in trabecular bone was significantly increased at 28 days post exposure to a single dose of uranium, and Bozal et al., 2005 observed that in Balb/c mice acute (48 h) exposure to uranium increased bone resorption in the metaphysis of the femoral bone (Bozal et al., 2005; Fukuda et al., 2006). Furthermore, an epidemiological study by Kurttio et al. (2005) reported an association between uranium exposure via drinking

Table 1
Uranium-induced adverse effects on bone development and maintenance.

Bone growth and maintenance process altered by uranium	Evidence of uranium induced alterations	Reference
Endochondral ossification	↓ Tibial metaphysis bone formation surface	Guglielmotti et al., 1984; Fukuda et al., 2006
	↓ Tibial bone length	Ubios et al., 1994
	↓ Tibial metaphysis bone volume	Ubios et al., 1994; Diaz-Sylvester et al., 2002; Pujadas Bigi and Ubios, 2007
	↓ Mandible growth (length and height)	
	↓ Femoral bone volume in metaphysis	Bozal et al., 2005
	↓ Femoral growth cartilage width	
	↓ Femoral cell proliferation in growth cartilage	
Intramembranous ossification	↓ Alveolar bone formation and volume in healing sockets	Guglielmotti et al., 1984, 1985; Guglielmotti et al., 1987; Ubios et al., 1990
	↓ Alveolar bone volume in healing sockets	Cabrini et al., 1984
Bone modeling and remodeling	↓ Mandibular bone formation in lingual side	Ubios et al., 1991; Pujadas Bigi et al., 2003, 2007
	↓ Mandibular bone formation in vestibular side	
	↓ Mandible growth (length and height)	Diaz-Sylvester et al., 2002; Ubios et al, 1994

water and increased serum levels of type I collagen carboxy terminal telopeptide, a marker of bone resorption (ATSDR, 2013; Kurttio et al., 2005).

Developmental toxicity studies have also demonstrated that uranium exposure during early life stages impairs skeletal development (Table S1). A dose-dependent association between uranium exposure and altered development of the skeletal system, including unossified sternebrae and reduced ossification in caudal, parietal, occipital, carpal, vertebral, and metatarsal bones, was reported in various studies where Swiss albino mice exposed during gestation (Bosque et al., 1992, 1993a,b; Domingo et al., 1989). The uranium-induced alterations in fetal bone development were among the most sensitive developmental effects observed in the developing mouse fetus (Bosque et al., 1993b; Domingo et al., 1989).

Overall, the available evidence from animal studies suggest that uranium exposure can interfere with intramembranous and endochondral ossification, bone modeling and remodeling, and promote bone resorption. Furthermore, early life stage studies demonstrate that uranium exposure impairs normal bone growth in developing individuals.

5. Potential mechanisms of uranium-induced toxicity in bone

The in vivo and in vitro studies described below have demonstrated that uranium can accumulate in osteoblasts, inhibit osteoblast differentiation and normal functions, and alter production and levels of Vitamin D (Fig. 1).

In vivo studies have demonstrated that uranium exposure can decrease cell proliferation in areas of endochondral ossification (Bozal et al., 2005), alter the cytoplasm and nuclei of active and inactive osteoblasts (Tasat et al., 2007), decrease the number of active osteoblasts (Bozal et al., 2005; Diaz Sylvester et al., 2002), and inhibit the expression of genes associated with normal bone development and mineralization (Wade-Gueye et al., 2012). Furthermore, in vitro studies have reported that uranium can induce and bind to osteoponin, a protein expressed in mineralized tissues which has been proposed to play a role in mineral homeostasis (Prat et al., 2010; Qi et al., 2014).

Studies using primary osteoblasts and immortalized human osteoblast cell lines indicate that uranium can accumulate in osteoblasts, promote cytotoxicity, alter cell phenotype, and reduce the activity of alkaline phosphatase a marker of osteoblast differentiation and bone mineralization (Milgram et al., 2008a,b; Tasat et al., 2007; Xiang et al., 2007). Uranium exposure has also been shown to increase reactive oxygen species (ROS) production osteoblasts (Tasat et al., 2007). Although the precise molecular mechanism for uranium-induced cellular responses has not been fully elucidated, Tasat et al. (2007) proposed that increased production of ROS may play a role in uranium-induced osteoblast toxicity. This proposed mechanism is supported by cell culture studies which have shown that excess ROS production can promote osteoblast toxicity and disrupt their differentiation (Bai et al., 2004; Mody et al., 2001).

These findings suggest that uranium disrupts osteoblast differentiation and inhibits their normal functions. As described above, osteoblasts are essential for bone formation, maintenance and recovery from injury. By decreasing osteoblast differentiation and proliferation, uranium exposure may alter the balance between the bone mineralizing activities regulated by osteoblasts, and the bone-resorptive activities of osteoclasts. This in turn may delay development of the skeletal system and promote increased bone fragility.

Animal studies have shown that uranium exposure may also interfere with bone growth and functions indirectly via altered metabolism and production of Vitamin D. Following short-term exposure to uranium in drinking water, significant decreases in the plasma levels of Vitamin D_3, potassium, and parathyroid hormone (a hormone which promotes renal Vitamin D_3 metabolism) were observed in adult rats (Tissandie et al., 2006). In a separate study, Tissandie et al. (2007) reported that nine months of uranium exposure in drinking water significantly decreased the plasma levels of hormonally active form of Vitamin D (1,25-(OH) $2D_3$) and the expression of CYP enzymes and nuclear receptor genes associated with Vitamin D_3 metabolism in the rat kidney and brain. However, circulating levels of PTH, 25 (OH)D_3 (the metabolic precursor of 1,25-(OH) $2D_3$), and calcium and phosphate

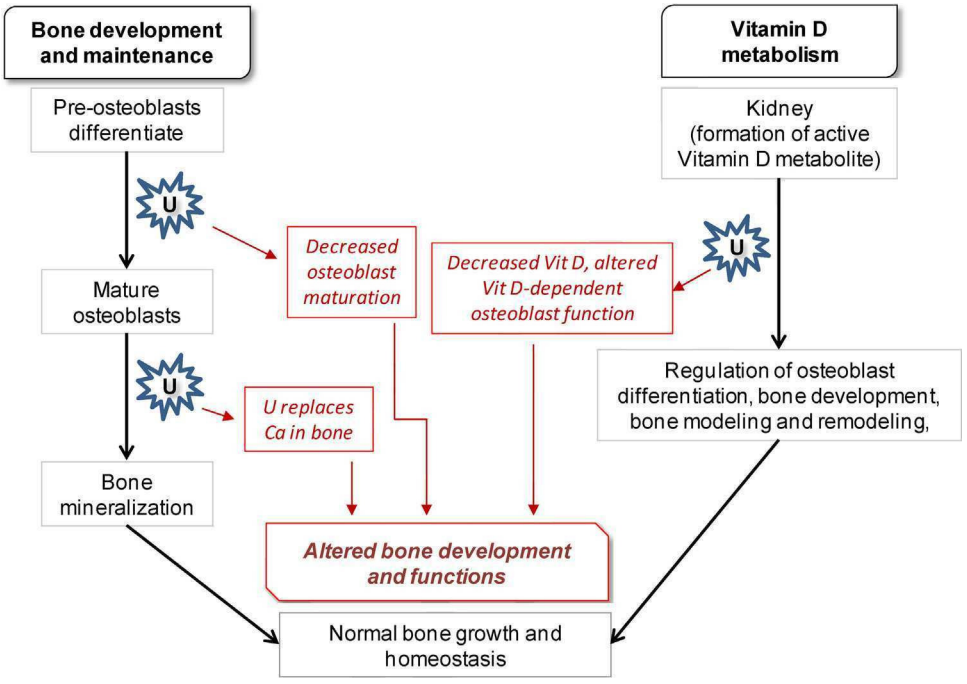

Fig. 1. Modes of action for uranium-induced alterations in normal bone functions and development.

concentrations were unaffected in the same study (Tissandie et al., 2007). Decreased enzymatic activity of cytochrome P450 27B1 (CYP27B1), which catalyzes renal biosynthesis of the active Vitamin D_3 metabolite (Prosser and Jones, 2004), was observed in rat kidneys following exposure to implanted uranium pellets (Yan et al., 2011). Uranium exposure has also been shown to significantly decrease VDR gene expression in the bones of young animals (Wade-Gueye et al., 2012). Furthermore, two epidemiological studies which evaluated the effects of depleted uranium exposure on Gulf War military personnel report increased urinary levels of calcium (McDiarmid et al., 2011), and altered serum levels of 1,25-(OH) $2D_3$ and PTH (McDiarmid et al., 2011, 2009). As described above, Vitamin D plays an essential role in regulation of mineral homeostasis and osteoblast functions. Inhibition of adequate VDR expression in bone cells could potentially reduce responsiveness to Vitamin D-regulated processes in bone such as osteoblast differentiation and bone mineralization. Overall, the evidence generated from animal and cell culture studies suggests that uranium exposure may promote bone toxicity directly by disrupting osteoblast development and functions and promoting cytotoxicity through increased ROS production, and indirectly by reducing renal metabolism of Vitamin D to its active metabolite, and reduced responsiveness to Vitamin D in osseous tissue (Fig. 1).

6. Discussion

Overall, evidence from animal and cell culture studies demonstrate that uranium exposure disrupts normal bone functions, including decreased endochondral and intramembranous ossification, and altered bone modeling and re-modeling. These responses result in delayed growth, increased bone resorption rates, reduced bone volume and density, and increased fragility. Furthermore, evidence from various animal studies suggest that early life stages are susceptible to uranium-induced osteotoxicity (Bosque et al., 1992, 1993a,b; Domingo et al., 1989; Pujadas Bigi et al., 2003; Pujadas Bigi and Ubios, 2007; Wade-Gueye et al., 2012).

The uranium-induced bone effects described above and the mechanisms associated with them are similar to those caused by exposure to cadmium and/or lead; heavy metals which are considered osteotoxic (ATSDR, 2012; Berglund et al., 2000; Bhattacharyya, 2009; Holz et al., 2007). Exposure to lead or cadmium is associated with impaired bone development, decreased mineralization and increased fragility (ATSDR, 2007, 2012; Ronis et al., 2001). Similar to uranium, animal studies have shown that exposure to these metals can promote bone toxicity directly by disrupting bone cell differentiation and inhibiting normal bone cell functions, and indirectly by altering renal metabolism of Vitamin D to its hormonally active form (Berglund et al., 2000; Holz et al., 2007). Furthermore, exposure to these metals can also cause disruptions in normal bone functions including fracture repair, endochondral ossification and bone modeling and remodeling; thus promoting increased bone fragility during early life stages and in the elderly (Berglund et al., 2000; Bhattacharyya, 2009; Carmouche et al., 2005; Holz et al., 2007). The overall consistency in the effects caused by uranium and known osteotoxic metals such as cadmium and lead further supports the conclusion that uranium is an osteotoxic heavy metal.

As described above, evidence from in vivo and cell culture experiments suggests that uranium exposure can directly affect normal bone function by targeting osteoblasts. Animal studies have reported that uranium exposure disrupts osteoblast differentiation and inhibits their function in areas of bone growth (Cabrini et al., 1984; Guglielmotti et al., 1985, 1984; Wade-Gueye et al., 2012) while cell culture studies report evidence of decreased osteoblast function and increased cytotoxicity (Milgram et al., 2008b; Tasat et al., 2007; Xiang et al., 2007). Furthermore, uranium has been shown to promote ROS production in a human osteoblast cell line (Tasat et al., 2007).

Uranium-induced toxicity to osteoblasts in sites of bone growth is relevant to early life stages as adequate osteoblast function is necessary for normal development of the skeletal system. The available evidence from developmental toxicity studies suggests that uranium can directly target osteoblasts, affect their differentiation and function, and delay bone development during prenatal and early postnatal life stages (Bosque et al., 1992, 1993a,b; Domingo et al., 1989; Pujadas Bigi et al., 2003; Wade-Gueye et al., 2012). Uranium has also been shown to cross the placenta and accumulate in the bones, liver and kidney of developing fetuses (Benson, 2001; Sanchez et al., 2006). Sanchez et al. (2006) reported that uranium accumulation in the bones of exposed fetuses was higher than in the fetal kidneys, an organ which is generally considered to be a primary target of uranium toxicity (Arzuaga et al., 2010; ATSDR, 2013). Uranium is also known to accumulate in areas of bone growth (Neuman et al., 1948; Rodrigues et al., 2013; Rowland and Farnham, 1969), where active calcification is occurring (de Rey et al., 1984; Durbin and Wrenn, 1975). Furthermore, ex-vivo studies using mouse preimplantation embryos (Kundt et al., 2000), and in vivo studies using the non-mammalian vertebrates *Danio rerio* and *Xenopus laevis* have shown that uranium exposure reduces embryo growth (Bourrachot et al., 2008; Mitchell et al., 2005). Taken together, the available studies provides evidence for a direct effect of uranium in developing animals. They strongly suggest that upon exposure uranium crosses the placenta, accumulates in fetal bones, and inhibits bone growth and development.

Additionally, an indirect pathway by which uranium could affect normal bone growth and functions may be through alterations in maternal Vitamin D metabolism. In vivo studies in rats have shown that uranium exposure can alter renal Vitamin D metabolism in adult and developing animals without significant renal kidney toxicity (Tissandie et al., 2007, 2006; Wade-Gueye et al., 2012; Yan et al., 2011). Gene expression and enzyme activity assays performed in these studies suggest that alterations in Vitamin D levels expression result from mRNA, protein, and activity of metabolic enzymes critical for production of the active Vitamin D metabolite.

Uranium-induced alterations in Vitamin D production and levels may result in reduced bone growth and mineralization during early life stages, and bone maintenance in the elderly. As described above, Vitamin D promotes increased mineral uptake and bone growth. Disorders in which Vitamin D metabolism and production is inhibited are characterized by reduced bone growth during fetal and early postnatal development (Bacchetta et al., 2012; Kaushal and Magon, 2013), and decreased bone mineral density in the elderly (Turner et al., 2012).

Uranium-induced alterations in maternal Vitamin D metabolism may also disrupt bone growth in the developing fetus. As discussed above, various developmental toxicity studies have reported that gestational exposure to uranium can impair skeletal development (Bosque et al., 1992, 1993a,b; Domingo et al., 1989). It has been suggested that some of the observed effects in developing fetuses are due, in part, to maternal toxicity (ATSDR, 2013; Domingo, 2001). Although there is no sufficient evidence to accurately determine which developmental effects are directly associated with maternal toxicity, uranium-induced changes in maternal production and levels of Vitamin D could contribute to the osteotoxicity observed in developing fetuses. Vitamin D is essential for fetal growth (Barrett and McElduff, 2010; Dror, 2011). Reduced maternal levels of Vitamin D during pregnancy can lead to decreased ossification in the developing human fetus, and has been shown to result in skeletal effects that persist through childhood, such as Rickets and low bone mineral density (Javaid et al., 2006;

Mahon et al., 2010; Viljakainen et al., 2010; Yorifuji et al., 2008). Uranium-induced disruption of maternal Vitamin D metabolism–resulting in decreased availability of the hormonally active Vitamin D metabolite–may thus cause fetal osteotoxicity. Studies evaluating the effects of uranium exposure on Vitamin D metabolism during pregnancy were not identified in the literature. Future studies should be aimed determining the potential role of uranium-induced alterations in maternal and fetal Vitamin D metabolism during this potentially susceptible life stage.

In addition to young individuals, the elderly may also represent a susceptible population to uranium-induced bone toxicity. During aging there is a shift in the ratio of bone mineralization versus erosion in bone remodeling. This results in decreased bone mineralization and increased bone fragility (Phan et al., 2004; Woodward et al., 2010). As discussed above, in vivo studies have shown that uranium exposure can alter bone remodeling resulting in increased resorption (Bozal et al., 2005; Fukuda et al., 2006; Guglielmotti et al., 1987; Kurttio et al., 2005; Ubios et al., 1991). Although there are no available studies on the potential effects of uranium exposure on aging bones, cadmium exposure has been shown to promote bone toxicity and increase bone fragility in elderly individuals (Bhattacharyya, 2009; Jarup et al., 1998) and to inhibit osteoblast functions while promoting osteoclast differentiation (Chen et al., 2009; Chen et al., 2012). Pb has also been shown to delay endochondral ossification and bone healing, and inhibit differentiation of osteoprogenitor cells (Carmouche et al., 2005). Given the similarities in the bone effects caused by exposure to these two metals, it is possible that uranium exposure may also promote bone resorption in exposed elderly individuals.

In conclusion, the available evidence from in-vivo and cell culture toxicity and mechanistic studies demonstrates that uranium exposure results in bone toxicity and that these effects may be caused by direct damage to osteoblast development and function, and Vitamin D metabolism. However, significant data gaps remain. Bone formation is a tightly regulated process which is controlled by transcription factors, cytokines and growth factors (Olsen et al., 2000; Yang, 2009), and the precise molecular and biochemical mechanisms by which uranium exposure inhibits osteoblast differentiation and bone mineralization have not been described. Furthermore, the potential osteotoxic effects of uranium exposure during pregnancy and in aging individuals are yet to be assessed. Finally, in addition to assessing the potential nephrotoxic effects of uranium in exposed human populations, epidemiological studies could also consider evaluating indicators of mineral homeostasis and bone health such as Vitamin D, BMD, and serum and urinary levels of biomarkers of bone formation and resorption.

Acknowledgements

Chase Kluemper (University of Kentucky), and Andrew Hotchkiss and Janice Lee (U.S. EPA) contributed to the development of this manuscript.

Appendix A. Supplementary data

Supplementary data associated with this article can be found, in the online version, at http://dx.doi.org/10.1016/j.toxlet.2015.05.006.

References

Adams, N., Spoor, N.L., 1974. Kidney and bone retention functions in the human metabolism of uranium. Phys. Med. Biol. 19, 460–471.
Anderson, P.H., Atkins, G.J., Turner, A.G., Kogawa, M., Findlay, D.M., Morris, H.A., 2011. Vitamin D metabolism within bone cells: effects on bone structure and strength. Mol. Cell. Endocrinol. 347, 42–47.
Anderson, P.H., Lam, N.N., Turner, A.G., Davey, R.A., Kogawa, M., Atkins, G.J., Morris, H.A., 2013. The pleiotropic effects of vitamin D in bone. J. Steroid Biochem. Mol. Biol. 136, 190–194.
Arruda-Neto, J.D., Guevara, M.V., Nogueira, G.P., Saiki, M., Cestari, A.C., Shtejer, K., Deppman, A., Pereira Filho, J.W., Garcia, F., Geraldo, L.P., Gouveia, A.N., Guzman, F., Mesa, J., Rodriguez, O., Semmler, R., Vanin, V.R., 2004. Long-term accumulation of uranium in bones of Wistar rats as a function of intake dosages. Radiat. Prot. Dosim. 112, 385–393.
Arzuaga, X., Rieth, S.H., Bathija, A., Cooper, G.S., 2010. Renal effects of exposure to natural and depleted uranium: a review of the epidemiologic and experimental data. J. Toxicol. Environ. Health B Crit. Rev. 13, 527–545.
ATSDR, 2007. Toxicological Profile for Lead. U.S. Department of Health and Human Services, Agency for Toxic Substances and Disease Registry (ATSDR), Atlanta, GA.
ATSDR, 2012. Toxicological Profile for Cadmium. U.S. Department of Health and Human Services, Agency for Toxic Substances and Disease Registry (ATSDR), Atlanta, GA.
ATSDR, 2013. Toxicological Profile for Uranium. U.S. Department of Health and Human Services, Agency for Toxic Substances and Disease Registry (ATSDR), Atlanta, GA.
Bacchetta, J., Harambat, J., Cochat, P., Salusky, I.B., Wesseling-Perry, K., 2012. The consequences of chronic kidney disease on bone metabolism and growth in children. Nephrol. Dial. Transp. 27, 3063–3071.
Bai, X.C., Lu, D., Bai, J., Zheng, H., Ke, Z.Y., Li, X.M., Luo, S.Q., 2004. Oxidative stress inhibits osteoblastic differentiation of bone cells by ERK and NF-kappaB. Biochem. Biophys. Res. Commun. 314, 197–207.
Barrett, H., McElduff, A., 2010. Vitamin D and pregnancy: an old problem revisited. Best Pract. Res. Clin. Endocrinol. Metab. 24, 527–539.
Benson, K., 2001. Evaluation of the health risks of embedded depleted uranium (DU) shrapnel on pregnancy and offspring development., in: U.S.A.M.R.a.M. Command (Ed.). Henry M. Jackson Foundation for the Advancement of Military Medicine Rockville, Maryland.
Berglund, M., Akesson, A., Bjellerup, P., Vahter, M., 2000. Metal-bone interactions. Toxicol. Lett. 112–113, 219–225.
Bhattacharyya, M.H., 2009. Cadmium osteotoxicity in experimental animals: mechanisms and relationship to human exposures. Toxicol. Appl. Pharmacol. 238, 258–265.
Bleise, A., Danesi, P.R., Burkart, W., 2003. Properties, use and health effects of depleted uranium (DU): a general overview. J. Environ. Radioact. 64, 93–112.
Bosque, M.A., Domingo, J.L., Corbella, J., 1992. Embryofetotoxicidad del uranio en ratones: variabilidad con el dia de exposicion. 1992 9, 107–110.
Bosque, M.A., Domingo, J.L., Llobet, J.M., Corbella, J., 1993a. Effectiveness of sodium 4,5-dihydroxybenzene-1,3-disulfonate (Tiron) in protecting against uranium-induced developmental toxicity in mice. Toxicology 79, 149–156.
Bosque, M.A., Domingo, J.L., Llobet, J.M., Corbella, J., 1993b. Embryotoxicity and teratogenicity of uranium in mice following subcutaneous administration of uranyl acetate. Biol. Trace Elem. Res. 36, 109–118.
Bourrachot, S., Simon, O., Gilbin, R., 2008. The effects of waterborne uranium on the hatching success, development, and survival of early life stages of zebrafish (Danio rerio). Aquat. Toxicol. 90, 29–36.
Bozal, C.B., Martinez, A.B., Cabrini, R.L., Ubios, A.M., 2005. Effect of ethane-1-hydroxy-1,1-bisphosphonate (EHBP) on endochondral ossification lesions induced by a lethal oral dose of uranyl nitrate. Arch. Toxicol. 79, 475–481.
Brugge, D., Buchner, V., 2011. Health effects of uranium: new research findings. Rev. Environ. Health 26, 231–249.
Cabrini, R.L., Gulielmotti, M.B., Ubios, A.M., 1984. Prevention of the toxic effect of uranium on bone by tetracycline. Acta Odontol. Latinoam. 1, 61–63.
Carmouche, J.J., Puzas, J.E., Zhang, X., Tiyapatanaputi, P., Cory-Slechta, D.A., Gelein, R., Zuscik, M., Rosier, R.N., Boyce, B.F., O'Keefe, R.J., Schwarz, E.M., 2005. Lead exposure inhibits fracture healing and is associated with increased chondrogenesis, delay in cartilage mineralization, and a decrease in osteoprogenitor frequency. Environ. Health Perspect. 113, 749–755.
Chen, X., Zhu, G., Gu, S., Jin, T., Shao, C., 2009. Effects of cadmium on osteoblasts and osteoclasts in vitro. Environ. Toxicol. Pharmacol. 28, 232–236.
Chen, X., Zhu, G., Jin, T., Zhou, Z., Gu, S., Qiu, J., Xiao, H., 2012. Cadmium stimulates the osteoclastic differentiation of RAW264.7 cells in presence of osteoblasts. Biol. Trace Elem. Res. 146, 349–353.
Clarke, B., 2008. Normal bone anatomy and physiology. Clin. J. Am. Soc. Nephrol. 3 (Suppl. (3)), S131–139.
Craft, E., Abu-Qare, A., Flaherty, M., Garofolo, M., Rincavage, H., Abou-Donia, M., 2004. Depleted and natural uranium: chemistry and toxicological effects. J. Toxicol. Environ. Health B Crit. Rev. 7, 297–317.
de Rey, B.M., Lanfranchi, H.E., Cabrini, R.L., 1984. Deposition pattern and toxicity of subcutaneously implanted uranium dioxide in rats. Health Phys. 46, 688–692.
Diaz Sylvester, P.L., Lopez, R., Ubios, A.M., Cabrini, R.L., 2002. Exposure to subcutaneously implanted uranium dioxide impairs bone formation. Arch. Environ. Health 57, 320–325.
Domingo, J.L., 2001. Reproductive and developmental toxicity of natural and depleted uranium: a review. Reprod. Toxicol. 15, 603–609.
Domingo, J.L., Paternain, J.L., Llobet, J.M., Corbella, J., 1989. The developmental toxicity of uranium in mice. Toxicology 55, 143–152.
Dror, D.K., 2011. Vitamin D status during pregnancy: maternal fetal, and postnatal outcomes. Curr. Opin. Obstet. Gynecol. 23, 422–426.
Durbin, P.W., Wrenn, M.E., 1975. Metabolism and effects of uranium in animals. Conference on Occupational Health Experience With Uranium, Arlington, VA, pp. 67–129.

Dusso, A.S., Brown, A.J., Slatopolsky, E., 2005. Vitamin D. Am. J. Physiol. Renal Physiol. 289, F8–28.
Eidson, A.F., 1994. The effect of solubility on inhaled uranium compound clearance: a review. Health Phys. 67, 1–14.
Ferguson, C., Alpern, E., Miclau, T., Helms, J.A., 1999. Does adult fracture repair recapitulate embryonic skeletal formation? Mech. Dev. 87, 57–66.
Fisenne, I.M., Welford, G.A., 1986. Natural U concentrations in soft tissues and bone of New York City residents. Health Phys. 50, 739–746.
Franz-Odendaal, T.A., 2011. Induction and patterning of intramembranous bone. Front. Biosci. 16, 2734–2746.
Fukuda, S., Ikeda, M., Chiba, M., Kaneko, K., 2006. Clinical diagnostic indicators of renal and bone damage in rats intramuscularly injected with depleted uranium. Radiat. Prot. Dosim. 118, 307–314.
Gerstenfeld, L.C., Cullinane, D.M., Barnes, G.L., Graves, D.T., Einhorn, T.A., 2003. Fracture healing as a post-natal developmental process: molecular, spatial, and temporal aspects of its regulation. J. Cell. Biochem. 88, 873–884.
Guglielmotti, M.B., Ubios, A.M., Cabrini, R.L., 1985. Alveolar wound healing alteration under uranyl nitrate intoxication. J. Oral Pathol. 14, 565–572.
Guglielmotti, M.B., Ubios, A.M., Cabrini, R.L., 1987. Morphometric study of the effect of a low dose of uranium on bone healing. Acta Stereol. 6, 357–366.
Guglielmotti, M.B., Ubios, A.M., de Rey, B.M., Cabrini, R.L., 1984. Effects of acute intoxication with uranyl nitrate on bone formation. Experientia 40, 474–476.
Haussler, M.R., Whitfield, G.K., Kaneko, I., Haussler, C.A., Hsieh, D., Hsieh, J.C., Jurutka, P.W., 2013. Molecular mechanisms of vitamin D action. Calcified Tissue Int. 92, 77–98.
Holz, J.D., Sheu, T.J., Drissi, H., Matsuzawa, M., Zuscik, M.J., Puzas, J.E., 2007. Environmental agents affect skeletal growth and development. Birth defects research. Part C. Embryo Today: Rev. 81, 41–50.
IAEA, 2008. Depleted Uranium. I.A.E. Agency, Vienna, Austria.
Jahangiri, L., Devlin, H., Ting, K., Nishimura, I., 1998. Current perspectives in residual ridge remodeling and its clinical implications: a review. J. Prosthet. Dent. 80, 224–237.
Jarup, L., Alfven, T., Persson, B., Toss, G., Elinder, C.G., 1998. Cadmium may be a risk factor for osteoporosis. Occup. Environ. Med. 55, 435–439.
Javaid, M.K., Crozier, S.R., Harvey, N.C., Gale, C.R., Dennison, E.M., Boucher, B.J., Arden, N.K., Godfrey, K.M., Cooper, C., 2006. Maternal vitamin D status during pregnancy and childhood bone mass at age 9 years: a longitudinal study. Lancet 367, 36–43.
Karsenty, G., 1999. The genetic transformation of bone biology. Genes Dev. 13, 3037–3051.
Kaushal, M., Magon, N., 2013. Vitamin D in pregnancy: a metabolic outlook. Indian J. Endocrinol. Metab. 17, 76–82.
Keith, L.S., Faroon, O.M., Fowler, B.A., 2007. Uranium. In: Nordberg, G.F., Fowler, B.A., Nordberg, M., Friberg, L.T. (Eds.), Handbook on the Toxicology of Metals. Elsevier, New York.
Komori, T., 2014. Mouse models for the evaluation of osteocyte functions. J. Bone Metab. 21, 55–60.
Kundt, M., Ubios, A.M., Cabrini, R.L., 2000. Effects of uranium poisoning on cultured preimplantation embryos. Biol. Trace Elem. Res. 75, 235–244.
Kurttio, P., Komulainen, H., Leino, A., Salonen, L., Auvinen, A., Saha, H., 2005. Bone as a possible target of chemical toxicity of natural uranium in drinking water. Environ. Health Perspect. 113, 68–72.
Lanske, B., Razzaque, M.S., 2007. Vitamin D and aging: old concepts and new insights. J. Nutr. Biochem. 18, 771–777.
Lariviere, D., Packer, A.P., Marro, L., Li, C., Chen, J., Cornett, R.J., 2007. Age dependence of natural uranium and thorium concentrations in bone. Health Phys. 92, 119–126.
Lariviere, D., Tolmachev, S.Y., Kochermin, V., Johnson, S., 2013. Uranium bone content as an indicator of chronic environmental exposure from drinking water. J. Environ. Radioact. 121, 98–103.
Mackie, E.J., 2003. Osteoblasts: novel roles in orchestration of skeletal architecture. Int. J. Biochem. Cell Biol. 35, 1301–1305.
Mackie, E.J., Ahmed, Y.A., Tatarczuch, L., Chen, K.S., Mirams, M., 2008. Endochondral ossification: how cartilage is converted into bone in the developing skeleton. Int. J. Biochem. Cell Biol. 40, 46–62.
Mahon, P., Harvey, N., Crozier, S., Inskip, H., Robinson, S., Arden, N., Swaminathan, R., Cooper, C., Godfrey, K., Group, S.W.S.S., 2010. Low maternal vitamin D status and fetal bone development: cohort study. J. Bone Mineral Res. 25, 14–19.
McDiarmid, M.A., Engelhardt, S.M., Dorsey, C.D., Oliver, M., Gucer, P., Gaitens, J.M., Kane, R., Cernich, A., Kaup, B., Hoover, D., Gaspari, A.A., Shvartsbeyn, M., Brown, L., Squibb, K.S., 2011. Longitudinal health surveillance in a cohort of Gulf War veterans 18 years after first exposure to depleted uranium. J. Toxicology Environ. Health Part A 74, 678–691.
McDiarmid, M.A., Engelhardt, S.M., Dorsey, C.D., Oliver, M., Gucer, P., Wilson, P.D., Kane, R., Cernich, A., Kaup, B., Anderson, L., Hoover, D., Brown, L., Albertini, R., Gudi, R., Squibb, K.S., 2009. Surveillance results of depleted uranium-exposed Gulf War I veterans: sixteen years of follow-up. J. Toxicol. Environmental Health Part A 72, 14–29.
Milgram, S., Carriere, M., Malaval, L., Gouget, B., 2008a. Cellular accumulation and distribution of uranium and lead in osteoblastic cells as a function of their speciation. Toxicology 252, 26–32.
Milgram, S., Carriere, M., Thiebault, C., Malaval, L., Gouget, B., 2008b. Cytotoxic and phenotypic effects of uranium and lead on osteoblastic cells are highly dependent on metal speciation. Toxicology 250, 62–69.
Mitchell, S.E., Caldwell, C.A., Gonzales, G., Gould, W.R., Arimoto, R., 2005. Effects of depleted uranium on survival, growth, and metamorphosis in the African clawed frog (*Xenopus laevis*). J. Toxicol. Environ. Health Part A 68, 951–965.
Mody, N., Parhami, F., Sarafian, T.A., Demer, L.L., 2001. Oxidative stress modulates osteoblastic differentiation of vascular and bone cells. Free Radical Biol. Med. 31, 509–519.
Neuman, W.F., Neuman, M.W., Mulryan, B.J., 1948. The deposition of uranium in bone; animal studies. J. Biol. Chem. 175, 705–709.
Norman, A.W., 2008. From vitamin D to hormone D: fundamentals of the vitamin D endocrine system essential for good health. Am. J. Clin. Nutr. 88, 491S–499S.
NRC, 2008. In: Council, N.R. (Ed.), Review of the Toxicologic and Radiologic Risks to Military Personnel from Exposures to Depleted Uranium During and after Combat. National Academy Press, Washington, D.C.
Olsen, B.R., Reginato, A.M., Wang, W., 2000. Bone development. Annu. Rev. Cell Dev. Biol. 16, 191–220.
Pellmar, T.C., Fuciarelli, A.F., Ejnik, J.W., Hamilton, M., Hogan, J., Strocko, S., Emond, C., Mottaz, H.M., Landauer, M.R., 1999. Distribution of uranium in rats implanted with depleted uranium pellets. Toxicol. Sci. 49, 29–39.
Phan, T.C., Xu, J., Zheng, M.H., 2004. Interaction between osteoblast and osteoclast: impact in bone disease. Histol. Histopathol. 19, 1325–1344.
Prado, G.R., Arruda-Neto, J.D., Sarkis, J.E., Geraldo, L.P., Muller, R.M., Garcia, F., Bittencourt-Oliveira, M.C., Guevara, M.V., Rodrigues, G., Mesa, J., Rodrigues, T.E., 2008. Evaluation of uranium incorporation from contaminated areas using teeth as bioindicators–a case study. Radiat. Prot. Dosimetry 130, 249–252.
Prat, O., Berenguer, F., Steinmetz, G., Ruat, S., Sage, N., Quemeneur, E., 2010. Alterations in gene expression in cultured human cells after acute exposure to uranium salt: Involvement of a mineralization regulator. Toxicol. In Vitro 24, 160–168.
Prosser, D.E., Jones, G., 2004. Enzymes involved in the activation and inactivation of vitamin D. Trends Biochem. Sci. 29, 664–673.
Pujadas Bigi, M.M., Lemlich, L., Mandalunis, P.M., Ubios, A.M., 2003. Exposure to oral uranyl nitrate delays tooth eruption and development. Health Phys. 84, 163–169.
Pujadas Bigi, M.M., Ubios, A.M., 2007. Catch-up of delayed tooth eruption associated with uranium intoxication. Health Phys. 92, 345–348.
Qi, L., Basset, C., Averseng, O., Quemeneur, E., Hagege, A., Vidaud, C., 2014. Characterization of UO2(2+) binding to osteopontin, a highly phosphorylated protein: insights into potential mechanisms of uranyl accumulation in bones. Metallomics 6, 166–176.
Rodrigues, G., Arruda-Neto, J.D., Pereira, R.M., Kleeb, S.R., Geraldo, L.P., Primi, M.C., Takayama, L., Rodrigues, T.E., Cavalcante, G.T., Genofre, G.C., Semmler, R., Nogueira, G.P., Fontes, E.M., 2013. Uranium deposition in bones of Wistar rats associated with skeleton development. Appl. Radiat. Isotopes 82, 105–110.
Ronis, M.J., Aronson, J., Gao, G.G., Hogue, W., Skinner, R.A., Badger, T.M., Lumpkin Jr., C.K., 2001. Skeletal effects of developmental lead exposure in rats. Toxicol. Sci. 62, 321–329.
Rowland, R.E., Farnham, J.E., 1969. The deposition of uranium in bone. Health Phys. 17, 139–144.
Sanchez, D.J., Belles, M., Albina, M.L., Gomez, M., Linares, V., Domingo, J.L., 2006. Exposure of pregnant rats to uranium and restraint stress: effects on postnatal development and behavior of the offspring. Toxicology 228, 323–332.
Seeman, E., 2009. Bone modeling and remodeling. Crit. Rev. Eukaryot. Gene Expr. 19, 219–233.
Shapiro, F., 2008. Bone development and its relation to fracture repair The role of mesenchymal osteoblasts and surface osteoblasts. Eur. Cells Mater. 15, 53–76.
Tasat, D.R., Orona, N.S., Mandalunis, P.M., Cabrini, R.L., Ubios, A.M., 2007. Ultrastructural and metabolic changes in osteoblasts exposed to uranyl nitrate. Arch. Toxicol. 81, 319–326.
Teti, A., 2011. Bone development: overview of bone cells and signaling. Curr. Osteoporos. Rep. 9, 264–273.
Tissandie, E., Gueguen, Y., Lobaccaro, J.M., Grandcolas, L., Voisin, P., Aigueperse, J., Gourmelon, P., Souidi, M., 2007. In vivo effects of chronic contamination with depleted uranium on vitamin D3 metabolism in rat. Biochim. Biophys. Acta 1770, 266–272.
Tissandie, E., Gueguen, Y., Lobaccaro, J.M., Paquet, F., Aigueperse, J., Souidi, M., 2006. Effects of depleted uranium after short-term exposure on vitamin D metabolism in rat. Arch. Toxicol. 80, 473–480.
Turner, A.G., Anderson, P.H., Morris, H.A., 2012. Vitamin D and bone health: Scandinavian journal of clinical and laboratory investigation. Supplementum 243, 65–72.
Ubios, A.M., Guglielmotti, M.B., Cabrini, R.L., 1990. Ethane 1-hydroxy-1, 1-diphosphonate (EHDP) counteracts the inhibitory effect of uranyl nitrate on bone formation. Arch. Environ. Health 45, 374–377.
Ubios, A.M., Guglielmotti, M.B., Steimetz, T., Cabrini, R.L., 1991. Uranium inhibits bone formation in physiologic alveolar bone modeling and remodeling. Environ. Res. 54, 17–23.
Ubios, A.M., Piloni, M.J., Marzorati, M., Cabrini, R.L., 1994. Bone growth is impaired by uranium intoxication. Acta Odontol. Latinoam. 8, 3–8.
Viljakainen, H.T., Saarnio, E., Hytinantti, T., Miettinen, M., Surcel, H., Makitie, O., Andersson, S., Laitinen, K., Lamberg-Allardt, C., 2010. Maternal vitamin D status determines bone variables in the newborn. J. Clin. Endocrinol. Metab. 95, 1749–1757.
Vortkamp, A., Pathi, S., Peretti, G.M., Caruso, E.M., Zaleske, D.J., Tabin, C.J., 1998. Recapitulation of signals regulating embryonic bone formation during postnatal growth and in fracture repair. Mech. Dev. 71, 65–76.

Wade-Gueye, N.M., Delissen, O., Gourmelon, P., Aigueperse, J., Dublineau, I., Souidi, M., 2012. Chronic exposure to natural uranium via drinking water affects bone in growing rats. Biochim. Biophys. Acta 1820, 1121–1127.
Woodward, J.C., Burkhardt, J.E., Lee, W., 2010. Bones and joints, In: Haschek, W.M., Rousseaux, C.G., Walling, M.A. (Eds.), Fundamentals of Toxicologic Pathology. second ed. Elsevier, New York, pp. 411–449.
Xiang, X., Zhu, G., Wang, L., Yan, M., Chen, X., 2007. Studies on the toxic effects of depleted uranium on osteoblast in vitro. J. Environ. Occup. Med. 24, 255–258.
Yan, M., Zhong, G., Gao, L., Xia, X., Wang, L., Hu, H., Weng, S., 2011. Effects of uranium depletion on 1alpha-hydroxylase in kidney of rats. Hum. Exp. Toxicol. 30, 786–790.
Yang, Y., 2009. Skeletal morphogenesis during embryonic development. Crit. Rev. Eukaryot. Gene expr. 19, 197–218.
Yorifuji, J., Yorifuji, T., Tachibana, K., Nagai, S., Kawai, M., Momoi, T., Nagasaka, H., Hatayama, H., Nakahata, T., 2008. Craniotabes in normal newborns: the earliest sign of subclinical vitamin D deficiency. J. Clin. Endocrinol. Metab. 93, 1784–1788.
Zhu, G., Tan, M., Li, Y., Xiang, X., Hu, H., Zhao, S., 2009. Accumulation and distribution of uranium in rats after implantation with depleted uranium fragments. J. Radiat. Res. (Tokyo) 50, 183–192.

From:	Strong, Jamie
To:	Arzuaga, Xabier
Subject:	RE: STAA award nomination for the uranium paper
Date:	Thursday, April 23, 2020 3:37:43 PM

I think that sounds right, hard to remember! I hope you are well and being safe!

From: Arzuaga, Xabier <Arzuaga.Xabier@epa.gov>
Sent: Tuesday, April 21, 2020 1:59 PM
To: Strong, Jamie <Strong.Jamie@epa.gov>
Subject: STAA award nomination for the uranium paper

Hi Jamie,
I hope that you guys are OK and staying healthy. We are doing well at home and have established a routine for the kids. So far its working well. They do their school work during the day and in the afternoons we will do something together. Julian and Sidney are also doing music and karate classes online. I have joined in for the karate and its lots of fun to do with a bunch of 6 year old kids. I am putting together an STAA award nomination for the uranium paper we published in 2015. Please let me know if you are agree with the estimated level of contribution below. Thanks and stay safe!
Xabier

- Jamie Strong; U.S. EPA, Office of Water
- Nominee's name: Xabier Arzuaga
- Publication title: "Modes of action associated with uranium induced adverse effects in bone function
- and development"
- I agree with my designated level of contribution: 15%

Xabier Arzuaga, PhD
Toxicologist
U.S. EPA, Office of Research and Development,
Center for Public Health and Environmental Assessment
1200 Pennsylvania Ave, NW (Mail Code 8601P) | Washington, DC 20460
RRB 71274 | Phone: (202) 564-1361
Email: arzuaga.xabier@epa.gov

From:	Gehlhaus, Martin
To:	Arzuaga, Xabier
Subject:	RE: STAA award nomination for the uranium paper
Date:	Tuesday, April 21, 2020 2:53:28 PM

Xabier!!! Great to hear from you. We're doing well... or as well as can be expected. My wife and I are working throughout the day and the kids have anywhere from 3 to 5 hours of school work... so we tend to fight over the WiFi. Like you and your family, we've settled into a routine to try and make the most of the situation.

I agree with estimated level of contribution.

Take care. Stay well.

Martin Gehlhaus

US Environmental Protection Agency
Region III
Superfund and Emergency Management Division
Risk Assessment Section
3SD52
1650 Arch Street
Philadelphia, PA 19103-2029
215-814-3359

From: Arzuaga, Xabier <Arzuaga.Xabier@epa.gov>
Sent: Tuesday, April 21, 2020 1:53 PM
To: Gehlhaus, Martin <Gehlhaus.Martin@epa.gov>
Subject: STAA award nomination for the uranium paper

Hi Martyn,
I hope that you guys are OK and staying healthy. We are doing well at home and have established a routine for the kids. So far its working well. They do their school work during the day and in the afternoons we will do something together. I am putting together an STAA award nomination for the uranium paper we published in 2015. Please let me know if you are agree with the estimated level of contribution below. Thanks and stay safe!
Xabier

- Martin Gehlhaus; U.S. EPA, Region 3
- Nominee's name: Xabier Arzuaga
- Publication title: "Modes of action associated with uranium induced adverse effects in bone function and
- development"
- I agree with my designated level of contribution: 20%

Xabier Arzuaga, PhD
Toxicologist
U.S. EPA, Office of Research and Development,
Center for Public Health and Environmental Assessment
1200 Pennsylvania Ave, NW (Mail Code 8601P) | Washington, DC 20460
RRB 71274 | Phone: (202) 564-1361
Email: arzuaga.xabier@epa.gov

This article was downloaded by: *[US EPA Environmental Protection Agency]*
On: *22 December 2010*
Access details: *Access Details: [subscription number 789514190]*
Publisher *Taylor & Francis*
Informa Ltd Registered in England and Wales Registered Number: 1072954 Registered office: Mortimer House, 37-41 Mortimer Street, London W1T 3JH, UK

Journal of Toxicology and Environmental Health, Part B
Publication details, including instructions for authors and subscription information:
http://www.informaworld.com/smpp/title~content=t713667286

Renal Effects of Exposure to Natural and Depleted Uranium: A Review of the Epidemiologic and Experimental Data

Xabier Arzuaga[a]; Susan H. Rieth[a]; Ambika Bathija[b]; Glinda S. Cooper[a]
[a] National Center for Environmental Assessment, U.S. Environmental Protection Agency, Washington, DC [b] Health and Ecological Criteria Division, Office of Science & Technology, U.S. Environmental Protection Agency, Washington, DC, USA

Online publication date: 17 December 2010

To cite this Article Arzuaga, Xabier , Rieth, Susan H. , Bathija, Ambika and Cooper, Glinda S.(2010) 'Renal Effects of Exposure to Natural and Depleted Uranium: A Review of the Epidemiologic and Experimental Data', Journal of Toxicology and Environmental Health, Part B, 13: 7, 527 — 545
To link to this Article: DOI: 10.1080/10937404.2010.509015
URL: http://dx.doi.org/10.1080/10937404.2010.509015

PLEASE SCROLL DOWN FOR ARTICLE

Full terms and conditions of use: http://www.informaworld.com/terms-and-conditions-of-access.pdf

This article may be used for research, teaching and private study purposes. Any substantial or systematic reproduction, re-distribution, re-selling, loan or sub-licensing, systematic supply or distribution in any form to anyone is expressly forbidden.

The publisher does not give any warranty express or implied or make any representation that the contents will be complete or accurate or up to date. The accuracy of any instructions, formulae and drug doses should be independently verified with primary sources. The publisher shall not be liable for any loss, actions, claims, proceedings, demand or costs or damages whatsoever or howsoever caused arising directly or indirectly in connection with or arising out of the use of this material.

Journal of Toxicology and Environmental Health, Part B, 13:527–545, 2010
ISSN: 1093-7404 print / 1521-6950 online
DOI: 10.1080/10937404.2010.509015

Taylor & Francis
Taylor & Francis Group

RENAL EFFECTS OF EXPOSURE TO NATURAL AND DEPLETED URANIUM: A REVIEW OF THE EPIDEMIOLOGIC AND EXPERIMENTAL DATA

Xabier Arzuaga[1], Susan H. Rieth[1], Ambika Bathija[2], Glinda S. Cooper[1]

[1]National Center for Environmental Assessment, U.S. Environmental Protection Agency, Washington, DC
[2]Health and Ecological Criteria Division, Office of Science & Technology, U.S. Environmental Protection Agency, Washington, DC, USA

Downloaded By: [US EPA Environmental Protection Agency] At: 17:09 22 December 2010

Elevated levels of naturally occurring uranium in groundwater have been found in small geographic areas throughout the world. Relevant research was reviewed pertaining to natural and depleted uranium (DU) exposure and nephrotoxicity, including epidemiologic community-based and occupational studies, studies of Gulf War veterans exposed to DU, and experimental studies in animals. Occupational cohort studies do not provide evidence of an increased risk of kidney-related mortality among uranium-exposed workers. However, occupational and community-based studies of populations chronically exposed to elevated drinking-water concentrations of uranium provide some evidence of adverse renal effects, as assessed by biomarkers of proximal tubule damage such as urinary levels of glucose, calcium, and various low-molecular-weight proteins. Indications of proximal tubule effects, as evidenced by increased urinary β_2-microglobulin and retinol binding protein levels, were also seen in the most recent follow-up surveillance study of Gulf War veterans exposed to DU. The reported β_2-microglobulin levels in these studies were generally considered to be within normal limits, but the long-term implications of the observed variation in these levels are not established. The kidney was observed to be a target of uranium toxicity following oral and implantation exposure routes in several animal species. The interpretation and importance of the observed changes in biomarkers of proximal tubule function are important questions that indicate the need for additional clinical, epidemiological, and experimental research.

Natural uranium (U) refers to uranium compounds with a naturally occurring composition of radioisotopes uranium-234, uranium-235, and uranium-238. Uranium is found in all soils and rock, with higher concentrations found in phosphate rock, lignite, and monazite sands (ATSDR, 1999). Uranium enrichment processes increase the concentration of U-235 from <1% to 2–4%. Depleted uranium (DU) refers to the less radioactive form of uranium remaining after enrichment. Depleted uranium is approximately 60% less radioactive than naturally occurring U because of decreased levels of U-235 (Bleise et al., 2003), and U has been used by the U.S. Department of Defense (DoD) and Armed Forces for various weapons systems since the late 1970s (Arfsten et al., 2001; Abu-Qare and Abou-Donia, 2002).

Elevated concentrations of U greater than 20 μg/L were detected in various Western groundwater systems and scattered pockets in the groundwaters of North Carolina, Maine, Connecticut, and other Eastern states (Orloff et al., 2004; U.S. EPA, 1985, 2000). Areas of high U concentrations in water are also found in many other countries globally, including Canada, Finland, the United Kingdom, and India (WHO, 2001). According

This article is not subject to U.S. copyright.
The views expressed are those of the authors and do not necessarily reflect the views or policies of the U.S. EPA.
Address correspondence to Glinda S. Cooper, PhD, National Center for Environmental Assessment 8601-P, U.S. Environmental Protection Agency, 1200 Pennsylvania Avenue, NW, Washington, DC 20460, USA. E-mail: cooper.glinda@epa.gov

Downloaded By: [US EPA Environmental Protection Agency] At: 17:09 22 December 2010

to biomonitoring data collected by the Centers for Disease Control (CDC, 2005) as part of the Third National Report on Human Exposure to Environmental Chemicals, the geometric mean concentration of U in urine for the U.S. population (ages 6 yr and older) for survey years 2001–2002 was 0.009 μg/L (95th percentile: 0.046 μg/L).

Craft et al. (2004) summarized data pertaining to a broad range of adverse health effects due to natural U and DU, including neurotoxicity, nephrotoxicity, reproductive effects, cancer, and effects on other systems. Renal effects were the focus of a recent case study of a family in western Connecticut describing the potential for nephrotoxicity from exposure to well water containing elevated levels of naturally occurring U, and the sensitivity of young children resulting from their increased exposure potential and their state of development (Magdo et al., 2007). In this review, research pertaining to U exposure and nephrotoxicity, focusing on the available epidemiologic data including (1) community-based and occupational studies of biomarkers of kidney damage, (2) occupational studies of kidney-related mortality, and (3) studies of soldiers exposed to DU, is presented. The animal nephrotoxicity and mechanism of action data have been reviewed previously (ATSDR, 1999); a summary of this and recent literature is also included later in this article.

STUDIES IN HUMANS

Measures of Renal Function

Kidney disease varies in severity from kidney failure requiring transplantation or dialysis to a subclinical, asymptomatic phase where some level of kidney damage may occur without detectable decreases in renal function. In clinical studies, such as prognostic studies of patients with diabetes or other conditions with a high risk of chronic kidney disease and its related complications, renal function has often been monitored by blood and 24-h urine samples allowing for the measurement of blood urea nitrogen (BUN) levels, total protein in the urine, and calculation of glomerular filtration rate (GFR). In community-based studies, less burdensome data collection techniques are usually required, resulting in the collection of a single urine sample at a study visit (a spot urine sample) or an overnight urine sample (i.e., first morning void). Another difference between clinical and community-based studies is that in the latter, it is more important that the methodology is able to accurately assess variability in the earliest phases of disease, when kidney function is still relatively high (Levey et al., 2009).

In addition to general measures of kidney function, other types of measures address specific types of damage that may occur. Larger molecules, such as albumin, are filtered by the glomeruli and reabsorbed by the proximal tubule through receptor mediated endocytosis (Birn and Christensen, 2006). Most of the albumin reabsorbed by the proximal tubule cells (approximately 95%) is returned to the plasma. The remaining amount is degraded in cell lysosomes and excreted in the urine (Comper et al., 2006). Glomerular and tubular injury may result in increased levels of urinary albumin. Tests of general glomerular function include creatinine clearance or GFR, as well as determination of urinary protein and urinary albumin concentrations, with the latter two measures reflecting the integrity of the glomerulus (i.e., the leakage of molecules through the filter). Damage to the proximal tubule decreases small-molecule reabsorption and results in increased urinary levels of glucose, calcium, and phosphate, and of low-molecular-weight proteins such as β_2-microglobulin, protein human complex forming (HC) [or α-microglobulin]), kappa chains, and retinol binding protein (Emeigh & Kinter, 2005; Seldén et al., 2009). β_2-Microglobulin is an endogenous low-molecular-mass protein (12 kD) that forms part of the class I major histocompatibility complex and is located on the surface of nucleated cells. During cell turnover β_2-microglobulin is released into the extracellular fluid and normally filtered by the glomerulus and reabsorbed in the proximal tubule (Bagshaw et al., 2007; Tolkoff-Rubin et al., 1988). Retinol binding protein (21 kD) is

primarily expressed in the liver and also reabsorbed by the proximal tubule (Bagshaw et al., 2007). Enzyme activity levels have also been used as markers of tissue damage at specific sites, with alkaline phosphatase (AP), *N*-acetyl-β-D-glucosaminidase (NAG), and γ-glutamyl transferase (GGT) reflecting proximal tubular tissue damage and other enzymes, such as lactate dehydrogenase (LDH), more indicative of damage to the distal tubule (Zalups et al., 1988; Emeigh 2005; Zamora et al., 2009; Seldén et al., 2009).

Downloaded By: [US EPA Environmental Protection Agency] At: 17:09 22 December 2010

Community-Based Studies

Several studies of populations chronically exposed to elevated drinking-water concentrations of U were conducted (Kurttio et al., 2002; Kurttio et al., 2006; Mao et al., 1995; Seldén et al., 2009; Zamora et al., 1998; Zamora et al., 2009). Three studies in Canada (in Saskatchewan, Quebec, and Nova Scotia), two in Finland, and one in Sweden evaluated renal function in communities with high concentrations of U in the drinking water supply (Table 1). Mean or median U concentrations in the drinking water of the exposed communities were approximately 7 μg/L in Sweden, 15–20 μg/L in Saskatchewan, 28 μg/L in Finland, 39 μg/L in Quebec (based on the maximum level measured over a 15-yr period), and more than 100 μg/L in Nova Scotia (Figure 1); corresponding values in the comparison nonexposed communities were <1 μg/L. Uranium concentrations in urine also varied considerably among these studies, with a median of 0.03 μg/L in Sweden, 0.078 μg/L in Finland, and 0.14 μg/L in Quebec.

The first of these studies, in Saskatchewan, measured urinary albumin in a first morning urine sample from 60 adults in 2 communities with elevated levels of U in drinking water (means of 14.7 and 19.6 μg/L) and 40 controls from a comparison (control) community (mean drinking water U concentration of 0.71 μg/L) (Mao et al., 1995). Cumulative intake was calculated as the product of concentration of U in water, average number of cups consumed per day, and years at current residence; the mean or range of this measure was not given. A correlation was seen between cumulative intake and urinary albumin, which was of marginal statistical significance when adjusting for age and diabetes history (Table 1).

Subsequent studies used a more extensive array of urinary and serological measures to assess kidney function. The studies from Canada were conducted in Nova Scotia (Zamora et al., 1998) and in a Quebec First Nations community (Zamora et al., 2009), with 30 and 54 exposed participants, respectively (Table 1). The study in Nova Scotia calculated a daily U intake based on the product of concentration of U in water or food and the amount consumed (based on 3-d food and water samples) and ranged from 3 to 570 μg/d in the exposed community and from <1 to 20 μg/d in the control community. Urinary U and glucose, protein, and creatinine concentrations were measured in a 24-h urine sample, and ß$_2$-microglobulin levels were measured in an overnight urine sample. Daily U intake correlated significantly with markers of proximal tubule injury: urinary glucose ($r_s = 0.40$; $p = 0.001$), AP ($r_s = 0.28$; $p = 0.05$), and ß$_2$-microglobulin ($r_s = 0.39$; $p = 0.01$). Weaker or no correlations were seen with urinary NAG activity ($r_s = 0.15$; 0.29), protein ($r_s = 0.17$; 0.23), creatinine ($r_s = 0.11$; 0.45), and LDH activity ($r_s = 0.02$; 0.89) levels, and a negative correlation coefficient was seen with GGT activity ($r_s = -0.22$; 0.12).

In Quebec, the study protocol was similar to that of the Nova Scotia study. Exposure was measured or calculated as the maximum water U concentration in prior 15 yr, cumulative intake in prior 15 yr (median 87 mg), cumulative intake in past 2.8 yr (median 22 mg), and U concentration in urine (median 0.14 μg/L) (Zamora et al., 2009). Adjusting exposure and renal biomarker measures for fluid intake, U concentration in urine was significantly correlated with GGT activity ($r_s = 0.37$) and ß$_2$-microglobulin ($r_s = 0.49$). Weaker correlations were seen with albumin ($r_s = 0.23$), glucose ($r_s = 0.14$), AP activity ($r_s = 0.15$), and NAG activity ($r_s = 0.15$).

Downloaded By: [US EPA Environmental Protection Agency] At: 17:09 22 December 2010

TABLE 1. Community-Based Studies of Markers of Renal Function in Relation to Exposure to Uranium in Drinking Water

Reference(s)	Study location and participants	Exposure measure(s)	Primary positive results
Canada			
Mao et al., 1995	Saskatchewan, Canada ($n = 40$ from one control community, $n = 60$ from two exposed communities). Mean age not reported, range 18 to 84 yr.	Cumulative intake[a] (range not given)	Cumulative intake correlated with urine albumin (per mmol creatinine levels, Beta = 0.13, $p = .03$; per mg/L, Beta = 2.19, $p = .07$), adjusting for age and diabetes history.
Zamora et al., 1998	Nova Scotia, Canada ($n = 30$ from a high exposure eommunity (water uranium concentrations >100 μg/L), $n = 20$ from a low exposure community (water uranium concentrations of <1 μg). Mean age 37, range 13 to 87 yr.	Uranium concentration in drinking water and daily intake[b]	Daily uranium intake correlated with markers of proximal tubule injury: urinary glucose ($r_s = 0.40$, $p = .001$), alkaline phosphatas ($r_s = 0.28$, $p = .05$), and ß$_2$-microglobulin ($r_s = 0.39$, $p = .01$).
Zamora et al., 2009	Quebec First Nations Community (Kitigan Zibi), Canada ($n = 54$). Mean age 38, range 12 to 73 yr.	Maximum water uranium concentration in past 15 yr, cumulative intake in past 15 yr, cumulative intake in past 2.8 yr, urinary uranium	In analyses adjusting exposure and renal biomarker measures for fluid intake, urinary uranium correlated with gamma glutamyl transferase ($r_s = 0.37$, $p = .0064$) and ß$_2$-microglobulin ($r_s = 0.49$, $p = .0047$).
Europe			
Kurttio et al., 2002	Southern Finland ($n = 325$ from areas with high water uranium levels). Mean age 52, range 15 to 82 yr.	Uranium concentration in drinking water, daily intake,[c] cumulative intake,[d] and urinary uranium	All uranium measures correlated with fractional excretion of calcium and increased systolic and diastolic blood pressure; urinary uranium measures also correlated with fractional excretion of phosphate and glucose.
Kurttio et al., 2006	Southern Finland ($n = 193$, subset of Kurttio et al. 2002). Mean age 56, range 18 to 81 yr.	Uranium concentration in drinking water, daily intake,[c] cumulative intake[d]	Glucose excretion associated with cumulative intake measure ($p = .02$); urinary uranium associated with increased systolic ($p = .01$) and diastolic blood pressure ($p = .07$).
Seldén et al., 2009	Arjäng, Sweden ($n = 301$ exposed, $n = 153$ controls). Mean age 51 (exposed) and 55 (controls), range 18 to 74 yr.	Uranium concentration in drinking water, cumulative intake,[d] urinary uranium	Significant correlation between urinary uranium concentrations and β2-microglobulin, protein HC, and kappa chains; in males, cumulative intake was associated with protein HC.

Note. See Figure 1 for more detailed description of water uranium concentrations in exposed communities.
[a]The product of concentration of uranium in the water, average number of cups consumed per day, and years at current residence.
[b]The product of concentration of uranium in the water or food and the amount consumed (based on 3-d food and water samples).
[c]The product of concentration of uranium in the water and volume used per day.
[d]The product of concentration of uranium in the water, volume used, and duration of water consumption.

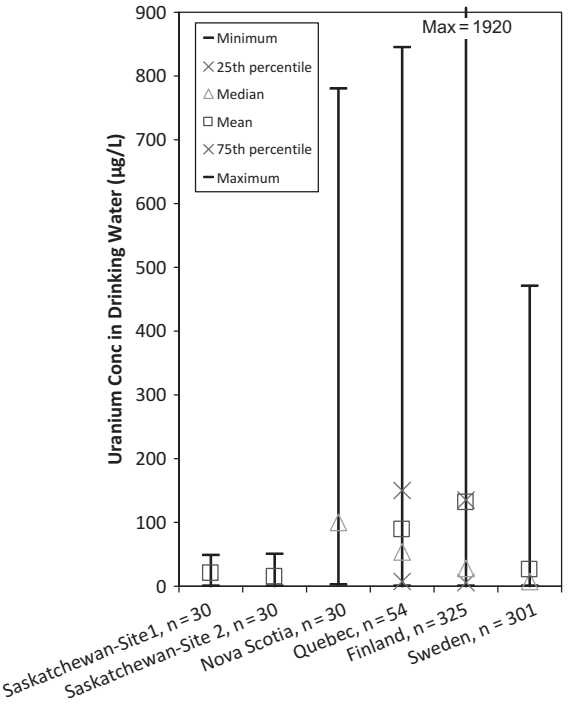

FIGURE 1. Uranium concentrations in drinking (μg/L) water in community studies. Saskatchewan sites 1 and 2, Mao et al. (1985), detection limit = 0.1 μg/L; Nova Scotia, Zamora et al. (1998), detection limit = 0.0006 μg/L; Quebec, Zamora et al. (2009), detection limit = 0.0006 μg/L (concentration values based on table of unadjusted data in Zamora et al., 2009); Finland, Kurttio et al. (2002, 2006), detection limit = 0.0004 μg/L; Sweden, Seldén et al. (2009), detection limit = 0.2 μg/L. Control community drinking water uranium concentrations were <1 μg/L.

Kurttio et al. (2002) conducted a study in 1999 of 325 individuals from areas in Finland with high uranium levels in the drinking water (Table 1). These individuals had used well water for at least 1 yr, and completed a questionnaire that included information on residential history and water consumption, allowing for calculation of measures of daily and cumulative U intake from water. A drinking-water sample (for measurement of U levels), overnight urine sample (for measurement of urinary U, glucose, creatinine, calcium, phosphate, and albumin), spot urine (for β_2-microglobulin measurement), and a nonfasting blood sample were collected. Daily intake ranged from <1 to 4128 μg/d (median 39 μg/d), cumulative intake ranged from <1 to 33,100 mg (median 129 mg), and U concentration in urine ranged from <1 to 5.65 μg/L (median 0.078 μg/L). Urinary U concentrations were correlated with fractional excretion of calcium (beta per 1 unit μg/mmol creatinine increase in urinary uranium = 1.5, 95% CI 0.6–2.3) and phosphate (beta = 13, 95% CI 1.4–25), and more weakly with glucose (beta = 0.7, 95% CI 0.4–1.8); associations with systolic and diastolic blood pressure (age, gender, body mass index, and smoking-adjusted beta = 6.8 and 8.5, respectively) were also seen. Kurttio et al. (2002) did not observe a relationship between U exposure and creatinine clearance, urinary albumin, or β_2-microglobulin. The high proportion (65%) of β_2-microglobulin values below the detection limit in the samples was a limitation of this analysis. In a subsequent study, Kurttio et al. (2006) recontacted the cohort in 2003; 222 (68%) lived in the same house as in 1999 and agreed to participate; 193 of these provided water, an overnight urine, and a blood sample for the follow-up study. β_2-Microglobulin was not measured in this study. Median daily intake of U from drinking water was 36 μg/L, similar to the mean of 39 μg/L in the baseline study reported by Kurttio et al. (2002). In the follow-up study, associations were only seen between urinary U concentrations and systolic and diastolic blood pressure, and between the cumulative intake measure and urinary glucose.

Another relatively large study included 301 participants from western Sweden living in areas with elevated levels of uranium in the drinking water obtained from wells and 151 controls from a nearby city using a city water supply (Seldén et al., 2009) (Table 1). Questionnaire data pertaining to drinking water consumption, smoking history, and other potential exposures were collected, and an overnight urine sample was collected from all participants; the members of the exposed groups and 15 randomly selected members of the control group also provided a water sample. Levels of cadmium (Cd), lead (Pb) and mercury (Hg) in the water samples were low (means ≤ 0.50 μg/L) and similar in both areas. The median U levels in the water were 6.7 and <0.20 μg/L in

Downloaded By: [US EPA Environmental Protection Agency] At: 17:09 22 December 2010

Downloaded By: [US EPA Environmental Protection Agency] At: 17:09 22 December 2010

the exposed and control samples, respectively, and the median U concentrations in urine were 0.03 and 0.0047 μg/L in exposed and controls, respectively. In the regression analyses adjusting for age, gender, and smoking and excluding 23 participants with diabetes, levels of low-molecular-weight proteins (β_2-microglobulin, kappa chains, and protein HC) were increased in relation to a 3-level variable for U concentrations in urine (<0.003, 0.003–0.0149 and ≥0.015 nmol/mmol creatinine). For β_2-microglobulin, the geometric mean was approximately 50% higher (i.e., ratio of geometric mean in the higher compared with lowest group = 1.48, 95% CI 1.03–2.13), and for kappa chains and protein HC, the elevations were 30% (ratio 1.32, 95% CI 1.04–1.68) and 20% (ratio 1.21, 95% CI 1.01–1.44), respectively. An association was also seen between protein HC and cumulative intake in males (ratio 1.40, 95% CI 1.08–1.81 in the middle category and 1.45, 95% CI 1.00–2.08) in the highest category of exposure). This pattern was not seen in females.

Occupational Exposure Studies

An occupational exposure study evaluating renal function in workers in a Colorado U mill also provides evidence of an association between natural U exposure and increased levels of urinary and serum β_2-microglobulin (Thun et al., 1985). In one area of this mill, the yellowcake drying and packaging area, exposure to air concentrations of U dust exceeded occupational standards for several years. Mean U concentrations in workers monitored were 65.2, 18.9, 20.5, and 19.1 μg/L urine in 1975, 1976, 1977, and 1978, respectively; these levels fell to means of 9.1 and 6.2 μg/L urine in 1980 and 1981 after the opening of a new mill in 1979. Workers who had worked at least 1 yr in the yellowcake area ($n = 30$) and workers in the crushing area ($n = 12$) were identified, and 39 of these 42 workers participated in the study. The exposure in the crushing area was to a less soluble form of U. A comparison group, matched by race, gender, and age (within 2 yr), was drawn from workers in a cement production plant in the area; 43 of the identified matches were recruited to the study but 7 of these were subsequently excluded because they had previously worked at the U mill. The final sample included 36 controls and 33 matched pairs. Cadmium levels were similar in the two groups, but blood Pb levels were higher among the controls (mean 0.45 and 0.78 μmol/L in exposed and controls, respectively). Renal function was evaluated through collection of an 8-h urine sample over the course of a workday, and midshift blood samples. Specific measures included serum creatinine and creatinine clearance as markers of glomerular functions and urinary β_2-microglobulin levels as markers of proximal tubular function. The ratio of the β_2-microglobulin clearance to creatinine clearance, denoted the fractional excretion, was calculated to represent the tubular component of β_2-microglobulin excretion. Urinary excretion of β_2-microglobulin was significantly increased in the workers compared with controls: where in the exposed group, mean (± standard deviation, SD) β_2-microglobulin concentration was 0.06 (± 0.38) mg/g creatinine, compared with 0.036 (± 0.031) in controls. Similar patterns were seen with measures expressed as micrograms per liter, micrograms per hour, and clearance (ml/min) (Table 2). Among the workers at the U plant, relative clearance of β_2-microglobulin was markedly correlated with duration of employment in the yellowcake area. In contrast, the tendency shown in the markers of glomerular function such as creatinine clearance was toward improved function in the exposed workers (Table 2).

Several cohort studies of workers at uranium processing facilities have examined mortality risk. Most of the detailed analyses focus on malignant diseases, but some data on mortality due to chronic nephritis (International Classification of Diseases, 9th revision, ICD-9, code 582) or other forms of renal disease are available (Table 3). The standardized mortality ratio of chronic nephritis among 8 cohort studies ranged from 0.67 to 1.88, each with relatively wide confidence intervals, and was approximately evenly distributed

TABLE 2. Renal Function Measures in Uranium Mill Workers and a Comparison Group of Workers From a Cement Plant (Thun et al., 1985)

	Uranium mill, exposed ($n = 39$)			Cement workers ($n = 36$)			
Variable	Mean	SD	Range	Mean	SD	Range	(p value)
β_2-Microglobulin[a]							
Serum (μg/ml)	2.05	0.46	1.28–3.40	1.83	0.26	1.36–2.40	(.01)
Urine (μg/L)	54.9	38.7	4.0–140.0	37.6	39.2	1.0–170.0	(.06)
Urine (μg/h)	4.40	2.99	0.36–13.63	2.50	2.05	0.18–10.01	(.002)
Urine (mg/g creatinine)	0.060	0.38	0.004–0.189	0.036	0.031	0.002–0.164	(.004)
Clearance (ml/min)	0.038	0.27	0.002–0.116	0.023	0.019	0.002–0.087	(.01)
Creatinine[b]							
Serum (mg/100 cm^3)	1.15	0.15	0.92–1.74	1.22	0.11	0.91–1.40	(.02)
Urine (mg/100 cm^3)	102.9	62.6	23.1–285.2	114.6	63.5	11.4–259.6	(.42)
Clearance (ml/min)[c]	95.6	20.6	48.8–172.2	88.4	13.0	39.1–116.6	(.08)
Relative clearance[d]	3.95	2.64	0.23–11.19	2.62	2.17	0.18–10.71	(.02)

[a]1 μg β_2-microglobulin = 1 μmol × 11,600.
[b]1 mg creatinine = 1 mmol × 113.12.
[c]Creatinine standardized to a body surface area of 1.73 m^2.
[d]β_2-Microglobulin clearance × 10^4/creatinine clearance.

Downloaded By: [US EPA Environmental Protection Agency] At: 17:09 22 December 2010

between estimates greater than 1 (Boice et al., 2008; Dupree-Ellis et al., 2000; Pinkerton et al., 2004), around 1 (Frome et al., 1990; McGeoghegan & Binks, 2000a), and less than 1 (Loomis & Wolf, 1996; McGeoghegan & Binks, 2000b; Polednak & Frome, 1981). The highest relative risk (standardized mortality ratio [SMR] = 1.88, based on 6 observed cases) was seen in the study by Dupres-Ellis et al. (2000), but the authors noted that the work environment of 4 of these cases was likely to have included high exposure to silica dust, which has also been linked to chronic kidney disease. None of these studies demonstrated an elevated risk for the broader category of genitourinary disease, and two studies observed a statistically significant decreased mortality risk (McGeoghegan & Binks, 2006; Loomis & Wolf, 1996).

Clinical Studies in Gulf War Veterans

Depleted uranium applications include armor plating for military vehicles, munitions used to penetrate armored targets, helicopter blade rotor tips, and aircraft landing gear. Approximately 10 and 300 tons of DU were expended by the U.S. Armed Forces during the Kosovo air campaign and the Persian Gulf War, respectively (Arfsten et al., 2001). Depleted uranium dusts and vapors, which may be inhaled or ingested, are generated during structure impact and perforation by DU munitions (Arfsten et al., 2001; Parkhurst & Guilmette, 2009). Several clinical studies evaluated the effects of exposure to DU in Gulf War veterans who had been mistakenly fired upon by U.S. forces in incidents that took place in February 1991. Exposure occurred via inhalation and ingestion of DU dust in the immediate aftermath of an incident, and through embedded metal fragments in some individuals who were hit by a high-density, penetrating device. In total, 74 soldiers who had been in or on an Army vehicle during one of these incidents have been followed through the Baltimore Veterans Affairs Depleted Uranium Follow-up program, initiated in 1993. This program has followed the majority of the approximately 90 soldiers involved in these incidents who survived and for whom contact information was available. After the initial study visit in 1994, biennial exams were conducted in 1997, 1999, 2001, and 2003 (reviewed in Squibb and McDiarmid, 2006), 2005, and 2007 (McDiarmid et al., 2007, 2009). The clinical and laboratory evaluations included 24-h urinary uranium concentration, with serum and urinary renal function measures. Examination of the 24-h urinary U concentration data over the 14-yr follow-up period revealed continued elevation of U, with levels ranging from 0.003

Downloaded By: [US EPA Environmental Protection Agency] At: 17:09 22 December 2010

TABLE 3. Studies of Noncancer Renal Disease Mortality Risk in Uranium Mill Workers

Reference(s)[a]	Sample size (*n*), inclusion criteria, follow-up, ICD revision[b]	All genitourinary disease			Chronic nephritis		
		Obs	Exp	SMR (CI)	Obs	Exp	SMR (95% CI)
Oak Ridge facilities							
Checkoway et al., 1988; Loomis and Wolf, 1996	*n* = 8116, Tennessee Eastman Corporation, Y-12 plant, Oak Ridge, TN. Worked ≥30 d between 1947 and 1974, began work after 1947. Follow-up through 1990. ICD-8.	15	NR	0.59 (0.33, 0.97)	5	NR	0.83 (0.27, 1.95)
Frome et al., 1990	*n* = 28,008 white males, Tennessee Eastman Corporation, several plants, Oak Ridge, TN. World War II workers. Worked ≥30 d before 1948 and did not work after January 1, 1948. Follow-up 1950 through 1979. ICD-8.	148	145.3	1.02 (*NR*)	52	52.65	0.99 (*NR*)
Polednak and Frome, 1981	*n* = 18,869 white males, Tennessee Eastman Corporation, Y-12 plant, Oak Ridge, TN. World War II workers. Worked ≥2 d between 1943 and 1947 and did not work after January 1, 1948. Follow-up through 1974. ICD-8.	63	99.04	0.64 (*NR*)	30	39.14	0.77 (*NR*)
Other U.S. facilities							
Boice et al., 2008	*n* = 718, Grants, NM uranium mill workers without mining experience and with likely exposure to uranium. Worked ≥6 mo between 1955 and 2004; 28% worked ≥5 yr. Follow-up through 2005. ICD-9.	NR			3	2.3	1.30 (0.27, 3.79)
Pinkerton et al., 2004; Waxweiler et al., 1983	*n* = 1484, white males, 7 mills, Colorado Plateau. Worked ≥1 year in mill, never worked in uranium mine, worked ≥1 d after 1940. 43% worked <3 yr. Follow-up through 1998. Total person-years = 49,925. ICD-9.	13	13.03	1.00 (0.53, 1.71)	8	5.91	1.35 (0.58, 2.67)
Dupree-Ellis et al., 2000	*n* = 2514, white males, Mallinckrodt Chemical Works, St. Louis, MO. Employed between 1942 and 1966. Average work duration 5.2 yr. Follow-up through 1993. ICD-8.	14	NR	0.95 (0.53, 1.54)	6	NR	1.88 (0.75, 3.81)
Ritz et al., 2000	*n* = 2218, males, Rocketdyne/Atomics International. Worked 1950–1993, monitored for radiation. Follow-up through 1994. Total person-years = 56,610. ICD-8.	5	6.44	0.78 (0.25, 1.81)	NR		
United Kingdom facilities							
McGeoghegan and Binks, 2000b	*n* = 19,454 (*n* = 13,950 radiation workers and *n* = 5489 nonradiation workers), Springfields, Lancashire, United Kingdom. Ever employed before 1996, follow-up through 1995. ICD-8.	Total: 42 67.32 0.62 (NR)[c] Rad: 28 48.94 0.57 (NR)[c] Non-rad: 14 18.38 0.76 (NR)			Total: 15 22.50 0.67 (NR) Rad: 10 16.48 0.61 (NR) Non-rad: 5 6.02 0.83 (NR) (disease category = chronic renal failure)		
McGeoghegan and Binks, 2000a	*n* = 12,544 (*n* = 3244 radiation workers and *n* = 9296 nonradiation workers), Capenhurst, Cheshire, United Kingdom. Ever employed before 1996, follow-up through 1995. ICD-8.	Total: 45 52.14 0.86 (NR) Rad: 7 7.13 0.98 (NR) Non-rad: 38 45.01 0.84 (NR)			Total: 19 17.17 1.1 (NR) Rad: 4 2.20 1.8 (NR) Non-rad:15 14.97 1.0 (NR) (disease category = chronic renal failure)		

Note. Abbreviations: Obs = observed; Exp = expected; CI = confidence interval; ICD = International Classification of Disease; NR = not reported; Rad = radiation workers; Non-rad = nonradiation workers.

[a]When more than one study is available for a cohort, the earlier references are noted but the results from the latest follow-up are provided in the table.

[b]In the studies using ICD-8, all genitourinary disease is based on codes 580–629 and chronic nephritis is based on code 582. In Pinkerton et al. (2004), all genitourinary disease is based on codes 580–629 and chronic nephritis is based on code 582–583 and 585–587. In Boice et al. (2008), the chronic nephritis category is based on code 580–589. McGeoghegan and Binks (2000a, 2000b) do not specify the codes used in their tables of results; all genitourinary disease and the chronic nephritis correspond, respectively, to their categories of genitourinary disease and chronic renal failure.

[c]Significant at $p < .01$.

Downloaded By: [US EPA Environmental Protection Agency] At: 17:09 22 December 2010

to 44.1 μg/g creatinine (Squibb & McDiarmid, 2006). Levels above 0.1 μg/g creatinine (the cut point used to define a high-exposure group) were found in most of the individuals who had retained DU shrapnel. Some indication of renal damage was seen in the 2001 assessment, with increased levels of urinary retinol binding protein (65.68 and 46.13 μg/g creatinine in the high- and low-exposure groups, respectively) and total protein (78.69 and 54.63 mg/g creatinine in the high- and low-exposure groups, respectively) (Table 4). Serum creatinine was quantitatively decreased, however, in the high-exposure group (mean 0.85 and 0.95 mg/dl in the high- and low-exposure groups, respectively). There was little evidence of renal damage in the 2003 and 2005 assessments. In the latest assessment conducted in 2007, however, a trend of elevated urinary retinol binding protein and increased urinary β_2-microglobulin levels was seen in the high-exposure compared with the low-exposure group (McDiarmid et al., 2009).

STUDIES IN ANIMALS

Studies in experimental animals involving different routes and durations of exposure support the conclusion that the kidney is likely to be a sensitive target organ for U toxicity. In addition, data from experimental animals suggest that U compounds of relatively higher solubility are associated with greater kidney damage (Craft et al., 2004; Dygert et al., 1949; Hindin et al., 2005; Maynard et al., 1953). In acute oral exposure studies with uranyl acetate (exposure duration ranging from 1–5 d) changes in kidney function, as evidenced by increases in urinary protein, blood creatinine, and BUN, were reported (Domingo et al., 1987; Ozmen & Yurekli, 1998). Renal damage reported in rabbits, rats, and dogs exposed to uranyl nitrate in the diet for 30 d or less included increased plasma protein plus degenerative changes (particularly of the proximal tubular epithelium and glomeruli) and necrosis (Goel et al., 1980; Maynard & Hodge 1949; Ortega et al., 1989).

The only investigation of chronic oral toxicity of U compounds is the series of experiments performed by Maynard and colleagues in support of the Manhattan Project (Maynard et al., 1953; Maynard & Hodge, 1949). Rats and dogs were exposed to uranyl fluoride, uranyl tetrachloride, uranyl nitrate hexahydrate, uranium dioxide, and uranium tetrafluoride in the diet (or in dogs by capsule if the diet became unpalatable) for 1 yr (dogs) or 2 yr (rats). Exposure protocols are described in Table 5. With the exception of exposure of rats to uranium dioxide, all uranium compounds produced some degee of renal toxicity, which was strongly influenced by compound solubility. For example, administration of 0.5% uranyl nitrate hexahydrate in the diet of rats (approximately 200 mg/kg-d U) produced degeneration of kidney tubules, necrosis, and regeneration. Serial sacrifices revealed that the tubular changes observed after 6 wk of exposure showed no appreciable progression even after 2 yr of exposure (Maynard et al., 1953). More recent subchronic (91-d) drinking-water studies of uranyl nitrate in the rat and rabbit (Gilman et al., 1998a, 1998b, 1998c; McDonald-Taylor et al., 1992, 1997) provide an examination of uranium compound toxicity at lower doses (0.06 to 54 mg/kg-d). See Table 5 for a more detailed summary of renal histopathologic changes reported by these investigators. McDonald-Taylor et al. (1992, 1997) reported histopathologic changes in kidney proximal tubules of rabbits at 1.7 mg/kg-d U, the lowest dose tested. Gilman et al. (1998b, 1998c) similarly reported histopathologic changes of the kidney at the lowest doses tested in rabbits and rats (0.05 and 0.06 mg/kg-d U, respectively). The incidences of renal histopathologic changes (including changes of the renal tubules, glomeruli, and interstitium) reported by Gilman et al. (1998b, 1998c), particular in the rat, were elevated at all dose levels; however, these changes showed a poor dose-response relationship and little if any rise in severity with increasing dose, despite a 600-fold range between the low and high doses used in this study and documentation of a rise in kidney uranium residues with

Downloaded By: [US EPA Environmental Protection Agency] At: 17:09 22 December 2010

TABLE 4. Renal Function Measures in Biennial Evaluations of Gulf War Veterans Exposed to Depleted Uranium in 1991

	Year of evaluation					
				2005		
	1999	2001	2003	Current exposure	Cumulative exposure	2007
n low exposure, *n* high exposure[a]	37, 13	26, 13	19, 13	24, 10	24, 10	25, 10
	p Value and direction of difference[b]					
Renal function measures—urinary						
Creatinine	0.07 H < L	0.29	0.31	0.24	0.08 H < L	0.43
Calcium		0.35	0.79	0.59	0.56	0.14 L < H
Phosphate (PO_4)		0.40	0.44	0.29	0.27	0.57
β_2-Microglobulin	0.27	0.78	0.53	0.22	0.83	0.11 H > L
Intestinal alkaline phosphatase			0.85	0.67	0.52	0.38
N-Acetyl β-glucosaminidase			0.38	0.96	0.90	0.32
Total protein	0.89	0.01 H > L	0.21	0.50	0.25	0.49
Microalbumin			0.85	0.40	0.32	0.17 H > L
Retinol binding protein	0.15 H > L	0.06 H > L	0.54	0.25	0.56	0.07 H > L
Renal function measures—serum						
Creatinine	0.14 H < L	0.03 H < L	0.11 H < L	0.72	0.56	0.11 H < L
Calcium		0.67	0.85	0.24	0.56	0.26
Phosphate (PO_4)		0.63	0.03 H > L	0.70	0.64	0.57
Uric acid	0.12 H < L	0.45	0.32	0.10 H < L	0.03 H < L	0.17 H > L

Note. Sources: McDiarmid et al. (2001), McDiarmid et al. (2004), McDiarmid et al. (2006), McDiarmid et al. (2007), and McDiarmid et al. (2009) for the 1999, 2001, 2003, 2005, and 2007 evaluations, respectively.

[a]Low (L) exposure defined as <0.10 μg uranium/g creatinine and high (H) defined as ≥0.10 μg uranium/g creatinine; *n* for specific assays may vary by 1–2 participants because of sample processing errors.

[b]Direction of difference given for tests in which the *p* value was ≤.20.

Downloaded By: [US EPA Environmental Protection Agency] At: 17:09 22 December 2010

TABLE 5. Summary of Subchronic and Chronic Oral Toxicity Studies of Uranium in Experimental Animals

Reference	Uranium compound	Species, sex, group size	Exposure conditions	Response and LOAEL
Subchronic studies				
McDonald-Taylor et al., 1992, 1997	Uranyl nitrate hexahydrate	Rabbit, New Zealand, M (3/group)	0, 24, 600 mg/L in drinking water (0, 1.7, 42 mg /kg-d U); 91 d. Followed by recovery periods of 0, 45, or 91 d	Kidney histopathology, including increases in glomerular basement membrane thickness and changes in proximal tubule cells seen in lowest dose group.
Gilman et al., 1998c	Uranyl nitrate hexahydrate	Rat, Sprague-Dawley, M & F (15/sex/group)	0, 0.96, 4.8, 24, 120, 600 mg/L in drinking water (M: 0, 0.06, 0.31, 1.52, 7.54, 36.7 mg /kg-d U; F: 0, 0.09, 0.42, 2.01, 9.98, 53.6 mg /kg-d U); 91 d	Histopathologic lesions of the kidney seen in lowest dose group; changes included dilation of tubules, apical displacement, and vesiculation of tubular nuclei and cytoplasmic vacuolation and degranulation in males and capsular sclerosis and reticulin sclerosis of tubular basement membranes and interstitial scarring in females.
Gilman et al., 1998b	Uranyl nitrate hexahydrate	Rabbit, New Zealand, M and F (10/sex/group)	M: 0, 0.96, 4.8, 24, 120, 600 mg/L in drinking water (0, 0.05, 0.20, 0.88, 4.82, 28.7 mg/kg-d U) F: 0, 4.8, 24, 600 mg/L in drinking water (0, 0.49, 1.32, 43.0 mg/kg-d U); 91 d	Histopathologic lesions of the kidney (male) seen in lowest dose group. Lesions included cytoplasmic vacuolation, anisokaryosis, and nuclear vesiculation.
Gilman et al., 1998a	Uranyl nitrate hexahydrate	Rabbit, SPF, M (5–8/group)	0, 24, 600 mg/L in drinking water (0, 1.4, 41.0 mg/kg-d U); 91 d followed by recovery periods of 0, 8, 14, 45, or 91 d	Histopathologic lesions of the kidney seen in 600 mg/L group, no attenuation of effect seen with any recovery period. Observed lesions included cytoplasmic vacuolation, anisokaryosis, nuclear hyperchromicity and vesiculation, tubular dilation, and reticulin sclerosis of the renal interstitial tissue.
Ortega et al., 1989	Uranyl acetate dihydrate	Rat, Sprague-Dawley, M (8/group)	0, 2, 4, 8, or 16 mg uranyl acetate dihydrate/kg-d (0, 1.1, 2.2, 3.4, 4.5, 9.0 mg/kg-d U); 28 d	Increase in total plasma protein seen in lowest dose group; urinary biochemical endpoints were not significantly altered by uranium treatment at any dose.

(Continued)

Downloaded By: [US EPA Environmental Protection Agency] At: 17:09 22 December 2010

TABLE 5. (Continued)

Reference	Uranium compound	Species, sex, group size	Exposure conditions	Response and LOAEL
Guéguen et al., 2007	Uranyl nitrate	Rat, Sprague-Dawley, M (3/group)	0, 40 mg/L in drinking water (0, 3.3 mg/kg-d U); 9 mo	Following single exposure to acetominophen, increased renal proximal tubular cell necrosis, increased gene expression of xenobiotic metabolizing enzymes in kidney relative to animals not exposed to uranium.
Chronic studies				
Maynard et al., 1953	Uranyl fluoride	Rat, Wistar, M and F (15–25/group)	0, 0.01, 0.05, 0.1, 0.15, 0.25, 0.5% in diet; up to 24 mo	Minimal renal changes in 0.15% diet group (~85 mg/kg-d U); marked tubular atrophy with later regeneration seen in 0.5% diet group (~280 mg/kg-d U)
	Uranyl nitrate hexahydrate		0, 0.01, 0.05, 0.1, 0.5, 1, 2% in diet; up to 24 mo	Slight traces of renal injury seen in 0.5% diet group (~200 mg/kg-d U); renal abnormalities (tubular atrophy, and increase in stroma and a narrowing of the cortex in 2% diet group (~700 mg/kg-d U)
	Uranium dioxide		0, 0.5, 2, 20% in diet; up to 24 mo	No effects seen at any dose
	Uranium tetrafluoride		0, 0.5, 2, 20% in diet; up to 24 mo	Mild renal tubular degeneration seen in 20% diet group (~9200 mg/kg-d U)

Downloaded By: [US EPA Environmental Protection Agency] At: 17:09 22 December 2010

dose. McDonald-Taylor et al. (1992, 1997) and Gilman et al. (1998a, 1998b, 1998c) reported a significant increase in ultrastructural and histopathological alterations associated with with tubular cell necrosis (Greaves, 2007; Walling, 1991) in U-exposed animals. These effects included thickening of the glomerular basement membrane. Neither McDonald-Taylor et al. (1992) nor Gilman et al. (1998a) found evidence of reversibility of kidney histopathologic changes after 91-d recovery periods.

The available subchronic and chronic oral toxicity studies on U compounds included limited evaluation of biomarkers of kidney function. Gilman et al. (1998a, 1998b, 1998c) examined urinary parameters in the rabbit, but not rat. In the first rabbit study Gilman et al. (1998b) measured various urinary parameters including levels of urea nitrogen, glucose, creatinine, total protein, and albumin as well as activities of LDH avtivity and NAG. Gilman et al. (1998a, 1998b, 1998c) found no marked effects after exposure to 29 mg U/kg-d for 91 d, but reported urinary parameter effects with the most persistent being increased glucose excretion in a second study in male rabbits exposed to 41 mg U/kg-d for 91 d (Gilman et al., 1998a). A dye clearance test used to assess renal function showed reduced rate of phenolsulfonphthalein excretion in male rabbits exposed to $\geq$ 120 mg/L uranyl nitrate (5 mg U/kg-d) but not in females (Gilman et al., 1998b). Rabbits exposed to lower levels of U in drinking water showed no marked changes in urinary parameters (Gilman et al., 1998a, 1998b).

Two animal studies that explored the renal effects of implanted DU particles in rats provide toxicity information relevant to the hazard associated with exposure of soldiers to embedded fragments of DU (Pellmar et al., 1998, 1999; Zhu et al., 2009). Pellmar et al. (1998, 1999) did not observe significant changes in biochemical or histologic markers of renal damage, while Zhu et al. (2009) reported that DU exposure led to increased renal damage as measured by light and electron microscopy including hypertrophy of epithelial cells, necrosis, fibrosis, increased mitochondria size, glomerulus thickening, and inflammatory-cell infiltration, and biochemical assays as evidenced by increased urinary β_2-microglobulin, albumin, serum creatinine, and BUN. Although both of these studies used similar methodologies for DU pellet implantation within the gastrocnemius muscle in the lower leg of Sprague-Dawley rats, the actual doses of implanted DU can not be compared based upon data provided. Pellmar et al. (1998, 1999) implanted rats with 0, 4, 10, and 20 U pellets (pellet weights not reported). Zhu et al. (2009) implanted rats with 0, 0.1, 0.2, and 0.3 g of DU fragments. After 6 mo of exposure, the highest renal U concentration reported by Pellmar et al. (1999) was 6920 $\pm$ 770 ng/g, while Zhu et al. (2009) reported a renal U concentration of 27,439 $\pm$ 2291 ng/g in the high-dose group. The differences in U-induced renal toxicity observed in these two studies may have been due to differences in U dose, tissue uptake, or diffusion from the implanted pellets.

STUDIES OF MECHANISMS OF RENAL TOXICITY

The cellular, molecular, and biochemical mechanisms for renal U uptake and toxicity have been previously reviewed (ATSDR, 1999). Recent studies using proximal and distal tubule cell lines (MDCK and LLC-PK_1 cells) suggest that U-induced renal toxicity is dependent on the formation of uranyl phosphate complexes, specifically $UO_2(PO_4)^-$ and $UO_2(HPO_4)$, and their uptake by the sodium dependent co-transporter NaPi-II and absorptive endocytosis (Muller et al., 2006, 2008). Furthermore, in vitro studies using isolated human and murine kidney cortex tubules suggest that U exposure inhibits cellular ATP content and gluconeogenesis through enzymatic inhibition of LDH, pyruvate carboxylase, glucose 6-phosphatase, and phoshoenolpyruvate carboxykinase. Toxicogenomic and proteomic studies using human renal HEK293 cells also suggest that U exposure altered expression of genes associated with calcium-dependent cell signaling such as IP3 cascade kinases PI4KII

Downloaded By: [US EPA Environmental Protection Agency] At: 17:09 22 December 2010

and PIK3R1, the intracellular calcium receptor calmodulin, and calmodulin-dependent proteins and cell trafficking pathways such as the potassium channel ABC subunits ATP6V1A1 and ABCC8 (Prat et al., 2005). Both in vivo and in vitro experiments showed that U exposure depleted cellular antioxidants such as glutathione (GSH) and glutathione reductase activity, increased reactive oxygen species (ROS) production and DNA damage, and promoted apoptosis (Banday et al., 2008; Linares et al., 2006; Thiebault et al., 2007). In vivo toxicogenomic studies reported that chronic exposure to U significantly enhanced expression of genes associated with oxidative stress responses such as superoxide dismutase 1 and ion transporters including NaPi-II and Slc34a1 (Taulan et al., 2004).

DISCUSSION

Some evidence of adverse renal effects, particularly with respect to biomarkers of proximal tubule damage, is seen in community-based studies of populations chronically exposed to elevated drinking water concentrations of U. The biomarker for which effects were most consistently seen was urinary levels of β_2-microglobulin (Zamora et al., 1998, 2009; Seldén et al., 2009). The study in Finland (Kurttio et al., 2002) did not demonstrate an association of toxicity to U with β_2-microglobulin levels. Prat et al. (2009) suggested that the calcium-dependent species seen in speciation analyses of the Finnish water samples may result in a low toxicity profile. It should also be noted, however, that 65% of the samples in Kurttio et al. (2002) were below the β_2-microglobulin limit of detection, and in contrast to the other studies, this measure was based on a spot urine rather than an overnight urine sample. β_2-Microglobulin was not included in the measurements used in the follow-up study in Finland (Kurttio et al., 2006). Thun et al. (1985) also reported strong associations between U exposure and β_2-microglobulin measures in urine and serum among workers in a U processing mill. Two of these studies included measures of other metals (Cd and Pb in Seldén et al. [2009] and Cd and Pb in Thun et al. [1985]), and there was no indication that the associations seen with U were the result of confounding by these other exposures. In addition, in the most recent follow-up surveillance study of Gulf War veterans exposed to DU, some indications of proximal tubule effects, as evidenced by increased urinary β_2-microglobulin and retinol binding protein levels, were noted (McDiarmid et al., 2009). Thus, although the subsets of renal tests, sensitivity of assays, and type of exposure measure varied across studies, as a group these studies show considerable consistency with respect to an indicator of proximal tubule damage and either measures of intake or U concentrations in urine. Occupational cohort studies do not provide evidence of an increased risk of kidney-related mortality among U-exposed workers. This outcome would be a relatively insensitive endpoint for the detection of renal damage, however, as it relies on cause of death as reported on death certificates. The reliability of this recording for chronic conditions, such as kidney disease, is much lower than for most cancers and acute events such as accidents and myocardial infarction (Harteloh et al., 2010).

Studies in experimental animals confirm that the kidney is a target of U toxicity following oral and implantation exposure. Both routes of exposure are relevant to human exposure situations. The available animal studies, however, provide an incomplete characterization of the dose-response relationship for kidney effects associated with chronic exposure at low environmental exposure levels. With the exception of early (1940s) studies conducted in support of the Manhattan Project (Dygert et al., 1949; Maynard et al., 1953; Maynard and Hodge, 1949), animal studies are generally limited to exposures of 90 d duration. Further, the majority of subchronic oral toxicity studies (Gilman et al., 1998a, 1998b, 1998c; McDonald-Taylor et al., 1992, 1997) of U compounds failed to identify a no-observed-adverse-effect level, and the kidney effects reported by some investigators (Gilman et al., 1998b, 1998c) did not exhibit a dose response. Investigation of clinical

biomarkers of renal toxicity in experimental animal studies is limited. Mechanistic studies suggest that cell toxicity may result from altered function of cell signaling pathways, increased ROS production, and depletion of endogenous cellular antioxidants.

In summary, various lines of evidence suggest that relatively low levels of U exposure may result in detectable changes in markers of renal damage in humans. The epidemiological studies do not provide evidence of clinically diagnosed kidney disease or renal failure within the exposed populations. Given the limited sample sizes and the potential selection of relatively healthy individuals in these types of community-based and occupational studies, the absence of the observation of this type of kidney disease is not surprising. Rather, these studies are better designed to examine associations within what would be considered the normal range of specific biomarkers of renal function. The question of the interpretation and importance of the observed effects of biomarkers of proximal tubule function is an important question that would benefit from additional clinical, epidemiological, and experimental research.

Downloaded By: [US EPA Environmental Protection Agency] At: 17:09 22 December 2010

REFERENCES

Abu-Qare, A. W., and Abou-Donia, M. B. 2002. Depleted uranium—The growing concern. *J. Appl. Toxicol*. 22:149–152.

Arfsten, D. P., Still, K. R., and Ritchie, G. D. 2001. A review of the effects of uranium and depleted uranium exposure on reproduction and fetal development. *Toxicol. Ind. Health* 17:180–191.

Agency for Toxic Substances and Disease Registry. 1999. *Toxicological profile for uranium*. Atlanta, GA: U.S. Department of Health and Human Services, Agency for Toxic Substances and Disease Registry. http://www.atsdr.cdc.gov/toxprofiles/tp150.pdf

Bagshaw, S. M., Langenberg, C., Haase, M., Wan, L., May, C. N., and Bellomo, R. 2007. Urinary biomarkers in septic acute kidney injury. *Intens. Care Med*. 33:1285–1296.

Banday, A. A., Priyamvada, S., Farooq, N., Yusufi, A. N., and Khan, F. 2008. Effect of uranyl nitrate on enzymes of carbohydrate metabolism and brush border membrane in different kidney tissues. *Food Chem. Toxicol*. 46:2080–2088.

Birn, H., and Christensen, E. I. 2006. Renal albumin absorption in physiology and pathology. *Kidney Int*. 69:440–449.

Bleise, A., Danesi, P. R., and Burkart, W. 2003. Properties, use and health effects of depleted uranium (DU): A general overview. *J. Environ. Radioact*. 64:93–112.

Boice, J. D., Jr., Cohen, S. S., Mumma, M. T., Chadda, B., and Blot, W. J. 2008. A cohort study of uranium millers and miners of Grants, New Mexico, 1979–2005. *J. Radiol. Prot*. 28:303–325.

Centers for Disease Control and Prevention. 2005. *Third national report on human exposure to environmental chemicals*. Atlanta, GA: U.S. Centers for Disease Control and Prevention. http://www.cdc.gov/exposurereport/pdf/thirdreport.pdf

Checkoway, H., Pearce, N., Crawford-Brown, D. J., and Cragle, D. L. 1988. Radiation doses and cause-specific mortality among workers at a nuclear materials fabrication plant. *Am. J. Epidemiol*. 127:255–266.

Comper, W. D., Hilliard, L. M., Nikolic-Paterson, D. J., and Russo, L.M. 2008. Disease-dependent mechanisms of albuminuria. *Am. J. Physiol. Renal Physiol*. 295:F1589–F1600.

Craft, E., Abu-Qare, A., Flaherty, M., Garofolo, M., Rincavage, H., and Abou-Donia, M. 2004. Depleted and natural uranium: Chemistry and toxicological effects. *J. Toxicol. Environ. Health B* 7:297–317.

Domingo, J. L., Llobet, J. M., Tomas, J. M., and Corbella, J. 1987. Acute toxicity of uranium in rats and mice. *Bull. Environ. Contam. Toxicol*. 39:168–174.

Dupree-Ellis, E., Watkins, J., Ingle, J. N., and Phillips, J. 2000. External radiation exposure and mortality in a cohort of uranium processing workers. *Am. J. Epidemiol*. 152:9195.

Dygert, H. P., LaBelle, C. W., Laskin, S., Pozzani, U. C., Roberts, E., Rothermel, J. J., Rothstein, A., Spiegl, C. J., Sprague, G. F., and Strokinger, H. E. 1949. Toxicity following inhalation. In *Pharmacology and Toxicology of Uranium Compounds*, eds. C. Voegtlin and H. C. Hodge, pp. 423–524.New York: McGraw-Hill.

Emeigh, S., and Kinter, L. 2005. Assessing renal effects of toxicants in vitro. In *Toxicology of the kidney*, 3rd ed., ed. J. Tarloff and L. Lash, pp 81–147. Washington, D.C.: CRC Press.

Emeigh Hart, S. 2005. Assessment of renal injury in vivo. *J. Pharmacol. Toxicol. Methods* 52:30–45.

Frome, E. L., Cragle, D. L., and McLain, R. W. 1990. Poisson regression analysis of the mortality among a cohort of World War II nuclear industry workers. *Radiat. Res*. 123:138–152.

Gilman, A. P., Moss, M. A., Villeneuve, D. C., Secours, V. E., Yagminas, A. P., Tracy, B. L., Quinn, J. M., Long, G., and Valli, V. E. 1998a. Uranyl nitrate: 91-Day exposure and recovery studies in the male New Zealand white rabbit. *Toxicol. Sci*. 41:138–151.

Gilman, A. P., Villeneuve, D. C., Secours, V. E., Yagminas, A. P., Tracy, B. L., Quinn, J. M., Valli, V. E., and Moss, M. A. 1998b. Uranyl nitrate: 91-Day toxicity studies in the New Zealand white rabbit. *Toxicol. Sci*. 41:129–137.

Gilman, A. P., Villeneuve, D. C., Secours, V. E., Yagminas, A. P., Tracy, B. L., Quinn, J. M., Valli, V. E., Willes, R. J., and Moss, M. A. 1998c. Uranyl nitrate: 28-day and 91-day toxicity studies in the Sprague-Dawley rat. *Toxicol. Sci*. 41:117–128.

Goel, K. A., Garg, V. K., and Garg, V. 1980. Histopathology of kidney of albino rat poisoned with uranyl nitrate. *Bull. Environ. Contam. Toxicol*. 24:9–12.

Greaves, P. 2007. *Histopathology of preclinical toxicity studies: Interpretation and relevance in drug safety evaluation*, 3rd ed., pp. 570–623. Boston: Academic Press.

Guéguen, Y., L. Grandcolas, C. Baudelin, S. Grison, E. Tissandié, J. R. Jourdain, F. Paquet, P. Voisin, J. Aigueperse, P. Gourmelon, and M. Souidi. 2007. Effect of acetaminophen administration to rats chronically exposed to depleted uranium. *Toxicology* 229:62–72.

Harteloh, P., de Bruin, K., and Kardaun, J. 2010. The reliability of cause-of-death coding in the Netherlands. *Eur. J. Epidemiol*. March 23 [Epub ahead of print].

Hindin, R., Brugge, D., and Panikkar, B. 2005. Teratogenicity of depleted uranium aerosols: A review from an epidemiological perspective. *Environ. Health* 4:17.

Kurttio, P., Auvinen, A., Salonen, L., Saha, H., Pekkanen, J., Makelainen, I., Vaisanen, S. B., Penttila, I. M., and Komulainen, H. 2002. Renal effects of uranium in drinking water. *Environ. Health Perspect*. 110:337–342. Erratum: *Environ. Health Perspect*. 111:632 (2003).

Kurttio, P., Harmoinen, A., Saha, H., Salonen, L., Karpas, Z., Komulainen, H., and Auvinen, A. 2006. Kidney toxicity of ingested uranium from drinking water. *Am. J. Kidney Dis*. 47:972–982.

Levey, A. S., Stevens, L. A., Schmid, C. H., Zhang, Y. L., Castro, A. F. 3rd, Feldman, H. I., Kusek, J. W., Eggers, P., Van Lente, F., Greene, T., and Coresh, J. 2009. A new equation to estimate glomerular filtration rate. *Ann. Intern. Med*. 150:604–612.

Linares, V., Belles, M., Albina, M. L., Sirvent, J. J., Sanchez, D. J., and Domingo, J. L. 2006. Assessment of the pro-oxidant activity of uranium in kidney and testis of rats. *Toxicol. Lett*. 167:152–161.

Loomis, D. P., and Wolf, S. H. 1996. Mortality of workers at a nuclear materials production plant at Oak Ridge, Tennessee, 1947–1990. *Am. J. Ind. Med*. 29:131–141.

Magdo, H. S., Forman, J., Graber, N., Newman, B., Klein, K., Satlin, L., Amler, R. W., Winston, J. A., and Landrigan, P. J. 2007. Grand rounds: Nephrotoxicity in a young child exposed to uranium from contaminated well water. *Environ. Health Perspect*. 115:1237–1241.

Mao, Y., Desmeules, M., Schaubel, D., Berube, D., Dyck, R., Brule, D., and Thomas, B. 1995. Inorganic components of drinking water and microalbuminuria. *Environ. Res*. 71:135–140.

Downloaded By: [US EPA Environmental Protection Agency] At: 17:09 22 December 2010

Downloaded By: [US EPA Environmental Protection Agency] At: 17:09 22 December 2010

Maynard, E. A., and Hodge, H. C. 1949. Study of toxicity of various uranium compounds when fed to experiment animals. In *Pharmacology and toxicology of uranium compounds*, eds. C. Voegtlin and H. C. Hodge, pp. 309–376. New York: McGraw-Hill.

Maynard, E. A., Downs, W. L., and Hodge, H. C. 1953. Oral toxicity of uranium compounds. In *Pharmacology and toxicology of uranium compounds*, eds. C. Voegtlin and H. C. Hodge, pp. 1221–1369. New York: McGraw-Hill.

McDiarmid, M. A., Squibb, K., Engelhardt, S., Oliver, M., Gucer, P., Wilson, P. D., Kane, R., Kabat, M., Kaup, B., Anderson, L., Hoover, D., Brown, L. D., Jacobson-Kram, D., and Depleted Uranium Follow-Up Program. 2001. Surveillance of depleted uranium exposed Gulf War veterans: Health effects observed in an enlarged "friendly fire" cohort. *J. Occup. Environ. Med*. 43:991–1000.

McDiarmid, M. A., Engelhardt, S., Oliver, M., Gucer, P., Wilson, P. D., Kane, R., Kabat, M., Kaup, B., Anderson, L., Hoover, D., Brown, L., Handwerger, B., Albertini, R. J., Jacobson-Kram, D., Thorne, C. D., and Squibb, K. S. 2004. Health effects of depleted uranium on exposed Gulf War veterans: A 10-year follow-up. *J. Toxicol. Environ. Health A* 67:277–296.

McDiarmid, M. A., Engelhardt, S. M., Oliver, M., Gucer, P., Wilson, P. D., Kane, R., Kabat, M., Kaup, B., Anderson, L., Hoover, D., Brown, L., Albertini, R. J., Gudi, R., Jacobson-Kram, D., Thorne, C. D., and Squibb, K. S. 2006. Biological monitoring and surveillance results of Gulf War I veterans exposed to depleted uranium. *Int. Arch. Occup. Environ. Health* 79:11–21.

McDiarmid, M. A., Engelhardt, S. M., Oliver, M., Gucer, P., Wilson, P. D., Kane, R., Cernich, A., Kaup, B., Anderson, L., Hoover, D., Brown, L., Albertini, R., Gudi, R., Jacobson-Kram, D., and Squibb, K. S. 2007. Health surveillance of Gulf War I veterans exposed to depleted uranium: updating the cohort. *Health Phys*. 93:60–73.

McDiarmid, M. A., Engelhardt, S. M., Dorsey, C. D., Oliver, M., Gucer, P., Wilson, P. D., Kane, R., Cernich, A., Kaup, B., Anderson, L., Hoover, D., Brown, L., Albertini, R., Gudi, R., and Squibb, K. S. 2009. Surveillance results of depleted uranium-exposed Gulf War I veterans: Sixteen years of follow-up. *J Toxicol Environ Health A* 72:14–29.

McDonald-Taylor, C. K., Bhatnagar, M. K., Gilman, A., Yagminas, A., and Singh, A. 1992. Uranyl nitrate-induced glomerular basement membrane alterations in rabbits: A quantitative analysis. *Bull. Environ. Contam. Toxicol*. 48:367–373.

McDonald-Taylor, C. K., Singh, A., and Gilman, A. 1997. Uranyl nitrate-induced proximal tubule alterations in rabbits: A quantitative analysis. *Toxicol. Pathol*. 25:381–389.

McGeoghegan, D., and Binks, K. 2000a. The mortality and cancer morbidity experience of workers at the Capenhurst uranium enrichment facility 1946–95. *J. Radiol. Prot*. 20:381–401.

McGeoghegan, D., and Binks, K. 2000b. The mortality and cancer morbidity experience of workers at the Springfields uranium production facility, 1946–95. *J. Radiol. Prot*. 20:111–137.

Muller, D., Houpert, P., Cambar, J., and Henge-Napoli, M. H. 2006. Role of the sodium-dependent phosphate co-transporters and of the phosphate complexes of uranyl in the cytotoxicity of uranium in LLC-PK1 cells. *Toxicol. Appl. Pharmacol*. 214: 166–177.

Muller, D. S., Houpert, P., Cambar, J., and Henge-Napoli, M. H. 2008. Role of the sodium-dependent phosphate cotransporters and absorptive endocytosis in the uptake of low concentrations of uranium and its toxicity at higher concentrations in LLC-PK1 cells. *Toxicol. Sci*. 101: 254–262.

Orloff, K. G., Mistry, K., Charp, P., Metcalf, S., Marino, R., Shelly, T., Melaro, E., Donohoe, A. M., and Jones, R. L. 2004. Human exposure to uranium in groundwater. *Environ. Res*. 94:319–326.

Downloaded By: [US EPA Environmental Protection Agency] At: 17:09 22 December 2010

Ortega, A., Domingo, J. L., Llobet, J. M., Tomas, J. M., and Paternain, J. L. 1989. Evaluation of the oral toxicity of uranium in a 4-week drinking-water study in rats. *Bull. Environ. Contam. Toxicol*. 42:935–941.

Ozmen, M., and Yurekli, M. 1998. Subacute toxicity of uranyl acetate in Swiss-albino mice. *Environ. Toxicol. Pharmacol*. 6:111–115.

Parkhurst, M. A., and Guilmette, R. A. 2009. Overview of the Capstone depleted uranium study of aerosols from impact with armored vehicles: Test setup and aerosol generation, characterization, and application in assessing dose and risk. *Health Phys*. 96:207–220.

Pellmar, T. C., Hogan, J. B., Benson, K. A., and Landauer, M. R. 1998. *Toxicological evaluation of depleted uranium in rats: Six-month evaluation point*. Bethesda, MD: Uniformed Services University of the Health Sciences. ADA410643.

Pellmar, T. C., Fuciarelli, A. F., Ejnik, J. W., Hamilton, M., Hogan, J., Strocko, S., Emond, C., Mottaz, H. M., and Landauer, M. R. 1999. Distribution of uranium in rats implanted with depleted uranium pellets. *Toxicol. Sci*. 49:29–39.

Pinkerton, L. E., Bloom, T. F., Hein, M. J., and Ward, E. M. 2004. Mortality among a cohort of uranium mill workers: An update. *Occup. Environ. Med*. 61:57–64.

Polednak, A. P., and Frome, E. L. 1981. Mortality among men employed between 1943 and 1947 at a uranium-processing plant. *J. Occup. Med*. 23:169–178.

Prat, O., Berenguer, F., Malard, V., Tavan, E., Sage, N., Steinmetz, G., and Quemeneur, E. 2005. Transcriptomic and proteomic responses of human renal HEK293 cells to uranium toxicity. *Proteomics* 5:297–306.

Prat, O., Vercouter, T., Ansoborlo, E., Fichet, P., Perret, P., Kurttio, P., and Salonen, L. 2009. Uranium speciation in drinking water from drilled wells in southern Finland and its potential links to health effects. *Environ. Sci. Technol*. 43:3941–3946.

Renault, S., Faiz, H., Gadet, R., Ferrier, B., Martin, G., Baverel, G., and Conjard-Duplany, A. 2010. Uranyl nitrate inhibits lactate gluconeogenesis in isolated human and mouse renal proximal tubules: A ^{13}C-NMR study. *Toxicol. Appl. Pharmacol*. 242:9–17.

Ritz, B., Morgenstern, H., Crawford-Brown, D., and Young, B. 2000. The effects of internal radiation exposure on cancer mortality in nuclear workers at Rocketdyne/Atomics International. *Environ. Health Perspect*. 108:743–751.

Seldén, A. I., Lundholm, C., Edlund, B., Hogdahl, C., Ek, B. M., Bergstrom, B. E., and Ohlson, C. G. 2009. Nephrotoxicity of uranium in drinking water from private drilled wells. *Environ. Res*. 109:486–494.

Squibb, K. S., and McDiarmid, M. A. 2006. Depleted uranium exposure and health effects in Gulf War veterans. *Philos. Trans. R. Soc. Lond. B Biol. Sci*. 361:639–648.

Taulan, M., Paquet, F., Maubert, C., Delissen, O., Demaille, J., and Romey, M. C. 2004. Renal toxicogenomic response to chronic uranyl nitrate insult in mice. *Environ. Health Perspect*. 112:1628–1635.

Thiebault, C., Carriere, M., Milgram, S., Simon, A., Avoscan, L., and Gouget, B. 2007. Uranium induces apoptosis and is genotoxic to normal rat kidney (NRK-52E) proximal cells. *Toxicol. Sci*. 98:479–487.

Thun, M. J., Baker, D. B., Steenland, K., Smith, A. B., Halperin, W., and Berl, T. 1985. Renal toxicity in uranium mill workers. *Scand. J. Work Environ. Health* 11:83–90.

Tolkoff-Rubin, N. E., Rubin, R. H., and Bonventre, J. V. 1988. Noninvasive renal diagnostic studies. *Clin. Lab. Med*. 8:507–526.

U. S. Environmental Protection Agency. 1985. *Nationwide occurrence of radon and other natural radioactivity in public water supplies*. Montgomery, AL: U. S. Environmental Protection Agency. EPA Number 520585008.

U. S. Environmental Protection Agency. 2000. *Radionuclides notice of data availability technical support document*. Washington, DC: U. S. Environmental Protection Agency.

http://www.epa.gov/OGWDW/radionuclides/pdfs/regulation_radionuclides_rulemaking_techsupportdoc.pdf

Walling, M. A. 1991. Morphologic manifestation of toxic cell injury. In *Handbook of toxicologic pathology*, vol. 2, eds. W. M. Haschek, C. G. Rousseaux, and M. A. Wallig, pp. 39–64. San Diego: Academic Press.

Waxweiler, R. J., Archer, V. E., and Roscoe, R. J. 1983. Mortality patterns among a retrospective cohort of uranium mill workers. In *Epidemiology applied to health physics, Sixteenth midyear topical meeting of the Health Physics Society*, Albuquerque, NM, pp. 428–435.

World Health Organization. 2001. *Depleted uranium sources, Exposure and health effects*. Geneva, Switzerland: World Health Organization. http://whqlibdoc.who.int/hq/2001/WHO_SDE_PHE_01.1.pdf

Zalups, R. K., Gelein, R. M., Morrow, P. E., and Diamond, G. L. 1988. Nephrotoxicity of uranyl fluoride in uninephrectomized and sham-operated rats. *Toxicol. Appl. Pharmacol*. 94:11–22.

Zamora M. L. L., Zielinski, J. M., Moodie, G. B., Falcomer, R. A. F., Hunt, W. C., and Capello, K. 2009. Uranium in drinking water: Renal effects of long-term ingestion by an Aboriginal community. *Arch. Environ. Occup. Health* 64:228–241.

Zamora, M. L., Tracy, B. L., Zielinski, J. M., Meyerhof, D. P., and Moss, M. A. 1998. Chronic ingestion of uranium in drinking water: A study of kidney bioeffects in humans. *Toxicol. Sci*. 43:68–77.

Zhu, G., Xiang, X., Chen, X., Wang, L., Hu, H., and Weng, S. 2009. Renal dysfunction induced by long-term exposure to depleted uranium in rats. *Arch. Toxicol*. 83:37–46.

Downloaded By: [US EPA Environmental Protection Agency] At: 17:09 22 December 2010

Table of Contents

General_Authors_Publications.....2
LI-266913_Makris_et_al_2016.....15
Record_of_agreement_-_Abbott.....53
Record_of_agreement_-_Arzuaga.....55
Record_of_agreement_-_Euling.....57
Record_of_agreement_-_Hogan.....59
Record_of_Agreement_-_Hotchkiss.....61
Record_of_agreement_-_Hunter.....63
Record_of_agreement_-_Jinot.....65
Record_of_agreement_-_John_Fox.....67
Record_of_agreement_-_Knudsen.....70
Record_of_agreement_-_Makris.....72
Record_of_agreement_-_Narotsky.....74
Record_of_agreement_-_Powers_(Parsons).....76
Record_of_agreement_(in_lieu)-_Scott.....78
Region_7_Meramec_Caverns_TCE_2016.....79

United States Environmental Protection Agency
Washington, DC 20460

STAA REPORT FOR THE SCIENTIST NOMINATIONS

General Information:

Nomination ID/App ID:	20-134
Research Category Primary:	Health Effects Research and Human Health Risk Assessment (HE)
Research Category Secondary:	
Laboratory/Office Name:	ORD
Nomination Entered By:	Susan Makris

Eligibility Checklist:

[Y] The nominated publication(s) has not been submitted to a previous STAA competition.

[Y] The nominated publication(s) was published on or before January 1, 2017 and on or after January 1,2012

[Y] The principal author was an EPA employee or a PHS employee assigned to EPA when the research was performed

[Y] The EPA authors (includes PHS employees assigned to EPA) contributed collectively a minimum of 50% toward the publication(s)

Nominating Official Name:	Kristina Chialton
Nominating Official Title:	SUPERVISORY BIOLOGIST
Nominating OfficialEmail:	thayer.kris@epa.gov
STAA Coordinator Name:	Kathleen Wiser
STAA Coordinator Email:	wiser.kathi@epa.gov

Justifications:

Justification 1:

The publication by Makris et al. (2016) addresses an issue that is critical to hazard evaluation, risk assessment, risk communication, and risk management for the chemical trichloroethylene (TCE), a volatile and widely used chlorinated solvent, specifically regarding regulatory decisions and actions that address a susceptible population, i.e., pregnant women and their fetuses. The available database of toxicology, epidemiology, and mechanistic information indicates that exposures to TCE during critical stages of prenatal development can potentially result in cardiac malformations. Based upon the weight of available evidence, the 2011 EPA TCE Integrated Risk Information System (IRIS) assessment established reference values for oral and inhalation exposure to TCE, using developmental cardiac defects from a controversial drinking water study in rats (Johnson et al., 2003).

In 2014, EPA initiated an Office of Research and Development (ORD) update on the potential for fetal cardiac defects resulting from TCE exposures. The ORD work group conducted a transparent systematic review of the data for all relevant studies, an extensive comparative analysis of the methodologies used to evaluate fetal cardiac abnormalities in published studies, and a rigorous evaluation of the benchmark dose modeling procedures and outcomes for cardiac malformations. Interviews with the lead author of the Johnson et al. (2003) publication led to enhanced characterization of the study methodologies, especially regarding the morphological evaluation of the fetuses. Additionally, a putative AOP was proposed by the ORD workgroup, linking developmental pathways with one of the notable cardiac malformations observed with TCE developmental exposure, i.e., ventricular septal defects. This was a novel and critical step forward in demonstrating the biological plausibility of the relationship between *in utero* TCE exposures and fetal cardiac malformations.

The results of this evaluation were first reported in a memo to Dr. Robert Kavlock (Acting Assistant Administrator of ORD), “TCE Developmental Cardiac Toxicity Assessment Update” dated April 30, 2014. The information was then shared with other Offices within the EPA, and it was used immediately in support of ongoing regulatory decisions.

The ORD work group subsequently published the expanded detailed findings from the TCE developmental toxicology update analyses in Makris et al. (2016), thus providing public access to the work group conclusions. The publication systematically reviews, evaluates, and synthesizes information on the individual studies, the lines of evidence (epidemiological, toxicological, *in vitro*, *in ovo*, and mechanistic/AOP), and integrates the

data into a cohesive, comprehensive, hypothesis-driven weight-of-evidence analysis that supports the Agency's conclusions on the potential for TCE exposures during *in utero* development to result in congenital heart defects (CHDs) in humans. Additionally, it clearly identifies strengths and limitations in the data, describes residual uncertainties, and ascribes levels of confidence in the conclusions. Issues raised in public comments about the adequacy of the Johnson et al. (2003) study for use in hazard characterization and reference value derivation are specifically addressed, and expanded information is provided on the study design and methodologies that were inadequately described in the published literature prior to the publication of the Makris et al. (2016) study.

Makris et al. (2016) remains a primary source of information on the evaluation of potential risk for cardiac malformations related to TCE exposure during pregnancy, and a basis of regulatory action. The evaluation of developmental cardiac malformations conducted by the ORD team of experts provided Program Offices, Regional Offices, and state environmental offices with an expanded rationale upon which to base health-protective risk assessment decisions and risk management practices regarding the exposure of pregnant women and their fetuses to TCE. Upon completion of the ORD developmental toxicity update assessment in 2014, OPPT immediately incorporated the conclusions into their TSCA Work Plan Chemical Risk Assessment for "Trichloroethylene: Degreasing, Spot Cleaning and Arts & Crafts Uses" (EPA Document No. 740R14002, June 2014; https://www.epa.gov/assessing-and-managing-chemicals-under-tsca/tsca-work-plan-chemical-risk-assessment-0). These commercial and consumer uses of TCE were banned based on the findings of excessive risk to pregnant women and their fetuses. Additionally, OLEM, EPA Regional Offices, and state environmental offices have utilized the ORD conclusions in support of regulatory decisions for Superfund sites and relative to vapor intrusion of TCE from contaminated soil and ground water in other localities. For example, EPA Region 7 directed the potentially responsible party at a groundwater contamination Superfund site in Franklin County, Mo., to perform additional work to protect workers and visitors from potentially harmful exposures to TCE vapors in nearby Meramec Caverns, a privately-owned tourist attraction near Stanton, MO. As a precautionary step, Meramec Caverns ceased cave tours from March 2016 to August 2016 while controls were instituted to reduce TCE vapor levels (USEPA Region 7 Fact Sheet, LaJolla Spring Cave Complex - Meramec Caverns, Stanton, Missouri, September 2016).

Justification 2A:

N/A

Justification 2B:

Michael Narotsky: 2016 Level III:

1) 2013: Comprehensive Assessment of a Chlorinated Drinking Water Concentrate in a Rat Multigenerational Reproductive Toxicity Study

2) 2015: Reproductive Toxicity of a Mixture of Regulated Drinking-Water Disinfection By-Products in a Multigenerational Rat Bioassay

Thomas Knudsen:

1) 2015: 2014 Level II for "ExpoCast High Throughput Framework for Rapid Prioritization of Human Exposure to Environmental Chemicals".

2) 2016: 2015 Level III for "Using High-Throughput Screening Assays to Profile Enzymatic and Receptor Signaling Activity of ToxCast Chemicals".

3) 2016: 2015 Level III for "Classifying Toxic and Therapeutic Mechanisms by Phenotypic Screening of ToxCast Chemicals".

4) 2016: 2015 Level III for "Development of a Novel Experimental System to Evaluate Predictive-Toxicity Signatures".

5) 2020: 2019 Level III for "A chemical and cheminformatics foundation for ToxCast & Tox21 research programs".

All other authors (Makris, Scott, Fox, Euling, Arzuaga, Hotchkiss, Hunter, Abbott, Narotsky, Parsons, Jinot, Hogan): no STAA nominations or awards in the past 5 years.

Justification 2C:

The current nomination is for a paper that addresses different subject matter than the papers for which Thomas Knudsen and Michael Narotsky were co-authors and that had been previously nominated for and received STAA awards.

Justification 2D:

N/A

Justification 2E:

Five of the co-authors of Makris et al, (2016) (Arzuaga, Euling, Hogan, Hotchkiss, Makris) are also co-authors on three publications on phthalate chemicals that are currently being nominated for STAA awards by Erin Yost (ORD). These are independent research projects with no overlap in subject matter.

Justification 3A:

1) Susan Makris was invited to participate in a Roundtable presentation on the assessment: “Trichloroethylene exposure and development of fetal cardiac malformations: What do the data tell us about inhalation exposures resulting from vapor intrusion and potential health risks to pregnant women?” at the Society of Toxicology 55th annual meeting, New Orleans, LA, March 13-17, 2016.

2) The publication by Makris et al. (2016) is cited extensively in external deliberations on regulatory decision-making for TCE. It clearly summarizes studies in the TCE developmental toxicology database, including the controversial study by Johnson et al. (2003), which is just one component of the extensive weight of evidence demonstrating that exposures to TCE at critical stages of prenatal development can result in cardiac malformations. Some organizations external to EPA support the EPA’s conclusions regarding cardiac malformation and the use of the Johnson et al (2003) study in risk calculations, yet other organizations do not. An example of this controversy was demonstrated at the March 2020 meeting of the EPA Scientific Advisory Committee for Chemicals (SACC) on the OPPT TCE Risk Evaluation. Public comments from environmental non-government organizations (NGOs), Safer Chemicals Healthy Families (SCHF), Environmental Health Strategy Center, Earthjustice, and Natural Resources Defense Council supported EPA’s conclusions regarding the weight of evidence for cardiac defects, while representative of industry consortia discounted the same evidence. Makris et al. (2016) was cited in the comments, demonstrating the relevance of this paper to the on-going discussion (Docket ID: EPA-HQ-OPPT-2019-0500; https://www.regulations.gov/document?D=EPA-HQ-OPPT-2019-0500-0001)

Justification 3B:

The Publisher (Elsevier) of Reproductive Toxicology assigned a special editor (Susan E. Maier, PhD, NIH) to manage the peer review process, since one of the co-authors of the paper, Thomas Knudsen, was Editor-in-Chief of the journal at that time. The editor assigned the paper to 3 independent, anonymous reviewers.

AUTHORS

Principal Author

Author Name:	Susan L. Makris	
Professional Title:		Salutation:
Email:	makris.susan@epa.gov	Organization:
Mailing Address:		
Street Line 1:		
City:		
Zip Code:		State:
At time of research was:	EPA Employee	
Separation Date:		
% of Effort:	13	

Contributing Author

Author Name:	Cheryl Siegel Scott (deceased)	
Professional Title:		Salutation:
Email:	scott.cheryl@epa.gov	Organization:
Mailing Address:		

Street Line 1:		
City:		
Zip Code:		State:
At time of research was:	Non EPA Personnel	
Separation Date:		
% of Effort:	8	

Contributing Author

Author Name:	Andrew Hotchkiss	
Professional Title:		Salutation:
Email:	hotchkiss.andrew@epa.gov	Organization:
Mailing Address:		
Street Line 1:		
City:		
Zip Code:		State:
At time of research was:	EPA Employee	
Separation Date:		
% of Effort:	8	

Contributing Author

Author Name:	Xabier Arzuaga	
Professional Title:		Salutation:
Email:	arzuaga.xabier@epa.gov	Organization:
Mailing Address:		

Street Line 1:		
City:		
Zip Code:		State:
At time of research was:	EPA Employee	
Separation Date:		
% of Effort:	8	

Contributing Author

Author Name:	John Fox	
Professional Title:		Salutation:
Email:	foxjff@yahoo.com	Organization:
Mailing Address:		
Street Line 1:		
City:		
Zip Code:		State:
At time of research was:	EPA Employee	
Separation Date:		
% of Effort:	8	

Contributing Author

Author Name:	Thomas Knudsen	
Professional Title:		Salutation:
Email:	knudsen.thomas@epa.gov	Organization:
Mailing Address:		

Street Line 1:		
City:		
Zip Code:		State:
At time of research was:	EPA Employee	
Separation Date:		
% of Effort:	8	

Contributing Author

Author Name:	Susan Euling	
Professional Title:		Salutation:
Email:	euling.susan@epa.gov	Organization:
Mailing Address:		
Street Line 1:		
City:		
Zip Code:		State:
At time of research was:	EPA Employee	
Separation Date:		
% of Effort:	8	

Contributing Author

Author Name:	Christina Parsons	
Professional Title:		Salutation:
Email:	parsons.christy@epa.gov	Organization:
Mailing Address:		

Street Line 1:		
City:		
Zip Code:		State:
At time of research was:	EPA Employee	
Separation Date:		
% of Effort:	5	

Contributing Author

Author Name:	Jennifer Jinot	
Professional Title:		Salutation:
Email:	jjinot@hotmail.com	Organization:
Mailing Address:		
Street Line 1:		
City:		
Zip Code:		State:
At time of research was:	EPA Employee	
Separation Date:	Mon Dec 31 00:00:00 GMT 2018	
% of Effort:	5	

Contributing Author

Author Name:	Karen Hogan	
Professional Title:		Salutation:
Email:	hogan.karen@epa.gov	Organization:
Mailing Address:		

Street Line 1:		
City:		
Zip Code:		State:
At time of research was:	EPA Employee	
Separation Date:		
% of Effort:	5	

Contributing Author

Author Name:	Barbara Abbott	
Professional Title:		Salutation:
Email:	abbott.barbara@att.net	Organization:
Mailing Address:		
Street Line 1:		
City:		
Zip Code:		State:
At time of research was:	EPA Employee	
Separation Date:	Tue Dec 31 00:00:00 GMT 2019	
% of Effort:	8	

Contributing Author

Author Name:	E. Sidney Hunter	
Professional Title:		Salutation:
Email:	hunter.sid@epa.gov	Organization:
Mailing Address:		

Street Line 1:		
City:		
Zip Code:		State:
At time of research was:	EPA Employee	
Separation Date:		
% of Effort:	8	

Contributing Author

Author Name:	Michael Narotsky	
Professional Title:		Salutation:
Email:	narotsky.michael@epa.gov	Organization:
Mailing Address:		
Street Line 1:		
City:		
Zip Code:		State:
At time of research was:	EPA Employee	
Separation Date:		
% of Effort:	8	

PUBLICATIONS

Publication 1:

Publication Title:	A systematic evaluation of the potential effects of trichloroethylene exposure on cardiac developmen
Publication Date:	Sat Aug 27 00:00:00 GMT 2016

Journal/Publication Method:	Reproductive Toxicology		
All Author(s):			
Volume:	65	Number:	1
Pages:	321-358	Immediately Index:	Immediately Index:
Citation ½ Life:	7.8	Impact Factor:	3.200

Reproductive Toxicology 65 (2016) 321–358

Contents lists available at ScienceDirect

Reproductive Toxicology

journal homepage: www.elsevier.com/locate/reprotox

Review

A systematic evaluation of the potential effects of trichloroethylene exposure on cardiac development

Susan L. Makris[a,*], Cheryl Siegel Scott[a], John Fox[a], Thomas B. Knudsen[d], Andrew K. Hotchkiss[b], Xabier Arzuaga[a], Susan Y. Euling[a], Christina M. Powers[e,1], Jennifer Jinot[a], Karen A. Hogan[a], Barbara D. Abbott[c], E. Sidney Hunter III[c], Michael G. Narotsky[c]

[a] U.S. Environmental Protection Agency, Office of Research and Development, National Center for Environmental Assessment, Washington, DC 20460, United States
[b] U.S. Environmental Protection Agency, Office of Research and Development, National Center for Environmental Assessment, Research Triangle Park, NC 27711, United States
[c] U.S. Environmental Protection Agency, Office of Research and Development, National Health and Environmental Effects Research Laboratory, Research Triangle Park, NC 27711, United States
[d] U.S. Environmental Protection Agency, Office of Research and Development, National Center for Computational Toxicology, Research Triangle Park, NC 27711, United States
[e] U.S. Environmental Protection Agency, Office of Transportation and Air Quality, Assessment and Standards Division, Ann Arbor, MI 48105, United States

ARTICLE INFO

Article history:
Received 10 March 2016
Received in revised form 27 July 2016
Accepted 25 August 2016
Available online 27 August 2016

Keywords:
Trichloroethylene
TCE
Cardiac
Malformations
AOP

ABSTRACT

The 2011 EPA trichloroethylene (TCE) IRIS assessment, used developmental cardiac defects from a controversial drinking water study in rats (Johnson et al. [51]), along with several other studies/endpoints to derive reference values. An updated literature search of TCE-related developmental cardiac defects was conducted. Study quality, strengths, and limitations were assessed. A putative adverse outcome pathway (AOP) construct was developed to explore key events for the most commonly observed cardiac dysmorphologies, particularly those involved with epithelial-mesenchymal transition (EMT) of endothelial origin (EndMT); several candidate pathways were identified. A hypothesis-driven weight-of-evidence analysis of epidemiological, toxicological, in vitro, in ovo, and mechanistic/AOP data concluded that TCE has the potential to cause cardiac defects in humans when exposure occurs at sufficient doses during a sensitive window of fetal development. The study by Johnson et al. [51] was reaffirmed as suitable for hazard characterization and reference value derivation, though acknowledging study limitations and uncertainties.

Published by Elsevier Inc. This is an open access article under the CC BY-NC-ND license (http://creativecommons.org/licenses/by-nc-nd/4.0/).

Contents

1. Introduction 322
2. Materials and methods 323
   2.1. Literature search update 323
   2.2. Study quality review 323
   2.3. Characterization of hazard and dose-response information 323

Abbreviations: AOP, adverse outcome pathway; BMD, benchmark dose; BMDS, Benchmark Dose Software; BMDL, 95% lower confidence limit on the benchmark dose; BMR, benchmark response; CHD, congenital heart defects; CI, confidence interval; DCA, dichloroacetic acid; IRIS, Integrated Risk Information System; EPA, U.S. Environmental Protection Agency; MGI, Mouse Genome Informatics; NTP, National Toxicology Program; POD, point of departure; TCA, trichloroacetic acid; TCE, trichloroethylene; WOE, weight of evidence (evidence integration).

* Corresponding author.
E-mail address: makris.susan@epa.gov (S.L. Makris).
[1] Affiliation during conduct of the data analysis: U.S. Environmental Protection Agency, Office of Research and Development, National Center for Environmental Assessment, Research Triangle Park, NC 27711, United States.

http://dx.doi.org/10.1016/j.reprotox.2016.08.014
0890-6238/Published by Elsevier Inc. This is an open access article under the CC BY-NC-ND license (http://creativecommons.org/licenses/by-nc-nd/4.0/).

2.4. Mechanistic data on developmental pathways and processes ... 323
2.5. Weight-of-evidence (WOE) evaluation ... 323
3. Results ... 323
3.1. Hazard for developmental cardiac defects ... 323
3.1.1. Epidemiological data ... 323
3.1.2. Toxicological data ... 327
3.1.3. Mechanistic data on developmental pathways and processes ... 343
3.1.4. Weight of evidence (WOE) for hazard ... 345
3.2. Dose-response assessment for developmental cardiac defects ... 345
3.2.1. Suitability of Johnson et al. [51] study for deriving a point of departure for a reference value ... 345
3.2.2. Dose-response modeling of the data from Johnson et al. [51] ... 345
3.2.3. Uncertainty in the point of departure (POD) ... 354
4. Discussion/conclusions ... 355
4.1. Updated characterization of available data and uncertainties ... 355
4.2. Expanded consideration of the mechanistic database ... 355
4.3. Documentation of the WOE evaluation (evidence integration) ... 356
4.4. Extended characterization of the dose-response modeling ... 356
Conflict of interest ... 356
Acknowledgements ... 356
References ... 356

1. Introduction

Trichloroethylene (TCE), CAS No. 79-01-6, is a volatile chemical and widely used chlorinated solvent that is frequently found in ground water and in soil at contaminated sites across the U.S. TCE ranks 16th among hazardous substances most commonly found at facilities on the federal National Priorities List [4]. At sites where groundwater is contaminated and depending upon site-specific circumstances, TCE exposures and accompanying human health risks may arise from: (1) movement of TCE vapors from subsurface locations into the indoor air of overlying and nearby buildings (i.e., vapor intrusion) [5]; and/or (2) use of groundwater as a source of drinking water, process water, or irrigation water. A number of health effects have been observed after exposure to TCE during development, e.g., decreased fetal survival, impaired growth, alterations in immune and nervous system function, and structural defects, including ocular and cardiac malformations [16]. Here we report on a focused review of the published literature, conducted to update the information and critically evaluate the available data relevant to the potential for cardiac defects resulting from developmental exposures to TCE. This effort was initiated because of concerns raised about study quality and application of the reference value to short term and pregnancy exposure scenarios.

EPA completed an IRIS Toxicological Review of TCE in September 2011 [87]. The most sensitive types of noncancer health effects identified in this assessment were developmental, renal, and immunological. A reference concentration (RfC)[2] of 0.0004 ppm (0.4 ppb or 2 $\mu g/m^3$) is derived in U.S. EPA [87], based on route-to-route extrapolated results from oral studies for the critical effects of heart malformations in rats and immunotoxicity in mice, further supported by route-to-route extrapolated results from an oral study of nephropathy in rats. The reference dose (RfD) for noncancer effects of 0.0005 mg/kg-day is based on the critical effects in oral studies of heart malformations in rats, adult immunological effects in mice, and developmental immunotoxicity in mice. The RfD is further supported by results from an oral study for the effect of toxic nephropathy in rats and route-to-route extrapolated results from an inhalation study for the effect of increased kidney weight in rats ([87]; pages 6–43).

After the final IRIS document was released, EPA and others realized that because fetal adverse outcomes could potentially result from short-term exposures or peaks in exposure during pregnancy, one of the two endpoints used to derive the RfC (the fetal cardiac defects) is particularly important when evaluating whether TCE exposure poses an immediate potential hazard and whether peak exposures are a potential health concern. A study by Johnson et al. [51], which reports the results of research on TCE in drinking water, including the findings of Dawson et al. [20], is included in the group of studies on which the reference values are based in the 2011 IRIS assessment, and is one of several lines of evidence regarding the hazard potential for developmental toxicity of TCE. Concerns have been raised about the Johnson et al. [51] study and EPA's use of this study for risk evaluation [1,90,38]. Specific needs to resolve these concerns include: (1) a systematic evaluation of study quality; (2) more details in the description of the study design (e.g., the source of concurrent controls); (3) a reexamination of the dose-response relationship for cardiac defects; and (4) an evaluation of the study results in light of other studies that did not observe cardiac defects after in utero exposures. In addition, concerns have been raised regarding the interpretation of the epidemiological database for cardiac defects associated with TCE exposures [13,1,90,38].

An updated literature search and analysis of the developmental cardiac toxicity data for TCE was conducted to address the identified issues and to provide a focused, rigorous, systematic scientific review of the available data on associations between exposure to TCE and fetal cardiac defects. The scope of this update and analysis was limited to the fetal cardiac defects observed following gestational exposures to TCE and/or its oxidative metabolites, dichloroacetic acid (DCA) and trichloroacetic acid (TCA), which have been specifically associated with cardiac malformations in rats [51,49,20,27,79,78], and does not include an update on other developmental effects after TCE exposure, i.e., fetal growth retardation, embryolethality, ocular malformations, developmental neurotoxicity, and developmental immunotoxicity. This update of the fetal cardiac effects includes (1) a systematic search to identify any recently published literature; (2) a detailed evaluation of the available data; (3) a hypothesis-driven assessment of the weight of evidence (evidence integration) for the association of TCE exposures with cardiac malformations; (4) a reexamination of the dose-response relationship for cardiac malformations; and (5) a transparent description of the evaluation. This process is aligned

[2] A reference concentration (RFC) or dose (RfD) is an estimate of a continuous inhalation exposure (daily oral exposure) for a chronic duration (up to a lifetime) to the human population (including sensitive subgroups) that is likely to be without an appreciable risk of deleterious effects during a lifetime.

with the [64] recommendations for systematic review, evidence integration (weight-of-evidence) evaluation, and presentation of information to increase transparency.

2. Materials and methods

2.1. Literature search update

A systematic literature search was conducted to identify all epidemiological, toxicological, and mechanistic studies relevant to cardiac defects associated with developmental exposure to TCE or its metabolites (TCA and DCA) that were published subsequent to the final systematic literature search conducted by EPA during completion of the 2011 IRIS assessment [87]. A date-delineated search of PubMed, Toxline, and Web of Science (WoS) was conducted (January 2010–January 2015), using search terms designed to identify any publications that addressed TCE or its specified metabolites. The search identified a total of 1769 unique citations, which were then screened using information contained in the title, abstract, and/or full text. Citations excluded from further consideration included studies that did not include an assessment of TCE or its metabolites, studies that did not directly assess or were not pertinent to the evaluation of cardiac development, and publications that did not include primary research data (e.g., reviews, press articles, meeting abstracts). The literature search did not identify any new experimental animal toxicology studies of fetal cardiac defects, but did identify two new epidemiological studies that assessed the association of TCE or chlorinated solvent exposures with cardiac defects [71,29] and two new studies that provided mechanistic information relevant to alterations of cardiac development following TCE (or metabolite) exposures [58,66].

2.2. Study quality review

For each epidemiological and toxicological study in the developmental toxicity database for TCE, whether previously included in the EPA TCE assessment [87] or newly identified in the updated literature search, a formal detailed review of study quality was conducted.

- Epidemiological data: Study quality evaluation criteria and a general format for capturing epidemiological study data and characterization have previously been developed by the IRIS program and are summarized in the *Guidelines for Developmental Toxicity Risk Assessment* [85]. These factors include study power, potential bias in data collection, selection bias, measurement biases associated with exposure and outcome, and consideration of potential confounding and effect modification. This format was used to summarize study information and observed strengths, biases, and confounding factors for each study. An independent review of the study quality conclusions presented here was conducted by a working group that included eight EPA experts in the field of epidemiology.
- Animal toxicology data: Study quality evaluation criteria for in vivo, in vitro, and avian in ovo developmental toxicology studies were developed specifically for this effort. These criteria included considerations described in U.S. EPA [85] and focused on the adequacy of study design and documentation of information on the test subjects (e.g., species, strain, source, sex, age/lifestage/embryonic stage), environment (e.g., husbandry, culture medium), test substance (e.g., identification, purity, analytical confirmation of stability and concentration), treatment (e.g., dose levels, controls, vehicle, group sizes, duration, route of administration), endpoints evaluated (e.g., schedule of evaluation, randomization and blinding procedures, assessment methods), and reporting (quality and completeness). Two separate reviewers conducted independent assessments of each in vivo mammalian study, and seven toxicologists independently evaluated study quality for four mammalian in vivo studies that had performed a detailed evaluation of developmental cardiac defects [15,51,28,20].

2.3. Characterization of hazard and dose-response information

- Hazard: Critical elements of the identified epidemiological and toxicological studies were extracted and summarized in tabular format. For epidemiological studies, the exposure measure and range, outcome classification, participant selection and comparability, consideration of likely confounding, data presentation and analysis, and sample size were summarized. For animal toxicology studies, the summary included information on the test subjects (species, strain, sex, number of animals assigned per group), exposure levels, timing, and duration, no-observed-adverse-effect levels (NOAELs), lowest-observed-adverse-effect levels (LOAELs), and treatment-related effects.
- Dose-response analysis: The cardiac malformation data [51] were reanalyzed using the Benchmark Dose Software (BMDS) nested logistic model that was used in the EPA TCE assessment [87] as well as other BMDS models to evaluate uncertainty related to model selection and modeling assumptions [88]. A benchmark response (BMR) of 0.01 (1%) extra risk was used, justified by the severity of the effect.

2.4. Mechanistic data on developmental pathways and processes

The 2011 IRIS assessment noted that many of the cardiac defects observed in humans and laboratory species (primarily rats and chickens) involved septal and valvular structures. To further characterize the potential for alterations in cardiac development, studies that evaluated aspects of valvulo-septal defects identified in the literature search, as well as mechanistic studies that had been included in the 2011 IRIS TCE assessment, were examined for relevant information. The search and data evaluation pointed to alterations in endocardial cushion formation and development. This prompted a search of the Mouse Genome Informatics (MGI) database (http://www.informatics.jax.org/) for genes associated with "abnormal cardiac epithelial to mesenchymal transition" [MP:0008825]. As a consequence, newer mechanistic concepts were explored.

2.5. Weight-of-evidence (WOE) evaluation

The WOE (evidence integration) for fetal cardiac defects was characterized according to the criteria described in the *Framework for Assessing Health Risk of Environmental Exposures to Children* [86], a scheme that was adapted from principles of causality assessment developed by [43]. Fig. 1 illustrates the components (key factors) included in the WOE analysis. Each participant in the review independently assessed the WOE, and through discussions arrived at a group consensus of the evidence supporting stronger and weaker weights of association for each key factor.

3. Results

3.1. Hazard for developmental cardiac defects

3.1.1. Epidemiological data

The epidemiological studies were reviewed for associations between maternal exposure to TCE and cardiac defects. Seven

Table 1
Study Summary and Quality Assessment for Epidemiologic Studies on TCE Exposure and Congenital Malformations.

Reference	Exposure Measure and Range	Outcome Classification	Participant Selection and Comparability	Consideration of Likely Confounding	Data Presentation and Statistical Analysis	Adequate Sample Size	Additional Comments
Ruckart et al. [71]	Individual level. Fate and transport, and water distribution modeling, TCE, up to 1400 ppb; other contaminates included vinyl chloride, 1,2-dichloroethylene, PCE, benzene. Average monthly concentration two months before and after conception.	Self-reported, verified by medical record; NTD, oral clefts prevalence, conotruncal heart defects[a].	United States. n = 12,598 live births among mothers residing at Camp Lejeune during pregnancy, identified from birth certificates and media campaign/referral, 1968 – 1985. Referents selected from children without a birth defect (~1:10 ratio), unmatched to cases. Excluded 54 cases due to lack of medical verification, refusal to provide medical records, and verified not to have the reported condition; 22 controls ineligible.	Bivariate analyses adjusted for mother's age, previous pregnancy, child's sex, child's sibling with a birth defect, father's occupational exposure to solvents, previous pregnancy, alcohol use, mother's employment status, use of prenatal vitamins, or maternal fevers.	Odds ratio and 95% confidence interval; unconditional logistic regression.	106 cases of NTDs, oral clefts and leukemia/non-Hodgkin lymphoma; medically-verified: 35 NTDs, 42 oral clefts; TCE exposed, 8 NTDs, 9 oral clefts.	Odds ratio not reported for conotruncal heart defects. Less than 3 conotruncal heart malformations observed.
Forand et al. [29]	Area level. Maternal residence in one of two contaminated areas at time of birth. Sample of 25% residences affected by soil vapor intrusion: Area 1, indoor air TCE, range−0.18–140 ug/m^3, median 16 ug/m^3; Area 2, indoor PCE, range 0.1 – 24 ug/m^3.	Congenital malformations[b], including cardiac (ICD−9 745.0–747.9[c]), in <2 year old children, NYSDOH Congenital Malformations Registry.	United States. n = 1440 live singleton births (1090 in TCE area, 350 in PCE area); referents, 1983–2000; 3.6 million births in New York State, excluding New York City.	Adjusted for mother's age, education, race, infant's sex, number of previous live births, and adequate prenatal care.	Rate ratios and 95% confidence intervals, Poisson regression.	61 children (44 in TCE area, 17 in PCE area) with at least one reportable birth defect. TCE area, 25 surveillance defects, 15 cardiac malformations (6 major, 3 conotruncal).	No births with NTDs or oral clefts.
Yauck et al. [94]	Area level. Maternal residence within 1.32 miles from at least one TCE emissions source at time of birth.	Cardiac malformations, excluding patent ductus arteriosus, persistent foramen ovale, or peripheral pulmonary stenosis, hospital medical record, Milwaukee Children's Hospital.	United States. n = 4025 infants, born 1997–1999; cases from hospital or birth records, population referents from birth certificates frequency matched by birth year; excluded infants ≤23weeks, if 24–26 weeks, died within 48 h of birth, or Down's syndrome diagnosis; one birth selected from multiple births.	Dichotomized by age (<38 years, ≥38 years); no differences found for race, ethnicity, maternal education, parity, number of prenatal visits, or cigarette use.	Odds ratio, logistic regression.	245 cases and 3780 controls; TCE exposed, 46 cases, 715 controls.	Pre-existing diabetes, chronic hypertension, and alcohol associated with outcome and not included in TCE statistical model. The poorly-defined exposure surrogate and lack of TCE exposure monitoring makes interpretation of results difficult.

Bove et al. [9]; Bove [8]	Area level. Maternal 1st trimester exposure to TCE, municipal water supply, 75 towns (55 ppb, maximum monthly estimate; 5% of study population above MCL of 5 ppb), other TTHMs.	Congenital malformations[d], including NTD, oral clefts and cardiac defects (ICD−9 745.0, 745.1, 745.2, 746.1, 746.3, 746.4, 746.7, 747.1, 747.3), NJDOH Birth Defects Registry and New Jersey fetal death certificates.	United States. n = 80,938 singleton live-born infants and 594 singleton fetal deaths, New Jersey birth and death records, 1985–1988.	Odds ratio adjusted if differed from unadjusted by ±15% for maternal age, race, education, parity prenatal care, previous stillbirth or miscarriage, and child's sex.	Odds ratio, logistic regression.	58 NTDs, 83 oral cleft, 108 major cardiac defects; TCE >10 ppb, 4 NTDs, 9 oral cleft defects, major cardiac defects, including ventricular septal defects, NR.	Effect measure estimates from univariate analysis did not differ by ±15% from multivariate analyses.
Goldberg et al. [35]	Family member exposed to municipal well water contaminated with TCE (range: 6–239 ppb), DCA, chromium.	Cardiac defects, medically diagnosed closest to birth date, excluding syndromes associated with cardiac abnormalities, supraventricular tachycardia or isolated ectopic cardiac beats without gross anatomic cardiac lesions, patent ductus arteriosus in premature infants, peripheral pulmonary stenosis and bicuspid aortic value without stenosis or regurgitation.	United States. n = 1363 live births, conceived between 1969 and 1987 whose parents live in Tucson Valley for 1 month before and during 1st trimester of pregnancy, identified from cardiologist's records, 218 lacking 1st trimester addresses, 406 disqualified, 31 not residing in Tucson during 1st trimester. Additional control groups: Groups 1 and 2 were current residents, selected using RDD in (a) proportion to all telephone numbers or (b) proportion to population with cardiac defects,	Compared to non-contaminated water area controls, more cases were Hispanic, case parents were less educated and were more likely blue-collar, and fathers were younger. No adjustment for potential confounders; possible bias introduced if differential selection between residents in contaminated area and rest of Tucson to cardiologist.	Prevalence rates, odds ratio.	707 families (246 exposed, 461 unexposed).	Population at risk not fully elucidated because did not include cases living in study area who were treated at hospitals outside Tucson area or subjects who moved during the study period. NR if interviewers were blinded. Use of family as a control group provides estimate of the proportion of households that had at one member who worked or resided in the contaminated are, not estimate of exposure prevalence in the birth population.
Lagakos et al. [56]	Maternal exposure during full period of pregnancy to 32 V0Cs detected in 1979 in two drinking water wells, including TCE: 267 μg/L, tetrachloro-ethylene: 21 μg/L, and chloroform: 12 μg/L.	Self-reported congenital malformations[e], including heart defects (ICD–9 425.3, 745.2, 745.4, 745.9, 746.6, 476.9, 747.1, 747.2, 785.2), 1960–1982.	United States. n = 6219 residences with telephones in Woburn, Massachusetts, 1149 refused interview and 60 non-English speaking; 4396 self-reported pregnancies.	Depending on outcome, adjusted for infant sex, maternal smoking during pregnancy, year pregnancy ended, maternal age, prior peri–natal death, prior low birth weight, and/or prior musculoskeletal anomaly.	Odds ratio, Cox proportional hazard.	3.467 pregnancies with infant living >7 days, 177 congenital anomalies, 5 pregnancies with mother receiving water from contaminated wells.	Self-reporting of outcomes, potential recall bias, and lack of exposure data for susceptible periods during pregnancy makes interpretation of results difficult.

Gm = grams; HCl = hydrochloric acid; IQ = interquartile; JEM = job-exposure-matrix; NR = not reported; NYSDOH = New York State Department of Health; RDD = random digit dialing; PCE = tetrachloroethylene; SES = socioeconomic status; TTHM = total trihalomethanes; VOC = voltile organic compounds.

[a] Ruckert et al. [71] also studied childhood leukemia and non-Hodgkin lymphoma.

[b] Forand et al. [29] also studied term low birthweight, pre–term birth, and fetal growth restriction.

[c] Infants with patent ductus arteriosus (ICD-9 747.0) included if birthweight ≥2500 gm.

[d] Bove et al. [9] and Bove [8] also studied low (<2500 gm) and very low birthweight (<1500 gm), small for gestational age, premature births examined but results not reported.

[e] Lagakos et al. [56] also studied perinatal death, low birth weight, and childhood disorders but did not report results.

Table 2
Consideration of Biases, Confounding, and Chance in TCE – Cardiac Defect Epidemiology Studies.

Reference	Selection bias	Information bias, Exposure	Information bias, Outcome	Recall bias	Chance	Confounding
Forand et al. [29] Cohort	Unlikely	Likely, area–level exposure assignment but soil vapor intrusion found throughout the TCE study area	Unlikely, birth defects registry study with medically-verified outcomes	Unlikely	No	Unlikely, adjusted for important maternal risk factors, including prenatal care but not folic acid intake
Yauck et al. [94] Case-control	Unlikely	Likely, area-level exposure assignment; poorly defined exposure surrogate	Unlikely, birth certificate and birth defects registry study	Unlikely	No	Likely, univariate statistical analyses not adjusted for maternal risk factors
Bove et al. [9]; Bove [8] Cohort	Unlikely	Likely, area–level exposure assignment	Unlikely, registry (birth, congenital malformation) study	Unlikely	Yes	Unlikely, univariate statistical analysis; effect estimate from multivariate analysis adjusted for important maternal risk factors, but not folic acid intake, not different by ±15% from univariate
Goldberg et al. [35] Prevalence	Likely. Two of three control groups are inappropriate and sparse details on selection of 3rd control group	Likely, area-level exposure assignment	Unlikely, cases identified from cardiologists files	Likely	No	Unable to assess; study lacks details of statistical analysis
Lagakos et al. [56] Prevalence	Unlikely	Likely, area-level exposure assessment	Likely, self-reported outcomes	Likely	Yes	Unlikely, age, education, race, prenatal care, and parity evaluated as potential confounders

reports from six epidemiological studies that investigated developmental cardiac birth defects in relation to estimated TCE exposure during pregnancy were identified in the literature [71,29,94,8,9,35,56]; five of the seven reports were reviewed in the EPA's 2011 Trichloroethylene Toxicological Review [87]. The publication by Forand et al. [29] analyzed the same study population described in the ATSDR [3,2] reports referenced in U.S. EPA [87]. Bove [8] and Bove et al. [9] report twice on the same study subjects. All of the studies examined outcomes in relation to oral exposures with the exception of the inhalation exposure studies from Forand et al. [29] and Yauck et al. [94]. The epidemiological study summaries and quality assessments are presented in Table 1. Consideration of bias, confounding, and chance are summarized in Table 2.

The studies were of different populations, living in different states, and of different epidemiological designs. Forand et al. [29] is a retrospective cohort study of 1440 live births among New York residents in an area contaminated with TCE via vapor intrusion. Bove [8]/Bove et al. [9] is a cross-sectional study of 80,938 singleton live-born infants and 594 singleton fetal deaths among residents in northern New Jersey receiving TCE in municipal water supplies. A strength of both studies is the use of state records, including State Birth Defects Registries with clinically verified outcomes that reduce information and subject recall bias, and the ability to control for potential confounding factors. Both of the studies observed an elevated relative risk estimate for major cardiac defects: a relative risk of 1.24 (a 50% confidence interval (CI) was reported: 0.75, 1.94) for >10 ppb TCE in municipal drinking water supplies compared to TCE exposure ≤1 ppb in Bove [8]/Bove et al. [9]; and an estimated relative risk of 2.40 (95% CI: 1.00, 5.77) compared to the rest of New York State, excluding New York City in Forand et al. [29]. Both studies report relative risk estimates for specific defects: 1.30 (50% CI: 0.88, 1.87) for ventricular septal defects and exposure to >5 ppb TCE in drinking water compared to <1 ppb (Bove [8]/Bove et al. [9]) and 4.91 (95% CI: 1.58, 15.24) for conotruncal defect in the TCE-contaminated area compared to the rest of New York State, excluding New York City [29]. Yauck et al. [94], a case-control study of 245 cases and 3780 controls, reported that living within 1.32 miles from at least one TCE emissions source in Wisconsin had a strong relative risk estimate of 6.2 (95% CI: 2.6, 14.5) for cardiac defects in infants born to mothers aged 38 years or older after controlling for potential confounding, but no association for cardiac defects was observed among infants of mothers aged less than 38 years (RR = 0.9, 95% CI: 0.6, 1.2). The original case-control study by Goldberg et al. [35] reported that the likelihood of family exposure to the contaminated water area among families with cardiac defects was three times that of exposure among randomly selected families in the same general locality. In a review article that included the Goldberg et al. [35] study, Bove et al. [7] calculated an unadjusted prevalence ratio of cardiac defects among residents of the contaminated area with first-trimester exposure compared with residents in uncontaminated areas of 2.58 (95% CI: 2.0, 3.4). Ruckart et al. [71] reported little detail on cardiac defects in a population exposed to TCE-contaminated water but noted a lower than expected number of conotruncal heart defects—although neither precise counts nor confidence intervals were reported, and the authors did not draw any conclusions concerning TCE exposure and the occurrence of all cardiac defects or conotruncal heart defects. Lagakos et al. [56] reported no association (p = 0.91) between exposure to TCE-contaminated water in Woburn, Massachusetts and a much larger categorical grouping of 'cardiovascular anomalies' which included heart murmurs (15 of 43 anomalies) and only 2 conotruncal heart defects.

Forand et al. [29] and Bove [8]/Bove et al. [9] provide evidence for an association between maternal TCE exposure and cardiac defects. A more mixed pattern of results is seen in three other studies with greater potential for bias and confounding [94,35,56]; however, the results of these studies are not necessarily inconsistent with the association observed by Forand et al. [29] or Bove [8]/Bove et al. [9] because, for the database as a whole, the epidemiological studies are imprecise in estimating effects due to the small number of cardiac defects. Additionally, information bias related

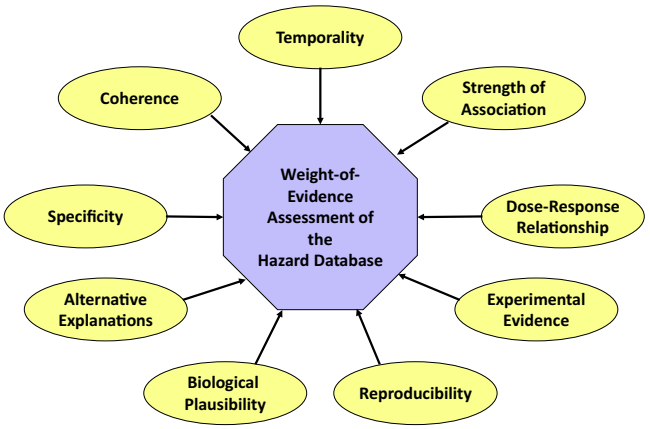

Fig. 1. Conceptual view of a Weight-of-Evidence evaluation. Considerations within a WOE evaluation of toxicity data are shown. The relative weight of each consideration can vary, based upon the data [86], Fig. 4-4). *Temporality* is the premise that the exposure must occur prior to the outcome. *Strength of association* is the consideration of study rigor and statistical power. *Variability analysis* considers the source of variability within individual studies. *Uncertainty analysis* considers information or data gaps in individual studies and in the comprehensive database of information. *Qualitative dose-response relationship* is the change in an effect, and the degree of the change, as a function of exposure or dose. *Experimental evidence* is the alterations in response or rate of response resulting from manipulation of exposure. *Reproducibility* is the observation of specific effects under varied conditions. *Biological plausibility* is the determination of whether an observed outcome could be attributed to the toxicological insult, given the currently known science. *Alternative or multiple explanations* are other explanations for the observed outcome(s) following the exposure of interest. *Specificity* refers to determination of the relationship between one exposure, the effect(s), and whether each effect is mediated through a single or alternative MOAs. *Coherence* is the extent to which the data are similar in outcome and exposure/dose and whether they support each biologically plausible hypothesis or MOA.

to the exposure assessment in these studies may provide alternative explanations for the apparent heterogeneity. As the exposure assessment methods in these studies are at an aggregate level based on locality (rather than based on individual-level measurements), one can assume that the incumbent exposure measurement error (also known as information bias) is non-differential with respect to cardiac defects. That is, any errors in exposure assessment are expected to be independent of case status. Such non-differential misclassification of exposure would typically result in bias towards the null [70] and limit the ability of the studies to detect some associations and possibly exposure-response relationships. None of the studies considered maternal folic acid intake, which may reduce the risk of cardiac defects [45] and is thus a potential confounder. Because TCE has been shown to induce folate deficiency in rats [22] and in workers [36], folate concentrations may be on the direct causal pathway from TCE exposure to cardiac defects. Thus it was methodologically appropriate for these studies not to control for folic acid/folate as that would have induced bias towards the null. Rather, women with low dietary intake of folic acid may represent a susceptible sub-group. Both Forand et al. [29] and Bove [8]/Bove et al. [9] adjust for other maternal risk factors, including adequate prenatal care, as potential confounding factors. Observations in the other studies are more uncertain compared to Forand et al. [29] and Bove [8]/Bove et al. [9], and the observed heterogeneity of results may be due to alternative explanations, such as bias, chance, or potential confounding. Use of hospital cases by Yauck et al. [94] and cases identified from cardiologists' records by Goldberg et al. [35] may introduce possible selection bias. It is difficult to evaluate control for potential confounding in Goldberg et al. [35] due to limited reporting in the publication. The self-reporting of outcome in Lagakos et al. [56] introduces uncertainty because of potential selective reporting.

In summary, epidemiologic data provide some support for the possible relationship between maternal TCE exposure and cardiac birth defects. Forand et al. [29] provide clear evidence of an association between living in an area contaminated by TCE via vapor intrusion and increased risk of conotruncal heart defects, and Bove [8]/Bove et al. [9] provide limited evidence for an association between maternal exposure to TCE, or the combination of TCE and other chlorinated solvents in drinking water, and cardiac defects. However, there are uncertainties in the interpretation of the epidemiological data on Bove [8]/Bove et al. [9] because of the small number of observed TCE-exposed cardiac defect cases, sparse reporting on TCE exposure and congenital heart defects (CHDs) in both publications, and the study's cross-sectional design that could not establish temporality. Two other studies with potential biases also observed elevated risk estimates between TCE exposure and cardiac defects [94,35] and these provide some corroboration of the observations in Forand et al. [29]. The lack of supporting evidence from Ruckart et al. [71] may be a consequence of the small number of reported cases. Additionally, because Lagakos et al. [56] examined a much more broadly defined set of outcomes, their findings are likely much less specific than conotruncal heart defects or even cardiac defects as reported by the other investigators.

The limited finding of an association between TCE exposure and conotruncal heart defects, in particular, and cardiac defects more generally has coherence with the broader epidemiological literature that reports association between maternal occupational exposure to degreasing solvents or to organic solvents and CHDs [11,34,93,83,84]. Although the reported associations between TCE exposure and increased risks of cardiac defects were observed in several studies [29,94,8,9,35], overall, these epidemiologic studies are not sufficient to establish a causal link between TCE exposure and cardiac defects in humans. This conclusion is consistent with other reviews of the epidemiological literature for TCE exposures and CHD [13,90,38]. Additional research could better characterize human exposures and health outcomes.

3.1.2. Toxicological data

The experimental toxicology database for the assessment of developmental cardiac defects resulting from TCE exposure includes in ovo chicken studies, in vitro assays, and rodent studies that assessed fetal morphology following in utero exposures to TCE or its oxidative metabolites. Summaries of studies that assessed cardiac development in mammalian laboratory animal models are presented in Table 3a (inhalation exposure to TCE), Table 3b (oral exposures to TCE), and Table 3c (oral exposures to DCA and TCA). Studies using non-mammalian or in vitro test systems to assess cardiac development following exposures to TCE, DCA, or TCA are summarized in Table 3d. Study strengths and limitations for the mammalian inhalation and oral studies of TCE or its metabolites (DCA or TCA) are summarized in Table 4. Exposure-response arrays for general categories of adverse developmental outcomes (decreased survival, decreased growth, and altered morphological development, including cardiac defects) are presented in Figs. 2–4 for studies with gestational inhalation exposures to TCE, oral exposures to TCE, and oral exposures to DCA and TCA (respectively). Incidence data for specific developmental findings are not presented herein since that information is summarized in the IRIS assessment [87].

3.1.2.1. Inhalation rodent and rabbit TCE studies. Five publications reported the conduct of studies in which TCE was administered by inhalation exposure to rats, using a prenatal developmental toxicity study design [15,42,39,21,74]. The studies by Hardin et al. [39] also included rabbits exposed to TCE, and the study by Schwetz et al. [74] also included mice exposed to TCE. None of these studies reported cardiac defects in fetuses following in utero exposures

Table 3a
Summary of mammalian in vivo toxicity studies assessing cardiac development — inhalation exposures.

Reference	Species/strain/ sex/number	Exposure level/ Duration[a]	NOAEL; LOAEL[b]	Effects
Carney et al. [15]	Rat, Sprague-Dawley, females, 27 dams/group	0, 50, 150, or 600 ppm (600 ppm = 3.2 mg/L)[c] (268.5, 805.5, 3222 mg/m^3) 6 h/d; GDs 6–20	Maternal NOAEL: 150 ppm (805.5 mg/m^3) Maternal LOAEL: 600 ppm (3222 mg/m^3) Developmental NOAEL: 600 ppm (3222 mg/m^3)	↓ Body weight gain (22% less than control) on GDs 6–9 at 600 ppm. No evidence of developmental toxicity, including heart defects.
Dorfmueller et al. [21]	Rat, Long-Evans, females, 30 dams/group	0 or 1800 ± 200 ppm (9674 ± 1075 mg/m^3)[c] 2 wks, 6 h/d, 5 d/wk; prior to mating and/or on GDs 0–20	Maternal NOAEL: 1800 ± 200 ppm (9674 ± 1075 mg/m^3) Developmental LOAEL: 1800 ± 200 ppm (9674 ± 1075 mg/m^3)	No maternal abnormalities. Statistically significant ↑ skeletal and soft tissue anomalies in fetuses from dams exposed during pregnancy only. No statistically significant treatment effects on behavior of offspring 10, 20, or 100 d postpartum. Body weight gains statistically significant ↓ in pups from dams with pre-gestational exposure.
Hardin et al. [39]	Rat, Sprague-Dawley, female, nominal 30/group	0 or 500 ppm (0 or 2685 mg/m^3) 6–7 h/d; GDs 1–19	Maternal NOAEL: 500 ppm (2685 mg/m^3) Developmental NOAEL: 500 ppm (2685 mg/m^3)	No maternal toxicity. No embryonic or fetal toxicity.
	Rabbit, New Zealand white, female, nominal 20/group	0 or 500 ppm (0 or 2685 mg/m^3) 6–7 h/d; GDs 1–24	Maternal NOAEL: 500 ppm (2685 mg/m^3) Developmental LOAEL: 500 ppm (2685 mg/m^3)	No maternal toxicity. Hydrocephaly observed in two fetuses of two litters, considered equivocal evidence of teratogenic potential.
Healy et al. [42]	Rat, Wistar, females, 31–32 dams/group	0 or 100 ppm (0 or 535 mg/m^3) 4 h/d; GDs 8–21	Maternal NOAEL: 100 ppm (535 mg/m^3) Developmental LOAEL: 100 ppm (535 mg/m^3)	No maternal abnormalities. Litters with total resorptions statistically significant ↑. Statistically significant ↓ fetal weight, and ↑ bipartite or absent skeletal ossification centers.
Schwetz et al. [74]	Rat, Sprague-Dawley, female, 20–35/group Mouse, Swiss-Webster, females, 30–40 dams/group	0 or 300 ppm (0 or 1611 mg/m^3) 7 h/d; GDs 6–15	Maternal LOAEL: 300 ppm (1611 mg/m^3) Developmental NOAEL: 300 ppm (1611 mg/m^3) Developmental LOAEL: 150 ppm (805.5 mg/m^3)	4–5% ↓ maternal body weight No embryonic or fetal toxicity; not teratogenic. Specific gravity of brains statistically significant ↓ at PNDs 0, 10, and 20–22. Similar effects at PNDs 20–22 in occipital cortex and cerebellum. No effects at 1 mo of age.

[a] To convert concentrations in air (at 25 °C) from ppm to mg/m^3: mg/m^3 = (ppm) × (molecular weight of the compound)/(24.45). For TCE: 1 ppm = 5.37 mg/m^3. 1000 mg/m^3 = 1 mg/L (air). Source: U.S. EPA, Technology Transfer Network – Air Toxics Web Site, http://www.epa.gov/ttnatw01/hlthef/tri-ethy.html, last accessed 08-06-15.
[b] NOAEL and LOAEL are based upon reported study findings.

to TCE; however, of these, only the Carney et al. [15] and Schwetz et al. [74] provided sufficient study detail to demonstrate that they were conducted in accordance with good laboratory practices and examined the fetuses using specific methods designed to detect abnormalities of cardiac development.

3.1.2.2. Oral rodent TCE studies. Six studies reported the results of oral administration of TCE to rodents during fetal development [51,28,61,62,20,18]. All studies were performed in rats, except Cosby and Dukelow [18] which used mice. In all of these rodent studies, TCE was administered by gavage, with the exception of the Dawson et al. [20] and Johnson et al. [51] studies, in which TCE was administered via drinking water. Only the two drinking water studies detected statistically significant treatment-related fetal cardiac defects.

The gavage studies by Fisher et al. [28], Narotsky et al. [62], and Narotsky and Kavlock [61] were conducted in accordance with good laboratory procedures. While Fisher et al. [28] conducted their cardiac evaluations with the same methods as described in Johnson et al. [51], and the first author of the Johnson et al. [51] paper participated as a member of the cardiac dissection team for the Fisher et al. [28] study, TCE-related cardiac defects were not detected. The studies by Narotsky et al. [62] and Narotsky and Kavlock [61] evaluated neonatal growth and viability, and examined cardiac and other soft tissue morphology only in pups that had died; no cardiac defects were reported. The study by Cosby and Dukelow [18] did not conduct a detailed assessment of cardiac development.

3.1.2.3. Oral rodent metabolite studies. Detailed information on the toxicokinetics of TCE is presented in the IRIS TCE assessment [87,Chap. 3]. Data in humans and rodents indicate that TCE crosses

Table 3b
Summary of mammalian in vivo toxicity studies assessing cardiac development—oral exposures.

Reference	Species/strain/ sex/number	Dose level/exposure duration[a]	Route/vehicle	NOAEL; LOAEL[b]	Effects
Cosby and Dukelow [18]	Mouse, B6D2F1, female, 28–62 dams/group	0, 24, or 240 mg/kg-d GDs 1–5, 6–10, or 11–15	Gavage in corn oil	Maternal NOAEL: 240 mg/kg-d Developmental NOAEL: 240 mg/kg-d	No maternal toxicity. No effects on embryonic or fetal development.
Dawson et al. [20]	Rat, Sprague-Dawley, 116 females allocated to 11 groups	0, 1.5, or 1100 ppm (mg/L) (0, 0.18 or 133 mg/kg-d) 2 mo before mating and/or during gestation	Drinking water	Maternal NOAEL: 1100 ppm (132 mg/kg-d) Developmental LOAEL: 1.5 ppm (0.18 mg/kg-d)	No maternal toxicity. Statistically significant ↑ in heart defects, primarily atrial septal defects, found at both dose levels in groups exposed prior to pregnancy and during pregnancy, as well as in group exposed to 1100 ppm dose during pregnancy only. No statistically significant ↑ in congenital heart defects in groups exposed prior to pregnancy only.
Fisher et al. [28]	Rat, Sprague-Dawley, female, 20–25 dams/group	0 or 500 mg/kg-d GDs 6–15	Gavage in soybean oil	Maternal NOAEL: 500 mg/kg-d Developmental NOAEL: 500 mg/kg-d	No maternal toxicity. No developmental toxicity. The incidence of heart malformations for fetuses from TCE-treated dams (3–5%) did not differ from negative controls. No eye defects observed.
Johnson et al. [51]	Rat, Sprague-Dawley, female, 9–13/group, 55 in control group	0, 2.5, 250, 1.5, or 1100 ppm (0, 0.00045, 0.048, 0.218, or 129 mg/kg-d)[d] GDs 0–22	Drinking water	Developmental NOAEL: 2.5 ppb (0.00045 mg/kg-d) Developmental LOAEL: 250 ppb[b] (0.048 mg/kg-d)	Statistically significant ↑ in percentage of abnormal hearts and the percentage of litters with abnormal hearts at ≥250 ppb.
Narotsky et al. [62]	Rat, F344, females, 8–12 dams/group	0, 10.1, 32, 101, 320, 475, 633, 844, or 1125 mg/kg-d GDs 6–15	Gavage in corn oil	Maternal LOAEL: 475 mg/kg-d	Statistically significant dose-related ↓ dam body weight gain at all dose levels on GDs 6–8 and 6–20. Delayed parturition at ≥475 mg/kg-d; ataxia at ≥633 mg/kg-d; mortality at 1125 mg/kg-d.
				Developmental NOAEL: 32 mg/kg-d Developmental LOAEL: 101 mg/kg-d	↑ full litter resorption and postnatal mortality at ≥425 mg/kg-d. Statistically significant prenatal loss at 1125 mg/kg-d. Pup body weight ↓ (not statistically significant) on PNDs 1 and 6. Statistically significant ↑ in pups with eye defects at 1125 mg/kg-d. Dose-related (not statistically significant) ↑ in pups with eye defects at ≥101 mg/kg-d.
Narotsky and Kavlock [61]	Rat, F344, females, 16–21 dams/group	0, 1125, or 1500 mg/kg-d GDs 6–19	Gavage in corn oil	Maternal LOAEL: 1125 mg/kg-d	Ataxia, ↓ activity, piloerection; dose-related ↓ body weight gain.
				Developmental LOAEL: 1125 mg/kg-d	Statistically significant ↑ full litter resorptions, ↓ live pups/litter; statistically significant ↓ pup body weight on PND 1; statistically significant ↑ incidences of microophthalmia and anophthalmia.

[a] For conversion of drinking water or dietary doses to mg/kg-d when no body weight or compound consumption data were available: mg/L in water x subacute conversion factor (0.121 for female rats, 0.191 for female mice); mg/L in water x subchronic conversion factor (0.093 for female rats, 0.164 for female mice); mg/kg (ppm) in feed x subacute conversion factor (0.117 for female rats, 0.224 for female mice); mg/kg (ppm) in feed x subchronic conversion factor (0.091 for female rats, 0.215 for female mice). For developmental studies, offspring duration of exposure was used; subacute conversion factor was applied unless otherwise noted. Reference: EFSA [25].

[b] NOAEL and LOAEL are based upon reported study findings.

Table 3c
DCA and TCA: Summary of mammalian in vivo toxicity studies assessing cardiac development—oral exposures.

Reference	Species/strain/ sex/number	Dose level/ exposure duration	Route/vehicle	NOAEL; LOAEL[a]	Effects
DCA					
Smith et al. [79]	Rat, Long Evans, female, 19–21 dams/group	A: 0, 14, 140, or 400 mg/kg-d B: 0, 900, 1400, 1900, or 2400 mg/kg-d GDs 6–15	Gavage in water	Maternal LOAEL: 14 mg/kg-d	Increased adjusted liver weight at ≥14 mg/kg-d; decreased body weight gain at ≥140 mg/kg-d; increased spleen and kidney weights at ≥400 mg/kg-d; mortality at ≥1400 mg/kg-day
				Developmental LOAEL: 140 mg/kg-d	Increased soft tissue malformations (primarily cardiovascular, e.g., defects between ascending aorta and right ventricle) at ≥140 mg/kg-d; decreased fetal weight and length at ≥400 mg/kg-d.; increased resorptions and increased orbital anomalies at ≥900 mg/kg-d
Fisher et al. [28]	Rat, Sprague-Dawley, female, 20 dams/group	0 or 300 mg/kg-d GDs 6–15	Gavage in water	Maternal LOAEL: 300 mg/kg-d	Decreased body weight gain
				Developmental LOAEL: 300 mg/kg-d	Decreased fetal weight; no significant difference from control in percent fetuses with cardiovascular malformations; no increased resorptions
Epstein et al. [27]	Rat, Long Evans, female, 7–10 dams/group	0 or 1900 mg/kg-d GDs 6–8, 9–11, or 12–15 0 or 2400 mg/kg-d GDs 10, 11, 12, or 13 0 or 3500 mg/kg-d GDs 9, 10, 11, 12, or 13	Gavage in water	Maternal LOAEL: Not characterized	Not reported
				Developmental LOAEL: 1900 mg/kg-d	Increased interventricular septal defects, membranous type, and high interventricular septal defects; fetal weight and survival data not reported
TCA					
Smith et al. [78]	Rat, Long Evans, female, 20–26 dams/group	0, 330, 800, 1200, or 1800 mg/kg-d GDs 6–15	Gavage in water	Maternal LOAEL: 330 mg/kg-d	Increased spleen and kidney weights; decreased body weight gain at ≥800 mg/kg-day.
				Developmental LOAEL: 330 mg/kg-d	Decreased fetal weight and length; soft tissue malformations (primarily cardiovascular, e.g., interventricular septal defect and levocardia, at incidences ranging from 5.4–95% in treated groups); increased postimplantation loss at ≥800 mg/kg-d; skeletal malformations, mainly orbital anomalies, at 1200 and 1800 mg/kg-day.
Fisher et al. [28]	Rat, Sprague-Dawley, female, 19 dams/group	0 or 300 mg/kg-d GDs 6–15	Gavage in water	Maternal LOAEL: 300 mg/kg-d	Decreased body weight gain
				Developmental LOAEL: 300 mg/kg-d	Decreased fetal weight; no significant difference from control in percent fetuses with cardiovascular malformations; no increased resorptions
Johnson et al. [49]	Rat, Long Evans, female, 55 control, 11 TCA	0 or 2730 ppm (291 mg/kg-d) GDs 1–22	Drinking water	Maternal LOAEL: 291 mg/kg-d	Decreased body weight gain
				Developmental LOAEL: 291 mg/kg-d	Decreased fetal weight; increased resorptions per litter; increased percent fetuses with abnormal hearts (10.5% vs 2.15% in controls)

[a] NOAEL and LOAEL are based upon reported study findings.

the placenta following maternal inhalation exposure. The major route of TCE biotransformation in humans and rodents is CYP-dependent oxidative metabolism. Metabolic saturation occurs at high oral dose levels in rodents (>1000 mg/kg-day), at much higher doses than those used in the Johnson et al. [51] study (i.e., ranging from 0.048 to 129 mg/kg-day). Tissue distribution experiments using various routes of administration produced time-course data of TCE tissue concentrations that were used to develop a PBPK model for all routes of exposure. Both the applied dose and the PBPK-modeled internal dose-metrics of the oxidative metabolites

Table 3d
Summary of non-mammalian and in vitro studies on TCE and metabolites (DCA and TCA) assessing cardiac development.

Reference	Species/strain/ sex/number	Dose level/ exposure duration	Route/vehicle	NOAEL; LOAEL[a]	Effects
Avian In Ovo					
Bross et al. [12]	Chicken, white leghorn, 20–24 embryos/group	TCE: 0, 1, 5, 10, or 25 μmol/egg Single injection on day 1 or 2	In ovo injection in mineral oil	Developmental LOAEL: 1 μmol	Decreased survival at ≥1 μmol; increased edema, light pigment, abnormal beak, club foot, and patchy feathers at ≥1 μmol; evisceration at ≥5 μmol; growth not affected; visceral (including cardiac) development was not assessed
Drake et al. [23]	Chicken, white leghorn, Babcock and Bovan strains, 32–46 embryos/group	TCE: 0, 0.2, 4, or 200 nmol/egg (0, 3, 60, or 3000 nM/egg) Single injections on HH13, HH15, HH17, and HH20; assessed on HH24 and HH30	In ovo injection in saline	Developmental LOAEL: 4 nmol	Decreased survival on HH30, increased proliferative index in outflow tract (OFT) and atrioventricular canal (AVC) cardiac cushion mesenchyme on HH24, increased mean cushion cellularity, and decreased blood flow on HH24 at ≥4 nmol;
		TCA: 0 or 4 nmol/egg (0 or 60 nM/egg) Injections on HH13, HH15, HH17, and HH20; assessed on HH24 and HH30	In ovo injection in saline	Developmental LOAEL: 4 nmol	Decreased survival on HH30, increased proliferative index in OFT and AVC cardiac cushion mesenchyme on HH24, increased mean cushion cellularity on HH24 at ≥4 nmol
Drake et al. [24]	Chicken, white leghorn, Bovan strain, 35–117 embryos/group	TCE and TCA: 0, 0.2, 2, 4, 20, or 200 nmol/egg (0, 3, 30, 60, 300, or 3000 nM/egg) Single injections on HH13, HH15, HH17, and HH20; assessed on HH18, HH21, and HH23	In ovo injection in saline	Developmental NOAEL: 0.2 nmol	No alterations in cardiac development on HH18, HH21, or HH23 were observed, since exposure was during period of cardiac specification rather than during period of valvuloseptal morphogenesis as in Drake et al. [23]
Elovaara et al. [26]	Chicken, white leghorn, SK 12 strain, 9–14 embryos/group	TCE: 0, 5, 25, 50, or 100 μmol/egg Single injection on day 2 or 6	In ovo injection in olive oil	Developmental LOAEL: 5 μmol	Increased malformations (exteriorization of viscera, edema, eye abnormalities, and skeletal abnormalities) in surviving 14- or 15-day embryos at ≥5 μmol; decreased survival, weight, and length at 100 μmol; visceral (including cardiac) development was not assessed
Loeber et al. [57]	Chicken, white leghorn, strain not reported, 91–128 treated embryos/group; 266-7 control embryos/group	TCE: 0, 5, 10, 15, 20, or 25 μM/egg Single injection on day 6, 12, 18, or 23; assessed at HH29, HH 34, or HH44	In ovo injection in saline or mineral oil	Developmental LOAEL: 10 μM	Overall increased cardiac malformations and embryo death in all treated embryos vs. control (categorized as ectomesenchymal tissue migration abnormalities, ECM abnormalities, and cell death abnormalities); increased percent embryos with cardiac malformations at ≥10 μM;
Rufer et al. [72]	Chicken, white leghorn, Hyline strain W36, 35–117 embryos/group	TCE: 0, 0.2, 4, 40, 200, or 2000 nmol/egg (0, 0.4, 8, 80, 400, or 4000 ppb/egg) Single injections on HH13, HH15, HH17, HH20, or HH24; assessed on HH24 and HH30	In ovo injection in saline	Developmental LOAEL: 4 nmol	Decreased survival on HH30 following exposure on HH15 or HH17 at ≥4 nmol; increased incidence of muscular ventricular septal defects (VSD) in embryos treated on HH 17 (related blood flow abnormalities confirmed by Doppler imaging); increased abnormalities of cardiac structure and function noted by echocardiography in HH28 treated embryos (incidence data not provided).

Table 3d (*Continued*)

Reference	Species/strain/ sex/number	Dose level/ exposure duration	Route/vehicle	NOAEL; LOAEL[a]	Effects
Zebra Fish					
Hassoun et al. [41]	Zebrafish (*Danio rerio*), 30 embryos/group	DCA: 0, 4, 8, 16, or 32 mM Exposed from 4 to 144 h post-fertilization (hpf)	Petri dish: 20 mL buffered water, with 60 mg sea salt/L	Developmental LOAEL: 4 mM	Dose-related increased mortality at ≥8 nM on 8–55 hpf; hatching delayed at 55 hpf in ≥8 mM; increased yolk sac edema at ≥8 nM; increased craniofacial (jaw and mouth) abnormalities at 80 hpf: 5% at 4 and 8 mM, 75% at ≥16 mM; skeletal muscle deformation and notochord/muscular lordosis at ≥16 mM by 144 hpf; abnormal feeding behavior at ≥4 mM by 144 hpf; increased heart rate at ≥16 mM at 32, 55, and 80 hpf and decreased heart rate with near cessation of peripheral blood flow at ≥16 mM at 144 hpf; increased superoxide anion and nitric oxide production at ≥4 nM by 80 hpf
Williams et al. [91]	Zebrafish (*Danio rerio*), 30 embryos/group	DCA: 0 or 32 mM (Ellagic acid groups were also conducted but are not described here) Exposed from 4 to 144 h post-fertilization (hpf)	Petri dish: 20 mL buffered water	Developmental LOAEL: 32 mM	At 32 mM: 100% mortality after 144 hpf; hatching rate delayed at 55 hpf; yolk sac and/or cardiac edema at 55–144 hpf; increased craniofacial (jaw and mouth) abnormalities at 80 hpf; skeletal muscle deformation and notochord/muscular lordosis by 144 hpf; abnormal feeding behavior at 144 hpf; increased heart rate at 32 and 55 hpf and decreased heart rate at 80 hpf with near cessation of peripheral blood flow at 144 hpf; increased superoxide anion at 144 hpf and nitric oxide by 55 hpf
In Vitro					
Hunter et al. [44]	Mouse, CD-1, 3–6 somites, 24 control and 10–18 treated embryos/group	DCA: 0,734, 1468, 4403, 4403, 5871, 7339, 11010, or 14680 μM 24 h exposure	Whole embryo culture	Developmental LOAEL: 5871 μM	Increased % malformations and % neural tube defects, decreased mean number of somites at ≥5871 μM; increased pharyngeal arch defects and **heart defects** at ≥7339 μM; increased rotational defects, eye defects, and somite dysmorphology at ≥11010 μM
	Mouse, CD-1, 3–6 somites, 106 control and 10–56 treated embryos/group	TCA: 0, 500, 1000, 2000, 3000, 4000, or 5000 μM 24 h exposure	Whole embryo culture	Developmental LOAEL: 2000 μM	Increased% malformations and% neural tube defects, decreased mean number of somites at ≥2000 μM; increased eye defects and **heart defects** at ≥3000 μM; increased somite dysmorphology at 4000 μM
Mishima et al. [60]	Chicken, white leghorn, strain not reported, HH13-14, 40–104 embryos/group	TCE: 0, 10, 40, or 80 ppm 24 h exposure	Whole embryo culture	Developmental LOAEL: 80 ppm	Decreased mesenchymal cell number in superior and inferior AV cushions at 80 ppm
Saillenfait et al. [73]	Rat, Sprague-Dawley, GD 10 explants, 4–7 somites, 20 embryos/group	TCE: 0, 2.5, 5, 10, 15, or 30 mM 46 h exposure	Whole embryo culture	Developmental LOAEL: 5 mM	Decreased yolk sac diameter, crown-rump length, head length, and% malformed (brain defects and reduction in embryonic axis) at ≥5 mM; increased malformations: bend in embryonic axis, reduction in first brachial arch, otic system defect, defective flexion, absence of hindlimb bud, delayed yolk sac circulation at ≥10 mM; increased eye defects and overall poor and abnormal development at ≥15 mM; no cardiac defects noted.

[a] NOAEL and LOAEL are based upon reported study findings.

Table 4
Study Quality Summary for Toxicology Studies that Assessed TCE Exposure and Developmental Effects.

Reference		Exposure Quality	Test Subjects	Study Design	Endpoints	Data & Statistics	Reporting
In Vivo Mammalian Inhalation Studies							
Carney et al. [15]	Strength	Ambient air control and 3 exposure groups; relevant route of administration and duration of exposure. Information on chemical source provided. Inhalation chamber characterized; dynamic airflow; mean chamber concentrations reported.	Species, strain, source, sex, age/lifestage/BW, reported. Randomly assigned to test groups prior to mating. Adequate sample size (27 litters/group).	GLP, guideline prenatal devtox study. All litters/fetuses evaluated. Fetal examination conducted without knowledge of treatment group.	Relevant maternal and fetal endpoints assessed. Fetal visceral exam used Staples method (examination of internal cardiac morphology) plus free-hand sectioning of head. Skeletal exam evaluated both bone and cartilage development.	Appropriate statistical methods; litter used as unit of statistical analysis.	Summary data for maternal and fetal endpoints reported.
	Limitation	Whole body exposure.					Individual maternal and fetal data NR.
Dorfmueller et al. [21]	Strength	Filtered ambient air control and 3 groups with a single high dose exposure level over various durations; relevant route of administration and duration of exposure. Information on chemical source provided. Inhalation chamber characterized; dynamic airflow; chamber concentrations monitored at 13 min intervals.	Species, strain, source, sex, age/lifestage/BW, reported. Randomly assigned to test groups. Adequate sample size (subset of 15 litters/group assigned to c-section).	Study included groups with exposures and assessments similar to EPA guideline.	Relevant maternal and fetal endpoints assessed. Fetal visceral exam used Wilson technique (free-hand sectioning of fetuses). Skeletal exam evaluated bone development.	Appropriate methods; litter used as unit of statistical analysis.	Summary data for maternal and fetal endpoints reported.
	Limitation	Technical grade solvent containing 99% TCE and 0.2% epichlorhydrin. Whole body exposure.		Information on facility certification NR. Non-random assignment (based upon uterine position) of 8 fetuses/litter to either skeletal or visceral exam; disposition of additional fetuses NR	Fetal visceral exam did not include in situ dissection and examination of cardiac morphology.		Individual maternal and fetal data NR.
Hardin et al. [39]	Strength	Control and 1 exposure group; relevant route of administration and duration of exposure.	Species, strain, sex, reported. Adequate sample size: target was 30 rats or 20 rabbits/group; report indicated difficulties in some studies resulting in 15 rabbits/group.	Study design similar to EPA guideline.	Relevant maternal and fetal endpoints assessed. Fetal visceral exam used Wilson technique (free-hand sectioning of 1/2 to 2/3 fetuses/litter). Skeletal exam evaluated bone development.		
	Limitation	Whole body exposure. Chemical characterization and source NR. Control exposure not characterized. Exposure chamber, conditions, and measurement of concentration NR. Duration of exposure not characterized for TCE.	Maternal source, age/lifestage/BW, and random assignment to test groups NR. Exact sample size NR.	Information on facility certification NR. The report summarized developmental toxicity testing for 9 chemicals including TCE; specific study design details for each test substance were NR.	The exact distribution of fetuses for visceral and skeletal evaluation NR. Random assignment to evaluation procedure NR. Whether Staples dissection method (examination of internal cardiac morphology) was used in the TCE studies was NR.	Statistical methods NR.	Study design details NR. Summary data for maternal and fetal endpoints NR. With the exception of a brain malformation in 2 rabbit fetuses, study findings for TCE were not discussed.

Table 4 (*Continued*)

Reference		Exposure Quality	Test Subjects	Study Design	Endpoints	Data & Statistics	Reporting
Healy et al. [42]	Strength	Ambient air control and 1 exposure group; relevant route of administration and duration of exposure. Information on chemical source provided. Inhalation chamber characterized; dynamic airflow; chamber concentrations monitored continuously.	Species, strain, source, sex, age/lifestage/BW, reported. Randomly assigned to test groups after mating. Adequate sample size (31 control, 32 treated litters).	Study design similar to EPA guideline. All fetuses assessed for external, visceral, and skeletal effects.	Relevant maternal and fetal endpoints assessed. Fetal visceral exam used fresh dissection and examination of internal organs. Skeletal exam evaluated bone development.	Appropriate statistical methods for some outcomes.	Summary data for maternal and fetal endpoints reported.
	Limitation	Whole body exposure. Chamber concentration data NR.		Information on facility certification NR. Exposure duration (4 h/day, GD 8–21) was insufficient in daily duration and did not cover the entire period of organogenesis. No indication that fetuses were examined without knowledge of treatment group.	Fetal visceral examination did not include brain or reproductive organs. Fetal cardiac exam did not include internal morphology.	No indication that litter was used as unit of statistical analysis for fetal anomalies.	Individual maternal and fetal data NR.
Schwetz et al. [74]	Strength	Filtered ambient air control and 1 exposure group; relevant route of administration and duration of exposure. Information on chemical source provided. Inhalation chamber characterized; dynamic airflow; chamber concentrations monitored continuously and mean concentrations reported.	Species, strain, sex, age/lifestage/BW, reported. Adequate sample size (30 control, 18 treated rats; 26 control, 12 treated mice).	Study design similar to EPA guideline. All fetuses assessed for external, visceral, and skeletal effects.	Relevant maternal and fetal endpoints assessed. Fetal visceral exam used Wilson technique (free-hand sectioning of 1/2 fetuses/litter) and skeletal exam evaluated bone development in ½ fetuses/litter. One fetus/litter randomly selected for whole-body sagittal sectioning and microscopic examination.	Appropriate statistical methods; litter used as unit of statistical analysis.	Summary data for some maternal and fetal endpoints reported.
	Limitation	Whole body exposure. 99.2% TCE; 0.76% inhibitors and impurities.	Animal source NR. Random assignment of maternal animals to test groups NR.	Information on facility certification NR. No indication that fetuses were examined without knowledge of treatment group.	Random assignment of fetuses to visceral or skeletal evaluation procedure NR. The use of in situ dissection and examination of cardiac morphology NR.		Maternal BW data NR. Individual maternal and fetal data NR.
In Vivo Mammalian Oral Studies							
Cosby and Dukelow [18]	Strength	Vehicle control and 2 treatment groups; relevant route of administration and duration of exposure. Information on chemical source provided. Formulations mixed immediately prior to dosing; formulation methods enhanced stability; concentration tested. Dose volume = 0.2 mL.	Species, strain, source, sex, age/lifestage/BW, reported. Adequate sample size (7–12 litters/control cohort, 10–12litters/treated cohort).	Study designed to examine effects on reproductive success and offspring birth and postnatal outcome.	Relevant maternal and offspring endpoints assessed. All pups examined. Random selection of litters for PND 43 postmortem evaluation.	Statistical analysis of data conducted.	Summary gestation index and litter size data reported.

	Limitation	Concentration data NR	Females non-randomly assigned to test groups (based on BW) after mating.	Corn oil vehicle. Dose duration (5 daily prenatal doses, initiating at GD 1, 6, or 11) do not cover the entire period of organogenesis. No indication that fetuses were examined without knowledge of treatment group.	Litter size standardization was implemented on PND 1 and 22; no indication of random selection of pups for culling.	Statistical methods not fully characterized. Replicate treatment data sets were pooled for tests of statistical significance. No indication that the litter was used as unit of statistical analysis.	Maternal BW and postmortem data NR. Offspring weight, length, external abnormalities, and postmortem data NR.
Dawson et al. [19]	Strength	Vehicle control and 2 treatment groups per metabolite; relevant duration of exposure. Information on chemical source provided.	Species, strain, source, sex, age/lifestage/BW, reported. Adequate sample size (10–17 dams/group).	Study designed specifically to assess fetal cardiac defects. Detailed fetal cardiac dissection, preservation, and examination methods provided.	Relevant fetal endpoints assessed. Fetal cardiac exam conducted without knowledge of treatment group. Positive cardiac findings were confirmed by unanimous agreement of study authors.		Individual and summary incidences of fetal cardiac defects reported.
	Limitation	Route of administration = intrauterine injection (not relevant to environmental exposures). Surgery was performed on GD 7 pregnant rats to insert osmotic pump. DCA and TCA purity, stability, concentration data NR	No indication of random assignment to test groups.	No information on laboratory certification status. Duration of study conduct NR.	Maternal observations consisted of monitoring for adverse consequences of surgery.	Statistical methods NR although significance was reported.	Fetal BW and length NR; variance for mean implant and resorption data not shown in bar graph; litter incidence of cardiac defects NR.
Dawson et al. [20][a]	Strength	Vehicle control and 2 treatment groups; relevant route of administration and duration of exposure. Information on chemical source provided; stability and concentration tested; formulation methods enhanced stability. Drinking water formulations mixed daily. WC measured daily. Dose calculations based on consumption, concentration, and TCE breakdown rates.	Species, strain, source, sex, age/lifestage/BW, reported. Randomly assigned to test groups after mating.	AAALAC-certified facility. Study designed specifically to assess fetal cardiac defects. Detailed fetal cardiac dissection, preservation, and examination methods provided.	Relevant maternal and fetal endpoints assessed. Fetal cardiac exam conducted without knowledge of treatment group. Positive cardiac findings were confirmed by unanimous agreement of study authors.	Individual fetal cardiac defect data were provided to EPA and analyzed using the litter as unit of statistical analysis.	Maternal endpoints reported for treated groups; individual fetal cardiac defects reported; litter associations for cardiac defects were provided to EPA.

Table 4 (*Continued*)

Reference		Exposure Quality	Test Subjects	Study Design	Endpoints	Data & Statistics	Reporting
	Limitation	Vehicle = tap water (unknown contaminants); possible imprecision in WC values since dams were group housed; TCE purity, stability, concentration data NR	No. of fetuses/group reported, but not number of litters;[b] however, Johnson et al. reported the number of litters in the control (n = 13–15) and TCE groups (n = 9–13).[a]	Study conducted over period of 3 years in 2 cohorts; study dates for control animals overlapped treated groups but were not exactly concurrent.	Fetal evaluation of non-cardiac findings (visceral and skeletal) was not described.	Statistical analysis conducted under contract by study authors did not use litter as unit of statistical analysis.[b]	Maternal FC, WC, clin obs, placental wt, necropsy data NR; fetal BW and length, external and skeletal data, and non-cardiac visceral data NR; variance for mean implant and resorption data NR; cardiac defects were not associated with litter of origin.[b]
Epstein et al. [27]	Strength	3 vehicle control groups and 3 treatment groups per exposure paradigm; relevant route of administration and durations of exposure (designed to identify critical developmental windows for cardiac defects). Information on chemical source provided; purity and stability confirmed; storage procedures enhanced stability.	Species, strain, source, sex, age/lifestage/BW, reported. Randomly assigned to test groups after mating. Adequate sample size (11–17 controls, 7–10 treated/group).	Study designed to identify critical windows of effects on cardiac development.	Relevant maternal and fetal endpoints assessed.	Statistical analysis of data conducted.	Incidence and mean (and %/litter) fetal cardiac data reported.
	Limitation			Information on facility certification NR. Study was conducted in 3 cohorts; dates of study conduct NR.	No indication that offspring were examined without knowledge of treatment group.	No indication if the litter was used as unit of statistical analysis.	Variance NR for mean data. Maternal data NR. Individual and summary implantation, resorption, fetal BW, length, sex, and external evaluation data NR.
Fisher et al. [28]	Strength	2 vehicle controls and 1 treatment group per test substance; relevant route of administration and duration of exposure. Information on chemical source provided; weekly stability and concentration tested; storage procedures enhanced stability. Dose volumes were based on maternal BW.	Species, strain, source, sex, age/lifestage/BW, reported. Randomly assigned to test groups after mating. Adequate sample size (19–25 litters/vehicle control or treated group, 12 litters/positive control group).	AAALAC-certified facility. Study designed specifically to assess fetal cardiac defects. All litters/fetuses evaluated. Fetuses were examined without knowledge of treatment group. Detailed fetal cardiac dissection, preservation, and examination methods provided. Positive control group was included. Cardiac dissection and evaluation team included Dr. Paula Johnson.	Relevant maternal and fetal endpoints assessed. Fetal cardiac exam conducted without knowledge of treatment group. Cardiac evaluation procedures were the same as those used in Dawson et al. [20] and Johnson et al. [51]; hearts were also stained with hematoxylin.	Appropriate statistical methods; litter used as unit of statistical analysis.	Summary data for maternal and fetal endpoints reported.
	Limitation	Stability schedule and data NR. Concentration not tested.					Individual maternal and fetal data NR.

Johnson et al. [49]	Strength	Vehicle control and 1 treatment level for each of 7 metabolites; relevant route of administration and duration of exposure. Administration methods enhanced stability. Drinking water formulations mixed daily. WC measured daily.	Species, strain, source, sex, age/lifestage/BW, reported. Number of dams (litters) reported: (55 controls, 10–20/high dose groups (4); 3–4/low dose groups (3).	AAALAC-certified facility. Study designed specifically to assess fetal cardiac defects. Detailed fetal cardiac dissection, preservation, and examination methods provided.	Relevant maternal and fetal endpoints assessed. Fetal cardiac exam conducted without knowledge of treatment group. Positive cardiac findings were confirmed by unanimous agreement of study authors.	Statistical methods provided. The litter was used as unit of statistical analysis.	Maternal mean WC, BW and uterine data reported; fetal mean resorptions and incidence of cardiac defects reported.
	Limitation	Information on source of test substances NR. WC values were for group housed dams(4/cage); purity, stability, concentration data NR	No indication that dams were randomly assigned to test groups. Control group was a combined cohort.[b]	Study dates for control animals overlapped treated groups but were not all concurrent.[b]	Fetal evaluation of non-cardiac visceral findings was not described.		Fetal BW and length, external data, and non-cardiac visceral data NR; litter incidence of cardiac malformations NR; variance for mean implantation and resorption data NR.
Johnson et al. [51,52]	Strength	Vehicle control and 4 treatment groups; relevant route of administration and duration of exposure. Information on chemical source provided; stability and concentration tested; formulation methods enhanced stability. Drinking water formulations mixed daily. WC measured daily. Dose calculations based on consumption, concentration, and TCE breakdown rates.	Species, strain, source, sex, age/lifestage/BW, reported. Randomly assigned to test groups after mating. Number of fetuses and litters, as well as dates of study conduct, are provided for each control and treated cohort. Control cohorts: n = 6–15); total control n = 55; TCE group cohorts: n = 9–13. Analysis of control cohort data was used to justify combining control cohorts.	AAALAC-certified facility. Study designed specifically to assess fetal cardiac defects. Detailed fetal dissection and cardiac preservation methods. All fetuses examined without knowledge of treatment group. Fetal evaluation methods were consistent across cohorts.	Relevant maternal and fetal endpoints assessed. Fetal cardiac exam conducted without knowledge of treatment group. Positive cardiac findings were confirmed by unanimous agreement of study authors.	Individual fetal cardiac defect data were provided to EPA and analyzed using the litter as unit of statistical analysis.	Individual fetal cardiac defects reported; litter associations for cardiac defects and maternal endpoints for treated groups; were provided to EPA.
	Limitation	TCE purity, stability, concentration NR Data derived from Dawson et al. [20] study were treated with tap water vehicle (unknown contaminants).	Some gaps in concurrency of treated groups and their controls resulted in part from random assignment procedures.	Animals were placed on study in small cohorts. Study conducted over period of 6 years in 5 cohorts; study data from 1994 to 1995 were combined with Dawson et al. [20] gestation-only data from 1989 to 1993 plus control data from metabolite studies conducted from 1992 to 1994. Study dates for control animals overlapped treated groups but were not exactly concurrent.	Fetal evaluation of non-cardiac findings (visceral and skeletal) was not described.	Statistical analysis conducted under contract by study authors did not consider litter effects.[b]	Maternal BW, FC, WC, clin obs, placental wt, necropsy data, resorptions and implantations NR; fetal BW and length, external and skeletal data, and non-cardiac visceral data NR; cardiac defects reported per 100-fetus basis, but not associated with litter of origin.[b]

Table 4 (*Continued*)

Reference		Exposure Quality	Test Subjects	Study Design	Endpoints	Data & Statistics	Reporting
Narotsky et al. [62]	Strength	Vehicle control and 4 treatment groups; relevant route of administration and duration of exposure. Information on chemical source provided; purity reported. Storage methods enhanced stability. Dose volumes based on GD6 BW.	Species, strain, source, sex, age/lifestage/BW, reported. Adequate sample size (8–12 dams/group).	AAALAC-certified facility. Modified Chernoff and Kavlock devtox screening study. Visceral examination of dead pups consisted of Wilson free-hand section of head and dissection of thoracic and abdominal organs.	Relevant maternal and fetal endpoints assessed.	Appropriate statistical methods; litter used as unit of statistical analysis.	Summary data for maternal and fetal endpoints reported.
	Limitation	Stability and concentration analysis NR	Random assignment to test group NR	Protocol did not require visceral or skeletal evaluation of live pups.			Individual maternal and fetal data NR.
Narotsky and Kavlock [61]	Strength	Vehicle control and 2 treatment groups; relevant route of administration and duration of exposure. Information on chemical source provided; purity reported. Storage methods enhanced stability. Dose volumes based on GD6 BW.	Species, strain, source, sex, age/lifestage/BW, reported. Assignment to test group after mating using unbiased procedure to ensure homogenous distribution of BWs. Adequate sample size (21 control, 16–17 treated/group).	AAALAC-certified facility. Modified Chernoff and Kavlock devtox screening study. Visceral examination of dead pups consisted of Wilson free-hand section of head and dissection of thoracic and abdominal organs.	Relevant maternal and fetal endpoints assessed.	Appropriate statistical methods; litter used as unit of statistical analysis.	Summary data for maternal and fetal endpoints reported.
	Limitation	Stability and concentration analysis NR		Protocol did not require visceral or skeletal evaluation of live pups.			Individual maternal and fetal data NR.
Smith et al. [78]	Strength	Vehicle control and 4 treatment groups; relevant route of administration and duration of exposure. Information on chemical source provided; purity, stability and concentration confirmed.	Species, strain, source, sex, age/lifestage/BW, reported. Randomly assigned to test groups. Adequate sample size (26 controls, 20–21 treated/group).	Study design similar to EPA guideline. All fetuses assessed for external findings; 2/3 fetuses assigned to visceral exam, and 1/3 fetuses assigned to skeletal exam (bone and cartilage).	Relevant maternal and fetal endpoints assessed.	Statistical analysis of data conducted.	Maternal BW, uterine, and organ weight data reported. Mean (±SD) fetal weight, length, and malformations reported; fetal malformation incidence data reported.
	Limitation	Stability and concentration data NR		Information on facility certification NR. No indication whether fetuses were randomly assigned to visceral or skeletal evaluation.	No indication that offspring were examined without knowledge of treatment group.	No indication if the litter was used as unit of statistical analysis.	Individual maternal and fetal data NR.
Smith et al. [79]	Strength	Vehicle control and 7 treatment groups; relevant route of administration and duration of exposure. Information on chemical source provided; purity, stability and concentration confirmed.	Species, strain, source, sex, age/lifestage/BW, reported. Randomly assigned to test groups. Adequate sample size (20 controls, 19–21 treated/group).	Study design similar to EPA guideline. All fetuses assessed for external findings; 2/3 fetuses assigned to visceral exam, and 1/3 fetuses assigned to skeletal exam (bone and cartilage).	Relevant maternal and fetal endpoints assessed.	Statistical analysis of data conducted.	Maternal BW and uterine data reported. Mean (±SD) fetal weight, length, and malformations reported; fetal malformation incidence data reported.
	Limitation	Stability and concentration data NR		Information on facility certification NR. No information provided regarding whether fetuses were randomly assigned to visceral or skeletal evaluation.	No indication that offspring were examined without knowledge of treatment group.	No indication if the litter was used as unit of statistical analysis.	Individual maternal and fetal data NR.

NR = Not Reported; BW = body weight; FC = food consumption; WC = water consumption.

[a] For Dawson et al. [20] and Johnson et al. [49], a number of study details were also provided in Johnson et al. [51,53,52]; Johnson [47].

[b] Additional information and/or data provided to EPA mitigated the limitations or uncertainties identified in the study report.

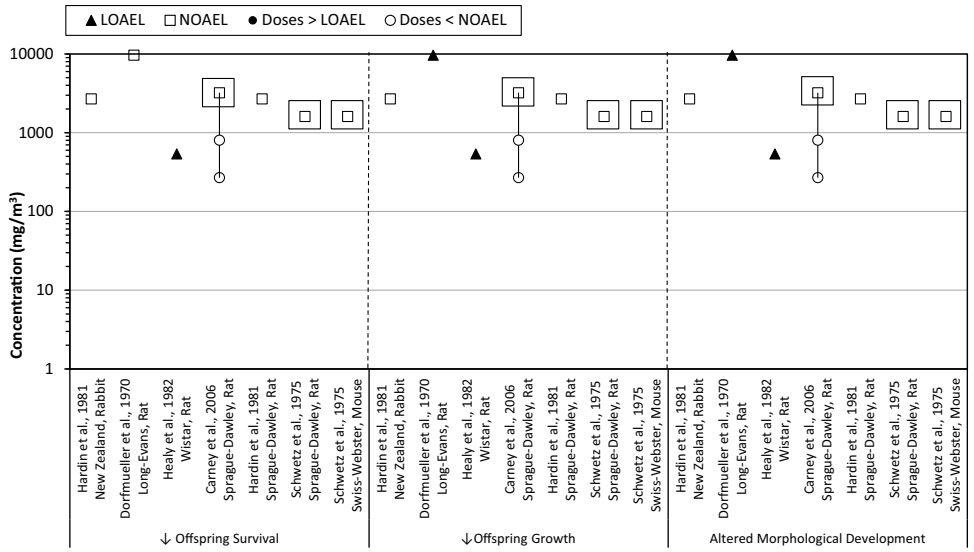

Fig. 2. TCE inhalation developmental toxicology studies. Effects on fetal/offspring survival, growth, and morphology following maternal inhalation exposures to TCE during gestation. Boxes indicate the doses at which maternal toxicity was observed.

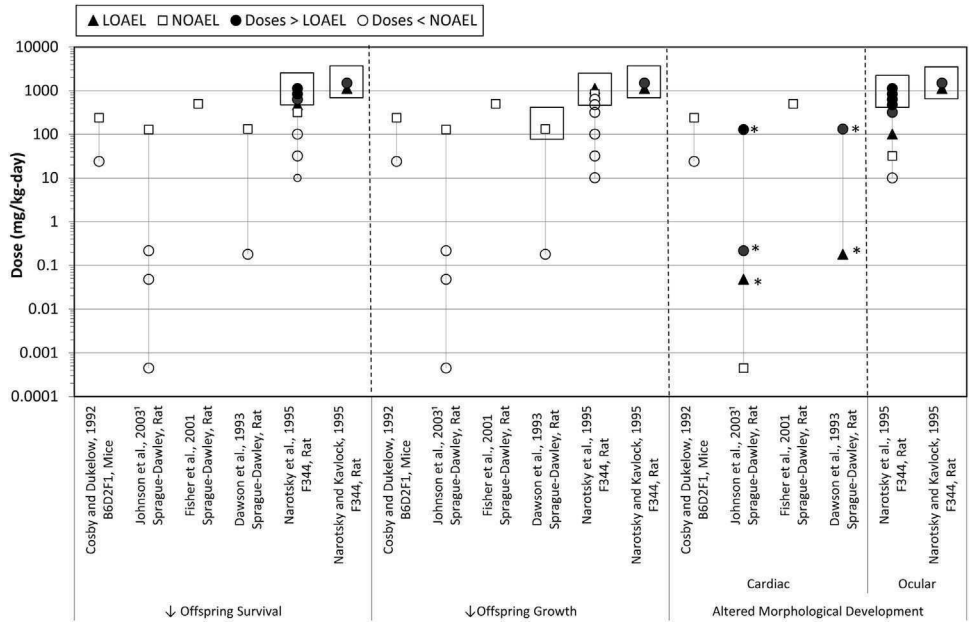

Fig. 3. TCE oral developmental toxicology studies. Effects on fetal/offspring survival, growth, and morphology following maternal oral exposures to TCE during gestation. Boxes indicate the doses at which maternal toxicity was observed. [1] Maternal toxicity was not reported in Johnson et al. [51]. * Doses at which cardiac defects were observed.

relevant to cardiac defects are presented in the TCE IRIS assessment [87], Tables 5–18).

Several studies were conducted in rats to examine the effects of developmental exposures to the TCE oxidative metabolites, DCA and TCA. Studies by Smith et al. [79] and Epstein et al. [27] observed cardiac defects following gavage administration of DCA during pregnancy. Smith et al. [78] and Johnson et al. [49] reported cardiac defects with TCA exposures administered during gestation via gavage or drinking water, respectively. However, a study by Fisher et al. [28] did not detect cardiac defects following gavage administration of DCA or TCA on GD 6–15. All of these studies used dissection methods that were designed to visualize the internal structures of the fetal heart. Other TCE metabolites were evaluated by Johnson et al. [49] and found not to elicit cardiac malformations following developmental exposures (i.e., carboxymethyl cysteine, dichloroacetaldehyde, dichloroethylene, dichlorovinyl cysteine, monochloroacetic acid, trichloroacetaldehyde, and trichloroethanol). Although the proximate toxicant which causes cardiac defects has not been identified, a recent study [6] identified 5-(1,2-dichlorovinyl)-L-cysteine as a key metabolite in placental effects of TCE, suggesting that further consideration of TCE metabolites may be warranted.

3.1.2.4. In ovo avian studies. Several studies examined cardiac development following in ovo administration of TCE to chicken embryos [72,24,23,57]. Abnormalities of cardiac structure and/or function were observed in each of these studies, at doses as low as 2–8 ppb. Defects in valvulo-septal development were similar to those that have been observed in rodents and humans, which is coherent given that early stages of cardiac development are similar across species [63].

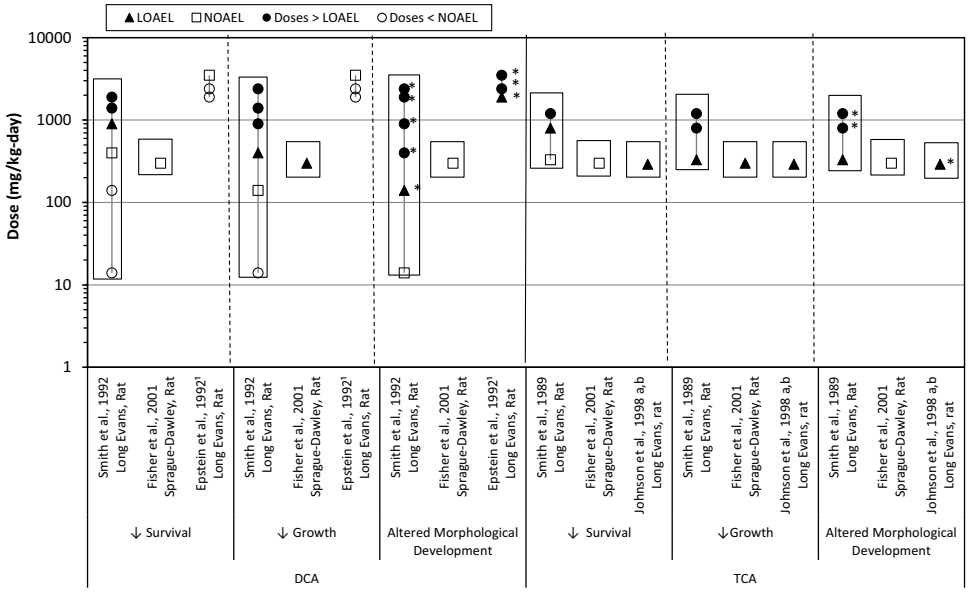

Fig. 4. DCA and TCA oral developmental toxicology studies. Effects on fetal/offspring survival, growth, and morphology following maternal oral exposures to TCE metabolites, DCA and TCA, during gestation. Boxes indicate the doses at which maternal toxicity was observed. [1]Maternal toxicity was not reported in Epstein et al. [27]. *Doses at which cardiac defects were observed.

3.1.2.5. In vitro assays. Whole embryo culture studies that examined cardiac development were conducted by Hunter et al. [44] using 3–6 somite mouse embryos exposed to DCA or TCA and by Mishima et al. [60] using HH 13-14 chicken embryos exposed to TCE. Dose-related alterations in cardiac development were observed in both of these models, although at high (not environmentally relevant) doses.

3.1.2.6. Evaluation of cardiac defects in the animal toxicology studies. As described, alterations in fetal cardiac development have been observed in rodent studies following in utero exposure to TCE and its oxidative metabolites. These findings are supported by the detection of cardiac anomalies in chicken embryos exposed to TCE in ovo, and in whole embryo cultures (mouse and chicken) of TCE and/or its metabolites. In spite of the concordant evidence that TCE has been associated with cardiac defects, controversy centers on the studies by Johnson et al. [51] and Dawson et al. [20], especially with respect to the study design and methods, reporting inadequacies, dose-response characteristics, and the lack of cardiac defect findings in other laboratory studies in rodents following gavage or inhalation exposures of TCE during development.

The Johnson et al. [51] publication reported the results of TCE drinking water exposures on fetal cardiac development in Sprague-Dawley rats from a 6-year-long academic research program. It included data on two TCE treatment groups studied in 1989–1991 that had previously been published by Dawson et al. [20], plus the data from two lower dose TCE treatment groups studied in 1994–1995. Cardiac malformation incidence data were compared between treated groups and combined control data from cohorts studied concurrent to treated groups over the course of the 6-year research program, including controls from studies on TCE metabolites, published in Johnson et al. [49]. Other information on the TCE studies reported in Johnson et al. [51] included published communications [40,50], errata [53,52], and individual cardiac malformation findings and evaluation methods provided to EPA by the primary study author (Dr. Paula Johnson, personal communications [47,48]). The Johnson et al. [51] paper summarized the combined results from the studies that administered TCE to pregnant rats at doses of 2.5 ppb, 250 ppb, 1.5 ppm, and 1100 ppm in drinking water throughout gestation. Fetal cardiac defects, primarily valvular and septal anomalies, were observed at ≥250 ppb.

The limitations and strengths of the toxicological studies were identified (details provided in Table 4). Limitations identified in the evaluation of the Johnson et al. [51] and Dawson et al. [20] studies presented here are consistent with the study design and reporting issues identified in the IRIS assessment [87], peer-reviewed publications such as Hardin et al. [38] and Watson et al. [90], and public comments submitted to the U.S. EPA [1]. The corresponding author for Johnson et al. [51] provided clarification on a number of topics and a detailed description of study methods beyond what had been previously published, including verification that concurrent controls were used for each of the treated groups (Fig. 5), information on fetal randomization and blinded cardiac evaluation procedures, and details of animal husbandry (Dr. Paula Johnson, personal communication, 2014). Subsequent to these discussions, the study author published an errata [53] to update the public record regarding methodological issues for Johnson et al. [51]. This information served to increase confidence in the study conduct and results. However, some study reporting and methodological details remain unknown, e.g., the precise dates that each individual control animal was on study, maternal body weight/food consumption and clinical observation data, and the detailed results of analytical chemistry testing for dose concentration. Additional possible sources of uncertainty identified for these studies include that the research was conducted over a 6-year period, that combined control data were used for comparison to treated groups, and that exposure characterization may be imprecise because tap (rather than distilled) drinking water was used in the Dawson et al. [20] study and because TCE intake values were derived from water consumption measures of group-housed animals. On the other hand, the strengths of this study include the examination of fetal hearts without knowledge of treatment (or control) group, standardized methods of fetal evaluation, examination of the gross (in situ) and internal structure of the fetal hearts by a group of three senior researchers/co-authors (P. Johnson, B. Dawson, and S. Goldberg), confirmation of cardiac anomalies by consensus agreement. In addition, individual fetal and litter cardiac abnormality data for treated groups were shared with EPA (Dr. Paula Johnson, personal

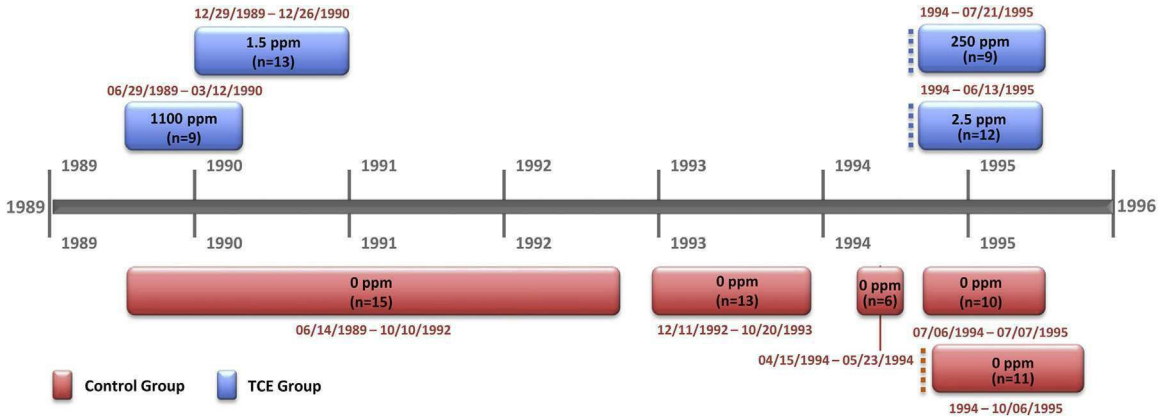

Fig. 5. Control vs. TCE treatment groups and dates of exposure. During the duration of the University of Arizona (UA) research program on TCE (1989–1995), a number of developmental toxicology studies were conducted on TCE and its metabolites. Control animals (red blocks) were on study when treated animals (blue blocks) were being exposed. The blocks are general representations of time frames and are not presented to exact scale. The dates that cohorts of animals were on study (as well as dose levels and the number of dams/litters for each cohort) are shown. In three cases, information on the exact month and day of animal receipt was not available (indicated by dotted lines). Exclusively pregnancy-only TCE-treated groups are included in this figure; however, other treatment regimens were also being conducted during the time period of 6/12/89 to 10/6/95 (i.e., 3 months pre-pregnancy-only, 2 months pre-pregnancy + pregnancy). Additionally, during this time period, TCE metabolites and other toxicokinetically related chemicals were studied: dichloroacetic acid (DCA), trichloroacetic acid (TCA), monochloroacetic acid (MCAA), trichloroethanol (TCEth), trichloroacetaldehyde (TCAld), dichloroacetaldehyde (DCAld), carboxy methylcystine (CMC), dichlorovinyl cystine (DCVC), dichloroethylene (DCE). The control animal cardiac malformation incidence data were combined for statistical comparison with incidence data for pregnancy-only TCE-treated groups. Sources of information used to compile this figure: [53,52,50,51,49,20].

communication (2008)), thereby facilitating independent statistical analysis of the data.

Inconsistencies in the results of studies that assessed cardiac development in rodents have been raised as an issue of particular concern. In the case of a number of these studies [61,62,18,42,39,21,74], a variety of animal species and strains, sources, and testing protocols were used (summarized in Table 5a), which precludes direct comparisons. For several of the older studies, information that would allow a valid comparison with the Johnson et al. [51] and Dawson et al. [20] studies is not reported. For example, detailed procedural details regarding fetal evaluation were not provided for Schwetz et al. [74], Dorfmueller et al. [21], Healy et al. [42], and Hardin et al. [39]. There is no indication whether fetuses were selected randomly for visceral evaluation, or whether they were examined without knowledge of treatment group (blinded assessment). Fetal cardiac evaluation methods were not elucidated in any detail, and the performance of fresh dissection of the heart to evaluate internal cardiac morphology was not mentioned. Hardin et al. [39] reported virtually no methodological information. In some studies, differences in overall study design limited meaningful cross-study comparison, e.g., due to limited exposure durations [18] or the evaluation of delivered PND 1 pups instead of fetuses [61,62]. The studies reported by Fisher et al. [28] and Carney et al. [15] were well-conducted developmental toxicity studies in rats and utilized procedures that facilitated evaluation of fetal cardiac morphology. Fisher et al. [28] and Carney et al. [15] did not observe treatment-related cardiac defects following TCE gavage or inhalation exposures, respectively, during gestation. Detailed examination of the study protocols (summarized in Table 5b) identified several variations in study design and conduct, including but not limited to differences in route of administration, and these differences may have contributed to the different study outcome as compared to Johnson et al. [51] and Dawson et al. [20]. In the case of the Fisher et al. [28] study, as previously noted, care was taken to follow the Johnson et al. [51] fetal evaluation procedures as closely as possible, yet a number of other differences in study design and conduct remained. For example, the source of the animals, the route of exposure, the vehicle/control substance, fetal cardiac tissue preservation methods, and some fetal cardiac evaluation procedures were different. A comparison of typical cardiac evaluation techniques used in developmental toxicology studies, illustrating some potential differences in resolution of abnormalities in the fetal heart, is presented in Table 6. This includes the procedures used by Carney et al. [15] and the procedures used by Dawson et al. [20], Johnson et al. [49], and Johnson et al. [51], as well as by Fisher et al. [28]. One possibility is that the procedural differences in fetal cardiac evaluation techniques could have contributed to differences in study outcome [90]. However, that explanation is not supported by two facts. First, the detailed description of the cardiac dissection and evaluation techniques (as reported in Dawson et al. [20] is sufficiently comparable to the procedures used by Carney et al. [15] (summarized in Table 6) to have facilitated visualization of overt cardiac malformations such as septal defects. Secondly, Fisher et al. [28] used the same cardiac evaluation techniques reported by Dawson et al. [20], Johnson et al. [49], and Johnson et al. [51], evaluated fetuses collaboratively with Dr. Johnson, and yet did not detect treatment-related incidences of cardiac defects.

In summary, Johnson et al. [51] and Dawson et al. [20] observed cardiac defects in fetal rats after gestational drinking water exposures to TCE. These findings have not been confirmed in studies with exposures to TCE during gestation that were conducted by other laboratories. However, none of the other studies have repeated precisely the same study design used by Johnson et al. [51] and Dawson et al. [20]. Differences in study methods such as the route of exposure, vehicle, source or strain of animals, or other unknown factors may have contributed to differences in the detection of cardiac malformations, and at this point in time, it would be impossible to identify the specific reason. Designing and conducting an exact replica of the Johnson et al. [51] study might be very difficult, if not impossible. For example, it is possible that the study animals used by Dawson et al. [19] and Johnson et al. [51] in the University of Arizona (UA) research program on TCE in drinking water may have been particularly susceptible to perturbation of cardiac development by TCE and its metabolites. The possibility of genetic drift in the strain/source of rats over the past 10–20 years might preclude designing and conducting a study with comparable results. Yet, such a susceptibility in the animal models used by Dawson et al. [20] and Johnson et al. [51] might have rendered those studies more (or less) predictive of responses in susceptible individuals in the human population, a difficult assumption to validate. In humans, cardiovascular malformations are common birth defects with both

Table 5a
Comparison of Methods Reported for Prenatal Developmental Toxicity Studies with TCE.

	Schwetz et al. [74]		Dorfmueller et al. [21]	Hardin et al. [39]		Healy et al. [42]	Cosby and Dukelow [18]	Narotsky and Kavlock [61]	Narotsky et al. [62]
Study Description/Objective									
Guideline-type [GT] or research [R] protocol	GT	GT	R	GT	GT	GT	R	R	R
Test Subjects									
Species	Rat	Mouse	Rat	Rat	Rabbit	Rat	Mouse	Rat	Rat
Strain	SD	SW	LE	WIS or SD	NZW	WIS	B6D2F1	Fischer 344	Fischer 344
Source (company)	NR	NR	CRL	NR	NR	NR	Jackson	Harlan	Harlan
Source (location)	NR	NR	NR	NR	NR	NR	Bar Harbor, ME	Indianapolis, IN	Indianapolis, IN
Dates of study conduct	NR	NR	NR	NR	NR	NR	NR	NR	NR
Day of mating confirmation (GD 0 or GD 1)	GD 0	GD 0	GD 1	NR	NR	NR	GD 1	GD 0	GD 0
Day of cesarean section	GD 21	GD 18	GD 21	GD 21	GD 30	GD 21	Delivered	Delivered	Delivered
Treatment									
Test Substance	TCE	TCE	TCE	TCE	TCE	TCE (Trilene)	TCE	TCE	TCE
Source	Dow	Dow	Dow	NR	NR	ICI	Aldrich	Aldrich	Aldrich
Purity (%)	99.24%	99.24%	99%	NR	NR	NR	NR	> 99%	> 99%
Route of administration	Inhalation a	Inhalation a	Inhalation a	Inhalation b	Inhalation b	Inhalation a	Gavage	Gavage	Gavage
Negative control (vehicle)	Filtered room air	Filtered room air	Filtered air	Air	Air	Ambient air	Corn oil	Corn oil	Corn oil
Positive control	N	N	N	N	N	N	N	N	N
No. of treated groups	1	1	1	1	1	1	2	2	4
Group size (litters/group)	30, 18	26, 12	8–12	(30)	(20)	31–32	(30)	16–21	8–12
Random assignment of test subjects to groups	NR	NR	Y	NR	NR	NR	NR	Y	NR
Dose period (duration)	GD 6–15	GD 6–15	GD 1–20	GD 1–19	GD 1–24	GD 8–21	GD 1–5, 6–10, or 11–15	GD 6–19	GD 6–15
Daily dosing schedule	7 h/day, 7 days/wk	7 h/day, 7 days/wk	6 h/day, 7 days/wk	6–7 h/day, 7 days/wk	6–7 h/day, 7 days/wk	4 h/day, days/wk NR	1x/day	1x/day	1x/day
Maternal evaluation									
In-life data (BW, FC, WC, and/or clinobs)	Y	Y	Y	NR	NR	Y	Y	Y	Y
Postmortem data (necropsy, organ wts, pathology, and/or CL)	Y	Y	Y	Y	Y	Y	Y	N	N
Fetal evaluation									
Implantations and resorptions (early and late)	Y	Y	Y	NR	NR	Y	N	N	N
Fetal weight, length, sex	Y	Y	Y	NR	NR	Y	Y (PND 1)	Y (PND 1)	Y (PND 1)
External fetal exam	Y	Y	Y	NR	NR	Y	Y (PND 1)	Y (PND 1)	Y (PND 1)
Percent fetuses (litters) evaluated for external findings	100 (100)	100 (100)	100 (100)	NR	NR	100 (100)	100 (100)	100 (100)	100 (100)
Visceral examination	Y	Y	Y	NR	Y c	Y	N	Y d	Y d
Percent fetuses (litters) evaluated for visceral findings	50 (100)	50 (100)	~33 (100) e	NR	NR	100 (100)	NA	NR (NR)	NR (NR)
Fresh dissection (in situ organ examination)	N	N	N	NR	NR	Y	N	N	Y f
Wilson exam (Bouins fixation, free-hand sections)	Y	Y	Y	NR	NR	N	N	Y	Y
Fetal cardiac examination methods	NR	NR	NR	NR	NR	NR	N	N	N
Fresh dissection and evaluation	NR	NR	NR	NR	NR	NR	N	N	N
Free-hand section of decalcified fetuses	Wilson	Wilson	Wilson	NR	NR	NR	N	Wilson d	Wilson d
Preservation	Bouin's immersion	Bouin's immersion	Bouin's immersion	NR	NR	NR	N	Bodian's immersion	Bodian's immersion
Confirmation of findings	NR	NR	NR	NR	NR	NR	N	N	N
Skeletal examination	Y	Y	Y	NR	NR	Y	N	N	N
Percent fetuses (litters) evaluated for skeletal findings	50 (100)	50 (100)	~33 (100) e	NR	NR	100 (100)	NA	NA	NA
Bone development	Y	Y	Y	NR	NR	Y	N	N	N
Cartilage development	N	N	N	NR	NR	N	N	N	N
Random selection of fetuses for visceral or skeletal evaluation	NR	NR	N	NR	NR	NA	N	N	N
Assessment of fetuses without knowledge of treatment group	NR	NR	NR	NR	NR	NR	N	N	N

This table only includes mammalian studies with prenatal TCE exposures and an evaluation of fetal morphology.
NR = not reported; NA = not applicable; Y = yes, N = No; DW = drinking water; GD = gestation day; PND = postnatal day; RA = retanoic acid; GLA = gluteraldehyde.
Test subject strain: SD = Sprague-Dawley, LE = Long Evans, WIS = Wistar, NZW = New Zealand White, SW = Swiss Webster.
Test subject Source: CRL = Charles River Laboratories, Jackson = Jackson Laboratories, Harlan = Harlan Laboratories.
Group sizes are range of actual group size (i.e., no. of dams) on study; numbers in parentheses () indicate target group size.
a = Whole-body exposure, dynamic air flow, analytical chamber concentrations.
b = Whole-body exposure, inadequately characterized.
c = Visceral examination was NR; however, brain malformations in TCE-treated rabbit fetuses were discussed.
d = Visceral examination of dead pups only; free-hand (Wilson's) sectioning of head only.
e = Four fetuses/litter were assigned to visceral examination and 4 fetuses/litter were assigned to skeletal examination. (33% is an estimate based upon the presumption of 12 fetuses/litter.)
f = Visceral evaluation of affected (i.e., abnormal) pups only.
Cardiac evaluation references: Staples exam: Stuckhardt and Poppe [82], Staples [80], Wilson [92]; University of AZ exam: Johnson et al. [51], Dawson et al. [20].

Table 5b
Comparison of Methods Reported for Prenatal Developmental Toxicity Studies with TCE.

	Dawson et al. [20]	Johnson et al. [51]	Fisher et al. [28]	Carney et al. [15]
Study Description/Objective				
GLP; guideline [G], or research [R] protocol	R	R	R	GLP, G
Test Subjects				
Species	Rat	Rat	Rat	Rat
Strain	SD	SD	SD	SD
Source (company)	Harlan	Harlan	CRL	CRL
Source (location	Indianapolis, IN	Indianapolis, IN	Raleigh, NC	Portage, MI
Dates of study conduct	1989–1990	1989–1995	NR	NR
Day of mating confirmation (GD 0 or GD 1)	NR	NR	GD 0	GD 0
Day of cesarean section	GD 22	GD 22	GD 21	GD 21
Treatment				
Test Substance	TCE	TCE	TCE	TCE
Source	Aldrich	Aldrich	Aldrich	Dow
Purity (%)	NR	NR	NR	99%
Route of administration	DW	DW	Gavage	Inhalation a
Negative control (vehicle)	Tap water	Distilled water	Soybean oil	Ambient air
Positive control	N	N	RA	N
No. of treated groups	2	4	1	3
Group size (litters/group)	9–15	9–12	19–25	27
Random assignment of test subjects to groups	Y	Y	Y	Y
Dose period (duration, gestation-only groups)	GD 1–22	GD 1–22	GD 6–15	GD 6–20
Daily dosing schedule	Ad libitum, 24 h/day	Ad libitum, 24 h/day	1x/day	6 h/day, 7 days/wk
Maternal evaluation				
In-life data (BW, FC, WC, and/or clinobs)	Y	Y	Y	Y
Postmortem data (necropsy, organ wts, pathology, and/or CL)	Y	Y	Y	Y
Fetal evaluation				
Implantations and resorptions (early and late)	Y	Y	Y	Y
Fetal weight, length, sex	Y	Y	Y	Y
External fetal exam	Y	Y	Y	Y
Percent fetuses (litters) evaluated for external findings	100 (100)	100 (100)	100 (100)	100 (100)
Visceral examination	Y	Y	Y	Y
Percent fetuses (litters) evaluated for visceral findings	100 (100)	100 (100)	100 (100)	50 (100)
Fresh dissection (in situ organ examination)	Y (heart)	Y (heart)	Y (heart)	Y (viscera)
Wilson exam (Bouins fixation, free-hand sections)	N	N	N	Y (head)
Fetal cardiac examination methods	Y	Y	Y	Y
Fresh dissection and evaluation	UA method	UA method	UA method	Staples exam
Free-hand section of decalcified fetuses	N	N	N	N
Preservation	GLA flush & immersion	GLA flush & immersion	formalin immersion	NR
Confirmation of findings	Y b	Y b	NR	NR
Skeletal examination	NR	NR	NR	Y
Percent fetuses (litters) evaluated for skeletal findings	NR	NR	NR	50 (100)
Bone development	NR	NR	NR	Y
Cartilage development	NR	NR	NR	Y
Random selection of fetuses for visceral or skeletal evaluation	NA	NA	NA	NA
Assessment of fetuses without knowledge of treatment group	Y	Y	Y	Y

This table only includes mammalian studies with prenatal TCE exposures and an evaluation of fetal morphology.
NR = not reported; NA = not applicable; Y = yes, N = No; DW = drinking water; GD = gestation day; RA = retanoic acid; GLA = gluteraldehyde; UA = University of Arizona.
Test subject strain: SD = Sprague-Dawley.
Test subject Source: CRL = Charles River Laboratories; Harlan = Harlan Laboratories.
Group sizes are range of actual group size (i.e., no. of dams) on study; numbers in parentheses () indicate target group size.
a = Whole-body exposure, dynamic air flow, analytical chamber concentrations.
b = Unanimous agreement of cardiac diagnoses by study investigators (a pathologist, a pediatric cardiologist, and a veterinarian) was required before a positive cardiac finding was diagnosed and recorded.
Cardiac evaluation references: Staples exam: Stuckhardt and Poppe [82], Staples [80]; University of AZ exam: Johnson et al. [51], Dawson et al. [20].

genetic predisposition and environmental exposures contributing to the multifactorial etiology [68].

3.1.3. Mechanistic data on developmental pathways and processes

Mechanistic mode-of-action data were discussed in the 2011 IRIS assessment [87] and provided one line of evidence regarding the potential for TCE to cause cardiac defects. There was not an explicit linkage to the developmental pathways and processes driving CHD in general or valvulo-septal defects in particular. To expand upon and refine this discussion, a preliminary conceptual model based on an Adverse Outcome Pathway (AOP) framework for CHD would be useful. Although such AOP elucidation is beyond the scope of the present review, data identified in the systematic literature search and MGI database search provides motivation for that future activity. Information upon which a preliminary AOP construct is based supports the biological plausibility that TCE exposures during development could lead to disruption of key processes in the development of cardiac valves and septa.

The most commonly reported cardiac defects associated with gestational exposures to TCE and its metabolites TCA and DCA in humans, rats, and chickens were valvulo-septal defects (atrial septal defects [ASDs], muscular and membranous ventricular septal defects [VSDs]) and pulmonary and aortic stenosis [16,29,94,51,49,8,9,20,19,35,57]. In particular, the period of valvulo-septal morphogenesis defines a window of TCE vulnerability in avian systems; thus an AOP anchored to this dysmorphology could identify relevant key events and key event relationships fol-

Table 6
Comparison of cardiac evaluation methods.

Method	Reference	Description
Wilson	Wilson [92]	• Immersion fixation of whole fetus in Bouin's solution • Free-hand serial sectioning of fetuses (approximately 2 mm thickness), including sections through the heart and great vessels
Staples	Staples [80]; Stuckhardt and Poppe [82]	• Dissection of unfixed decapitated or anesthetized fetus • Examination of external structure of the heart and great vessels • Examination in situ of internal structure of the heart via two cuts: ○ Incision made beginning to the right of the ventral midline surface of the heart at the apex and extending anteriorly and ventrally into the pulmonary artery (exposing the tricuspid valve between the right atrium and right ventricle and the 3 cusps of the semilunar valve of the pulmonary artery); the interventricular septum examined for defects. ○ Incision made starting to the left of the ventral midline surface at the apex and extending thorough the left ventricle into the ascending aorta (exposing the bicuspid valve between the left atrium and left ventricle and the 3 cusps of the semilunar valves of the aorta).
University of AZ	Dawson et al. [20]; Johnson et al. [51]	• Examination of the great vessels in situ, including pulmonary venous attachment to the left atrium and cranial and caudal vena caval connections to the right atrium • Removal of the heart from the thorax; the heart is flushed and then immersion fixed with 2% gluteraldehyde • Dissection of unfixed fetus • Examination of external structure of the heart from dorsal and ventral aspects • Examination of internal structure of the heart and vessels: ○ Right atrial appendage excised to evaluate the atrial septum for defects (left atrial appendage removed if the atrial septum is not adequately visualized) ○ Aorta and pulmonary vessels evaluated for course, caliber, and orientation, then excised at valve rings ○ All remaining atrial tissue removed to expose pulmonary, aortic, tricuspid, and mitral valves; location of coronary ostium noted; each valve probed for patency, and formation of each valve leaflet examined. ○ Incision made ventrally through the tricuspid valve to the apex of the heart. Another incision made through the pulmonary valve toward the apex of the heart and joining the cut made through the tricuspid valve. Incision made from each edge of the mitral valve toward the apex, and the left ventricular free wall removed (allowing complete visualization of the ventricular septum for evaluation of defects).

lowing exposure to TCE during the vulnerable period. In normal cardiac development, valvulo-septal morphogenesis is driven by mesenchymal cells in the regions of the atrioventricular canal (AVC) and outflow tract (OFT) regions. AVC cushions are formed as mesenchymal cells are derived from squamosal endothelial cells by epithelial-mesenchymal transition [EMT], specifically of endothelial origin [EndMT], and invade and populate the cardiac jelly matrix. These mesenchymal cells subsequently proliferate and differentiate to form the AV valves and membranous septum. They also contribute to patterning the myocardium via directing vascular flow. Evidence points to a stepwise EndMT cascade involving the following key events [46,54,89]:

- initiation of EndMT by signal molecules elaborated from myocardial cells into the cardiac jelly;
- disassembly of cell–cell junctions between squamosal endothelial cells in the endocardium;
- delamination by loss of polarity, cytoskeletal rearrangement, and breakdown of basal lamina;
- invasion of cardiac jelly by newly motile mesenchymal cells;
- proliferation of trans-differentiated mesenchyme to 'cellularize' and remodel the cardiac jelly;
- patterning of the AV myocardium by flow-mediated remodeling of the looped heart;
- differentiation of cardiac valves and membranous septum.

A search of the MGI database (http://www.informatics.jax.org/) for abnormalities in cardiac EMT identified mouse knockouts with developmental phenotypes similar to those reported for avian studies with TCE, implicating the possibility of disruption of the following genetic signals and responses by TCE exposure during cardiac development. Candidate genes implicated pathways such as TGF-beta signaling, ephrin signaling, Notch signaling, the VEGF pathway, and RXR signaling. Potential molecular initiating events, not yet evaluated experimentally, may involve a cellular initiation of vascular inflammatory signals, perhaps through an LXR/RXR-mediated effect on cholesterol homeostasis, vulnerability to reactive oxygen species (ROS) [91,41,28], or disruption of the downstream consequences of VEGF signaling [65].

In support of disruption of EndMT being a potential key event in TCE-induced valvulo-septal defects, embryonic TCE exposure has been associated with inhibition of cell–cell separation and mesenchymal formation [10], alterations in mesenchymal cell migration [60,75] and alterations in endocardial proliferation patterns [24]. In ovo studies have shown that TCE and TCA can alter cushion formation, cardiac function, and embryo survival [23], and cushion cellularity can be altered as a function of concentration, duration, and timing of exposure. The ephrin-EPH system might be of high relevance to an AOP for TCE-induced valvulo-septal defects. Loss of Ephrin-A1 in mice, a ligand for class A Eph receptor tyrosine kinases, results in thickened aortic and mitral valves. These embryos display hypercellularity in outflow tract endocardial cushions and elevated mesenchymal marker expression, suggesting that excessive numbers of cells undergo EMT [30]. Ephrin-A1 and its cognate receptor (EphA3) are expressed in adjacent cells in the developing endocardial cushions. In contrast to the ligand, functional inactivation of EphA3 results in hypoplasia of AVC endocardial cushions with fewer migrating mesenchymal cells [81]. As such, disruption of Ephrin-A1 ligand or EphA3 receptor function impacts endocardial cushion formation in different ways, potentially leading to hypercellularity or hypocellularity, respectively. Both effects have been described in in vitro models of TCE-induced effects on endocardial cushions. Endocardial disruption may have additional or downstream consequences on the developing heart,

related to dysregulation of cellular Ca2+ fluxes and cardiac contractility [58,66,59,14,76,17] or to alterations in cardiac hemodynamics [72].

3.1.4. Weight of evidence (WOE) for hazard

The WOE (evidence integration) for fetal cardiac defects was characterized according to the criteria described in *A Framework for Assessing Health Risk of Environmental Exposures to Children* [86], a scheme that is derived from principles of causality assessment developed by Hill [43]. The key components (factors) of the WOE analysis were: temporality, strength of association, variability analysis, uncertainty analysis, qualitative dose-response, experimental evidence, reproducibility (consistency), biological plausibility, alternative or multiple explanations, specificity, and coherence (Fig. 1). Independent assessments of the WOE were conducted by reviewers, and a group consensus of the evidence supporting stronger and weaker weights of association for each key factor was derived. The evidence supporting stronger and weaker weight of association for each key factor is presented in Table 7.

Despite the recognized uncertainties and limitations in the TCE database, the evidence supports a conclusion that TCE has the potential to cause cardiac defects in humans when exposure occurs at sufficient doses during a sensitive period of fetal development. This conclusion is warranted by the data that demonstrate or suggest a potential hazard to cardiac development, including epidemiological studies, developmental toxicology studies in rodents with TCE and its metabolites (DCA and TCA), avian in ovo studies, in vitro assays, and mechanistic data that form the basis of a preliminary conceptual model of an AOP for valvuloseptal defects resulting from TCE exposures. Limitations within the database that increase the uncertainties regarding this conclusion are acknowledged. These limitations are described in detail above. The epidemiological studies provide evidence of associations between TCE, or TCE and other chlorinated solvents, and cardiac defects, but these studies have limitations related mainly to exposure measurement error and lower statistical power due to the rarity of cardiac defects. The rodent developmental toxicology studies conducted by Dawson et al. [20], Johnson et al. [51], and Johnson et al. [49] that reported cardiac defects resulting from TCE (and metabolite) drinking water exposures have study design and reporting limitations. Additionally, two good quality (GLP) inhalation and gavage rodent studies conducted in other laboratories, Carney et al. [15] and Fisher et al. [28], respectively, have not detected cardiac defects.

In accordance with the Guidelines for Developmental Toxicity Risk Assessment [85], the database is considered to be adequate to support categorization of the health-related database for hazard and dose-response, with the determination that there is "Sufficient Experimental Animal Evidence" and "Limited Human Data" for developmental cardiac toxicity. This category "includes data from experimental animal studies and/or limited human data that provide convincing evidence for the scientific community to judge that a potential for developmental toxicity exists." The minimum evidence that would be necessary to determine whether there is or is not sufficient evidence of developmental toxicity is the existence of appropriate, well-conducted animal studies. The overall TCE database met this criterion, although limitations and uncertainties in the primary study used in dose response [51] are acknowledged.

3.2. Dose-response assessment for developmental cardiac defects

Given the hazard conclusion that (despite uncertainties and limitation in the database) TCE has the potential to cause cardiac defects in humans when exposure occurs at sufficient doses during a sensitive period of fetal development, the next critical issue addressed by this update is the dose-response assessment.

3.2.1. Suitability of Johnson et al. [51] study for deriving a point of departure for a reference value

The Johnson et al. [51] study is the only available study potentially useable for dose-response analysis of fetal cardiac defects. On the whole, the Johnson et al. [51] study is considered suitable for use in deriving a POD for the following reasons. The study has an appropriate design. It was conducted by a relevant route of exposure (drinking water), covered the entire period of gestation which subsumes the developmental window for the initiation of cardiac defects, and tested multiple exposure levels. Further support was derived from the finding of a robust, statistically significant dose-response relationship. Additionally, this judgement took into consideration the strengths and limitations of the study and uncertainties identified in the WOE analysis.

The study was conducted over a period of 6 years, with exposed animals and their concurrent controls distributed across time. This design is not problematic per se; clinical trials and epidemiological studies are frequently conducted similarly, with staggered entry of subjects [31,69]. An important consideration to address is the potential for increased variability among litters owing to temporal drift and other possible factors.

Overdispersion, or greater variation among litters than is expected based on within-litter variation among offspring, can be dealt with by a standard method for clustered data [77,33,55,32,67]. This method deals effectively with between-litter variation from all sources, assuming that within-litter variation (conditional on the litter-mean) is approximately binomial. This method was applied for significance tests and dose-response analyses (discussed below).

Another concern about the study design is that the two highest exposure levels and their associated controls were observed in 1989–93, and the two lowest exposures and their controls were observed during 1993–1995 (Table 8; [53,52]). This raises a question whether temporal change rather than exposures can account for the observed responses. We also note that the two highest TCE doses and their controls, reported originally in Dawson et al. [20], used tap water as a vehicle and drinking water source. Hypothetically, if teratogens in tapwater did increase cardiac defects, that would likely increase the control response and perhaps impede the ability to observe a significant increase.

Employing all of the data, there is a highly significant ($P < 0.001$) increasing dose-response trend (Fig. 6) based on a Cochran-Armitage trend test after adjusting for overdispersion. The trend is also significant ($P < 0.04$) when the highest dose is dropped. The temporal disjunction between the middle and high dose groups prompts further examination. There is no significant trend for the two low-dose groups and their controls. When the two high dose groups and related controls (Table 8) were considered separately, a significant trend ($P < 0.03$) was found.

Confidence that data from Johnson et al. [51] represent a real response is supported by the increasing trend in response (Fig. 6), and the observations of higher percentages of cardiac malformations elicited by higher doses (500 mg/kg-day and higher) in studies of rats exposed to TCE metabolites, TCA and DCA [27,79,78]. The highest dose in the Johnson et al. [51] study lies at the lower end of doses that elicited substantial responses in these other studies. Thus, a hypothesis that the Johnson data represent a false positive or an anomalous dose-response pattern seems implausible, based on trend tests and comparison with studies that used higher doses.

3.2.2. Dose-response modeling of the data from Johnson et al. [51]

Dose-response modeling of the cardiac malformation data from Johnson et al. [51] was conducted using the nested log-logistic and other BMDS models (http://www.epa.gov/ncea/bmds/) and a BMR of 0.01 (1%) extra risk, the BMR level that was used in the EPA 2011 TCE assessment [87].

Table 7
WOE Evaluation of the Potential for Development Exposures to TCE to Result in Cardiac Defects.

Key Factor[a,b]	Type of evidence considered	Data	Evidence for stronger weight of association	Evidence for weaker weight of association	Comments or Null Evidence
Temporality	Timing of exposures and response	Tox	Studies in various species in which TCE (or metabolites DCA or TCA) were administered during a sensitive period of in utero cardiac development resulted in morphological and/or functional alterations. • Drinking water administration of TCE to rats on GD 1–22 resulted in a statistically significant treatment-related increase in the incidence of cardiac defects [51,20]. • Drinking water administration of TCA (the TCE oxidative metabolite) to rats on GD 1–22 resulted in a statistically significant treatment-related increase in the incidence of cardiac defects [49]. Gavage administration of TCE metabolites (DCA and TCA) on GD 6–15 [78] or of DCA during discrete windows of time within GD 6–15 [27] resulted in treatment-related increases in the incidences of cardiac defects. • Avian in ovo studies that administered TCE or TCA during the period of valvuloseptal morphogenesis (e.g., HH 15–20) resulted in altered cardiac morphology and/or function [72,23]. • A study of DCA exposure to zebra fish [41] demonstrated evidence of a disruption in cardiac development (pericardial edema and altered heart rate). • Mouse whole embryo culture studies of DCA and TCA administered at the period of 3–6 somites detected cardiac defects [44]; a chicken whole embryo culture study of TCE administered at HH 13–14 detected alterations in AV cushion [60]. • Avian atrioventricular canal cell culture (HH 16) study found evidence of inhibited endothelial cell separation and early events of mesenchymal cell formation in the heart following TCE exposures [10].	Some in vivo or in vitro studies rodent studies in which TCE (or metabolites DCA or TCA) was administered during a sensitive period of in utero cardiac development resulted in no morphological alterations. • Gavage administration of TCE or metabolites (DCA and TCA) to rats on GD 6–15 did not result in treatment-related cardiac defects [28]. • Inhalation exposures of TCE to rats on GD 6–20 [15] or to rats and mice on GD 6–15 [74] did not result in treatment-related cardiac defects.	• NE

	Exposure occurs before outcomes onset	Epi	• Four cohort or case-control studies consider temporality [71,29,94,35]. Three studies observed an association between the TCE exposure surrogate and major cardiac defects [29,94,35]. An association with conotruncal defects, specifically, was observed in Forand et al. [29].	• Temporality was not considered in Bove [8]/Bove et al. [9], Goldberg et al. [35], or Lagakos et al. [56].	• The small numbers of conotruncal heart defects in Ruckart et al. [71] precluded any analysis of this endpoint and TCE exposure.
Strength of association	Study quality, including study strengths and limitations	Tox	• For Johnson et al. [51], Dawson et al. [20], and Johnson et al. [49], all of which detected cardiac malformations, study quality strengths include randomized assignment to test group, detailed description of fetal cardiac dissection and evaluation procedures, evaluation of fetal hearts without knowledge of treatment group, and confirmation of all cardiac defects by consensus of 3 experts. Statistical analysis of data from this study was appropriately conducted by EPA statisticians using individual fetal and litter data that were provided by the study author. • The power of detection in the Johnson et al. [51] study was enhanced by the use of historical controls that did not demonstrate a temporal shift in cardiac defects. A significant dose related trend in cardiac defects was observed even without large group sizes. • A strong association of exposure to response was observed at high dose levels in multiple studies that identified cardiac defects. In Johnson et al. [51] there was a highly significant positive trend for cardiac defects. • Potential confounding factors exist in studies that did not identify cardiac defects (e.g., different routes of exposure, the use of different rodent strains or suppliers across studies, and the use of soybean oil as a vehicle in Fisher et al. [28].	• For Johnson et al. [51] major study quality limitations include the use of data pooled from separate study cohorts conducted over an approximately 6-year period, the use of tap water as the vehicle for some of control and treated groups (as reported by Dawson et al. [20] with no characterization of possible contaminants and incomplete reporting of study methods and results. • While Dawson et al. [20] indicated that levels of TCE in dose formulations were tested by gas chromatography, the analytical findings were not reported. Johnson et al. [51] did not report whether dose formulations were analyzed. Further, levels of TCE were not assessed in the vehicle control water; therefore, it is plausible that TCE contaminated the water and that doses were actually higher than measured. • The Dawson et al. [20] and Johnson et al. [51] studies estimated doses based on the average water consumption. This method does not provide precise information to calculate TCE dose because variability in drinking water consumption among dams is not characterized. • The dose selection for Johnson et al. [51] resulted in a NOAEL that is approximately 700-fold lower than the next highest dose. • Some studies that did not identify treatment-related cardiac defects following developmental exposures to TCE, e.g., Carney et al. [15], Fisher et al. [28], and Schwetz et al. [74], were well-conducted and adequately-reported GLP and/or guideline studies with no substantive limitations identified. • One study [28] attempted to replicate the methods used in the Johnson et al. [51] study, utilizing the same fetal cardiac dissection and evaluation techniques, and including one of the Johnson et al. [51] study authors in the assessment team, yet found no treatment-related cardiac defects.	• Some studies that reported no cardiac defects following TCE gestational exposures [61,62,42,39] or avian in ovo studies [12,26] did not indicate that detailed evaluation of fetal hearts was conducted. • A rat whole embryo culture study of TCE administered at the period of 4–7 somites detected no cardiac defects in a study by [73]; however, the study methods indicate that there was no evaluation of the embryonic heart.

Table 7 (*Continued*)

Key Factor[a,b]	Type of evidence considered	Data	Evidence for stronger weight of association	Evidence for weaker weight of association	Comments or Null Evidence
	Magnitude of the effect measure	Epi	• Increased risk estimates between all or major cardiac defects ranged from 1.24 (95% CI: 0.75, 1.94) to 2.40 (95% CI: 1.27, 3.62) observed in 3 studies [29,9,35]. Stronger associations, observed with the TCE exposure surrogate for conotruncal defects and ventricular septal defects than for major cardiac defects, a broader category [29,9]. A fourth study observed an increased risk estimate of 6.2 (95% CI: 2.6, 14.5) for cardiac defects in infants of mothers aged ≥38 years and maternal residence within 1.32 miles from at least one TCE emissions source [94].	• No association in Yauck et al. [94] in mothers <38 years of age and maternal residence within 1.32 miles from at least one TCE emissions source nor in Lagakos et al. [56], which does not observe an association with cardiac defects. Alternative reasons such as lower statistical power may explain these observations.	• NE
Variability analysis	Sources of within- and cross-study variability that contribute to uncertainty	Tox	• Johnson et al. [51] test subject source, husbandry, and randomization procedures were consistent across all cohorts, i.e., including Dawson et al. [20] and metabolite studies Johnson et al. [51]. Fetal cardiac evaluation methodology, which included evaluation without knowledge of treatment group and confirmation of all cardiac anomalies by 3 expert scientists, was also consistently applied across cohorts and studies from the UA laboratory. This had the result of reducing intra- and inter-study variability in the assessment. • Johnson et al. [51] reported that cardiac defect incidences were consistent across all control cohorts (55 litters over approximately 6 years). An EPA review of the available control data did not observe unusual heterogeneity in prevalence of malformations. • Studies that reported cardiac defects following administration of metabolites (DCA and TCA) used randomized assignment of maternal animals to test group, thus reducing intra-study variability. • Although Dawson et al. [20] and Johnson et al. [51] identified cardiac defects following exposures to TCE during development, Carney et al. [15], Fisher et al. [28], and Schwetz et al. Schwetz et al. (2006) did not find treatment-related cardiac abnormalities. This may be the result of differences in the study design and assessment methods. This includes such aspects as animal strain, age, source, exposure route and vehicle, duration of exposure, and cardiac evaluation methods.	• The Johnson et al. [51] study reported data from several cohorts of animals, which were on study over a period of approximately 6 years. The data included control cohorts, some of which were concurrent and some that were non-concurrent to the TCE-treated groups [53,52]. Data that definitively link the individual control litter response data with each particular cohort are no longer available for independent examination. • Different study outcomes were observed in studies that had many similarities in study design and conduct, i.e., Dawson et al. [20] and Johnson et al. [51] identified exposure related cardiac defects while Fisher et al. [28] did not. In the Fisher et al. [28] study, care was taken to ensure that the same cardiac evaluation methods were used as in the Dawson et al. [20] and Johnson et al. [51] studies, including fetal evaluation with knowledge of treatment group, and one of the study authors of Johnson et al. [51] participated in the fetal examination. • The use of soy bean oil in the Fisher et al. [28] study vs. water vehicle and control for Johnson et al. [51] and Dawson et al. [20] studies. • The Johnson et al. [51] and Dawson et al. [20] studies did not calculate variability in TCE dose by measuring individual dam water consumption.	• Based upon the toxicokinetic profile of TCE [87], it is considered unlikely that toxicokinetic factors contributed significantly to differences in response across study protocols.

	Sources of within- and cross-study variability that contribute to uncertainty	Epi	• NE (not considered in Hill analysis)	• NE (not considered in Hill analysis)	• Studies examined different populations, exposure levels, gradients, and media. Additionally, different sets of strengths and uncertainties in this set of studies would contribute to observed cross-study variability.
Uncertainty analysis	Missing information or data gaps, within and across studies	Tox	• For the studies conducted by the UA laboratory [51,20] that identified cardiac defects following exposures to TCE, DCA, or TCA, detailed descriptions of evaluation methods for assessment of cardiovascular effects were provided. • Individual fetal and litter cardiac findings data, as well as detailed information on study conduct and fetal evaluation methods, were provided to the EPA for Johnson et al. [51] and Dawson et al. [20].	• The publications for studies conducted by the UA laboratory that identified cardiac defects following exposures to TCE, DCA, or TCA [51,49,20] did not report essential study details, and generally did not include summaries of maternal data or fetal data for endpoints other than cardiac defects. • For well-conducted studies that did not detect cardiac defects following developmental exposures to TCE or metabolites [15,28] adequate descriptions of study methodology and summary data for maternal and fetal findings were reported. • Mechanistic data for alterations in cardiac development are limited and do not identify initiating events for the putative AOP.	• NE
	Missing information or data gaps, within and across studies	Epi	• NE (not considered in Hill [43] analysis)	• NE (not considered in Hill analysis)	• NE
Qualitative dose-response	Association between exposure/dose and degree of effect	Tox	• Alterations in cardiac development were observed in multiple studies at high dose levels following TCE, DCA, or TCA exposures [51,49,20,79,78]. • The incidence of cardiovascular effects increased as a function of dose in Johnson et al. [51]. • An association between exposure to TCE (or DCA or TCA) and alterations in cardiac development was reported in various animal models, i.e., LE and SD rats, CD-1 mice, chicken embryos, and zebra fish [23,24,91,41,51,20,79,78]. • A BMDL for Johnson et al. [51] was derived by EPA statisticians from individual cardiac defect data provided to EPA. Litter contribution to the outcome of interest was incorporated in the analysis. A significant dose-response trend was identified, whether or not the high dose value was included in the analysis.	• The dose response for cardiac defects identified by Johnson et al. [51] could only be fit to a model with elimination of the high dose data from the analysis. The lowest dose tested had a zero response for cardiac defects, below the historical control incidence. The doses tested were spaced over several orders of magnitude, with wide gaps. • Carney et al. [15] was the only other study in the database that evaluated developmental effects of TCE over multiple dose levels. In that study, no fetal toxicity and minimal maternal toxicity was reported.	• TCE doses tested in Johnson et al. [51] and Dawson et al. [20] (drinking water): 2.5 ppb, 250 ppb, 1.5 ppm, or 1100 ppm (0, 0.00045, 0.048, 0.218, or 129 mg/kg-day) • TCE doses tested in Fisher et al. [28] (gavage): 500 mg/kg-day • TCE doses tested in Carney et al. [15] (inhalation): 50, 150, or 600 ppm (268.5, 805.5, or 3222 mg/m^3)

Table 7 (*Continued*)

Key Factor[a,b]	Type of evidence considered	Data	Evidence for stronger weight of association	Evidence for weaker weight of association	Comments or Null Evidence
	Exposure-response gradient: Association between exposure/dose and degree of effect	Epi	• NE	• Goldberg et al. [35] and Lagakos et al. [56] examined exposure-response; none observed.	• NE
Experimental evidence	Hypothesis testing: manipulation of exposure scenario with resulting alterations in response	Tox	• A study by [27] administered the metabolite DCA to rats on varied days of gestation and identified critical windows of exposure for eliciting cardiac developmental defects. • No statistically significant increases in congenital heart defects were observed in groups of rats that were exposed to TCE prior to pregnancy only [20]. • Drake et al. [24] demonstrated that cardiac defects did not occur in chick embryos exposed to TCE and TCA during the period of cardiac specification (approximately GD 6 in rats) rather than the period of valvuloseptal morphogenesis.	• Studies in rodents that administered TCE via drinking water detected an increase in fetuses with cardiac defects [51,20]; studies that administered TCE via other routes (gavage and inhalation) were negative for this response [15,28,74]. • In a whole embryo culture (WEC) study of DCA and TCA [44], that identified cardiac defects, the acid nature of DCA and TCA may have impacted dysmorphogenesis.	• Studies that manipulated the gestational exposure period were not conducted with TCE.
	Association not observed once exposure ceases	Epi	• NE	• No differences between observed and expected numbers of cardiac defect cases once wells were closed in contaminated area [35].	• NE
Reproducibility [Consistency]	Reproducibility: Corroboration across studies, labs, routes of exposure, species, etc.	Tox	• Studies that administered TCE in drinking water to rats on GD 1–22 were conducted over a period of approximately 6 years by researchers at the same academic facility (UA, Tucson) used the same cardiac evaluation methods and identified treatment and dose-related cardiac malformations [51,49,20]. A preliminary screening study that utilized intrauterine administration of TCE also detected cardiac defects [20]. The types of cardiac malformations observed were similar across study cohorts and treatment groups throughout the duration of the research program. • Studies on TCE metabolites (TCA and TCA) conducted in other laboratories [27,79,78] identified cardiac defects similar to those observed in the UA studies. • Cardiac septal anomalies were observed in avian in ovo studies [72,23], and in WEC assays [60,44] with TCE and/or metabolite exposures. Zebrafish studies also demonstrated evidence of alterations in cardiac development [91,41].	• Studies conducted in other laboratories than UA and that administered TCE by gavage or inhalation [15,28,74] did not identify statistically significant increases in cardiac defects. Fisher et al. [28] used the same cardiac evaluation methods as the UA lab.	• Studies that did not identify cardiac defects with TCE and/or metabolite exposures [15,28,74] did not replicate all aspects of the Johnson et al. [51] study, even though Fisher et al. [28] used the same cardiac evaluation techniques as [51] and Dawson et al. [20], and therefore provide only limited evidence of lack of reproducibility.

	Consistency: Association observed in different populations, places, time and circumstances.	Epi	• Association between cardiac defects and TCE exposure surrogate observed in four studies. These studies were of different populations living in different states (NY, NJ) and covered slightly different time periods (1983–2000, 1985–1988) [29,8,9]. Two other studies of weaker designs were of different populations and carried out in two different locations in the United States, and provide supporting evidence [94,35].	• Lagakos et al. [56] compared a pregnancy receiving contaminated residential well water to a pregnancy not receiving residential water from contaminated wells and does not observed an association between cardiac defects and contaminated drinking water.	• NE
Biological plausibility	Observed outcome can be attributed to toxic insult given the known science	Tox	• Avian in ovo studies and atrioventricular cell culture studies support the biological plausibility of effects of TCE on cardiac development, given that early chick heart development is similar to mammalian (including human), particularly regarding the role of the cardiac cushion in septation [63]. • Preliminary exploration of a possible adverse outcome pathway (AOP) has resulted in a reasonable conceptual model for TCE-induced congenital heart defects. In this construct, the vulnerable period is defined by endocardial morphogenesis. Endothelial–mesenchyme transition (EMT) is disrupted in the area of the atrioventricular canal, leading to septal defects. Studies in knockout mice have suggested the possible disruption of genetic signals and response by TCE exposure during cardiac development. Candidate genes have implicated pathways such as TGF-beta, ephrins, Notch signaling, VEGF pathway, and RXR signaling. Potential molecular initiating events may involve a cellular initiation of vascular inflammatory signals, perhaps through an LXR/RXR-mediated effect on cholesterol homeostasis, vulnerability to reactive oxygen species or disruption of the downstream consequences of VEGF signaling.	• A definitive AOP for TCE-induced cardiac defects, including a putative initiating event, has not yet been characterized. Additional mechanistic data are needed to support the hypothesized AOP. • There are insufficient mechanistic data to characterize additional potential MOAs other than that hypothesized in the AOP construct.	• It is possible that multiple modes of action are involved in alterations to cardiac development.

Table 7 (*Continued*)

Key Factor[a,b]	Type of evidence considered	Data	Evidence for stronger weight of association	Evidence for weaker weight of association	Comments or Null Evidence
	Observed association plausible given the known science	Epi	• NE	• NE	• In vitro and in vivo animal studies report cardiac defects with TCE and TCE-metabolite exposure.
Alternative or multiple explanations	Other possible explanations for observed outcome after the exposure of interest	Tox	• Given the presumed contribution of both environmental exposures and genetic predisposition in human congenital heart disease [68], it is possible that the test subjects used in the Johnson et al. [51] study and others conducted in that laboratory may have been particularly susceptible to alterations in cardiac development. • Other contributing factors or confounding factors were not specifically identified in the evaluated in-vivo studies. • It is possible that the absence of treatment-related cardiac defects in well-conducted TCE studies [15,28] or metabolite studies [28] was due to confounding variables such as differences in strain/source of animal model, route of exposure, toxicokinetics, vehicle [e.g., soybean oil in Fisher et al. [28]], or differences in cardiac evaluation methods. • It is unlikely that the cardiac defects observed by Johnson et al. [51] were an artifact of the evaluation procedures used, since a study by Fisher et al. [28], using the same fetal cardiac evaluation procedures, did not identify an association between TCE exposure and the incidence of cardiac defects.	• There is a possibility that cardiac defects detected in the Dawson et al. [20] study were associated in part with the use of tap water as a control vehicle (i.e., possible presence of contaminants).	• NE
	Other possible explanations for observed outcome after the exposure of interest (not considered in Hill analysis)	Epi	• Potential maternal risk factors were adjusted in statistical analysis in Forand et al. [29] and Yauck et al. [94] or were not found in statistical analyses to influence observed association by ±15% [8,9].	• Potential for confounding from another exposure given the poor exposure definition in Yauck et al. [94]. The positive association in Goldberg et al. [35] may result from likely selection biases in controls.	• NE

Specificity	Single cause and effect relationship resulting from exposure to test substance	Tox	• Cardiac defects in rats appear to be attributable to direct chemical exposure to TCE or metabolites (DCA or TCA) and are unlikely to be the result of secondary effect of maternal toxicity. Johnson et al. [51] reported that TCE exposure via drinking water to pregnant rats did not result in maternal toxicity. Carney et al. [15] reported minimal decreases in body weight gain in dams, with no adverse fetal outcomes. In fetuses, there was no indication of TCE-related fetal weight deficits, external or skeletal anomalies, or of soft tissue alterations other than cardiac defects in Johnson et al. [51], nor in any other study. • The majority of the cardiac malformations following TCE exposures to rats [20] or chicks [72,23] during sensitive periods of cardiac development were ventricular septal defects, valve defects, or outflow tract abnormalities. Mechanistic data suggest a common etiology (disruption of the cardiac cushion formation) for the observed cardiac defects [10].	• Studies conducted in other laboratories than UA and that administered TCE by gavage or inhalation [15,28,74] did not identify cardiac defects. Fisher et al. [28] used the same cardiac evaluation methods as the UA lab. • The cardiac defects detected in the Dawson et al. [20] study might have been related to the use of tap water as a vehicle (i.e., possible contaminants).	NE
	Single cause and effect relationship resulting from exposure to test substance	Epi	• NE	• Specificity not as critical compared to other Hill aspects since outcomes may have several risk factors. Maternal risk factors, specifically chemical risk factors, associated with cardiac defects in infants have not been well studied.	• NE
Coherence	Summary: Extent to which data are similar in outcome and exposure across database	Tox	• Multiple studies were conducted at UA [51,49,20], in which rats were administered TCE or metabolites DCA or TCA in drinking water on GD 1–22 and for which study design and cardiac evaluation methodologies were consistent. The outcomes of these studies (detection of cardiac defects, particularly septal defects, valve abnormalities, and outflow tract anomalies) are consistent across these studies. Additionally, these outcomes are supported by the results of avian in ovo and in vitro studies, studies with TCE metabolites (DCA and TCA) in rodents, in vitro whole embryo culture studies, and mechanistic data.	• Developmental toxicity studies with TCE that were conducted in other laboratories [15,28,74] administered TCE to rats of other strains or sources, using different routes of exposure (inhalation or gavage), administered on different days of gestation (i.e., not including GD 1–6) than the UA studies and did not identify cardiac defects. No other study in the TCE database reported cardiac defects at the low dose levels reported by Johnson et al. [51].	• NE
	Cause and effect interpretation should not conflict with the generally known facts of the natural history and biology of the disease	Epi	• Associations in epidemiologic studies of cardiac defects and maternal occupational exposure to degreasing solvents or to organic solvents [34,93,83,84].	• NE	• NE

NE = No relevant evidence.
HH = Hamburger-Hamilton stages of chick development [37].
UA = University of Arizona.
Tox = Animal toxicology studies; Epi = Epidemiological studies.
Key Factor References.
[a] U.S. EPA [86].
[b] Hill [43].

Table 8
Data analysis of cardiac abnormalities reported by Johnson et al. [51].

Conc. in drinking water, ppm	0	0	0	0.0025	0.250	1.5	1100
Dose, mg/kg-d	0	0	0	0.00045	0.048	0.218	129
Internal dose metric[a]	0	0	0	0.00031	0.033	0.15	88
Dates	1989–93	1993–95	all	1994–95	1994–95	1989–90	1989–90
N (litters)[b]	20	35	55	12	9	13	9
N (fetuses)[b]	232	374	606	144	110	181	105
N (fetuses with cardiac defect)[b]	7	6	13	0	5	9	11
p (fetuses with cardiac defect)	0.0302	0.0160	0.0215	0	0.0455	0.0497	0.1048

[a] Total Oxidative Metabolism per unit (body weight)$^{3/4}$; units are mg/wk-kg$^{3/4}$.
[b] For the purpose of this analysis, the control litters (fetuses) were designated as belonging to the 1989-93 or 1993-95 cohorts based upon an analysis of the numbers of control animals assigned to study, the incidences of cardiac malformations reported, and individual animal identification numbers Dawson et al. [20]; Johnson [51,52,48]; Johnson (2008); Paula Johnson, personal communication.

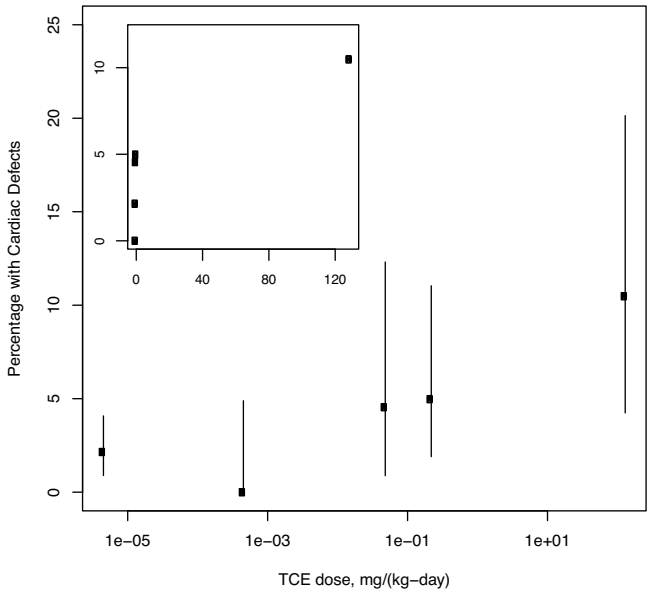

Fig. 6. Percent of Offspring with Cardiac Defects [51]. The dose is on log scale. The inset figure shows the same data on the untransformed scale. Confidence limits (95%) for percentages are also shown. The solid points identify the treated groups and the open points identify the control.

The nested dose-response model accounts for overdispersion using a beta-binomial model [88]. To confirm that approach, we also applied a suite of models for dichotomous binomial data after adjusting the data for clustering, using an estimated design effect of 1.53 [77,33,55,67].

Given the uncertainties in the dose-response analysis related to the nature of the data, the confidence in the POD based on Johnson et al. [51] has limitations. Overall, however, the POD derived in the 2011 TCE assessment [87], which used an approach consistent with standard U.S. EPA dose-response practices, remains a reasonable choice.

Several sources of uncertainty related to modeling assumptions were examined:

(1) Do the data have a plateau at less than 100% response? The evidence is equivocal and does not permit a clear answer. Considering the confidence intervals for responses in Fig. 6, it is not clear whether the response reaches a plateau or increases more gradually. A number of National Toxicology Program (NTP) studies of developmental toxicity also have a low but significant maximum response, although they differ in apparent pattern of response.[3] A model with a plateau is plausible, but would not substantially change the general conclusion and results. (We used the dichotomous-Hill model in BMDS, which allows a plateau to be estimated.)
(2) Is it better to drop or retain the high dose? For the 2011 TCE assessment [87], the high dose was dropped on the strength of an examination of residuals at the low doses for the nested model. The decision to drop the high dose is confirmed in this re-examination, using non-nested dichotomous models (adjusted for intralitter correlation using estimated design effects [33]). Dropping the high dose leads to higher model goodness of fit and better fit in the region of the BMD_{01} and BMD_{05}.
(3) Are there sufficient data in the low-dose region and near the BMD_{01} to permit reliable inference about the dose-response curve shape (which influences the BMD and BMDL)? BMD inference at the 1% extra-risk level is highly uncertain, because BMD and BMDL values vary by several orders of magnitude depending on the modeling assumptions. This is attributed in part to the lack of monotonicity at the lowest dose and the apparent supralinearity of the overall exposure-response relationship. Additional doses would be required to better specify the curve shape in the low-dose region. More reliable inference can be made for higher BMRs.

3.2.3. Uncertainty in the point of departure (POD)

There is substantial model and parameter uncertainty at the 1% level of extra risk, although 1% is the appropriate BMR based on severity of the effect (i.e., cardiac malformations). These uncertainties can be attributed primarily to having too few data points in the low-dose range, where more data would be required to adequately characterize the dose-response shape. Uncertainty decreases for higher BMR levels (5% and 10% extra risk), although 10% exceeds the range of the data for some models.

- The $BMDL_{01}$ 0.0207 mg/kg-day (BMD_{01} 0.0646) for the nested log-logistic model selected in the 2011 TCE assessment (with slope constrained and without the high dose group) [87] provides a compromise value from the range of BMDLs derived from the variety of models examined.
- With a 5% BMR (i.e., 5-fold greater), the BMDL for the nested log-logistic model ($BMDL_{05}$ 0.108 mg/kg-day; BMD_{05} 0.337) [87] is about 5-fold higher than the 2011 $BMDL_{01}$.
- Model-averaged $BMDL_{01}$ or $BMDL_{05}$ for dichotomous models (using a Rao-Scott transformation to adjust for intra-litter

[3] These NTP studies have a significant increase in malformations and maximum response less than 10%: TER86091, mice, MeDOPA; TER84054, rabbits, Carbon disulphide; TER82079, rats, Gentian Violet; TER84063, rats, DEHP; TER84111, mice, theophylline. http://tools.niehs.nih.gov/ntp.tox/index.cfm?fuseaction=ntpsearch.allchemicalsforstudy&searchterm=Developmental.

correlation; [33]) with the high dose dropped to achieve better fit in the low-dose range yielded the following values: BMD_{01} 0.0809 mg/kg-day and $BMDL_{01}$ 0.0225 mg/kg-day, BMD_{05} 0.282 mg/kg-day and $BMDL_{05}$ 0.178 mg/kg-day. This option yields results similar to that of the modeling approach used in the 2011 TCE assessment [87].
- The LOAEL/NOAEL approach, although there is also uncertainty about defining a POD with this approach, uses either the second highest dose (0.218 mg/kg-day) or the next lower dose (0.048 mg/kg-day) as a POD. These are biologically plausible as LOAELs because the apparent extra risk values calculated from the observed responses of 2.9% and 2.5%, respectively, exceed 1%, the level identified as a suitable BMR.

In summary, additional dose-response analyses were performed to characterize the uncertainty in the POD. Alternative PODs were derived based on use of alternative models, alternative BMR levels, or alternative procedures (such as a LOAEL/NOAEL approach), each with different strengths and limitations. These alternatives were within about an order of magnitude of the POD derived in the 2011 TCE assessment [87].

Overall, taking into account the Johnson et al. [51] study design, strengths and limitations, and uncertainties in the WOE, and in spite of any reservations based upon considerations pertaining to confidence in the dose response, a majority of the expert participants in this update project agreed that the Johnson et al. [51] study was suitable for use in deriving a POD. The majority of the participants agreed that the results of the present analysis are consistent with and further support the dose-response conclusions of the 2011 IRIS TCE assessment [87].

4. Discussion/conclusions

This updated systematic review and analysis was conducted to address the potential for exposure to TCE and its metabolites during critical windows of development to result in cardiac defects. The review developed: (1) an updated characterization of the available data and uncertainties in the TCE database for cardiac defects, (2) an expanded consideration of the mechanistic database that may support future research to develop an AOP for cardiac defects resulting from TCE exposures, (3) documentation of data and WOE evaluations (evidence integration) for hazard, and (4) an extended characterization of the dose-response modeling.

4.1. Updated characterization of available data and uncertainties

One of the goals of this review was to identify any new data (i.e., postdating the last literature search performed for the EPA 2011 TCE document [87]) that address cardiac malformations associated with exposures to TCE, DCA, and TCA. A total of 1769 unique citations were identified and screened for relevance. Of these, only two additional epidemiological studies and two mechanistic studies met the established inclusion criteria. We found no animal toxicology studies (in vivo, in vitro, or in ovo) that evaluated cardiac defects with TCE (or metabolite) exposures and that had been published since January 2010.

The epidemiological and toxicological studies that had been considered in the 2011 TCE document [87] and the new studies that were identified were evaluated for study quality in a transparent and consistent manner, utilizing multiple reviewers with relevant expertise. Study strengths were identified. The epidemiological studies were examined in detail for considerations of bias, confounding, and chance. Study flaws, inadequacies, and limitations were described for the toxicological studies. These analyses formed the basis for characterizing uncertainties in the epidemiological and toxicological databases.

Several epidemiological studies observed evidence of an association between TCE exposures and CHDs. This was found to be coherent with broader epidemiological literature reporting an association between maternal occupational exposure to degreasing solvents or organic solvents and cardiac defects. The available database of epidemiologic studies provided some support for an association but is not sufficient to establish a causal link.

Evaluation of the toxicological data included targeted attention given to studies and issues that have been portrayed as controversial in the published literature. This was particularly in regard to the findings of cardiac defects identified by Dawson et al. [20] and Johnson et al. [51]. A number of potential concerns associated with these studies were dispelled, e.g., that inadequate or inappropriate cardiac evaluation methods were used, control animals were not on study concurrently with treated animals, fetuses were not randomly assigned to evaluations, cardiac examinations were conducted with knowledge of treatment group, and statistical analysis of cardiac malformation data was inappropriate. Detailed comparisons of methods used in the various developmental toxicology studies to evaluate potential cardiac defects helped to facilitate this analysis as well as to identify differences between the studies that found cardiac defects with TCE exposures [51,20] and similarly-conducted studies that did not [15,28]. The detailed methodological evaluation led to the conclusion that differences in study methods (e.g., route of exposure, vehicle, animal source or strain, or other factors) may have contributed to differences in the detection of cardiac malformations, an issue that can no longer be definitively resolved. As noted previously in the 2011 TCE document [87], some limitations of these studies were found to be unresolvable, yet resulting uncertainties were not judged to compromise the use of the studies for hazard characterization and dose-response assessment.

4.2. Expanded consideration of the mechanistic database

Mechanistic data were considered as part of the WOE analysis for the 2011 TCE assessment [87]. However, those data did not provide a linkage to the developmental pathways and processes responsible for observed cardiac defects. Further consideration of data identified in the literature search and the MGI database motivated exploration of the potential for identifying a preliminary conceptual model of an AOP framework. It was proposed that an AOP anchored to the primary dysmorphologies associated with gestational TCE, DCA, and TCA exposure (i.e., valvulo-septal defects, muscular and membranous ventral septal defects, and pulmonary and aortic stenosis) might identify key events and relationships. In this construct, the vulnerable period is defined by endocardial morphogenesis. Endothelial–mesenchyme transition (EMT) is disrupted in the area of the atrioventricular canal, leading to septal defects. Studies in knockout mice have suggested the possible disruption of genetic signals and response by TCE exposure during cardiac development. Candidate genes have implicated pathways such as TGF-beta signaling, ephrin signaling, Notch signaling, the VEGF pathway, and RXR signaling. Potential molecular initiating events may involve a cellular initiation of vascular inflammatory signals, perhaps through an LXR/RXR-mediated effect on cholesterol homeostasis, vulnerability to reactive oxygen species or disruption of the downstream consequences of VEGF signaling. Although these hypothetical initiating events have not yet been experimentally investigated, the disruption of EndMT is well-supported as a potential key event in valvulo-septal defects induced by TCE exposures. Even at this preliminary stage of AOP development, the potential construct provides support for the biological plausibility of TCE exposures resulting in cardiac defects, and it is a significant achievement in defining research needs. Further

research can provide opportunities to improve understanding of the mechanism, including exploring linkages between proposed AOPs for molecular targets and cellular processes underlying early heart development, and using alternative experimental models and methods to evaluate effects of TCE and its metabolites.

4.3. Documentation of the WOE evaluation (evidence integration)

A structured approach to the WOE evaluation for both epidemiological and toxicological hazard was conducted according to the precepts of a published EPA evidence integration framework [86] that is based upon criteria established by Hill [43]. The hypothesis-based evidence for stronger and weaker weight of association was summarized and evaluated.

Overall, the WOE supported the conclusion that TCE exposure at sufficient doses during prenatal development has the potential to cause cardiac defects in humans. In Johnson et al. [51], the lowest dose to rats that resulted in these outcomes was 0.048 mg/kg-day TCE in drinking water.

This conclusion is based upon multiples lines of evidence:

- Epidemiological studies that identified a clear association between cardiac defects and maternal TCE exposures via vapor intrusion [29] and limited evidence for an association of TCE, or TCE in combination with other solvents, in drinking water (Bove [8]/Bove et al. [9]).
- Toxicology studies with TCE from one laboratory [51,20] that identified treatment and dose-related defects in cardiac development in rats following maternal drinking water exposures, although study design and reporting deficiencies were noted, and other laboratories were unable to replicate the findings using different routes of exposure [15,28].
- Toxicology studies with metabolites of TCE from two laboratories that observed defects in cardiac development in rats after maternal high-dose gavage or drinking water exposure to DCA [79,27] or TCA [78,49].
- In ovo studies from two laboratories [72,23,24,57] that found defects in cardiac structure or function in chicken embryos resulting from low-dose TCE exposures that disrupted valvulo-septal development (a process highly conserved across species, including humans)
- In vitro assays (whole embryo culture studies) from two laboratories that identified alterations in cardiac development with high doses of TCE [60] or its metabolites DCA and TCA [44] exposures to chicken or mouse embryos, respectively.
- Mechanistic data, including a putative AOP construct, that is consistent with the potential for TCE to cause cardiac defects and supports the biological plausibility of an effect on cardiac development with exposure to TCE.

The evidence was characterized as "Sufficient Experimental Animal Evidence" and "Limited Human Evidence" in accordance with the *Guidelines for Developmental Toxicity Risk Assessment* [85].

4.4. Extended characterization of the dose-response modeling

The dose-response relationship for cardiac defects in the Johnson et al. [51] study is robust and statistically significant. The study design is unusual when compared with standard guideline developmental toxicology protocols. Treated and concurrent control animals were evaluated over a 6-year period, there was a temporal gap between the 2 lower dose groups and the 2 higher dose groups. The possibility of increased variability among litters due to temporal drift and perhaps other factors across time (overdispersion), was dealt with by using a standard method for clustered data. The dose-response trend was found to be highly significant after adjusting for overdispersion. Because the maximal observed response was 10%, models with plateaus of less than 100% were investigated and were found to not substantially change the general conclusions and results. Confidence in the dose-response relationship is supported by the increasing trend in response and by metabolite studies that demonstrate findings at higher dose levels. Despite uncertainties in the dose-response analysis, the use of the Johnson et al. [51] study for dose-response assessment remains a reasonable choice.

Conflict of interest

The authors declare that there are no conflicts of interest.

Acknowledgements

This manuscript is dedicated to the memory of Cheryl Siegel Scott (1955–2014). In her role as an epidemiologist at the Environmental Protection Agency, National Center for Environmental Assessment, Cheryl contributed significantly to the 2011 IRIS TCE assessment, and to the developmental epidemiology evaluation that forms a cornerstone of this review.

The authors thank Weihsueh Chiu (Texas A&M University, College of Veterinary Medicine and Biomedical Sciences, College Station, TX 77843) and Jamie Strong (EPA/OW, Washington, DC) for contributions to earlier drafts of the manuscript and Mafruz Haque (EPA/ORD/NCEA, Washington, DC) and Robert Kavlock (EPA/ORD, Washington, DC) for contributions to figures.

References

[1] AIA (Aerospace Industries Association), Comments on the EPA toxicological review of TCE: developmental effects, Project No. 0904539.00, Available online at http://www.regulations.gov/#!documentDetail;D=EPA-HQ-ORD-2009-0791-0009.
[2] ATSDR (Agency for Toxic Substances and Disease Registry), Health Consultation: Endicott Area Investigation: Health Statistics Review: Cancer and Birth Outcome Analysis, Endicott Area, Town of Union, Broome County, New York, U.S. Department of Health and Humans Services, Atlanta, GA, 2006 http://www.atsdr.cdc.gov/HAC/pha/EndicottAreaInvestigation/EndicottHealthStatsReviewHC052606.pdf.
[3] ATSDR (Agency for Toxic Substances and Disease Registry), Health Consultation: Health Statistics Review Follow-up: Cancer and Birth Outcome Analysis: Endicott Area Investigation, Endicott Area, Town of Union, Broome County, New York, U.S. Department of Health and Human Services, Atlanta, GA, 2008 http://www.atsdr.cdc.gov/hac/pha//EndicottAreaInvestigationFollowUp/EndicottAreaHC051508.pdf.
[4] ATSDR (Agency for Toxic Substances and Disease Registry), The Priority List of Hazardous Substances That Will Be the Subject of Toxicological Profiles [ATSDR Tox Profile], CDC Agency for Toxic Substances and Disease Registry, Atlanta, GA, 2013 http://www.atsdr.cdc.gov/SPL/index.html.
[5] ATSDR (Agency for Toxic Substances and Disease Registry), Public Health Statement on Trichloroethylene [ATSDR Tox Profile], CDC Agency for Toxic Substances and Disease Registry, Atlanta, GA, 2014 http://www.atsdr.cdc.gov/ToxProfiles/tp19-c1-b.pdf.
[6] E. Boldenow, I. Hassan, M.C. Chames, C. Xi, R. Loch-Caruso, The trichloroethylene metabolite S-(1,2-dichlorovinyl)-l-cysteine butnot trichloroacetate inhibits pathogen-stimulated TNF-in humanextraplacental membranes in vitro, Reprod. Toxicol. 52 (2015) 1–6, http://dx.doi.org/10.1016/j.reprotox.2015.01.007.
[7] F. Bove, Y. Shim, P. Zeitz, Drinking water contaminants and adverse pregnancy outcomes: a review [Review], Environ. Health Perspect. 110 (2002) 61–74.
[8] F.J. Bove, Public drinking water contamination and birthweight, prematurity, fetal deaths, and birth defects, Toxicol. Ind. Health 12 (1996) 255–266.
[9] F.J. Bove, M.C. Fulcomer, J.B. Klotz, J. Esmart, E.M. Dufficy, J.E. Savrin, Public drinking water contamination and birth outcomes, Am. J. Epidemiol. 141 (1995) 850–862.
[10] A. Boyer, W. Finch, R. Runyan, Trichloroethylene inhibits development of embryonic heart valve precursors in vitro, Toxicol. Sci. 53 (2000) 109–117.
[11] J.D. Brender, M.U. Shinde, F.B. Zhan, X. Gong, P.H. Langlois, Maternal residential proximity to chlorinated solvent emissions and birth defects in offspring: a case-control study, Environ. Health 13 (96) (2014), http://dx.doi.org/10.1186/1476-069x-13-96.
[12] G. Bross, D. Difranceisco, M.E. Desmond, The effects of low dosages of trichloroethylene on chick development, Toxicology 28 (1983) 283–294, http://dx.doi.org/10.1016/0300-483x(83)90002-1.
[13] J. Bukowski, Critical review of the epidemiologic literature regarding the association between congenital heart defects and exposure to

trichloroethylene, Crit. Rev. Toxicol. 44 (2014) 581–589, http://dx.doi.org/10.3109/10408444.2014.910755.
[14] P.T. Caldwell, P.A. Thorne, P.D. Johnson, S. Boitano, R.B. Runyan, O. Selmin, Trichloroethylene disrupts cardiac gene expression and calcium homeostasis in rat myocytes, Toxicol. Sci. 104 (2008) 135–143, http://dx.doi.org/10.1093/toxsci/kfn078.
[15] E.W. Carney, B.A. Thorsrud, P.H. Dugard, C.L. Zablotny, Developmental toxicity studies in Crl:CD (SD) rats following inhalation exposure to trichloroethylene and perchloroethylene, Birth Defects Res. B Dev. Reprod. Toxicol. 77 (2006) 405–412, http://dx.doi.org/10.1002/bdrb.20091.
[16] W.A. Chiu, J. Jinot, C.S. Scott, S.L. Makris, G.S. Cooper, R.C. Dzubow, A.S. Bale, M.V. Evans, K.Z. Guyton, N. Keshava, J.C. Lipscomb, S. Barone Jr., J.F. Fox, M.R. Gwinn, J. Schaum, J.C. Caldwell, Human health effects of trichloroethylene: key findings and scientific issues [Review], Environ. Health Perspect. 121 (2013) 303–311, http://dx.doi.org/10.1289/ehp.1205879.
[17] J.M. Collier, O. Selmin, P.D. Johnson, R.B. Runyan, Trichloroethylene effects on gene expression during cardiac development, Birth Defects Res. A Clin. Mol. Teratol. 67 (2003) 488–495, http://dx.doi.org/10.1002/bdra.10073.
[18] N.C. Cosby, W.R. Dukelow, Toxicology of maternally ingested trichloroethylene (TCE) on embryonal and fetal development in mice and of TCE metabolites on in vitro fertilization, Fundam. Appl. Toxicol. 19 (1992) 268–274.
[19] B. Dawson, P. Johnson, S. Goldberg, J. Ulreich, Cardiac teratogenesis of trichloroethylene and dichloroethylene in a mammalian model, J. Am. Coll. Cardiol. 16 (1990) 1304–1309.
[20] B. Dawson, P. Johnson, S. Goldberg, J. Ulreich, Cardiac teratogenesis of halogenated hydrocarbon-contaminated drinking water, J. Am. Coll. Cardiol. 21 (1993) 1466–1472, http://dx.doi.org/10.1016/0735-1097(93)90325-U.
[21] M.A. Dorfmueller, S.P. Henne, R.G. York, R.L. Bornschein, J.M. Manson, Evaluation of teratogenicity and behavioral toxicity with inhalation exposure of maternal rats to trichloroethylene, Toxicology 14 (1979) 153–166.
[22] J. Dow, T. Green, Trichloroethylene induced vitamin B(12) and folate deficiency leads to increased formic acid excretion in the rat, Toxicology 146 (2000) 123–136, http://dx.doi.org/10.1016/S0300-483X(00)00156-6.
[23] V. Drake, S. Koprowski, J. Lough, N. Hu, S. Smith, Trichloroethylene exposure during cardiac valvuloseptal morphogenesis alters cushion formation and cardiac hemodynamics in the avian embryo, Environ. Health Perspect. 114 (2006) 842–847.
[24] V.J. Drake, S.L. Koprowski, N. Hu, S.M. Smith, J. Lough, Cardiogenic effects of trichloroethylene and trichloroacetic acid following exposure during heart specification of avian development, Toxicol. Sci. 94 (2006) 153–162, http://dx.doi.org/10.1093/toxsci/kfl083.
[25] EFSA (European Food Safety Authority), Guidance on selected default values to be used by the EFSA Scientific Committee, Scientific Panels and Units in the absence of actual measured data, EFSA J. 10 (2012) 2579, http://dx.doi.org/10.2903/j.efsa.2012.2579.
[26] E. Elovaara, K. Hemminki, H. Vainio, Effects of methylene chloride, trichloroethane, trichloroethylene, tetrachloroethylene and toluene on the development of chick embryos, Toxicology 12 (1979) 111–119, http://dx.doi.org/10.1016/0300-483x(79)90037-4.
[27] D.L. Epstein, G.A. Nolen, J.L. Randall, S.A. Christ, E.J. Read, J.A. Stober, M.K. Smith, Cardiopathic effects of dichloroacetate in the fetal Long-Evans rat, Teratology 46 (1992) 225–235, http://dx.doi.org/10.1002/tera.1420460306.
[28] J. Fisher, S. Channel, J. Eggers, P. Johnson, K. MacMahon, C. Goodyear, G. Sudberry, D. Warren, J. Latendresse, L. Graeter, Trichloroethylene, trichloroacetic acid, and dichloroacetic acid: do they affect fetal rat heart development, Int. J. Toxicol. 20 (2001) 257–267.
[29] S.P. Forand, E.L. Lewis-Michl, M.I. Gomez, Adverse birth outcomes and maternal exposure to trichloroethylene and tetrachloroethylene through soil vapor intrusion in New York State, Environ. Health Perspect. 120 (2012) 616–621, http://dx.doi.org/10.1289/ehp.1103884.
[30] L.A. Frieden, T.A. Townsend, D.B. Vaught, D.M. Delaughter, Y. Hwang, J.V. Barnett, J. Chen, Regulation of heart valve morphogenesis by Eph receptor ligand, ephrin-A1, Dev. Dyn. 239 (2010) 3226–3234, http://dx.doi.org/10.1002/dvdy.22458.
[31] L.M. Friedman, C.D. Furberg, D. DeMets, Fundamentals of Clinical Trials, 4th ed., Springer-Verlag, New York, NY, 2010, http://dx.doi.org/10.1007/978-1-4419-1586-3.
[32] K.Y. Fung, D. Krewski, J.N. Rao, A.J. Scott, Tests for trend in developmental toxicity experiments with correlated binary data, Risk Anal. 14 (1994) 639–648, http://dx.doi.org/10.1111/j.1539-6924.1994.tb00277.x.
[33] K.Y. Fung, L. Marro, D. Krewski, A comparison of methods for estimating the benchmark dose based on overdispersed data from developmental toxicity studies, Risk Anal. 18 (1998) 329–342, http://dx.doi.org/10.1111/j.1539-6924.1998.tb01299.x.
[34] S.M. Gilboa, T.A. Desrosiers, C. Lawson, P.J. Lupo, T.J. Riehle-Colarusso, P.A. Stewart, E. van Wijngaarden, M.A. Waters, A. Correa, N.B.D.P. Stud, Association between maternal occupational exposure to organic solvents and congenital heart defects, National Birth Defects Prevention Study, 1997–2002, Occup. Environ. Med. 69 (2012) 628–635, http://dx.doi.org/10.1136/oemed-2011-100536.
[35] S.J. Goldberg, M.D. Lebowitz, E.J. Graver, S. Hicks, An association of human congenital cardiac malformations and drinking water contaminants, J. Am. Coll. Cardiol. 16 (1990) 155–164.
[36] T. Green, J. Dow, C. Ong, V. Ng, H. Ong, Z. Zhuang, X. Yang, L. Bloemen, Biological monitoring of kidney function among workers occupationally exposed to trichloroethylene, Occup. Environ. Med. 61 (2004) 312–317, http://dx.doi.org/10.1136/oem.2003.007153.
[37] V. Hamburger, H.L. Hamilton, A series of normal stages in the development of the chick embryo, J. Morphol. 88 (1951) 49–92, http://dx.doi.org/10.1002/jmor.1050880104.
[38] B. Hardin, B. Kelman, R. Brent, Trichloroethylene and dichloroethylene: a critical review of teratogenicity [Review], Birth Defects Res. A Clin. Mol. Teratol. 73 (2005) 931–955, http://dx.doi.org/10.1002/bdra.20192.
[39] B.D. Hardin, G.P. Bond, M.R. Sikov, F.D. Andrew, R.P. Beliles, R.W. Niemeier, Testing of selected workplace chemicals for teratogenic potential, Scand. J. Work. Environ. Health 7 (1981) 66–75.
[40] B.D. Hardin, B.J. Kelman, R.L. Brent, Trichloroethylene and cardiac malformations [Letter], Environ. Health Perspect. 112 (2004) A607–A608.
[41] E. Hassoun, C. Kariya, F. Williams, Dichloroacetate-induced developmental toxicity and production of reactive oxygen species in zebrafish embryos, J. Biochem. Mol. Toxicol. 19 (2005) 52–58, http://dx.doi.org/10.1002/jbt.20051.
[42] T.E.J. Healy, T.R. Poole, A. Hopper, Rat fetal development and maternal exposure to trichloroethylene 100 ppm, Br. J. Anaesth. 54 (1982) 337–341.
[43] A.B. Hill, The environment and disease: association or causation? Proc. R. Soc. Med. 58 (1965) 295–300.
[44] E. Hunter, E. Rogers, J. Schmid, A. Richard, Comparative effects of haloacetic acids in whole embryo culture, Teratology 54 (1996) 57–64, http://dx.doi.org/10.1002/(SICI)1096-9926(199606)54:2<57:AID-TERA1>3.0.CO;2-1.
[45] K.J. Jenkins, A. Correa, J.A. Feinstein, L. Botto, A.E. Britt, S.R. Daniels, M. Elixson, C.A. Warnes, C.L. Webb, Noninherited risk factors and congenital cardiovascular defects: current knowledge: a scientific statement from the American Heart Association Council on cardiovascular disease in the young, Circulation 115 (2007) 2995–3014, http://dx.doi.org/10.1161/CIRCULATIONAHA.106.183216.
[46] B. Jensen, T. Wang, V.M. Christoffels, A.F.M. Moorman, Evolution and development of the building plan of the vertebrate heart [Review], BBA—Mol. Cell Res. 1833 (2013) 783–794, http://dx.doi.org/10.1016/j.bbamcr.2012.10.004.
[47] P. Johnson, Personal communication from Paula Johnson, University of Arizona, to Susan Makris, U.S. EPA, 26 August 2008. Available online, 2008.
[48] P. Johnson, Personal communication from Paula Johnson, University of Arizona, to Susan Makris, U.S. EPA, 21 February 2014. Available online, 2014.
[49] P.D. Johnson, B.V. Dawson, S.J. Goldberg, Cardiac teratogenicity of trichloroethylene metabolites, J. Am. Coll. Cardiol. 32 (1998) 540–545, http://dx.doi.org/10.1016/s0735-1097(98)00232-0.
[50] P.D. Johnson, B.V. Dawson, S.J. Goldberg, M.Z. Mays, Trichloroethylene: Johnson et al.'s response [Letter], Environ. Health Perspect. 112 (2004) A608–A609, http://dx.doi.org/10.1289/ehp.112-a608.
[51] P.D. Johnson, S.J. Goldberg, M.Z. Mays, B.V. Dawson, Threshold of trichloroethylene contamination in maternal drinking waters affecting fetal heart development in the rat, Environ. Health Perspect. 111 (2003) 289–292.
[52] P.D. Johnson, S.J. Goldberg, M.Z. Mays, B.V. Dawson, Erratum: threshold of trichloroethylene contamination in maternal drinking waters affecting fetal heart development in the rat [Erratum], Environ. Health Perspect. 113 (2005) A18.
[53] P.D. Johnson, S.J. Goldberg, M.Z. Mays, B.V. Dawson, et al., Erratum: Erratum for Johnson [Environ Health Perspect 113:A18 (2005)], Environ. Health Perspect. 122 (2014) A94, http://dx.doi.org/10.1289/ehp.122-a94.
[54] J.C. Kovacic, N. Mercader, M. Torres, M. Boehm, V. Fuster, Epithelial-to-mesenchymal and endothelial-to-mesenchymal transition: from cardiovascular development to disease [Review], Circulation 125 (2012) 1795–1808, http://dx.doi.org/10.1161/CIRCULATIONAHA.111.040352.
[55] D. Krewski, Y. Zhu, A simple data transformation for estimating benchmark doses in developmental toxicity experiments, Risk Anal. 15 (1995) 29–39, http://dx.doi.org/10.1111/j.1539-6924.1995.tb00090.x.
[56] S.W. Lagakos, B.J. Wessen, M. Zelen, An analysis of contaminated well water and health effects in Woburn, Massachusetts, J. Am. Stat. Assoc. 81 (1986) 583–596.
[57] C. Loeber, M. Hendrix, S. Diez De Pinos, S. Goldberg, Trichloroethylene: a cardiac teratogen in developing chick embryos, Pediatr. Res. 24 (1988) 740–744, http://dx.doi.org/10.1203/00006450-198812000-00018.
[58] O. Makwana, L. Ahles, A. Lencinas, O.I. Selmin, R.B. Runyan, Low-dose trichloroethylene alters cytochrome P450-2C subfamily expression in the developing chick heart, Cardiovasc. Toxicol. 13 (2013) 77–84, http://dx.doi.org/10.1007/s12012-012-9180-0.
[59] O. Makwana, N.M. King, L. Ahles, O. Selmin, H.L. Granzier, R.B. Runyan, Exposure to low-dose trichloroethylene alters shear stress gene expression and function in the developing chick heart, Cardiovasc. Toxicol. 10 (2010) 100–107, http://dx.doi.org/10.1007/s12012-010-9066-y.
[60] N. Mishima, S. Hoffman, E.G. Hill, E.L. Krug, Chick embryos exposed to trichloroethylene in an ex ovo culture model show selective defects in early endocardial cushion tissue formation, Birth Defects Res. A Clin. Mol. Teratol. 76 (2006) 517–527, http://dx.doi.org/10.1002/bdra.20283.
[61] M.G. Narotsky, R.J. Kavlock, A multidisciplinary approach to toxicological screening: II. Developmental toxicity, J. Toxicol. Environ. Health 45 (1995) 145–171, http://dx.doi.org/10.1080/15287399509531987.
[62] M.G. Narotsky, E.A. Weller, V.M. Chinchilli, R.J. Kavlock, Nonadditive developmental toxicity in mixtures of trichloroethylene, di(2-ethylhexyl) phthalate, and heptachlor in a 5x5x5 design, Fundam. Appl. Toxicol. 27 (1995) 203–216, http://dx.doi.org/10.1093/toxsci/27.2.203.

[63] NRC (National Research Council), Assessing the Human Health Risks of Trichloroethylene: Key Scientific Issues, The National Academies Press, Washington, DC, 2006 http://www.nap.edu/catalog.php?record_id=11707.
[64] NRC, Chapter 7: a roadmap for revision, in: Review of the Environmental Protection Agency's Draft IRIS Assessment of Formaldehyde, The National Academies Press, Washington, D.C, 2011 http://www.nap.edu/catalog.php?record_id=13142.
[65] J. Ou, Z. Ou, D. Mccarver, R. Hines, K. Oldham, A. Ackerman, K. Pritchard, Trichloroethylene decreases heat shock protein 90 interactions with endothelial nitric oxide synthase: implications for endothelial cell proliferation, Toxicol. Sci. 73 (2003) 90–97, http://dx.doi.org/10.1093/toxsci/kfg062.
[66] B. Palbykin, J. Borg, P.T. Caldwell, J. Rowles, A.J. Papoutsis, D.F. Romagnolo, O.I. Selmin, Trichloroethylene induces methylation of the Serca2 promoter in H9c2Cells and embryonic heart, Cardiovasc. Toxicol. 11 (2011) 204–214, http://dx.doi.org/10.1007/s12012-011-9113-3.
[67] J.N.K. Rao, A.J. Scott, A simple method for the analysis of clustered binary data, Biometrics 48 (1992) 577–585, http://dx.doi.org/10.2307/2532311.
[68] A.A. Richards, V. Garg, Genetics of congenital heart disease, Curr. Cardiol. Rev. 6 (2010) 91–97, http://dx.doi.org/10.2174/157340310791162703.
[69] K. Rothman, S. Greenland, T. Lash, Modern Epidemiology, 3rd ed., Lippincott Williams & Wilkins, Philadelphia, PA, 2008.
[70] K.J. Rothman, S. Greenland, Modern epidemiology, in: Modern Epidemiology, 2nd ed., Lippincott, Williams, & Wilkins, Philadelphia, PA, 1998.
[71] P.Z. Ruckart, F.J. Bove, M. Maslia, Evaluation of exposure to contaminated drinking water and specific birth defects and childhood cancers at Marine Corps Base Camp Lejeune, North Carolina: a case-control study, Environ. Health 12 (104) (2013), http://dx.doi.org/10.1186/1476-069x-12-104.
[72] E.S. Rufer, T.A. Hacker, G.R. Flentke, V.J. Drake, M.J. Brody, J. Lough, S.M. Smith, Altered cardiac function and ventricular septal defect in avian embryos exposed to low-dose trichloroethylene, Toxicol. Sci. 113 (2010) 444–452, http://dx.doi.org/10.1093/toxsci/kfp269.
[73] A.M. Saillenfait, I. Langonne, J.P. Sabate, Developmental toxicity of trichloroethylene, tetrachloroethylene and four of their metabolites in rat whole embryo culture, Arch. Toxicol. 70 (1995) 71–82, http://dx.doi.org/10.1007/bf02733666.
[74] B.A. Schwetz, B.K.J. Leong, P.J. Gehring, The effect of maternally inhaled trichloroethylene, perchloroethylene, methyl chloroform, and methylene chloride on embryonal and fetal development in mice and rats, Toxicol. Appl. Pharmacol. 32 (1975) 84–96, http://dx.doi.org/10.1016/0041-008x(75)90197-0.
[75] O. Selmin, P. Thorne, P. Caldwell, P. Johnson, R. Runyan, Effects of trichloroethylene and its metabolite trichloroacetic acid on the expression of vimentin in the rat H9c2 cell line, Cell Biol. Toxicol. 21 (2005) 83–95, http://dx.doi.org/10.1007/s10565-005-0124-3.
[76] O.I. Selmin, P.A. Thorne, P.T. Caldwell, M.R. Taylor, Trichloroethylene and trichloroacetic acid regulate calcium signaling pathways in murine embryonal carcinoma cells p19, Cardiovasc. Toxicol. 8 (2008) 47–56, http://dx.doi.org/10.1007/s12012-008-9014-2.
[77] M.M. Shoukri, M.A. Chaudhary, Analysis of Correlated Data with SAS and R: Third Edition, Chapman & Hall/CRC, Boca Raton, FL, 2007 https://www.crcpress.com/Analysis-of-Correlated-Data-with-SAS-and-R-Third-Edition/Shoukri-Chaudhary/9781584886198.
[78] M.K. Smith, J.L. Randall, E.J. Read, J.A. Stober, Teratogenic activity of trichloroacetic acid in the rat, Teratology 40 (1989) 445–451, http://dx.doi.org/10.1002/tera.1420400506.
[79] M.K. Smith, J.L. Randall, E.J. Read, J.A. Stober, Developmental toxicity of dichloroacetate in the rat, Teratology 46 (1992) 217–223, http://dx.doi.org/10.1002/tera.1420460305.
[80] R.E. Staples, Detection of visceral alterations in mammalian fetuses [Abstract], Teratology 9 (1974) A37A38.
[81] L.J. Stephen, A.L. Fawkes, A. Verhoeve, G. Lemke, A. Brown, A critical role for the EphA3 receptor tyrosine kinase in heart development, Dev. Biol. 302 (2007) 66–79, http://dx.doi.org/10.1016/j.ydbio.2006.08.058.
[82] J.L. Stuckhardt, S.M. Poppe, Fresh visceral examination of rat and rabbit fetuses used in teratogenicity testing, Teratog. Carcinog. Mutagen. 4 (1984) 181–188, http://dx.doi.org/10.1002/tcm.1770040203.
[83] J. Tikkanen, O. Heinonen, Maternal exposure to chemical and physical factors during pregnancy and cardiovascular malformations in the offspring, Teratology 43 (1991) 591–600, http://dx.doi.org/10.1002/tera.1420430614.
[84] J. Tikkanen, O.P. Heinonen, Cardiovascular malformations and organic solvent exposure during pregnancy in Finland, Am. J. Ind. Med. 14 (1988) 1–8, http://dx.doi.org/10.1002/ajim.4700140102.
[85] U.S. EPA (U.S. Environmental Protection Agency), Guidelines for Developmental Toxicity Risk Assessment. (EPA/600/FR-91/001), U.S. Environmental Protection Agency, Risk Assessment Forum, Washington, DC, 1991 http://cfpub.epa.gov/ncea/cfm/recordisplay.cfm?deid=23162.
[86] U.S. EPA (U.S. Environmental Protection Agency), A Framework for Assessing Health Risk of Environmental Exposures to Children. (EPA/600/R-05/093F), U.S. Environmental Protection Agency, Office of Research and Development, National Center for Environmental Assessment, Washington, DC, 2006 http://cfpub.epa.gov/ncea/cfm/recordisplay.cfm?deid=158363.
[87] U.S. EPA (U.S. Environmental Protection Agency), Toxicological review of trichloroethylene (CASRN 79-01-6) in support of summary information on the Integrated Risk Information System (IRIS) [EPA Report]. (EPA/635/R-09/011F), 2011, Washington, DC http://www.epa.gov/iris/supdocs/0199index.html.
[88] U.S. EPA (U.S. Environmental Protection Agency), Benchmark dose software (BMDS). Version 2.5.0.82 [build: 5/17/2014] [BMDS], U.S. Environmental Protection Agency, National Center for Environmental Assessment, Washington, DC, 2014, Retrieved from http://www.epa.gov/ncea/bmds/.
[89] A. von Gise, W.T. Pu, Endocardial and epicardial epithelial to mesenchymal transitions in heart development and disease [Review], Circ. Res. 110 (2012) 1628–1645, http://dx.doi.org/10.1161/circresaha.111.259960.
[90] R.E. Watson, C.F. Jacobson, A.L. Williams, W.B. Howard, J.M. DeSesso, Trichloroethylene-contaminated drinking water and congenital heart defects: a critical analysis of the literature [Review], Reprod. Toxicol. 21 (2006) 117–147, http://dx.doi.org/10.1016/j.reprotox.2005.07.013.
[91] F.E. Williams, T.J. Sickelbaugh, E. Hassoun, Modulation by ellagic acid of DCA-induced developmental toxicity in the zebrafish (Danio rerio), J. Biochem. Mol. Toxicol. 20 (2006) 183–190, http://dx.doi.org/10.1002/jbt.20135.
[92] J.G. Wilson, Methods for administering agents and detecting malformations in experimental animals, in: J. Warkany (Ed.), Teratology: Principles and Techniques, 8 ed., University of Chicago Press, Chicago, IL, 1965, pp. 262–267.
[93] P.D. Wilson, C.A. Loffredo, A. Correa-Villaseñor, C. Ferencz, Attributable fraction for cardiac malformations, Am. J. Epidemiol. 148 (1998) 414–423.
[94] J.S. Yauck, M.E. Malloy, K. Blair, P.M. Simpson, D.G. Mccarver, Proximity of residence to trichloroethylene-emitting sites and increased risk of offspring congenital heart defects among older women, Birth Defects Res. A Clin. Mol. Teratol. 70 (2004) 808–814, http://dx.doi.org/10.1002/bdra.20060.

Makris, Susan

From: Barbara Abbott <abbott.barbara@att.net>
Sent: Thursday, April 23, 2020 3:10 PM
To: Makris, Susan; Euling, Susan; Hotchkiss, Andrew; Arzuaga, Xabier; Knudsen, Thomas; Hunter, Sid; Narotsky, Michael; Parsons, Christy; Fox, John; Hogan, Karen; jjinot@hotmail.com
Subject: Re: STAA award application

Greetings Sue,
I agree with your percent contribution as shown in the table for my contribution to the publication that you are nominating for a STAA award. I have not been nominated or received an award in the previous 5 years. As shown I retired in 2019.
I expect that this email response is a required part of the application so I will refrain from extraneous communications, but wish you well in these challenging days.

Regards, Barbara Abbott

Sent from AT&T Yahoo Mail on Android

On Thu, Apr 23, 2020 at 1:45 PM, Makris, Susan <Makris.Susan@epa.gov> wrote:

Greetings esteemed coauthors! Our publication on "A systematic evaluation of the potential effects of trichloroethylene exposure on cardiac development", published in 2016, is still eligible to be nominated for a STAA award. I plan to submit the award nomination by the Apr 30 deadline. I propose the following percent contributions. Please respond to this email ASAP, and indicate 1) if you agree with the percent contribution assigned to you, and 2) whether you have been nominated for or have won a STAA award within the past 5 years. Thank you in advance for your prompt attention to this task! Sue

Coauthors	Percent Contribution	Agree w/% (Yes/No)	Nominated for STAA award in past 5 yrs (Yes/No)	Won STAA award in past 5 yrs (Yes/No)
Susan L. Makris	13			
Cheryl Siegel Scott (D)	8			
John Fox (E)	8			
Thomas B. Knudsen	8			
Andrew K. Hotchkiss	8			
Xabier Arzuaga	8			
Susan Y. Euling	8			
Christina M. Powers (Parsons)	5			
Jennifer Jinot (R)	5			
Karen A. Hogan (E)	5			

Barbara D. Abbott (R)	8			
E. Sidney Hunter, III	8			
Michael G. Narotsky	8			
Total	100			

D = deceased

R = retired

E = emeritus

Susan Makris

USEPA/ORD/CPHEA, 1200 Pennsylvania Ave. NW, Mailcode 8623R, Washington, DC 20460

202-564-7332 (O), 202-697-2621 (M), 202-564-0296 (F), makris.susan@epa.gov

Courier address: Ronald Reagan Bldg., 1300 Pennsylvania Ave. NW, Rm 71280, Washington, DC 20004

Makris, Susan

From: Arzuaga, Xabier
Sent: Thursday, April 23, 2020 2:34 PM
To: Makris, Susan
Subject: RE: STAA award application

Hi Sue,
Thank you very much for organizing this. I agree with the percent contribution. Also, I have not been nominated for an STAA award, but Erin is also submitting the DIBP paper and I am a co-author on that paper. Thanks!
Xabier

From: Makris, Susan <Makris.Susan@epa.gov>
Sent: Thursday, April 23, 2020 1:45 PM
To: Euling, Susan <Euling.Susan@epa.gov>; Hotchkiss, Andrew <Hotchkiss.Andrew@epa.gov>; Arzuaga, Xabier <Arzuaga.Xabier@epa.gov>; Knudsen, Thomas <Knudsen.Thomas@epa.gov>; Hunter, Sid <Hunter.Sid@epa.gov>; Narotsky, Michael <Narotsky.Michael@epa.gov>; Parsons, Christy <Parsons.Christy@epa.gov>; Fox, John <Fox.John@epa.gov>; Hogan, Karen <Hogan.Karen@epa.gov>; abbott.barbara@att.net; jjinot@hotmail.com
Subject: STAA award application

Greetings esteemed coauthors! Our publication on "A systematic evaluation of the potential effects of trichloroethylene exposure on cardiac development", published in 2016, is still eligible to be nominated for a STAA award. I plan to submit the award nomination by the Apr 30 deadline. I propose the following percent contributions. Please respond to this email ASAP, and indicate 1) if you agree with the percent contribution assigned to you, and 2) whether you have been nominated for or have won a STAA award within the past 5 years. Thank you in advance for your prompt attention to this task! Sue

Coauthors	Percent Contribution	Agree w/% (Yes/No)	Nominated for STAA award in past 5 yrs (Yes/No)	Won STAA award in past 5 yrs (Yes/No)
Susan L. Makris	13			
Cheryl Siegel Scott (D)	8			
John Fox (E)	8			
Thomas B. Knudsen	8			
Andrew K. Hotchkiss	8			
Xabier Arzuaga	8			
Susan Y. Euling	8			
Christina M. Powers (Parsons)	5			
Jennifer Jinot (R)	5			
Karen A. Hogan (E)	5			
Barbara D. Abbott (R)	8			
E. Sidney Hunter, III	8			
Michael G. Narotsky	8			
Total	100			
D = deceased R = retired				

E = emeritus

Susan Makris
USEPA/ORD/CPHEA, 1200 Pennsylvania Ave. NW, Mailcode 8623R, Washington, DC 20460
202-564-7332 (O), 202-697-2621 (M), 202-564-0296 (F), makris.susan@epa.gov
Courier address: Ronald Reagan Bldg., 1300 Pennsylvania Ave. NW, Rm 71280, Washington, DC 20004

Makris, Susan

From: Euling, Susan
Sent: Thursday, April 23, 2020 2:58 PM
To: Makris, Susan
Subject: RE: STAA award application

Thank you for your hard work on the application.

I agree with the percentage and I do not think I was part of a STAA award in the last 5 years.

Sue

From: Makris, Susan <Makris.Susan@epa.gov>
Sent: Thursday, April 23, 2020 1:45 PM
To: Euling, Susan <Euling.Susan@epa.gov>; Hotchkiss, Andrew <Hotchkiss.Andrew@epa.gov>; Arzuaga, Xabier <Arzuaga.Xabier@epa.gov>; Knudsen, Thomas <Knudsen.Thomas@epa.gov>; Hunter, Sid <Hunter.Sid@epa.gov>; Narotsky, Michael <Narotsky.Michael@epa.gov>; Parsons, Christy <Parsons.Christy@epa.gov>; Fox, John <Fox.John@epa.gov>; Hogan, Karen <Hogan.Karen@epa.gov>; abbott.barbara@att.net; jjinot@hotmail.com
Subject: STAA award application

Greetings esteemed coauthors! Our publication on "A systematic evaluation of the potential effects of trichloroethylene exposure on cardiac development", published in 2016, is still eligible to be nominated for a STAA award. I plan to submit the award nomination by the Apr 30 deadline. I propose the following percent contributions. Please respond to this email ASAP, and indicate 1) if you agree with the percent contribution assigned to you, and 2) whether you have been nominated for or have won a STAA award within the past 5 years. Thank you in advance for your prompt attention to this task! Sue

Coauthors	Percent Contribution	Agree w/% (Yes/No)	Nominated for STAA award in past 5 yrs (Yes/No)	Won STAA award in past 5 yrs (Yes/No)
Susan L. Makris	13			
Cheryl Siegel Scott (D)	8			
John Fox (E)	8			
Thomas B. Knudsen	8			
Andrew K. Hotchkiss	8			
Xabier Arzuaga	8			
Susan Y. Euling	8			
Christina M. Powers (Parsons)	5			
Jennifer Jinot (R)	5			
Karen A. Hogan (E)	5			
Barbara D. Abbott (R)	8			
E. Sidney Hunter, III	8			
Michael G. Narotsky	8			
Total	100			
D = deceased R = retired E = emeritus				

Susan Makris
USEPA/ORD/CPHEA, 1200 Pennsylvania Ave. NW, Mailcode 8623R, Washington, DC 20460
202-564-7332 (O), 202-697-2621 (M), 202-564-0296 (F), makris.susan@epa.gov
Courier address: Ronald Reagan Bldg., 1300 Pennsylvania Ave. NW, Rm 71280, Washington, DC 20004

Makris, Susan

From: Hogan, Karen
Sent: Thursday, April 23, 2020 1:56 PM
To: Makris, Susan
Subject: RE: STAA award application

Hi Sue, Great that the paper is eligible! I agree with having the lowest percent contribution, and would take a lower amount so that the lead author gets more appropriate credit, but assume that 5% is the lowest option.
Thanks for taking this on,
Karen

From: Makris, Susan <Makris.Susan@epa.gov>
Sent: Thursday, April 23, 2020 1:45 PM
To: Euling, Susan <Euling.Susan@epa.gov>; Hotchkiss, Andrew <Hotchkiss.Andrew@epa.gov>; Arzuaga, Xabier <Arzuaga.Xabier@epa.gov>; Knudsen, Thomas <Knudsen.Thomas@epa.gov>; Hunter, Sid <Hunter.Sid@epa.gov>; Narotsky, Michael <Narotsky.Michael@epa.gov>; Parsons, Christy <Parsons.Christy@epa.gov>; Fox, John <Fox.John@epa.gov>; Hogan, Karen <Hogan.Karen@epa.gov>; abbott.barbara@att.net; jjinot@hotmail.com
Subject: STAA award application

Greetings esteemed coauthors! Our publication on "A systematic evaluation of the potential effects of trichloroethylene exposure on cardiac development", published in 2016, is still eligible to be nominated for a STAA award. I plan to submit the award nomination by the Apr 30 deadline. I propose the following percent contributions. Please respond to this email ASAP, and indicate 1) if you agree with the percent contribution assigned to you, and 2) whether you have been nominated for or have won a STAA award within the past 5 years. Thank you in advance for your prompt attention to this task! Sue

Coauthors	Percent Contribution	Agree w/% (Yes/No)	Nominated for STAA award in past 5 yrs (Yes/No)	Won STAA award in past 5 yrs (Yes/No)
Susan L. Makris	13			
Cheryl Siegel Scott (D)	8			
John Fox (E)	8			
Thomas B. Knudsen	8			
Andrew K. Hotchkiss	8			
Xabier Arzuaga	8			
Susan Y. Euling	8			
Christina M. Powers (Parsons)	5			
Jennifer Jinot (R)	5			
Karen A. Hogan (E)	5	Yes	No	No
Barbara D. Abbott (R)	8			
E. Sidney Hunter, III	8			
Michael G. Narotsky	8			
Total	100			
D = deceased R = retired E = emeritus				

Susan Makris
USEPA/ORD/CPHEA, 1200 Pennsylvania Ave. NW, Mailcode 8623R, Washington, DC 20460
202-564-7332 (O), 202-697-2621 (M), 202-564-0296 (F), makris.susan@epa.gov
Courier address: Ronald Reagan Bldg., 1300 Pennsylvania Ave. NW, Rm 71280, Washington, DC 20004

Makris, Susan

From: Hotchkiss, Andrew
Sent: Thursday, April 23, 2020 3:35 PM
To: Makris, Susan
Subject: RE: STAA award application

Hi Sue,

I hope all is well with you. Seems like forever since we have been able to catch up.

Thanks for submitting this. I am fine with what you list below and, to my knowledge, this and the phthalate STAA are the only STAAs I have been nominated for in the last 5 years.

Best regards,
Andrew

From: Makris, Susan <Makris.Susan@epa.gov>
Sent: Thursday, April 23, 2020 1:45 PM
To: Euling, Susan <Euling.Susan@epa.gov>; Hotchkiss, Andrew <Hotchkiss.Andrew@epa.gov>; Arzuaga, Xabier <Arzuaga.Xabier@epa.gov>; Knudsen, Thomas <Knudsen.Thomas@epa.gov>; Hunter, Sid <Hunter.Sid@epa.gov>; Narotsky, Michael <Narotsky.Michael@epa.gov>; Parsons, Christy <Parsons.Christy@epa.gov>; Fox, John <Fox.John@epa.gov>; Hogan, Karen <Hogan.Karen@epa.gov>; abbott.barbara@att.net; jjinot@hotmail.com
Subject: STAA award application

Greetings esteemed coauthors! Our publication on "A systematic evaluation of the potential effects of trichloroethylene exposure on cardiac development", published in 2016, is still eligible to be nominated for a STAA award. I plan to submit the award nomination by the Apr 30 deadline. I propose the following percent contributions. Please respond to this email ASAP, and indicate 1) if you agree with the percent contribution assigned to you, and 2) whether you have been nominated for or have won a STAA award within the past 5 years. Thank you in advance for your prompt attention to this task! Sue

Coauthors	Percent Contribution	Agree w/% (Yes/No)	Nominated for STAA award in past 5 yrs (Yes/No)	Won STAA award in past 5 yrs (Yes/No)
Susan L. Makris	13			
Cheryl Siegel Scott (D)	8			
John Fox (E)	8			
Thomas B. Knudsen	8			
Andrew K. Hotchkiss	8			
Xabier Arzuaga	8			
Susan Y. Euling	8			
Christina M. Powers (Parsons)	5			
Jennifer Jinot (R)	5			
Karen A. Hogan (E)	5			
Barbara D. Abbott (R)	8			
E. Sidney Hunter, III	8			

Michael G. Narotsky	8			
Total	100			
D = deceased R = retired E = emeritus				

Susan Makris
USEPA/ORD/CPHEA, 1200 Pennsylvania Ave. NW, Mailcode 8623R, Washington, DC 20460
202-564-7332 (O), 202-697-2621 (M), 202-564-0296 (F), makris.susan@epa.gov
Courier address: Ronald Reagan Bldg., 1300 Pennsylvania Ave. NW, Rm 71280, Washington, DC 20004

Makris, Susan

From: Hunter, Sid
Sent: Thursday, April 23, 2020 1:51 PM
To: Makris, Susan
Subject: RE: STAA award application

Good Mornin'
8%- I agree
No STAA nominations
THANK YOU for doing this!
sid

From: Makris, Susan <Makris.Susan@epa.gov>
Sent: Thursday, April 23, 2020 1:45 PM
To: Euling, Susan <Euling.Susan@epa.gov>; Hotchkiss, Andrew <Hotchkiss.Andrew@epa.gov>; Arzuaga, Xabier <Arzuaga.Xabier@epa.gov>; Knudsen, Thomas <Knudsen.Thomas@epa.gov>; Hunter, Sid <Hunter.Sid@epa.gov>; Narotsky, Michael <Narotsky.Michael@epa.gov>; Parsons, Christy <Parsons.Christy@epa.gov>; Fox, John <Fox.John@epa.gov>; Hogan, Karen <Hogan.Karen@epa.gov>; abbott.barbara@att.net; jjinot@hotmail.com
Subject: STAA award application

Greetings esteemed coauthors! Our publication on "A systematic evaluation of the potential effects of trichloroethylene exposure on cardiac development", published in 2016, is still eligible to be nominated for a STAA award. I plan to submit the award nomination by the Apr 30 deadline. I propose the following percent contributions. Please respond to this email ASAP, and indicate 1) if you agree with the percent contribution assigned to you, and 2) whether you have been nominated for or have won a STAA award within the past 5 years. Thank you in advance for your prompt attention to this task! Sue

Coauthors	Percent Contribution	Agree w/% (Yes/No)	Nominated for STAA award in past 5 yrs (Yes/No)	Won STAA award in past 5 yrs (Yes/No)
Susan L. Makris	13			
Cheryl Siegel Scott (D)	8			
John Fox (E)	8			
Thomas B. Knudsen	8			
Andrew K. Hotchkiss	8			
Xabier Arzuaga	8			
Susan Y. Euling	8			
Christina M. Powers (Parsons)	5			
Jennifer Jinot (R)	5			
Karen A. Hogan (E)	5			
Barbara D. Abbott (R)	8			
E. Sidney Hunter, III	8			
Michael G. Narotsky	8			
Total	100			
D = deceased R = retired E = emeritus				

Susan Makris
USEPA/ORD/CPHEA, 1200 Pennsylvania Ave. NW, Mailcode 8623R, Washington, DC 20460
202-564-7332 (O), 202-697-2621 (M), 202-564-0296 (F), makris.susan@epa.gov
Courier address: Ronald Reagan Bldg., 1300 Pennsylvania Ave. NW, Rm 71280, Washington, DC 20004

Makris, Susan

From: Jennifer Jinot <jjinot@hotmail.com>
Sent: Friday, April 24, 2020 9:20 AM
To: Makris, Susan
Subject: Re: STAA award application

Hi, Sue. Hope you're doing well. I am fine with the contribution. And, sorry, I don't recall whether or not I was nominated for or awarded an staa award in the past 5 years. It's possible, but I'm not sure. Definitely not in the past two and a half years! But beyond that I don't remember. Thanks for attempting this! And take care. jj

Get Outlook for Android

From: Makris, Susan <Makris.Susan@epa.gov>
Sent: Thursday, April 23, 2020 1:45:16 PM
To: Euling, Susan <Euling.Susan@epa.gov>; Hotchkiss, Andrew <Hotchkiss.Andrew@epa.gov>; Arzuaga, Xabier <Arzuaga.Xabier@epa.gov>; Knudsen, Thomas <Knudsen.Thomas@epa.gov>; Hunter, Sid <Hunter.Sid@epa.gov>; Narotsky, Michael <Narotsky.Michael@epa.gov>; Parsons, Christy <Parsons.Christy@epa.gov>; Fox, John <Fox.John@epa.gov>; Hogan, Karen <Hogan.Karen@epa.gov>; abbott.barbara@att.net <abbott.barbara@att.net>; jjinot@hotmail.com <jjinot@hotmail.com>
Subject: STAA award application

Greetings esteemed coauthors! Our publication on "A systematic evaluation of the potential effects of trichloroethylene exposure on cardiac development", published in 2016, is still eligible to be nominated for a STAA award. I plan to submit the award nomination by the Apr 30 deadline. I propose the following percent contributions. Please respond to this email ASAP, and indicate 1) if you agree with the percent contribution assigned to you, and 2) whether you have been nominated for or have won a STAA award within the past 5 years. Thank you in advance for your prompt attention to this task! Sue

Coauthors	Percent Contribution	Agree w/% (Yes/No)	Nominated for STAA award in past 5 yrs (Yes/No)	Won STAA award in past 5 yrs (Yes/No)
Susan L. Makris	13			
Cheryl Siegel Scott (D)	8			
John Fox (E)	8			
Thomas B. Knudsen	8			
Andrew K. Hotchkiss	8			
Xabier Arzuaga	8			
Susan Y. Euling	8			
Christina M. Powers (Parsons)	5			
Jennifer Jinot (R)	5			
Karen A. Hogan (E)	5			
Barbara D. Abbott (R)	8			
E. Sidney Hunter, III	8			
Michael G. Narotsky	8			
Total	100			
D = deceased R = retired				

E = emeritus

Susan Makris
USEPA/ORD/CPHEA, 1200 Pennsylvania Ave. NW, Mailcode 8623R, Washington, DC 20460
202-564-7332 (O), 202-697-2621 (M), 202-564-0296 (F), makris.susan@epa.gov
Courier address: Ronald Reagan Bldg., 1300 Pennsylvania Ave. NW, Rm 71280, Washington, DC 20004

From: John Fox
To: Makris, Susan
Subject: Re: STAA award application
Date: Friday, April 24, 2020 2:02:29 PM

Sorry, i overlooked the questions!
More formalin:

1) if you agree with the percent contribution assigned to you,
YES

2) whether you have been nominated for or have won a STAA award within the past 5 years.
NO

_____
On Friday, April 24, 2020, 12:57:42 PM EDT, Makris, Susan <makris.susan@epa.gov> wrote:

Hi John, Thanks for the info, and for the levity! But could you also please respond to my email more formally and specifically answer the 2 questions, since your response is needed as documentation for the nomination process. We can catch up again later! Sue

Susan Makris

USEPA/ORD/CPHEA, 1200 Pennsylvania Ave. NW, Mailcode 8623R, Washington, DC 20460

202-564-7332 (O), 202-697-2621 (M), 202-564-0296 (F), makris.susan@epa.gov

Courier address: Ronald Reagan Bldg., 1300 Pennsylvania Ave. NW, Rm 71280, Washington, DC 20004

From: Makris, Susan
Sent: Thursday, April 23, 2020 1:45 PM
To: Euling, Susan <Euling.Susan@epa.gov>; Hotchkiss, Andrew <Hotchkiss.Andrew@epa.gov>; Arzuaga, Xabier <Arzuaga.Xabier@epa.gov>; Knudsen, Thomas <Knudsen.Thomas@epa.gov>; Hunter, Sid <Hunter.Sid@epa.gov>; Narotsky, Michael <Narotsky.Michael@epa.gov>; Parsons, Christy <Parsons.Christy@epa.gov>; Fox, John <Fox.John@epa.gov>; Hogan, Karen <Hogan.Karen@epa.gov>; abbott.barbara@att.net; jjinot@hotmail.com
Subject: STAA award application

Greetings esteemed coauthors! Our publication on "A systematic evaluation of the potential effects of trichloroethylene exposure on cardiac development", published in 2016, is still eligible to be nominated for a STAA award. I plan to submit the award nomination by the Apr 30 deadline. I propose the following percent contributions. Please respond to this email ASAP, and indicate 1) if you agree with the percent contribution assigned to you, and 2) whether you have been nominated for or have won a STAA award within the past 5 years. Thank you in advance for your prompt attention to this task! Sue

Coauthors	Percent Contribution	Agree w/% (Yes/No)	Nominated for STAA award in past 5 yrs (Yes/No)	Won STAA award in past 5 yrs (Yes/No)
Susan L. Makris	13			
Cheryl Siegel Scott (D)	8			
John Fox (E)	8			
Thomas B. Knudsen	8			
Andrew K. Hotchkiss	8			
Xabier Arzuaga	8			
Susan Y. Euling	8			
Christina M. Powers (Parsons)	5			
Jennifer Jinot (R)	5			
Karen A. Hogan (E)	5			
Barbara D. Abbott (R)	8			
E. Sidney Hunter, III	8			
Michael G. Narotsky	8			
Total	100			
D = deceased R = retired E = emeritus				

Susan Makris

USEPA/ORD/CPHEA, 1200 Pennsylvania Ave. NW, Mailcode 8623R, Washington, DC 20460

202-564-7332 (O), 202-697-2621 (M), 202-564-0296 (F), makris.susan@epa.gov

Courier address: Ronald Reagan Bldg., 1300 Pennsylvania Ave. NW, Rm 71280, Washington, DC 20004

Makris, Susan

From: Knudsen, Thomas
Sent: Thursday, April 23, 2020 3:17 PM
To: Makris, Susan; Euling, Susan; Hotchkiss, Andrew; Arzuaga, Xabier; Hunter, Sid; Narotsky, Michael; Parsons, Christy; Fox, John; Hogan, Karen; abbott.barbara@att.net; jjinot@hotmail.com
Subject: RE: STAA award application

Sue,

See box below
Good luck!

Thomas B. Knudsen, PhD
Developmental Systems Biologist
Computational Toxicology and Bioinformatics Branch
Biomolecular and Computational Toxicology Division
Center for Computational Toxicology and Exposure
Office of Research and Development
U.S. Environmental Protection Agency
TEL: 919-541-9776
CELL: 919-698-4308
EMAIL: knudsen.thomas@epa.gov
If I am not the Federal Contracting Officer or Representative (CO/COR) on your contract please DO NOT consider this technical direction (TD). Any TD will be formally identified and/or documented from your CO or COR.

From: Makris, Susan <Makris.Susan@epa.gov>
Sent: Thursday, April 23, 2020 1:45 PM
To: Euling, Susan <Euling.Susan@epa.gov>; Hotchkiss, Andrew <Hotchkiss.Andrew@epa.gov>; Arzuaga, Xabier <Arzuaga.Xabier@epa.gov>; Knudsen, Thomas <Knudsen.Thomas@epa.gov>; Hunter, Sid <Hunter.Sid@epa.gov>; Narotsky, Michael <Narotsky.Michael@epa.gov>; Parsons, Christy <Parsons.Christy@epa.gov>; Fox, John <Fox.John@epa.gov>; Hogan, Karen <Hogan.Karen@epa.gov>; abbott.barbara@att.net; jjinot@hotmail.com
Subject: STAA award application

Greetings esteemed coauthors! Our publication on "A systematic evaluation of the potential effects of trichloroethylene exposure on cardiac development", published in 2016, is still eligible to be nominated for a STAA award. I plan to submit the award nomination by the Apr 30 deadline. I propose the following percent contributions. Please respond to this email ASAP, and indicate 1) if you agree with the percent contribution assigned to you, and 2) whether you have been nominated for or have won a STAA award within the past 5 years. Thank you in advance for your prompt attention to this task! Sue

Coauthors	Percent Contribution	Agree w/% (Yes/No)	Nominated for STAA award in past 5 yrs (Yes/No)	Won STAA award in past 5 yrs (Yes/No)
Susan L. Makris	13			
Cheryl Siegel Scott (D)	8			
John Fox (E)	8			
Thomas B. Knudsen	8	Yes	Yes	Yes
Andrew K. Hotchkiss	8			
Xabier Arzuaga	8			
Susan Y. Euling	8			

Christina M. Powers (Parsons)	5			
Jennifer Jinot (R)	5			
Karen A. Hogan (E)	5			
Barbara D. Abbott (R)	8			
E. Sidney Hunter, III	8			
Michael G. Narotsky	8			
Total	100			
D = deceased R = retired E = emeritus				

Susan Makris
USEPA/ORD/CPHEA, 1200 Pennsylvania Ave. NW, Mailcode 8623R, Washington, DC 20460
202-564-7332 (O), 202-697-2621 (M), 202-564-0296 (F), makris.susan@epa.gov
Courier address: Ronald Reagan Bldg., 1300 Pennsylvania Ave. NW, Rm 71280, Washington, DC 20004

Makris, Susan

From: Makris, Susan
Sent: Thursday, April 30, 2020 7:35 AM
To: Makris, Susan
Subject: FW: STAA award application

I agree with the percent contribution of 13%. I have not been nominated for or won a STAA award within the past 6 years. Susan Makris

Susan Makris
USEPA/ORD/CPHEA, 1200 Pennsylvania Ave. NW, Mailcode 8623R, Washington, DC 20460
202-564-7332 (O), 202-697-2621 (M), 202-564-0296 (F), makris.susan@epa.gov
Courier address: Ronald Reagan Bldg., 1300 Pennsylvania Ave. NW, Rm 71280, Washington, DC 20004

From: Makris, Susan
Sent: Thursday, April 23, 2020 1:45 PM
To: Euling, Susan <Euling.Susan@epa.gov>; Hotchkiss, Andrew <Hotchkiss.Andrew@epa.gov>; Arzuaga, Xabier <Arzuaga.Xabier@epa.gov>; Knudsen, Thomas <Knudsen.Thomas@epa.gov>; Hunter, Sid <Hunter.Sid@epa.gov>; Narotsky, Michael <Narotsky.Michael@epa.gov>; Parsons, Christy <Parsons.Christy@epa.gov>; Fox, John <Fox.John@epa.gov>; Hogan, Karen <Hogan.Karen@epa.gov>; abbott.barbara@att.net; jjinot@hotmail.com
Subject: STAA award application

Greetings esteemed coauthors! Our publication on "A systematic evaluation of the potential effects of trichloroethylene exposure on cardiac development", published in 2016, is still eligible to be nominated for a STAA award. I plan to submit the award nomination by the Apr 30 deadline. I propose the following percent contributions. Please respond to this email ASAP, and indicate 1) if you agree with the percent contribution assigned to you, and 2) whether you have been nominated for or have won a STAA award within the past 5 years. Thank you in advance for your prompt attention to this task! Sue

Coauthors	Percent Contribution	Agree w/% (Yes/No)	Nominated for STAA award in past 5 yrs (Yes/No)	Won STAA award in past 5 yrs (Yes/No)
Susan L. Makris	13			
Cheryl Siegel Scott (D)	8			
John Fox (E)	8			
Thomas B. Knudsen	8			
Andrew K. Hotchkiss	8			
Xabier Arzuaga	8			
Susan Y. Euling	8			
Christina M. Powers (Parsons)	5			
Jennifer Jinot (R)	5			
Karen A. Hogan (E)	5			
Barbara D. Abbott (R)	8			
E. Sidney Hunter, III	8			
Michael G. Narotsky	8			
Total	100			
D = deceased				

R = retired
E = emeritus

Susan Makris
USEPA/ORD/CPHEA, 1200 Pennsylvania Ave. NW, Mailcode 8623R, Washington, DC 20460
202-564-7332 (O), 202-697-2621 (M), 202-564-0296 (F), makris.susan@epa.gov
Courier address: Ronald Reagan Bldg., 1300 Pennsylvania Ave. NW, Rm 71280, Washington, DC 20004

Makris, Susan

From: Narotsky, Michael
Sent: Thursday, April 23, 2020 2:12 PM
To: Makris, Susan
Subject: RE: STAA award application

Hi Sue,

Thank you for doing this!

I'm fine with the percent contributions. I won (along with 18 coauthors) a Level III STAA in 2016. I filled in the table below.

I will keep my fingers crossed (except when washing hands)!

All the best,
Mike

From: Makris, Susan <Makris.Susan@epa.gov>
Sent: 23 April, 2020 1:45 PM
To: Euling, Susan <Euling.Susan@epa.gov>; Hotchkiss, Andrew <Hotchkiss.Andrew@epa.gov>; Arzuaga, Xabier <Arzuaga.Xabier@epa.gov>; Knudsen, Thomas <Knudsen.Thomas@epa.gov>; Hunter, Sid <Hunter.Sid@epa.gov>; Narotsky, Michael <Narotsky.Michael@epa.gov>; Parsons, Christy <Parsons.Christy@epa.gov>; Fox, John <Fox.John@epa.gov>; Hogan, Karen <Hogan.Karen@epa.gov>; abbott.barbara@att.net; jjinot@hotmail.com
Subject: STAA award application

Greetings esteemed coauthors! Our publication on "A systematic evaluation of the potential effects of trichloroethylene exposure on cardiac development", published in 2016, is still eligible to be nominated for a STAA award. I plan to submit the award nomination by the Apr 30 deadline. I propose the following percent contributions. Please respond to this email ASAP, and indicate 1) if you agree with the percent contribution assigned to you, and 2) whether you have been nominated for or have won a STAA award within the past 5 years. Thank you in advance for your prompt attention to this task! Sue

Coauthors	Percent Contribution	Agree w/% (Yes/No)	Nominated for STAA award in past 5 yrs (Yes/No)	Won STAA award in past 5 yrs (Yes/No)
Susan L. Makris	13			
Cheryl Siegel Scott (D)	8			
John Fox (E)	8			
Thomas B. Knudsen	8			
Andrew K. Hotchkiss	8			
Xabier Arzuaga	8			
Susan Y. Euling	8			
Christina M. Powers (Parsons)	5			
Jennifer Jinot (R)	5			
Karen A. Hogan (E)	5			
Barbara D. Abbott (R)	8			

E. Sidney Hunter, III	8			
Michael G. Narotsky	8	Yes	Yes	Yes
Total	100			
D = deceased R = retired E = emeritus				

Susan Makris
USEPA/ORD/CPHEA, 1200 Pennsylvania Ave. NW, Mailcode 8623R, Washington, DC 20460
202-564-7332 (O), 202-697-2621 (M), 202-564-0296 (F), makris.susan@epa.gov
Courier address: Ronald Reagan Bldg., 1300 Pennsylvania Ave. NW, Rm 71280, Washington, DC 20004

Makris, Susan

From: Parsons, Christy
Sent: Thursday, April 23, 2020 4:00 PM
To: Makris, Susan
Subject: RE: STAA award application

Hi Sue,

Wonderful to hear from you and thanks very much for your work to nominate this publication.

My responses are in the table below.

Hope you are doing well and staying healthy –
Christy

From: Knudsen, Thomas <Knudsen.Thomas@epa.gov>
Sent: Thursday, April 23, 2020 3:17 PM
To: Makris, Susan <Makris.Susan@epa.gov>; Euling, Susan <Euling.Susan@epa.gov>; Hotchkiss, Andrew <Hotchkiss.Andrew@epa.gov>; Arzuaga, Xabier <Arzuaga.Xabier@epa.gov>; Hunter, Sid <Hunter.Sid@epa.gov>; Narotsky, Michael <Narotsky.Michael@epa.gov>; Parsons, Christy <Parsons.Christy@epa.gov>; Fox, John <Fox.John@epa.gov>; Hogan, Karen <Hogan.Karen@epa.gov>; abbott.barbara@att.net; jjinot@hotmail.com
Subject: RE: STAA award application

Sue,

See box below
Good luck!

Thomas B. Knudsen, PhD
Developmental Systems Biologist
Computational Toxicology and Bioinformatics Branch
Biomolecular and Computational Toxicology Division
Center for Computational Toxicology and Exposure
Office of Research and Development
U.S. Environmental Protection Agency
TEL: 919-541-9776
CELL: 919-698-4308
EMAIL: knudsen.thomas@epa.gov
If I am not the Federal Contracting Officer or Representative (CO/COR) on your contract please DO NOT consider this technical direction (TD). Any TD will be formally identified and/or documented from your CO or COR.

From: Makris, Susan <Makris.Susan@epa.gov>
Sent: Thursday, April 23, 2020 1:45 PM
To: Euling, Susan <Euling.Susan@epa.gov>; Hotchkiss, Andrew <Hotchkiss.Andrew@epa.gov>; Arzuaga, Xabier <Arzuaga.Xabier@epa.gov>; Knudsen, Thomas <Knudsen.Thomas@epa.gov>; Hunter, Sid <Hunter.Sid@epa.gov>; Narotsky, Michael <Narotsky.Michael@epa.gov>; Parsons, Christy <Parsons.Christy@epa.gov>; Fox, John <Fox.John@epa.gov>; Hogan, Karen <Hogan.Karen@epa.gov>; abbott.barbara@att.net; jjinot@hotmail.com
Subject: STAA award application

Greetings esteemed coauthors! Our publication on "A systematic evaluation of the potential effects of trichloroethylene exposure on cardiac development", published in 2016, is still eligible to be nominated for a STAA

award. I plan to submit the award nomination by the Apr 30 deadline. I propose the following percent contributions. Please respond to this email ASAP, and indicate 1) if you agree with the percent contribution assigned to you, and 2) whether you have been nominated for or have won a STAA award within the past 5 years. Thank you in advance for your prompt attention to this task! Sue

Coauthors	Percent Contribution	Agree w/% (Yes/No)	Nominated for STAA award in past 5 yrs (Yes/No)	Won STAA award in past 5 yrs (Yes/No)
Susan L. Makris	13			
Cheryl Siegel Scott (D)	8			
John Fox (E)	8			
Thomas B. Knudsen	8	Yes	Yes	Yes
Andrew K. Hotchkiss	8			
Xabier Arzuaga	8			
Susan Y. Euling	8			
Christina M. Powers (Parsons)	5	Yes	No	No
Jennifer Jinot (R)	5			
Karen A. Hogan (E)	5			
Barbara D. Abbott (R)	8			
E. Sidney Hunter, III	8			
Michael G. Narotsky	8			
Total	100			
D = deceased R = retired E = emeritus				

Susan Makris
USEPA/ORD/CPHEA, 1200 Pennsylvania Ave. NW, Mailcode 8623R, Washington, DC 20460
202-564-7332 (O), 202-697-2621 (M), 202-564-0296 (F), makris.susan@epa.gov
Courier address: Ronald Reagan Bldg., 1300 Pennsylvania Ave. NW, Rm 71280, Washington, DC 20004

Documentation of % completion for Cheryl Siegel Scott

I, Susan Makris, verify that Cheryl Siegel Scott contributed 8% to the paper by Makris et al (2016). Cheryl passed away in 2014, prior to publication of the paper. The Acknowledgements on page 356 of the paper state:

This manuscript is dedicated to the memory of Cheryl Siegel Scott (1955–2014). In her role as an epidemiologist at the Environmental Protection Agency, National Center for Environmental Assessment, Cheryl contributed significantly to the 2011 IRIS TCE assessment, and to the developmental epidemiology evaluation
that forms a cornerstone of this review.

Region 7

Iowa
Kansas
Missouri
Nebraska
Nine Tribal Nations

Fact Sheet

September 2016

LaJolla Spring Cave Complex - Meramec Caverns
Stanton, Missouri

INTRODUCTION

This fact sheet provides a brief overview of environmental testing and actions taken to address trichloroethylene vapors at the LaJolla Spring Cave Complex—Meramec Caverns near Stanton, Mo.

BACKGROUND

In March 2016, EPA Region 7 directed the potentially responsible party at a groundwater contamination Superfund site in Franklin County, Mo., to perform additional work to protect workers and visitors from potentially harmful exposures to trichloroethylene (TCE) vapors in nearby Meramec Caverns, a privately-owned tourist attraction near Stanton, Mo.

As a precautionary step, Meramec Caverns, also known as the LaJolla Springs Cave Complex, decided to cease cave tours in March 2016 while the potentially responsible party (TRW Automotive U.S., LLC) instituted controls to reduce TCE vapor levels. This work included:

--Installation of a set of air lock doors separating the upper level of the caverns from the lower level of the caverns;

--Installation of air scrubbers in the front portion of the cave including the gift shop/cafeteria; and

--Installation of two ventilation shafts to modify airflow in the back portion of the cave, while also redirecting the natural airflow away from the air lock door system.

As a result of this work, tours in the front of the cave resumed in June 2016, and the cave was fully reopened for tours in August 2016.

Since the controls were implemented, air testing has indicated that TCE vapors are below levels of health concern in the cave. EPA will continue to monitor air testing results periodically to verify that TCE concentrations remain below levels of health concern.

CONTAMINATION HISTORY

TCE vapors in the cave likely originate from two sources: the former TRW/Ramsey facility in

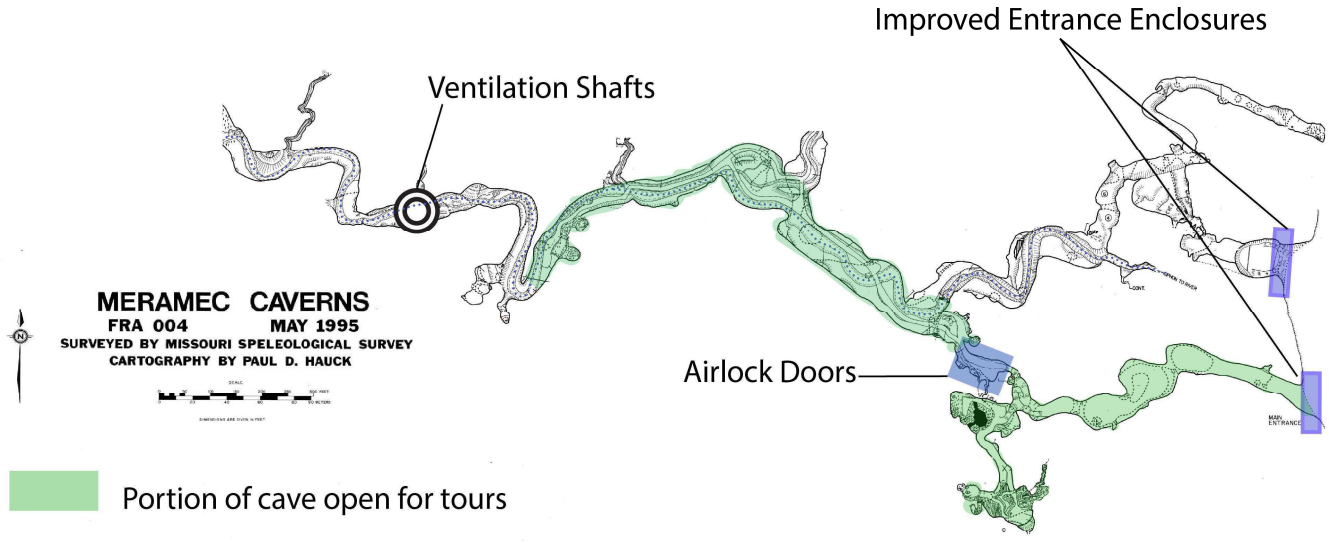

30284642

downtown Sullivan and the Sullivan Landfill.

Both of these facilities are associated with the Oak Grove Village Well Superfund Site, which became part of EPA's National Priorities List in 2002. The former TRW/Ramsey facility environmental cleanup is managed by the Missouri Department of Natural Resources' (MDNR) Resource Conservation and Recovery Act (RCRA) program.

TCE contamination in the area's groundwater has been under investigation since 1986, when it was first detected by MDNR during routine sampling of a well. From October 2002 to January 2005, EPA and MDNR sampled air in Meramec Caverns. In 2003, samples showed TCE concentrations above levels of health concern. The cave owner took immediate steps to increase air flow within the cave, and samples collected in 2004 and 2005 showed those actions had decreased TCE concentrations to acceptable levels.

In 2011, EPA issued a toxicological evaluation for TCE based on the best available science at that time. This comprehensive evaluation, which underwent extensive external peer review, identified potential adverse health effects at lower concentrations of TCE than used in the past. The health effects that may occur following exposure to the lowest concentrations of TCE include heart malformations in the fetus and adverse effects on the immune system.

EPA, the Agency for Toxic Substances and Disease Registry (ATSDR), MDNR and the Missouri Department of Health and Senior Services (MDHSS) met with the cave owner in December 2014 to discuss a MDHSS health consultation released on Dec. 12, 2014, regarding TCE air concentrations in the cave air. The health consultation recommendations included the following: (1) Inform workers of elevated TCE concentrations in the cave air, and potential health risks associated with TCE inhalation; and (2) Implement permanent measures to mitigate vapor intrusion into the cave as soon as possible.

Since December 2014, EPA has conducted sampling and overseen the implementation of a number of actions intended to address the TCE levels in the cave. In February 2016, based on new data from late 2015, ATSDR recommended to EPA that TCE exposures to employees in Meramec Caverns be stopped until the levels were brought below levels of health concern.

At that time, EPA met with the cave's owner and multiple partner agencies, including MDHSS, as well as MDNR and ATSDR, to determine appropriate health-based benchmarks and specific actions that could be taken to protect the health of the cave's workers and visitors.

In March 2016, the owner of Meramec Caverns proactively closed the cave for tours while controls were being installed. After installation of these controls were completed, including the installation of air scrubbers and ventilation shafts, as well as other protective measures, the front portion of the cave reopened in June 2016. The back portion of the cave reopened for tours in August 2016.

GOING FORWARD

EPA is requiring the Potentially Responsible Party (TRW Automotive U.S., LLC) to perform routine air monitoring to verify that the controls in place are effectively maintaining TCE vapors below levels of health concern. EPA will continue to evaluate the data to determine the frequency of future tests.

If future tests indicate that TCE vapor concentrations are not being sustained below levels of health concern, EPA will recommend re-closure if necessary to protect human health.

ADDITIONAL INFORMATION

Technical documents, maps, and other site related information is available online at: https://semspub.epa.gov/src/collection/07/SC34273

Research, to date, and letters exchanged by the participating entities are also included in the above website.

For additional information, please contact Tonya Howell at 913-551-7589 or at howell.tonya@epa.gov.

For media inquiries, please contact Angela Brees at 913-551-7940 or brees.angela@epa.gov.

Table of Contents

General_Authors_Publications.....2
LI-266872_final_Hsieh_Zepp_2019.....12
LI-266872_Hsieh_and_Zepp_Supporting_Information.....23
LI-266872_Record_of_Agreement_Hsieh.....36
LI-266872_Record_of_Agreement_Zepp.....37
LI-266872_Justification_for_Principal_Author.....39
Justification_for_Principal_Author.....40
Record_of_Agreement_Zepp.....41
Resignees_Report.....43

United States Environmental Protection Agency
Washington, DC 20460

STAA REPORT FOR THE SCIENTIST NOMINATIONS

General Information:

Nomination ID/App ID:	20-135
Research Category Primary:	Monitoring and Measurement Methods (MM)
Research Category Secondary:	Transport and Fate (TF)
Laboratory/Office Name:	ORD
Nomination Entered By:	Richard Zepp

Eligibility Checklist:

[Y] The nominated publication(s) has not been submitted to a previous STAA competition.

[Y] The nominated publication(s) was published on or before January 1, 2017 and on or after January 1,2012

[Y] The principal author was an EPA employee or a PHS employee assigned to EPA when the research was performed

[Y] The EPA authors (includes PHS employees assigned to EPA) contributed collectively a minimum of 50% toward the publication(s)

Nominating Official Name:	Timothy Watkins
Nominating Official Title:	DIRECTOR, NERL
Nominating OfficialEmail:	watkins.tim@epa.gov
STAA Coordinator Name:	Kathleen Wiser
STAA Coordinator Email:	wiser.kathi@epa.gov

Justifications:

Justification 1:

The nomination is related to one of the EPA Administrator's Core Mission Objectives which is to "ensure new and existing chemicals and pesticides are reviewed for their potential risks to human health and the environment and actions are taken when necessary". From the regulatory perspective many engineered nanomaterials (ENMs) are regarded as "chemical substances" under the Toxic Substances Control Act (TSCA). EPA's mission includes evaluation of ENMs prior to their use by EPA's Office of Pollution Prevention and Toxics (OPPT). Thus, EPA is required to gather information about these materials including exposure and release information. The evaluations of these commercial submissions examine consumer exposures to ENMs, where both hard data and exposure models are largely absent or inapplicable. For these reasons this nomination includes particularly useful evaluations relevant to EPA's mission. This STAA nomination contributes to EPA's CSS research on monitoring and modeling of environmental release of ENMs and its assessment of human and ecological exposures to ENMs. In addition, the research contributes to the US National Nanotechnology Initiative (NNI) which helps coordinate US government research on engineered nanomaterials (ENMs). EPA plays a key role in the NNI research on environmental health and safety of ENMs. The research described in this STAA application was highlighted as one of the products to be delivered by ORD from the FY19 CSS Emerging Materials and Technology research in this area. This work is also directly relevant to the current research and regulatory efforts of sister Agencies and Departments such as Consumer Products Safety Commission (CPSC), National Institute of Occupational Safety and Health (NIOSH) and NIST who are also heavily engaged in evaluating human exposures to ENMs.

Our research effort focused on Graphene Oxide (GO) , a rapidly growing carbon nanomaterial. We used GO used to develop generalizable approaches for research on this class of emerging chemicals. GO is an important precursor to graphene, a one-atom thick, two-dimensional nanomaterial made of a special type of carbon that has received unprecedented attention as a result of its fundamental properties and broad applications. The oxygen functionalities of GO enhance dispersibility in the aqueous phase, making it suitable for biomedical applications in biosensor and drug carrier materials and in environmental and energy applications such as photocatalysis or as sorbents for toxic pollutant removal and water splitting. Available results have shown that GO is more reactive in water than other carbon nanomaterials such as carbon nanotubes. As a reactive nanomaterial, GO does not maintain its pristine form in the environment. For example, reduction of GO to reduced graphene oxide (rGO) is one of its primary transformation pathways. Both GO and rGO are transformed on exposure to sunlight, but rGO is much less reactive and thus builds up and persists in the environment. One of the potential main pathways for transformations of these graphene derivatives involves reactions with reactive oxygen species (ROS) produced by sunlight-induced photoreactions of natural substances such as the dissolved organic

matter in lakes, rivers, and the ocean. This nomination provides creative new approaches for quantifying reactions of graphene derivatives in aquatic environments with three ROS: **hydroxyl radicals**, **singlet oxygen**, and **superoxide radical anions**. Reactions mediated by ROS are generally referred to as "indirect" photoreactions. Current research suggests that the reactivity of GO in indirect photoreactions may be crucial to regulating long-term exposure to rGO, the

long-lived reduction product of GO. Our objectives here were to develop methods for quantifying the rates of reaction of GO and rGO via these indirect pathways. The methods were used to provide data for simulations of the fate of GO and other nanomaterials in aquatic environments using modeling tools such as WASP8.

Commercially available single-layer GO was used in the research. Reduced rGO was synthesized by irradiating a GO dispersion in an Atlas Suntest CPS+ solar simulator. Both GO and rGO were dispersed in water by mild sonication then irradiated in a solar simulator (equipped with 1 kW Xenon arc lamp) for different time intervals. The carbon contents of GO and rGO dispersions were determined by measuring the dissolved organic carbon (DOC) which was used as the concentration index. Reactive oxygen species were photoproduced and quantified using techniques that were developed in our laboratory. **Hydroxyl radicals** were produced by photo-Fenton reaction in a rotating-turntable merry-go-round reactor (MGRR) equipped with a Hanovia medium pressure mercury lamp and a temperature-controlled circulating water bath (25 ± 2°C). The reaction samples contained $Fe(ClO_4)_3$, H_2O_2, and GO (or rGO) (~ 4 mg-C/L) at pH4. Steady state concentrations of OH radicals were measured by following reactions of the OH-probes *p*-chlorobenzoic acid or terephthalic acid. The second order rate constant for reaction of GO or rGO with hydroxyl was determined by normalizing the observed first-order rate constant for GO degradation to the OH concentration. Alternatively, competition kinetics studies involving additions of hydroxyl scavengers (chemicals that react at well-defined rates with hydroxyl radicals) were used to estimate second order rate constants for reaction of GO or rGO with hydroxyl). **Singlet oxygen**, an excited form of ordinary oxygen, was produced by irradiation of Rose Bengal as a photosensitizer. Steady-state singlet oxygen concentrations were determined by dividing the pseudo-first-order decay rate of furfuryl alcohol (FFA, 0.1 mM) by its rate constant for reaction with singlet oxygen. The second-order rate constant between GO and singlet oxygen was determined by quantitation of the effects of added GO or rGO on the steady state singlet oxygen concentration. **Superoxide anion** was produced by the chemical reaction between phenazine methosulfate and reduced-form -nicotinamide adenine dinucleotide (NADH). Superoxide production was confirmed by formation of XTT (35 - 75 μM) formazan, a known product. The second-order rate constant of reaction of GA with superoxide was calculated by the inhibitory effect of GO or the formation of XTT formazan. This reaction was followed by changes in the absorbance of XTT formazan at 470 nm.

Major challenges in exposure assessment of graphene-based ENMs are their stability and susceptibility to different reactive reagents in environment. This study provides new data and equations that apply to rates of sunlight-induced transformations of GO and its reduced form, rGO, in water. Although singlet oxygen is a widely-observed ROS produced on sunlight-irradiation of the aquatic environment, our study demonstrated that reaction with singlet oxygen had a negligible effect on transformation of GO with no effect on DOC, UV-vis spectra or particle size. In contrast, the results indicated that hydroxyl radicals can quickly degrade not only GO, but also the less reactive rGO. The data show that rGO has a similar reactivity to hydroxyl radical as GO. Reaction with hydroxyl radicals resulted in mineralization of GO, with

loss of color and formation of photoluminescent products. Reaction with superoxide ions slightly reduced GO. Together, these results suggest that an integrated understanding of ROS distribution and GO reactivity with ROS is needed to better assess long-term exposure to GO and rGO. It may also prove valuable in designing GO or rGO in environmental applications because high hydroxyl radical reactivity indicates stability of these types of nanomaterials cannot be overlooked when used as catalysts or carriers.

To summarize, the methods developed by in this nominated research provide useful approaches for providing data that can be used to predict the rates of transformations of graphene and other nanomaterials in aquatic environments. Importantly, as risk is a function of the inherent hazards of a substance and the actual potential for exposure, data on transformation dynamics from commercially relevant nanomaterials are a valuable starting point for consideration in fate and transport modeling, exposure assessment, and risk assessment frameworks. For example, water quality models such as WASP8.1 can use data and relationships from these studies for simulating the behavior of nanomaterials in aquatic environments and WASP is one of the most widely used water quality models in the world.

Justification 2A:

N/A

Justification 2B:

2019

Richard Zepp. ““Sunlight-Driven Reduction of Silver Ions by Natural Organic Matter.” 2019, Honorable Mention

2018:

n/a

2017:

Richard Zepp. “Understanding the fate and transport of human adenovirus in environmental matrices.” 2017, Level I

Richard Zepp. “Measuring the impact of light exposure on transformations and aggregation of emerging chemicals.” 2017, Level III

Richard Zepp. “Probing Photosensitization by Functionalized Carbon Nanotubes. “2017, Honorable Mention

2016:

n/a

2015:

Richard Zepp, “Photoreactivity of Unfunctionalized Single-Wall Carbon Nanotubes Involving Hydroxyl Radical: Chiral Dependency and Surface Coating Effect”, 2015, Honorable Mention

2014:

Richard Zepp, “Release Characteristics of Selected Carbon Nanotube Polymer Composites”, 2014, Level III

Justification 2C:

The multipart nomination by Richard Zepp and co-workers. “Measuring the impact of light exposure on transformations and aggregation of emerging chemicals.” 2017, Level III includes discussion of direct photoreactions of graphene oxide. This earlier paper differed significantly from the nominated Hsieh/Zepp paper which provides methods for measuring

concentrations of ROS, equations that describe the kinetics of reactions between ROS and GO, and data for the rates of reaction of the ROS with GO and its reduction product, rGO

Justification 2D:

There is Supplemental Information submitted for the nomination by Hsieh and Zepp, but this has not been previously used in any STAA nominations..

Justification 2E:

Zepp is a co-author on the nomination by Boyes et al "Comprehensive framework for evaluating the environmental health and safety implications of engineered nanomaterials."

This nomination is based on a review article that was published several years before the paper by Hsieh and Zepp was published. It is a great review but there is little overlap between the two papers.

Justification 3A:

The authors were invited to present talks on the material covered by nominated paper at several national and international meetings during the 5-year period prior to submission of this nomination:

- Invited to a symposium on “Environmental Applications and Implications of Graphene Based Nanomaterials” during the Environmental Chemistry Division at the National Meeting of the American Chemical Society, Boston in August 2015. Was lead speaker.
- Invited to present this research at Johns Hopkins University on "Interactions of Natural Organic Matter with Photochemical Reactions of Carbon Nanoparticles in Aquatic Environments” in February 2016
- Presented at the National American Chemical Society Meeting in San Francisco, April 2017
- Presented at the SETAC World Congress meeting, Orlando November 2016
- Presented at the National American Chemical Society Meeting, Washington DC August 2017
- Presented at the Fall Meeting of the American Geophysical Union, Wahington DC; December 2018
- Presented at the National American Chemical Society Meeting in New Orleans, March 2019
- Invited to be presented at the National American Chemical Society Meeting in Philadelphia March 2020; postponed until 2021 due to coronavirus problem
- Presented at UNEP meetings in New Zealand, September 2019 and Vermont during September 2018

Justification 3B:

The paper was reviewed and accepted for publication by three peer reviewers of Environmental Science: Nano a premier international journal that is one of the most desirable publications for environmental research. *Environmental Science: Nano* has a high impact factor of 7.704, reflective of the quality of its external review process. In addition, the research was subjected to peer review of papers and discussions by the authors and other participants at the national and international scientific meetings on nanomaterials and environmental science noted in Section 3A. The paper was internally reviewed for content and policy implications by Dr. Tim Buckley, NERL/EMMD Director.

AUTHORS

Principal Author

Author Name:	Richard G. Zepp		
Professional Title:		Salutation:	Dr.
Email:	zepp.richard@epa.gov	Organization:	
Mailing Address:			
Street Line 1:	1270 Founders Lake Drive		
City:	Athens		
Zip Code:	30606	State:	GA
At time of research was:	EPA Employee		
Separation Date:			
% of Effort:	50		

Contributing Author

Author Name:	Hsin-Se Hsieh		
Professional Title:		Salutation:	Dr.
Email:	hsinse@gmail.com	Organization:	
Mailing Address:			
Street Line 1:	No 3 Zhenping Lane, Erlin Township, Changhua County, Taiwan, 52666		
City:			
Zip Code:		State:	
At time of research was:	Non EPA Personnel		
Separation Date:			
% of Effort:	50		

PUBLICATIONS

Publication 1:

Publication Title:	Reactivity of Graphene Oxide with Reactive Oxygen Species (Hydroxyl Radical, Singlet Oxygen, and Sup		
Publication Date:	Tue Dec 01 00:00:00 GMT 2020		
Journal/Publication Method:	Environmental Science: Nano		
All Author(s):			
Volume:	6	Number:	12
Pages:	3734-3744	Immediately Index:	Immediately Index:
Citation ½ Life:	6.9	Impact Factor:	7.704

Environmental Science Nano

PAPER

Check for updates

Cite this: *Environ. Sci.: Nano*, 2019, **6**, 3734

Reactivity of graphene oxide with reactive oxygen species (hydroxyl radical, singlet oxygen, and superoxide anion)†

Hsin-Se Hsieh [a] and Richard G. Zepp *[b]

Received 22nd June 2019,
Accepted 9th October 2019

DOI: 10.1039/c9en00693a

rsc.li/es-nano

Increases in the production and applications of graphene oxide (GO), coupled with reports of its toxic effects, are raising concerns about its health and ecological risks. To better understand GO's fate and transport in aquatic environments, we investigated its reactivity with three major reactive oxygen species (ROS): $HO^{\bullet}$, $^1O_2$, and $O_2^{\bullet-}$. Second-order degradation rate constants were calculated on the loss of dissolved organic carbon (DOC) and steady-state concentration of individual ROS species. Absolute second-order rate constants were determined by competition kinetics to be 6.24×10^4, 8.65×10^2, and 0.108 mg-C^{-1} L s^{-1} for $HO^{\bullet}$, $^1O_2$, and $O_2^{\bullet-}$, respectively. Photoreduced GO products had a similar reactivity to $HO^{\bullet}$ as GO, with rate constants comparable to polycyclic aromatic compounds, but about two times higher than dissolved organic matter on a per carbon basis. Reaction with $HO^{\bullet}$ resulted in decomposition of GO, with loss of color and formation of photoluminescent products. In contrast, reaction with $^1O_2$ showed no effect on DOC, UV-vis spectra or particle size, while reaction with $O_2^{\bullet-}$ slightly reduced GO. These results demonstrate that interactions with ROS will affect GO's persistence in water and should be considered in exposure assessment or environmental application of GO.

Environmental significance

Major challenges in exposure assessment of graphene-based nanomaterials are evaluations of their stability and susceptibility to different reactive reagents in the environment. Our study demonstrated that reaction with singlet oxygen in the aquatic environment had a negligible effect on transformation of GO although it is normally two- to three-orders of magnitude more concentrated than $HO^{\bullet}$. In contrast, hydroxyl radical attack quickly degraded not only GO, but also the less photoreactive rGO, the main photoproduct of GO. Together, these results suggest that an integrated understanding of ROS distribution and GO reactivity with ROS is needed to better assess long-term exposure to GO and rGO in the environment and in designing GO or rGO for environmental applications.

Introduction

Graphene-based nanomaterials have attracted attention from many disciplines including electronics, composite materials and energy, and from environmental and biomedical applications.[1–3] Graphene oxide (GO) is of particular interest due to its economical production and its versatility for transformation into other graphene-based materials such as reduced graphene oxide or graphene quantum dots.[4–6] Given the rapid advances in mass production of GO and potential increases in exposure, coupled with various toxic effects,[7,8] health and ecological risk concerns have emerged. To assess exposure risk, there must be a better understanding of fate and transport of GO in aquatic environments, especially persistence under different environmental conditions.[9] Research suggests that reactivity of GO in indirect photolysis or reactions with environmental reactive reagents (*e.g.*, enzymatic oxidation) may be crucial to regulating long-term exposure.[10,11]

In natural waters, singlet oxygen ($^1O_2$), superoxide anion ($O_2^{\bullet-}$), and hydroxyl radical ($HO^{\bullet}$) are three major reactive oxygen species (ROS). In sunlit waters, steady-state concentrations for $^1O_2$, $O_2^{\bullet-}$, and $HO^{\bullet}$ ranged from 10^{-12}–10^{-13} M, 10^{-9}–10^{-12} M, and 10^{-15}–10^{-18} M, respectively.[12] Additionally, $HO^{\bullet}$ can be generated in reactions between reduced-form metals (*e.g.*, Fe(II)) or minerals (*e.g.*, iron oxide) with H_2O_2.[13,14] Due to the extensive presence of H_2O_2 – some of which is produced by biological sources – metal-catalyzed $HO^{\bullet}$ sources may dominate transformation of contaminants

[a] *National Research Council Associate, National Exposure Research Laboratory, U.S. Environmental Protection Agency, Athens, Georgia 30605, USA*
[b] *National Exposure Research Laboratory, Exposure Methods & Measurement Division, U.S. Environmental Protection Agency, Athens, Georgia 30605, USA. E-mail: zepp.richard@epa.gov; Tel: +1 (706) 355 8117*

† Electronic supplementary information (ESI) available. See DOI: 10.1039/c9en00693a

This journal is © The Royal Society of Chemistry 2019

in waters where UV light irradiation is limited.[15] ROS reactivity of various carbon nanomaterials has been reported. Fullerene (C_{60}) reacts with $^1O_2$ at a rate constant of (0.69 ± 0.28) mg-C^{-1} L s^{-1}, presumably *via* physical quenching.[16] Exposure of $^1O_2$ to photo-excited C_{60} leads to formation of fullerene oxides.[17] Scavenging abilities of fullerenols and carbon nanotubes (CNT) toward $HO^{\bullet}$, $^1O_2$, and $O_2^{\bullet-}$ have been confirmed by spin trapping.[18,19] Other product studies of CNT reactions show that reactions with $^1O_2$ resulted in both surface oxide formation and decarboxylation, while reaction with $HO^{\bullet}$ caused continuous loss of carboxyl groups and evolution of CO_2.[20]

Reactivities of GO with ROS are interesting for their relevance to applications, toxicity, and transformation in biological and natural systems. For example, $HO^{\bullet}$ was proposed as oxidant for degrading GO into graphene quantum dots, supported by evidences of microscopy (TEM and AFM), spectroscopy (XPS and Raman) and mass spectrometry.[21,22] Additionally, $HO^{\bullet}$ was suggested as the major species responsible for decomposition of GO in solar irradiation and ozonation.[23–26] To estimate the reaction rate constant, Hou *et al.* irradiated 100 mM H_2O_2 to produce $HO^{\bullet}$ and measured the resulting DOC decay of GO.[10] The reported value is uncertain, however, due to coexistence of direct photolysis and $HO^{\bullet}$ reaction. GO itself may generate $^1O_2$ *via* photolysis[23,27,28] or by catalytic decomposition of H_2O_2,[29] a ubiquitous ROS species in natural waters. While $^1O_2$ was reported to mediate the photooxidation of graphene,[30] reactivity of GO with $^1O_2$ is not yet confirmed. Extracellular $O_2^{\bullet-}$ was reported to reduce GO in saline solution in the dark,[31] but there is also a knowledge gap on the rate of the reduction reaction. Only limited studies are available for quantifying the rate of reactions between GO and individual ROS, especially in the absence of direct photolysis.

Here, we present a detailed study on reactivity of GO with three different types of ROS, using both competition kinetics of ROS and degradation kinetics of DOC measurement. The objective was to provide rate constants and equations for GO reactions with ROS to provide meaningful data for modeling fate and transport of this emerging carbon-based nanomaterial in aquatic environments.[32]

Materials and methods

Materials

Single-layer graphene oxide (GO) with a 2 mg mL^{-1} concentration in pure water was purchased from Cheap Tubes Inc. (Brattleboro, VT). According to the supplier, the GO was manufactured by the modified Hummer's method[33] and contains 35–42% carbon content. Stock dispersions of GO were prepared by dispersing the purchased GO in water, with a low-energy ultrasonic bath (M5800, Branson Ultrasonics, Danbury, CT) for 5 min at room temperature. Photoreduced GO (rGO) was prepared by irradiating a 40 mg L^{-1} GO dispersion in an Atlas SunTest CPS+ solar simulator equipped with a 1 kW xenon arc lamp (Mount Prospect, IL) for different time intervals (1–7 d). The carbon contents of GO and rGO dispersions were determined by measuring the dissolved organic carbon (DOC) and using it as the concentration index. The DOC-normalized UV-vis absorbance of GO and rGO are provided in ESI† Fig. S1. Other characterizations of GO and rGO have been previously reported.[34] All chemicals were reagent grade and used as received from Sigma-Aldrich (St. Louis, MO) or Fisher Sci. (Pittsburgh, PA); detailed information of chemicals is provided in ESI.† Aqueous solutions or dispersions were prepared with water purified by a Millipore Milli-Q Synthesis system (18.2 MΩ cm at 25 °C).

Reaction with hydroxyl radical

$HO^{\bullet}$ was produced by photo-Fenton reaction in a rotating-turntable merry-go-round reactor (MGRR) equipped with a Hanovia medium pressure mercury lamp and a temperature-controlled circulating water bath (25 ± 2 °C).[15] The 436 nm monochromatic light was isolated with a combination of Corning 3–73 and 5–58 filters. The light intensity at 436 nm was measured as 0.0063 mol photons per L h^{-1}, using ferrioxalate actinometry within test tubes (Pyrex 9826, 5 mL sample).[35] In the degradation experiments, reaction samples contained $Fe(ClO_4)_3$ (15 μM), H_2O_2 (10 mM), and GO (or rGO) (~4 mg-C L^{-1}) at pH 4. Fe concentration was confirmed by the 1,10-phenanthroline method after being reduced by hydroxylamine hydrochloride.[36] The observed first-order degradation rate constant of GO, $k_{obs,DOC}$ (s^{-1}), was measured by DOC decay in the samples. Steady-state $HO^{\bullet}$ concentration, $[HO^{\bullet}]_{ss}$ (M), was determined by dividing the observed pseudo-first-order decay rate constant of *para*-chlorobenzoic acid (*p*CBA, 1.5 μM), added in separate samples, by the rate constant of *p*CBA with $HO^{\bullet}$ (5.2×10^9 M^{-1} s^{-1}).[37] The apparent degradation rate constant of GO with $HO^{\bullet}$, $k^{obs}_{HO^{\bullet},GO}$ (M^{-1} s^{-1}), was calculated using eqn (1) and (2):

$$\begin{aligned} d[DOC]_{GO}/dt &= -k^{obs}_{HO^{\bullet},GO} \times [HO^{\bullet}]_{ss} \times [DOC]_{GO} \\ &= -k_{obs,DOC} \times [DOC]_{GO} \end{aligned} \quad (1)$$

$$k^{obs}_{HO^{\bullet},GO} = k_{obs,DOC}/[HO^{\bullet}]_{ss} \quad (2)$$

where $[DOC]_{GO}$ (mg-C L^{-1}) is the dissolved carbon content of GO or rGO.

In competition kinetics, with methanol (MeOH) as the major scavenger, the absolute second-order rate constant of GO with $HO^{\bullet}$ was determined by adding varied amounts of GO to reaction solutions containing sodium oxalate (60 μM), $Fe(ClO_4)_3$ (1.5 μM), *p*CBA (0.5 μM), MeOH (50 μM) and H_2O_2 (50 μM) at pH 5.4 ± 0.1. The steady-state concentration of $HO^{\bullet}$ was corrected with SFs to account for differences in inner-filtering effects, according to eqn (3) and (4):[38]

$$[HO^{\bullet}]_{ss} = [HO^{\bullet}]_{obs}/SF \quad (3)$$

$$SF = \frac{1 - 10^{-a_\lambda L}}{2.303\ (a_\lambda L)} \quad (4)$$

where a_λ (cm^{-1}) is the absorbance coefficient of samples at 436 nm and L (cm) is the average optical pathlength for the test tubes (~1 cm).

The second-order rate constant between GO and $HO^\bullet$, $k_{HO^\bullet,GO}$ (mg-C^{-1}L s^{-1}), was determined by the standard competition kinetics equation:

$$\frac{[HO^\bullet]_{ss,0}}{[HO^\bullet]_{ss}} = 1 + \frac{k_{HO^\bullet,GO}}{\sum (k_{HO^\bullet,Si}[S_i])}[DOC]_{GO} \quad (5)$$

where $[HO^\bullet]_{ss,0}$ is the steady-state $HO^\bullet$ concentration in the absence of GO; $k_{HO^\bullet,Si}$ (M^{-1} s^{-1}) is the rate constant of each $HO^\bullet$ scavenger in the system; and $[S_i]$ (M) is the concentration of each individual scavenger, including *p*CBA, oxalate, H_2O_2, and MeOH ($k_{HO^\bullet,Si}$ = 5.2 × 10^9, 1.0 × 10^7, 2.7 × 10^7, and 9.7 × 10^8 M^{-1} s^{-1}, respectively).[39]

For comparison, $k_{HO^\bullet,GO}$ was also examined by using terephthalic acid (TPA, 20 μM) to replace MeOH as the major $HO^\bullet$ scavenger, and other reagents remained at the same concentrations without added *p*CBA.[40] The relationship between $HO^\bullet$ concentration and formation of 2-hydroxyterephthalic acid (HTA), a hydroxylated product of TPA by $HO^\bullet$, was used to calculate the $k_{HO^\bullet,GO}$ by:

$$\frac{\Delta FL_{425,0}}{\Delta FL_{425}} = \frac{[HO^\bullet]_{ss,0}}{[HO^\bullet]_{ss}} = 1 + \frac{k_{HO^\bullet,GO}}{\sum (k_{HO^\bullet,Si}\cdot[S_i])}[DOC]_{GO} \quad (6)$$

where ΔFL_{425} and $\Delta FL_{425,0}$ are the fluorescence intensities (counts) of HTA in samples with and without GO, respectively, and $[S_i]$ is the concentration of oxalate, H_2O_2, and TPA ($k_{HO^\bullet,TPA}$ = 3.3 × 10^9 M^{-1} s^{-1}).[40]

Reaction with singlet oxygen

$^1O_2$ was generated by irradiating rose bengal (RB, 0.5 μM) as a photosensitizer. Solutions were adjusted to pH 5.3 ± 0.2 by 0.1 N NaOH solution and irradiated with a monochromatic light at 546 nm in the same MGRR, with a combination of Corning 3–68 and 4–72 filters. Light intensity was measured at 0.018 mol photons per L h^{-1} by the same ferrioxalate actinometry method.[34] The half-life of RB upon exposure to light with this irradiance was 3.75 h, determined by the decay of its characteristic absorbance at 549 nm. Steady-state $^1O_2$ concentrations, $[^1O_2]_{ss}$ (M), were obtained by dividing the pseudo-first-order decay rate of furfuryl alcohol (FFA, 0.1 mM) by its rate constant for reaction with $^1O_2$ ($k_{^1O_2,FFA}$ = 1.2 × 10^8 M^{-1} s^{-1}).[40] $[^1O_2]_{ss}$ was also corrected with light-screening factors described in eqn (3), using the combined absorbance of RB and GO (or rGO) at 546 nm. The second-order rate constant between GO and $^1O_2$, $k_{^1O_2,GO}$, attributed to both physical and chemical quenching, was determined by eqn (7):

$$\frac{[^1O_2]_{ss,0}}{[^1O_2]_{ss}} = 1 + \frac{k_{^1O_2,GO}}{\sum (k_{^1O_2,Si}\cdot[S_i])}[DOC]_{GO} \quad (7)$$

where $[^1O_2]_{ss,0}$ is the steady-state $^1O_2$ concentration in the absence of GO; $k_{^1O_2,\ Si}$ (M^{-1} s^{-1}) is the rate constant of $^1O_2$ scavenger in the system; and $[S_i]$ is the concentration of individual scavenger ($k_{^1O_2,H_2O}\cdot[H_2O]$ = 2.5 × 10^5 s^{-1}).[41]

To evaluate potential GO transformation due to reaction with $^1O_2$, GO characterization was examined during a reaction course of 56 h. Considering that RB was gradually photobleached, extended $^1O_2$ production was achieved by sequentially adding RB in a stepwise dose increment of 0.5 μM every 8 h.

Reaction with superoxide anion

$O_2^{\bullet-}$ was chemically produced using phenazine methosulfate (PMS, 2 μM) to catalyze the oxidation of reduced-form β-nicotinamide adenine dinucleotide (NADH, 20–100 μM) in air-saturated solutions at pH 8.[42] $O_2^{\bullet-}$ production was confirmed by formation of XTT (35–75 μM) formazan, a product of the reaction between $O_2^{\bullet-}$ and XTT.[43] The second-order rate constant of GO with $O_2^{\bullet-}$, $k_{O_2^{\bullet-},\ GO}$ (mg-C^{-1} L s^{-1}), was calculated by the inhibitory effect of GO on formation of XTT formazan (eqn (8)):

$$\frac{\Delta A_{470,0}}{\Delta A_{470}} = 1 + \frac{k_{O_2^{\bullet-},GO}}{k_{O_2^{\bullet-},XTT}\cdot[XTT]}[DOC]_{GO} \quad (8)$$

where $k_{O_2^{\bullet-},\ XTT}$ (M^{-1} s^{-1}) is the reaction rate constant between $O_2^{\bullet-}$ and XTT; ΔA_{470} and $\Delta A_{470,0}$ are absorbances of XTT formazan *via* reaction with $O_2^{\bullet-}$ in dispersions with and without GO, respectively. Superoxide dismutase (SOD), an enzyme that catalyzes the dismutation of $O_2^{\bullet-}$ to H_2O_2, was used to determine whether the increased absorbance was due to $O_2^{\bullet-}$. In solutions of XTT, NADH, and PMS at pH 8, the self-disproportionation of $O_2^{\bullet-}$ to H_2O_2 is negligible (k = 6 × 10^4 M^{-1} s^{-1})[44] because of high reactivity of XTT ($k_{O_2^{\bullet-},XTT}$ = 8.59 × 10^4 M^{-1} s^{-1})[43] and slow production rate of $O_2^{\bullet-}$ (NADH oxidation rate constant = 0.255 min^{-1}). In the absence of scavengers, $O_2^{\bullet-}$ would eventually disproportionate to H_2O_2. Therefore, the H_2O_2 yield in the NADH/PMS (without XTT) in the presence of varied amounts of GO was used as supportive evidence for the reaction between GO and $O_2^{\bullet-}$.

Analyses

*p*CBA and FFA were analyzed in an Agilent 1200 HPLC coupled with a diode array detector (DAD) at 230 nm and 219 nm, respectively. HTA was analyzed in the same HPLC with a fluorescence detector (FLD) (excitation 315 nm, emission 425 nm).[40] XTT formazan was monitored at 470 nm in a Perkin Elmer Lambda 35 spectrophotometer equipped with 1 cm quartz cuvette. H_2O_2 concentration in the NADH/PMS systems was measured by the DPD/HRP assay at 551 nm, as described previously.[45] DOC was analyzed in a TOC-V_{CPH} analyzer (Shimadzu, Japan), using non-purgeable organic carbon (NPOC) mode with potassium hydrogen phthalate as the standard. Spectroscopic analyses of GO were carried out in Lambda 35 spectrophotometer for UV-vis absorbance and Horiba Fluorolog 3 fluorometer for photoluminescence (PL),

 This journal is © The Royal Society of Chemistry 2019

both with 1 cm light path quartz cuvettes. Hydrodynamic size was measured on a Zetasizer Nano ZS (Malvern Instruments Ltd., Worcestershire, UK), using a dynamic light-scattering technique with a 633 nm He–Ne laser. Except in DOC measurement, samples used for GO characterization were filtered through Millipore Amicon Ultra-4 centrifugal filters (10k MWCO for RB and 3k MWCO for $Fe(ClO_4)_3$, H_2O_2, NADH, and PMS), *via* centrifugation at 4500 × *g*, for 40 minutes. Filtered GO concentrates were washed with water *via* the same centrifugal filtration procedure for 5 cycles, then re-dispersed in water to initial volume. The recovery of GO in this ultrafiltration process was 92.6% for 3k filter and 90.1% for 10k filter, found by comparing the 230 nm absorbance of filtered to non-filtered suspensions.

Results and discussion

Reactivity with hydroxyl radical (HO•)

To minimize interference by direct photolysis of GO on determining its reactivity with HO•, we chose a visible light of 436 nm for initiating the photo-Fenton reaction to generate HO• by reaction of Fe(II) (from photoreaction of Fe(III) complexes) with H_2O_2. Preliminary experiments showed there was no DOC decay for GO under 48 h irradiation at wavelengths longer than 405 nm in the MGRR (Fig. S2†).

DOC decay of GO (10 mg L^{-1}, ~4 mg-C L^{-1}) in pH 4 dispersions containing $Fe(ClO_4)_3$ and H_2O_2, under irradiation at 436 nm are shown in Fig. 1a. No DOC decrease was observed in the dark control or in systems without added Fe (*i.e.*, H_2O_2 alone). In systems with added $Fe(ClO_4)_3$ alone, a slight reduction of DOC was observed, presumably caused by Fenton reaction related to the small yield of H_2O_2, a self-disproportionated product of $O_2^{\bullet-}$, produced from photolysis of GO.[23] The pseudo-first-order decay rate constant of DOC decay in this control, however, is 25 times smaller than in the experiment with both $Fe(ClO_4)_3$ and H_2O_2. These results suggested that direct photolysis is negligible and DOC reduction was mainly due to the reaction with HO• generated from photo-Fenton reaction. Indeed, the steady-state concentration of HO• was calculated as 7.6×10^{-14} M using the observed pseudo-first-order degradation rate of *p*CBA (see inset in Fig. 1a). The reaction of GO with HO• resulted in a continuous decrease in the UV-vis absorbance, as shown in Fig. 1b; this differs from the previous indirect photolysis study in which absorbance increased at the beginning due to direct photolysis.[10] It is consistent with the argument that observed DOC decay was due to GO oxidation by HO•, and is further supported by the inhibitory effect of MeOH, a HO• scavenger, on the decrease of GO absorbance at 230 nm (Fig. S3†). Note that addition of MeOH did not totally prevent degradation, which could be due to the locally-high concentration of Fe on the GO surface (see later discussion). Even though both DOC and UV-vis spectra decreased, Fig. 2 shows that reacted GO products exhibited strong photoluminescence (in the range of 400–480 nm) upon excitation by light with wavelengths between 250–450 nm. A

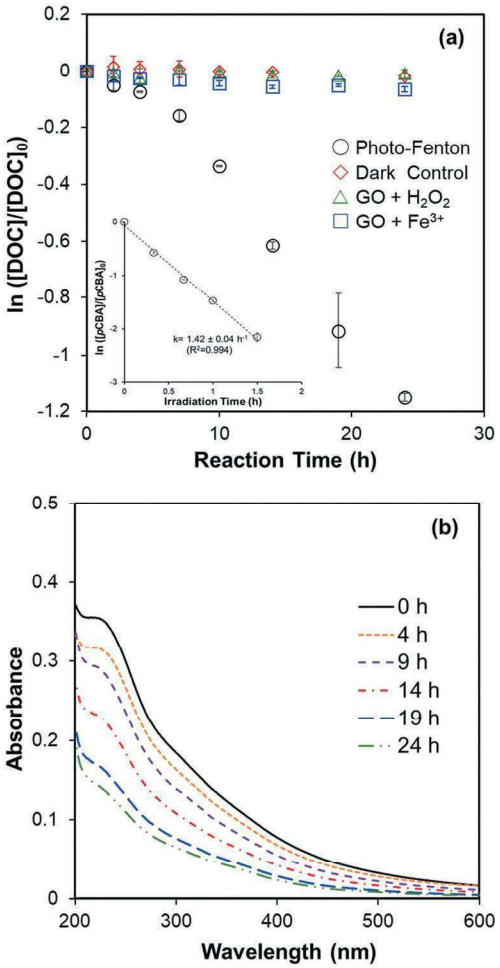

Fig. 1 (a) Degradation of GO (10 mg L^{-1}) in the pH 4 dispersions with: Fenton reagent (15 μM $Fe(ClO_4)_3$ and 10 mM H_2O_2) (○), 10 mM H_2O_2 (△), 15 μM $Fe(ClO_4)_3$ (□) under irradiation at 436 nm. The dark control samples containing the same Fenton reagents were placed in the dark (◇). The inset shows the pseudo-first-order decay of added *p*CBA (1.5 μM) in the photo-Fenton sample. (b) UV-vis spectra of HO• reacted GO after removing Fenton reagents by ultrafiltration.

similar fluorescence pattern has been reported previously[10,21] from the fragmentation of GO flakes by HO•, confirmed with qualitative characterization (*e.g.*, TEM, AFM, and XPS *etc.*) and mass spectrometry.

Fig. S4a† shows the DOC decay of rGO and Fig. S4b† shows the decay of *p*CBA, obtained from separated experiments in which HO• was produced by irradiating dispersions containing rGO, $Fe(ClO_4)_3$ and H_2O_2 at 436 nm. Both DOC and *p*CBA decays are well-fitted with pseudo-first-order kinetics in dispersions containing rGO, indicating that HO• reached steady state status in the systems and contributed to first-order decay of the DOCs of GO and rGO (eqn (1) and (2)). The observed first-order DOC decay rate ($k_{obs,DOC}$), steady-state HO• concentration ($[HO^{\bullet}]_{ss}$), and the computed apparent second-order degradation rate constants of GO and rGO in reaction with HO•, are summarized in Table 1. We analyzed DOC data in Fig. 1a by calculating rate constants for the initial loss (0–7 h) and subsequent more

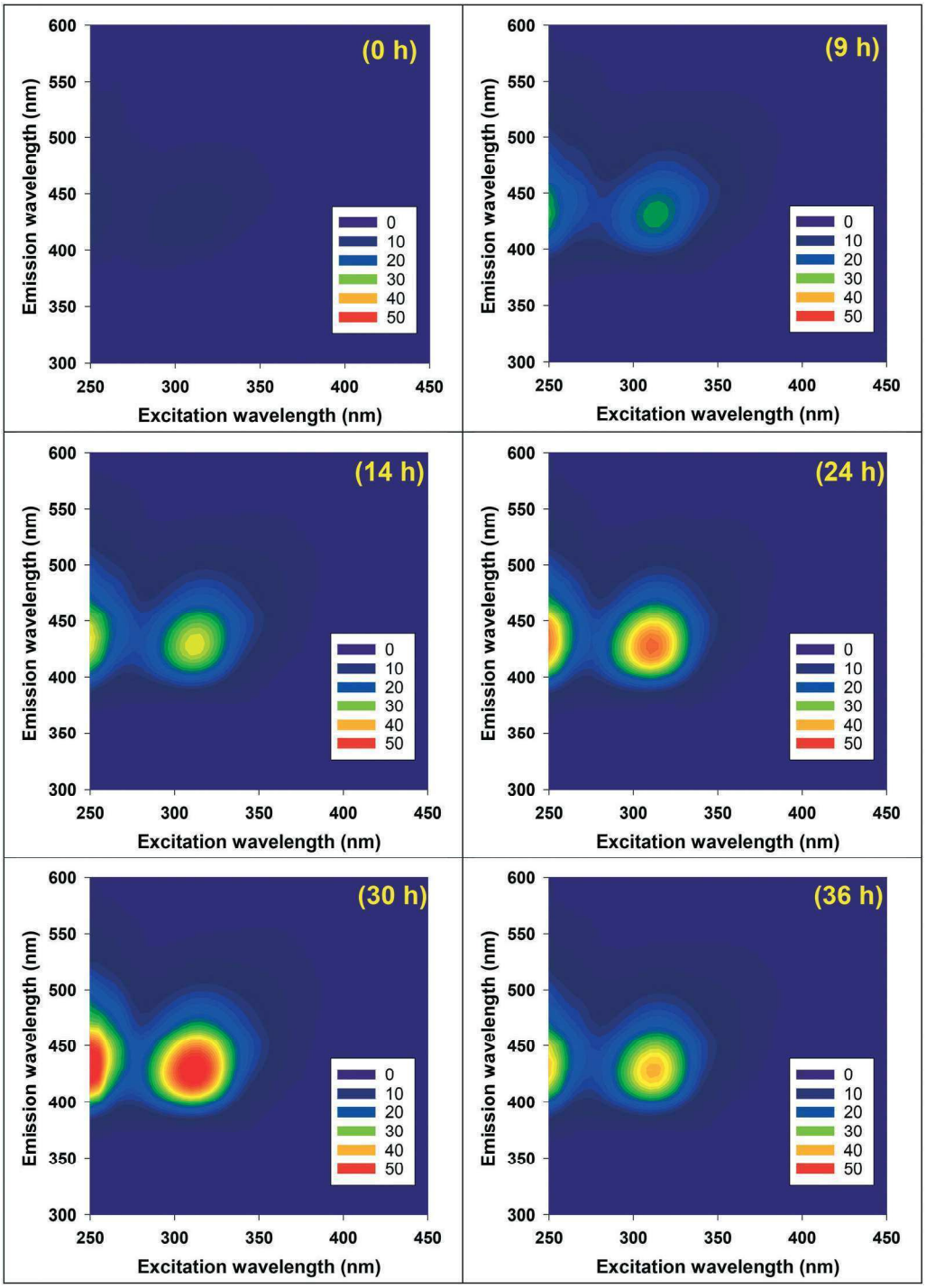

Fig. 2 Excitation-emission matrices of HO˙ reacted GO (10 mg L^{-1} initially) in the condition described in Fig. 1a. Intensity units are quinine sulfate equivalents after removing water Raman and Rayleigh scattering peaks.

rapid loss (during the 7–24 h interval). Degradation rate constants for GO are 0.8×10^8 M^{-1} s^{-1} for the first 7 h, and 2.2×10^8 M^{-1} s^{-1} thereafter. The time-dependence indicates that different oxidation mechanisms may be involved, presumably due to susceptibility of different functionalities to HO˙ attack. For rGO, the second-order degradation rate constant appeared to be dependent on previous irradiation time in the solar simulator. The value decreased from 1.78×10^8 M^{-1} s^{-1} for 1D-rGO to 0.74×10^8 M^{-1} s^{-1} for 7D-rGO, based on DOC data in the 0–13 h interval. We suspect this is because GO was photoreduced to rGO quickly (<1 d), and further irradiation caused photooxidation of rGO to form more oxidized functionalities (*e.g.*, carboxyl and phenyl) which are normally less reactive with HO˙. Further

 This journal is © The Royal Society of Chemistry 2019

Table 1 Apparent degradation rate constants for the reactions of GO and photo-reduced GO (rGO) with HO• produced in the pH 4 photo-Fenton system described in Fig. 1a. Standard errors are calculated from the linear regression of $\ln(C/C_0)$ where C is [DOC] and [*p*CBA] separately

	$k_{obs,DOC}$[a] (h^{-1})	$k_{obs,pCBA}$[a] (h^{-1})	$[HO^•]_{ss}$ ($\times 10^{-14}$ M)	$k^{obs}_{HO^•,GO}$[b] ($\times 10^8$ M^{-1} s^{-1})
GO (0–7 h)	0.022 ± 0.002	1.42 ± 0.04	7.6 ± 0.2	0.81 ± 0.08
GO (7–24 h)	0.059 ± 0.003	1.42 ± 0.04	7.6 ± 0.2	2.16 ± 0.13
1D-rGO	0.036 ± 0.002	1.04 ± 0.03	5.6 ± 0.2	1.80 ± 0.11
2D-rGO	0.033 ± 0.002	1.17 ± 0.05	6.3 ± 0.3	1.47 ± 0.11
4D-rGO	0.026 ± 0.001	1.51 ± 0.02	8.0 ± 0.1	0.90 ± 0.04
7D-rGO	0.027 ± 0.002	1.89 ± 0.09	10.1 ± 0.5	0.74 ± 0.07

[a] Pseudo-first-order decay rates for DOC and *p*CBA, respectively. [b] The second-order degradation rate constant was calculated by eqn (2).

investigation is warranted, however. Compared to the previous study which used solar irradiated H_2O_2 as HO• source, second-order degradation rate constants reported here are only 0.14–0.43 times the previous one (5.1×10^8 M^{-1} s^{-1}).[10] This difference may be a result of error in determining the rate of direct photolysis in a previous study where the DOC decay did not follow a first-order pattern very well. In other words, the rate of direct photolysis might be underestimated when a pseudo-first-order decay model was used to fit the DOC decay for a long period. In contrast, the experiment presented here avoided direct photolysis of GO by using photo-Fenton reaction at 436 nm, which certainly improved the accuracy of the determined indirect rate constant.

Useful information for evaluating the persistence of GO and rGO subjected to attack by HO• is provided in Table 1. The use of DOC, however, cannot explicitly represent reactivity of GO with HO• because HO• attack does not necessarily involve mineralization of carbon grids. Competition kinetics was therefore used to determine the absolute second-order rate constant for reaction with HO•. For competition kinetics to be valid, it is assumed that production of HO• was not affected by the target material. In acid solutions of $Fe(ClO_4)_3$, however, GO was found to catalyze the photoreduction of Fe(III) to Fe(II) under irradiation at 436 nm (Fig. 3a), presumably due to electron transfer from irradiated GO to the complexed Fe(III). An increased steady-state concentration of HO• was subsequently observed when H_2O_2 was present (Fig. 3b). This may explain why adding MeOH (10 mM) did not totally prevent GO degradation in the photo-Fenton system (Fig. S3†), since the HO• generated by GO-catalyzed Fenton reaction is spatially close to GO and readily reacts with it before diffusing to be scavenged by MeOH. This also suggests that complexation of Fe with GO may be an important pathway for degradation of GO in aquatic environments containing high concentrations of Fe.

Based on eqn (5), the catalytic effect of GO on Fe reduction resulted in an unrealistic, negative second-order rate constant for the reaction between GO and HO• when GO concentration was below 5 mg L^{-1} (~2 mg-C L^{-1}). The catalytic effect of GO was then eliminated by adding sodium oxalate (60 μM) to chelate Fe, and the Fe concentration was decreased to 1.5 μM to avoid complexation between GO and Fe. The Fenton reaction was mainly driven by ligand-to-metal charge transfer from oxalate to Fe, which efficiently reduced Fe(III) to Fe(II) and produced HO• at a constant rate under irradiation at 436 nm.[15] Reactivity of HO• scavengers may limit application of competition kinetics when HO• production is not uniform. As a benchmark, we used *tert*-butanol (*t*-BuOH) as a control; a linear relationship

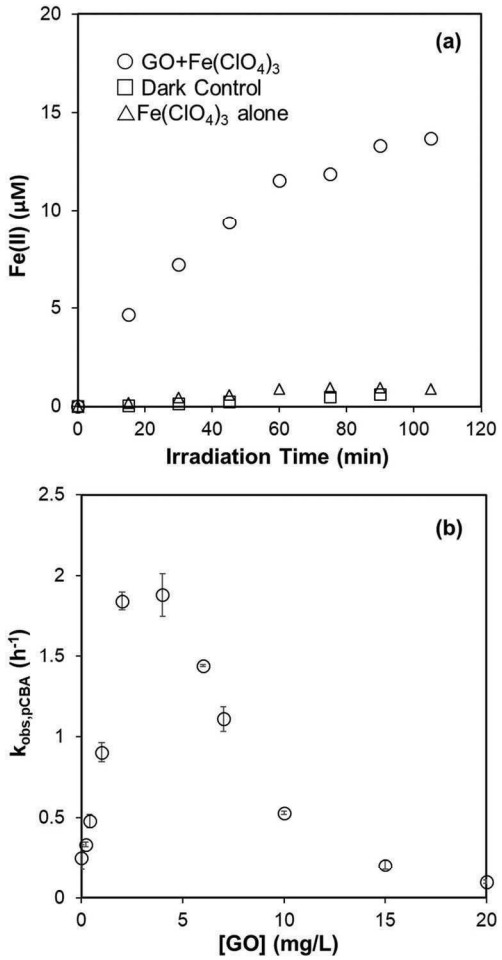

Fig. 3 (a) Production of Fe(II) in the pH 4 suspension of 20 mg L^{-1} GO and 100 μM $Fe(ClO_4)_3$ under irradiation at 436 nm. Fe(II) concentration was determined by 1,10-phenanthroline complexing method, using the absorbance at 510 nm. (b) Pseudo-first-order decay rate of *p*CBA (1 μM) in the photo-Fenton system (5 μM $Fe(ClO_4)_3$ and 20 μM H_2O_2, pH = 4) under irradiation at 436 nm.

between added *tert*-butanol and $[HO^{\bullet}]_{ss,0}/[HO^{\bullet}]_{ss}$ was observed in the presence of 50 μM MeOH (Fig. S5a†). The calculated $k_{HO^{\bullet},t\text{-BuOH}}$ of 6.15 ± 0.32 × 10^8 M^{-1} s^{-1} agreed well with the previously reported value of 6 × 10^8 M^{-1} s^{-1},[38] indicating that, in this oxalate/Fe/H_2O_2 system, the error from using *p*CBA-measured $[HO^{\bullet}]_{ss}$ for competition kinetics is minimized.

A linear relationship between dosed GO amount and $[HO^{\bullet}]_{ss,0}/[HO^{\bullet}]_{ss}$ in the same oxalate/Fe/H_2O_2 system – when *p*CBA (0.5 μM) was used to measure steady-state HO• concentration – is shown in Fig. 4a, supporting that GO's catalytic effect was negligible. A similar linear relationship was observed for HTA fluorescence when TPA was used as the major HO• scavenger (Fig. 4b). Results of competitive kinetics for rGO are provided in Fig. S5b–e.† Second-order rate constants (calculated by eqn (5)) for the reaction between GO (or rGO) with HO• are summarized in Table 2. The rate constant for GO is (6.24 ± 0.13) × 10^4 mg-C^{-1} L s^{-1}. When HTA fluorescence (Fig. 4b) and eqn (6) are used, the rate constant is calculated to be (6.93 ± 0.22) × 10^4 mg-C^{-1} L s^{-1}. The two values are within ~10% error, but much smaller than that reported for graphene (3.67 × 10^5 mg-C^{-1} L s^{-1}).[46] Rate constants for rGO were in the range of (8.59–5.89) × 10^4 mg-C^{-1} L s^{-1}, decreasing with extended duration in the previous solar irradiation period and agreeing with the trend of DOC degradation rate constants listed in Table 1. Overall, these values are comparable to most polycyclic aromatic hydrocarbons (*e.g.*, 7.8 × 10^4 mg-C^{-1} L s^{-1} for pyrene and 7.5 × 10^4 mg-C^{-1} L s^{-1} for biphenyl),[47] but two to three times higher than dissolved organic matter (DOM) in water systems ((2.7 ± 0.77) × 10^4 mg-C^{-1} L s^{-1}).[48]

Table 2 Absolute second-order rate constants and calculated *R* squared value for GO and rGO with HO• in the pH 5.4 photo-Fenton system described in Fig. 4a

	$k_{HO^{\bullet},GO}$ (×10^4 mg-C^{-1} L s^{-1})	*R* squared
GO	6.24 ± 0.13	0.987
1D-rGO	8.59 ± 0.32	0.966
2D-rGO	7.43 ± 0.48	0.894
4D-rGO	6.98 ± 0.39	0.927
7D-rGO	5.89 ± 0.31	0.917

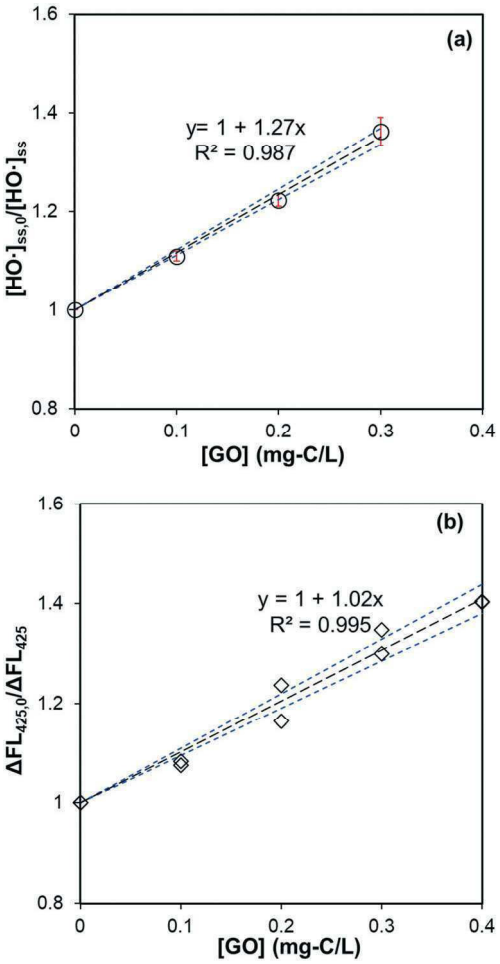

Fig. 4 (a) Effect of GO on the steady-state HO• concentration in the system of sodium oxalate (60 μM), $Fe(ClO_4)_3$ (1.5 μM), H_2O_2 (50 μM), MeOH (50 μM), and *p*CBA (0.5 μM) under irradiation at 436 nm. The slope is significantly different from zero (p = 0.002) and the standard deviation of the slope is 0.04. (b) Effect of GO on the fluorescence of HTA produced in the system of sodium oxalate (60 μM), $Fe(ClO_4)_3$ (1.5 μM), H_2O_2 (50 μM), TPA (20 μM) under irradiation at 436 nm. The slope is significantly different from zero (p < 0.001) and the standard deviation of the slope is 0.03. Black dotted lines represent the linear regression fit, and the blue dotted lines are 95% confidence bands.

Reactivity with singlet oxygen ($^1O_2$)

Irradiation of 0.5 μM RB at 546 nm light generated a steady-state $^1O_2$ concentration ($[^1O_2]_{ss}$) of 1.33 × 10^{-12} M within 80 minutes. As irradiation extended, RB photo-bleached (first-order rate constant of 0.185 h^{-1}) and the $^1O_2$ production rate decreased accordingly. Therefore, competition kinetics experiments were carried out in the span of 80 minutes. The

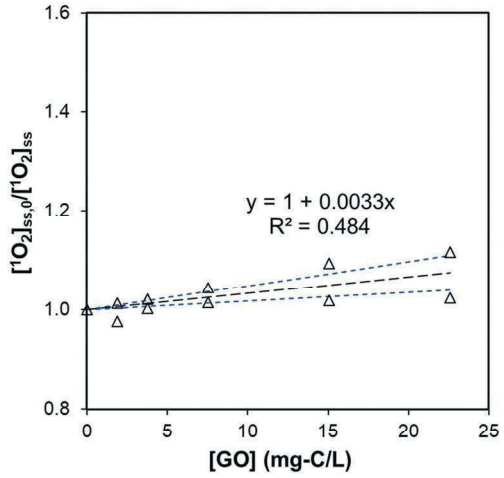

Fig. 5 Effect of GO on the steady-state concentration of $^1O_2$, generated by irradiating 0.5 μM RB at 546 nm (pH = 5.3 ± 0.2). The slope is significantly different from zero (p = 0.017) and the standard deviation of the slope is 0.0007. Black dotted lines represent the linear regression fit, and the blue dotted lines are 95% confidence bands.

This journal is © The Royal Society of Chemistry 2019

effect of GO concentration on the $[^1O_2]_{ss}$ in the solutions of pH 5.3 ± 0.2 is shown in Fig. 5. Multiplying the slope and its standard deviation by the combined rate constant of $^1O_2$ with H_2O and FFA, the absolute second-order rate constant for the reaction of GO with $^1O_2$ was calculated to be 865 ± 183 mg-C^{-1} L s^{-1}, which is about two orders of magnitude lower than the reaction with HO$^{\bullet}$. Because concentrations of $^1O_2$ in natural water could be two or three orders of magnitude higher than HO$^{\bullet}$, we further examined whether reaction with $^1O_2$ would result in any transformation of GO. In the continuous production of $^1O_2$ *via* stepwise dose of RB into the irradiated sample, the average $^1O_2$ concentration in the system containing 10 mg L^{-1} GO was calculated as:

$$\frac{[^1O_2]_{ave} = \int_0^{T_{step}} [^1O_2]_{ini} e^{-k_{RB}t} dt}{T_{step}} \quad (9)$$

where $[^1O_2]_{ini}$ is the steady-state $^1O_2$ concentration at the first 80 minutes (1.33×10^{-12} M), k_{RB} is the observed photobleaching rate of RB (0.185 h^{-1}), and T_{step} (h) is the time interval between each dose. With a stepwise dose every 8 h, the $[^1O_2]_{ave}$ is calculated to be 6.9×10^{-13} M. In 56 h experiments, there was no DOC decrease for GO after subtracting the DOC in the control of RB alone from the DOC in GO + RB solutions to ($k_{obs,DOC} < 10^{-4}$ h^{-1}), as shown in Fig. S6a;† this resulted in an apparent second-order degradation constant less than 4×10^4 M^{-1} s^{-1}. Besides DOC, measurements of UV-vis spectra, hydrodynamic size, and photoluminescence also show that GO remained intact (Fig. S6b and S7†), suggesting the chemical reaction between GO and $^1O_2$ is negligible. In contrast, the effect of GO on decreasing the steady-state $^1O_2$ concentration produced by RB was mainly due to physical quenching. This is similar to the reported reaction between C_{60} and $^1O_2$, despite the three-order discrepancy in second-order rate constant (865 mg-C^{-1} L s^{-1} *vs.* 0.69 mg-C^{-1} L s^{-1}),[16] yet different from results of CNTs in which $^1O_2$ was reported to cause surface oxidation.[20] We believe this is the first report of GO being chemically inert to photo-generated $^1O_2$.

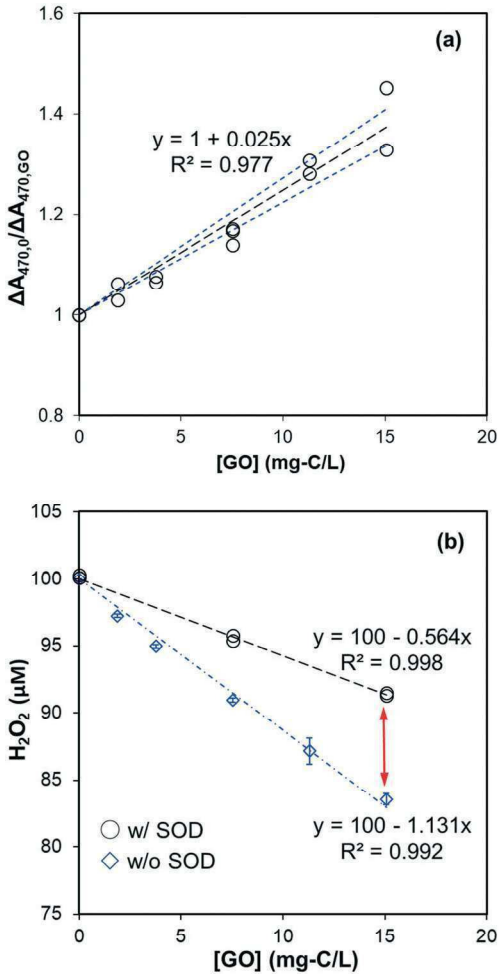

Fig. 6 (a) GO effect on XTT formazan formation by $O_2^{\bullet-}$ in the system of NADH (30 μM), PMS (2 μM), and XTT (50 μM) at pH 8. The slope is significantly different from zero ($p < 0.001$) and the standard deviation of the slope is 0.002. Black dotted lines represent the linear regression fit, and the blue dotted lines are 95% confidence bands. (b) Effect of SOD (40 U mL^{-1}) on the H_2O_2 formation in the pH 8 phosphate buffered dispersions containing NADH (100 μM), PMS (2 μM), and GO. The difference indicated by the red arrow is attributed to scavenging of $O_2^{\bullet-}$ by GO.

Reactivity with superoxide anion ($O_2^{\bullet-}$)

Reactivity of GO with $O_2^{\bullet-}$ was investigated by its competitive effect on the formation of soluble XTT formazan. We chose XTT as the $O_2^{\bullet-}$ probe rather than nitro blue tetrazolium (NBT^{2+}) because the negatively-charged formazan product prevents coagulation with GO. That GO inhibited the formation of $O_2^{\bullet-}$-reduced XTT formazan in the NADH/PMS is shown in Fig. 6a. The second-order rate constant for the reaction of GO with $O_2^{\bullet-}$, $k_{O_2^{\bullet-},GO}$, was calculated to be 0.108 ± 0.004 mg-C^{-1} L s^{-1} by multiplying the slope in Fig. 6a by the rate constant of XTT with $O_2^{\bullet-}$, based on eqn (8). To limit direct reaction between XTT and reduced PMS and obtain measurable change in the absorbance, the XTT concentration used in these experiments was not high enough for eqn (8) to be exactly valid (*i.e.*, [XTT] was not constant during reaction). If the decrease of XTT over time was considered, the $k_{O_2^{\bullet-},GO}$ was calculated as 0.078 mg-C^{-1} L s^{-1} by using least square-fitting to minimize the sum of squared error (SSE) between predicted and measured $\Delta A_{470,0}/\Delta A_{470}$. Interested readers are referred to ESI† for further details.

To observe the transformation of GO caused by $O_2^{\bullet-}$ reaction, GO was found to be slowly reduced with increasing absorbance in the visible wavelength region (Fig. S8†). Spectral change was only partially attributed to $O_2^{\bullet-}$, however, as the addition of SOD (40 U mL^{-1}) did not totally inhibit absorbance increase which indicates a direct reaction between GO and reduced PMS or NADH. This raised the question of whether inhibition of XTT formazan (Fig. 6a) was due to decreased $O_2^{\bullet-}$ yield in the presence of GO. To test it, we compared the effect of XTT concentration on formation of XTT formazan. If inhibition on XTT formazan was due to decreased production of $O_2^{\bullet-}$, the slope of $\Delta A_{470,0}/\Delta A_{470}$

should remain constant at different XTT concentrations. Increasing XTT from 35 μM to 75 μM resulted, however, in a proportional decrease in slope from 0.0345 to 0.018 mg-C^{-1} L (as shown in Fig. S9†), suggesting that inhibition on XTT formazan was mainly due to competition between GO and XTT for $O_2^{\bullet-}$. Using slopes in Fig. S9,† the calculated rate constant was in the range of 0.095–0.116 mg-C^{-1} L s^{-1}, consistent with the value obtained from Fig. 6a, despite different NADH concentrations (30 μM *vs.* 20 μM).

The effect of GO on the final H_2O_2 concentration in the NADH/PMS system (without XTT) is shown in Fig. 6b. H_2O_2 concentration linearly decreased with increased GO, indicating GO acted as an electron sink in the system. This excludes the possibility that GO inhibited the formation of XTT formazan by simply shutting down electrons from $O_2^{\bullet-}$ to form H_2O_2. Meanwhile, decreased H_2O_2 concentration was significantly recovered by adding SOD to the system, suggesting that $O_2^{\bullet-}$ was competitively consumed by GO – presumably by forming chemical bonding or one-electron reduction of GO, consistent with increased GO absorbance in the range of visible wavelength (Fig. S8†). A similar finding based on XPS, FTIR and Raman analysis[31] demonstrated the $O_2^{\bullet-}$-reduction of GO. Since reduction of GO to rGO could greatly change its hydrophilicity and bioaccumulation properties, further study is needed to clarify evolution of GO from exposure to superoxide anion.

Environmental implications

Major challenges in exposure assessment of graphene-based nanomaterials are their stability and susceptibility to different reactive reagents in environment. Our study demonstrated that reaction with $^1O_2$ had a negligible effect on transformation of GO, although its steady-state concentration in aquatic environments is normally two- to three-orders of magnitude higher than HO$^\bullet$. In contrast, HO$^\bullet$ attack quickly degraded not only GO, but also the less photoreactive rGO. Together, these results suggest that an integrated understanding of ROS distribution and GO reactivity with ROS is needed to better assess long-term exposure of GO and rGO. It may also prove valuable in designing GO or rGO in environmental applications because high HO$^\bullet$ reactivity indicates stability of these types of nanomaterials cannot be overlooked when they are used as catalysts or carriers. Nevertheless, further study is still needed to clarify the detailed mechanisms of GO degradation by individual ROS, including the identification of reacted products.

Conflicts of interest

There are no conflicts of interest to declare.

Acknowledgements

This article has been reviewed in accordance with the U.S. Environmental Protection Agency's (U.S. EPA) peer and administrative review policies and approved for publication. Mention of trade names or commercial products does not constitute an endorsement or recommendation for use by the U.S. EPA. We thank F. Rauschenberg, Senior Service America, Inc., for editorial assistance.

References

1 K. S. Novoselov, V. I. Fal'ko, L. Colombo, P. R. Gellert, M. G. Schwab and K. Kim, A roadmap for graphene, *Nature*, 2012, **490**, 192–200.
2 M. Xu, T. Liang, M. Shi and H. Chen, Graphene-like two-dimensional materials, *Chem. Rev.*, 2013, **113**, 3766–3798.
3 F. Perreault, A. Fonseca de Faria and M. Elimelech, Environmental applications of graphene-based nanomaterials, *Chem. Soc. Rev.*, 2015, **44**, 5861–5896.
4 D. Chen, H. Feng and J. Li, Graphene oxide: preparation, functionalization, and electrochemical applications, *Chem. Rev.*, 2012, **112**, 6027–6053.
5 Y. Zhu, S. Murali, W. Cai, X. Li, J. W. Suk, J. R. Potts and R. S. Ruoff, Graphene and Graphene Oxide: Synthesis, Properties, and Applications, *Adv. Mater.*, 2010, **22**, 3906–3924.
6 S. Park and R. S. Ruoff, Chemical methods for the production of graphenes, *Nat. Nanotechnol.*, 2009, **4**, 217–224.
7 Q. Zhang, Z. Wu, N. Li, Y. Pu, B. Wang, T. Zhang and J. Tao, Advanced review of graphene-based nanomaterials in drug delivery systems: Synthesis, modification, toxicity and application, *Mater. Sci. Eng., C*, 2017, **77**, 1363–1375.
8 A. B. Seabra, A. J. Paula, R. de Lima, O. L. Alves and N. Duran, Nanotoxicity of graphene and graphene oxide, *Chem. Res. Toxicol.*, 2014, **27**, 159–168.
9 J. Zhao, Z. Wang, J. C. White and B. Xing, Graphene in the aquatic environment: adsorption, dispersion, toxicity and transformation, *Environ. Sci. Technol.*, 2014, **48**, 9995–10009.
10 W.-C. Hou, W. M. Henderson, I. Chowdhury, D. G. Goodwin, X. Chang, S. Martin, D. H. Fairbrother, D. Bouchard and R. G. Zepp, The contribution of indirect photolysis to the degradation of graphene oxide in sunlight, *Carbon*, 2016, **110**, 426–437.
11 G. P. Kotchey, B. L. Allen, H. Vedala, N. Yanamala, A. A. Kapralov, Y. Y. Tyurina, J. Klein-Seetharaman, V. E. Kagan and A. Star, The Enzymatic Oxidation of Graphene Oxide, *ACS Nano*, 2011, **5**, 2098–2108.
12 J. M. Burns, W. J. Cooper, J. L. Ferry, D. W. King, B. P. DiMento, K. McNeill, C. J. Miller, W. L. Miller, B. M. Peake, S. A. Rusak, A. L. Rose and T. D. Waite, Methods for reactive oxygen species (ROS) detection in aqueous environments, *Aquat. Sci.*, 2012, **74**, 683–734.
13 W. P. Kwan and B. M. Voelker, Rates of hydroxyl radical generation and organic compound oxidation in mineral-catalyzed Fenton-like systems, *Environ. Sci. Technol.*, 2003, **37**, 1150–1158.
14 B. A. Southworth and B. M. Voelker, Hydroxyl Radical Production via the Photo-Fenton Reaction in the Presence of Fulvic Acid, *Environ. Sci. Technol.*, 2003, **37**, 1130–1136.

 This journal is © The Royal Society of Chemistry 2019

15 R. G. Zepp, B. C. Faust and J. Hoigne, Hydroxyl Radical Formation in Aqueous Reactions (Ph 3-8) of Iron(II) with Hydrogen-Peroxide - the Photo-Fenton Reaction, *Environ. Sci. Technol.*, 1992, **26**, 313–319.

16 J. W. Arbogast, A. P. Darmanyan, C. S. Foote, F. N. Diederich, R. L. Whetten, Y. Rubin, M. M. Alvarez and S. J. Anz, Photophysical properties of sixty atom carbon molecule (C60), *J. Phys. Chem.*, 1991, **95**, 11–12.

17 D. I. Schuster, P. S. Baran, R. K. Hatch, A. U. Khan and S. R. Wilson, The role of singlet oxygen in the photochemical formation of $C_{60}O$, *Chem. Commun.*, 1998, 2493–2494, DOI: 10.1039/A806603E.

18 J.-J. Yin, F. Lao, P. P. Fu, W. G. Wamer, Y. Zhao, P. C. Wang, Y. Qiu, B. Sun, G. Xing, J. Dong, X.-J. Liang and C. Chen, The scavenging of reactive oxygen species and the potential for cell protection by functionalized fullerene materials, *Biomaterials*, 2009, **30**, 611–621.

19 I. Fenoglio, M. Tomatis, D. Lison, J. Muller, A. Fonseca, J. B. Nagy and B. Fubini, Reactivity of carbon nanotubes: Free radical generation or scavenging activity?, *Free Radical Biol. Med.*, 2006, **40**, 1227–1233.

20 X. Qu, P. J. Alvarez and Q. Li, Photochemical transformation of carboxylated multiwalled carbon nanotubes: role of reactive oxygen species, *Environ. Sci. Technol.*, 2013, **47**, 14080–14088.

21 H. Bai, W. T. Jiang, G. P. Kotchey, W. A. Saidi, B. J. Bythell, J. M. Jarvis, A. G. Marshall, R. A. S. Robinson and A. Star, Insight into the Mechanism of Graphene Oxide Degradation via the Photo-Fenton Reaction, *J. Phys. Chem. C*, 2014, **118**, 10519–10529.

22 X. J. Zhou, Y. Zhang, C. Wang, X. C. Wu, Y. Q. Yang, B. Zheng, H. X. Wu, S. W. Guo and J. Y. Zhang, Photo-Fenton Reaction of Graphene Oxide: A New Strategy to Prepare Graphene Quantum Dots for DNA Cleavage, *ACS Nano*, 2012, **6**, 6592–6599.

23 T. Du, A. S. Adeleye, T. Zhang, C. Jiang, M. Zhang, H. Wang, Y. Li, A. A. Keller and W. Chen, Influence of light wavelength on the photoactivity, physicochemical transformation, and fate of graphene oxide in aqueous media, *Environ. Sci.: Nano*, 2018, **5**, 2590–2603.

24 T. Du, A. S. Adeleye, T. Zhang, N. Yang, R. Hao, Y. Li, W. Song and W. Chen, Effects of ozone and produced hydroxyl radicals on the transformation of graphene oxide in aqueous media, *Environ. Sci.: Nano*, 2019, **6**, 2484–2494.

25 L. Duan, T. Zhang, W. Song, C. Jiang, Y. Hou, W. Zhao, W. Chen and P. J. J. Alvarez, Photolysis of graphene oxide in the presence of nitrate: implications for graphene oxide integrity in water and wastewater treatment, *Environ. Sci.: Nano*, 2019, **6**, 136–145.

26 Y. Gao, X. Ren, X. Zhang and C. Chen, Environmental fate and risk of ultraviolet- and visible-light-transformed graphene oxide: A comparative study, *Environ. Pollut.*, 2019, **251**, 821–829.

27 A. S. Adeleye, X. Wang, F. Wang, R. Hao, W. Song and Y. Li, Photoreactivity of graphene oxide in aqueous system: Reactive oxygen species formation and bisphenol A degradation, *Chemosphere*, 2018, **195**, 344–350.

28 F. F. Zhao, S. C. Wang, Z. L. Zhu, S. G. Wang, F. F. Liu and G. Z. Liu, Effects of oxidation degree on photo-transformation and the resulting toxicity of graphene oxide in aqueous environment, *Environ. Pollut.*, 2019, **249**, 1106–1114.

29 D. M. Wang, Y. Zhang, L. L. Zheng, X. X. Yang, Y. Wang and C. Z. Huang, Singlet Oxygen Involved Luminol Chemiluminescence Catalyzed by Graphene Oxide, *J. Phys. Chem. C*, 2012, **116**, 21622–21628.

30 X. G. Hu, M. Zhou and Q. X. Zhou, Ambient Water and Visible-Light Irradiation Drive Changes in Graphene Morphology, Structure, Surface Chemistry, Aggregation, and Toxicity, *Environ. Sci. Technol.*, 2015, **49**, 3410–3418.

31 H. Zhao, C. Zhang, Y. Wang, W. Chen and P. J. J. Alvarez, Self-Damaging Aerobic Reduction of Graphene Oxide by Escherichia coli: Role of GO-Mediated Extracellular Superoxide Formation, *Environ. Sci. Technol.*, 2018, **52**, 12783–12791.

32 Y. Han, C. D. Knightes, D. Bouchard, R. Zepp, B. Avant, H. S. Hsieh, X. Chang, B. Acrey, W. M. Henderson and J. Spear, Simulating graphene oxide nanomaterial phototransformation and transport in surface water, *Environ. Sci.: Nano*, 2019, **6**, 180–194.

33 W. S. Hummers and R. E. Offeman, Preparation of Graphitic Oxide, *J. Am. Chem. Soc.*, 1958, **80**, 1339.

34 W. C. Hou, I. Chowdhury, D. G. Goodwin, Jr., W. M. Henderson, D. H. Fairbrother, D. Bouchard and R. G. Zepp, Photochemical transformation of graphene oxide in sunlight, *Environ. Sci. Technol.*, 2015, **49**, 3435–3443.

35 C. G. Hatchard and C. A. Parker, A New Sensitive Chemical Actinometer. II. Potassium Ferrioxalate as a Standard Chemical Actinometer, *Proc. R. Soc. London, Ser. A*, 1956, **235**, 518–536.

36 J. W. Stucki and W. L. Anderson, The Quantitative Assay of Minerals for Fe2+ and Fe3+ Using 1,10-Phenanthroline: I. Sources of Variability1, *Soil Sci. Soc. Am. J.*, 1981, **45**, 633–637.

37 M. S. Elovitz and U. von Gunten, Hydroxyl Radical/Ozone Ratios During Ozonation Processes. I. The Rct Concept, *Ozone: Sci. Eng.*, 1999, **21**, 239–260.

38 C. Hu, F. E. Muller-Karger and R. G. Zepp, Absorbance, absorption coefficient, and apparent quantum yield: A comment on common ambiguity in the use of these optical concepts, *Limnol. Oceanogr.*, 2002, **47**, 1261–1267.

39 G. V. Buxton, C. L. Greenstock, W. P. Helman and A. B. Ross, Critical Review of rate constants for reactions of hydrated electrons, hydrogen atoms and hydroxyl radicals (·OH/·O−) in Aqueous Solution, *J. Phys. Chem. Ref. Data*, 1988, **17**, 513–886.

40 M. Saran and K. H. Summer, Assaying for hydroxyl radicals: Hydroxylated terephthalate is a superior fluorescence marker than hydroxylated benzoate, *Free Radical Res.*, 1999, **31**, 429–436.

41 W. R. Haag and J. Hoigne, Singlet Oxygen in Surface Waters. 3. Photochemical Formation and Steady-State Concentrations in Various Types of Waters, *Environ. Sci. Technol.*, 1986, **20**, 341–348.

42 V. Ponti, M. U. Dianzani, K. Cheeseman and T. F. Slater, Studies on the reduction of nitroblue tetrazolium chloride mediated through the action of NADH and phenazine methosulphate, *Chem.-Biol. Interact.*, 1978, **23**, 281–291.
43 M. W. Sutherland and B. A. Learmonth, The Tetrazolium Dyes MTS and XTT Provide New Quantitative Assays for Superoxide and Superoxide Dismutase, *Free Radical Res.*, 1997, **27**, 283–289.
44 B. H. J. Bielski, D. E. Cabelli, R. L. Arudi and A. B. Ross, Reactivity of HO2/O−2 Radicals in Aqueous Solution, *J. Phys. Chem. Ref. Data*, 1985, **14**, 1041–1100.
45 H. S. Hsieh, R. Wu and C. T. Jafvert, Light-independent reactive oxygen species (ROS) formation through electron transfer from carboxylated single-walled carbon nanotubes in water, *Environ. Sci. Technol.*, 2014, **48**, 11330–11336.
46 J. G. Radich and P. V. Kamat, Making Graphene Holey. Gold-Nanoparticle-Mediated Hydroxyl Radical Attack on Reduced Graphene Oxide, *ACS Nano*, 2013, **7**, 5546–5557.
47 M. E. Lindsey and M. A. Tarr, Inhibition of hydroxyl radical reaction with aromatics by dissolved natural organic matter, *Environ. Sci. Technol.*, 2000, **34**, 444–449.
48 P. L. Brezonik and J. Fulkerson-Brekken, Nitrate-induced photolysis in natural waters: Controls on concentrations of hydroxyl radical photo-intermediates by natural scavenging agents, *Environ. Sci. Technol.*, 1998, **32**, 3004–3010.

 This journal is © The Royal Society of Chemistry 2019

Supporting Information

Reactivity of Graphene Oxide with Reactive Oxygen Species (Hydroxyl Radical, Singlet Oxygen, and Superoxide Anion)

Hsin-Se Hsieh[†], *Richard Zepp*[*,††]

[†]National Research Council Associate, National Exposure Research Laboratory, Ecosystem Research Division, U.S. Environmental Protection Agency, Athens, Georgia 30605, United States

[††]National Exposure Research Laboratory, Ecosystem Research Division, U.S. Environmental Protection Agency, Athens, Georgia 30605, United States

*Corresponding author. Phone: (706)355-8117. E-mail: zepp.richard@epa.gov

Pages: 13

Figures: S1-S9

Chemicals

Iron(III) perchlorate hydrate (<0.005% Cl^-), rose bengal (RB, 92%), furfuryl alcohol (FFA, 98%), 4-chlorobenzoic acid (pCBA, 99%), terephthalic acid (TPA, 98%), 2-hydroxyterephthalic acid (HTA, 97%), potassium hydrogen phthalate (99.95%), *N,N*-diethyl-*p*-phenylenediamine sulfate salt (DPD, 98%), 1,10-Phenanthroline (99%), β-Nicotinamide adenine dinucleotide reduced disodium salt hydrate (NADH, 97%), phenazine methosulfate (PMS, 90%), XTT sodium salt (90%), Nitrotetrazolium blue chloride (NBT^{2+}, 98%), horseradish peroxidase (HRP), superoxide dismutase (SOD) from bovine erythrocytes were obtained from Sigma-Aldrich (St. Louis, MO)**.** Sodium oxalate, hydrogen peroxide (30%), hydroxylamine hydrochloride (96%), Potassium Phosphate Monobasic, and Potassium Phosphate Dibasic were purchased from Thermo Fisher Scientific Inc. (Pittsburgh, PA).

Competition Kinetics for Superoxide Anion

At pH 8, the 2 μM PMS-catalyzed oxidation of NADH to $O_2^{\cdot-}$ followed pseudo-first-order kinetics, with a rate constant k_{NADH} of 0.255 min^{-1} in the presence of probe (NBT or XTT),

$$NADH \xrightarrow{PMS, k_{NADH}} O_2^{\cdot-} \quad (1)$$

The time-dependent $O_2^{\cdot-}$ production rate and NADH concentration are expressed as

$$P_{O_2^{\cdot-}} = -\frac{d[NADH]}{dt} = k_{NADH}[NADH] \quad (2)$$

$$[NADH] = [NAHD]_0 e^{-k_{NADH}t} \quad (3)$$

For the second-order reaction of $O_2^{\cdot-}$ with XTT and GO,

$$O_2^{\cdot-} + XTT \xrightarrow{k_{XTT}} XTT\ Formazan \quad (4)$$

$$O_2^{\cdot-} + GO \xrightarrow{k_{GO}} Product \quad (5)$$

The total $O_2^{\cdot-}$ scavenging rate and XTT formazan (MF) production rate are written as

$$S_{O_2^{\cdot-}} = (k_{XTT}[XTT] + k_{GO}[GO])[O_2^{\cdot-}] \quad (6)$$

$$P_{MF} = k_{XTT}[XTT][O_2^{\cdot-}] \quad (7)$$

$$-\frac{d[XTT]}{dt} = k_{XTT}[XTT][O_2^{\cdot-}] \quad (8)$$

Using quasi-steady-state approximation (QSSA), $P_{O_2^{\cdot-}} = S_{O_2^{\cdot-}}$

$$2k_{NADH}[NADH] = (k_{XTT}[XTT] + k_{GO}[GO])[O_2^{\cdot-}] \quad (9)$$

$$[O_2^{\cdot-}] = \frac{2k_{NADH}[NADH]}{k_{XTT}[XTT]+k_{GO}[GO]} \quad (10)$$

Using $[O_2^{\cdot-}]$ in eq 10, to substitute it in eq 7

$$P_{MF} = \frac{(k_{XTT}[XTT])(k_{NADH}[NADH])}{k_{XTT}[XTT]+k_{GO}[GO]} \quad (11)$$

The absorbance ratio of MF in the absence and presence of GO equals the integral of MF production rate, which could be simplified as eteq? 12:

$$\frac{\Delta A_{470,0}}{\Delta A_{470}} = \frac{\int P_{MF,0}dt}{\int P_{MF}dt} = \frac{\int (k_{\mathrm{NADH}}[NADH])dt}{\int\left(\frac{(\mathrm{k_{XTT}[XTT]})(k_{NADH}[NADH])}{\mathrm{k_{XTT}[XTT]+k_{GO}[GO]}}\right)dt} = \frac{\int ([NADH]_0 e^{-k_{NADH}t})\,dt}{\int\left(\frac{(\mathrm{k_{XTT}[XTT]})([NADH]_0 e^{-k_{NADH}t})}{\mathrm{k_{XTT}[XTT]+k_{GO}[GO]}}\right)dt}$$

$$\frac{\Delta A_{470,0}}{\Delta A_{470}} = \frac{\int (e^{-k_{NADH}t})\,dt}{\int\left(\frac{(e^{-k_{NADH}t})}{1+(\mathrm{k_{GO}[GO]/\,k_{XTT}[XTT]})}\right)dt} \qquad (12)$$

in which $[XTT]_{t+dt} = [XTT]_t - \left\{\frac{k_{\mathrm{NADH}}([NADH]_0 e^{-k_{NADH}t})}{1+(\mathrm{k_{GO}[GO]/\,k_{XTT}[XTT]}_t)}\right\}dt$ by combining eq 8 and 10.

Since there is only one unknown parameter, k_{GO}, in each competition experiment for $O_2^{\cdot-}$, the k_{GO} value could be obtained from least square-fitting by minimizing the sum of squared error (SSE) between predicted and measured $\Delta A_{470,0}/\Delta A_{470}$.

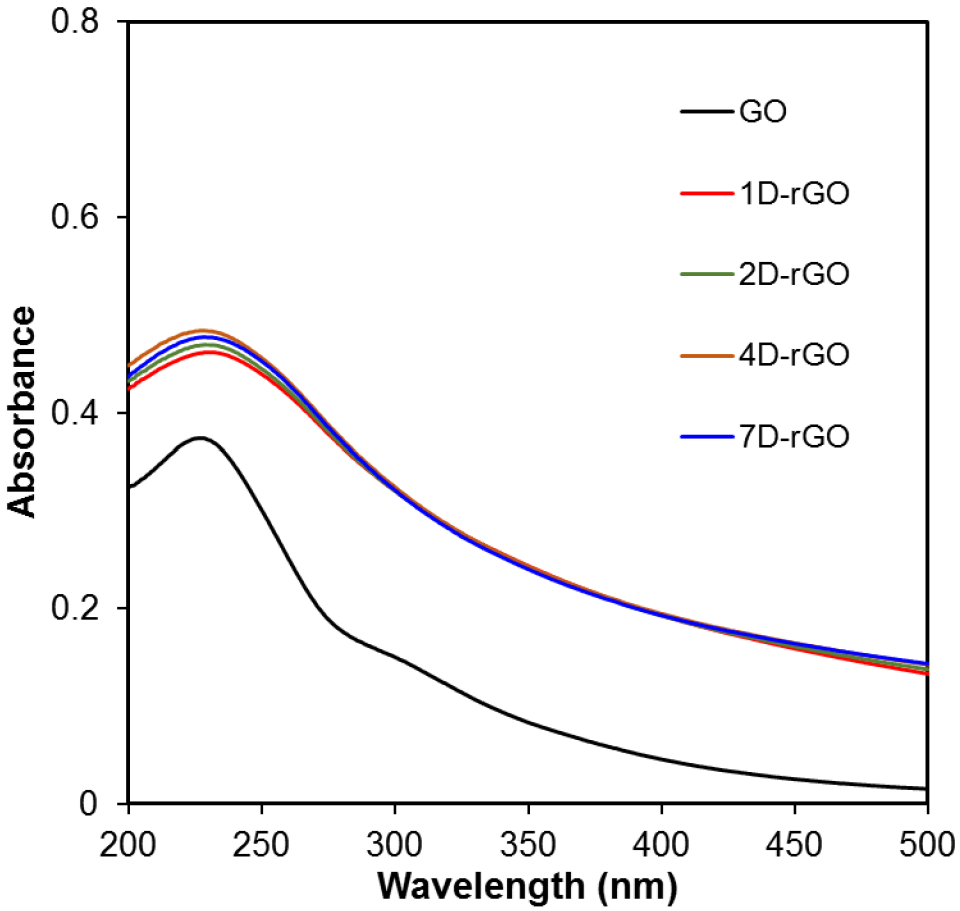

60

61 Figure S1. UV-vis absorbance of GO and photoreduced GO (rGO) at constant DOC concentration

62 (4 mg-C/L).

63

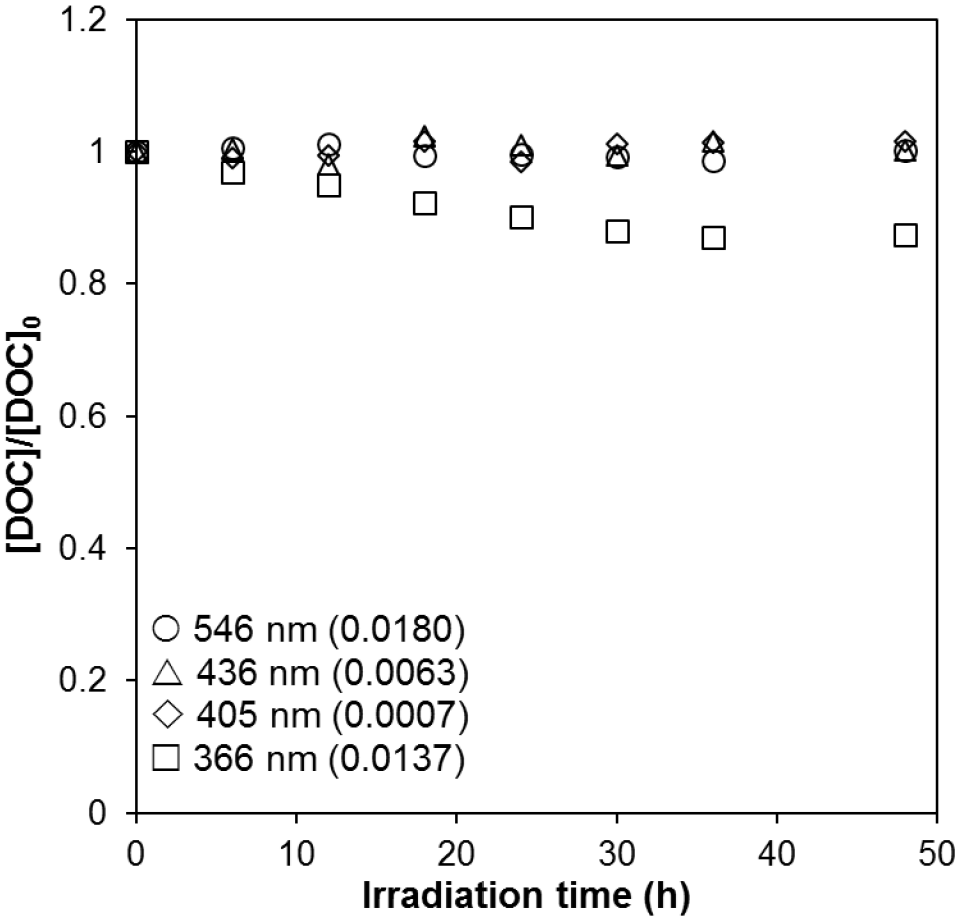

Figure S2. Temporal DOC trend of GO dispersions (15 mg/L) under exposure to light with different wavelengths in MGRR. Values in parentheses are the light intensities in mol photons L^{-1} h^{-1} in 5 mL solution, determined by ferrioxalate actinometry.

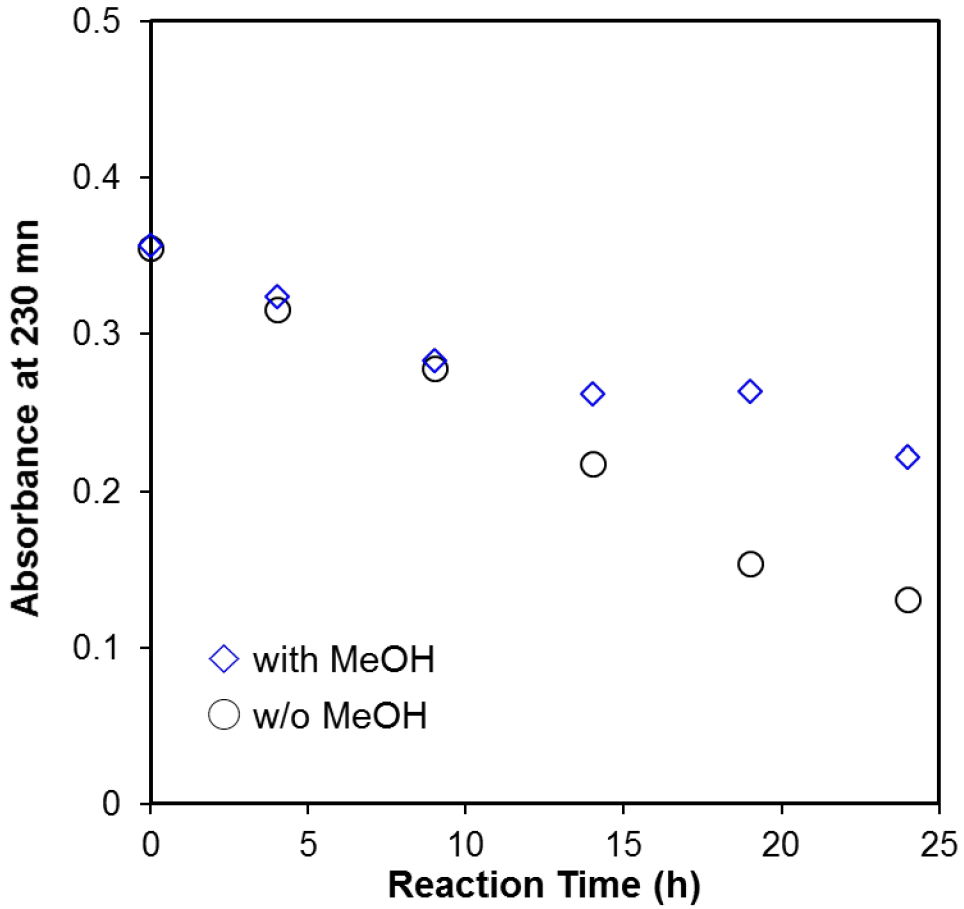

70

71 Figure S3. Effect of MeOH (10 mM) on the decrease of GO absorbance at 230 nm in the reaction

72 with HO• produced by photo-Fenton reaction as described in Figure 1a.

73

74

75

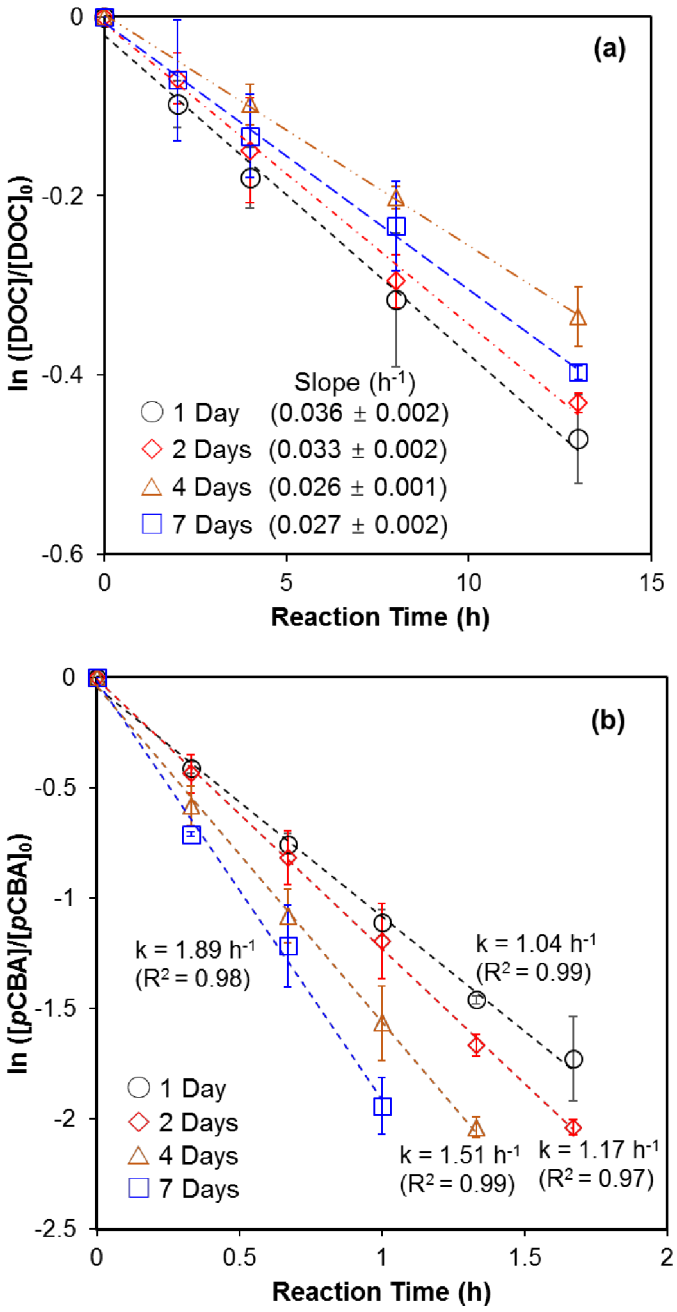

76

77 Figure S4. (a) DOC decays of photoreduced GO (rGO, ~ 4 mg-C/L) in pH 4 dispersions containing
78 15 μM $Fe(ClO_4)_3$ and 10 mM H_2O_2 under irradiation at 436 nm. (b) Decay of *p*CBA (1.5 μM)
79 added in the samples described in (a). Legends in both figures indicate how long the rGO had
80 previously irradiated in full-spectrum solar simulator (Atlas CPS+).

81

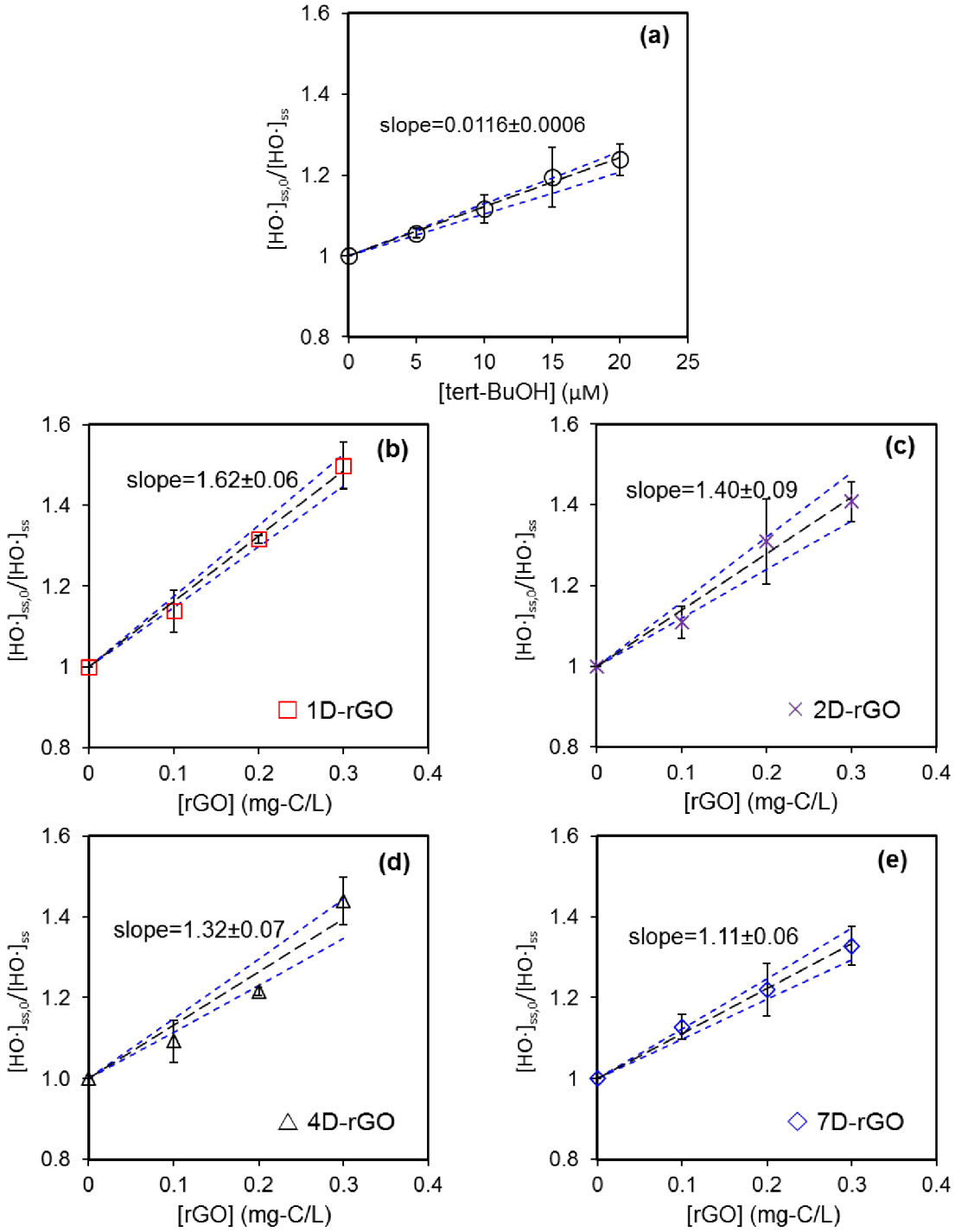

Figure S5. Effect of tert-butanol and rGO on steady state HO• concentrations in the system of sodium oxalate (60 μM), $Fe(ClO_4)_3$ (1.5 μM), H_2O_2 (50 μM), MeOH (50 μM), and *p*CBA (0.5 μM) irradiated at 436 nm. Black dotted lines represent the linear regression fit, and the blue dotted lines are 95% confidence bands.

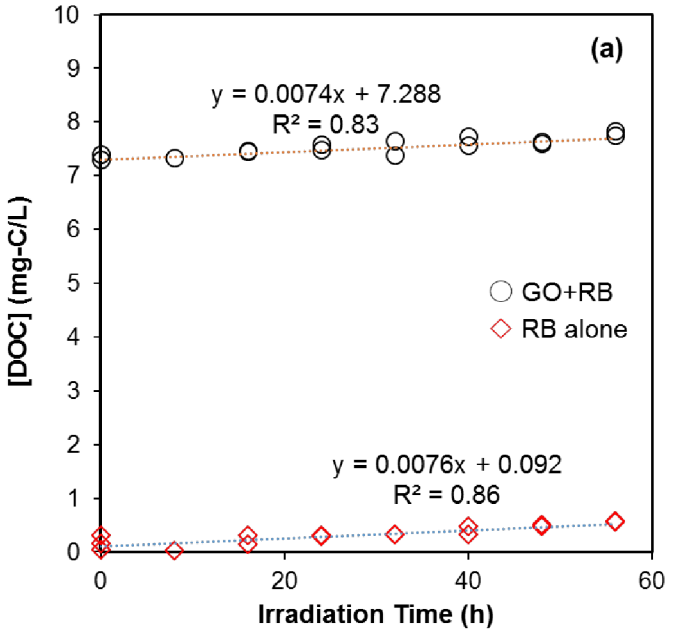

86

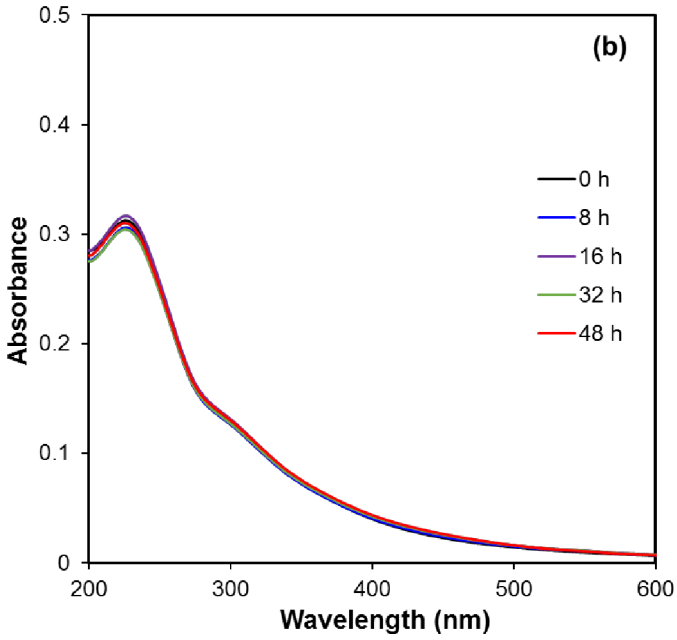

87

88 Figure S6. (a) DOC in the RB control samples and mixtures of GO (20 mg/L) and RB under
89 irradiation at 546 nm. The increase of DOC in mixtures was attributed to the step-wise dose of RB
90 (0.5 μM per 8 h). (b) UV-vis spectra of GO (10 mg/L) after continuous exposure to $^1O_2$ ($[^1O_2]_{ave}$
91 ~ 6.9×10^{-13} M) produced by photosensitization of step-wise dosed RB (0.5 μM per 8 h) under
92 irradiation at 546 nm. Before UV-vis measurement, reacted RB was removed by ultrafiltration.

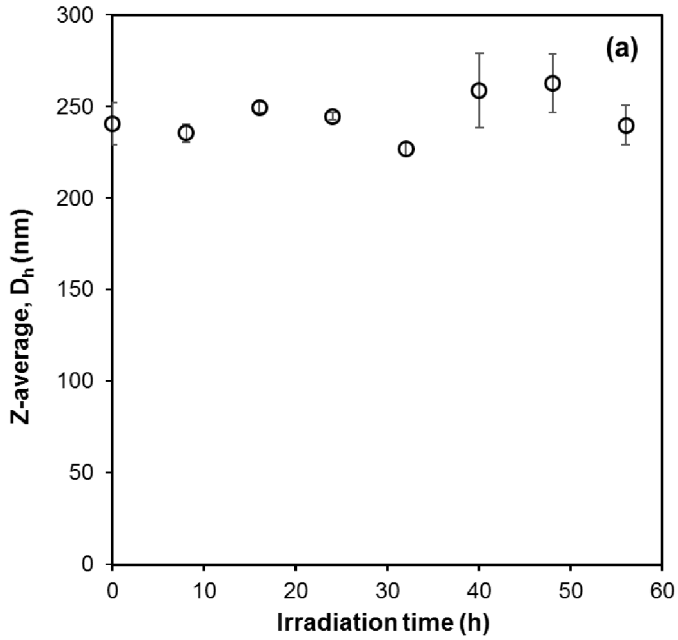

93

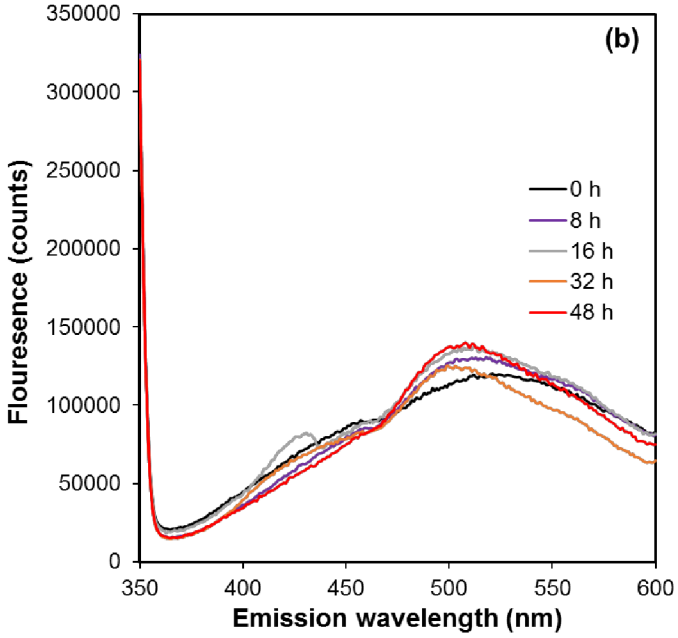

94

95

96 Figure S7. (a) Hydrodynamic diameter of GO after continuous exposure to $^1O_2$ produced by

97 photosensitization of step-wise dosed RB (0.5 μM per 8 h) under irradiation at 546 nm (c)

98 Fluorescence of $^1O_2$ reacted GO with excitation at 310 nm. Before measurement, reacted RB was

99 removed by ultrafiltration.

100

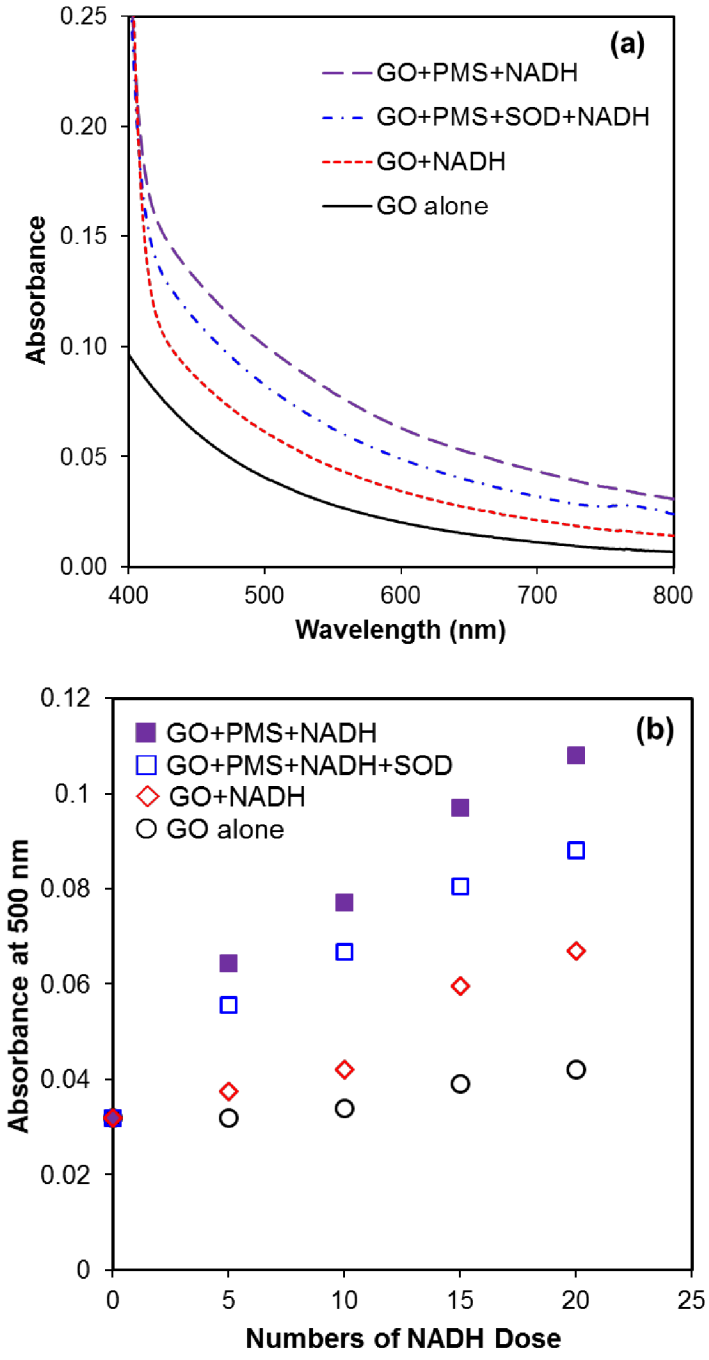

101

102 Figure S8. (a) Final absorbances of GO (15 mg/L) in the pH 8 dispersions containing PMS (1μM)
103 and (or) SOD (40 U/mL) after sequentially adding NADH in a stepwise dose increment of 100 μM
104 every 30 min for totally 20 times. (b) Temporal trends of GO absorbance at 500 nm. Note that the
105 absorbance has been normalized to same sample volume (6 mL).

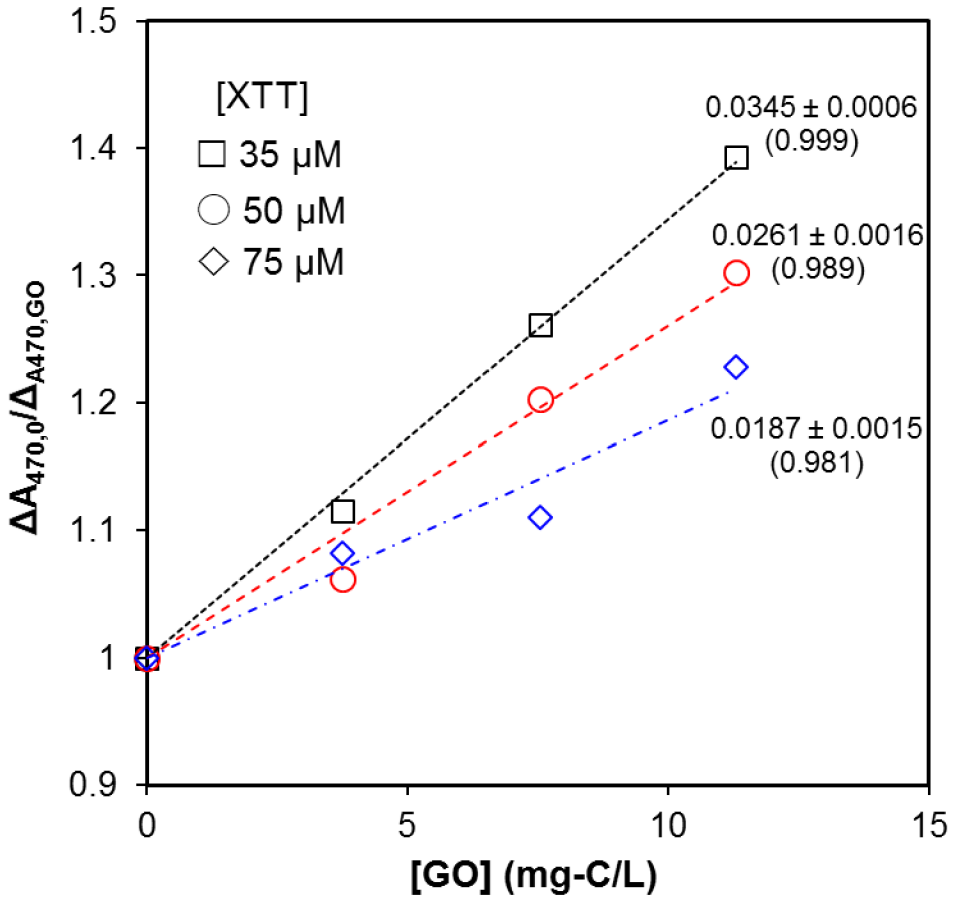

106

107 Figure S9. Inhibitory effect of GO on the formation of XTT formazan by superoxide anion in the

108 presence of different initial XTT concentration (NADH = 20 µM; PMS = 2 µM; pH = 8).

Zepp, Richard

From: Hsin Se Hsieh <hsinse@gmail.com>
Sent: Tuesday, April 28, 2020 8:14 AM
To: Richard Zepp; Zepp, Richard
Cc: Hsin Se Hsieh
Subject: Credit of scientific work

Dear Richard,

This email serves as a proof that I am in agreement with my designated percentage of 50% contribution as stated on the 2020 Scientific and Technological Achievement Awards Nomination Form for our paper "Reactivity of Graphene Oxide with Reactive Oxygen Species (Hydroxyl Radical, Singlet Oxygen, and Superoxide Anion."

Let me know if there is anything I can help.

Best,

Hsinse
--
謝心色
Hsin-Se Hsieh
Tel:(886)921-899136
hsinse@gmail.com

From:

Sent To:

Subject: Re: EPA award

I am in agreement with my designated percentage ot 50% contribution as stated on the 2020 Scientific and Technological Achievement Awards Nomination Form for our paper " Reactivity of Graphene Oxide with Reactive Oxygen Species (Hydroxyl Radical, Singlet Oxygen, and Superoxide Anion)."

Richard G Zepp

Justification for Principal Author

This paper was a joint effort by the candidate, Dr. Richard G. Zepp, and Dr. Hsin-Se Hsieh, a National Research Council Associate at NERL-EMMD (now NERL-CEMM). Zepp provided overall direction for this research, and most of the experiments were conducted in his laboratory. He was involved in acquiring, setting up the optical equipment, designing the experiments, and the writing of the paper. Whenever contributions are comparable, Dr. Zepp encourages graduate student collaborators to be lead authors.

Justification for Principal Author

This paper was a joint effort by the candidate, Dr. Richard G. Zepp, and Dr. Hsin-Se Hsieh, a National Research Council Associate at NERL-EMMD (now NERL-CEMM). Zepp provided overall direction for this research, and most of the experiments were conducted in his laboratory. He was involved in acquiring, setting up the optical equipment, designing the experiments, and the writing of the paper. Whenever contributions are comparable, Dr. Zepp encourages graduate student collaborators to be lead authors.

From:

Sent To:

Subject: Re: EPA award

I am in agreement with my designated percentage ot 50% contribution as stated on the 2020 Scientific and Technological Achievement Awards Nomination Form for our paper " Reactivity of Graphene Oxide with Reactive Oxygen Species (Hydroxyl Radical, Singlet Oxygen, and Superoxide Anion)."

Richard G Zepp

Zepp, Richard

From: Hsin Se Hsieh <hsinse@gmail.com>
Sent: Tuesday, April 28, 2020 8:14 AM
To: Richard Zepp; Zepp, Richard
Cc: Hsin Se Hsieh
Subject: Credit of scientific work

Dear Richard,

This email serves as a proof that I am in agreement with my designated percentage of 50% contribution as stated on the 2020 Scientific and Technological Achievement Awards Nomination Form for our paper "Reactivity of Graphene Oxide with Reactive Oxygen Species (Hydroxyl Radical, Singlet Oxygen, and Superoxide Anion."

Let me know if there is anything I can help.

Best,

Hsinse
--
謝心色
Hsin-Se Hsieh
Tel:(886)921-899136
hsinse@gmail.com

Table of Contents

General_Authors_Publications.....2
LI-266785_Publication_3D_2019_final.....8
Record_of_Percentage_Agreement_?_Dean_Lay.....15
Record_of_Percentage_Agreement_-_Phillip_Potter.....16
Record_of_Percentage_Agreement_?_Slawomir_Lomnicki.....17
Record_of_Percentage_Agreement-Al-Abed.....18
Publication_3D_2019_final.....19

United States Environmental Protection Agency
Washington, DC 20460

STAA REPORT FOR THE SCIENTIST NOMINATIONS

General Information:

Nomination ID/App ID:	20-137
Research Category Primary:	Other Environmental Research (OR)
Research Category Secondary:	Control Systems and Technology (CS);Health Effects Research and Human Health Risk Assessment (HE)
Laboratory/Office Name:	ORD
Nomination Entered By:	Souhail Al-Abed

Eligibility Checklist:

[N] The nominated publication(s) has not been submitted to a previous STAA competition.

[N] The nominated publication(s) was published on or before January 1, 2017 and on or after January 1,2012

[N] The principal author was an EPA employee or a PHS employee assigned to EPA when the research was performed

[N] The EPA authors (includes PHS employees assigned to EPA) contributed collectively a minimum of 50% toward the publication(s)

Nominating Official Name:	Kirk Scheckel
Nominating Official Title:	SUPERVISORY PHYSICAL SCIENTIST
Nominating OfficialEmail:	scheckel.kirk@epa.gov
STAA Coordinator Name:	Kathleen Wiser
STAA Coordinator Email:	wiser.kathi@epa.gov

Justifications:

Justification 1:

Polymers used in 3D printing are known to emit hazardous materials when heated. While the emissions from pristine polymers and some filaments have been studied, many filaments contain additives that may influence their hazardous emissions. For example, carbon nanotubes (CNTs) are added to some filaments to confer structural and electrical properties and are likely to interact with volatile organic compound (VOC) emissions. This research used a commercially-available CNT-containing 3D printer filament to investigate the effect of CNTs on VOC emissions during the printing process. While the presence of CNTs caused a slight overall decrease in the total VOC emissions, there was a shift towards more hazardous compounds being emitted. These findings should influence future studies on 3D printer emissions to include additives such as CNTs, metals, and dyes.

Justification 2A:

If research has been invited for presentation at national/international societies. The following invited presentations resulted from this research:

· Potter, P. M. VOC Emissions and Formation Mechanisms from Carbon Nanotube Composites During 3D Printing. Poster presentation at the 257th American Chemical Society National Meeting, Orlando, Mar 31st-Apr 4th, 2019.

· Al-Abed, S. R. VOC Emissions Influenced by Polymer Additives in 3D Printing. Poster presentation at Global Summit on Regulatory Science 2019, Milan, Sep 24-26, 2019.

Justification 2B:

1. Unique source of funding for research

All funding came from the intramural research budget of the EPA Office of Research and Development

2. Any awards Internal/External to EPA that were received for the research

None to date

3. Number of times the publication has been downloaded/viewed

4. How many times it has been cited (Google Scholar)

Publication	Number of downloads/views	Number of citations (Google Scholar)
Potter et al., 2019	779	4

Justification 2C:

Justification 2D:

Justification 2E:

Justification 3A:

Justification 3B:

AUTHORS

Principal Author

Author Name:	Souhail R. Al-Abed		
Professional Title:		Salutation:	Dr.
Email:	al-abed.souhail@epa.gov	Organization:	

Mailing Address:			
Street Line 1:	26 Martin Luther King Drive West		
City:	Cincinnati		
Zip Code:	45268	State:	OH
At time of research was:	EPA Employee		
Separation Date:			
% of Effort:	50		

Contributing Author

Author Name:	Phillip Potter		
Professional Title:		Salutation:	Dr.
Email:		Organization:	
Mailing Address:			
Street Line 1:			
City:			
Zip Code:		State:	
At time of research was:	Non EPA Personnel		
Separation Date:			
% of Effort:	20		

Contributing Author

Author Name:	Slawomir Lomnicki		
Professional Title:		Salutation:	Dr.
Email:	slomni1@lsu.edu	Organization:	

Mailing Address:			
Street Line 1:			
City:			
Zip Code:		State:	
At time of research was:	Non EPA Personnel		
Separation Date:			
% of Effort:	15		

Contributing Author

Author Name:	Dean Lay		
Professional Title:		Salutation:	Mr.
Email:	deanjlay@gmail.com	Organization:	
Mailing Address:			
Street Line 1:			
City:			
Zip Code:		State:	
At time of research was:	Non EPA Personnel		
Separation Date:			
% of Effort:	15		

PUBLICATIONS

Publication 1:

Publication Title:	VOC emissions and formation mechanisms from carbon nanotube composites during 3D printing

Publication Date:	Thu Feb 28 00:00:00 GMT 2019		
Journal/Publication Method:	Environmental Science and Technology		
All Author(s):			
Volume:	53	Number:	8
Pages:	4364-4370	Immediately Index:	Immediately Index:
Citation ½ Life:	7.1	Impact Factor:	7.149

Environmental Science & Technology

Article

Cite This: Environ. Sci. Technol. 2019, 53, 4364−4370

pubs.acs.org/est

VOC Emissions and Formation Mechanisms from Carbon Nanotube Composites during 3D Printing

Phillip M. Potter,[†] Souhail R. Al-Abed,*[,‡] Dean Lay,[§] and Slawomir M. Lomnicki[§]

[†]Oak Ridge Institute for Science and Education (ORISE) and [‡]National Risk Management Research Laboratory (NRMRL), U.S. Environmental Protection Agency, Cincinnati, Ohio 45268, United States

[§]Department of Environmental Sciences, Louisiana State University, Baton Rouge, Louisiana 70803, United States

Supporting Information

ABSTRACT: A commercially available, 3D printer nanocomposite filament of carbon nanotubes (CNTs) and acrylonitrile−butadiene−styrene (ABS) was analyzed with respect to its VOC emissions during simulated fused deposition modeling (FDM) and compared with a regular ABS filament. VOC emissions were quantified and characterized under a variety of conditions to simulate the thermal degradation that takes place during FDM. Increasing the residence time and temperature resulted in significant increases in VOC emissions, and the oxygen content of the reaction gas influenced the VOC profile. In agreement with other studies, the primary emitted VOC was styrene. Multiple compounds are reported in this work for the first time as having formed during FDM, including 4-vinylcyclohexene and 2-phenyl-2-propanol. Our results show that printing 222.0 g of filament is enough to surpass the reference concentration for inhalation exposure of 1 mg/m^3 according to the EPA's Integrated Risk Information System (IRIS). The presence of CNTs in the filament influenced VOC yields and product ratios through three types of surface interactions: (1) adsorption of O_2 on CNTs lowers the available O_2 for oxidation of primary backbone cleavage intermediates, (2) adsorption of styrene and other VOCs to CNTs leads to surface-catalyzed degradation, and (3) CNTs act as a trap for certain VOCs and prevent them from entering vapor emissions. While the presence of CNTs in the filament lowered the total VOC emission under most experimental conditions, they increased the emission of the most hazardous VOCs, such as α-methylstyrene and benzaldehyde. The present study has identified an increased risk associated with the use of CNT nanocomposites in 3D printing.

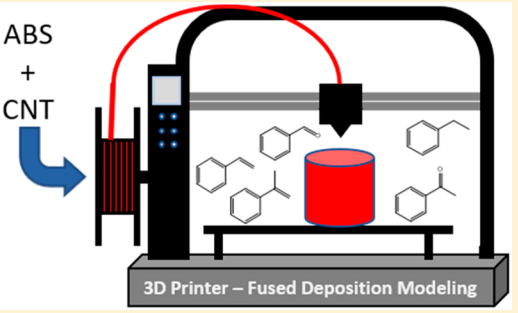

INTRODUCTION

There is a growing concern over hazardous emissions from 3D printers using fused deposition modeling (FDM) as they become more affordable and enter more workplaces and consumer households. Three-dimensional printers operate at borderline temperatures of thermal degradation reactions for polymer filament feedstock. Despite design efforts to limit exposure, printing emissions are still a threat to user health.[1] Emissions from FDM can be grouped into two categories: particulate matter (PM) and gas-phase compounds. Particulate matter emitted from 3D printers has been studied across a variety of size ranges,[2−10] including nanoparticle emission.[11−15] Studies involving gas-phase compounds usually concern volatile organic compounds (VOCs). While some studies quantify total VOCs,[3,7] there have been few attempts to fully characterize and quantify VOC emissions.[5,6,16,17]

Acrylonitrile−butadiene−styrene (ABS) is a common polymer used in FDM (Figure 1). Thermal degradation of ABS has been studied in the past under conditions of extrusion[18] and incineration.[19] Three-dimensional printing filaments often contain additives to adjust their physicochemical properties. Common additives include dyes, plasticizers, stabilizers, wood particles, metal particles, and carbon allotropes. Many of these additives can either degrade into VOCs or contribute to their formation. The effects of many filament additives on VOC emissions during FDM has not been studied.

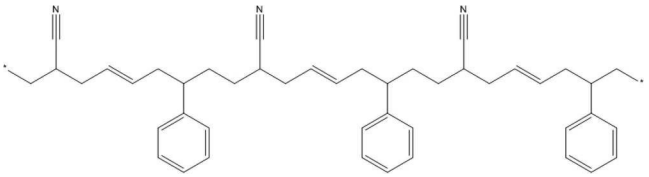

Figure 1. Typical structure of colinear ABS polymer.

Nanocomposites consisting of carbon nanotubes (CNTs) and a variety of polymers can be made with unique mechanical and electrical properties.[20,21] These CNT nanocomposites are used with 3D printers to produce conductive electrical components.[22] Despite the increasing usage of CNT nano-

Received: February 4, 2019
Revised: March 12, 2019
Accepted: March 15, 2019
Published: March 15, 2019

Downloaded via US EPA RESEARCH TRIANGLE PARK on April 16, 2019 at 14:30:50 (UTC).
See https://pubs.acs.org/sharingguidelines for options on how to legitimately share published articles.

© 2019 American Chemical Society

DOI: 10.1021/acs.est.9b00765
Environ. Sci. Technol. 2019, 53, 4364−4370

composites, their influence on hazardous VOC emissions during FDM has not been investigated. The adsorptive properties of CNTs have also been extensively studied on VOCs,[23] including aromatic species.[24,25] A thorough understanding of the role CNTs play in VOC formation in thermal processes is critical to limiting health risks to 3D printer users.

In this work, two commercially available 3D printer filaments, consisting of an ABS−CNT nanocomposite and a plain ABS, were subjected to thermal conditions that simulate FDM. VOC emissions from the simulated printing were quantified and characterized to determine the effect of CNT addition on hazardous emissions.

MATERIALS AND METHODS

Three-dimensional printer filaments were purchased from 3DXTech. The ABS filament is from the standard ABS product line, and the nanocomposite ABS−CNT filament is from the 3DXNano ESD product line. The ABS−CNT filament is advertised to contain CNTs, but the concentration is not reported. Quartz sample baskets were made in the LSU Chemistry Department glass-blowing shop. Pure reference standards used for quantification were purchased from Sigma-Aldrich and dissolved in dichloromethane (DCM) to create calibration curves. HPLC-grade DCM was purchased from Fisher Scientific.

All degradation experiments were performed using the System for Thermal Diagnostic Studies (STDS).[26] The STDS is a custom-built, modular instrument that has been previously used to provide thermal conditions for combustion of various waste components.[27,28] A diagram for the STDS can be found in the Supporting Information (Figure S1). The STDS consists of a ceramic furnace and quartz reactor housed within a gas chromatograph (GC) oven. Gas-phase compounds leaving the reactor pass through a heated transfer line into the injection port of a second GC where they are separated and detected by a mass spectrometer (MS). The advantages of the STDS include being a closed system with direct transfer of products into the detection module, which minimizes sample loss and increases detection sensitivity. Approximately 50−100 mg of filament was weighed and placed in a quartz sample holder basket (15 mm × 4 mm i.d.) above the heated reactor. For pyrolysis experiments, the sample was purged with N_2 at room temperature for 3 min. The sample was then lowered into the preheated reactor, and pyrolysis began. During reaction, the second, analytical GC oven was kept at −60 °C to condense all compounds that passed through the 280 °C transfer line. Gas flow rate was set at each temperature to maintain a vapor residence time in the reactor of approximately 0.2 s. After reaction completion, the transfer line was removed from the injection port of the second GC and analysis of the reaction products began. Analysis of reaction products was conducted using an Agilent 6890N GC equipped with a DB5-MS column (30 m × 0.25 mm × 0.25 μm) and a 5973N MS with an electron impact (EI) ion source set at 70 eV. The temperature program was as follows: −60 °C initial temperature held for 0.5 min, followed by heating at a rate of 15 °C/min to 130 °C, held for 1 min, heated to 225 °C at a rate of 25 °C/min, and finally heated to 300 °C at 10 °C/min and held for 7 min, giving a total runtime of 32.47 min. The GC inlet and MS quadrupole temperatures were 280 and 150 °C, respectively. The split/splitless inlet was set to a constant split flow of 10 mL/min. The carrier gas used was ultrahigh-purity helium (UHP, 99.999%) at a constant column flow of 1.0 mL/min. However, during sample collection, the flow of N_2 through the transfer line was high enough to increase the column flow to 2 mL/min or above, with the remainder going out the split vent. The mass spectrometer was operated in total ion count mode (TIC) over a mass scan range of 50−500 amu. Identification of pyrolysis products was performed using the Wiley and NIST libraries and by comparison of retention times with those of purchased standard compounds. VOC emissions were calculated by dividing the emitted mass of each VOC by the mass of filament used in the experiment and reported as μg/g. Additional information on the quantification methods and method detection limits can be found in the Supporting Information. Mass loss was calculated by weighing the filament prior to reaction and dividing by the filament mass after reaction.

Reaction conditions were selected to simulate common 3D printer parameters. The manufacturer recommended printing temperatures are 220−240 °C for the ABS filament and 230−260 °C for the ABS−CNT filament. A printing temperature of 230 °C was selected for consistency between samples, but users often change printing temperatures to alter printed objects, and extruder nozzles are unlikely to heat uniformly. To account for user preference and nozzle construction, degradation experiments were also performed at 200 and 300 °C. The residence time in the heated area of the printer is based on the feed rate of the filament and the length of the extruder nozzle. Feed rate is often changed by the user to affect the quality of the printed object. Residence times of 1 and 3 min were investigated. The design of 3D printer nozzles can lead to oxygen-deprived conditions inside the nozzle where melted filament is exposed to the highest temperatures. To better understand the role of oxygen in the thermal degradation of 3D printer filament, experiments were carried out in both pyrolytic (N_2) and oxidative (4% O_2/N_2) conditions.

RESULTS AND DISCUSSION

Degradation Products. Thermogravimetric studies of ABS polymer do not show any significant mass loss at temperatures below 325 °C.[29] Despite mass loss during these experiments being very low (<1% for all experiments), simulated FDM has yielded emissions of several VOCs. The major components of VOC emissions from simulated 3D printing are shown in Table 1, and their associated structures are presented in Table S1. All of these compounds, except for 2,6-di-*tert*-butylquinone and 2,4-di-*tert*-butylphenol, have been

Table 1. Major Components of VOC Emissions from Thermal Degradation of ABS 3D Printer Filament

compound	source
4-vinylcyclohexene	butadiene monomer dimerization
ethylbenzene	polymer backbone cleavage
styrene	unreacted monomer/backbone cleavage
isopropylbenzene	polymer backbone cleavage
benzaldehyde	oxidation of backbone cleavage intermediate
α-methylstyrene	polymer backbone cleavage
tetramethylsuccinonitrile	polymerization byproduct
acetophenone	oxidation of backbone cleavage intermediate
2-phenyl-2-propanol	oxidation of backbone cleavage intermediate
2,6-di-*tert*-butylquinone	2,4-di-*tert*-butylphenol degradation
2,4-di-*tert*-butylphenol	polymer UV stabilizer

DOI: 10.1021/acs.est.9b00765
Environ. Sci. Technol. 2019, 53, 4364−4370

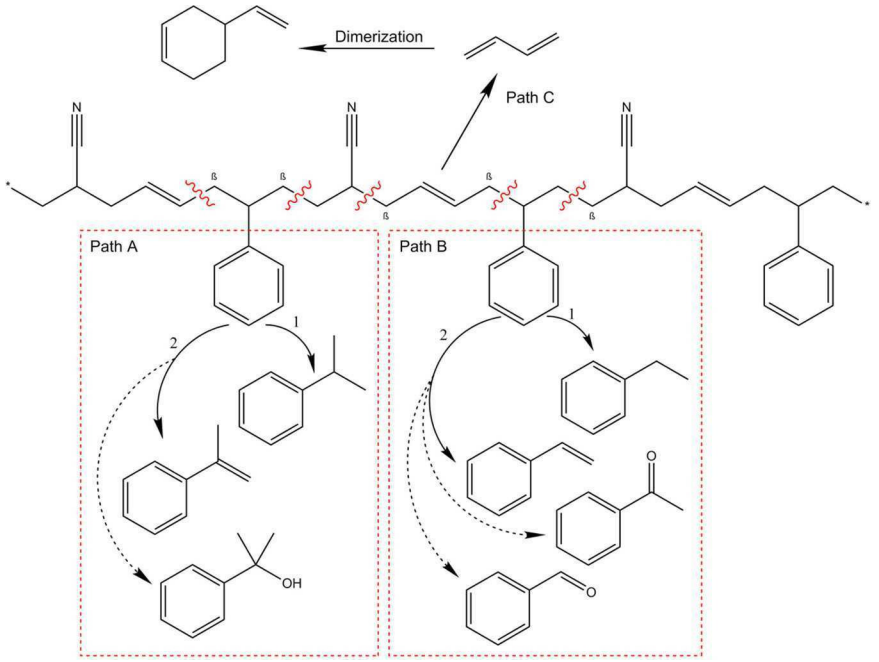

Figure 2. Pathways of the low-temperature depolymerization of ABS filament. Solid arrows signify primary polymer backbone degradation products. Dashed arrows signify secondary products formed by the oxygenation of primary products.

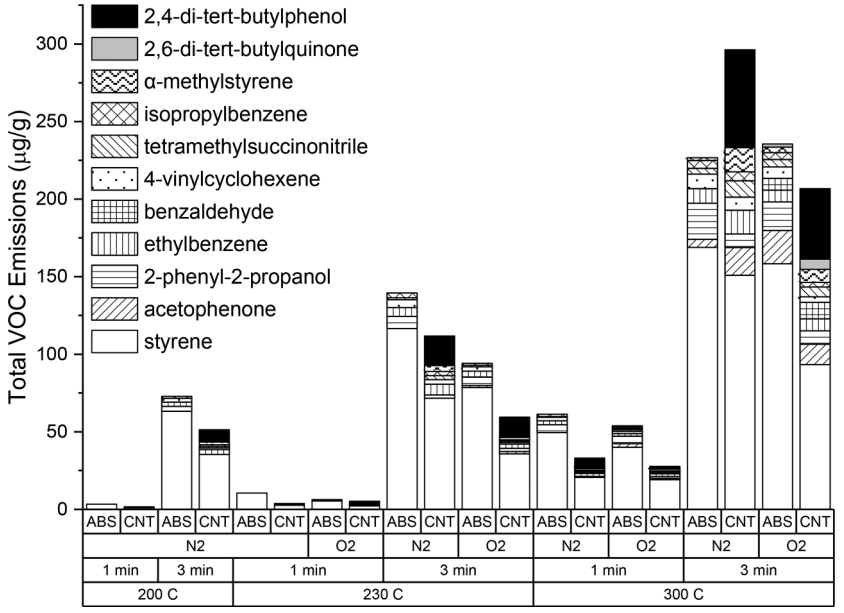

Figure 3. VOC emissions from thermal degradation of ABS and ABS−CNT composite. Experiment names are generated from the temperature + residence time + reaction gas + filament type.

found in previous studies involving ABS incineration and heated extrusion.[18,19] Studies involving VOC emissions from ABS filament have shown different compound profiles and VOC concentrations obtained from similar filaments from different manufacturers.[5] The emitted VOCs in the current experiments are likely the result of either desorption of unreacted monomer from the polymer matrix or slow degradation/depolymerization of the ABS polymer. In this work, styrene comprises a significant portion of total VOC emissions and justifies the assumption of trapped monomer as the primary VOC emission. Tetramethylsuccinonitrile (TMSN) and 2,4-di-*tert*-butylphenol, a polymerization by-product and polymer stabilizer, respectively, are likely part of the polymer synthesis process and volatilized during heating.

Other compounds, unlikely to be present in pristine polymer material, were also detected. Ethylbenzene is the most commonly reported styrene degradation product,[5,6,11,16] but in this work we also report 4-vinylcyclohexene, isopropylbenzene, benzaldehyde, α-methylstyrene, acetophenone, and 2-phenyl-2-propanol. Figure 2 presents proposed pathways to the observed thermal degradation products of ABS at low temperatures. On the basis of the proposed pathways, the depolymerization process is initiated through the cleavage of polymer backbone at β-carbons with respect to either phenyl or nitrile groups. The VOC sources in Table 1 are inferred

DOI: 10.1021/acs.est.9b00765
Environ. Sci. Technol. 2019, 53, 4364−4370

from these pathways based on where cleavage occurred on the polymer backbone and whether additional oxygen atoms have been incorporated into their structure.

VOC Emission. Emissions for VOCs from different reaction temperatures, residence times, and oxygen contents are shown in Figure 3. Complete data tables are presented in the Supporting Information (Table S2). Interestingly, some oxygenated products were observed under pyrolytic conditions such as acetophenone and benzaldehyde. This may suggest that oxygen is adsorbed to the polymer matrix.

Role of Residence Time. For all measured conditions, increasing the residence time from 1 to 3 min led to increased yields of all observed products. As seen in Figure 3, the increase in VOC emissions was not directly proportional to the increase in residence time. For 200 and 230 °C, styrene emission increased by an order of magnitude when increasing the residence time from 1 to 3 min. At 300 °C, tripling the residence time increased styrene emission by a factor of approximately four. The significant increase in the effect of residence time seen at lower temperatures could indicate that a residence time of 1 min is too short for accurate analysis due to the time needed for the filament to equilibrate to the reactor temperature. Therefore, the results for experiments with a residence time of 3 min are more accurate predictions of actual printer emissions.

Role of Temperature. Extrusion temperature in 3D printers is typically selected through a combination of user preference and manufacturer suggestions. Extrusion temperature both is the most commonly adjusted printing parameter and had the most significant effect on VOC emissions. Across all parameter combinations, higher temperature resulted in higher yields of every individual VOC. Figure 4 compares VOC emissions from ABS filament in pure N_2 at 200, 230, and 300 °C for 3 min.

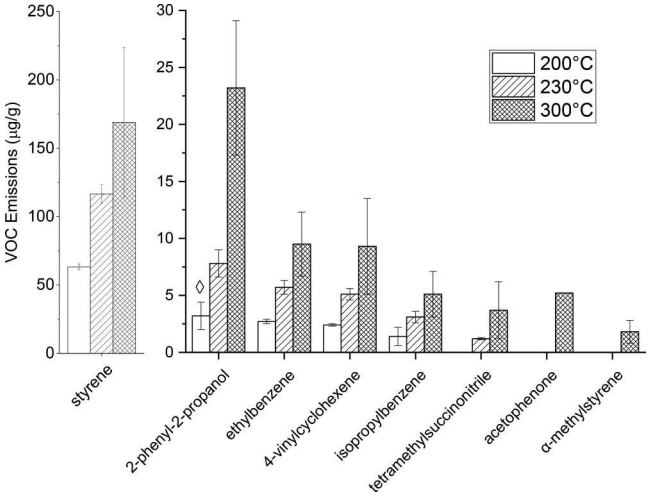

Figure 4. Individual VOC emissions from pyrolysis of ABS filament for 3 min in pure N_2 at 200, 230, and 300 °C. Error bars represent ± one standard deviation. ◊ = below method detection limit.

Acetophenone and α-methylstyrene were typically not detected until 300 °C under pyrolytic conditions. However, both acetophenone and α-methylstyrene were formed at 230 °C by the addition of O_2 and CNTs, respectively. Despite temperature having the greatest effect, no individual parameter can be used to predict VOC emissions.

Role of Oxygen. Depending on the design of the extruder nozzle, melted filament may be exposed to oxygen-deprived conditions prior to exiting the nozzle into air. Thus, the construction of extruder nozzles likely yields emissions that include products formed under both oxidative and oxygen-deprived conditions. The presence of oxygen in the reaction gas led to lower levels of emitted styrene and certain degradation products (Table S2), primarily those that do not contain oxygen in their formula. This decrease in emission can be explained by (1) oxidation of polymer decomposition products to low molecular weight products not analyzed in this study (CO, CO_2, and compounds with less than six carbons) and (2) increased formation of oxygen-containing acetophenone and benzaldehyde. Contrary to acetophenone and benzaldehyde (Figure 2, Path B), 2-phenyl-2-propanol yield (Figure 2, Path A) is not affected by addition of gas-phase O_2. This may indicate that polymer-adsorbed oxygen plays a key role in Path A, while gas-phase O_2 forms secondary products in Path B.

Role of Carbon Nanotubes. Studies have indicated that incorporation of single-walled CNTs into ABS decreases the activation energy of thermal degradation by up to 6 kcal/mol.[30] The mechanism of this effect is not clear. The presence of CNTs in the filament affected both the total VOC emission and the VOC profile. Overall, addition of CNTs slightly decreased the emissions of VOCs (Figure 3), except for the sample treated at 300 °C/3 min/N2, which showed the highest emission due to the drastically increased emission of UV stabilizer 2,4-di-*tert*-butylphenol. Figure 5 shows emissions of five VOCs that best exemplify the differences between ABS and ABS−CNT filament degradation. Despite still being the most prevalent VOC, styrene emissions decreased in the presence of CNTs (Figure 5A) except for pyrolytic conditions at 300 °C, where the difference between ABS and ABS−CNT was insignificant.

The sum of the products of Path A decomposition (Figure 2) did not change significantly for the ABS−CNT samples; however, the product distribution within this group was altered. The formation of α-methylstyrene was increased (Figure 5B), and 2-phenyl-2-propanol was significantly suppressed (Figure 5C). This change in product ratio away from oxygenated products is explained by a change in available oxygen in the system, possibly due to strong adsorption of O_2 on CNTs.

Figure 6 shows the VOC yields of Path A and Path B products only, with the exclusion of styrene and benzaldehyde. Styrene is not included in the Path B product sum to compensate for the presence of unreacted monomer, and benzaldehyde was removed due to only being formed at the highest temperature. The similarities between Path A and Path B after the removal of styrene and benzaldehyde, particularly in the CNT-containing filament, leads to the conclusion that the majority of styrene emissions is from unreacted monomer and not polymer backbone cleavage. Figure 6 also indicates that CNTs do not have a significant effect on the preference for Path A or Path B. The decrease in styrene emission in the presence of CNTs is therefore likely due to adsorption and subsequent surface-catalyzed degradation of unreacted styrene monomer on CNTs. There may even be a synergistic effect between adsorption of both O_2 and VOCs on the surface of CNTs as several compounds show significantly lower yields when both O_2 and CNTs are present, including 2-phenyl-2-propanol, acetophenone, and isopropylbenzene.

DOI: 10.1021/acs.est.9b00765
Environ. Sci. Technol. 2019, 53, 4364−4370

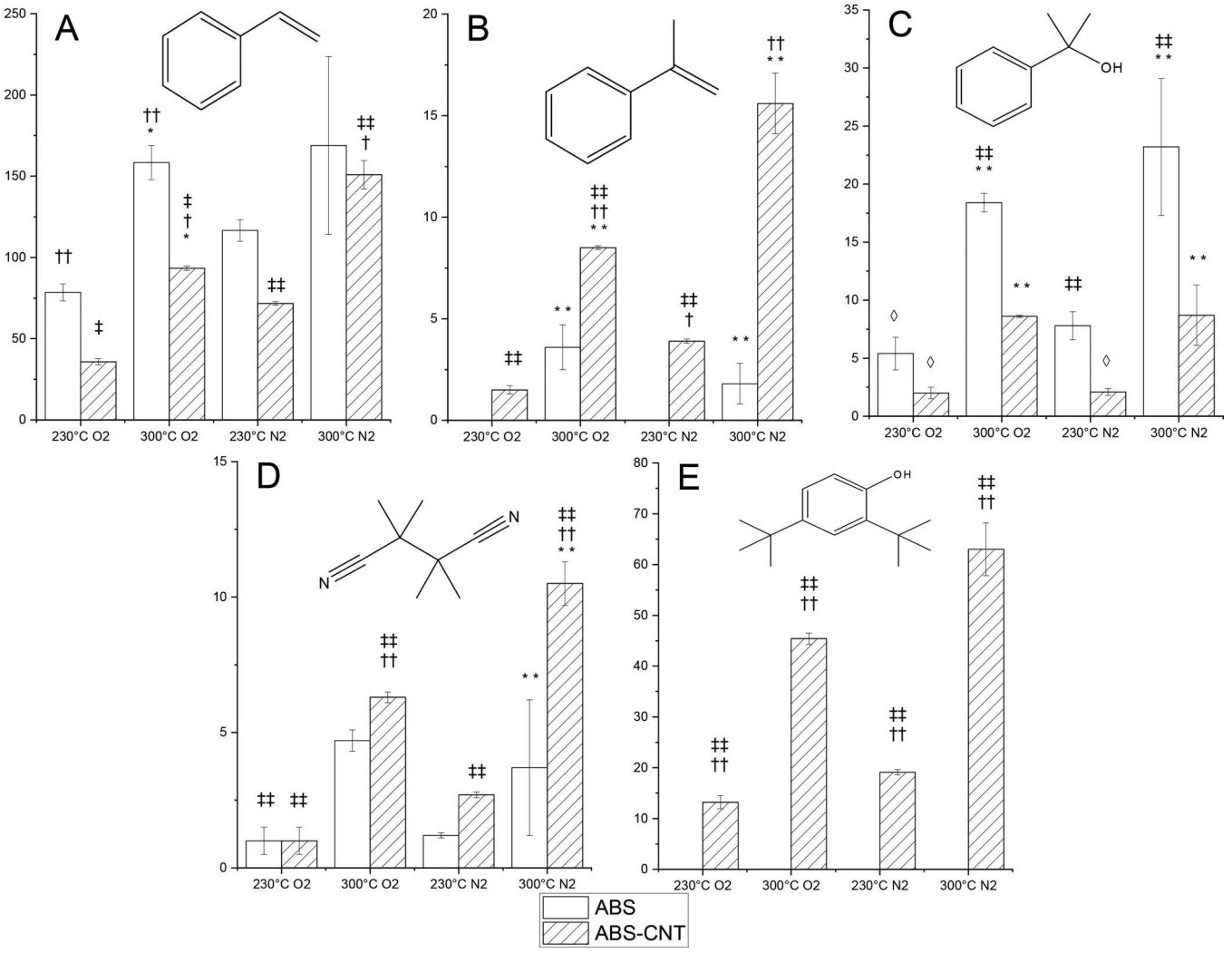

Figure 5. Influence of CNTs on emissions of (a) styrene, (b) α-methylstyrene, (c) 2-phenyl-2-propanol, (d) tetramethylsuccinonitrile, and (e) 2,4-di-*tert*-butylphenol. All values are in μg/g. ‡ = statistical significance between 230 and 300 °C, † = statistical significance between O2 and N2, * = statistical significance between ABS and ABS−CNT, and ◊ = below method detection limit. Single symbol represents p value of <0.05, and double symbol represents p value of <0.01. Statistical significance determined using ANOVA with a posthoc Tukey test. Error bars are ± one standard deviation.

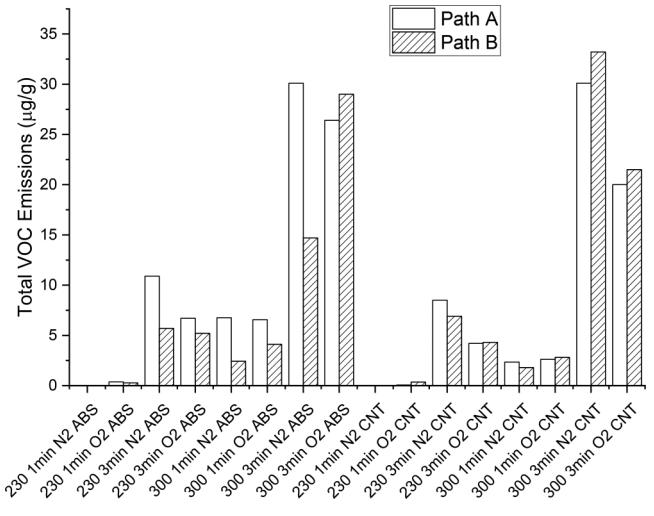

Figure 6. VOC emissions from Path A and Path B of the mechanism in Figure 2. Unreacted monomer styrene removed from all conditions and benzaldehyde removed from 300 °C/3 min/O_2.

CNTs could also be acting as sinks for certain VOCs. Significantly lower yields for certain VOCs, such as 2-phenyl-2-propanol, could be due to an increased affinity for adsorption of phenolic compounds on CNTs.[24] This would mean that formation of these VOCs is not necessarily affected by CNTs but that they are not detected once adsorbed to CNTs.

There is evidence that three types of surface interactions may be responsible for the effect of CNTs on VOC emissions: (1) strong adsorption of O2 on CNTs, lowering the amount of O2 available for reaction with polymer backbone cleavage intermediates, (2) adsorption of unreacted monomer styrene to CNTs yielding different products compared to Path A and Path B, and (3) increased affinity for certain aromatics leading to CNTs acting as sinks for particular VOCs. These three interactions can occur independently, compete, or even exhibit synergy in altering VOC emissions.

Some VOC emissions are not the result of polymer degradation. As seen in Figure 5D, TMSN was emitted in greater concentrations in the presence of CNTs. TMSN is a polymerization byproduct from the radical initiator 2,2′-azobis-isobutyronitrile. Interestingly, a new group of VOCs was

DOI: 10.1021/acs.est.9b00765
Environ. Sci. Technol. 2019, 53, 4364−4370

observed for ABS−CNT filaments: 2,4-di-*tert*-butylphenol and 2,6-di-*tert*-butylquinone. Shown in Figure 5E, 2,4-di-*tert*-butylphenol was only emitted from ABS−CNT filament. 2,4-Di-*tert*-butylphenol is a common polymer stabilizer that protects from UV damage. The structural and mechanical changes caused by the addition of CNTs to ABS could necessitate a different polymer formulation that incorporates different polymerization initiators and stabilizers. It is not clear whether this stabilizer is only added to ABS−CNT or if the presence of CNTs triggers the release.

Environmental Implications. The Integrated Risk Information System (IRIS) is an EPA-created tool for categorizing chemicals and their associated health hazards. IRIS contains entries for five of the measured VOCs from this study, and three entries contain a reference concentration for inhalation exposure (RfC). Table 2 shows the IRIS RfC values for styrene, ethylbenzene, and isopropylbenzene (in IRIS as cumene). The IRIS RfC for styrene is 1 mg/m^3, which could be easily reached after printing a few hundred grams of filament depending on room size and ventilation. VOCs whose formation is increased by CNTs also pose known inhalation hazards, such as α-methylstyrene[31] and benzaldehyde.[32]

Table 2. IRIS RfC Values for VOCs Emitted during 3D Printing[a]

compound	RfC (mg/m^3)	printed mass to achieve RfC (g)
styrene	1	222.0
ethylbenzene	1	2451.0
cumene/isopropylbenzene	0.4	2586.0

[a]Calculated "printed mass to achieve RfC" values based on highest emission of individual VOC and a 37.5 m^3 unventilated room.

The increasing utility and decreasing price of 3D printing is leading to greater numbers of printers in households and workplaces and, therefore, increased exposure of users to hazardous emissions. Understanding the printing parameters that have the greatest influence on VOC emissions can lead to printer designs and that limit these emissions and recommended printing locations that limit exposure to users. This work has shown that filament additives such as CNTs can influence VOC emissions, and their use in 3D printing should be reevaluated. CNTs increase formation of more hazardous VOC emissions and, if emitted in particulate, pose an added inhalation hazard as adsorption sites for VOCs.

The variety of filament additives currently available on the market includes wood fiber, transition metal particles, organic dyes, metal-containing dyes, nanomaterials, and phosphorescent materials. Many of these materials either contain VOCs or may catalyze VOC formation at printing temperatures. Future work will involve prioritizing the risk posed by these additives and investigating their influence on VOC emissions. There is also a need to address particulate emissions from 3D printers. While the STDS is not designed for particulate matter collection, we are exploring other experimental setups to capture and characterize particulate emissions with respect to their morphology, metal content, and adsorbed organic species. As the popularity of 3D printing grows and applications spread from industry to the household, there is a critical need to investigate filament additives to assess their health risks.

■ ASSOCIATED CONTENT

Supporting Information

The Supporting Information is available free of charge on the ACS Publications website at DOI: 10.1021/acs.est.9b00765.

Additional methods, instrument diagram, calibration curves, and data table (PDF)

■ AUTHOR INFORMATION

Corresponding Author

*Phone: (513) 569-7849. Fax: (513) 569-7879. E-mail: alabed.souhail@epa.gov.

ORCID

Souhail R. Al-Abed: 0000-0002-5595-1300

Notes

The authors declare no competing financial interest.

■ ACKNOWLEDGMENTS

This research was funded and conducted by the National Risk Management Research Laboratory of the U.S. Environmental Protection Agency (EPA), Cincinnati, OH. This project was supported, in part, by appointments in the Research Participation Program at the Office of Research and Development (ORD), EPA administered by the Oak Ridge Institute for Science and Education (92431601) through an interagency agreement between the DOE and the EPA. This manuscript was subjected to EPA internal reviews and quality assurance approval. The research results presented in this paper do not necessarily reflect the views of the Agency or its policy. Mention of trade names or products does not constitute endorsement or recommendation for use.

■ REFERENCES

(1) Stefaniak, A. B.; LeBouf, R. F.; Duling, M. G.; Yi, J.; Abukabda, A. B.; McBride, C. R.; Nurkiewicz, T. R. Inhalation exposure to three-dimensional printer emissions stimulates acute hypertension and microvascular dysfunction. *Toxicol. Appl. Pharmacol.* **2017**, *335*, 1−5.

(2) Stephens, B.; Azimi, P.; El Orch, Z.; Ramos, T. Ultrafine particle emissions from desktop 3D printers. *Atmos. Environ.* **2013**, *79*, 334−339.

(3) Afshar-Mohajer, N.; Wu, C. Y.; Ladun, T.; Rajon, D. A.; Huang, Y. Characterization of particulate matters and total VOC emissions from a binder jetting 3D printer. *Building and Environment* **2015**, *93*, 293−301.

(4) Zhou, Y.; Kong, X. R.; Chen, A. L.; Cao, S. J. Investigation of Ultrafine Particle Emissions of Desktop 3D Printers in the Clean Room. *Procedia Eng.* **2015**, *121*, 506−512.

(5) Azimi, P.; Zhao, D.; Pouzet, C.; Crain, N. E.; Stephens, B. Emissions of Ultrafine Particles and Volatile Organic Compounds from Commercially Available Desktop Three-Dimensional Printers with Multiple Filaments. *Environ. Sci. Technol.* **2016**, *50* (3), 1260−1268.

(6) Steinle, P. Characterization of emissions from a desktop 3D printer and indoor air measurements in office settings. *J. Occup. Environ. Hyg.* **2016**, *13* (2), 121−132.

(7) Mendes, L.; Kangas, A.; Kukko, K.; Molgaard, B.; Saamanen, A.; Kanerva, T.; Flores Ituarte, I. F.; Huhtiniemi, M.; Stockmann-Juvala, H.; Partanen, J.; Hameri, K.; Eleftheriadis, K.; Viitanen, A. K. Characterization of Emissions from a Desktop 3D Printer. *J. Ind. Ecol.* **2017**, *21*, S94−S106.

(8) Rao, C. C.; Gu, F.; Zhao, P.; Sharmin, N.; Gu, H. B.; Fu, J. Z. Capturing PM2.5 Emissions from 3D Printing via Nanofiber-based Air Filter. *Sci. Rep.* **2017**, *7*, 10366.

(9) Stabile, L.; Scungio, M.; Buonanno, G.; Arpino, F.; Ficco, G. Airborne particle emission of a commercial 3D printer: the effect of

DOI: 10.1021/acs.est.9b00765
Environ. Sci. Technol. 2019, 53, 4364−4370

filament material and printing temperature. *Indoor Air* **2017**, *27* (2), 398−408.
(10) Vance, M. E.; Pegues, V.; Van Montfrans, S.; Leng, W.; Marr, L. C. Aerosol Emissions from Fuse-Deposition Modeling 3D Printers in a Chamber and in Real Indoor Environments. *Environ. Sci. Technol.* **2017**, *51* (17), 9516−9523.
(11) Kim, Y.; Yoon, C.; Ham, S.; Park, J.; Kim, S.; Kwon, O.; Tsai, P. J. Emissions of Nanoparticles and Gaseous Material from 3D Printer Operation. *Environ. Sci. Technol.* **2015**, *49* (20), 12044−12053.
(12) Deng, Y. L.; Cao, S. J.; Chen, A. L.; Guo, Y. S. The impact of manufacturing parameters on submicron particle emissions from a desktop 3D printer in the perspective of emission reduction. *Building and Environment* **2016**, *104*, 311−319.
(13) Yi, J. H.; LeBouf, R. F.; Duling, M. G.; Nurkiewicz, T.; Chen, B. T.; Schwegler-Berry, D.; Virji, M. A.; Stefaniak, A. B. Emission of particulate matter from a desktop three-dimensional (3D) printer. *J. Toxicol. Environ. Health, Part A* **2016**, *79* (11), 453−465.
(14) Kwon, O.; Yoon, C.; Ham, S.; Park, J.; Lee, J.; Yoo, D.; Kim, Y. Characterization and Control of Nanoparticle Emission during 3D Printing. *Environ. Sci. Technol.* **2017**, *51* (18), 10357−10368.
(15) Zhang, Q.; Wong, J. P. S.; Davis, A. Y.; Black, M. S.; Weber, R. J. Characterization of particle emissions from consumer fused deposition modeling 3D printers. *Aerosol Sci. Technol.* **2017**, *51* (11), 1275−1286.
(16) Stefaniak, A. B.; LeBouf, R. F.; Yi, J. H.; Ham, J.; Nurkewicz, T.; Schwegler-Berry, D. E.; Chen, B. T.; Wells, J. R.; Duling, M. G.; Lawrence, R. B.; Martin, S. B.; Johnson, A. R.; Virji, M. A. Characterization of chemical contaminants generated by a desktop fused deposition modeling 3-dimensional Printer. *J. Occup. Environ. Hyg.* **2017**, *14* (7), 540−550.
(17) Floyd, E. L.; Wang, J.; Regens, J. L. Fume emissions from a low-cost 3-D printer with various filaments. *J. Occup. Environ. Hyg.* **2017**, *14* (7), 523−533.
(18) Contos, D. A.; Holdren, M. W.; Smith, D. L.; Brooke, R. C.; Rhodes, V. L.; Rainey, M. L. Sampling and Analysis of Volatile Organic-Compounds Evolved during Thermal-Processing of Acrylonitrile-Butadiene-Styrene Composite Resins. *J. Air Waste Manage. Assoc.* **1995**, *45* (9), 686−694.
(19) Shapi, M. M.; Hesso, A. Gas-Chromatographic Mass-Spectrometric Analysis of Some Potential Toxicants Amongst Volatile Compounds Emitted during Large-Scale Thermal-Degradation of Poly(Acrylonitrile Butadiene Styrene) Plastic. *J. Chromatogr., Biomed. Appl.* **1991**, *562* (1−2), 681−696.
(20) Coleman, J. N.; Khan, U.; Blau, W. J.; Gun'ko, Y. K. Small but strong: A review of the mechanical properties of carbon nanotube-polymer composites. *Carbon* **2006**, *44* (9), 1624−1652.
(21) Breuer, O.; Sundararaj, U. Big returns from small fibers: A review of polymer/carbon nanotube composites. *Polym. Compos.* **2004**, *25* (6), 630−645.
(22) Acquah, S. F. A.; Leonhardt, B. E.; Nowotarski, M. S.; Magi, J. M.; Chambliss, K. A.; Venzel, T. E. S.; Delekar, S. D.; Al-Hariri, L. A. Carbon Nanotubes and Graphene as Additives in 3D Printing. *Carbon Nanotubes-Current Progress of Their Polymer Composites*; InTech, 2016; pp 227−251.
(23) Ren, X. M.; Chen, C. L.; Nagatsu, M.; Wang, X. K. Carbon nanotubes as adsorbents in environmental pollution management: A review. *Chem. Eng. J.* **2011**, *170* (2−3), 395−410.
(24) Lin, D. H.; Xing, B. S. Adsorption of phenolic compounds by carbon nanotubes: Role of aromaticity and substitution of hydroxyl groups. *Environ. Sci. Technol.* **2008**, *42* (19), 7254−7259.
(25) Zhang, S. J.; Shao, T.; Kose, H. S.; Karanfil, T. Adsorption of Aromatic Compounds by Carbonaceous Adsorbents: A Comparative Study on Granular Activated Carbon, Activated Carbon Fiber, and Carbon Nanotubes. *Environ. Sci. Technol.* **2010**, *44* (16), 6377−6383.
(26) Rubey, W. A.; Grant, R. A. Design Aspects of a Modular Instrumentation System for Thermal Diagnostic Studies. *Rev. Sci. Instrum.* **1988**, *59* (2), 265−269.
(27) Kibet, J.; Khachatryan, L.; Dellinger, B. Molecular Products and Radicals from Pyrolysis of Lignin. *Environ. Sci. Technol.* **2012**, *46* (23), 12994−13001.
(28) Nganai, S.; Lomnicki, S.; Dellinger, B. Ferric Oxide Mediated Formation of PCDD/Fs from 2-Monochlorophenol. *Environ. Sci. Technol.* **2009**, *43* (2), 368−373.
(29) Polli, H.; Pontes, L. A. M.; Araujo, A. S.; Barros, J. M. F.; Fernandes, V. J. Degradation behavior and kinetic study of ABS polymer. *J. Therm. Anal. Calorim.* **2009**, *95* (1), 131−134.
(30) Yang, S. Y.; Rafael Castilleja, J.; Barrera, E. V.; Lozano, K. Thermal analysis of an acrylonitrile-butadiene-styrene/SWNT composite. *Polym. Degrad. Stab.* **2004**, *83* (3), 383−388.
(31) Morgan, D. L.; Mahler, J. F.; Kirkpatrick, D. T.; Price, H. C.; O'Connor, R. W.; Wilson, R. E.; Moorman, M. P. Characterization of inhaled alpha-methylstyrene vapor toxicity for B6C3F1 mice and F344 rats. *Toxicol. Sci.* **1999**, *47* (2), 187−194.
(32) Laham, S.; Broxup, B.; Robinet, M.; Potvin, M.; Schrader, K. Subacute Inhalation Toxicity of Benzaldehyde in the Sprague-Dawley Rat. *Am. Ind. Hyg. Assoc. J.* **1991**, *52* (12), 503−510.

DOI: 10.1021/acs.est.9b00765
Environ. Sci. Technol. 2019, 53, 4364−4370

From: Dean Lay
To: Al-Abed, Souhail
Subject: Record of Percentage Agreement – Dean Lay
Date: Wednesday, April 29, 2020 3:38:57 PM

Name: Dean Lay

Organization: Louisiana State University

Nominee's name: Souhail Al-Abed

Title: VOC Emissions and Formation Mechanisms from Carbon Nanotube Composites during 3D Printing

I agree with the following designated percentage of contribution:

Souhail Al-Abed	50%
Phillip Potter	20%
Slawomir Lomnicki	15%
Dean Lay	15%

From: Potter, Phillip
To: Al-Abed, Souhail
Subject: Record of Percentage Agreement - Phillip Potter
Date: Wednesday, April 29, 2020 4:25:00 PM

Name: Phillip Potter
Organization: Oak Ridge Institute for Science and Education
Nominee's name: Souhail Al-Abed
Title: VOC Emissions and Formation Mechanisms from Carbon Nanotube Composites during 3D Printing

I agree with the following designated percentage of contribution:

Souhail Al-Abed	50%
Phillip Potter	20%
Slawomir Lomnicki	15%
Dean Lay	15%

Thank you,
Phillip Potter

Phillip Potter, Ph.D.
Research Fellow | Center for Environmental Solutions and Emergency Response
U.S. Environmental Protection Agency
5995 Center Hill Avenue | Cincinnati, OH 45224
513-487-2683 | potter.phillip@epa.gov

From: Slawomir Lomnicki
To: Al-Abed, Souhail
Subject: Record of Percentage Agreement – Slawomir Lomnicki
Date: Tuesday, April 28, 2020 12:39:52 PM

Name: Slawomir Lomnicki
Organization: Louisiana State University
Nominee's name: Souhail Al-Abed
Title: VOC Emissions and Formation Mechanisms from Carbon Nanotube Composites during 3D Printing

I agree with the following designated percentage of contribution:

Souhail Al-Abed	50%
Phillip Potter	20%
Slawomir Lomnicki	15%
Dean Lay	15%

LSU

Slawo Lomnicki
Assistant Professor
Department of Environmental Sciences
Louisiana State University
1251 Energy Coast & Environment Bldg., Baton Rouge, LA 70803
office 225-578-8147
slomni1@lsu.edu | lsu.edu | http://www.environmental.lsu.edu

Project Leader
LSU Superfund Research Center
Louisiana State University
338 CHoppin Hall, Baton Rouge, LA 70803
office 225-578-4054
slomni1@lsu.edu | lsu.edu | http://www.srp.lsu.edu

2020 STAA Nomination

Category: Other Environmental Research (OR)

Record of Percentage Agreement

Each author contributed to the manuscript according to the following percentages:

Author	Eligible	Total proportion effort (%)
Al-Abed, S. R.	yes	50
Potter, P. M.	yes	20
Lomnicki, S. M.	yes	15
Lay, D. J.	yes	15

Nominated Publication:

Potter, P. M., Al-Abed, S. R., Lay, D., & Lomnicki, S. M. (2019). VOC emissions and formation mechanisms from carbon nanotube composites during 3D printing. *Environmental science & technology, 53*(8), 4364-4370. doi: 10.1021/acs.est.9b00765

Environmental Science & Technology

Article

Cite This: Environ. Sci. Technol. 2019, 53, 4364−4370

pubs.acs.org/est

VOC Emissions and Formation Mechanisms from Carbon Nanotube Composites during 3D Printing

Phillip M. Potter,[†] Souhail R. Al-Abed,*[,‡] Dean Lay,[§] and Slawomir M. Lomnicki[§]

[†]Oak Ridge Institute for Science and Education (ORISE) and [‡]National Risk Management Research Laboratory (NRMRL), U.S. Environmental Protection Agency, Cincinnati, Ohio 45268, United States

[§]Department of Environmental Sciences, Louisiana State University, Baton Rouge, Louisiana 70803, United States

Supporting Information

ABSTRACT: A commercially available, 3D printer nanocomposite filament of carbon nanotubes (CNTs) and acrylonitrile−butadiene−styrene (ABS) was analyzed with respect to its VOC emissions during simulated fused deposition modeling (FDM) and compared with a regular ABS filament. VOC emissions were quantified and characterized under a variety of conditions to simulate the thermal degradation that takes place during FDM. Increasing the residence time and temperature resulted in significant increases in VOC emissions, and the oxygen content of the reaction gas influenced the VOC profile. In agreement with other studies, the primary emitted VOC was styrene. Multiple compounds are reported in this work for the first time as having formed during FDM, including 4-vinylcyclohexene and 2-phenyl-2-propanol. Our results show that printing 222.0 g of filament is enough to surpass the reference concentration for inhalation exposure of 1 mg/m^3 according to the EPA's Integrated Risk Information System (IRIS). The presence of CNTs in the filament influenced VOC yields and product ratios through three types of surface interactions: (1) adsorption of O_2 on CNTs lowers the available O_2 for oxidation of primary backbone cleavage intermediates, (2) adsorption of styrene and other VOCs to CNTs leads to surface-catalyzed degradation, and (3) CNTs act as a trap for certain VOCs and prevent them from entering vapor emissions. While the presence of CNTs in the filament lowered the total VOC emission under most experimental conditions, they increased the emission of the most hazardous VOCs, such as α-methylstyrene and benzaldehyde. The present study has identified an increased risk associated with the use of CNT nanocomposites in 3D printing.

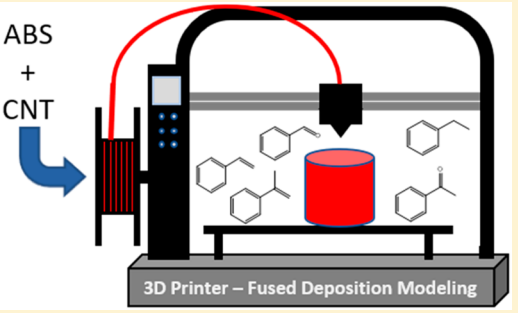

INTRODUCTION

There is a growing concern over hazardous emissions from 3D printers using fused deposition modeling (FDM) as they become more affordable and enter more workplaces and consumer households. Three-dimensional printers operate at borderline temperatures of thermal degradation reactions for polymer filament feedstock. Despite design efforts to limit exposure, printing emissions are still a threat to user health.[1] Emissions from FDM can be grouped into two categories: particulate matter (PM) and gas-phase compounds. Particulate matter emitted from 3D printers has been studied across a variety of size ranges,[2−10] including nanoparticle emission.[11−15] Studies involving gas-phase compounds usually concern volatile organic compounds (VOCs). While some studies quantify total VOCs,[3,7] there have been few attempts to fully characterize and quantify VOC emissions.[5,6,16,17]

Acrylonitrile−butadiene−styrene (ABS) is a common polymer used in FDM (Figure 1). Thermal degradation of ABS has been studied in the past under conditions of extrusion[18] and incineration.[19] Three-dimensional printing filaments often contain additives to adjust their physicochemical properties. Common additives include dyes, plasticizers, stabilizers, wood particles, metal particles, and carbon allotropes. Many of these additives can either degrade into VOCs or contribute to their formation. The effects of many filament additives on VOC emissions during FDM has not been studied.

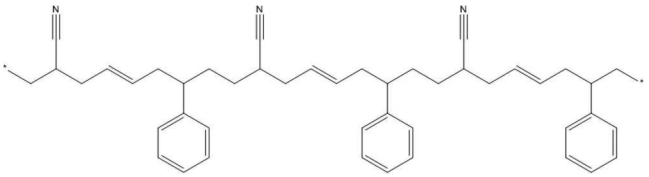

Figure 1. Typical structure of colinear ABS polymer.

Nanocomposites consisting of carbon nanotubes (CNTs) and a variety of polymers can be made with unique mechanical and electrical properties.[20,21] These CNT nanocomposites are used with 3D printers to produce conductive electrical components.[22] Despite the increasing usage of CNT nano-

Received: February 4, 2019
Revised: March 12, 2019
Accepted: March 15, 2019
Published: March 15, 2019

Downloaded via US EPA RESEARCH TRIANGLE PARK on April 16, 2019 at 14:30:50 (UTC).
See https://pubs.acs.org/sharingguidelines for options on how to legitimately share published articles.

© 2019 American Chemical Society

DOI: 10.1021/acs.est.9b00765
Environ. Sci. Technol. 2019, 53, 4364−4370

composites, their influence on hazardous VOC emissions during FDM has not been investigated. The adsorptive properties of CNTs have also been extensively studied on VOCs,[23] including aromatic species.[24,25] A thorough understanding of the role CNTs play in VOC formation in thermal processes is critical to limiting health risks to 3D printer users.

In this work, two commercially available 3D printer filaments, consisting of an ABS−CNT nanocomposite and a plain ABS, were subjected to thermal conditions that simulate FDM. VOC emissions from the simulated printing were quantified and characterized to determine the effect of CNT addition on hazardous emissions.

MATERIALS AND METHODS

Three-dimensional printer filaments were purchased from 3DXTech. The ABS filament is from the standard ABS product line, and the nanocomposite ABS−CNT filament is from the 3DXNano ESD product line. The ABS−CNT filament is advertised to contain CNTs, but the concentration is not reported. Quartz sample baskets were made in the LSU Chemistry Department glass-blowing shop. Pure reference standards used for quantification were purchased from Sigma-Aldrich and dissolved in dichloromethane (DCM) to create calibration curves. HPLC-grade DCM was purchased from Fisher Scientific.

All degradation experiments were performed using the System for Thermal Diagnostic Studies (STDS).[26] The STDS is a custom-built, modular instrument that has been previously used to provide thermal conditions for combustion of various waste components.[27,28] A diagram for the STDS can be found in the Supporting Information (Figure S1). The STDS consists of a ceramic furnace and quartz reactor housed within a gas chromatograph (GC) oven. Gas-phase compounds leaving the reactor pass through a heated transfer line into the injection port of a second GC where they are separated and detected by a mass spectrometer (MS). The advantages of the STDS include being a closed system with direct transfer of products into the detection module, which minimizes sample loss and increases detection sensitivity. Approximately 50−100 mg of filament was weighed and placed in a quartz sample holder basket (15 mm × 4 mm i.d.) above the heated reactor. For pyrolysis experiments, the sample was purged with N_2 at room temperature for 3 min. The sample was then lowered into the preheated reactor, and pyrolysis began. During reaction, the second, analytical GC oven was kept at −60 °C to condense all compounds that passed through the 280 °C transfer line. Gas flow rate was set at each temperature to maintain a vapor residence time in the reactor of approximately 0.2 s. After reaction completion, the transfer line was removed from the injection port of the second GC and analysis of the reaction products began. Analysis of reaction products was conducted using an Agilent 6890N GC equipped with a DB5-MS column (30 m × 0.25 mm × 0.25 μm) and a 5973N MS with an electron impact (EI) ion source set at 70 eV. The temperature program was as follows: −60 °C initial temperature held for 0.5 min, followed by heating at a rate of 15 °C/min to 130 °C, held for 1 min, heated to 225 °C at a rate of 25 °C/min, and finally heated to 300 °C at 10 °C/min and held for 7 min, giving a total runtime of 32.47 min. The GC inlet and MS quadrupole temperatures were 280 and 150 °C, respectively. The split/splitless inlet was set to a constant split flow of 10 mL/min. The carrier gas used was ultrahigh-purity helium (UHP, 99.999%) at a constant column flow of 1.0 mL/min. However, during sample collection, the flow of N_2 through the transfer line was high enough to increase the column flow to 2 mL/min or above, with the remainder going out the split vent. The mass spectrometer was operated in total ion count mode (TIC) over a mass scan range of 50−500 amu. Identification of pyrolysis products was performed using the Wiley and NIST libraries and by comparison of retention times with those of purchased standard compounds. VOC emissions were calculated by dividing the emitted mass of each VOC by the mass of filament used in the experiment and reported as μg/g. Additional information on the quantification methods and method detection limits can be found in the Supporting Information. Mass loss was calculated by weighing the filament prior to reaction and dividing by the filament mass after reaction.

Reaction conditions were selected to simulate common 3D printer parameters. The manufacturer recommended printing temperatures are 220−240 °C for the ABS filament and 230−260 °C for the ABS−CNT filament. A printing temperature of 230 °C was selected for consistency between samples, but users often change printing temperatures to alter printed objects, and extruder nozzles are unlikely to heat uniformly. To account for user preference and nozzle construction, degradation experiments were also performed at 200 and 300 °C. The residence time in the heated area of the printer is based on the feed rate of the filament and the length of the extruder nozzle. Feed rate is often changed by the user to affect the quality of the printed object. Residence times of 1 and 3 min were investigated. The design of 3D printer nozzles can lead to oxygen-deprived conditions inside the nozzle where melted filament is exposed to the highest temperatures. To better understand the role of oxygen in the thermal degradation of 3D printer filament, experiments were carried out in both pyrolytic (N_2) and oxidative (4% O_2/N_2) conditions.

RESULTS AND DISCUSSION

Degradation Products. Thermogravimetric studies of ABS polymer do not show any significant mass loss at temperatures below 325 °C.[29] Despite mass loss during these experiments being very low (<1% for all experiments), simulated FDM has yielded emissions of several VOCs. The major components of VOC emissions from simulated 3D printing are shown in Table 1, and their associated structures are presented in Table S1. All of these compounds, except for 2,6-di-*tert*-butylquinone and 2,4-di-*tert*-butylphenol, have been

Table 1. Major Components of VOC Emissions from Thermal Degradation of ABS 3D Printer Filament

compound	source
4-vinylcyclohexene	butadiene monomer dimerization
ethylbenzene	polymer backbone cleavage
styrene	unreacted monomer/backbone cleavage
isopropylbenzene	polymer backbone cleavage
benzaldehyde	oxidation of backbone cleavage intermediate
α-methylstyrene	polymer backbone cleavage
tetramethylsuccinonitrile	polymerization byproduct
acetophenone	oxidation of backbone cleavage intermediate
2-phenyl-2-propanol	oxidation of backbone cleavage intermediate
2,6-di-*tert*-butylquinone	2,4-di-*tert*-butylphenol degradation
2,4-di-*tert*-butylphenol	polymer UV stabilizer

DOI: 10.1021/acs.est.9b00765
Environ. Sci. Technol. 2019, 53, 4364−4370

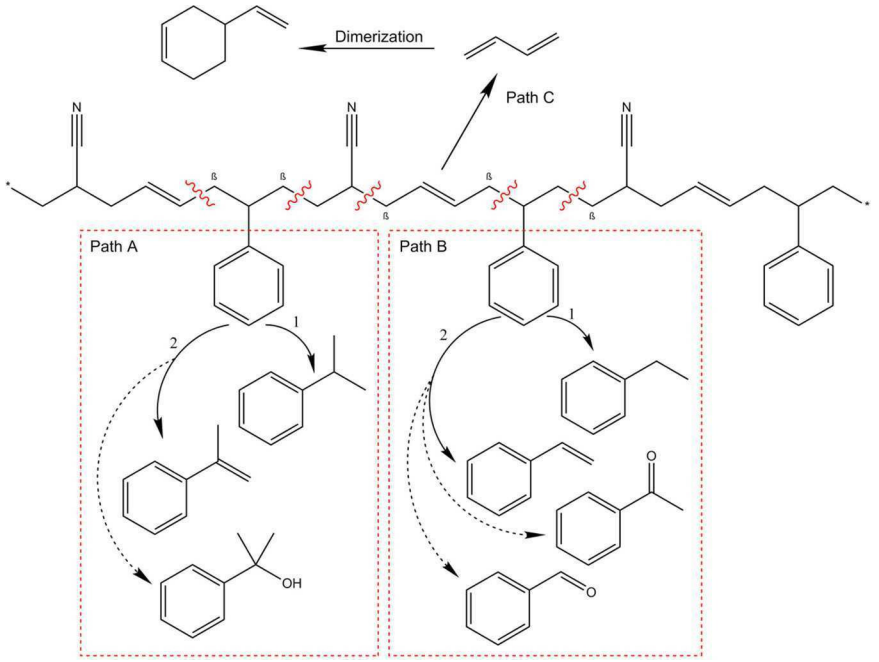

Figure 2. Pathways of the low-temperature depolymerization of ABS filament. Solid arrows signify primary polymer backbone degradation products. Dashed arrows signify secondary products formed by the oxygenation of primary products.

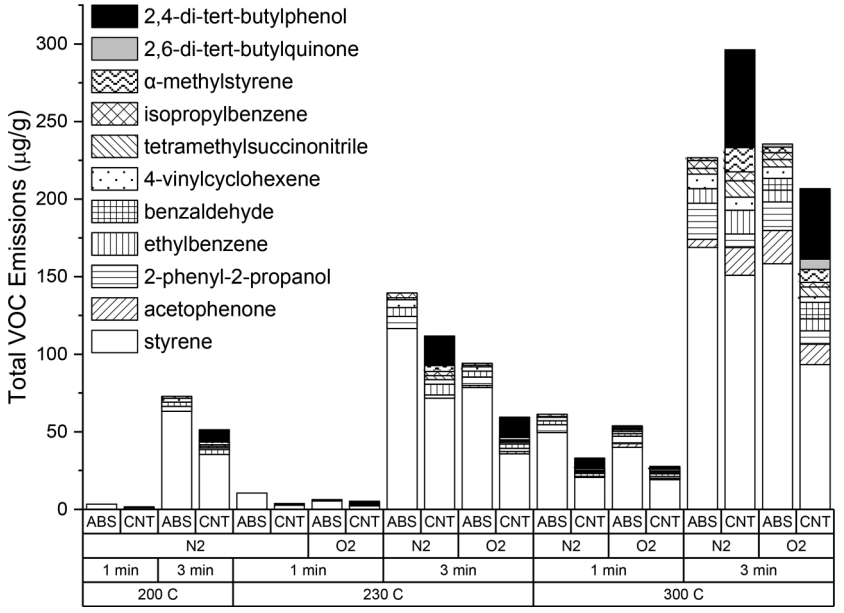

Figure 3. VOC emissions from thermal degradation of ABS and ABS−CNT composite. Experiment names are generated from the temperature + residence time + reaction gas + filament type.

found in previous studies involving ABS incineration and heated extrusion.[18,19] Studies involving VOC emissions from ABS filament have shown different compound profiles and VOC concentrations obtained from similar filaments from different manufacturers.[5] The emitted VOCs in the current experiments are likely the result of either desorption of unreacted monomer from the polymer matrix or slow degradation/depolymerization of the ABS polymer. In this work, styrene comprises a significant portion of total VOC emissions and justifies the assumption of trapped monomer as the primary VOC emission. Tetramethylsuccinonitrile (TMSN) and 2,4-di-*tert*-butylphenol, a polymerization by-product and polymer stabilizer, respectively, are likely part of the polymer synthesis process and volatilized during heating.

Other compounds, unlikely to be present in pristine polymer material, were also detected. Ethylbenzene is the most commonly reported styrene degradation product,[5,6,11,16] but in this work we also report 4-vinylcyclohexene, isopropylbenzene, benzaldehyde, α-methylstyrene, acetophenone, and 2-phenyl-2-propanol. Figure 2 presents proposed pathways to the observed thermal degradation products of ABS at low temperatures. On the basis of the proposed pathways, the depolymerization process is initiated through the cleavage of polymer backbone at β-carbons with respect to either phenyl or nitrile groups. The VOC sources in Table 1 are inferred

DOI: 10.1021/acs.est.9b00765
Environ. Sci. Technol. 2019, 53, 4364−4370

from these pathways based on where cleavage occurred on the polymer backbone and whether additional oxygen atoms have been incorporated into their structure.

VOC Emission. Emissions for VOCs from different reaction temperatures, residence times, and oxygen contents are shown in Figure 3. Complete data tables are presented in the Supporting Information (Table S2). Interestingly, some oxygenated products were observed under pyrolytic conditions such as acetophenone and benzaldehyde. This may suggest that oxygen is adsorbed to the polymer matrix.

Role of Residence Time. For all measured conditions, increasing the residence time from 1 to 3 min led to increased yields of all observed products. As seen in Figure 3, the increase in VOC emissions was not directly proportional to the increase in residence time. For 200 and 230 °C, styrene emission increased by an order of magnitude when increasing the residence time from 1 to 3 min. At 300 °C, tripling the residence time increased styrene emission by a factor of approximately four. The significant increase in the effect of residence time seen at lower temperatures could indicate that a residence time of 1 min is too short for accurate analysis due to the time needed for the filament to equilibrate to the reactor temperature. Therefore, the results for experiments with a residence time of 3 min are more accurate predictions of actual printer emissions.

Role of Temperature. Extrusion temperature in 3D printers is typically selected through a combination of user preference and manufacturer suggestions. Extrusion temperature both is the most commonly adjusted printing parameter and had the most significant effect on VOC emissions. Across all parameter combinations, higher temperature resulted in higher yields of every individual VOC. Figure 4 compares VOC emissions from ABS filament in pure N_2 at 200, 230, and 300 °C for 3 min.

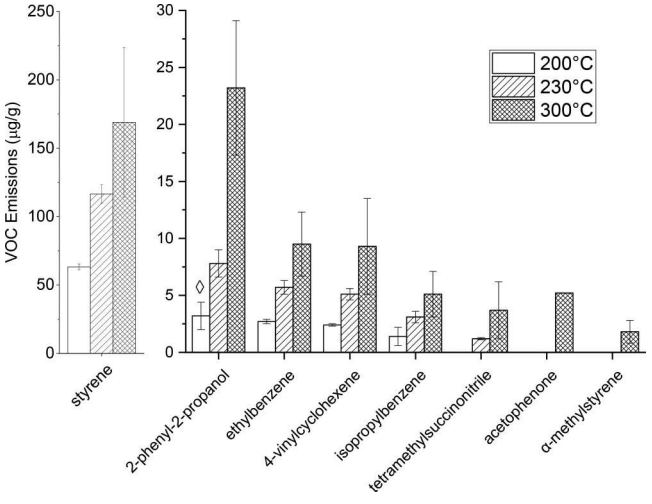

Figure 4. Individual VOC emissions from pyrolysis of ABS filament for 3 min in pure N_2 at 200, 230, and 300 °C. Error bars represent ± one standard deviation. ◊ = below method detection limit.

Acetophenone and α-methylstyrene were typically not detected until 300 °C under pyrolytic conditions. However, both acetophenone and α-methylstyrene were formed at 230 °C by the addition of O_2 and CNTs, respectively. Despite temperature having the greatest effect, no individual parameter can be used to predict VOC emissions.

Role of Oxygen. Depending on the design of the extruder nozzle, melted filament may be exposed to oxygen-deprived conditions prior to exiting the nozzle into air. Thus, the construction of extruder nozzles likely yields emissions that include products formed under both oxidative and oxygen-deprived conditions. The presence of oxygen in the reaction gas led to lower levels of emitted styrene and certain degradation products (Table S2), primarily those that do not contain oxygen in their formula. This decrease in emission can be explained by (1) oxidation of polymer decomposition products to low molecular weight products not analyzed in this study (CO, CO_2, and compounds with less than six carbons) and (2) increased formation of oxygen-containing acetophenone and benzaldehyde. Contrary to acetophenone and benzaldehyde (Figure 2, Path B), 2-phenyl-2-propanol yield (Figure 2, Path A) is not affected by addition of gas-phase O_2. This may indicate that polymer-adsorbed oxygen plays a key role in Path A, while gas-phase O_2 forms secondary products in Path B.

Role of Carbon Nanotubes. Studies have indicated that incorporation of single-walled CNTs into ABS decreases the activation energy of thermal degradation by up to 6 kcal/mol.[30] The mechanism of this effect is not clear. The presence of CNTs in the filament affected both the total VOC emission and the VOC profile. Overall, addition of CNTs slightly decreased the emissions of VOCs (Figure 3), except for the sample treated at 300 °C/3 min/N2, which showed the highest emission due to the drastically increased emission of UV stabilizer 2,4-di-*tert*-butylphenol. Figure 5 shows emissions of five VOCs that best exemplify the differences between ABS and ABS−CNT filament degradation. Despite still being the most prevalent VOC, styrene emissions decreased in the presence of CNTs (Figure 5A) except for pyrolytic conditions at 300 °C, where the difference between ABS and ABS−CNT was insignificant.

The sum of the products of Path A decomposition (Figure 2) did not change significantly for the ABS−CNT samples; however, the product distribution within this group was altered. The formation of α-methylstyrene was increased (Figure 5B), and 2-phenyl-2-propanol was significantly suppressed (Figure 5C). This change in product ratio away from oxygenated products is explained by a change in available oxygen in the system, possibly due to strong adsorption of O_2 on CNTs.

Figure 6 shows the VOC yields of Path A and Path B products only, with the exclusion of styrene and benzaldehyde. Styrene is not included in the Path B product sum to compensate for the presence of unreacted monomer, and benzaldehyde was removed due to only being formed at the highest temperature. The similarities between Path A and Path B after the removal of styrene and benzaldehyde, particularly in the CNT-containing filament, leads to the conclusion that the majority of styrene emissions is from unreacted monomer and not polymer backbone cleavage. Figure 6 also indicates that CNTs do not have a significant effect on the preference for Path A or Path B. The decrease in styrene emission in the presence of CNTs is therefore likely due to adsorption and subsequent surface-catalyzed degradation of unreacted styrene monomer on CNTs. There may even be a synergistic effect between adsorption of both O_2 and VOCs on the surface of CNTs as several compounds show significantly lower yields when both O_2 and CNTs are present, including 2-phenyl-2-propanol, acetophenone, and isopropylbenzene.

DOI: 10.1021/acs.est.9b00765
Environ. Sci. Technol. 2019, 53, 4364−4370

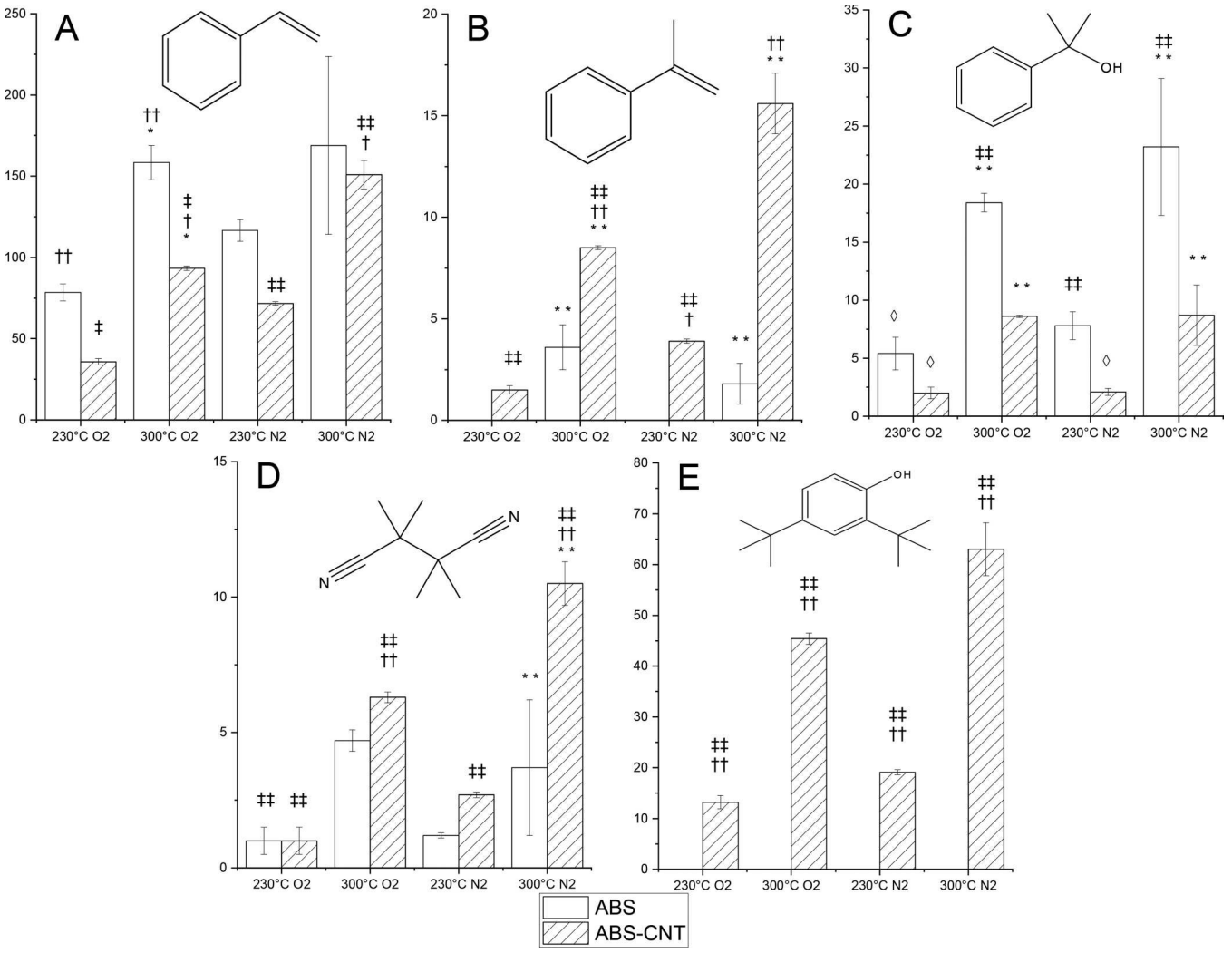

Figure 5. Influence of CNTs on emissions of (a) styrene, (b) α-methylstyrene, (c) 2-phenyl-2-propanol, (d) tetramethylsuccinonitrile, and (e) 2,4-di-*tert*-butylphenol. All values are in μg/g. ‡ = statistical significance between 230 and 300 °C, † = statistical significance between O2 and N2, * = statistical significance between ABS and ABS−CNT, and ◊ = below method detection limit. Single symbol represents p value of <0.05, and double symbol represents p value of <0.01. Statistical significance determined using ANOVA with a posthoc Tukey test. Error bars are ± one standard deviation.

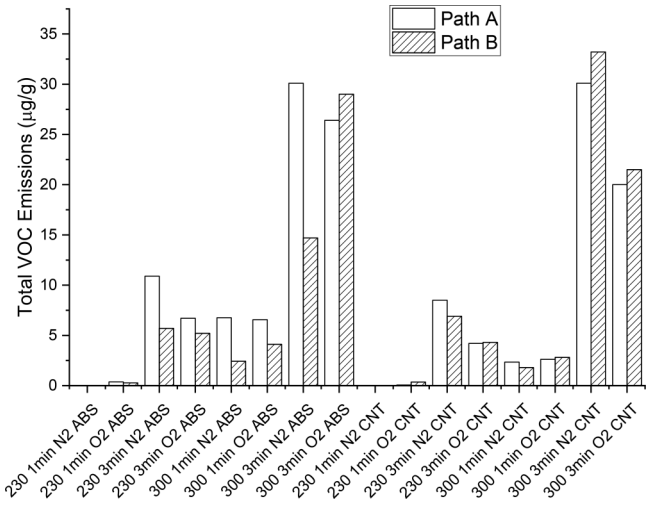

Figure 6. VOC emissions from Path A and Path B of the mechanism in Figure 2. Unreacted monomer styrene removed from all conditions and benzaldehyde removed from 300 °C/3 min/O_2.

CNTs could also be acting as sinks for certain VOCs. Significantly lower yields for certain VOCs, such as 2-phenyl-2-propanol, could be due to an increased affinity for adsorption of phenolic compounds on CNTs.[24] This would mean that formation of these VOCs is not necessarily affected by CNTs but that they are not detected once adsorbed to CNTs.

There is evidence that three types of surface interactions may be responsible for the effect of CNTs on VOC emissions: (1) strong adsorption of O2 on CNTs, lowering the amount of O2 available for reaction with polymer backbone cleavage intermediates, (2) adsorption of unreacted monomer styrene to CNTs yielding different products compared to Path A and Path B, and (3) increased affinity for certain aromatics leading to CNTs acting as sinks for particular VOCs. These three interactions can occur independently, compete, or even exhibit synergy in altering VOC emissions.

Some VOC emissions are not the result of polymer degradation. As seen in Figure 5D, TMSN was emitted in greater concentrations in the presence of CNTs. TMSN is a polymerization byproduct from the radical initiator 2,2′-azobis-isobutyronitrile. Interestingly, a new group of VOCs was

DOI: 10.1021/acs.est.9b00765
Environ. Sci. Technol. 2019, 53, 4364−4370

observed for ABS−CNT filaments: 2,4-di-*tert*-butylphenol and 2,6-di-*tert*-butylquinone. Shown in Figure 5E, 2,4-di-*tert*-butylphenol was only emitted from ABS−CNT filament. 2,4-Di-*tert*-butylphenol is a common polymer stabilizer that protects from UV damage. The structural and mechanical changes caused by the addition of CNTs to ABS could necessitate a different polymer formulation that incorporates different polymerization initiators and stabilizers. It is not clear whether this stabilizer is only added to ABS−CNT or if the presence of CNTs triggers the release.

Environmental Implications. The Integrated Risk Information System (IRIS) is an EPA-created tool for categorizing chemicals and their associated health hazards. IRIS contains entries for five of the measured VOCs from this study, and three entries contain a reference concentration for inhalation exposure (RfC). Table 2 shows the IRIS RfC values for styrene, ethylbenzene, and isopropylbenzene (in IRIS as cumene). The IRIS RfC for styrene is 1 mg/m^3, which could be easily reached after printing a few hundred grams of filament depending on room size and ventilation. VOCs whose formation is increased by CNTs also pose known inhalation hazards, such as α-methylstyrene[31] and benzaldehyde.[32]

Table 2. IRIS RfC Values for VOCs Emitted during 3D Printing[a]

compound	RfC (mg/m^3)	printed mass to achieve RfC (g)
styrene	1	222.0
ethylbenzene	1	2451.0
cumene/isopropylbenzene	0.4	2586.0

[a]Calculated "printed mass to achieve RfC" values based on highest emission of individual VOC and a 37.5 m^3 unventilated room.

The increasing utility and decreasing price of 3D printing is leading to greater numbers of printers in households and workplaces and, therefore, increased exposure of users to hazardous emissions. Understanding the printing parameters that have the greatest influence on VOC emissions can lead to printer designs and that limit these emissions and recommended printing locations that limit exposure to users. This work has shown that filament additives such as CNTs can influence VOC emissions, and their use in 3D printing should be reevaluated. CNTs increase formation of more hazardous VOC emissions and, if emitted in particulate, pose an added inhalation hazard as adsorption sites for VOCs.

The variety of filament additives currently available on the market includes wood fiber, transition metal particles, organic dyes, metal-containing dyes, nanomaterials, and phosphorescent materials. Many of these materials either contain VOCs or may catalyze VOC formation at printing temperatures. Future work will involve prioritizing the risk posed by these additives and investigating their influence on VOC emissions. There is also a need to address particulate emissions from 3D printers. While the STDS is not designed for particulate matter collection, we are exploring other experimental setups to capture and characterize particulate emissions with respect to their morphology, metal content, and adsorbed organic species. As the popularity of 3D printing grows and applications spread from industry to the household, there is a critical need to investigate filament additives to assess their health risks.

■ ASSOCIATED CONTENT

Supporting Information

The Supporting Information is available free of charge on the ACS Publications website at DOI: 10.1021/acs.est.9b00765.

Additional methods, instrument diagram, calibration curves, and data table (PDF)

■ AUTHOR INFORMATION

Corresponding Author

*Phone: (513) 569-7849. Fax: (513) 569-7879. E-mail: alabed.souhail@epa.gov.

ORCID

Souhail R. Al-Abed: 0000-0002-5595-1300

Notes

The authors declare no competing financial interest.

■ ACKNOWLEDGMENTS

This research was funded and conducted by the National Risk Management Research Laboratory of the U.S. Environmental Protection Agency (EPA), Cincinnati, OH. This project was supported, in part, by appointments in the Research Participation Program at the Office of Research and Development (ORD), EPA administered by the Oak Ridge Institute for Science and Education (92431601) through an interagency agreement between the DOE and the EPA. This manuscript was subjected to EPA internal reviews and quality assurance approval. The research results presented in this paper do not necessarily reflect the views of the Agency or its policy. Mention of trade names or products does not constitute endorsement or recommendation for use.

■ REFERENCES

(1) Stefaniak, A. B.; LeBouf, R. F.; Duling, M. G.; Yi, J.; Abukabda, A. B.; McBride, C. R.; Nurkiewicz, T. R. Inhalation exposure to three-dimensional printer emissions stimulates acute hypertension and microvascular dysfunction. *Toxicol. Appl. Pharmacol.* **2017**, *335*, 1−5.

(2) Stephens, B.; Azimi, P.; El Orch, Z.; Ramos, T. Ultrafine particle emissions from desktop 3D printers. *Atmos. Environ.* **2013**, *79*, 334−339.

(3) Afshar-Mohajer, N.; Wu, C. Y.; Ladun, T.; Rajon, D. A.; Huang, Y. Characterization of particulate matters and total VOC emissions from a binder jetting 3D printer. *Building and Environment* **2015**, *93*, 293−301.

(4) Zhou, Y.; Kong, X. R.; Chen, A. L.; Cao, S. J. Investigation of Ultrafine Particle Emissions of Desktop 3D Printers in the Clean Room. *Procedia Eng.* **2015**, *121*, 506−512.

(5) Azimi, P.; Zhao, D.; Pouzet, C.; Crain, N. E.; Stephens, B. Emissions of Ultrafine Particles and Volatile Organic Compounds from Commercially Available Desktop Three-Dimensional Printers with Multiple Filaments. *Environ. Sci. Technol.* **2016**, *50* (3), 1260−1268.

(6) Steinle, P. Characterization of emissions from a desktop 3D printer and indoor air measurements in office settings. *J. Occup. Environ. Hyg.* **2016**, *13* (2), 121−132.

(7) Mendes, L.; Kangas, A.; Kukko, K.; Molgaard, B.; Saamanen, A.; Kanerva, T.; Flores Ituarte, I. F.; Huhtiniemi, M.; Stockmann-Juvala, H.; Partanen, J.; Hameri, K.; Eleftheriadis, K.; Viitanen, A. K. Characterization of Emissions from a Desktop 3D Printer. *J. Ind. Ecol.* **2017**, *21*, S94−S106.

(8) Rao, C. C.; Gu, F.; Zhao, P.; Sharmin, N.; Gu, H. B.; Fu, J. Z. Capturing PM2.5 Emissions from 3D Printing via Nanofiber-based Air Filter. *Sci. Rep.* **2017**, *7*, 10366.

(9) Stabile, L.; Scungio, M.; Buonanno, G.; Arpino, F.; Ficco, G. Airborne particle emission of a commercial 3D printer: the effect of

DOI: 10.1021/acs.est.9b00765
Environ. Sci. Technol. 2019, 53, 4364−4370

filament material and printing temperature. *Indoor Air* **2017**, *27* (2), 398−408.
(10) Vance, M. E.; Pegues, V.; Van Montfrans, S.; Leng, W.; Marr, L. C. Aerosol Emissions from Fuse-Deposition Modeling 3D Printers in a Chamber and in Real Indoor Environments. *Environ. Sci. Technol.* **2017**, *51* (17), 9516−9523.
(11) Kim, Y.; Yoon, C.; Ham, S.; Park, J.; Kim, S.; Kwon, O.; Tsai, P. J. Emissions of Nanoparticles and Gaseous Material from 3D Printer Operation. *Environ. Sci. Technol.* **2015**, *49* (20), 12044−12053.
(12) Deng, Y. L.; Cao, S. J.; Chen, A. L.; Guo, Y. S. The impact of manufacturing parameters on submicron particle emissions from a desktop 3D printer in the perspective of emission reduction. *Building and Environment* **2016**, *104*, 311−319.
(13) Yi, J. H.; LeBouf, R. F.; Duling, M. G.; Nurkiewicz, T.; Chen, B. T.; Schwegler-Berry, D.; Virji, M. A.; Stefaniak, A. B. Emission of particulate matter from a desktop three-dimensional (3D) printer. *J. Toxicol. Environ. Health, Part A* **2016**, *79* (11), 453−465.
(14) Kwon, O.; Yoon, C.; Ham, S.; Park, J.; Lee, J.; Yoo, D.; Kim, Y. Characterization and Control of Nanoparticle Emission during 3D Printing. *Environ. Sci. Technol.* **2017**, *51* (18), 10357−10368.
(15) Zhang, Q.; Wong, J. P. S.; Davis, A. Y.; Black, M. S.; Weber, R. J. Characterization of particle emissions from consumer fused deposition modeling 3D printers. *Aerosol Sci. Technol.* **2017**, *51* (11), 1275−1286.
(16) Stefaniak, A. B.; LeBouf, R. F.; Yi, J. H.; Ham, J.; Nurkewicz, T.; Schwegler-Berry, D. E.; Chen, B. T.; Wells, J. R.; Duling, M. G.; Lawrence, R. B.; Martin, S. B.; Johnson, A. R.; Virji, M. A. Characterization of chemical contaminants generated by a desktop fused deposition modeling 3-dimensional Printer. *J. Occup. Environ. Hyg.* **2017**, *14* (7), 540−550.
(17) Floyd, E. L.; Wang, J.; Regens, J. L. Fume emissions from a low-cost 3-D printer with various filaments. *J. Occup. Environ. Hyg.* **2017**, *14* (7), 523−533.
(18) Contos, D. A.; Holdren, M. W.; Smith, D. L.; Brooke, R. C.; Rhodes, V. L.; Rainey, M. L. Sampling and Analysis of Volatile Organic-Compounds Evolved during Thermal-Processing of Acrylonitrile-Butadiene-Styrene Composite Resins. *J. Air Waste Manage. Assoc.* **1995**, *45* (9), 686−694.
(19) Shapi, M. M.; Hesso, A. Gas-Chromatographic Mass-Spectrometric Analysis of Some Potential Toxicants Amongst Volatile Compounds Emitted during Large-Scale Thermal-Degradation of Poly(Acrylonitrile Butadiene Styrene) Plastic. *J. Chromatogr., Biomed. Appl.* **1991**, *562* (1−2), 681−696.
(20) Coleman, J. N.; Khan, U.; Blau, W. J.; Gun'ko, Y. K. Small but strong: A review of the mechanical properties of carbon nanotube-polymer composites. *Carbon* **2006**, *44* (9), 1624−1652.
(21) Breuer, O.; Sundararaj, U. Big returns from small fibers: A review of polymer/carbon nanotube composites. *Polym. Compos.* **2004**, *25* (6), 630−645.
(22) Acquah, S. F. A.; Leonhardt, B. E.; Nowotarski, M. S.; Magi, J. M.; Chambliss, K. A.; Venzel, T. E. S.; Delekar, S. D.; Al-Hariri, L. A. Carbon Nanotubes and Graphene as Additives in 3D Printing. *Carbon Nanotubes-Current Progress of Their Polymer Composites*; InTech, 2016; pp 227−251.
(23) Ren, X. M.; Chen, C. L.; Nagatsu, M.; Wang, X. K. Carbon nanotubes as adsorbents in environmental pollution management: A review. *Chem. Eng. J.* **2011**, *170* (2−3), 395−410.
(24) Lin, D. H.; Xing, B. S. Adsorption of phenolic compounds by carbon nanotubes: Role of aromaticity and substitution of hydroxyl groups. *Environ. Sci. Technol.* **2008**, *42* (19), 7254−7259.
(25) Zhang, S. J.; Shao, T.; Kose, H. S.; Karanfil, T. Adsorption of Aromatic Compounds by Carbonaceous Adsorbents: A Comparative Study on Granular Activated Carbon, Activated Carbon Fiber, and Carbon Nanotubes. *Environ. Sci. Technol.* **2010**, *44* (16), 6377−6383.
(26) Rubey, W. A.; Grant, R. A. Design Aspects of a Modular Instrumentation System for Thermal Diagnostic Studies. *Rev. Sci. Instrum.* **1988**, *59* (2), 265−269.
(27) Kibet, J.; Khachatryan, L.; Dellinger, B. Molecular Products and Radicals from Pyrolysis of Lignin. *Environ. Sci. Technol.* **2012**, *46* (23), 12994−13001.
(28) Nganai, S.; Lomnicki, S.; Dellinger, B. Ferric Oxide Mediated Formation of PCDD/Fs from 2-Monochlorophenol. *Environ. Sci. Technol.* **2009**, *43* (2), 368−373.
(29) Polli, H.; Pontes, L. A. M.; Araujo, A. S.; Barros, J. M. F.; Fernandes, V. J. Degradation behavior and kinetic study of ABS polymer. *J. Therm. Anal. Calorim.* **2009**, *95* (1), 131−134.
(30) Yang, S. Y.; Rafael Castilleja, J.; Barrera, E. V.; Lozano, K. Thermal analysis of an acrylonitrile-butadiene-styrene/SWNT composite. *Polym. Degrad. Stab.* **2004**, *83* (3), 383−388.
(31) Morgan, D. L.; Mahler, J. F.; Kirkpatrick, D. T.; Price, H. C.; O'Connor, R. W.; Wilson, R. E.; Moorman, M. P. Characterization of inhaled alpha-methylstyrene vapor toxicity for B6C3F1 mice and F344 rats. *Toxicol. Sci.* **1999**, *47* (2), 187−194.
(32) Laham, S.; Broxup, B.; Robinet, M.; Potvin, M.; Schrader, K. Subacute Inhalation Toxicity of Benzaldehyde in the Sprague-Dawley Rat. *Am. Ind. Hyg. Assoc. J.* **1991**, *52* (12), 503−510.

DOI: 10.1021/acs.est.9b00765
Environ. Sci. Technol. 2019, 53, 4364−4370

Table of Contents

General_Authors_Publications.....2
LI-266786_Gwinn_et_al_AJPH2017303771.....12
CMP_Science_Committee__Thank_You!.....21
Gwinn_et_al_AJPH2017303771.....22
Record_of_Agreement_-_David_Bussard.....31
Record_of_Agreement_-_Kacee_Deener.....32
Record_of_Agreement_-_Maureen_R_Gwinn.....35
Record_of_Agreement_-_Robert_J_Kavlock.....37
Record_of_Agreement_-_Wayne_E_Cascio.....39
Greenberg_AJPH2017303844.....42
AJPH_-_STAA_justification_Clean_4292020_final_v3.....45
Record_of_Agreement_-_Daniel_A_Axelrad.....49
Record_of_Agreement_-_Thomas_A_Burke.....50
Record_of_Agreement_-_Tina_Bahadori.....52
Gwinn_AJPH_STAA_-_record_of_agreement_explanation.....54
Record_of_Agreement_-_Russell_Thomas.....55

STAA REPORT FOR THE SCIENTIST NOMINATIONS

General Information:

Nomination ID/App ID:	20-138
Research Category Primary:	Health Effects Research and Human Health Risk Assessment (HE)
Research Category Secondary:	Integrated Risk Assessment (IR)
Laboratory/Office Name:	ORD
Nomination Entered By:	Maureen Gwinn

Eligibility Checklist:

[Y] The nominated publication(s) has not been submitted to a previous STAA competition.

[Y] The nominated publication(s) was published on or before January 1, 2017 and on or after January 1,2012

[Y] The principal author was an EPA employee or a PHS employee assigned to EPA when the research was performed

[Y] The EPA authors (includes PHS employees assigned to EPA) contributed collectively a minimum of 50% toward the publication(s)

Nominating Official Name:	Reeder Sams
Nominating Official Title:	DEPUTY DIRECTOR FOR MANAGEMENT, NERL
Nominating OfficialEmail:	sams.reeder@epa.gov
STAA Coordinator Name:	Kathleen Wiser
STAA Coordinator Email:	wiser.kathi@epa.gov

Justifications:

Justification 1:

EPA's progress under Strategic Goal 1 of A Cleaner, Healthier Environment and Goal 3: Greater Certainty, Compliance, and Effec scientific assessments that inform decision making. This challenge has been amplified for chemical assessments that inform actions the Toxic Substances Control Act (TSCA), Clean Water Act (CWA), Safe Drinking Water Act (SDWA), and the Superfund-relatec calculations have created significant uncertainties and have even brought some assessments to a grinding halt. The nominated publi reframes chemical risk assessment to enable rather than hamper environmental and public health decision making. As EPA moves a platform for considering how new data streams can shape the future of chemical risk assessment. It proposes a path for using the fu alternatives to animal testing, new approach methods, and innovative approaches to integrate different data streams. The publicatio enhance, and deliver chemical risk assessments for the thousands of chemicals and pollutants in the safety evaluation pipeline, inclu projects with EPA Program Offices have been developed where the viability of this proposed paradigm shift is being explored and of this paper also emphasizes the importance of taking a public health approach in considering chemical and pollutant exposure. Th risk factors, including genetic, behavioral and environmental. While EPA regulates through a traditional risk assessment lens and h other federal and state agencies or health care professionals may be responsible for managing other risk factors of disease that have this paper provides a framework for EPA to partner with other public health organizations to more effectively target disease burden collaborating with EPA's Office of Air and Radiation to do this around the issue of pollutant exposures and cardiovascular disease behavioral factors, but also by certain environmental factors. By using the principles articulated in this paper, EPA has been able to address this disease. For example, the Department of Health and Human Services' MillionHearts Initiative has incorporated increas effects as a criterion for success in its MillionHearts Hospital and Healthcare Recognition Program. Additionally, through partnersh professional organizations, EPA has been able to deliver important public health information about the environmental contributors healthcare professional practitioners.

Justification 2A:

Not Applicable

Justification 2B:

Not applicable

Justification 2C:

Not applicable

Justification 2D:

Not applicable

Justification 2E:

Not applicable

Justification 3A:

News media coverage:

Although there is no known media coverage, this manuscript was included as the cover article for the journal in 2017 when publish editor, Dr. Michael R. Greenberg, distinguished professor at the Edward J. Bloustein School of Planning and Public Policy, Rutgers participate in a podcast discussion with the associate editor regarding the potential impact of this work.

1. Cover article (https://ajph.aphapublications.org/doi/10.2105/AJPH.2017.303771)

2. Journal editorial (https://ajph.aphapublications.org/doi/10.2105/AJPH.2017.303844)

3. Invited Podcast (https://soundcloud.com/alfredomorabia/ajph-podcast-of-the-july-2017-issue-english)

Invited presentations:

Based on this publication, there have been multiple invitations to present this work.

1. Health Canada Chemical Management Plan Science Committee meeting, November 2018; (Thank you letter attached).

2. 2017 National Environmental Health Association invited session

a. Gwinn MR, Bahadori T, Deener KC. Session on Risk Assessment at a Crossroads: A Portfolio Approach to Protect Public Hea Rapids, MI July 10-13, 2017.

3. Society of Toxicology (SOT) 57th Annual Meeting and ToxExpo, a Contemporary Concepts in Toxicology workshop on the "To

a. Cascio WE, "Aging and Increased Susceptibility to Environmental Toxicants". San Antonio, TX, March 10, 2018

4. National Institute of Environmental Health Sciences sponsored symposium "Understanding the Combined Effects of Environm as a Model"

a. Cascio WE, "Overview of the Atherosclerosis and Chemical Stressors", Research Triangle Park, NC, April 3, 2018

Other Evidence:

1. Health Canada (HC) and Environment and Climate Change Canada (ECCC) through the Chemicals Management Plan (CMP) a roadmap for implementing a public health/population health approach to support chemical risk assessment and management in https://www.canada.ca/en/health-canada/services/chemical-substances/chemicals-management-plan/science-committee/meeting-

2. This paper is part of the curriculum in Risk Sciences at Johns Hopkins, specifically as a roadmap for the future of health risk. I of public health, and invited presentations at Johns Hopkins, invited Deans lectures at Drexel University, University of Colorado, R Sewell Lecture in Environmental Health at Columbia University Mailman School of Public Health.

3. The manuscript has an Attention Score in the top 25% of all research outputs scored by Altmetric. It has had 19 citations in Sc and has a field-weighted citation impact of 3.72. A value greater than 1.00 means that document is more cited than expected acco publication; document type, and disciplines associated with its source. (https://apha.altmetric.com/details/20293499/citations). Acc since publication (https://scholar.google.com/scholar?um=1&ie=UTF-8&lr&cites=12958655616865832005) and there have been 2 https://www.researchgate.net/publication/317016558_Chemical_Risk_Assessment_Traditional_vs_Public_Health_Perspectives).

Justification 3B:

The research was published in the peer reviewed journal American Journal of Public Health (AJPH), a key journal in the field of pu is ranked #4 of 156 titles in the Public, Environmental and Occupational Health category in the Social Sciences Citation Index and edition. *AJPH* rose among peer journals in the Science Citation Index to No. 12 in 2018, up from No. 16 in 2017. And in the Social https://www.apha.org/news-and-media/news-releases/ajph-news-releases/2019/impact-factor-2019). The peer review process at A peer reviewers, and peer reviewers do not know the authors of the papers they are reviewing. Reviewed papers usually receive ca by the responsible associate editor, deputy editor, and editor-in-chief. Initial screening results in rejection of the majority of manusc are selected for review, the time to first decision is about three months. Overall time from submission to acceptance, which include aspires to select, through peer review, the highest quality science and public health practice–related manuscripts. To achieve this, must be thorough, objective, and fair. Every aspect of this process involves important ethical principles and decisions. The reputat researchers, reviewers, editors, public health practitioners, research subjects, funding agencies, and administrators of public healt possible AJPH policies to ensure the ethical treatment of all participants in the publication process.

AUTHORS

Principal Author

Author Name:	Maureen R. Gwinn	
Professional Title:		Salutation:
Email:	gwinn.maureen@epa.gov	Organization:
Mailing Address:		
Street Line 1:		
City:		
Zip Code:		State:
At time of research was:	EPA Employee	
Separation Date:		
% of Effort:	12	

Contributing Author

Author Name:	Kacee Deener	
Professional Title:		Salutation:
Email:	deener.kathleen@epa.gov	Organization:
Mailing Address:		
Street Line 1:		
City:		
Zip Code:		State:
At time of research was:	EPA Employee	
Separation Date:		

% of Effort: 12

Contributing Author

Author Name: David A Bussard

Professional Title: Salutation:

Email: bussard.david@epa.gov Organization:

Mailing Address:

Street Line 1:

City:

Zip Code: State:

At time of research was: EPA Employee

Separation Date:

% of Effort: 10

Contributing Author

Author Name: Russell S Thomas

Professional Title: Salutation:

Email: thomas.russell@epa.gov Organization:

Mailing Address:

Street Line 1:

City:

Zip Code: State:

At time of research was: EPA Employee

Separation Date:

% of Effort:	10	

Contributing Author

Author Name:	Tina Bahadori	
Professional Title:		Salutation:
Email:	bahadori.tina@epa.gov	Organization:
Mailing Address:		
Street Line 1:		
City:		
Zip Code:		State:
At time of research was:	EPA Employee	
Separation Date:		
% of Effort:	10	

Contributing Author

Author Name:	Wayne E Cascio	
Professional Title:		Salutation:
Email:	cascio.wayne@epa.gov	Organization:
Mailing Address:		
Street Line 1:		
City:		
Zip Code:		State:
At time of research was:	EPA Employee	
Separation Date:		

% of Effort:	10	

Contributing Author

Author Name:	Thomas A Burke	
Professional Title:		Salutation:
Email:	tburke1@jhu.edu	Organization:
Mailing Address:		
Street Line 1:		
City:		
Zip Code:		State:
At time of research was:	Non EPA Personnel	
Separation Date:	Fri Jan 20 00:00:00 GMT 2017	
% of Effort:	12	

Contributing Author

Author Name:	Daniel A Axelrad	
Professional Title:		Salutation:
Email:	axelrad.daniel@epa.gov	Organization:
Mailing Address:		
Street Line 1:		
City:		
Zip Code:		State:
At time of research was:	EPA Employee	
Separation Date:		

% of Effort:	10	

Contributing Author

Author Name:	David Dix	
Professional Title:		Salutation:
Email:	dix.david@epa.gov	Organization:
Mailing Address:		
Street Line 1:		
City:		
Zip Code:		State:
At time of research was:	Non EPA Personnel	
Separation Date:		
% of Effort:	2	

Contributing Author

Author Name:	Robert J Kavlock	
Professional Title:		Salutation:
Email:	rkavlock@icloud.com	Organization:
Mailing Address:		
Street Line 1:		
City:		
Zip Code:		State:
At time of research was:	Non EPA Personnel	
Separation Date:	Fri Nov 03 00:00:00 GMT 2017	

% of Effort:	12

PUBLICATIONS

Publication 1:

Publication Title:	Chemical Risk Assessment: Traditional vs Public Health Perspectives
Publication Date:	Sat Jul 01 00:00:00 GMT 2017
Journal/Publication Method:	American Journal of Public Health
All Author(s):	
Volume:	107
Pages:	1032-1039
Citation ½ Life:	9.8

Chemical Risk Assessment: Traditional vs Public Health Perspectives

Preventing adverse health effects of environmental chemical exposure is fundamental to protecting individual and public health. When done efficiently and properly, chemical risk assessment enables risk management actions that minimize the incidence and effects of environmentally induced diseases related to chemical exposure. However, traditional chemical risk assessment is faced with multiple challenges with respect to predicting and preventing disease in human populations, and epidemiological studies increasingly report observations of adverse health effects at exposure levels predicted from animal studies to be safe for humans. This discordance reinforces concerns about the adequacy of contemporary risk assessment practices for protecting public health.

It is becoming clear that to protect public health more effectively, future risk assessments will need to use the full range of available data, draw on innovative methods to integrate diverse data streams, and consider health endpoints that also reflect the range of subtle effects and morbidities observed in human populations.

Considering these factors, there is a need to reframe chemical risk assessment to be more clearly aligned with the public health goal of minimizing environmental exposures associated with disease. (*Am J Public Health.* 2017;107:1032–1039. doi:10.2105/AJPH.2017.303771)

Maureen R. Gwinn, PhD, Daniel A. Axelrad, MPP, Tina Bahadori, ScD, David Bussard, BA, Wayne E. Cascio, MD, Kacee Deener, MPH, David Dix, PhD, Russell S. Thomas, PhD, Robert J. Kavlock, PhD, and Thomas A. Burke, PhD, MPH

See also Greenberg, p. 1020.

For the past several decades, human health risk assessment has been a pillar of environmental health protection. In general, the products of risk assessment have been numerical risk values derived from animal toxicology studies of observable effects at high doses of individual chemicals. Although this approach has contributed to our understanding of overt health outcomes from chemical exposures, it does not always match our understanding from epidemiology studies of the consequences of real-world exposures in human populations, which are characterized by exposure to multiple pollutants, often chronically, at concentrations that can fluctuate over wide ranges; susceptible populations and life stages; potential interactions between chemicals and nonchemical stressors and background disease states; and lifestyle factors that modify exposures (e.g., airtight houses).[1] These and other issues are particularly important when determining risk of complex diseases, such as cardiovascular disease.

Ten years ago, the National Research Council offered a new paradigm for evaluating the safety of chemicals on the basis of chemical characterization, testing using a toxicity pathway approach, and modeling and extrapolating the dose–response relationship from in vitro testing, all embedded in a risk context and considering population-based data and exposure.[2] Efforts such as the Tox21 Consortium[3,4] and ToxCast program[5] have helped us better understand the biological interactions of large numbers of chemicals using high-throughput assay systems, and we are witnessing early adoption of new technologies and approaches for screening chemicals for integrated testing.[6]

Several other factors are also changing the way environmental health professionals think about chemical risks and how to most effectively protect public health, especially for complex diseases like cardiovascular disease. It is estimated that intrinsic factors (e.g., those that result in mutations stemming from random errors in DNA replication) account for only 10% to 30% of many common cancers.[7] Similarly, only 30% to 40% of birth defects can be attributed to known causes such as genetics, fetal alcohol syndrome, maternal smoking, and folate insufficiency.[8] Other studies have concluded that nongenetic environmental factors and gene by environment interactions are the primary causes of chronic diseases.[9] The ability to evaluate and quantify the role of environmental factors on public health is a clear opportunity, but it is limited by the lack of readily available models for prominent clinical outcomes.

CURRENT CHALLENGES

Understanding public health risk from environmental chemical exposures is complicated by many factors, such as population variability and susceptibility, long latencies between critical exposures and disease manifestations, and background environmental exposures. Issues of population variability and susceptibility are poorly understood and difficult to characterize and incorporate into risk assessments. For example, a person's unique microbiome may modulate his or her response to environmental exposures.[10,11] Although studies are limited in this emerging area, knowledge about the

ABOUT THE AUTHORS

At the time of the writing of this article, all of the authors were with the US Environmental Protection Agency, Washington, DC.

Correspondence should be sent to Maureen R. Gwinn, PhD DABT ATS, Office of Research and Development, US Environmental Protection Agency, 1300 Pennsylvania Ave NW, Ronald Reagan Building, Room 41205, MC 8101R, Washington, DC 20460 (e-mail: gwinn.maureen@epa.gov). Reprints can be ordered at http://www.ajph.org by clicking the "Reprints" link.

This article was accepted March 2, 2017.
doi: 10.2105/AJPH.2017.303771

microbiome may inform inter-individual variability and unexplained susceptibility observed in populations. Scientists have begun to appreciate the role of the microbiome in the lack of reproducibility and interpretability of animal studies.[12]

Another example is the effects of early life environmental exposures on health outcomes later in life. Advances in the field of epigenetics have revealed that developmental exposure to endocrine disrupting chemicals can alter epigenetic programming of gene regulation and thus may play a role in the risk of obesity later in life.[13] Similar to microbiome research, studies in this area are limited, and a better understanding of the link between chemical exposure, epigenetic gene regulation, and health outcomes through epidemiological research can help us better address factors that are currently difficult to account for in traditional risk assessment. Finally, there are also methodological challenges in determining attributable risks in populations with background environmental exposures, as these background exposures may change the population health baselines or affect the response of the target chemical. Other examples of important factors to incorporate in risk assessments can be found in Table 1.

OPPORTUNITIES FOR USING MULTIPLE DATA TYPES

Concurrent with these challenges, science and technology are advancing rapidly and in ways that create opportunities for risk assessment. Public health disciplines help us understand how baseline health status can influence the effect of population-level chemical exposures. We also need to consider how environmental pollutants may contribute to overall disease burden for endpoints not traditionally considered in chemical risk assessment (e.g., metabolic disorders, autism). New methods in epidemiological research help us evaluate complex interactions among multifactorial causes of disease ranging from macro (societal, neighborhood) to micro (molecular) factors, relevance of exposures during sensitive life stages, and a better understanding of interrelatedness of disease across the life span.[14]

Advances in high-throughput technologies and computational modeling (e.g., ToxCast, Tox21, and ExpoCast efforts) are providing data on hazard and exposure potential for a large number of data-poor chemicals. The increased generation of data for both hazard and exposure from these advances can be used to better understand the biological pathways that lead to adverse health effects in ways that were not possible in the past. But linking these observations to specific disease endpoints is challenging because the translation of effects across levels of biological organization is not well understood. One approach with the potential to advance our understanding of how chemical exposures can affect health is the use of adverse outcome pathways, which integrate various types of biological information to link molecular initiating events to downstream key events and ultimately unwanted health outcomes.[15,16]

TABLE 1—Examples of Current Risk Assessment Challenges and Opportunities

Risk Assessment Challenge	Description	Impact on Risk Assessment	Public Health Opportunity
Molecular initiating events and subsequent key events in adverse outcome pathways	Early biological changes or precursor effects in response to chemical exposures may be identified by in vitro, animal, or epidemiological studies	Useful for qualitative and quantitative understanding of ultimate health effect of early biological changes	Improved public health protection without need for long-term toxicology or epidemiology studies
Background exposures	Population exposures to a myriad of environmental chemicals at low concentrations	Exposures to background chemicals may affect response to target chemical exposures and may change population health baselines	Increased public health protection if baseline exposures are taken into account when determining prevention strategies
Nonchemical stressors	Physical and psychosocial stressors, including noise, temperature, socioeconomic status, social stress, and limited resources	Impact on baseline susceptibility and potential effect modification	Potential role in cumulative assessment, improved identification of vulnerable populations, potential target for public health interventions (e.g., stress management)
Early life determinants of health	Biological characteristics and exposures that can determine chronic and lifelong health outcomes	Effect of exposures during early life may play a role in later disease states (e.g., endocrine disruptors, epigenetic changes)	Potential for early life interventions for prevention and management of later disease
Baseline health status	Individual health status, with a focus on potential health susceptibilities	Baseline health status may affect response to additional environmental chemical exposures	Increased public health protection if baseline health status is taken into account
Microbiome	Microorganisms that reside within and on our bodies and interact with the environment	Exposure modification, susceptibility and resilience to environmental pollutants, important as an early life determinant of health	Potential targets for prevention and intervention, management of allergic responses, and precision risk management

To fully realize the potential of adverse outcome pathway–based approaches and to integrate biological findings across disciplines, we must strengthen our ability to detect precursor events in human populations and to identify biologically relevant exposure metrics, ideally measurable in individuals. Another advancement that has a great potential to advance our understanding of data-poor chemicals is the use of nontesting approaches (e.g., quantitative structure–activity relationship) that allow us to predict toxicity when adequate testing data are absent—especially when we combine knowledge of chemical structural features and in vitro bioactivity determinations. Advances in the development of chemical libraries, cheminformatics, and read-across predictions and integration with molecular data and adverse outcome pathways have significantly improved their application and predictive capacity, which will allow more comprehensive assessment of the health effects of exposures.[17,18]

Effectively predicting population risk by integrating a variety of data streams (e.g., epidemiology, toxicology, high-throughput testing) and considering multiple sources and pathways of exposure can better inform environmental public health decisions. Advances in technology and computational capabilities have fostered new opportunities for generating and analyzing molecular, animal, and human data on effects and exposures, which can be integrated

TABLE 2—Data Streams and Opportunities and Challenges for Informing Risk Assessment

Data Type	Description	Opportunity	Challenge
Nontesting data	Nontesting approaches, such as quantitative structure–activity relationship models and read-across allow us to predict toxicity when adequate testing data are absent	Advances in the field have significantly improved their application and predictive capacity	Developing principles for acceptance, for characterizing and incorporating uncertainties into predictions, and for developing objective metrics of performance
Molecular	Biochemical and cell-based bioactivity data and "omics-based" data on thousands of chemicals	Can help inform our understanding of the health outcomes of environmental exposures, using data that are potentially more human relevant	Lack of scientific consensus on inferring hazard from bioactivity in vitro assay and omics-based data and providing quantitative dose–response information on exposure metrics
Animal	Traditional animal testing provides a hazard based point of departure for risk assessments	Targeted animal testing can be performed on the basis of the results of bioactivity data to focus on key health outcomes	Potential uncertainties with using traditional animal testing to estimate human risk (e.g., extrapolating from animal to human or high to low doses and accounting for human population variability and life stage susceptibility)
Human	Epidemiological and other human data support holistic assessment of the effects of chemical exposures on public health	Newer exposure science and statistical techniques advance the understanding of human variability that can be obtained from epidemiology and individual sequencing; understanding effect modification by nonchemical stressors and baseline health status	Often limited mechanistic and dose–response data, and exposure misclassification can bias results to the null; possibility of unmeasured confounders often undermines confidence in observed associations, and it may require multiple studies and many years to rule out chance, bias, and confounding as possible explanations for observed associations
Exposure	Exposure characterization that captured the variability in time, space, and within and across populations; better toxicokinetic data link external to internal dosimetry and relevant environmental exposure concentrations with biological significance	Targeted and nontargeted biomonitoring, application of sensors, and other new technologies are greatly advancing population exposure characterization; high-throughput exposure models allow exposure predictions on thousands of chemicals with associated uncertainty	Estimating and incorporating the inter- and intraindividual variability in exposures into current designs of toxicity testing and risk assessments; extrapolating relevant target tissue and organ dose information from external exposures and in vitro assays; accounting for multiple exposures; sample collection, data management, and analysis; and covering or extrapolating to a broader chemical space
Digital data	The ongoing revolution in social media use and communication has provided a new source of data used in exposure science and environmental epidemiology for local and timely information about disease and health dynamics	A significant source of untapped data	The collection and application of these data have significant ethical implications that need to be understood and managed, particularly taking into account personal identifiable information; methods to evaluate the quality of the data and build confidence in the applications are needed

into chemical risk assessments. At the same time, probabilistic and high-throughput approaches for risk assessment have been advancing. Table 2 highlights various data types available and challenges in applying these data types to inform risk assessment.

A PUBLIC HEALTH PERSPECTIVE

A public health perspective for chemical risk assessment would approach risk assessment from a new lens. It would address population health with a focus on the health and societal burden of disease; use and integrate all available types of data—including traditional toxicology, human epidemiological findings, and newer and emerging data streams and information, such as digital epidemiology,[19] high-throughput and high-content data, and adverse outcome pathways; and draw on public health approaches, such as attributable risk or relative risk. This new perspective may be especially important for some historically challenging aspects of risk assessment, such as understanding cumulative risks of exposures to multiple chemical and nonchemical stressors. Internationally, scientists have raised concerns about the large number of ubiquitous chemicals people are exposed to and called for rethinking approaches to evaluating the health effects of chemicals.[16] Figure 1 presents a conceptual model for a public health perspective for risk assessment.

Although approaching assessments from the perspective of health outcomes may be challenging, it provides the opportunity to evaluate exposures and effects across the life span that are relevant to population health. Advances in science and technology, such as adverse outcome pathway development, the broader availability of chemical and biological data, and the applications of statistical and bioinformatics tools, bring this previously aspirational approach well within reach.[20]

EXAMPLE: CARDIOVASCULAR DISEASE

A public health approach may inform the challenge of cardiovascular disease. Cardiovascular disease is the number 1 cause of mortality worldwide and is a major US public health burden.[21,22] Annual costs of cardiovascular disease in the United States were estimated to be $317 billion in 2011 and 2012, considering direct medical costs and lost productivity because of premature mortality.[22] This estimate is likely to substantially underestimate the social cost of cardiovascular disease because of limitations in the estimation of indirect costs associated with morbidity and premature mortality.[23]

Although much is known about the biochemical and behavioral risk factors associated with cardiovascular disease, particularly compared with other diseases and health conditions, the traditional risk factors fail to account for 10% to 25% of its prevalence.[24] Environmental factors, including air pollution[25] and chemical exposures[26] are thought to contribute to the unexplained fraction. Although mortality stemming from cardiovascular disease has decreased over the past few decades in the developed world as a result of reductions in behavioral risk factors, the rising prevalence of obesity and diabetes might account for the deceleration in the rate of improvement in annual cardiovascular mortality in the United States over the past few years.[27]

There is an urgent need to better understand the biological pathways through which environmental exposures to chemical and nonchemical stressors act to stimulate and accelerate atherosclerosis and promote adverse cardiovascular health effects. Applying the adverse outcome pathway framework,[28] the initial molecular response to a chemical exposure will often be receptor

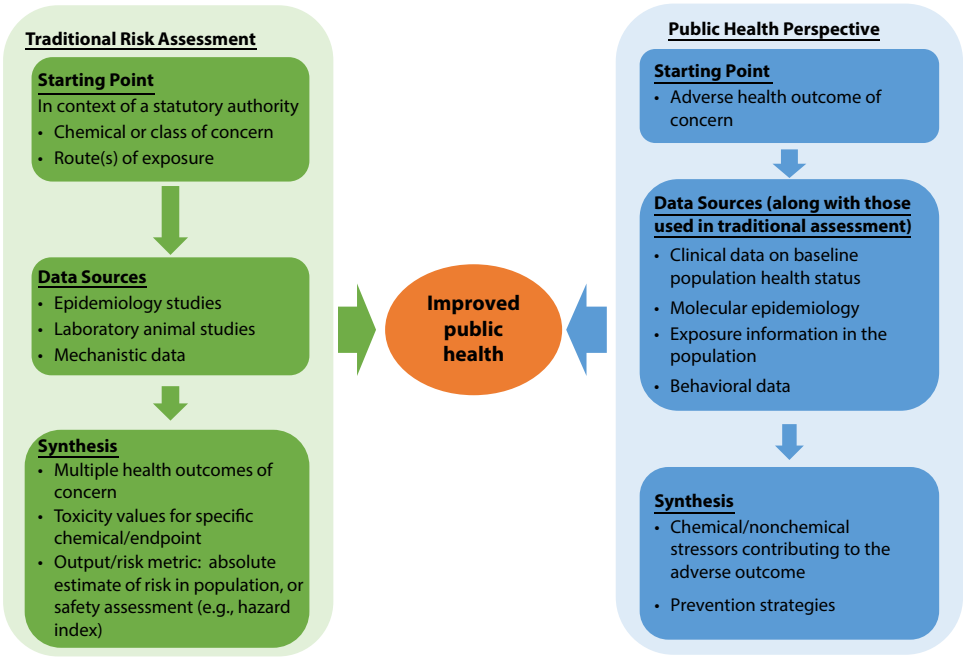

Note. This conceptual model illustrates how the starting point in a public health–focused risk assessment would differ from that of traditional risk assessment. In traditional risk assessment, the starting point is focused on specific chemicals or classes of chemicals of concern, with multiple data streams saying what the critical effects from that chemical are. A public health perspective would focus on the adverse health outcome of concern with multiple data streams, informing our understanding of hazard and exposure in the context of public health decisions related to that outcome and not necessarily focused on just 1 chemical or class of chemicals.

FIGURE 1—Conceptual Model for a Public Health Perspective for Chemical Risk Assessment

activation and changes in metabolism and, ultimately, changes in tissue and organ function. Such changes can be modified by both intrinsic (e.g., gender, age, genetic, and epigenetic background) and extrinsic factors (e.g., coexposures to other chemical and nonchemical stressors; Figure 2). Over time, these changes produce subclinical effects, such as changes in electrical and mechanical cardiac function, vascular function, and nonobstructive atherosclerotic vascular changes. With the persistence of metabolic changes that stimulate the progression of vascular disease, clinical cardiovascular events such as heart attacks, strokes, heart failure, and abnormal heart rhythms follow.

To date, the most comprehensive application of this approach has been in the study of population-level health effects of air pollution exposure.[28] Epidemiological data at the population level has provided support that air pollutant exposure (e.g., ambient particular matter and NO_2) accelerates the development and progression of coronary atherosclerosis.[25] Xenobiotic metals such as arsenic, cadmium, lead, and mercury are also associated with atherosclerosis.[29] Gene–environment interaction alters the risk of vascular disease[30]; for example, the residential proximity to highways (representing exposure to a mixture of traffic-related air pollutants) is associated with peripheral vascular disease, which is modified by the gene encoding bone morphogenic protein.[7,31]

Because of the complexity of the drivers of atherosclerosis, a medical model treating blood pressure and high cholesterol and advising dietary modification and exercise will be inadequate to fully address this disease. Likewise, identifying the chemicals that increase risk on an individual basis will be inadequate to prevent vascular disease. Instead an integrated systems approach is

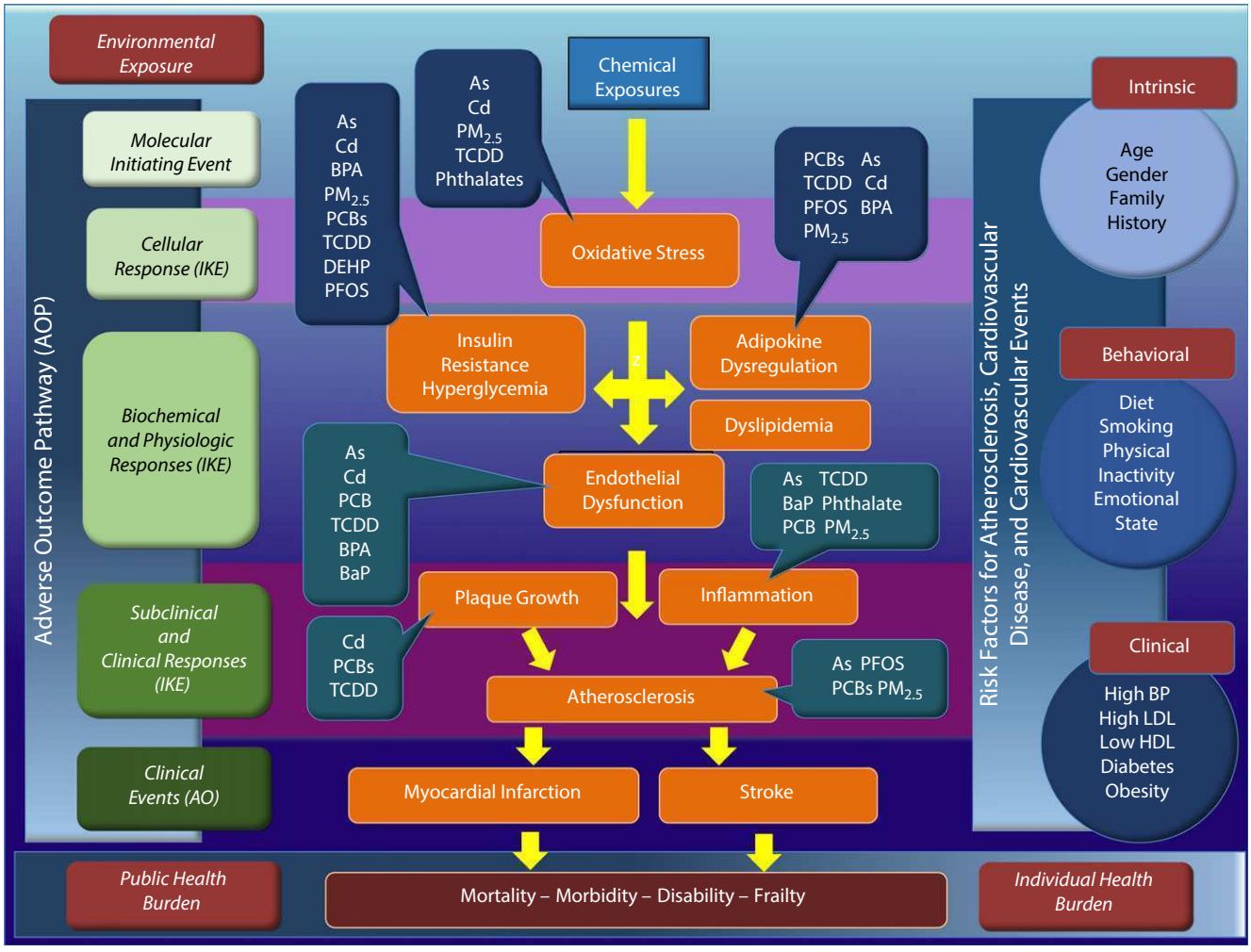

Source. Action of specific chemicals and metals adapted from Kirkley and Sargis.[26]

Note. As = Arsenic; AO = adverse outcome; BaP = benzo[a]pyrene; BPA = bisphenol A; Cd = Cadmium; DEHP = di(2-ethylhexyl) phthlate; DES = diethylstilbestrol; HDL = high-density lipoprotein; IKE = intermediate key event; LDL = low-density lipoprotein; PCB = polychlorinated biphenyl; PFOS = perfluorooctane sulfonic acid; $PM_{2.5}$ = particulate matter ≤ 2.5 μm; TCDD = tetrachlorodibenzo-p-dioxin. This figure illustrates the biological pathway leading from exposure to adverse cardiovascular outcomes for a variety of chemicals. On the left-hand side of the figure these pathways are linked to the adverse outcome pathway, and on the right-hand side of the figure we see the traditional risk factors for adverse cardiovascular outcomes.

FIGURE 2—Adverse Outcome Pathway for Cardiovascular Outcomes

needed to fully account for all known risk factors and formulate the problem to define the most effective strategy to decrease individual risk and societal burden. Accomplishing this will require clinical data that fully reflect a population under consideration as well as exposures to traditional risk factors, biomonitoring data documenting exposures to multiple chemicals, and molecular responses from in vitro and in vivo studies indicative of the activation of biochemical pathways that accelerate atherosclerosis.

Although this approach might not be practical currently, it is not unrealistic to think about future states where it could become standard practice. Our proposed innovative approach to chemical risk assessment is occurring contemporaneously during the formative stages of the National Institutes of Health–sponsored Precision Medicine Initiative, which will drive integration of genomics, data sciences, and bioinformatics as the basis for improved individual health care, disease prevention, and public health. The Affordable Care Act has accelerated electronic medical record adoption in health care practices and hospital systems, potentially offering a valuable source of information for population-level health monitoring. Recent research has used big data to study the early stages of disease and better classify and predict disease progression and could be used to inform personalized medicine to optimize wellness in healthy populations.[32–34]

Moreover, the anticipated integration and development of technologies and analytical tools have the potential to improve public health and increase the spatial and temporal resolution of environmental health surveillance. The establishment of a long-term representative precision medicine cohort, if integrated with the proposed National Biomonitoring Network,[35] could have enormous benefit in helping us understand the relationship between chemical exposures and disease and in managing some of the most challenging clinical problems more effectively.

Applying this framework would potentially expand our understanding of the origins of vascular disease and its progression, helping define strategies for primary prevention to thwart the initiation of the process we ultimately call atherosclerosis. Thus, such a framework would provide new and ongoing insights into the associations between environmental exposures that contribute the greatest burden to public health. This approach would facilitate accounting for sensitive populations and could inform suggested individual health or behavioral measures in which there have been past exposures or in which current exposure cannot be reduced enough to protect those most at risk.

CONCLUSIONS

The proposed conceptual model is grounded in public health principles and focused on identifying the greatest opportunity to reduce environmental exposures to improve health outcomes. Along with traditional risk assessment, this perspective can better inform public health decision-making. Although there are clear benefits to operating within a public health–focused framework and moving away from individual chemicals and apical endpoints, there are also challenges.

Informing Decision-Making

Since the 1980s, the Environmental Protection Agency's decision-making has been grounded on traditional risk assessments that are conducted within the constraints of the Environmental Protection Agency's statutes and programs. Although program-targeted risk assessments will remain an important component, the disease-based approach draws on information in a holistic fashion that cuts across organizational and legal boundaries, integrating traditional inputs and newer data streams. These assessments will provide decision-makers with critical information to inform exposure-reduction efforts to affect the selected health outcomes and, ultimately, improve public health. Because those exposure-reduction efforts would take place within the existing statutory construct, an important implementation step would be to move from findings of disease-based risk assessments to assessments of specific risk management actions under the relevant statutory authorities.

Priorities for Screening and Testing

A health outcome–focused framework can inform priorities for screening and testing the toxicity of chemicals. Efforts to develop and synthesize approaches for screening large numbers of chemicals using high-throughput toxicity testing and exposure prediction should continue to provide data for data-poor chemicals. For example, in the recently announced Cancer Moonshot,[36] high-throughput approaches could screen a large set of chemicals for potential carcinogenicity and identify a suite of chemicals for additional animal toxicity testing.

Examining noncancer endpoints will also be challenging, which is why developing adverse outcome pathways and networks to contextualize and interpret nonapical hazard data in relation to population health is of increasing value. Epidemiology studies can be designed to inform and validate high-throughput testing approaches by identifying both chemical stressors and nonchemical stressors that modify responses to chemical exposures; they can also be designed to test relationships between disease and early markers of exposure and biological response (e.g., epigenetic changes).

The Impact of Cumulative Exposures

Although cumulative risk assessment has been of high interest for the past few decades, putting cumulative assessment approaches into practice has been challenging. This framework provides a new construct for considering cumulative risk. By focusing on a health endpoint of concern, one could consider the multiple exposures that may contribute to a health outcome. Past National Research Council recommendations have encouraged assessors to evaluate the combined effects of exposures to all chemicals that affect a common adverse outcome, for example, male reproductive development.[37] Challenges include gaining adequate understanding of individual chemical effects to group chemicals by health outcome. Increased research into the biological pathways by which chemicals affect health status can help inform approaches for estimating the joint effect of chemicals without

testing all permutations or combinations.

One example of an alternative approach is health impact assessment, which uses a systems approach to array data sources and analytic methods and considers input from stakeholders to determine potential effects of a proposed action or decision on the health of a population and the distribution of those effects in the population.[38] Using health impact assessment approaches for chemical risk assessments made through this framework can offer a method to organize various data streams that can influence our understanding of a health effect, inform potential multiple contributors to adverse health outcomes, and provide recommendations to decision-makers for monitoring and managing these outcomes.

Consider Public Health Concepts

This new approach takes a systematic view of collective factors that contribute to a health outcome or disease state, including those that are not regulated by a single federal entity. Any single health outcome may be influenced by multiple factors beyond chemical exposures, such as nutrition, genetics, and social stressors. Because those factors are not regulated, it is important for environmental regulatory agencies to understand what fraction of the disease burden is influenced by the regulated environmental exposure.

Public health approaches, such as attributable risk, can help inform this understanding. Challenges may include incorporating these approaches, which are typically used in epidemiology, to animal and advanced toxicity testing data; ensuring adequate training with the approaches; and communicating risk in a way that acknowledges the influence of nonregulated factors.

Public Health Implications

Understanding the health effects of chemicals has real implications for public health. This proposed approach for chemical risk assessment starts at the health endpoint and incorporates multiple data streams, including data developed using newer technologies such as high-throughput screening. In parallel with more traditional risk assessment approaches, this will lead to a better understanding of mechanisms of single chemicals as well as cumulative exposures that lead to specific disease endpoints.

This new lens will need to be applied to the complete risk assessment process—problem formulation, data considerations, and data synthesis through multipathway methods, including cumulative assessment and health impact assessment—with an eye to the prevention of adverse effects. This approach draws on the best available science to improve our understanding of the health effects of environmental chemicals and informs decision-making to prevent, reduce, or mitigate exposure and ultimately improve public health. AJPH

CONTRIBUTORS

M. R. Gwinn led the compilation of text and revisions of the article. M. R. Gwinn and K. Deener led creation of Figure 1. M. R. Gwinn, K. Deener, and R. J. Kavlock led the creation of Table 1. D. A. Axelrad, T. Bahadori, D. Bussard, R. S. Thomas, and R. J. Kavlock led the drafting of text on challenges and opportunities. T. Bahadori, R. S. Thomas, and R. J. Kavlock led the creation of Table 2. W. E. Cascio led the creation of Figure 2. W. E. Cascio and K. Deener led the drafting of text on public health. R. J. Kavlock and T. A. Burke led the discussions and outlined the article. All authors contributed to discussions of the concepts behind this article and contributed text to the various sections.

ACKNOWLEDGMENTS

The authors would like to acknowledge the assistance of Laura Romano in preparing the article.

Note. The views expressed in this article are those of the authors and do not necessarily reflect the views or policies of the US Environmental Protection Agency.

REFERENCES

1. Birnbaum LS, Burke TA, Jones JJ. Informing 21st-century risk assessments with 21st-century science. *Environ Health Perspect*. 2016;124(4):A60–A63.

2. National Research Council. *Toxicity Testing in the 21st Century: A Vision and a Strategy*. Washington, DC: National Academies Press; 2007.

3. Kavlock RJ, Austin CP, Tice RR. Toxicity testing in the 21st century: implications for human health risk assessment. *Risk Anal*. 2009;29(4):485–487; discussion 492–497. [Comment on Toxicity testing in the 21st century: implications for human health risk assessment. *Risk Anal*. 2009]

4. Tice RR, Austin CP, Kavlock RJ, Bucher JR. Improving the human hazard characterization of chemicals: a Tox21 update. *Environ Health Perspect*. 2013; 121(7):756–765.

5. Kavlock R, Chandler K, Houck K, et al. Update on EPA's ToxCast program: providing high throughput decision support tools for chemical risk management. *Chem Res Toxicol*. 2012;25(7):1287–1302.

6. Browne P, Judson RS, Casey WM, Kleinstreuer NC, Thomas RS. Screening chemicals for estrogen receptor bioactivity using a computational model. *Environ Sci Technol*. 2015;49(14):8804–8814.

7. Wu S, Powers S, Zhu W, Hannun YA. Substantial contribution of extrinsic risk factors to cancer development. *Nature*. 2016;529(7584):43–47.

8. Weinhold B. Environmental factors in birth defects: what we need to know. *Environ Health Perspect*. 2009;117(10): A440–A447.

9. Rappaport SM, Barupal DK, Wishart D, Vineis P, Scalbert A. The blood exposome and its role in discovering causes of disease. *Environ Health Perspect*. 2014;122(8):769–774.

10. Dietert RR, Silbergeld EK. Biomarkers for the 21st century: listening to the microbiome. *Toxicol Sci*. 2015;144(2): 208–216.

11. Patterson AD, Turnbaugh PJ. Microbial determinants of biochemical individuality and their impact on toxicology and pharmacology. *Cell Metab*. 2014; 20(5):761–768.

12. Servick K. Of mice and microbes. *Science*. 2016;353(6301):741–743.

13. Stel J, Legler J. The role of epigenetics in the latent effects of early life exposure to obesogenic endocrine disrupting chemicals. *Endocrinology*. 2015;156(10): 3466–3472.

14. Buck Louis GM, Bloom MS, Gatto NM, Hogue CR, Westreich DJ, Zhang C. Epidemiology's continuing contribution to public health: the power of "then and now." *Am J Epidemiol*. 2015;181(8): e1–e8.

15. Ankley GT, Bennett RS, Erickson RJ, et al. Adverse outcome pathways: a conceptual framework to support ecotoxicology research and risk assessment. *Environ Toxicol Chem*. 2010;29(3):730–741.

16. Goodson WH III, Lowe L, Carpenter DO, et al. Assessing the carcinogenic potential of low-dose exposures to chemical mixtures in the environment: the challenge ahead. *Carcinogenesis*. 2015; 36(suppl 1):S254–S296.

17. Mansouri K, Abdelaziz A, Rybacka A, et al. CERAPP: Collaborative Estrogen Receptor Activity Prediction Project. *Environ Health Perspect*. 2016;124(7): 1023–1033.

18. Judson R, Houck K, Martin M, et al. Analysis of the effects of cell stress and cytotoxicity on in vitro assay activity across a diverse chemical and assay space. *Toxicol Sci*. 2016;153(2):409. [Erratum in Analysis of the effects of cell stress and cytotoxicity on in vitro assay activity across a diverse chemical and assay space. *Toxicol Sci*. 2016]

19. Bakker KM, Martinez-Bakker ME, Helm B, Stevenson TJ, et al. Digital epidemiology reveals global childhood disease seasonality and the effects of immunization. *Proc Natl Acad Sci USA*. 2016; 113(24):6689–6694.

20. National Academies of Sciences, Engineering, and Medicine. *Using 21st Century Science to Improve Risk-Based Evaluations*. Washington, DC: National Academies Press; 2017.

21. Moran AE, Forouzanfar MH, Roth GA, et al. Temporal trends in ischemic heart disease mortality in 21 world regions, 1980 to 2010: the Global Burden of Disease 2010 study. *Circulation*. 2014; 129(14):1483–1492.

22. Mozaffarian D, Benjamin EJ, Go AS, et al. Heart disease and stroke statistics—2016 update: a report from the American Heart Association. *Circulation*. 2016; 133(4):e38–e360.

23. US Environmental Protection Agency. *Guidelines for Preparing Economic Analyses*. Washington, DC; 2010.

24. Kannel WB, Vasan RS. Adverse consequences of the 50% misconception. *Am J Cardiol*. 2009;103(3):426–427.

25. Kaufman JD, Adar SD, Barr RG, et al. Association between air pollution and

coronary artery calcification within six metropolitan areas in the USA (the Multi-Ethnic Study of Atherosclerosis and Air Pollution): a longitudinal cohort study. *Lancet*. 2016;388(10045): 696–704.

26. Kirkley AG, Sargis RM. Environmental endocrine disruption of energy metabolism and cardiovascular risk. *Curr Diab Rep*. 2014;14(6):494.

27. Sidney S, Quesenberry CP Jr, Jaffe MG, et al. Recent trends in cardiovascular mortality in the United States and public health goals. *JAMA Cardiol*. 2016; 1(5):594–599.

28. Cosselman KE, Navas-Acien A, Kaufman JD. Environmental factors in cardiovascular disease. *Nat Rev Cardiol*. 2015;12(11):627–642.

29. Solenkova NV, Newman JD, Berger JS, et al. Metal pollutants and cardiovascular disease: mechanisms and consequences of exposure. *Am Heart J*. 2014; 168(6):812–822.

30. Zanobetti A, Baccarelli A, Schwartz J. Gene-air pollution interaction and cardiovascular disease: a review. *Prog Cardiovasc Dis*. 2011;53(5):344–352.

31. Ward-Caviness CK, Neas LM, Blach C, et al. Genetic variants in the bone morphogenic protein gene family modify the association between residential exposure to traffic and peripheral arterial disease. *PLoS One*. 2016;11(4):e0152670.

32. Dinov ID, Heavner B, Tang M, et al. Predictive big data analytics: a study of Parkinson's disease using large, complex, heterogeneous, incongruent, multisource and incomplete observations. *PLoS One*. 2016;11(8):e0157077.

33. Hood L, Lovejoy JC, Price ND. Integrating big data and actionable health coaching to optimize wellness. *BMC Med*. 2015;13:4.

34. Khoury MJ, Evans JP. A public health perspective on a national precision medicine cohort: balancing long-term knowledge generation with early health benefit. *JAMA*. 2015;313(21): 2117–2118.

35. Association of Public Health Laboratories. *National Biomonitoring Plan*. Silver Spring, MD; 2015.

36. Mitchell E. Moonshot toward a cure for cancer. *J Natl Med Assoc*. 2016;108(2): 104–105.

37. National Research Council. *Phthalates and Cumulative Risk Assessment: The Tasks Ahead*. Washington, DC: National Academies Press; 2008.

38. National Research Council. *Improving Health in the United States: The Role of Health Impact Assessment*. Washington, DC: National Academies Press; 2011.

This article has been cited by:

1. Susanna H. Wegner, Caroline L. Pinto, Caroline L. Ring, John F. Wambaugh. 2020. High-throughput screening tools facilitate calculation of a combined exposure-bioactivity index for chemicals with endocrine activity. *Environment International* **137**, 105470. [Crossref]
2. Nur H. Orak, Mitchell J. Small, Marek J. Druzdzel. 2019. Bayesian network-based framework for exposure-response study design and interpretation. *Environmental Health* **18**:1. . [Crossref]
3. Keely Maxwell, Bryan Hubbell, Emily Eisenhauer. 2019. Institutional insights on integrating social and environmental science for solutions-driven research. *Environmental Science & Policy* **101**, 97-105. [Crossref]
4. Sean Watford, Stephen Edwards, Michelle Angrish, Richard S. Judson, Katie Paul Friedman. 2019. Progress in data interoperability to support computational toxicology and chemical safety evaluation. *Toxicology and Applied Pharmacology* **380**, 114707. [Crossref]
5. R.R. Boyles, A.E. Thessen, A. Waldrop, M.A. Haendel. 2019. Ontology-based data integration for advancing toxicological knowledge. *Current Opinion in Toxicology* **16**, 67-74. [Crossref]
6. Annie von Eyken, Daniel Furlong, Samareh Arooni, Fred Butterworth, Jean-François Roy, Jerry Zweigenbaum, Stéphane Bayen. 2019. Direct injection high performance liquid chromatography coupled to data independent acquisition mass spectrometry for the screening of antibiotics in honey. *Journal of Food and Drug Analysis* **27**:3, 679-691. [Crossref]
7. Marissa B. Kosnik, David M. Reif. 2019. Determination of chemical-disease risk values to prioritize connections between environmental factors, genetic variants, and human diseases. *Toxicology and Applied Pharmacology* 114674. [Crossref]
8. Hanna K.L. Johansson, Julie Boberg, Marianne Dybdahl, Marta Axelstad, Anne Marie Vinggaard. 2019. Chemical risk assessment based on in vitro and human biomonitoring data: A case study on thyroid toxicants. *Current Opinion in Toxicology* **15**, 8-17. [Crossref]
9. Philippe Grandjean. 2018. Delayed discovery, dissemination, and decisions on intervention in environmental health: a case study on immunotoxicity of perfluorinated alkylate substances. *Environmental Health* **17**:1. . [Crossref]
10. Axel Mie, Christina Rudén, Philippe Grandjean. 2018. Safety of Safety Evaluation of Pesticides: developmental neurotoxicity of chlorpyrifos and chlorpyrifos-methyl. *Environmental Health* **17**:1. . [Crossref]
11. Kathleen C. Deener, Jason D. Sacks, Ellen F. Kirrane, Barbara S. Glenn, Maureen R. Gwinn, Thomas F. Bateson, Thomas A. Burke. 2018. Epidemiology: a foundation of environmental decision making. *Journal of Exposure Science & Environmental Epidemiology* **28**:6, 515-521. [Crossref]
12. Esben Budtz-Jørgensen, Philippe Grandjean. 2018. Application of benchmark analysis for mixed contaminant exposures: Mutual adjustment of perfluoroalkylate substances associated with immunotoxicity. *PLOS ONE* **13**:10, e0205388. [Crossref]
13. Sean M. Watford, Rachel G. Grashow, Vanessa Y. De La Rosa, Ruthann A. Rudel, Katie Paul Friedman, Matthew T. Martin. 2018. Novel application of normalized pointwise mutual information (NPMI) to mine biomedical literature for gene sets associated with disease: Use case in breast carcinogenesis. *Computational Toxicology* **7**, 46-57. [Crossref]
14. Lesa L. Aylward. 2018. Integration of biomonitoring data into risk assessment. *Current Opinion in Toxicology* **9**, 14-20. [Crossref]
15. Bernard D. Goldstein. 2018. Solution-focused risk assessment. *Current Opinion in Toxicology* **9**, 35-39. [Crossref]
16. Han Li, Siliang Yuan, Guanyong Su, Meng Li, Qiangwei Wang, Guonian Zhu, Robert J. Letcher, Yufei Li, Zhihua Han, Chunsheng Liu. 2017. Whole-Life-Stage Characterization in the Basic Biology of Daphnia magna and Effects of TDCIPP on Growth, Reproduction, Survival, and Transcription of Genes. *Environmental Science & Technology* **51**:23, 13967-13975. [Crossref]
17. Philippe Grandjean, Martine Bellanger. 2017. Calculation of the disease burden associated with environmental chemical exposures: application of toxicological information in health economic estimation. *Environmental Health* **16**:1. . [Crossref]
18. Michael R. Greenberg. 2017. Risk Analysis in the 21st Century: Adapting to New Challenges and Opportunities. *American Journal of Public Health* **107**:7, 1020-1021. [Citation] [Full Text] [PDF] [PDF Plus]
19. Carol Jagger. 2017. Educational Disparities in Adult Disability: Person, Place, Policies, and Family. *American Journal of Public Health* **107**:7, 1021-1022. [Citation] [Full Text] [PDF] [PDF Plus]

From: Norman, Christine (HC/SC)
To: Deener, Kathleen
Cc: CMP Science / PGPC (HC/SC)
Subject: CMP Science Committee: Thank You!
Date: Wednesday, December 05, 2018 3:50:52 PM

Dear Kacee,

On behalf of Health Canada and Environment and Climate Change Canada, I would like to extend our appreciation and gratitude for taking time out of your busy schedule to participate in the face-to-face CMP Science Committee meeting last week.

Your presentation and contribution to the deliberations were both relevant, and highly respected by the committee. You played a significant role in the realisation of our meeting objectives, by providing input for each of the charge questions and contributing to the development of the Committee Report.

Once again, thank you for your valuable time, contribution and expertise towards this forward thinking topic.

Kind regards,

Christine Norman
Director – Directrice
Exisiting Substances Risk Assessment Bureau - Bureau de l'évaluation des risques pour les substances existantes
Healthy Environments and Consumer Safety Branch - Direction générale de la santé environnementale et de la sécurité des consommateurs
Health Canada - Santé Canada
Tel: (613) 948-7451 / Tél: (613) 948-7451
Email / Courriel: christine.norman@canada.ca

Chemical Risk Assessment: Traditional vs Public Health Perspectives

Preventing adverse health effects of environmental chemical exposure is fundamental to protecting individual and public health. When done efficiently and properly, chemical risk assessment enables risk management actions that minimize the incidence and effects of environmentally induced diseases related to chemical exposure. However, traditional chemical risk assessment is faced with multiple challenges with respect to predicting and preventing disease in human populations, and epidemiological studies increasingly report observations of adverse health effects at exposure levels predicted from animal studies to be safe for humans. This discordance reinforces concerns about the adequacy of contemporary risk assessment practices for protecting public health.

It is becoming clear that to protect public health more effectively, future risk assessments will need to use the full range of available data, draw on innovative methods to integrate diverse data streams, and consider health endpoints that also reflect the range of subtle effects and morbidities observed in human populations.

Considering these factors, there is a need to reframe chemical risk assessment to be more clearly aligned with the public health goal of minimizing environmental exposures associated with disease. (*Am J Public Health.* 2017;107:1032–1039. doi:10.2105/AJPH.2017.303771)

Maureen R. Gwinn, PhD, Daniel A. Axelrad, MPP, Tina Bahadori, ScD, David Bussard, BA, Wayne E. Cascio, MD, Kacee Deener, MPH, David Dix, PhD, Russell S. Thomas, PhD, Robert J. Kavlock, PhD, and Thomas A. Burke, PhD, MPH

See also Greenberg, p. 1020.

For the past several decades, human health risk assessment has been a pillar of environmental health protection. In general, the products of risk assessment have been numerical risk values derived from animal toxicology studies of observable effects at high doses of individual chemicals. Although this approach has contributed to our understanding of overt health outcomes from chemical exposures, it does not always match our understanding from epidemiology studies of the consequences of real-world exposures in human populations, which are characterized by exposure to multiple pollutants, often chronically, at concentrations that can fluctuate over wide ranges; susceptible populations and life stages; potential interactions between chemicals and nonchemical stressors and background disease states; and lifestyle factors that modify exposures (e.g., airtight houses).[1] These and other issues are particularly important when determining risk of complex diseases, such as cardiovascular disease.

Ten years ago, the National Research Council offered a new paradigm for evaluating the safety of chemicals on the basis of chemical characterization, testing using a toxicity pathway approach, and modeling and extrapolating the dose–response relationship from in vitro testing, all embedded in a risk context and considering population-based data and exposure.[2] Efforts such as the Tox21 Consortium[3,4] and ToxCast program[5] have helped us better understand the biological interactions of large numbers of chemicals using high-throughput assay systems, and we are witnessing early adoption of new technologies and approaches for screening chemicals for integrated testing.[6]

Several other factors are also changing the way environmental health professionals think about chemical risks and how to most effectively protect public health, especially for complex diseases like cardiovascular disease. It is estimated that intrinsic factors (e.g., those that result in mutations stemming from random errors in DNA replication) account for only 10% to 30% of many common cancers.[7] Similarly, only 30% to 40% of birth defects can be attributed to known causes such as genetics, fetal alcohol syndrome, maternal smoking, and folate insufficiency.[8] Other studies have concluded that nongenetic environmental factors and gene by environment interactions are the primary causes of chronic diseases.[9] The ability to evaluate and quantify the role of environmental factors on public health is a clear opportunity, but it is limited by the lack of readily available models for prominent clinical outcomes.

CURRENT CHALLENGES

Understanding public health risk from environmental chemical exposures is complicated by many factors, such as population variability and susceptibility, long latencies between critical exposures and disease manifestations, and background environmental exposures. Issues of population variability and susceptibility are poorly understood and difficult to characterize and incorporate into risk assessments. For example, a person's unique microbiome may modulate his or her response to environmental exposures.[10,11] Although studies are limited in this emerging area, knowledge about the

ABOUT THE AUTHORS

At the time of the writing of this article, all of the authors were with the US Environmental Protection Agency, Washington, DC.

Correspondence should be sent to Maureen R. Gwinn, PhD DABT ATS, Office of Research and Development, US Environmental Protection Agency, 1300 Pennsylvania Ave NW, Ronald Reagan Building, Room 41205, MC 8101R, Washington, DC 20460 (e-mail: gwinn.maureen@epa.gov). Reprints can be ordered at http://www.ajph.org by clicking the "Reprints" link.

This article was accepted March 2, 2017.
doi: 10.2105/AJPH.2017.303771

microbiome may inform inter-individual variability and unexplained susceptibility observed in populations. Scientists have begun to appreciate the role of the microbiome in the lack of reproducibility and interpretability of animal studies.[12]

Another example is the effects of early life environmental exposures on health outcomes later in life. Advances in the field of epigenetics have revealed that developmental exposure to endocrine disrupting chemicals can alter epigenetic programming of gene regulation and thus may play a role in the risk of obesity later in life.[13] Similar to microbiome research, studies in this area are limited, and a better understanding of the link between chemical exposure, epigenetic gene regulation, and health outcomes through epidemiological research can help us better address factors that are currently difficult to account for in traditional risk assessment. Finally, there are also methodological challenges in determining attributable risks in populations with background environmental exposures, as these background exposures may change the population health baselines or affect the response of the target chemical. Other examples of important factors to incorporate in risk assessments can be found in Table 1.

OPPORTUNITIES FOR USING MULTIPLE DATA TYPES

Concurrent with these challenges, science and technology are advancing rapidly and in ways that create opportunities for risk assessment. Public health disciplines help us understand how baseline health status can influence the effect of population-level chemical exposures. We also need to consider how environmental pollutants may contribute to overall disease burden for endpoints not traditionally considered in chemical risk assessment (e.g., metabolic disorders, autism). New methods in epidemiological research help us evaluate complex interactions among multifactorial causes of disease ranging from macro (societal, neighborhood) to micro (molecular) factors, relevance of exposures during sensitive life stages, and a better understanding of interrelatedness of disease across the life span.[14]

Advances in high-throughput technologies and computational modeling (e.g., ToxCast, Tox21, and ExpoCast efforts) are providing data on hazard and exposure potential for a large number of data-poor chemicals. The increased generation of data for both hazard and exposure from these advances can be used to better understand the biological pathways that lead to adverse health effects in ways that were not possible in the past. But linking these observations to specific disease endpoints is challenging because the translation of effects across levels of biological organization is not well understood. One approach with the potential to advance our understanding of how chemical exposures can affect health is the use of adverse outcome pathways, which integrate various types of biological information to link molecular initiating events to downstream key events and ultimately unwanted health outcomes.[15,16]

TABLE 1—Examples of Current Risk Assessment Challenges and Opportunities

Risk Assessment Challenge	Description	Impact on Risk Assessment	Public Health Opportunity
Molecular initiating events and subsequent key events in adverse outcome pathways	Early biological changes or precursor effects in response to chemical exposures may be identified by in vitro, animal, or epidemiological studies	Useful for qualitative and quantitative understanding of ultimate health effect of early biological changes	Improved public health protection without need for long-term toxicology or epidemiology studies
Background exposures	Population exposures to a myriad of environmental chemicals at low concentrations	Exposures to background chemicals may affect response to target chemical exposures and may change population health baselines	Increased public health protection if baseline exposures are taken into account when determining prevention strategies
Nonchemical stressors	Physical and psychosocial stressors, including noise, temperature, socioeconomic status, social stress, and limited resources	Impact on baseline susceptibility and potential effect modification	Potential role in cumulative assessment, improved identification of vulnerable populations, potential target for public health interventions (e.g., stress management)
Early life determinants of health	Biological characteristics and exposures that can determine chronic and lifelong health outcomes	Effect of exposures during early life may play a role in later disease states (e.g., endocrine disruptors, epigenetic changes)	Potential for early life interventions for prevention and management of later disease
Baseline health status	Individual health status, with a focus on potential health susceptibilities	Baseline health status may affect response to additional environmental chemical exposures	Increased public health protection if baseline health status is taken into account
Microbiome	Microorganisms that reside within and on our bodies and interact with the environment	Exposure modification, susceptibility and resilience to environmental pollutants, important as an early life determinant of health	Potential targets for prevention and intervention, management of allergic responses, and precision risk management

To fully realize the potential of adverse outcome pathway–based approaches and to integrate biological findings across disciplines, we must strengthen our ability to detect precursor events in human populations and to identify biologically relevant exposure metrics, ideally measurable in individuals. Another advancement that has a great potential to advance our understanding of data-poor chemicals is the use of nontesting approaches (e.g., quantitative structure–activity relationship) that allow us to predict toxicity when adequate testing data are absent—especially when we combine knowledge of chemical structural features and in vitro bioactivity determinations. Advances in the development of chemical libraries, cheminformatics, and read-across predictions and integration with molecular data and adverse outcome pathways have significantly improved their application and predictive capacity, which will allow more comprehensive assessment of the health effects of exposures.[17,18]

Effectively predicting population risk by integrating a variety of data streams (e.g., epidemiology, toxicology, high-throughput testing) and considering multiple sources and pathways of exposure can better inform environmental public health decisions. Advances in technology and computational capabilities have fostered new opportunities for generating and analyzing molecular, animal, and human data on effects and exposures, which can be integrated

TABLE 2—Data Streams and Opportunities and Challenges for Informing Risk Assessment

Data Type	Description	Opportunity	Challenge
Nontesting data	Nontesting approaches, such as quantitative structure–activity relationship models and read-across allow us to predict toxicity when adequate testing data are absent	Advances in the field have significantly improved their application and predictive capacity	Developing principles for acceptance, for characterizing and incorporating uncertainties into predictions, and for developing objective metrics of performance
Molecular	Biochemical and cell-based bioactivity data and "omics-based" data on thousands of chemicals	Can help inform our understanding of the health outcomes of environmental exposures, using data that are potentially more human relevant	Lack of scientific consensus on inferring hazard from bioactivity in vitro assay and omics-based data and providing quantitative dose–response information on exposure metrics
Animal	Traditional animal testing provides a hazard based point of departure for risk assessments	Targeted animal testing can be performed on the basis of the results of bioactivity data to focus on key health outcomes	Potential uncertainties with using traditional animal testing to estimate human risk (e.g., extrapolating from animal to human or high to low doses and accounting for human population variability and life stage susceptibility)
Human	Epidemiological and other human data support holistic assessment of the effects of chemical exposures on public health	Newer exposure science and statistical techniques advance the understanding of human variability that can be obtained from epidemiology and individual sequencing; understanding effect modification by nonchemical stressors and baseline health status	Often limited mechanistic and dose–response data, and exposure misclassification can bias results to the null; possibility of unmeasured confounders often undermines confidence in observed associations, and it may require multiple studies and many years to rule out chance, bias, and confounding as possible explanations for observed associations
Exposure	Exposure characterization that captured the variability in time, space, and within and across populations; better toxicokinetic data link external to internal dosimetry and relevant environmental exposure concentrations with biological significance	Targeted and nontargeted biomonitoring, application of sensors, and other new technologies are greatly advancing population exposure characterization; high-throughput exposure models allow exposure predictions on thousands of chemicals with associated uncertainty	Estimating and incorporating the inter- and intraindividual variability in exposures into current designs of toxicity testing and risk assessments; extrapolating relevant target tissue and organ dose information from external exposures and in vitro assays; accounting for multiple exposures; sample collection, data management, and analysis; and covering or extrapolating to a broader chemical space
Digital data	The ongoing revolution in social media use and communication has provided a new source of data used in exposure science and environmental epidemiology for local and timely information about disease and health dynamics	A significant source of untapped data	The collection and application of these data have significant ethical implications that need to be understood and managed, particularly taking into account personal identifiable information; methods to evaluate the quality of the data and build confidence in the applications are needed

into chemical risk assessments. At the same time, probabilistic and high-throughput approaches for risk assessment have been advancing. Table 2 highlights various data types available and challenges in applying these data types to inform risk assessment.

A PUBLIC HEALTH PERSPECTIVE

A public health perspective for chemical risk assessment would approach risk assessment from a new lens. It would address population health with a focus on the health and societal burden of disease; use and integrate all available types of data—including traditional toxicology, human epidemiological findings, and newer and emerging data streams and information, such as digital epidemiology,[19] high-throughput and high-content data, and adverse outcome pathways; and draw on public health approaches, such as attributable risk or relative risk. This new perspective may be especially important for some historically challenging aspects of risk assessment, such as understanding cumulative risks of exposures to multiple chemical and nonchemical stressors. Internationally, scientists have raised concerns about the large number of ubiquitous chemicals people are exposed to and called for rethinking approaches to evaluating the health effects of chemicals.[16] Figure 1 presents a conceptual model for a public health perspective for risk assessment.

Although approaching assessments from the perspective of health outcomes may be challenging, it provides the opportunity to evaluate exposures and effects across the life span that are relevant to population health. Advances in science and technology, such as adverse outcome pathway development, the broader availability of chemical and biological data, and the applications of statistical and bioinformatics tools, bring this previously aspirational approach well within reach.[20]

EXAMPLE: CARDIOVASCULAR DISEASE

A public health approach may inform the challenge of cardiovascular disease. Cardiovascular disease is the number 1 cause of mortality worldwide and is a major US public health burden.[21,22] Annual costs of cardiovascular disease in the United States were estimated to be $317 billion in 2011 and 2012, considering direct medical costs and lost productivity because of premature mortality.[22] This estimate is likely to substantially underestimate the social cost of cardiovascular disease because of limitations in the estimation of indirect costs associated with morbidity and premature mortality.[23]

Although much is known about the biochemical and behavioral risk factors associated with cardiovascular disease, particularly compared with other diseases and health conditions, the traditional risk factors fail to account for 10% to 25% of its prevalence.[24] Environmental factors, including air pollution[25] and chemical exposures[26] are thought to contribute to the unexplained fraction. Although mortality stemming from cardiovascular disease has decreased over the past few decades in the developed world as a result of reductions in behavioral risk factors, the rising prevalence of obesity and diabetes might account for the deceleration in the rate of improvement in annual cardiovascular mortality in the United States over the past few years.[27]

There is an urgent need to better understand the biological pathways through which environmental exposures to chemical and nonchemical stressors act to stimulate and accelerate atherosclerosis and promote adverse cardiovascular health effects. Applying the adverse outcome pathway framework,[28] the initial molecular response to a chemical exposure will often be receptor

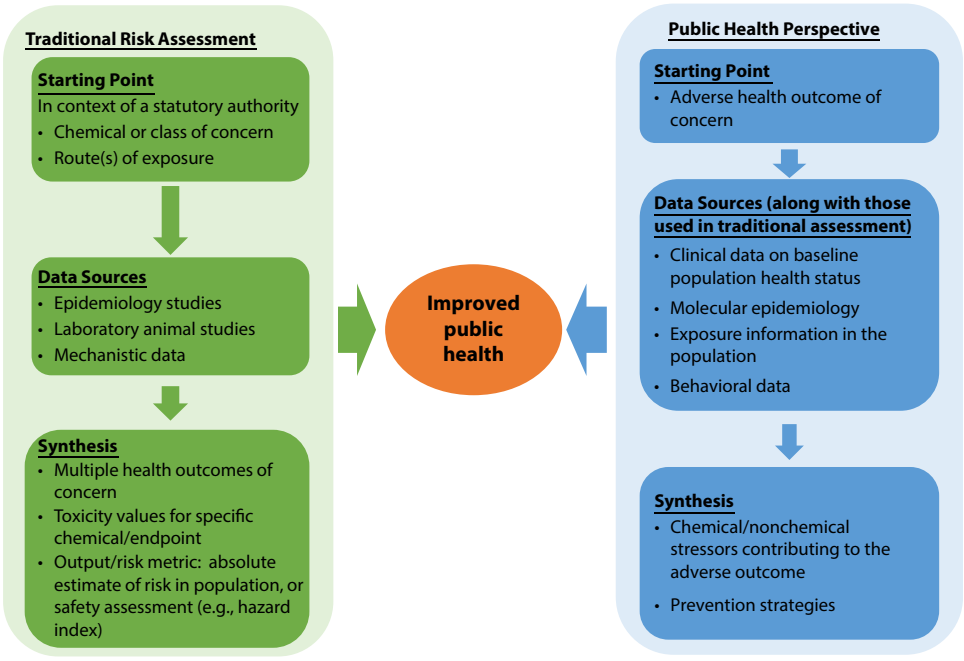

Note. This conceptual model illustrates how the starting point in a public health–focused risk assessment would differ from that of traditional risk assessment. In traditional risk assessment, the starting point is focused on specific chemicals or classes of chemicals of concern, with multiple data streams saying what the critical effects from that chemical are. A public health perspective would focus on the adverse health outcome of concern with multiple data streams, informing our understanding of hazard and exposure in the context of public health decisions related to that outcome and not necessarily focused on just 1 chemical or class of chemicals.

FIGURE 1—Conceptual Model for a Public Health Perspective for Chemical Risk Assessment

activation and changes in metabolism and, ultimately, changes in tissue and organ function. Such changes can be modified by both intrinsic (e.g., gender, age, genetic, and epigenetic background) and extrinsic factors (e.g., coexposures to other chemical and nonchemical stressors; Figure 2). Over time, these changes produce subclinical effects, such as changes in electrical and mechanical cardiac function, vascular function, and nonobstructive atherosclerotic vascular changes. With the persistence of metabolic changes that stimulate the progression of vascular disease, clinical cardiovascular events such as heart attacks, strokes, heart failure, and abnormal heart rhythms follow.

To date, the most comprehensive application of this approach has been in the study of population-level health effects of air pollution exposure.[28] Epidemiological data at the population level has provided support that air pollutant exposure (e.g., ambient particular matter and NO_2) accelerates the development and progression of coronary atherosclerosis.[25] Xenobiotic metals such as arsenic, cadmium, lead, and mercury are also associated with atherosclerosis.[29] Gene–environment interaction alters the risk of vascular disease[30]; for example, the residential proximity to highways (representing exposure to a mixture of traffic-related air pollutants) is associated with peripheral vascular disease, which is modified by the gene encoding bone morphogenic protein.[7,31]

Because of the complexity of the drivers of atherosclerosis, a medical model treating blood pressure and high cholesterol and advising dietary modification and exercise will be inadequate to fully address this disease. Likewise, identifying the chemicals that increase risk on an individual basis will be inadequate to prevent vascular disease. Instead an integrated systems approach is

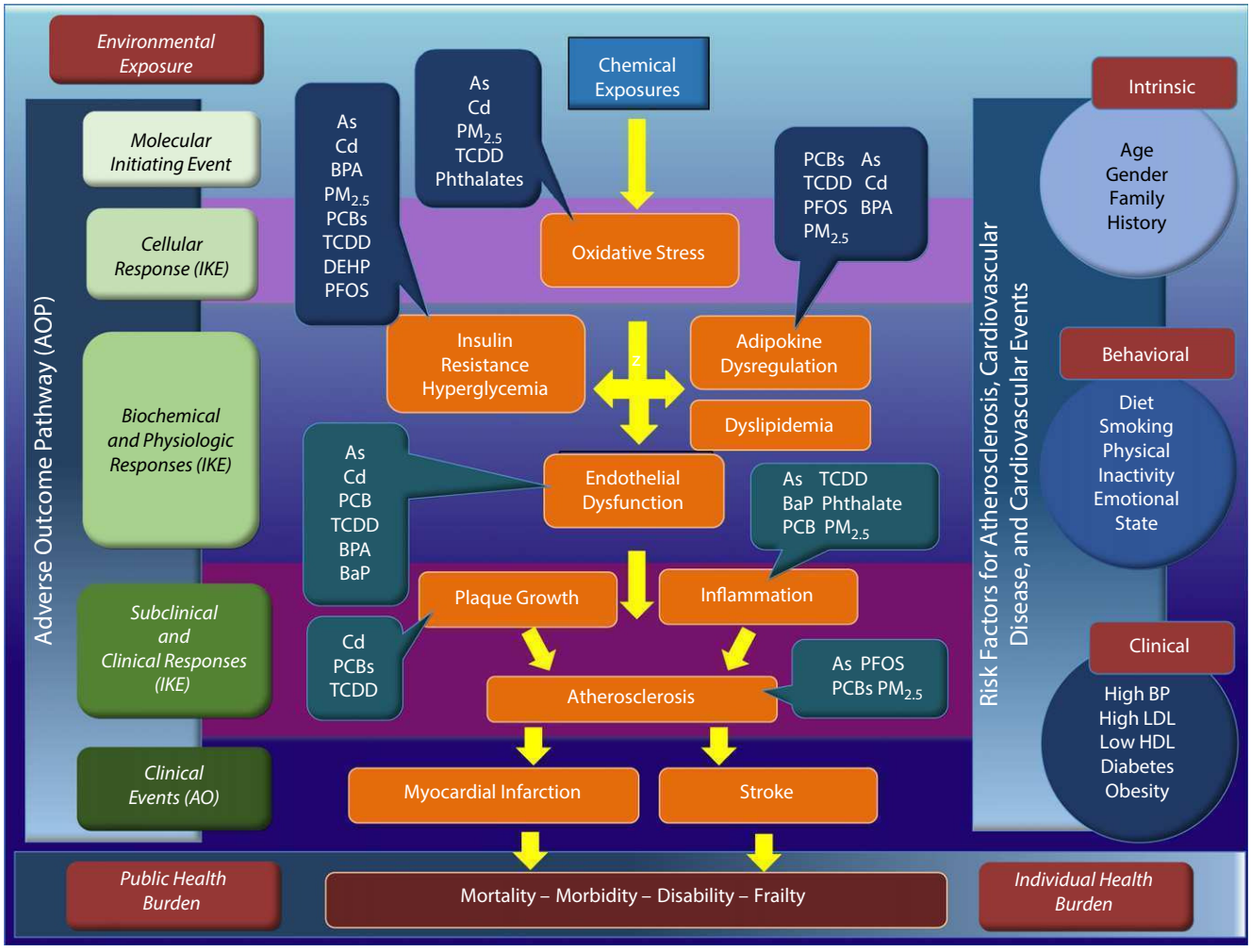

Source. Action of specific chemicals and metals adapted from Kirkley and Sargis.[26]

Note. As = Arsenic; AO = adverse outcome; BaP = benzo[a]pyrene; BPA = bisphenol A; Cd = Cadmium; DEHP = di(2-ethylhexyl) phthlate; DES = diethylstilbestrol; HDL = high-density lipoprotein; IKE = intermediate key event; LDL = low-density lipoprotein; PCB = polychlorinated biphenyl; PFOS = perfluorooctane sulfonic acid; $PM_{2.5}$ = particulate matter ≤ 2.5 μm; TCDD = tetrachlorodibenzo-p-dioxin. This figure illustrates the biological pathway leading from exposure to adverse cardiovascular outcomes for a variety of chemicals. On the left-hand side of the figure these pathways are linked to the adverse outcome pathway, and on the right-hand side of the figure we see the traditional risk factors for adverse cardiovascular outcomes.

FIGURE 2—Adverse Outcome Pathway for Cardiovascular Outcomes

needed to fully account for all known risk factors and formulate the problem to define the most effective strategy to decrease individual risk and societal burden. Accomplishing this will require clinical data that fully reflect a population under consideration as well as exposures to traditional risk factors, biomonitoring data documenting exposures to multiple chemicals, and molecular responses from in vitro and in vivo studies indicative of the activation of biochemical pathways that accelerate atherosclerosis.

Although this approach might not be practical currently, it is not unrealistic to think about future states where it could become standard practice. Our proposed innovative approach to chemical risk assessment is occurring contemporaneously during the formative stages of the National Institutes of Health–sponsored Precision Medicine Initiative, which will drive integration of genomics, data sciences, and bioinformatics as the basis for improved individual health care, disease prevention, and public health. The Affordable Care Act has accelerated electronic medical record adoption in health care practices and hospital systems, potentially offering a valuable source of information for population-level health monitoring. Recent research has used big data to study the early stages of disease and better classify and predict disease progression and could be used to inform personalized medicine to optimize wellness in healthy populations.[32–34]

Moreover, the anticipated integration and development of technologies and analytical tools have the potential to improve public health and increase the spatial and temporal resolution of environmental health surveillance. The establishment of a long-term representative precision medicine cohort, if integrated with the proposed National Biomonitoring Network,[35] could have enormous benefit in helping us understand the relationship between chemical exposures and disease and in managing some of the most challenging clinical problems more effectively.

Applying this framework would potentially expand our understanding of the origins of vascular disease and its progression, helping define strategies for primary prevention to thwart the initiation of the process we ultimately call atherosclerosis. Thus, such a framework would provide new and ongoing insights into the associations between environmental exposures that contribute the greatest burden to public health. This approach would facilitate accounting for sensitive populations and could inform suggested individual health or behavioral measures in which there have been past exposures or in which current exposure cannot be reduced enough to protect those most at risk.

CONCLUSIONS

The proposed conceptual model is grounded in public health principles and focused on identifying the greatest opportunity to reduce environmental exposures to improve health outcomes. Along with traditional risk assessment, this perspective can better inform public health decision-making. Although there are clear benefits to operating within a public health–focused framework and moving away from individual chemicals and apical endpoints, there are also challenges.

Informing Decision-Making

Since the 1980s, the Environmental Protection Agency's decision-making has been grounded on traditional risk assessments that are conducted within the constraints of the Environmental Protection Agency's statutes and programs. Although program-targeted risk assessments will remain an important component, the disease-based approach draws on information in a holistic fashion that cuts across organizational and legal boundaries, integrating traditional inputs and newer data streams. These assessments will provide decision-makers with critical information to inform exposure-reduction efforts to affect the selected health outcomes and, ultimately, improve public health. Because those exposure-reduction efforts would take place within the existing statutory construct, an important implementation step would be to move from findings of disease-based risk assessments to assessments of specific risk management actions under the relevant statutory authorities.

Priorities for Screening and Testing

A health outcome–focused framework can inform priorities for screening and testing the toxicity of chemicals. Efforts to develop and synthesize approaches for screening large numbers of chemicals using high-throughput toxicity testing and exposure prediction should continue to provide data for data-poor chemicals. For example, in the recently announced Cancer Moonshot,[36] high-throughput approaches could screen a large set of chemicals for potential carcinogenicity and identify a suite of chemicals for additional animal toxicity testing.

Examining noncancer endpoints will also be challenging, which is why developing adverse outcome pathways and networks to contextualize and interpret nonapical hazard data in relation to population health is of increasing value. Epidemiology studies can be designed to inform and validate high-throughput testing approaches by identifying both chemical stressors and nonchemical stressors that modify responses to chemical exposures; they can also be designed to test relationships between disease and early markers of exposure and biological response (e.g., epigenetic changes).

The Impact of Cumulative Exposures

Although cumulative risk assessment has been of high interest for the past few decades, putting cumulative assessment approaches into practice has been challenging. This framework provides a new construct for considering cumulative risk. By focusing on a health endpoint of concern, one could consider the multiple exposures that may contribute to a health outcome. Past National Research Council recommendations have encouraged assessors to evaluate the combined effects of exposures to all chemicals that affect a common adverse outcome, for example, male reproductive development.[37] Challenges include gaining adequate understanding of individual chemical effects to group chemicals by health outcome. Increased research into the biological pathways by which chemicals affect health status can help inform approaches for estimating the joint effect of chemicals without

testing all permutations or combinations.

One example of an alternative approach is health impact assessment, which uses a systems approach to array data sources and analytic methods and considers input from stakeholders to determine potential effects of a proposed action or decision on the health of a population and the distribution of those effects in the population.[38] Using health impact assessment approaches for chemical risk assessments made through this framework can offer a method to organize various data streams that can influence our understanding of a health effect, inform potential multiple contributors to adverse health outcomes, and provide recommendations to decision-makers for monitoring and managing these outcomes.

Consider Public Health Concepts

This new approach takes a systematic view of collective factors that contribute to a health outcome or disease state, including those that are not regulated by a single federal entity. Any single health outcome may be influenced by multiple factors beyond chemical exposures, such as nutrition, genetics, and social stressors. Because those factors are not regulated, it is important for environmental regulatory agencies to understand what fraction of the disease burden is influenced by the regulated environmental exposure.

Public health approaches, such as attributable risk, can help inform this understanding. Challenges may include incorporating these approaches, which are typically used in epidemiology, to animal and advanced toxicity testing data; ensuring adequate training with the approaches; and communicating risk in a way that acknowledges the influence of nonregulated factors.

Public Health Implications

Understanding the health effects of chemicals has real implications for public health. This proposed approach for chemical risk assessment starts at the health endpoint and incorporates multiple data streams, including data developed using newer technologies such as high-throughput screening. In parallel with more traditional risk assessment approaches, this will lead to a better understanding of mechanisms of single chemicals as well as cumulative exposures that lead to specific disease endpoints.

This new lens will need to be applied to the complete risk assessment process—problem formulation, data considerations, and data synthesis through multipathway methods, including cumulative assessment and health impact assessment—with an eye to the prevention of adverse effects. This approach draws on the best available science to improve our understanding of the health effects of environmental chemicals and informs decision-making to prevent, reduce, or mitigate exposure and ultimately improve public health. AJPH

CONTRIBUTORS

M. R. Gwinn led the compilation of text and revisions of the article. M. R. Gwinn and K. Deener led creation of Figure 1. M. R. Gwinn, K. Deener, and R. J. Kavlock led the creation of Table 1. D. A. Axelrad, T. Bahadori, D. Bussard, R. S. Thomas, and R. J. Kavlock led the drafting of text on challenges and opportunities. T. Bahadori, R. S. Thomas, and R. J. Kavlock led the creation of Table 2. W. E. Cascio led the creation of Figure 2. W. E. Cascio and K. Deener led the drafting of text on public health. R. J. Kavlock and T. A. Burke led the discussions and outlined the article. All authors contributed to discussions of the concepts behind this article and contributed text to the various sections.

ACKNOWLEDGMENTS

The authors would like to acknowledge the assistance of Laura Romano in preparing the article.

Note. The views expressed in this article are those of the authors and do not necessarily reflect the views or policies of the US Environmental Protection Agency.

REFERENCES

1. Birnbaum LS, Burke TA, Jones JJ. Informing 21st-century risk assessments with 21st-century science. *Environ Health Perspect*. 2016;124(4):A60–A63.

2. National Research Council. *Toxicity Testing in the 21st Century: A Vision and a Strategy*. Washington, DC: National Academies Press; 2007.

3. Kavlock RJ, Austin CP, Tice RR. Toxicity testing in the 21st century: implications for human health risk assessment. *Risk Anal*. 2009;29(4):485–487; discussion 492–497. [Comment on Toxicity testing in the 21st century: implications for human health risk assessment. *Risk Anal*. 2009]

4. Tice RR, Austin CP, Kavlock RJ, Bucher JR. Improving the human hazard characterization of chemicals: a Tox21 update. *Environ Health Perspect*. 2013; 121(7):756–765.

5. Kavlock R, Chandler K, Houck K, et al. Update on EPA's ToxCast program: providing high throughput decision support tools for chemical risk management. *Chem Res Toxicol*. 2012;25(7):1287–1302.

6. Browne P, Judson RS, Casey WM, Kleinstreuer NC, Thomas RS. Screening chemicals for estrogen receptor bioactivity using a computational model. *Environ Sci Technol*. 2015;49(14):8804–8814.

7. Wu S, Powers S, Zhu W, Hannun YA. Substantial contribution of extrinsic risk factors to cancer development. *Nature*. 2016;529(7584):43–47.

8. Weinhold B. Environmental factors in birth defects: what we need to know. *Environ Health Perspect*. 2009;117(10): A440–A447.

9. Rappaport SM, Barupal DK, Wishart D, Vineis P, Scalbert A. The blood exposome and its role in discovering causes of disease. *Environ Health Perspect*. 2014;122(8):769–774.

10. Dietert RR, Silbergeld EK. Biomarkers for the 21st century: listening to the microbiome. *Toxicol Sci*. 2015;144(2): 208–216.

11. Patterson AD, Turnbaugh PJ. Microbial determinants of biochemical individuality and their impact on toxicology and pharmacology. *Cell Metab*. 2014; 20(5):761–768.

12. Servick K. Of mice and microbes. *Science*. 2016;353(6301):741–743.

13. Stel J, Legler J. The role of epigenetics in the latent effects of early life exposure to obesogenic endocrine disrupting chemicals. *Endocrinology*. 2015;156(10): 3466–3472.

14. Buck Louis GM, Bloom MS, Gatto NM, Hogue CR, Westreich DJ, Zhang C. Epidemiology's continuing contribution to public health: the power of "then and now." *Am J Epidemiol*. 2015;181(8): e1–e8.

15. Ankley GT, Bennett RS, Erickson RJ, et al. Adverse outcome pathways: a conceptual framework to support ecotoxicology research and risk assessment. *Environ Toxicol Chem*. 2010;29(3):730–741.

16. Goodson WH III, Lowe L, Carpenter DO, et al. Assessing the carcinogenic potential of low-dose exposures to chemical mixtures in the environment: the challenge ahead. *Carcinogenesis*. 2015; 36(suppl 1):S254–S296.

17. Mansouri K, Abdelaziz A, Rybacka A, et al. CERAPP: Collaborative Estrogen Receptor Activity Prediction Project. *Environ Health Perspect*. 2016;124(7): 1023–1033.

18. Judson R, Houck K, Martin M, et al. Analysis of the effects of cell stress and cytotoxicity on in vitro assay activity across a diverse chemical and assay space. *Toxicol Sci*. 2016;153(2):409. [Erratum in Analysis of the effects of cell stress and cytotoxicity on in vitro assay activity across a diverse chemical and assay space. *Toxicol Sci*. 2016]

19. Bakker KM, Martinez-Bakker ME, Helm B, Stevenson TJ, et al. Digital epidemiology reveals global childhood disease seasonality and the effects of immunization. *Proc Natl Acad Sci USA*. 2016; 113(24):6689–6694.

20. National Academies of Sciences, Engineering, and Medicine. *Using 21st Century Science to Improve Risk-Based Evaluations*. Washington, DC: National Academies Press; 2017.

21. Moran AE, Forouzanfar MH, Roth GA, et al. Temporal trends in ischemic heart disease mortality in 21 world regions, 1980 to 2010: the Global Burden of Disease 2010 study. *Circulation*. 2014; 129(14):1483–1492.

22. Mozaffarian D, Benjamin EJ, Go AS, et al. Heart disease and stroke statistics—2016 update: a report from the American Heart Association. *Circulation*. 2016; 133(4):e38–e360.

23. US Environmental Protection Agency. *Guidelines for Preparing Economic Analyses*. Washington, DC; 2010.

24. Kannel WB, Vasan RS. Adverse consequences of the 50% misconception. *Am J Cardiol*. 2009;103(3):426–427.

25. Kaufman JD, Adar SD, Barr RG, et al. Association between air pollution and

coronary artery calcification within six metropolitan areas in the USA (the Multi-Ethnic Study of Atherosclerosis and Air Pollution): a longitudinal cohort study. *Lancet*. 2016;388(10045): 696–704.

26. Kirkley AG, Sargis RM. Environmental endocrine disruption of energy metabolism and cardiovascular risk. *Curr Diab Rep*. 2014;14(6):494.

27. Sidney S, Quesenberry CP Jr, Jaffe MG, et al. Recent trends in cardiovascular mortality in the United States and public health goals. *JAMA Cardiol*. 2016; 1(5):594–599.

28. Cosselman KE, Navas-Acien A, Kaufman JD. Environmental factors in cardiovascular disease. *Nat Rev Cardiol*. 2015;12(11):627–642.

29. Solenkova NV, Newman JD, Berger JS, et al. Metal pollutants and cardiovascular disease: mechanisms and consequences of exposure. *Am Heart J*. 2014; 168(6):812–822.

30. Zanobetti A, Baccarelli A, Schwartz J. Gene-air pollution interaction and cardiovascular disease: a review. *Prog Cardiovasc Dis*. 2011;53(5):344–352.

31. Ward-Caviness CK, Neas LM, Blach C, et al. Genetic variants in the bone morphogenic protein gene family modify the association between residential exposure to traffic and peripheral arterial disease. *PLoS One*. 2016;11(4):e0152670.

32. Dinov ID, Heavner B, Tang M, et al. Predictive big data analytics: a study of Parkinson's disease using large, complex, heterogeneous, incongruent, multisource and incomplete observations. *PLoS One*. 2016;11(8):e0157077.

33. Hood L, Lovejoy JC, Price ND. Integrating big data and actionable health coaching to optimize wellness. *BMC Med*. 2015;13:4.

34. Khoury MJ, Evans JP. A public health perspective on a national precision medicine cohort: balancing long-term knowledge generation with early health benefit. *JAMA*. 2015;313(21): 2117–2118.

35. Association of Public Health Laboratories. *National Biomonitoring Plan*. Silver Spring, MD; 2015.

36. Mitchell E. Moonshot toward a cure for cancer. *J Natl Med Assoc*. 2016;108(2): 104–105.

37. National Research Council. *Phthalates and Cumulative Risk Assessment: The Tasks Ahead*. Washington, DC: National Academies Press; 2008.

38. National Research Council. *Improving Health in the United States: The Role of Health Impact Assessment*. Washington, DC: National Academies Press; 2011.

This article has been cited by:

1. Susanna H. Wegner, Caroline L. Pinto, Caroline L. Ring, John F. Wambaugh. 2020. High-throughput screening tools facilitate calculation of a combined exposure-bioactivity index for chemicals with endocrine activity. *Environment International* **137**, 105470. [Crossref]
2. Nur H. Orak, Mitchell J. Small, Marek J. Druzdzel. 2019. Bayesian network-based framework for exposure-response study design and interpretation. *Environmental Health* **18**:1. . [Crossref]
3. Keely Maxwell, Bryan Hubbell, Emily Eisenhauer. 2019. Institutional insights on integrating social and environmental science for solutions-driven research. *Environmental Science & Policy* **101**, 97-105. [Crossref]
4. Sean Watford, Stephen Edwards, Michelle Angrish, Richard S. Judson, Katie Paul Friedman. 2019. Progress in data interoperability to support computational toxicology and chemical safety evaluation. *Toxicology and Applied Pharmacology* **380**, 114707. [Crossref]
5. R.R. Boyles, A.E. Thessen, A. Waldrop, M.A. Haendel. 2019. Ontology-based data integration for advancing toxicological knowledge. *Current Opinion in Toxicology* **16**, 67-74. [Crossref]
6. Annie von Eyken, Daniel Furlong, Samareh Arooni, Fred Butterworth, Jean-François Roy, Jerry Zweigenbaum, Stéphane Bayen. 2019. Direct injection high performance liquid chromatography coupled to data independent acquisition mass spectrometry for the screening of antibiotics in honey. *Journal of Food and Drug Analysis* **27**:3, 679-691. [Crossref]
7. Marissa B. Kosnik, David M. Reif. 2019. Determination of chemical-disease risk values to prioritize connections between environmental factors, genetic variants, and human diseases. *Toxicology and Applied Pharmacology* 114674. [Crossref]
8. Hanna K.L. Johansson, Julie Boberg, Marianne Dybdahl, Marta Axelstad, Anne Marie Vinggaard. 2019. Chemical risk assessment based on in vitro and human biomonitoring data: A case study on thyroid toxicants. *Current Opinion in Toxicology* **15**, 8-17. [Crossref]
9. Philippe Grandjean. 2018. Delayed discovery, dissemination, and decisions on intervention in environmental health: a case study on immunotoxicity of perfluorinated alkylate substances. *Environmental Health* **17**:1. . [Crossref]
10. Axel Mie, Christina Rudén, Philippe Grandjean. 2018. Safety of Safety Evaluation of Pesticides: developmental neurotoxicity of chlorpyrifos and chlorpyrifos-methyl. *Environmental Health* **17**:1. . [Crossref]
11. Kathleen C. Deener, Jason D. Sacks, Ellen F. Kirrane, Barbara S. Glenn, Maureen R. Gwinn, Thomas F. Bateson, Thomas A. Burke. 2018. Epidemiology: a foundation of environmental decision making. *Journal of Exposure Science & Environmental Epidemiology* **28**:6, 515-521. [Crossref]
12. Esben Budtz-Jørgensen, Philippe Grandjean. 2018. Application of benchmark analysis for mixed contaminant exposures: Mutual adjustment of perfluoroalkylate substances associated with immunotoxicity. *PLOS ONE* **13**:10, e0205388. [Crossref]
13. Sean M. Watford, Rachel G. Grashow, Vanessa Y. De La Rosa, Ruthann A. Rudel, Katie Paul Friedman, Matthew T. Martin. 2018. Novel application of normalized pointwise mutual information (NPMI) to mine biomedical literature for gene sets associated with disease: Use case in breast carcinogenesis. *Computational Toxicology* **7**, 46-57. [Crossref]
14. Lesa L. Aylward. 2018. Integration of biomonitoring data into risk assessment. *Current Opinion in Toxicology* **9**, 14-20. [Crossref]
15. Bernard D. Goldstein. 2018. Solution-focused risk assessment. *Current Opinion in Toxicology* **9**, 35-39. [Crossref]
16. Han Li, Siliang Yuan, Guanyong Su, Meng Li, Qiangwei Wang, Guonian Zhu, Robert J. Letcher, Yufei Li, Zhihua Han, Chunsheng Liu. 2017. Whole-Life-Stage Characterization in the Basic Biology of Daphnia magna and Effects of TDCIPP on Growth, Reproduction, Survival, and Transcription of Genes. *Environmental Science & Technology* **51**:23, 13967-13975. [Crossref]
17. Philippe Grandjean, Martine Bellanger. 2017. Calculation of the disease burden associated with environmental chemical exposures: application of toxicological information in health economic estimation. *Environmental Health* **16**:1. . [Crossref]
18. Michael R. Greenberg. 2017. Risk Analysis in the 21st Century: Adapting to New Challenges and Opportunities. *American Journal of Public Health* **107**:7, 1020-1021. [Citation] [Full Text] [PDF] [PDF Plus]
19. Carol Jagger. 2017. Educational Disparities in Adult Disability: Person, Place, Policies, and Family. *American Journal of Public Health* **107**:7, 1021-1022. [Citation] [Full Text] [PDF] [PDF Plus]

April 30, 2020

Subject: Record of Percentage Agreement (Maureen R. Gwinn)

From: David A. Bussard
ORD-OSAPE

STAA Nomination by Maureen Gwinn: Risk Analysis in the 21st Century: Adapting to New Challenges and Opportunities

Nominated Publication: Chemical Risk Assessment: Traditional vs Public Health Perspectives

I agree with my designated percentage of contribution to this project as listed below.

M. Gwinn – 12%
K. Deener – 12%
T. Burke – 12%
R. Kavlock -12%
W. Cascio – 10%
T. Bahadori – 10%
R. Thomas – 10%
D. Bussard – 10%
D. Axelrad – 10%
D. Dix - 2%

From: Deener, Kathleen
To: Gwinn, Maureen
Subject: RE: STAA questions - please confirm via email on percentage of effort
Date: Thursday, April 30, 2020 11:02:39 AM

Subject: Record of Percentage Agreement (Maureen R. Gwinn)

Kacee Deener
ORD-OSAPE
STAA Nomination by Maureen Gwinn: Risk Analysis in the 21st Century: Adapting to New Challenges and Opportunities
Nominated Publication: Chemical Risk Assessment: Traditional vs Public Health Perspectives

I agree with my designated percentage of contribution to this project as listed below.

Kacee Deener, MPH
Deputy Director, Office of Science Advisor, Policy and Engagement
Office of Research and Development
US Environmental Protection Agency
(ph) 202.564.1990 | (mobile) 202.510.1490
deener.kathleen@epa.gov

From: Gwinn, Maureen <gwinn.maureen@epa.gov>
Sent: Thursday, April 30, 2020 10:56 AM
To: Axelrad, Daniel <Axelrad.Daniel@epa.gov>; Cascio, Wayne <Cascio.Wayne@epa.gov>; Deener, Kathleen <Deener.Kathleen@epa.gov>; Bahadori, Tina <Bahadori.Tina@epa.gov>; Bussard, David <Bussard.David@epa.gov>; Thomas, Russell <Thomas.Russell@epa.gov>; tburke1@jhu.edu; Robert Kavlock <rkavlock@icloud.com>
Subject: STAA questions - please confirm via email on percentage of effort
Importance: High

Hi team –

Working on the STAA Submission, and didn't realize we needed this for the submission. Can you please confirm your agreement with the percentage of effort for your role in this publication? I am not sure what to do about David Dix as I have no contact information, but we'll do our best. Also, if you have any preference on how your name should be on the citation (e.g., Kathleen v Kacee?, include middle initial?, specific salutation?) please let me know.

Sorry for the last minute!

The form of your response should look as follows (using myself as an example):

Subject: Record of Percentage Agreement (Maureen R. Gwinn)

Maureen R. Gwinn
ORD-CCTE
STAA Nomination by Maureen Gwinn: Risk Analysis in the 21st Century: Adapting to New Challenges and Opportunities
Nominated Publication: Chemical Risk Assessment: Traditional vs Public Health Perspectives

I agree with my designated percentage of contribution to this project as listed below.

Proposed record of agreement (truly a team effort!):

M. Gwinn – 12%
K. Deener – 12%
T. Burke – 12%
R. Kavlock -12%
W. Cascio – 10%
T. Bahadori – 10%
R. Thomas – 10%
D. Bussard – 10%
D. Axelrad – 10%
D. Dix - 2%

Details from the STAA guidance is also below.

- Record of Percentage Agreement: The nomination package must include a Record of Percentage Agreement document from each author listed on the nomination form. This document may be submitted in the form of an e-mail or signed letter, which states that the co-author agrees with the total percentage of effort listed beside his or her name entered in the nomination form. The document should list "Record of Percentage Agreement" in the subject line, followed by the coauthor's first and last name. The body of the document should contain the co-author's name and organization, the nominee's name, the title(s) of the nominated publication(s), and a brief statement that the author agrees with his or her designated percentage of contribution. (Note: A Record of Percentage Agreement document is required for single-author nominations.)

Thanks!

Maureen

Maureen R. Gwinn, PhD DABT ATS
Division Director
Biomolecular and Computational Toxicology Division
Center for Computational Toxicology and Exposure
Office of Research and Development
US Environmental Protection Agency
109 TW Alexander Drive MC D-143-02
Durham, NC 27711

Office: 919-541-3794

Cell: 703-434-9093

From:	Gwinn, Maureen
To:	Axelrad, Daniel; Cascio, Wayne; Deener, Kathleen; Bahadori, Tina; Bussard, David; Thomas, Russell; tburke1@jhu.edu; Robert Kavlock
Subject:	STAA questions - please confirm via email on percentage of effort
Date:	Thursday, April 30, 2020 10:55:00 AM
Attachments:	AJPH - STAA justification_Clean_4.29.2020 final v2.docx
Importance:	High

Hi team –

Working on the STAA Submission, and didn't realize we needed this for the submission. Can you please confirm your agreement with the percentage of effort for your role in this publication? I am not sure what to do about David Dix as I have no contact information, but we'll do our best. Also, if you have any preference on how your name should be on the citation (e.g., Kathleen v Kacee?, include middle initial?, specific salutation?) please let me know.

Sorry for the last minute!

The form of your response should look as follows (using myself as an example):

> Subject: Record of Percentage Agreement (Maureen R. Gwinn)
>
> Maureen R. Gwinn
> ORD-CCTE
> STAA Nomination by Maureen Gwinn: Risk Analysis in the 21st Century: Adapting to New Challenges and Opportunities
> Nominated Publication: Chemical Risk Assessment: Traditional vs Public Health Perspectives
>
> I agree with my designated percentage of contribution to this project as listed below.

Proposed record of agreement (truly a team effort!):

M. Gwinn – 12%
K. Deener – 12%
T. Burke – 12%
R. Kavlock -12%
W. Cascio – 10%
T. Bahadori – 10%
R. Thomas – 10%
D. Bussard – 10%
D. Axelrad – 10%
D. Dix - 2%

Details from the STAA guidance is also below.

- Record of Percentage Agreement: The nomination package must include a Record of Percentage Agreement document from each author listed on the nomination form. This document may be submitted in the form of an e-mail or signed letter, which states that the co-author agrees with

the total percentage of effort listed beside his or her name entered in the nomination form. The document should list “Record of Percentage Agreement” in the subject line, followed by the coauthor’s first and last name. The body of the document should contain the co-author’s name and organization, the nominee’s name, the title(s) of the nominated publication(s), and a brief statement that the author agrees with his or her designated percentage of contribution. (Note: A Record of Percentage Agreement document is required for single-author nominations.)

Thanks!

Maureen

Maureen R. Gwinn, PhD DABT ATS
Division Director
Biomolecular and Computational Toxicology Division
Center for Computational Toxicology and Exposure
Office of Research and Development
US Environmental Protection Agency
109 TW Alexander Drive MC D-143-02
Durham, NC 27711

Office: 919-541-3794
Cell: 703-434-9093

From: Robert Kavlock
To: Gwinn, Maureen
Subject: Re: STAA questions - please confirm via email on percentage of effort
Date: Thursday, April 30, 2020 11:29:06 AM

I confirm the percentage effort.

Sent from my iPad

> On Apr 30, 2020, at 10:56 AM, Gwinn, Maureen <gwinn.maureen@epa.gov> wrote:
>
> Hi team –
>
> Working on the STAA Submission, and didn't realize we needed this for the submission. Can you please confirm your agreement with the percentage of effort for your role in this publication? I am not sure what to do about David Dix as I have no contact information, but we'll do our best. Also, if you have any preference on how your name should be on the citation (e.g., Kathleen v Kacee?, include middle initial?, specific salutation?) please let me know.
>
> Sorry for the last minute!
>
> The form of your response should look as follows (using myself as an example):
>
> > Subject: Record of Percentage Agreement (Maureen R. Gwinn)
> >
> > Maureen R. Gwinn
> > ORD-CCTE
> > STAA Nomination by Maureen Gwinn: Risk Analysis in the 21st Century: Adapting to New Challenges and Opportunities
> > Nominated Publication: Chemical Risk Assessment: Traditional vs Public Health Perspectives
> >
> > I agree with my designated percentage of contribution to this project as listed below.
>
> **Proposed record of agreement (truly a team effort!):**
>
> M. Gwinn – 12%
> K. Deener – 12%
> T. Burke – 12%

R. Kavlock -12%
W. Cascio – 10%
T. Bahadori – 10%
R. Thomas – 10%
D. Bussard – 10%
D. Axelrad – 10%
D. Dix - 2%

Details from the STAA guidance is also below.

<!--[if !supportLists]-->• <!--[endif]-->Record of Percentage Agreement: The nomination package must include a Record of Percentage Agreement document from each author listed on the nomination form. This document may be submitted in the form of an e-mail or signed letter, which states that the co-author agrees with the total percentage of effort listed beside his or her name entered in the nomination form. The document should list "Record of Percentage Agreement" in the subject line, followed by the coauthor's first and last name. The body of the document should contain the co-author's name and organization, the nominee's name, the title(s) of the nominated publication(s), and a brief statement that the author agrees with his or her designated percentage of contribution. (Note: A Record of Percentage Agreement document is required for single-author nominations.)

Thanks!

Maureen

Maureen R. Gwinn, PhD DABT ATS
Division Director
Biomolecular and Computational Toxicology Division
Center for Computational Toxicology and Exposure
Office of Research and Development
US Environmental Protection Agency
109 TW Alexander Drive MC D-143-02
Durham, NC 27711

Office: 919-541-3794
Cell: 703-434-9093

<AJPH - STAA justification_Clean_4.29.2020 final v2.docx>

From: Cascio, Wayne
To: Gwinn, Maureen
Subject: Record of Percentage Agreement (Wayne E. Cascio)
Date: Thursday, April 30, 2020 11:10:21 AM

Hi Maureen – Here is the information requested to complete our application.

Wayne E. Cascio
ORD-CPHEA
STAA Nomination by Maureen Gwinn: Risk Analysis in the 21st Century: Adapting to New Challenges and Opportunities
Nominated Publication: Chemical Risk Assessment: Traditional vs Public Health Perspectives

I agree with my designated percentage of contribution to this project as listed below.

Proposed record of agreement (truly a team effort!):

M. Gwinn – 12%
K. Deener – 12%
T. Burke – 12%
R. Kavlock -12%
W. Cascio – 10%
T. Bahadori – 10%
R. Thomas – 10%
D. Bussard – 10%
D. Axelrad – 10%
D. Dix - 2%

Many thanks, Wayne

Wayne E. Cascio, MD, FACC | Director | Center for Public Health and Environmental Assessment | Office of Research and Development | U.S. Environmental Protection Agency | Research Triangle Park, NC 27711 | Phone: 919.541.2508 | Cell: 919.627.3762|

From: Gwinn, Maureen <gwinn.maureen@epa.gov>
Sent: Thursday, April 30, 2020 10:56 AM
To: Axelrad, Daniel <Axelrad.Daniel@epa.gov>; Cascio, Wayne <Cascio.Wayne@epa.gov>; Deener, Kathleen <Deener.Kathleen@epa.gov>; Bahadori, Tina <Bahadori.Tina@epa.gov>; Bussard, David <Bussard.David@epa.gov>; Thomas, Russell <Thomas.Russell@epa.gov>; tburke1@jhu.edu; Robert Kavlock <rkavlock@icloud.com>
Subject: STAA questions - please confirm via email on percentage of effort
Importance: High

Hi team –

Working on the STAA Submission, and didn't realize we needed this for the submission. Can you

please confirm your agreement with the percentage of effort for your role in this publication? I am not sure what to do about David Dix as I have no contact information, but we'll do our best. Also, if you have any preference on how your name should be on the citation (e.g., Kathleen v Kacee?, include middle initial?, specific salutation?) please let me know.

Sorry for the last minute!

The form of your response should look as follows (using myself as an example):

> Subject: Record of Percentage Agreement (Maureen R. Gwinn)
>
> Maureen R. Gwinn
> ORD-CCTE
> STAA Nomination by Maureen Gwinn: Risk Analysis in the 21st Century: Adapting to New Challenges and Opportunities
> Nominated Publication: Chemical Risk Assessment: Traditional vs Public Health Perspectives
>
> I agree with my designated percentage of contribution to this project as listed below.

Proposed record of agreement (truly a team effort!):

M. Gwinn – 12%
K. Deener – 12%
T. Burke – 12%
R. Kavlock -12%
W. Cascio – 10%
T. Bahadori – 10%
R. Thomas – 10%
D. Bussard – 10%
D. Axelrad – 10%
D. Dix - 2%

Details from the STAA guidance is also below.

- Record of Percentage Agreement: The nomination package must include a Record of Percentage Agreement document from each author listed on the nomination form. This document may be submitted in the form of an e-mail or signed letter, which states that the co-author agrees with the total percentage of effort listed beside his or her name entered in the nomination form. The document should list "Record of Percentage Agreement" in the subject line, followed by the coauthor's first and last name. The body of the document should contain the co-author's name and organization, the nominee's name, the title(s) of the nominated publication(s), and a brief statement that the author agrees with his or her designated percentage of contribution. (Note: A Record of Percentage Agreement document is required for single-author nominations.)

Thanks!

Maureen

Maureen R. Gwinn, PhD DABT ATS
Division Director
Biomolecular and Computational Toxicology Division
Center for Computational Toxicology and Exposure
Office of Research and Development
US Environmental Protection Agency
109 TW Alexander Drive MC D-143-02
Durham, NC 27711

Office: 919-541-3794
Cell: 703-434-9093

Risk Analysis in the 21st Century: Adapting to New Challenges and Opportunities

See also Gwinn et al., p. 1032.

During the late 1970s, there was widespread concern that many chemicals in commerce caused cancer or promoted it. In addition, the US government was concerned about operations of commercial nuclear power plants, which at that time seemed destined to increase from approximately 100 plants to 10 times that number. Hazardous waste disposal was a third widely publicized national human health and environmental issue. In response to these concerns, the US government charged the newly created Environmental Protection Agency (EPA) and the Nuclear Regulatory Commission (NRC) with developing a scientific basis for assessing and managing associated risks.[1,2]

In response, a group of primarily scientists and engineers developed the Society for Risk Analysis (SRA). The SRA quickly expanded to include members from Europe, Asia, and selected other nations. The following 6 questions are a convenient way of presenting how risk analysts study a possible threat; the first 3 cover risk assessment, and the last 3 cover risk management[1]:

1. What can go wrong?
2. What are the chances that something with important consequences will go wrong?
3. What are the consequences if something does go wrong?
4. How can consequences be prevented or reduced?
5. How can recovery be enhanced if the event occurs?
6. How can key local officials, expert staff, and the public organize and be informed to reduce risk and concern, and increase trust and confidence?

These six questions represent the systematic approach of risk analysis, covering ecological health, and the social, political, legal, and economic consequences of risks and their management. They became core elements of risk analysis as the field matured, with epidemiologists, toxicologists, and engineers, as well as sociologists, anthropologists, ethicists, economists, and psychologists broadening SRA membership.

The aerospace, medical, military, oil, and rail industries have become heavily vested in risk analysis. Recently, the fields of oral health and criminal justice have begun to apply the tools of risk analysis. Despite having some limitations, the field has carved out an important niche, providing scientifically based information about human health and environmental risk to decision-makers.

BIG DATA APPLICATIONS TO CUMULATIVE RISK

I have worked on many risk analyses, and the frustration I face is not having enough high-quality data. Sometimes, no data are available for analysis, and best estimates rely on professional judgement. Other times, data might be available, but it might not be representative of the problem being studied. This issue is addressed in this issue of *AJPH* by Gwinn et al.[3] (p. 1032) and nine other current or former EPA employees. Their article describes how risk assessment will be expanded in the 21st century by increased monitoring in multiple environments, storing the data in formats that are compatible with other data sets, and widely circulating these data. The data can then be used to investigate complex multifactor hypotheses about the contribution of chemical risks to disease.

The Gwinn et al.[3] approach allows for the formulation of models that simulate multi-exposure environments rather than the current set of analytical tools that examine one chemical at a time. The authors assert that using big data to explore cumulative risk may lead to the reduction of environmental exposures from multiple chemical agents and nonchemical stressors. They provide the example of heart disease, and identify specific organ targets and genetic expressions that need further exploration. Their approach is clearly applicable to the exploration of other complex health outcomes (e.g., children's behavioral disorders or obesity).

The big data approach faces challenges, particularly in removing traditional turf and legal barriers that exist between agencies and their subunits that maintain data sets. We must overcome these issues if we are to adopt a new paradigm that presents a holistic view of health and disease. I firmly believe this can be done, because it already has already been done in other branches of science.

SYSTEMS MODELING AND CUMULATIVE RISK

Understanding relationships among behavioral, environmental, and social risk factors requires sophisticated systems modeling

ABOUT THE AUTHOR

Michael R. Greenberg is with the Edward J. Bloustein School of Planning and Public Policy, Rutgers University, New Brunswick, New Jersey.

Correspondence should be sent to Michael R. Greenberg, PhD, 33 Livingston Avenue, Edward J. Bloustein School of Planning and Public Policy, Rutgers University, New Brunswick, NJ 08901-1958 (e-mail: mrg@ejb.rutgers.edu). Reprints can be ordered at http://www.ajph.org by clicking the "Reprints" link.

This editorial was accepted April 8, 2017.

doi: 10.2105/AJPH.2017.303844

that link these factors with health outcomes and each other. Risk analysts have a long history of such efforts in regard to asbestos, mercury, radiation, and many others toxins.[1,2] What is exciting today is that the promise of big data will allow us to build stronger models based on many more factors that influence outcomes than were available in the past.

CUMULATIVE RISK AND ENVIRONMENTAL JUSTICE

Neither cumulative risk nor systems thinking are new to this *Journal*. I found more than two dozen articles about cumulative risk and systems in the *Journal,* many of which are recent. What is different about the article by Gwinn et al. is that it lays out a plan for using big data to make progress in our understanding of multiple risks. Having served on an EPA Environmental Justice Science Advisory Board committee and having studied cumulative risk and environmental justice for many years, I believe that the ideas in this article are implementable at this time, not across the entire nation, but in selected neighborhoods. The place to try out database development, intersection, and modeling of human health impacts is in neighborhoods with concentrations of industry, warehousing, and transportation.

For instance, Newark, New Jersey, has neighborhoods with populations that are more than 80% African American and Latino American, and who are disproportionately poor. Newark passed the first environmental justice ordinance that we are aware of in the United States. The ordinance requires applicants for a new site to provide data about their proposals for local review.[4] However, for the ordinance to work, this city and many others like it across the United States need technical support that logically should come from federal and state environmental protection agencies. Will they get it? I am doubtful because of proposed budget cuts and other constraints placed on the EPA.[5,6] From the perspective of environmental and social justice, to postpone or even repudiate these important potentially path-breaking opportunities would be a serious miscarriage of social justice. AJPH

Michael R. Greenberg, PhD

ACKNOWLEDGMENTS

I thank Dona Schneider of Rutgers University for careful editing and Editor-in-Chief Alfredo Morabia, MD, PhD, for encouraging me to write this editorial.

REFERENCES

1. Greenberg M. *Explaining Risk Analysis: Protecting Health and the Environment*. New York, NY: Earthscan/Routledge; 2017.

2. Greenberg M, Goldstein B, Anderson E, Dourson M, Landis W, North DW. Whither risk assessment: new challenges and opportunities a third of a century after the Red Book. *Risk Anal.* 2015;35(11):1959–1968.

3. Gwinn M, Axelrad D, Bahadori T, et al. A public health perspective on 21st century risk assessment. *Am J Public Health*. 2017;107(7):1032–1039.

4. City of Newark. Newark Passes Innovative Environmental Justice Ordinance. July 15, 2016. Available at: http://www.ci.newark.nj.us/news/newark-passes-innovative-environmental-justice-ordinance. Accessed March 30, 2017.

5. Samet JM, Burke T, Goldstein B. The Trump administration and the environment—heed the science. *N Engl J Med*. 2017;376(12):1182–1188.

6. McCarthy G, Burke TA. We need a strong Environmental Protection Agency: it's about public health! *Am J Public Health*. 2017;107(5):649–651.

Educational Disparities in Adult Disability: Person, Place, Policies, and Family

See also Montez et al., p. 1101.

Declines in functioning, both mental and physical, and subsequent inability to live independently are key concerns of older people as they age. Over the past few decades, the United States and the United Kingdom have seen increases in the prevalence of mild disability, especially among women, leading to reductions in years spent disability-free.[1,2] In addition to this overall worsening situation, socioeconomic disparities in disability remain large in both countries.

At a national level, the United Kingdom has tended to use occupation- or neighborhood-based measures to explore differences in health and disability between socioeconomic groups; however, education, which generally changes little after early adulthood, suffers less from reverse causation. Nevertheless, there is a strong correlation between education and both middle- and later-life socioeconomic status measures given that increased education leads to greater job opportunities and higher incomes, as well as healthier lifestyles and better health outcomes.

Over the past two decades in England, the change in the compulsory school-leaving age from 14 years to 15 years and greater opportunities for university education have resulted in decreases in the prevalence and incidence of dementia[3] and a real reduction of years with cognitive impairment among women[2] in more older, recent cohorts. Furthermore, education was the sole socioeconomic measure differentiating disability pathways among individuals aged 85 to 90 years in the Newcastle 85+ Study.[4]

PLACE

If there is evidence for the far-reaching effects of education through to very old age, it seems obvious that we have to maximize educational opportunities for all individuals. However, education is not only executed at an individual level. In this issue of *AJPH*, Montez et al.

ABOUT THE AUTHOR

Carol Jagger is with the Institute of Health & Society, Newcastle University, Newcastle upon Tyne, England.

Correspondence should be sent to Carol Jagger, PhD, Institute for Health & Society, Campus for Ageing and Vitality, Newcastle University, Newcastle upon Tyne, NE4 5PL United Kingdom (e-mail: carol.jagger@ncl.ac.uk). Reprints can be ordered at http://www.ajph.org by clicking the "Reprints" link.

This editorial was accepted April 13, 2017.

doi: 10.2105/AJPH.2017.303859

This article has been cited by:

1. Michelle Bell, Michael R. Greenberg. 2018. Climate Change and Human Health: Links Between History, Policy, and Science. *American Journal of Public Health* **108**:S2, S54-S55. [Citation] [Full Text] [PDF] [PDF Plus]

STAA justification: Chemical Risk Assessment: Traditional vs Public Health Perspectives

Maureen R. Gwinn, PhD, Daniel A. Axelrad, MPP, Tina Bahadori, ScD, David Bussard, BA, Wayne E. Cascio, MD, Kacee Deener, MPH, David Dix, PhD, Russell S. Thomas, PhD, Robert J. Kavlock, PhD, and Thomas A. Burke, PhD, MPH

1. Explain how the nominated papers represent research that is innovative and important in advancing the scientific knowledge or technology relevant to EPA's mission. It is important to provide a clear and compelling explanation of the relevance, and impact of the research to EPA's mission (for example, the relevance of the research to one of EPA's Strategic Goals may be described):

EPA's progress under Strategic Goal 1 of A Cleaner, Healthier Environment and Goal 3: Greater Certainty, Compliance, and Effectiveness often hinges on the Agency's ability to produce scientific assessments that inform decision making. This challenge has been amplified for chemical assessments that inform actions under every major statute in EPA's jurisdiction, including the Toxic Substances Control Act (TSCA), Clean Water Act (CWA), Safe Drinking Water Act (SDWA), and the Superfund-related laws. Controversies around data limitations and statistical calculations have created significant uncertainties and have even brought some assessments to a grinding halt. The nominated publication presents a pragmatic and practical paradigm shift that reframes chemical risk assessment to enable rather than hamper environmental and public health decision making. As EPA moves away from vertebrate animal testing, this paper provides a platform for considering how new data streams can shape the future of chemical risk assessment. It proposes a path for using the full range of available data, including data mining approaches, alternatives to animal testing, new approach methods, and innovative approaches to integrate different data streams. The publication shows how this full range of data can be used to shape, enhance, and deliver chemical risk assessments for the thousands of chemicals and pollutants in the safety evaluation pipeline, including those under the new TSCA program. Several pilot projects with EPA Program Offices have been developed where the viability of this proposed paradigm shift is being explored and examined under different environmental statutes. The framing of this paper also emphasizes the importance of taking a public health approach in considering chemical and pollutant exposure. There are many disease states that are associated with numerous risk factors, including genetic, behavioral and environmental. While EPA regulates through a traditional risk assessment lens and has responsibility for mitigating environmental exposures, other federal and state agencies or health care professionals may be responsible for managing other risk factors of disease that have an environmental component. The approach articulated in this paper provides a framework for EPA to partner with other public health organizations to more effectively target disease burden. EPA's Office of Research and Development has been collaborating with EPA's Office of Air and Radiation to do this around the issue of pollutant exposures and cardiovascular disease risk. Cardiovascular disease risk is influenced by genetic and behavioral factors, but also by certain environmental factors. By using the principles articulated in this paper, EPA has been able to form partnerships with federal and state agencies to begin to address this disease. For example, the Department of Health and Human Services' MillionHearts Initiative has incorporated increasing awareness for physicians of particle pollution's adverse effects as a criterion for success in its MillionHearts Hospital and Healthcare Recognition Program. Additionally, through partnerships with state and local public health agencies and healthcare professional organizations, EPA has been able to deliver important public health information about the

environmental contributors to cardiovascular disease risk to frontline public health and healthcare professional practitioners.

2. The EPA's current STAA guidelines prohibit resubmission of publications nominated for STAA awards in previous years. Please provide the following information:

a. If multiple publications are submitted, provide a comprehensive explanation of the relationship and links between subject matter among the different nominated publications. For example, the discussion could describe how one publication builds on the results of a second publication:

Not applicable

b. List the previous five years STAA nominations and associated publications for each EPA author. Categorize the list by author and include publication title, year, and award:

Not applicable

c. Provide a description of how this nomination's publication(s) differ from previous (last 5 years) and current nominations(s) by the author(s):

Not applicable

d. Indicate whether previously submitted supplemental information is listed as supplemental information for the current nomination:

No previously submitted supplemental information.

e. If any of the authors have submitted a concurrent nomination to another Research Category, provide sufficient justification to distinguish the difference between nominations:

Not applicable

3. Provide evidence of recognition of the contribution from outside EPA:

News media coverage:

Although there is no known media coverage, this manuscript was included as the cover article for the journal in 2017 when published, with a special editorial on the article from the associate editor, Dr. Michael R. Greenberg, distinguished professor at the Edward J. Bloustein School of Planning and Public Policy, Rutgers University. The journal also invited the lead author to participate in a podcast discussion with the associate editor regarding the potential impact of this work.

1. Cover article (https://ajph.aphapublications.org/doi/10.2105/AJPH.2017.303771)
2. Journal editorial (https://ajph.aphapublications.org/doi/10.2105/AJPH.2017.303844)
3. Invited Podcast (https://soundcloud.com/alfredomorabia/ajph-podcast-of-the-july-2017-issue-english)

Invited presentations:

Based on this publication, there have been multiple invitations to present this work.

1. Health Canada Chemical Management Plan Science Committee meeting, November 2018; (Thank you letter attached).
2. 2017 National Environmental Health Association invited session
    a. Gwinn MR, Bahadori T, Deener KC. Session on Risk Assessment at a Crossroads: A Portfolio Approach to Protect Public Health. *National Environmental Health Association*. Grand Rapids, MI July 10-13, 2017.
3. Society of Toxicology (SOT) 57th Annual Meeting and ToxExpo, a Contemporary Concepts in Toxicology workshop on the "Toxicological Concerns in Older Adults: A Neglected Majority"
    a. Cascio WE, "Aging and Increased Susceptibility to Environmental Toxicants". San Antonio, TX, March 10, 2018
4. National Institute of Environmental Health Sciences sponsored symposium "Understanding the Combined Effects of Environmental Chemical and Non-Chemical Stressors: Atherosclerosis as a Model"
    a. Cascio WE, "Overview of the Atherosclerosis and Chemical Stressors", Research Triangle Park, NC, April 3, 2018

Other Evidence:

1. Health Canada (HC) and Environment and Climate Change Canada (ECCC) through the Chemicals Management Plan (CMP) used this paper as the basis to explore the development of a roadmap for implementing a public health/population health approach to support chemical risk assessment and management in Canada. https://www.canada.ca/en/health-canada/services/chemical-substances/chemicals-management-plan/science-committee/meeting-records-reports/committee-report-november-28-29-2018.html

2. This paper is part of the curriculum in Risk Sciences at Johns Hopkins, specifically as a roadmap for the future of health risk. It has also been incorporated into lectures at multiple schools of public health, and invited presentations at Johns Hopkins, invited Deans lectures at Drexel University, University of Colorado, Rutgers University, University of Wisconsin and the Annual Sewell Lecture in Environmental Health at Columbia University Mailman School of Public Health.

3. The manuscript has an Attention Score in the top 25% of all research outputs scored by Altmetric. It has had 19 citations in Scopus which corresponds to the 95th percentile for the field and has a field-weighted citation impact of 3.72. A value greater than 1.00 means that document is more cited than expected according to the average. It takes into account: The year of publication; document type, and disciplines associated with its source. (https://apha.altmetric.com/details/20293499/citations). According to Google Scholar, this paper has been cited 26 times since publication (https://scholar.google.com/scholar?um=1&ie=UTF-8&lr&cites=12958655616865832005) and there have been 285 reads of this paper on ResearchGate (https://www.researchgate.net/publication/317016558_Chemical_Risk_Assessment_Traditional_vs_Public_Health_Perspectives).

4. Provide an explanation of the external peer review process used to evaluate the scientific merit of the nominated publications (this is particularly important):

The research was published in the peer reviewed journal American Journal of Public Health (AJPH), a key journal in the field of public health. The AJPH impact factor for 2018 is 5.381. AJPH is ranked #4 of 156 titles in the Public, Environmental and Occupational Health category in the Social Sciences Citation Index and #16 of 179 titles for the same category in the Science edition. *AJPH* rose among peer journals in the Science Citation Index to No. 12 in 2018, up from No. 16 in 2017. And in the Social Science Citation Index, the journal was ranked No. 6. (https://www.apha.org/news-and-media/news-releases/ajph-news-releases/2019/impact-factor-2019). The peer review process at AJPH is a double-blind process. Authors do not know the peer reviewers, and peer reviewers do not know the authors of the papers they are reviewing. Reviewed papers usually receive careful scrutiny by three reviewers and additional assessment by the responsible associate editor, deputy editor, and editor-in-chief. Initial screening results in rejection of the majority of manuscripts within two weeks of submission. For those papers that are selected for review, the time to first decision is about three months. Overall time from submission to acceptance, which includes revisions by the authors, is about six months. AJPH aspires to select, through peer review, the highest quality science and public health practice–related manuscripts. To achieve this, the entire peer review and publication process of the AJPH must be thorough, objective, and fair. Every aspect of this process involves important ethical principles and decisions. The reputation of AJPH depends on the trust of readers, authors, researchers, reviewers, editors, public health practitioners, research subjects, funding agencies, and administrators of public health policy. This trust is enhanced by describing as explicitly as possible AJPH policies to ensure the ethical treatment of all participants in the publication process.

CITATION: Please propose an appropriate citation **reflecting the value of the work to the EPA** that will be printed on the award certificate for winning STAA nominations. Keep in mind that the word "for" will precede the citation on the actual certificate. Use "Initial Caps" format. For example, "Effect of Benzene on Adult Population". Do ***not*** use the title of the publication, do ***not*** exceed 120 characters including spaces (in Microsoft Word, use "File", "Properties", "Statistics" to get a character count; include spaces), and do ***not*** use italics, underlines, or special characters.

"Risk Analysis in the 21st Century: Adapting to New Challenges and Opportunities"

From: Axelrad, Daniel
To: Gwinn, Maureen
Subject: Record of Percentage Agreement (Daniel A. Axelrad)
Date: Thursday, April 30, 2020 12:54:05 PM

Daniel A. Axelrad
OP-NCEE
STAA Nomination by Maureen Gwinn: Risk Analysis in the 21st Century: Adapting to New Challenges and Opportunities
Nominated Publication: Chemical Risk Assessment: Traditional vs Public Health Perspectives

I agree with my designated percentage of contribution to this project as listed below.

M. Gwinn – 12%
K. Deener – 12%
T. Burke – 12%
R. Kavlock -12%
W. Cascio – 10%
T. Bahadori – 10%
R. Thomas – 10%
D. Bussard – 10%
D. Axelrad – 10%
D. Dix - 2%

From: Dr. Thomas A. Burke
To: Gwinn, Maureen
Cc: Axelrad, Daniel; Cascio, Wayne; Deener, Kathleen; Bahadori, Tina; Bussard, David; Thomas, Russell; Robert Kavlock
Subject: Re: STAA questions - please confirm via email on percentage of effort
Date: Thursday, April 30, 2020 1:10:01 PM

Looks good to me. It was really a great team effort.

Sent from my iPhone

> On Apr 30, 2020, at 10:58 AM, Gwinn, Maureen <gwinn.maureen@epa.gov> wrote:
>
> Hi team –
>
> Working on the STAA Submission, and didn't realize we needed this for the submission. Can you please confirm your agreement with the percentage of effort for your role in this publication? I am not sure what to do about David Dix as I have no contact information, but we'll do our best. Also, if you have any preference on how your name should be on the citation (e.g., Kathleen v Kacee?, include middle initial?, specific salutation?) please let me know.
>
> Sorry for the last minute!
>
> The form of your response should look as follows (using myself as an example):
>
> > Subject: Record of Percentage Agreement (Maureen R. Gwinn)
> >
> > Maureen R. Gwinn
> > ORD-CCTE
> > STAA Nomination by Maureen Gwinn: Risk Analysis in the 21st Century: Adapting to New Challenges and Opportunities
> > Nominated Publication: Chemical Risk Assessment: Traditional vs Public Health Perspectives
> >
> > I agree with my designated percentage of contribution to this project as listed below.
>
> **Proposed record of agreement (truly a team effort!):**
>
> M. Gwinn – 12%
> K. Deener – 12%
> T. Burke – 12%
> R. Kavlock -12%

W. Cascio – 10%
T. Bahadori – 10%
R. Thomas – 10%
D. Bussard – 10%
D. Axelrad – 10%
D. Dix - 2%

Details from the STAA guidance is also below.

<!--[if !supportLists]-->• <!--[endif]-->Record of Percentage Agreement: The nomination package must include a Record of Percentage Agreement document from each author listed on the nomination form. This document may be submitted in the form of an e-mail or signed letter, which states that the co-author agrees with the total percentage of effort listed beside his or her name entered in the nomination form. The document should list "Record of Percentage Agreement" in the subject line, followed by the coauthor's first and last name. The body of the document should contain the co-author's name and organization, the nominee's name, the title(s) of the nominated publication(s), and a brief statement that the author agrees with his or her designated percentage of contribution. (Note: A Record of Percentage Agreement document is required for single-author nominations.)

Thanks!

Maureen

Maureen R. Gwinn, PhD DABT ATS
Division Director
Biomolecular and Computational Toxicology Division
Center for Computational Toxicology and Exposure
Office of Research and Development
US Environmental Protection Agency
109 TW Alexander Drive MC D-143-02
Durham, NC 27711

Office: 919-541-3794
Cell: 703-434-9093

<AJPH - STAA justification_Clean_4.29.2020 final v2.docx>

From: Bahadori, Tina
To: Gwinn, Maureen
Subject: Trying again: STAA information
Date: Thursday, April 30, 2020 1:15:30 PM

Subject: Record of Percentage Agreement (Tina Bahadori)

Tina Bahadori
ORD-OSAPE
STAA Nomination by Maureen Gwinn: Risk Analysis in the 21st Century: Adapting to New Challenges and Opportunities
Nominated Publication: Chemical Risk Assessment: Traditional vs Public Health Perspectives

I agree with my designated percentage of contribution to this project as listed below.

From: Gwinn, Maureen <gwinn.maureen@epa.gov>
Sent: Thursday, April 30, 2020 10:56 AM
To: Axelrad, Daniel <Axelrad.Daniel@epa.gov>; Cascio, Wayne <Cascio.Wayne@epa.gov>; Deener, Kathleen <Deener.Kathleen@epa.gov>; Bahadori, Tina <Bahadori.Tina@epa.gov>; Bussard, David <Bussard.David@epa.gov>; Thomas, Russell <Thomas.Russell@epa.gov>; tburke1@jhu.edu; Robert Kavlock <rkavlock@icloud.com>
Subject: STAA questions - please confirm via email on percentage of effort
Importance: High

Hi team –

Working on the STAA Submission, and didn't realize we needed this for the submission. Can you please confirm your agreement with the percentage of effort for your role in this publication? I am not sure what to do about David Dix as I have no contact information, but we'll do our best. Also, if you have any preference on how your name should be on the citation (e.g., Kathleen v Kacee?, include middle initial?, specific salutation?) please let me know.

Sorry for the last minute!

The form of your response should look as follows (using myself as an example):

Subject: Record of Percentage Agreement (Maureen R. Gwinn)

Maureen R. Gwinn
ORD-CCTE
STAA Nomination by Maureen Gwinn: Risk Analysis in the 21st Century: Adapting to New Challenges and Opportunities
Nominated Publication: Chemical Risk Assessment: Traditional vs Public Health Perspectives

I agree with my designated percentage of contribution to this project as listed below.

Proposed record of agreement (truly a team effort!):

M. Gwinn – 12%
K. Deener – 12%
T. Burke – 12%
R. Kavlock -12%
W. Cascio – 10%
T. Bahadori – 10%
R. Thomas – 10%
D. Bussard – 10%
D. Axelrad – 10%
D. Dix - 2%

Details from the STAA guidance is also below.

- Record of Percentage Agreement: The nomination package must include a Record of Percentage Agreement document from each author listed on the nomination form. This document may be submitted in the form of an e-mail or signed letter, which states that the co-author agrees with the total percentage of effort listed beside his or her name entered in the nomination form. The document should list "Record of Percentage Agreement" in the subject line, followed by the coauthor's first and last name. The body of the document should contain the co-author's name and organization, the nominee's name, the title(s) of the nominated publication(s), and a brief statement that the author agrees with his or her designated percentage of contribution. (Note: A Record of Percentage Agreement document is required for single-author nominations.)

Thanks!

Maureen

Maureen R. Gwinn, PhD DABT ATS
Division Director
Biomolecular and Computational Toxicology Division
Center for Computational Toxicology and Exposure
Office of Research and Development
US Environmental Protection Agency
109 TW Alexander Drive MC D-143-02
Durham, NC 27711

Office: 919-541-3794
Cell: 703-434-9093

Record of Agreement

We have included all records of agreement we currently have, although not all are in the full format. I hope that as individual emails that would be sufficient. One co-author, Dr. David Dix, left the Agency soon after we started this project and I have not had contact with him. We likely will not get feedback from him on this award nomination.

Thank you

Maureen Gwinn

From: Thomas, Russell
To: Gwinn, Maureen
Subject: RE: Record of Percentage Agreement (Russell Thomas)
Date: Thursday, April 30, 2020 1:27:52 PM

Im fine with it

From: Gwinn, Maureen <gwinn.maureen@epa.gov>
Sent: Thursday, April 30, 2020 1:27 PM
To: Thomas, Russell <Thomas.Russell@epa.gov>
Subject: Record of Percentage Agreement (Russell Thomas)

Rusty – can you send the below back to me if you are in agreement? Then I can submit and move this on. Thanks. Maureen

> Subject: Record of Percentage Agreement (Russell Thomas)
>
> Russell Thomas
> ORD-CCTE
> STAA Nomination by Maureen Gwinn: Risk Analysis in the 21st Century: Adapting to New Challenges and Opportunities
> Nominated Publication: Chemical Risk Assessment: Traditional vs Public Health Perspectives
>
> I agree with my designated percentage of contribution to this project as listed below.

From: Gwinn, Maureen <gwinn.maureen@epa.gov>
Sent: Thursday, April 30, 2020 10:56 AM
To: Axelrad, Daniel <Axelrad.Daniel@epa.gov>; Cascio, Wayne <Cascio.Wayne@epa.gov>; Deener, Kathleen <Deener.Kathleen@epa.gov>; Bahadori, Tina <Bahadori.Tina@epa.gov>; Bussard, David <Bussard.David@epa.gov>; Thomas, Russell <Thomas.Russell@epa.gov>; tburke1@jhu.edu; Robert Kavlock <rkavlock@icloud.com>
Subject: STAA questions - please confirm via email on percentage of effort
Importance: High

Hi team –

Working on the STAA Submission, and didn't realize we needed this for the submission. Can you please confirm your agreement with the percentage of effort for your role in this publication? I am not sure what to do about David Dix as I have no contact information, but we'll do our best. Also, if you have any preference on how your name should be on the citation (e.g., Kathleen v Kacee?, include middle initial?, specific salutation?) please let me know.

Sorry for the last minute!

The form of your response should look as follows (using myself as an example):

> Subject: Record of Percentage Agreement (Maureen R. Gwinn)
>
> Maureen R. Gwinn
> ORD-CCTE
> STAA Nomination by Maureen Gwinn: Risk Analysis in the 21st Century: Adapting to New Challenges and Opportunities
> Nominated Publication: Chemical Risk Assessment: Traditional vs Public Health Perspectives
>
> I agree with my designated percentage of contribution to this project as listed below.

Proposed record of agreement (truly a team effort!):

M. Gwinn – 12%
K. Deener – 12%
T. Burke – 12%
R. Kavlock -12%
W. Cascio – 10%
T. Bahadori – 10%
R. Thomas – 10%
D. Bussard – 10%
D. Axelrad – 10%
D. Dix - 2%

Details from the STAA guidance is also below.

- Record of Percentage Agreement: The nomination package must include a Record of Percentage Agreement document from each author listed on the nomination form. This document may be submitted in the form of an e-mail or signed letter, which states that the co-author agrees with the total percentage of effort listed beside his or her name entered in the nomination form. The document should list "Record of Percentage Agreement" in the subject line, followed by the coauthor's first and last name. The body of the document should contain the co-author's name and organization, the nominee's name, the title(s) of the nominated publication(s), and a brief statement that the author agrees with his or her designated percentage of contribution. (Note: A Record of Percentage Agreement document is required for single-author nominations.)

Thanks!

Maureen

Maureen R. Gwinn, PhD DABT ATS
Division Director
Biomolecular and Computational Toxicology Division
Center for Computational Toxicology and Exposure
Office of Research and Development
US Environmental Protection Agency
109 TW Alexander Drive MC D-143-02

Durham, NC 27711

Office: 919-541-3794
Cell: 703-434-9093

Table of Contents

General_Authors_Publications.....2
LI-266819_OczkowskiEtAl_16_productivity_comparison.....18
LI-266822_OczkowskiEtAl_18_Nbay_isotopes.....36
Record_of_Agreement_coauthors.....53

STAA REPORT FOR THE SCIENTIST NOMINATIONS

General Information:

Nomination ID/App ID:	20-139
Research Category Primary:	Ecological Research (ER)
Research Category Secondary:	Monitoring and Measurement Methods (MM)
Laboratory/Office Name:	ORD/CEMM/ACESD
Nomination Entered By:	Autumn Oczkowski

Eligibility Checklist:

[Y] The nominated publication(s) has not been submitted to a previous STAA competition.

[Y] The nominated publication(s) was published on or before January 1, 2017 and on or after January 1,2012

[Y] The principal author was an EPA employee or a PHS employee assigned to EPA when the research was performed

[Y] The EPA authors (includes PHS employees assigned to EPA) contributed collectively a minimum of 50% toward the publication(s)

Nominating Official Name:	Wayne Munns
Nominating Official Title:	SUPERVISORY ECOLOGIST
Nominating OfficialEmail:	munns.wayne@epa.gov
STAA Coordinator Name:	Kathleen Wiser
STAA Coordinator Email:	wiser.kathi@epa.gov

Justifications:

Justification 1:

The nominated work was developed in response to the Agency's mission to provide for clean and safe water (currently objective 1.2 of the FY18-FY22 strategic plan). The United States has long had a nutrient pollution problem, where excess nutrient loads from human sources like sewage and fertilizers have had a host of negative impacts on coastal ecosystems, including harmful algal blooms and anoxic and hypoxic waters. The Safe and Sustainable Waters Resources (SSWR) National Research Program was developed, in part, to protect and restore aquatic ecosystems to adhere to the congressional mandates found in the Clean Water Act and other legislation. Recent restoration efforts have been increasingly successful, with more waterbodies switching into a 'recovery' mode. There is now a pressing need to understand what recovery looks like, how long it takes, and how best to measure it. The research done in this nomination was developed as part of the SSWR research program, where we sought to critically assess the fundamental underpinnings of how aquatic ecosystem response trajectories to nutrient reductions are measured. In order to improve and refine our management actions, we must learn how coastal waterbodies respond to and recover from efforts to reduce human nutrient loads. The nominated work provides some of the fundamental baseline necessary to assess response and recovery work. The two manuscripts are the product of the synthesis of a wide number of studies and many thousands of individual measurements taken across decades. They provide new information about which ecological parameters are appropriate to use and what they are (and are not) able to tell us.

Over the past decade, nutrient inputs to Narragansett Bay have decreased by more than half. Sewage treatment plants (STPs) discharging into the bay were upgraded to tertiary treatment with the goal of improving estuarine water quality and reducing the duration and extent of low-oxygen zones associated with sewage nutrient-supported production. Little is known about how phytoplankton production responds to major nutrient reductions and a team at our division has been actively monitoring the ecosystem recovery. As we began to document production responses in Narragansett Bay, we found a critical, fundamental knowledge gap in how we measure production. There is no feasible way to directly measure ecosystem production, so ecologists rely on indirect measurements. Oczkowski et al. (2016) takes a critical look at these measurements and uses both *in situ* data and those from large mesocosm nutrient enrichment experiments conducted in the early 1980s to compare the efficacy of chlorophyll concentrations, nutrient concentrations, cell

counts, rates of ^{14}C productivity, dissolved oxygen, and pH in representing net ecosystem production. Dissolved oxygen and pH were able to reliably track net ecosystem production and, contrary to paradigm, ^{14}C productivity and chlorophyll concentrations were not. These results should fundamentally change how we view, and measure, estuarine response and recovery to water quality improvements in all estuaries.

In Oczkowski et al. (2018), we build on the work presented in Oczkowski et al. (2016) by combining nutrient concentration and Secchi depth data with measurements of naturally occuring nitrogen (N) and carbon (C) stable isotopes in particulate matter, seaweeds, and hard clams from Narragansett Bay. Stable isotopes can add an additional level of insight into N sources and bay productivity (the rate of production). We synthesized data from 22 datasets collected over 44 years, from 1972 to 2016, spanning the range of before, during, and after the water quality improvements. While the impacts of the sewage treatment plant upgrades were not detectible in either the dissolved N concentrations or water clarity (Secchi) data, the stable isotope results clearly reflected the upgrades. The more recent N isotope measurements in the plants and animals reflected the advanced treatment and the C isotopes indicated that productivity may have declined in Narragansett Bay. Stable isotopes allowed us to see changes that would otherwise not be detectable. To our knowledge, isotopes have only been used in this context in the Baltic and in Moreton Bay, Australia. While these other studies observed an increased incorporation of offshore ‘natural’ N after N-reductions, Oczkowski et al (2018) made it clear that Narragansett Bay production is still predominantly supported by sewage N.

Justification 2A:

Two publications are submitted as part of this nomination. Both manuscripts seek to identify the best ways to assess coastal ecosystem response to major management efforts to reduce anthropogenic nitrogen loads to estuaries. The first publication (Oczkowski et al. 2016) synthesizes data from experimental mesocosms and more recent field collections to determine which common ecological measurements best reflect ecosystem changes. The second paper builds on this effort by demonstrating how stable isotope measurements provide additional, critical insight into how estuaries recover from nutrient pollution.

Justification 2B:

n/a

Justification 2C:

n/a

Justification 2D:

n/a

Justification 2E:

Lead author Autumn Oczkowski is also a coauthor on another nomination entitled: Linking ecosystem services to vector-borne disease in San Juan Bay Estuary, Puerto Rico. This work, which includes two manuscripts (given at the end of this justification), sought to link wetland ecosystem services to mosquito-vectored diseases in the San Juan Bay Estuary in San Juan, Puerto Rico. The two nominations are quite different. One looks to improve understanding of the relationships between vector borne illnesses, environmental quality, and ecosystem services in a tropical wetland. The other is addressing the impact of nitrogen reductions associated with sewage treatment plant upgrades on temperate estuarine water quality.

Manuscripts associated with the concurrent nomination:

Yee, S. H., D. A. Yee, R. de Jesús Crespo, A. Oczkowski, F. Bai, and S. Friedman (2019). Linking Water Quality to *Aedes aegypti* and Zika in Flood-Prone Neighborhoods. EcoHealth 16:191-209 https://doi.org/10.1007/s10393-019-01406-6

De Jesús Crespo, R., P. Méndez Lázaro, and S.H. Yee (2018) Linking wetland ecosystem services to vector borne disease: Dengue fever in San Juan Bay Estuary,

Puerto Rico. Wetlands 39: 1281-1293.
https://doi.org/10.1007%2Fs13157-017-0990-5

Justification 3A:

The work conducted as part of this nomination has been of great interest to the broader academic community. Many researchers were surprised to see how poorly some of the most commonly used ecological measurements seemed to reflect estuarine ecosystem processes. As a result, the lead author was asked to present on this at six different academic institutions over a period of four years. The manuscripts have been downloaded a total of almost 1200 times (601 times for Oczkowski et al. 2016 and 596 times for Oczkowski et al. 2018) from the journal Estuaries and Coasts, which is widely read by the coastal ecology and management communities. They have also been cited nine times. Dr. Oczkowski was invited to give the plenary talk, and present this work, at a meeting hosted by the Narragansett Bay Estuary Program on “The State of Narragansett Bay and its Watershed” in October 2017. While the EPA ultimately canceled the presentation, the invitation to give the keynote presentation at such a large event does demonstrate the influence and importance of the nominated research.

INVITED PRESENTATIONS RELATED TO STAA NOMINATION:

A. Oczkowski. 2014. Human impacts on coastal environments—exploring at the boundaries of disciplines. Boston University in Boston, MA.

A. Oczkowski, C. Oviatt, S. Nixon. 2014. Monitoring the productivity of coastal ecosystems: when simpler is better. EPA Seminar at the Atlantic Ecology Division. Narragansett, RI.

A. Oczkowski. 2014. Human impacts on coastal environments—exploring at the boundaries of disciplines. The University of Kentucky in Lexington, KY (Voted top-ranked speaker for the semester by the students).

A. Oczkowski. 2015. Monitoring the productivity of our changing coastal ecosystems, and the case of Narragansett Bay. The Ecosystems Center at the Marine Biological Laboratory in Woods Hole, MA.

A. Oczkowski. 2016. Monitoring the productivity of our changing coastal ecosystems and the case of Narragansett Bay. The Chesapeake Biological Laboratory, University of Maryland, Solomons, MD.

A. Oczkowski, C. Schmidt, S. Robinson, A. Hanson, D. Cobb, J. Krumholz, R. McKinney. 2018. How major reductions in nitrogen loads have impacted the Narragansett Bay Ecosystem. University of Massachusetts Dartmouth School for Marine Science and Technology. New Bedford, MA

A. Oczkowski, C. Schmidt, A. Hanson, D. Cobb, J. Krumholz, S. Robinson, C. McManus, J. Grear, R. Pruell, B. Taplin, A. Pimenta, R. McKinney. 2018. How major reductions in nitrogen loads have impacted the Narragansett Bay Ecosystem. University of Rhode Island Graduate School of Oceanography. Narragansett, RI

ADDITIONAL PRESENTATIONS RELATED TO STAA NOMINATION:

A. Oczkowski, C. Oviatt, S. Nixon. 2013. Monitoring the productivity of coastal ecosystems: when simpler is better. SWN Symposium. http://www.gso.uri.edu/swn-symposium. Narragansett, RI.

A. Oczkowski, C. Oviatt, S. Nixon. 2013. Monitoring the productivity of coastal ecosystems: when simpler is better. The 6th International Nitrogen Conference, Kampala, Uganda.

A. Oczkowski, C. Oviatt, S. Nixon. 2014. Monitoring the productivity of coastal ecosystems using pH: when simpler is better. New England Estuarine Research Society. Salem, MA.

Justification 3B:

Both manuscripts were submitted to, and ultimately accepted by, Estuaries and Coasts. They followed EPA management clearance processes as well as the journal's peer-review and editorial processes.

AUTHORS

Contributing Author

Author Name:	Jason Krumholz		
Professional Title:		Salutation:	Dr.
Email:	jkrumholz@gmail.com	Organization:	
Mailing Address:			
Street Line 1:			
City:			
Zip Code:		State:	
At time of research was:	Non EPA Personnel		
Separation Date:			
% of Effort:	2		

Principal Author

Author Name:	Autumn J. Oczkowski		
Professional Title:		Salutation:	Dr.
Email:	oczkowski.autumn@epa.gov	Organization:	
Mailing Address:			
Street Line 1:			
City:			
Zip Code:		State:	
At time of research was:	EPA Employee		
Separation Date:			
% of Effort:	60		

Contributing Author

Author Name:	Kenneth Miller		
Professional Title:		Salutation:	
Email:	kenneth.m.miller@gdit.com	Organization:	
Mailing Address:			
Street Line 1:			
City:			
Zip Code:		State:	
At time of research was:	Non EPA Personnel		
Separation Date:			
% of Effort:	5		

Contributing Author

Author Name:	Donald Cobb	
Professional Title:		Salutation:
Email:	cobb.donald@epa.gov	Organization:
Mailing Address:		
Street Line 1:		
City:		
Zip Code:		State:
At time of research was:	EPA Employee	
Separation Date:		
% of Effort:	2	

Contributing Author

Author Name:	Christopher Hunt	
Professional Title:		Salutation:
Email:	chunt@unh.edu	Organization:
Mailing Address:		
Street Line 1:		
City:		
Zip Code:		State:
At time of research was:	Non EPA Personnel	
Separation Date:		
% of Effort:	7	

Contributing Author

Author Name:	Courtney Schmidt		
Professional Title:		Salutation:	Dr.
Email:	courtney.schmidt@nbep.org	Organization:	
Mailing Address:			
Street Line 1:			
City:			
Zip Code:		State:	
At time of research was:	Non EPA Personnel		
Separation Date:			
% of Effort:	5		

Contributing Author

Author Name:	Adam Pimenta		
Professional Title:		Salutation:	
Email:	pimenta.adam@epa.gov	Organization:	
Mailing Address:			
Street Line 1:			
City:			
Zip Code:		State:	
At time of research was:	EPA Employee		
Separation Date:			
% of Effort:	2		

Contributing Author

Author Name:	Scott Nixon		
Professional Title:		Salutation:	Dr.
Email:	swn@uri.edu	Organization:	
Mailing Address:			
Street Line 1:			
City:			
Zip Code:		State:	
At time of research was:	Non EPA Personnel		
Separation Date:			
% of Effort:	1		

Contributing Author

Author Name:	Emily Santos		
Professional Title:		Salutation:	
Email:	emily.santos@humboldt.edu	Organization:	
Mailing Address:			
Street Line 1:			
City:			
Zip Code:		State:	
At time of research was:	Non EPA Personnel		
Separation Date:			
% of Effort:	3		

Contributing Author

Author Name:	Alana Hanson		
Professional Title:		Salutation:	
Email:	hanson.alana@epa.gov	Organization:	
Mailing Address:			
Street Line 1:			
City:			
Zip Code:		State:	
At time of research was:	EPA Employee		
Separation Date:			
% of Effort:	3		

Contributing Author

Author Name:	Leslie Smith		
Professional Title:		Salutation:	Dr.
Email:	leslie.smith@youroceanconsulting.com	Organization:	
Mailing Address:			
Street Line 1:			
City:			
Zip Code:		State:	
At time of research was:	Non EPA Personnel		
Separation Date:			
% of Effort:	1		

Contributing Author

Author Name:	Rick McKinney		
Professional Title:		Salutation:	Dr.
Email:	mckinney.rick@epa.gov	Organization:	
Mailing Address:			
Street Line 1:			
City:			
Zip Code:		State:	
At time of research was:	EPA Employee		
Separation Date:			
% of Effort:	3		

Contributing Author

Author Name:	Candace Oviatt		
Professional Title:		Salutation:	Dr.
Email:	coviatt@uri.edu	Organization:	
Mailing Address:			
Street Line 1:			
City:			
Zip Code:		State:	
At time of research was:	Non EPA Personnel		
Separation Date:			
% of Effort:	3		

Contributing Author

Author Name:	Leanna Heffner		
Professional Title:		Salutation:	Dr.
Email:	leanna@nwblcc.org	Organization:	
Mailing Address:			
Street Line 1:			
City:			
Zip Code:		State:	
At time of research was:	Non EPA Personnel		
Separation Date:			
% of Effort:	1		

Contributing Author

Author Name:	Sandra Robinson		
Professional Title:		Salutation:	
Email:	robinson.sandra@epa.gov	Organization:	
Mailing Address:			
Street Line 1:			
City:			
Zip Code:		State:	
At time of research was:	EPA Employee		
Separation Date:			
% of Effort:	1		

Contributing Author

Author Name:	Joaquin Chaves		
Professional Title:		Salutation:	Dr.
Email:	joaquin.e.chavescedeno@nasa.gov	Organization:	
Mailing Address:			
Street Line 1:			
City:			
Zip Code:		State:	
At time of research was:	Non EPA Personnel		
Separation Date:			
% of Effort:	1		

PUBLICATIONS

Publication 1:

Publication Title:	Comparing measures of estuarine ecosystem production in a temperate New England estuary		
Publication Date:	Wed Jun 01 00:00:00 GMT 2016		
Journal/Publication Method:	Estuaries and Coasts		
All Author(s):			
Volume:	39	Number:	1
Pages:	1827-1844	Immediately Index:	Immediately Index:
Citation ½ Life:	4.7	Impact Factor:	2.686

Publication 2:

Publication Title:	How the distribution of anthropogenic nitrogen has changed in Narragansett Bay (RI, USA) following m		
Publication Date:	Thu Jul 12 00:00:00 GMT 2018		
Journal/Publication Method:	Estuaries and Coasts		
All Author(s):			
Volume:	41	Number:	1
Pages:	2260-2276	Immediately Index:	Immediately Index:
Citation ½ Life:	4.7	Impact Factor:	2.686

Estuaries and Coasts (2016) 39:1827–1844
DOI 10.1007/s12237-016-0113-1

Comparing Measures of Estuarine Ecosystem Production in a Temperate New England Estuary

Autumn Oczkowski[1] · Christopher W. Hunt[2] · Kenneth Miller[3] · Candace Oviatt[4] · Scott Nixon[4] · Leslie Smith[5]

Received: 31 July 2015 / Revised: 18 May 2016 / Accepted: 19 May 2016 / Published online: 1 June 2016
© Coastal and Estuarine Research Federation (outside the USA) 2016

Abstract Anthropogenic nutrient enrichments and concerted efforts at nutrient reductions, compounded with the influences of climate change, are likely changing the net ecosystem production (NEP) of our coastal systems. To quantify these changes, scientists monitor a range of physical, chemical, and biological parameters sampled at various frequencies. Water column chlorophyll concentrations are arguably the most commonly used indicator of net phytoplankton production, as well as a coarse indicator of NEP. We compared parameters that estimate production, including chlorophyll, across an experimental nutrient gradient and in situ in both well-mixed and stratified estuarine environments. Data from an experiment conducted in the early 1980s in mesocosms designed to replicate a well-mixed mid-Narragansett Bay (Rhode Island) water column were used to correlate changes in chlorophyll concentrations, pH, dissolved oxygen (O_2), dissolved inorganic nitrogen, phosphate, and silicate concentrations, cell counts, and ^{14}C carbon uptake measurements across a range of nutrient enrichments. The pH, O_2, nutrient, and cell count measurements reflected seasonal cycles of spring blooms followed by late summer/early fall respiration periods across nutrient enrichments. Chlorophyll concentrations were more variable and rates of ^{14}C productivity were inconsistent with observed trends in nutrient concentrations, pH, and O_2 concentrations. Similar comparisons were made using data from a well-mixed lower Narragansett Bay station and a more stratified upper Narragansett Bay station in 2007 and 2008. Trends among pH, O_2, and nutrient concentration parameters were similar to those observed in the mesocosm dataset, suggesting that continuous free water measurements of pH and O_2 seem to reliably reflect ecosystem metabolism and, while not perfect measures, may be underused indicators of NEP.

Keywords pH · Dissolved oxygen · Production · Estuary · Eutrophication · Nutrients · Ecosystem

Communicated by David G. Kimmel

Electronic supplementary material The online version of this article (doi:10.1007/s12237-016-0113-1) contains supplementary material, which is available to authorized users.

✉ Autumn Oczkowski
oczkowski.autumn@epa.gov

[1] Atlantic Ecology Division, US Environmental Protection Agency, 27 Tarzwell Dr., Narragansett, RI 02882, USA

[2] Ocean Process Analysis Laboratory, University of New Hampshire, Durham, NH 03824, USA

[3] CSC, 6361 Walker Lane, Suite 300, Alexandria, VA 22310, USA

[4] Graduate School of Oceanography, University of Rhode Island, Narragansett, RI 02882, USA

[5] Your Ocean Consulting, LLC, 9924 Rainbow Drive, Knoxville, TN 37922, USA

Introduction

Humans have had an indelible influence on coastal ecosystems, with actions often resulting in eutrophication, which is the enhancement of gross primary productivity associated with an increased supply of nutrients (Nixon 1995). Productivity is the rate of production of a constituent (i.e., the amount of carbon or organic matter generated over a certain period of time), while production is the stock of that constituent (e.g., the total carbon or organic matter present at a given time, Cloern et al. 2014). As regulators and managers work to mitigate the flow of nutrients to the coast, there are more and more examples of ecosystems undergoing oligotrophication, where reductions in nutrient supplies impact gross and net ecosystem production, often in unexpected ways (e.g., Duarte et al. 2009; Nixon

2009). For example, in Narragansett Bay, Rhode Island, where nutrient inputs are dominated by point sources, all of the major sewage treatment plants discharging to the estuary and associated tributaries have upgraded, or are in the process of upgrading, to tertiary treatment (Krumholz 2012). Tertiary treatment will reduce inputs of nitrogen (N), the primary limiting nutrient in the estuary, from 16-20 to ≤8 mg l^{-1} (Krumholz 2012). As there is little historical context within which to evaluate the response of an ecosystem to nutrient reductions of this magnitude, this is an opportunity to assess how nutrient reductions will impact food webs and water quality (e.g., Borja et al. 2010; Duarte et al. 2009; Kemp et al. 2009; Nixon et al. 2009).

Overprinted on the ecosystem response to changing nutrient loads are the impacts of climate change, including rising sea levels and warming waters (e.g., Sallenger et al. 2012; Yin et al. 2009) as well as other more subtle changes such as the increasing frequency of large storms (Kunkel et al. 2013; Redmond and Abatzoglou 2014) and ocean acidification (Zeebe 2012). As researchers struggle to gauge the impacts of these changes during an era of ever-tightening budgets, there is a need to reassess how we measure and monitor changes in estuarine production and determine which tools may yield reliable observations of future changes.

To understand the impacts of changing nutrient inputs and climate on coastal ecosystems and food webs, scientists have traditionally sought to characterize the amount and type (e.g., phytoplankton, macroalgae, seagrass, kelp) of primary production in the ecosystem (e.g., Glibert et al. 2014; Greening et al. 2014). The abundance of primary producers is controlled by a complex interplay of abiotic factors such as nutrient supply, light, and temperature as well as by top-down grazing. It has been generally demonstrated that increasing nutrient supplies result in higher primary production, subsequently resulting in higher secondary production (Nixon 1982; Nixon and Buckley 2002), at least up to a point (Breitburg et al. 2009a, b; Oczkowski and Nixon 2008). Coastal ecologists and ecosystem managers, concerned with the response of ecosystem processes to human influences, want to quantify and monitor these impacts, typically by quantifying the base of the food chain: the primary producers. Because food chains are dynamic, the phytoplankton present in the water column at any given time are not the total population produced, rather those left after consumption by higher trophic levels. Abundance measures do not account for energy consumed via maintenance respiration. We frame our subsequent discussions of water column productivity using the following operational definitions:

$$\mathrm{NEP} = \mathrm{NPP} - R_{\mathrm{hetero}} \quad (1)$$

$$\mathrm{NPP} = \mathrm{GPP} - R_{\mathrm{auto}} \quad (2)$$

Where NEP is net ecosystem production, R_{hetero} is heterotrophic respiration, NPP is net primary production, GPP is gross primary production, and R_{auto} is autotrophic respiration. Specifically, this work compares and contrasts different methods for estimating NEP. We acknowledge that there is no direct or "correct" way of measuring NEP, NPP, or GPP; thus there is no "right answer" against which to compare other measures. The goal of this work is to identify the method best suited to addressing the question: How do we monitor the net ecosystem production of an estuary or coastal system in response to large perturbations like major nutrient reductions?

There is a long history of developing methods and techniques to measure primary production and respiration well-documented elsewhere (for example, Williams et al. 2002). In particular, work has focused on determining whether systems were net heterotrophic (consumption > production) or autotrophic (production > consumption). The first efforts at quantifying net ecosystem productivity (the rate of production), were based on measures of dissolved oxygen (O_2) made via discrete water collection and subsequent Winkler titration (Clesceri et al. 1990; Winkler 1888). By quantifying O_2 concentration changes between dawn and dusk measurements, the net amount of productivity could be estimated, with the difference between dusk and dawn yielding an estimate of respiration. The advent of Steeman Nielsen's ^{14}C method, in which radioactive carbon uptake by phytoplankton was directly measured, was widely considered a major breakthrough as the high sensitivity of the method allowed for the quantification of production in oligotrophic (low productivity) systems. However, the question of whether net (productivity–respiration) or gross productivity (total productivity) was measured has been a source of some discussion (Cloern et al. 2014; Marra 2009; Peterson 1980). The ^{14}C method for quantifying productivity rates is still widely used, with data feeding into ecological models such as the light·biomass (BZI) models (e.g., Brush and Brawley 2009; Cole and Cloern 1984).

Primary production is also estimated using measures of chlorophyll concentrations via two methods; discrete measurement using a fluorometer (DOE 1994) and via probes, which measure in situ water column fluorescence (e.g., Stoffel and Kiernan 2009). When using total chlorophyll content in a unit of water as a means to assess NPP, a representative chlorophyll/carbon ratio is assumed (i.e., Eppley 1968; Ryther and Yentsch 1958; Williams and Murdoch 1966). Neither fluorescence-based measurements nor the ^{14}C method account for phytoplankton consumed by zooplankton nor the contributions from other primary producers including macroalgae, seagrass, and kelp. Finally, some scientists have adapted H.T. Odum's open water method for measuring net production using data-logging oxygen probes (e.g., Caffrey 2004; Caffrey et al. 2014; Howarth et al. 2014; Mortazavi et al. 2012).

With researchers using different measures of production and productivity—often interchangeably—across a wide range of coastal systems and under increasing pressure to

monitor, model, and characterize these systems, it is important to periodically reassess these measures and what they tell us. While there has already been some thoughtful comparison among measures of NEP, such comparisons focus on some, but not all, of the measures discussed here (e.g., Alvarez-Fernandez and Riegman 2014; Bender et al. 1987; Howarth and Michaels 2000). Given an increasing need to use pre-existing data to support models and decision support tools designed to predict future production, we believe that a re-evaluation of commonly used production measures is important. While conducted more than 30 years ago, data from the Marine Ecosystems Research Laboratory (MERL) experiments provide the opportunity for such a comparison across a wide range of nutrient enrichment. Observations from MERL were consistent with available water quality data collected in 2007 and 2008 in nearby Narragansett Bay, Rhode Island. We suggest that free water pH and O_2 methods should be employed more frequently in assessments of coastal production and respiration, whether as high-frequency measures of net production or as baseline information from which to compare different aspects of production, such as chlorophyll concentrations, cell counts, or ^{14}C incubations.

Methods

MERL Mesocosm Experiment (1981–1983)

The MERL nutrient enrichment experiment was carried out from 1 June 1981 to 26 September 1983 in a series of fiberglass mesocosms designed to replicate the mid-Narragansett Bay water column. This experiment is described in detail in Frithsen et al. (1985a, b) and Nixon et al. (2015). The mesocosms were 1.83 m in diameter and contained a 5-m water column and 0.37 m of intact benthic sediments collected from the nearby bay. Estuarine water was pumped into each tank at a rate designed to mimic the long-term mean residence time of the adjacent bay (27 days; Pilson 1985). Three mesocosms served as controls while the remaining six were treated with incrementally increasing amounts of inorganic nitrogen (N), phosphorous (P), and silica (Si) in a ratio of 12.80 N:1.00 P:0.91 Si; the ratio was based on measured sewage effluent (Nixon 1981). The lowest level of nutrient enrichment (1X mesocosm) was meant to approximate the daily, areal-weighted input of nutrients into the entire Narragansett Bay from sewage and runoff (Frithsen et al. 1985a). In the 1X mesocosm 7.57 mmol of N, 0.591 mmol of P, and 0.54 mmol of Si were added daily. The 2X mesocosm received double this amount and the 4X mesocosm, quadruple. While there were some additional mesocosms that underwent even more extreme enrichment as part of this experiment, they are not included in this manuscript as only the control (C), 1X, 2X, and 4X mesocosms spanned the feasible range of nutrient inputs to this ecosystem (as based on Nixon et al. 2008).

Measurements of water column nitrate + nitrite (NO_3 + NO_2), ammonia (NH_3), phosphate (PO_4), and dissolved silica (DSi) were made weekly, during a mixing cycle, with a Technicon Autoanalyzer and following the methods of Solorzano (1969), Wood et al. (1967), Hager et al. (1972) and Brewer and Riley (1965) (Table 1). Samples for chlorophyll-a (subsequently referred to as chlorophyll) were also collected on the same day as water samples for nutrient analysis and analyzed using the method outlined in Yentsch and Menzel (1963), as modified by Lorenzen (1966). Diel measures of oxygen and pH were made weekly following a dawn-dusk-dawn cycle. Oxygen was measured via the Winkler method (Carritt and Carpenter 1966) and estimates of daily system production were made from the oxygen measurements and were corrected for diffusive flux (Frithsen et al. 1985a). To compare dawn-dusk-dawn measures of productivity and respiration to ^{14}C-based rate measures, they were converted to carbon units (g C m^{-2} day^{-1}) using a photosynthetic quotient of 1.2 and respiratory quotient of 1.1. These values were based on comparisons from this dataset (Oviatt et al. 1986b).

The pH values were measured using an Orion Ross combination electrode and a Beckman Model 71 m. All of the pH data presented in this manuscript are given in the National Bureau of Standards scale (or pH_{NBS}). Working buffers (pH 4, 7, and 9, all ±0.02) for standardization were made monthly and placed in a water bath set at the temperature of the mesocosms. A check of the electrode was done before each measurement in a pH 7 buffer. To quantify the potential influence of water temperature on pH values, alkalinity, ambient pH, salinity, and in situ temperature data were input to the CO2SYS program (Lewis and Wallace 1998) to calculate dissolved inorganic carbon (DIC) concentrations. These DIC concentrations, together with the original alkalinity and salinity values, were re-input to CO2SYS in order to derive the pH at 12 °C for all mesocosm treatments.

The ^{14}C incubations were conducted on alternate weeks to O_2 and pH sampling and methods were based on Steemann-Nielsen (1952). Water samples were collected, zooplankton filtered out using a 200-μm mesh, and samples were treated with radioactive carbon (^{14}C). Bottles were suspended at five depths (0.1, 0.5, 1, 2.5, and 4.5 m) in each mesocosm from 10:00 hours to 16:00 hours (Keller 1986). Hourly production per square meter of surface water was calculated by following Strickland and Parsons (1972) (Table 1) where hourly measures of ^{14}C uptake were converted to daily estimates using parameters derived from a photosynthesis-light (P-I) curve (Keller 1986). Light data available in Frithsen et al. (1985b) indicated that the mean 1 % light level ranged from 4.17 ± 0.70 m in the control mesocosm to 2.98 ± 0.60 m in the 4X treatment. Given that the water column was 5 m, growth from benthic primary producers was not considered.

Table 1 A list of parameters measured as part of the Marine Ecosystem Research Laboratory (MERL) nutrient enrichment experiment as well as those measured at two locations in Narragansett Bay in 2007 and 2008. Sampling frequency and sampling location within the water column are also given. Nutrient measurements include dissolved inorganic nitrogen (DIN), phosphate (PO_4), and dissolved silica (DSi). The final column represents our best estimate of what these different parameters are actually measuring, albeit net ecosystem production (NEP), net primary production (NPP), or gross primary production (GPP)

Measurement	Frequency	Water column position	Production measure[a]
MERL nutrient enrichment experiment (1981–1983)			
nutrients	weekly	surface	NEP
chlorophyll	weekly	surface	NEP[b]
oxygen	weekly	surface	NEP[c]
pH_{NBS}	weekly	surface	NEP
^{14}C	alternate weeks	bottles suspended at 5 depths	NPP, GPP[d]
cell counts	weekly	mix of surface, mid, and bottom	NEP[b]
Lower Narragansett Bay station (2007–2008)			
pH_{NBS}	15 min	surface	NEP
oxygen	15 min	surface	NEP
fluorescence (chlorophyll)	15 min	surface	NEP[b]
chlorophyll	monthly[e]	1 m below surface and at chlorophyll maximum	NEP[b]
^{14}C	monthly[e]	1 m below surface and at chlorophyll maximum	NPP, GPP[d]
nutrients	weekly	surface	NEP
Providence-Seekonk River estuary station (May–Dec. 2007 & May–Nov. 2008)			
pH_{NBS}	15 min	surface, bottom	NEP
oxygen	15 min	surface, bottom	NEP
fluorescence (chlorophyll)	15 min	surface, bottom	NEP[b]
nutrients	~twice monthly	surface, bottom	NEP

[a] Samples were not necessarily collected for this purpose

[b] For phytoplankton component of production only

[c] While oxygen concentration data were measured, they were used to calculate rates of productivity, both are presented in this study

[d] These measures represent productivity, not production

[e] Twice monthly from May through August. Sampling ended in August 2008

Weekly water samples were collected to determine phytoplankton species composition. Equal volumes of water were drawn from surface, mid, and bottom depths and combined. Samples were size fractionated into cell sizes greater and less than 10 μm. The <10 μm portion was counted live using a Fuchs-Rosenthal hemocytometer (Oviatt et al. 1989).

Narragansett Bay Data (2007–2008)

High-frequency pH, dissolved oxygen, and chlorophyll data were available from the University of Rhode Island's Graduate School of Oceanography (GSO at 41° 29.535′ N, 71° 25.137′ W) for 2007 and 2008 (Table 1). The quality assurance plan describing the sensors used is available online (QAPP NBFSMN 2014). During these years, some ^{14}C and discrete chlorophyll concentration data were also available (NBFSMN 2014; Smith 2011). Fifteen-minute measurements of pH, dissolved oxygen, and chlorophyll were used to create daily average values (measurement details are available at NBFSMN 2014). Water samples were collected 1 m below the surface and at the depth of the chlorophyll maximum for chlorophyll and ^{14}C analysis. Details of the ^{14}C uptake measurements are described in Smith (2011). For chlorophyll analysis, water was filtered through glass fiber filters and the filters were subsequently extracted in a 90 % acetone solution for 24 h and analyzed on a Turner 10-AU fluorometer. Weekly nutrient concentration (dissolved inorganic nitrogen (DIN), PO_4, DSi) data were collected at the surface (MERL 2015).

To assess a more stratified water column, high-frequency pH, O_2, and chlorophyll (as fluorescence) data from the summers of 2007 (May 24 to Dec 5) and 2008 (May 8 to Nov 9) from the Providence-Seekonk River Estuary (Bullock Reach buoy at 41° 44.434′ N, 71° 22.480′ W) were examined (NBFSMN 2014) (Table 1). As described earlier, 15-min measurements were used to create daily averages. Surface and bottom data (~7-m deep and 1 m above the sediment) were available and presented separately. Nutrient concentrations were measured twice a month at the Bullock Reach buoy by the

Narragansett Bay Commission (NBC 2016). In this dataset, multiple DIN and PO_4 results were censored due to the original result falling below the detection limit.

Statistics

Statistical correlation analyses were performed using SAS 9.2 and NCSS9 software. For the analyses, only MERL mesocosm O_2 and pH results from the first dawn measurements were used. All other MERL and Narragansett Bay results were used as reported in the analyses, with the exception of one MERL 2X mesocosm chlorophyll data point and one Narragansett Bay silica data point. In these two cases, the results deviated strongly from the neighboring results, even in the context of seasonality and appear to be transcription errors. While no explanation could be identified for the unusual results, a sensitivity analysis indicated that removing these two results did not affect the statistical significance of any correlations.

Associations between nutrients and production parameters in the MERL and GSO data were assessed using Pearson product moment correlations, with statistical significance assessed at the 95 % confidence level. The distributions of the results were tested for normality using both statistical and graphical methodologies. In order to meet the assumption of normality for the Pearson product moment correlation, fluorescence, chlorophyll, DIN, and ^{14}C results from the Narragansett Bay dataset, and the chlorophyll and phytoplankton counts from the MERL dataset, were log (base 10) transformed prior to performing any analyses. For the Narragansett Bay Bullock Reach data, due to a higher frequency of non-detects among the DIN and orthophosphate measurements, the non-parametric Spearman Rank correlation was used instead of the parametric Person correlations.

To assess whether any associations between nutrients and production parameters occurred after a time lag, cross-correlation analyses were performed for the MERL and Narragansett Bay data (GSO and Bullock Reach; Fig. 1). Analyses were based on calculated weekly mean concentrations to enable evaluating all parameters using a consistent time interval despite the differing sample collection/analysis frequencies. As ^{14}C and cell counts were measured less frequently, these data were included and analyzed as monthly means. To minimize the effect of seasonality on the non-zero lags, data were modeled using seasonal AR(1) time series models, with first differencing (Box and Jenkins 1976), in which a model was fit to each variable that described the seasonal variation of the data, but not any other increasing, decreasing, or other non-seasonal trends. Therefore, model residuals correspond to the results after the seasonal component has been removed, but still included any other patterns found in the original results, including interrelationships across variables. As a result, the correlations at non-zero lags would not be biased by the concurrence of the seasonal cycles of the two variables.

In addition to evaluating the nutrients and physical parameters individually, multiple regression models were fit to compare the overall association between chlorophyll concentrations for MERL (fluorescence for GSO) and nutrients, pH, and O_2. For each data set, a full regression model was fit with chlorophyll/fluorescence as the dependent variable and individual nutrients (including all possible two-way and three-way interactions) as independent variables. A second model was fit using O_2, pH, and its interaction term as independent variables. The adjusted *R*-squared value was determined in each case as it estimates the total variability of the productivity parameter explained by the independent variables. The adjusted *R*-squared value does not automatically increase with each additional independent variable added to the model, allowing for more direct comparisons. An adjusted *R*-squared value generated using the O_2/pH model that was comparable to the *R*-squared value generated using the nutrient model would indicate that a similar amount of predictive information could be obtained using O_2/pH. To avoid bias, only sampling events for which results were obtained for all nutrients and physical parameters were included in this assessment. All transformations used for the regression models were the same as those used for the correlation analyses. However, because only 16 days from the Bullock's Reach sampling included all parameters, which would likely result in model over-fitting when including all nutrients and interaction terms were included, these data were excluded from the analysis.

Results

MERL Mesocosms

Inorganic Measurements

Across the range of nutrient enrichment (C to 4X), seasonal variations in pH and O_2 were consistent with the well-established seasonal patterns of phytoplankton biomass in the bay (e.g., Oviatt et al. 1986a), which were largely based on observations of cell abundances and chlorophyll concentrations and supported by inverse relationships with nutrient concentrations. Narragansett Bay was characterized by a spring bloom of diatoms that, at least up until the early 1980s when these experiments were conducted (e.g., Nixon et al. 2009), occurred in late February/early March (Keller and Riebesell 1989; Pratt 1965). The pH and O_2 measurements closely correlated with one another ($p < 0.0001$ and correlations factors >0.9; Table S1, Figs. 2 and 3), indicating that the inhaling and exhaling of the mesocosms were linked. Highest pH values and O_2 concentrations occurred in February

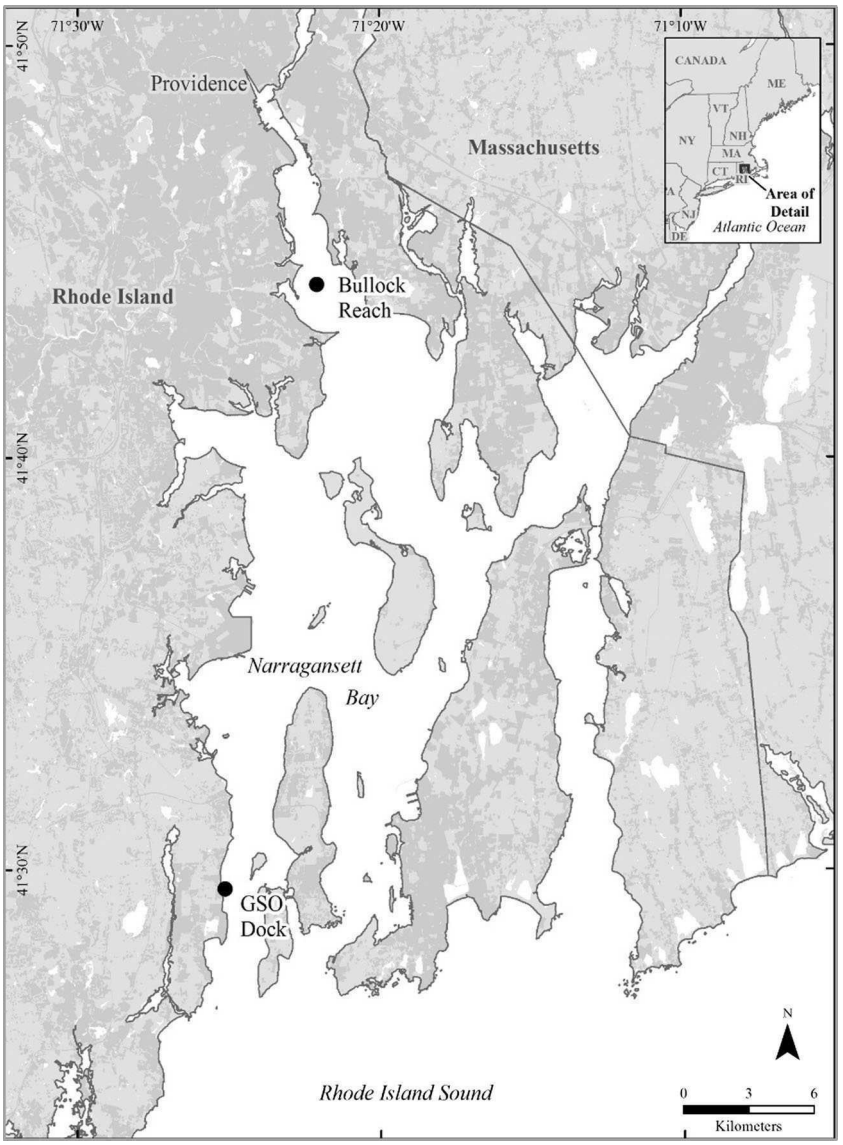

Fig. 1 Map of Narragansett Bay showing the locations of the MERL Mesocosm experiments (at the GSO Dock) and the mid and upper Narragansett Bay monitoring stations (GSO Dock and Bullock Reach, respectively). *Darker shaded land areas* indicate developed landscapes and *lighter shaded areas* indicate undeveloped regions

and March in both 1982 and 1983 (Fig. 2). The reverse was true during periods of presumed low production and/or respiration in the late summer and fall.

When the pH and O_2 values were greatest, concentrations of DIN, PO_4, and DSi were low (Fig. 2). There was a significant negative correlation between nutrient levels, particularly DSi, and both pH and O_2 and, in general, the strength of this correlation increased with level of enrichment (Table S1). The seasonality that characterized the pH and O_2 data was also reflected in the nutrient data, in which nutrient concentrations were drawn down to values close to zero in the winter, starting in January, and concentrations only rose again beginning in the late summer and early fall, when respiration presumably exceeded production. Nutrient concentrations remained high until another spring bloom appeared (Oviatt et al. 1986a; Pratt 1965).

Biotic Measurements

Chlorophyll concentrations reflected the mesocosm enrichments, ranging from 0.9 to 22.4 mg l^{-1} in the control, 0.8 to 58.2 mg l^{-1} in the 1X, 0 to 80.3 mg l^{-1} in the 2X, and 1.7 to 112.8 mg l^{-1} in the 4X mesocosms. Chlorophyll concentrations were significantly ($p < 0.0001$) in phase with pH and O_2, and increases in chlorophyll concentrations were associated with a decline in nutrient concentrations ($p < 0.0001$, with the exception of chlorophyll and DSi in the control tank, where $p = 0.01$) (Table S1, Fig. 4). While the highest chlorophyll concentrations corresponded to peaks in pH and O_2, the chlorophyll data were more variable during the bloom periods. Chlorophyll concentrations greater than 15–20 mg l^{-1} were always associated with periods of high production according to measurements of

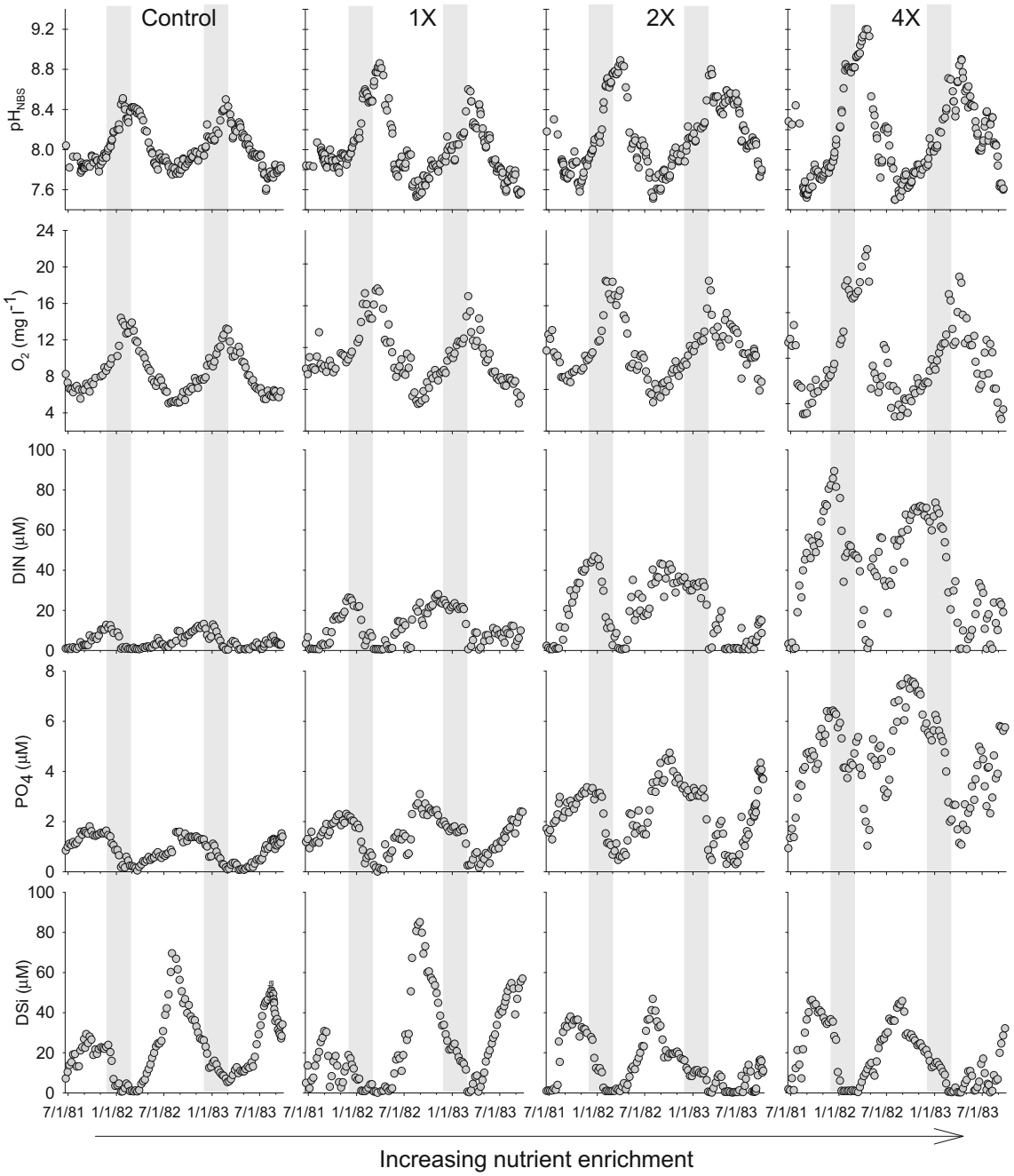

Fig. 2 The pH, dissolved oxygen (O_2), dissolved inorganic nitrogen (DIN), phosphate (PO_4) and silicate (DSi) data for the MERL Control (C) to 4X treatments. *Graph columns* represent data from mesocosms across increasing enrichment (from *left* to *right*). *Shaded areas* denote winter months (December, January, and February) and were included for orientation

pH, O_2, and nutrients, but the chlorophyll measurements within those periods varied widely, for example ranging >100 mg l^{-1} in the 4X tank during a bloom (Fig. 4).

In all of the mesocosms, cell counts ranged over four orders of magnitude per 1 ml of water. The phytoplankton populations across all mesocosms, particularly during the winter-spring blooms, were largely composed of diatoms, specifically *Skeletonema* spp. which was consistent with the adjacent Narragansett Bay at that time (Frithsen et al. 1985b; Nixon et al. 2009; Pratt 1965). There were statistically significant correlations between cell counts and all other parameters in the 2X and 4X mesocosms (Fig. 5, Table S1); however, cell counts were often not significantly correlated to pH, O_2, and DSi in the C and 1X mesocosms. Overall, however, species composition was similar across treatments, particularly during bloom periods (Frithsen et al. 1985b; Oviatt et al. 1986a).

Measurements of ^{14}C-based rates of carbon uptake did not begin until July 1982, or roughly halfway through the MERL

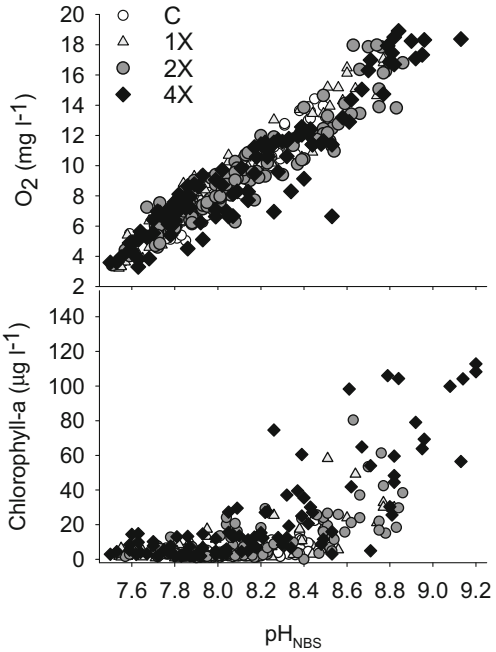

Fig. 3 *Top panel* shows O_2 data plotted against pH for the MERL mesocosm Control (C), 1X, 2X, and 4X treatments. *Bottom panel* shows chlorophyll-a values plotted against pH for the four treatments

experiment. Because of this, we did not include those data in our correlation analyses and discuss only our observations (Fig. 5). We also considered them in the context of the estimated rates of daily system production and respiration that were based on the dawn-dusk-dawn oxygen measurements (Fig. 6).

A Case Study of Narragansett Bay

The Well-Mixed Water Column

To determine whether our observations from the MERL mesocosms were still relevant in a contemporary well-mixed water column (mid-Narragansett Bay is either well mixed or very weakly stratified and the lower bay is well mixed) (Spaulding and Swanson 2008), we compiled a dataset for 2 years (2007 and 2008) from adjacent Narragansett Bay as pH, O_2, nutrients, ^{14}C, and both discrete measurements of chlorophyll and fluorescence data were available, albeit at different sampling frequencies (Fig. 7). The weekly mean pH and O_2 were most closely correlated to one another ($p < 0.0001$, correlation factor = 0.776), and both were also significantly and negatively correlated with nutrient concentrations (pH vs. fluorescence: $p = 0.001$, pH vs. all other nutrients: $p < 0.0001$, O_2 vs. PO_4 and DSi: $p < 0.0001$, and O_2 vs. DIN: $p = 0.002$) (Table S2). In contrast, O_2 and fluorescence data were not significantly correlated over the 2 years. As the discrete chlorophyll and ^{14}C data were obtained less frequently, they were compared to the other parameters using monthly bins (Table S3) because nutrient and discrete chlorophyll sampling were intended to represent the conditions for the month and not just the specific day that was sampled. Reassuringly, discrete chlorophyll measurements were most closely correlated with in situ fluorescence (correlation factor = 0.749, $p = 0.0001$). But the only other significant correlation was with DIN (−0.527, $p = 0.0171$) (Table S3).

While there were stronger correlations between the ^{14}C measurements and the other parameters, these correlations were opposite of the expected direction. The ^{14}C data were negatively correlated with pH (correlation factor = −0.615, $p = 0.0039$) and O_2 (−0.691, $p = 0.0008$), but positively correlated with PO_4 (0.465, $p = 0.0389$) and DSi (0.567, $p = 0.0092$) (Table S3). The amount of ^{14}C uptake by phytoplankton should be greatest when production is greatest, as there would be more cells to take up the carbon. Productive periods, such as a phytoplankton bloom, should result in more dissolved inorganic carbon removal (and associated increases in particulate ^{14}C retention and pH) and more water column O_2. While pH and O_2 were consistent with the patterns observed in the larger dataset, the ^{14}C data were not.

Bullock Reach, a More Stratified Water Column

At Bullock Reach, in upper Narragansett Bay, both pH and O_2 data were available for surface and bottom depths (~6.5 m from bottom) for the 2007 and 2008 growing seasons (Fig. 8). In both years, there was a clear decoupling of surface and bottom data in the summer months (roughly June through September) and a reconvergence of values later in the fall. When surface and bottom O_2 and pH data were plotted against one another, there was a linear trend similar to those observed in the MERL experiments and in the lower bay, but the stratification was evident (Fig. 9). In general, the lowest pH and O_2 values were associated with summer bottom waters and highest pH and O_2 with summer surface waters. The mid-range points that overlapped tended to be spring and fall data.

The pH, O_2, and chlorophyll (as fluorescence) data were highly correlated ($p < 0.0001$, Table S4). While both the DIN and PO_4 were correlated to pH ($p = 0.017$ and $p = 0.003$), only DIN was significantly correlated to chlorophyll concentrations ($p = 0.008$) and neither nutrient was correlated to O_2. Of course, the strength of these relationships (or lack thereof) may be influenced, at least in part, by the much smaller number of discretely collected nutrient samples compared to the buoy data ($n = 17$ vs. $n \geq 300$, respectively). However, there were enough nutrient samples to observe that DIN concentrations were lower in the summer than they were in the spring and early fall. The highest DIN concentrations observed at this upper bay station were akin to those from the 2X tank of the MERL mesocosms. Like the 2X tank, concentrations dropped close to zero in the summer, when the system is considered most productive, and rose back up in the late fall (Oviatt et al. 1986a) (Fig. 8).

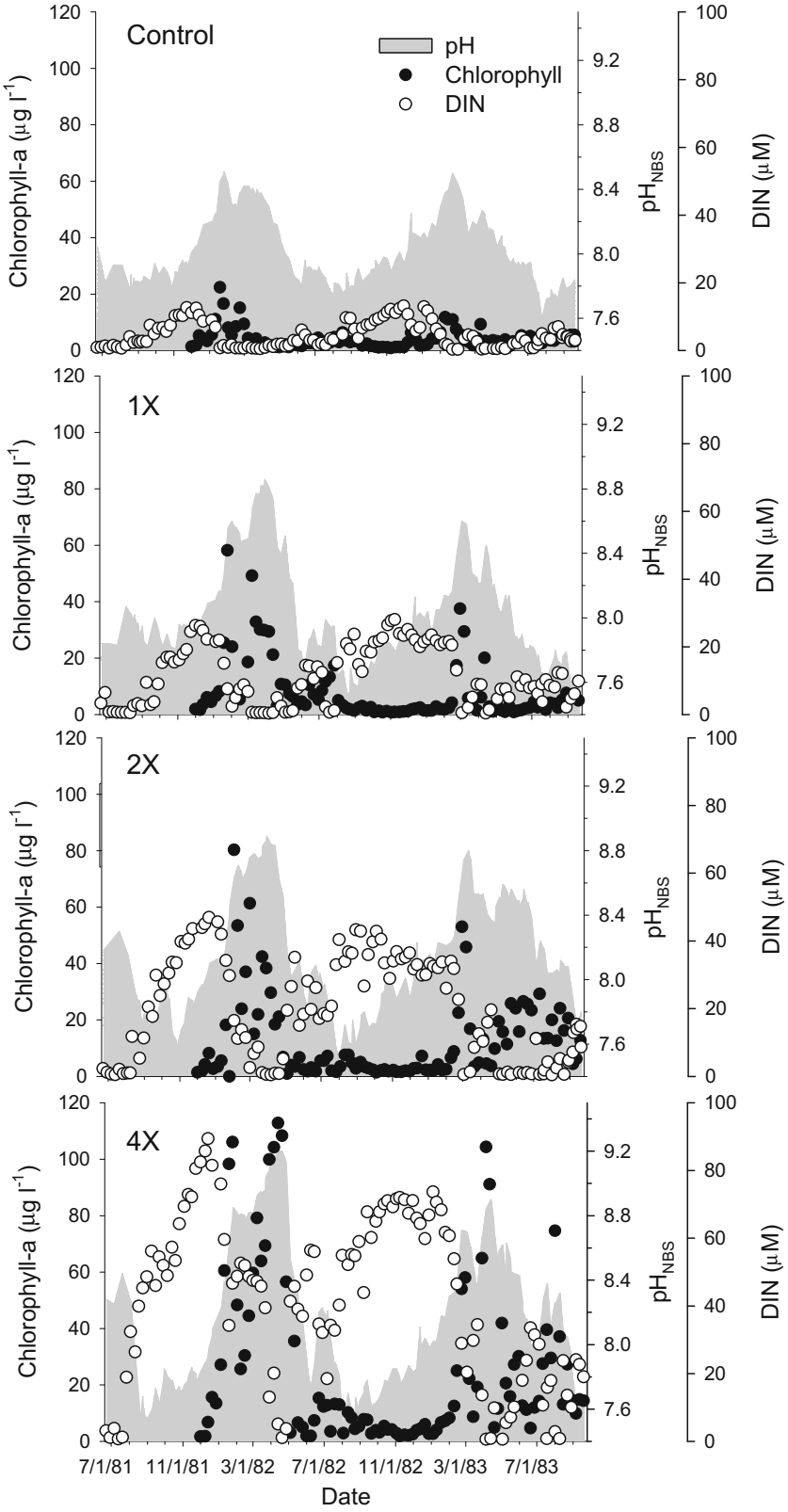

Fig. 4 Chlorophyll-a, DIN, and pH (*shaded area*) time series data for each MERL treatment

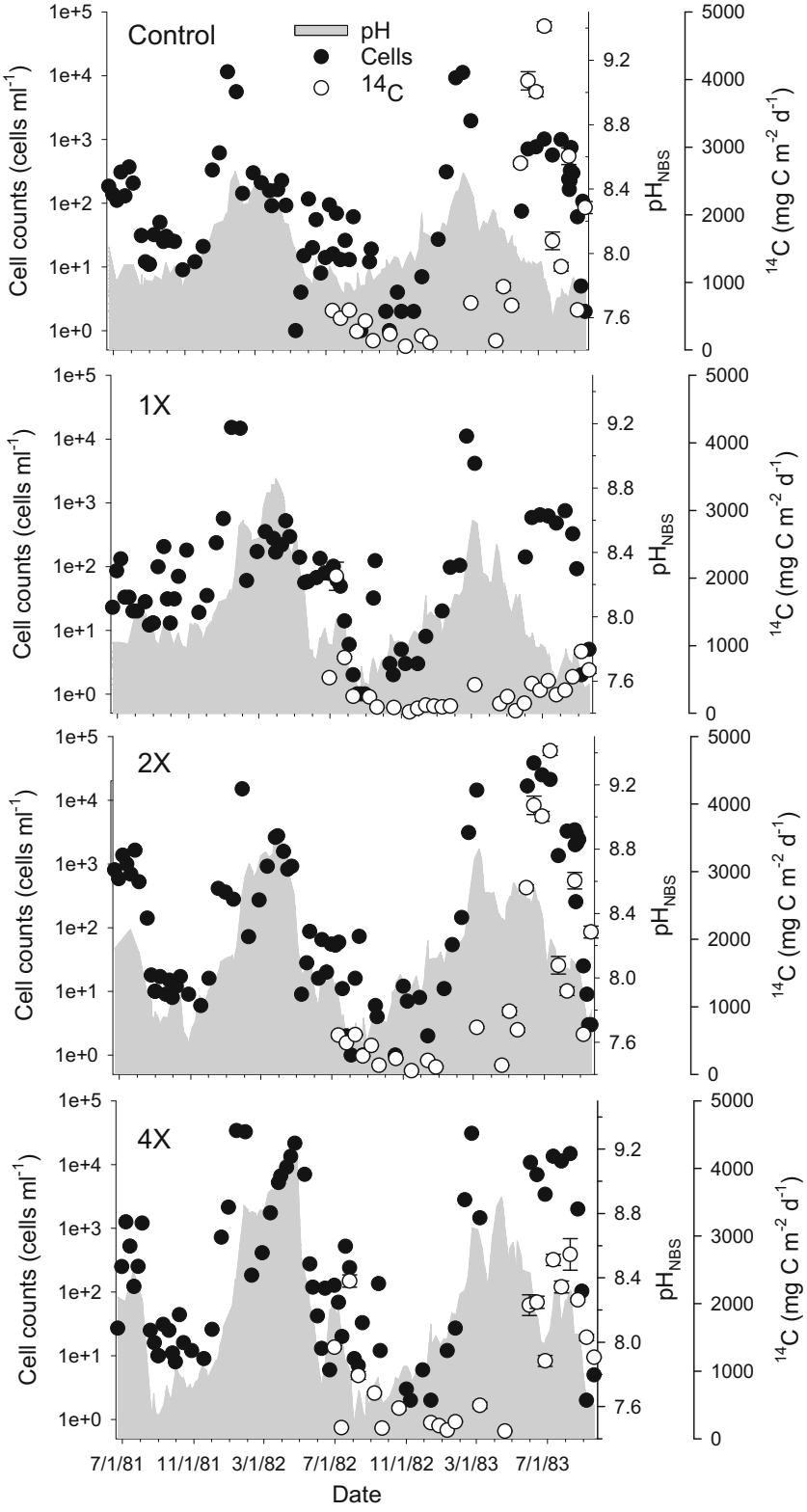

Fig. 5 The phytoplankton cell count (e.g., cells) and ^{14}C data, with pH as shaded area in the background, for the MERL mesocosm treatments

Multiple Regression Models

The adjusted *R*-squared values obtained from the physical parameter and nutrient models ranged between 27.4 % (for the GSO fluorescence) and 60.4 % (MERL 4X chlorophyll) (Table S5). The adjusted *R*-squared values calculated using the nutrient models ranged between 27.4 % (GSO fluorescence) and 66.4 % (MERL 2X chlorophyll). For chlorophyll, the nutrients

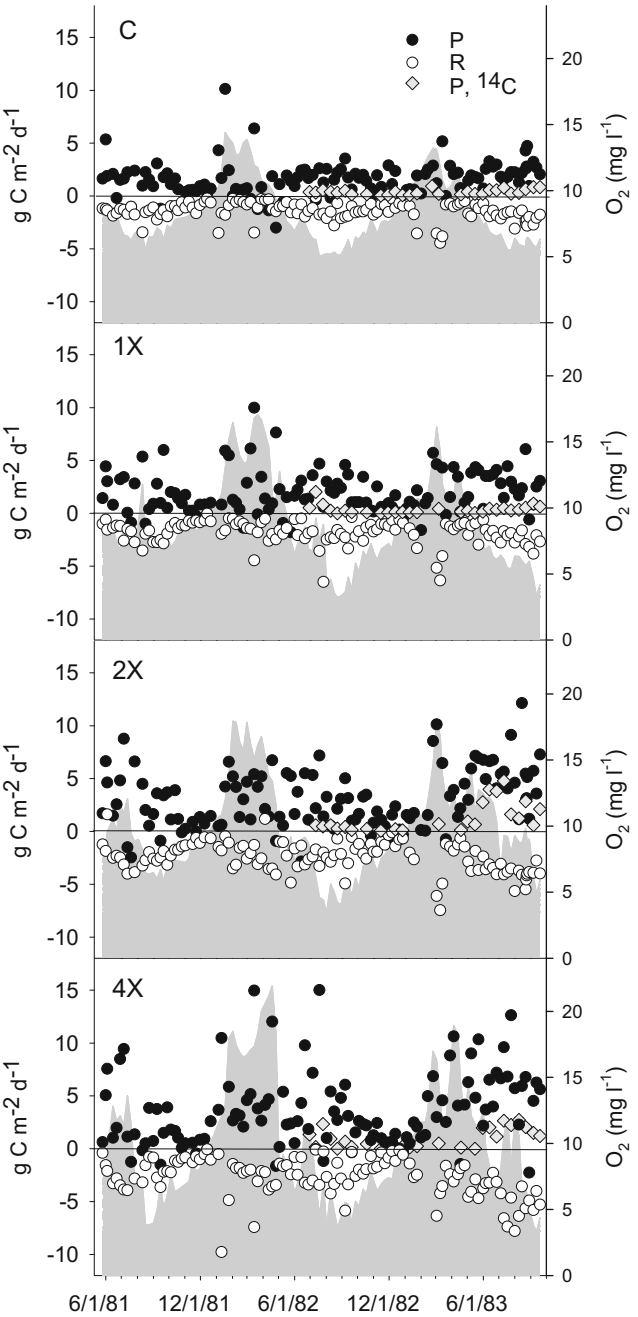

Fig. 6 Productivity in the control (C), 1X, 2X, and 4X MERL mesocosms. Rates of productivity (*closed circle*) and respiration (*open circle*) were calculated from measured dawn-dusk-dawn oxygen measurements, corrected for diffusive flux, and converted to carbon units using ratios given in Oviatt et al. (1986b). Productivity values based on ^{14}C uptake are also given (*diamonds*). Dissolved oxygen concentrations, measured at the first dawn, are shown as a *shaded area*, for reference. The respiration value on January 18, 1982, in the 4X mesocosm (−21.40 g C m^{-2} day^{-1}) was not included in this figure

explained a greater proportion of observed variability in the 1X and 2X tanks, and a smaller proportion of the observed variability in the control and 4X tanks. For the GSO data, both the nutrients and physical parameters were relatively poor predictors of fluorescence, with both yielding *R*-squared values less than 30 %.

Discussion

Observations from the MERL Mesocosms

The range in pH was quite wide across the mesocosm enrichments, from about 7.5 to 9.2, which is similar to lower Narragansett Bay, where pH typically ranges from about 7.6 to 8.6 over the course of a year (Hinga 1992). For perspective, pH in the open ocean typically varies <0.1 (e.g., Duarte et al. 2013; Hoffman et al. 2011). In each of the experimental mesocosms, the pH values covaried with O_2 (Table S1, Fig. 3), a relationship which has been well-documented elsewhere (e.g., Wallace et al. 2014). Seawater pH is primarily controlled by the components of the CO_2 system (collectively known as DIC) in seawater, although temperature and salinity also influence pH (Pilson 1998). Photosynthesis reduces CO_2, increasing the pH of the water column in estuarine areas of high NEP. Inputs of CO_2, such as those released into the water column during the consumption of organic matter through respiration, and possibly via anthropogenic CO_2 contributions associated with climate change, cause a decline in pH. In productive coastal systems, DIC concentrations are largely driven by production and/or respiration of the ecosystem (Duarte et al. 2009). Additionally, the pH is influenced by changes in temperature and salinity. The impacts of all of these factors are difficult to separate out, but appear to be less than that of production and respiration (Nixon et al. 2015). While the impacts of ocean acidification are difficult to discern, given the dynamic range of pH, the decline in pH in surface ocean waters attributable to acidification is on the order of 0.1 (Hoffman et al. 2011). Salinity ranges in the mesocosms (and Lower Narragansett Bay) are quite narrow, from 26 to 33, while seasonal water temperatures span a much broader range, generally from 0 to 23 °C (Fulweiler et al. 2015; NBFSMN 2014); however, this wide ranging temperature has a fairly minor impact on pH values. To assess how much of the observed pH variation could be attributable to seasonal shifts in temperature, we calculated the pH at 12 °C for our dataset (according to Nixon et al. 2015) and found that the difference between the in situ pH and the pH at the constant temperature was generally <0.15 (the maximum difference was, for two data points, 0.17, calculated via Lewis and Wallace 1998).

Despite having a faster rate of air-sea gas exchange, the O_2 concentration data reflect the same metabolic trends. Dissolved oxygen is released during production and consumed as organic matter is broken down by microorganisms. Of course, an estuary is not a closed system and pH and O_2 values can be influenced by exchange with other water bodies (advection) and the atmosphere (Hoffman et al. 2011; Kemp and Testa 2011; Nixon et al. 2015) and, as recent work has demonstrated, can vary substantially over the course of a day (Howarth et al. 2014). These exchange rates vary with factors

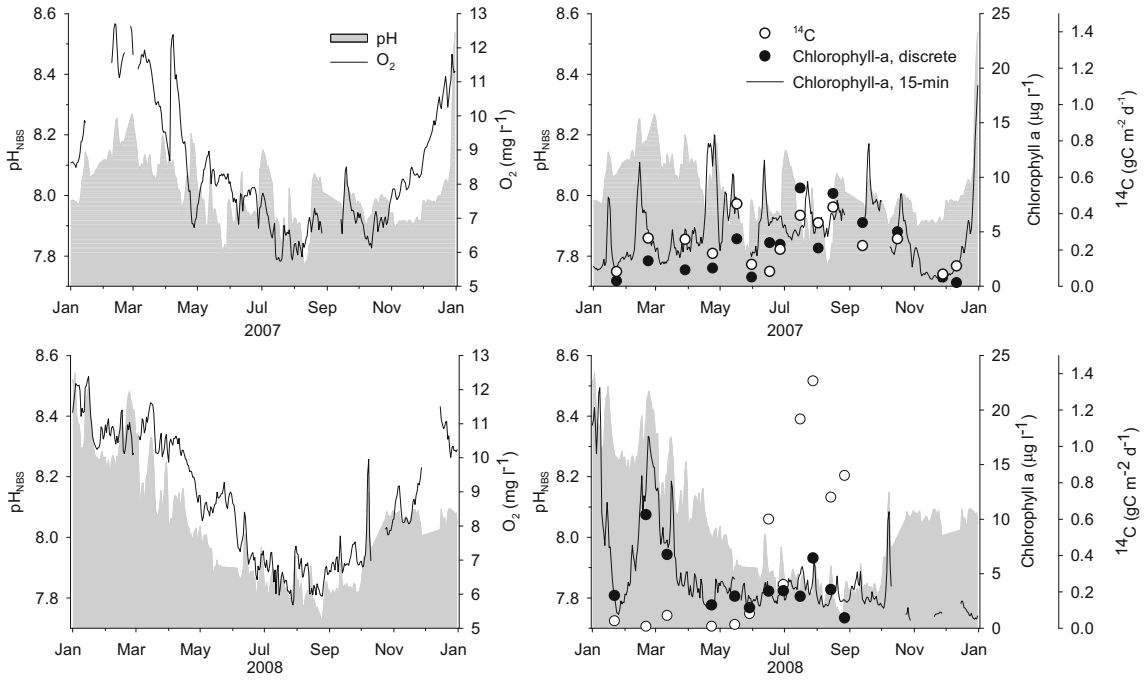

Fig. 7 Available data for a lower Narragansett Bay monitoring station (GSO, 41 29.535′, 71 25.137′) for 2007 (*left panels*) and 2008 (*right panels*). pH data are shown as a *gray filled area* in all panels, ^{14}C and chlorophyll-a (both discrete and from in situ fluorescence) are shown in the *top graphs* and dissolved oxygen (O_2) concentrations a given as a *solid line* in the bottom graphs

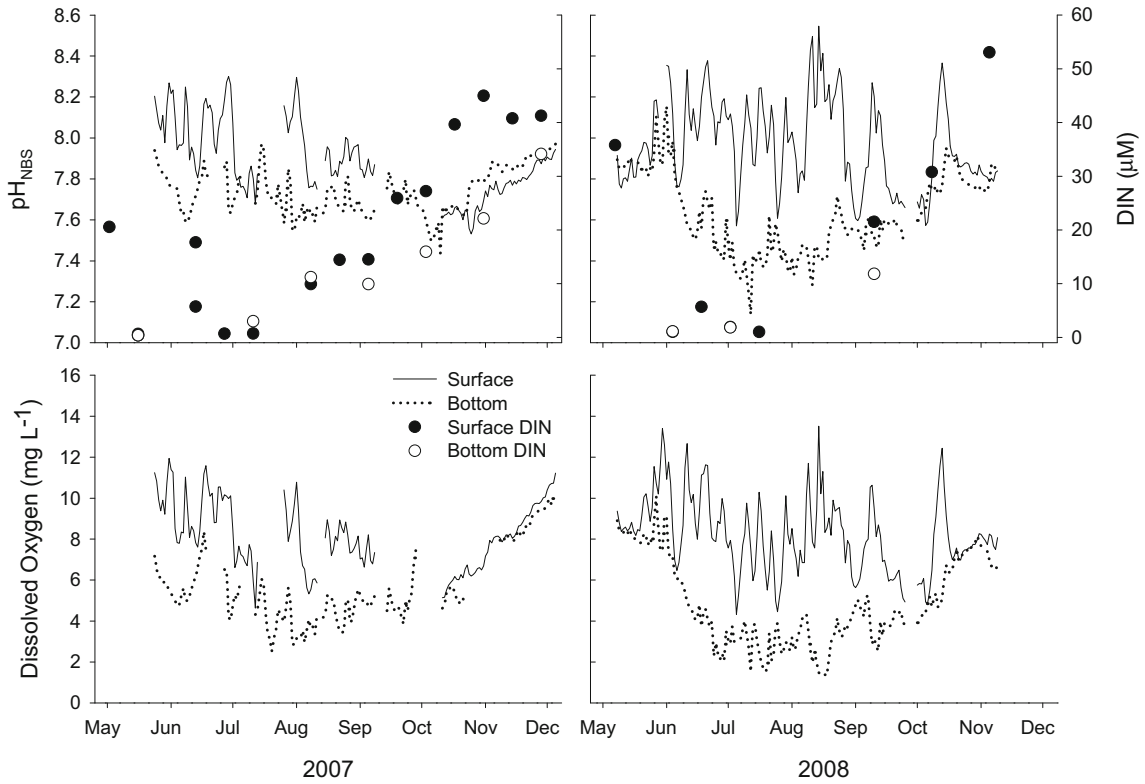

Fig. 8 Available data for the Upper Narragansett Bay Bullock Reach station. Note that the *x*-axes span from May to December and do not represent the whole year. *Top graphs* show surface (*solid line*) and bottom (*dashed line*) pH values as well as surface and bottom DIN data, which were available at a twice monthly sampling frequency. *Bottom panels* present surface (*solid line*) and bottom (*dashed line*) O_2 concentration data (NBC 2016; NBFSMN 2014)

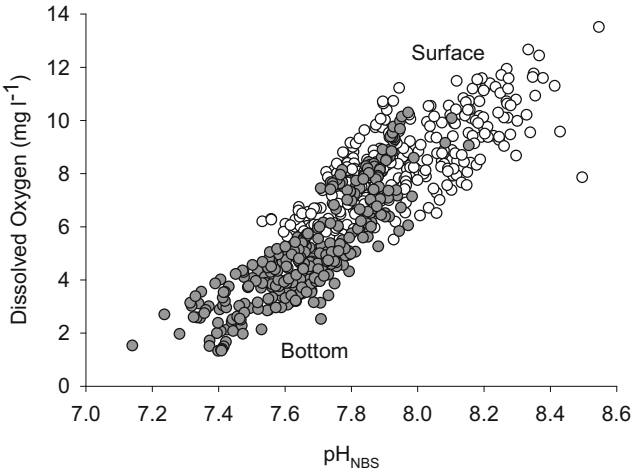

Fig. 9 Mean daily pH data are plotted against mean daily O_2 concentrations for Bullock Reach, in Upper Narragansett Bay from the summers of 2007 and 2008. Surface measurements are shown as *open circles* and bottom water measurements are shown as *filled circles*

like temperature, wind speed, surface films, rain, bottom-generated turbulence, surface turbulence, turbidity, and fetch. The parameterization of exchange rates varies significantly in the literature (e.g., Abril et al. 2009; Borges et al. 2004; Ho et al. 2011; Raymond and Cole 2001; Zappa et al. 2007). In the case of the MERL experiments, the lip of the mesocosms further decreased air-sea gas exchange rates by protecting the water surface from the full impact of the wind. The boundary layer thickness in the mesocosms (560 ± 90 μm) was more than three times thicker than Narragansett Bay (60–180 μM when winds were 1.8–3.3 m s^{-1}; Bopp et al. 1981; Nixon et al. 1980). The air-sea fluxes of O_2 and CO_2 are also often dependent on estuarine and landscape geomorphology, where the rate of flux is influenced by water depth and exposure. For example, in two shallow (<1.5 m depth) estuaries near Waquoit Bay, MA, calculated air-sea fluxes accounted for between 5 and 50 % of the apparent daytime production in the summer (Kremer et al. 2003). Another study of 22 estuaries estimated that fluxes were greater in shallow water, accounting for about 25 % of the oxygen flux in waters 1-m deep, but less than 5 % of the flux in 8-m deep waters (Caffrey 2004). The water column in the MERL mesocosms was 5-m deep (Frithsen et al. 1985a). Considering the much slower exchange rate of CO_2, the close agreement between pH and O_2 suggests that the effects of air-sea fluxes in and out of the mesocosms were relatively minor.

Considering the internal consistency of the nutrient, O_2, and pH datasets, we found it surprising that the chlorophyll data during periods of peak production were so variable, although others have shown chlorophyll-a to be a weak indicator of phytoplankton biomass (e.g., Alvarez-Fernandez and Riegman 2014; Kruskopf and Flynn 2006). Overall, if we accept that nutrient concentrations, pH, and O_2 values tracked NEP in the MERL mesocosms, then chlorophyll measurements made via discrete water sample collections were able to detect periods of high production, but depending on sampling frequency and timing, may have failed to capture or reflect the full bloom period (Figs. 3 and 4). Cell counts were undertaken to identify which species of phytoplankton were present and to measure their relative abundances; these counts were not made with the intent to assess net production, but rather to characterize the phytoplankton community. Counts were highly correlated to all of the other parameters in the more enriched 2X and 4X mesocosms (Table S1). Correlations were not as strong in the C and 1X mesocosms, suggesting that lower density populations were more difficult to characterize based on the weekly sampling. However, at the higher levels of nutrient enrichment, both chlorophyll concentrations and cell counts were highly correlated to the other parameters.

The ^{14}C measurements are much more challenging to interpret, as determining exactly what the measurement represents is complicated in itself (Peterson 1980). Because the zooplankton, or at least a portion of the zooplankton, is filtered out of the samples, ^{14}C uptake rates reflect a combination of net and gross phytoplankton production (Cloern et al. 2014; Peterson 1980; Oviatt et al. 1986b). For context, weekly measurements of dawn-dusk-dawn oxygen concentrations were used to calculate rates of daily productivity (dawn to dusk) and respiration (dusk to dawn) (Frithsen et al. 1985a). Established photosynthetic and respiratory quotients (1.2 and 1.1) were used to convert from oxygen to carbon, so values could be compared to the ^{14}C dataset (Oviatt et al. 1986b). The oxygen-based measurements represent system apparent productivity (SAP) or the net productivity of the whole mesocosm (e.g., Nixon et al. 1986). While scrubbed frequently (approximately weekly), growth on the sides of the mesocosms accounted for about 10 % of the total production (Oviatt et al. 1986b). The ^{14}C uptake rates reflect carbon uptake by phytoplankton in the absence of grazers, the SAP measurements, like the O_2 concentrations, reflect the whole mesocosm. This may explain why the ranges of rates for net productivity and respiration are greater in the oxygen-based measurements across all of the treatments (Fig. 6). These ranges increased with nutrient enrichment, indicating that the mesocosms had a high production efficiency (Cloern et al. 2014). Overall, a distinction should be made between daily or seasonal differences in the amount of primary producers present in the water column (stock) and the quantification of the rate at which these changes occur. These measures provide two different pieces of information.

Results from the MERL experiments suggest that, while ^{14}C may be a preferred method for estimating net daily productivity by phytoplankton, periodic discrete ^{14}C measurements do not sensitively track shifts in whole system production over monthly or seasonal periods, particularly when compared to pH and O_2 concentration measurements (Figs. 2 and 5). In the case of the MERL nutrient enrichment experiment, the highest rates of

^{14}C uptake did not coincide with the 1983 spring bloom, when there were more phytoplankton in the water column (Fig. 5). Rates of ^{14}C uptake appeared greater during periods presumed to have high respiration (and lower production) than they did during periods with high pH, O_2 concentrations, and chlorophyll. This apparent poor relationship may not be especially surprising as ^{14}C measures phytoplankton productivity and autotrophic respiration as the rate of radioactive carbon uptake by a subsample of the phytoplankton population (in the absence of larger zooplankton) over a specific interval of time (often a day). Growth rates and associated carbon fixation vary with nutrient availability, temperature, species composition, and growth phase of the phytoplankton (e.g., Halsey et al. 2010; López-Sandoval et al. 2014) and the accuracy could be influenced by methodological factors (e.g., Cloern et al. 2014) We further speculate that, during bloom periods, the growth of the phytoplankton could have been nutrient limited in the non-mixed bottles. This is in contrast to changes in pH, O_2, and nutrient concentrations, which respond to the overall net water column processes, including the activities of all producers and consumers (Fig. 5). Carbon uptake rates (as ^{14}C) typically are integrated throughout the water column, using dissipating light curves, and the information resulting from this method is often used to assess phytoplankton dynamics (e.g., Nixon et al. 2009; Oviatt et al. 2002), including in the establishment of photosynthetic quotients, which allows the conversion between units of carbon and oxygen (e.g., Smith et al. 2012). This method was never intended to monitor net ecosystem changes (or NEP) at weekly to seasonal timescales, and it has been successfully used to compare mean annual NEP both within (Oviatt et al. 2002) and across systems (Cloern et al. 2014). While phytoplankton growth and subsequent ^{14}C uptake rates may be limited by nutrient availability during bloom periods, depending on the method used, the impact of these underestimates could be dampened when considering annual averages of ^{14}C-based productivity. Overall, we suggest that what is actually measured is production potential, i.e., the potential growth rate of phytoplankton in idealized conditions (absence of predators, physical forcing held constant), under fixed nutrient conditions.

Narragansett Bay, 2007–2008

To assess how representative the observations from the MERL mesocosms were to a modern water column, we repeated our analyses with data from the lower west passage of Narragansett Bay, just offshore of the mesocosms location, 25 years after the nutrient enrichment experiment was conducted. During the intervening decades, significant changes in the Bay and its ecosystem have been documented as the result of climate change and management practices (e.g., Fulweiler et al. 2015; Smith et al. 2010). Nixon et al. (2009 and references therein) synthesized the plankton dynamics in the lower bay and associated phenological changes over the past 50+ years, and observed changes in species composition and abundance, particularly in the summer months. There has been a shift from winter-spring *Skeletonema* spp. blooms, like those observed in the MERL dataset, and smaller summer flagellate blooms, to a smaller or absent winter-spring bloom and much larger summer blooms of diatoms, including *Skeletonema* spp. (Borkman 2002; Nixon et al. 2009). These changes among and across years are important to document, especially in the context of climate change and the recent nutrient reductions to Narragansett Bay (Krumholz 2012; Smith et al. 2010). The complexities of these co-occurring impacts highlight the need for an assessment of not just high-resolution net productivity fluxes or production estimates, but other measures such as continued cell counts, phytoplankton species identification and rates of ^{14}C uptake, which could change with species composition or nutrient availability.

Overall, the correlations observed among parameters in the MERL mesocosms held for the more modern water column (Fig. 7). pH and O_2 trended similarly and were highly correlated with one another. This was consistent with observations for other northeast estuaries, including Narragansett Bay in the summer of 2013 (Wallace et al. 2014). Both of these parameters were also significantly inversely correlated with nutrients (Table S2). In situ fluorescence-based chlorophyll measurements were only weakly correlated to pH, were not significantly correlated to O_2, but were well correlated with discrete chlorophyll measurements (Table S2). In 2008, the ^{14}C carbon uptake measurements were particularly inconsistent and difficult to interpret, where rates were lowest during the traditional winter spring bloom period and greatest in the summer and early fall, when all other parameters indicated low production and high respiration (Fig. 7, Table S3).

An Example from a More Stratified Water Column

The MERL mesocosms were designed to be vertically well-mixed in order to replicate the well-mixed lower and mid-Narragansett Bay. However, it is useful to assess our observations (and generalizations) from a well-mixed water column in the context of a more stratified system, to see how decoupled production and respiration compare. The upper portion of the bay, and in particular the Providence-Seekonk River Estuary, has a more traditional density-driven estuarine circulation and is stratified during the summer growing season (Spaulding and Swanson 2008). This stratification is one of the many factors contributing to low oxygen bottom waters in the summer (Bergondo et al. 2005; Codiga et al. 2009; Spaulding and Swanson 2008). Seasonal hypoxia has been a cause for great concern throughout the region, and provided the impetus to upgrade all the major sewage treatment plants to tertiary treatment (N removal; RIDEM 2005).

The summer stratification is clearly reflected in both the pH and O_2 data, particularly in 2008, with the water column appearing more well-mixed after about October in both years as surface and bottom values overlap (Fig. 8). These data support the well-documented observation of summer net production in the surface waters and net respiration in the bottom waters of this portion of the estuary (e.g., Deacutis 2008; Wallace et al. 2014). In this dataset, DIN and PO_4 were significantly correlated with pH (but not O_2), where high pH values in the summer surface water were associated with low nutrient concentrations (Table S4). These concentrations, particularly of DIN, rose steadily into the fall (Fig. 8). Given the correlation between pH and O_2, we speculate that the lack of significant correlation between O_2 and nutrient concentrations may be, at least in part, due to the paucity of nutrient concentration data ($n = 17$; Table S4). But, if we accept that pH is an accurate reflection of NEP, then the DIN concentration data can potentially be used in conjunction with the pH data to assess how N-limited the system is and how changes to nutrient sources over time impact overall production.

Monitoring NEP

Each of the parameters presented, either directly or indirectly, measure some aspect of estuarine production and were designed and developed to address a specific research need. As the concept of ecosystems developed in ecology, scientists were particularly interested in understanding whether different types of ecosystems were net producers or consumers of organic matter, i.e., net autotrophic or net heterotrophic (e.g., Golley 1993). These first studies sought to measure the flow of carbon through the systems and to compare the inputs to the outputs. Discrete dawn-dusk type carbon and oxygen measurements were not intended to monitor daily or episodic production; rather, they provided information that was used to make an assessment of net production over a discrete period of time (e.g., Oviatt et al. 1986b). The measurements often formed the basis of more complex calculations developed to characterize whole water column or estuarine metabolism (e.g., Oviatt et al. 1981, 1986b). To paraphrase Staehr et al. (2012), these metabolism studies were intended to compare rates across ecosystems, look at organic matter transfer within and among adjacent systems, to look at ecosystem-level responses to perturbations, and aid in the development of biogeochemical and trophic models.

Later, the ^{14}C method was developed to address questions of net autotrophy or net heterotrophy in low-productivity waters, as it directly quantified carbon uptake by phytoplankton. While this technique may be useful for assessing rates of C uptake for specific water columns or calculating annual measures of C produced, the data from the MERL mesocosms suggest that, while sensitive to daily rates of C uptake, ^{14}C rates are not appropriate for capturing shorter term fluctuations in production in these dynamic systems (Table S3, Fig. 5).

Discrete chlorophyll measurements roughly track fluctuations in production in the MERL mesocosms, as suggested by the pH, O_2, DIN, PO_4, and DSi data, where the highest chlorophyll values corresponded to bloom periods. But, the chlorophyll time series were not as closely correlated to these other variables as we had expected. Regression models found that nutrients could only predict 29–66 % the variance in chlorophyll and pH/O_2 models could similarly predict 27–60 %. By assuming that chlorophyll concentrations would reflect phytoplankton production, we also assumed that all phytoplankton have roughly the same amount of chlorophyll in their cells over their life cycles. The MERL and Narragansett Bay 2007–2008 datasets, as well as the work of others, indicate that this may be a precarious assumption. With the advent of in situ sensor packages that measure water column fluorescence, we have often relied on fluorescence and chlorophyll measurements to monitor and assess ecosystem production and bound periods characterized by high production or high respiration. But, these sensor packages also commonly measure pH, O_2, temperature, and salinity.

We suggest that pH and dissolved oxygen concentration measurements are efficient, cost-effective tools for high-resolution continuous monitoring of net production and respiration, particularly when data are collected from the surface and bottom of the water column. They are also integrative and easy to obtain. Although they do not directly characterize the producers themselves, the data from the MERL mesocosm experiments and Narragansett Bay suggest that they sensitively reflect phytoplankton blooms.

There is no perfect or correct production measure; even the most direct methods fail to capture the entire system. For example, the potential impacts of temperature, salinity, advection, and air-sea exchange must also be considered when assessing pH and O_2 measurements. Thus, we must deliberately select the parameters that are best suited to address the questions or challenges we face. If the goal is to monitor the changes in production of a system within and across seasons and across years, we suggest that the ability to easily generate more frequent pH and O_2 data more than compensates for the uncertainties associated with each parameter. Also, these high-resolution pH and O_2 data could be used to inform when and where to focus sampling efforts for measures of chlorophyll, cell counts, nutrients, and ^{14}C, each of which provide unique and useful insights into the production dynamics of the system. As Oviatt et al. (1986b) wrote, “every measure of primary production has its own complexities” and should be considered in the context of other supporting information. Carefully calibrated buoy pH and O_2 data, often available online, can provide an important context, or baseline, of the net ecosystem production from which to consider the information provided by other primary production measures.

Acknowledgments We would like to thank all of the scientists and support staff who contributed to the MERL mesocosm experiments and the development of such thorough datasets that are still used, even after 30 years. The manuscript was improved by feedback from Dr. Jason Grear, Dr. Richard Pruell, Roxanne Johnson, and three anonymous reviewers. This is ORD Tracking Number ORD-013005 of the Atlantic Ecology Division, National Health and Environmental Effects Research Laboratory, Office of Research and Development, US Environmental Protection Agency. Although the research described in this article has been funded in part by the US Environmental Protection Agency, it has not been subjected to Agency review. Therefore, it does not necessarily reflect the views of the Agency. Mention of trade names or commercial products does not constitute endorsement or recommendation for use.

References

Abril, G., M.V. Commarieu, A. Sottolichio, P. Bretel, and F. Guerin. 2009. Turbidity limits gas exchange in a large macrotidal estuary. *Estuarine, Coastal and Shelf Science* 83: 342–348.

Alvarez-Fernandez, S., and R. Riegman. 2014. Chlorophyll in North Sea coastal and offshore waters does not reflect long term trends of phytoplankton biomass. *Journal of Sea Research* 91: 35–44.

Bender, M., K. Grande, K. Johnson, J. Marra, P.J.L. Williams, J. Sieburth, M. Pilson, C. Langdon, G. Hitchcock, J. Orchardo, C. Hunt, and P. Donaghay. 1987. A comparison of four methods for determining planktonic community production. *Limnology and Oceanography* 32: 1085–1098.

Bergondo, D.L., D.R. Kester, H.E. Stoffel, and W.L. Woods. 2005. Time-series observations during the low sub-surface oxygen events in Narragansett Bay during summer 2001. *Marine Chemistry* 97: 90–103.

Bopp, R.F., P.H. Santschi, Y.-H. Li, and B.L. Deck. 1981. Biodegredation and gas-exchange of gaseous alkanes in model estuarine ecosystems. *Organic Geochemistry* 3: 9–14.

Borges, A.V., B. Delille, L.-S. Schiettecatte, F. Gazeau, G. Abril, and M. Frankignoulle. 2004. Gas transfer velocities of CO2 in three European estuaries (Randers Fjord, Scheldt, and Thames). *Limnology and Oceanography* 49: 1630–1641.

Borja, Á., D.M. Dauer, M. Elliott, and C.A. Simenstand. 2010. Medium- and long-term recovery of estuarine and coastal ecosystems: patterns, rates, and restoration effectiveness. *Estuaries and Coasts* 33: 1249–1260.

Borkman, D. 2002. Analysis and simulation of skeletonema costatum (Grev.) Clev Annual Abundance patterns in lower Narragansett Bay 1959 to 1996. Ph.D. thesis. Graduate School of Oceanography, University of Rhode Island, Narragansett, RI, 395 pp.

Box, G.E.P., and G.M. Jenkins. 1976. *Time series analysis—forecasting and control*. San Francisco: Holden Day.

Breitburg, D.L., J.K. Craig, R.S. Fulford, K.A. Rose, W.R. Boynton, D. Brady, B.J. Ciotti, R.J. Diaz, K.D. Friedland, J.D. Hagy III, D.R. Hart, A.H. Hines, E.D. Houde, S.E. Kolesar, S.W. Nixon, J.A. Rice, D.H. Secor, and T.E. Targett. 2009a. Nutrient enrichment and fisheries exploitation: interactive effects on estuarine living resources and their management. *Hydrobiologia* 629: 31–47.

Breitburg, D.L., D.W. Hondorp, L.A. Davias, and R.J. Diaz. 2009b. Hypoxia, nitrogen, and fisheries: integrating effects across local and global landscapes. *Annual Review of Marine Science* 1: 329–349.

Brewer, P.G., and J.P. Riley. 1965. The automatic determination of nitrate in seawater. *Deep-Sea Research* 12: 765–772.

Brush, M.J., and J.W. Brawley. 2009. Adapting the light · biomass (BZI) models of phytoplankton primary production to shallow marine ecosystems. *Journal of Marine Systems* 75: 227–235.

Caffrey, J.M. 2004. Factors controlling net ecosystem metabolism in U.S. estuaries. *Estuaries and Coasts* 27: 90–101.

Caffrey, J.M., M.C. Murrell, K.S. Amacker, J.W. Harper, S. Phipps, and M.S. Woodrey. 2014. Seasonal and inter-annual patterns in primary production, respiration, and net ecosystem metabolism in three estuaries in the Northeast Gulf of Mexico. *Estuaries and Coasts* 37: S222–S241.

Carritt, D.E., and J.H. Carpenter. 1966. Comparison and evaluation of currently employed modifications of the Winkler method for determining dissolved oxygen in sea water. *Journal of Marine Research* 24: 286–318.

Clesceri, L.S., A.E. Greenberg, and R.R. Trussell. 1990. *Selected physical and chemical standard methods for students*, 17th ed. Washington D.C.: American Public Health Association.

Cloern, J.E., S.Q. Foster, and A.E. Kleckner. 2014. Phytoplankton primary production in the world's estuarine-coastal ecosystems. *Biogeosciences* 11: 2477–2501.

Codiga, D.L., H.E. Stoffel, C.F. Deacutis, S. Kiernan, and C.A. Oviatt. 2009. Narragansett Bay hypoxic event characteristics based on fixed-site monitoring network time series: intermittency, geographic distribution, spatial synchronicity, and interannual variability. *Estuaries and Coasts* 32: 621–641.

Cole, B.E., and J.E. Cloern. 1984. Significance of biomass and light availability to phytoplankton productivity in San Francisco Bay. *Marine Ecology Progress Series* 17: 15–24.

Deacutis, C.F. 2008. Evidence of ecological impacts from excess nutrients in Upper Narragansett Bay. In *Science for ecosystem-based management Narragansett Bay in the 21st century*, ed. A. Desbonnet and B.A. Costa-Pierce, 349–381. New York: Springer.

DOE. 1994. Handbook of methods for the analysis of the various parameters of the carbon dioxide system in sea water. In *Version 2*. eds. A. G. Dickson and C. Goyet. ORNL/CDIAC-74DOE. http://cdiac.ornl.gov/oceans/DOE_94.pdf. Accessed 7 May 2015.

Duarte, C.M., D.J. Conley, J. Carsensen, and M. Sánchez-Camacho. 2009. Return to Neverland: shifting baselines affect eutrophication restoration targets. *Estuaries and Coasts* 32: 29–36.

Duarte, Carlos M., Iris E. Hendriks, Tommy S. Moore, Ylva S. Olsen, Alexandra Steckbauer, Laura Ramajo, Jacob Carstensen, Julie A. Trotter, and Malcolm McCulloch. 2013. Is ocean acidification an open-ocean syndrome? Understanding anthropogenic impacts on seawater pH. *Estuaries and Coasts* 36: 221–236.

Eppley, R.W. 1968. An incubation method for estimating the carbon content of phytoplankton in natural waters. *Limnology and Oceanography* 13: 574–582.

Frithsen, J.B., A.A. Keller, M.E.Q. Pilson. 1985a. Effects of inorganic nutrient additions in coastal areas: a mesocosm experiment data report. Volume 1. MERL Series, Report No. 3. University of Rhode Island. Kingston, RI.

Frithsen, J.B., P.A. Lane, A.A. Keller, and M.E.Q. Pilson. 1985b. Effects of inorganic nutrient additions in coastal areas: a mesocosm experiment data report. Volume 2. MERL Series, Report. No. 4. The University of Rhode Island, Kingston, RI.

Fulweiler, R.W., A.J. Oczkowski, K.M. Miller, C.A. Oviatt, and M.E.Q. Pilson. 2015. Whole truths vs. half truths—and the search for clarity in long-term water temperature records. *Estuarine, Coastal and Shelf Science* 157: A1–A6.

Glibert, P.M., D.C. Hinkle, B. Sturgis, and R.V. Jesien. 2014. Eutrophication of a Maryland/Virginia Coastal Lagoon: a tipping point, ecosystem changes, and potential causes. *Estuaries and Coasts* 37: S128–S146.

Golley, F.B. 1993. *A history of the ecosystem concept in ecology*. New Haven: Yale University Press.

Greening, H., A. Janicki, E.T. Sherwood, R. Pribble, and J.O.R. Johansson. 2014. Ecosystem responses to long-term nutrient management in an urban estuary: Tampa Bay, Florida, USA. *Estuarine, Coastal and Shelf Science* 151: A1–A16.

Hager, S.W., E.L. Atlas, L.I. Fordon, A.W. Mantyla, and P.K. Park. 1972. A comparison at sea of manual and autoanalyzer analyses of

phosphate, nitrate, and silicate. *Limnology and Oceanography* 17: 931–937.

Halsey, K.H., A.J. Milligan, and M.J. Behrenfeld. 2010. Physiological optimization underlies growth rate-independent chlorophyll-specific gross and net primary production. *Photosynthesis Research* 103: 125–137.

Hinga, K.R. 1992. Co-occurrence of dinoflagellate blooms and high pH in marine enclosures. *Marine Ecology Progress Series* 86: 181–187.

Ho, D.T., P. Schlosser, and P.M. Orton. 2011. On factors controlling airwater gas exchange in a large tidal river. *Estuaries and Coasts* 34: 1103–1116.

Hoffman, G.E., J.S. Smith, K.S. Johnson, U. Send, L.A. Levin, F. Micheli, A. Paytan, N.N. Price, B. Peterson, Y. Takeshita, P.G. Matson, E.D. Crook, K.J. Kroeker, M.C. Gambi, E.B. Rivest, C.A. Frieder, P.C. Yu, and T.R. Martz. 2011. High-frequency dynamics of ocean pH: a multi-ecosystem comparison. PLoS ONE 6: e28983.

Howarth, R.W., and A.F. Michaels. 2000. The measurement of primary production in aquatic ecosystems. In *Methods in ecosystem science*, ed. O.E. Sala, 72–85. New York: Springer.

Howarth, Robert W., Melanie Hayn, Roxanne M. Marino, Neil Ganju, Kenneth Foreman, Karen McGlathery, Anne E. Giblin, Peter Berg, and Jeffrey D. Walker. 2014. Metabolism of a nitrogen-enriched coastal marine lagoon during the summertime. *Biogeochemistry* 118: 1–20.

Keller, A.A. 1986. Modeling the productivity of natural phytoplankton populations using mesocosm data along a nutrient gradient. Ph.D. Dissertation. University of Rhode Island.

Keller, A.A., and U. Riebesell. 1989. Phytoplankton carbon dynamics during a winter-spring diatom bloom in an enclosed marine ecosystem: Primary production, biomass, and loss rates. *Marine Biology* 103: 131–142.

Kemp, W.M., and J.M. Testa. 2011. Metabolic balance between ecosystem production and consumption. In *Treatise on estuaries and coastal science*, vol. 7, ed. E. Wolansky and D. McLusky, 83–118. Oxford: Elsevier Ltd.

Kemp, W.M., J.M. Testa, D.J. Conley, D. Gilbert, and J.D. Hagy. 2009. Temporal responses of coastal hypoxia to nutrient loading and physical controls. *Biogeosciences* 6: 2985–3008.

Kremer, J.N., A. Reischauer, and C. D'Avanzo. 2003. Estuary-specific variation in the air-water gas exchange coefficient for oxygen. *Estuaries* 26: 829–836.

Krumholz, J.S. 2012. Spatial and temporal patterns in nutrient standing stock and mass-balance in response to load reductions in a temperate estuary. Ph.D. Dissertation, University of Rhode Island.

Kruskopf, M., and K.J. Flynn. 2006. Chlorophyll content and fluorescence responses cannot be used to gauge reliably phytoplankton biomass, nutrient status or growth rate. *New Phytologist* 169: 525–536.

Kunkel K.E., and 24 others. 2013. Monitoring and understanding trends in extreme storms. *Bulletin of the American Meteorological Society* 94: 499–514.

Lewis, E., and D. W.R. Wallace. 1998. Program developed for CO_2 system ORNL/CDIAC-105, Carbon Dioxide Information Analysis Center, Oak Ridge National Laboratory, US Department of Energy, Oak Ridge, Tennessee.

López-Sandoval, D.C., T. Rodríguez-Ramos, P. Cermeño, C. Sobrino, and E. Marañón. 2014. Photosynthesis and respiration in marine phytoplankton: relationship with cell size, taxonomic affiliation, and growth phase. *Journal of Experimental Marine Biology and Ecology* 457: 151–159.

Lorenzen, C.J. 1966. A method for the continuous measurement of *in vivo* chlorophyll concentrations. *Deep Sea Research* 13: 223–227.

Marra, J. 2009. Net and gross productivity: weighing in with ^{14}C. *Aquatic Microbial Ecology* 56: 123–131.

MERL. 2015. http://www.gso.uri.edu/merl/merl.html. Accessed 7 May 2015.

Mortazavi, B., A.A. Riggs, J.M. Caffrey, H. Genet, and S.W. Phipps. 2012. The contribution of benthic nutrient regeneration to primary production in a shallow eutrophic estuary, Weeks Bay, Alabama. *Estuaries and Coasts* 35: 862–877.

Narragansett Bay Fixed-Site Monitoring Network (NBFSMN) 2014. Rhode Island Department of Environmental Management, Office of Water Resources. Data available at www.dem.ri.gov/bart.

NBC 2016. Narragansett Bay Commission nutrient monitoring. http://snapshot.narrabay.com/app/WaterQualityInitiatives/NutrientMonitoring. Accessed 24 May 2016.

Nixon, S.W. 1981. Remineralization and nutrient cycling in coastal marine ecosystems. In *Estuaries and nutrients*, ed. B.J. Neilson and L.E. Cronin, 111–138. Clifton: Humana Press.

Nixon, S.W. 1982. Nutrient dynamics, primary production and fisheries yields of lagoons. *Oceanologica Acta*, Special Issue: 357–371.

Nixon, S.W. 1995. Coastal marine eutrophication: a definition, social causes, and future concerns. *Ophelia* 41: 199–219.

Nixon, S.W. 2009. Eutrophication and the macroscope. *Hydrobiologia* 629: 5–19.

Nixon, S.W., and B.A. Buckley. 2002. "A strikingly rich zone"—nutrient enrichment and secondary production in coastal marine ecosystems. *Estuaries* 25: 782–796.

Nixon, S.W., D. Alonso, M.E.Q. Pilson and B.A. Buckley. 1980. Turbulent mixing in aquatic microcosms. In *Microcosms in ecological research*, ed. J. Giesy, 818–849. U.S. Department of Energy, CONF-781101.

Nixon, S.W., C.A. Oviatt, J. Frithsen, and B. Sullivan. 1986. Nutrients and the productivity of estuarine and coastal marine ecosystems. *Journal of the Limnological Society of South Africa* 12: 43–71.

Nixon, S.W., B. Buckley, S. Granger, L. Harris, A. Oczkowski, R. Fulweiler, and L. Cole. 2008. Nutrient (N and P) inputs to Narragansett Bay: Past, present, and future. In *Science for ecosystem-based management Narragansett Bay in the 21st century*, ed. A. Desbonnet and B.A. Costa-Pierce, 101–176. New York: Springer.

Nixon, S.W., R.W. Fulweiler, B.A. Buckley, S.L. Granger, B.L. Nowicki, and K.M. Henry. 2009. The impact of changing climate on phenology, productivity, and benthic-pelagic coupling in Narragansett Bay. *Estuarine, Coastal and Shelf Science* 82: 1–18.

Nixon, S.W., A.J. Oczkowski, M.E.Q. Pilson, L. Fields, C.A. Oviatt, and C.W. Hunt. 2015. On the response of pH to inorganic nutrient enrichment in well-mixed coastal marine waters. *Estuaries and Coasts* 38: 232–241.

Oczkowski, A., and S. Nixon. 2008. Increasing nutrient concentrations and the rise and fall of a coastal fishery; a review of data from the Nile Delta, Egypt. *Estuarine, Coastal and Shelf Science* 77: 309–319.

Oviatt, C., B. Buckley, and S. Nixon. 1981. Annual metabolism in Narragansett Bay calculated from survey field measurements and microcosm observations. *Estuaries* 4: 167–175.

Oviatt, C.A., A.A. Keller, P.A. Sampou, and L.L. Beatty. 1986a. Patterns of productivity during eutrophication: a mesocosm experiment. *Marine Ecology Progress Series* 28: 69–80.

Oviatt, C.A., D.T. Rudnick, A.A. Keller, P.A. Sampou, and G.T. Almquist. 1986b. A comparison of system (O_2 and CO_2) and C-14 measurements of metabolism in estuarine mesocosms. *Marine Ecology Progress Series* 28: 57–67.

Oviatt, C.A., P. Lane, F. French III, and P. Donaghay. 1989. Phytoplankton species and abundance in response to eutrophication in coastal marine mesocosms. *Journal of Plankton Research* 11: 1223–1244.

Oviatt, C.A., A.A. Keller, and L. Reed. 2002. Annual primary production in Narragansett Bay with no bay-wide winter-spring phytoplankton bloom. *Estuarine, Coastal and Shelf Science* 54: 1013–1026.

Peterson, B.J. 1980. Aquatic primary productivity and the ^{14}C-CO_2 method: A history of the productivity problem. *Annual Review of Ecology and Systematics* 11: 359–385.

Pilson, M.E.Q. 1985. On the residence time of water in Narragansett Bay. *Estuaries* 8: 2–14.

Pilson, M.E.Q. 1998. *An introduction to the chemistry of the sea*, 1st ed. Cambridge: Cambridge University Press.

Pratt, D.M. 1965. The winter-spring diatom flowering in Narragansett Bay. *Limnology Oceanography* 10: 173–184.

QAPP NBFSMN. 2014. Quality assurance project plan for the Narragansett bay fixed site monitoring network. Available at: http://www.dem.ri.gov/pubs/qapp/nbfsmn.pdf. Accessed 6 May 2015.

Raymond, P.A., and J.J. Cole. 2001. Gas exchange in rivers and estuaries: choosing a gas transfer velocity. *Estuaries* 24: 312–317.

Redmond, K.T., and J.T. Abatzoglou. 2014. Current climate and recent trends. In *Climate change in North America*, ed. G. Ohring, 53–94. Switzerland: Springer International Publishing.

RIDEM. 2005. Plan for managing nutrient loadings to Rhode Island Waters. RI General Law § 46-12-3(25).

Ryther, J.H., and C.S. Yentsch. 1958. Primary production of continental shelf waters off New York. *Limnology and Oceanography* 3: 327–338.

Sallenger, A.H., K.S. Doran, and P.A. Howd. 2012. Hotspot of accelerated sea-level rise on the Atlantic coast of North America. *Nature Climate Change* 2: 884–888.

Smith, L.M. 2011. Impacts of spatial and temporal variation of water column production and respiration on hypoxia in Narragansett Bay. Ph.D. Dissertation, University of Rhode Island.

Smith, L.M., S. Whitehouse, and C.A. Oviatt. 2010. Impacts of climate change on Narragansett Bay. *Northeast Naturalist* 17: 77–90.

Smith, L.M., C.M. Silver, and C.A. Oviatt. 2012. Quantifying variation in water column photosynthetic quotient with changing field conditions in Narragansett Bay, RI, USA. *Journal of Plankton Research* 34: 437–442.

Solorzano, L. 1969. Determination of ammonia in natural waters by the phenol hypochlorite method. *Limnology and Oceanography* 14: 799–801.

Spaulding, M.L., and C. Swanson. 2008. Circulation and transport dynamics in Narragansett Bay. In *Science for ecosystem-based management Narragansett Bay in the 21st century*, ed. A. Desbonnet and B.A. Costa-Pierce, 233–279. New York: Springer.

Staehr, P.A., J.M. Testa, W.M. Kemp, J.J. Cole, K. Sand-Jensen, and S.V. Smith. 2012. The metabolism of aquatic ecosystems: history, applications, and future challenges. *Aquatic Science* 74: 15–29.

Steemann-Nielsen, E. 1952. The use of radioactive 14C for measuring organic production in the sea. *Journal du Conseil pour l'exploration de la Mer* 18: 117–140.

Stoffel, H., and S. Kiernan. 2009. Narragansett Bay fixed-site monitoring network: final report on activities during 2005–2008. Available at: http://www.dem.ri.gov/bart/pdf/nbfsmin.pdf, accessed 20 Feb 2015.

Strickland, J.D.H., and T.R. Parsons. 1972. A practical handbook of seawater analysis. Fisheries Research Board of Canada, Bulletin No. 167.

Wallace, R.B., H. Baumann, J.S. Grear, R.C. Aller, and C.J. Gobler. 2014. Coastal ocean acidification: the other eutrophication problem. *Estuarine, Coastal and Shelf Science* 148: 1–13.

Williams, R.B., and M.B. Murdoch. 1966. Phytoplankton production and chlorophyll concentration in the Beaufort Channel, North Carolina. *Limnology and Oceanography* 11: 73–82.

Williams, P.J., B. Le, D.N. Thomas, and C.S. Reynolds. 2002. *Phytoplankton productivity carbon assimilation in marine and freshwater ecosystems*. Oxford: Blackwell Science Ltd.

Winkler, L.W. 1888. Die Bestimmung des in Wasser gelösten Sauerstoffen. *Berichte der Deutschen Chemischen Gesellschaft* 21: 2843–2855.

Wood, E.D., F.A.J. Armstrong, and F.A. Richards. 1967. Determination of nitrate in sea water by cadmium-copper reduction to nitrite. *Journal of the Marine Biological Association of the United Kingdom* 47: 23–31.

Yentsch, C.S., and D.W. Menzel. 1963. A method for the determination of phytoplankton chlorophyll and phaeophytin by fluorescence. *Deep Sea Research* 10: 221–231.

Yin, J., M.E. Schlesinger, and R.J. Stouffer. 2009. Model projections of rapid sea-level rise on the northeast coast of the United States. *Nature Geoscience* 2: 262–266.

Zappa, C.J., W.R. McGillis, P.A. Raymond, J.B. Edson, E.J. Hintsa, H.J. Zemmelink, J.W.H. Dacey, and D.T. Ho. 2007. Environmental turbulent mixing controls on air-water gas exchange in marine and aquatic systems. *Geophysical Research Letters* 34: L10601.

Zeebe, R. 2012. History of seawater carbonate chemistry, atmospheric CO2, and ocean acidification. *Annual Review of Earth and Planetary Sciences* 40: 141–165. doi:10.1146/annurev-earth-042711-105521.

Estuaries and Coasts (2018) 41:2260–2276
https://doi.org/10.1007/s12237-018-0435-2

How the Distribution of Anthropogenic Nitrogen Has Changed in Narragansett Bay (RI, USA) Following Major Reductions in Nutrient Loads

Autumn Oczkowski[1] · Courtney Schmidt[2] · Emily Santos[3] · Kenneth Miller[4] · Alana Hanson[1] · Donald Cobb[1] · Jason Krumholz[5] · Adam Pimenta[1] · Leanna Heffner[6] · Sandra Robinson[1] · Joaquín Chaves[7] · Rick McKinney[1]

Received: 21 December 2017 / Revised: 26 June 2018 / Accepted: 28 June 2018 / Published online: 12 July 2018
© This is a U.S. government work and not under copyright protection in the U.S.; foreign copyright protection may apply 2018

Abstract

Over the past decade, nitrogen (N) loads to Narragansett Bay have decreased by more than 50%. These reductions were, in large part, the direct result of multiple wastewater treatment facility upgrades to tertiary treatment, a process which employs N removal. Here, we document ecosystem response to the N reductions and assess how the distribution of sewage N in Narragansett Bay has changed from before, during, and shortly after the upgrades. While others have observed clear responses when data were considered annually, our seasonal and regional comparisons of pre- and post-tertiary treatment dissolved inorganic nitrogen (DIN) concentrations and Secchi depth data, from bay-wide surveys conducted periodically from the early 1970s through 2016, resulted in only a few subtle differences. Thus, we sought to use stable isotope data to assess how sewage N is incorporated into the ecology of the Bay and how its distribution may have changed after the upgrades. The nitrogen ($\delta^{15}N$) and carbon ($\delta^{13}C$) stable isotope measurements of particulate matter served as a proxy for phytoplankton, while macroalgae served as short-term integrators of water column bio-available N, and hard clams (*Mercenaria mercenaria*) as integrators of water column production. In contrast to other estuarine stable isotope studies that have observed an increased influence of isotopically lower marine N when sewage N is reduced, the opposite has occurred in Narragansett Bay. The tertiary treatment upgrades have increased the effluent $\delta^{15}N$ values by at least 2‰. The plants and animals throughout Narragansett Bay have similarly increased by 1–2‰, on average. In contrast, the $\delta^{13}C$ values measured in particulate matter and hard clams have declined by about the same amount. The $\delta^{15}N$ results indicated that, even after the N reductions, sewage N still plays an important role in supporting primary and secondary production throughout the bay. However, the $\delta^{13}C$ suggests that overall net production in Narragansett Bay has decreased. In the 5 years after the major wastewater treatment facilities came on-line for nutrient removal, oligotrophication has begun but sewage remains the dominant source of N to Narragansett Bay.

Keywords Stable isotope · $\delta^{15}N$ · Eutrophication · Sewage treatment plant · Wastewater treatment facility · Tertiary treatment · Ecosystem response · Oligotrophication

Communicated by Carolyn A. Currin

✉ Autumn Oczkowski
oczkowski.autumn@epa.gov

[1] US EPA, Atlantic Ecology Division, 27 Tarzwell Dr., Narragansett, RI 02882, USA

[2] Narragansett Bay Estuary Program – NEIWPCC, 235 Promenade St. Suite 310, Providence, RI 02908, USA

[3] Geology, Humboldt State University, 1 Harpst St, Arcata, CA 95521, USA

[4] CSRA LLC, 6361 Walker Lane Suite 300, Alexandria, VA 22310, USA

[5] McLaughlin Research Corporation, 132 Johnnycake Hill Rd, Middletown, RI 02842, USA

[6] Western Alaska Landscape Conservation Cooperative, US Fish and Wildlife Service, 1011 E. Tudor Rd, Anchorage, AK 99503, USA

[7] Science Systems and Applications, Inc., NASA Goddard Space Flight Center, 8800 Greenbelt Rd, Greenbelt, MD 20771, USA

Introduction

In what has been labeled as a "Grand Ecological Experiment" (Nixon et al. 2008) for the improvement of water quality, anthropogenic nitrogen loadings have been drastically reduced into Narragansett Bay (Rhode Island, USA) over the past decade. Starting in 2006, all major wastewater treatment facilities (WWTFs) began removing nitrogen (N) from effluent by upgrading from secondary to tertiary treatment (NBEP 2017). The initial target of 50% N reduction was met in 2012, and between 2013 and 2015, additional facilities have upgraded for a total reduction of 62% in sewage N loads from rivers and a 47% reduction in direct WWTF discharges into the bay since 2000. A recent, post-upgrade budget calculated the total N load from rivers and sewage to this N-limited system at 3570×10^3 kg year^{-1} (NBEP 2017), down from an estimated 8131×10^3 kg year^{-1} for 1982 to 1983 (Nixon et al. 2008). Total phosphorous (P) loads have similarly declined from 1053×10^3 kg year^{-1} in 1982–1983 to 332×10^3 kg year^{-1} in 2013–2015 (NBEP 2017). Recent work by Oviatt et al. (2017) has documented reductions in mean annual nutrient concentrations along the length of Narragansett Bay as well as decreases in the duration of hypoxia and in system apparent production. Narragansett Bay has a long history of human influence (Nixon et al. 2008), and the recent large-scale reduction in N loading provides a unique opportunity to continue to document recovery of the system.

Narragansett Bay (Fig. 1) is a fairly straightforward research estuary. The bay has a narrow salinity gradient. From Conimicut Point at the top of the Upper Bay to its mouth, it ranges from about 29 to 32 and is generally considered to be partially stratified to well mixed (Kremer and Nixon 1978; Spaulding and Swanson 2008). The relatively small freshwater inputs primarily enter at the head of the bay via the Providence River Estuary. Sewage remains the largest single source of nutrients to Narragansett Bay, with 12 WWTFs discharging directly to the bay and 25 others that discharge to tributaries (NBEP 2017). The bulk of the sewage enters the Providence-Seekonk River Estuary and Upper Bay because the northern portion of the Bay watershed is more urban. Between 2000 and 2010, the sewage N loads that discharged directly to the Providence River Estuary and its tributaries were about 60–70% of the total sewage loads to the bay (NBEP 2017). Most geochemical and ecological parameters that we measure reflect a gradient from the urban head of the bay to the mouth. This includes chlorophyll and nutrient concentrations (e.g., Oviatt et al. 2002), metals (in sediment, Wells et al. 2000), benthic community structure (Perez et al. 1999), and a suite of emerging contaminants (Cantwell et al. 2017).

There have been measurements of stable isotopes of nitrogen (δ^{15}N) and carbon (δ^{13}C) made periodically in Narragansett Bay from the early 1980s (e.g., Garber 1982; Gearing et al. 1991) to the present in both coastal salt marshes (e.g., McKinney et al. 2001; Pruell et al. 2006) and open estuarine waters (Chaves 2004; Oczkowski et al. 2008; Schmidt 2014). Measurements of δ^{15}N often reflect anthropogenic inputs, where higher values are indicative of human or animal sources and lower values are associated with lower impact (e.g., Fry 2006). Because of this, the highest δ^{15}N values in Narragansett Bay would be expected in the Providence River—the area of the bay most closely associated with direct and indirect sewage input (Fig. 1). However, Chaves (2004) reported higher values in the Upper Bay, measured in particulate matter (PM), than in either the Providence River Estuary or Lower Bay. The isotopically lighter values measured in the Providence River Estuary could have been reflecting preferential uptake of the lighter ^{14}N over ^{15}N in this nutrient-rich environment. Lower δ^{15}N values in the Providence River Estuary, relative to Upper Narragansett Bay, were also measured in PM, macroalgae, fish, and shellfish prior to the WWTF upgrades (e.g., Oczkowski et al. 2008; Pruell and Taplin 2015; Pruell et al. 2017). Chaves (2004) also suggested that the lower δ^{15}N values measured at the mouth of Narragansett Bay were reflecting shelf N influences in this N-limited environment. In contrast to the observed trends in PM-δ^{15}N, Oczkowski et al. (2008) did not observe a gradient in the mainstem of Narragansett Bay in either δ^{15}N or δ^{13}C values measured in the tissues of hard clams (*Mercenaria mercenaria*), which are located in the sediment and filtering food as it passes. They did, however, find a clear gradient in macroalgae where δ^{15}N values decreased down the bay. It was hypothesized that the clams in Narragansett Bay were largely consuming sewage-supported phytoplankton formed in the Upper Bay. The macroalgae integrated δ^{15}N values associated with the in situ bio-available dissolved N, which reflected a mixing gradient from isotopically high (δ^{15}N) sewage-enriched Upper Bay waters to isotopically lower shelf water nitrogen. Pruell and Taplin (2015) also observed patterns similar to those seen in the macroalgae in young-of-year winter flounder (*Pseudopleuronectes americanus*) collected from near-shore locations.

Stable isotopes are tools that, when considered in conjunction with other water quality and ecological data, allow one to track how the anthropogenic N is distributed through an ecosystem and to quantify responses to major perturbations. There are only a few studies that have used a stable isotope approach to assess the ecological response to nutrient reduction. In a Baltic Sea embayment, a major WWTF was upgraded to tertiary treatment by 1998 (Savage and Elmgren 2004). The δ^{15}N in the macroalga *Fucus vesiculosus* declined with distance from the sewage outfall, and there was a substantial decrease in δ^{15}N values throughout the embayment after a tertiary treatment upgrade reduced N loads by about 85% (Savage and Elmgren 2004). The post-reduction δ^{15}N values were roughly 4‰ lower than earlier measurements,

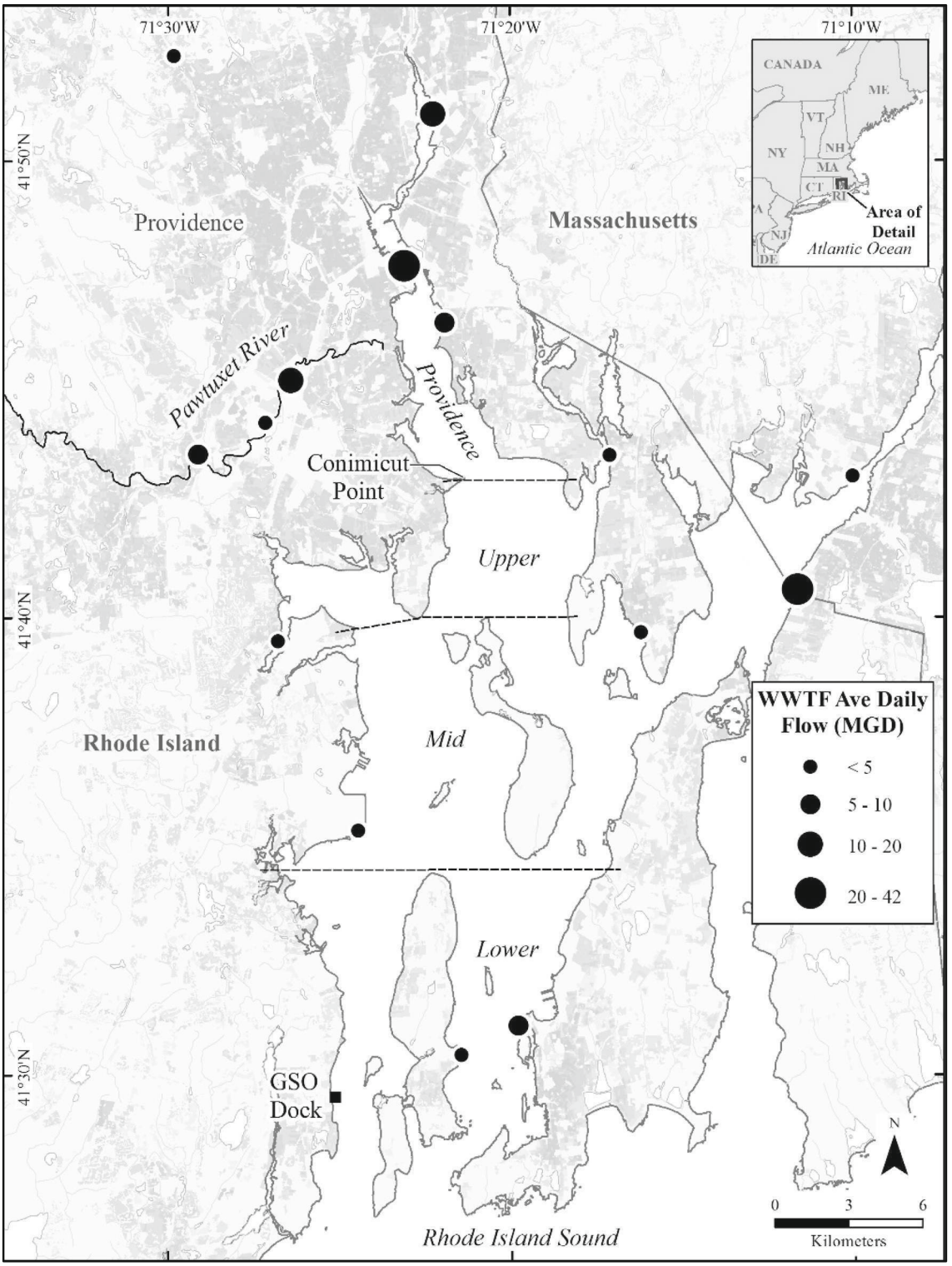

Fig. 1 Map showing the Providence River Estuary and the upper, middle, and lower regions of Narragansett Bay. Markers on the map depict the volume of discharge (in millions of gallons per day or MGD) from wastewater treatment facilities (WWTF)

reflecting proportionally more of a marine influence. Similar observations occurred in Moreton Bay, Australia, after a 50% reduction in N loads, for the red macroalga *Catenella nipae* (Costanzo et al. 2005) and in the Moreton Bay estuarine tributaries as measured in filamentous algae and shore crabs (Pitt et al. 2009). While only a few studies have been completed, they provide insight into what might be expected in Narragansett Bay in response to its N load reductions.

Given the foundation of stable isotope studies in this region and our ongoing research, we used these tools to understand how the bay responded to the nutrient reductions in sewage effluent in the first 5 years after the improvements. Prior to the upgrades, secondary treated effluent had $\delta^{15}N$ values of about 6.1 ± 0.8 and $11.2 \pm 0.5‰$ in nitrate and ammonium, respectively (DiMilla 2011). While the dissolved inorganic N (DIN) in the secondary effluent shifted back and forth from being ammonia dominated to nitrate dominated, the DIN in the tertiary effluent is predominantly nitrate with an average value of 13.4‰ (Schmidt et al. 2016). While the N load from the WWTFs decreased by more than half, the $\delta^{15}N$ of the DIN load increased. Recent work has shown that $\delta^{15}N$ values in juvenile flounder in Upper Narragansett Bay increased significantly between 2002 and 2004 and 2012–2014 (Pruell et al. 2017).

We used stable isotopes of N and C to identify how the distribution of sewage N has changed in Narragansett Bay since the WWTF upgrades. In addition to nutrient concentrations and measures of Secchi depth, we focused on water column PM, which is a mix of phytoplankton and other water column particulates, and macroalgae, which integrate water column nutrients over longer time periods. We also used filter feeding hard clams as a sentinel of the food web by measuring $\delta^{15}N$ and $\delta^{13}C$ in their tissues. We hypothesized that the $\delta^{15}N$ values of primary and secondary producers in the Upper Bay would increase to reflect the shift in source $\delta^{15}N$ and that the Middle and Lower Bay $\delta^{15}N$ values in the plant and animal tissues would decrease to reflect offshore N contributions. We also expected to see declines in $\delta^{13}C$ values in particulate matter and hard clams in those samples collected after the N reductions as they would reflect decreases in net production associated with lower N inputs (e.g., Oczkowski et al. 2010; Oczkowski et al. 2014). Our results were inconsistent with our hypothesis that the $\delta^{15}N$ in the estuary would look more marine following the sewage N reductions and support the observation that sewage is still the dominant N source to the bay's food web (NBEP 2017). But, the $\delta^{13}C$ data from the clams and particulate matter support observations of an overall decrease in production (e.g., Oviatt et al. 2017). Given how different Narragansett Bay looks from other coastal ecosystems that have experienced similar nutrient reductions, we provide important context for how ecosystem responses to large-scale source reductions should be considered.

Methods

Water Clarity Measurements

We compiled Secchi depth measurements (in m), as a proxy for water clarity, from a number of different sources (Table 1). All of the monthly values from 1997 to 1998 were converted from light attenuation coefficient data (K_d; m^{-1}) to estimates of Secchi depth, where Secchi depth was approximated as $1.7 \div K_d$ (Poole and Atkins 1929; Oviatt et al. 2002). About 10% of values from the Narragansett Bay Commission (NBC) dataset for the Providence River Estuary were estimated from K_d (NBEP 2017). As part of the Narragansett Bay Fixed Site Monitoring Network (NBFSMN), the Graduate School of Oceanography (GSO) at the University of Rhode Island also recorded K_d values from nine stations in our sampling area from 2006 to 2015, which were converted to measurements of water column clarity (from m^{-1} to m). Given that we were focused on the impacts during the growing season, we excluded winter Secchi data from our analyses.

Particulate Matter and Nutrients

Recent samples for particulate matter and nutrients were collected as part of the Bay Ecosystem Time Series (BETS) efforts led by the US EPA's Atlantic Ecology Division. Additional nitrate plus nitrite ($NO_3^- + NO_2^-$) and ammonium (NH_4^+) concentration data, collectively known as dissolved inorganic N or DIN, were available from several additional sources, where Narragansett Bay was sampled over a range of locations and at different frequencies (see Table 1). Samples were collected approximately monthly, although extensive ice cover prevented sampling in some winter months, at eight stations (Tables 1 and 2) from 17 January 2014 to 7 December 2016. Using a 5-L Niskin bottle, the surface, middle, and bottom of the water column were sampled. Water was decanted into acid-washed 1-L bottles, which were then stored in the dark, on ice, until they were transported back to the laboratory. There, two replicates of approximately 400 mL of sample water were filtered through pre-combusted glass fiber filters. The exact volume of water filtered was noted as it varied with water particulate content.

Some of the filtrate was decanted into acid-stripped scintillation vials which were then frozen until samples could be analyzed for inorganic nutrient concentrations. We used an Astoria-Pacific Astoria 2 continuous-flow analyzer (Astoria-Pacific, Clackamas, OR, USA) to measure nitrate plus nitrite ($NO_3^- + NO_2^-$) and ammonium (NH_4^+) concentrations. The $NO_3^- + NO_2^-$ was measured via cadmium reduction (US EPA method 353.2), and the NH_4^+ concentrations were measured using EPA method 350.1. Samples were calibrated against a five-point standard curve, check standards were run every 15 samples, and Milli-Q blanks were run every 10 samples.

To determine stable isotope values of the particulate matter, filters were dried in a 60 °C oven for at least 24 h. Once dry, they were pelletized and C and N isotope compositions were determined using an Elementar Vario Micro elemental analyzer connected to a continuous flow Isoprime 100 isotope ratio mass spectrometer (Elementar Americas, Mt. Laurel, NJ). Replicate analyses of isotopic standard reference materials

Table 1 The time spans in which data were collected are given for each parameter, as well as the source of each dataset

Time span	Frequency	No. of stations	Water column position	Source
Secchi				
April 1997–April 1998	Twice monthly	15[a]		Oviatt et al. (2002)
July 2007–November 2015	Variable, but roughly weekly	10[b]		NBEP (2017)
August 2008–August 2009 & July 2013–February 2016	Variable, but roughly twice monthly from June to October	9[c]		GSO/NBFSMN
January 2014–December 2016	Monthly	8		This study
Dissolved inorganic nitrogen				
July 1972–August 1973	Twice monthly	13	Surface and bottom	Kremer and Nixon (1978)
September 1979–September 1980	Twice monthly	6	Surface	Oviatt and Pastore (1980)
June 2000–December 2002	Variable[a]	Variable[d]	Surface	Chaves (2004)
November 2011–November 2012	Monthly	9	Surface and bottom	Schmidt (2014)
March 2006–December 2012 & January 2013-June 2016	Monthly and twice monthly in June, July, August, and September	12	Surface	Krumholz (2012); Oviatt, personal communication
January 2014–December 2016	Monthly	8	Surface, middle, and bottom	This study
Particulate matter				
June 2000–September 2001	Variable[a]	Variable[d]	Surface	Chaves (2004)
August 2004–November 2005	Five sampling events	Ranged from 1 to 10	Surface	DiMilla (2006)
January 2014–December 2016	Monthly	8	Surface, middle, and bottom	This study
Macroalgae[e]				
September 2006		16		Oczkowski et al. (2008)
8 January 2007–8 January 2008		24		This study
July 2012		23		Schmidt (2014)
September 2015		21		This study
August 2016		12		This study
Hard clams[e]				
June–September 2005		10		Oczkowski et al. (2008) and DiMilla (2006)
August–October 2012		15		Schmidt (2014)
June 2015–December 2016		10		This study

[a] Sixteen stations were sampled. We included 15 in our analysis as we excluded a Greenwich Bay station

[b] All stations are in the Providence River, with the exception of one station that was immediately to the south

[c] Omitting two Greenwich Bay stations and one station in Mt. Hope Bay. One station, included in the analysis, had only three data points

[d] Sampling frequencies across stations ranged from single events at some stations to four times per week at select stations

[e] Discrete sampling events

Table 2 Station locations for water samples collected from the top, middle, and bottom of the water column at each of eight locations as part of the ongoing Bay Ecosystem Time Series (BETS) research effort

Station no.	Latitude	Longitude	Spatial category
1	41.76109	− 71.3783	Providence River Estuary
2	41.69886	− 71.3263	Upper Bay
3	41.65884	− 71.38687	Upper Bay
4	41.59823	− 71.38174	Middle Bay
5	41.49254	− 71.41158	Lower Bay
6	41.64164	− 71.31014	Upper Bay
7	41.56658	− 71.31102	Middle Bay
8	41.49481	− 71.35384	Lower Bay

Resultant water clarity and dissolved inorganic nitrogen concentration data, as well as particulate stable isotope data, from these stations, are presented in this manuscript

USGS 40 ($\delta^{13}C = -26.39‰$, $\delta^{15}N = -4.52‰$) and USGS 41 ($\delta^{13}C = 37.63‰$, $\delta^{15}N = 47.57‰$) were used to normalize isotopic values of working standards (blue mussel homogenate) to the air ($\delta^{15}N$) and Vienna Pee Dee Belemnite ($\delta^{13}C$) scales (Paul et al. 2007). Isotope values are expressed in δ notation following the formula $\delta X\ (‰) = [(R_{sample} / R_{standard}) - 1] \times 10^3$, where X is ^{13}C or ^{15}N and R is $^{13}C/^{12}C$ or $^{15}N/^{14}N$ isotopic ratio, respectively. Working standards were analyzed after every 24 samples to monitor instrument performance and check data normalization. The precision of the laboratory standards was better than ± 0.3‰ for C and N.

Particulate $\delta^{15}N$ values given in Chaves (2004) and DiMilla (2006) were measured via the US EPA Atlantic Ecology Division's Carlo-Erba NA 1500 Series II elemental analyzer interfaced with a Micromass Optima mass spectrometer. Further, while particulate samples were also collected by Schmidt (2014), the sampling methods and analyses were different enough that direct comparisons to the other data were not appropriate; thus, they were not included in these analyses.

Macroalgae

Samples were collected at low tide from rocky outcrops and the bases of lighthouses positioned mid-channel throughout Narragansett Bay. The goal was to collect samples from below the water line and away from the coast, and any associated seeps, so that the $\delta^{15}N$ values of the macroalgae would be representative of the water column $\delta^{15}N$. Collected samples were stored in plastic bags, in the dark and on ice, until they were processed in the lab. Samples were separated by genus and, where possible, species, rinsed with deionized water, and all visible epiphytes were removed. In some cases, when we were unsure of the genus or species, subsamples were frozen and later identified by macroalgal experts (Carol Thornber or Lindsay Green, personal communication). Clean samples were dried in a 60 °C oven for at least 24 h and then ground to a fine powder using a mortar and pestle. Ground samples were stored in acid-washed scintillation vials until analysis on the Carlo-Erba NA 1500 Series II elemental analyzer interfaced with a Micromass Optima mass spectrometer, as described for particulate matter.

Analytical methods were also the same across all sampling periods, except the 2015 and 2016 samples were analyzed on an Isoprime 100 isotope ratio mass spectrometer interfaced with a Micro Vario Elemental Analyzer. In some cases, macroalgal samples were frozen until they could be processed. Freezing macroalgae does not have an impact on $\delta^{15}N$ values (Oczkowski et al. 2015).

Hard Clams

Hard clams (*M. mercenaria*), known locally as quahogs, were first collected subtidally in 2005 and 2006 from throughout Narragansett Bay. Resultant data were presented in Oczkowski et al. (2008) and DiMilla (2006). Briefly, the foot muscle was removed from individual clams, rinsed with deionized water, and dried in a 60 °C oven. Dried tissues were ground to a fine powder using a mortar and pestle and stored in acid-washed scintillation vials until analysis. These methods were repeated again by Schmidt (2014) and in 2015 and 2016, as part of this study (Table 1). Note that the hard clams collected in 2015 were collected manually from shallow, subtidal near-shore waters. In contrast, the other clams were collected via dredge by the Rhode Island Department of Environmental Management and, in a few cases in 2005, by scuba divers (DiMilla 2006; Oczkowski et al. 2008; Schmidt 2014).

Hard clam samples collected prior to 2015 were analyzed on the Carlo-Erba NA 1500 Series II elemental analyzer interfaced with a Micromass Optima mass spectrometer, and the more recent samples were measured on the Isoprime 100 isotope ratio mass spectrometer interfaced with a Micro Vario Elemental Analyzer. Analytical techniques were the same as those described in the "Macroalgae" section.

Statistics

To explore the impact of the WWTF upgrades on the $\delta^{15}N$ and $\delta^{13}C$ spatially, seasonally, and over time, we used a series of linear regression models, with the exception of the comparison of our particulate matter data to those of Chaves (2004). In this latter case, an analysis of variance (ANOVA) was used because we did not include a continuous variable for latitude in our analysis. The sewage plant upgrade effect was examined in the models by categorizing sampling events as pre-, post-, and during upgrade, where the pre category included all data from before 2012, before most of the WWTFs upgraded to tertiary treatment, during included data from the transitional period of 2012–2013, and post included any data from 2014 to

the present. When supported by the model fit and data, a three-level ordinal variable was used for the upgrade variable; otherwise, two indicator (binary) variables were used, with pre-upgrade used as a reference category. When sampling occurred throughout the year, seasonality was included in the models using multiple indicator variables. Because the head and mouth of the Bay are oriented north to south, spatial effects were first evaluated by including the latitude of the sampling location in the models. This allowed spatial effects to be quantified as a function of distance. For the Secchi and DIN evaluations, we did not assume a linear effect with latitude. Instead, locations were categorized as Providence (PVD), Upper, Middle, and Lower Bay and fit as separate indicator variables within the model. Additional explanatory variables specific to a given sample type, such as the macroalgal color and water column position of particulate matter samples, were included as indicator variables in the associated models. Interactions among explanatory variables were included in all models; when interactions were statistically significant, pairwise comparisons were made between combinations of the two interacting variables using the Bonferroni correction. Data were evaluated for compliance with the normal distribution assumption using the Shapiro-Wilk statistical test and graphical evaluations such as histograms and quantile-quantile plots. Based on these results, the assumption of a normal distribution was determined to be valid for stable isotope results for each of the measured matrices. For Secchi and DIN, the assumption of a normal distribution was not met; however, the assumption of a lognormal distribution was, and therefore, these results were natural log-transformed prior to performing the analyses for these parameters. Median and mean Secchi and DIN values of untransformed data are presented for descriptive purposes (Table 3). All analyses were performed at the 95% confidence level, and all analyses were performed using SAS version 9.2 software.

Results

Water Clarity

We compared Secchi data from before 2012 to data after 2014. The WWTF upgrades were ongoing over the course of a few years, but two of the largest dischargers upgraded in 2012 and 2013, making 2013 the first full year of achievement (NBEP 2017). Given the skewedness of the dataset, we looked for

Table 3 Results of a comparison between Secchi depth (m) and DIN concentrations (μM) from before the upgrades ("pre," before 2012) and after ("post," 2014 and after)

Period	Region	Secchi							DIN						
			Raw values			LN-transformed				Raw values			LN-transformed[a]		
		n	Median	Mean	SD	Mean	SD	Signif.	n	Median	Mean	SD	Mean	SD	Signif.
Region															
Pre	Lower	88	4.15	4.40	1.49	1.43	0.30	Pre > post	507	1.08	4.94	9.89	0.22	1.76	
Post		69	3.50	3.60	1.15	1.23	0.32		195	1.87	2.90	2.81	0.59	1.04	
Pre	Mid	138	2.99	3.24	0.79	1.15	0.23		390	0.80	5.09	8.84	0.14	1.93	Post > pre
Post		102	2.89	3.12	1.42	1.05	0.42		169	2.44	3.63	3.76	0.67	1.23	
Pre	Upper	72	2.56	2.77	0.81	0.98	0.29		22	4.00	9.35	11.34	0.66	2.53	
Post		53	2.60	2.92	1.44	0.96	0.49		22	4.27	5.76	4.23	1.52	0.69	
Pre	PVD	474	2.02	2.06	0.83	0.64	0.42		232	17.11	20.03	17.75	2.14	1.73	Pre > post
Post		500	1.77	1.96	0.86	0.58	0.44		101	8.36	10.25	9.15	1.54	1.63	
Season															
Pre	Spring	287	2.60	2.74	1.27	0.90	0.48	Pre > post	385	0.53	5.82	12.53	− 0.21	2.02	Post > pre
Post		214	1.88	2.35	1.19	0.74	0.46		196	1.72	3.50	5.16	0.61	1.08	
Pre	Summer	288	2.11	2.20	0.98	0.69	0.47	Pre > post	522	1.12	4.91	9.56	0.27	1.71	
Post		307	1.67	1.82	0.92	0.50	0.44		172	1.84	3.10	3.76	0.41	1.34	
Pre	Autumn	197	2.77	2.99	1.26	1.02	0.39		244	13.78	18.59	15.04	2.53	1.01	Pre > post
Post		203	3.00	3.15	1.12	1.08	0.38		119	7.69	9.42	6.90	1.92	0.93	

The number of samples are given under the "*n*" column. We present the median, means, and standard deviations (SD) of the raw (untransformed) data as well as the means and SD of the LN-transformed values. When differences in the LN-transformed means were significantly different, they were noted under the column "Signif." Comparisons are presented for both regions (Lower Bay, Middle Bay, Upper Bay, Providence River Estuary) (Fig. 1) as well as by season, where spring is April through June, summer is July through September, and fall is October through December. Winter data were excluded from the Bonferroni correction pairwise comparisons

[a] Surface water concentrations only. Values in μM

statistical differences only in the LN-transformed data. Based on a three-factor ANOVA model with upgrade statues (pre vs. post), region, and season (spring, summer, fall), all effects were significant ($p < 0.001$), but differences in the LN-transformed means were small (≤ 0.2), especially given the standard deviations (~0.4). In the Lower Bay, Secchi depth was significantly more shallow (lower values indicating a less clear water column) than it was before the upgrades (Table 3) and Secchi depth was also significantly shallower after the upgrades in both the spring and summer.

Nutrients

We used the same statistical ANOVA model to evaluate the nutrient data that was used to analyze the Secchi dataset. All effects, including all two-factor interactions, of LN-transformed data were significant ($p < 0.001$, based on the model term F tests) in surface water DIN concentrations. Only in the Providence River Estuary was there a significant decline in DIN concentrations after the upgrades (Table 3). In Mid-Narragansett Bay, DIN concentrations were significantly higher after 2014. These differences may have been biased by very different numbers of samples, where $n = 390$ in the Middle Bay prior to and $n = 169$ after upgrades, which could be influenced by inter-annual variability. Only in spring were post-upgrade DIN concentrations throughout the bay significantly higher than those measured before 2012. In the fall, post-upgrade DIN concentrations were lower when compared to before the nutrient reductions took place.

Particulate Matter

The $\delta^{15}N$ values of the PM were homogenous throughout the water column, with surface, middle, and bottom samples similar for most of the sampling periods (e.g., Fig. 2). Our statistical multiple linear regression model found an interaction ($p = 0.042$ for the model interaction term significance test) between latitude and depth, where the change in $\delta^{15}N$ was greater in the bottom waters, with increasing latitude. Estimated differences among depths were less than 0.3‰. While values throughout the water column generally ranged from 5 to 15‰, there were some notable outliers. Samples collected on 1 May 2015 had elevated $\delta^{15}N$ values at the Lower Bay stations 5, 7, and 8, where the highest values were measured in the bottom waters. Also, on 28 June 2016, there was one very high bottom water $\delta^{15}N$ value observed at station 8. We suggest that this last exceptionally high value may have reflected some sort of contamination, but have included it in our results (although not in our statistical analyses).

There were significant seasonal differences, where $\delta^{15}N$ values were greater in the summer and fall, compared to winter, based on the above model's season indicator variables' significance tests (Fig. 3). To explore the magnitude of these differences, we used the results of our regression analysis to estimate mean $\delta^{15}N$ above winter values for each season (including spring) and for each region of the bay (Providence River Estuary, Upper Bay, Middle Bay, and Lower Bay; Fig. 3). The magnitude of difference between spring and winter and between summer and winter decreased down the bay, while the difference between fall and winter showed the opposite trend. To explore whether this down bay increase in fall $\delta^{15}N$ values might be attributable to production or recycled particulate N, we performed the same statistical analyses with the $\delta^{13}C$ data and observed trends that were consistent with those seen for $\delta^{15}N$ (Fig. 3).

When comparing the PM data collected in 2000–2002 to those collected in 2014–2016, our statistical model identified a number of interactions, namely, between the two time periods and season and between latitude and season. Positive seasonal differences between the 2014–2016 dataset and the 2000–2002 dataset were clear, both in space and time (Fig. 4). In general, the most pronounced differences were observed in the fall. These differences were on the order of 2.2‰. Summer and spring differences ranged from about 1.8 to 2.0‰, with a subtle gradient from Upper to Lower Bay. Differences between datasets were < 0.3‰ in the winter.

High-resolution (approximately weekly) PM data collected from 2000 to 2002 (Chaves 2004) at a station in the lower west passage of Narragansett Bay were compared to data collected between 2014 and 2016. When a separate statistical two-factor ANOVA model was fit using data from this location, a significant time period/season interaction was observed ($p = 0.0382$ for the model interaction term F test). Bonferroni pairwise comparisons of the period-specific seasonal difference indicated that there were no significant seasonal differences in the 2000–2002 dataset, but that fall $\delta^{15}N$ values were greater than spring and winter in the more recent dataset. When comparing the two datasets on a seasonal basis, there were significant increases in $\delta^{15}N$ values in the spring, summer, and fall, but no significant differences in the winter. Overall, while there were gaps in the datasets, they do illustrate the differences between $\delta^{15}N$ values measured in particulate matter from two time series collected 15 years apart and before and after major perturbations to the nutrient regime of Narragansett Bay (Fig. 5).

Macroalgae

The $\delta^{15}N$ values ranged from about 6 to 16‰ over the length of Narragansett Bay (Fig. 6). Because we used attached macroalgae as a passive sampler and integrator of bioavailable water column N, we grouped the macroalgae, which were identified to the genus or species level, by color: brown (Phaeophyta), green (Chlorophyta), and red (Rhodophyta). The brown algae consisted primarily of fucoids (e.g., *Fucus spiralis*, *Fucus vesiculosus*), the green primarily of ulvoids,

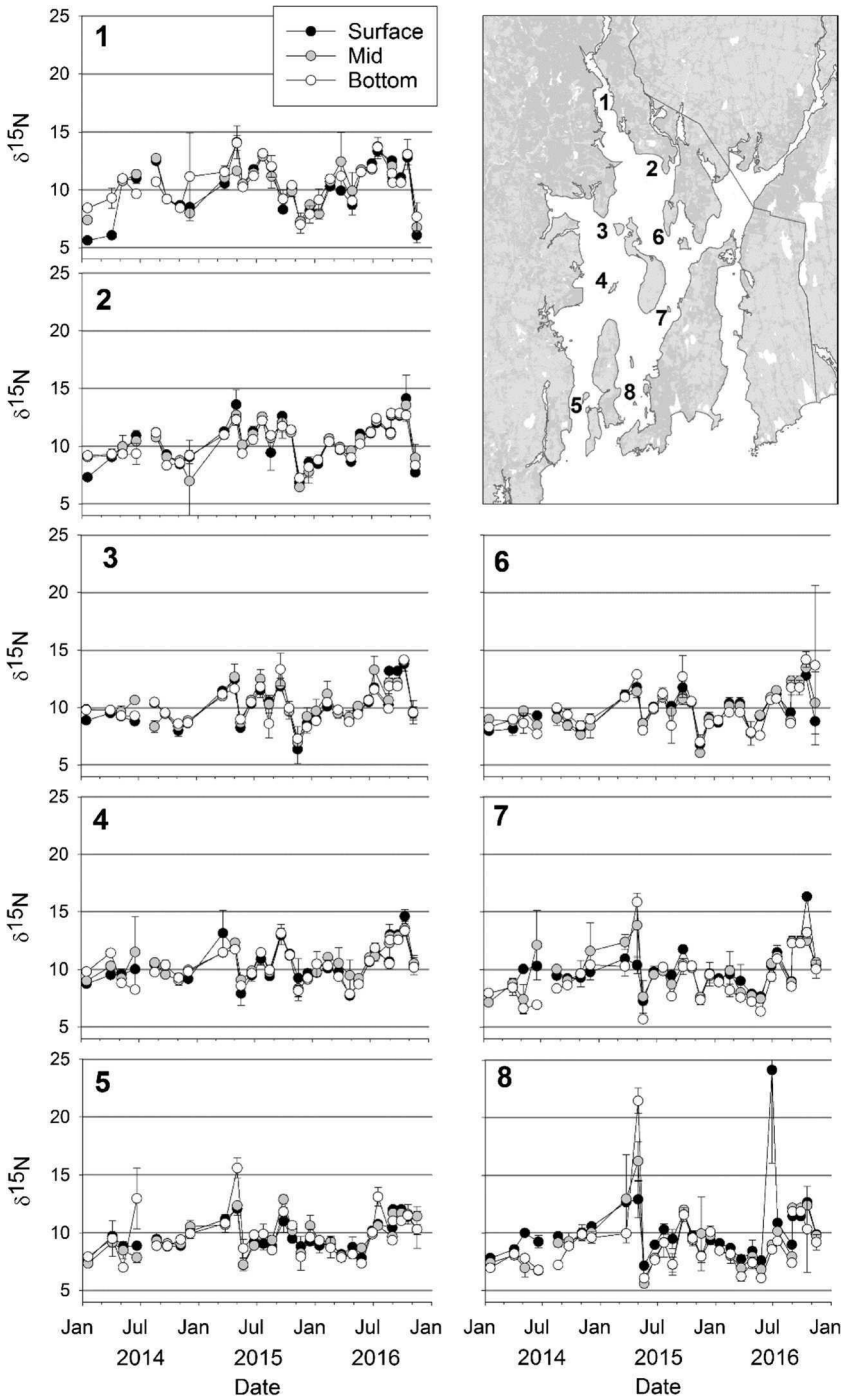

Fig. 2 The $\delta^{15}N$ values of particulate matter (PM) from January 2014 through November 2016 are given for eight stations in Narragansett Bay. PM was sampled from water collected at the surface, middle, and bottom of the water column at each location. Station locations are given in the inset map

and the red primarily of *Grateloupia turuturu* and *Polysiphonia* sp. The green macroalgae were the most readily available throughout the bay and Providence River Estuary, although all three groups were present at all sampling locations in the bay proper. When considering the overall means of all macroalgae collected in the bay as a whole, there were clear increases in $\delta^{15}N$ values among the three time periods (Figs. 6 and 7).

As macroalgae were collected in the late summer and early fall, no seasonal comparisons could be made. However, based on a multiple linear regression model including latitude and separate indicator variables for color and time period, there were significant differences among colors (red, green, brown), time periods (2005–2007, 2012, 2015–2016), and with latitude ($p < 0.001$ for all comparisons based on the regression parameter estimate significance tests). Overall, the $\delta^{15}N$ of the macroalgae decreased significantly with latitude, with the statistical model estimating a decrease of 0.7‰ per 0.1° latitude, or an overall 1.4‰ decrease down the bay.

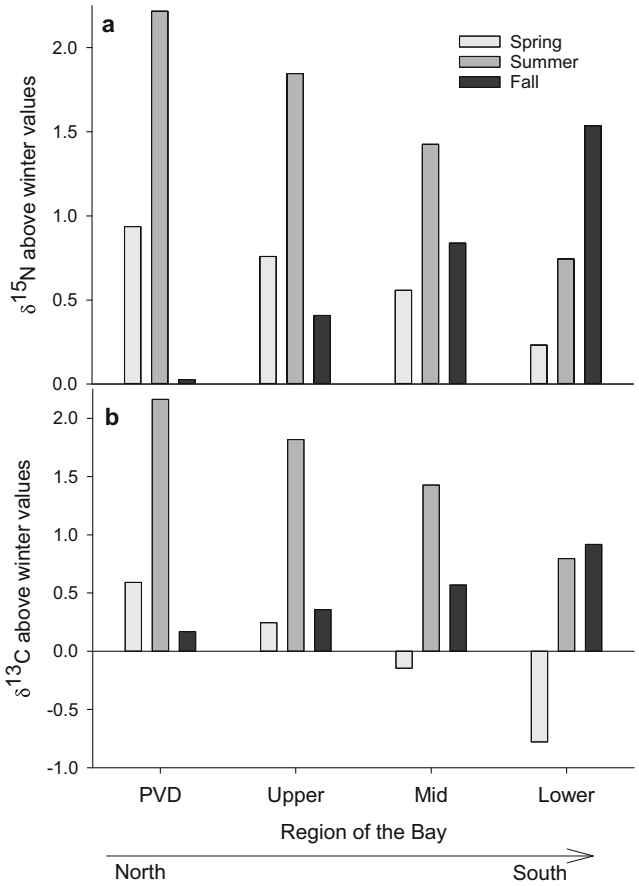

Fig. 3 Seasonal differences among PM $\delta^{15}N$ data (**a**) and $\delta^{13}C$ values (**b**) are presented as the statistical model estimated mean difference between spring, summer, or fall and winter values. Data were divided into regions of the bay where PVD is the Providence River Estuary and upper, middle, and lower refer to the regions of Narragansett Bay (see Fig. 1). WWTFs are not practicing tertiary treatment in the winter months, when temperatures are cold

Values for $\delta^{15}N$ increased over time. Between consecutive time periods, there was an average increase of 1.4‰ for brown macroalgae, 0.6‰ for green macroalgae, and 0.8‰ for red macroalgae from pre-2012 to 2012–2013 and

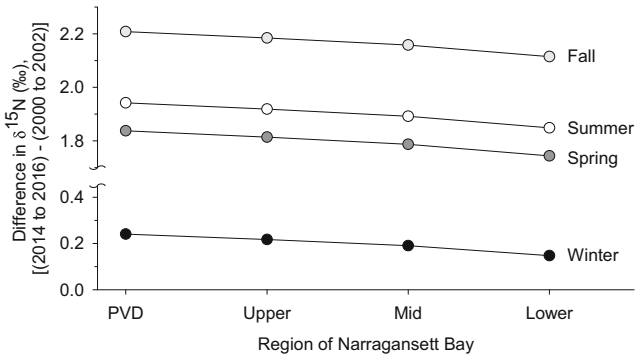

Fig. 4 The statistical model estimated mean differences between PM $\delta^{15}N$ values measured in 2014–2016 and in 2000–2002 (collected by Chaves 2004) broken out by season and region of Narragansett Bay

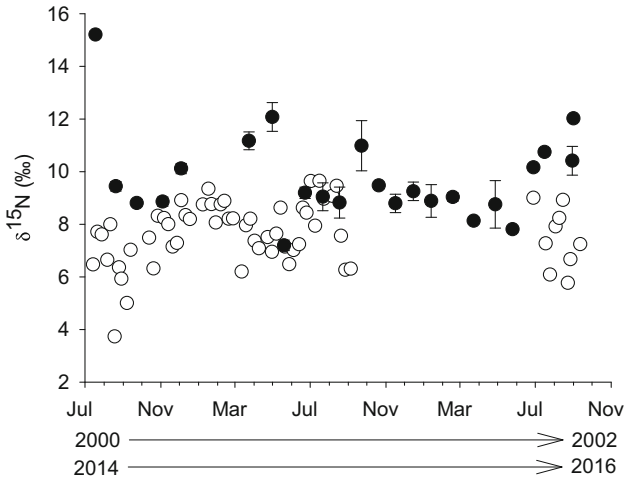

Fig. 5 Individual $\delta^{15}N$ PM values for samples collected by Chaves (2004), just off the GSO dock, identified in Fig. 1, and as part of this study at station 5, identified in Fig. 2. Closed circles represent data collected as part of this study (2014–2016) while open circles represent samples collected by Chaves (2004; 2000–2002)

2012–2013 to post-2013. This translates to overall increases of 2.8, 1.2, and 1.5‰ for brown, green, and red macroalgae over the decade between the first and last sampling periods (Fig. 7).

Hard Clams

Tissue $\delta^{15}N$ values ranged from approximately 11 to 16‰, where the lowest measured values were from clams collected in the Providence River Estuary in 2005–2006. Conversely, the highest measured values were also from clams collected in the Providence River Estuary in 2015–2016. Throughout the rest of the bay, differences among regional means were subtle, with mean values ranging from 12.9‰ (Upper Bay, pre-2012) to 13.9‰ (Upper Bay, post-2013) (Fig. 8). While the periods during and after the upgrades were not significantly different, both were different from pre-upgrade (pre-2012). The magnitudes of these differences varied significantly depending on location in the bay, where the differences were the most pronounced in the Providence River Estuary and Upper Narragansett Bay (Fig. 9). Differences between time periods were negligible in the Lower Bay. In contrast to the increased $\delta^{15}N$ values over time observed throughout the rest of our datasets, the statistical model estimated a slight decrease (0.3‰) in $\delta^{15}N$ between the earliest (pre-2102) and most recent (post-2013) clam datasets in the Lower Bay (Fig. 9).

Carbon stable isotope data were available for some of the 2005–2006 clams as well as for the 2015–2016 clams. Because $\delta^{13}C$ data were only available for two of the time periods, and due to the spatial patterns observed for $\delta^{15}N$, separate two-sample *t* test comparisons of $\delta^{13}C$ between the

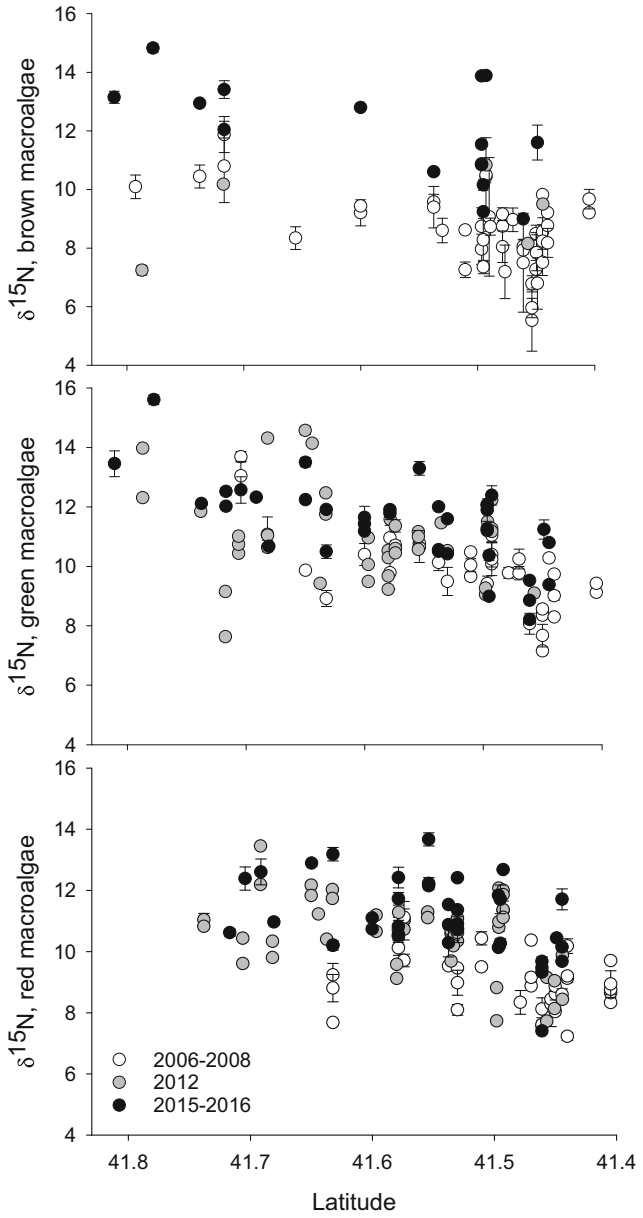

Fig. 6 Macroalgal $\delta^{15}N$ values from samples attached to rocky outcrops, organized by latitude. The higher-latitude samples were collected from the head of the bay, and lower-latitude samples are from the mouth. Samples were organized by color, where brown macroalgae are shown in the *top panel*, green in the *middle*, and red in the *bottom panel*. Samples were collected over three different sampling periods: before (2006–2008), during (2012), and after (2015–2016) the WWTF upgrades. Details on data sources are given in Table 1

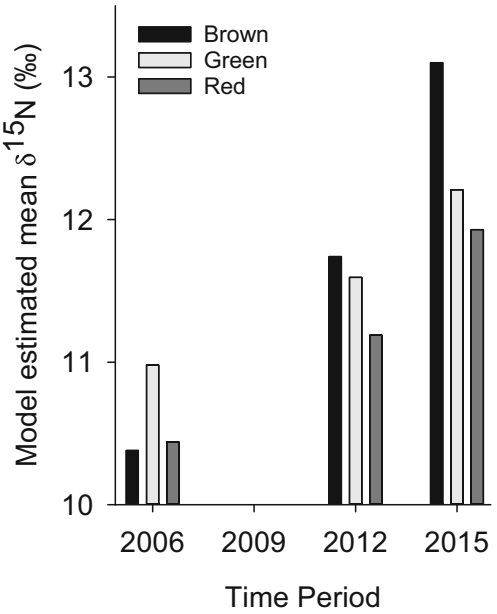

Fig. 7 Statistical model based estimates of mean estimated macroalgal $\delta^{15}N$ values in tissues, by color, over time

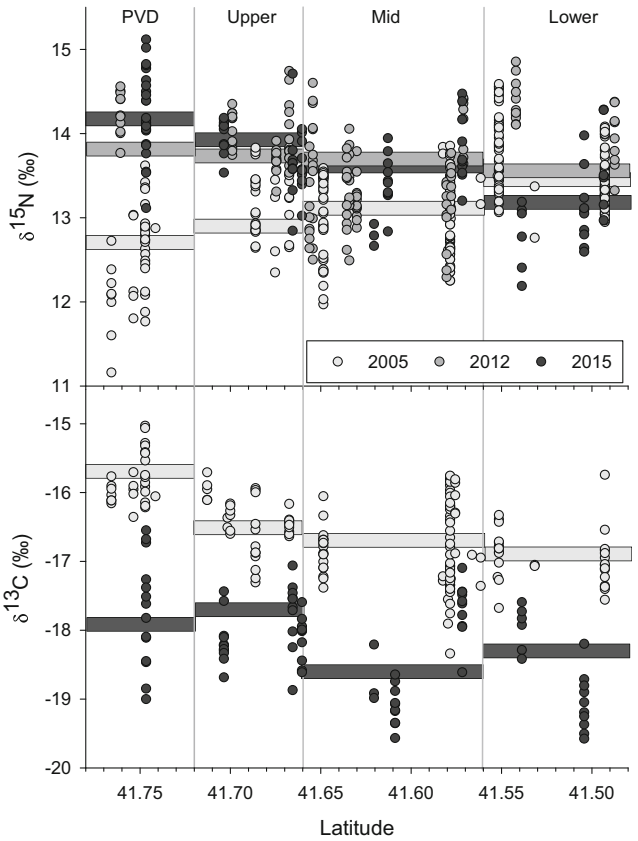

Fig. 8 Hard clam (*Mercenaria mercenaria*) $\delta^{15}N$ values, with distance down Narragansett Bay expressed as latitude. Individual clam measurements are given as circles, and horizontal bars represent statistical model-estimated mean $\delta^{15}N$ values for each region of the bay. PVD is the Providence River Estuary and upper, middle, and lower refer to the regions of the bay as defined in Fig. 1

two periods were run for each subarea. There were clear differences between periods for each region, where the more recent data had significantly lower $\delta^{13}C$ values than the 2005–2006 clams ($p < 0.0001$ for each region) (Fig. 8). Overall, clams from 2015 to 2016 were at least 1‰ lower, on average, than they were in 2005–2006 where mean differences between the two time periods ranged from 1.2‰ in the Upper Bay to 2.2‰ in the Providence River Estuary.

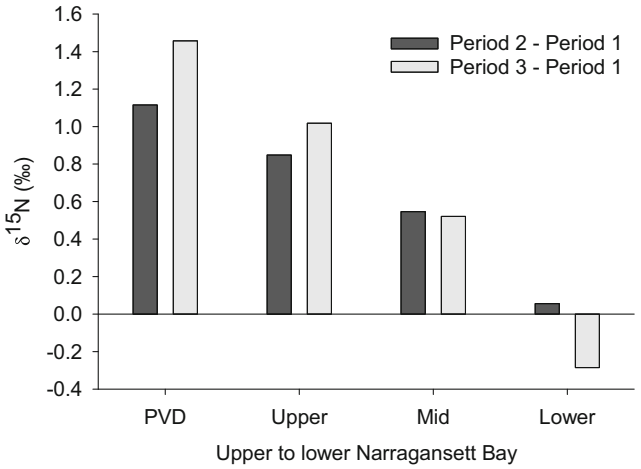

Fig. 9 Model estimated mean differences between periods for hard clam (*Mercenaria mercenaria*) $\delta^{15}N$ values where the pre-upgrade period (period 1) is represented by the 2005 clams, during the upgrades by the 2012 (period 2), and post-upgrades by the clams collected in 2015–2016 (period 3). Differences are given by region of the bay where PVD is the Providence River Estuary and upper, lower, and middle represent regions of the bay, from north to south

Discussion

Narragansett Bay has been highly impacted by human activities for more than 200 years, with the bulk of the nutrient loads entering at the head of the bay from sewage (Nixon 2008). Given the time span of fertilization, the recent WWTF N reductions have been akin to turning off the tap, reducing loads to the lowest ever measured in the system. However, in the first 4 years following the reductions, the impact of the WWTF reductions on nutrient concentrations in the bay has been complex. Oviatt et al. (2017) observed pronounced declines in annual concentrations of nitrogen, particularly in the Providence River Estuary, and our seasonal analyses found significant, albeit small, declines in surface water DIN concentrations in the Providence River Estuary, coincident with the upgrades. But these water column reductions did not persist throughout the bay proper in our dataset. In one region, mean concentrations significantly increased. Overall, median DIN concentrations were very low south of the Providence River Estuary (< 5 μM), both before and after upgrades (Table 3). Nutrient concentrations in Narragansett Bay have always been low during the growing season, even when the bay was heavily fertilized by secondary treated waste (Oviatt 2008; Krumholz 2012; Schmidt 2014). While the water column DIN concentrations in our analyses did not clearly reflect the source reductions, probably because they have always been very low during the growing season, this does not mean that the upgrades are not impacting the overall net production of this N-limited ecosystem.

Comparisons of Secchi depth measurements from before and after the upgrades also showed small differences, again with counter-intuitive results, where in some locations and in some seasons, Secchi depth was slightly shallower after the upgrades. While these differences were statistically significant, we suggest that they may not be ecologically significant, especially given the regional scale of the analyses, the heterogeneity of sampling frequencies and sites among the different data sources, and imprecise conversions of some of the data from light attenuation coefficients to Secchi depths. However, the results are consistent with the more detailed analyses presented in NBEP (2017). That report documents a steady improvement in water column clarity in the Lower Bay from 1972 to 1997, coincident with the decline in chlorophyll concentrations (e.g., Nixon et al. 2009). However, no improvement was seen between 2004 and 2014 (the time spanning the N reductions). In the northern part of the bay, there was a strong inter-annual variability in water clarity, but with no trends. In the summer months, variability in water column clarity was attributed to rainfall, where wet summers were associated with lower water clarity (NBEP 2017). Climate and other variables may mask the influence of water quality improvements associated with sewage upgrades, and as responses are ongoing, clear discernment of ecosystem response to the nutrient reductions will likely occur over a longer timescale than we report here (e.g., Boesch 2002; Greening and Janicki 2006).

Narragansett Bay is N-limited, particularly during the growing season (e.g., Oviatt et al. 1995; Kremer and Nixon 1978; Pilson 1985a), and despite eutrophication in the Upper Bay and Providence River Estuary, secondary production is often food limited in the late summer and fall (e.g., Durbin and Durbin 1981; Grassle and Grassle 1984; Rudnick et al. 1985; Campbell 1993). Water column DIN concentrations are very low during this time, frequently < 2 μM, throughout the bay. If bio-available N is quickly taken up by primary producers, then measurements of remaining water column N concentrations would not be the best indicator of anthropogenic N distribution in Narragansett Bay, particularly during the growing season. Further, while measurements of water clarity are useful for monitoring bay changes, particulate matter can be stirred up during storms, temporarily reducing water column visibility. Also, plankton (and particulate matter) at a station are not necessarily formed at that location, as they drift with the tides. While the residence time of water in Narragansett Bay is on the order of a month (Pilson 1985b), near-surface residual currents are ~5 cm s^{-1} (Kincaid et al. 2008). We calculate transport times on the order of 7 days from Upper to Lower Bay (distance ~30 km). Thus, it is possible, and even probable, that water clarity measurements at a Middle or Lower Bay station are impacted by phytoplankton formed in the Upper Bay, supported by sewage N (e.g., Melrose et al. 2014). Changes in water clarity and production, or lack thereof, may also be influenced by longer-term incremental drivers associated with changes in climate. Surface water chlorophyll concentrations in the bay have been declining for more than

50 years (Borkman and Smayda 2009; Nixon et al. 2009; Borkman and Smayda 2016; NBEP 2017). The decreases have been attributed to increased water column stratification, and subsequently reduced benthic-pelagic coupling due to warmer waters, decreased winds, and warmer, cloudier winters (Pilson 1991; Oviatt 2004; Nixon et al. 2009; Fulweiler et al. 2015). While direct measurements of nutrient concentrations and water clarity can indicate the net impact of these factors, stable isotopes can tease out changing N sources from more long-term stressors associated with climate change. The $\delta^{15}N$ values have changed as the source has changed (Schmidt et al. 2016) while any changes in $\delta^{13}C$ could reflect changes in net production (Oczkowski et al. 2014; Oczkowski et al. 2018).

We propose that the stable isotope data provide the necessary insight to assess changes as bioavailable N is quickly incorporated into primary and secondary production. Spatial trends in $\delta^{15}N$ values in juvenile winter flounder (*Pseudopleuronectes americanus*) are consistent with our hypothesis that biota in the Providence River Estuary would have elevated $\delta^{15}N$ values after the treatment plant upgrades (Pruell et al. 2017). Higher $\delta^{15}N$ values in the Providence River Estuary where DIN concentrations were also high (> 10 μM) were likely due to both the elevated $\delta^{15}N$ values of the source (sewage) N and the decrease in the abundance of bioavailable N. In the latter case, less N available would reduce the ability of the primary producers to preferentially select the metabolically more favorable ^{14}N over ^{15}N (e.g., York et al. 2007; Oczkowski et al. 2008; Thornber et al. 2008; Pruell et al. 2017). We also observed elevated macroalgal $\delta^{15}N$ values in the Providence River Estuary (e.g., Fig. 6).

In fact, macroalgal $\delta^{15}N$ values increased throughout the Bay across the three different sampling periods (2005–2007, 2012, 2015–2016). The macroalgae, which were fixed to rocky outcrops, integrated in situ water column bio-available N; they were autochthonous samplers of water column DIN-$\delta^{15}N$. The clear down-bay gradients in macroalgae $\delta^{15}N$ values were consistent over our sampling period, even though the overall values increased over time (Fig. 6). While there were differences among color, they all reflected a mixing gradient of high sewage $\delta^{15}N$ values at the head of the bay to lower $\delta^{15}N$ values at the mouth. Most of the green macroalgae (*Ulva* sp.) were annuals and integrated $\delta^{15}N$ values in water column DIN over a period of days. Some red species, as well as all the brown species sampled, were perennial, with tissue turnover times and N uptake rates that were slower than they were for *Ulva* sp. (Pedersen and Borum 1996; Thornber et al. 2008; Raimonet et al. 2013), perhaps explaining differences among divisions. While the magnitude of change in $\delta^{15}N$ values over time differed among the divisions, they presented a consistent picture of N dynamics in Narragansett Bay, with $\delta^{15}N$ values indicative of tertiary treated sewage. A 2013–2015 nutrient budget for Narragansett Bay calculated that WWTFs are still the dominant source of N to the bay, accounting for 55% of the total N loading (NBEP 2017).

The PM dataset further supports these observations. Our statistical model looked at differences among seasons and regions of the bay (Providence River Estuary, Upper Bay, Middle Bay, Lower Bay) and indicated that there were some clear differences in the spring, summer, and fall PM $\delta^{15}N$ values among the different regions, across the whole dataset. Winter PM $\delta^{15}N$ values did not differ spatially, presumably because low temperatures and shorter day lengths reduced both primary production and WWTF N removal. The statistical model estimated differences between $\delta^{15}N$ values in the spring and winter, summer and winter, and fall and winter. There were significant down-bay gradients in the spring and summer data, where the difference between spring and winter ranged from 0.9‰ in the Providence River Estuary to 0.2‰ in the Lower Bay and the difference between summer and winter ranged from 2.2 to 0.7‰ (Fig. 3). In contrast to these expected down-bay gradients, differences between fall and winter displayed the opposite trend, with the Providence River Estuary being essentially 0‰ and increasing to 1.5‰ in the Lower Bay. To better understand why the fall data trends were so different, we performed the same analyses using available $\delta^{13}C$ measurements as they can reflect net ecosystem production, where higher values are associated with high levels of production (e.g., Oczkowski et al. 2014; Oczkowski et al. 2018). The $\delta^{13}C$ data exhibited the same spatial trends as the $\delta^{15}N$. We speculate that the fall gradient towards higher $\delta^{15}N$ and $\delta^{13}C$ values in the Lower Bay may reflect resuspension of recently deposited organic matter associated with rougher fall weather which would likely show a down-bay gradient like the down-bay gradient in vertical mixing (e.g., Spaulding and Swanson 2008). Or they could be reflecting a seasonal shift as tertiary treatment supported Upper Bay plankton were transported down the bay during the same season that N removal rates decreased in the WWTFs. The N removal in the facilities is temperature dependent, with lower rates associated with colder weather (NBEP 2017). The spring $\delta^{15}N$ values were closest to the winter values. In contrast, the summer values, for both $\delta^{15}N$ and $\delta^{13}C$, were much higher than winter and occurred when Narragansett Bay was food limited and DIN concentrations were near zero (Oviatt 2008; Schmidt 2014; Fig. 4). Overall, $\delta^{15}N$ values have increased more than 1.5‰ throughout the bay during the spring, summer, and fall between 2000 and 2002 and 2014–2016 (Figs. 4 and 5).

Based on their study of clam and macroalgal samples collected in 2006, Oczkowski et al. (2008) suggested that sewage-supported plankton, grown in the Upper Bay and transported down-bay, were a significant food source for hard clams (*M. mercenaria*) throughout Narragansett Bay. The clam $\delta^{15}N$ values were homogenous throughout the bay, and the authors estimated that as much as half of the N in the clam tissues could be of sewage origin. The clams collected as part

of this study, as well as those collected in 2012, support this hypothesis. Clams, like the macroalgae, showed substantial increases in $\delta^{15}N$ values in the Providence River Estuary. The statistical model-estimated mean values for this system were 12.7, 13.8, and 14.2‰, for the periods 2005, 2012, and 2015–2016, respectively (Fig. 8). Differences among sampling periods, with higher values associated with more recent years, narrowed down the bay (from Upper Bay to Middle Bay to Lower Bay). The Lower Bay means ranged from 13.2‰ in 2015–2016 to 13.6‰ in 2005–2006. The slight decrease in Lower Bay $\delta^{15}N$ values could be reflecting increased contributions of shelf N. If this is the case, then differences could be more pronounced over time (Figs. 8 and 9).

While the $\delta^{15}N$ values in clams, as well as in particulate matter and macroalgae, suggest that sewage is still an important source of N to Narragansett Bay, an observation supported by current nutrient budgets (NBEP 2017), the $\delta^{13}C$ values in the clams indicate that the net production in the bay has declined. There were substantial decreases in $\delta^{13}C$ values between 2005 and 2006 and 2015–2016 (Fig. 8), on the order of 1–2‰, on average. Others have demonstrated that $\delta^{13}C$ values can reflect net ecosystem production, with higher $\delta^{13}C$ values indicating more productive systems and vice versa (e.g., Oczkowski et al. 2010; Oczkowski et al. 2018). As the decreases in $\delta^{13}C$ values were also consistent with longer-term observations of declining chlorophyll values in the bay (Nixon et al. 2009; Fulweiler and Heiss 2014), we cannot specifically identify the WWTF upgrades as the only driver of the changes in $\delta^{13}C$ values.

A Synthesis of Ecological Responses

While sewage N loads have been reduced by more than half, the predominant source of N to Narragansett Bay is still from WWTFs (NBEP 2017). Our analyses found that, when considered seasonally and regionally, water column DIN concentrations have decreased and water clarity appears to have (slightly) improved in the Providence River Estuary. The stable isotope results illustrate how sewage N still plays an important role in supporting the plants and animals in the ecosystem. While we had expected that the 2015–2016 samples collected in the Lower Bay to more closely reflect marine N sources, the only evidence of this was in the hard clam data where the decrease in $\delta^{15}N$ values between the earliest and most recent data was ~0.3‰. Except for the Lower Bay clams, the $\delta^{15}N$ values throughout Narragansett Bay have increased over time. This is particularly pronounced in the Providence River Estuary, where increases were typically > 1‰. Of course, the upgrades were recent and it is too soon to fully assess the legacy effects of more than a century of heavy nutrient fertilization on the ecosystem. However, dramatic declines occurred in nutrients, turbidity, and chlorophyll concentrations in the year after sewage diversion in Kaneohe Bay, Hawaii (Smith et al. 1981), although the response of Tampa Bay to nutrient reductions occurred over a longer time period (years to decades) and response was also influenced by weather conditions (Greening and Janicki 2006). A mesocosm study by Oviatt et al. (1984) concluded that water column recovery rates in the "grossly polluted" Providence River Estuary could occur on a short timescale (< 1 year). Mesocosms designed to replicate Mid-Narragansett Bay conditions were outfitted with intact, structurally undisturbed sediments from the Providence River Estuary, a Middle Bay location, and offshore. After 5 months, the behavior of the Providence River treatments, including seasonal dynamics of plankton and benthic fauna, were more similar to the other treatments than they were to the in situ Providence River Estuary conditions (Oviatt et al. 1984). A partially to well-mixed water column and fairly short residence times surely contribute to more efficient recoveries.

Recycling of N and any associated isotope transformations are impossible to tease out of our bulk analyses, but it is unlikely that benthic N cycling is driving the observed isotope changes. Surface water chlorophyll concentrations and the amount of freshly deposited organic matter are the best predictors of sediment N cycling in Narragansett Bay (Fulweiler and Heiss 2014). Chlorophyll concentrations have been declining over the past 50 years, indicating long-term declines in plankton production (Fulweiler and Heiss 2014), and further declines in nutrient loads associated with the WWTF upgrades also appear to be decreasing bay-wide production (e.g., Oviatt et al. 2017), observations supported by our $\delta^{13}C$ dataset. Declines in chlorophyll and production are frequently observed after major nutrient reductions (Boesch 2002), but the challenge in this system is separating responses from long-term trends. There are no apparent long-term temporal trends in N_2 fluxes or rates of sediment oxygen demand (the latter is a good indicator of organic matter loading) at two stations in Narragansett Bay (Fulweiler et al. 2016; Fulweiler, personal communication). The work of Oviatt et al. (1984) suggests that legacy nutrient regeneration is unlikely to be the primary drivers of the observed stable isotope trends while the observations of Fulweiler and Heiss (2014) indicate that rates of N cycling have not increased. Lower N loads could lead to more tightly recycled bio-available N and associated elevated $\delta^{15}N$ values (e.g., Brandes and Devol 1997; Granger et al. 2004; Granger et al. 2010). But, if this were the primary driver, we would expect to see down-bay gradients in $\delta^{15}N$ values lessen or even reverse as N was continuously recycled as it moves through the bay.

The results presented here are like the few other studies that have used stable isotopes to document estuarine ecological response to WWTF upgrades to tertiary treatment (and N removal) in the sense that responses were swift (within years) and distinct (e.g., Smith et al. 1981). But, this study also differs from those studies. For example, in Moreton Bay, researchers observed that $\delta^{15}N$ values decreased after the

WWTF upgrades, reflecting more marine sources (Costanzo et al. 2005; Pitt et al. 2009). Savage and Elmgren (2004) made similar observations in the Himmerfjärden Bay of the Baltic Sea. In both examples, declines in $\delta^{15}N$ values were substantial, about 4–6‰. In contrast, we saw $\delta^{15}N$ values increase throughout the Bay by 1‰ or more. While sewage N loads to Narragansett Bay have decreased considerably, they remain the largest source of N to the estuary. This, in conjunction with the documented increases in sewage effluent $\delta^{15}N$ values, supports our suggestion that Narragansett Bay is still heavily influenced by sewage N loads (Fig. 10; NBEP 2017). Our study supports the hypothesis put forth in Oczkowski et al. (2008) that sewage supported production in the Upper Bay is an important food source to the middle and lower portions of the bay.

The reduction in N loads was a relatively discrete (few year) event that co-occurred during other long-term changes in the ecology and phenology of Narragansett Bay. As Duarte et al. (2009) cautioned, the results of this study should be considered in the context of shifting baselines and concurrent changes in other stressors. There is substantial documentation of increased variability in seasonal plankton dynamics, including shifts in the timing of some annual phytoplankton blooms, from the late winter to the summer, as well as declines in the magnitude of blooms since the 1960s and particularly after the nutrient reductions (Nixon et al. 2009; Oviatt et al. 2017). Zooplankton are better positioned to graze down these warmer weather phytoplankton blooms, which decreases the amount of organic matter reaching the benthos (Oviatt et al. 2002). Others have documented declines in benthic nutrient fluxes and speculate on the potentially important role of N fixation in the future, particularly in the lower parts of the bay (see Nixon et al. 2009). While N fixation could supply the Narragansett Bay water column with a significant amount of "new" N, which would have $\delta^{15}N$ values close to 0‰, we do not see evidence of this in the stable isotope data, but recognize that the system is ever-changing and the response to the reductions is probably ongoing. Our current assessment could serve as a recovery baseline from which to observe N dynamics as ecosystem oligotrophication continues. While the $\delta^{15}N$ data do not reflect the lower values associated with marine contributions or N fixation, the $\delta^{13}C$ data, particularly for the clams, are consistent with the observations of declining productivity (e.g., Li and Smayda 2001; Nixon et al. 2009; Fulweiler and Heiss 2014; Oviatt et al. 2017).

In the 5 years after the major WWTFs came on-line for nutrient removal, and just over a decade since the process began, net production may have decreased, and the process of oligotrophication begun. But, current nutrient budgets show that sewage remains the dominant source of N to Narragansett Bay (NBEP 2017) and our stable isotope data demonstrate that it still plays an important role in supporting primary and secondary ecosystem production.

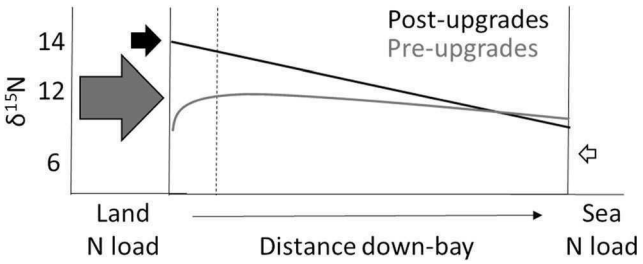

Fig. 10 Conceptual model of $\delta^{15}N$ dynamics based on the results of this study. The light gray line represents the $\delta^{15}N$ values in plants and animals in Narragansett Bay before the sewage upgrades. The black line represents the situation with tertiary treatment. The dashed line denotes the mouth of the Providence River Estuary (to the *left*) and downstream Narragansett Bay proper (to the *right*). The arrows were designed to represent the primary N loads. Their size is roughly proportional to the size of the annual loads (gray arrow = pre-upgrade sewage N loads, black arrow = post-upgrade, white arrow = shelf contributions). The points of the arrows represent the approximate $\delta^{15}N$ values of the sources

Acknowledgements The late coastal ecologist Scott Nixon was fond of saying that the wise studied lakes, the less-wise studied rivers, where water flowed in one direction, and only the most foolish studied estuaries where water moved in all directions, changing over the course of a day. This has never been truer when trying to assess the impacts of oligotrophication. We would like to thank the Rhode Island Department of Environmental Management for providing hard clams to us for more than a decade. We would also like to thank Mike Charpentier for creating Fig. 1, Steve Granger for the assistance in the field during those first collections in the mid-2000s, and to Scott Nixon and Candace Oviatt for all of the valuable data that they have collected, and information and wisdom that they have provided, over the years. Thanks to Lindsey Fields for measuring the DIN concentrations and Rebecca Robinson for the support to C. Schmidt. We are grateful to Carol Thornber and Lindsay Green of the University of Rhode Island for their help with identifying macroalgae. This manuscript has been improved by input from Roxanne Johnson, Rose Martin, and Brenda Rashleigh. This is ORD tracking number ORD-023673. The views expressed in this article are those of the authors and do not necessarily represent the views or polices of the US Environmental Protection Agency, NEIWPCC, nor of the McLaughlin Research Corporation. Any mention of trade names, products, or services does not imply an endorsement by the US government or the US Environmental Protection Agency. The EPA does not endorse any commercial products, services, or enterprises.

References

Boesch, D.F. 2002. Challenges and opportunities in reducing nutrient over-enrichment of coastal ecosystems. *Estuaries* 25 (4): 886–900.

Borkman, D.G., and T. Smayda. 2009. Multidecadal (1959–1997) changes in Skeletonema abundance and seasonal bloom patterns in Narragansett Bay, Rhode Island, USA. *Journal of Sea Research* 61 (1-2): 84–94.

Borkman, D.G., and T.J. Smayda. 2016. Coincident patters of waste water suspended solids reduction, water transparency increase, and chlorophyll decline in Narragansett Bay. *Marine Pollution Bulletin* 107 (1): 161–169.

Brandes, J.A., and A.H. Devol. 1997. Isotopic fractionation of oxygen and nitrogen in coastal marine sediments. *Geochimica et Cosmochimica Acta* 61 (9): 1793–1801.

Campbell, R.G. 1993. Studies of feeding behavior, development, and food limitation in first feeding nauplii of the copepod *Acartia tonsa* (Copepoda: Calanoida). Ph.D. Dissertation, Graduate School of Oceanography, University of Rhode Island, Narragansett, Rhode Island.

Cantwell, M.G., D.R. Katz, J.C. Sullivan, K. Ho, and R.M. Burgess. 2017. Temporal and spatial behavior of pharmaceuticals in Narragansett Bay, Rhode Island, United States. *Environmental Toxicology and Chemistry* 36 (7): 1846–1855.

Chaves, J. E. 2004. Potential use of 15N to assess nitrogen sources and fate in Narragansett Bay. Ph.D. Dissertation, Graduate School of Oceanography, University of Rhode Island, Narragansett, Rhode Island.

Costanzo, S.D., J. Udy, B. Longstaff, and A. Jones. 2005. Using nitrogen stable isotope ratios ($\delta^{15}N$) of macroalgae to determine the effectiveness of sewage upgrades: Changes in the extent of sewage plumes over four years in Moreton Bay, Australia. *Marine Pollution Bulletin* 51 (1-4): 212–217.

DiMilla, P.A., 2006. Using stable nitrogen isotopes to characterize and evaluate nitrogen sources to Greenwich Bay, RI and their influence on isotopic signatures in estuarine organisms. MS Thesis, University of Rhode Island, Kingston, RI.

DiMilla, P.A., S.W. Nixon, A.J. Oczkowski, M.A. Altabet, and R.A. McKinney. 2011. Some challenges of an "upside down" nitrogen budget– Science and management in Greenwich Bay, RI (USA). *Marine Pollution Bulletin* 62 (4): 672–680.

Duarte, C.M., D.J. Conley, J. Carstensen, and M. Sánchez-Camacho. 2009. Return to *Neverland*: Shifting baselines affect eutrophication restoration targets. *Estuaries and Coasts* 32 (1): 29–36.

Durbin, A.G., and E.G. Durbin. 1981. Standing stock and estimated production rates of phytoplankton and zooplankton in Narragansett Bay, R. *I. Estuaries* 4 (1): 24–41.

Fry, B. 2006. Stable isotope ecology. Springer science+business media, LLC, New York, New York.

Fulweiler, R.W. and E.M. Heiss. 2014. (Nearly) a decade of directly measured sediment N_2 fluxes: What can Narragansett Bay tell us about the global ocean nitrogen budget? 27: 184–195.

Fulweiler, R.W., A.J. Oczkowski, K.M. Miller, C.A. Oviatt, and M.E.Q. Pilson. 2015. Whole truths vs. half truths— And a search for clarity in long-term water temperature records. *Estuarine, Coastal, and Shelf Science* 157: A1–A6.

Fulweiler, R.W., H.E. Emery, and T.J. Maguire. 2016. A workflow for reproducing mean benthic gas fluxes. *Earth and Space Science* 3 (8): 318–325.

Garber, J. H. 1982. 15N-Tracer and Other Laboratory Studies of Nitrogen Remineralization in Sediments and Waters from Narragansett Bay, Rhode Island. Dissertation, University of Rhode Island, Kingston, RI.

Gearing, P.J., J.N. Gearing, J.T. Maughan, and C.A. Oviatt. 1991. Isotopic distribution of carbon from sewage sludge and eutrophication in the sediments and food web of estuarine ecosystems. *Environmental Science and Technology* 25 (2): 295–301.

Granger, J., D.M. Sigman, J.A. Needoba, and P.J. Harrison. 2004. Coupled nitrogen and oxygen isotope fractionation of nitrate during assimilation by cultures of marine phytoplankton. *Limnology and Oceanography.* 49 (5): 1763–1773.

Granger, J., D.M. Sigman, M.M. Rohde, M.T. Maldonade, and P.D. Tortell. 2010. N and O isotope effects during nitrate assimilation by unicellular prokaryotic and eukaryotic plankton cultures. *Geochimica et Cosmochimica Acta.* 74 (3): 1030–1040.

Grassle, J.P. and J.F. Grassle. 1984. The utility of studying the effects of pollutants on single species populations in benthos of mesocosms and coastal ecosystems. In Concepts in marine pollution measurements, ed, H.White. Maryland Sea Grant College Park, College Park, Maryland.

Greening, H., and A. Janicki. 2006. Toward reversal of eutrophic conditions in a subtropical estuary: Water quality and seagrass response to nitrogen load reductions in Tampa Bay, Florida, USA. *Environmental Management* 38 (2): 163–178.

Kincaid, K., D. Bergondo, and K. Rosenberger. 2008. Circulation and exchange between lower Narragansett Bay and Rhode Island sound. In *Science for ecosystem-based management: Narragansett Bay in the 21st century springer*, ed. B. Costa-Pierce and A. Desbonet, 301–324. New York: Verlag.

Kremer, J.N., and S.W. Nixon. 1978. *A coastal marine ecosystem, simulation and analysis*. New York: Springer-Verlag.

Krumholz, J.S. 2012. Spatial and temporal patterns in nutrient standing stock and mass-balance in response to load reductions in a temperate estuary. Ph.D. Dissertation, University of Rhode Island.

Li, Y., and T.J. Smayda. 2001. A chlorophyll time series for Narragansett Bay: Assessment of the potential effect of tidal phase on measurement. *Estuaries and Coasts* 24: 328–336.

McKinney, R.A., W.G. Nelson, M.A. Charpentier, and C. Wigand. 2001. Ribbed mussel nitrogen isotope signatures reflect nitrogen sources in coastal salt marshes. *Ecological Applications* 11 (1): 203–214.

Melrose, D.C., J.S. Krumholz, and M.C. McManus. 2014. Measuring changes in total phytoplankton-sized particle volume over time as a proxy for primary production and food availability in narragansett Bay, RI. Proceedings of the 34th Milford Aquaculture Seminar. *Journal of Shellfish Research* 33: 541–565.

Narragansett Bay Estuary Program (NBEP). 2017. State of Narragansett Bay and Its Watershed. Technical Report, Providence, RI. http://nbep.org/the-state-of-our-watershed/technicalreport/. Accessed 19 December 2017.

Nixon, S.W., B. Buckley, S. Granger, L. Harris, A. Oczkowski, R. Fulweiler, and L. Cole. 2008. Nutrient (N and P) inputs to Narragansett Bay: Past, present, and future. In *Science for ecosystem-based management Narragansett Bay in the 21st century*, ed. A. Desbonnet and B.A. Costa-Pierce, 101–176. New York: Springer.

Nixon, S.W., R.W. Fulweiler, B.A. Buckley, S.L. Granger, B.L. Nowicki, and K.M. Henry. 2009. The impact of changing climate on phenology, productivity, and benthic-pelagic coupling in Narragansett Bay. Estuarine, coastal, and shelf. *Science* 82: 1–18.

Oczkowski, A., S. Nixon, K. Henry, P. DiMilla, M. Pilson, S. Granger, B. Buckley, C. Thornber, R. McKinney, and J. Chaves. 2008. Distribution and trophic importance of anthropogenic nitrogen in Narragansett Bay: An assessment using stable isotopes. *Estuaries and Coasts* 31 (1): 53–69.

Oczkowski, A.J., M.E.Q. Pilson, and S.W. Nixon. 2010. A marked gradient in $\delta^{13}C$ values of clams *Mercenaria mercenaria* across a marine embayment may reflect variations in ecosystem metabolism. *Marine Ecology Progress Series* 414: 145–153.

Oczkowski, A., E. Markham, A. Hanson, and C. Wigand. 2014. Carbon stable isotopes as indicators of coastal eutrophication. *Ecological Applications* 24 (3): 457–466.

Oczkowski, A., C.S. Thornber, E.E. Markham, R. Rossi, A. Ziegler, and S. Rinehart. 2015. Testing sample stability using four storage methods and the macroalgae *Ulva* and *Gracilaria*. *Limnology and Oceanography: Methods* 13: 9–14.

Oczkowski, A., B. Taplin, R. Pruell, A. Pimenta, R. Johnson, and J. Grear. 2018. Carbon stable isotope values in plankton and mussels reflect changes in carbonate chemistry associated with nutrient enhanced net production. Frontiers in Marine Science 5 https://doi.org/10.3389/fmars.2018.00043.

Oviatt, C.A. 2004. The changing ecology of temperate coastal waters during a warming trend. *Estuaries* 27 (6): 895–904.

Oviatt, C.A. 2008. Impacts of nutrients on Narragansett Bay productivity: A gradient approach. In *Science for ecosystem-based management: Narragansett Bay in the 21st century*, ed. A. Desbonnet and B.A. Costa-Pierce, 523–544. New York: Springer.

Oviatt, C.A., and R. Pastore. 1980. *Some aspects of water quality in and pollution sources to the Providence River. Report for region 1 EPA September 1979–September 1980. Contract #68–04-1002*, 02203. Boston, MA: United States Environmental Protection Agency.

Oviatt, C.A., M.E.Q. Pilson, S.W. Nixon, J.B. Frithsen, D.T. Rudnick, J.R. Kelly, J.F. Grassle, and J.P. Grassle. 1984. Recovery of a polluted estuarine system: A mesocosm experiment. *Marine Ecology Progress Series* 16: 203–217.

Oviatt, C., P. Doering, B. Nowicki, L. Reed, J. Cole, and J. Frithsen. 1995. An ecosystem level experiment on nutrient limitation in temperate coastal marine environments. *Marine Ecology Progress Series* 116: 171–179.

Oviatt, C.A., A.A. Keller, and L. Reed. 2002. Annual primary production in Narragansett Bay with no bay-wide winter-spring phytoplankton bloom. *Estuarine, Coastal and Shelf Science* 54 (6): 1013–1026.

Oviatt, C., L. Smith, J. Krumholz, C. Coupland, H. Stoffel, A. Keller, M.C. McManus, and L. Reed. 2017. Managed nutrient reduction impacts on nutrient concentrations, water clarity, primary production, and hypoxia in a north temperate estuary. *Estuarine, Coastal, and Shelf Science* 199: 25–34.

Paul, D., G. Skrzypek, and I. Fórizs. 2007. Normalization of measured stable isotopic compositions to isotope reference scales – A review. *Rapid Communications in Mass Spectrometry* 21 (18): 3006–3014.

Pedersen, M.F., and J. Borum. 1996. Nutrient control of algal growth in estuarine waters. Nutrient limitation and the importance of nitrogen requirements and nitrogen storage among phytoplankton and species of macroalgae. *Marine Ecology Progress Series* 142: 261–272.

Perez, K.T., E.W. Davey, R.H. Moore, P.R. Burn, M.S. Rosol, J.A. Cardin, R.L. Johnson, and D.N. Kopans. 1999. Application of computer-aided tomography (CT) to the study of estuarine benthic communities. *Ecological Applications* 9 (3): 1050–1058.

Pilson, M.E.Q. 1985a. Annual cycles of nutrients and chlorophyll in Narragansett Bay, Rhode Island. *Journal of Marine Research* 43 (4): 849–873.

Pilson, M.E.Q. 1985b. On the residence time of water in Narragansett Bay. *Estuaries* 8 (1): 2–14.

Pilson, M.E.Q. 1991. Aspects of Climate Around Narragansett Bay. NBP-91-64. pp. 59. http://nbep.org/publications/NBP-91-64.pdf. Accessed 19 December 2017.

Pitt, K.A., R.M. Connolly, and P. Maxwell. 2009. Redistribution of sewage-nitrogen in estuarine food webs following sewage treatment upgrades. *Marine Pollution Bulletin* 58 (4): 573–580.

Poole, H., and W.R.G. Atkin. 1929. Photo-electric measurements of submarine illumination throughout the year. *Journal of the Marine Biological Association of the United Kingdom* 16 (01): 297–324.

Pruell, R.J., and B.K. Taplin. 2015. Carbon and nitrogen isotope ratios of juvenile winter flounder as indicators of inputs to estuarine systems. *Marine Pollution Bulletin* 101 (2): 624–631.

Pruell, R.J., B.K. Taplin, J.L. Lake, and S. Jayaraman. 2006. Nitrogen isotope ratios in estuarine biota collected along a nutrient gradient in Narragansett Bay, Rhode Island, USA. *Marine Pollution Bulletin* 52 (6): 612–620.

Pruell, R.J., B.K. Taplin, and K.M. Miller. 2017. Trends in nitrogen isotope ratios of juvenile winter flounder reflect changing nitrogen inputs to Rhode Island, USA estuarine systems. *Marine Pollution Bulletin* 118 (1-2): 41–47.

Raimonet, M., G. Guillou, F. Mornet, and P. Richard. 2013. Macroalgae $\delta^{15}N$ values in well-mixed estuaries: Indicator of anthropogenic nitrogen input or macroalgae metabolism? Estuarine, coastal, and shelf. *Science* 119: 126–138.

Rudnick, D.T., R. Elmgren, and J.B. Frithsen. 1985. Meiofaunal prominence and benthic seasonality in a coastal marine ecosystem. *Oecologia* 67 (2): 157–168.

Savage, C., and R. Elmgren. 2004. Macroalgal (*Fucus vesiculosus*) $\delta^{15}N$ values trace decrease in sewage influence. *Ecological Applications* 14 (2): 517–526.

Schmidt, C.E. 2014. Investigation of nitrogen cycling using stable nitrogen and oxygen isotopes in Narragansett Bay, RI. Dissertation, University of Rhode. Island, Kingston, RI.

Schmidt, C.E., R.S. Robinson, L. Fields, and S.W. Nixon. 2016. Changes to nitrate isotopic composition of waste water treatment effluent and rivers after upgrades to tertiary treatment in the Narragansett Bay watershed, RI. *Marine Pollution Bulletin* 104 (1-2): 61–69.

Smith, S.V., W.J. Kimmerer, E. Laws, R.E. Brock, and T.W. Walsh. 1981. Kaneohe Bay sewage diversion experiment: Perspectives on ecosystem responses to nutritional perturbation. *Pacific Science* 35: 279–395.

Spaulding, S.L. and C. Swanson. 2008. Circulation and transport dynamics in Narragansett Bay. *In Science for ecosystem-based management Narragansett Bay in the 21st century*, ed. A. Desbonnet and B.A. Costa-Pierce, 233–279. New York: Springer.

Thornber, C.S., P. DiMilla, S.W. Nixon, and R.A. McKinney. 2008. Natural and anthropogenic nitrogen uptake by bloom-forming macroalgae. *Marine Pollution Bulletin* 56 (2): 261–269.

Wells, M.L., G.J. Smith, and K.W. Bruland. 2000. The distribution of colloidal and particulate bioactive metals in Narragansett Bay RI. *Marine Chemistry* 71 (1-2): 143–163.

York, J., G. Tomasky, and I. Valiela. 2007. Stable isotopic detection of ammonium and nitrate assimilation by phytoplankton in the Waquoit Bay estuarine system. *Limnology and Oceanography* 52 (1): 144–155.

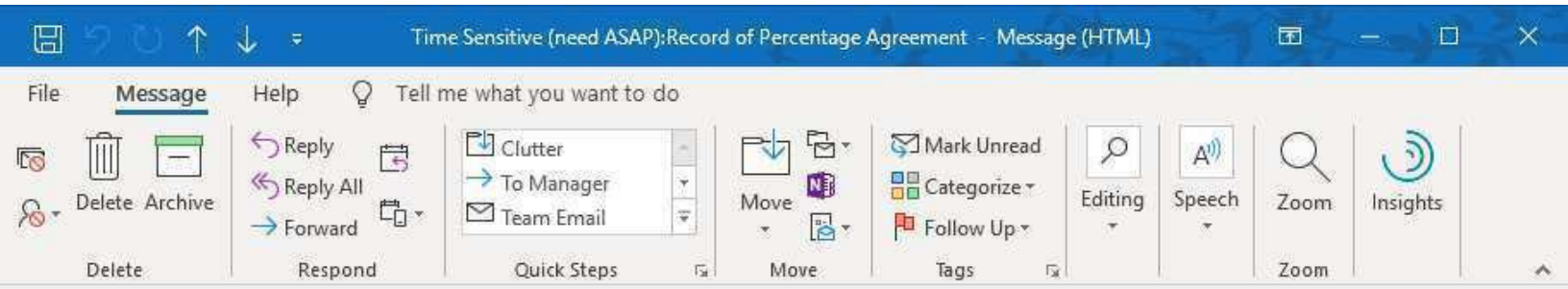

Time Sensitive (need ASAP):Record of Percentage Agreement

Oczkowski, Autumn

Reply | Reply All | Forward | ...

To Chris Hunt; Miller, Kenneth M; Courtney Schmidt; Emily A Santos; Hanson, Alana; McKinney, Rick; Candace Oviatt; Cobb, Donald; Jason Krumholz; Pimenta, Adam; Leslie Smith; Leanna Heffner; **+2 others**

Mon 4/27/2020 2:29 PM

Retention Policy 10 years (Capstone approach) (10 years) Expires 4/25/2030

You forwarded this message on 4/28/2020 12:26 PM.

Hi everyone.

Two of our journal articles are being nominated for a US EPA award for Science and Technical Achievement. As part of the nomination, I need a concurrence from each of you on your Percent Contribution to both articles. Note below I just took the Average across both papers for each article (last two columns). **The Nomination is due on this coming Wednesday, 4/29**.

If you are ok with your percentage, **please just Reply to Me with an "I concur"**. If you'd like more information on the award nomination or to discuss further, let me know.

Thanks,

Autumn

Oczkowski et al. 2016		Oczkowski et al. 2018		Overall Contribution		
Coauthor	% Contribution	Coauthor	% Contribution	Coauthor	% Contribution	Coauthor Affiliation
Oczkowski	70	Oczkowski	50	Autumn Oczkowski	60	ORD/ACESD
Hunt	15	Schmidt	10	Christopher Hunt	7.5	University of New Hampshire
Miller	5	Santos	6	Kenneth Miller	5.5	CSRA, LLC
Oviatt	5	Miller	6	Courtney Schmidt	5	Narragansett Bay Estuary Program
Nixon	3	Hanson	6	Emily Santos	3	Humboldt State University
Smith	2	Cobb	5	Alana Hanson	3	ORD/ACESD
		Krumholz	4	Rick McKinney	3	ORD/ACESD
		Pimenta	4	Candace Oviatt	2.5	University of Rhode Island
		Heffner	1	Don Cobb	2.5	ORD/ACESD
		Robinson	1	Jason Krumholz	2	McLaughlin Research Corporation
		Chaves	1	Adam Pimenta	2	ORD/ACESD
		McKinney	6	Scott Nixon	1.5	University of Rhode Island
				Leslie Smith	1	Your Ocean Consulting, LLC
				Leanna Heffner	0.5	Western Alaska Landscape Conservation Cooperative
				Sandra Robinson	0.5	ORD/ACESD
				Joaquin Chaves	0.5	NASA Goddard Space Flight Center

Re: Time Sensitive (need ASAP):Record of Percentage Agreement

CH

Chris Hunt <chunt@unh.edu>(Chris Hunt via gmail.com)

To Oczkowski, Autumn

Reply | Reply All | Forward | ...

Mon 4/27/2020 2:33 PM

Retention Policy 10 years (Capstone approach) (10 years) Expires 4/25/2030

You replied to this message on 4/27/2020 2:38 PM.
The actual sender of this message is different than the normal sender. Click here to learn more.

I concur!! I'm also amazing I'm your most-contributing coauthor- your EPA colleagues need to step up their game.

On Mon, Apr 27, 2020 at 2:28 PM Oczkowski, Autumn <Oczkowski.Autumn@epa.gov> wrote:

Caution - External Email

Hi everyone.

Two of our journal articles are being nominated for a US EPA award for Science and Technical Achievement. As part of the nomination, I need a concurrence from each of you on your Percent Contribution to both articles. Note below I just took the Average across both papers for each article (last two columns). **The Nomination is due on this coming Wednesday, 4/29**.

If you are ok with your percentage, **please just Reply to Me with an "I concur"**. If you'd like more information on the award nomination or to discuss further, let me know.

Thanks,

Autumn

RE: Time Sensitive (need ASAP):Record of Percentage Agreement

MK

Miller, Kenneth M <kenneth.m.miller@gdit.com>(Miller, K

To Oczkowski, Autumn

Reply | Reply All | Forward | ...

Mon 4/27/2020 2:32 PM

Retention Policy 10 years (Capstone approach) (10 years) Expires 4/25/2030

You replied to this message on 4/27/2020 2:32 PM.
The actual sender of this message is different than the normal sender. Click here to learn more.

Autumn,

I concur (and congratulations!)

Ken

KEN MILLER
Statistician
General Dynamics Information Technology
6361 Walker Lane, Suite 300
Alexandria, VA 22310
Phone: (703) 485-4332
Email: Kenneth.m.miller@gdit.com

Please note new phone number and email address

From: Oczkowski, Autumn <Oczkowski.Autumn@epa.gov>
Sent: Monday, April 27, 2020 2:29 PM
To: Chris Hunt <chunt@unh.edu>; Miller, Kenneth M <Kenneth.M.Miller@csra.com>; Courtney Schmidt

RE: Time Sensitive (need ASAP):Record of Percentage Agreement

CS

Courtney Schmidt <Courtney.Schmidt@nbep.org>
To Oczkowski, Autumn

Reply | Reply All | Forward | ...

Mon 4/27/2020 3:08 PM

Retention Policy 10 years (Capstone approach) (10 years) Expires 4/25/2030

You replied to this message on 4/27/2020 3:18 PM.

I concur.

From: Oczkowski, Autumn <Oczkowski.Autumn@epa.gov>
Sent: Monday, April 27, 2020 2:29 PM
To: Chris Hunt <chunt@unh.edu>; Miller, Kenneth M <kenneth.m.miller@gdit.com>; Courtney Schmidt <Courtney.Schmidt@nbep.org>; Emily A Santos <Emily.Santos@humboldt.edu>; Hanson, Alana <Hanson.Alana@epa.gov>; McKinney, Rick <Mckinney.Rick@epa.gov>; Candace Oviatt <coviatt@uri.edu>; Cobb, Donald <Cobb.Donald@epa.gov>; Jason Krumholz <jkrumholz@gmail.com>; Pimenta, Adam <Pimenta.Adam@epa.gov>; Leslie Smith <leslie.smith@youroceanconsulting.com>; Leanna Heffner <heffnergso@gmail.com>; Robinson, Sandra <Robinson.Sandra@epa.gov>; 'Joaquin Chaves' <quincho1969@gmail.com>
Subject: Time Sensitive (need ASAP):Record of Percentage Agreement

Hi everyone.
Two of our journal articles are being nominated for a US EPA award for Science and Technical Achievement. As part of the nomination, I need a concurrence from each of you on your Percent Contribution to both articles. Note below I just took the Average across both papers for each article (last two columns). **The Nomination is due on this coming Wednesday, 4/29**.
If you are ok with your percentage, **please just Reply to Me with an "I concur"**. If you'd like more information on the award nomination or to discuss further, let me know.
Thanks,
Autumn

All folders are up to date. Connected to: Microsoft Exchange 100%

Re: Time Sensitive (need ASAP):Record of Percentage Agreement

Reply | Reply All | Forward | ...

EA

Emily A Santos <Emily.Santos@humboldt.edu>
To Oczkowski, Autumn

Mon 4/27/2020 2:48 PM

Retention Policy 10 years (Capstone approach) (10 years) Expires 4/25/2030

You replied to this message on 4/27/2020 2:57 PM.

I, Emily Santos, concur.

On Mon, Apr 27, 2020 at 11:28 AM Oczkowski, Autumn <Oczkowski.Autumn@epa.gov> wrote:

> Hi everyone.
>
> Two of our journal articles are being nominated for a US EPA award for Science and Technical Achievement. As part of the nomination, I need a concurrence from each of you on your Percent Contribution to both articles. Note below I just took the Average across both papers for each article (last two columns). **The Nomination is due on this coming Wednesday, 4/29**.
>
> If you are ok with your percentage, **please just Reply to Me with an "I concur"**. If you'd like more information on the award nomination or to discuss further, let me know.
>
> Thanks,
>
> Autumn

RE: Time Sensitive (need ASAP):Record of Percentage Agreement

Hanson, Alana
To Oczkowski, Autumn

Reply | Reply All | Forward | ...

Mon 4/27/2020 2:53 PM

Retention Policy 10 years (Capstone approach) (10 years) Expires 4/25/2030

You replied to this message on 4/27/2020 2:58 PM.

I concur.

From: Oczkowski, Autumn <Oczkowski.Autumn@epa.gov>
Sent: Monday, April 27, 2020 2:29 PM
To: Chris Hunt <chunt@unh.edu>; Miller, Kenneth M <kenneth.m.miller@gdit.com>; Courtney Schmidt <Courtney.Schmidt@nbep.org>; Emily A Santos <Emily.Santos@humboldt.edu>; Hanson, Alana <Hanson.Alana@epa.gov>; McKinney, Rick <Mckinney.Rick@epa.gov>; Candace Oviatt <coviatt@uri.edu>; Cobb, Donald <Cobb.Donald@epa.gov>; Jason Krumholz <jkrumholz@gmail.com>; Pimenta, Adam <Pimenta.Adam@epa.gov>; Leslie Smith <leslie.smith@youroceanconsulting.com>; Leanna Heffner <heffnergso@gmail.com>; Robinson, Sandra <Robinson.Sandra@epa.gov>; 'Joaquin Chaves' <quincho1969@gmail.com>
Subject: Time Sensitive (need ASAP):Record of Percentage Agreement

Hi everyone.
Two of our journal articles are being nominated for a US EPA award for Science and Technical Achievement. As part of the nomination, I need a concurrence from each of you on your Percent Contribution to both articles. Note below I just took the Average across both papers for each article (last two columns). **The Nomination is due on this coming Wednesday, 4/29**.
If you are ok with your percentage, **please just Reply to Me with an "I concur"**. If you'd like more information on the award nomination or to discuss further, let me know.
Thanks,
Autumn

RE: Time Sensitive (need ASAP):Record of Percentage Agreement

Reply | Reply All | Forward | ...

MR McKinney, Rick
To Oczkowski, Autumn

Mon 4/27/2020 4:10 PM

Retention Policy 10 years (Capstone approach) (10 years) Expires 4/25/2030

You replied to this message on 4/27/2020 4:10 PM.

I concur.

From: Oczkowski, Autumn <Oczkowski.Autumn@epa.gov>
Sent: Monday, April 27, 2020 2:29 PM
To: Chris Hunt <chunt@unh.edu>; Miller, Kenneth M <kenneth.m.miller@gdit.com>; Courtney Schmidt <Courtney.Schmidt@nbep.org>; Emily A Santos <Emily.Santos@humboldt.edu>; Hanson, Alana <Hanson.Alana@epa.gov>; McKinney, Rick <Mckinney.Rick@epa.gov>; Candace Oviatt <coviatt@uri.edu>; Cobb, Donald <Cobb.Donald@epa.gov>; Jason Krumholz <jkrumholz@gmail.com>; Pimenta, Adam <Pimenta.Adam@epa.gov>; Leslie Smith <leslie.smith@youroceanconsulting.com>; Leanna Heffner <heffnergso@gmail.com>; Robinson, Sandra <Robinson.Sandra@epa.gov>; 'Joaquin Chaves' <quincho1969@gmail.com>
Subject: Time Sensitive (need ASAP):Record of Percentage Agreement

Hi everyone.
Two of our journal articles are being nominated for a US EPA award for Science and Technical Achievement. As part of the nomination, I need a concurrence from each of you on your Percent Contribution to both articles. Note below I just took the Average across both papers for each article (last two columns). **The Nomination is due on this coming Wednesday, 4/29**.
If you are ok with your percentage, **please just Reply to Me with an "I concur"**. If you'd like more information on the award nomination or to discuss further, let me know.
Thanks,
Autumn

Re: Time Sensitive (need ASAP):Record of Percentage Agreement

Reply | Reply All | Forward | ...

CO

Candace Oviatt <coviatt@uri.edu>
To Oczkowski, Autumn

Mon 4/27/2020 3:32 PM

Retention Policy 10 years (Capstone approach) (10 years) Expires 4/25/2030

You replied to this message on 4/27/2020 3:34 PM.

Hi Autumn,
I concur.
Good luck, Candace

On Monday, April 27, 2020, Oczkowski, Autumn <Oczkowski.Autumn@epa.gov> wrote:

> Hi everyone.
>
> Two of our journal articles are being nominated for a US EPA award for Science and Technical Achievement. As part of the nomination, I need a concurrence from each of you on your Percent Contribution to both articles. Note below I just took the Average across both papers for each article (last two columns). **The Nomination is due on this coming Wednesday, 4/29**.
>
> If you are ok with your percentage, **please just Reply to Me with an "I concur"**. If you'd like more information on the award nomination or to discuss further, let me know.
>
> Thanks,
>
> Autumn

All folders are up to date. Connected to: Microsoft Exchange 100%

RE: Time Sensitive (need ASAP):Record of Percentage Agreement

Reply | Reply All | Forward | ...

CD

Cobb, Donald
To Oczkowski, Autumn

Mon 4/27/2020 2:43 PM

Retention Policy 10 years (Capstone approach) (10 years) Expires 4/25/2030

You replied to this message on 4/27/2020 2:43 PM.

I concur.

Thanks Miss Autumn.

From: Oczkowski, Autumn <Oczkowski.Autumn@epa.gov>
Sent: Monday, April 27, 2020 2:29 PM
To: Chris Hunt <chunt@unh.edu>; Miller, Kenneth M <kenneth.m.miller@gdit.com>; Courtney Schmidt <Courtney.Schmidt@nbep.org>; Emily A Santos <Emily.Santos@humboldt.edu>; Hanson, Alana <Hanson.Alana@epa.gov>; McKinney, Rick <Mckinney.Rick@epa.gov>; Candace Oviatt <coviatt@uri.edu>; Cobb, Donald <Cobb.Donald@epa.gov>; Jason Krumholz <jkrumholz@gmail.com>; Pimenta, Adam <Pimenta.Adam@epa.gov>; Leslie Smith <leslie.smith@youroceanconsulting.com>; Leanna Heffner <heffnergso@gmail.com>; Robinson, Sandra <Robinson.Sandra@epa.gov>; 'Joaquin Chaves' <quincho1969@gmail.com>
Subject: Time Sensitive (need ASAP):Record of Percentage Agreement

Hi everyone.
Two of our journal articles are being nominated for a US EPA award for Science and Technical Achievement. As part of the nomination, I need a concurrence from each of you on your Percent Contribution to both articles. Note below I just took the Average across both papers for each article (last two columns). **The Nomination is due on this coming Wednesday, 4/29**.
If you are ok with your percentage, **please just Reply to Me with an "I concur"**. If you'd like more information on the award

Re: Time Sensitive (need ASAP):Record of Percentage Agreement

Reply | Reply All | Forward | ...

JK

Jason Krumholz <jkrumholz@gmail.com>
To Oczkowski, Autumn
Mon 4/27/2020 3:50 PM

Retention Policy 10 years (Capstone approach) (10 years) Expires 4/25/2030

You replied to this message on 4/27/2020 4:04 PM.

I concur

On Mon, Apr 27, 2020 at 2:28 PM Oczkowski, Autumn <Oczkowski.Autumn@epa.gov> wrote:

> Hi everyone.
>
> Two of our journal articles are being nominated for a US EPA award for Science and Technical Achievement. As part of the nomination, I need a concurrence from each of you on your Percent Contribution to both articles. Note below I just took the Average across both papers for each article (last two columns). **The Nomination is due on this coming Wednesday, 4/29**.
>
> If you are ok with your percentage, **please just Reply to Me with an "I concur"**. If you'd like more information on the award nomination or to discuss further, let me know.
>
> Thanks,
>
> Autumn

Oczkowski et al. 2016	Oczkowski et al. 2018	Overall Contribution	

RE: Time Sensitive (need ASAP):Record of Percentage Agreement

PA

Pimenta, Adam
To Oczkowski, Autumn

Reply | Reply All | Forward | ...

Mon 4/27/2020 3:10 PM

Retention Policy 10 years (Capstone approach) (10 years) Expires 4/25/2030

You replied to this message on 4/27/2020 3:18 PM.

I concur.

Adam R. Pimenta
US EPA - Atlantic Coastal Environmental Sciences Division
Narragansett, Rhode Island
P: 401-782-9675

From: Oczkowski, Autumn
Sent: Monday, April 27, 2020 2:29 PM
To: Chris Hunt <chunt@unh.edu>; Miller, Kenneth M <kenneth.m.miller@gdit.com>; Courtney Schmidt <Courtney.Schmidt@nbep.org>; Emily A Santos <Emily.Santos@humboldt.edu>; Hanson, Alana <Hanson.Alana@epa.gov>; McKinney, Rick <Mckinney.Rick@epa.gov>; Candace Oviatt <coviatt@uri.edu>; Cobb, Donald <Cobb.Donald@epa.gov>; Jason Krumholz <jkrumholz@gmail.com>; Pimenta, Adam <Pimenta.Adam@epa.gov>; Leslie Smith <leslie.smith@youroceanconsulting.com>; Leanna Heffner <heffnergso@gmail.com>; Robinson, Sandra <Robinson.Sandra@epa.gov>; 'Joaquin Chaves' <quincho1969@gmail.com>
Subject: Time Sensitive (need ASAP):Record of Percentage Agreement

Hi everyone.
Two of our journal articles are being nominated for a US EPA award for Science and Technical Achievement. As part of the nomination, I need a concurrence from each of you on your Percent Contribution to both articles. Note below I just took the

Scott Nixon passed away in 2012. His contribution to the Oczkowski et al. 2016 was posthumous, so no contribution approval form is available.

Re: Time Sensitive (need ASAP):Record of Percentage Agreement

LS

Leslie Smith <leslie.smith@youroceanconsulting.com>
To Oczkowski, Autumn

Reply | Reply All | Forward | ...

Tue 4/28/2020 6:00 AM

Retention Policy 10 years (Capstone approach) (10 years) Expires 4/26/2030

You replied to this message on 4/28/2020 6:20 AM.

I concur.

I hope you and your family are safe and healthy in these interesting times!

Take care,
Leslie

> On Apr 27, 2020, at 2:28 PM, Oczkowski, Autumn <Oczkowski.Autumn@epa.gov> wrote:
>
> Hi everyone.
> Two of our journal articles are being nominated for a US EPA award for Science and Technical Achievement. As part of the nomination, I need a concurrence from each of you on your Percent Contribution to both articles. Note below I just took the Average across both papers for each article (last two columns). **The Nomination is due on this coming Wednesday, 4/29**.
> If you are ok with your percentage, **please just Reply to Me with an "I concur"**. If you'd like more information on the award nomination or to discuss further, let me know.
> Thanks,
> Autumn

Re: FW: Time Sensitive (need ASAP):Record of Percentage Agreement

Reply | Reply All | Forward | ...

LH

Leanna Heffner <leanna.heffner@gmail.com>
To Oczkowski, Autumn

Tue 4/28/2020 2:34 PM

Retention Policy 10 years (Capstone approach) (10 years) Expires 4/26/2030

Wow this is really cool Autumn!! And yes you are right, I don't check my other email address often, so this is the best one to reach me at.

I concur with both of those percentages and I'm still just honored to be included given my small contribution. :)

Have you been able to go back to work yet and move forward on your research? Alaska is the first state that has started reopening certain things...effectively trying to cautiously test reopening the economy partially while not overwhelming our healthcare system. But since my job can be done remotely, I'm guessing I'll be working from home in this bathrobe for months!

Big Nixon-sis hugs,
L

On Tue, Apr 28, 2020 at 8:26 AM Oczkowski, Autumn <Oczkowski.Autumn@epa.gov> wrote:

> Hey Leanna,
>
> I sent this to an email address that you might not check. Could you look at this and get back to me??
>
> Thanks,
>
> Autumn

RE: Time Sensitive (need ASAP):Record of Percentage Agreement

Reply | Reply All | Forward | ...

RS

Robinson, Sandra
To Oczkowski, Autumn

Mon 4/27/2020 2:50 PM

Retention Policy 10 years (Capstone approach) (10 years) Expires 4/25/2030

You replied to this message on 4/27/2020 2:57 PM.

I concur.

From: Oczkowski, Autumn <Oczkowski.Autumn@epa.gov>
Sent: Monday, April 27, 2020 2:29 PM
To: Chris Hunt <chunt@unh.edu>; Miller, Kenneth M <kenneth.m.miller@gdit.com>; Courtney Schmidt <Courtney.Schmidt@nbep.org>; Emily A Santos <Emily.Santos@humboldt.edu>; Hanson, Alana <Hanson.Alana@epa.gov>; McKinney, Rick <Mckinney.Rick@epa.gov>; Candace Oviatt <coviatt@uri.edu>; Cobb, Donald <Cobb.Donald@epa.gov>; Jason Krumholz <jkrumholz@gmail.com>; Pimenta, Adam <Pimenta.Adam@epa.gov>; Leslie Smith <leslie.smith@youroceanconsulting.com>; Leanna Heffner <heffnergso@gmail.com>; Robinson, Sandra <Robinson.Sandra@epa.gov>; 'Joaquin Chaves' <quincho1969@gmail.com>
Subject: Time Sensitive (need ASAP):Record of Percentage Agreement

Hi everyone.
Two of our journal articles are being nominated for a US EPA award for Science and Technical Achievement. As part of the nomination, I need a concurrence from each of you on your Percent Contribution to both articles. Note below I just took the Average across both papers for each article (last two columns). **The Nomination is due on this coming Wednesday, 4/29**.
If you are ok with your percentage, **please just Reply to Me with an "I concur"**. If you'd like more information on the award nomination or to discuss further, let me know.
Thanks,
Autumn

All folders are up to date. Connected to: Microsoft Exchange 100%

Re: Time Sensitive (need ASAP):Record of Percentage Agreement

JC

Joaquin Chaves <quincho1969@gmail.com>
To Oczkowski, Autumn

Reply | Reply All | Forward | ...

Mon 4/27/2020 4:50 PM

Retention Policy 10 years (Capstone approach) (10 years) Expires 4/25/2030

You replied to this message on 4/28/2020 6:17 AM.

I concur. Good luck

On Mon, Apr 27, 2020 at 2:28 PM Oczkowski, Autumn <Oczkowski.Autumn@epa.gov> wrote:

> Hi everyone.
>
> Two of our journal articles are being nominated for a US EPA award for Science and Technical Achievement. As part of the nomination, I need a concurrence from each of you on your Percent Contribution to both articles. Note below I just took the Average across both papers for each article (last two columns). **The Nomination is due on this coming Wednesday, 4/29**.
>
> If you are ok with your percentage, **please just Reply to Me with an "I concur"**. If you'd like more information on the award nomination or to discuss further, let me know.
>
> Thanks,
>
> Autumn

Oczkowski et al. 2016	Oczkowski et al. 2018	Overall Contribution	

Table of Contents

General_Authors_Publications.....2
LI-266902_economic_impacts_of_env_regulation.....15
STAA2020_Ferris_RPA.....55
STAA2020_Marten_RPA.....56
STAA2020_Garbaccio_RPA.....57
STAA2020_Wolverton_RPA.....58

United States Environmental Protection Agency
Washington, DC 20460

STAA REPORT FOR THE SCIENTIST NOMINATIONS

General Information:

Nomination ID/App ID:	20-140
Research Category Primary:	Environmental Policy and Decision-Making Studies (EP)
Research Category Secondary:	Review Articles (RA)
Laboratory/Office Name:	AO
Nomination Entered By:	Maryann Wolverton

Eligibility Checklist:

[Y] The nominated publication(s) has not been submitted to a previous STAA competition.

[Y] The nominated publication(s) was published on or before January 1, 2017 and on or after January 1,2012

[Y] The principal author was an EPA employee or a PHS employee assigned to EPA when the research was performed

[Y] The EPA authors (includes PHS employees assigned to EPA) contributed collectively a minimum of 50% toward the publication(s)

Nominating Official Name:	Brett Snyder
Nominating Official Title:	
Nominating OfficialEmail:	snyder.brett@epa.gov
STAA Coordinator Name:	Kathleen Wiser
STAA Coordinator Email:	wiser.kathi@epa.gov

Justifications:

Justification 1:

Concern regarding the economic impacts of environmental regulations has been part of the public dialogue since the beginning of the U.S. EPA. Although environmental regulations reduce emissions of harmful pollutants, thus generating health and other benefits for the American public, they also raise industry production costs because they require changes in production processes that would otherwise not be undertaken. A fundamental question constantly faced by EPA is how to balance the improvements in environmental quality that come with more stringent regulations against its costs, particularly when they are unevenly distributed. Debate over this issue continues today.

The nominated article brings much needed evidence-based clarity and structure to the debate over the economic impacts of environmental regulation. Often cited evidence on the effect of environmental policies are based on inconsistent and incomplete measures of their impact to individual households through the economy. For example, changes in gross domestic product and productivity are commonly referenced as evidence of the impact of environmental regulation on the U.S. economy, despite being only a partial measure of the impact on society's well-being and masking important distributional considerations. The nominated article places the existing empirical evidence within a more expansive definition of economic impacts to bring clarity to what is, and is not, known about the effect of environmental regulations overall and how those impacts differ across households. In providing a comprehensive discussion of these issues, the nominated article allows the EPA to reflect the latest evidence in its analyses, including which types of economic impacts are possible to quantify along with a broad sense of their direction and magnitude.

The nominated article reviews and combines lessons from early studies to find measurable but not severe effects on the national economy from environmental regulation. While price increases due to regulatory requirements outweighed the stimulative effect of investments in pollution abatement, they nearly offset one another. However, the synthesis finds evidence that such offsetting effects mask serious impacts on local labor markets due to the regional and industry concentration of plant closures. Establishing the connection between these seemingly different national versus local impact characterizations is important for policymakers to have a

robust understanding of how regulations have affected households through changes in the prices and quantities of goods, plant openings and closures, barriers of entry for new firms, or impacts on small businesses.

To understand what these earlier findings may mean for impacts of future regulations, the nominated article synthesizes and connects a substantial body of recent work that has examined industry-specific effects of environmental regulation on the productivity, plant location, and employment decisions of pollution-intensive firms. Contrary to some of the early impacts of environmental regulations, recent econometric-based studies found relatively small or no effect on sector-specific productivity and employment on existing firms. However, this branch of literature has found that firms were less likely to open plants in locations subject to more stringent regulation compared to other U.S. locations. In contrast, studies that used economy-wide models to explicitly account for sectoral linkages and intertemporal effects found substantial sector-specific effects due to environmental regulation, including in sectors that were not directly regulated. These connections established by the nominated article highlight the importance of how seemingly hidden costs of regulations are key to understanding how the impacts of regulation are distributed across the country.

The nominated article notes that it is useful to also think about the overall impacts of environmental regulation on the economy through the lens of benefit-cost analysis. The net change in social welfare that households experience is calculated by summing all of the benefits from the regulation and subtracting all of the costs it imposes. The costs represent the total burden that a regulation imposes on the economy, which include the value lost to society of goods and services that will no longer be produced and consumed as resources are reallocated toward pollution abatement. The benefits include changes in health and improvements in hard to measure environmental benefits such as the functioning of an ecosystem. While this approach does not speak to how the costs of regulation are distributed across sectors, it has the advantage of explicitly weighing the benefits of environmental improvements against their costs. If benefits are greater than costs, then overall social welfare is improved.

When conducting such exercises, the nominated article stresses that it is important to anticipate the ways that environmental improvements may either directly improve the productivity of

economic factors – such as through the increased productivity of outdoor workers – or change the composition of the economy as firms and households change their behavior. If individuals are healthier, for example, they may choose to reallocate their time between work and leisure. While estimating the effects of pollution on production and household behavior can be challenging, studies that have partially accounted for this interconnection have found substantial impacts of improvements in environmental quality on the overall economy. For example, one study estimated that the social cost of the Clean Air and Clean Water Acts was more than 50% greater than the compliance cost estimate. While the greatest impacts of the regulation fell on the directly regulated sectors, sectors that were not directly regulated but supplied key intermediate goods experienced significant negative impacts on output and labor productivity.

The nominated article identifies several important issues regarding the impacts of environmental regulation on the U.S. economy that remain unresolved. In particular, it identifies the need for a unifying structural framework for understanding the economic impacts of environmental regulation. However, quantifying the distribution of the costs and benefits of regulation raises several methodological and empirical challenges. For instance, firms make many decisions regarding whether to expand or reduce production at existing facilities or whether to open new facilities. These decisions have implications for when and how many workers are hired, the wages and benefits offered, and the number of hours worked, which are then linked to the productivity of firms, sectors, and ultimately the overall economy. The lack of an overarching structural framework that coherently links individual decisions to their macroeconomic implications hinders the ability to follow these pathways of effects and to understand the net effects on a sector, household, or the economy as a whole.

Another research gap discussed by the nominated article is the need to consider not only the distribution of costs but also benefits. However, folding benefits into the evaluation of economic impacts is complicated. An analyst needs to understand to what extent certain types of households differentially benefit from reductions in emissions. Another important consideration is whether workers enjoy health improvements that enhance their productivity and change their consumption and investment behavior over time.

Justification 2A:

n/a

Justification 2B:

2013 Cycle

Shadbegian R, **Wolverton A**. 2010. Location decisions of polluting plants: theory, empirical evidence, and consequences. *International Review of Environmental and Resource Economics* 4(1):1-49. Award: Level II

2015 Cycle

Marten, A., and Newbold, S. 2012. Estimating the Social Cost of Non-CO2 GHG Emissions: Methane and Nitrous Oxide. *Energy Policy* 51: 957-972. Award: Level 3.

2016 Cycle

Greenstone M, Kopits E, **Wolverton A**. 2013. Estimating the social cost of carbon for use in U.S. federal rulemakings: a methodology and interpretation. Review of Environmental Economics and Policy 7(1):23-46. Award: Level 3.

Kopits E, **Marten A**, **Wolverton A**. 2013. Incorporating ‘catastrophic’ climate change into policy analysis. *Climate Policy* DOI 10.1080/14693062.2014.864947. Award: Honorable mention.

Newbold S, Griffiths C, Moore C, **Wolverton A**, Kopits E. 2013. A rapid assessment model for understanding the social cost of carbon. Climate Change Economics 4(1). DOI 10.1142/S2010007813500012 Award: Honorable mention.

Marten, A., and Newbold, S. 2013. Temporal Resolution and DICE, Nature Climate Change. *Nature Climate Change* 3: 526 – 527. Award: Honorable mention.

2017 Cycle

Marten, A., and Newbold, S. 2014. The value of information for integrated assessment models of climate change. *Journal of Environmental Economics and Management* 68:111-123. Award: Level 3.

Marten, A. 2014. The Role of Scenario Uncertainty in Estimating the Benefits of Carbon Mitigation. *Climate Change Economics*. Award: Level 3.

Kopits E, McGartland A, Morgan C, Pasurka C, Shadbegian R, Simon N, Simpson RD, **Wolverton A.** 2014. Retrospective Cost Analysis of EPA Regulations: A Case Study Approach. Journal of Benefit-Cost Analysis, 5(2), (2014), 173-193. Award: Level 3.

Wolverton A. 2014. Retrospective evaluation of costs associated with methyl bromide critical use exemptions for open field strawberries in California. *Journal of Benefit Cost Analysis* 5 (2). Award: Level 3.

Marten A, Kopits E, Griffiths C, Newbold S, **Wolverton A.** 2014. Incremental CH4 and N2O Mitigation Benefits Consistent with the US Government's SC-CO2 Estimates. *Climate Policy,* 15(2), pp. 272-298. Award: Level 3.

Ferris A, Shadbegian R, **Wolverton A.** 2014. The Effect of Environmental Regulation on Power Sector Employment: Phase I of the Title IV SO2 Trading Program." Journal of the Association of Environmental and Resource Economists. 1(4) 521-553. Award: Level 3.

2018-2019 Cycle

Condon, N, Klemick, H., and **Wolverton, A.** 2015. Impacts of ethanol policy on corn prices: A review and meta-analysis of recent evidence. *Food Policy* 51: 63-73. Award: Level 3.

Klemick, H, Kopits, E., and **Wolverton, A.** Potential Barriers to Improving Energy Efficiency in Commercial Buildings: The Case of Supermarket Refrigeration. *Journal of Benefit-Cost Analysis* 8(1): 115-145. Award: Honorable mention.

Klemick, H, Kopits, E., Sargent, K, and **Wolverton, A.** Heavy-Duty Trucking and the Energy Efficiency Paradox: Evidence from Focus Groups and Interviews. *Transportation Research Part A: Policy and Practice* 17: 154-166. Award: Honorable mention.

Justification 2C:

The current package focuses on the economic impacts of U.S. environmental regulations. It is distinct from past nominations by the authors, and there are no other current nominations by the same authors. Previous nominations by the authors focused on evidence of the energy efficiency paradox, measuring impacts of ethanol policy on corn prices, conducting retrospective analysis of the cost of EPA regulations, estimating the employment impacts of the SO_2 cap-and-trade policy on electric utilities, valuing changes in greenhouse gas emissions, understanding polluting plant location decisions, and quantifying catastrophic climate impacts.

Justification 2D:

n/a

Justification 2E:

n/a

Justification 3A:

The nominated paper, "The Impacts of Environmental Regulation on the U.S. Economy," is published in the *Oxford Research Encyclopedia of Environmental Economics*, which includes a globally diverse set of articles on a wide range of topics related to how and why environmental issues influence economic activity and the effects of economics on the environment. The editorial board for the *Oxford Research Encyclopedia of Environmental Economics* consists of a set of highly regarded economists: Dr. James R. Kahn, Washington and Lee University and the Federal University of Amazonas; Dr. Dan Biller, World Bank; Dr. John Whitehead, Appalachian State University; and Dr. Rawshan Ara Begum, Kumamoto University, Japan. The Encyclopedia makes this knowledge available to a wide range of natural and social scientists, as

well as educators, students, researchers and practitioners. Articles published in the Encyclopedia are also available online as part of the *Oxford Research Encyclopedia of Environmental Science*, which received over 1 million online views or visits between April 2018 and April 2020.

The published and working versions of the nominated paper have attracted wide readership and interest. According to the journal's website, "The Impacts of Environmental Regulation on the U.S. Economy" has been viewed or visited over 13,000 times since it was posted online. Research Gate indicates that the published paper has 373 reads from its website. The paper has been cited in three published research studies and two dissertations. In addition, the NCEE Working Paper version of the study, "The Impacts of Environmental Regulation on the U.S. Economy," was downloaded from the EPA by non-EPA users 881 times between March 2019 and March 2020, and was the most downloaded working paper and the third most downloaded document from the National Center for Environmental Economics (NCEE) website during this time period. Research Gate reports 199 reads from its website.

The nominated publication, "The Impacts of Environmental Regulation on the U.S. Economy," stems from efforts to inform a 2015-2017 Science Advisory Board (SAB) review about the role of economy-wide models for examining the costs, benefits, and economic impacts of an EPA air regulation. The authors presented to the SAB on these topics several times during the SAB review process and received compliments from panelists for the care and expertise they displayed on these topics. The nominated publication uses information that was assembled for the SAB panel as a starting point for initiating a broader review and discussion of the literature.

Citations of the nominated article

Arbuckle, M., and M. Mercer 2020. Economic outlook and the gender gap in attitudes about climate change. *Population and the Environment*. March.

Golovanov, E., L. Mikhalina, and K. Ekimova. 2017. *Role and Importance of Environmental Pressure in the System of Regional Economic Security*. December.

Gupta, V., and Y. Zheng. 2020. Investigando a gestão do desempenho Ambiental. *Revista Brasileira de Gestão de Negócios* 22(1). Three essays on environment, economics and politics

Justification 3B:

The Oxford Research Encyclopedia of Environmental Economics uses a single-blind referee process. All contributions are assessed by the editor and reviewed by independent expert reviewers. The authors responded to the comments by incorporating changes into the manuscript, which was then reevaluated prior to acceptance for publication.

AUTHORS

Principal Author

Author Name:	Ann Wolverton		
Professional Title:		Salutation:	Dr.
Email:	wolverton.ann@epa.gov	Organization:	
Mailing Address:			
Street Line 1:	1200 Pennsylvania Avenue Northwest, MC 1809T		
City:	Washington		
Zip Code:	20460	State:	DC

At time of research was:	EPA Employee		
Separation Date:			
% of Effort:	25		

Contributing Author

Author Name:	Alex Marten		
Professional Title:		Salutation:	Dr.
Email:	marten.alex@epa.gov	Organization:	
Mailing Address:			
Street Line 1:	1200 Pennsylvania Avenue Northwest, MC 1809T		
City:	Washington		
Zip Code:	20460	State:	DC
At time of research was:	EPA Employee		
Separation Date:			
% of Effort:	25		

Contributing Author

Author Name:	Ann E. Ferris		
Professional Title:		Salutation:	Dr.
Email:	ferris.ann@epa.gov	Organization:	
Mailing Address:			
Street Line 1:	1200 Pennsylvania Avenue Northwest, MC 1809T		
City:	Washington		

Zip Code:	20460	State:	DC
At time of research was:	EPA Employee		
Separation Date:			
% of Effort:	25		

Contributing Author

Author Name:	Richard Garbaccio		
Professional Title:		Salutation:	Dr.
Email:	garbaccio.richard@gmail.com	Organization:	
Mailing Address:			
Street Line 1:			
City:			
Zip Code:		State:	
At time of research was:	EPA Employee		
Separation Date:	Mon Dec 31 00:00:00 GMT 2018		
% of Effort:	25		

PUBLICATIONS

Publication 1:

Publication Title:	The Impacts of Environmental Regulation on the U.S. Economy		
Publication Date:	Fri Sep 01 00:00:00 GMT 2017		
Journal/Publication Method:	Oxford Research Encyclopedia of Environmental Economics		
All Author(s):			
Volume:	n/a	Number:	n/a

Pages:	1-40	Immediately Index:	Immediately Index:
Citation ½ Life:	n/a	Impact Factor:	n/a

The Impacts of Environmental Regulation on the U.S. Economy

Ann E. Ferris, Richard Garbaccio, Alex Marten, and Ann Wolverton

Subject: Policy, Governance, and Law, Environmental Economics
Online Publication Date: Sep 2017 DOI: 10.1093/acrefore/9780199389414.013.396

Summary and Keywords

Concern regarding the economic impacts of environmental regulations has been part of the public dialogue since the beginning of the U.S. EPA. Even as large improvements in environmental quality occurred, government and academia began to examine the potential consequences of regulation for economic growth and productivity. In general, early studies found measurable but not severe effects on the overall national economy. Although price increases due to regulatory requirements outweighed the stimulative effect of investments in pollution abatement, they nearly offset one another. However, these studies also highlighted potentially substantial effects on local labor markets due to the regional and industry concentration of plant closures.

More recently, a substantial body of work examined industry-specific effects of environmental regulation on the productivity of pollution-intensive firms most likely to face pollution control costs, as well as on plant location and employment decisions within firms. Most econometric-based studies found relatively small or no effect on sector-specific productivity and employment, though firms were less likely to open plants in locations subject to more stringent regulation compared to other U.S. locations. In contrast, studies that used economy-wide models to explicitly account for sectoral linkages and intertemporal effects found substantial sector-specific effects due to environmental regulation, including in sectors that were not directly regulated.

It is also possible to think about the overall impacts of environmental regulation on the economy through the lens of benefit-cost analysis. While this type of approach does not speak to how the costs of regulation are distributed across sectors, it has the advantage of explicitly weighing the benefits of environmental improvements against their costs. If benefits are greater than costs, then overall social welfare is improved. When conducting such exercises, it is important to anticipate the ways in which improvements in environmental quality may either directly improve the productivity of economic factors—such as through the increased productivity of outdoor workers—or change the composition of the economy as firms and households change their behavior. If individuals are healthier, for example, they may choose to reallocate their time between work and leisure. Although introducing a role for pollution in production and household behavior can be challenging,

PRINTED FROM the OXFORD RESEARCH ENCYCLOPEDIA, ENVIRONMENTAL SCIENCE (oxfordre.com/environmentalscience) (c) Oxford University Press USA, 2020. All Rights Reserved. Personal use only; commercial use is strictly prohibited (for details see Privacy Policy and Legal Notice).

date: 27 April 2020

studies that have partially accounted for this interconnection have found substantial impacts of improvements in environmental quality on the overall economy.

Keywords: economic impacts, environmental regulation, economic productivity, employment, plant location, social welfare, health benefits

In the 1960s increased awareness and concern about the negative consequences of environmental pollution on human health and ecosystems spurred a national approach to environmental policy and regulation in the United States (Griswald, 2012). The U.S. Council on Environmental Quality (U.S. CEQ) was formed in 1970 to advise the president on the environment, and the first Earth Day took place in April of that same year, with over 20 million Americans participating. Both the National Environmental Policy Act and the Clean Air Act were also signed into law in 1970, significantly expanding the federal government's role in controlling air pollution. The U.S. Environmental Protection Agency (U.S. EPA) was established on December 2, 1970, to implement the requirements of these two major pieces of legislation (Lewis, 1985). The Clean Water Act followed in 1972.[1]

Although environmental regulations reduce emissions of harmful pollutants, thus generating health and other benefits for the American public, they also raise a plant's production costs because they require installation and operation of pollution controls or changes in production processes that would otherwise not be undertaken. Almost immediately, the ability to balance environmental protection and the costs of pollution control requirements was tested. In 1971, the U.S. EPA Administrator, William D. Ruckelshaus, rejected the timetable submitted for bringing Union Carbide's Marietta, Ohio, plant into compliance with Clean Air Act requirements. Union Carbide responded by threatening to lay off a large number of workers. The U.S. EPA negotiated with the company on its emissions reduction schedule while preserving workers' jobs. This was done without compromising the environmental goal of reducing sulfur dioxide emissions at the plant, which declined 70% by April 1972 (Lewis, 1985).

From the beginning it also has been recognized that the potential negative effects on overall economic growth, productivity, and employment, as well as on specific industries should be considered alongside the positive consequences of improving environmental quality. In part, this balanced approach was likely motivated by the significant slowdown in U.S. productivity growth, uptick in inflation, and, by the mid-1970s, doubling of the unemployment rate that coincided with the expansion of federal oversight into areas such as environmental quality.[2] To better understand the potential effects of environmental regulation on the economy several government reports were commissioned to investigate the potential impacts on a wide array of measures, including national economic growth, industries and firms, employment, and consumers (e.g., U.S. CEQ, 1971). As data became available to study the impact of regulations retrospectively, the academic community also weighed in with studies of its own.

In the United States, current practice in federal government economic analyses of environmental regulation is to explicitly weigh the gains to society from environmental protection against the costs, measured in terms of changes in net social welfare. At the same

PRINTED FROM the OXFORD RESEARCH ENCYCLOPEDIA, ENVIRONMENTAL SCIENCE (oxfordre.com/environmentalscience) (c) Oxford University Press USA, 2020. All Rights Reserved. Personal use only; commercial use is strictly prohibited (for details see Privacy Policy and Legal Notice).

date: 27 April 2020

time, economic analyses continue to examine how those welfare changes are distributed throughout the economy. Although a particular environmental regulation may result in an overall net gain to society, this may not be true for particular subsets of the economy. Understanding who is positively and negatively impacted by a particular policy is important when contemplating policy options.

This article is organized as follows. Section I summarizes research on the part of the federal government into the economic impacts of U.S. environmental regulation. Building on this early work, Section 2 discusses the academic literature on the impacts of environmental regulation on overall productivity and growth, and Section 3 reviews the literature on impacts to particular sectors of the economy, with specific emphasis on industry productivity, labor markets, and plant entry and exit decisions. Section 4 discusses expanding the notion of overall economic impacts to think about welfare effects of environmental regulation. Section 5 describes efforts to explicitly consider benefits when modeling the economy-wide welfare effects of environmental regulation. Section 6 concludes by discussing several areas ripe for additional research.

Early Government Studies on the Economic Impacts of Environmental Regulation

In the early 1970s, as the U.S. began to implement the Clean Air and Clean Water Acts, there was limited information available on how environmental regulation might impact the economy (Haveman & Smith, 1978). To help fill this gap, President Nixon directed the U.S. CEQ, U.S. EPA, and the U.S. Department of Commerce, with guidance from the Council of Economic Advisers, to study the macroeconomic and microeconomic impacts of air and water pollution control costs. The first report, released in 1972, summarized a macroeconomic study and several microeconomic studies with the goal of developing a better understanding of the nature and magnitude of the potential impacts of environmental regulations on the economy as a whole and on individual industries and regions (U.S. CEQ et al., 1972). The underlying studies summarized by the report were described as initial analytic efforts that helped shed light on the paucity of available data on pollution abatement at that time (Haveman & Smith, 1978; Portney, 1981). Given their groundbreaking nature the underlying studies were subsequently published in an academic journal (see Evans, 1973; Russell, 1973; Dorfman, 1973). The general conclusion from the report was that pollution control costs “would not seriously threaten the long-run economic viability of the industrial activities examined,” though it also noted that since such impacts can be measured they are not “inconsequential” (U.S. CEQ et al., 1972).

The results of the macroeconomic study indicated that the national economy would be significantly, though not “severely” impacted by pollution abatement costs to implement the Clean Air Act. Pollution abatement costs were assumed to affect the economy through higher product prices and new demand for pollution abatement equipment and services. In the absence of adjustments in macroeconomic monetary or fiscal policy, price increases outweighed the stimulative effect of investments in pollution abatement, reducing the

PRINTED FROM the OXFORD RESEARCH ENCYCLOPEDIA, ENVIRONMENTAL SCIENCE (oxfordre.com/environmentalscience) (c) Oxford University Press USA, 2020. All Rights Reserved. Personal use only; commercial use is strictly prohibited (for details see Privacy Policy and Legal Notice).

date: 27 April 2020

growth rate of U.S. Gross National Product (GNP) by 0.3 percentage points and increasing the unemployment rate by 0.1 to 0.2 percentage points over the 1972 to 1976 period. However, the study also showed that employment declines were nearly offset by increased employment created by pollution control investments. When monetary and fiscal policy adjustments were incorporated, they offset the slowdown in GNP and increase in unemployment but at the cost of more rapid inflation and a further decline in the balance of international trade (U.S. CEQ et al., 1972).[3]

The microeconomic studies summarized in the report were based on analyses of the economic impacts of environmental regulations on eleven specific industries (e.g., auto manufacturing, pulp and paper, petroleum refining). Consistent with the macroeconomic study, the authors characterized the results as indicating that none of the industries studied would be "severely impacted" (i.e., the long term viability of these industries was not seriously threatened). The report estimated that for some industries prices will increase (by an annual average of between zero and 2% over the 1972 to 1976 period, depending on the industry), indicating some pass-through of costs. However, it also concluded that "profits will decline for some firms in most of the industries because firms will not be able to pass on the full cost of pollution abatement to consumers in the form of higher prices" (U.S. CEQ et al., 1972).

The early interaction between the newly created U.S. EPA and Union Carbide also highlighted a concern that environmental regulations could result in the layoff of workers at particular plants or even plant closures. However, as with other economic impacts, there was no empirical literature available that could provide a basis for estimates of national employment impacts associated with newly promulgated environmental regulations. The 1972 report summarized results from the microeconomic studies related to plant closures and employment effects. Of the approximately 12,000 plants in the industries studied, approximately 200–300 plants would be likely to close between 1972 and 1976 due to environmental regulations. However, the report noted that many of these plants were likely to have closed anyway because they were economically vulnerable for other reasons (U.S. CEQ et al., 1972). The employment impact from the projected plant closures was estimated to be approximately 50,000 to 125,000 jobs lost between 1972 and 1976 or about 1% to 4% of total employment in those industries. This would amount to an increase in national unemployment of approximately 0.05% (U.S. CEQ et al., 1972). The report warned, however, that the impact could be substantially higher if the economy was not at full employment. It is important to note that these estimates were not a net impact, since they did not include the number of people who found work in these industries over the same time period.

While the microeconomic studies in the 1972 report focused only on regulated industries, the macroeconomic study aimed to include all sectors of the economy, including pollution abatement activities. Macroeconomic impact modeling conducted as part of subsequent government reports found that growth in pollution abatement activities had a stimulative impact on the U.S. economy—creating additional jobs and decreasing the unemployment rate—relative to what would have occurred absent regulation (U.S. CEQ, 1979; DRI,

PRINTED FROM the OXFORD RESEARCH ENCYCLOPEDIA, ENVIRONMENTAL SCIENCE (oxfordre.com/environmentalscience) (c) Oxford University Press USA, 2020. All Rights Reserved. Personal use only; commercial use is strictly prohibited (for details see Privacy Policy and Legal Notice).

date: 27 April 2020

1981). Another U.S. CEQ report suggested that more efficient plants may have expanded production to make up for plants that closed (U.S. CEQ, 1978).

Initial concern about widespread job loss in the economy was, to a large degree, alleviated by empirical evidence. Based on self-reports from affected industries, the U.S. EPA found 118 plant closures between 1971 and 1977, affecting over 21,900 employees, were reportedly due to environmental regulations.[4] This estimate is about half the size of the minimum estimate projected in the 1972 report (U.S. CEQ, 1978; Haveman & Smith, 1978). The Department of Commerce also surveyed plant closings due to pollution control requirements and found 131 of them between 1974 and 1977, noting that 75% of permanent closings were not solely due to environmental regulation. As the economy improved over this time period, the number of plant closings reported each year also declined (Rutledge, Drieling, & Dunlap, 1978). Another Department of Commerce survey indicated that in over 60% of plant closures, plant age or facility obsolescence was a contributing factor (Segal & Dunlap, 1977). The 1978 U.S. CEQ report observed that closures were more likely to occur at plants that were older, smaller, less-efficient, and marginally profitable absent pollution control requirements (U.S. CEQ, 1978).

Although effects of environmental regulation on the overall U.S. labor market were not as substantial as anticipated, these reports acknowledged that individual plant “closures and the unemployment that they cause may be significant for the communities that they affect” (U.S. CEQ, 1978). In particular, substantial industry- and location-specific effects may occur due to the geographic concentration of plant closures in “older industrial towns already suffering from relatively high unemployment rates” (U.S. CEQ, 1978). Data collected by the U.S. EPA demonstrate that layoffs between 1971 and 1982 that were due, at least partially, to environmental regulation were concentrated in the primary metals, chemical, pulp and paper, and food processing industries. About 40% of the layoffs occurred in the upper Midwest, and another 28% occurred in the Northeast (U.S. EPA, 1982).

Academic Literature on Impact of Environmental Regulation on Overall Productivity and Growth

A key concern that motivated research into the impacts of environmental regulation on the economy was the significant slowdown in productivity growth that occurred at the same time as expansion of federal oversight into the environmental arena (Gray, 2015).[5] Initial interest by academic economists built on government-sponsored studies conducted in the early 1970s (e.g., U.S. CEQ et al., 1972). Using data on the costs of air and water pollution abatement and Solow growth accounting, Denison (1978, 1979)—a founder of growth accounting and an economist at the Brookings Institution at the time—was one of the first to empirically assess the impact of environmental regulations on productivity growth (i.e., the rate at which output per unit of input increases over time).[6] Denison esti-

PRINTED FROM the OXFORD RESEARCH ENCYCLOPEDIA, ENVIRONMENTAL SCIENCE (oxfordre.com/environmentalscience) (c) Oxford University Press USA, 2020. All Rights Reserved. Personal use only; commercial use is strictly prohibited (for details see Privacy Policy and Legal Notice).

date: 27 April 2020

mated that compared to the long-run growth rate of output per unit of input from 1948 to 1973 of just under 2%, environmental regulations resulted in an annual decline of between—0.10 and -0.20 percentage points between 1969 and 1978.

Christainsen and Haveman (1981A, 1981B) questioned several aspects of the data, methodology, and interpretation in Denison's growth accounting studies. They constructed indices for "regulatory intensity," based on the cumulative number of major pieces of public regulatory legislation, including, but not limited to environment (Christainsen & Haveman, 1981A). They used these indices to econometrically estimate the contribution of federal regulatory requirements to the slowdown in the growth of labor productivity. They concluded that regulations were responsible for between 12% and 21% of the 1.3 percentage point slowdown in productivity for manufacturing during 1973–1977, relative to the 1958–1965 period. Separately, based on their own work and a survey of other studies, Christainsen and Haveman (1981B) estimated that between 8 and 12% of the productivity slowdown could be attributed specifically to the cost of meeting environmental regulations.

About a decade later, Jorgenson and Wilcoxen (1990) used a computable general equilibrium (CGE) model to examine the impact of environmental regulations on the long-run growth of the U.S. economy. CGE models simulate the workings of a market economy and can be used to capture how the imposition of a regulation ripples through the entire economy, affecting both individual sectors and economy-wide aggregates. Jorgenson and Wilcoxen's dynamic CGE model divided the U.S. economy into 35 sectors, with behavioral parameters estimated from a time-series data set. Comparing steady states with and without environmental regulation, they estimated that regulation had reduced the level of real GNP by 2.6%. During the period 1973–1985, they estimated that the growth rate of GNP had been reduced by 0.2%. By sector, they found that pollution controls had the largest effects on chemicals, coal mining, motor vehicles, petroleum refining, primary metals, and pulp and paper. Using the same model, Jorgenson and Wilcoxen (1993) estimated that the Clean Air Act Amendments of 1990 would reduce the level of GNP by an additional 0.6%.

Academic Literature on Economic Impacts of Environmental Regulation on Specific Sectors

While the overall effect of environmental regulation on productivity and economic growth continue to be metrics of interest, effects on different subsets of the economy are also highly relevant when gauging the impacts of regulation. For instance, one might wish to understand how prices and quantities of goods in affected sectors respond to regulation, or whether the costs of meeting the requirements of a regulation results in plant closures, additional barriers of entry for new firms, or particularly large impacts on small businesses. Likewise, it might be important to understand how a regulation affects ener-

PRINTED FROM the OXFORD RESEARCH ENCYCLOPEDIA, ENVIRONMENTAL SCIENCE (oxfordre.com/environmentalscience) (c) Oxford University Press USA, 2020. All Rights Reserved. Personal use only; commercial use is strictly prohibited (for details see Privacy Policy and Legal Notice).

date: 27 April 2020

gy production and prices, employment in particular sectors, and the ability of consumers to switch to available substitutes or absorb increased prices for certain products.

Federal agencies promulgating new regulations are required by statute or Executive Order to estimate some of these impacts. For instance, Executive Order 13563 states: “Our regulatory system must protect public health, welfare, safety, and our environment while promoting economic growth, innovation, competitiveness, and job creation. It must be based on the best available science.” Executive Order 13211 requires, to the extent permitted by law, that agencies prepare a statement of energy effects when a regulatory action is expected to significantly affect energy supply, distribution, or use. The Regulatory Flexibility Act directs agencies to pay particularly close attention to the economic impacts of regulation on small businesses.

Although there is a wide range of economic impacts of potential interest to policymakers and the public when evaluating the effects of an environmental regulation, this entry focuses on only a subset of these. Specifically, this article summarizes the empirical literature on productivity impacts in pollution-intensive industries, the potential effect of environmental regulation on plant location and the U.S. labor market.

Productivity Studies

With little to suggest environmental regulations were a large drag on overall productivity growth, researchers began to investigate whether pollution-intensive industries newly subject to regulation experienced more significant productivity impacts. One early study by Gollop and Roberts (1983) estimated the effect of sulfur dioxide emissions regulation on productivity growth in the electric power industry from 1973 to 1979.[7] They estimated that the overall impact of the regulations on constrained utilities, which incurred both increased fuel and capital costs, to be an average decline in annual productivity growth of almost 0.6 percentage points per year. As the period of analysis also corresponded with a sharp rise in fuel costs, a key empirical challenge was to separate fuel switching induced by the regulation—from high- to low-sulfur coal—from the general rise in fuel prices.

Gray (1987) represented another important early study of the effect of environmental regulation on the productivity growth of pollution-intensive industries. He econometrically estimated the impact of federal environmental and occupational safety and health regulations on total factor productivity (TFP) growth for a wide array of manufacturing industries for the years 1958 to 1978.[8] (Total factor productivity is the amount of output produced as a function of all plant inputs, including labor, capital, materials, and energy.) He found that 30% of the slowdown in TFP growth could be attributed to the imposition of government regulations. However, only about one third of the 30% was specifically attributable to environmental regulations.

Similarly, Barbera and McConnell (1990) estimated the impact of environmental regulations on TFP for five of the most polluting industries. For the paper industry, they found that pollution abatement accounted for 30% of the decline in TFP in 1970–1980 compared to 1960–1970. For the chemical, iron and steel, and stone, clay, and glass indus-

PRINTED FROM the OXFORD RESEARCH ENCYCLOPEDIA, ENVIRONMENTAL SCIENCE (oxfordre.com/environmentalscience) (c) Oxford University Press USA, 2020. All Rights Reserved. Personal use only; commercial use is strictly prohibited (for details see Privacy Policy and Legal Notice).

date: 27 April 2020

tries estimates ranged from a 10% to 12% decline, while TFP actually increased for nonferrous metals over this time period. Unlike previous work, the authors were able to differentiate between direct effects (i.e., the need to increase total inputs for the same level of output when increasing abatement) and indirect effects (i.e., potential changes in the production function, which may be positive or negative).

Economists have continued to use detailed industry- and plant-specific data to investigate the effects of environmental regulations on pollution-intensive industries, while improving on the empirical techniques of early studies. In general, they continued to find relatively small or no effect of environmental regulation on firm- or plant-level productivity. For instance, Repetto, Rothman, Faeth, and Austin (1997) asserted that there is a bias in traditional measures of productivity because a reduction in bad outputs (pollution) is not accounted for in those measures. When Domazlicky and Weber (2004) accounted for polluting outputs they found that while there were costs associated with environmental regulations for the six chemical sectors investigated, they were not correlated with a reduction in productivity.

Berman and Bui (2001B) also pointed out a number of potential problems with earlier studies. First, heterogeneity bias may exist as dirtier plants may also be less productive, making abatement appear to reduce productivity. (The opposite effect may occur for cleaner plants.) Second, abatement expenditures may be difficult to classify and may overstate the true economic costs of environmental regulation. To avoid these problems, the authors construct a TFP measure for U.S. refineries in the Los Angeles air basin using physical quantities. Although abatement costs were high due to strict air quality regulations, they found that refinery productivity actually rose during the 1987 to 1992 time period in the Los Angeles air basin, in contrast to declining productivity for refineries in other parts of the country that were not subject to the regulations.

Several studies are notable because of their use of sophisticated empirical techniques and detailed U.S. plant-level data from the U.S. Census of Manufactures and the Pollution Abatement and Cost Expenditure (PACE) survey.[9] Gray and Shadbegian (2003) examined how the impact of pollution abatement costs on productivity varies by type of pulp and paper mill over the 1979–1990 period. They found significant impacts on productivity for integrated mills, though not for non-integrated mills. They found no significant differences between older and newer plants. For the same time period, Shadbegian and Gray (2005) considered effects on paper mills, refineries, and steel mills and found that abatement expenditures generally had no significant effect on the productivity of non-abatement inputs. As in their previous paper, they examined subgroups of plants, those with dirtier production technologies and with more end-of-line abatement, but they did not find significant differences. Becker (2011) and Greenstone, List, and Syverson (2012) relied on differences in environmental stringency across counties in and out of attainment with the National Ambient Air Quality Standards to identify the impact of environmental regulation on the productivity of manufacturing plants. Becker (2011) found no statistically significant effect on productivity for plants in counties with higher environmental costs. Greenstone et al. (2012) estimated that for plants in heavily polluting industries, the

PRINTED FROM the OXFORD RESEARCH ENCYCLOPEDIA, ENVIRONMENTAL SCIENCE (oxfordre.com/environmentalscience) (c) Oxford University Press USA, 2020. All Rights Reserved. Personal use only; commercial use is strictly prohibited (for details see Privacy Policy and Legal Notice).

date: 27 April 2020

nonattainment designation was associated with a 2.4% decline in TFP among plants that emitted the targeted pollutants. Estimated separately, ozone and carbon monoxide–emitting plants in nonattainment counties had productivity losses of about 2%. Sulfur dioxide emitters saw no significant change in TFP. TSP emitting plants experienced a productivity increase of about 1.0%.

Plant Entry and Exit Decisions

Another key question that has arisen in the literature is whether compliance costs due to environmental regulations affect plant location decisions. Some U.S. counties—geographic and governmental jurisdictions within each state—face more stringent regulations when they are out of attainment with the National Ambient Air Quality Standards (NAAQS) for criteria air pollutants (e.g., particulate matter, ozone). In addition, because states frequently are responsible for implementing and enforcing federal regulations it is possible that differences in monitoring and enforcement may cause the costs of compliance to vary across states.

Bartik (1985) is an important early paper in the plant location literature because it sets out the analytic framework for how differences in costs across locations influence siting decisions. Levinson (1996) extended this framework to explicitly consider the role of environmental regulatory costs. If compliance costs differ across locations or by type of plant, this can influence firm-level decisions about where to locate new plants and how to shift production among existing plants. Relying mainly on cross-sectional data, early empirical studies did not find evidence that environmental regulations affected U.S. plant location decisions (e.g., Carlton, 1983; McConnell & Schwab, 1990; Levinson, 1996). However, later studies that had access to panel data and more refined empirical techniques to better account for spatial correlation across locations, omitted variable bias, and plant- and location-specific effects found that higher compliance costs had a significant, negative effect on plant location, particularly in the most pollution-intensive industries (Shadbegian & Wolverton, 2010).[10]

Among the panel studies, it is relatively common to use attainment status with one or more NAAQS regulations as a proxy for environmental regulatory stringency. Henderson (1996) found evidence that manufacturing plants that were relatively high emitters of volatile organic compounds and nitrogen oxides were less likely to locate in counties out of attainment with the ozone NAAQS and that a county that came into attainment with the ozone NAAQS (and therefore was no longer subject to additional regulatory scrutiny) attracted about 8% more plants than a county that did not change status. Kahn (1997) found that manufacturing plants were less likely to close in counties out of attainment for particulate matter. However, conditional on remaining open, these plants grew more slowly over the 1982 to 1988 period.

Examining four polluting manufacturing industries, Becker and Henderson (2000) estimated that counties out of attainment with the ozone NAAQS attracted 26%–45% fewer plants than counties in attainment between 1967 and 1992. In addition, they found that

PRINTED FROM the OXFORD RESEARCH ENCYCLOPEDIA, ENVIRONMENTAL SCIENCE (oxfordre.com/environmentalscience) (c) Oxford University Press USA, 2020. All Rights Reserved. Personal use only; commercial use is strictly prohibited (for details see Privacy Policy and Legal Notice).

date: 27 April 2020

the further out of attainment a county, the larger the estimated loss in new plants. In a similar study, Millimet and List (2004) examined how ozone attainment status affected plant entry and exit in pollution-intensive industries in New York from 1980 to 1990. They found that factors such as a higher proportion employed in manufacturing, smaller populations, and higher wages help mitigate the effects of nonattainment on plant entry and exit. Condliffe and Morgan (2009) found that nonattainment with the ozone NAAQS had, on average, a statistically negative effect on plant entry in U.S. counties between 1996 and 1998, but that this effect was mainly concentrated in the more pollution-intensive manufacturing industries.

List, McHone, and Millimet (2003) is one of the few studies to examine the impact of attainment status on the relocation of existing plants. Using data from New York, they found that a county that changed ozone attainment status between 1980 and 1990 experienced over a 50% change in the flow of newly relocating plants. In particular, counties out of attainment and therefore subject to more stringent environmental standards attracted significantly fewer relocating plants than counties in attainment.

Labor Market Impacts

The potential employment impacts of environmental policy have been of concern since the Clean Air Act first was implemented, and interest continues. Analytically, the impacts of environmental regulation on employment are quite difficult to disentangle from other economic changes and conditions that affect employment. Because environmental regulation shifts economic activity toward less-polluting activities, employment impacts are a mix of potential declines and gains over time, across regions, and across industries of the economy. In addition to impacts on the directly regulated sectors, environmental regulations often increase demand for pollution control equipment and services needed for compliance. Moreover, a regulation that increases the costs of a primary input such as electricity may cause a decrease in the demand for labor in energy-intensive industries.

Microeconomic theory of production and factor demand describes how firms adjust their demand for inputs, such as labor, in response to changes in economic conditions. Researchers have used this framework to represent pollution abatement requirements as changes in quasi-fixed factors of production (Berman & Bui, 2001A), an increase in the price of pollution (Greenstone, 2002), an increase in pollution abatement costs (Morgenstern, Pizer, & Shih, 2002), an emissions tax (Holland, 2012), an increase in the price of capital (Deschênes, 2014), or an increase in energy prices (Deschênes, 2012). Impacts on firm-level labor demand can be decomposed into substitution and output effects. The substitution effect measures a change in employment as the firm responds to a change in input price, holding output constant. For example, with only capital and labor inputs, if the price of capital increases, the firm will substitute toward increased use of labor to produce the same level of output. With three or more productive factors, the substitution effect depends on the cross-elasticities of labor demand. The change in input price may also change the firm’s marginal cost of production, which then may affect the firm’s profit-maximizing level of output. The output effect measures how employment changes as the

PRINTED FROM the OXFORD RESEARCH ENCYCLOPEDIA, ENVIRONMENTAL SCIENCE (oxfordre.com/environmentalscience) (c) Oxford University Press USA, 2020. All Rights Reserved. Personal use only; commercial use is strictly prohibited (for details see Privacy Policy and Legal Notice).

date: 27 April 2020

firm adjusts output to maximize profits, while holding relative input shares constant. As the output and substitution effects may be both positive, negative, or some combination, theory alone cannot predict the sign of the total impact of regulation on labor demand at regulated firms.

Overall, the economics literature finds little evidence that environmental regulations have had a significant impact on employment in regulated sectors and generally does not speak to the sign or magnitude of the overall effect of regulation on national employment.[11] Berman and Bui (2001A) examined the impact of local air quality regulations on employment in manufacturing plants relative to similar plants that did not face the same regulations. They found that even though regulations impose large costs on plants, they had a statistically insignificant effect on employment. Ferris, Shadbegian, and Wolverton (2014) also used a quasi-experimental empirical approach, and found that relative to similar but unregulated plants, employment impacts from Phase I of the sulfur dioxide cap-and-trade program were close to zero for regulated utilities. Gray, Shadbegian, Wang, and Meral (2014) found that pulp mills subject to certain air and water regulations experienced relatively small, and not always statistically significant, decreases in employment. Curtis (FORTHCOMING) found a small negative impact of the nitrogen oxides cap-and-trade program on manufacturing employment, with impacts primarily occurring through decreased hiring rates, rather than increased separation rates. Sheriff, Ferris, and Shadbegian (2016) found negative impacts of ozone regulations on employment at electric utilities, with no accompanying changes in electricity generation, possibly indicating labor-saving technical change.

Other research on employment effects in regulated sectors, such as Greenstone (2002) and Walker (2011, 2013), suggest that counties subject to stricter air quality regulation may generate fewer manufacturing jobs than less regulated ones. However, because they identified employment impacts by comparing nonattainment to similar attainment areas, employment impacts are likely overstated; they are “double counted” to the extent that regulation caused plants to locate in one area of the country rather than another (Greenstone, 2002). List, Millimet, Fredriksson, and McHone (2003) found some evidence that this type of geographic relocation may be occurring. Kahn and Mansur (2013) examined manufacturing employment impacts of air regulations by pairing a regulated county with a neighboring, less regulated county, while controlling for differences in electricity price and labor regulation. They found limited evidence that air regulations caused employment to be lower on net within a county-border-pair. Although regulation may cause labor to relocate across a border, since one county’s loss is another’s gain, such shifts cannot be transformed into an estimate of a national impact on employment.

If employment impacts are anticipated in related but not directly regulated sectors, then a general equilibrium approach would likely better capture those impacts. However, existing CGE models used to analyze the overall impacts of environmental regulation almost always assume full employment. One way to incorporate involuntary unemployment into CGE models as an equilibrium condition has been to use a reduced form approach consistent with the notion that frictions in the marketplace prevent wages from adjusting to

PRINTED FROM the OXFORD RESEARCH ENCYCLOPEDIA, ENVIRONMENTAL SCIENCE (oxfordre.com/environmentalscience) (c) Oxford University Press USA, 2020. All Rights Reserved. Personal use only; commercial use is strictly prohibited (for details see Privacy Policy and Legal Notice).

date: 27 April 2020

their market-clearing level. Modelers often specify a wage curve, based on the empirical observation of Blanchflower and Oswald (1994), that real wages are a decreasing function of the unemployment rate. This approach amounts to an exogenous assumption regarding the amount of unemployment within the labor market.

Dissou and Sun (2013) specified a wage curve to examine the welfare and employment implications of different ways of recycling revenues from a carbon cap-and-trade system. They found relatively small effects on employment for low- and high-skilled workers across scenarios, noting that this is unsurprising given that carbon-intensive industries tend to use relatively more capital than labor (i.e., as such, one would expect them to shed more capital than labor in response to the policy). Likewise, Rivers (2013) incorporated a wage curve into a highly stylized three-sector static CGE model to examine the employment implications of renewable energy policies. Rivers found that subsidies increase equilibrium unemployment. Böhringer, Rivers, Rutherford, and Wigle (2012) used a CGE model to assess the labor market impacts of a feed-in-tariff policy in the electricity market in Ontario. They found that while increasing employment in "green" manufacturing, the policy had the opposite effect on employment in the rest of the economy and increased the unemployment rate overall. The authors acknowledged that external effects and technical change are ignored in the static model, and in certain cases their inclusion might produce a different outcome. Böhringer, Keller, and van der Werf (2013) used a CGE model of Germany to investigate the impacts of renewable energy promotion. They found that the possibilities for enhancing welfare and employment are quite limited, hinging crucially on the subsidy rate and financing mechanism.

CGE models that explicitly model wage-setting mechanisms often adopt labor market models from the labor economics literature. There are a number of wage-setting mechanisms, including efficiency wages, collective wage-bargaining, job search and matching models, as well as explicit incorporation of other types of wage rigidities. The efficiency wage model is predicated on the idea that employers can increase worker productivity by paying above-market wages. In the collective wage-bargaining model above-market wages result from negotiations between firms and trade unions with some degree of market power. Job search-and-matching models assume that finding a job requires time and effort and is inherently stochastic. The higher the ratio of unemployed to vacancies, the lower the probability of finding a job.[12]

Balistreri (2002) laid out a methodology for incorporating two salient features of the job search and matching model into a CGE framework: "(1) supplying labor for production is costly in terms of the foregone reservation wage and an individual's chance of not being matched to a job (i.e., becoming unemployed); and (2) there is an externality by which the risk of an individual not being matched is affected by the aggregate behavior of other agents." He then demonstrated how this formulation of the job search and matching model operates within a dynamic CGE model of the United States when simulating a cap-and-trade policy to reduce carbon emissions.[13] Babiker and Eckaus (2007) introduced wage rigidities by limiting sectoral labor mobility and sectoral wage adjustment in a multi-region global CGE model. Dixon, Johnson, and Rimmer (2011) allowed for potential disequi-

PRINTED FROM the OXFORD RESEARCH ENCYCLOPEDIA, ENVIRONMENTAL SCIENCE (oxfordre.com/environmentalscience) (c) Oxford University Press USA, 2020. All Rights Reserved. Personal use only; commercial use is strictly prohibited (for details see Privacy Policy and Legal Notice).

date: 27 April 2020

librium in the U.S. labor market by specifying three states: employed, unemployed, and not in the labor force where employed labor is differentiated by industry, occupation, and region. The model also assumed a cost associated with changing employment states (Dixon & Rimmer, 2002).

Expanding the Notion of Overall Economic Impacts to Think about Social Welfare

Although changes in gross domestic or gross national product (GDP or GNP) and productivity have often been reported by government and academics as a metric for understanding the overall impact of an environmental regulation on the U.S. economy, they also have long recognized its shortcomings as a way to capture the full effects of policy on social well-being or welfare.

Executive orders signed under Presidents Nixon and Ford, directed federal agencies to evaluate the potential effects of new regulation on the economy through the conduct of "Quality of Life Reviews" and "Inflation Impact Statements" (Morgenstern, 1997; OMB, 1997). The stated objective of a Quality of Life Review was to minimize the burden of environmental regulations on businesses. Inflation Impact Statements were broader; their purpose was to monitor agency activity for potentially inflationary actions and to conduct an inflation impact analysis (OMB, 1997). Economists hired to oversee these analyses concluded, however, that a regulation could not be inflationary unless its costs to society exceeded its benefits. As a result, they began conducting benefit-cost analyses (BCAs) of new, major regulations as a way to meet executive order requirements.[14]

A BCA that quantifies the social benefits and costs associated with a regulation seeks to answer the question, is it theoretically possible for the "gainers" from the policy to fully compensate the "losers" and still remain better off (U.S. EPA, 2010).[15] In this context, the measure used to gauge a regulation's effect on the economy is the net change in social welfare that households experience. The net change in welfare is derived "by summing all of the benefits that accrue as a result of a policy change (including spillover effects) less costs imposed by the policy on society (including externalities)" (U.S. EPA, 2010). Since spillovers and externalities are nonmarket transactions, quantifying private costs and benefits is not a sufficient proxy for estimating the costs and benefits of a new regulation to society. Social cost represents the total burden that a regulation will impose on the economy. It is defined as the sum of all opportunity costs incurred as a result of a regulation, where an opportunity cost is the value lost to society of all goods and services that will not be produced and consumed in the presence of regulation as resources are reallocated away from consumption and production activities toward pollution abatement (U.S. EPA, 2010). Social benefits are also measured in terms of opportunity cost (OMB, 1997).[16]

PRINTED FROM the OXFORD RESEARCH ENCYCLOPEDIA, ENVIRONMENTAL SCIENCE (oxfordre.com/environmentalscience) (c) Oxford University Press USA, 2020. All Rights Reserved. Personal use only; commercial use is strictly prohibited (for details see Privacy Policy and Legal Notice).

date: 27 April 2020

Why Move Beyond Impacts on Productivity and GDP to Consider Effects on Economic Welfare?

GNP or GDP has been recognized as “a flawed measure of economic welfare” because a number of factors that affect one’s quality of life are not included, such as leisure, health status, crime, and the environmental quality, among others (Jones & Klenow, 2016).[17] In addition, these measures may be misleading due to double counting. For example, a regulation that requires firms to invest in new capital in a given year will result in a large increase in the investment component of GDP. However, capital also affects the availability of goods and services that can be consumed over a much longer time period, which is also captured in the consumption component of GDP (Paltsev & Capros, 2013). To avoid double counting, studies sometimes report changes in household consumption as an indicator of social welfare. However, as with GDP, this measure excludes consideration of how a new policy affects leisure and other quality of life factors such as environmental quality.[18] Another previously discussed alternative, economic productivity, is narrowly focused on the degree to which a policy affects the amount of output that can be produced using a given amount of inputs.

Economists use the concepts of equivalent variation (EV) and compensating variation (CV) to explore how a policy affects social well-being. Both of these are monetary measures of the change in utility brought about by changes in prices and incomes. The difference between them depends on whether one assumes the policy change has already occurred (EV), or is not yet in place (CV). For instance, EV measures what a consumer would be willing to pay to avoid an increase in prices (and thus, a decline in real income) resulting from a regulation going into effect. In contrast, CV measures how much a consumer would need to be compensated to accept changes in prices and income such that the consumer achieves the same level of utility experienced prior to the policy shock. In addition, changes in welfare encompass more than just market activities—for instance, there is a monetary value to leisure.

Literature on the Social Cost of U.S. Environmental Regulation

Hazilla and Kopp (1990) is an early example of a study that examined the welfare impact of environmental regulations on the economy. Relying on a 36-sector dynamic CGE model, they estimated the social cost of the U.S. Clean Air and Clean Water Acts for 1981 to 1990 expressed in terms of compensating variation.[19] They found that all sectors of the economy were affected, with the greatest impacts of the regulation falling on electric utilities, motor vehicles, crude oil and natural gas, primary metals, and chemicals. Sectors that were not directly regulated but supplied key intermediate goods also experienced significant negative impacts on output and labor productivity. Their estimate of the social cost of the regulations (about $980 billion) was more than 50% greater than the U.S. EPA’s equivalent engineering cost estimate. Hazilla and Kopp (1990) noted the importance of this result since “very few policymakers have recognized that social costs can ex-

PRINTED FROM the OXFORD RESEARCH ENCYCLOPEDIA, ENVIRONMENTAL SCIENCE (oxfordre.com/environmentalscience) (c) Oxford University Press USA, 2020. All Rights Reserved. Personal use only; commercial use is strictly prohibited (for details see Privacy Policy and Legal Notice).

date: 27 April 2020

ceed private expenditures.” They state that the difference between the two measures is “a direct result of household behavior in which leisure is substituted for consumption.”

Two studies by the U.S. EPA on the benefits and costs of the Clean Air Act demonstrate how impacts on the economy differ when expressed in terms of economic welfare relative to GNP. The U.S. EPA (1997) relied on the CGE model used in Jorgenson and Wilcoxen (1990) to retrospectively examine the sectoral impacts and aggregate effects of the Clean Air Act from 1970 to 1990. As measured by changes in prices and output, the sectors most impacted were motor vehicles, petroleum refining, and electricity generation. The aggregate effect on GNP was estimated as a reduction in the long-run rate of GNP growth of 0.2%, with the 1990 level of GNP 1 percent lower than in the no-control scenario. The impact on social welfare, measured in terms of equivalent variation, was considerably smaller than the change in GNP, even though benefits of the Clean Air Act were not included in the CGE model.

The U.S. EPA (2011) study of the prospective effects of the Clean Air Act Amendments from 1990 to 2020 used a dynamic, forward-looking 35-sector CGE model. It found substantial secondary effects of compliance costs on the overall economy, a large portion of which likely result from energy price increases and the diversion of capital from activities that enhance long-term productivity to investment in pollution control equipment in the industrial sector. Once again, it found that GDP is not a particularly good measure of the welfare impact of a policy. In a cost-only scenario (i.e., no benefits included), GDP in 2020 was $108 billion lower than in the no-control case, while social welfare, measured as equivalent variation, was 25% smaller than the effect on GDP (about $82 billion lower than in the no control case) due to the reallocation of some of the household’s time to leisure instead of labor. Unlike the U.S. EPA’s retrospective analysis, an additional scenario included some of the health benefits of the Clean Air Act. We discuss these in the next section.

Incorporating Benefits into Economy-Wide Modeling of Welfare Effects from Environmental Regulation

Due to the many ways in which economic activity is linked to environmental quality it is not possible to provide a full accounting of the effect of environmental policy on economic productivity and social well-being without also taking into account the beneficial effects and their impact on the economy. As policies change the environment they may either directly improve the productivity of economic factors (e.g., reduced depreciation from acidic deposition, increased productivity of outdoor workers) or change the composition of the economy as firms and households change their behavior (e.g., labor-leisure choices).

PRINTED FROM the OXFORD RESEARCH ENCYCLOPEDIA, ENVIRONMENTAL SCIENCE (oxfordre.com/environmentalscience) (c) Oxford University Press USA, 2020. All Rights Reserved. Personal use only; commercial use is strictly prohibited (for details see Privacy Policy and Legal Notice).

date: 27 April 2020

There has been growing awareness that these interconnections between the environment and the economy are important for understanding the net effect of a policy on the economy and overall social well-being (Carbone & Smith, 2013). However, introducing a role for the environment into production and household behavior at an economy-wide scale is an area of applied analysis that is still developing. The suite of studies that have partially incorporated pollution into these types of frameworks have found substantial impacts on the overall economy of improvements in environmental quality. This section discusses the ways in which improvements in environmental quality can have a significant effect on economic activity and literature that explicitly accounts for the relationship between pollution and productivity when estimating the social welfare of air regulations.

Relationship Between Pollution and Productivity

Although much of the initial literature focused on the connection between economic activity and compliance with environmental regulations, recent work has shown that understanding the way benefits from improving environmental quality interact with economic activity is also important for understanding the overall impacts of regulation. In fact, many estimates of the benefits associated with environmental policies leverage changes in market activity that complement household consumption of nonmarket goods and services as environmental quality varies. For example, households' willingness to pay for environmental improvements are commonly estimated based on the way spatial and/or temporal variation in environmental quality affects housing prices due to its influence on housing demand (Palmquist, 2005). Similarly, studies leveraging observed housing market behavior in response to variation in environmental amenities, have estimated households' willingness to pay for improvements in health (Gayer, Hamilton, & Viscusi, 2002). Benefits from improvements in environmental quality are also routinely estimated from consumers' willingness to trade-off other consumption for improved environmental quality in their recreation decisions (Phaneuf & Smith, 2005).

Human health has an important and direct connections with both economic activity and environmental quality. Degredation of environmental quality, such as air pollution, can increase the incidence of premature mortality (Levy, Baxter, & Schwartz, 2009; Fann et al., 2012; Tagaris et al., 2009). While vulnerable populations such as children and the elderly are particularly susceptible to the effects of pollution, environmental degradation also impacts the mortality rate of working age individuals, thereby having a direct effect on labor force participation (U.S. EPA, 2011). Similarly, the morbidity effects of pollution can impact labor supply due to effect on sick days taken (i.e., the extensive margin), as well as worker productivity while on the job (i.e., the intensive margin) (e.g., Vennemo, 1997).[20] Restrictions on an individual's time endowment also affects the proportion allocated to work versus leisure activities. Pollution-related morbidity effects also increase demand for medical goods and services, which means those resources are not available for other productive uses in the economy (Matus, Yang, Paltsev, Reilly, & Nam, 2008). Although the size of these resource shifts may be relatively small, consideration of their ef-

PRINTED FROM the OXFORD RESEARCH ENCYCLOPEDIA, ENVIRONMENTAL SCIENCE (oxfordre.com/environmentalscience) (c) Oxford University Press USA, 2020. All Rights Reserved. Personal use only; commercial use is strictly prohibited (for details see Privacy Policy and Legal Notice).

date: 27 April 2020

fect on economic activity may still be warranted, particularly given the highly distorted state of health-care markets.

In addition, environmental degradation affects the health of children in ways that are potentially different than for adults. First, children can be more vulnerable to pollution due to normal childhood activities and behavior patterns. According to U.S. EPA (2013A), “Children generally eat more food, drink more water, and breathe more air relative to their size than adults do, and consequently may be exposed to relatively higher amounts of environmental contaminants.” Second, children may be more vulnerable to pollution because they are still developing physically and may, therefore, be more easily harmed. The effects of environmental quality on children’s health impacts economic activity through multiple channels. In a dynamic setting, changes in the health risks faced by children, in the form of mortality and development, can have long-term implications for the economy through impacts on future labor supply and worker productivity. Furthermore, pollution-related illnesses in children can affect labor supply when parents and guardians have to take time off from work to provide care (Salkever, 1982).

Changes in environmental quality also impact the availability and productivity of other inputs to production. For example, atmospheric and deposition effects of air pollution can lead to materials damages, thereby increasing the depreciation rate of physical capital (U.S. EPA, 1999; Saha & Eckelman, 2014) and causing damages to buildings and structures of cultural and historical significance (Grosclaude & Soguel, 1994), which may impact regional tourism (Kling, Revier, & Sable, 2004). Similarly, air pollution has the potential to affect agriculture and forestry through its direct effect on vegetation via induced foliar injury, reduced annual growth rates, and induced root loss (U.S. EPA, 2007). Visible foliar injury can reduce the desirability of leafy crops, (e.g., spinach, lettuce) and ornamentals (e.g., petunias, geraniums, poinsettias). Discoloration and early shedding of leaves from air pollution, can also have notable welfare effects in areas where foliage is highly valued (e.g., scenic vistas, fall foliage).

Literature Incorporating Benefits into Economy-Wide Analysis of Environmental Regulation

It has been estimated that environmental regulations prevent substantial numbers of premature deaths ever year and have a significant effect on rates of morbidity (U.S. EPA, 2011). A number of researchers have modeled the way these improvements in human health may interact with the economy using CGE models. Several of the initial studies were conducted in Europe. Vennemo (1997) was one of the first to incorporate environmental externalities into an applied CGE model of the Norwegian economy. Morbidity associated with air pollution was assumed to impact labor supply at both the extensive and intensive margins and was modeled as pollutant specific labor shocks. While the early work of Vennemo was limited in its ability to capture some of the complex connections between the economy and the environment, it provided insights into their potential impor-

PRINTED FROM the OXFORD RESEARCH ENCYCLOPEDIA, ENVIRONMENTAL SCIENCE (oxfordre.com/environmentalscience) (c) Oxford University Press USA, 2020. All Rights Reserved. Personal use only; commercial use is strictly prohibited (for details see Privacy Policy and Legal Notice).

date: 27 April 2020

tance. Environmental feedbacks significantly reduced consumption of goods and services as well as overall social welfare.

A decade later, Mayeres and van Regemorter (2008) studied the effect of health impacts from air pollution on the European economy. Their study pushed the science forward by incorporating some aspects of mortality, morbidity, and non-health impacts of air pollution from the energy sector as non-separable elements of households' utility functions in a general equilibrium framework. In other words, the study allowed for the behavior of households to be affected by changes in health status and environmental quality. Morbidity was modeled as both reducing households' time endowment directly and as a labor productivity shock. By modeling a portion of the labor morbidity effect as a shock to labor productivity, Mayeres and van Regemorter attempted to capture the role of paid sick leave, whereby some households will remain financially whole in the face of changes in morbidity, while firms see a change in the productivity of their labor force. The study also incorporated the medical costs of pollution-induced mortality and morbidity more fully into the model by considering the effect of air pollution on private and public spending for medical services and household's time endowments within a bi-directional coupling of the economy and the environment.

Researchers in the United States also began to incorporate health impacts from air pollution into a prominent multiregion, global CGE model (i.e., the Emission Prediction and Policy Analysis [EPPA] model). To date, the health effects version of the model has been used to study the impact of historical ozone and particulate matter air pollution in the U.S. (Matus et al., 2008), Europe (Nam, Selin, Reilly, & Paltsev, 2010), and China (Matus et al., 2012), and future ozone pollution globally (Selin et al., 2009). To incorporate premature mortality, the model accounted for the damages to households in terms of total factor consumption, including leisure, while also accounting for the cumulative economic effect of reduced labor, consumption, and investment associated with premature mortality. To incorporate pollution-induced morbidity, the model accounted for the reduced time available for labor and/or leisure, the increased demand for medical services, and cumulative economic effects from those changes.

Two studies have estimated how including the benefits of air pollution regulation affects social welfare. Matus et al. (2008) estimated that by 2000 air pollution regulations in the United States provided a welfare improvement (measured in terms of equivalent variation) of nearly $400 billion [1997$], with households being willing to pay another $250 billon [1997$] to avoid the remaining damages from air pollution.[21] They also estimated that consumption of final goods was 5.4% higher in 2000 due to improvements in air quality than in a world without those environmental policies. The U.S. EPA conducted a similar study looking at the expected economy-wide impacts of all regulations promulgated thus far under the Clean Air Act Amendments (U.S. EPA, 2011). The study modeled two scenarios in a CGE framework: a "cost-only" scenario that introduced the compliance costs of the regulations into the model, and a "labor force-adjusted" scenario that modeled both the costs and some human health benefits, specifically the mortality risk and morbidity reductions expected to accrue to the labor force as an increase in their avail-

PRINTED FROM the OXFORD RESEARCH ENCYCLOPEDIA, ENVIRONMENTAL SCIENCE (oxfordre.com/environmentalscience) (c) Oxford University Press USA, 2020. All Rights Reserved. Personal use only; commercial use is strictly prohibited (for details see Privacy Policy and Legal Notice).

date: 27 April 2020

able time endowment. The scenario also included expected reductions in the demand for medical services as a result of reduced morbidity.

Figure 1. Economy-Wide Impacts of the Clean Air Act Amendments.

Source: U.S. EPA (2011).

The U.S. EPA's analysis highlights a number of important insights. First, it showed how important accounting for the beneficial impacts of environmental policies are when trying to assess their economic impacts. When accounting for the human health impacts of the policy the expected effect on GDP was less than half of what it was when only compliance costs were considered. Inclusion of health benefits in the control case also reduced negative impacts on sectors such as electricity, mining, and minerals and increased the positive impacts on sectors such as computer equipment manufacturing. Second, as previously discussed, it demonstrated that GDP is not a particularly good measure of the welfare impact of a policy. Recall that, even when only considering the costs of the policy, the change in GDP was significantly different than the change in welfare. Figure 1 shows that this issue is exacerbated once the human health impacts of the policy are included. In the initial years the impact of the policy on GDP was negative while the policy was immediately welfare improving (with this effect growing over time). This is primarily driven by changes in the time endowment, which allows households to engage in more leisure while also supplying more labor, increasing both consumption and welfare.

As already mentioned, other nonmarket impacts of environmental policies may also be important for determining effects on social welfare. For example, Finnoff and Tschirhart (2008) coupled ecological and economic general equilibrium models of the Alaskan economy with a food web model of Alaska's marine ecosystem to study the economic impacts of regulating commercial fishing. They found potentially notable general equilibrium effects due to the direct effects in the regulated sector and indirect effects on the tourism sector. In addition, while most of the primary factors (capital and labor) utilized in the directly regulated industry resided outside of Alaska, they found that the domestic labor market was affected due to reductions in real income as well as changes in the tourism sector.[22]

Carbone and Smith (2013) tested the quantitative importance of general equilibrium welfare effects when there are changes in human health, nonmarket ecosystem services, and non-use existence services that result from improving environmental quality. Specifically, they added sector-specific sulfur and nitrogen oxide emissions factors that have effects

PRINTED FROM the OXFORD RESEARCH ENCYCLOPEDIA, ENVIRONMENTAL SCIENCE (oxfordre.com/environmentalscience) (c) Oxford University Press USA, 2020. All Rights Reserved. Personal use only; commercial use is strictly prohibited (for details see Privacy Policy and Legal Notice).

date: 27 April 2020

on lakes and forests through acidic deposition, along with negative human health impacts to a CGE model. They also included two non-market services associated with recreational fisheries and tree cover and a non-use existence value associated with general habitat services. The authors conducted a series of experiments to compare the welfare change with and without the general equilibrium effects from changes in air quality improvements. For a policy resulting in a 40% emissions reduction, roughly the magnitude of reductions from the Clean Air Act Amendments, and focusing only on improvements to recreational fisheries, they found that including general equilibrium effects increases the estimate of the welfare improvement by 12% to 55%.[23] These results led the authors to conclude that even when the value of nonmarket services is a small fraction of the aggregate value of the economy, the general equilibrium effects stemming from how changes in environmental quality affect household behavior may be notable.

Case Study: Removing Lead from Gasoline

Lead had been used by refiners as an additive in gasoline to increase octane levels and improve engine performance since the 1920s. This practice led to high levels of lead in the atmosphere and soil. Studies in the early 1980s increasingly tied lead exposure to negative health effects in children (e.g., learning problems, hyperactivity, and lower IQ) and adults (e.g., increased blood pressure and hypertension). In addition, automobile manufacturers were required to install catalytic converters in new cars beginning with the 1975 model year to reduce emissions of hydrocarbons, nitrogen oxides, and carbon monoxide. However, catalytic converters lose their effectiveness when exposed to lead.

To protect public health, particularly children in urban areas, and to address complications for catalytic converters, the U.S. EPA required retailers to begin selling some amount of unleaded gasoline in 1974. As awareness of the health impacts of lead exposure grew, so did demand for more rapid removal of lead from gasoline. In 1982 the U.S. EPA promulgated a tradable performance standard that established a system of property rights for lead use, which could be traded between refiners in order to lower costs. The standard was made tradable in part due to concerns that small refiners might find it difficult to meet the new standards and would benefit from additional flexibility (Hahn & Hester, 1989). In 1985 the U.S. EPA further tightened the standards. In addition to trading, the U.S. EPA allowed refiners to bank emissions reductions across quarters in that first year of the more stringent program. Lead in gasoline was banned completely in 1996.

PRINTED FROM the OXFORD RESEARCH ENCYCLOPEDIA, ENVIRONMENTAL SCIENCE (oxfordre.com/environmentalscience) (c) Oxford University Press USA, 2020. All Rights Reserved. Personal use only; commercial use is strictly prohibited (for details see Privacy Policy and Legal Notice).

date: 27 April 2020

Ex-post assessments found that trading and banking were used extensively. Larger refiners tended to reduce lead in their fuel, generating extra permits, and then sold these rights to smaller refiners with relatively higher refining costs. Banking provisions were mainly utilized by large refiners, though smaller refiners also benefited from this flexibility since it increased the pool of permits available for purchase (Hahn & Hester, 1989). While researchers did not rely on the econometric and general equilibrium modeling approaches discussed in other sections of this article, the limited data available indicate substantial cost savings (Newell & Rogers, 2006). Hahn and Hester (1989) stated that "it is reasonable to estimate that the cost savings to refiners from lead rights trading and banking amounted to hundreds of millions of dollars." Kerr and Newell (2003) also found evidence that periods when the trading and banking provisions were used corresponded with more rapid adoption of octane-enhancing technologies to replace the use of lead.

Systematic ex-ante benefit-cost estimates are not available for the early lead phasedown program, but the U.S. EPA conducted extensive benefit-cost analysis for the 1985 regulation (U.S. EPA, 1985). For 1986 to 1988, benefits of a ten-fold reduction in lead content were estimated to outweigh costs about 12 to 1 (e.g., in 1986, benefits of $7.8 billion compared to costs of $600 million in 1983 dollars). When blood pressure-related benefits to adults, which were estimated with less certainty, were excluded from the analysis benefits still exceeded costs 2 to 1 (Nichols, 1997). The finding of sizable net benefits associated with phasing out lead in gasoline is remarkable given the knowledge gaps at the time. The U.S. EPA was only able to quantify avoided costs of medical care and remedial education for children with blood levels above a certain threshold. The willingness to pay for avoided lasting health and cognitive impacts were not included in the analysis but would likely have been of a larger magnitude than the included benefits (Keohane & Olmstead, 2007). In a recent study, Wolfe et al. (2016) found that economy-wide feedbacks of cognitive damages from leaded aviation fuel, still in use in the United States, are also significant. In particular, they found economy-wide welfare losses using a dynamic CGE model were 54% larger than static partial equilibrium estimates.

Significant Outstanding Research Questions

There are a number of important questions regarding the impacts of environmental regulation on the U.S. economy that remain unresolved. We briefly discuss several, emphasiz-

PRINTED FROM the OXFORD RESEARCH ENCYCLOPEDIA, ENVIRONMENTAL SCIENCE (oxfordre.com/environmentalscience) (c) Oxford University Press USA, 2020. All Rights Reserved. Personal use only; commercial use is strictly prohibited (for details see Privacy Policy and Legal Notice).

date: 27 April 2020

ing their saliency to ongoing public debate and the need for renewed attention in the research arena.

Unifying Structural Framework for Understanding Economic Impacts of Environmental Regulation

Analyses of major regulation traditionally focus on estimating the overall costs and benefits of a policy to society. The distribution of those costs and benefits is also of great interest but such analyses face a number of methodological and empirical challenges. Identifying the particular sectors or subsectors affected, how costs are passed through to households and firms, and the ways in which households and firms respond can be quite difficult to analyze, and sometimes results in unexpected effects (Kolstad, 1999, 2014). Decisions regarding whether to expand or reduce production at existing facilities or whether to open new facilities have implications for when and how many workers are hired. Likewise, labor input decisions may manifest as changes in how many workers are hired or laid off, the types of workers hired or laid off, the wages and benefits offered, or the number of hours worked. These decisions, in turn, are linked to the productivity of firms, sectors, and ultimately the overall economy.

Based on the existing literature and the relative magnitude of environmental regulations compared to the size of the U.S. economy, one would anticipate that for most environmental regulations, economic impacts likely have limited or no macroeconomic implications (Arrow et al., 1996; Ferris et al., 2014).[24] However, lack of an overarching structural framework that coherently links individual decisions to their macroeconomic implications also hinders the ability to analyze potential economy-wide impacts of environmental regulation.

Separating out the effects of environmental regulation from the myriad of other phenomena affecting consumption and production decisions also is an ongoing challenge. In terms of employment impacts, it has long been observed that even a large-scale air regulation is unlikely to have a noticeable impact on aggregate net U.S. employment. Instead, labor in affected sectors would primarily be reallocated from one productive use to another, and national employment effects from regulation would be small and transitory (e.g., as workers move from one job to another) (Arrow et al., 1996). Given the literature to-date, this is also likely to be true when evaluating the effects of environmental regulation on productivity or plant entry and exit decisions.

If the economy is operating at less than full employment, economic theory does not clearly indicate either magnitude or direction of the total impact (Schmalansee & Stavins, 2011). For example, an early government sponsored macroeconomic study (U.S. CEQ et al., 1972) estimated that pollution abatement spending was stimulative to employment in the U.S. at a time of less than full employment. Likewise, the Congressional Budget Office identified U.S. EPA regulations that reduce mercury from power plants and hazardous air pollutants from industrial boilers and process heaters as potentially leading to short-run net increases in economic growth and employment, driven by capital investments to com-

PRINTED FROM the OXFORD RESEARCH ENCYCLOPEDIA, ENVIRONMENTAL SCIENCE (oxfordre.com/environmentalscience) (c) Oxford University Press USA, 2020. All Rights Reserved. Personal use only; commercial use is strictly prohibited (for details see Privacy Policy and Legal Notice).

date: 27 April 2020

ply with the regulations (CBO, 2011). An important fundamental research question is how to accommodate slackness in the economy—when labor and other resources are not fully and efficiently employed—as a structural feature in economic models. This feature may be important in evaluating the impact of large-scale environmental regulation on employment (Smith, 2012, 2015).[25]

Incorporating Benefits into Welfare and Economic Impact Analyses

To describe the complete incidence of a regulation, one should consider not only the distribution of costs but also benefits. However, folding benefits into the evaluation of economic impacts is complicated. An analyst would need to understand to what extent certain types of households differentially benefit from reductions in emissions. Another important consideration would be whether workers enjoy health improvements that enhance their productivity, thus reducing the long-term impact of the regulation on producers and labor. In practice, the evaluation of how costs and benefits are distributed across economic sectors are usually evaluated separately.

Note that absent a credible way to represent environmental externalities in a general equilibrium model—or the benefits that accrue to society from mitigating them—an assessment of the welfare and economic impacts derived from this approach are incomplete. The research studying the importance of incorporating the environment in analyses of the economic effects of environmental policies is still developing, though the results have thus far been robust in the conclusion that estimates of the overall economic impacts of a policy will be significantly biased if only the costs of compliance are included.

Although the beneficial impacts of environmental policies need to be incorporated in an assessment of their economy-wide effects to achieve unbiased results, there are numerous technical challenges to developing robust linkages between the economy and the environment. For example, to date the primary approach to including mortality risk reductions in CGE models has been to increase the time endowment based on the expected change in the population. Based on the typical assumption of homothetic preferences in these models and the relatively small size of such shocks compared to the size of the labor force, this approach values the change in the mortality risk reduction at approximately the wage rate. While analytically convenient, this time endowment approach undervalues households' willingness to pay for mortality risk reductions by an order of magnitude (Smith, 2012). The discrepancy in how households' preference regarding mortality risk are captured raises questions about how this difference affects forecasts of behavioral changes in response to changes in mortality risk. This is an area of future research that will be important for improving our understanding of how human health impacts of environmental policies feedback into the economy.

In addition, as noted by Antoine et al. (2008) and Carbon and Smith (2013), there are a number of data challenges with linking the environment and the economy in applied general equilibrium models. The CGE model requires benchmark estimates of the value for each of the inputs to activities, including the nonmarket inputs supplied by the environ-

PRINTED FROM the OXFORD RESEARCH ENCYCLOPEDIA, ENVIRONMENTAL SCIENCE (oxfordre.com/environmentalscience) (c) Oxford University Press USA, 2020. All Rights Reserved. Personal use only; commercial use is strictly prohibited (for details see Privacy Policy and Legal Notice).

date: 27 April 2020

ment. However, these inputs are often not observed, or at least not recorded, in national economic account statistics. Even in the United States, national or regional data for the time spent engaged in these activities is not complete. Also, the literature has yet to provide readily available estimates for elasticities that relate the ability for households to substitute between land and other market goods when providing activities involving the environment, such as recreation services, and their ability to substitute between these and other activities in their utility function. The fine spatial resolution at which policies impact the environment also presents unique data and methodological challenges as applied general equilibrium models are often resolved at a fairly aggregate level.

Understanding Labor Productivity Effects

Environmental regulation may also affect labor supply and productivity or employees' ability to work. While the theoretical framework for analyzing labor supply and productivity effects is analogous to that for labor demand (decomposing a wage change from a consumer's perspective into income and substitution effects), it is more difficult to study empirically. Although this literature faces empirical challenges, particularly in terms of requiring detailed individual-level labor data for the separation of impacts of reduced exposure to pollution from other factors influencing labor productivity, early work supported by the U.S. EPA found that air quality improvements led to reductions in lost work days (e.g., Ostro, 1987) and increased labor productivity for outdoor workers (Crocker & Horst, 1981). More recently, there has been some limited evidence that worker productivity may improve with better ambient air quality and worsen on days with higher pollution (Graff Zivin & Neidell, 2012; Chang, Graff Zivin, Gross, & Neidell, 2016).

Valuing Employment Impacts in Benefit-Cost Analysis

The standard approach in regulatory analysis has been to analyze employment as an economic impact. However, the great recession in the 2000s spurred new interest in considering the question of whether employment impacts also should be considered as a social cost of regulation (Ferris & McGartland, 2013). Rogerson (2015) notes that an economy-wide model that explicitly accounts for the labor market already incorporates employment effects into its welfare calculation through changes in how the household values consumption and leisure in the utility function. For instance, in the case where a policy lowers employment, it also likely lowers output and consumption but increases leisure. The only way to weigh the cost of lower consumption against the benefit of higher leisure is through a utility function that explicitly values both. Rogerson goes on to observe that this need not apply only to a model with full employment and no price rigidities.

With less than full employment due to a preexisting wage rigidity, the model will reflect that leisure is valued less than employment by households. When Rogerson (2015) examined whether welfare calculations in a highly stylized model are affected by assumptions about how quickly the labor market responds to a policy shock, he finds that the size of the labor response has little effect. This is because of the offsetting effects on leisure.

PRINTED FROM the OXFORD RESEARCH ENCYCLOPEDIA, ENVIRONMENTAL SCIENCE (oxfordre.com/environmentalscience) (c) Oxford University Press USA, 2020. All Rights Reserved. Personal use only; commercial use is strictly prohibited (for details see Privacy Policy and Legal Notice).

date: 27 April 2020

Even at full employment affected sectors may experience transitory effects as workers change jobs (Arrow et al., 1996; Smith, 2015; Kuminoff, Schoellman, & Timmins, 2015). For example, some workers may need to retrain or relocate in anticipation of the new requirements or require time to search for new jobs, while shortages in some sectors or regions could bid up wages to attract workers. It is important to recognize that these adjustments can entail local labor disruptions, and although the aggregate impact on the national workforce is expected to be small, localized changes in employment can still have negative impacts on some individuals and communities and positive impacts on others. If these types of adjustment costs are substantial, excluding them may underestimate the social cost of regulation.[26]

Empirical Evidence of the Porter Hypothesis

Based mainly on case studies, Porter (1991) and Porter and van der Linde (1995) argued that well designed environmental regulations could "trigger innovation that may partially or more than fully offset the costs of complying with them." While agreeing with some of Porter and van der Linde's (1995) arguments, such as the desirability of market-based regulation, Palmer, Oates, and Portney (1995) criticized the "Porter hypothesis" as not being broadly generalizable and argued that most regulations have costs to society and should be subject to a benefit-cost test.

Jaffe and Palmer (1997) distinguished "narrow," "weak," and "strong" versions of the Porter hypothesis. The narrow version is simply the argument frequently made by economists that flexible regulatory policies give firms greater incentives to innovate and thus are better than prescriptive regulations. The weak version is the argument that properly designed environmental regulations may stimulate innovations that may not have existed otherwise. In the strong version, it is argued that well-designed regulations can spur firms into innovating to such an extent that they can both comply with the regulation and increase profits, creating a win-win situation. Ambec, Cohen, Elgie, and Lanoie (2013) reviewed empirical evidence for and against the validity of the Porter hypothesis. For the weak version, they conclude that on balance evidence exists that "there is a positive link between environmental regulation and innovation, although the strength of the link varies." For the strong version of the Porter hypothesis, they found that the majority of studies were not supportive.

In spite of their conclusions, Ambec et al. (2013) noted that "we continue to find conflicting evidence concerning the Porter Hypothesis, alternative theories that might explain it, and oftentimes a misunderstanding of what the Porter Hypothesis does and does not say." They point to the need for additional research that relies on longitudinal data, the value of improved data and methodologies that better pinpoint the mechanisms by which regulation can lead to innovation, which in turn may increase or decrease costs, and the need for a better understanding of the role of non-regulatory approaches such as reporting or voluntary programs in spurring innovation in abatement technologies.

PRINTED FROM the OXFORD RESEARCH ENCYCLOPEDIA, ENVIRONMENTAL SCIENCE (oxfordre.com/environmentalscience) (c) Oxford University Press USA, 2020. All Rights Reserved. Personal use only; commercial use is strictly prohibited (for details see Privacy Policy and Legal Notice).

date: 27 April 2020

Acknowledgment

Any opinions and conclusions expressed herein are those of the author(s) and do not necessarily represent the views of the U.S. Environmental Protection Agency.

Suggested Readings

Arrow, K. J., Cropper, M. L., Eads, G. C., Hahn, R. W., Lave, L. B., Noll, R. G., et al. (1996). Benefit-cost analysis in environmental, health, and safety regulation: A statement of principles. American Enterprise Institute, the Annapolis Center, and Resources for the Future. Retrieved from **https://www.aei.org/wp-content/uploads/2014/04/-benefitcost-analysis-in-environmental-health-and-safety-regulation_161535983778.pdf**.

Carbone, J. C., & Smith, V. K. (2013). Valuing nature in a general equilibrium. *Journal of Environmental Economics and Management*, *66*(1), 72–89.

Coglianese, C., Finkel, A. M., & Carrigan, C. (Eds.). (2013). *Does regulation kill jobs?* Philadelphia: University of Pennsylvania Press.

Graff Zivin, J. S., & Neidell, M. J. (2013). Environment, health, and human capital, *Journal of Economic Literature*, *51*(3), 689–730.

Gray, W. B. (2015). Environmental regulations and business decisions. *IZA World of Labor*, *187*, 1–10.

Jaffe, A. B., Peterson, S. R., Portney, P. R., & Stavins, R. N. (1995). Environmental regulation and the competitiveness of U.S. manufacturing: What does the evidence tell us? *Journal of Economic Literature*, *33*(1), 132–163.

Lewis, J. (1985). The birth of EPA. *EPA Journal*, *11*(9), 6–11.

Matus, K., Yang, T., Paltsev, S., Reilly, J. M., & Nam, K. M. (2008). Toward integrated assessment of environmental change: Air pollution health effects in the USA. *Climatic Change*, *88*(1), 59–92.

Morgenstern, R. D. (1997). *Economic analyses at EPA: Assessing regulatory impact*. Washington, DC: Resources for the Future.

Palmer, K., Oates, W. E., & Portney, P. R. (1995). Tightening environmental standards: The benefit-cost or the no-cost paradigm? *Journal of Economic Perspectives*, *9*(4), 119–132.

Portney, P. R. (1981). The macroeconomic impacts of federal environmental regulation. *Natural Resources Journal*, *21*, 459–488.

Repetto, R. D., Rothman, D., Faeth, P., & Austin, D. (1997). Has environmental protection really reduced productivity? *Challenge*, *40*(1), 46–57.

PRINTED FROM the OXFORD RESEARCH ENCYCLOPEDIA, ENVIRONMENTAL SCIENCE (oxfordre.com/environmentalscience) (c) Oxford University Press USA, 2020. All Rights Reserved. Personal use only; commercial use is strictly prohibited (for details see Privacy Policy and Legal Notice).

date: 27 April 2020

Shadbegian, R. J., & Wolverton, A. (2010). Location decisions of U.S. polluting plants: Theory, empirical evidence, and consequences. *International Review of Environmental and Resource Economics*, *4*, 1–49.

Smith, V. K. (2012). Reflections: In search of crosswalks between macroeconomics and environmental economics. *Review of Environmental Economics and Policy*, *6*(2), 298–317.

Smith, V. K. (2015). Should benefit–cost methods take account of high unemployment? Symposium introduction. *Review of Environmental Economics and Policy*, *9*(2), 165–178.

U.S. CEQ, U.S. Environmental Protection Agency (U.S. EPA), U.S. Department of Commerce. (1972). *The economic impact of pollution control: A summary of recent studies*. Retrieved from **https://nepis.epa.gov/Exe/ZyPURL.cgi?Dockey=2000T77Y.txt**.

U.S. EPA. (2010). *Guidelines for preparing economic analyses*. EPA 240-R-10-001. Retrieved from **https://www.epa.gov/environmental-economics/guidelines-preparing-economic-analyses**.

U.S. EPA. (2011). *The benefits and costs of the Clean Air Act 1990 to 2020*. EPA Report to Congress. Retrieved from **https://www.epa.gov/clean-air-act-overview/benefits-and-costs-clean-air-act-1990-2020-second-prospective-study**.

References

Ambec, S., Cohen, M. A., Elgie, S., & Lanoie, P. (2013). The Porter hypothesis at 20: Can environmental regulation enhance innovation and competitiveness? *Review of Environmental Economics and Policy*, *7*(1), 2–22.

Antoine, B., Gurgel, A., & Reilly, J. M. (2008). Will recreation demand for land limit biofuels production? *Journal of Agricultural & Food Industrial Organization*, *6*(2), 1–29.

Arrow, K. J., Cropper, M. L., Eads, G. C., Hahn, R. W., Lave, L. B., Noll, R. G., et al. (1996). *Benefit-cost analysis in environmental, health, and safety regulation: A statement of principles*. American Enterprise Institute, the Annapolis Center, and Resources for the Future. Retrieved from **https://www.aei.org/wp-content/uploads/2014/04/-benefitcost-analysis-in-environmental-health-and-safety-regulation_161535983778.pdf**.

Babiker, M., & Eckaus, R. S. (2007). Unemployment effects of climate policy. *Environmental Science and Policy*, *10*, 600–609.

Balistreri, E. J. (2002). Operationalizing equilibrium unemployment: A general equilibrium external economies approach. *Journal of Economic Dynamics and Control*, *26*, 347–374.

Barbera, A. J., & McConnell, V. D. (1990). The impact of environmental regulations on industry productivity: Direct and indirect effects. *Journal of Environmental Economics and Management*, *18*, 50–65.

PRINTED FROM the OXFORD RESEARCH ENCYCLOPEDIA, ENVIRONMENTAL SCIENCE (oxfordre.com/environmentalscience) (c) Oxford University Press USA, 2020. All Rights Reserved. Personal use only; commercial use is strictly prohibited (for details see Privacy Policy and Legal Notice).

date: 27 April 2020

Bartik, T. J. (1985). Business location decisions in the United States: Estimates of the effects of unionization, taxes, and other characteristics of states. *Journal of Business and Economic Statistics*, *3*(1), 14–22.

Becker, R. A. (2011). Local environmental regulation and plant-level productivity. *Ecological Economics*, *70*, 2513–2522.

Becker, R. A., & Henderson, J. V. (2000). Effects of air quality regulations on polluting industries. *Journal of Political Economy*, *108*(2), 379–421.

Berman, E., & Bui, L. T. (2001a). Environmental regulation and labor demand: Evidence from the South Coast air basin. *Journal of Public Economics*, *79*(2), 265–295.

Berman, E., & Bui, L. T. (2001b). Environmental regulation and productivity: Evidence from oil refineries. *Review of Economics and Statistics*, *83*(3), 498–510.

Blanchflower, D., & Oswald, A. (1994). *The wage curve*. Cambridge, MA: MIT Press.

Boeters, S., & Savard, L. (2013). The labor market in computable general equilibrium models. In P. B. Dixon & D. W. Jorgenson (Eds.), *Handbook of Computable General Equilibrium Modeling*. Waltham, MA: Elsevier.

Böhringer, C., Keller, A., & van der Werf, E. (2013). Are green hopes too rosy? Employment and welfare impacts of renewable energy promotion. *Energy Economics*, *36*(C), 277–285.

Böhringer, C., Rivers, N. J., Rutherford, T. F., & Wigle, R. (2012). Green jobs and renewable electricity policies: Employment impacts of Ontario's feed-in tariff. *B.E. Journal of Economic Analysis and Policy*, *12*(1), 1–40.

Brauer, M., Blair, J., & Vedal, S. (1996). Effect of ambient ozone exposure on lung function in farm workers. *American Journal of Respiratory and Critical Care Medicine*, *154*, 981–987.

Carbone, J. C., & Smith, V. K. (2013). Valuing nature in a general equilibrium. *Journal of Environmental Economics and Management*, *66*(1), 72–89.

Carlton, D. W. (1983). The location and employment choices of new firms: An econometric model with discrete and continuous endogenous variables. *Review of Economics and Statistics*, *65*(3), 440–449.

Chang, T., Graff Zivin, J. S., Gross, T., & Neidell, M. J. (2016). Particulate pollution and the productivity of pear packers. *American Economic Journal: Economic Policy*, *8*(3), 141–169.

Christainsen, G. B., & Haveman, R. H. (1981a). Public regulations and the slowdown in productivity growth. *American Economic Review*, *71*(2), 320–325.

PRINTED FROM the OXFORD RESEARCH ENCYCLOPEDIA, ENVIRONMENTAL SCIENCE (oxfordre.com/environmentalscience) (c) Oxford University Press USA, 2020. All Rights Reserved. Personal use only; commercial use is strictly prohibited (for details see Privacy Policy and Legal Notice).

date: 27 April 2020

Christainsen, G. B., & Haveman, R. H. (1981b). The contribution of environmental regulations to the slowdown in productivity growth. *Journal of Environmental Economics and Management*, *8*, 381–390.

Coglianese, C., Finkel, A. M., & Carrigan, C. (Eds.). (2013). *Does regulation kill jobs?* Philadelphia: University of Pennsylvania Press.

Condliffe, S., & Morgan, O. A. (2009). The effects of air quality regulations on the location decisions of pollution-intensive manufacturing plants. *Journal of Regulatory Economics*, *36*, 83–93.

Congressional Budget Office (CBO) (2011). Policies for increasing economic growth and employment in 2012 and 2013. Statement of D. W. Elmendorf, Director, before the Senate Budget Committee, Retrieved from **http://www.cbo.gov/sites/default/files/11-15-Outlook_Stimulus_Testimony.pdf**.

Crocker, T. D., & Horst, R. L., Jr. (1981). Hours of work, labor productivity, and environmental conditions: A case study. *Review of Economics and Statistics*, *63*(3), 361–368.

Curtis, E. M. (Forthcoming). Who loses under power plant cap and trade programs? The labor market effects of the NOx budget trading program. *Review of Economics and Statistics*. Posted online June 18, 2017.

Dale, L. (1970, August 12). Nixon's inflation alert. *New York Times*. Retrieved from **http://www.nytimes.com/1970/08/12/archives/nixons-inflation-alert-adviser-mccracken-suggests-blame-lies-in.html**.

Davis, S. J., & von Wachter, T. (2011). Recessions and the costs of job loss. *Brookings Papers on Economic Activity*, *43*(2), 1–55.

Denison, E. F. (1978). Effects of selected changes in the institutional and human environment upon output per unit of input. *Survey of Current Business*, *58*(1), 21–43.

Denison, E. F. (1979). Pollution abatement programs: Estimates of their effect upon output per unit of input, 1975–78. *Survey of Current Business*, *59*(8) (Part 1), 58–59.

Deschênes, O. (2012). Climate policy and labor markets. In D. Fullerton & C. Wolfram (Eds.), *The design and implementation of U.S. climate policy*. Chicago: University of Chicago Press.

Deschênes, O. (2014). Environmental regulations and labor markets. *IZA World of Labor*, *22*, 1–10.

Dissou, Y., & Sun, Q. (2013). GHG mitigation policies and employment: A CGE analysis with wage rigidity and application to Canada. *Canadian Public Policy*, *39*, S53–S65.

Dixon, P. B., Johnson, M., & Rimmer, M. T. (2011). Economy-wide effects of reducing illegal immigrants in U.S. employment. *Contemporary Economic Policy*, *29*(1), 14–30.

PRINTED FROM the OXFORD RESEARCH ENCYCLOPEDIA, ENVIRONMENTAL SCIENCE (oxfordre.com/environmentalscience) (c) Oxford University Press USA, 2020. All Rights Reserved. Personal use only; commercial use is strictly prohibited (for details see Privacy Policy and Legal Notice).

date: 27 April 2020

Dixon, P. B., & Rimmer, M. T. (2002). USAGE-ITC: Theoretical structure. Retrieved from **https://www.gtap.agecon.purdue.edu/resources/download/958.pdf**.

Domazlicky, B. R., & Weber, W. L. (2004). Does environmental protection lead to slower productivity growth in the chemical industry? *Environmental and Resource Economics*, *28*, 301–324.

Dorfman, R. (1973). Discussion. *American Economic Review*, *63*(2), 253–256.

Data Resources, Inc (DRI). (1981). The macroeconomic impact of federal pollution control programs: 1981 assessment. Report for the U.S. EPA. July 17.

Evans, M. K. (1973). A forecasting model applied to pollution control costs. *American Economic Review*, *63*(2), 244–252.

Fann, N., Lamson, A. D., Anenburg, S. C., Wesson, K., Risley, D., & Hubbell, B. J. (2012). Estimating the national public health burden associated with exposure to ambient PM2.5 and ozone. *Risk Analysis*, *32*(1), 81–95.

Ferris, A. E., & McGartland, A. (2013). A research agenda for improving the treatment of employment impacts in regulatory impact analysis. In C. Coglianese, A. M. Finkel, & C. Carrigan (Eds.), *Does regulation kill jobs?* (pp. 170–189). Philadelphia: University of Pennsylvania Press.

Ferris, A. E., Shadbegian, R. J., & Wolverton, A. (2014). The effect of environmental regulation on power sector employment: Phase I of the Title IV SO2 trading program. *Journal of the Association of Environmental and Resource Economists*, *1*(4), 521–553.

Finnoff, D. C., & Tschirhart, J. (2008). Linking dynamic economic and ecological general equilibrium models. *Resource and Energy Economics*, *30*(2), 91–114.

Fleurbaey, M. (2009). Beyond GDP: The quest for a measure of social welfare. *Journal of Economic Literature*, *47*(4), 1029–1075.

Gayer, T., Hamilton, J. T., & Viscusi, W. K. (2002). The market value of reducing cancer risk: Hedonic housing prices with changing information. *Southern Economic Journal*, *69*(2), 266–289.

Gollop, F. M., & Roberts, M. J. (1983). Environmental regulations and productivity growth: The case of fossil-fueled electric power generation. *Journal of Political Economy*, *91*(4), 654–674.

Graff Zivin, J. S., & Neidell, M. J. (2012). The impact of pollution on worker productivity. *American Economic Review*, *102*(7), 3652–3673.

Gray, W. B. (1987). The cost of regulation: OSHA, EPA and the productivity slowdown. *American Economic Review*, *77*(5), 998–1006.

PRINTED FROM the OXFORD RESEARCH ENCYCLOPEDIA, ENVIRONMENTAL SCIENCE (oxfordre.com/environmentalscience) (c) Oxford University Press USA, 2020. All Rights Reserved. Personal use only; commercial use is strictly prohibited (for details see Privacy Policy and Legal Notice).

date: 27 April 2020

Gray, W. B. (2015). Environmental regulations and business decisions. *IZA World of Labor*, *187*, 1–10.

Gray, W. B., & Shadbegian, R. J. (2003). Plant vintage, technology, and environmental regulation. *Journal of Environmental Economics and Management*, *46*, 384–402.

Gray, W. B., Shadbegian, R. J., Wang, C., & Meral, M. (2014). Do EPA regulations affect labor demand? Evidence from the pulp and paper industry. *Journal of Environmental Economics and Management*, *68*(1), 188–202.

Greenstone, M. (2002). The impacts of environmental regulations on industrial activity: Evidence from the 1970 and 1977 Clean Air Act Amendments and the Census of Manufactures. *Journal of Political Economy*, *110*(6), 1175–1219.

Greenstone, M., List, J. A., & Syverson, C. (2012). The effects of environmental regulation on the competitiveness of U.S. manufacturing. NBER Working Paper Series 18392, National Bureau of Economic Research.

Griswald, E. (2012, September 21). How ‘silent spring’ ignited the environmental movement. *New York Times*. Retrieved from **http://www.nytimes.com/2012/09/23/magazine/how-silent-spring-ignited-the-environmental-movement.html**.

Grosclaude, P., & Soguel, N. C. (1994). Valuing damage to historic buildings using a contingent market: A case study of road traffic externalities. *Journal of Environmental Planning and Management*, *37*, 279–287.

Hahn, R. W., & Hester, G. L. (1989). Marketable permits: Lessons for theory and practice. *Ecology Law Quarterly*, *16*, 380–391.

Hanley, N., & Spash, C. L. (1993). *Cost-benefit analysis and the environment*. Vermont: Elgar.

Haveman, R. H., & Smith, V. K. (1978). Investment, inflation, unemployment, and the environment. In P. Portney (Ed.), *Current issues in U.S. environmental policy*. Washington, DC: Resources for the Future.

Hazilla, M., & Kopp, R. J. (1990). Social costs of environmental quality regulations: A general equilibrium analysis. *Journal of Political Economy*, *98*(4), 853–873.

Henderson, J. V. (1996). Effects of air quality regulation. *American Economic Review*, *86*(4), 789–813.

Holland, S. P. (2012). Spillovers from climate policy to other pollutants. In D. Fullerton & C. Wolfram (Eds.), *The design and implementation of U.S. climate policy*. Chicago: University of Chicago Press.

PRINTED FROM the OXFORD RESEARCH ENCYCLOPEDIA, ENVIRONMENTAL SCIENCE (oxfordre.com/environmentalscience) (c) Oxford University Press USA, 2020. All Rights Reserved. Personal use only; commercial use is strictly prohibited (for details see Privacy Policy and Legal Notice).

date: 27 April 2020

Hoppe, P., Prami, G., Rabe, G., Lindner, J., Fruhmann, G., & Kessel, R. (1995). Environmental ozone field study on pulmonary and subjective responses of assumed risk groups. *Environmental Research*, *71*(2), 109–121.

Jaffe, A. B., & Palmer, K. (1997). Environmental regulation and innovation: A panel data study. *Review of Economics and Statistics*, *79*(4), 610–619.

Jaffe, A. B., Peterson, S. R., Portney, P. R., & Stavins, R. N. (1995). Environmental regulation and the competitiveness of U.S. manufacturing: What does the evidence tell us? *Journal of Economic Literature*, *33*(1), 132–163.

Jones, C. I., & Klenow, P. J. (2016). Beyond GDP? Welfare across countries and time. *American Economic Review*, *106*(9), 2426–2457.

Jorgenson, D. W., & Wilcoxen, P. J. (1990). Environmental regulation and U.S. economic growth. *Rand Journal of Economics*, *21*(2), 314–340.

Jorgenson, D. W., & Wilcoxen, P. J. (1993). The economic impact of the Clean Air Act Amendments of 1990. *Energy Journal*, *141*, 159–182.

Kahn, M. E. (1997). Particulate pollution trends. *Regional Science and Urban Economics*, *1*, 87–107.

Kahn, M. E., & Mansur, E. T. (2013). Do local energy prices and regulation affect the geographic concentration of employment? *Journal of Public Economics*, *101*, 105–114.

Kendrick, D. A. (1993). In memoriam: Edward F. Denison. *Review of Income and Wealth*, *39*(1), 117–119.

Keohane, N. O., & Olmstead, S. M. (2007). *Markets and the environment*. Washington, DC: Island.

Kerr, S., & Newell, R. G. (2003). Policy-induced technology adoption: Evidence from the U.S. lead phasedown. *Journal of Industrial* Economics, *51*(3), 317–343.

Kling, R. W., Revier, C. F., & Sable, K. (2004). Estimating the public good value of preserving a local historic landmark: The role of non-substitutability and citizen information. *Urban Studies*, *41*(10), 2025–2041.

Kolstad, C. D. (1999). *Environmental economics*. Oxford: Oxford University Press.

Kolstad, C. D. (2014). Who pays for climate regulation? *SIEPR Policy Brief*. Stanford, CA: Stanford Institute for Economic Policy Research, Stanford University.

Kuminoff, N. V., Schoellman, T., & Timmins, C. D. (2015). Environmental regulations and the welfare effects of job layoffs in the United States: A spatial approach. *Review of Environmental Economics and Policy*, *9*(2), 198–218.

PRINTED FROM the OXFORD RESEARCH ENCYCLOPEDIA, ENVIRONMENTAL SCIENCE (oxfordre.com/environmentalscience) (c) Oxford University Press USA, 2020. All Rights Reserved. Personal use only; commercial use is strictly prohibited (for details see Privacy Policy and Legal Notice).

date: 27 April 2020

Levinson, A. (1996). Environmental regulations and manufacturers' location choices: Evidence from the Census of Manufactures. *Journal of Public Economics*, *62*, 5–29.

Levy, J. I., Baxter, L. K., & Schwartz, J. (2009). Uncertainty and variability in health-related damages from coal-fired power plants in the United States. *Risk Analysis*, *29*(7), 1000–1014.

Lewis, J. (1985). The birth of EPA. *EPA Journal*, *11*(9), 6–11.

List, J. A., McHone, W. W., & Millimet, D. L. (2003). Effect of air quality regulation on the destination choice of relocating plants. *Oxford Economic Papers*, *55*, 657–678.

List, J. A., Millimet, D. L., Fredriksson, P. G., & McHone, W. W. (2003). Effects of environmental regulations on manufacturing plant births: Evidence from a propensity score matching estimator. *The Review of Economics and Statistics*, *85*(4), 944–952.

Mark, J. (1978). Testimony before the Congressional Joint Economic Committee. In *Special study on economic change: Hearings before the Joint Economic Committee, Congress of the United States, Part 2* (pp. 476–486). Washington, DC: U.S. Government Printing Office.

Matus, K., Yang, T., Paltsev, S., Reilly, J. M., & Nam, K. M. (2008). Toward integrated assessment of environmental change: Air pollution health effects in the USA. *Climatic Change*, *88*(1), 59–92.

Matus, K., Nam, K.-M., Selin, N. E., Lamsal, L. N., Reilly, J. M., & Paltsev, S. (2012). Health damages from air pollution in China. *Global Environmental Change*, *22*(1), 55–66.

Mayeres, I., & van Regemorter, D. (2008). Modeling the health related benefits of environmental policies and their feedback effects: A CGE analysis for the EU countries with GEM-E3. *Energy Journal*, *29*(1), 135–150.

McConnell, V. D., & Schwab, R. M. (1990). The impact of environmental regulation on industry location decisions: The motor vehicle industry. *Land Economics*, *66*(1), 67–81.

Millimet, D. L., & List, J. A. (2004). The case of the missing pollution haven hypothesis. *Journal of Regulatory Economics*, *26*(3), 239–262.

Morgenstern, R. D. (1997). The legal and institutional setting for economic analysis at EPA. In R. D. Morgenstern (Ed.), *Economic analyses at EPA: Assessing regulatory impact* (pp. 5–23). Washington, DC: Resources for the Future.

Morgenstern, R. D., Pizer, W. A., & Shih, J. S. (2002). Jobs versus the environment: An industry level perspective. *Journal of Environmental Economics and Management*, *43*, 412–436.

Nam, K. M., Selin, N. E., Reilly, J. M., & Paltsev, S. (2010). Measuring welfare loss caused by air pollution in Europe: A CGE analysis. *Energy Policy*, *38*, 5059–5071.

PRINTED FROM the OXFORD RESEARCH ENCYCLOPEDIA, ENVIRONMENTAL SCIENCE (oxfordre.com/environmentalscience) (c) Oxford University Press USA, 2020. All Rights Reserved. Personal use only; commercial use is strictly prohibited (for details see Privacy Policy and Legal Notice).

date: 27 April 2020

Newell, R. G., & Rogers, K. (2006). The market-based lead phasedown. In J. Freeman & C. Kolstad (Eds.), *Moving to markets in environmental regulation: Lessons from twenty years of experience*. Oxford: Oxford University Press.

Nichols, A. L. (1997). Lead in gasoline. In R. D. Morgenstern (Ed.), *Economic analyses at EPA: Assessing regulatory impact* (pp. 49–86). Washington, DC: Resources for the Future.

Office of Management and Budget (OMB). (1997). *Report to Congress on the Costs and Benefits of Federal Regulations*. Executive Office of the President. Retrieved from **https://www.whitehouse.gov/omb/inforeg_chap1**.

Ostro, B. D. (1987). Air pollution and morbidity revisited: A specification test. *Journal of Environmental Economics and Management*, *14*, 87–98.

Palmer, K., Oates, W. E., & Portney, P. R. (1995). Tightening environmental standards: The benefit-cost or the no-cost paradigm? *Journal of Economic Perspectives*, *9*(4), 119–132.

Palmquist, R. B. (2005). Property value models. In K. G. Mäler & J. R. Vincent (Eds.), *Handbook of environmental economics* (Vol. 2, pp. 763–819). Amsterdam, The Netherlands: Elsevier.

Paltsev, S., & Capros, P. (2013). Cost concepts for climate change mitigation. *Climate Change Economics*, *4*(1), 1340003-1-1340003-26.

Phaneuf, D. J., & Smith, V. K. (2005). Recreation demand models. In K. G. Mäler & J. R. Vincent (Eds.), *Handbook of environmental economics* (Vol. 2, pp. 671–761). Amsterdam, The Netherlands: Elsevier.

Porter, M. E. (1991). America’s green strategy. *Scientific American*, *264*(4), 168.

Porter, M. E., & van der Linde, C. (1995). Toward a new conception of the environment competitiveness relationship. *Journal of Economic Perspectives*, *9*(4), 97–118.

Portney, P. R. (1981). The macroeconomic impacts of federal environmental regulation. *Natural Resources Journal*, *21*, 459–488.

Repetto, R. D., Rothman, D., Faeth, P., & Austin, D. (1997). Has environmental protection really reduced productivity? *Challenge*, *40*(1), 46–57.

Rivers, N. (2013). Renewable energy and unemployment: A general equilibrium analysis. *Resource and Energy Economics 35*, 467–485.

Rogerson, R. (2015). A macroeconomic perspective on evaluating environmental regulations. *Review of Environmental Economics and Policy*, *9*(2), 219–238.

Russell, C. S. (1973). Application of microeconomic models to regional environmental quality management. *American Economic Review*, *63*(2), 236–243.

PRINTED FROM the OXFORD RESEARCH ENCYCLOPEDIA, ENVIRONMENTAL SCIENCE (oxfordre.com/environmentalscience) (c) Oxford University Press USA, 2020. All Rights Reserved. Personal use only; commercial use is strictly prohibited (for details see Privacy Policy and Legal Notice).

date: 27 April 2020

Rutledge, G. L., Drieling, F. J., & Dunlap, B. C. (1978). Capital expenditures by business for pollution abatement, 1973–77 and planned 1978. *Survey of Current Business*, *58*(6), 33–38.

Saha, M., & Eckelman, M. J. (2014). Urban scale mapping of concrete degradation from projected climate change. *Urban Climate*, *9*, 101–114.

Salkever, D. S. (1982). Children's health problems: Implications for parental labor supply and earnings. In V. Fuchs (Ed.), *Economic aspects of health* (pp. 221–252). Chicago: University of Chicago Press.

Schmalansee, R. L., & Stavins, R. N. (2011, March). *A guide to economic and policy analysis for the transport rule*. White Paper. Commissioned by Exelon Corporation. Retrieved from **http://www.analysisgroup.com/uploadedfiles/content/insights/publishing/2011_stavinsschmalansee_transportrulereport.pdf**.

Segal, F. W., & Dunlap, B. C. (1977). Capital expenditures by business for pollution abatement, 1976 and planned 1977. *Survey of Current Business*, *57*(6), 13–15.

Selin, N. E., Wu, S., Nam, K.-M., Reilly, J. M., Paltsev, S., Prinn, R. G., et al. (2009). Global health and economic impacts of future ozone pollution. *Environmental Research Letters*, *4*, 1–9.

Shadbegian, R. J., & Gray, W. B. (2005). Pollution abatement expenditures and plant-level productivity: A production function approach. *Ecological Economics*, *54*, 196–208.

Shadbegian, R. J., & Wolverton, A. (2010). Location decisions of U.S. polluting plants: Theory, empirical evidence, and consequences. *International Review of Environmental and Resource Economics*, *4*, 1–49.

Sheriff, G., Ferris, A. E., & Shadbegian, R. J. (2016). How did air quality standards affect employment and generation at U.S. power plants? The importance of stringency, implementation, and timing. NCEE Working Paper, #15-01. National Center for Environmental Economics, U.S. EPA.

Smith, V. K. (2012). Reflections: In search of crosswalks between macroeconomics and environmental economics. *Review of Environmental Economics and Policy*, *6*(2), 298–317.

Smith, V. K. (2015). Should benefit–cost methods take account of high unemployment? Symposium introduction. *Review of Environmental Economics and Policy*, *9* (2), 165–178.

Stiglitz, J. E., Sen, A. K., & Fitoussi, J. P. (2009, September). *Report by the Commission on the Measurement of Economic Performance and Social Progress*. Commission of inquiry, France.

Tagaris, E., Liao, K.L., DeLucia, A. J., Deck, L., Amar, P., & Russell, A. G. (2009). Potential impact of climate change on air-pollution related human health effects. *Environmental Science and Technology*, *43*(3), 4979–4988.

PRINTED FROM the OXFORD RESEARCH ENCYCLOPEDIA, ENVIRONMENTAL SCIENCE (oxfordre.com/environmentalscience) (c) Oxford University Press USA, 2020. All Rights Reserved. Personal use only; commercial use is strictly prohibited (for details see Privacy Policy and Legal Notice).

date: 27 April 2020

The White House. (1993). *Executive Order 12866: Regulatory Planning and Review*, 58 Fed. Reg. 51735.

U.S. Council on Environmental Quality (U.S. CEQ). (1971). *Environmental quality—1971*. Washington, DC: U.S. Government Printing Office.

U.S. CEQ. (1978). *Environmental quality—1978*. Washington DC: U.S. Government Printing Office.

U.S. CEQ. (1979). *Environmental quality—1979*. Washington, DC: U.S. Government Printing Office.

U.S. CEQ, U.S. Environmental Protection Agency (U.S. EPA), U.S. Department of Commerce. (1972). *The economic impact of pollution control: A summary of recent studies*. Retrieved from **https://nepis.epa.gov/Exe/ZyPURL.cgi?Dockey=2000T77Y.txt**.

U.S. EPA. (1982). *Economic dislocation early warning system: 1980–1982 quarterly report*. Washington DC: U.S. EPA.

U.S. EPA. (1985). *Costs and benefits of reducing lead in gasoline: Final regulatory impact analysis*. Retrieved from **https://yosemite.epa.gov/ee/epa/eerm.nsf/vwan/ee-0034-1.pdf/%24file/ee-0034-1.pdf**.

U.S. EPA. (1997). *The benefits and costs of the Clean Air Act, 1970 to 1990*. Prepared for U.S. Congress. Retrieved from **https://www.epa.gov/sites/production/files/2015-06/documents/contsetc.pdf**.

U.S. EPA. (1999). *The benefits and costs of the Clean Air Act 1990 to 2010*. EPA Report to Congress. Retrieved from **http://www.epa.gov/cleanairactbenefits/1990-2010/chap1130.pdf**.

U.S. EPA. (2007). *Review of the national ambient air quality standards for ozone: Policy assessment of scientific and technical information*. EPA-452/R-07-007. Retrieved from **http://www.epa.gov/ttn/naaqs/standards/ozone/data/2007_07_ozone_staff_paper.pdf**.

U.S. EPA. (2010). *Guidelines for preparing economic analyses*. EPA 240-R-10-001. Retrieved from **https://www.epa.gov/environmental-economics/guidelines-preparing-economic-analyses**.

U.S. EPA. (2011). *The benefits and costs of the Clean Air Act 1990 to 2020*. EPA Report to Congress. Available at **https://www.epa.gov/clean-air-act-overview/benefits-and-costs-clean-air-act-1990-2020-second-prospective-study**.

U.S. EPA. (2013a). *America's children and the environment*, Third edition. EPA 240-R-13-001. Retrieved from **http://www.epa.gov/envirohealth/children/pdfs/ACE3_2013.pdf**.

PRINTED FROM the OXFORD RESEARCH ENCYCLOPEDIA, ENVIRONMENTAL SCIENCE (oxfordre.com/environmentalscience) (c) Oxford University Press USA, 2020. All Rights Reserved. Personal use only; commercial use is strictly prohibited (for details see Privacy Policy and Legal Notice).

date: 27 April 2020

U.S. EPA. (2013b). *Integrated science assessment for ozone and related photochemical oxidants*. EPA 600/R-10/076F. Retrieved from **http://ofmpub.epa.gov/eims/eimscomm.getfile?p_download_id=511347**.

Vennemo, H. (1997). A Dynamic applied general equilibrium model with environmental feedbacks. *Economic Modeling*, *14*(1), 99–154.

Walker, W. R. (2011). Environmental regulation and labor reallocation. *American Economic Review*, *101*(2), 442–447.

Walker, W. R. (2013). The transitional costs of sectoral reallocation: Evidence from the Clean Air Act and the workforce. *Quarterly Journal of Economics*, *128*(4), 1787–1835.

Wolfe, P. J., Giang, A., Ashok, A., Selin, N. E., & Barrett, S. R. H. (2016). Costs of IQ loss from leaded aviation gasoline emissions. *Environmental Science and Technology*, *50*, 9026–9033.

Notes:

(1.) For instance, *Silent Spring* by Rachel Carson, which documented the use and potentially detrimental effects of pesticide use and is credited with the eventual ban of DDT, was published in 1962. In Ohio, the Cuyahoga River had become so polluted that it caught fire in 1969.

(2.) Growth in labor productivity (i.e., output per worker hour) fell from an average annual rate of 3.4 percent from 1947 through 1966 to about 2.2 percent from 1966 through 1973 and further to about 1.5 percent from 1973 through 1977 (Mark, 1978). The Nixon Administration also issued an “inflation alert” in 1970 due to increases in wages and other prices but did not identify a particular cause (Dale, 1970). The national unemployment rate also climbed from 3.6 percent in 1968 to 7.7 percent in 1976.

(3.) While the analysis only explicitly considered costs, the report qualitatively discussed the benefits of improved environmental quality such as increased agricultural output, increased productivity and work hours, and health improvements.

(4.) Between 1978 and 1982, 37 additional plants were identified as being shut down due in part to environmental regulatory requirements, affecting another 11,000 jobs (U.S. EPA, 1982).

(5.) Other hypotheses included shifts in industrial composition, changes in labor force composition, a slowdown in capital-labor ratio improvements, and a leveling off of research and development expenditures.

(6.) These studies were part of a larger research project by Edward Denison investigating the wide range of reasons for the productivity slowdown, published by Brookings Institution in 1979 as a book, *Accounting for Slower Economic Growth: The United States in the*

PRINTED FROM the OXFORD RESEARCH ENCYCLOPEDIA, ENVIRONMENTAL SCIENCE (oxfordre.com/environmentalscience) (c) Oxford University Press USA, 2020. All Rights Reserved. Personal use only; commercial use is strictly prohibited (for details see Privacy Policy and Legal Notice).

date: 27 April 2020

1970s. For more information on Denison's contributions to national growth accounting, see Kendrick (1993).

(7.) They constructed an index of regulatory intensity as a function of the severity of the emission standard, the extent of enforcement, and the unconstrained emission rate relevant to each utility.

(8.) Gray (1987) used annual pollution control operating costs as a measure of environmental regulation and level of enforcement effort directed toward each industry as a measure of occupational safety and health regulation.

(9.) The PACE survey collected plant-level data on the capital and operating costs of meeting major environmental regulations annually between 1973 and 1994, and then again in 1999 and 2005. Many researchers have called for its resumption to assist in the conduct of plant-level analysis to inform policy debates (e.g., Gray, 2015). No other comparable data source on compliance costs exists.

(10.) For a detailed review of the literature on U.S. environmental regulation and plant location decisions, see Shadbegian and Wolverton (2010), which includes topics not discussed here such as the potential effects of environmental regulation on international competitiveness and whether location decisions are influenced by environmental justice considerations. Also see Jaffe, Peterson, Portney, and Stavins (1995), and Gray (2015).

(11.) See Coglianese, Finkel, and Carrigan (2013) for a more in-depth summary of recent literature, which supports the conclusion that environmental regulations have resulted in no or relatively modest effects on employment.

(12.) See Boeters and Savard (2013) for a detailed discussion of different models of unemployment and calibration issues encountered when incorporating them into a CGE model.

(13.) Balistreri (2002) showed that a higher elasticity of substitution between labor and leisure led to larger and more persistent impacts on unemployment. Likewise, the higher the share of leisure relative to labor, the larger the impact on unemployment. A lower share of workers that were already matched to a job and a higher turnover rate reduced the impacts on unemployment. In addition, higher elasticities of scale on employment resulted in larger changes in unemployment, while higher elasticities of scale on the unemployment rate reduced the response.

(14.) The notion that one should attempt to quantify the societal costs and benefits of a federal regulation has much older origins. As early as 1902, the Bureau of Land Reclamation and U.S. Army Corps of Engineers used benefit-cost analysis (Hanley & Spash, 1993).

(15.) Agencies conducts BCAs for all rules deemed economically significant or particularly novel. Economically significant rules are defined by E.O. 12866 as those with costs and benefits of at least $100 million (nominal) in a single year. The E.O. directs agencies to "select those approaches that maximize net benefits (including potential economic, environmental, public health and safety, and other advantages; distributive impacts; and equi-

PRINTED FROM the OXFORD RESEARCH ENCYCLOPEDIA, ENVIRONMENTAL SCIENCE (oxfordre.com/environmentalscience) (c) Oxford University Press USA, 2020. All Rights Reserved. Personal use only; commercial use is strictly prohibited (for details see Privacy Policy and Legal Notice).

date: 27 April 2020

ty), unless a statute requires another regulatory approach" (The White House, 1993). This objective, that a policy's net benefits be positive, is referred to as the Potential Pareto criterion (U.S. EPA, 2010).

(16.) Beginning in the 1960s, environmental economics began to develop techniques for measuring what individuals are willing to pay for a particular non-market environmental or health benefit (Hanley & Spash, 1993). See EPA (2010) for more information on specific techniques commonly used for this purpose.

(17.) GDP is defined as the sum of the value (price times quantity) of all market goods and services produced in the economy and is equal to Consumption + Investment + Government + (Exports—Imports). Because GDP is viewed as a relatively poor indicator of social welfare, there is an active discussion of ways to move national account metrics closer to a measure of well-being (e.g., Stiglitz, Sen, & Fitoussi, 2009; Fleurbaey, 2009).

(18.) Paltsev and Capros (2013) noted that the direction of the difference between effects of a policy as measured by GDP versus consumption varies with time period and scenario in some models. They also note that the extent to which welfare and consumption measures differ depends on what is assumed about the responsiveness of labor supply to changes in wage rates.

(19.) CGE models are recognized as being "best suited for estimating the cost of policies that have large economy-wide impacts, especially when indirect and interaction effects are expected to be significant" (U.S. EPA, 2010).

(20.) Outdoor workers may be particularly vulnerable to health impacts associated with air pollution due to increased exposure (U.S. EPA, 2013b; Brauer, Blair, & Vedal, 1996; Hoppe et al., 1995). In addition, studies have found empirical evidence that air quality is a significant determinant of productivity for a subset of workers (Crocker & Horst, 1981; Graff Zivin & Neidell, 2012).

(21.) The results presented by Matus et al. (2008) are gross estimates and do not include the costs of compliance with the environmental regulations that produce the human health improvements.

(22.) While Antoine, Gurgel, and Reilly (2008) did not consider benefits, they examined the importance of including nonmarket goods and services provided by the environment when analyzing the cost of biofuel policies. They directly introduced nonmarket recreation services into a CGE model and found that the inclusion of a competing demand for unmanaged forests (for outdoor recreation) lowered the amount of land converted to biofuel production. The authors found this trade-off associated with nonmarket services to be a potentially important component for characterizing the social cost of mitigation policy, increasing the welfare costs by around 20% in years where biofuels were considered a relatively cost-effective mitigation strategy by the model.

PRINTED FROM the OXFORD RESEARCH ENCYCLOPEDIA, ENVIRONMENTAL SCIENCE (oxfordre.com/environmentalscience) (c) Oxford University Press USA, 2020. All Rights Reserved. Personal use only; commercial use is strictly prohibited (for details see Privacy Policy and Legal Notice).

date: 27 April 2020

(23.) Carbone and Smith (2013) recalibrated the model depending on whether the welfare measure includes general equilibrium effects and for different sets of substitution elasticities so that the marginal WTP implicit in the model remained in line with empirical estimates. The lower end of the range assumed greater substitutability relative to the reference case; the higher end of the range assumed stronger complementarity than in the reference case.

(24.) Ferris et al. (2014) observed that “spending on pollution abatement capital [in the electricity sector] represented about 0.5% of revenues from total retail sales of electricity in 1999. This is roughly consistent with other heavily regulated industries: pollution abatement capital costs for US manufacturing plants were roughly 0.4% of total shipments, while they were about 1% for pulp and paper, steel, and oil refining in 2005.”

(25.) EPA sponsored a workshop in 2012, “Advancing the Theory and Methods for Understanding Employment Effects of Environmental Regulation.” Several papers were subsequently published in the peer-reviewed literature, including Smith (2015), Rogerson (2015), and Kuminoff et al. (2015).

(26.) Several empirical studies have indicated that transition costs for displaced workers may be larger than previously thought (Davis & von Wachter, 2011; Smith, 2015).

Ann E. Ferris

U.S. Environmental Protection Agency

Richard Garbaccio

U.S. Environmental Protection Agency

Alex Marten

U.S. Environmental Protection Agency

Ann Wolverton

U.S. Environmental Protection Agency

PRINTED FROM the OXFORD RESEARCH ENCYCLOPEDIA, ENVIRONMENTAL SCIENCE (oxfordre.com/environmentalscience) (c) Oxford University Press USA, 2020. All Rights Reserved. Personal use only; commercial use is strictly prohibited (for details see Privacy Policy and Legal Notice).

date: 27 April 2020

Klemick, Heather

From: Ferris, Ann
Sent: Wednesday, April 29, 2020 2:35 PM
To: Wolverton, Ann
Cc: Klemick, Heather
Subject: Record of Percentage Agreement for Ann Ferris for 2019 STAA nomination

Record of Percentage Agreement for Ann Ferris for 2019 STAA nomination.

NOMINATED PUBLICATION:

Ferris, A., Garbaccio, R., Marten, A., and A. Wolverton. 2017. The Impacts of Environmental Regulation on the U.S. Economy. *Oxford Research Encyclopedia of Environmental Economics*. Oxford University Press.
.

[Ferris 25%, Garbaccio 25%, Marten 25%, Wolverton 25%]

OVERALL PERCENTAGE ALLOCATION:
Ferris: 25/100 = 25%
Garbaccio: 25/100 = 25%
Marten: 25/100 = 25%
Wolverton: 25/100 = 25%

I agree with my designated percentage contribution of 25%.

Ann

Klemick, Heather

From: Marten, Alex
Sent: Thursday, April 30, 2020 9:36 AM
To: Wolverton, Ann
Cc: Klemick, Heather
Subject: RE: Record of Percentage Agreement for Alex Marten for 2019 STAA nomination.

Record of Percentage Agreement for Alex Marten for 2019 STAA nomination.

NOMINATED PUBLICATION:

Ferris, A., Garbaccio, R., Marten, A., and A. Wolverton. 2017. The Impacts of Environmental Regulation on the U.S. Economy. *Oxford Research Encyclopedia of Environmental Economics*. Oxford University Press.
.

[Ferris 25%, Garbaccio 25%, Marten 25%, Wolverton 25%]

OVERALL PERCENTAGE ALLOCATION:
Ferris: 25/100 = 25%
Garbaccio: 25/100 = 25%
Marten: 25/100 = 25%
Wolverton: 25/100 = 25%

I agree with my designated percentage contribution of 25%.

Alex

Klemick, Heather

From: Richard Garbaccio <garbaccio.richard@gmail.com>
Sent: Wednesday, April 29, 2020 1:24 PM
To: Wolverton, Ann
Cc: Klemick, Heather
Subject: Re: Record of Percentage Agreement for Richard Garbaccio for 2019 STAA nomination.

Record of Percentage Agreement for Richard Garbaccio for 2019 STAA nomination.

NOMINATED PUBLICATION:

Ferris, A., Garbaccio, R., Marten, A., and A. Wolverton. 2017. The Impacts of Environmental Regulation on the U.S. Economy. Oxford Research Encyclopedia of Environmental Economics. Oxford University Press.

.

[Ferris 25%, Garbaccio 25%, Marten 25%, Wolverton 25%]

OVERALL PERCENTAGE ALLOCATION:

Ferris: 25/100 = 25%

Garbaccio: 25/100 = 25%

Marten: 25/100 = 25%

Wolverton: 25/100 = 25%

I agree with my designated percentage contribution of 25%.

Richard

Klemick, Heather

From: Wolverton, Ann
Sent: Tuesday, April 28, 2020 12:22 PM
To: Klemick, Heather
Subject: Record of Percentage Agreement for Ann Wolverton for 2019 STAA nomination

Record of Percentage Agreement for Ann Wolverton for 2019 STAA nomination.

NOMINATED PUBLICATION:

Ferris, A., Garbaccio, R., Marten, A., and A. Wolverton. 2017. The Impacts of Environmental Regulation on the U.S. Economy. Oxford Research Encyclopedia of Environmental Economics. Oxford University Press.
.

[Ferris 25%, Garbaccio 25%, Marten 25%, Wolverton 25%]

OVERALL PERCENTAGE ALLOCATION:
Ferris: 25/100 = 25%
Garbaccio: 25/100 = 25%
Marten: 25/100 = 25%
Wolverton: 25/100 = 25%

I agree with my designated percentage contribution of 25%.

Ann

Table of Contents

General_Authors_Publications.....2
LI-266939_Ghimire_et_al_2017.....13
Ghimire_et_al_2017.....26
Ghimire_et_al_2017_JCP_Record_of_%_contribution.....39
Ghimire_et_al_2017_SI.....40
RE__JCP_municipal_RWH_publication_award_nomination_Ingwersen.....77
ARCSA_letter_of_support.....78
ARCSA.....79

STAA REPORT FOR THE SCIENTIST NOMINATIONS

General Information:

Nomination ID/App ID:	20-141
Research Category Primary:	Industry and the Environment (IE)
Research Category Secondary:	Energy and the Environment (EE);Sustainability and Innovation (SI)
Laboratory/Office Name:	ORD
Nomination Entered By:	John Johnston

Eligibility Checklist:

[Y] The nominated publication(s) has not been submitted to a previous STAA competition.

[Y] The nominated publication(s) was published on or before January 1, 2017 and on or after January 1,2012

[Y] The principal author was an EPA employee or a PHS employee assigned to EPA when the research was performed

[Y] The EPA authors (includes PHS employees assigned to EPA) contributed collectively a minimum of 50% toward the publication(s)

Nominating Official Name:	Brian Schumacher
Nominating Official Title:	CHEMIST
Nominating OfficialEmail:	schumacher.brian@epa.gov
STAA Coordinator Name:	Kathleen Wiser
STAA Coordinator Email:	wiser.kathi@epa.gov

Justifications:

Justification 1:

Rainwater harvesting has gained acceptance nationally and globally as both a viable solution to address water scarcity and a climate change adaptation strategy. Rainwater harvesting is one example of green infrastructure, which is an Agency priority as carried out by the Office of Water and supported by the Office of Research and Development Safe and Sustainable Water Resources (SSWR) Strategic Research Action Plan (2016-2019). The Water Infrastructure Improvement Act states “The Administrator shall promote the use of green infrastructure in, and coordinate the integration of green infrastructure into, permitting and enforcement under this Act, planning efforts, research, technical assistance, and funding guidance of the Environmental Protection Agency.” Signed into law in 2019, it mandates the “Administrator shall ensure that the Office of Water coordinates efforts to increase the use of green infrastructure with… State, tribal, and local governments and the private sector.” The Green Infrastructure Models and Tools Program/Project 5.02 in the SSWR National Research Program was designed to address the research and development needs of the Agency. According to the National Academies’ 2015 report *Using Graywater and Stormwater to Enhance Local Water Supplies: An Assessment of Risks, Costs, and Benefits*, “Chronic and episodic water shortages are becoming common in many regions of the United States, and urban population growth in water scarce regions further compounds the challenges.” Rainwater harvesting can augment conventional water supply systems to provide for non-potable uses such as toilet flushing and irrigation, and serve as a sustainable, decentralized, and more cost-effective solution to water management challenges. However, the human and ecological health impacts and life cycle costs of rainwater harvesting are not well characterized for commercial buildings. The authors conducted life cycle analysis of a commercial rainwater harvesting system and compared it to a municipal water supply system adapted to Washington, D.C. Eleven life cycle impact assessment indicators were assessed, with a functional unit of 1 m3 of rainwater and municipal water delivery system for toilets and urinals in a four-story commercial building with 1000 employees. Their study showed that the benchmark commercial rainwater harvesting system outperformed the municipal system in all categories except Ozone Depletion. Sensitivity and performance analyses revealed pump and pumping energy to be key contributors to most impact categories, which further guides trade-off analysis with respect to energy intensities. Trade-off analysis revealed that commercial rainwater harvesting performed better than the municipal system in Ozone Depletion if rainwater harvesting energy intensity was less than the municipal supply by at least 0.86 kWh/m3 (249% of the benchmark municipal energy usage at 0.35 kWh/m3). This novel contribution provided a transparent set of publicly available life cycle inventory unit processes as well as a comprehensive suite of life cycle impact assessment results relevant to water resource decision making, with a methodology that can be extended to additional locations.

This nominated paper was the outcome of a successful collaboration with the nonprofit American Rainwater Catchment Systems Association (ARCSA, www.arcsa.org) and was delivered to the SSWR as Product 5.02A.3 in 2018. The results from the study, particularly the impact of pumping energy on life cycle impacts and the need to "right-size" a system, were key findings of interest to ARCSA. The EPA authors credited the success of the effort to the engagement of a private sector stakeholder to help both in problem definition as well as in guiding the potential solution, also providing design and material data to the analysis. Although ARCSA initially contacted the EPA because of their interest in life cycle impact assessment methodology, their goal in becoming a partner was to increase the relevance of the research to their professional society by designing a case study that would be of greater interest generally and viewed as more "realistic" to practitioners. The resulting collaboration and paper not only furthered the EPA's mission but also the mission of ARCSA.

Justification 2A:

n/a

Justification 2B:

Ghimire, S.R., Johnston, J.M., Ingwersen, W.W. and Hawkins, T.R., 2014. Life cycle assessment of domestic and agricultural rainwater harvesting systems. Environmental Science & Technology, 48(7):4069-4077.

STAA Award Level Level II, 2016

Justification 2C:

Ghimire et al. (2014) presented a life cycle impact assessment methodology for optimized, domestic and agricultural rainwater harvesting systems, comparing conventional water supplies, municipal water supplies and well water irrigation systems to serve as examples. The nominated publication of Ghimire et al. (2017) addressed the life cycle impacts of a commercial rainwater harvesting system design provided by the non-profit organization ARCSA for a typical commercial building in a large U.S. city (compared to a municipal water supply system adapted to Washington, D.C). The case study, system design, life cycle inventory material data and

impact assessment are unique to the nominated publication. Although ARCSA reached out to the EPA to express interest in the methodology of Ghimire et al. (2014), their goal in becoming a partner was to increase the relevance of the research to their professional society by designing a case study that would be of greater interest generally and viewed as more "realistic" to practitioners.

Justification 2D:

n/a

Justification 2E:

n/a

Justification 3A:

According to Google Scholar, as of April 19, 2020, the nominated publication has been cited 36 times (excluding self citation). This is across 20 countries including the U.S.:

Concha Larrauri, P., Campos Gutierrez, J.P., Lall, U. and Ennenbach, M., 2020 A City Wide Assessment of the Financial Benefits of Rainwater Harvesting in Mexico City. JAWRA Journal of the American Water Resources Association. **U.S.**

Rahman, A., Snook, C., Haque, M.M. and Hajani, E., 2020. Use of design curves in the implementation of a rainwater harvesting system. Journal of Cleaner Production, p.121292. **Australia**

Rodríguez, C.A.P., 2020. Comunidades sostenibles: construcción de canales de recolección de agua lluvia con material PET. (Sustainable communities: channel construction rainwater harvesting PET materials). Centro Sur, 4(1), pp.30-41. **Ecuador**

Semaan, M., 2020. A Novel Approach to Communal Rainwater Harvesting for Single-Family Housing: A Study of Tank Size, Reliability, and Costs (Doctoral dissertation, Virginia Tech). **U.S.**

Asadi, S., Nazari-Heris, M., Nasab, S.R., Torabi, H. and Sharifironizi, M., 2020. An Updated Review on Net-Zero Energy and Water Buildings: Design and Operation. In Food-Energy-Water Nexus Resilience and Sustainable Development (pp. 267-290). Springer, Cham. **U.S. and Iran**

Nashait, A.F., Jasim, O.Z., Ismail, M.M. and Saad, F.H., 2020. Integrating various satellite images for identification of the water bodies through using machine learning: A case study of Salah Adin, Iraq. **Iraq**

Nnaji, C.C. and Aigbavboa, C., 2020. A Scenario-Driven Assessment of the Economic Feasibility of Rainwater Harvesting Using Optimized Storage. Water Resources Management, pp.1-16. Nigeria and South Africa

de Souza, T.D. and Ghisi, E., 2020. Harvesting rainwater from scaffolding platforms and walls to reduce potable water consumption at buildings construction sites. Journal of Cleaner Production, p.120909. **Brazil**

Sousa, V., Silva, C.M. and Meireles, I., 2019. Performance of water efficiency measures in commercial buildings. Resources, Conservation and Recycling, 143, pp.251-259. **Portugal**

Husain, D., Garg, P. and Prakash, R., 2019. Ecological footprint assessment and its reduction for industrial food products. International Journal of Sustainable Engineering, pp.1-13. **India**

Eränen, R., 2019. Vattenförsörjning i skärgården: Regnvatteninsamling och infiltration till grundvattenmagasin. Independent thesis Advanced level (professional degree), Luleå University of Technology, Department of Civil, Environmental and Natural Resources Engineering. **Sweden**

Severis, R.M., da Silva, F.A., Wahrlich, J., Skoronski, E. and Simioni, F.J., 2019. Economic analysis and risk-based assessment of the financial losses of domestic rainwater harvesting systems. Resources, Conservation and Recycling, 146, pp.206-217. **Brazil**

Yaqub, G., Hamid, A. and Asghar, S., 2019. Rain water quality assessment as air quality indicator in Pakistan. Bangladesh Journal of Scientific and Industrial Research, 54(2), pp.161-168. **Pakistan**

Zanni, S., Cipolla, S.S., di Fusco, E., Lenci, A., Altobelli, M., Currado, A., Maglionico, M. and Bonoli, A., 2019. Modeling for sustainability: Life cycle assessment application to evaluate environmental performance of water recycling solutions at the dwelling level. Sustainable Production and Consumption, 17, pp.47-61. **Italy**

Jia, X., Li, Z., Tan, R.R., Foo, D.C., Majozi, T. and Wang, F., 2019. Interdisciplinary contributions to sustainable water management for industrial parks. **China, South Africa, the Philippines, Malaysia**

Leong, J.Y.C., Balan, P., Chong, M.N. and Poh, P.E., 2019. Life-cycle assessment and life-cycle cost analysis of decentralised rainwater harvesting, greywater recycling and hybrid rainwater-greywater systems. Journal of Cleaner Production, 229, pp.1211-1224. **Malaysia**

Tavakol-Davani, H., Rahimi, R., Burian, S.J., Pomeroy, C.A., McPherson, B.J. and Apul, D., 2019. Combining Hydrologic Analysis and Life Cycle Assessment Approaches to Evaluate Sustainability of Water Infrastructure: Uncertainty Analysis. Water, 11(12), p.2592. **U.S.**

Faragò, M., Brudler, S., Godskesen, B. and Rygaard, M., 2019. An eco-efficiency evaluation of community-scale rainwater and stormwater harvesting in Aarhus, Denmark. Journal of Cleaner Production, 219, pp.601-612. **Denmark**

Marinoski, A.K. and Ghisi, E., 2019. Environmental performance of hybrid rainwater-greywater systems in residential buildings. Resources, Conservation and Recycling, 144, pp.100-114. **Brazil**

Pavolová, H., Bakalár, T., Kudelas, D. and Puškárová, P., 2019. Environmental and economic assessment of rainwater application in households. Journal of cleaner production, 209, pp.1119-1125. **Slovak Republic**

Yan, X., Ward, S., Butler, D. and Daly, B., 2018. Performance assessment and life cycle analysis of potable water production from harvested rainwater by a decentralized system. Journal of Cleaner Production, 172, pp.2167-2173. **UK and Republic of Ireland**

Li, Y., Huang, Y., Ye, Q., Zhang, W., Meng, F. and Zhang, S., 2018. Multi-objective optimization integrated with life cycle assessment for rainwater harvesting systems. Journal of hydrology, 558, pp.659-666. **China**

Teston, A., Geraldi, M.S., Colasio, B.M. and Ghisi, E., 2018. Rainwater harvesting in buildings in Brazil: A literature review. Water, 10(4), p.471. **Brazil**

Zhang, S., Zhang, J., Jing, X., Wang, Y., Wang, Y. and Yue, T., 2018. Water saving efficiency and reliability of rainwater harvesting systems in the context of climate change. Journal of Cleaner Production, 196, pp.1341-1355. **China**

Lani, N.H.M., Syafiuddin, A., Yusop, Z. and bin Mat Amin, M.Z., 2018. Performance of small and large scales rainwater harvesting systems in commercial buildings under different reliability and future water tariff scenarios. Science of The Total Environment, 636, pp.1171-1179. **Malaysia**

Dijk, S., 2018. Performance assessment of citywide rainwater harvesting strategies in New York City (Master's thesis, University of Twente). **The Netherlands and the U.S.**

Antunes, L.N., Ghisi, E. and Thives, L.P., 2018. Permeable pavements life cycle assessment: a literature review. Water, 10(11), p.1575. **Brazil**

Tavakol-Davani, H., Burian, S.J., Butler, D., Sample, D., Devkota, J. and Apul, D., 2018. Combining Hydrologic Analysis and Life Cycle Assessment Approaches to Evaluate Sustainability of Water Infrastructure. Journal of Irrigation and Drainage Engineering, 144(11), p.05018006. **U.S. and U.K**.

Moore, T.L., Rodak, C.M., Ahmed, F. and Vogel, J.R., 2018. Urban stormwater characterization, control and treatment. Water Environment Research, 90(10), pp.1821-1871. **U.S.**

Zanni, S., Cipolla, S.S., di Fusco, E. and Lenci, A`, 2018. Modeling for sustainability: Life cycle assessment application to evaluate environmental performance of water recycling solutions at the dwelling level. Sustainable Production and Consumption 17 (2019) 47-61 **Italy**

Rose, H.S., Upshaw, C.R. and Webber, M.E., 2018. Evaluating Energy and Cost Requirements for Different Configurations of Off-Grid Rainwater Harvesting Systems. Water, 10(8), p.1024. **U.S.**

Wasserstein, B., 2018. Water Utilities Objectives Evaluation of Single Family Residence Greywater Systems (Doctoral dissertation, Duke University). **U.S.**

Bangale, M.C., Patil, M.C., Waghule, M.S., Kharat, M.A., Sabale, P.D. and Yadav, S.J., 2018. Design of Rooftop Rainwater Harvesting in Nimgaon Village-A Case Study of Junnar Tahsil. International Research Journal of Engineering and Technology,05 (05). **India**

Ghisi, E., Colasio, B.M., Geraldi, M. and Teston, A., 2017. Rainwater Harvesting in Buildings in Brazil: A Literature Review. In Multidisciplinary Digital Publishing Institute Proceedings (Vol. 2, No. 5, p. 186). **Brazil**

Allison, L., Davis, B. and Kaminsky, J., 2017. Rainwater Irrigation Systems: Recommendations for UW Seattle. **U.S.**

Ghisi, E., Colasio, B.M., Geraldi, M. and Teston, A., 2017 Rainwater Harvesting in Buildings in Brazil: A Literature Review Proceedings 2017, 1, x; doi: www.mdpi.com/journal/proceedings **Brazil**

Justification 3B:

We followed the external review process of the Journal of Cleaner Production and edited the manuscript in response to all peer reviewer comments. We responded to their comments in a summary letter and provided a revised submission according to the decision of the Managing Editor for acceptance with revision.

AUTHORS

Principal Author

Author Name:	John M. Johnston		
Professional Title:		Salutation:	Dr.
Email:	johnston.johnm@epa.gov	Organization:	
Mailing Address:			
Street Line 1:			
City:			
Zip Code:		State:	
At time of research was:	EPA Employee		
Separation Date:			
% of Effort:	30		

Contributing Author

Author Name:	Santosh Ghimire		
Professional Title:		Salutation:	Dr.
Email:	sghimire02@gmail.com	Organization:	
Mailing Address:			
Street Line 1:			
City:			
Zip Code:		State:	
At time of research was:	Non EPA Personnel		
Separation Date:			
% of Effort:	40		

Contributing Author

Author Name:	Wesley Ingwersen		
Professional Title:		Salutation:	Dr.
Email:	ingwersen.wesley@epa.gov	Organization:	
Mailing Address:			
Street Line 1:			
City:			
Zip Code:		State:	
At time of research was:	EPA Employee		
Separation Date:			
% of Effort:	20		

Contributing Author

Author Name:	Sarah Sojka		
Professional Title:		Salutation:	Dr.
Email:	ssojka@randolphcollege.edu	Organization:	
Mailing Address:			
Street Line 1:			
City:			
Zip Code:		State:	
At time of research was:	Non EPA Personnel		
Separation Date:			
% of Effort:	10		

PUBLICATIONS

Publication 1:

Publication Title:	Life cycle assessment of a commercial rainwater harvesting system compared with a municipal water su		
Publication Date:	Mon Feb 06 00:00:00 GMT 2017		
Journal/Publication Method:	Journal of Cleaner Production		
All Author(s):			
Volume:	151	Number:	0
Pages:	74-86	Immediately Index:	Immediately Index:
Citation ½ Life:	4.40	Impact Factor:	6.395

Journal of Cleaner Production 151 (2017) 74–86

Contents lists available at ScienceDirect

Journal of Cleaner Production

journal homepage: www.elsevier.com/locate/jclepro

Life cycle assessment of a commercial rainwater harvesting system compared with a municipal water supply system

Santosh R. Ghimire [a], John M. Johnston [b, *], Wesley W. Ingwersen [c], Sarah Sojka [d]

[a] ORISE Postdoctoral Research Participant, U.S. Environmental Protection Agency, Office of Research and Development, 960 College Station Rd., Athens, GA 30605, USA
[b] U.S. Environmental Protection Agency, Office of Research and Development, 960 College Station Rd., Athens, GA 30605, USA
[c] U.S. Environmental Protection Agency, Office of Research and Development, 26 W. Martin Luther King Dr., Cincinnati, OH 45268, USA
[d] Randolph College, 2500 Rivermont Ave., Lynchburg, VA 24503, USA

ARTICLE INFO

Article history:
Received 20 December 2016
Received in revised form
3 February 2017
Accepted 3 February 2017
Available online 6 February 2017

Keywords:
Life cycle assessment
Commercial rainwater harvesting
Municipal water supply
Energy intensity

ABSTRACT

Building upon previously published life cycle assessment (LCA) methodologies, we conducted an LCA of a commercial rainwater harvesting (RWH) system and compared it to a municipal water supply (MWS) system adapted to Washington, D.C. Eleven life cycle impact assessment (LCIA) indicators were assessed, with a functional unit of 1 m^3 of rainwater and municipal water delivery system for toilets and urinals in a four-story commercial building with 1000 employees. Our assessment shows that the benchmark commercial RWH system outperforms the MWS system in all categories except Ozone Depletion. Sensitivity and performance analyses revealed pump and pumping energy to be key components for most categories, which further guides LCIA tradeoff analysis with respect to energy intensities. Tradeoff analysis revealed that commercial RWH performed better than MWS in Ozone Depletion if RWH's energy intensity was less than that of MWS by at least 0.86 kWh/m^3 (249% of the benchmark MWS energy usage at 0.35 kWh/m^3). RWH also outperformed MWS in Metal Depletion and Freshwater Withdrawal, regardless of energy intensities, up to 5.51 kWh/m^3. An auxiliary commercial RWH system with 50% MWS reduced Ozone Depletion by 19% but showed an increase in all other impacts, which were still lower than benchmark MWS system impacts. Current models are transferrable to commercial RWH installations at other locations.
Published by Elsevier Ltd. This is an open access article under the CC BY license (http://creativecommons.org/licenses/by/4.0/).

1. Introduction

Approximately 5–20% of the global population is predicted to live under absolute water scarcity (<500 m^3/person/year) up until the point of a 2 °C increase in mean global temperature, and a higher percentage as temperatures rise further (Schewe et al., 2014). The climate change impact and the 21st century's mega-droughts with longer duration may result in unprecedented water scarcity from the southwestern to the southeastern U.S., and to other parts of the world, which is driving the global search for alternate water sources (USGCRP, 2012; Ault et al., 2016; USEPA, 2016a). Rainwater harvesting (RWH) is receiving renewed interest as a green infrastructure practice in the face of necessary adaptation to global climate change (USGCRP, 2012; Ghimire et al., 2014). RWH has been used for drinking water and agricultural irrigation since 11,500 BCE in North America and 4500 BCE in Asia (Pandey et al., 2003; Mays et al., 2013; Ghimire and Johnston, 2015). Other potential benefits of RWH include reduced impacts on the environment and human health, reduced stormwater runoff and combined sewer overflows, and economic viability (Ghimire et al., 2012; Wang and Zimmerman, 2015). In practice the implementation of RWH has remained a challenge. This is due primarily to a lack of understanding of its environmental and human health impacts (criteria pollutants from material selection and energy use) and partly due to the lack of regulations governing RWH practices. Although state regulations and statutes continue to favor RWH (ARCSA, 2016; Harvesth2o, 2016; NCSL, 2016), the U.S. Environmental Protection Agency (EPA) reported “there are currently no federal regulations governing rainwater harvesting for non-potable use, and the policies and regulations enacted at the state and local levels vary widely from one location to another” (USEPA, 2013a).

* Corresponding author.
E-mail addresses: sghimire02@gmail.com (S.R. Ghimire), Johnston.JohnM@epa.gov (J.M. Johnston), Ingwersen.Wesley@epa.gov (W.W. Ingwersen), ssojka@randolphcollege.edu (S. Sojka).

http://dx.doi.org/10.1016/j.jclepro.2017.02.025
0959-6526/Published by Elsevier Ltd. This is an open access article under the CC BY license (http://creativecommons.org/licenses/by/4.0/).

Studies worldwide have explored RWH life cycle cost impacts (Roebuck et al., 2011), water savings potential (Ghisi et al., 2009; Domenech and Sauri, 2011; Ward et al., 2012), water quality and health risks (Lye, 2002; Domenech et al., 2012), optimal designs (Sample and Liu, 2014), energy intensity versus economic and CO_2 emissions (Gurung and Sharma, 2014; Siems and Sahin, 2016), hydrologic impacts (Ghimire and Johnston, 2013), and climate change adaptation (Pandey et al., 2003). Of particular interest is the life cycle environmental and human health criteria air pollutant impacts of RWH. Life cycle assessment (LCA) has been widely used since its inception in the late 1960s in diverse sectors to assess environmental and human health impacts in a cradle-to-grave approach that avoids or minimizes unintended consequences (Hunt et al., 1996; ISO, 2006b, a; Meyer and Upadhyayula, 2013; Ingwersen et al., 2016). Use of LCA to assess RWH systems is also increasing. Previous studies focused on residential small and large building systems that vary by region; however, findings varied by design parameters and data sources, as demonstrated by the following examples. Crettaz et al. (1999) performed an LCA on RWH for clothes washing and toilet flushing in Switzerland and reported RWH as energetically favorable if pumping energy intensity for municipal drinking water was greater than 0.8 kWh/m^3. Angrill et al. (2012) reported life cycle impacts of RWH for laundry use in compact urban densities were generally lower than in diffused settings in Spain. Morales-Pinzón et al. (2015) reported a lower life cycle global warming potential of RWH than tap water for toilet flushing and clothes washing in a single-family house if the average storage tank was smaller than 2 m^3.

In the U.S., interest in RWH is growing due to increased droughts as well as its environmental benefits (Thomas et al., 2014; Sojka et al., 2016). An energy and greenhouse gas (GHG) emission analysis of RWH in a university building in Ohio reported RWH as a viable option with GHG emission payback periods higher than the energy payback periods but contradicted the results of Anand and Apul (2011) due to difference in data sources (process-based versus Economic Input Output life cycle assessment data) (Devkota et al., 2015). Wang and Zimmerman (2015) assessed life cycle climate change, fossil fuel depletion, and eutrophication impacts of RWH for office buildings in 14 large cities across the U.S., from Boston, Massachusetts to Seattle, Washington, and reported that reduced eutrophication and combined sewer flows varied with location.

Ghimire et al. (2014) published an LCA of domestic and agricultural RWH systems that compared conventional water supplies, municipal water supplies and well water irrigation systems in the southeastern U.S. The American Rainwater Catchment Systems Association then contacted the authors about conducting a similar study for a commercial RWH system. Comprehensive understanding of the life cycle implications of commercial RWH systems is only in its infancy but is important for informing urban water management planning and decision making. Consequently, we conducted an LCA of a typical commercial RWH system in an average size commercial building sited in a large U.S. city (EIA, 2016) and combined this with scenario and sensitivity analysis, with the intention of providing more generalizable life cycle implications of commercial RWH systems.

1.1. Objective, scope, and novelty

Our objective is to conduct an LCA of a commercial RWH system and compare it to a municipal water supply (MWS), hereafter called benchmark commercial RWH and MWS systems. Eleven life cycle impact assessment (LCIA) indicators were calculated per functional unit of 1 m^3 of rainwater and municipal water delivery for flushing toilets and urinals in a four-story commercial building with 1000 employees. These included Acidification, Energy Demand, Eutrophication, Fossil Depletion, Freshwater Withdrawal, Global Warming, Human Health Criteria, Metal Depletion, Ozone Depletion, Smog, and Evaporative Water Consumption. LCIA sensitivity was addressed for (i) storage tank materials and volume, (ii) energy usage or energy intensity, (iii) water demand, (iv) water loss, (v) system service life, and (vi) an auxiliary commercial RWH system augmented with MWS. The LCA system boundary spans cradle-to-grave, excluding the distribution of both systems' components from final manufacture to point of use and disposal phases for lack of comparable data (see Supplementary Material or SM 1 for additional details). This study provides a comprehensive LCA of commercial RWH to inform RWH planning and decision making, with standards and regulations at state and local levels governing urban water management decisions (USEPA, 2013a). The life cycle inventory (LCI) and LCA models are generally transferrable in recreating LCA models of other commercial RWH and MWS systems by obtaining appropriate LCI data. The following sections describe methods, tools, databases and assumptions and results, with concluding remarks on potential implications for commercial RWH design and planning.

2. Methods and tools

2.1. Site selection

Washington, D.C. was selected as the study site primarily due to readily available data on the MWS system, precipitation record and commercial RWH design. While the commercial RWH system was designed for local precipitation patterns, the analysis required extensive data on an existing urban MWS system compatible with existing life cycle data for MWS. The EPA conducted a study of the Cincinnati MWS system that uses the Ohio River as a source with chlorine disinfection (Cashman et al., 2014). Data were developed in a modular and reusable fashion to be reconfigured and customized for other regions. Study area selection criteria included a large urban area with similar source water characteristics, treatment processes and distribution architecture to Cincinnati, Ohio, as well as publically available data on the water supply system and sufficient precipitation record. Other U.S. cities considered included Los Angeles, Phoenix, Austin, Chicago and Atlanta. Although water demand for Washington, D.C. (benchmark MWS system) was slightly higher $\approx$ 1.1 times Cincinnati MWS system demand, it has comparable treatment system and distribution pipe network composition (Ductile Iron pipe >90%).

2.2. Definition of the benchmark commercial RWH and MWS systems

The American Rainwater Catchment Systems Association provided the design for a commercial RWH system from one of its member companies to be configured for a typical urban system. This design was customized for flushing 40 toilets and 15 urinals in a four-story commercial building with 1000 people, adapted to Washington, D.C. (Fig. 1 and Table 1, see SM 1 and 2 for additional details).

Key design parameters and assumptions used in the benchmark commercial RWH system analysis were:

- Total water demand for flushing all urinals and toilets for the building was estimated at 2653 m^3/y (2685 gallons/day): high-efficiency urinal demand at 0.47 L per flush (l/f) or 0.125 gallon/flush (g/f), and high-efficiency toilet demand at 4.8 l/f or 1.28 g/f (AWE, 2016);

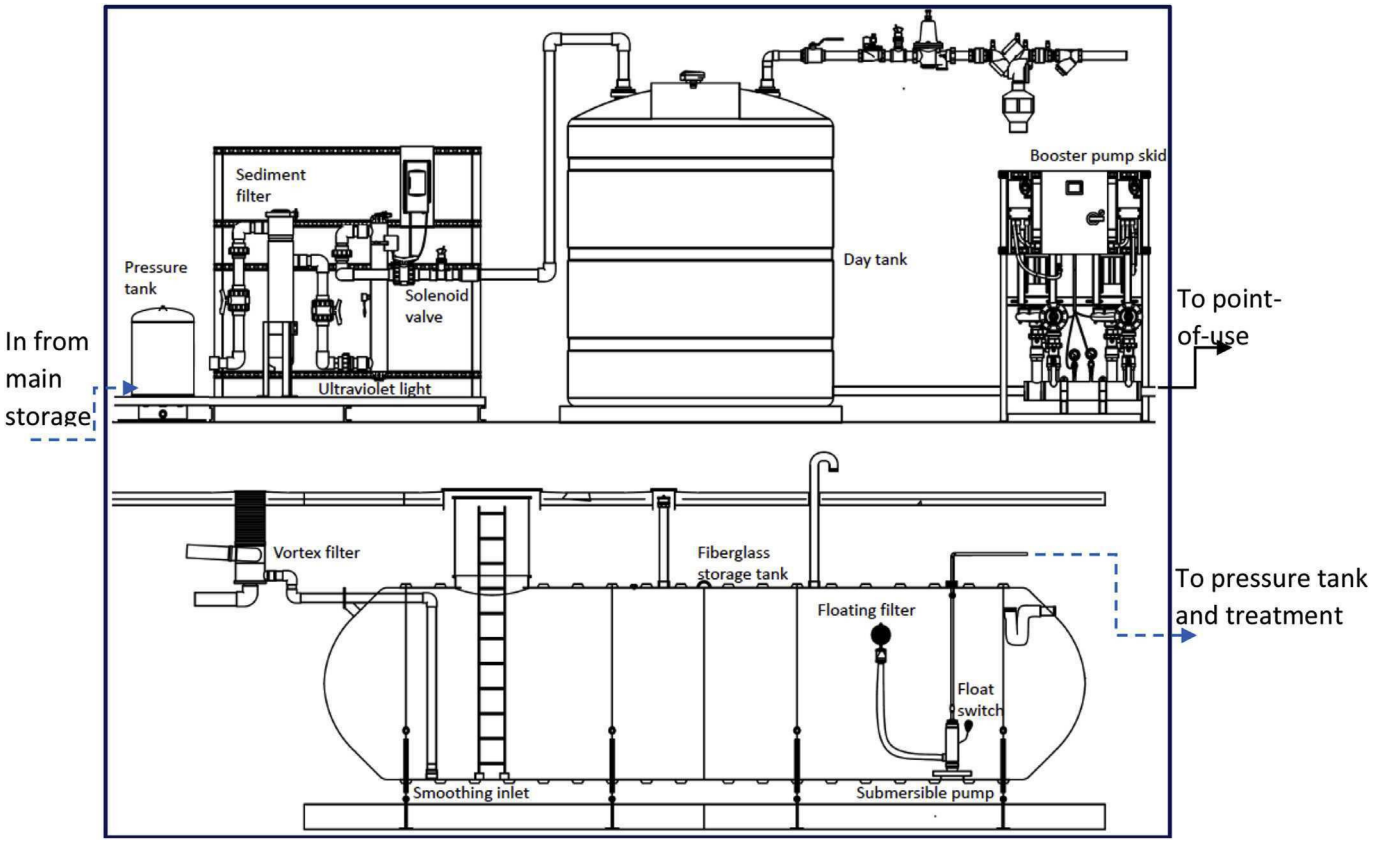

Fig. 1. Schematic of commercial rainwater harvesting system (designed by Rainwater Management Solutions).

- Storage tank volume was designed at 76 m^3 (20,000 gallons), supplying 77% of total volumetric water demand (RMS, 2009) (see SM 1 for additional details);
- The benchmark commercial RWH system met 77% of total toilet and urinal water demand (77% of 2653 m^3/y = 2042.81 m^3/y) and an auxiliary commercial RWH system was operated with support of MWS to meet additional demand;
- Pumping energy intensity was estimated at 0.19 kWh/m^3 (see SM 1 for additional details);
- Water loss throughout the system was 5%;
- Service life of the system was 50 years and components with shorter service lives were replaced at the end of their service lives;
- Distribution of system components from final manufacture to point of use and disposal were excluded from LCA.

The benchmark MWS system was defined using available information from the District of Columbia Water and Sewer Authority (DCWSA, 2015) and Baltimore District, U.S. Army Corps of Engineers (USACE, 2016) (Fig. 2 and SM 2).

The District of Columbia Water and Sewer Authority (DC Water) purchased 100% of drinking water from the Washington Aqueduct operated by the Baltimore District, U.S. Army Corps of Engineers. The Washington Aqueduct collected, purified and pumped drinking water to three jurisdictions, including DC Water, Arlington County, Virginia, and Fairfax County Water Authority, Virginia (USACE, 2016). Washington Aqueduct owned and operated two treatment plants, Dalecarlia and McMillan (source water: Potomac River), an intake pumping facility, and three water storage facilities. Seventy-two percent of total treated water from the two plants (i.e., 72% × 192,052,776 m^3/y) was sold to DC Water in 2012. DC Water consisted of 2092 km (1300 miles) of pipes, eight water storage facilities, four pumping stations, and 36,000 valves. Thus, DC Water (benchmark MWS system) was a combination of District of Columbia Water and Sewer Authority-owned and Washington Aqueduct-owned facilities. Key design parameters and assumptions pertaining to the benchmark MWS system were:

- The two water treatment plants of Washington Aqueduct produced 192,052,776 m^3/y or 139 million gallons of water per day and 72% of the treated water from the Aqueduct sold to DC Water;
- Water loss throughout the system was 24%, based on sold to pumped ratio of 76% in 2008 (DCWSA, 2008);
- Water treatment options were consistent with average U.S. water treatment;
- MWS energy intensity was estimated at 0.35 kWh/m^3 combining two energy uses: Washington Aqueduct energy use (0.20 kWh/m^3) included electricity required to pump source water and energy throughout the water treatment plants and DC Water services pumping energy use (0.15 kWh/m^3) for transporting the treated water (see SM 1 for additional details);
- All infrastructure had service lives of 100 years except the pump with 15-y service life, replaced at the end of its service life;
- Distribution of the system components from final manufacture to point of use and disposal were excluded from LCA.

2.2.1. Functional unit

To facilitate comparison of water supply from two different sources, 1 m^3 of water supply was defined as the functional unit for annual water supply and service lives of system components.

Table 1
Description of the major components of benchmark commercial rainwater harvesting system and life cycle inventory.

Main component	Sub-component	Material (unit)	Amount	Lifetime (y)	LCI data source
Vortex Filter	Housing	polypropylene (kg)	47.7	40	Ecoinvent (2012)
	Lid	aluminum (kg)	3.6	40	Ecoinvent (2012)
	Intermediate ring	stainless steel (kg)	7.3	40	Ecoinvent (2012)
	Filter insert	stainless steel (kg)	4.1	40	Ecoinvent (2012)
Smoothing inlet	Smoothing inlet	stainless steel (kg)	3.2	40	Ecoinvent (2012)
Floating filter	Filter assembly	stainless steel (kg)	0.7	15	Ecoinvent (2012)
	Hose	food grade reinforced plastic hose (kg)	2.3	15	Ecoinvent (2012)
	Floating ball	polyethylene (kg)	0.2	15	Ecoinvent (2012)
Main pump, 1 hp	Main pump	primarily stainless steel (kg)	18.0	15	Ghimire et al. (2014)
Booster pump, 1 hp	A booster pump	primarily stainless steel (kg)	18.0	15	Ghimire et al. (2014)
Level switch	Float switch and cable	polypropylene (Housing) (kg)	0.9	12.5	Ecoinvent (2012)
Pressure tank	Tank	rolled steel (16 gauge), butyl rubber, copolymer polypropylene (kg)	16.4	50	Ecoinvent (2012)
Bag filter	Bag filter	polypropylene (kg)	0.2	15	Ecoinvent (2012)
	Filter housing	polypropylene (kg)	4.6	15	Ecoinvent (2012)
Ultraviolet (UV) light chamber	Housing	316L stainless steel (kg)	14.6	11	Ecoinvent (2012)
	Bulbs	quartz (kg)	0.9	11	Ecoinvent (2012)
	Quartz sleeves	fused silica (kg)	0.5	11	Ecoinvent (2012)
Solenoid Valve	Valve	brass (kg)	0.5	7.5	Ecoinvent (2012)
Day Tank	high-density polyethylene (HDPE)	PE pipe equivalent length 181 m (kg)	43.2	50	NIST (2013)
Ultrasonic level transmitter (sensor)	Housing (LU20 Model)	polypropylene (kg)	0.9	15	Ecoinvent (2012)
Pipe, collection	2 in Polyvinyl chloride (PVC)	water supply 2 in 1 m - PVC cradle-to-gate (m)	61.0	50	NIST (2013)
Pipe, supply	1.5 in chlorinated PVC	HCWD 1.5 in 1 m- CPVC cradle-to-gate (m)	152.0	50	NIST (2013)
Storage Tank	Fiberglass (FG) Storage Tank	glass fibre (kg)	2773.0	50	NIST (2013)
	Two FG Access Riser (36 in diameter, 3 ft tall)	glass fibre (kg)	113.6	50	Ecoinvent (2012)
	Two FG Access Collars (36 in)	glass fibre (kg)	113.6	50	Ecoinvent (2012)
	Two overflow pipe (8 in 2 ft)	water supply 8 in 1 m - PE cradle-to-gate (kg)	2.3	50	NIST (2013)
Energy usage	Pumping energy	electricity, at residential user (kWh/m^3)	0.19	N/A	Cashman et al. (2014)

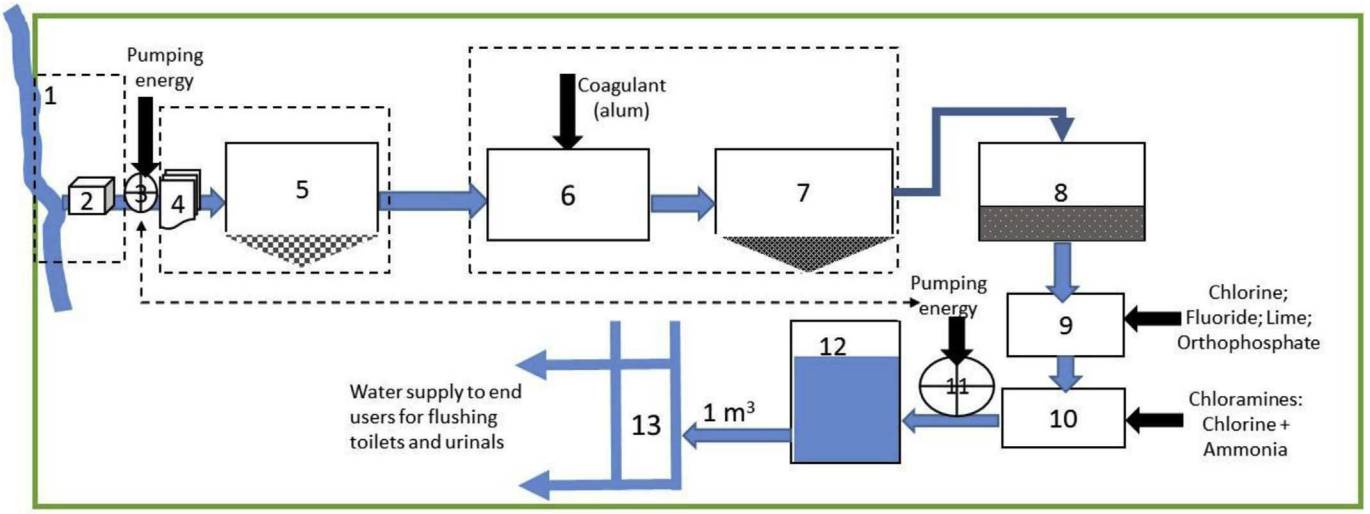

Fig. 2. Washington, D.C. municipal water supply system. Number Key: (1) Source water (Potomac River); (2) Source water acquisition infrastructure; (3) Acquisition pump; (4) Screening infrastructure; (5) Pre-sedimentation (natural settling in a pre-treatment storage); (6) Flocculation; (7) Sedimentation (coagulated particles); (8) Filtration (sand filter); (9) Primary Disinfection (Gaseous Chlorine, Lime addition, Fluorination, Orthophosphate); (10) Secondary Disinfection: Chloramines; (11) Distribution Pump (four); (12) Storage Tanks (eleven); (13) Water pipe network (based on District of Columbia Water and Sewer Authority (DCWSA, 2015) and Baltimore District, U.S. Army Corps of Engineers (USACE, 2016)).

Standardization by 1 m^3 enabled comparison of LCIA scores regardless of volumetric water supply, because material input is linearly related to volumetric water supply. In addition, accounting for service lives of system components addressed the issue of product replacement.

2.3. Development of LCI and LCA models

Primary data collected on commercial RWH included design components (Table 1, also see SM 2). Similarly, primary data were collected on the benchmark MWS system for system components,

Table 2
Sensitivity analysis scenarios.

Commercial RWH system	MWS (Washington D.C. water) system
Storage tank material (Polyethylene and Fiberglass)	–
Commercial RWH energy intensities (0.19–5.51 kWh/m^3)	MWS energy intensities (0.35–10.15 kWh/m^3)
Storage tank volume (from 0.25 to 4.5 × benchmark volume)	–
Commercial RWH demand (10%–100% of benchmark demand)	–
Commercial RWH system water loss (0%–30%)	DC Water system water loss (0%–30%)
System service life (50 years versus 75 years)	System service life (100 years)
Auxiliary commercial RWH system (0%–90% MWS)	–

amount of material and energy use, and water demand from the District of Columbia Water and Sewer Authority (DCWSA, 2015) and Baltimore District, U.S. Army Corps of Engineers (USACE, 2016) (see SM 2 for details on LCI). The LCI of the benchmark systems was compiled using Building for Environmental and Economic Sustainability (BEES) (NIST, 2013), Ecoinvent (2012) version 2.2, U.S. LCI database (NREL, 2013), and Cincinnati drinking water treatment and distribution systems collected from a previous study (Cashman et al., 2014). There are limitations to using the Ecoinvent database, a European LCI, in the U.S. because results would be sensitive to data quality and material type. However, data availability is a major consideration, such that the LCI and LCA utilized data and methods from a domestic RWH study in the southeastern U.S (Ghimire et al., 2014). as well as the LCI of the Cincinnati MWS system (Cashman et al., 2014).

2.4. Life cycle impact assessment (LCIA)

LCIA methods included combining the Tool for the Reduction and Assessment of Chemical and Other Environmental Impacts or, TRACI 2.1 (USEPA, 2013b), with the ReCiPe's Metal Depletion and Fossil Depletion (Goedkoop et al., 2012), Water Footprint's Evaporative Water Consumption and Freshwater Withdrawal (WFN, 2009), and the non-renewable Cumulative Energy Demand of Ecoinvent (Hischier et al., 2010). TRACI 2.1 methods included were Global Warming, Ozone Depletion, Smog, Human Health Criteria (air pollutants), Eutrophication, and Acidification. Human health (cancer) and ecotoxicity indicators were excluded due to lack of high quality life cycle data for release to air and water, consistent with Ingwersen et al. (2016). OpenLCA (2016) version 1.4.2, an open source LCA software (GreenDelta © 2016) was used for all LCIA calculations in conjunction with LCIA methods and LCI databases.

LCIA percentage contributions of the benchmark systems and their components were analyzed. LCIA sensitivity analysis was conducted for various scenarios (Table 2) which further guided LCIA tradeoff analysis with respect to energy intensities and the auxiliary commercial RWH system. Sensitivity and tradeoff LCIA results were normalized for each impact category by maximum LCIA score (see SM 4 for the details on LCIA normalization).

LCIA tradeoff of the auxiliary commercial RWH system, augmented with 10%–90% MWS, was assessed by summing the

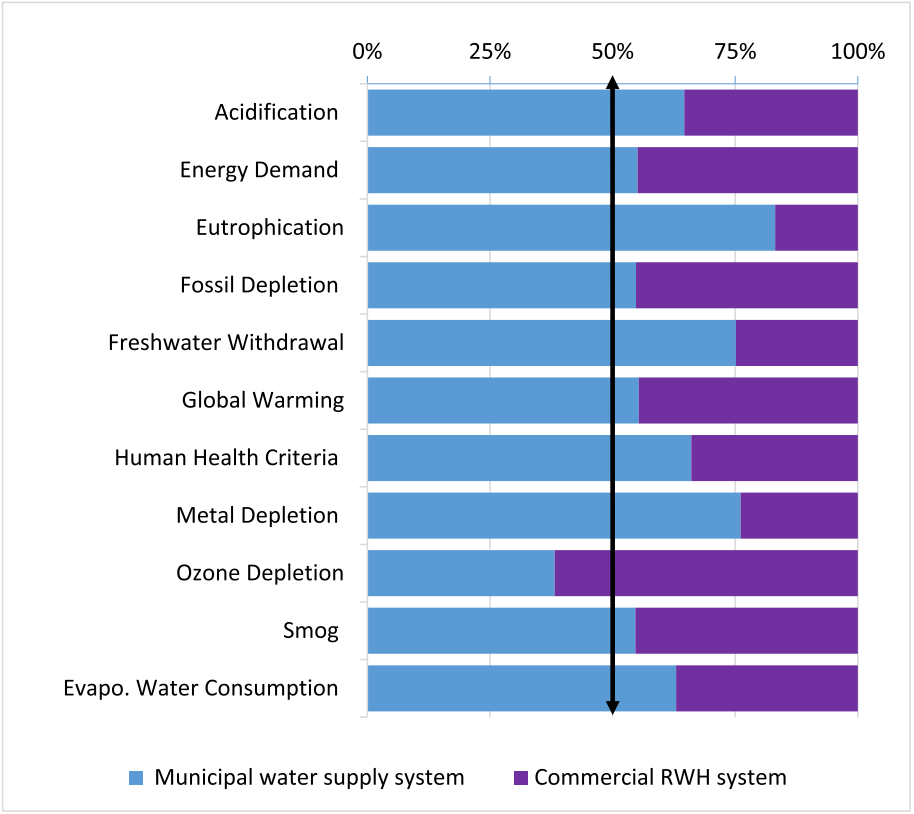

Fig. 3. Comparison of life cycle impacts of the benchmark commercial rainwater harvesting system to the municipal water supply system adapted to Washington, D.C. (vertical arrow indicates the threshold 50%).

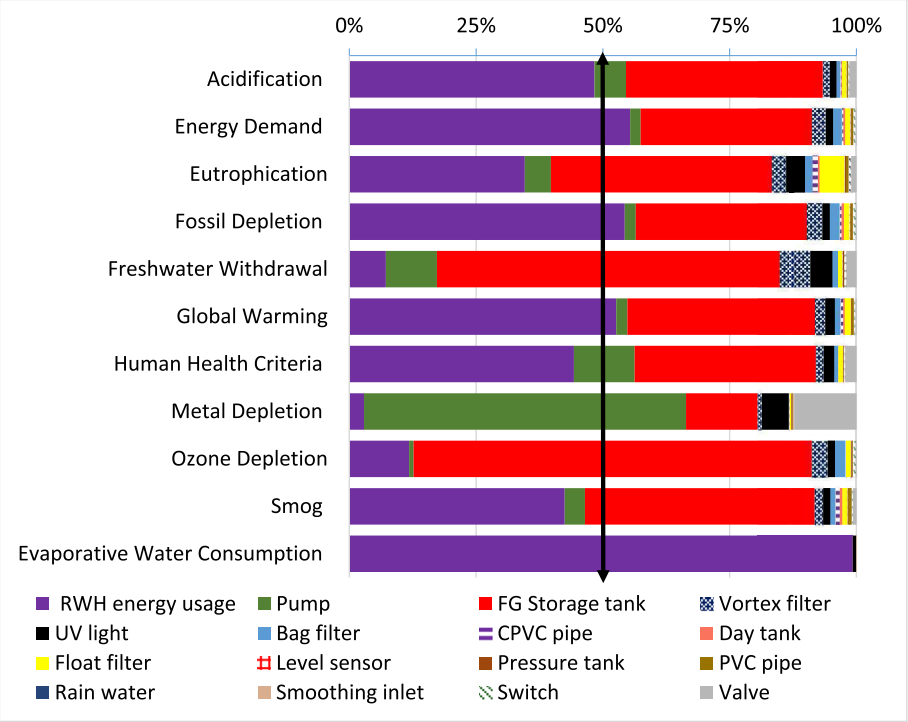

Fig. 4. Percentage comparison of life cycle impacts showing the performance of commercial rainwater harvesting (RWH) system components. Note: RWH energy usage includes pumping energy at the commercial RWH storage tank (vertical arrow indicates the threshold 50%).

fractional impacts of both systems delivering 1 m^3 of water supply (Equation (1)):

$$I_{aux} = p_c \times I_c + p_m \times I_m \quad (1)$$

for each impact categoryI_{aux} = the auxiliary system's impact (impact/m^3 of water supply), $.I_c$ = the benchmark commercial RWH system's impact (impact/m^3 of water supply), $.I_m$ = the benchmark MWS system's impact (impact/m^3 of water supply), $.p_c$ and p_m are commercial RWH and MWS percentage (in decimal) such that

$$p_c + p_m = 1 \quad (2)$$

Equation (1) was applied to estimate the impacts of the auxiliary commercial RWH system using the functional unit impacts of both benchmark systems; e.g., if a commercial RWH system supplied 70% of total demand (i.e., $p_c = 0.7$), then the value of I_{aux} would be 0.7 × benchmark commercial RWH system impact, I_c, + 0.3 × municipal water supply impact, I_m. Functional unit impacts per 1 m^3 water delivery were calculated, with inputs linearly related to volumetric water supply.

3. Results and discussion

3.1. Performance analysis

LCIA percentage contribution analysis showed that the benchmark commercial RWH system performed better than (<40%) or equivalent to (45%–55%) the MWS system in all impact categories except Ozone Depletion at 62% (Fig. 3).

Commercial RWH was slightly better than or equivalent to (at 45%, assuming a margin of error) MWS for Energy Demand, Fossil Depletion, Global warming, and Smog and better than MWS in 6 impact categories, ranging from 65% (Acidification) to 83% (Eutrophication). Percentage comparison of component-specific LCIA revealed energy usage to be the dominant contributor of both systems (Figs. 4–5). Commercial RWH energy usage (pumping energy) and storage tank collectively dominated (>50%) in all but Metal Depletion, ranging from 74.8% (Freshwater Withdrawal), 89.6% (Global Warming), to 99.2% (Evaporative Water Consumption). The commercial RWH storage tank (Fiberglass) dominated in Ozone Depletion (78.5%) and Freshwater Withdrawal (67.6%). MWS energy usage (treatment plant operation and water transport) dominated (>50%) in five categories, ranging from 60.3% (Smog) to 99.7% (Evaporative Water Consumption). The pump dominated in Metal Depletion impact of both systems, 63.5% in commercial RWH and 84.8% in MWS. Source water acquisition contributed to total MWS Freshwater Withdrawal impact at 64.8%, and primary and secondary disinfection together contributed to Eutrophication and Ozone Depletion impacts at 79.2% and 51.1%. All other commercial RWH system components were below 15%, and the remaining MWS system components were <10% (Figs. 4–5). Detailed values of LCIA of benchmark systems and their components are included in SM 2.

3.2. Sensitivity analysis

Normalized LCIA of energy usage revealed linear impact variation, confirming linearity in LCIA scores consistent with linear LCA models (Fig. 6). For purposes of this analysis, impact variation were grouped as Mild slope, e.g., Metal Depletion; Moderate slope, e.g., Freshwater Withdrawal; or High slope, e.g., Evaporative Water Consumption (Fig. 6a–b).

The rate of change of impacts across LCIA categories was consistent with the dominant components. For example, in the case of commercial RWH energy usage, Evaporative Water Consumption and Fossil Depletion fell under High slope because pumping energy dominated those impacts; Ozone Depletion and Freshwater

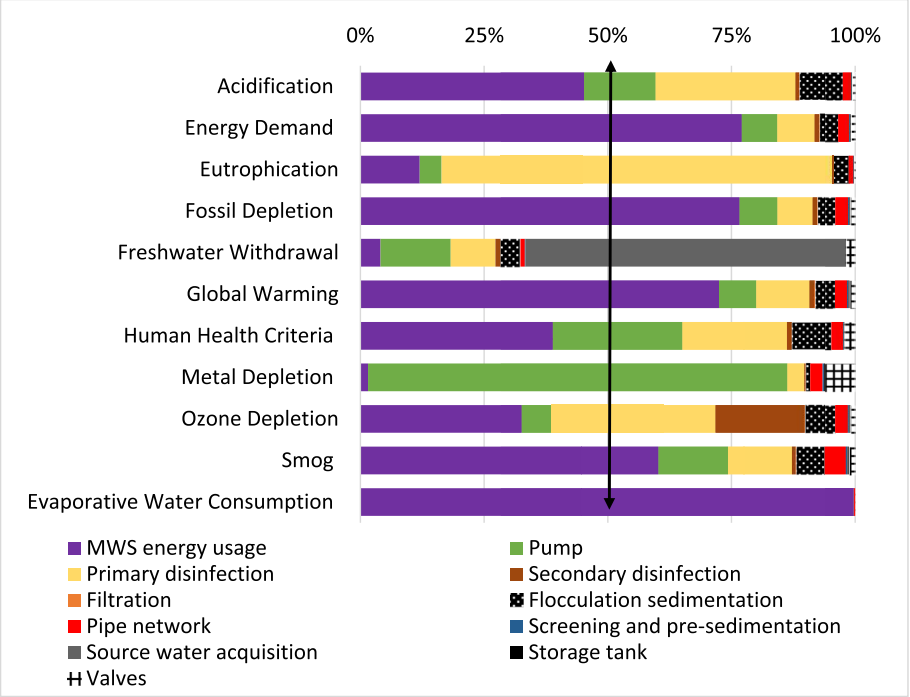

Fig. 5. Percentage comparison of life cycle impacts showing the performance of municipal water supply (MWS) system components. Note: MWS energy usage includes electricity required to pump in source water, energy throughout the water treatment plants, and pumping energy for transporting treated water (vertical arrow indicates the threshold 50%).

Withdrawal fell under Moderate slope because of storage tank. LCIA scores, normalized with respect to maximum scores of the storage tank, showed that fiberglass material dominated nine impact categories, while polyethylene (PE) tank dominated Energy Demand and Fossil Depletion (see SM 4). The fiberglass storage tank material was deemed appropriate for underground placement as designed by Rainwater Management Solutions. In practice, tank material is selected to meet system requirements and impact focus. Linear slopes were also observed in commercial RWH storage tank volume, water demand, water loss, and auxiliary commercial RWH system sensitivity analyses (SM 4). Additional sensitivity analysis results of storage tank materials and volume, water demand, water loss, system service life and auxiliary commercial RWH system, as well as a closer look at the LCIA release contributing processes of commercial RWH storage tank, pumping energy and pump, are provided in SM 3–4.

3.3. The LCIA tradeoffs of the systems

Energy usage or energy intensity sensitivity analysis revealed conditional LCIA tradeoffs of commercial RWH and MWS systems to energy requirements (Fig. 7a–k). Using regression equations (Fig. 7, Table 3), LCIA tradeoffs can be predicted for the two systems when energy intensity is known.

For Ozone Depletion, commercial RWH outperformed MWS if commercial RWH pumping energy intensity (E_c) was less than MWS energy intensity (E_m), $E_c + 0.86 \leq E_m$. For example, for $E_c = 0.19$ kWh/m^3 and $E_m = 1.05$ kWh/m^3, Ozone Depletion scores of commercial RWH and MWS systems were estimated at 4.1×10^{-8} kgCFC11 eq/m^3 and 4.2×10^{-8} kgCFC11 eq/m^3. Commercial RWH outperformed in Metal Depletion and Freshwater Withdrawal impacts, regardless of energy intensities analyzed. In Human Health Criteria and Eutrophication impacts, commercial RWH outperformed MWS, depending on energy intensities, if $E_c \leq E_m$. Commercial RWH outperformed in all other impact categories such as Energy Demand, if $E_c + 0.09 \leq E_m$. Mean Absolute Percentage Error (MAPE) of predicting LCIA impact scores using commercial RWH Tradeoff equations ranged from 0.26% (Evaporative Water Consumption) to 1.20% (Ozone Depletion) (Table 3; also see SM 4 for additional details on MAPE). In the case of MWS Tradeoff equations, MAPE ranged from 0.12% (Smog) to 2.40% (Metal Depletion). MAPE was selected as an appropriate, transparent statistic for comparing fit of the equations instead of another statistic such as coefficient of determination (R^2), thus avoiding any potential model exaggeration as reported by Birnbaum (1973).

Auxiliary commercial RWH system sensitivity analysis provided additional insights into LCIA tradeoffs. The impacts of the auxiliary system increased linearly with the percentage increase of MWS, as explained by Equation (1), except for Ozone Depletion with the reverse relationship due to the greater Ozone Depletion impact of benchmark commercial RWH system than MWS. An auxiliary commercial RWH system with 50% MWS reduced Ozone Depletion by 19%, but with an increase in all other impacts ranging from 10% Smog, 11% Energy Demand, 35% Evaporative Water Consumption, to 197% Eutrophication with respect to the benchmark commercial RWH system (Table 4). All increases were below benchmark MWS system impacts though, by as much as 8% Smog to 40% Eutrophication.

The benchmark commercial RWH storage tank volume of 76 m^3 (20,000 gallons) was estimated using a traditional behavioral and mass balance model, a spreadsheet-based, time series modeling approach (RMS, 2009). Two tank materials were evaluated by LCIA score, PE versus fiberglass, utilizing BEES and Ecoinvent data sources. Storage tank material and volume depends on the system requirement, annual precipitation and impact focus. In addition, infrastructure characteristics such as pump efficiencies, number of stories in a building and system head, as well as geographic characteristics such as location and water demand, water sources, treatment processes and storage options influence pumping energy intensities. Variations with sensitivity analyses of commercial RWH

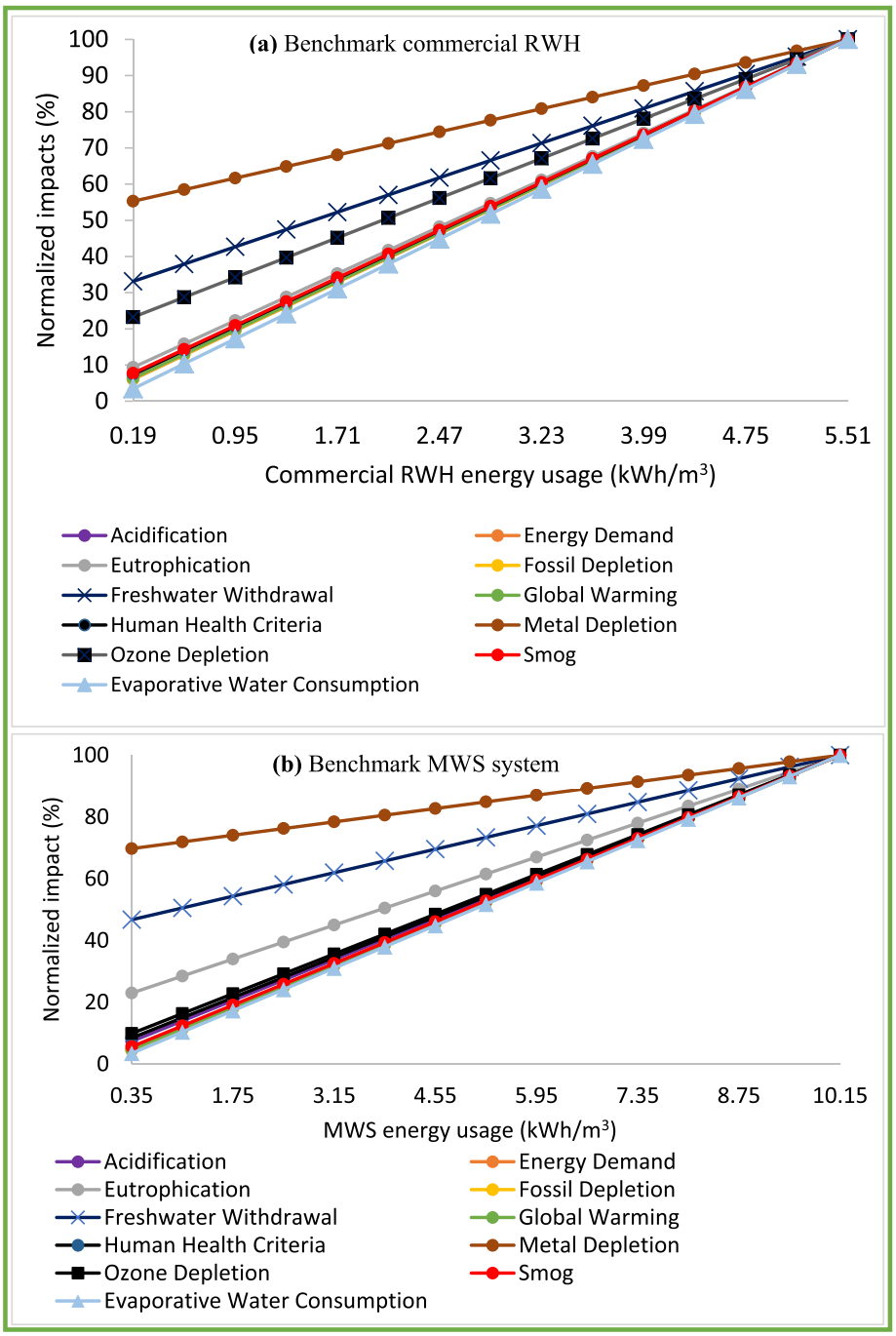

Fig. 6. Sensitivity analysis of energy usage to life cycle impacts of (a) benchmark commercial rainwater harvesting (RWH) system and (b) benchmark municipal water supply (MWS) system.

energy intensities (0.19 kWh/m^3 to a hypothetical value of 5.51 kWh/m^3) and MWS energy intensities (0.35 kWh/m^3 to a hypothetical value of 10.15 kWh/m^3) were addressed by capturing theoretical and empirical commercial RWH pumping energy (0.20 kWh/m^3 to 4.9 kWh/m^3) (Retamal et al., 2009; Vieira et al., 2014) and average national MWS pumping energy estimates (0.396 kWh/m^3 to high intensity water source desalination of 3.17 kWh/m^3) (Pabi et al., 2013; Wang and Zimmerman, 2015). Although alternative disinfection options were not the focus of current study, it is important to note that primary and secondary disinfection dominated Eutrophication and Ozone Depletion impacts of the MWS system. Therefore, appropriate information on disinfection technology is important in comparing impacts with a commercial RWH system.

The benchmark MWS system used chlorination similar to a majority of U.S. water systems—eighty-five percent of the water treatment plants in the U.S. were using chlorine by 1941, and today all drinking water filtration in the U.S. is accompanied by chlorination or other disinfection technologies such as ozonation and UV light (Sedlak, 2014).

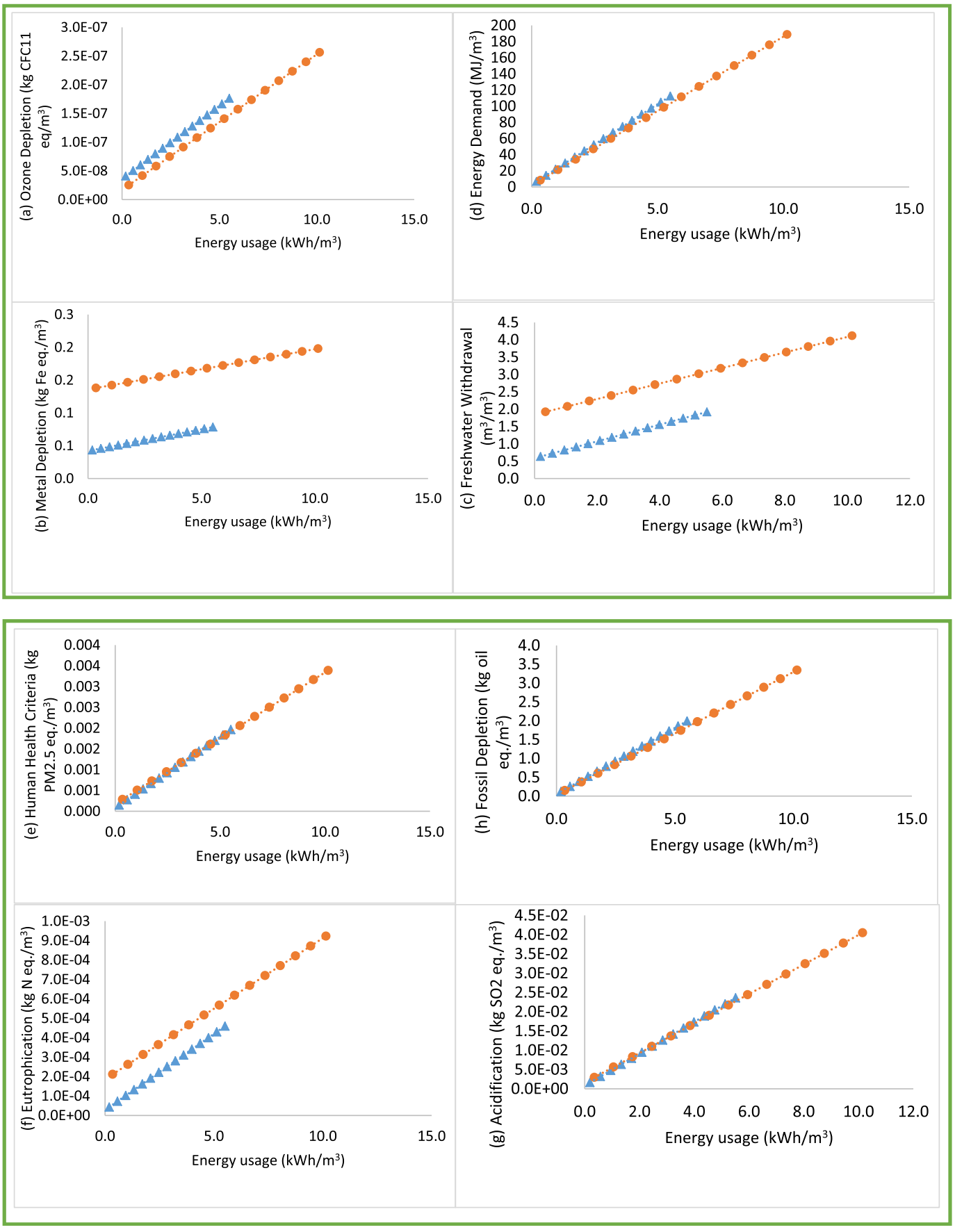

Fig. 7. LCIA tradeoff analysis for a range of energy intensities in commercial rainwater harvesting (RWH) and municipal water supply (MWS) systems: (a) Ozone Depletion, (b) Metal Depletion, (c) Freshwater Withdrawal, and (d) Energy Demand categories. Legend: Triangles = commercial RWH system and Circles = MWS system, (e) Human Health Criteria, (f) Eutrophication, (g) Acidification, and (h) Fossil Depletion. Legend: Triangles = commercial RWH system and Circles = MWS system, (i) Global warming, (j) Evaporative water consumption and (k) Smog.

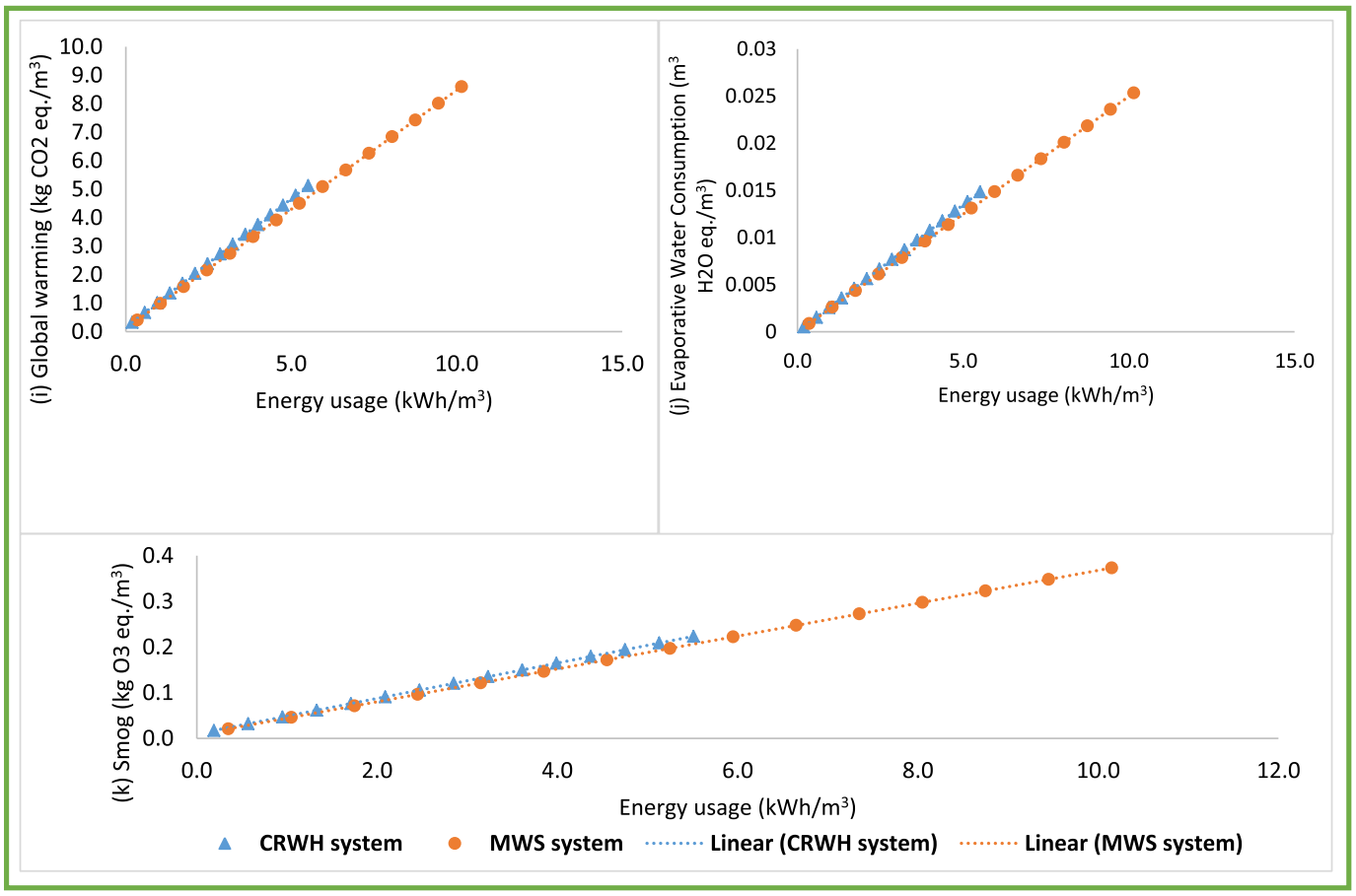

Fig. 7. (*continued*).

4. Summary and study implications

In addition to assessing the comprehensive life cycle environmental and human health impacts of a commercial RWH system compared to a MWS system, we addressed sensitivity of LCIA impact scores to storage tank material and volume, energy usage, water demand, water loss, system service life and an auxiliary commercial RWH system augmented with MWS. The LCA system boundary spans cradle-to-grave, excluding distribution of both systems' components from final manufacture to point of use and disposal phases.

Our analyses revealed that the benchmark commercial RWH performed better or equivalent (45–55%) to MWS in all impact categories except Ozone Depletion. Sensitivity analyses of energy usage, water demand, water loss, and storage tank volume confirmed linearity trends in LCIA scores. Additional sensitivity analyses showed that storage tank with fiberglass material dominated in nine of the 11 impact categories, except in Energy Demand and Fossil Depletion. Annual LCIA impacts for the commercial RWH system with longer service life (75 y) were lower than that of the system with shorter service life (50 y). An auxiliary commercial RWH system augmented with 50% MWS reduced Ozone Depletion impact by 19% showing increases in all other impacts. The LCIA tradeoff equations with respect to energy usage revealed conditional LCIA tradeoffs with energy requirements.

This study informs RWH planning and decision making through a comprehensive LCA of a commercial RWH system, with standards and regulations at the state and local level (USEPA, 2013a). LCA models are transferrable to other commercial RWH installations and study implications are summarized:

- A suite of 11 LCIA impact categories, as well as sensitivity analyses, provided insights into LCIA impact tradeoffs. The importance of LCIA impact categories and dominant components, especially material selection and energy usage, should be considered.
- Commercial RWH fiberglass storage tank material dominated (>50%) in Ozone Depletion and Freshwater Withdrawal impact categories. Selecting PE instead of fiberglass to reduce Ozone Depletion impact may be an option, although a PE tank may not be as appropriate for underground placement because it also necessitates greater Energy Demand and Fossil Depletion than fiberglass. Sensitivity of the data source was evaluated by performing an example LCIA of commercial RWH storage tank materials, fiberglass and PE with Ecoinvent (2012) and the BEES database (NIST, 2013). A data quality assessment of LCI by defining representativeness (including temporal, geographic, technological aspects, and completeness of data) would provide insight into variation in data (ISO, 2006b; USEPA, 2016b); however, it was beyond the scope of this study.
- Commercial RWH pumping energy usage was the most dominant component; therefore, eliminating or reducing pumping energy is key to reducing commercial RWH impacts. An alternate energy mix (e.g., solar) can minimize impacts of a dominant release contributor.
- Regression equations are useful for estimating impact tradeoffs of alternatives. Benchmark MWS treatment practices were consistent with typical U.S. surface water treatment, thus

Table 3
Life Cycle Impact Assessment (LCIA) tradeoff equations with respect to energy intensities (X, kWh/m^3). X_c and X_m are commercial rainwater harvesting (RWH) and municipal water supply (MWS) system energy intensities; Y = LCIA impact score; MAPE = Mean Absolute Percentage Error.

LCIA impact category	Tradeoff condition	Commercial RWH LCIA tradeoff equation	MAPE (%) (commercial RWH equation)	MWS LCIA tradeoff equation	MAPE (%) (MWS equation)
Acidification	$X_c + 0.05 \leq X_m$	$Y = 4.1 \times 10^{-3} X + 8.4 \times 10^{-4}$	0.60	$Y = 3.8 \times 10^{-3} X + 1.6 \times 10^{-3}$	0.82
Energy Demand	$X_c + 0.09 \leq X_m$	$Y = 2.0 \times 10^{1} X + 3.0 \times 10^{0}$	0.52	$Y = 1.8 \times 10^{1} X + 1.9 \times 10^{0}$	2.20
Eutrophication	$X_c \leq X_m$	$Y = 7.8 \times 10^{-5} X + 2.8 \times 10^{-5}$	0.35	$Y = 7.3 \times 10^{-5} X + 1.9 \times 10^{-4}$	1.10
Fossil Depletion	$X_c + 0.07 \leq X_m$	$Y = 3.5 \times 10^{-1} X + 5.6 \times 10^{-2}$	0.45	$Y = 3.3 \times 10^{-1} X + 3.5 \times 10^{-2}$	1.22
Freshwater Withdrawal	Regardless of X	$Y = 2.4 \times 10^{-1} X + 5.9 \times 10^{-1}$	0.32	$Y = 2.2 \times 10^{-1} X + 1.8 \times 10^{0}$	2.15
Global Warming	$X_c + 0.05 \leq X_m$	$Y = 9.0 \times 10^{-1} X + 1.5 \times 10^{-1}$	0.48	$Y = 8.4 \times 10^{-1} X + 1.1 \times 10^{-1}$	0.38
Human Health Criteria	$X_c \leq X_m$	$Y = 3.4 \times 10^{-4} X + 8.2 \times 10^{-5}$	0.38	$Y = 3.2 \times 10^{-4} X + 1.7 \times 10^{-4}$	0.66
Metal Depletion	Regardless of X	$Y = 6.6 \times 10^{-3} X + 4.2 \times 10^{-2}$	0.15	$Y = 6.1 \times 10^{-3} X + 1.4 \times 10^{-1}$	2.40
Ozone Depletion	$X_c + 0.86 \leq X_m$	$Y = 2.5 \times 10^{-8} X + 3.6 \times 10^{-8}$	1.20	$Y = 2.4 \times 10^{-8} X + 1.7 \times 10^{-8}$	1.38
Smog	$X_c + 0.05 \leq X_m$	$Y = 3.9 \times 10^{-2} X + 1.0 \times 10^{-2}$	0.52	$Y = 3.6 \times 10^{-2} X + 8.3 \times 10^{-3}$	0.12
Evaporative Water Consumption	$X_c + 0.05 \leq X_m$	$Y = 2.7 \times 10^{-3} X + 4.3 \times 10^{-6}$	0.26	$Y = 2.5 \times 10^{-3} X + 2.6 \times 10^{-6}$	0.13

applicable to other MWS systems that use surface water such as New York City (York, 2016), Austin (Water, 2010), and Seattle (2016). Accurate information on water treatment and energy use is imperative, and caution must be exercised when estimating the impacts of an energy-efficient MWS system because these systems require significantly less energy than energy-intensive ones (e.g., water source desalination and water transportation).

- LCIA tradeoffs exist due to variations in system requirements such as energy intensities and tank size for different rainfall and water demands. While component performance findings can help to improve the design of a specific component, slopes and tradeoff results focus on target impacts of a commercial RWH system.
- Appropriate storage tank volume, water demand, and energy intensity may be determined by considering a threshold point to minimize commercial RWH impacts using slope zone curves. For example, a hypothetical threshold at 50% water demand may be as efficient, with a relatively small variation in slope beyond the threshold. A dramatic increase in impacts was found below 50% of water demand due to input flow inefficiency.
- A threshold can also be devised for an auxiliary commercial RWH system operation. A 50% auxiliary commercial RWH system outperformed MWS in all LCIA categories except Ozone Depletion. Different thresholds determined from the regression equations can be set for different energy intensities.
- Regulatory requirements on water quality, water withdrawal and plumbing codes can also influence impacts due to component size, material, and treatment standards and should be considered when designing a commercial RWH system. When implemented at the watershed-scale, the potential impacts of commercial RWH on freshwater balance, water quality, runoff and sewer overflow, groundwater level (and economic viability) need further attention. Human health (cancer) and ecotoxicity impacts in addition to the cradle-to-cradle analysis are additional research needs.

Table 4
Life Cycle Impact Assessment (LCIA) tradeoff scores of auxiliary commercial rainwater harvesting (RWH) system, augmented with municipal water supply (MWS) from 10% to 90%. I_c and I_m refer to the LCIA impact score per cubic meter water supply of benchmark commercial RWH and MWS systems; % differences are reported for a 50% auxiliary commercial RWH system with respect to I_c given by: $[(I_c$ —Impact value @ 0.5)$/I_c]$ x 100.

Impact category	Unit	Benchmark LCIA values		MWS fraction and LCIA scores of the auxiliary commercial RWH system									% Difference @ 50% MWS
		MWS (I_m)	Commercial RWH (I_c)	0.1	0.2	0.3	0.4	0.5	0.6	0.7	0.8	0.9	
Acidification	kg SO2 eq	3.0E-03	1.6E-03	1.8E-03	1.9E-03	2.0E-03	2.2E-03	2.3E-03	2.4E-03	2.6E-03	2.7E-03	2.8E-03	−41
Energy Demand	MJ	8.4E+00	6.8E+00	7.0E+00	7.1E+00	7.3E+00	7.4E+00	7.6E+00	7.7E+00	7.9E+00	8.1E+00	8.2E+00	−11
Eutrophication	kg N eq	2.1E-04	4.3E-05	6.0E-05	7.7E-05	9.4E-05	1.1E-04	1.3E-04	1.4E-04	1.6E-04	1.8E-04	2.0E-04	−197
Fossil Depletion	kg oil eq	1.5E-01	1.2E-01	1.3E-01	1.3E-01	1.3E-01	1.3E-01	1.4E-01	1.4E-01	1.4E-01	1.4E-01	1.5E-01	−11
Freshwater Withdrawal	m^3	1.9E+00	6.4E-01	7.6E-01	8.9E-01	1.0E+00	1.2E+00	1.3E+00	1.4E+00	1.5E+00	1.7E+00	1.8E+00	−101
Global Warming	kg CO2 eq	4.0E-01	3.3E-01	3.3E-01	3.4E-01	3.5E-01	3.6E-01	3.6E-01	3.7E-01	3.8E-01	3.9E-01	4.0E-01	−12
Human Health Criteria	kg PM2.5 eq	2.9E-04	1.5E-04	1.6E-04	1.7E-04	1.9E-04	2.0E-04	2.2E-04	2.3E-04	2.4E-04	2.6E-04	2.7E-04	−47
Metal Depletion	kg Fe eq	1.4E-01	4.3E-02	5.3E-02	6.2E-02	7.2E-02	8.1E-02	9.1E-02	1.0E-01	1.1E-01	1.2E-01	1.3E-01	−109
Ozone Depletion	kg CFC11 eq	2.5E-08	4.1E-08	3.9E-08	3.8E-08	3.6E-08	3.5E-08	3.3E-08	3.2E-08	3.0E-08	2.8E-08	2.7E-08	19
Smog	kg O3 eq	2.1E-02	1.7E-02	1.8E-02	1.8E-02	1.8E-02	1.9E-02	1.9E-02	1.9E-02	2.0E-02	2.0E-02	2.1E-02	−10
Evaporative Water Consumption	m^3 H2O eq	8.8E-04	5.2E-04	5.5E-04	5.9E-04	6.2E-04	6.6E-04	7.0E-04	7.3E-04	7.7E-04	8.0E-04	8.4E-04	−35

Acknowledgements

This research was supported in part by an appointment to the Postdoctoral Research Program at the U.S. Environmental Protection Agency (EPA), Office of Research and Development, Athens, GA, USA, administered by the Oak Ridge Institute for Science and Education through Interagency Agreement Number DW8992298301 between the U.S. Department of Energy and the U.S. Environmental Protection Agency. Although this document has been reviewed in accordance with EPA policy and approved for publication, it may not necessarily reflect official Agency policy. Mention of trade names or commercial products does not constitute endorsement or recommendation for use. The preliminary findings of this study were presented at the American Rainwater Catchment Systems Association 2015 Conference, Long Beach, California, and at the American Center for Life Cycle Assessment LCA XVI Conference 2016, Charleston, South Carolina. The authors thank Fran Rauschenberg (Senior Environmental Employee) and Scott R. Unger (EPA) for technical editing and review, and two anonymous reviewers for their constructive comments that improved the manuscript. The authors also thank Heather Kinkade and James Derstler (American Rainwater Catchment Systems Association) for their support and contribution in data collection. Sarah Sojka's contributions include design and sizing of the commercial RWH system, research on the MWS system, product information, and manuscript review. Sarah was not involved in the calculation of life cycle impacts or assignment of the range of values for pumping energy. Sarah is a former employee of Rainwater Management Solutions and remains affiliated with the company through her husband (a partner in the company) and a cooperative grant for commercialization research.

Appendix A. Supplementary data

Supplementary data related to this article can be found at http://dx.doi.org/10.1016/j.jclepro.2017.02.025.

References

Anand, C., Apul, D.S., 2011. Economic and environmental analysis of standard, high efficiency, rainwater flushed, and composting toilets. J. Environ. Manag. 92, 419–428.
Angrill, S., Farreny, R., Gasol, C.M., Gabarrell, X., Vinolas, B., Josa, A., Rieradevall, J., 2012. Environmental analysis of rainwater harvesting infrastructures in diffuse and compact urban models of Mediterranean climate. Int. J. Life Cycle Assess. 17, 25–42.
ARCSA, 2016. Laws, Rules & Codes. www.arcsa.org/?page=273 (April 12, 2016).
Ault, T.R., Mankin, J.S., Cook, B.I., Smerdon, J.E., 2016. Relative impacts of mitigation, temperature, and precipitation on 21st-century megadrought risk in the American Southwest. Sci. Adv. 2.
AWE, 2016. Office Building Introduction. www.allianceforwaterefficiency.org/office_buildings.aspx (April 13, 2016).
Birnbaum, M.H., 1973. The devil rides again: correlation as an index of fit. Psychol. Bull. 79, 239.
Cashman, S., Gaglione, A., Mosley, J., Weiss, L., Hawkins, T.R., Ashbolt, N.J., Cashdollar, J., Xue, X., Ma, C., Arden, S., 2014. Environmental and Cost Life Cycle Assessment of Disinfection Options for Municipal Drinking Water Treatment. U.S. Environmental Protection Agency, Cincinnati, OH USA.
Crettaz, P., Jolliet, O., Cuanillon, J.M., Orlando, S., 1999. Life cycle assessment of drinking water and rain water for toilets flushing. J. Water Serv. Res. Technol.-Aqua 48, 73–83.
DCWSA, 2008. Independent Engineering Inspection of the District of Columbia Water and Sewer Authority's Wastewater and Water Systems (District of Columbia Water and Sewer Authority Washington DC).
DCWSA, 2015. About Drinking Water Quality in Washington, DC. www.dcwater.com/drinking_water/about.cfm (September 3, 2015).
Devkota, J., Schlachter, H., Apul, D., 2015. Life cycle based evaluation of harvested rainwater use in toilets and for irrigation. J. Clean. Prod. 95, 311–321.
Domenech, L., Han, H.J., Sauri, D., 2012. Rainwater harvesting for human consumption and livelihood improvement in rural Nepal: benefits and risks. Water Environ. J. 26, 465–472.
Domenech, L., Sauri, D., 2011. A comparative appraisal of the use of rainwater harvesting in single and multi-family buildings of the Metropolitan Area of Barcelona (Spain): social experience, drinking water savings and economic costs. J. Clean. Prod. 19, 598–608.
Ecoinvent, 2012. Ecoinvent Centre. www.ecoinvent.org (July 2, 2012).
EIA, 2016. 2012 CBECS Survey Data. www.eia.gov/consumption/commercial/data/2012/#b2 (January 22, 2014).
Ghimire, S.R., Johnston, J.M., 2013. Impacts of domestic and agricultural rainwater harvesting systems on watershed hydrology: a case study in the Albemarle-Pamlico river basins (USA). Ecohydrol. Hydrobiol. 13, 159–171.
Ghimire, S.R., Johnston, J.M., 2015. Traditional knowledge of rainwater harvesting compared to five modern case studies. In: Karvazy, K., Webster, V. (Eds.), World Environmental and Water Resources Congress 2015. American Society of Civil Engineers, USA, pp. 182–193.
Ghimire, S.R., Johnston, J.M., Ingwersen, W.W., Hawkins, T.R., 2014. Life cycle assessment of domestic and agricultural rainwater harvesting systems. Environ. Sci. Technol. 48, 4069–4077.
Ghimire, S.R., Watkins Jr., D.W., Li, K., 2012. Life cycle cost assessment of a rain water harvesting system for toilet flushing. Water Sci. Technol. Water Supply 12, 309–320.
Ghisi, E., Tavares, D.D., Rocha, V.L., 2009. Rainwater harvesting in petrol stations in Brasilia: potential for potable water savings and investment feasibility analysis. Resour. Conservat. Recycl. 54, 79–85.
Goedkoop, M.H., Huijbregts, M., Schryver, A., Struijs, J., Zelm, R., 2012. ReCiPe 2008-A Life Cycle Impact Assessment Method Which Comprises Harmonised Category Indicators at the Midpoint and the Endpoint Level. Ministry of Housing, Spatial Planning and Environment, Netherlands.
Gurung, T.R., Sharma, A., 2014. Communal rainwater tank systems design and economies of scale. J. Clean. Prod. 67, 26–36.
Harvesth2o, 2016. Regulations & Statutes. www.harvesth2o.com/statues_regulations.shtml (April 11, 2016).
Hischier, R.A.H.-J.B., Büsser, S., Doka, G., Frischknecht, R., Kleijer, A., Leuenberger, M., Nemecek, T., Simons, A., 2010. Documentation of Changes Implemented in Ecoinvent Data v2.2 Swiss Centre for LCI (Switzerland).
Hunt, R.G., Franklin, W.E., Hunt, R.G., 1996. LCA — How it came about. Int. J. Life Cycle Assess. 1, 4–7.
Ingwersen, W., Gausman, M., Weisbrod, A., Sengupta, D., Lee, S.-J., Bare, J., Zanoli, E., Bhander, G.S., Ceja, M., 2016. Detailed life cycle assessment of Bounty® paper towel operations in the United States. J. Clean. Prod. 131, 509–522.
ISO, 2006a. Environmental Management — Life Cycle Assessment — Principles and Framework, ISO 14040. International Organization for Standardization, Switzerland.
ISO, 2006b. Environmental Management — Life Cycle Assessment — Requirements and Guidelines, ISO 14044. International Organization for Standardization, Switzerland.
Lye, D.J., 2002. Health risks associated with consumption of untreated water from household roof catchment systems. JAWRA J. Am. Water Resour. Assoc. 38, 1301–1306.
Mays, L., Antoniou, G., Angelakis, A., 2013. History of water cisterns: legacies and lessons. Water-Sui. 5, 1916–1940.
Meyer, D.E., Upadhyayula, V.K., 2013. The use of life cycle tools to support decision making for sustainable nanotechnologies. Clean. Technol. Environ. Policy 1–16.
Morales-Pinzón, T., Rieradevall, J., Gasol, C.M., Gabarrell, X., 2015. Modelling for economic cost and environmental analysis of rainwater harvesting systems. J. Clean. Prod. 87, 613–626.
NCSL, 2016. State Rainwater Harvesting Laws and Programs. www.ncsl.org/research/environment-and-natural-resources/rainwater-harvesting.aspx (April 11, 2016).
NIST, 2013. Building for Environmental and Economic Sustainability (BEES). www.nist.gov/el/economics/BEESSoftware.cfm (February 15, 2013).
NREL, 2013. U.S. Life Cycle Inventory Database. National Renewable Energy Laboratory (NREL). www.lcacommons.gov/nrel/search (September 30, 2013).
OpenLCA, 2016. openLCA 1.4.2. http://www.openlca.org/ (January 20, 2012).
Pabi, S., Amarnath, A., Goldstein, R., Reekie, L., 2013. Electricity Use and Management in the Municipal Water Supply and Wastewater Industries.
Pandey, D.N., Gupta, A.K., Anderson, D.M., 2003. Rainwater harvesting as an adaptation to climate change. Curr. Sci. 85, 46–59.
Retamal, M., Glassmire, J., Abeysuriya, K., Turner, A., White, S., 2009. The Water-energy Nexus: Investigation into the Energy Implications of Household Rainwater Systems. Institute for Sustainable Futures, University of Technology, Sydney.
RMS, 2009. Tank Sizing Spreadsheet. Rainwater Management Solutions (Salem, VA).
Roebuck, R.M., Oltean-Dumbrava, C., Tait, S., 2011. Whole life cost performance of domestic rainwater harvesting systems in the United Kingdom. Water Environ. J. 25, 355–365.
Sample, D.J., Liu, J., 2014. Optimizing rainwater harvesting systems for the dual purposes of water supply and runoff capture. J. Clean. Prod. 75, 174–194.
Schewe, J., Heinke, J., Gerten, D., Haddeland, I., Arnell, N.W., Clark, D.B., Dankers, R., Eisner, S., Fekete, B.M., Colón-González, F.J., 2014. Multimodel assessment of water scarcity under climate change. Proc. Natl. Acad. Sci. 111, 3245–3250.
Seattle, C.o., 2016. Water System Overview. www.seattle.gov/Util/MyServices/Water/AbouttheWaterSystem/WaterSystemOverview/index.htm (March 23, 2016).
Sedlak, D., 2014. Water 4.0: the Past, Present, and Future of the World's Most Vital Resource. Yale University Press, U.S.A.
Siems, R., Sahin, O., 2016. Energy intensity of residential rainwater tank systems: exploring the economic and environmental impacts. J. Clean. Prod. 113,

251–262.
Sojka, S., Younos, T., Crawford, D., 2016. Modern urban rainwater harvesting systems: design, case studies, and impacts. In: Younos, T., Parece, E.T. (Eds.), Sustainable Water Management in Urban Environments. Springer International Publishing, Cham, Switzerland, pp. 209–234.
Thomas, R.B., Kirisits, M.J., Lye, D.J., Kinney, K.A., 2014. Rainwater harvesting in the United States: a survey of common system practices. J. Clean. Prod. 75, 166–173.
USACE, 2016. Washington Aqueduct. www.nab.usace.army.mil/Missions/WashingtonAqueduct.aspx (April 13, 2016).
USEPA, 2013a. Rainwater Harvesting Conservation, Credit, Codes, and Cost Literature Review and Case Studies. Office of Water. U.S. Environmental Protection Agency, Washington, DC.
USEPA, 2013b. Tool for the Reduction and Assessment of Chemical and Other Environmental Impacts (TRACI). www.epa.gov/nrmrl/std/traci/traci.html (July 2, 2013).
USEPA, 2016a. Adapting to Climate Change Southeast. https://www.epa.gov/arc-x (October 17, 2016).
USEPA, 2016b. Guidance on Data Quality Assessment for Life Cycle Inventory Data. U.S. Environmental Protection Agency, Ohio, USA.
USGCRP, 2012. Regional Climate Impacts: Southeast, U.S. Global Change Research Program. www.globalchange.gov/publications/reports/scientific-assessments/us-impacts/regional-climate-change-impacts/southeast (January 19, 2012).
Vieira, A.S., Beal, C.D., Ghisi, E., Stewart, R.A., 2014. Energy intensity of rainwater harvesting systems: a review. Renew. Sustain. Energy Rev. 34, 225–242.
Wang, R., Zimmerman, J.B., 2015. Economic and environmental assessment of office building rainwater harvesting systems in various U.S. cities. Environ. Sci. Technol. 49, 1768–1778.
Ward, S., Memon, F.A., Butler, D., 2012. Performance of a large building rainwater harvesting system. Water Res. 46, 5127–5134.
Water, A., 2010. City of Austin Municipal Water Supply Overview (City of Austin, Texas, USA).
WFN, 2009. Water Footprint Manual Enschede. The Netherlands Water Footprint Network, The Netherlands.
York, T.C.o.N., 2016. History of New York City's Water Supply System. www.nyc.gov/html/dep/html/drinking_water/history.shtml (March 23, 2016).

Journal of Cleaner Production 151 (2017) 74–86

Contents lists available at ScienceDirect

Journal of Cleaner Production

journal homepage: www.elsevier.com/locate/jclepro

Life cycle assessment of a commercial rainwater harvesting system compared with a municipal water supply system

Santosh R. Ghimire [a], John M. Johnston [b, *], Wesley W. Ingwersen [c], Sarah Sojka [d]

[a] ORISE Postdoctoral Research Participant, U.S. Environmental Protection Agency, Office of Research and Development, 960 College Station Rd., Athens, GA 30605, USA
[b] U.S. Environmental Protection Agency, Office of Research and Development, 960 College Station Rd., Athens, GA 30605, USA
[c] U.S. Environmental Protection Agency, Office of Research and Development, 26 W. Martin Luther King Dr., Cincinnati, OH 45268, USA
[d] Randolph College, 2500 Rivermont Ave., Lynchburg, VA 24503, USA

ARTICLE INFO

Article history:
Received 20 December 2016
Received in revised form
3 February 2017
Accepted 3 February 2017
Available online 6 February 2017

Keywords:
Life cycle assessment
Commercial rainwater harvesting
Municipal water supply
Energy intensity

ABSTRACT

Building upon previously published life cycle assessment (LCA) methodologies, we conducted an LCA of a commercial rainwater harvesting (RWH) system and compared it to a municipal water supply (MWS) system adapted to Washington, D.C. Eleven life cycle impact assessment (LCIA) indicators were assessed, with a functional unit of 1 m^3 of rainwater and municipal water delivery system for toilets and urinals in a four-story commercial building with 1000 employees. Our assessment shows that the benchmark commercial RWH system outperforms the MWS system in all categories except Ozone Depletion. Sensitivity and performance analyses revealed pump and pumping energy to be key components for most categories, which further guides LCIA tradeoff analysis with respect to energy intensities. Tradeoff analysis revealed that commercial RWH performed better than MWS in Ozone Depletion if RWH's energy intensity was less than that of MWS by at least 0.86 kWh/m^3 (249% of the benchmark MWS energy usage at 0.35 kWh/m^3). RWH also outperformed MWS in Metal Depletion and Freshwater Withdrawal, regardless of energy intensities, up to 5.51 kWh/m^3. An auxiliary commercial RWH system with 50% MWS reduced Ozone Depletion by 19% but showed an increase in all other impacts, which were still lower than benchmark MWS system impacts. Current models are transferrable to commercial RWH installations at other locations.
Published by Elsevier Ltd. This is an open access article under the CC BY license (http://creativecommons.org/licenses/by/4.0/).

1. Introduction

Approximately 5–20% of the global population is predicted to live under absolute water scarcity (<500 m^3/person/year) up until the point of a 2 °C increase in mean global temperature, and a higher percentage as temperatures rise further (Schewe et al., 2014). The climate change impact and the 21st century's mega-droughts with longer duration may result in unprecedented water scarcity from the southwestern to the southeastern U.S., and to other parts of the world, which is driving the global search for alternate water sources (USGCRP, 2012; Ault et al., 2016; USEPA, 2016a). Rainwater harvesting (RWH) is receiving renewed interest as a green infrastructure practice in the face of necessary adaptation to global climate change (USGCRP, 2012; Ghimire et al., 2014). RWH has been used for drinking water and agricultural irrigation since 11,500 BCE in North America and 4500 BCE in Asia (Pandey et al., 2003; Mays et al., 2013; Ghimire and Johnston, 2015). Other potential benefits of RWH include reduced impacts on the environment and human health, reduced stormwater runoff and combined sewer overflows, and economic viability (Ghimire et al., 2012; Wang and Zimmerman, 2015). In practice the implementation of RWH has remained a challenge. This is due primarily to a lack of understanding of its environmental and human health impacts (criteria pollutants from material selection and energy use) and partly due to the lack of regulations governing RWH practices. Although state regulations and statutes continue to favor RWH (ARCSA, 2016; Harvesth2o, 2016; NCSL, 2016), the U.S. Environmental Protection Agency (EPA) reported “there are currently no federal regulations governing rainwater harvesting for non-potable use, and the policies and regulations enacted at the state and local levels vary widely from one location to another” (USEPA, 2013a).

* Corresponding author.
E-mail addresses: sghimire02@gmail.com (S.R. Ghimire), Johnston.JohnM@epa.gov (J.M. Johnston), Ingwersen.Wesley@epa.gov (W.W. Ingwersen), ssojka@randolphcollege.edu (S. Sojka).

http://dx.doi.org/10.1016/j.jclepro.2017.02.025
0959-6526/Published by Elsevier Ltd. This is an open access article under the CC BY license (http://creativecommons.org/licenses/by/4.0/).

Studies worldwide have explored RWH life cycle cost impacts (Roebuck et al., 2011), water savings potential (Ghisi et al., 2009; Domenech and Sauri, 2011; Ward et al., 2012), water quality and health risks (Lye, 2002; Domenech et al., 2012), optimal designs (Sample and Liu, 2014), energy intensity versus economic and CO_2 emissions (Gurung and Sharma, 2014; Siems and Sahin, 2016), hydrologic impacts (Ghimire and Johnston, 2013), and climate change adaptation (Pandey et al., 2003). Of particular interest is the life cycle environmental and human health criteria air pollutant impacts of RWH. Life cycle assessment (LCA) has been widely used since its inception in the late 1960s in diverse sectors to assess environmental and human health impacts in a cradle-to-grave approach that avoids or minimizes unintended consequences (Hunt et al., 1996; ISO, 2006b, a; Meyer and Upadhyayula, 2013; Ingwersen et al., 2016). Use of LCA to assess RWH systems is also increasing. Previous studies focused on residential small and large building systems that vary by region; however, findings varied by design parameters and data sources, as demonstrated by the following examples. Crettaz et al. (1999) performed an LCA on RWH for clothes washing and toilet flushing in Switzerland and reported RWH as energetically favorable if pumping energy intensity for municipal drinking water was greater than 0.8 kWh/m^3. Angrill et al. (2012) reported life cycle impacts of RWH for laundry use in compact urban densities were generally lower than in diffused settings in Spain. Morales-Pinzón et al. (2015) reported a lower life cycle global warming potential of RWH than tap water for toilet flushing and clothes washing in a single-family house if the average storage tank was smaller than 2 m^3.

In the U.S., interest in RWH is growing due to increased droughts as well as its environmental benefits (Thomas et al., 2014; Sojka et al., 2016). An energy and greenhouse gas (GHG) emission analysis of RWH in a university building in Ohio reported RWH as a viable option with GHG emission payback periods higher than the energy payback periods but contradicted the results of Anand and Apul (2011) due to difference in data sources (process-based versus Economic Input Output life cycle assessment data) (Devkota et al., 2015). Wang and Zimmerman (2015) assessed life cycle climate change, fossil fuel depletion, and eutrophication impacts of RWH for office buildings in 14 large cities across the U.S., from Boston, Massachusetts to Seattle, Washington, and reported that reduced eutrophication and combined sewer flows varied with location.

Ghimire et al. (2014) published an LCA of domestic and agricultural RWH systems that compared conventional water supplies, municipal water supplies and well water irrigation systems in the southeastern U.S. The American Rainwater Catchment Systems Association then contacted the authors about conducting a similar study for a commercial RWH system. Comprehensive understanding of the life cycle implications of commercial RWH systems is only in its infancy but is important for informing urban water management planning and decision making. Consequently, we conducted an LCA of a typical commercial RWH system in an average size commercial building sited in a large U.S. city (EIA, 2016) and combined this with scenario and sensitivity analysis, with the intention of providing more generalizable life cycle implications of commercial RWH systems.

1.1. Objective, scope, and novelty

Our objective is to conduct an LCA of a commercial RWH system and compare it to a municipal water supply (MWS), hereafter called benchmark commercial RWH and MWS systems. Eleven life cycle impact assessment (LCIA) indicators were calculated per functional unit of 1 m^3 of rainwater and municipal water delivery for flushing toilets and urinals in a four-story commercial building with 1000 employees. These included Acidification, Energy Demand, Eutrophication, Fossil Depletion, Freshwater Withdrawal, Global Warming, Human Health Criteria, Metal Depletion, Ozone Depletion, Smog, and Evaporative Water Consumption. LCIA sensitivity was addressed for (i) storage tank materials and volume, (ii) energy usage or energy intensity, (iii) water demand, (iv) water loss, (v) system service life, and (vi) an auxiliary commercial RWH system augmented with MWS. The LCA system boundary spans cradle-to-grave, excluding the distribution of both systems' components from final manufacture to point of use and disposal phases for lack of comparable data (see Supplementary Material or SM 1 for additional details). This study provides a comprehensive LCA of commercial RWH to inform RWH planning and decision making, with standards and regulations at state and local levels governing urban water management decisions (USEPA, 2013a). The life cycle inventory (LCI) and LCA models are generally transferrable in recreating LCA models of other commercial RWH and MWS systems by obtaining appropriate LCI data. The following sections describe methods, tools, databases and assumptions and results, with concluding remarks on potential implications for commercial RWH design and planning.

2. Methods and tools

2.1. Site selection

Washington, D.C. was selected as the study site primarily due to readily available data on the MWS system, precipitation record and commercial RWH design. While the commercial RWH system was designed for local precipitation patterns, the analysis required extensive data on an existing urban MWS system compatible with existing life cycle data for MWS. The EPA conducted a study of the Cincinnati MWS system that uses the Ohio River as a source with chlorine disinfection (Cashman et al., 2014). Data were developed in a modular and reusable fashion to be reconfigured and customized for other regions. Study area selection criteria included a large urban area with similar source water characteristics, treatment processes and distribution architecture to Cincinnati, Ohio, as well as publically available data on the water supply system and sufficient precipitation record. Other U.S. cities considered included Los Angeles, Phoenix, Austin, Chicago and Atlanta. Although water demand for Washington, D.C. (benchmark MWS system) was slightly higher $\approx$ 1.1 times Cincinnati MWS system demand, it has comparable treatment system and distribution pipe network composition (Ductile Iron pipe >90%).

2.2. Definition of the benchmark commercial RWH and MWS systems

The American Rainwater Catchment Systems Association provided the design for a commercial RWH system from one of its member companies to be configured for a typical urban system. This design was customized for flushing 40 toilets and 15 urinals in a four-story commercial building with 1000 people, adapted to Washington, D.C. (Fig. 1 and Table 1, see SM 1 and 2 for additional details).

Key design parameters and assumptions used in the benchmark commercial RWH system analysis were:

- Total water demand for flushing all urinals and toilets for the building was estimated at 2653 m^3/y (2685 gallons/day): high-efficiency urinal demand at 0.47 L per flush (l/f) or 0.125 gallon/flush (g/f), and high-efficiency toilet demand at 4.8 l/f or 1.28 g/f (AWE, 2016);

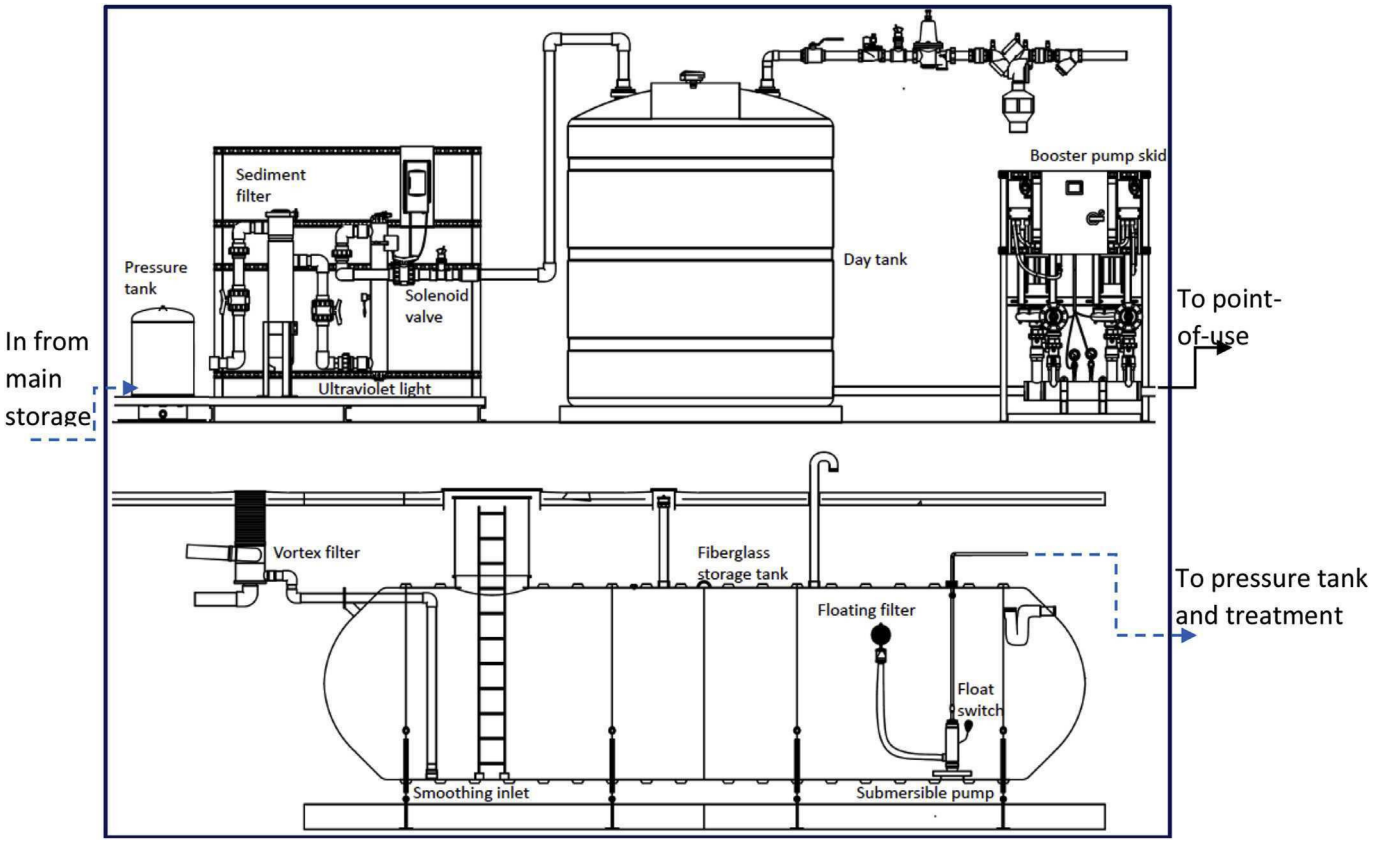

Fig. 1. Schematic of commercial rainwater harvesting system (designed by Rainwater Management Solutions).

- Storage tank volume was designed at 76 m^3 (20,000 gallons), supplying 77% of total volumetric water demand (RMS, 2009) (see SM 1 for additional details);
- The benchmark commercial RWH system met 77% of total toilet and urinal water demand (77% of 2653 m^3/y = 2042.81 m^3/y) and an auxiliary commercial RWH system was operated with support of MWS to meet additional demand;
- Pumping energy intensity was estimated at 0.19 kWh/m^3 (see SM 1 for additional details);
- Water loss throughout the system was 5%;
- Service life of the system was 50 years and components with shorter service lives were replaced at the end of their service lives;
- Distribution of system components from final manufacture to point of use and disposal were excluded from LCA.

The benchmark MWS system was defined using available information from the District of Columbia Water and Sewer Authority (DCWSA, 2015) and Baltimore District, U.S. Army Corps of Engineers (USACE, 2016) (Fig. 2 and SM 2).

The District of Columbia Water and Sewer Authority (DC Water) purchased 100% of drinking water from the Washington Aqueduct operated by the Baltimore District, U.S. Army Corps of Engineers. The Washington Aqueduct collected, purified and pumped drinking water to three jurisdictions, including DC Water, Arlington County, Virginia, and Fairfax County Water Authority, Virginia (USACE, 2016). Washington Aqueduct owned and operated two treatment plants, Dalecarlia and McMillan (source water: Potomac River), an intake pumping facility, and three water storage facilities. Seventy-two percent of total treated water from the two plants (i.e., 72% × 192,052,776 m^3/y) was sold to DC Water in 2012. DC Water consisted of 2092 km (1300 miles) of pipes, eight water storage facilities, four pumping stations, and 36,000 valves. Thus, DC Water (benchmark MWS system) was a combination of District of Columbia Water and Sewer Authority-owned and Washington Aqueduct-owned facilities. Key design parameters and assumptions pertaining to the benchmark MWS system were:

- The two water treatment plants of Washington Aqueduct produced 192,052,776 m^3/y or 139 million gallons of water per day and 72% of the treated water from the Aqueduct sold to DC Water;
- Water loss throughout the system was 24%, based on sold to pumped ratio of 76% in 2008 (DCWSA, 2008);
- Water treatment options were consistent with average U.S. water treatment;
- MWS energy intensity was estimated at 0.35 kWh/m^3 combining two energy uses: Washington Aqueduct energy use (0.20 kWh/m^3) included electricity required to pump source water and energy throughout the water treatment plants and DC Water services pumping energy use (0.15 kWh/m^3) for transporting the treated water (see SM 1 for additional details);
- All infrastructure had service lives of 100 years except the pump with 15-y service life, replaced at the end of its service life;
- Distribution of the system components from final manufacture to point of use and disposal were excluded from LCA.

2.2.1. Functional unit

To facilitate comparison of water supply from two different sources, 1 m^3 of water supply was defined as the functional unit for annual water supply and service lives of system components.

Table 1
Description of the major components of benchmark commercial rainwater harvesting system and life cycle inventory.

Main component	Sub-component	Material (unit)	Amount	Lifetime (y)	LCI data source
Vortex Filter	Housing	polypropylene (kg)	47.7	40	Ecoinvent (2012)
	Lid	aluminum (kg)	3.6	40	Ecoinvent (2012)
	Intermediate ring	stainless steel (kg)	7.3	40	Ecoinvent (2012)
	Filter insert	stainless steel (kg)	4.1	40	Ecoinvent (2012)
Smoothing inlet	Smoothing inlet	stainless steel (kg)	3.2	40	Ecoinvent (2012)
Floating filter	Filter assembly	stainless steel (kg)	0.7	15	Ecoinvent (2012)
	Hose	food grade reinforced plastic hose (kg)	2.3	15	Ecoinvent (2012)
	Floating ball	polyethylene (kg)	0.2	15	Ecoinvent (2012)
Main pump, 1 hp	Main pump	primarily stainless steel (kg)	18.0	15	Ghimire et al. (2014)
Booster pump, 1 hp	A booster pump	primarily stainless steel (kg)	18.0	15	Ghimire et al. (2014)
Level switch	Float switch and cable	polypropylene (Housing) (kg)	0.9	12.5	Ecoinvent (2012)
Pressure tank	Tank	rolled steel (16 gauge), butyl rubber, copolymer polypropylene (kg)	16.4	50	Ecoinvent (2012)
Bag filter	Bag filter	polypropylene (kg)	0.2	15	Ecoinvent (2012)
	Filter housing	polypropylene (kg)	4.6	15	Ecoinvent (2012)
Ultraviolet (UV) light chamber	Housing	316L stainless steel (kg)	14.6	11	Ecoinvent (2012)
	Bulbs	quartz (kg)	0.9	11	Ecoinvent (2012)
	Quartz sleeves	fused silica (kg)	0.5	11	Ecoinvent (2012)
Solenoid Valve	Valve	brass (kg)	0.5	7.5	Ecoinvent (2012)
Day Tank	high-density polyethylene (HDPE)	PE pipe equivalent length 181 m (kg)	43.2	50	NIST (2013)
Ultrasonic level transmitter (sensor)	Housing (LU20 Model)	polypropylene (kg)	0.9	15	Ecoinvent (2012)
Pipe, collection	2 in Polyvinyl chloride (PVC)	water supply 2 in 1 m - PVC cradle-to-gate (m)	61.0	50	NIST (2013)
Pipe, supply	1.5 in chlorinated PVC	HCWD 1.5 in 1 m- CPVC cradle-to-gate (m)	152.0	50	NIST (2013)
Storage Tank	Fiberglass (FG) Storage Tank	glass fibre (kg)	2773.0	50	NIST (2013)
	Two FG Access Riser (36 in diameter, 3 ft tall)	glass fibre (kg)	113.6	50	Ecoinvent (2012)
	Two FG Access Collars (36 in)	glass fibre (kg)	113.6	50	Ecoinvent (2012)
	Two overflow pipe (8 in 2 ft)	water supply 8 in 1 m - PE cradle-to-gate (kg)	2.3	50	NIST (2013)
Energy usage	Pumping energy	electricity, at residential user (kWh/m^3)	0.19	N/A	Cashman et al. (2014)

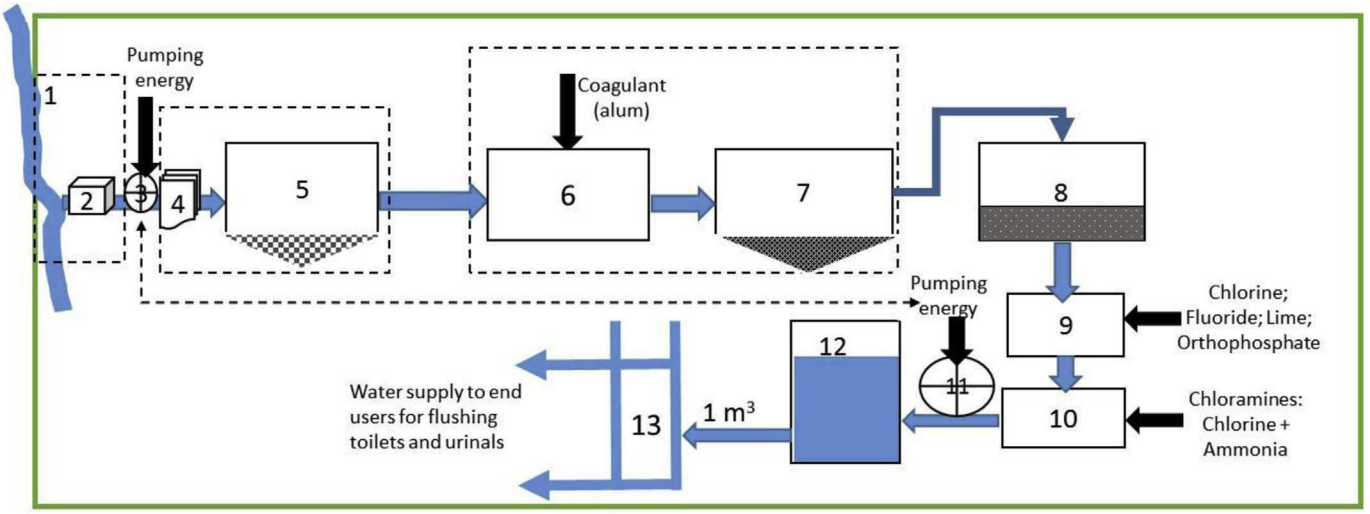

Fig. 2. Washington, D.C. municipal water supply system. Number Key: (1) Source water (Potomac River); (2) Source water acquisition infrastructure; (3) Acquisition pump; (4) Screening infrastructure; (5) Pre-sedimentation (natural settling in a pre-treatment storage); (6) Flocculation; (7) Sedimentation (coagulated particles); (8) Filtration (sand filter); (9) Primary Disinfection (Gaseous Chlorine, Lime addition, Fluorination, Orthophosphate); (10) Secondary Disinfection: Chloramines; (11) Distribution Pump (four); (12) Storage Tanks (eleven); (13) Water pipe network (based on District of Columbia Water and Sewer Authority (DCWSA, 2015) and Baltimore District, U.S. Army Corps of Engineers (USACE, 2016)).

Standardization by 1 m^3 enabled comparison of LCIA scores regardless of volumetric water supply, because material input is linearly related to volumetric water supply. In addition, accounting for service lives of system components addressed the issue of product replacement.

2.3. Development of LCI and LCA models

Primary data collected on commercial RWH included design components (Table 1, also see SM 2). Similarly, primary data were collected on the benchmark MWS system for system components,

Table 2
Sensitivity analysis scenarios.

Commercial RWH system	MWS (Washington D.C. water) system
Storage tank material (Polyethylene and Fiberglass)	–
Commercial RWH energy intensities (0.19–5.51 kWh/m^3)	MWS energy intensities (0.35–10.15 kWh/m^3)
Storage tank volume (from 0.25 to 4.5 × benchmark volume)	–
Commercial RWH demand (10%–100% of benchmark demand)	–
Commercial RWH system water loss (0%–30%)	DC Water system water loss (0%–30%)
System service life (50 years versus 75 years)	System service life (100 years)
Auxiliary commercial RWH system (0%–90% MWS)	–

amount of material and energy use, and water demand from the District of Columbia Water and Sewer Authority (DCWSA, 2015) and Baltimore District, U.S. Army Corps of Engineers (USACE, 2016) (see SM 2 for details on LCI). The LCI of the benchmark systems was compiled using Building for Environmental and Economic Sustainability (BEES) (NIST, 2013), Ecoinvent (2012) version 2.2, U.S. LCI database (NREL, 2013), and Cincinnati drinking water treatment and distribution systems collected from a previous study (Cashman et al., 2014). There are limitations to using the Ecoinvent database, a European LCI, in the U.S. because results would be sensitive to data quality and material type. However, data availability is a major consideration, such that the LCI and LCA utilized data and methods from a domestic RWH study in the southeastern U.S (Ghimire et al., 2014). as well as the LCI of the Cincinnati MWS system (Cashman et al., 2014).

2.4. Life cycle impact assessment (LCIA)

LCIA methods included combining the Tool for the Reduction and Assessment of Chemical and Other Environmental Impacts or, TRACI 2.1 (USEPA, 2013b), with the ReCiPe's Metal Depletion and Fossil Depletion (Goedkoop et al., 2012), Water Footprint's Evaporative Water Consumption and Freshwater Withdrawal (WFN, 2009), and the non-renewable Cumulative Energy Demand of Ecoinvent (Hischier et al., 2010). TRACI 2.1 methods included were Global Warming, Ozone Depletion, Smog, Human Health Criteria (air pollutants), Eutrophication, and Acidification. Human health (cancer) and ecotoxicity indicators were excluded due to lack of high quality life cycle data for release to air and water, consistent with Ingwersen et al. (2016). OpenLCA (2016) version 1.4.2, an open source LCA software (GreenDelta © 2016) was used for all LCIA calculations in conjunction with LCIA methods and LCI databases.

LCIA percentage contributions of the benchmark systems and their components were analyzed. LCIA sensitivity analysis was conducted for various scenarios (Table 2) which further guided LCIA tradeoff analysis with respect to energy intensities and the auxiliary commercial RWH system. Sensitivity and tradeoff LCIA results were normalized for each impact category by maximum LCIA score (see SM 4 for the details on LCIA normalization).

LCIA tradeoff of the auxiliary commercial RWH system, augmented with 10%–90% MWS, was assessed by summing the

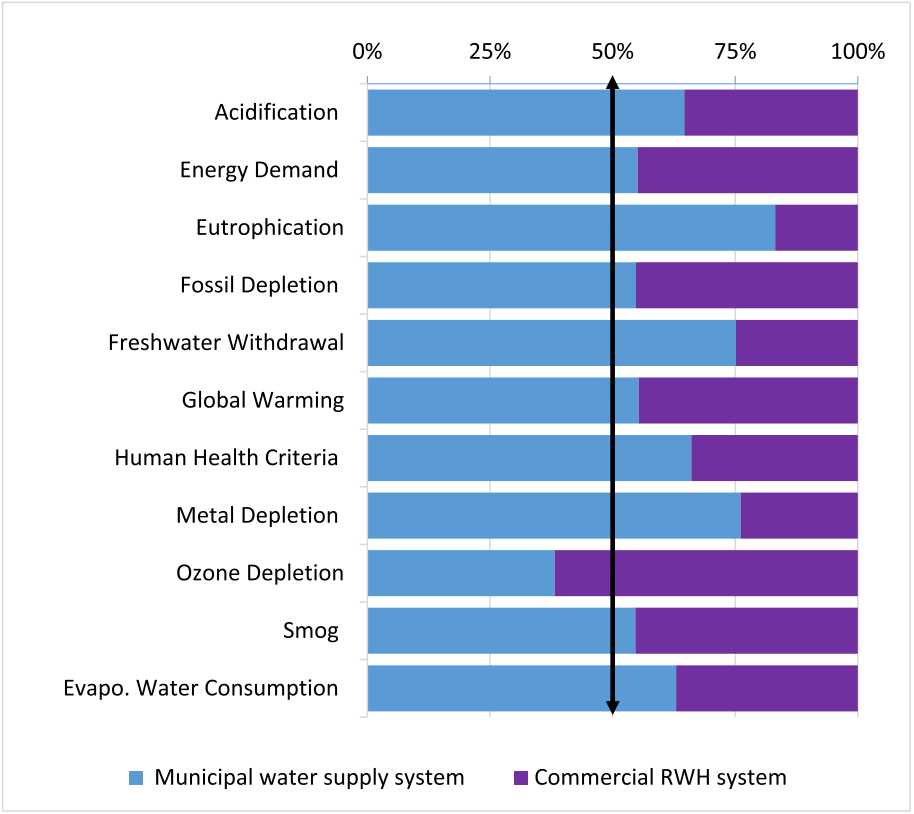

Fig. 3. Comparison of life cycle impacts of the benchmark commercial rainwater harvesting system to the municipal water supply system adapted to Washington, D.C. (vertical arrow indicates the threshold 50%).

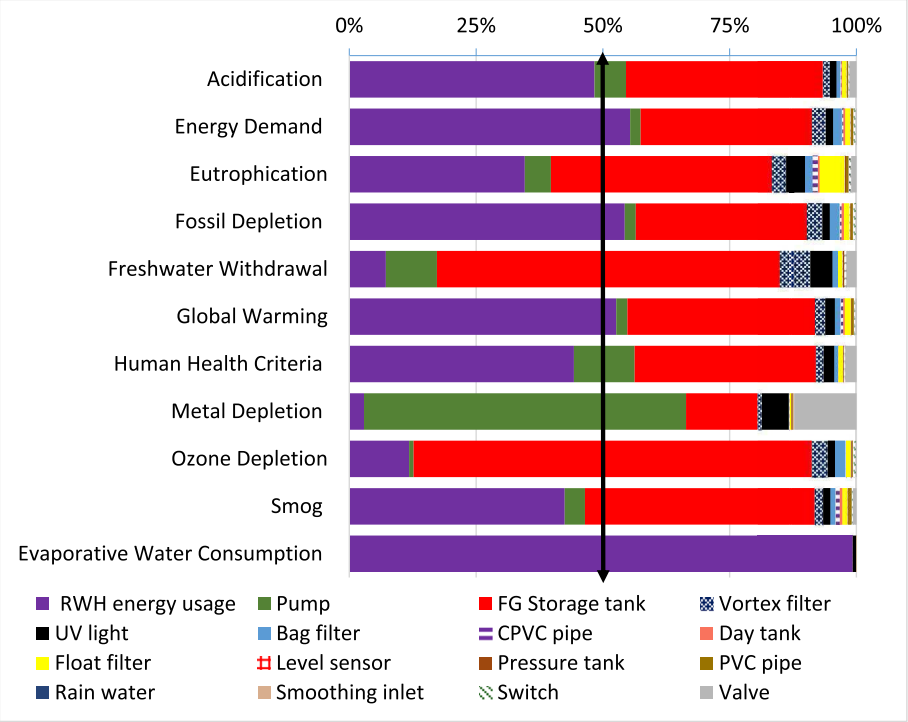

Fig. 4. Percentage comparison of life cycle impacts showing the performance of commercial rainwater harvesting (RWH) system components. Note: RWH energy usage includes pumping energy at the commercial RWH storage tank (vertical arrow indicates the threshold 50%).

fractional impacts of both systems delivering 1 m^3 of water supply (Equation (1)):

$$I_{aux} = p_c \times I_c + p_m \times I_m \quad (1)$$

for each impact categoryI_{aux} = the auxiliary system's impact (impact/m^3 of water supply), $.I_c$ = the benchmark commercial RWH system's impact (impact/m^3 of water supply), $.I_m$ = the benchmark MWS system's impact (impact/m^3 of water supply), $.p_c$ and p_m are commercial RWH and MWS percentage (in decimal) such that

$$p_c + p_m = 1 \quad (2)$$

Equation (1) was applied to estimate the impacts of the auxiliary commercial RWH system using the functional unit impacts of both benchmark systems; e.g., if a commercial RWH system supplied 70% of total demand (i.e., $p_c = 0.7$), then the value of I_{aux} would be 0.7 × benchmark commercial RWH system impact, I_c, + 0.3 × municipal water supply impact, I_m. Functional unit impacts per 1 m^3 water delivery were calculated, with inputs linearly related to volumetric water supply.

3. Results and discussion

3.1. Performance analysis

LCIA percentage contribution analysis showed that the benchmark commercial RWH system performed better than (<40%) or equivalent to (45%–55%) the MWS system in all impact categories except Ozone Depletion at 62% (Fig. 3).

Commercial RWH was slightly better than or equivalent to (at 45%, assuming a margin of error) MWS for Energy Demand, Fossil Depletion, Global warming, and Smog and better than MWS in 6 impact categories, ranging from 65% (Acidification) to 83% (Eutrophication). Percentage comparison of component-specific LCIA revealed energy usage to be the dominant contributor of both systems (Figs. 4–5). Commercial RWH energy usage (pumping energy) and storage tank collectively dominated (>50%) in all but Metal Depletion, ranging from 74.8% (Freshwater Withdrawal), 89.6% (Global Warming), to 99.2% (Evaporative Water Consumption). The commercial RWH storage tank (Fiberglass) dominated in Ozone Depletion (78.5%) and Freshwater Withdrawal (67.6%). MWS energy usage (treatment plant operation and water transport) dominated (>50%) in five categories, ranging from 60.3% (Smog) to 99.7% (Evaporative Water Consumption). The pump dominated in Metal Depletion impact of both systems, 63.5% in commercial RWH and 84.8% in MWS. Source water acquisition contributed to total MWS Freshwater Withdrawal impact at 64.8%, and primary and secondary disinfection together contributed to Eutrophication and Ozone Depletion impacts at 79.2% and 51.1%. All other commercial RWH system components were below 15%, and the remaining MWS system components were <10% (Figs. 4–5). Detailed values of LCIA of benchmark systems and their components are included in SM 2.

3.2. Sensitivity analysis

Normalized LCIA of energy usage revealed linear impact variation, confirming linearity in LCIA scores consistent with linear LCA models (Fig. 6). For purposes of this analysis, impact variation were grouped as Mild slope, e.g., Metal Depletion; Moderate slope, e.g., Freshwater Withdrawal; or High slope, e.g., Evaporative Water Consumption (Fig. 6a–b).

The rate of change of impacts across LCIA categories was consistent with the dominant components. For example, in the case of commercial RWH energy usage, Evaporative Water Consumption and Fossil Depletion fell under High slope because pumping energy dominated those impacts; Ozone Depletion and Freshwater

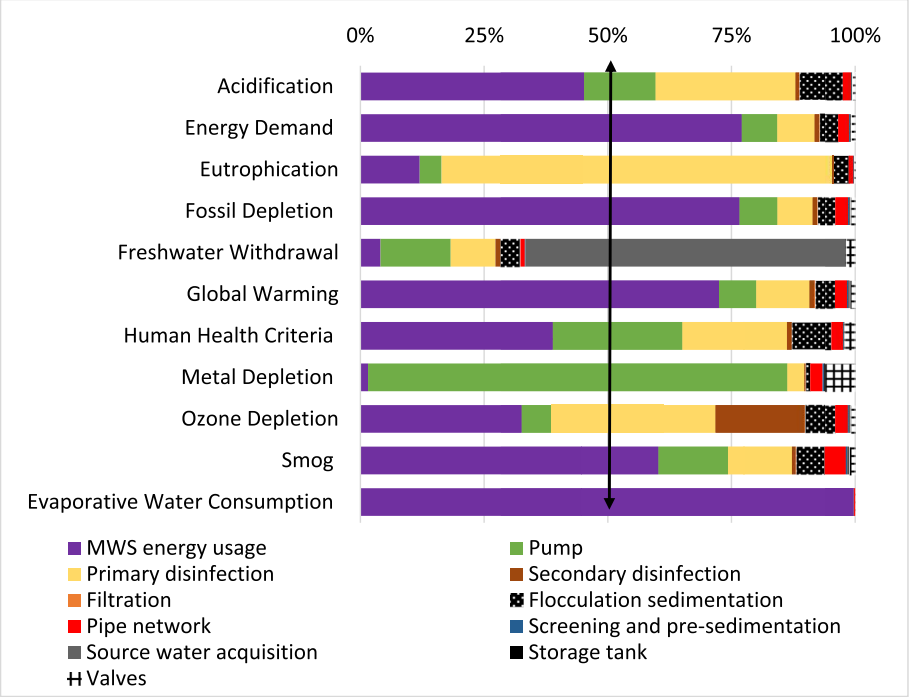

Fig. 5. Percentage comparison of life cycle impacts showing the performance of municipal water supply (MWS) system components. Note: MWS energy usage includes electricity required to pump in source water, energy throughout the water treatment plants, and pumping energy for transporting treated water (vertical arrow indicates the threshold 50%).

Withdrawal fell under Moderate slope because of storage tank. LCIA scores, normalized with respect to maximum scores of the storage tank, showed that fiberglass material dominated nine impact categories, while polyethylene (PE) tank dominated Energy Demand and Fossil Depletion (see SM 4). The fiberglass storage tank material was deemed appropriate for underground placement as designed by Rainwater Management Solutions. In practice, tank material is selected to meet system requirements and impact focus. Linear slopes were also observed in commercial RWH storage tank volume, water demand, water loss, and auxiliary commercial RWH system sensitivity analyses (SM 4). Additional sensitivity analysis results of storage tank materials and volume, water demand, water loss, system service life and auxiliary commercial RWH system, as well as a closer look at the LCIA release contributing processes of commercial RWH storage tank, pumping energy and pump, are provided in SM 3–4.

3.3. The LCIA tradeoffs of the systems

Energy usage or energy intensity sensitivity analysis revealed conditional LCIA tradeoffs of commercial RWH and MWS systems to energy requirements (Fig. 7a–k). Using regression equations (Fig. 7, Table 3), LCIA tradeoffs can be predicted for the two systems when energy intensity is known.

For Ozone Depletion, commercial RWH outperformed MWS if commercial RWH pumping energy intensity (E_c) was less than MWS energy intensity (E_m), $E_c + 0.86 \leq E_m$. For example, for $E_c = 0.19$ kWh/m^3 and $E_m = 1.05$ kWh/m^3, Ozone Depletion scores of commercial RWH and MWS systems were estimated at 4.1×10^{-8} kgCFC11 eq/m^3 and 4.2×10^{-8} kgCFC11 eq/m^3. Commercial RWH outperformed in Metal Depletion and Freshwater Withdrawal impacts, regardless of energy intensities analyzed. In Human Health Criteria and Eutrophication impacts, commercial RWH outperformed MWS, depending on energy intensities, if $E_c \leq E_m$. Commercial RWH outperformed in all other impact categories such as Energy Demand, if $E_c + 0.09 \leq E_m$. Mean Absolute Percentage Error (MAPE) of predicting LCIA impact scores using commercial RWH Tradeoff equations ranged from 0.26% (Evaporative Water Consumption) to 1.20% (Ozone Depletion) (Table 3; also see SM 4 for additional details on MAPE). In the case of MWS Tradeoff equations, MAPE ranged from 0.12% (Smog) to 2.40% (Metal Depletion). MAPE was selected as an appropriate, transparent statistic for comparing fit of the equations instead of another statistic such as coefficient of determination (R^2), thus avoiding any potential model exaggeration as reported by Birnbaum (1973).

Auxiliary commercial RWH system sensitivity analysis provided additional insights into LCIA tradeoffs. The impacts of the auxiliary system increased linearly with the percentage increase of MWS, as explained by Equation (1), except for Ozone Depletion with the reverse relationship due to the greater Ozone Depletion impact of benchmark commercial RWH system than MWS. An auxiliary commercial RWH system with 50% MWS reduced Ozone Depletion by 19%, but with an increase in all other impacts ranging from 10% Smog, 11% Energy Demand, 35% Evaporative Water Consumption, to 197% Eutrophication with respect to the benchmark commercial RWH system (Table 4). All increases were below benchmark MWS system impacts though, by as much as 8% Smog to 40% Eutrophication.

The benchmark commercial RWH storage tank volume of 76 m^3 (20,000 gallons) was estimated using a traditional behavioral and mass balance model, a spreadsheet-based, time series modeling approach (RMS, 2009). Two tank materials were evaluated by LCIA score, PE versus fiberglass, utilizing BEES and Ecoinvent data sources. Storage tank material and volume depends on the system requirement, annual precipitation and impact focus. In addition, infrastructure characteristics such as pump efficiencies, number of stories in a building and system head, as well as geographic characteristics such as location and water demand, water sources, treatment processes and storage options influence pumping energy intensities. Variations with sensitivity analyses of commercial RWH

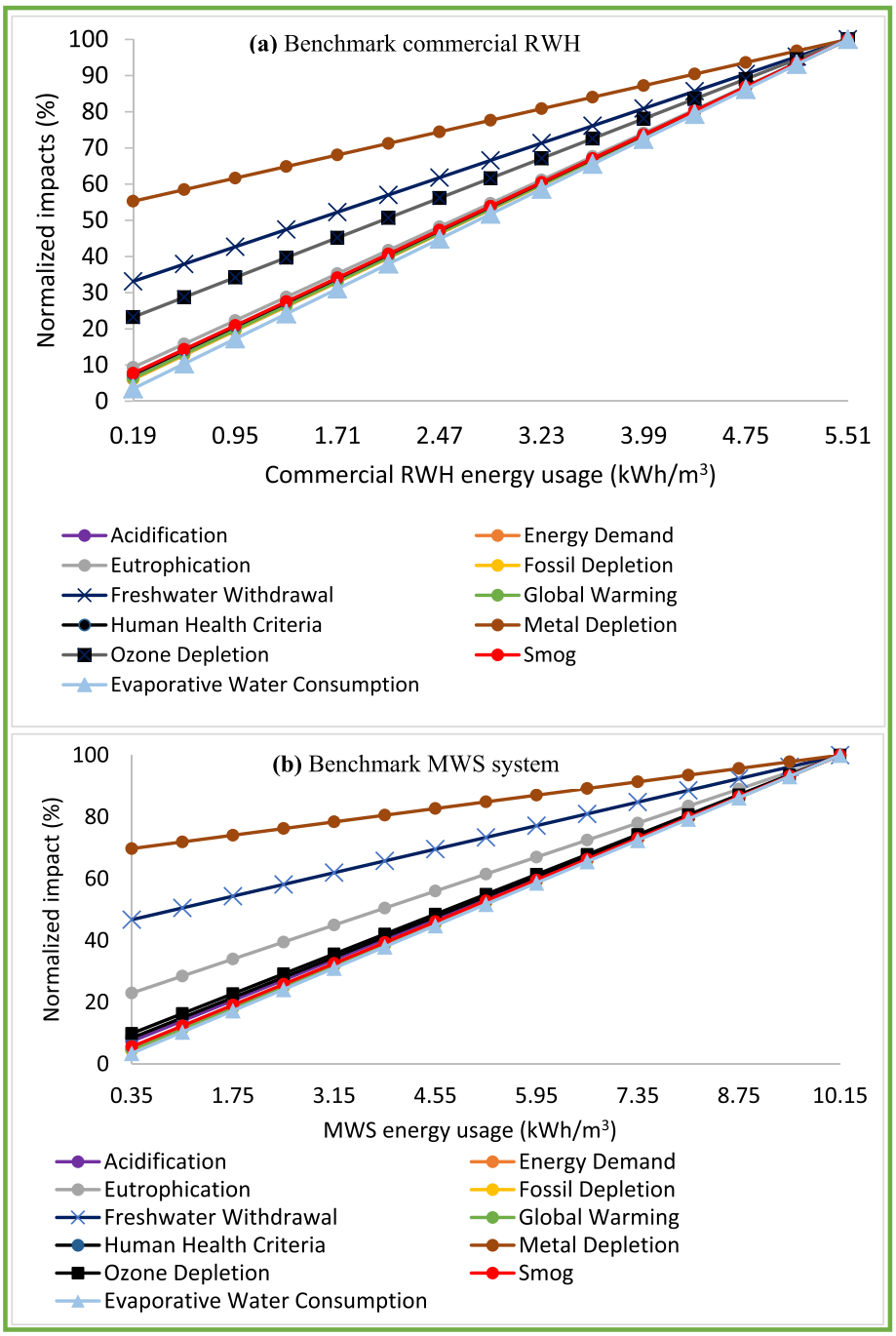

Fig. 6. Sensitivity analysis of energy usage to life cycle impacts of (a) benchmark commercial rainwater harvesting (RWH) system and (b) benchmark municipal water supply (MWS) system.

energy intensities (0.19 kWh/m^3 to a hypothetical value of 5.51 kWh/m^3) and MWS energy intensities (0.35 kWh/m^3 to a hypothetical value of 10.15 kWh/m^3) were addressed by capturing theoretical and empirical commercial RWH pumping energy (0.20 kWh/m^3 to 4.9 kWh/m^3) (Retamal et al., 2009; Vieira et al., 2014) and average national MWS pumping energy estimates (0.396 kWh/m^3 to high intensity water source desalination of 3.17 kWh/m^3) (Pabi et al., 2013; Wang and Zimmerman, 2015). Although alternative disinfection options were not the focus of current study, it is important to note that primary and secondary disinfection dominated Eutrophication and Ozone Depletion impacts of the MWS system. Therefore, appropriate information on disinfection technology is important in comparing impacts with a commercial RWH system.

The benchmark MWS system used chlorination similar to a majority of U.S. water systems—eighty-five percent of the water treatment plants in the U.S. were using chlorine by 1941, and today all drinking water filtration in the U.S. is accompanied by chlorination or other disinfection technologies such as ozonation and UV light (Sedlak, 2014).

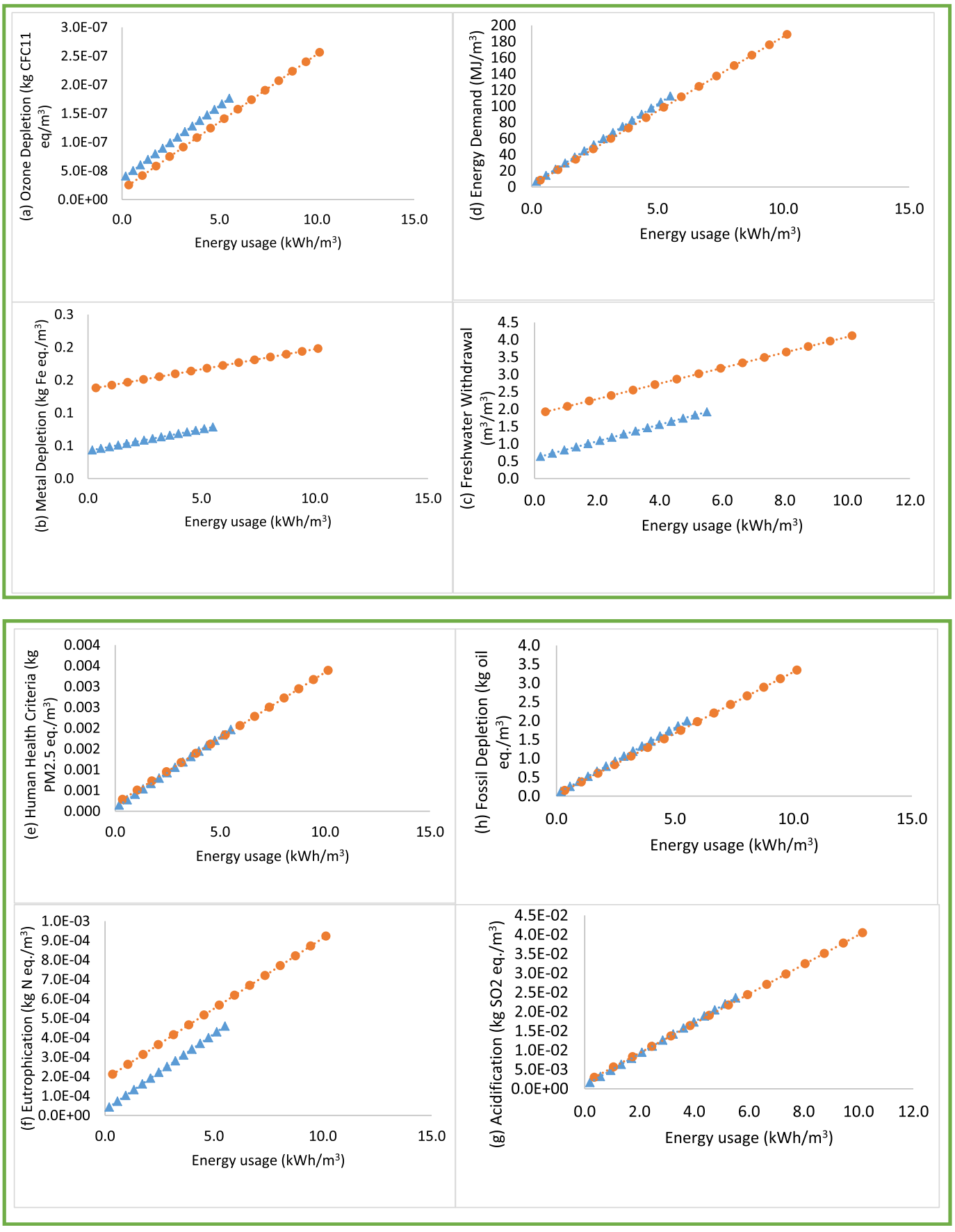

Fig. 7. LCIA tradeoff analysis for a range of energy intensities in commercial rainwater harvesting (RWH) and municipal water supply (MWS) systems: (a) Ozone Depletion, (b) Metal Depletion, (c) Freshwater Withdrawal, and (d) Energy Demand categories. Legend: Triangles = commercial RWH system and Circles = MWS system, (e) Human Health Criteria, (f) Eutrophication, (g) Acidification, and (h) Fossil Depletion. Legend: Triangles = commercial RWH system and Circles = MWS system, (i) Global warming, (j) Evaporative water consumption and (k) Smog.

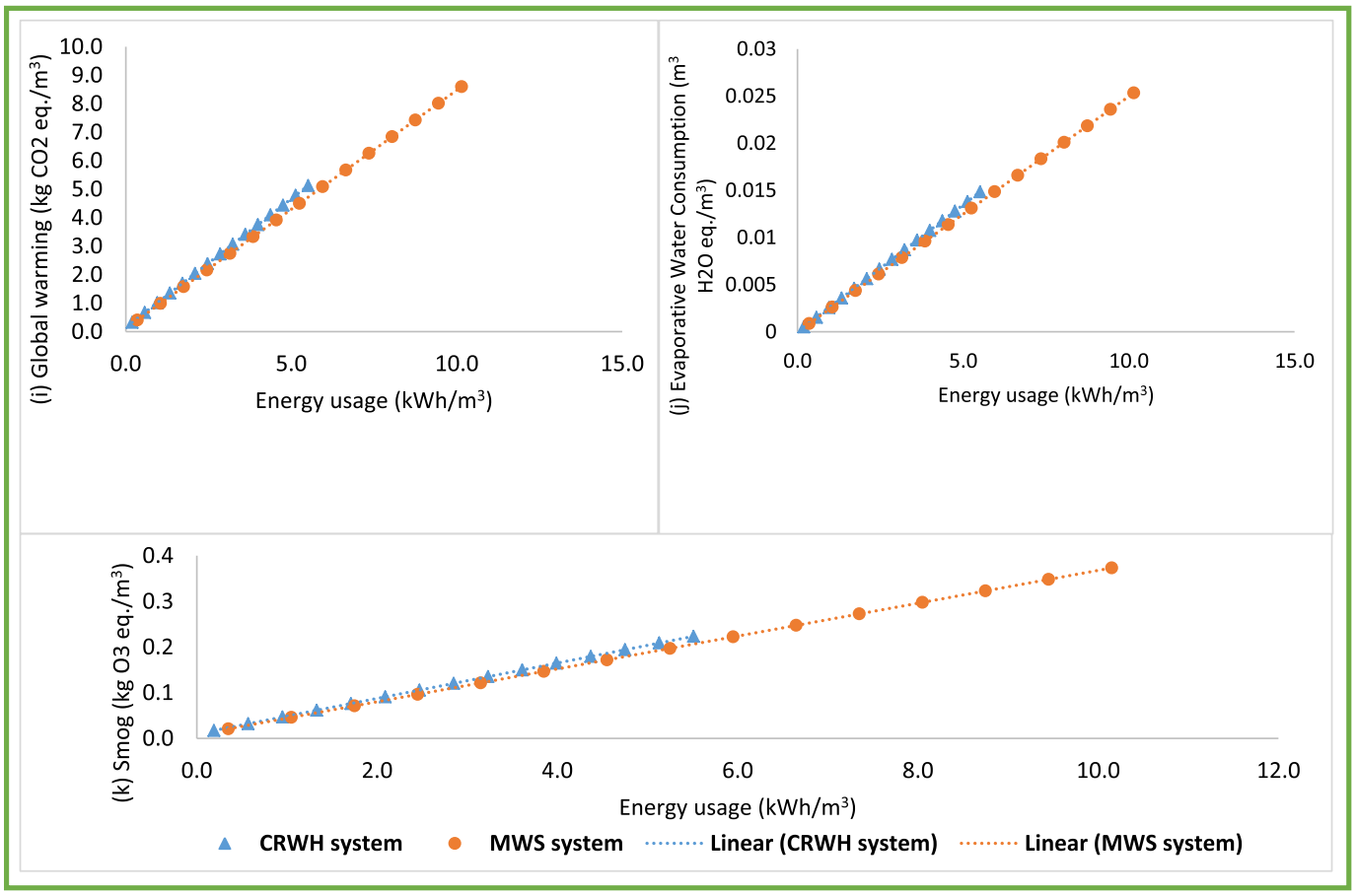

Fig. 7. (*continued*).

4. Summary and study implications

In addition to assessing the comprehensive life cycle environmental and human health impacts of a commercial RWH system compared to a MWS system, we addressed sensitivity of LCIA impact scores to storage tank material and volume, energy usage, water demand, water loss, system service life and an auxiliary commercial RWH system augmented with MWS. The LCA system boundary spans cradle-to-grave, excluding distribution of both systems' components from final manufacture to point of use and disposal phases.

Our analyses revealed that the benchmark commercial RWH performed better or equivalent (45–55%) to MWS in all impact categories except Ozone Depletion. Sensitivity analyses of energy usage, water demand, water loss, and storage tank volume confirmed linearity trends in LCIA scores. Additional sensitivity analyses showed that storage tank with fiberglass material dominated in nine of the 11 impact categories, except in Energy Demand and Fossil Depletion. Annual LCIA impacts for the commercial RWH system with longer service life (75 y) were lower than that of the system with shorter service life (50 y). An auxiliary commercial RWH system augmented with 50% MWS reduced Ozone Depletion impact by 19% showing increases in all other impacts. The LCIA tradeoff equations with respect to energy usage revealed conditional LCIA tradeoffs with energy requirements.

This study informs RWH planning and decision making through a comprehensive LCA of a commercial RWH system, with standards and regulations at the state and local level (USEPA, 2013a). LCA models are transferrable to other commercial RWH installations and study implications are summarized:

- A suite of 11 LCIA impact categories, as well as sensitivity analyses, provided insights into LCIA impact tradeoffs. The importance of LCIA impact categories and dominant components, especially material selection and energy usage, should be considered.
- Commercial RWH fiberglass storage tank material dominated (>50%) in Ozone Depletion and Freshwater Withdrawal impact categories. Selecting PE instead of fiberglass to reduce Ozone Depletion impact may be an option, although a PE tank may not be as appropriate for underground placement because it also necessitates greater Energy Demand and Fossil Depletion than fiberglass. Sensitivity of the data source was evaluated by performing an example LCIA of commercial RWH storage tank materials, fiberglass and PE with Ecoinvent (2012) and the BEES database (NIST, 2013). A data quality assessment of LCI by defining representativeness (including temporal, geographic, technological aspects, and completeness of data) would provide insight into variation in data (ISO, 2006b; USEPA, 2016b); however, it was beyond the scope of this study.
- Commercial RWH pumping energy usage was the most dominant component; therefore, eliminating or reducing pumping energy is key to reducing commercial RWH impacts. An alternate energy mix (e.g., solar) can minimize impacts of a dominant release contributor.
- Regression equations are useful for estimating impact tradeoffs of alternatives. Benchmark MWS treatment practices were consistent with typical U.S. surface water treatment, thus

Table 3
Life Cycle Impact Assessment (LCIA) tradeoff equations with respect to energy intensities (X, kWh/m^3). X_c and X_m are commercial rainwater harvesting (RWH) and municipal water supply (MWS) system energy intensities; Y = LCIA impact score; MAPE = Mean Absolute Percentage Error.

LCIA impact category	Tradeoff condition	Commercial RWH LCIA tradeoff equation	MAPE (%) (commercial RWH equation)	MWS LCIA tradeoff equation	MAPE (%) (MWS equation)
Acidification	$X_c + 0.05 \leq X_m$	$Y = 4.1 \times 10^{-3} X + 8.4 \times 10^{-4}$	0.60	$Y = 3.8 \times 10^{-3} X + 1.6 \times 10^{-3}$	0.82
Energy Demand	$X_c + 0.09 \leq X_m$	$Y = 2.0 \times 10^{1} X + 3.0 \times 10^{0}$	0.52	$Y = 1.8 \times 10^{1} X + 1.9 \times 10^{0}$	2.20
Eutrophication	$X_c \leq X_m$	$Y = 7.8 \times 10^{-5} X + 2.8 \times 10^{-5}$	0.35	$Y = 7.3 \times 10^{-5} X + 1.9 \times 10^{-4}$	1.10
Fossil Depletion	$X_c + 0.07 \leq X_m$	$Y = 3.5 \times 10^{-1} X + 5.6 \times 10^{-2}$	0.45	$Y = 3.3 \times 10^{-1} X + 3.5 \times 10^{-2}$	1.22
Freshwater Withdrawal	Regardless of X	$Y = 2.4 \times 10^{-1} X + 5.9 \times 10^{-1}$	0.32	$Y = 2.2 \times 10^{-1} X + 1.8 \times 10^{0}$	2.15
Global Warming	$X_c + 0.05 \leq X_m$	$Y = 9.0 \times 10^{-1} X + 1.5 \times 10^{-1}$	0.48	$Y = 8.4 \times 10^{-1} X + 1.1 \times 10^{-1}$	0.38
Human Health Criteria	$X_c \leq X_m$	$Y = 3.4 \times 10^{-4} X + 8.2 \times 10^{-5}$	0.38	$Y = 3.2 \times 10^{-4} X + 1.7 \times 10^{-4}$	0.66
Metal Depletion	Regardless of X	$Y = 6.6 \times 10^{-3} X + 4.2 \times 10^{-2}$	0.15	$Y = 6.1 \times 10^{-3} X + 1.4 \times 10^{-1}$	2.40
Ozone Depletion	$X_c + 0.86 \leq X_m$	$Y = 2.5 \times 10^{-8} X + 3.6 \times 10^{-8}$	1.20	$Y = 2.4 \times 10^{-8} X + 1.7 \times 10^{-8}$	1.38
Smog	$X_c + 0.05 \leq X_m$	$Y = 3.9 \times 10^{-2} X + 1.0 \times 10^{-2}$	0.52	$Y = 3.6 \times 10^{-2} X + 8.3 \times 10^{-3}$	0.12
Evaporative Water Consumption	$X_c + 0.05 \leq X_m$	$Y = 2.7 \times 10^{-3} X + 4.3 \times 10^{-6}$	0.26	$Y = 2.5 \times 10^{-3} X + 2.6 \times 10^{-6}$	0.13

applicable to other MWS systems that use surface water such as New York City (York, 2016), Austin (Water, 2010), and Seattle (2016). Accurate information on water treatment and energy use is imperative, and caution must be exercised when estimating the impacts of an energy-efficient MWS system because these systems require significantly less energy than energy-intensive ones (e.g., water source desalination and water transportation).

- LCIA tradeoffs exist due to variations in system requirements such as energy intensities and tank size for different rainfall and water demands. While component performance findings can help to improve the design of a specific component, slopes and tradeoff results focus on target impacts of a commercial RWH system.
- Appropriate storage tank volume, water demand, and energy intensity may be determined by considering a threshold point to minimize commercial RWH impacts using slope zone curves. For example, a hypothetical threshold at 50% water demand may be as efficient, with a relatively small variation in slope beyond the threshold. A dramatic increase in impacts was found below 50% of water demand due to input flow inefficiency.
- A threshold can also be devised for an auxiliary commercial RWH system operation. A 50% auxiliary commercial RWH system outperformed MWS in all LCIA categories except Ozone Depletion. Different thresholds determined from the regression equations can be set for different energy intensities.
- Regulatory requirements on water quality, water withdrawal and plumbing codes can also influence impacts due to component size, material, and treatment standards and should be considered when designing a commercial RWH system. When implemented at the watershed-scale, the potential impacts of commercial RWH on freshwater balance, water quality, runoff and sewer overflow, groundwater level (and economic viability) need further attention. Human health (cancer) and ecotoxicity impacts in addition to the cradle-to-cradle analysis are additional research needs.

Table 4
Life Cycle Impact Assessment (LCIA) tradeoff scores of auxiliary commercial rainwater harvesting (RWH) system, augmented with municipal water supply (MWS) from 10% to 90%. I_c and I_m refer to the LCIA impact score per cubic meter water supply of benchmark commercial RWH and MWS systems; % differences are reported for a 50% auxiliary commercial RWH system with respect to I_c given by: $[(I_c$ —Impact value @ 0.5)$/I_c]$ x 100.

Impact category	Unit	Benchmark LCIA values		MWS fraction and LCIA scores of the auxiliary commercial RWH system									% Difference @ 50% MWS
		MWS (I_m)	Commercial RWH (I_c)	0.1	0.2	0.3	0.4	0.5	0.6	0.7	0.8	0.9	
Acidification	kg SO2 eq	3.0E-03	1.6E-03	1.8E-03	1.9E-03	2.0E-03	2.2E-03	2.3E-03	2.4E-03	2.6E-03	2.7E-03	2.8E-03	−41
Energy Demand	MJ	8.4E+00	6.8E+00	7.0E+00	7.1E+00	7.3E+00	7.4E+00	7.6E+00	7.7E+00	7.9E+00	8.1E+00	8.2E+00	−11
Eutrophication	kg N eq	2.1E-04	4.3E-05	6.0E-05	7.7E-05	9.4E-05	1.1E-04	1.3E-04	1.4E-04	1.6E-04	1.8E-04	2.0E-04	−197
Fossil Depletion	kg oil eq	1.5E-01	1.2E-01	1.3E-01	1.3E-01	1.3E-01	1.3E-01	1.4E-01	1.4E-01	1.4E-01	1.4E-01	1.5E-01	−11
Freshwater Withdrawal	m^3	1.9E+00	6.4E-01	7.6E-01	8.9E-01	1.0E+00	1.2E+00	1.3E+00	1.4E+00	1.5E+00	1.7E+00	1.8E+00	−101
Global Warming	kg CO2 eq	4.0E-01	3.3E-01	3.3E-01	3.4E-01	3.5E-01	3.6E-01	3.6E-01	3.7E-01	3.8E-01	3.9E-01	4.0E-01	−12
Human Health Criteria	kg PM2.5 eq	2.9E-04	1.5E-04	1.6E-04	1.7E-04	1.9E-04	2.0E-04	2.2E-04	2.3E-04	2.4E-04	2.6E-04	2.7E-04	−47
Metal Depletion	kg Fe eq	1.4E-01	4.3E-02	5.3E-02	6.2E-02	7.2E-02	8.1E-02	9.1E-02	1.0E-01	1.1E-01	1.2E-01	1.3E-01	−109
Ozone Depletion	kg CFC11 eq	2.5E-08	4.1E-08	3.9E-08	3.8E-08	3.6E-08	3.5E-08	3.3E-08	3.2E-08	3.0E-08	2.8E-08	2.7E-08	19
Smog	kg O3 eq	2.1E-02	1.7E-02	1.8E-02	1.8E-02	1.8E-02	1.9E-02	1.9E-02	1.9E-02	2.0E-02	2.0E-02	2.1E-02	−10
Evaporative Water Consumption	m^3 H2O eq	8.8E-04	5.2E-04	5.5E-04	5.9E-04	6.2E-04	6.6E-04	7.0E-04	7.3E-04	7.7E-04	8.0E-04	8.4E-04	−35

Acknowledgements

This research was supported in part by an appointment to the Postdoctoral Research Program at the U.S. Environmental Protection Agency (EPA), Office of Research and Development, Athens, GA, USA, administered by the Oak Ridge Institute for Science and Education through Interagency Agreement Number DW8992298301 between the U.S. Department of Energy and the U.S. Environmental Protection Agency. Although this document has been reviewed in accordance with EPA policy and approved for publication, it may not necessarily reflect official Agency policy. Mention of trade names or commercial products does not constitute endorsement or recommendation for use. The preliminary findings of this study were presented at the American Rainwater Catchment Systems Association 2015 Conference, Long Beach, California, and at the American Center for Life Cycle Assessment LCA XVI Conference 2016, Charleston, South Carolina. The authors thank Fran Rauschenberg (Senior Environmental Employee) and Scott R. Unger (EPA) for technical editing and review, and two anonymous reviewers for their constructive comments that improved the manuscript. The authors also thank Heather Kinkade and James Derstler (American Rainwater Catchment Systems Association) for their support and contribution in data collection. Sarah Sojka's contributions include design and sizing of the commercial RWH system, research on the MWS system, product information, and manuscript review. Sarah was not involved in the calculation of life cycle impacts or assignment of the range of values for pumping energy. Sarah is a former employee of Rainwater Management Solutions and remains affiliated with the company through her husband (a partner in the company) and a cooperative grant for commercialization research.

Appendix A. Supplementary data

Supplementary data related to this article can be found at http://dx.doi.org/10.1016/j.jclepro.2017.02.025.

References

Anand, C., Apul, D.S., 2011. Economic and environmental analysis of standard, high efficiency, rainwater flushed, and composting toilets. J. Environ. Manag. 92, 419–428.
Angrill, S., Farreny, R., Gasol, C.M., Gabarrell, X., Vinolas, B., Josa, A., Rieradevall, J., 2012. Environmental analysis of rainwater harvesting infrastructures in diffuse and compact urban models of Mediterranean climate. Int. J. Life Cycle Assess. 17, 25–42.
ARCSA, 2016. Laws, Rules & Codes. www.arcsa.org/?page=273 (April 12, 2016).
Ault, T.R., Mankin, J.S., Cook, B.I., Smerdon, J.E., 2016. Relative impacts of mitigation, temperature, and precipitation on 21st-century megadrought risk in the American Southwest. Sci. Adv. 2.
AWE, 2016. Office Building Introduction. www.allianceforwaterefficiency.org/office_buildings.aspx (April 13, 2016).
Birnbaum, M.H., 1973. The devil rides again: correlation as an index of fit. Psychol. Bull. 79, 239.
Cashman, S., Gaglione, A., Mosley, J., Weiss, L., Hawkins, T.R., Ashbolt, N.J., Cashdollar, J., Xue, X., Ma, C., Arden, S., 2014. Environmental and Cost Life Cycle Assessment of Disinfection Options for Municipal Drinking Water Treatment. U.S. Environmental Protection Agency, Cincinnati, OH USA.
Crettaz, P., Jolliet, O., Cuanillon, J.M., Orlando, S., 1999. Life cycle assessment of drinking water and rain water for toilets flushing. J. Water Serv. Res. Technol.-Aqua 48, 73–83.
DCWSA, 2008. Independent Engineering Inspection of the District of Columbia Water and Sewer Authority's Wastewater and Water Systems (District of Columbia Water and Sewer Authority Washington DC).
DCWSA, 2015. About Drinking Water Quality in Washington, DC. www.dcwater.com/drinking_water/about.cfm (September 3, 2015).
Devkota, J., Schlachter, H., Apul, D., 2015. Life cycle based evaluation of harvested rainwater use in toilets and for irrigation. J. Clean. Prod. 95, 311–321.
Domenech, L., Han, H.J., Sauri, D., 2012. Rainwater harvesting for human consumption and livelihood improvement in rural Nepal: benefits and risks. Water Environ. J. 26, 465–472.
Domenech, L., Sauri, D., 2011. A comparative appraisal of the use of rainwater harvesting in single and multi-family buildings of the Metropolitan Area of Barcelona (Spain): social experience, drinking water savings and economic costs. J. Clean. Prod. 19, 598–608.
Ecoinvent, 2012. Ecoinvent Centre. www.ecoinvent.org (July 2, 2012).
EIA, 2016. 2012 CBECS Survey Data. www.eia.gov/consumption/commercial/data/2012/#b2 (January 22, 2014).
Ghimire, S.R., Johnston, J.M., 2013. Impacts of domestic and agricultural rainwater harvesting systems on watershed hydrology: a case study in the Albemarle-Pamlico river basins (USA). Ecohydrol. Hydrobiol. 13, 159–171.
Ghimire, S.R., Johnston, J.M., 2015. Traditional knowledge of rainwater harvesting compared to five modern case studies. In: Karvazy, K., Webster, V. (Eds.), World Environmental and Water Resources Congress 2015. American Society of Civil Engineers, USA, pp. 182–193.
Ghimire, S.R., Johnston, J.M., Ingwersen, W.W., Hawkins, T.R., 2014. Life cycle assessment of domestic and agricultural rainwater harvesting systems. Environ. Sci. Technol. 48, 4069–4077.
Ghimire, S.R., Watkins Jr., D.W., Li, K., 2012. Life cycle cost assessment of a rain water harvesting system for toilet flushing. Water Sci. Technol. Water Supply 12, 309–320.
Ghisi, E., Tavares, D.D., Rocha, V.L., 2009. Rainwater harvesting in petrol stations in Brasilia: potential for potable water savings and investment feasibility analysis. Resour. Conservat. Recycl. 54, 79–85.
Goedkoop, M.H., Huijbregts, M., Schryver, A., Struijs, J., Zelm, R., 2012. ReCiPe 2008-A Life Cycle Impact Assessment Method Which Comprises Harmonised Category Indicators at the Midpoint and the Endpoint Level. Ministry of Housing, Spatial Planning and Environment, Netherlands.
Gurung, T.R., Sharma, A., 2014. Communal rainwater tank systems design and economies of scale. J. Clean. Prod. 67, 26–36.
Harvesth2o, 2016. Regulations & Statutes. www.harvesth2o.com/statues_regulations.shtml (April 11, 2016).
Hischier, R.A.H.-J.B., Büsser, S., Doka, G., Frischknecht, R., Kleijer, A., Leuenberger, M., Nemecek, T., Simons, A., 2010. Documentation of Changes Implemented in Ecoinvent Data v2.2 Swiss Centre for LCI (Switzerland).
Hunt, R.G., Franklin, W.E., Hunt, R.G., 1996. LCA — How it came about. Int. J. Life Cycle Assess. 1, 4–7.
Ingwersen, W., Gausman, M., Weisbrod, A., Sengupta, D., Lee, S.-J., Bare, J., Zanoli, E., Bhander, G.S., Ceja, M., 2016. Detailed life cycle assessment of Bounty® paper towel operations in the United States. J. Clean. Prod. 131, 509–522.
ISO, 2006a. Environmental Management — Life Cycle Assessment — Principles and Framework, ISO 14040. International Organization for Standardization, Switzerland.
ISO, 2006b. Environmental Management — Life Cycle Assessment — Requirements and Guidelines, ISO 14044. International Organization for Standardization, Switzerland.
Lye, D.J., 2002. Health risks associated with consumption of untreated water from household roof catchment systems. JAWRA J. Am. Water Resour. Assoc. 38, 1301–1306.
Mays, L., Antoniou, G., Angelakis, A., 2013. History of water cisterns: legacies and lessons. Water-Sui. 5, 1916–1940.
Meyer, D.E., Upadhyayula, V.K., 2013. The use of life cycle tools to support decision making for sustainable nanotechnologies. Clean. Technol. Environ. Policy 1–16.
Morales-Pinzón, T., Rieradevall, J., Gasol, C.M., Gabarrell, X., 2015. Modelling for economic cost and environmental analysis of rainwater harvesting systems. J. Clean. Prod. 87, 613–626.
NCSL, 2016. State Rainwater Harvesting Laws and Programs. www.ncsl.org/research/environment-and-natural-resources/rainwater-harvesting.aspx (April 11, 2016).
NIST, 2013. Building for Environmental and Economic Sustainability (BEES). www.nist.gov/el/economics/BEESSoftware.cfm (February 15, 2013).
NREL, 2013. U.S. Life Cycle Inventory Database. National Renewable Energy Laboratory (NREL). www.lcacommons.gov/nrel/search (September 30, 2013).
OpenLCA, 2016. openLCA 1.4.2. http://www.openlca.org/ (January 20, 2012).
Pabi, S., Amarnath, A., Goldstein, R., Reekie, L., 2013. Electricity Use and Management in the Municipal Water Supply and Wastewater Industries.
Pandey, D.N., Gupta, A.K., Anderson, D.M., 2003. Rainwater harvesting as an adaptation to climate change. Curr. Sci. 85, 46–59.
Retamal, M., Glassmire, J., Abeysuriya, K., Turner, A., White, S., 2009. The Water-energy Nexus: Investigation into the Energy Implications of Household Rainwater Systems. Institute for Sustainable Futures, University of Technology, Sydney.
RMS, 2009. Tank Sizing Spreadsheet. Rainwater Management Solutions (Salem, VA).
Roebuck, R.M., Oltean-Dumbrava, C., Tait, S., 2011. Whole life cost performance of domestic rainwater harvesting systems in the United Kingdom. Water Environ. J. 25, 355–365.
Sample, D.J., Liu, J., 2014. Optimizing rainwater harvesting systems for the dual purposes of water supply and runoff capture. J. Clean. Prod. 75, 174–194.
Schewe, J., Heinke, J., Gerten, D., Haddeland, I., Arnell, N.W., Clark, D.B., Dankers, R., Eisner, S., Fekete, B.M., Colón-González, F.J., 2014. Multimodel assessment of water scarcity under climate change. Proc. Natl. Acad. Sci. 111, 3245–3250.
Seattle, C.o., 2016. Water System Overview. www.seattle.gov/Util/MyServices/Water/AbouttheWaterSystem/WaterSystemOverview/index.htm (March 23, 2016).
Sedlak, D., 2014. Water 4.0: the Past, Present, and Future of the World's Most Vital Resource. Yale University Press, U.S.A.
Siems, R., Sahin, O., 2016. Energy intensity of residential rainwater tank systems: exploring the economic and environmental impacts. J. Clean. Prod. 113,

251–262.
Sojka, S., Younos, T., Crawford, D., 2016. Modern urban rainwater harvesting systems: design, case studies, and impacts. In: Younos, T., Parece, E.T. (Eds.), Sustainable Water Management in Urban Environments. Springer International Publishing, Cham, Switzerland, pp. 209–234.
Thomas, R.B., Kirisits, M.J., Lye, D.J., Kinney, K.A., 2014. Rainwater harvesting in the United States: a survey of common system practices. J. Clean. Prod. 75, 166–173.
USACE, 2016. Washington Aqueduct. www.nab.usace.army.mil/Missions/WashingtonAqueduct.aspx (April 13, 2016).
USEPA, 2013a. Rainwater Harvesting Conservation, Credit, Codes, and Cost Literature Review and Case Studies. Office of Water. U.S. Environmental Protection Agency, Washington, DC.
USEPA, 2013b. Tool for the Reduction and Assessment of Chemical and Other Environmental Impacts (TRACI). www.epa.gov/nrmrl/std/traci/traci.html (July 2, 2013).
USEPA, 2016a. Adapting to Climate Change Southeast. https://www.epa.gov/arc-x (October 17, 2016).
USEPA, 2016b. Guidance on Data Quality Assessment for Life Cycle Inventory Data. U.S. Environmental Protection Agency, Ohio, USA.
USGCRP, 2012. Regional Climate Impacts: Southeast, U.S. Global Change Research Program. www.globalchange.gov/publications/reports/scientific-assessments/us-impacts/regional-climate-change-impacts/southeast (January 19, 2012).
Vieira, A.S., Beal, C.D., Ghisi, E., Stewart, R.A., 2014. Energy intensity of rainwater harvesting systems: a review. Renew. Sustain. Energy Rev. 34, 225–242.
Wang, R., Zimmerman, J.B., 2015. Economic and environmental assessment of office building rainwater harvesting systems in various U.S. cities. Environ. Sci. Technol. 49, 1768–1778.
Ward, S., Memon, F.A., Butler, D., 2012. Performance of a large building rainwater harvesting system. Water Res. 46, 5127–5134.
Water, A., 2010. City of Austin Municipal Water Supply Overview (City of Austin, Texas, USA).
WFN, 2009. Water Footprint Manual Enschede. The Netherlands Water Footprint Network, The Netherlands.
York, T.C.o.N., 2016. History of New York City's Water Supply System. www.nyc.gov/html/dep/html/drinking_water/history.shtml (March 23, 2016).

From: Ingwersen, Wesley
To: Johnston, JohnM; Dr. Santosh R. Ghimire; ssojka@randolphcollege.edu
Subject: RE: JCP municipal RWH publication award nomination
Date: Tuesday, April 28, 2020 12:41:08 PM
Attachments: image006.png
image007.png

Greetings to all. Thanks John for this nomination. I agree with the %. I would be very curious to know if ARCSA or anyone else working in RHW (practically or policy wise and not just research studies) has built on our findings.

Best,
Wes

From: Johnston, JohnM <Johnston.JohnM@epa.gov>
Sent: Tuesday, April 28, 2020 12:18 PM
To: Dr. Santosh R. Ghimire <sghimire02@gmail.com>; Ingwersen, Wesley <ingwersen.wesley@epa.gov>; ssojka@randolphcollege.edu
Subject: JCP municipal RWH publication award nomination

Hello Santosh, Wes and Sarah – Hope you are all staying safe and healthy in these challenging times. In preparation for a possible EPA STAA (Scientific and Technical Achievement Award) paper nomination, please reply to this email that you agree with percentage contribution:

S. Ghimire 40%
J. Johnston 30%
W. Ingwersen 20%
S. Sojka 10%

The deadline for submission is this week. I'll send a draft of the nomination narrative for review. The 2014 *ES&T* paper this work was inspired by received a Level II award in the 2016 round. Because of the ARCSA collaboration on this effort we hope it does similarly. It already has 40 citations according to Google Scholar (incl. self cites). We lost touch with Heather Kincade after it was published, so would be great to find out what if anything happened within ARCSA, because they initiated the study.

Thanks,
John

John M. Johnston PhD | Chief, Landscape and Aquatic Systems Modeling Branch | Environmental Processes Division | Center for Environmental Measurement and Modeling | US Environmental Protection Agency | Athens, GA | Office: +01 706.355.8300 | Cell: +01 706.206.1485 |

From: Sarah Sojka
To: Santosh Ghimire
Cc: Johnston, JohnM; Ingwersen, Wesley
Subject: Re: JCP municipal RWH publication award nomination
Date: Tuesday, April 28, 2020 1:59:55 PM
Attachments: ATT00001.txt

Hello all-

The percentages look good. I am on the board of directors on the ARCSA Foundation. A few years ago, ARCSA merged with the Texas Rainwater Catchment Systems Association and reorganized into a 501(c)3 organization (the Foundation) and a 501(c) 6 organization (ARCSA). I do not know if anyone has done followup research, but I know that the findings from the study, particularly the impact of pumping energy on lifecycle impacts and the need to "right-size" a system, have been important for many members of the organization. If a statement of the value of the research for ARCSA is important/useful, I can definitely work on that.

Thanks,
Sarah

Sarah L. Sojka

Associate Professor

Coordinator of Online Programs

Department of Environmental Studies and Science

Department of Physics and Engineering

C: 434.242.0298

On Tue, Apr 28, 2020 at 1:20 PM Santosh Ghimire <sghimire02@gmail.com> wrote:

> Hi John,
> I agree with the percentages.
>
> Thank you,
> Sincerely,
> ---
> *Santosh R. Ghimire, Ph.D., M. ASCE*
> 140 Caroline Ct

Circleville, OH 43113

Mobile: (706) 207-0323
GoogleScholar: http://scholar.google.com/citations?user=OFBscEEAAAAJ&hl=en&oi=ao

(Sent from my iPhone)

> On Apr 28, 2020, at 12:18 PM, Johnston, JohnM <Johnston.JohnM@epa.gov> wrote:
>
> <image001.gif>
>
> Hello Santosh, Wes and Sarah – Hope you are all staying safe and healthy in these challenging times. In preparation for a possible EPA STAA (Scientific and Technical Achievement Award) paper nomination, please reply to this email that you agree with percentage contribution:
>
> S. Ghimire 40%
>
> J. Johnston 30%
>
> W. Ingwersen 20%
>
> S. Sojka 10%
>
> The deadline for submission is this week. I'll send a draft of the nomination narrative for review. The 2014 *ES&T* paper this work was inspired by received a Level II award in the 2016 round. Because of the ARCSA collaboration on this effort we hope it does similarly. It already has 40 citations according to Google Scholar (incl. self cites). We lost touch with Heather Kincade after it was published, so would be great to find out what if anything happened within ARCSA, because they initiated the study.
>
> Thanks,
>
> John
>
> John M. Johnston PhD | Chief, Landscape and Aquatic Systems Modeling Branch | Environmental Processes Division | Center for Environmental Measurement and Modeling | US Environmental Protection Agency | Athens, GA | Office: +01 706.355.8300 | Cell: +01 706.206.1485 |

<image002.png>
<image003.png>
<image004.jpg>

SUPPLEMENTARY MATERIAL

Title: Life Cycle Assessment of a Commercial Rainwater Harvesting System Compared with a Municipal Water Supply System

Santosh R. Ghimire [1], John M. Johnston[2], Wesley W. Ingwersen[3], and Sarah Sojka[4]*

[1]ORISE Postdoctoral Research Participant, U.S. Environmental Protection Agency, Office of Research and Development, 960 College Station Rd., Athens, GA 30605, USA

E-Mail: sghimire02@gmail.com

[2]U.S. Environmental Protection Agency, Office of Research and Development, 960 College Station Rd., Athens, GA 30605, USA

*Corresponding E-Mail: Johnston.JohnM@epa.gov

[3]U.S. Environmental Protection Agency, Office of Research and Development, 26 W. Martin Luther King Dr., Cincinnati, OH 45268, USA

E-Mail: Ingwersen.Wesley@epa.gov

[4]Randolph College, 2500 Rivermont Ave., Lynchburg, VA 24503, USA

E-Mail: ssojka@randolphcollege.edu

Number of pages: 31

Number of Figures: 16

Number of Tables: 4

Supplementary Material 1 (SM 1) describes the life cycle assessment system boundary, calculation of pumping energy, and sizing of the commercial rainwater harvesting storage tank. SM 2 provides additional details on the life cycle inventory and life cycle assessment of the benchmark commercial rainwater harvesting and municipal water supply systems. SM 3 includes

additional information on the benchmark system component performance analyses. SM 4 provides additional information on sensitivity analyses.

SM 1: Benchmark Systems Definition and Assumptions

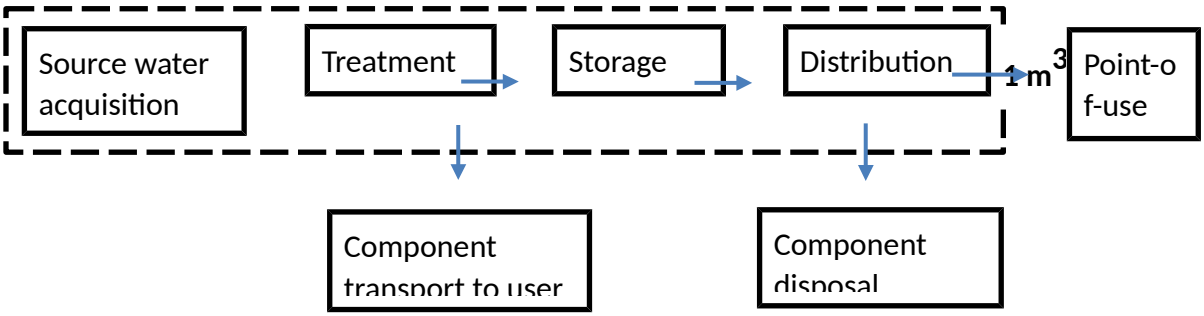

Fig. S1. Life Cycle Assessment system boundary of commercial rainwater harvesting (RWH) and municipal water supply (MWS) systems. Source water for commercial RWH and MWS systems is provided by surface water and rainwater. Figure adapted with permission from (Ghimire et al., 2014). Copyright (2014) American Chemical Society.

Benchmark commercial rainwater harvesting (RWH) system pumping energy estimation

Pumping energy intensity (i.e., energy use per unit volume of water, kWh/m^3), E_{crwh} of commercial RWH system, was expressed as:

$$E_{crwh} = \left(\frac{P_{crwh}}{Q_h} \right) \quad \text{(S1)}$$

where

E_{crwh} = Pumping energy intensity per cubic meter water supply (kWh/m^3)

$P_{crwh} = ¿$ Power (kW) consumed by the pump, estimated using power equation, which also incorporated safety factor of output power, α, consistent with Cheng (2002):

$$P_{crwh} = \left(\frac{Q \, x \gamma \, x \, H}{1000 \, x \, \eta_1 \, x \, \eta_2} \right) (1 + \alpha) \qquad \text{(S2)}$$

where

Q = capacity of the pump (1.18 x 10^{-04} m^3/s)

Pump capacity, Q, was estimated by the average daily demand for flushing toilets and urinals for 1,000 employees (500 male and 500 female) in a typical four-story U.S. commercial building, using high-efficiency urinal demand at 0.47 liter/flush (l/f) or 0.125 gallon/flush (g/f) and high-efficiency toilet demand at 4.8 l/f or 1.28 g/f (AWE, 2016). These demands were lower than the EPA WaterSense® maximum average flush rate criteria at 1.9 l/f or 0.5 g/f for water efficiency urinal fixture (USEPA, 2009). Each male employee used 2 urinals and 1 toilet and female employees used 3 toilets every work day, resulting in water flow rate of 1.18 x 10^{-04} m^3/s [i.e., 500 x (2 x 0.125+1.28 x 1) +500 x (3 x 1.28) = 2,685 gallons/day =1.18 x 10^{-04} m^3/s]. The system operated 260 days per year (5 days per week x 52 weeks per year).

γ = specific weight of water (9,807 N/m^3)

H = total pump head (38.2 m) = static head (8.1 m + 0.254 m) + pressure head (21.12 m) + friction losses; with friction losses at 30% of static head and pressure head (i.e., 0.3 x 29.48 m = 8.8 m) (Fig. S2)

η_1 = pump efficiency (0.65)

η_2 = Mechanical transmission efficiency (1.00)

α = safety factor of output power (0.2)

The parameters η_1, η_2, α, and friction losses were consistent with Cheng (2002).

The estimated pumping energy per m^3 commercial RWH supply was 0.19 kWh/m^3.

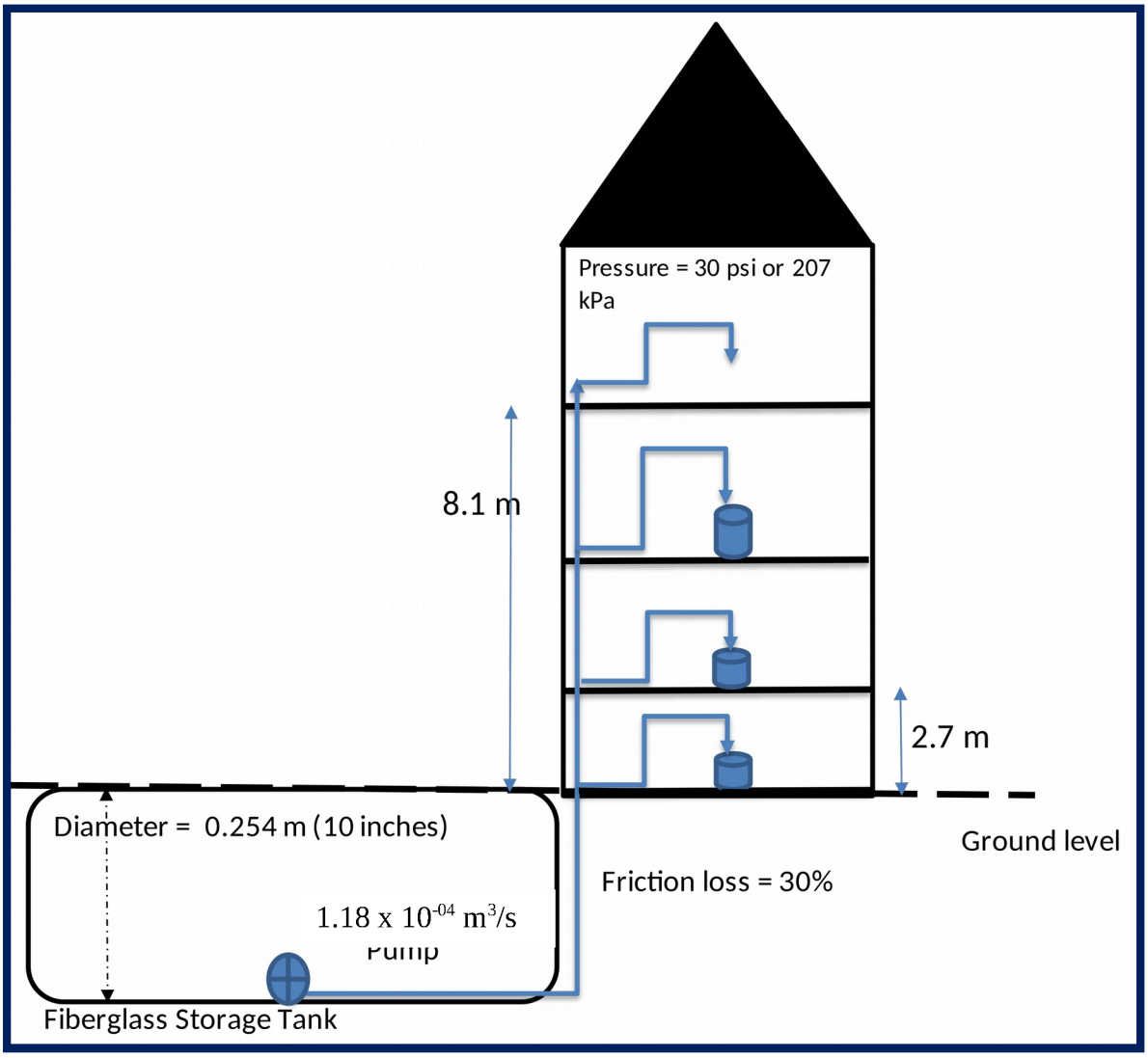

Fig. S2. Commercial rainwater harvesting system configuration depicting the major parameters used for pumping energy estimation (not to scale).

Commercial RWH energy intensity varies by water demand and system design. In an Australian study, for example, empirical pumping energy ranged from 0.9 kWh/m^3 for household non-potable use to 4.9 kWh/m^3 for potable use (Retamal et al., 2009). Others have considered theoretical pumping energy at 0.44 kWh/m^3 for a three-story office building in U.S. cities (Wang

and Zimmerman, 2015) and 0.54 kWh/m^3 for an office building in the UK (Ward et al., 2012). A literature review by Vieira et al. (2014) reported median theoretical energy intensity at 0.20 kWh/m^3, which was much lower than other empirical values.

Benchmark MWS system energy intensity estimation

We estimated the benchmark MWS energy intensity at 0.35 kWh/m^3 by combining two energy use sources: Washington Aqueduct energy use (0.20 kWh/m^3) (Equation S3) and DC Water services energy use (0.15 kWh/m^3) (Equation S4). The Washington Aqueduct energy intensity, E_{DC1} (0.20 kWh/m^3), was estimated using volume of water sold to customers and actual energy costs in FY 2012:

$$E_{DC1} = \frac{C_e}{V \, x \, R_e} \tag{S3}$$

where

E_{DC1} = Washington Aqueduct energy intensity (kWh/m^3)

C_e = actual Washington Aqueduct energy costs in FY 2012 ($/y) (obtained from Washington Aqueduct) (WA, 2012)

V = volume of water sold to customers in FY 2012: 192,871,598.3 m^3/y or 50,951.3 MG/y obtained from Washington Aqueduct) (WA, 2012)

R_e = District of Columbia commercial electric rate in 2012 ($0.1202/kWh), obtained from U.S. Energy Information Administration or EIA's 2012 average monthly commercial bill (USEIA, 2016)

DC Water services energy use intensity, E_{DC2} (0.15 kWh/m^3), was estimated using available energy use data from the District Department of the Environment (DDOE, 2010) and DC water supply volume in 2012:

$$E_{DC2}=\frac{E_e}{V} \quad \text{(S4)}$$

where

E_e = DC Water services energy use in 2006 (20,534,096 kWh, obtained from District Department of the Environment) (DDOE, 2010)

V = DC Water supply in 2012 (139,796,630 m^3), obtained from Washington Aqueduct (WA, 2012)

We note that the MWS system's energy intensity varies with water sources and pumping, treatment processes, and storage options, which may be higher if the embedded energy is considered; for example, 4.9 kWh/m^3 for medium water utility in southern California with 83% imported water (NAP, 2015). Estimated pumping electric energy use by the U.S. public water supply industry, community water systems in 2011 ranged from 0.42 kWh/m^3 surface water to 0.55 kWh/m^3 groundwater to 3.17 kWh/m^3 desalination water, as reported by Electric Power Research Institute and Water Research Foundation (Pabi et al., 2013).

Benchmark commercial RWH storage tank sizing

Rainwater Management Solutions provided a design for commercial RWH storage tank (76 m^3 or 20,000 gallons) using a spreadsheet-based, time series modeling approach (RMS, 2009) that builds on traditional behavioral and mass balance models (Fewkes, 2000; Liaw and Tsai, 2004; Villarreal and Dixon, 2005; Mitchell, 2007; Roebuck and Ashley, 2007). Eighteen

scenarios, representing 18 different tank sizes, were modeled using eight-year daily precipitation data, from January 1, 2000 to December 31, 2007, obtained from the National Climatic Data Center for Ronald Reagan National Airport. The average annual precipitation during this period (104 cm) was comparable to the average annual precipitation for the entire period of record (101 cm, 1948-2014). Note that the station was in operation for part of 2015, but a full year of data was not obtained, and 1948 and 1956 were excluded because data was missing for one or more months. The date range chosen to model the RWH system included one unusually dry year (2001, 76 cm of precipitation) and one unusually wet year (2003, 151 cm of precipitation) and therefore represented variability in precipitation with a relatively short period for modeling.

Runoff volume from the roof of a commercial RWH building on day t (RV_t, gallons per day) was calculated as:

$$RV_t = A \times 0.62 \times (P_t - 0.01) \times E \quad \text{(S5)}$$

where

A = roof area in plan view (ft^2)

P_t = precipitation depth on day t (in per day), and

E = collection efficiency factor (0.9 was used for this study).

A conversion factor of 0.62 was used to convert inch x ft^2 to gallons, based on a rule-of-thumb of 0.62 gallons of rainwater collection per square foot of roof area per inch rainfall (TWDB, 2005). Because RWH systems are typically designed so that the “first flush” is diverted from the tank, the first 0.01 in of rainfall on each day was subtracted from the precipitation depth of 0.01 in. This depth is equivalent to 5 gallons per 1,000 ft^2 of roof area, similar to rules-of-thumb used in designing RWH systems (TWDB, 2005; Boulware et al., 2009).

Overflow volume on day t (O_t) is calculated using a "spill before supply" approach:

$$O_t = T_{t-1} + RV_t - S \quad \text{(S6)}$$

where

S = maximum storage capacity (gallons).

Withdrawals from the system were calculated as a daily demand (D_t) of 2,685 gallons. Water use was calculated assuming 1,000 occupants (five days per week, 8 hours per day), high efficiency fixtures (0.125 g/f urinals and 1.28 g/f toilets), and an equal number of male and female occupants. We assumed 2 urinals and 1 toilet uses per male occupant per day and 3 toilet uses per female occupant per day. The volume of harvested rainwater supplied each day (RS_t in gallons) is calculated as:

$$RS_t = D_t \qquad If\ D_t \leq T_{t-1} - LW + RV_t - O_t \quad \text{(S7)}$$

$$RS_t = T_{t-1} - LW + RV_t - O_t \qquad If\ D_t > T_{t-1} - LW + RV_t - O_t \quad \text{(S8)}$$

These values were used to calculate tank water level as

$$T_t = T_{t-1} + RV_t - O_t - RS_t \quad \text{(S9)}$$

LW is a low-water cut-off level (5% of the total tank volume) and T is the water level in the tank, both in gallons, and t is time in days. This method replicated shut-down of the system when the tank's water level was low. System performance was evaluated based on volumetric reliability, or the percent of yearly demand supplied by harvested rainwater (rainwater supplied/total demand). Overflow volume per year was the average sum of O_t per year (gallons). A counter identified each day the modeled system overflows and each day the modeled system was not able to meet 100% of demand ("dry" days). Average counts of these days per year were presented as "Overflow days (per year)" and "Dry days (per year)," respectively.

The tank size selected for the LCA was 76 m^3 (20,000 gallons) based on the modeling approach detailed above (Fig. S3). Annually, this tank size would supply an average of 77% of the total estimated demand: 0.77 x 2,653 m^3y^{-1} = 2,042.81 m^3y^{-1} of harvested rainwater. Additional water demand for flushing toilets and urinals would be supplied by the municipal system. Larger tank sizes can meet more of the demand with less runoff but also require more materials, excavation and higher costs for construction. We assumed that the MWS system provided enough pressure head for a building necessary for the additional water demand, thus no extra pumps required.

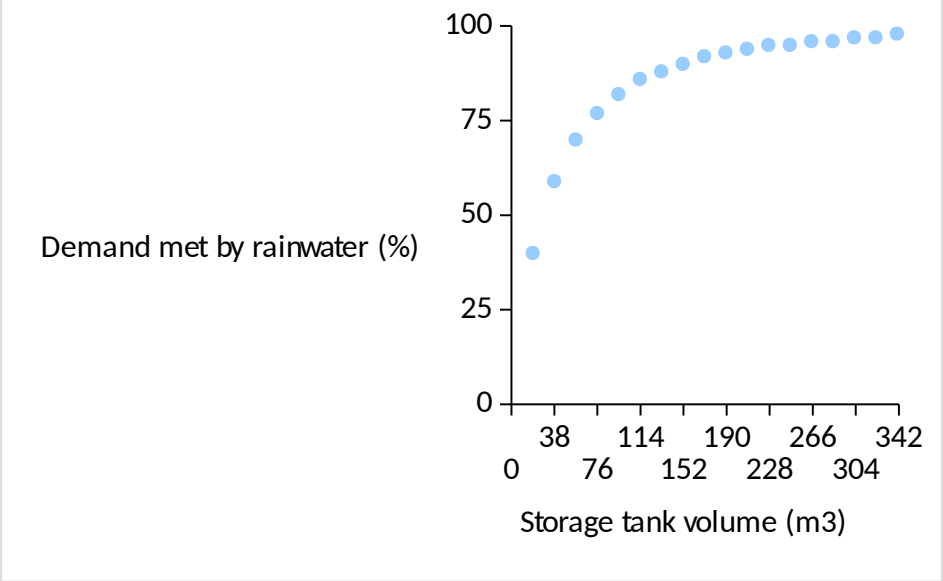

Fig. S3. Percentage demand met by a storage tank in a rainwater harvesting system (adapted with permission from RMS, 2009).

SM 2: LCA of the Benchmark Systems

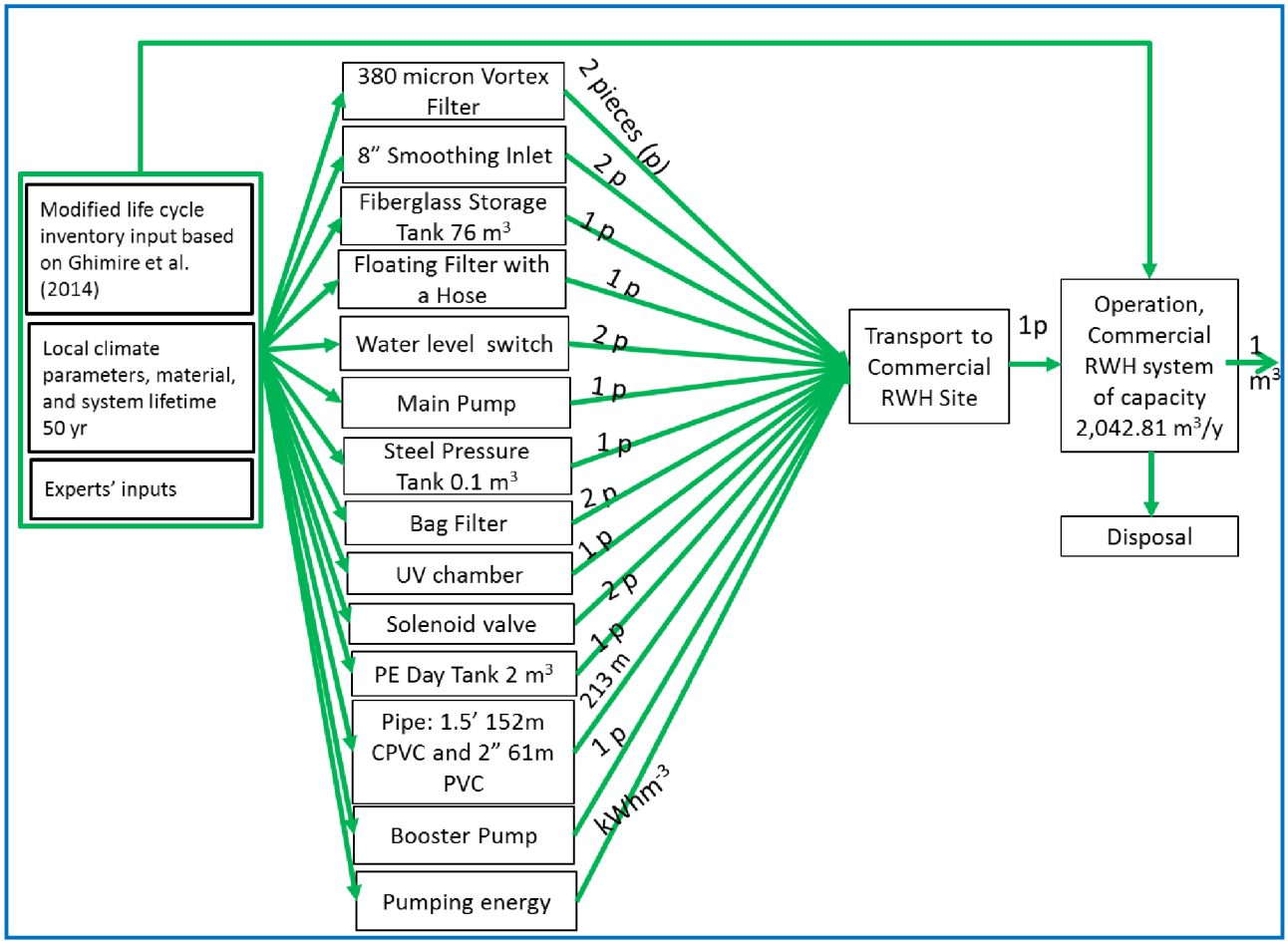

Fig. S4. Life Cycle Assessment model of commercial rainwater harvesting system. Figure adapted with permission from (Ghimire et al., 2014). Copyright (2014) American Chemical Society.

Table S1

Description of the major components of benchmark municipal water supply system and life cycle inventory (LCI).

Main component	Sub-component	Material (unit)	Amount	Service life (year)	LCI data source
Source water acquisition	Potomac River	Water (m^3)	1.003	N/A	N/A
	Source water acquisition infrastructure	Pipes, concrete, brick, excavation, reinforcing steel, Limestone (various units)	2.401E-07 m/m^3 pipes to 4.865E-03 kg/m^3 Limestone	100	Cashman et al. (2014)
Pump	Acquisition and distribution	primarily stainless steel (pieces)	24.00	15	Ghimire et al. (2014)
Energy usage	Acquisition at water treatment plants and water distribution electricity	electricity, at industrial user (kWh/m^3)	0.350	N/A	DDOE (2010); WA (2012); Cashman et al. (2014); USEIA (2016)
Screening and pre-sedimentation	Screening and grit removal infrastructure	Pipes, reinforced concrete, excavation, chromium steel, cast iron, high density polyethylene, aluminum, copper, and steel low alloyed (various units)	3.116E-08 m/m^3 pipes to 9.781E-05 kg/m^3 steel low alloyed	100	Cashman et al. (2014)
	Sedimentation infrastructure	Pipes, excavation, brick (various units)	1.633E-07 m/m^3 pipes to 3.699E-04 kg/m^3 brick	100	Cashman et al. (2014)
Flocculation and sedimentation	Flocculation	Alum coagulant, flocculation infrastructure, polyDADMAC (various units)	2.907E-07 m/m^3 pipes to 3.590E-02 lb av/m^3 Alum	100	Cashman et al. (2014)
	Sedimentation	Sedimentation infrastructure (various units)	1.633E-07 m/m^3 pipes to 3.699E-04 kg/m^3 brick	100	Cashman et al. (2014)
Filtration	Sand	sand, at mine (kg/m^3)	6.870E-03	100	Ecoinvent (2012) ; Cashman et al. (2014)
	Filtration infrastructure	Pipes, concrete, excavation, reinforcing steel (various units)	1.277E-07 m/m^3 pipes to 7.954E-05 kg/m^3 reinforcing steel	100	Cashman et al. (2014)
Primary disinfection	Primary disinfection	Quicklime, lime addition infrastructure, sodium tripolyphosphate, Fluorination, and gaseous chlorine (various	2.705E-03 kg/m^3 Quicklime to 9.376E-03 lb av/m^3 hydrogen fluoride	N/A	Cashman et al. (2014)

		units)			
Secondary disinfection	Ammonia	Ammonia, partial oxidation, liquid (kg/m^3)	4.762E-04	N/A	USEPA (1999); Ecoinvent (2012)
	Chlorine	Chlorine, gaseous (kg/m^3)	2.000E-03	N/A	Ecoinvent (2012); DCWSA (2015)
Storage tank	Tanks (11 units)	Concrete (m^3/m^3)	3.201E-08	100	DCWSA (2008); Ross (2013) ; Cashman et al. (2014)
		Steel (kg/m^3)	6.442E-05	100	DCWSA (2008); Ross (2013); Cashman et al. (2014)
		Excavation (m^3/m^3)	1.604E-05	100	DCWSA (2008) ; Ross (2013); Cashman et al. (2014)
Pipe network	Cast iron (1,772 km)	Cast iron (km/m^3)	1.282E-07	100	DCWSA (2008, 2013); Ecoinvent (2012); NIST (2013)
	Ductile iron (211.3 km)	Ductile iron (km/m^3)	1.528E-08	100	DCWSA (2008); Cashman et al. (2014)
	Steel (46.0 km)	Proxy Ductile Iron (km/m^3)	3.329E-09	100	DCWSA (2008); Ecoinvent (2012)
	Reinforced and prestressed concrete (56.5 km)	Reinforced and prestressed concrete (km/ m^3)	4.085E-09	100	DCWSA (2008); Ecoinvent (2012)
	Other (6.3 km)	PVC (km/m^3)	4.539E-10	100	DCWSA (2008); Ecoinvent (2012)
Valves	36,000 Valves	Steel (kg/m^3)	2.203E-03	100	DCWSA (2008); Cashman et al. (2014)

The life cycle impact assessment (LCIA) scores of the benchmark commercial RWH and MWS systems are provided in Tables S2 and S3.

Table S2

Life Cycle Impact Assessment scores of benchmark commercial rainwater harvesting (RWH) system and components. PVC = polyvinyl chloride; CPVC = chlorinated PVC; FG = fiberglass; UV = ultraviolet.

	Life cycle impact categories and units										
Component	Acidification kg SO2 eq	Energy Demand MJ	Eutrophication kg N eq	Fossil Depletion kg oil eq	Freshwater Withdrawal m^3	Global Warming kg CO2 eq	Human Health Criteria kg PM2.5 eq	Metal Depletion kg Fe eq	Ozone Depletion kg CFC11 eq	Smog kg O3 eq	Evapo. Water Consumption m^3 H2O eq
Bag filter	1.2E-05	1.1E-01	6.6E-07	2.4E-03	6.8E-03	3.5E-03	1.0E-06	3.1E-05	8.4E-10	1.6E-04	3.5E-11
CPVC pipe	3.9E-06	2.5E-02	4.3E-07	5.4E-04	6.3E-05	2.0E-03	1.0E-07	4.7E-05	5.4E-11	1.5E-04	4.4E-13
Day tank	2.1E-06	2.4E-02	1.5E-07	5.5E-04	1.7E-06	8.4E-04	4.0E-08	3.2E-06	5.3E-14	9.0E-05	4.8E-16
Energy usage	7.8E-04	3.8E+00	1.5E-05	6.7E-02	4.6E-02	1.7E-01	6.5E-05	1.3E-03	4.8E-09	7.4E-03	5.1E-04
FG storage tank	6.3E-04	2.3E+00	1.9E-05	4.2E-02	4.3E-01	1.2E-01	5.2E-05	6.1E-03	3.2E-08	7.9E-03	3.5E-09
Float filter	1.3E-05	6.5E-02	2.1E-06	1.3E-03	5.3E-03	3.8E-03	1.2E-06	1.2E-04	3.7E-10	1.6E-04	8.7E-08
Level sensor	1.1E-06	1.1E-02	6.3E-08	2.2E-04	6.5E-04	3.4E-04	9.8E-08	3.0E-06	8.0E-11	1.6E-05	3.3E-12
Pressure tank	1.2E-06	6.8E-03	8.4E-08	1.2E-04	1.5E-03	3.5E-04	1.7E-07	1.1E-04	4.9E-11	1.4E-05	1.7E-07
Pump	1.0E-04	1.4E-01	2.2E-06	2.7E-03	6.4E-02	7.2E-03	1.8E-05	2.8E-02	3.6E-10	6.9E-04	7.8E-09
PVC pipe	2.9E-06	2.3E-02	2.0E-07	5.0E-04	5.8E-05	1.3E-03	4.2E-08	4.4E-05	4.7E-11	1.2E-04	4.1E-13
Rain water	0.0E+00	0.0E+00	0.0E+00	0.0E+00	0.0E+00	0.0E+00	0.0E+00	0.0E+00	0.0E+00	0.0E+00	0.0E+00
Smoothing inlet	6.6E-07	3.2E-03	5.1E-08	5.6E-05	9.1E-04	1.9E-04	9.9E-08	7.6E-05	1.8E-11	7.5E-06	1.1E-07
Switch	3.3E-06	3.1E-02	1.8E-07	6.5E-04	1.9E-03	9.7E-04	2.8E-07	8.6E-06	2.3E-10	4.5E-05	9.6E-12
UV light	2.1E-05	1.0E-01	1.6E-06	1.8E-03	2.8E-02	6.1E-03	3.1E-06	2.3E-03	5.7E-10	2.5E-04	3.5E-06
Valve	2.3E-05	9.5E-03	4.4E-07	1.6E-04	1.3E-02	5.5E-04	3.2E-06	5.3E-03	4.6E-11	1.2E-04	2.2E-09
Vortex filter	2.4E-05	1.9E-01	1.2E-06	3.8E-03	3.8E-02	6.7E-03	2.3E-06	3.7E-04	1.3E-09	3.0E-04	4.1E-07
RWH system (Total)	1.6E-03	6.8E+00	4.3E-05	1.2E-01	6.4E-01	3.3E-01	1.5E-04	4.3E-02	4.1E-08	1.7E-02	5.2E-04

Table S3

Life Cycle Impact Assessment scores of benchmark municipal water supply (MWS) system and components.

Impact category	Life cycle impact categories and units										
	Acidification	Energy Demand	Eutrophication	Fossil Depletion	Freshwater Withdrawal	Global Warming	Human Health Criteria	Metal Depletion	Ozone Depletion	Smog	Evapo. Water Consumption
Component	kg SO2 eq	MJ	kg N eq	kg oil eq	m^3	kg CO2 eq	kg PM2.5 eq	kg Fe eq	kg CFC11 eq	kg O3 eq	m^3 H2O eq
Energy usage	1.3E-03	6.4E+00	2.5E-05	1.1E-01	7.8E-02	2.9E-01	1.1E-04	2.1E-03	8.3E-09	1.3E-02	8.7E-04
Filtration	1.7E-06	6.6E-03	6.4E-08	1.3E-04	1.2E-03	5.5E-04	2.1E-07	1.0E-04	2.6E-11	3.3E-05	3.7E-08
Flocculation sedimentation	2.6E-04	3.2E-01	6.5E-06	5.4E-03	7.7E-02	1.6E-02	2.3E-05	1.2E-03	1.5E-09	1.2E-03	2.4E-07
Pipe network	4.8E-05	1.8E-01	2.0E-06	3.8E-03	1.7E-02	9.8E-03	6.7E-06	3.5E-03	6.4E-10	9.0E-04	1.5E-06
Primary disinfection	8.4E-04	6.3E-01	1.7E-04	1.1E-02	1.7E-01	4.3E-02	6.0E-05	4.7E-03	8.4E-09	2.7E-03	6.3E-07
Pump	4.3E-04	6.0E-01	9.4E-06	1.1E-02	2.7E-01	3.0E-02	7.5E-05	1.2E-01	1.5E-09	2.9E-03	3.3E-08
Screening and pre-sedimentation	2.9E-06	1.3E-02	1.1E-07	2.8E-04	2.2E-03	7.6E-04	3.9E-07	3.9E-04	4.8E-11	5.9E-05	8.5E-08
Secondary disinfection	2.2E-05	7.7E-02	6.3E-07	1.3E-03	1.8E-02	4.1E-03	2.7E-06	2.5E-04	4.6E-09	1.5E-04	1.4E-10
Source water acquisition	3.3E-06	1.5E-02	1.2E-07	3.0E-04	1.2E+00	1.0E-03	2.5E-07	7.7E-05	7.2E-11	6.3E-05	1.3E-07
Storage tank	6.7E-07	2.4E-03	2.2E-08	4.9E-05	1.1E-03	1.6E-04	1.8E-07	2.5E-04	9.5E-12	1.1E-05	2.2E-11
Valves	1.9E-05	7.5E-02	5.5E-07	1.5E-03	3.5E-02	4.7E-03	6.2E-06	8.4E-03	2.5E-10	2.6E-04	7.5E-10
MWS system (Total)	3.0E-03	8.4E+00	2.1E-04	1.5E-01	1.9E+00	4.0E-01	2.9E-04	1.4E-01	2.5E-08	2.1E-02	8.8E-04

SM 3: Performance Analysis of Benchmark Systems Components

Release contribution of benchmark commercial RWH storage tank to Ozone Depletion

A Sankey diagram illustrates percentage contributions of different flows in commercial RWH storage tank (fiberglass) product system to Ozone Depletion impact. Two major flows contributing to the Ozone Depletion impact of storage tank product system were injection moulding (~73.5%) and glass fibre (~26.5%) (Fig. S5).

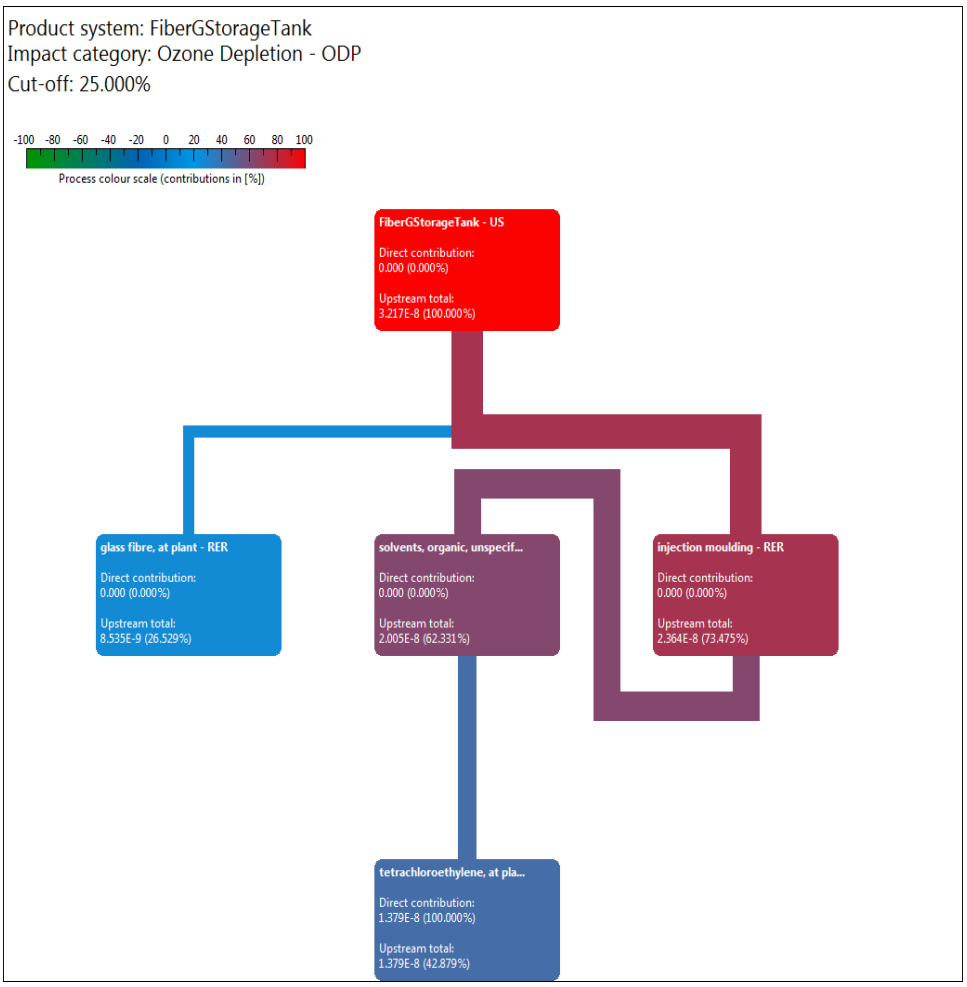

Fig. S5. Sankey diagram revealing the percentage contribution of different flows in the benchmark commercial rainwater harvesting storage tank product system's Ozone Depletion impact category (diagram generated using openLCA with cut-off at 25%) (OpenLCA, 2016).

A closer look at the processes showed that tetrachloroethylene process contributed 42.9% of the storage tank Ozone Depletion impact originating from the injection moulding (Fig. S6), and tetrachloroethylene and dichloromethane (needed for injection moulding of storage tank) contributed to 62.1% of Ozone Depletion (S6).

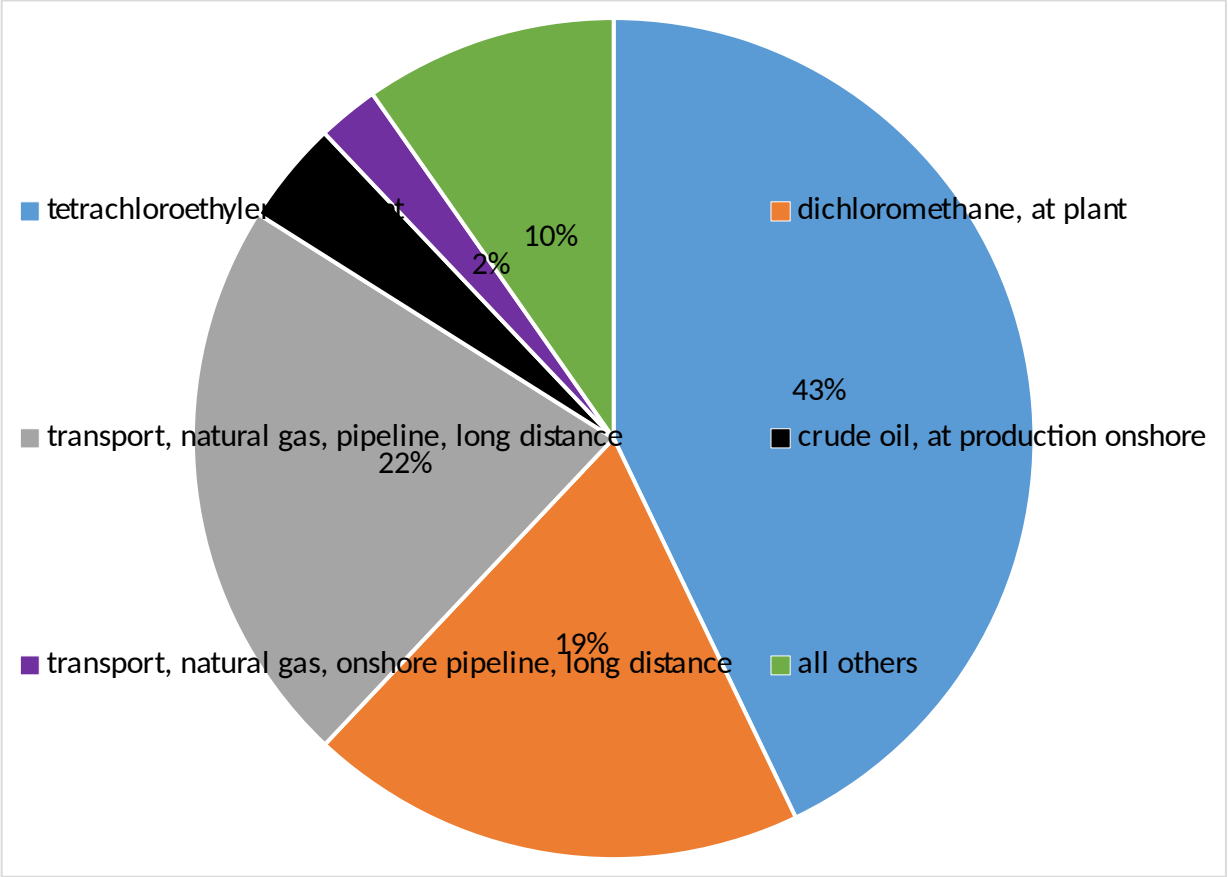

Fig. S6. Major release contributors of benchmark commercial rainwater harvesting fiberglass storage tank to Ozone Depletion impact category. All others include contributing flows lower than 2% individually such as transport (natural gas, pipeline, long distance), crude oil (at production onshore), uranium (enriched 3.0% at enrichment plant), etc. totaling <10%.

Release contribution of benchmark commercial RWH storage tank to Freshwater Withdrawal

A closer look at the processes of commercial RWH storage tank showed electricity, hydropower at run-of-river power plant as the major contributing process (93.8%) to Freshwater Withdrawal impact (Fig. S7).

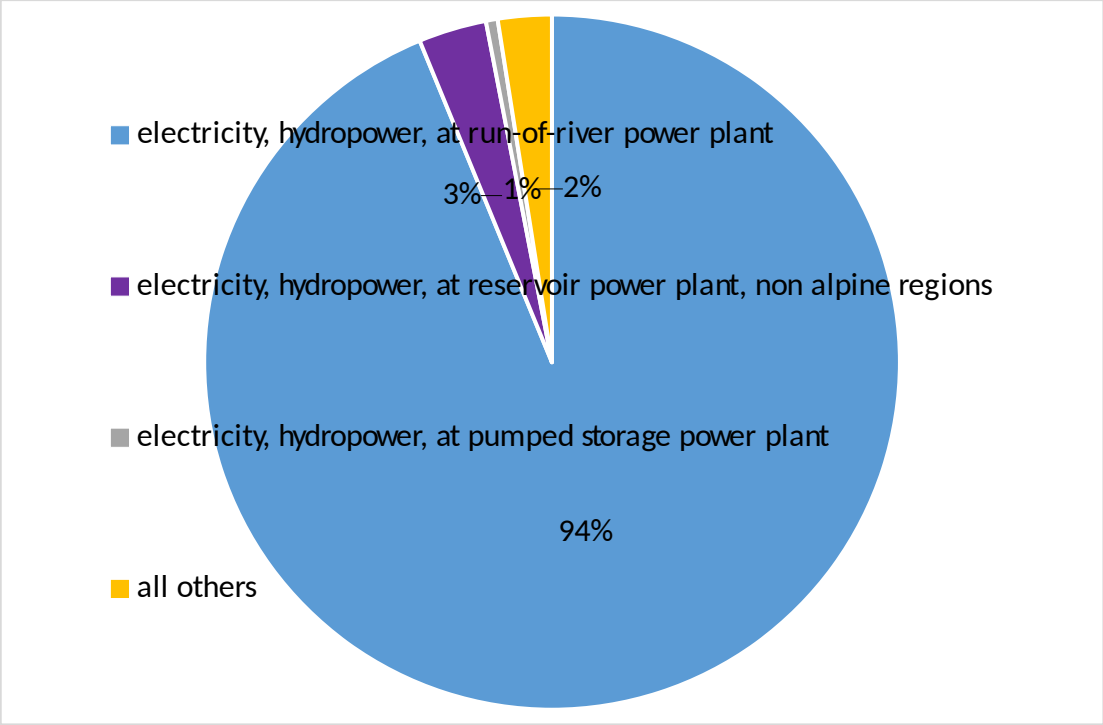

Fig. S7. Release contributors to fiberglass storage tank Freshwater Withdrawal impact. All others include contributing flows lower than 1% individually such as electricity and hydropower at pumped storage power plant, etc. totaling <3%.

Top five process contributors to benchmark commercial RWH energy usage

A further analysis of commercial RWH energy usage (pumping energy) processes revealed electricity, coal as dominant process for five impact categories: Acidification (74.3%),

Eutrophication (49%), Global Warming (67.8%), Human Health Criteria (68.9%), and Smog (55.4%) (Fig. S8).

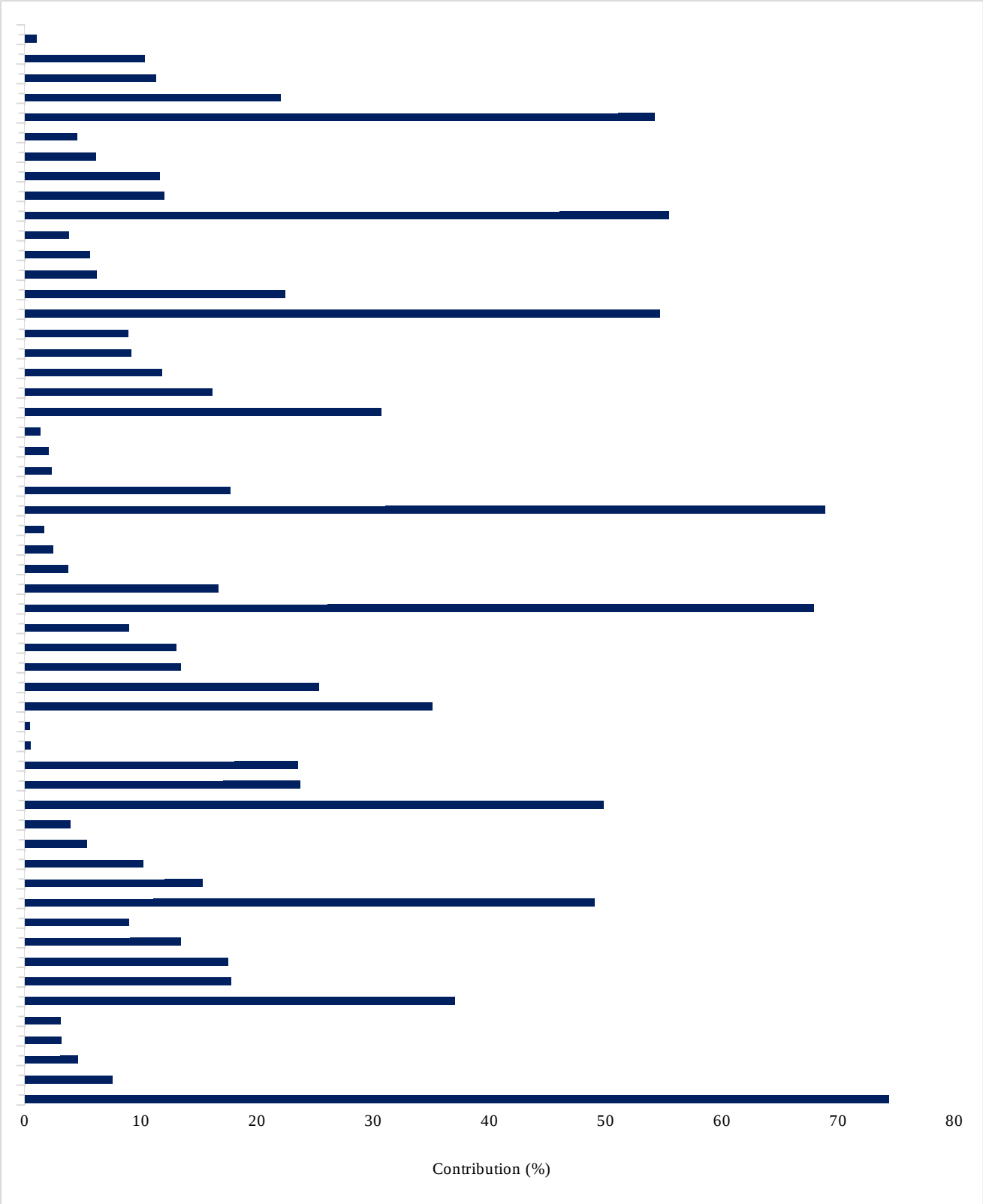
0
10
20
30
40
50
60
70
80
Contribution (%)

Fig. S8. Top five process contributors to benchmark commercial rainwater harvesting system pumping energy life cycle impact categories.

Release contribution of benchmark commercial RWH pump to Metal Depletion

A closer look at the processes of commercial RWH pump to the dominant Metal Depletion impact indicated copper concentrate as the major (68.0%) release contributor (Fig. S9).

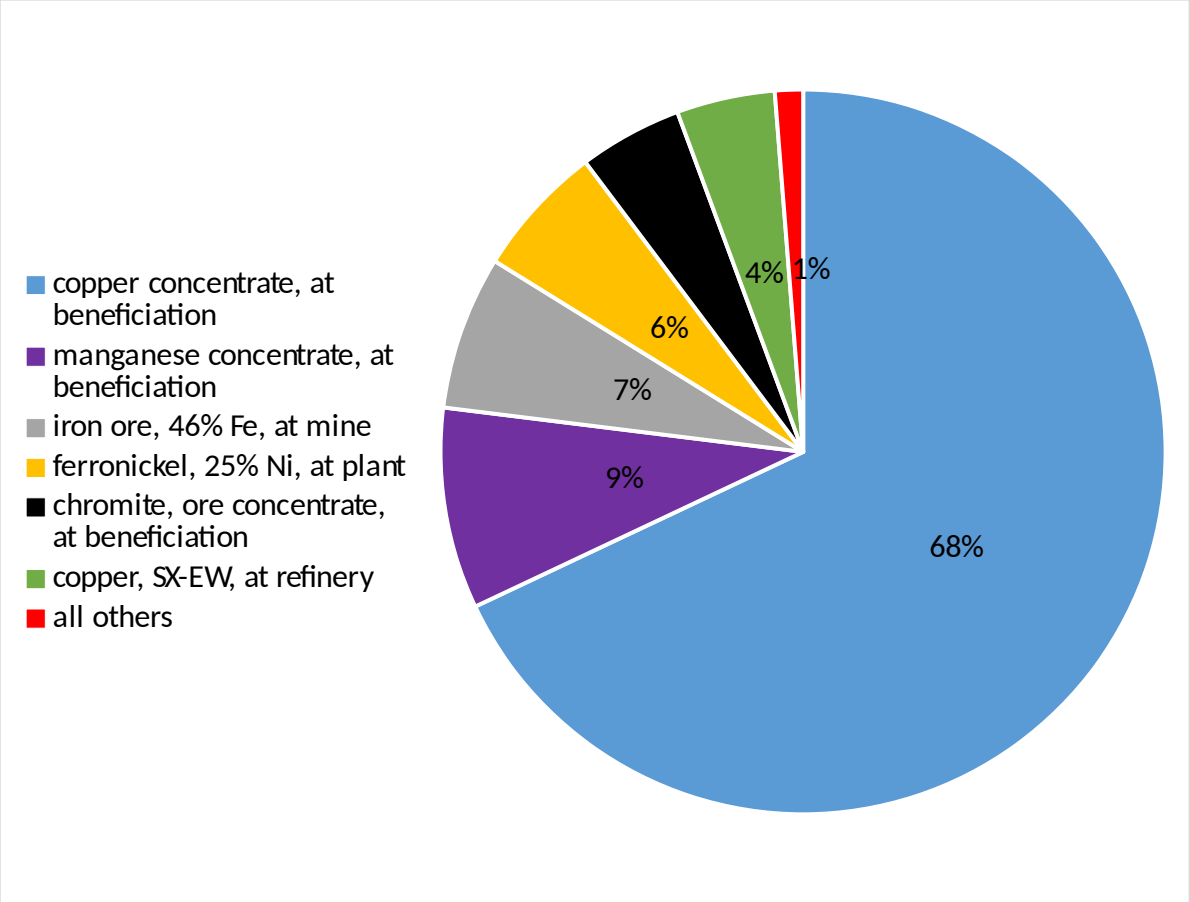

Fig. S9. Major release contributors of benchmark commercial rainwater harvesting system Pump to Metal Depletion impact category. All others include contributing flows lower than 1% individually, such as Molybdenum concentrate, main product tin, at regional storage, etc. totaling <2%.

SM 4: Sensitivity Analysis of Benchmark Systems

Sensitivity of storage tank materials on the LCIA of commercial RWH system

Table S4
Description of Storage tank materials.

Main component	Sub-component	Material	Mass (kg)	Source
Fiberglass (FG) Storage Tank and accessories	FG Storage Tank	Glass fibre	2,773	Ecoinvent (2012)
	Two FG Access Riser (36 in Diameter 3 ft tall)	Glass fibre	113.6	Ecoinvent (2012)
	Two FG Access Collars (36 in Diameter)	Glass fibre	113.6	Ecoinvent (2012)
	Two overflow pipe (8 in Diameter 2 ft high-density polyethylene or HDPE)	Water supply 1 in 1 m - PE cradle-to-gate: equivalent length of 4 x 8 ft x 0.3048 m/ft = 9.75 m	2.3	NIST (2013)
Polyethylene (PE) Storage Tank and accessories (BEES database)	PE Storage Tank	Water supply 1 in 1 m - PE cradle-to-gate: equivalent length 10,507 m @ 0.16 lb/ft	2,506	NIST (2013); Plastic-Mart (2016)
	Two PE Access Riser (36 in Diameter 3 ft tall)	Water supply 1 in 1 m - PE cradle-to-gate: equivalent length of 36 x 2 x 3 ft x 0.3048 m/ft	15.7	NIST (2013)
	Two PE Access Collars (36 in Diameter x 3 ft)	Water supply 1 in 1 m - PE cradle-to-gate: equivalent length of 36 x 2 x 3 ft x 0.3048 m/ft	15.7	NIST (2013)
	Two overflow pipe (8 in 2 ft HDPE)	Water supply 8 in 1 m - PE cradle-to-gate: equivalent length of 8 x 2 x 2 ft x 0.3048 m/ft	2.3	NIST (2013)
PE Storage Tank and accessories (Ecoinvent database)	PE Storage Tank	Polyethylene, HDPE, granulate, at plant	2,506	Ecoinvent (2012); (Plastic-Mart, 2016)
	Two PE Access Riser (36 in Diameter 3 ft tall)	Polyethylene, HDPE, granulate, at plant	15.7	Ecoinvent (2012)
	Two PE Access Collars (36 in Diameter)	Polyethylene, HDPE, granulate, at plant	15.7	Ecoinvent (2012)

Two overflow pipe (8 in 2 ft long HDPE)	Polyethylene, HDPE, granulate, at plant: @ (0.16 lb/ft x 8 x 4 ft x 1kg/2.2 lb)	2.3	NIST (2013)

We performed an LCIA of commercial RWH storage tank (76 m^3) materials, fiberglass and polyethylene (PE) with Ecoinvent (2012) and the Building for Environmental and Economic Sustainability (BEES) database of the National Institute of Standards and Technology (NIST, 2013) (Table S4).

The LCIA of the storage tanks (fiberglass and PE materials) indicated mixed results: fiberglass dominated in nine impact categories and PE dominated in the remaining two, Energy Demand and Fossil Depletion, regardless of data source (Fig. S10).

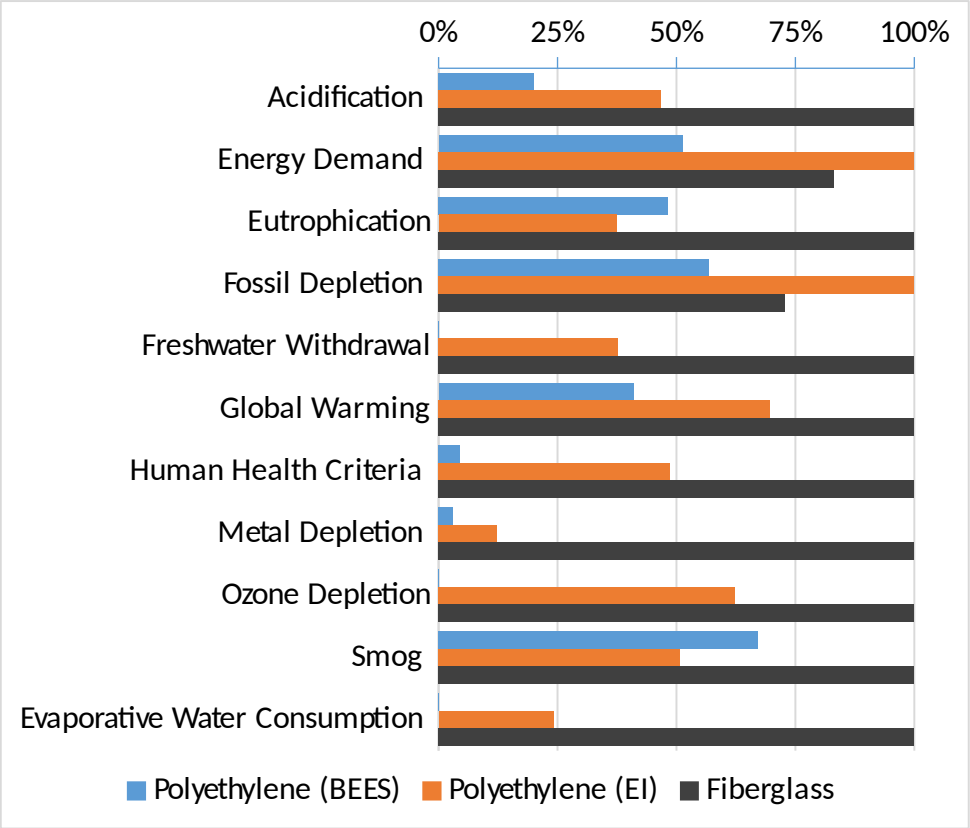

Fig. S10. Life Cycle Impact Assessment **(**LCIA) comparison of commercial rainwater harvesting storage tank materials fiberglass and polyethylene with two different data sources, the Building for Environmental and Economic Sustainability (BEES) database and Ecoinvent database (EI). LCIA impact scores were normalized by maximum value per category.

Sensitivity of storage tank volume on the LCIA of commercial RWH system

We varied the benchmark commercial RWH storage tank volume from 19 m^3 to 342 m^3 (0.25 to 4.5 times the benchmark volume of 76 m^3), keeping system demand and other design parameters unchanged. The maximum volume of 342 m^3 (i.e., 4.5 x 76 m^3) equals 100% of water demand met by commercial RWH. The normalized LCIA with respect to maximum impact at

342 m^3 revealed linear variation in impacts with zones of Mild, Moderate, and High slopes (Fig. S11), similar to energy usage variation zones.

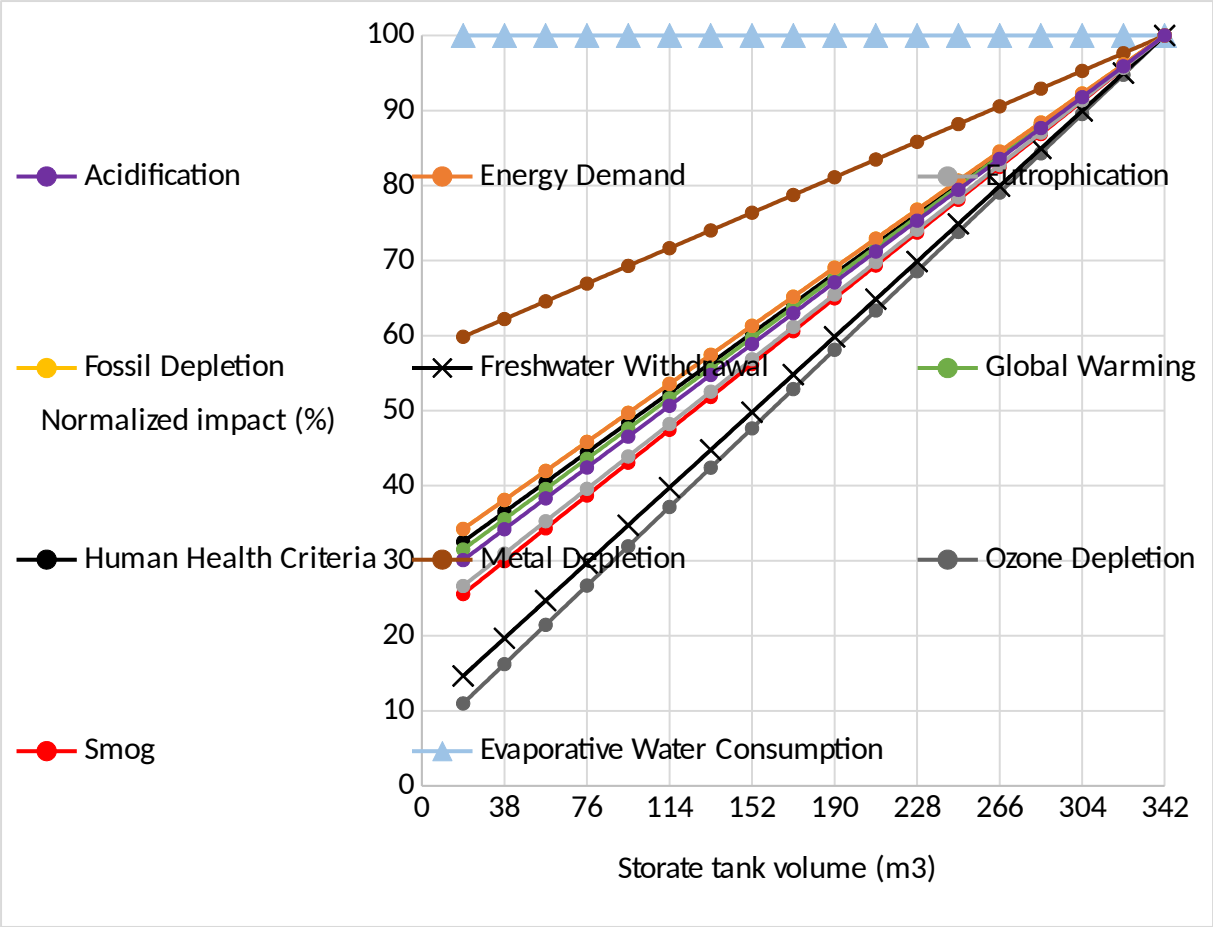

Fig. S11. Sensitivity analysis of commercial rainwater harvesting (RWH) storage tank volume variation to Life Cycle Impact Assessment (LCIA) of benchmark commercial RWH system. LCIA impact scores were normalized by maximum value of 342 m^3.

The storage tank's Evaporative Water Consumption impact was found to be insensitive to the commercial RWH system because its actual Evaporative Water Consumption (3.46×10^{-9} m^3) was negligible when compared to commercial RWH's 0.00051 m^3 (Fig. S12). Further, the Ecoinvent 2.2 database was not comprehensive in its inclusion of evaporative water losses, partially contributing to underestimates of actual Evaporative Water Consumption.

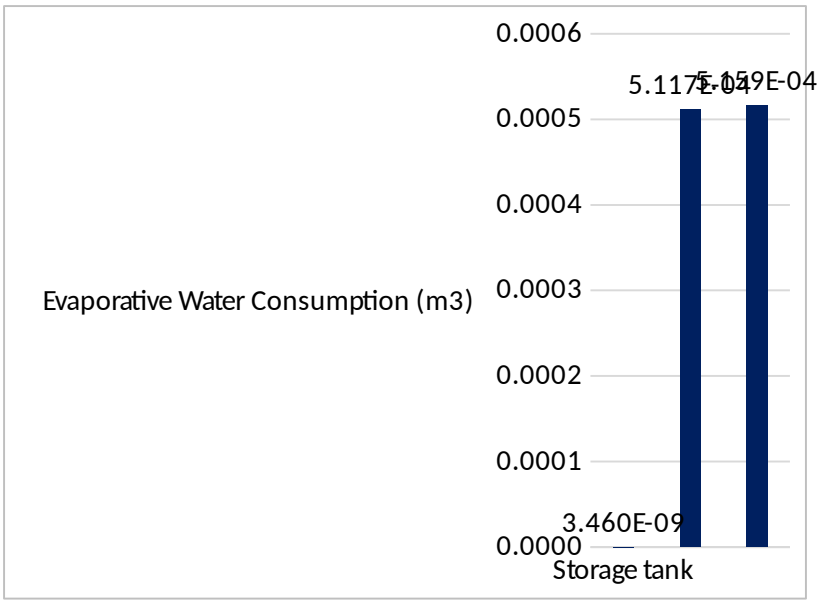

Fig. S12. Comparison of Evaporative Water Consumption impact of commercial rainwater harvesting (RWH) system with storage tank and pumping energy.

Sensitivity of water demand on the LCIA of commercial RWH system

We varied the benchmark commercial RWH system water demand (2,653 m^3/y) from 265.3 m^3/y to 2,653 m^3/y (10% to 100%). Each commercial RWH component input except pump and pumping energy was influenced by this variation because flow inputs for the components were normalized by water demand. Pump and pumping energy intensity were kept constant, regardless of the demand variation range. Because input flows of each component were normalized by water demand, the impacts also varied inversely (Fig. S13a, b).

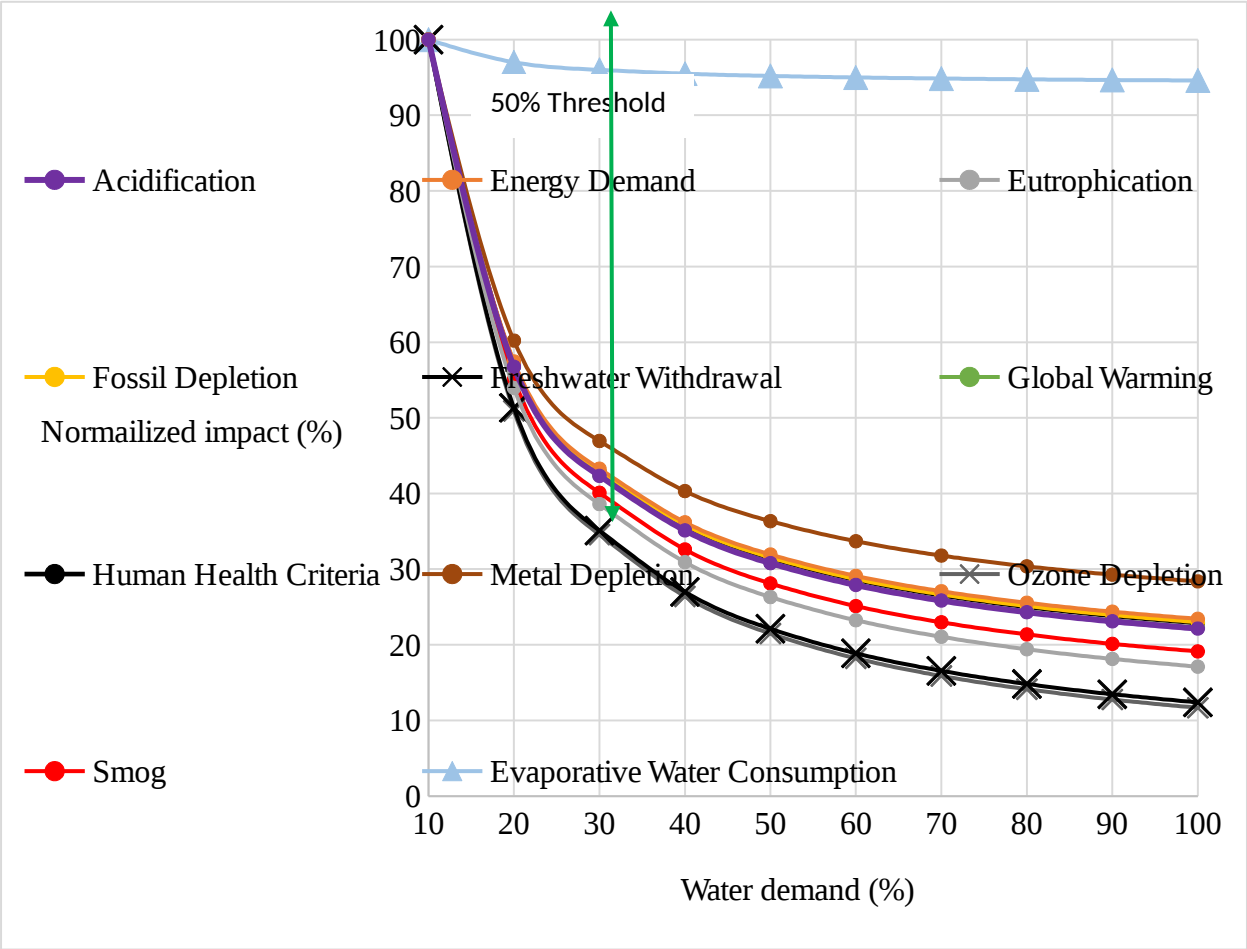

Fig. S13 a. Sensitivity analysis of benchmark commercial rainwater harvesting system annual water demand variation (10%-100% of total system demand at 2,653 m^3/y) to Life Cycle Impact Assessment (LCIA). LCIA impacts were normalized by maximum value at lowest annual water demand of 10% of 2,653 m^3/y.

Notice that the high variation zone was still Ozone Depletion impact because the storage tank was the dominant component for this category; the minor variation in Evaporative Water Consumption slope occurred for the same reason discussed in the storage tank sensitivity analysis in Fig. S12.

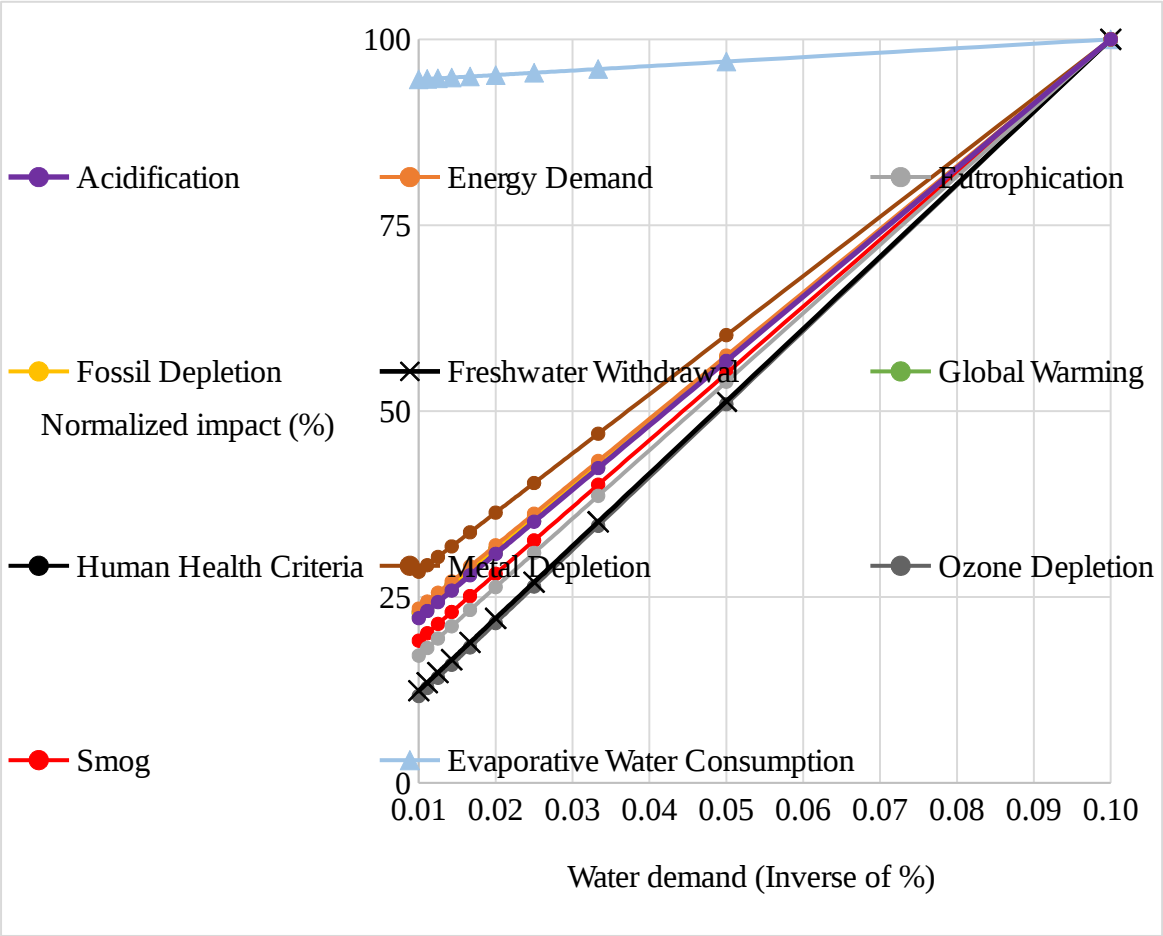

Fig. S13 b. Sensitivity analysis of benchmark commercial rainwater harvesting system annual water demand variation with inverse scale of percentage (i.e., from 1/10% to 1/100% of benchmark system demand at 2,653 m^3/y) to Life Cycle Impact Assessment (LCIA). LCIA impacts were normalized by maximum value at lowest annual water demand of 10% of 2,653 m^3/y.

Sensitivity of water losses on the LCIA of commercial RWH and MWS systems

We varied water losses from 0% to 30% throughout the benchmark commercial RWH and MWS systems. Normalized LCIA results with respect to maximum impact values at 30% water loss in benchmark systems indicated linear variation in all impacts which was expected

due to the corresponding linear variation in input flows. Because water loss linearly altered the input of each component, LCIA impacts also varied for both systems (Fig. S14); sensitivity of water loss to Ozone Depletion impact is presented as an example, and all other impact categories followed the same trend (not shown).

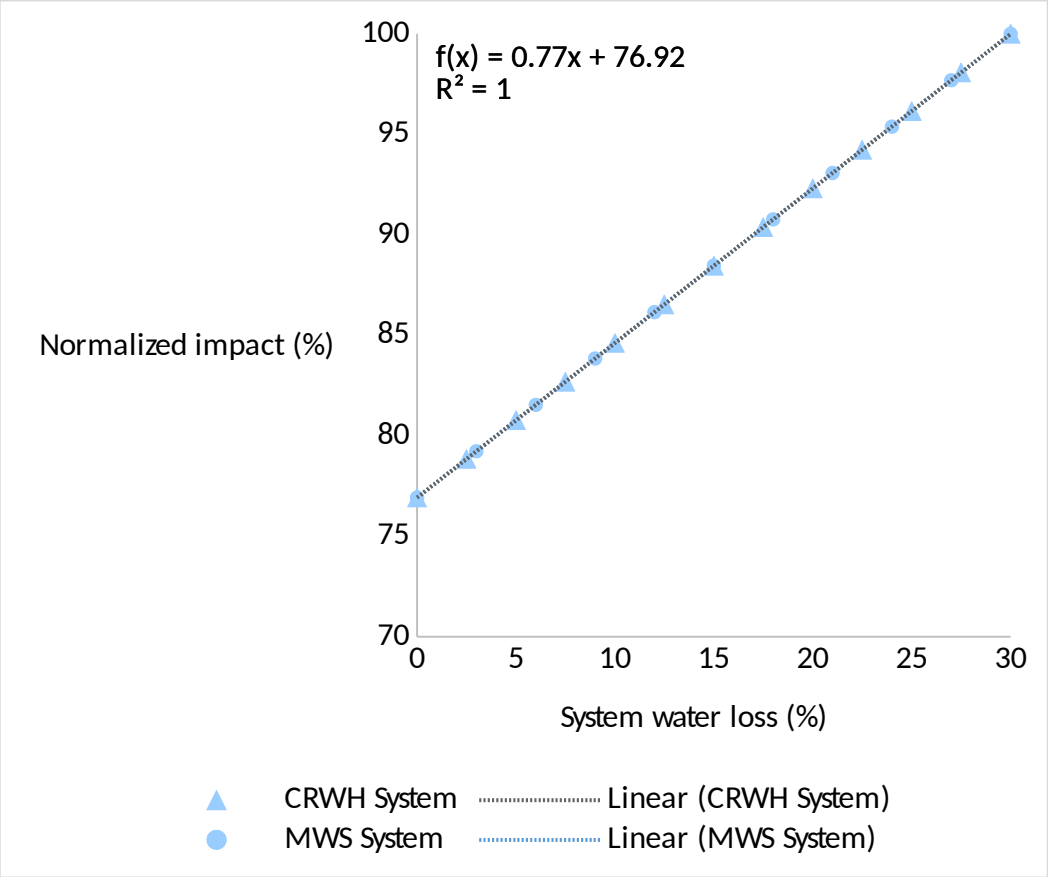

Fig. S14. Sensitivity analysis of water losses in benchmark commercial rainwater harvesting (CRWH) and municipal water supply (MWS) systems. Ozone Depletion impact normalized with respect to maximum Ozone Depletion impact, with highest water losses at 30%.

Sensitivity of service life on the LCIA of commercial RWH system

We performed the sensitivity analysis of benchmark commercial RWH system to service lives of 50 and 75 years. Annual LCIA results were normalized with respect to maximum impact

values at shorter service life of 50 years. Analysis showed lower annual LCIA impacts for the commercial RWH system with a higher service life of 75 years ranging from 66.9% (Evaporative Water Consumption) to 99.0% (Metal Depletion) (Fig. S15).

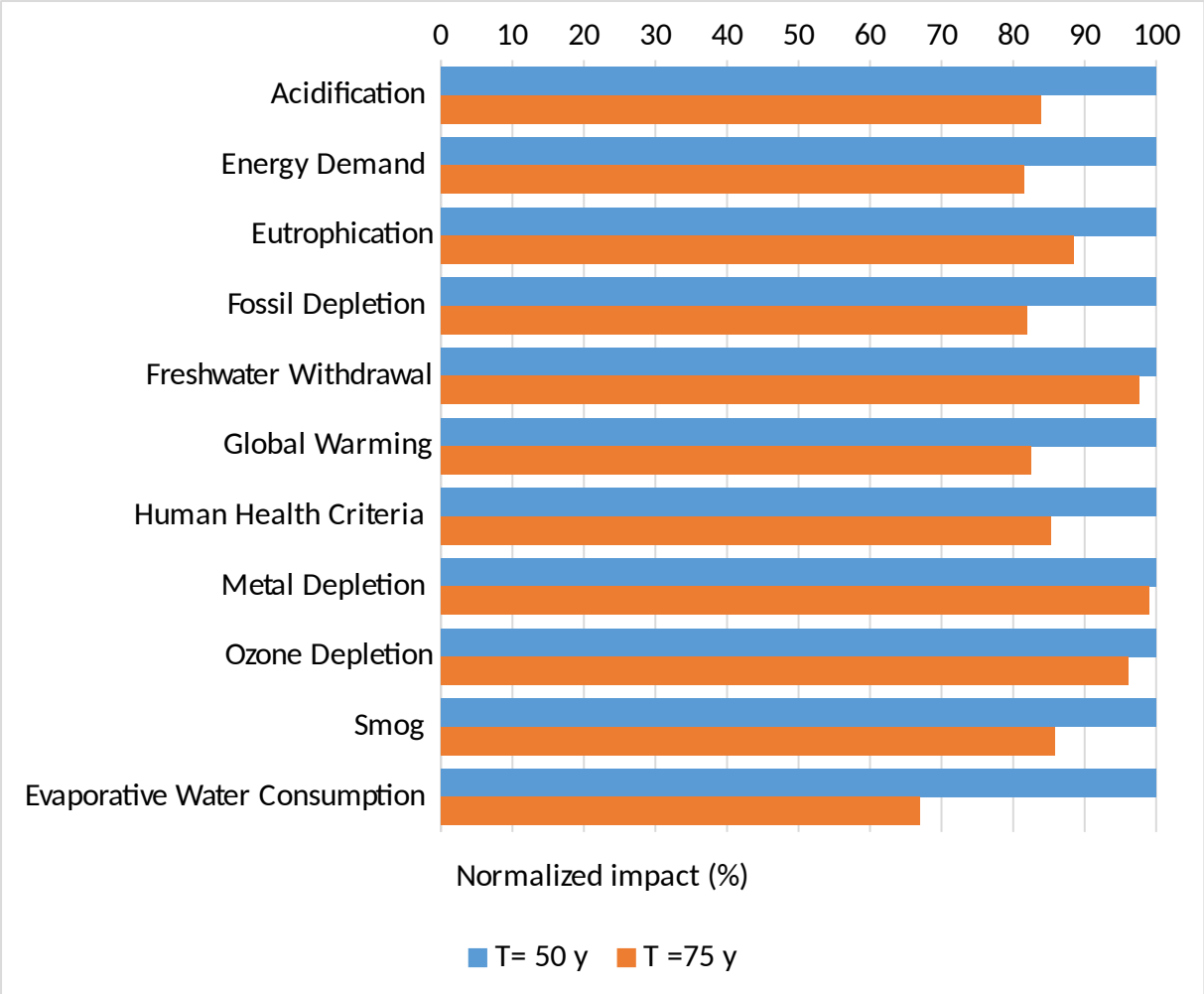

Fig. S15. Sensitivity of benchmark commercial rainwater harvesting system to system service life, T. Annual Life Cycle Impact Assessment (LCIA) scores were normalized by maximum LCIA scores at T = 50 year (y).

Tradeoff analysis of auxiliary commercial RWH system augmented with municipal water supply

Analysis of the auxiliary commercial RWH system provided additional insights into LCIA tradeoffs. An auxiliary commercial RWH with 50% MWS reduced Ozone Depletion impact by 19% showing increases in all other impacts with respect to benchmark commercial

RWH impacts (Fig. S16). The slope of auxiliary commercial RWH system's Ozone Depletion impact was reversed because the benchmark commercial RWH system's Ozone Depletion impact was greater than that of the MWS system.

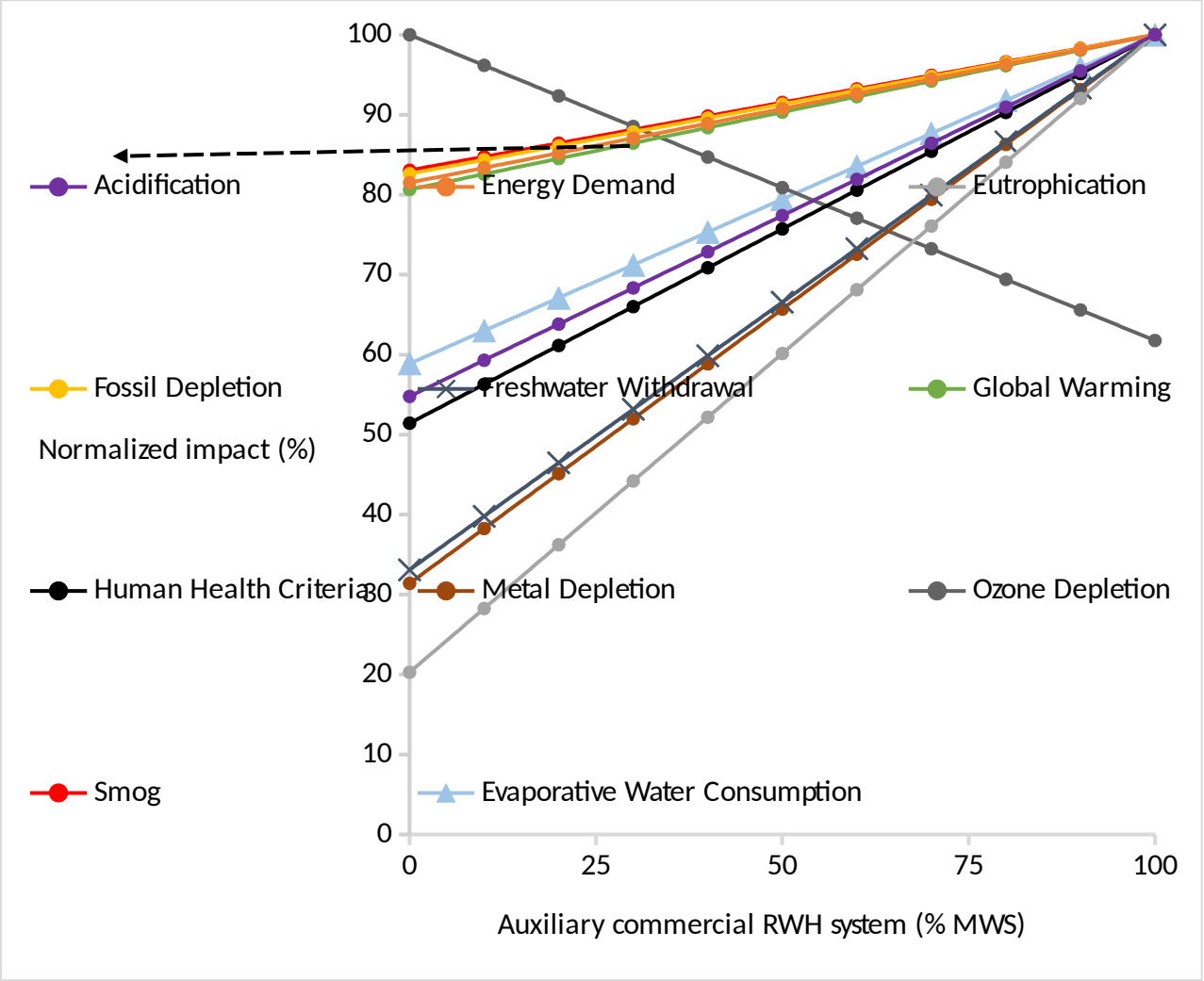

Fig. S16. Tradeoff analysis of an auxiliary commercial rainwater harvesting (RWH) system augmented with municipal water supply (MWS). Life Cycle Impact Assessment (LCIA) scores were normalized by maximum LCIA value at 100% MWS.

LCIA normalization

For all analyses, the normalized impact was calculated with respect to maximum impact, as given by Equation (S10):

$$I_n = \frac{I}{I_{max}} x\,100 \tag{S10}$$

where for a specified LCIA impact category,

I_n = normalized impact (dimensionless, %)

I_{max} = maximum impact (impact/m^3)

I = current impact (impact/m^3)

Mean absolute percentage error (MAPE)

Mean absolute percentage error (MAPE) was estimated as:

$$MAPE = \frac{100}{n} x \sum_{n=1}^{15} ¿\,\frac{¿}{M}\,¿\,M - F \vee ¿ \tag{S11}$$

where

n = Number of variants (15)

M = Modeled LCIA score

F = Forecast LCIA score using the tradeoff equation

REFERENCES

AWE, 2016. Office Building Introduction. www.allianceforwaterefficiency.org/office_buildings.aspx (April 13, 2016).

Boulware, E.B., Pope, T., Lye, D., Kniffen, B., Wheeler, J., Morris, W., Jennings, R., Shultz, J., Winters, W., Daily, C., Knight, J., 2009. Rainwater catchment design and installation standards. American Rainwater Catchment Systems Association and American Society of Plumbing Engineers, USA.

Cashman, S., Gaglione, A., Mosley, J., Weiss, L., Hawkins, T.R., Ashbolt, N.J., Cashdollar, J., Xue, X., Ma, C., Arden, S., 2014. Environmental and cost life cycle assessment of disinfection options for municipal drinking water treatment. U.S. Environmental Protection Agency, Cincinnati, OH USA.

Cheng, C.-L., 2002. Study of the inter-relationship between water use and energy conservation for a building. Energy and Buildings 34, 261-266.

DCWSA, 2008. Independent Engineering Inspection of the District Of Columbia Water and Sewer Authority's Wastewater and Water Systems. District of Columbia Water and Sewer Authority Washington DC.

DCWSA, 2013. Independent Engineering Inspection of DC Water's Wastewater and Water Systems, findings and recommendations, Final Report. District of Columbia Water and Sewer Authority Washington DC.

DCWSA, 2015. Chlorine, Disinfection Performance. www.dcwater.com/waterquality/chlorine.cfm, (Oct. 7, 2015).

DDOE, 2010. District of Columbia Greenhouse Gas Emissions Inventory 2006 Emissions Baseline. District Department of the Environment, Washington, DC.

Ecoinvent, 2012. Ecoinvent Centre. www.ecoinvent.org (July 2, 2012).

Fewkes, A., 2000. Modelling the performance of rainwater collection systems: towards a generalised approach. Urban Water 1, 323-333.

Ghimire, S.R., Johnston, J.M., Ingwersen, W.W., Hawkins, T.R., 2014. Life Cycle Assessment of Domestic and Agricultural Rainwater Harvesting Systems. Environmental Science & Technology 48, 4069-4077.

Liaw, C.H., Tsai, Y.L., 2004. Optimum storage volume of rooftop rain water harvesting systems for domestic use. Wiley Online Library.

Mitchell, V.G., 2007. How important is the selection of computational analysis method to the accuracy of rainwater tank behaviour modelling? Hydrol Process 21, 2850-2861.

NAP, 2015. Using Graywater and Stormwater to Enhance Local Water Supplies: An Assessment of Risks, Costs, and Benefits. The National Academies of Sciences, Engineering, and Medicine, Washington, DC.

NIST, 2013. Building for Environmental and Economic Sustainability (BEES). www.nist.gov/el/economics/BEESSoftware.cfm (Feb 15, 2013).

OpenLCA, 2016. openLCA 1.4.2. www.openlca.org/.

Pabi, S., Amarnath, A., Goldstein, R., Reekie, L., 2013. Electricity Use and Management in the Municipal Water Supply and Wastewater Industries.

Plastic-Mart, 2016. 20000 Gallon Vertical Plastic Storage Tank. www.plastic-mart.com/product/6470/20000-gallon-vertical-plastic-storage-tank-43825 (Aug. 2, 2016).

Retamal, M., Glassmire, J., Abeysuriya, K., Turner, A., White, S., 2009. The Water-Energy Nexus: Investigation into the Energy Implications of Household Rainwater Systems. Institute for Sustainable Futures, University of Technology, Sydney.

RMS, 2009. Tank sizing spreadsheet. Rainwater Management Solutions, Salem, VA.

Roebuck, R., Ashley, R., 2007. Predicting the hydraulic and life-cycle cost performance of rainwater harvesting systems using a computer based modelling tool. Water Practice and Technology 2, wpt2007046.

Ross, R.B., 2013. Metallic materials specification handbook. Springer Science & Business Media.

TWDB, 2005. The Texas Manual on Rainwater Harvesting, 3rd ed. Texas Water Development Board, Austin, USA.
USEIA, 2016. Electric Sales, Revenue, and Average Price www.eia.gov/electricity/sales_revenue_price/index.cfm (April 13, 2016).
USEPA, 1999. Alternative Disinfectants and Oxidants Guidance Manual. Office of Water, U.S. Environmental Protection Agency, Washington DC.
USEPA, 2009. WaterSense Specification for Flushing Urinals. www3.epa.gov/watersense/docs/urinal_finalspec508.pdf (August 14, 2009).
Vieira, A.S., Beal, C.D., Ghisi, E., Stewart, R.A., 2014. Energy intensity of rainwater harvesting systems: A review. Renewable and Sustainable Energy Reviews 34, 225-242.
Villarreal, E.L., Dixon, A., 2005. Analysis of a rainwater collection system for domestic water supply in Ringdansen, Norrköping, Sweden. Building and Environment 40, 1174-1184.
WA, 2012. Washington Aqueduct Annual Financial Report Fiscal Year 2012. Finance and Accounting Office, Washington Aqueduct, Washington, DC.
Wang, R., Zimmerman, J.B., 2015. Economic and environmental assessment of office building rainwater harvesting systems in various U.S. cities. Environ Science& Technol 49, 1768-1778.
Ward, S., Butler, D., Memon, F.A., 2012. Benchmarking energy consumption and CO2 emissions from rainwater-harvesting systems: an improved method by proxy. Water and Environment Journal 26, 184-190.

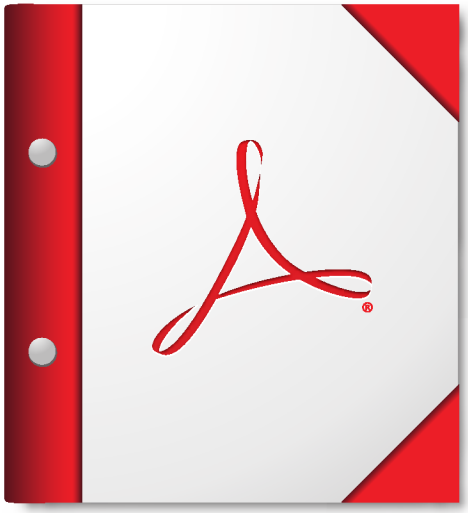

For the best experience, open this PDF portfolio in Acrobat X or Adobe Reader X, or later.

Get Adobe Reader Now!

ARCSA® FOUNDATION

and

ARCSA®
AMERICAN RAINWATER CATCHMENT SYSTEMS ASSOCIATION

May 1, 2020

Dear STAA Selection Committee:

The ARCSA Foundation is dedicated to expanding and sharing knowledge about rainwater harvesting systems to encourage the smart adoption of rainwater harvesting to maximize environmental benefit while protecting human health. When designed, installed and maintained correctly, rainwater-harvesting systems can reduce the strain on municipal water supplies and private groundwater sources, reduce storm water runoff, and reduce energy consumption for water treatment and distribution. However, research on how to appropriately design, install and maintain these systems is lacking. One particular issue is a disconnect between researchers and the rainwater harvesting industry. This often leads to results that are not applicable in the industry. The nominated research paper (Ghimire et al, 2017) stands in stark contrast to this overall trend. The results of the paper provide valuable insight into designing systems to maximize their environmental benefit and minimize the environmental impacts. These findings have helped guide an increasing emphasis on "right-sizing" systems. Research such as this helps move rainwater harvesting beyond simple rain barrels to larger-scale systems with greater environmental benefits.

American Rainwater Catchment Systems Association Foundation

Name: Jim Urtz, President

Signature: Jim Urtz Date: May 1, 2020

American Rainwater Catchment Systems Association

Name: James M. Majerowicz, President

Signature: James M. Majerowicz Date: May 1, 2020

ARCSA® FOUNDATION

and

ARCSA®
AMERICAN RAINWATER CATCHMENT SYSTEMS ASSOCIATION

May 1, 2020

Dear STAA Selection Committee:

The ARCSA Foundation is dedicated to expanding and sharing knowledge about rainwater harvesting systems to encourage the smart adoption of rainwater harvesting to maximize environmental benefit while protecting human health. When designed, installed and maintained correctly, rainwater-harvesting systems can reduce the strain on municipal water supplies and private groundwater sources, reduce storm water runoff, and reduce energy consumption for water treatment and distribution. However, research on how to appropriately design, install and maintain these systems is lacking. One particular issue is a disconnect between researchers and the rainwater harvesting industry. This often leads to results that are not applicable in the industry. The nominated research paper (Ghimire et al, 2017) stands in stark contrast to this overall trend. The results of the paper provide valuable insight into designing systems to maximize their environmental benefit and minimize the environmental impacts. These findings have helped guide an increasing emphasis on "right-sizing" systems. Research such as this helps move rainwater harvesting beyond simple rain barrels to larger-scale systems with greater environmental benefits.

American Rainwater Catchment Systems Association Foundation

Name: Jim Urtz, President

Signature: Jim Urtz Date: May 1, 2020

American Rainwater Catchment Systems Association

Name: James M. Majerowicz, President

Signature: James M. Majerowicz Date: May 1, 2020

Table of Contents

General_Authors_Publications.....2
LI-267138_Trebitz_Hoffman_TAFS2015.....18
LI-267139_Sierszen_et_al_JGLR_2019.....40
LI-267141_Schoen_etal_LimnolOceanogr_2016.....49
Record_of_Percentage_Agreement_Cooper.....63
Record_of_Percentage_Agreement_Hoffman.....64
Record_of_Percentage_Agreement_Kosiara.....65
Record_of_Percentage_Agreement_Schoen.....66
Record_of_Percentage_Agreement_Sierszen.....67
Record_of_Percentage_Agreement_Trebitz.....68
Record_of_Percentage_Agreement_Uzarski.....69

STAA REPORT FOR THE SCIENTIST NOMINATIONS

General Information:

Nomination ID/App ID:	20-142
Research Category Primary:	Ecological Research (ER)
Research Category Secondary:	Monitoring and Measurement Methods (MM)
Laboratory/Office Name:	ORD
Nomination Entered By:	Joel Hoffman

Eligibility Checklist:

[Y] The nominated publication(s) has not been submitted to a previous STAA competition.

[Y] The nominated publication(s) was published on or before January 1, 2017 and on or after January 1,2012

[Y] The principal author was an EPA employee or a PHS employee assigned to EPA when the research was performed

[Y] The EPA authors (includes PHS employees assigned to EPA) contributed collectively a minimum of 50% toward the publication(s)

Nominating Official Name:	Joel Hoffman
Nominating Official Title:	SUPERVISORY BIOLOGIST
Nominating OfficialEmail:	hoffman.joel@epa.gov
STAA Coordinator Name:	Kathleen Wiser
STAA Coordinator Email:	wiser.kathi@epa.gov

Justifications:

Justification 1:

Ecosystem services accounting allows actual or potential environmental changes to be evaluated in terms of their likely effects on humans. Fishery support is a prominent ecosystem service attributed to aquatic systems and refers to providing spawning, foraging, and refuge habitat to species that are exploited for recreational fishing or commercial harvest. While this concept is broadly accepted, it remains a scientific challenge to quantify this ecosystem service in coastal zones where fish production is related to a mosaic of wetland, river, and open-water habitats; and human utilization of that production, while extensive, is distributed widely over user groups and over a spatial extent far larger than any specific habitat element. Coastal wetlands in the Laurentian Great Lakes exemplify a complex fishery support situation, with a variety of commercially and recreationally valuable fish species using them for nursery, rearing, foraging, and spawning habitat but also spending substantial time out in the open lake. Further, human user groups value diverse aspects of the fishery, including dockside value (commercial harvesters), trophy size and catchability (sport anglers), and eating quality (family and subsistence fishers). Addressing this challenge requires improved association of coastal wetland species with available commercial and recreational fisheries data, as well as improved methods for associating coastal wetland habitat use with specific life stages (larvae, juvenile, adult) and habitat function. The pair of nominated papers showcase the EPA/ORD effort to address coastal-zone fishery support from two distinct but complimentary angles – one paper conceptually links harvested fish species with coastal wetland usage to assess the magnitude of fishery support, while the other empirically links harvestable fish species to multiple potential habitats to determine which hydrogeomorphic settings most strongly foster cross-habitat support.

The Trebitz and Hoffman (2015) paper focuses on establishing associations between fisheries data and coastal wetland habitat use. The approach was to combine recreational and commercial harvest data with coastal wetland survey data to identify fishery-relevant, wetland-using species; then to examine their exploitation and life history patterns to determine how multispecies fishery support can be decomposed into more homogeneous and measurable components; and finally to examine relationships of those components to coastal wetland condition to identify ecosystem service changes associated with habitat degradation and restoration. The key findings of this paper are that at least 21 Great Lakes fish species that are

directly harvested or that serve as prey for harvested species are regular users of coastal wetlands, that >50% of the commercial fishery (ca. 11,000 metric tons annually) and >80% of the recreational fishery (ca. 4.3 million fish annually) in the Great Lakes is accounted for by wetland-using species, and that wetland degradation is associated with a shift from dominance by commercially and recreationally high-values species in high quality wetlands to dominance by

low-value rough species in impacted wetlands, implying that restoring coastal wetlands can improve both commercial and recreational fisheries in the Great Lakes.

The Sierszen et al. (2019) paper focuses on quantifying fish production across a gradient of hydrogeomorphic settings to determine for which species and which ecological settings cross-habitat fishery-support is most likely to occur. The approach relied on an improved ecological tracer method (described in the Schoen et al. (2016) supporting article) to dissect habitat use for multiple fishery-relevant species caught in both coastal wetland and nearshore areas. The author list includes collaborators who helped to collect specimens and environmental data in some of the wetlands; EPA ORD authors Michael Sierszen (retired) and Joel Hoffman led the design and analysis of the data as well as the drafting of the manuscript. The key findings are that use of resources from multiple habitats by high-value fish species was widespread, particularly in morphologically open and hydrologically connected coastal settings, and that outwelling nutrition from coastal wetlands is important to support fish production but so is nearshore energy imported into wetlands either by water movements or fish movements. The findings support the need to protect or restore lost inter-habitat connections in the Great Lakes coastal zone in order to maintain and improve Great Lakes fisheries.

The work represents a substantial scientific advancement in our understanding of how coastal wetlands provide ecosystem services in the Great Lakes, and thereby aids bi-national resource management, including recreational fisheries and commercial harvest. For example, Hoffman and Trebitz (2015) was recently cited in an Interagency Ecological Restoration Quality Committee seminar addressing coastal wetland restoration success. The presenter was a Canadian resource manager from the Central Lake Ontario Conservation Authority.

<u>Supplemental Items:</u>

Schoen, L.S., J.J. Student, J.C. Hoffman, M. Sierszen, and D.G. Uzarski. 2016. Reconstructing fish movements between coastal wetland and nearshore habitats of the Great Lakes. Limnology and Oceanography 61 (5):1800-1813.

This supplemental article is foundational to the Sierszen et al. (2019) nominated article, demonstrating how various chemical tracers in fish bones and tissues can be used to reconstruct movements of fish between open nearshore waters and Great Lakes coastal wetlands. We made this article supplementary simply because the author composition excludes it from STAA eligibility. The non-EPA authors on this supplementary nomination are supported under the Great Lakes Restoration Initiative to conduct Great Lakes-wide coastal wetland monitoring.

Justification 2A:

The pair of nominated papers showcase the EPA/ORD effort to address coastal-zone fishery support from two distinct but complimentary angles – one paper conceptually links harvested fish species with coastal wetland usage to assess the magnitude of fishery support (Trebitz and Hoffman 2015), while the other empirically links harvestable fish species to multiple potential habitats to determine which hydrogeomorphic settings most strongly foster cross-habitat support (Siersen et al. 2019). Specifically, Trebitz and Hoffman (2015) conclude that a key information need to advance the quantification of fisheries support in coastal habitats is "better data on fish origins and movements" to pair with the fisheries data. The Sierszen et al. (2019) was designed to meet this need.

Justification 2B:

Joel Hoffman

Hoffman, J.C., J.R. Kelly, G.S. Peterson, and A.M. Cotter. 2015. Landscape-scale food webs of fish nursery habitat along a river-coast mixing zone. Estuaries and Coasts 38 (4):1335–1349. **STAA Honorable Mention 2015, Approach to Understand and Classify Nutrient and Energy Sources to Coastal Ecosystems**.

Bellinger, B.J., J.C. Hoffman, T.R. Angradi, D.W. Bolgrien, M. Starry, C. Elonen, T. Jicha, L. Lehto, L. Monson, M.S. Pearson, L. Anderson, and B.H. Hill. 2016. Water quality in the St. Louis River Area of Concern, Lake Superior: historical and current conditions and delisting implications. Journal of Great Lakes Research 42(1):28-38. **STAA Honorable Mention 2016, Supporting AOC Decision-Making**.

Hoffman, J.C., J. Schloesser, A.S. Trebitz, G. Peterson, M. Gutsch, H. Quinlan, and J.R. Kelly. 2016. Sampling design for early detection of aquatic invasive species in Great Lakes ports. Fisheries 41(1):26-37. **STAA Level 3 Award 2019, On-the-ground implementation of early detection monitoring**.

Trebitz, A.S., J.C. Hoffman, G. Grant, T. Billehus, and E.M. Pilgrim. 2015. Potential for DNA-based identification of Great Lakes aquatic fauna: match and mismatch between organism inventories and DNA barcode libraries. Scientific Reports 5:12162. **STAA Level 3 Award 2019**, **, On-the-ground implementation of early detection monitoring**.

Trebitz, A.S., J.C. Hoffman, J.A. Darling, E.M. Pilgrim, J.R. Kelly, E.A. Brown, W.L. Chadderton, S.P. Egan, E.K. Grey, S.A. Hashsham, K.E. Klymus, A.R. Mahon, J.L. Ram, M. Schultz, C.A. Stepien and J.C. Schardt. 2017. Early detection monitoring for aquatic non-indigenous species: Optimizing surveillance, incorporating advanced technologies, and identifying research needs. Journal of Environmental Management 202 (Part 1):299-310. **STAA Level 3 Award 2019, On-the-ground implementation of early detection monitoring**.

Michael Sierszen

N/A

Anett Trebitz

Hoffman, J.C., J. Schloesser, A.S. Trebitz, G. Peterson, M. Gutsch, H. Quinlan, and J.R. Kelly. 2016. Sampling design for early detection of aquatic invasive species in Great Lakes ports. Fisheries 41(1):26-37. **STAA Level 3 Award 2019, On-the-ground implementation of early detection monitoring**.

Trebitz, A.S., J.C. Hoffman, G. Grant, T. Billehus, and E.M. Pilgrim. 2015. Potential for DNA-based identification of Great Lakes aquatic fauna: match and mismatch between organism inventories and DNA barcode libraries. Scientific Reports 5:12162. **STAA Level 3 Award 2019**, **, On-the-ground implementation of early detection monitoring**.

Trebitz, A.S., J.C. Hoffman, J.A. Darling, E.M. Pilgrim, J.R. Kelly, E.A. Brown, W.L. Chadderton, S.P. Egan, E.K. Grey, S.A. Hashsham, K.E. Klymus, A.R. Mahon, J.L. Ram, M. Schultz, C.A. Stepien and J.C. Schardt. 2017. Early detection monitoring for aquatic non-indigenous species: Optimizing surveillance, incorporating advanced technologies, and identifying research needs. Journal of Environmental Management 202 (Part 1):299-310. **STAA Level 3 Award 2019, On-the-ground implementation of early detection monitoring**.

Justification 2C:

STAA Honorable Mention 2015, Approach to Understand and Classify Nutrient and Energy Sources to Coastal Ecosystems. This earlier award demonstrates the approach using stable isotope tracers in fish tissue to assign production of fish to either wetland or nearshore habitat.

STAA Honorable Mention 2016, Supporting AOC Decision-Making. This nomination highlighted ecological research supporting impairment assessment needs for the EPA Area of Concern program.

STAA Level 3 Award 2019, On-the-ground implementation of early detection monitoring. This award addressed ORD research to develop an aquatic invasive species early detection monitoring program in the Great Lakes.

Justification 2D:

N/A

Justification 2E:

N/A

Justification 3A:

1. Citations for each publication nominated

Trebitz, A.S. and J.C. Hoffman. 2015. Coastal wetland support of Great Lakes fisheries: Progress from concept to quantification. Transactions of the American Fisheries Society 144 (2):352-372.

Impact factor: 2-year factor is 1.563, 5-year factor is 1.781

Citation ½ life: 15.8

Immediacy Index: 0.344

Sierszen, M.E., L.S. Schoen, J.M. Kosiara, J.C. Hoffman, M.J. Cooper, and D.G. Uzarski. 2019. Relative contributions of nearshore and wetland habitats to coastal food webs in the Great Lakes. Journal of Great Lakes Research 45(1):129-137.

Impact factor: 2-year factor is 2.175, 5-year factor is 2.464

Citation ½ life: 8.0

Immediacy Index: 0.771

2. If research has been invited for presentation at national/international societies

Joel Hoffman and Michael Sierszen were both invited to give numerous seminars and presentations at international conferences based on this work:

Hoffman, J.C. 2016. Fringe benefit: Value of restoring coastal wetlands

for Great Lakes fisheries. Department of Fisheries, Wildlife and Conservation Biology Seminar, University of Minnesota, St. Paul, March 31.

Hoffman, J.C. 2015. Coastal migrations of Great Lakes fishes and implications for resource management. Water Resource Science Seminar, University of Minnesota, Duluth, November 30.

Hoffman, J.C., A.S. Trebitz, G.S. Peterson, A.M. Cotter, and J.R. Kelly. 2014. Progress towards understanding the importance of coastal wetland nursery habitat to Great Lakes fisheries support. 144th Annual Meeting of the American Fisheries Society, Quebec City, Quebec, Canada, August 17-21.

Sierszen, M.E. 2017. Food web analysis using stable isotope mixing models. Institute for Great Lakes Research, Central Michigan University, Mt. Pleasant, Michigan, October.

Sierszen, M.E. 2018. Food web analysis using stable isotope mixing models. Cornell Biological Field Station, Cornell University, Bridgeport, New York, June.

3. Unique source of funding for research

ORD research was funded through the Research Action Plan. The non-EPA co-authors on this nomination were supported by the Great Lakes Research Initiative and EPA as part of the Great Lakes Coastal Wetland Monitoring Program (https://www.greatlakeswetlands.org/).

4. Any awards Internal/External to EPA that were received for the research

None

5. Number of times the publication has been downloaded/viewed

Based on ResearchGate, the Trebitz and Hoffman (2015) article has been downloaded 266 times, and the Sierszen et al. (2019) article has been downloaded 112 times.

6. How many times it has been cited (Google Scholar)

According to Google Scholar, the Trebitz and Hoffman (2015) article has been cited 17 times, and the Sierszen et al. article, which was published in 2019, has yet to be cited.

The supplemental Schoen et al. (2016) article has been cited 18 times.

7. Letters of Recommendation

None.

Justification 3B:

Both articles underwent EPA/ORD's internal peer review process, followed by full external peer review at their respective journals.

AUTHORS

Principal Author

Author Name:	Joel C. Hoffman		
Professional Title:		Salutation:	Dr.
Email:	hoffman.joel@epa.gov	Organization:	
Mailing Address:			
Street Line 1:	6201 Congdon Blvd		
City:	Duluth		
Zip Code:	55804	State:	Minnesota
At time of research was:	EPA Employee		

Separation Date:			
% of Effort:	25		

Contributing Author

Author Name:	Anett Trebitz		
Professional Title:		Salutation:	Dr.
Email:	trebitz.anett@epa.gov	Organization:	
Mailing Address:			
Street Line 1:	6201 Congdon Boulevard		
City:	Duluth		
Zip Code:	55804	State:	MN
At time of research was:	EPA Employee		
Separation Date:			
% of Effort:	25		

Contributing Author

Author Name:	Michael Sierszen		
Professional Title:		Salutation:	Dr.
Email:	mesierszen@gmail.com	Organization:	
Mailing Address:			
Street Line 1:	6201 Congdon Boulevard		
City:	Duluth		
Zip Code:	55804	State:	MN
At time of research was:	EPA Employee		

Separation Date:	Fri Jun 08 00:00:00 GMT 2018		
% of Effort:	25		

Contributing Author

Author Name:	Matthew Cooper		
Professional Title:		Salutation:	Dr.
Email:	mcooper@northland.edu	Organization:	
Mailing Address:			
Street Line 1:			
City:			
Zip Code:		State:	
At time of research was:	Non EPA Personnel		
Separation Date:			
% of Effort:	5		

Contributing Author

Author Name:	Donald Uzarski		
Professional Title:		Salutation:	Dr.
Email:	uzars1dg@cmich.edu	Organization:	
Mailing Address:			
Street Line 1:			
City:			
Zip Code:		State:	
At time of research was:	Non EPA Personnel		

Separation Date:			
% of Effort:	5		

Contributing Author

Author Name:	Lee Schoen		
Professional Title:		Salutation:	Mr.
Email:	schoenl1@michigan.gov	Organization:	
Mailing Address:			
Street Line 1:			
City:			
Zip Code:		State:	
At time of research was:	Non EPA Personnel		
Separation Date:			
% of Effort:	10		

Contributing Author

Author Name:	Jessica Kosiara		
Professional Title:		Salutation:	Ms.
Email:	jessica_kosiara@fws.gov	Organization:	
Mailing Address:			
Street Line 1:			
City:			
Zip Code:		State:	
At time of research was:	Non EPA Personnel		

Separation Date:

% of Effort: 5

PUBLICATIONS

Publication 1:

Publication Title:	Coastal wetland support of Great Lakes fisheries: Progress from concept to quantification		
Publication Date:	Wed Mar 04 00:00:00 GMT 2015		
Journal/Publication Method:	Transactions of the American Fisheries Society		
All Author(s):			
Volume:	144	Number:	2
Pages:	352-372	Immediately Index:	Immediately Index:
Citation ½ Life:	15.8	Impact Factor:	1.563

Publication 2:

Publication Title:	Relative contributions of nearshore and wetland habitats to coastal food webs in the Great Lakes		
Publication Date:	Mon Nov 19 00:00:00 GMT 2018		
Journal/Publication Method:	Journal of Great Lakes Research		
All Author(s):			
Volume:	45	Number:	1
Pages:	129-137	Immediately Index:	Immediately Index:

Citation ½ Life:	8.0	Impact Factor:	2.175

Publication 3:

Publication Title:	Reconstructing fish movements between coastal wetland and nearshore habitats of the Great Lakes		
Publication Date:	Fri Jul 01 00:00:00 GMT 2016		
Journal/Publication Method:	Limnology and Oceanography		
All Author(s):			
Volume:	61	Number:	5
Pages:	1800-1813	Immediately Index:	Immediately Index:
Citation ½ Life:	not available	Impact Factor:	4.325

This article was downloaded by: [US EPA Library], [J. C. Hoffman]
On: 09 March 2015, At: 06:16
Publisher: Taylor & Francis
Informa Ltd Registered in England and Wales Registered Number: 1072954 Registered office: Mortimer House, 37-41 Mortimer Street, London W1T 3JH, UK

Transactions of the American Fisheries Society

Publication details, including instructions for authors and subscription information:
http://www.tandfonline.com/loi/utaf20

Coastal Wetland Support of Great Lakes Fisheries: Progress from Concept to Quantification

Anett S. Trebitz[a] & Joel C. Hoffman[a]

[a] U.S. Environmental Protection Agency, Mid-Continent Ecology Division, 6201 Congdon Boulevard, Duluth, Minnesota 55804, USA

Published online: 04 Mar 2015.

CrossMark

Click for updates

To cite this article: Anett S. Trebitz & Joel C. Hoffman (2015) Coastal Wetland Support of Great Lakes Fisheries: Progress from Concept to Quantification, Transactions of the American Fisheries Society, 144:2, 352-372, DOI: 10.1080/00028487.2014.982257

To link to this article: http://dx.doi.org/10.1080/00028487.2014.982257

PLEASE SCROLL DOWN FOR ARTICLE

Taylor & Francis makes every effort to ensure the accuracy of all the information (the "Content") contained in the publications on our platform. However, Taylor & Francis, our agents, and our licensors make no representations or warranties whatsoever as to the accuracy, completeness, or suitability for any purpose of the Content. Any opinions and views expressed in this publication are the opinions and views of the authors, and are not the views of or endorsed by Taylor & Francis. The accuracy of the Content should not be relied upon and should be independently verified with primary sources of information. Taylor and Francis shall not be liable for any losses, actions, claims, proceedings, demands, costs, expenses, damages, and other liabilities whatsoever or howsoever caused arising directly or indirectly in connection with, in relation to or arising out of the use of the Content.

This article may be used for research, teaching, and private study purposes. Any substantial or systematic reproduction, redistribution, reselling, loan, sub-licensing, systematic supply, or distribution in any form to anyone is expressly forbidden. Terms & Conditions of access and use can be found at http://www.tandfonline.com/page/terms-and-conditions

Transactions of the American Fisheries Society 144:352–372, 2015
American Fisheries Society 2015
ISSN: 0002-8487 print / 1548-8659 online
DOI: 10.1080/00028487.2014.982257

ARTICLE

Coastal Wetland Support of Great Lakes Fisheries: Progress from Concept to Quantification

Anett S. Trebitz* and Joel C. Hoffman
U.S. Environmental Protection Agency, Mid-Continent Ecology Division, 6201 Congdon Boulevard, Duluth, Minnesota 55804, USA

Downloaded by [US EPA Library], [J. C. Hoffman] at 06:16 09 March 2015

Abstract

Fishery support is recognized as a valuable ecosystem service provided by aquatic systems, but it is harder to quantify than to describe conceptually. In this paper, we combine data on fish inhabiting Great Lakes coastal wetlands (GLCWs) with information on commercial and recreational harvest and the piscivore forage base to develop quantitative understanding of the multiple species involved in direct and indirect fishery support of this complex fishery. We then examine patterns of species co-occurrence and life history and relationships to GLCW conditions in order to identify fishery support metrics useful in aggregating species patterns and evaluating management outcomes. Our criteria for wetland prevalence (≥10% occurrence) and fishery importance (≥1% of recreational or commercial harvest in one or more of the Great Lakes or having a major forage fish role) yielded 21 wetland-using, fishery-relevant species representing multiple taxonomic groups and life history attributes. Wetland-using species are estimated to make up half the biomass and 60% of the dollar value of the fish landed commercially and ~80% of the fish numbers harvested recreationally. All of the GLCWs studied supported species of interest to recreational and commercial fishers but with widely varying composition. A few key habitat characteristics (e.g., vegetation structure) are broadly predictive of the types of sport and panfish present, with more degraded GLCWs generally supporting abundant but lower-value taxa (rough-fish species) and less degraded GLCWs supporting fewer but higher-value taxa (sport and panfish species). No single taxonomic or functional metric seems adequate to capture the diversity of fishery-relevant species supported by GLCWs; fishery support needs to be understood and managed in a multimetric context.

Ecosystem services accounting allows actual or potential environmental changes to be evaluated in terms of their likely effects on humans (National Research Council 2005; Farber et al. 2006; Palmer and Filoso 2009). Fishery support is a prominent ecosystem service attributed to aquatic systems and refers to providing spawning, foraging, and refuge habitat to species that are exploited for recreational fishing or commercial harvest (Holmlund and Hammer 1999; Barbier et al. 2011). Unfortunately, while fishery support is readily understood as a concept, how best to actually measure complex cases of fishery support is far from established. The sources of complexity in fishery support can arise from a number of factors, including the diversity of fish species and human user groups involved and the spatial extent and connectivity of the ecosystem (Barbier et al. 2011; Engle 2011; Tallis et al. 2012).

Coastal wetlands in the Laurentian Great Lakes exemplify a complex fishery support situation. Great Lakes coastal wetlands (GLCWs) are used by a large suite of fish species, including many with recognized sport and commercial importance (Jaworski and Raphael 1978; Jude and Pappas 1992; Sierszen et al. 2012b), whose high biological productivity and diversity contribute to food webs extending across a much broader nearshore zone (Wetzel 1992; Brazner et al. 2000; Vadeboncoeur et al. 2011). Human user groups in the Great Lakes value diverse aspects of the fishery, including biomass and dockside value (commercial harvesters), trophy size (sport anglers), and catchability and eating quality (family and

*Corresponding author: trebitz.anett@epa.gov
Received May 16, 2014; accepted October 15, 2014

Downloaded by [US EPA Library], [J. C. Hoffman] at 06:16 09 March 2015

subsistence fishers). As with coastal habitats elsewhere (Able 2005; Manson et al. 2005; Jordan et al. 2012), the spatial scale over which GLCW fishery support plays out is complicated because the various fish species can move among GLCWs and other habitats on a seasonal, ontogenetic, or facultative basis and because fishing activities often take place outside the GLCWs themselves and are assessed and managed over broad spatial scales (e.g., Brazner et al. 2001; Murphy et al. 2012).

Among the questions that need to be addressed to develop fishery support metrics for such complex situations are which species to include, what kinds of measurement endpoints are informative, and how to establish the linkage between specific ecosystems and the broader spatial scales over which ecological services are realized. There is also the question of how fishery support metrics relate to ecosystem conditions and potential management actions. This is a subject of considerable current interest for Great Lakes coastal habitats, since the ongoing Great Lakes Restoration Initiative (GLRI 2010) is supporting expanded efforts to remediate environmental impacts and improve ecological condition. Many GLRI projects are directed at the coastal margin, which is most directly affected by shoreline development (e.g., urbanization and hydrologic alteration) and watershed-derived stressors such as sedimentation and nutrient loading (Vadeboncoeur et al. 2011; Niemi et al. 2007; Allan et al. 2013). Developing quantifiable metrics of fishery support would provide a basis for prioritizing management actions and tracking the benefits of such restoration projects (Wainger and Mazzotta 2011).

Ideally, fishery support accounting would work with endpoints that can be quantified as a standing stock or a rate (growth or production) per unit area (Bell 1997; Wainger and Boyd 2009; Engle 2011) as a basis for evaluating changes in fishable biomass or size. However, growth or production data are time-consuming to collect and thus rarely obtained in synoptic surveys. Rather, the typical fish survey produces count and occurrence data from a standardized sampling effort meant to index assemblage composition and the relative abundance of species. Establishing endpoints of value to human users (e.g., the presence of a target species) can be sufficient to link an ecosystem condition with an ecological outcome (e.g., improved habitat for that species) for which human preferences can be measured (Wainger and Mazzotta 2011). Index data may therefore be useful for fishery service accounting and can offer a robust avenue for evaluating fish–habitat relationships because of their ability to smooth over some of the variability due to sampling gear, location, and time (Steen et al. 2008). Community-level analyses of such index data have shown that GLCW fish composition is substantially affected by habitat and watershed conditions (e.g., Brazner and Beals 1997; Seilheimer and Chow-Fraser 2007; Arend and Bain 2008; Trebitz et al. 2009a). However, species composition data must be translated into metrics of fishery support to predict the ecosystem services implications of proposed management actions affecting GLCWs. To date, analyses focusing on fishery-relevant species and endpoints are lacking for GLCWs.

Our goals in this paper are to add quantitative detail toward understanding which Great Lakes species are both fishery relevant and wetland users and to ascertain their patterns of co-occurrence and life history in order to identify multispecies fishery support metrics that are useful in differentiating among GLCW types and conditions. We speak of GLCWs as providing "direct" fishery support when they harbor species that are sought, caught, and harvested by commercial harvesters or recreational anglers (whether the fish are captured in the wetland or elsewhere) and as providing "indirect" fishery support when they harbor forage fish available for consumption by other fishes inhabiting the broader nearshore zone. Our approach was to combine recreational and commercial harvest data with GLCW survey data to identify fishery-relevant, wetland-using species; to examine their exploitation and life history patterns to determine how multispecies fishery support can be decomposed into more homogeneous and measurable components; and finally to examine relationships to GLCW condition in order to identify metrics that are useful in tracking ecosystem service changes associated with habitat degradation and restoration.

We acknowledge that our approach does not address some of the recalcitrant questions related to fish habitat, such the extent to which GLCWs are essential and what portion of the harvested biomass or production can be attributed to them (Rose 2000; Able 2005; Levin and Stunz 2005; Rosenfield and Hatfield 2011). Also, we focus exclusively on the supply side of fishery support ecosystem services and do not address the equally complex problem of assigning values to the benefits that humans derive from a fishery (e.g., Whitehead et al. 2005; Brander et al. 2006; Spangenberg and Settele 2010). Nevertheless, our analysis constitutes substantial progress in refining our understanding of the associations between GLCWs and the multiple fishery-relevant species that inhabit them, thereby moving fishery support from a purely conceptual basis toward operationally applicability. The issues discussed in the context of GLCWs are equally relevant to complex cases of fishery support in other aquatic ecosystem types and locations (e.g., salt marshes, seagrass beds, and mangroves: Manson et al. 2005; Sheaves 2009; Engle 2011; Vasconcelos et al. 2011).

METHODS

Our analyses of patterns for fishery-relevant, wetland-using fish species relies primarily on data from 58 GLCWs surveyed via electrofishing over the summers of 2002–2004 (details in Trebitz et al. 2009a). This data set included lacustrine, riverine, and protected-type GLCWs on all five Great Lakes, with sites being chosen to span a gradient of agricultural use and urbanization in the watershed (Danz et al. 2005). Our sampling was conducted from mid to late summer, as is typical of GLCW fish surveys. Fish were sampled at five to seven

separate locations per wetland (standardized 10-min electrofishing effort per station, or 50–70 min of effort per wetland). The sampling effort was distributed proportionally to the available vegetated and open-water habitat. Catches were enumerated by species and by age-class (young-of-year, yearling, or adult) based on size distributions. Supporting water quality and habitat data were also collected.

Establishing wetland use and fishery importance.—We operationally defined species that are both wetland using and fishery relevant as those that we found in at least 10% of the GLCWs surveyed that also met certain recreational and commercial harvest thresholds. The 10% occurrence criterion was to ensure that we only included species with sufficient data that their distribution and prevalence patterns could be assessed. For additional perspective, we compiled published species data from ichthyoplankton surveys of GLCWs. Such data demonstrate spawning and nursery use of GLCWs and are especially relevant for fish species not detected in adult and juvenile summer surveys owing to sampling gear (typically fyke nets or electrofishing) or temporal biases. Because we found larval fish data for relatively few GLCWs and mostly reported in general terms (e.g., presence only, spatially aggregated), we did not set a criterion for occurrence frequency in listing species (but applied the same harvest thresholds).

We identified wetland-using species having direct fishery importance using recent recreational and commercial fishing data compiled by various management agencies (Table 1). We classified the harvest level for each species in each lake into four tiers: "dominant" for species making up a larger percentage of the harvest than any other species; "major" for those comprising $\geq$10% of the total; "minor" for those comprising 1.0–10% of the total; and "trace" for those comprising $<$1.0% of the total, based on the number harvested in recreational fishing and the biomass landed in commercial fishing. We used tiers rather than actual quantities because of the large range in productivity across the lakes and the variation in assessment methods and spatial and temporal coverage among data sources (Table 1). A species had to attain at least minor recreational or commercial harvest in at least one lake to be retained in our analyses. When fishery data were aggregated across taxa (e.g., "sunfish" rather than individual species), we applied the harvest level to all potential species meeting the criteria of $\geq$10% occurrence in GLCWs. For the commercial fishing data, we also computed the average price and percent of the total biomass and dollar value attributable to each species. To do so, we summed U.S. and Canadian data without regard to year, assuming that among-year differences were unimportant. No currency conversion was applied, since the exchange rate lay between US$0.95 and $1.05 per Canadian dollar for all of 2011 and 2012. We did not attempt to assign a dollar value to species of recreational importance given the much greater complexity of evaluating recreational enjoyment as opposed to commercial values and landings (e.g., Gordon et al. 1973; Provencher and Bishop 1997).

We identified fish species having indirect fishery importance in the Great Lakes (i.e., as forage for sport fish) as those wetland-using species that are significant components of coastal predator diets or pelagic prey fish surveys, based on the scientific literature. We excluded sedentary, demersal species (e.g., sculpins) because they are unlikely to move (and thus transfer energy) between GLCWs and nearshore environments even if prevalent in both habitats.

Evaluating wetland associations.—We characterized GLCW associations for the wetland-using, fishery-relevant species using our own survey data and life history information from the literature. First, general distribution and prevalence patterns were evaluated to determine which fishery-relevant species are most commonly encountered, how many such species typically occur, and how their composition varies across GLCWs. Then, to address the extent to which GLCW condition affects fishery support, relationships between the species and wetland environmental characteristics were examined at two spatial scales: the wetland scale and the scale of sampling locations within wetlands (hereafter, station scale). Finally, we examined the patterns in various potential summary metrics of fishery support suggested by the taxonomic and life history patterns for the fishery-relevant species.

At the wetland scale, the relationships of species to categorical environmental variables were analyzed by means of box plots and analysis of variance (ANOVA) and relationships to numerical environmental variables were analyzed by linear regression. We also computed the richness of the fishery-relevant species in four categories: sport fish, panfish, rough fish, and forage fish. Patterns in the assemblage of fishery-relevant species were examined using nonmetric multidimensional scaling (NMDS) ordination, with Bray–Curtis similarity as the distance metric. To facilitate graphical depiction of fish composition patterns, we focused on results from a two-dimensional ordination (a three-dimensional ordination explained only 7% more variability). The ordinations combined all age-classes, since trial ordinations that examined young-of-year and juvenile–adult fish separately were qualitatively similar. Overlay vectors to the ordination were generated for the individual species, for richness for the four species categories, and for the environmental variables by computing the Pearson correlation between each of these variables and the first and second ordination axis scores and using the resulting values as x- and y-coordinates for the endpoints of the vectors radiating from the origin. Encounter probability (the percent of sampling locations within each GLCW at which a species was captured) was used as the species-level variable for all of the wetland-scale analyses because encounter probability is interpretable in terms of fishing opportunity and presents a useful compromise between high-variability abundance data and low-information occurrence data (Sheaves et al. 2012).

Downloaded by [US EPA Library], [J. C. Hoffman] at 06:16 09 March 2015

TABLE 1. Sources and details for fishery harvest data. The commercial data are comprehensive, whereas the recreational data are from surveys with varying focal species, user groups, and temporal and spatial coverage. The recreational data are on a number basis unless stated otherwise.

Source	Lake (area)	Year	Details
		Commercial	
OMNR 2013a	Erie (Canada)	2012	All landings, biomass and dollar value
OMNR 2013b	Huron (Canada)	2012	All landings, biomass and dollar value
OMNR 2013c	Ontario (Canada)	2012	All landings, biomass and dollar value
OMNR 2013d	Superior (Canada)	2011	All landings, biomass and dollar value
NMFS database[a]	Five lakes (U.S.)	2011	All landings, biomass and dollar value
		Recreational	
OMNR 2013a	Erie (Canada)	2012	Angler diaries
Ohio DNR 2012	Erie (Ohio)	2011	Creel: boat fishing only, selected species
MDNR database[b]	Huron (Saginaw Bay)	2011	Creel and charter reporting: ice, boat, shore fishing
Breidert 2011	Michigan (U.S.)	2010	Biomass basis
Hanson 2012	Michigan: (U.S.)	2011	Creel: recreational anglers, selected species
Masterson and Eggold 2012	Michigan (Wisconsin)	2011	Creel, charter reporting, mail survey: boat and shore fishing, selected species
Lantry and Eckert 2012	Ontario (New York)	2011	Creel: boat fishing only
Zunker 2013	Superior (Wisconsin)	2012	Creel and charter reporting; ice and boat fishing
DFO 2008[c]	Four lakes (Canada)	2005	Mail survey

[a]Available: www.st.nmfs.noaa.gov/commercial-fisheries/commercial-landings/other-specialized-programs/great-lakes-landings/index.
[b]Available: www.dnr.state.mi.us/CharterCreel/Default.aspx.
[c]Included despite data age because it was most recent Canada-side data available for three of the lakes.

Downloaded by [US EPA Library], [J. C. Hoffman] at 06:16 09 March 2015

At the station scale, the relationships of species to categorical environmental variables were analyzed graphically and by cross-tabulation, while the relationships to numerical environmental variables were analyzed via logistic regression. Station-scale analyses were pursued only for species with enough data for this to be meaningful, operationally defined as species found in ≥25% of the GLCWs, in all five Great Lakes, and for which we caught ≥100 individuals. Station-scale analyses used presence/absence as the data format and only included GLCWs in which the species was found, so that absences reflected station characteristics rather than broader distribution patterns. We did not use abundance data (e.g., catch per effort) for these analyses because they often fail to meet distributional assumptions (Francis et al. 2005; Valavanis et al. 2008) and lead to a more complicated hierarchical data structure for stations nested within wetlands (Wagner et al. 2006). For species with enough data (at least five presences per predictor variable), station-scale analyses were conducted separately for young-of-year and for older fish (juveniles and adults combined), so that differences across life stages could be examined.

Wetland-scale and station-scale analyses focused on a small set of the available environmental variables chosen a priori to have relevance to fish, minimal collinearity, and potential for manipulation by GLCW restoration or management. The numerical variables (measured at the station scale, averaged to the wetland scale) were turbidity (nephelometric turbidity units; an index of water clarity), fetch (m [$\log_{10}$ transformed]; an index of wind-and-wave exposure), sediment density (g/cm^3; higher densities are sandier), and a submerged- and floating-leaf vegetation structure index (higher levels indicate denser cover and more growth forms; Brazner and Beals 1997); see Trebitz et al. (2009a) for computation details on all these variables. We also considered one categorical descriptor at the wetland scale (protected, riverine, or lacustrine wetland; Albert et al. 2005) and one at the station scale (channelized, lake-like, or backbay station; Trebitz et al. 2009a). For the ordination analyses only, we included additional environmental variables (as overlay vectors) to provide a more comprehensive picture of GLCW conditions. These were plankton chlorophyll *a* (an index of water clarity and productivity), three anthropogenic disturbance metrics (percent natural land cover in the watershed, percent natural land cover in the 100-m buffer around the GLCW, and an agricultural intensity index calculated from county and 8-digit HUC data; Danz et al. 2005), and two additional vegetation structure metrics (the maximum depth of submerged plant growth and a nuisance plant density index based primarily on the emergent taxa *Phragmites* (common reeds), *Typha* (cattails), and purple loosestrife *Lythrum salicaria*; Trebitz and Taylor 2007). Two potentially fish-relevant environmental variables that we did not include were dissolved oxygen (since earlier work had shown that it explains GLCW fish composition only at very small spatial scales, e.g., among vegetation beds; Trebitz et al.

2009b); and water temperature. Water temperature is confounded with a latitudinal anthropogenic disturbance gradient across the Great Lakes basin (population density and agricultural intensity both increase to the south; Trebitz et al. 2009a), and the basinwide distribution of the fish species considered here suggests that water temperature is not the primary driver of their abundance patterns.

Finally, we examined potential guild-level fishery support metrics (e.g., groupings based on species composition or traits such as sport fish or warmwater species), with the goal of identifying metrics that usefully aggregate species-specific information while preserving patterns relevant to different human user groups and GLCW conditions. We depict the results with radar plots (polar coordinate plots in which points are specified by angle and distance from the origin rather than the usual *x*- and *y*-values), with the level of the fishery support metric given by the distance from the origin and the angle matching that of the GLCW in the earlier NMDS ordination. The guild metrics were constructed by summing encounter probabilities across the relevant species using adults only for taxonomic combinations (to focus on harvestable fish) but all life stages for life history combinations (the usual procedure in computing fish guild metrics for biotic integrity analyses; Fausch et al. 1990). We obtained a macrohabitat classification from an analysis of Great Lakes fish species done by Jude and Pappas (1992), with the groupings that we used being "coastal" (their rankings of 32–66), "weak wetland" (their rankings of 67–90), and "strong wetland" (their rankings of 90–113). We compiled life history information relevant to wetland affinity (i.e., littoral tendency, substrate preference, vegetation use, and thermal preference) from Becker (1983), Coker et al. (2001), and Lane et al. (1996a, 1996b). We classified fish as obligate wetland users if they rely on aquatic vegetation to spawn or for nursery habitat and as facultative wetland users otherwise.

RESULTS

Wetland-Using Species of Direct Fishery Importance

We identified 18 fish species (Table 2) that had at least a 10% frequency of occurrence in GLCWs (our criteria for wetland using) and that made up at least 1% of the recreational or commercial harvest in one or more Great Lakes (our criteria for direct fishery importance). Collectively, these species made up 48% of the landed biomass and accounted for 63% of the dollar value of all species harvested commercially across the Great Lakes in 2011 or 2012 (Table 3), as estimated from

TABLE 2. Great Lakes coastal wetland–using fishes with direct importance to recreational or commercial fishing, organized by general fishing category. Importance by lake (E = Erie, H = Huron, M = Michigan, O = Ontario, and S = Superior) is coded as follows: dominant (largest percentage of the harvest of any species) = bold with asterisks; major (>10% of the harvest) = bold and underlined; minor (1–10% of the harvest) = ordinary type; and trace (<1% of the harvest) = in parentheses. The basis is biomass for commercial harvests but numbers for recreational harvests.

Species	Commercial importance					Recreational importance				
Sport fish										
Channel Catfish	E	H	(M)			(E)	H		O	(S)
Largemouth Bass						E	H		O	S
Northern Pike		(H)		O	(S)	(E)	H	(M)	(O)	S
Smallmouth Bass	(E)	(H)				E	**H**	M	O	S
Yellow Perch	***E***	H	(M)	***O***	(S)	***E***	***H***	***M***	***O***	**S**
Walleye[a]	**E**	H	(M)	O	(S)	E	**H**	M	**O**	***S***
White Bass	**E**	(H)	(M)	(O)		E	(H)			
White Perch	E	(H)	(M)	O		(E)	(H)	(M)		
Panfish										
Black Crappie[b]		(H)		O		(E)	H	(M)	**O**	(S)
Rock Bass	(E)	(H)		O		(E)	**H**		O	
Sunfish (3 species)[c]	(E)			**O**		E	H	(M)	O	
Rough fish										
Black/Brown Bullhead[d]	(E)	(H)		O						
Common Carp	E	(H)	(M)	(O)						
Freshwater Drum	E	(H)		O		(E)	(H)			
Gizzard Shad	(E)									
White Sucker	(E)	(H)		O			(H)			

[a]Walleyes dominate the Canadian side of Lake Superior harvest only.

[b]Black Crappies meet our GLCW prevalence criteria but White Crappies do not; the fishery harvest data do not differentiate between the two species.

[c]Sunfish meeting the GLCW prevalence criteria and of interest to anglers are Pumpkinseeds, Bluegills, and Green Sunfish; some fishery harvest sources differentiate among the species but others do not.

[d]Black and Brown Bullheads are difficult to differentiate (Rutkayová et al. 2013) and thus are combined in our data.

Downloaded by [US EPA Library], [J. C. Hoffman] at 06:16 09 March 2015

TABLE 3. Percentages of Great Lakes–wide total commercially landed biomass and dollar value and average prices for wetland-using species. Numbers reflect combined NMFS and OMNR data for 2011 or 2012 across all five Great Lakes. Species are listed in order of decreasing percent biomass or price.

Species	% Biomass	% Dollar value	Price ($/kg)
Sport fish			
Yellow Perch	18.2	36.0	5.16
Walleye	10.6	18.5	4.55
White Bass	8.0	4.3	1.40
White Perch	6.0	2.8	1.21
Channel Catfish	1.7	0.5	0.76
Northern Pike	0.1	<0.1	0.58
Panfish			
Black Crappie	<0.1	<0.1	7.20
Sunfish (3 species)	0.1	0.1	2.79
Rock Bass	<0.1	<0.1	1.17
Rough fish			
Freshwater Drum	1.7	0.3	0.41
Common Carp	1.3	0.3	0.56
Black/Brown Bullhead	0.2	0.1	0.74
White Sucker	<0.1	<0.1	0.20
Gizzard Shad	0.1	<0.1	0.07
All of above species	48.0	62.9	

Downloaded by [US EPA Library], [J. C. Hoffman] at 06:16 09 March 2015

NOAA and OMNR databases and reports (Table 1). The total biomass of wetland-using species landed commercially exceeded 11,000 metric tons, with the vast majority coming from Lake Erie. The total number of fish from wetland-using species harvested recreationally in just Canadian waters in 2005 exceeded 4 million, with roughly half of those coming from Lake Erie (Table 4). The percentage of the commercial harvest accounted for by wetland-using species varied widely among lakes (>70% in Lakes Erie and Ontario, ~10% in Lake Huron, ≤1.0% in Lakes Michigan and Superior), but the majority of the recreational harvest was due to wetland-using species in all the lakes (Table 4).

Yellow Perch *Perca flavescens* is the most important wetland-using species for Great Lakes fisheries. The species is ubiquitous in GLCWs, occurring more frequently than any other fishery-relevant species (Brazner and Beals 1997; Seilheimer and Chow-Fraser 2007; Arend and Bain 2008; Trebitz et al. 2009a). Yellow Perch comprised 32% of the total fish harvested recreationally across Canadian Great Lakes waters in 2005 (DFO 2008)—a rate three times higher than that of any other species. Yellow Perch also comprised 36% of the dollar value and 18% of the biomass landed in commercial fisheries across all five Great Lakes in 2010–2011 (Table 3)—a dollar value higher than that of any other species and a landed biomass second only to that of Lake Whitefish *Coregonus clupeaformis*. Yellow Perch are particularly important to commercial fishing in Lakes Erie and Ontario (>25% of the harvested biomass) and to recreational fishing in Lakes Erie and Huron (>75% of the harvest; DFO 2008; Ohio DNR 2012; OMNR 2013a), but they also make up at least 25% of

TABLE 4. Estimated percentages of the total recreational and commercial harvest across the Great Lakes comprised of the wetland-using fish species from Table 2. Commercial harvests reflect combined NMFS and OMNR data for 2011 and 2012; recreational harvest data are from a Canada-side 2005 survey (DFO 2008) that does not cover Lake Michigan (cross-lake comparisons for more recent recreational fishing data are difficult because of variations in methodology).

	Commercial harvest		Recreational harvest	
Lake	Biomass (metric tons)	Percent	Number (thousands)	Percent
Erie	10,313	72.2	2,248,469	95
Huron	407	11.1	1,022,878	71
Michigan	28	1.0		
Ontario	184	84.0	803,739	76
Superior	1.6	<0.1	237,861	61
All 5 lakes	10,933	48.0	4,312,947	82

the recreational harvest in portions of Lakes Michigan, Ontario, and Superior (Lantry and Eckert 2012; Hanson 2012; Masterson and Eggold 2012; Zunker 2013).

Seventeen other wetland-using species are important fishery targets in the Great Lakes. Walleye *Sander vitreus* have major recreational importance in three of the lakes (Table 2) and comprised 11% of the commercial biomass and 19% of the dollar value in 2010–2011 (Table 3). White Bass *Morone chrysops* and White Perch *Morone americana* each exceeded 5% of the landed biomass and 2% of the dollar value, with commercial landings coming from four lakes and recreational harvests in three lakes (Tables 2, 3). Channel Catfish *Ictalurus punctatus* are commercially landed in three lakes and recreationally harvested in four of them (Table 2). Smallmouth Bass *Micropterus dolomieu* and Northern Pike *Esox lucius* have recreational importance in all five lakes as well as some commercial harvest (Table 2). The Largemouth Bass *Micropterus salmoides* is the only wetland-using sport fish lacking commercial importance, but it is harvested recreationally in four lakes (Table 2). Rock Bass *Ambloplites rupestris*, Black Crappie *Pomoxis nigromaculatus*, and sunfish *Lepomis* spp. each attain major recreational or commercial importance in at least one lake and are harvested in several more (Table 2). The sunfish species of most interest to recreational anglers are Pumpkinseed *L. gibbosus* and Bluegill *L. macrochirus*, but large Green Sunfish *L. cyanellus* are also fished (Becker 1983). Four wetland-using rough-fish species attain at least minor commercial importance in Lakes Erie or Ontario, although rough-fish harvests only reach trace levels in Lakes Huron and Michigan (Table 2). Some Freshwater Drum *Aplodinotus grunniens* and White Sucker *Catostomus commersonii* are also recreationally harvested, while bullheads (*Ameiurus* spp.) and Common Carp *Cyprinus carpio* are commercially harvested only. Gizzard Shad *Dorosoma cepedianum* are commercially harvested only in Lake Erie and only at trace levels (i.e., below our 1.0% criterion); however, we include this species in Table 2 because of its numerical dominance in the GLCWs of Lake Erie and its role in indirect fishery support.

Wetland-Using Species of Indirect Fishery Importance

We identified five wetland-using, mobile, small-bodied fish species capable of providing indirect fishery support as forage for nearshore piscivores. These are Yellow Perch and Gizzard Shad (already in Table 2), plus Spottail Shiner *Notropis hudsonius*, Emerald Shiner *Notropis atherinoides*, and Alewife *Alosa pseudoharengus*, which have 40, 32, and 28% frequencies of occurrence, respectively, in our GLCW data set. Alewife, Emerald Shiner, Spottail Shiner, and young-of-year Yellow Perch are considered important pelagic forage species in multiple Great Lakes, while young-of-year Gizzard Shad are important in Lake Erie (Jude and Tesar 1985; Knight and Vondracek 1993; Rand and Stewart 1998; Zhao et al. 2013; J. S. Schaeffer, T. P. O'Brien, and S. Lenart [paper presented at the Great Lakes Fish Commission, Lake Huron Committee meeting, 2012]). Yellow Perch and Gizzard Shad thus provide both indirect fishery support (as young of year) and direct fishery support (as adults).

Larval Surveys as Additional Evidence for Wetland Use

All of the species classified as wetland using based on regular occurrence in adult and juvenile fish surveys were also found in GLCWs as larvae. Importantly, additional species were found as larvae that rarely or never appear in adult and juvenile surveys. Most notable among these from a fishery perspective are *Coregonus* species and Rainbow Smelt *Osmerus mordax*. Rainbow Smelt ranks third (after Yellow Perch) in commercially landed biomass across the Great Lakes according to NMFS and OMNR data, with harvests being particularly important in Lake Erie (24%), and attains major recreational harvest in Lake Superior (DFO 2008; Zunker 2013). Identification of larval *Coregonus* to species is difficult (Auer 1982), but those from GLCWs likely include Lake Whitefish and Cisco *C. artedi*, since these are the most widespread and shallow-water oriented of the coregonines (Scott and Crossman 1973; Gamble et al. 2011). Lake Whitefish represent the largest portion (biomass) of the species harvested commercially from Lakes Michigan, Huron, and Superior and experience some recreational harvest, whereas Ciscoes dominate the commercial harvest in Lake Ontario and are a close second to Lake Whitefish in Lake Superior (NMFS and OMNR data; DFO 2008; Zunker 2013). The other fishery-relevant species caught as larvae (Table 5) but not reported in Table 2 are rough fishes with only trace commercial importance (Bowfin *Amia calva*, Quillback *Carpiodes cyprinus*, Bigmouth Buffalo *Ictiobus cyprinellus*, and Burbot *Lota lota*).

Wetland Prevalence and Life History Patterns for Fishery-Relevant Species

Among the 21 species caught in our survey and identified as providing direct or indirect fishery support, the highest GLCW occurrence rates are for Yellow Perch (>90%), followed by Pumpkinseed, White Sucker, and Common Carp (each >70%) and Largemouth Bass, Northern Pike, Bullheads, Rock Bass, and Bluegill (each ≥60%; Table 6). Twenty of the twenty-one species were found in GLCWs in all five Great Lakes. Gizzard Shad were not found in Lake Superior but nevertheless were more numerous across all 58 GLCWs combined that any other species (due to extremely high catches in Lake Erie); Yellow Perch were the next most numerically abundant species across the data set. We caught at least one of the eight sport fish species in every GLCW, with some wetlands yielding as many as six (Table 7). The average richness of sport fish exceeded three in the GLCWs of all lakes except Lake Huron, where the average was only 2.3. All GLCWs harbored at least one of the five panfish species, with the average between two and three in all lakes. All GLCWs also

Downloaded by [US EPA Library], [J. C. Hoffman] at 06:16 09 March 2015

TABLE 5. Fishery-relevant species for which larvae have been documented in GLCWs within various lakes. The taxonomic resolution is to the least common denominator across studies. All studies commenced sampling in April or May, continued for at least 2 months, and used fine-mesh pushed or towed nets (except Cooper et al. 2012, which used light traps).

Species	Erie[a]	Huron[b]	Michigan[c]	Ontario[d]	Superior[e]
Found regularly as adults or juveniles:					
Black/Brown Bullhead	xx		xx	xx	xx
Channel Catfish	xx				xx
Alewife/Gizzard Shad	xx	xx	xx	xx	
Black Crappie	xx	xx	xx	xx	xx
Common Carp/Goldfish	xx	xx	xx	xx	xx
Freshwater Drum	xx	xx		xx	xx
Largemouth Bass		xx	xx		
Northern Pike		xx	xx	xx	xx
Rainbow Smelt	xx	xx		xx	xx
Rock Bass		xx	xx	xx	xx
Smallmouth Bass		xx	xx	xx	xx
Sunfish	xx	xx	xx	xx	xx
Yellow Perch	xx	xx	xx	xx	xx
Walleye	xx				xx
White/Longnose Sucker[f]	xx	xx	xx	xx	xx
White Perch/White Bass	xx			xx	xx
Not found regularly as adults or juveniles:					
Bigmouth Buffalo	xx				
Bowfin			xx		
Burbot		xx	xx		xx
Cisco/Lake Whitefish	xx	xx	xx		xx
Quillback	xx				
Rainbow Smelt	xx	xx		xx	xx

[a]Ohio shore GLCWs: Cooper et al. (1981); Mizera et al. (1981); Johnson (1989); Krupa (2003).
[b]Les Cheneaux Islands and Saginaw Bay area GLCWs: O'Gorman (1983); Höök et al. (2001); Cooper et al. (2012).
[c]Two Michigan shore GLCWs: Jude et al. (1981); Chubb and Liston (1986).
[d]New York shore and Toronto area GLCWs: Lewis and Patch (1982); Klumb et al. (2003).
[e]Wisconsin shore GLCWs: Tanner et al. (2004); Hoffman et al. (2012); Hoffman, unpublished.
[f] Longnose Suckers *Catostomus catostomus* are not fishery relevant. They are listed here only because they cannot be differntiated from White Suckers as larvae.

harbored at least one of the five rough-fish species, with the average richness being substantially higher in Lake Erie than in the other lakes (Table 7). The average richness of forage species was lowest in Lake Huron GLCWs (Table 7). The richnesses of sport, pan-, rough-, and forage fish were essentially uncorrelated (all $r < 0.3$).

The 21 fish species vary considerably in the life history traits relevant to understanding their use of GLCWs and in the potential for developing guild metrics relevant to fishery support. Eleven are classified as having a warm thermal preference, but there are also 9 having cool thermal preference and one each having cold–cool and cold preferences (Table 6). All of the species are somewhat or predominantly littoral, but 11 are coastal associated and only 10 weakly or strongly wetland associated. Only four of the species are obligate wetland users (requiring vegetation for spawning or nurseries), although most have vegetation affinity (Table 6). Among the nine species with ≥50% occurrence in the GLCWs, the one consistent trait is that all are littoral with moderate or high vegetation affinity (Table 6). None of the pelagic forage species exhibits a warm thermal preference or obligate wetland use, which is to be expected. There was little congruence among the various dimensions along which life history can be classified (Table 6). For example, the thermal guild categories did not align consistently with the habitat association categories, nor did wetland dependency align with the life history categories; and obligate vegetation spawners like Northern Pike and Common Carp were classified as coastal associated rather than wetland associated based on their macrohabitat use patterns.

Environmental Associations for Fishery-Relevant Species

Ordinations of encounter probability data produced species vectors radiating throughout the ordination space (Figure 1), reflecting considerable variation in the makeup of fishery-relevant species across GLCWs. The two-dimensional ordination depicted had a stress of 0.20 and explained 79% of the among-wetland variability. The GLCWs from Lakes Superior,

Downloaded by [US EPA Library], [J. C. Hoffman] at 06:16 09 March 2015

TABLE 6. Summary of life history traits for 24 coastal wetland–using species of direct or indirect fishery relevance, in order of percent occurrence in our GLCW survey. See text for categorization details.

Species	Occurrence (%)	Thermal guild	Macrohabitat association	Wetland use	Wetland-related life history
			Sport fish		
Yellow Perch	93	Cool	Coastal	Facultative	Often littoral, moderate veg affinity
Largemouth Bass	67	Warm	Weak wet	Obligate	Littoral, high veg affinity
Northern Pike	67	Cool	Coastal	Obligate	Littoral, high veg affinity
Smallmouth Bass	38	Warm	Coastal	Facultative	Often littoral, but only sparse veg
Walleye	28	Cool	Coastal	Facultative	Often littoral, but low veg affinity
White Perch	14	Warm	Weak wet	Facultative	Somewhat littoral
White Bass	10	Warm	Strong wet	Facultative	Somewhat littoral, age-0 veg affinity
Channel Catfish	10	Warm	Coastal	Facultative	Somewhat littoral, low veg affinity
			Panfish		
Pumpkinseed	79	Warm	Weak wet	Obligate	Littoral, high veg affinity
Rock Bass	64	Cool	Weak wet	Facultative	Littoral, age-0 veg affinity
Bluegill	60	Warm	Weak wet	Facultative	Littoral, high veg affinity
Black Crappie	33	Cool	Coastal	Facultative	Littoral, high veg affinity
Green Sunfish	16	Warm	Strong wet	Facultative	Littoral, high veg affinity
			Rough fish		
White Sucker	72	Cool	Coastal	Facultative	Littoral, age-0 veg affinity
Common Carp	71	Warm	Coastal	Obligate	Littoral, high veg affinity
Black/Brown Bullhead	67	Warm	Strong wet	Facultative	Littoral, high veg affinity
Gizzard Shad	33	Cool	Weak wet	Facultative	Littoral, high veg affinity
Freshwater Drum	22	Warm	Weak wet	Facultative	Somewhat littoral, age-0 veg affinity
			Forage fish		
Yellow Perch[a]	93	Cool	Coastal	Facultative	Often littoral, moderate veg affinity
Spottail Shiner	40	Cold–cool	Coastal	Facultative	Age-0 veg affinity, adults pelagic/littoral
Gizzard Shad[a]	33	Cool	Weak wet	Facultative	Littoral, high veg affinity
Emerald Shiner	32	Cool	Coastal	Facultative	Age-0 veg affinity, adults pelagic/littoral
Alewife	28	Cold	Coastal	Facultative	Littoral, low veg affinity

[a]The entries for Yellow Perch and Gizzard Shad are repeated under forage fish due to the dual roles of these species.

Downloaded by [US EPA Library], [J. C. Hoffman] at 06:16 09 March 2015

Ontario, and Erie each form a cluster, whereas those from Lakes Michigan and Huron span much more ordination space, indicating more diverse composition (Figure 1). All species ordinated were found in at least four of the five Great Lakes, so the ordination reflects prevalence patterns rather than simply extent of range. Overlay vectors suggest a primary axis of variation related to eutrophication and anthropogenic disturbance (highest values in the lower left quadrant) and a secondary axis related to substrate type and vegetation structure (highest values in the upper left and right quadrants; Figure 1). Rough-fish richness and three of the five rough-fish species were oriented toward eutrophication–disturbance. Forage-fish richness and two of the five forage species also aligned with the eutrophication–disturbance axis, while one

TABLE 7. Mean wetland-scale richness (ranges in parentheses) of groups of fishery-relevant species, summarized by lake. Table 6 lists the species contributing to each group.

Lake	Number of wetlands	Sport fish	Panfish	Rough fish	Forage fish
Erie	6	3.3 (2–5)	2.8 (2–4)	4.3 (3–6)	3.5 (2–5)
Huron	6	2.3 (1–3)	2.5 (1–4)	2.5 (1–4)	1.5 (0–3)
Michigan	17	3.2 (1–6)	2.4 (1–4)	3.2 (1–6)	2.1 (0–4)
Ontario	12	3.2 (2–4)	2.8 (2–4)	3.0 (2–4)	2.0 (1–3)
Superior	17	3.2 (2–5)	2.2 (1–4)	2.0 (1–3)	2.2 (1–4)
All 5 lakes	58	3.1 (1–6)	2.5 (1–4)	2.8 (1–6)	2.2 (0–5)

Downloaded by [US EPA Library], [J. C. Hoffman] at 06:16 09 March 2015

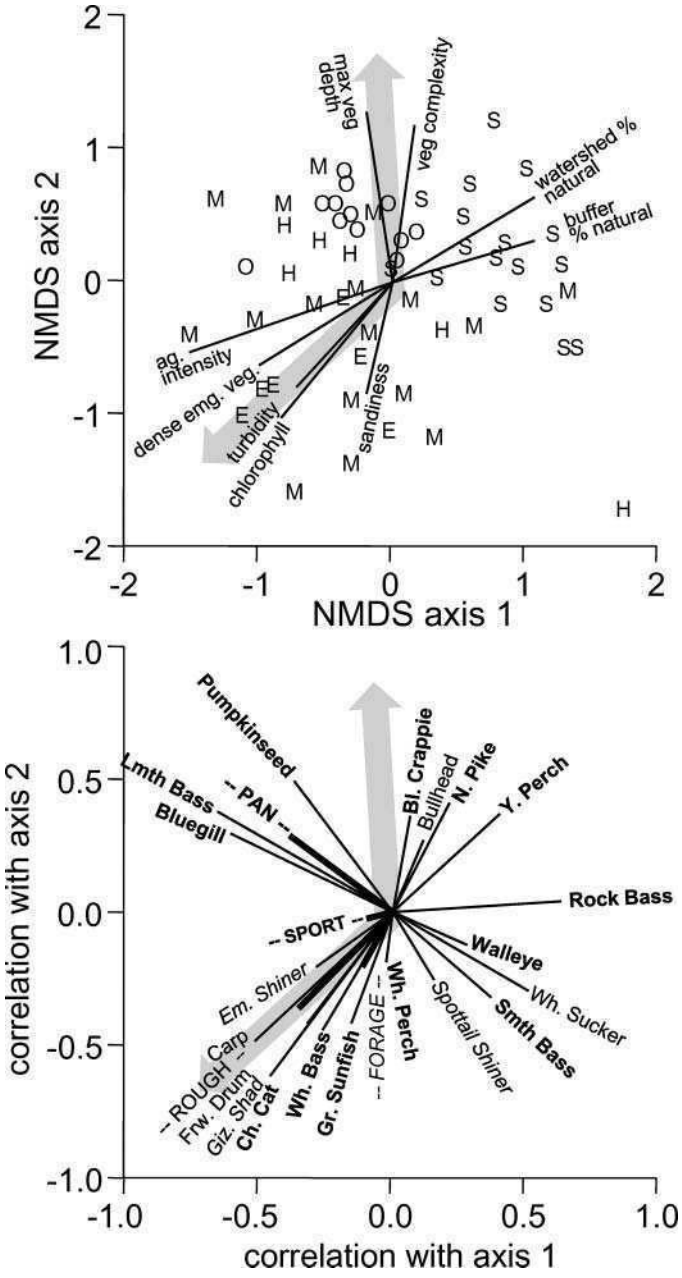

FIGURE 1. NMDS ordination of wetland-scale encounter probability for 24 fishery-relevant species. The top panel shows the positions of GLCWs coded by lake (E = Erie, H = Huron, M = Michigan, O = Ontario, and S = Superior) overlain with vectors showing the correlation with environmental variables. The bottom panel shows overlay vectors for all species (thin lines) except Alewifes (for which the vector is too short to depict) as well as group richness (thick lines), with the names of sport fish and panfish in bold, those of rough fish in ordinary type, and those of forage fish in italics. In both panels the wide gray arrows summarize the two general axes of environmental variation, the one oriented to the lower left being related to eutrophication and anthropogenic disturbance and the other being related to vegetation structure.

species (Alewife) was uncorrelated with the ordination. Panfish richness and three of the five panfish species aligned with increasing vegetation structure. Sport fish richness had little correlation with the ordination because of the disparate orientations of the component species.

The results of analyses relating individual species to environmental variables broadly reflected the patterns in the ordination but revealed further details relevant to how GLCW condition affects fishery support. Species ordinating in the upper left quadrant consistently had positive responses to vegetation structure at both wetland and station scales (Table 8), highlighting this as an influential environmental variable. Despite a strong association between turbidity and the overall eutrophication–disturbance gradient, negative associations to turbidity were few (Table 8), which is consistent with a general tolerance for turbidity by GLCW fish species (Trebitz et al. 2007). Fetch and sediment density ("sandiness") were rarely predictors at the wetland scale but were at the station scale for several species (Table 8). There were few differences among GLCW types (lacustrine, protected, or riverine) in species encounter probabilities, but more species had presence/absence patterns related to station type (lakelike, backbay, or channel; Table 8). Several species showed contrasting station-scale response patterns between life stages, with young-of-year tending to be more open-area oriented than older fish based on station type and fetch relationships (e.g., Largemouth Bass, Yellow Perch, Rock Bass, White Sucker, and Common Carp; Table 8).

Potential Guild Metrics of Fishery Support

Radar plots suggest that fishing-related groupings have some potential for organizing GLCW fishery support patterns. Encounter rates for adult sport fish were highest in GLCWs in the upper, well-vegetated radar plot quadrants (Figure 2a), and those for adults of the three panfish species of most interest to anglers (Black Crappie, Bluegill, and Pumpkinseed) were highest in GLCWs in the upper left quadrants (Figure 2b). Encounter rates for adult rough fish (mostly of interest to commercial fishing) were highest in GLCWs in the lower left, eutrophic–disturbed quadrant (Figure 2c). Only some of the potential taxonomic aggregations usefully distinguished among GLCWs. Encounter rates for adult Smallmouth Bass and Largemouth Bass were highest in upper left quadrant GLCWs (Figure 2d), but those for percids (Walleye and Yellow Perch) were distributed more or less evenly across the radar-plot space while those for adult *Morone* spp. (White Bass and White Perch) were nonzero in only a few GLCWs (not shown).

Groupings based on life history traits do not have much potential to organize fishery-support differences among GLCWs. The GLCW points were more or less uniformly distributed across the radar plots for the groupings of direct fishery-support species illustrated (wetland-associated species, obligate wetland spawners, species with a warm thermal preference, and vegetation-associated sport and panfish; Figure 3) as well as for other trait-based

TABLE 8. Wetland- and station-scale environmental associations, presented clockwise by species position within the ordination. The up and down arrows indicate positive and negative responses, respectively, with arrow thickness indicating significance (thin: $P < 0.05$; thick: $P < 0.005$) for the numerical predictors (Turb = turbidity, Veg = vegetation structure, fetch, and Sand = sediment density). Station-scale analyses are presented by age-group: 0 (young of year), older (juveniles and adults), all, or na (insufficient data). Three species—Alewife, Walleye, and White Perch—are not listed because there were no significant predictors for them.

	Wetland-scale predictors					Station-scale predictors					
Species	GLCW type	Turb	Veg	Fetch	Sand	Age	Station type	Turb	Veg	Fetch	Sand
Upper left quadrant											
Bluegill			↑			Older	Backbay↑		⇓	↑	
Largemouth Bass			⇑			0	Channel↓		⇓	⇓	
						Older					
Pumpkinseed			⇑			Older	Lakelike↑		↑	↑	↓
Age-0 sunfish[a]			⇑			0	Lakelike↑		⇓		⇓
Upper right quadrant											
Black Crappie						All	Backbay↓				
Northern Pike	Lacustrine↓		↑			0					
						Older					
Black/Brown Bullhead					⇓	0					↓
						Older	Channel↓				⇓
Yellow Perch		↓	↑			0	Lakelike↑		↑	↑	
						Older		⇓	⇑		
Rock Bass		↓				0					
						Older	Lakelike↓			⇓	↑
Lower right quadrant											
White Sucker						0					
						Older	Lakelike↓			⇓	⇓
Smallmouth Bass	Protected↓	↓	↓			0			↓		
						Older			↓		↓
Spottail Shiner			↓	↓	↓	All	Backbay↓		↓	↑	
Lower left quadrant											
Green Sunfish			↓			na					
Channel Catfish	Riverine↑					na					
White Bass		⇑				na					
Gizzard Shad		⇑	↑			na					
Freshwater Drum		⇑			↑	na					
Common Carp		⇑		⇑		0	Backbay↓	↓	⇓	↑	
						Older	Lakelike↓	↑			
Emerald Shiner		⇑				All	Backbay↓		↓		

[a] Bluegill and Pumpkinseed combined.

Downloaded by [US EPA Library], [J. C. Hoffman] at 06:16 09 March 2015

combinations examined (not illustrated), and trial plots summing just adults rather than all life stages were no clearer. For forage species, there was a pattern of higher encounters with vegetation-associated species in lower left quadrant GLCWs driven largely by Gizzard Shad (not shown), but other useful life history trait–related patterns were not evident.

DISCUSSION

Our goals were to refine our understanding of which Great Lakes species are both fishery relevant and wetland using, to examine their patterns of co-occurrence and life history with an eye toward developing useful metrics for multispecies fishery support, and to examine the relationships between GLCW condition and fishery support in the context of potential management actions. We discuss our progress toward each of these goals below.

Prominent Fishery-Relevant, Wetland-Using Species

We identified eight sport fish, five panfish, and five roughfish species meeting the criteria of having at least 10% occurrence across GLCWs and representing at least 1% of the

Downloaded by [US EPA Library], [J. C. Hoffman] at 06:16 09 March 2015

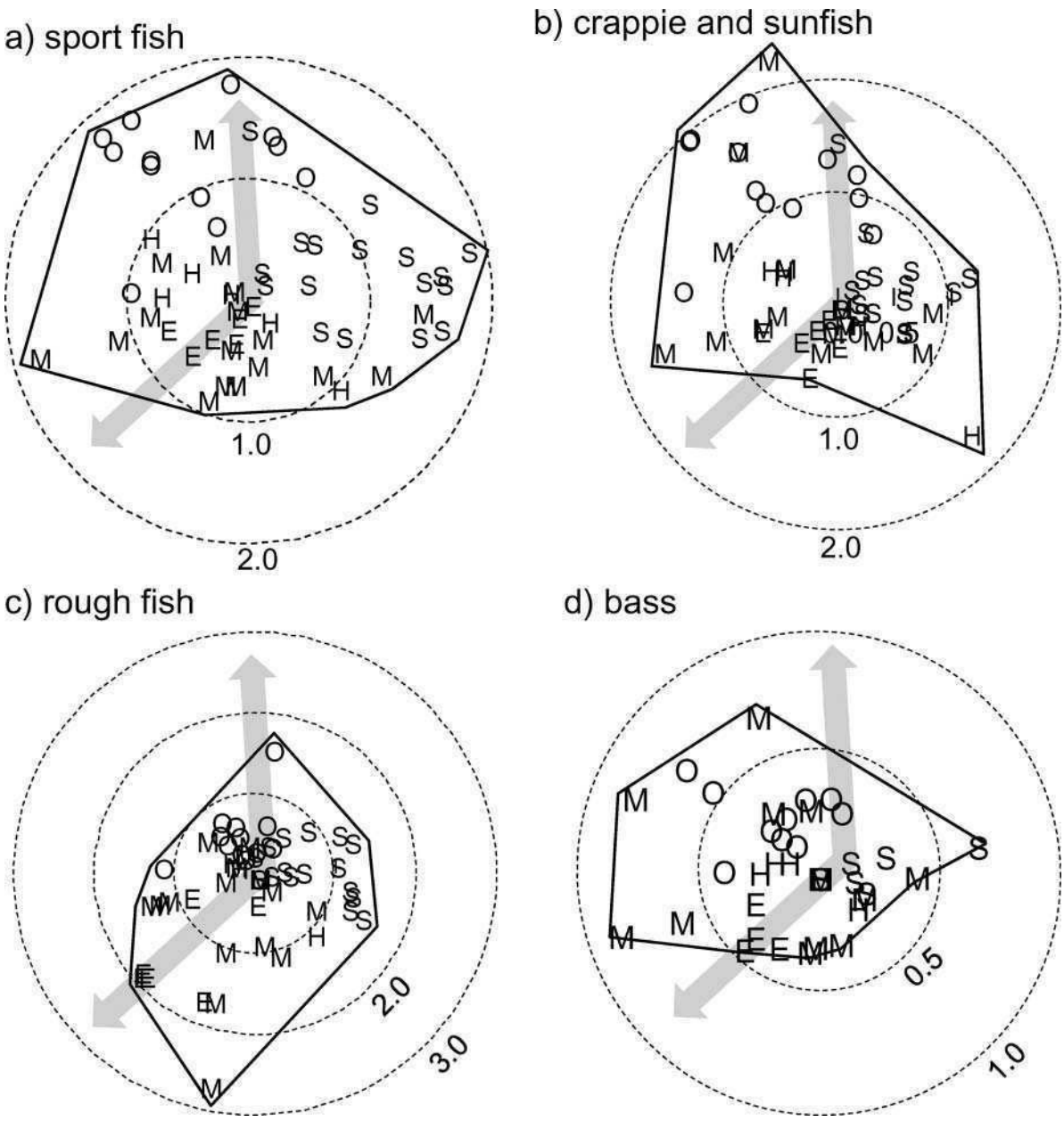

FIGURE 2. Radar plots showing the summed probabilities of encountering an adult fish in various taxonomic or fishing-relevance categories. Panel **(a)** shows any of eight sport fish species, panel **(b)** Black Crappies, Bluegills, and Pumpkinseeds, panel **(c)** any of five rough-fish species, and panel **(d)** Largemouth and Smallmouth Bass. The GLCWs (letter symbols) are plotted at the same angles from the origin as in the ordination but with the radial distance reflecting the encounter probability (further from the origin = higher probability). The rings show the distance scale, the polygons enclose the extent of the data points, and the wide gray arrows indicate the two general axes of environmental variation from the ordination.

recreational or commercial harvest in at least one lake, thereby adding quantitative detail to the long-recognized importance of GLCWs in supporting fishery-relevant species (Jaworski and Raphael 1978; Herdendorf et al. 1981; Jude and Pappas 1992). While Yellow Perch is the most prominent wetland-using species in terms of sport and commercial importance, other wetland-using species popular with recreational anglers include Largemouth Bass, Smallmouth Bass, Walleye, Northern Pike, Channel Catfish, Black Crappie, Bluegill, and Pumpkinseed, while almost all of the rough-fish species landed commercially in the Great Lakes are users of GLCWs.

Estimates that ~50% of the commercial harvest (biomass) and >80% of the recreational harvest (numbers) across the Great Lakes are comprised of species that use wetlands suggest that the GLCW role in direct fishery support is large. Simply combining fishery harvest data with information on wetland use is obviously insufficient to quantify the portion deriving from wetland-driven recruitment or productivity,

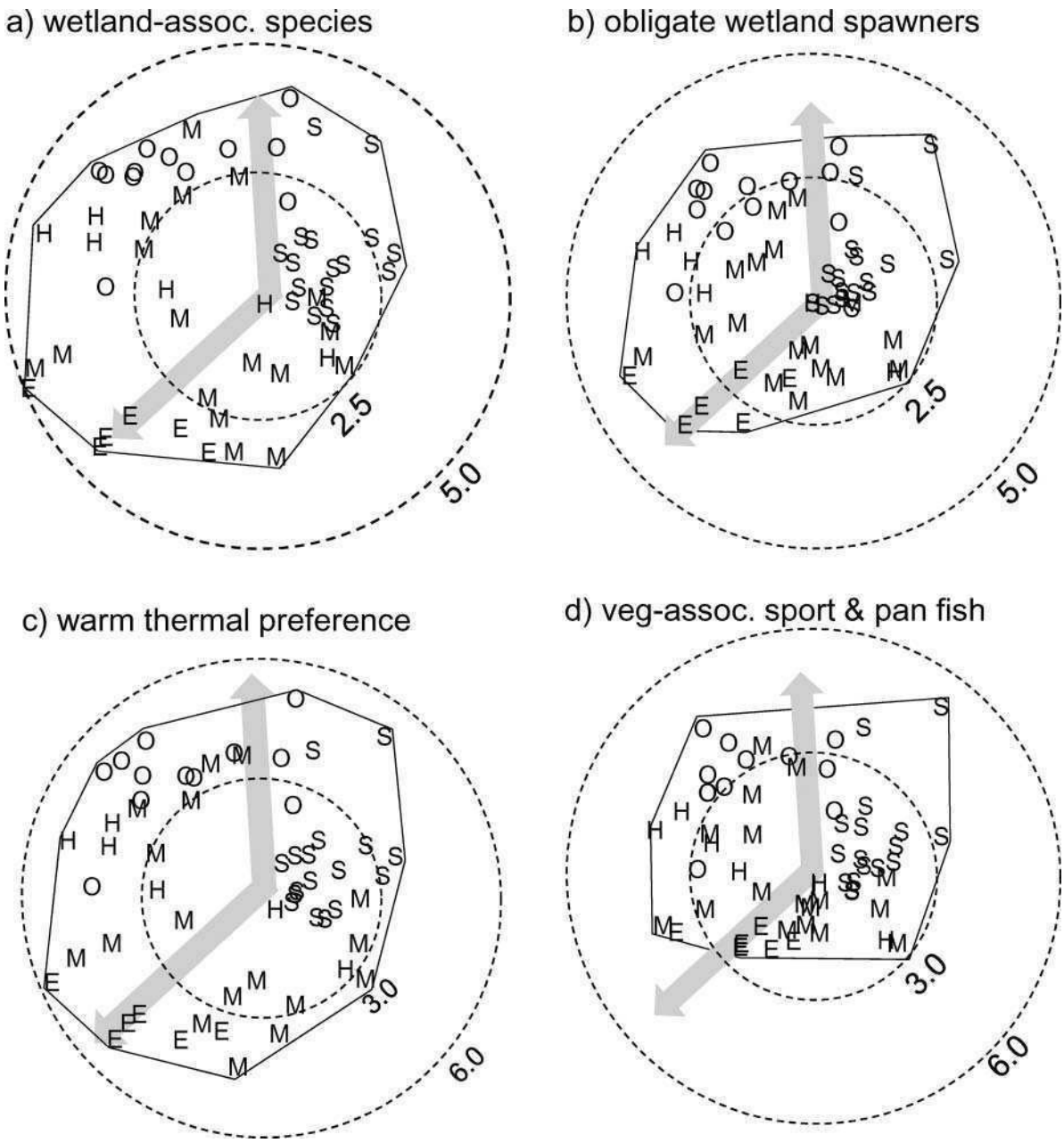

FIGURE 3. Radar plots showing the summed probabilities of encountering any life stage of a species with direct fishery importance in various life history categories derived from Table 5. Panel **(a)** shows species having a weak or strong wetland association, panel **(b)** species that are obligate wetland spawners, panel **(c)** species having a warm thermal preference, and panel **(d)** sport fish or panfish with high or young-of-year vegetation affinity. See Figure 2 for additional details.

especially since the harvested species also use other coastal habitats. However, the GLCW contribution is likely substantial based on the high areal productivity of wetlands. Shallow-water habitat in the Great Lakes is a small portion of the total lake area (~3%), and an even smaller portion is littoral (i.e., vegetated; Wetzel 1992); yet littoral habitat is estimated to represent 14–37% of the basinwide primary productivity, with areal productivity in areas with mixed submerged, floating, and emergent vegetation (i.e., wetlands) more than five times that of littoral habitats having only submerged vegetation (Brazner et al. 2000). Furthermore, a positive correlation between lakewide wetland area and Great Lakes commercial fish harvest has been reported (Brazner et al. 2000).

The GLCWs also provide indirect fishery support for sport fish species that may not use them directly. Wetland-using forage species, notably Emerald Shiner, Spottail Shiner, Gizzard Shad, and Alewife, are important diet items for nearshore

Downloaded by [US EPA Library], [J. C. Hoffman] at 06:16 09 March 2015

Downloaded by [US EPA Library], [J. C. Hoffman] at 06:16 09 March 2015

pelagic predators such as salmonids (e.g., Brandt 1986; Jude et al. 1987). Also, the harvest data compiled in this paper do not include fish caught for sale as live bait, another indirect contribution to Great Lakes fisheries (baitfish species include White Sucker, Emerald Shiner, and Spottail Shiner; Kerr 2012).

Almost all of the species commercially harvested from the Great Lakes are destined for human consumption (T. Goniea, Michigan Department of Natural Resources, T. Johnson, Ontario Ministry of Natural Resources, and R. Kinnunen, Michigan Sea Grant, personal communications). Sport and panfish sold as restaurant and retail-counter fare bring higher prices and make up more of the harvest on a dollar basis than a biomass basis, whereas rough fish sold in ethnic food markets bring lower prices and make up more of the harvest on a biomass basis than a dollar basis (Table 3). Gizzard Shad is the exception (it is sold primarily as crab bait), explaining the lower price for it than all the other commercial species. Harvest data, however, have limitations for representing fish value, particularly for recreational fishing. For example, angler interest in fishing for Largemouth and Smallmouth Bass and Northern Pike is higher than the harvest suggests (because of catch-and-release regulations and anglers' persisting even when their success is low; Bence and Smith 1999; DFO 2008; USFWS and USCB 2012), whereas the harvest of White Perch and White Bass is more opportunistic than targeted (Ohio DNR 2012). Great Lakes recreational fishery data probably underestimate the importance of sunfish and crappie species because assessments tend to emphasize the ice-free season and large-boat access points. Shore-based anglers report a greater tendency to seek sunfish than do boat-based anglers (Palla 2011), and at least in Lake Superior crappie tend to be targets in ice-fishing rather than summer angling (J. Lindgren, Minnesota Department of Natural Resources, personal communication). A national-scale angler preference survey (USFWS and USCB 2012) found that sunfish and crappie were broadly popular fishing targets even though the largest fishing-related expenditures (e.g., guide services and multiday trips) were directed at sport fish.

Our list of wetland-using species providing fishery support is conservative. For example, the recreationally important Muskellunge *Esox masquinongy* and the commercially harvested Bigmouth Buffalo are obligate vegetation spawners and thus wetland dependent, but they were omitted because of their low occurrence in our survey (~5%). Goldfish *Carassius auratus* and some redhorse sucker species (*Moxostoma* spp.) meet our wetland prevalence criterion but were not included because their commercial harvest is low. Quillback have commercial importance in Lake Erie but their occurrence was only 6% in our cross-lake survey. Surveys targeting distribution patterns on a lake-specific scale might include these species (e.g., Bigmouth Buffalo and Quillback occur frequently in Lake Erie GLCWs). Our compilation of larval fish data suggests that additional species might meet the criteria for being wetland-using if GLCW fish surveys were better timed to detect species for which the adults are present only briefly (e.g., in spring) to breed. Given their large commercial importance, finding *Coregonus* species and Rainbow Smelt in GLCWs as larvae but not at older life stages points to a potentially very important but poorly documented fishery support.

With respect to indirect fishery support, we only included species that are prominent in pelagic forage fish surveys or predator diet studies. We suspect these forage fish surveys underestimate the contribution of species that stay in very shallow waters, as this is an environment not easily sampled. Yellow Perch, for example, are not reported as being present in recent nearshore forage fish assessments for Lake Superior (e.g., Johnson et al. 2004; Gamble et al. 2011) despite being numerically dominant in a study of exchange between a Lake Superior GLCW and the adjacent nearshore area (Brazner et al. 2001). Brazner et al. (2001) also found frequent wetland–nearshore exchange for forage-sized Golden Shiner *Notemigonus crysoleucas* and Blacknose Shiner *Notropis heterolepis*, additional common GLCW species that likely provide some indirect fishery support. Stable isotope and otolith microelement analyses offer tools for getting at exchanges and habitat use patterns (Brazner et al. 2004; Hoffman et al., in press), but studies relevant to addressing fishery support in the Great Lakes are just beginning.

Useful Summary Metrics of GLCW Fishery Support?

The wetland-using, fishery-relevant species vary considerably in life history traits and environmental associations. While this means that GLCWs across a broad geographic and condition gradient are capable of providing meaningful fishery support, it also raises the problem of how to best quantify that support across species and fishery categories in order to ascertain the important patterns. We are not aware of good solutions to this problem in the fishery support literature; studies typically focus on a single fishery segment and either look at species (sometimes genera or families) one at a time or at very broad aggregations of catch (e.g., Manson et al. 2005; Vasconcelos et al. 2011; Sheaves et al. 2012; Blandon and zu Ermgassen 2014; Seitz et al. 2014). We saw the problem of quantifying multispecies, multi–user group fishery support as analogous to that of translating the concept of biological integrity into measurable indicators (e.g., Karr and Chu 1999), which led us to explore metrics based on taxonomic and functional groupings similar to those that have proven to be of value in biological integrity assessment.

Metrics that combine species that are related taxonomically or that are defined in terms of fishery user groups have some potential for organizing GLCW fishery support patterns. Radar plots depicting among-wetland patterns in encounter probability (i.e., the percentage of sampling locations where a species occurred) show some clear spatial patterns, especially for sport and rough-fish species; however, efforts to aggregate fishery-

Downloaded by [US EPA Library], [J. C. Hoffman] at 06:16 09 March 2015

relevant species via encounter probability summation had variable success. Combining the three panfish species of most interest to anglers (Bluegill, Pumpkinseed, and Black Crappie) conveniently also combined species with similar orientations in the ordination while excluding the opposing Rock Bass and Green Sunfish and produced a strong signal in the radar plots. However, Yellow Perch and Walleye (i.e., the Percidae) were not nearly as useful in the radar plots when combined despite their having similar orientations in the ordination and potentially similar appeal to anglers. Quantification based on richness was generally not helpful because combining enough species to obtain adequate range resulted in species with opposing occurrence patterns trading off in the calculations. For example, the orientation of the vectors for sport fish species was so diverse that overall sport fish richness had no meaningful pattern.

Functional metrics of the type generally included in fish-based biotic integrity indices (Fausch et al. 1990; Simon 1998) were generally not useful in organizing patterns of fishery support. Tolerance metrics did not discern among GLCWs because all of the fishery-relevant species are at least moderately tolerant of turbidity (Trebitz et al. 2007) and otherwise adapted to a wide variety of water quality conditions (Jude and Pappas 1992). Dietary categories essentially duplicated categorizing by fishing type, since the sport fish are piscivores, the panfish feed primarily on macroinvertebrates, and the rough fish are largely omnivores. Spawning guild metrics also did little to move classification beyond taxonomic and fishery groupings; for example, nest guarding is characteristic of both bass and sunfish. Even summarizing species encounter probabilities within life history traits related directly to the use of GLCWs (e.g., thermal preference, vegetation association, and wetland dependence; Table 6) did little to organize the patterns of fishery support, as evidenced by point clouds with no obvious spatial bias in the radar plots (Figure 3).

Are "Wetland Dependence" and "Poster-Child Species" Useful?

The presence of charismatic species may serve as public-friendly endpoints that people can readily value. For this reason and because single-species fisheries are more tractable to quantify, studies of fishery support have tended to focus on individual taxa for which both exploitation and habitat associations are well understood (e.g., penaeid shrimp in estuaries and mangroves; salmon *Oncorhynchus* spp. in Pacific Northwest coastal zone, blue crabs *Callinectes sapidus* in seagrass beds; Manson et al. 2005; Engle 2011; Jordan et al. 2012). Were we to nominate a representative fishery-support species for GLCWs, Yellow Perch is an obvious candidate given its high abundance and frequency of occurrence, its prominence in commercial and sport harvests, and its role as a forage species. However, Yellow Perch are not restricted to wetland environments either by life history or prevalence (they are equally abundant in nearshore/beach and GLCW habitats; Brazner and Beals 1997), and recent studies suggest that the species separates into primarily wetland-resident and primarily lake-resident populations having only weak connectivity (Janetski et al. 2013; Schoen 2013). Thus, while GLCW-derived Yellow Perch are known to play an ecological role in the Great Lakes, the species does not demonstrate that GLCWs are necessary to support Great Lakes fisheries.

In fact, the concept of wetland dependence among Great Lakes fish species is not a good match with GLCW use (as Table 6 illustrates). Fish have ontogeny and plasticity in habitat use that make essential fish habitat difficult to quantify (e.g., Levin and Stunz 2005; Kimirei et al. 2011), and even for species for which certain habitats are crucial those habitats may be neither limiting nor ones in which much time is spent (Minns et al. 1996; Rosenfield 2003). Thus, there is a need to characterize the interactions between GLCWs and other nearshore habitats analogous to that recognized for other coastal habitats (e.g., mangroves and salt marshes) in the context of the coastal ecosystem mosaic (Manson et al. 2005; Sheaves 2009). Furthermore, there is geographic variability in the Great Lakes with respect to how strongly fish species are wetland associated, as discrete GLCWs provide the only littoral habitat in some areas (e.g., Lake Superior) whereas entire coastal regions are littoral in character elsewhere (e.g., western Lake Erie and Green Bay). Nevertheless, the evidence of the spawning of multiple fishery-relevant species in GLCWs demonstrates that these habitats do contribute to overall fish populations and the use of multiple habitats (including GLCWs) for spawning–rearing can be a valuable risk-hedging strategy. Acknowledging that the spatial scale over which fishery-relevant species and their fisheries operate extends well beyond the GLCWs is not at odds with valuing GLCWs for fishery support. Increased attention to quantifying the spatial distribution of fishing effort and harvest would help establish the link between GLCW availability/condition and fishery support.

Focusing on "poster child" species or life history traits thought to coincide with wetland dependence (e.g., an affinity for quiescent or warm water, vegetated habitat, and organic substrates) sells short the diversity of fishery-relevant species that GLCWs support. The alternative is to embrace this diversity by evaluating entire suites of species despite the complexity this entails and by continuing to work toward useful multimetric characterization of fishery support. Species-specific assessments should be chosen for their value in understanding wetland–lake connectivity and the effects of ecological conditions. For example, despite the lack of clear wetland dependence or a requirement for vegetation on the part of Yellow Perch, the within-wetland encounter rates for this species were strongly and negatively correlated with the anthropogenic disturbance gradient in our ordination, making it a potentially useful indicator species.

Downloaded by [US EPA Library], [J. C. Hoffman] at 06:16 09 March 2015

GLCW Fishery Support in Relation to Wetland Characteristics and Condition

Great Lakes coastal wetlands are naturally heterogeneous, with differences in hydromorphology, substrate type, and vegetation structure leading to broad differences in the fish communities supported. The natural variability in GLCWs can generally be described as a continuum ranging from those in sheltered settings that tend to be deep and morphologically complex with organic sediments and vegetation that is abundant and diverse in form to those in exposed settings that tend to be shallower and morphologically simpler with sandier substrates and vegetation that is sparser and more monotypic. Like coastal ecosystems worldwide, GLCWs are also subject to stressors stemming from shoreline and watershed land-use practices (nutrient and sediment inputs, shoreline hardening, hydrologic alteration, recreational overuse, and the proliferation of nuisance species) that affect their physical and biological structures. Changes particularly relevant to fish assemblages include declining water clarity, degraded vegetation, and altered trophic pathways (Whillans 1996; Deegan 2002; Jude et al. 2005; Seitz et al. 2014).

Evans et al. (1987) characterize the overall productivity of lakes as depending on nutrient and energy inputs but the distribution of that production as driven by habitat conditions and biotic interactions. The same can be said of support for fish in GLCWs, as is readily apparent in our ordination of fishery-relevant species. As the most eutrophic and most littoral of the Great Lakes, Lake Erie would be expected to support the largest number and biomass of littoral fish. However, the fish composition in that lake is strongly biased toward rough-fish species of lesser commercial value and limited recreational interest. The GLCWs in other eutrophic settings (e.g., Green Bay and Saginaw Bay) are similar to those of Lake Erie with respect to species composition. In less eutrophic, less disturbed areas of the Great Lakes, yields of wetland-using, fishery-relevant species are lower but distributed more toward the sport and panfish species that bring high dockside prices and recreational interest. Depending on the characteristics of the individual GLCWs (and the broader biogeography), the fishery-relevant species supported are likely to divide into a warmer-water, phytophilic group (e.g., sunfish, Largemouth Bass, Black Crappie, and Northern Pike) and a cooler-water, lithophilic group (e.g., Smallmouth Bass, Walleye, and Rock Bass), although some species like Yellow Perch are prevalent in both.

These patterns suggest some ability to manage the nature of fishery support in GLCWs through protection and restoration. In a broad sense, anything that ameliorates degraded vegetation structure in GLCWs is likely to enhance conditions for the more desirable panfish and sport fish species. Poor water clarity resulting from nutrient and sediment loading is strongly implicated in the loss of the structurally diverse vegetation (Lougheed et al. 2001; Albert and Minc 2004) that is important to many sport and pan fish species (Randall et al. 1996; Smokorowski and Pratt 2007) and in shifting energy flow from benthic pathways and visual feeders (often sport and panfish) toward planktonic pathways and tactile/filter feeders (often rough fish; Sierszen et al. 2012a). As is evident from the "dense emergent vegetation" vector in our ordination (Figure 1), the proliferation of invasive plant species such as *Typha* and *Phragmites* is associated with nutrient loading and hydrologic alteration (Frieswyk and Zedler 2007; Tulbure and Johnston 2010) and can negatively affect the habitat for ambush piscivores such as Northern Pike and Largemouth Bass. Shoreline clearing and hardening are also associated with degraded vegetation structure in GLCWs (e.g., Trebitz et al. 2009b; Uzarski et al. 2009) and tend to reduce spawning habitat (Reed and Pereira 2009). Disruption of the normal connectivity between GLCWs and the adjacent lakes is another condition that is detrimental to support for fishery-relevant species (Johnson et al. 1997; Jude et al. 2005). Restoring hydrologic connectivity is a major thrust of restoration on marine coasts (e.g., Montalto and Steenhuis 2004) and is expected to enhance the number and size of fishery-relevant species in GLCWs (Bouvier et al. 2009). Nutrient and sediment control, invasive plant removal, and the reversal of shoreline hardening and hydrologic alterations are all part of the suite of restoration efforts currently proposed in the Great Lakes coastal areas (GLRI 2010), some with the express purpose of improving fisheries.

As a tangible example of potential restoration outcomes, consider the differences in fishery-relevant species encounter rates between the GLCWs within Lake Michigan that ordinated in a quadrant associated with high anthropogenic disturbance (lower left) and those associated with well-developed vegetation structure (upper left and right). While the among-GLCW variability is considerable, restoration actions that alter the vegetation structure from that typical of disturbed wetlands to that typical of well-vegetated wetlands could lead to an approximate doubling of the encounter rate for fishable-size (adult) bass, crappie, and sunfish but a halving of that for rough fish (Figure 4). This would clearly benefit recreational anglers, who value bass and panfish but have little interest in rough fish; for commercial fishing the shift away from rough fish and toward panfish would bring reduced landed biomass but higher dockside values. There was no difference in Yellow Perch encounter rates between the above GLCW groups, but other studies suggest that water quality improvements (especially in lacustrine coastal wetlands) would also roughly double the abundance of Yellow Perch (Leach et al. 1977; Parker et al. 2012). We chose Lake Michigan deliberately for the above example because its coastline spans the broadest disturbance gradient within the Great Lakes (Niemi et al. 2007) and the GLCW groups being compared are geographically and morphologically similar enough that shifts in ordination position between them are plausible. Predictions of restoration outcomes within some of the other Great Lakes are more difficult due to their less-prominent disturbance gradients (less "signal"

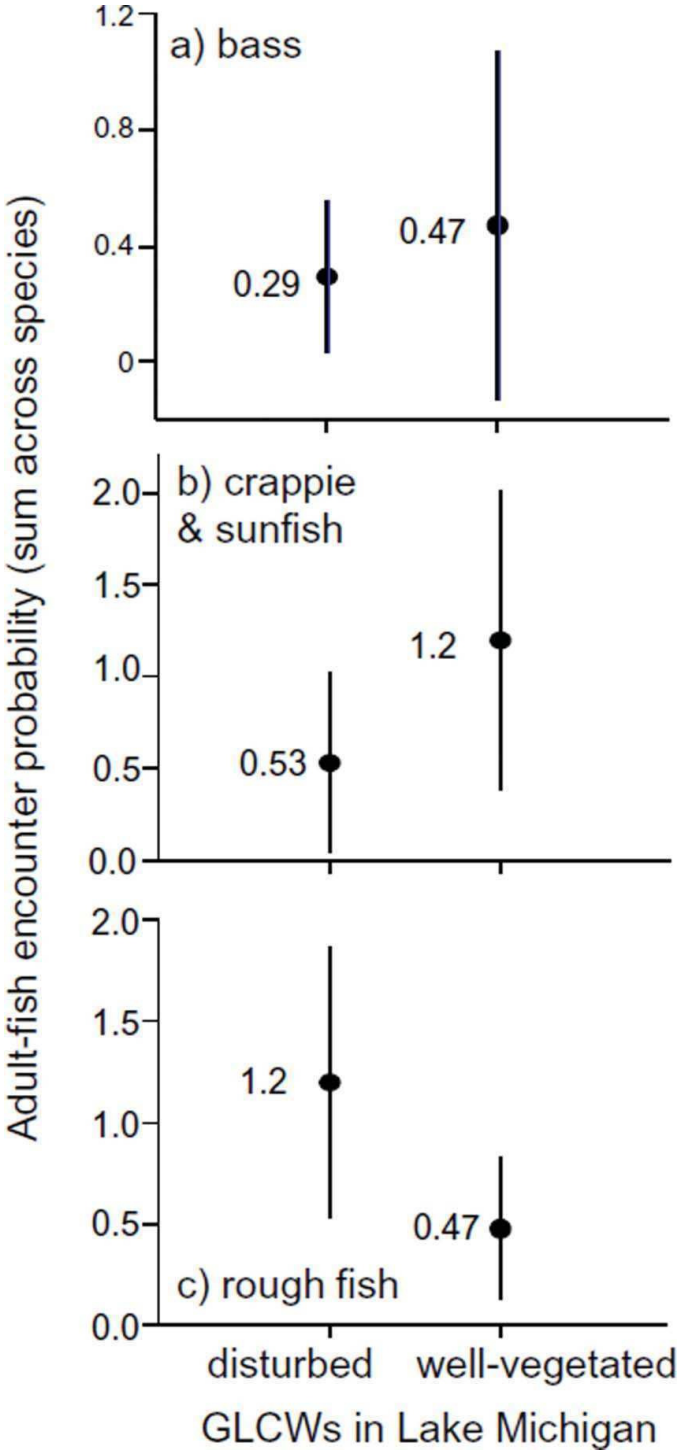

FIGURE 4. Comparison of encounter probabilities among Lake Michigan GLCWs falling into the disturbed (lower left; $N = 8$) ordination quadrant with ones falling into the well-vegetated (upper left and upper right; $N = 4$) ordination quadrants from Figure 1 for **(a)** Largemouth or Smallmouth Bass, **(b)** Black Crappies, Bluegills, or Pumpkinseeds, and **(c)** the five rough-fish species. The circles denote averages and the vertical bars 95% confidence intervals.

relative to "noise"). Ultimately, developing a framework for assessing the responses of fishery-relevant species on a regional scale is desirable because the cumulative effect of small-scale habitat degradation can be substantial impact over broader coastal regions (Jordan et al. 2009) and because habitat protection and restoration maintain fish communities and the diversity of fishing opportunities across broader scales than just individual ecosystems (Rahel 2002; Sheaves 2009).

Summary and Conclusions

Great Lakes coastal wetlands exemplify a complex fishery support situation. At least 21 fish species that are directly harvested or that serve as prey for other harvested species are regular users of GLCWs; they represent diverse taxonomic groups and life history traits; and they are fished for by multiple human user groups well beyond the GLCWs themselves. Our criteria of a minimum level of GLCW use and fishery importance make this list of species conservative; including species with more biogeographically restricted distributions or temporal use patterns not picked up by summer adult/juvenile fish surveys (e.g., larvae) would reveal additional fishery-relevant species supported by GLCWs. We have shown that synoptic survey data reveal patterns in fishery-relevant species associated with differences in the physical environments and ecological conditions of GLCWs that can be interpreted in terms of differences in fishing opportunity. For example, we can predict that management actions that lead to improved vegetation structure by controlling nutrient loading and other anthropogenic stressors will increase the rates of encounter with wetland-associated pan- and sport fish while lowering those with rough fish. Quantifying fishery support for GLCWs and other complex situations (such as those found in marine coastal ecosystems) is usefully viewed as a multispecies, multimetric problem that synoptic survey data can help solve. Our estimates that ~50% of the commercial and ~80% of the recreational fishery harvest in the Great Lakes is accounted for by wetland-using species would benefit from additional studies linking roving fish and spatially distributed fisheries back to GLCWs. The key information needs closely parallel those expressed for understanding fishery support in other coastal habitats (e.g., Able et al. 2005; Manson et al. 2005) and include fishery harvest data with higher spatial and temporal resolutions in order to match the ecologically relevant scales of habitat use; better data on fish origins and movements; and data documenting differential growth, mortality, and recruitment among alternative habitats.

ACKNOWLEDGMENTS

We thank Michael Sierszen, John Brazner, David Jude, Edward Rutherford, and Don Schreiner for conversations that helped shape our thinking; staff from various fish management agencies for helping locate data reports; and the MED coastal

Downloaded by [US EPA Library], [J. C. Hoffman] at 06:16 09 March 2015

wetland team for generating fish composition and habitat data. The views expressed in this paper are those of the authors and do not necessarily reflect the views or policies of the U.S. Environmental Protection Agency.

REFERENCES

Able, K. W. 2005. A reexamination of fish estuarine dependence: evidence for connectivity between estuarine and ocean habitats. Estuarine, Coastal, and Shelf Science 64:5–17.

Albert, D. A., and L. D. Minc. 2004. Plants as regional indicators of Great Lakes coastal wetland health. Aquatic Ecosystem Health Management 7:233–247.

Albert, D. A., D. A. Wilcox, J. W. Ingram, and T. A. Thompson. 2005. Hydrogeomorphic classification for Great Lakes coastal wetlands. Journal of Great Lakes Research 31(Supplement 1):129–46.

Allan, J. D., P. B. McIntyre, S. D. P. Smith, B. S. Halpern, G. Boyer, A. Buchsbaum, A. Burton, L. Campbell, L. Chadderton, J. Ciborowski, P. Doran, T. Eder, D. M. Infante, L. B. Johnson, C. G. Joseph, A. L. Marino, A. Prusevich, J. Read, J. Rose, E. Rutherford, S. Sowa, and A. D. Steinman. 2013. Joint analysis of stressors and ecosystems services to enhance restoration effectiveness. Proceedings of the National Academy of Sciences of the USA 110:372–377.

Arend, K. K., and M. B. Bain. 2008. Fish communities in coastal freshwater ecosystems: the role of the physical and chemical setting. BMC Ecology [online serial] 8:23.

Auer, N. A. 1982. Identification of larval fishes of the Great Lakes basin with emphasis on the Lake Michigan drainage. Great Lakes Fishery Commission, Special Publication 82-3, Ann Arbor, Michigan.

Barbier, E. B., S. D. Hacker, C. Kennedy, E. W. Koch, A. C. Stier, and B. R. Silliman. 2011. The value of estuarine and coastal ecosystem services. Ecological Monographs 81:169–193.

Becker, G. C. 1983. Fishes of Wisconsin. University of Wisconsin Press, Madison.

Bell, F. W. 1997. The economic valuation of saltwater marsh supporting marine recreational fishing in the southeastern United States. Ecological Economics 21:243–254.

Bence, J. R., and K. D. Smith. 1999. An overview of recreational fisheries of the Great Lakes. Pages 259–305 *in* W. W. Taylor and C. P. Ferreri, editors. Great Lakes fishery policy and management: a binational perspective. Michigan State University Press, East Lansing.

Blandon, A., and P. S. E. zu Ermgassen. 2014. Quantitative estimate of commercial fish enhancement by seagrass habitat in southern Australia. Estuarine, Coastal, and Shelf Science 141:1–8.

Bouvier, L. D., K. Cottenie, and S. E. Doka. 2009. Aquatic connectivity and fish metacommunities in wetlands of the lower Great Lakes. Canadian Journal of Fisheries and Aquatic Sciences 66:933–948.

Brander, L. M., R. J. Florax, and J. E. Vermaat. 2006. The empirics of wetland valuation: a comprehensive summary and a meta-analysis of the literature. Environmental Resource Economics 33:223–250.

Brandt, S. B. 1986. Food of trout and salmon in Lake Ontario. Journal of Great Lakes Research 12:200–205.

Brazner, J. C., and E. W. Beals. 1997. Patterns in fish assemblages from coastal wetland and beach habitat in Green Bay, Lake Michigan: a multivariate analysis of abiotic and biotic forcing factors. Canadian Journal of Fisheries and Aquatic Sciences 54:1743–1761.

Brazner, J. C., S. E. Campana, D. K. Tanner, and S. T. Schram. 2004. Reconstructing habitat use and wetland nursery origin of Yellow Perch from Lake Superior using otolith elemental analysis. Journal of Great Lakes Research 30:492–507.

Brazner, J. C., M. E. Sierszen, J. R. Keough, and D. K. Tanner. 2000. Assessing the ecological importance of coastal wetlands in a large-lake context. Internationale Vereinigung für Theoretische und Angewandte Limnologie Verhandlungen 27:1950–1961.

Brazner, J. C., D. K. Tanner, and J. A. Morrice. 2001. Fish-mediated nutrient and energy exchange between a Lake Superior coastal wetland and its adjacent bay. Journal of Great Lakes Research 27:98–111.

Breidert, B. 2011. Harvest of fishes from Lake Michigan during 2010. Report to Great Lakes Fishery Commission, Lake Michigan Committee, Ann Arbor, Michigan.

Chubb, S. L., and C. R. Liston. 1986. Density and distribution of larval fishes in Pentwater Marsh, a coastal wetland on Lake Michigan. Journal of Great Lakes Research 12:332–343.

Coker, G. A., C. B. Portt, and C. K. Minns. 2001. Morphological and ecological characteristics of Canadian freshwater fishes. Canadian Manuscript Report of Fisheries Aquatic Sciences 2554.

Cooper, C. L., W. C. Bartholomew, C. R. Herdendorf, J. M. Reutter, and F. L. Snyder. 1981. Limnetic larval fish of the Maumee and Sandusky River estuaries. Journal of Great Lakes Research 7:51–54.

Cooper, M. J., K. F. Gyekis, and D. G. Uzarski. 2012. Edge effects on abiotic conditions, zooplankton, macroinvertebrates, and larval fishes in Great Lakes fringing marshes. Journal of Great Lakes Research 38:142–151.

Danz, N. P., R. R. Regal, G. J. Niemi, V. J. Brady, T. Hollenhorst, L. B. Johnson, G. E. Host, J. M. Hanowski, C. A. Johnston, T. Brown, J. Kingston, and J. R. Kelly. 2005. Environmentally stratified sampling design for the development of Great Lakes environmental indicators. Environmental Monitoring and Assessment 102:41–65.

Deegan, L. A. 2002. Lessons learned: the effects of nutrient enrichment on the support of nekton by seagrass and salt marsh ecosystems. Estuaries 25:727–742.

DFO (Department of Fisheries and Oceans). 2008. Survey of recreational fishing in Canada: selected results for the Great Lakes fishery 2005. DFO, Ottawa.

Engle, V. D. 2011. Estimating the provision of ecosystem services by Gulf of Mexico coastal wetlands. Wetlands 31:179–193.

Evans, D. O., B. A. Henderson, N. J. Bax, T. R. Marshall, R. T. Oglesby, and W. J. Christie. 1987. Concepts and methods of community ecology applied to freshwater fisheries management. Canadian Journal of Fisheries and Aquatic Sciences 44(Supplement):S448–S470.

Farber, S., R. Costanza, D. L. Childers, K. Erickson, K. Gross, M. Grove, C. S. Hopkinson, J. Kahn, S. Pincetl, A. Troy, P. Warren, and M. Wilson. 2006. Linking ecology and economics for ecosystem management. Bioscience 56:121–133.

Fausch, K. D., J. Lyons, J. R. Karr, and P. L. Angermeyer. 1990. Fish communities as indicators of environmental degradation. Pages 123–144 *in* S. M. Adams, editor. Biological indicators of stress in fish. American Fisheries Society, Symposium 8, Bethesda, Maryland.

Francis, M. P., M. A. Morrison, J. Leathwick, C. Walsh, and C. Middleton. 2005. Predictive models of small fish presence and abundance in northern New Zealand harbours. Estuarine, Coastal, and Shelf Science 64:419–435.

Frieswyk, C. B., and J. B. Zedler. 2007. Vegetation change in Great Lakes coastal wetlands: deviation from the historical cycle. Journal of Great Lakes Research 33:366–380.

Gamble, A. E., T. R. Hrabik, J. D. Stockwell, and D. L. Yule. 2011. Trophic connections in Lake Superior, part II. The nearshore fish community. Journal of Great Lakes Research 37:550–560.

GLRI (Great Lakes Restoration Initiative). 2010. Great Lakes Restoration Initiative action plan, FY2010–FY2014. Available: greatlakesrestoration.us/pdfs/glri_actionplan.pdf. (January 2015).

Gordon, D., D. W. Chapman, and T. C. Bjornn. 1973. Economic evaluations of sport fisheries: what do they mean? Transactions of the American Fishery Society 102:293–311.

Hanson, D. 2012. 2011 Lake Michigan recreational fishery trends by region. Lake Michigan Committee Meeting, Windsor, Ontario. Available: http://www.in.gov/dnr/fishwild/files/fw-Lake_Michigan_Recreational_Creel_Report_2011.pdf. (January 2015).

Downloaded by [US EPA Library], [J. C. Hoffman] at 06:16 09 March 2015

Herdendorf, C. E., S. M. Hartley, and M. D. Barnes, editors. 1981. Fish and wildlife resources of the Great Lakes coastal wetlands within the United States, volume 1. Overview. U.S. Fish and Wildlife Service Report FWS/OBS-81/02-v1.

Hoffman, J. C., J. R. Kelly, G. S. Peterson, and A. M. Cotter. In press. Landscape-scale food webs of fish nursery habitat along a river–coast mixing zone. Estuaries and Coasts. DOI: 10.1007/s12237-014-9880-8.

Hoffman, J. C., J. R. Kelly, G. S. Peterson, A. M. Cotter, M. A. Starry, and M. E. Sierszen. 2012. Using δ^{15}N in fish larvae as an indicator of watershed sources of anthropogenic nitrogen: response at multiple spatial scales. Estuaries and Coasts 35:1453–1467.

Holmlund, C., and M. Hammer. 1999. Ecosystem services generated by fish populations. Ecological Economics 29:253–368.

Höök, T. O., N. M. Eagan, and P. W. Webb. 2001. Habitat and human influences on larval fish assemblages in northern Lake Huron coastal marsh bays. Wetlands 21:281–291.

Janetski, D. J., C. R. Ruetz, Y. Bhagat, and D. F. Clapp. 2013. Recruitment dynamics of age-0 Yellow Perch in a drowned river mouth lake: assessing synchrony with nearshore Lake Michigan. Transactions of the American Fisheries Society 142:505–514.

Jaworski, E., and C. N. Raphael. 1978. Fish, wildlife, and recreational values of Michigan's coastal wetlands. Report to Michigan Department of Natural Resources, Ypsilanti.

Johnson, D. L. 1989. Lake Erie wetlands: fisheries considerations. Pages 257–273 *in* K. A. Krieger, editor. Lake Erie estuarine systems: issues, resources, status, and management. National Oceanic and Atmospheric Administration, Estuary-of-the-Month Seminar Series 14, Washington, D.C..

Johnson, D. L., W. E. Lynch, and T. W. Morrison. 1997. Fish communities in a diked Lake Erie wetland and an adjacent undiked area. Wetlands 17:43–54.

Johnson, T. B., M. H. Hoff, A. S. Trebitz, C. R. Bronte, T. D. Corry, J. F. Kitchell, S. T. Lozano, D. M. Mason, J. V. Scharold, S. T. Schram, and D. R. Schreiner. 2004. Spatial patterns in assemblage structures of pelagic forage fish and zooplankton in western Lake Superior. Journal of Great Lakes Research 30(Supplement 1):395–406.

Jordan, S. J., T. O. O'Higgins, and J. A. Dittmar. 2012. Ecosystem services of coastal habitats and fisheries: multiscale ecological and economic models in support of ecosystem-based management. Marine Coastal Fisheries: Dynamics, Management, and Ecosystem Science [online serial] 4:573–586.

Jordan, S. J., L. M. Smith, and J. A. Nestlerode. 2009. Cumulative effects of coastal habitat alterations on fishery resources: towards prediction at regional scales. Ecology and Society [online serial] 14(1):16.

Jude, D., D. Albert, D. G. Uzarski, and J. Brazner. 2005. Lake Michigan's coastal wetlands: distribution, biological components with emphasis on fish, and threats. Pages 439–477 *in* T. Edsall and M. Munawar, editors. State of Lake Michigan: ecology, health, and management. Backhuys Publishers, Ann Arbor, Michigan.

Jude, D. J., and J. Pappas. 1992. Fish utilization of Great Lakes coastal wetlands. Journal of Great Lakes Research 18:651–672.

Jude, D. J., T. L. Rutecki, C. P. Madenjian, G. E. Noguchi, P. P. Schneeberger, S. A. Klinger, G. G. Godun, and M. H. Winnel. 1981. The physical, chemical, and biological nature of Pigeon Lake, a Lake Michigan coastal lake. University of Michigan, Great Lakes Research Division, Special Report 78, Ann Arbor.

Jude, D. J., and F. J. Tesar. 1985. Recent changes in the inshore forage fish of Lake Michigan. Canadian Journal of Fisheries and Aquatic Sciences 42:1154–1157.

Jude, D. J., F. J. Tesar, S. F. Deboe, and T. J. Miller. 1987. Diet and selection of major prey species by Lake Michigan salmonines, 1973–1982. Transactions of the American Fisheries Society 116:677–691.

Karr, J. R., and E. W. Chu. 1999. Restoring life in running waters: better biological monitoring. Island Press, Washington, D.C.

Kerr, S. J. 2012. The management of bait in Ontario: a review. Ontario Ministry of Natural Resources, Peterborough.

Kimirei, I. A., I. Nagelkerken, B. Griffioen, C. Wagner, and Y. D. Mgaya. 2011. Ontogenetic habitat use by mangrove/seagrass-associated coral reef fishes shows flexibility in time and space. Estuarine, Coastal, and Shelf Science 92:47–58.

Klumb, R. A., L. G. Rudstam, E. L. Mills, C. P. Schneider, and P. M. Sawyko. 2003. Importance of Lake Ontario embayments and nearshore habitats as nurseries for larval fishes with emphasis on Alewife (*Alosa pseudoharengus*). Journal of Great Lakes Research 29:181–198.

Knight, R. L., and B. Vondracek. 1993. Changes in prey fish populations in western Lake Erie, 1969–88, as related to Walleye, *Stizostedion vitreum*, predation. Canadian Journal of Fisheries and Aquatic Sciences 50:1289–1298.

Krupa, K. A. 2003. Larval fish exchange between Lake Erie and a coastal marsh. Master's thesis. Ohio State University, Columbus.

Lane, J. A., C. B. Portt, and C. K. Minns. 1996a. Nursery habitat characteristics of Great Lakes fishes. Canadian Manuscript Report of Fisheries and Aquatic Sciences 2338.

Lane, J. A., C. B. Portt, and C. K. Minns. 1996b. Spawning habitat characteristics of Great Lakes fishes. Canadian Manuscript Report of Fisheries and Aquatic Sciences 2368.

Lantry, J. R., and T. H. Eckert. 2012. 2011 Lake Ontario fishing boat survey. New York State Department of Environmental Conservation, Albany.

Leach, J. H., M. G. Johnson, J. R. M. Kelso, J. Hartmann, W. Nümann, and B. Entz. 1977. Responses of percid fishes and their habitats to eutrophication. Journal of the Fisheries Research Board of Canada 34:1964–1971.

Levin, P. S., and G. W. Stunz. 2005. Habitat triage for exploited fishes: can we identify essential "essential fish habitat"? Estuarine, Coastal, and Shelf Science 64:70–78.

Lewis, L. M., and S. P. Patch. 1982. Lake Ontario shoreline protection study report: Sage Creek Marsh. U.S. Fish and Wildlife Service, Cortland, New York.

Lougheed, V. S., B. Crosbie, and P. Chow-Fraser. 2001. Primary determinants of macrophyte community structure in 62 marshes across the Great Lakes basin: latitude, land use, and water quality effects. Canadian Journal of Fisheries and Aquatic Sciences 58:1603–1612.

Manson, F. J., N. R. Loneragan, G. A. Skilleter, and S. R. Phinn. 2005. An evaluation of the evidence for linkages between mangroves and fisheries: a synthesis of the literature and identification of research directions. Oceanography and Marine Biology: an Annual Review 43:485–515.

Masterson, C., and B. Eggold. 2012. Wisconsin's 2011 open-water sportfishing effort and harvest from Lake Michigan and Green Bay. Wisconsin Department of Natural Resources, Publication FH-830-12, Milwaukee.

Minns, C. K., R. G. Randall, J. E. Moore, and V. W. Cairns. 1996. A model simulating the impact of habitat supply limits on Northern Pike, *Esox lucius*, in Hamilton Harbour, Lake Ontario. Canadian Journal of Fisheries and Aquatic Sciences 53(Supplement 1):20–34.

Mizera, J. J., C. L. Cooper, and C. E. Herdendorf. 1981. Limnetic larval fish in the nearshore zone of the western basin of Lake Erie. Journal of Great Lakes Research 7:62–64.

Montalto, F. A., and T. S. Steenhuis. 2004. The link between hydrology and restoration of tidal marshes in the New York–New Jersey estuary. Wetlands 24:414–425.

Murphy, S., N. Collins, S. E. Doka, and B. J. Fryer. 2012. Evidence of Yellow Perch, Largemouth Bass, and Pumpkinseed metapopulations in coastal embayments of Lake Ontario. Environmental Biology of Fishes 95:213–226.

National Research Council. 2005. Valuing ecosystem services: towards better environmental decision making. National Academies Press, Washington, D.C.

Niemi, G. J., J. R. Kelly, and N. P. Danz. 2007. Environmental indicators for the coastal region of the North American Great Lakes: introduction and prospectus. Journal of Great Lakes Research 33(Supplement 3):1–12.

O'Gorman, R. 1983. Distribution and abundance of larval fish in the nearshore waters of western Lake Huron. Journal of Great Lakes Research 9:14–22.

Downloaded by [US EPA Library], [J. C. Hoffman] at 06:16 09 March 2015

Downloaded by [US EPA Library], [J. C. Hoffman] at 06:16 09 March 2015

Ohio DNR (Department of Natural Resources). 2012. Ohio's Lake Erie fisheries 2011. Ohio DNR, Federal Aid in Fish Restoration, Project f-69-P, Annual Status Report, Fairport and Sandusky.

OMNR (Ontario Ministry of Natural Resources). 2013a. 2012 status of major stocks. OMNR, Wheatley.

OMNR (Ontario Ministry of Natural Resources). 2013b. Lake Huron commercial fishing summary for 2012. OMNR, Owen Sound.

OMNR (Ontario Ministry of Natural Resources). 2013c. Lake Ontario fish communities and fisheries: 2012 annual report of the Lake Ontario management unit. OMNR, Picton.

OMNR (Ontario Ministry of Natural Resources). 2013d. Lake Superior commercial fishing summary for 2011. OMNR, Lake Superior Report TR-LSA-2013-nn, Owen Sound.

Palla, J. S. 2011. Lake Michigan 2010 creel survey report. Indiana Department of Natural Resources, Indianapolis.

Palmer, M. A., and S. Filoso. 2009. Restoration of ecosystem services for environmental markets. Science 325:575–576.

Parker, A. D., M. J. Cooper, C. R. Ruetz, D. P. Coulter, and D. G. Uzarski. 2012. Chemical and physical factors associated with Yellow Perch abundance in Great Lakes coastal wetlands: patterns within and among wetland types. Wetlands Ecology and Management 20:137–150.

Provencher, B., and R. C. Bishop. 1997. An estimable dynamic model of recreation behavior with an application to Great Lakes angling. Journal of Environmental Economics and Management 33:107–127.

Rahel, F. J. 2002. Homogenization of freshwater faunas. Annual Reviews in Ecology and Systematics 33:291–315.

Rand, P. S., and D. J. Stewart. 1998. Dynamics of salmonine diets and foraging in Lake Ontario, 1983–1993: a test of a bioenergetic model prediction. Canadian Journal of Fisheries and Aquatic Sciences 55:307–317.

Randall, R. G., C. K. Minns, V. W. Cairns, and J. E. Moore. 1996. The relationship between an index of fish production and submerged macrophytes and other habitat features at three littoral areas in the Great Lakes. Canadian Journal of Fisheries and Aquatic Sciences 53(Supplement 1):35–44.

Reed, J. R., and D. L. Pereira. 2009. Relationship between shoreline development and nest site selection by Black Crappie and Largemouth Bass. North American Journal of Fisheries Management 29:943–948.

Rose, K. R. 2000. Why are quantitative relationships between environmental quality and fish populations so elusive? Ecological Applications 10:367–385.

Rosenfield, J. 2003. Assessing the habitat requirements of stream fishes: an overview and evaluation of different approaches. Transactions of the American Fisheries Society 132:953–968.

Rosenfield, J. S., and T. Hatfield. 2011. Information needs for assessing critical habitat of freshwater fish. Canadian Journal of Fisheries and Aquatic Sciences 63:683–698.

Rutkayová, J., R. Biskup, R. Harant, V. Šlechta, and J. Koščoet, 2013. *Ameiurus melas* (Black Bullhead): morphological characteristics of new introduced species and its comparison with *Ameiurus nebulosus* (Brown Bullhead). Reviews in Fish Biology and Fisheries 23:51–68.

Schoen, L. S. 2013. Wetland–nearshore habitat coupling in the Great Lakes: reconstructing fish movements among Great Lakes coastal wetlands. Master's thesis. Central Michigan University, Mount Pleasant.

Scott, W. B., and E. J. Crossman. 1973. Freshwater fishes of Canada. Fisheries Research Board of Canada, Ottawa.

Seilheimer, T. S., and P. Chow-Fraser. 2007. Application of the wetland fish index to northern Great Lakes marshes, with emphasis on Georgian Bay coastal wetlands. Journal of Great Lakes Research 33(Supplement 3):154–171.

Seitz, R. D., H. Wennhage, U. Bergström, R. N. Lipcius, and T. Ysebaert. 2014. Ecological value of coastal habitats for commercially and ecologically important species. ICES Journal of Marine Science 71:648–665.

Sheaves, M. 2009. Consequences of ecological connectivity: the coastal ecosystem mosaic. Marine Ecology Progress Series 391:107–115.

Sheaves, M., R. Johnston, and R. M. Connolly. 2012. Fish assemblages as indicators of estuary ecosystem health. Wetlands Ecology and Management 20:477–490.

Sierszen, M. E., J. C. Brazner, A. M. Cotter, J. A. Morrice, G. S. Peterson, and A. S. Trebitz. 2012a. Watershed and lake influences on the energetic base of coastal wetland food webs across the Great Lakes basin. Journal of Great Lakes Research 38:418–428.

Sierszen, M. E., J. A. Morrice, A. S. Trebitz, and J. C. Hoffman. 2012b. A review of selected ecosystems services provided by coastal wetlands of the Laurentian Great Lakes. Aquatic Ecosystem Health Management 15:92–106.

Simon, T. P. 1998. Assessing the sustainability and biological integrity of water resources using fish communities. CRC Press, Boca Raton, Florida.

Smokorowski, K. E., and T. C. Pratt. 2007. Effect of change in physical structure and cover on fish and fish habitat in freshwater ecosystems: a review and meta-analysis. Environmental Reviews 15:12–41.

Spangenberg, J. H., and J. Settele. 2010. Precisely incorrect? Monetising the value of ecosystem services. Ecological Complexity 7:327–337.

Steen, P. J., T. G. Zorn, P. W. Seelbach, and J. S. Schaeffer. 2008. Classification tree models for predicting distribution of Michigan stream fish from landscape variables. Transactions of the American Fisheries Society 137:976–996.

Tallis, H., S. E. Lester, M. Ruckelshaus, M. Plummer, K. McLeod, A. Guerry, S. Andelman, M. Caldwell, M. Conte, S. Copps, D. Fox, R. Fujita, S. Gaines, G. Gelfenbaum, B. Gold, P. Kareiva, C. Kim, K. Lee, M. Papenfus, S. Redman, B. Silliman, L. Wainger, and C. White. 2012. New metrics for managing and sustaining the ocean's bounty. Marine Policy 36:303–306.

Tanner, D. K., J. C. Brazner, V. J. Brady, and R. R. Regal. 2004. Habitat associations of larval fish in a Lake Superior coastal wetland. Journal of Great Lakes Research 30:349–359.

Trebitz, A. S., J. C. Brazner, V. J. Brady, R. Axler, and D. K. Tanner. 2007. Turbidity tolerances of Great Lakes coastal wetland fishes. North American Journal of Fisheries Management 27:619–633.

Trebitz, A. S., J. C. Brazner, N. P. Danz, M. S. Pearson, G. S. Peterson, D. K. Tanner, D. L. Taylor, C. W. West, and T. Hollenhorst. 2009a. Geographic, anthropogenic, and habitat influences on Great Lakes coastal wetland fish assemblages. Canadian Journal of Fisheries and Aquatic Sciences 66:1328–1342.

Trebitz, A. S., J. C. Brazner, M. S. Pearson, G. S. Peterson, D. K. Tanner, and D. L. Taylor. 2009b. Patterns in habitat and fish assemblages within Great Lakes coastal wetlands and implications for sampling design. Canadian Journal of Fisheries and Aquatic Sciences 66:1343–1354.

Trebitz, A. S., and D. L. Taylor. 2007. Exotic and invasive aquatic plants in Great Lakes coastal wetlands: distribution and relation to watershed land use and plant richness and cover. Journal of Great Lakes Research 33:705–721.

Tulbure, M. G., and C. A. Johnston. 2010. Environmental conditions promoting nonnative *Phragmites australis* expansion in Great Lakes coastal wetlands. Wetlands 30:577–587.

USFWS (U.S. Fish and Wildlife Service) and USCB (U.S. Census Bureau). 2012. 2011 National survey of fishing, hunting, and wildlife-associated recreation. USFWS and USCB, Report FHW/11-NAT, Washington, D.C.

Uzarski, D. G., T. M. Burton, R. E. Kolar, and M. J. Cooper. 2009. The ecological impacts of fragmentation and vegetation removal in Lake Huron's coastal wetlands. Aquatic Ecosystem Health and Management 12:45–62.

Valavanis, V. D., G. J. Pierce, A. F. Zuur, A. Palialexis, A. Saveliev, I. Katara, and J. Wang. 2008. Modelling essential fish habitat based on remote sensing, spatial analysis, and GIS. Hydrobiologia 612:5–20.

Vadeboncoeur, Y., P. McIntyre, and M. J. Vander Zanden. 2011. Borders of biodiversity: life at the edge of the world's large lakes. BioScience 61:526–537.

Vasconcelos, R. P., P. Reis-Santos, M. J. Costa, and H. N. Cabral. 2011. Connectivity between estuaries and marine environment: integrating metrics to assess estuarine function. Ecological Indicators 11:1123–1133.

Wagner, T., D. B. Hayes, and M. T. Bremigan. 2006. Accounting for multilevel data structures in fisheries data using mixed models. Fisheries 31:180–187.

Wainger, L. A., and J. W. Boyd. 2009. Valuing ecosystem services. Pages 92–111 *in* K. McLeod and H. Leslie, editors. Ecosystem-based management for the oceans. Island Press, Washington, D.C.

Wainger, L., and M. Mazzotta. 2011. Realizing the potential of ecosystem services: a framework for relating ecological changes to economic benefits. Environmental Management 48:710–733.

Wetzel, R. G. 1992. Wetlands as metabolic gates. Journal of Great Lakes Research 18:529–532.

Whillans, T. H. 1996. Historic and comparative perspectives on rehabilitation of marshes as habitat for fish in the lower Great Lakes basin. Canadian Journal of Fisheries and Aquatic Sciences 53(Supplement 1):58–66.

Whitehead, J. C., P. A. Groothuis, R. Southwick, and P. Foster-Turley. 2005. Measuring the economic benefits of Saginaw Bay coastal marsh with revealed and stated preference methods. Journal of Great Lakes Research 35:430–437.

Zhao, Y., P. M. Kocovsky, and C. P. Madenjian. 2013. Development of a stock–recruitment model and assessment of biological reference points for the Lake Erie Walleye fishery. North American Journal of Fishery Management 33:956–964.

Zunker, C. 2013. Wisconsin's 2012 Lake Superior creel survey report. Wisconsin Department of Natural Resources, Bayfield.

Downloaded by [US EPA Library], [J. C. Hoffman] at 06:16 09 March 2015

Journal of Great Lakes Research 45 (2019) 129–137

Contents lists available at ScienceDirect

Journal of Great Lakes Research

journal homepage: www.elsevier.com/locate/jglr

Relative contributions of nearshore and wetland habitats to coastal food webs in the Great Lakes

Michael E. Sierszen [a,*], Lee S. Schoen [b], Jessica M. Kosiara [b], Joel C. Hoffman [a], Matthew J. Cooper [c,1], Donald G. Uzarski [b]

[a] U.S. Environmental Protection Agency, Office of Research and Development, National Health and Environmental Effects Laboratory, Mid-Continent Ecology Division, 6201 E. Congdon Boulevard, Duluth, MN 55804, USA
[b] Central Michigan University, Institute for Great Lakes Research, CMU Biological Station and Department of Biology, Mount Pleasant, MI 48859, USA
[c] Department of Biological Sciences, University of Notre Dame, Notre Dame, IN 46556, USA

ARTICLE INFO

Article history:
Received 8 March 2018
Accepted 2 November 2018
Available online 19 November 2018

Communicated by: Noel Urban

Keywords:
Great Lakes
Food webs
Coastal habitats
Stable isotopes
Otoliths

ABSTRACT

Hydrologic linkages among coastal wetland and nearshore areas allow coastal fish to move among the habitats, which has led to a variety of habitat use patterns. We determined nutritional support of coastal fishes from 12 wetland-nearshore habitat pairs using stable isotope analyses, which revealed differences among species and systems in multi-habitat use. Substantial (proportions > 0.30) nutrition often came from the habitat other than that in which fish were captured. Nearshore subsidies to coastal wetlands indicate wetlands are not exclusively exporters of energy and materials; rather, there is reciprocity in the mutual energetic support of nearshore and wetland food webs. Coastal wetland hydrogeomorphology influenced the amount of multi-habitat use by coastal fishes. Fishes from systems with relatively open interfaces between wetland and nearshore habitats exhibited less nutritional reliance on the habitat in which they were captured, and higher use of resources from the adjacent habitat. Comparisons of stable isotope analyses of nutrition with otolith analyses of occupancy indicated nutritional sources often corresponded with habitat occupancy; however, disparities among place of capture, otolith analyses, and nutritional analyses indicated differences in the types of support those analyses inform. Disparities between occupancy information and nutritional information can stem from movements for support functions other than foraging. Together, occupancy information from otolith microchemistry and nutritional information from stable isotope analyses provide complementary measures of the use of multiple habitats by mobile consumers. This work underscores the importance of protecting or restoring a diversity of coastal habitats and the hydrologic linkages among them.

Published by Elsevier B.V. on behalf of International Association for Great Lakes Research. This is an open access article under the CC BY-NC-ND license (http://creativecommons.org/licenses/by-nc-nd/4.0/).

Introduction

Identifying the habitats and resources that support production in aquatic ecosystems is essential to understand system dynamics and to identify priorities for ecosystem protection. Lacustrine food webs have been shown to rely on resources from a combination of benthic, pelagic, and littoral habitats (Hecky and Hesslein, 1995; Schindler and Scheuerell, 2002; Vander Zanden and Vadeboncoeur, 2002). Although coupling among habitats has been emphasized for smaller lakes (e.g., Schindler and Scheuerell, 2002), multihabitat interactions have been shown to be integral to even the world's largest lakes (Eshenroder et al., 1999; Sierszen et al., 2014; Stockwell et al., 2014). In large lakes, adjacent habitats can be linked by energy flux (i.e., a physical exchange, such as carbon export from a coastal wetland to the nearshore; Bouchard, 2007), animal movements (i.e., a biological exchange, such as nearshore fish larvae settling in coastal wetlands; Hoffman et al., 2015a), or both.

Coastal wetlands are especially valuable systems; they are highly productive habitats that are coupled with less-productive nearshore waters (Uzarski et al., 2005) and produce a wide array of ecosystem services, which include the support of Great Lakes fisheries (Sierszen et al., 2012b; Trebitz and Hoffman, 2015). Hydrologic linkages among Great Lakes nearshore and coastal wetland habitats allow coastal fish to move among the habitats for various life-support functions such as feeding, spawning, and thermal and oxygen refuge (e.g., Parker et al., 2012), which has led to a variety of habitat use patterns (Jude and Pappas, 1992). Fine-scale microchemical analyses of yellow perch otoliths revealed life-history strategies that rely upon using those habitat linkages, including annual migrations between nearshore and wetlands, wetland residence, nearshore residence, and combinations thereof (Schoen et al., 2016).

* Corresponding author.
E-mail address: mesierszen@gmail.com (M.E. Sierszen).
[1] Present address: Burke Center for Freshwater Innovation, Northland College, Ashland, WI 54806 USA.

https://doi.org/10.1016/j.jglr.2018.11.006
0380-1330/Published by Elsevier B.V. on behalf of International Association for Great Lakes Research. This is an open access article under the CC BY-NC-ND license (http://creativecommons.org/licenses/by-nc-nd/4.0/).

A variety of approaches have been applied to examine the ways various lake habitats support aquatic food webs. Significant contributions of benthic habitats to whole-lake food webs have been demonstrated using fish diets (Schindler and Scheuerell, 2002), measures of primary, bacterial, and secondary productivity (Vadeboncoeur et al., 2002), stable isotope analyses (Hecky and Hesslein, 1995), and combinations of diet and stable isotope methods (Vander Zanden and Vadeboncoeur, 2002). To quantify the importance of benthic, pelagic, and littoral habitats to support higher consumers in large lakes, stable isotope analyses (Sierszen et al., 2014) and a combination of bioenergetics modeling and stable isotope analyses (Stockwell et al., 2014) have been brought to bear.

In the Laurentian Great Lakes, movement of fishes among habitats has been tracked using mark-recapture methods, radio telemetry, and bioacoustics (reviewed by Landsman et al., 2011). The roles of coastal wetland and nearshore habitats in the nutrition and life-history of fishes have been explored using fish sampling (Jude and Pappas, 1992; Brazner et al., 2001; Meixler et al., 2005), stable isotope analyses (Sierszen et al., 2012a; Hoffman et al., 2015a), and otolith microchemical analyses (Brazner et al., 2004; Pangle et al., 2010; Schoen et al., 2016). We focus on the latter three techniques, as each provides useful and potentially different types of information on the ways aquatic habitats support fishes. Location of capture provides a basic level of information on habitat occupancy, but the duration of habitat use and the life functions supported by the habitat may not be apparent based on those measures alone (Cunjak et al., 2005). Otolith analyses also provide occupancy information, at time scales ranging from days to lifetimes, but also without revealing the type of support provided by the habitats (Hogan et al., 2007). Stable isotope analyses provide information on nutritional support at seasonal or annual time scales depending on growth rate (Vander Zanden et al., 2015), but with less information on occupancy.

We recognized that the degree to which exchanges occur between coastal wetland and nearshore habitats can be influenced by the hydrology and morphology of their interface (Polis et al., 1997; Keough et al., 1999; Morrice et al., 2011). We therefore designed this study to include sites with a range of hydrogeomorphology in selected coastal systems of lakes Huron and Michigan. Our primary objectives were therefore to quantify the nutritional support of coastal fishes by coastal wetland and nearshore habitats; to contrast nutritional support with occupancy measures of habitat use; and to examine the influence of coastal hydrogeomorphology on multi-habitat nutrition.

Methods

We collected fish and primary consumer (zooplankton and benthic invertebrate) samples from 12 wetland-nearshore pairings in Lake Michigan, northern Lake Huron, and Saginaw Bay (Fig. 1). Each site consisted of a nearshore area (3–5 m depth) adjacent to a coastal wetland (1–2 m depth). The sites were selected to represent the most common hydrogeomorphic wetland types of lakes Michigan and Huron as described in Albert et al. (2005). Hydrogeomorphic categories used in this study include barred drowned river mouth wetland, protected (embayment) lacustrine wetland, and open (non-embayment) lacustrine wetland, in order of increasing wave exposure and potential mixing with nearshore water. We selected sites based upon the distribution of hydrogeomorphic types in the basin and chose three drowned river mouth systems in Lake Michigan, three protected (embayment) lacustrine wetlands in Les Cheneaux of northern Lake Huron, and six open (non-embayment) lacustrine wetlands distributed among Thunder Bay and Saginaw Bay on Lake Huron (Table 1). To further characterize the degree to which the systems were exposed to waves and susceptible to exchange with the lakes, we calculated modified effective fetch and maximum fetch according to Howes et al. (1999). All samples were collected between 15 June and 15 August 2012; fish and invertebrate samples were collected concurrently at each site. We collected wetland and nearshore zooplankton using triplicate 100 m subsurface horizontal tows with a 40 cm diameter, 80 μm mesh plankton net. In the wetlands, care was taken not to include benthic biota and detritus by avoiding sediments and macrophytes. Plankton tows were taken before fish and benthos sampling that might have suspended sediments and epiphytes. In the few cases when benthic or epiphytic materials were encountered, the sample was discarded, the net rinsed, and the tow was retaken. Nearshore tows were taken in at least 3 m depth to avoid benthic materials, and outside river plumes (where present) and far enough offshore to avoid wetland influence. Plankton samples were sieved onto 50 μm mesh Nitex filters, rinsed with deionized water, and frozen pending analysis. We collected macroinvertebrates using 500 μm mesh D-net sweeps within all vegetation zones (cf. Uzarski et al., 2004; Uzarski et al., 2017) in each wetland. Nearshore benthic macroinvertebrates were collected using PONAR grabs taken along three transects parallel to shore. Macroinvertebrates were sorted by taxon and then frozen pending analysis. To ensure that primary consumers were used to establish the food web baselines, we omitted predatory taxa (e.g., odonates) as well as those whose $\delta^{15}N$ indicated they occupied higher trophic positions.

The Michigan Department of Natural Resources sampled nearshore fish using experimental gill-nets set in nearshore habitats adjacent to wetland habitats. However, no fish were collected from Pentwater nearshore. We sampled wetland fish with a combination of modified fyke-nets and boat electrofishing. After collection, fish were placed on ice and frozen within 24 h. In the lab, muscle tissue samples were taken from anterior dorsal portions of individual fish. For smaller specimens, we analyzed whole fillets. Fish and invertebrate tissue samples were rinsed in deionized water, dried at 55 °C, ground, and 0.5 mg packed into a tin capsule for stable isotope analysis. Samples were analyzed for $\delta^{13}C$ and $\delta^{15}N$ values using a Costech 4010 EA (Costech analytical Technologies Inc., Valencia, CA, U.S.A.) and Thermo Delta Plus XP isotope ratio mass spectrometer (Thermo Fisher Scientific Inc., Waltham, MA, U.S.A.). We analyzed 68 zooplankton samples, 277 benthic invertebrate samples, and 448 fish samples. The analytical error, expressed as the standard deviation of the stable isotope values of replicate analyses of reference materials, was 0.18 for $\delta^{13}C$ and 0.21 for $\delta^{15}N$. Reference materials included walleye *Sander vitreus* muscle tissue used throughout the project to determine instrument precision and drift, as well as a commercially-obtained sulfanilamide standard (Sigma-Aldrich; $\delta^{13}C = -28.58$; $\delta^{15}N = -3.1$), which yielded the same estimates of precision as the walleye standard.

We quantified the nutritional contributions of wetland and nearshore food-web pathways to the common species of fishes collected using mean isotope values of zooplankton, benthos, and fishes in a multisource dual-isotope mixing model (IsoSource 1.3.1; Phillips and Gregg, 2003; Phillips et al., 2005). IsoSource is an iterative probabilistic model that calculates source contributions to a stable isotope mixture when the number of sources is too large to permit a unique solution (i.e., number of sources > number of isotope systems + 1). All possible combinations of each source are examined in small increments, and combinations that sum to the observed mixture within a small tolerance (ca. 0.1‰) are considered feasible solutions. Each multivariate solution (i.e., each combination of source contributions that satisfies the model tolerance) is equally valid. However, each source has a univariate distribution of possible contributions, and the frequency of occurrence of a particular contribution in that distribution reflects the likelihood of that proportional contribution (Semmens et al., 2013). Correct reporting of model results requires that the distribution of feasible solutions be described (Phillips and Gregg, 2003). When a distribution of source contributions is well constrained (i.e., it has a relatively narrow range of possible contributions) and symmetrical, the mean (i.e., the most frequent contribution of that source) describes the most likely contribution, and the standard deviation may be used to express dispersion about the mean. Distribution characteristics determine whether the mean, median or mode reflects the most likely value, and whether standard deviations, confidence intervals and quartiles are best used

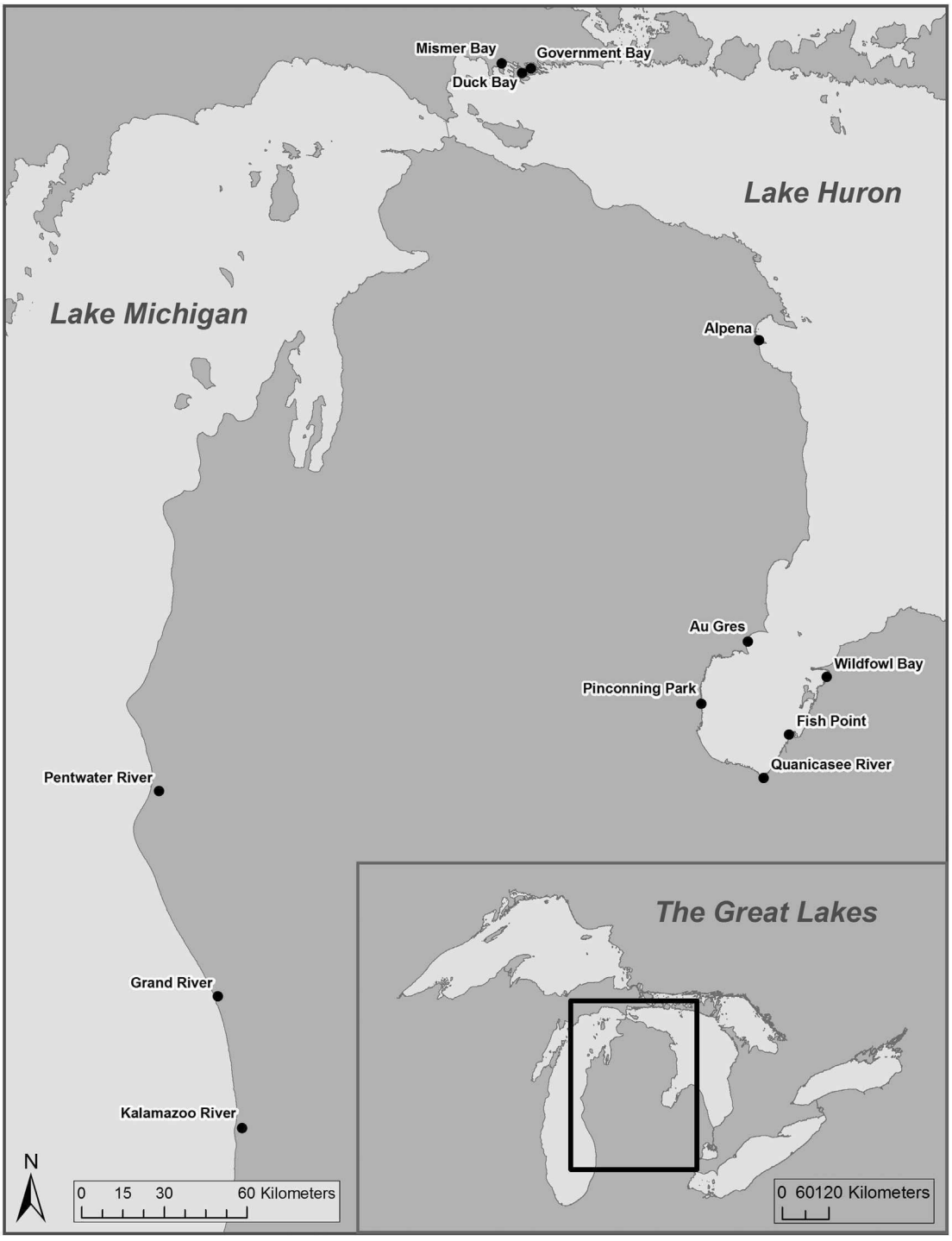

Fig. 1. Location of sampling sites on lakes Michigan and Huron.

to express dispersion. Because source distributions are often skewed, we used medians and quartiles to describe source contributions, expressed as nutrition obtained through nearshore food-web pathways by summing contributions of nearshore zooplankton and benthos sources.

Calculating isotope mixing across trophic levels requires knowledge of trophic fractionation of isotopes (i.e., the ^{15}N and ^{13}C enrichment of a consumer relative to its food). We used a nitrogen isotope fractionation factor of 3.4‰ (Cabana and Rasmussen, 1994) and carbon isotope fractionation of 1.0‰ (Vander Zanden and Rasmussen, 2001). Those factors were used to adjust fish isotope values according to the trophic position of each fish sample, as calculated from the difference in $\delta^{15}N$ between the food web base (mean of nearshore and wetland benthos and plankton sources) and the fish. To verify that those calculations were realistic, we compared our calculated trophic positions with those from FishBase (www.fishbase.org) and those calculated using both diet and stable isotope techniques (Vander Zanden et al., 1997).

We modelled the diets of fish species that were common in the wetland and nearshore habitats, which resulted in a total of 114 species-habitat combinations. We used several approaches to evaluate the degree to which fish were nutritionally supported by wetland and nearshore habitats during recent (seasonal or annual) life history. First, if the proportion of nearshore nutrition obtained from the mixing model was in the vicinity of 0.5, it would mean that the consumer obtained

Table 1
Study sites, locations (cf. Fig. 1), wetland hydrogeomorphic type, and estimates of exposure to lake waves (modified effective fetch and maximum fetch, km).

Site	Location	HGM type	Mod. eff. fetch	Max fetch
Grand River	Lake Michigan	Drowned River Mouth	0.0099	1.4
Kalamazoo River	Lake Michigan	Drowned River Mouth	0.0072	0.61
Pentwater River	Lake Michigan	Drowned River Mouth	0.0310	2.2
Government Bay	Les Cheneaux	Protected Lacustrine	1.87	3.78
Duck Bay	Les Cheneaux	Protected Lacustrine	0.42	2.4
Mismer Bay	Les Cheneaux	Protected Lacustrine	0.1105	6.27
Wildfowl Bay	Saginaw Bay	Open Lacustrine	20.53	29.3
Au Gres	Saginaw Bay	Open Lacustrine	37.03	43
Pinconning	Saginaw Bay	Open Lacustrine	12.22	22
Quanicassee	Saginaw Bay	Open Lacustrine	38.09	255.8
Fish Point	Saginaw Bay	Open Lacustrine	21.45	40.65
Alpena	Thunder Bay	Open Lacustrine	167.32	176

equivalent support from the two habitats. Therefore, mid-range (e.g., 0.4–0.6) values suggest high degrees of multihabitat support, whereas high (primarily nearshore nutrition) and low (primarily wetland nutrition) values indicate predominantly single-habitat support. Second, if fish from the two adjacent habitats had similar distributions of nearshore nutrition, it would suggest common foraging histories, either by traveling between the habitats or by an interaction of the habitats through hydrologic mixing or movement of prey. We tested for differences between wetland-caught and nearshore-caught fish using two-sample *t*-tests of arcsine-transformed data. Finally, if fish with high proportions of nutrition from one of the habitats were captured in the other habitat, it was an obvious (though not quantitative) indication of multihabitat use. These measures were compared among wetland sites that differed in hydrogeomorphic type and fetch exposure to the nearshore. We examined the influence of wetland type on sources of nutrition to wetland- and nearshore-caught fish by testing for differences in nearshore nutrition among fish from systems differing in hydrogeomorphic type, modified effective fetch (MEF), and maximum fetch (MaxF). We pooled fish species within each habitat and arcsine-transformed proportions of nearshore nutrition for their use in ANOVA.

We examined the influence of fish species on multiple-habitat use by comparing the intraspecific range of nearshore nutrition across systems. If fish species determined the degree to which they obtained nutrition from multiple habitats - for example, if species A fed mostly from wetland habitat and species B consistently fed from both habitats - we would expect each species to have a relatively narrow range in their proportions of nearshore nutrition when compared among all sites. Also, those ranges would differ in their magnitudes, with species A having low proportions of nearshore nutrition and species B having values near 0.5. Conversely, if fish species did not determine amount of multihabitat feeding, and foraging behavior varied with location, we would expect a relatively broad range in proportion of nearshore nutrition when compared among sites. We compared the range of median values for each species across sites and expressed the overall variability at each habitat as the difference between the 1st quartile associated with the minimum median value and the 3rd quartile associated with the maximum median value. We limited this analysis to species that were collected in four or more systems.

In an earlier study (Schoen et al., 2016), we used otolith microchemical analyses to trace movement patterns between wetland and nearshore habitats by yellow perch collected from the same sites as in this study. Otolith analyses revealed several life-history patterns in habitat use, including exclusive wetland residence, wetland use as juveniles followed by nearshore residence as adults, annual migrations between habitats, and combinations thereof. We have now enhanced that analysis by discriminating annual migrants that primarily used wetland habitats from those that primarily used lake habitats, according to amount of intra-annual growth accumulated in each habitat based on otolith ring analysis. We compared the estimates of wetland and nearshore habitat use according to time spent in those habitats (based on otolith analyses) with habitat use according to nutritional support (based on stable isotope mixing model results) by comparing the two measures for the same individual yellow perch. We also included fish for which we had stable isotope data but no microchemistry data, to a total of 124 individual yellow perch. We used the output of the isotope mixing model from individual yellow perch to address four objectives: 1) to determine whether life-history category predicted nutrition; 2) to test whether wetland-caught and nearshore-caught fish had similar nutritional sources (as above); 3) to test for discrepancies between habitat of capture and habitat of dominant nutritional support; and 4) to test for the influence of wetland hydrogeomorphology on the contributions of multiple habitats to fish nutrition.

Results

Wetland primary consumers analyzed for stable isotope ratios to characterize wetland benthic sources included amphipods, isopods, chironomids, mayflies, and snails. Richness of primary consumers in nearshore habitats was lower, but amphipods, oligochaetes, and chironomids were the most abundant taxa and plentiful enough to characterize nearshore benthic sources. Zooplankton were collected from each habitat but were not characterized taxonomically. Bulk zooplankton samples could therefore have contained taxa that varied in trophic position, which could add uncertainty to our calculations of the trophic positions of higher consumers; however, our trophic position estimates were in agreement with other published estimates (see below).

Fish species commonly collected in wetland habitats for stable isotope analysis included yellow perch *Perca flavescens*, rock bass *Ambloplites rupestris*, bluegill *Lepomis macrochirus*, pumpkinseed *Lepomis gibbosus*, largemouth bass *Micropterus salmoides*, smallmouth bass *Micropterus dolomieu*, northern pike *Esox lucius*, walleye *Sander vitreus*, bowfin *Amia calva*, black bullhead *Ameiurus melas*, brown bullhead *Ameiurus nebulosus*, bluntnose minnow *Pimephales notatus*, and round goby *Neogobius melanostomus*. Fishes captured in nearshore habitats included those species as well as lean lake trout *Salvelinus namaycush*, lake whitefish *Coregonus clupeaformis*, and freshwater drum *Aplodinotus grunniens*. Although ours was not a comprehensive collection, it includes major common species typical of Great Lakes coastal habitats (Jude and Pappas, 1992; Keough et al., 1996; Brazner, 1997).

We did not adjust $\delta^{13}C$ values for lipid content prior to use in the mixing model. The ratio of carbon:nitrogen in our fish samples were generally <3.5 and in rare instances exceeded 4.0. At low C:N values such as these, normalization of $\delta^{13}C$ for lipid content is not recommended (e.g., Hoffman et al., 2015b) and would not influence isotope mixing results. Further, use of lipid-corrected fish values in the mixing model would have required arithmetic correction of invertebrate values, which has been shown to be unreliable (Logan et al., 2008; Kiljunen et al., 2006).

Stable isotope analyses

Across sites, we found a consistent difference between wetland and nearshore habitats in the $\delta^{13}C$ values of their respective biota. At Lake Michigan drowned river mouth wetlands and Les Cheneaux protected lacustrine wetland sites, nearshore primary consumers were generally ^{13}C-enriched relative to wetland primary consumers (Fig. 2a, b, Electronic Supplementary Material (ESM) Table S1). However, at four open lacustrine wetlands (Alpena, Pinconning, Wildfowl Bay, and Fish Point) nearshore primary consumers were ^{13}C-depleted relative to those of wetland habitats (Fig. 2c, ESM Table S1). Fish caught in the nearshore and wetland habitats at the Lake Michigan drowned river mouth systems often had $\delta^{13}C$ values that corresponded with those of

primary consumers from the habitat of capture. In contrast, at many open and protected lacustrine wetland sites, the $\delta^{13}C$ values of nearshore- and wetland-caught fish were interspersed (e.g., Fig. 2b). At every site except the Grand River, and in 51 of 128 species-habitat combinations (40%), the range in fish $\delta^{13}C$ was outside that of the primary consumers in the habitat of capture (ESM Table S1), indicating the fish might have obtained substantial nutritional support from a habitat other than that of capture.

At one open and two protected lacustrine wetland sites (Au Gres, Mismer Bay, and Government Bay), nearshore and wetland zooplankton samples had nearly identical stable isotope ratios. In contrast, wetland benthic invertebrates were ^{13}C-depleted relative to nearshore benthos. This suggests there may have been strong hydrologic mixing between wetland and nearshore waters at these sites. In those cases, three sources were used in the mixing model (nearshore benthos, wetland benthos, zooplankton) and half of the zooplankton contribution to fish nutrition from the mixing model was attributed to nearshore habitats.

Comparisons of our calculated fish trophic positions to previously published estimates showed them to be in good agreement (Table 2). This is important, as trophic position was used along with trophic fractionation factors to standardize fish $\delta^{13}C$ and $\delta^{15}N$ values prior to use in the mixing model. Inclusion of juveniles resulted in lower trophic position estimates for some species.

Isotope mixing

Frequently, the habitat in which fish were captured supplied the majority of their nutrition as estimated through isotope mixing; however, substantial support (proportions > 0.30) often came from the adjacent habitat. Of the 113 species-habitat pairs, 37 (33%) had less than half of their nutrition originating from their habitat of capture, based on median values (Table S2).

Wetland-caught fish species at the drowned river mouth wetland sites on Lake Michigan had significantly lower amounts of nearshore-based nutrition than did nearshore-caught fish. There were significant differences in the amount of nearshore nutrition between wetland-caught and nearshore-caught fish (all fish species pooled) at the Grand River site ($p = 0.039$) and the Kalamazoo River site ($p < 0.001$), indicating differences in foraging patterns between nearshore and wetland fish and relatively little food-web exchange between habitats. Wetland-caught fish tended to have proportions of nearshore nutrition ≤ 0.4, and nearshore fish tended to have proportions of nearshore nutrition ≥ 0.6 (e.g., Fig. 3a; Table S2). At Pentwater, wetland-caught fish had low proportions (≤0.4) of nearshore nutrition. No nearshore fish were collected at Pentwater.

At the open and protected lacustrine wetland sites of Saginaw Bay, Alpena, and Les Cheneaux, proportions of nutrition from the nearshore for most fish species were near the middle of the range, with no statistical difference between fish caught in nearshore and conspecifics caught in wetland habitats (Fig. 3b, c; ESM Table S2). Only two of the nine lacustrine wetlands (the open lacustrine site at Wildfowl Bay, $p = 0.003$, and the protected lacustrine site at Mismer Bay, $p = 0.018$; two-sample *t*-tests; all fish species pooled within habitats) showed significant differences between the nutritional sources of wetland- and nearshore-caught fish, indicating differences in foraging habits between fish from the two habitats.

Estimates of wetland exposure to lake waves differed among hydrogeomorphic types. The drowned river mouth systems had the lowest MEF and MaxF values among all study sites, protected lacustrine sites were intermediate, and open lacustrine sites had the highest MEF and MaxF values (Table 1). Proportions of nearshore nutrition in wetland-caught fish (all species pooled within hydrogeomorphic types) differed significantly among types (ANOVA, $p < 0.001$; $F = 10.897$; $r^2 = 0.230$), with fish from drowned river mouth systems having significantly lower nearshore nutrition than those from protected or open lacustrine sites.

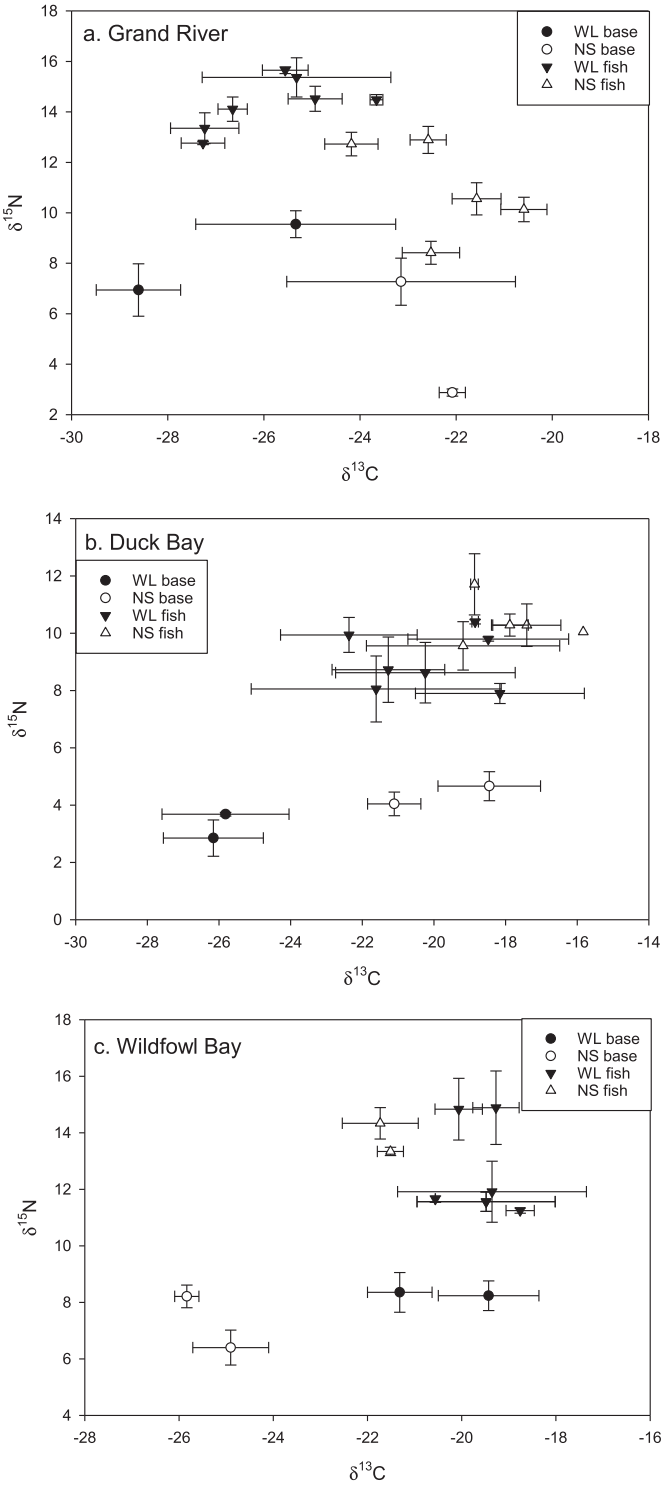

Fig. 2. $\delta^{13}C$ and $\delta^{15}N$ values of biota from three representative wetland-nearshore sites: a) at the Grand River drowned river mouth site on Lake Michigan; b) at the Duck Bay protected lacustrine wetland site on northern Lake Huron's Les Cheneaux region; c) at the Wildfowl Bay lacustrine wetland site on Lake Huron's Saginaw Bay. Black dots: wetland primary consumers (zooplankton and benthos); black triangles: wetland fishes; open circles: nearshore primary consumers; open triangles: nearshore fishes.

Nearshore nutrition did not differ significantly between wetland fish from protected and open lacustrine sites. Nearshore nutrition in wetland-caught fish increased significantly with MEF ($p < 0.001$; $F = 6.034$; $r^2 = 0.509$) and MaxF ($p < 0.001$; $F = 6.034$; $r^2 = 0.509$). Nearshore nutrition in nearshore-caught fish differed significantly among all hydrogeomorphic types, with highest nearshore nutrition in drowned

Table 2
Comparison of trophic position (TP) calculated in this study with those from the literature: diet-based estimates in FishBase (www.fishbase.org), and diet- and stable isotope (SI)-based estimates from Vander Zanden et al. (1997); VZ).

Fish species	TP this study	TP FishBase (diet)	TP VZ (diet)	TP VZ (SI)
Walleye	3.6–4.7	4.5 ± 0.0	3.9–4.5	4.1–4.9
Largemouth bass	3.2–5.3	3.8 ± 0.4	3.6–4.5	3.9–4.4
Yellow perch	2.6–4.6	3.7 ± 0.2	3.5–4.5	3.0–4.3
Bluegill	3.1–4.6	3.2 ± 0.2		
Northern pike	3.6–4.0	4.1 ± 0.4	4.2–4.5	3.4–4.5
Smallmouth bass	2.9–4.5	3.6 ± 0.2	3.5–4.5	3.6–4.7
Rock bass	3.4–4.8	3.4 ± 0.2	3.5–4.1	3.5–4.4
Pumpkinseed	3.0–3.5	3.3 ± 0.1	3.0–3.5	2.8–4.2
Black bullhead	2.9–4.1	3.8 ± 0.4		
Bowfin	3.6–4.8	3.8 ± 0.7		
Round goby	3.0–3.9	3.3 ± 0.1		

river mouth systems and lowest nearshore nutrition in open lacustrine sites ($p < 0.001$; $F = 15.512$; $r^2 = 0.478$). Nearshore nutrition in nearshore-caught fish decreased significantly with MEF ($p < 0.001$; $F = 6.642$; $r^2 = 0.719$) and MaxF ($p < 0.001$; $F = 6.642$; $r^2 = 0.719$).

Comparing the influence of fish species on sources of nutrition across sites, yellow perch and rock bass caught in wetland habitats tended to have lower median values of nearshore nutrition than did nearshore-caught conspecifics, whereas northern pike median values were similar in wetland and nearshore habitats (Table 3). The medians for wetland-caught yellow perch (and largemouth bass and bluegill, which were caught only in wetlands) indicated predominantly wetland nutrition (overall proportions 0.05–0.61); whereas, nearshore-caught yellow perch and rock bass tended toward nearshore nutrition (proportions 0.43–0.98); northern pike from both habitats and nearshore walleye had median values that bracketed 0.5, indicating a strong mix of nutrition from both habitats. The range of values for each species varied from 0.49 for wetland northern pike to 0.69 for wetland rock bass. These broad ranges suggest variable habitat support across systems, i.e., that site had a relatively strong effect on the amount of multi-habitat support of species. For a more comprehensive view of the variability in these data, see ESM Table S2.

Otolith-isotope comparison

Yellow perch individuals classified as wetland residents via otolith microchemistry ($n = 6$) had median proportions of nearshore nutrition ranging from 0.005 to 0.44 based on isotope mixing; those classified as nearshore residents ($n = 12$) had nearshore nutrition from 0.42 to 0.96 (ESM Table S3). Overall, 5/6 (83%) of the individuals classified as wetland residents had most (proportions > 0.50) of their nutrition from wetland habitats and 10/12 (83%) of individual yellow perch classified as nearshore residents had most of their nutrition from the nearshore. Annual migrants classified as primarily using nearshore habitats ($n = 16$) obtained from 0.05 to 0.995 nearshore nutrition, and 81% of them had >0.50 of their nutrition from nearshore habitats; annual migrants classified as primarily using wetland habitats ($n = 20$) had from 0 to 0.96 nearshore nutrition, and 70% of those individuals had >0.50 of their nutrition from wetland habitats. Young-of-year ($n = 38$), which we were unable to classify reliably from otolith microchemistry, had median estimates of nearshore nutrition that ranged from zero to 0.995. Of those fish, 18% were captured in wetland habitats but had high proportions of nearshore nutrition based on the stable isotope mixing model, indicating that young-of-year routinely move between habitats.

Individual yellow perch at drowned river mouth sites obtained high proportions of their nutrition from their habitat of capture (Fig. 4a; ESM Table S3). As observed in the species-level analyses, individual yellow perch at protected and open lacustrine wetland sites had variable amounts of nearshore nutrition, often mid-range, indicating substantial inputs from both habitats (Fig. 4b, c). There were significant differences

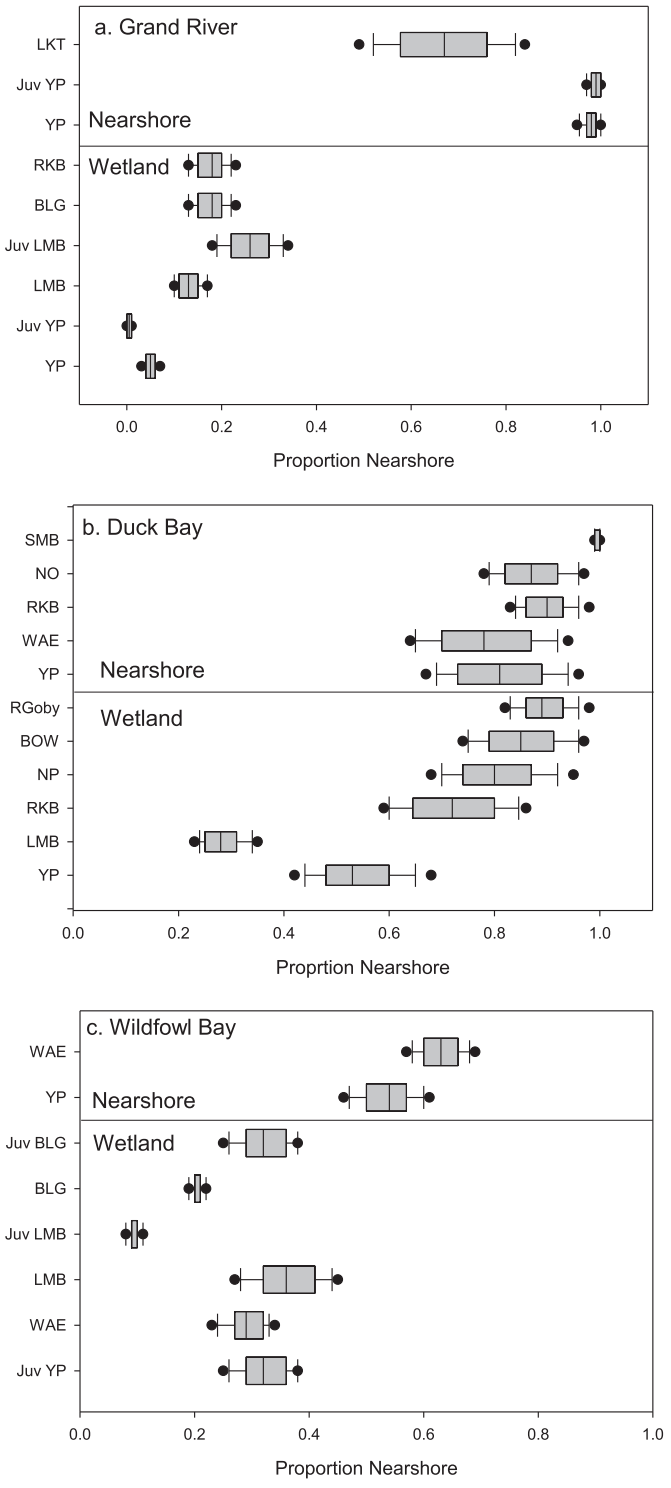

Fig. 3. Mixing model results expressed as proportion nearshore-derived nutrition for fish species sampled from nearshore habitats (upper panels) and wetland habitats (lower panels) at the same three representative sites as in Fig. 1. Species abbreviations as in Table 1. Boxes span 1st to 3rd quartiles, with vertical line at median; whiskers indicate 10th and 90th percentiles; dots indicate 5th and 95th percentiles.

in the proportion of nearshore nutrition between nearshore-caught and wetland-caught individual yellow perch at the Grand River ($p < 0.001$) and Kalamazoo River ($p = 0.006$) drowned river mouth sites, but no significant differences at any of the lacustrine wetland sites. At drowned river mouth sites, 30 of 32 (94%) had more than half of their nutrition matching the habitat in which they were captured. At lacustrine

Table 3
Excerpt from Table S2. Median proportions of nearshore nutrition of fish species (YP = yellow perch; NP = northern pike; RKB = rock bass; LMB = largemouth bass; BLG = bluegill; WAE = walleye) from wetland (WL) and nearshore (NS) habitats. Quartile range indicates the span between the first quartile associated with the minimum median value and the third quartile associated with the maximum median value, and reflect relative variability in nutritional support among sites.

Site	WL YP	NS YP	WL NP	NS NP	WL RKB	NS RKB	WL LMB	WL BLG	NS WAE
Grand R.	0.05	0.98			0.18		0.13	0.18	
Kalamazoo R.	0.39	0.88			0.13		0.39	0.14	
Pentwater R.	0.27				0.29		0.52	0.27	
Duck Bay	0.53	0.81	0.80	0.87	0.72	0.90	0.28		0.78
Mismer Bay	0.41	0.90		0.69	0.63	0.75			0.67
Government Bay	0.61	0.44	0.41	0.39	0.39	0.45			0.37
Pinconning	0.41	0.83	0.63				0.34		0.82
Wildfowl		0.54					0.36	0.21	0.63
Quanicassee	0.60	0.68	0.63				0.61	0.51	0.66
Au Gres	0.05	0.47	0.41				0.31		0.41
Fish Point		0.77			0.56		0.55	0.32	0.57
Alpena		0.43		0.53		0.65			0.45
Min–max	0.05–0.61	0.43–0.98	0.41–0.80	0.39–0.87	0.13–0.72	0.45–0.90	0.13–0.61	0.14–0.51	0.37–0.82
Quartile range	0.63	0.65	0.49	0.59	0.69	0.55	0.64	0.53	0.54

wetland sites, 58 of 92 (63%) of individuals captured had over half of their nutrition matching the habitat in which they were captured.

Occupancy based on habitat of capture and life-history patterns identified from otolith analyses often predicted the major habitat supporting fish nutrition, but there were notable exceptions. For numerous individual yellow perch, the habitat providing most of their nutrition was not the habitat in which they were captured or in which they spent most of their time based upon otolith microchemical analyses (Table 4). For example, we captured yellow perch in the nearshore that were classified as migrants primarily using the nearshore, but which had very little nearshore diet contributions (e.g., at Duck Bay). We also captured fish in the nearshore that were classified as migrants that primarily used wetlands, but which had high nutritional support from the nearshore (e.g., at Pinconning). We captured one fish in the Quanicassee wetland that was classified as a nearshore resident but which had almost no nearshore diet contribution. This suggests the fish was targeting prey that were exported to the nearshore, or there was an error in either the otolith classification or the isotope mixing model.

Discussion

Our analyses shed light on the contributions coastal wetland and lake habitats make to the nutrition of coastal fishes and advance our understanding of factors that influence multi-habitat use by coastal fishes in large lakes. Among the places and fish species we examined, use of resources from multiple habitats was widespread. It was also reciprocal in that fish caught in both wetland and nearshore often obtained substantial amounts of nutrition from the alternative habitat. Our quantification of food web subsidies from coastal wetlands to the nearshore is consistent with the characterization of coastal wetlands as energy-rich systems that export resources to adjacent zones (Odom, 1968; Wetzel, 1992; Brazner et al., 2000). Further, our results go beyond the "outwelling" perspective of wetlands as sources of energy and materials (Odom, 1968; see also Polis et al., 1997) because there is reciprocity in the mutual energetic support of nearshore and wetland habitats. Our measures of nearshore contributions to wetland biota concur with earlier estimates from coastal habitats in the other Laurentian Great Lakes (Sierszen et al., 2012a; Hoffman et al., 2015a) and enhance our recognition of interacting organisms and resources among intact Great Lakes habitats.

Discrepancies between results of different measures of habitat resource use are particularly informative to our understanding of how fishes use habitat. Capture of fish in habitats that did not provide the majority of their nutrition may reflect relatively short-term (e.g., diel) occupancy, emigration from nursery habitats by young-of-year (e.g., Brazner et al., 2001), or feeding on prey resources that were exported from adjacent areas. Similarly, when otolith analyses indicate patterns in movement or occupancy that are not reflected in nutrition, it can relate to movement for life functions other than feeding, such as spawning migration (when little feeding is done) or to access thermal or other physiological refugia. Movements of Atlantic salmon into tributary waters for thermal refuge were tracked through telemetry, but were not reflected in stable isotope values (Cunjak et al., 2005). Also, seasonal movements among different habitats may sometimes not be reflected in otolith profiles due to seasonal depression of otolith accretion (Clement et al., 2014).

The majority of variability we measured in coastal fish stable isotope values was in $\delta^{13}C$, which was often outside the measured range of primary consumers in the habitat of capture. Differences between the $\delta^{13}C$ of coastal wetland and nearshore biota can be traced to differences in the $\delta^{13}C$ of dissolved inorganic carbon in those habitats (Keough et al., 1996, 1998). Higher trophic-level consumers with $\delta^{13}C$ values outside those of their capture habitat have been described in other coastal systems of lakes Superior, Michigan, Erie, and Ontario (Keough et al., 1996; Hoffman et al., 2010; Sierszen et al., 2012a), and may be expected given accounts of movements among coastal habitats by Great Lakes fishes (Jude and Pappas, 1992; Brazner et al., 2001; Landsman et al., 2011; Midwood and Chow-Fraser, 2015). These conditions necessitated our use of all wetland and nearshore sources in the isotope mixing model.

Wetland hydrogeomorphology influenced the use of multiple habitats by coastal fishes. Analyses of variance among wetland classes and across measures of wetland exposure to nearshore waters revealed consistent patterns in the use of resources from nearshore and wetland. As the interface between wetland and nearshore became more open to exchange (i.e., from drowned river mouth to protected lacustrine to open lacustrine wetland, and at higher measures of modified effective fetch and maximum fetch) fish from both habitats exhibited less nutritional reliance on the habitat in which they were captured, and higher use of resources from the adjacent habitat. Boundary conditions can influence their accessibility and the amount of habitat coupling by mobile consumers (Dolson et al., 2009). In earlier analyses, a Great Lakes coastal wetland separated from the lake by a large barrier spit had a food web isotopically dissimilar to that of the adjacent nearshore (Keough et al., 1996), whereas there was complete isotopic overlap between the food webs of a morphologically open coastal wetland and nearshore waters (Brazner et al., 2000).

Fish species appeared to differ somewhat in their support from multiple habitats. Yellow perch and rock bass (and largemouth bass and bluegill, which were only captured in wetlands) tended toward support from their site of capture, whereas northern pike and walleye had stronger tendencies toward multi-habitat support. Nonetheless, all species

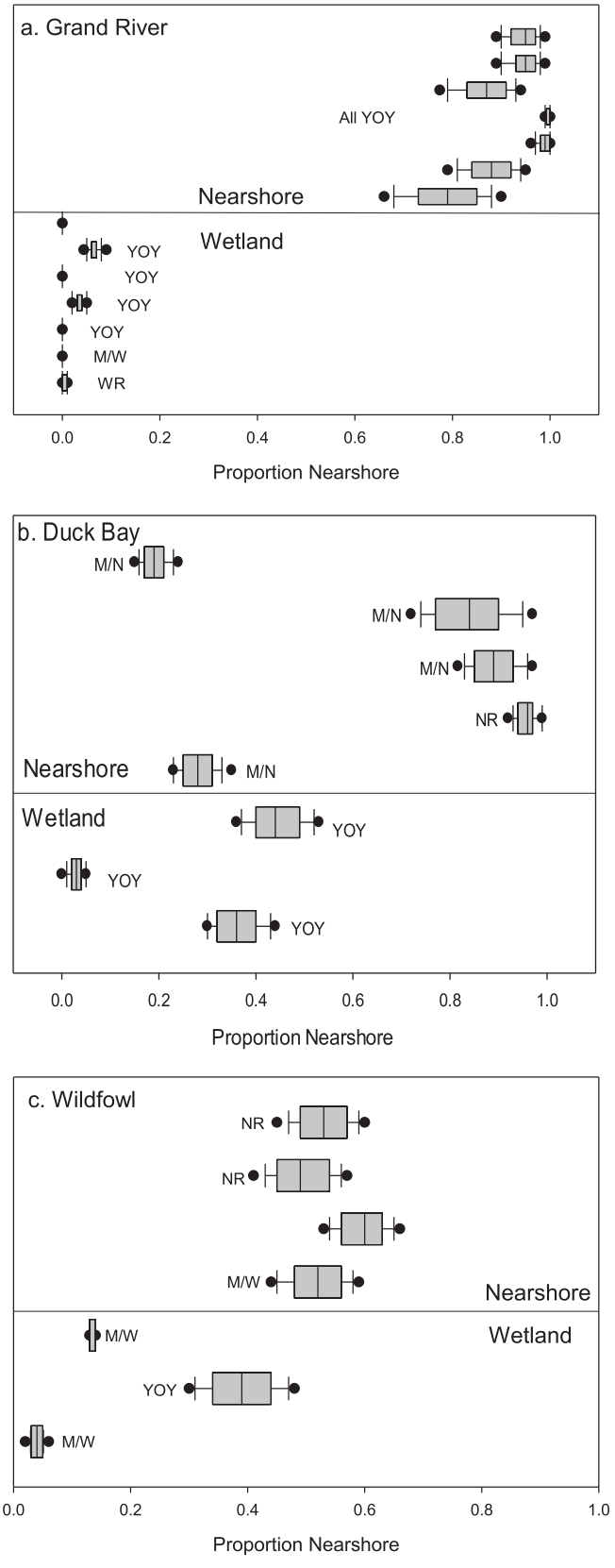

Fig. 4. Mixing model results for individual yellow perch sampled from nearshore and wetland habitats at the three representative sites; box dimensions as in Fig. 3. Life-history habitat categories determined from otolith microchemical analyses indicated next to the boxes: WL (wetland resident); NR (nearshore resident); M/N (annual migrant between habitats using mostly nearshore); M/W (annual migrant using mostly wetland); YOY (young-of-year). When no life-history type is indicated, otoliths were not analyzed.

Table 4
Excerpt from Table S3. Individual yellow perch for which the habitat of occupancy, based on place of capture (Capt. Hab.) or life history classification from otolith microchemical analyses (LH), did not provide most of the nutrition based on stable isotope mixing model results. Capture habitat was wetland (W) or nearshore (N); life history classifications are wetland resident (WR), nearshore resident (NR), annual migrants (M/W for primarily wetland use; M/N for primarily nearshore use) and young of year (Y). Proportion nearshore nutrition given as median (1st quartile, 3rd quartile).

Site	Capt. hab.	LH	Prop. nearshore
Duck	N	M/N	0.28 (0.25, 0.31)
	N	M/N	0.19 (0.17, 0.21)
Mismer	W	Y	0.65 (0.62, 0.66)
Government	W		0.71 (0.65, 0.77)
	N	NR	0.42 (0.32, 0.53)
	N		0.31 (0.30, 0.32)
Pinconning	W	Y	0.65 (0.53, 0.76)
	W	Y	0.83 (0.77, 0.90)
	W	Y	0.59 (0.48, 0.70)
	W		0.87 (0.82, 0.92)
	W		0.71 (0.59, 0.82)
	W		0.77 (0.69, 0.87)
	N	M/W	0.85 (0.78, 0.91)
	N	M/W	0.93 (0.90, 0.96)
Quanicassee	W	Y	0.995 (0.99, 1.00)
	W	Y	0.72 (0.65, 0.81)
	W	Y	0.995 (0.99, 1.00)
	W		0.63 (0.50, 0.76)
	W	M/N	0.05 (0.03, 0.07)
Au Gres	N		0.43 (0.40, 0.46)
Fish Point	W		0.68 (0.56, 0.79)
	W	Y	0.55 (0.39, 0.70)
	W		0.61 (0.47, 0.74)
	W	Y	0.66 (0.53, 0.78)

we examined had wide ranges in their nutrition across sites, indicating that site had a relatively strong effect on foraging patterns.

At the Lake Michigan and Les Cheneaux sites, nearshore primary consumers and most nearshore fish were ^{13}C-enriched relative to wetland biota, a pattern commonly observed in other Great Lakes coastal wetlands attributable to respiration and remineralization of carbon in wetland habitats (Keough et al., 1996, 1998; Sierszen et al., 2012a). In wetlands situated on Saginaw Bay and Thunder Bay (Alpena), nearshore biota were ^{13}C-depleted relative to those of wetland habitats. This suggests that the nearshore food webs in those bays were influenced by ^{13}C-depleted inputs from the Saginaw River and Thunder Bay River, respectively, which probably carried strong heterotrophic signals. Alternatively, high productivity in those wetlands may have resulted in decreased C isotope fractionation during C uptake and photosynthesis, and led to ^{13}C enrichment of wetland biota.

Understanding the use of aquatic habitats in the Great Lakes is valuable to fishery management and to identify critical habitats for protection and restoration (Landsman et al., 2011). Our findings enhance our understanding of the ways multiple habitats support food webs in large lakes. They also indicate that complementary types of information are provided by these different measures of habitat use. The reciprocity we found in the support of coastal fishes by adjacent habitats, revealed by nutritional and occupancy information, and the role of hydrogeomorphology in regulating those interactions, are valuable advancements. Coastal fishes in the Great Lakes use a mosaic of interacting habitats, and hydrologic linkages among those habitats maintain diversity of fishes, which act as metacommunities (Bouvier et al., 2009; Sierszen et al., 2012a; Midwood and Chow-Fraser, 2015). The use of restored access to spawning and nursery habitats by coastal fish (e.g., Oele et al., 2015) makes a compelling argument for restoration of lost inter-habitat connections. Our results substantiate the value of protecting coastal habitats and restoring coastal wetlands that are hydrologically connected to the Great Lakes.

Supplementary data to this article can be found online at https://doi.org/10.1016/j.jglr.2018.11.006.

Acknowledgements

We thank David Clapp, Dave Fielder, Bill Wellenkamp, and the Michigan Department of Natural Resources Fisheries Division for assisting in fish collections, and Ryan Wheeler, Tom Langer, Bridget Wheelock, Lindsey Adams, and Kaley Genther for assisting in the collection and preparation of samples for analysis. Thanks to John Brazner and the journal reviewers for critical comments that substantially improved the manuscript. The research described in this article has been funded in part by the U.S. Environmental Protection Agency as part of the Great Lakes Restoration Initiative under proposal EPA GLNPO-2010-H-3-984-758 and the Great Lakes Fish and Wildlife Restoration Act under FWS Agreement Number: F14AP00520. The research was also supported by the Garden Club of America Coastal Wetlands Award, Center for Coastal Resources Management at the Virginia Institute of Marine Science, College of William and Mary. The views expressed in this article are those of the authors and do not necessarily reflect the views or policies of the U.S. EPA, Michigan DNR, or Michigan DEQ. This paper is Contribution Number 112 of the Central Michigan University Institute for Great Lakes Research.

References

Albert, D.A., Wilcox, D.A., Ingram, J., Thompson, T.A., 2005. Hydrogeomorphic classification for Great Lakes coastal wetlands. J. Great Lakes Res. 31 (Suppl. 1), 129–146. https://doi.org/10.1016/S0380-1330(05)70294-X.

Bouchard, V., 2007. Export of organic matter from a coastal freshwater wetland to Lake Erie: an extension of the outwelling hypothesis. Aquat. Ecol. 41, 1–7.

Bouvier, L.D., Cottenie, K., Doka, S.E., 2009. Aquatic connectivity and fish metacommunities in wetlands of the lower Great Lakes. Can. J. Fish. Aquat. Sci. 66, 933–948.

Brazner, J.C., 1997. Regional, habitat, and human development influences on coastal wetland and beach fish assemblages in Green Bay, Lake Michigan. J. Great Lakes Res. 23, 36–51.

Brazner, J.C., Sierszen, M.E., Keough, J.R., Tanner, D.K., 2000. Assessing the ecological importance of coastal wetlands in a large lake context. Verh. Internat. Verein. Limnol. 27, 1950–1961.

Brazner, J.C., Tanner, D.K., Morrice, J.A., 2001. Fish-mediated nutrient and energy exchange between a Lake Superior coastal wetland and its adjacent bay. J. Great Lakes Res. 27, 98–111.

Brazner, J.C., Campana, S.E., Tanner, D.K., Schram, S.T., 2004. Reconstructing habitat use and wetland nursery origin of yellow perch from Lake Superior using otolith elemental analysis. J. Great Lakes Res. 30, 492–507.

Cabana, G., Rasmussen, J.B., 1994. Modeling food chain structure and contaminant bioaccumulation using stable nitrogen isotopes. Nature 372, 255–257.

Clement, M., Chiasson, A.G., Veinott, Gl., Cairns, D.K., 2014. What otolith microchemistry and stable isotope analysis reveal and conceal about anguillid eel movements across salinity boundaries. Oecologia 175, 1143–1153.

Cunjak, R.A., Roussel, J.-M., Gray, M.A., Dietrich, J.P., Cartwright, D.F., Munkittrick, K.R., Jardine, T.D., 2005. Using stable isotope analysis with telemetry or mark-recapture data to identify fish movement and foraging. Oecologia 144, 636–646.

Dolson, R., McCann, K., Rooney, N., Ridgway, M., 2009. Lake morphometry predicts the degree of habitat coupling by a mobile predator. Oikos 118, 1230–1238.

Eshenroder, R., Sideleva, V.G., Todd, T.N., 1999. Functional convergence among pelagic sculpins of Lake Baikal and deepwater ciscoes of the Great Lakes. J. Great Lakes Res. 25, 847–855.

Hecky, R.E., Hesslein, R.H., 1995. Contributions of benthic algae to lake food webs as revealed by stable isotope analysis. J. N. Am. Benthol. Soc. 14, 631–653.

Hoffman, J.C., Peterson, G.S., Cotter, A.M., Kelly, J.R., 2010. Using stable isotope mixing in a Great Lakes coastal tributary to determine food web linkages in young fishes. Estuar. Coasts 33, 1391–1405.

Hoffman, J.C., Kelly, J.R., Peterson, G.S., Cotter, A.M., 2015a. Landscape-scale food webs of fish nursery habitat along a river-coast mixing zone. Estuar. Coasts 38, 1335–1349.

Hoffman, J.C., Sierszen, M.E., Cotter, A.M., 2015b. Fish tissue lipid-C:N relationships for correcting $\delta^{13}C$ values and estimating lipid content in aquatic food-web studies. Rapid Commun. Mass Spectrom. 29, 2069–2077.

Hogan, Z., Baird, I.G., Radtke, R., Vander Sanden, M.J., 2007. Long distance migration and marine habitation in the tropical Asian catfish, *Pangasius krempfi*. J. Fish Biol. 71, 818–832.

Howes, D.E., Morris, M., Zacharias, M., 1999. British Columbia Estuary Mapping System. Resources Inventory Committee, Province of British Columbia, Canada 0-7726-3911-6.

Jude, D.J., Pappas, J., 1992. Fish utilization of Great Lakes coastal wetlands. J. Great Lakes Res. 18, 651–672.

Keough, J.R., Sierszen, M.E., Hagley, C.A., 1996. Analysis of a Lake Superior coastal food web with stable isotope techniques. Limnol. Oceanogr. 41, 136–146.

Keough, J.R., Hagley, C.A., Ruzycki, E., Sierszen, M.E., 1998. $\delta^{13}C$ composition of primary producers and role of detritus in a freshwater coastal ecosystem. Limnol. Oceanogr. 43, 734–740.

Keough, J.R., Thompson, T.A., Guntenspergen, G.R., Wilcox, D.A., 1999. Hydrogeomorphic factors and ecosystem responses in coastal wetlands of the Great Lakes. Wetlands 19, 821–834.

Kiljunen, M., Grey, J., Sinisalo, T., Harrod, C., Immonen, H., Jones, R.I., 2006. A revised model for lipid-normalizing values from aquatic organisms, with implications for isotope mixing models. J. Appl. Ecol. 43, 1213–1222.

Landsman, S.J., Nguyen, V.M., Gutowsky, L.F.G., Gobin, J., Cook, K.V., Binder, T.R., Lower, N., McLaughlin, R.L., Cooke, S.J., 2011. Fish movement and migration studies in the Laurentian Great Lakes: research trends and knowledge gaps. J. Great Lakes Res. 37, 365–379.

Logan, J.M., Jardine, T.D., Miller, T.J., Bunn, S.E., Cunjak, R.A., Lutcavage, M.E., 2008. Lipid corrections in carbon and nitrogen stable isotope analyses: comparison of chemical extraction and modelling methods. J. Anim. Ecol. 77, 838–846.

Meixler, M.S., Arend, K.K., Bain, M.B., 2005. Fish community support in wetlands within protected embayments of Lake Ontario. J. Great Lakes Res. 31 (Suppl. 1), 188–196.

Midwood, J.D., Chow-Fraser, P., 2015. Connecting coastal marshes using movements of resident and migratory fishes. Wetlands 35, 69–79.

Morrice, J.A., Trebitz, A.S., Kelly, J.R., Sierszen, M.E., Cottter, A.M., Hollenhorst, T., 2011. Determining sources of water to Great Lakes coastal wetlands: a classification approach. Wetlands 31, 1199–1213.

Odom, E.P., 1968. A research challenge: evaluating the productivity of coastal and estuarine water. Proceedings of the Second Sea Grant Conference. Univ. of Rhode Island, pp. 63–64.

Oele, D.L., Hogan, J.D., McIntire, P.B., 2015. Chemical tracking of northern pike migrations: if we restore access to breeding habitat, will they come? J. Great Lakes Res. 41, 853–861.

Pangle, K.L., Ludsin, S.A., Fryer, J.J., 2010. Otolith microchemistry as a stock identification tool for freshwater fishes: testing its limits in Lake Erie. Can. J. Fish. Aquat. Sci. 67, 1475–1489.

Parker, A.D., Cooper, M.J., Ruetz III, C.R., Coulter, D.P., Uzarski, D.G., 2012. Chemical and physical factors associated with yellow perch abundance in Great Lakes coastal wetlands: patterns within and among wetland types. Wetl. Ecol. Manag. 20, 137–150.

Phillips, D.L., Gregg, J.W., 2003. Source partitioning using stable isotopes: coping with too many sources. Oecologia 136, 261–269.

Phillips, D.L., Newsome, S.D., Gregg, J.W., 2005. Combining sources in stable isotope mixing models: alternative methods. Oecologia 144, 520–527. https://doi.org/10.1007/s00442-004-1816-8 (PMID:15711995).

Polis, G.A., Anderson, W.B., Holt, R.D., 1997. Toward an integration of landscape and food web ecology: the dynamics of spatially subsidized food webs. Annu. Rev. Ecol. Syst. 28, 289–316.

Schindler, D.E., Scheuerell, M.D., 2002. Habitat coupling in lake ecosystems. Oikos 98, 177–189.

Schoen, L.S., Student, J.J., Hoffman, J.C., Sierszen, M.E., Uzarski, D.G., 2016. Reconstructing fish movements between coastal wetland and nearshore habitats of the Great Lakes. Limnol. Oceanogr. 61, 1800–1813.

Semmens, B.X., Ward, E.J., Parnell, A.C., Phillips, D.L., Bearhop, S., Inger, R., Jackson, A., Moore, J.W., 2013. Statistical basis and outputs of stable isotope mixing models: comment on fry (2013). Mar. Ecol. Prog. Ser. 490, 285–289.

Sierszen, M.E., Brazner, J.C., Cotter, A.M., Morrice, J.A., Peterson, G.S., Trebitz, A.S., 2012a. Watershed and lake influences on the energetic base of coastal wetland food webs across the Great Lakes Basin. J. Great Lakes Res. 38, 418–428.

Sierszen, M.E., Morrice, J.A., Trebitz, A.S., Hoffman, J.C., 2012b. A review of selected ecosystem services provided by coastal wetlands of the Laurentian Great Lakes. Aquat. Ecosys. Health Manag. 15, 92–106.

Sierszen, M.E., Hrabik, T.R., Stockwell, J.D., Cotter, A.M., Hoffman, J.C., Yule, D.L., 2014. Depth gradients in food-web processes linking habitats in large lakes: Lake Superior as an exemplar ecosystem. Freshw. Biol. 59, 2122–2136.

Stockwell, J.D., Yule, D.L., Hrabik, T.R., Sierszen, M.E., Isaac, E.J., 2014. Habitat coupling in a large lake system: delivery of an energy subsidy by an offshore planktivore to the nearshore zone of Lake Superior. Freshw. Biol. 59, 1197–1212.

Trebitz, A.M., Hoffman, J.C., 2015. Coastal wetland support of Great Lakes fisheries: progress from concept to quantification. Trans. Am. Fish. Soc. 144, 352–372.

Uzarski, D.G., Burton, T.M., Genet, J.A., 2004. Validation and performance of an invertebrate index of biotic integrity for Lakes Huron and Michigan fringing wetlands during a period of lake level decline. Aquat. Ecosys. Health Manag. 7 (2), 269–288.

Uzarski, D.G., Burton, T.M., Cooper, M.J., Ingram, J.W., Timmermans, S.T.A., 2005. Fish habitat use within and across wetland classes in coastal wetlands of the five Great Lakes: development of a fish-based index of biotic integrity. J. Great Lakes Res. 31 (Suppl. 1), 171–187.

Uzarski, D.G., Brady, V.J., Cooper, M.J., Wilcox, D.A., Albert, D.A., Axler, R., Bostwick, P., Brown, T.A., Ciborowski, J.J.H., Danz, N.P., Gathman, J., Gehring, T., Grabas, G., Garwood, A., Howe, R., Johnson, L.B., Lamberti, G.A., Moerke, A., Murry, B., Niemi, G., Norment, C.J., Ruetz III, C.R., Steinman, A.D., Tozer, D., Wheeler, R., O'Donnell, T.K., Schneider, J.P., 2017. Standardized measures of coastal wetland condition: implementation at the Laurentian Great Lakes basin-wide scale. Wetlands 37, 15–32. https://doi.org/10.1007/s13157-016-0835-7.

Vadeboncoeur, Y., Vander Zanden, M.J., Lodge, D.M., 2002. Putting the lake back together: reintegrating benthic pathways into lake food web models. Bioscience 52, 44–54.

Vander Zanden, M.J., Rasmussen, J.B., 2001. Variation in $\delta^{15}N$ and $\delta^{13}C$ trophic fractionation: implications for aquatic food web studies. Limnol. Oceanogr. 46, 2061–2066.

Vander Zanden, M.J., Vadeboncoeur, Y., 2002. Fishes as integrators of benthic and pelagic food webs in lakes. Ecology 83, 2152–2161.

Vander Zanden, M.J., Cabana, G., Rasmussen, J.B., 1997. Comparing trophic position of freshwater fish calculated using stable nitrogen isotope ratios ($\delta^{15}N$) and literature dietary data. Can. J. Fish. Aquat. Sci. 54, 1142–1158.

Vander Zanden, M.J., Clayton, M.K., Moody, E.K., Solomon, C.T., Weidel, B.C., 2015. Stable isotope turnover and half-life in animal tissues: a literature synthesis. PLoS One 10, e0116182. https://doi.org/10.1371/journal.pone.0116182.

Wetzel, R.G., 1992. Wetlands as metabolic gates. J. Great Lakes Res. 18, 529–532.

LIMNOLOGY
and
OCEANOGRAPHY

ASLO

Limnol. Oceanogr. 61, 2016, 1800–1813
© 2016 Association for the Sciences of Limnology and Oceanography
doi: 10.1002/lno.10340

Reconstructing fish movements between coastal wetland and nearshore habitats of the Great Lakes

Lee S. Schoen,*[1] James J. Student,[2] Joel C. Hoffman,[3] Michael E. Sierszen,[3] Donald G. Uzarski[1]

[1]Department of Biology, Institute for Great Lakes Research, Central Michigan University, Mount Pleasant, Michigan
[2]Center for Elemental and Isotopic Analysis, College of Science and Technology, Central Michigan University, Mount Pleasant, Michigan
[3]US Environmental Protection Agency, Office of Research and Development, National Health and Environmental Effects Research Laboratory, Mid-Continent Ecology Division, Duluth, Minnesota

Abstract

The use of resources from multiple habitats has been shown to be important to the production of aquatic consumers. To quantify the support of Great Lakes coastal wetland (WL) and nearshore (NS) habitats to yellow perch, we used otolith microchemistry to trace movements between the habitats. WL and NS water and fish samples were collected from lakes Huron and Michigan for water and otolith trace element analysis. Recently deposited otolith-edge Sr : Ca and Ba : Ca from otoliths were strongly correlated with the chemistry of the water in which fish were caught. In general, Sr : Ca and Ba : Ca in otoliths were significantly greater for individuals collected from WL areas. Because of these observed chemical differences between WL and NS habitats, quadratic discriminant function analysis (QDFA) was used to classify individuals with high accuracy to the habitat from which they were collected. We then combined the predictive abilities of QDFA with the otolith chemistry transect data that represents an individuals' entire life, to classify habitat use through each fish's life. Our results suggest larval use of WL habitats as well as three life histories for adult yellow perch. These strategies include (1) fish utilizing WL once annually (2) WL residents (3) WL residence as juveniles followed by movement to nearshore as adults. This application represents a novel use of transect otolith microchemistry to reconstruct fish movements between freshwater environments across entire life spans at fine scales. These results suggest that regular movements of fish may facilitate the production of coastal fishes in the Great Lakes.

Introduction

Our understanding of the production dynamics of aquatic systems has been substantially advanced through the perspective of multi-habitat support of consumers. Across a wide range of lake sizes, fish have been found to use resources from a combination of benthic, pelagic, and littoral habitats (Schindler and Scheuerell 2002; Vander Zanden and Vadeboncoeur 2002). In large lakes around the world, native macroinvertebrate and fish species such as opossum shrimp (*Mysis diluviana*), kiyi (*Coregonus kiyi*) and lake trout (*Salvelinus namaycush*) have evolved to feed in a combination of benthic and pelagic habitats through diel vertical migration (Ahrenstorff et al. 2011; Sierszen et al. 2014).

Similarly, littoral (e.g., coastal wetland) and nearshore food webs can be strongly coupled. This idea can be traced back to the work of Lindeman (1942) and the marine coastal wetland carbon "outwelling" hypothesis originally proposed by Odum (1968) which suggested that coastal marsh production exceeds the metabolic needs of local wetland (WL) consumers and is exported to nearshore (NS) food webs. Great Lakes coastal wetland habitats are analogous to coastal marine systems in that they are extremely productive habitats with direct hydrologic connections to less productive offshore waters (Uzarski et al. 2005). This connectivity facilitates the use of resources from multiple habitats by coastal consumers; however, measures of multi-habitat support have ranged widely, both among systems and within species (e.g., Schindler and Scheuerell 2002; Sierszen et al. 2012).

In general, the use of the resources from numerous aquatic habitats is accomplished by movements of fish among the habitats (Schindler and Scheuerell 2002; Vander Zanden and Vadeboncoeur 2002; Ahrenstorff et al. 2011). In

*Correspondence: schoelee@gmail.com

Additional Supporting Information may be found in the online version of this article.

the Great Lakes, coastal wetlands support more than 80 species of fish, including 30 species of nearshore game fish (Jude and Pappas 1992). This likely represents an ecologically important, understudied linkage between wetland and nearshore environments. For example, Brazner et al. (2001) documented emigration of thousands of young-of-year yellow perch (*Perca flavescens*), northern pike (*Esox luscious*) and emerald shiner (*Notropis atherinoides*) from a Lake Superior coastal wetland, subsidizing predators of the nearshore food web with energy and nutrients from the wetland nursery habitat. Similarly, adult predatory fish movements represent a potentially strong mechanism behind multiple-habitat use due to their highly mobile and flexible foraging tactics (Schindler and Scheuerell 2002; McCann et al. 2005). However, very little is known about the frequency and duration of wetland habitat use by Great Lakes fishes (Jude and Pappas 1992). Therefore, to fully understand the support of fish by wetland and nearshore habitats, it is critical to assess movements of juvenile and adult fish between coastal habitats.

Several methods have evolved to track fish movements including net surveys, mark-recapture and radio frequency tagging (Pangle et al. 2010). While these methods are particularly effective in tracking short-term, fine-scale movements, they have logistical limits in studies exploring spatially and temporally large-scale movements. A more comprehensive approach for understanding such movements involves the use of trace element microchemistry in fish otoliths. Otoliths or "ear stones" are internal structures used by fish for hearing and balance and grow in daily increments or rings which are visible using a variety of optical methods (Campana and Thorrold 2001). Although they are composed mainly of calcium carbonate ($CaCO_3$), various trace elements can substitute to replace Ca, of which several (i.e., Sr and Ba) are incorporated relative to their availability in the water at the time of otolith growth (Pangle et al. 2010; Zeigler and Whitledge 2010). Therefore, if sufficient gradients in these trace elements exist between two or more habitats of interest, the chronological order and frequency of time spent in different habitats can be revealed by analyzing for trace elements across the entire growth history of the otolith. For instance, studies have commonly used laser ablation inductively coupled plasma mass spectrometry (LA-ICP-MS) to reconstruct where a fish resided by analyzing the chemical constituents of its otolith from its core (formed during embryonic development) to its edge (formed just prior to capture and death).

In this study, we employ LA-ICP-MS otolith microchemistry as a tool for tracking movements of fish between Great Lakes nearshore and coastal wetland habitats to examine habitat use and variation in life history strategies. This study represents a novel application of transect-based otolith microchemistry, and to our knowledge this is one of the first comprehensive studies to reconstruct movements of fish between coastal wetland and nearshore habitats of the Great Lakes across entire lifespans.

Methods

Habitat reconstruction focused on yellow perch because of its economic and ecological importance as a forage fish and recreational game fish. Its mobile behavior and abundance in Great Lakes WL and NS habitats was also a major reason for its selection (Beletsky et al. 2007; Blackwell and Kaufman 2012).

Fish and water samples were collected from 12 WL-NS pairings in Lake Michigan, northern Lake Huron and Saginaw Bay (Fig. 1). Each site consisted of a NS area (3–5 m depth) adjacent to a WL area (<1 m depth). The sites were selected to represent the most common hydrogeomorphic WL types of Lakes Michigan and Huron as described in Albert et al. (2005). Hydrogeomorphic categories used in this study include riverine WL, protected (embayment) lacustrine WL and open (non-embayment) lacustrine WL, in order of increasing wave exposure and Great Lakes mixing. Sites were chosen based upon the distribution of hydrogeomorphic types in the basin and included three riverine systems in Lake Michigan (Grand River, Kalamazoo River, and Pentwater River), four lacustrine WL in northern Lake Huron (Duck Bay, Mismer Bay, Government Bay, and Alpena) and five lacustrine WL in Saginaw Bay (AuGres, Pinconning Park, Quanicassee River, Fish Point, and Wildfowl Bay).

Water samples were collected at each of the 12 sites 15 June 2012–15 August 2012. Wetland and nearshore water samples were collected to evaluate relationships between water and otolith chemistry and to examine variation in trace element chemistries between WL and NS habitats. At each site, two WL samples were taken from within dominant vegetation types and two additional NS samples were taken beyond the boundary of WL vegetation, or outside of the visible river plume in Lake Michigan drowned river mouth sites. Distances between WL and NS water stations were dependent upon river discharge, shoreline slope and the expanse of wetland vegetation. In general, distances ranged from 1 to 2 miles in Lake Michigan drowned river mouth complexes to 0.5–4.0 miles in Lake Huron fringing wetlands. Water sampling was limited to a single event and elements of interest included strontium (Sr), barium (Ba), sodium (Na), magnesium (Mg), potassium (K), manganese (Mn), lead (Pb), and Calcium (Ca) (Pangle et al. 2010). Water samples were collected and processed using a modified protocol described in Shiller (2003). Briefly, samples were collected using acid washed equipment, filtered through 0.45 μm acid washed filters and preserved in a 2.0% solution of nitric acid. Samples were refrigerated until analysis.

Elemental analysis of water samples was conducted at the Center for Elemental and Isotopic Analysis (CELISA) at Central Michigan University utilizing sector field inductively

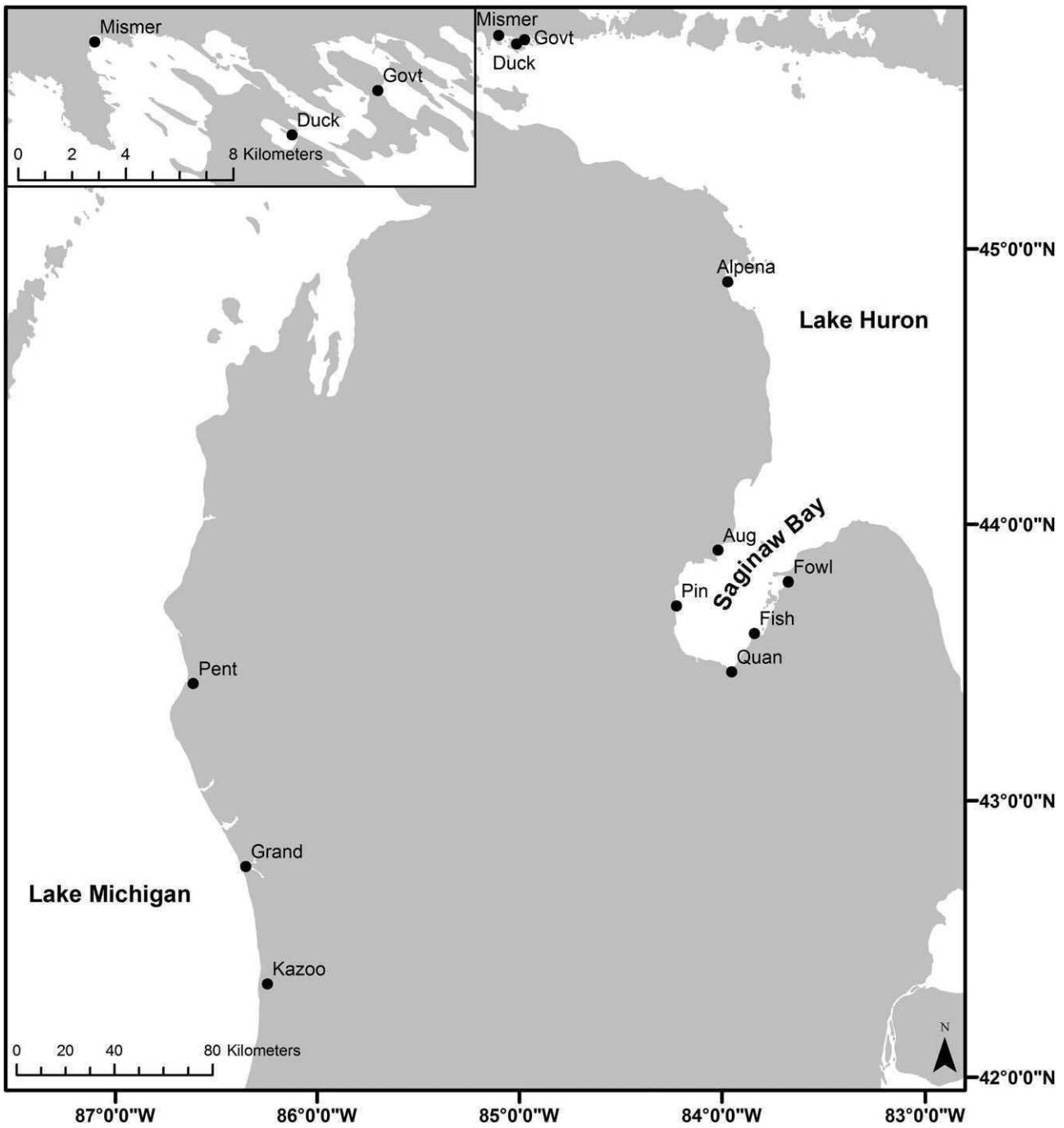

Fig. 1. Location of sampling sites from Lakes Michigan and Huron, including Saginaw Bay. WL and NS site pairs marked by black dots. Northern Lake Huron sites enlarged separately to show sampling locations.

coupled plasma mass spectrometer (SF-ICP-MS). See Supporting Information Table S2 for operating parameters. Water samples were analyzed within 6 months of collection. Before analysis, 9.9 mL of each preserved water sample was spiked with 100 mL of an internal standard of Indium115 to correct for instrumental drift during analysis and calibrations. Minimum detection limits of 0.003ppb (Pb), 0.012ppb (Mn), 0.013ppb (Cu), 0.016ppb (Ba), 0.099ppb (Sr), 14.6ppb (Mg), 16.6ppb (K), 22.6ppb (Na), and 32.5ppb (Ca) were calculated based on 3× the cps of the average laboratory blanks.

All yellow perch were collected 15 June 2012–15 August 2012. A minimum of three yellow perch were sought from each habitat (i.e., six per site) regardless of size. However, no yellow perch were collected from the Alpena WL or

Pentwater NS. WL fish were collected with a combination of modified fyke nets and boat electrofishing. NS fish were collected by the Michigan DNR using experimental gill nets set in NS habitats adjacent to WL habitats. After collection, fish were placed on ice and frozen within 24 h of collection. In the lab, sagittal otoliths were removed, cleaned of any tissue in ultrapure water and stored in clean polypropylene micro centrifuge tubes. Otolith sections were then prepared by mounting otoliths in Epo-fix® epoxy resin and sectioning them through the transverse plane with a low-speed wafering saw to a thickness of 400 μm. After sectioning, otoliths were polished to the plane of the core with 600 and 1200 grit SiC paper and 1 μm Alumina polishing film. Sections were then mounted to analysis slides, sonicated for 10 min in ultrapure water, and dried in a laminar flow hood until analysis.

Otolith sections were analyzed at Central Michigan University at CELISA using LA-ICP-MS. See Supporting Information Table S3 for specific instrument types and their operating parameters. According to previous studies, we analyzed otoliths for strontium (Sr), barium (Ba), magnesium (Mg), manganese (Mn), copper (Cu), Zinc (Zn), and lead (Pb) (Pangle et al. 2010; Zeigler and Whitledge 2010). Otoliths were either analyzed on a line passing through the core or in select cases the transect line angle was changed to avoid obvious fractures. Laser ablation transects were always selected perpendicular to growth annuli. Prior to each otolith analysis, an 80 μm-wide pre-cleaning ablation raster was conducted using two laser pulses along each transect segment.

The analysis of 5–6 otoliths (depending on transect lengths) were bracketed by 3 NIST 612 glass standard analyses used for determining trace element concentrations. Measured trace element concentrations were processed using the Iolite software Trace Element Internal Standardization Routine (Hellstrom et al. 2008). For every sample and standard analysis, 40–50 s of carrier gas blank was measured prior to laser ablation for background corrections. Ca was used as a pseudo-internal standard at 40 wt.% as in stoichiometric calcium carbonate relative to NIST 612 glass concentration values reported by Pearce et al. (1997). The Iolite software calculates limits of detection for each analysis. For simplicity, the mean limits of detection for all analyzed otoliths for Mg, Mn, Cu, Zn, Sr, Ba, and Pb were 0.364, 0.253, 0.080, 0.139, 0.061, 0.059, and 0.008 $\mu g \times g^{-1}$, respectively. After ablation, all otoliths were imaged using a Nikon SMZ 1000 dissecting microscope equipped with a Digital Sight (DS-Fi2) 10× digital camera and NIS-Elements Viewer sofware to measure positions of the core and annuli along the laser transect to label these regions on the resulting trace element transect data.

Prior to all statistical analyses, elemental concentrations in water and otoliths were converted into molar equivalents and normalized to $\mu molX \times molCa^{-1}$ where "X" is the element of interest. These data are represented as X : Ca throughout the remainder of the text. Elements were excluded from statistical analysis if they fell below detection limits in over half of our water or otolith samples. We analyzed data by region (i.e., Lake Michigan, northern Lake Huron and Saginaw Bay) in all of our analyses to account for differences among underlying geology, land use and hydrogeomorphic types of WLs (i.e., riverine, open embayment, protected embayment). We also assumed that fish would be able to travel within each of our sampling regions and wanted to identify within-region variation. All statistical analyses were performed in R 2.15.1. An α of 0.05 was used for all statistical tests.

To identify a suite of trace elements to be used for habitat use reconstruction, it was necessary to identify elements (1) whose chemistry in the otolith was positively correlated with water chemistry and (2) whose chemistry in the outer otolith was significantly different in fish collected from WL as opposed to NS habitats, while being relatively consistent among WLs within each region. Relationships between dissolved trace element and otolith trace element chemistry were determined using least-squares regressions between average outer otolith chemistry from each sampling location and elemental chemistry of the water from which the fish were caught. The mean outer 10 μm of data from each otolith was used in the regressions since this portion had stable signal and should reflect the most recent several weeks of environmental chemistry (Zeigler and Whitledge 2010).

The otolith-edge chemistry of elements that showed significant, positive relationships with local water chemistry were compared for WL and NS-caught fish. These comparisons were made, by region, using one way analyses of variance (ANOVAs), followed by Tukey's HSD tests for multiple comparisons. We also tested for differences in combined elemental signatures using multivariate analyses of variance (MANOVAs). We treated individual fish as replicates, since their otolith-edge chemistry reflects the previous several weeks of movement within the habitat from which they were collected. WL fish and water samples were pooled by site within each region, whereas nearshore fish and water samples were pooled within each region because of a limited sample size of nearshore fish and because we assumed the nearshore water samples were well mixed. In all tests, we assumed distributions were normal because sample sizes were too small to test for significance, while ANOVA and MANOVA are robust to departures from normality.

To distinguish between WL and NS habitat use in otolith trace element transects it was necessary to determine an elemental threshold or "fingerprint" for WL and NS habitats within each region. It is not possible to do this with the elemental water chemistry, since otolith chemistry does not exactly follow that of the surrounding water due to physiological processes (Dorval et al. 2007). As a result, traditional interpretation of fish movements through spectra has been qualitative (i.e., peaks or valleys in elemental concentrations

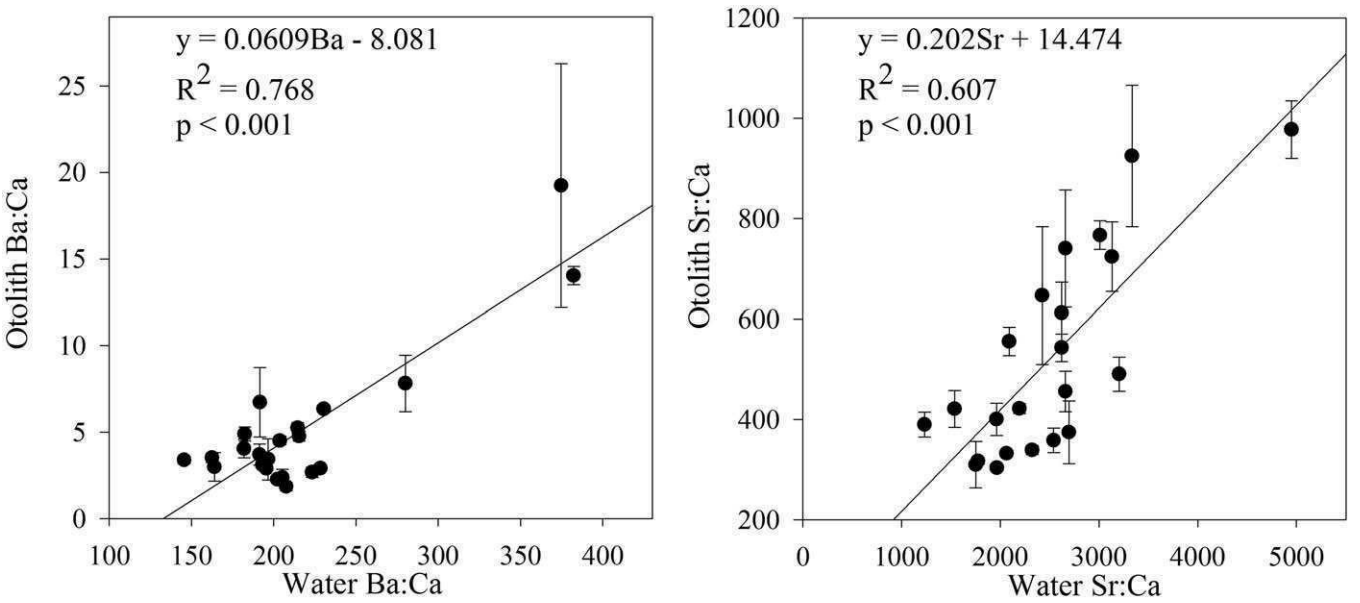

Fig. 2. Least squares regression between water and otolith-edge Sr : Ca (left) and Ba : Ca (right). Data points are sample means ± 1 S.E. No fish were collected from Alpena WL or Pentwater River WL and these sites are excluded from the regressions.

or oscillations are interpreted as movements). Instead, we developed a suite of habitat reconstruction elements as outlined above, and used the chemistry of these elements in the otolith-edge of WL and NS-caught fish to develop elemental signatures for WL and NS habitat within Lake Michigan, northern Lake Huron, and Saginaw Bay. We then verified the classification accuracy of each regional model using a leave-one-out jackknifing procedure to determine how accurate each models was for each habitat type. After using this jackknifing procedure, we used a binomial distribution to assess whether jackknife classification accuracies were significantly better than random (i.e., 50% wetland, 50% nearshore) assignment, within each region. The resulting regional models were then applied to individual points along each otolith transect using the predict function to classify regions along laser transects as representing WL or NS habitat use.

Results

Lead and Manganese were below detection limit in several waters samples and most otoliths, and were excluded from our analysis. After normalizing each element to molar equivalents of Ca, mean Sr : Ca and Ba : Ca in water and otoliths showed positive linear relationships (Figs. 2A,B; $p < 0.001$, $R^2 = 0.607$ and $p < 0.001$, $R^2 = 0.768$ respectively). No relationships were found for Mg : Ca, Cu : Ca or Zn : Ca and these elements were not included in subsequent analyses. We detected differences in Sr : Ca and/or Ba : Ca between WL and NS habitats within all regions (Fig. 3; ANOVA, $p < 0.001$). Otolith Sr : Ca was significantly higher in otoliths from WL fish than from NS fish from Lake Michigan (Fig. 3A), northern Lake Huron (Fig. 3C) and Saginaw Bay (Fig. 3E), with the exception of Wildfowl Bay WL (Saginaw Bay), Government Bay WL (northern Lake Huron), and the Kalamazoo River WL (Lake Michigan). In general, mean Ba : Ca in otoliths of WL fish was also higher than NS fish. Otolith Ba : Ca was statistically higher than NS otoliths from the Quanicassee River (Saginaw Bay; Fig. 3B), Duck Bay (northern Lake Huron; Fig. 3D) and the Kalamazoo River and Grand Rivers (Lake Michigan; Fig. 3F).

Sr : Ca and Ba : Ca from otoliths were used for multivariate and discriminant analyses based upon these ANOVA results. After combining Sr : Ca and Ba : Ca as elemental fingerprints for wetland and nearshore habitats, wetland habitats were significantly different than nearshore habitats in Saginaw Bay (MANOVA; df = 1, $F = 21.456$, $p < 0.001$), northern Lake Huron (MANOVA; df = 1, $F = 4.2486$, $p = 0.02105$) and Lake Michigan (MANOVA; df = 1, $F = 18.76$, $p < 0.001$). The inclusion of Sr : Ca and Ba : Ca in the QDFA models of WL and NS otolith chemistry in Lake Michigan, northern Lake Huron and Saginaw Bay also increased the classification accuracy within those regions based upon the jackknifing model verification. Therefore, otolith-edge Sr : Ca and Ba : Ca were combined in a QDFA to develop predictive models of WL and NS otolith chemistry, by region. Otolith chemistry of WL and NS fish were classified with 8–100% accuracy based upon jackknifing results (Table 1). Compared with a binomial distribution, these WL an dNS classification accuracies were significantly better than random assignment for Saginaw Bay, northern Lake Huron and Lake Michigan ($p < 0.001$, $p = 0.0497$, $p < 0.001$, respectively).

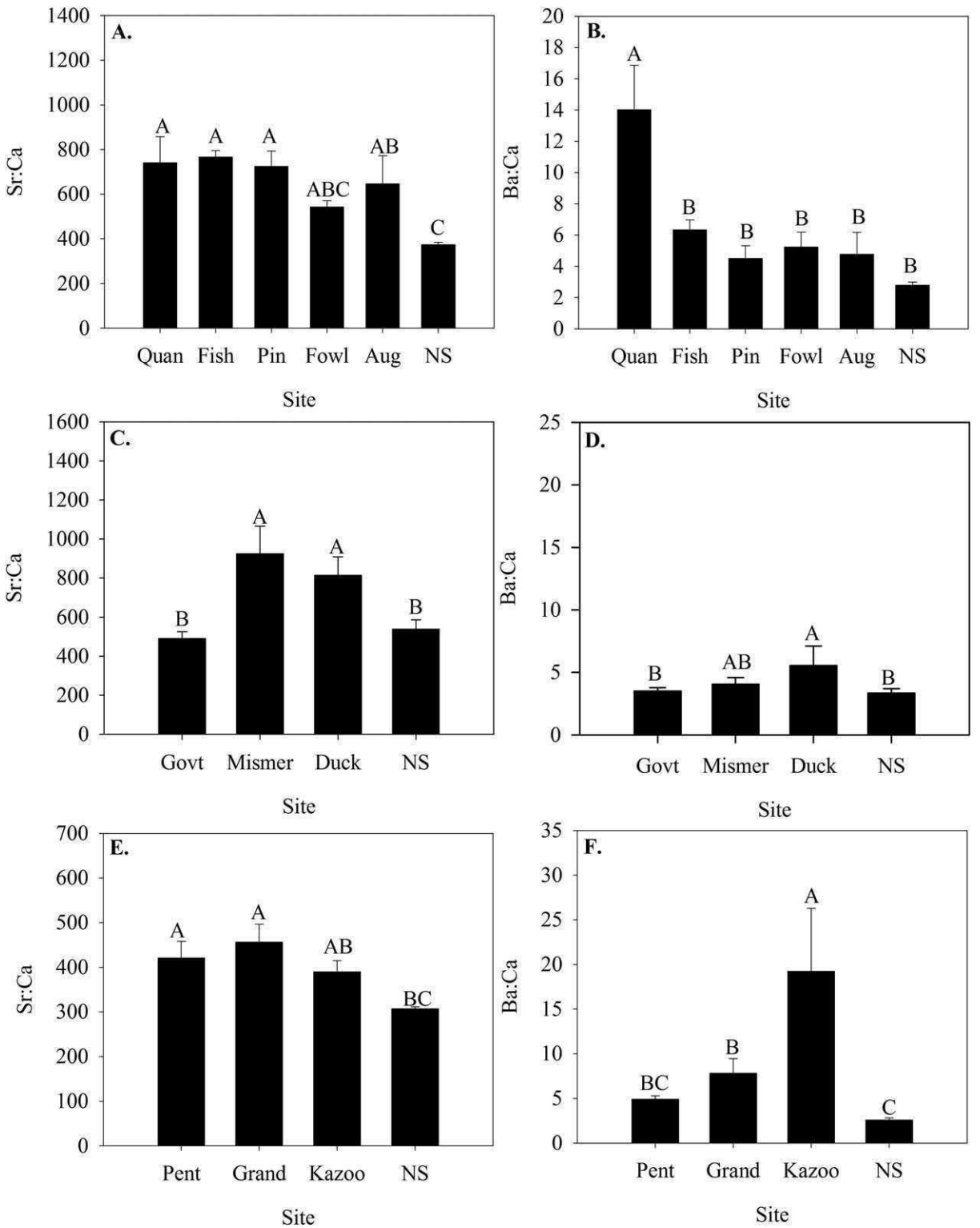

Fig. 3. Mean otolith Sr : Ca and Ba : Ca values (± 1 S.E.) for habitats in Saginaw Bay in (top; **A**, **B**), northern Lake Huron (middle; **C**, **D**) and Lake Michigan (bottom; **E**, **F**). Means marked with the same letter are not significantly different (ANOVA followed by Tukey's HSD test, $p < 0.05$). Nearshore samples were pooled within each region for the analysis. From left to right, sites include the Quanicassee River mouth, Fish Point, Wildfowl Bay, AuGres and nearshore (Saginaw Bay), Government Bay, Mismer Bay, Duck Bay and nearshore (Northern Lake Huron) and the Pentwater River, Grand River, Kalamazoo River and nearshore (Lake Michigan). Nearshore samples were combined in the analyses for comparisons.

Table 1. Results of Linear Discriminant Function Analysis (QDFA) classification accuracy of fish to habitat of capture (i.e., wetland (WL) or nearshore (NS)) by region, using a leave-one-out jackknife procedure. Predictive models were constructed using otolith-edge Sr : Ca and Ba : Ca.

Source Location	Assigned location		% fish classified correctly
Saginaw Bay			
	NS	WL	
NS			
AuGres	4	0	100
Pinconning	3	0	100
Quanicassee	5	0	100
Fish Point	3	0	100
Wildfowl Bay	5	0	100
WL			
AuGres	1	5	83
Pinconning	0	7	100
Quanicassee	0	4	100
Fish Point	0	3	100
Wildfowl Bay	1	2	67
Northern Lake Huron			
	NS	WL	
NS			
Duck Bay	5	0	100
Mismer Bay	2	0	100
Government Bay	3	0	100
Alpena	4	0	100
WL			
Duck Bay	0	8	100
Mismer Bay	4	5	56
Government Bay	12	1	8
Alpena	—	—	N/A
Lake Michigan			
	NS	WL	
NS			
Grand River	13	1	93
Kalamazoo River	5	0	100
Pentwater River	—	—	N/A
WL			
Grand River	1	8	89
Kalamazoo River	0	3	100
Pentwater River	3	5	63

Nearly all yellow perch otoliths analyzed in this study produced a common pattern in early-life otolith chemistry before the first annulus, including a core area with elevated Ba and a spike in Sr : Ca and Ba : Ca between the core and annulus one (Fig. 4A). When applying the QDFA models to these transect data, the core and intermediate peak between the core and annulus one were typically classified as WL use (Fig. 4B). All estimation of WL and NS habitat use were created by (1) plotting Sr : Ca along laser transects and (2) applying the QDFA model to transect data to estimate whether otolith growth regions represented WL or NS chemistry as shown in Fig. 3B, combining Sr : Ca and Ba : Ca as predictors of habitat use.

Any fish greater than 2 yr of age (i.e., with two annuli) was classified as adult and these otoliths were used in life history analysis of Great Lakes yellow perch. Consequently, 61 yellow perch were included in the adult habitat use reconstruction analysis. After applying the QDFA model to these adult transects, adult yellow perch subjectively grouped into three distinct patterns outside of the first annulus (Fig. 5A–C). In life history 1, elemental chemistries demonstrated WL use once per year (Fig. 5A, $n = 36$). In scenario 2, otolith chemistry transects indicated WL habitat use year-round or a movement of fish between WL and NS habitats twice per year (Fig. 5B, $n = 13$). In scenario 3, otolith transects demonstrated a WL use as an adult between annuli 1 and 3 and predominantly NS use beyond this stage (Fig. 5C, $n = 13$).

Dissolved WL and NS trace element comparisons of Sr : Ca and Ba : Ca from water samples are shown in Fig. 6. While otolith Sr : Ca, and Ba : Ca were consistently higher within WL habitats, dissolved Sr : Ca and Ba : Ca were more variable among WL and NS sites. Within Saginaw Bay, Sr : Ca was significantly higher than the NS within Pinconning and Fish Point WL (Fig. 6A). Dissolved Sr : Ca within northern Lake Huron WL was not statistically greater than the NS at any site (Fig. 6C). Within Lake Michigan, WL Sr : Ca was higher than the NS within the Grand River only (Fig. 6E). Within Lake Michigan, Kalamazoo River WL Sr : Ca was significantly lower than NS Sr : Ca (Fig. 6E). Within Saginaw Bay, dissolved Ba : Ca was statistically higher than the NS in the Quanicassee River WL only (Fig. 6B). Within northern Lake Huron, dissolved NS Ba : Ca was equal to WL Ba : Ca with the exception of Government Bay WL, where it was statistically lower than the NS (Fig. 6D). In Lake Michigan, dissolved Ba : Ca was significantly greater than the NS in the Kalamazoo River WL and Grand River WL (Fig. 6F).

Discussion

Otolith chemistry is a rapidly evolving tool used to reconstruct environmental histories and fish movements across areas with different chemical signatures. This technology is commonly applied to explore fish movements across coarse spatial boundaries with distinct chemical differences such as freshwater-saltwater movements of pacific salmon (Zimmerman and Reeves 2000). Key advances in the application of otolith microchemistry in freshwater systems have included work by Bronte et al. (1996) and Brazner et al. (2004*a*) which documented site-specific otolith signatures for wetland and nearshore spawning locations utilizing micro-milling or whole-otolith based methods of otolith sampling. In contrast

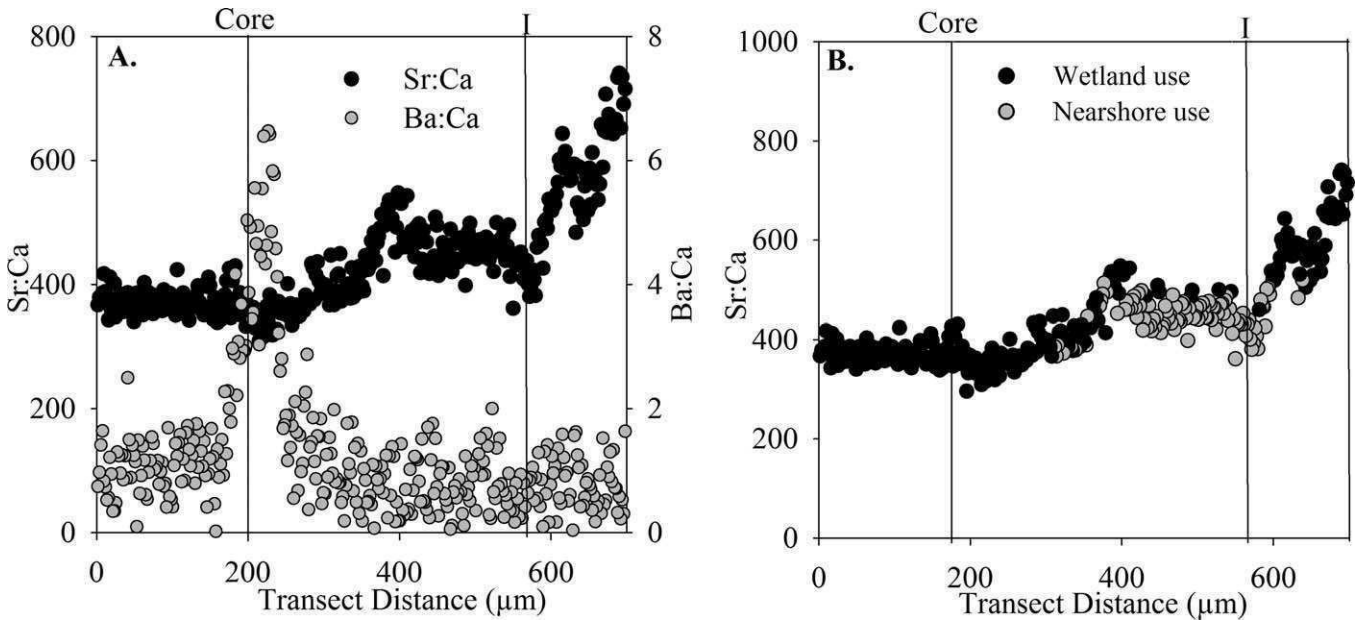

Fig. 4. **(A)** Sr : Ca and Ba : Ca for an age 1+ yellow perch. Raw data plotted, without WL and NS classifications by QDFA. **(B)** Classification of predicted WL and NS habitat use from otolith in Fig. 3A based upon linear discriminant function analysis (QDFA). Data points represent Sr : Ca across otolith transect. WL habitat use is indicated by dark circles, NS habitat use indicated by light circles. Core and annuli indicated by vertical bars.

to these studies, the goal of the current research was to develop "general" wetland and nearshore fingerprints to quantify movements between these habitats. In addition, by using LA-ICM-MS to sample otoliths, the current research was able to analyze material from discrete zones (i.e., across annuli) in order to quantify changes in habitat use over across entire lifecycles. Future studies may be able to build upon our research by identifying the use of specific wetlands as described in (Brazner et al. 2004a; Brazner et al. 2004b); however, this technique remains largely untested within the Great Lakes.

Positive relationships between otolith-edge Sr : Ca and Ba : Ca and water chemistry are consistent with previous Great Lakes research (Zeigler and Whitledge 2010). However, we found no evidence suggesting that water chemistry of Mn : Ca or Mg : Ca influence the levels of Mn : Ca or Mg : Ca in yellow perch otoliths of the Great Lakes and these elements. This may be because Ba : Ca and Sr : Ca are primarily influenced by water chemistry whereas other elements may be influenced by factors such as physiological regulation and/or diet (Dorval et al. 2007; Gibson-Reinemer et al. 2009).

In our analysis of Great Lakes water chemistry, it was apparent that dissolved Sr : Ca and Ba : Ca were not always higher in wetland habitats of Lake Michigan, northern Lake Huron and Saginaw Bay - even at wetland sites where otolith Sr : Ca and/or Ba : Ca was elevated. In addition to influence of water chemistry, previous studies have associated changes in otolith chemistry to changes in temperature, salinity and growth rate and interactions among trace elements (Dorval et al. 2007; Gibson-Reinemer et al. 2009; Collingsworth et al. 2010). Other studies have suggested a link between ontogenetic changes and the inclusion of trace elements in marine otoliths (i.e., Brophy et al. 2004; Walther et al. 2010). Therefore, elevated Sr : Ca and Ba : Ca in otoliths of fish occupying wetland habitats may be driven by the combined effects of local trace element chemistry, interactions with other elements, temperature and individual growth rates. To our knowledge, research on the effects of these conditions on otolith chemistry is extremely limited in freshwater fishes (i.e., Collingsworth et al. 2010); therefore, additional experiments are necessary before we can determine how these conditions influence freshwater otolith chemistry.

The predictive QDFA models of wetland and nearshore otolith chemistry had a high level of accuracy in predicting wetland and nearshore otolith chemistries within each region using Sr : Ca and Ba : Ca. However, based upon the jackknifing results, we found that there may be coastal wetland habitats whose otolith chemistry cannot be reliably distinguished from the nearshore with a high degree of accuracy (i.e., AuGres WL, Wildfowl Bay WL and Government Bay WL). Our results suggest that the dissolved trace element chemistries of these wetlands are characterized by low Sr : Ca and Ba : Ca, similar to that of the nearshore. We speculate that otolith microchemistry may not be able to reliably detect fish movements between Great Lakes nearshore habitats and open embayment wetland habitats, which are known to have high wave exposure and mixing with pelagic water (Albert et al. 2005).

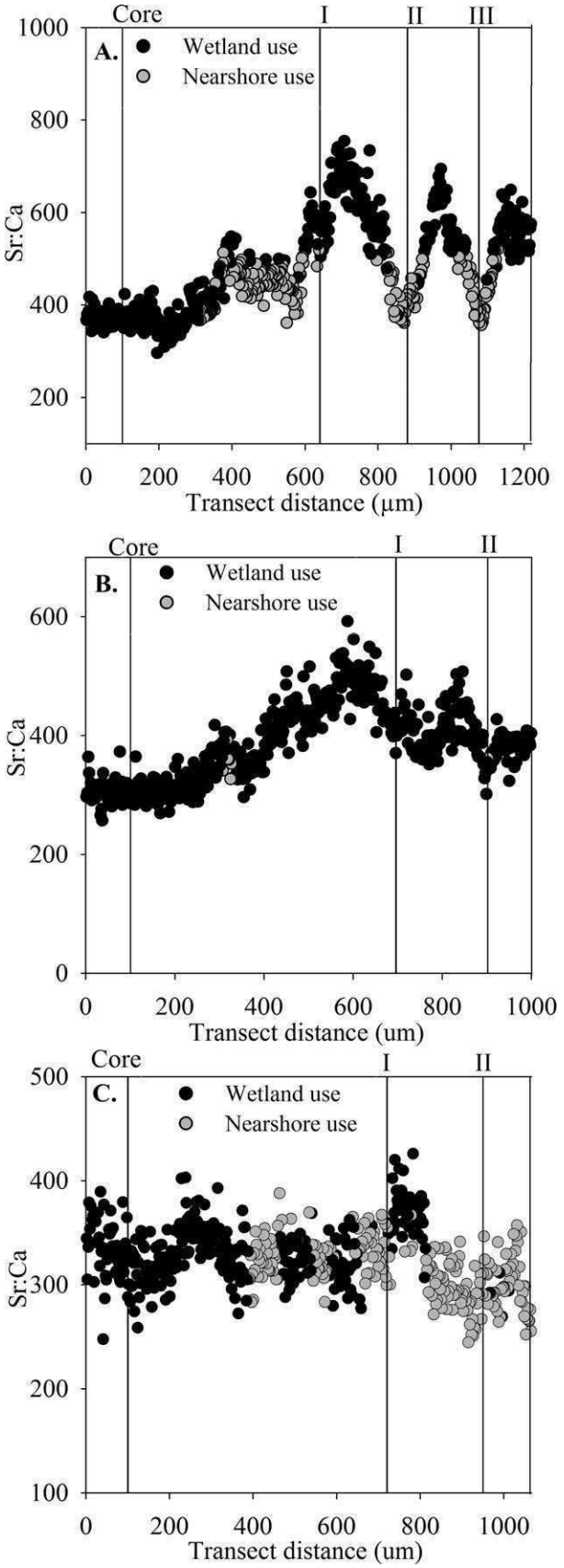

Elevated Ba : Ca in the core region along each transect was classified as wetland use based upon the QDFA models. However, this does not necessarily indicate wetland habitat use in the primordial otolith region. It is possible that elevated barium a relic of initial otolith calcification wherein higher levels of minor trace elements are incorporated for this protein-demanding process (Zhang and Runham 1992). Spikes in Ba, Mn and other elements in this zone may also be a general characteristic of otoliths created by maternal signatures as described in Ruttenberg et al. (2005) and Roy et al. (2013). In addition, we found elevated Sr : Ca and Ba : Ca outside of the core region in the area between the core and annulus one. Great Lakes yellow perch have a pelagic larval stage which may last 80 d, after which larvae return to littoral vegetation (Beletsky et al. 2007). We suspect that this return to wetland habitat is documented in yellow perch otoliths by a spike in Sr : Ca and Ba : Ca between the core the first annulus. This portion of the otolith likely corresponds to the time when fish are moving back offshore during winter, possibly for thermal refugia.

Adult yellow perch subjectively grouped into at least three life histories based upon our analysis. The most common history was single, annual use of wetland habitats, most likely for spawning. The position of wetland signatures along transects often coincided with the annuli, which are typically formed in June or July each year in the northern hemisphere (Blackwell and Kaufman 2012). This is consistent with previous research which suggests that yellow perch spawn among wetland vegetation each spring, before traveling offshore to form schools as adults (Robillard and Marsden 2001; Roberge et al. 2002).

Individuals exhibiting the second life-history of bi-annual or year-round use of wetland habitats may be staying in them, particularly as juveniles, to forage and/or to avoid predators. Many prey of yellow perch use wetlands as a predation refuge because prey species have lower aerobic demands than predators and wetland habitats tend to have lower oxygen (Robb and Abrahams 2002). Although diet analyses were not included in this study, it is also possible that individuals are occupying coastal wetlands to forage on insects, which are highly abundant in structurally complex wetland habitats (Uzarski et al. 2005; Cooper et al. 2014). However, it should be noted that none of the fish classified into this category were greater than 4 yr of age; therefore, it is possible that we are overestimating the abundance of this

Fig. 5. Results of QDFA-estimated WL and NS habitat use in three representative yellow perch based upon concentrations of Sr: Ca and Ba: Ca. Data points represent Sr: Ca across otolith transect; WL habitat use is indicated by dark circles, NS habitat use is indicated by light circles. Core and annuli indicated by vertical bars. Axes within each panel use different scales. **(A)** Fish utilizing WLs once per year; **(B)** WL resident; **(C)** WL use followed by movement nearshore as adult.

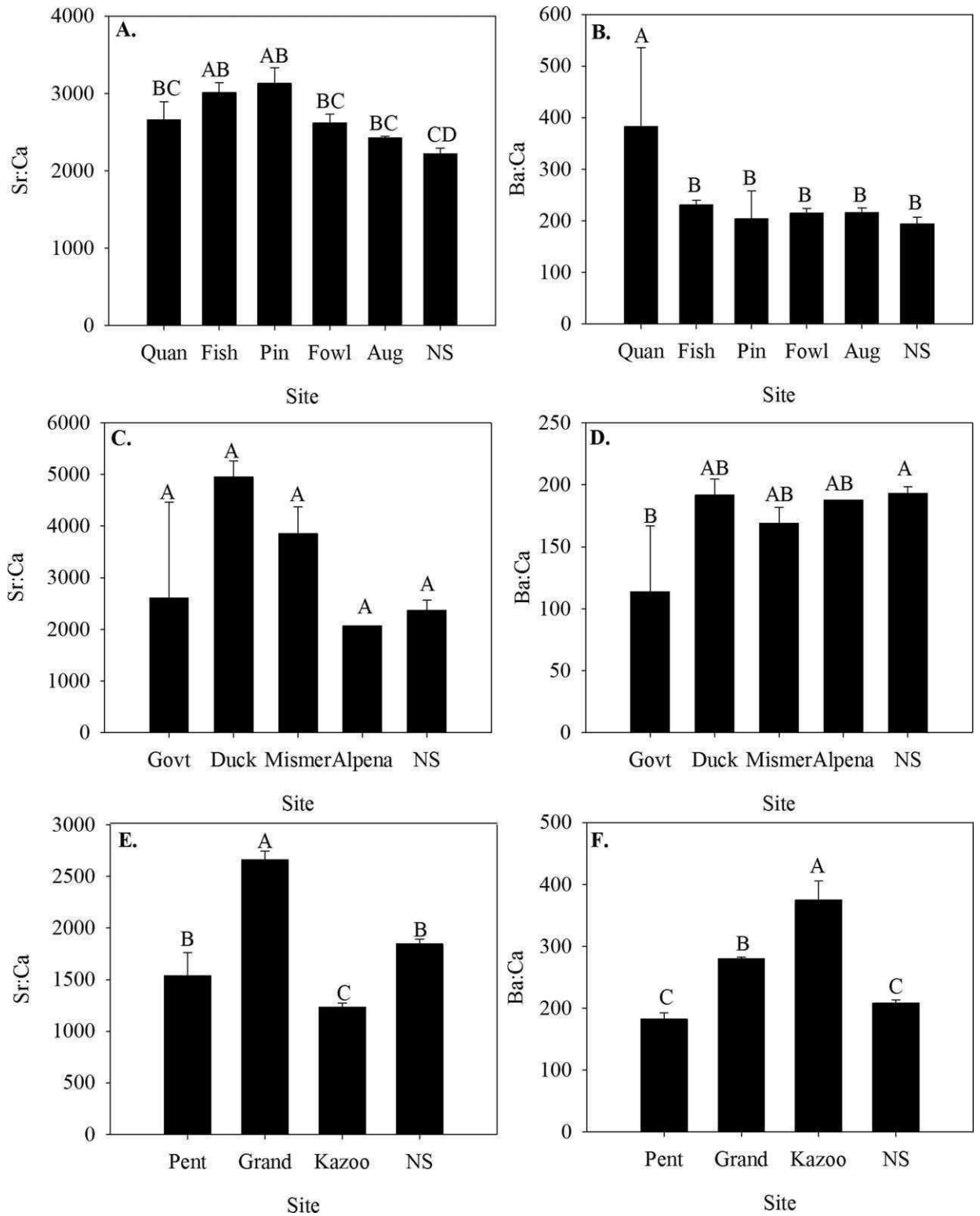

Fig. 6. Mean dissolved Sr : Ca and Ba : Ca values (± 1 S.E.) for habitats in Saginaw Bay (top; **A**, **B**), northern Lake Huron (middle; **C**, **D**) and Lake Michigan (bottom; **E**, **F**) habitats. Means marked with the same letter are not significantly different (ANOVA followed by Tukey's HSD test, $p < 0.05$). From left to right, sites include the Quanicassee River mouth, Fish Point, Wildfowl Bay, AuGres and nearshore (Saginaw Bay), Government Bay, Duck Bay, Mismer Bay, Alpena and nearshore (Northern Lake Huron) and the Pentwater River, Grand River, Kalamazoo River and nearshore (Lake Michigan). Nearshore samples were pooled in the analyses.

life history because some of these fish may have eventually moved to nearshore habitats as adults.

The third life history of nearshore residence was a combination of wetland use as juveniles (age 1–2) and movement to the nearshore as adults. Although yellow perch typically spawn in vegetated wetland habitats, they have been observed to spawn in nearshore waters of Lake Michigan with cobble substrate (Robillard and Marsden 2001). Parker et al. (2009) found genetic, morphological and dietary differences between yellow perch inhabiting deep nearshore habitats and those using shallow wetland areas of the Great Lakes. Similarly, Janetski et al. (2013) found irregular relationships between wetland and nearshore yellow perch recruitment in Lake Michigan, suggesting that connectivity between these habitats may be limited. Our data are consistent with a nearshore contingent of Great Lakes yellow perch, confirming the existence of such as life history. Similarly, this pattern may also suggest that young yellow perch may be moving nearshore later in life as adults when physical conditions in the wetland are no longer favorable for growth, which may be analogous to partial migration in saltwater fishes (Kerr et al. 2009).

We also observed small spikes in Sr : Ca and Ba : Ca within otolith transects, below the wetland- nearshore threshold value established by the QDFA. These peaks may hold information regarding short-term wetland visits (<20 d) that may go unnoticed in our analysis due to spatial resolution limitations related to laser ablation parameters. Higher temporal resolution in LA-SF-ICP-MS transects may be achieved in future studies if higher-concentration elements such as Sr, Ba, and Ca were the only elements of interest, while utilizing smaller laser beam diameters and faster scan rates. Alternatively, these peaks could indicate changes in environmental conditions such as annual Great Lakes temperature fluctuations or changes diet (Elsdon and Gillanders 2004; Collingsworth et al. 2010).

One limitation to the current study is that we did not include additional habitat types in our analysis of wetland and nearshore habitat use. Although it is possible that yellow perch are moving into habitats that were not included in the analysis (i.e., offshore habitats), it has been suggested that yellow perch are an intermediate Great Lakes species, using nearshore areas as adults and wetland habitat for spawning and nursery purposes (Wei et al. 2004). Previous studies of yellow perch have shown that yellow perch typically occupy nearshore, open water habitats (Roberge et al. 2002; Hoffman and Trebitz 2015) and move to shallow water each spring to spawn in cobble reefs or wetland vegetation before moving back to deeper water (Robillard and Marsden 2001; Roberge et al. 2002). Therefore, it is unlikely that the fish in this analysis are frequenting offshore habitats of the Great Lakes.

In addition, our analyses were based upon a limited set of water and fish samples collected during a single summer season. Although Pangle et al. (2010) showed stable interannual trace element signatures within Lake Erie tributaries, previous research has demonstrated seasonal and annual variability in dissolved trace elements based upon factors such as precipitation (Shiller 1997; Negrel and Pauwels 2004). Therefore, we acknowledge that variability in Great Lakes trace element chemistry and otolith microchemistry may warrant further investigation. If water and fish samples were collected over a long enough period of time, site-specific elemental "libraries" could be developed to correct for any interannual and intraannual variability in these signatures as suggested in Pangle et al. (2010).

Conclusions

Coastal fish surveys have suggested that Great Lakes fish communities use coastal wetlands disproportionate to their availability (Jude and Pappas 1992; Wei et al. 2004). However, few studies have attempted to quantify movements of fish between these habitat types (i.e., Brazner et al. 2001). Our methods quantify the frequency and duration of this habitat use across entire life spans and suggest complex life histories for yellow perch including (1) individuals that visit wetlands temporarily each spring (2) prolonged wetland-residence; and (3) individuals that utilize coastal wetlands as juveniles before moving to the nearshore as adults.

The results of this study have important implications for the successful management of the Great Lakes ecosystem, including yellow perch stocks. Application of this technique may be useful for other ecologically important species. With respect to yellow perch, our data suggest a variety of life history strategies within the Great Lakes that may be driven by factors associated with wetland and nearshore habitat use, such as predation risk or food (Robb and Abrahams 2002). The importance of predation, food availability, physiological costs and growth potential have been found to influence salmonid movements (Metcalfe 1998; Mangel and Stamps 2001) although the importance of these factors in driving life histories in Great Lakes fish populations has not been explored.

To our knowledge this is the most comprehensive evaluation of life history strategies in Great Lakes yellow perch. Our results illustrate the importance of coastal wetland and nearshore habitats for larval fish, juveniles and adults. Together, these analyses suggest that wetland and nearshore food webs of the Great Lakes support fish through frequent movements between habitats. These movements may be related to processes such as egg deposition (Stockwell et al. 2014), cross-habitat foraging as adults (McCann et al. 2005) or emigration as larvae or juveniles from wetlands, subsidizing wetland and nearshore food webs with energy from adjacent habitats.

References

Ahrenstorff, T. D., T. R. Hrabik, J. D. Stockwell, D. L. Yule, and G. G. Sass. 2011. Seasonally dynamic diel vertical migrations of Mysis diluviana, coregonine fishes, and siscowet lake trout in the pelagia of western Lake Superior. Trans. Am. Fish. Soc. **140**: 1504–1520. doi:10.1080/00028487.2011.637004

Albert, D. A., D. A. Wilcox, J. Ingram, and T. A. Thompson. 2005. Hydrogeomorphic classification for Great Lakes coastal wetlands. J. Great Lakes Res. **31**: 129–146. doi:10.1016/S0380-1330(05)70294-X

Beletsky, D., D. M. Mason, D. J. Schwab, E. S. Rutherford, J. Janssen, D. F. Clapp, and J. M. Dettmers. Biophysical model of larval yellow perch advection and settlement in Lake Michigan. 2007. J. Great Lakes Res. **33**: 842–866. doi:10.3394/0380-1330(2007)33[842:BMOLYP]2.0.CO;2

Blackwell, B. G., and T. M. Kaufman. 2012. Timing of yellow perch annulus formation and relationship between fish and otolith lengths. N. Am. J. Fish. Manag. **32**: 239–248. doi:10.1080/02755947.2012.672364

Brazner, J. C., D. K. Tanner, and J. A. Morrice. 2001. Fish-mediated nutrient and energy exchange between a Lake Superior coastal wetland and its adjacent bay. J. Great Lakes Res. **27**: 98–111. doi:10.1016/S0380-1330(01)70625-9

Brazner, J. C., S. E. Campana, and D. K. Tanner. 2004a. Habitat fingerprints for Lake Superior coastal wetlands derived from elemental analysis of yellow perch otoliths. Trans. Am. Fish. Soc. **133**: 692–704. doi:10.1577/T03-091.1

Brazner, J. C., S. E. Campana, D. K. Tanner, and S. T. Schram. 2004b. Reconstructing habitat use and wetland nursery origin of yellow perch from Lake Superior using otolith elemental analysis. J. Great Lakes Res. **30**: 492–507. doi:10.1016/S0380-1330(04)70365-2

Bronte, C. R., R. J. Hesselberg, J. A. Showsmith, and M. H. Hoff. 1996. Discrimination among spawning concentrations of Lake Superior lake herring based on trace element profiles in sagittae. Trans. Am. Fish. Soc. **125**: 852–859. doi:10.1577/1548-8659(1996)125<0852:DASCOL>2.3.CO;2

Brophy, D., T. E. Jeffries, and B. S. Danilowicz. 2004. Elevated manganese concentrations at the cores of the clupeid otoliths : Possible environmental, physiological, or structural origins. Mar. Biol. **144**: 779–786. doi:10.1007/s00227-003-1240-3

Campana, S. E., and S. R. Thorrold. 2001. Otoliths, increments and elements : Keys to a comprehensive understanding of fish populations. Can. J. Fish. Aquat. Sci. **58**: 30–38. doi:10.1139/f00-177

Collingsworth, P. D., J. J. Van Tassell, J. W. Olesk, and E. A. Marschall. 2010. Effects of temperature and elemental concentration on the chemical composition of juvenile yellow perch (Perca flavescens) otoliths. Can. J. Fish. Aquat. Sci. **67**: 1187–1196. doi:10.1139/F10-050

Cooper, M. J., G. A. Lamberti, and D. G. Uzarski. 2014. Spatial and temporal trends in invertebrate communities of Great Lakes coastal wetlands, with emphasis on Saginaw Bay of Lake Huron. J. Great Lakes Res. **40**: 168–182. doi:10.1016/j.jglr.2013.12.003

Dorval, E., C. M. Jones, R. Hannigan, and J. van Monfrans. 2007. Relating otolith chemistry to surface water chemistry in a coastal plain estuary. Can. J. Fish. Aquat. Sci. **64**: 411–424. doi:10.1139/F07-015

Elsdon, T. S., and B. M. Gillanders. 2004. Fish otolith chemistry influenced by exposure to multiple environmental variables. J. Exp. Mar. Biol. Ecol. **313**: 269–284. doi:10.1016/j.jembe.2004.08.010

Friedrich, L. A., and N. M. Halden. 2010. Determining exposure history of northern pike and walleye to tailings effluence using trace metal uptake in otoliths. Environ. Sci. Technol. **44**: 1551–1558. doi:10.1021/es903261q

Gibson-Reinemer, D. K., B. M. Johnson, P. J. Martinez, D. L. Winkelman, A. E. Koenig, and J. D. Woodhead. 2009. Elemental signatures in otoliths of hatchery Rainbow Trout (Oncorhynchus mykiss) : Distinctiveness and utility for detecting origins and movement. Can. J. Fish. Aquat. Sci. **66**: 513–524. doi:10.1139/F09-015

Hellstrom, J., C. Paton, J. D. Woodhead, and J. M. Hergt. 2008. Iolite : Software for spatially resolved LA-(quad and MC) ICPMS analysis. Short Course Ser. - Mineral. Assoc. Can. **40**: 343–348.

Hoffman, J. C., and A. S. Trebitz. 2015. Coastal wetland support of great lakes fisheries : Progress from concept to quantification. Trans. Am. Fish. Soc. **144**: 352–372. doi:10.1080/00028487.2014.982257

Janetski, D. J., C. R. Ruetz, and Y. Bhagat. 2013. Recruitment dynamics of age-0 yellow perch in a drowned River Mouth Lake : Assessing synchrony with nearshore Lake Michigan. Trans. Am. Fish. Soc. **142**: 505–515. doi:10.1080/00028487.2012.756432

Jude, D. J., and J. Pappas. 1992. Fish utilization of Great Lakes coastal wetlands. J. Great Lakes Res. **18**: 651–672. doi:10.1016/S0380-1330(92)71328-8

Kerr, L. A, H. S. David, and M. P. Philip. 2009. Partial Migration of Fishes as Exemplified by the Estuarine-Dependent White Perch. Fisheries **34**: 114–123. doi:10.1577/1548-8446-34.3.114

Lindeman, R.L. 1942. The trophic dynamic aspect of ecology. Ecology **23**: 399–418. doi:10.1007/BF02464428

Mangel, M., and J. Stamps. 2001. Tradeoffs between growth and mortality and the maintenance of individual variation in growth. Evol. Ecol. Res. **3**: 583–593.

McCann, K. S., J. B. Rasmussen, and J. Umbanhowar. 2005. The dynamics of spatially coupled food webs. Ecol. Lett. **8**: 513–523. doi:10.1111/j.1461-0248.2005.00742.x

Metcalfe, N. B. 1998. The interaction between behavior and physiology in determining life history patterns in Atlantic salmon (Salmo salar). Can. J. Fish. Aquat. Sci. **55**: 93–103. doi:10.1139/d98-005

Negrel, P., and H. Pauwels. 2004. Interactions between different groundwaters in Brittany catchments (France): Characterizing multiple sources through strontium and sulphur isotope tracing. Water Air Soil Pollut. **151**: 261–285. doi:10.1023/B:WATE.0000009912.04798.b7

Odum, E. P. 1968. A research challenge : Evaluating the productivity of coastal and estuarine water. Proceedings of the Second Sea Grant Conference. Univ. of Rhode Island, pp. 63–64.

Pangle, K. L, S. A. Ludsin, and B. J. Fryer. 2010. Otolith microchemistry as a stock identification tool for freshwater fishes : Testing its limits in Lake Erie. Can. J. Fish. Aquat. Sci. **67**: 1475–1489. doi:10.1139/F10-076

Parker, A. D., C. A. Stepian, O. J. Sepulveda-Villet, C. B. Ruehl, and D. G. Uzarski. 2009. The interplay of morphology, habitat, resource use, and genetic relationships in young yellow perch. Trans. Am. Fish. Soc. **138**: 899–914. doi:10.1577/T08-093.1

Pearce, N. J. G., W. T. Perkins, J. A. Westgate, M. P. Gorton, and S. E. Jackson. 1997. A compilation of new and published major and trace element data for NIST SRM 610 and NIST SRM 612 glass reference materials. Geostand. Newsl. **21**: 115–144. doi:10.1111/j.1751-908X.1997.tb00538.x

Robb, T., and M. V. Abrahams. 2002. The influence of hypoxia on risk of predation and habitat choice by the fathead minnow, *Pimephales promelas*. Behav. Ecol. Sociobiol. **52**: 25–30. doi:10.1126/science.288.5467.854

Roberge, M., T. Slaney, and C. K. Minns. 2002. Life history characteristics of freshwater fishes occurring in British Columbia, with major emphasis on lake habitat characteristics. Can. Man. Rep. Fish. Aquat. Sci. **2611**: 107–108f.

Robillard, S. R., and E. Marsden. 2001. Spawning substrate preferences of yellow perch along a sand–cobble shoreline in southwestern Lake Michigan. N. Am. J. Fish. Manag. **21**: 208–215. doi:10.1577/1548 8675(2001)021<0208:SSPOYP>2.0.CO;2

Roy, A., A. J. Frisch, C. Syms, S. R. Thorrold, and G. P. Jones. 2013. Retention of a transgenerational marker (137Barium) in tissues of adult female anemonefish and assessment of physiological stress. Environ. Biol. Fish. **94**: 459–466. doi:10.1007/s10641-012-0029-y

Ruttenberg, B. I., and others. 2005. Elevated levels of trace elements in cores of otoliths and their potential for use as natural tags. Mar. Ecol. Prog. Ser. **297**: 273–281. doi:10.3354/meps297273

Schindler, D. E., and M. D. Scheuerell. 2002. Habitat coupling in lake ecosystems. Oikos **98**: 177–189. doi:10.1034/j.1600-0706.2002.980201.x

Shiller, A. M. 1997. Dissolved trace elements in the Mississippi River : Seasonal, interannual, and decadal variability. Geochim. Cosmochim. Acta. **61**: 4321–4330. doi:10.1016/S0016-7037(97)00245-7

Shiller, A. M. 2003. Syringe filtration methods for examining dissolved and colloidal trace elemental distributions in remote field locations. Environ. Sci. Technol. **37**: 3953–3957. doi:10.1021/es0341182

Sierszen, M. E., J. C. Brazner, A. M. Cotter, J. A. Morrice, G. S. Peterson, and A. S. Trebitz. 2012. Watershed and lake influences on the energetic base of coastal wetland food webs across the Great Lakes Basin. J. Great Lakes Res. **38**: 418–428. doi:10.1016/j.jglr.2012.04.005

Sierszen, M. E., T. R. Hrabik, J. D. Stockwell, A. M. Cotter, J. C. Hoffman, and D. L. Yule. 2014. Depth gradients in food-web processes linking habitats in large lakes : Lake Superior as an exemplar ecosystem. Freshwat. Biol. **59**: 2122–2136. doi:10.1111/fwb.12415

Stockwell, J. D., D. L. Yule, T. R. Hrabik, M. E. Sierszen, and E. J. Isaac. 2014. Habitat coupling in a large lake system : Delivery of an energy subsidy by an offshore planktivore to the nearshore zone of Lake Superior. Freshw. Biol. **59**: 1197–1212. doi:10.1111/fwb.12340

Uzarski, D. G., T. M. Burton, M. J. Cooper, J. W. Ingram, and S. T. A. Timmermans. 2005. Fish habitat use within and across wetland classes in coastal wetlands of the five Great Lakes : Development of a fish-based index of biotic integrity. J. Great Lakes Res. **31**: 171–187. doi:10.1016/S0380-1330(05)70297-5

Vander Zanden, M. J., and Y. Vadeboncoeur. 2002. Fishes as integrators of benthic and pelagic food webs in lakes. Ecology **83**: 2152–2161. doi:10.1890/0012-9658(2002)083[2152:FAIOBA]2.0.CO;2

Walther, B. D., M. J. Kingsford, M. D. O'Callaghan, and M. T. McCulloch. 2010. Interactive effects of ontogeny, food ration and temperature on elemental incorporation in otoliths of a coral reef fish. Environ. Biol. Fish. **89**: 441–451. doi:10.1007/s10641-010-9661-6

Wei, A., P. Chow-Fraser, and D. Albert. 2004. Influence of shoreline features on fish distribution in the Laurentian Great Lakes. Can J. Fish. Aquat. Sci. **61**: 1113–1123. doi:10.1139/f04-061

Zeigler, J. M., and G. W. Whitledge. 2010. Assessment of otoliths chemistry for identifying source environment of fishes in the lower Illinois River, Illinois. Hyrobiologia **638**: 109–119. doi:10.1080/19425120.2012.675967

Zhang, Z., and N. W. Runham. 1992. Initial development of Oregochromis niloticus (Teleostei, Cichlidae) otoliths. J. Zool. (London) **227**: 465–478. doi:10.1111/j.1469-7998.1992.tb04407.x

Zimmerman, C. E., and G. H. Reeves. 2000. Population structure of sympatric anadromous and nonanadromous Oncorhynchus mykiss : Evidence from spawning surveys and

otoliths microchemistry. Can. J. Fish. Aquat. Sci. **57**: 2152–2162. doi:10.1139/f00-192

Acknowledgments

We thank David Clapp, Dave Fielder, Bill Wellenkamp and the Michigan Department of Natural Resources Fisheries Division for assisting in fish collections as well as Ryan Wheeler, Tom Langer, Bridget Ziola, Lindsey Adams and Kaley Genther for assisting in the collection and preparation of samples for analysis. We also thank Jonathon Launspach for his help creating maps. The research described in this article has been funded in part by the U.S. Environmental Protection Agency as part of the Great Lakes Restoration Initiative under proposal EPA GLNPO-2010-H-3-984-758 titled GLIC : Implementing Great Lakes Coastal Wetland Monitoring. The research was also supported by the Garden Club of America Coastal Wetlands Award Selection Committee, Center for Coastal Resources Management at the Virginia Institute of Marine Science, College of William and Mary. The views expressed in this article are those of the authors and do not necessarily reflect the views or policies of the Michigan DNR, DEQ or the U.S. EPA. This paper is Contribution Number 73 of the Central Michigan University Institute for Great Lakes Research.

Submitted 29 June 2015
Revised 8 February 2016
Accepted 20 April 2016

Associate editor : Stephanie Hampton

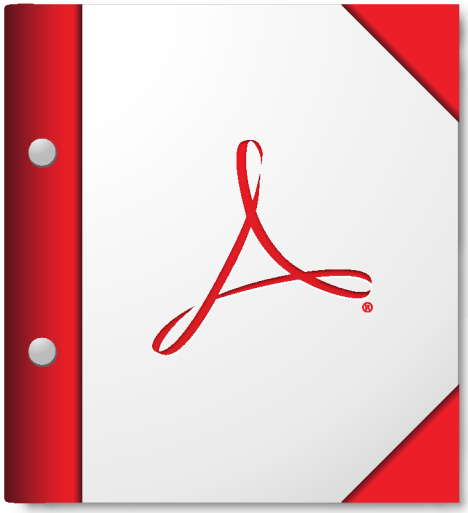

For the best experience, open this PDF portfolio in Acrobat X or Adobe Reader X, or later.

Get Adobe Reader Now!

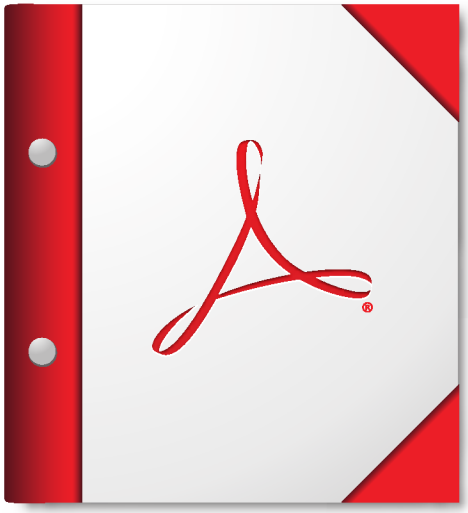

For the best experience, open this PDF portfolio in Acrobat X or Adobe Reader X, or later.

Get Adobe Reader Now!

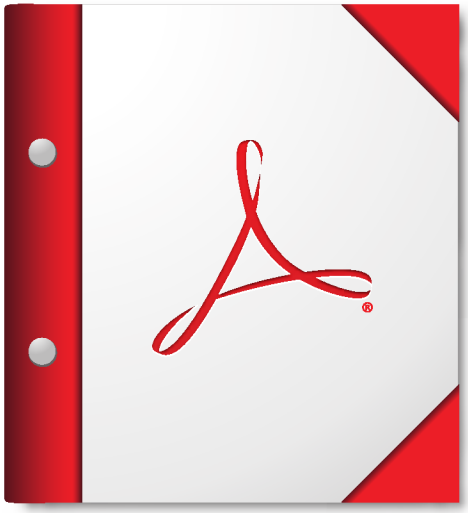

For the best experience, open this PDF portfolio in Acrobat X or Adobe Reader X, or later.

Get Adobe Reader Now!

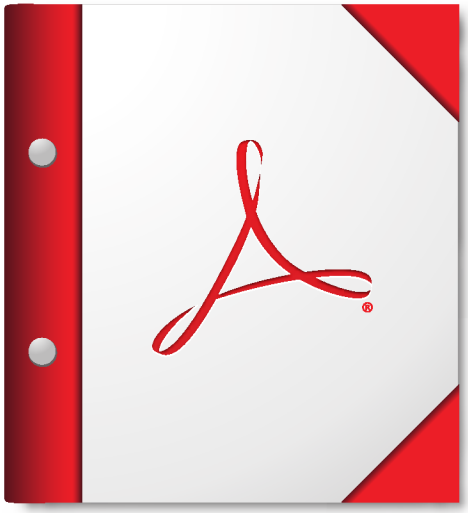

For the best experience, open this PDF portfolio in Acrobat X or Adobe Reader X, or later.

Get Adobe Reader Now!

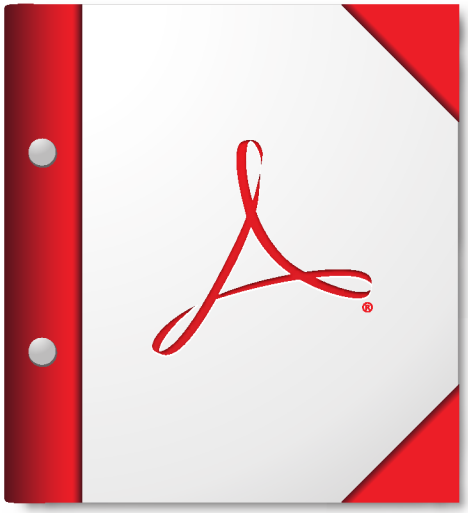

For the best experience, open this PDF portfolio in Acrobat X or Adobe Reader X, or later.

Get Adobe Reader Now!

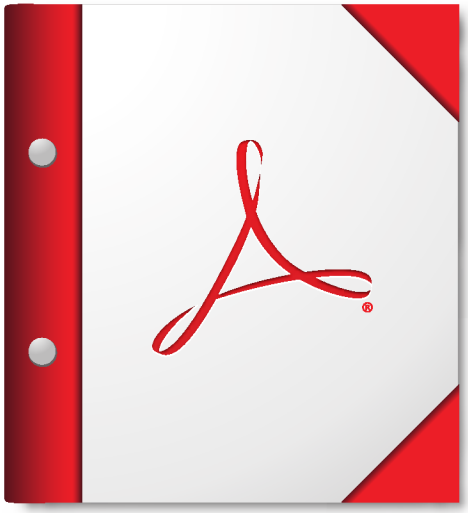

For the best experience, open this PDF portfolio in Acrobat X or Adobe Reader X, or later.

Get Adobe Reader Now!

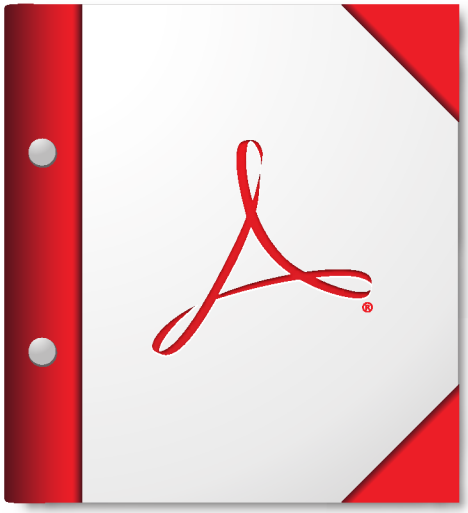

For the best experience, open this PDF portfolio in Acrobat X or Adobe Reader X, or later.

Get Adobe Reader Now!